Polyhedron Vol. 9, No. 1, pp. 1–9, 1990
Printed in Great Britain

0277–5387/90 $3.00+.00
© 1989 Pergamon Press plc

THE USE OF FLUORINE-19 NMR DATA IN THE DETERMINATION OF THE ELECTRON DENSITY ON THE BENZENE RING IN ARENE METAL COMPLEXES

NATALIYA A. OGORODNIKOVA* and DMITRII N. KRAVTSOV

A. N. Nesmeyanov Institute of Organoelement Compounds, The U.S.S.R. Academy of Sciences, Vavilov Street 28, Moscow, U.S.S.R.

(*Received* 16 *January* 1989; *accepted* 4 *May* 1989)

Abstract—Linear relationships between the ^{19}F NMR chemical shifts of *p*-substituted *p'*-fluorobiphenyls and the theoretically calculated net charges, Δq_t, Δq_π and Δq_σ, on the *p*-carbon atoms of the substituted benzenes were established. A method for evaluating the net charge on the benzene ring in non-paramagnetic η^6-arene metal complexes, based on the ^{19}F NMR data for respective *p*-fluorophenyl derivatives, is presented. For arene metal complexes, the benzene net charges are: +0.26e for $[Cr(CO)_3(\eta\text{-}C_6H_6)]$, +0.11e for $[Cr(CO)_2(PPh_3)(\eta\text{-}C_6H_6)]$, +0.12e for $[Cr(CO)_2(AsPh_3)(\eta\text{-}C_6H_6)]$ (benzene) and +0.42e for $[Fe(\eta\text{-}C_5H_5)(\eta\text{-}C_6H_6)]PF_6$ (CH_3NO_2, acetone). For these complexes, the data obtained give evidence for the total charge shift in the arene → ML_n direction. This method has the advantage of producing reasonable results without using complicated calculations. The validity of the method is confirmed by comparison of the data obtained with the results of physical investigations and the relative reactivity of the free and coordinated arenes.

We have previously proposed[1–3] an approach for examining the η^5-cyclopentadienyl metal compounds which enables one to characterize the metal–ring bond with respect to its polarity and stability.

An analogous strategy may be developed for η^6-arene metal complexes. The present work focusses on the first stage of the problem, namely, on the evaluation of the polarity of the metal–ring bond in arene metal complexes in terms of the net charges.

As in the case of cyclopentadienyl compounds,[1] the present method for estimating the net charge on the benzene ring in arene metal complexes on the basis of fluorine shielding in respective *p*-fluorobenzene derivatives stems from the known linear relationships between theoretically calculated net charges and ^{19}F NMR chemical shifts in the substituted benzenes.[4,5] The above linear dependences for a benzene system have suggested that a linear correlation should also exist in a biphenyl system. Indeed, we have shown that good linear relationships are observed between ^{19}F chemical shifts in *p*-substituted *p'*-fluorobiphenyls and the net charges on the *p*-carbon atom in the substituted benzenes.

* Author to whom correspondence should be addressed.

EXPERIMENTAL

Data on the fluorine chemical shift in *p*-fluorobiphenyl are available in the literature.[6–9] With a view to obtaining the mean value of the fluorine chemical shift for *p*-fluorobiphenyl in a larger set of solvents normally used for organometallic compounds, than that in ref. 6 (Table 1, column 3), we recorded the ^{19}F chemical shift of 4-$FC_6H_4C_6H_4F$-4′ in different solvents relative to fluorobenzene (Table 1, column 4) and, making use of the data[7] on the chemical shift induced by a fluorine substituent (Table 1, column 5), we have calculated the ^{19}F chemical shift of *p*-fluorobiphenyl for nine different solvents relative to fluorobenzene (Table 1, column 6). The mean value of the fluorine chemical shift for *p*-$FC_6H_4C_6H_5$ in 11 widely varying solvents is calculated to be 2.79 ± 0.17 ppm (here and below a positive sign corresponds to the upfield shift); this value slightly differs from that obtained by Taft *et al.*[6] (2.75 ± 0.22 ppm).

We have borrowed the data for dioxane and methanol solutions of *p*-$FC_6H_4C_6H_5$ from ref. 6 owing to the close agreement between our values (Table 1, column 6) and those reported by Taft *et al.*[6] for cyclohexane, CCl_4 and acetone solutions

Table 1. ^{19}F NMR chemical shifts[a] in 4-$RC_6H_4C_6H_4F$-4′

N	Solvent	R = H[6b]	R = F	SCS for R = F[7c]	R = H
1	Cyclohexane	3.00	2.75	0.27	3.02
2	CCl_4	2.90	2.69	0.28	2.97
3	Benzene		2.82	0.12	2.94
4	THF		2.76	0.08	2.84
5	Acetone	2.70	2.63	0.08	2.71[d]
6	CH_3CN		2.53	0.06	2.59
7	DMF		2.64	0.03	2.67
8	DMSO		2.48	0.00	2.48
9	CH_2Cl_2		2.68	0.10	2.78
10	Dioxane	2.90			2.90[6]
11	Nitrobenzene	2.10			
12	CH_3OH	2.80			2.80[6]
	The mean value	2.75			2.79
	Standard error	±0.22			±0.17

[a] Recorded in ppm relative to C_6H_5F, the positive sign indicates the upfield shift.

[b] For ~ 5% solutions relative to C_6H_5F as an internal standard, experimental error ±0.08 ppm.[6]

[c] For solutions of concentration ⩽ 0.03 M.[7]

[d] In ref. 9, the value of the fluorine chemical shift of *p*-$FC_6H_4C_6H_5$ relative to C_6H_5F is equal to 2.72 ppm (deuteroacetone).

(see Table 1, column 3). The data[6] for the $C_6H_5NO_2$ solution were not included due to the possible ability of nitrobenzene, as an electron acceptor, to specifically interact with the solute to form charge-transfer complexes.

A Bruker WP-200 spectrometer was used for 188.31 ^{19}F NMR spectra. Locking was accomplished on the deuterium signal of D_2O, introduced into a 5 mm NMR tube. The sample solution was inserted into a 4 mm sealed ampoule in the tube, and ^{19}F shifts for ~ 0.2 M solutions were referenced to C_6H_5F at the same concentration and in the same solvent, and presented without correction for volume diamagnetic susceptibility. The accuracies of the ^{19}F chemical shifts are ±0.01 ppm or better.

RESULTS

The relationship between the ^{19}F shifts in p-fluorobiphenyls and the change in electron density on the benzene ring

Comparison of the data on the fluorine chemical shifts for 4-$RC_6H_4C_6H_4F$-4′ (R = NO_2, CN, F, H, CH_3, OH, NH_2; see Table 2) with the calculated[4] net charges on the *p*-carbon atoms in RC_6H_5 (Δq_π, Δq_σ, Δq_t; Table 3) has shown that there are linear relationships between the ^{19}F chemical shifts of *p*-substituted *p*′-fluorobiphenyls and the net charges, Δq_π, Δq_σ, Δq_t, on the *p*-carbon atom in the substituted benzenes (*r* is 0.966, 0.960 and 0.974, respectively; Table 4).

The relationship between the ^{19}F shifts in p-fluorophenyl-substituted arene metal complexes and the change in electron density on the benzene ring in non-substituted arene metal complexes

The above linear correlations led us to conclude that the fluorophenyl fragment can serve as a reference for determining the electron density on the carbon atom carrying this fragment. In turn, this allows a linear relationship between the ^{19}F chemical shift in *p*-fluorophenyl-substituted arene metal complexes and the net charge on the benzene ring in the above complexes to be postulated.

Indeed, by taking into consideration the symmetry of a benzene ligand in arene metal complexes, one may obtain the net charge on the ring by mere multiplication of the CH-fragment charge, f_{CH}, by six. As far as the charge distribution in the CH-fragment itself is concerned, different possibilities are conceivable. One may neglect the changes in charge-transfer along the C—H σ-bond and consider that the charge on the hydrogen atom remains

Table 2. Fluorine chemical shifts (ppm) in 4-$RC_6H_4C_6H_4F$-4′

N	R	Solvent	Relative to p-$FC_6H_4C_6H_5$[7]	Relative to C_6H_5F
1	NO_2	Cyclohexane	−3.11	−0.09[a]
2	CN	Cyclohexane	−2.71	0.31[a]
3	F	Cyclohexane	−0.27	2.75[a]
4	H	Cyclohexane		3.02
5	CH_3	$(CD_3)_2CO$		3.21[b]
6	OH	$(CD_3)_2CO$		4.12[b]
7	NH_2	Cyclohexane	1.99	5.01[a]

[a] Estimated by using the fluorine chemical shift of p-$FC_6H_4C_6H_5$ (3.02 ppm) relative to fluorobenzene (cyclohexane) (Table 1, column 6).

[b] 4-Substituted 4′-fluorobiphenyls were obtained by UV irradiation of RC_6H_4I in C_6H_5F or FC_6H_4I in C_6H_5R; the reaction mixture was evaporated, the residue was dissolved in deuteroacetone and inserted into an NMR tube. Measurements on solutions of individual compounds were not carried out.[9,10]

Table 3. The net charges on the p-carbon atom in RC_6H_4[4]

N	R		Δq_π[a]	Δq_σ[a]	Δq_t[a]
1	NO_2		0.043	−0.087	−0.044
2	CN		0.028	−0.078	−0.050
3	F		−0.021	−0.050	−0.071
4	H		0	−0.063	−0.063
5	CH_3		−0.012	−0.056	−0.068
6	OH		−0.039	−0.039	−0.078
		sq[b]	−0.057[d]	−0.029[d]	−0.086[d]
7	NH_2	pyr[c]	−0.035[d]	−0.042[d]	−0.077[d]

[a] The values of Δq are given relative to 1 for q_π, relative to 5 for q_σ and relative to 6 for q_t; the negative sign points to an increase in electron density.

[b] For a planar configuration of $H_2NC_6H_5$.

[c] For a pyramidal configuration of the nitrogen atom in $H_2NC_6H_5$.

[d] Following the authors of ref. 4, who used the mean value of the calculated charges for a planar and non-planar configuration of the nitrogen atom to plot correlations with ^1H, ^{13}C and ^{19}F NMR shifts, in calculations we have also used the mean value.

Table 4. Parameters of correlation equations $\Delta q = b(\delta\ ^{19}F)+a$

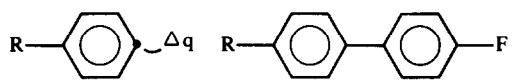

R = NO_2, CN, F, H, CH_3, OH, NH_2

$\Delta q = b(\delta\ ^{19}F)+a$	r	S
$\Delta q_\pi = -0.0170(\delta\ ^{19}F)+0.0378$	0.966	0.010
$\Delta q_\sigma = 0.0097(\delta\ ^{19}F)-0.0839$	0.960	0.006
$\Delta q_t = -0.0073(\delta\ ^{19}F)-0.0462$	0.974	0.004

unchanged (f_H = constant). On the contrary, it is possible to consider the charge distribution on the CH-fragment to be invariable (f_H/f_C = constant). Finally, one may consider an intermediate assumption to be the most plausible [$f_H = f_H^0 + k(f_C - f_C^0)$].

Either of these viewpoints suggests that the existence of a linear relationship between the fluorine chemical shift of the corresponding fluorophenyl-substituted compounds and the electron density on the carbon atom bound to the fluorophenyl fragment should result in a linear dependence between the fluorine shift and the net charge on the CH-fragment, f_{CH}.

To plot the linear dependence of the benzene net charges in arene metal complexes on fluorine screening in respective p-fluorophenyl derivatives, at least two reference points with known charge values must be available. For such points, we have chosen benzene and the cyclopentadienyl anion against the ^{19}F chemical shifts of p-fluorobiphenyl and a free p-fluorophenylcyclopentadienyl anion.[11] It is not possible unfortunately to compare ^{19}F chemical shifts for cation and anion radicals of p-fluorobiphenyl with fluorine screening in non-paramagnetic fluorophenyl-substituted arene metal complexes.* The net charge on the CH-fragment

* For the same reason, to establish any relationships between chemical shift and charge density in the frame of the NMR method, a number of monocyclic aromatic 6π-electron systems, $C_5H_5^-$, C_6H_6 and $C_7H_7^+$, are under comparison (see, for example refs 12–14 and references therein).

in a free cyclopentadienyl anion is equal to −0.2 (corresponds to the fluorine shift value, 17.9 ppm, for *p*-fluorophenylcyclopentadienyllithium and sodium in hexamethylphosphoramide[11]), and the net charge on the benzene CH-fragment is equal to zero (δ ^{19}F for *p*-$FC_6H_4C_6H_5$ is 2.79 ppm; Table 1), giving rise to eq. (1) and the equivalent eq. (2). The latter represents our definition of the net charge on the benzene ring in arene metal complexes which fixes this charge via the ^{19}F chemical shift of their *p*-fluorophenyl-substituted derivatives:

$$f_{CH} = -0.0132(\delta\ ^{19}F)+0.0369 \qquad (1)$$

$$f_{C_6H_6} = -0.0792(\delta\ ^{19}F)+0.2214, \qquad (2)$$

where f_{CH} is the net charge on the CH-fragment and $f_{C_6H_6}$ refers to the benzene net charge in arene metal complexes (in a.u.); δ ^{19}F denotes the fluorine chemical shift of the respective *p*-fluorophenyl derivatives (in ppm relative to fluorobenzene).

Data on ^{19}F chemical shifts for some *p*-fluorobiphenyl metal complexes are available in the literature[15–17] (Table 5). In accordance with eq. (2), the net charge on the benzene ligand in benzene tricarbonyl chromium is equal to +0.26e (in benzene), and substitution of the *n*-donor triphenylphosphine or -arsine group for a CO ligand leads to a positive charge decrease (i.e. an increase in electron density) on the ring to +0.11 and +0.12, respectively (in benzene). The electron-withdrawing action of $CpFe^+$ on the benzene ring is much stronger than that of a $Cr(CO)_3$ group, hence, the net charge on the benzene ligand in the benzene-(cyclopentadienyl)iron cation is equal to +0.42e (CH_3NO_2, acetone; Table 5). The data obtained give evidence on the total charge displacement in the arene → ML_n direction in arene metal complexes, and are in a good agreement with results of physical investigations and the relative reactivity of the free and coordinated arenes.

DISCUSSION

Comparison of the net charges obtained on the benzene ring in arene metal complexes with those given by quantum-chemical calculations is difficult due to discord in the latter results; on the benzene ring in benzene tricarbonyl chromium: +0.572[18] (SCCC MO); +0.261[19] (SCCC MO); +0.102[20] (INDO); +0.06[21] (CNDO/2); −0.078[22] (CNDO/2); −0.133[23] (SCCC MO); −0.84[24] (*ab initio*); for the benzene(cyclopentadienyl)iron cation: +0.654[25] (INDO); +0.888[26] (INDO). The ESCA data are consistent with the positive charges being based on the arene carbon atoms in benzene

Table 5. The net charges on the benzene ring (a.u.) in arene metal complexes

Compound	Solvent	δ ^{19}F[a]	References	$f_{C_6H_6}$[b]
$[Cr(CO)_3(\eta\text{-}C_6H_6)]$	Benzene	−0.50	15[c]	+0.261
	Benzene	−0.55	16[d]	+0.265
	$CDCl_3$	−1.19	15[c]	+0.316
	DMSO	−0.44	16[d]	+0.256
	Benzene–$HClO_4$ (0.3N)–CH_3COOH (98%) (1:1:4)	−0.55	16[d]	+0.265
$[Cr(CO)_2(PPh_3)(\eta\text{-}C_6H_6)]$	Benzene	+1.41	15[c]	+0.110
	$CDCl_3$	+1.08	15[c]	+0.136
$[Cr(CO)_2(AsPh_3)(\eta\text{-}C_6H_6)]$	Benzene	+1.35	15[c]	+0.115
	$CDCl_3$	+0.95	15[c]	+0.146
$[Fe(\eta\text{-}C_5H_5)(\eta\text{-}C_6H_6)]PF_6$	CH_3NO_2	−2.53	17[e]	+0.422
	Acetone	−2.45	17[e]	+0.415

[a] For corresponding $[ML_n(\eta^6\text{-}C_6H_5C_6H_4F\text{-}p)]$ in ppm relative to C_6H_5F; the positive sign indicates the upfield shift.

[b] For the linear relation $f_{C_6H_6} = -0.0792\ (\delta\ ^{19}F)+0.2214$, the net charges in terms of our definition are accurate to ±0.0792 ($\Delta\delta$ ^{19}F) (for $\Delta\delta$ ^{19}F see footnotes *c*, *d* and *e*) and, hence, the accuracy of all the given values is not less than ±0.008e.

[c] Relative to the external standard of C_6H_5F;[15] the measurements are accurate to ±0.1 ppm.

[d] The accuracy of the measurement cited in ref. 16 is ±0.05 ppm.

[e] The accuracy of the measurements cited in ref. 17 is ±0.08 ppm.

tricarbonyl chromium and substituted arene complexes.[27-30]

Relevance of X-ray crystallographic and dipole measurements

A remarkably large value of the dipole moment in benzene tricarbonyl chromium (4.31 D, cyclohexane;[31] 4.38 D, heptane;[32] 4.56 D, cyclohexane[33]) and the substituent effects on dipole moments in the substituted analogues (for these, the values range from 3.5 to 6.3 D, benzene) are attributed to electron charge drift from the arene ligand to the carbonyl groups via the metal atom.[31-39] The dipole moment of monosubstituted benzene complexes differs from the vectorial sum $\mu[Cr(CO)_3(C_6H_6)]+\mu(C_6H_5X) = \mu_O+\mu_X$; in the complexes, both the components, μ_O and μ_X, adopt modified values.[34,38] According to the values of dipole moments in symmetrical *p*-disubstituted complexes[31-34,36,38] (with the μ_X component equal to zero), electron-releasing substituents cause an increase in the μ_O component, whereas electron-withdrawing substituents exert an opposite effect; hence, μ_O can reflect a degree of electron displacement from the arene ligand to the carbonyl groups.[38]

Unfortunately, the value of these quantitative measurements is, as yet, unclear. The method used for determining dipole moments suffers from inherent complications (see, for instance refs 33–38). In addition, the dipole moments of arene tricarbonyl chromium complexes, to a great extent, are solvent-dependent; the maximum values are observed in solvents such as dioxane and the minimum—in heptane; benzene gives intermediate values.[32,35]

This peculiarity in behaviour of arene tricarbonyl chromium complexes has been explained by Strohmeier in the early 1960s as being due to the formation of donor–acceptor compounds between a solvent and the π-complex whose aromatic ring can act a potential electron acceptor.[32,35] On the other hand, benzene tricarbonyl chromium compounds were shown to form charge-transfer complexes with electron acceptors rather than with electron donors.[40-43] A study of the molecular complex of (η^6-anisole)$Cr(CO)_3$ and 1,3,5-trinitrobenzene (1,3,5-TNB) by X-ray crystallography,[43] performed in 1966, has revealed a structure of "face-to-face" stacking of the benzene rings of coordinated anisole and 1,3,5-TNB, which is similar to the complexes with the free arenes; therefore, by analogy with organic compounds, the examination of dipole moments in arene tricarbonyl chromium complexes was carried out in benzene[37,38] and even in dioxane.[39]

Only in 1981 did Japanese authors[44] prove, on the basis of electronic absorption spectra, that tricarbonyl (η^6-[2.2]paracyclophane)chromium and even chromium–carbonyl complexes without an η^6-coordinated aromatic ring, $(Me_3PCr(CO)_5$, $Ph_3PCr(CO)_5$, $[Ph_2PCH_2CH_2PPh_2]Cr(CO)_4)$, form charge-transfer complexes with 1,3,5-TNB which are closely related to the complexes of benzene tricarbonyl chromium. The aforementioned authors supposed that, in solution, the acceptor molecule sits beneath the base of the pyramid formed by three metal–carbonyl bonds; by revising the results of Carter *et al.*,[43] they showed that in the crystal where a molecule of (anisole)$Cr(CO)_3$ is sandwiched between two 1,3,5-TNB molecules, the distance (4.70 Å) between the chromium and the centre of the 1,3,5-TNB in contact with the carbonyl groups is, in fact, shorter than the distance (5.14 Å) between chromium and the 1,3,5-TNB located on the η^6-coordinated anisole. An analogous result was obtained by X-ray analysis of the molecular complex of (phenanthrene)tricarbonyl chromium with 1,3,5-TNB.[45]

The formation of complexes between (benzene)$Cr(CO)_3$ and electron donor molecules has eventually been discovered.[46] The 1 : 1 complex formation between benzene-d_6 and $[Cr(CO)_3(\eta$-arene)], where arene is C_6H_5R (R = H, Me, OMe, Cl) and $C_{10}H_8$, has been observed by ^1H NMR spectroscopy. It is notable that the value of the equilibrium constant in the case of the $[Cr(CO)_3(\eta$-$C_6H_6)]$–benzene-d_6 system is almost identical to that found for the nitrobenzene–benzene-d_6 system.

Consequently, the data on the dipole moments of arene tricarbonyl chromium compounds in benzene and dioxane do not reflect an intrinsic polarity of the organometallic derivatives under investigation but the polarity of their complexes with the solvent, the force of the interaction being controlled by the arene structure (for instance, by substituents inserted into the ring).

Thus, arene tricarbonyl chromium compounds were shown[46] to be a relatively rare example of molecules which can reveal both electron donor and electron acceptor properties during charge-transfer complex formation. It should be noted that in these complexes electron flow from the benzene ligand to the carbonyl groups is in accord with their ability to form complexes with electron acceptor and electron donor molecules (based on carbonyl groups and the coordinated benzene ring, respectively).

The data available (see Table 5) show that by changing the solvent from $CHCl_3$ to benzene for arene–carbonyl complexes of chromium, fluorine

shielding is increased, i.e. in our opinion, an increase in electron density occurs on the ring (Table 5); this can be treated as a direct consequence of a molecular complex being formed with the donor benzene molecule. Substitution of the electron donor triphenylphosphine for a CO group in $[Cr(CO)_3(C_6H_6)]$ also brings about an increase in electron density on the benzene ring (from +0.26 to +0.11e, benzene; Table 5), a low-frequency shift of the CO stretching vibrations (ν(CO) for $[Cr(CO)_3(C_6H_6)]$ 1891, 1970 and for $[Cr(CO)_2(PPh_3)(C_6H_6)]$ 1825, 1884 cm^{-1} (CH_2Cl_2)[48]) and a corresponding decrease in dipole moment of the molecule (for $[Cr(CO)_3(C_6H_6)]$, μ is 4.81[32,36] ÷ 5.08[34] and for $[Cr(CO)_2(PPh_3)(C_6H_6)]$, μ is 4.13 D[49] (in benzene).

Charge density correlation with other indicators such as pK_a and S-coefficients

Traditional chemical methods for investigation, in most cases, provide evidence for the electron-withdrawing effect of the ML_n unit on the benzene ring upon complexation. From this viewpoint, arene tricarbonyl chromium complexes[50,51] and the benzene(cyclopentadienyl)iron cation[52] have been thoroughly considered in the reviews. We shall focus our attention on the most essential examples and emphasize some important points.

A classical approach, involving an acidity/basicity comparison of coordinated and free acids and amines, demonstrates that upon coordination with the $Cr(CO)_2PPh_3$ group, the acidity of the benzoic acid is increased by *ca* 0.4 pK_a units,[53] with the $Cr(CO)_3$ group—by *ca* 0.9 pK_a units[47] and with the $CpFe^+$ group—by *ca* 2.7 pK_a units[54] (50% aqueous ethanol); coordination of aniline with the $Cr(CO)_3$ group lowers its basicity by approximately 1.6 pK_a units (potentiometry, 82% aqueous ethanol)[55] and with the $CpFe^+$ group—by 5.6 pK_a units (spectrophotometry, H_2SO_4).[56] An alternative classical approach is based on the determination of the electron effects of organometallic groups as substituents. Here again the variation in the σ_I and σ_R^0 constants, as calculated from ^{19}F chemical shifts for corresponding *m*- and *p*-fluorophenyl derivatives by the Taft method, in proceeding from a free Ph group (σ_I+0.08; σ_R^0−0.09; "inert" solvents[57]) to that coordinated with $Cr(CO)_2PPh_3$ and $Cr(CO)_2AsPh_3$ fragments (σ_I+0.13, σ_R^0+0.048 and σ_I+0.13; σ_R^0+0.043, respectively; $CDCl_3$[15]) and further with the $Cr(CO)_3$ and $CpFe^+$ units (σ_I+0.27; σ_R^0+0.005; $CDCl_3$[15] and σ_I+0.38; σ_R^0 +0.01 respectively; acetone[17]) speaks for a pronounced increase in the electron-withdrawing action of the phenyl group 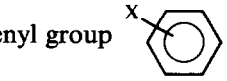 in the series: X = H < π-$Cr(CO)_2PPh_3$ ≈ π-$Cr(CO)_2AsPh_3$ < π-$Cr(CO)_3$ < π-$CpFe^+$. As was expected, our data indicate that electron density on the benzene ring decreases in the same order: $f_{C_6H_6}$ = 0; +0.14; +0.15; +0.32 ($CDCl_3$); +0.42e (acetone) (Table 5).

Discussion of kinetics effects

Some cyclopentadienyl and arene metal complexes are known to stabilize the adjacent charged centres.

An increase in the ability of the benzene ring to stabilize the adjacent carbanionic centres on coordination with the ML_n fragment (see, for example refs 58–61) is consistent with our results.

On the contrary, what is surprising is a sharp enhancement in the ability of the coodinated benzene ring to stabilize the adjacent carbocationic centres.

Solvolysis of $BtCH_2Cl$ and BtCH(Cl)Ph (Bt designates benzene tricarbonyl chromium) in aqueous acetone (S_N1) proceeds 10^5 and 10^3 times as fast as that of the corresponding free benzyl analogues;[62] the rate of non-catalysed isomerization of $BtCH_2SCN$ to $BtCH_2NCS$ (via $BtCH_2^+$) is increased by a factor of more than 2.5×10^4 compared to $PhCH_2SCN$.[63] A mechanism for stabilization of α-carbocationic centres by an electron-withdrawing benzene tricarbonyl chromium group is under discussion. The INDO MO calculations for $[Cr(CO)_3(\eta\text{-}C_6H_5CH_2)]^+$ and a free benzyl cation[64] did not confirm either of the following assumptions: direct interaction of the lone pair electrons on the chromium atom with the cationic centre or stabilization by π-conjugation of the α-carbonium atom with the ring.[50]

Substantial enhancement of the ability of the phenyl group to stabilize the α-carbocationic centres upon complexation with the $Cr(CO)_3$ unit clearly demonstrates an ambivalent ability of benzene tricarbonyl chromium to behave not only as an electron-withdrawing group, but also as an electron-releasing group. A systematic study of the dipole moments of (benzene)$Cr(CO)_3$ and a number of its methyl- and *t*-butyl-substituted derivatives in cyclohexane (which was not reported until 1985[33]) has shown that molecular optical anisotropy, as determined from the experimental molar Kerr constants (in cyclohexane), for all the complexes examined is opposite in sign to that predicted from additivity of the anisotropies of the component arene and $Cr(CO)_3$ fragments. These authors[33] came to

the conclusion that the electron system of the chromium–arene bond is highly polarizable along the bond and provides a channel of relatively free electron movement between the arene and $Cr(CO)_3$. Now it is worth mentioning that the dipole moments[31–39] and the CO stretching frequencies for substituted benzene tricarbonyl chromium complexes (see, for example, refs 50 and 51, and refs therein) can be both larger or smaller than for benzene tricarbonyl chromium, depending on the donor–acceptor character of the inserted substituents. Analogously, the ability of the benzene tricarbonyl chromium group to stabilize carbocations varies over a wide range, decreasing as the cation stability increases. The pK_R^+ values for the ionization equilibria (in aqueous acids)

$$R^+ + H_2O \overset{K_{R^+}}{\rightleftharpoons} ROH + H^+$$

for Ph_2CH^+, $PhCHBt^+$ and Bt_2CH^+ are equal to -13.3, -10.4 and -9.5, respectively, whereas $FcCHBt^+$ (Fc is ferrocenyl) is noticeably less stable than $FcCHPh^+$ (pK_{R^+} equals -1.0 and 0.49, respectively).[65]

The study on relative acelation rates for $[Cr(CO)_3(RC_6H_5)]$ (R = H, Me, Et, *i*-Pr, *t*-Bu) and free arenes under Friedel–Crafts conditions ($MeCOCl$, $AlCl_3$, CH_2Cl_2) indicated that the complexed arenes are far less reactive compared to the free molecules, owing to electron-withdrawing effects of the $Cr(CO)_3$ unit.[66,67]

The mechanism of electrophilic substitution in cyclopentadienyl and arene metal complexes is under discussion;[68] it should be emphasized that a decrease in reactivity of the coordinated benzene upon electrophilic substitution falls into line with a pronounced decrease in electron density on the benzene ring on coordination (up to +0.32, $CDCl_3$; Table 5). Similarly, the rate of electrophilic isotope exchange of the benzene tricarbonyl chromium aromatic hydrogen, occurring in media of high acidity such as $BF_3/D_2O/CF_3CO_2D/D_2SO_4$, is seven orders of magnitude lower than that of benzene.[69] By contrast, replacement of one carbonyl group by a triphenylphosphine ligand increases the rate of H/D exchange by three orders of magnitude, which allows the exchange to be performed in less acidic CF_3CO_2D.[69] This is in accord with an increase in electron density on the ring in $[Cr(CO)_2(PPh_3)(C_6H_6)]$ (up to +0.14, $CDCl_3$) compared with benzene tricarbonyl chromium (+0.32, $CDCl_3$, Table 5).

Upon nucleophilic aromatic substitution, the complexed arenes, on the contrary, are far more reactive than the free ones. (It is of note that an activating effect of halo-arene coordination to the metals often exceeds the influence of strong electron-withdrawing substituents introduced into the ring.) The synthetic potential of such reactions is well recognized, the mechanism being, perhaps, more involved than that of S_NAr reactions has attracted more attention.[50–52,68,70] Kinetic studies on the reactions of the complexed halo-arenes with the methoxide ion in methanol (refs 68, 70, 71 and refs therein) agree with a two-step mechanism for the addition–elimination process where the nucleophilic addition appears to be a rate-determining step. Chlorobenzene tricarbonyl chromium was shown to be more reactive than chlorobenzene by a factor of *ca* 10^{11},[68] and $[CpFe(C_6H_5Cl)]^+$ is approximately 10^5 times as reactive as chlorobenzene tricarbonyl chromium.[71] Replacement of PPh_3 for a CO group in chlorobenzene tricarbonyl chromium substantially hinders the chlorine substitution. Exchange of the chlorine in $[Cr(CO)_3(C_6H_5Cl)]$ upon interaction with NaOMe in a MeOH–THF mixture (3:2) readily occurs at 62.5°C over 7 h, whereas $[Cr(CO)_2(PPh_3)(C_6H_5Cl)]$ remains unchanged under these conditions.[72] As in the case of electrophilic substitution reactions, these data are again in accord with the net charge values on the benzene ring which we have obtained for the parent non-substituted molecules: 0 for benzene, +0.14e for $[Cr(CO)_2(PPh_3)(C_6H_6)]$, +0.32e for $[Cr(CO)_3(C_6H_6)]$ and +0.42e for $[CpFe(C_6H_6)]^+$ (Table 5). The same electron mechanisms are presumably responsible for the electron-withdrawing effects of π-$Cr(CO)_2PPh_3$, π-$Cr(CO)_3$ and π-$CpFe^+$ fragments on the benzene ring of arene metal complexes in the ground state, and for stabilization of transition states in electrophilic substitution and nucleophilic addition in the arene ring (which is the rate-determining step in the nucleophilic substitution of $[L_nM(C_6H_5Hal)]$ with MeO^- in MeOH, see above).

Therefore, we can conclude that the values obtained for the net charges on the benzene ring in arene complexes of transition metals agree well with all the data under consideration.

Acknowledgement—The authors with to thank N. P. Gambaryan for valuable discussion.

REFERENCES

1. N. A. Ogorodnikova and A. A. Koridze, *Polyhedron* 1983, **2**, 941.
2. N. A. Ogorodnikova, A. A. Koridze, E. I. Fedin and P. V. Petrovskii, *Izv. Akad. Nauk SSSR, Ser. Khim.* 1983, 2047.
3. N. A. Ogorodnikova and D. N. Kravtsov, *Polyhedron* 1985, **4**, 311.

4. W. J. Hehre, R. W. Taft and R. D. Topsom, *Prog. Phys. Org. Chem.* 1976, **12**, 159.
5. G. E. Maciel and J. J. Natterstad, *J. Chem. Phys.* 1965, **42**, 2427.
6. R. W. Taft, E. Price, I. R. Fox, I. C. Lewis, K. K. Andersen and G. T. Davis, *J. Am. Chem. Soc.* 1963, **85**, 3146.
7. S. K. Dayal and R. W. Taft, *J. Am. Chem. Soc.* 1973, **95**, 5595.
8. M. J. S. Dewar and A. P. Marchand, *J. Am. Chem. Soc.* 1966, **88**, 3318.
9. J. Kelm and K. Strauss, *Spectrochim. Acta* 1981, **37A**, 689.
10. E. C. Herrmann, G.-A. Hoyer and J. Kelm, *Spectrochim. Acta* 1982, **38A**, 1057.
11. N. A. Ogorodnikova, A. A. Koridze and S. P. Gubin, *J. Organomet. Chem.* 1981, **215**, 293.
12. R. N. Young, *Prog. NMR Spectrosc.* 1979, **12**, 261.
13. G. L. Nelson and E. A. Williams, *Prog. Phys. Org. Chem.* 1976, **12**, 229.
14. J. W. Emsley, J. Feeney and L. H. Sutcliffe, *High Resolution Nuclear Magnetic Resonance Spectroscopy*, Vols 1 and 2. Pergamon Press, Oxford (1965 and 1966).
15. T. E. Bitterwolf, *Polyhedron* 1983, **2**, 675.
16. V. S. Khandkarova, S. P. Gubin and B. A. Kvasov, *J. Organomet. Chem.* 1970, **23**, 509.
17. A. N. Nesmeyanov, I. F. Leshchova, Yu. A. Ustynyuk, Ye. I. Sirotkina, I. N. Bolesova, L. S. Isaeva and N. A. Vol'kenau, *J. Organomet. Chem.* 1970, **22**, 689.
18. D. A. Brown, N. J. Fitzpatrick and N. J. Mathews, *J. Organomet. Chem.* 1975, **88**, C27.
19. D. G. Carroll and S. P. McGlynn, *Inorg. Chem.* 1968, **7**, 1285.
20. M. Coletta, G. Cranozzi and G. Rigatti, *Inorg. Chim. Acta* 1977, **24**, 195.
21. J. Y. Saillard, D. Grandjean, F. Choplin and G. Kaufmann, *J. Molec. Struct.* 1974, **23**, 362.
22. N. J. Fitzpatrick, J.-M. Savariault and J.-F. R. Labarre, *J. Organomet. Chem.* 1977, **127**, 325.
23. D. A. Brown, J. P. Chester, N. J. Fitzpatrick and I. J. King, *Inorg. Chem.* 1977, **16**, 2497.
24. M. F. Guest, I. H. Hillier, B. R. Higginson and D. R. Lloyd, *Molec. Phys.* 1975, **29**, 113.
25. O. I. Belchenko, P. V. Schastnev and V. S. Bashurova, *J. Organomet. Chem.* 1980, **187**, 375.
26. D. W. Clack and L. A. P. Kane-Maguire, *J. Organomet. Chem.* 1979, **174**, 199.
27. J. A. Connor, L. M. R. Derrick and I. H. Hillier, *J. Chem. Soc., Faraday Trans.* II 1974, **70**, 941.
28. J. A. Connor, *J. Organomet. Chem.* 1975, **94**, 195.
29. F. Kinomura, T. Tamura, I. Watanabe, Y. Yokoyama and S. Ikeda, *Bull. Chem. Soc. Jpn* 1976, **49**, 3544.
30. C. Azokpota, C. Pommier, Y. Limouzin and J. C. Maire, *J. Organomet. Chem.* 1976, **117**, 349.
31. E. O. Fischer and S. Schreiner, *Chem. Ber.* 1959, **92**, 938.
32. W. Strohmeier and H. Hellmann, *Ber. Buns. Ges.* 1963, **67**, 190.
33. M. J. Aroney, M. K. Cooper, R. K. Pierens, S. J. Platten and S. W. Filipczuk, *J. Organomet. Chem.* 1985, **295**, 333.
34. E. W. Randal and L. E. Sutton, *Proc. Chem. Soc. (Lond.)* 1959, 93.
35. W. Strohmeier and D. Hobe, *Z. Electrochem.* 1960, **64**, 945.
36. W. Strohmeier and H. Hellmann, *Chem. Ber.* 1963, **96**, 2859.
37. K. Öfele, *Chem. Ber.* 1966, **99**, 1732.
38. H. Lumbroso, C. Segard and B. Roques, *J. Organomet. Chem.* 1973, **61**, 249.
39. M. J. Aroney, M. K. Cooper, P. A. Englert and R. K. Pierens, *J. Molec. Struct.* 1981, **77**, 99.
40. G. Huttner, E. O. Fischer, R. D. Fischer, O. L. Carter, A. T. McPhail and G. A. Sim, *J. Organomet. Chem.* 1966, **6**, 288.
41. H. Kobayashi, M. Kobayashi and Y. Kaizu, *Bull. Chem. Soc. Jpn* 1973, **46**, 3109.
42. H. Kobayashi, M. Kobayashi and Y. Kaizu, *Bull. Chem. Soc. Jpn* 1975, **48**, 1222.
43. O. L. Carter, A. T. McPhail and G. A. Sim, *J. Chem. Soc. A* 1966, 822.
44. H. Kobayashi, K. Kobayashi and Y. Kaizu, *Inorg. Chem.* 1981, **20**, 4135.
45. R. De Lal, J. Seyerl, L. Zsolnai and G. Huttner, *J. Organomet. Chem.* 1979, **175**, 185.
46. W. J. Bland, R. Davis and J. L. A. Durrant, *J. Organomet. Chem.* 1982, **234**, C20.
47. B. Nicholls and M. C. Whiting, *J. Chem. Soc.* 1959, 551.
48. V. I. Losilkina, M. N. Estekhina, N. K. Baranetskaya and V. N. Setkina, *J. Organomet. Chem.* 1986, **299**, 187.
49. W. Strohmeier and H. Hellmann, *Ber. Buns. Phys. Chem.* 1964, **68**, 481.
50. R. Devis and L. A. P. Kane-Maguire, *Comprehensive Organometallic Chemistry* (Edited by G. Wilkinson, F. G. A. Stone and E. B. Abel), Vol. 3, pp. 953–1077. Pergamon Press, Oxford (1982).
51. A. Solladié-Cavallo, *Polyhedron* 1985, **4**, 901.
52. D. Astruc, *Tetrahedron* 1983, **39**, 4027.
53. G. Jaouen and R. Dabard, *J. Organomet. Chem.* 1973, **61**, C36.
54. A. N. Nesmeyanov, N. A. Vol'kenau and Ye. L. Sirotkina, *Izv. Akad. Nauk SSSR, Ser. Khim.* 1967, 1170.
55. E. O. Fischer, K. Öfele, H. Essler, W. Fröhlich, J. P. Mortensen and W. Semmlinger, *Chem. Ber.* 1958, **91**, 2763.
56. A. N. Nesmeyanov, N. A. Vol'kenau, I. N. Bolesova and L. S. Isayeva, *Izv. Akad. Nauk SSSR, Ser. Khim.* 1968, 2416.
57. Yu. A. Zhdanov and V. I. Minkin, *Korrelyatsionny Analiz v Organicheskoi Khimii.* Rostov University Press, U.S.S.R. (1966).
58. W. S. Trahanovsky and R. J. Card, *J. Am. Chem. Soc.* 1972, **94**, 2897.
59. J. F. Helling and W. A. Hendrickson, *J. Organomet. Chem.* 1977, **141**, 99.
60. R. G. Sutherland, B. R. Steele, K. J. Demchuk and C. C. Lee, *J. Organomet. Chem.* 1979, **181**, 411.

61. C. C. Lee, B. R. Steele, K. J. Demchuk and R. G. Sutherland, *Can. J. Chem.* 1979, **57**, 946.
62. J. D. Holmes, D. A. K. Jones and R. Pettit, *J. Organomet. Chem.* 1965, **4**, 324.
63. A. Ceccon, *J. Organomet. Chem.* 1971, **29**, C19.
64. D. W. Clack and L. A. P. Kane-Maguire, *J. Organomet. Chem.* 1978, **145**, 201.
65. A. Ceccon, A. Gobbo and A. Venzo, *J. Organomet. Chem.* 1978, **162**, 311.
66. G. E. Herberich and E. O. Fischer, *Chem. Ber.* 1962, **95**, 2803.
67. W. R. Jackson and W. B. Jennings, *J. Chem. Soc. B* 1969, 1221.
68. W. E. Watts, *Comprehensive Organometallic Chemistry* (Edited by G. Wilkinson, F. G. A. Stone and E. B. Abel), Vol. 8, Chap. 59, pp. 1013–1071. Pergamon Press, Oxford (1982).
69. V. N. Setkina, N. K. Baranetskaya, A. G. Ginzburg, V. I. Zdanovich, M. N. Nefedova and D. N. Kursanov, *J. Organomet. Chem.* 1973, **61**, 287.
70. V. V. Litvak and V. D. Shteingarts, *Izv. Sib. Otd. Akad. Nauk SSSR, Ser. Khim.* 1983, **9**, 59.
71. A. C. Knipe, S. J. McCuinness and W. E. Watts, *J. Chem. Soc., Perkin Trans.* II 1981, 193.
72. R. Iwata and I. Ogata, *J. Chem. Soc. Jpn* 1969, **90**, 1156.

Polyhedron Vol. 9, No. 1, pp. 11–22, 1990
Printed in Great Britain

0277–5387/90 $3.00+.00
© 1989 Pergamon Press plc

η^3-ALLYL COMPLEXES OF TUNGSTEN—I. PREPARATION AND REACTIONS OF $[(\eta^3\text{-}C_3H_5)_3WCl]_2$

R. BENN, T. H. BROCK, M. C. F. B. DIAS,* P. W. JOLLY,† A. RUFIŃSKA, G. SCHROTH, K. SEEVOGEL and B. WASSMUTH

Max-Planck-Institut für Kohlenforschung, D-4330 Mülheim a.d. Ruhr, F.R.G.

(*Received* 3 *July* 1989; *accepted* 31 *July* 1989)

Abstract—An improved synthesis of $(\eta^3\text{-}C_3H_5)_4W$ from $W(OPh)_6$ and allylmagnesium bromide is reported. The further reaction with HX (X = Cl, Br) or iodine leads to $[(\eta^3\text{-}C_3H_5)_3WX]_2$ compounds, which in turn react with donor ligands to form the adducts $(\eta^3\text{-}C_3H_5)_3W(L)X$. Treatment of $(\eta^3\text{-}C_3H_5)_3W(PMe_3)Cl$ with RMgX (R = Me, Et) produces the tungsten–alkyl compounds $(\eta^3\text{-}C_3H_5)_3W(PMe_3)R$.

Although $(\eta^3\text{-}C_3H_5)_4W$ (**1**) was first isolated by Oberkirch and Wilke over 25 years ago as one of a series of homoleptic η^3-allyl–transition metal compounds,[1,2] its inaccessibility has resulted in an almost complete neglect of its chemistry which is apparently limited to the report in a patent of the reaction with HCl[3] and its use as a catalyst component for polymerization reactions.[4,5]

As part of a programme aimed at extending the chemistry of the η^3-allyl complexes of the Group VI metals, we have developed an improved synthesis for **1**, and in this and the following publication we present some of its reactions. This paper is concerned with the conversion into the $(\eta^3\text{-}C_3H_5)_3WX$ system and the further reaction with donor ligands.

RESULTS AND DISCUSSION

The original synthesis of $(\eta^3\text{-}C_3H_5)_4W$ (**1**) from WBr_5 and allylmagnesium chloride, in ether at room temperature, is tedious and unreliable and the yield varies between a high of 20% and zero.[1] This can be increased to *ca* 30% by reacting WCl_6 in THF at 60°C,[5] however, in both cases the product is contaminated with an oil (presumably the result of the tungsten-catalysed oligomerization of liberated alkenes or the ring-opening oligomerization of THF) which is difficult to remove. The situation can, however, be improved by reacting $W(OPh)_6$ with allylmagnesium bromide in THF at 60°C [eq. (1)]: the yield is consistently *ca* 60% and practically no oily side-products are formed:

$$W(OPh)_6 + 6C_3H_5MgBr \rightarrow \underset{(\mathbf{1})}{(\eta^3\text{-}C_3H_5)_4W} + C_6H_{10} + 6Mg(OPh)Br. \quad (1)$$

$(\eta^3\text{-}C_3H_5)_4W$ is a pale yellow, crystalline solid which is soluble in most organic solvents and which can be sublimed at 60°C in high vacuum. The compound decomposes above *ca* 100°C and is slowly oxidized in air. NMR spectroscopic investigations have shown that both $(\eta^3\text{-}C_3H_5)_4Mo$ and $(\eta^3\text{-}C_3H_5)_4W$ have similar structures, that the four allyl groups are magnetically equivalent and that they are bonded asymmetrically to the metal atom.[6] We have recently reported the crystal structure of $(\eta^3\text{-}C_3H_5)_3MoOAc$[7] and one may suppose that the tetra-η^3-allyl derivatives of tungsten and molybdenum have the structure shown below (Fig. 1) in which the allyl groups are arranged pair-wise in a distorted tetrahedral manner around the central metal atom.

$(\eta^3\text{-}C_3H_5)_4W$ reacts with gaseous HCl in pentane at −78°C with the initial protonolysis of one allyl group to give $[(\eta^3\text{-}C_3H_5)_3WCl]_2$ (**2**) [eq. (2)]:

$$2(\eta^3\text{-}C_3H_5)_4W + 2HCl \rightarrow \underset{(\mathbf{2})}{[(\eta^3\text{-}C_3H_5)_3WCl]_2} + 2C_3H_6. \quad (2)$$

It is essential that this reaction be carried out in the presence of a large excess of HCl but, since further reaction occurs in an uncontrollable manner, the

* Present address: Instituto Superior Técnico, Univ. Técnica de Lisboa, Portugal.

† Author to whom correspondence should be addressed.

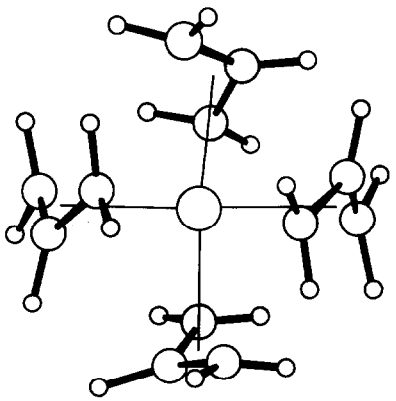

Fig. 1. The proposed structure for $(\eta^3\text{-}C_3H_5)_4M$ (M=Mo, W).

product must be isolated as quickly as possible. The bromide, $[(\eta^2\text{-}C_3H_5)_3WBr]_2$ (**3**), can be prepared in an analogous reaction with gaseous HBr, while the iodide $[(\eta^3\text{-}C_3H_5)_3WI]_2$ (**4**) is accessible through reaction of **1** with iodine in ether. Neither the reaction of **1** with Br_2 nor with HI led to the desired products; instead material with a high halogen content is obtained which has not been investigated further. It did not prove possible to prepare the fluoride; treatment of **1** with HF led to decomposition, while no reaction was observed between the chloride and NaF or AgF. The stability of the $(\eta^3$-allyl$)_3WX$ compounds decreases in the order Cl > Br > I, the iodide decomposing above *ca* −40°C.

Addition of one equivalent of $AlCl_3$ to a suspension of the chloride, **2**, in toluene produces a brown solution whose ^1H NMR spectrum (see Table 1) indicates the presence of three η^3-allyl groups and which is assumed to contain the binuclear species **5** [eq. (3)] by analogy to similar reactions involving $(\eta^3\text{-}C_3H_5)_3MoCl$[7] and $(\eta^6\text{-}MeC_6H_5)(\eta^3\text{-}C_3H_5)WCl$[8] and $AlCl_3$ or $EtAlCl_2$.

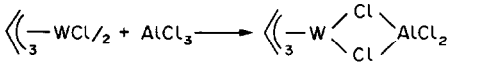

2 **5** (3)

The corresponding $(\eta^3$-allyl$)_3W$–acetate (**6**), –trifluoroacetate (**7**) and –acetylacetonate (**8**) have been prepared from the chloride by anion exchange reactions with silver acetate, thallium trifluoroacetonate and thallium acetylacetonate, respectively. The ^1H NMR spectrum of the acetylacetonate indicates that it is formed as a mixture of two isomers in the ratio 73 : 27.

Adducts **9**–**14** are formed by reacting the chloride with P-, N- or C-donor ligands [eq. (4)]:

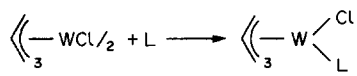

(4)

9, L = PF_3; **10**, L = PMe_3
11, L = $P(OMe)_3$; **12**, L = pyridine
13, L = MeCN; **14**, L = C_4H_9NC

The product of the reaction with 1,2-bis(dimethylphosphino)ethane is the binuclear species **15** in which the bidentate ligand bridges the two metal atoms. Trimethylphosphine adducts (**16**, **17**) to $[(\eta^3\text{-}C_3H_5)_3WBr]_2$ and $[(\eta^3\text{-}C_3H_5)_3WI]_2$ have also been prepared.

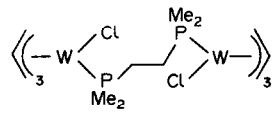

15

Reaction of $(\eta^3\text{-}C_3H_5)_3W(P(OMe)_3)Cl$ (**11**) with further phosphite and lithium-sand resulted in the formation of a yellow compound, **18**, whose NMR spectroscopic data (A_2B spin system in the ^{31}P NMR spectrum, equivalent but asymmetric η^3-allyl groups in the ^1H NMR spectrum—see Experimental) indicate that it has a structure in which the ligands are arranged in a trigonal bipyramidal manner around the central metal atom with the allyl groups occupying the apices [eq. (5)]. Similar behaviour has been reported for the corresponding molybdenum system.[7]

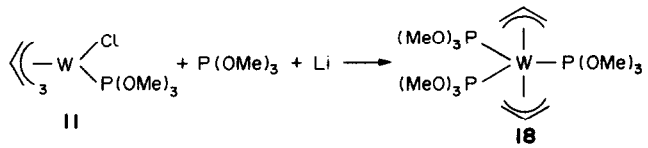

11 **18** (5)

Reaction of the trimethylphosphine adduct, **10**, with Grignard reagents led to the formation of the tungsten–methyl and –ethyl compounds, **19** and **20** [eq. (6)]. These pale yellow compounds are relatively stable, decomposing slowly at room temperature.

$(\eta^3\text{-}C_3H_5)_3W(PMe_3)Cl + RMgI \rightarrow$
(10)
$(\eta^3\text{-}C_3H_5)_3W(PMe_3)R + MgICl.$ (6)
(19, R = Me; **20**, R = Et)

Table 1. ^{1}H NMR data of the $(\eta^3\text{-}C_3H_5)_3W(L)X$ compounds[a]

Compound	Solvent, Temperature (°C)	δ_{meso}(H*n*,m)	δ_{anti}(H*n*,m)	δ_{syn}(H*n*,m)	*J*(Hz)	Miscellaneous
$(\eta^3\text{-}C_3H_5)_3WCl$ **(2)**	d_8-THF, −30	5·32 (H1,m) 4·44 (H11,m) 4·28 (H21,m)	0·92 (H4,dd) 1·37 (H5,dd) 3·6 (H14,dd) 0·36 (H15,dd) 1·43 (H24,dd) 2·89 (H25,dd)	2·57 (H2,m) 2·64 (H3,m) 2·47 (H12,dd) 1·13 (H13,m) 3·55 (H22,dd) 3·04 (H23,m)	*J*(1,2) 8·7, *J*(1,3) 8·9, *J*(1,4) 12·3, *J*(1,5) 13·1, *J*(2,3) 2·8, *J*(2,4) 2·7, *J*(3,5) 2·8. *J*(11,12) 8·4, *J*(11,13) 8·4, *J*(11,14) 11·8, *J*(11,15) 10·2, *J*(12,13) 2·4, *J*(12,14) 0, *J*(13,15) *ca* 2·8. *J*(21,22) *ca* 8·2, *J*(21,23) 7·4, *J*(21,24) 11·9, *J*(21,25) 11·4, *J*(22,23) 2·5, *J*(22,24) 0, *J*(23,25) 2·5.	
$(\eta^3\text{-}C_3H_5)_3WBr$ **(3)**	d_8-THF, −30	5·50 (H1,m) 4·73 (H11,m) 4·28 (H21,m)	0·97 (H4,dd) *ca* 0·9 (H5,dd) *ca* 1·8 (H14) 3·39 (H15,m) *ca* 3·6 (H24) 0·71 (H25,dd)	2·90 (H2,m) 2·57 (H3,m) 3·81 (H12,m) 3·30 (H13,m) 2·29 (H22,dd) 1·21 (H23,m)	*J*(1,2) 8·4, *J*(1,3) 8·3, *J*(1,4) 12·0, *J*(1,5) *ca* 12·6, *J*(2,3) 3·6, *J*(2,4) 3·6, *J*(3,5) *ca* 3·6. *J*(11,12) 8·2, *J*(11,13) 7·9, *J*(11,15) *ca* 12, *J*(12,13) 2·3, *J*(13,15) *ca* 2·7. *J*(21,22) 8·6, *J*(21,23) 8·5, *J*(21,25) 10·1, *J*(22,23) 2·8, *J*(22,25) 2·8.	
$(\eta^3\text{-}C_3H_5)_3WI$ **(4)**	d_8-THF, −30	5·62 (H1,m) 5·17 (H11,m) 4·26 (H21,m)		3·15 (H2,m) 2·15 (H3,m) 4·06 (H12,dd) 2·26 (H22,dd) 1·29 (H23,m)		
$(\eta^3\text{-}C_3H_5)_3WCl_2AlCl_2$ **(5)**	d_8-toluene, −50	5·54 (H1,m) 4·41 (H11,m) 3·37 (H21,m)	2·95 (H4,dd) 1·32 (H5,dd) 2·1 (H14,br) 1·59 (H15,dd) 3·58 (H24,d) 0·10 (H25,dd)	3·35 (H2,d) 3·42 (H3,d) 2·1 (H12,br) 1·87 (H13,br) 1·69 (H22,dd) 0·02 (H23,dd)	*J*(1,2) 8·0, *J*(1,3) 8·8, *J*(1,4) 12·0, *J*(1,5) 12·7. *J*(11,12) 9·2, *J*(11,13) 8·4, *J*(11,14) 11·1, *J*(11,15) 13·3. *J*(21,22) 8·6, *J*(21,23) 8·3, *J*(21,24) 11·8, *J*(21,25) 9·9.	
$(\eta^3\text{-}C_3H_5)_3WO_2CMe$ **(6)**	d_8-THF, −40	5·28 (H1,m) 4·70 (H11,m) 4·06 (H21,m)	1·15 (H4,dd) 0·60 (H5,d) 3·61 (H14)	2·82 (H2,m) 2·74 (H3,m) 2·46 (H12,dd)	*J*(1,2) 8·6, *J*(1,3) 8·6, *J*(1,4) 13·8, *J*(1,5) 11·0, *J*(2,3) 2·8, *J*(2,4) 2·4, *J*(3,5) *ca* 3·0.	

Table 1. (*continued*)

Compound	Solvent, Temperature (°C)	δ_{meso}(H*n*,m)	δ_{anti}(H*n*,m)	δ_{syn}(H*n*,m)	*J*(Hz)	Miscellaneous
			0·35 (H15,d) 3·28 (H24,br) 1·53 (H25,d)	3·46 (H22,m) 3·34 (H23,m)	*J*(11,12) 8·6, *J*(11,13) *ca* 8·8, *J*(11,14) *ca* 10·9, *J*(11,15) 10·4, *J*(12,13) 2·7. *J*(21,22) 7·9, *J*(21,23) 8·5, *J*(21,24) 11·4, *J*(21,25) 12·5, *J*(22,23) 2·4, *J*(22,24) 2·3.	
$(\eta^3\text{-}C_3H_5)_3WO_2CCF_3$ (**7**)	d_6-acetone, −80	5·62 (H1,m) 5·04 (H11,m) 4·38 (H21,m)	1·14 (H4,dd) 0·54 (H5,dd) 3·87 (H14,d) 0·39 (H15,dd) 3·47 (H24,dd) 1·73 (H25,d)	2·97 (H2,m) 2·93 (H3,m) 2·56 (H12,dd) 0·98 (H13,m) 3·70 (H22,dd) 3·40 (H23,dd)	*J*(1,2) 8·8, *J*(1,3) 8·6, *J*(1,4) 13·7, *J*(1,5) 10·6, *J*(2,3) 2·9, *J*(2,4) 2·7, *J*(3,5) 3·5. *J*(11,12) 8·6, *J*(11,13) 8·6, *J*(11,14) 11·4, *J*(11,15) 11·0, *J*(12,13) *ca* 2·5, *J*(12,14) *ca* 0, *J*(13,15) *ca* 3·0. *J*(21,22) 8·0, *J*(21,23) 8·6, *J*(21,24) 11·6, *J*(21,25) 12·6, *J*(22,23) *ca* 2·2, *J*(22,24) *ca* 2·6, *J*(23,25) 0.	
$(\eta^3\text{-}C_3H_5)_3W(acac)$ (**8a**) 73%	d_6-acetone, −80	5·63 (H1,m) 4·92 (H11,m) 4·04 (H21,m)	1·89 (H4,dd) 0·76 (H5,dd) 3·75 (H14,d) 0·31 (H15,dd) 1·61 (H24,d) 3·03 (H25,dd)	2·52 (H2,m) 2·43 (H3,m) 2·29 (H12,dd) 0·97 (H13,m) 2·97 (H22,m) 2·95 (H23,m)	*J*(1,2) 9·4, *J*(1,3) 8·9, *J*(1,4) 13·2, *J*(1,5) 12·2, *J*(2,3) 2·7, *J*(2,4) *ca* 2·0, *J*(3,5) *ca* 2·4. *J*(11,12) 8·6, *J*(11,13) 8·5, *J*(11,14) 11·6, *J*(11,15) 10·4, *J*(12,13) 2·7, *J*(12,14) 0, *J*(13,15) *ca* 2·9. *J*(21,22) *ca* 7·6, *J*(21,23) 8·4, *J*(21,24) 12·2, *J*(21,25) *ca* 10·8, *J*(22,23) 2·2, *J*(22,24) 0·0, *J*(23,25) *ca* 1·8.	5·34 (s,CH) 1·84 (s,M) 1·72 (s,Me)
$(\eta^3\text{-}C_3H_5)_3W(acac)$ (**8b**) 27%	d_6-acetone, −80	5·37 (H1,m) 4·78 (H11,m) 4·04 (H21,m)	1·08 (H4,dd) 0·51 (H5,dd) 3·54 (H14,d) 0·31 (H15,dd) 1·49 (H24,d) 3·24 (H25,dd)	2·76 (H2,m) 2·81 (H3,m) 2·42 (H12) 0·88 (H13,m) 3·25 (H22,dd) 3·42 (H23,m)	*J*(1,2) 8·6, *J*(1,3) 8·7, *J*(1,4) 13·8, *J*(1,5) 11·1, *J*(2,3) 3·0, *J*(2,4) 2·8, *J*((3,5) *ca* 2·2. *J*(11,12) 8·6, *J*(11,13) 8·7, *J*(11,14) 11·2, *J*(11,15) *ca* 10·4, *J*(12,13) *ca* 2·8, *J*(12,14) 0, *J*(13,15) *ca* 2·8.	4·31 (s,CH) 2·01 (s,Me) 1·67 (s,Me)

					J(21,22) 8·6, J(21,23) 8·0, J(21,24) 12·7, J(21,25) 11·7, J(22,23) 2·4, J(22,24) 0, J(23,25) 2·3.	
(η^3-C_3H_5)$_3$W(PF_3)Cl **(9)**	d_8-THF, −80	5·15 (H1,m) 5·12 (H11,m) 4·33 (H21,m)	2·00 (H4,d) 1·48 (H5,d) 3·76 (H14,d) 1·14 (H15,m) 2·37 (H24,dd) 0·29 (H25,d)	3·66 (H2,d) 2·89 (H3,t) 3·58 (H12) 3·52 (H13) 2·64 (H22,dd) 1·94 (H23,d)	J(1,2) 9·2, J(1,3) 9·0, J(1,4) 13·7, J(1,5) 11·6, J(2,3) *ca* 2, J(3,5) *ca* 2. J(11,12) *ca* 8·3, J(11,13) 8·3, J(11,14) 12·0, J(11,15) 11·9, J(12,13) 2·5, J(13,15) 2·8. J(21,22) 8·4, J(21,23) 8·8, J(21,24) 12·7, J(21,25) 10·4, J(22,23) 2·0, J(23,25) 2. J(2,P) 0, J(3,P) 9·0, J(4,P) *ca* 0, J(5,P) 0. J(13,P) 16·2, J(14,P) 0, J(15,P) 7·8. J(22,P) 14·2, J(23,P) *ca* 0, J(24,P) 4·8, J(25,P) 0.	
(η^3-C_3H_5)$_3$W(PMe_3)Cl **(10)**	d_6-acetone, −30	4·88 (H1,m) 4·82 (H11,m) 4·05 (H21,m)	2·47 (H4,m) 1·14 (H5,m) 3·25 (H14,m) 0·72 (H15,m) 2·26 (H24,m) −0·01 (H25,dd)	3·19 (H2,m) 2·41 (H3,m) 3·20 (H12,m) 2·89 (H13,m) 2·32 (H22,m) 1·64 (H23,m)	J(1,2) 9·4, J(1,3) 9·1, J(1,4) 13·6, J(1,5) 11·6, J(2,3) 2·0, J(2,4) 1·4, J(2,5) 1·4, J(3,4) 0·9, J(3,5) 2·2, J(4,5) 1·3. J(11,12) 8·1, J(11,13) 8·2, J(11,14) 11·1, J(11,15) 11·7, J(12,13) 2·6, J(12,14) *ca* 0·7, J(12,15) 0·7, J(13,15) 2·4. J(21,22) 8·5, J(21,23) 8·5, J(21,24) 11·4, J(21,25) 10·4, J(22,23) 2·6, J(22,24) *ca* 0·7, J(22,25) 0·7, J(23,24) 0·7, J(23,25) *ca* 2·6. J(1,P) 1·4, J(2,P) 0, J(3,P) 6·6, J(4,P) *ca* 0·7, J(5,P) *ca* 0, J(6,P) 9·2. J(11,P) 4·3, J(12,P) 0, J(13,P) 13·0, J(14,P) *ca* 0, J(15,P) 8·3. J(21,P) *ca* 0, J(22,P) 12·0, J(23,P) 0·9, J(24,P) 4·2, J(25,P) 0.	1·56 (d,PMe, J(P,H) 9·2)

Table 1. (*continued*)

Compound	Solvent, Temperature (°C)	δ_{meso}(H*n*,m)	δ_{anti}(H*n*,m)	δ_{syn}(H*n*,m)	*J*(Hz)	Miscellaneous
$(\eta^3\text{-}C_3H_5)_3W(P(OMe)_3)Cl$ **(11)**	CD_2Cl_2, −30	5·09 (H1,m) 4·67 (H11,q) 3·80 (H21,m)	3·4 (H4,d) 0·81 (H5,d) 2·28 (H14,d) 1·39 (H15,d) 2·46 (H24,d) 0·02 (H25,d)	3·4 (H2,d) 3·4 (H3,d) 3·29 (H12,d) 2·65 (H13,d) 1·55 (H22,d) 2·46 (H23,d)	*J*(1,2) 8·1, *J*(1,3) 8·1, *J*(1,4) 11·5, *J*(1,5) 11·7. *J*(11,12) 9·5, *J*(11,13) 9·1, *J*(12,13) 2·0, *J*(11,14) 13·7, *J*(12,14) 1·8, *J*(13,14) 0·8, *J*(11,15) 11·5, *J*(12,15) 1·1, *J*(13,15) 2·2, *J*(14,15) 1·6. *J*(21,22) 8·8, *J*(22,23) 2·5, *J*(21,24) 10·6, *J*(22,24) 2·5, *J*(21,25) 10·1. *J*(1,P) 5·0, *J*(5,P) 7·1. *J*(11,P) 2·0, *J*(12,P) 0·8, *J*(13,P) 7·9, *J*(14,P) 1·1, *J*(15,P) 4. *J*(22,P) 0, *J*(23,P) > 0, *J*(24,P) 0. *J*(25,P) 0.	3·79 (Me,d, *J*(P,H) 9·6)
$(\eta^3\text{-}C_3H_5)_3W(py)Cl$ **(12)**	CD_2Cl_2, −30	5·20 (H1,m) 5·14 (H11,q) 4·84 (H21,q)	2·16 (H4,d) 2·83 (H5,d) 3·42 (H14,d) 1·40 (H15,d) 3·70 (H24,d) 0·43 (H25,d)	2·65 (H2,d) 2·61 (H3,d) 3·58 (H12,d) 2·90 (H13,d) 2·28 (H22,dd) 1·14 (H23,t)	*J*(1,2) 9·2, *J*(1,3) 9·3, *J*(1,4) 11·6, *J*(1,5) 13·5. *J*(11,12) 8·0, *J*(11,13) 8·5, *J*(11,14) 10·2, *J*(11,15) 10·4. *J*(21,22) 8·5, *J*(21,23) 8·4, *J*(21,24) 11·8, *J*(21,25) 10·2.	8·96 (*o*-H,py,d) 7·28 (*m*-H,py,t) 7·75 (*p*-H,py,t)
$(\eta^3\text{-}C_3H_5)_3W(CNC_4H_9)Cl$ **(14)**	d_8-THF, 27	5·35 (H1,m) 4·77 (H11,m) 3·91 (H21,m)	2·98 (H4,d) 0·91 (H5,d) 2·51 (H14,d) 1·88 (H15,d) 2·71 (H24,d) 0·14 (H25,d)	3·33 (H2,dd) 3·29 (H3,dd) 3·25 (H12,dd) 2·44 (H13,dd) 2·44 (H22,dd) 1·55 (H23,dd)	*J*(1,2) *ca* 8·1, *J*(1,3) 8·2, *J*(1,4) 11·3, *J*(1,5) 11·8, *J*(2,3) 2·6. *J*(11,12) *ca* 9·2, *J*(11,13) *ca* 9·2, *J*(11,14) 13·6, *J*(11,15) 11·9, *J*(12,13) *ca* 2·0. *J*(21,22) *ca* 8·4, *J*(21,23) *ca* 8·3, *J*(21,24) 11·6, *J*(21,25) 9·4, *J*(22,23) *ca* 2·3.	3·85 (NCH_2, *J*(H,H) 6·3), *ca* 1·7 (C_2H_4). 0·98 (Me,t, *J*(H,H) 7·2).
$[(\eta^3\text{-}C_3H_5)_3WCl]_2$ $(Me_2PC_2H_4PMe_2)$ **(15)**	d_8-THF, −30	4·85 (H1,m) 4·79 (H11,m) 4·01 (H21,m)	2·53 (H4,d) 1·20 (H5, br) 0·73 (H15,m) 0·0 (H25, br)	2·94 (H13,m) 1·6 (H23)		1·53 (PMe_2)
$(\eta^3\text{-}C_3H_5)_3W(PMe_3)Br$ **(16)**	d_8-THF, 27	5·24 (H1,m) 4·68 (H11,m) 3·99 (H21,m)	3·37 (H4,m) 0·64 (H5,m) 3·18 (H14,m) 1·79 (H15,m)	3·51 (H2,m) 2·84 (H3,m) 3·13 (H12,m) 2·30 (H13,m)	*J*(1,2) 8·1, *J*(1,3) 8·3, *J*(1,4) 11·0, *J*(1,5) 11·9, *J*(2,3) 2·5, *J*(2,4) 0·8, *J*(2,5) 0·8, *J*(3,5) 2·2, *J*(4,5) 0·8. *J*(11,12) 9·6, *J*(11,13) 9·1,	1·65 (PMe,d, *J*(P,H) 8·9).

			2·28 (H24,m) 0·05 (H25,d)	2·19 (H22)	J(11,14) 13·5, J(11,15) 11·5, J(12,13) 2·2, J(12,14) 1·8, J(12,15) 1·2, J(13,14) 0·9, J(13,15) 2·1, J(14,15) 1·8. J(21,22) 8·5, J(21,23) 8·5, J(21,24) 11·3, J(21,25) 10·3, J(22,23) 2·6, J(22,24) 0·7. J(1,P) 4·3, J(2,P) 0, J(3,P) 13·0, J(4,P) *ca* 0, J(5,P) 8·0. J(11,P) 1·4, J(12,P) 0, J(13,P) 6·9, J(14,P) 1·1. J(21,P) 0, J(22,P) 11·8, J(24,P) *ca* 4, J(25,P) *ca* 0.	
$(\eta^3\text{-}C_3H_5)_3W(PMe_3)I$ **(17)**	d_8-THF, 27	4·49 (H1,m) 5·80 (H11,m) 4·07 (H21,m)	4·26 (H4,m) 2·65 (H5,m) 0·50 (H15,m) 2·35 (H24,m) 0·12 (H25,dd)	2·26 (H3,m) 3·89 (H12,m) 2·78 (H13,m) 2·12 (H22,m)		1·83 (PMe,d)
$(\eta^3\text{-}C_3H_5)_3W(PMe_3)Me$ **(19)**	d_8-THF, −80	4·45 (H1,m) 3·96 (H11,m) 4·26 (H21,m)	0·58 (H4,dd) 2·42 (H14,dd) −0·17 (H15,dd) −0·19 (H25,m)	2·84 (H3,dd) 2·80 (H12,m) 1·64 (H23,dd)		1·38 (PMe,d), −1·24 (WMe,d,J(P,H) *ca* 12·5)
$(\eta^3\text{-}C_3H_5)_3W(PMe_3)Et$ **(20)**	d_8-THF, −30	4·38 (H1,m) 4·16 (H11,m) 4·10 (H21,m)	0·48 (H4,br) 1·68 (H5,d) −0·20 (H14,dd) 2·06 (H15,dd) 2·57 (H25,d) −0·12 (H24,m)	2·01 (H2,m) 2·76 (H3,dd) 1·64 (H12,m) 2·16 (H13,m) 2·14 (H22,m) 2·68 (H23,dd)	J(1,2) 9·4, J(1,3) 10·0, J(1,4) 10·7, J(1,5) 13·1, J(2,3) *ca* 1·0, J(2,4) 2·5. J(11,12) 8·3, J(11,13) 8·7, J(11,14) 11·0, J(11,15) 11·7, J(12,13) 2·5, J(12,14) 2·0. J(21,22) 7·6, J(21,23) 7·3, J(21,24) 9·7, J(21,25) 10·5, J(22,23) 3·0, J(21,25) 2·6. J(1,P) 1·7, J(2,P) 5·2. J(11,P) 0, J(12,P) *ca* 1, J(13,P) 10·8. J(15,P) 4·2. J(21,P) 5·7, J(22,P) 14·6, J(24,P) 10·5.	1·37 (PMe,d, J(P,H) 8·0), 0·75 (CMe,dd, J(H,H) 7·7/7·8), −0·09/−1·64, (WCH_2,m, J(H,P) 21·7/9·5, ^2J(H,H) −13·5, ^3J(H,H) 7·7/7·8).

[a] 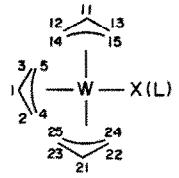

SPECTROSCOPIC INVESTIGATIONS

The structure of the $[(\eta^3\text{-}C_3H_5)_3WX]_2$ compounds **(2)**–**(4)** is not known. Conventionally they would be regarded as dimeric with the halide atoms bridging the tungsten atoms and this assumption is supported by their dissolution upon adding $AlCl_3$ in toluene. However, a monomeric structure cannot be ruled out particularly in view of the large number of stable organometallic compounds in which the metal atom has only 16-electrons in its valence shell, while the mass spectra all show a signal assignable to a monomeric species $[(\eta^3\text{-}C_3H_5)_3WX]^+$ with no higher fragments being detected. The IR spectra of these compounds have been recorded between −90 and −30°C (see Experimental) and compared to those of the trimethylphosphine adducts (**10**, **16**, **17**). The strongest absorption is assigned to the W—X stretching frequency. Although there is a shift to shorter wavelengths upon forming the PMe_3-adducts, there is insufficient data available to decide whether the absorptions should be assigned to terminal or bridging halide atoms. In the absence of a crystal structure determination, we will assume that the compounds are dimeric.

The complexity of the ^1H NMR spectra of the various $(\eta^3\text{-}C_3H_5)_3W$ compounds reported in this publication (see, for example, Fig. 2 and Table 1) is a result of the inequivalence and asymmetric bonding of the three allyl groups: the 15 allylic hydrogen atoms generate 15 multiplets. The hydrogen atoms have been assigned to a particular allyl group by means of homo-decoupling and the assignment of the *meso*-, *syn*- and *anti*-protons is based upon experience, the chemical shift (frequently $\delta meso\text{-H} > \delta syn\text{-H} > \delta anti\text{-H}$) and the ^1H–^1H-coupling constants [frequently ^3J(*meso*-H, *syn*-H) ~8–9 Hz, ^3J(*meso*-H, *anti*-H) ~10–13 Hz; ^3J(*syn*-H, *anti*-H) <5 Hz]. A full stereochemical assignment has, however, not been attempted.

The ^{183}W chemical shifts of compounds **10**, **16**, **17** and **19** have been measured using indirect two-dimensional (^{31}P, ^{183}W) NMR spectroscopy[9] and in all cases only one tungsten chemical shift is observed. The δ ^{183}W values lie within the range observed for other tungsten(IV) complexes.[10] The halogen dependence is normal and is associated with the effect of the electronegativity of the substituents upon the charge density dependence of the nuclear shielding term.

EXPERIMENTAL

All experiments were carried out under an atmosphere of argon. Solvents (ether, THF, pentane, toluene) were dried and freed from dissolved oxygen by distillation from diethylmagnesium. Acetonitrile and CH_2Cl_2 were dried with P_4O_{10}, hexane with $CaCl_2$, d_8-THF with K/Na-alloy and d_6-acetone with a 0·4 nm molecular sieve.

The NMR spectra were measured on Bruker–FT machines: ^1H NMR, mainly WM 400 (400·13 MHz), ^{31}P NMR, mainly WP 80 (32·4 MHz), ^{13}C NMR, mainly WM 300 (75·5 MHz). The ^{183}W NMR spectra were recorded with a WM 400 machine at the ^{183}W-resonance of 16·6 MHz by

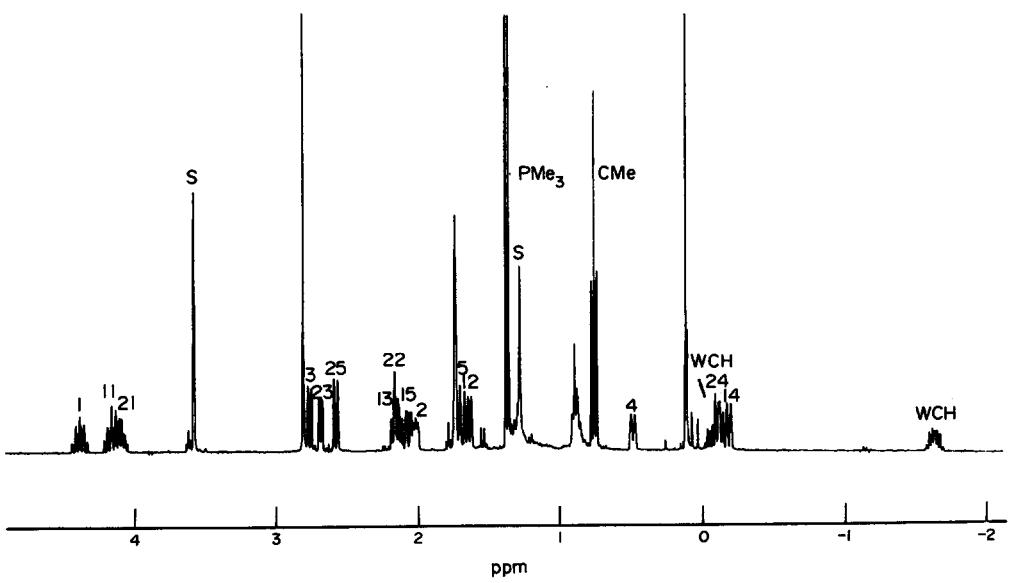

Fig. 2. The ^1H NMR spectrum of $(\eta^3\text{-}C_3H_5)_3W(PMe_3)Et$ (**20**) (d_8-THF, −30°C); S = solvent, for assignment see Table 1, footnote *a*.

means of indirect 2D–^{31}P–^{183}W-correlated NMR spectroscopy using an aqueous solution of sodium tungstate as the external standard.

IR spectra were recorded with a Nicolet–FT–IR 7199 as a KBr mull (4000–400 cm^{-1}) or as a polyethylene mull (400–100 cm^{-1}). Raman spectra were recorded with a Coderg-LTR-800. Mass spectra were measured at 70 eV with a Varian CH-5.

Microanalyses were carried out by Dornis and Kolbe, Microanalytical Laboratory, Mülheim a.d. Ruhr.

$(\eta^3\text{-}C_3H_5)_4W$ (1)

Allylmagnesium bromide (11·8 g, 81·3 mmol) was dissolved in THF (150 cm^3) at 60°C and $W(OPh)_6$ (80 g, 10·8 mmol)[11] was added over 5 min. The solution was kept at 60°C for 1 h, cooled and evaporated to dryness at room temperature. The pale beige residue was dried *in vacuo* for 14 h and extracted with 4 × 100 cm^3 of pentane. The pentane solution was evaporated and the pale yellow product crystallized five times from hexane to remove completely the magnesium salts. Yield 2·33 g (62% theory). Found: C, 41·4; H, 5·9; W, 52·6. Calc. for $C_{12}H_{20}W$: C, 41·4; H, 5·8; W, 52·8%.

IR (KBr, −50°C): ν 3080, 3020, 3010, 1498, 1470, 1310, 1235, 1205, 1012, 905, 585. Raman (−30°C): ν 1498, 1235, 1205, 1012, 585, 360. MS: m/z 348 [M^+], 306 [$M^+ - C_3H_6$], 301 (100%), 275, 261, 42, 41, 39. ^{1}H NMR (d_8-toluene): δ 3·89 (H1, m), 2·82 (H2, m), 1·66 (H3, m), 2·82 (H4, m), −0·19 (H5, m), J(1,2) 8·5, J(1,3) 8·5, J(1,4) 13·0, J(1,5) 10·5, J(2,3) 1·8, J(3,5) 1·8—For numbering scheme, see Table 1. ^{13}C NMR (d_8-toluene): δ 99·4 (*meso*-C1), 61·19/43·07 (CH_2), J(C1, H) 156, J(C2/3, H), 160/152, ^1J(C2/3, W) 7·4/13·8. ^{183}W NMR (d_8-toluene, 166 MHz): δ −3186.

The compound can also be prepared in 29–45% yield by reacting allylmagnesium bromide with WCl_6 (12 : 1) in THF at 60°C, followed by removal of the solvent and extraction of the residue with pentane. Oily side-products were removed by treating the solution with active charcoal and the compound was isolated by repeated recrystallization from pentane.

$[(\eta^3\text{-}C_3H_5)_3WCl]_2$ (2)

$(\eta^3\text{-}C_3H_5)_4W$ (3·0 g, 8·62 mmol) was dissolved in pentane (350 cm^3) and the solution cooled to −78°C. Dry gaseous HCl was passed over the stirred solution for 20 min. The resulting yellow product was isolated and washed with cold pentane. Pure samples were obtained by repeatedly suspending the compound in ether at −78°C, warming the solution briefly to room temperature and precipitating the compound at −78°C until the ether solution was pale yellow. The product was dried *in vacuo* at −78°C and decomposes rapidly if warmed above 0°C. Yield 1·49 g (50% theory). Found: C, 31·6; H, 4·3; Cl, 10·3; W, 53·7. Calc for $C_9H_{15}ClW$: C, 31·6; H, 4·4; Cl, 10·4; W, 53·7%.

IR (KBr, −45°C): ν 3080–3025, 1500, 1012, 585. FIR (polyethylene, −80°C): ν(WCl) 251—see text. MS: m/z 342 (M^+), 300 ($M^+ - C_3H_6$), 272, 109, 42, 41 (100%). ^{1}H NMR spectrum: see Table 1. Magnetic susceptibility (−80°C): diamagnetic.

$[(\eta^3\text{-}C_3H_5)_3WBr]_2$ (3)

$(\eta^3\text{-}C_3H_5)_4W$ (0·20 g, 0·57 mmol) was dissolved in pentane (150 cm^3) at −78°C and treated with gaseous HBr for 15 min. A beige–brown solid precipitated immediately and was isolated, washed with pentane (5 × 40 cm^3) and dried for 2 days *in vacuo*. The compound was isolated as a dark beige voluminous powder and decomposes slowly above −20°C. Yield 0·13 g (58% theory). Found: C, 27·8, H, 3·8; Br, 20·7; W, 47·6. Calc. for $C_9H_{15}BrW$: C, 27·9; H, 3·9; Br, 20·6; W, 47·5%.

IR (KBr, −50°C): ν 3080–3025, 1500, 1010, 596. FIR (polyethylene, −90°C): ν(WBr) 170. MS: m/z 386 (M^+), 356 ($M^+ - 42$), 80, 79, 42, 41 (100%). ^{1}H NMR spectrum: see Table 1.

$[(\eta^3\text{-}C_3H_5)_3WI]_2$ (4)

$(\eta^3\text{-}C_3H_5)_4W$ (0·73 g, 2·10 mmol) was dissolved in ether (60 cm^3) at −78°C. Iodine (0·27 g, 1·05 cm^3) dissolved in ether (10 cm^3) was added slowly to the stirred solution, which was left for a further 14 h at −78°C. The precipitated beige–brown solid was isolated and washed with pentane (4 × 50 cm^3) at −78°C and dried *in vacuo*. Yield 0·52 g (57% theory). Found: C, 24·7; H, 3·7; I, 29·1; W, 42·4. Calc. for $C_9H_{15}IW$: C, 24·9; H, 3·5; I, 29·2; W, 42·4%.

IR (KBr, −50°C): ν 3080–3025, 1498, 1010, 590. FIR (polyethylene, −90°C): ν(WI) 149. MS: m/z 434 (M^+), 392 ($M^+ - 42$), 301 (100%), 261, 42. ^{1}H NMR spectrum: see Table 1.

$(\eta^3\text{-}C_3H_5)_3WCl_2AlCl_2$ (5)

This compound is presumed to be present in the brown solution formed upon reacting $[(\eta^3\text{-}C_3H_5)_3WCl]_2$ with $AlCl_3$ (1 : 1) in d_8-toluene.

^{1}H NMR spectrum: see Table 1.

$(\eta^3\text{-}C_3H_5)_3WO_2CMe$ (6)

$[(\eta^3\text{-}C_3H_5)_3WCl]_2$ (2·90 g, 8·47 mmol) was stirred in ether (60 cm^3) with silver acetate (1·41 g, 8·45 mmol) at −20°C for 8 days. The solvent was distilled off *in vacuo* and the residue extracted with pentane (4 × 30 cm^3) at −30°C. The combined extract was evaporated and the resulting yellow solid recrystallized from hexane at −30°C. A second fraction was obtained by treating the mother liquor with active charcoal to remove oily impurities. The compound is relatively stable and is not immediately oxidized by air. Combined yield 2·32 g (75% theory). Found: C, 36·1; H, 5·0; W, 50·1. Calc. for $C_{11}H_{18}O_2W$: C, 36·1; H, 5·0; W, 50·2%.

IR (KBr, −45°C): *v* 3080–3000, 1530 (OAc), 1480 (OAc), 1465, 1375, 1010, 585. MS: *m/z* 366 (M^+), 342 (M^+ −42), 281, 253, 60, 43 (100%), 41. ^1H NMR spectrum: see Table 1.

$(\eta^3\text{-}C_3H_5)_3WO_2CCF_3$ (7)

$[(\eta^3\text{-}C_3H_5)_3WCl]_2$ (0·95 g, 2·77 mol) was stirred in ether (60 cm^3) with thallium trifluoroacetate (0·87 g, 2·74 mmol) at −40°C for 4 days. The reaction mixture was filtered to remove TlCl, evaporated to dryness and the product dissolved in pentane at −50°C and precipitated out at −78°C. A second impure fraction could be obtained by reacting the mother liquor with Avicel. The compound decomposes above −40°C. Yield 0·50 g (43% theory). Found: C, 31·3; H, 3·7; F, 13·7; W, 43·6. Calc. for $C_{11}H_{15}F_3O_2W$: C, 31·5; H, 3·6; F, 13·6; W, 43·8%.

IR (film, RT): *v* 3080–3000; 1670 (CO), 1610 (CO), 1498, 1210, 1165, 1015, 600, 585. MS: *m/z* 420 (M^+), 378 (M^+ −42), 69, 50, 42, 41, 39 (100%). ^1H NMR spectrum: see Table 1.

$(\eta^3\text{-}C_3H_5)_3W(acac)$ (8)

$[(\eta^3\text{-}C_3H_5)_3WCl]_2$ (0·96 g, 2·80 mmol) was stirred in dichloromethane (50 cm^3) with thallium acetylacetonate (0·85 g, 2·80 mmol) at −40°C for 18 h. The solvent was removed *in vacuo* and the residue extracted with pentane (3 × 40 cm^3) at −40°C. The combined extract was concentrated and cooled to −78°C to give the product as a bright yellow solid. The compound decomposes at room temperature. Yield 0·68 g (60% theory). Found: C, 41·3; H, 5·5; W, 45·1. Calc. for $C_{14}H_{22}O_2W$: C, 41·4; H, 5·5; W, 45·3%.

IR (KBr, −45°C): *v* 3080–3000, 1598 (CO), 1525 (CO), 1498, 1370, 1012, 580. MS: *m/z* 406 (M^+), 364 (M^+ −42), 42, 41 (100%). ^1H NMR spectrum: see Table 1. The compound is formed as a mixture of two isomers in the ratio 73:27.

$(\eta^3\text{-}C_3H_5)_3W(PF_3)Cl$ (9)

Trifluorophosphine was passed over a solution of $[(\eta^3\text{-}C_3H_5)_3WCl]_2$ (0·15 g, 0·43 mmol) in ether (30 cm^3) at −50°C. A yellow solution was formed from which the compound was isolated as a pale yellow solid. Yield 0·18 g (95% theory). The instability of the compound prevented its analysis.

^1H NMR spectrum: see Table 1. ^{31}P NMR (d_8-THF, −30°C): δ 113·7 (dt, *J*(P,F) 1334·6, *J*(P,W) 350·9).

$(\eta^3\text{-}C_3H_5)_3W(PMe_3)Cl$ (10)

Trimethylphosphine (5 cm^3, 47·7 mmol) was added dropwise at −30°C with stirring to $[(\eta^3\text{-}C_3H_5)_3WCl]_2$ (1·0 g, 2·92 mmol). A yellow solid was formed immediately. The excess phosphine was removed *in vacuo* and the residue dissolved in ether. The compound crystallized out at −30°C as a yellow solid and a second fraction was obtained by concentrating the mother liquor. The compound is stable at room temperature and does not react with air. Yield 1·20 g (98% theory). Found: C, 34·3; H, 6·0; Cl, 8·4; P, 7·3; W, 43·9. Calc. for $C_{12}H_{24}ClPW$: C, 34·4; H, 5·8; Cl, 8·5; P, 7·4; W, 43·9%.

IR (KBr, RT): *v* 3080–3020, 1500, 1425, 1015, 935, 595. FIR (polyethylene, RT): *v*(WCl) 206. MS: *m/z* 418 (M^+), 376 (M^+ −42), 76, 41 (100%). ^1H NMR spectrum: see Table 1. ^{13}C NMR (d_8-THF, RT): δ 101·6 (C-*meso*), 67·4 (C-1), 55·4 (C-2)-allyl-1; 95·1 (C-*meso*), 64·9 (C-1), 47·9 (C-2)-allyl-2; 88·4 (C-*meso*), 63·0 (C-1), 41·7 (C-2)-allyl-3; 14·8 (PMe, *J*(C,P) *ca* 30·5). ^{31}P NMR (d_8-THF, −30°C): δ −29·1. 2D-^{31}P-^{183}W NMR (d_8-THF, 27°C): δ −2263 (^1J(P,W) 173·5).

$(\eta^3\text{-}C_3H_5)_3W(P(OMe)_3)Cl$ (11)

Trimethylphosphite (2 cm^3, 16·9 mmol) was added to $[(\eta^3\text{-}C_3H_5)_3WCl]_2$ (0·55 g, 1·59 mmol) at −30°C. The reaction mixture was stirred for 30 min and the excess phosphite removed *in vacuo*. The residue was washed with pentane (5 × 5 cm^3) at −80°C and dissolved in ether (20 cm^3) at −30°C. The resulting green solution was concentrated and cooled to −50°C. The product precipitated as a pale green solid. Yield 0·51 g (68·7% theory). Found: C, 30·9; H, 5·2; Cl, 7·6; P, 6·6; W, 39·4. Calc. for $C_{12}H_{24}ClO_3PW$: C, 30·8; H, 5·2; Cl, 7·6; P, 6·7; W, 39·6%.

IR (KBr, −30°C): *v* 3040, 1495, 1100–1000, 1005, 575. ^1H NMR spectrum: see Table 1.

$(\eta^3\text{-}C_3H_5)_3W(py)Cl$ (**12**)

$[(\eta^3\text{-}C_3H_5)_3WCl]_2$ (0·55 g, 1·59 mmol) was suspended in pyridine (2·2 cm^3) at −30°C and dichloromethene (20 cm^3) was added. The reaction mixture was stirred for 30 min, the solution evaporated and the resulting yellow–green residue washed with ether (3 × 2 cm^3) and dried *in vacuo*. Yield 0·48 g (71·6% theory). Found: C, 39·9; H, 4·8; Cl, 8·4; N, 3·3; W, 43·6. Calc. for $C_{14}H_{20}ClNW$: C, 39·8; H, 4·8; Cl, 8·3; N, 3·4; W, 33·7%.

IR (KBr, −30°C): *v* 3060, 3010, 1600, 1485, 1440, 1060, 1020, 1010, 760, 700. ^1H NMR spectrum: see Table 1.

$(\eta^3\text{-}C_3H_5)_3W(NCMe)Cl$ (**13**)

$[(\eta^3\text{-}C_3H_5)_3WCl]_2$ (0·59 g, 1·72 mmol) was suspended in acetonitrile (4 cm^3) and dichloromethene (15 cm^3) was added at −50°C. The resulting solution was stirred for 5 h, warmed to −30°C and concentrated to 5 cm^3, to give a white solid which was washed with acetonitrile and ether and dried under high vacuum. Yield 0·46 g (69·7% theory). Found: C, 34·5; H, 4·7; Cl, 9·2; N, 3·7; W, 47·9. Calc. for $C_{11}H_{18}ClNW$: C, 34·5; H, 4·8; Cl, 9·3; N, 3·5; W, 47·8%.

IR (KBr, −30°C): *v* 3060, 2318 (NC), 2280(NC), 1495, 1015. ^1H NMR (CD_2Cl_2, −30°C): δ 3·95 (*anti*-H), 0·56 (*anti*-H), 0·41 (*anti*-H), 2·20 (Me), 2·39 (Me). The compound is formed as a mixture of two isomers (55 : 45).

$(\eta^3\text{-}C_3H_5)_3W(CNC_4H_9)Cl$ (**14**)

$[(\eta^3\text{-}C_3H_5)_3WCl]_2$ (1·34 g, 3·91 mmol) and *n*-butylisocyanide (0·42 cm^3, 4·0 mmol) were suspended in ether (30 cm^3) at −78°C and stirred for 5 days. The resulting grey–beige suspension was evaporated to dryness at −78°C and the residue washed with pentane (2 × 20 cm^3) at −30°C and dried *in vacuo*. Yield 1·56 g (94% theory). Found: C, 39·7; H, 5·0; Cl, 8·5; N, 3·4; W, 43·3. Calc. for $C_{14}H_{24}ClNW$: C, 39·5; H, 5·7; Cl, 8·3; N, 3·3; W, 43·2%.

IR (KBr, −50°C): *v* 3080–3025, 2205 (CN), 1498, 1465, 1010, 590. MS: *m/z* 425 (M^+), 383 (M^+ −42), 300, 86 (100%), 42, 41. ^1H NMR spectrum: see Table 1.

$[(\eta^3\text{-}C_3H_5)_3WCl]_2(Me_2PC_2H_4PMe_2)$ (**15**)

$[(\eta^3\text{-}C_3H_5)_3WCl]_2$ (0·59 g, 1·72 mmol) and 1,2-bis(dimethylphosphino)ethane (0·26 g, 1·74 mmol) were stirred at −60°C in ether (50 cm^3) for 6 days. The reaction mixture was evaporated *in vacuo* at −30°C and the resulting grey–beige residue washed with pentane (3 × 30 cm^3). Yield 0·61 g (85% theory). Found: C, 34·6; H, 5·7; Cl, 8·4; P, 7·3; W, 43·9. Calc. for $C_{24}H_{46}Cl_2P_2W_2$: C, 34·5; H, 5·6; Cl, 8·5; P, 7·4; W, 44·0%.

IR (KBr, −50°C): *v* 3080–3025, 1498, 1430, 1015, 940, 595. MS: *m/z* 449, 95, 55, 42, 41. ^1H NMR spectrum: see Table 1. ^{31}P NMR (d_8-THF, 27°C): δ −19·3, ^1J(P,P) 12·6, ^1J(P,W) 169·9.

$(\eta^3\text{-}C_3H_5)_3W(PMe_3)Br$ (**16**)

$[(\eta^3\text{-}C_3H_5)_3WBr]_2$ (0·24 g, 0·62 mmol) was suspended in ether (4 cm^3) at −60°C and treated with trimethylphosphine (0·30 cm^3, 2·87 mmol). The reaction temperature was allowed to reach 0°C over 8 h. The solvent was removed at −40°C *in vacuo* and the beige residue was recrystallized from ether. Yield 0·27 g (94% theory). Found: C, 31·2; H, 5·3; Br, 17·2; P, 6·6; W, 39·6. Calc. for $C_{12}H_{24}BrPW$: C, 31·1; H, 5·2; Br, 17·3; P, 6·7; W, 39·7%.

IR (KBr, −25°C); *v* 3080–3025, 1498, 1420, 1010, 960. FIR (polyethylene, −90°C): *v*(WBr) 133. MS: *m/z* 462 (M^+), 420 (M^+ −42), 76, 61, 42, 41 (100%). ^1H NMR spectrum: see Table 1. ^{31}P NMR (d_8-THF, 25°C): δ −34·3, *J*(P,W) 171·5. 2D–^{31}P–^{183}W (d_8-THF, 25°C): δ ^{183}W −2244.

$(\eta^3\text{-}C_3H_5)_3W(PMe_3)I$ (**17**)

$[(\eta^3\text{-}C_3H_5)_3WI]_2$ (0·20 g, 0·46 mmol) was suspended in ether (5 cm^3) at −60°C and treated with trimethylphosphine (0·25 cm^3, 2·39 mmol). The reaction mixture was allowed to warm to −30°C over 3 h and the resulting solution was filtered and evaporated to dryness at −40°C to give the product as a yellow powder. Yield 0·22 g (93% theory). Found: C, 28·4; H, 5·0; I, 24·7; P, 6·0; W, 35·9. Calc. for $C_{12}H_{24}IPW$: C, 28·3; H, 4·7; I, 24·9; P, 6·1; W, 36·1%.

IR (KBr, 25°C): *v* 3080–3025, 1495, 1425, 1010, 945. FIR (polyethylene, −50°C): *v*(WI) < 100. MS: *m/z* 510 (M^+), 468 (M^+ −42), 76, 61, 42, 41 (100%). ^1H NMR spectrum: see Table 1. ^{31}P NMR (d_8-THF, 25°C): δ −40·0, ^1J(P,W) 170·9. 2D–^{31}P–^{183}W NMR (d_8-THF, 25°C): δ ^{183}W −2172.

$(\eta^3\text{-}C_3H_5)_2W(P(OMe)_3)_3$ (**18**)

$(\eta^3\text{-}C_3H_5)_3W(P(OMe)_3)Cl$ (0·43 g, 0·92 mmol) and trimethylphosphite (2·5 cm^3, 21 mmol) were dissolved in THF (40 cm^3) at −30°C. Excess lithium powder was added and the solution stirred at −50°C for 18 h. The unreacted lithium was filtered off and the solution was evaporated to

dryness. The solid residue was extracted with ether (20 cm^3) at −30°C and the extract evaporated to dryness to give the product which was washed repeatedly with pentane. Yield 0·19 g (41·8% theory).

^1H NMR (d_8-toluene, −80°C): δ 5·36 (H1, br), 2·19 (H2, t), 2·39 (H3, d), 1·74 (H4, d), 1·35 (H5, d), 3·45 (Me, d), 3·35 (Me, s), J(1,2) 5·9, J(1,3) 5·6, J(2,3) 3·8, J(1,4) 7·6, J(1,5) 7·1, J(Me,P) 9·8, ΣJ(Me′,P) 8·6. ^{31}P NMR (d_8-toluene, 50°C): δ_P 159·0, $\delta_{P'}$, 141·3, J(P,W) 486·5, J(P′,W) 445·9, J(P,P′) 44·2.

$(\eta^3\text{-}C_3H_5)_3W(PMe_3)Me$ (**19**)

$(\eta^3\text{-}C_3H_5)_3W(PMe_3)Cl$ (0·30 g, 0·72 mmol) was dissolved in ether (50 cm^3) at −30°C and methylmagnesium iodide in ether (0·22 cm^3, 0·72 mmol) was added dropwise. The reaction mixture was stirred for 12 h, the solvent removed *in vacuo* and the residue extracted with pentane (4 × 30 cm^3) at −30°C. Cooling the concentrated extract gave the product as a yellow powder. Yield 0·19 g (66% theory). Found: C, 39·3; H, 6·9; P, 7·6; W, 46·4. Calc. for $C_{13}H_{27}PW$: C, 39·2; H, 6·8; P, 7·8; W, 46·2%.

IR (KBr, 25°C): ν 3080–3025, 1498, 1475, 1425, 1012, 940, 598. MS: m/z 398 (M^+), 383 (M^+ −Me), 355, 302, 276, 76, 61 (100%), 42, 41. ^1H NMR spectrum: see Table 1. ^{31}P NMR (d_8-THF, −80°C): δ −26·4, ^1J(P,W) 166·0, 2D–^{31}P–^{183}W NMR (d_8-THF, 27°C): δ ^{183}W −2999.

$(\eta^3\text{-}C_3H_5)_3W(PMe_3)Et$ (**20**)

$(\eta^3\text{-}C_3H_5)_3W(PMe_3)Cl$ (0·63 g, 1·50 mmol) was dissolved in ether (100 cm^3) at −24°C and treated dropwise with ethylmagnesium iodide in ether (1·0 cm^3, 1·50 mmol). The reaction mixture was stirred for a further 16 h, the solvent evaporated *in vacuo* and the residue extracted with pentane (5 × 20 cm^3) at −30°C. The compound was obtained as a yellow powder by cooling the concentrated extract. Yield 0·48 g (77% theory). Found: C, 40·9; H, 6·9; P, 7·4; W, 44·5. Calc. for $C_{14}H_{29}PW$: C, 40·8; H, 7·1; P, 7·5; W, 44·6%.

IR (KBr, 25°C): ν 3080–3025, 1498, 1425, 1012, 950, 598. MS: m/z 412 (M^+), 370 (M^+ −42), 366, 328, 76, 61, 42, 41, 29, 28, 27 (100%). ^1H NMR spectrum: see Table 1. ^{31}P NMR (d_8-THF, 30°C): δ −28·0, ^1J(P,W) 179·4.

REFERENCES

1. W. Oberkirch, Dissertation, Techn. Hochschule Aachen (1963).
2. G. Wilke, B. Bogdanović, P. Heimbach, W. Keim, M. Kröner, W. Oberkirch, K. Tanaka, E. Steinrücke, D. Walter and H. Zimmermann, *Angew. Chem.* 1966, **78**, 157.
3. G. Wilke (Studiengesellschaft Kohle mbH), Ger. 1,197,453 (1963).
4. See for example, E. L. Vollershtein, S. I. Beiln and B. A. Dolgoplosk, *Dokl. Akad. Nauk. SSSR* 1972, **202**, 1071; Y. I. Ermakov, B. N. Kuznetsov and A. N. Startsevi, *Kinet. Katal.* 1974, **15**, 539; I. A. Oreshkin, L. T. Red'kina, V. L. Makovetskii, E. I. Tinyakova and B. A. Dolgoplosk, *Vysokoml. Soedin. Ser. B.* 1972, **14**, 384.
5. J. P. Candlin and H. Thomas, *Adv. Chem. Ser.* 1974, **132**, 212.
6. R. Benn, A. Rufińska and G. Schroth, *J. Organomet. Chem.* 1981, **217**, 91.
7. R. Benn, S. Holle, P. W. Jolly, C. Krüger, C. C. Romão, M. J. Romão, A. Rufińska and G. Schroth, *Polyhedron* 1986, **5**, 461.
8. P. R. Brown, F. G. N. Cloke, M. L. H. Green and N. J. Hazel, *J. Chem. Soc., Dalton Trans.* 1983, 1075.
9. R. Benn, A. Rufińska, *Magn. Reson. Chem.* 1988, **26**, 895.
10. M. Minelli, J. H. Enmark, R. T. C. Brownlee, M. J. O'Connor and A. G. Wedd, *Coord. Chem. Rev.* 1985, **68**, 169.
11. H. Funk and W. Baumann, *Z. Anorg. Allg. Chem.* 1937, **231**, 264.

Polyhedron Vol. 9, No. 1, pp. 23–34, 1990
Printed in Great Britain

0277–5387/90 $3.00+.00
© 1989 Pergamon Press plc

η^3-ALLYL COMPLEXES OF TUNGSTEN—II. REACTION OF $[(\eta^3\text{-}C_3H_5)_3WCl]_2$ WITH ORGANOMAGNESIUM COMPOUNDS

R. BENN, T. H. BROCK, P. W. JOLLY,* A. RUFIŃSKA and G. SCHROTH

Max-Planck-Institut für Kohlenforschung, D-4330 Mülheim a.d. Ruhr, F.R.G.

(*Received* 3 *July* 1989; *accepted* 31 *July* 1989)

Abstract—$[(\eta^3\text{-}C_3H_5)_3WCl]_2$ reacts with alkylmagnesium halides to give $(\eta^3\text{-}C_3H_5)_3WR$ species in which the β-H-atoms of the alkyl group interact with the metal atom in an agostic manner. $(\eta^3\text{-}C_3H_5)_3WEt$ reacts with trimethylphosphine with intramolecular protonation of an allyl group to give $(\eta^3\text{-}C_3H_5)_2(\eta^2\text{-}CH_2:CH_2)W(PMe_3)_2$ with elimination of propene, and with butylisocyanide with insertion into the W—Et bond to give $(\eta^3\text{-}C_3H_5)_3(\eta^2\text{-}EtC:NC_4H_9)W$. Methyl-substituted allylmagnesium halides react with $[(\eta^3\text{-}C_3H_5)_3WCl]_2$ to give $(\eta^3\text{-}C_3H_5)_3(\eta^3\text{-}MeC_3H_4)W$ and $(\eta^3\text{-}C_3H_5)_3(\eta^3\text{-}1,3\text{-}Me_2C_3H_3)W$ as a mixture of isomers.

In the preceding publication we described the preparation of $[(\eta^3\text{-}C_3H_5)_3WCl]_2$ (**1**) from $(\eta^3\text{-}C_3H_5)_4W$ and gaseous HCl and the further reaction with trimethylphosphine and alkylmagnesium halides to give $(\eta^3\text{-}C_3H_5)_3W(PMe_3)R$ species.[1] Here we discuss the course of reaction in the absence of donor ligands.

RESULTS AND DISCUSSION

$[(\eta^3\text{-}C_3H_5)_3WCl]_2$ (**1**) reacts readily with alkylmagnesium halides to give yellow compounds having the composition $(\eta^3\text{-}C_3H_5)_3WR$ [**2–7**, eq. (1)]:

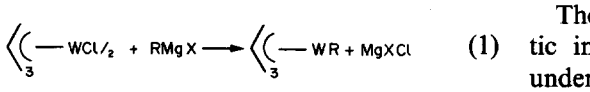

(1)

R=Et, **2**; R=CH_2CD_3, **3**; R=C_3H_7, **4**;
R=C_3H_7-*i*, **5**; R=C_4H_9, **6**; R=C_5H_{11}, **7**

The thermal stability and the yield of these compounds decrease with increasing length of the alkyl chain and whereas the ethyl compound, **2**, can be handled briefly at 0°C, the pentenyl derivative, **7**, decomposes at this temperature within a few seconds. A 3-butenyl derivative, **8**, could not be obtained pure and we were unable to isolate a cyclohexyl derivative. The NMR spectroscopic results described in the following section indicate that the compounds have a structure in which the β-H atoms of the alkyl group interact with the metal in an agostic manner,[2] e.g. **2**. However, in contrast to the analogous molybdenum system,[3] rotation of the β-alkyl group with proton-exchange could not be frozen out on the NMR time scale even at −125°C.

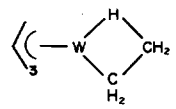

2

The importance of the 2-electron, 3-centred agostic interaction in stabilizing the compounds is underlined by attempts to prepare $(\eta^3\text{-}C_3H_5)_3WMe$ (**9**): the reaction between **1** and methylmagnesium iodide produced a violet compound which could not be obtained analytically pure and which decomposed if warmed above −78°C. The ^1H NMR spectrum of this species (δ 4.91/4.31/3.54 (*syn*-H), *ca* 0.1/0.3 (*anti*-H), 0.74 (s, Me, d_8-THF, −80°C), the mass spectrum (*m/z* 322, M^+) and the IR spectrum are consistent with the presence of **9** and moreover, the addition of trimethylphosphine to the reaction mixture led to the formation of $(\eta^3\text{-}C_3H_5)_3W(PMe_3)Me$ (spectroscopic comparison) which we had previously prepared by reacting $(\eta^3\text{-}C_3H_5)_3W(PMe_3)Cl$ with methylmagnesium iodide.[1] Related compounds containing a Me_3C- or $(Me_3Si)_3C$-group could not be prepared.

* Author to whom correspondence should be addressed.

The $(\eta^3\text{-}C_3H_5)_3WR$ compounds do not react with alkenes, alkynes or CO with insertion into the W—C bond. In the case of the propyl, **4**, and butyl, **6**, derivatives it has been shown spectroscopically that a slow reaction occurs with ethylene (1.1 at, −50°C, 8 days) to give the ethyl derivative, **2**. This reaction is presumably the result of alkene exchange in an intermediate $(\eta^3\text{-}C_3H_5)_3$(alkene)WH species; the less strongly bonded substituted alkene being displaced by ethylene [eq. (2)]:

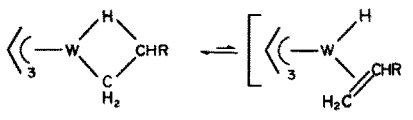

4, 6

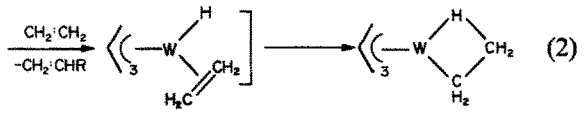

(2)

2

In contrast, the ethyl derivative **2** does react with butylisocyanide with insertion into the W—C bond and compound **10** containing an η^2-N-butylpropyliminoacyl group is formed [eq. (3)]. This reaction presumably involves the initial formation of an adduct which reacts further with isonitrile insertion.

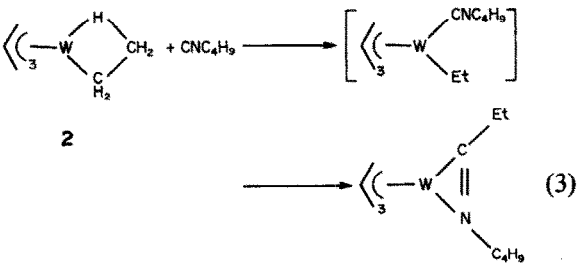

2

(3)

10

The suggested structure for **10** is supported by a comparison of the IR and ^{13}C NMR data (ν(C:N) 1680, δ(C:N) 211.5) with, for example, those for a related molybdenum compound $CpMo(CO)_2(\eta^2$-MeC:NMe: (ν(C:N) 1720, δ(C:N) 195.2), as well as for $CpMo(CO)_2(P(OMe)_3)(\eta^1$-PhC:NMe): ($\nu$(C:N) 1570, δ(C:N) 155.5).[4,5]

$(\eta^3\text{-}C_3H_5)_3WEt$ (**2**) reacts at low temperature with trimethylphosphine. The product is not, however, the expected adduct $(\eta^3\text{-}C_3H_5)_3W(PMe_3)Et$, instead intramolecular protonation of an allyl group by the agostic hydrogen atom occurs to give $(\eta^3\text{-}C_3H_5)_2(\eta^2\text{-}CH_2\text{:}CH_2)W(PMe_3)_2$ [eq. (4)]. The initial isolated product is an unsymmetrical isomer (**11**; ^{31}P NMR, ABX-spin system) which rearranges above −40°C to a symmetrical form (**12**; ^{31}P NMR, A_2X-spin system), whereby the mutual arrangement of the two allyl groups in these species has not been established.

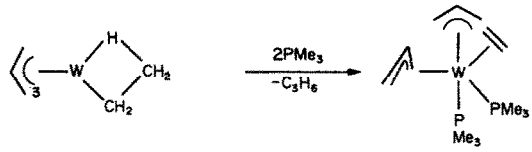

2 **11**

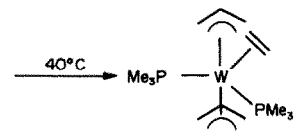

(4)

12

A similar reaction is observed with bis(dimethylphosphino)ethane, but in this case the product, $(\eta^3\text{-}C_3H_5)_2(\eta^2\text{-}CH_2\text{:}CH_2)W(Me_2PC_2H_4PMe_2)$ (**13**), has an unsymmetrical structure related to **11** and moreover, shows no tendency to rearrange.

Reaction of $[(\eta^3\text{-}C_3H_5)_3WCl]_2$ with allylmagnesium halides does not lead to compounds containing an η^1-allyl group, instead the allyl group isomerizes and the mixed tetra(η^3-allyl)tungsten compounds: $(\eta^3\text{-}C_3H_5)_3(\eta^3\text{-}2\text{-}MeC_3H_4)W$ (**14**), $(\eta^3\text{-}C_3H_5)_3(\eta^3\text{-}1\text{-}MeC_3H_4)W$ (**15**) and $(\eta^3\text{-}C_3H_5)_3(\eta^3\text{-}1,3\text{-}Me_2C_3H_3)W$ (**16**) are formed. Compounds **15** and **16** are formed as a mixture of two isomers. The NMR spectroscopic investigations indicate that in the case of the 1-methylallyl system, **15**, the methyl group occupies a *syn* position in both isomers and that these differ in the arrangement of the substituted allyl group with respect to the other three allyl groups. The isomers containing an η^3-1,3-$Me_2C_3H_3$ group differ in the configuration of the methyl groups: in **16a** these both occupy a *syn* position while in **16b** one methyl group is *syn* and the other *anti*.

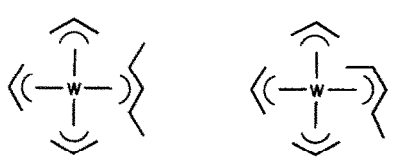

16a **16b**

The arrangement of the allyl groups with respect to each other has been confirmed in these compounds by COSY and NOESY experiments (see below) which indicate that the organic ligands adopt a pseudo-tetrahedral arrangement around the central metal atom similar to that suggested for $(\eta^3\text{-}C_3H_5)_4W$.[1]

Table 1. ^{1}H NMR data for $(\eta^3\text{-}C_3H_5)_3WR$ and related compounds

Compound	Solvent, temperature (°C)	δ_{meso}(H*n*,m)	δ_{syn}(H*n*,m)	δ_{anti}(H*n*,m)	*J*(Hz)	Miscellaneous
$(\eta^3\text{-}C_3H_5)_3WCH_2CH_3$[a] (2)	d_8-THF, −80	4.11 (H1,m) 3.88 (H11,m) 3.28 (H21,m)	3.15 (H2,m) 1.54(H3,m) 2.51 (H12,dd) 1.45 (H13,m) 2.83 (H22,dd) 3.21 (H23,m)	2.43 (H4,dd) −0.59 (H5,dd) 3.35 (H14,d) 0.33 (H15,dd) 0.87 (H24,d) 2.56 (H25,dd)	*J*(1,2) 8.0, *J*(1,3) 7.4, *J*(1,4) 12.4, *J*(1,5) 10.6, *J*(2,3) 3.2, *J*(2,4) 3.2, *J*(3,5) 3.2. *J*(11,12) 8.0, *J*(11,13) 8.3, *J*(11,14) 12.5, *J*(11,15) 10.0, *J*(12,13) 2.3, *J*(12,14) 0, *J*(13,15) 2.2. *J*(21,22) 8.6, *J*(21,23) 8.3, *J*(21,24) 11.8, *J*(21,25) 12.3, *J*(22,23) 3.0, *J*(22,24) 0, *J*(23,25) 2.6.	2.08/1.36 (WCH_2, dd/dq, ^2J(H,H) −5.6, ^3J(H,H) 7.0/7.0), −2.95 (CMe, dd, ^3J(H,H) 7.0).
$(\eta^3\text{-}C_3H_5)_3WCH_2CD_3$[a] (3)	d_8-THF, −80	4.15 (H1,m) 3.93 (H11,m) *ca* 3.2 (H21)	*ca* 3.2 (H2) 1.53 (H3,m) *ca* 2.5 (H12) 1.45 (H13,m) 2.80 (H22,m) *ca* 3.2 (H23)	*ca* 3.2 (H2) −0.64 (H5,dd) 3.33 (H14,dd) 0.30 (H15,dd) 0.82 (H24,dd) *ca* 2.5 (H25)		2.02/1.30 (WCH_2, d/d)
$(\eta^3\text{-}C_3H_5)_3WCH_2CH_2CH_3$[a] (4)	d_6-acetone, −80	4.15 (H1,m) 3.82 (H11,m) 3.50 (H2,m)	3.14 (H2,m) 1.56 (H3,m) 2.46 (H12,dd) 1.35 (H13,m) 3.33 (H22,m) 2.84 (H23,dd)	2.47 (H4,dd) −0.32 (H5,dd) 3.24 (H14,d) 0.23 (H15,dd) 2.54 (H24,dd) 0.91 (H25,d)	*J*(1,2) 7.9, *J*(1,3) 7.3, *J*(1,4) 12.4, *J*(1,5) 10.2, *J*(2,3) 3.4, *J*(2,4) 3.1, *J*(3,5) 3.2, *J*(4,5) *ca* 0. *J*(11,12) 8.0, *J*(11,13) 8.4, *J*(11,14) 12.4, *J*(11,15) 9.7, *J*(12,13) 2.3, *J*(12,14) 0, *J*(13,15) *ca* 1.9. *J*(21,22) 8.4, *J*(21,23) 8.5, *J*(21,24) 12.7, *J*(21,25) 11.9, *J*(22,23) 2.9, *J*(22,24) 2.7, *J*(23,25) 0.	1.28/2.07 (WCH_2, dt/dt, ^2J(H,H) −6.6, ^3J(H,H) *ca* 6.6/6.6), −3.42 (WHC, br), −4.19 (C*H*Me, br), 0.85 (Me dd, ^3J(H,H) 6.0/6.0)
$(\eta^3\text{-}C_3H_5)_3WCHMe_2$[a] (5)	d_6-acetone, −80	4.0 (H1,m) 3.93 (H11,m) *ca* 3.1 (H21)	1.49 (H3,m) 2.50 (H12,m) 1.34 (H13,m) 2.74 (H23,m)	2.53 (H4,m) −0.50 (H5,dd) 3.33 (H14,dd) 0.27 (H15,dd) 0.74 (H25,d)		2.20 (WCH, m), −2.84 (WHC, br), 1.69 (CMe, d)

Table 1. (*continued*)

Compound	Solvent, temperature (°C)	δ_{meso}(H*n*,m)	δ_{syn}(H*n*,m)	δ_{anti}(H*n*,m)	*J*(Hz)	Miscellaneous
$(\eta^3\text{-}C_3H_5)_3WC_4H_9\text{-}n$[a] **(6)**	d_6-acetone, −80	4.14 (H1,m) 3.84 (H11,m) 3.50 (H21,m)	3.14 (H2,m) 1.54 (H3,m) 2.48 (H12,dd) 1.35 (H13,m) 3.34 (H22,m) 2.82 (H23,dd)	2.41 (H4,dd) −0.37 (H5,dd) 3.26 (H14,d) 0.23 (H15,dd) 2.55 (H24,dd) 0.90 (H25,d)	*J*(1,2) 7.9, *J*(1,3) 7.4, *J*(1,4) 12.4, *J*(1,5) 10.3, *J*(2,3) 3.3, *J*(2,4) *ca* 3.3, *J*(3,5) *ca* 3.3. *J*(11,12) 8.3, *J*(11,13) 8.3, *J*(11,14) *ca* 12.5, *J*(11,15) *ca* 9.8, *J*(12,13) *ca* 2.2, *J*(12,14) 0, *J*(13,15) *ca* 2.2. *J*(21,22) 8.4, *J*(21,23) 8.4, *J*(21,24) 12.5, *J*(21,25) 11.7, *J*(22,23) 2.9, *J*(22,24) 2.8, *J*(23,25) 0.	1.25/*ca* 2.05 (m, WCH_2). −3.64 (WHC, m), −4.04 (CH, m), 0.77 (Me, t, ^3J(H,H) 7.4), 1.18 (MeCH_2, m).
$(\eta^3\text{-}C_3H_5)_3WC_4H_8CH_3$[a] **(7)**	d_8-THF, −80	4.13 (H1,m) 3.83 (H11,m) 3.56 (H21,m)	3.18 (H2,m) 1.58 (H3,m) 2.51 (H21,dd) *ca* 3.32 (H22) 2.87 (H23,dd)	2.37 (H4,dd) −0.34 (H5,dd) *ca* 3.32 (H14) 0.30 (H15,dd) 2.60 (H24,dd)		2.11 (WCH_2, dt), −3.86 (WHC, br), 0.83 (Me, t)
$(\eta^3\text{-}C_3H_5)_3WC_2H_4CH\text{:}CH_2$[b] **(8)**	d_8-THF, −50	4.50 (H12,m) 3.79 (H11,m) *ca* 4.15 (H21)		−0.30 (H5,dd) −0.48 (H15,dd) 0.30 (H24,dd)		−3.86 (WHC, br), 5.76 (CH:, m), 4.94 (H_2C:, m)
$(\eta^3\text{-}C_3H_5)_3W(\eta^2\text{-EtC:}NC_4H_9)$[c] **(10)**	d_8-THF, −40	4.08 (H1,m) 3.49 (H11,m) 2.94 (H21,m)	3.12 (H2,m) 1.91 (H3,m) 2.23 (H12,dd) 1.19 (H13,m) 3.79 (H22,m) 2.10 (H23,m)	2.12 (H4,dd) −0.77 (H5,dd) 2.76 (H14,dd) −0.19 (H15,dd) 3.06 (H24,dd) 0.70 (H25,d)	*J*(1,2) 8.1, *J*(1,3) 8.0, *J*(1,4) 12.8, *J*(1,5) 10.5, *J*(2,3) 2.6, *J*(2,4) 2.3, *J*(3,5) 2.7. *J*(11,12) 7.8, *J*(11,13) 8.3, *J*(11,14) 11.0, *J*(11,15) 9.4, *J*(12,13) 2.5, *J*(12,14) *ca* 0, *J*(12, 15) 2.1. *J*(21,22) 8.7, *J*(21,23) 8.6, *J*(21,24) 13.0, *J*(21,25) 12.0, *J*(22,23) 1.8, *J*(22,24) *ca* 1.2	3.22 (H6, m), 3.03 (H7, m), 2.92 (H8, td) 2.74 (H9, td), 1.28 (H10, dd), *ca* 1.3 (H16-19), 1.28 (H20, t), *J*(6,7) −12.5, *J*(6,16) 6.0, *J*(6,17) 9.0, *J*(7,16) *ca* 5.4, *J*(7,17) *ca* 8.8, *J*(8,9) −14.6, *J*(8,10) 7.8, *J*(9,10) 7.4, *J*(18,20) *ca* 7.1, *J*(19,20) 7.1

$(\eta^3\text{-}C_3H_5)_2(\eta^2\text{-}CH_2{:}CH_2)W(PMe_3)_2$[d] **(11)**	d_8-THF, −40	4.3 (H1,m)	1.67 (H2,m) 0.13 (H3,m)	0.65 (H4,m) 0.94 (H5,m)	*J*(1,2) 6.5, *J*(1,3) 6.9, *J*(1,4) 9.0, *J*(1,5) 9.2, *J*(2,3) 3.9, *J*(2,4) 2.4. *J*(1,P) 8.8, *J*(2,P) 6.5, *J*(4,P) 11.2, *J*(5,P) 9.6.	1.9 (PMe, d, *J*(P,H) 5.6), 1.06 (H-6), −0.02 (H-7, m). *J*(7,P) 2.7, *J*(6,6′) 9.1, *J*(6,7) −2.6, *J*(6,7′) 9.8, *J*(7,7′) 9.0.
$(\eta^3\text{-}C_3H_5)_2(\eta^2\text{-}CH_2{:}CH_2)W(PMe_3)_2$[e] **(12)**	d_8-THF, −40	4.40 (H1,m) 0.95 (H11,m)	2.87 (H2,dd) 1.89 (H3,m) 2.17 (H12,m) 0.20 (H13,m)	2.30 (H4,dd) −1.07 (H5,dd) 1.62 (H14,m) 0.71 (H15,dd)	*J*(1,2) 7.7, *J*(1,3) 7.5, *J*(1,4) 10.8, *J*(1,5) 9.6, *J*(2,3) 2.7, *J*(3,5) 1.3. *J*(11,12) 6.0, *J*(11,14) 8.4, *J*(11,15) 8.1, *J*(12,13) 2.8. *J*(1,P) 14.5, *J*(2,P) 1.3, *J*(3,P) 18.5, *J*(4,P) 3.2. *J*(11,P) 6.6, *J*(12,P) *ca* 6.2, *J*(14,P) *ca* 16.	1.46 (PMe-20, d, *J*(H,P) 7.2), 1.05 (PMe-30, d, *J*(H,P) 5.7), 0.21 (H-16, m), −1.59m (H-17,m).
$(\eta^3\text{-}C_3H_5)_2(\eta^2\text{-}CH_2{:}CH_2)$ $W(Me_2PC_2H_4PMe_2)$[f] **(13)**	d_8-THF, −50	4.49 (H1,m)	2.55 (H2)	2.22 (H4,dd) −1.05 (H5,dd)		1.58/1.42 (Me-20/20′, d) 1.17/0.55 (Me-30/30′, d)
$(\eta^3\text{-}C_3H_5)_3(\eta^3\text{-}2\text{-}MeC_3H_4)W$ **(14)**	d_8-THF, −80	4.32 (H1,m) 4.25 (H11,m) 3.95 (H21,m)	2.05 (H2,m) 1.87 (H12,m)	−0.40 (H5,br) −0.33 (H15,br)	*J*(1,2) *ca* 8.8, *J*(1,3) *ca* 8.8, *J*(1,4) 11.0, *J*(1,5) 13.2. *J*(11,12) 8.7, *J*(11,13) 8.7, *J*(11,14) 11.0, *J*(11,15) 13.0. *J*(21,22) 8.6, *J*(21,23) 8.6, *J*(21,24) *ca* 11.6, *J*(21,25) *ca* 11.6.	2.48/1.41 (br/br, *syn*-H), 2.27 (Me, s).
$(\eta^3\text{-}C_3H_5)_3(\eta^3\text{-}1\text{-}MeC_3H_4)W$[g] **(15a)** (39%)	d_6-acetone, −80	4.81 (H1,m) 4.26 (H11,m) 4.17 (H21,m)	2.63 (H2,m) 1.81 (H3,m) 3.16 (H12,m) 1.78 (H13,m) 3.04 (H22,m) 1.85 (H23,m)	2.78 (H4,m) −0.17 (H5,m) 2.47 (H14,m) −0.37 (H15,m) 3.10 (H24,m) −0.19 (H25,m)	*J*(1,2) 8.8, *J*(1,3) 8.9, *J*(1,4) 13.0, *J*(1,5) 11.0, *J*(2,3) 1.8, *J*(2,4) *ca* 1.5, *J*(2,5) *ca* 1.0, *J*(3,4) *ca* 1.0, *J*(3,5) ≠ 0, *J*(4,5) 1.0. *J*(11,12) 8.7, *J*(11,14) *ca* 11.5, *J*(11,15) *ca* 10.5, *J*(12,13) 2.2, *J*(12,14) *ca* 1.3, *J*(12,15) *ca* 0.7, *J*(13,14) *ca* 1.3, *J*(13,15) ≠ 0, *J*(14,15) *ca* 1.3. *J*(21,22) 8.8, *J*(21,23) 8.6, *J*(21,24) 13.1, *J*(22,23) 2.1, *J*(22,24) *ca* 0.9, *J*(22,25) *ca* 0.9, *J*(23,24) ≠ 0, *J*(23,25) *ca* 2.5, *J*(24,25) ≠ 0.	4.39 (H31, m) 2.73 (H32, m), 1.49 (Me-33, dd), 2.50 (H34,m) 0.27 (H35,m). *J*(31,32) 8.8, *J*(31,33) ≠ 0, *J*(31,34) 12.0, *J*(31,35) 11.5, *J*(32,34) *ca* 1.7, *J*(32,35) *ca* 0.9, *J*(33,35) 6.2, *J*(34,35) *ca* 1.3, *J*(5,35) ≠ 0, *J*(15,25) ≠ 0.

Table 1. (*continued*)

Compound	Solvent, temperature (°C)	δ_{meso}(H*n*,m)	δ_{syn}(H*n*,m)	δ_{anti}(H*n*,m)	*J*(Hz)	Miscellaneous
$(\eta^3\text{-}C_3H_5)_3(\eta^3\text{-}1\text{-}MeC_3H_4)W^h$ **(15b)** (61%)	d_6-acetone, −80	4.49 (H1,m) 4.23 (H11,m) 4.26 (H21,m)	2.77 (H2,m) 1.80 (H3,m) 3.05 (H12,m) 2.06 (H13,m) 2.97 (H22,m) 1.97 (H23,m)	2.44 (H4,m) −0.14 (H5,m) 2.96 (H14,m) −0.23 (H15,m) 2.80 (H24,m) −0.33 (H25,m)	*J*(1,2) 8.8, *J*(1,3) 8.6, *J*(1,4) 12.6, *J*(1,5) 10.8, *J*(2,3) 2.2, *J*(2,4) *ca* 0.9, *J*(2,5) *ca* 0.9, *J*(3,4) ≠ 0, *J*(3,5) *ca* 2.4, *J*(4,5) ≠ 0. *J*(11,12) 8.6, *J*(11,13) 8.5, *J*(11,14) 12.6, *J*(11,15) 11.0, *J*(12,13) 2.2, *J*(12,14) *ca* 0.9, *J*(12,15) *ca* 0.9, *J*(13,14) ≠ 0, *J*(13,15) *ca* 2.4, *J*(14,15) ≠ 0. *J*(21,22) 8.8, *J*(21,23) 8.6, *J*(21,24) 13.1, *J*(21,25) *ca* 10.7, *J*(22,23) 2.1, *J*(22,24) *ca* 0.9, *J*(22,25) *ca* 0.9, *J*(23,24) ≠ 0, *J*(23,25) *ca* 2.3, *J*(24,25) ≠ 0.	4.13 (H31, m), 1.89 (Me-32, d), 1.69 (H33, m), 3.73 (H34, m), −0.45 (H35, m) *J*(31,32) ≠ 0, *J*(31,33) 8.6, *J*(31,34) 12.6, *J*(31,35) 10.0, *J*(32,34) 6.1, *J*(32,35) ≠ 0, *J*(33,34) ≠ 0. *J*(5,15) ≠ 0. *J*(5,25) ≠ 0.
$(\eta^3\text{-}C_3H_5)_3(\eta^3\text{-}1,3\text{-}Me_2C_3H_3)W^i$ **(16a)** (44%)	d_8-THF, −30	4.87 (H1,m) 4.36 (H11,m) 4.23 (H21,m)	2.68 (H2,m) 1.99 (H3,m) 2.86 (H12,m) 1.79 (H13,m) 3.09 (H22,m) 1.89 (H23,m)	2.79 (H4,m) −0.28 (H5,m) 2.58 (H14,m) −0.18 (H15,m) 2.41 (H24,m) −0.58 (H25,m)	*J*(1,2) 8.7, *J*(1,3) 8.7, *J*(1,4) 12.9, *J*(1,5) 11.1, *J*(2,3) 2.0, *J*(2,4)+*J*(2,5) *ca* 1.0, *J*(3,5) 2.6. *J*(11,12) 8.8, *J*(11,13) *ca* 8.6, *J*(11,14) 12.7, *J*(11,15) 10.7, *J*(12,13) 2.2, *J*(12,14)+*J*(12,15) 1.0, *J*(13,15) 2.2. *J*(21,22) *ca* 8.8, *J*(21,23) *ca* 8.5, *J*(21,24) 12.9, *J*(21,25) 10.5, *J*(22,23) 2.1, *J*(22,24)+*J*(22,25) 1.1, *J*(23,25) 2.5.	4.28 (H31, m) 1.92 (Me-32, d), 1.51 (Me-33, d), 3.25 (H34, m), −0.13 (H35, m) *J*(31,34) 12.0, *J*(31.35) 10.4, *J*(32,34) 6.1, *J*(33,35) 6.3, *J*(34,35) 1.2, *J*(25,35) ≠ 0.
$(\eta^3\text{-}C_3H_5)_3(\eta^3\text{-}1,3\text{-}Me_2C_3H_3)W^j$ **(16b)** (56%)	d_8-THF, −30	4.62 (H1,m) 4.13 (H11,m)	2.77 (H2,m) 1.77 (H3,m)	2.85 (H4,m) −0.13 (H5,m)	*J*(1,2) *ca* 9.2, *J*(1,3) 8.6, *J*(1,4) 13.4, *J*(1,5) 11.1, *J*(2,3) 1.8,	4.33 (H31, m) 3.53 (H32, dd), 1.52 (Me-33, d),

4.11 (H21,m)	3.14 (H12,m) 1.41 (H13,m) 2.77 (H22,m) 1.71 (H23,m)	2.26 (H14,m) −0.07 (H15,m) 3.24 (H24,m) −0.25 (H25,m)	$J(2,4)+J(2,5)$ 1.1, $J(3,5)$ 2.6. $J(11,12)$ 8.4, $J(11,13)$ 8.2, $J(11,14)$ 12.7, $J(11,15)$ 10.1, $J(12,13)$ 2.5, $J(12,14)+J(12,15)$ 0.7, $J(13,15)$ 2.9. $J(21,22)$ *ca* 8.7, $J(21,23)$ 8.6, $J(21,24)$ 13.2, $J(21,25)$ 10.5, $J(22,23)$ *ca* 1.9, $J(22,24)+J(22,25)$ 0.9, $J(23,25)$ 2.5.	1.45 (Me-34, d), 0.63 (H35, dd). $J(31,32)$ 9.3, $J(31,35)$ 12.1, $J(32,34)$ 6.7, $J(32,35)$ 0.7, $J(33,35)$ 6.2. $J(15,25) \neq 0$.

a

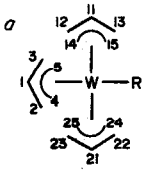

b

Provisional assignment

c

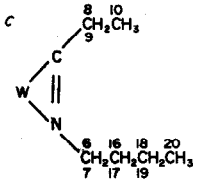

d

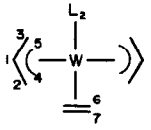

e

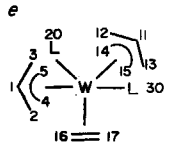

f

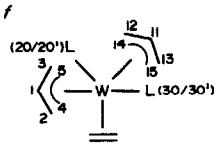

g

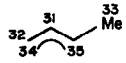

h

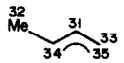

i

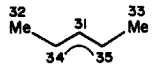

j

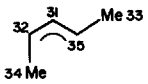

SPECTROSCOPIC INVESTIGATIONS

The structural identification of the compounds described above is based largely upon the interpretation of the NMR spectra and this is discussed in more detail here. The ^{1}H NMR spectroscopic data have been listed in Table 1.

Of particular interest in the NMR spectra of the $(\eta^3\text{-}C_3H_5)_3WR$ compounds are those signals due to the agostic system. We will limit ourselves to discussing briefly the ethyl compound $(\eta^3\text{-}C_3H_5)_3WEt$ (**2**). The ^{13}C NMR spectrum of this compound shows, in addition to nine signals for the three inequivalent allyl groups, a signal at 25.6 ppm(t) which is assigned to the metal-bonded methylene group (C-10) and a signal at −1.2 ppm(q) which is assigned to the methyl group (C-11, J(C,H) 122). The ^{1}H NMR spectrum consists of 15 signals for the allylic hydrogen atoms, signals at 2.08 and 1.36 ppm which are assigned to the methylene hydrogen atoms (H-6, H-7) and a high field doublet at −2.95 ppm which is associated with the methyl group (H-8). This signal broadens on cooling the sample to −125°C but, in contrast to the analogous molybdenum systems,[3] it did not prove possible to stop the exchange process. The IR spectrum of **2** has a characteristic absorption at 2328 cm^{-1} (m) which is assigned to the agostic system and indicates a significant weakening of the C—H bond. This absorption is as expected shifted to 1736 cm^{-1} ($\Delta\nu$ 592 cm^{-1}) in the deuterated compound $(\eta^3\text{-}C_3H_5)_3WCH_2CD_3$ (**3**). Deuteration also causes a shift of two further signals out of the 3000 cm^{-1} area to 2237 and 2137 cm^{-1}. Comparison of the combined data with other systems indicates that we are dealing here with a typical example of an agostic system.[2]

The NMR spectra of $(\eta^3\text{-}C_3H_5)_3(\eta^3\text{-}1\text{-}$

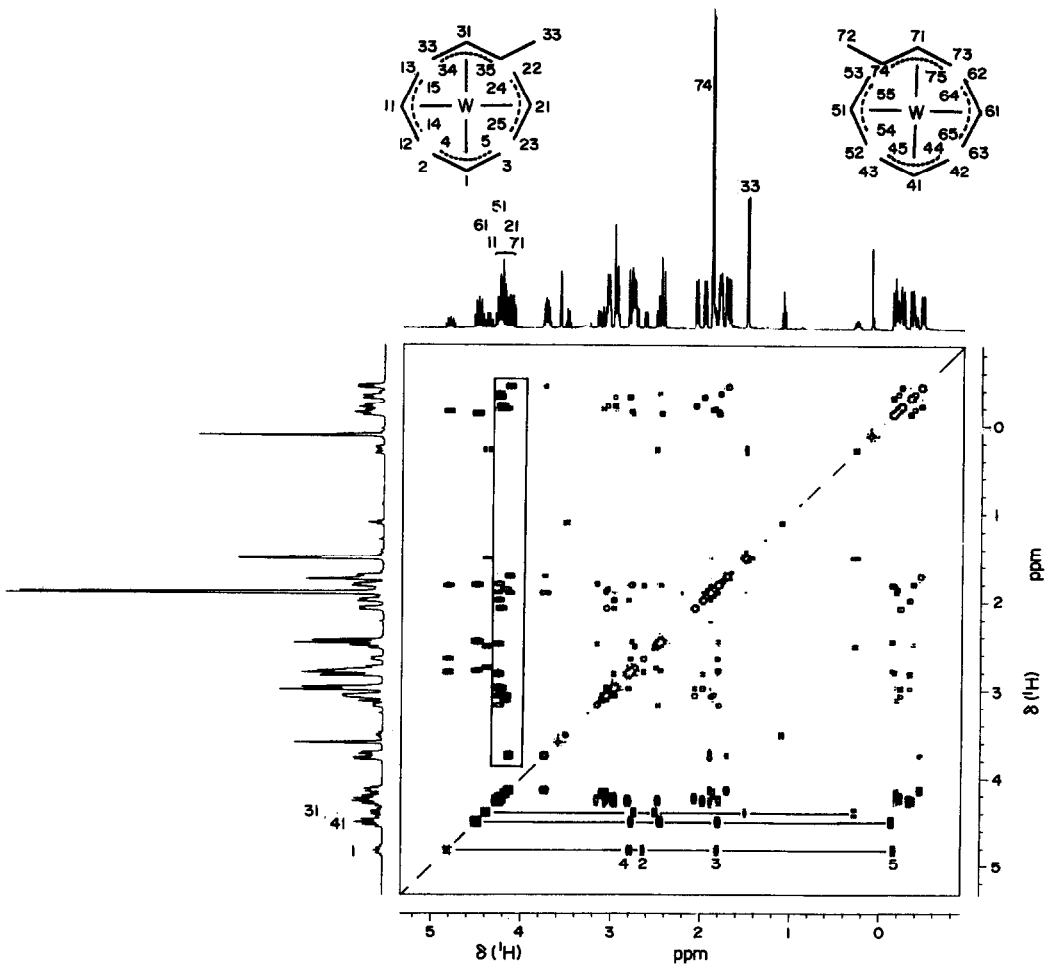

Fig. 1. 400.13 MHz COSY spectrum (symmetrized) of **15** in d_8-THF at 243 K. The data points in the F_1-direction are derived from 512 spectra each consisting of eight scans. The external one-dimensional spectrum is shown at the top of the figure and the internal projection of the two-dimensional matrix is shown in the F_1-dimension.

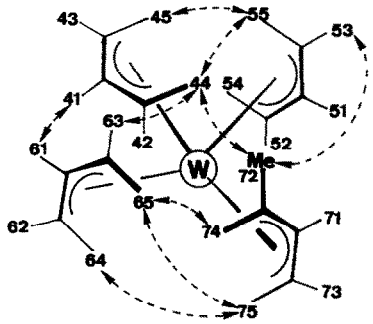

Fig. 2. Suggested structure for the major $(\eta^3\text{-}C_3H_5)_3(\eta^3\text{-}1\text{-}MeC_3H_4)W$ isomer (**15a**) based upon a two-dimensional NOE experiment carried out at 243 K. The NOE interactions are indicated by the dotted arrows.

$MeC_3H_4)W$ (**15**) and $(\eta^3\text{-}C_3H_5)_3(\eta^3\text{-}1,3\text{-}Me_2C_3H_3)W$ (**16**), which are both formed as a mixture of two isomers, contain a multitude of signals. For example, the ^1H NMR spectrum of **15** consists of 40 signals all of which have been identified and assigned using two-dimensional COSY and NOESY techniques.[6] The COSY spectrum is shown in Fig. 1 and allows the position of the methyl group and each individual allylic proton to be immediately assigned.

The stereochemical arrangement of the allyl group for the major isomer, **15a**, can be deduced from the NOESY spectrum and the results are summarized in Fig. 2.

The assignment of the ^{13}C NMR spectrum of **10**, **15** and **16** is based upon the chemical shifts, the values for J(C,W) and the two-dimensional (^1H, ^{13}C) spectra. The methyl groups in the two isomers of **15** give rise to two signals at 14.7(q) and 19.0(q) ppm in the ^{13}C NMR spectrum, while those for **16** appear as two pairs at 14.4(q)/19.0(q) and 14.6(q)/21.3(q). The arrangement of the methyl groups (*syn* or *anti*) follows from the H,H-coupling constants in the substituted allyl group and the values are reproduced schematically below.

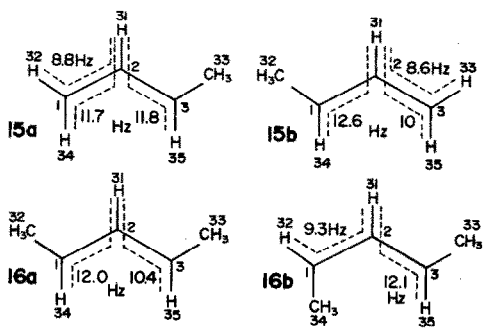

As can be seen from the data, in both **15a** and **15b** the methyl group occupies a *syn* position and consequently the only difference between these two isomers is the arrangement of the 1-methylallyl group (Me at C-1 or C-3) with respect to the other three allyl groups in the distorted tetrahedron. In the case of **16**, the coupling constants suggest that the isomers differ in the *syn* or *anti* position of one of the methyl groups. Interestingly, a third isomer in which the *syn*-methyl group is at C-1 and the *anti*-methyl group at C-3 is not observed and underlines the steric restrictions placed upon the system by the asymmetric arrangement of the allyl groups around the metal atom.

EXPERIMENTAL

The experimental conditions and spectrometers used have been described earlier.[1]

$(\eta^3\text{-}C_3H_5)_3WEt$ (2)

$[(\eta^3\text{-}C_3H_5)_3WCl]_2$ (1.30 g, 3.80 mmol) was stirred in ether at −78°C and treated with a solution of ethylmagnesium bromide in ether (2.10 cm^3, 3.50 mmol). The solution was stirred for a further 15 min at −78°C, the solvent was removed under high vacuum and the residue extracted with pentane (4×30 cm^3). The solvent, after being treated with Avicel was evaporated to give the product as a yellow powder which decomposes above 0°C. Yield 1.03 g (81% theory). Found: C, 39.0; H, 6.0; W, 54.7%. Calc. for $C_{11}H_{20}W$: C, 39.3; H, 6.0; W, 54.7%.

IR (KBr, −50°C): ν 3080, 3025, 2238, 1495, 1012, 590. MS: m/z 336(M^+), 308(M^+-28), 294(M^+-42), 280, 41, 28, 27 (100%). ^1H NMR spectrum: see Table 1. ^{13}C NMR (d_8-THF, −30°C): δ 97.0 (C-21, J(C,H), 162), 96.7 (C-11, J(C,H) 157), 94.9 (C-1, J(C,H) 160), 75.9 (C-23, J(C,H) 155, J(C,W) 8.9), 56.1 (C-13, J(C,H) 146/158, J(C,W) 20.3), 55.6 (C-2, J(C,H) 156, J(C,W) 14.1), 44.1 (C-3, J(C,H) 156, J(C,W) 10.5), 41.0 (C-12, J(C,H) 154/161, J(C,W) 11.3), 35.8 (C-22, J(C,H) 156, J(C,W) 16.3), 25.6 (C-6, J(C,H) 146, J(C,W) 31.5), −1.2 (C-7, J(C,H) 122)—numbering scheme shown below.

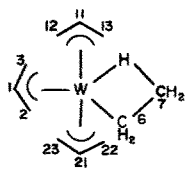

$(\eta^3\text{-}C_3H_5)_3WCH_2CD_3$ (3)

Prepared as above from $[(\eta^3\text{-}C_3H_5)_3WCl]_2$ and 2,2,2-trideuteroethylmagnesium chloride. Yield

76% theory. Found: C, 39.0; H/D, 7.1; W, 54.0. Calc. for $C_{11}H_{17}D_3W$: C, 38.7; H/D, 6.8; W, 54.2%.

IR (KBr, −50°C): *v* 3080–3025, 2237, 2134, 1736, 1495, 1012, 595. MS: *m/z* 339(M^+), 309(M^+-30), 307, 262 (100%), 39, 30, 27. ^{1}H NMR spectrum: see Table 1.

$(\eta^3\text{-}C_3H_5)_3WC_3H_7\text{-}n$ (4)

Prepared as above from $[(\eta^3\text{-}C_3H_5)_3WCl]_2$ and *n*-propylmagnesium chloride. Yield 68% theory. Found: C, 41.1; H, 6.2; W, 52.6. Calc. for $C_{12}H_{22}W$: C, 41.2; H, 6.3; W, 52.5%.

IR (KBr, −50°C): *v* 3080–3025, 2330, 1498, 1470, 1375, 585. MS: *m/z* 350(M^+), 308(M^+-42), 42, 41 (100%), 27. ^{1}H NMR spectrum: see Table 1.

$(\eta^3\text{-}C_3H_5)_3WC_3H_7\text{-}i$ (5)

Prepared as above from $[(\eta^3\text{-}C_3H_5)_3WCl]_2$ and *iso*-propylmagnesium chloride. Yield 47% theory. Found: C, 41.0; H, 6.4; W, 52.4. Calc. for $C_{12}H_{22}W$: C, 41.2; H, 6.3; W, 52.5%.

IR (KBr, −50°C): *v* 3080–3025, 2330, 1498, 1470, 1375, 585. MS: *m/z* 350(M^+), 308(M^+-42), 302, 276, 262, 42, 41 (100%). ^{1}H NMR spectrum: see Table 1.

$(\eta^3\text{-}C_3H_5)_3WC_4H_9\text{-}n$ (6)

Prepared as above from $[(\eta^3\text{-}C_3H_5)_3WCl]_2$ and *n*-butylmagnesium bromide. Yield 72% theory. Found: C, 42.8; H, 6.5; W, 49.8. Calc. for $C_{13}H_{24}W$: C, 42.9; H, 6.6; W, 50.5%.

IR (KBr, −50°C) *v* 3080–3025, 2330, 1498, 1460, 1375, 1012, 585. MS: *m/z* 364(M^+), 308(M^+-56), 56, 41 (100%). ^{1}H NMR spectrum: see Table 1.

$(\eta^3\text{-}C_3H_5)_3WC_5H_{11}\text{-}n$ (7)

Prepared as above from $[(\eta^3\text{-}C_3H_5)_3WCl]_2$ and *n*-pentenylmagnesium bromide. Yield 58% theory. Found: C, 44.7; H, 6.8; W, 48.6. Calc. for $C_{14}H_{26}W$: C, 44.5; H, 6.9; W, 48.6%.

IR (KBr, −55°C): *v* 3080–3025, 2330, 1498, 1465, 1370, 1012, 590. MS: *m/z* 378(M^+), 302, 262, 42 (100%), 41. ^{1}H NMR spectrum: see Table 1.

$(\eta^3\text{-}C_3H_5)_3W(\eta^2\text{-}EtC:NC_4H_9\text{-}n)$ (10)

$(\eta^3\text{-}C_3H_5)_3WEt$ (0.25 g, 0.74 mmol) was dissolved in ether at −78°C, treated with *n*-butylisocyanide (0.077 cm^3, 0.74 mol) and stirred for 12 h. The solvent was evaporated at −30°C under high vacuum to give the product as a yellow–brown solid. Yield 0.24 g (78% theory). Found: C, 46.0; H, 7.1; N, 3.4; W, 43.7. Calc. for $C_{16}H_{29}NW$: C, 45.8; H, 7.0; N, 3.3; W, 43.8%.

IR (KBr, 25°C): *v* 3080–3025, 1090(C:N), 1502, 1480, 1375, 1008, 602. MS: *m/z* 419(M^+), 377(M^+-42), 332, 42, 41 (100%), 27. ^{1}H NMR spectrum: see Table 1. ^{13}C NMR (d_8-THF, −40°C): δ 211.54 (C-7, *J*(C,W) 40.5), 108.67 (C-21, *J*(C,H) 161), 98.22 (C-1, *J*(C,H) 161), 92.20 (C-11, *J*(C,H) 161), 64.32 (C-23, *J*(C,H) 156, *J*(C,W) 10.6), 61.50 (C-13, *J*(C,H) 156/144, *J*(C,W) 16.7), 61.19 (C-3, *J*(C,H) 152, *J*(C,W) 12.7), 45.24 (C-2, *J*(C,H) 157, *J*(C,W) 11.6), 45.12 (C-22, *J*(C,H) 163/152, *J*(C,W) 11.2), 42.61 (C-6, *J*(C,H) 136), 33.35 (C-16, *J*(C,H) 128), 30.39 (C-12, *J*(C,H) 162/151, *J*(C,W) 16.7), 26.63 (C-8, *J*(C,H) 127), 21.77 (C-18, *J*(C,H) 127), 14.46 (C-20, *J*(C,H) 125), 11.15 (C-9, *J*(C,H) 127)—numbering scheme shown below.

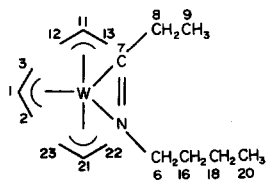

$(\eta^3\text{-}C_3H_5)_2(\eta^2\text{-}CH_2:CH_2)W(PMe_3)_2$ (11, 12)

$(\eta^3\text{-}C_3H_5)_3WEt$ (0.30 g, 0.89 mol) was dissolved in ether (20 cm^3) at −78°C, treated with trimethylphosphine (5.0 cm^3, 4.78 mmol) and stirred for 12 h. The solvent and unreacted phosphine were removed under high vacuum to give the product as a yellow powder. Yield 0.33 g (83% theory). Found: C, 37.7; H, 7.3; P, 14.1; W, 41.1. Calc. for $C_{14}H_{32}P_2W$: C, 37.7; H, 7.2; P, 13.9; W, 41.2%.

IR (KBr, −50°C): *v* 3080–3025, 1475, 1470, 1425, *ca* 1200, 935, 594. MS: *m/z* 466(M^+), 404(M^+-42), 342, 76, 61, 59 (100%), 42, 28. ^{1}H NMR spectrum: see Table 1; Compound **11** rearranges at −40°C to give **12**. ^{31}P NMR (d_8-THF, −30°C): **12** A_2X spectrum (X = ^{183}W) δ −22.9, ^1J(P,W) 228.1; **11** ABX spectrum δ −31.7, −36.7, ^1J(P,W) 217.5, ^1J(P′,W) 175.1, *J*(P,P′) 31.2.

$(\eta^3\text{-}C_3H_5)_2(\eta^2\text{-}CH_2:CH_2)W(Me_2PC_2H_4PMe_2)$ (13)

$(\eta^3\text{-}C_3H_5)_3WEt$ (0.17 g, 0.51 mmol) was dissolved in ether (30 cm^3) at −30°C, treated with 1,2-bis(dimethylphosphino)ethane (0.082 cm^3, 0.51 mmol) and stirred for 12 h. The solvent was evaporated under high vacuum and the residue analysed spectroscopically.

IR (KBr, −60°C): *v* 3080–3025, 1475, 1470, 1425, *ca* 1200, 935, 602. MS: *m/z* 444(M^+),

402(M^+-42), 150, 135, 122, 42, 41. ^{1}H NMR spectrum: see Table 1. ^{31}P NMR (d_8-THF, −30°C): δ 20.3, 4.3, ^1J(P,W) 229.5; ^1J(P′,W) 168.5, ^1J(P,P′) 7.6.

(η^3-C_3H_5)$_3$(η^3-2-MeC_3H_4)W (14)

[(η^3-C_3H_5)$_3$WCl]$_2$ (0.58 g, 1.70 mmol) was suspended in ether (100 cm^3) at −78°C and 2-methylpropenylmagnesium chloride in ether (9.0 cm^3, 1.71 mmol) was added dropwise over 20 min. The reaction mixture was stirred for 90 min, evaporated to dryness at −78°C and the residue extracted with pentane (2 × 50 cm^3). The extract was evaporated at −78°C under high vacuum to give the product as a yellow solid. Yield: 0.29 g (47% theory). Found: C, 43.2; H, 6.3; W, 50.5. Calc. for $C_{13}H_{22}W$: C, 43.1; H, 6.1; W, 50.8%.

IR (KBr, −50°C): ν 3080–3025, 1498, 1445, 1435, 1365, 1020, 1010, 590, 555. MS: m/z 362(M^+), 320(M^+-42), 315 (100%), 55, 41. ^{1}H NMR spectrum: see Table 1.

(η^3-C_3H_5)$_3$(η^3-1-MeC_3H_4)W (15)

[(η^3-C_3H_5)$_3$WCl]$_2$ (1.98 g, 5.78 mmol) was suspended in ether (100 cm^3) at −78°C and 2-butenylmagnesium chloride in ether (35 cm^3, 5.25 mmol) was added dropwise over 2.5 h. The reaction mixture was stirred for 3 h, the solvent evaporated and the residue extracted with pentane (3 × 40 cm^3) at −30°C. The solvent was concentrated and cooled to give the product as yellow crystals. Yield 1.76 g (93% theory). Found: C, 43.1; H, 6.2; W, 50.7. Calc. for $C_{13}H_{22}W$: C, 43.1; H, 6.1; W, 50.8%.

IR (KBr, −50°C): ν 3085–3020, 1498, 1375, 1010, 585. MS: m/z 364(M^++2), 362(M^+), 320($M-42$), 318 (100%), 41. ^{1}H NMR spectrum: see Table 1; the compound is formed as a mixture of two isomers (39:61). ^{13}C NMR (d_8-THF, −30°C): δ 102.60 (C-31, J(C,H) 155), 100.78 (C-21, J(C,H) 166), 100.23 (C-11, J(C,H) 160), 95.33 (C-1, J(C,H) 159), 72.43 (C-35, J(C,H) 154, J(C,W) 8.6), 63.11 (C-13, J(C,W) 15.6), 62.46 (C-23), 61.48 (C-3, J(C,W) 15.3), 45.27 (C-12, J(C,H) 158, J(C,W) 8.9), 45.02 (C-22, J(C,H) 160, J(C,W) 6.8), 42.07 (C-2, J(C,H) 159, J(C,W) 7.7), 36.33 (C-32, J(C,H) 158, J(C,W) 11.1), 14.75 (C-33, J(C,H) 125)—isomer **a**, 27%; 102.93 (C-1, J(C,H) 160), 102.68 (C-31, J(C,H) 155), 100.37 (C-21, J(C,H) 159), 99.13 (C-11, J(C,H) 159), 62.84 (C-3, J(C,H) 144), J(C,W) 13.4), 62.62 (C-23, J(C,H) 145, J(C,W) 14.4), 62.34 (C-34, J(C,H) 157), 60.96(C-13, J(C,H) 148, J(C,W) 15.2), 57.38 (C-33, J(C,H) 151, J(C,W) 18.1), 46.90 (C-2, J(C,H) 158, J(C,W) 11.0), 44.21 (C-12, J(C,H) 159, J(C,W) 8.0), 43.91 (C-22, J(C,H) 159, J(C,W) 6.9), 19.03 (C-32, J(C,H) 126)—isomer **b**, 73%—numbering scheme shown below.

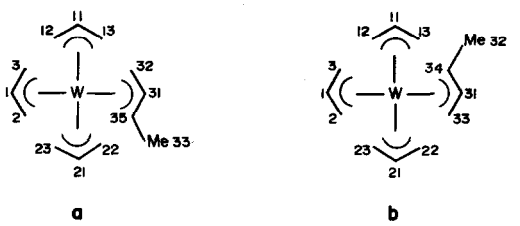

(η^3-C_3H_5)$_3$(η^3-1,3-$Me_2C_3H_3$)W (16)

[(η^3-C_3H_5)$_3$WCl]$_2$ (1.15 g, 3.36 mmol) was suspended in ether (40 cm^3) at −78°C and treated with a solution of pent-3-enylmagnesium bromide in ether (6.0 cm^3, 3.02 mmol). The reaction mixture was stirred for 3 h, the solvent evaporated under high vacuum and the residue extracted with pentane (4 × 30 cm^3) at −78°C. The extract was concentrated and cooled to give the product as yellow crystals. Yield 0.81 g (71% theory). Found: C, 44.8; H, 6.4; W, 48.6. Calc. for $C_{14}H_{24}W$: C, 44.7; H, 6.4; W, 48.9%.

IR (KBr, −45°C): ν 3080–3025, 1498, 1370, 1015, 585. MS: m/z 376(M^+), 334(M^+-42), 41 (100%). ^{1}H NMR spectrum: see Table 1; the compound is formed as a mixture of two isomers (44:56). ^{13}C NMR (d_8-THF, −30°C): δ 106.21 (C-31, J(C,H) 155), 103.49 (C-11, J(C,H) 160), 101.27 (C-21, J(C,H) 159), 94.17 (C-1, J(C,H) 159), 65.63 (C-35, J(C,H) 160, J(C,W) 12.2), 64.54 (C-23, J(C,W) 16.3), 62.69 (C-13, J(C,H) 147), 61.16 (C-3, J(C,H) 153, J(C,W) 14.3), 52.44 (C-34, J(C,H) 158, J(C,W) 7.1), 47.69 (C-12, J(C,W) 10.2), 45.55 (C-22, J(C,W) 8.1), 42.43 (C-2, J(C,H) 159, J(C,W) 10.2), 19.07 (Me-32, J(C,H) 126), 14.42 (Me-33, J(C,H) 125)—isomer **a**, 37%; 102.47 (C-31, J(C,H) 158), 101.99 (C-21, J(C,H) 159), 99.26 (C-11, J(C,H) 160), 98.82 (C-1, J(C,H) 159), 71.63 (C-35, J(C,H) 153, J(C,W) 7.1), 62.58 (C-3, J(C,H) 147), 61.70 (C-23, J(C,H) 152, J(C,W) 14.2), 60.84 (C-13, J(C,H) 148, J(C,W) 19.3), 51.55 (C-32, J(C,H) 149, J(C,W) 14.2), 49.68 (C-22, J(C,H) 148, J(C,W) 9.2), 45.01 (C-12, J(C,W) 7.1), 43.32 (C-2, J(C,H) 160, J(C,W) 6.2), 21.29 (Me-34, J(C,H) 127), 14.54 (Me-33, J(C,H) 125)—isomer **b**, 63%—numbering scheme shown below.

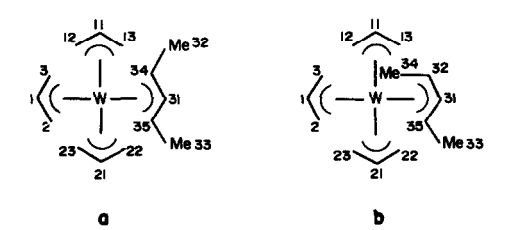

REFERENCES

1. R. Benn, T. H. Brock, M. C. F. B. Dias, P. W. Jolly, A. Rufińska, G. Schroth, K. Seevogel and B. Wassmuth, *Polyhedron* 1989, **9**, 11.
2. M. Brookhart, M. L. H. Green and L.-L. Wong, *Prog. Inorg. Chem.* 1988, **36**, 1.
3. R. Benn, S. Holle, P. W. Jolly, R. Mynott and C. C. Romão, *Angew. Chem.* 1986, **98**, 555.
4. R. D. Adams and D. F. Chodosh, *J. Am. Chem. Soc.* 1977, **99**, 6544.
5. R. D. Adams and D. F. Chodosh, *Inorg. Chem.* 1978, **17**, 41.
6. R. R. Ernst, G. Bodenhausen and A. Wokaun, *Principles of Nuclear Magnetic Resonance in One and Two Dimensions*. Claredon Press, Oxford (1987); R. Benn and H. Günther, *Angew. Chem. Int. Edn Engl.* 1983, **22**, 350.

Polyhedron Vol. 9, No. 1, pp. 35–45, 1990
Printed in Great Britain

0277–5387/90 $3.00+.00
© 1989 Pergamon Press plc

SYNTHESIS OF POLYPHOSPHINE LIGANDS CONTAINING TRIMETHYLENE LINKAGES AND PLATINUM(II)–POLYPHOSPHINE COMPLEXES

LISA M. GREEN* and DEVON W. MEEK†

Department of Chemistry, The Ohio State University, Columbus, OH 43210, U.S.A.

(*Received* 24 *February* 1989; *accepted* 7 *August* 1989)

Abstract—The addition of lithium diisopropylamide (LDA) to solutions of 1-bromo-3-chloropropane and a primary or secondary phosphine in THF at −78°C provides a new, inexpensive and time efficient method for the synthesis of high-purity 3-chloropropylphosphines in high yield. The monophosphine intermediate $C_6H_5P[CH_2CH_2CH_2Cl]_2$ was used for the synthesis of the known chelating triphosphine ligands $C_6H_5P[CH_2CH_2CH_2P(C_6H_5)_2]_2$ (ttp) and $C_6H_5P[CH_2CH_2CH_2P(C_6H_{11})_2]_2$ (Cyttp). This method was extended to the synthesis of two new polyphosphine ligands that contain electron-withdrawing groups, i.e. $(p\text{-}CF_3C_6H_4)_2PCH_2CH_2CH_2P(H)C_6H_5$ (CF_3PPH) and $C_6H_5P[CH_2CH_2CH_2P(p\text{-}CF_3C_6H_4)_2]_2$ (CF_3ttp). Platinum(II) complexes of CF_3PPH and CF_3ttp were synthesized and the spectral properties of these complexes are compared to known platinum(II) complexes.

Following the pioneering work of Mann and Millar[1–3] on the syntheses of trivalent phosphorus derivatives, many tertiary phosphines have become available and these compounds have become important ligands in coordination chemistry and catalysis.[4] Research in our laboratory has focused on the chemistry of polyphosphine ligands containing trimethylene linkages,[4–6] which have proven to be valuable chelating agents for Group VIII metal ions. A properly designed chelating polyphosphine ligand can accentuate the special effects of phosphine ligands as it simultaneously provides: (1) more control on the coordination number, stoichiometry and stereochemistry of the resulting metal complexes; (2) an increased basicity (or nucleophilicity) at the metal centre; (3) slower intra- and intermolecular exchange processes; and (4) detailed structural and bonding information in the form of metal–phosphorus and phosphorus–phosphorus coupling constants.

The chemistry of polyphosphine ligands has been slower to evolve than the monophosphine analogues, primarily because the synthetic procedures for their preparation are more complicated. During the past 15 years several synthetic strategies have begun to emerge.[7–15] However, the straightforward coupling reaction between 3-chloropropylphosphines and phosphide nucleophiles is still the most common method for preparing many common polyphosphine ligands (Scheme 1). The range of application of this method has been limited by the stability of the 3-chloropropylphosphine intermediates which have been available only with bulky substituents such as phenyl or cyclohexyl on phosphorus. In addition, this method has a number of disadvantages: (1) the synthesis of 3-chloropropylphosphine intermediates, $R_2PCH_2CH_2CH_2Cl$, requires a 10-fold excess of 1,3-dichloropropane to inhibit subsequent substitution of both Cl atoms to form $R_2PCH_2CH_2CH_2PR_2$; (2) 1,3-dichloropropane is expensive; (3) impurities, such as phosphine oxides, disubstituted species, e.g. $R_2PCH_2CH_2CH_2PR_2$, and $R_2PCH_2CH_2CH_2P(H)Ph$ are generated; (4) the ligands require purification by column chromatography and vacuum distillation; and (5) the method is time consuming.

* Author to whom correspondence should be addressed. Current address: Amoco Oil Company. P.O. Box 400, Naperville, IL 60566, U.S.A.

† Deceased, 7 December 1988.

$$R_2PH + CH_3CH_2CH_2CH_2Li \longrightarrow LiPR_2 + CH_3CH_2CH_2CH_3$$

$$LiPR_2 + \text{xs } ClCH_2CH_2CH_2Cl \longrightarrow R_2PCH_2CH_2CH_2Cl$$

$$R'PH_2 + 2CH_3CH_2CH_2CH_2Li \longrightarrow Li_2PR' + 2CH_3CH_2CH_2CH_3$$

$$2R_2PCH_2CH_2CH_2Cl + Li_2PR' \longrightarrow R'P[CH_2CH_2CH_2PR_2]_2$$

Scheme 1.

This paper presents a new, general method for the synthesis of 3-chloropropylphosphine intermediates, ttp and Cyttp. In addition, this method is extended to the synthesis of two new chelating phosphine ligands, 3-bis(4-trifluoromethylphenylphosphino)propylphenylphosphine (CF_3 PPH) and bis(3-bis(4-trifluoromethylphenylphosphino)propyl)phenylphosphine (CF_3ttp), which contain the electron-withdrawing CF_3 group in the *para* position of the phenyl ring. The syntheses of platinum(II) complexes of CF_3PPH and CF_3ttp are described.

EXPERIMENTAL

(a) *General procedures*

Reagent grade chemicals were used without further purification where possible. 1-Bromo-3-chloropropane was purified by distillation from anhydrous $MgSO_4$ under Ar and diisopropylamine was purified by distillation from anhydrous BaO under Ar. The purchased phosphines, which were sealed under an Ar atmosphere, were used without further purification. Stock solutions of lithium diisopropylamide were prepared[16] in hexane and titrated[17] using published procedures. Reagent grade solvents were purified by distillation under N_2 over the appropriate drying agents.[18] Distilled water and absolute ethanol were purged with an Ar stream for 20 min prior to use. General procedures for the manipulation of air-sensitive compounds, under an Ar atmosphere, were used in the following synthetic procedures.[19]

The ^{31}P NMR spectra were recorded on a Bruker HX-90 FT spectrometer operating at 36.43 MHz in 10 mm tubes fitted with co-axial inserts containing trimethylphosphate in d_6-acetone or on a Bruker AM-250 FT spectrometer operating at 101.256 MHz in 5 mm tubes. The $^{31}P\{^1H\}$ NMR spectra are referenced to external 85% phosphoric acid. The ^1H NMR spectra were recorded on a Bruker WP-80 FT spectrometer operating at 80.07 MHz or on a Bruker AM-250 FT spectrometer operating at 250.134 MHz in 5 mm tubes. The ^1H spectra are referenced to external TMS. The ^{13}C NMR spectra were recorded on a Bruker MSL-300 FT spectrometer operating at 75.479 MHz in 10 mm tubes or on a Bruker AM-250 FT spectrometer operating at 62.896 MHz in 5 mm tubes. The $^{13}C\{^1H\}$ NMR spectra are referenced to external TMS. IR spectra were recorded neat or as Nujol mulls between KBr or CsI plates on a Perkin–Elmer model 283B grating spectrometer and the spectra were referenced to the sharp 1601 cm^{-1} peak of a polystyrene film.

(b) *Synthesis of polyphosphine ligands and ligand intermediates*

(1) *Synthesis of* $(C_6H_5)_2PCH_2CH_2CH_2Cl$. A stock solution of 0.547 M LDA (22.5 cm^3, 12.3 mmol) was added dropwise over a 15 min period to a solution of $(C_6H_5)_2PH$ (2.00 cm^3, 11.5 mmol) and $Br(CH_2)_3Cl$ (1.20 cm^3, 12.0 mmol) in 40 cm^3 of THF cooled to −78°C in a dry ice–isopropanol bath. The solution was warmed to room temperature and the solvent was removed *in vacuo*. The yellow–orange oil was dissolved in 30 cm^3 of toluene and hydrolysed with 30 cm^3 of water. After 10 min of rapid stirring, the organic layer was transferred to a flask containing anhydrous $MgSO_4$. The aqueous layer was extracted three times with 15 cm^3 aliquots of toluene and the extracts were combined over anhydrous $MgSO_4$ and dried overnight. The solution was filtered through neutral alumina (60 mesh) on a Schlenk frit to remove the $MgSO_4$ and the solvent was removed *in vacuo* to give a clear pale yellow oil. Yield: 2.86 g, 95.0%. $^{31}P\{^1H\}$ NMR data: $\delta P = -17.4$ ppm. $R_f = 1.4$ in 1:1 toluene–hexane solvent mixtures.

(2) *Synthesis of* $(CH_3CH_2)_2PCH_2CH_2CH_2Cl$. This compound was prepared like (1), starting with a stock solution of 0.2398 M LDA (34.0 cm^3, 8.15 mmol), 0.070 g (7.8 mmol) of $(CH_3CH_2)PH$ and 0.80 cm^3 (8.1 mmol) of $Br(CH_2)_3Cl$ in 20 cm^3 of THF which was cooled to −78°C in a dry ice–isopropanol bath. Yield: 0.62 g, 48%. $^{31}P\{^1H\}$ NMR data: $\delta P = -24.6$ ppm.

(3) *Synthesis of* $C_6H_5P(CH_2CH_2CH_2Cl)_2$. This compound was prepared like (1), starting with a

stock solution of 0.654 M LDA (65.0 cm^3, 42.5 mmol), 2.30 cm^3 (20.9 mmol) of $C_6H_5PH_2$ and 4.10 cm^3 (41.5 mmol) of $Br(CH_2)_3Cl$ in 150 cm^3 of THF which was cooled to −78°C in a dry ice–isopropanol bath. The resulting oil was heated *in vacuo* for several hours at 45°C to remove all volatile materials. Yield: 5.40 g, 100%. $^{31}P\{^1H\}$ NMR data: $\delta P = -26.6$ ppm. $R_f = 2.0$ in 1:1 toluene–hexane solvent mixtures.

(4) *Synthesis of* $(C_6H_5)(H)PCH_2CH_2CH_2Cl$. This compound was prepared like (1), starting with a stock solution of 0.2398 M LDA (29.0 cm^3, 18.7 mmol), 2.00 cm^3 (18.2 mmol) of $(C_6H_5)PH_2$ and 1.80 cm^3 (18.2 mmol) of $Br(CH_2)_3Cl$ in 40 cm^3 of THF which was cooled to −78°C in a dry ice–isopropanol bath. The liquid was purified by Kugelrohr distillation. Yield: 3.40 g, 100%. ^{31}P NMR data: $\delta P = -53.9$ ppm, $^1J(P—H) = 208$ Hz.

(5) *Synthesis of* $(C_6H_{11})(H)PCH_2CH_2CH_2Cl$. This compound was prepared like (1), starting with a stock solution of 0.645 M LDA (24.0 cm^3, 15.5 mmol), 2.00 cm^3 (15.1 mmol) of $(C_6H_{11})PH_2$ and 1.50 cm^3 (15.1 mmol) of $Br(CH_2)_3Cl$ in 40 cm^3 of THF which was cooled to −78°C in a dry ice–isopropanol bath. The colourless liquid was purified by Kugelrohr distillation. Yield: 2.35 g, 78.6%. ^{31}P NMR data: $\delta P = -51.9$ ppm, $^1J(P—H) = 193$ Hz.

(6) *Synthesis of* $C_6H_5P[CH_2CH_2CH_2P(C_6H_5)_2]_2$, ttp. A stock solution of 1.6 M *n*-BuLi (120 cm^3, 192 mmol) was added dropwise, over a 1 h period, to a solution of $(C_6H_5)_2PH$ (31.6 cm^3, 182 mmol) in 800 cm^3 of THF cooled to 0°C. The red solution was stirred for an additional 30 min and then it was added dropwise, over a 2.5 h period, to a solution of $C_6H_5P(CH_2CH_2CH_2Cl)_2$ (23.88 g, 90.75 mmol) in 200 cm^3 of diethyl ether. The resulting bright orange solution was stirred overnight and then refluxed for 6 h. The solvent was removed *in vacuo*, and the resulting yellow–orange oil was dissolved in 300 cm^3 of toluene and hydrolysed with 100 cm^3 of absolute ethanol followed by 400 cm^3 of water. After 30 min of rapid stirring, the organic layer was transferred to a flask containing anhydrous $MgSO_4$. The aqueous layer was extracted three times with 150 cm^3 aliquots of toluene, and the extracts were combined over anhydrous $MgSO_4$ and dried overnight. The solution was filtered through neutral alumina (60 mesh) on a Schlenk frit to remove the $MgSO_4$ and the solvent was removed *in vacuo* to give a white oil. Yield: 51 g, 100%. $^{31}P\{^1H\}$ NMR data: $\delta PPh = -28.7$ ppm, $\delta PPh_2 = -18.1$ ppm. $R_f = 8.1$ in 1:1 toluene–hexane solvent mixtures.

(7) *Synthesis of* $C_6H_5P[CH_2CH_2CH_2P(C_6H_{11})_2]_2$, Cyttp. This triphosphine was prepared by a procedure analogous to that used for ttp, (method 6), by starting with a stock solution of 1.6 M *n*-BuLi (100 cm^3, 160 mmol) and a solution of $(C_6H_{11})_2PH$ (33.5 cm^3, 153 mmol) in 600 cm^3 of THF which was cooled to 0°C. This compound required only 1 h of reflux (as compared to 6 h for ttp) in order to completely react. Yield: 40 g, 91%. $^{31}P\{^1H\}$ NMR data: $\delta PPh = -27.7$ ppm, $\delta PCy_2 = -7.2$ ppm. $R_f = 6.2$ in 1:1 toluene–hexane solvent mixtures.

(8) *Synthesis of* $(p\text{-}CF_3C_6H_4)_2PH$. A Grignard solution of 4-bromobenzotrifluoride was prepared by the dropwise addition of a solution containing 31.0 cm^3 (221 mmol) of 4-bromobenzotrifluoride in 100 cm^3 of diethyl ether to 5.83 g (240 mmol) of Mg turnings and a crystal of I_2 in 50 cm^3 of diethyl ether. Gentle heat was applied to initiate the reaction and 100 cm^3 of additional diethyl ether were added. The resulting Grignard solution was filtered through celite on a frit and the filtrate was cooled to 0°C. A solution of 10.0 cm^3 (77.6 mmol) of diethyl phosphite in 100 cm^3 of diethyl ether was added dropwise to the Grignard solution. The resulting viscous solution was refluxed for 2 h (40–50°C) during which it became thick and waxy. The waxy mixture was cooled to 0°C and it was slowly hydrolysed with 150 cm^3 of an aqueous 10% HCl solution. The hydrolysed solution was warmed to room temperature, the layers were allowed to separate and the deep red organic layer was transferred to a flask containing anydrous $MgSO_4$. The aqueous layer was extracted six times with 50 cm^3 aliquots of benzene. The organic layers were combined over anhydrous $MgSO_4$ and dried overnight. The red solution was filtered to remove the $MgSO_4$ and the solvent was removed *in vacuo*. The resulting red oil was dissolved in 200 cm^3 of diethyl ether and the solution was cooled to 0°C. Solid lithium aluminium hydride (3.03 g, 79.8 mmol) was added *very slowly*, via a solid addition funnel, to the cold red solution; gas bubbles evolved (**NOTE**: extreme caution should be exercised when using solid lithium aluminium hydride due to its corrosive, highly flammable nature). The cold slurry was stirred for 1 h and then hydrolysed slowly with 6 cm^3 of water, 6 cm^3 of an aqueous 10% NaOH solution, and then by 12 cm^3 of water. The slurry was warmed to room temperature and the orange phosphine solution was filtered into a flask containing anhydrous $MgSO_4$. The remaining salts were washed six times with 30 cm^3 aliquots of benzene and the aliquots were combined over anhydrous $MgSO_4$ and dried. The orange solution was filtered through a Schlenk frit to remove the $MgSO_4$ and the solvent was removed from the filtrate *in vacuo* to yield an orange oil. The clear liquid product, $(p\text{-}CF_3C_6H_4)_2PH$, was extracted from the orange oil by Kugelrohr dis-

tillation. Yield: 13.9 g, 58.6%. ^{31}P NMR data: $\delta P = -42.2$ ppm, $^{1}J(P—H) = 227$ Hz.

(9) *Synthesis of* $(p\text{-}CF_3C_6H_4)_2PCH_2CH_2CH_2Cl$. A stock solution of 0.2398 M LDA (83.0 cm^3, 19.9 mmol) was added dropwise, over a 3.5 h period, to a solution of 6.08 g (18.9 mmol) of $(p\text{-}CF_3C_6H_4)_2PH$ and 1.90 cm^3 (19.2 mmol) of $Br(CH_2)_3Cl$ in 150 cm^3 of THF cooled to −78°C in a dry ice–isopropanol bath. The resulting solution was allowed to warm slowly in the dry ice–isopropanol bath and it was stirred overnight at room temperature. The solvent was removed *in vacuo*, and the resulting yellow oil was redissolved in 100 cm^3 of toluene and hydrolysed with 120 cm^3 of water. The organic layer was transferred to a flask containing anhydrous $MgSO_4$. The aqueous layer was extracted four times with 50 cm^3 aliquots of toluene. The extracts were combined over anhydrous $MgSO_4$ and dried overnight. The solution was filtered through a small amount of neutral alumina (60 mesh) on a Schlenk frit to remove the $MgSO_4$. The solvent was removed from the clear, colourless filtrate *in vacuo* to give a clear oil. The oil was warmed *in vacuo* to remove all volatile materials. Yield: 7.54 g, 100%. $^{31}P\{^{1}H\}$ NMR data: $\delta P = -16.7$ ppm.

(10) *Synthesis of* $(p\text{-}CF_3C_6H_4)_2PCH_2CH_2CH_2P(H)C_6H_5$, CF_3PPH. A stock solution of 0.523 M LDA (38.0 cm^3, 19.9 mmol) diluted with 40 cm^3 of hexane was added slowly, dropwise to a solution of 7.54 g (18.9 mmol) of $(p\text{-}CF_3C_6H_4)_2PCH_2CH_2CH_2Cl$ and 2.10 cm^3 (18.9 mmol) of $C_6H_5PH_2$ in 200 cm^3 of THF cooled to −78°C in a dry ice–isopropanol bath. The resulting red solution was allowed to warm to room temperaure and it was stirred overnight. The solution was refluxed for 3 h (80°C) and then the solvent was removed *in vacuo* to give a light orange oil. The oil was dissolved in 200 cm^3 of toluene and hydrolysed with 200 cm^3 of water. The yellow organic layer was transferred to a flask containing anhydrous $MgSO_4$. The aqueous layer was extracted four times with 50 cm^3 aliquots of toluene and the extracts were combined over $MgSO_4$ and dried overnight. The solution was filtered through neutral alumina (60 mesh) on a Schlenk frit to remove the $MgSO_4$ and the solvent was removed from the filtrate *in vacuo* to give a white oil. The oil was heated *in vacuo* for 1 h to remove volatile materials. Yield: 7.13 g, 79.8%. ^{31}P NMR data: $\delta HPPh = -54.5$ ppm, $^{1}J(P—H) = 207$ Hz, $\delta P(p\text{-}CF_3C_6H_4)_2 = -16.6$ ppm.

(11) *Synthesis of* $C_6H_5P[CH_2CH_2CH_2P(p\text{-}CF_3C_6H_4)_2]_2$, CF_3ttp. This triphosphine was prepared by a procedure analogous to that used for CF_3PPH, (method 10), by starting with a stock solution of 0.525 M LDA (34.0 cm^3, 17.8 mmol) diluted with 40 cm^3 of hexane, 6.34 g (15.9 mmol) of $(p\text{-}CF_3C_6H_4)_2PCH_2CH_2CH_2Cl$ and 0.90 cm^3 (8.2 mmol) of $C_6H_5PH_2$ in 300 cm^3 of THF cooled to −78°C in a dry ice–isopropanol bath. The oil was gently heated *in vacuo* to remove remaining volatile materials. Yield: 5.5 g, 82%. $^{31}\{^{1}H\}P$ NMR data: $\delta PPh = -28.0$ ppm, $\delta P(p\text{-}CF_3C_6H_4)_2 = -16.9$ ppm.

(c) *Synthesis of platinum complexes of* CF_3PPH *and* CF_3ttp

(1) *Synthesis of* $PtCl_2(CF_3PPH)$. A solution of 0.30 M CF_3PPH ligand in benzene (1.8 cm^3, 0.54 mmol) was added to a slurry containing 0.2032 g (0.5431 mmol) of $PtCl_2COD$[20] and 1 drop of a 6 M HCl solution in 20 cm^3 of benzene. A yellow colour was observed which quickly disappeared and a white solid precipitated. The solution was concentrated under an Ar stream to 1 cm^3 and then 10 cm^3 of hexane were added to complete the precipitation of the white solid. The white solid was collected on a Schlenk frit, washed twice with 2.0 cm^3 aliquots of hexane and dried *in vacuo*. Yield: 0.37 g, 92%. Calc. (Found): C, 37.4(37.4); H, 2.7(3.0); Cl, 9.6(9.4); F, 15.4(15.2); P, 8.4(8.2).

(2) *Synthesis of* $[PtCl(CF_3ttp)]Cl$. A stock solution of 0.10 M CF_3ttp ligand in benzene (14.0 cm^3, 1.40 mmol) was added to a slurry containing 0.52 g (1.40 mmol) of $PtCl_2COD$[20] in 40 cm^3 of benzene via a syringe. A faint yellow colour appeared and then a fine white solid precipitated. The slurry was refluxed for 3 h and then it was concentrated *in vacuo* to one-half its initial volume. The white solid was collected by vacuum filtration, washed with benzene and diethyl ether and dried in a desiccator. Yield: 1.5 g, 62%. Calc. (Found): C, 43.6(43.1); H, 3.0(3.4); Cl, 6.4(6.8); P, 8.4(8.0).

RESULTS AND DISCUSSION

(a) *Synthesis of phosphine ligands*

Traditionally, 3-chloropropylphosphines have been prepared by adding the lithium salt of the appropriate phosphine (Cy_2PH or Ph_2PH) to an excess of 1,3-dichloropropane (1 : 10 molar ratio) over a 15–24 h period (Scheme 1).[8] The triphosphine ligands were prepared by coupling reactions between the 3-chloropropylphosphine intermediates and phosphide nucleophiles. We have developed a new method for the synthesis of 3-chloropropylphosphines and polydentate phosphine ligands (Schemes 2 and 3) which is less expensive, requires less operator time and results in

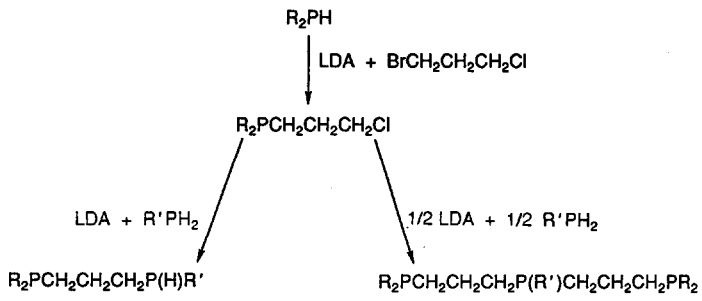

Scheme 2.

high-yield, high-purity products. The route is based on work by Kyba and co-workers on the synthesis of phosphino macrocycles.[21,22]

Compared to the original procedure for the synthesis of 3-chloropropylphosphines,[7,8] we have implemented two important modificiations. First, 1-bromo-3-chloropropane has been substituted for 1,3-dichloropropane. The bromine atom of 1-bromo-3-chloropropane undergoes nucleophilic substitution reactions faster than chlorine, consequently, a more selective substitution reaction and minimization of disubstitution of 1,3-dichloropropane, which is a side reaction that commonly occurs in the original method, can be accomplished. Replacing *n*-BuLi with LDA is the second modification of the original method.[7,8] Because LDA is a more sterically hindered, weaker base than *n*-BuLi, it can be used to generate the lithium organophosphides (i.e. R_2PLi) *in situ* at cold temperatures (*ca* $-78°C$) in the presence of 1-bromo-3-chloropropane or 3-chloropropylphosphine intermediates. Hence, the reaction procedures for generating 3-chloropropylphosphines and polydentate phosphine ligands are now one-step, one-flask reactions.

The new method of preparing 3-chloropropylphosphines (Scheme 2) leads to $(C_6H_5)_2PCH_2CH_2CH_2Cl$ in near quantitative yield from $(C_6H_5)_2PH$. The spectral data agreed with previously reported data for this compound.[8,23] The purity of $(C_6H_5)_2PCH_2CH_2CH_2Cl$ was tested using thin-layer chromatography; no trace impurities were observed. This method also leads to $(CH_3CH_2)_2PCH_2CH_2CH_2Cl$ from diethyl phosphine, however, traces of solvent remained in the product after vacuum distillation. It was characterized by its $^{31}P\{^1H\}$ NMR and IR spectra. Reactions of $[(CH_3)_2CH]_2PH$ and $(C_6H_{11})_2PH$ with 1-bromo-3-chloropropane in the presence of LDA did not give clean samples of the known compounds $[(CH_3)_2CH]_2PCH_2CH_2CH_2Cl$[24] and $(C_6H_{11})_2PCH_2CH_2CH_2Cl$,[8] apparently because of the high basicity of these phosphines and their significant steric requirements.[25]

The reaction of $C_6H_5PH_2$ with two equivalents each of 1-bromo-3-chloropropane and LDA yields $C_6H_5P(CH_2CH_2CH_2Cl)_2$ in near quantitative yield and high purity. The ^1H and $^{31}P\{^1H\}$ NMR data for this compound have been reported previously by Kyba and co-workers,[19] the $^{13}C\{^1H\}$ NMR data

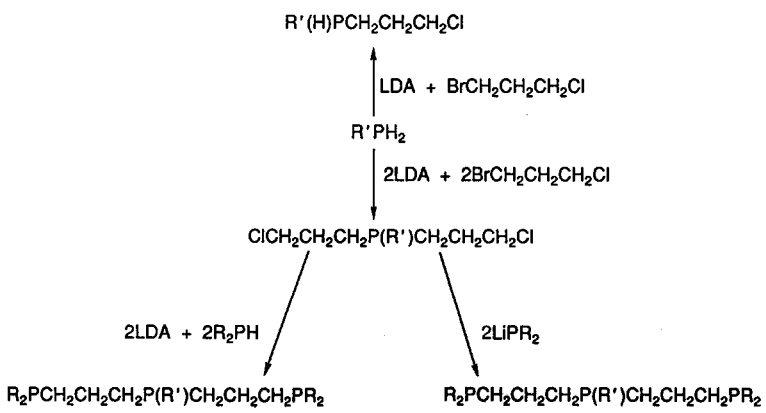

Scheme 3.

are reported in Table 1. The compound was tested for trace impurities by thin-layer chromatography; no impurities were detected. A similar reaction was used to prepare $C_6H_{11}P(CH_2CH_2CH_2Cl)_2$ from $C_6H_{11}PH_2$. However, only 17% (based on ^{31}P NMR intensities) of the desired product was formed ($\delta^{31}P = -20.8$ ppm); the major product was the monoalkylated species, $C_6H_{11}(H)PCH_2CH_2CH_2Cl$ ($^{31}P = -51.9$ ppm).

The monoalkylated compounds $C_6H_5(H)PCH_2CH_2CH_2Cl$ and $C_6H_{11}(H)PCH_2CH_2CH_2Cl$, were prepared by addition of one equivalent each of LDA and 1-bromo-3-chloropropane to the corresponding primary phosphine (Scheme 3). These ligands are bifunctional due to reactive P—H and C—Cl bonds, hence they are useful intermediates for the synthesis of chelating polydentate ligands. IR spectra for both species exhibit characteristic P—H stretching absorptions; in addition, the doublets due to P—H spin–spin coupling in the ^1H NMR spectra confirm the presence of the P—H bond. The data are reported in Table 2.

As a result of the new procedures for the synthesis of 3-chloropropylphosphines, a new method, utilizing $C_6H_5P(CH_2CH_2CH_2Cl)_2$, can be envisioned for the synthesis of the chelating triphosphine ligands ttp and Cyttp (Scheme 3). Samples of ttp and Cyttp were obtained in high yield. The purities of ttp and Cyttp were tested by thin-layer chromatography and $^{31}P\{^1H\}$ and ^1H NMR spectroscopy. The $^{31}P\{^1H\}$ and ^1H NMR data for Cyttp and ttp corroborated data reported previously for these ligands.[8] The $^{13}C\{^1H\}$ NMR data for ttp agreed with those reported by Arapac and Dahlenburg,[23] the $^{13}C\{^1H\}$ data for Cyttp is reported in Table 1.

We have extended the above synthetic procedures to the synthesis of two new ligands, CF_3PPH and CF_3ttp, which incorporate an electron-withdrawing CF_3 group in the *para* position of the phenyl rings on the terminal phosphorus atom. The first step in preparing these new ligands is the synthesis of a new secondary phosphine, bis[4-(trifluoromethyl)-phenyl]phosphine, $(p\text{-}CF_3C_6H_4)_2PH$. Kapoor and co-workers[26–28] have generated secondary phosphines containing electron-withdrawing groups (i.e. $(p\text{-}FC_6H_4)_2PH$, $(m\text{-}FC_6H_4)_2PH$ and $(m\text{-}CF_3C_6H_4)_2PH$), and incorporated these phosphines into bidentate ligands; however, $(p\text{-}CF_3C_6H_4)_2PH$ has not been reported. Based on Hammett substituent constants, a CF_3 group in the *para* position of a benzene ring is more electron-attracting ($\sigma = 0.54$) than the same group in the *meta* position of a benzene ring ($\sigma = 0.43$).[29] Thus, the $(p\text{-}CF_3C_6H_4)_2P$ group incorporated into a chelating triphosphine ligand will provide the greatest contrast to ttp.

Kapoor and co-worker's[26–28] method for preparing secondary phosphines involves isolation of the secondary phosphine oxides (i.e. $(p\text{-}FC_6H_4)_2P(O)H$, $(m\text{-}FC_6H_4)_2P(O)H$ and $(m\text{-}CF_3C_6H_4)_2P(O)H$). Although the oxide of bis[4-(trifluoromethyl)phenyl]phosphine has been reported,[30] the synthetic details provided were very vague. The method reported here for the synthesis of (*p*-

Table 1. $^{13}C\{^1H\}$ NMR data[a] for 3-chloropropylphosphines and Cyttp

Data	$(C_6H_5)P[(CH_2)_3Cl]_2$	$C_6H_5(H)P(CH_2)_3Cl$	$C_6H_{11}(H)P(CH_2)_3Cl$	Cyttp
Phenyl ring				
P—C	137.0 d (13)	135.6 d (11)		138.6 d (15)
o-C	132.4 d (20)	134.0 d (16)		132.5 d (19)
m-C	128.6 d (6.4)	129.1 d (5.8)		128.2 d (5.3)
p-C	129.3 s	128.8 s		128.6 s
Cyclohexyl ring				
P—C		32.4 br	33.3 d (12)	
o-C		31.5 d (7.2)	29.0 d (7.2)	
m-C		27.4 d (9.5)	27.3 d	
p-C		26.7 s	26.5 s	
Trimethylene chain				
P—C	29.1 d (15)	32.1 d (7.9)	32.3 d (12)	30.3 t (23)
—C—	25.4 d (11)	20.9 d (13)	16.0 d (13)	24.8 t (33)
C—Cl	45.7 d (13)	45.9 d (9.3)	46.1 d (11)	

[a] Chemical shifts are in ppm. Coupling constants (in parentheses) are in Hz. s = singlet, d = doublet, br = broad, t = pseudo-triplet (overlapping doublet of doublets). Coupling constants for pseudo triplets are $^1J(P—C) + {}^3J(P—C)$. Solvent: $(CD_3)_2CO$.

Table 2. ^{31}P NMR, ^{1}H NMR and diagnostic IR data[a] for 3-chloropropylphosphines

Phosphine	^{31}P (ppm)	^{1}H (ppm)	IR (cm^{-1})
$C_6H_5P(CH_2CH_2CH_2Cl)_2$[b]	−26.6	7.42 (m) 5H 3.55 (m) 4H 1.79 (m) 8H	1588 (C=C) 1560 (C=C) 1488 (Ph—P) 648 (C—Cl)
$C_6H_5(H)P(CH_2)_3Cl$[c]	−53.9 ^{1}J(P—H) = 208	7.52 (m) 7.34 (m) 4.15 (d) 1H J(P—H) = 207 Hz 3.60 (t) 2H J(H—H) = 6.3 Hz 1.89 (m) 4H	2290 (P—H) 1590 (C=C) 1488 (Ph—P) 648 (C—Cl)
$C_6H_{11}(H)P(CH_2)_3Cl$[c]	−51.9 ^{1}J(P—H) = 193	3.64 (t) 2H J(H—H) = 6.4 Hz 2.94 (d) 1H J(P—H) = 194 Hz 1.77 (m) 10H 1.26 (m) 5H	2270 (P—H) 645 (C—Cl)

[a] d = doublet, m = multiplet, t = triplet. ^{31}P NMR spectra recorded in THF.
[b] CD_2Cl_2 solvent.
[c] $(CD_3)_2CO$ solvent.

$CF_3C_6H_4)_2PH$ does not rely on the isolation of the phosphine oxide, but incorporates an *in situ* reduction of the oxide to form the desired secondary phosphine.

The first three steps in the synthesis of (p-$CF_3C_6H_4)_2PH$; the formation of a Grignard, followed by addition of diethyl phosphite to the Grignard solution and subsequent reaction with a strong acid, are standard procedures for the synthesis of secondary phosphine oxides.[31,32] The presence of the phosphine oxide, (p-$CF_3C_6H_4)_2P(O)H$, can be detected *in situ* by ^{31}P NMR spectroscopy (δP = 16.4 ppm, ^{1}J(P—H) = 495 Hz). The final step of the scheme involves an *in situ* reduction of the phosphine oxide with $LiAlH_4$[31] to form the secondary phosphine. The clear liquid product, (p-$CF_3C_6H_4)_2PH$, has been characterized by ^{31}P and ^{1}H NMR and IR spectroscopies (Table 3) and $^{13}C\{^{1}H\}$ NMR spectroscopy (Table 4).

The second step in preparing CF_3PPH and CF_3ttp is the synthesis of the 3-chloropropylphosphine intermediate, (p-$CF_3C_6H_4)_2PCH_2CH_2CH_2Cl$. Reactions involving the secondary phosphine, (p-$CF_3C_6H_4)_2PH$, are complicated by side reactions which involve the CF_3 group and n-BuLi or LDA to give uncharacterized products. These complications have also been observed by Higgins and Levason.[34] By employing dilute solutions of LDA and by adding LDA very slowly to a solution of (p-$CF_3C_6H_4)_2PH$ and 1-bromo-3-chloropropane, these side reactions can be eliminated and high yields of (p-$CF_3C_6H_4)_2PCH_2CH_2CH_2Cl$ are obtained. The NMR and IR spectroscopic data for (p-$CF_3C_6H_4)_2PCH_2CH_2CH_2Cl$ are given in Tables 3 and 4.

Reactions of (p-$CF_3C_6H_4)_2PCH_2CH_2CH_2Cl$ with one equivalent each of LDA and $C_6H_5PH_2$ give the bidentate ligand (p-$CF_3C_6H_4)_2PCH_2CH_2CH_2P(H)C_6H_5$, CF_3PPH (Scheme 3). The synthesis of CF_3ttp is similar to the procedure used to prepare CF_3PPH, however, two equivalents each of $(C_6H_5)_2PH$ and LDA are used. The ^{1}H NMR and IR spectroscopic data for these ligands are given in Table 3 and the $^{13}C\{^{1}H\}$ NMR data are given in Table 4.

(b) *Synthesis of platinum complexes of* CF_3PPH *and* CF_3ttp

In order to compare the coordination properties of metal complexes coordinated to the new chelating phosphine ligands that contain (p-$CF_3C_6H_4)_2P$ groups, and to complete the characterization of these ligands, platinum complexes of CF_3PPH and CF_3ttp were prepared. The platinum complex of CF_3PPH, $PtCl_2(CF_3PPH)$, was pre-

Table 3. $^{31}P\{^1H\}$ NMR, ^1H NMR and diagnostic IR data[a] for $(p\text{-}CF_3C_6H_4)_2PH$, $(p\text{-}CF_3C_6H_4)_2P(CH_2)_3Cl$, CF_3PPH and CF_3ttp

Phosphine		$^{31}P\{^1H\}$ (ppm)	^1H (ppm)	IR (cm^{-1})
$(p\text{-}CF_3C_6H_4)_2PH$		−42.2	7.45 (m) 8H 5.15 (d) 1H ^1J(P—H) = 222 Hz	2290 (P—H) 1610 (C=C) 1499 (P—Ph) 1125 (CF_3)
$(p\text{-}CF_3C_6H_4)_2P(CH_2)_3Cl$		−16.7	7.72 (m) 8H 3.71 (m) 2H 2.38 (m) 2H 1.92 (m) 2H	1611 (C=C) 1500 (P—Ph) 1150 (CF_3) 650 (C—Cl)
CF_3PPH[b]	PhPH	−54.5	7.68 (m)	2280 (P—H)
	$(p\text{-}CF_3C_6H_4)_2P$	−16.6	7.45 (m) 7.31 (m) 4.10 (ddd) ^1J(P—H) = 207 Hz ^3J(H—H) = 5.9 Hz ^3J(H—H) = 7.8 Hz 2.31 (m) 2.00 (m) 1.59 (m)	1608 (C=C) 1150 (CF_3)
CF_3ttp[c]	PhP	−28.0	7.47 (m) 20H	1609 (C=C)
	$(p\text{-}CF_3C_6H_4)_2P$	−16.9	2.17 (m) 4H 1.81 (m) 4H 1.48 (m) 4H	1120 (CF_3)

[a] $^{31}P\{^1H\}$ and 1H NMR spectra were recorded in $(CD_3)_2CO$. m = multiplet; d = doublet.
[b] Poor integration due to small residual impurities.
[c] $^{31}P\{^1H\}$ NMR spectrum recorded in CD_2Cl_2.

Table 4. $^{13}C\{^1H\}$ NMR data[a] for $(p\text{-}CF_3C_6H_4)_2PH$, $(p\text{-}CF_3C_6H_4)_2P(CH_2)_3Cl$, CF_3PPH and CF_3ttp

Data	$(p\text{-}CF_3C_6H_4)_2PH$	$(p\text{-}CF_3C_6H_4)_2P(CH_2)_3Cl$	CF_3PPH	CF_3ttp
—PC_6H_5				
P—C			135.1 d (12)	138.4 d (16)
o-C			133.5 d (16)	132.9 d (19)
m-C			128.3 d (5.8)	128.8 d (7.3)
p-C			128.0 s	129.4 s
—$P(p\text{-}CF_3C_6H_4)_2$				
P—C	140.4 d (13)	143.8 d (17)	143.0 d (18)	143.7 t (30)[b,c]
o-C	135.3 d (17)	133.4 d (19)	132.8 d (19)	133.6 d (11)
		125.8 m		133.3 d (11)
m-C	126.3 s	131.0 q (32)	125.0 m	125.6 m
p-C[d]	131.5 q (33)		130.5 q (32)	131.1 q (32)
		125.5 q (272)	131.0 q (32)	
—CF_3	125.2 q (272)		128.6 q (272)	124.6 q (272)
Methylene-C				
PhP—C		29.6 d (18)	24.2 dd (16, 9.0)[e]	29.4 t (24)[c]
—C—		24.9 d (13)	24.4 t (25)[c]	22.7 t (32)[c]
CF_3PhP—C		45.8 d (16)	28.4 dd (14, 7.2)[e]	30.0 t (25)[c]

[a] d = doublet, dd = doublet of doublets, m = multiplet, q = quartet, s = singlet, t = pseudo-triplet. Solvent: $(CD_3)_2CO$; CF_3ttp, CD_2Cl_2.
[b] The two phenyl rings on phosphorus are inequivalent.
[c] Coupling constant (in parentheses) is ^1J(P—C) + ^3J(P—C).
[d] Coupling is due to the fluorine atoms on the CF_3 group.
[e] [^1J(P—C), ^3J(P—C)].

Table 5. ^{31}P NMR data[a] for $PtCl_2(CF_3PPH)$ and $[PtCl(CF_3ttp)]Cl$

Complex	δP_1	δP_2	^1J[Pt—P(1)]	^1J[Pt—P(2)]	^1J[P(1)—P(2)]	^1J[P(1)—H]
$PtCl_2(CF_3PPH)$[b]	−29.0	−5.2	3199	3422		480
$[PtCl(CF_3ttp)]Cl$	−20.9	−2.8	3025	2229	27	

[a] Chemical shifts are in ppm, coupling constants are in Hz. The HPPh and the PhP groups are labelled P(1). The R_2P groups are labelled P(2).
[b] Solvent = $(CD_3)_2CO$.
[c] Solvent = CD_3NO_2.

pared from $PtCl_2COD$[20] [eq. (1)] using a procedure similar to the method used to prepare $PtCl_2(PPH)$ (PPH = $(C_6H_5)CH_2CH_2CH_2P(H)C_6H_5$) and $PtCl_2(CyPPH)$ (CyPPH = $(C_6H_{11})_2PCH_2CH_2CH_2P(H)C_6H_5$):[35]

$$PtCl_2COD + CF_3PPH \longrightarrow PtCl_2(CF_3PPH) + COD. \quad (1)$$

The $^{31}P\{^1H\}$ NMR spectrum of $PtCl_2(CF_3PPH)$ is a first-order AM spin system, and it consists of two doublets with the corresponding ^{195}Pt satellites (Fig. 1, Table 5). In order to evaluate the inductive effect of the $(p\text{-}CF_3C_6H_4)_2P$ groups, the ^{31}P NMR data obtained for $PtCl_2(CF_3PPH)$ are compared to data[34] for $PtCl_2(PPH)$ and $PtCl_2(CyPPH)$. The ^{31}P chemical shift of the $(p\text{-}CF_3C_6H_4)_2P$ group (−5.2 ppm) shifts to slightly higher field than the $(C_6H_5)_2P$ group (−5.7 ppm) of $PtCl_2(PPH)$. However, the effect is minimal. The electronegative effect of the $p\text{-}CF_3C_6H_4$ groups is also observed in the one-bond coupling constant, ^1J[Pt—P(2)], which is slightly larger for the $(p\text{-}CF_3C_6H_4)_2P$ group of $PtCl_2(CF_3PPH)$ [^1J[Pt—P(2)] = 3422 Hz vs 3403 Hz for the $(C_6H_5)_2P$ group of $PtCl_2(PPH)$]. However, the effect is not as dramatic as the difference between the platinum–phosphorus coupling of $PtCl_2(CyPPH)$ (^1J[Pt—P(2)] = 3303 Hz) and $PtCl_2(PPH)$ (^1J[Pt—P(2)] = 3403 Hz).

The platinum complex of the triphosphine ligand CF_3ttp, $[PtCl(CF_3ttp)]Cl$, was prepared also from $PtCl_2COD$ [eq. (2)] by use of a procedure similar to the method[36] employed for the synthesis of [PtCl(ttp)]Cl:

$$PtCl_2COD + CF_3ttp \longrightarrow [PtCl(CF_3ttp)]Cl + COD. \quad (2)$$

The $^{31}P\{^1H\}$ NMR spectrum of $[PtCl(CF_3ttp)]Cl$ is a first-order A_2M spin system, and it consists of a triplet and the corresponding ^{195}Pt satellites and a doublet and the corresponding ^{195}Pt satellites (Fig. 2, Table 5). Once again, the ^{31}P chemical shift of the $(p\text{-}CF_3C_6H_4)_2P$ groups (−2.8 ppm) is slightly down-

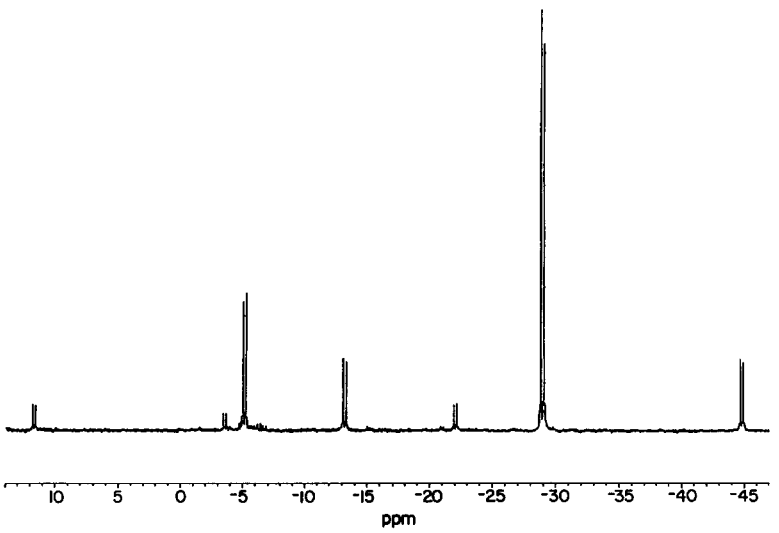

Fig. 1. 250 MHz $^{31}P\{^1H\}$ NMR spectrum of $PtCl_2(CF_3PPH)$ in d_6-acetone.

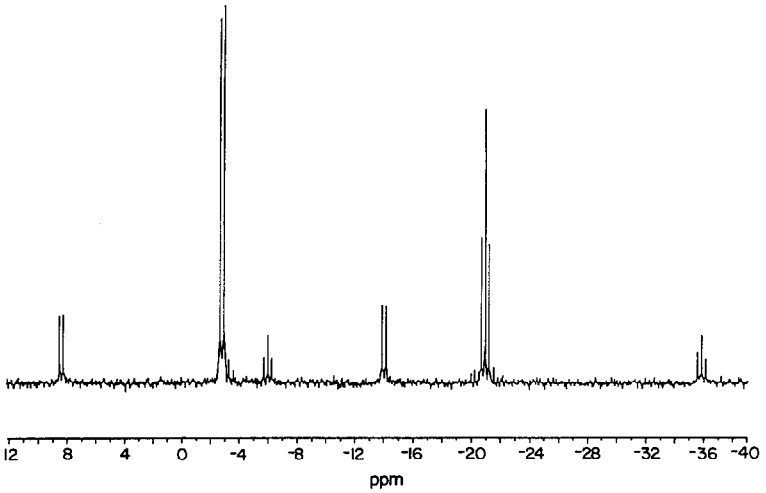

Fig. 2. 250 MHz $^{31}P\{^1H\}$ NMR spectrum of [PtCl(CF_3ttp)]Cl in CD_3NO_2.

field from the chemical shift of the $(C_6H_5)_2P$ groups (−3.9 ppm) of [PtCl(ttp)]Cl due to the electron-withdrawing effect of the *p*-$CF_3C_6H_4$ groups. In addition, the ^1J[Pt—P(2)] coupling constant for [PtCl(CF_3ttp)]Cl (^1J[Pt—P(2)] = 2264 Hz) is larger than the same coupling constant for [PtCl(ttp)]Cl (^1J[Pt—P(2)] = 2229 Hz). However, like $PtCl_2$(CF_3PPH), the difference between the ^1J[Pt—P(2)] coupling constants of [PtCl(CF_3ttp)]Cl and [PtCl(ttp)]Cl is not as dramatic as the difference between [PtCl(ttp)]Cl (^1J[Pt—P(2)] = 2229 Hz) and [PtCl(Cyttp)]Cl[36] (^1J[Pt—P(2)] = 2152 Hz).

In conclusion, the electron-withdrawing character of the *p*-CF_3 group on the phenyl ring of CF_3PPH and CF_3ttp is small compared to the difference in electron-withdrawing character between aryl and alkyl substituted phosphorus atoms in ttp and Cyttp, and PPH and CyPPH. Also, the *p*-CF_3 group does not impart increased solubility to the platinum complexes of CF_3PPH and CF_3ttp, relative to the platinum complexes of PPH and ttp.

Acknowledgements—The authors are grateful to the Amoco Foundation for a Graduate Fellowship to L.M.G. during 1986–1987, and to the Ohio State University for a University Fellowship to L.M.G. and for purchase of the Bruker MSL-300 NMR spectrometer. We would also like to thank Johnson Matthey for loan of the Pt metal.

REFERENCES

1. F. G. Mann and I. T. Millar, *J. Chem. Soc.* 1951, 2205.
2. F. G. Mann and I. T. Millar, *J. Chem. Soc.* 1952, 3039.
3. F. G. Mann and I. T. Millar, *J. Chem. Soc.* 1952, 4453.
4. R. M. Mason and D. W. Meek, *Angew. Chem. Int. Ed., Engl.* 1978, **17**, 183.
5. D. W. Meek, D. L. DuBois and J. Tiethof, *Adv. Chem. Ser.* 1976, 150.
6. D. W. Meek and T. J. Mazanec, *Accts Chem. Res.* 1981, **14**, 266.
7. T. E. Nappier, D. W. Meek, R. M. Kirchner, R. M. and J. A. Ibers, *J. Am. Chem. Soc.* 1973, **95**, 4194.
8. R. Uriarte, T. J. Mazanec, K. D. Tau and D. W. Meek, *Inorg. Chem.* 1980, **19**, 79.
9. R. D. Waid and D. W. Meek, *Organometallics* 1983, **2**, 932.
10. R. D. Waid and D. W. Meek, *Inorg. Chem.* 1984, **23**, 778.
11. M. Baacke, O. Stelzer and V. Wray, *Chem. Ber.* 1980, **113**, 1356.
12. M. Baacke, S. Hietkamp, J. Morton and O. Stelzer, *Chem. Ber.* 1981, **114**, 2568.
13. B. N. Diel and A. D. Norman, *Phos. Sulf.* 1982, **12**, 227.
14. B. N. Diel, R. C. Haltiwanger and A. D. Norman, *J. Am. Chem. Soc.* 1982, **104**, 4700.
15. M. Antberg, C. Prengel and L. Dahlenburg, *Inorg. Chem.* 1984, **23**, 4170.
16. H. O. House, W. V. Phillips, T. S. B. Sayer and C. Yau, *J. Org. Chem.* 1978, **43**, 700.
17. S. C. Watson and J. F. Eastham, *J. Organomet. Chem.* 1967, **9**, 165.
18. D. F. Shriver, *The Manipulation of Air-sensitive Compounds*. Krieger, Malabar, Florida (1982).
19. D. D. Perrin, W. L. F. Armarego and D. R. Perrin, *Purification of Laboratory Chemicals*. Pergamon Press Inc., New York (1966).
20. H. C. Clark and L. E. Manzer, *J. Organomet. Chem.* 1973, **59**, 411.
21. E. P. Kyba, A. M. John, S. B. Brown, C. W. Hudson, M. J. McPhaul, A. Harding, K. Larsen, S.

Niedzwiecki and R. E. Davis, *J. Am. Chem. Soc.* 1980, **102**, 139.
22. E. P. Kyba and S. Liu, *Inorg. Chem.* 1985, **24**, 1613.
23. E. Arapac and L. Dahlenburg, *Z. Naturforsch.* 1980, **35b**, 196.
24. H. Sommer, S. Hietkamp and O. Stelzer, *Chem. Ber.* 1984, **117**, 3414.
25. C. A. Tolman, *Chem. Rev.* 1977, **77**, 313.
26. P. N. Kapoor and L. M. Venanzi, *Helv. Chim. Acta* 1977, **60**, 2824.
27. P. N. Kapoor, D. D. Pathak, G. Gaur and M. Kutty, *J. Organomet. Chem.* 1984, **276**, 167.
28. P. N. Kapoor, R. N. Kapoor, D. D. Pathak and G. Gaur, *Inorg. Chim. Acta* 1986, **112**, 153.
29. A. Streitwieser, Jr. and C. H. Heathcock, *Introduction to Organic Chemistry*, 2nd edn, pp. 1131, 1197–1198. Macmillan, New York (1981).
30. M. Grayson, C. E. Farley and C. A. Streuli, *Tetrahedron* 1967, **23**, 1065.
31. B. B. Hunt and B. C. Saunders, *J. Chem. Soc.* 1957, 2413.
32. H. R. Hays, *J. Org. Chem.* 1968, **33**, 3690.
33. K. B. Mallion and F. G. Mann, *J. Chem. Soc.* 1964, 6121.
34. S. J. Higgins and W. Levason, *Inorg. Chem.* 1985, **24**, 1105.
35. R. D. Waid and D. W. Meek, *Inorg. Chem.* 1984, **23**, 778.
36. R. D. Waid, PhD dissertation, The Ohio State University (1982).
37. K. D. Tau, PhD dissertation, The Ohio State University (1978).

Polyhedron Vol. 9, No. 1, pp. 47–51, 1990
Printed in Great Britain

0277–5387/90 $3.00+.00
© 1989 Pergamon Press plc

SYNTHESIS, THERMAL DECOMPOSITION AND POWDER DIFFRACTION DATA OF AMMONIUM DECAFLUOROURANATE(VI), $(NH_4)_4UF_{10}$

SVETOZAR MILIĆEV* and BRANKO DRUŽINA

J. Stefan Institute, Edvard Kardelj University, Ljubljana, Yugoslavia

and

BOGDAN VOLAVŠEK

Faculty of Technical Sciences, University of Maribor, Yugoslavia

(*Received* 8 *June* 1989; *accepted* 4 *August* 1989)

Abstract—The synthesis of $(NH_4)_4UF_{10}$ is described. Thermal decomposition proceeds through four steps giving $(NH_4)_3UF_8$ at 200°C, $(NH_4)UF_6$ at 280°C, $(NH_4)U_3F_{13}$ at 380°C and finally UF_4 at 600°C. $(NH_4)UF_6$ decomposes through an intermediate to UF_4 and not directly. Powder data of $(NH_4)_4UF_{10}$ were indexed on the basis of a monoclinic cell [a = 12.87(2), b = 8.36(2), c = 13.60(7) Å, β = 121.5(3)°].

In 1984 we reported the synthesis and vibrational spectra of $(NH_4)_4UF_{10}$.[1] This is, as far as we are aware, the first monomeric hexavalent uranium compound with so high a coordination number (larger than eight). There were reports[2] of attempted syntheses of such a species, but in our case the Raman spectrum of a definitely stoichiometric diamagnetic compound clearly indicates a coordination number larger than eight, and the broad IR N—H stretching absorption showing moderate hydrogen bonding suggests a distorted UF_{10}^{4-} ion, with one of the fluorine atoms having significant ionic character. The radius of hexavalent uranium[3] should be comparable for higher coordination numbers with the intramolecular nonbonded atomic radius of fluorine,[4] allowing space for even more than 10 fluorine atoms. Nevertheless, it is an unexpected result (see also the discussion on the unlikeliness of nonacoordination in isolated anions of actinide fluorides in ref. 5). We report more details of the synthesis, the thermal behaviour and the powder diffraction data of the compound. Attempts to prepare a single crystal suitable for X-ray structure determination were unsuccessful.

* Author to whom correspondence should be addressed.

EXPERIMENTAL

Synthesis

White $(NH_4)_4UF_{10}$ was synthesized by the procedure, described previously.[1] The results were better if the argon arc-welded copper vessel equipped with a Teflon packed nickel valve containing $(NH_4)_4UF_8$ and XeF_2 in excess (added by sublimation) was held at 55°C for a prolonged time, even for a few days. For reliable synthesis, one should start from very active UF_4, with a large specific surface (obtained by thermal decomposition[6] of $(N_2H_5)UF_5$), from which $(NH_4)_4UF_8$ is prepared.[7] More coarse UF_4, prepared by the usual hydrofluorination[8] of UO_2, results in $(NH_4)_4UF_8$ of insufficient purity, giving, at the end, impure and very unstable $(NH_4)_4UF_{10}$. $(NH_4)_4UF_{10}$ decomposes rapidly in air, changing colour to green. Found: U, 47.9; $(NH_4)^+$, 13.9; F, 37.7. Calc. for $(NH_4)_4UF_{10}$: U, 47.6; $(NH_4)^+$, 14.4; F, 38.0%.

Thermoanalysis

A 100 mg sample was referenced on a Mettler TA–1 thermoanalyser against a 100 mg sample of α-Al_2O_3. The heating rate was 4°C min^{-1} in a

Table 1. Powder diffraction data of $(NH_4)_4UF_{10}$, of its first decomposition product at 200°C, of $(NH_4)_4UF_8$ and of $(NH_4)_3UF_8$

$(NH_4)_4UF_8$[7]		$(NH_4)_4UF_{10}$				$(NH_4)_3UF_8$[10]		Product at 200°C	
d(Å)	I	$d_{(obs)}$	I	$d_{(calc)}$	hkl	d(Å)	I	d(Å)	I
		8.39	w	8.36	010				
		6.97	w	6.78	011				
		6.01	w	5.80	002				
5.80	vs							5.61	w
5.54	m					5.56	100	5.49	vs
		5.45	vs	5.48	200				
		5.05	w	5.11	111				
4.74	mw	4.76	vs	4.76	012	4.77	40	4.74	m
4.64	s								
		4.15	m	4.18	020				
3.70	ms								
3.60	w	3.64	w	3.66	300				
3.56	ms								
3.40	mw	3.38	s	3.39	022	3.37	60	3.37	s
3.34	mw								
3.25	m								
3.19	mw	3.16	w	3.16	103				
		3.05	w	3.06	301				
2.95	vw								
2.92	w	2.897	m	2.899	004	2.90	50	2.88	ms
2.87	m								
2.79	w–b	2.756	w	2.752	320				
2.67	mw								
2.62	m	2.630	w	2.638	22–4				
2.52	w	2.514	w	2.512	032				
2.43	mw								
2.39	m	2.404	m	2.402	401	2.41	15	2.39	m?
		2.365	w	2.361	13–3				
2.33	w								
2.29	mw	2.295	w	2.293	420				
2.27	w								
2.23	w								
2.19	m	2.197	m	2.199	223	2.21	20	2.19	m
2.16	w								
2.11	m–b	2.143	m	2.142	204	2.15	20	2.07	w
2.06	mw	2.089	m	2.090	040				
2.03	w	2.025	w	2.029	412				
2.00	vw	1.976	w	1.967	042				
1.97	ms	1.956	m	1.955	430	1.96	40	1.96	m
1.94	w								
1.91	m	1.898	m	1.896	233				
		1.856	m	1.860	134	1.86	30b	1.85	ms
		1.770	w	1.768	502				
		1.628	m	1.628	522	1.63	15	1.63	m
		1.608	m	1.607	052	1.61	10	1.60	mw
		1.525	m	1.525	235				

Unit cell[9] of $(NH_4)_4UF_8$: monoclinic, $a = 13.126$, $b = 6.692$, $c = 13.717$ Å, $\beta = 121.32°$, $V = 1029$ Å^3; unit cell of $(NH_4)_4UF_{10}$ (this paper): monoclinic, $a = 12.87(2)$, $b = 8.36(2)$, $c = 13.60(7)$ Å, $\beta = 121.5(3)°$; $V = 1248$ Å^3.

Intensities of $(NH_4)_4UF_{10}$ and of the decomposition product are estimated visually.

stream of dried argon (5 $dm^3 h^{-1}$). The DTA range was 10 μV and the DTG range was 10 mg min^{-1}.

Thermal decomposition was also followed, confirming the results of the Mettler thermoanalyser, by weighing 2 g of $(NH_4)_4UF_{10}$ into a Ni crucible (100 cm^3) in an Ar dry-box. The crucible was held at successive temperatures for 1 h at each step (starting at 60°C, with steps of 10°C). Volatile products were pumped off in a dynamic vacuum. At each stage it was cooled down and samples were taken for powder data and chemical analysis.

Powder data

Debye–Scherrer X-ray diffraction patterns were obtained from a sample sealed in a quartz capillary using graphite monochromatized Cu-K_α radiation on an Enraf–Delft instrument. Intensities were estimated visually.

RESULTS AND DISCUSSION

In the series of known ammonium fluorouranates, $(NH_4)_4UF_{10}$ has the highest NH_4:U mol ratio and the highest valency state of uranium. Of the possible NH_4:U mol ratios for uranium in IV, V and VI valency states, only the lowest two (1:1 and 2:1) are fully represented by six compounds.[7,9,10] Within the higher ratios (3:1 and 4:1) there are, except for $(NH_4)_4UF_{10}$, only two compounds known; $(NH_4)_3UF_8$[9] and $(NH_4)_4UF_8$,[7] both synthesized by heating NH_4F and the fluoride of uranium in the proper valency state. This is not surprising since higher NH_4:F

Table 2. Powder diffraction data of decomposition products of $(NH_4)_4UF_{10}$ at 280, 380 and 600°C

Product at 280°C		$(NH_4)UF_6$[10]		Product at 380°C		$(NH_4)U_3F_{13}$[7]		Product at 600°C		UF_4 (ASTM data)	
d(Å)	I	d(Å)	I	d(Å)	I	d(Å)	I	d(Å)	I	d(Å)	I
5.76	s	5.81	100b			8.2	vw	4.19	s	4.213	10
4.12	vs	4.13	80	7.88	vw	7.9	m	4.16	m	4.183	6
4.06	m	3.99	30	7.28	w	7.2	mw–b	3.92	m	3.957	6
3.22	s	3.30	80	6.55	w			3.70	m	3.728	8
		2.96	10	5.53	w	5.50	m	3.52	m	3.555	6
2.91	m	2.88	50			5.37	w	3.39	w	3.374	4
2.65	w	2.64	20	4.54	vw	4.51	mw			3.299	6
		2.62	20	4.20	m	4.19	m	3.26	m	3.276	5
2.40	w	2.38	10	3.94	m	3.98	w			2.798	5
		2.35	10	3.71	s	3.70	w			2.782	1
2.22	s	2.20	70b			3.63	ms			2.705	3
2.10	m	2.07	30	3.55	m	3.50	ms	2.68	w	2.689	4
1.98	w	2.00	10	3.35	vw	3.34	ms			2.666	2
1.91	m	1.90	30	3.28	s	3.23	ms			2.580	1
		1.87	10	3.13	w	3.09	mw	2.47	vw	2.471	2
1.86	m	1.85	35			3.04	vw			2.454	1
1.82	m	1.81	30	2.82	w	2.89	ms	2.11	w	2.121	3
		1.77	10	2.69	m	2.68	m			2.109	2
1.71	w	1.75	10			2.62	mw			2.095	4
				2.59	w	2.56	m	2.06	m	2.068	7
				2.47	wd			2.00	m	2.001	6
						2.40	vw	1.94	m	1.977	4
						2.34	mw	1.87	m		
						2.25	mw–b				
				2.17	w	2.15	mw				
				2.12	w	2.11	w				
				2.07	m	2.08	mw				
				2.00	m	2.02	s				
				1.990	w	1.995	m				
				1.946	m	1.945	s				

Intensities of the decomposition products are estimated visually.

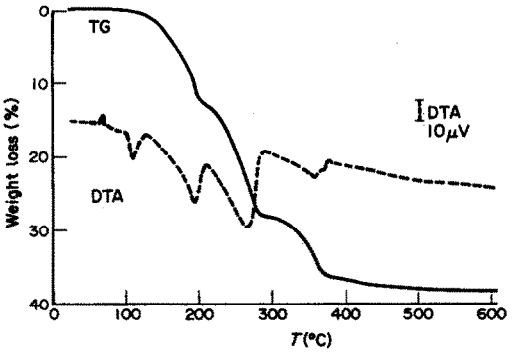

Fig. 1. TG and DTA curves of $(NH_4)_4UF_{10}$, as determined by a Mettler TA–1 thermoanalyser.

Table 3. Thermal decomposition of $(NH_4)_4UF_{10}$

		Calculated weight loss in %	Measured weight[a] loss in %
	$(NH_4)_4UF_{10}$		
200°C	$(NH_4)_3UF_8$	11.2	11.9
280°C	$(NH_4)UF_6$	26.0	27.5
380°C	$(NH_4)U_3F_{13}$	34.7	36.2
600°C	UF_4	37.2	38.0

[a] Results of a Mettler TA–1 thermoanalyser.

ratios and higher valency states tend to make these compounds increasingly less stable. The synthesis of $(NH_4)_4UF_{10}$ by oxidizing $(NH_4)_4UF_8$ with XeF_2 under very mild conditions is a new approach in the chemistry of these compounds, which in this case, using the proper starting compounds, overcame the problem of stability.

The powder diffraction data of $(NH_4)_4UF_8$ from which $(NH_4)_4UF_{10}$ was prepared, of $(NH_4)_4UF_{10}$ itself and of its first proved decomposition product at 200°C, identified as $(NH_4)_3UF_8$, are of a similar kind (Table 1). Such a degree of similarity was already observed in some potassium, and also in sodium fluorouranates. It was suggested that variations in valency and coordination of the actinide ions may leave their positions virtually unchanged.[5] Probably this is also happening in our case, particularly as the synthesis of $(NH_4)_4UF_{10}$ from $(NH_4)_4UF_8$ occurs through a relatively mild fluorinating agent under mild conditions. Powder data of $(NH_4)_4UF_{10}$ were indexed on the basis of a monoclinic unit cell. Its dimensions are similar to those[9] of $(NH_4)_4UF_8$ (Table 1), with the *b* axis significantly enlarged (by more than 25%).

$(NH_4)_4UF_{10}$ decomposes through three steps (at 200, 280 and 380°C) (Fig. 1) in which we could clearly identify the intermediate products by weight loss and powder data (Tables 1 and 2) and through a fourth at 600°C to UF_4. Additionally, we always noticed on the Mettler thermoanalyser an endothermic effect at *ca* 110°C, accompanied with a small weight loss, and the powder data at 110°C showed a mixture of $(NH_4)_4UF_{10}$ and an unknown compound. Nevertheless, we were not able to isolate this intermediate, even by slowly decomposing $(NH_4)_4UF_{10}$ in bulk. The actual decomposition path is not surprising. Uranium is reduced in the first step to a valency of V and in the third to IV. The N:U ratio diminishes from 4:1 to 3:1, 1:1 and in the last intermediate to 1:3. The 3:1 compound, $(NH_4)_3UF_8$, is known, and although its thermal decomposition was not investigated in detail, it has been observed[9] that on heating it under certain conditions, $(NH_4)UF_6$ was obtained. This is in accordance with our decomposition path. But it has not yet been observed that $(NH_4)UF_6$ decomposes through an intermediate to UF_4.[12] This last intermediate, $(NH_4)U_3F_{13}$, is identical with the last intermediate in the decomposition of $(NH_4)_4UF_8$,[7] where it was obtained from $(NH_4)UF_5$.

Acknowledgements—We are grateful to Professor B. Žemva for helpful discussions, to Mrs A. Rahten for taking the thermal decomposition curves and to Mrs B. Sedej for making chemical analyses. The financial support of the Research Community of Slovenia is gratefully acknowledged.

REFERENCES

1. B. Družina, S. Milićev and J. Slivnik, *J. Chem. Soc., Chem. Commun.* 1984, 363.
2. H. Martin and A. Albers, *Naturwissenschaften* 1946, **33**, 370; H. Martin, A. Albers and H.-P. Dust, *Z. Anorg. Allg. Chem.* 1951, **265**, 128; I. Peka, *Coll. Czech. Chem. Commun.* 1965, **30**, 217; 1966, **31**, 4245; I. Peka, L. Sedlakova and F. Sykora, *Coll. Czech. Chem. Commun.* 1966, **31**, 4449; I. Peka and P. Horaček, *Coll. Czech. Chem. Commun.* 1967, **32**, 426; V. Rak and P. Horaček, *Coll. Czech. Chem. Commun.* 1973, **38**, 42; M. Iwasaki, N. Ishikawa and K. Ohwada, *Abstr. IXth Int. Symp. Fluorine Chem.*, Avignon (1979); *J. Inorg. Nucl. Chem.* 1978, **40**, 503.
3. R. D. Shannon and C. T. Prewitt, *Acta Cryst.* 1969, **B25**, 925; 1970, **B26**, 1046.
4. L. S. Bartell, *J. Chem. Phys.* 1960, **32**, 827; C. Glidewell, *Inorg. Chim. Acta* 1975, **12**, 219.
5. R. A. Penneman, R. R. Ryan and A. Rosenzweig, *Struct. Bond. Berlin* 1973, **13**, 1.

6. J. A. Lukjanichev, N. S. Nikolajev and J. N. Mikhajlov, *Zh. Neorg. Khim.* 1963, **7**, 1617; B. Frlec, *J. Inorg. Nucl. Chem.* 1967, **29**, 2112; M. Milojević, J. Slivnik and P. Glavič, *NIJS-P-211* 1967, 1.
7. R. Benz, R. M. Douglas, F. M. Kruse and R. A. Penneman, *Inorg. Chem.* 1963, **2**, 799.
8. J. J. Katz and E. Rabinowitch, *The Chemistry of Uranium*, p. 361. McGraw-Hill, New York (1951).
9. R. A. Penneman, G. D. Sturgeon and L. B. Asprey, *Inorg. Chem.* 1964, **3**, 126.
10. B. Volavšek, *Croat. Chem. Acta* 1961, **33**, 181; R. A. Penneman, L. B. Asprey and G. Sturgeon, *J. Am. Chem. Soc.* 1962, **84**, 4608; R. Bougon, P. Charpin, J. P. Desmoulin and J. G. Malm, *Inorg. Chem.* 1976, **15**, 2532.
11. A. Rosenzweig and D. T. Cromer, *Acta Cryst.* 1970, **B26**, 38.
12. Nguyen-Nghi, A. J. Dianoux, H. Marquet-Ellis and P. Plurien, *C.R. Acad. Sci., Paris* 1965, **260**, 2229.

Polyhedron Vol. 9, No. 1, pp. 53–61, 1990
Printed in Great Britain

0277–5387/90 $3.00+.00
© 1989 Pergamon Press plc

REORIENTATIONAL PROCESSES IN SOLID $(C_6H_6)_2Cr$, $(C_6H_6)Cr(CO)_3$ AND $(C_6H_5Me)Cr(CO)_3$

DARIO BRAGA* and FABRIZIA GREPIONI

Dipartimento di Chimica "G. Ciamician", Università di Bologna, via F. Selmi 2, 40126 Bologna, Italy

(*Received* 13 *June* 1989; *accepted* 4 *August* 1989)

Abstract—The reorientational motion of the benzene rings in solid $(C_6H_6)_2Cr$ (**1**) and $(C_6H_6)Cr(CO)_3$ (**2**) and of the tricarbonyl group in solid $(C_6H_5Me)Cr(CO)_3$ (**3**), proposed on the basis of solid-state NMR experiments (wide-line ^1H and ^{13}C MAS) is studied by means of the pairwise potential energy method. Starting from the known crystal structures of the three species, relative potential energy barriers to motion and root mean square librational amplitudes at the bottom of the potential energy wells are evaluated and compared with the available anisotropic displacement parameters of the atoms involved in the process. The results show that the crystal packing in **2** and **3** forbids rotation of the $Cr(CO)_3$ group as a whole, while benzene reorientation encounters low potential energy barriers in both **1** and **2**, in agreement with the spectroscopic information. An alternative interpretation of the dynamic behaviour shown by **3**, based on large amplitude librations of both C_6H_5Me and $Cr(CO)_3$ groups, is put forward.

There is an increasing awareness that the understanding of the dynamic behaviour shown by many organometallic species in the solid state depends on combined efforts of both spectroscopic and diffraction methods.[1] The motion of groups of atoms or of entire molecules in a molecular crystal is controlled primarily by the distribution of the molecules within the crystal lattice, that is to say by the complicated balance of attractive and repulsive intermolecular forces at work between each atom and the environment.[2] Without this idea in mind it is difficult to understand the reasons for many, sometimes contradictory, dynamic processes in the condensed state of matter when compared with analogous behaviour in solution. For instance, $Fe_3(CO)_{12}$ and $Ru_3(CO)_{12}$, which in solution undergo CO-exchange at very low temperature,[3] are, respectively, "dynamic"[4] and "static"[5] in the solid state; while the *cis*- and *trans*-isomers of $(C_5H_5)_2Fe_2(CO)_4$, which interconvert via CO-bridge opening in solution,[6] show "static" CO's and rapidly rotating C_5H_5 ligands in the solid.[7]

Difficulties also arise from the conceptual difference between a spectroscopic experiment which yields time-averaged structural information depending on the working frequency span, and a diffraction experiment which operates an average over time and space of the entire content of the crystal lattice under examination.[8,9] Recently, it has been possible to demonstrate that the results of X-ray or neutron diffraction and solid-state NMR spectroscopy can be correlated by examining the dynamic information contained in the anisotropic displacement parameters (atomic "thermal" parameters, hereafter a.d.p.) in the light of spectroscopic results.[1,10]

A similar approach has also been applied to investigate the relationship between diffraction data and solution behaviour of a high nuclearity rhodium cluster.[11]

Moreover, semi-quantitative methods for the evaluation of the potential energy (p.e. hereafter) terms associated with molecule or fragment reorientations, widely employed in organic solid-state chemistry, have proved their extreme usefulness in the study of the collective effect of the molecules packed in a crystal on the occurrence of dynamic processes in solid organometallic species,[1,12] at least in cases where *intra*-molecular interactions play a limited role.

* Author to whom correspondence should be addressed.

In this paper the procedures mentioned above are applied to three closely related species: $(C_6H_6)_2Cr$ (**1**), $(C_6H_6)Cr(CO)_3$ (**2**) and $(C_6H_5Me)Cr(CO)_3$ (**3**), whose crystal structures are well documented by room- and low-temperature or neutron diffraction studies,[13-17] and whose solid-state dynamic behaviours have been studied either by wideline proton NMR (**1**, **2**)[18,19a] or by ^{13}C MAS NMR (**3**).[20] Results of quasi-elastic neutron scattering and of low-frequency Raman vibrational studies are also available for **2**.[19b] On the basis of the spectroscopic studies benzene reorientation around the molecular axes has been proposed for **1** and **2**,[18,19] while rotation of the tricarbonyl group has been invoked for **3**.[20]

Our purpose is to investigate the control exerted by the crystal packing on such dynamic processes in terms of p.e. barriers to motion, and to study the "shape" of the p.e. wells associated with the ground-state structures. In order to evaluate preferential displacement directions, use will also be made of the a.d.p.[21] of the atoms involved in the motions (when the available data are found of sufficient quality).

Finally, an alternative interpretation of the dynamic behaviour shown by **3**, which does not require rotation of the whole $Cr(CO)_3$ unit in the solid but only large amplitude librations of both the C_6H_5Me and $Cr(CO)_3$ fragments around their equilibrium positions, is proposed.

METHODS

The p.e. terms associated with molecular fragment reorientation of solid, neutral transition metal complexes or clusters can be evaluated by the pairwise p.e. method widely used in organic solid-state chemistry.[22] The method is well documented and will not be described in detail. The reader seeking more details of the computational procedures is referred to refs 23–26, while refs 1 and 27 contain more information about their application to organometallic species. The basic assumption is that the crystal packing of such species is dominated by purely van der Waals' interactions with no contribution of an ionic nature arising from permanent ionic charges or bond polarities. The p.e. is thus obtained as a simple function of the intermolecular separation in the crystal by summing up repulsive and attractive intermolecular energy terms between a reference molecule and the surrounding ones falling within a 10 Å cutoff and distributed by space group symmetry. The values of the coefficients to be used in the p.e. expression

$$\text{p.e.} = \sum_i \sum_j (A\, e^{-Br_{ij}} - Cr_{ij}^{-6})$$

for hydrogen, carbon and oxygen atoms are taken from the current literature.[24,26] The metal atom contribution is not taken into account. We have previously shown[1,27] that this rather drastic simplification affects only the values of the p.e. minima (the metal atoms contributing a constant attractive background), while it has no effect on the "shape" of the p.e. wells or on the heights of the p.e. barriers we are interested in (which are obviously dominated by the most external atoms). On the other hand, it must be stressed that we have no means for a correct evaluation of the "true" potential energy of an organometallic molecule in a crystal. We have chosen, by comparing closely related species of similar geometry and containing the same metal, to work on a *relative* scale. This is why the attention will be focused on the *relative* heights of the p.e. barriers (ΔE) and on changes in the p.e. profiles caused by temperature on crystals of the same species.

On these grounds, it should be clear that without "exterior" information, from spectroscopic methods, this kind of approach might have little to say. When such information is available, however, the feed-back to the comprehension of the averaging mechanisms at work in the solid state becomes of paramount importance.[28]

Atomic coordinates and space groups for all the species discussed herein were taken from the original structural reports (see Table 1 and refs therein). In the cases of **1** and **2**, where the molecules lie on crystallographic symmetry elements, the crystals were described in sub-groups of the actual space groups as required in order to operate on the entire molecules,[29] while keeping the packing distribution unaltered. Reorientations were performed by $\pm 180°$ rigid-body rotations of the molecular fragments or entire molecules around appropriately defined molecular axes and by calculating the p.e. values at 10° steps. The molecular packing was considered static during the motion, in such a way that the environment around the reorienting fragment retains the space-group symmetry and no cooperation by neighbouring molecules is involved. Because this limitation is known to cause an overestimation of the p.e. barriers,[30] the effect of cooperation was carefully explored in the controversial case of **3** (see below). This was carried out by allowing the first neighbouring molecules around the reference one to have the same kind of motion as the latter, and surrounding such a "molecular cluster" by an outer shell of static molecules in order to avoid undue freedom of the inner ones. Potential energy minimization was then performed by the steepest-descent method until convergence occurred.[30]

Table 1. Summary of crystallographic details, space group treatment and packing coefficients for **1(a,b)**, **2(a,b)** and **3**

$(C_6H_6)_2Cr$	**1a**	**1b**
Method, *T*, reference	X-ray, r.t., 13	X-ray, 100 K, 14
Space group[a]	$Pa\bar{3}(P2_12_12_1)$	$Pa\bar{3}(P2_12_12_1)$
a (Å)	9.667	9.553
V(cell) (Å^3)	904.2	871.8
Packing coefficient	0.54	0.57
$(C_6H_6)Cr(CO)_3$	**2a**	**2b**
Method, *T*, reference	X-ray, r.t., 15	Neutron, 78 K, 16
Space group[a]	$P2_1/m(P2_1)$	$P2_1/m(P2_1)$
a (Å)	6.17(2)	6.010(4)
b (Å)	11.07(4)	10.918(6)
c (Å)	6.57(2)	6.504(4)
β (°)	101.5(1)	100.60(5)
V(cell) (Å^3)	439.7	419.5
Packing coefficient	0.60	0.63
$(C_6H_5Me)Cr(CO)_3$	**3**	
Method, *T*, reference	X-ray, r.t., 17	
Space group	$P2_12_12_1$	
a (Å)	11.109(4)	
b (Å)	7.231(3)	
c (Å)	12.206(4)	
V(cell) (Å^3)	980.5	
Packing coefficient	0.60	

[a] Non-isomorphous subgroups of lower symmetry used to treat the molecules as independent units (see text) are reported in parentheses.

Because p.e. calculations are very sensitive to the atomic positions, hydrogen atoms of the C_6H_6 (**1** and **2**) and C_6H_5Me groups (**3**) were added in calculated, neutron-derived positions (C—H, 1.08 Å), with the exception of **2a** (see Table 1) whose original coordinates from the neutron diffraction study were used. All calculations were performed by using a slightly modified version of the program OPEC.[23] The relative p.e., ΔE = p.e. − p.e.$_{min}$, where p.e. is obtained as a function of the rotation angle and p.e.$_{min}$ is its minimum value (which invaraibly corresponds to the observed structure), is shown in Figs 1, 2 and 3 for **1**, **2** and **3**, respectively (see next section). The scale of energy is not the same in the three graphs.

In order to put this on a semi-quantitative basis the comparison of the p.e. wells corresponding to 0° rotation, root mean square (r.m.s.) librational amplitudes were evaluated as suggested by Shmueli and Kroon,[31] from the expression $\langle\varphi^2\rangle^{1/2} = kT/2c$, where k is Boltzmann's constant and the coefficient c is obtained by a least-squares fit of the polynomial

$$E(\varphi) = a + b\varphi + c\varphi^2 + d\varphi^3 + c\varphi^4$$

near the bottom of the p.e. well. The anharmonic contribution to libration (contained in the fourth and fifth coefficients) is not considered at the present stage of this study, although it can be anticipated that it appears to be relevant in **2** and **3** at room temperature. Finally, packing coefficients were calculated from the ratio $(V_{mol}Z)/V_{cell}$, where V_{mol} is evaluated by the method of intersecting caps from Kitaigorodsky.[2] Van der Waals radii taken from the literature (C, 1.75; O, 1.40; H, 1.15 Å) were used,[32] while the chromium atom was attributed a radius of 2.15 Å. Once again these choices allow comparison of the packing efficiency of the molecules in the crystals on a relative basis.[33] Packing coefficients provide, *inter alia*, an alternative and straightforward way of looking at the effects of a temperature decrease on the crystal packing.

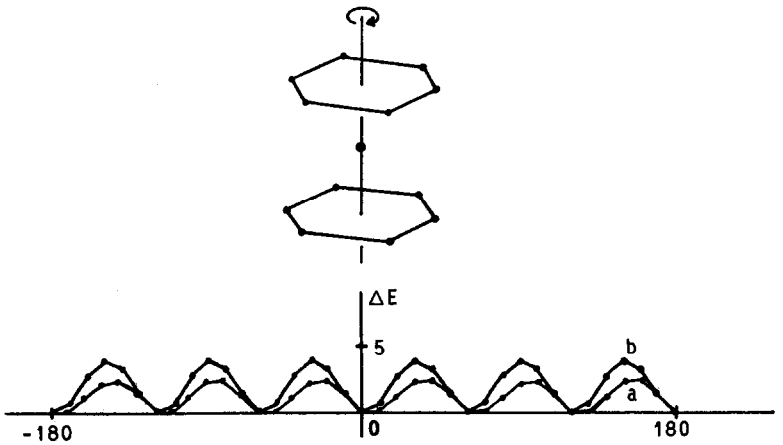

Fig. 1. Relative p.e. (ΔE, kcal mol^{-1}) vs angle of benzene in-plane rotation (°) in $(C_6H_6)_2Cr$, at (a) r.t. and (b) 100 K.

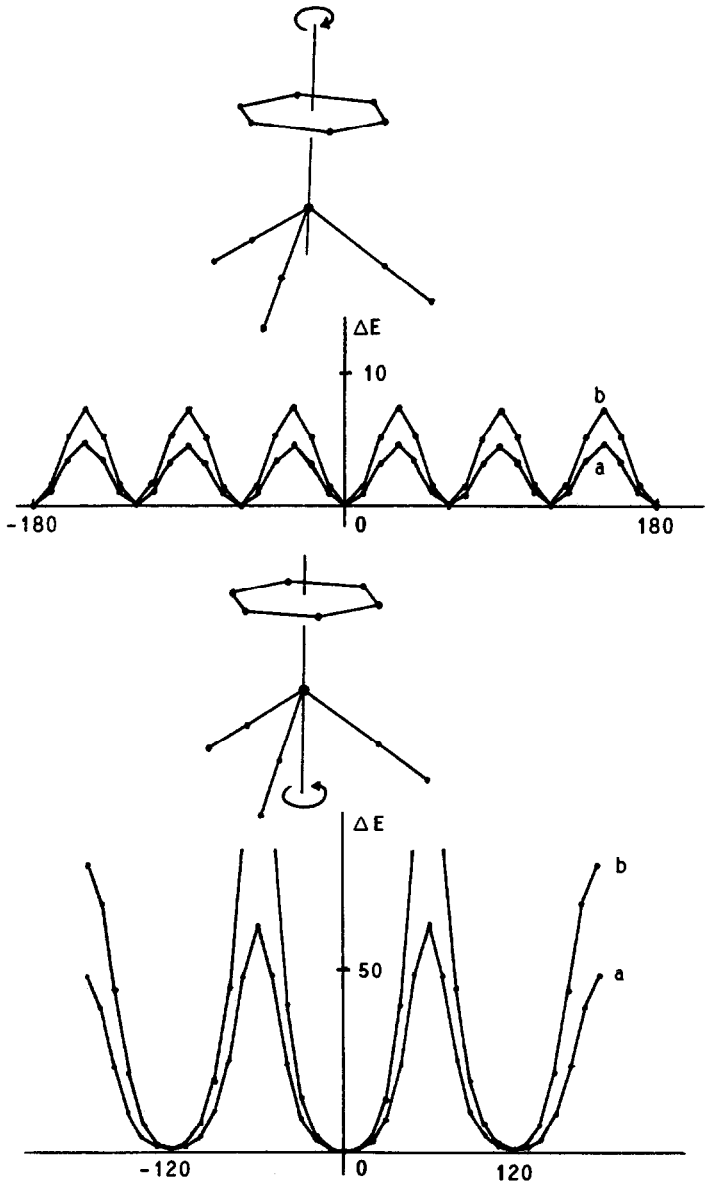

Fig. 2. Relative p.e. (ΔE, kcal mol^{-1}) vs angle of rotation around the molecular axis for benzene (top) and for $Cr(CO)_3$ group (bottom) in $(C_6H_6)Cr(CO)_3$ at (a) r.t. and (b) 78 K. The scale of energy is not the same in the two graphs.

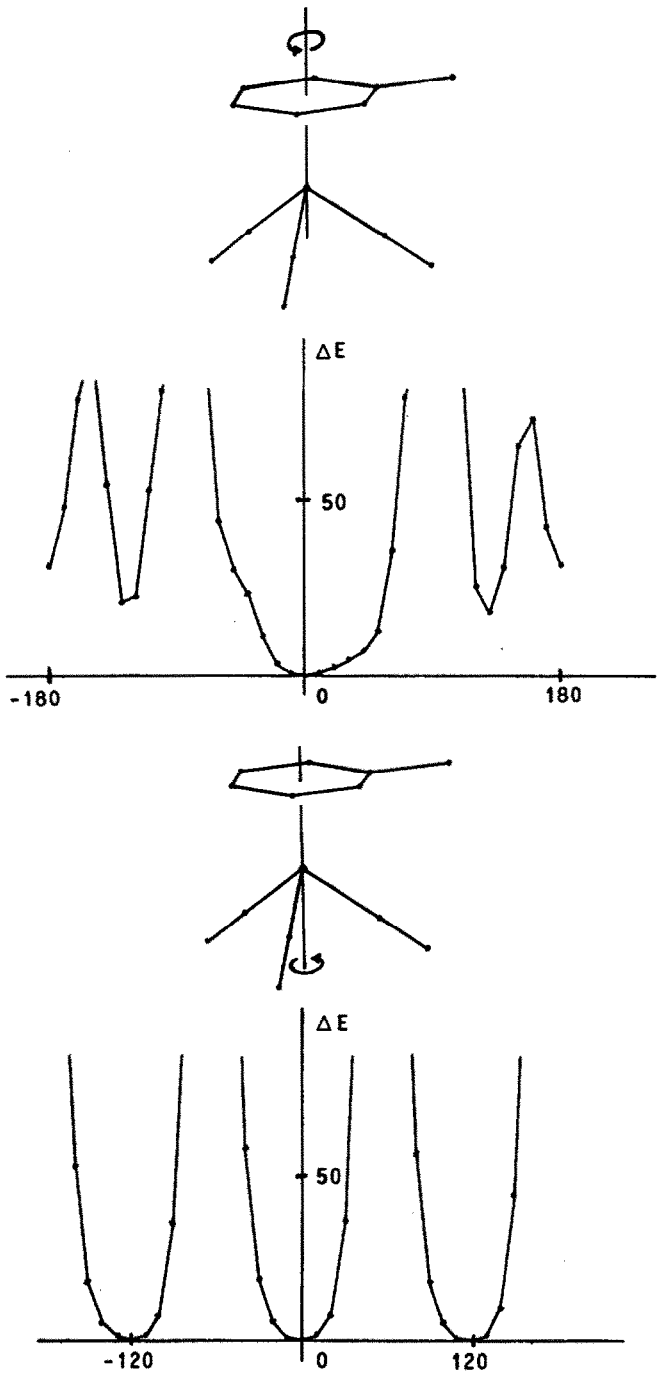

Fig. 3. Relative potential energy (ΔE, kcal mol^{-1}) vs angle of rotation (°) for toluene (top) and $Cr(CO)_3$ group (bottom) in $(C_6H_5Me)Cr(CO)_3$.

RESULTS AND DISCUSSION

Dynamic processes in solid $(C_6H_6)_2Cr$ **(1)**, $(C_6H_6)Cr(CO)_3$ **(2)** *and* $(C_6H_5Me)Cr(CO)_3$ **(3)**

Dibenzene chromium has been the subject of many structural studies, mainly owing to the controversy on its molecular symmetry (D_{3d}/D_{6h}) in the solid state.[34] As listed in Table 1, we have adopted the room-temperature (r.t.) coordinates first reported by Jellinek in 1963 (**1a**),[13] and the low-temperature (100 K) X-ray determination coordinates (**1b**).[14] The dynamic behaviour in solid $(C_6H_6)_2Cr$ has been ascertained by wideline NMR spectroscopy providing evidence that the arene groups undergo "essentially free rotation" about

Table 2. Potential energy barriers (kcal mol^{-1}) and r.m.s. librational amplitudes (°)[a] for **1**, **2** and **3**

$(C_6H_6)_2Cr$	**1a**, r.t.	**1b**, 100 K
p.e. barrier	2.0	3.9
r.m.s. librational amplitude	7.5	3.4
$(C_6H_6)Cr(CO)_3$	**2a**, r.t.	**2b**, 78 K
(C_6H_6) rotation		
p.e. barrier	4.6	7.5
r.m.s. lib. ampl.	5.6	2.2
$Cr(CO)_3$ rotation		
p.e. barrier	73.0	134.5
r.m.s. lib. ampl.	8.0	2.7
$(C_6H_5Me)Cr(CO)_3$	**3**, r.t.	
(C_6H_5Me) rotation		
p.e. barrier	192.3	
r.m.s. lib. ampl.	7.6	
$Cr(CO)_3$ rotation		
p.e. barrier	301.8	
r.m.s. lib. ampl.	5.7	

[a] Anharmonic contribution is not considered in the calculation of the r.m.s. librational amplitudes (see text).

the principal molecular axis in the temperature range 178–381 K.[18]

Similar behaviour has been detected in solid $(C_6H_6)Cr(CO)_3$ (**2**), in the range 77–439 K.[19a] An activation energy of 4.2 kcal mol^{-1}, obtained from spin–lattice relaxation times, has been reported for the process. Comparable values have been obtained from quasi-elastic neutron scattering (3.9 kcal mol^{-1} at 300 K) and from Raman spectroscopy (4.7 kcal mol^{-1} at 300 K, 6.2 kcal mol^{-1} at 120 K).[19b] Results of two independent structural studies are available for **2**: a r.t. determination (**2a**),[15] and a combined X-ray/neutron refinement carried out at 78 K (**2b** in Table 1).[16]

While the C_6H_6 groups show essentially the same behaviour on the NMR time scale in **1** and **2**, it has been suggested that the $Cr(CO)_3$ unit of this latter species is static because of the steric hindrance to rotation caused by the spatial distribution of the CO groups.[19a]

$(C_6H_5Me)Cr(CO)_3$ (**3**) has been recently studied by ^{13}C MAS NMR. In order to account for the spectral features observed in the temperature range 196–333 K,[20] the authors have invoked a rotational motion of the $Cr(CO)_3$ unit while the C_6H_5Me ligand remains static. From line-width analysis a rotational energy barrier of 15.5 kcal mol^{-1} has been obtained for the process.[20] The close relationship between the structures of **2** and **3** and the difference in their solid-state dynamic behaviour prompted us to the investigation of the proposed equilibration mechanisms. Figure 1 shows a comparison of the p.e. barriers calculated for **1a** and **1b** for a complete rotation of the arene group around the molecular axis. Barrier heights and r.m.s. librational amplitudes are listed in Table 2.

The p.e. profiles show minima of almost identical energies every 60° rotation, corresponding to jumps by the carbon atoms to the neighbouring positions. The p.e. barrier for each rotational jump increases from 2.0 to 3.9 kcal mol^{-1} on decreasing the temperature to 100 K. This change is accompanied by a decrease of the r.m.s. librational amplitudes from 7.5 to 3.5° which indicates that the p.e. well at r.t. is not only less deep but also somewhat flatter.

The same trend in barrier heights and r.m.s. librational amplitudes is found for C_6H_6 rotation in **2** (see Fig. 2, top) on passing from r.t. (**2a**) (4.6 kcal mol^{-1}, 5.6°) to 78 K (**2b**) (7.5 kcal mol, 2.2°). The slight increase of the p.e. barrier to benzene rotation in **2**, with respect to **1**, can be attributed to the different packing requirements of the $(CO)_3$ group in the former molecule with respect to the flat benzene rings in **1**, as also shown by the value of the packing coefficient, which is larger for **2** than for **1** (see Table 2).

As shown in Fig. 2 (bottom), rotation of the $Cr(CO)_3$ unit around the molecular axis in **2** is prevented by high p.e. barriers centred at $\pm 60°$ from the minimum. Minima of equivalent energy are otherwise observed at $\pm 120°$, which correspond to site "exchange" between the CO ligands in accord with the three-fold symmetry. Therefore a rotational motion of this kind is not possible for **2**. The barrier height, however, shows the expected decrease on passing from 78 K to r.t. The r.m.s. librational amplitudes indicate that the librational freedom of the $Cr(CO)_3$ unit increases extensively with the temperature (more than for the C_6H_6 ligand), although rotational jumps are forbidden by the steeply rising walls of the p.e. well. It is worth noting, at this stage, that the lowering of the p.e. barrier to motion, caused by a temperature increase in both **1** and **2**, is invariably accompanied by an increase of the r.m.s. librational amplitudes. This is an indication that, although there is no direct relationship between barrier height and extent of motion at the bottom of the p.e. well, the barrier decrease allows the atoms to "spend more time" further away from the equilibrium positions. In agreement with this observation the a.d.p. of the C_6H_6 and $(CO)_3$ groups in **2** are found to be larger at r.t. than at 78 K (see Fig. 4), thus providing an important indication that such parameters reflect, at least in the present case, true atomic motion and

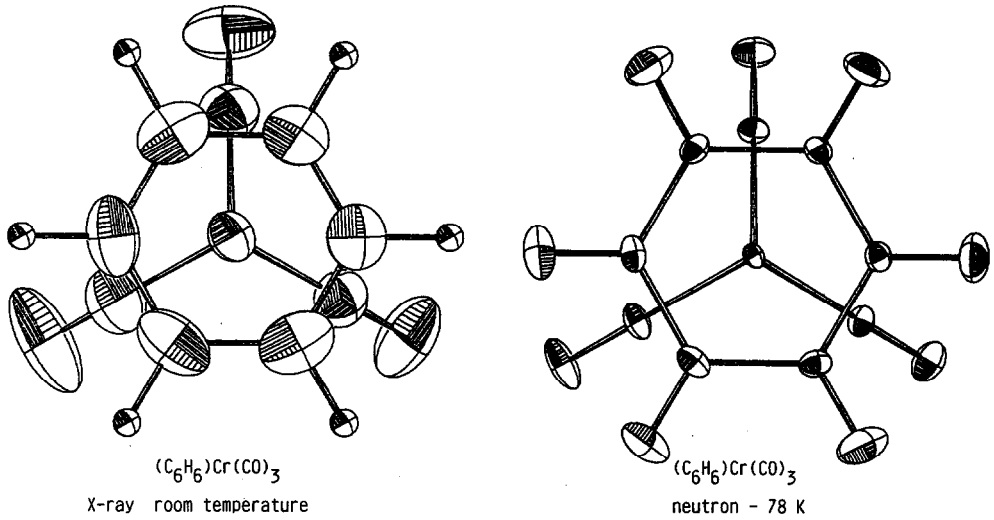

Fig. 4. Comparison of a.d.p. for $(C_6H_6)Cr(Co)_3$ at r.t. and 78 K (from refs 15 and 16).

not static disorder.[35] The same relationship between a.d.p. and p.e. barriers had previously been found for C_5H_5 reorientation in the *cis*- and *trans*-isomers of $(C_5H_5)_2Fe_2(CO)_4$.[1] Furthermore, in accordance with a preferential libration of the two fragments around the molecular symmetry axis, the a.d.p. for **2** clearly shows the presence of a strongly anisotropic librational motion around the three-fold axis (r.m.s. amplitudes obtained from thermal motion analysis are 7.7 and 3.5° around the three-fold axis, and 3.7 and 1.8° around the other axes for **2a** and **2b**, respectively).[15,16]

Let us now consider $(C_6H_5Me)Cr(CO)_3$. Potential energy profiles for independent rotations of the C_6H_5Me and $Cr(CO)_3$ units around the three-fold axis of this latter fragment are shown together in Fig. 3. [It should be pointed out that this axis is neither a molecular symmetry axis (the molecule possesses only *m*-symmetry) nor an inertia axis of the molecule, but rather the "coordination" axis of the chromium atom.] It appears that both C_6H_5Me and $Cr(CO)_3$ fragment reorientations are forbidden. However, as seen for **2**, minima at $\pm 120°$ are found which correspond to the three CO positions of the $Cr(CO)_3$ group.

These results play against the proposed rotation of the $Cr(CO)_3$ unit as the equilibration mechanism at work in solid **3**. As mentioned in the previous section, cooperation to the motion by the molecules surrounding the reference one was tested for **3** by allowing: (a) rigid-body rotation of the molecule as a whole around its major inertia axis; (b) rigid-body rotation around the "coordination" axis; and (c) reorientation of the two fragments as described above but in a cooperating environment.[30] In no cases were the p.e. barriers found to decrease significantly with respect to those obtained in a static environment.

Let us examine the p.e. wells in more detail (see Fig. 3). The calculated p.e. remains below the reference activation energy (*ca* 16 kcal mol^{-1}) yielded by the MAS experiment on **3**[20] within large angular ranges [-33, $+50°$ for C_6H_5Me; -28, $+24°$ for $Cr(CO)_3$]. This is an indication that the crystal packing, while effectively blocking reorientation of the two fragments, does allow extensive angular displacements from their equilibrium positions. It is also worth noting that the two p.e. wells are asymmetric with respect to the origin (0° rotation), although in opposite directions. On these premises and by taking advantage of the "exterior" spectroscopic information, which clearly indicates that an averaging mechanism is operating in solid **3**, we suggest that what is really taking place in the solid state is an extensive *swinging* of the two fragments in opposite directions around the chromium coordination axis. Such an extremely large amplitude librational motion can easily afford an exchange mechanism between the observed "*cis*" rotameric configuration and the one in which the CO's are staggered with respect to the ring atoms ($\pm 15°$ torsions of the two fragments, see Fig. 5). Incidentally, this latter rotameric configuration is the one observed in solid **2**. In the absence of exchange processes, the staggered configuration in **3** is expected to give rise to three resonances for the CO

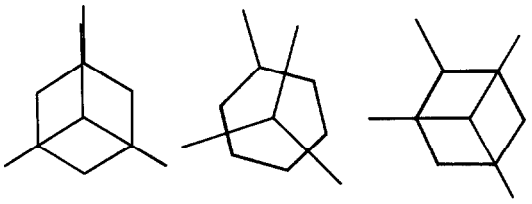

Fig. 5. Schematic representation of the proposed mechanism of interconversion (rotation of the two moieties in opposite directions) between the different rotameric configurations of $(C_6H_5Me)Cr(CO)_3$ in the solid state. The "*cis*" configuration is the one observed in the solid state.

groups. As the temperature is increased the limiting "*trans*" configuration may also be attained ($\pm 30°$ torsions, see Fig. 5), thus further contributing to the spectral features above coalescence (298 K).[20] In such a way the equilibration mechanism between the various rotameric configurations ("*cis*" eclipsed, staggered, "*trans*" eclipsed) does not necessitate full rotational freedom of either fragments. On decreasing the temperature, the swinging motion is reduced and finally stopped and a static structure is seen on the NMR time scale.

We trust that a full assessment of this phenomenon will be made possible by collection of low-temperature diffraction data of **3** [or of the analogous species $(C_6H_5Me)Mo(CO)_3$[20]] which is presently under way.

Finally, it is interesting to speculate on the fact that **2** might show similar behaviour under MAS NMR experimental conditions. We have, in fact, shown that the $Cr(CO)_3$ unit in **2** behaves in very much the same way as in **3**, possessing a very large librational freedom in its crystal. Therefore we can predict that a large amplitude librational motion of the tricarbonyl group will accompany rotation of the benzene ring in **2**.

CONCLUSIONS

We have shown that information of a dynamic nature can be extracted either from a.d.p. alone, when data collected at different temperatures are available, or by studying the molecular organization within the crystal lattice and the way in which the crystal packing controls the reorientational motions. The atom–atom p.e. method appears to be a powerful complementary tool to investigate such dynamic processes. What is more, the method, although based on several non-trivial approximations, is able to provide reliable semi-quantitative criteria to discriminate between genuine rotational freedom and large amplitude librational motions in the solid state. It should be stressed that both p.e. calculations and thermal motion analysis can be carried out by simply taking advantage of the *entire* structural information (atomic positions but also a.d.p. and crystal packing) yielded by a conventional diffraction experiment of reasonable quality. On this basis, we would like to emphasize that the commonplace belief that "X-ray diffraction techniques can not detect dynamic processes occurring in the solid state" should be definitively put aside.

Acknowledgements—It is a pleasure to thank Professor H.-B. Bürgi (Bern) and Professor A. Gavezzotti (Milano) for many useful discussions. Financial support by Consiglio Nazionale delle Ricerche is acknowledged.

REFERENCES

1. D. Braga, F. Grepioni and C. Gradella, *J. Chem. Soc., Dalton Trans.* 1989, 1721.
2. A. I. Kitaigorodsky, *Molecular Crystals and Molecules*. Academic Press, New York (1973).
3. E. Band and E. L. Muetterties, *J. Am. Chem. Soc.* 1978, **78**, 639.
4. (a) H. Dorn, B. E. Hanson and E. Motell, *Inorg. Chim. Acta* 1981, **54**, L71; (b) B. E. Hanson, C. E. Lisic, J. T. Petty and G. Iannacone, *Inorg. Chem.* 1984, **25**, 4062.
5. S. Aime, M. Botta, R. Gobetto, D. Osella and L. Milone, *Inorg. Chim. Acta* 1988, **146**, 151.
6. (a) O. Gausow, A. R. Burke and W. D. Vernon, *J. Am. Chem. Soc.* 1972, **94**, 2550; (b) R. D. Adams and F. A. Cotton, *J. Am. Chem. Soc.* 1973, **95**, 6589.
7. H. C. Dorn, B. E. Hanson and E. Motell, *J. Organomet. Chem.* 1982, **224**, 181.
8. (a) E. L. Muetterties, *Inorg. Chem.* 1965, **4**, 769; (b) E. Band and E. L. Muetterties, *Chem. Rev.* 1978, **78**, 639.
9. R. E. Benfield, D. Braga and B. F. G. Johnson, *Polyhedron* 1988, **7**, 2549.
10. C. E. Anson, R. E. Benfield, A. W. Bott, B. F. G. Johnson, D. Braga and E. A. Marseglia, *J. Chem. Soc., Chem. Commun.* 1988, 889.
11. D. Braga and B. T. Heaton, *J. Chem. Soc., Chem. Commun.* 1987, 608.
12. J. Sanz-Aparicio, S. Martinez-Carrera, S. Garcia-Blanco and A. Conde, *Acta Cryst.* 1988, **B44**, 259.
13. F. Jellinek, *J. Organomet. Chem.* 1963, **1**, 43.
14. E. Keulen and F. Jellinek, *J. Organomet. Chem.* 1966, **5**, 490.
15. M. F. Bailey and L. F. Dahl, *Inorg. Chem.* 1965, **4**, 1314.
16. B. Rees and P. Coppens, *Acta Cryst.* 1973, **B29**, 2516.
17. F. van Meurs and H. van Koningsveld, *J. Organomet. Chem.* 1977, **131**, 423.
18. S. E. Anderson, *J. Organomet. Chem.* 1974, **71**, 263.
19. (a) P. Delise, G. Allegra, E. R. Mognaschi and A.

Chierico, *J. Chem. Soc., Faraday Trans. II* 1975, **71**, 207; (b) K. Chhor and G. Lucazen, *J. Raman Spectrosc.* 1982, **13**, 235.
20. G. Wagner and B. E. Hanson, *Inorg. Chem.* 1987, **26**, 2019.
21. J. D. Dunitz, V. Schomaker and K. N. Trueblood, *J. Phys. Chem.* 1988, **92**, 856.
22. (a) A. J. Pertsin and A. I. Kitaigorodski, *The Atom–Atom Potential Method*, Springer, Berlin (1987); (b) A. Gavezzotti and M. Simonetta; in *Organic Solid State Chemistry* (Edited by G. R. Desiraju). Elsevier, Amsterdam (1987).
23. A. Gavezzotti, *J. Am. Chem. Soc.* 1983, **105**, 5220.
24. A. Gavezzotti and M. Simonetta, *Acta Cryst.* 1975, **A31**, 165.
25. A. Gavezzotti, *Nouv. J. Chim.* 1982, **6**, 443.
26. A. Gavezzotti and M. Simonetta, *Chem. Rev.* 1981, **82**, 1.
27. D. Braga and F. Grepioni, *Polyhedron* 1989, **8**, 2237.
28. (a) M. C. Etter, R. C. Hoye and G. M. Vojta, *Cryst. Rev.* 1988, **1**, 281; (b) C. A. Fyfe and R. E. Wasylishen, *Solid State Chemistry Techniques* (Edited by A. K. Cheetham and P. Day), Chap. 6, p. 190. Clarendon, Oxford (1987).
29. *International Tables for X-ray Crystallography*, Vol. I. Reidel, Dordrecht, Holland (1983).
30. A. Gavezzotti and M. Simonetta, *Acta Cryst.* 1976, **A32**, 997.
31. (a) U. Shmueli and P. A. Kroon, *Acta Cryst.* 1974, **A30**, 768; (b) U. Shmueli and I. Goldberg, *Acta Cryst.* 1973, **B29**, 2466.
32. A. Bondi, *J. Phys. Chem.* 1964, **68**, 441.
33. D. Braga and F. Grepioni, *Acta Cryst. B* 1989, **B45**, 378.
34. (a) M. F. Bailey and L. F. Dahl, *Inorg. Chem.* 1965, **4**, 1298; (b) J. A. Ibers, *J. Chem. Phys.* 1964, **40**, 3129; (c) F. A. Cotton, W. A. Dollase and J. S. Wood, *J. Am. Chem. Soc.* 1963, **85**, 1543.
35. E. Maverick and J. D. Dunitz, *Molec. Phys.* 1987, **2**, 451.

Polyhedron Vol. 9, No. 1, pp. 63–68, 1990
Printed in Great Britain

0277–5387/90 $3.00+.00
© 1989 Pergamon Press plc

POLY(BENZOTRIAZOLYL)BORATES—I. LIGAND SYNTHESIS AND CHARACTERIZATION

FERGUS J. LALOR,† S. M. MILLER and (in part) N. GARVEY

Department of Chemistry, University College, Cork, Republic of Ireland

(*Received* 13 *June* 1989; *accepted* 4 *August* 1989)

Abstract—The preparation and characterization of the new potassium poly(azolyl)borate salts $KH_2B(C_6H_4N_3)_2$, $KHB(C_6H_4N_3)_3$ and $KB(C_6H_4N_3)_4$ ($C_6H_4N_3$ = benzotriazolyl) and their thallium(I) derivatives is described. ^{13}C NMR spectroscopy identifies the anions as the N(1)-regioisomers and suggests a similar structure for the tetrakis(indazolyl)borate anion $[B(C_7H_5N_2)_4]^-$. The unexpected regioisomerism of the anions—which differs from that of related species—is attributed to the importance of electronic effects.

Heating a mixture of pyrazole or its C-substituted derivatives (i.e. Hpz*) with an alkali metal tetrahydroborate salt leads to elimination of hydrogen and the formation of B—N bonds:

$$BH_4^- + n\text{Hpz}^* \xrightarrow{\Delta} [H_{4-n}B(\text{pz}^*)_n]^- + nH_2. \quad (1)$$

In his pioneering studies of this reaction Trofimenko[1] demonstrated that the resulting anionic poly(1-pyrazolyl)borates possess unusual ligand characteristics, combining aspects of the properties of classical σ-bonding chelating ligands such as acetylacetonate with those of the π-bonding cyclopentadienide anion. The results summarized in several recent reviews[2] testify to a continuing growth of interest in these compounds. The poly(1-pyrazolyl)borate anions may be considered to be a subgroup of a wider class of ligands which are potentially accessible via the reaction of BH_4^- with heterocyclic compounds containing both an acidic ring NH group and an adjacent ring heteroatom with at least one available lone pair of elecrons. The range of such compounds reported to date consists of derivatives of indazole,[3] nitroindazoles,[4,5] imidazoles,[6,7] benzimidazole[6] and 1,2,4-triazole.[1] In a number of cases[1,4,5] the ligand itself has not been isolated but was characterized in the form of its transition metal complexes. None of these ligands nor their derived complexes have been structurally characterized by X-ray crystallographic methods and there is only a single report[8] of the formation of an organometallic derivative. Recent work in their laboratories has shown that the chemical properties of organometallic complexes containing poly(1-pyrazolyl)borate ligands may be dramatically altered by relatively minor changes in the substitution pattern of the pyrazole ring[9] and this has impelled us to investigate the behaviour of organometallic complexes of analogous ligand systems with modified steric and/or electronic properties. In this communication we describe the preparation and characterization of a new series of poly(azolyl)borate ligands derived from benzotriazole. The ligating properties of the new compounds will be discussed in a forthcoming paper.[10] Some of the results described here have been published in an abbreviated form.[11]

RESULTS AND DISCUSSION

When an intimate mixture of benzotriazole and potassium borohydride (*ca* 4–5 : 1 molar ratio) is heated in a closed system, melting and evolution of hydrogen takes place at *ca* 90°C. If this temperature is maintained the gas evolution ceases after *ca* one equivalent of hydrogen has been released. However, work-up at this stage gave no evidence for the formation of a mono(benzotriazolyl)borate anion (see below). Further heating causes a second equivalent of hydrogen to be evolved between *ca* 98–130°C, a third between 170–200°C, and a fourth between 240–260°C. Work-up at each stage gave the

† Author to whom correspondence should be addressed.

potassium salts of the bis-, tris-, and tetrakis (benzotriazolyl)borates $K[H_2B(C_6H_4N_3)_2]$ (**1**), $K[HB(C_6H_4N_3)_3]$ (**2**) and $K[B(C_6H_4N_3)_4]$ (**3**), respectively ($C_6H_4N_3$ = benzotriazolyl). Only the bis-derivative **1** and unreacted KBH_4 could be detected when the reaction was interrupted after evolution of a single equivalent of hydrogen. The new poly(benzotriazolyl)borates are white (**1**, **2**) or off-white (**3**) solids and were isolated in *ca* 75–80% yield. Purification by crystallization was not satisfactory but traces of unreacted benzotriazole could be removed by washing with boiling methylcyclohexane. Prolonged heating with this solvent or attempts to sublime out unreacted benzotriazole under high vacuum appeared to cause slow decomposition. Both the bis- and tris(benzotriazolyl) compounds **1** and **2** are hygroscopic and the presence of water could be detected by IR and NMR spectroscopy in samples which had been dried at *ca* 80°C *in vacuo*. Microanalytical data (Table 1) were in agreement with the formulation of both these compounds as monohydrates. All three potassium salts were readily converted into the analogous anhydrous thallium(I) derivatives $Tl[H_2B(C_6H_4N_3)_2]$ (**4**), $Tl[HB(C_6H_4N_3)_3]$ (**5**) and $Tl[B(C_6H_4N_3)_4]$ (**6**). Acidification of an aqueous solution of **2** with acetic acid yielded an unstable off-white solid which was insoluble in all the usual organic solvents except dimethylsulphoxide in which it decomposed with evolution of gas. Microanalytical data (Table 1) were in approximate agreement with a formulation as the trihydrate of the parent acid of **2** i.e. $H[HB(C_6H_4N_3)_3]\cdot 3H_2O$ (**7**). Further attempts to characterize the material were not successful.

Since benzotriazole exists as a mixture of N(1)—H and N(2)—H tautomers, B—N bond formation (in the reaction with borohydride anion) can occur potentially at either of these atoms with

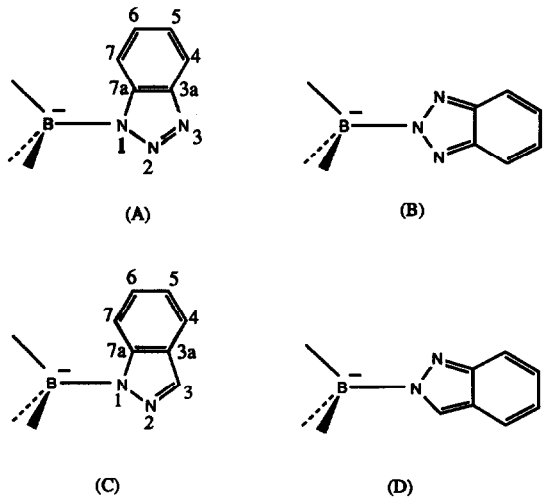

Fig. 1. Regioisomeric structures and numbering system for (benzotriazolyl)- and (indazolyl)borates.

formation of one or other of the pair of regioisomeric structures A and B, illustrated in Fig. 1. A similar possibility of regioisomerism exists for the reaction of the borohydride anion with 3-monosubstituted pyrazoles. In all such systems studied to date, the reaction is strictly regiospecific. The critical factor appears to be the degree of steric crowding at the boron since the regioisomer with the ring-substituent in the more remote 3-position is formed exclusively.[12] We, therefore, anticipated that compounds **1**–**6** would exist in the B—N(2) regioisomeric form (i.e. B, Fig. 1) in which steric hindrance at boron is minimized. The structures of **1**–**6** were readily established by ^{13}C NMR spectroscopy. Six distinct carbon resonances would be predicted for exclusively N(1)-bonded regioisomers as against three for the more symmetrical N(2)-bonded alterna-

Table 1. Yield, melting point and analytical data

Compound	Yield (%)	Melting point (°C)	Analysis—% found (calc.) C	H	N
$K[H_2B(C_6H_4N_3)_2]\cdot H_2O$ (**1**)	81	170–175	47.3 (47.1)	3.4 (3.9)	27.1 (27.4)
$K[HB(C_6H_4N_3)_3]\cdot H_2O$ (**2**)	76	120–125 dec.	50.9 (51.1)	3.6 (3.6)	30.0 (29.8)
$K[B(C_6H_4N_3)_4]$ (**3**)	76	310 dec.	55.7 (55.2)	3.2 (3.1)	31.8 (32.2)
$Tl[H_2B(C_6H_4N_3)_2]$ (**4**)	58	200–202	31.7 (31.8)	2.6 (2.2)	18.3 (18.5)
$Tl[HB(C_6H_4N_3)_3]$ (**5**)	77	240–245 dec.	37.4 (37.9)	2.6 (2.3)	22.3 (22.1)
$Tl[B(C_6H_4N_3)_4]$ (**6**)	64	310 dec.	41.9 (41.9)	2.4 (2.3)	24.1 (24.4)
$H[HB(C_6H_4N_3)_3]\cdot 3H_2O$ (**7**)	51	145–150 dec.	49.4 (51.3)	3.9 (4.8)	31.6 (29.9)
$K[B(C_7H_5N_2)_4]$ (**8**)	70	310 dec.	64.6 (64.9)	3.8 (3.9)	21.7 (21.6)
$Tl[B(C_7H_5N_2)_4]$ (**9**)	85	240 dec.	49.5 (49.2)	2.9 (2.9)	16.2 (16.4)

tive and nine for structures with both forms of bonding. The fully-decoupled ^{13}C NMR spectra of complexes **1–5** are summarized in Table 2. (The thallium tetrakis(benzotriazolyl)borate compound, **6**, was insufficiently soluble in the usual solvents for its spectrum to be recorded.) All of the compounds studied give similar six-line spectra and they are therefore shown to involve N(1)-bonded benzotriazolyl groups. (Assignment of the resonances in the spectra of **1–5** to individual carbon atoms was made by reference to the very similar spectrum of 1-methylbenzotriazole.[13])

The ^1H NMR spectra of complexes **1–5** (see Experimental) were all similar in showing a complicated series of resonances in the aromatic region, generally separable into two highly asymmetric multiplets centred on *ca* δ 7.5 and 8.0 ppm. The observed pattern is compatible with the proposed N(1)-bonded structures in that the more symmetrical N(2)-regioisomers should exhibit a relatively simple AA^1BB^1 spectrum, similar to that of 2-methylbenzotriazole.[14] Apart from the absorption at *ca* 3400 cm^{-1}, characteristic of water of hydration in **1** and **2**, and ν(BH) bands in **1** (2450, 2430, 2390 cm^{-1}, broad) and **2** (2480 cm^{-1}), the IR spectra of the potassium salts **1–3** (KBr disc) show considerable similarity in the 1600–650 cm^{-1} region. Noticeable differences from the spectra of benzotriazole itself are medium to strong bands at *ca* 1490, 1450, 1350, 1290 and 1270 cm^{-1}, as well as strong bands at *ca* 1145, 1127, 1057 and (in **3**) 930 and 840 cm^{-1} which are either weak or absent in the spectrum of the free heterocycle. The IR spectra of the thallium salts **4–6** in pressed polyethylene discs are virtually identical to those of the potassium salts in KBr.

The series of (indazolyl)- and (nitroindazolyl)borate ligands described by Zaidi and coworkers[3–5] possess the same potential for regioisomerism as do the (benzotriazolyl)borates (i.e. C and D of Fig. 1). This possibility receives no mention in the original literature, where B—N(1) bonding is assumed without explicit discussion of evidence in favour of that conclusion. While our results with benzotriazole do suggest that the structurally similar indazole would also form the N(1)-regioisomer we have attempted to gather more definite evidence on the point. The tetrakis(indazolyl) borate salt $K[B(C_7H_5N_2)_4]$ (**8**) ($C_7H_5N_2$ = indazolyl) was prepared in improved yield and purity by a modification of the published procedure and was readily converted into its thallium(I) derivative (**9**). We chose compound **8** as the most sterically crowded of the (indazolyl)borates and, therefore, the most likely to exist wholly or partly as the N(2)-regioisomer. Since the structure of **8** may not be deduced directly from its ^{13}C NMR spectrum (see below), we attempted to grow crystals suitable for an X-ray crystallographic study but were not successful. Neither could crystals of suitable quality be obtained of the thallium salt **9** which, like its benzotriazolyl analogue **6**, is insoluble in

Table 2. ^{13}C NMR data

Compound	C(3)	C(3a)	C(4)	C(5)	C(6)	C(7)	C(7a)
$K[H_2B(C_6H_4N_3)_2]$ (**1**)[a]	—	146.84	118.64	122.60	125.27	114.09	139.11
$Tl[H_2B(C_6H_4N_3)_2]$ (**4**)[b]	—	146.58	118.38	124.42	126.63	114.68	139.43
$K[HB(C_6H_4N_3)_3]$ (**2**)[c]	—	145.32	118.18	123.45	126.37	112.21	137.94
$Tl[HB(C_6H_4N_3)_3]$ (**5**)[c]	—	145.34	119.16	124.20	127.54	112.28	137.80
$K[B(C_6H_4N_3)_4]$ (**3**)[a]	—	147.88	119.10	123.45	126.37	114.16	138.98
1-Methylbenzotriazole[d]	—	146.50	119.80	124.10	127.50	110.50	134.20
1-Methylindazole[d]	132.90	124.90	121.40	120.80	126.50	109.80	140.70
$\Delta\delta$[e]		1.38	−0.70	−0.65	−1.13	3.66	4.78
Calculated for **8**[f]	—	126.28	120.70	120.15	125.37	113.46	145.48
$K[B(C_7H_5N_2)_4]$ (**8**)[a]	133.75[g]	126.24[h]	119.94	119.48	124.16	115.13	146.09[g]

[a] Spectrum recorded in acetone-d_6.
[b] Spectrum recorded in methanol-d_4.
[c] Spectrum recorded in chloroform-d.
[d] Data from ref. 13(a), recorded in acetone-d_6. The reported assignments of C(5) and C(6) in 1-methylbenzotriazole have been interchanged—see text.
[e] δC(3)–δC(1-methylbenzotriazole)—see text.
[f] δC(1-methylindazole) + $\delta\Delta$—see text.
[g] Quartet—see text.
[h] Broad resonance—see text.

common organic solvents. The IR spectrum of **8** shows strong bands at 1450, 1410, 1325, 1260, 1155, 1140, 1100 and 820 (broad) cm^{-1} which are either absent or of low intensity in the spectrum of indazole. The IR spectrum of **9** is similar to that of **8**. A singlet in the ^1H NMR spectrum of **8** in acetone-d_6, integrating for four protons, is assigned to the unique proton at C(3) of the indazole nucleus and indicates that all four indazolyl groups are equivalent in the anion. The protons of the benzene portion of the indazolyl nucleus appear as a pair of complex multiplets centred on δ 6.8 (4H) and 7.7 (12H) ppm, respectively. Because the inherent asymmetry of the indazole nucleus is such that—unlike **1**–**6**—neither N(1)—B nor N(2)—B regioisomers of **8** possess a plane of symmetry bisecting the aromatic ring, the ^1H NMR spectrum cannot be simply interpreted in terms of the regioisomeric structure of the anion. A similar problem affects the ^{13}C NMR spectrum of **8** which is summarized in Table 2. The observed seven-line spectrum is compatible with either regioisomer and the positions of the resonances themselves are sufficiently close to those of both 1- and 2-methylindazole[13a] to prevent any firm conclusion being drawn as to the structure present. Extrapolation from the ^{13}C NMR spectrum of the potassium tetrakis(1-benzotriazolyl) borate (**3**), however, does provide some tentative evidence in favour of an analogous structure for **8**. From a comparison of the spectra of $K[B(1\text{-}C_6H_4N_3)_4]$ (**2**) and 1-methylbenzotriazole[13b] in acetone-d_6 we can derive a set of empirical correction factors, $\Delta\delta$, reflecting the change in chemical shift of the carbon nuclei on formal replacement of the N(1)–methyl group by the N(2)—B bond in **3**. Applying these correction factors to the ^{13}C NMR spectrum of 1-methyl indazole† produces calculated chemical shift values for **8** which are in good agreement with the observed spectrum (Table 2). While not to be regarded as proof, we believe that this result is strongly suggestive of an N(1)-bonded regioisomeric structure for **8** and, by extension, for the other reported indazolylborate ligands. A further interesting aspect of the ^1H decoupled ^{13}C NMR spectrum of **8** is the observation that the resonances of C(3) and C(7a) appear as two broadened quartets with a line-separation of *ca* 3.0 Hz. In addition, the singlet resonance of C(3a) is also noticeably broadened. We ascribe the splitting of the C(3) and C(7a) resonances to long-range coupling with the ^{11}B nucleus (80.22%, $I = 3/2$). While such coupling is not unexpected in four-coordinate anionic boron compounds,[15] it is strange that it is not observed in the spectrum of the closely related $K[B(1\text{-}C_6H_4N_3)_4]$ (**3**). The broadening of all three resonances is likely to be due to the effects of partial quadrupolar collapse of the coupling.[16]

With the regiospecificity of the benzotriazole–borohydride reaction firmly established as involving B—N(1) bonding and with the probability being that the reaction with indazoles follows the same pattern, we are left with a question: Why does the regiospecificity of this reaction depart from well-established precedent and produce the most sterically crowded anion, even in the highly congested tetrakis(azolyl)borates? We believe that the answer lies in a trade-off between steric and electronic effects in the anions. While N(2)—B bonding minimizes steric crowding, it does so at the expense of forcing the heterocycle into a quinonoid form with a resulting loss of aromatic delocalization energy. It seems clear that this produces an unacceptable net destabilization of the anion. It remains to be seen whether we can force the formation of the N(2)-bonded isomers by making the heterocycle even more sterically demanding, e.g. by the introduction of substituents at C(4) and C(7).

EXPERIMENTAL

Potassium borohydride, benzotriazole and indazole were commercially available. KBH_4 was dried *in vacuo* at 110°C for 12 h before use. Benzotriazole was recrystallized from benzene and indazole was sublimed in high vacuum. IR spectra were recorded on Perkin–Elmer 257 and 628 spectrophotometers. ^1H and ^{13}C NMR spectra were measured on Perkin–Elmer Hitachi R20-A and Jeol FX-60 instruments operating at ambient temperature and are referenced to internal trimethylsilane. Elemental

† The data in ref. 13(b) were chosen for comparison with the spectrum of **3** because of the common solvent employed for the two measurements. We note that this paper does not explain the origin of the assignments of the individual resonances to particular carbon atoms. The quoted assignments for C(5) and C(6) differ by 4.1 and −2.7 ppm, respectively, from the resonances assigned to these carbon atoms in ref. 13(a) where the individual assignments are justified. The measurements in ref. 13(a) were made on solutions in deuterochloroform. Comparison of the data on compounds common to both studies and of spectra recorded in both solvents and quoted in ref. 13(b) shows that a solvent shift of *ca* 1.0 ppm is to be expected for the carbon nuclei in question and that resonances measured in chloroform are invariably displaced to high field with respect to those determined in acetone. We conclude that the assignments for C(5) and C(6) quoted in ref. 13(b) are in error. Since the anomaly is removed if the assignments are simply reversed, this is assumed in the subsequent discussion.

analyses were determined by the staff of the Microanalytical Laboratory of University College, Cork.

Potassium dihydrobis(1-benzotriazolyl)borate monohydrate (**1**)

Finely powdered benzotriazole (10.0 g, 84 mmol) and potassium borohydride (1.13 g, 21 mmol) were intimately mixed in a three-necked, round-bottomed flask fitted with a magnetic stirring bar, a nitrogen inlet valve, a thermocouple well and a 30-cm air condenser, the top of which was connected to a wet-test meter. Thermocouple probes for a digital thermometer and temperature-control device were placed in the well which extended close to the bottom of the flask. The apparatus was flushed with nitrogen, sealed off from the atmosphere and placed in an oil-bath. Gentle heating to *ca* 100°C with stirring caused the mixture to melt with vigorous evolution of gas. When *ca* 470 cm^3 of gas (*ca* 21 mmol) had been evolved the rate of gas evolution slackened considerably. The temperature was slowly raised to 130°C during which a further 470 cm^3 of gas were measured before the evolution ceased once more. Nitrogen was admitted to the apparatus and the melt was allowed to cool slightly before being poured into *ca* 250 cm^3 of stirred toluene. The fine white precipitate of $K[H_2B(C_6H_4N_3)_2]\cdot H_2O$ (**1**) which formed after a few minutes was collected by filtration, washed with 2×50 cm^3 of hot toluene and dried *in vacuo* over P_4O_{10}. Yield, 5.23 g, 81%. The compound is soluble in water and acetone but insoluble in chloroform and dichloromethane. The ^1H NMR spectrum in acetone-d_6 consists of a pair of broad unsymmetrical complex multiplets centred on δ 7.75 and 8.40 ppm and integrating for equal numbers of protons.

Potassium hydrotris(1-benzotriazolylborate)monohydrate (**2**)

The general procedure was as described above for **1** except that heating was continued at *ca* 130°C and the reaction mixture eventually solidified. On raising the temperature to 170°C, the mixture melted again and between this temperature and 200°C a further 470 cm^3 of hydrogen was slowly evolved. Work-up as described for **1** produced 9.0 g (76%) of **2**. Compound **2** is soluble in water, alcohols, acetone, chloroform and dichloromethane but insoluble in petroleum. The ^1H NMR spectra in chloroform-d consisted of a single broad complex multiplet centred on *ca* δ 7.7 ppm.

Potassium tetrakis(1-benzotriazolyl)borate (**3**)

The general procedure was as described for **2** but employing 12.5 g (100 mmol) of benzotriazole, i.e. a 1 : 5 ratio of KBH_4 to triazole. From 200°C the temperature was raised to *ca* 260°C and held there for 24 h during which *ca* 470 cm^3 of hydrogen was released. Work-up as before yielded a brown solid which was dissolved in hot methanol, heated with activated charcoal and reprecipitated with water to yield 8.34 g (76%) of pure $K[B(1\text{-}C_6H_4N_3)_4]$ (**3**). Compound **3** is soluble in acetone and alcohols but insoluble in water, chloroform and dichloromethane. The ^1H NMR spectrum in acetone-d_6 showed two multiplets centred on δ 7.4 and 8.4 ppm and integrating for four and 12 protons, respectively.

Preparation of the thallium(I) derivatives (**4**–**6**)

A solution of the potassium(benzotriazolyl) borate in distilled water (**1**, **2**) or methanol (**3**) was treated with an equimolar quantity of thallium(I) formate in distilled water. A white precipitate usually formed immediately but occasionally an oil was formed which converted into a fine white solid when kept at 0°C overnight. $Tl[H_2B(1\text{-}C_6H_4N_3)_2]$ (**4**) and $Tl[HB(1\text{-}C_6H_4N_3)_3]$ (**5**) were recrystallized from methanol–water and chloroform–petroleum, respectively, while $Tl[B(1\text{-}C_6H_4N_3)_4]$ (**6**) was microanalytically pure as formed. Compound **4** is soluble in methanol only, while compound **5** is also soluble in chloform and dichloromethane. Compound **6** is insoluble in all common organic solvents. The ^1H NMR spectra of **4** and **5** are similar to those of the potassium analogues.

Potassium tetrakis(1-indazolyl)borate (**8**)

The literature preparation of **8** involves heating a 1 : 4 mixture of KBH_4 and indazole to 215°C, but the quoted volume of hydrogen evolved appears to be in error.[3c] In our hands, these conditions did not prove successful. Three equivalents of hydrogen were evolved while the mixture was heated slowly to *ca* 200°C but continued heating at this temperature or slightly above caused it to solidify and carbonize and no further hydrogen was released. In contrast, gradual heating of a 1 : 5 mixture of reactants, 0.84 g KBH_4 (15.6 mmol) and 9.2 g indazole (78 mmol), and holding the mixture at 220°C for 24 h caused the elimination of *ca* 1.2 litres of hydrogen (*ca* 86% of the theoretical volume) before there was any sign of solidification and carbonization. Work-up as described for the benzotriazolylborates gave crude **8** as a yellow solid.

Recrystallization of the yellow product from a mixture of ethanol and 1-hexene gave **8** in *ca* 70% yield as an off-white microanalytically pure solid. The material described by earlier workers is yellow, has a lower m.p. than our product, was isolated in only 48% yield and gives microanalytical results outside the normally acceptable limits.[3c] Compound **8** is soluble in alcohol and acetone but only sparingly so in chloroform and dichloromethane. It is insoluble in water and hydrocarbons. The ^{1}H NMR spectrum is described in the text. The thallium(I) derivative **9** was prepared as described for the benzotriazole analogue.

Acknowledgement—We are grateful to Professor M. D. Curtis of the Chemistry Department, The University of Michigan at Ann Arbor for providing facilities during the writing of this paper.

REFERENCES

1. S. Trofimenko, *J. Am. Chem. Soc.* 1967, **89**, 3170.
2. S. Trofimenko, *Prog. Inorg. Chem.* 1986, **34**, 116; K. Niedenzu and S. Trofimenko, *Top. Curr. Chem.* 1986, **131**, 1; A. Shaver, *Comprehensive Coordination Chemistry* (Edited by G. Wilkinson, R. D. Gillard and J. A. McCleverty), Vol. 2, p. 245. Pergamon Press, Oxford (1987).
3. (a) S. A. A. Zaidi and M. A. Neyazi, *Transition Met. Chem.* 1979, **4**, 164; (b) K. S. Siddiqi, M. A. Neyazi, Z. A. Siddiqi, S. J. Majid and S. A. A. Zaidi, *Ind. J. Chem.* 1982, **21A**, 932; (c) K. S. Siddiqi, M. A. Neyazi and S. A. A. Zaidi, *Synth. React. Inorg. Met.-Org. Chem.* 1981, **11**, 253.
4. Z. A. Siddiqi, S. Khan and S. A. A. Zaidi, *Synth. React. Inorg. Met.-Org. Chem.* 1982, **12**, 433; 1983, **13**, 425.
5. Z. A. Siddiqi, S. Khan, K. S. Siddiqi and S. A. A. Zaidi, *Synth. React. Inorg. Met.-Org. Chem.* 1984, **14**, 303.
6. S. Chao and C. E. Moore, *Analytica Chim. Acta* 1978, **100**, 457; D. C. Hockman, C. E. Moore, J. L. Huston and S. Chao, *Analyt. Lett.* 1981, **14**, 719.
7. S. A. A. Zaidi, T. A. Khan and Z. A. Siddiqi, *Synth. React. Inorg. Met.-Org. Chem.* 1984, **14**, 717; *Bull. Soc. Chim. Fr.* 1984, **5–6**, 149.
8. S. A. A. Zaidi, S. A. Shaheer, S. R. A. Zaidi and M. Shakir, *Ind. J. Chem.* 1986, **25A**, 863.
9. T. Desmond, F. J. Lalor, G. Ferguson, B. Ruhl and M. Parvez, *J. Chem. Soc., Chem. Commun.* 1983, 55.
10. F. J. Lalor, S. Miller and G. Ferguson, in preparation.
11. F. J. Lalor, S. Miller and N. Garvey, *J. Organomet. Chem.* 1988, **356**, C57.
12. S. Trofimenko, J. C. Calabrese and J. S. Thompson, *Inorg. Chem.* 1987, **26**, 1507; K. Niedenzu, P. M. Niedenzu and K. R. Warner, *Inorg. Chem.* 1985, **24**, 1604; T. J. Desmond, F. J. Lalor, G. Ferguson and M. Parvez, *J. Organomet. Chem.* 1984, **277**, 91; W. H. McCurdy, *Inorg. Chem.* 1975, **14**, 2292.
13. (a) M. Begtrup, R. M. Claramunt and J. Elguero, *J. Chem. Soc., Perkin II* 1978, 99; (b) L. Stefaniak, *Org. Mag. Reson.* 1978, **11**, 385.
14. M. H. Palmer, R. H. Findlay, S. M. F. Kennedy and P. S. McIntyre, *J. Chem. Soc., Perkin II* 1975, 1695.
15. J. D. Odom, *Comprehensive Organometallic Chemistry* (Edited by G. Wilkinson, F. G. A. Stone and E. W. Abel), p. 253. Pergamon Press, Oxford (1982).
16. L. W. Hall, D. W. Lowman, P. D. Ellis and J. Odom, *Inorg. Chem.* 1975, **14**, 580.

Polyhedron Vol. 9, No. 1, pp. 69–74, 1990
Printed in Great Britain

0277–5387/90 $3.00+.00
© 1989 Pergamon Press plc

URANIUM POLY(PYRAZOL-1-YL)BORATE COMPLEXES: X-RAY CRYSTAL STRUCTURES OF $UCl_2Cp[HB(3,5\text{-}Me_2Pz)_3]$ AND $UCl_3[HB(3,5\text{-}Me_2Pz)_3]$

ÂNGELA DOMINGOS,* NOÉMIA MARQUES and A. PIRES DE MATOS

Departamento de Química, ICEN, LNETI, 2686 Sacavém Codex, Portugal

(*Received* 26 *June* 1989; *accepted* 4 *August* 1989)

Abstract—The crystal and molecular structures of $UCl_2Cp[HB(3,5\text{-}Me_2Pz)_3]$ (**1**) and $UCl_3[HB(3,5\text{-}Me_2Pz)_3]$ (**2**) have been determined by single crystal X-ray diffraction. Compound **1** crystallizes in space group $P\bar{1}$, $a = 10.770(1)$, $b = 11.146(5)$, $c = 11.820(4)$ Å, $\alpha = 114.53(2)$, $\beta = 91.70(2)$, $\gamma = 107.45(2)°$, $V = 1211.77$ Å^3, $Z = 2$; compound **2** crystallizes in space group $P2_1/c$, $a = 8.173(1)$, $b = 14.279(3)$, $c = 19.167(7)$ Å, $\beta = 100.17(2)°$, $V = 2201.71$ Å^3, $Z = 4$. In both compounds the uranium centre is six-coordinate and displays octahedral geometry, close to C_s symmetry for complex **1** and to C_{3v} symmetry for complex **2**. For compound **1** the average U—Cl, U—N and U—C(Cp) bond distances are 2.60(1), 2.51(2) and 2.74(1) Å; for **2** the average U—Cl and U—N bond distances are 2.56(1) and 2.43(1) Å.

Since the synthesis and X-ray structural characterization of $UCl_3[HB(3,5\text{-}Me_2Pz)_3](THF)$,[1] actinide poly(pyrazolyl)borate chemistry has experienced a continuing progress. Although derivatives of this complex with cyclopentadienide, dialkylamides, alkoxides and aryloxides have been described,[2–4] few structural data are available on these complexes. These include the seven-coordinate $UCl(OC_6H_5)_2[HB(3,5\text{-}Me_2Pz)_3](THF)$ complex[4] and the related eight-coordinate $UCl(OBu^t)(HBPz_3)_2$ and $UCl(OC_6H_5)(HBPz_3)_2$ complexes.[5]

During the course of our investigation on uranium poly(pyrazolyl)borate compounds we have found that the ligand $[HB(3,5\text{-}Me_2Pz)_3]$ can be used as a probe in ^1H NMR spectroscopy. In particular, the ^1H NMR spectra of the previously reported $UCl_2Cp[HB(3,5\text{-}Me_2Pz)_3]$ and $UCl_3[HB(3,5\text{-}Me_2Pz)_3]$ complexes[2] exhibited signals which were consistent with C_s and C_{3v} point symmetries, respectively. In order to verify if the structures found in solution were the same in the solid state, we have undertaken the X-ray crystallographic study of these compounds.

EXPERIMENTAL

The syntheses and characterization of **1** and **2** have been reported earlier.[2]

Crystals of the compounds suitable for X-ray diffraction were obtained by slow diffusion of *n*-pentane into saturated solutions of $UCl_2Cp[HB(3,5\text{-}Me_2Pz)_3]$ in THF and of $UCl_3[HB(3,5\text{-}Me_2Pz)_3](THF)$ in CH_2Cl_2, at room temperature. The crystals were sealed in thin-walled glass capillaries in a nitrogen-filled glove-box.

Data were collected at room temperature on an Enraf–Nonius Cad 4 diffractometer with graphite-monochromatized Mo-K_α radiation, in the $1.5 < \theta < 25°$ range, using a ω–2θ scan mode. Crystal data, data collection and refinement for both complexes are presented in Table 1. Data reduction was carried out using the Enraf–Nonius program; for complex **1** a decay of 80% (in 83.3 h) in the intensities of three standard reflections monitored every 100 measurements was observed and linearly corrected; empirical absorption corrections were applied based on ψ scans. The structures were solved by Patterson and Fourier methods and refined by full-matrix least-squares.[6] All non-hydrogen atoms were refined anisotropically, and the contributions of the hydrogen atoms were included in calculated positions, not refined but con-

* Author to whom correspondence should be addressed.

Table 1. Crystallographic data

Compound	$UCl_2Cp[HB(3,5\text{-}Me_2Pz)_3]$ (1)	$UCl_3[HB(3,5\text{-}Me_2Pz)_3]$ (2)
Formula	$C_{20}H_{27}BN_6Cl_2U$	$C_{15}H_{22}BN_6Cl_3U$
Formula weight	671.16	641.01
Crystal system	Triclinic	Monoclinic
Space group	$P\bar{1}$	$P2_1/c$
a (Å)	10.770(1)	8.173(1)
b (Å)	11.146(5)	14.279(3)
c (Å)	11.820(4)	19.167(7)
α (°)	114.53(2)	90
β (°)	91.70(2)	100.17(2)
γ (°)	107.45(2)	90
V (Å^3)	1211.77	2201.71
Z	2	4
D_{calc} (g cm^{-3})	1.839	1.934
Linear absorbance coefficient (cm^{-1}) (M_o-K_α)	66.18	73.94
Decay corrections, min., max.	1.0003, 2.2618	—
Range in absorbance correction factors	0.7728, 0.9987	0.7405, 0.9986
Number of unique data [$F_o > 3\sigma(F_o)$]	3110	3454
Number of parameters refined	278	242
Final R, R_w	0.038, 0.037	0.029, 0.032

strained to ride on their carbon atoms with group U_{iso} values assigned. A weighting scheme $W = (\sigma^2(F_o)+0.0001F_o^2)^{-1}$ was used in both structures. In the final difference Fourier maps the highest peaks were 1.84 and 1.11 e Å^{-3} for compounds **1** and **2**, respectively, close in both cases to the uranium atom. Atomic scattering factors and anomalous dispersion terms were taken from *International Tables for X-ray Crystallography*.

Tables of final atomic positional and thermal parameters, full lists of bond lengths and angles, equations of mean-least-square planes and tables of F_o/F_c values have been deposited as supplementary material with the Editor.

RESULTS AND DISCUSSION

Figures 1 and 2 show perspective views of the molecules with their atomic numbering schemes. Molecule **1** has approximately C_s symmetry with a non-crystallographic mirror plane passing through uranium, boron, pyrazolyl (2) and C_3(Cp). Molecule **2** has approximately C_{3v} symmetry.

By considering that the Cp ligand occupies a single coordination site, the coordination geometry about uranium is, in both compounds, octahedral. The three nitrogens of the tridentate pyrazolyl borate ligand occupy one three-fold face while the remaining ligands form the staggered triangular face on the other side of the central atom. However, in view of the rigid nature of the tripodal ligand and of its relatively small bite (1.24 for **1** and 1.25 for **2**), distortions from the regular octahedron are observed in both compounds. The twist angles between the two previous triangular faces are 57.8 and 58.4° for complex **1** and **2**, respectively, close to 60° as observed in the regular octahedron. The planes of these two faces are inclined by 2.9 and 3.2°, respectively, for **1** and **2**. The angles at the metal atom from the pyrazolyl donor atoms are much lower than 90°, allowing the opening of the face formed by the other ligands. In fact, the N—U—N angles are 73.5(2), 85.0(2), 72.6(2)° (av. 77.0°) and 79.2(2), 76.3(2), 76.3(2)° (av. 77.3°) for complexes **1** and **2**, respectively; the Cl—U—Cl/Cp angles in complex **1** are 91.2(2), 99.9(3), 102.0(3)° (av. 97.7°), while for complex **2** the corresponding Cl—U—Cl angles are 96.4(2), 99.6(2), 95.0(2)° (av. 97.0°). Thus, a higher distortion from the regular octahedron is observed for the mixed-Cp derivative. Figures 3 and 4 show views of the molecules emphasizing the octahedral geometry of the inner coordination sphere.

Selected bond lengths and bond angles are given in Tables 2 and 3. Slightly longer U—Cl and U—N bond lengths are observed for the Cp derivative (average 2.60(1), 2.51(2) Å compared with 2.56(1), 2.43(1) Å for **2**), probably due to the replacement of a chlorine atom by the more sterically demanding

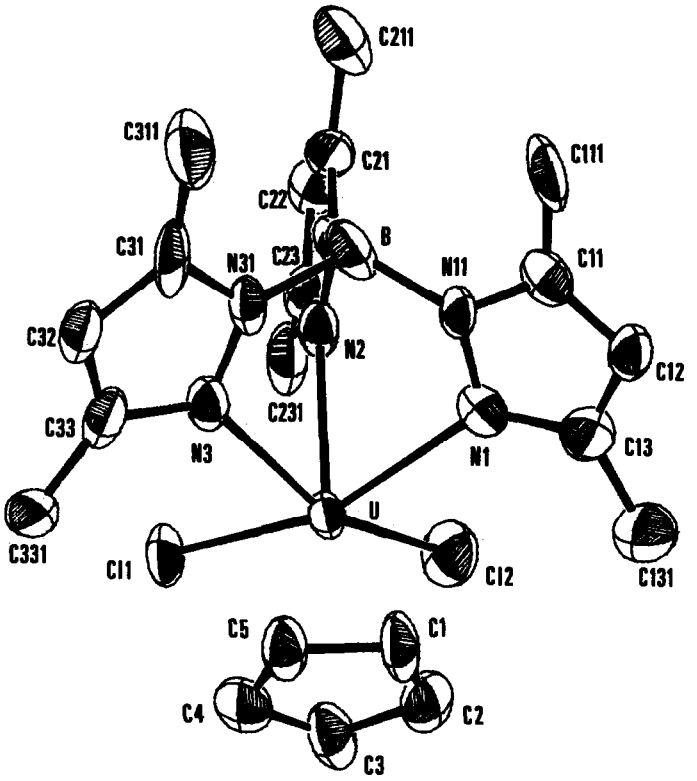

Fig. 1. ORTEP plot of $UCl_2Cp[HB(3,5\text{-}Me_2Pz)_3]$ with 50% probability thermal ellipsoids.

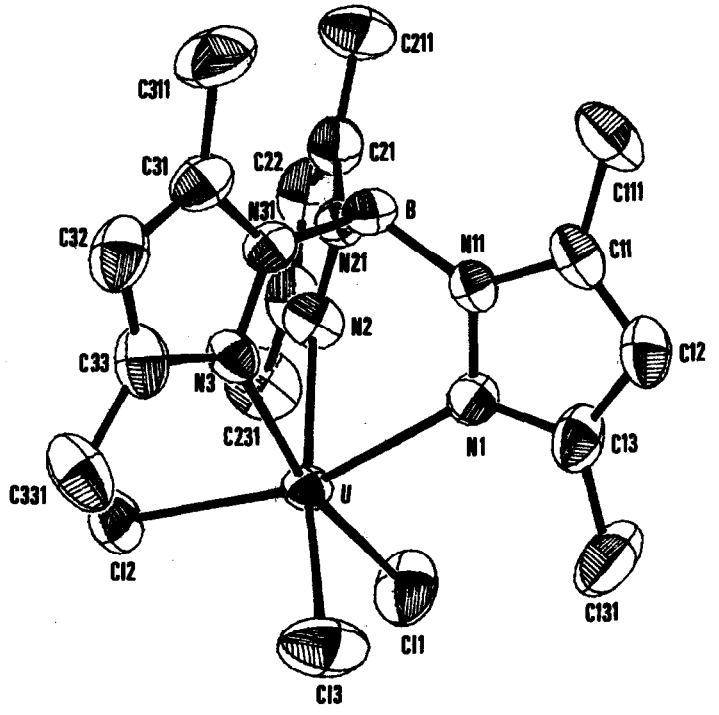

Fig. 2. ORTEP plot of $UCl_3[HB(3,5\text{-}Me_2Pz)_3]$ with 50% probability thermal ellipsoids.

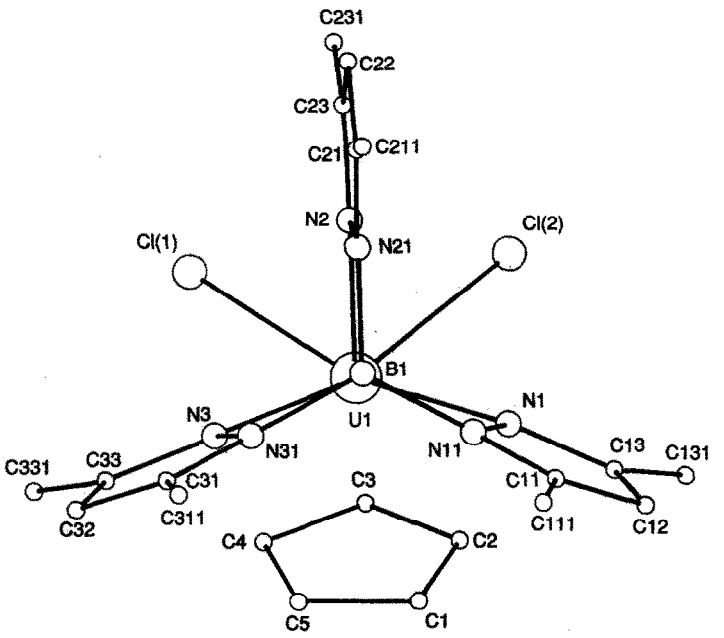

Fig. 3. A B–U view (PLUTO) of $UCl_2Cp[HB(3,5\text{-}Me_2Pz)_3]$.

Cp ligand. Compound **2** has slightly shorter U—Cl and U—N bond distances compared with the values of 2.60(1) and 2.49(2) Å in seven-coordinate $UCl_3[HB(3,5\text{-}Me_2Pz)_3](THF)$, which is consistent with the smaller effective radius of uranium in a lower coordinate complex. The angles at the uranium centre in **1** are also affected by the bulkier Cp, as can be seen with the values of the Cl—U—Cl/Cp and N—U—N angles.

The U—Cp and the C—C(Cp) bond lengths (average 2.74(1) and 1.40(1) Å, respectively) are in the range observed in other cyclopentadienyl com-

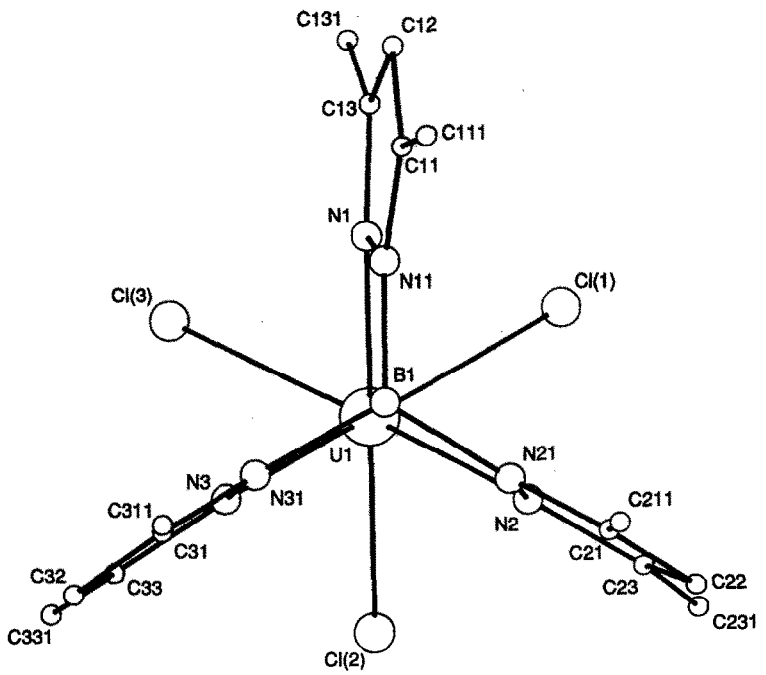

Fig. 4. A B–U view (PLUTO) of $UCl_3[HB(3,5\text{-}Me_2Pz)_3]$.

Table 2. Selected bond lengths (Å) and bond angles (°) for $UCl_2Cp[HB(3,5\text{-}Me_2Pz)_3]$

U—N(1)	2.531(9)		U—Cl(1)	2.588(3)	
U—N(2)	2.499(7)		U—Cl(2)	2.601(3)	
U—N(3)	2.504(7)				
U—C(1)	2.738(8)		C(1)—C(2)	1.40(1)	
U—C(2)	2.737(9)		C(2)—C(3)	1.39(1)	
U—C(3)	2.734(9)		C(3)—C(4)	1.41(1)	
U—C(4)	2.751(9)		C(4)—C(5)	1.39(1)	
U—C(5)	2.741(8)		C(5)—C(1)	1.39(1)	
av. U—C	2.74(1)		U—Cp[a]	2.468	
B—N(11)	1.53(1)	B—N(21)	1.56(1)	B—N(31)	1.55(1)
N(1)—N(11)	1.40(1)	N(2)—N(21)	1.38(1)	N(3)—N(31)	1.37(1)
N(1)—C(13)	1.35(1)	N(2)—C(23)	1.35(1)	N(3)—C(33)	1.37(1)
N(11)—C(11)	1.32(1)	N(21)—C(21)	1.35(1)	N(31)—C(31)	1.37(1)
C(11)—C(111)	1.50(1)	C(21)—C(211)	1.49(1)	C(31)—C(311)	1.48(1)
C(11)—C(12)	1.36(1)	C(21)—C(22)	1.38(1)	C(31)—C(32)	1.39(1)
C(12)—C(13)	1.37(1)	C(22)—C(23)	1.37(1)	C(32)—C(33)	1.35(1)
C(13)—C(131)	1.51(1)	C(23)—C(231)	1.48(1)	C(33)—C(331)	1.48(1)
av. B—N	1.55(2)	av. N—C	1.35(2)	av. C—CH_3	1.49(2)
av. N—N	1.38(2)	av. C—C	1.37(1)		
N(1)—U—N(2)	73.5(3)		N(1)—U—Cl(1)	160.6(3)	
N(1)—U—N(3)	85.0(3)		N(1)—U—Cl(2)	87.5(3)	
N(2)—U—N(3)	72.6(3)		N(1)—U—Cp	99.3(3)	
Cl(1)—U—Cl(2)	91.2(2)		N(2)—U—Cl(1)	87.1(3)	
Cp—U—Cl(1)	99.9(3)		N(2)—U—Cl(2)	85.9(3)	
Cp—U—Cl(2)	102.0(3)		N(2)—U—Cp	169.2(3)	
N(11)—B—N(21)	110.6(7)		N(3)—U—Cl(1)	89.3(3)	
N(11)—B—N(31)	113.0(6)		N(3)—U—Cl(2)	158.4(3)	
N(21)—B—N(31)	108.6(8)		N(3)—U—Cp	99.1(3)	

[a] Cp = centroid of cyclopentadienyl.

Table 3. Selected bond lengths (Å) and bond angles (°) for $UCl_3[HB(3,5\text{-}Me_2Pz)_3]$

U—N(1)	2.439(5)		U—Cl(1)	2.555(2)	
U—N(2)	2.430(5)		U—Cl(2)	2.548(3)	
U—N(3)	2.433(5)		U—Cl(3)	2.568(3)	
B—N(11)	1.529(8)	B—N(21)	1.553(8)	B—N(31)	1.544(8)
N(1)—N(11)	1.377(6)	N(2)—N(21)	1.382(7)	N(3)—N(31)	1.380(7)
N(1)—C(13)	1.349(8)	N(2)—C(23)	1.356(8)	N(3)—C(33)	1.351(8)
N(11)—C(11)	1.341(8)	N(21)—C(21)	1.338(7)	N(31)—C(31)	1.343(7)
C(11)—C(111)	1.488(9)	C(21)—C(211)	1.465(10)	C(31)—C(311)	1.510(10)
C(11)—C(12)	1.378(9)	C(21)—C(22)	1.372(10)	C(31)—C(32)	1.380(9)
C(12)—C(13)	1.365(9)	C(22)—C(23)	1.371(10)	C(32)—C(33)	1.375(9)
C(13)—C(131)	1.510(9)	C(23)—C(231)	1.515(10)	C(33)—C(331)	1.504(10)
av. B—N	1.542(12)	av. N—C	1.352(4)	av. C—CH_3	1.50(2)
av. N—N	1.380(3)	av. C—C	1.373(5)		
N(1)—U—N(2)	79.2(2)		N(1)—U—Cl(1)	91.1(2)	
N(1)—U—N(3)	76.3(2)		N(1)—U—Cl(2)	168.6(2)	
N(2)—U—N(3)	76.3(2)		N(1)—U—Cl(3)	92.2(2)	
Cl(1)—U—Cl(2)	96.4(2)		N(2)—U—Cl(1)	90.5(2)	
Cl(1)—U—Cl(3)	99.6(2)		N(2)—U—Cl(2)	92.1(2)	
Cl(2)—U—Cl(3)	95.0(2)		N(2)—U—Cl(3)	166.9(2)	
N(11)—B—N(21)	110.2(5)		N(3)—U—Cl(1)	163.2(2)	
N(11)—B—N(31)	110.4(5)		N(3)—U—Cl(2)	94.6(2)	
N(21)—B—N(31)	109.5(5)		N(3)—U—Cl(3)	92.1(2)	

plexes.[7,8] The pyrazolyl and the Cp rings are planar, with root mean-square deviations from their least-square planes of 0.0102, 0.0049, 0.0136 and 0.0042 Å (pyrazolyl (1), (2) (3) and Cp). The angle between the plane of the Cp and the plane of the donor atoms of the pyrazolyl ligand is 123.3°. The Cp and the pyrazolyl (2) ring are nearly perpendicular, the angle between their least-square planes being 90.94°.

For compound **2**, each of the three pyrazolyl rings is also planar, with root mean-square deviations from their least-square planes of 0.0116, 0.0066, and 0.0144 Å.

There are no short intermolecular contacts in both compounds. The closest intramolecular non-bonded contacts are, in compound **1**, 3.29 and 3.41 Å for Cl(1)···C(4) and Cl(2)···C(2) and 3.18, 3.14 Å for N(1)···C(1) and N(3)···C(5).

REFERENCES

1. R. G. Ball, F. Edelmann, J. G. Matisons, J. Takats, N. Marques, J. Marçalo, A. Pires de Matos and K. W. Bagnall, *Inorg. Chim. Acta* 1987, **132**, 137.
2. J. Marçalo, N. Marques, A. Pires de Matos and K. W. Bagnall, *J. Less-Common. Met.* 1986, **122**, 219.
3. N. Marques, J. Marçalo, A. Pires de Matos, I. Santos and K. W. Bagnall, *Inorg. Chim. Acta* 1987, **137**, 309.
4. Â. Domingos, J. Marçalo, N. Marques, A. Pires de Matos, J. Takats and K. W. Bagnall, *J. Less-Common Met.* 1989, **149**, 271.
5. Â. Domingos, A. Pires de Matos and I. Santos, *J. Less-Common Met.* 1989, **149**, 279.
6. G. M. Sheldrick, SHELX Crystallographic Program. University of Cambridge (1976).
7. R. D. Ernst, W. J. Kennelly, C. S. Day, V. W. Day and T. J. Marks, *J. Am. Chem. Soc.* 1979, **101**, 2656.
8. K. W. Bagnall, F. Benetollo, G. Bombiero and G. De Paoli, *J. Chem. Soc., Dalton Trans.* 1984, 67.

Polyhedron Vol. 9, No. 1, pp. 75–79, 1990
Printed in Great Britain

0277–5387/90 $3.00+.00
Pergamon Press plc

THE SYNTHESIS OF DICOPPER–HEXAOSMIUM CLUSTERS; X-RAY STRUCTURE ANALYSIS OF THE NEW HETERONUCLEAR CLUSTER DIANION $[Cu_2Os_6(CO)_{18}I_2]^{2-}$ AS ITS $[PPh_3Me]^+$ SALT

MICHAEL P. DIEBOLD, BRIAN F. G. JOHNSON and JACK LEWIS*

University Chemical Laboratory, Lensfield Road, Cambridge CB2 1EW, U.K.

and

MARY McPARTLIN* and HAROLD R. POWELL

School of Chemistry, The Polytechnic of North London, Holloway Road, London N7 8DB, U.K.

(*Received* 19 *July* 1989; *accepted* 11 *August* 1989)

Abstract—The dianion $[Os_6(CO)_{18}]^{2-}$ (**1**) reacts with $[Cu(NCMe)_4]^+$ to form $[Os_6(CO)_{18}(CuNCMe)_2]$ (**2**). Treatment of **1** with $[(PPh_3Me)I]$ followed by reaction with $[Cu(NCMe)_4]^+$ gives $[Os_6(CO)_{18}(CuI)_2]^{2-}$ (**3**). An X-ray crystal structure determination of **3** shows that a hexaosmium octahedral arrangement has opposite faces capped by CuI groups. Both **2** and **3** are susceptible to (CuL) loss in the presence of nucleophiles such as organophosphines, THF or acetonitrile.

Reactions of carbonyl cluster anions with mononuclear cationic metal complexes usually give clusters in which one or more electrophiles are simply added to the anionic complex as, for example, in the formation of $[Os_{10}C(CO)_{24}(CuNCMe)]^-$ and $[Os_{10}C(CO)_{24}(CuNCMe)_2]$ from the reaction of the decaosmium dianion $[Os_{10}C(CO)_{24}]^{2-}$ with $[Cu(NCMe)_4]^+$.[1] However, condensation reactions between anionic carbonyl clusters and electrophilic mononuclear metal complexes may also occur, and are an important route for the formation of very large heteronuclear carbonyl complexes.[2–4] A number of clusters with core stoichiometry $M_6M'_2$ have been synthesized by the reaction of M_6 carbonyl anions (M = Rh,[5] Ru,[6–8] Os[4,9]) with $M'L_n$ cations such as $[Cu(NCMe)_4]^+$, $[AuPPh_3]^+$. A variety of metal core geometries have been found for these clusters, including those in which the heterometal atoms are directly bound to one another,[6] and those in which these atoms are on opposite sides of the M_6 polyhedra.[4,5,7] We now report two new $M_6M'_2$ compounds, $[Os_6(CO)_{18}(CuNCMe)_2]$ (**2**) and $[Os_6(CO)_{18}(CuI)_2]^{2-}$ (**3**), in which the opposite faces of the octahedral cluster dianion, **1**, are capped by the CuL ligands.

* Authors to whom correspondence should be addressed.

RESULTS AND DISCUSSION

Reaction of the $[Ph_3PMe]^+$ salt of the hexaosmium dianion $[Os_6(CO)_{18}]^{2-}$ (**1**) with $[Cu(NCMe)_4]^+$ in CH_2Cl_2 or acetone (Scheme 1) gives a product which we tentatively identify as

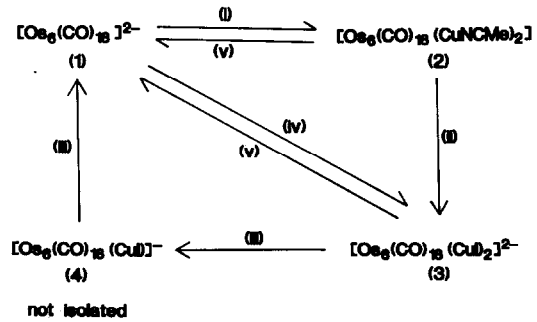

Scheme 1. (i) Excess $[Cu(NCMe)_4]^+$; (ii) e.g. CsI; (iii) rapid addition of dppm; (iv) excess $[PPh_3MeI]$ followed by excess $[Cu(NCMe)_4]^+$; (v) donor molecules, e.g. THF, MeCN.

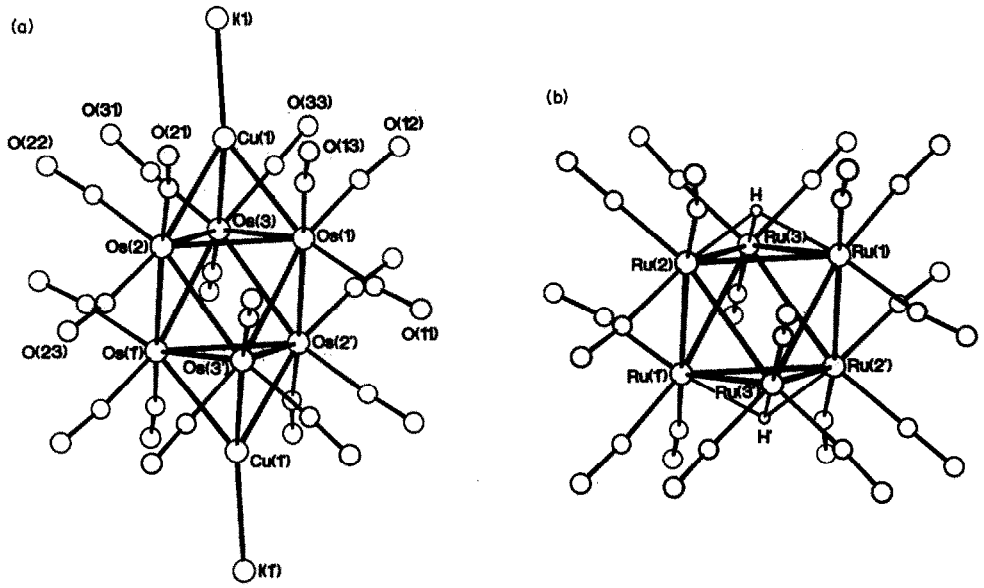

Fig. 1. The structures of (a) the dianion $[Cu_2Os_6(CO)_{18}I_2]^{2-}$ (**3**) and (b) the dihydride $[H_2Ru_6(CO)_{18}]^{2-}$ (**6**) (from ref. 13). In the numbering scheme for **3** the carbonyl carbon atoms have the same number as the relevant oxygen atoms.

$[Os_6(CO)_{18}(CuNCMe)_2]$ (**2**). Isolation and characterization of **2** is hampered by its instability; for example, this compound decomposes to **1** on silica TLC plates. Fast-atom bombardment (FAB) mass spectra of solutions of **2** gave $[Os_6(CO)_{18}]$ as the largest fragment, and in acetone **2** reacted with the halide salts of IR windows to produce the dianions $[Os_6(CO)_{18}(CuX)_2]^{2-}$ (X = Br or I), which were identified by their IR spectra. Our formulation of **2** as $[Os_6(CO)_{18}(CuNCMe)_2]$ is based primarily on the observation that further reaction with $[PPh_3Me]I$ gave the dianion **3**, and on the similarity of the IR spectrum of **2** to that of the dianion, **3**, which has been fully characterized by X-ray structure analysis (*vide infra*).

The dianion, **3**, was also somewhat unstable, and its reaction with donor molecules such as amines or organophosphines, or its dissolution in THF or acetonitrile regenerates the dianion $[Os_6(CO)_{18}]^{2-}$ quantitatively. An intermediate, **4**, is observed in the reaction with phosphines (see Experimental); the major IR peaks of **4** are at frequencies between those in **1** and **3**, which is consistent with this compound being the monoanion $[Os_6(CO)_{18}(CuI)]^-$. IR peaks at energies similar to those of **4** have also been observed for a mixture of **1** and **3** in dichloromethane, although an accurate measurement of these absorptions was not possible as they overlap with those of **1** and **3**.

X-ray structure analysis of **3** establishes the overall structure shown in Fig. 1(a), and selected bond lengths and interbond angles are given in Table 1.

Table 1. Selected bond lengths (Å) and interbond angles (°) for **3**

Os(1)—Os(2)	2.937(1)	Os(1)—Os(3)	2.955(1)
Os(2)—Os(3)	2.938(1)	Os(1)—Os(2)	2.867(1)
Os(1)—Os(3)	2.884(1)	Os(2)—Os(3)	2.871(1)
Os(1)—Cu	2.661(2)	Os(2)—Cu	2.667(2)
Os(3)—Cu	2.643(2)	Cu—I	2.447(2)
Os—C(carbonyl) (range)	1.845–1.925(18)		

Os(3)—Os(1)—Os(2)	59.8(1)	Cu—Os(1)—Os(2)	56.7(1)
Cu—Os(1)—Os(3)	55.9(1)	Os(3)—Os(2)—Os(1)	60.4(1)
Cu—Os(2)—Os(1)	56.4(1)	Cu—Os(2)—Os(3)	56.0(1)
Os(2)—Os(3)—Os(1)	59.8(1)	Cu—Os(3)—Os(1)	56.4(1)
Cu—Os(3)—Os(2)	56.8(1)	Os(2)—Cu—Os(1)	66.9(1)
Os(3)—Cu—Os(1)	67.7(1)	Os(3)—Cu—Os(2)	67.2(1)
I—Cu—Os(1)	140.9(1)	I—Cu—Os(2)	139.3(1)
I—Cu—Os(3)	140.5(1)	Os—C—O (range)	173–176(2)

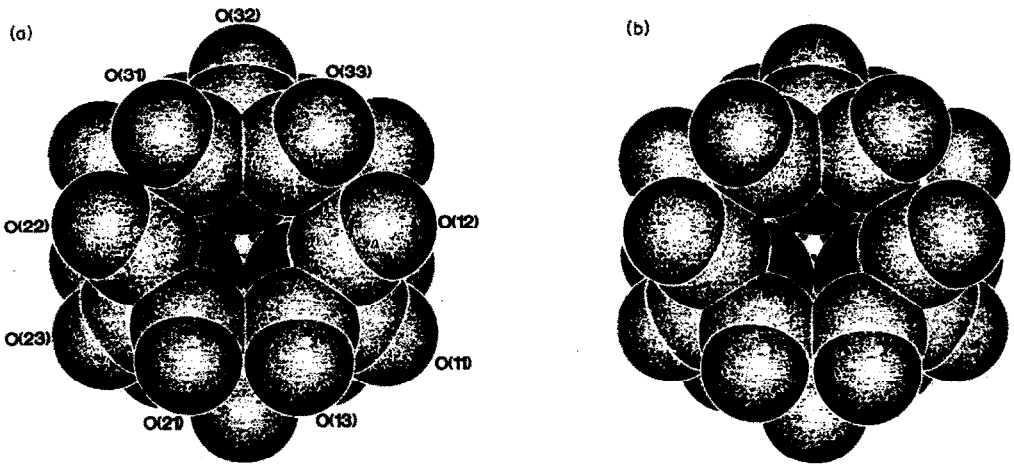

Fig. 2. Computed space filling models of (a) $[Cu_2Os_6(CO)_{18}I_2]^{2-}$ and (b) $[H_2Ru_6(CO)_{18}]^{2-}$. The μ_3-Cu and μ_3-H are not included and the metal atoms have been calculated with covalent radii.

The metal framework of **3** consists of an Os_6 octahedron with the copper atoms capping opposite faces, giving a similar metal core to that in $[Ru_6(CO)_{18}(CuC_6H_5CH_3)_2]$[7] and $[Os_6(CO)_{18}(AuPMe_3)_2]$ (**5**).[10] Overall, the molecule has virtual D_{3d} symmetry although the crystallographic symmetry is only C_i. The isolobal analogy between Group IB metals and the hydride ligand in clusters is well established,[11] and it is possibly surprising that **3** adopts a completely different Os_6 framework from the capped square pyramidal geometry of its dihydrido analogue $[Os_6(CO)_{18}H_2]$.[12] However, the overall structure of **3** does bear a remarkable similarity to that of the related dihydride ruthenium cluster $[Ru_6(CO)_{18}(\mu_3\text{-}H)_2]$ (**6**) shown in Fig. 1(b).[13] An alternative arrangement, in which the two copper atoms are bonded to each other has been observed, for example, in the ruthenium compound $[Ru_6C(CO)_{18}(CuNCMe)_2]$.[6] In **3**, as in the *trans*-capped cluster $[Ru_6(CO)_{18}(CuC_6H_5CH_3)_2]$,[7] the metal–metal bonds of the capped faces (mean 2.943(1) Å) are somewhat longer than those of the other edges (mean 2.874(1) Å), and are very close in value to the analogous bridged and unbridged lengths in the dihydride $[Ru_6(CO)_{18}(\mu_3\text{-}H)_2]$ (2.954 and 2.867 Å, respectively).[13] An unanticipated similarity in the steric requirement of the hydrogen and the copper ligands is evident in the computed space-filling models shown in Fig. 2(a) and (b).

The two symmetry related Cu—I vectors lie close to the virtual S_6 axis of the molecule; two of the Cu—Os bond distances do not differ significantly (Os(1)—Cu and Os(2)—Cu, mean 2.664(2) Å), but the third is rather shorter (Os(3)—Cu 2.643(2) Å).

A number of reactions of **2** and **3** were tried in an attempt to form even higher nuclearity clusters. Further reaction of **3** with electrophiles such as $[Cu(NCMe)_4]^+$ and $[AuPPh_3]^+$ does not occur. This may be attributed to steric factors, because although the carbonyl ligands can accommodate two groups, this causes surface ligand congestion [Fig. 2(a)]. Reaction of heteronuclear clusters with cluster dianions has sometimes been shown to lead to formation of giant clusters,[3] but substitution reactions of the acetonitrile ligands in **2** by $[Os_6(CO)_{18}]^{2-}$ does not occur. We are currently investigating the possibility that less sterically demanding nucleophiles, such as $[Os(CO)_4]^{2-}$ or $[Mn(CO)_5]^-$, may be capable of displacing the NCMe ligands.

EXPERIMENTAL

All manipulations were carried out in open flasks. $[Os_6(CO)_{18}]$[14] and $[NEt_4]_2[Os_6(CO)_{18}]$[15] were prepared according to standard literature procedures. Triphenylphosphine and bis(diphenylphosphinomethane) (dppm) were used as purchased. All solvents were distilled prior to use. IR spectra were recorded on a Perkin–Elmer 1710 and FAB mass spectra were recorded on a Kratos MS890.

Preparation of $[Os_6(CO)_{18}(CuNCMe)_2]$ (**2**)

$[Cu(NCMe)_4][PF_6]$ (30 mg, 0.094 mmol) was added to a solution of $[NEt_4]_2[Os_6(CO)_{18}]$ (20 mg, 0.010 mmol) in 10 cm^3 of acetone. After 20 min the solvent was removed on a rotary evaporator and the orange residue was extracted with CH_2Cl_2. Attempts to purify **2** by chromatography resulted in decomposition to $[Os_6(CO)_{18}]^{2-}$ (**1**). IR: ν(CO) in CH_2Cl_2: 2038s, 2022m, 1983w(br) cm^{-1}. FAB m/z: 1656 corresponding to $(Os_6(CO)_{18})$.

Preparation of $[PPh_3Me]_2[Os_6(CO)_{18}(CuI)_2]$ (3)

Dichloromethane (20 cm^3) was added to $Os_6(CO)_{18}$ (30 mg, 0.018 mmol) and $[PPh_3Me]I$ (100 mg, 0.250 mmol). After 2 h $[Cu(NCMe)_4][PF_6]$ (48 mg, 0.15 mmol) was added and the solution stirred for an additional 2 h. The solution was then filtered and the solvent was removed *in vacuo*. The remaining solid was taken up in the minimum of acetone. Methanol was added and the resulting orange precipitate was collected by filtration. Yield: 26 mg, 0.010 mmol, 56%. IR: ν(CO) in CH_2Cl_2: 2029s, 2015m, 1959w(br) cm^{-1}. FAB *m/z*: 1656 ($Os(CO)_{18}$). Found: C, 26.4; H, 1.6. Calc.: C, 26.1; H, 1.4%.

Other reactions of **2**

The acetonitrile ligands in **2** were easily replaced by weak nucleophiles such as halides. Reactions of **2** with stronger nucleophiles (e.g.) phosphines resulted in the loss of the $[Cu(NCMe)]^+$ groups and formation of $[Os_6(CO)_{18}]^{2-}$ (**1**).

Reactions of **3**

In separate experiments, compound **3** (5 mg) in CH_2Cl_2 (10 cm^3) was reacted with slightly more than 2 equivalents of $[Os_6(CO)_{18}]^{2-}$, dppm or PPh_3. No reaction was observed with $[Os_6(CO)_{18}]^{2-}$. With the phosphines, $[Os_6(CO)_{18}]^{2-}$ (**1**) was always the ultimate product, although an unisolated intermediate **4** was often identified in the IR spectrum (ν(CO) in CH_2Cl_2: 2018s, 2006m, 1946w(br) cm^{-1}). Compound **4** could be made virtually quantitatively (as determined by IR) by rapid addition of dppm to a solution of **3**. However, after a few minutes **1** began to form, and **4** disappeared completely within 0.5 h. Compound **3** was also reacted with THF and acetonitrile by dissolution in the neat solvent, and in both cases only **1** was detected in the IR spectrum.

Crystal data for **1**

$C_{56}H_{36}Cu_2I_2O_{18}Os_6P_2$, $M = 2580.92$, triclinic, space group $P\bar{1}$ (no. 2), $a = 14.218(3)$, $b = 12.369(3)$, $c = 10.073(2)$ Å, $\alpha = 88.18(2)$, $\beta = 91.31(2)$, $\gamma = 113.52(4)°$, $U = 1623.61$ $Å^3$, $Z = 1$, $D_c = 2.64$ g cm^{-3}, $F(000) = 1166$. An orange crystal of size $0.22 \times 0.22 \times 0.35$ mm, μ(Mo-K_α) = 132.93 cm^{-1}, was used in the data collection.

Data collection

Data were collected in the θ-range 3–25°, with a scan width of 0.80°, using the technique described previously.[16] Equivalent reflections were merged to give 4119 data with $I/\sigma(I) > 3.0$.

Structure solution and refinement[17]

The coordinates of the three independent osmium atoms were deduced from a Patterson synthesis, and the remaining non-hydrogen atoms were located from subsequent difference-Fourier syntheses. The methyl and phenyl groups of the counterion were constrained to idealized geometry (C—C 1.395 and C—H 1.08 Å); the hydrogen atoms were given a common isotropic thermal parameter of 0.1 $Å^2$. Absorption corrections were applied to the data after initial refinement with isotropic thermal parameters for all atoms.[18] The non-hydrogen atoms were assigned anisotropic thermal parameters in the final cycles of full-matrix refinement which converged at $R = 0.0385$ and $R' = 0.0402$, with weights of $w = 1/\sigma^2 F_o$ assigned to the individual reflections.

Acknowledgements—We thank NATO (M.P.D.) and the SERC (H.R.P.) for financial support.

REFERENCES

1. B. F. G. Johnson, J. Lewis, W. J. H. Nelson, M. D. Vargas, D. Braga, K. Henrick and M. McPartlin, *J. Chem. Soc., Dalton Trans.* 1986, 975.
2. B. T. Heaton, L. Strona, S. Martinengo, D. Strumolo, V. G. Albano and D. Braga, *J. Chem. Soc., Dalton Trans.* 1983, 2175; A. Ceriotti, F. Demartin, G. Longoni, M. Manassero, G. Piva and M. Sansoni, *Angew. Chem. Int. Edn. Engl.* 1985, **24**, 697.
3. S. R. Drake, K. Henrick, B. F. G. Johnson, J. Lewis, M. McPartlin and J. Morris, *J. Chem. Soc., Chem. Commun.* 1986, 928.
4. M. D. Vargas and J. Nicholls, *Adv. Inorg. Chem. Radiochem.* 1986, **30**, 123.
5. V. G. Albano, D. Braga, S. Martinengo, P. Chini, M. Sansoni and D. Strumolo, *J. Chem. Soc., Dalton Trans.* 1980, 52.
6. J. S. Bradley, R. L. Pruett, E. Hill, G. B. Ansell, M. E. Leonowicz and M. A. Modrick, *Organometallics* 1982, **1**, 748.
7. C. B. Ansell, M. A. Modrick and J. S. Bradley, *Acta Cryst.* 1984, **C40**, 365; P. G. Jones, *Acta Cryst.* 1986, **C42**, 1099.
8. S. R. Bunkhall, H. D. Holden, B. F. G. Johnson, J. Lewis, G. N. Pain, P. R. Raithby and M. J. Taylor, *J. Chem. Soc., Chem. Commun.* 1984, 25.
9. C. Couture and D. H. Farrar, *J. Chem. Soc., Chem. Commun.* 1985, 197.
10. P. R. Raithby, personal communication.
11. J. W. Lauher and K. Wald, *J. Am. Chem. Soc.* 1981, **103**, 7648; K. P. Hall and D. M. P. Mingos, *Prog. Inorg. Chem.* 1984, **32**, 237.

12. M. McPartlin, C. R. Eady, B. F. G. Johnson and J. Lewis, *J. Chem. Soc., Chem. Commun.* 1976, 883.
13. M. R. Churchill and J. Wormald, *J. Am. Chem. Soc.* 1971, **93**, 5670.
14. C. R. Eady, B. F. G. Johnson and J. Lewis, *J. Chem. Soc., Dalton Trans.* 1975, 2606.
15. C. R. Eady, B. F. G. Johnson and J. Lewis, *J. Chem. Soc., Chem. Commun.* 1976, 302.
16. M. K. Cooper, P. J. Guerney and M. McPartlin, *J. Chem. Soc., Dalton Trans.* 1982, 757.
17. G. M. Sheldrick, SHELX 76 program for crystal structure determination. University of Cambridge, U.K. (1976).
18. N. Walker and D. Stuart, *Acta Cryst.* 1983, **A39**, 158.

Polyhedron Vol. 9, No. 1, pp. 81–98, 1990
Printed in Great Britain

0277–5387/90 $3.00+.00
© 1989 Pergamon Press plc

OXOVANADIUM(IV) AND AMINO ACIDS—III.* THE SYSTEM L-ASPARTIC ACID+VO^{2+}; A POTENTIOMETRIC AND SPECTROSCOPIC STUDY

J. COSTA PESSOA, R. L. MARQUES and L. F. VILAS BOAS

Centro de Química Estrutural, Complexo I, Instituto Superior Técnico, 1096 Lisboa, Portugal

and

R. D. GILLARD†

Department of Chemistry, University of Wales, P.O. Box 912, Cardiff CF1 3TB, Wales, U.K.

(*Received* 28 *November* 1988 ; *accepted* 16 *August* 1989)

Abstract—The equilibria in the system L-aspartic acid $+VO^{2+}$ in aqueous solution for $1.5 \leqslant pH \leqslant 11$ have been studied by a combination of pH-potentiometric and spectroscopic methods [electron paramagnetic resonance (EPR), visible absorption and circular dichroism (CD)]. For $pH > 4$, high ligand-to-metal ratios were used. The results of the various methods are made self-consistent, then rationalized assuming an equilibrium model including the species MDH_2, MDH, MD, MD_2H_3, MD_2H and MD_2 (where H_2D denotes L-aspartic acid) and several hydrolysis products; their formation constants and individual electronic spectra (isotropic and CD) are given. Plausible isomeric structures for each of the stoichiometries are discussed.

Although knowledge of the complex equilibria of VO^{2+} in the presence of amino acids is relevant in understanding its possible interaction with likely biological ligands, few reliable data exist.

The first part of this study[1] introduced our work and gave detailed results for the system (L-Ala)+VO^{2+} in the pH range 2–12. Part II[2] concerned the L-serine and L-threonine+VO^{2+} systems. The present paper describes our study of the L-Asp+VO^{2+} system, which combined the results of potentiometric and spectroscopic techniques. Part of this work has been presented in a preliminary form.[3]

Some work has been published concerning the L-Asp+VO^{2+} system.[4–7] Tewari and Srivastava[4] determined $\log\beta(ML) = 8.98$, $\log\beta(ML_2) = 14.47$ and $\log\beta(ML_3) = 19.89$, based on titration in the range $3.2 < pH < 8.6$ with $L/M = 4$ and $C_{VO} = 10^{-3}$ M. Even assuming no precipitation of vanadyl hydroxide and/or oxidation in those conditions, the observed values of $\bar{n}$ probably arise from extensive hydrolysis and not the formation of ML_3 complexes. Tak *et al.*[5] determined $\log\beta(ML) = 8.39$ and $\log\beta(ML_2) = 14.44$, based on titration with $C_{VO} = C_{Asp} = 5\times10^{-3}$ M (C_{VO} and C_{Asp} denote total concentration of oxovanadium(IV) and aspartic acid, respectively), in the pH range 3–11. Clearly, one would expect vanadyl hydroxide precipitation and/or oxidation in these conditions.

Johnson and Shepherd[7] recorded EPR spectra at room temperature of solutions containing L-Asp and VO^{2+} (C_{VO}, C_{Asp} and pH unspecified), detecting only one species; it had $A_0 = 96$ gauss. In solutions containing glycine (Gly) and VO^{2+}, where $VO(GlyO)_2$ would predominate, $A_0 = 98$ gauss. Assuming in both cases N_2O_2 coordination in the equatorial plane, they concluded that the decrease by 2 gauss in A_0 is owing to the axial coordination of a β-COO^- group.

* For Parts I and II, see refs 1 and 2, respectively.

† Author to whom correspondence should be addressed.

Our results with the L-Asp + VO^{2+} system differ completely from those for the L-Ala,[1] L-Thr,[2] L-Cys, D-Pen (Pen = penicillamine)[8] and L-glutamic acid[9] systems over practically the whole pH range studied (1.6–11). This probably results from coordination of the β-COO^- group at quite low pH ($\sim$2) (coordination of the α-COO^- group starts at pH < 2).

Several experimental difficulties in systems involving oxovanadium(IV) + amino acids are discussed in Part I.[1] Between pH 4 and 8, relatively high ligand-to-metal (L/M ratios) must be used to avoid extensive hydrolysis of VO^{2+} and eventually precipitation of $VO(OH)_2$. However, such precipitation and/or the presence of a soluble oxovanadium(IV) hydrolysis product for pH $\gtrsim$5 is clearly not so important in the present system as for other amino acids, and much lower L/M ratios may be used.

Since pK_{a1} (α-COOH), pK_{a2} (β-COOH) and pK_{a3} (R—NH_3^+) can easily be determined, the calculated formation constants correspond to the general reaction:

$$xM^{2+} + yD^{2-} + zH^+ \rightleftharpoons M_xD_yH_z. \qquad (1)$$

We abbreviate L-aspartic acid as H_2D and the aspartate ion is then D^{2-}. For the formulation $(VO)_x(AspO)_y(H)_z$ we normally use the abbreviation $M_xD_yH_z$. For each $M_xD_yH_z$ proposed in our final equilibrium model, possible structures are discussed.

When needed we also abbreviate L-alanine and L-serine as HA and HS, and alaninate and serinate as A^- and S^-, respectively.

MATERIALS AND METHODS

For the refinement of formation constants and calculation of spectra of individual species the MINIQUAD,[10] SUPERQUAD[11] and the SQUAD[12] programs were used. In order to estimate formation constants to use as initial values for MINIQUAD and SUPERQUAD we followed a procedure described later which is summarized in Table 1.

All solutions were prepared in an inert atmosphere (high purity dinitrogen passed through soda-lime and glass wool). All measurements were performed at 25°C with solutions containing 2.25 M $NaNO_3$. The instruments used and calibration procedure for pH measurements were described in Part I.[1] We continue to assume that the EMF values (E) depend on $[H^+]$ according to

$$E = E^{ol} + Q \log [H^+] + J_H[H^+] + J_{OH}[OH^-].$$

The maximum pH value for the titration curves of solutions containing L-Asp + VO^{2+} was 8.4.

Seven titration curves ($4.7 \times 10^{-3} \lesssim C_{Asp} \lesssim 80 \times 10^{-3}$ M) (C_{Asp}—total aspartic acid concentration) were obtained to determine the protonation constants in 2.25 M $NaNO_3$; NaOH (2.2 M) was used in most cases. As $J_H \sim 20$, the corrections in the acid range are only significant for pH < 2.0.

As for the systems L-Ala, L-Ser and L-Thr + VO^{2+},[1,2] two types of titration curves were obtained: those involving measurements in the range 2.2 $\lesssim$ pH $\lesssim$ 4.2 (with 0.9 $\lesssim$ L/M $\lesssim$ 4 and $2.3 \times 10^{-3} \lesssim C_{VO} \lesssim 5.0 \times 10^{-3}$ M) and those involving pH measurements in the range 4.5 $\lesssim$ pH $\lesssim$ 8.4 (12 $\lesssim$ L/M $\lesssim$ 26 and $1.3 \times 10^{-3} \lesssim C_{VO} \lesssim 2.6 \times 10^{-3}$ M).

A total of 80 visible absorption spectra and 90 CD spectra (visible region) were used for the calculation of spectra of individual species, with concentrations in the ranges $4 \times 10^{-3} \lesssim C_{VO} \lesssim 5.0 \times 10^{-2}$ M and 0.013 $\lesssim C_{Asp} \lesssim$ 0.17 M, respectively. Ligand-to-metal ratios were in the range 0.4 $\lesssim$ L/M $\lesssim$ 26.

RESULTS

EPR spectra

The EPR spectra recorded with frozen "solutions" containing L-Asp and VO^{2+} at 77 K are typical VO^{2+} axial spectra. The field region that corresponds to $A_\parallel$ and $M_I = 5/2$ and 7/2 gives more information about the type and number of species present.

In Fig. 1, we include the high-field region of the EPR spectra of frozen "solutions" containing L-Asp + VO^{2+} with a L/M ratio of 10 at several values of pH. Analysing Figure 1 in terms of the distinct EPR components DI to DV detected and the corresponding g and A values (a single EPR component, e.g. DI, may well, of course, arise from different vanadium complexes with approximately the same g and A parameters):

(i) for pH $\lesssim$ 3, the spectra of solutions containing L-Asp + VO^{2+} with L/M = 10.0 are of the same type as those for solutions of L-Ala + VO^{2+} with L/M = 53.9;[1]
(ii) for pH $\gtrsim$ 3, the spectra differ from those for the systems involving L-Ala, L-Ser, L-Thr, L-Cys and D-Pen + VO^{2+} at similar pH values.

For DI, DIII and DIV, we estimate[12,13] $g_\parallel \sim$ 1.938, 1.937 and 1.943 and $A_\parallel \sim$ 179, 173 and 161×10^{-4} cm^{-1}, respectively. Although the $g_\parallel$ values seem rather low, this could suggest a $VO(O_4)$

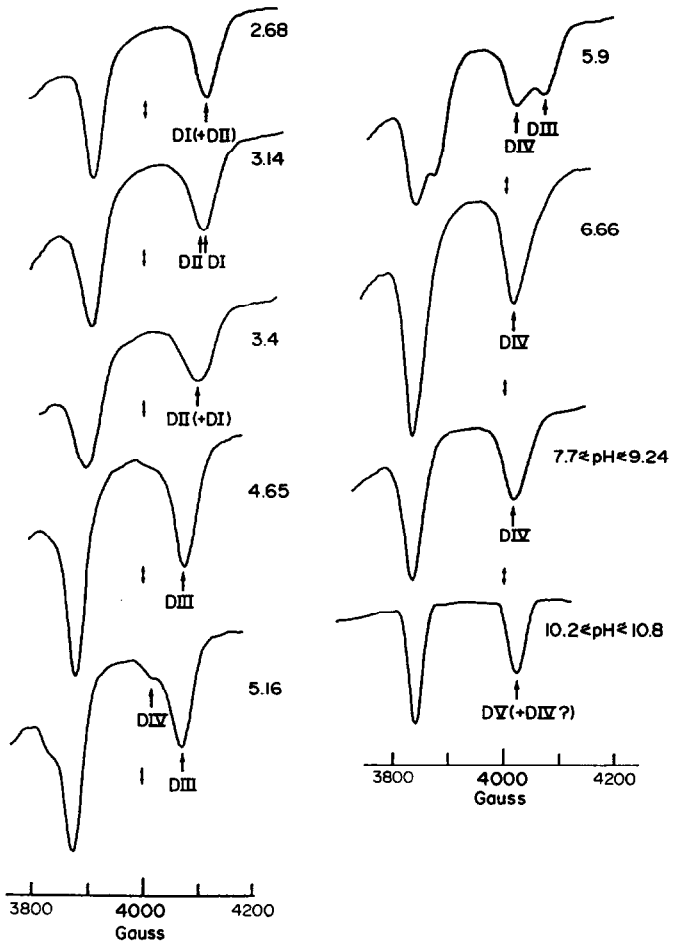

Fig. 1. High field range (3800–4200 gauss) of the first derivative EPR spectra at 77 K of frozen "solutions" containing L-Asp and VO^{2+} with a L/M ratio of 10.0. The total vanadium concentration is in the range $(1.1–1.5) \times 10^{-2}$ M. Gain and modulation are in the range $(2.5–3.2) \times 10^5$ and 1.6–3.2 depending on the spectra. pH values are indicated and ↕ represents a field marker for 4000 gauss.

coordination for those species which give rise to DI and to DIII and a $VO(N_2O_2)$ coordination for DIV.

CD and visible absorption spectra

Most visible and CD spectra for the L-Asp+VO^{2+} system differ completely from those for the systems containing L-Ala, L-Ser, L-Thr, L-Cys, D-Pen and L-Glu+VO^{2+} under similar experimental conditions.

Figure 2 includes visible spectra of L-Asp+VO^{2+} solutions with a L/M ratio of 12.9. As the pH increases, band II gradually separates from band I revealing a progressive increase in the ligand field around VO^{2+}. Although the L/M value is rather low, at pH ~ 3.4 band II is no longer a shoulder on band I. For solutions of L-Ala+VO^{2+} with L/M = 53.9 a similar situation occurs only for pH > 4.6.

Over the range $6.8 \lesssim pH \lesssim 8.5$, the spectra almost coincide and λ_{max} for bands I and II are ~740 and ~538 nm, respectively. For pH > 8.6, the increase in ε_m for $450 < \lambda < 600$ nm suggests hydrolysis of VO^{2+}.

Figures 3 and 4 include CD spectra of L-Asp+VO^{2+} solutions with L/M = 12.9. Only for $pH \lesssim 2.2$ may one observe similarities with spectra in the systems containing L-Ala, L-Ser and L-Thr+VO^{2+}.[1,2] For pH > 2.2, the spectra are completely different, which means that the type of complexes formed and their coordination geometries also differ.

In the range $6.8 \lesssim pH \lesssim 8.0$, the CD, visible and EPR spectra of solutions containing L-Asp+VO^{2+} with high L/M values coincide (Fig. 5). This probably means that 100% of oxovanadium(IV) is in the form of a single species. Its CD and visible spectra are therefore known, which simplifies the calculations with the SQUAD program.

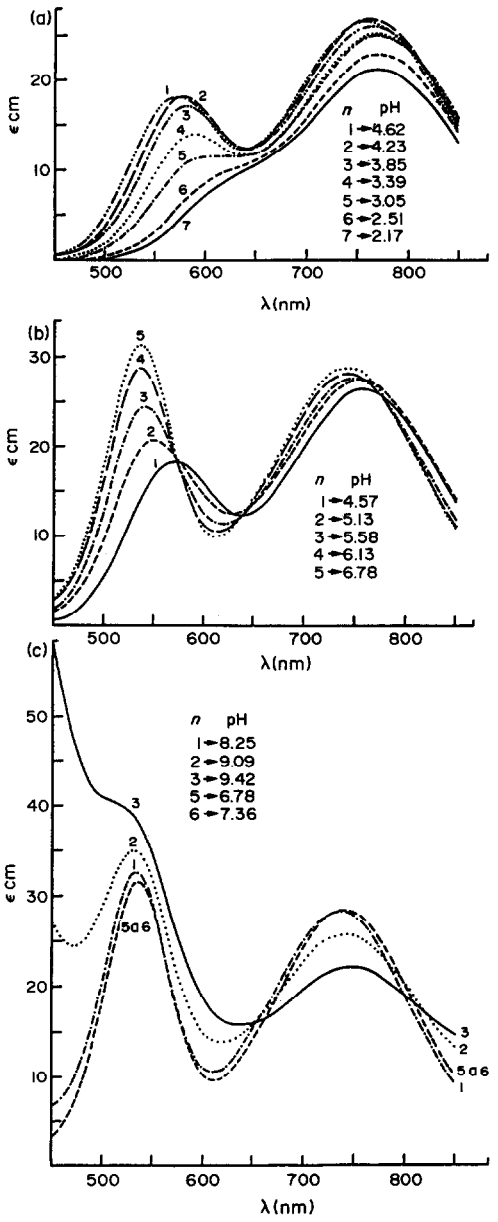

Fig. 2. Visible spectra of solutions containing L-Asp+VO^{2+} with the L/M ratio of 12.9 and $C_{VO} = (8–12) \times 10^{-3}$ M. The pH corresponding to each spectrum is indicated. The CD spectra for the same solutions are shown in Figs 3 and 4.

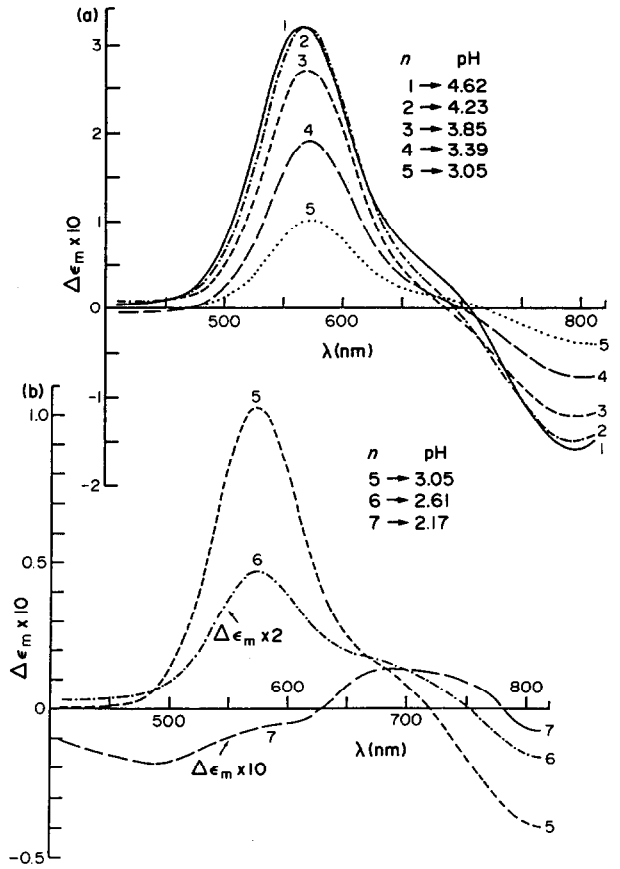

Fig. 3. Circular dichroism spectra of solutions containing L-Asp+VO^{2+} with the L/M of 12.9 and $C_{VO} = (8–12) \times 10^{-3}$ M. The isotropic absorption spectra of these solutions are shown in Fig. 2.

For pH $\gtrsim$ 11, the $\Delta\varepsilon_m$ values in the range $400 < \lambda < 800$ nm are zero; therefore no aspartate is coordinated to VO^{2+}.

Visible and CD spectra have also been recorded at fixed pH (pH = 1.6, 2.18, 3.06 and 5.4) for varying amino acid-to-vanadium ratios, and at fixed L/M values (1.0 and 2.0) varying the pH. Figures 6 and 7 include some of these spectra.

The visible spectra of solutions at pH 1.6 are similar to the spectrum of $[VO(H_2O)_5]^{2+}$ and the changes of the ε_m values as L/M increases are not pronounced. Some corresponding CD spectra are shown in Fig. 6(a). These are relatively similar to those recorded with L-Ala+VO^{2+} for pH 2.62[1] although—in the present case—the band with $\Delta\varepsilon < 0$ is relatively more important.

The visible spectra of solutions at pH 2.18 are also similar to the spectrum of $[VO(H_2O)_5]^{2+}$, but band II is more pronounced and the ε_m values increase with L/M. The corresponding CD spectra are shown in Fig. 6(b). The relative importance of the band with $\lambda_{max} \sim 700$ nm ($\Delta\varepsilon > 0$) increases with L/M. This can be explained only by the existence of at least two optically active complexes with differing L/M stoichiometry, probably 1 : 1 and 2 : 1, the 2 : 1 complex being responsible for the band with $\varepsilon_{max} \sim 700$ nm.

The visible spectra of solutions at pH 3.06 [Fig. 7(a)] change significantly as L/M increases. The corresponding CD spectra [Fig. 7(b)] manifest a general increase of the [$\Delta\varepsilon_m$] values with L/M; however the spectral profile remains the same.

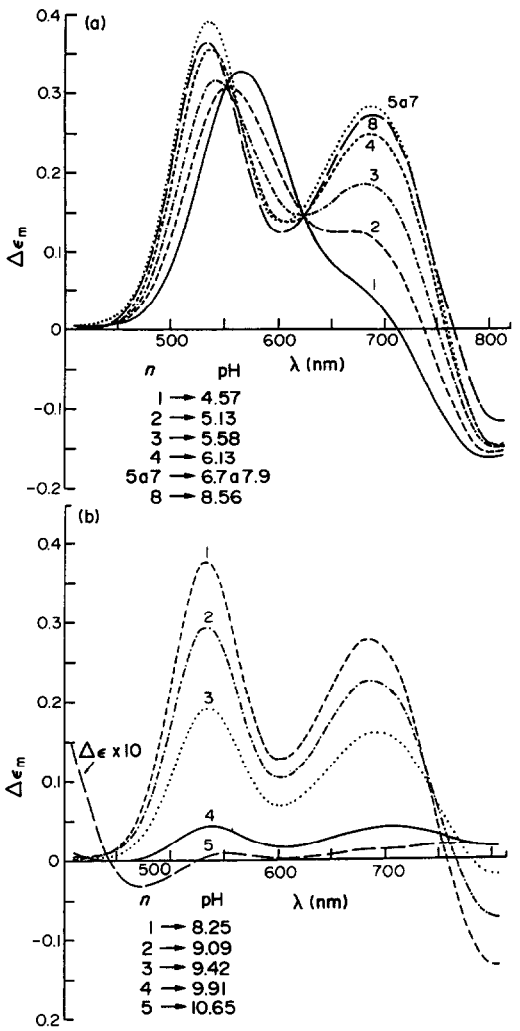

Fig. 4. Circular dichroism spectra of solutions containing L-Asp+VO^{2+} with L/M of 12.9 and $C_{VO} = (1.0–1.2) \times 10^{-2}$ M. The isotropic absorption spectra of these solutions are shown in Fig. 2.

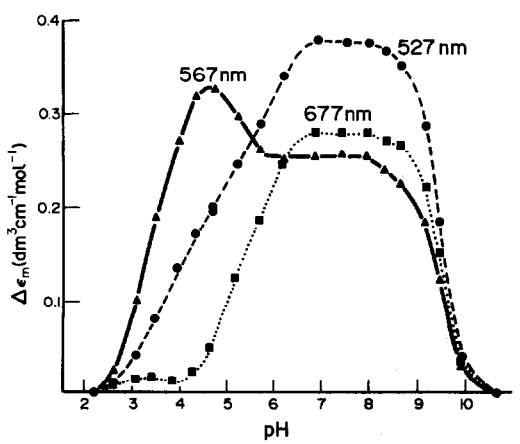

Fig. 5. Change with pH of the $\Delta\varepsilon_m$ values of L-Asp+VO^{2+} solutions with a L/M ratio of 12.9 from Figs 3 and 4 at three different wavelengths.

The visible spectra of solutions with L/M = 1 or 2 change significantly as the pH varies from 1.7 to 4; one starts with spectra similar to the spectrum of $VO(H_2O)_5^{2+}$ but values of ε_m gradually increase and bands I and II become distinct. For pH > 3, the two bands are quite distinct. For pH $\gtrsim$ 3.2, the ε_m values in the range 450 $\lesssim \lambda \lesssim$ 550 nm are greater for the solutions with L/M = 1. This effect probably results from VO^{2+} hydrolysis, $(VO)_2(OH)_2^{2+}$ being formed, which is less important for the solutions with L/M = 2. The CD spectra of the corresponding solutions with L/M = 2 are shown in Fig. 8. At pH 1.78, the CD spectrum is similar to those of Fig. 6(a) but for pH > 2 the pattern changes completely.

Several CD spectra were recorded with solutions containing L-aspartic acid-β-methyl ester and VO^{2+} in the range 1.5 $\lesssim$ pH $\lesssim$ 3.8 with a 1 : 1 mole ratio. The ester was probably partially hydrolysed and hydrolysis also took place while the spectra were being recorded. However the spectra for pH $\lesssim$ 2 may be explained assuming coordination of the α-COO^- group since they resemble those for 1 : 1 solutions of L-Ala+VO^{2+}.[1] For pH > 2, the spectra are consistent with the existence of two types of complexes (**A** and **B**) both contributing to the overall Cotton effect:

A—a VO^{2+}–L-aspartate-β-methyl ester complex with a CD spectrum similar to those obtained in the L-Ala+VO^{2+} system for pH > 2;

B—a VO^{2+}–L-aspartate complex with a CD spectrum similar to those shown in Fig. 8(b).

In spite of the ester hydrolysis, these experiments clearly show that for aspartate the β-COO^- group is certainly involved in the coordination to VO^{2+} for pH > 2.

Potentiometry

The protonation constants calculated by the MINIQUAD[10] and SUPERQUAD[11] programs practically coincide. From SUPERQUAD, for L-Asp in solutions containing 2.25 M $NaNO_3$ (at 25°C): $pK_{a1} = 2.124$, $pK_{a2} = 3.881$ and $pK_{a3} = 9.771$ values, used in all calculations.

Figure 9 shows formation curves calculated for three of the titration curves with "low" L/M values.

The EMF readings are no longer stable for pH $\gtrsim$ 4.0 and 4.6 for titration curves with L/M = 0.897 and 3.92, respectively. As for the L-Ala, L-Ser and L-Thr+VO^{2+} system under similar conditions, such instability is probably due to oxidation and/or extensive hydrolysis of oxovanadium(IV). No precipitation was detected in these cases.

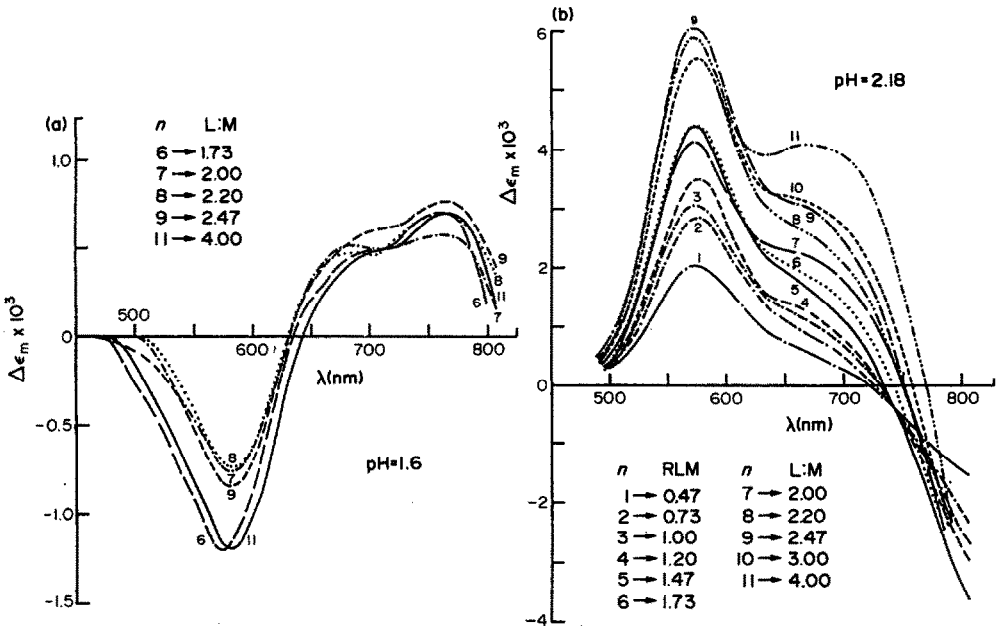

Fig. 6. Circular dichroism spectra of solutions containing L-Asp + VO^{2+} with varying L/M and fixed pH. (a) pH ~ 1.6 and $C_{VO} = (1.8–2.8) \times 10^{-2}$ M; (b) pH ~ 2.18 and $C_{VO} = (2.4–2.8) \times 10^{-2}$ M.

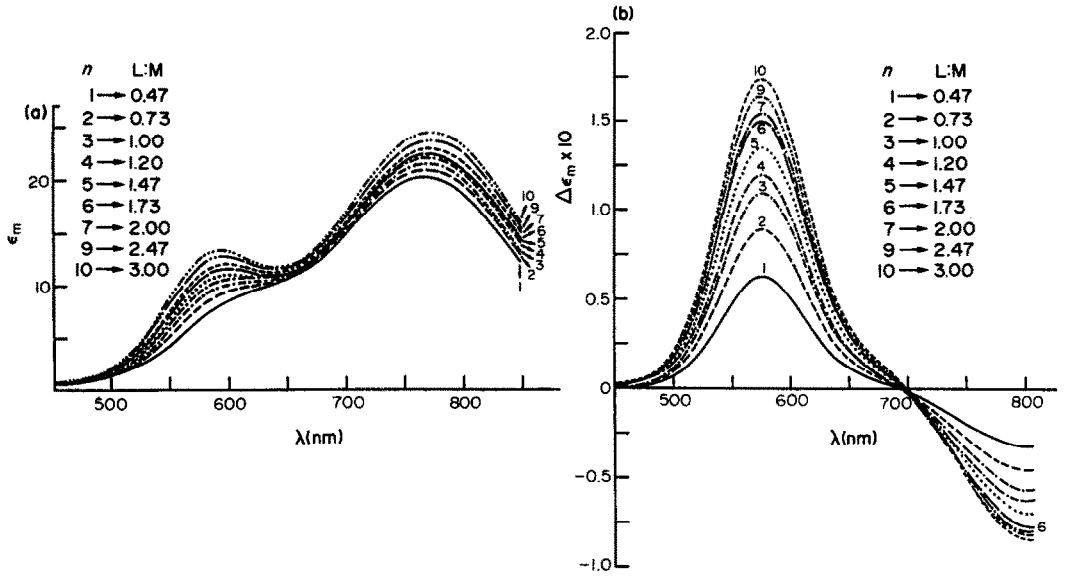

Fig. 7. Visible absorption (a) and CD spectra (b) of solutions containing L-Asp and VO^{2+} at pH 3.06 with varying L/M [$C_{VO} = (2.6–2.7) \times 10^{-2}$ M].

Comparing the formation curves in Fig. 9:

(i) The $\bar{n}$ values are higher than those calculated from titration curves in the other systems (L-Ala, L-Ser, L-Thr, L-Cys and D-Pen + VO^{2+}) in similar conditions.

(ii) For different C_{VO} and C_{Asp}, the formation curves do not coincide; this probably results from formation of protonated complexes (e.g. MDH_2, MDH, MD_2H, etc.).

(iii) Values for $\bar{n} > 1$ are obtained, which may indicate either that species like MD and MD_2H predominate, or more complex situations: e.g. MD_2H and/or M_2H_{-2} form in parallel with protonated complexes such as MD_2H_2 and MD_2H_3 (and eventually dimeric complexes).

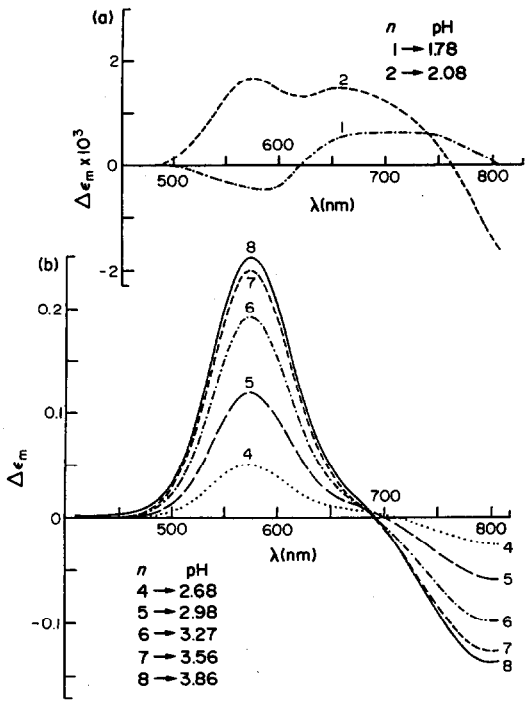

Fig. 8. Circular dichroism spectra of solutions containing L-Asp+VO^{2+} with the L/M ratio of 2.0 and $C_{VO} = (2.5–2.7) \times 10^{-2}$ M. The pH corresponding to each spectrum is indicated.

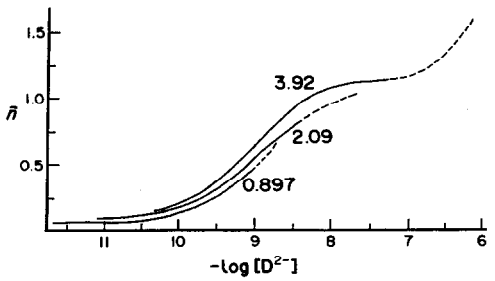

Fig. 9. Formation curves calculated for three titration curves with "low" L/M values. The dashed lines correspond to "titration points" where the EMF readings were no longer stable. The ligand-to-metal ratios are indicated.

For titration curves with "high" L/M values, $\bar{n} \sim 2.0$ for pH $\gtrsim$ 7.0. This indicates that MD_2H and MD_2 form.

Calculations

Potentiometry. Calculations involving the refinement of β_{xyz} values of all possible species (i.e. $M_xL_yH_z$ with x, y and z quite general) always gave results with no physical meaning. We therefore started with the titration curves corresponding to "low" L/M values (1–4). The results of all calculations may be summarized as follows:

(i) Consistent formation constants for MDH, MD and MD_2H are always calculated with low standard deviations for all equilibrium models tested.

(ii) Species MDH_2 is normally accepted and the corresponding $\log\beta$ is obtained with an intermediate standard deviation (SD). As for the systems with L-Ala, L-Ser, L-Thr, L-Cys, D-Pen and L-Glu+VO^{2+} [1,2,8,9] this species is important in describing the system. The sizeable SD values probably result from the L-Asp being mainly in the H_2D form in the pH range 2.2–3.5, so that no H^+ is involved in the formation of MDH_2.

(iii) Species MD_2H_4, MD_2H_3, MD_2H_2, MD_2, M_2D_2 and MDH_{-1} are accepted in some models but with a relatively high SD; in other cases they are rejected. The inclusion of any has practically no effect on the χ^2 and σ values. These species probably form but not in significant amounts in the experimental conditions used.

(iv) No other stoichiometries were accepted in any of the calculations with the SUPERQUAD program.

We conclude that only MDH_2, MDH, MD and MD_2H form in significant amounts in the conditions used to record the titration curves with "low" L/M values. Therefore we used SUPERQUAD to refine simultaneously: $\log\beta_{112}$, $\log\beta_{111}$, $\log\beta_{110}$ and $\log\beta_{121}$. Once these were calculated, the values for $\log\beta_{112}$ and $\log\beta_{111}$ were considered correct and included as fixed constants in all further calculations with MINIQUAD and SUPERQUAD. Analysing all results obtained now including all available titration curves (with high and "low" L/M values):

(i) Formation constants (β_{110} and β_{121}) for species MD and MD_2H are always derived with values practically coincident with those obtained using only the titration curves with "low" L/M values; the corresponding SD's are low.

(ii) A consistent value for the formation constant of MD_2 is always obtained with a low SD.

(iii) Species MD_2H_3 is usually accepted and β_{123} is consistently calculated with an intermediate SD, but models not including this species seem equally acceptable.

(iv) Species MDH_{-1}, M_2D_2, $M_2D_2H_{-1}$ and MDH_{-2} are normally rejected.

(v) Species MD_2H_4 and MD_2H_2 are not obtained in a consistent manner; the SD's are large and these species are frequently rejected. Probably

they do not exist in significant amounts in the experimental conditions used.

(vi) When included, species M_2D_3 is frequently accepted and the corresponding models normally have a reasonable χ^2 value.

Overall, from the calculations with MINIQUAD and SUPERQUAD, species with stoichiometries MDH_2, MDH, MD, MD_2H and MD_2 certainly exist. The potentiometric results are not clear in deciding if MD_2H_3 and/or M_2D_3 form or not. The values obtained for the formation constants of all these species, χ^2 and σ are almost unaffected whether MD_2H_2 is included or not.

From the potentiometric results we selected three models (I, II and III) included in Table 1. It is not possible to choose among these three on the sole basis of these calculations with MINIQUAD and SUPERQUAD. However, by incorporating spectroscopic results, the choice can be made.

Spectrometry. If M_2D_3 existed with log $\beta_{230} \sim 28.6$, this stoichiometry would be quite important in the pH ranges 5–9: it would then be impossible to explain why the visible and CD spectra of solutions with L/M = 12.9 do not change in the range 6.8–7.9 and why, at pH ~ 5.4, the visible and CD spectra with $7 \lesssim$ L/M $\lesssim 26$ practically coincide. Therefore, model III in Table 1 (which includes M_2D_3) is unable to explain the experimental visible and CD spectra and will not be discussed further.

In choosing between models I and II, one is deciding if MD_2H_3 exists.

As mentioned above, the CD spectra in Fig. 6(b) can only be explained if a species with an aspartate–vanadium stoichiometry of two gradually forms as L/M increases. The only 2:1 complexes that may form in significant amounts at pH ~2.2 are MD_2H_4 and MD_2H_3. Since the potentiometric results suggest that MD_2H_4 does not form in these conditions, these CD spectra indicate that MD_2H_3 should indeed be included in the equilibrium model. Furthermore, when SQUAD is used to calculate the visible or CD spectra of the several species that may exist, the SD in the absorbance data and spectra calculated and the sum of squares of the (experimental − calculated) spectra are much better for model II than for model I. Therefore MD_2H_3 must be included in the equilibrium model.

According to model II (and I), for solutions with high L/M values in the range $4.5 \lesssim$ pH $\lesssim 8$ the main stoichiometries are MD_2H and MD_2. MD and MD_2H_2 (if it is included) are in much lower concentrations. Using experimental visible and CD spectra in the range $4.5 \lesssim$ pH $\lesssim 7.8$ and $9.4 \lesssim$ L/M $\lesssim 25.7$, the visible and CD spectra for MD_2H and MD_2 may be very easily calculated with SQUAD and obtained with very low SD. These calculated spectra are included in Fig. 10.

Once these visible (and CD) spectra of MD_2H and MD_2 are known, they can be considered as fixed and included in the input file of SQUAD, to

Table 1. Compositions and formation constants of the species in the L-Asp+VO^{2+} system, assuming various equilibrium models (I–III) and for L-Asp+Cu^{2+} system (IV and V). Values for log β_{xyz} of eq. (1) are given[a]

	Species	I	II	III	IV[b]	V[c]
1	MDH_2	15.55	15.55	15.55	12.48	—
2	MDH	12.56	12.56	12.56	8.80	12.82
3	MD	9.05	9.05 (0.03)	9.05	—	9.08
4	MD_2H	21.49	21.49 (0.02)	21.49	—	21.21
5	MD_2	16.25	16.25 (0.2)	16.25	15.96	16.25
6	MD_2H_3	[d]	27.77 (0.3)	[e]	—	—
7	M_2D_3	[d]	[d]	28.6 (0.2)	—	—
8	MD_2H_2	[d]	24–25	[d]	—	25.15
9	MD_2H_4	[d]	29	[d]	—	—
10	M_2D_2	[d]	19–20	[d]	—	—
11	MDH_{-1}	[d]	2–3	[d]	—	—

[a] In the L-Asp+VO^{2+} system species 1–5 certainly form. Species 8–11 are not necessary to explain the experimental potentiometric results.

[b] From ref. 26 (T = 25°C and I = 0.2 M in KCl).

[c] From ref. 25 (T = 25°C and I = 0.10 M in KNO_3).

[d] Not included in calculations on this model.

[e] If β_{123} is included as a constant to be refined it is accepted with log $\beta_{123} \sim 27.8$; β_{123}, σ and χ^2 are not greatly affected by this.

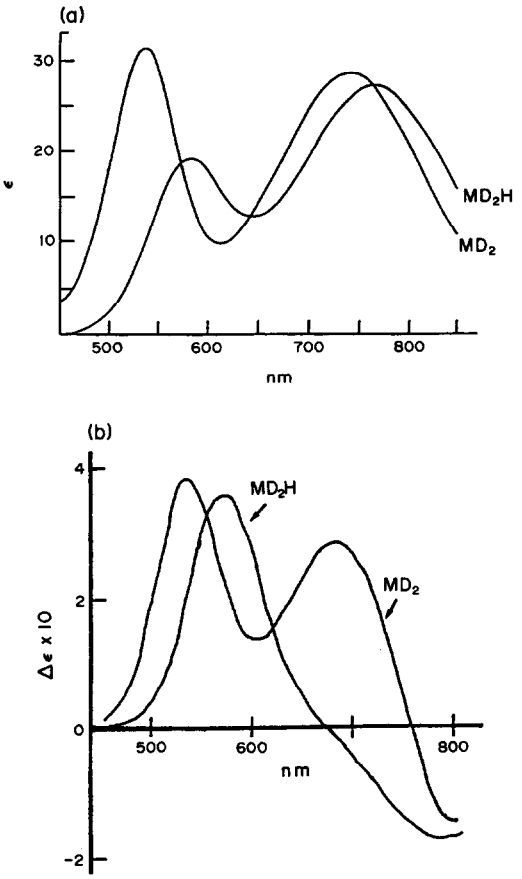

Fig. 10. Visible absorption (a) and CD (b) spectra (calculated using the SQUAD[10] program) for species MD_2H and MD_2, using the formation constants in model II—Table 1, and experimental visible and CD spectra in the pH and L/M ranges 4.5–7.8 and 9.4–25.7, respectively.

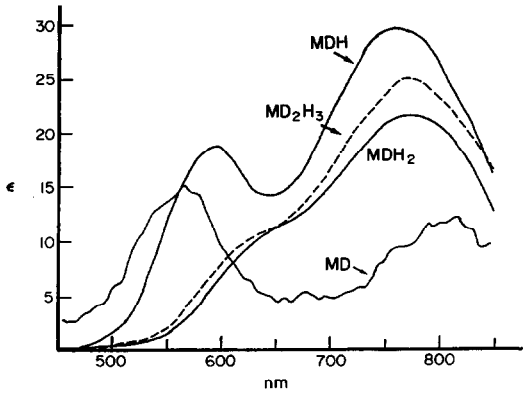

Fig. 11. Visible absorption spectra (calculated using the SQUAD[10] program) for species MDH_2, MDH, MD and MD_2H_3 using the formation constants in model II—Table 1, and experimental visible spectra in the pH and L/M ranges 1.6–3.9 and 0.47–12.9, respectively. The SD of the calculated ε_{xyz} values follow the order: $\varepsilon_{110} \gg \varepsilon_{111} > \varepsilon_{123}, \varepsilon_{112}$. As for Figs 10 and 12, all spectra are represented exactly as they were obtained using SQUAD. For MD the irregularities do not represent vibrational structure but are the result of the high SD associated with the ε_{110} values.

help calculate the visible (and CD) spectra of the species that predominate in the range $1.5 \lesssim pH \lesssim 4$. The problem is not simple; this is a rather narrow range of pH and the spectra of the four species MDH_2, MDH, MD_2H and MD_2H_3 must be calculated. Further, MDH and MD_2H_3 have "parallel concentrations" (i.e. their concentration ratio is constant).

While the ε_{xyz} values for several species in the range $450 < \lambda < 850$ nm all have the same order of magnitude, the $\Delta\varepsilon_{xyz}$ values may be quite different and for a given solution the contribution to the experimental $\Delta\varepsilon_m$ values of a species that exists in a low concentration may be as important as the contribution of another species that exists in high concentration. Therefore small errors in the formation constants may introduce large errors in the calculated $\Delta\varepsilon_{xyz}$ values.

This probably accounts for the fact that—while for the visible spectra the results are quite satisfactory and the calculated visible spectra are reasonably well defined (except for MD (Fig. 11), where the SD of the ε_{110} values are relatively high)—the results for the CD spectra are not so good.

The calculated CD spectra show differences as the pH range of the experimental spectra included is expanded from $1.6 \lesssim pH \lesssim 3$ to $1.6 \lesssim pH \lesssim 3.9$. In fact, while the CD spectra of MDH_2, MDH and MD_2H_3 are calculated in a consistent manner and with relatively low SD values (Fig. 12), the spectrum for MD is calculated with very high $\Delta\varepsilon_{110}$ and SD values. The SD's of the calculated $\Delta\varepsilon_{111}$ values are always intermediate between those of $\Delta\varepsilon_{112}$, $\Delta\varepsilon_{123}$ and those of $\Delta\varepsilon_{110}$. If the pH of the experimental spectra included is <3.4 then spectrum MD(1) in Fig. 12 is obtained. However, if the experimental spectra up to pH 3.9 are also used, the spectrum derived for MD changes (spectrum MD(2) in Fig. 12).

DISCUSSION

Speciation

The equilibrium model—the set of species that should be included to explain all the experimental potentiometric and spectroscopic results (with plausible values for their formation constants)—is contained in Table 1 (model II). For low L/M ratios, other complex species might possibly be important.

Figure 13 gives the concentration distribution

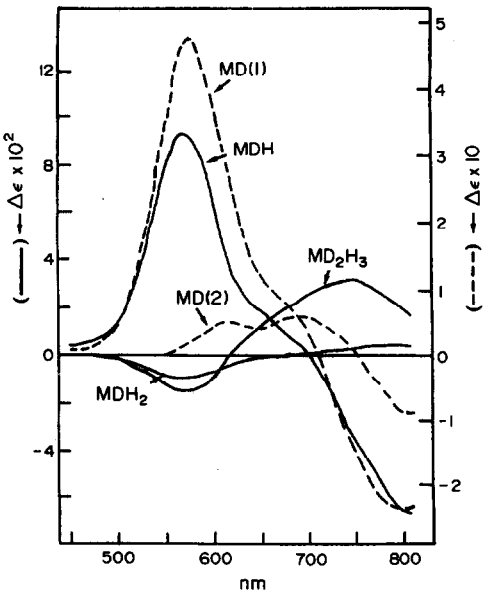

Fig. 12. Circular dichroism spectra (calculated using the SQUAD[10] program) for species MDH_2, MDH, MD and MD_2H_3 using the formation constants in model II—Table 1, and experimental CD spectra in the pH and L/M ranges 1.6–3.9 and 0.47–12.9, respectively. The SD of the calculated $\Delta\varepsilon_{xyz}$ values follow the order: $\Delta\varepsilon_{110} \gg \Delta\varepsilon_{111} > \Delta\varepsilon_{123}$, $\Delta\varepsilon_{112}$. The $\Delta\varepsilon_{xyz}$ values should only be considered as an order of magnitude and are not exact values.

calculated for L/M = 12.9 and a total oxovanadium(IV) concentration of 0.01 M.

As the pK_a values of α- and β-COOH are relatively low and VO^{2+} has a strong affinity for oxygen-containing ligands,[14,15] the complexes that form generally differ from those in the systems containing VO^{2+} with L-Ala, L-Ser, L-Thr, L-Cys, D-Pen and L-Glu.[1,2,8,9] Besides, and exceptionally in the present case, a relatively low L/M ratio (e.g. 10) is adequate to avoid precipitation of $VO(OH)_2 \cdot xH_2O$ and/or extensive hydrolysis of the Asp–VO^{2+} complexes.

The experimental CD spectra obtained in the range $3 \lesssim pH \lesssim 4.6$ and the MD_2H spectrum calculated are relatively similar to those recorded in the L-malate+VO^{2+} system[16] with L/M = 38 in the range $3 \lesssim pH \lesssim 5$. The only differences are:

(i) bands I and II in the L-malate+VO^{2+} system are observed at ~745 and 550 nm, respectively, and

(ii) the pattern of the CD bands are (+, +, −) in the L-Asp+VO^{2+} system and (+, −) (or probably: +, −, −) in the L-Mal+VO^{2+} system, the separation of the d_{xz}, d_{yz} levels being greater in the former system.

On a semi-quantitative basis, the concentration distribution shown explains the evolution of the visible and CD spectra of Figs 2–8, i.e. that the spectra are unchanged in the pH range 6.8–8.0.

For solutions with L/M = 12.9, Fig. 13 shows that for $pH \gtrsim 3$ the MD_2H stoichiometry begins to predominate. $|\Delta\varepsilon_{121}|$ is high, explaining why there is such a rapid evolution of the CD spectra in the pH range 2–4.

We emphasize that the contribution of MD_2H to the CD spectra is so pronounced that we can not eliminate the possibility that a small error in β_{121} or in the pH of the solutions may result in incorrectly calculated CD spectra for MDH and MD (similar to the dominant spectrum of MD_2H).

In solutions containing L-Asp+VO^{2+} with

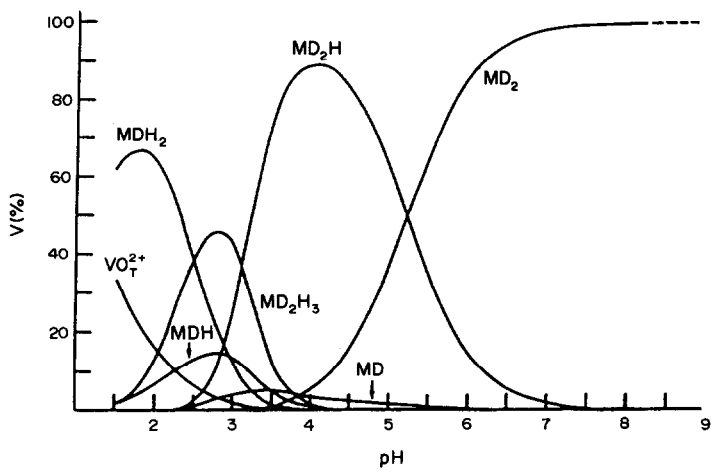

Fig. 13. Concentration distributions of the complexes formed in the VO^{2+} + L-Asp system in solutions with C_{VO} = 0.01 M and L/M = 12.9, calculated using the β_{xyz} values of model II—Table 1. The EPR components abbreviated as DIII and DIV in Fig. 1, correspond to MD_2H and MD_2 stoichiometries, respectively.

L/M = 12.9, the hydrolysis of MD_2 starts for pH $\gtrsim$ 8 and for pH $\gtrsim$ 10.5 there is almost no aspartate coordinated to oxovanadium(IV). Apart from a slight shift of band I to longer wavelengths as the pH increases, for pH $\lesssim$ 10 nothing suggests the formation of intermediate species in the "complete" hydrolysis of MD_2.

In the pH range 8–10, there is a drastic decrease of the $|\Delta\varepsilon_m|$ values but for 450 $\lesssim \lambda \lesssim$ 750 nm the type of spectra recorded is always the same. This suggests that hydrolysis of MD_2 may involve an intermediate (e.g. MD_2H_{-1}) with the same coordination geometry in the equatorial plane. For the solutions with L/M = 12.9 there is no indication of any complex with a stoichiometry MDH_{-n}. If this does occur, its $\Delta\varepsilon_{11-n}$ must be such that its contribution to the observed CD spectra is not obvious.

On a quantitative basis, the visible and CD spectra calculated by SQUAD using the formation constants of Table 1 and the visible and CD spectra of Figs 10–12 practically coincide with the corresponding experimental spectra.

Structures

A most valuable indication of structure for each $M_xD_yH_z$ species in the L-Asp + VO^{2+} system comes from comparison of its measured β, visible and CD spectra with those obtained or estimated for other systems. We consider four possible modes of coordination:

Group 1—the α-COO^- group (aspartate acting as a monodentate ligand) and/or both α-COO^- and $-NH_2$ groups (aspartate bidentate). Comparison should be with the L-Ala[1] and/or L-Ser[2] + VO^{2+} systems.

Group 2—the α-COO^- and β-COO^- groups. Ideally, comparison should be with the system succinate + VO^{2+},[17–19] where a seven-membered ring is also involved. However, those are EPR results and mainly qualitative; we may more usefully compare our results with the malonate + VO^{2+} systems.[20]

Group 3—the NH_2 and β-COO^- groups: a six-membered ring may form. Ideally, comparisons should be made with results obtained from the β-Ala + VO^{2+} system.

Group 4—L-Asp acting as a tridentate ligand. Comparisons to give predicted formation constants are difficult, because there are so few results from other L-Asp + M systems (e.g. M = Cu^{2+}) or other VO^{2+} systems with suitable ligands.

Virtually no information is available from visible and CD spectra of suitable VO^{2+} complexes except for the L-Ala[1] and L-Ser[2] + VO^{2+} systems. We will therefore compare available values of β_{xyz}, defined as in eq. (1). We first estimate values of β_{xyz} for each possible structure to compare with those in Table 1.

To compare with the L-Ser + VO^{2+} system, one should consider

$$xM + yL' + zH^+ \overset{\beta'_{xyz}}{\rightleftharpoons} M_xL'_yH_z, \qquad (2)$$

where $L' = NH_2CH(CH_2COOH)COO^-$.

To compare with dicarboxylate systems,[19,20] we must consider:

$$xM + yL^* + zH^+ \overset{\beta^*_{xyz}}{\rightleftharpoons} M_xL^*_yH_z, \qquad (3)$$

where $L^* = NH_3^+CH(CH_2COO^-)COO^-$.

For structures of group 1 complexes, the linear plot based on the pK_a (NH_3^+) and pK_a (α-COOH) provides estimated constants (included in Table 2) $\log\beta'_{xyz}$ (Asp) from each known $\log\beta_{xyz}$ (Ser)[2] for the $M_xS_yH_z$.

A similar plot based on the pK_a's of the R-COOH

Table 2. Estimation of formation constants for aspartato–VO^{2+} complexes with a coordination geometry similar to complexes formed in the L-Ser + VO^{2+} system

$M_xS_yH_z$[a] stoichiometry	$\log\beta_{xyz}$ (L-ser)[b]	$\log\beta'_{xyz}$ estimated	Calculation of β_{xyz} (L-asp)[c]	$\log\beta_{xyz}$ estimated	$M_xD_yH_z$ stoichiometry
MSH	10.37	10.7	$\beta' \times (K_{a2})^{-1}$	14.6	MDH_2
MS	6.38	6.6	$\beta' \times (K_{a2})^{-1}$	10.5	MDH
MS_2H	16.44	17	$\beta' \times (K_{a2})^{-2}$	24.8	MD_2H_3
MS_2	11.70	12.1	$\beta' \times (K_{a2})^{-2}$	19.9	MD_2H_2
$M_2S_2H_{-2}$	4.99	5.1	$\beta' \times (K_{a2})^{-2}$	12.9	M_2D_2
MS_2H_2	19.9	20.6	$\beta' \times (K_{a2})^{-2}$	28.4	MD_2H_4
$M_2S_2H_{-3}$	−1.23	−1.3	$\beta' \times (K_{a2})^{-2}$	6.5	$M_2D_2H_{-1}$

[a] S = L-serinate$^-$.
[b] From ref. 2.
[c] pK_{a2} = pK_a (β-COOH) = 3.88.

Table 3. Estimation of formation constants for aspartato complexes with a coordination geometry similar to complexes formed in the succinato[19] and malonato[20] systems

$M_xL_yH_z$[a] stoichiometry	$\log \beta_{xyz}$[b] (malonato or succinato)	$\log \beta^*_{xyz}$ estimated	Calculation of β_{xyz} (L-aspartate)[c]	$\log \beta_{xyz}$ estimated	$M_xD_yH_z$ stoichiometry
ML	{5.59 / 3.66(suc)}	{4.4 / 3.1}	$\beta^* \times (K_{a3})^{-1}$	{14.2 / 12.9}	MDH
ML_2	9.48	7.4	$\beta^* \times (K_{a3})^{-2}$	26.9	MD_2H_2
MLH_{-1}	0.52	0.4	$\beta^* \times (K_{a3})^{-1}$	10.2	MD
MLH	6.20	4.9	$\beta^* \times (K_{a3})^{-1}$	14.7	MDH_2
ML_2H_{-1}	2.56	2.0	$\beta^* \times (K_{a3})^{-2}$	21.5	MD_2H

[a] In this context, L = malonate^{2-} or succinate^{2-}.
[b] All log β's for malonate except the one with succinate.
[c] $pK_{a3} = pK_a(NH^+_3) = 9.77$.

groups gives estimated constants β^*_{xyz} (included in Table 3) for aspartato complexes with "group 2" structures similar to the succinato[19]– or malonato[20]–VO^{2+} complexes.

To estimate the constants which would correspond to aspartato–VO^{2+} structures of group 3 requires the unknown β_{xyz} for the system β-Ala+VO^{2+}. We use values for Cu^{2+} or Ni^{2+}.[21] Here, β_{110} (L-Ala)/β_{110} (β-Ala) ~ 10 and β_{120} (L-Ala)/β_{120} (β-Ala) ~ 10^2, so we estimate log β_{111} ~ 9.5 and log β_{122} ~ 17.4 for complexes of VO^{2+} coordinating via the β-COO^- and —NH_2 groups.

We now discuss (on the basis of Figs 14 and 15) the structures for each stoichiometry in model II—Table 1. Potentiometry alone cannot distinguish between different structures of the same stoichiometry, except in favourable cases. Table 4 includes possible structures for each stoichiometry $M_xD_yH_z$ and the corresponding estimated β_{xyz}.

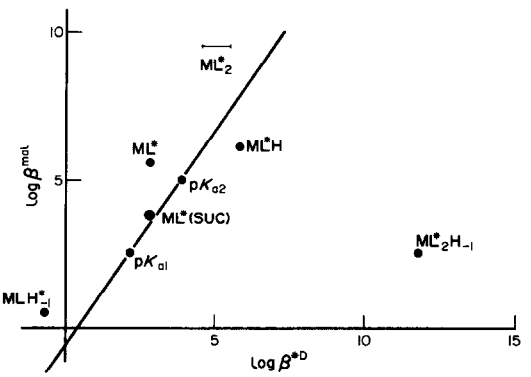

Fig. 15. Representation of $\log \beta_{xyz}$(Mal) vs $\log \beta^*_{xyz}$(L-Asp). The β^*_{xyz}(L-Asp) are defined according to eq. (3) and were obtained multiplying the β_{xyz} values by $(K_{a3})^{-y}$. The straight line is based solely on the pK_a of the COOH groups of the two ligands.

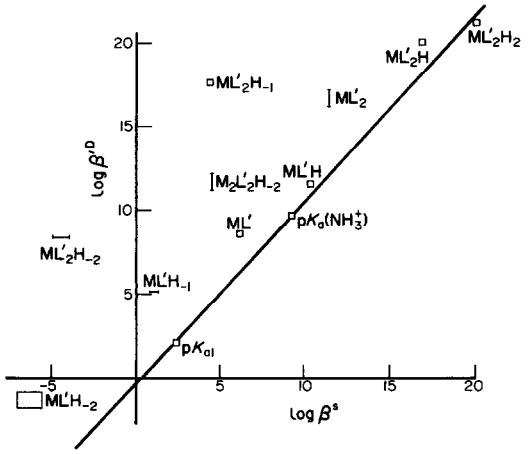

Fig. 14. Representation of $\log \beta'_{xyz}$(L-Asp vs $\log \beta_{xyz}$(L-Ser).[2] The β'_{xyz}(L-Asp) are defined according to eq. (2) and were obtained by multiplying the β_{xyz} values by $(K_{a2})^{-y}$. The straight line is based solely on the pK_a(α-COOH) and $pK_a(NH^+_3)$ values for the amino acids.

MDH_2. This stoichiometry probably has the α-COO^- group equatorial. Writing the formation as

$$VO^{2+} + nH_2D \rightleftharpoons VO(H_2D)^{2+}_n, \qquad (4)$$

K_1 ~ 78, higher than for Gly (14.8),[22] L-Ala (15.6),[1] L-Ser (12.5) and L-Thr (12.9).[2] The point [log β'_{112} (Asp), log β_{111} (Ser)] in Fig. 14 is slightly above the line. Higher values of K_1 (300–480) have also been obtained for the 1:1 complex VO^{2+}–lactate, another case where coordination involving only the R-COO^- group is expected.[23,24]

The visible spectra of MD_2 for L-Ala,[1] L-Ser,[2] and L-Asp are alike. However, the CD spectrum (Fig. 12) is different and is like that of the bidentate 1:1 L-alaninate (MA stoichiometry). This CD spec-

trum and the high value of K_1 suggest either that another complex should be included in the model (e.g. with MD_2H_4 stoichiometry) or that in $VO(H_2D)(H_2O)_n^{2+}$ (i.e. MDH_2) there is some favourable interaction of the β-COOH group with a coordinated water molecule, stabilizing a structure "similar" to that of a bidentate amino acid.

We give our reasons for preferring the latter explanation, i.e. for excluding MD_2H_4, which would correspond to two aspartate ligands coordinated via the α-COO^-.

In the L-Ala,[1] L-Ser and L-Thr[2] + VO^{2+} systems (and[25] in L-lactic acid + VO^{2+}) the corresponding species have been considered to exist. In the L-Asp + VO^{2+} system, a value for β_{124} has been refined in some models but with a high SD and much less consistently. It is possible to calculate potentiometric formation constants for the stoichiometries MDH_2 and especially for MD_2H_4 only because in this pH range part of the aspartic acid exists as H_3D^+. MD_2H_4 does not form in significant concentrations in our conditions. For conditions which would favour MD_2H_4 (pH ~ 2, L/M = 12.9), MDH and MD_2H_3 are quite important and probably "repress" its formation.

MDH. This corresponds to MA and MS stoichiometries in the L-Ala and L-Ser + VO^{2+} systems. However, the visible spectrum and especially the CD spectrum (Figs 11 and 12) are quite different from those for MA[1] and MS;[2] thus the structure of MDH is different.

Table 4 includes its possible structures. The point [log β_{110} (Suc), log β_{111} (Asp)] is near the line in Fig. 15. The EPR spectra also suggest a $VO(O_4)$ coordination geometry in this pH range. Thus all the results indicate that the MDH stoichiometry involves complexes with the α- and β-COO^- groups coordinated, both probably equatorial.

While MDH_2 and MD_2H_4 have not been included in equilibrium models for the L-Asp + Cu^{2+} system, CuDH is normally considered.[25-27]

MD_2H_3. The visible spectrum (Fig. 11) is similar to that of $[VO(H_2O)_5]^{2+}$. However, its CD spectrum differs from that expected for structure[1,2] **XXVII** implied by this and $|\Delta\varepsilon_{123}| \gg |\Delta\varepsilon_{112}|$.

The estimated formation constants for **XII** and **XIII** (Table 4) would be ~24.8 and 28. Our measured log β_{123} = 27.77 favouring **XIII** and the EPR spectra where MD_2H_3 is one of the most important species indicate $VO(O_4)$ coordination. However, structures such as **XXVIII** and **XXIX** cannot be ruled out.

MD. This is never important in any solutions used for spectra. Visible and CD spectra MD(1) are ill-defined but mutually consistent: λ_{max} (visible) are ~560 and 810 nm, and in the CD spectrum, ~570 ($\Delta\varepsilon > 0$) and ~800 ($\Delta\varepsilon > 0$).

Some plausible structures **VII–IX** are included in Table 4. We choose **IX** by elimination. Structure **VII** is similar to those of MA and MS. The CD for MD differs completely from those for MA[1] and MS[2] and the point [log β'_{110} (Asp), log β_{111} (Ser)] (Fig. 14) is well above the line, so **VII**, the structure for MA and MS, is not correct for MD.

For **VIII**, the estimated formation constant is too low. In Fig. 15, the point [log β_{111}(Mal), log β^*_{110} (Asp)] is well above the line, i.e. the structures for VO(Mal) and VO(Asp) differ. Structure **IX** is likely because it has an estimated formation constant close to that measured for β_{110}(Asp) suggesting that aspartate is tridentate. Other donor atoms could of course be coordinated equatorial.

Tridentate coordination of aspartate is familiar elsewhere. The formation constant of Cu(Asp) is considerably greater than those of Cu(Gly) and Cu(norvalinate), evidence for tridentate coordination,[26] although NMR relaxation suggested that aspartate interacted through —NH_2 and β-COO^- groups.[28] Several solid Cu^{2+} and Ni^{2+} complexes e.g. $[Cu(L\text{-}Asp)(Im)]\cdot 2H_2O$,[29] $[Cu(L\text{-}Asp)(Phen)(H_2O)]\cdot 4H_2O$,[30] $[Ni(L\text{-}Asp)(H_2O)_2]$[31] and $[Ni(L\text{-}Asp)(Im)_3]$,[32] contain terdentate aspartate, where Im = imidazole and Phen = 1,10-phenanthroline.

MD_2H_2. Structures are included in Table 4 with estimated formation constants. The log β_{122} for some models is ~24–25, suggesting that if MD_2H_2 does form, it does not involve N_2O_2 equatorial coordination.

The point [log β_{120}(Mal), log β^*_{122}(Asp)] in Fig. 15 is well above the line, so the structures in solution of $VO(Mal)_2^{2-}$ and $VO(HAsp)_2$ (if it forms) differ. Solid $(H_2tmen)\cdot[VO(Mal)_2(H_2O)]\cdot 2H_2O$[33] ($H_2tmen$ = N,N,N′,N′-tetramethylethylenediamine)

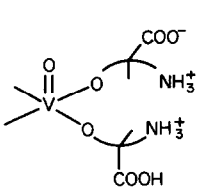

(XXVII)

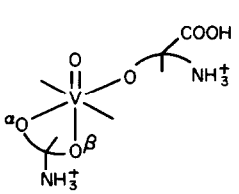

(XXVIII)

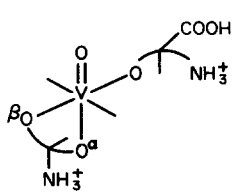

(XXIX)

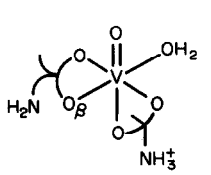

(XXX)

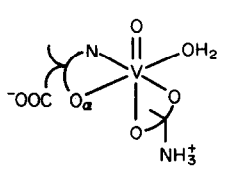

(XXXI)

Table 4. Estimated formation constants for particular isomeric structures of several micro-species within a given $M_xD_yH_z$ stoichiometry, compared with the measured constants for that stoichiometry

	Structure		Estimated formation constant Log β	
MDH_2 (15.55)[c]	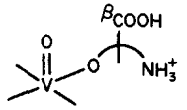	(I)	14.6 14.7	Table 2 Table 3
MD_2H_4 (29)[c]	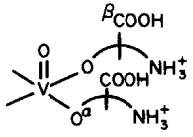	(II)	~28.4	Table 2
MDH (12.56)[c]	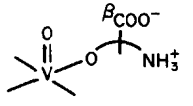	(III)	10.5	$\simeq \beta^{I}_{112} \cdot K_{a2}$
	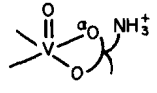	(IV)	14.2 12.9	Table 3 (malonate) Table 3 (succinate)
	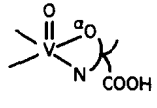	(V)	10.5	Table 2
	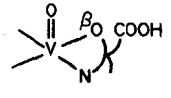	(VI)	~9.5	$\sim \beta^{V}/10$ (see text)
MD (9.05)[c]	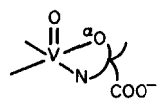	(VII)	7.5	$\sim \beta^{V} \cdot K^{C\,b}_{a2}$
	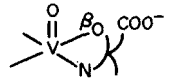	(VIII)	~5.8	$\simeq \beta^{VI} \cdot K^{C\,b}_{a1}$
	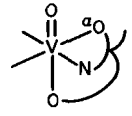	(IX)	~9(?)	$\beta^{IX} \gg \beta^{VIII}$
MDH_{-1} (2–3)[c]	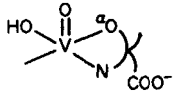	(X)	~1.5	$\sim \beta^{Ala}_{11-1}$
	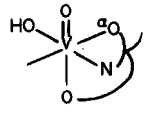	(XI)	~4(?)	$\beta^{XI} \gg \beta^{X}$
MD_2H_3 (27.77)[c]	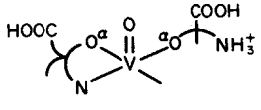	(XII)	24.8	Table 2
	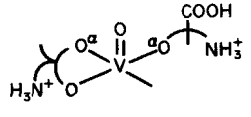	(XIII)	~28	$\simeq \beta^{VI} \cdot \beta^{I}$

MD_2H_2 (24–25)[c]	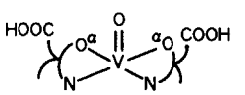	(XIV)	19.9	Table 2
	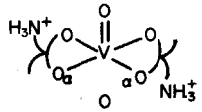	(XV)	26.9 ~25	Table 3 assuming: $\beta^{Mal}_{120}/\beta^{Suc}_{120} \sim (\beta^{Mal}_{110}/\beta^{Suc}_{110})^{2a}$
	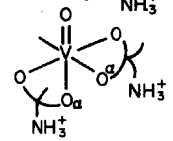	(XVI)	?	$\beta^{XVI} < \beta^{XV}$ (?)
	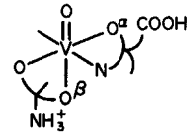	(XVII)	?	$\beta^{XVII} < \beta^{XV}$ (?)
MD_2H (21.49)[c]	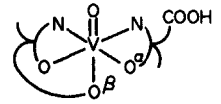	(XVIII)	~19.5(?)	$\beta^{XVIII} > \beta^{XIV} \cdot K^{C}_{a2}{}^{b}$
	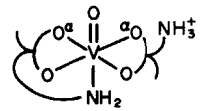	(XIX)	~21.5(?)	$\beta^{XIX} > \beta^{XV} \cdot K^{C}_{a3}{}^{b}$
	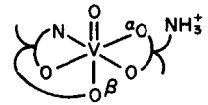	(XX)	~21(?)	$\beta^{XX} = ?$
	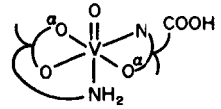	(XXI)	~21(?)	$\beta^{XXI} = ?$
MD_2 (16.25)[c]	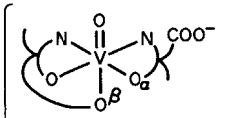	(XXII)	~16.5(?)	$\beta^{XXII} \simeq \beta^{XVIII} \cdot K^{C}_{a2}{}^{b}$
	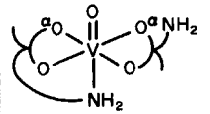	(XXIII)	~13.5(?)	$\beta^{XXIII} \simeq \beta^{XIX} \cdot K^{C}_{a3}{}^{b}$
	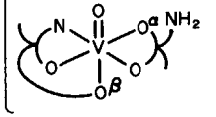	(XXIV)	~13.5(?)	$\beta^{XXIV} \simeq \beta^{XX} \cdot K^{C}_{A3}{}^{b}$
M_2D_2 (19–20)[c]	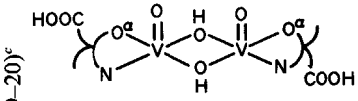	(XXV)	12.3	Table 2
	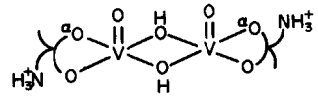	(XXVI)	(?)	$\beta^{XXVIII} > \beta^{XXV}$ (?)

[a] There is no published formation constant for β_{120}(succinate); $\log\beta$ for **XV** was therefore estimated assuming $(\beta_{120}(\text{malonate})/\beta_{120}(\text{succinate}) \simeq [\beta_{110}(\text{malonate})/\beta_{110}(\text{succinate})]^2$.

[b] $pK_{a1}{}^{c}$, $pK_{a2}{}^{c}$ and pK_{a3} are the dissociation constants of coordinated aspartic acid (coordination involving the other groups), which we assume to be ~2, ~3 and ~8, respectively. If the dissociation of the coordinated ligand is followed by the coordination of that group, we assume that the corresponding $\log\beta$ increases by 2–3 units.

[c] The measured formation constants (Table 1, model II) are written as $\log\beta$ alongside the stoichiometry of the macro-species to which they refer.

[d] For many stoichiometries, and particularly for species involving chelated L-aspartate, the orientation of the oxygen of oxovanadium relative to the substituents on the asymmetric carbon atom of the chelated amino acid gives further isomeric possibilities: we discuss these elsewhere but pay no heed to them here.

Table 5. Spectroscopic properties for each band of each species $(VO)_x(D)_y(H^+)_z$ and concordance with the EPR spectra (Fig. 1)

Species	λ_{max}	ε	$\Delta\varepsilon$	$\lvert\Delta\varepsilon/\varepsilon\rvert$[a]	λ_{max}	ε	$\Delta\varepsilon$	$\lvert\Delta\varepsilon/\varepsilon\rvert$[a]	EPR component
MDH_2	~630 (?) 565	~9 —	— −0.0094	0.0010	770 ~785	21.7 —	— 0.0048	0.0002	DI (and DII?)[b]
MDH	593 565	19.0 —	— 0.094	0.0049	750 ≳800	29.8 —	— ~−0.066	0.0022	DI+DII[b]
MD[c]	~560	~15	—		~810	~12	—		
	(1) ~570	—	0.466	(1) 0.031	(1) ~800	—	(1) ~−0.257	(1) 0.0055	[e]
	(2) ~610	—	0.053	(2) 0.0035	(2) 695 [d]	—	(2) 0.060[d]	(2) 0.0050	
					(3) 800	—	(3) −0.090	(2) 0.0075	
MD_2H_3	~630 ~570	~11 —	— −0.0152	0.0014	775 745	25.1 —	— 0.032	0.0013	DII (and DI?)[b]
MD_2H	581 575	19.3 —	— 0.36	0.019	768 780	27.1 —	— −0.172	0.0063	DIII
MD_2	537	31.5	0.382	0.012	738 688 [d] ~805	28.6 — —	— 0.282 [d] −0.142	0.0099 0.0050	DIV

[a] Approximate asymmetry factor calculated for each band according to: $\Delta\varepsilon$ (at λ_{max})/ε (at λ_{max}).

[b] The g and A parameters for the EPR components abbreviated as DI and DII are not sufficiently different to be distinguished as distinct peaks. As pH increases the peaks corresponding to $A_{\parallel} = 5/2$ and $7/2$ gradually shift to lower strength and no clear concordance can be established.

[c] Two types of spectra [(1) and (2)] were obtained for MD (see Fig. 12). The λ and $\Delta\varepsilon$ were calculated with quite high SD.

[d] Two bands of opposite sign are observed in the CD spectrum; these partly cancel.

[e] In the experimental conditions corresponding to the speciation of Fig. 13, from which these electronic spectra were derived, MD would not be detected in the EPR spectra.

contains the oxygens of the COO^- groups in equatorial positions, though this is not necessarily relevant to the solution geometry of the ion.

Brookes and Pettit[25] included the MD_2H_2 stoichiometry in the equilibrium model for the L-Asp+Cu^{2+} system, but earlier potentiometric work[26,27] did not. In the L-Ala,[1] L-Ser and L-Thr[2]+VO^{2+} systems, the corresponding species is the most important in the pH ranges 5–7 for solutions with high L/M ratios, and probably involves an equatorial N_2O_2 coordination. However, in the L-Asp+VO^{2+} system, species of this stoichiometry are apparently unimportant in our conditions.

MD_2H. MD_2H is the most important stoichiometry in the pH range 3–6 with L/M = 12.9 (Fig. 13), and has EPR spectrum DIII. Some possible structures for MD_2H are included in Table 4. The CD spectrum of MD_2H (Fig. 10) differs completely from those for MA_2[1] and MS_2.[2] Thus, the EPR spectra, and the β_{121} value eliminate **XVIII**. Structures **XXX** and **XXXI** cannot be utterly ruled out, although the other structures **XIX–XXI** involving terdentate aspartate seem more plausible.

MD_2 (giving DIV in EPR). This is the most important stoichiometry in the pH range 6–9 with L/M = 12.9 (Fig. 13). Its values of $g_\parallel$ and $A_\parallel$ suggest a N_2O_2 equatorial coordination. Band II in its visible spectrum is at 537 nm, lower than for MD_2H, so the ligand field increases from MD_2H to MD_2 (consistent with the EPR spectra): equatorial coordination of one or two R—NH_2 groups is certainly involved; structures like **XXIII** may be ruled out.

Its CD spectrum (Fig. 10) shows three bands (450–800 nm). The splitting of the d_{xz},d_{yz} levels is thus clearly observed, partly because one transition has $\Delta\varepsilon > 0$ and the other $\Delta\varepsilon < 0$ (and cf. Table 5). In the isotropic spectrum, two bands only are observed, with band I broader than band II, as usual. The splitting in the CD spectrum suggests that the equatorial coordination does not involve *cis* ligands. This effect has been seen in the visible spectrum, in low symmetry complexes involving other coordinating groups,[15] but the perturbation in ligand field induced here by the coordination of R—COO^- and R—NH_2 groups is probably not so large.

Acknowledgements—J.C.P. and L.F.V.B. thank the Instituto Nacional de Investigação Científica, Fundação Calouste Gulbenkian and the British Council for financial support. R.D.G. acknowledges the grant of study leave which has contributed to this programme.

REFERENCES

1. J. Costa Pessoa, L. F. Vilas Boas, R. D. Gillard and R. J. Lancashire, *Polyhedron* 1988, **7**, 1245.
2. J. Costa Pessoa, R. D. Gillard and L. F. Vilas Boas, *XXVI Int. Conf. Coord. Chem.*, Portugal, Porto (August 1988), Abstr. C45; *Polyhedron*, 1989, **8**, 1173.
3. R. D. Gillard, R. Marques, J. Costa Pessoa and L. Vilas Boas, *Comunicação 5CP12*. 9° Encontro Nacional de Química, Coimbra (1986).
4. R. C. Tewari and M. N. Srivastava, *Talanta* 1973, **20**, 133.
5. S. G. Tak, O. P. Sunar and C. P. Trivedi, *J. Ind. Chem. Soc.* 1972, **49**, 121.
6. M. K. Singh and M. N. Srivastava, *J. Inorg. Nucl. Chem.* 1972, **34**, 2081.
7. C. R. Johnson and R. E. Shepherd, *Bioinorg. Chem.* 1978, **8**, 115.
8. J. Costa Pessoa and L. Vilas Boas, 1980-Autumn Meeting—Chemical Society, University College, Cardiff (1980).
9. J. L. Antunes, J. Costa Pessoa, R. D. Gillard and L. F. Vilas Boas, unpublished results.
10. A. Sabatini, A. Vacca and P. Gans, *Talanta*, 1974, **21**, 53; P. Gans, A. Sabatini and A. Vacca, *Inorg. Chim. Acta* 1976, **18**, 237.
11. P. Gans, A. Sabatini and A. Vacca, *Inorg. Chim. Acta* 1983, **79**, 219; P. Gans, A. Sabatini and A. Vacca, *J. Chem. Soc., Dalton Trans.* 1985, 1195.
12. D. J. Leggett and W. A. E. McBryde, *Analyt. Chem.* 1975, **47**, 1065; D. J. Leggett, *Analyt. Chem.* 1977, **49**, 276; D. J. Leggett, S. L. Kelly, L. R. Shine, Y. T. Wu, D. Chang and K. M. Kadish, *Talanta* 1983, **30**, 579.
13. N. D. Chasteen, in *Biological Magnetic Resonance* (Edited by L. J. Berliner and J. Reuben), Vol. 3, p. 53. Plenum Press, New York (1981).
14. L. Casella, M. Gullotti, A. Pintar, S. Colonna and A. Manfredi, *Inorg. Chim. Acta* 1988, **144**, 89.
15. L. F. Vilas Boas and J. Costa Pessoa, in *Comprehensive Coordination Chemistry* (Edited by G. Wilkinson, R. D. Gillard and J. A. McCleverty), Vol. 3, pp. 453–583. Pergamon Press, Oxford (1987).
16. J. Costa Pessoa, L. F. Vilas Boas and M. H. Teixeira, to be published.
17. D. B. McPhail and B. A. Goodman, *J. Chem. Soc., Faraday Trans.* 1987, **83**, 3513.
18. S. P. Singh and J. P. Tandon, *Acta Chim. Acad. Sci. Hung.* 1974, **80**, 425.
19. G. Micera and A. Dessi, *J. Inorg. Biochem.* 1988, **33**, 99.
20. I. Nagypál and I. Fábián, *Inorg. Chim. Acta* 1982, **61**, 109.
21. R. M. Smith, R. J. Motekaitis and A. E. Martell, *Inorg. Chim. Acta* 1985, **103**, 73; R. M. Smith and A. E. Martell, *Critical Stability Constants*. Plenum Press, New York: (a) 1976, Vol. 2; (b) 1982, Vol. 5 (1st Supplement).
22. I. Fábián and I. Nagypál, *Inorg. Chim. Acta* 1982, **62**, 193.
23. R. Reeder and P. H. Rieger, *Inorg. Chem.* 1971, **10**, 1258.
24. K. M. Jones and E. Larsen, *Acta Chem. Scand.* 1965, **19**, 1205.

25. G. Brookes and L. D. Pettit, *J. Chem. Soc., Dalton Trans.* 1977, 1918.
26. I. Nagypál, A. Gergeley and E. Farkas, *J. Inorg. Nucl. Chem.* 1974, **36**, 699.
27. J. H. Ritsma, *Rev. Trav. Chim.* 1975, **94**, 210.
28. S. Khazaeli and R. E. Viola, *J. Inorg. Biochem.* 1984, **22**, 33.
29. L. Antolini, G. Marcotrigiano, L. Menabue, G. C. Pellacani and M. Saladini, *Inorg. Chem.* 1982, **21**, 2263.
30. L. Antolini, L. P. Battaglia, A. Bonamartini Corradi, G. Marcotrigiano, L. Menabue, G. C. Pellacani, M. Saladini and M. Sola, *Inorg. Chem.* 1986, **25**, 2901.
31. L. Antolini, L. Menabue, G. C. Pellacani and G. Marcotrigiano, *J. Chem. Soc., Dalton Trans.* 1982, 2541.
32. L. P. Battaglia, A. Bonamartini Corradi, L. Antolini, G. Marcotrigiano, L. Menabue and G. C. Pellacani, *J. Am. Chem. Soc.* 1982, **104**, 2407.
33. A. Pajunen and S. Pajunen, *Acta Cryst.* 1980, **B36**, 2425.

Polyhedron Vol. 9, No. 1, pp. 99–105, 1990
Printed in Great Britain

0277–5387/90 $3.00+.00
© 1989 Pergamon Press plc

KINETICS AND MECHANISM OF THE OXIDATION OF DIETHYLENETRIAMINEPENTAACETATOCOBALTATE(II) BY PERIODATE

MERVAT H. ABU-ELENIEN, N. I. AL-SHATTI, MOHAMED A. HUSSEIN and YOUSIF SULFAB*

Department of Chemistry, Kuwait University, P.O. Box 5969 Safat, 13060 Safat, Kuwait

(*Received* 27 *February* 1989; *accepted* 16 *August* 1989)

Abstract—The kinetics of the oxidation of Co^{II}DTPA (DTPA = diethylenetriaminepentaacetate) by periodate in acetate buffer showed the formation of a long-lived intermediate. The formation of the intermediate exhibited a first-order dependence on the Co^{II} complex concentration. The variation of the pseudo-first-order rate constant, k_{obs}, with periodate concentration at constant $[H^+]$, $[CH_3CO_2^-]$, ionic strength and temperature, is governed by eq. (i):

$$k_{obs} = \frac{a[IO_4^-]^2}{b + c[IO_4^-]}. \quad \text{(i)}$$

The decrease in the magnitude of k_{obs} with increasing acetate ion concentration seems to be due to its coordination with the Co^{II} complex. The value of k_{obs} increases with decreasing pH, indicating that the protonated form of the Co^{II} complex is the more reactive species. A mechanism consistent with the kinetic results is proposed.

Oxidation of organic substrates by periodate ion proceeds through the formation of cyclic intermediates when bridging groups (e.g. OH, NH_2 and CO) are in the 1,2-positions.[1] Oxygen atom transfer with the formation of HOI as an intermediate was invoked in periodate oxidation of the iodide ion.[2] Thus, it seems that periodate oxidations proceed via an inner-sphere mechanism.

Inner-sphere electron-transfer was also suggested in the reactions of the aqua-ions vanadium(IV)[3] and iron(II)[4] and some (aminopolycarboxylato) cobalt(II) complexes with periodate. The formation of intermediates in the iron(II),[4] $[Co^{II}EDTA]^{2-}$ (EDTA = ethylenediaminetetraacetate),[5] $[Co^{II}HEDTA]^-$ [HEDTA = N-(2-hydroxyethyl)ethylenediaminetriacetate],[6] Co^{II}EDDA (EDDA = ethylenediaminediacetate)[6] and $[Co^{II}NTA]^-$ (NTA = nitrilotriacetate)[7] oxidations lends support to this mechanism. Additional support for this mechanism may also be drawn from a consideration of the rate laws for the oxidation of $[Co^{II}EDTA]^{2-}$, $[Co^{II}HEDTA]^-$ and Co^{II}EDDA. The rate law for the $[Co^{II}EDTA]^{2-}/IO_4^-$ reaction requires a rapid equilibrium preceding the slow intramolecular electron-transfer step. The kinetics of the oxidation of both $[Co^{II}HEDTA]^-$ and Co^{II}EDDA by IO_4^- proceed by two parallel pathways;[6] one first-order in each reactant and the other first-order in each cobalt(II) complex and second-order in the oxidant concentration. The pathway which is first-order in each reactant concentration, almost certainly, proceeds via an inner-sphere electron-transfer process. This is necessitated by the pathway showing a second-order dependence on $[IO_4^-]$ since a rapid pre-equilibrium between both $[Co^{II}HEDTA]^-$ and Co^{II}EDDA with IO_4^- is required to account for the termolecular reaction.[8]

The second-order dependence on the reductant concentration observed in periodate oxidation of $Cr(H_2O)_6^{3+}$ [9] and in one pathway of $Fe(H_2O)_6^{2+}$,[4] where two one-electron-transfers in a single activated complex were proposed, seems to support an inner-sphere mechanism. Two-electron-transfer is believed to be obtained by way of this mechanism.

* Author to whom correspondence should be addressed.

A common mechanism for the oxidation of aminopolycarboxylatocobalt(II) complexes is further supported by an excellent isokinetic relationship obtained on plotting composite $\Delta H^{\ddagger}$ vs composite $\Delta S^{\ddagger}$.[7] The composite $\Delta H^{\ddagger}$ and $\Delta S^{\ddagger}$ values contain contributions from the pre-equilibrium step between periodate and the cobalt(II) complexes as well as from the intramolecular electron-transfer step.

In this study we report the kinetics of the oxidation of (diethylenetriaminepentaacetato) cobaltate(II), $Co^{II}DTPA$, by periodate. This study furnishes direct kinetic evidence for inner-sphere oxidation by periodate.

EXPERIMENTAL

Materials and solutions

Reagent grade sodium metaperiodate was used for preparing fresh solutions by weight and these were wrapped with aluminium foil to avoid photochemical decomposition.[10] Cobalt(II) nitrate was standardized against EDTA volumetrically.[11] A stock solution of the ligand, DTPA, was prepared as the disodium salt by weighing the acid and neutralizing with the appropriate amount of sodium hydroxide. Sodium acetate and sodium nitrate solutions were prepared by weight from reagent grade chemicals. A stock solution of acetic acid was made up by dilution and standardized against sodium hydroxide.

Apparatus

A Unicam SP 8000 spectrophotometer equipped with thermostatted cell holders was used for recording the UV–vis absorption spectrum of the product of oxidation of $Co^{II}DTPA$ and for monitoring the change in absorbance of the product as a function of time. The pH of the reaction was measured using a Radiometer digital pH meter model PHM 62.

Kinetics measurements

The kinetics of oxidation of $Co^{II}DTPA$ by IO_4^- was carried out under pseudo-first-order conditions with $[IO_4^-] \geqslant 20\,[Co^{II}DTPA]$. $Co^{II}DTPA$ solutions were made up by adding a 10% excess of the ligand to the Co^{II} solution immediately before each kinetic run as this complex was reported to be air sensitive.[12] However, over the pH 4–5 range, where the kinetics of the reactions were investigated, no significant air oxidation of the cobalt(II) complex was observed.

The formation of the intermediate was followed either at 564 nm or at 380 nm, where appreciable changes in absorbance were observed. The final absorbance (A_∞) was constant at each of these wavelengths for a period of 30 min and decreased by 0.01 units absorbance 1 h after the reaction was complete at 564 nm. The conversion of the Co^{III} intermediate was not studied in detail.

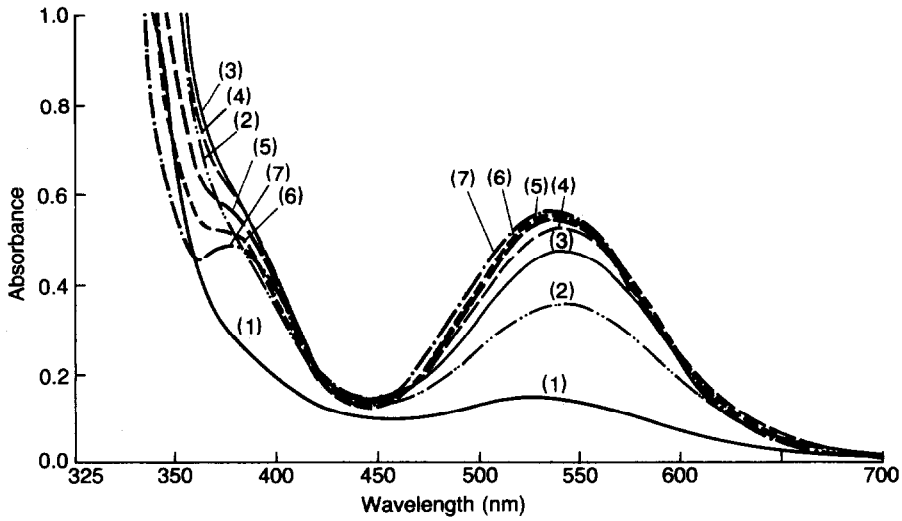

Fig. 1. Change in absorbance as a function of time. Curves 1–6 were recorded at 3, 6, 10, 16, 28 and 60 min, respectively, from the time of starting the reaction. Curve 7 shows the absorbance of the final Co^{III} product. $[Co^{II}DTPA] = 5.0 \times 10^{-4}$ M, $[IO_4^-] = 0.03$ M, pH = 4.10, $\mu = 0.55$ M and $T = 25°C$ (4 cm path length).

Reaction product

The UV–vis absorption spectrum of the oxidation of $Co^{II}DTPA$ by periodate is shown in Fig. 1. It is evident from this spectrum that this reaction proceeds via the formation of an intermediate which is slowly converted to a final product. A similar behaviour was found in the oxidation of $[Co^{II}EDTA]^{2-}$, $[Co^{II}HEDTA]^{-}$, $Co^{II}EDDA$ and $[Co^{II}NTA]^{-}$ by the same oxidant.[5-7] The final product showed two peaks at 377 and 538 nm. These peaks are almost identical to those exhibited by $[Co^{III}(HEDTA)(H_2O)]$[6] and it thus seems that the final product of the oxidation of $Co^{II}DTPA$ by periodate has a pentacoordinated DTPA.

RESULTS

Figure 1 shows that the oxidation of $Co^{II}DTPA$ by periodate leads to the formation of an intermediate Co^{III} product which slowly converts to the final Co^{III} product at pH 4.10. The final product is fully formed when the reaction solution is left overnight.

Under conditions of a large excess of $[IO_4^-]$ at fixed pH, ionic strength and temperature, plots of $\ln(A_\infty - A_t)$ against time were linear up to $\geqslant 90\%$ of reaction (correlation coefficient >0.99). The results in Table 1 show that the magnitude of the pseudo-first-order rate constant, k_{obs}, does not vary with the initial concentration of the Co^{II} complex. A first-order dependence on $[Co^{II}DTPA]_T$ is deduced. The magnitude of k_{obs} was not affected by changes of the wavelength at which the reaction was followed.

Table 2 shows that the variation of k_{obs} with $[IO_4^-]$ is not linear. A plot of $k_{obs}/[IO_4^-]$ vs $[IO_4^-]$, using the results in Table 2, is curved. However, a plot of $[IO_4^-]/k_{obs}$ vs $[IO_4^-]^{-1}$ is linear with an intercept, as shown in Fig. 2. The dependence of k_{obs} on $[IO_4^-]$ is consistent with eq. (1) which can be rearranged to the form of eq. (2):

$$k_{obs} = \frac{a[IO_4^-]^2}{b + c[IO_4^-]} \quad (1)$$

$$[IO_4^-]/k_{obs} = \frac{c}{a} + \frac{b}{a[IO_4^-]}. \quad (2)$$

From eq. (2) and Fig. 2 it could be shown that the intercept is $I = c/a$ and the slope is $S = b/a$. The values of I and S were calculated, using a linear least-squares fit to eq. (2), as 8.77 ± 0.16 M s and $(8.64 \pm 0.17) \times 10^{-2}$ M^2 s, respectively, at pH 4.52, $[CH_3CO_2^-] = 0.50$ M, $\mu = 0.55$ M and $T = 25.0°C$.

The results in Table 3 show that k_{obs} decreases with increasing pH. The decrease in k_{obs} over the pH 4.0–4.5 range is very small. At pH $\geqslant 5$, however, the value of k_{obs} was greatly decreased. From plots

Table 1. First-order dependence on $[Co^{II}DTPA]_T$[a]

10^4 $[Co^{II}DTPA]$ (M)	10^3 k_{obs} (s^{-1})
2.0	1.35±0.03
4.0	1.49±0.01
5.0	1.39±0.01[b]
6.0	1.62±0.02
8.0	1.44±0.01
10.0	1.54±0.01

[a] $[IO_4^-] = 0.02$ M; pH = 4.53±0.01; $\mu = 0.55$ M ($CH_3CO_2Na + NaNO_3$); $[CH_3CO_2^-] = 0.50$ M, $T = 25°C$, $\lambda = 564$ nm, [b] $\lambda = 380$ nm.

Table 2. Variation of the pseudo-first-order rate constant for the $Co^{II}DTPA/IO_4^-$ reaction with $[IO_4^-]$[a]

10^2 $[IO_4^-]$ (M)	10^3 k_{obs} (s^{-1})
0.50	0.19±0.02
0.80	0.42±0.01
1.20	0.76±0.01
1.60	1.12±0.01
2.00	1.54±0.02
2.40	2.01±0.02
3.20	2.72±0.03
4.00	3.57±0.08
5.00	4.73±0.09

[a] $[Co^{II}DTPA] = 5.0 \times 10^{-4}$ M, $\mu = 0.55$ M, $[CH_3CO_2^-] = 0.50$ M, $T = 25.0°C$, pH = 4.52 and $\lambda = 564$ nm.

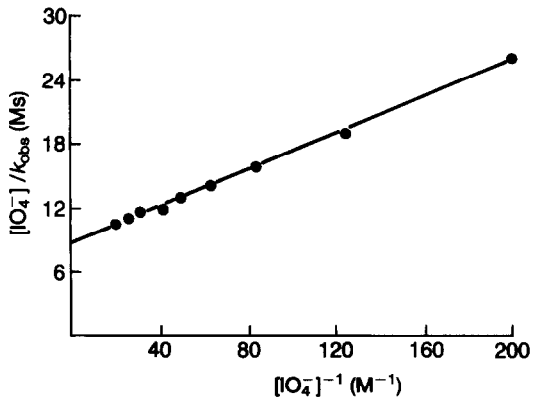

Fig. 2. Plot of $[IO_4^-]/k_{obs}$ vs $[IO_4^-]^{-1}$ of the results in Table 2.

Table 3. Effect of pH on the pseudo-first-order rate constant at different periodate concentrations[a]

pH	10^2 [IO_4^-] (M)	10^3 k_{obs} (s^{-1})
4.10	0.5	0.16±0.02
	1.5	1.00±0.01
	2.0	1.59±0.02
	3.0	2.63±0.02
	4.5	4.15±0.05
4.35	0.5	0.15±0.01
	2.8	2.48±0.02
	5.0	4.81±0.05
	6.0	5.83±0.27
	7.0	6.85±0.15
5.05	1.0	0.50±0.01
	2.0	1.15±0.01
	3.0	1.81±0.02
	4.0	2.45±0.02
	5.0	3.15±0.04

[a] $[Co^{II}DTPA]_T = 5.0 \times 10^{-4}$ M, $\mu = 0.55$ M, $[CH_3CO_2^-] = 0.50$ M, $T = 25.0$°C.

similar to that in Fig. 2, the values of I and S at different pH values were calculated and these are collected in Table 4. A plot of I vs $[H^+]^{-1}$, shown in Fig. 3, was found to be linear with an intercept $I_1 = 6.34 \pm 0.18$ M s and a slope, $S_1 = (7.60 \pm 0.30) \times 10^{-5}$ M^2 s.

The effect of the acetate ion on the reaction rate was investigated over the concentration range 0.10–0.50 M at fixed reaction conditions. The results in Table 5 show that k_{obs} decreases with increasing acetate ion concentration. The variation of k_{obs} with $[CH_3CO_2^-]$ is governed by eq. (3), where a plot of $1/k_{obs}$ vs $[CH_3CO_2^-]$ is linear:

$$1/k_{obs} = 1/k^0 + 1/k'[CH_3CO_2^-]. \quad (3)$$

The values of $1/k^0$ and $1/k'$ at various periodate

Table 4. Variation of the intercept (I) and the slope (S) with pH

pH	I (M s)	S (M^2 s)
4.10	7.55±0.42	0.115±0.004
4.35	7.85±0.42	0.126±0.005
4.52	8.77±0.16	0.086±0.002
5.05	14.92±0.08	0.051±0.002

$[CH_3CO_2^-] = 0.50$ M, $\mu = 0.55$ M and $T = 25.0$°C.

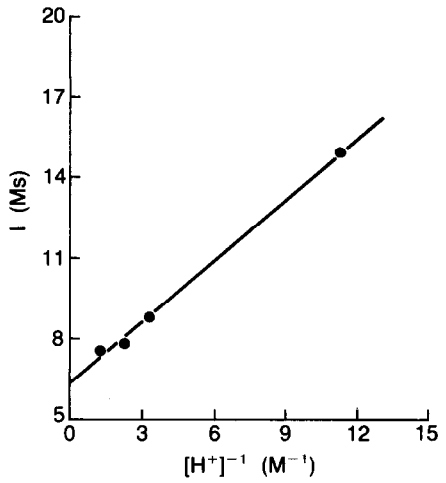

Fig. 3. Variation of intercept, I, with $[H^+]^{-1}$.

concentrations were obtained from a linear least-squares fit to eq. (3). The values of k^0 and k' are collected in Table 6. The dependence of k^0 on $[IO_4^-]$ obeyed eq. (2) as plots of $[IO_4^-]/k^0$ vs $[IO_4^-]^{-1}$ at 15, 20 and 25°C are linear with an intercept, I_2, and a slope, S_2. The parameter k' seems to have a second-order dependence on $[IO_4^-]$ with the results at 25°C showing the best fit.

Table 5. Effect of acetate ion concentration on the pseudo-first-order rate constant at various $[IO_4^-]$ and temperatures at pH = 3.98 and $\mu = 0.55$ M

$[CH_3CO_2^-]$ (M)	$[IO_4^-]$ (M)	10^3 k_{obs} (s^{-1}) 0.01	0.02	0.03	0.04	0.05
		$T = 25.0$°C				
0.10		1.03	2.53	3.97	5.47	7.37
0.20		0.98	2.24	3.66	5.33	7.03
0.30		0.81	2.09	3.58	4.95	6.67
0.40		0.73	1.93	3.32	4.62	6.53
0.50			1.84	3.05	4.50	6.32
		$T = 20.0$°C				
0.10			1.81	3.09	4.54	5.76
0.20			1.68	2.70	4.01	5.50
0.30			1.54	2.54	3.84	5.28
0.40			1.36	2.31	3.67	5.15
0.50			1.28	2.21	3.38	4.77
		$T = 15.0$°C				
0.10			1.27	2.15	3.05	4.25
0.20			1.16	1.90	2.83	4.14
0.30			1.03	1.82	2.68	4.02
0.40			0.98	1.76	2.40	3.58
0.50			0.94	1.59	2.32	3.38

Table 6. Values of k^0 and k' derived from the variation of the pseudo-first-order rate constant with $[CH_3CO_2^-]$ at various periodate concentrations and temperatures

$10^2\,[IO_4^-]$ (M)	$10^3\,k^0$ (s^{-1})	$10^3\,k'$ ($M^{-1}\,s^{-1}$)
	$T = 25.0°C$	
1.0	1.25±0.09	0.71±0.11
2.0	2.73±0.06	2.70±0.17
3.0	4.31±0.12	5.56±0.61
4.0	5.92±0.12	9.25±0.89
5.0	7.63±0.08	17.86±1.35
	$T = 20.0°C$	
2.0	2.07±0.07	1.66±0.13
3.0	3.35±0.09	3.12±0.23
4.0	4.82±0.14	5.74±0.60
5.0	6.10±0.14	13.29±2.03
	$T = 15.0°C$	
2.0	1.38±0.05	1.38±0.14
3.0	2.30±0.08	2.67±0.32
4.0	3.33±0.08	3.72±0.29
5.0	4.30±0.04	5.49±0.17

DISCUSSION

The oxidation of Co^{II}DTPA by periodate proceeds via the formation of an intermediate Co^{III} product as is evident from Fig. 1. This behaviour is analogous to that observed in the oxidation of the Co^{II} complexes of EDTA,[5] HEDTA,[6] EDDA[6] and NTA[7] by the same oxidant. The intermediate Co^{III} product of the oxidation of Co^{II}DTPA converts to the final product with a half-life >3 h.

The structure of Co^{II} complexes of DTPA in solution, until recently, has not been reported. It was shown by an NMR study that the three nitrogens of deprotonated DTPA coordinate to Co^{II} and that proton addition decreases the number of coordinated nitrogens.[13] This is in agreement with the structure proposed by Chabarek *et al.*[14] for Cu^{II} DTPA complexes, where three nitrogens and one carboxylate group coordinate in the unprotonated form and two nitrogens and two carboxylate groups coordinate in the protonated form. Huchital and Hodges[12] proposed that in the unprotonated form of the Co^{II} complex, three nitrogens and three carboxylate groups are bound to the metal ion as shown in Fig. 4(A). Protonation of this complex, it is believed, would occur at a terminal nitrogen resulting in the formation of a free iminodiacetate group, leaving only two nitrogens and three carboxylate groups coordinated to Co^{II} as in Fig. 4(B). The sixth coordination site would be occupied by a water molecule. The two forms, (A) and (B), are in equilibrium with each other with an acid dissociation constant $\sim 10^{-5}$ M.[12]

The protonated form (B), of the Co^{II}DTPA complex seems to be the reactive species since the magnitude of the pseudo-first order rate constant decreased with increasing pH. The unprotonated form reacts very slowly with periodate. The decrease in the value of k_{obs} with increasing acetate ion concentration most likely arises from coordination of this ion with the protonated form (B) by replacing the water molecule. Substitution of a coordinated H_2O by an acetate ion was reported in the $[Co^{II}(NTA)(H_2O)_2]^-$ complex.[7]

A mechanism for the oxidation of Co^{II}DTPA by IO_4^- could be described by the reaction scheme in eqs (4)–(8):

$$[Co^{II}DTPA]^{3-} + H^+ \rightleftharpoons [Co^{II}(DTPAH)(H_2O)]^{2-} \quad K_a \quad (4)$$

$$[Co^{II}(DTPAH)(H_2O)]^{2-} + CH_3CO_2^- \rightleftharpoons [Co^{II}(DTPAH)(CH_3CO_2)]^{3-} + H_2O \quad K_1 \quad (5)$$

$$[Co^{II}(DTPAH)(H_2O)]^{2-} + IO_4^- \rightleftharpoons [Co^{II}(DTPAH)(IO_4)]^{3-} + H_2O \quad K_2 \quad (6)$$

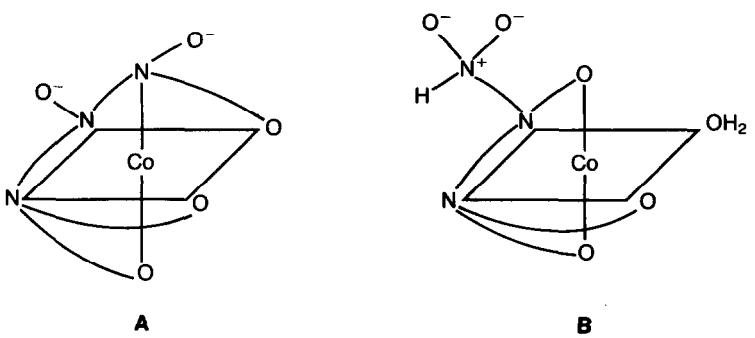

Fig. 4. Structural forms of Co^{II}DTPA complexes.

$$[Co^{II}(DTPAH)(IO_4)]^{3-} + IO_4^- \rightleftharpoons [Co^{II}(DTPAH)(IO_4)_2]^{4-} \quad K_3 \quad (7)$$

$$[Co^{II}(DTPAH)(IO_4)_2]^{4-} \rightarrow [(DTPAH)(IO_4)Co^{III}—I^{VI}]^{4-}. \quad k_{et} \quad (8)$$

In this mechanism it is assumed that the species $[Co^{II}(DTPAH)(IO_4)]^{3-}$ has a negligible contribution towards the formation of an intermediate Co^{II} product. Separate kinetic runs at pH ~ 6, where the hexacoordinated form (A) is the dominant species, are extremely slow. It could therefore be concluded that a reaction pathway involving form (A) and IO_4^- is of minor importance. The formation of $[Co^{II}(DTPAH)(IO_4)_2]^{4-}$ requires that in addition to the replacement of H_2O, an acetate group be set free with DTPA functioning as a tetradentate ligand. Inner-sphere electron-transfer is supported by the formation of the intermediate which exhibited high absorption below 400 nm. This high absorption may arise from ligand-to-metal (LTM) charge-transfer, in this case I^{VI} to Co^{III}. An outer-sphere electron-transfer between $[Co^{II}(DTPAH)(IO_4)]^{3-}$ and IO_4^- is not expected to show the formation of an intermediate with LTM charge-transfer. The I^{VI} in the intermediate would be coordinated to Co^{III} via an oxygen atom. Second-order dependence on $[IO_4^-]$ is not unique to this system; it was found in the oxidation of $[Co^{II}HEDTA]^-$,[6] $Co^{II}EDDA$[6] and V^{IV}.[15]

The rate law given in eq. (9) is derived from the above mechanism assuming that K_3 is small:

$$\frac{d[Co^{III}]}{dt} = \frac{k_{et}K_aK_2K_3[H^+][Co^{II}]_T[IO_4^-]^2}{1+K_a[H^+]+(K_1+K_1K_a[H^+])[CH_3CO_2^-]+(K_2+K_2K_a[H^+])[IO_4^-]^-}. \quad (9)$$

The dependence of k_{obs} on $[IO_4^-]$, $[H^+]$ and $[CH_3CO_2^-]$ is given in eq. (10),

$$k_{obs} = \frac{k_{et}K_aK_2K_3[H^+][IO_4^-]^2}{1+K_a[H^+]+(K_1+K_1[H^+])[CH_3CO_2^-]+(K_2+K_2K_a[H^+])[IO_4^-]}. \quad (10)$$

At fixed $[H^+]$ and $[CH_3CO_2^-]$, eq. (10) could be rearranged to the form of eq. (11) which is identical to the experimental form of eq. (2),

$$[IO_4^-]/k_{obs} = \frac{K_2+K_2K_a[H^+]}{k_{et}K_aK_2K_3[H^+]} + \frac{1+K_a[H^+]+(K_1+K_1K_a[H^+])[CH_3CO_2^-]}{k_{et}K_aK_2K_3[H^+][IO_4^-]}. \quad (11)$$

From eqs (2) and (11) it can be shown that the plot of $[IO_4^-]/k_{obs}$ vs $[IO_4^-]^{-1}$ should be linear with an intercept and a slope given by eqs (12) and (13), respectively:

$$\text{Intercept} = I = c/a = \frac{1+K_a[H^+]}{k_{et}K_aK_3[H^+]} \quad (12)$$

$$\text{Slope} = S = b/a = \frac{1+K_a[H^+]+(K_1+K_1K_a[H^+])[CH_3CO_2^-]}{k_{et}K_aK_2K_3[H^+]}. \quad (13)$$

The variation of the intercept, I, with $[H^+]$ is given by eq. (14) which is consistent with the variation of I with $[H^+]$ shown in Fig. 3:

$$I = \frac{1}{k_{et}K_3} + \frac{1}{k_{et}K_aK_3[H^+]}. \quad (14)$$

From eq. (14) a plot of I vs $[H^+]^{-1}$ gives an intercept $I_1 = 1/k_{et}K_3$ and a slope, $S_1 = 1/k_{et}K_aK_3$. The value of K_a, the protonation constant for the $Co^{II}DTPA$ complex, is calculated from I_1/S_1 as $(8.34 \pm 0.3) \times 10^4$ M^{-1} which is in excellent agreement with the pK_a value of 4.92 reported for this complex.[12]

Equation (10) could be rearranged to the form of eq. (15) which would account for the linear dependence of $1/k_{obs}$ on $[CH_3CO_2^-]$ at fixed $[IO_4^-]$ and $[H^+]$.

$$1/k_{obs} = \frac{1+K_a[H^+]+(K_2+K_aK_2[H^+])[IO_4^-]}{k_{et}K_aK_2K_3[H^+][IO_4^-]^2} + \frac{(K_1+K_1K_a[H^+])[CH_3CO_2^-]}{k_{et}K_aK_2K_3[H^+][IO_4^-]^2}. \quad (15)$$

A comparison of eqs (3) and (15) shows that:

$$k^0 = \frac{k_{et}K_aK_2K_3[H^+][IO_4^-]^2}{1+K_a[H^+]+(K_2+K_aK_2[H^+])[IO_4^-]} \quad (16)$$

and

$$k' = \frac{k_{et}K_aK_2K_3[H^+][IO_4^-]^2}{(K_1+K_1K_a[H^+])}. \quad (17)$$

From eq. (16) a plot of $[IO_4^-]/k^0$ vs $[IO_4^-]^{-1}$ should be linear with an intercept I_2 and a slope S_2 given in eqs (18) and (19), respectively:

$$\text{Intercept} = I_2 = \frac{1+K_a[H^+]}{k_{et}K_aK_3[H^+]} \quad (18)$$

$$\text{Slope} = S_2 = \frac{1+K_a[H^+]}{k_{et}K_aK_2K_3[H^+]}. \quad (19)$$

The magnitude of K_2 is obtained from I_2/S_2 as

372 ± 37, 146 ± 15 and 99 ± 6 M^{-1} at 25, 20 and 15°C, respectively. The decrease in the value K_2 with decreasing temperature indicates that entry of the periodate ion is an endothermic process. From the slope of the plot k' vs $[IO_4^-]^2$ of eq. (17) and S_2 of eq. (19) the value of K_1 is calculated as ~ 8 M^{-1} at 25°C. Nearly the same value is obtained when the same slope is used with eq. (18) and substituting K_2 as 372 M^{-1} at 25°C.

In the reaction of $Co^{II}DTPA$ with $Fe^{III}(CN)_6^{3-}$ it was proposed that form (B) does not decompose to final products.[12] In the reaction reported here, however, the conversion of the intermediate to the final product may occur via the coordination of free carboxylate group at one site and by a water molecule at the other. Thus, I^{VII} or I^{VI} may be attacked by a water molecule and hydrolysis takes place without Co—O bond cleavage. Periodate is known to exchange oxygen atoms with water quite rapidly.[16]

Acknowledgement—Financial support for this work, provided under grant SC09 by the Research Council of Kuwait University, is greatly appreciated.

REFERENCES

1. G. J. Buist, *Comprehensive Chemical Kinetics* (Edited by C. H. Bamford and C. F. H. Tripper), Vol. 6, Ch. 5, pp. 435–456. Elsevier, Amsterdam (1972).
2. A. Indelli, F. Ferranti and F. Secco, *J. Phys. Chem.* 1966, **70**, 631.
3. Y. Sulfab and A. I. Abu-Shadi, *Inorg. Chim. Acta* 1977, **21**, 115.
4. F. R. El-Eziri and Y. Sulfab, *Inorg. Chim. Acta* 1977, **25**, 15.
5. A. Y. Kassim and Y. Sulfab, *Inorg. Chim. Acta* 1977, **24**, 247.
6. A. A. Abdel-Khalek and Y. Sulfab, *J. Inorg. Nucl. Chem.* 1981, **43**, 3257.
7. M. A. Hussein, A. A. Abdel-Khalek and Y. Sulfab, *J. Chem. Soc., Dalton Trans.* 1983, 317.
8. R. G. Wilkins, *The Study of Kinetics and Mechanism of Reactions of Transition Metal Complexes*, p. 64. Allyn and Bacon, Boston (1974).
9. A. Y. Kassim and Y. Sulfab, *Inorg. Chem.* 1981, **20**, 506.
10. F. S. H. Head and H. A. Standing, *J. Chem. Soc.* 1952, 1457.
11. A. I. Vogel, *A Textbook of Quantitative Inorganic Analysis*, 3rd edn., p. 443. Longmans, London (1961).
12. D. H. Huchital and R. J. Hodges, *Inorg. Chem.* 1973, **12**, 1004.
13. L. L. Grazynski and B. J. Trzebiatowska, *Coord. Chem.* 1980, **10**, 159.
14. S. Chabarek, A. E. Frost, M. A. Doran and N. J. Bicknell, *J. Inorg. Nucl. Chem.* 1959, **11**, 184.
15. D. J. B. Galliford and J. M. Ottaway, *Analyst* 1972, **91**, 415.
16. K. Kustin and Lieberman, *J. Phys. Chem.* 1964, **68**, 3869.

Polyhedron Vol. 9, No. 1, pp. 107–111, 1990
Printed in Great Britain

0277–5387/90 $3.00+.00
© 1989 Pergamon Press plc

A PM3 SCF–MO STUDY OF THE STRUCTURE AND BONDING IN THE CAGE SYSTEMS S_4N_4 AND S_4N_4X ($X = N^+$, N^-, S, N_2S, P^+, C, Si, B^- AND Al^-)

HENRY S. RZEPA* and J. DEREK WOOLLINS

Department of Chemistry, Imperial College, London SW7 2AY, U.K.

(*Received* 6 *April* 1989; *accepted* 16 *August* 1989)

Abstract—Short S—S interactions in S_4N_4 and related S···S bridged systems S_4N_4X ($X = N^+$, N^-, N_2S, S, P^+, B^-) are rationalized in terms of localized orbitals derived using the PM3 semi-empirical SCF–MO method. Two localized orbitals which correspond to an S—S single bond and to one of the two lone pairs on X can be identified when the bridging group is associated with six valence electrons ($X = N^-$, S). In contrast, two valence isomers are found for the four electron substitutents ($X = N^+$, P^+, C, Si, B^- and Al^-) which differ in having *either* an S—S bond (the closed form) *or* a lone pair on X (the open form). As the electronegativity of X decreases, the closed form is increasingly favoured in energy, being the lowest energy isomer for $X = B^-$, Al^- or Si. Unusual structures with X = Si and Al^- in particular are predicted.

In both the gas and the solid state, tetrasulphur tetranitride (S_4N_4) exists in a cage geometry of D_{2d} symmetry, involving a square-planar arrangement of nitrogen atoms and an approximately tetrahedral arrangement of sulphur atoms exhibiting significant S—S bonding interactions.[1] The bonding in S_4N_4 specifically has been discussed in many papers, of which a particularly appropriate explanation involving a localized orbital approach is that due to Gopinathan and Whitehead,[2] and subsequently discussed by Palmer.[3] A related series of cage molecules S_4N_4X is known[1] which can be considered to be derived from S_4N_4 by bridging one of the two S···S bonds with $X = N^-$, N_2S or N^+. In these compounds, the remaining S—S bonding interaction is retained with the first two substituents but is entirely lost with $X = N^+$. In this paper, we extend such an approach to these cage systems, employing the PM3 semi-empirical SCF–MO method,[4] and investigating a range of four and six electron substituents X.

RESULTS AND DISCUSSION

A number of theoretical analyses of S_4N_4 and related molecules have been reported at *ab initio* and semi-empirical SCF–MO levels.[2,3] Gopinathan and Whitehead[2] were the first to analyse an SCF–MO wavefunction in terms of localized orbitals using the CNDO–BW method and similar subsequent calculations at the *ab initio* level gave essentially the same result.[3] These studies established several features of the bonding in S_4N_4. Importantly, the inclusion of *d*-orbitals in the basis set was found not to be necessary unless a quantitative description of the molecular geometry is required, and would not be expected to modify any bonding scheme qualitatively.[3] Thus *s*/*p* basis orbital localization schemes indicated that of the 44 valence electrons in S_4N_4, 16 occupy the eight S—N bonds, eight correspond to sulphur lone pairs, 16 to two lone pairs each on nitrogen and four to two S—S bonds (resonance structure **1**). A further refinement which is not obvious from a resonance structure such as **1** is that the two lone pairs on nitrogen are actually quite different in character, one of these overlapping with the two adjacent sulphur atoms to give appreciable p_π–p_π S=N=S double bond character. This scheme provides a rationalization for the relatively short experimental S—S distance of 2.58 Å observed for S_4N_4.

We wished to extend this analysis to molecules of the type S_4N_4X. However, the Gopinathan and Whitehead CNDO–BW procedure was applied

* Author to whom correspondence should be addressed.

without geometry optimization, and so cannot be used to predict molecular geometries and relative enthalpies of formation of new species for which no molecular structure is available. Geometry optimization at the *ab initio* level would in turn require considerable computer resources for such species. Recently a new semi-empirical SCF–MO procedure termed PM3 has been reported[4] which is computationally much faster than the *ab initio* level and which is reported to reproduce both the energies and molecular geometries of a wide range of "hypervalent" compounds. The method represents a significant advance over older semi-empirical procedures such as MNDO, but is based only on the use of an *s/p* orbital basis set. For this reason, we wished to establish firstly that PM3 yields a similar interpretation of the bonding in S_4N_4 to that described above and, if so, to use this technique to investigate the series of cage molecules S_4N_4X.

(i) *The parent molecule* S_4N_4

At the PM3 level, the parent molecule S_4N_4 is a stable minimum with D_{2d} symmetry, the calculated Hessian matrix having only positive eigenvalues.[5] This compares with the results obtained using the earlier MNDO method, which predicted this structure not to be a stable minimum.[6] Somewhat surprisingly, the "inverse" structure in which the four nitrogen atoms are tetrahedral is 29.4 kcal mol^{-1} lower in energy using PM3, a result not obtained at, for example, the *ab initio* level.[3] This particular failing may be associated with the tendency of nitrogen in the PM3 parametrization to significantly underestimate rotational barriers in species such as amides.[5] For comparison between systems containing the same number of S—N bonds, such an error might be expected to cancel. The PM3 calculated S···S bonding and S···S edge distances for the "normal" isomer of S_4N_4 are similar to the experimental values (Table 1), with the calculated S—N distances (1.69 Å) being longer than those observed (1.59 Å), but nevertheless significantly shorter than typical calculated S—N single bond lengths.

The scheme introduced by Perkins and Stewart[7] was used to obtain localized orbitals. In this terminology, a localization index (LI) of 1.0 indicates a one-centre (lone pair) orbital, and a value of 2.0 a two-centre covalent bond. Our results using PM3 are in complete agreement with earlier treatments,[2,3] showing S_4N_4 to have one lone pair orbital localized almost entirely (LI $\leqslant$ 1.11) on each of the S and N atoms and eight S—N covalent σ type orbitals (LI $\sim$ 2.1). Four of the remaining 12 electrons are associated with two S—S localized orbitals (LI $\sim$ 2.1). The last eight electrons correspond to four further nitrogen lone pairs, but with a value of the localization index (1.37) that indicates significant π type interactions with *two* adjacent sulphur atoms and hence partial p_π–p_π S=N=S bonding. A σ/π partitioning of the PM3 wavefunction[5] also confirms this result, with predicted S—N π bond orders of 0.24. The associated short S—S distance is due to compression by the SNS unit, rather than to specific S—S bonding.

(ii) *The six electron groups* $X = N^-$, S, N_2S

The predicted PM3 structures for S_4N_4X also reproduce the known trends in bond lengths (Table 1). With $X = N^-$ and particularly for N_2S, shorter S···S distances than in S_4N_4 are predicted. The largest discrepancy with experiment is for $X = N^-$, where all six S—S edges are known to have similar lengths, whereas the calculation predicts two sets of values differing by 0.43 Å. Localized orbital analysis of these systems for the six electron substituents, $X = N^-$, S and N_2S, reveals in each case one S—S localized orbital of the type found for S_4N_4 and π

Table 1. Calculated PM3 properties for S_4N_4 and S_4N_4X

X	None	N^+	N^-	S	N_2S
ΔH_f[a]	81.0	268.4	−14.3	85.5	70.3
S—S[b]	2.638 (2.58)	4.393 (4.01)	2.492 (2.73)	2.480	2.430 (2.43)
S—S_{edge}[c]	2.878 (2.69)	3.077 (2.81)	2.923 (2.71)	2.966	3.007
Localized Orbital[d]	1.375 (85.0)	1.866 (68.5)	1.221 (90.4)	1.262 (88.9)	1.259 (89.0)

[a] Standard calculated heat of formation, in kcal mol^{-1}.

[b] S—S distance, in Å. Experimental values are given in parentheses.

[c] Length of other edge in S_4 unit.

[d] Localization index of highest energy localized orbital.[7] Percentage contribution from nitrogen is given in parentheses.

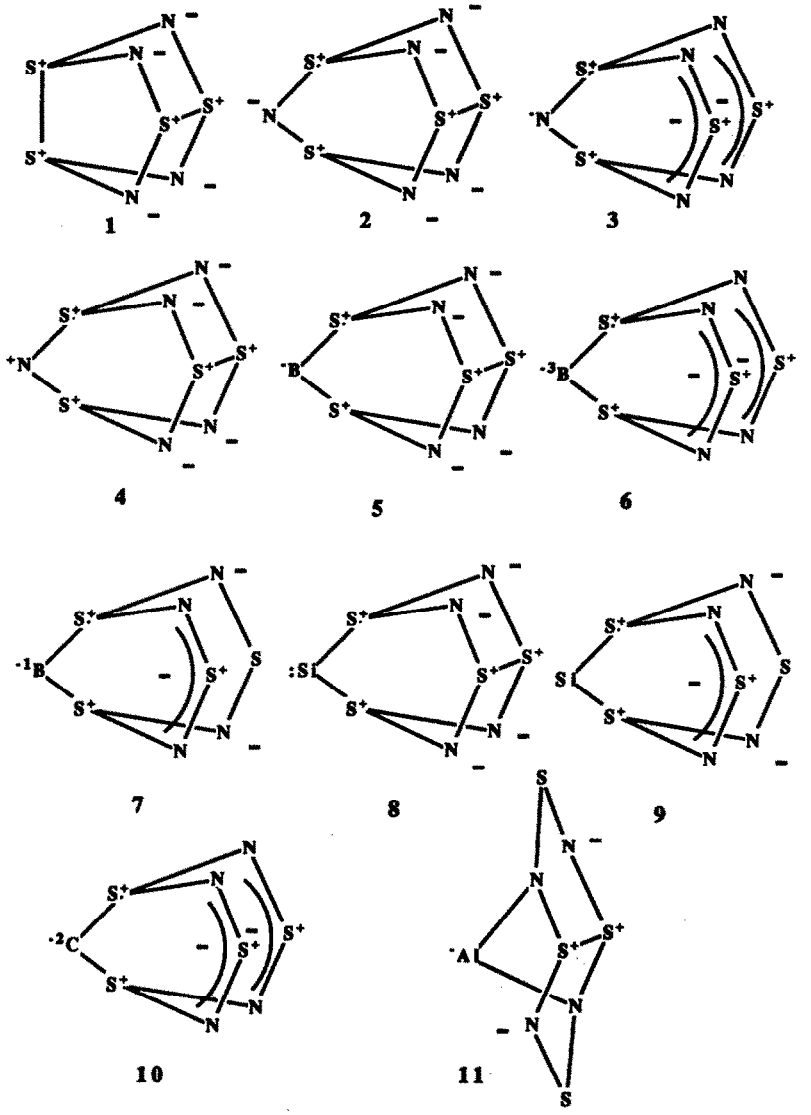

type lone pairs on each nitrogen atom, as well as two lone pairs (for $X = N^-$) for the bridging group. This corresponds approximately to resonance structure **2**. The six electrons associated with, for example, $X = N^-$, plus the two electrons from the adjacent S—S bond result in eight valence electrons for group X, leaving the remaining S—S bond intact.

(iii) *The four electron groups* $X = N^+$, P^+, C, Si, B^-, Al^-

For the known substitutent $X = N^+$, the S—S bond length is correctly predicted to correspond to a long non-bonding interaction (Table 1). Unlike $X = N^-$, no S—S localized orbital is revealed with $X = N^+$ and what were largely four nitrogen lone pairs in S_4N_4 become essentially four two-centre orbitals (LI = 1.87) corresponding to S=N π bonds (Table 1). These S—N bonds are calculated (1.60 Å) to be significantly shorter than the length in S_4N_4 itself. As with $X = N^-$, a localized lone pair on the bridging "N^+" substituent is found and the bonding can be approximated by **3**. Electron counting indicates that the N^+ substituent has only four valence electrons, which together with the two electrons from the adjacent S—S bond would give a bridging six electron nitrenium ion. The electronegativity of such a group is clearly greater than that of the remaining S—S bond, and hence the two electrons associated with this bond are transferred to the N^+ to increase the valence electrons of X to eight. The S—S region no longer has two associated electrons, and the resultant S—S bond length is typical of a non-bonding interaction.

This analysis raises the possibility that these two electrons may partition either on group X, or between the S—S region, but not both! We were indeed able to locate a series of second stationary points for a range of four electron groups (Fig. 1).

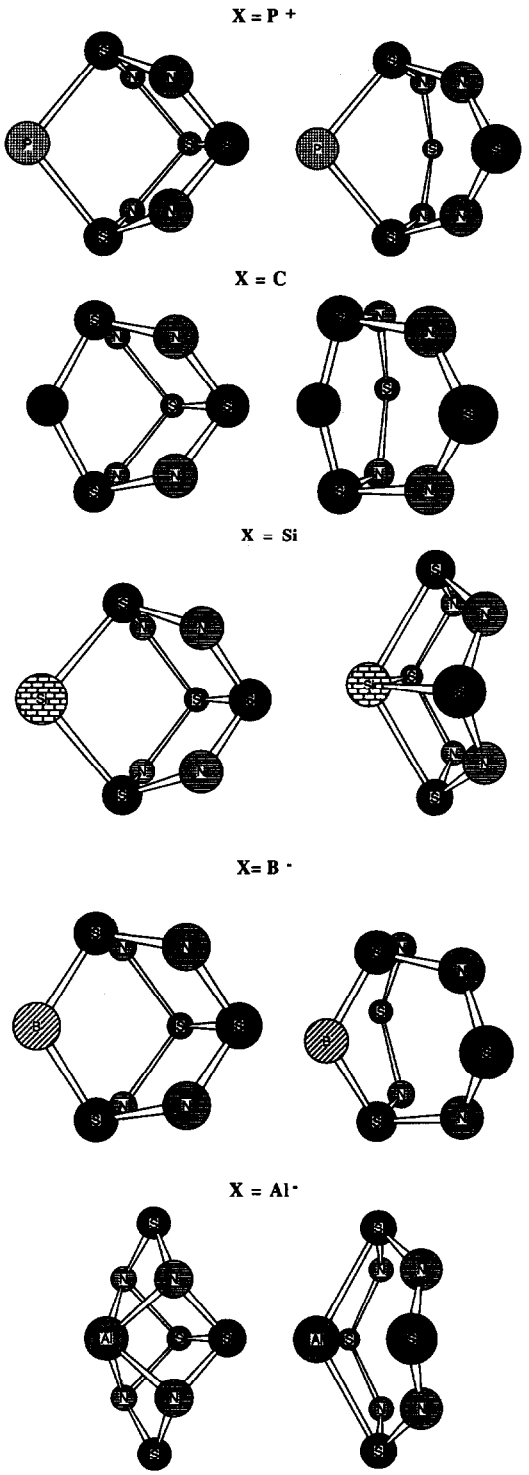

Fig. 1. Structural forms of the cyclic systems S_4N_4X.

That for $X = N^+$ (Table 2) has localized orbitals which show the presence only of an S—S single bond and no second nitrogen lone pair. However, the energy of this "closed" valence isomer is sufficiently high that it is unlikely to be experimentally accessible. This does raise the possibility that less electronegative bridging groups than N^+ might result in the alternative valence isomers being more stable. For example, the analogue $X = P^+$ shows a much smaller energy difference between the two valence isomers (Table 2). With the isoelectronic group $X = B^-$, the stability reverses completely, and the isomer **5** containing an S—S bond is predicted to be *more* stable than the open form. If the analogy with $X = N^+$ were to be followed, this open form would have a formal 3^- charge on the boron as in **6**. However, the localized orbitals show not two but *one* lone pair on boron, corresponding to the alternative resonance form **7**. No minimum corresponding to **6** could be located. Indeed the calculated boron charge for **7** reveals only a small negative value (−0.33). Presumably, the low nuclear charge on boron cannot compensate for the considerable electron repulsion resulting from two adjacent lone pairs in **6**. A similar situation is predicted for the neutral group X = Si, where the closed form **8** is closely analogous to divalent silylene systems, and represents an interesing candidate for isolation. The open form with X = Si has only one localized lone pair giving a formally six electron silicon species. However, the structure of this open form is quite different from the B^- analogue (Fig. 1), with four equal weak ($r_{Si—S}$ 2.47 Å) bonds predicted to each sulphur atom and overall four-fold symmetry corresponding to two or more equal contributions from resonance forms such as **9**. With the substituent X = C, the closed isomer is in fact the high energy form, consistent with the known relative instability of carbenes relative to the silylenes. The open isomer in this case actually corresponds to an eight electron carbon, with a calculated charge on this atom of −1.80 and, as such, is unlikely to represent an isolable species. The Al^-

Table 2. Relative PM3 calculated energies of open and closed forms for S_4N_4X with four electron bridging groups X

X	ΔH_{Closed}[a]	ΔH_{Open}[b]
N^+	98.7 (2.65)	0.0 (4.39) [268.4]
P^+	32.4 (2.54)	0.0 (4.36) [293.1]
C	49.6 (2.50)	0.0 (4.35) [142.1]
Si	−7.8 (2.44)	0.0 (4.24) [118.4]
B^-	−7.8 (2.45)	0.0 (4.67) [62.2]
Al^-	−7.3 (2.44)	0.0 (4.39) [−81.4]

[a] Energy relative to open form, in kcal mol^{-1}. The S—S bond distances are given in parentheses in Å.

[b] Enthalpy of formation of open isomer in square brackets.

homologue has a similar electronic structure for the open form, with a calculated charge of −1.25 on Al. The closed isomer however adopts another unique geometry, with four equal Al—N bonds (2.017 Å) corresponding to an average of resonance forms such as **11**.

In conclusion, we have shown that analysis of the unusual bonding in these types of third period caged compounds, using a combination of the PM3 SCF–MO procedure and orbital localization schemes, can result in valuable insight into the bonding of such species and the prediction of unusual geometries for several of the substituents.

Acknowledgement—We thank the SERC for the award of a grant for graphics equipment, including a Vaxstation 3200, on which all the calculations were performed.

REFERENCES

1. J. D. Woollins, *Non Metal Rings, Cages and Clusters*. Wiley, Chichester (1988).
2. M. S. Gopinathan and M. A. Whitehead, *Can. J. Chem.* 1975, **53**, 1343.
3. (a) R. H. Findlay, M. H. Palmer, A. J. Downes, R. G. Egdell and R. Evans, *Inorg. Chem.* 1980, **19**, 1307; (b) See R. G. Haddon, S. R. Wasserman, F. Wudl and G. R. J. Williams, *J. Am. Chem. Soc.* 1980, **102**, 6687 for a discussion of the role of *d* functions in *ab initio* calculations on hypervalent sulphur species.
4. J. J. P. Stewart, *J. Comp. Chem.* 1989, **10**, 209, 221.
5. J. J. P. Stewart, MOPAC 5.0 program system; Quantum Chemistry Program Exchange, Bloomington, Indiana (1989). For a comprehensive discussion of the MOPAC program system, including a definition of all terms in the Hamiltonian and PM3 parameter sets, see J. J. P. Stewart, *J. Comp. Aided Molec. Design* (1989), in press. Molecular structures were drawn using the Chem3D program available for a Macintosh computer from Cambridge Scientific Computing, using a locally written interface from MOPAC.
6. P. J. Dunn and H. S. Rzepa, *J. Chem. Soc., Perkin Trans. 2* 1987, 1669; for other applications of the MNDO procedure to analysis of bonding in S—N systems, see H. S. Rzepa and J. D. Woollins, *J. Chem. Soc., Dalton Trans.* 1988, 3051; R. M. Bannister and H. S. Rzepa, *J. Chem. Soc., Dalton Trans.* 1989, 1609.
7. P. G. Perkins and J. J. P. Stewart, *J. Chem. Soc., Faraday Trans. 2* 1982, **78**, 285; see also T. A. Modro, H. S. Rzepa and J. Symes, *J. Chem. Soc., Perkin Trans. 2* 1987, 767 for a MNDO application of this localization scheme to transition state bonding.

Polyhedron Vol. 9, No. 1, pp. 113–118, 1990
Printed in Great Britain

0277–5387/90 $3.00+.00
© 1989 Pergamon Press plc

KINETICS OF OXIDATION OF ASCORBIC ACID BY OCTACYANOMOLYBDATE(V) IN AQUEOUS METHANOL—A COMPARATIVE STUDY

R. A. EL-ZARU* and H. A. HODALI

Department of Chemistry, Faculty of Science, University of Jordan, Amman, Jordan

(*Received* 24 *April* 1989; *accepted* 17 *August* 1989)

Abstract—The oxidation of ascorbic acid (AH_2) by octacyanomolybdate(V) in a buffered acidic aqueous methanolic medium has been studied and compared with that of hexacyanoferrate(III) and octacyanotungstate(V). The reaction has been found to be first-order with respect to both oxidant concentration and ascorbic acid concentration. The dependence on acidity suggested a rate law of the form:

$$-d[OX]/2dt = (k_a + k_b/[H^+])[OX][AH_2],$$

where k_a is the rate constant of the reaction with molecular ascorbic acid and approximately equals zero for $[Fe(CN)_6]^{3-}$ and $[W(CN)_8]^{3-}$ and k_b is the rate constant of the reaction with the ascorbate anion. The rate measurements for the three oxidants were used to calculate the entropies and enthalpies of activation. The differences in the rates of oxidation of ascorbic acid by the three oxidants, which are in the order $Mo^V \gg Fe^{III} > W^V$, are discussed.

The oxidation of ascorbic acid (AH_2), to dehydroascorbic acid (A), has been the subject of interest for many years.[1–6] With its 1,2-enediol group, ascorbic acid is a powerful reducing agent and is widely used as a reductometric reagent in the titration of various oxidants:

$$AH_2 + 2[OX] \rightarrow A + 2H^+ + 2[RED].$$

On the other hand, many methods for the quantitative determination of ascorbic acid by a variety of oxidizing agents have been described.[7–11] Particular interest has been devoted to the use of potassium hexacyanoferrate(III) in the oxidimetric determination of ascorbic acid in acidic, neutral, and alkaline media.[12] In line with our interest in the kinetics of the oxidation of acyloins (1,2-enediol),[13–15] this kinetic study has been undertaken to compare the rates of oxidation of ascorbic acid with the cyano complexes of Mo^V, Fe^{III} and W^V in acidic aqueous methanol medium. The study is an attempt to obtain additional information about the mechanism, thermodynamic and reactivity parameters of the reactions of these oxidants with ascorbic acid. This might help the selection and choice of the optimum conditions in the use of these cyano complexes in the titrimetric determination of ascorbic acid and other related compounds.

EXPERIMENTAL

Materials

The L-ascorbic acid and $K_3Fe(CN)_6$ used in this investigation were B.D.H. Analar grade and were used without further purification. The cyano complexes, $K_4W(CN)_8 \cdot 2H_2O$, $K_4Mo(CN)_8 \cdot 2H_2O$,[16] $Cs_3W(CN)_8 \cdot 2H_2O$ and $Cs_3Mo(CN)_8 \cdot 2H_2O$[17] were prepared by literature methods. The latter were pure after only one crystallization and were used as primary standards. Analytical grade reagents and doubly distilled water were used throughout the measurements. The aqueous methanolic solutions of ascorbic acid and the oxidizing agent were freshly prepared and bubbled with purified nitrogen for a period of 10 min before use. The desired buffer solutions for varying the pH of the reaction medium were prepared by mixing suitable

* Author to whom correspondence should be addressed.

volumes of 0.05 M potassium hydrogen phthalate and 0.1 M HCl (pH = 2.2–3.0) or 0.2 M KCl and 0.2 M HCl (pH = 1.0–1.6). The pH was measured with a Metrohm 632 pH meter. The measured pHs were corrected for 50% v/v aqueous methanol using the relationship:[18] $pH_{corr.} = pH_{meas.} + 0.08$.

Kinetic measurements

The reactions were carried out in buffered acidic aqueous methanol (50% v/v) using a thermostatted bath to regulate the temperature to ±0.2°C. The ionic strength was adjusted to a constant value of 0.06 M (for $K_3Fe(CN)_6$ and $Cs_3W(CN)_8 \cdot 2H_2O$) or 0.12 M (for $Cs_3Mo(CN)_8 \cdot 2H_2O$) by the addition of NaCl. The progress of the reaction was followed by measuring the absorbance (A_t) of the unconsumed $[Mo(CN)_8]^{3-}$, $[Fe(CN)_6]^{3-}$ and $[W(CN)_8]^{3-}$ at 390, 420 and 357 nm, respectively. The experiments were carried out with a thermostatted Unicam SP8-500 spectrophotometer. Solutions of ascorbic acid and the cyano complexes were protected from light during the preparation and kinetic measurements.

Stoichiometry

By maintaining stoichiometric amounts (1 : 2) of ascorbic acid and the oxidizing agent and performing spectrophotometric measurements at the proper wavelength, the following stoichiometric equation[19] was found to hold for the three oxidants:

$$H_2A + 2[M(CN)_n]^{3-} = A + 2[M(CN)_n]^{4-} + 2H^+.$$

Where $n = 6$, M = Fe; $n = 8$, M = Mo or W. The dehydroascorbic acid was identified by TLC as the final product.

RESULTS AND DISCUSSION

The oxidation of ascorbic acid was investigated at a constant concentration of hydronium ion and at a constant ionic strength. The concentration of the oxidants $[Mo(CN)_8]^{3-}$, $[Fe(CN)_6]^{3-}$ and $[W(CN)_8]^{3-}$ were kept constant at 1.0×10^{-3} M while ascorbic acid concentrations were varied to fulfil pseudo first-order conditions. The results for the three oxidants are shown in Table 1 and pseudo first-order plots for $[Mo(CN)_8]^{3-}$ are linear to about 80% of the reaction (Fig. 1). Similar plots were obtained for $[Fe(CN)_6]^{3-}$ and $[W(CN)_8]^{3-}$.

Absorption measurements carried out at stoichiometric amounts of the reactants ($[OX]^{3-}$: $[H_2A] = 2:1$) and at different pH values are shown in Table 2. The second-order plots for $[Mo(CN)_8]^{3-}$ are also linear for about 80% completion (Fig. 2), thus confirming a first-order dependence on both reactants. Similar plots were also obtained for $[Fe(CN)_6]^{3-}$ and $[W(CN)_8]^{3-}$. The second-order rate constant (k') has been found to depend on $[H^+]$ (Table 2). It is found that k' decreases with increasing acidity (other variables were constant). Plots of k' vs $1/[H^+]$ are straight lines (Fig. 3) with a positive intercept in the case of $[Mo(CN)_8]^{3-}$ and almost with zero intercept in the cases of both $[Fe(CN)_6]^{3-}$ and $[W(CN)_8]^{3-}$.

From these results, the reaction of ascorbic acid with the cyano complexes under study, in buffered 50% v/v aqueous methanol is considered to proceed via two parallel pathways and the overall mechanism for the reaction can be represented by eqs (1)–(4):

$$AH_2 \overset{K_1}{\rightleftharpoons} AH^- + H^+ \quad (1)$$

$$AH_2 + [OX]^{3-} \xrightarrow{k_2} AH\cdot + [OX]^{4-} + H^+ \quad (2)$$

Table 1. Observed rate constants for the oxidation of ascorbic acid[a]

	$[Mo(CN)_8]^{3-}$[b]		$[Fe(CN)_6]^{3-}$[c]		$[W(CN)_8]^{3-}$[c]	
$10^3\,[AH_2]$	$10^3\,k_1$ (s^{-1})	$k'_1 = k_1/[AH_2]$ ($M^{-1}\,s^{-1}$)	$10^3\,k_1$ (s^{-1})	$k'_1 = k_1/[AH_2]$ ($M^{-1}\,s^{-1}$)	$10^3\,k_1$ (s^{-1})	$k'_1 = k_1/[AH_2]$ ($M^{-1}\,s^{-1}$)
2.00	3.68	1.84	—	—	—	—
3.00	5.50	1.83	2.25	0.750	1.72	0.572
4.00	7.25	1.81	3.02	0.753	2.30	0.575
5.00	9.25	1.85	3.83	0.766	2.87	0.573
6.00	—	—	4.58	0.763	3.47	0.578
Average		1.83 ± 0.02		0.758 ± 0.008		0.575 ± 0.003

[a] $[Mo(CN)_8^{3-}] = [Fe(CN)_6^{3-}] = [W(CN)_8^{3-}] = 1.0 \times 10^{-3}$ M, $t = 10$°C.
[b] $[H^+] = 1.0$ M, $I = 0.12$ M.
[c] pH = 2.2, $I = 0.06$ M.

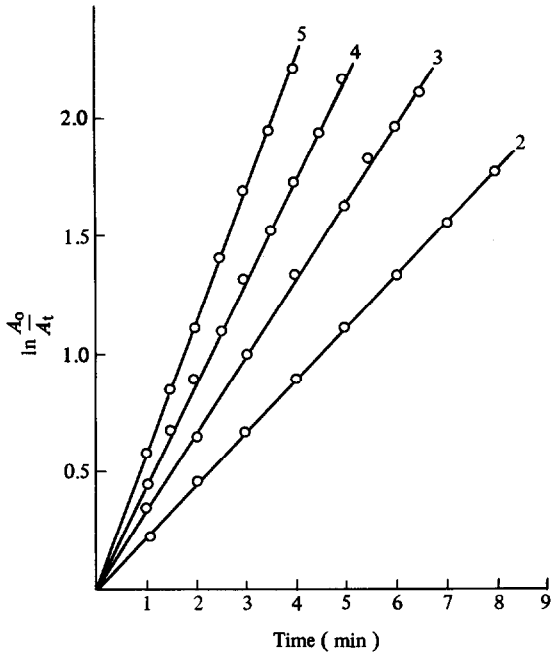

Fig. 1. Plots of $\ln(A_o/A_t)$ vs time for the oxidation of ascorbic acid by $[Mo(CN)_8]^{3-}$ at different concentrations of ascorbic acid.

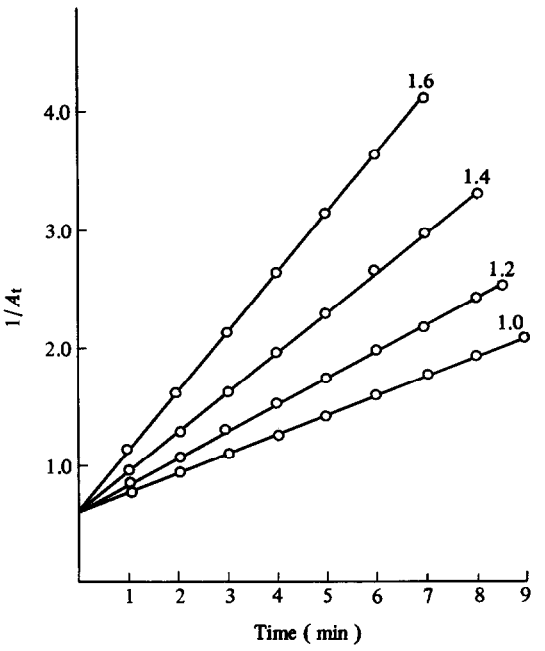

Fig. 2. Plots of $(1/A_t)$ vs time at different pH values. Acid dependence of oxidation of ascorbic acid by $[Mo(CN)_8]^{3-}$.

$$AH^- + [OX]^{3-} \xrightarrow{k_3} AH\cdot + [OX]^{4-} \quad (3)$$

$$AH\cdot + [OX]^{3-} \xrightarrow{\text{fast}} A + [OX]^{4-} + H^+. \quad (4)$$

In view of the above scheme and assuming a stationary steady-state condition for the radical, the following rate law can be readily derived.

$$-d[OX^{3-}]/2dt = (k_2 + K_1k_3/[H^+])[AH_2][OX^{3-}] \quad (5)$$

and

$$-d[OX^{3-}]/dt = (k_a + k_b/[H^+])[AH_2][OX^{3-}] \quad (6)$$

$$= (k_a + k')[AH_2][OX^{3-}], \quad (7)$$

where

$$k' = k_b/[H^+]$$

and

$k_a = 0$ for $[Fe(CN)_6]^{3-}$ and $[W(CN_8]^{3-}$.

From plots of k' vs $1/[H^+]$ (Fig. 3) the values of k_b at constant temperature (15°C) and constant ionic strength (0.06 M for $[Fe(CN)_6]^{3-}$ and $[W(CN)_8]^{3-}$; 0.12 M for $[Mo(CN)_8]^{3-}$), are:

$$k_b([Mo(CN)_8]^{3-}) = 0.310\ s^{-1}$$

$$*k_b([Mo(CN)_8]^{3-})_{corr.} = 0.258\ s^{-1}$$

$$k_b([Fe(CN)_6]^{3-}) = 4.97 \times 10^{-3}\ s^{-1}$$

$$*k_b([Fe(CN)_6]^{3-})_{corr.} = 4.17 \times 10^{-3}\ s^{-1}$$

$$k_b([W(CN)_8]^{3-}) = 2.87 \times 10^{-3}\ s^{-1}$$

$$*k_b[W(CN)_8]^{3-})_{corr.} = 2.42 \times 10^{-3}\ s^{-1}.$$

The first dissociation constant[19] of ascorbic acid (K_1) corrected for 50% v/v aqueous methanol at 15°C was found to be 6.7×10^{-5} and 6.9×10^{-5} M at $I = 0.06$ and 0.12 M, respectively. Therefore,

$$k_3([Mo(CN)_8]^{3-}) = 1.58 \times 10^4\ M^{-1}\ s^{-1}$$

$$k_3([Fe(CN)_6]^{3-}) = 2.63 \times 10^2\ M^{-1}s^{-1}$$

$$k_3([W(CN)_8]^{3-}) = 1.53 \times 10^2\ M^{-1}s^{-1}.$$

The variation of rate constant with ionic strength was investigated in the presence of NaCl and for a range of ionic strengths (from $I = 1.0$–1.3 M for $[Mo(CN)_8]^{3-}$ and $I = 0.06$–0.12 M for $[Fe(CN)_6]^{3-}$ and $[W(CN)_8]^{3-}$). Plots of $\log k'$ vs $\sqrt{I}$ for the above three oxidants are straight lines with slopes of +2.6, +3.0 and +1.7, respectively. Thus the addition of neutral salts accelerates the rate of the reaction and

* Corrected for the pH measured in 50% v/v aqueous methanol.

Table 2. Acidic dependence of oxidation of ascorbic acid[a]

1/[H⁺]	$[Mo(CN)_8]^{3-}$[b] k' ($M^{-1}s^{-1}$)	$[Fe(CN)_6]^{3-}$[c] k' ($M^{-1}s^{-1}$)	$[W(CN)_8]^{3-}$[c] k' ($M^{-1}s^{-1}$)
10.00	4.35	—	—
15.85	6.00	—	—
25.12	9.05	—	—
39.81	13.8	—	—
1.59×10^{2}	—	0.412	0.320
2.51×10^{-2}	—	0.978	0.623
3.98×10^{-2}	—	1.50	—
5.01×10^{-2}	—	—	1.35
6.31×10^{-2}	—	2.79	—
7.08×10^{-2}	—	—	1.87
1.00×10^{-3}	—	4.61	2.77

[a] $[Mo(CN)_8^{3-}] = [Fe(CN)_6^{3-}] = [W(CN)_8^{3-}] = 1.0\times10^{-3}$ M, $[AH_2] = 5.0\times10^{-4}$ M, $t = 15°C$, k' values are obtained from plots of $1/A_t$ vs time.
[b] $I = 0.12$ M.
[c] $I = 0.060$ M.

Table 3. Ionic strength dependence[a]

I (M)	$[Mo(CN)_8]^{3-}$[b] $10^3 k_1$ (s^{-1})	$[Fe(CN)_6]^{3-}$[c] $10^3 k_1$ (s^{-1})	$[W(CN)_8]^{3-}$[d] $10^3 k_1$ (s^{-1})
0.060	—	2.15	1.72
0.080	—	2.78	2.00
0.100	—	3.50	2.28
0.120	—	4.28	2.57
1.00	5.50	—	—
1.10	7.50	—	—
1.20	9.53	—	—
1.30	12.6	—	—

[a] $[Mo(CN)_8^{3-}] = [Fe(CN)_6^{3-}] = [W(CN)_8^{3-}] = 1.0\times10^{3}$ M, $[AH_2] = 3.0\times10^{-3}$ M, $t = 10°C$.
[b] $[H^+] = 1.0$ M, $\Delta\log k/\Delta\sqrt{I} = 2.60$.
[c] pH = 2.2, $\Delta\log k/\Delta\sqrt{I} = 2.96$.
[d] pH = 2.2, $\Delta\log k/\Delta\sqrt{I} = 1.72$.

indicates a positive salt effect. A slope of +3.0 for $[Fe(CN)_6]^{3-}$ confirms that the reaction takes place through the interaction of a −3 and −1 charged species.[20] However, in the case of $[Mo(CN)_8]^{3-}$ and $[W(CN)_8]^{3-}$, slopes of +2.6 and +1.7 indicate the formation of ion-pairing[21] such as $Na_n[M(CN)_8]^{n-3}$ ($n = 0.4$, M = Mo; $n = 1.3$, M = W) in the activated complex.

Reactions were investigated at 5, 10, 15 and 20°C at 5:1 molar ratios of ascorbic acid to oxidant, constant pH (2.2) and constant ionic strength. From the observed data, enthalpies and entropies of activation were obtained (Table 4) using Eyring's equation, from plots of $-\log k/T$ vs $1/T$, where k is the pseudo first-order rate constant (Fig. 4). Values of $\Delta H^{\ddagger}$ and $\Delta S^{\ddagger}$ were obtained from the slopes and intercepts, respectively.

The rate of oxidation of ascorbic acid with $[Mo(CN)_8]^{3-}$ has been found to be exceptionally faster than that with $[Fe(CN)_6]^{3-}$ or $[W(CN)_8]^{3-}$ under similar conditions. The calculated relative rates of the three oxidants at pH = 2.2, $I = 0.06$ M,

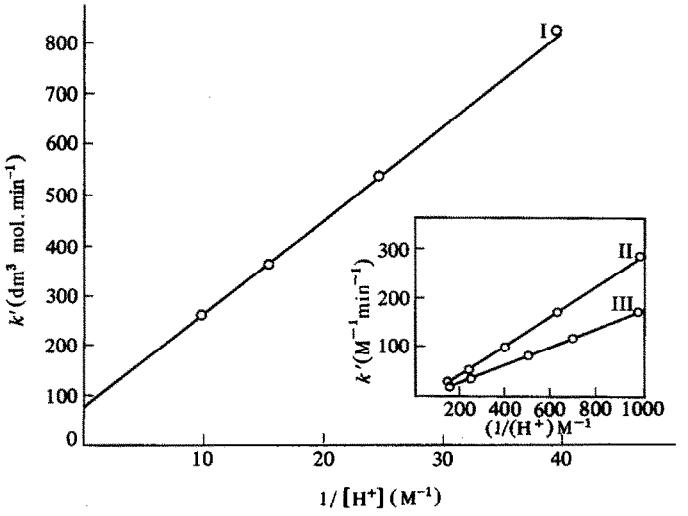

Fig. 3. Plots of k' vs $1/[H^+]$ for the oxidation of ascorbic acid by $[Mo(CN)_8]^{3-}$ (I), $[Fe(CN)_6]^{3-}$ (II) and $[W(CN)_8]^{3-}$ (III).

Table 4. Rate constants at different temperatures. Enthalpies and entropies of activation (average values)[a]

Complex	k_1 (min^{-1})	$10^3 k_1$ (s^{-1})	t (°C)	$\Delta H^{\ddagger}$ (kJ mol^{-1})	$\Delta S^{\ddagger}$ (J K^{-1} mol^{-1})
$[Mo(CN)_8]^{3-}$[b]	0.254	4.23	5	33.0	−111
	0.333	5.55	10		
	0.433	7.22	15		
	0.556	9.26	20		
$[Fe(CN)_6]^{3-}$[c]	0.0920	1.53	5	41.5	−105
	0.129	2.15	10		
	0.178	2.97	15		
	0.248	4.14	20		
$[W(CN)_8]^{3-}$[c]	0.0750	1.25	5	36.7	−102
	0.101	1.68	10		
	0.135	2.25	15		
	0.184	3.07	20		

[a] $[Mo(CN)_8^{3-}] = [Fe(CN)_6^{3-}] = [W(CN)_8^{3-}] = 1.0 \times 10^{-3}$ M, $[AH_2] = 5.0 \times 10^{-4}$ M.
[b] $[H^+] = 1.0$ M, $I = 1.0$ M.
[c] pH = 2.2, $I = 0.060$ M.

and 15°C are:

$$k'(M^{-1}s^{-1}) = \underset{27.5}{[Mo(CN)_8]^{3-}} \gg \underset{0.412}{[Fe(CN)_6]^{3-}} > \underset{0.320}{[W(CN)_8]^{3-}}.$$

The high reactivity of $[Mo(CN)_8]^{3-}$ could be explained in view of the following facts. First, the ability of $[Mo(CN)_8]^{3-}$ to oxidize both the ascorbate monoanion (AH^-) and the undissociated ascorbic acid (AH_2) as shown clearly in the plot of k' vs $1/[H^+]$ (Fig. 3). In this figure straight lines are obtained with intercepts close to zero in the case of $[Fe(CN)_6]^{3-}$ and $[W(CN)_8]^{3-}$ but with a positive intercept in the case of $[Mo(CN)_8]^{3-}$. This is also consistent with the higher reduction potential[3] of $[Mo(CN)_8]^{3-}$ compared with $[Fe(CN)_6]^{3-}$ or $[W(CN)_8]^{3-}$.

The second factor seems to be the closest

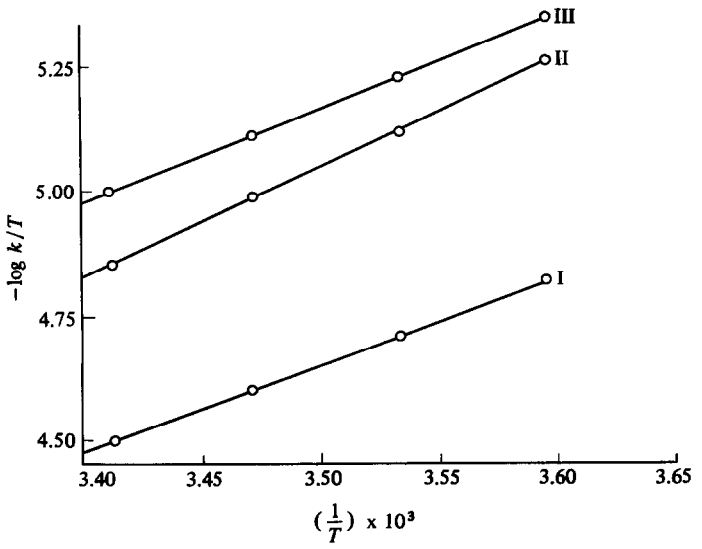

Fig. 4. Plots of $-\log k/T$ vs $(1/T)$ for $[Mo(CN)_8]^{3-}$ (I), $[Fe(CN)_6]^{3-}$ (II) and $[W(CN)_8]^{3-}$ (III).

approach between the reacting species in the activated complex. This is shown by the values of $\Delta S^{\ddagger}$, with $[Mo(CN)_8]^{3-}$ having the most negative value. Also, in favour of the highest reactivity for $[Mo(CN)_8]^{3-}$ is the smallest value of $\Delta H^{\ddagger}$ (Table 4).

Acknowledgement—The financial support of the Department of Graduate Studies and Research, University of Jordan, is acknowledged.

REFERENCES

1. L. Erdey and C. Svehla, *Chemist Analyst* 1963, **52**, 24.
2. A. G. Lappin, M. C. M. Laranjira and L. Youde-Owei, *J. Chem. Soc., Dalton Trans.* 1981, 721.
3. E. Pelizzetti, E. Mentasti and E. Pramauro, *Inorg. Chem.* 1978, **17**, 1181.
4. E. Pelizzetti, E. Mentasti and E. Pramauro, *Inorg. Chem.* 1976, **15**, 2898.
5. V. S. Mehrotra, M. C. Agrawal and S. P. Mushran, *J. Phys. Chem.* 1969, **73**, 1996.
6. M. M. Taqui Khan and A. E. Martell, *J. Am. Chem. Soc.* 1969, 4668.
7. K. K. Verma, A. Jain and R. Rawat, *J. Ass. Off. Analyt. Chem.* 1984, **67**, 262.
8. K. K. Verma, *Talanta* 1982, **29**, 41.
9. K. K. Verma and A. K. Gulati, *Analyt. Chem.* 1980, **52**, 2336.
10. A. Srivastava and S. Rose, *Talanta* 1977, **24**, 517.
11. D. Gupta, P. D. Sharma and Y. K. Gupta, *Talanta* 1975, **22**, 913.
12. G. S. Sastry and G. G. Rao, *Talanta* 1971, **19**, 212.
13. R. A. El-Zaru and H. A. Hodali, *Dirasat* 1988, **XV**, 108.
14. R. A. El-Zaru and A. A. Jarrar, *Egypt. J. Chem.* 1977, **20**, 603.
15. A. A. Jarrar, R. A. El-Zaru and A. S. Shahin, *Arab. J. Sci. Engng* 1988, **13**, 65.
16. J. C. Leipoldt, L. D. C. Bok and P. J. Cilliers, *Z. Anorg. Allg. Chem.* 1974, **407**, 350.
17. L. D. Bok, J. G. Leipoldt and S. S. Basson, *Z. Anorg. Allg. Chem.* 1975, **415**, 81.
18. R. G. Bates and R. A. Robinson, *Chemical Physics of Ionic Solutions* (Edited by B. C. Conway), ch. 12. Wiley, New York (1964); E. Kozakoova and B. Csefalvayova, *Chem. Zvesti* 1980, **34**, 610.
19. R. A. El-Zaru and A. Jarrar, *Chem. Ind.* 1977, 741.
20. M. H. Ford-Smith and J. H. Rawsthorne, *J. Chem. Soc. A* 1969, 160.
21. J. G. Leipoldt, L. D. C. Bok, A. J. Van Wyk and C. R. Dennis, *J. Inorg. Nucl. Chem.* 1977, **39**, 2019.

Polyhedron Vol. 9, No. 1, pp. 119–124, 1990
Printed in Great Britain

0277–5387/90 $3.00+.00
© 1989 Pergamon Press plc

A STUDY OF THE REACTION BETWEEN CHROMIUM(III) HEXAAMMINE AND GLYCINE IN A MELT

PAUL O'BRIEN* and NIGEL B. SELLERS

Department of Chemistry, Queen Mary College, University of London, Mile End Road, London E1 4NS, U.K.

(*Received* 23 *June* 1989; *accepted* 17 *August* 1989)

Abstract—Powdered mixtures of glycine and $[Cr(NH_3)_6](NO_3)_3$ melt and react at temperatures between 130 and 180°C to produce a glassy, purple material $[Cr(NH_3)_3(O_2CCH_2NH_3)_3](NO_3)_3$ (**I**), which on dissolution in water, yields *fac*-$[Cr(glyO)_3]$ (**II**) as a precipitate. The initial reaction between the ammine and glycine had previously been reported to occur in the solid state. The method has been used to prepare fully deuterated **II**.

For some time we have been interested, both in the reactions of various coordination complexes in the solid state[1–4] and in the coordination chemistry of chromium(III).[5–8] We were consequently intrigued by the report of an alleged solid state reaction between powdered mixtures of glycine and $[Cr(NH_3)_6](NO_3)_3$, which could be used to prepare *fac*-tris-glycinatochromium(III)[9] and, by extension, a series of related tris-amino acidates.[10] We have re-investigated this reaction and our results show that the reaction proceeds in a melt and apparently stops after three molecules of ammonia have been lost. The dissolution in water of the glass obtained on cooling the reaction mixture leads to the precipitation of red **II**.[9] The method can be used to prepare this complex on a small scale; such syntheses are often a problem with chromium(III).[7] The procedure has been used to prepare the complex from fully deuterated glycine, which may be a useful compound for ^2H NMR studies.[11]

RESULTS AND DISCUSSION

Initial experiments and observations

Preliminary experiments rapidly confirmed that heating a 3:1 mixture of glycine and $[Cr(NH_3)_6](NO_3)_3$ (142°C, 20 min) yielded a purple material **I**. **I** was glassy on cooling to room temperature and was readily soluble in cold water. On standing overnight a precipitate of **II** was obtained. The fact that **I** appeared glassy led us to observe the course of the reaction using a hot stage microscope.

Mixtures of glycine and $[Cr(NH_3)_6](NO_3)_3$ (3:1) were prepared by direct weighing and ground for 5 min in an agate mill. On heating (*ca* 5°C min^{-1}) the mixture clearly melted at *ca* 135°C, just after the decomposition of the ammine had started. This experiment was repeated using a range of glycine to hexaammine ratios and melting was observed for compositions between 40 and 90 mol % of glycine. These results are summarized in Fig. 1 and Table 1. Clearly some kind of a reactive eutectic mixture is formed by mixtures of glycine and $[Cr(NH_3)_6](NO_3)_3$, which is surprising as both of the compounds are polar species which decompose, char (glycine) or deaminate ($[Cr(NH_3)_6](NO_3)_3$), before melting. In isothermal experiments, on the hot stage microscope, we observed that there was a slight induction time, during which some reaction occurred before melting and these results are summarized in Table 1.

Thermal studies

Thermogravimetric analysis (10°C min^{-1}, static air) of various samples of glycine and $[Cr(NH_3)_6](NO_3)_3$ confirmed that the reaction proceeded with the loss of three equivalents of ammonia under a variety of reaction conditions. Typical results are shown in Fig. 2. The reaction in the melt occurs at

* Author to whom correspondence should be addressed.

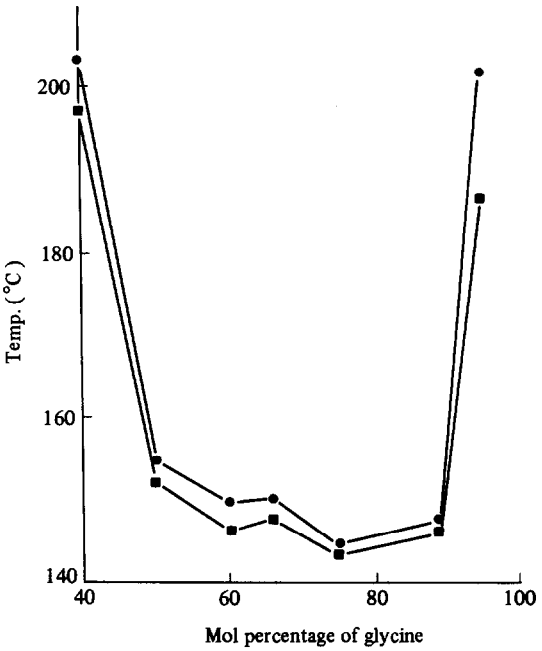

Fig. 1. Melting behaviour of various mixtures of $[Cr(NH_3)_6](NO_3)_3$ and glycine: ■ initial appearance of liquid; ● final disappearance of solid.

a lower temperature than the deammination of the hexaammine (170°C)[12] or the decomposition of glycine (245°C), when heated separately under similar conditions. Differential thermal analysis of mixtures of glycine and the hexaammine (10°C min^{-1}, static air) resulted in the traces shown in Fig. 2. Two endotherms are observed, the second of these (extrapolated onset temperature 154°C) is concurrent with the reaction in the melt. The first (extrapolated onset temperature 106°C) occurs before melting and is independent of any mass loss. This may be associated with some sintering of the fine powders of glycine and the hexaammine; no changes in the IR spectra of such samples are detected (4000–400 cm^{-1}).

Isothermal studies of the decomposition were then carried out to investigate the effect of varying the temperature and the composition of the reaction mixture on the reaction rate. The progress of the reaction was plotted as α vs time (α, fraction of reaction, $\alpha = 1$, 100% reaction, corresponding to the loss of three molecules of ammonia from each hexaammine). Figure 3 shows some typical results for various temperatures and compositions. The reaction profile is approximately linear ($0.15 > \alpha > 0.75$) and attempts to fit the whole profile to successive first-order reactions produced ill-defined results. Reaction profiles were similar at temperatures between 134 and 151°C and estimated zero-order rate constants for the reaction are summarized in Table 1. Rate constants derived from experiments under a wide range of conditions are shown on the Arrhenius plot, Fig. 4. The activation energy derived from this plot is *ca* 115 kJ mol^{-1}. The reaction of the hexaammine with alanine was exactly similar. These results indicate:

(1) a zero-order rate, relatively independent of the amino acid concentration in the melt (Table 1, 1:3–1:8 ratios of chromium complex to glycine, Fig. 4);

(2) a zero-order rate, relatively independent of the amino acid used (Table 2);

(3) a fairly high enthalpy of activation and an entropy of activation close to zero.

Taken together the results suggest that the reaction in the melt may proceed by a dissociative reaction

Table 1. Characterization of reaction in melt and zero-order rate constants

[Gly]:[Cr]	Temperature (°C)	Time to completion (10^3 s)	Time to melt (s)	% Reaction in melt	10^3k (s^{-1})
3:1	134	8.4	365	95.6	0.197
	139	5.4	260	95.2	0.240
	148	2.4	140	94.2	0.690
	159	1.02	—	—	1.618
5:1	142	2.52	240	89.5	0.544
	147	1.50	220	85.4	0.814
	153	1.02	125	87.5	1.315
8:1	141	5.04	—	—	—
	148	1.62	—	—	—
	151	1.32	—	—	—

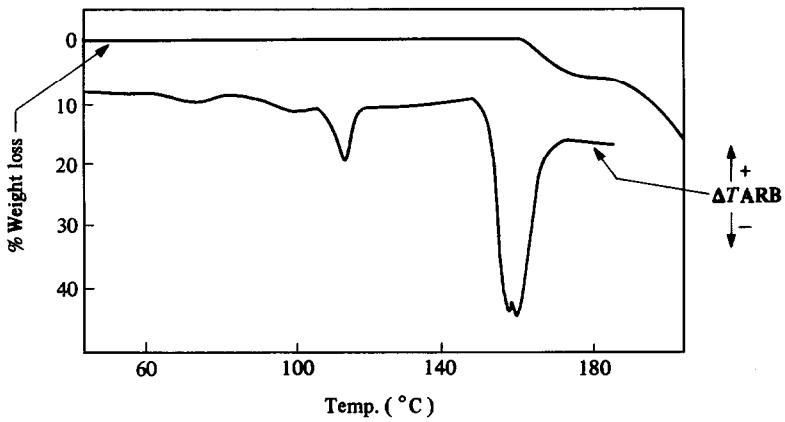

Fig. 2. Typical DTA and TGA, for a 3 : 1 [gly] : [Cr] mixture.

in which the rate-determining step is the loss of ammonia molecules from the ammine complex. Thus it resembles, in being dissociative, the reaction of glycine with $[Cr(NH_3)_5H_2O]^{3+}$, as studied by Sykes *et al.*,[13] in which water is lost dissociatively. Given the markedly different conditions of the reaction (melt vs aqueous solution) the activation parameters are remarkably similar to those for the aquopentammine, an enthalpy of activation of 106 kJ mol^{-1}, compared to our value of *ca* 115 kJ mol^{-1} and an entropy of activation close to zero (Table 2). The linearity of plots of α vs time for the majority of the reaction suggests the ammonia molecules are lost at a similar rate from each of the intermediate complexes in the reaction.

IR and electronic spectra

The IR and electronic spectra are summarized in Tables 3 and 4. The IR spectra of the mixture before heating is simply an addition of the spectra of free glycine and the hexaammine nitrate, all of the bands can be assigned by reference to the literature (Table 3). After heating, the spectrum is considerably modified. The antisymmetric stretch of the COO^- group is shifted from 1604 cm^{-1} in the mixture to 1659 cm^{-1} in the product and the new position is consistent with coordination of the carboxylate function to the metal.[14] New bands are also observed at 534, 518 and 412 cm^{-1} and may be assigned tentatively to M—O stretches.[14] The

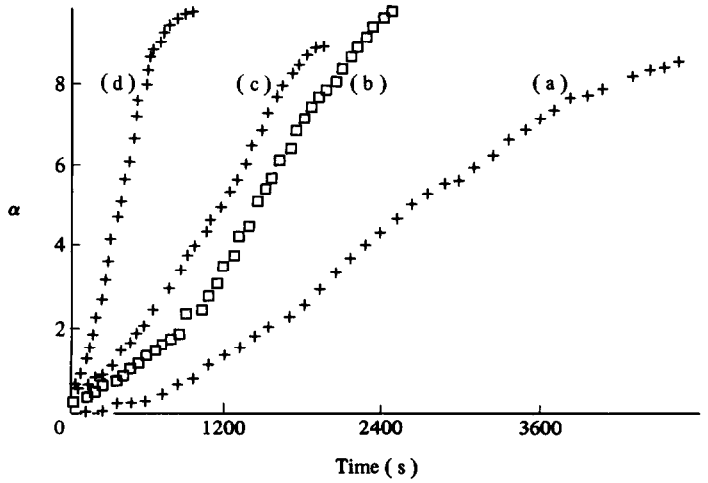

Fig. 3. Typical results of isothermal gravimetric experiments (calculated with $\alpha = 1.00$ for the loss of three mols of ammonia per hexaammine); (a) [gly] : [Cr] 3 : 1 139°C; (b) [gly] : [Cr] 3 : 1 145°C; (c) [gly] : [Cr] 3 : 1 148°C; (d) [gly] : [Cr] 5 : 1 142°C.

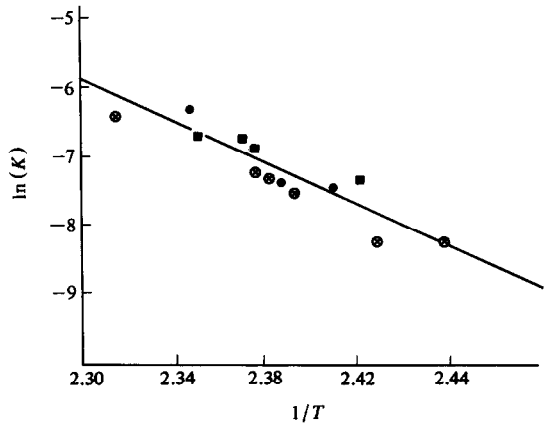

Fig. 4. Arrhenius plot of the various zero-order rate constants: ⊗ [gly]:[Cr] 3:1; ● [gly]:[Cr] 5:1; □ [gly]:[Cr] 8:1.

modes of vibration associated with the NH_3^+ of glycine remain essentially unchanged; 1587, 1142, 518 cm^{-1} (Table 3).

The electronic spectra of various complexes with chromophores from CrN_6 to CrN_3O_3 are summarized in Table 3; the lowest energy *d–d* transition ($^4A_{1g} \rightarrow {}^4T_{2g}$ in O_h symmetry) gives an approximate measure of the ligand field strength.[15] The initial product of the reaction, **I**, can be assigned as a CrN_3O_3 chromophore. The fact that the lowest energy transition is not split suggests a facial arrangement of the donor atoms.[5,16]

Taken together with the thermo-analytical results the spectroscopic data support the formulation of the intermediate as a ring open facial complex of zwitterionic glycine and chromium(III).

Preparation of deuterated $[Cr(gly)_3]$

The method proved to be a facile way of preparing fully deuterated *fac*-$[Cr(gly)_3]$ from solid D_5-glycine and the hexaammine. Small scale preparations (see Experimental) were feasible and deuteration was confirmed by IR spectroscopy.

CONCLUSIONS

The reaction between chromium hexaammine and glycine proceeds in a melt. Earlier suggestions that this was a solid state reaction are erroneous. The fact that this reaction proceeds in a homogeneous phase explains why the reaction effectively stops after the reaction of three mols of glycine with the hexaammine, i.e. at the electrically neutral N_3O_3 chromophore (the overall complex is presumably charged due to pendant $-NH_3^+$ groups). This material **I** presumably ring closes in aqueous solution to give substantial yields of the red *fac*-tris-glycinatochromium(III) complex. The method is useful for preparing this complex on a small scale and has been used to prepare the fully deuterated complex.

EXPERIMENTAL

Materials

Reagent grade D_5-glycine was purchased from Goss Chemicals, all other reagents were purchased from B.D.H. Chemicals Ltd. $[Cr(NH_3)_6](NO_3)_3$ was prepared by the literature method.[17]

Physical measurements

Electronic spectra were recorded with a Perkin–Elmer 330 spectrophotometer; IR spectra were recorded on a Mattson Polaris FT–IR spectrometer; as Nujol mulls or KBr disks (*ca* 2%, 200 mg). Thermogravimetric studies were carried out using a Stanton Redcroft TG-750 (in static air). Differential thermal analysis was undertaken using a DTA 671B, calibrated with high purity indium metal.

Table 2. Parameters derived from thermal analysis

[Gly]:[Cr]	ΔH^a (kJ mol^{-1})	E_a (kJ mol^{-1})	$\Delta H^{\ddagger b}$ (kJ mol^{-1})	$\Delta S^{\ddagger b}$ (J K^{-1} mol^{-1})
3:1	170	116 (12)	129 (11)	−1.33
5:1	—	115 (12)	113 (8)	−38.33
8:1	—	101 (40)	107 (15)	−45.64
All data	—	115 (16)	—	—
[Ala]:[Cr] 3:1	245	145 (23)	148 (19)	—

Errors are one standard deviation.

[a] Per mol of chromium(III).

[b] Calculated as described in ref. 18.

Table 3. IR spectra

Reaction mixture	Product (glass)	Assignment	Literature glycine[a] ($[Cr(NH_3)_6]$[a])
	1659	$\nu_a(COO^-)$	1610
1604	1642		
	1627	$\delta_a(NNH)$	(1630)
1526	1587	$\delta_d(NH_3^+)$	1585
1404	1406	$\nu_s(COO^-)$	1413
1383	1385	$\nu_a(NO_3^-)$	1390[b]
	1375		
	1362		
1334	1355	$\rho_w(CH_2)$	1333
1312	1312	$\delta_s(NH_3)$	(1307)
1132	1142	$\mu_r(NH_3^+)$	1131
1112	1132		1110
1034	1038	$\nu_a(CCN)$	1033
	949	$\mu_r(CH_2)$	
911	916		910
893	832	$\nu_s(CCN)$	893
	826		
758	754	$\mu_r(NH_3)$	(748)
	717		
698	694	$\mu_w(COO^-)$	694
608	668	$\delta(COO^-)$	607
504	599	$\mu_r(COO^-)$	504
	578	$\nu(MO)$	(545)
	534		
	518	$\mu_t(NH_3^+)$	516
	476	$\nu(MN)$	(495, 473, 456)
	465		
	412	$\nu(MO)$	415[a]

[a] For details of assignments see ref. 14, ν, stretching, μ_w, wagging, μ_r, rocking, μ_t, twisting, δ, in-plane bending deformation.

[b] Band due to nitrate (see ref. 19), the reference ammine spectrum is the chloride salt, see [a].

Methods

Mixtures ([gly]:[Cr], 3:1; 5:1; 8:1; and [ala]:[Cr], 3:1) were prepared by direct weighing of the components, glycine or alanine and the hexaammine. The mixture was preground in an agate mortar and ground to a fine mixture in an agate mill (Speci-Mill, Specac) for 5–10 min. This procedure led to reproducible results in kinetic and other experiments. All mixtures were used immediately and reaction was followed by thermogravimetry. In general, the mixtures used lost the equivalent of 3 mols of ammonia per mol of chromium. There was some slight evidence of further reaction in the 8:1 [gly]:[Cr] mixtures. Activation parameters were calculated as described by Edwards *et al.*[18]

Table 4. Electronic spectra[a]

Compound	Energy	
$[Cr(NH_3)_6]^{3+}$	21.6	28.3
$[Cr(NH_3)_6]^{3+}$/glycine (1:3 before heating)	21.7	28.6
Purple glass (I) (cooled to RT)	19.6	26.1
fac-$[Cr(glyO)_3]$	19.2	25.3

[a] $10^3 \times cm^{-1}$, by diffuse reflectance, for the two lowest energy bands.

Preparation of fully deuterated fac-$[Cr(gly_3)]$

$[Cr(NH_3)_6](NO_3)_3$ (0.43 g) and deuterated glycine (0.3 g) were ground together with pestle and mortar and then ground in an agate mill for 10 min.

The mixture was placed in an oven for 45 min at 135°C. The glass formed was dissolved in deuterium oxide and the solution left overnight, after which time red crystals of deuterated *fac*-[$Cr(gly)_3$] had precipitated. These were filtered off, washed with D_2O, and air dried. Yields, based on chromium, were 30–40%.

Acknowledgements—N.B.S. thanks the SERC for a research studentship. We also thank the University of London, Central Research Fund for their support of our work.

REFERENCES

1. P. O'Brien, *Polyhedron* 1983, **2**, 233.
2. P. O'Brien, *Transition Met. Chem.* 1980, **5**, 314.
3. P. O'Brien, *Inorg. Chim. Acta* 1981, **55**, L27.
4. P. O'Brien, *Polyhedron* 1986, **5**, 659.
5. M. Abdullah, J. Barrett and P. O'Brien, *J. Chem. Soc., Dalton Trans.* 1984, 1647.
6. J. Barrett, P. O'Brien and J. Pedrosa de Jesus, *Polyhedron* 1985, **1**, 4.
7. L. F. Larkworthy, K. B. Nolan and P. O'Brien, *Comprehensive Coordination Chemistry* (Edited by G. Wilkinson, R. D. Gillard and J. A. McCleverty), Chap. 35. Pergamon Press, Oxford (1987).
8. M. Abdullah, J. Barrett and P. O'Brien, *J. Chem. Soc., Dalton Trans.* 1985, 2085.
9. H. Oki and K. Otsuka, *Bull. Chem. Soc. Jpn.* 1976, **49**, 1841.
10. H. Oki, *Bull. Chem. Soc. Jpn.* 1977, **50**, 680.
11. W. D. Wheeler and J. I. Legg, *Inorg. Chem.* 1984, **23**, 3798.
12. W. W. Wendlandt and C. Y. Chou, *J. Inorg. Nucl. Chem.* 1964, **26**, 943.
13. T. Tamasami, R. S. Taylor and A. G. Sykes, *Inorg. Chem.* 1976, **15**, 2318.
14. K. Nakamoto, *Infrared And Raman Spectra of Inorganic And Coordination Compounds*, 4th edn, pp. 192, 234, and 245. John Wiley, Interscience, New York (1972).
15. R. G. Wilkins and M. G. Williams, *Modern Coordination Chemistry* (Edited by J. Lewis and R. G. Wilkins), p. 187. Interscience, New York (1960).
16. M. Watabe, H. Yano, Y. Odaka and H. Kobayashi, *Inorg. Chem.* 1981, **20**, 3623.
17. A. L. Oppegard and J. C. Bailar Jr, *Inorg. Synth.* 1950, **3**, 153.
18. J. O. Edwards, F. Monacelli and G. Ortaggi, *Inorg. Chim. Acta* 1974, **11**, 47.
19. B. M. Gatehouse, S. E. Livingstone and R. S. Nyholm, *J. Chem. Soc.* 1957, 4222.

Polyhedron Vol. 9, No. 1, pp. 125–128, 1990
Printed in Great Britain

0277–5387/90 $3.00+.00
© 1989 Pergamon Press plc

SYNTHESIS, CHARACTERIZATION AND ^{1}H NMR (EXPERIMENTAL AND THEORETICAL) SPECTRAL STUDIES OF SOME NEUTRAL AND ANIONIC COMPLEXES OF DIPHENYL TIN ISOCYANATE CHLORIDE

P. C. SRIVASTAVA,* A. TRIVEDI and P. SINGH

Chemistry Department, Lucknow University, Lucknow-226007, India

(*Received* 3 *August* 1989; *accepted* 17 *August* 1989)

Abstract—Neutral adducts and anionic complexes of $Ph_2Sn(NCO)Cl$ of the general formula $Ph_2Sn(NCO)Cl \cdot nL$ ($n = 1$, L = 2,2′-bipyridyl, Me_4NCl; $n = 2$, L = DMSO and DMF) have been isolated. These complexes have been characterized through elemental analysis, molecular weight, molar conductance, IR and ^{1}H NMR data. Experimental ^3J [$Sn^{119}CCH(O)$] ($^3J_{exp.}$) has been computed from the ^{1}H NMR spectra and it has been observed that there is an increase in $^3J_{exp.}$ ($Ph_2Sn(NCO)Cl$) on complexation. Further, $^3J[Sn^{119}CCH(O)]$ has been calculated ($^3J_{theor.}$) and it is seen that there is close agreement between $^3J_{theor.}$ and $^3J_{exp.}$ values.

Diphenyl tin mixed halide pseudohalides [$Ph_2Sn(X)X'$] (X = NCO, NCS, N_3; X′ = Cl, Br) were recently reported by us.[1] We also reported another complex, $Ph_2Sn(NCS)Br \cdot 2DMSO$. Thus, the coordination chemistry of these diphenyl tin mixed halide pseudohalides has not been studied in detail and no coordination compound of $Ph_2Sn(NCO)Cl$ is known. Therefore, we prepared coordination compounds of $Ph_2Sn(NCO)Cl$ with DMSO, DMF and 2,2′-bipyridyl yielding neutral complexes $Ph_2Sn(NCO)Cl \cdot nL$ ($n = 1$, L = 2,2′-bipyridyl; $n = 2$, L = DMSO and DMF) and with $[Me_4N]^+[Cl]^-$ yielding anionic complexes $[Me_4N]^+$ $[Ph_2Sn(NCO)Cl_2]^-$. These complexes have been characterized through elemental analysis, molecular weight, molar conductance, IR and ^{1}H NMR data.

The ^{1}H NMR spectral data have been interpreted in terms of *o*-, *m*- and *p*-phenyl proton chemical shifts and ^3J[SnCCH(*ortho*)] coupling constants (^3J). Semi-empirical calculations have been made for $^3J_{theor.}$ and correlated with experimentally observed $^3J_{exp.}$ for these complexes. It is observed that there is an increase in coupling constant $^3J[Sn^{119}CCH(O)]$ of $Ph_2Sn(NCO)Cl$ on complexation.

* Author to whom correspondence should be addressed.

EXPERIMENTAL

Ph_3SnCl (E. Merck), ICl (E. Merck), KNCO and Lewis bases (BDH) used in the present investigation, were procured commercially. $Ph_3Sn(NCO)$ was prepared according to the reported method.[2] $Ph_2Sn(NCO)Cl$ was prepared by the cleavage of $Ph_3Sn(NCO)$ with ICl in chloroform[1] and the physico-chemical measurements were carried out as before.[1]

The complexes were prepared by the interaction of $Ph_2Sn(NCO)Cl$ with ligands under nitrogen in the following manner:

$$Ph_2Sn(NCO)Cl + nL \rightarrow Ph_2Sn(NCO)Cl \cdot nL$$

($n = 1$, L = 2,2′-bipyridyl, Me_4NCl; $n = 2$, L = DMSO and DMF).

A typical preparation of the complex $Ph_2Sn(NCO)Cl \cdot 2,2'$-bipyridyl is described below.

Preparation of $Ph_2Sn(NCO)Cl \cdot 2,2'$-*bipyridyl*

$Ph_2Sn(NCO)Cl$ (1.00 g, 2.85 mmol) was taken in ~30 cm^3 of anhydrous acetone. To this 2,2′-bipyridyl (0.44 g, 2.85 mmol) was added in ~20 cm^3 of the same solvent. The resulting reaction mixture was stirred for 1 h, refluxed for 3 h and excess solvent was removed by distillation. To the remaining ~4–5 cm^3 of the solution petroleum ether (40–60°C) was added. The complex formed

was separated, washed with petroleum ether (40–60°C) and dried *in vacuo* (yield 0.80 g, 55.55%).

RESULTS AND DISCUSSION

The complexes with their characterization data are listed in Table 1. These complexes are white, crystalline solids and are soluble in DMF, DMSO, nitrobenzene and chloroform+DMSO solvent mixtures. They are sharp melting, thermally stable and sensitive to atmospheric oxygen and moisture.

The molar conductance of a 10^{-3} M solution in DMSO at 30°C and molecular weight of these complexes in nitrobenzene indicate the monomeric and non-electrolytic nature of the neutral complexes,[3,4] whereas $[Me_4N]^+[Ph_2Sn(NCO)Cl_2]^-$ is a 1 : 1 electrolyte. The Van't Hoff factor (i) = 2.05 indicates the presence of two ions in the solution.

IR spectra

In $Ph_2Sn(NCO)Cl$, the cyanate group bonded by nitrogen is evident by the presence of a strong band corresponding to $\nu_{asym.}NCO$ at 2230 cm^{-1}. In potassium cyanate, the $\nu_{asym.}NCO$ appears at 2165.[6] A shift to higher wave number has been found to occur for the N-bonded cyanate group and a shift to lower wave number occurs for the O-bonded NCO group.[7,8] Thus from the above values of $\nu_{asym.}NCO$, it is evident that the bonding of the NCO group has taken place through nitrogen, indicating Sn—NCO bonding, in agreement with earlier reports.[9-12]

In the neutral and anionic complexes synthesized, $\nu_{asym.}NCO$ appears as a strong band at 2205 ± 5 cm^{-1}. Thus, a negative shift of about 25 ± 5 cm^{-1} indicates an increase in the coordination number of tin.[13] The $\nu_{sym.}NCO$ is found at 1322 ± 13 cm^{-1} and δNCO is found at 622 ± 13 cm^{-1}.

In order to decide the coordination site in DMSO adducts, the (S=O) stretching absorption frequencies is of diagnostic value. The νSO in free DMSO has been assigned at 1050 cm^{-1}.[14] In the adduct the νSO is found at 940 cm^{-1}. A distinct negative shift of the (S=O) stretching frequency is observed, which proves (Sn ← O) bonding in the complex.[1,14-16] In the complex $Ph_2Sn(NCO)Cl$ with DMF, the νCO in free DMF appears at 1666 cm^{-1} while in the adduct νCO is found at 1645 cm^{-1}. The shift to lower wave number indicates coordination through the oxygen atom of the carbonyl group of the ligand.[17]

In the case of 2,2′-bipyridyl, C=C, C=N and ring stretching appear at 1582, 1560 and 1540 cm^{-1}. On coordination through both nitrogens of the ligand, these bands show a positive shift and appear

Table 1. Characterization data for neutral and anionic complexes of $Ph_2Sn(NCO)Cl$

Number	Complex	Melting point (°C)	Yield (%)	Molecular weight obs. (calc.)	Molar conductance (Ω^{-1} cm^2 mol^{-1})	Elemental analysis (%), Obs. (Calc.) C	H	N	Cl[a]	Sn
1	$Ph_2Sn(NCO)Cl\cdot2DMSO$	160	59.72	495 (506.31)	12.4	40.2 (40.3)	4.3 (4.3)	2.7 (2.8)	7.0 (7.0)	23.4 (23.5)
2	$Ph_2Sn(NCO)Cl\cdot2DMF$	158	67.37	480 (496.19)	9.8	43.9 (43.5)	4.8 (4.8)	8.4 (8.5)	7.1 (7.1)	23.9 (23.9)
3	$Ph_2Sn(NCO)Cl\cdot2,2'$-bipyridyl	220	55.55	475 (506.19)	10.3	54.3 (54.2)	3.4 (3.5)	8.2 (8.3)	7.0 (7.0)	23.3 (23.4)
4	$[Me_4N]^+[Ph_2Sn(NCO)Cl_2]^-$	189	63.35	224 (459.69)	58.5	44.2 (44.4)	4.7 (4.8)	6.0 (6.1)	15.4 (15.4)	25.6 (25.8)

[a] Estimated volumetrically by Volhard's method.[5]

at 1610, 1600 and 1545 cm^{-1}, respectively, in the spectrum of the adduct, in agreement with the observations of previous workers.[18-20]

^1H *NMR spectra*

The ^1H NMR spectra of the complexes of $Ph_2Sn(NCO)Cl$ with DMSO and DMF show two multiplets centred at 7.69 and 7.09, and 7.85 and 7.45 ppm, respectively; the lower field multiplet corresponding to *o*-phenyl protons and the higher field multiplet corresponding to *m*- and *p*-phenyl protons.[21-23] The singlet for CH_3 protons appears at 2.35 ppm in the case of DMSO whereas in DMF two singlets centred at 2.90 and 3.02 ppm appear for $—CH_3$ protons [$—N(CH_3)_2$]. The $—(CH_3)_2$ doublet separation is 10.8 Hz. In the case of free DMF, two singlets are centred at 2.79 and 2.94 ppm, the doublet separation is 9.0 Hz.[24] The aldehyde proton of DMF appears at *ca* 7.90 ppm[24] but in the complex it is probably smothered by the multiplets of the phenyl protons. The experimental ^3J[SnCCH(O)] for the $Ph_2Sn(NCO)Cl \cdot 2DMSO$ complex is 85.20 Hz, whereas for the $Ph_2Sn(NCO)Cl \cdot 2DMF$ complex its value is 84.60 Hz.

The ^1H NMR of the anionic complex $[Me_4N]^+[Ph_2Sn(NCO)Cl_2]^-$ shows two multiplets centred at 8.19 and 7.45 ppm due to the *o*-protons, and the *m*- and *p*-protons of the phenyl groups, respectively, and a singlet at 3.25 ppm is due to the CH_3 protons. The experimental ^3J[SnCCH(O)] for this anionic complex is 78.30 Hz.

The integration of the peak areas corresponds to the proposed stoichiometry of the above complexes.

Semi-empirical calculations

On the basis of the Scherr and Oliver relationship,[25] the theoretical value of the metal proton coupling constant of R_4M type compounds may be calculated. Since the metal proton coupling constant depends upon (i) the hybridization and (ii) electronegativity of the groups attached to the metal,[26a] it is obvious that the value of J for all those related derivatives which possess the same hybridization as that of R_4M ([e.g. R_nMX_{4-n} or $[R(R')]_n\ MX_{4-n}$ or $R_nM\ [(X')X]_{4-n}$) type compounds where (n = 1–4), could be obtained by including the electronegativity term (Δx). It is thus possible to conceive the general relationship:

$$^3J\text{ compound} = {}^3JR_4M \pm A\Delta x, \qquad (1)$$

where A is a constant, $\Delta x = \Sigma x_A - \Sigma x_B$;
Σx_A = sum of electronegativities of the groups attached to the metal in the compound whose J is to be calculated;
Σx_B = sum of the electronegativities of the groups attached to the metal in the parent compound (R_4M). Thus ^3J of $Ph_2Sn(X')X$ (X = Cl, X' = NCO) will be given by the following relationship:

$$^3JPh_2Sn(NCO)Cl = {}^3JPh_4Sn + A\Delta x. \qquad (2)$$

^3J of Ph_4Sn equals 68.17 Hz has been previously reported by us.[22] The value of Δx ($\Delta x = \Sigma x_A - \Sigma x_B$ = 12.39 − 9.96 = 2.43) in $Ph_2Sn(NCO)Cl$ is 2.43. Assuming that the constant A = 3, ^3J of $Ph_2Sn(NCO)Cl$

$$= 68.17 + 3 \times 2.43$$
$$= 68.17 + 7.29$$
$$= 75.46 \text{ Hz}.$$

The theoretical value of ^3J of $Ph_2Sn(NCO)Cl$ is in close agreement with the experimentally observed 75.60 Hz; ^3J value for $Ph_2Sn(NCO)Cl$.

$^3J_{theor.}$ *of the complexes of* $Ph_2Sn(NCO)Cl$

As stated above, the coupling constant mainly depends upon (i) hybridization or *S*-character and (ii) electronegativity of the group attached to the metal.[26a] Therefore, both these factors should be taken into consideration when calculating the coupling constants of the complexes of $Ph_2Sn(NCO)Cl$. However, it has been established in the case of the adducts of Me_3SnCl by Bolles and Drago[27] that the total amount of tin *S*-orbital participation in bonding in the adduct and free Me_3SnCl is constant. We believe that a similar situation exists in the complexes of $Ph_2Sn(NCO)Cl$ and free $Ph_2Sn(NCO)Cl$ and conclude that the change in the coupling constant of $Ph_2Sn(NCO)Cl$ on complex formation will occur because of the electronegativity of the groups surrounding the tin metal atom. Thus $^3J_{theor.}$ for the complexes could be obtained by the following relationship:

$$^3J\text{ complex} = {}^3JPh_2Sn(NCO)Cl + A'n\chi p_{X'}, \qquad (3)$$

where constant A' is equal to unity, in the present study; n = number of ligating atoms = 1 and 2; $\chi p_{X'}$ = electronegativity of the ligating atom X' on the Pauling scale.

The theoretically calculated ^3J values of the (neutral and anionic) complexes of $Ph_2Sn(NCO)Cl$ using eq. (3) are listed in Table 2 and are in close agreement with the experimental values of ^3J.

Although the calculations are crude because the ring current effect which would also affect the values of coupling constant has not been taken into account, there is reasonably good agreement between the theoretical and experimental values of ^3J. Such calculations on the complexes of

Table 2. ^{1}H NMR data of neutral and anionic complexes of $Ph_2Sn(NCO)Cl$

Number	Complex	C_6H_5 protons (δ) (ppm) *o*-protons	*m*- and *p*-protons	CH_3-protons (ppm)	$^3J_{exp.}$ (Hz)	$^3J_{theor.}$ (Hz)
1[a]	$Ph_2Sn(NCO)Cl \cdot 2DMSO$	7.69(m)	7.09(m)	2.35(s)	85.20	86.54
2	$Ph_2Sn(NCO)Cl \cdot 2DMF$	7.85(m)	7.45(m)	2.90(s) 3.02(s)	84.60	86.54
4	$[Me_4N]^+[Ph_2Sn(NCO)Cl_2]^-$	8.19(m)	7.45(m)	3.25(s)	78.30	78.41

Multiplicity; m = multiplet; s = singlet.

(i) The position of the phenyl multiplets is the approximate centre of the multiplet.

[a](ii) The spectrum of this complex is at 60 MHz, the rest are at 90 MHz.

(iii) $\chi p_{X'}$ = electronegativity of X′ atom of the ligand bound to tin; χp of oxygen (sp^2 hybrid orbital of DMSO and DMF, 5.54,[26b], 2.95.[26b]

$Ph_2Sn(NCO)Cl$ have been performed for the first time and form a basis for calculating the coupling constants of several such complexes. Furthermore, there is an increase in $^3J_{theor.}$ and $^3J_{exp.}$ values of $Ph_2Sn(NCO)Cl$ on complexation. This could serve as a general parameter for predicting coordination through ^{1}H NMR spectral studies.

Acknowledgements—The authors are thankful to the Regional Sophisticated Instrumentation Centre in CDRI, Lucknow, for elemental analysis, IR and NMR spectral data. Two of us (A.T.) and (P.S.) are thankful to C.S.I.R. and U.G.C., New Delhi, for financial support.

REFERENCES

1. P. C. Srivastava, S. K. Srivastava and S. B. Sharma, *Can. J. Chem.* 1985, **63**, 329.
2. A. S. Mufti and R. C. Poller, *J. Chem. Soc.* 1965, 5055.
3. W. J. Geary, *Coord. Chem. Rev.* 1971, **7**, 81.
4. N. N. Greenwood, B. P. Straughan and A. E. Wilson, *J. Chem. Soc. A* 1968, 2209.
5. A. I. Vogel, *Quantitative Inorganic Analysis*, p. 267. Longman, London (1975).
6. A. Maki and J. C. Decius, *J. Chem. Phys.* 1959, **31**, 772.
7. A. Sabatini and I. Bertini, *Inorg. Chem.* 1965, **4**, 959.
8. J. L. Burmeister, E. A. Deardroff, A. Jensen and V. H. Christiansen, *Inorg. Chem.* 1970, **9**, 58.
9. A. H. Norbury and A. I. P. Sinha, *J. Chem. Soc. A* 1968, 1598.
10. A. H. Norbury, *Adv. Inorg. Chem. Radiochem.* 1975, **17**, 231.
11. D. Forster and D. M. L. Goodgame, *J. Chem. Soc.* 1965, 1286.
12. S. K. Srivastava, PhD thesis, University of Lucknow, India (1981).
13. J. H. Holloway, G. P. McQuillan and D. S. Ross, *J. Chem. Soc. A* 1969, 2505.
14. N. P. Crawford and G. A. Nelson, *J. Chem. Soc. A* 1969, 1049.
15. H. G. Langer and A. H. Blut, *J. Organomet. Chem.* 1966, **5**, 288.
16. G. Vicentini and L. B. Zinner, *Inorg. Nucl. Chem. Lett.* 1971, **7**, 967.
17. R. Makhija and M. Onyszchuk, *J. Organomet. Chem.* 1977, **15**, 261.
18. A. A. Schilt and R. C. Taylor, *J. Inorg. Nucl. Chem.* 1959, **9**, 211.
19. A. J. Carty and D. G. Tuck, *J. Chem. Soc. A* 1966, 1081.
20. S. P. Sinha, *Spectrochim. Acta* 1964, **20**, 879.
21. W. C. Sau, L. A. Carpino and R. R. Holmes, *J. Organomet. Chem.* 1980, **197**, 181.
22. P. C. Srivastava and S. K. Srivastava, *Spectrochim. Acta* 1984, **40A**, 607.
23. P. C. Srivastava and S. K. Srivastava, *Spectrochim. Acta* 1985, **41A**, 687.
24. R. M. Silverstein, G. C. Bassler and T. C. Morril, *Spectrometric Identification of Organic Compounds* p. 241. Wiley, New York (1981).
25. P. A. Scherr and J. P. Oliver, *J. Am. Chem. Soc.* 1972, **94**, 8026.
26. J. E. Huheey, *Inorganic Chemistry*, (a) p. 407 and (b) pp. 162–163. Harper and Row, London (1978).
27. T. F. Bolles and R. S. Drago, *J. Am. Chem. Soc.* 1966, **88**, 5730.

Polyhedron Vol. 9, No. 1, pp. 129–135, 1990
Printed in Great Britain

0277–5387/90 $3.00+.00
© 1989 Pergamon Press plc

FURTHER STUDIES OF THE KINETIC COORDINATION TEMPLATE EFFECT IN THE METAL-ION CATALYSED FORMATION OF ARYLPHOSPHONIUM SALTS

DAVID W. ALLEN* and PAUL E. CROPPER

Department of Chemistry, Sheffield City Polytechnic, Pond Street, Sheffield S1 1WB, U.K.

(*Received* 4 *April* 1989; *accepted* 15 *August* 1989)

Abstract—The reactions of a series of bis-imines (derived from *o*-bromobenzaldehyde and α,ω-diamines) with tertiary phosphines in the presence of nickel(II) bromide in ethanol proceed with replacement of the *o*-halogen to form the related bis(arylphosphonium) salts, each *o*-haloarylimino moiety providing a kinetic coordination template for the substitution process. Only for bis-imines able to form five-, six- or seven-membered chelate systems with the metal ion is the substitution reaction inhibited or the yield reduced. Kinetic template effects in arylphosphonium salt formation have also been observed in the related reactions of 2,3-bis(*o*-chlorophenyl)quinoxaline, 1-(N-benzylidene)amino-8-bromonaphthalene and *o*-iodobenzoic acid. The structural requirements of the coordination template are discussed in the light of these and earlier results.

We have shown that the *o*-haloaryl imines (**1**, R^1 = H or Me; R^2 = aryl or benzyl; X = Cl, Br or I) undergo facile replacement of the *o*-halogen on heating under reflux in ethanol with tertiary phosphines in the presence of nickel(II) bromide to form the related arylphosphinium salts (**2**; R^1 = H or Me; R^2 = aryl or benzyl; R^3 = alkyl or aryl).[1] The corresponding *p*-haloarylimines are inert under these conditions. Related regiospecific replacement of halogen under mild conditions occurs in the nickel(II) and copper(II) promoted reactions of tertiary phosphines[2] (and trialkylphosphites)[3,4] with *o*-haloarylazo dyestuffs (**3**; R^1 = H or Me; R^2 = H or NHAc) and the bipyridyl system (**4**)[5] and in the nickel (II) promoted reactions of the 2-(2-bromophenyl)benzimidazole (**5**).[6] We have suggested that these reactions involve the operation of a kinetic template effect in which metal-ion promoted replacement of the halogen *ortho* to the imino groups is assisted by coordination of the metal to

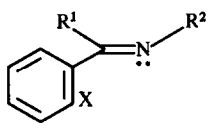

(1)

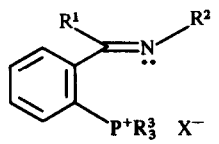

(2)

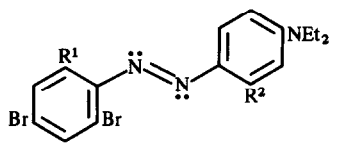

(3)

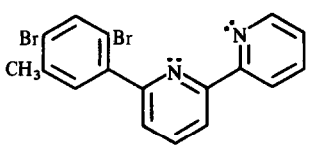

(4)

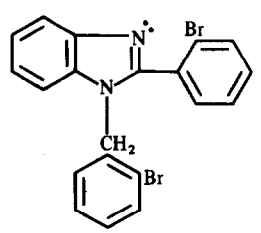

(5)

* Author to whom correspondence should be addressed.

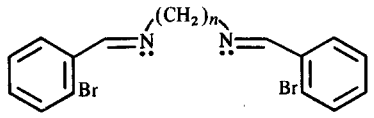

(6)

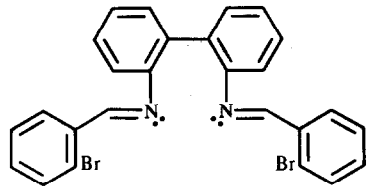

(7)

the imino-nitrogen atom. We have also shown that introduction of a second donor atom or group into the substituent R^2 present at the imino-nitrogen of related imines inhibits these reactions, presumably owing to the diversion of the metal ion in other modes of coordination. Thus, e.g. the bis-imines (**6**, $n = 2$) and (**7**) undergo hydrolysis rather than phosphonium salt formation on heating in ethanol with tertiary phosphines in the presence of nickel(II) bromide. In this paper, we report related studies of a range of bis-imines in which diversion of the metal ion by chelation becomes less likely and also studies of the reactions of some new kinetic template systems.

RESULTS AND DISCUSSION

The synthesis of a range of bis-imines (**6**; $n = 0$, 3–8 or 12) was achieved by heating together the appropriate α,ω-diamine (1 mol equiv.) with *o*-bromobenzaldehyde in ethanol. The ^{1}H NMR spectra of these compounds exhibited the characteristic signal at *ca* δ 8.6 corresponding to the imino protons. On heating the bis-imines under reflux in ethanol with triphenylphosphine in the presence of a catalytic amount of nickel(II) bromide, the related bis(phosphonium) salts (**8**) and (**9**; $n = 3$–8, or 12) were isolated. The yield of the salt from the trimethylene-bridged template (**6**; $n = 3$) was significantly lower than from the other bis-imine templates, presumably reflecting competition for the metal ion catalyst by chelation to form a six-membered ring system. The constitution of the bis (phosphonium) salts was confirmed by ^{1}H and ^{31}P NMR studies, the integrated spectra being consistent with the introduction of two phosphine moieties. ^{31}P NMR spectra exhibited only one signal in each case at 24–26 ppm (characteristic of tetraarylphosphonium salts). Apart from the bis(triphenylphosphonio) salt derived from the bis(azine) (**6**; $n = 0$) great difficulty has been experienced in characterizing the above alkylene-bridged salts by microanalysis. Repeated microanalyses of these compounds, although within acceptable limits for %H and %N, gave consistently low %C results, possibly as a consequence of the difficulty in ensuring full combustion of such materials or as a result of their hygroscopic nature. Attempts to characterize them by analysis following conversion to the related mercury(II) bromide adducts, i.e. R_4P^+ $HgBr_3^-$, also failed to give acceptable microanalytical data. However, from the above spectroscopic data, it is clear that as the tendency for the alkylene-bridged bis(imines) to act as chelating ligands towards the metal ion decreases, then each *o*-haloarylimine functions independently of the other in promoting the template-substitution process. Predictably, the two aryl-bridged bis-

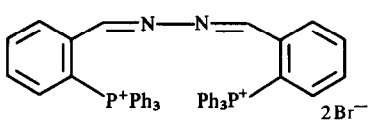

(8)

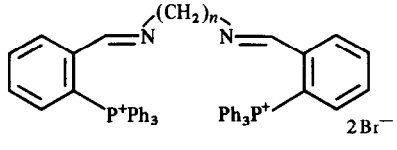

(9)

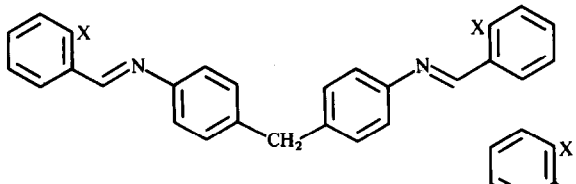

(10)

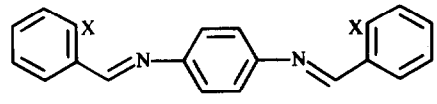

(11)

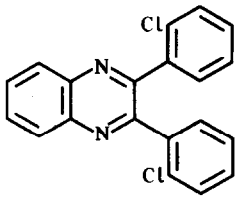

(12)

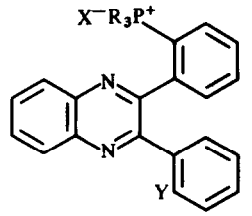

(13)

$(R_3P)_2NiCl_2$

(14)

imines (**10**; X = Br) and (**11**; X = Br), also behaved normally in the nickel(II) catalysed reactions with tertiary phosphines in giving the related bis(phosphonium) salts (**10** and **11**; X = $Ph_3P^+Br^-$ or $Bu_3^+PBr^-$) in good yield.

We have also explored the reactivity of a series of new potential template molecules towards tertiary phosphines in the presence of nickel(II) or copper(II) ions. The synthesis of the 2,3-disubstituted quinoxaline (**12**) was achieved by heating together equimolar amounts of 2,2′-dichlorodibenzoyl and *o*-phenylenediamine in ethanol, the product crystallizing on cooling in quantitative yield.

On heating the quinoxaline (**12**) in ethanol with excess triphenylphosphine or tributylphosphine in the presence of nickel(II) chloride, the colourless phosphonium salts (**13**; R = Ph or Bu, X = Br, Y = $PR_3^+Br^-$ or Cl) were produced in good yields.

No reaction occurred in the absence of nickel(II) chloride or in the presence of copper(II) acetate as the sole catalyst.

The ^{31}P NMR spectra of both products exhibited two signals (of differing intensities) with chemical shifts of 26.7 and 25.2 ppm (R = Ph; in a 3 : 1 ratio) and 34.2 and 32.6 ppm (R = Bu; in a 3 : 4 ratio), respectively. It is likely that these signals arise from a mixture of mono- and diphosphonium salts since **12** contains two possible reaction sites where the substitution reaction could occur. Integration of the ^1H NMR spectra of these products lent support to this suggestion. It was not possible to separate the mixed salts into the mono- and di-species. Isolation of the diphosphonium salts (**13**; R = Ph or Bu, X = Br^-, Y = $R_3P^+Br^-$) was only possible when the quinoxaline was heated in ethanol with the preformed nickel(II) phosphine complexes (**14**; R = Ph and Bu) and an additional quantity of the free phosphine (1 mol equiv.). The latter complexes were prepared by mixing together nickel(II) chloride (1 mol equiv.), dissolved in hot ethanol with the appropriate tertiary phosphine (2.2 mol equiv.), dissolved in ethanoic acid.[7]

The reaction of equimolar amounts of the quinoxaline (**12**) with (**14**) but excluding the extra mol of tertiary phosphine, again led to a mixture of the mono- and diphosphonium salts.

The reaction of the 8-bromo-1-iminonaphthalene (**15**) (prepared by the condensation of 1-amino-8-bromonaphthalene with benzaldehyde in ethanol) with triphenylphosphine also gave a phosphonium salt (**16**) when heated under reflux in ethanol with nickel(II) bromide. Again, no reaction occurred in the absence of nickel(II), and copper(II) acetate failed to catalyse the reaction. In contrast, *neither* 1-amino-8-bromonaphthalene *nor* the reduction product (**17**) of the imine (**15**) functioned as active templates, again indicating rather specific requirements of the donor centre in the template system as was also apparent in systems related to **1**.[1]

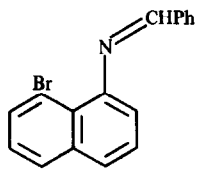

(15)

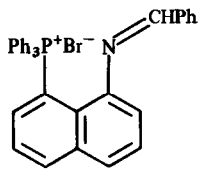

(16)

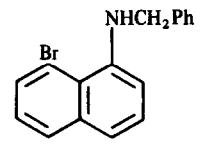

(17)

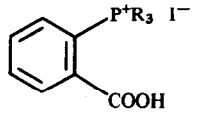

(18)

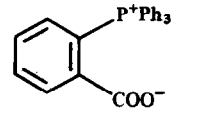

(19)

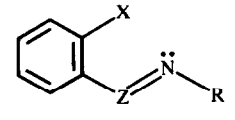

(20)

Whereas the reactions of both *o*-chloro- and *o*-bromobenzoic acids with triphenylphosphine or tributylphosphine in the presence of *either* nickel(II) bromide *or* copper(II) acetate failed to give rise to phosphonium salts, the related reactions of *o*-iodobenzoic acid in the presence of nickel(II) bromide gave the phosphonium salts (**18**; R = Ph or Bu) and for R = Ph, the related betaine (**19**).

The ^{31}P NMR spectrum of the product from the reaction with triphenylphosphine exhibited two signals of equal intensity at 26.2 ppm corresponding to the expected phosphonium salt (**18**) and 21.7 ppm, respectively, corresponding to the betaine (**19**). Addition of a strong acid to the solution resulted in the loss of the signal at 21.7 ppm, thus confirming that this signal was due to the presence of **19**. The ^{31}P NMR of the butylphosphonium salt (**18**; R = Bu) exhibited a signal at 33.2 ppm. Copper(II) acetate failed to catalyse these substitution reactions.

Other simple derivatives of *o*-iodobenzoic acid e.g. the corresponding methyl ester, amide, or hydrazide, did not function as active templates in the presence of either nickel(II) or copper(II) catalysts.

All the molecules which promote a kinetic template effect in arylphosphonium salt formation, with the exception of the 1,8-disubstituted naphthalene (**15**) and *o*-iodobenzoic acid, conform to the generalized structure (**20**) which we suggested earlier on the basis of our studies of the reactions of a series of *o*-haloarylimines.[1]

It is also necessary to recognize the role of the group bound to the sp^2-hybridized nitrogen atom. For the imine substrates (**20**; Z = CR) this is clearly of importance, since it has been shown that the presence of bulky groups at the nitrogen, *or* the presence of an additional donor within that group, which can divert the metal from its catalytic role, have adverse effects on the substitution reaction.[1] In the case of the azo dyestuffs and the *o*-halophenylbipyridyl substrate (**4**), the presence of additional donors does not seem to matter.

There is also a crucial interrelation between the template and the specific metal ion which is required. In general, for donors with only one donor atom, only nickel(II) is effective as the catalyst [as for the *o*-haloarylimines (**1**),[1] the benzimidazole (**5**)[6] and the quinoxaline (**12**)], whereas for the two donor systems, e.g. the *o*-halophenylbipyridyl system (**4**)[5] and many of the azo dyestuffs (**3**),[2] the reactions are catalysed by both copper(II) and nickel(II) ions.

Only two other types of effective template are left, the oxygen donor system of *o*-iodobenzoic acid and the 1,8-haloiminonaphthalene (**15**) which do not conform to the general design (**20**). It is interesting that the reactions of these single donor templates are catalysed solely by nickel(II) ions. It is clear that the oxygen template of *o*-iodobenzoic acid is at the margin of reactivity, since if the halogen is changed to bromine or chlorine, or if the acid function is methylated or converted to the amide/hydrazide derivative, then the template reactivity disappears. The "unexpected" reactivity of the haloiminonaphthalene (**15**) can doubtless be attributed to the 1,8- (or *peri*-) position of the substituents on the naphthalene ring. In view of the geometry of the naphthalene system, substituents located at these positions are in much closer proximity than similar substituents located *ortho* to each other on a benzene ring. This closer proximity has been responsible for the appearance of several unique properties of *peri*-substituted naphthalenes. Such "proximity effects" have been observed in *peri*-cyclization reactions[8] as well as in the *peri*-effects on 1,2-cyclizations[9] and investigations of the chemical reactivity of *peri*-substituted naphthalene derivatives.[10–12,13]

EXPERIMENTAL

^{31}P NMR spectra were recorded on a Bruker WP80SY instrument. Chemical shifts are reported with respect to 85% orthophosphoric acid as external standard; shifts to high frequency are positive in sign. ^1H NMR spectra were recorded on the same instrument, and chemical shifts are reported on the δ scale with respect to tetramethylsilane as internal standard in deuteriochloroform solution.

Preparation of potential templates

The following compounds were prepared as previously described: 8-bromo-1-naphthylamine,[14] bis(tertiary phosphine) nickel(II) chloride (**14**; R = Ph or Bu),[7] 2-iodomethylbenzoate[15] and 2-iodobenzamide.[16] 2-Halobenzoic acids were obtained commercially.

The synthesis of the bis-imines

These were prepared by heating together 2-bromobenzaldehyde (2 mol) with the appropriate α-ω diamine (1 mol) in refluxing ethanol for 60–90 min. Compounds (**10**) and (**11**) were prepared using the same conditions with replacement of the α-ω diamine by 4,4′-methylenedianiline, and *p*-phenylenediamine, respectively. In all cases, the bis-imines crystallized on cooling and were purified by recrystallization.

N,N′-bis-(2-bromobenzylidene)azine (**6**; $n = 0$). This was isolated as yellow crystals (98%), m.p.

177°C (from $CHCl_3$–EtOH) (Found: C, 45.7; H, 2.6; N, 7.5. $C_{14}H_{10}N_2Br_2$ requires: C, 45.9; H, 2.7; N, 7.6%), δ^1H($CDCl_3$): 8.6 (s, 2H), 8.1–7.1 (m, 8ArH) ppm.

N,N′ - bis - (2 - bromobenzylidene)propane - 1,3 - diamine (**6**; $n = 3$). (88%) m.p. 65°C (from EtOH) (Found: C, 50.0; H, 3.9; N, 6.9. $C_{17}H_{16}N_2Br_2$ requires: C, 50.0; H, 3.9; N, 6.9%), δ^1H($CDCl_3$): 8.6 (s, 2H), 8.1–7.2 (m, 8ArH), 3.8 (t, 4H), 2.1 (q, 2H) ppm.

N,N′ - bis - (2 - bromobenzylidene)butane - 1,4 - diamine (**6**; $n = 4$). (81%), m.p. 51°C (from EtOH) (Found: C, 51.2; H, 4.3; N, 6.5. $C_{18}H_{18}N_2Br_2$ requires: C, 51.2; H, 4.3; N, 6.6%), δ^1H($CDCl_3$): 8.6 (s, 2H), 8.1–7.2 (m, 8ArH), 3.7 (s, 4H), 1.8 (s, 4H) ppm.

N,N′ - bis - (2 - bromobenzylidene)pentane - 1,5 - diamine (**6**; $n = 5$). This was obtained as a pale cream solid (74%), m.p. 48°C (from EtOH) (Found: C, 52.3; H, 4.6; N, 6.3. $C_{19}H_{20}N_2Br_2$ requires: C, 52.3; H, 4.6; N, 6.4%), δ^1H($CDCl_3$): 8.6 (s, 2H), 8.1–7.2 (m, 8ArH), 3.7 (t, 4H), 1.8 (q, 6H) ppm.

N,N′ - bis - (2 - bromobenzylidene)hexane - 1,6 - diamine (**6**; $n = 6$). (85%), m.p. 73°C (from EtOH) (Found: C, 53.4; H, 4.9; N, 6.1. $C_{20}H_{22}N_2Br_2$ requires: C, 53.3; H, 4.9; N, 6.2%), δ^1H($CDCl_3$): 8.6 (s, 2H), 8.1–7.1 (m, 8ArH), 3.6 (t, 4H), 1.6 (m, 8H) ppm.

N,N′ - bis - (2 - bromobenzylidene)heptane - 1,7 - diamine (**6**; $n = 7$). (73%), m.p. 48°C (from EtOH) (Found: C, 54.5; H, 5.2; N, 6.0. $C_{21}H_{24}N_2Br_2$ requires: C, 54.3; H, 5.2; N, 6.0%), δ^1H ($CDCl_3$): 8.6 (s, 2H), 8.1–7.2 (m, 8ArH), 3.6 (t, 4H), 1.6 (m, 10H) ppm.

N,N′ - bis - (2 - bromobenzylidene)octane - 1,8 - diamine (**6**; $n = 8$). (81%), m.p. 52°C (from EtOH) (Found: C, 55.3; H, 5.5; N, 5.9. $C_{22}H_{26}N_2Br_2$ requires: C, 55.2; H, 5.5; N, 5.8%), δ^1H($CDCl_3$): 8.6 (s, 2H), 8.1–7.2 (m, 8ArH), 3.7 (t, 4H), 1.1 (m, 12H) ppm.

N,N′ - bis - (2 - bromobenzylidene)dodecane - 1,12 - diamine (**6**; $n = 12$). This was obtained as pale yellow crystals (65%), m.p. 53°C (from EtOH) (Found: C, 58.5; H, 6.4; N, 5.2. $C_{26}H_{34}N_2Br_2$ requires: C, 58.4; H, 6.4; N, 5.2%), δ^1H($CDCl_3$): 8.6 (s, 2H), 8.1–7.1 (m, 8ArH), 3.7 (t, 4H), 1.5 (m, 20H) ppm.

N,N′ - bis - (2 - bromobenzylidene)4,4′ - diaminodiphenylmethane (**10**). This was isolated as pale yellow crystals (83%), m.p. 142°C (from EtOH) (Found: C, 60.7; H, 3.7; N, 5.2. $C_{27}H_{20}N_2Br_2$ requires: C, 60.9; H, 3.8; N, 5.3%), δ^1H($CDCl_3$): 8.8 (s, 2H), 8.3–7.2 (m, 16ArH), 4.0 (s, 2H) ppm.

N,N′ - bis - (2 - bromobenzylidene)1,4 - diaminobenzene (**11**). This was obtained as bright yellow crystals (92%), m.p. 157°C (from petrol 60:40) (Found: C, 54.3; H, 3.1; N, 6.1. $C_{20}H_{14}N_2Br_2$ requires: C, 54.3; H, 3.2; N, 6.3%), δ^1H($CDCl_3$): 8.9 (s, 2H), 8.4–7.3 (m, 12ArH) ppm.

The synthesis of other potential templates

2,3-*Bis*(2-*chlorophenyl*)*quinoxaline* (**12**). To a stirred solution of *o*-phenylene diamine (2.2 g, 0.02 mol) in ethanol (50 cm^3) 2,2′-dichlorodibenzoyl (5.58 g, 0.02 mol) was added. The solution was heated under reflux under nitrogen for 2 h. On cooling, pale cream crystals formed. These were recrystallized from ethanol to give the 2,3-bis-(2-chlorophenyl)quinoxaline (6.9 g, 98%), m.p. 116–118°C (from EtOH) (Found: C, 68.5; H, 3.4; N, 8.0. $C_{20}H_{12}N_2Cl_2$ requires: C, 68.4; H, 3.4; N, 8.0%).

1-(*N-benzylidene*)*amino*-8-*bromonaphthalene* (**15**). A mixture of 8-bromo-1-naphthylamine (1.0 g, 4.5×10^{-3} mol) and benzaldehyde (0.48 g, 4.5×10^{-3} mol) in ethanol (10 cm^3) with a catalytic amount of *p*-toluene sulphonic acid was heated under reflux under nitrogen for 2 h. After filtration, the solid was recrystallized (0.9 g, 59%), m.p. 97°C (from MeOH) (Found: C, 66.1; H, 4.0; N, 4.4. $C_{17}H_{12}NBr$ requires: C, 65.8; H, 3.9; N, 4.5%), δ^1H($CDCl_3$): 8.4 (s, 1H), 8.1–6.8 (m, 11ArH) ppm.

1-*Bromo*-8-*benzylaminonaphthalene*. To a solution of 1-(N-benzylidene)amino-8-bromonaphthalene (0.5 g) in ethanol (5 cm^3) was added sodium borohydride (0.5 g) and the mixture heated under reflux for 1 h. The resulting solution was poured into water, and the amine extracted into ether. Evaporation of the dried ether extract gave an oil. δ^1H($CDCl_3$): 4.5 (s, 2H, $PhCH_2$), and 6.5–8.0 (m, 7H); *m/z* 300 (M^+).

2-*Iodobenzhydrazide*. (Prepared by a modification of a general procedure.[17]) To a flask containing redistilled thionyl chloride (32.6 g, 20 cm^3, 0.28 mol), 2-iodobenzoic acid (10 g, 0.04 mol) was added slowly and the mixture heated on a water bath for 30 min. On addition of all the acid the mixture was heated for a further 30 min. Isolation of the crude acid chloride was achieved by distilling off the excess thionyl chloride. On standing overnight red crystals of 2-iodobenzoylchloride formed. The crystals were filtered and washed with petrol (9.17 g, 86%). The crude acid chloride (5.0 g, 0.02 mol) was added dropwise, with excessive stirring, to a freezing solution of hydrazine hydrate (25 cm^3, 64% w/v). Following the exothermic reaction, the hydrazide crystallized out on standing. After filtration, the product was recrystallized giving 2-iodobenzhydrazide (3.1 g, 63%), m.p. 192°C (Found: C, 33.0; H, 2.6; N, 10.1. $C_7H_7ON_2I$

requires: C, 32.1; H, 2.7; N, 10.7%), δ^1H($(CD_3)_2CO$): 10.0 (s, 1H), 7.9 (d, 1ArH), 7.4 (m, 3ArH), 2.1 (s, 2H) ppm.

Preparation of bis-phosphonium salts

General procedure for the reactions of bis-imines with phosphines. The bis-imine (10^{-3} mol), tertiary phosphine (5×10^{-3} mol) and nickel(II) bromide (2×10^{-4} mol equiv.) were heated together under reflux in ethanol (10 cm^3) in a nitrogen atmosphere for 5–8 h and the progress of the reaction was monitored by TLC (Kieselgel; $CHCl_3$–EtOH (90 : 10) as the eluant). The reaction mixture was then poured into water (50 cm^3) containing KBr (0.5 g), and extracted with ether (2×20 cm^3) in order to remove non-ionic impurities. The aqueous layer was then extracted with chloroform (3×10 cm^3) and discarded. The chloroform layer was dried ($MgSO_4$) and evaporated. The oily residue was then triturated several times with sodium-dried ether until it solidified. On filtration, most of the bis-phosphonium salts, when in contact with the atmosphere, changed almost instantaneously from light-brown solids into dark-brown sticky amorphous compounds. Several of the bis-phosphonium salts that were not hygroscopic were recrystallized from chloroform–ethyl acetate (except as stated otherwise). Characterization by microanalysis proved to be impossible on the hygroscopic salts even on conversion to their related mercuric bromide, tetrafluoroborate, perchlorate or picrate salts. The following salts have been characterized:

N,N′ - bis - (2 - triphenylphosphoniobenzylidene) azine dibromide (**8**). This was isolated as bright yellow crystals (70%), m.p. 300°C (from $CHCl_3$–ether) (Found: C, 63.3; H, 4.6; N, 3.0. $C_{50}H_{40}N_2Br_2P_2 \cdot 3H_2O$ requires: C, 63.6; H, 4.9; N, 3.0), δ^{31}P($CDCl_3$): 26.34 ppm; δ^1H($CDCl_3$): 8.6 (s, 2H), 8.2–7.1 (m, 38ArH) ppm.

N,N′ - bis - (2 - triphenylphosphoniobenzylidene) propane - 1,3 - diamine dibromide. (**9**; $n = 3$). This was isolated as a brown hygroscopic solid (~ 25%), δ^{31}P($CDCl_3$): 24.60 ppm; δ^1H($CDCl_3$): 8.65 (s, 2H), 8.2–7.2 (m, 38ArH), 2.2 (t, 4H), 0.4 (qn, 2H) ppm.

N,N′ - bis - (2 - triphenylphosphoniobenzylidene) butane - 1,4 - diamine dibromide. (**9**; $n = 4$). This was isolated as a brown hygroscopic solid (65%), δ^1H($CDCl_3$): 8.7 (s, 2H), 8.1–7.0 (m, 38ArH), 2.2 (s, 4H), 0.8 (s, 4H) ppm.

N,N′ - bis - (2 - triphenylphosphoniobenzylidene) pentane - 1,5 - diamine dibromide. (**9**; $n = 5$). This was isolated as a brown hygroscopic solid (~ 60%), δ^{31}P($CDCl_3$): 24.68 ppm; δ^1H($CDCl_3$): 8.6 (s, 2H), 8.2–7.2 (m, 38ArH), 2.5 (t, 4H), 0.5 (q, 6H) ppm.

N,N′-bis - (2 - triphenylphosphoniobenzylidene) hexane - 1,6 - diamine dibromide. (**9**; $n = 6$). This was isolated as a brown hygroscopic solid (~ 68%), δ^{31}P($CDCl_3$): 24.69 ppm; δ^1H($CDCl_3$): 8.8 (s, 2H), 8.5–7.4 (m, 38ArH), 2.2 (t, 4H), 0.8 (m, 8H) ppm.

N,N′ - bis - (2 - triphenylphosphoniobenzylidene) heptane - 1,7 - diamine dibromide. (**9**; $n = 7$). This was isolated as a hygroscopic brown solid (~ 70%), δ^{31}P($CDCl_3$): 24.78 ppm; δ^1H($CDCl_3$): 8.5 (s, 2H), 8.2–7.1 (m, 38ArH), 2.6 (t, 4H), 0.7 (m, 10H) ppm.

N,N′ - bis - (2 - triphenylphosphoniobenzylidene) octane - 1,8 - diamine dibromide. (**9**; $n = 8$). This was isolated as a brown hygroscopic solid (~ 62%), δ^{31}P($CDCl_3$): 24.69 ppm; δ^1H($CDCl_3$): 8.6 (s, H), 8.1–7.2 (m, 38ArH), 2.7 (t, 4H), 0.7 (m, 12H) ppm.

N,N′ - bis - (2 - triphenylphosphoniobenzylidene) dodecane - 1,12 - diamine dibromide. (**9**; $n = 12$). This was isolated as a brown hygroscopic solid (~ 63%), δ^{31}P($CDCl_3$): 25.05 ppm; δ^1H($CDCl_3$): 8.35 (s, 2H), 8.1–7.3 (m, 38ArH), 2.7 (t, 4H), 0.8 (m, 20H) ppm.

N,N′ - bis - (2 - triphenylphosphoniobenzylidene) 4,4′-diaminodiphenylmethane dibromide. (**10**; X = $Ph_3P^+Br^-$). This was isolated as yellow crystals (70%), m.p. > 300°C (from EtOH–EtOAc) (Found: C, 67.1; H, 4.6; N, 2.5. $C_{63}H_{50}N_2Br_2P_2 \cdot 4H_2O$ requires: C, 67.0; H, 5.1; N, 2.5%), δ^{31}P($CDCl_3$): 25.89 ppm; δ^1H($CDCl_3$): 8.65 (s, 2H), 8.2–7.2 (m, 38ArH), 6.75–5.95 (8ArH) (deceptively simple $[AX]_2$ system), 3.65 (s, 2H) ppm. (Found: $(M - {}^{81}Br)^+$, 975.2647. $C_{63}H_{50}N_2P_2Br_2$ requires: $(M - {}^{81}Br)^+$, 975.2632).

N,N′ - bis - (2 - tributylphosphoniobenzylidene) 4,4′-diaminodiphenylmethane dibromide. (**10**; X = $Bu_3P^+Br^-$). This was isolated as yellow crystals (67%), m.p. > 300°C (from $CHCl_3$–EtOAc) (Found: C, 63.8; H, 7.9; N, 2.9. $C_{51}H_{74}N_2Br_2P_2$ requires: C, 64.1; H, 8.0; N, 2.9%), δ^{31}P($CDCl_3$): 34.01 ppm; δ^1H($CDCl_3$): 8.8 (s, 2H), 8.0 (m, 8ArH), 7.3 (s, 8ArH), 4.1 (s, 2H), 2.95 (m, 12H), 1.50 (m, 24H), 0.8 (m, 18H) ppm.

N,N′ - bis - (2 - triphenylphosphoniobenzylidene) 1,4 - diaminobenzene dibromide. (**11**; X = $Ph_3P^+Br^-$). This was isolated as orange crystals (76%), m.p. > 300°C (from $CHCl_3$–EtOAc) (Found: C, 67.6; H, 4.6; N, 2.8: $C_{56}H_{44}N_2Br_2P_2 \cdot 2H_2O$ requires: C, 67.1; H, 4.8; N, 2.8%) δ^{31}P($CDCl_3$): 25.86 ppm; δ^1H($CDCl_3$) 8.75 (s, 2H) 7.9–7.3 (m, 42ArH) ppm.

N,N′ - bis - (2 - tributylphosphoniobenzylidene) 1,4 - diaminobenzene dibromide. (**11**; X = Bu_3P^+

Br^-). This was isolated as an orange hygroscopic solid, $\delta^{31}P(CDCl_3)$: 33.60 ppm; $\delta^1H(CDCl_3)$: 8.7 (s, 2H), 8.1–7.3 (m, 12ArH), 2.80 (m, 12H), 1.40 (m, 24H), 0.9 (m, 18H) ppm.

General preparation of quinoxaline diphosphonium salts

The quinoxaline (10^{-3} mol), bis(tertiary phosphine) nickel(II) chloride (10^{-3} mol) and an extra mol of the appropriate tertiary phosphine were heated together under reflux in ethanol in a nitrogen atmosphere for 6–8 h. The product isolation procedure described above was employed and the following salts were isolated:

2,3 - *Bis* - (2 - *triphenylphosphoniophenyl)quinoxaline dibromide.* (**13**; R = Ph; X = Br; Y = $Ph_3P^+Br^-$). A cream solid (50%), m.p. 270°C decomposes (from $CHCl_3$–EtOAc) (Found: C, 69.1; H, 4.9: $C_{56}H_{42}N_2Cl_2P_2$. $CHCl_3$ requires: C, 68.8; H, 4.3%), $\delta^{31}P(CDCl_3)$: 26.73 ppm.

2,3-*Bis*-(2-*tributylphosphoniophenyl)quinoxaline dibromide.* (**13**; R = Bu; X = Br; Y = $Bu_3P^+Br^-$). A cream solid was collected (41%), m.p. 240°C (from $CHCl_3$–ether) (Found: C, 64.3; H, 8.4; N, 3.3. $C_{44}H_{66}N_2Cl_2P_2 \cdot 4H_2O$ requires: C, 63.8; H, 8.9; N, 3.4%), $\delta^{31}P(CDCl_3)$: 32.96 ppm; $\delta^1H(CDCl_3)$: 8.1 (m, 4ArH), 7.6 (m, 8ArH), 2.85 (m, 12H), 1.45 (m, 24H), 0.8 (m, 18H) ppm.

Preparation of mono-phosphonium salts

General procedure. The template (10^{-3} mol), tertiary phosphine (3×10^{-3} mol) and nickel(II) bromide (2×10^{-3} mol) were heated together under reflux in ethanol (10 cm^3) in a nitrogen atmosphere for 6–8 h. The phosphonium salt products were isolated as described above, except that the aqueous solutions of the salts derived from 2-iodobenzoic acid were acidified with hydriodic acid prior to extraction with chloroform.

2 - *Carboxyphenyltriphenylphosphonium iodide.* (**18**; R = Ph). This was isolated as a cream coloured solid (44%), m.p. 120°C (from $CHCl_3$–EtOAc) (Found: C, 57.2; H, 4.7. $C_{25}H_{20}IO_2P \cdot H_2O$ requires: C, 56.8; H, 4.2%), $\delta^{31}P(CDCl_3)$: 26.18 ppm; $\delta^1H(CDCl_3)$: 9.8 (s, 1H), 7.8 (m, 19ArH) ppm.

2 - *Carboxyphenyltributylphosphonium iodide.* (**18**; R = Bu). This was obtained as a light-brown solid (56%), m.p. 184°C (from $CHCl_3$–ether) (Found: C, 51.2; H, 7.5. $C_{19}H_{32}IO_2P$ requires: C, 50.7; H, 7.1%), $\delta^{31}P(CDCl_3)$: 34.98 ppm; $\delta^1H(CDCl_3)$: 9.7 (s, 1H), 8.6–7.7 (m, 4ArH), 2.7 (m, 6H), 1.5 (m, 12H), 0.9 (m, 9H) ppm.

8 - (*N - benzylidene)amino - 1 - naphthyltriphenylphosphonium bromide* (**16**). This was isolated as a pale yellow solid 67%), m.p. 90–95°C decomposes (from $CHCl_3$–EtOAc) (Found: C, 72.2; H, 4.7; N, 2.4. $C_{35}H_{27}N_1P_1Br_1$ $0.5H_2O$ requires: C, 72.3; H, 4.8; N, 2.4%), $\delta^{31}P(CDCl_3)$: 24.1 ppm; $\delta^1H(CDCl_3)$: 8.5 (d, 1H), 8.3–6.3 (m, 26ArH) ppm.

Acknowledgement—We thank the SERC for a studentship (to P.E.C.).

REFERENCES

1. D. W. Allen, P. E. Cropper, P. G. Smithurst, P. R. Ashton and B. F. Taylor, *J. Chem. Soc., Perkin Trans. I* 1986, 1989.
2. D. W. Allen, I. W. Nowell, L. A. March and B. F. Taylor, *J. Chem. Soc., Perkin Trans. I* 1984, 2523.
3. N. Hall and R. Price, *J. Chem. Soc., Perkin Trans. I* 1979, 2634.
4. J. A. Connor, D. Dubowski, A. C. Jones and R. Price, *J. Chem. Soc., Perkin Trans. I* 1982, 1143.
5. D. W. Allen, P. E. Cropper and I. W. Nowell, *Polyhedron* 1989, **8**, 1039.
6. D. W. Allen, P. E. Cropper and I. W. Nowell, *J. Chem. Res.(S)* 1987, 298, (M) 2562.
7. L. M. Venanzi, *J. Chem. Soc.* 1958, 719.
8. R. L. Letsinger and J. A. Gilpin, *J. Org. Chem.* 1964, **29**, 243.
9. H. Bendas and C. J. Djerassi, *J. Am. Chem. Soc.* 1956, **78**, 2474.
10. R. Lesser, A. Glaser and G. Aczel, *Justus Liebigs Annln. Chem.* 1914, **402**, 31.
11. G. Suld and A. P. Stuart, *J. Org. Chem.* 1964, **29**, 2939.
12. H. G. Rule and H. M. Turner, *J. Chem. Soc.* 1935, 317.
13. V. Balasubramaniyan, *Chem. Rev.* 1966, **66**, 567.
14. L. F. Fieser and A. M. Seligman, *J. Am. Chem. Soc.* 1939, **61**, 137.
15. L. Kahovec and J. Wagner, *Mschr. Chem.* 1943, **74**, 279.
16. J. S. Pizey and R. L. Wain, *J. Sci. Fd Agric.* 1959, **10**, 577.
17. A. I. Vogel, *Textbook of Practical Organic Chemistry*, 4th edn, pp. 498–561. Longman, London (1978).

Polyhedron Vol. 9, No. 1, pp. 137–141, 1990
Printed in Great Britain

0277–5387/90 $3.00+.00
© 1989 Pergamon Press plc

KINETICS AND MECHANISM OF THE REACTION OF NITRILOTRIACETATOCHROMIUM(III) WITH SOLOCHROME YELLOW 2G

ZHANG HUALIN* and ZHANG XU

Department of Chemistry, Fudan University, Shanghai, China

(*Received* 16 *May* 1989; *accepted after revision* 22 *August* 1989)

Abstract—The kinetics of the mixed-ligand complex formation reaction of [Cr(NTA)(H_2O)(H_2O/OH)] (NTA = nitrilotriacetic acid) with Solochrome Yellow 2G [salt of 2-hydroxy-5-[4-sulphophenyl)azo]benzoic acid, $Na(C_{13}H_9N_2O_6S \cdot 2H_2O)$] were investigated in the pH range 5–7 at 40°C and ionic strength 0.1 mol dm^{-3} ($NaClO_4$). The protonation constant of [Cr(NTA)(H_2O)(OH)] at these conditions was determined photometrically and the value $K_a = 2.69 \times 10^5$ mol^{-1} dm^3 was obtained. TLC was also used to monitor the reaction. The pseudo-first-order rate constants (k_{obs}) were found to follow the equation:

$$k_{obs}^{-1} = b_i + a_i C_{Cr(NTA)}^{-1}$$

where a_i and b_i were varied with pH. The results conform to the following scheme:

$$\begin{array}{lll} [Cr(NTA)(H_2O)_2] + HL^{2-} \overset{Q_1}{\rightleftharpoons} [Cr(NTA)(H_2O)(HL)]^{2-} & \xrightarrow{k_1} & H_3O^+ \\ K_a \Big\| \Big\downarrow & & [Cr(NTA)L]^{3-} + \\ [Cr(NTA)(H_2O)(OH)]^- + HL^{2-} \overset{Q_2}{\rightleftharpoons} [Cr(NTA)(OH)(HL)]^{3-} & \xrightarrow{k_2} & H_2O \end{array}$$

and hence gives:

$$b_i = \frac{Q_1 K_a [H^+] + Q_2}{Q_1 K_a k_1 [H^+] + k_2 Q_2}; \quad a_i = \frac{K_a [H^+] + 1}{Q_1 K_a k_1 [H^+] + k_2 Q_2}.$$

The constants of mixed-ligand formation reaction determined were:

$$Q_1 = 1970\ mol^{-1}\ dm^3, \quad Q_2 = 650\ mol^{-1}\ dm^3,$$
$$k_1 = 2.3 \times 10^{-2}\ s^{-1}, \quad k_2 = 1.7 \times 10^{-2}\ s^{-1}.$$

The values of the Q_1, Q_2 and TLC results indicate that the reaction underwent two consecutive steps which involved a rapid formation of the monodentate coordinated dye intermediate followed by the rate-determining ring closure. Similar to TAPP, EDTA etc. as a primary ligand, the coordination of NTA can also greatly enhance the reaction activity of chromium(III) to form the mixed-ligand complex. It can be explained by the increasing electron density of the central chromium(III) and the hydrogen bond formation between the free oxy ion and the adjacent coordinated water.

Azo dyes are widely used in the dyeing industry and chromium(III) azo dye complexes are common mordant dyes.[1] Substitution inertness of $[Cr(H_2O)_6]^{3+}$ is well known.[2] However, it was reported that the anation reactions of $[Cr^{III}Y(H_2O)_n]$, Y represents NH_3 and $C_2O_4^{2-}$, with unidentate ligands are about 10 times faster than that of $[Cr(H_2O)_6]^{3+}$.[3] Moreover, in the case of porphin[4] or EDTA[5] as primary ligand, the rates of anation of the secondary ligand to the chromium(III) complex

* Author to whom correspondence should be addressed.

increases by three to six orders of magnitude. Few studies on the substitution reactions of chromium(III) with dyes have been reported[6] and the kinetic behaviour of chromium(III) mixed-ligand complexes containing azo dyes has not been noticed. The thermodynamic equilibria of reactions of Solochrome Yellow 2G with metal ions have been investigated extensively, but the kinetic and mechanism studies on complexation reactions between them have not been reported so far. In the present work, the kinetics and mechanism of the reaction which involves mixed-ligand complex formation between $[Cr(NTA)(H_2O)(H_2O/OH)]$ and Solochrome Yellow 2G (NaH_2L) have been studied in order to learn how the primary ligand, NTA, affects the lability of chromium(III).

EXPERIMENTAL

Materials

Solochrome Yellow 2G was prepared by following a procedure published elsewhere[7] and the purity was checked by elemental analysis.

$(NH_4)[Cr(NTA)(H_2O)(OH)]\cdot 2H_2O$ was synthesized by the known method.[8] The chromium analysis and visible spectrum of the complex were in good agreement with those in the literature.[8]

All other chemicals used were analytical reagent grade. All solutions were made in deionized water.

Apparatus

Spectra and absorbance of prepared solutions were recorded using a UV-240 recording spectrophotometer (Shimadzu, Japan). The pH measurements were made using a PHM84 research pH meter (Radiometer, Copenhagen).

Visible spectra

The absorption spectra of Solochrome Yellow 2G, CrNTA complexes and their mixture (Cr (NTA)–Solochrome Yellow 2G = 10 : 1) are shown in Fig. 1. Spectral observation indicates the light yellow species of Solochrome Yellow 2G HL^{2-} [Fig. 1(a)] which exists in the pH range 5–7 changes to the orange species, L^{3-} [Fig. 1(b)] in solution at pH 11. Figure 1(c) and (d) are the absorption spectra of $[Cr(NTA)(H_2O)(OH)]^-$ and $[Cr(NTA)(H_2O)_2]$, respectively. Figure 1(e) and (f) show the spectra of a mixture of Cr(NTA) and Solochrome Yellow 2G at pH 6.5 at the beginning of mixing and after completion of the reaction. By comparison of the curves in Fig. 1 it is shown that curve (e) is similar to curve (a), while curve (f) is closed to curve (b) which reveals that Solochrome Yellow 2G in the reaction product is a bidentate ligand. Hence, the reaction kinetics were followed by monitoring the growth in absorbance due to the bidentate Solochrome Yellow 2G mixed-ligand complex at 400 nm and the K_a of $[Cr(NTA)(H_2O)(OH)]$ was determined at 555 nm.

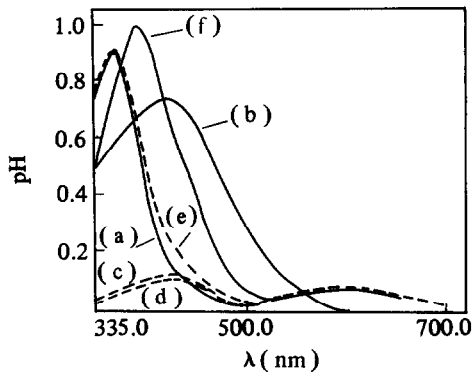

Fig. 1. The absorption spectra of Solochrome Yellow 2G, Cr(NTA) complexes and their mixture at different pH. (a) Solochrome Yellow 2G; $c = 3\times10^{-4}$ mol dm^{-3}, pH = 5–7; (b) Solochrome Yellow 2G; $c = 3\times10^{-4}$ mol dm^{-3}, pH = 11; (c) $[Cr(NTA)(H_2O)_2]$; $c = 3\times10^{-3}$ mol dm^{-3}; (d) $[Cr(NTA)(H_2O)(OH)]^-$; $c = 3\times10^{-3}$ mol dm^{-3}; (e) Solochrome Yellow 2G; $c = 3\times10^{-4}$ mol dm^{-3}, pH = 6.5, 2 min after mixing; (f) 24 h after mixing.

K_a *of* $[Cr(NTA)(H_2O)(OH)]$

The protonation constant of $[Cr(NTA)(H_2O)(OH)]$ was determined photometrically by the published method[9] at 40°C and $\mu = 0.1$ ($NaClO_4$). The equilibrium constant K_a is given as 2.69×10^5 mol^{-1} dm^3.

Kinetic measurements

The curve of the anation reaction in the pH range 5–7 at 40°C and an ionic strength of 0.1 ($NaClO_4$) was followed by observing the increase in absorbance at 400 nm, where the product and the reactants differ appreciably. All experiments were carried out in excess of Cr(NTA) complex and the pseudo-first-order rate constants, k_{obs}, were computed from the gradients of the linear plots of $\ln(A_\infty - A_t)$ vs time by means of a least-squares program. The concentration of Solochrome Yellow 2G is 3.36×10^{-5} mol dm^{-3} and the concentration of Cr(NTA) complex ranges from 3.40×10^{-4} to 12.8×10^{-4} mol dm^{-3}.

TLC analysis

The chromatography of samples was carried out using a silica gel 60 F_{254} (E. Merck) chromatosheet

and ethanol was applied as the developing solvent. The colour and R_f value of Solochrome Yellow 2G (pH 5, HL^{2-}) and Cr(NTA) complex were light yellow, 0.53, purple and zero, respectively. The mixed solution of the Cr(NTA) complex and Solochrome Yellow 2G (10 : 1) at pH 5 was spotted at (a) $t = 2$ min, (b) $t = 1$ h and (c) $t = 24$ h after mixing and then chromatographed. The chromatograms showed the constituents in the reaction mixture were separated to form two or three well-defined zones with different colours. Three coloured spots were shown in situations (a) and (b), the colours and R_f values were as follows: light yellow, 0.48; orange, 0.30; and purple, zero. However, the light yellow substance disappeared and another two coloured species still remained in situation (c). Moreover, the colour intensity of the light yellow species decreased until it disappeared when the reaction time increased and the colour intensity of the orange substance increased with increasing reaction time. Hence, it is reasonable to assume that the orange and purple species are the final product; $[Cr(NTA)L]^{3-}$ and remaining Cr(NTA) complex. The light yellow species which formed quickly when the reactants were mixed and has a R_f value close to HL^{2-} may be assumed to be a steady intermediate.

RESULTS AND DISCUSSION

The pseudo-first-order rate constants, k_{obs}, were measured at various pH values and concentrations of the Cr(NTA) complex. The results are listed in Table 1.

Table 1 shows that k_{obs} decreases with an increase of pH at a given concentration of Cr(NTA), while it increases with an increase of Cr(NTA) concentration at the same pH. In the pH range studied, the plots of k_{obs}^{-1} vs $[Cr(NTA)]_T^{-1}$ at interpolated pH values were linear and some examples are shown in Fig. 2; the slopes, a_i, and intercepts, b_i, of the straight lines were both increased with the increase of pH.

According to the acid dissociation constant of Solochrome Yellow 2G and K_a of $[Cr(NTA)(H_2O)(OH)]$, we can consider that the main species of these in the pH range 5–7 are HL^{2-}, $[Cr(NTA)(H_2O)(OH)]^-$ and $[Cr(NTA)(H_2O)_2]$. As a result of the consistent dependence of k_{obs} on the Cr(NTA) complex concentrations and pH of solutions with an ion-pair mechanism, the complexation reaction probably progresses along the following two parallel paths:

$$[Cr(NTA)(H_2O)_2] + HL^{2-} \overset{Q_1}{\rightleftharpoons} I_1 \xrightarrow{k_1} [Cr(NTA)L]^{3-} \quad (1)$$

$$K_a \uparrow\downarrow$$

$$[Cr(NTA)(H_2O)(OH)]^- + HL^{2-} \overset{Q_2}{\rightleftharpoons} I_2 \xrightarrow{k_2} [Cr(NTA)L]^{3-}. \quad (2)$$

Table 1. Pseudo-first-order rate constants k_{obs} (s^{-1}) for the reaction of Solochrome Yellow 2G with Cr(NTA) at different concentrations of Cr(NTA) and pH values

	Concentration of Cr(NTA) 3.40×10^{-4} mol dm^{-3}						
pH	7.70	6.92	6.71	6.05	5.76	5.50	4.70
$10^3 k_{obs}$	2.2	2.8	3.4	4.8	5.1	5.9	6.8
	Concentration of Cr(NTA) 4.90×10^{-4} mol dm^{-3}						
pH	7.05	6.72	6.39	6.02	5.83	5.44	5.02
$10^3 k_{obs}$	3.2	4.2	5.4	6.5	7.1	7.9	8.6
	Concentration of Cr(NTA) 6.70×10^{-4} mol dm^{-3}						
pH	6.90	6.65	6.41	6.20	5.90	5.54	5.31
$10^3 k_{obs}$	4.8	5.6	6.6	7.2	8.0	9.0	9.4
	Concentration of Cr(NTA) 9.00×10^{-4} mol dm^{-3}						
pH	6.94	6.67	6.34	5.94	5.53	5.21	
$10^3 k_{obs}$	5.6	6.5	7.8	9.1	10.1	10.6	
	Concentration of Cr(NTA) 1.28×10^{-3} mol dm^{-3}						
pH	7.06	6.82	6.35	6.12	5.85	5.41	
$10^3 k_{obs}$	5.5	6.7	8.9	10.5	10.6	11.5	

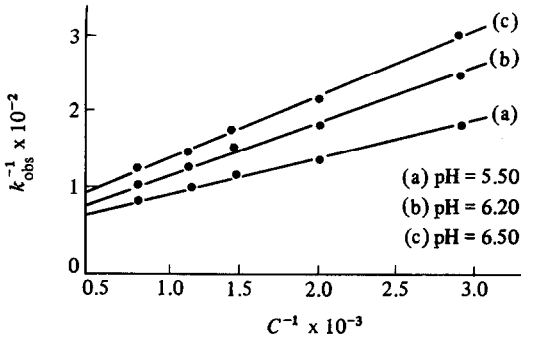

Fig. 2. Linear dependence of k_{obs}^{-1} on $[Cr(NTA)]_T^{-1}$ at different pH.

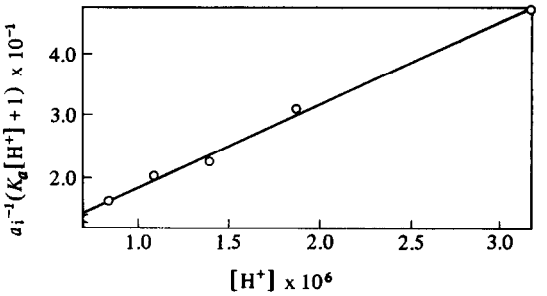

Fig. 3. A plot of $a_i^{-1}(K_a[H^+]+1)$ vs $[H^+]$.

The rate equation derived on the basis of the above mechanism under the pseudo-first-order conditions is given by eq. (3):

$$\frac{d \ln [Cr(NTA)L]}{dt} = k_{obs}[NaH_2L]_T$$

and

$$k_{obs} = \frac{(Q_1K_ak_1[H^+]+k_2Q_2)[Cr(NTA)]_T}{1+K_a[H^+]+(Q_1K_a[H^+]+Q_2)[Cr(NTA)]_T}, \quad (3)$$

where $[NaH_2L]_T$ and $[Cr(NTA)]_T$ are the total concentrations of Solochrome Yellow 2G and Cr(NTA) complex added. Equation (3), on arrangement, gives eq. (4) which satisfies the observed results (Fig. 2):

$$k_{obs}^{-1} = \frac{Q_1K_a[H^+]+Q_2}{Q_1K_ak_1[H^+]+k_2Q_2} + \frac{K_a[H^+]+1}{Q_1K_ak_1[H^+]+k_2Q_2} \times \frac{1}{[Cr(NTA)]_T}. \quad (4)$$

Hence, the slope, a_i, and intercept, b_i, can be expressed as eqs (5) and (6):

$$a_i = \frac{K_a[H^+]+1}{Q_1K_ak_1[H^+]+k_2Q_2} \quad (5)$$

and

$$b_i = \frac{Q_1K_a[H^+]+Q_2}{Q_1K_ak_1[H^+]+k_2Q_2}, \quad (6)$$

which on arrangement give eqs (7) and (8)

$$\frac{K_a[H^+]+1}{a_i} = Q_1K_ak_1[H^+]+k_2Q_2 \quad (7)$$

and

$$b_i(A_1[H^+]+B_1) = Q_1K_a[H^+]+Q_2. \quad (8)$$

Figures 3 and 4 show a plot of $a_i^{-1}(K_a[H^+]+1)$ and $b_i(A_1[H^+]+B_1)$ as a function of $[H^+]$, which give straight lines, and the straight lines obtained have the slopes $A_1 = Q_1K_ak_1$, $A_2 = Q_1K_a$ and intercepts $B_1 = k_2Q_2$, $B_2 = Q_2$. From the slopes and intercepts we can obtain k_1, k_2 and Q_1, Q_2. The results are listed in Table 2.

The calculation of electrostatic interaction involving the 0, 2− and 1−, 2− charges (we ignore the negative charge on the SO_3^- group), as developed by Fuoss, shows that the ion-pair formation constants, K_0, are less than 0.2.[10] However, the Q_1 and Q_2 values obtained for the present system far exceed the K_0 calculated and can be compared with the stability constants of the chromium(III) acetate complex (log K_1 = 4.67, log K_2 = 2.52, log K_3 = 2.69).[11] Hence, it may be reasonable to assume that I_1 and I_2 could not be ion-pairs, but rapidly formed intermediates, $[Cr(NTA)(H_2O)(HL)]^{2-}$ and $[Cr(NTA)(OH)(HL)]^{3-}$, in which only the carboxylate of HL^{2-} is coordinated to chromium(III). $Q_1 > Q_2$ indicates that the coordinated hydroxyl group weakens the coordinate ability of central metal chromium(III). Furthermore, the TLC results also supported the process in which the carboxylate complex formed rapidly and then gradually changed to the product, i.e. the mixed-ligand complex formation reaction underwent two consecutive steps; the rapid formation of unidentate carboxylate complex and then the slow chelate ring closure. Consequently, it is suggested that the rate-determing step is chelate ring closure

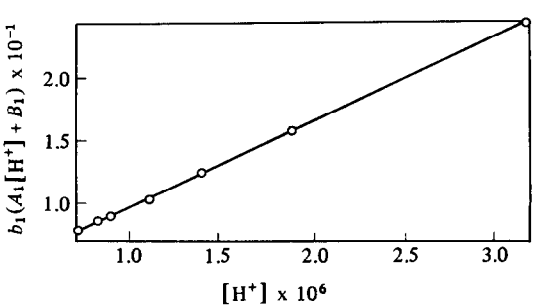

Fig. 4. A plot of $b_i(A_1[H^+]+B_1)$ vs $[H^+]$.

Table 2. Resolved rate constants for formation of the [Cr(NTA)L] complex

$A_1(1.2\pm0.1)\times10^7$	$B_1(11.0\pm0.5)$
$A_2(5.3\pm0.1)\times10^8$	$B_2(650\pm9)$
$k_1(2.3\pm0.2)\times10^{-2}\ s^{-1}$	$Q_1(1970\pm40)\ mol^{-1}\ dm^3$
$k_2(1.7\pm0.1)\times10^{-2}\ s^{-1}$	$Q_2(650\pm9)\ mol^{-1}\ dm^3$

and the rate constants of carboxylate complex formation k_1 are far greater than those of the second step ($k_{I_1} \gg 2.3\times10^{-2}$, $k_{I_2} \gg 1.7\times10^{-2}$).

It is well known that the substitution reactions of chromium(III) ion are inert. But the reaction activity can increase greatly for mixed-ligand complex formation reactions from the coordinated chromium(III) ion, the rate constants of the anation reaction of $[Cr(TAPP)(H_2O)_2]$ with NCS^- and $[Cr(EDTA)(H_2O)]$ with OAc^- are 1.56×10^{-2} $mol^{-1}\,dm^3\,s^{-1}$[4] and $3\ mol^{-1}\,dm^3\,s^{-1}$,[5] respectively, and they are $10^{3.6}$ and 10^5 times faster than that of $[Cr(H_2O)_6]^{3+}$.[12,13] In our work, the rate constants for the anation reaction of $[Cr(NTA)(H_2O)_2]$ and $[Cr(NTA)(H_2O)(OH)]^-$ with the carboxylate of Solochrome Yellow 2G are much greater than $2.3\times10^{-2}\ mol^{-1}\ dm^3\ s^{-1}$. This fact indicates that NTA can labilize the anation reaction of chromium (III) also. The results can be explained reasonably by the increasing electron density of the central chromium(III) owing to the electron donation from NTA, and this makes it more like a labile chromium(II) ion.[3] On the other hand, the free oxy ion existing in the complex ion can act as a nucleophile to form a hydrogen bond with adjacent coordinated water to weaken the $Cr—OH_2$ bond and this makes it easy for the water to leave.

Acknowledgement—This work was supported by the National Natural Science Foundation of China.

REFERENCES

1. Zhang Zhaolin and Zhang Yulin, *Jing Chu Luo He Ran Liao*, p. 101. Chemical Industry Press, Beijing (1986).
2. F. A. Cotton and G. Wilkinson, *Advanced Inorganic Chemistry*, p. 1189. Wiley, New York (1980).
3. K. R. Ashley, J. G. Leipoldt and V. K. Joshi, *Inorg. Chem.* 1980, **19**, 1608.
4. J. G. Leipoldt and H. Meyer, *Polyhedron* 1987, **6**, 1361.
5. H. Ogino, T. Watanabe and N. Tanaka, *Inorg. Chem.* 1975, **14**, 2093.
6. N. F. Kosenko, T. V. Malkova and K. B. Yatsimiskii, *Tr. Ivanov. Khim.-tekhnol. In-ta* 1976, **20**, 22.
7. V. P. Gupta, *Ind. J. Chem.* 1982, **21A**, 546.
8. A. Uehara, E. Kyuno and R. Tsuchiya, *Bull. Chem. Soc. Jpn* 1967, **40**, 2322.
9. H. M. N. H. Irving and R. H. Al-Jarrah, *Analytica Chim. Acta* 1972, **60**, 347.
10. R. D. Cannon, *Electron Transfer Reactions*, p. 103. Butterworths, London (1980).
11. T. C. Matts and P. Moore, *J. Chem. Soc. A* 1971, 1632.
12. C. Postmus and E. L. King, *J. Phys. Chem.* 1955, **59**, 1217.
13. S. C. Tyagl and A. A. Khan, *J. Inorg. Nucl. Chem.* 1979, **41**, 1447.

Polyhedron Vol. 9, No. 1, pp. 143–146, 1990
Printed in Great Britain

0277–5387/90 $3.00+.00
© 1989 Pergamon Press plc

COMMUNICATION

MONOTUNGSTONONAVANADATE AND *MER*-TRITUNGSTOTRIVANADATE

OLIVER W. HOWARTH* and JEREMY J. HASTINGS

Department of Chemistry, University of Warwick, Coventry CV4 7AL, U.K.

(*Received* 7 *September* 1989; *accepted* 21 *September* 1989)

Abstract—Two new tungstovanadates, $[WV_9O_{28}]^{5-}$ and *mer*-$[W_3V_3O_{19}]^{5-}$, have been identified in equilibrated aqueous solutions. ^{51}V–^{51}V COSY spectra support structures analogous to known molybdovanadates, although the tungstovanadate species more readily support a higher anionic charge.

Several tungstovanadates [tungsten(VI), vanadium(V)] have been reported in the solid state and also in aqueous solution, where they persist for some time after dissolution before chemical equilibrium is reached. These species include three with the Lindqvist structure,[1] $[W_5VO_{19}]^{3-}$, $\delta_V = -522.9$; *cis*-$[W_4V_2O_{19}]^{4-}$, $\delta_V = -508.3$; its monoprotonated form, $\delta_V = -526$ ($pK_a \approx 2.7$) and *fac*-$[W_3V_3O_{19}]^{5-}$, $\delta_V = -500$.[2] At lower pH there are also many Keggin-type species,[2] such as $[V \cdot V_2W_{10}O_{40}]^{5-}$, with a central tetrahedral vanadium and a full range of isomeric forms.

An alternative approach to the investigation of tungstovanadates is to work with fully equilibrated solutions, preferably at more than one temperature, and over a wide range of pH and metal ratios. This approach has been used with simple vanadates,[3] peroxo-[4] and sulphidovanadates[5] and molybdovanadates.[6] In this latter case the dominant species at a high V–Mo ratio were $[MoV_9O_{28}]^{5-}$, its protonated form ($pK_a \approx 2.8$, 0.6 mol dm^{-3} NaCl), and *cis*- and *trans*-$[Mo_2V_8O_{28}]^{4-}$, each with the decavanadate structure.[7] At lower V–Mo ratios a wide variety of species are found,[8,9] including $[Mo_5VO_{19}]^{3-}$ and *cis*-$[Mo_4V_2O_{19}]^{4-}$ ($pK_a = 3.9$) but not $[Mo_3V_3O_{19}]^{5-}$. However, Keggin structures are only found in small amounts. We report here two major new species apparent from a similar investigation of the tungstovanadate system, which are found in the medium pH range 3–7, alongside the (5,1) and *cis*-(4,2)† species reported earlier.

$[WV_9O_{28}]^{5-}$ AND $[HWV_9O_{28}]^{4-}$

Figure 1 shows the ^{51}V NMR spectrum of a pH 4.97 solution raised to 99°C, with 20 mmol dm^{-3} of tungsten and 80 mmol dm^{-3} of vanadium. The sharp peak at −503.5 ppm arises from *cis*-(4,2), with weaker peaks from decavanadate (0,10) at −418.3, −495.4 and (in part) −511.6 ppm. The broad peak at −564 ppm arises from exchange-averaged tetrahedral vanadate species. The remaining peaks are in the area ratios 2:2:2:1:1:1, and Table 1 shows their shifts to be close to those of $[MoV_9O_{28}]^{5-}$. Figure 2, part of a ^{51}V–^{51}V COSY spectrum[6] at pH 3.56, reveals the connectivities of the vanadium atoms in this species. The full spectrum also shows the connectivities (1,9)1–2, 1–3 and 5-6, albeit more weakly. A *fac*-(3,3) peak prob-

Table 1.

Peak	$[WV_9O_{28}]^{5-}$	$[MoV_9O_{28}]^{5-}$
1[a]	−428[b]	−425[b]
2[a]	−496.3	−495.5
3[a]	−507.8	−505
4	−513.8	−514.9
5	−518.6	−516.2
6	−525.7	−525.3

[a] Two vanadium atoms per molecule.
[b] δ_V (ppm), referred to $VOCl_3$ capillary, 20°C.

* Author to whom correspondence should be addressed.

† (*n*,*m*) is shorthand for the species $[W_nV_mO_x]^{(2x-6n-5m)-}$.

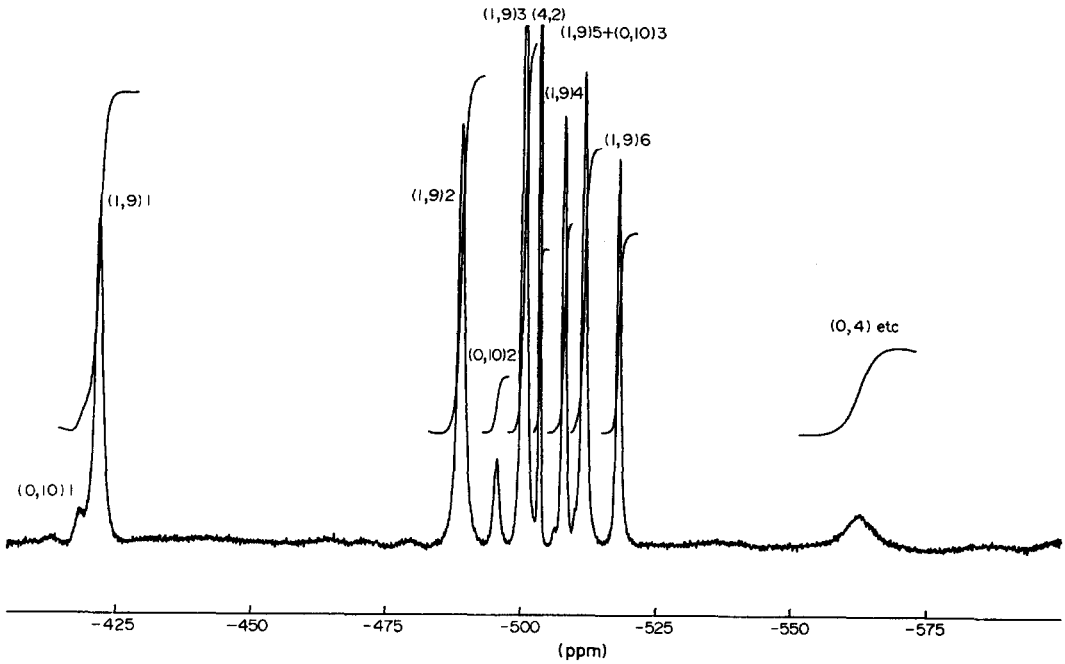

Fig. 1. ^{51}V NMR spectrum at pH 4.97, 99°C, 20 and 80 mmol dm^{-3} in tungsten and vanadium, respectively, showing predominantly $[WV_9O_{28}]^{5-}$.

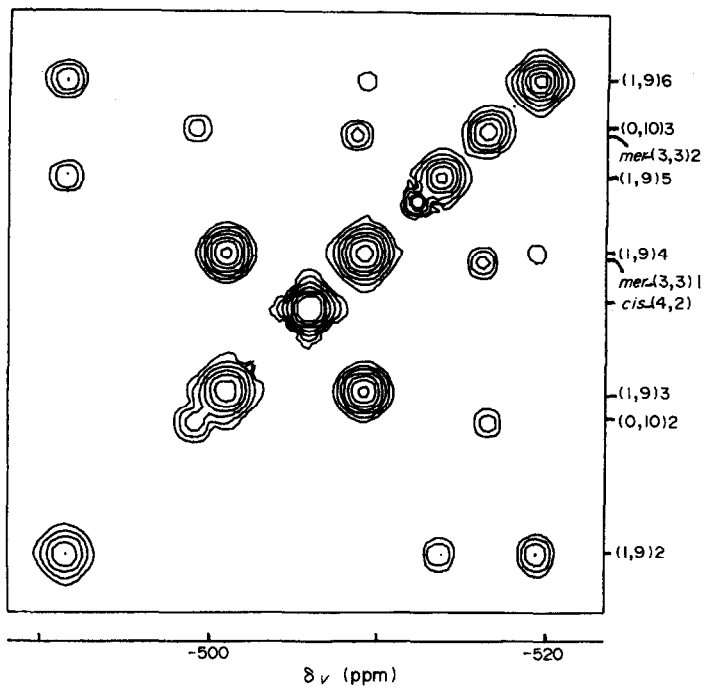

Fig. 2. 99°C ^{51}V–^{51}V COSY-90 spectrum of $[WV_9O_{28}]^{5-}$, together with some $[W_5VO_{19}]^{3-}$, $[W_4V_2O_{19}]^{4-}$ and *fac*- and *mer*-$[HW_3V_3O_{19}]^{4-}$. 400 mmol dm^{-3} in vanadium, 125 mmol dm^{-3} in tungsten; pH 3.56.

ably lies under the (1,9)3 peak, but of course has no coupling to reveal it. Thus the (1,9) tungstovanadate must be isostructural with the corresponding (1,9) molybdovanadate, and have the structure shown in Fig. 3. At lower pH the species protonates, and although decomposition occurs before protonation is complete, the pK_a (20°C) is *ca* 2.3.

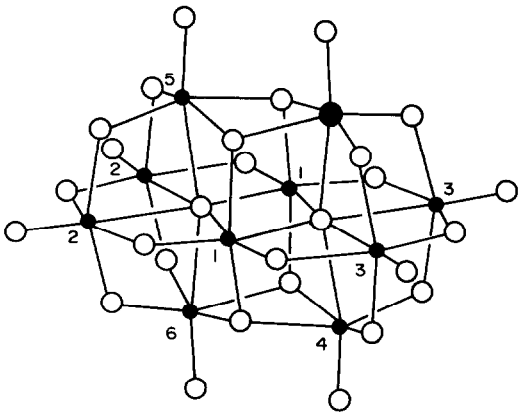

Fig. 3. Structure of $[WV_9O_{28}]^{5-}$ (● = W, • = V, ○ = O).

MER-$[W_3V_3O_{19}]^{5-}$

Figure 4 shows the ^{51}V NMR spectrum of a pH 6.51 solution, raised to 99°C, with 50 mmol dm^{-3} of both tungsten and vanadium. The dominant peaks are those from *cis*-(4,2) (truncated in the figure) and tetrahedral (0,*n*) species. Weak peaks from (1,9) are also apparent. There is also a peak at −496.7 ppm arising from *fac*-(3,3). The (4,2) and *fac*-(3,3) peaks at 20°C arise at −511.4 and −501.4 ppm, respectively, and thus correspond adequately with the values reported by Leparulo-Loftus and Pope.[2] They also have the correct relative dependence upon the tungsten–vanadium ratio.

However, two further peaks also appear strongly in Fig. 4, at −504.7 and −509.2 ppm, in the area ratio 1 : 2. The corresponding 20°C values are −513 and −518 ppm. The latter resonance was observed but not explained by Pope.[2] They have the same dependence on concentration and metal ratio as the *fac*-(3,3) peak, and show a strong ^{51}V–^{51}V coupling in COSY spectra (see Fig. 2 for one example). We therefore propose that they arise from *mer*-(3,3) (Fig. 5). The ^{51}V shifts of the resonances are consistent with Pope's observation[2] that a neighbouring VO_6 octahedron increases δ_V. They decrease below pH 6.5, at the onset of protonation.

CONCLUSIONS

Although the tungstovanadate species mirror the molybdovanadates in many ways, there are also significant differences. Judging from the relative proportions of species under comparable conditions, tungsten fits somewhat less readily into the decavanadate structure than does molybdenum. Indeed, we have little evidence yet for (2,8) tungstovanadate species. In contrast, tungstovanadate Keggin species are more stable than molybdovanadate Keggins.

Also, in all the cases where isostructural species exist, the pK_a is lower in the tungsten case [(1,9), 2.3 vs 2.8; (2,4) 2.7 vs 3.9].[6,9] Concomitantly, (3,3) species are only found with tungsten. Evidently the tungstovanadate species prefer to bear a higher

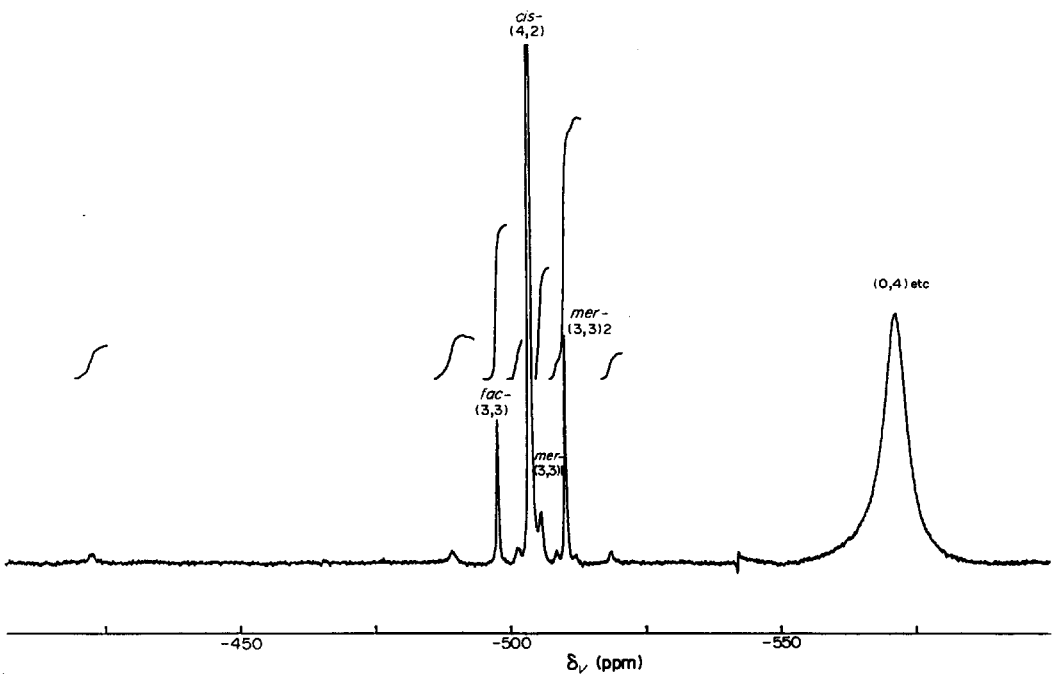

Fig. 4. ^{51}V NMR spectrum at pH 6.51, 99°C, 50 mmol dm^{-3} in tungsten and vanadium, showing predominantly $[W_4V_2O_{28}]^{4-}$, tetrahedral vanadates and *fac*- and *mer*-$[W_3V_3O_{28}]^{5-}$.

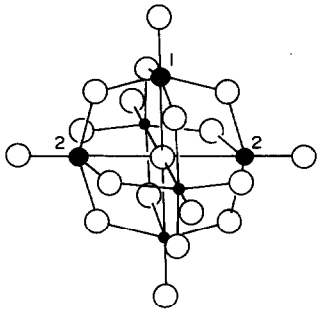

Fig. 5. Structure of *mer*-$[W_3V_3O_{28}]^{5-}$ (● = W, • = V, ○ = O).

anionic charge, perhaps because of stronger π-bonding from oxygen to tungsten.

EXPERIMENTAL

^{51}V NMR spectra were obtained at 105.2 MHz on a Bruker WH400 spectrometer, typically with 2000 transients. ^{51}V–^{51}V COSY-90 spectra[6] were obtained at 99°C to minimize linewidths. All pH values refer to the solutions at 20°C.

Acknowledgement—We thank Lage Pettersson for helpful discussion.

REFERENCES

1. I. Lindqvist, *Arkiv. Kemi.* 1952, **5**, 247.
2. M. A. Leparulo-Loftus and M. T. Pope, *Inorg. Chem.* 1987, **26**, 2112.
3. E. Heath and O. W. Howarth, *J. Chem. Soc., Dalton Trans.* 1981, 1105.
4. A. T. Harrison and O. W. Howarth, *J. Chem. Soc., Dalton Trans.* 1985, 1173.
5. A. T. Harrison and O. W. Howarth, *J. Chem. Soc., Dalton Trans.* 1986, 1405.
6. O. W. Howarth, L. Pettersson and I. Andersson, *J. Chem. Soc., Dalton Trans*, 1989, 1915.
7. A. G. Swallow, F. R. Ahmed and W. H. Barnes, *Acta Cryst.* 1966, **21**, 397.
8. R. I. Maksimovskaya and N. N. Chumachenko, *Polyhedron* 1987, **6**, 1813.
9. O. W. Howarth, L. Pettersson and I. Andersson, to be published.

Polyhedron Vol. 9, No. 1, p. 147, 1990
Pergamon Press plc. Printed in Great Britain

BOOK REVIEW

Gmelin Handbook of Inorganic Chemistry, 8th edn, Boron Compounds, Formula Index for 3rd Supplement Volumes 1–4. Springer, Berlin, 1988. ISBN 3-540-93576-2. 960.0 DM.

Volumes 1–4 of the 3rd supplement covered compounds between boron and hydrogen, boron and oxygen, boron and nitrogen or fluorine, and boron and chlorine, bromine, iodine, sulphur, selenium and tellurium, and carboranes, respectively, all up to the end of 1984. The present volume provides, in 240 pages, the index to their listings.

The first column of the tabulation gives the empirical formula of the compound, the second gives the linear molecular formulae, and the third gives the page reference in the appropriate volume. The authors are R. Warncke with R. Bohrer, H. Hartwig, R. Jonuschat, B. Kalbskopf, R. Nohl, V. Nohl, H.-J. Richter-Ditten and P. Velić.

This will enhance the value of these volumes to people working in the field of boron chemistry.

Department of Chemistry
University College London
20 Gordon Street
London WC1 HOAJ, U.K.

A. G. DAVIES

Polyhedron Vol. 9, No. 2/3, pp. 149, 1990
Pergamon Press plc. Printed in Great Britain

FOREWORD

Having been "asked" by Malcolm Chisholm to act as a guest editor for a Polyhedron Symposium-in-Print on "main group chemistry, or something" one is left with the problem of narrowing this brief so as to cover something a little more manageable in scope. The choice of the chemistry of the heavier group III (13) elements aluminium, gallium and indium arose from the desire to put together a multi-disciplinary symposium which would inform and stimulate as wide a readership as possible. The often quoted, renewed interest in the chemistry of aluminium, gallium and indium is perhaps unique in that it does, indeed, cover many areas of research: inorganic, biological, organic, organometallic and solid-state chemistry. The breadth and quality of papers submitted are, I believe, due testament to this.

I have tried to give the authors as much freedom as possible in the style and content of their contributions, allowing for both timely reviews and original research to be presented. The papers are not placed in any specific order. I have, however, tried to group together related topics.

I would like to acknowledge the help of Professor Malcolm Chisholm (Executive Editor), Miss Sheryl Fellows (Polyhedron Production Editor) and Mr Mark Perigard (my secretary) for their advice and assistance with this symposium.

A. R. BARRON

Polyhedron Vol. 9, No. 2/3, pp. 151–161, 1990
Printed in Great Britain

0277–5387/90 $3.00+.00
© 1990 Pergamon Press plc

COMPARISON OF LIGANDS OF DIFFERING DENTICITY AND BASICITY FOR THE *IN VIVO* CHELATION OF ALUMINIUM AND GALLIUM

DAVID J. CLEVETTE*† and CHRIS ORVIG*

Department of Chemistry, University of British Columbia, 2036 Main Mall, Vancouver, British Columbia V6T 1Y6, Canada

Abstract—Twenty-eight chelating ligands for aluminium, gallium and indium have been evaluated as binders of the M^{3+} ions in a simple human blood plasma model. Effective formation constants (at pH 7.4) and values of pM ($-\log[M^{3+}]$) were not found to be convenient tools for the comparison of all ligands under certain conditions. Speciation modelling allowed a direct comparison amongst ligands of the binding efficacy towards these metal ions under blood plasma conditions (50 μM transferrin sites, 0.1 M citrate, pH 7.4, 25°C). Applications of speciation computer modelling to animal studies are also discussed.

We are interested in the speciation and chelation of the trivalent metal ions of aluminium, gallium and indium *in vivo*. The presence of abnormally high concentrations of aluminium in the nuclei of brain cells of Alzheimer disease patients[1,2] and the inherent neurotoxicity of aluminium,[3] as well as the wide use of radioisotopes of gallium and indium as diagnostic agents in nuclear medicine, have spawned considerable interest in the chelation chemistry of these metal ions in recent years. This Symposium-in-print is a testament in general to the burgeoning chemistry of the group 13 (IIIA) elements.

In vivo chelation of Al, Ga and In requires a basic chemical knowledge of the properties of the potential chelating ligand. If the purpose of the ligand is decorporation of the ion then considerable water solubility is needed in addition to high thermodynamic stability of the metal–ligand complex. If a complex is to be a radioactive imaging agent, lipophilicity is usually necessary to prevent washout and the stability should be such that the complex is not demetallated before it reaches its ultimate biological target. Thus, the determination of thermodynamic stability constants is a critical component of the design of complexes which will interact with biological systems in any manner.

Since we are involved in ligand design and synthesis, we have found it necessary to compare the metal-binding affinities of ligands which we have prepared with those of ligands in the literature (Fig. 1). Often it is difficult to compare directly formation constants of different ligands for a metal ion because of variations in denticity and in the number of ionizable protons. Our approach to ligand comparisons has been adopted from that pioneered by Perrin and co-workers[4,5] and refined extensively by May and Williams.[6,7] In this contribution we demonstrate a very simple blood plasma model which we have found extremely useful in comparing ligands which bind the group 13 metal ions.

THE METAL IONS

The coordination chemistry of Al, Ga and In in aqueous solution reflects the acidity of these trivalent metal ions, M^{3+}. Infinite dilution pK_a values for the hydrolysis reaction (1)

$$[M(H_2O)_6]^{3+} = [M(OH)(H_2O)_5]^{2+} + H^+ \quad (1)$$

are, in order of decreasing acidity, 2.6 for Ga, 3.9 for In and 5 for Al.[8] This is a measure of the bond strength between the metal ion and the oxygen atoms from bound water molecules. The stronger the M—O bond, the weaker the O—H bond, and the acidity increases. The reason that Ga and In are more acidic than Al has been explained classically in terms of the relative deshielding of the positive metal centres of Ga and In by the more diffuse *d*-electrons, with a concomitant higher effective

* Authors to whom correspondence should be addressed.
† Present address: Department of Chemistry, Doane College, Crete, NE 68333, U.S.A.

nuclear charge. The great affinity of the Al^{3+}, Ga^{3+} and In^{3+} ions for oxygen donor ligands has been well documented[9,10] and this paper concentrates in large part on ligands of this type.

We have used a large number of formation constants from the literature to calculate linear free energy relationships (LFERs) for the formation constants of two similar metal ions with each of two groups of ligands. The two groups of ligands are ligands which incorporate exclusively oxygen-donor groups and those which incorporate both oxygen and nitrogen coordinating atoms. (The

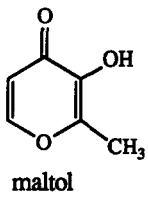

maltol

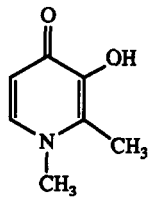

Hdpp

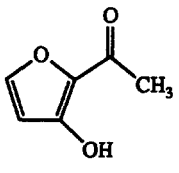

isomaltol

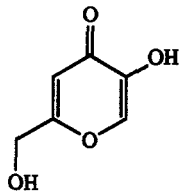

kojic acid

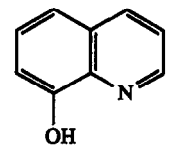

oxine

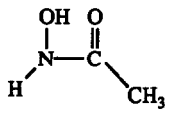

acetohydroxamic acid = aha

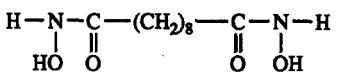

C_8-dihydroxamic acid = C_8-dha

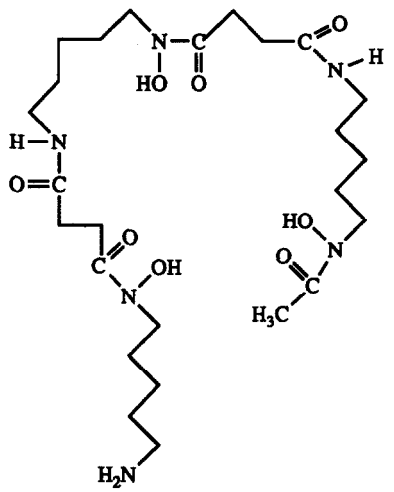

desferriferrioxamine-B = df-B

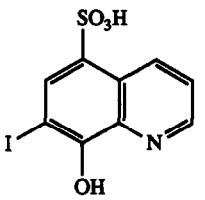

ferron

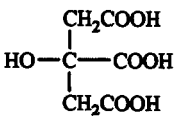

citric acid

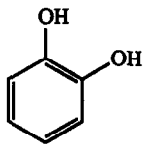

catechol

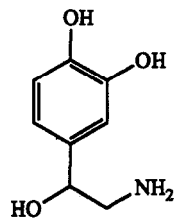

norepinephrine = norepi

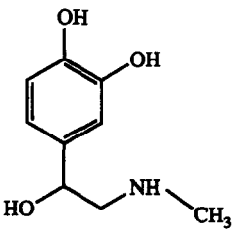

epinephrine = epi

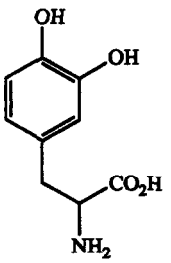

L-dopa

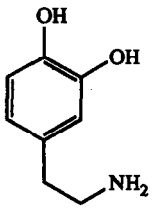

dopamine

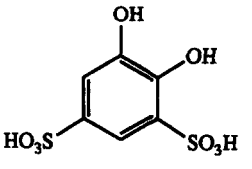

tiron

Fig. 1. The ligands.

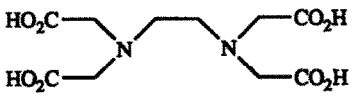

edta

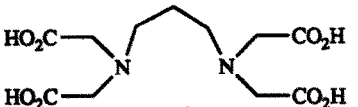

tmdta

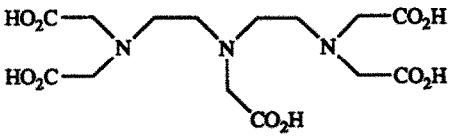

dtpa

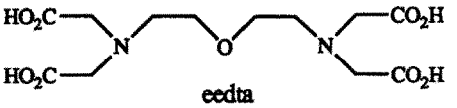

eedta

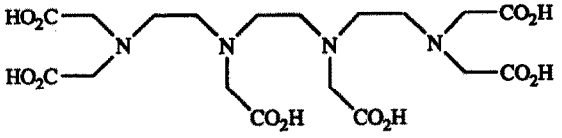

ttha

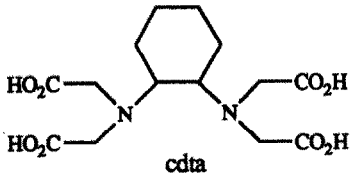

cdta

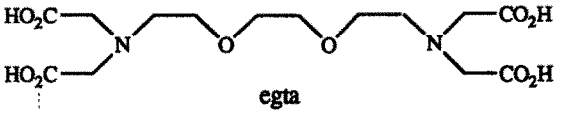

egta

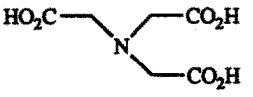

nta

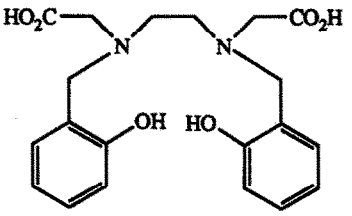

hbed

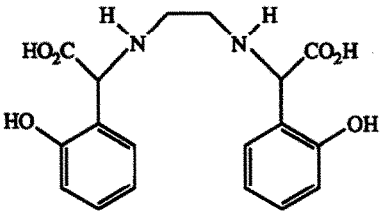

ehpg

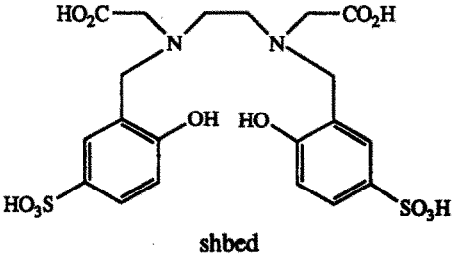

shbed

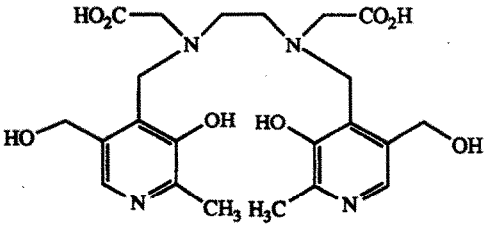

pled

Fig. 1—*continued.*

complexation of the ferric ion has been extensively studied; Fe^{3+}, with a pK_a of ~ 2.5,[8] is a convenient reference metal ion for the group 13 ions.[11–13]) Constants for Al, Ga and In were plotted individually versus Fe^{III} and the linear equations were found for O-donor ligands to be (with regression coefficients R):

$$\log K_{Al} = (0.795)\log K_{Fe} + 0.02 \quad R = 0.994 \quad (2)$$

$$\log K_{Ga} = (0.954)\log K_{Fe} - 0.65 \quad R = 0.987 \quad (3)$$

$$\log K_{In} = (0.970)\log K_{Fe} + 0.68 \quad R = 0.996 \quad (4)$$

and for O,N-donor ligands:

$$\log K_{Al} = (0.617)\log K_{Fe} + 2.48 \quad R = 0.929 \quad (5)$$

$$\log K_{Ga} = (0.991)\log K_{Fe} - 0.57 \quad R = 0.959 \quad (6)$$

$$\log K_{In} = (1.034)\log K_{Fe} - 0.73 \quad R = 0.994. \quad (7)$$

The slopes of these plots give a relative ordering of the affinity towards O- or O,N-donor ligands. The slope with O,N ligands for Al^{3+} is lower than that with O ligands, whereas the reverse is true for Ga^{3+} and In^{3+}. The slopes of the O-donor LFERs give the relative affinity as Fe > In > Ga ≫ Al. Indium is misplaced before Ga when compared with the order of metal ion acidities and this might be explained by size considerations. Indium forms stronger complexes than Fe (slope > 1) with the O,N-donor ligands in this study; they are mostly hexadentate ligands (edta derivatives) with large "bites" which tend to favour In chelation.

THE LIGANDS

In describing the equilibrium between a metal ion and a ligand, a formation constant (K' or K) is reported either in terms of the reaction with the fully protonated ligand [HL—eq. (8)]:

$$M + HL = ML + H \quad K' = \frac{[ML][H]}{[M][HL]} \quad (8)$$

or more commonly, with the fully deprotonated ligand [L—eq. (9)]:

$$M + L = ML \quad K = \frac{[ML]}{[M][L]} \quad (9)$$

where charges have been omitted for clarity. Direct comparison of constants (either K or K') for a set of ligands with a metal ion does not demonstrate the differences in binding strength at a particular pH. The competition between H^+ and M^{n+} for the ligand must be considered and the fraction of protonated ligand at any specific pH becomes very important.

An effective, or conditional, formation constant is one that corrects K or K' by the fraction of ligand deprotonated at a particular pH,[14,15]

$$K_{eff(pH)} = \alpha K \quad (10)$$

or

$$\log K_{eff(pH)} = \log K + \log \alpha, \quad (11)$$

where α is the fraction of deprotonated ligand ($0 < \alpha \leqslant 1$) as governed by the pK_a values. (Similarly, one may obtain $\log K_{eff(pH)} = \log K' - \log \alpha$.) This provides a more direct comparison of formation constants within a set of ligands (of same denticity) at a set pH value (obviously, pH 7.4 is commonly chosen). In Table 1, $\log K_{eff(7.4)}$ values are given for some multidentate O-donor ligands that are known[9] to be reasonable chelators for trivalent metal ions in aqueous solution. For consistency, these values were calculated from formation constants* determined as close to 25°C and 0.15 M ionic strength (isotonic) as possible. Table 2 presents similar calculations for bidentate ligands. Each ligand (except transferrin) is shown in Fig. 1. The discussion is limited to ligands with C or N atoms adjacent to the bonding O atoms (phosphate ligands are not considered, *vide infra*).

Another commonly used comparison of the strengths of metal–ligand complexes is the pM value. The pM is the negative log of the concentration of the free metal ion (i.e. the negative log of the concentration of $Al(H_2O)_6^{3+}$, $Ga(H_2O)_6^{3+}$ or $In(H_2O)_6^{3+}$). This value is computed from formation constants at a given pH (again, often 7.4) with known total metal and ligand concentrations. Commonly, pM is calculated for a solution containing 1 μM total metal and 10 μM ligand. These concentration levels are used to calculate pM values at pH 7.4 for the ligands listed in Tables 1 and 2. The higher the pM value, the stronger the chelator. Values of pM allow a direct comparison between ligands of different denticities as long as each ligand prevents hydrolysis of the metal ion. Figure 2 graphs the pM "excess" over that allowed by hydrolysis for a selected set of ligands with Al^{3+}, Ga^{3+} and In^{3+} at pH 7.4. (Care must be taken in comparing pM values such that the ligand-to-metal ratio is the same; if the ligand–metal ratio increases, the pM value increases accordingly.) When comparing pM values with weaker ligands, the hydroxide ion (OH^-) limits the upper amount of free metal ion in solution (i.e. the lower limit on pM) so that weak ligands have the same pM value as does OH^-. Water may be excluded from the calculations in order to compare the relative strength of these

* All formation constants have been taken from ref. 9 unless otherwise stated.

Table 1. Values of pM and log K_{eff} for the multidentate ligands with Al^{3+}, Ga^{3+} and In^{3+}. log K_{eff} is the effective formation constant at pH 7.4 calculated from data obtained from ref. 9, unless otherwise indicated. Values of pM are calculated for 1 μM total metal and 10 μM total ligand at pH 7.4 and 25°C. The minimum pM values allowed by hydrolysis are 12.6 (Al), 18.4 (Ga), and 15.3 (In)[a]

	Al		Ga		In	
Ligand	log K_{eff}	pM	log K_{eff}	pM	log K_{eff}	pM
df-B	19.5[b]	20.4	23.5[b]	24.4	15.9[b]	16.9
C_8dha	11.7[b]	13.0	NR		NR	
cdta	14.5	15.4	18.2	19.2	23.8	24.7
edta	13.7	14.7	18.9	19.9	22.1	23.1
dtpa	14.4	15.3	20.1	20.9	24.8	25.6
egta	10.4	12.6	NR		NR	
tmdta	12.5	13.6	17.0	18.6	17.4	18.4
ttha	15.8	16.8	NR		NR	
eedta	NR		17.5	18.7	22.0	22.9
pled	NR		23.0	23.9	17.2	18.2
hbed	NR		29.8	30.8	29.9	30.9
shbed	NR		28.3	29.3	20.2	21.2
ehpg	NR		24.3	25.3	17.1	18.1
nta	9.1	12.6	11.5	18.4	14.6	15.3
citrate	7.2[c]	13.3	10.0	18.4	NR	
Tf	13.5 (12.5)[d]	14.5	20.3 (19.3)[e]	20.9	30.5 (25.5)[f]	31.1

[a] NR = not reported.
[b] Reference 40.
[c] Reference 20.
[d] Reference 12.
[e] Reference 41.
[f] Reference 22.

Table 2. Values of pM and log β_{3eff} for the bidentate ligands with Al^{3+}, Ga^{3+} and In^{3+} calculated as in Table 1. Values of pM are also calculated for 1 μM total metal and 10 μM total ligand at pH 7.4 and 25°C[a]

	Al		Ga		In	
Ligand	log β_{3eff}	pM	log β_{3eff}	pM	log β_{3eff}	pM
aha	15.6	12.6	NR		NR	
oxine	NR		33.3	23.8	28.2	18.7
ferron	19.4	12.6	28.7	19.5	29.8	20.4
catechol	15.4	12.6	NR		NR	
dopamine	17.1[b]	12.6	NR		NR	
L-dopa	16.9[b]	12.6	NR		NR	
epi	18.2[b]	12.6	NR		NR	
norepi	18.4[b]	12.6	NR		NR	
tiron	24.9[b]	15.8	NR		NR	
kojic acid	18.1	12.6	NR		NR	
maltol	18.4	12.6	NR		NR	
isomaltol	14.5[c]	12.6	16.4[c]	18.4	14.8[c]	15.3
Hdpp	24.9[d]	15.4	31.0[e]	21.6	25.5[e]	16.2

[a] NR = not reported.
[b] Reference 31.
[c] Reference 42.
[d] Reference 43.
[e] Reference 36.

weaker ligands; however, as Martell and Motekaitis have pointed out,[16] these results are irrelevant to a real situation.

Comparison of $\log K_{eff}$ values can determine the differences among the weaker ligands as well as the stronger ones; however, this is limited in that it cannot be used to directly compare ligands of varying denticities. There does exist a linear relationship between $\log K_{eff}$ (or $\log \beta_{3eff}$) and pM for those ligands that prevent hydrolysis. For ML complexes (Table 1), $\log K_{eff}$ was close to pM -1.1 while for ML_3 complexes $\log \beta_{3eff}$ was close to pM $+9.0$. (Citrate was not included; an anomalously high pM is found because of the formation of ternary hydroxo–citrato–metal complexes.) The slopes of these pM vs $\log K_{eff}/\log \beta_{3eff}$ correlations are found to be (and can be analytically derived as) unity in both cases; however, the intercept differs by $\sim 10^{10}$ which is why a comparison of multi- and bidentate ligands using $\log K_{eff}$ or $\log \beta_{3eff}$ values is not useful.

Although the pM "excess" approach of Fig. 2 works for many ligands, we sought through speciation modelling a direct comparison of all types of ligands regardless of denticity, number of ionizable protons, or relative binding strength.

BLOOD PLASMA SPECIATION MODELLING

Ultimately, the speciation of a metal in the presence of potential chelators will provide insights into

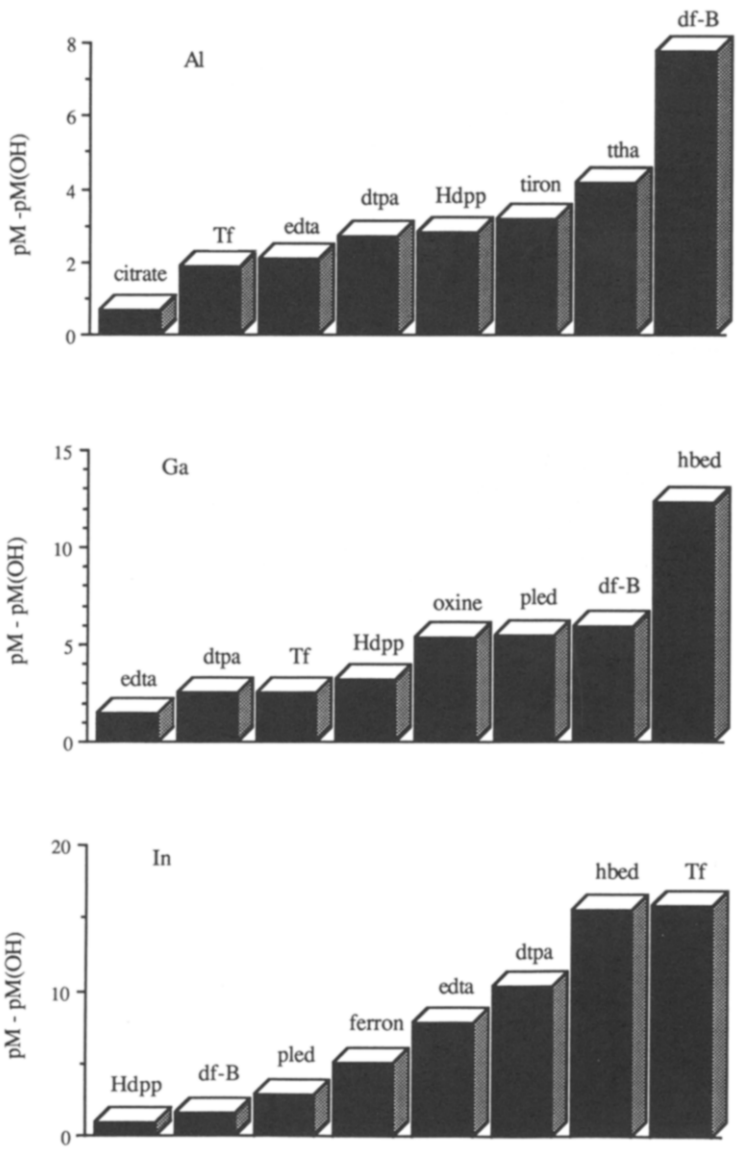

Fig. 2. The pM "excess" [pM − pM(OH)] plotted for a select group of ligands for Al (top), Ga (middle) and In (bottom) systems at pH 7.4 and 25°C.

the *in vivo* behaviour. The multi-equilibrium blood plasma model chosen for the speciation of Al^{3+}, Ga^{3+} and In^{3+} contains citrate (0.1 mM) and transferrin (abbreviated Tf, a two-sited protein[17] present at 37 μM) which are assumed to be the principal low molecular weight and high molecular weight chelators of trivalent metal ions in blood plasma, respectively.[15,18] Only 30% of the sites on Tf are saturated with Fe^{3+},[19] and the ferric ion is assumed to remain complexed with Tf in the presence of other chelating agents for modelling purposes. This leaves 50 μM empty sites on Tf available for chelation with Al, Ga or In. Transferrin binding constants in the literature are measured as effective formation constants at pH 7.4 under a quantified excess of bicarbonate. These are listed and referenced in Table 1 (one constant for each site). Citrate equilibrium constants are taken from refs 20 and 21 for Al and Ga, respectively. The often quoted first binding constant for In with Tf ($10^{30.5}$)[22] is anomalously high and is most likely inaccurate. Other workers have deduced the first formation constant for In with Tf to be $10^{23.8}$[23] or $10^{18.8}$.[24] Since values for this constant are discrepant (there may be a bicarbonate dependence), this discussion is limited to the speciation modelling of Al and Ga. (Iron is a concern in modelling Al and Ga,[13] so we have compared some calculations which include separate concentrations of Fe^{3+} and Tf and we have found results very similar to those for the simple model with 50 μM empty Tf sites.) Human serum albumin was not included in the model because of a lack of good numbers for Al-binding and because it is generally agreed not to be a good competitor for Al in the presence of the other ligands commonly found in blood.[15,18] Phosphate, although present in total at about 1.5 mM in plasma (as $H_2PO_4^-$ and HPO_4^{2-}), was excluded from the model because of a lack of reliable formation constant data which consider hydrolysis. Data and constants recorded at 25°C are compared as these are the most prevalent in the literature.[9] Not many potentiometric studies have been carried out at 37°C.

The calculated speciation distribution in our blood plasma model for Al and Ga in the absence of exogenous ligands is shown in Fig. 3. Ga^{3+} should be completely complexed by Tf; however, a significant amount of Al^{3+} may be complexed by citrate in the form of $Al(OH)(H_{-1}Cit)^{2-}$. There are no reports of a similar citrate species of Ga^{3+}; the Ga–citrate system[21] has not been studied in nearly as much detail as has the Al–citrate system.[20,25–30] It should be noted that the distribution of the Al^{3+} ion between citrate and Tf depends on whether the total Al concentration is above the saturation level of Tf (50 μM). If it is more then Al^{3+} would be bound to citrate (*vide infra*). There have been discrepancies in the speciation of the Al–citric acid–H_2O system. In a review of Al–citrate studies current in 1986, Martin[29] agreed with Motekaitis and Martell[27] that the major species present at pH 7.4 was $Al(H_{-1}Cit)^-$, while subsequently both $Al(H_{-1}Cit)^-$ and $Al(OH)(H_{-1}Cit)^{2-}$ (the major form at pH 7.4) were found by Öhman.[20] The latter complex was also postulated by Martin[18] in his reconsideration of the available data. We use Öhman's results[20] in our blood plasma model. Based on the protocol of Fig. 3, the results of Martin,[18] Motekaitis and Martell,[27] and Öhman[20] all give percentages of total Al as citrate in the 13–16 range.

The concentration required for each ligand in Table 1 to complex Al or Ga in the presence of citrate and Tf in the blood plasma model has been calculated. The results are presented visually in ligand competition diagrams; these plot the percentage of the metal ion complexed with a particular ligand against the concentration of ligand. For Al^{3+} (Fig. 4), the diagram is divided into two regions,

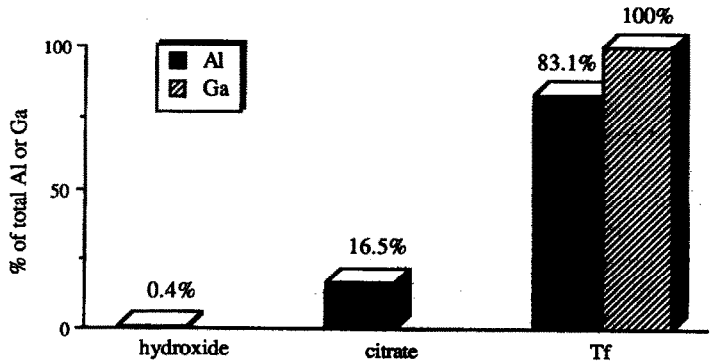

Fig. 3. Calculated blood plasma distribution of 1 μM total Al or Ga between 0.1 mM total citrate and 50 μM available Tf binding sites at pH 7.4 and 25°C.

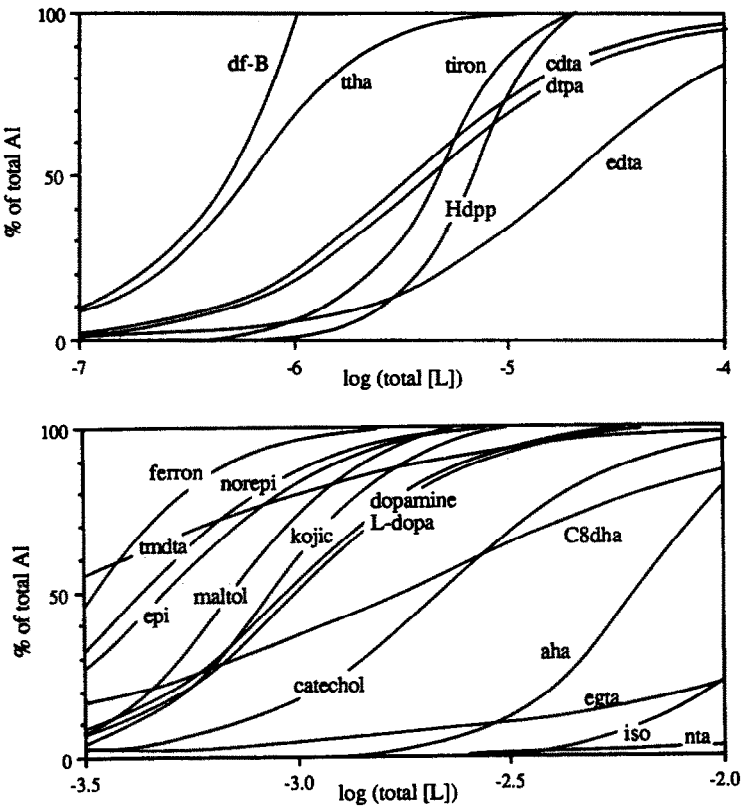

Fig. 4. Plots of the total ligand concentration required to complex a dilute (< 50 μM) solution of Al in the presence of 0.1 mM citrate and 50 μM available Tf binding sites at pH 7.4 and 25°C. The top figure shows those ligands that require < mM concentration levels, while the ligands in the bottom figure require ⩾ mM levels.

those of low (μM) and high (mM) concentrations. The ligands of particular relevance to chemistry in plasma are those that do not require a large excess (< mM) to complex Al (or Ga) in the presence of citrate and transferrin. For Al, those ligands include the multidentate ligands desferriferrioxamine-B (a trihydroxamate siderophore), edta and its derivatives ttha, cdta and dtpa (aminocarboxylates), and the bidentate ligands tiron (a disulphonated catechol) and Hdpp (a 3-hydroxy-4-pyridinone). The curves in Fig. 4 for the bidentate ligands have steeper slopes than those for the multidentate ligands. The thermodynamics of forming a 3 : 1 complex versus a 1 : 1 complex dictate that a large excess of a multidentate ligand is required to complex 80–100% of the metal ion, whereas only a small excess of multidentate ligand is required in the 0–20% range. The chelate effect mandates that the multidentate ligands should require a lower concentration than a bidentate ligand to completely bind the metal ion if the binding groups are similar. It is interesting to note that the two bidentate ligands Hdpp and tiron (both of which benefit from considerable resonance stabilization that increases the negative charge on the binding oxygens) compete with edta and its derivatives in the binding of Al^{3+} in our plasma model.

The more weakly complexing ligands for Al^{3+} in Fig. 4 require at least millimolar concentrations in the blood to complex a significant amount of the ion. The poorer ligands include the neurologically active catecholamines dopamine, L-dopa, epinephrine and norepinephrine.[31] In the brain, Tf and citrate are present in vanishingly small quantities; therefore it seems plausible that these ligands could compete with weaker ligands (such as hydroxide) for Al and Ga in the brain.

Comparison of the analogous results for Ga^{3+} (Fig. 5) with those for Al^{3+} shows that the curves for a given ligand are generally shifted to the right (higher concentrations required) in the Ga diagram. The ratio of log K_{eff}(Ga/Al) for Tf is 1.50, while the same ratio (log K_{eff} or log β_{3eff}) is 1.31 ± 0.11 with all other ligands in Tables 1 and 2. (This is significantly different at the 98% level based on unpaired t-tests.) Hence it is more difficult to remove Ga from Tf than it is to remove Al from Tf with the same ligand. For example, an edta concentration of 10 μM in the

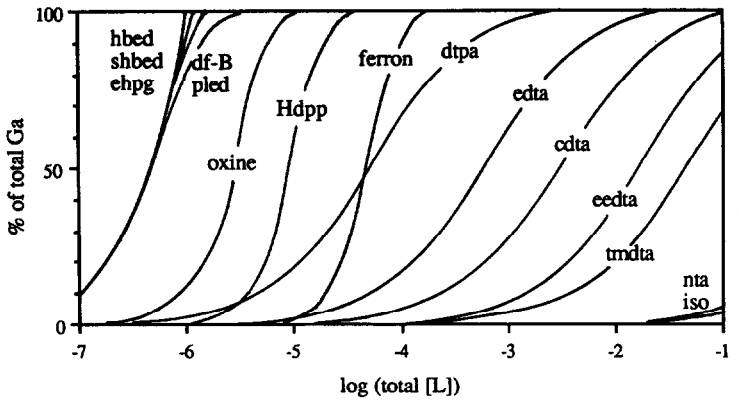

Fig. 5. Plots of the ligand concentrations required to complex a dilute (< 50 μM) solution of Ga in the presence of 0.1 mM citrate and 50 μM available Tf binding sites at pH 7.4 and 25°C.

blood should complex approx. 30% of Al^{3+}, but would complex less than 3% of Ga^{3+} under the same conditions. Great care should be taken when using Ga^{3+} biodistributions as a marker for Al^{3+} in the blood unless a large excess of ligand is present.

Martell and co-workers have determined very high stability constants for some edta derivatives with Ga^{3+}, Fe^{3+} and In^{3+} (hbed, shbed, ehpg and pled).[9,24] A recent reevaluation[32] of the pled formation constants has detailed some of the difficulties in obtaining accurate formation constants with these ligands because the numbers are so large. As is shown in Fig. 5, because of the high formation constants, these ligands (along with df-B) are excellent candidates for Ga chelation. Welch, Martell and co-workers[33,34] and Hunt[35] have been studying them. The next best set of ligands are the bidentate ligands, oxine, Hdpp and ferron. Oxine (8-hydroxyquinoline), a well-known chelator of trivalent metal ions,[9] is widely used in nuclear medicine with isotopes of Ga and In, and is a gravimetric agent for Al. Dtpa and edta both complex > 50% of the total Ga at 1 mM ligand concentration in blood plasma. We have examined the biodistribution of complexes of Hdpp and some of its analogues.[36]

These curves allow the determination of the ligand concentration required to retain a certain percentage of the metal ion in the metal–ligand complex in human blood plasma. The quantity R_n is the amount of ligand (in μM) required to complex n% of 1 μM metal ion at pH 7.4 in a solution of 0.1 mM citrate and 50 μM available Tf binding sites (R_n = [total ligand]/1 μM total metal). Tables 3 and 4 list, for Al^{3+} and Ga^{3+} respectively, R_{20}, R_{50} and R_{90} values for the ligands in this study. For those ligands with $R_n > 1$ (not the best ligands), the R_n values are independent of the metal ion concentration when the latter is below 1 μM and the R_n values are nearly independent in the range 1–50 μM (50 μM being the concentration at which all the empty sites of Tf should be saturated). What is really being measured is the competition between excesses of ligands for a small quantity of metal ion. As long as the concentration of the metal ion is low (a good assumption with biomedical applications), these values may be taken as the lower limit of concentration (in μM) required to retain the given percentage of the ion as the metal–ligand complex

Table 3. Comparison of calculated ligand complexation with Al^{3+} in the blood plasma model consisting of 1 μM Al^{3+}, 0.1 mM citrate, 50 μM empty Tf sites, pH 7.4, and 25°C. R_n is the ratio of total ligand concentration to total metal concentration required to complex n% of the metal

Ligand	R_{20}	R_{50}	R_{90}
df-B	0.20	0.50	0.90
ttha	0.20	0.60	2.2
tiron	2.4	4.7	11
Hdpp	3.7	6.5	13
cdta	1.0	3.5	30
dtpa	1.1	4.3	36
edta	4.7	19	180
ferron	210	340	720
norepi	230	440	1200
epi	260	500	1300
maltol	450	720	1500
kojic acid	540	870	1800
tmdta	66	260	2500
dopamine	490	950	2600
L-dopa	500	1000	2800
catechol	1100	2200	6400
aha	3900	6300	13,000
C_8-dha	420	1800	19,000
isomaltol	9400	15,000	32,000
egta	10,000	40,000	$> 10^5$
nta	$> 10^5$	$> 10^5$	$> 10^5$

Table 4. Comparison of calculated ligand complexation with Ga^{3+} as in Table 3

Ligand	R_{20}	R_{50}	R_{90}
hbed	0.20	0.50	0.90
shbed	0.20	0.50	0.90
ehpg	0.20	0.50	0.90
df-B	0.20	0.52	1.1
pled	0.21	0.55	1.4
oxine	1.5	2.9	5.6
Hdpp	5.3	9.1	19
ferron	29	47	100
dtpa	13	52	470
edta	150	610	5600
cdta	810	3300	31,000
eedta	4000	16,000	$> 10^5$
tmdta	11,000	46,000	$> 10^5$
nta	$> 10^5$	$> 10^5$	$> 10^5$
isomaltol	$> 10^5$	$> 10^5$	$> 10^5$

in the blood plasma. For example, a 13 μM Hdpp solution in blood plasma should complex about 90% of 1 μM Al^{3+}, whereas it would take a 1.3 or 1.5 mM (100-fold increase) epinephrine or maltol solution to complex a comparable percentage of Al^{3+}. Similarly, df-B would complex 100% Al with a slight excess over 1 μM. With the very powerful chelating agents, df-B, hbed, shbed and ehpg, these R_n values do not represent the lower limit of concentration. Much lower total metal concentrations would have to be considered to calculate the lower limits.

APPLICATIONS

Obviously in applying the above calculations from *in vitro* data to *in vivo* behaviour, certain limitations are unavoidable. Almost all *in vivo* laboratory work with Al^{3+} and Ga^{3+} is conducted in mice, rats or rabbits, not people. Physiological differences (pH concentrations) from humans will render the above calculations less precise and, regardless of species, Fe^{3+} transport has been assumed to be governed by human transferrin. Temperature differences may alter slightly the actual concentrations required but should not affect the relative ligand positions unduly. Kinetics have been ignored as workers are just beginning to address[37] this aspect in the calculation of the biological chelation of metal ions.

We have performed two *in vivo* ^{67}Ga biodistribution studies in laboratory mice,[36] in which Hdpp solutions were injected (by tail vein) such that the ligand concentrations in the blood plasma were 0.2 μM in one study and 4.0 mM in the other ($\approx 10^{-12}$ M $^{67}Ga^{3+}$ in the blood in each study). Based on the R_n values in Table 4, $^{67}Ga^{3+}$ would be removed to Tf in dilute Hdpp but $^{67}Ga^{3+}$ would be retained as $^{67}Ga(dpp)_3$ in the concentrated case. With the concentrated solution, we found a significant difference (99% level by unpaired *t*-tests) in the biodistribution of eight organs from those animals that were injected with a weak complexing agent (citrate).[36] The Ga–citrate biodistribution was the same as that of ^{67}Ga–Tf (lots of liver),[38] while the concentrated Ga–Hdpp preparation was cleared very rapidly via the kidneys. With the dilute Hdpp injection, no difference from the citrate biodistribution was found; the dilute Hdpp biodistribution also reflected that of Ga–Tf. These results support the predictions based on the above calculations. In fact, nothing less than a 100-fold increase over the dilute case, to 20 μM Hdpp, should have altered the biodistribution drastically.

In a recent study of oral administration,[39] tris-(maltolato)aluminium(III) was found to transport Al^{3+} across the gastrointestinal tract into the blood plasma in rabbits much more effectively than aluminium chloride or aluminium citrate. Assuming that the Al found in the blood was transported in the form of the tris(maltolato) complex, the nature of the Al speciation in the blood after the transport was of considerable interest because the urine of the rabbits showed abnormally high Al levels for a month after the single oral administration. The Al concentration in the blood (average of five animals) peaked at 67 μM, 1–3 h after administration (by AAS). Based on three molecules of maltol per Al^{3+} ion, there were 200 μM maltol in the blood. From Table 3 it can be estimated that 720 μM maltol would be required to complex 50% of Al. Speciation modelling using the plasma model presented in this contribution estimates that only 6.4% of the Al should remain as maltol-containing species (Fig. 6), the remainder being distributed between citrate complexes and transferrin. (Transport and storage due to protein saturation would be consistent with the long biological half-life.) The same calculation with Hdpp instead of maltol as the complexing agent shows that about 94% of the Al should be complexed with Hdpp in the blood (Fig. 6). (Hdpp is also bidentate and monoprotic and thus also forms an Al^{3+} complex which possesses a net neutral charge.)

Calculations such as these have prompted us to examine a variety of 3-hydroxy-4-pyridinones as *in vivo* chelating agents for Al and Ga transport. The blood plasma model presented here is crude when compared with a more comprehensive system such as "fully-loaded" ECCLES,[6] but for

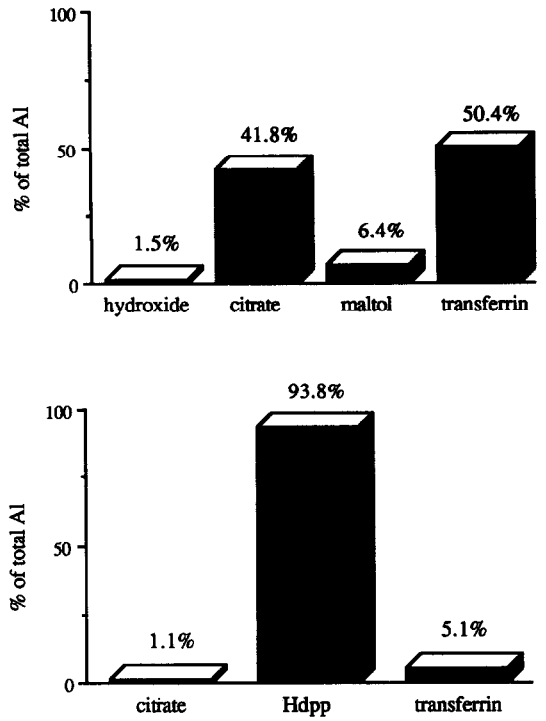

Fig. 6. Calculated distribution of 67 μM Al in blood plasma (citrate and Tf at pH 7.4). The top figure includes 200 μM maltol, while the bottom figure includes 200 μM Hdpp.

estimations of relative metal binding it has proven invaluable.

Acknowledgements—We wish to acknowledge the British Columbia Health Care Research Foundation and the Natural Sciences and Engineering Research Council of Canada for operating grants, Professor W. R. Harris for helpful discussions and a preprint of ref. 12, and to Dr G. Berthon for a preprint of ref. 30.

REFERENCES

1. D. P. Perl, *Environ. Health Perspect.* 1985, **63**, 149.
2. D. R. Crapper McLachlan, *Neurobiol. Aging* 1986, **7**, 525.
3. L. Liss (Ed.), *Aluminum Neurotoxicity*. Pathotox Publishers, Park Forest South, Illinois (1980).
4. P. S. Hallman, D. D. Perrin and A. E. Watt, *Biochem. J.* 1971, **121**, 549.
5. D. D. Perrin and R. P. Agarwal, *Metal Ions Biol. Syst.* 1973, **2**, 168.
6. P. M. May, P. W. Linder and D. R. Wiliams, *J. Chem. Soc., Dalton Trans.* 1977, 588.
7. P. M. May and D. R. Williams, *FEBS Lett.* 1977, **78**, 134.
8. C. F. Baes Jr. and R. E. Mesmer, *The Hydrolysis of Cations*. John Wiley, New York (1976).
9. A. E. Martell and R. M. Smith, *Critical Stability Constans*, Vols 1–6. Plenum Press, New York (1974–1989).
10. R. G. Pearson, *Inorg. Chem.* 1988, **27**, 734.
11. W. R. Harris, *Biochemistry* 1986, **25**, 803.
12. W. R. Harris and J. Sheldon, *Inorg. Chem.*, in press.
13. A. L. Crumbliss and J. M. Garrison, *Comments Inorg. Chem.* 1988, **8**, 1.
14. The concept of correcting stability constants for competing ions was first introduced in J. Schubert, *Ann. Rev. Nucl. Sci.* 1955, **5**, 369.
15. R. B. Martin, *Clin. Chem.* 1986, **32**, 1797.
16. A. E. Martell and R. J. Motekaitis, *J. Inorg. Biochem.* 1989, **36**, 347: Abstract N010, *Int. Conf. Bioinorg. Chem.*, Boston, Massachusetts (July 1989).
17. N. D. Chasteen, *Coord. Chem. Rev.* 1977, **22**, 1.
18. R. B. Martin, *Metal Ions Biol. Syst.* 1988, **24**, 1.
19. N. D. Chasteen, *Adv. Inorg. Biochem.* 1983, **5**, 201.
20. L.-O. Öhman, *Inorg. Chem.* 1988, **27**, 2565.
21. W. R. Harris and A. E. Martell, *Inorg. Chem.* 1976, **15**, 713.
22. S. Kulprathipanja, D. J. Hnatowich, R. Beh and D. Elmaleh, *Int. J. Nucl. Med. Biol.* 1979, **6**, 138.
23. D. J. Lurie, F. A. Smith and A. Shukri, *Int. J. Appl. Radiat. Isotopes* 1985, **36**, 57.
24. C. J. Bannochie and A. E. Martell, *J. Am. Chem. Soc.* 1989, **111**, 4735.
25. G. E. Jackson, *S. Afr. J. Chem.* 1982, **35**, 89.
26. L.-O. Öhman and S. Sjöberg, *J. Chem. Soc., Dalton Trans.* 1983, 2513.
27. R. J. Motekaitis and A. E. Martell, *Inorg. Chem.* 1984, **23**, 18.
28. J. E. Gregor and H. K. J. Powell, *Aust. J. Chem.* 1986, **39**, 1851.
29. R. B. Martin, *J. Inorg. Biochem.* 1986, **28**, 181.
30. M. Venturini and G. Berthon, *J. Inorg. Biochem.*, in press.
31. T. Kiss, I. Sóvágó and R. B. Martin, *J. Am. Chem. Soc.* 1989, **111**, 3611.
32. R. J. Motekaitis, Y. Sun and A. E. Martell, *Inorg. Chim. Acta* 1989, **159**, 29.
33. M. A. Green, M. J. Welch, C. J. Mathias, P. Taylor and A. E. Martell, *Nucl. Med. Biol.* 1985, **12**, 381.
34. C. J. Mathias, Y. Sun, M. J. Welch, M. A. Green, J. A. Thomas, K. R. Wade and A. E. Martell, *Nucl. Med. Biol.* 1988, **15**, 69.
35. F. C. Hunt, *Nucl. Med. Biol.* 1988, **15**, 651, 659.
36. D. J. Clevette, D. M. Lyster, W. O. Nelson, T. Rihela, G. A. Webb and C. Orvig, *Inorg. Chem.*, in press.
37. M. M. Jones and P. M. May, *Inorg. Chim. Acta* 1987, **138**, 67.
38. S. M. Larson, *Semin. Nucl. Med.* 1978, **8**, 193.
39. T. P. A. Kruck, A. Boyd, C. Orvig and D. R. Crapper McLachlan, submitted for publication.
40. A. Evers, R. D. Hancock, A. E. Martell and R. J. Motekaitis, *Inorg. Chem.* 1989, **28**, 2189.
41. W. R. Harris and V. L. Pecoraro, *Biochemistry* 1983, **22**, 292.
42. T. G. Lutz, D. J. Clevette, S. J. Rettig and C. Orvig, *Inorg. Chem.* 1989, **28**, 715.
43. D. J. Clevette, W. O. Nelson, A. Nordin, C. Orvig and S. Sjöberg, *Inorg. Chem.* 1989, **28**, 2079.

Polyhedron Vol. 9, No. 2/3, pp. 163–170, 1990
Printed in Great Britain

0277–5387/90 $3.00+.00
© 1990 Pergamon Press plc

ALUMINIUM, GALLIUM AND INDIUM IN BIOLOGICAL FLUIDS—A COMPUTER MODEL OF BLOOD PLASMA

GRAHAM E. JACKSON

Department of Chemistry, University of Cape Town, Rondebosch 7700, South Africa

Abstract—A computer model of the solution equilibria involving Al^{3+}, Ga^{3+} and In^{3+} in blood plasma has been constructed and used to investigate the *in vivo* fate of these metal ions. The effect of a series of chelating agents on the species distribution of Al^{3+} is reported. Chemical explanations are given for a number of clinical observations on the use of $^{67}Ga^{3+}$ and $^{111}In^{3+}$ in nuclear medicine.

In recent years, as evidenced by this special publication, there has been a renaissance in the chemistry of aluminium, gallium and indium. Because of their favourable decay characteristics and availability, $^{67,68}Ga^{3+}$ and $^{111}In^{3+}$ have been used in nuclear medicine, but it is only recently that the significance of the aqueous chemistry of these metal ions has been recognized. The biological importance of the sister elemental Al^{3+} has long been ignored. However, this element has now been linked to the aetiology of a number of neurological and skeletal disorders in man. First recognized in patients undergoing long-term haemodyalisis the effects of aluminium are now known to be more widespread.[1–8]

This paper investigates, using a computer model of blood plasma, the aqueous chemistry of Al^{3+}, Ga^{3+} and In^{3+}. Whereas these three metal ions show very similar chemical behaviours, their *in vivo* functions differ considerably from each other. Aluminium can be regarded as a polluting metal *in vivo*, whereas gallium and indium are clinically very useful. For this reason the metal ions are discussed separately.

COMPUTER MODEL OF BLOOD PLASMA

May *et al.*[9,10] have published a computer model of blood plasma and have used this model to explain several clinical observations.[11] The model consists of 40 ligands, nine metal ions and *ca* 5000 complexes. To this model we have added the appropriate formation constants for Al^{3+}, Ga^{3+} and In^{3+}. These constants were, as far as possible, abstracted from the literature.[12] In cases where the same constants had been published by several authors the values of these constants were evaluated critically. In cases where a complex was potentially important, but for which no constants were available, values were estimated. This was done mainly using linear free-energy relationships[13] between Al^{3+}, Ga^{3+}, In^{3+} and Fe^{3+}, but in certain cases appropriate interpolations were made based on chemical analogies. Amino acid complexes of Al^{3+} and Ga^{3+} were not included in the model as previous experiments have shown these complexes to be unimportant.[14] The final set of constants used in this simulation study is given in Table 1. The constants for the chelating agents N,N′-bis(*o*-hydroxylbenzyl)ethylenediamine-N,N′-diacetic acid (HBED),[29,30] ethylene-1,2-bis(*o*-hydroxyphenylglycine) (EHPG),[12] desferrioxamine (DFO),[31,32] N,N′-bis(pyridoxyl)ethylenediamine-N,N′-diacetic acid (PLED),[29,33] N-phosphonomethylglycine (PMG),[34] 1,2-dihydroxybenzene-3,5-disulphonate (TIRON),[35] ethylenedinitrilo-N,N′-diacethylhydroxamic-N,N′-diacetic acid (EDDO)[12] and catechol (CAT)[36] were obtained from the literature and used without modification.

Mixed-ligand (ternary) complex formation occurs widely in systems containing metal ions and two or more different ligands. These complexes have been shown to be important in blood plasma.[37] Since very little data are available on ternary complex formation of Al^{3+}, Ga^{3+} and In^{3+} the relevant binary constants were used to calculate the ternary constants. This was achieved using the prescan facilities (MIX)[38] of the computer program ECCLES with a ternary stabilization factor of 1.0.

Table 1. Binary Al^{3+} and Ga^{3+} stability constants used in the blood model

L	p	q	r	log β	Reference	L	p	q	r	log β	Reference
						Al^{3+}					
Tartrate	1	1	−1	1.18	15	Fluoride	1	1	0	7.01	12
	1	2	0	7.65	15		1	2	0	12.75	12
	1	1	−2	−3.97	15		1	3	0	17.02	12
	1	2	−1	3.93	15		1	4	0	19.72	12
	1	2	−3	−8.74	15		1	5	0	20.91	12
	1	3	−4	−26.8	15						
	1	3	−6	−39.5	15	Phosphate	1	1	0	11.4	27
							1	1	1	20.5	28
Transferrin	1	1	0	12.9	16		1	1	2	25.8	
	2	1	0	25.2	16	Cysteinate	1	2	0	6.43	28
Salicylate	1	1	0	12.7	17	Malonate	1	1	0	6.3	14
	1	2	0	23.11	17		1	2	0	11.1	14
	1	2	−1	15.51	17		1	3	0	13.3	14
	1	2	−2	6.19	17		1	1	−1	0.79	14
							1	2	−2	−7.42	14
Oxalate	1	1	0	5.02	14						
	1	2	0	9.33	14	Citrate[a]	1	1	0	8.0	18
	1	3	0	12.41	14		1	1	−1	4.6	19
	1	1	−1	−0.51	14		1	1	1	10.2	20
	1	1	−2	−8.59	14		1	2	0	13.0	
						Succinate	1	1	−1	−0.25	14
Carbonate	2	1	−4	−20.4	25		2	1	−1	2.88	14
	3	1	−5	−22.7	25		1	1	−2	−5.19	14
Hydroxide	1	0	−1	−5.10	23	HBED	1	1	0	29.4	[b]
	1	0	−2	−10.4	26						
	1	0	−3	−15.9	25	EHPG	1	1	0	25.2	[b]
	1	0	−4	−24.1		EDDO	1	1	0	16.6	[b]
	3	0	−11	−54.8			1	1	1	20.6	[b]
	6	0	−15	−49.5			1	1	2	22.6	[b]
	8	0	−22	−76.5			1	1	−1	9.7	[b]
						Ga^{3+}					
Phosphate	1	1	1	18.8	12	Oxalate	1	1	0	6.45	12
	1	1	0	10.0	[b]		1	2	0	12.38	12
	1	1	2	19.5	12		1	3	0	17.86	12
							1	1	−1	2.0	[b]
Citrate[a]	1	1	1	11.6	21		1	1	−2	−4.0	[b]
	1	1	−1	7.1	22						
	1	1	0	10.02		Malonate	1	1	0	2.4	[b]
	1	2	0	15.3	[b]		1	2	0	3.6	[b]
						Transferrin	1	1	0	20.3	13
Hydroxide	1	0	−1	−3.31	23		2	1	0	39.6	[b]
	1	0	−2	−6.76	24						
	1	0	−3	−11.16	24	Salicylate	1	1	0	16.1	21
	1	0	−4	−17.17	24	Tartrate	1	1	0	18.5	21

[a] Neutral ligand H_3 citrate.
[b] Estimated.

Table 2. Important ternary Al^{3+} and Ga^{3+} stability constants used to construct the blood model. Other ternary constants calculated automatically using MIX[24]

Species	log β	Reference
$[Al(citrate)(malonate)]^{2-}$	12.05	[a]
$[Al(citrate)(salicylate)]^{2-}$	20.0	[a]
$[Al(citrate)(oxalate)]^{2-}$	11.2	[a]
$[Al(citrate)(cysteinate)]^{2-}$	14.9	28
$[Al(HPO_4)(malonate)]^{-}$	25.3	28
$[Al(H_2PO_4)(malonate)]$	30.6	28
$[Al(HPO_4)(salicylate)]^{-}$	29.56	28
$[Al(H_2PO_4)(salicylate)]$	34.16	39
$[Al(HPO_4)(oxalate)]^{-}$	24.8	[a]
$[Al(H_2PO_4)(oxalate)]$	28.3	39
$[Al(HPO_4)_2(oxalate)]^{3-}$	42.1	39
$[Al(HPO_4)(cysteinate)]^{-}$	15.66	[a]
$[Al(HPO_4)(citrate)]^{2-}$	26.5	39
$[Al(H_2PO_4)(citrate)]^{-}$	30.38	39
$[Al(HPO_4)(OH)]$	28.6	[a]
$[Al(HPO_4)(OH)_2]^{-}$	32.8	[a]
$[Al(H_2PO_4)(OH)]^{+}$	33.5	[a]
$[Al(H_2PO_4)(OH)_2]$	41.0	[a]
$[Al(H_2PO_4)(OH)_3]^{-}$	45.8	[a]
$[Ga(HPO_4)(OH)]$	27.3	[a]
$[Ga(HPO_4)(OH)_2]^{-}$	35.0	[a]
$[Ga(H_2PO_4)(OH)]^{+}$	28.5	[a]
$[Ga(H_2PO_4)(OH)_2]$	37.4	[a]
$[Ga(H_2PO_4)(OH)_3]^{-}$	44.7	[a]
$[Ga(HPO_4)(oxalate)]^{-}$	24.7	[a]
$[Ga(H_2PO_4)(oxalate)]$	25.4	[a]
$[Ga(HPO_4)(citrate)]^{2-}$	26.5	[a]
$[Ga(H_2PO_4)(citrate)]^{-}$	30.38	[a]

[a] Estimated.

In addition to this automatic calculation of ternary stability constants, the constants given in Table 2 were calculated[40] and included in the model.

Aluminium

Aluminium readily undergoes extensive hydrolysis in aqueous solution forming an insoluble salt $Al(OH)_3$. Being amphoteric at higher pH this salt redissolves to form $[Al(OH)_4]^-$. In the presence of phosphate aluminium can also form the highly insoluble complex $Al(OH)_2(H_2PO_4)$. Based on the solubility products and stability constants of these two complexes it is possible to calculate the concentration at which they will begin to precipitate (or the solution becomes supersaturated). The solubility product, K_{sp}, of amorphous $Al(OH)_3$ is given by:[23]

$$K_{sp} = [Al^{3+}]/(H^+)^3 = 10^{10.7},$$

while the equilibrium constant β_3 for the reaction

$$Al(H_2O)_3^{3+} = Al(OH)_3 + 3H^+$$

is given by[26]

$$\beta_3 = [Al(OH)_3](H^+)^3[Al^{3+}]^{-1} = 10^{-15.9}.$$

Substituting the solubility product expression into this equation we get for the maximum concentration of $Al(OH)_3$

$$[Al(OH)_3]_{max} = \beta_3 K_{sp} = 10^{-5.2} \text{ mol dm}^{-3}.$$

At pH 7.4 the highest permitted concentration of free Al^{3+} from amorphous $Al(OH)_3$ is $10^{10.7} \times 10^{-3\times 7.4} = 10^{-11.5}$ mol dm^{-3}. Similarly, the concentration of $Al(OH)_2(H_2PO_4)$ at which precipitation occurs can be calculated.[41]

$$K_{sp} = [Al^{3+}][H_2PO_4^-][H^+]^{-2} = 10^{-1.5}$$

and[27]

$$\beta = \frac{[Al(H_2PO_4)(OH)_2][H^+]^2}{[Al^{3+}][H_2PO_4^-]} = 10^{-3.6},$$

therefore, $[Al(H_2PO_4)(OH)_2]_{max} = \beta K_{sp} = 10^{-5.1}$ mol dm^{-3}.

At pH 7.4 in blood plasma with a total phosphate concentration of 1.6 mmol dm^{-3} the concentration of $H_2PO_4^-$ is estimated, using the computer model, to be 2.1×10^{-5} mol dm^{-3}. This leads to an estimated maximum free Al^{3+} concentration permitted by $[Al(H_2PO_4)(OH)_2]$ of 2.5×10^{-12} mol dm^{-3}. If no account is taken of metal ion, particularly Ca^{2+}, binding, then the concentration of $H_2PO_4^-$ becomes 2.8×10^{-4} mol dm^{-3} and the maximum free Al^{3+} concentration is estimated to be 1.8×10^{-13} mol dm^{-3}.

The avidity of transferrin for Al^{3+} has been measured, under physiological conditions, to be 12.9 and 12.3 for log K_1 and log K_2, respectively.[16] At 1 μmol total Al^{3+} per litre of plasma, Martin[41] has shown that this leads to a permitted free Al^{3+} concentration of $10^{-14.6}$ mol dm^{-3}. However, if competition with the other components of blood plasma is taken into account a lower free metal concentration is obtained. At pH 7.4 our results have shown that within the total aluminium concentration range 10^{-13}–10^{-5} mol dm^{-3}, *ca* 50% of the aluminium is bound to transferrin in the 1 : 1 complex. Using this information, after suitable manipulation of the relevant equation we arrive at the conclusion that the free Al^{3+} concentration is $\sim 10^{-9} \times [Al^{3+}]_{Total}$. At a total Al^{3+} concentration of 1 μmol this means a free Al^{3+} concentration of 10^{-15} mol dm^{-3}.

Since Al^{3+} readily undergoes hydrolysis in aqueous solution its complexes are likely to be similarly affected. In certain cases this has been explicitly determined, but in the majority of cases stability

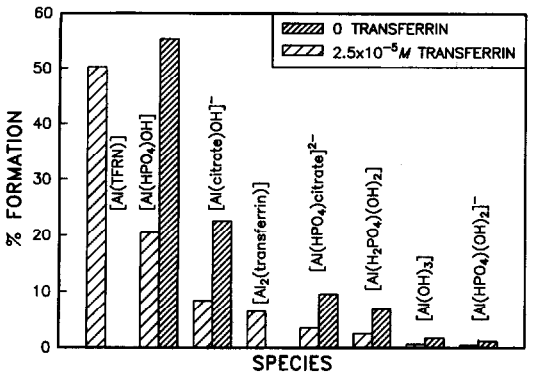

Fig. 1. Calculated blood plasma species distribution of Al^{3+}. Total $[Al^{3+}] = 10^{-9}$ mol dm^{-3}, [transferrin sites] $= 2.5 \times 10^{-5}$ mol dm^{-3}, [phosphate] = 1.6 mmol dm^{-3}, other component concentrations taken from ref. 9.

constants have been determined under acid conditions where little or no hydrolysis takes place. In these cases hydrolysis constants for the complexes have been estimated (see Table 1).[39] Similarly Al^{3+} forms very stable binary[27,42] and ternary phosphate[28,39] complexes. Because of the high plasma concentration of phosphate ($\sim$ 1.6 mmol dm^{-3}) it is important that these ternary complexes be included in any model of plasma (see Table 2).

Figure 1 shows the calculated species distribution of Al^{3+} in blood plasma. This distribution is independent of aluminium concentration within the range 10^{-13}–10^{-5} mol dm^{-3}. Since transferrin uptake of the metal is inevitable, but slow, we have considered the species distribution before and after equilibrium with this protein becomes established. In the absence of transferrin binding the neutral $[Al(HPO_4)OH]$ species predominates. This is contrary to a previous analysis[43] in which citrate complexes were predicted to predominate. Once transferrin binding is included in the calculation, the concentration of the low molecular weight species decreases but their relative distribution remains fairly constant. The effect of the transferrin is to decrease the amount of Al^{3+} available to the low molecular weight pool.

The effect of pH upon the Al^{3+} species distribution is shown in Fig. 2. At low pH the $[Al(H_2PO_4)]^{2+}$ species is formed exclusively. The concentration of this species decreases with increasing pH such that at pH 5 it accounts for only 1% of the total aluminium. Between pH 4 and 6.5 the $[Al(H_2PO_4)citrate]^-$ species predominates. As the pH is raised this species deprotonates to give $[Al(HPO_4)citrate]^{2-}$. Between pH 6 and 8, $[Al(citrate)OH]^-$ and hydrolysed phosphate complexes predominate. Beyond pH 8 hydroxy–aluminium species are formed.

The potential toxicity of aluminium has led to the development of protocols for its removal from the body. Clinical success has been limited.[44] At present the reagent of choice is desferrioxamine,[45,46] a naturally occurring siderophore. Since the primary objective in decreasing the body burden of Al^{3+} is to increase urinary excretion of the metal ion, we have tested, using our computer model, the effect of various chelating agents upon the Al^{3+} species distribution. Various chelating agents have been investigated using the Plasma Mobilizing Index,[11] *PMI*, which is defined as the increase in the low molecular weight concentration of a metal ion brought about by a chelating agent relative to the metal ion concentration in the absence of the chelating agent. Figure 3 shows the *PMI*

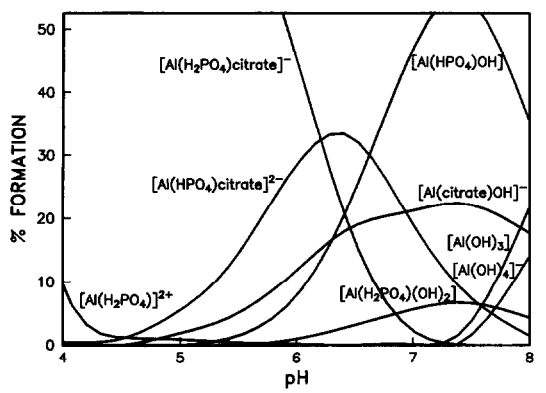

Fig. 2. Calculated low molecular weight blood plasma species distribution of Al^{3+} as a function of pH. Total $[Al^{3+}] = 10^{-9}$ mol dm^{-3}, [phosphate] = 1.6 mmol dm^{-3}, other component concentrations taken from ref. 9.

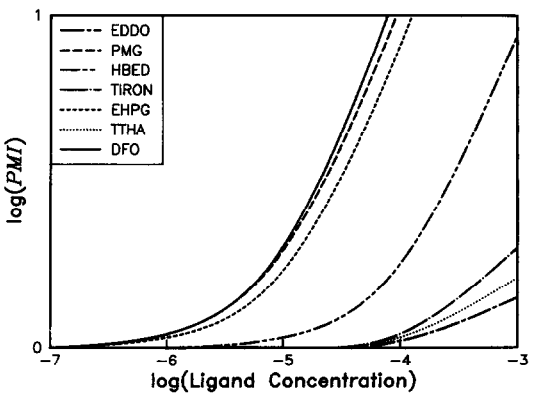

Fig. 3. Plasma Mobilizing Index of Al^{3+} with several chelating ligands. Fixed free $[Al^{3+}] = 10^{-14}$ mol dm^{-3}, [phosphate] = 1.6 mmol dm^{-3}, other component concentrations taken from ref. 9.

curves for the various reagents tested. The polyaminopolycarboxylates (EDTA, DTPA, CDTA etc.) showed little or no mobilization below a concentration of 10^{-3} mol dm^{-3}. Only with the analogue triethylenetetramine hexa-acetic acid (TTHA) did mobilization occur at this concentration. A similar mobilization was exhibited by the substituted catechol TIRON and the hydroxamate EDDO. Of intermediate ability was HBED. Good mobilization was exhibited by the catechol derivative EHPG and the phosphonate PMG. These calculations were based on a free Al^{3+} concentration of 10^{-14} mol dm^{-3}. If this concentration is lowered the Al^{3+} *PMI* curves shown in Fig. 3 will move to the left, but their position relative to each other will remain unchanged.

Desferrioxamine, which is clinically used to increase Al^{3+} excretion,[46] was found to be the most efficient mobilizer of Al^{3+}. This is true, however, only if the equilibrium constants of Garrison and Crumbliss[31] are used in the calculations. If the much lower equilibrium constants of Schwarzenbach[32] are used instead, desferrioxamine is predicted to give rise to little or no aluminium mobilization.

Clinically, several side effects have been noted with the use of desferrioxamine to increase urinary excretion of aluminium. Figure 4 shows the effect of the chelating ligands considered in this study on the low molecular weight concentration of Zn^{2+} and Fe^{3+}. As expected the catechol derivatives, HBED and EHPG, cause a large increase in the low molecular weight concentration of Fe^{3+} but only a small increase in the low molecular weight concentration of Zn^{2+}. A much larger increase in Zn^{2+} mobilization was shown by the polyaminopolycarboxylate TTHA. Of the chelating ligands considered, DFO appears to have the most potential as an *in vivo* Al^{3+} chelating agent. This ligand causes the largest increase in low molecular weight Al^{3+} yet has very little effect on the Fe^{3+} or Zn^{2+} biodistribution. If the concentration of Al^{3+} is lowered, DFO will begin to mobilize Fe^{3+} such that in the absence of Al^{3+} extensive Fe^{3+} mobilization occurs. This has been observed clinically. With a high (> 200 μmol dm^{-3}) plasma concentration of Al^{3+}, DFO preferentially causes Al^{3+} excretion,[47] but with a high plasma concentration of Fe^{3+} (haemosiderosis, β-thalassemia) DFO treatment results in increased Fe^{3+} excretion.[48]

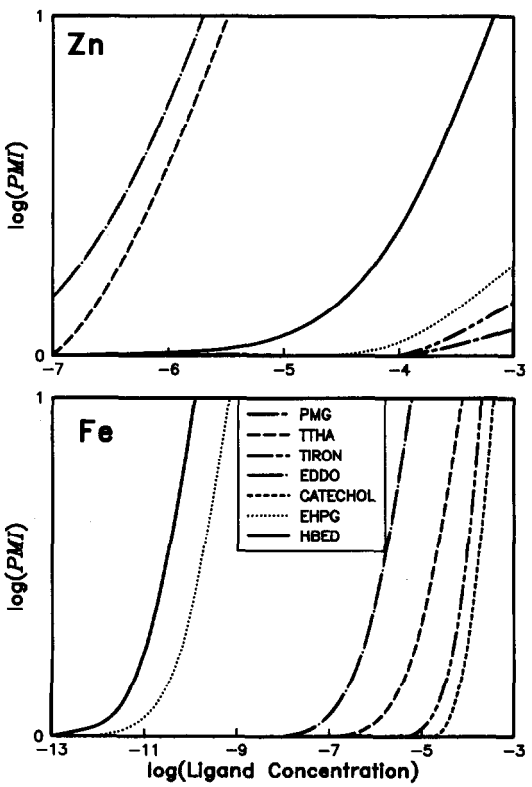

Fig. 4. Plasma Mobilizing Index curves for Fe^{3+} and Zn^{2+} with several chelating agents. Fixed free $[Fe^{3+}] = 10^{-23}$ and fixed free $[Zn^{2+}] = 10^{-9}$ mol dm^{-3}.

Gallium and indium

Like Al^{3+}, In^{3+} and Ga^{3+} undergo extensive hydrolysis in aqueous solution[23,24] forming the insoluble salts $In(OH)_3$ and $Ga(OH)_3$. It is for this reason that the radionuclides ^{67}Ga and ^{111}In are supplied with a high background concentration of acid or citrate. Based on the solubility products of these two salts ($10^{-35.3}$ and 10^{-37}, respectively)[23] the maximum solution concentration of $In(OH)_{3(aq)}$ and $Ga(OH)_{3(aq)}$ can be estimated to be 2×10^{-9} and 5×10^{-9} mol dm^{-3}, respectively. This is higher than the maximum concentration of the insoluble phosphate salts, $InPO_4$ ($K_{sp} = 10^{-21.6}$)[12] and $GaPO_4$ ($K_{sp} = 10^{-21}$),[12] which is estimated to be $10^{-11.6}$ and 10^{-11} mol dm^{-3}, respectively. At pH 7.4, in blood plasma, the maximum concentration of free Ga^{3+} and In^{3+} permitted by $Ga(OH)_3$ and $In(OH)_3$ is $\sim 10^{-18}$ and 10^{-16} mol dm^{-3}, respectively, whereas the maximum free concentration permitted by $GaPO_4$ and $InPO_4$ is 3×10^{-13} and 7×10^{-15} mol dm^{-3}, respectively.

In nuclear medicine scanning procedures, in the absence of carrier Ga^{3+}, blood, $^{67 \text{ or } 68}Ga^{3+}$ concentrations are between 1 and 100 pmol, depending on the procedure and administered dose. At this concentration, our computer model of blood plasma shows the metal ion is bound almost exclusively to transferrin. The predominant low molecular weight complexes are hydrolysed phosphate and citrate complexes. At mg/kg levels, $Ga(NO_3)_3$ has been found to be effective in a variety of murine

tumour models.[49] Preclinical studies showed the dose-limiting toxicity to be renal. In addition, while not the method of choice, high levels of carriers Ga^{3+} have been used in bone scanning.[50] At these elevated levels of Ga^{3+} the transferrin binding sites are saturated and the excess Ga^{3+} is distributed as shown in Table 3. At these high concentrations the solubility of $Ga(OH)_3$ and $GaPO_4$ is exceeded and the formation of colloidal gallium is expected. Clinically[51] rapid excretion in the urine and deposition in the bone is seen at mg/kg levels of Ga^{3+}. Other agents which block binding sites on transferrin, e.g. carrier levels of scandium[52] or hyperferremia associated with whole-body X-ray irradiation,[53] have a similar effect on Ga^{3+} biodistribution.

^{67}Ga as the citrate complex is used extensively as a tumour imaging agent.[54] Computer simulation shows that even with an elevated citrate concentration (10^{-3} mol dm^{-3}) the Ga–citrate complexes are not able to survive in plasma and release the $^{67}Ga^{3+}$ to transferrin. It is the labelled transferrin which is accumulated by the tumour. This conclusion is supported by clinical observations.[55] Addition of carrier Ga^{3+} or Fe^{3+} displaces the $^{67}Ga^{3+}$ from the transferrin complex, resulting in increased excretion and a lower tumour uptake of the radioactive isotope.

Recently, numerous ligands have been designed for the selective chelation of radionuclides.[33,56,57] Since the major *in vivo* chelator of Ga^{3+} and In^{3+} is transferrin, we have calculated the ability of a range of chelating agents to remove the metal ions from this protein. The results for Ga^{3+} are given in Fig. 5 in the form of *PMI* curves. The substituted catechol derivatives HBED, PLED and EHPG are able to prevent protein binding of Ga^{3+} at very low ligand concentrations. Desferrioxamine is also predicted to be a strong *in vivo* chelator of Ga^{3+}. DTPA, its analogues, and TIRON are ineffective at removing Ga^{3+} from transferrin.

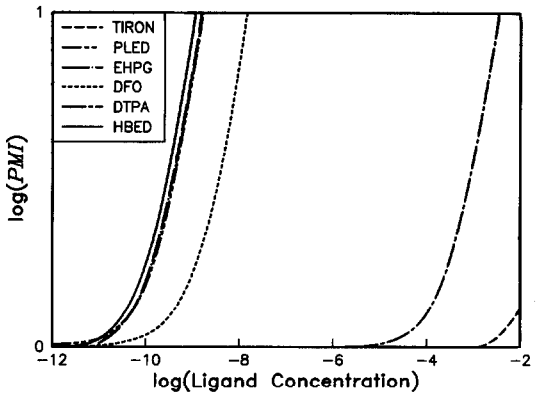

Fig. 5. Plasma Mobilizing Index curves for Ga^{3+} with several chelating agents. Fixed free $[Ga^{3+}] = 10^{-24}$ mol dm^{-3}. Total $[Ga^{3+}]$ in absence of chelating agent = $\sim 10^{-10}$ mol dm^{-3}.

Simple hydroxamic acids form stable Ga^{3+} complexes. Our simulation studies have shown, however, that these complexes are not stable enough *in vivo* to prevent exchange of Ga^{3+} with transferrin. Animal studies[58] support this conclusion in that the biodistribution of $^{67}Ga^{3+}$–hydroxamic acid complexes follow closely the distribution of ^{67}Ga–citrate.

Attempts have been made to use DTPA as a complexing agent for $^{67}Ga^{3+}$ and $^{111}In^{3+}$ radioimaging.[59] Alternatively DTPA, as the anhydride, has been coupled to proteins as a means of radiolabelling the macromolecule.[60] These attempts have to a large extent been unsuccessful. DTPA is unable to prevent loss of the metal ion *in vivo*.[61] Computer simulation of this system has shown that the metal ion in the Ga^{3+} DTPA complex is lost to transferrin. The driving force for this reaction is the high *in vivo* concentration of Ca^{2+} which displaces Ga^{3+} from its DTPA complex. As a check of our blood plasma model the species distribution of Ca was calculated and compared with measured values obtained in the literature, a satisfactory agreement being obtained (Table 4). The fact that $^{111}In^{3+}$ labelled DTPA and EDTA protein conjugates have been used clinically[62,63] can be attributed to the slow decomposition of these complexes relative to the duration of the diagnostic procedure. Any dissociation though leads to increased background radiation and hence decreased contrast. Similar results have been obtained with $^{67}Cu^{2+}$ labelled DTPA– and EDTA–protein conjugates.[64] The fast exchange kinetics of Cu^{2+}, however, limit the clinical usefulness of these complexes. Here our computer model predicts that the metal ion is lost to albumin.

Table 3. Calculated species distribution of Ga^{3+} complexes in blood plasma. Total $[Ga^{3+}] = 0.18$ mmol dm^{-3}, total [phosphate] = 1.6 mmol dm^{-3}, other component concentrations taken from ref. 9

Species	Concentration (mol dm^{-3})	Total Ga^{3+} (%)
$[Ga(OH)_4]^-$	1.3×10^{-4}	70.3
$[Ga_2(TFRN)]$	2.5×10^{-5}	26.6
$[Ga(OH)_3]$	4.9×10^{-7}	2.9
$[Ga(TFRN)]$	2.5×10^{-8}	0.3
$[Ga(HPO_4)(OH)_2]$	1.0×10^{-8}	0.0
$[Ga(OH)_2]^+$	5.4×10^{-9}	0.0
$[Ga]^{3+}_{free}$	5.0×10^{-17}	0.0

Table 4. Calculated and observed citrate species concentrations present in blood plasma. Component concentrations taken from ref. 9

Complex	Concentration (mol dm^{-3}) Calculated	Observed[59]
Ca–citrate	0.058	0.038
Mg–citrate	0.032	0.044
Na–citrate	0.031	0.039

Finally, at a DFO concentration of 10^{-5} mol dm^{-3} our computer model predicts that 81% of Ga^{3+} will be complexed to DFO and 19% bound to transferrin. Clinical studies have shown, however, that the ^{67}Ga labelled DFO–IgG conjugate is stable *in vivo* with no loss of radionuclide after incubation with serum or following intravenous injection.[65] The high charge and stability of the Ga–DFO complex is consistent with the rapid renal excretion of the metal ion. DFO is used to reduce ^{67}Ga background radiation from the blood-pool in diagnostic imaging.[66]

In conclusion, in this study we have used computer simulation in an attempt to explain and predict the *in vivo* fate of Al^{3+}, Ga^{3+} and In^{3+} complexes. However a word of caution is necessary. Computer models are only as good as the data upon which they are based. Many of the constants used in this study have been estimated or determined under inappropriate conditions. Also, kinetic factors which affect the metal ion species distribution have not been taken into account. Much work therefore needs to be done on the aqueous chemistry of Al^{3+}, Ga^{3+} and In^{3+} to improve our model. Notwithstanding these limitations, our model has been successful in explaining many clinically observed phenomena.

Acknowledgements—Financial support of the University of Cape Town Research and Ethics and Research Committees is gratefully acknowledged.

REFERENCES

1. W. Griswold, V. Reznik, S. Mendova, D. Trauner and A. Alfrey, *Pediatrics* 1983, **71**, 56.
2. S. Andreoli, J. Bergstein and D. Sherrard, *New Engl. J. Med.* 1984, **310**, 1079.
3. R. Garruto, R. Fukatsu, R. Yanagihara, D. Gajdusek, G. Hook and C. Fiori, *Proc. Nat. Acad. Sci. USA* 1984, **81**, 1875.
4. D. Perl, *Environ. Health Perspect.* 1985, **63**, 149.
5. R. Wurtman, *Sci. Am.* 1985, **252**, 62.
6. R. Garruto and Y. Yase, *Trends Neuroscience* 1986, **9**, 368.
7. D. Perl and A. Brody, *Science* 1980, **208**, 297.
8. J. Meyer and W. Thomas, *Kidney Int.* 1986, **29**, s20.
9. P. M. May, D. R. Williams and P. W. Linder, *J. Chem. Soc., Dalton Trans.* 1977, 588.
10. G. Berthon, B. Hacht, M. Blais and P. M. May, *Inorg. Chim. Acta* 1986, **125**, 219.
11. P. M. May and D. R. Williams, *FEBS Lett.* 1977, **78**, 134.
12. A. E. Martell and R. M. Smith, *Critical Stability Constants*, Vols 1–4. Plenum Press, New York (1974–1979).
13. S. Moerlein and M. Welch, *Int. J. Nucl. Med. Biol.* 1981, **8**, 277.
14. G. Jackson and A. Cosgrove, *S. Afr. J. Chem.* 1982, **35**, 93.
15. M. Walser, *J. Clin. Invest.* 1961, **40**, 723.
16. R. Martin, Y. Savory, S. Brown, R. Bertholf and M. Wills, *Clin. Chem.* 1987, **33**, 405.
17. L. Öhman and S. Sjöberg, *Acta Chem. Scand.* 1983, **A37**, 875.
18. R. Martin, *J. Inorg. Biochem.* 1986, **28**, 181.
19. L. Öhman, *Inorg. Chem.* 1988, **27**, 2565.
20. G. Jackson, *S. Afr. J. Chem.* 1982, **35**, 89.
21. N. Skorik and A. Artish, *Russ. J. Inorg. Chem.* 1985, **38**, 1130.
22. W. Harris and A. Martell, *Inorg. Chem.* 1976, **15**, 713.
23. C. Baes and R. Mesmer, *The Hydrolysis of Cations*. John Wiley, New York (1976).
24. P. Brown, *J. Chem. Soc., Dalton Trans.* 1989, 399.
25. L. Öhman and W. Forsling, *Acta Chem. Scand.* 1981, **A35**, 795.
26. G. Berthon and M. Venturini, *J. Chem. Soc., Dalton Trans.* 1987, 1145.
27. G. Jackson and K. Voyi, *S. Afr. J. Chem.* 1988, **41**, 17.
28. S. Ramamoorthy and P. Manning, *J. Inorg. Nucl. Chem.* 1975, **37**, 363.
29. C. Taliaferro and A. Martell, *Inorg. Chem.* 1985, **24**, 2408.
30. W. Harris and A. Martell, *Inorg. Chem.* 1976, **15**, 713.
31. J. Garrison and A. Crumbliss, *Inorg. Chim. Acta* 1987, **138**, 61.
32. G. Schwarzenbach and F. Schwarzenbach, *Helv. Chim. Acta* 1963, **46**, 1390.
33. R. Motekaitis, Y. Sun and A. Martell, *Inorg. Chim. Acta* 1989, **159**, 29.
34. R. Motekaitis and A. Martell, *J. Coord. Chem.* 1985, **14**, 139.
35. T. Kiss, I. Sóvágó and R. Martin, *J. Am. Chem. Soc.* 1989, **111**, 3611.
36. R. Motekaitis and A. Martell, *J. Am. Chem. Soc.* 1984, **23**, 18.
37. H. Sigel, in *Advances in Solution Chemistry* (Edited by I. Bertim, L. Lunazzi and A. Dei). Plenum Press, New York (1981).
38. P. M. May, PhD thesis, University of St Andrews (1980).

39. P. Arp and W. Meyer, *Can. J. Chem.* 1985, **63**, 3357.
40. Y. Marcus and I. Eliezer, *Coord. Chem. Rev.* 1969, **44**, 273.
41. R. Martin, *Clin. Chem.* 1986, **32**, 1797.
42. G. Jackson and K. Voyi, *Polyhedron* 1987, **6**, 2095.
43. P. May, J. Slatter and G. Berthon, *Trace Element Metabolism in Man and Animals 5th Proceedings* (Edited by C. Mills, I. Bremmer and J. Chester), p. 542. CAB, Slough (1985).
44. P. May and R. Bulman, *Prog. Med. Chem.* 1983, **20**, 225.
45. P. Ackrill, A. Ralston, J. Day and K. Hodge, *Lancet ii*, 1980, 692.
46. T. Chang and P. Barre, *Lancet ii*, 1983, 1051.
47. D. Verbeelen, J. Smeyers-Verbeke, I. Van Hooff, A. Van Der Straeten and G. Roy, *Kidney Int.* 1986, **30**, 68.
48. A. Martell, W. Anderson and D. Badman (Eds), *Development of Iron Chelators for Clinical Use.* Elsevier, New York (1981).
49. B. Foster, K. Clagett-Carr, D. Hoth and B. Leyland-Jones, *Cancer Treat. Rep.* 1986, **70**, 1311.
50. C. Williams, in *Bone Scintigraphy* (Edited by E. Silberstein), p. 17. Futura, New York (1984).
51. H. Bruner, R. Hayes and J. Perkinson, *Radiology* 1953, **61**, 602.
52. R. Hayes, *Int. J. Nucl. Med. Biol.* 1983, **10**, 257.
53. W. Bradley, P. Alderson, W. Eckelman, R. Hamilton and J. Weiss, *J. Nucl. Med.* 1978, **19**, 204.
54. G. Saha, in *Essentials of Nuclear Medicine Science* (Edited by W. Hladik, G. Saha and K. Study), p. 3. Williams and Wilkins, Baltimore (1987).
55. K. Scholacker, W. Franke, E. Henke, W. Fromm, G. Maka and G. Beyer, *Eur. J. Nucl. Med.* 1986, **11**, 345.
56. M. Kappel, V. Pecoraro and K. Raymond, *Inorg. Chem.* 1985, **24**, 2447.
57. C. Taliaferro and A. Martell, *J. Coord. Chem.* 1984, **13**, 249.
58. J. Herscheid, G. Knops and M. Hoekstra, *Nucl. Med. Commun.* 1986, **7**, 53.
59. F. Hosain, R. Reba and H. Wagner, *Radiology* 1969, **93**, 1135.
60. C. Meares, *Nucl. Med. Biol.* 1986, **13**, 311.
61. S. Yek, C. Meares and D. Goodwin, *J. Radioanal. Chem.* 1979, **53**, 327.
62. D. Scheinberg, M. Strand and O. Gansow, *Science* 1982, **215**, 1511.
63. D. Hnatowich, W. Layne, R. Childs, D. Lanteigne, M. Davis, T. Griffin and P. Doherty, *Science* 1983, **220**, 613.
64. W. Cole, S. DeNardo, C. Meares, M. McCall, G. DeNardo, A. Epstein, H. O'Brien and M. Moi, *Nucl. Med. Biol.* 1986, **13**, 363.
65. C. Motta-Hennessy, S. Eccles, C. Dean and G. Coghlan, *Eur. J. Nucl. Med.* 1985, **11**, 240.
66. S. Larson, J. Rasey, Z. Grunbaum and D. Allen, *Radiology* 1979, **130**, 241.

Polyhedron Vol. 9, No. 2/3, pp. 171–187, 1990
Printed in Great Britain

0277–5387/90 $3.00+.00
© 1990 Pergamon Press plc

ALUMINIUM COMPLEXES OF HYDROXYALIPHATIC AND HYDROXYAROMATIC LIGANDS IN AQUEOUS SYSTEMS—SOME PROBLEMS AND SOLUTIONS

ARTHUR E. MARTELL,* RAMUNAS J. MOTEKAITIS and ROBERT M. SMITH

Department of Chemistry, Texas A&M University, College Station, TX 77843–3255, U.S.A.

Abstract—The stabilities of aluminium(III) complexes of ligands with hard oxygen donors are analysed and an up-to-date compilation of critical stability constants of aluminium(III) complexes of hydroxyaliphatic and hydroxyaromatic chelating agents is presented. The interferences with complex formation caused by hydrolysis of the metal ion to form soluble mononuclear and polynuclear hydroxo complexes, and by aluminium(III) hydroxide precipitation, are illustrated. In view of contradictory reports in the literature, a unified treatment of aluminium(III) citrate complexes is presented, and the formation of stable and metastable forms of mononuclear and ternuclear hydroxo citrate complexes is illustrated. The limitations in the use of normal formation constants for representing equilibrium data involving ligands with very high pK's is explained, and the use of hydrogen ion displacement equilibrium constants for such systems is recommended. Comparison of the effectiveness of several ligands for aluminium(III) complexation shows that desferriferrioxamine B (Desferal®)†, recommended for the treatment of aluminium(III) overload is by far the superior ligand over a very broad pH range.

The aquo aluminium(III) ion is the "hardest" of the trivalent ions commonly found in biological systems and the environment. Its effective ionic radius of 0.54 Å is considerably smaller than other commonly encountered trivalent metal ions (Table 1) such as Fe^{3+} (0.64 Å) and In^{3+} (0.80 Å). Trivalent boron, with an ionic radius of 0.23 Å, does not occur as an electropositive ion in aqueous solution.

Because of its small ionic radius, aluminium(III) polarizes solvated water molecules very strongly, giving rise to several hydrolytic species (hydroxo complexes), which are described by the equilibrium constants presented in Table 2. The monohydroxo complex, $Al(OH)(H_2O)_n^{2+}$, formed in the first

* Author to whom correspondence should be addressed.

† Desferal® is the trademark of Ciby–Geigy Co., Basel.

Table 1. Hydrolysis constants and solubility products of trivalent metal ions of biochemical and biomedical interest

Metal ion	Ionic[a] radius(Å)	Log K[b]		
		[MOH]/[M][OH][c]	[M][OH]^3[d]	[M(OH)$_4$]/[M][OH]^4[d]
Al^{3+}	0.54	8.5	−33.5	33.4
Ga^{3+}	0.62	11.0	−37	39.4
Fe^{3+}	0.64	11.3	−38.8	—
In^{3+}	0.80	9.5	−36.9	33.8
Gd^{3+}	0.94[e]	5.4	−25.7	—

[a] Reference 1.
[b] Reference 2.
[c] 25.0°C and 0.10 M ionic strength.
[d] 25.0°C and 0.00 M ionic strength.
[e] For six-coordinate Gd^{3+}, 1.05 if eight-coordinate; 1.10 if nine-coordinate.

Table 2. Critical equilibrium constants of aluminium(III) complexes at 25.0°C and 0.10 M ionic strength

Ligand	Protonation constants	Quotient, Q	Log Q	References
HOH, HL	13.78	$[ML]/[M][L]$	8.47	3, 4, 5
		$[ML_2]/[M][L]^2$	16.65	
		$[ML_3]/[M][L]^3$	(26.9)	
		$[ML_4]/[M][L]^4$	(33.7)	
		$[M_3L_4]/[M]^3[L]^4$	41.99	
		$[M_{13}O_4L_{24}]/[M]^{13}[L]^{32}$	335.8	
HF, HL	2.94	$[ML]/[M][L]$	6.43	6, 7, 8, 9,
		$[ML_2]/[M][L]^2$	11.63	10, 11, 12
		$[ML_3]/[M][L]^3$	15.5	
		$[ML_4]/[M][L]^4$	18.3	
		$[M(OH)L]/[MOH][L]$	6.13	
		$[M(OH)L_2]/[MOH][L]^2$	10.36	
		$[M(OH)_3L][OH]/[M(OH)_4][L]$	−3.73	
Lactic acid, HL OH $CH_3CHCOOH$	3.61[a]	$[ML]/[M][L]$	2.36[a]	13
		$[ML_2]/[M][L]^2$	4.42[a]	
		$[ML_3]/[M][L]^3$	5.8[a]	
Malic acid, H_2L OH $HOOCCH_2CHCOOH$	4.45,[b] 3.15[b]	$[ML]/[M][L]$	3.32[b]	14
Citric acid, H_3L COOH $HOOCCH_2CCH_2COOH$ OH	5.70, 4.35, 2.90	$[ML]/[M][L]$	7.98	15, 16, 17
		$[MHL]/[ML][H]$	2.94	
		$[ML]/[MH_{-1}L][H]$	3.31[c]	
		$[MH_{-1}L]/[M(H_{-1}L)(OH)][H]$	6.23[a,c]	
		$[M_3(OH)(H_{-1}L)_3]/[M]^3[L]^3$	14.43[a,c]	
		$[M_3(OH)_4(H_{-1}L)_3][H]^7/[M]^3[L]^3$	−10.91[a,c]	
HIDA, H_2L CH_2CH_2OH $HOOCCH_2NHCH_2COOH$	8.68, 2.20	$[ML]/[M][L]$	7.74	18
D-Gluconic acid, HL HO OH OH $HOCH_2CHCHCHCHCOOH$ OH	3.44	$[ML/[M][L]$	1.98	16
		$[ML]/[MH_{-1}L][H]$	2.87[c]	
		$[MH_{-1}L]/[MH_{-3}L][H]^2$	9.29[c]	
Bicine, HL $HOCH_2CH_2$ $HOCH_2CH_2NCH_2COOH$	8.11, 1.7	$[MHL]/[M][HL]$	3.38	16
		$[MHL]/[MH_{-2}L][H]^3$	13.72[c]	
DL-Tartaric acid, H_2L OH $HOOCCHCHCOOH$ OH	3.97, 2.82	$[ML_2]/[M][L]^2$	7.65	16
		$[MH_{-1}L][H]/[M][L]$	1.18[c]	
		$[MH_{-1}L]/[MH_{-2}L][H]$	5.15[c]	
		$[ML_2]/[MH_{-1}L_2][H]$	3.72[c]	
		$[MH_{-1}L_2]/[MH_{-3}L_2][H]^2$	12.67[c]	
		$[MH_{-4}L_3][H]^4/[M][L]^3$	−15.92[c]	
		$[MH_{-4}L_3]/[MH_{-5}L_3][H]$	10.89[c]	
		$[MH_{-5}L_3]/[MH_{-6}L_3][H]$	12.7[c]	

Table 2—*continued*

Ligand	Protonation constants	Quotient, Q	Log Q	References
Salicylic acid, H_2L 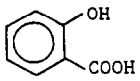	13.4,[d] 2.81[d]	$[ML][H]/[M][HL]$ $[ML_2][H]/[ML][HL]$ $[ML_3][H]/[ML_2][HL]$	−0.2[d] −2.8[d] −6.5[d]	19, 20
Sulphoxine, H_2L 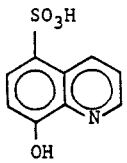	8.42, 3.95	$[ML]/[M][L]$ $[ML_2]/[M][L]^2$ $[ML_3]/[M][L]^3$	9.2 17.6 24.7	21
Maltol, HL 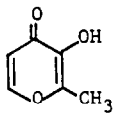	8.42[a]	$[ML]/[M][L]$ $[ML_2]/[M][L]^2$ $[ML_3]/[M][L]^3$ $[M_2(OH)_2L_2][H]^2/[M]^2[L]^2$	8.25[a] 14.26[a] 20.16[a] 8.02[a,c]	22
3-Hydroxy-2-methyl-4-pyridinone, HL 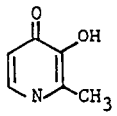	9.80, 3.65	$[ML]/[M][L]$ $[ML_2]/[M][L]^2$ $[ML_3]/[M][L]^3$	11.87 22.54 32.05	23
Catechol, H_2L 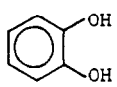	13.3, 8.30	$[ML][H]^2/[M][H_2L]$ $[ML_2][H]^2/[ML][H_2L]$ $[ML_3][H]^2/[ML_2][H_2L]$ $[MHL_2]/[ML_2][H]$ $[MHL_3]/[ML_3][H]$	−6.0 −9.10 −13.61 6.05 8.05	16, 24
4-Sulphocatechol, H_3L 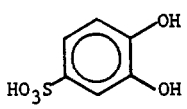	12.8,[d] 8.50[d]	$[ML][H]^2/[M][H_2L]$ $[ML_2][H]^2/[ML][H_2L]$ $[ML_3][H]^2/[ML_2][H_2L]$	−4.7[d] −8.0[d] −12.0[d]	20
Tiron, H_4L 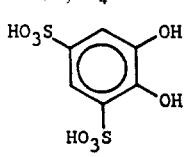	12.5, 7.62	$[ML][H]^2/[M][H_2L]$ $[ML_2][H]^2/[ML][H_2L]$ $[ML_3][H]^2/[ML_2][H_2L]$	−3.21 −6.2 −10.0	25–27 28
Chromotropic acid, H_4L 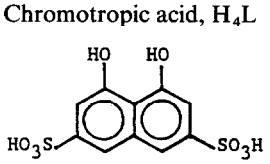	—,[e] 5.39[d]	$[ML][H]^2/[M][H_2L]$ $[ML_2][H]^2/[ML][H_2L]$	−3.82[d] −8.25[d]	20, 29, 30
Dopamine, H_2L 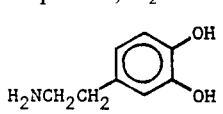	13.1, 10.36, 8.88	$[MHL]/[M][HL]$ $[M(HL)_2]/[M][HL]^2$ $[M(HL)_3]/[M][HL]^3$	13.32 23.99 30.63	28[f]

Table 2—*continued*

Ligand	Protonation constants	Quotient, Q	Log Q	References
L-DOPA, H_3L 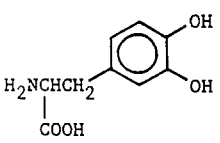	13.4, 9.81, 8.75, 2.20	[MHL]/[M][HL] $[M(HL)_2]/[M][HL]^2$ $[M(HL)_3]/[M][HL]^3$	12.72 22.62 28.43	28[f]
Acetohydroxamic acid, HL 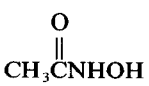	9.36[d]	[ML]/[M][L] $[ML_2]/[M][L]^2$ $[ML_3]/[M][L]^3$	7.95[d] 15.29[d] 21.47[d]	31
Desferriferrioxamine B H_3L 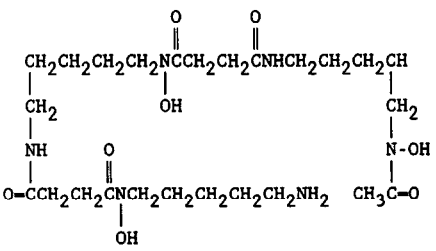	10.79, 9.55, 8.96, 8.32	[MHL]/[M][HL] [MHL]/[ML][H] $[MH_2L]/[MHL][H]$	24.14 9.43 1.2	32

[a] 25.0°C, 0.6.
[b] 29.0°C, 1.0.
[c] Proton may involve ligand hydroxyl group.
[d] 20.0°C, 0.1.
[e] Too high for measurement.
[f] These constants are not available in Reference 28. They were obtained on our request from one of the authors (T. Kiss).

step, is converted to several more complex hydrolytic species as the pH is increased. The following complexes listed in Table 2 have been detected: $Al(OH)_2^+$, $Al_3(OH)_4^{5+}$, $Al(OH)_3$ (insoluble), $Al(OH)_4^-$, and the unique polynuclear complex $Al_{13}O_4(OH)_{24}^{7+}$. The rates of formation of the polynuclear complexes are quite slow, and the complexes may persist in solution for long periods of time as metastable species even when the pH has been changed to the conditions where they are no longer the most stable complexes.

A review of the early literature on the coordination chemistry of aluminium(III) reveals considerable stability data of questionable validity. In many cases the strong hydrolytic tendencies of aluminium(III) had not been considered in data processing and in deciding on the complex species present in solution. Workers at that time were not completely aware of the tendency of aluminium(III) to form long-lasting yet metastable hydrolytic complexes which may persist for hours or even days.

The slowness of substitution reactions in the coordination sphere of aluminium(III) is further aggravated when the donors are multidentate ligands, which involve steric effects as well as cooperative donor group coordination about the metal ions. Equilibrium measurements of aluminium(III)–ligand interactions are almost invariably slow, and studies that do not take this factor into account are generally in error.

EFFECTIVE LIGAND DONOR GROUPS FOR ALUMINIUM(III)

Because aluminium(III) is probably the "hardest" metal ion frequently encountered in aqueous complex systems, it is apparent that it is most strongly bound by ligands with hard donor groups. The most effective donor groups are therefore, negative oxygen donors, having a single negative charge, HO^- or RO^-, but even more effective is the oxide O^{2-} ion. Thus the hydroxide ion (Tables 1 and 2) forms many complexes of aluminium(III), while the oxide anion, which is more difficult to generate (i.e. to replace both H^+ ions from water) may be

found in polymeric hydrolytic species bridging two (or more) aluminium(III) ions.

The fluoride ion is also small, negative and isoelectronic with OH^-. It is seen in Table 2, however, that binding of fluoride to aluminium(III), while quite strong, is considerably weaker than that of hydroxide ion. This difference is due to the polarity of the hydroxide ion, whereby its negative charge is directed toward the electron acceptor (the metal ion), whereas the fluoride ion is more symmetrical. Thus the metal ion sees less negative charge density with fluoride binding than it does with hydroxide coordination.

ORGANIC LIGANDS

The following are some of the donor groups which are most frequently present in organic ligands which have been found to be very effective in binding aluminium(III) in aqueous solution, presented in the order of decreasing hardness, which is also the order of decreasing metal ion affinity.

Monodentate donor groups

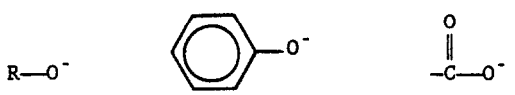

Alkoxide $\gtrsim 14$ Phenoxide ~ 10 Carboxylate ~ 4

The following are some of the more frequently encountered bidentate pairs containing these donor groups. They are found in both natural and synthetic ligands which are effective for aluminium(III) and other trivalent metal ions (e.g. siderophores).

Bidentate combinations

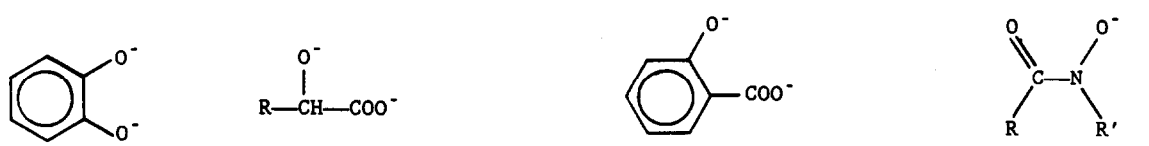

Catecholate ~ 22 Hydoxy acid anion ~ 18 Aromatic hydroxy acid anion ~ 16 Hydroxamate ~ 9

Hard donor groups also have very high affinities for the hardest positive ion of all—the hydrogen ion—so that coordination of a metal ion such as Al^{3+} with these donor groups in aqueous solution always involves strong competition with hydrogen ions. The intensity of that competition for the hard oxygen donors presented above is measured quantitively by the log protonation constants (pK's) listed under each donor (ΣpK is given for the bidentate pairs). These protonation constants also provide a quantitative measure of the hardness of each monodentate donor and the pK sum indicates the hardness of the bidentate donor pairs.

A survey of the literature indicates that organic ligands having sufficient affinity for Al^{3+} to form complexes stable enough to resist its strong hydrolytic tendencies (and consequent precipitation) are generally multidentate and contain arrangements of several donor groups selected from the hard oxygen donors listed above. Table 2 contains a new up-to-date compilation of the critical (selected) equilibrium constants for the aluminium(III) complexes of various types of ligands with the functional groups of interest. A variety of ligands is selected so that the complexes listed represent a considerable variation of structural types and a wide range of stabilities. In order to keep the table within limits, many well-known ligands having structures very similar to those listed have been omitted. The successive log protonation constants are presented in the order of decreasing pK's. In most cases, the normal stability constants (as log values) are given, corresponding to reaction of the aquo metal ion with the most basic (most fully deprotonated) form of the ligand as indicated by eq. (1):

$$Al^{3+} + L^{n-} \rightleftharpoons AlL^{(3-n)+}$$

$$K = [AlL^{(3-n)+}]/[Al^{3+}][L^{n-}]. \quad (1)$$

When possible, stability constants are presented in this form, but such is not always the case. For ligands with very hard donor groups it is sometimes not possible to determine or calculate the concentration of the most basic form of the ligands, L^{n-}, because the highest pK's are too high for accurate measurement in aqueous solution. Since one or more of the highest protonation constants are either unknown or inaccurately known, calculation of the value of log K_1 is either not possible, or the value is an inaccurate estimate. This difficulty is circumvented by listing equilibrium constants for the displacement of hydrogen ions, as in eqs (2) and (3), in place of the normal stability constants:

$$Al^{3+} + HL^{(n-1)-} \rightleftharpoons AlL^{(3-n)+} + H^+$$

$$K_1^H = [AlL^{(3-n)+}][H^+]/[Al^{3+}][HL^{(n-1)-}] \quad (2)$$

$$Al^{3+} + H_2L^{(n-2)-} \rightleftharpoons AlL^{(3-n)+} + 2H^+$$

$$K_2^H = [AlL^{(3-n)+}][H^+]^2/[Al^{3+}][H_2L^{(n-2)-}]. \quad (3)$$

These equilibrium constants [eqs (2) and (3)] can be determined with the full precision of the potentiometric methods in the p[H] range 2–12, with no dependence on the uncertain values of the ligand protonation constants measured above p[H] 12. The potentiometric procedure, and the limitations involved are described in detail elsewhere.[33] An alternate type of formalism is now employed for expressing stability constants for ligands with pK's too high to measure. This procedure designates the most basic form of the ligand attainable in aqueous solution by titration with alkali metal hydroxide as L^{n-}, and subtracting any additional protons displaced by the metal ions by the formalism $H_{-1}L^{(n+1)-}$, $H_{-2}L^{(n+2)-}$, etc. This procedure makes a clear distinction between protons that may be titrated with base in aqueous solution and the additional protons displaced by metal ions. It is seen in Table 2 that displacement reactions such as eqs (2) and (3) have been employed to describe equilibria between the aluminium(III) ion with catechol and catechol derivatives, and that the proton subtraction formalism is also used for several complexes.

The main reason why potentiometric pH measurements cannot be carried out accurately above pH 12 and below pH 2 (for 0.10 M ionic strength) is that the liquid junction potentials change considerably in the presence of high concentrations of hydrogen ion or hydroxide ion. This may be avoided in some cases when the protonated and unprotonated ligands differ considerably in UV–vis absorbance, as with phenols and some catechols. In such cases the extent of dissociation can be measured spectrophotometrically while the $[H^+]$, $[OH^-]$ concentrations are determined from the stoichiometry of the solution. Even this method has its limitations, however. For a solution at 0.10 M ionic strength, a pK of 13.0 with equal concentrations of ligand acid and basic forms (maximum buffering), the hydroxide ion concentration would be approximately 0.2 M, so that the ionic strength is greatly exceeded merely due to this anion alone. It is obvious that under these conditions the ionic strength cannot be controlled and the equilibrium constant cannot be determined accurately.

This problem was encountered with aluminium(III) complexes of L-DOPA and its analogues in a paper by Kiss *et al.*[28] In this case the ionic strength was "controlled with KCl" to 0.2 M. The value of $\log K_1^H$ (first protonation constant) of L-DOPA was given as 13.4, quite properly with one significant figure. If it is realized, however, that hydroxide ion concentration at p[H] 13.4 is nearly 0.5 M, which is probably in addition to the 0.2 M KCl present, it is seen that the ionic strength is way out of control, even if lower concentrations of base were employed. Thus the uncertainty in the 13.4 value is considerable. Unfortunately, the authors used this high pK to calculate the stability constant, β_3 as 38.36, implying considerable accuracy, in spite of the uncertainty in the ligand protonation constants. It would have been better to eliminate the high pK's from the metal ion equilibria and express them more accurately as proton displacement reactions, as is done in Table 2. The more precise proton displacement constants can be used for accurate equilibrium calculations of molecular species formed in interactions of the Al^{III}–L-DOPA complexes with other ligands and metal ions.

ALIPHATIC HYDROXYL GROUPS AS LIGANDS

The aliphatic alkoxide donor has such high proton affinity that in some molecules it remains protonated and does not combine with Al^{3+} even at extremely high pH, while on the other hand in other ligands it is an effective partner in aluminium(III) coordination. Proton binding in aliphatic alcohols is so strong that simple alkoxide complexes of Al^{3+} resulting from proton dissociation are not formed, nor are the bis-alkoxides such as complexes of ethyleneglycolate, $^-O—CH_2CH_2—O^-$. (In the latter case, complexes do form with the very hard B^{3+} centre, which was noted above as not forming an electropositive ion in aqueous solution.) However, alkoxide donor groups participate in coordination of hard metal ions such as Al^{3+}, with proton dissociation, when they function in conjunction with other donor groups, which are more easily dissociated (less hard), so that the chelate effect provides sufficient incremental metal ion affinity to overbalance the strong proton affinity. Common examples are tartaric acid and citric acid, which complex metal ions through adjacent alkoxide and carboxylate donor groups.

In many cases it is difficult to determine by equilibrium measurements whether the displacement of a hydrogen ion occurs at the aliphatic hydroxyl group or at a coordinated water molecule, as follows:

Thus far most of the evidence presented has been indirect or circumstantial, such as the occurrence of strong coordination with the alkoxyl group, and lack of strong coordination in its absence, and argu-

ments based on relative hydrolytic tendencies of metal ions, such as in the case of aluminium(III) citrate described below.[16]

MICROSCOPIC EQUILIBRIA OF CATECHOL COMPLEXES

Much has been stated in recent publications that the knowledge of microscopic equilibrium constants is essential for the "proper" interpretation of metal ion [including aluminium(III)] complexes of ligands containing phenolic and catechol donor groups. While microscopic equilibrium constants are interesting and useful in the interpretation of metal complex equilibria in solution, and knowledge of the structures of individual microspecies in solution is useful in the interpretation of protonation constants and metal ion stability constants, they are certainly not necessary for the accurate determination of equilibrium constants and stability constants of solution components, and for measuring the thermodynamic parameters for the conversion of one component to another. An interesting example is the acid–base equilibria and the formation of aluminium(III) complexes of L-DOPA, recently described by Kiss *et al.*[28] The ligand, designated as H_3L, dissociates in three steps, in accordance with Scheme 1. H_3L itself actually consists of four microspecies, the one shown, and three species with the carboxyl protonated and one of the other three donor groups deprotonated. The concentrations of these latter three species can be estimated from the differences in pK's of the carboxylate and the other proton acceptors as about 10^{-6} times the concentration of the species H_3L indicated in the scheme, and hence they can be ignored without appreciable error, thus greatly simplifying the microscopic treatment of the remaining species present. In the paper by Kiss *et al.*,[28] the difference between $H_2L_a^-$ and $H_2L_b^-$ were ignored and grouped together as a single species. The total concentrations of these two species was estimated from the change in phenolate (catecholate) absorbance in going from H_3L to $[H_2L_a^- + H_2L_b^-]$. It was not stated if the absorbances measured were considered to involve equal contributions from the two microspecies, or whether it was merely assumed that an average value would be satisfactory. In any case these authors reported a pseudo microscopic distribution constant $[H_2L_c^-]/([H_2L_a^-]+[H_2L_b^-])$ of 1/1.6. In the first deprotonation step the ammonium group is somewhat less dissociated than the sum of the two phenolic groups (i.e. the catechol group).

The product of the second deprotonation consists of three microspecies, but a single species was assumed.[28] The elimination of HL_c^{2-} is reasonable since its concentration is about 10^{-4} of that of the sum of $[HL_a^{2-}]$ and $[HL_b^{2-}]$. Although ignored at this point, its existence at low concentrations was invoked later in the paper[28] to calculate a special microscopic aluminium(III) stability constant. The grouping of the two phenolate forms together for the microscopic treatment of both H_2L^- and HL^{2-} was convenient, because there does not exist at the present time experimental data for determining the relative concentrations of these two species.

For the aluminium(III) complexes of L-DOPA, six distinct complexes may be determined directly from potentiometric p[H] measurements. Three of these macrospecies are $AlHL^+$, $Al(HL)_2^-$ and $Al(HL)_3^{3-}$, in which the aluminium(III) ion is recognized as combining with the catecholate donor groups, with the proton moving entirely to the α-amino group. The other three are the stepwise dissociation constants of $Al(HL)_3^{3-}$. Unfortunately, these dissociation constants for the complexes of the monoprotonated ligand were not reported by Kiss *et al.*[28] The formation reactions of these three complexes overlap, but the individual constants can easily be sorted out and calculated by modern computer methods. At higher pH, the complex $Al(HL)_3^{3-}$ undergoes three successive dissociations to eventually form the completely deprotonated complex, as follows:

$$Al(HL)_3^{3-} \overset{9.75}{\rightleftharpoons} AlL(HL)_2^{2-} \overset{10.15}{\rightleftharpoons}$$

$$AlHL(L)_2 \overset{10.65}{\rightleftharpoons} AlL_3.$$

These pK's differ approximately by the calculated statistical values (log 3 units) showing that they have little influence on each other. The pK's (protonation constants) are in the pH range accessible by potentiometry and the values reported are reliable.

The formation constants of the protonated complexes, which can be measured accurately, were not given in the paper. Instead, the overall constants, β_1, β_2 and β_3 were reported.[28] These constants involve combination of the metal ion with the fully deprotonated ligand, which cannot be determined accurately (such calculations required pK_{3a} which is known only approximately).

With respect to microscopic equilibria involving aluminium(III) complexes, Kiss *et al.*[28] chose to estimate the concentrations of species HL_c^{2-}, and from this calculate what they term as "proper" stability constants with this microspecies, obtained log values of 16.03, 13.21 and 9.12 for $[Al(HL)^+]/[Al^{3+}][HL_c^{2-}]$, $[Al(HL)_2^-]/[Al(HL)^+][HL_c^{2-}]$, and $[Al(HL)_3^{3-}]/[Al(HL)_2^-][HL_c^{2-}]$, respectively. While such constants are interesting for comparison with

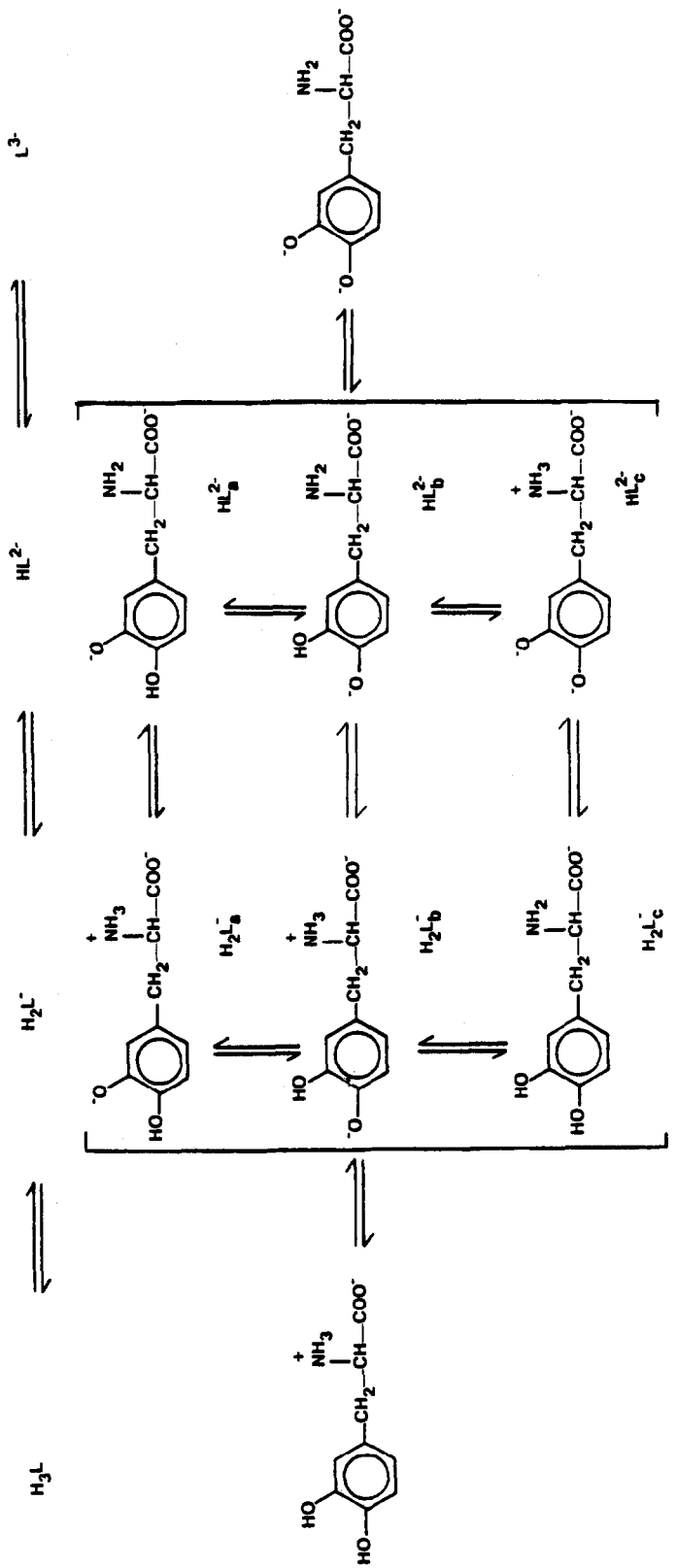

Scheme 1. Microscopic acid–base equilibria of L-DOPA.

binding constants of other ligands such as catechol, it should be remembered that they are approximations and cannot (in fact need not) be employed for the calculation of metal complex species in solution. (Although the original experimental data were accurate, the derived microscopic constants are only estimates, requiring the inaccurate value of pK_{3a} and an "estimated" pK for the microspecies HL_c^{2-}.)

METASTABLE EQUILIBRIA

The tendency of aluminium(III) ions to form several hydrolytic species leads to the formation of mononuclear and polynuclear hydroxo complexes, indicated in Table 2. The small size of the Al^{3+} ion, the strong interactions with the hydroxide ion and the tendency of the hydroxide ion to bridge Al^{3+} centres to form polynuclear arrays—all contribute to very slow attainment of equilibrium. Thus the experience of the author and his associates, and the reports of other investigators[15,17] indicate that complex formation of aluminium(III) complexes of simple ligands may take hours, or up to a day, to come to equilibrium. For this reason the conversion of polynuclear hydroxo complexes to still larger oligomeric species which are necessary precursors of the macromolecular polymer, solid $Al(OH)_3$, takes still longer, so that soluble hydroxo complexes may be maintained almost indefinitely under conditions such that solid aluminium hydroxide is the thermodynamically stable species. Such solutions revert back to the true equilibrium state (i.e. precipitation occurs) if they are seeded with solid hydrous aluminium hydroxide. The nature of the complexes that form in such metastable solutions, and their relative concentrations are expressed by the equilibrium constants in Table 2. In order to describe these metastable systems in greater detail two sets of species distribution curves calculated from the data in Table 2 are presented for the same solutions, with and without the use of K_{sp} for solid aluminium(III) hydroxide.

Relative molar concentrations of aluminium(III) species at a total analytical concentration of 1.00×10^{-6} M, with the concentration of the complex $Al(OH)_3$ plotted as a soluble (supersaturated) complex, are illustrated in Fig. 1. At this dilution polynuclear species are not represented in the succession of increasingly hydroxylated complexes, all of which are monodentate. At a T_M of 1.0×10^{-3} M, however, the polymeric complex $Al_{13}(OH)_{32}^{7+}$, sometimes written as the partially dehydrated form $Al_{13}O_4(OH)_{24}^{7+}$, dominates the system from p[H] 5 to 8, as indicated in Fig. 2. When the equilibria between the species formed includes the solid phase, the distribution curves are very different. Figure 3 shows that the solid precipitate is present from pH 4.5 to 10, and dominates the system over most of that range. Precipitation provides the driving force for conversion of aluminium(III) species to $Al(OH)_3$. It is also seen that the excess solid maintains a constant concentration of the soluble $Al(OH)_3$ complex (at saturation). An interesting aspect of the distribution curves in Fig. 3 is the fact that the free aluminium(III) in solution under precipitation conditions is around 5×10^{-8} M (as the $Al(OH)_3$ complex), a not insignificant con-

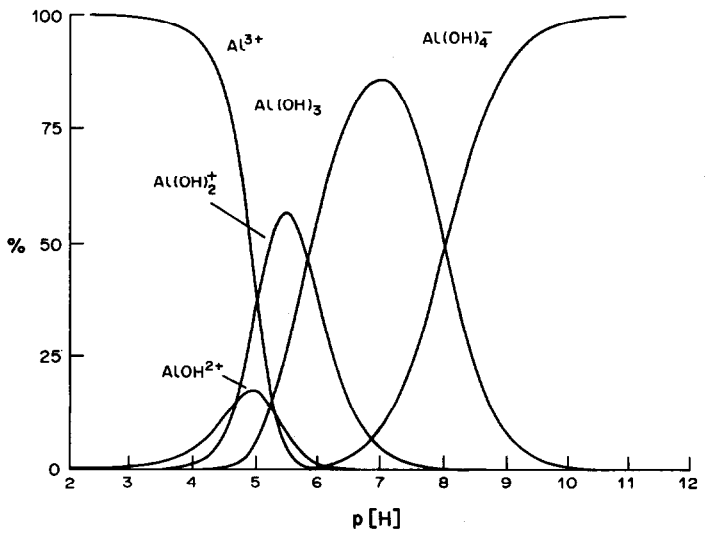

Fig. 1. Relative molar concentrations of hydrolytic species formed from the aquo aluminium(III) ion as a function of $-\log[H^+]$. Total analytical concentration of aluminium(III) species is 1.00×10^{-6} M. The concentration of $Al(OH)_3$ is plotted as a supersaturated solution. $T = 25.0°C$, $\mu = 0.100$ M.

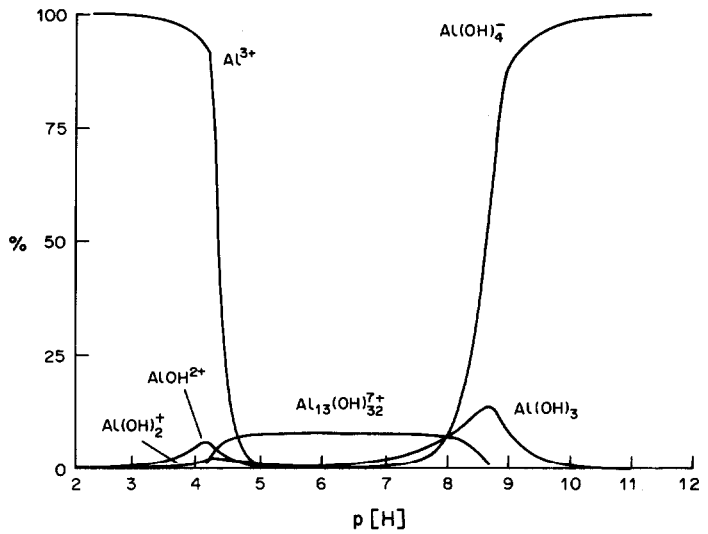

Fig. 2. Relative molar concentrations of hydrolytic species formed from the aquo aluminium(III) ion as a function of $-\log[H^+]$. Total analytical concentration of aluminium(III) species is 1.00×10^{-3} M. The molar concentration of $Al_{13}(OH)_{32}$ constitutes 98.8% of the aluminium(III) present. The concentration of $Al(OH)_3$ is plotted as a supersaturated solution. $T = 25.0°C$, $\mu = 0.100$ M.

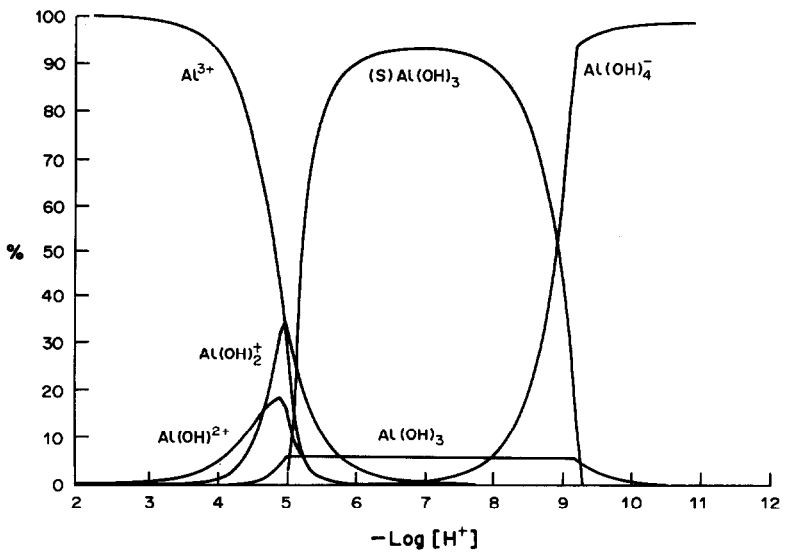

Fig. 3. Relative molar concentrations of hydrolytic species formed from the aquo aluminium(III) ion as a function of $-\log[H^+]$. Total analytical concentration of aluminium(III) species is 1.00×10^{-6} M. (S)$Al(OH)_3$ represents the relative quantity of precipitate. $T = 25°C$; $\mu = 0.100$ M.

centration, which indicates that aluminium(III) is free to move about in aqueous solution in the environment, in the absence of more effective precipitating agents.

Because of the presence of fluoride in natural waters, it is of interest to consider what happens to aluminium(III) hydrolysis in the presence of the F^- ion. Figure 4, calculated from the data in Table 2, indicates considerable formation of fluoride complexes in acid solution. Comparison with Fig. 3 shows that fluoride narrows the pH range of $Al(OH)_3$ precipitation considerably, and increases the pH of initial precipitation of $Al(OH)_3$ by a full unit. It is obvious from these effects that the fluoride ion greatly increases the concentration and mobility of aluminium(III) in natural waters.

TYPICAL HYDROXY ORGANIC LIGANDS AND THEIR ALUMINIUM(III) COMPLEXES

The data in Table 2 indicate the affinities of a wide variety of hydroxy aliphatic and hydroxy aromatic

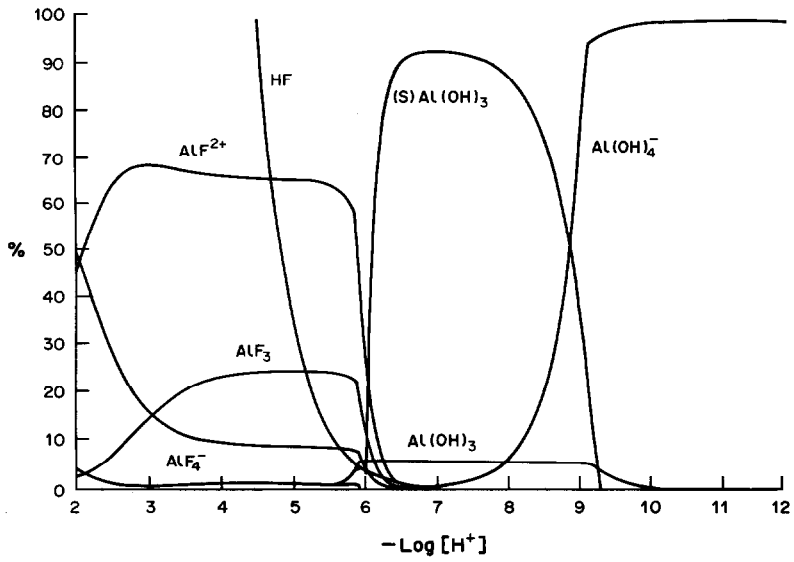

Fig. 4. Relative molar concentrations of complex species formed from 1.0×10^{-6} M aquo aluminium(III) ion and 5.0×10^{-5} M fluoride ion. (S)Al(OH)$_3$ represents the relative quantity of precipitated Al(OH)$_3$. $T = 25.0°C$; $\mu = 0.100$ M.

ligands for aluminium(III). These data may be employed to determine the speciation (at equilibrium) of aluminium(III) in systems containing two or more competing ligands. In all cases, the use of ligand pK's and aluminium(III) hydrolysis constants in the equilibrium analysis takes the corresponding side reactions (hydroxo complexing and proton competition) into account, and the relative effectiveness of the coordinating ligands thus depends on many factors, as indicated above, and are not easily judged by the magnitudes of the stability constants themselves.

Because of space limitations, this analysis of aluminium(III) speciation in complex systems is restricted to several well-known ligands of some importance in aluminium(III) chemistry: citric acid, EDTA, catechol, and a hydroxamic acid, desferriferrioxamine B (DFB). Citric acid forms several interesting complexes of aluminium(III), and is present in blood serum and other biological fluids. EDTA is a well-known universal chelating agent with surprisingly high aluminium(III) affinity. Catechol has the highest affinity for aluminium(III) by virtue of its hard oxygen donors, but its coordination with metal ions is countered by high proton affinity. Hydroxamic acids such as DFB have weaker (less hard) oxygen donors but have the advantage of relatively low proton affinities compared to catechols.

Citrate complexes

The chemistry of aluminium(III)–citrate complexes has been characterized by much inconsistent data and conflicting interpretations. This situation is due at least in part to the fact that substitution reactions, equilibria with hydrolytic species and the formation of hydroxo-bridged polynuclear species, are extremely slow. A definitive paper on aluminium(III) citrate, and other hydroxy acid complexes of aluminium(III) was that of Motekaitis and Martell,[16] who demonstrated that the potentiometric equilibrium data, obtained over a wide range of conditions, may be explained by three aluminium(III) complexes **1**, **2** and **3**, the 1 : 1 complex AlL (citric acid = H_3L), and its protonated ($AlHL^+$) and deprotonated ($AlH_{-1}L^-$) forms. The protonation site in AlL is suggested as a carbonyl group, thus liberating the aliphatic alkoxy group for strong aluminium(III) coordination through hydrogen ion displacement. The coordinate bond strength of this configuration was considered strong enough to withstand addition of a second proton, which is indicated as going to a second carboxyl group in $AlHL^+$, **2**. Deprotonation of AlL results in the completely deprotonated complex $AlH_{-1}L^-$, **3**, in which all four donor oxygens are considered to be coordinated to aluminium(III). Strong evidence for the involvement of the ligand hydroxyl group in **1** and **3** was demonstrated by Motekaitis and Martell from potentiometric equilibrium measurements. At p[H] values considerably below 4, the potentiometric equilibrium data show the neutralization of one more proton than the three available from the carboxylic acid groups of the ligand. This neutralization reaction is complete well below the p[H] value of the first hydrolysis step of the uncoordinated (aquo) aluminium(III) ion, so

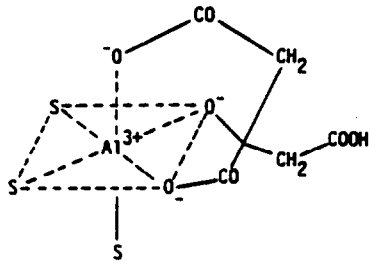

1

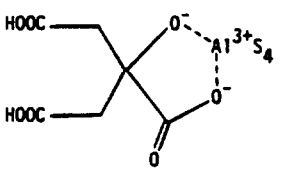

2

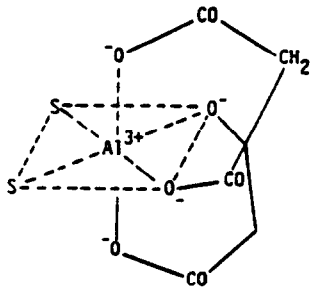

3

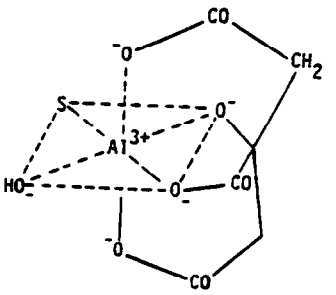

4

that it could not come from coordinated water, and deprotonation of the aliphatic hydroxyl group is the only other possibility. Moreover, it was found that potentiometric data for higher ratios (2 : 1, 3 : 1) of the ligand to metal ion are fully explained by the mononuclear species and the protonation equilibria of the free, uncoordinated excess ligand, so that there is no need to invoke 2 : 1 or 3 : 1 ligand to metal species for the aluminium(III)–citrate system.

The above reasoning based on potentiometric data and hydrolytic tendencies of aluminium(III) demonstrates the presence of the ligand deprotonated aliphatic hydroxyl donor in both ML and $MH_{-1}L^{-}$. Further comparisons[16] with other citrate complexes of other metal ions, and aluminium(III) complexes of other hydroxy ligands suggests that the complex MHL^{+} also contains the deprotonated ligand hydroxyl donor and two protonated carboxyl groups.

Detailed and exhaustive potentiometric studies of the aluminium(III)–citrate system by Ohman and Sjöberg,[15] and Ohman[17] have demonstrated the formation of additional complex species, mainly at somewhat higher pH and considerably higher complex concentration: a trinuclear complex which slowly forms, with up to 20 h required to reach equilibrium, $Al_3(OH)(H_{-1}L)_3^{4-}$. This species dominates the solution from p[H] 3 to 8, at 10^{-3} M concentration, when the system is allowed a long period of time to come to equilibrium. Another, less stable ternuclear complex, $Al_3(OH)_4(H_{-1}L)_3^{7-}$, was detected at higher pH, as well as an additional mononuclear complex, $Al(OH)(H_{-1}L)^{2-}$ (**4**). The formation of polynuclear complexes are of course very sensitive to concentration, as may be seen from the distribution curves, Figs 5 and 6, for 1 : 1 aluminium(III)–citrate solutions at 1.0×10^{-3} and 1.0×10^{-6} M. It is seen that the polynuclear complexes which are dominant at the higher concentration are completely absent when the solution is diluted 1000-fold.

It is quite possible that the potentiometric measurements that have led to the detection of the hydrolytic aluminium(III)–citrate species, $Al_3(OH)(H_{-1}L)_3^{4-}$, $Al_3(OH)_4(H_{-2}L)_3^{7-}$ and $Al(OH)(H_{-1}L)^{2-}$, have in fact been dealing with metastable equilibria, as described above. The distribution curves in Figs 5 and 6 were calculated without consideration of the possibility of $Al(OH)_3$ precipitation, and indeed the authors[15,17] were very careful in excluding data taken from solutions containing even a trace of a solid phase. On the other hand, if one recalculates the distribution in Fig. 5 taking the K_{sp} of $Al(OH)_3$ into consideration, a completely different picture emerges (Fig. 7). The concentrations of $Al_3(OH)(H_{-1}L)_3^{4-}$ and $Al(OH)(H_{-1})^{2-}$ are greatly reduced, and the less stable trinuclear species $Al_3(OH)_4(H_{-1}L)_3^{7-}$ is completely eliminated.

Aluminium(III)–*catechol complexes*

As suggested above, of the common ligands available for binding aluminium(III), the stability of the aluminium(III)–catechol complexes is the highest. However, its full effectiveness cannot be observed

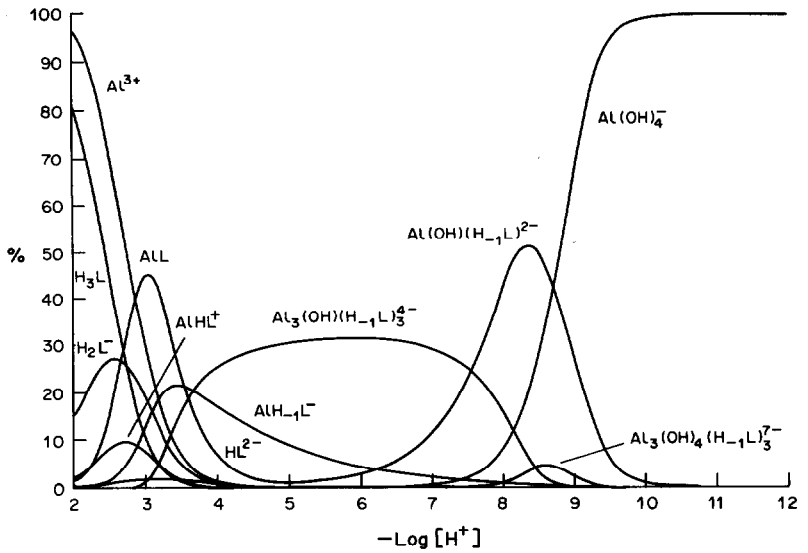

Fig. 5. Relative molar concentrations of complex species formed from 1.00×10^{-3} M aquo aluminium(III) and 1.00×10^{-3} M citric acid as a function of p[H]. The $Al(OH)_3$ formed (max %, 0.1) is considered as remaining in solution. $T = 25.0°C$; $\mu = 0.100$ M.

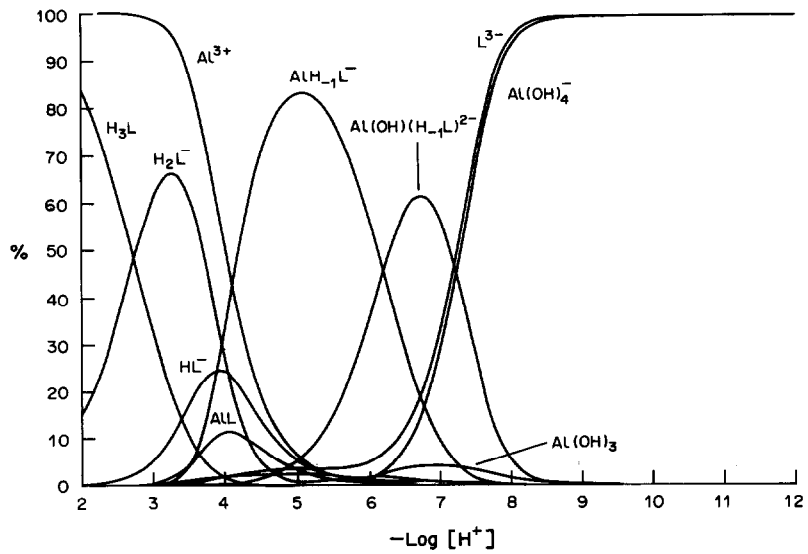

Fig. 6. Relative molar concentrations of complex species formed from 1.00×10^{-6} M aquo aluminium(III) and 1.00×10^{-6} M citric acid as a function of p[H]. The $Al(OH)_3$ formed (max %, 3.9) is considered as remaining in solution. $T = 25.0°C$; $\mu = 0.100$ M.

except at high pH, because of its high pK's, and consequent strong competition by hydrogen ions, even in alkaline solution. The first protonation constant of the catecholate ligand is too high to be measured accurately, and the conventional stability constants based on catechol = H_2L, which require both pK's for calculation [eq. (1)], cannot be reported with accurate constants. More accurate equilibrium data may be obtained for hydrogen ion displacement reactions. These factors may be perceived in the pK's and stability constants listed in Table 3.

EDTA has surprisingly high affinity for aluminium(III), with a binding constant of $10^{16.3}$. Part of the high affinity is due to the formation of a stable hydroxo complex (pK 5.87) so that the monohydroxo species is the most stable form above pH 6. In competition with citric acid the EDTA complexes dominate, and very little aluminium(III) citrate forms. Species distribution curves of a 1 : 1 : 1 aluminium(III)–citrate–EDTA system[34] shows that aluminium(III)–citrate never forms to more than about 15% of the total, and is present only in acid solution.

Table 3. pK's and stability constants of aluminium(III)–catecholate complexes (catechol = H_2L)

Equilibrium quotients and log K values				Reference
$\frac{[HL^-]}{[L^{2-}][H^+]}$	13.7[a]	$\frac{[H_2L]}{[HL^-][H^+]}$	9.37[a]	24
$\frac{[AlL^+]}{[Al^{3+}][L^{2-}]}$	16.9[a]	$\frac{[AlL_2^-]}{[AlL^+][L^{2-}]}$	13.6[a]	24
$\frac{[AlL^{3-}]_3}{[AlL_2^-][L^{2-}]}$	8.9[a]			24
$\frac{[AlL^+][H^+]^2}{[Al^{3+}][H_2L]}$	−6.08[b]	$\frac{[AlL_2^-][H^+]^2}{[AlL^+][H_2L]}$	−9.18[b]	16
$\frac{[AlL^{3-}][H^+]^2}{[AlL_2^-][H_2L]}$	−13.52[b]	$\frac{[AlHL_2]}{[AlL_2^-][H^+]}$	6.05[b]	16

[a] T = 20°C, 0.10 M.
[b] T = 25°C, 0.10 M.

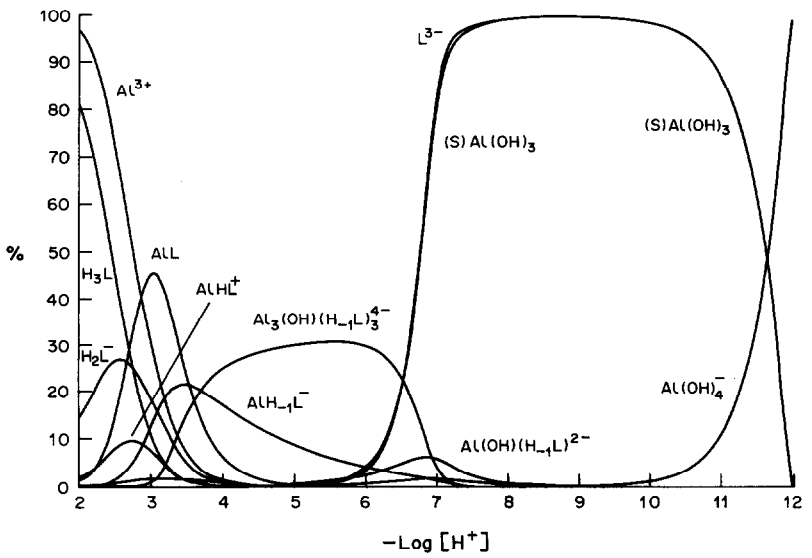

Fig. 7. Relative molar concentrations of complex species formed from 1.00×10^{-3} M aquo aluminium(III) and 1.00×10^{-3} M citric acid as a function of p[H]. (S)$Al(OH)_3$ represents the relative quantity of precipitated $Al(OH)_3$. T = 25.0°C; μ = 0.100 M.

When EDTA competes with catechol for aluminium(III), however, the catechol dominates, although only at high pH, where there is less proton competition. The distribution curves of the 1 : 1 : 3 aluminium(III)–EDTA–catechol system [a 3 M ratio of catechol is needed to supply six donor groups to aluminium(III)], illustrated in Fig. 8, show that the aluminium(III)–EDTA chelates are the major species up to pH 8.5. Beyond that the 3 : 1 aluminium(III)–catechol complex dominates up to and above pH 12, with only minimal interference by $Al(OH)_4^-$.

The Desferriferrioxamine B–aluminium(III) *complex*

Desferriferrioxamine B (Desferal® DFB) is a microbial siderophore which has long been used for the treatment of Cooley's anaemia.[35,36] It is now also being used for the treatment of aluminium overload.[37] Because of its medicinal importance it is of interest to compare its affinity for aluminium(III) with that of other ligands. The stability constant for the aluminium(III) chelate, formed in accordance with the following reaction, has been reported

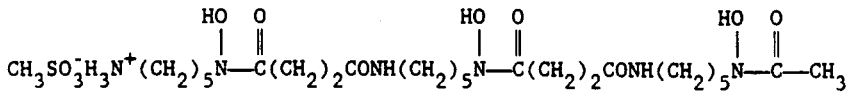

Desferriferrioxamine B, methanesulphonate salt

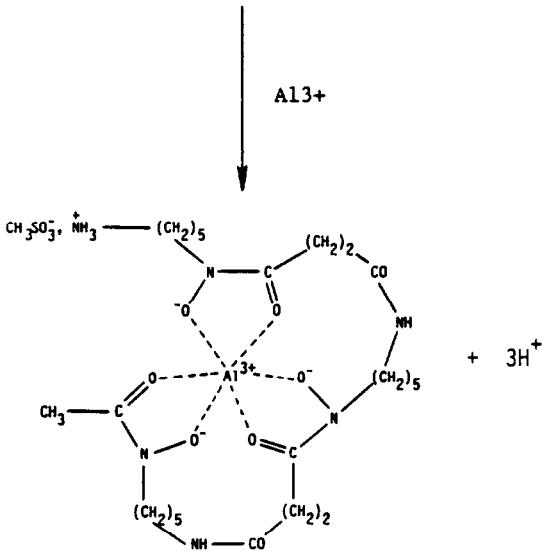

recently[28] as $10^{24.14}$ for the species with a protonated terminal aliphatic amino group. It is this form which exists at physiological pH. With these data it is possible to calculate the species present in solutions containing DFB and a competing chelating agent.

$$\log\left(\frac{[\mathrm{AlHL}^{+}]}{[\mathrm{Al}^{3+}][\mathrm{HL}^{2-}]}\right) = 24.14$$

$$\log\left(\frac{[\mathrm{AlHL}^{+}]}{[\mathrm{AlL}][\mathrm{H}^{+}]}\right) = 9.43.$$

Figures 9 and 10 clearly demonstrate the remarkable affinity of DFB for aluminium(III). The aluminium(III)–DFB chelate predominates over the EDTA chelate between pH 3 and 11.5 (Fig. 9), with the latter ([MHE]+[ME^{-}]) accounting for about 50% of the metal ion only below pH 3, and dis-

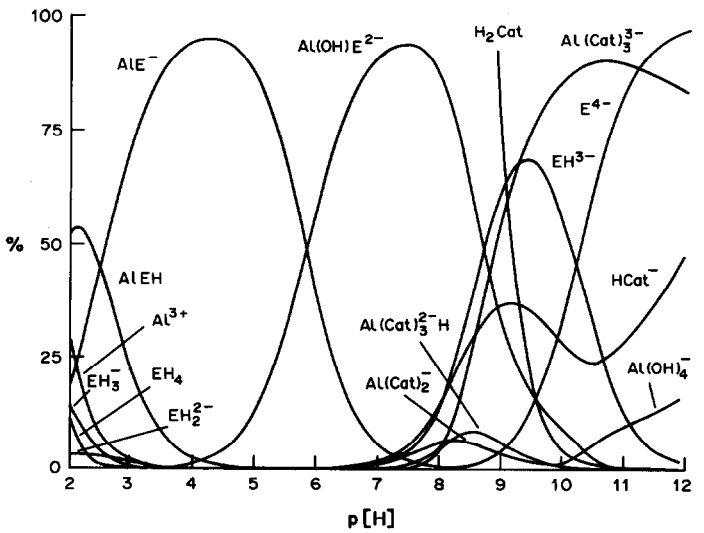

Fig. 8. Relative molar concentrations of complex species formed as a function of $-\log[H^{+}]$ in a solution containing the total analytical concentrations, aluminium(III), 1.00×10^{-3} M; pyrocatechol, 3.00×10^{-3} M; EDTA, 1.00×10^{-3} M; $T = 25.00°C$; $\mu = 0.100$ M; Cat = dinegative catechol anion and E is tetranegative EDTA anion.

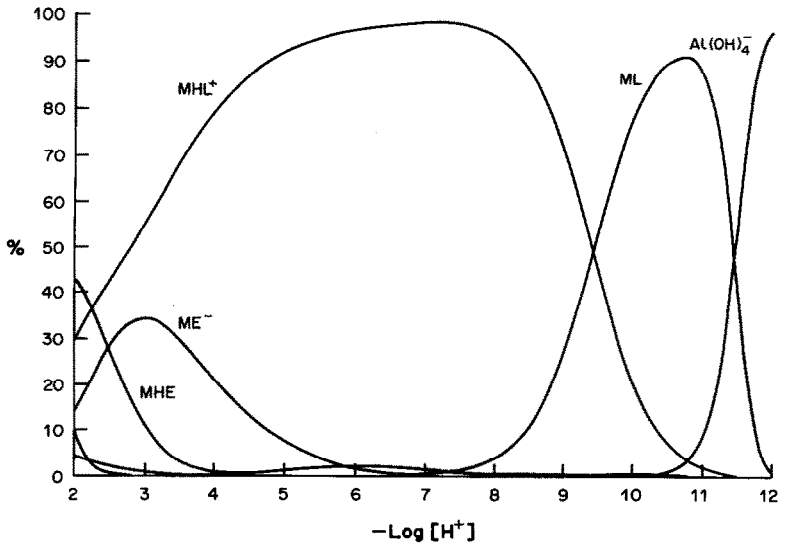

Fig. 9. DFB more effective than EDTA for binding aluminium(III). EDTA = H_4E; DFB = H_3L or H_4L^+; $Al^{3+} = M^{3+}$. Total concentrations of components, $T_{EDTA} = T_{DFB} = T_{Al^{III}} = 0.0010$ M; $T = 25.0°C$, $\mu = 0.100$ M (KCl).

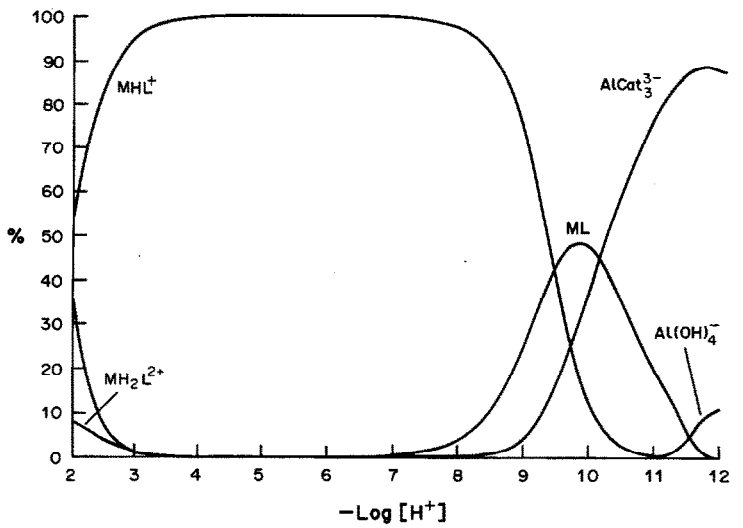

Fig. 10. Catechol more effective than DFB only at very high pH. DFB = H_3L—H_4L^+; catechol = H_2Cat; $Al^{3+} = M^{3+}$. Total concentrations $T_{DFB} = T_{Al^{III}} = 1.0 \times 10^{-3}$ M; $T_{Cat} = 3.0 \times 10^{-3}$ M; $T = 25.0°C$, $\mu = 0.100$ M(KCl).

appearing entirely at and above pH 6. The aluminium(III)–DFB chelate is eventually converted to $Al(OH)_4^-$, but only above pH 11. Even with catechol as a competing ligand (Fig. 10), the aluminium(III)–DFB complex predominates over the entire pH range from pH 2 to 10, and is the only complex present at physiological pH. Only above pH 9 does the catechol ligand begin to grow in, but it does not become the major aluminium(III) complex until the pH is increased to above 10.

Acknowledgement—The research was supported by a grant, A-259, from The Robert A. Welch Foundation.

REFERENCES

1. R. D. Shannon, *Acta Cryst.* 1976, **A32**, 751.
2. R. M. Smith and A. E. Martell, *Critical Stability Constants*, Vols 4 and 6. Plenum Press, New York (1976, 1989).
3. H. Kubota, PhD Dissertation. University of Wisconsin (1956).
4. P. L. Brown, R. N. Sylva, G. E. Batley and J. Ellis, *J. Chem. Soc., Dalton Trans.* 1985, 1967.
5. M. Pesavento, A. Profumo, C. Riolo and T. Soldi, *Analyst* 1989, **114**, 623.
6. W. M. Latimer and W. L. Jolly, *J. Am. Chem. Soc.* 1953, **75**, 1548.

7. E. L. King and P. K. Gallagher, *J. Phys. Chem.* 1959, **36**, 1073.
8. E. W. Baumann, *J. Inorg. Nucl. Chem.* 1969, **31**, 3155.
9. R. P. Agarwal and E. C. Moreno, *Talanta* 1971, **18**, 873.
10. Y. Couturier, *Bull. Soc. Chim. Fr.* 1986, 171.
11. A. Yuchi, K. Ueda, H. Wada and G. Nakagawa, *Anal. Chim. Acta* 1986, **186**, 313.
12. A. Yuchi, H. Hotta, H. Wada and G. Nakagawa, *Bull. Chem. Soc. Jpn* 1987, **60**, 1379.
13. E. Marklund, S. Sjöberg and L. O. Ohman, *Acta Chem. Scand.* 1986, **A40**, 367.
14. M. K. Misra and R. K. Nanda, *J. Ind. Chem. Soc.* 1965, **42**, 267.
15. L. O. Ohman and S. Sjöberg, *J. Chem. Soc., Dalton Trans.* 1983, 2513.
16. R. J. Motekaitis and A. E. Martell, *Inorg. Chem.* 1984, **23**, 18.
17. L. O. Ohman, *Inorg. Chem.* 1988, **27**, 2565.
18. R. Lewis and G. N. Nancollas, unpublished results.
19. B. Das and S. Aditya, *J. Ind. Chem. Soc.* 1959, **36**, 473.
20. L. Havelkova and M. Bartusek, *Coll. Czech. Chem. Commun.* 1969, **34**, 530.
21. K. Hayashi, T. Ohsawa, K. Okamoto, J. Hidaka and H. Einago, *J. Coord. Chem.* 1983, **12**, 243.
22. T. Hedlund and L. O. Ohman, *Acta Chem. Scand.* 1988, **A42**, 702.
23. D. J. Clevette, W. O. Nelson, A. Nordin, C. Orvig and S. Sjöberg, *Inorg. Chem.* 1989, **28**, 2079.
24. J. A. Kennedy and H. K. J. Powell, *Aust. J. Chem.* 1985, **38**, 659.
25. R. Nasanen and J. Veivo, *Suomen Kem.* 1956, **B29**, 213.
26. R. Nasanen, *Acta Chem. Scand.* 1957, **11**, 1308.
27. A. Yuchi, N. Yanai, H. Wada and G. Nakagawa, *Analyst* 1988, **113**, 1405.
28. T. Kiss, I. Sovago and R. B. Martin, *J. Am. Chem. Soc.* 1989, **111**, 3611.
29. O. Jantti, *Suomen Kem.* 1957, **B30**, 136.
30. V. T. Athavale, N. Mahadevan, P. K. Mathur and R. M. Sathe, *J. Inorg. Nucl. Chem.* 1967, **29**, 1947.
31. G. Anderegg, F. L'Eplattenier and G. Schwarzenbach, *Helv. Chim. Acta* 1963, **46**, 1400.
32. A. Evers, R. D. Hancock, A. E. Martell and R. J. Motekaitis, *Inorg. Chem.* 1989, **28**, 2189.
33. A. E. Martell and R. J. Motekaitis, *Determination and Use of Stability Constants.* VCH Publishers, New York (1989).
34. A. E. Martell and R. J. Motekaitis, in *The Environmental Chemistry and Toxicology of Aluminium* (Edited by T. E. Lewis), pp. 3–17. Lewis Publishers, Chelsea, Michigan (1989).
35. J. B. Neilands, in *Development of Iron Chelators for Clinical Use* (Edited by A. E. Martell, W. F. Anderson and D. G. Badman), pp. 13–31. Elsevier, New York (1981).
36. M. E. De Broe, in *Proceedings International Chelation Conference* (Edited by M. Rubin). Georgetown University, Washington D.C. (20–22 July 1989).
37. A. E. Martell, R. J. Motekaitis, I. Murase, L. F. Sala, R. Stoldt, C. Y. Ng, H. Rosenkrantz and J. J. Metterville, *Inorg. Chim. Acta* 1987, **138**, 231.

Polyhedron Vol. 9, No. 2/3, pp. 189–192, 1990
Printed in Great Britain

0277–5387/90 $3.00+.00
© 1990 Pergamon Press plc

2,3-DIPHOSPHOGLYCERATE BINDING OF Zn^{2+} AND Al^{3+}

IMRE SÓVÁGÓ and TAMÁS KISS

Department of Inorganic and Analytical Chemistry, Lajos Kossuth University, H-4010 Debrecen, Hungary

and

R. BRUCE MARTIN

Chemistry Department, University of Virginia, Charlottesville, VA 22903, U.S.A.

Abstract—The blood red cell contains millimolar amounts of 2,3-diphosphoglycerate, yet no metal ion stability constants appear to have been determined. We show that in the free ligand the 2-phospho group is about six times more basic than the 3-phospho group. We have determined the stability constants for the binding of Zn^{2+} which occurs at about 0.2 mM in the red cell, and of Al^{3+} which reduces red cell size and inhibits haemoglobin synthesis. At physiological pH both metal ions occur predominantly as MA_2 complexes. The free Zn^{2+} concentration permitted within the red cell by the 2:1 complex is about 0.3 μm. 2,3-Diphosphoglycerate binds Al^{3+} strongly enough so that at equilibrium there should be comparable concentrations of Al^{3+} on both sides of the red cell membrane.

In addition to well-known dementias and osteodystrophy, toxicity due to aluminium has also been associated with anaemia.[1] The cause of Al^{3+}-induced anaemia is uncertain: iron levels are normal, but the red blood cells are reduced in size (microcytosis), and the condition improves upon use of reduced Al^{3+} levels in dialysis fluids.[2–4] Al^{3+} lowers haemoglobin levels,[5] and it has been suggested that the metal ion interferes with haemoglobin synthesis.[6] In the blood plasma, the predominant small molecule Al^{3+} carrier is citrate,[7,8] while the major protein carrier is transferrin.[7,9,10] If a pathway exists for Al^{3+} transport from the plasma to inside the red cell, 2,3-diphosphoglycerate (DPG), $^{-2}O_3POCH_2CH(COO^-)OPO_3^{2-}$, present at 2–4 mM concentration, seems likely to be the predominant small ligand. Since on a molar basis, the amount of DPG considerably exceeds haemoglobin, with which it interacts in the deoxygenated form, Al^{3+} levels probably would not rise high enough to withdraw significant quantities of DPG from interacting with haemoglobin. However, a DPG complex of Al^{3+} may become an active deleterious species. Since we know of no stability constant information with the important DPG ligand, we have determined its stability constants with Al^{3+} and Zn^{2+}. Zn^{2+} occurs at a concentration of 0.2 mM in the red cell, and much of it may occur as a DPG complex. Mg^{2+} and Ca^{2+}, also present in the red cell, bind more weakly to DPG, and their stabilities have not been determined.

EXPERIMENTAL

The pentasodium salt of 2,3-diphospho-D-glyceric acid was purchased from Sigma Chemical Company in St. Louis Mo. Potentiometric titrations were performed with a Radiometer PHM 64 pH meter and a TTA 80 automatic titration unit equipped with G2040B glass and K4040 calomel electrodes. Precipitation occurs even at 6:1 molar ratios of DPG to Al^{3+}. The DPG concentration was 6 mM and the metal ion concentrations were adjusted to give DPG-to-metal ion molar ratios of 2, 3 and 4 for Zn^{2+} and 8, 9 and 10 for Al^{3+}. At these ratios precipitation occurs above pH 8.5 for Zn^{2+} and pH 7.5 for Al^{3+}. In the soluble region, fits between experimental and calculated (PSEQUAD[11]) titration curves were excellent. The temperature used was 25°C and the ionic strength was controlled with 0.2 M KCl. All pH meter readings were made on a concentration scale. To convert pK_a values in this paper to the more common mixed scale based on NBS buffers,[12]

add 0.13 log units. Metal ion stability constants require no conversion.

RESULTS

Table 1 shows the overall stability constants in the standard log β_n format. Under the experimental conditions MA complexes of penta-anionic DPG and either Zn^{2+} or Al^{3+} were not detected; protonated complexes such as MA_2H intervene. Inspection of Table 1 reveals that Al^{3+} complexes bind significantly more strongly to DPG than does Zn^{2+}. This behaviour is typical of many ligands containing mainly oxygen donor atoms.[7]

From the log β values in the footnote to Table 1 the successive concentration pK_a values from dianionic DPG are 3.19, 5.96 and 7.14 to give the penta-anionic ligand designated A. Successive stability constants for binding to monoprotonated ligand species AH are for Zn^{2+}, log $K_1 = 3.24$ and log $K_2 = 2.46$, and for Al^{3+}, log $K_1 = 5.98$ and log $K_2 = 4.16$. Successive deprotonations from the protonated 2 : 1 complex $MA_2H_2 \rightarrow MA_2H \rightarrow MA_2$ occur with concentration pK_a values of 5.45 and 6.94 for Zn^{2+}, and of 5.64 and 6.32 for Al^{3+}. In the case of Zn^{2+}, MA_2 forms MA_2H_{-1} with p$K_a = 8.44$, either by proton loss from a coordinated water molecule or by coordination of a hydroxide ion.

Figures 1 and 2 show the species distribution curves for DPG complexes of Zn^{2+} and Al^{3+}.

Table 1. 2,3-Diphosphoglycerate acidity constants and Zn^{2+} and Al^{3+} complex stability constants (log β)[a]

Species	Zn^{2+}	Al^{3+}
MAH	10.38	13.12
MA_2H_2	19.98	24.42
MA_2H	14.53	18.78
MA_2	7.59	12.46
MA_2H_{-1}	−0.85	—

[a] At 25°C and 0.2 M ionic strength. Standard deviations are less than 0.03 log units. For protonation of the penta-anionic ligand A we obtain the following concentration log β values: HA, 7.14; H_2A, 13.10; and H_3A, 16.29.

DISCUSSION

We can assign the pK_a values to the functional groups in 2,3-diphosphoglyceric acid by comparing its values with those of two model compounds. The first two ionizations occurring from a neutral DPG molecule are essentially strong acid deprotonations from each of the phosphate groups, yielding the dianionic species $^{-}HO_3POCH_2CH(COOH)OPO_3H^{-}$. To assist comparisons on a common pH scale, we add 0.13 log units (for 0.20 ionic strength) to the concentration pK_a constants reported in this paper, to obtain the mixed constants commonly appearing in the literature. Thus the successive mixed pK_a values from the dianionic DPG species become 3.32, 6.09 and 7.27. These values may be compared directly with successive pK_a values of 3.55 and 7.0 reported for 2-phosphoglyceric acid[13] and of 3.5 and 6.25 for 3-phosphoglyceric acid,[14] all values were obtained under similar but not identical conditions. Since glyceric acid[15] has a p$K_a = 3.5$,

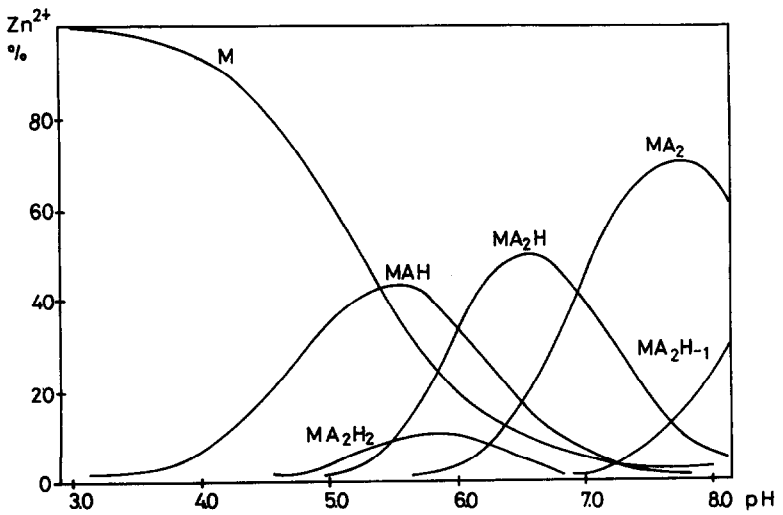

Fig. 1. Species distribution curves for 2 mM total zinc(II) and 6 mM 2,3-diphosphoglycerate using the constants in Table 1. The symbol A refers to the penta-anionic ligand, so that MA_2 bears a net eight-minus charge.

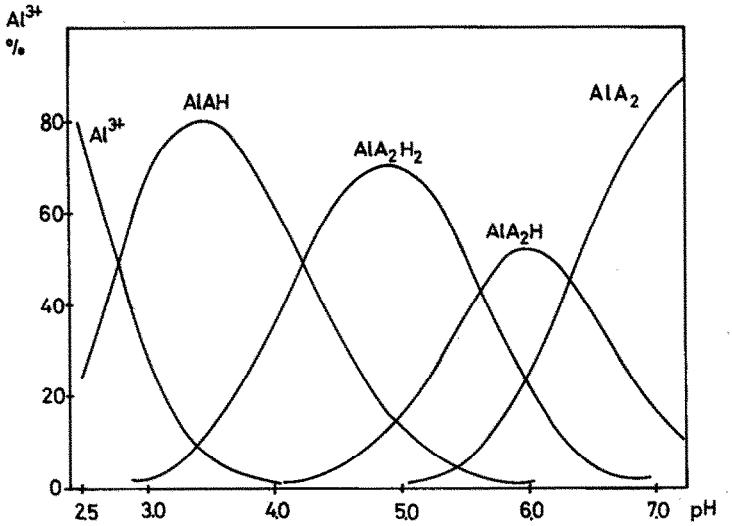

Fig. 2. Species distribution curves for 0.6 mM total aluminium(III) and 6 mM 2,3-diphosphoglycerate using the constants in Table 1. The symbol A refers to the penta-anionic ligand, so that AlA_2 bears a net seven-minus charge.

the deprotonation with pK_a ranging from 3.32 to 3.55 in the three phosphoglyceric acids may be identified mainly with the carboxylic acid group. The two remaining DPG pK_a values of 6.09 and 7.27 pertain to both phosphate groups. Comparison with the values for 2- and 3-phosphoglyceric acids suggests that in DPG the $pK_a = 6.09$ corresponds predominantly to deprotonation of the 3-phosphate group and the $pK_a = 7.27$ predominantly to the 2-phosphate group. Thus the main monoprotonated DPG tautomer is $^{-2}O_3POCH_2CH(COO^-)OPO_3H^-$.

A more quantitative analysis confirms the last conclusion. We set up the usual microconstant scheme for the last two phosphate ionizations in DPG with the last subscript on a microconstant (small k) indicating the group undergoing deprotonation. Thus we have $10^{-6.09} = K_2 = k_2 + k_3$, $10^{7.27} = K_3^{-1} = k_{23}^{-1} + k_{32}^{-1}$, and $K_2K_3 = k_2k_{23} = k_3k_{32} = 10^{-13.36}$. If we allow a 0.3 log unit intrinsic interaction between the phosphate groups $pk_{23} - pk_3 = pk_{32} - pk_2 = 0.3$, we find $pk_3 = 6.16$, $pk_2 = 6.92$, $pk_{32} = 7.20$ and $pk_{23} = 6.44$. In monoprotonated DPG the ratio of deprotonated 3-phosphate to deprotonated 2-phosphate groups is given by $k_3/k_2 = 6$. The negatively-charged carboxylate group renders the closer 2-phosphate group more basic than the 3-phosphate group.

Stability constant comparisons indicate that metal ion binding to phosphoglyceric acids involves more than the carboxylate group. For Zn^{2+} binding, the first stability constant logs are glycerate,[15] 1.8; 3-phosphoglycerate,[14] 2.9; 2-phosphoglycerate,[13] 3.4; and DPG, 3.24 to the monoprotonated species AH. The much weaker metal ion binding in glycerate indicates phosphate involvement in all the other ligands. The 0.5 log unit stronger Zn^{2+} binding favouring 2- over 3-phosphoglycerate may be accounted for by a combination of the 0.8 log unit greater basicity of the phosphate group in 2-phosphoglycerate and its ability to form a seven-membered phosphate–carboxylate chelate ring vs an eight-membered chelate ring in 3-phosphoglycerate.

We may estimate a stability constant for Zn^{2+} binding to a single phosphate group species in MAH of DPG from a linear relationship found for Zn^{2+} binding to simple phosphate esters,[16] $\log K = 0.35\ pK_a$. For a $pK_a = 6.1$ we estimate $\log K = 2.1$. Since the observed stability constant is $\log K = 3.24$, the strengthening by about one log unit indicates that Zn^{2+} is not simply complexed to a single phosphate but is chelated by DPG.

Additional insights into the structures of the 2:1 DPG complexes may be obtained by considering the successive pK_a values for deprotonations in the series $MA_2H_2 \rightarrow MA_2H \rightarrow MA_2$. For Al^{3+} the successive mixed pK_a values of 5.77 and 6.45 differ by 0.68, little more than the statistical difference of 0.60, and the average value of 6.1 is close to the microconstant value ($pk_3 = 6.16$) for the 3-phosphate group in the free ligand. Thus the most straightforward interpretation is that of the carboxylate and 2-phosphate groups in both DPG molecules chelating Al^{3+} and deprotonations taking place from the two unchelated 3-phosphate groups. In this complex the Al^{3+} is chelated by a minor tautomer of the monoprotonated DPG. A

full analysis of a situation in which a metal ion binds to a minor tautomer appears in a study of Al^{3+} binding to catecholamines.[17]

This simple structural interpretation of the 2:1 DPG complexes of Al^{3+} appears inadequate to account for the corresponding Zn^{2+} complexes. The successive mixed pK_a values of 5.58 and 7.07 differ by 1.5 log units with the first value less and the second value greater than the corresponding values of Al^{3+}. The $pK_a = 7.07$ for deprotonation to give MA_2 is in the range of microconstants for deprotonation of the more basic 2-phosphate group in the free ligand, while the $pK_a = 5.45$ value is significantly more acidic than any free ligand phosphate microconstant. This low value may be due to chelation of a 3-phosphate group upon its deprotonation. The pK_a values for the 2:1 DPG complexes suggest that increases in ligand denticity and Zn^{2+} coordination number occur upon successive deprotonations in the MA_2H_2 complex. After forming the MA_2 complex, Zn^{2+} picks up a hydroxide ion with mixed $pK_a = 8.57$ to yield MA_2H_{-1}.

Figures 1 and 2 show that under physiological conditions neutral solutions of DPG contain predominantly the fully deprotonated MA_2 species for both Zn^{2+} and Al^{3+}. Under conditions of excess of a relatively strong binding ligand in the MA_2 complex region, we may approximate the free metal ion concentration by $[M] \simeq C_M/(\beta_2 C_A^2)$ where C_M and C_A are the total metal ion and ligand concentrations, respectively. The log β_2 values (Table 1) are 7.6 for Zn^{2+} and 12.5 for Al^{3+}. Taking the red cell total DPG concentration as 4 mM and the total Zn^{2+} concentration as 0.2 mM, we find permitted free $[Zn^{2+}] \simeq 0.3$ μM. For a total Al^{3+} concentration of 1 μM we find the free $[Al^{3+}] \simeq 2 \times 10^{-14}$ M. This value is comparable to the free Al^{3+} concentration allowed in the blood plasma by citrate or transferrin.[7,10] Stronger mixed complexes not considered here may form within the red cell. Therefore, at equilibrium there should be comparable concentrations of Al^{3+} on both sides of the red cell membrane.

Acknowledgement—This research was supported by a grant from the NIEHS (ES04446).

REFERENCES

1. M. R. Wills and J. Savory, *Lancet* 1983, **ii**, 29.
2. A. I. K. Short, R. J. Winney and J. S. Robson, *Proc. EDTA*, 1980, **17**, 226.
3. J. A. O'Hare and D. J. Murnaghan, *N. Engl. J. Med.* 1982, **306**, 654.
4. M. Touam, F. Martinez, B. Lacour, R. Bourdon, J. Zingraff, S. DiGiulio and T. Drueke, *Clin. Nephrol.* 1983, **19**, 295.
5. P. Altman, F. Marsh, D. Plowman and J. Cunningham, *Lancet* 1988, **i**, 1012.
6. L. Kaiser and K. A. Schwartz, *Am. J. Kid. Dis.* 1985, **6**, 348.
7. R. B. Martin, *Metal Ions Biol. Syst.* 1988, **24**, 1.
8. R. B. Martin, *J. Inorg. Biochem.* 1986, **28**, 181.
9. R. B. Martin, J. Savory, S. Brown, R. L. Bertholf and M. R. Wills, *Clin. Chem.* 1987, **33**, 405.
10. R. B. Martin, *Clin. Chem.* 1986, **32**, 1797.
11. L. Zekany and I. Nagypal, in *Computational Methods for the Determination of Stability Constants* (Edited by D. Leggett). Plenum Press, New York (1985).
12. R. G. Bates, *Pure Appl. Chem.* 1985, **57**, 531.
13. F. Wold and C. E. Ballou, *J. Biol. Chem.* 1957, **227**, 301.
14. M. Larsson-Raznikiewicz, *Eur. J. Biochem.* 1972, **30**, 579.
15. R. K. Cannan and A. Kibrick, *J. Am. Chem. Soc.* 1938, **60**, 2314.
16. S. S. Massoud and H. Sigel, *Inorg. Chem.* 1988, **27**, 1447.
17. T. Kiss, I. Sóvágó and R. B. Martin, *J. Am. Chem. Soc.* 1989, **111**, 3611.

Polyhedron Vol. 9, No. 2/3, pp. 193–197, 1990
Printed in Great Britain

0277–5387/90 $3.00+.00
Pergamon Press plc

ALUMINOSILICATE STABILITIES UNDER BLOOD PLASMA CONDITIONS

R. BRUCE MARTIN

Chemistry Department, University of Virginia, Charlottesville, VA 22903, U.S.A.

Abstract—Aluminosilicates occur in the core of plaques in the brains of Alzheimer victims, This paper shows that under conditions prevailing in the blood plasma, the free Al^{3+} concentrations permitted by six aluminosilicates ($6–100 \times 10^{-14}$ M) are competitive with those from citrate and transferrin at 10 μM or greater total aluminium concentrations. With equilibria in a competitive range, kinetic effects play a significant role. Aluminosilicates probably form at bound Al^{3+} sites bathed in a silicic acid-containing fluid.

Up to 20% each of aluminium and silicon co-reside as aluminosilicates in the cores of senile plaques found extracellularly in the brains of individuals with Alzheimer's disease.[1] This paper compares the solubility properties of six aluminosilicate systems with the combining capabilities of other aluminium ligands that occur in the blood plasma. Reliable equilibrium data are difficult to obtain in aluminosilicate systems. Results reported by geochemists applicable to fresh waters of low ionic strength are adjusted to apply to the 0.16 ionic strength of blood plasma and the activity H^+ scale used by most chemists and all biochemists. These adjustments are identical to those made earlier.[2,3]

RESULTS

Silicic acid, $Si(OH)_4$, occurs at about 20 μM in the blood plasma.[4] It loses its first proton with $pK_a = 9.6$; hence only the acidic form occurs in neutral solutions. The plasma concentration is sufficiently low that only mononuclear silicic acid matters; there is no tendency to form amorphous or colloidal silica. The anions of silicic acid bind Mg^{2+} and Ca^{2+} so weakly[5] that a negligible amount of their complexes occurs in blood plasma. Only in insoluble silicates do significant interactions with metal ions take place.

Before discussing insoluble aluminosilicates, we consider the extent of soluble complex formation between Al^{3+} and silicic acid. The stability constant for the soluble complex of Al^{3+} with silicic acid remains unknown, but an estimate may be derived from the known stability constant of Fe^{3+}. (Since Al^{3+} does not exhibit the UV spectral changes that Fe^{3+} does in different environments, measurement of the stability constant for Al^{3+} binding to silicic acid is difficult.) For the displacement equilibrium

$$Fe^{3+} + Si(OH)_4 \rightleftharpoons FeOSi(OH)_3^{2+} + H^+$$

a reported stability constant at 25°C and 0.1 ionic strength is $K_{1H} = 0.25$.[6] Taking $pK_a = 9.6$ for silicic acid, we deduce that the stability constant for the iron complex is $\log K_{1Fe} = 9.0$. Stability constants for Al^{3+} complexes have been found to be linearly related to those of Fe^{3+} by $\log K_1(Al^{3+}) = 0.3 + 0.71 \log K_1(Fe^{3+})$; this correlation is obeyed by hydroxide ion.[3] Applying this equation to silicic acid we find for the Al^{3+} complex, $\log K_1 = 6.7$ and $\log K_{1H} = -2.9$. In acidic and neutral solutions where $pH \ll pK_a = 9.6$, we obtain for the conditional stability constant described by

$$K_{1c} = [AlOSi(OH)_3^{2+}]/[Al^{3+}][Si(OH)_4],$$

$\log K_{1c} = \log K_1 - pK_a + pH = 6.7 - 9.6 + 7.4 = 4.5$ at pH 7.4. With ambient 20 μM silicic acid the molar ratio of bound to unbound Al^{3+} becomes

$$[AlOSi(OH)_3^{2+}]/[Al^{3+}] = 10^{4.5} \times 10^{-4.7} = 0.6.$$

Thus we estimate that in the plasma the amount of Al^{3+} bound to the monoanion of silicic acid is about 60% of the free aqueous Al^{3+}.

Several studies disagree over the Al/Si molar ratio, r, in synthetic aluminosilicates. The variations probably arise from differences in solution conditions used in the preparations. A non-dialysable species with $r = 2$(imogolite) formed from pH 4.5 to 5.5 when the silicic acid concentration exceeded 0.1 mM,[7,8] five times that found in the plasma. The same laboratory reports $r < 1$ in alkaline solutions.[9] Another study shows r dropping from very high values near pH 5 and levelling off to $r = 3$–

4 near pH 7.[10] This study also reported that citrate inhibited aggregation but not formation of aluminosilicates. At pH 6.6 experiments showed a switch of Al^{3+} binding from silicate to phosphate when the latter is present.[10] This last result agrees with conclusions reached below. Finally, a reversible, metastable, amorphous aluminosilicate exhibits a variable r that rises from pure silica with $r = 0$ at pH 2 and increases with pH, reaching $r = 3.0$ at pH 7.33.[11] Thus, although the last two studies reveal similar r values at pH 7.4, they differ depending on whether the trend from acidic solutions shows r decreasing or increasing. Extensive quantitative information provided in the last study permits its analysis in greater detail.

According to one study, the Al and Si concentrations in natural waters are controlled by reversible formation of a metastable, amorphous aluminosilicate whose composition depends upon pH: high Si, low Al at low pH, and low Si, high Al at high pH.[11] The reversible dissolution of the amorphous aluminosilicate may be written as

$$(SiO_2)_{1-f}(Al(OH)_3)_f + 3fH^+ \rightleftharpoons (1-f)Si(OH)_4 + fAl^{3+} + (5f-2)H_2O, \quad (1)$$

where f is the fraction of solid that contains Al and $1-f$ the fraction that contains Si. The ratio of Al to Si in the solid is given by $r = f/(1-f)$.

From analyses of solutions, the fraction f in the variable composition solid is well approximated by a linear relation between f and pH[11] that may be written as

$$f = -0.24 + 0.135\,pH. \quad (2)$$

At pH 1.8, $f = 0$ and the solid silicic acid contains no Al. At pH 9.2, $f = 1$ and the solid $Al(OH)_3$ contains no Si. The right-hand ordinate of Fig. 1 shows f, the fraction of Al in the solid, for the straight line that rises from pH 4 to 9. For equimolar Al and Si, $f = 0.50$, and eq. (2) yields pH = 5.5. For $f = 0.75$, eq. (2) yields pH = 7.33, close to that of blood plasma; we employ $f = 0.75$ and $r = f/(1-f) = 3.0$ in subsequent calculations. Corresponding to the pH values along the abscissa, r values for the metastable aluminosilicate appear across the top of Fig. 1.

An equilibrium solubility constant for the reversible reaction may be written as

$$K_s = K_{Si}^{1-f}K_{Al}^{f} = [Si(OH)_4]^{1-f}[Al^{3+}]^f/(H^+)^{3f}, \quad (3)$$

where we use concentrations in the numerator and activity for H^+. From analyses of solutions at low ionic strength the data suggest $K_{Si} = (Si(OH)_4) = 10^{-3.0}$ and $K'_{Al} = (Al^{3+})/(H^+)^3 = 8.7$, where the parentheses indicate activities.[11] To adjust to the

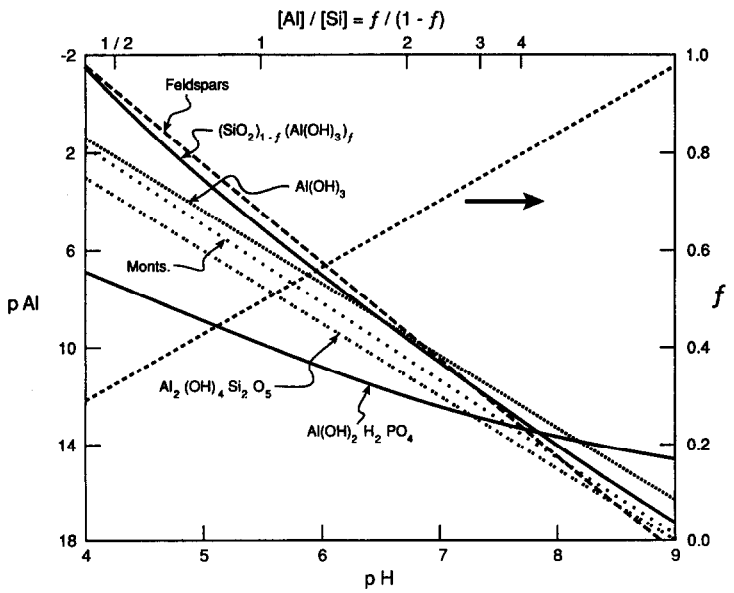

Fig. 1. Negative logarithm of free Al^{3+} molar concentration, pAl, permitted by eight insoluble Al compounds as a function of pH. Starting in the upper left hand corner the eight compounds are two feldspars, variable composition metastable aluminosilicate, amorphous aluminium hydroxide, two montmorillonites (Monts), kaolinite and variscite. The left hand pAl ordinate applies to the six descending curves. The mole fraction aluminium, f, for the metastable aluminosilicate is represented by the ascending straight line with f values on the right hand ordinate. The ratio $r = f/(1-f) =$ [Al]/[Si] in the metastable component appears across the top of the figure. The f and r values apply only to the variable composition metastable aluminosilicate. Dashes indicate straight lines.

molar concentration scale at 0.16 ionic strength, we use the above K_{Si} for uncharged $Si(OH)_4$, and adjust K'_{Al} to $K_{Al} = [Al^{3+}]/(H^+)^3 = 10^{9.7}$, similar to earlier adjustments.[2,3]

Solving the solubility constant, eq. (3), for the free aqueous Al^{3+} concentration, we obtain

$$[Al^{3+}] = (H^+)^3 10^{9.7}(10^{-3.0}/[Si(OH)_4])^{1/r}, \quad (4)$$

where $r = f/(1-f)$. At pH 7.33 when $r = 3.0$, and without a common ion, we find $[Si(OH)_4] = 4.6 \times 10^{-11}$ M and $[Al^{3+}] = 14 \times 10^{-11}$ M. For the latter value, the negative logarithm of the free $[Al^{3+}]$ is pAl = 9.9.

In the blood plasma the $Si(OH)_4$ concentration is close to 20 μM[4] so we now fix this quantity and solve eq. (4) for the free Al^{3+} concentration in solutions of different acidities. Figure 1 shows the results in the form of a plot of the negative logarithm of the free $[Al^{3+}]$, pAl, as a function of $4 < pH < 9$. The descending curve for the metastable aluminosilicate begins in the uppermost left corner of Fig. 1. Lower free Al^{3+} concentrations, greater pAl, appear closer to the bottom of Fig. 1. At pH 7.4 of blood plasma with 20 μM silicic acid and $r = 3.0$, eq. (4) yields pAl = 12.0. This value is listed as the second entry in Table 1.

Table 1 lists the negative logarithm of the free Al^{3+} concentration as pAl under blood plasma conditions. For amorphous $Al(OH)_3$, $K_s = [Al^{3+}]/(H^+)^3 = 10^{10.7}$ was used as in previous articles.[2,3] This value representing an adjustment of a low ionic strength value to 0.16 ionic strength and an activity H^+ scale has recently received confirmation in a study performed at 0.6 ionic strength.[12]

Table 1. Negative logarithm of free Al^{3+} molar concentration under blood plasma conditions[a]

	pAl
Amorphous $Al(OH)_3$	11.5
Metastable $SiO_2(Al(OH)_3)_3$	12.0
Anorthite, $CaAl_2Si_2O_8$	12.0
Albite, $NaAlSi_3O_8$	12.2
Ca-montmorillonite, $CaAl_{14}Si_{22}O_{60}(OH)_{12}$	12.4
Na-montmorillonite, $NaAl_7Si_{11}O_{30}(OH)_6$	12.7
Variscite, $Al(OH)_2H_2PO_4$	12.9
Gibbsite, $Al(OH)_3$	13.0
Kaolinite, $Al_2(OH)_4Si_2O_5$	13.2
0.1 mM Citrate	13.4[b]
Transferrin	13.6[c]

[a] pH 7.4, 0.16 ionic strength, 20 μM $Si(OH)_4$, 140 mM Na^+, 1.3 mM Ca^{2+} and 2 mM total phosphate.

[b] 10 μM total Al^{3+}.

[c] 10 μM total Al^{3+} with 50 μM unoccupied transferrin sites.

Adjustment of this high ionic strength value to 0.16 ionic strength and the activity H^+ scale yields a K_s constant identical to the above. This value is 10 times greater than that found for the best linear fit to experimental points over a range of compositions in the low ionic strength variable composition, metastable aluminosilicate study. As a result the straight line for amorphous $Al(OH)_3$ in Fig. 1 rides 1.0 log unit higher than a line consistent with the metastable aluminosilicates. For the slowly forming crystalline gibbsite form of $Al(OH)_3$ the $K_s = 10^{9.2}$, so that pAl is 1.5 log units greater than that for amorphous $Al(OH)_3$. The gibbsite pAl value appears near the bottom of Table 1.

The pAl values in Table 1 refer to the negative logarithm of the hexaaquo Al^{3+}. Since most solvated Al at $pH > 6.2$ occurs as tetrahedral $Al(OH)_4^-$, the total solvated Al concentration is much greater. At pH 7.4 we calculate[3,2] the molar ratio $[Al(OH)_4^-]/[Al^{3+}] = 2.5 \times 10^6$. Thus for a solution saturated with amorphous $Al(OH)_3$ at pH 7.4, we find from Table 1 pAl = 11.5, and calculate $[Al^{3+}] = 3 \times 10^{-12}$ M and $[Al(OH)_4^-] = 8$ μM. Though the free hexaaquo Al^{3+} species enters calculations, at $pH > 6.2$ the tetrahedral $Al(OH)_4^-$ species should be the starting point for discussions of Al speciation.

Silica was introduced into solutions containing $Al(OH)_3$ and after lengthy aging to achieve equilibrium, the results analysed in terms of a solid equivalent to halloysite (kaolinite).[13] The reverse of the synthesis reaction is

$$Al_2(OH)_4Si_2O_5 + 6H^+ \rightleftharpoons 2Al^{2+} + 2Si(OH)_4 + H_2O,$$

for which the solubility constant may be defined as

$$K_s = [Al^{3+}][Si(OH)_4]/(H^+)^3,$$

where the brackets represent concentrations. At a fixed silicic acid concentration we may write

$$K_s/[Si(OH)_4] = [Al^{3+}]/(H^+)^3, \quad (5)$$

which is of the same form as the previous K_s equation. In order to stabilize halloysite against microcrystalline gibbsite the silicic acid concentration must be 150 μM.[13] This value is 7.5 times the 20 μM $Si(OH)_4$ that occurs in blood plasma. Two factors may reduce or even invert this factor.[13] Formation of a well-organized kaolinite would require a nine-fold lower silicic acid concentration. Moreover, gibbsite forms with difficulty in biological systems, and amorphous $Al(OH)_3$ is more than 10 times more soluble than gibbsite. These results suggest that in extracellular fluids formation of halloysite and especially kaolinite become favoured in

comparison with amorphous $Al(OH)_3$. These comparisons are borne out by the quantitative results in Table 1.

We may apply eq. (5) to kaolinite by adjusting the low ionic strength K_s[14] to concentration at 0.16 ionic strength to obtain $K_s = 10^{4.3}$. With $Si(OH)_4$ held at 20 μM eq. (5) may be solved for $[Al^{3+}]$ as a function of H^+. The results plotted as pAl vs pH appear in Fig. 1. Both kaolinite and amorphous $Al(OH)_3$ solubilities exhibit an identical dependence on $(H^+)^3$, and both display a slope of three in Fig. 1. The straight line for kaolinite shows a lower free Al^{3+} than does the line for amorphous $Al(OH)_3$.

The plagioclase feldspars constitute a continuous series of six aluminium silicate mixtures in a common triclinic lattice from $NaAlSi_3O_8$ (albite) to $CaAl_2Si_2O_8$ (anorthite). Equilibrium constants for the terminal members of the series establish their stabilities relative to kaolinite.[15] We combine these constants with our kaolinite value adjusted to blood plasma conditions. For albite we obtain

$$NaAlSi_3O_8 + 4H^+ + 4H_2O \rightleftharpoons Na^+ + Al^{3+} + 3Si(OH)_4,$$

for which

$$K_b = [Na^+][Al^{3+}][Si(OH)_4]^3/(H^+)^4 = 10^{2.4}. \quad (6)$$

For anorthite we write

$$0.5CaAl_2Si_2O_8 + 4H^+ \rightleftharpoons 0.5Ca^{2+} + Al^{3+} + Si(OH)_4,$$

for which

$$K_n = [Ca^{2+}]^{0.5}[Al^{3+}][Si(OH)_4]/(H^+)^4 = 10^{11.5}. \quad (7)$$

We now substitute into eqs (6) and (7) the blood plasma conditions of 140 mM Na^+, 1.3 mM Ca^{2+}, and 20 μM $Si(OH)_4$ to obtain for albite

$$[Al^{3+}] = 10^{17.4}(H^+)^4 \quad (8)$$

which gives at pH 7.4, pAl = 12.2, and for anorthite

$$[Al^{3+}] = 10^{17.6}(H^+)^4 \quad (9)$$

which yields at pH 7.4, pAl = 12.0. The pair of pAl values appear in Table 1. Equations (8) and (9) exhibit identical fourth power dependencies on H^+ and constant terms that differ by only 0.2 log units. The average result of pAl = 4pH − 17.5 appears as the straight line labelled Feldspars in Fig. 1.

A treatment similar to that for the Feldspars may be applied to Na– and Ca–montmorillonites. The compositions appear in Table 1. Equilibrium constants for conversion to kaolinite have been tabulated.[15] We obtain for the Na compound, pAl = 10.5–3.14 pH, and for the Ca compound, pAl = 10.8–3.14 pH. Since the pair of equations display an identical pH dependence (22/7) and exhibit constant terms within 0.3 log units of each other, we plot an average of the two in Fig. 1 with the label Monts. Separate entries for the two-layered montmorillonites appear in Table 1.

Figure 1 also plots the pAl curve for insoluble variscite, $Al(OH)_2H_2PO_4$. For this salt the free Al^{3+} concentration from pH 3 to 11 is given by[2,3]

$$[Al^{3+}] = (H^+)[(H^+) + 10^{-6.77}]/30Tp,$$

where the total phosphate concentration, Tp, is taken as 2 mM, typical of that in blood plasma. The variscite curve is the lowest one in Fig. 1 over most of the pH range, and this insoluble salt permits the lowest free Al^{3+} concentration until pH 7.2 when the variscite curve crosses that for kaolinite. At pH > 7.2 kaolinite permits a lower free Al^{3+} concentration than does variscite. Between 7.2 < pH < 8.1 the curve for variscite crosses all the other pAl curves in Fig. 1.

DISCUSSION

The results of this paper dispel much of the mystery regarding appearance of aluminosilicates in senile plaques. Near a blood plasma pH of 7.4, also typical of other body fluids external to cells, Fig. 1 and Table 1 show that six aluminosilicates display comparable affinities for Al^{3+}. The lower free Al^{3+} (higher pAl) allowed by variscite at low pH no longer prevails in neutral solutions. The physiological pH region shows the greatest congestion of pAl curves in Fig. 1. The equilibrium constants used to define the curves in Fig. 1 are made only with difficulty on heterogeneous systems. The systems used to determine the equilibrium constants are much simpler than blood plasma. In the plasma, kinetic effects become more important and supersaturation occurs. The crystalline gibbsite form of $Al(OH)_3$ is unlikely to form in the plasma. Although the presence of organic molecules often hinders precipitation processes, aged, neutral solutions containing silicic acid and $Al(OH)_4^-$ at 25°C gave well-formed kaolinite plates in the presence of 5 μM quercetin (an organic flavone), while no plates were found in parallel experiments without quercetin.[16]

Values for pAl taken as a pH 7.4 slice through Fig. 1 appear in Table 1. The free Al^{3+} concentrations permitted by the six aluminosilicates range from (6 to 100) × 10^{-14} M. Table 1 also lists additional pAl values, including those for amorphous and crystalline (gibbsite) $Al(OH)_3$, variscite, and the ligands citrate and transferrin.

Blood plasma contains two strong ligands that bind Al^{3+} in soluble complexes. Citrate (at 0.1 mM

in plasma) is the strongest small molecule Al^{3+} ligand[2,3,17] and transferrin the strongest protein Al^{3+} binder.[2,3,18] Table 1 lists pAl values for binding of 10 μM total Al, an amount typical of an Al excess condition. These last two pAl values in Table 1 are comparable with the previous ones. The free Al^{3+} concentration is proportional to the total metal ion concentration. For each doubling of the total Al concentration, the pAl values for citrate and transferrin decrease by 0.3 log units. Thus for 20 μM total Al, pAl values in Table 1 for citrate and transferrin become 13.1 and 13.3, respectively. A difference of 0.5 pM units between two entries in Table 1 means that the stronger binding ligand of greater pAl allows 1/3 the free Al^{3+} concentration of the weaker binding ligand. Therefore, at Al levels of 10 μM and greater, citrate and transferrin no longer sequester Al^{3+} sufficiently to prevent its precipitation as an aluminosilicate. In the cerebrospinal fluid with little citrate and no transferrin, Al^{3+} is complexed weakly by other ligands,[19] and the tendency toward aluminosilicate formation becomes much greater than in the plasma.

By what process do aluminosilicate plaques form? A possible scenario is that Al^{3+} first binds at sites on phosphorylated proteins, the most likely matrix forming Al^{3+} site.[20] Al^{3+} at these sites is bathed in excess silicic acid which reacts with the Al^{3+}, sometimes releasing it, forming some kind of amorphous aluminosilicate that possibly rearranges to a less soluble form. Once formed, the aluminosilicate may become coated with protective agents stabilizing a non-equilibrium status. By this scenario Al remains the primary culprit in formation of aluminosilicate plaques. The inverse process is unlikely because there are no evident silicic acid sites without Al^{3+}. Nature holds many aluminosilicates; it will be interesting to learn the composition of aluminosilicates in plaques. As mentioned above, a well-formed kaolinite forms slowly but more rapidly in the presence of an organic compound. Of the many other aluminosilicates those containing Na^+, Ca^{2+}, or Mg^{2+} may be important, as these ions are relatively concentrated in the blood.

The analysis and conclusions in this paper are based on systems at equilibrium or in metastable equilibrium. Though mentioned, kinetic effects are hard to include in extended analysis. This problem occurs in all biological systems. Many substances that theoretically should precipitate in body fluids do not readily do so. When they occasionally do, we consider the result an abnormality, such as kidney stones, gallstones, gout and atherosclerotic plaques. The Ca^{2+} concentration in extracellular fluids is more than 200 times greater than the saturation concentration from hydroxyapatite.[21] On an equilibrium basis body fluids should contain many more precipitates and gels. Their precipitation evidently requires a nucleation site with appropriate geometry. In the case of aluminosilicates, an abnormally phosphorylated protein in the brain[22,23] may provide the requisite nucleation site.

Acknowledgement—This research was supported by a grant from the NIEHS (ESO4446).

REFERENCES

1. J. M. Candy, A. E. Oakley, J. Klinowski *et al.*, *Lancet* 1986, **1**, 354.
2. R. B. Martin, *Clin. Chem.* 1986, **32**, 1797.
3. R. B. Martin, *Metal Ions Biol. Syst.* 1988, **24**, 1.
4. J. W. Dobbie and M. J. B. Smith, in *Silicon Biochemistry*, p. 194. Ciba Foundation Symposium 121, John Wiley, New York (1986).
5. P. H. Santschi and P. W. Schindler, *J. Chem. Soc., Dalton Trans.* 1974, 181.
6. L. L. Olson and C. R. O'Melia, *J. Inorg. Nucl. Chem.* 1973, **35**, 1977.
7. V. C. Farmer, in *Silicon Biochemistry*, p. 4. Ciba Foundation Symposium 121, John Wiley, New York (1986).
8. V. C. Farmer and A. R. Fraser, *J. Soil Sci.* 1982, **33**, 737.
9. V. C. Farmer, A. R. Fraser and J. M. Fait, *Geochem. Cosmochim. Acta* 1979, **43**, 1417.
10. J. D. Birchall and J. S. Chappell, *Clin. Chem.* 1988, **34**, 265.
11. T. Paces, *Geochem. Cosmochim. Acta* 1978, **42**, 1487.
12. L. Ohman, *Inorg. Chem.* 1989, **28**, 3629.
13. J. D. Hem, C. E. Roberson, C. J. Lind and W. L. Polzer, Geological Survey Water-Supply Paper 1827-E. U.S. Government Printing Office (1973).
14. C. T. Driscoll, J. P. Baker, J. J. Bisogni and C. L. Schofield, in *Geological Aspects of Acid Deposition* (Edited by O. P. Bricker), p. 55. Butterworth, London (1984).
15. W. Stumm and J. J. Morgan, *Aquatic Chemistry*, p. 400. Wiley-Interscience, New York (1970).
16. J. D. Hem and C. J. Lind, *Science* 1974, **184**, 1171.
17. R. B. Martin, *J. Inorg. Biochem.* 1986, **28**, 181.
18. R. B. Martin, J. Savory, S. Brown, R. L. Bertholf and M. R. Wills, *Clin. Chem.* 1987, **33**, 405.
19. T. Kiss, I. Sovago and R. B. Martin, *J. Am. Chem. Soc.* 1989, **111**, 3611.
20. M. M. Esiri and R. J. P. Williams, *Neurobiol. Ageing* 1987, **7**, 581.
21. R. B. Martin, *Metal Ions Biol. Syst.* 1984, **17**, 1.
22. N. H. Sternberger, L. A. Sternberger and J. Ulrich, *Prog. Natl. Acad. Sci.* 1985, **82**, 4274.
23. I. Grundke-Iqbal, K. Iqbal, Y. Tung, M. Quinlan, H. M. Wisniewski and L. I. Binder, *Proc. Natl. Acad. Sci.* 1986, **83**, 4913.

Polyhedron Vol. 9, No. 2/3, pp. 199–205, 1990
Printed in Great Britain

0277–5387/90 $3.00+.00
© 1990 Pergamon Press plc

EQUILIBRIUM AND STRUCTURAL STUDIES OF SILICON(IV) AND ALUMINIUM(III) IN AQUEOUS SOLUTION—XXIII. A POTENTIOMETRIC STUDY OF THE COMPOSITION AND STABILITY OF ALUMINIUM COMPLEXES WITH NITRILOTRIACETIC ACID

LARS-OLOF ÖHMAN

Department of Inorganic Chemistry, University of Umeå, S-901 87 Umeå, Sweden

Abstract—Equilibria between H^+, aluminium(III) and nitrilotriacetic acid [$N(CH_2COOH)_3$, H_3L] were studied in 0.6 M Na(Cl) medium at 25°C. The measurements were performed as EMF titrations (glass electrode) within the limits $1.4 \leqslant -\log[H^+] \leqslant 9.4$; $0.0006 \leqslant B \leqslant 0.04$ M; $0.0007 \leqslant C \leqslant 0.04$ M and $0.25 \leqslant C/B \leqslant 5$ (B and C stand for the total concentrations of aluminium(III) and nitrilotriacetic acid, respectively). All data can be explained with a series of mononuclear species $AlL(H_2O)_2^0$ ($\log \beta_{-3,1,1} = -1.853 \pm 0.007$), $AlL(OH)(H_2O)^-$ ($\log \beta_{-4,1,1} = -7.28 \pm 0.026$) and $AlL(OH)_2^{2-}$ ($\log \beta_{-5,1,1} = -15.47 \pm 0.032$) together with a dimer of $AlL(OH)(H_2O)^-$, i.e. $Al_2(OH)_2L_2^{2-}$ ($\log \beta_{-8,2,2} = -12.74 \pm 0.038$). (The formulae given are based on an assumed resemblance with species found in the solid state.) The acidity constants of nitrilotriacetic acid were studied in separate titrations ($0.003 \leqslant C \leqslant 0.02$ M) and were found to be $\log \beta_{-1,0,1} = -1.74 \pm 0.023$, $\log \beta_{-2,0,1} = -4.04 \pm 0.015$ and $\log \beta_{-3,0,1} = -12.95 \pm 0.016$. All equilibrium constants given are defined according to the general reaction $pH^+ + aAl^{3+} + rH_3L \rightleftarrows H_pAl_q(H_3L)_r^{p+3q}$ and the uncertainties reported are $3\sigma(\log \beta_{p,q,r})$. Data were analysed with the least-squares computer program LETAGROPVRID. In a series of calculations with the modelling program SOLGASWATER, the potential ability of the nitrilotriacetate ion to increase the solubility of gibbsite, is illustrated.

In a current research project at this department, the ability of Al^{3+} to form complexes with ligands of geo- and biochemical relevance is being investigated. The goal of our studies performed with ligands of geochemical importance, is to gain a better understanding of the processes affecting the mobility and acute toxicity of this element in natural waters influenced by natural or anthropogenic acidity[1] ("acid rain"). Correspondingly, the intention behind our studies of biochemically interesting ligands, is to provide data of relevance to aluminium-toxicological studies in man.[1]

As these aims put certain demands on the experimental conditions under which the data must be collected, i.e. at low concentrations and near-neutral pH-values, we spend a lot of effort collecting and analysing data with as large a variation in pH, aluminium and ligand concentration and aluminium–ligand ratio as possible. Through these studies the common occurrence of mono- and polynuclear mixed Al–OH–ligand complexes has been demonstrated.[2–4] Furthermore, in several of the systems studied, the occurrence of ternary solid phases has been identified near the precipitation boundary of aluminium hydroxide.[5–7]

The aim of the present investigation is to interpret the complexation features of nitrilotriacetic acid, NTA, towards Al^{3+}. As the sodium salt of this compound is a commonly used additive in washing powder (as a detergent builder) in several countries, it can be regarded as a potential anthropogenic complex former in the biosphere. Furthermore, as it has recently been shown that NTA under certain circumstances forms a water-soluble, net-neutral species with Al^{3+},[8] there is a risk that NTA might induce an elevated aluminium-toxicity towards aquatic biocenoses and superior organisms.

A final reason for undertaking this investigation is the need from clinical chemists and biochemists for a well-defined system to set the free Al^{3+} concentration when for instance the binding constants of Al^{3+} to transferrin are evaluated[9] or when the

influence of Al^{3+} on the promotion of tubulin into microtubules is being studied.[10] The formal analogy between pH-buffers for proper pH-control and aluminium–ligand systems for Al^{3+} control has been discussed by Martin,[11] who also illustrated this point with NTA and citrate as two suitable complex formers. In view of the complexity and time-dependence of the reactions between Al^{3+} and citrate ions[12,13] as compared to those reported in the Al^{3+}–NTA system, NTA promises to be a much better choice of buffer than citrate in such studies.

Several reports on the complexation of NTA to Al^{3+} have appeared in the literature.[14–16] In none of these articles has, however, the experimental data base been wide enough to permit a comprehensive and unbiased search for a speciation model. Furthermore, since the deprotonation and aluminium-complexation of NTA commence at very low pH-values, comparable to the behaviour of oxalic acid,[3] an investigation of this system with the potentiometric method places very high demands on the analytical precision as well as on the measuring equipment.

EXPERIMENTAL

Chemicals and analysis

Nitrilotriacetic acid, NTA [$N(CH_2COOH)_3$, H_3L] (Merck p.a.), was used after drying at 80°C. Stock solutions were prepared by dissolving H_3L and sodium chloride in water and the L content was determined potentiometrically. The titrated amount was in good agreement (within 0.1%) with the value expected from weighing. Stock solutions of sodium chloride and aluminium chloride, as well as the dilute hydrochloric acid and sodium hydroxide solutions, were prepared and standardized as described earlier.[17]

Apparatus

The automatic system for precise EMF titrations, the thermostat and the electrodes have been described earlier.[17]

Temperature and medium

The measurements were carried out at 25.00 ± 0.05°C in a constant ionic medium of 0.6 M Na(Cl).

Method

The present investigation was carried out as a series of potentiometric titrations. The titration procedures, including a special procedure to calibrate the glass electrode, have been described in earlier papers.[17,18] The reproducibility and reversibility of equilibria were tested by performing both forward (increasing $-\log[H^+]$ by means of additions of OH^-) and backward (decreasing $-\log[H^+]$ with H^+) titrations. The acidity constants of nitrilotriacetic acid were determined in separate titrations.

The three-component titrations were performed at a constant ratio between the total concentration of aluminium (B) and nitrilotriacetic acid (C). The upper $-\log[H^+]$ limits in these titrations were set by the formation of a precipitate or by the appearance of extremely sluggish equilibria. These phenomena were presumed to originate from the precipitation and polynuclear hydrolysis of aluminium, respectively.

Data treatment

In order to visualize experimental results, the data sets Z_c vs $-\log[H^+]$ were calculated and some of them are presented in Fig. 1; Z_c is defined as the average number of OH^- ions reacted per nitrilotriacetic acid and is given by the relation $Z_c = (h - H - k_w h^{-1})/C$, where $h = [H^+]$ and H denotes the total concentration of protons calculated over the zero level H_2O, Al^{3+} and H_3L. The term $k_w h^{-1}$, where k_w is the ionic product of water in 0.6 M Na(Cl) medium, corresponds to the free concentration of hydroxide ions. These curves reflect the total complexation behaviour of the system, comprising binary [eqs (1) and (2)] as well as ternary [eq. (3)] equilibria:

$$H_3L \rightleftarrows H_{3-n}L^{n-} + nH^+ \quad (\beta_{-n,0,1};\ n = 1, 2 \text{ and } 3) \tag{1}$$

$$pH^+ + qAl^{3+} \rightleftarrows H_pAl_q^{p+3q} \quad (\beta_{p,q,0}) \tag{2}$$

$$pH^+ + qAl^{3+} + rH_3L \rightleftarrows H_pAl_q(H_3L)_r^{p+3q} \quad (\beta_{p,q,r}). \tag{3}$$

For the acidity constants of nitrilotriacetic acid [i.e. eq. (1)], results from separate experiments will be used, while for the hydrolytic equilibria of Al^{3+} [i.e. eq. (2)], results obtained in earlier papers of this series[13,19,20] will be used. This hydrolytic scheme of Al^{3+} comprises the species $[Al(OH)]^{2+}$ (log $\beta_{-1,1,0} = -5.52$), $Al(OH)_2^+$ (log $\beta_{-2,1,0} = -11.3$), $Al(OH)_3$ (log $\beta_{-3,1,0} = -17.3$), $Al(OH)_4^-$ (log $\beta_{-4,1,0} = -23.46$), $Al_3(OH)_4^{5+}$ (log $\beta_{-4,3,0} = -13.57$) and $Al_{13}O_4(OH)_{24}^{7+}$ (log $\beta_{-32,13,0} = -109.2$).

In the evaluation of the three-component experimental data [i.e. eq. (3)] the binary complex models were considered as known and all effects above this

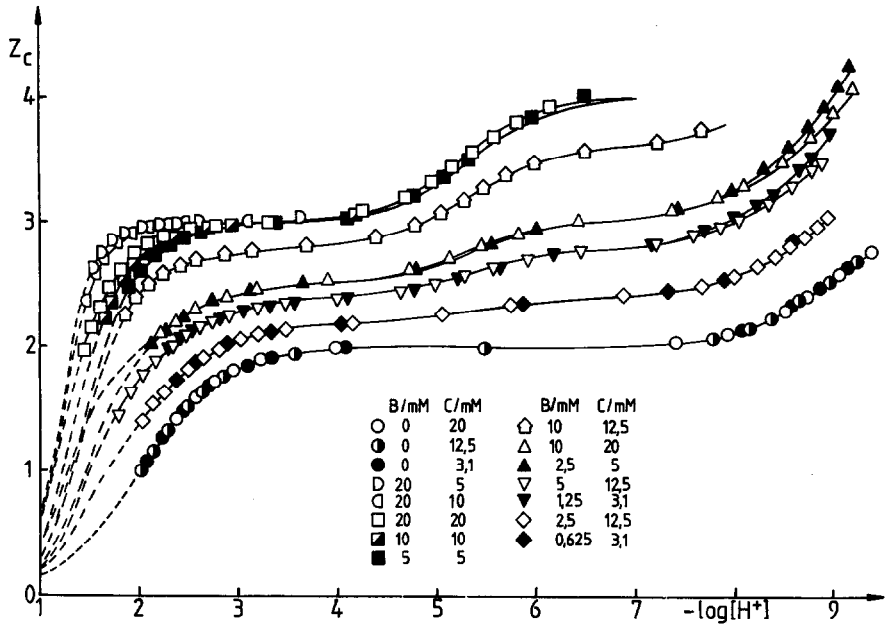

Fig. 1. Part of the experimental data plotted as curves $Z_c(-\log[H^+])$. All symbols represent initial concentrations and the lines have been calculated using the set of proposed constants in Table 1. The dashed lines at low $-\log[H^+]$ denote extrapolated values where no measurements have been performed.

level treated as being caused by ternary species. The mathematical analysis of data was performed with the least-squares computer program LETAGROPVRID[21] (version ETITR[22,23]). The *p,q,r*-triplets and corresponding equilibrium constants that "best" fit the experimental data were determined by minimizing the error squares sum $U = \Sigma(H_{calc} - H_{exp})^2$, where H_{calc} and H_{exp} denote calculated and experimental values of the analytical H^+ concentrations, respectively. The standard deviations $\sigma(H)$ and $3\sigma(\log \beta_{p,q,r})$ obtained in the LETAGROP calculations, were defined and calculated according to Sillén.[24,25] The computations were performed on a CD Cyber 850 computer.

DATA, CALCULATIONS AND RESULTS

Binary H^+–H_3L *equilibria*

The data comprise 99 experimental points collected via three potentiometric titrations within the range $0.003 \leqslant C \leqslant 0.020$ M and $2.0 \leqslant -\log[H^+] \leqslant 9.4$. The LETAGROP calculation ended at $\sigma(H) = 0.06 \times 10^{-3}$ M and the following equilibrium constants were obtained: $\log(\beta_{-1,0,1} \pm 3\sigma) = -1.744 \pm 0.023$, $\log(\beta_{-2,0,1} \pm 3\sigma) = -4.037 \pm 0.015$, $\log(\beta_{-3,0,1} \pm 3\sigma) = -12.950 \pm 0.016$.

Ternary H^+–Al^{3+}–H_3L *equilibria*

These data comprise 15 titrations (462 experimental points) within the ranges $0.0006 \leqslant B \leqslant 0.040$ M, $0.0007 \leqslant C \leqslant 0.040$ M and $1.4 \leqslant -\log[H^+] \leqslant 9.2$. The following C/B ratios have been covered: 0.25, 0.5, 1, 1.25, 2, 2.5 and 5. In order to visualize experimental data, Z_c vs $-\log[H^+]$ were calculated and some of these data are illustrated in Fig. 1. From the fact that Z_c values exceeding the value of three are obtained, it can be directly concluded that the formation of aluminium hydrolytic products and/or ternary aluminium–nitrilotriacetate–hydroxide complexes are significant. On the basis of this plot, the evaluation of data was accordingly divided into three parts, corresponding to data with $-\log[H^+] \leqslant 3.2$; $3.2 \leqslant -\log[H^+] \leqslant 6.5$ and $-\log[H^+] \geqslant 6.5$, respectively.

In the first calculation, performed on data with $-\log[H^+] \leqslant 3.2$, the stability constants for the species $(-1, 1, 1)^{2+}$, $(-2, 1, 1)^+$ and $(-3, 1, 1)^0$ were simultaneously varied. It did, however, turn out that only the stability constant for $(-3, 1, 1)^0$ attained a positive value ($\log(\beta_{-3,1,1} \pm 3\sigma) = -1.852 \pm 0.005$), i.e. the species AlH_2L^{2+} and $AlHL^+$ were rejected. This value for AlL^0 was then regarded as known when data with $3.2 \leqslant -\log[H^+] \leqslant 6.5$ were examined.

From the shapes of the $Z_c(-\log[H^+])$ curves in this region it was directly concluded that the species $(-4, 1, 1)^-$ had to be the predominating one. As these curves, however, also showed a small but systematic dependence on total concentrations, it was also apparent that a simultaneous formation of the corresponding dimer, $(-8, 2, 2)^{2-}$, had to be taken into consideration. For this reason, the original data base was supplemented with two titrations at $C/B = 1$ and $Z_c = 3.50$, the first in which an initially $B = C = 0.040$ M solution was titrated with pure ionic medium and a second in which the burette and vessel solutions were switched. Through these titrations it was found that on increasing $B = C$ from 0.7×10^{-3} to 40×10^{-3} M, $-\log[H^+]$ decreased from 5.40 to 5.12, i.e. a clearly measurable effect. On all data in this region, a LETAGROP calculation was then performed in which the formation constants for $(-4, 1, 1)^-$ and $(-8, 2, 2)^{2-}$ were simultaneously refined. The result of this calculation [$\log(\beta_{-4,1,1} \pm 3\sigma) = -7.26 \pm 0.035$; $\log(\beta_{-8,2,2} \pm 3\sigma) = -12.75 \pm 0.048$; $U = 3.95$], as compared to the results obtained when only one of the complexes was considered [$\log(\beta_{-4,1,1} \pm 3\sigma) = -7.01 \pm 0.019$, $U = 30.2$; $\log(\beta_{-8,2,2} \pm 3\sigma) = -12.36 \pm 0.036$, $U = 41.8$] showed that both of these species were needed to give a satisfactory fit to the data.

Finally, with $C/B \geqslant 1.25$, it was found that a species with an even higher degree of deprotonation was formed (cf. Fig. 1). These data were fully explained by the appearance of a species with the composition $(-5, 1, 1)^{2-}$. The LETAGROP calculation on these data gave $\log(\beta_{-5,1,1} \pm 3\sigma) = -15.46 \pm 0.031$.

To obtain the "best" equilibrium constants for all ternary species, a final calculation was performed in which the equilibrium constants for all species detected above were co-refined on all data. This calculation ended at $\sigma(H) = 0.13 \times 10^{-3}$ M and with the equilibrium constants given in Table 1. With this final model, no remaining systematic deviations could be observed.

In order to visualize the amounts of the different species, the computer program SOLGASWATER,[26] equipped with plotting procedures, has been used to calculate some distribution diagrams. These are presented in Fig. 2.

DISCUSSION

Equilibria and structures

The present investigation has shown that nitrilotriacetic acid (NTA, H_3L) at 25°C and in a 0.6 M Na(Cl) medium titrates as a triprotic weak acid with successive pK_a values of 1.74, 2.30 and 8.91. The surprisingly high value of pK_{a_3} can probably be explained by the appearance of NTA as a zwitterion in aqueous solution, i.e. one of the three protons is actually positioned on the imino nitrogen group. A qualitative observation which gives support to this assumption is the fact that the solubility of NTA is significantly increased in the presence of excess strong acid.

In its interaction with the aluminium ion, the present study has shown that the first complex NTA forms is the uncharged species $H_{-3}Al(H_3L)$. A previously reported species[14] $H_{-2}Al(H_3L)^+$ could not be verified and is probably an artifact caused by experimental difficulties at the low $-\log[H^+]$ values at which it was interpreted.

According to a recent report[8] on the structure of $H_{-3}Al(H_3L)$, the nitrilotriacetate ion acts as a tribasic, tetradentate (via the three carboxylate groups and the imino group) ligand in its interaction with Al^{3+} and that, accordingly, this species should be written $AlL(H_2O)_2^0$. Since the ligand thus occu-

Table 1. Binary and ternary complexes in the three-component system H^+–Al^{3+}–NTA. The formation constants are related according to the reaction $pH^+ + qAl^{3+} + rH_3L \rightleftarrows H_pAl_q(H_3L)_r^{p+3q}$, where H_3L stands for nitrilotriacetic acid

Number of titrations/ Number of points	p	q	r	Tentative formula	$\log(\beta_{pqr} \pm 3\sigma)$
3/99	−1	0	1	H_2L^-	−1.74±0.023
	−2	0	1	HL^{2-}	−4.04±0.015
	−3	0	1	L^{3-}	−12.95±0.016
15/462	−3	1	1	$AlL(H_2O)_2^0$	−1.853±0.007
	−4	1	1	$AlL(OH)(H_2O)^-$	−7.28±0.026
	−5	1	1	$AlL(OH)_2^{2-}$	−15.47±0.032
	−8	2	2	$Al_2(OH)_2L_2^{2-}$	−12.74±0.038

pies four of the six coordination positions around the aluminium ion, the absence of a bis-ligand complex in this system can be readily understood.

Also, in view of the appearance of $AlL(H_2O)_2^0$, it is logical to assume that the two succeeding species $H_{-4}Al(H_3L)^-$ and $H_{-5}Al(H_3L)^{2-}$ are hydrolysis products of this species, i.e. that they should be written $AlL(OH)(H_2O)^-$ and $AlL(OH)_2^{2-}$, respectively. The corresponding pK_a values for $AlL(H_2O)_2^0$ and $AlL(OH)(H_2O)^-$ then becomes 5.43 and 8.19.

These values are considerably lower than those previously determined for $Al(salicylate)_2^-$ (7.60, 9.32)[18] or $Al(H^{-1}\ citrate)^-$ (6.2).[13] In fact, the acidity of $AlL(H_2O)_2^0$ exceeds the acidity of $Al(H_2O)_6^{3+}$ ($pK_a = 5.52$).[19] The reason for this high acidity is uncertain but a possible explanation is the high electron demand from the coordinated imino

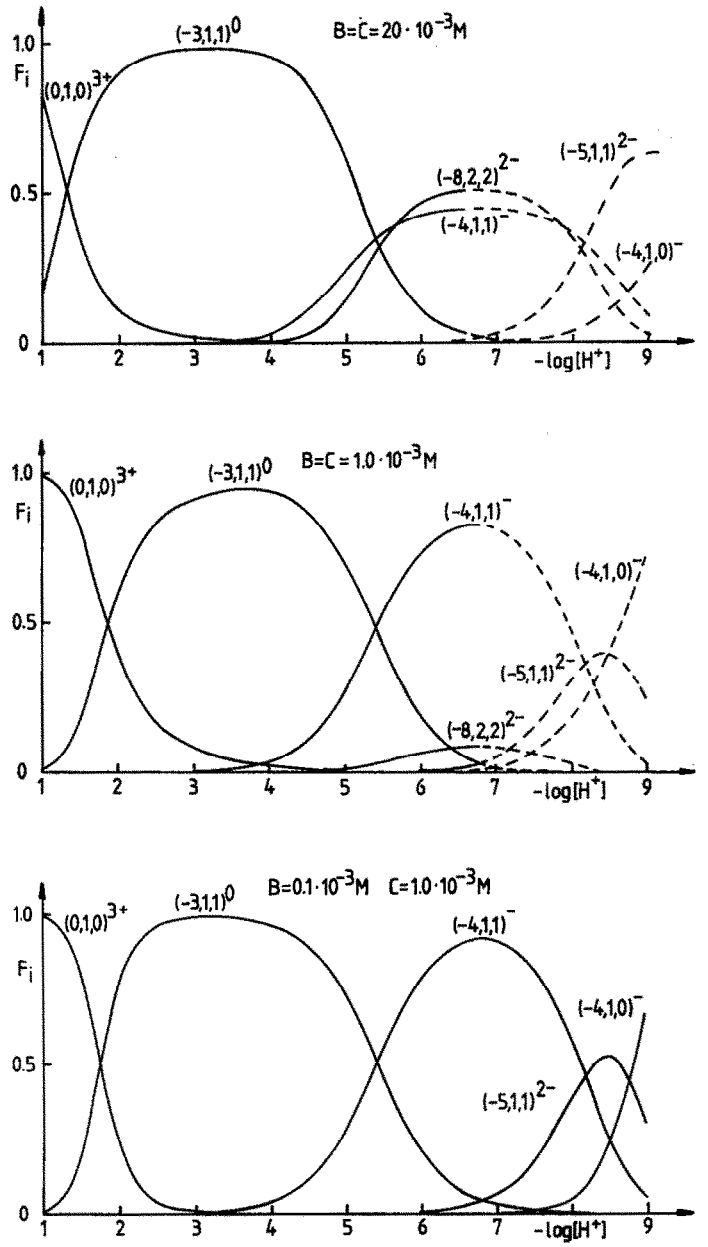

Fig. 2. Distribution diagrams $F_i(-\log[H^+])$. F_i is defined as the ratio between aluminium(III) in a species and the total aluminium(III). The calculations were performed with the computer program SOLGASWATER using the equilibrium constants given in Table 1. Dashed curves denote precipitation ranges.

group. This hypothesis is supported by the fact that the Al—OH_2 distance for the water molecule coordinated *trans* to the nitrogen in $AlL(H_2O)_2^0$ (1.829 Å)[8] is shorter than the corresponding distance in $Al(H_2O)_6Cl_3$ (1.88 Å).[27]

Also with regard to the dimer $H_{-8}Al_2(H_3L)_2^{2-}$, the structure report cited above[8] provides its structure in the solid state. This species is shown to consist of two AlL-units bridged by a dihydroxo bridge, i.e. $Al_2(OH)_2L_2^{2-}$, thus creating an octahedral coordination around both aluminium ions. By writing the formation of this species as $2AlL(OH)(H_2O)^- \rightleftarrows Al_2(OH)_2L_2^{2-} + 2H_2O$, log $K = 1.82$, the connection with its corresponding monomer is emphasized. From the resulting equilibrium constant, it can furthermore be concluded that the monomer dominates in solutions with $B = C < 15 \times 10^{-3}$ M. The pronounced concentration dependence of the dimer is also illustrated in Fig. 2 where it is shown that the formation of $Al_2(OH)_2L_2^{2-}$ is negligible at $B = 10^{-4}$ and $C = 10^{-3}$ M.

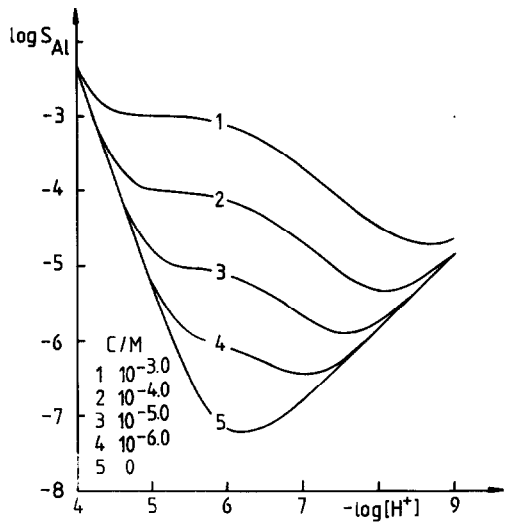

Fig. 3. Solubility of gibbsite (log* $K_{so} = 9.6$) expressed as log S_{Al} vs $-\log[H^+]$ for different total concentrations of nitrilotriacetic acid, C.

Modelling calculations

The concentration of aluminium under most natural conditions is regulated by the occurrence of secondary formed hydroxo phases. Therefore, the potential ability of a given ligand to affect its aquatic behaviour can be suitably indicated via computerized modelling in which aluminium hydroxide or some clay mineral, e.g. kaolinite ($Al_2(OH)_4Si_2O_5$), is used as a solubility regulating phase. Under such conditions, the presence of a complex-forming substance will raise the total solubility of the solid phase but leave concentrations of Al^{3+} and hydrolytic species unaffected.

In Fig. 3, the ability of various amounts of NTA to increase the solubility of gibbsite (log* $K_{so} = 9.6$)[28] is illustrated. From this figure it can be concluded that even very low concentrations of NTA can be expected to cause a substantial solubilization of gibbsite in near-neutral solutions. Compared to previously investigated ligands within the present series,[29] it can be stated that the complexation strength of the nitrilotriacetate ion is somewhat weaker than that of the citrate ion[13] but considerably stronger than that of the oxalate ion,[3] especially in slightly alkaline solutions.

From Fig. 4, which correspondingly gives areas for the predominating aluminium-containing species in solutions equilibrated with gibbsite, it can be concluded that the solubilization in near-neutral solutions is mainly caused by the occurrence of the species $Al(OH)L^-$. In this figure also, the restricted predominance of $Al_2(OH)_2L_2^{2-}$ to solutions of high ligand concentrations is emphasized.

With regard to human bio-uptake considerations, a main concern has been devoted to the occurrence of water-soluble, net-neutral species of low (<650) molecular weight,[11,30] as these might pass cell membranes via a passive diffusion mechanism.[31] The formation of such aluminium species with citrate,[13] tartrate[32] and maltolate[33] has been suggested[11] as the reason why these substances ele-

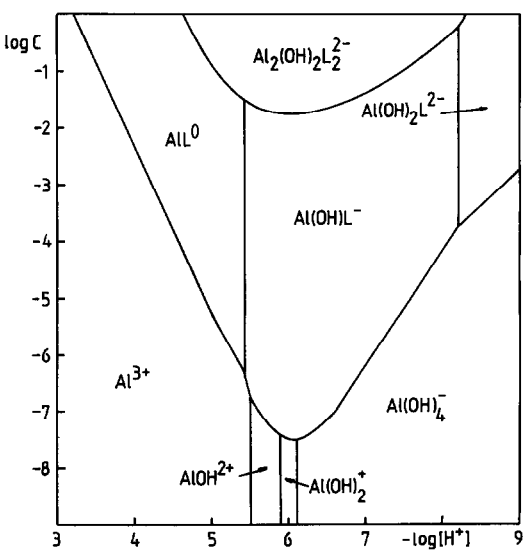

Fig. 4. Predominance area diagram showing the dominating aqueous aluminium species in equilibrium with gibbsite as a function of log C and $-\log[H^+]$.

vate the bio-availability[34] and toxicity[35,36] of aluminium. Also in the present system, the formation of such a species is highly predominant (cf. Figs 2 and 4) in slightly acidic solutions. It is therefore probable that nitrilotriacetate ions may also cause an elevated aluminium absorption from the gastrointestinal tract.

Acknowledgement—This work forms part of a programme which is financially supported by the Swedish Natural Science Research Council.

REFERENCES

1. H. Sigel and A. Sigel (Eds), *Metal Ions in Biological Systems*, Vol. 24, Aluminium and its role in biology. Marcel Dekker, New York (1988).
2. L.-O. Öhman and S. Sjöberg, *Polyhedron* 1983, **2**, 1329.
3. S. Sjöberg and L.-O. Öhman, *J. Chem. Soc., Dalton Trans.* 1985, 2665.
4. E. Marklund, L.-O. Öhman and S. Sjöberg, *Acta Chem. Scand.* 1989, **43**, 641.
5. L.-O. Öhman and S. Sjöberg, *Acta Chem. Scand.* 1982, **A36**, 47.
6. H. Bilinski, L. Horvath, N. Ingri and S. Sjöberg, *Geochim. Cosmochim. Acta* 1985, **50**, 1911.
7. T. Hedlund, H. Bilinski, L. Horvath, N. Ingri and S. Sjöberg, *Inorg. Chem.* 1988, **27**, 1370.
8. G. C. Valle, G. G. Bombi, B. Corain, M. Favarato and P. Zatta, *J. Chem. Soc., Dalton Trans.* 1989, 1513.
9. R. B. Martin, J. Savory, S. Brown, R. L. Bertholf and M. R. Wills, *Clin. Chem.* 1987, **33**, 405.
10. T. L. MacDonald, W. G. Humphreys and R. B. Martin, *Science* 1987, **236**, 183.
11. R. B. Martin, *Clin. Chem.* 1986, **32**, 1797.
12. L.-O. Öhman and S. Sjöberg, *J. Chem. Soc., Dalton Trans.* 1983, 2513.
13. L.-O. Öhman, *Inorg. Chem.* 1988, **27**, 2565.
14. T. R. Bhat, R. R. Das and J. Shankar, *Ind. J. Chem.* 1967, **5**, 324.
15. M. M. Taqui Khan and A. Hussein, *Ind. J. Chem.* 1980, **19A**, 50.
16. A. Napoli, *Ann. Chim. (Rome)* 1984, **74**, 699.
17. L.-O. Öhman and S. Sjöberg, *Acta Chem. Scand.* 1981, **A35**, 201.
18. L.-O. Öhman and S. Sjöberg, *Acta Chem. Scand.* 1983, **A37**, 875.
19. L.-O. Öhman and W. Forsling, *Acta Chem. Scand.* 1981, **A35**, 795.
20. L.-O. Öhman, S. Sjöberg and N. Ingri, *Acta Chem. Scand.* 1983, **A37**, 561.
21. N. Ingri and L.-G. Sillén, *Ark. Kemi* 1964, **23**, 97.
22. R. Arnek, L.-G. Sillén and O. Wahlberg, *Ark. Kemi* 1969, **31**, 353.
23. P. Brauner, L.-G. Sillén and R. Whiteker, *Ark. Kemi* 1969, **31**, 365.
24. L.-G. Sillén, *Acta Chem. Scand.* 1962, **16**, 159.
25. L.-G. Sillén and B. Warnqvist, *Ark. Kemi* 1969, **31**, 341.
26. G. Eriksson, *Anal. Chim. Acta* 1979, **112**, 375.
27. D. R. Buchanan and P. M. Harris, *Acta Cryst.* 1968, **B24**, 954.
28. C. F. Baes and R. E. Mesmer, *The Hydrolysis of Cations*. Wiley, New York (1976).
29. L.-O. Öhman and S. Sjöberg, in *Metal Speciation* (Edited by J. R. Kramer and H. A. Allen), Chap. 1. Lewis Publishers, Chelsea (1988).
30. M. M. Finnegan, T. G. Lutz, W. O. Nelson, A. Smith and C. Orvig, *Inorg. Chem.* 1987, **26**, 2171.
31. V. A. J. Levin, *J. Med. Chem.* 1980, **23**, 682.
32. E. Marklund and L.-O. Öhman, *J. Chem. Soc., Dalton Trans.*, accepted for publication.
33. T. Hedlund and L.-O. Öhman, *Acta Chem. Scand.* 1988, **A42**, 702.
34. P. Slanina, W. Frech, L.-G. Ekström, L. Lööf, S. Slorach and A. Cedergren, *Clin. Chem.* 1986, **32**, 539.
35. U. DeBoni, A. Otvos, J. W. Scott and D. R. Crapper, *Acta Neuropath.* 1976, **35**, 285.
36. D. R. McLachlan, *Neurobiol. Aging* 1986, **7**, 525.

Polyhedron Vol. 9, No. 2/3, pp. 207–214, 1990
Printed in Great Britain

0277–5387/90 $3.00+.00
Pergamon Press plc

SPECTROSCOPIC STUDIES OF GALLIUM COMPLEXES IN SOLUTION

MICHAEL J. TAYLOR*

Department of Chemistry, University of Auckland, Private Bag, Auckland, New Zealand

Abstract—High-field ^{71}Ga NMR spectra at 122.03 MHz of aqueous solutions of Ga^{3+} in the presence of oxyanions reveal sulphate, phosphate or citrate complexes. In halogen acid solutions the $[Ga(H_2O)_6]^{3+}$ signal is accompanied by that of a mixture of $[GaX_n(H_2O)_{4-n}]^{3-n}$ (X = Cl or Br; n = 1–4) from which a single NMR peak is observed. Aqueous solutions of $[GaCl_4]^-$ and $[GaBr_4]^-$ in combination yield one peak due to mixed halides undergoing ligand exchange. The diethyl ether extract of this solution displays the five signals of the complex acids $H^+(aq)[GaCl_nBr_{4-n}]^-$ (n = 0–4). The Raman spectrum of this system provides a set of $\nu(Ga—Cl)_{sym}$ and $\nu(Ga—Br)_{sym}$ frequencies. The ^{17}O chemical shift of the $[H_9O_4]^+$ ion occurs at 15 ppm. Attempts to investigate the halogen exchange process of gallium mixed-halide species by a two-dimensional ^{71}Ga NMR technique are described. ^{71}Ga NMR spectra of mixed-ligand halide/thiocyanate complexes are attributable to species $[GaX_n(NCS)_{4-n}]^-$ (X = Cl or Br; n = 0–4). Chemical shift trends show the gallium(III) shielding order, Cl < NCS < Br < I.

Gallium forms a variety of soluble complexes[1] and, like aluminium, has an extensive and complicated hydrolysis chemistry.[2] Stability constants have been determined for various systems,[3] but there is often uncertainty about the total coordination number, the extent of inner- and outer-shell solvation, and the structure of the gallium(III) complexes formed by a given ligand. The behaviour of gallium(III) with simple and chelating ligands is a relatively undeveloped aspect of post-transition element chemistry, and many of the species which are thought to exist are inadequately characterized.

Complex formation plays an important part in the analytical chemistry of gallium, and has a specific function in the mechanism of solvent extraction of gallium(III).[4] The discovery that radioactive ^{67}Ga administered as the citrate becomes localized in soft tumour tissue[5] has prompted extensive clinical research, with corresponding efforts to elucidate the fundamental chemistry pertaining to the use of gallium complexes in disease diagnosis.[6–8] The *in vivo* behaviour of Ga^{3+} vis-à-vis Al^{3+} and Fe^{3+} requires thorough study of the species formed by this element, especially in aqueous solutions at near neutral pH.

This paper is directed towards the better understanding of the coordination chemistry of gallium to which structural studies, especially those of solutions by multinuclear NMR and Raman spectroscopy, can contribute.

EXPERIMENTAL

Materials

Stock 2.5 mol dm^{-3} solutions of gallium(III) in HCl or HBr were prepared by dissolving a known weight of powered gallium metal in concentrated hydrochloric or hydrobromic acid, and finally heating the solution to ensure the oxidation of any gallium(II) species.[9] Excess aqueous ammonia was added to a portion of gallium(III) in HCl solution and the precipitate of $Ga(OH)_3$ was washed to remove chloride. Portions of freshly prepared, wet $Ga(OH)_3$ were dissolved in the appropriate acids to obtain solution of gallium(III) nitrate, sulphate, phosphate or citrate. $Bu_4N[GaCl_4]$ and $Bu_4N[GaBr_4]$ were prepared as described previously.[10]

Solvent extracts were obtained by shaking 5 cm^3 of the gallium(III) aqueous halogen acid solution with an equal volume of diethyl ether. Laboratory grade diethyl ether was used without purification.

*Address for correspondence until May 1990: c/o Department of Chemistry, Royal Holloway and Bedford New College, Egham Hill, Egham, Surrey TW20 0EX, U.K.

Spectroscopy

^{71}Ga NMR spectra were recorded at 122.03 MHz using a 10-mm broadband probe in a Bruker AM400 spectrometer at 295 K. 4K data points were collected over 100,000 Hz using a 60° pulse (10 μs) and a pulse recycle time of 20 ms. Spectra were processed with 10–20 Hz line broadening. Two-dimensional NOESY-type spectra were obtained using a standard pulse sequence with 90° mixing and detection pulses. 128 increments of 512 data points each, were collected and processed with shifted sine-bell window functions in both dimensions. Mixing times were varied, in separate experiments, from 1 to 50 ms. Cross peaks were detected only with a mixing time of 10 ms. ^{71}Ga spectra are referenced to $Ga(NO_3)_3$ in D_2O/HNO_3. ^{17}O NMR spectra were recorded at 54.24 MHz using a 10 mm broadband probe. 4K data points were collected over 85,000 Hz using a 50° pulse (11 μs) and a pulse recycle time of 0.11 s. Spectra were processed with 20–50 Hz line broadening. ^{17}O spectra were referenced to external H_2O at 295 K.

Raman spectra were excited by 488.0 nm radiation from a Coherent Radiation CR4 Ar^+ laser and recorded with a Jasco R300 Raman spectrometer.

RESULTS AND DISCUSSION

Aqueous gallium solutions with oxyanion ligands

Aqueous solutions contain the aquagallium cation $[Ga(H_2O)_6]^{3+}$. It is a labile species with a lifetime to the exchange of a water molecule of 5.6×10^{-4} s at 25°C.[11] A value of 6.1 ± 0.2 has been measured for the coordination number of gallium(III) ions by means of ^{17}O NMR studies.[11,12] ^{1}H NMR studies also support the existence of $[Ga(H_2O)_6]^{3+}$.[13] The hexaqua cation undergoes self-hydrolysis to $[Ga(OH)(H_2O)_5]^{2+}$ with the hydrolysis constant $pK_{1,1} = 2.6$.[2] Further reaction yields $[Ga(OH)_2(H_2O)_4]^+$ ($pK_{1,2} \sim 7.5$).[14] The hexaqua cation is the reference standard for ^{71}Ga NMR measurements ($\delta = 0$ ppm). Because of hydrolysis the line width of this resonance varies with pH. When hydrolysis is suppressed by the addition of acid, the $[Ga(H_2O)_6]^{3+}$ resonance has a minimum line width of 53 Hz but this increases greatly above pH 1.[15] Interaction of gallium(III) with perchlorate may contribute to the line broadening, but there is no other evidence of association between Ga^{3+} and ClO_4^-. Addition of base to gallium(III) solutions produces a signal with a line width of *ca* 300 Hz and a chemical shift of 233 ppm which is that of $[Ga(OH)_4]^-$.[16,17]

A 1.0 mol dm^{-3} solution of gallium(III) nitrate gives a single ^{71}Ga NMR line due to $[Ga(H_2O)_6]^{3+}$. Broadening of the line in nitric acid may be due to exchange processes with gallium-containing species of lower symmetry, such as $[Ga(NO_3)(H_2O)_5]^{2+}$. Gallium(III) solutions in sulphuric acid show a hexaquagallium signal which broadens from 150 to 400 Hz with an increase of H_2SO_4 concentration.[17] In this case a second signal occurs 13 ppm upfield of the $[Ga(H_2O)_6]^{3+}$ line and increases in intensity with sulphuric acid concentration to account for almost 50% of the gallium in a solution of $Ga_2(SO_4)_3$ in 8 mol dm^{-3} H_2SO_4, the spectrum of which is given in Fig. 1(a). Assuming bidentate attachment of the sulphate ion, a possible six-coordinate structure is $[Ga(SO_4)(H_2O)_4]^+$.

The ^{71}Ga NMR spectra of gallium(III) solutions in phosphoric acid have a markedly different appearance from the nitrate or sulphate solutions and consist of a very broad signal. In *ca* 0.5 mol dm^{-3} gallium(III) phosphate solution this band has a half-width exceeding 5000 Hz and extends from +75 to −100 ppm, Fig. 1(b). The $[Ga(H_2O)_6]^{3+}$

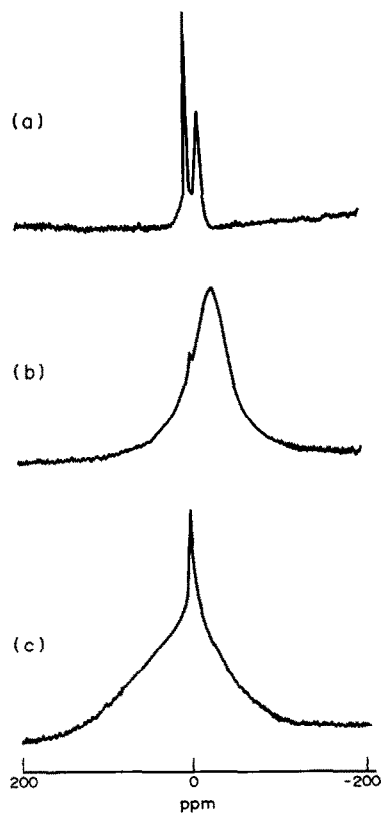

Fig. 1. ^{71}Ga NMR spectra: (a) aqueous gallium(III) sulphate in 8 mol dm^{-3} H_2SO_4; (b) aqueous gallium(III) phosphate solution; (c) aqueous gallium(III) citrate solution.

peak at 0 ppm is detected as a shoulder on the main band. The separate signal shows that exchange reactions between the hexaqua cation and gallium phosphate complexes are slow on the NMR timescale. The gallium phosphate band centre moves from -20 to -30 ppm on adding H_3PO_4 to the solution, which demonstrates that several Ga^{3+} phosphate species are involved but provides little information as to their structures. Glickson and co-workers,[7] using ^{31}P NMR, have detected as many as four gallium-containing species each giving a distinct peak, and consider that $[Ga(H_3PO_4)]^{3+}$ and $[Ga(H_2PO_4)]^{2+}$ are two of the principal complexes formed in this system. The likelihood of water molecules in the coordination sphere should be considered in assigning structures to these complexes. Gallium citrate has also been studied in the context of cellular binding of gallium(III), and the inhibition of this process by citrate and other buffers. There is support for 1 : 1 gallium–citrate complexes and also gallium citrate polymers.[6] The ^{71}Ga NMR evidence of complex formation was indirect and depended on loss of intensity of the hexaquagallium peak. The gallium citrate resonance was broadened beyond detection in spectra obtained at 27.45 MHz. Figure 1(c) shows the ^{71}Ga NMR spectrum of a gallium citrate solution recorded at 122.03 MHz in which the sharp peak due to $[Ga(H_2O)_6]^{3+}$ co-exists with a very broad peak extending from $+150$ to -100 ppm (centre *ca* $+25$ ppm), which presumably arises from gallium citrate complexes. Further work, including the investigation of solutions at low temperature to slow the rate of chemical exchange reactions, is needed to ascertain the number and identity of the species concerned, and ^{1}H, ^{13}C, and ^{17}O NMR spectra should be brought to bear on the problem.[18,19] The extension of NMR studies to biologically active systems of greater complexity has made good use of variable-pH ^{27}Al NMR and variable-temperature ^{1}H NMR, but attempts to employ ^{71}Ga NMR have been less successful.[8] Only resonances of gallium in a rather symmetrical local environment are sharp enough to be detected, as shown by the results for systems with simple ligands.

Aqueous gallium halide solutions

Gallium(III) exists in conc. HCl solution as the tetrahedral complex anion $[GaCl_4]^-$, and the corresponding complexes, $[GaBr_4]^-$ and $[GaI_4]^-$, are formed in HBr or HI solutions. All three of these complexes are well characterized by various methods, including Raman spectra.[1,20] The ^{71}Ga NMR signal of gallium in conc. HCl occurs at 245 ppm, close to the value for the $[GaCl_4]^-$ ion in CH_3CN (250 ppm).[21] Without a large excess of chloride, the ^{71}Ga NMR spectrum of aqueous gallium chloride shows a strong, sharp signal due to $[Ga(H_2O)_6]^{3+}$ and a second much broader signal between 150 and 250 ppm whose position depends on the Cl–Ga ratio in the solution.[16] Figure 2(a) is a typical high-field NMR spectrum of this system. The second signal probably arises from a rapid equilibrium between $[GaCl_4]^-$ and other chloro complexes, $[GaCl_n(H_2O)_{4-n}]^{3-n}$ ($n = 1$–3). The situation is similar to that of gallium(III) chloride in acetonitrile where the gallium ion exists as $[Ga(CH_3CN)_6]^{3+}$, which gives a NMR signal at -75 ppm, accompanied by $[GaCl_4]^-$ formed by autocomplexing.[21] Figure 2(b) illustrates the behaviour of gallium(III) in HBr solutions. Again there is evidence of a mixture of complexes, $[GaBr_n(H_2O)_{4-n}]^{3-n}$, which is converted into one complex, $[GaBr_4]^-$ ($\delta = 65$ ppm), when excess bromide is added.

Investigations by Lincoln *et al.*[22] of chloride exchange on gallium(III) in concentrated aqueous chloride solutions have shown that the dynamics of this process can be rationalized in terms of an associative exchange of chloride on $[GaCl_4]^-$. The energetics of formation of the transition state are more favourable for a tetrahedral than an octahedral species. This is borne out by the fact that the rate constant for chloride exchange of $[GaCl_4]^-$ is as high as 10^6 s^{-1},[22] whereas that of the aqua-

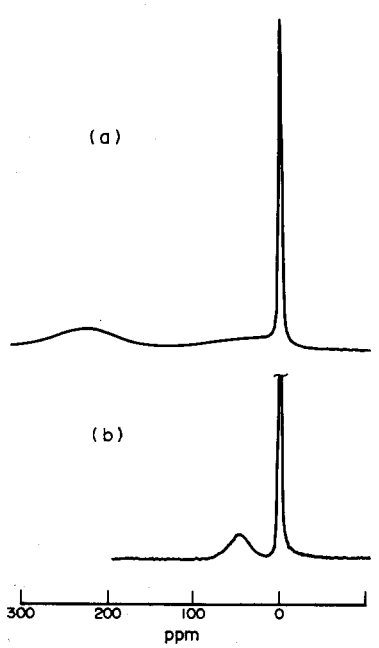

Fig. 2. ^{71}Ga NMR spectra: (a) aqueous gallium(III) chloride in 4 mol dm^{-3} HCl; (b) aqueous gallium(III) bromide in 4 mol dm^{-3} HBr.

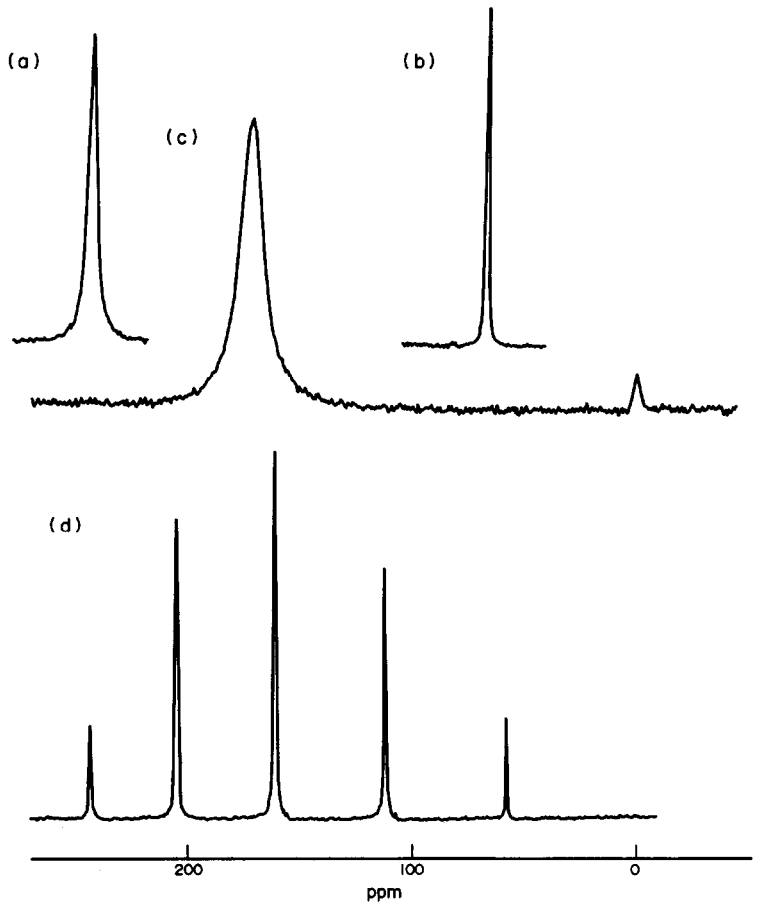

Fig. 3. ^{71}Ga NMR spectra: (a) aqueous gallium(III) chloride in 8 mol dm^{-3} HCl; (b) aqueous gallium(III) bromide in 8 mol dm^{-3} HBr; (c) aqueous gallium(III) chloride plus bromide mixture with [HCl] = 4 mol dm^{-3} and [HBr] = 4 mol dm^{-3}; (d) diethyl ether extract of the aqueous phase shown in (c). Chemical shifts: $[GaCl_4]^-$, 245; $[GaCl_3Br]^-$, 206; $[GaCl_2Br_2]^-$, 162; $[GaClBr_3]^-$, 112; $[GaBr_4]^-$, 57 ppm.

ligand in $[Ga(H_2O)_6]^{3+}$ is *ca* 10^4 s^{-1} at the same temperature.[11] Since the tetrahedral complex is highly labile it is not surprising to find, as first noted by Colton *et al.*,[23] that a mixture of $(GaCl_4]^-$ and $[GaBr_4]^-$ in aqueous solution gives only an exchange-averaged signal, indicating rapid halogen exchange on the NMR time scale. Figure 3 gives the ^{71}Ga NMR spectrum at 122.03 MHz of an equimolar $[GaCl_4]^-$ and $[GaBr_4]^-$ mixture showing the band which replaces the signals of $[GaCl_4]^-$ at 245 ppm and $[GaBr_4]^-$ at 65 ppm, when these species are observed separately. The presence of a small amount of $[Ga(H_2O)_6]^{3+}$ is indicated by the small peak close to 0 ppm. Under the conditions of a temperature of 295 K and an operating frequency of 122.03 MHz the exchange-averaged signal has a line width of 1200 Hz, which is some 1000 Hz greater than the line width of the $[GaCl_4]^-$ or $[GaBr_4]^-$ peaks in aqueous solution at the same temperature. The signals of the halide complexes are separated by 23,000 Hz in the present spectra. These data allow an estimate of the exchange rate, k, for ligand scrambling of 8×10^5 s^{-1}, using $k = \pi\Delta\nu^2/2\Delta W$, where $\Delta\nu$ is the signal separation and ΔW is the line broadening due to exchange.[24] This is in close agreement with the value of 10^6 s^{-1} for chloride exchange in $[GaCl_4]^-$ in aqueous acid solution obtained by ^{35}Cl NMR methods.[22] The average signal from the Ga/Cl/Br aqueous solution is ascribed to the mixture of species $[GaCl_nBr_{4-n}]^-$ (where n = 0–4), and as expected this peak changes its position if the composition of the mixture is varied.

Gallium halide complex anions in non-aqueous solutions and solvent extracts

Several groups have carried out ^{71}Ga NMR studies of the anionic gallium(III) chloride, bromide

and iodide mixed-halide complexes.[10,23,25] Distinct peaks are observed in acetonitrile or dichloromethane solutions, and chemical shifts have been obtained for the 15 possible four-coordinate halide species $[GaCl_xBr_yI_z]^-$ (where $x+y+z=4$). Obviously this implies that the ligand exchange reactions between the individual members of the series are slow on the NMR time scale, and in fact these reactions are slow enough that their progress can be followed by NMR after mixing a given pair of complexes, $[GaX_4]^-$ and $[GaY_4]^-$.[10] The previously reported spectra of the gallium(III) mixed-halide anions were obtained with NMR spectrometers operating at 27.45 MHz[10] or 30.36 MHz[23] for ^{71}Ga, and under these conditions some overlapping of the bands of chemically distinct complexes was evident. In the present work the ^{71}Ga NMR spectrum of the same mixture of anions, as Bu_4N^+ salts in dichloromethane or in acetonitrile, was recorded at 122.03 MHz. All 15 species were present, and the signals which were overlapping in the earlier spectra (those of the pairs $[GaCl_3I]^-$ and $[GaClBr_3]^-$, $[GaCl_2BrI]^-$ and $[GaBr_4]^-$, and $[GaCl_2I_2]^-$ and $[GaBr_3I]^-$) were now resolved to the level of the base line, Fig. 4. This work confirmed the previous assignments and chemical shift values.[10,23]

Gallium(III) is efficiently extracted from aqueous hydrogen halide solutions by ether and ketone solvents. Extraction takes place in the form of an ion-pair complex $H^+[GaX_4]^-$ (where X = Cl, Br, or I), as has been demonstrated by vibrational spectra.[4,26] ^{71}Ga NMR results provide further support for this mechanism. The diethyl ether extract of a gallium(III) solution in 8 mol dm^{-3} HCl gives a signal at 245 ppm due to $[GaCl_4]^-$ and that of a gallium(III) solution in 8 mol dm^{-3} HBr gives a signal at 58 ppm due to $[GaBr_4]^-$. Extraction of the combined aqueous solution, gallium(III) in 4 mol dm^{-3} HCl and 4 mol dm^{-3} HBr, yielded an ether phase whose ^{71}Ga NMR spectrum is given in Fig. 3(d). This shows the five separate peaks due to the species $[GaCl_nBr_{4-n}]^-$ (where $n = 0$–4) with relative intensities close to the statistical ratio of 1:4:6:4:1. The spectrum is in contrast to that of the aqueous phase prior to extraction, which consists of one rather broad band extending from 150 to 200 ppm [Fig. 3(c)]. Evidently the halide exchange, which is rapid in the aqueous solution, becomes very much slower when the species are transferred to the low dielectric constant medium of the diethyl ether phase.

An attempt was made to determine the rate of ligand exchange between the gallium mixed-halide complexes by using a two-dimensional NMR technique. This approach can be employed to investigate intermolecular scrambling reactions and has been successfully applied, using ^{119}Sn NMR spectra, to study the kinetics and mechanism of halide redistribution in a mixture of $SnCl_4$ and $SnBr_4$.[27] In this two-dimensional experiment, halide scrambling causes magnetization transfer between the various spin-labelled sites, which gives rise to cross peaks in the spectrum. A series of such experiments, using different magnetization mixing times, gives rise to cross peaks of varying intensity. This allows interpretation of the exchange kinetics. ^{119}Sn is a spin 1/2 nucleus with a T_1 relaxation time in the order of several seconds, and so presents a favourable case for this type of experiment. We are not aware of this technique having been applied to

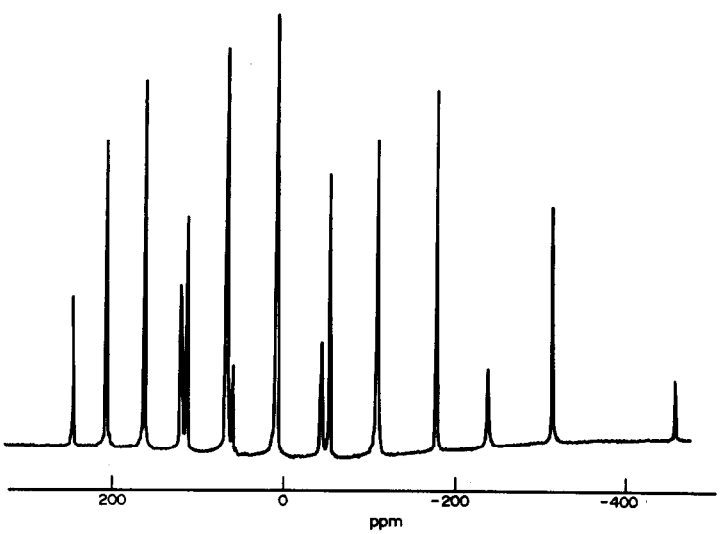

Fig. 4. ^{71}Ga NMR spectrum of a mixture of the complexes $[GaY_nY_{4-n}]^-$ and $[GaX_2YX]^-$ (where X, Y or Z = Cl, Br or I) in dichloromethane. For the chemical shift data see ref. 10.

nuclei other than spin 1/2 systems, but thought it worthwhile to test the possibility of using the ^{71}Ga nucleus which has a spin of 3/2 and a short relaxation time in the millisecond range. The details of the parameters which were tried are given in the Experimental. Problems were encountered principally because the nuclear relaxation time tends to be short in comparison with the time for chemical exchange between sites (the gallium atoms of pairs of the mixed-halide complex anions). This was certainly the case when the $[GaCl_nBr_{4-n}]^-$ mixtures were present in a diethyl ether extract, or in dichloromethane solution. Acetonitrile offered a more promising medium to which small amounts of water could be added to increase the polarity, and hence the rate of reaction, while retaining the separate NMR signals of the chemically distinct species. In this solvent we obtained a cross peak between $[GaCl_4]^-$ and $[GaCl_3Br]^-$ although various factors, including the composition of the particular sample which was relatively deficient in bromide, meant that a full set of off-diagonal peaks could not be detected. The observation of a cross peak is consistent with a halide exchange mechanism which involves association between the reacting species, perhaps via a four-centred transition state as suggested for the $SnCl_4/SnBr_4$ example.[27] In that example the rate of halide exchange from $SnCl_4$ to $SnCl_3Br$ was shown to be significantly greater than that of $SnBr_4$ to $SnClBr_3$. This may explain why the only cross peak seen in the present work was that between the pair $[GaCl_4]^-$ and $[GaClBr_3]^-$.

The two-dimensional ^{71}Ga NMR experiment was also attempted using as the sample a mixture of $[GaCl_4]^-$ and $[GaBr_4]^-$ (as Bu_4N^+ salts) in methanol containing a small amount of water. No cross peaks could be found, although all five halide complexes were present and a separate peak near 0 ppm revealed that part of the gallium now existed as $[Ga(H_2O)_6]^{3+}$. In this spectrum the chemical shifts of the species $[GaCl_nBr_{4-n}]^-$ had almost the same values as in other solvents. However, the line widths were increased by *ca* 1000 Hz, implying a life-time of the tetrahalogallate complex of less than 1 ms.

NMR spectra of ^{17}O at natural abundance can be detected easily using a high-field spectrometer and used to investigate cation solvation.[28] In the present work ^{17}O NMR spectra at 54.42 MHz were recorded from samples of the diethyl ether extracts containing $H^+(solv)[GaCl_4]^-$ or $H^+(solv)[GaBr_4]^-$ to gain information on the cationic complex. The spectrum contains a peak at 7 ppm from Et_2O[29] and a peak at 15 ppm (line width 200 Hz) due to water molecules associated with the hydrogen ion. Measurements of the amount of water which accompanies the ion-pair complex during this type of solvent extraction[20] suggest that the cation is $[H_9O_4]^+$, i.e. the H_3O^+ ion to which three additional water molecules are hydrogen bonded. The downfield shift of the ^{17}O resonance by 15 ppm from the value in liquid water at neutral pH reflects the influence of the H^+ cation on the associated water molecules within the highly acidic species $[H_9O_4]^+$.

Raman studies of gallium(III) *mixed-halide systems*

The Raman spectra of gallium(III) solutions in concentrated HCl, or concentrated HBr, are those of $[GaCl_4]^-$ and $[GaBr_4]^-$, respectively.[20] The spectrum of a mixture of these two solutions contains bands in the 400–200 cm^{-1} range assignable to the ν(Ga—Cl) and ν(Ga—Br) stretching modes of the mixed-halide complexes $[GaCl_nBr_{4-n}]^-$ (where $n = 0$–4). Because the time scale of vibrational spectroscopy is very much shorter than that of NMR there is no possibility of averaging between the signals of the individual members of the series of complexes. An additional band at 560 cm^{-1} is reasonably assigned to ν(Ga—O) stretching of the $[Ga(H_2O)_6]^{3+}$ ion.[30]

The Raman spectrum of the diethyl ether extract of the mixed-chloride/-bromide system, whose composition was known from the NMR investigation, was similar to that of the aqueous solution prior to extraction. Measurement of the spectrum of the ether extract furnished the frequencies of the gallium(III) mixed-halide complexes in Table 1. Only an incomplete set was known from earlier work.[31,32]

Gallium thiocyanate complex anions

Gallium(III) forms two types of thiocyanato complexes,[1] $[Ga(NCS)_4]^-$ and $[Ga(NCS)_6]^{3-}$. These contain nitrogen-bonded NCS^- and the choice in solid compounds seems to be dictated by the nature, and particularly the size, of the counter-ion. In the present study an attempt was made to observe the ^{71}Ga NMR spectrum of $(Et_4N)_3[Ga(NCS)_6]$ in acetonitrile as solvent. Only a very broad band was obtained which may indicate that partial dis-

Table 1. Stretching frequencies (cm^{-1}) of mixed-halide complex anions of gallium(III)

Complexes	$\nu(Ga—Br)_{sym}$	$\nu(Ga—Cl)_{sym}$
$[GaCl_4]^-$	—	345
$[GaCl_3Br]^-$	274	362
$[GaCl_2Br_2]^-$	250	376
$[GaClBr_3]^-$	228	388
$[GaBr_4]^-$	210	—

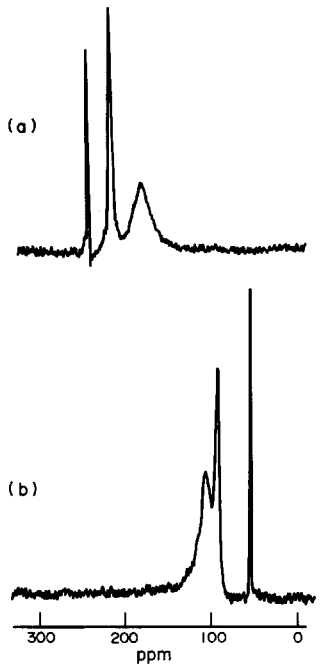

Fig. 5. ^{71}Ga NMR spectra: (a) gallium(III) chloride plus thiocyanate mixture in acetonitrile; (b) gallium(III) bromide plus thiocyanate mixture in acetonitrile.

sociation of $[Ga(NCS)_6]^{3-}$ occurs to give a mixture of four- and six-coordinate thiocyanato complexes.

Mixed-ligand halide/thiocyanate complexes were also investigated. ^{71}Ga NMR chemical shift data have been reported for the series $[GaX_n(NCS)_{4-n}]^-$ (where X = Cl or I; n = 1–3).[33] Dissolution of potassium thiocyanate in a solution of $Bu_4N[GaCl_4]$ in acetonitrile led to a mixture with the ^{71}Ga NMR spectrum shown in Fig. 5(a). Sharp peaks due to $[GaCl_4]^-$ at 247 ppm and $[GaCl_3(NCS)]^-$ at 220 ppm were accompanied by a broad peak at 185 ppm responsible for the remaining gallium. The position of the broad peak depends on the amount of thiocyanate present and this signal can be attributed to an exchange-averaged mixture of $[GaCl_2(NCS)_2]^-$ and $[GaCl(NCS)_3]^-$, the individual chemical shifts of which have been observed at 194 and 157 ppm, respectively.[34] Similar results were obtained by adding NCS^- to $[GaBr_4]^-$ in CH_3CN solution, Fig. 5(b). The $[GaBr_4]^-$ signal is at 61 ppm and a new sharp peak at 99 ppm is assigned to $[GaBr_3(NCS)]^-$. The remaining peak at *ca* 120 ppm is broad and appears to be the exchange-averaged signal of $[GaBr_2(NCS)_2]^-$, $[GaBr(NCS)_3]^-$ and perhaps $[Ga(NCS)_4]^-$. The present results enable thiocyanate to be placed between chloride and bromide in the order in which the ligands confer shielding of the gallium nucleus. The sequence of increased shielding, Cl < NCS < Br < I, is consistent with the "hard acid" character of the Ga^{3+} ion which bonds to the thiocyanate ligand through nitrogen rather than sulphur.

Acknowledgements—The author thanks Dr J. M. Coddington for the NMR measurements, and the New Zealand University Grants' Committee and Medical Research Council for equipment grants.

REFERENCES

1. M. J. Taylor, in *Comprehensive Coordination Chemistry* (Edited by G. Wilkinson, R. D. Gillard and J. A. McCleverty), Vol. 3, Chap. 25.1. Pergamon Press, Oxford (1987).
2. C. F. Baes Jr and R. E. Mesmer, *The Hydrolysis of Cations*. Wiley-Interscience, New York (1976).
3. L. G. Sillén and A. E. Martell, *Stability Constants of Metal Ion Complexes*. The Chemical Society, London. Special Publication No. 17 (1964); No. 25 (1971).
4. M. J. Taylor, *J. Chem. Soc. A* 1968, 1780.
5. C. L. Edwards and R. L. Hayes, *J. Nucl. Med.* 1969, 103.
6. J. D. Glickson, T. P. Pitner, J. Webb and R. A. Gams, *J. Am. Chem. Soc.* 1975, **97**, 1679.
7. R. E. Lenkinski, C. H. F. Chang and J. D. Glickson, *J. Am. Chem. Soc.* 1978, **100**, 5383.
8. W. O. Nelson, T. B. Karpishin, S. J. Rettig and C. Orvig, *Inorg. Chem.* 1988, **27**, 1045.
9. C. A. Evans, K.-H. Tan, S. P. Tapper and M. J. Taylor, *J. Chem. Soc., Dalton Trans.* 1973, 988.
10. B. R. McGarvey, M. J. Taylor and D. G. Tuck, *Inorg. Chem.* 1981, **20**, 2010.
11. D. Fiat and R. E. Connick, *J. Am. Chem. Soc.* 1968, **90**, 608.
12. T. J. Swift, O. G. Fritz Jr and T. A. Stephenson, *J. Chem. Phys.* 1967, **46**, 406.
13. A. Fratiello, R. E. Lee and R. E. Schuster, *Inorg. Chem.* 1970, **9**, 82.
14. P. L. Brown, *J. Chem. Soc., Dalton Trans.* 1989, 399.
15. J. W. Akitt and D. Kettle, *Magn. Reson. Chem.* 1989, **27**, 377.
16. J. W. Akitt, N. N. Greenwood and A. Storr, *J. Chem. Soc.* 1965, 4410.
17. J. Kodweiss, D. Köhnlein, G. Kössler, O. Lutz, W. Messner, K. R. Mohn, A. Nolle, G. Nothaft, P. Ruppert, N. Steinhauser, D. Zepf, E. Haid and W. Schich, *Z. Naturfor.* 1986, **41a**, 471.
18. C. H. F. Chang, T. P. Pitner, R. E. Lenkinski and J. D. Glickson, *J. Am. Chem. Soc.* 1977, **99**, 5858.
19. J. E. Gregor and H. K. J. Powell, *Aust. J. Chem.* 1986, **39**, 1851.
20. K. Schug and L. I. Katzin, *J. Phys. Chem.* 1962, **66**, 907.
21. S. F. Lincoln, *Aust. J. Chem.* 1972, **25**, 2705.
22. S. F. Lincoln, A. C. Sandercock and D. R. Stranks, *J. Chem. Soc., Dalton Trans.* 1975, 669.

23. R. Colton, D. Dakternieks and J. Hauenstein, *Aust. J. Chem.* 1981, **34**, 949.
24. J. Sandström, *Dynamic NMR Spectroscopy*. Academic Press, London (1982).
25. V. P. Tarasov, V. I. Privalov, G. A. Kirakosyan and Y. A. Buslaev, *Z. Naturfor.* 1983, **38b**, 1173.
26. R. J. H. Clark, B. Crociani and A. Wasserman, *J. Chem. Soc. A* 1970, 2458.
27. R. Ramachandran, C. T. G. Knight, R. J. Kirkpatrick and E. Oldfield, *J. Magn. Reson.* 1985, **65**, 136.
28. J. M. Coddington, R. F. Howe and M. J. Taylor, *Inorg. Chim. Acta*, in press.
29. J. Mason, *Multinuclear NMR*. Plenum Press, New York (1987).
30. S. P. Best, J. K. Beattie and R. S. Armstrong, *J. Chem. Soc., Dalton Trans.* 1984, 2611.
31. R. Rafaeloff and A. Silberstein-Hirsh, *Spectrochim. Acta* 1975, **31A**, 183.
32. A. N. Grigor'ev, A. I. Grigor'ev, F. M. Spridonov, L. M. Mikheeva and L. N. Komissarova, *Russ. J. Inorg. Chem.* (*Engl. Transl.*) 1977, **22**, 508.
33. F. W. Wehrli, *Annu. Rep. NMR Spectrosc.* 1979, **9**, 125.
34. V. P. Tarasov, S. P. Petrosyants, G. A. Kirakosyan and Y. A. Buslaev, *Koord. Khim.* 1980, **6**, 52.

Polyhedron Vol. 9, No. 2/3, pp. 215–222, 1990
Printed in Great Britain

0277–5387/90 $3.00+.00
© 1990 Pergamon Press plc

KINETIC STUDIES OF LIGAND SUBSTITUTION REACTIONS OF ALUMINIUM, GALLIUM AND INDIUM

KAZUO SAITO*

Graduate School, International Christian University, Osawa, Mitaka 181, Japan

and

AKIRA NAGASAWA

Chemistry Department, Faculty of Science, Tohoku University, Aoba, Sendai 980, Japan

Abstract—The mechanism of ligand substitution reactions of tervalent ion complexes of these main group elements has been mostly discussed on the basis of activation parameters, including volume of activation, but the experimental work has been almost limited to the reactions of unidentate ligands. We have undertaken kinetic studies of the ligand isotopic exchange of tris(β-diketonato) complexes by the isotope labelling method and compared the mechanism and rate of substitution with those in the literature. Mutual relationships among the activation parameters are also discussed.

Substitution reactions of these main group metal complexes have drawn rather limited attention of coordination chemists. Since Taube first advocated the idea of substitution lability and inertness in 1952,[1] the complexes of tervalent metal ions of aluminium, gallium and indium had been explicitly understood to be substitution labile until *ca* 1960. One of the present authors studied the exchange of ^{69}Ga and ^{114m}In between the tervalent aqua ions and their complexes with EDTA in aqueous solution.[2,3] The rates were immeasurably low at pH 2–8 and 2–10 for the Ga and In systems, respectively. They exhibited different dependencies upon H^+ and OH^- concentration in the pH regions below 2 and above 8 or 10, respectively, but were always independent of the concentration of the aqua ions. Their complexes with the related multidentate ligand *N*-2-hydroxyethylethylene-diamine-*N*,*N*′,*N*′-triacetate gave essentially similar results.[2,4] We considered, rather simply, that the rate was governed by the ease with which the metal–ligand bond was broken. [$\Delta H^{\ddagger}$(kJ mol^{-1}), 92 and 104 at pH 1.5 and 63 and 75 at pH 8 and 10 for the Ga and In complexes, respectively].

Since then, a considerable amount of work was performed on the substitution reactions of the complexes of tervalent Al, Ga and In. The systems studied in aqueous solutions include the replacement of the aqua ligand, not only by a simple unidentate ligand such as sulphate (with Al[5,6]), but also by bi- and multidentate chelating agents such as salicylate (with Al[7] and Ga[8]), its derivatives (Al,[9] Ga[10]), citrate (Al[11]), aromatic dyes used as metal indicators in analytical chemistry (Al,[12–15] Ga[16] and In[17,18]) and tropolone[19] and its 3-isopropyl derivative.[20] There has been a good deal of discussion about the comparison of lability among the three metal ions and the mechanism of substitution. Most dispute has been based on the activation enthalpies and entropies, and on the dependence of the rate-constant upon the concentration of incoming ligands.

Through these studies, it was made clear that there is an overall trend towards greater rates in the order Al, Ga and In. It was also found that the hydrolysed species, $[M(OH)(H_2O)_5]^{2+}$, undergo anation reaction faster than the aqua ions, $[M(H_2O)_6]^{3+}$, by more than two orders of magnitude, and the reason is attributed to the mutual

* Author to whom correspondence should be addressed.

Abbreviations: acac, enolate anion of acetylacetone; bzbz, enolate anion of dibenzoylmethane; hfac, enolate anion of hexafluoroacetylacetone; tfac, enolate anion of trifluoroacetylacetone; Htrp, tropolone; Hipt, 3-isopropyltropolone; DMF, dimethylformamide; DMSO, dimethylsulphoxide; THF, tetrahydrofuran; TMP, trimethylphosphate; dmf, dmso, thf, and tmp represent the ligand.

ligand interaction due to the OH^- ligand (Al,[21] Ga[22]).

The substitution lability and the reaction mechanism of the metal complexes as an intrinsic property of the metal ion are best discussed on the basis of the results of ligand isotopic exchange reactions, because such reactions involve no net change of the existing species in the reaction system. Since Fiat and Connick gave the result of their pioneering experiment in the 1960's,[23] a significant amount of work has been performed on the kinetics of exchange between solvated molecules and bulk solvent, mostly by the NMR relaxation method. The results are summerized in Table 1.

The usefulness of activation volume in discussing the mechanism of substitution reactions was nicely demonstrated in recent review with a huge accumulation of experimental data.[29,30] It seems most promising to make use of the $\Delta V^{\ddagger}$ data for ligand isotopic exchange reactions for clarifying the mechanism of substitution. Merbach and his co-workers successfully applied such a consideration to the solvated tervalent ions of Al, Ga and In.[21,22,25-28] These studies, however, are limited to unidentate ligands. The only available $\Delta V^{\ddagger}$ data involving bidentate ligands are those for the anation of tropolone upon hexaaqua,[19] and of 3-isopropyltropolone upon hexakis (dmso) complexes of Al and Ga.[20] Since the rate-determining step of these anation reactions is claimed to be the formation of the first M—O (tropolone) bond, these systems may be included in the anation of unidentate ligands.

KINETIC STUDIES OF LIGAND ISOTOPIC EXCHANGE OF TRIS(ACETYLACETONATO) COMPLEXES

We have been undertaking kinetic studies of the isotopic exchange of a variety of tris(acetylacetonato) complexes of tervalent metal ions by the use of acetylacetone [^{14}C] in organic solvents, including neat acetylacetone (Hacac).[31] This method is useful only for slow reactions, and the available data are limited because of the experimental difficulty. Complexes with chelating ligands, however, often exhibit a different rate and mechanism of substitution from those of the complexes with unidentate ligands. Hence, such work must complement the other studies mentioned above, particularly when the data of activation volume are available. On the basis of such results we proposed a universal empirical parameter "metal ion lability constant" which indicates the lability of tervalent metal ions, including Al, Ga and In.[32]

Our data, which is related to Al, Ga and In, are listed in Table 2. Tris(bidentate) type complexes often undergo fluxional site exchange and the rate has been estimated by the observation of the NMR signals of ^1H or ^{19}F at various temperatures. These data are summarized in Table 3.

Mechanism of substitution

Related reactions. When Fiat and Connick gave the enthalpies and entropies of activation for the exchange of coordinated water molecules in aqueous solution,[23] a dissociative and an associative mechanism were envisaged for Al^{3+} and Ga^{3+} complexes, respectively. Recent data of the volume of activation suggest a dissociative nature for the substitution mechanism of both ions. New data for the entropy of activation were added to the exchange of water[21,22] and there now seems to be a rather unanimous understanding that the complexes of both tervalent ions undergo ligand exchange through a dissociative (D) or a dissociative interchange (I_d) mechanism. Discrimination between D and I_d is discussed on a stereochemical basis; the greater the ionic radius of the central metal ion and the less bulky the ligand, the greater the extent to which the incoming ligand participates in the formation of the transition state. It is claimed that such a trend is reflected in the decrease of entropy of activation.

The data in Table 3 are understood to indicate that the fluxional site exchange takes place through an intra-molecular mechanism. The activation parameters are thought to reflect the ease with which one M—O bond is broken to give a reaction intermediate, which undergoes fluxional rearrangement to result in isomerization or racemization. Although not explicitly discussed, a modestly positive entropy of activation is in accord with the discussion given above, that the dissociative break of the M—O bond should be the rate-determining step. (The big positive $\Delta S^{\ddagger}$ for the racemization of $[Al(acac)_3]$ in mixed pentane–ethanol or –diethyl ether are unusual.[39] A recent study on the resolution and racemization in methanol gave no $\Delta S^{\ddagger}$ value.[44])

Ligand exchange of acetylacetonate. The process of this ligand exchange was discussed elsewhere[32] and is given here only briefly (Fig. 1). The observed first-order rate constant k_0 is proportional to the concentration of water (<0.15 mol kg^{-1}) and is expressed by eq. (1):

$$\text{Rate} = k_0[Al(acac)_3] = [Al(acac)_3](k_1 + k_2[H_2O]). \quad (1)$$

For the exchange to take place, proton transfer between $acac^-$ and Hacac is essential and most

Table 1. Activation parameters of ligand exchange reactions of tervalent metal complexes with unidentate ligands

No.	Compound	Reagent	Solvent	k^{298}[a] (s^{-1})	$\Delta H^{\ddagger}$ (kJ mol^{-1})	$\Delta S^{\ddagger}$ (J mol^{-1} K^{-1})	$\Delta V^{\ddagger}$ (cm^3 mol^{-1})	Mechanism	Reference
1	$Al(H_2O)_6^{3+}$	H_2O	H_2O	31	—	—	—	—	24
2	$Al(H_2O)_6^{3+}$	H_2O	H_2O	0.13	113	+117	—	*D*	23
3	$Al(H_2O)_6^{3+}$	H_2O	H_2O	1.29	85	+42	+5.7	*D, I*	21
4	$Al(dmso)_6^{3+}$	dmso	CD_3NO_2	0.30	83	+22	+15.6	*D*	25
5	$Al(dmf)_6^{3+}$	dmf	CD_3NO_2	0.05	88	+28	+13.6	*D*	25
6	$Al(tmp)_6^{3+}$	tmp	CD_3NO_2	0.78	85	+38	+22.5	*D*	26
7	$Al(dmso)_6^{3+}$	Hipt[b]	DMSO	0.22 M^{-1}	82	+19	+12.2	*D*	20
8	$Ga(H_2O)_6^{3+}$	H_2O	H_2O	1800	26	−92	—	*A*	23
9	$Ga(H_2O)_6^{3+}$	H_2O	H_2O	400	67	+30	+5.0	*I*	22
10	$Ga(OH)(H_2O)_5^{2+}$	H_2O	H_2O	14 M^{-1}	111	+150	+7.7	*I*	22
11	$Ga(dmso)_6^{3+}$	dmso	CD_3NO_2	1.87	73	+3.5	+13.1	*I, D*	25
12	$Ga(dmf)_6^{3+}$	dmf	DMF	1.7	61	−34	—	*A*	27
13	$Ga(dmf)_6^{3+}$	dmf	CD_3NO_2	1.72	85	+45	+7.9	*D*	25
14	$Ga(tmp)_6^{3+}$	tmp	CD_3NO_2	6.4	77	+27	+20.9	*D*	26
15	$Ga(dmso)_6^{3+}$	Hipt[b]	DMSO	37 M^{-1}	74	+34	+10.6	*D*	20
16	$Ga(H_2O)_6^{3+}$	Htrp[b]	H_2O	38 M^{-1}	61	−12	+4.0	*I*	19
17	$Ga(OH)(H_2O)_5^{2+}$	Htrp[b]	H_2O	8200 M^{-1}	29	−74	+2.4	*I*	19
18	$In(H_2O)_6^{3+}$	H_2O	H_2O	4×10^4	(19)	—	—	—	28
19	$In(tmp)_6^{3+}$	tmp	CD_3NO_2	7.6 M^{-1}	33	−118	−21.4	*I*	26
20	$In(dmso)_6^{3+}$	Hipt[b]	DMSO	1.9×10^4	37	−40	−0.1	*I*	20
21	$In(dmf)_6^{3+}$	Hipt[b]	DMF	3.5×10^5	36	−18	+0.3	*I*	20
22	$Sc(tmp)_6^{3+}$	tmp	CD_3NO_2	39 M^{-1}	21	−143	−18.7	*A, I*	26
23	$Sc(tmp)_6^{3+}$	tmp	TMP	736	34	−76	−23.8	*A, I*	26

[a] M^{-1} unit represents second-order rate constants.

[b] For the anation of tropolone and its derivative, formation of the first M—O bond is rate-determining.

Table 2. Kinetic data of ligand isotopic exchange of tris(β-dikctonato) complexes of aluminium, gallium and indium

No.	Compound	Solvent	k^{298}[a] (s^{-1})	$\Delta H^{\ddagger}$ (kJ mol^{-1})	$\Delta S^{\ddagger}$ (J mol^{-1} K^{-1})	$\Delta V^{\ddagger}$ (cm^3 mol^{-1})	Reference
1	$Al(acac)_3$	Hacac	9.1×10^{-5}	85	−38	+10	33
2	$Al(acac)_3$	Hacac	k_2 1.4×10^{-3} M^{-1}	79	−34	+5	33
3	$Al(acac)_3$	toluene	~0	—	—	—	34
4	$Al(acac)_3$	toluene	k_2 2.7×10^{-4} M^{-1}	80	−16	—	34
5	$Al(acac)_3$	$CH_3COOC_2H_5$	1.07×10^{-6}	90[e]	−51	—	34
6	$Al(acac)_3$	$CH_3COOC_2H_5$	k_2 4.6×10^{-4} M^{-1}			—	34
7	$Al(acac)_3$	THF	1×10^{-6}	89[e]	−33	—	35
8	$Al(acac)_3$	THF	k_2 3.3×10^{-4} M^{-1}			—	35
9	$Al(bzbz)_3$[b]	THF	1×10^{-8}[d]	108[e]	−7	—	36
10	$Al(bzbz)_3$	THF	k_2 3.2×10^{-5} M^{-1}			—	36
11	$Ga(acac)_3$[b]	THF	$\leqslant4\times10^{-6}$	79[e]	−55	—	37
12	$Ga(acac)_3$	THF	k_2 4.2×10^{-3} M^{-1}				37
13	$Ga(acac)_3$	Hacac	1.6×10^{-3}	67	−71	—	38
14	$In(acac)_3$[c]	Hacac	~2	47	−84	—	38
15	$Sc(acac)_3$[c]	Hacac	60	36	−88	—	[f]

[a] k_2, second-order rate constant for the water assisted path. $k_0 = k_1 + k_2[H_2O]$.

[b] Observed first-order rate constant increases with the increase in Hacac concentration in THF.

[c] By NMR relaxation method; [In] = 0.001–0.1 M, [Hacac] = 0.1–2 M, [Sc] = 0.5 M. The rate was measured in acetonitrile containing Hacac and extrapolated to neat Hacac concentration (9.4 M).

[d] At 273°C.

[e] The activation parameters were measured for k_0. Since the contribution of k_1 is very small they are thought to be those for the k_2 value.

[f] Y. Hatakeyama, H. Kido, M. Harada, H. Tomiyasu and H. Fukutomi, *Inorg. Chem.* 1986, **27**, 992.

Table 3. Kinetic data of fluxional site-exchange of tris(β-diketinato) complexes of aluminium, gallium and indium

No.	Compound	Solvent	T (°C)	k_1 (s^{-1})	$\Delta H^{\ddagger}$ (kJ mol^{-1})	$\Delta S^{\ddagger}$ (J mol^{-1} K^{-1})	Method[a]	Reference
1	$Al(acac)_3$	C_2H_5OH–C_5H_{12}	—	—	134	+227	CD	39
2	$Al(acac)_3$	$(C_2H_5)_2O$–C_5H_{12}	−1	1.9×10^{-4}	128	+211	CD	39
3	$Al(acac)_3$	CH_3OH	10	0.007	(92)[b]	—	CD	44
4	$Al(tfac)_3$	$CDCl_3$	103	34	(99)[b]	—	^{19}F	40
5	$Al(tfac)_3$	$CDCl_3$	84.5	0.65	114	+68	^{1}H	41
6	$Al(acac)_2(hfac)$	CH_2Cl_2	25	8.0	(77)[b]	+42	^{1}H	42
7	$Al(acac)_2(bzbz)$	o-$C_6H_4Cl_2$	25	0.0022[c]	(92)[b]	+3.7	^{1}H	42
8	$Al(acac)(hfac)_2$	C_6H_6	25	0.84[c]	(80)[b]	+12	^{19}F	42
9	$Al(acac)(hfac)_2$	CH_2Cl_2	25	0.86[c]	(90)[b]	+45	^{19}F	42
10	$Al(acac)(hfac)_2$	$C_6H_5NO_2$	25	1.5[c]	(82)[b]	+24	^{19}F	42
11	$Ga(tfac)_3$	$CDCl_3$	61.5	38	(87)[b]	—	^{19}F	40
12	$Ga(tfac)_3$	$CDCl_3$	44.7	0.98	91	+41	^{1}H	41
13	$Ga(acac)_2(hfac)$	CH_2Cl_2	25	770[c]	(64)[b]	+16	^{19}F	42
14	$Ga(acac)_2(hfac)$	CH_2Cl_2	25	980	61	+7	^{19}F	43
15	$Ga(acac)_2(bzbz)$	C_6H_6	25	0.077[c]	(85)[b]	+9	^{1}H	42
16	$Ga(acac)_2(bzbz)$	C_6H_6	25	0.088	87	+14	^{1}H	43
17	$In(tfac)_3$	$CDCl_3$	< −57	> 36	(< 57)[b]	—	^{19}F	40

[a] CD = circular dichroism, ^{1}H, ^{19}F NMR relaxation with these nuclei.

[b] Values in parentheses, Arrhenius activation energy.

[c] Extrapolated values.

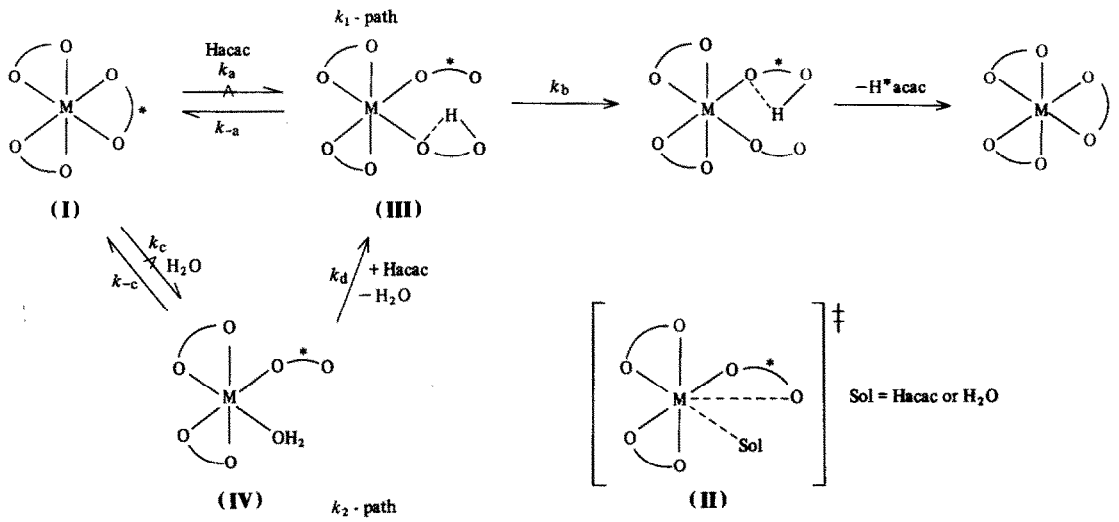

Fig. 1. Plausible mechanism of the ligand exchange of [Al(acac)$_3$] (**I**) in acetylacetone (Hacac). Asterisks denote the ^{14}C-labelling and arrows with circumflexes show the rate-determining step.

likely proceeds on the intermediate, **III**, which has two bidentate, one unidentate acac$^-$ and one unidentate Hacac as ligands. A very small deuterium isotope effect ($k_H:k_D$ ratio, 1.6 and 1.5 for the k_1 and k_2 paths, respectively) excludes the possibility of rate-determining proton transfer. Hence, the k_1 is related to the rate of individual reaction steps (Fig. 1) by eq. (2):

$$k_1 = k_a k_b/(k_{-a}+k_b), \qquad (2)$$

where $k_b/(k_{-a}+k_b)$ represents the branching ratio at the intermediate **III**. We have considered that the formation of **III** from the original complex **I** is the rate-determining step, and have illustrated the structure of a plausible transition state, **II**, in Fig. 1. The water-assisted path may be interpreted by considering a route through **IV** (Fig. 1), i.e. the breaking of the Al—O bond is facilitated by the water molecule to give **IV**, which quickly reacts with Hacac to give **III**.

A characteristic feature of our experimental results is that the entropy of the activation values is always negative throughout the systems for Al, Ga and In. We have discussed that the rate-determining step in the spontaneous path is the first breaking of the Al—O bond to give intermediate **III**.[31] Since the $\Delta V^\ddagger$ values for the spontaneous and water-assisted exchange of acetylacetonate in neat Hacac are moderately positive, we consider that the breaking of the Al—O bond takes place through a dissociative mechanism, most likely to be the I_d mechanism.[33] Although $\Delta V^\ddagger$ values are not available for the experiments in other solvents, absence of the dependence of the rate upon the Hacac concentration supports the dissociative nature of the ligand exchange.

The large differences between our $\Delta S^\ddagger$ values (Table 2) and those in the literature (Table 1) should be interpreted by considering the different nature of the ligands. One of the reasons for a negative $\Delta S^\ddagger$ should be due to the I_d (not D) nature of the mechanism. Since Hacac (and naturally acac$^-$, too) is a bulky ligand, an I_d-like mechanism is feasible, as discussed, for the substitution of unidentate ligands. There should be, however, an additional contribution based on the nature of our particular reaction.

An I_d mechanism suggests the approach of free Hacac to the central metal ion during the rate-determining step. Such access is not only motivated by the electrostatic interaction between Al^{3+} and incoming Hacac, but also by the stacking between incoming Hacac and coordinated acac$^-$. After the breaking of one Al—O bond, that particular acac$^-$ ligand does not become entirely free, but is linked to the Al^{3+} ion through the other Al–O bond. This is the reason why the backward reaction (rate constant, k_{-a}, cf. Fig. 1) takes place, and the branching ratio of eq. (2) contributes to the overall reaction rate. Both forward and backward reactions between **I** and **III** have a common transition state and a decrease in the branching ratio does not change the $\Delta H^\ddagger$ value but only decreases the $\Delta S^\ddagger$ value. (These interactions are not involved in the reactions in Tables 1 and 3.) Quantitative assessment of such contributions is difficult but the magnitude should be big enough to make the $\Delta S^\ddagger$ values negative.

Comparison of the rates

We have found a linear relationship on the log–log scale between the first-order rate constants of the ligand exchange of tris(acetylacetonato) complexes in Hacac and those of the water exchange of hexaaqua complexes of 12 kinds of tervalent main group and transition metal ion. (When such data were missing, first-order rate-constants of relevant reactions were used in their places.)[32] This fact implies that each ion has its own characteristic lability and each ligand exchange reaction has its own characteristic velocity. Thus first-order rate-constants of a given ligand exchange reaction can be expressed by eq. (3),

$$\log(k_1/s^{-1}) = \sigma + \kappa, \qquad (3)$$

where σ and κ are empirical parameters representing the individual lability of the metal ion and the individuality of the given ligand exchange, respectively. Ligand exchange reactions have their own enthalpies of activation and hence, different temperature coefficients of the rate from one another. Therefore, comparison of the rate constants at one temperature gives only approximate values of σ, which may be expressed by the integer or half integer.

By setting the κ value of water exchange of aqua complexes in water to zero, σ values of tervalent metal ions were estimated on the linear log–log diagram involving 12 tervalent metal ions by the method of least squares. Thus, tervalent ions of Al, Ga and In are given σ values 0.5, 2 and 5, respectively. (The same diagram gave κ values of -4.5 and -1 for the exchange of $acac^-$ in Hacac and of dmf in dimethylformamide, respectively.) These σ values may represent the relative lability of tervalent ions of these three main group elements.

Acknowledgements—The authors thank the Editor, Professor A. R. Barron, for inviting us to join this interesting Symposium-in-Print. They are also indebted to our collaborators who have participated in the laborious kinetic studies by the isotope labelling method, whose names are in the references.

REFERENCES

1. H. Taube, *Chem. Rev.* 1952, **50**, 69.
2. K. Saito and M. Tsuchimoto, *J. Inorg. Nucl. Chem.* 1961, **23**, 71.
3. K. Saito and M. Tsuchimoto, *J. Inorg. Nucl. Chem.* 1963, **25**, 1245.
4. K. Saito and M. Tsuchimoto, *Bull. Chem. Soc. Japan* 1962, **35**, 367; 1963, **36**, 1073.
5. H. Strehlow and G. Busse, *Ber. Bunsen-Ges. Phys. Chem.* 1984, **88**, 467.
6. A. Walsleben and H. Strehlow, *J. Sol. Chem.* 1985, **14**, 881.
7. F. Secco and M. Verturini, *Inorg. Chem.* 1978, **14**, 1975.
8. R. B. Jordan, *Inorg. Chem.* 1983, **22**, 4160.
9. B. Perlmutter-Hayman and E. Tapuhi, *Inorg. Chem.* 1979, **18**, 875.
10. R. Corligi, F. Secco and M. Verturini, *Inorg. Chem.* 1982, **21**, 2992.
11. M. A. Lopez-Quintela, W. Knoche and J. Veith, *J. Chem. Soc., Faraday Trans. I* 1984, **80**, 2313.
12. K. Hayashi, K. Okamoto, J. Hidaka and H. Einaga, *J. Chem. Soc., Dalton Trans.* 1982, 1377.
13. S. Schoenherr, R. Bertram and H. Goerz, *Z. Anorg. Allg. Chem.* 1983, **503**, 193.
14. R. Caminiti, A. Lai, G. Saba and G. Crisponi, *Chem. Phys. Lett.* 1983, **97**, 180.
15. I. Ohkura, K. Fujiwara, K. Okamoto, J. Hidaka and H. Einaga, *J. Coord. Chem.* 1984, **13**, 221.
16. A. L. Shvarz, L. S. Molochnikov, T. M. Ivanova, G. N. Zviadadze, B. K. Radionov and B. E. Dzevitskii, *Zh. Fiz.-Khim.* 1983, **57**, 2292.
17. B. Perlmutter-Hayman, F. Secco and M. Venturini, *Inorg. Chem.* 1985, **24**, 3828.
18. E. Montasti, C. Baiocchi and L. J. Kirschenbaum, *J. Chem. Soc., Dalton Trans.* 1985, 2615.
19. S. Yamada, A. Iwanaga, S. Funahashi and M. Tanaka, *Inorg. Chem.* 1984, **23**, 3528.
20. K. Ishihara, S. Funahashi and M. Tanaka, *Inorg. Chem.* 1986, **25**, 2898.
21. D. Hugi-Cleary, L. Helm and A. E. Merbach, *Helv. Chim. Acta* 1985, **68**, 545.
22. D. Hugi-Cleary, L. Helm and A. E. Merbach, *J. Am. Chem. Soc.* 1987, **109**, 4444.
23. D. Fiat and R. E. Connick, *J. Am. Chem. Soc.* 1968, **90**, 608.
24. H. W. Baldwin and H. Taube, *J. Chem. Phys.* 1960, **33**, 206.
25. C. Ammann, P. Moore, A. E. Merbach and C. H. McAteer, *Helv. Chim. Acta* 1980, **63**, 268.
26. A. E. Merbach, *Pure Appl. Chem.* 1982, **54**, 1479.
27. W. G. Mobius and N. A. Matowiyoff, *Inorg. Chem.* 1969, **8**, 725.
28. G. E. Glass, W. E. Schwabacher and R. S. Tobias, *Inorg. Chem.* 1968, **7**, 2471.
29. T. Asano and W. J. le Noble, *Chem. Rev.* 1978, **78**, 457.
30. R. van Eldik, T. Asano and W. J. le Noble, *Chem. Rev.* 1989, **89**, 549.
31. K. Saito, H. Kido and A. Nagasawa, *Coord. Chem. Rev.* 1990, **100**, in press.
32. H. Kido and K. Saito, *J. Am. Chem. Soc.* 1988, **110**, 3187.
33. A. Nagasawa, H. Kido, T. M. Hattori and K. Saito, *Inorg. Chem.* 1986, **25**, 4330.
34. K. Saito and K. Masuda, *Bull. Chem. Soc. Japan* 1970, **43**, 119.
35. K. Saito and K. Masuda, *Bull. Chem. Soc. Japan* 1968, **41**, 384.

36. K. Matsuzawa and K. Saito, *Bull. Chem. Soc. Japan* 1973, **46**, 2777.
37. C. Chatterjee, K. Matsuzawa, H. Kido and K. Saito, *Bull. Chem. Soc. Japan* 1974, **47**, 2809.
38. H. Kido and Y. Hatakeyama, Unpublished.
39. B. Nordén and I. Jonaš, *Inorg. Nucl. Chem. Lett.* 1976, **12**, 33.
40. R. C. Fay and T. S. Piper, *Inorg. Chem.* 1964, **3**, 348.
41. D. L. Grossmann and D. T. Haworth, *Inorg. Chim. Acta* 1984, **84**, L17.
42. D. A. Case and T. J. Pinnavaia, *Inorg. Chem.* 1971, **10**, 482.
43. T. J. Pinnavaia, J. M. Sebeson and D. A. Case, *Inorg. Chem.* 1969, **8**, 644.
44. Y. Okamoto, E. Yashima and K. Hatada, *J. Chem. Soc., Chem. Commun.* 1984, 1051.

Polyhedron Vol. 9, No. 2/3, pp. 223–226, 1990
Printed in Great Britain

0277–5387/90 $3.00+.00
© 1990 Pergamon Press plc

A NEW PREPARATIVE METHOD FOR VARIOUS METAL ENOLATES

KEIJI MARUOKA, NAOKI HIRAYAMA and HISASHI YAMAMOTO*

Department of Applied Chemistry, Nagoya University, Chikusa, Nagoya 464-01, Japan

Abstract—A variety of metal enolates including magnesium, boron, aluminium, zinc and gallium have been prepared from α-iodo carbonyl compounds and organometallic reagents under mild conditions. The metal enolates thus obtained have been utilized for the stereoselective aldol reaction with aldehydes with the object of elucidating the influence of metal and solvent effects on the erythro/threo selectivity.

Metal enolates are undoubtedly one of the most valuable intermediates in organic synthesis and a number of preparative methods have been developed for generating a variety of metal enolates.[1] Lithium enolates are most commonly employable and produced from carbonyl compounds with lithium dialkylamides or from enol silyl ethers with methyllithium in ethereal solvents.[2] Boron enolates, which are indispensable in aldol chemistry, are obtained from carbonyl compounds and dialkylboron triflates in the presence of tertiary amines.[3] Other metal enolates such as magnesium, zinc, titanium, zirconium, etc., were conveniently prepared from the corresponding lithium enolates by ligand exchange with metal halides.[4] In most methodologies, the metal enolates suffer from the co-existence of side-products such as amines, ammonium salts and inorganic metal salts that might influence the reactivity and selectivity in the subsequent reaction with electrophiles.[1] Here we wish to disclose a new method for preparing various metal enolates which involves the reaction of α-iodo carbonyl compounds with organometallic reagents as illustrated in Scheme 1.[5–7] In this methodology, the only side-product is alkyl iodide that, if necessary, can be readily removed from the reaction system by simple vacuum evaporation.[8]

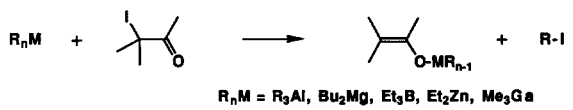

Scheme 1.

When *trans*-4-*tert*-butyl-2-iodocyclohexanone[9] in CH_2Cl_2 was treated with Me_3Al (1.2 equiv.) in hexane, at −40°C for 1.5 h and at −20°C for 1.5 h, 4-*tert*-butylcyclohexanone was obtained in 69% yield after acidic work-up. Other organometallic reagents such as Bu_2Mg, Et_3B, R_3Al (R = Et, *i*-Bu), Et_2Zn and Me_3Ga are equally effective for dehalogenation of α-iodo ketones (Table 1). However, α-bromo ketones were totally recovered under similar conditions to those described above. As revealed in Table 1, the α-iodo ester is also susceptible towards dehalogenation. It should be noted that α-iodo carbonyl substrates such as α-iodoacetophenone are not employable due to the facile self-condensation resulting predominantly in formation of the aldol adduct, 1,3-diphenyl-3-hydroxy-4-iodo-1-propanone. This finding suggests the *in situ* generation of the metal enolate and alkyl halide as depicted in Scheme 1, and hence prompted us to investigate the stereoselective aldol reaction of these metal enolates with aldehydes with the object of elucidating the influence of metal and solvent effects on the erythro/threo selectivity. The selected data are listed in Table 2 where a direct comparison can be made for the influence of the metal on the degree of diastereoselection. For a given metal little enhancement in stereoselectivity was observed on changing the polarity of the solvent from toluene to THF (entries 2–4 and 7–9). In contrast, in a given solvent there appears to be a large metal effect (entries 3, 6, 10 and 11). It is apparent that the boron enolates are superior to the corresponding aluminium, zinc and gallium enolates in stereoselective bond construction. This tendency is even more clear with isobutyraldehyde as an electrophile except for the case of zinc enolates (entries 12–15).

In a similar fashion, the aldol condensation of ester enolate with aldehyde appears to be feasible.

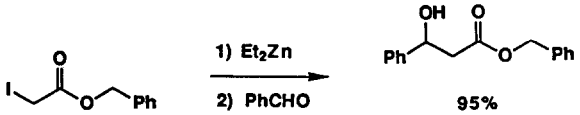

* Author to whom correspondence should be addressed.

Table 1. Dehalogenation of α-iodo carbonyl compounds[a]

Entry	Substrate	Reagent[b] (equiv.)	Conditions (°C, h)	Per cent yield[c]
1	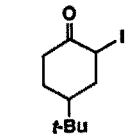	Me_3Al (1.2)	−40, 1.5; −20, 1.5	69
2		Et_3Al (1.2)	−78, 0.5; −40, 0.5	65
3		*i*-Bu_3Al (1.2)	−78, 1	57
4		Et_3B (1.2)	−78, 1.3	70
5		Bu_2Mg (1.2)	−78, 0.5	66
6		Et_2Zn (2)	−78, 0.3	63
7		Me_3Ga (2)	25, 1	53
8	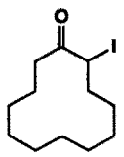	Me_3Al (1.2)	0, 0.5	90
9		Et_3B (1.2)	−78, 2; −40, 0.3	72
10		Et_2Zn (2)	−78, 0.3	95
11	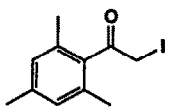	Me_3Al (1.2)	−20, 0.5	88
12		Et_2Zn (2)	−78, 0.8	95
	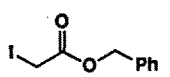	Et_2Zn (2)	−78, 0.25	94

[a] The reaction was carried out in CH_2Cl_2 and quenched with dil. HCl.
[b] Used as a hexane solution.
[c] Isolated yield.

Table 2. Aldol reaction of various metal enolates[a]

Entry	Reagent (equiv.)	Solvent	Conditions[b] (°C, h)	Per cent yield[c] (ratio)
	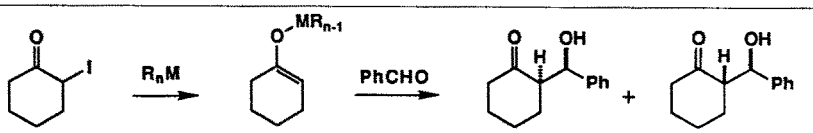			
1	Me_3Al (1.2)	CH_2Cl_2	−78, 2	43 (3:2)
2	Me_3Al (2)	Toluene	−78, 0.5	57 (3:2)
3	Me_3Al (2)	CH_2Cl_2	−78, 2	57 (3:2)
4	Me_3Al (2)	CH_2Cl_2–ether	−20, 1	59 (3:2)
5	Et_3Al (2)	CH_2Cl_2	−78, 2	50 (3:2)
6	Et_3B (1.2)	CH_2Cl_2	−78, 2	57 (1:3)
7	Et_3B (2)	CH_2Cl_2	−78, 2	82 (1:3)
8	Et_3B (2)	CH_2Cl_2–ether	−20, 4; 0, 0.7	89 (1:4)
9	Et_3B (2)	CH_2Cl_2–THF	−40, 3	81 (1:4)
10	Et_2Zn (2)	CH_2Cl_2	−78, 2	51 (1:1.7)
11	Me_3Ga (2)	CH_2Cl_2	−40, 1	52 (1:1)
	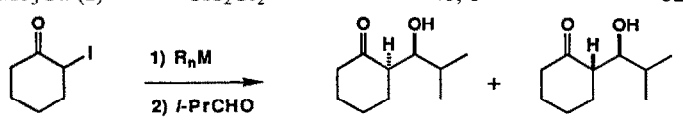			
12	Me_3Al (2)	CH_2Cl_2	−78, 0.7	57 (1:2)
13	Me_3Al (2)	CH_2Cl_2–ether	−20, 0.5	51 (1:4)
14	Et_3B (2)	CH_2Cl_2	−78, 2	59 (1:24)
15	Et_2Zn (2)	CH_2Cl_2	−78, 2	52 (1:24)

[a] The metal enolates were prepared under the same conditions as described in Table 1 and treated with 2 equiv. of aldehyde.
[b] Isolated yield.
[c] The erythro/threo ratio was determined by ^1H NMR analysis.

EXPERIMENTAL

General

IR spectra were recorded on a Hitachi 260-10 spectrometer. ^{1}H NMR spectra were measured on a Varian GEMINI-200 (200 MHz) spectrometer. Reactions involving air- or moisture-sensitive compounds were conducted in appropriate round-bottomed flasks with magnetic stirring bars under an atmosphere of dry argon. In experiments requiring dry solvents, ether and THF were freshly distilled from sodium metal using benzophenone ketyl as indicator. Hexane and toluene were dried over sodium metal. Methylene chloride was stored over 4-Å molecular sieves. Organometallic reagents such as R_3Al (R = Me, Et and *i*-Bu), Et_3B, Bu_2Mg, Et_2Zn and Me_3Ga were obtained from Toyo Stauffer Chemical Company Ltd, Japan.

Preparation of α-iodo carbonyl compounds

trans-4-*tert*-Butyl-2-iodocyclohexanone,[8] 2-iodocyclododecanone, 2-iodo-2′,4′,6′-trimethylacetophenone and 2-iodocyclohexanone[7] were synthesized from the corresponding ketones by sequential treatment with lithium diisopropylamide, trimethylsilyl chloride and N-iodosuccinimide in THF. Benzyl iodoacetate was prepared by reaction of bromoacetyl bromide and benzyl alcohol with triethylamine in CH_2Cl_2 and subsequent halogen exchange with sodium iodide in acetone.

Dehalogenation of α-iodo carbonyl compounds

A representative reaction is as follows. A 2 M hexane solution of Me_3Al (0.6 mmol) was added, at −78°C, to a solution of *trans*-4-*tert*-butyl-2-iodocyclohexanone (0.5 mmol) in CH_2Cl_2 (2 cm^3) and the resulting mixture was stirred at −40°C for 1.5 h and at −20°C for 1.5 h. The mixture was poured into 1 N HCl and extracted with CH_2Cl_2. The combined CH_2Cl_2 extracts were concentrated and purified by column chromatography on silica gel (ether–hexane as eluant) to furnish 4-*tert*-butylcyclohexanone in 69% yield.

Other dehalogenation experiments were carried out in a similar manner to describe the above and the results are listed in Table 1.

Aldol reaction of 2-iodocyclohexanone with aldehydes

A typical procedure is provided by the synthesis of 2-(α-hydroxybenzyl)cyclohexanone with Me_3Al (entry 3). The dimethylaluminium enolate of cyclohexanone (0.5 mmol) in CH_2Cl_2 (2 cm^3) was prepared as described above. To this solution was added, at −78°C, benzaldehyde (1 mmol). The resulting solution was stirred at −78°C for 2 h and poured into 1 N HCl. The crude product was extracted with CH_2Cl_2, concentrated and purified by column chromatography on silica gel to furnish an erythro/threo mixture of 2-(α-hydroxybenzyl)cyclohexanone in 57% yield. The ^{1}H NMR spectrum of the aldol products showed the ratio of the erythro and threo isomers to be 3 : 2. This analysis was based on an absorption due to the benzylic proton peaks at δ4.73 and 5.30. Column chromatography on silica gel (ether–hexane = 1 : 4) separated two isomers. The first fraction was the erythro isomer: IR (CCl_4): 3570 cm^{-1} (OH), 1700 cm^{-1} (C=O); ^{1}H NMR ($CDCl_3$): δ7.20–7.40 (5H, m, aryl CH), 5.41 (1H, broad t, CH—O), 3.05 (1H, d, J = 3.2 Hz, OH), 2.27–2.67 (3H, m, CH_2C=O and CHC=O), 1.38–2.18 (6H, m, CH_2); mass m/z(%): 77 (100), 186 (2.5, $M^+ - 18$); m.p. 103–105°C (recrystallized from hexane–ethyl acetate; ref. 10 m.p. 103.5–104.5°C). From the second fraction the threo isomer was obtained: IR (CCl_4): 3570 cm^{-1} (OH), 1690 cm^{-1} (C=O); ^{1}H NMR ($CDCl_3$): δ7.25–7.43 (5H, m, aryl CH), 4.80 (1H, d, J = 9.0 Hz, CH—O), 3.99 (1H, s, OH), 2.28–2.70 (3H, m, CH_2C=O and CHC=O), 1.18–1.83 (6H, m, CH_2); mass m/z(%): 77 (100), 186 (3.5, $M^+ - 18$); m.p. 75.5–77.5°C (recrystallized from hexane; ref. 10 m.p. 75°C).

Similarly, the erythro/threo ratio of 2-(1-hydroxy-2-methylpropyl)cyclohexanone was determined by ^{1}H NMR analysis based on an absorption due to the hydroxy methyne proton peaks at δ3.74 and 3.56.

REFERENCES

1. (a) H. O. House, *Modern Synthetic Reactions*, 2nd edn. W. A. Benjamin, Menlo Park (1972); (b) J. K. Rasmussen, *Synthesis* 1977, 91; (c) T. Mukaiyama, *Pure Appl. Chem.* 1983, **55**, 1749; (d) D. A. Evans, in *Asymmetric Synthesis* (Edited by J. D. Morrison), Vol. 3, pp. 1–110. Academic Press, New York (1984); (e) T. Mukaiyama, *Pure Appl. Chem.* 1986, **58**, 505.
2. (a) T. Oishi, *Kagaku No Ryoiki* 1972, **26**, 453; (b) G. Stork, *Pure Appl. Chem.* 1975, **43**, 553; (c) D. Seebach, *Angew. Chem. Int. Edn Engl.* 1988, **27**, 1624.
3. I. Paterson, *Chem. Ind.* 1988, **27**, 1624. See also: (a) S. Masamune, W. Choi, F. A. J. Kerdesky and B. Imperiali, *J. Am. Chem. Soc.* 1981, **103**, 1566; (b) D. A. Evans, J. Bartroli and T. L. Shih, *J. Am. Chem. Soc.* 1981, **103**, 2127; (c) S. Masamune, T. Sato, B. Kim and T. A. Wollmann, *J. Am. Chem. Soc.* 1986, **108**, 8279; (d) I. Paterson and C. K. McClure, *Tetrahedron Lett.* 1987, **28**, 1229.

4. (a) D. A. Evans and L. R. McGee, *Tetrahedron Lett.* 1980, **21**, 3975; (b) Y. Yamamoto and K. Maruyama, *Tetrahedron Lett.* 1980, **21**, 4607; (c) M. T. Reetz and R. Peter, *Tetrahedron Lett.* 1981, **22**, 4691; (d) D. A. Evans and L. R. McGee, *J. Am. Chem. Soc.* 1981, **103**, 2876; (e) D. L. Comins and J. D. Brown, *Tetrahedron Lett.* 1984, **25**, 3297; (f) Y. Ito, T. Katsuki and M. Yamaguchi, *Tetrahedron Lett.* 1984, **25**, 6015; (g) T. Katsuki and M. Yamaguchi, *Tetrahedron Lett.* 1985, **26**, 5807; (h) C. Siegel and E. R. Thornton, *Tetrahedron Lett.* 1986, **27**, 457.
5. For synthetic utility of the halogenophilicity of organoaluminium reagents, see: (a) K. Maruoka, Y. Fukutani and H. Yamamoto, *J. Org. Chem.* 1985, **50**, 4412; (b) K. Maruoka, H. Sano and H. Yamamoto, *Chem. Lett.* 1985, 1689.
6. For the Et_2AlCl-promoted Reformatsky reaction of α-bromo ketones and aldehydes in the presence of Zn, see: K. Maruoka, S. Hashimoto, Y. Kitagawa, H. Yamamoto and H. Nozaki, *Bull. Chem. Soc. Jpn* 1980, **53**, 3301.
7. The Et_3B-induced Reformatsky type reaction of α-halo ketones with aldehyde has been advanced: K. Nozaki, K. Oshima and K. Utimoto, *Tetrahedron Lett.* 1988, **29**, 1041; For the R_3Sb-mediated aldol reaction, see: Y. Huang, C. Chen and Y. Shen, *J. Chem. Soc., Perkin Trans. I* 1988, 2855.
8. Aluminium enolates can be generated by reaction of specific ketones such as trityl ketones with Me_3Al. See: M. Ertas and D. Seebach, *Helv. Chim. Acta* 1985, **68**, 961.
9. R. D'Ascoli, M. D'Auria, L. Nucciarelli, G. Piancatelli and A. Scettri, *Tetrahedron Lett.* 1980, **21**, 4521.
10. T. Mukaiyama, K. Banno and K. Narasaka, *J. Am. Chem. Soc.* 1974, **96**, 7503.

Polyhedron Vol. 9, No. 2/3, pp. 227–231, 1990
Printed in Great Britain

0277–5387/90 $3.00+.00
© 1990 Pergamon Press plc

THE EFFECT OF ALUMINIUM ALKOXIDES ON SINGLE ELECTRON TRANSFER REACTIONS. A CONVENIENT SYNTHETIC ROUTE TO (N,N-DIALKYLCARBOMOYL)GERMANES

A. V. SELEZNEV, D. A. BRAVO-ZHIVOTOVSKII,* T. I. VAKUL'SKAYA and M. G. VORONKOV

Institute of Organic Chemistry, Siberian Branch of the U.S.S.R. Academy of Sciences, 664033 Irkutsk, U.S.S.R.

Abstract—Aluminium alkoxides are shown to prominently influence the selectivity of reactions involving a single electron transfer (SET) stage. Triethylgermyllithium (**I**) reacts with amides $R_2NC(O)X$ (*II*) (X = Cl, OMe, NMe_2, Ph) by a mechanism which includes a free-radical stage. The radical anion salt of N,N-diethylbenzamide, which is thermally stable in hydrocarbons, was detected. An efficient synthesis of the interesting reagents, (N,N-dialkylcarbamoyl)germanes, based on the reaction of **I** with **II** (*X* = Cl, OMe), in the presence of an equimolar amount of $(s\text{-BuO})_3Al$, has been developed.

Metal alkoxides often influence the reactions of various organomagnesium and organolithium compounds. Some recent papers in this field deserve mention. McGarrity *et al.* have shown that a mixed *n*-butyllithium–lithium *n*-butylate aggregate is more reactive than a tetrameric *n*-butyllithium in reactions with benzaldehyde.[1]

The effect of lithium and magnesium 2-ethoxyethoxides on the reactions with participation of organolithium compounds and Grignard reagents has been studied.[2,3] The addition of these agents to dimethylformamide followed by the Oppenauer oxidation of $RCH(OM)NMe_2$ leads to an acceptable yield of N,N-dialkylamides if the reaction is carried out in the presence of one of the above mentioned alkoxides. In the absence of alkoxides, no successful carboxamidation of the reagent takes place. In the authors' opinion, the roles of alkoxides are the catalysis of the Oppenauer oxidation and stabilization of the $RCH(OM)NMe_2$ intermediate. The stabilization is performed via involvement of the intermediate into the alkoxide cluster.

In the presence of magnesium 2-ethoxyethoxide, the *n*-butyllithium metallating ability sharply drops. The additives of this alkoxide are shown to facilitate the yield of organolithium compounds in the synthesis of the latter from alkyl halides and lithium metal in THF.[3]

Some aluminium alkoxide/organolithium reagent systems have been studied. Ashby and Noding have examined the selectivity of methylation of 4-tert-butylcyclohexanone with methyllithium in diethyl ether in the presence of various alkoxides including $(i\text{-PrO})_3Al$.[4] The latter does not affect the axial alcohol–equatorial alcohol ratio whereas a t-BuOLi additive increases this ratio.

The addition of organolithium reagents to α,β-unsaturated ketones occurs preferably at the 1,4-position if bis(2,6-di-tert-butyl-4-alkylphenoxide) methylaluminium was previously added to the ketone.[5]

Analysis of the literature data allows us to conclude that lithium, magnesium and aluminium alkoxides do affect the reactivity of organolithium compounds. However, the character of this effect cannot be predicted, as a rule, due to the scarcity of any systematic research in this field.

RESULTS AND DISCUSSION

We have studied the effect of aluminium and lithium alkoxides on the reaction of **I** with **II** in hydrocarbons, eq. (1).

* Author to whom correspondence should be addressed.

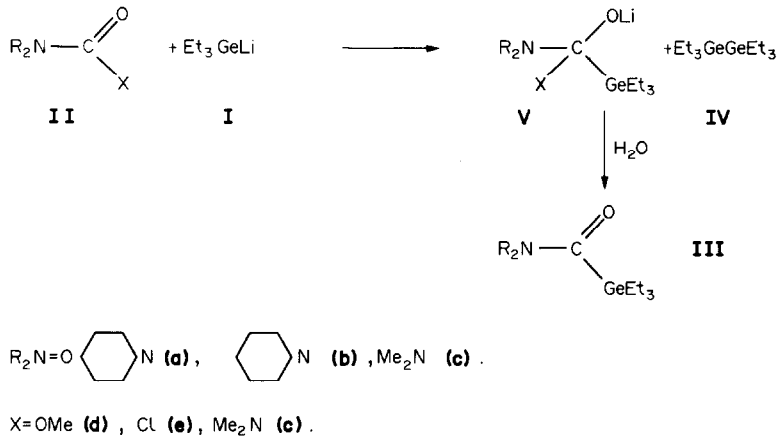

(1)

The reaction displays insufficient selectivity with respect to carbamoylgermane (**III**). The interaction of compound **I** with substrate **IIc,e** in hexane at −50°C leads to 9% of (N,N-dimethylcarbamoyl)triethylgermane and 72% of hexaethyldigermane (**IV**) with a **III** : **IV** ratio of 0.13.[6]

It should be noted that the carbamoylgermanes, **III**, represent a scanty and poorly studied class of organogermanium compounds. This is, firstly, due to synthetic problems.[6] Our research has suggested a synthetic route to these organogermanium compounds.

Addition of equimolar quantities of aluminium or lithium alkoxides changes the reaction selectivity (Table 1). The reaction results depend upon both the metal in the alkoxide and the alkoxy group.

The **III** : **IV** ratio changes over time. Thus, in the reaction with **IIb,d** it is 3.8 after 15 min, whereas 20 h later, this value is 0.4, the total conversion increasing simultaneously. Evidently, the intermediate **V** is the product of a reversible addition reaction, formed under kinetically controlled conditions.

Compound **I** and t-BuOLi give a non-volatile complex, $Et_3GeLi \cdot 3t\text{-}BuOLi$, which is insoluble in hexane. Examination of the mass spectra of an analogous relatively volatile silicon complex, $Me_3Si\text{-}Li \cdot 3t\text{-}BuOLi$, shows the latter to be aggregated in an associate, $(Me_3SiLi)_2(t\text{-}BuOLi)_6$.[7] Compound **I** and $(s\text{-}BuO)_3Al$ form a non-volatile complex of approximate composition $Et_3GeLi \cdot 1.5(s\text{-}BuO)_3Al$, which is insoluble in hexane.

Table 1. The effect of alkoxide on the **III** : **IV** ratio in the reaction of **I** with 1-carbomethoxymorpholine at 20°C[a]

Alkoxide	**III** : **IV** ratio after 15 min	Conversion (%)
—	1.6	100
$(n\text{-}BuO)_3Al$	2.0	60
$(s\text{-}BuO)_3Al$	8.5	32
$(t\text{-}BuO)_3Al$	0.8	81
s-BuOLi	1.6	57
t-BuOLi	0.3	100

[a] Hexane–benzene solution (1 : 1, v/v).

The reaction seems to follow a radical pathway (Scheme 1). This suggestion is valid since metal alkoxides favour electron transition and can be involved in it.[8] They are also able to efficiently stabilize the radical-anion[9] due to insertion of the latter into the alkoxide aggregate. The *k*, *l* and *m* symbols in the Scheme indicate the associative nature of the reagents and intermediates under consideration.[10–13]

Previously, a possible retention of associate alkyllithium structures in the reaction with ethylbenzoates and an accelerating effect of EtOLi have been reported.[14]

The radical pathway of the reaction is proved by ESR-detected paramagnetism of the reaction mixtures. The ESR spectrum of a mixture of **I** and **IIa,d** at −70°C shows a broad signal without hyperfine components. At −30°C the signal disappears. The ESR spectrum of the **I** : **IIc,e** mixture displays a strongly broadened triplet (Fig. 1). The signals in the spectrum do not disappear for some time (0.25 h), even at room temperature. The signal broadening is caused by a high degree of association of **I** and the intermediate radical ion pairs[10,13] in inert solvents at negative temperatures.

Unexpectedly, we have observed fairly well resolved ESR spectra of N,N-diethylbenzamide radical anions in the reactions of elemento-organolithium compounds with N,N-diethylbenzamide (**VI**), at room temperature. These reactions proceed in hydrocarbons according to a scheme analogous to that described above, giving (benzoyl) triethylgermane after the hydrolysis of the corresponding $PhC(OLi)(GeEt_3)NEt_2$.[15] Triethylsilyl-

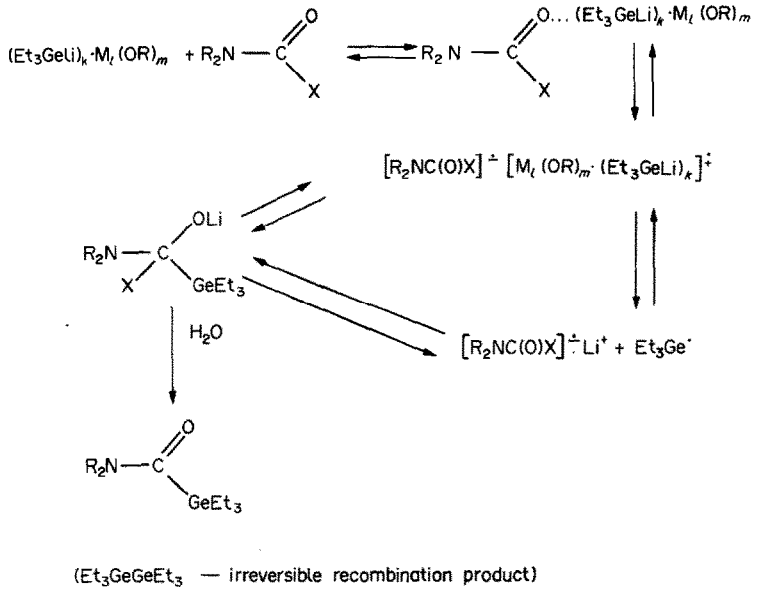

Scheme 1.

lithium and **VI** in a hexane–toluene mixture give an ESR spectrum (Fig. 2) showing HFS: $^2H_p \times {}^3H_o \times {}^3H_m \times {}^3N$ with constants 9.84, 5.19, 2.63 and 1.25 G $\{[PhC(O)NEt_2]^-Li^+\}$. The spectrum of a mixture of triethylgermylpotassium and **VI** in benzene contains a quintet of $^2H_p \times {}^3H_o$ with constants 7.56 and 4.86 G $\{[PhC(O)NEt_2]^-K^+\}$; HFS: $^2H_p \times {}^3H_o \times {}^3H_m \times {}^3N$ and constants 7.56, 4.86, 1.5 and 0.7 G. (The last two figures are obtained from a simulated spectrum.)

Reagent **I** completely reduces substrate **VI** in the HMPA–THF mixture. The latter spectrum shows a hyperfine structure $^2H_p \times {}^3H_o \times {}^3H_m \times {}^5H_{Et} \times {}^3N$ with constants 7.92, 4.86, 1.2, 0.6 and 0.6 G, respectively. This spectrum of the N,N-diethylbenzamide radical anion is in good agreement with that of the radical anion produced electrochemically.[16]

The N,N-diethylbenzamide radical anion is thermally stable in both hydrocarbon and solvating media. In hydrocarbons at room temperature the signal intensity of the spectra does not change much over 2–3 days. It should be noted that in the reaction of **I** with **VI**, since the reducing system of **I** is relatively weak in hydrocarbons,[17] the adduct : digermane ratio is 9.0, which means a minimal formation of reduced products in a free-radical reaction. A stronger reducing agent, triethylgermylpotassium, in benzene gives a 1.0 ratio and in HMPA only traces of adduct were detected. A similar result is observed if one increases the electron-withdrawing ability of the substrate instead of the reducibility of the organometallic reagent (Table 2).

Among the amides studied, **IIc,e** is the strongest

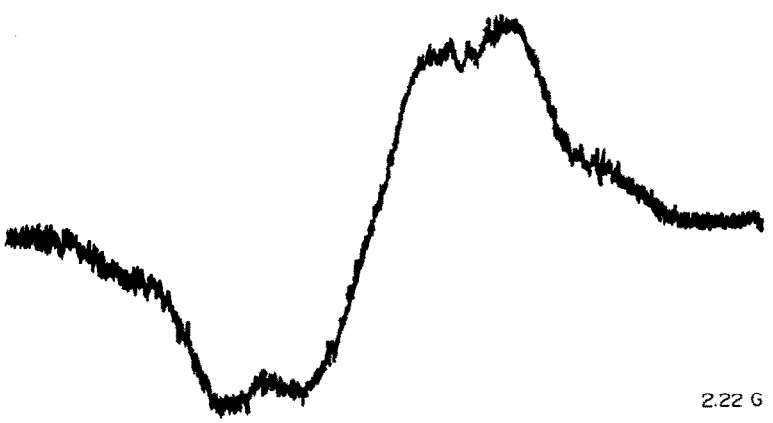

Fig. 1. ESR spectrum of a mixture of reagent **I** and **IIa,d**.

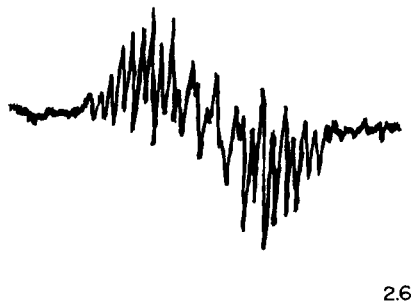

Fig. 2. ESR spectrum of the N,N-diethylbenzamide radical anion $[PhC(O)NEt_2]^{\cdot-}Li^+$ in a hexane–toluene solution.

electron acceptor, and the minimal **III**:**IV** ratio was fixed in the reaction with this substrate. A (s-BuO)$_3$Al additive only slowed down the reaction. (s-BuO)$_3$Al is highly efficient in reactions with the less electron-withdrawing but more basic amides **IIa,d**, **IIb,d** and **IIc,e**. This fact allows us to offer a preparative synthesis of **III**; a considerably simpler one than that employed previously.[18]

The dependence of the reaction results from the nature of the alkoxide and substrate and is caused by the formation of a triple complex, $R_2NC(O)X(Et_3GeLi)_kM_l(OR)_m$, whose stability governs further conversion. The stability of this complex increases with an increase in the substrate basicity. The different effects of aluminium and lithium alkoxides is related to the higher coordination possibility of the aluminium atom, which leads to strengthening of the triple complex. The rigid steric demands of the alkoxy groups can be explained by the fact that the latter are responsible for both the triple complex stability and the probability of intra-complex transformations (at a cluster cell level).

Table 2. Dependence of the **III**:**IV** product ratio upon the structure of substrate in the reaction of **I** with **II**

Substrate	(s-BuO)$_3$Al, equimolar amount	**III**:**IV** for 15 min	Conversion (%)
IIa,d	—	1.6	100
	1	8.5	32
IIb,d	—	0.8	94
	0.5	0.4	70
	1	3.8	41
IIc,e	—	1.1	100
	0.25	6.0	40
	1	—	0
IIc,c	—	0.1	100
	1	0.1	15

The approach of the donor molecule to the $(Et_3GeLi)_kM_l(OR)_m$ associate is most hindered with tert-butoxy groups.

EXPERIMENTAL

All tests were performed in evacuated systems. Quantitative determination of aluminium was carried out by gravimetry with 8-oxyquinoline.[19] IR spectra were recorded on a Specord 75 IR spectrometer as thin films. ^1H and ^{13}C NMR spectra were run on a JEOL FX-90Q spectrometer, chemical shifts are given against TMS. ESR spectra were recorded on RE-1307 and Radiopan instruments. ESR spectra simulation was performed by a modified program.[20] Mass spectra were recorded on a Varian MAT-212 instrument (70 eV). GLC analysis was performed on a Chrom-5 chromatograph.

Reaction of **I** *with* **II** *in the presence of the corresponding alkoxide (general procedure)*

To a degassed solution of alkoxide in hexane a solution of **I** in benzene was added. As a result, an amorphous transparent precipitate was formed. If 0.25 mol of alkoxide was added, the precipitate dissolved immediately. When (*n*-BuO)$_3$Al was used, no precipitate was observed at all.

To the resultant reagent the corresponding amide, **II**, was added and the whole mixture was shaken. An exothermic reaction took place. After 15 min an aliquot of the reaction mixture was taken and hydrolysed, and the **III**:**IV** ratio was determined by GLC data. Complete analysis of the mixture was performed by GLC–MS.

Synthesis of **IIIa**

To a degassed solution of (s-BuO)$_3$Al (2.43 g, 9.86 mmol) in 18 cm^3 of hexane a solution of **I** (1.65 g, 9.9 mmol) in 15 cm^3 of benzene was added, which simultaneously gave an amorphous transparent precipitate. To the resultant reagent, compound **IIa,d** was added and the mixture was stirred, first at room temperature (1 h) and then at 70–80°C (3 h). The reaction mixture was left overnight and then it was treated with 2 cm^3 of water. The aluminium hydroxide precipitate was separated by centrifugation, then it was extracted twice with benzene. The supernatant layer and extracts were dried over anhydrous sodium sulphate. A yellow liquid which was stable in air was isolated, 1.45 g (54%), by fractionation at a reduced pressure. The yellow colour was caused by a slight impurity of bis(triethylgermyl)ketone, since the product is normally colourless. B.p. 115–118°C/1–2 mm Hg. Found:

C, 48.90; H, 8.17; Ge, 25.12; N, 5.12. Calc. for $C_{11}H_{23}GeNO_2$: C, 48.24; H, 8.46; Ge, 26.50; N, 5.11%. Mass spectrum (*m/z*, ion): 275 M^+, 247 (M^+-28), 161 ($M^+-C(O)N(CH_2CH_2)_2O$), 86 ($M^+-C(O)GeEt_3$). ^1H NMR ($CDCl_3$; δ, ppm): 1.05 m, 15H, Et_3Ge; 3.59 m, 8H, $N(CH_2CH_2)_2O$. ^{13}C NMR ($CDCl_3$; δ, ppm): 182.7 C=O; 66.4 CH_2O; 66.0 CH_2O; 45.5 CH_2N; 39.5 CH_2N; 7.98 $—CH_2Ge$; 4.4 CH_3CH_2Ge. IR (ν, cm^{-1}): 1575 (C=O).

Synthesis of **IIIb**

To the reagent obtained from **I** (1.4 g, 8.4 mmol) and $(s\text{-}BuO)_3Al$ (2.0 g, 8.1 mmol) in a mixture of hexane–benzene (1 : 1, v/v), amide **IIb,d** (1.2 g, 8.4 mmol) was added. The reaction mixture was stirred at room temperature for 40 min and then treated with water. Further operations were performed as described above. As a result, 0.75 g (33%) of yellow liquid was obtained. B.p. 105–108°C/1 mm Hg. Found: C, 53.48; H, 9.16; Ge, 26.79; N, 4.58. Calc. for $C_{12}H_{25}GeNO$: C, 53.00; H, 9.27; Ge, 26.70; N, 5.15%. Mass spectrum (*m/z*, ion): 273 M^+, 245 (M^+-28), 161 ($M^+-C(O)N(CH_2CH_2)_2CH_2$), 84 ($M^+-C(O)GeEt_3$). ^1H NMR ($CDCl_3$; δ, ppm): 1.04 m, 15H, Et_3Ge; 1.60 m, 6H, $—CH_2CH_2CH_2—$; 3.38 m, 2H, CH_2N; 3.54 m, 2H, CH_2N. ^{13}C NMR (CDC_3; δ, ppm): 183.7 C=O; 47.1 CH_2N; 40.7 CH_2N; 27.2, 25.7, 25.0 $—CH_2CH_2CH_2—$; 9.0 $—CH_2Ge$; 5.4 $CH_3—CH_2Ge$. IR (ν, cm^{-1}): 1580 (C=O).

REFERENCES

1. J. F. McGarrity, C. A. Ogle, Z. Brich and H. R. Loosli, *J. Am. Chem. Soc.* 1985, **107**, 1810.
2. C. G. Screttas and B. R. Steele, *J. Org. Chem.* 1988, **53**, 5151.
3. C. G. Screttas and B. R. Steele, *J. Org. Chem.* 1989, **54**, 1013.
4. E. C. Ashby and S. A. Noding, *J. Org. Chem.* 1979, **44**, 4371.
5. K. Maruoka, K. Nonoshita and H. Yamamoto, *Tetrahedron Lett.* 1987, **28**, 5723.
6. S. D. Pigarev, *Disstsii Akad. Nauk.* 1988, Irkutsk.
7. A. V. Seleznev, D. A. Bravo-Zhivotovskii, I. D. Kalikhman, V. Yu. Vitkovskii, O. B. Bannikova, M. G. Voronkov and N. S. Vyazankin, *Metallo-organ. Khim.* 1988, **1**, 689.
8. E. C. Ashby, D.-H. Bae, W.-S. Park, R. N. Depriest and W.-Y. Su, *Tetrahedron Lett.* 1984, **25**, 5107.
9. C. G. Screttas and M. Micha-Screttas, *J. Am. Chem. Soc.* 1987, **109**, 7573.
10. V. I. Korsunsky, M. B. Taraban, T. V. Leshina, O. I. Margorskaya and N. S. Vyazankin, *J. Organomet. Chem.* 1981, **215**, 179.
11. D. C. Bradley, R. C. Mehrotra and D. P. Gaur, *Metal Alkoxides*. Academic Press, London (1978).
12. K. S. Chen, F. Bertini and J. K. Kochi, *J. Am. Chem. Soc.* 1973, **95**, 1340.
13. N. Hirota, *J. Am. Chem. Soc.* 1967, **89**, 32.
14. M. A. Al-Aseer, B. D. Allison and S. G. Smith, *J. Org. Chem.* 1985, **50**, 2715.
15. D. A. Bravo-Zhivotovskii, S. D. Pigarev, I. D. Kalikhman, O. A. Vyazankina and N. S. Vyazankin, *J. Organomet. Chem.* 1983, **248**, 51.
16. J. Voss and F. R. Bruhn, *Justus Liebigs Annln Chem.* 1979, 1931.
17. D. A. Bravo-Zhivotovskii, O. A. Kruglaya and N. S. Vyazankin, *Zh. Obshch. Khim.* 1980, **50**, 2144.
18. D. A. Bravo-Zhivotovskii, S. D. Pigarev, O. A. Vyazankina, A. S. Medvedeva, L. P. Saphronova and N. S. Vyazankin, *Izv. AN SSSR Ser. Khim.* 1984, 1897.
19. W. F. Hillebrand and G. E. F. Lundell, *Applied Inorganic Analysis*, 2nd edn. John Wiley, New York (1953).
20. Yu. A. Kruglyak, G. G. Dyadusha, V. A. Kuprievich, L. M. Podol'skaya and G. I. Kagan, *Methods for Calculating Electronic Structure and Spectra of the Molecule*. Naukova Dumka, Kiev (1969).

Polyhedron Vol. 9, No. 2/3, pp. 233–237, 1990
Printed in Great Britain

0277–5387/90 $3.00+.00
© 1990 Pergamon Press plc

STERICALLY CROWDED ARYLOXIDE COMPOUNDS OF ALUMINIUM—REACTIVITY OF COORDINATED BENZALDEHYDE

MICHAEL B. POWER and ANDREW R. BARRON*

Department of Chemistry, Harvard University, 12 Oxford Street, Cambridge, MA 02138, U.S.A.

Abstract—The interaction of aluminium complexes containing the sterically hindered phenoxide ligand 2,6-di-*tert*-butyl-4-methylphenoxide (BHT) with benzaldehyde has been investigated. Interaction of benzaldehyde with $AlR(BHT)_2$ leads to the Lewis acid–base adduct $AlMe(BHT)_2[O{=}C(H)Ph]$, R = Me. When R = Et, reduction of coordinated benzaldehyde is observed. The addition of benzaldehyde to $AlMe_2(BHT)$ leads to the formation of the acetophenone complex, $AlMe_2(BHT)[O{=}C(Me)Ph]$. A mechanism for this unique aldehyde to ketone transformation is proposed. The dimeric compound $[AlEt(BHT)(OCH_2Ph)]_2$ is formed from the interaction of $AlEt_2(BHT)$ and benzaldehyde.

Organoaluminium compounds are of synthetic importance in organic chemistry,[1] in particular the reactions of alkyl aluminium compounds with organic carbonyls. These reactions are often complicated because of the presence of multiple reaction pathways and the dimeric nature of many organoaluminium compounds. Recent work reported in the literature[2–4] has focused on the use of monomeric aluminium complexes, derived from the sterically hindered 2,6-di-*tert*-butyl-4-methylphenol (BHT-H, from the trivial name butylated hydroxytoluene), as bulky Lewis acids for the modification of the reactivity of coordinated ketones.

We report here the reaction of benzaldehyde with the organoaluminium aryloxide compounds $AlR_x(BHT)_{3-x}$ (R = Me, Et; x = 1, 2) (Scheme 1).

RESULTS AND DISCUSSION

The interaction of $AlMe(BHT)_2$[5] with benzaldehyde in pentane allows the isolation of the Lewis acid–base complex $AlMe(BHT)_2[O{=}C(H)Ph]$ (**1**), as a bright orange crystalline solid. As has been observed[5] for other complexes of $AlMe(BHT)_2$, compound **1** can be handled in air for several minutes without appreciable decomposition.

The ^1H NMR signal for the aluminium methyl ligand of **1** (δ +0.73 ppm) is downfield of that found for $AlMe(BHT)_2$ (δ −0.43 ppm).[5] This downfield shift is consistent with an increase in p character in the Al—C bond in going from a planar sp^2 to a tetrahedral sp^3 aluminium centre.[6]

The complex shows a decreased carbonyl stretch, ν(CO), in the IR spectrum and a downfield shift in the ^{13}C NMR spectrum for the carbonyl α-carbon, in comparison to the "free" ligand, consistent with coordination of the organic carbonyl to aluminium. An upfield shift for the α-proton of benzaldehyde on coordination to $AlMe(BHT)_2$ is perhaps an indication of the increased hydridic nature of the proton.

Adduct formation is not observed between benzaldehyde and $AlEt(BHT)_2$; instead, reduction of the aldehyde occurs to give a coordinated alkoxide. Interaction of $AlEt(BHT)_2$[7] with one equivalent of benzaldehyde results in an equimolar mixture of $AlEt(BHT)_2$ and $Al(BHT)_2(OCH_2Ph)[O{=}C(H)Ph]$ (**2**). If, however, the reaction is carried out with two equivalents of benzaldehyde, **2** is the only product observed. All NMR and IR spectroscopy (see Experimental) are consistent with the proposed structure of **2**.

Compound **2** is presumably formed as a result of the reduction of one coordinated benzaldehyde with the concomitant elimination of ethylene [eq. (1)], followed by the subsequent coordination of a second benzaldehyde molecule [eq. (2)]:

$$AlEt(BHT)_2 + O{=}C(H)Ph \longrightarrow \text{“}Al(BHT)_2(OCH_2Ph)\text{”} + C_2H_4. \quad (1)$$

$$\text{“}Al(BHT)_2(OCH_2Ph)\text{”} + O{=}C(H)Ph \longrightarrow Al(BHT)_2(OCH_2Ph)[O{=}C(H)Ph]. \quad (2)$$

* Author to whom correspondence should be addressed.

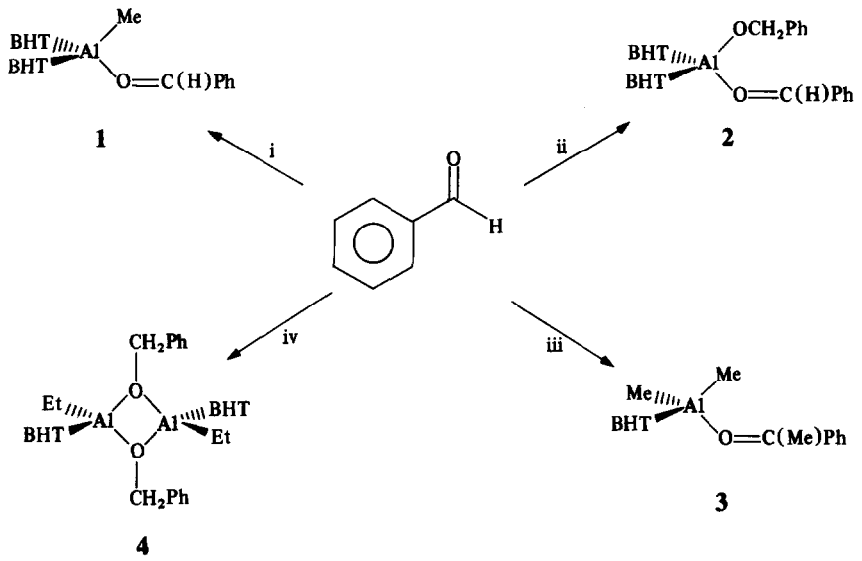

Scheme 1. (i) $AlMe(BHT)_2$; (ii) $AlEt(BHT)_2$; (iii) $AlMe_2(BHT)$; (iv) $AlEt_2(BHT)$.

Because the steric bulk of the two BHT ligands in $AlEt(BHT)_2$ would preclude the formation of any dimeric species, the reduction must occur in an intra-molecular fashion,[1] presumably involving a cyclic six-membered transition state (**I**).

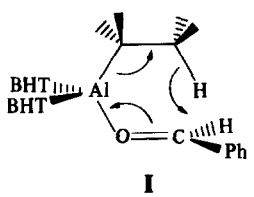

I

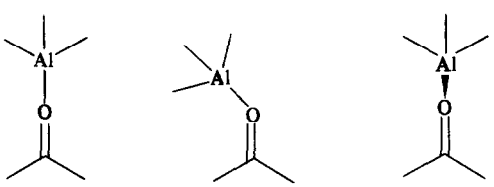

II **III** **IV**

An organocarbonyl group can coordinate to a Lewis acid such as aluminium, by one of three modes of bonding, sp (**II**), sp^2 (**III**) and via the C=O π-bond (**IV**).

Theoretical calculations for the model system $H_3Al(O{=}CH_2)$ have predicted that sp^2 coordination (**II**) is energetically favoured,[7] yet Ittel and co-workers have reported the X-ray structure of the methyltolueneoate complex of $AlEt_2(BHT)$ in which the carbonyl is coordinated perpendicular to the π-nodal plane of the ester (**IV**).[8] It is not inconceivable, therefore, that such a coordination mode would be accessible for the transition state **I**.

The room temperature ^1H NMR spectrum of an equimolar solution of $AlMe_3$ and BHT-H contains a single peak due to Al—Me protons;[5,8] integration consistent with the stoichiometry $AlMe_2(BHT)$. If, however, the sample is cooled to $-80°C$, four peaks are observed that have been assigned as $AlMe(BHT)_2$, $AlMe_2(BHT)$, $Al_2Me_5(BHT)$ and Al_2Me_6.[5,8] It is proposed, therefore, that two concurrent disproportionations occur in solution [eqs (3) and (4)]:

$$Al_2Me_5(BHT) \rightleftharpoons 0.5Al_2Me_6 + AlMe_2BHT \quad (3)$$

$$3AlMe_2(BHT) \rightleftharpoons Al_2Me_5(BHT) + AlMe(BHT)_2. \quad (4)$$

Despite the presence of these equilibria we have shown that the reaction of an equimolar solution of $AlMe_3$ and BHT-H at room temperature with Lewis bases (L) results in the formation of the Lewis acid–base adduct $AlMe_2(BHT)(L)$.[5,9] We have, therefore, investigated the reaction of this equilibrium mixture with benzaldehyde.

Addition of one equivalent of benzaldehyde to an equimolar mixture of $AlMe_3$ and BHT-H at room temperature, in the presence of diethyl ether, results in the isolation of $AlMe_2(BHT)[O{=}C(Me)Ph]$ (**3**), in *ca* 60% yield (Scheme 1). Compound **3** can be made directly by the interaction of acetophenone in place of benzaldehyde (see Experimental).

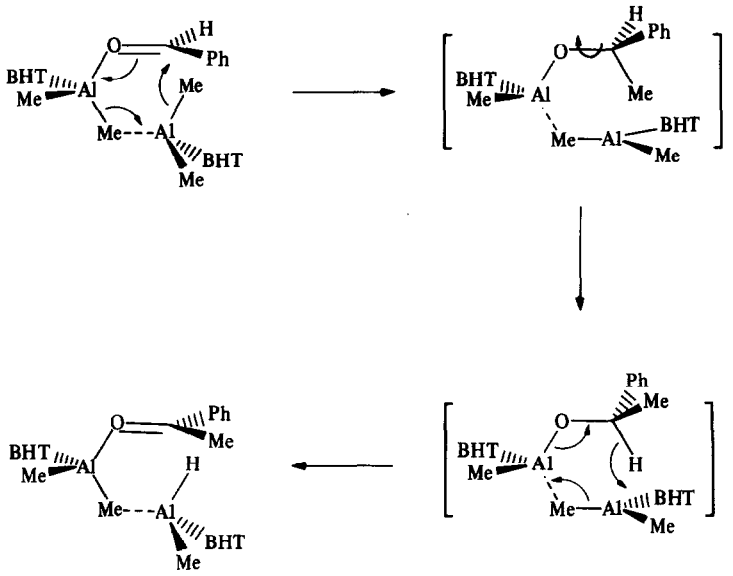

Scheme 2.

The conversion of an aldehyde to the corresponding methylketone in a single step, represents, we believe, a unique reaction in organic chemistry and we are presently investigating the generality of this C—C bond formation.

In order to obtain stoichiometric conversion of the benzaldehyde to acetophenone, 1.5 equivalents of "$AlMe_2(BHT)$" are required; suggesting that the aldehyde coordinates to one molecule of $AlMe_2$(BHT) while a second equivalent acts as the methyl source. A speculative mechanism for this transformation based on previously reported alkylations of ketones via dimeric intermediates is proposed in Scheme 2. The presence of a transient species, formed immediately on mixing $AlMe_2(BHT)$ and benzaldehyde, with a peak at δ 5.11 ppm in the ^1H NMR, is consistent with the presence of a OCH(Me)Ph ligand.[9]

The interaction of benzaldehyde with $AlEt_2$(BHT)[7] does not result in a clean reaction. We can conclude from the NMR data, however, that the major product arises from the reduction of the coordinated benzaldehyde, to give AlEt(BHT)(OCH_2Ph) (**4**) (see Experimental). There is no evidence for the further coordination of benzaldehyde to **4**. We propose therefore that **4** is dimeric involving bridging alkoxides (Scheme 1).[10]

EXPERIMENTAL

Microanalyses were performed by Oneida Research Services Inc., Whitesboro, New York. Melting points were determined in sealed capillaries and are uncorrected. IR spectra (4000–600 cm^{-1}) were recorded on a Perkin–Elmer 137 grating spectrometer as Nujol mulls. NMR spectra, in C_6D_6, were recorded on Bruker AM-250 (^1H) and AM-300 (^{13}C) spectrometers (δ in ppm relative to $SiMe_4$). All manipulations were carried out under nitrogen. Solvents were dried, distilled and degassed before use.

Trimethylaluminium and triethylaluminium were used as 2.0 M and 1.0 M solutions in hexane, respectively. $AlMe(BHT)_2$ and $AlEt(BHT)_2$ were prepared by literature procedures.[5,7]

$AlMe(BHT)_2[O{=}C(H)Ph]$ (1)

To a pentane (40 cm^3) solution of $AlMe(BHT)_2$ (2.00 g, 4.16 mmol) was added a pentane (30 cm^3) solution of benzaldehyde (0.46 cm^3, 4.16 mmol). A deep red solution resulted, from which an orange solid precipitated after 1 h of stirring. Filtration, followed by recrystallization from hexane (−20°C) resulted in crystals. Yield *ca* 80%; m.p. 107–108°C. Found: C, 77.3; H, 9.5. Calc. for $C_{38}H_{55}O_3Al$: C, 77.8; H, 9.4%.

IR (Nujol, NaCl, cm^{-1}): 1630 (s), 1600 (s), 1575 (s), 1530 (w), 1320 (m), 1250 (s), 1200 (s), 1170 (m), 1120 (m), 1020 (m), 950 (w), 900 (sh), 890 (s), 860 (s), 840 (s), 800 (w), 770 (m), 750 (m), 660 (s).

NMR (δ, C_6D_6). ^1H: 8.86 (1H, s, O=C*H*), 7.31 [2H, d, J(H—H) = 7.5 Hz, *o*-C_6H_2], 7.20 (4H, s, BHT, C_6H_2), 6.90 [1H, t, J(H—H) = 7.5 Hz, *p*-C_6H], 6.69 [2H, t, J(H—H) = 7.5 Hz, *m*-C_6H_2], 2.29 (6H, s, CH_3), 1.66 (36H, s, CCH_3), 0.73 (3H, s, Al—CH_3). ^{13}C: 201.67 (*C*=O), 154.87 (O—*C*, BHT), 140.02 (*C*—C=O), 139.08 (*o*-*C*, BHT),

134.17 (*o-C*, PhCHO), 132.70 (*m-C*, PhCHO), 129.61 (*p-C*, PhCHO), 126.40 (*m-C*, BHT), 125.89 (*p-C*, BHT), 35.45 (CH_3, BHT), 31.89 [$C(CH_3)_3$, BHT], 21.40 [$C(CH_3)_3$, BHT], −6.08 (Al—CH_3).

$Al(BHT)_2(OCH_2Ph)[O{=}C(H)Ph]$ (2)

To $AlEt(BHT)_2$ (2.0 g, 4.04 mmol) in pentane (30 cm^3) at room temperature was added benzaldehyde (0.94 cm^3, 8.08 mmol) in pentane (30 cm^3). The resulting deep red solution was allowed to stir for 24 h. The solution was then reduced in volume *in vacuo* and then cooled to −20°C. This yielded a deep red microcrystalline solid. Yield: *ca* 70%; m.p. 110–112°C. Found: C, 76.9; H, 8.6. Calc. for $C_{43}H_{39}O_4Al$: C, 77.4; H, 8.9%.

IR (Nujol, NaCl, cm^{-1}): 1620 (s), 1595 (s), 1570 (m), 1355 (w), 1310 (m), 1290 (sh), 1260 (s), 1225 (s), 1210 (sh), 1165 (m), 1120 (m), 1075 (w), 1020 (w), 950 (w), 905 (s), 885 (m), 855 (m), 840 (m), 800 (w), 765 (m), 755 (m), 710 (m), 690 (m), 670 (s), 640 (m).

NMR (δ, C_6D_6). ^1H: 9.07 (1H, s, C*H*O), 7.40 [2H, d, J(H—H) = 7.5 Hz, *o*-C_6H_2], 7.30 [2H, d, J(H—H) = 7.5 Hz, *o*-C_6H_2], 7.20 (4H, s, C_6H_2, BHT), 7.09 (1H, t, J = 7.5 Hz, *p*-C_6H), 6.90 (1H, t, J = 7.5 Hz, *p*-C_6H), 6.68 (2H, t, J = 7.5 Hz, *m*-C_6H_2), 5.09 (2H, s, OCH_2Ph), 2.27 (6H, s, CH_3), 1.69 (36H, s, CCH_3). ^{13}C: 203.95 (*C*=O), 154.45 (O—*C*, BHT), 144.8 (*C*—CH_2O), 139.87 (*C*—C=O), 139.12 (*o-C*, BHT), 134.25 (*o-C*, PhCHO), 132.53 (*m-C*, PhCHO), 129.47 (*p-C*, PhCHO), 128.41 (*o-C*, $PhCH_2O$), 127.55 (*m-C*, $PhCH_2O$), 126.75 (*p*-C, $PhCH_2O$), 126.41 (*m-C*, BHT), 126.24 (*p-C*, BHT), 65.95 (CH_2), 35.50 (CH_3, BHT), 31.70 [$C(CH_3)_3$, BHT], 21.37 [$C(CH_3)_3$, BHT].

$AlMe_2(BHT)[O{=}C(Me)Ph]$ (3)

Method 1. To a solution of BHT-H (2.2 g, 10.0 mmol) in pentane (25 cm^3) was added $AlMe_3$ (5 cm^3, 10.0 mmol) in hexane. After the solution was stirred for 0.5 h, acetophenone (1.23 cm^3, 10.0 mmol) was added. A yellow precipitate gradually formed as the addition proceeded. The reaction mixture was then stirred for 1 h. Filtration, followed by washing with pentane (2 × 20 cm^3), and drying *in vacuo* gave an orange solid. Yield: *ca* 90%.

Method 2. To a solution of $AlMe_2(BHT)$ (5.70 mmol), prepared as described above, in the presence of Et_2O was added benzaldehyde (0.63 cm^3, 5.70 mmol) at room temperature. A deep orange–red coloured solution formed immediately. Removal of the solvent *in vacuo* yielded an oily residue, which when washed with pentane (15 cm^3), formed a yellow solid. Yield: *ca* 60%; m.p. 106–107°C. Found: C, 74.8; H, 9.1. Calc. for $C_{25}H_{37}O_2Al$: C, 75.7; H, 9.4%.

IR (Nujol, NaCl, cm^{-1}); 1625 (s), 1600 (m), 1575 (m), 1310 (sh), 1275 (s), 1220 (w), 1200 (sh), 1185 (m), 1100 (w), 1020 (w), 965 (w), 865 (s), 780 (w), 755 (w), 710 (m), 670 (s), 600 (m).

NMR (δ, C_6D_6). ^1H: 7.50 [2H, d, J(H—H) = 7.5 Hz, *o*-C_6H_2], 7.29 (2H, s, C_6H_2, BHT), 6.98 [1H, t, J(H—H) = 7.5 Hz, *p*-C_6H], 6.76 [2H, t, J(H—H) = 7.5 Hz, *m*-C_6H_2], 2.38 (3H, s, CH_3), 2.12 (3H, s, $OCCH_3$), 1.65 (18H, s, CCH_3), −0.05 (6H, s, Al—CH_3). ^{13}C: 210.71 (*C*=O), 155.75 (O—*C*, BHT), 138.77 (*o-C*, BHT), 137.42 (*C*—C=O), 134.39 (*o-C*, Ph), 131.12 (*m-C*, Ph), 129.01 (*p-C*, Ph), 126.09 (*m-C*, BHT), 125.15 (*p-C*, BHT), 35.11 (CH_3, BHT), 31.30 [$C(CH_3)_3$, BHT], 26.0 (CH_3, PhMeCO), 21.53 [$C(CH_3)_3$, BHT], −5.52 (Al—CH_3).

$AlEt(BHT)(OCH_2Ph)$ (4)

To an equimolar mixture of $AlEt_3$ (5.28 cm^3, 5.28 mmol) and BHT-H (1.16 g, 5.28 mmol) in pentane (30 cm^3) was added a pentane (20 cm^3) solution of benzaldehyde (0.58 cm^3, 5.28 mmol). The resulting deep orange solution was stirred overnight during which time it lightened in colour to pale orange. The resulting solution was evaporated to dryness *in vacuo* to leave an orange oil.

NMR (δ, C_6D_6) Crude mixture, ^1H: 7.30 [2H, d, J(H—H) = 7.5 Hz, *o*-C_6H_2], 7.21 (2H, s, C_6H_2, BHT), 7.03 [1H, t, J(H—H) = 7.5 Hz, *p*-C_6H_2], 6.98 [2H, t, J(H—H) = 7.5 Hz, *m*-C_6H_2] 5.17 (2H, s, OCH_2Ph), 2.33 (3H, s, CH_3), 1.47 (18H, s, CCH_3), 1.02 (3H, t, J(H—H) = 7.5 Hz, Al—CH_2CH_3), 0.08 [2H, q, J(H—H) = 7.5 Hz, Al—CH_2CH_3]. ^{13}C: 154.03 (O—*C*, BHT), 138.42 (*o-C*, BHT), 136.5 (*C*—CH_2O, OCH_2Ph), 129.94 (*o-C*, Ph), 129.29 (*m-C*, Ph), 128.68 (*p-C*, Ph), 126.22 (*m-C*, BHT), 125.77 (*p-C*, BHT), 68.48 (OCH_2Ph), 35.28 (CH_3, BHT), 31.81 [$C(CH_3)_3$, BHT], 21.52 [$C(CH_3)_3$, BHT], 9.54 (CH_3, Al—Et), 1.76 (CH_2, Al—Et).

Acknowledgements—Financial support of this work is provided by the donors of the Petroleum Research Fund, administered by the American Chemical Society under grant No. 20082-G5, ICI Wilton Materials Research Centre, U.K. and ICI Americas, Wilmington DE, U.S.A.

REFERENCES

1. See J. R. Zietz, G. C. Robinson and K. L. Lindsay, *Comprehensive Organometallic Chemistry* (Edited by G. Wilkinson, F. G. A. Stone and E. W. Abel), Vol. 7, Ch. 46. Pergamon Press, Oxford (1982).

2. K. Manuoka, T. Itoh, M. Sakuria and H. Yamamoto, *J. Am. Chem. Soc.* 1988, **110**, 3588.
3. A. J. Stern and J. S. Swenton, *J. Chem. Soc., Chem. Commun.* 1988, 1255.
4. K. Maruoka, Y. Arari and H. Yamamoto, *J. Am. Chem. Soc.* 1988, **110**, 2650.
5. M. D. Healy, D. A. Wierda and A. R. Barron, *Organometallics* 1988, **7**, 2543.
6. A. R. Barron, *J. Chem. Soc., Dalton Trans.* 1988, 3047.
7. A. P. Stevens, R. Mulhaupt, W. Fultz, J. Calabrese, W. Robbins and S. D. Ittel, *Organometallics* 1988, **7**, 409.
8. T. J. LePage and K. B. Wiberg, *J. Am. Chem. Soc.* 1988, **110**, 6642.
9. M. D. Healy, M. B. Power and A. R. Barron, unpublished results.
10. T. Mole, *Aust. J. Chem.* 1966, **19**, 373.

Polyhedron Vol. 9, No. 2/3, pp. 239–243, 1990
Printed in Great Britain

0277–5387/90 $3.00+.00
Pergamon Press plc

BUTYL METAL ARYLOXIDES, ARYLAMIDES, AND SULPHUR AND PHOSPHORUS ANALOGUES—II.* SYNTHESIS AND CHARACTERIZATION OF NOVEL BULKY ALKOXIDES AND ARYLOXIDES OF ALUMINIUM; X-RAY STRUCTURE OF $[Al(\mu\text{-}OCH_2Ar)Me_2]_2$ (Ar = $C_6H_2Bu^t_3$-2,4,6)

BEKIR ÇETINKAYA, PETER B. HITCHCOCK, HATAM A. JASIM, MICHAEL F. LAPPERT† and HUGH D. WILLIAMS

School of Chemistry and Molecular Sciences, University of Sussex, Brighton BN1 9QJ, U.K.

Abstract—The alkoxide, (2,4,6-tri-t-butylbenzoxo)dimethylaluminium, $[Al(\mu\text{-}OCH_2Ar)Me_2]_2$ (Ar = $C_6H_2Bu^t_3$-2,4,6), (**1**), has been prepared from the corresponding benzyl alcohol $ArCH_2OH$ and trimethylaluminium in C_6H_{14} at *ca* 25°C. Even using an excess of the alcohol, only one of the methyl groups of $AlMe_3$ was replaceable under these conditions. By contrast, using the bulky phenol Ar′OH (Ar′ = $C_6H_3Bu^t_2$-2,6) and an excess of $AlMe_3$ yielded the bis-aryloxide, bis-[2,6-di(t-butyl)phenoxo]methylaluminium, $AlMe(OAr')_2$ (Ar′ = $C_6H_3Bu^t_2$-2,6), (**2**). The less hindered phenol Ar″OH (Ar″ = $C_6H_3Bu^t_2$-2,4) and an excess of $AlMe_3$ gave the expected aryloxide, (2,4-di-t-butylphenoxo)dimethylaluminium, $AlMe_2(OAr'')$ (Ar″ = $C_6H_3Bu^t_2$-2,4) (**3**). Compounds **1**–**3** have been characterized spectroscopically and in the case of the crystalline alkoxide **1**, also by X-ray crystallography; some selected geometric parameters are: Al—O 1.841(3) and 1.858(2), Al—C 1.939(5) and 1.959(6), Al···Al′ 2.84, O···O 2.37 Å; O—Al—O′ 79.8(1), Al—O—Al′ 100.2(1)°. Complex **1** has the structure $[AlMe_2(\mu\text{-}OCH_2Ar)]_2$, both as the solid and at 30°C in C_6D_6 solution. Less complete data on the aryloxides **2** and **3** suggest that the former is a monomer, whereas the latter is a dimer, probably by virtue of OAr″-bridging.

We have been interested for a long time in making compounds containing sterically hindered ligands. Our earlier work on the aryloxides bearing t-butyl substituents in the 2- and 6-positions is summarized in ref. 1. Complexes which we have investigated in this context have involved Li, Na, Mg, Ti^{III}, Ti^{IV}, Zr^{IV}, Rh^{I} (affording a tautomeric η^5-cyclohexadienonyl complex), Ge^{II}, Sn^{II}, Pb^{II}, P^{III}, Sc^{III}, Y^{III}, La^{III}, Pr^{III}, Nd^{III}, Dy^{III}, Ho^{III}, Er^{III}, Yb^{II}, Yb^{III}, Th^{IV} and U^{IV}.

Three 2,6-di-t-butylphenols are readily available having the formula 2,6-Bu^t_2-4-R-C_6H_2OH (R = H, Me, or Bu^t), because they are used as antioxidants. They have proved to be the source of interesting metal aryloxides which in general are hydrocarbon-soluble and often are available in an unusually low metal oxidation state and/or coordination number and have a low degree of molecular aggregation. For example, whereas the lanthanide elements (Ln) are characterized by having large ionic radii and hence normally form complexes having high Ln coordination numbers, the appropriate lanthanum(III) aryloxides are the three-coordinate complexes $[Ln(OC_6H_2Bu^t_2\text{-}2,6\text{-}R\text{-}4)_3]$,[2] and related ytterbium(II) aryloxides have a four- or five-coordinate metal environment, $[Yb(OAr''')_2(L)_n]$ (Ar‴ = $C_6H_2Bu^t_2$-2,6-Me-4; $n = 2$ and L = Et_2O or THF; or $n = 3$ and L = THF).[3] Another reason why such aryloxides have proved to be of interest is that a methyl group of one or more of the *o*-Bu^t groups is capable of participating in cyclometallation reactions.[4]

There are previous records of the use of two of these phenols in aluminium chemistry. The reaction between $AlPh_3$ and OAr (Ar = $C_6H_2Bu^t_3$-2,4,6) yielded $AlPh_{3-n}(OAr)_n$ ($n = 1$ or 2); it was proposed that the reaction proceeds by a free radical pathway on the basis of ESR data and the detection of biphenyl.[5] The monomeric compounds

* For Part I, see ref. 1a.

† Author to whom correspondence should be addressed.

$AlR_2(OAr''')$ (R = Me or Bu^i) and $AlBu^i(OAr''')_2$ were prepared from the appropriate alkyl AlR_3 and Ar'''OH,[6] while $AlMe_2Cl$ and Ar'''OH afforded $[AlMe(\mu\text{-}Cl)(OAr''')]_2$.[7] The reaction between various aluminium alkyls and Ar'''OH was followed by NMR[8] in the $AlMe_3$/Ar'''OH system; the compounds $Al_2Me_5(OAr''')$, $AlMe_2(OAr''')$ and $AlMe(OAr''')_2$ (monomeric in crystal; X-ray) were identified and some have application in synthesis and as catalysts for polymerization of C_3H_6.[8] X-ray data are also available on $AlMe_2(OAr''')(PMe_3)$ and $[NHMe_3][AlCl_2(Me)OAr''']$.[9]

The benzylic alcohol $ArCH_2OH$ has not, as far as we are aware, been used previously as a source of metal alkoxides. The intervention of the methylene group between the *ipso*-carbon and the OH group no doubt alleviates the steric effects of the two t-butyl groups in the 2- and 6-positions. A cyclometallation reaction involving one of the methyl groups of a metal complex L_nMOCH_2Ar would result in the formation of a seven-membered C_5OAl ring fused to the 1,2-positions of the aromatic nucleus; such a ring might well have been expected to be strainless.

EXPERIMENTAL

Materials, measurements and techniques

(2,4,6-Tri-t-butyl)benzyl alcohol was prepared according to a published synthesis.[10] Manipulative procedures of air-sensitive materials and the purification of the phenols were described in Part I.[1a] High resolution electron impact mass spectra and NMR spectra were run on a Kratos MS80RF and a Bruker WP80 or Bruker WM360 instrument, respectively.

Synthesis of **1**

A solution of the benzyl alcohol (2.65 g, 9.60 mmol) in hexane (25 cm^3) was slowly added to a solution of trimethylaluminium (2.4 mmol Al_2Me_6) in hexane (4.8 cm^3). An exothermic reaction took place and a gas was evolved. After stirring for *ca* 2 h, volatiles were removed *in vacuo*. The residue was dissolved in warm hexane (25 cm^3) and the suspension was filtered. The filtrate gave white needles of **1** (1.1 g, 94%) (Found: C, 75.0; H, 10.4. Calc. for $C_{21}H_{37}AlO$: C, 75.9; H, 11.1%). ^{1}H NMR (C_6D_6): 0.60 (s, 12H, $AlMe_2$), 1.40 (s, 18H, *p*-Bu^t), 1.50 (s, 36H, *o*-Bu^t), 5.52 (s, 4H, CH_2Ar), 7.6 [s, 4H, 3,4-*H*(Ar)].

Synthesis of **2**

2,6-Di-t-butylphenol was distilled at 100°C and 10^{-3} torr prior to use. The distillate solidified upon cooling. Trimethylaluminium (20 cm^3, 2 mol dm^{-3}, 400 mmol) was added to a hexane solution (150 cm^3) of the phenol (5.00 g, 24 mmol). The reaction mixture was warmed to 60°C for 8 h, then stirred for 24 h at *ca* 25°C and filtered. The filtrate was concentrated (to *ca* 10 cm^3) and cooled (−78°C) to give white crystals of **2** (4.1 g, 74%), m.p. 95–97°C (Found: C, 77.1; H, 9.4. Calc. for $C_{29}H_{45}AlO_2$: C, 76.9; H, 10.0%). The white crystals rapidly turned dark green in air.

Synthesis of **3**

2,4-Di-t-butylphenol was distilled at 120°C and 5×10^{-3} torr prior to use. The preparation, scale and work-up were as described for the bisaryloxide **2**. Crystals of **3** (4.3 g, 68%), m.p. 158–159°C, were obtained from hexane. The mass spectrum gave the following peaks (*m/z*) (assignments in parentheses): 509 $[\{AlMe_2(OAr'')\}_2\text{-}Me]^+$; 262 $[\{AlMe_2(OAr'')\}]^+$; 247 $[AlMe(OAr'')]^+$ and 232 $[Al(OAr'')]^+$.

X-ray structure of **1**

X-Ray quality crystals of the alkoxide **1** were recrystallized from *n*-hexane at −30°C. A crystal of dimensions *ca* $0.40\times0.20\times0.22$ mm was mounted and sealed under argon in a Lindemann capillary. Intensities for $+h\pm k\pm l$ reflections with $2<\theta<25°$ were measured in the $\theta/2\theta$ mode with a scan width of $\Delta\theta=(0.8+0.35\tan\theta)°$, with a maximum scan time of 1 min.

Two standard reflections monitored every hour showed no significant variation. Data were corrected for Lp effects but not for absorption and, after averaging any equivalent reflections, 2663 reflections with $|F^2|>\sigma(F^2)$ were used in the structure refinement. The values of $\sigma(F^2)$ were taken as $[\sigma^2(I)+0.02(I)^2]^{1/2}$/Lp.

Crystal data. $C_{42}H_{74}Al_2O_2$, $M=665.02$, triclinic, $a=10.043(2)$, $b=10.399(2)$, $c=12.446(2)$ Å, $\alpha=103.50(1)$, $\beta=98.41(2)$, $\gamma=113.63(1)°$, $U=1115.3$ Å^3, $Z=1$, $D_c=0.99$ g cm^{-3}, $F(000)=368$. Monochromated Mo-K_α radiation, $\lambda=0.71069$ Å, $\mu=0.90$ cm^{-1}. Space group $P\bar{1}$.

The structure was solved by direct methods using the MULTAN program.[11] The Al, O and C atoms were refined with anisotropic temperature factors by full-matrix least-squares. The H atoms were initially located by a difference map and then refined isotropically, except for those in the 4-Bu^t group which were fixed at calculated positions (C—H, 1.08

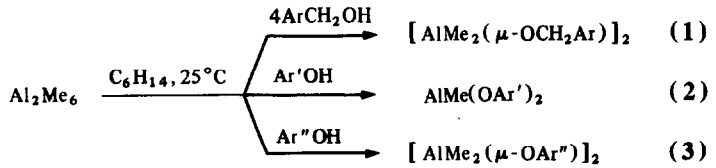

Scheme 1. Reactions of Al_2Me_6 with 2,4,6-$Bu^t_3C_6H_2CH_2OH$ ($ArCH_2OH$), 2,6-di-t-butylphenol (Ar'OH) or 2,4-di-t-butylphenol (Ar"OH).

Å). Refinement converged at $R = 0.074$, $R' = 0.087$ when the maximum shift/error was 0.3 and the weighting scheme was $w = 1/\sigma^2(F)$. A final difference map showed no peaks at > 0.5 e Å^{-3}. The structure solution and refinement were carried out using a PDP 11/34 computer and the Enraf–Nonius Structure Determination Package. Scattering factors for neutral atoms were taken from ref. 12. Tables of atom coordinates, thermal parameters and remaining bond lengths and angles are available from the Cambridge Crystallographic Data Centre. A list of final structure factors is available from one of the authors (P.B.H.).

RESULTS AND DISCUSSION

The routes to the new aluminium alkoxides and aryloxides **1–3** are summarized in Scheme 1. Selected interatomic distances and angles for the alkoxide **1** are in Table 1, the molecular structure being illustrated in Fig. 1 together with the atom numbering scheme.

Noteworthy features relating to the formation of the alkoxide **1** are, firstly, that reaction with an excess of the benzylic alcohol $ArCH_2OH$ under ambient conditions did not lead to further substitution of a methyl group on aluminium and, secondly,

Table 1. Selected intramolecular distances (Å) and angles (°) with ESDs in parentheses for $[Al(\mu\text{-}OCH_2Ar)Me_2]_2$ (Ar = $C_6H_2Bu^t_3$-2,4,6) (**1**)

(a) Bonds

Al—O	1.841(3)	Al—O'[a]	1.858(2)
Al—C(20)	1.939(5)	Al—C(21)	1.959(6)
O—C(19)	1.443(4)	C(19)—C(1)	1.507(4)
C(1)—C(2)	1.412(5)	C(1)—C(6)	1.410(5)
C(2)—C(3)	1.378(5)	C(2)—C(7)	1.554(6)
C(3)—C(4)	1.383(6)	C(4)—C(5)	1.375(5)
C(4)—C(8)	1.526(5)	C(5)—C(6)	1.384(5)
C(6)—C(9)	1.552(6)	C(7)—C(10)	1.530(7)
C(7)—C(11)	1.541(6)	C(7)—C(12)	1.549(6)
C(8)—C(16)	1.423(9)	C(8)—C(17)	1.421(11)
C(8)—C(18)	1.340(10)	C(9)—C(13)	1.520(8)
C(9)—C(14)	1.543(8)	C(9)—C(15)	1.547(5)

(b) Angles

O—Al—O'[a]	79.8(1)	O—Al—C(20)	118.5(2)
O—Al—C(21)	117.1(2)	O'—Al—C(20)[a]	110.3(2)
O'—Al—C(21)[a]	110.4(1)	C(20)—Al—C(21)	114.8(2)
Al—O—Al'[a]	100.2(1)	Al—O—C(19)	134.5(2)
Al'—O—C(19)[a]	125.3(2)	O—C(19)—C(1)	108.9(3)
C(19)—C(1)—C(2)	119.6(2)	C(19)—C(1)—C(6)	119.8(3)
C(2)—C(1)—C(6)	120.1(3)	C(1)—C(2)—C(3)	117.3(4)
C(1)—C(2)—C(7)	123.3(3)	C(3)—C(2)—C(7)	119.1(3)
C(2)—C(3)—C(4)	123.4(3)	C(3)—C(4)—C(5)	116.6(4)
C(3)—C(4)—C(8)	121.6(3)	C(5)—C(4)—C(8)	121.7(4)
C(4)—C(5)—C(6)	123.5(4)	C(1)—C(6)—C(5)	117.2(3)
C(1)—C(6)—C(9)	122.8(3)	C(5)—C(6)—C(9)	119.6(4)

[a] Symmetry element, ', is $-x, -y, -z$.

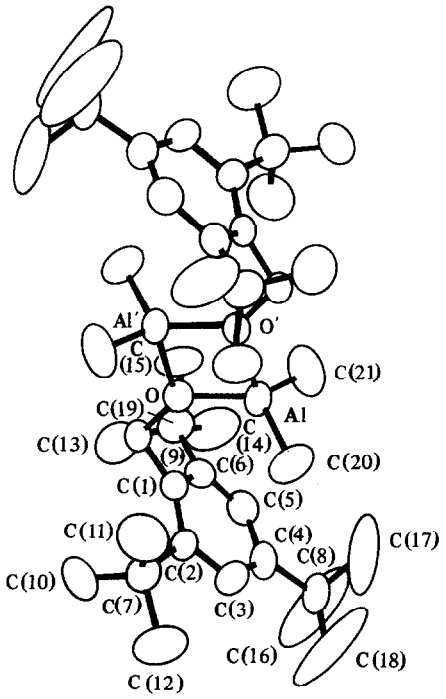

Fig. 1. The molecular structure and atom numbering scheme for crystalline $[Al(\mu\text{-}OCH_2C_6H_2Bu^t_3\text{-}2,4,6)Me_2]_2$ (**1**).

that the compound was at least moderately thermally stable and showed no inclination to undergo cyclometallation below 100°C. Regarding the lack of reactivity with an excess of the alcohol, this may reflect the strength of the bridging and the limited nucleophilicity of the reagent. NMR data showed no evidence of dissociation of the dimer in solution. The fact that bridging is through the oxygen rather than involving one of the methyl groups attached to the aluminium is not surprising. Related compounds include $[AlMe_2(\mu\text{-}OBu^t)]_2$ (**4**),[13] $[AlBr_2(\mu\text{-}OSiMe_3)]_2$ (**5**)[14] and $[AlMe_2(\mu\text{-}OAlMe_2)]$ (**6**).[15]

The reactions involving the two phenols were carried out using an excess of trimethylaluminium because we sought to obtain the mono-aryloxides. Rather similar reaction conditions were employed to those for the benzoxide, namely the use of a hydrocarbon solvent at ambient temperature. Nevertheless, unexpectedly, the more hindered phenol Ar′OH (Ar′ = $C_6H_3Bu^t_2$-2,6) reacted to yield the bisaryloxide **2**. This suggests that Ar′OH reacts much faster with $AlMe_2(OAr')$ than with $AlMe_3$, perhaps because the former, unlike the latter, is a monomer, as established by X-ray crystallography for the related compound $AlMe(OC_6H_2Bu^t_2\text{-}2,6\text{-}Me\text{-}4)_2$.[8] Consistent with this is the observation that the isomeric and less hindered phenol Ar″OH (Ar″ = $C_6H_3Bu^t_2$-2,4) gave the mono-substituted compound **3**, which is believed to be a dimer and, based on analogy with complex **1**, is formulated as having the structure $[AlMe_2(\mu\text{-}OAr'')]_2$. The evidence for the dimeric formulation comes from the EI mass spectrum which shows the highest peak corresponding to a dimeric parent (*P*) minus a methyl, $(P-Me)^+$.

The aryloxide **3** was reasonably stable in air. By contrast, the bisaryloxide **2** rapidly turned dark green upon exposure to the atmosphere, consistent with the monomer formulation. Heating either the melt of **2** at 200°C for 1 h, or a benzene solution under reflux for 30 days, provided no evidence for cyclometallation, but only slight decomposition. Likewise, the monoaryloxide **3** did not eliminate methane when heated in a benzene solution under reflux for 3 weeks; under these conditions, $AlMe_2(NHAr)$ gave the cyclometallated product $AlMe(NHAr)$.[16]

The centrosymmetric dimeric crystalline molecule **1** (Fig. 1) has a planar Al_2O_2 framework. The four-membered ring mean plane bisects the two methyl groups bonded to the aluminium atom. The carbon atom C(19) bonded to the oxygen atom is *ca* 0.03 Å below the plane. The aromatic plane [C(1) to C(6)] forms an angle of 89.3° with the Al_2O_2 plane. The central carbon atoms C(7) and C(9) of the 2- and 6-Bu^t groups are *ca* 0.35 and 0.37 Å below the aromatic plane, respectively, whilst C(19) is *ca* 0.54 Å above the aromatic plane, as a result of the steric strain.

The Al—O and Al—O′ bond lengths of 1.841(3) and 1.858(2) Å, respectively, are similar to that [1.864(6) Å] found by electron diffraction in the same ring in gaseous **4**,[13] but are significantly longer than those found in crystalline **5** [1.80(2) Å],[14] or **6** [1.80(2) Å].[15] The C—O bond distance, 1.443(4) Å, is unexceptional. The intramolecular non-bonded Al···Al′ distance, 2.84 Å, is similar to that found in gaseous **4**, 2.82 Å,[13] while the corresponding non-bonded O···O′ distance of 2.37 Å is slightly shorter than that in **4**, 2.44 Å; this may be a reflection of steric effects. The internal angles within the Al_2O_2 ring are rather similar to those found in gaseous **4**, that at aluminium, 79.8(1)°, being smaller than that at oxygen, 100.2(2)°; these values may be compared with those of 81.9(7) and 98.1(7)° for the corresponding angles in **4**.[13]

The tetrahedral coordination environment at the Al atom is extremely irregular, as evident from the following values: O—Al—O′ 79.8(1), O—Al—C(20) 118.2(5), O—Al—C(21) 117.1(2) and C(20)—Al—C(21) 114.8(2)°. The sum of the angles at the O atom is 360°; corresponding to a trigonal planar environment at O.

The two substituted benzyl groups on the O atom are in a mutually *trans* position.

The endocyclic angles at the 2-, 4- and 6-C atoms of the Ar group are smaller than those in the other positions, presumably because of the bulky substituents.

Acknowledgements—We are grateful to the EEC (Simulation Contract: ST200335), SERC (H.D.W.) and the Government of Iraq (H.A.J.) for their support.

REFERENCES

1. (a) A. W. Duff, R. A. Kamarudin, M. F. Lappert and R. J. Norton, *J. Chem. Soc., Dalton Trans.* 1986, 489; (b) A. Antiñolo, G. S. Bristow, G. K. Campbell, A. W. Duff, P. B. Hitchcock, R. A. Kamarudin, M. F. Lappert, R. J. Norton, N. Sarjudeen, D. J. W. Winterborn, J. L. Atwood, W. E. Hunter and H. Zhang, *Polyhedron* 1989, **8**, 1601.
2. P. B. Hitchcock, M. F. Lappert and A. Singh, *J. Chem. Soc., Chem. Commun.* 1983, 1499; P. B. Hitchcock, M. F. Lappert and R. G. Smith, *Inorg. Chim. Acta* 1987, **139**, 183.
3. G. B. Deacon, P. B. Hitchcock, S. A. Holmes, M. F. Lappert, P. MacKinnon and R. H. Newnham, *J. Chem. Soc., Chem. Commun.* 1989, 935.
4. cf. I. P. Rothwell, *Polyhedron* 1985, **4**, 177.
5. E. Müller, P. Ziemek and A. Rieker, *Tetrahedron Lett.* 1964, 207; A. Rieker, *Angew. Chem. Int. Ed. Engl.* 1964, **3**, 654.
6. K. B. Starowieyski, S. Pasynkiewicz and M. Skowrońska-Ptasińska, *J. Organomet. Chem.* 1975, **90**, C4.
7. M. Skowrońska-Ptasińska, K. B. Starowieyski, S. Pasynkiewicz and M. Carewska, *J. Organomet. Chem.* 1978, **160**, 403.
8. J. M. Bollinger, M. B. Comisarow, C. A. Cupas and G. A. Olah, *J. Am. Chem. Soc.* 1967, **89**, 5687.
9. A. P. Shreve, R. Mulhaupt, W. Fultz, J. Calabrese, W. Robbins and S. D. Ittel, *Organometallics* 1988, **7**, 409.
10. M. D. Healy, D. A. Wierda and A. R. Barron, *Organometallics* 1988, **7**, 2543.
11. G. Germain, P. Main and M. M. Woolfson, *Acta Cryst.* 1971, **A27**, 360.
12. *International Tables for X-Ray Crystallography*, Vol. 4. Kynoch Press, Birmingham (1974).
13. A. Haaland and O. Stokbeland, *J. Organomet. Chem.* 1975, **94**, 345.
14. M. Bonamico, G. Dessy and C. Ercolani, *J. Chem. Soc., Chem. Commun.* 1966, 24.
15. J. L. Atwood and M. J. Zaworotko, *J. Chem. Soc., Chem. Commun.* 1983, 302.
16. P. B. Hitchcock, H. A. Jasim, M. F. Lappert and H. D. Williams, *Polyhedron* 1989, **9**, 245.

Polyhedron Vol. 9, No. 2/3, pp. 245–251, 1990
Printed in Great Britain

0277–5387/90 $3.00+.00
Pergamon Press plc

BULKY METAL ARYLOXIDES, ARYLAMIDES AND SULPHUR AND PHOSPHORUS ANALOGUES—III.* ALUMINIUM COMPOUNDS DERIVED FROM 2,4,6-TRI-t-BUTYLANILINE; X-RAY STRUCTURE OF $[AlMe\{\mu\text{-}NHC_6H_2Bu^t_2\text{-}4,6\text{-}C(Me)_2CH_2\text{-}2\}]_2$

PETER B. HITCHCOCK, HATAM A. JASIM, MICHAEL F. LAPPERT† and HUGH D. WILLIAMS

School of Chemistry and Molecular Sciences, University of Sussex, Brighton BN1 9QJ, U.K.

Abstract—Treatment of $AlMe_3$ with $ArNH_2$ ($Ar = C_6H_2Bu^t_3$-2,4,6) in C_6H_{14} at 60°C afforded $[AlMe_2(\mu\text{-}NHAr)]_2$ (**1**). Heating the amide **1** either at 200°C for 3 h or (NMR) in C_6D_6 at 80°C for 3 weeks in a sealed tube led to methane elimination and formation of the cyclometallated compound $[AlMe\{\mu\text{-}NHC_6H_2Bu^t_2\text{-}4,6\text{-}C(Me)_2CH_2\text{-}2\}]_2$ (**2**); unexpectedly, the hydrogen atom abstracted from the NHAr ligand of **1** originated from the 2-t-butyl group rather than the NH. Deuterolysis of **2** yielded $D_2NC_6H_2Bu^t_2$-4,6-$C(Me)_2CH_2D$-2. $AlCl_3$ and $ArNH_2$ gave the 1:1 adduct $AlCl_3(NH_2Ar)$ (**3**), which upon heating either at 150°C and 10^{-4} torr or (NMR) in C_6D_6 at 80°C for 24 h gave isobutene and the retro-Friedel Crafts product $AlCl_3(NH_2C_6H_3Bu^t_2$-2,4) (**4**). An excess of LiNHAr did not react with $AlMe_3$, but with $AlCl_3$ furnished $Al(NHAr)_2Cl$ (**5**). The X-ray structure of the cyclometallated compound **2** showed it to be a pentacyclic centrosymmetric dimer, containing a central $(AlN)_2$ square [⟨Al—N⟩ 1.965(6) Å], with the adjacent six-membered unsaturated alumino-heterocycles in a twisted boat conformation, one below and the other above the $(AlN)_2$ plane and the two anilido ligands in a *transoid* arrangement. The preparation of the metal anilides M(NHAr) [M = Li (**6**), $SiMe_3$ (**7**) or $SnMe_3$ (**8**)] is described.

We have introduced the sterically demanding arylamido ligand NHAr ($Ar = C_6H_2Bu^t_3$-2,4,6) into coordination chemistry in the context of complexes of Li,[1,2] B,[3] Sn^{II},[1] P^{III},[4,5] As^{III},[4,5] P^{III}/Li,[5] P^{III}/Al^5 and Ni^{II}.[1]

Secondary amido–metal complexes L_nM—NHR are much less well known than tertiary analogues (L_nM—NRR′), because of their frequently encountered intermolecular amine elimination to form the bis(metallo)amine L_nM—N(R)—ML_n;[6] a bulky group R, such as R = Ar, is expected to hinder such an associative decomposition pathway. Alternatively, the amide L_nM—NHR, by virtue of its NH proton, may participate in alkane elimination, as in the conversion of an alkylaminoalane into an alkyliminoalkane [e.g.[7] *cis*- or *trans*-$\{AlMe_2(\mu\text{-}NHPr^i)\}_2 \rightarrow$ *trans*-$\{AlMe(\mu\text{-}NPr^i)\}_{4 \text{ or } 7}$].

The NHAr ligand is of further interest because of its potential for geometrical isomerism; for example, $[Li(\mu\text{-}NHAr)(OEt_2)]_2$ has the two aryl groups arranged in a *transoid* fashion.[1] Another feature, directly attributable to its substantial steric requirements, is the capacity of the ligand NHAr to stabilize unusual partners; e.g. the compounds $B(NHAr)X_2$ (X = F, Cl, or NH_2) were found to be unexpectedly thermally stable with respect to HX elimination.[3]

The reaction between trimethylaluminium and a series of anilines was first investigated by Smith and co-workers.[8] They observed that the reaction between $AlMe_3$ and the aniline $R'NH_2$ afforded $[AlMe_2(NHR')]_m$ ($m = 2$ for $R' = 2\text{-}MeC_6H_4$; X-ray), which on heating, yielded $[AlMe(NR')]_n$ [$n = 6$ for R′ = Ph (**I**) (see Scheme 1); X-ray] [R′ = R′ 2- or 4-MeC_6H_4, or 2,6-$Me_2C_6H_3$]. Using the more sterically hindered 2,6-di(isopropyl)aniline Ar″NH_2, Power and co-workers found that the ambient temperature product $[AlMe_2(\mu\text{-}NHAr'')]_2$ upon heating at 170°C afforded the iminoalane $[AlMe(\mu\text{-}NAr'')]_3$ (**II**) (Scheme 1); this was of special interest, because it

* For Part II, see ref. 13.

† Author to whom correspondence should be addressed.

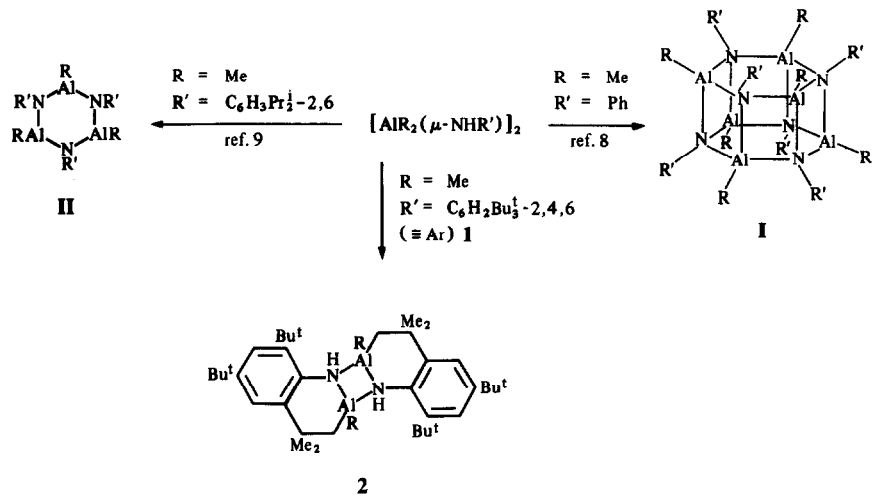

Scheme 1. Thermolysis products of three arylamino(dimethyl)alanes; in each case methane was the co-product.

provided the first example of an Al—N compound having both Al and N in a three-coordinate environment, an AlN borazine analogue.[9] Curiously we have found[10] that for the even more sterically crowded 2,4,6-tri-t-butylaniline system, an iminoalane was not observed but instead **1** afforded the cyclometallated product (**2**) (Scheme 1); these results are now presented in full.

Cyclometallation in the context of a 2,4,6-tri-t-butylphenyl derivative of P^{III} (**III**) [R = CH(SiMe$_3$)$_2$][11] or As^{III} (**IV**)[5] had previously been noted; and the topic has been reviewed in the context of 2,6-di-t-butylphenoxometal complexes.[12] However, the complexes [AlMe$_2$(μ-OC$_6$H$_3$Bu$^t_2$-2,4)]$_2$ were thermally stable.[13] A rare example of a cyclometallation in aluminium chemistry is the formation of **V** by thermolysis of 2-phenyl-1-(diphenylalumino)benzene.[14]

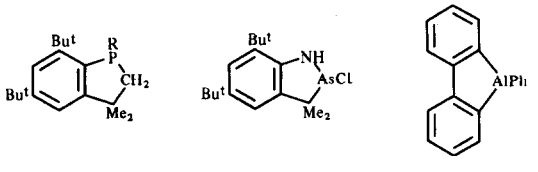

The chemistry[15] and spectroscopy[16] of base adducts of AlCl$_3$ is well documented. The crystalline pyridine adduct of AlCl$_3$ has the structure [AlCl$_2$(py)$_4$][AlCl$_4$].[17]

Numerous chloro(amino)alanes and chloro(imino)alanes are known,[6] such as the dimeric AlCl(NMe$_2$)$_2$[18] and the tetrameric AlCl(NPr^i).[19]

EXPERIMENTAL

Materials, measurements and techniques

2,4,6-Tri-t-butylaniline, ArNH$_2$ (from ArH, via ArNO$_2$),[20] and [Li(μ-NHAr)(OEt$_2$)]$_2$[1] were prepared by published methods. Manipulative procedures for the air-sensitive aluminium compounds and their precursors were described in Part II;[13] IR, NMR and EI mass spectra were obtained using Perkin–Elmer FT1700, Bruker WP80 or WM360 and Kratos MS80RF, respectively.

Synthesis of Li(NHAr) (**6**)

LiBu^n in hexane (20 cm^3, 1.5 mol dm^{-3}, 30 mmol) was syringed into a solution containing the freshly sublimed ArNH$_2$ (6.00 g, 22.98 mmol) in hexane (100 cm^3) at *ca* 25°C. A white precipitate was immediately formed. The reaction mixture was refluxed for 3 h, cooled and filtered. The insoluble 2,4,6-tri-t-butylanilidolithium (**6**) (5.6 g, 92%), m.p. *ca* 300°C (decomp.), was washed with hexane (20 cm^3) to remove any residual n-butyl-lithium and then pumped dry. In repeat experiments, the yield was in the range 85–95%. Compound **6** was not sublimable at 250°C and 10^{-4} torr without complete decomposition.

Synthesis of Me$_3$Si(NHAr) (**7**)

Freshly distilled chloro(trimethyl)silane (1.05 cm^3, 0.90 g, 8.37 mmol) was added to a solution of **6** (2.2 g, 8.24 mmol) and triethylamine (5 cm^3) in

diethyl ether (150 cm^3). The reaction mixture was refluxed for 3 days and the precipitated LiCl was filtered off. Volatiles were removed from the filtrate *in vacuo*. The residue comprised 2,4,6-tri-t-butylanilino(trimethyl)silane (**7**) (2.39 g, 87%), m.p. 88°C (Found: C, 75.8; H, 11.5; N, 4.3. Calc. for $C_{21}H_{39}NSi$: C, 75.6; H, 11.8; N, 4.1%); it was purified by sublimation at 130°C and 10^{-3} torr.

Synthesis of $Me_3Sn(NHAr)$ (**8**)

The procedure was that used for the preparation of the anilinosilane (**7**), using **6** (1.00 g, 3.74 mmol), triethylamine (5 cm^3) and chloro(trimethyl)tin (1.00 g, 5.02 mmol). The 2,4,6-tri-t-butylanilido(trimethyl)tin (**8**) (1.16 g, 73%), m.p. 66–67°C, was crystallized from hexane at −30°C, but with difficulty, due to its high solubility; it sublimed at 250°C and 10^{-4} torr, but there was extensive decomposition.

Synthesis of **1**

A trimethylaluminium solution in hexane (10 cm^3, 2 mol dm^{-3}, 20 mmol) was added (10 min) to a hexane solution (100 cm^3) of $ArNH_2$ (4.00 g, 15.3 mmol). A white precipitate gradually (30 min) formed. The reaction mixture was heated with stirring at 60°C for 48 h and filtered whilst warm. Cooling the filtrate yielded colourless crystals of 2,4,6-tri-t-butylanilino(dimethyl)alane (**1**) (3.40 g, 89%), m.p. 241–244°C. ^1H NMR (C_6D_6): −0.38 (s, 6H, $AlMe_2$), 1.37 (s, 18H, 2-, 4- and 6-Bu^t), 3.8 (br, 1H, NH), 7.37 (s, 2H, 3- and 5-H).

Synthesis of
$[AlMe\{\mu\text{-}NHC_6H_2Bu^t_2\text{-}4,6\text{-}C(Me)_2CH_2\text{-}2\}]_2$ (**2**)

The anilinoalane **1** (4.00 g, 12.6 mmol) was slowly heated for *ca* 4 h at 210°C, using a Wood's alloy bath. Some foaming was observed. The cooled residue was crystallized from hexane (50 cm^3, −78°C) to furnish colourless crystals of the cyclometallated aminoalane **2** (2.5 g, 66%), m.p. 240–243°C [Found: *M* (Signer method in Et_2O), 294. $C_{18}H_{29}AlN$ requires *M*, 301]. IR (Nujol): ν(N—H) 3349(vs) cm^{-1}. ^1H and $^{13}C\{^1H\}$ NMR data are summarized in Figs 1 and 2, respectively.

In a separate experiment, the anilinoalane **1** was heated at 80°C in a sealed NMR tube. After 3 weeks, the cyclometallation to produce **2** was 75% complete. After a further 1 week, no trace of **1** was detectable.

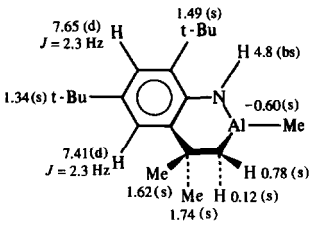

Fig. 1. Assignments of the ^1H NMR signals of **2**; spectrum at 360 MHz and 305 K.

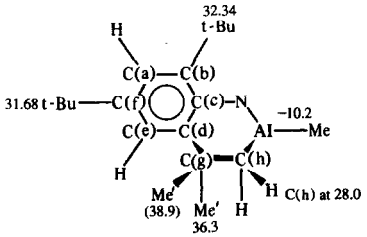

Fig. 2. Assignments of the $^{13}C\{^1H\}$ NMR signals of **2**; spectrum at 90.67 MHz and 305 K; chemical shifts only for the methyl groups of the Bu^t groups are shown.

Deuterolysis of the cyclometallated aminoalane **2**

Deuterium oxide (1 cm^3) was added dropwise to a solution of compound **2** (0.4 g, 1.33 mmol) in diethyl ether (30 cm^3). An immediate white precipitate was formed. After stirring for 3 days, the ether was removed *in vacuo* and the residue extracted into hexane (30 cm^3). The extract was concentrated and cooled to give colourless crystals of $D_2NC_6H_2Bu^t_2$-4,6-$C(Me)_2CH_2D$-2, m.p. 139°C (m.p. 137°C for the deuterium-free aniline). IR (Nujol) (trideuterated amine): ν(N—D) at 2620(m) and 2520(m) cm^{-1} [cf. for the deuterium-free amine, ν(N—H) at 3510(m) and 3440(m) cm^{-1}]. MS for the deuterium-free amine gave (*m/z*, e = 1): P^+ at 261.2457 ($C_{18}H_{31}N$ requires 261.2456) and $(P-Me)^+$ at 246.2221 [$(P-Me)^+$ requires 246.2222]; the trideuterated amine gave $(P-Me)^+$ at 249.2410 [$C_{17}H_{25}D_3N$ requires $(P-Me)^+$ at 249.2387].

Synthesis of $AlCl_3(NH_2Ar)$ (**3**)

Aluminium trichloride (1.3 g, 9.74 mmol) (sublimed twice prior to use) was added to freshly sublimed $ArNH_2$ (2.2 g, 8.43 mmol) in toluene (100 cm^3). The reaction mixture was stirred for 48 h and filtered. The filtrate upon concentration (to *ca* 20 cm^3) yielded colourless needles of **3** (2.6 g, 74%), m.p. 140°C (Found: C, 53.9; H, 8.3; N, 3.2. Calc. for $C_{18}H_{31}AlCl_3N$: C, 54.7; H, 7.9; N, 3.5%). IR (Nujol): ν(N—H) 3380(s) and 3150(br) cm^{-1},

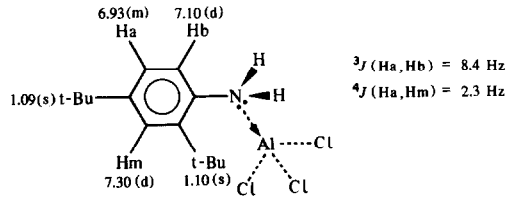

Fig. 3. Assignments of the ^{1}H NMR signals of **4**; spectrum at 80 MHz and 305 K.

$\nu(AlCl_3)$ 570(s) cm^{-1}. ^{1}H NMR data are summarized in Fig. 3.

Thermolysis of **3**, *a retro-Friedel Crafts reaction*

The adduct **3** (0.5 g, 1.26 mmol) was slowly heated for 3 h *in vacuo* at 150°C at 10^{-4} torr in a sublimation apparatus. This yielded white crystals of the sublimate $AlCl_3(H_2NC_6H_3Bu^t_2$-2,4) (**4**) (0.2 g, 47%), m.p. 110–115°C (Found: C, 48.5; H, 6.5; N, 4.2. Calc. for $C_{14}H_{23}AlCl_3N$: C, 49.6; H, 6.8; N, 4.1%). IR (Nujol): ν(N—H) 3315(s), $\nu(AlCl_3)$ 570(s) and 290(s) cm^{-1}. MS (*m/z*, e = 1; assignments in parentheses): 337 and 339 (P^+), 281 and 283 ($P-Bu)^+$, 148 $[C_6H_4(t\text{-}Bu)NH_2]^+$ and 133 $[\{C_6H_4(t\text{-}Bu)NH_2\}-Me]^+$.

In another experiment, a solution of **3** in C_6D_6 was heated at 80°C in a sealed NMR tube. After 24 h no trace of **3** was detected; complete conversion into **4** and 2-methylpropene had been effected.

Synthesis of $Al(NHAr)_2Cl$ (**5**)

LiNHAr (2.29 g, 8.57 mmol) was added to freshly sublimed $AlCl_3$ (0.4 g, 2.99 mmol) in toluene (100 cm^3) and diethyl ether (20 cm^3). The reaction mixture was stirred for 6 days, whereafter volatiles were removed *in vacuo*. The residue was extracted into hexane (50 cm^3). The extract was concentrated and cooled (to *ca* 30 cm^3 at 5°C) to afford colourless crystals of the di(anilido)aluminium chloride **5** (1.8 g, 36%), m.p. 199–201°C (Found: C, 74.6; H, 10.2; N, 4.3. Calc. for $C_{36}H_{60}AlClN_2$: C, 74.1; H, 10.3; N, 4.8%). IR (Nujol): ν(N—H) 3430(s) cm^{-1}.

X-ray structure of
$[AlMe\{\mu\text{-}NHC_6H_2Bu^t_2\text{-}4,6\text{-}C(Me)_2CH_2\text{-}2\}]_2$ (**2**)

X-ray quality crystals of the cyclometallated anilide **2** were crystallized from n-hexane at −30°C. A crystal of dimensions *ca* 0.20 × 0.30 × 0.15 mm was mounted and sealed under argon in a Lindemann capillary. Intensities of $+h \pm k \pm l$ reflections with $2 < \theta < 55°$ were measured in the $\theta/2\theta$ mode with a scan width of $\Delta\theta = (0.8+0.14\tan\theta)$ and a maximum scan time of 1 min.

Two standard reflections monitored every hour showed no significant variation. Data were corrected for Lp effects but not for absorption and, after averaging any equivalent reflections, 2711 reflections with $|F^2| > \sigma(F^2)$ were used in the structure refinement. The values of $\sigma(F^2)$ were taken as $[\sigma^2(I)+(0.02I)^2]^{1/2}$/Lp.

Crystal data. $C_{38}H_{64}Al_2N_2$, $M = 602.95$, triclinic, $a = 9.309(2)$, $b = 9.860(1)$, $c = 22.132(4)$ Å, $\alpha = 80.03(2)$, $\beta = 81.43(2)$, $\gamma = 73.84(1)°$, $U = 1910.7$ Å^3, $Z = 2$, $D_c = 1.044$ g cm^{-3}, $F(000) = 664$, Cu-K_α radiation (Ni filter), $\lambda = 1.5418$ Å, $\mu = 8.4$ cm^{-1}. Space group $P\bar{1}$.

The structure was solved by direct methods using the MULTAN program.[21] The Al, N and C atoms were refined with anisotropic temperature factors by full-matrix least-squares. The H atoms were placed at calculated positions (C—H = 1.08 Å) and held fixed with a common isotropic temperature of $B = 8.0$ Å^2. Refinement converged at $R = 0.083$, $R' = 0.095$ when the maximum shift/error was 6.9 and the weighting scheme was $w = 1/\sigma^2(F)$. A final difference map was everywhere < 0.44 e Å^{-3}. The structure solution and refinement were carried out using a PDP 11/34 computer and the Enraf–Nonius Structure Determination Package. Scattering factors were taken from ref. 22. Tables of atom coordinates, thermal parameters and remaining bond lengths and angles are available from the Cambridge Crystallographic Data Centre. A list of final structure factors is available from one of the authors (P.B.H.).

RESULTS AND DISCUSSION

The reactions leading to the new compounds **1**–**8** are summarized in Scheme 2.

The formation of *trans*-$[AlMe_2(\mu\text{-}NHAr)]_2$ (**1**) by aminolysis of trimethylaluminium with an equivalent portion of 2,4,6-tri-t-butylaniline ($ArNH_2$) is unexceptional. The structure of **1** has not been unambiguously elucidated. It is based on analogy with data from the literature[6–9] and on the ^{1}H NMR spectrum, which showed that the following pairs were magnetically equivalent: (i) the methyls on Al, (ii) the 2- and 6-Bu^t groups of Ar and (iii) the 3- and 5-hydrogens of Ar. In diethyl ether, compound **1** appeared to be the monomer $AlMe_2(NHAr)(OEt_2)_n$.

The thermolysis of the aminoalane **1** afforded the cyclometallated aminoalane **2**. This is surprising, as an iminoalane was expected: cf. the formation of the crystallographically characterized compounds **I** and **II**, from apparently analogous reactions of $[AlMe_2(\mu\text{-}NHPh)]_2$ and $[AlMe_2(\mu\text{-}NHC_6H_3Pr^i_2$-2,6)]$_2$, respectively (Scheme 1).

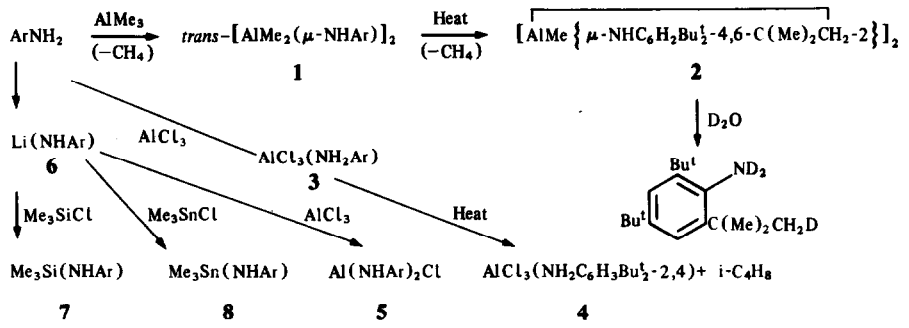

Scheme 2. Reactions of 2,4,6-tri-t-butylaniline ($ArNH_2$) leading to the aluminium derivatives **1**–**5**, and some related reactions.

The formation of **2** from **1** demonstrates an unusual cyclization in aluminium chemistry, involving unprecedented aliphatic C—H bond cleavage. It is remarkable that the methane elimination from **1** results from capture of a C*H* rather than the N*H* hydrogen by an aluminium-bound methyl group. This is attributed to a steric, rather than an electronic, effect. As for the latter, it is well known that Al—Me bonds are readily cleaved by protic reagents; the NH proton of **1** is in all probability acidic (cf. the two related reactions in Scheme 1), as is the case in P(NHAr)(:NAr) which is readily N-deprotonated by treatment with $LiBu^n$ or $AlMe_3$.[5]

The evidence for the structure of the cyclometallated anilinoalane (**2**) rests ultimately on single crystal X-ray diffraction data, *vide infra*. The ^1H and $^{13}C\{^1H\}$ NMR spectra are readily assigned, Figs 1 and 2, respectively. The fact that the pair of *C*-methyl substituents in the $AlNC_4$ ring are diastereotopic is consistent with this ring being non-planar (boat-shaped in the crystal). The presence of the NH protons is inferred both from the ^1H NMR and the IR spectra, ν(NH) 3349 cm^{-1}.

Confirmation of the cyclometallation was further demonstrated by the deuterolysis of **2** (Scheme 2). It is interesting that the *N,N*-dideuteration of $ArNH_2$ was slow, the half-life of ArNHD in C_6D_6 in the presence of D_2O being > 1 day at 300 K. This is attributed to the steric protection afforded by the 2- and 6-Bu^t groups.

The chlorobis(anilino)alane $AlCl(NHAr)_2$ (**5**) was obtained from $AlCl_3 + 2Li(NHAr)$, but was not accessible from $AlCl_3(NH_2Ar)$ (**3**). Thermolysis of **3**, did not cause the expected dehydrochlorination, but instead the retro-Friedel Crafts product, **4**, was obtained in quantitative yield.

Compound **4** was identified *inter alia* by its ^1H NMR spectrum; for assignments, see Fig. 3. The formation of **4** was shown to be accompanied by 2-methylpropene elimination, derived site-selectively from the 2-Bu^t group of **3**. When the thermolysis of **3** was carried out in C_6D_6, no $C_6D_5Bu^t$ was formed. This retro-Friedel Crafts reaction for a Group 13 metal halide–arylamine complex appears to be unprecedented. A dealkylation has been observed in a Fries rearrangement.[23]

The X-ray structure of **2** reveals two independent dimers, each lying on a crystallographic inversion centre, the mid-point of the almost square AlNAlN ring. The molecular geometry and atom numbering scheme for one of the dimers is illustrated in Fig. 4; they have the same basic features, hence the following discussion will refer to only one of the dimers. Selected geometric parameters are in Table 1.

The dimensions of the planar AlNAlN ring are very similar to those in $[AlMe_2(\mu\text{-}NMe_2)]_2$ [AlN: 1.948(7) and 1.967(7) Å, Al···Al 2.823 and N···N 2.735 Å],[24] or $[AlMe_2(\mu\text{-}NHC_6H_4Me\text{-}2)]_2$ [AlN: 1.949(7) and 1.965(7) Å].[8] The tetrahedral coor-

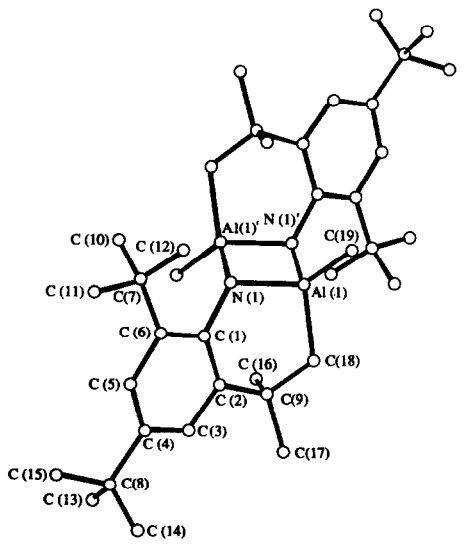

Fig. 4. The molecular structure and atom numbering scheme for crystalline **2**. Only one of the two independent molecules is shown.

Table 1. Selected intramolecular distances (Å) and angles (°) for **2** with ESDs in parentheses

(a) Bonds

Al(1)—N(1)	1.957(6)	Al(1)—N(1′)	1.973(6)
Al(1)—C(18)	1.933(8)	Al(1)—C(19)	1.966(11)
N(1)—C(1)	1.497(9)	C(1)—C(2)	1.418(9)
C(1)—C(6)	1.398(8)	C(2)—C(3)	1.419(10)
C(2)—C(9)	1.527(9)	C(3)—C(4)	1.368(9)
C(4)—C(5)	1.375(10)	C(4)—C(8)	1.581(11)
C(5)—C(6)	1.423(10)	C(9)—C(18)	1.572(13)
Al(2)—N(2)	1.973(6)	Al(2)—C(35)	1.945(8)
Al(2)—C(38)	1.944(9)	N(2)—C(20)	1.465(10)
C(20)—C(21)	1.436(11)	C(20)—C(25)	1.412(9)
C(21)—C(22)	1.389(12)	C(21)—C(28)	1.564(10)
C(22)—C(23)	1.390(10)	C(23)—C(24)	1.391(12)
C(23)—C(27)	1.549(13)	C(24)—C(25)	1.391(12)
C(25)—C(26)	1.567(12)	C(26)—C(35)	1.542(12)
Al(2)—N(2″)	1.956(7)		

(b) Angles

N(1)—Al(1)—N(1′)	88.1(3)	N(1)—Al(1)—C(18)	99.8(3)
N(1)—Al(1)—C(19)	120.9(3)	N(1′)—Al(1)—C(18)	113.9(3)
N(1′)—Al(1)—C(19)	115.1(3)	C(18)—Al(1)—C(19)	115.5(4)
Al(1)—N(1)—Al(1′)	91.9(2)	Al(1)—N(1)—C(1)	118.8(4)
Al(1)—N(1′)—C(1′)	124.2(5)	N(1)—C(1)—C(2)	120.3(5)
N(1)—C(1)—C(6)	117.2(6)	C(2)—C(1)—C(6)	122.4(6)
C(1)—C(2)—C(3)	115.5(6)	C(1)—C(2)—C(9)	128.4(6)
C(3)—C(2)—C(9)	116.1(6)	C(2)—C(3)—C(4)	123.7(7)
C(3)—C(4)—C(5)	118.7(7)	C(3)—C(4)—C(8)	120.7(6)
C(5)—C(4)—C(8)	120.5(6)	C(4)—C(5)—C(6)	122.0(6)
C(1)—C(6)—C(5)	117.4(6)	C(1)—C(6)—C(7)	125.4(6)
C(5)—C(6)—C(7)	117.1(5)	N(2)—Al(2)—N(2″)	87.8(3)
N(2)—Al(2)—C(35)	98.6(3)	N(2)—Al(2)—C(38)	121.3(3)
N(2″)—Al(2)—C(35)	116.5(3)	N(2″)—Al(2)—C(38)	112.9(3)
C(35)—Al(2)—C(38)	116.2(3)	Al(2)—N(2)—Al(2″)	92.2(3)
Al(2)—N(2)—C(20)	120.2(4)	Al(2)—N(2″)—C(20″)	120.8(4)
N(2)—C(20)—C(21)	118.1(6)	N(2)—C(20)—C(25)	122.5(7)
C(21)—C(20)—C(25)	119.3(7)	C(20)—C(21)—C(22)	118.0(6)
C(20)—C(21)—C(28)	123.3(7)	C(22)—C(21)—C(28)	118.7(7)
C(21)—C(22)—C(23)	123.2(8)	C(22)—C(23)—C(24)	117.4(8)
C(22)—C(23)—C(27)	120.0(8)	C(24)—C(23)—C(27)	122.5(7)
C(23)—C(24)—C(25)	122.6(7)	C(20)—C(25)—C(24)	119.1(7)
C(20)—C(25)—C(26)	126.2(7)	C(24)—C(25)—C(26)	114.7(6)

Symmetry element ′ is $\bar{x}$, $1-y$, $1-z$.
Symmetry element ″ is $1-x$, $1-y$, z.

dination environment at Al is extremely irregular: N(1)AlN(1)′ 88.1(3), N(1)AlC(18) 99.8(3), N(1)Al(1)C(19) 120.9(3) and C(18)Al(1)C(19) 115.5(4)°; likewise the nitrogen environment is also distorted tetrahedral.

The anilido ligands are mutually *transoid* and there is disorder in the Me moieties of the 4-Bu^t groups of dimer (a) only. Each of the two six-membered rings NAlC(18)C(9)C(2)C(1) containing the Al atoms is in a twisted boat conformation, one being below and the other above the $(AlN)_2$ plane; C(1) and C(18) are *ca* 0.98 and 1.74 Å above the $(AlN)_2$ plane. The methyl group bonded to Al is 1.48 Å out of the $(AlN)_2$ plane in a direction opposite to that of the six-membered ring. The C(1)—C(6) plane forms an angle of 105.7° with respect to the $(AlN)_2$ plane in dimer (a), while in dimer (b) this angle is 103.2°.

The endocyclic angles at the substituted carbons of the aromatic ring are smaller than the others, presumably because of steric effects. The central carbon atoms of the *o*-Bu^t group, C(7), lies in the

aromatic plane; while C(9), the central carbon of the CMe_2 moiety, is *ca* 0.11 Å above the plane and the N atom is *ca* 0.17 Å below the plane.

Acknowledgements—We are grateful to SERC (H.D.W.) and the government of Iraq (H.A.J.) for grants.

REFERENCES

1. B. Çetinkaya, P. B. Hitchcock, M. F. Lappert, M. C. Misra and A. J. Thorne, *J. Chem. Soc., Chem. Commun.* 1984, 148.
2. T. Fjeldberg, P. B. Hitchcock, M. F. Lappert and A. J. Thorne, *J. Chem. Soc., Chem. Commun.* 1984, 822.
3. P. B. Hitchcock, H. A. Jasim, M. F. Lappert and H. D. Williams, *J. Chem. Soc., Chem. Commun.* 1984, 662.
4. P. B. Hitchcock, M. F. Lappert, A. K. Rai and H. D. Williams, *J. Chem. Soc., Chem. Commun.* 1986, 1633.
5. P. B. Hitchcock, H. A. Jasim, M. F. Lappert and H. D. Williams, *J. Chem. Soc., Chem. Commun.* 1986, 1634.
6. Cf. M. F. Lappert, P. P. Power, A. R. Sanger and R. C. Srivastava, *Metal and Metalloid Amides*. Ellis Horwood, Chichester (1980); M. Cesari and S. Cucinella, in *The Chemistry of Inorganic Homo- and Heterocycles* (Edited by I. Haiduc and D. W. Sowerby), Vol. 1, Ch. 6. Academic Press, London (1987).
7. S. Amirkhalili, P. B. Hitchcock, A. D. Jenkins and J. D. Smith, *J. Chem. Soc., Dalton Trans.* 1981, 377; G. Del Piero, M. Cesari, G. Dozzi and A. Mazzei, *J. Organomet. Chem.* 1977, **129**, 281; S. Cucinella, T. Salvatori, C. Busetto and M. Cesari, *J. Organomet. Chem.* 1976, **21**, 137.
8. A.-A. I. Al-Wassil, P. B. Hitchcock, S. Sarisaban, J. D. Smith and C. L. Wilson, *J. Chem. Soc., Dalton Trans.* 1985, 1929.
9. K. M. Waggoner, H. Hope and P. P. Power, *Angew. Chem. Int. Ed. Engl.* 1988, **27**, 1699.
10. H. D. Williams, D.Phil. thesis, University of Sussex (1985).
11. B. Çetinkaya, P. B. Hitchcock, M. F. Lappert, A. J. Thorne and H. Goldwhite, *J. Chem. Soc., Chem. Commun.* 1982, 691.
12. I. P. Rothwell, *Polyhedron* 1985, **4**, 177.
13. B. Çetinkaya, P. B. Hitchcock, H. A. Jasim, M. F. Lappert and H. D. Williams, *Polyhedron* 1990, **9**, 239.
14. J. J. Eisch and W. C. Kaska, *J. Am. Chem. Soc.* 1962, **84**, 1502; 1966, **88**, 2976.
15. Cf. N. N. Greenwood and K. Wade, in *Friedel Crafts and Related Reactions* (Edited by G. A. Olah), Vol. 1, Ch. 7. Wiley, New York (1963).
16. I. M. Vezyosi, A. F. Zanoli and G. Peyronel, *Spectrochim. Acta* 1981, **37A**, 593.
17. P. Pullmann, K. Hensen and J. W. Bats, *Z. Naturfor.* 1982, **37B**, 1312.
18. J. K. Ruff, *J. Am. Chem. Soc.* 1961, **83**, 2835.
19. H. Nöth and P. Wolfgardt, *Z. Naturfor.* 1976, **31B**, 697.
20. L. R. C. Barclay and E. E. Betts, *Can. J. Chem.* 1955, **33**, 672; J. Burgers, M. A. Hoefnagel, P. E. Verkade, H. Visser and B. M. Wepster, *Rec. Trav. Chim. Pays-Bas* 1958, **77**, 491.
21. G. Germain, P. Main and M. M. Woolfson, *Acta Cryst.* 1971, **A27**, 360.
22. *International Tables for X-Ray Crystallography*, Vol. 4. Kynoch Press, Birmingham (1974).
23. R. Martin, *Bull. Soc. Chim. Fr.* 1973, **12**, 4694.
24. G. M. McLaughlin, G. A. Sim and J. D. Smith, *J. Chem. Soc., Dalton Trans.* 1972, 2197.

Polyhedron Vol. 9, No. 2/3, pp. 253–255, 1990
Printed in Great Britain

0277–5387/90 $3.00+.00
© 1990 Pergamon Press plc

KINETIC CONTROL IN THE ALCOHOLYSIS REACTION INVOLVING HEXAKISDIMETHYLAMIDODIALUMINIUM AND TERT-BUTANOL. PREPARATION, CRYSTAL AND MOLECULAR STRUCTURES OF $Al(OBu^t)_3(HNMe_2)$ AND $Al_2(NMe_2)(OBu^t)_5$

MALCOLM H. CHISHOLM,* VINCENT F. DiSTASI and WILLIAM E. STREIB

Department of Chemistry and Molecular Structure Center, Indiana University, Bloomington, IN 47405, U.S.A.

Abstract—Addition of excess Bu^tOH to hydrocarbon solutions of $Al_2(NMe_2)_6$ yields $Al(OBu^t)_3(HNMe_2)$ and $Al_2(OBu^t)_6$ as kinetic and thermodynamic products, respectively, by way of a remarkably persistent intermediate $Al_2(NMe_2)(OBu^t)_5$.

The addition of alcohols to metal amides provides a general route to metal alkoxides and often is successful where other routes based on metathetic reactions involving metal halides fail.[1] We report here some observations of the addition of Bu^tOH to $Al_2(NMe_2)_6$[2] that reveal some rather interesting mechanistic aspects of the alcoholysis reaction leading to $Al_2(OBu^t)_6$.[3]

Addition of excess Bu^tOH (as the benzene/Bu^tOH azeotrope, 37% by weight Bu^tOH) to hydrocarbon solutions of $Al_2(NMe_2)_6$ generates an exothermic reaction. Removal of the solvent under a dynamic vacuum yields a white solid $Al(OBu^t)_3(HNMe_2)$ that sublimes at 40–50°C, 10^{-1} torr (house vacuum).† Crystals of $Al(OBu^t)_3(HNMe_2)$ were obtained from toluene at −15°C. In the solid state there are two crystallographically-independent hydrogen bonded dimers $[Al(OBu^t)_3(HNMe_2)]_2$, each having a centre of symmetry‡ (see Fig. 1). The two crystallographically different monomer units $Al(OBu^t)_3(HNMe_2)$ differ little with respect to the central AlO_3N core. The greatest variation in structural parameters is associated with the Al—O—C angles.

$Al(OBu^t)_3(HNMe_2)$ loses $HNMe_2$ in refluxing toluene with an N_2 purge, and the white crystalline compound $Al_2(OBu^t)_6$ is obtained upon subsequent crystallization at −15°C. $Al_2(OBu^t)_6$ does not react with $HNMe_2$(excess) in hydrocarbon solutions at room temperature and by ^1H NMR in benzene-d_6

* Author to whom correspondence should be addressed.

† Dry and oxygen-free solvents and atmospheres (N_2) were used throughout. Satisfactory elemental analyses have been obtained for C, H and N. ^1H NMR data at 22°C, 300 MHz in C_6D_6: $Al(OBu^t)_3(HNMe_2)$: OBu^t, δ 1.46, s, 27H; $HNMe_2$, δ 1.84, d, 6H, $^3J_{HH}$ = 6.3 Hz; $Al_2(NMe_2)(OBu^t)_5$: NMe_2, δ 2.41, s, 6H; OBu^t, δ 1.50, s, 9H; δ 1.37, s, 36H.

‡ Crystal data for $Al(OBu^t)_3(HNMe_2)$ at −155°C: a = 17.244(2), b = 13.033(1), c = 17.674(2) Å, β = 111.16(1)°, Z = 8, D_{calc} = 1.045 g cm^{-3} and space group $P2_1/c$. Of 5947 reflections collected using Mo-K_α ($6° < 2\theta < 45°$), 4853 reflections were unique and the 4003 reflections having $F > 3\sigma(F)$ were used in the full least-squares refinement leading to $R(F)$ = 0.058 and $R_w(F)$ = 0.062. The hydrogen atoms were refined isotropically; all other atoms were refined anisotropically. The unit cell contains two independent $Al(OBu^t)_3(HNMe_2)$ molecules. Each molecule is present as a symmetry related hydrogen-bonded dimer. There is a disorder in one of the Bu^t groups in one molecule involving carbons numbered 23–25 and hydrogen atoms 35–43. Crystal data for $Al_2(NMe_2)(OBu^t)_5$ at −159°C: a = 9.967(2), b = 15.016(3), c = 9.874(1) Å, α = 91.99(1), β = 95.61(1), γ = 97.14(1)°, Z = 2, D_{calc} = 1.056 g cm^{-3} and space group $P\bar{1}$. Of the 4501 reflections collected, 3822 reflections were unique and the 2786 reflections having $F > 3\sigma(F)$ were used in the refinement leading to $R(F)$ = 0.059 and $R_w(F)$ = 0.068. There appears to be a disorder among the hydrogen atoms of the C(17) and C(22) Bu^t ligands. All hydrogen atoms were placed in calculated positions and were assigned thermal parameters equal to one plus the isotropic equivalent of the atom to which they were bonded. In the final least-squares refinement, the non-hydrogen atoms were varied with anisotropic thermal parameters. General operating procedures have been previously described: M. H. Chisholm, K. Folting, J. C. Huffman and C. C. Kirkpatrick, *Inorg. Chem.* 1984, **23**, 1021. Fractional coordinates have been deposited with the Director, Cambridge Crystallographic Data Centre.

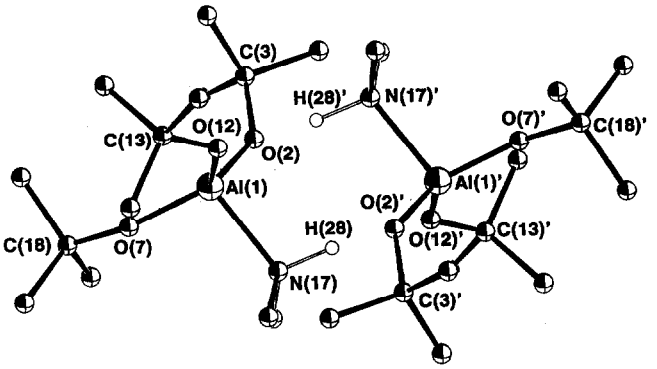

Fig. 1. An ORTEP drawing of one of the hydrogen-bonded (H(28)---O(2)′) centrosymmetric dimers found in the unit cell of $Al(OBu^t)_3(HNMe_2)$. Selected distances (Å) are: Al(1)—O(2), Al(1)—O(7), Al(1)—O(12) and Al(1)—N(17) = 1.711(2), 1.699(2), 1.744(2) and 1.977(3) and the angles (°) at Al(1) involving O(2) to O(7), —O(12) and —N(17) are 120.7(1), 114.4(1) and 98.0(1) and O(7) to O(12), —N(17) are 113.8(1) and 103.4(1), respectively.

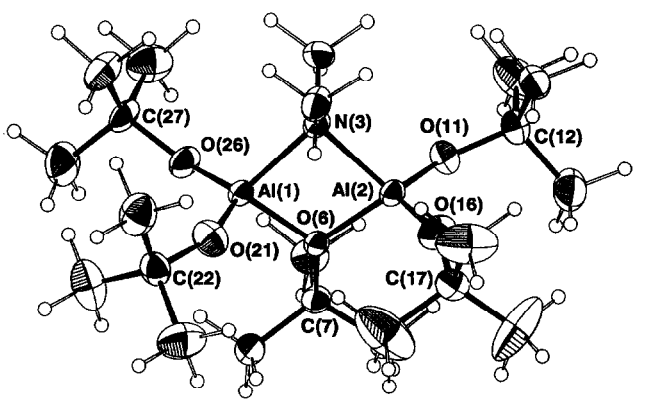

Fig. 2. An ORTEP drawing of the $Al_2(NMe_2)(OBu^t)_5$ molecule. Selected bond distances (Å) and angles (°) are: Al(1)—N(3), Al(1)—O(6), Al(1)—O(21), Al(1)—O(26) = 1.942(4), 1.819(3), 1.676(4), 1.690(4); Al(2)—N(3), Al(2)—O(6), Al(2)—O(11), Al(2)—O(16) = 1.943(4), 1.823(3), 1.697(3) and 1.671(3); O(6)—Al(1)—N(3) = 84.3(1), O(6)—Al(2)—N(3) = 84.2(1), Al(1)—O(6)—Al(2) = 98.8(1) and Al(1)—N(3)—Al(2) = 90.9(2).

the signals associated with $HNMe_2$ and $Al_2(OBu^t)_6$ are quite distinct. Thus it appears that $Al(OBu^t)_3(HNMe_2)$ is the kinetic product of the alcoholysis reaction involving $Al_2(NMe_2)_6$ and tert-BuOH, and $Al_2(OBu^t)_6$ is the thermodynamic product.

A plausible explanation of the above seemed to be that $Al(OBu^t)_3(HNMe_2)$ had a memory of the last step in the alcoholysis reaction, namely the alcoholysis of a bridged compound of formula $Al_2(\mu\text{-}NMe_2)_2(OBu^t)_4$. This notion led us to examine the alcoholysis reaction by both NMR tube experiments at low temperatures and also on the bench top with varying equivalents of added Bu^tOH. From these studies it became apparent that there is a kinetically persistent intermediate in the formation of $Al(OBu^t)_3(HNMe_2)$ but it is $Al_2(\mu\text{-}NMe_2)(\mu\text{-}OBu^t)(OBu^t)_4$ and not $Al_2(\mu\text{-}NMe_2)_2(OBu^t)_4$. $Al_2(NMe_2)(OBu^t)_5$ is the major product of the reaction between $Al_2(NMe_2)_6$ and Bu^tOH (4–5 equiv), and is present for considerable periods (2–6 h) in the presence of an excess of Bu^tOH at room temperature. $Al_2(NMe_2)(OBu^t)_5$ was crystallized from toluene at −15°C. The presence of the bridging NMe_2 and OBu^t ligands, inferred from ^1H NMR data,* was confirmed by the single crystal X-ray determination† (see Fig. 2).

Thus the kinetically slow alcoholysis step

* See footnote † on page 253.

† See footnote ‡ on page 253.

involves the replacement of the bridging NMe_2 ligand in $Al_2(NMe_2)(OBu^t)_5$. This must surely yield 1 equiv of $Al(OBu^t)_3(HNMe_2)$ and a reactive fragment $Al(OBu^t)_3$, which under reaction conditions reacts preferentially with liberated $HNMe_2$ present in solution rather than dimerizing to form $Al_2(OBu^t)_6$, the thermodynamic product.

Alcoholysis reactions involving the less sterically demanding alcohols, cyclohexanol and isopropanol are kinetically more labile and do not reveal such insight into the related steps of NMe_2 for OR substitution. The anticipated dimeric structure of $Al_2(OBu^t)_6$ has been confirmed by a single crystal X-ray structure and will be reported in a full account of this work.

Acknowledgement—We thank the National Science Foundation for support of this work.

REFERENCES

1. D. C. Bradley, R. C. Mehrotra and P. D. Gaur, in *Metal Alkoxides*. Academic Press, New York (1978).
2. J. Ruff, *J. Am. Chem. Soc.* 1961, **83**, 2835.
3. W. Wayne and H. Adkins, *Org. Synth.* 1941, **21**, 8; *Collective Volumes* 196, **3**, 48.

Polyhedron Vol. 9, No. 2/3, pp. 257–263, 1990
Printed in Great Britain

0277–5387/90 $3.00+.00
© 1990 Pergamon Press plc

STRUCTURAL AND SPECTROSCOPIC CHARACTERIZATION OF THE COMPOUNDS $[Al(NMe_2)_3]_2$, $[Ga(NMe_2)_3]_2$, $[(Me_2N)_2Al\{\mu\text{-}N(H)1\text{-}Ad\}]_2$ (1-Ad = 1-ADAMANTANYL) AND $[\{Me(\mu\text{-}NPh_2)Al\}_2NPh(\mu\text{-}C_6H_4)]$

K. M. WAGGONER, M. M. OLMSTEAD and P. P. POWER*

Department of Chemistry, University of California, Davis, CA 95616, U.S.A.

Abstract—The compounds $[Al(NMe_2)_3]_2$ (**1**), $[Ga(NMe_2)_3]_2$ (**2**), $[(Me_2N)_2Al\{\mu\text{-}N(H)1\text{-}Ad\}]_2$ (**3**) and $[\{Me(\mu\text{-}NPh_2)Al\}_2NPh(\mu\text{-}C_6H_4)]\cdot 0.5PhMe$ (**4**) have been structurally and spectroscopically characterized by X-ray crystallography, ^1H, ^{13}C, ^{27}Al, ^{69}Ga and ^{71}Ga NMR. A new synthesis is also provided for the previously known compound **1**. The structures of **1** and **2** are the first reported structures of tris-dialkylamides of aluminium or gallium. Both possess dimeric structures in the solid with dimethylamide bridges and distorted tetrahedral geometry at the metal. The terminal $-NMe_2$ groups display significant deviation from planarity in both compounds. The transamination reaction between **1** and 1 equiv. of 1-$AdNH_2$ affords **3** in high yield. The compound **4** was synthesized by treatment of $AlMe_3$ with 2 equiv. of $HNPh_2$ in refluxing toluene. The *ortho*-metallated product, **4**, is somewhat surprising in view of the prior synthesis of $Al(NPh_2)_3$ via a similar reaction. Crystal data at 130 K with Mo-K_α ($\lambda = 0.71069$ Å) radiation are as follows; **1**, triclinic, $a = 7.224(3), b = 8.545(3), c = 8.792(3)$ Å, $\alpha = 61.61(2), \beta = 85.02(3), \gamma = 88.76(3)°$, $Z = 1$, space group $P\bar{1}$, $R = 0.041$; **2**, triclinic, $a = 7.306(4)$, $b = 8.514(4)$, $c = 8.809(4)$ Å, $\alpha = 61.11(3), \beta = 85.13(4), \gamma = 89.14(4)°$, space group $P\bar{1}$, $Z = 1$, $R = 0.035$; **3**, monoclinic, $a = 8.420(5)$, $b = 18.487(6)$, $c = 10.319(5)$ Å, $\beta = 108.44(4)°$, space group $P2_1/c$, $Z = 2$, $R = 0.047$; **4**, monoclinic, $a = 16.069(6)$, $b = 13.053(5)$, $c = 16.424(4)$ Å, $\beta = 97.57(2)°$, space group $P2_1/c$, $Z = 4$, $R = 0.066$.

Compounds involving Al—N bonds have been studied for many years.[1,2] Although they are of interest in their own right they have also attracted attention because of their possible applications in catalysis,[3] as reducing agents[4] and as synthetic intermediates.[5] More recently they have engendered interest as precursors for a low temperature route to aluminium nitride.[6] Currently, aluminium amides (aminoalanes) constitute, perhaps, the most important class of Al—N compounds although the related iminoalanes $(RAlNR')_n$ display a wider variety of interesting structures whose chemistry has only been partially developed.[7,8] The structures of aluminium amides have also attracted considerable attention. A characteristic feature of most of the structures reported to date is their association through bridging of the amide ligands.[1,2] In spite of this interest there are a number of classes of aluminium amides of fundamental importance which have not been adequately characterized and on which more information, expecially structural, is desirable. For example, there are no data currently available for monomeric aminoalanes of formula $R_2AlNR'_2$. These compounds are isoelectronic to the corresponding B—P and Si—C multiply bonded compounds $R_2PBR'_2$[9] and $R_2SiCR'_2$[10] which are of considerable current interest. In addition, the number of structurally characterized trisamide derivatives of Al or the heavier main group III congeners is very few. For example, there is only one instance of a structurally characterized trisamide of Al,[11] Ga,[12] In[12] or Tl.[13]

In this paper, we report the structural characterization of compounds $[M(NMe_2)_3]_2$ (M = Al **1**, M = Ga **2**), $[(Me_2N)_2Al\{\mu\text{-}N(H)1\text{-}Ad\}]_2$ (**3**) and $[\{Me(\mu\text{-}NPh_2)Al\}_2NPh(\mu\text{-}C_6H_4)]\cdot 0.5$ PhMe (**4**). The unusual *ortho*-metallated compound **4** was synthesized during the alkane elimination reaction between 2 equiv. of $HNPh_2$.

* Author to whom correspondence should be addressed.

EXPERIMENTAL

General procedures

All reactions were performed using modified Schlenk techniques under an inert atmosphere of N_2. Solvents were freshly distilled from drying agents and degassed before use. $HNMe_2$ (Matheson), $HNPh_2$, H_2N(1-Ad), $AlCl_3$, $AlMe_3$ (Aldrich) and $GaCl_3$ (Strem) were used as received. $LiNMe_2$ was synthesized by the passage of dry $HNMe_2$ through *n*-BuLi (0.8 M) in hexane and isolation of the precipitated $LiNMe_2$ by filtration. NMR data were recorded in C_6D_6 solution on a General Electric QE-300 spectrometer. All compounds gave satisfactory C, H and N analysis.

Preparation of $[Al(NMe_2)_3]_2$ (**1**)[14] *and* $[Ga(NMe_2)_3]_2$ (**2**).[15] A hexane (40 cm^3) slurry of $LiNMe_2$ (30 mmol, 1.53 g) was added slowly, with stirring, to a cooled (ice bath) hexane (40 cm^3) solution of $AlCl_3$ (10 mmol, 1.33 g). The reaction mixture was allowed to warm to room temperature and stirred for a further 10 h. After filtration the solution was concentrated under reduced pressure to a volume of *ca* 20 cm^3. Cooling in a $-20°C$ freezer afforded **1** as colourless crystals. Yield, 1.28 g, 80.5%. M.p. = 88–89°C (ref. 14 = 87–89°C). ^1H NMR:[14] $\delta = 2.34$ (s, μ-NMe_2), 2.68(s); ^{13}C NMR: $\delta = 41.98$, 42.2 (μ-NMe_2); ^{27}Al NMR: $\delta = 107$ ($\nu_{1/2} = 840$ Hz).

$[Ga(NMe_2)_3]_2$ was synthesized in an identical manner as described in the literature[15] to afford the product as colourless crystals. Yield, 1.6 g, 79.6%. M.p. 90–91°C (ref. 15 = 90–92°C). ^1H NMR:[15] $\delta = 2.46$ (s, μ-NMe_2), 2.84(s); ^{13}C NMR: $\delta = 43.97$, 44.35 (μ-NMe_2); ^{69}Ga NMR: $\delta = 274$ ($\nu_{1/2} = 29000$ Hz); ^{71}Ga NMR: $\delta = 276$ ($\nu_{1/2} = 8400$ Hz).

Preparation of $[(Me_2N)_2Al\{\mu\text{-}N(H)1\text{-}Ad\}]_2$ (**3**). A toluene (30 cm^3) solution of H_2N(1-Ad) (0.3 g, 2 mmol) was added to a toluene (20 cm^3) solution of **1** (2 mmol, 0.318 g). The mixture was then refluxed for 18 h. The solution was slowly (over 4 h) allowed to cool to room temperature whereupon colourless crystals of the product, **3**, were observed to form. Yield, 0.36 g, 68%. M.p. dec. slowly > 350°C. ^1H NMR: $\delta = 0.3$ (s, tentative NH), $\delta = 1.9$ (complex multiplets due to 1-Ad group), $\delta = 2.75$ (s, NMe_2); ^{13}C NMR: $\delta = 30.55$, 36.54, 41.41, 45.30 (complex pattern owing to 1-Ad and NMe_2 groups); ^{27}Al NMR was not observed owing to poor solubility of **3** in C_6D_6.

Preparation of $[\{Me(\mu\text{-}NPh_2)Al\}_2NPh(\mu\text{-}C_6H_4)]\cdot 0.5PhMe$ (**4**). A toluene solution (30 cm^3) of $HNPh_2$ (10 mmol, 1.69 g) was added to a toluene (20 cm^3) solution of $AlMe_3$ (5 mmol, 2.5 cm^3 of a 2 M $AlMe_3$ solution in toluene). The mixture was then refluxed for 18 h. Upon cooling the solution was concentrated under reduced pressure to incipient crystallization. Filtration followed by cooling overnight in a $-20°C$ freezer afforded the product **4** as colourless crystals. Yield, 2.46 g (4.19 mmol), 83.7%. M.p. = 201–202°C. ^1H NMR: $\delta = -0.3$ (s, μ-AlMe), $\delta = 0.12$ (s, AlMe), $\delta = 1.8$ (s, Me, PhMe), $\delta = 5.78$–7.32 (complex multiplets); ^{13}C NMR: complex series of peaks observed between $\delta = 113.6$ and 136.86; ^{27}Al NMR: $\delta = 152$ ($\nu_{1/2} = 16000$ Hz).

X-ray crystallography

All X-ray data were collected on a Syntex $P2_1$ diffractometer equipped with a graphite monochromator and a locally modified LT-1 device for low temperature work. Important crystallographic parameters and refinement data are provided in Table 1. An omega scan method was used as described in ref. 16. Crystallographic programs used were those of SHELXTL, Version 5, installed on a Data General Eclipse computer. Scattering factors were from common sources.[17] An absorption correction was applied by using the method described in ref. 18. Final refinement was carried out using an isotropic thermal parameter for all non-hydrogen atoms and a riding model for the inclusion of hydrogen atoms in which the hydrogen isotropic thermal parameters were set at 1.2 times those for the bonded carbon. All compounds were coated with a layer of hydrocarbon oil upon removal from the Schlenk tube. A suitable crystal was selected, attached to a glass fibre with silicone grease and immediately placed in the low temperature nitrogen stream. The important metric features of **1**–**4** are provided in Table 2.

RESULTS

The compounds **1** and **2** were synthesized in excellent yields by treatment of the metal trihalide with three equivalents of $LiNMe_2$. The novel compound **3** was obtained in high yield by the transamination reaction between H_2N(1-Ad) with **1**. The *ortho*-metallated compound **4** was synthesized by treatment of $AlMe_3$ with 2 equiv. of $HNPh_2$.

Description of the structures of **1**–**4**

Drawings of structures **1** and **2** are presented in Figs 1 and 2. Important bond distances and angles for **1** and **2** are provided in Table 2. The compounds are isomorphous and they have very similar centrosymmetric, dimeric structures with dimethyl-

Table 1. Crystallographic data for the structural analyses of **1–4**

	1	**2**	**3**	**4**
Formula	$C_{12}H_{36}Al_2N_6$	$C_{12}H_{36}Ga_2N_6$	$C_{28}H_{56}Al_2N_6$	$C_{38}H_{35}Al_2N_3 \cdot 0.5C_7H_8$
Formula weight	318.42	403.90	530.76	633.74
Temperature (K)	130	130	130	130
Crystal system	Triclinic	Triclinic	Monoclinic	Monoclinic
a (Å)	7.224(3)	7.306(4)	8.420(5)	16.069(6)
b (Å)	8.545(3)	8.514(4)	18.487(6)	13.053(5)
c (Å)	8.792(3)	8.809(4)	10.319(5)	16.424(4)
α (°)	61.61(2)	61.11(3)	—	—
β (°)	85.02(3)	85.13(4)	108.44(4)	97.57(2)
γ (°)	88.76(3)	89.14(4)	—	—
V (Å^3)	475.5(3)	477.8(4)	1526(1)	3415(2)
Space group	$P\bar{1}$	$P\bar{1}$	$P2_1/c$	$P2_1/c$
Z	1	1	2	4
$D_{calc.}$ (g cm^{-3})	1.11	1.40	1.16	1.33
μ (cm^{-1})	1.52	29.7	1.19	1.15
2θ range (°)	0–55	0–55	0–50	0–50
Number of observed reflections	1620, $I > 3\sigma(I)$	1875, $I > 2\sigma(I)$	1467, $I > 3\sigma(I)$	3613, $I > 2\sigma(I)$
Number of variables	109	109	175	410
R, R_w	0.041, 0.044	0.035, 0.037	0.047, 0.048	0.066, 0.063

amide bridges. The metals possess a distorted tetrahedral coordination with the angles at the metal varying from 88.2(1) to 114.9(1)° in **1** and from 87.7(1) to 117.2(1)° in the case of **2**. The terminal and bridging Al—N distances average 1.802(2) and 1.965(2) Å, and the corresponding Ga—N bond lengths average 1.855(4) and 2.013(3) Å. The M_2N_2 cores display only minor distortions from perfectly square configurations. In both **1** and **2** the N—C distances in the bridging -NMe_2 groups are 0.03–0.04 Å longer than they are in the terminal groups. In addition, the angle between the normals to the NC_2 planes in the terminal -NMe_2 groups is 74.8° in **1** and 73.8° in **2**. The terminal -NMe_2 groups display small but significant distortions from planarity that are greatest in the gallium species. The sum of the nitrogen angles in the terminal-NMe_2 groups in **1** are: N(2) = 356.4°,

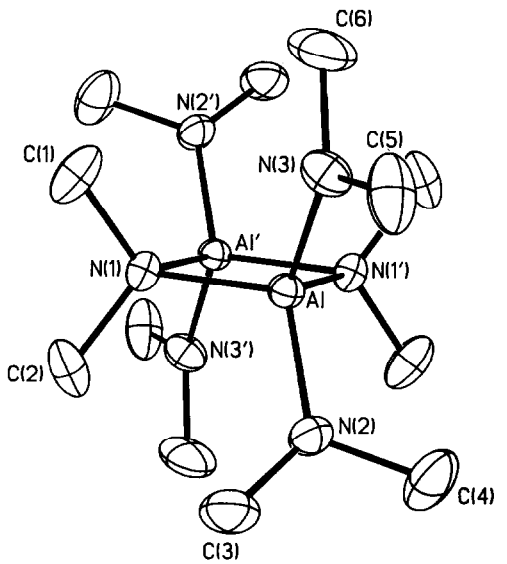

Fig. 1. Structure of $[Al(NMe_2)_3]_2$ (**1**).

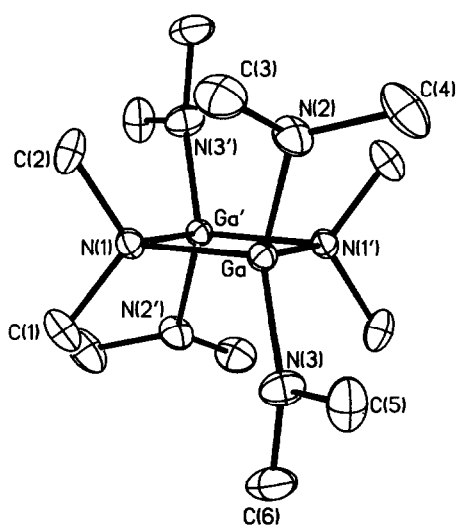

Fig. 2. Structure of $[Ga(NMe_2)_3]_2$ (**2**).

Table 2. Important bond distances (Å) and angles (°) for **1–4**

1		**2**		**3**		**4**	
Al—N(1)	1.951(2)	Ga—N(1)	2.005(2)	Al—N(1)	1.957(3)	Al(1)—N(1)	1.842(3)
Al—N(2)	1.805(2)	Ga—N(2)	1.861(4)	Al—N(2)	1.796(4)	Al(1)—N(2)	1.991(4)
Al—N(3)	1.799(2)	Ga—N(3)	1.849(4)	Al—N(3)	1.789(3)	Al(1)—N(3)	1.990(3)
Al—N(1)′	1.979(2)	Ga—N(1)′	2.021(3)	Al—N(1)′	1.938(3)	Al(2)—N(2)	2.002(3)
N(1)—C(1)	1.487(4)	N(1)—C(1)	1.478(5)	N(1)—C(1)	1.498(4)	Al(2)—N(3)	1.992(4)
N(1)—C(2)	1.493(3)	N(1)—C(2)	1.487(6)	N(1)—H	0.77(4)	Al(1)—C(37)	1.947(4)
N(2)—C(3)	1.456(3)	N(2)—C(3)	1.450(6)	N(2)—C(11)	1.447(5)	Al(2)—C(38)	1.954(4)
N(2)—C(6)	1.450(4)	N(2)—C(4)	1.453(4)	N(2)—C(12)	1.446(5)	Al(2)—C(2)	1.955(4)
Al···Al	2.822	Ga···Ga	2.902	Al···Al	2.864	N(2)—C(13)	1.464(5)
						N(2)—C(19)	1.468(5)
N(1)—Al—N(1)′	88.2(1)	N(1)—Ga—N(1)′	87.7(1)	N(1)—Al—N(1)′	85.3(1)	N(1)—C(7)	1.443(5)
Al—N(1)—Al′	91.8(1)	Ga—N(1)—Ga′	92.3(1)	Al—N(1)—Al′	94.7(1)	N(1)—C(1)	1.412(5)
C(3)—N(2)—C(4)	109.8(2)	C(3)—N(2)—C(4)	109.7(3)	C(11)—N(2)—C(12)	110.3(3)	C(1)—C(2)	1.426(6)
Al—N(2)—C(3)	126.9(2)	Ga—N(2)—C(3)	121.2(3)	Al—N(2)—C(11)	128.1(2)	C(2)—C(3)	1.396(6)
Al—N(2)—C(4)	119.7(2)	Ga—N(2)—C(4)	119.2(3)	Al—N(2)—C(12)	121.5(3)	C(3)—C(4)	1.398(6)
C(1)—N(1)—C(2)	106.7(2)	C(1)—N(1)—C(2)	107.6(3)			C(4)—C(5)	1.379(7)
						C(9)—C(10)	1.380(7)
						Al···Al	2.683
						Al(1)—N(2)—Al(2)	84.5(1)
						Al(1)—N(3)—Al(2)	84.7(1)
						N(2)—Al(1)—N(3)	85.7(1)
						N(2)—Al(2)—N(3)	85.4(1)
						Al(1)—N(1)—C(1)	125.4(3)
						Al(1)—N(1)—C(7)	117.9(3)
						Al(2)—C(2)—C(1)	123.9(3)
						C(2)—C(1)—N(1)	117.9(4)

N(3) = 358.8° and in **2** they are 350.2 and 357.5°. Thus, N(2) and N(3) deviate 0.172 and 0.065 Å from the AlC(4)C(5) and AlC(5)C(6) planes and in the gallium compound the corresponding deviations are 0.288 and 0.145 Å. The Al···Al separation is 2.822 Å; the Ga···Ga distance is significantly greater at 2.902 Å.

The structure of **3** is illustrated in Fig. 3. It has many similarities to that of **1**. The molecule possesses an inversion centre with bridging -N(H)1-Ad ligands. The coordination of the aluminium is distorted tetrahedral with the angles at the metal varying from 85.3(1) to 120.2(2)°. The terminal Al—N distances average 1.793(4) Å and the bridging bond lengths average 1.948(3) Å. The internal angles in the Al_2N_2 core are 85.3(1)° at aluminium and 94.7(1)° at nitrogen. The angle between the normals to the NC_2 in the terminal -NMe_2 group is 72°. The Al···Al separation is 2.864 Å.

The structure of **4** comprises a central $\{AlMe(\mu\text{-}NPh_2)\}_2$ core in which one of the aluminiums is also bonded to a terminal -NPh_2 group which in turn is linked to the remaining Al through an Al—C bond to one of its *ortho*-carbons. The structure includes a half molecule of toluene packed around an inversion centre. The presence of this molecule was confirmed by ^1H NMR data. Important bond distances and angles are provided in Table 2, and the structure is illustrated in Fig. 4. Both aluminiums possess distorted tetrahedral configurations. However, Al(1) differs from Al(2) in that it is bound to three nitrogens and one carbon whereas Al(2) is bonded to two nitrogens and two carbons. Within the central Al_2N_2 core the Al—N distances average 1.994(4) Å. However, the Al(1)—N distances are marginally shorter than the Al(2)—N bonds. The terminal Al(1)—N(1) distance is 1.842(4) Å. The

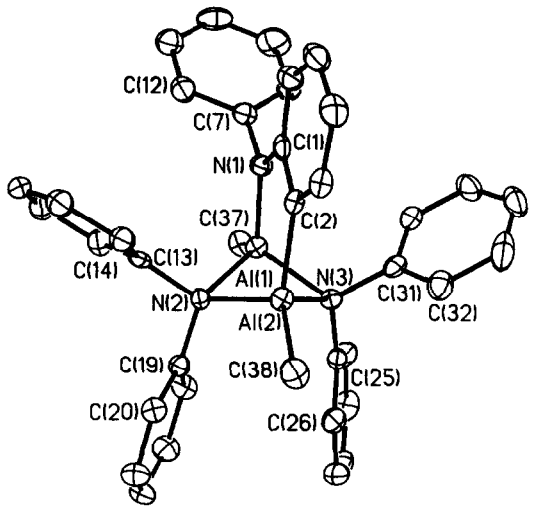

Fig. 4. Structure of $[\{Me(\mu\text{-}NPh_2)Al\}_2NPh(\mu\text{-}C_6H_4)]$ (**4**).

two Al—C(methyl) bonds are 1.947(4) Å for Al(1) and 1.954(4) Å for Al(2) and the Al(2)—(C)phenyl distance, 1.955(4) Å, is not statistically different. The Al_2N_2 core is non-planar and there is a distance of 0.3 Å between the Al(1)···Al(2) and N(2)···N(3) vectors. The atoms Al(1), N(1), C(1), C(2), Al(2) are virtually coplanar, and this plane, which includes the C(1) phenyl ring, is almost perpendicular (88.7°) to the N(2)···N(3) vector. There are large asymmetries in the angles at N(2) and N(3). For example, C(13)—N(2)···N(3) and C(31)—N(3)···N(2) angles average 147.6° whereas the C(19)—N(2)···N(3) and C(25)—N(3)···N(2) angles average 103.3°. In other words the (phenyl) C—N···N angles on the side of the *ortho*-metallated $N(Ph)C_6H_4$ group are more open by about 34°.

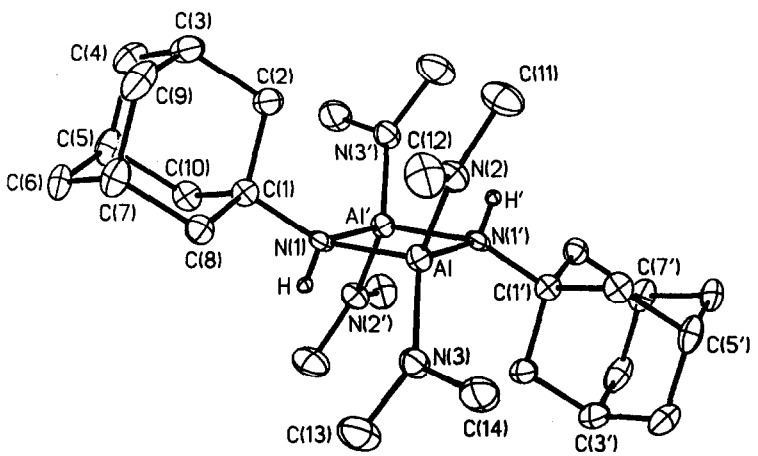

Fig. 3. Structure of $[(Me_2N)_2Al\{\mu\text{-}NCH)1\text{-}Ad\}]_2$ (**3**)

DISCUSSION

The X-ray crystal structures of **1** and **2** represent, apparently, the first structures of neutral tris-dialkylamides of aluminium and gallium. Both compounds **1** and **2** have been known for a number of years. However, the only other triamides of aluminium or gallium that have been structurally characterized are the bulky silylamide derivatives $M[N(SiMe_3)_2]_3$ (M = Al[11] or Ga[14]). These are monomeric, whereas both **1** and **2** are dimeric. The difference in structure is presumably due to the difference in size between $-NMe_2$ and $-N(SiMe_3)_2$. The ready availability of the acceptor *p*-orbitals and the relatively large size of both aluminium and gallium encourage dimerization in the case of the $-NMe_2$ ligand. On the other hand, in the case of the smaller boron atom a monomeric structure is observed for $B(NMe_2)_3$.[19] Longer N—C distances are observed in the bridging $-NMe_2$ groups presumably because of the change in hybridization from sp^2 to sp^3. The M—N bond lengths for $Al[N(SiMe_3)_2]_3$[11] and $Ga[N(SiMe_3)_2]_3$[12] are 1.78(1) and 1.857(8) Å, respectively. These distances are comparable to the terminal M—N bonds found in **1** and **2**. Longer M—N bonds would have been expected in the latter owing to the higher coordination number of the metal. It has been argued that the bond distances in the trisilylamide complexes are lengthened somewhat owing to the large size of these groups. Another explanation for the longer bonds concerns the silyl nitrogen substituents. In the case of these ligands, N⇄Si bonding competes with and may reduce N⇄M bonding. These arguments may have some validity since it appears that the bridging lengths in **1** and **2** are relatively normal when compared to other four-coordinate aluminium and gallium compounds containing the $-NMe_2$ group. For example, the bridging Al—N bonds in the dimer $(Cl_2AlNMe_2)_2$ are 1.961(6) Å long.[20] In $(Me_2AlNMe_2)_2$ they are 1.955 Å[21] and in the trimer $(H_2AlNMe_2)_3$[22] they are a little shorter at 1.93 Å. Similar observations are possible in the case of the gallium species **2**. However, the structure of the closely related $(H_2GaNMe_2)_2$[23] gives a Ga—N bond length of 2.027(4) Å which is very close to the value observed in **2**. The geometry of the terminal ligands in **1** and **2** is also of significant interest. All the terminal nitrogens show deviation from planarity and this is a rare phenomenon in metal amide chemistry. It has not, to our knowledge, been well established in other main group metal $-NMe_2$ derivatives.[23] Some non-planarity at nitrogen has however been observed in certain phosphorus amides and in geometrically restricted ligand systems.[24] It is notable that the greater deviation is observed in the gallium compound. It is thus arguable that the more diffuse *d*-orbitals in gallium may not participate in N→M interactions to as great an extent as those in the aluminium compound. This reduction might lead to the observed differences in pyramidicity. An alternative explanation is that the barriers to deformation of the nitrogen centres are small (cf. low inversion of NH_3) and crystal packing effects may give rise to the small deviations that are observed.

The reaction between **1** and 1 equiv. of H_2N(1-Ad) gives an excellent yield of the transaminated product **3**. The -N(H)1-Ad groups were observed exclusively in the bridging position and in a *trans*-configuration. A consequence of the asymmetric substitution of the bridging nitrogen atom is the tilting of the AlN(2)N(3) plane by 9.3° from the perpendicular relative to the AlN(1)Al′N(1)′ core. The tilt is, as expected, toward the least crowded (N—H) groups on both sides of the Al_2N_2 plane. The reasons for the preference of the -N(H)1-Ad ligand for the bridging position are not clear. However, it may be that the basicity of the -N(H)1-Ad ligand is greater than that of the $-NMe_2$ group and is more likely to bridge for that reason. It is unlikely that steric effects play a major role since apparently the $-NMe_2$ group readily behaves as a bridging ligand without undue steric crowding as observed in **1** and **2**. It is also perhaps noteworthy that the aluminiums are further apart in **3** than they are in **1** which is suggestive of slightly greater crowding in **3**.

The compound **4** was obtained as a somewhat unexpected product from the reaction of $AlMe_3$ with 2 equiv. of $HNPh_2$. Moreover, the product **4** is the major one from this reaction. Compounds related to **4** which have already been reported in the literature are $Al(NPh_2)_3$,[14(b)] $Al_2Me_5(\mu\text{-}NPh_2)$ **(5)**[25] and $(Me_2AlNPh_2)_2$.[26] All were synthesized by alkane elimination using various aluminium alkyls. However, no *ortho*-metallated products were observed in any of these cases. To our knowledge only one aluminium compound involving *ortho*-metallation of an $-NPh_2$ has been reported. This is the species $Cl_2AlN(Ph)(\mu\text{-}C_6H_4)Al(Cl)N(Ph)(\mu\text{-}C_6H_4)Al(Cl)NPh_2$ which was characterized on the basis of Raman and ^1H NMR spectroscopy.[27] The compound **5** has been characterized by X-ray crystallography and has an interesting dimeric structure with both a methyl and a $-NPh_2$ bridge. The complex **4** also possesses a dimeric structure and, owing to the different coordination of each aluminium, there is asymmetry in the bond distances and angles in the Al_2N_2 core. The Al(1) centre bonded to three nitrogens and one carbon has the longer bonds

owing perhaps to its greater electron density. For example, the terminal Al(1)—N(1) distance in **4** is 1.842(4) Å whereas in **1** and **3** they are about 1.8 Å long. The bridging Al—N bonds in **4** are also marginally longer than they are in **1** or **3**. Surprisingly, the three Al—C bonds have almost equal lengths even though a shorter Al(2)—C(2) bond might have been predicted on the basis of the sp^2 hybridization at carbon. Another interesting feature of this structure is that the C—C bonds in the C(1) phenyl ring are, on average, longer than those in the other five phenyl rings. There is also some evidence for an alternating pattern in the C—C ring distances suggesting some lessening of delocalization in the *ortho*-metallated ring. Although this is consistent with the somewhat lengthened average C—C bond length, it is difficult to account for this phenomenon in terms of any multiple bonding with aluminium since this bond is not unusually short.

Acknowledgements—We are grateful to the National Science Foundation for financial support and to R. A. Bartlett for technical assistance and for helpful advice and discussions.

REFERENCES

1. M. F. Lappert, A. R. Sanger, R. C. Srivastava and P. P. Power, *Metal and Metalloid Amides*. Ellis-Horwood, Chichester, U.K. (1980).
2. T. Mole and E. A. Jeffrey, *Organoaluminium Compounds*. Elsevier, Amsterdam (1972).
3. S. A. Snam, *Belg. Pat.* 1965, 654,406; *Swiss Pat.* 1967, 434749.
4. S. Cesca, M. Santoslasi, W. Marconi and N. Palladino, *Ann. Chim.* (Rome) 1965, **54**, 704.
5. H. Nöth and E. Wiberg, *Fortschr. Chem. Forsch.* 1967, **8**, 323.
6. J. F. Janik, E. N. Duesler and R. T. Paine, *Inorg. Chem.* 1987, **26**, 4341; L. V. Interrante, G. A. Sigel, M. Garbauskas, C. Hejna and G. A. Slack, *Inorg. Chem.* 1989, **28**, 252.
7. M. Cesari and S. Cucinella, in *The Chemistry of Inorganic Homo- and Heterocycles* (Edited by I. Haiduc and D. B. Sowerby), Vol. I, p. 167. Academic Press, London (1987).
8. S. Amirkhalili, P. B. Hitchcock and J. D. Smith, *J. Chem. Soc., Dalton Trans.* 1979, 1206.
9. X. Feng, M. M. Olmstead and P. P. Power, *Inorg. Chem.* 1986, **25**, 4613.
10. A. G. Brook, S. C. Nyburg, F. Abdesaken, B. Gutekunst, G. Gutekunst, R. K. M. R. Kallury, Y. C. Poon, Y.-M. Chang and W. Wong-Ng, *J. Am. Chem. Soc.* 1982, **104**, 5667.
11. G. M. Sheldrick and W. S. Sheldrick, *J. Chem. Soc. A* 1969, 2279.
12. H. Bürger, J. Cichon, U. Goetze, U. Wannagat and H. J. Wismar, *J. Organomet. Chem.* 1971, **31**, 1; Structure given in P. G. Eller, D. C. Bradley, M. B. Hursthouse and D. W. Meek, *Coord. Chem. Rev.* 1977, **24**, 1.
13. P. Krommes and J. Lorberth, *J. Organomet. Chem.* 1977, **131**, 415; R. Allmann, W. Henke, P. Krommes and J. Lorberth, *J. Organomet. Chem.* 1978, **162**, 283.
14. (a) E. Wiberg and A. May, *Z. Naturf.* 1955, **10b**, 234; (b) P. Longi, G. Mazzanti and G. Bernardini, *Gazz. Chim. Ital.* 1960, **90**, 180; (c) J. K. Ruff, *J. Am. Chem. Soc.* 1961, **83**, 2835; (d) E. C. Ashby and R. A. Kovar, *Inorg. Chem.* 1971, **10**, 893.
15. H. Nöth and P. Konrad, *Z. Naturf.* 1975, **30b**, 681.
16. H. Hope, in *A.C.S. Symposium Series No. 357* (Edited by A. L. Wayda and M. Darensbourg), Ch. 10. A.C.S. Washington, D.C. (1987).
17. *International Tables for X-ray Crystallography*, Vol. IV. Kynoch Press, Birmingham, U.K. (1974).
18. XABS: the method obtains an empirical absorption tensor for an expression relating F_o and F_c: B. Moezzi, PhD dissertation, University of California, Davis (1987).
19. A. H. Clark and G. A. Anderson, *J. Chem. Soc., Chem. Commun.* 1969, 1082.
20. T. C. Barthe, A. Haaland and D. P. Novak, *Acta Chem. Scand.* 1975, **28A**, 273.
21. H. Hess, A. Hinderer and S. Z. Steinhauser, *Z. Anorg. Chem.* 1970, **377**, 1; K. Gosling, G. M. McLaughlin, G. A. Sim and J. D. Smith, *J. Chem. Soc., Chem. Commun.* 1970, 1617; *J. Chem. Soc., Dalton Trans.* 1972, 2197.
22. K. N. Semenenko, E. B. Lobkovskii and A. L. Doronsinskii, *J. Struct. Chem.* 1972, **13**, 696.
23. P. L. Barten, A. J. Downs, D. W. H. Rankin and H. E. Robertson, *J. Chem. Soc., Dalton Trans.* 1985, 807.
24. C. Rømming and J. Songstad, *Acta. Chem. Scand.* 1978, **A32**, 689 and 1979, **A33**, 187; M. M. Olmstead, P. P. Power and M. Viggiano, *J. Am. Chem. Soc.* 1983, **105**, 2927; M. Lattman, M. M. Olmstead, P. P. Power, D. W. H. Rankin and H. E. Robinson, *Inorg. Chem.* 1988, **27**, 3012; See also in P. Molinie, R. Brec, J. Rouxel and P. Herpun, *Acta Cryst.* 1973, **29B**, 925.
25. V. R. Magnusson and G. D. Stucky, *J. Am. Chem. Soc.* 1969, **91**, 2544.
26. M. Kawai, T. Ogawa and H. Hiroto, *Bull. Chem. Soc. Jpn* 1964, **37**, 1302; N. Wiberg, W. Baumersten and P. Zahn, *J. Organomet. Chem.* 1972, **36**, 267, 277.
27. H. Hoberg, *Annalen* 1972, **766**, 142.

Polyhedron Vol. 9, No. 2/3, pp. 265–276, 1990
Printed in Great Britain

0277–5387/90 $3.00+.00
© 1990 Pergamon Press plc

POLY(PYRAZOLYL)HYDROBORATO AND POLY(PYRAZOLYL)METHANE ALUMINIUM ALKYL DERIVATIVES

ADRIAN LOONEY and GERARD PARKIN*

Department of Chemistry, Columbia University, NY 10027, U.S.A.

Abstract—Bis- and tris(pyrazolyl)hydroborato aluminium methyl derivatives, $\{\eta^3$-HB(3,5-$Me_2pyz)_3\}Al(CH_3)_2$, $\{\eta^2$-HB(3-$Bu^tpyz)_3\}Al(CH_3)_2$ and $\{\eta^2$-H_2B(3-$Bu^tpyz)_2\}Al(CH_3)_2$ have been prepared by metathesis of $Al(CH_3)_3$ with either $K\{HB(3,5\text{-}Me_2pyz)_3\}$, $Tl\{HB(3\text{-}Bu^tpyz)_3\}$ or $K\{H_2B(3\text{-}Bu^tpyz)_2\}$, respectively. In contrast to the formation of these 1 : 1 complexes, the isostructural but neutral ligand $HC(pyz)_3$ readily coordinates three equivalents of $(CH_3)_3Al$ giving $\{HC(pyz)_3\}[Al(CH_3)_3]_3$. ^1H NMR studies provide evidence for the formation of the mono- and bis-complexes $\{HC(pyz)_3\}[Al(CH_3)_3]$ and $\{HC(pyz)_3\}[Al(CH_3)_3]_2$ as products of the reaction of $HC(pyz)_3$ with less than three equivalents of $Al(CH_3)_3$. The aluminium–carbon bonds of $\{\eta^3$-HB(3,5-$Me_2pyz)_3\}Al(CH_3)_2$ are readily cleaved by H_2O to give $\{\eta^3$-HB(3,5-$Me_2pyz)_3\}Al(OH)_2$ and CH_4. However, the reaction of $\{\eta^3$-HB(3,5-$Me_2pyz)_3\}Al(CH_3)_2$ with D_2O gives CH_4 in addition to CH_3D and thus demonstrates that a secondary process involving coupling of the aluminium–methyl ligand with one of the hydrogen atoms of the pyrazolyl methyl group must be competitive with the direct reaction of the aluminium–carbon bond with D_2O. The complex $\{\eta^2$-H_2B(3-$Bu^tpyz)_2\}Al(CH_3)_2$ undergoes a unimolecular rearrangement of the bis(3-t-butylpyrazolyl)hydroborato ligand to give the more stable isomer, $\{\eta^2$-H_2B(3-Bu^tpyz)(5-Bu^tpyz)$\}Al(CH_3)_2$. The kinetics of this rearrangement are first-order with the activation parameters $\Delta H^\ddagger = 34.5(8)$ kcal mol^{-1} and $\Delta S^\ddagger = 6(2)$ e.u. and the proposed mechanism consists of steps involving a 1,2-shift of the t-butylpyrazolyl group.

There has been a long-standing interest in aluminium alkyl derivatives which has stemmed from their importance as co-catalysts in the Ziegler–Natta polymerization of olefins[1] and also as reagents in organic synthesis.[2] More recently, these derivatives have shown promise for producing thin films of pure metal by chemical vapour deposition,[3] thus providing a means of forming conductive contacts on silicon-based devices.[4] Furthermore, aluminium alkyl derivatives have also found use as precursors in the controlled synthesis of materials, e.g. aluminium nitride ceramics.[5] A detailed understanding of the structures of organoaluminium derivatives and the mechanisms of their transformations at the molecular level is critical if these processes are to be truly controlled. In this respect, the coordination chemistry of aluminium alkyls with multidentate macrocyclic and non-macrocyclic nitrogen, oxygen and sulphur ligands is an area of considerable current interest. Alkylaluminium derivatives of these ligands are frequently complex molecules that are either oligomeric or multinuclear, in which each of the donor sites coordinates to an individual aluminium centre. For example, coordination of macrocyclic amines, crown ethers and crown thioethers to $Al(CH_3)_3$ results in the formation of complex mono-, bis-, tris- and tetrakis(trimethylaluminium) derivatives, e.g. $[Al(CH_3)_3][12]aneS_4$,[6] $[Al(CH_3)_3]_4[12]aneS_4$,[7] $[Al(CH_3)_3]_4[14]aneN_4Me_4$,[8] $[Al(CH_3)_3]_2$[dibenzo-18-crown-6],[9] $[Al(CH_3)_3]_3$[dibenzo-18-crown-6],[10] $[Al(CH_3)_3]_4$[18-crown-6],[10] $[Al(CH_3)_3]_4$[15-crown-5],[9] $[Al(CH_3)_3]_2$[12-crown-4],[11] $[Al(CH_3)_3]_2$[dicyclohexyl-18-crown-6][12] and $[Al(CH_3)_3][14]aneS_4$[13] and also a variety of more unusual complexes, e.g. $[Al(CH_3)]_2[C_{10}H_{20}N_4][Al(CH_3)_3]_2$, $[(CH_3)_2AlCl]_2[Al\cdot C_{10}H_{20}N_4][Al(CH_3)_2]$ and $[Al(CH_3)][C_8H_{19}N_4][Al(CH_3)_2]$.[14] Thus, chelation of multidentate ligands to a *single* aluminium alkyl centre is rather rare, of which the macrocyclic phthalocyanine derivatives $Al(C_{22}H_{23}N_4)(CH_2CH_3)_2$ and $Al(C_{22}H_{22}N_4)(CH_2CH_3)$[15] and the non-

* Author to whom correspondence should be addressed.

macrocyclic tetradentate Schiff-base* complexes Al(SALEN)(C_2H_5), Al(SALOPHEN)(C_2H_5), Al(SALPN)(C_2H_5), Al(ACEN)(C_2H_5) and Al(ACEN)(C_2H_5)$_2$ are examples.[16] We have recently described the synthesis and reactivity of tris(pyrazolyl)hydroboratomagnesium alkyl complexes.[17] In particular, these studies have shown that coordination of the {η^3-tris(pyrazolyl)hydroborato} ligand to magnesium provides well-defined monomeric complexes that are suitable for mechanistic investigations and also exhibit novel reaction pathways. Therefore, we wished to extend these studies to aluminium alkyl derivatives and this paper describes synthetic and mechanistic studies of alkylaluminium complexes containing poly(pyrazolyl)hydroborato and poly(pyrazolyl)-methane co-ligands.

RESULTS AND DISCUSSION

Synthesis of alkyl derivatives

(1) *Preparation of bis- and tris(pyrazolyl)hydroborato aluminium alkyl derivatives.* The tris(pyrazolyl)hydroborato aluminium methyl derivatives {η^3-HB(3,5-Me_2pyz)$_3$}Al(CH_3)$_2$ and {η^2-HB(3-Bu^{t}pyz)$_3$}Al(CH_3)$_2$ are readily prepared by metathesis of Al(CH_3)$_3$ with either K{HB(3,5-Me_2pyz)$_3$},[18] (3,5-Me_2pyz = 3,5-$C_3N_2(CH_3)_2H$) or Tl{HB(3-Bu^{t}pyz)$_3$}[19] (3-Bu^{t}pyz = 3-$C_3N_2Bu^tH_2$), respectively [eqs (1) and (2)]:

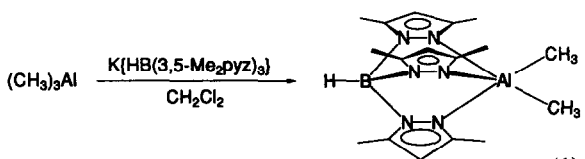

(1)

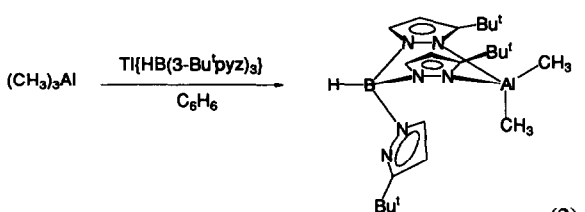

(2)

* SALEN, SALOPHEN and SALPN are the 2 : 1 condensation products of salicylaldehyde with ethylenediamine, *o*-phenylenediamine and propylenediamine, respectively, and ACEN is the 2 : 1 condensation product of acetylacetone with ethylenediamine.

† Calculations have estimated that decomposition of $TlCH_3$ by either disproportionation to thallium and Tl(CH_3)$_3$ or by reductive coupling to give thallium and C_2H_6 are thermodynamically favoured.[20]

The reaction of (CH_3)$_3$Al with Tl{HB(3-Bu^{t}pyz)$_3$} is also accompanied by the deposition of thallium metal, which is presumably a decomposition product of unstable $TlCH_3$.†

The tris(t-butylpyrazolyl)hydroborato aluminium methyl derivative has been characterized by NMR spectroscopy as the four-coordinate η^2-complex, {η^2-HB(3-Bu^{t}pyz)$_3$}Al(CH_3)$_2$. For example, the ^{1}H NMR spectrum (in benzene-d_6) shows two sets of t-butylpyrazolyl groups (δ 1.26 and 1.53 ppm) in the ratio 2 : 1 and two inequivalent Al—CH_3 groups (δ 0.01 and −0.11 ppm) in the ratio 1 : 1. In contrast, the ^{1}H and ^{13}C NMR spectra (in benzene-d_6) of the tris(3,5-dimethylpyrazolyl) hydroborato aluminium methyl derivative indicate only one environment for both Al—CH_3 and 3,5-dimethylpyrazolyl groups. The Al—CH_3 group is observed at δ −0.05 and −7.1 ppm ($^1J_{C-H}$ = 113 Hz) in the ^{1}H and ^{13}C NMR spectra, respectively. Variable-temperature ^{1}H NMR studies down to *ca* −90°C show no indication of inequivalent pyrazolyl or methyl groups. This data cannot unequivocally distinguish between the structure in solution as five-coordinate {η^3-HB(3,5-Me_2pyz)$_3$}Al(CH_3)$_2$, or highly fluxional four-coordinate {η^2-HB(3,5-Me_2pyz)$_3$}Al(CH_3)$_2$. However, the complex [{η^3-HB(3,5-Me_2pyz)$_3$}$_2$Al][$AlCl_4$] which possesses two {η^3-tris(3,5-dimethylpyrazolyl)hydroborato} ligands has recently been reported[21] and thus provides a precedence for the five-coordinate, η^3-description, i.e. {η^3-HB(3,5-Me_2pyz)$_3$}Al(CH_3)$_2$. Other evidence in favour of the η^3-description of {η^3-HB(3,5-Me_2pyz)$_3$}Al(CH_3)$_2$ is that the structurally characterized four-coordinate gold complex, {η^2-HB(pyz)$_3$}Au(CH_3)$_2$ (pyz = $C_3N_2H_3$), which also exhibits only one pyrazolyl group environment in the ^{1}H NMR spectrum at room temperature, exhibits the fully frozen-out spectrum at −90°C.[22] Thus, if {HB(3,5-Me_2pyz)$_3$}Al(CH_3)$_2$ is four-coordinate in solution, it must possess significantly lower barriers to rearrangement than both {η^2-HB(pyz)$_3$}Au(CH_3)$_2$ and {η^2-HB(3-Bu^{t}pyz)$_3$}Al(CH_3)$_2$. The activation barrier ($\Delta G^{\ddagger}$) for the rearrangement process for {η^2-HB(3-Bu^{t}pyz)$_3$}Al(CH_3)$_2$ has been estimated by magnetization transfer studies to be 17(2) kcal mol^{-1} at 40°C.

The formation of an η^2-complex for the tris(t-butylpyrazolyl)hydroborato derivative, rather than an η^3-complex, is not surprising in terms of the steric demands of the tris(t-butylpyrazolyl)hydroborato ligand. The cone angles of the tris(pyrazolyl) hydroborato ligands {η^3-HB(pyz)$_3$}, {η^3-HB(3,5-Me_2pyz)$_3$} and {η^3-HB(3-Bu^{t}pyz)$_3$} have been estimated. as 184, 224 and 244°C, respectively, and the tris(t-butylpyrazolyl)hydroborato ligand

has been described as effectively restricting a metal to having a maximum coordination number of four.[23]

The related bis(t-butylpyrazolyl)hydroborato complex, $\{\eta^2\text{-}H_2B(3\text{-}Bu^tpyz)_2\}Al(CH_3)_2$, is synthesized by the analogous reaction of $(CH_3)_3Al$ with $K\{H_2B(3\text{-}Bu^tpyz)_2\}$ [eq. (3)]:

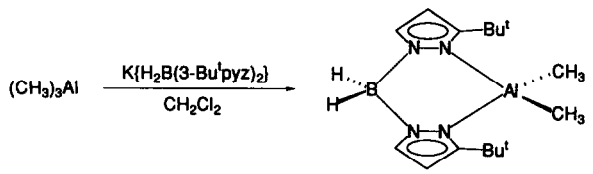

(3)

Only one type of Al—CH_3 and t-butylpyrazolyl groups are observed in both the ^1H and ^{13}C NMR spectra of $\{\eta^2\text{-}H_2B(3\text{-}Bu^tpyz)_2\}Al(CH_3)_2$. Thus, the Al—$CH_3$ group is observed at δ −0.06 ppm in the ^1H NMR spectrum (in benzene-d_6) and the t-butylpyrazolyl group appears as a singlet at δ 1.30 ppm, corresponding to the t-butyl substituent, and two doublets at δ 5.83 and 7.39 ppm ($^3J_{H-H}$ = 2.2 Hz), corresponding to the pyrazolyl hydrogens at the four- and five-positions, respectively. Assignment of the pyrazolyl resonances at δ 5.83 and 7.39 has been completed using Nuclear Overhauser enhancement experiments.

^{27}Al NMR has been suggested as a probe for determining the coordination number of aluminium[24] and the ^{27}Al NMR spectra of $\{\eta^3\text{-HB}(3,5\text{-}Me_2pyz)_3\}Al(CH_3)_2$ and $\{\eta^2\text{-}H_2B(3\text{-}Bu^tpyz)_2\}Al(CH_3)_2$ show broad resonances at δ 133 (ω = 5000 Hz) and 140 (ω = 5000 Hz) ppm (relative to $Al(acac)_3$), respectively, with the four-coordinate complex having the slightly larger chemical shift.

$\{\eta^2\text{-}H_2B(3\text{-}Bu^tpyz)_2\}Al(CH_3)_2$ has also been obtained from the reaction of $(CH_3)_2AlCl$ with $K\{H_2B(3\text{-}Bu^tpyz)_2\}$, thus demonstrating that metathesis of the chloride ligand is favoured over the alkyl ligand [eq. (4)]:

$$(CH_3)_2AlCl \xrightarrow[CH_2Cl_2]{K\{H_2B(3\text{-}Bu^tpyz)_2\}} \{\eta^2\text{-}H_2B(3\text{-}Bu^tpyz)_2\}Al(CH_3)_2. \quad (4)$$

(2) *The reaction of* $(CH_3)_3Al$ *with tris(pyrazolyl) methane.* Treatment of $HC(pyz)_3$[25] with more than three equivalents of $(CH_3)_3Al$ allows the complex $\{HC(pyz)_3\}[Al(CH_3)_3]_3$ to be isolated [eq. (5)]:

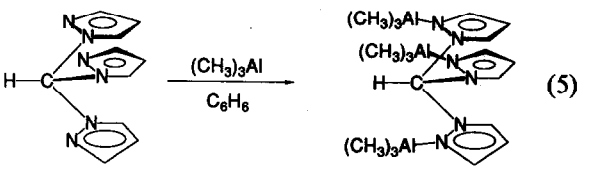

(5)

Hence, in contrast to the formation of monomeric mononuclear aluminium alkyl derivatives using poly(pyrazolyl)hydroborato ligands, the isostructural but neutral poly(pyrazolyl)methane ligand readily coordinates to three aluminium alkyl centres.

In order to investigate the formation of mono- and bis(trimethylaluminium) complexes as intermediates in the formation of the tris-adduct, $\{HC(pyz)_3\}[Al(CH_3)_3]_3$, the reaction between $(CH_3)_3Al$ and $HC(pyz)_3$ in benzene-d_6 has been monitored using ^1H NMR spectroscopy at room temperature, as shown in Figs 1 and 2. The spectra have been obtained as a function of the $(CH_3)_3Al:HC(pyz)_3$ molar ratio. The results show that upon increasing the molar ratio of $(CH_3)_3Al:HC(pyz)_3$, there is a smooth shift of the resonances of the hydrogen atoms of the pyrazolyl and methine groups. The tris(pyrazolyl) methane resonances that are most sensitive are those of the methine hydrogen, $HC(pyz)_3$ (i.e. H_a) and the doublet at δ 7.21 in the free ligand (i.e. H_{dorb}), which shift to low and high field, respectively, upon increasing the $(CH_3)_2Al:HC(pyz)_3$ molar ratio. Interestingly, H_{dorb} is relatively insensitive to the concentration of $(CH_3)_3Al$ until the molar ratio of $(CH_3)_3Al:HC(pyz)_3$ reaches *ca* 1 : 1, after which it shifts dramatically to high field (*vide infra*). The shifts of the pyrazolyl resonances are also accompanied by a shift of the resonance of the coordinated $(CH_3)_3Al$ to higher field. These changes in chemical shift level off at a molar ratio of $(CH_3)_3Al:HC(pyz)_3$ of 3 : 1, as shown in Fig. 2. Removal of the solvent (and excess $(CH_3)_3Al$) *in vacuo* from samples containing up to a 3 : 1 molar ratio, followed by redissolving in benzene-d_6 regenerates the original spectrum. However, samples with molar ratios greater than 3 : 1 give spectra corresponding to the 3 : 1 product after performing this procedure. These results demonstrate that $HC(pyz)_3$ may coordinate up to three equivalents of $(CH_3)_3Al$ via the three nitrogen atom donors [eq. (6)]:

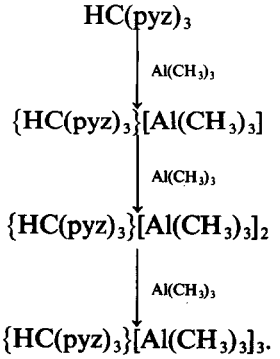

(6)

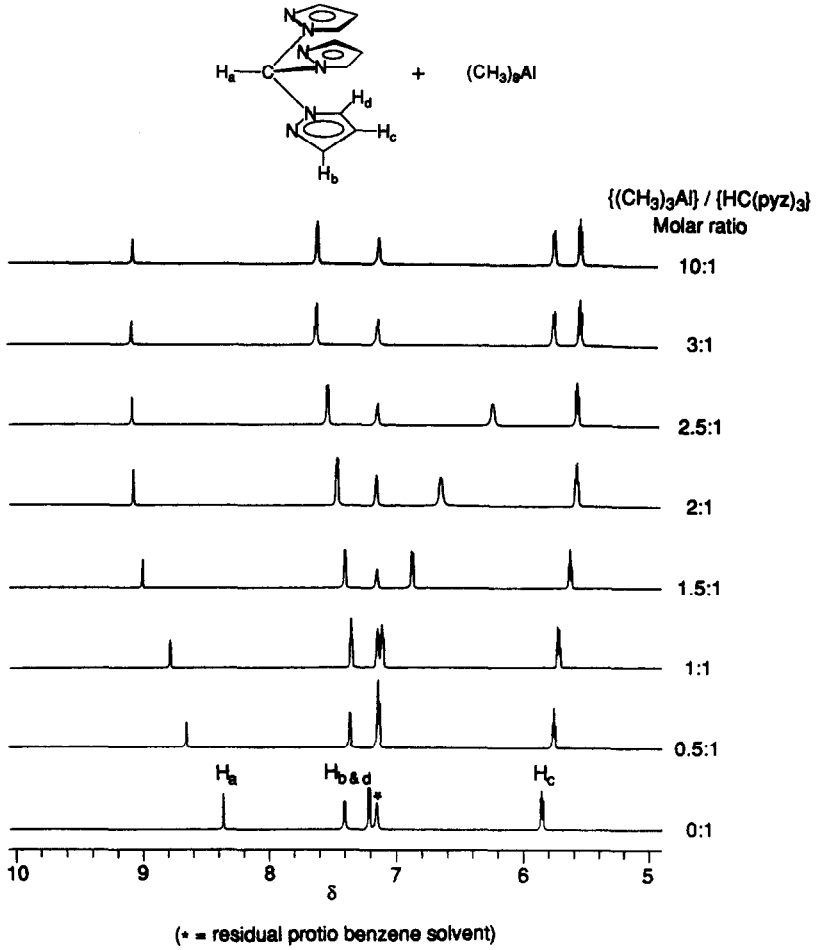

Fig. 1.

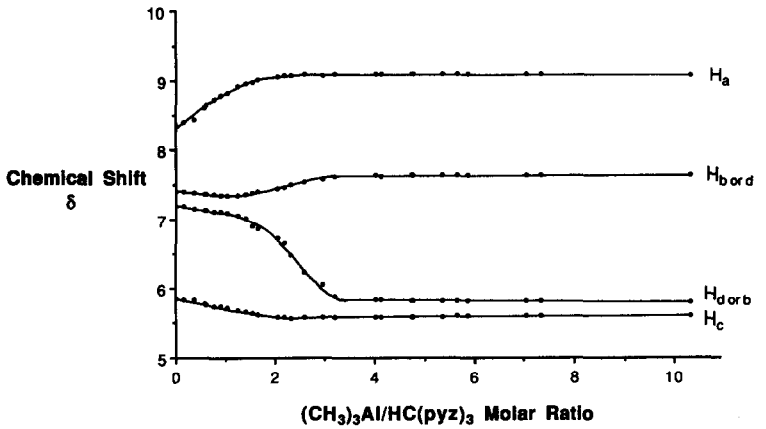

Fig. 2.

The room temperature ^1H NMR spectra of solutions derived from stoichiometric and non-stoichiometric amounts of $HC(pyz)_3$ and $(CH_3)_3Al$ show only one type of pyrazolyl and $(CH_3)_3Al$ environment at each $(CH_3)_3Al:HC(pyz)_3$ molar ratio, thus suggesting that the $(CH_3)_3Al$ is highly mobile and may readily transfer between the mono-, bis- and tris(trimethylaluminium)tris(pyrazolyl)-methane complexes. Although the mono- and bis-complexes cannot be unequivocally observed, the irregular variation of the chemical shifts of the pyrazolyl hydrogens provides evidence for

the existence of such complexes in solution. For example, as shown in Fig. 2, whereas the resonance attributed to $\{HC(pyz)_3\}$ (i.e. H_a) shifts progressively to low field, the pyrazolyl resonance H_{bord} shifts initially to high field until a molar ratio $(CH_3)_2Al:HC(pyz)_3$ of *ca* 1 : 1 is reached, at which point it shifts to low field. Similarly, the pyrazolyl resonance H_{dorb} initially shifts slowly to high field until a molar ratio for $(CH_3)_3Al:HC(pyz)_3$ of *ca* 1 : 1 is reached, at which point the shift to high field is more dramatic. If the solutions contained only the tris-complex $\{HC(pyz)_3\}[Al(CH_3)_3]_3$ and free ligand $HC(pyz)_3$ in rapid exchange, then a regular variation of each of the chemical shifts, H_a, H_{bord}, H_c and H_{dorb}, would have been predicted. These conclusions are supported by the observation that lowering the temperature of a solution of molar ratio $(CH_3)_3Al:HC(pyz)_3$ *ca* 2 : 1 to −60°C results in the broadening of the resonances of the pyrazolyl hydrogens, but unfortunately the low temperature limit was not achieved. Thus, while it is likely that the product of composition, $\{HC(pyz)_3\}[Al(CH_3)_3]_3$, consists of three $(CH_3)_3Al$ units bonded to the three pyrazolyl nitrogen atom donors, for the products $\{HC(pyz)_3\}[Al(CH_3)_3]$ and $\{HC(pyz)_3\}[Al(CH_3)_3]_2$ the data do not permit distinction between chelation, e.g. $\{\eta^3\text{-}HC(pyz)_3\}[Al(CH_3)_3]$ and unidentate coordination, e.g. $\{\eta^1\text{-}HC(pyz)_3\}[Al(CH_3)_3]$.

Reactivity and mechanistic studies

(1) *Reaction of* $\{HB(3,5\text{-}Me_2pyz)_3\}Al(CH_3)_2$ *with* H_2O. The reaction of $\{HB(3,5\text{-}Me_2pyz)_3\}Al(CH_3)_2$ with water results in cleavage of both aluminium–carbon bonds to give the dihydroxy derivative $\{HB(3,5\text{-}Me_2pyz)_3\}Al(OH)_2$ and methane [eq. (7)]. A monohydroxy aluminium complex, $Al(C_{22}H_{22}N_4)OH$, has recently been reported.[15]

$$\{HB(3,5\text{-}Me_2pyz)_3\}Al(CH_3)_2 + 2H_2O \longrightarrow \{HB(3,5\text{-}Me_2pyz)_3\}Al(OH)_2 + 2CH_4. \quad (7)$$

Similarly, the deuteriated comlex $\{HB(3,5\text{-}Me_2pyz)_3\}Al(OD)_2$ may be prepared by the treatment of $\{HB(3,5\text{-}Me_2pyz)_3\}Al(CH_3)_2$ with D_2O. The ^1H NMR spectrum (in benzene-d_6) of $\{HB(3,5\text{-}Me_2pyz)_3\}Al(OH)_2$ possesses a resonance at δ 15.95 ppm which is absent for the complex $\{HB(3,5\text{-}Me_2pyz)_3\}Al(OD)_2$ and is thus assigned to the Al–OH group. A broad IR absorption at *ca* 3300 cm^{-1} (KBr disc) for $\{HB(3,5\text{-}Me_2pyz)_3\}Al(OH)_2$ shifts to *ca* 2380 cm^{-1} for $\{HB(3,5\text{-}Me_2pyz)_3\}Al(OD)_2$ ($\nu_H/\nu_D = 1.4$) and is thus assigned to the AlO–H stretch. The hydrolysis reaction has also been examined using $^{17}OH_2$ (*ca* 45% enriched).

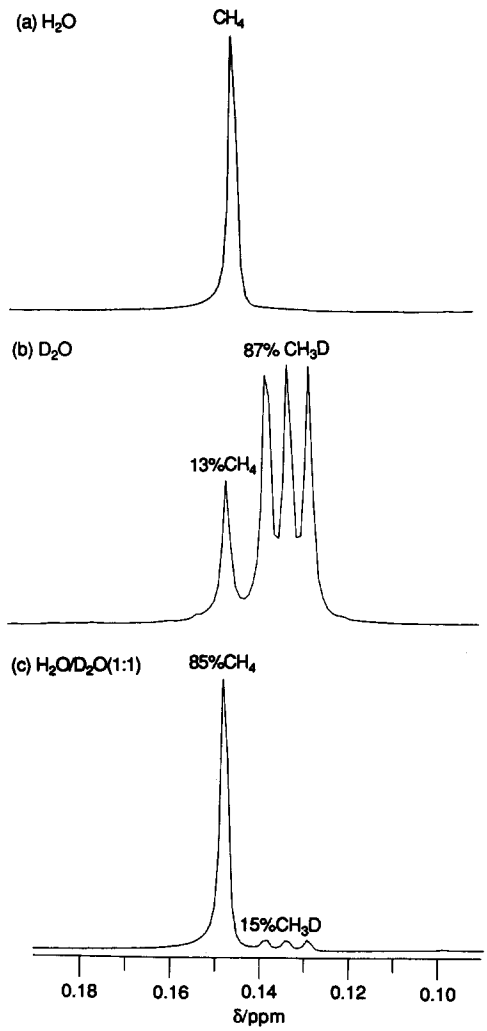

Fig. 3.

Unfortunately, a ^{17}O NMR resonance could not be observed for the product, presumably as a result of quadrupolar broadening.

The reaction of $\{HB(3,5\text{-}Me_2pyz)_3\}Al(CH_3)_2$ with D_2O is of particular interest since the methane eliminated is not solely CH_3D, the product of direct attack by D_2O at the Al–C bond. Figure 3 shows the ^1H NMR spectrum (400 MHz, benzene-d_6) of the methane eliminated from (a) $\{HB(3,5\text{-}Me_2pyz)_3\}Al(CH_3)_2$ with H_2O, (b) $\{HB(3,5\text{-}Me_2pyz)_3\}Al(CH_3)_2$ with D_2O (99.8%) and (c) $\{HB(3,5\text{-}Me_2pyz)_3\}Al(CH_3)_2$ with excess of a mixture of $H_2O:D_2O$ (1 : 1 molar ratio). Remarkably, the reaction between $\{HB(3,5\text{-}Me_2pyz)_3\}Al(CH_3)_2$ and D_2O generates significant quantities (*ca* 13%) of CH_4 (Scheme 1). The ^2H NMR spectrum of the product of $\{HB(3,5\text{-}Me_2pyz)_3\}Al(CH_3)_2$ and D_2O was measured in order to determine the source of the extra hydrogen in the CH_4 and demonstrates that one of the methyl groups of the pyrazolyl

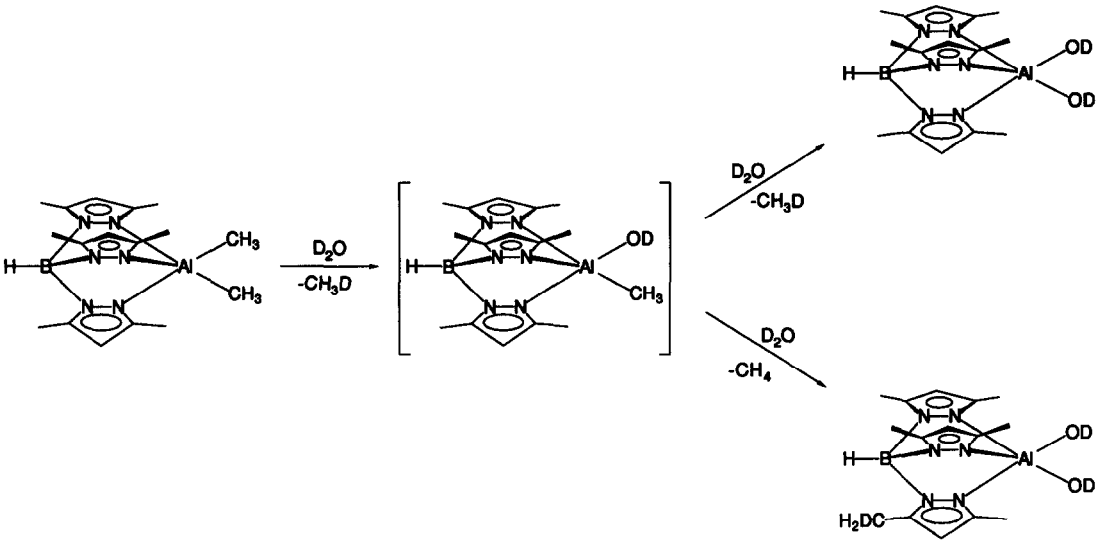

Scheme 1.

groups is selectively enriched in deuterium. These results suggest that the formation of CH_4 in the reaction of $\{HB(3,5\text{-}Me_2pyz)_3\}Al(CH_3)_2$ with D_2O may arise by a coupling of the aluminium–methyl ligand with one of the hydrogen atoms of the pyrazolyl methyl group and that this process must be competitive with the direct reaction of the aluminium–carbon bond with D_2O. Although we can not identify which one of the two methyl group substituents is attacked in this manner, a potential mechanism for this competitive formation of CH_4 vs CH_3D is illustrated in Scheme 2, in which abstraction of a hydrogen atom from one of the methyl groups of the tris(3,5-dimethylpyrazolyl)-hydroborato ligand by the Al—CH_3 group occurs. Similar abstractions of hydrogen from ligand methyl groups have been observed in other systems.[26] Models suggest that metallation of one of the dimethylpyrazolyl groups by the aluminium centre would be more favourable after initially dissociating one of the pyrazolyl groups from the aluminium. In view of the competitive elimination of CH_4 in the reaction with D_2O, an upper limit of $k_H : k_D = 5.3$ has been estimated for the kinetic isotope effect for the hydrolysis by examining the ratio of $CH_4 : CH_3D$ eliminated in the reaction with excess $H_2O : D_2O$ (1 : 1 molar ratio).

(2) 3,5 *Isomerization of the bis*(3-t-butylpyrazolyl)*hydroborato ligand.* The methyl complex $\{\eta^2\text{-}H_2B(3\text{-}Bu^tpyz)_2\}Al(CH_3)_2$ undergoes a rearrangement of the bis(3-t-butylpyrazolyl)hydroborato ligand upon heating at *ca* 100°C to give the more stable isomer, $\{\eta^2\text{-}H_2B(3\text{-}Bu^tpyz)(5\text{-}Bu^tpyz)\}Al(CH_3)_2$, as shown in eq. (8):

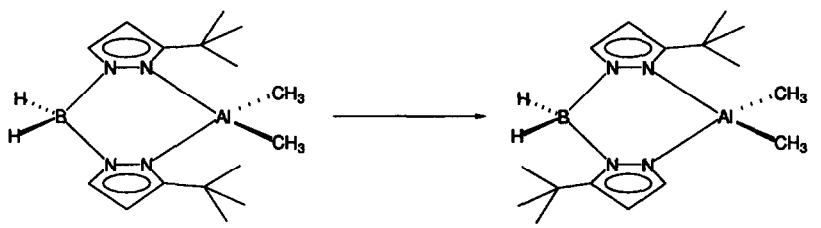

(8)

The ^1H NMR spectrum of the rearranged isomer, $\{\eta^2\text{-}H_2B(3\text{-}Bu^tpyz)(5\text{-}Bu^tpyz)\}Al(CH_3)_2$, in benzene-$d_6$ shows a single resonance at δ −0.01 ppm for the $Al(CH_3)_2$ groups and two sets of resonances for the t-butylpyrazolyl groups. The pyrazolyl hydrogens of each of these t-butylpyrazolyl groups has been identified by nuclear Overhauser enhancement experiments (see Table 1). Although we cannot unequivocally distinguish which set of resonances corresponds to the (3-t-butylpyrazolyl) and (5-t-butylpyrazolyl) groups, comparison with the ^1H NMR spectrum of $\{\eta^2\text{-}H_2B(3\text{-}Bu^tpyz)_2\}Al(CH_3)_2$ suggests that the sets of resonances at δ 1.35, 5.85 and 7.41 and δ 1.22, 5.74 and 7.33 are assigned to the (3-t-butylpyrazolyl) and (5-t-butylpyrazolyl) groups, respectively.

Similar rearrangement processes have also been observed for copper and cobalt complexes of a related ligand system, i.e. $\{\eta^3\text{-}HB(3\text{-}Pr^ipyz)_3\} \rightarrow \{\eta^3\text{-}HB(3\text{-}Pr^ipyz)_2(5\text{-}Pr^ipyz)\}$.[27] A potential mech-

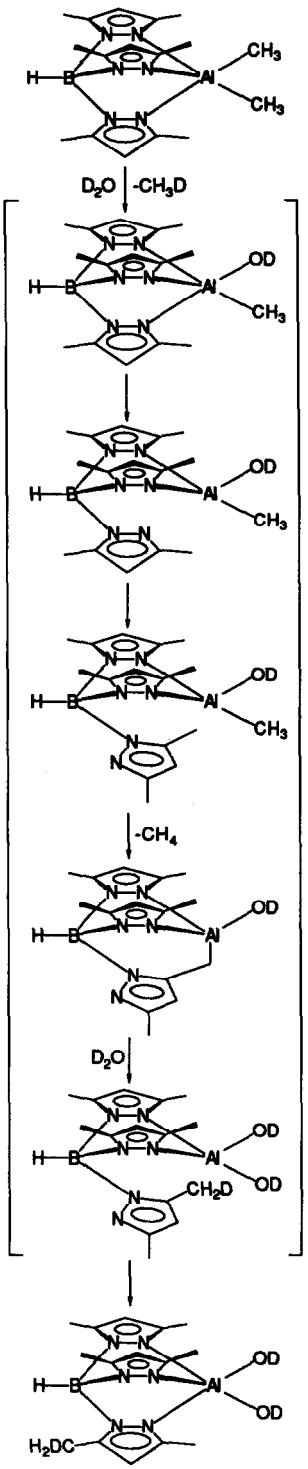

Scheme 2.

anism for this apparent 1,3-migration of the alkyl group (either Bu^t or Pr^i) from the 3-position to the 5-position of the pyrazolyl ring may involve an indirect process involving a 1,2-shift of the boron substituent from N(1) to N(2) [or alternatively of the aluminium substituent from N(2) to N(1)], as shown in Scheme 3.

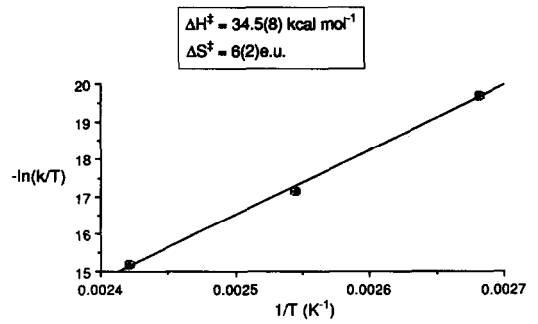

Fig. 4.

In order to obtain more information about the nature of the above 3,5-rearrangement process, we have examined the kinetics of the transformation of $\{\eta^2\text{-}H_2B(3\text{-}Bu^tpyz)_2\}Al(CH_3)_2$ to $\{\eta^2\text{-}H_2B(3\text{-}Bu^tpyz)(5\text{-}Bu^tpyz)\}Al(CH_3)_2$. The data show that the reaction exhibits first-order kinetics over *ca* 3 half-lives. First-order kinetics have also been confirmed by the observation that the same rate constant (within experimental error) is obtained for solutions of initial concentration 63 and 6.3 mmol. The temperature-dependence of the rate constant has been measured over a 40°C temperature range (Table 2), from which the activation parameters $\Delta H^{\ddagger} = 34.5(8)$ kcal mol^{-1} and $\Delta S^{\ddagger} = 6(2)$ e.u. have been derived (Fig. 4). In particular, the small positive value of $\Delta S^{\ddagger}$ suggests that the transition state is not highly ordered, consistent with the proposed mechanism involving dissociation of one of the pyrazolyl groups.

CONCLUSIONS

Poly(pyrazolyl)hydroborato aluminium methyl derivatives, $\{\eta^3\text{-}HB(3,5\text{-}Me_2pyz)_3\}Al(CH_3)_2$, $\{\eta^2\text{-}HB(3\text{-}Bu^tpyz)_3\}Al(CH_3)_2$ and $\{\eta^2\text{-}H_2B(3\text{-}Bu^tpyz)_2\}Al(CH_3)_2$, have been prepared by metathesis of $Al(CH_3)_3$ with either $K\{HB(3,5\text{-}Me_2pyz)_3\}$, $Tl\{HB(3\text{-}Bu^tpyz)_3\}$ or $K\{H_2B(3\text{-}Bu^tpyz)_2\}$, respectively. In contrast to the formation of these 1 : 1 complexes, the isostructural but neutral ligand $HC(pyz)_3$ readily coordinates up to three equivalents of $(CH_3)_3Al$ giving $\{HC(pyz)_3\}[Al(CH_3)_3]_3$.

The aluminium–carbon bonds of $\{\eta^3\text{-}HB(3,5\text{-}Me_2pyz)_3\}Al(CH_3)_2$ are readily cleaved by H_2O to give $\{\eta^3\text{-}HB(3,5\text{-}Me_2pyz)_3\}Al(OH)_2$ and CH_4. However, the reaction of $\{\eta^3\text{-}HB(3,5\text{-}Me_2pyz)_3\}Al(CH_3)_2$ with D_2O demonstrates that a secondary process involving coupling of the aluminium–methyl ligand with one of the hydrogen atoms of the pyrazolyl methyl group must be competitive with the direct reaction of the aluminium–carbon bond with D_2O.

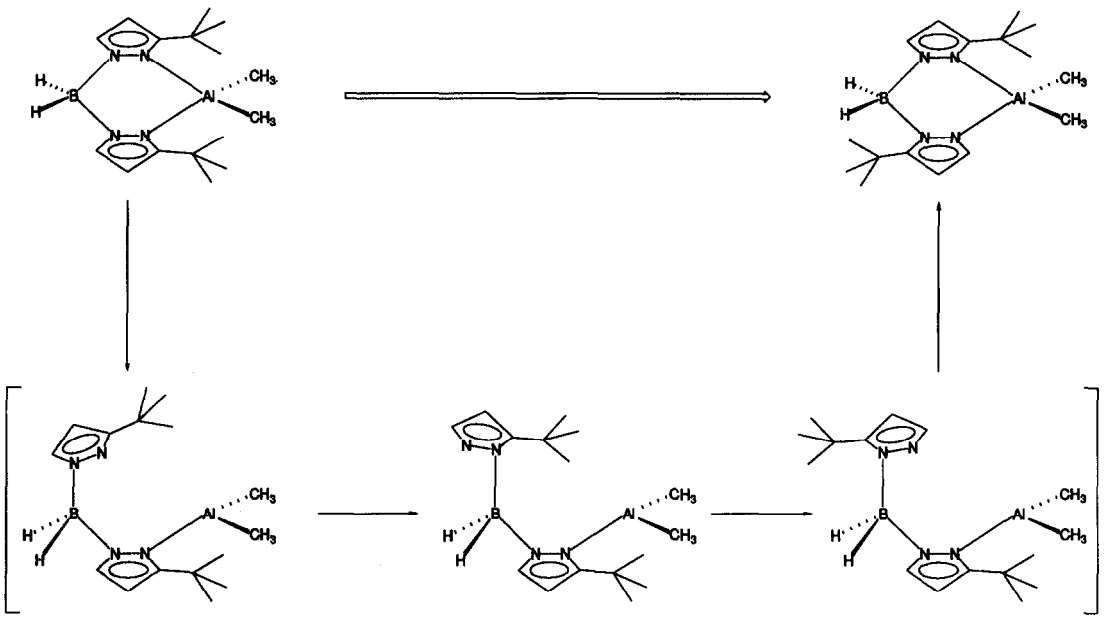

Scheme 3.

The complex $\{\eta^2\text{-}H_2B(3\text{-}Bu^tpyz)_2\}Al(CH_3)_2$ has been shown to undergo a unimolecular rearrangement of the bis(3-t-butylpyrazolyl)hydroborato ligand to give the more stable isomer, $\{\eta^2\text{-}H_2B(3\text{-}Bu^tpyz)(5\text{-}Bu^tpyz)\}Al(CH_3)_2$. The kinetics of this rearrangement are first-order with the activation parameters $\Delta H^{\ddagger} = 34.5(8)$ kcal mol^{-1} and $\Delta S^{\ddagger} = 6(2)$ e.u. and the proposed mechanism consists of steps involving a 1,2-shift of the t-butylpyrazolyl group.

EXPERIMENTAL

General considerations

All manipulations were performed using a combination of glovebox, high-vacuum or Schlenk techniques.[28] Solvents were purified and degassed by standard procedures. ^1H, ^2H, ^{13}C, ^{17}O and ^{27}Al NMR spectra were measured on Varian VXR 200, 300 and 400 spectrometers. IR spectra were recorded as KBr discs or Nujol mulls on a Perkin–Elmer 1420 spectrophotometer. Elemental analyses were obtained from Galbraith Laboratories, Inc. (Knoxville, Tennessee, U.S.A.) and Desert Analytics (Tucson, Arizona, U.S.A.).

$K\{HB(3,5\text{-}Me_2pyz)_3\}$,[18] $Tl\{HB(3\text{-}Bu^tpyz)_3\}$,[20] $K\{H_2B(3\text{-}Bu^tpyz)_2\}$[18] and $HC(pyz)_3$[25] were prepared as described previously.

Preparation of $\{\eta^3\text{-}HB(3,5\text{-}Me_2pyz)_3\}Al(CH_3)_2$

A solution of $(CH_3)_3Al$ in hexane (2.0 M, 2.5 cm^3, 5 mmol) was added to a stirred suspension of $K\{HB(3,5\text{-}Me_2pyz)_3\}$ (1.0 g, 2.97 mmol) in CH_2Cl_2 (30 cm^3) at room temperature. The $K\{HB(3,5\text{-}Me_2pyz)_3\}$ dissolved and was replaced by a fine white precipitate. The mixture was filtered after 1 h. The solvent was removed from the filtrate under reduced pressure giving $\{HB(3,5\text{-}Me_2pyz)_3\}Al(CH_3)_2$ as a white solid (0.47 g, 45%) which may be recrystallized from toluene. Found: C, 53.5; H, 7.6; N, 22.8. Calc.: C, 57.6; H, 7.9; N, 23.7%. IR data (Nujol mull, KBr plates, cm^{-1}): 2505 (ν_{B-H}).

Preparation of $\{\eta^2\text{-}HB(3\text{-}Bu^tpyz)_3\}Al(CH_3)_2$

$(CH_3)_3Al$ (0.3 cm^3, 3.1 mmol) was added to a solution of $Tl\{HB(3\text{-}Bu^tpyz)_3\}$ (1.0 g, 1.7 mmol) in C_6H_6 at room temperature, giving a black deposit of thallium metal. The mixture was filtered after 15 min. The solvent was removed from the filtrate under reduced pressure giving $\{\eta^2\text{-}HB(3\text{-}Bu^tpyz)_3\}Al(CH_3)_2$ as a white solid (0.36 g, 48%) which may be recrystallized from pentane. Found: C, 55.8; H, 8.7; N, 20.2. Calc.: C, 63.0; H, 9.2; N, 19.2%. IR data (Nujol mull, KBr plates, cm^{-1}): 2465 (ν_{B-H}).

Preparation of $\{\eta^2\text{-}H_2B(3\text{-}Bu^tpyz)_2\}Al(CH_3)_2$

A solution of $(CH_3)_3Al$ in hexane (2.0 M, 6 cm^3, 12 mmol) was added to a solution of $K\{H_2B(3\text{-}Bu^tpyz)_2\}$ (500 mg, 1.7 mmol) in CH_2Cl_2 (80 cm^3) at room temperature giving a fine white precipitate. The mixture was filtered after 10 min. The solvent

Table 1. ^{1}H and ^{13}C NMR data[a]

Compound	Assignment	δ (ppm)	Coupling (Hz)
$\{\eta^3$-HB(3,5-Me_2pyz)$_3\}$Al$(CH_3)_2$	^{1}H *NMR*		
	η^3-HB$\{C_3N_2H(CH_3)_2\}_3$		
	1 CH_3	2.11	s
	1 CH_3	2.16	s
	η^3-HB$\{C_3N_2H(CH_3)_2\}_3$	5.50	s
	η^3-HB$\{C_3N_2N(CH_3)_2\}_3$	—	
	Al$(CH_3)_2$	−0.05	s
	^{13}C *NMR* (*in* C_7D_8)		
	η^3-HB$\{C_3N_2H(CH_3)_2\}_3$		
	1 C	12.6	q, $^{1}J_{C-H} = 128$
	1 C	13.3	q, $^{1}J_{C-H} = 128$
	η^3-HB$\{C_3N_2H(CH_3)_2\}_3$		
	1 C	106.9	d, $^{1}J_{C-H} = 172$
	1 C	145.9	s
	1 C	149.3	s
	η^3-HB$\{C_3N_2H(CH_3)_2\}_3$		
	Al$(CH_3)_2$	−7.1	q, $^{1}J_{C-H} = 113$
$\{\eta^2$-HB(3-Bu^{t}pyz)$_3\}$Al$(CH_3)_2$	^{1}H *NMR*		
	η^2-HB$\{C_3N_2C(CH_3)_3\}_3$		
	1 $C(CH_3)_3$	1.53	s
	2 $C(CH_3)_3$	1.26	s
	η^2-HB$\{C_3N_2H_2C(CH_3)_3\}_3$		
	2 H	5.81	d, $^{3}J_{H-H} = 2.4$
	2 H	7.44	d, $^{3}J_{H-H} = 2.4$
	1 H	6.21	d, $^{3}J_{H-H} = 2.2$
	1 H	7.32	d, $^{3}J_{H-H} = 2.2$
	η^2-HB$\{C_3N_2H_2C(CH_3)_3\}_3$	—	
	Al$(CH_3)_2$		
	1 CH_3	0.01	s
	1 CH_3	−0.11	s
	^{13}C *NMR*		
	η^2-HB$\{C_3N_2H_2C(CH_3)_3\}_3$		
	1 $C(CH_3)_3$	31.2	
	2 $C(CH_3)_3$	31.4	
	η^2-HB$\{C_3N_2H_2C(CH_3)_3\}_3$		
	1 C	—	
	2 C	—	
	η^2-HB$\{C_3N_2H_2C(CH_3)_3\}_3$		
	1 C	101.8	
	1 C	135.8	
	1 C	—	
	2 C	105.2	
	2 C	138.9	
	2 C	166.6	
	Al$(CH_3)_2$	—	
$\{\eta^2$-H_2B(3-Bu^{t}pyz)$_2\}$Al$(CH_3)_2$	^{1}H *NMR*		
	η^2-H_2B$\{C_3N_2H_2C(CH_3)_3\}_2$	1.30	s
	η^2-H_2B$\{C_3N_2H_2C(CH_3)_3\}_2$		
	1 H	5.83	d, $^{3}J_{H-H} = 2.2$
	1 H	7.39	d, $^{3}J_{H-H} = 2.2$
	η^2-H_2B$\{C_3N_2H_2C(CH_3)_3\}_2$	—	
	AlCH_3	0.06	s

Table 1 (*Continued*).

Compound	Assignment	δ (ppm)	Coupling (Hz)
	^{13}C *NMR*		
	η^2-$H_2B\{C_3N_2H_2C(CH_3)_3\}_2$	31.5	q, $^1J_{C-H} = 126$
	η^2-$H_2B\{C_3N_2H_2C(CH_3)_3\}_2$	31.6	dct (partial resolution), $^2J_{C-H} = ca$ 5 Hz
	η^2-$H_2B\{C_3N_2H_2C(CH_3)_3\}_2$		
	1 C	104.3	d, $^1J_{C-H} = 175$ d, $^2J_{C-H} = 9$
	1 C	138.4	d, $^1J_{C-H} = 187$ d, $^2J_{C-H} = 6$
	1 C	166.5	s
	$AlCH_3$	−2.9	q, $^1J_{C-H} = 114$
$\{\eta^2$-H_2B(3-Bu^{t}pyz)(5-Bu^{t}pyz)$\}Al(CH_3)_2$	^{1}H *NMR*		
	$\{3$-$C_3N_2H_2C(CH_3)_3\}$ $\{3$-$C_3N_2H_2C(CH_3)_3)\}$	1.35	s
	1 $H_{(4\,posn)}$	5.85	d, $^3J_{H-H} = 2.2$
	1 $H_{(5\,posn)}$	7.41	d, $^3J_{H-H} = 2.2$
	$\{5$-$C_3N_2H_2C(CH_3)_3\}$	1.22	s
	$\{5$-$C_3N_2H_2C(CH_3)_3\}$		
	1 $H_{(4\,posn)}$	5.74	d, $^3J_{H-H} = 2.2$
	1 $H_{(5\,posn)}$	7.33	d, $^3J_{H-H} = 2.2$
	η^2-$H_2B\{C_3N_2H_2C(CH_3)_3\}_2$	—	
	$AlCH_3$	−0.01	s
	^{13}C *NMR*		
	η^2-$H_2B\{C_3N_2H_2C(CH_3)_3\}_2$		
	1 C	30.0	
	1 C	30.8	
	η^2-$H_2B\{C_3N_2H_2C(CH_3)_3\}_2$		
	1 C	—	
	1 C	—	
	η^2-$H_2B\{C_3N_2H_2C(CH_3)_3\}_2$		
	1 C	102.8	
	1 C	103.5	
	1 C	138.6	
	1 C	139.4	
	1 C	159.0	
	1 C	165.5	
	$AlCH_3$	−5.2	
$\{HC(pyz)_3\}[Al(CH_3)_3]_3$	^{1}H *NMR*		
	$HC(C_3N_2H_3)_3$		
	1 H	5.54	t, $^3J_{H-H} = 2.5$
	1 H	5.95	d, $^3J_{H-H} = 2.5$
	1 H	7.58	d, $^3J_{H-H} = 2.5$
	$HC(C_3N_2H_3)_3$	9.09	s
	$Al(CH_3)_3$	−0.47	s
	^{13}C *NMR*		
	$HC(C_3N_2H_3)_3$		
	1 C	145.4	d
	1 C	132.5	d
	1 C	108.8	d
	$HC(C_3N_2H_3)_3$	80.7	d
	$Al(CH_3)_3$	−6.9	q

[a] In C_6D_6. Abbreviations: s = singlet, d = doublet, t = triplet, q = quartet, spt = septet, dct = dectet.

Table 2. Rate constants and activation parameters for the isomerization of $\{\eta^2\text{-}H_2B(3\text{-}Bu^tpyz)_2\}Al(CH_3)_2$ to $\{\eta^2\text{-}H_2B(3\text{-}Bu^tpyz)(5\text{-}Bu^tpyz)\}Al(CH_3)_2$

T (K)	k (s^{-1})	$\Delta G^{\ddagger}$ (kcal mol^{-1})
373	$1.04(5) \times 10^{-6}$	32.2(1)
393	$1.40(7) \times 10^{-5}$	32.0(1)
413	$1.04(5) \times 10^{-4}$	32.0(1)

$\Delta H^{\ddagger} = 34.5(8)$ kcal mol^{-1}; $\Delta S^{\ddagger} = 6(2)$ e.u.

was removed from the filtrate under reduced pressure giving $\{\eta^2\text{-}H_2B(3\text{-}Bu^tpyz)_2\}Al(CH_3)_2$ as a white solid (200 mg, 38%). Found: C, 60.0; H, 8.7; N, 17.1. Calc.: C, 60.7; H, 9.6; N, 17.7%. IR data (Nujol mull, KBr plates, cm^{-1}): 2470 (ν_{B-H}).

Reaction of $K\{H_2B(3\text{-}Bu^tpyz)_2\}$ *with* $(CH_3)_2AlCl$

A solution of $(CH_3)_2AlCl$ in hexane (1 M, 0.42 cm^3, 0.42 mmol) was added to a solution of $K\{H_2B(3\text{-}Bu^tpyz)_2\}$ (100 mg, 0.33 mmol) in CH_2Cl_2 (25 cm^3) at room temperature giving a fine white precipitate. The mixture was filtered after 10 min and the solvent was removed from the filtrate under reduced pressure giving $\{\eta^2\text{-}H_2B(3\text{-}Bu^tpyz)_2\}Al(CH_3)_2$ as a white solid (47 mg, 44%) which was identified by ^1H NMR spectroscopy.

Preparation of $\{HB(3,5\text{-}Me_2pyz)_3\}Al(OH)_2$

H_2O (0.02 cm^3, 1.1 mmol) was added to a solution of $\{HB(3,5\text{-}Me_2pyz)_3\}Al(CH_3)_2$ (200 mg, 0.56 mmol) in C_6H_6 (20 cm^3). The solvent was removed from the solution under reduced pressure giving $\{HB(3,5\text{-}Me_2pyz)_3\}Al(OH)_2$ as a white solid (90 mg, 45%). Found: C, 49.6; H, 6.7; N, 22.3. Calc.: C, 50.3; H, 6.8; N, 23.5%. IR data (Nujol mull, KBr plates, cm^{-1}): 3300 (very broad) (ν_{O-H}), 2480 (ν_{B-H}).

Similar procedures were followed for the reactions with D_2O, $H_2{}^{17}O$ and $H_2{}^{18}O$.

The reactions between $\{HB(3,5\text{-}Me_2pyz)_3\}Al(CH_3)_2$ and H_2O and D_2O were also carried out in benzene-d_6 and monitored by ^1H NMR spectroscopy.

Isomerization of $\{\eta^2\text{-}H_2B(3\text{-}Bu^tpyz)_2\}Al(CH_3)_2$ *to* $\{\eta^2\text{-}H_2B(3\text{-}Bu^tpyz)(5\text{-}Bu^tpyz)\}Al(CH_3)_2$

A solution of $\{\eta^2\text{-}H_2B(3\text{-}Bu^tpyz)_2\}Al(CH_3)_2$ (*ca* 50 mg, 0.16 mmol) in benzene (2 cm^3) was heated at 140°C for 1 day. The solvent was removed under reduced pressure giving $\{\eta^2\text{-}H_2B(3\text{-}Bu^tpyz)(5\text{-}Bu^tpyz)\}Al(CH_3)_2$ as a white solid (*ca* 40 mg, 80%).

Kinetics of the rearrangement of $\{\eta^2\text{-}H_2B(3\text{-}Bu^tpyz)_2\}Al(CH_3)_2$ *to* $\{\eta^2\text{-}H_2B(3\text{-}Bu^tpyz)(5\text{-}Bu^tpyz)\}Al(CH_3)_2$

Reactions were followed using ^1H NMR spectroscopy by monitoring the decrease in intensity of the t-butyl resonance of the starting complex, $\{\eta^2\text{-}H_2B(3\text{-}Bu^tpyz)_2\}Al(CH_3)_2$, in benzene-$d_6$ solutions (63 mM and 6.3 mM) in sealed 5 mm NMR tubes. Reaction temperatures were maintained by using temperature baths which were constant to within ± 0.1°C. $\Delta G^{\ddagger}(T)$ was calculated from the Eyring equation, $\Delta G^{\ddagger} = RT\ln(\kappa k_B T/kh)$, assuming a transmission coefficient, κ, of 1. Plots of $\ln(k/T)$ vs $1/T$ were constructed to yield the activation parameters $\Delta H^{\ddagger} = 34.5(8)$ kcal mol^{-1} and $\Delta S^{\ddagger} = 6(2)$ e.u.

Preparation of $\{HC(pyz)_3\}[Al(CH_3)_3]_3$

A solution of $HC(pyz)_3$ (200 mg, 0.93 mmol) in C_6H_6 (20 cm^3) was treated with excess $(CH_3)_2Al$ (1.5 ml, 20.8 mmol). The mixture was filtered after 15 min at room temperature and the solvent was removed under reduced pressure giving $\{HC(pyz)_3\}[Al(CH_3)_3]_3$ as a white solid (260 mg, 65%). IR data (Nujol mull, KBr plates, cm^{-1}): 3140 (ν_{C-H}).

REFERENCES

1. H. Sinn and W. Kaminsky, *Adv. Organomet. Chem.* 1980, **18**, 99.
2. (a) E. Negishi, *Organometallics in Organic Synthesis*, Vol. 1. Wiley, New York (1980); (b) D. Seyferth (Ed.), *New Applications of Organometallic Reagents in Organic Synthesis*. Elsevier, Amsterdam (1976).
3. (a) C. F. Powell, J. H. Oxley and J. M. Blocher Jr (Eds), *Vapor Deposition*. Wiley, New York (1966); (b) W. Kern and V. S. Ban, in *Thin Film Processes*, p. 257. Academic Press, New York (1978).
4. (a) B. E. Bent, R. G. Nuzzo and L. H. Dubois, *Mater. Res. Soc. Symp. Proc.* 1988, **101**, 177; (b) M. J. Cooke, R. A. Heinecke, R. C. Stern and J. W. C. Maes, *Solid State Technol.* 1982, **25**, 62; (c) M. L. Green, R. A. Levy, R. G. Nuzzo and E. Coleman, *Thin Solid Films* 1984, **114**, 367; (d) R. A. Levy, M. L. Green and P. K. Gallagher, *J. Electrochem. Soc.* 1984, **131**, 2175.
5. (a) L. V. Interrante, L. E. Carpenter, C. Whitmarsh, W. Lee and G. Slack, *Mater. Res. Soc. Symp. Proc.* 1986, **73**, 986; (b) N. Kuramoto and H. Taniguchi, *J. Mater. Sci. Lett.* 1984, **3**, 471.
6. G. H. Robinson and S. A. Sangokoya, *J. Am. Chem. Soc.* 1988, **110**, 1494.
7. S. A. Sangokoya, B. Lee, W. T. Pennington and G. H. Robinson, *J. Coord. Chem.* 1989, **19**, 331.
8. G. H. Robinson, H. Zhang and J. L. Atwood, *J. Organomet. Chem.* 1987, **331**, 153.

9. J. L. Atwood, D. C. Hrncir, R. Shakir, M. S. Dalton, R. D. Priester and R. D. Rogers, *Organometallics* 1982, **1**, 1021.
10. J. L. Atwood, R. D. Priester, R. D. Rogers and L. G. Canada, *J. Incl. Phenom.* 1983, **1**, 61.
11. G. H. Robinson, S. G. Bott, H. Elgamal, W. E. Hunter and J. L. Atwood, *J. Incl. Phenom.* 1985, **3**, 65.
12. G. H. Robinson, W. E. Hunter, S. G. Bott and J. L. Atwood, *J. Organomet. Chem.* 1987, **326**, 9.
13. G. H. Robinson, H. Zhang and J. L. Atwood, *Organometallics* 1987, **6**, 887.
14. (a) G. H. Robinson, M. F. Self, S. A. Sangokoya and W. T. Pennington, *J. Am. Chem. Soc.* 1989, **111**, 1520; (b) G. H. Robinson, S. A. Sangokoya, F. Moise and W. T. Pennington, *Organometallics* 1988, **7**, 1887; (c) G. H. Robinson and S. A. Sangokoya, *Organometallics* 1988, **7**, 1453; (d) G. H. Robinson, E. S. Appel, S. A. Sangokoya, H. Zhang and J. L. Atwood, *J. Coord. Chem.* 1988, **17**, 373; (e) G. H. Robinson, F. Moise, W. T. Pennington and S. A. Sangokoya, *J. Cryst. Spectrosc. Res.* 1988, **18**, 387; (f) G. H. Robinson and S. A. Sangokoya, *J. Am. Chem. Soc.* 1987, **109**, 6852; (g) G. H. Robinson, A. D. Rae, C. F. Campana and S. K. Byram, *Organometallics* 1987, **6**, 1227.
15. V. L. Goedken, H. Ito and T. Ito, *J. Chem. Soc., Chem. Commun.* 1984, 1453.
16. S. J. Dzugan and V. L. Goedken, *Inorg. Chem.* 1986, **25**, 2858.
17. R. Han, A. Looney and G. Parkin, *J. Am. Chem. Soc.* 1989, **111**, 7276.
18. S. Trofimenko, *J. Am. Chem. Soc.* 1966, **88**, 1842.
19. S. Trofimenko, J. C. Calabrese and J. S. Thompson, *Inorg. Chem.* 1987, **26**, 1507.
20. P. Schwerdtfeger, P. D. W. Boyd, G. A. Bowmaker, H. G. Macj and H. Oberhammer, *J. Am. Chem. Soc.* 1989, **111**, 15.
21. A. H. Cowley, C. J. Carrano, R. L. Geerts, R. A. Jones and C. M. Nunn, *Angew. Chem. Int. Ed. Engl.* 1988, **27**, 277.
22. A. J. Canty, N. J. Minchin, J. M. Patrick and A. H. White, *Aust. J. Chem.* 1983, **36**, 1107.
23. (a) S. Trofimenko, J. C. Calabrese and J. S. Thompson, *Inorg. Chem.* 1987, **26**, 1507; (b) E. Frauendorfer and H. Brunner, *J. Organomet. Chem.* 1982, **240**, 371.
24. R. Benn, A. Rufinska, H. Lehmkohl, E. Janssen and C. Kruger, *Angew. Chem. Int. Ed. Engl.* 1983, **22**, 779.
25. S. Trofimenko, *J. Am. Chem. Soc.* 1970, **92**, 5118.
26. (a) M. E. Thompson, S. M. Baxter, A. R. Bulls, B. J. Burger, M. C. Nolan, B. D. Santarsiero, W. P. Schaefer and J. E. Bercaw, *J. Am. Chem. Soc.* 1987, **109**, 203; (b) C. McDade, J. C. Green and J. E. Bercaw, *Organometallics* 1982, **1**, 1629; (c) G. Parkin and J. E. Bercaw, *Organometallics* 1989, **8**, 1172.
27. S. Trofimenko, J. C. Calabrese, P. J. Domaille and J. S. Thompson, *Inorg. Chem.* 1989, **28**, 1091.
28. (a) J. P. McNally, V. S. Leong and N. J. Cooper, *Am. Chem. Soc. Symp. Ser.* 1987, **357**, 6; (b) B. J. Burger and J. E. Bercaw, *Am. Chem. Soc. Symp. Ser.* 1987, **357**, 79.

Polyhedron Vol. 9, No. 2/3, pp. 277–282, 1990
Printed in Great Britain

0277–5387/90 $3.00+.00
© 1990 Pergamon Press plc

SYNTHESIS AND MOLECULAR STRUCTURE OF A BIS[DI(ALKYL)ALANYL]METHANE; $R_2Al—CH_2—AlR_2$ [R = $CH(SiMe_3)_2$]

MARCUS LAYH and WERNER UHL*

Institut für Anorganische Chemie der Universität Stuttgart, Pfaffenwaldring 55, FRG-7000 Stuttgart 80, F.R.G.

Abstract—Reaction of $Cl_2Al—CH_2—AlCl_2$ with lithium-bis(trimethylsilyl)methyl in *n*-pentane yields $[(Me_3Si)_2CH]_2Al—CH_2—Al[CH(SiMe_3)_2]_2$ (**1**), the first stable organometallic derivative of the starting tetrahalide. The crystal structure of **1** shows monomeric molecules with two trigonal planar coordinated metal atoms. The coordination sphere of the central carbon atom deviates significantly from tetrahedral geometry with an Al—C—Al angle of 129.6°. Further experiments for the synthesis of methylene bridged dialanes were not successful with R = mesityl, *tert*-butyl, tris(trimethylsilyl)methyl and trimethylsilyl.

Organometallic compounds of aluminium which contain a methylene bridge between two aluminium atoms have been isolated and well characterized only for the tetrachloro and tetrabromo derivatives.[1] These compounds are easily synthesized by the reaction of dichloro or dibromo methane with elemental aluminium [eq. (1)] and are potential starting materials for the preparation of the corresponding tetra(alkyl)alanes by metathesis with lithium alkyls. There are, however, only a few and discouraging reports in the literature dealing with such reactions: lithium–methyl or lithium– ethyl[2,3] give products of unknown composition, probably mixtures of the symmetrically substituted tri(alkyl)alanes and oligomeric or polymeric methylene bridged species.[3] Distillation leads to complete decomposition into triorganyls, AlR_3.

$$4Al + 4CH_2Cl_2 \longrightarrow 2Cl_2Al—CH_2—AlCl_2 + \text{“}CH_2{=}CH_2\text{”} \quad (1)$$

Recently we succeeded in the synthesis of a dialane(4) with an aluminium–aluminium bond, kinetically stabilized by the high sterical shielding of four bulky bis(trimethylsilyl)methyl groups.[4] This ligand appears to be also suitable for obtaining a stable molecule containing the $Al—CH_2—Al$ fragment, because it should prevent the formation of intermediates with coordination numbers higher than three at the metal atoms and therefore the dismutation process, as it occurs with the methyl or ethyl derivatives.

Interestingly there are two recent reports[5] concerning the addition of Al—H bonds to alkynes. which should lead to molecules with three aluminium atoms bonded to one carbon atom. Unfortunately the products were not isolated and only investigated by hydrolysis experiments, therefore they need further characterization.

$[(Me_3Si)_2CH]_2Al—CH_2—Al[CH(SiMe_3)_2]_2$ (1)

Compound **1** is best obtained by reaction of lithium-bis(trimethylsilyl)methyl with $Cl_2Al—CH_2—AlCl_2$ in a molar ratio of 4:1 in *n*-pentane. Since the synthesis of the lithium compound takes place in diethyl ether,[6] the solvent was completely removed by distillation and the remaining solid evacuated for several hours at room temperature until a final pressure of 10^{-3} torr was reached. A suspension of the prepared ether-free lithium-organyl in *n*-pentane was then treated at −50°C with solid $Cl_2Al—CH_2—AlCl_2$ (only slightly soluble in hydrocarbons) to produce, after warming to room temperature and recrystallization from *n*-pentane, the title compound **1** [eq. (2)] in 45% yield. Solubility of the colourless crystals of **1** is high in *n*-pentane but only moderate in benzene, in which, cryoscopically, a monomeric molecular weight was observed. The ^1H NMR spectrum shows three signals with intensities of 36:2:1. The resonance of the central bridging CH_2-group is shifted to high field ($\delta = -0.55$ ppm) and broadened due to the quadrupole moment of aluminium. Very pure fractions of **1**, obtained after repeated recrystallization,

* Author to whom correspondence should be addressed.

reveal a splitting of the $SiMe_3$ singulet into three lines with intensities of 1:2:1. This effect may be due to hindered rotation about the bonds between the aluminium atoms and the central carbon atom, and we assume a staggered conformation of the alanyl substituents (see, also, crystal structure below). Compound **1** is thermally very resistant and melts at 152°C without decomposition.

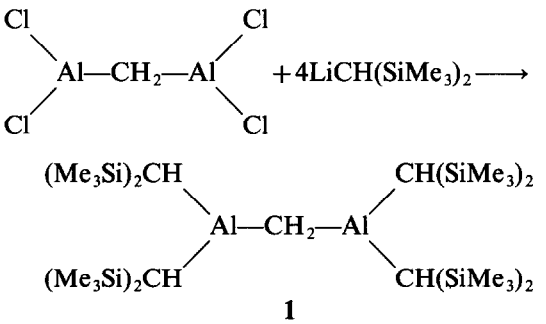

1

$+4LiCl.$ (2)

Because of the low yield, the mother liquor remaining after the isolation of **1** was investigated. A yellow liquid of high viscosity was left after removal of the solvent. Its ^1H NMR spectrum showed, besides some small signals, mainly the resonances of **1** and lithium-bis(trimethylsilyl)methyl in a 1:1 ratio. We did not succeed, however, in isolating a second fraction of crystalline **1**. The surplus lithium compound led us to extend the time of reaction and even to work in boiling solvent, but in no experiment did we find a higher yield than mentioned above. Tris[bis(trimethylsilyl) methyl]alane, $Al[CH(SiMe_3)_2]_3$, expected as a dismutation product, was not detectable.

Other ligands

Subsequent to the successful synthesis of **1** we tried to obtain further organometallic derivatives containing the Al—CH_2—Al fragment. The reaction of lithium–*tert*-butyl with the starting tetrahalide leads to complete decomposition of the lithium compound via β-elimination into lithium hydride and *iso*-butene, without any detectable attack at the halogen alane. This result is in accord with observations made in similar experiments with alkyl alanes or alkyl halogenalanes.[7,8] Mesityl-Grignard produces trimesitylalane[9] as the only isolable product in 30% yield. Lithium–tris(trimethylsilyl)methyl—only available as an etherate[10]—reacts in the presence of the halogen alane with complexed tetrahydrofuran or tetramethylethylenediamine, thereby forming tris(trimethylsilyl)methane, $HC(SiMe_3)_3$.

Reaction with lithium–trimethylsilyl $LiSiMe_3$, also does not lead to the desired compound. A brown oil was obtained, from which after repeated recrystallization colourless, highly air-sensitive crystals of $Li[Al(SiMe_3)_4]$ (**2**) were isolated in 35% yield applied to $LiSiMe_3$. In addition to usual characterization, this result was ascertained through the specific reaction of aluminium tribromide with four equivalents of $LiSiMe_3$ [eq. (3)] yielding the analytically and spectroscopically identical product:

$$AlBr_3 + 4LiSiMe_3 \longrightarrow Li[Al(SiMe_3)_4] + 3LiBr. \quad (3)$$

2

The synthesis of **2**, in 35% yield, has already been described in the literature[11] starting from aluminium amalgam, trimethylchlorosilane and lithium metal, although in parts the published properties of **2** differ significantly from our observations. Therefore, we repeated the characterization. The trimethylsilyl alanate is easily soluble in non-polar solvents like *n*-pentane and sublimes in a closed capillary under normal pressure at 220°C before melting. Cryoscopic molecular weight measurement reveals a non-dissociated, monomeric molecule in benzene solution.

There is only one further lithium derivative which reacts with the starting halogen alane to form a methylene bridged dialane. This is lithium–(trimethylsilyl)methyl, $LiCH_2SiMe_3$; but the product will not be discussed in this report for two reasons: first, in solution with benzene it shows an equilibrium between monomeric and dimeric species and we hope to get crystals suitable for X-ray diffraction to prove whether this compound is dimeric in solid state. Second, in solution, it decomposes slowly at room temperature to unknown solid products, and a thorough study of this reaction may lead to a better understanding of the dismutation processes already mentioned for the methyl and ethyl derivatives.

MOLECULAR STRUCTURE OF 1

Single crystals suitable for X-ray diffraction studies were grown directly from the reaction mixture at 0°C. Buerger precession photos indicated the centrosymmetric orthorhombic space group *Pcca* with four molecules in the unit cell and half a molecule in the asymmetric unit. Further details of structure determination and refinement are listed in Table 2 (Experimental). All positions of the hydrogen atoms were found in a Fourier synthesis and refined isotropically to reasonable values.

Figure 1 shows a stereoscopic view of one molecule of **1**. It is located on a crystallographic two-

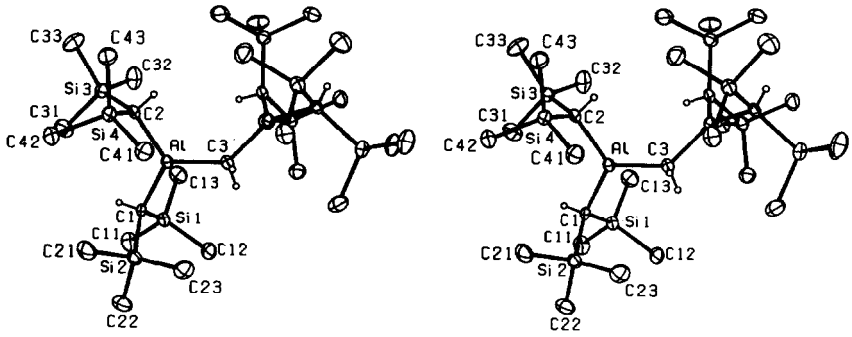

Fig. 1. ORTEP[29] stereo diagram of **1** with labelling scheme. The atoms are represented by 40% probability thermal ellipsoids. The hydrogen atoms have been omitted for clarity except for the four α-H (with arbitrary radius) of the element–organic substituents. They clearly show the orientation of the ligands.

fold axis bisecting the angles H—C—H and Al—C—Al at the central carbon atom C(3) and transferring both halves of the molecule into one another. The bis(trimethylsilyl)methyl substituents at one aluminium atom are arranged in such a way that the inner C—H bonds point in one direction, so that one hydrogen is in the neighbourhood of the trimethylsilyl groups of the second ligand. This arrangement corresponds to that found in tetrakis[bis(trimethylsilyl)methyl]dimetal(4) derivatives of aluminium,[4] gallium[12] and indium[13] as well as in $In[CH(SiMe_3)_2]_3$[14] and $\{Sn[CH(SiMe_3)_2]_2\}_2$,[15] but differs from the conformation in (TMEDA) $Li(\mu\text{-}Br)_2In[CH(SiMe_3)_2]_2$[13] or in $K\{Cl_2Al[CH(SiMe_3)_2]_2\}$.[8] Unlike the just mentioned dimetal(4) derivatives of Al, Ga and In, the central atoms Al, C(1), C(2), C(3) and the symmetrically dependent atoms do not lie in a plane. Instead, we observe a nearly staggered conformation of the two alanyl substituents (torsion angles C(1)—Al···Al′—C(1)′ 113.1°; C(2)—Al···Al′—C(2)′ 74.9°). The aluminium atom lies only 1.6 pm above the plane defined by the three inner carbon atoms; this fact and the sum of the three angles, C—Al—C (360.0°), verifies a nearly ideal planar coordination.

The angles at the central carbon atom, C(3), show significant deviations from the values expected for sp^3 atoms with Al—C—Al 129.6° (Table 1). Steric repulsion between the bulky substituents cannot be the only reason for this, because the usual lengthening of the corresponding Al—C bond is not observed, but a very short bond length of 193.8 pm is found. This is 2 pm shorter than the terminal Al—C bonds. Tri(organyl)alanes usually have Al—C bond lengths longer than 195 pm: e.g. $(AlMe_3)_2$ 195.3 pm,[16] tri(mesityl)alane 199.5 pm,[9] $Al(CH_2C_6H_5)_3$ 198.9 pm.[17] Shorter distances are observed only in dimeric tri(cyclopropyl)alane (192.8–195.9 pm,[18] the shortest one to a disordered cyclopropyl group) and in compounds with at least one electronegative substituent at aluminium: e.g. $(Me_2AlCl)_2$ 193.5 pm,[19] $[Cl_2Al—CH(SiMe_3)_2]_2$ 191.2 pm,[8] $K[MeAlCl_3]$ 193.9 pm[20] and $[(C_5Me_5)AlMeCl]_2$ (Al—Me) 191.6 pm.[21]

A possible explanation for the large angle at C(3), on the one hand, and the short Al—C(3) distance, on the other, is the separation of charge due to the high difference in electronegativities between aluminium and carbon. Both aluminium atoms lead to an accumulation of negative charge at the central carbon atom. Additional coulombic attraction should therefore decrease the Al—C distance and repulsion between the positively charged metal atoms should increase the Al—C—Al angle. Furthermore, hyperconjugation has to be considered between the C—H bonds at the central carbon atom, C(3), and the empty *p*-orbitals of both aluminium atoms, because each of the two C—H σ-bonds is nearly parallel to one of these orbitals (torsion angles: C(1)—Al—C(3)—H(3) −95.3°; C(2)—Al—C(3)—H(3) 83.1°).

Recently the crystal structures of similar methylene bridged indium compounds $Cl_2In—CH_2—InCl_2 \cdot 2TMEDA$ and $Cl(Br)In—CH_2—InCl_2 \cdot 2TMEDA$ were published.[22] They also show large angles at the central carbon atom of 117.6 and 117.5°.

EXPERIMENTAL

Preparation of **1**

A suspension of 8.43 g (0.0507 mol) of ether-free lithium–bis(trimethylsilyl)methyl in 100 cm^3 of *n*-pentane was treated at −50°C with 2.66 g (0.0127 mol) of solid $Cl_2Al—CH_2—AlCl_2$. After warming to room temperature and stirring for 19 h, the lithium

Table 1. Listing of selected bond lengths (pm), bond angles (°) and torsion angles (°) for **1**

Al—C(3)	193.8(1)	Al—C(1)	195.5(2)
		Al—C(2)	195.8(2)
C(1)—Si(1)	186.0(2)	C(2)—Si(3)	186.1(2)
C(1)—Si(2)	187.2(2)	C(2)—Si(4)	187.2(2)
Al—C(3)—Al′	129.6(2)	Al—C(1)—Si(1)	110.7(1)
H(3)—C(3)—H(3)′	101(1)	Al—C(1)—Si(2)	116.8(1)
C(3)—Al—C(1)	119.41(9)	Al—C(2)—Si(3)	119.0(1)
C(3)—Al—C(2)	118.61(9)	Al—C(2)—Si(4)	109.6(1)
C(1)—Al—C(2)	121.97(9)	Si(1)—C(1)—Si(2)	114.8(1)
		Si(3)—C(2)—Si(4)	117.2(1)

	$n=1$	$n=2$	$n=3$
C(1)—Si(1)—C(1*n*)	112.6(1)	111.6(1)	110.3(1)
C(1)—Si(2)—C(2*n*)	110.2(1)	113.8(1)	110.9(1)
C(2)—Si(3)—C(3*n*)	111.9(1)	110.5(1)	112.4(1)
C(2)—Si(4)—C(4*n*)	110.2(1)	112.1(1)	113.0(1)

C(1)—Al—C(3)—Al′	138.50(8)	C(3)—Al—C(1)—H(1)	−172(1)
C(2)—Al—C(3)—Al′	−43.14(9)	C(3)—Al—C(2)—H(2)	16(1)
C(1)—Al—C(3)—H(3)	−95.3(9)	C(3)—Al—C(1)—Si(1)	−61.4(1)
C(2)—Al—C(3)—H(3)	83.1(9)	C(3)—Al—C(1)—Si(2)	72.4(1)
C(2)—Al—C(1)—H(1)	10(1)	C(3)—Al—C(2)—Si(3)	129.3(1)
C(1)—Al—C(2)—H(2)	−165(1)	C(3)—Al—C(2)—Si(4)	−91.8(1)

Al′ and H(3)′ generated by $-x; y; 1/2-z$.

Table 2. Cell data and details of the structure solution for **1**

Formula	$Al_2Si_8C_{29}H_{78}$
Crystal system	Orthorhombic
Space group	*Pcca* (No. 54[24])
Z	4
Packing coefficient (%)[25]	69
Melting point (°C)	152
Temperature (°C)	-120 ± 3
a (pm)	2282.0(4)
b (pm)	1700.9(2)
c (pm)	1164.6(2)
Volume (10^{-30} m^3)	4520.3
μ (10^2 cm^{-1}); no absorption correction	2.9
Crystal size	$0.7\times0.8\times0.3$ mm
Diffractometer	Syntex $P2_1$
Radiation	Mo-K_α; 0.71069
2θ scan range	$2.0° \leqslant 2\theta \leqslant 55°$
Octant used	$0 \leqslant h \leqslant 29$
	$0 \leqslant k \leqslant 22$
	$0 \leqslant l \leqslant 15$
Type of data collection; scan width	ω-scan; 2.0°
Standard reflections	2 per every 100 reflections
Unique reflections	5188
Observed reflections; $I > 2\sigma(I)$	4169
Parameters refined	333
Programs used	SHELXS86;[26] direct method
	XRAY76[27]
Scattering factors of neutral atoms[28]	
Full-matrix least-squares	
$R = \Sigma\|\|F_o\|-\|F_c\|\|/\Sigma\|F_o\|$	0.044
$R_w = [\Sigma w(\|F_o\|-\|F_c\|)^2/\Sigma wF_o^2]^{1/2}$; $w = 1/\sigma F(o)$	0.019
Maximum residual electron density (10^{30} e m^{-3})	0.4

chloride was filtered off. Compound **1** crystallized from the solution after partial removal of the solvent *in vacuo* and cooling to 0°C. Yield: 4.0 g (45%); colourless crystals. Melting point (closed capillary; argon): 152°C. Molecular weight (cryoscopically in benzene): calc. 705.6; found; 670. ^1H NMR spectrum (in C_6D_6): $\delta = 0.30$ ppm ($SiMe_3$); $\delta = -0.22$ ppm ($CHSiMe_3$); $\delta = -0.50$ ppm ($Al—CH_2—Al$). ^{13}C NMR spectrum (in C_6D_6): $\delta = 5.9$ ppm ($SiMe_3$); $\delta = 13.2$ ppm ($CHSiMe_3$); Al—C—Al not found. IR spectrum (in paraffin; CsBr windows; cm^{-1}): 1250 s δCH_3; 1050 m, 1010 m $\delta[CH(Si_2)]$ and $\rho(CH_2)$; 950 vw, 920 m, 840 vs, 780 m, 750 m all $\rho[CH_3(Si)]$; 710 vw, 645 m, 630m, 610 vw all $\nu(SiC_3)$; 555 w, 520 w, 510 w, 475 w all ν(AlC).

Preparation of **2**

1.23 g (0.0046 mmol) of aluminium tribromide dissolved in 200 cm^3 of *n*-pentane were treated at −70°C with 38.8 cm^3 of a solution of $LiSiMe_3$ (0.0184 mol; 0.475 M) in *n*-hexane.[23] After warming to room temperature and stirring for a further 3 h the dark brown reaction mixture was filtered and the solvent removed *in vacuo*. Compound **2** sublimes out of the remaining oil at 10^{-3} torr and 65°C. Yield: 0.95 g (63%); colourless crystals; spontaneously inflammable in air. **2** sublimes in a closed capillary under argon with normal pressure at a temperature of 220°C without melting. Molecular weight (cryoscopically in benzene): calc. 326.7; found 345. Mass spectrum (20 eV; 325 K): 326.1 (44%) M^+; 253.1 (100%) $LiAl(SiMe_3)_3$. ^1H NMR spectrum (in C_6D_6): $\delta = 0.21$ ppm. ^{13}C NMR spectrum (in C_6D_6): $\delta = 4.5$ ppm. IR spectrum (in paraffin; CsBr windows; cm^{-1}): 1247 s, 1235 s, 1213 m $\delta(CH_3)$; 1089 vw, 1052 w; 925 m, 900 m, 830 vs, 750 m all $\rho(CH_3)$; 670 s, 655 s, 609 s $\nu(SiC_3)$; 518 w,br., 455 w,br. ν(LiSi); 400 w, 375 w $\nu(AlSi_4)$ or $\delta(SiC_3)$. Raman spectrum (crystals in capillary; 488 nm; cm^{-1}): 1256 m, 1238 m $\delta(CH_3)$; 870 m, 840 m,br. $\rho(CH_3)$; 682 s, 658 s $\nu_{as}(SiC_3)$; 620 s, 608 s $\nu_s(SiC_3)$; 438 w; 384 m $\nu_{as}(AlSi_4)$; 315 s $\nu_s(AlSi_4)$; 264 w, 227 m $\delta(SiC_3)$; 158 vs $\rho(SiC_3)$; 115 m $\delta(AlSi_4)$.

Crystal data, X-ray data and structure refinement

Table 2 lists all information about unit cell parameters, data acquisition and structure refinement for compound **1**.

REFERENCES

1. M. R. Ort and E. H. Mottus, *J. Organomet. Chem.* 1973, **50**, 47.
2. H. Lehmkuhl and R. Schäfer, *Tetrahedron Lett.* 1966, 2315.
3. E. C. Ashby and R. S. Smith, *J. Organomet. Chem.* 1982, **225**, 71.
4. W. Uhl, *Z. Naturf.* 1988, **43B**, 1113.
5. A. V. Kuchin, S. A. Markova and G. A. Tolstikov, *Izv. Akad. Nauk SSSR* 1988, 1448; A. V. Kuchin, S. A. Markova, S. I. Lomakina and G. A. Tolstikov, *Zh. Obshch. Khim.* 1988, **58**, 1567.
6. P. J. Davidson, D. H. Harris and M. F. Lappert, *J. Chem. Soc., Dalton Trans.* 1976, 2268.
7. W. Uhl, *Z. Anorg. Allg. Chem.* 1989, **570**, 37.
8. W. Uhl, unpublished.
9. W. Seidel, *Z. Anorg. Allg. Chem.* 1985, **524**, 101; J. J. Jerius, J. M. Hahn, A. F. M. M. Rahman, O. Mols, W. H. Ilsley and J. P. Oliver, *Organometallics* 1986, **5**, 1812.
10. M. A. Cook, C. Eaborn, A. E. Jukes and D. R. M. Walton, *J. Organomet. Chem.* 1970, **24**, 529.
11. L. Rösch and G. Altnau, *Chem. Ber.* 1979, **112**, 3934.
12. W. Uhl, M. Layh and T. Hildenbrand, *J. Organomet. Chem.* 1989, **364**, 289.
13. W. Uhl, M. Layh and W. Hiller, *J. Organomet. Chem.* 1989, **368**, 139.
14. A. J. Carty, M. J. S. Gynane, M. F. Lappert, S. J. Miles, A. Singh and N. J. Taylor, *Inorg. Chem.* 1980, **19**, 3637.
15. D. E. Goldberg, P. B. Hitchcock, M. F. Lappert, K. M. Thomas, A. J. Thorne, T. Fjeldberg, A. Haaland and B. E. R. Schilling, *J. Chem. Soc., Dalton Trans.* 1986, 2387.
16. R. G. Vranka and E. L. Amma, *J. Am. Chem. Soc.* 1967, **89**, 3121; J. C. Huffman and W. E. Streib, *J. Chem. Soc., Chem. Commun.* 1971, 911.
17. A. F. M. M. Rahman, K. F. Siddiqui and J. P. Oliver, *Organometallics* 1982, **1**, 881.
18. J. W. Moore, D. A. Sanders, P. A. Scherr, M. D. Glick and J. P. Oliver, *J. Am. Chem. Soc.* 1971, **93**, 1035; W. H. Ilsley, M. D. Glick, J. P. Oliver and J. W. Moore, *Inorg. Chem.* 1980, **19**, 3572.
19. K. Brendhaugen, A. Haaland and D. P. Novak, *Acta Chem. Scand. A* 1974, **28**, 45.
20. J. L. Atwood, D. C. Hrncir and W. R. Newberry, *Cryst. Struct. Commun.* 1974, **3**, 615.
21. P. R. Schonberg, R. T. Paine and C. F. Campana, *J. Am. Chem. Soc.* 1979, **101**, 7726.
22. M. A. Khan, C. Peppe and D. G. Tuck, *Organometallics* 1986, **5**, 525.
23. L. Rösch, G. Altnau, E. Hahn and H. Havemann, *Z. Naturf.* 1981, **36B**, 1234; W. Biffar, H. Nöth and R. Schwerthöffer, *Liebigs Ann. Chem.* 1981, 2067.
24. *International Tables for X-Ray Crystallography*, 3rd edn, Vol. 1. Kynoch Press, Birmingham (1969).
25. A. I. Kitaigorodskii, *Organic Chemical Crystallography*. Consultants Bureau, New York (1961).
26. G. M. Sheldrick, *Crystallographic Computing 3*,

(Edited by G. M. Sheldrick, C. Krüger and R. Goddard), University Press, Oxford (1985).
27. J. M. Stewart, *The X-Ray System*, Version 1976. University of Maryland (1976).
28. D. T. Cromer and J. B. Mann, *Acta Cryst.* 1968, **24A**, 321; R. F. Stewart, E. R. Davidson and W. T. Simpson, *J. Chem. Phys.* 1965, **42**, 3175.
29. C.-K. Johnson, ORTEP, Report ORNL-3794. Oak Ridge National Laboratory, Oak Ridge, Tennessee (1965).

Polyhedron Vol. 9, No. 2/3, pp. 283–287, 1990
Printed in Great Britain

0277–5387/90 $3.00+.00
© 1990 Pergamon Press plc

SYNTHESIS AND CRYSTAL STRUCTURE OF A MIXED BIS(ARENE)GALLIUM(I) COMPLEX: DIMERIC (η^6-1,2,4,5-TETRAMETHYLBENZENE) (η^6-TOLUENE)GALLIUM(I) TETRACHLOROGALLATE(III)

H. SCHMIDBAUR,* R. NOWAK, B. HUBER and G. MÜLLER

Anorganisch-chemisches Institut der Technischen Universität München, Lichtenbergstraße 4, D-8046 Garching, F.R.G.

Abstract—The title compound (η^6-1,2,4,5-tetramethylbenzene)(η^6-toluene)gallium(I) tetrachlorogallate(III) (**1**) crystallizes from dilute solutions of equimolar quantities of gallium(I) tetrachlorogallate(III) and 1,2,4,5-tetramethylbenzene (durene) in toluene on slow cooling to 0°C. More concentrated solutions yield the 1 : 1 complex (1,2,4,5-$C_6H_2Me_4$)$Ga^+GaCl_4^-$ (**2**). The crystals of compound **1** contain centrosymmetrical dimers, $\{[(\eta^6\text{-}C_6H_2Me_4)(\eta^6\text{-}C_6H_5Me)Ga]GaCl_4\}_2$, in which each gallium(I) centre is hexahapto-bonded to one durene and one toluene molecule. The two aromatic hydrocarbons of these bent-sandwich moieties form an interplane angle of 58°. With a metal-to-ring distance of 2.642 Å, the durene ring is much closer to the Ga^+ atom than the toluene ring (3.039 Å). The Ga^+ atoms are bridged via two slightly distorted $GaCl_4^-$ tetrahedra through contacts with three of the four chlorine atoms. The structure resembles that of the $[(C_6H_6)_2Ga]GaX_4$ complexes with X = Cl, Br.

Salts of the low-valent heavy Group 13 metal cations with counter-ions of low polarizability are unique in showing high solubility in aromatic hydrocarbons.[1] Extensive work in recent years has provided evidence that these phenomena have their origin in the formation of arene complexes of gallium(I), indium(I) and thallium(I), in which the metal is η^6-bonded to the aromatic system, i.e. with the metal positioned exactly above the ring centre in most cases.[2–7] Apart from the 1 : 1 stoichiometry with only one arene in the first coordination sphere of the metal, an increasing number of bent-sandwich complexes with a 2 : 1 ratio of arene-to-metal has been discovered. As a rule, the two aromatic rings show an interplane angle of *ca* 60° in these complexes, with counter-ion contacts of the metal roughly in the plane bisecting the interarene angle. This mode of coordination was first detected for the benzene adducts of $Ga[GaCl_4]$[2] and $Ga[GaBr_4]$,[3] but has meanwhile also been found even in complex networks with donors like the small cyclophanes.[8–9] Compounds of the alternative 1 : 2 stoichiometry arene–metal, with a metal on both sides of a given arene ring, seems to be restricted to the neighbouring elements in Groups 14 and 15.[10] An extreme situation of arene coordination has been reached in the complex of gallium(I) with the large-ring [2,2,2]-paracyclophane, however, where the metal is no less than η^{18}-bonded to the carbon atoms of three benzene rings.[11]

We report here the synthesis and structure determination of a dimeric bent-sandwich gallium(I) complex, in which each metal is η^6-coordinated to two benzene molecules with a different pattern of methyl substitution. This complex is of interest since it allows a direct comparison of metal bonding to ligands with different donor capacity, as determined by the inductive effect of the substituents. There is only one precedent for this situation,[12] with both toluene and hexaethylbenzene present at the gallium(I) centre. The extreme steric crowding at the C_6Et_6 ligand makes this example rather special, however, and a study was therefore initiated with ligand combinations where the steric bulk should play a minor rôle.

SYNTHESIS AND PROPERTIES OF COMPLEXES

Gallium(I) tetrachlorogallate(III) dissolves readily in anhydrous toluene to give a solution probably

* Author to whom correspondence should be addressed.

containing toluene complexes of unknown stoichiometry and structure which have not yet been isolated. $Ga[GaCl_4]$ can also be dissolved in solutions of 1,2,4,5-tetramethylbenzene (durene) in toluene on heating. Rapid cooling of these mixtures containing high concentrations of durene and the gallium salt to room temperature leads to the separation of a heavy liquid phase which is difficult to crystallize. Slow cooling to *ca* 0°C (refrigerator) gives a fine microcrystalline precipitate which analyses as the 1:1 complex of durene and $Ga[GaCl_4]$, m.p. 15–16°C. Its structure could not be determined. From dilute solutions in toluene a macrocrystalline product can be crystallized on cooling to 0°C, whose microanalysis data indicate the presence of the title compound with mixed arenes present (m.p. 5°C). The transparent, colourless crystals are extremely hygroscopic, and decomposition starts immediately on contact with air. The black colour developed, thereby, indicates disproportionation to metallic gallium. The ^1H NMR spectrum of benzene solutions shows the resonances of toluene and durene in a 1:1 molar intensity ratio.

Experiments with benzene–durene mixtures gave only oily products which were not characterized any further.

Table 1. Crystal data and structure solution of the compound $\{[(\eta^6\text{-}1,2,4,5\text{-}C_6H_2Me_4)(\eta^6\text{-}C_6H_5Me)Ga]GaCl_4\}_2$

Formula	$C_{17}H_{22}Ga_2Cl_4$
M_r	507.617
Space group	$P\bar{1}$ (No. 2)
a (Å)	9.821(1)
b (Å)	11.214(1)
c (Å)	11.287(1)
α (°)	90.59(1)
β (°)	115.11(1)
γ (°)	101.56(1)
V (Å^3)	1096.4
Z	2
ρ_{calc} (g cm^{-3})	1.537
μ (Mo-K_α) (cm^{-1})	29.4
T (°C)	−60
Number of measured reflections	4302
Number of unique reflections	4272
Number of observed reflections	3030
Number of refined parameters	208
R^a	0.044
R_w^b	0.037
$\Delta\rho_{final}$ (e/Å^3) (max/min)	+0.64/−0.63

$^a R = \Sigma(\|F_o\|-|F_c\|)/\Sigma|F_o|$.
$^b R_w = [\Sigma w(|F_o|-|F_c|)^2/\Sigma wF_o^2]^{1/2}$, $w = 1/\sigma^2(F_o)$.

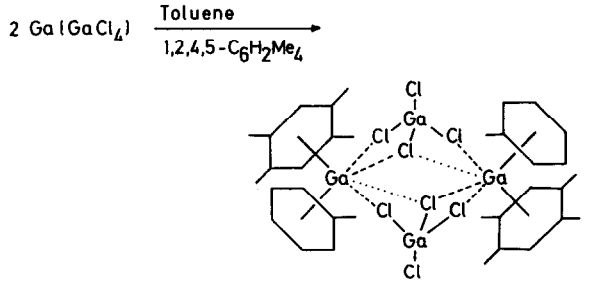

DETERMINATION AND DESCRIPTION OF THE CRYSTAL STRUCTURE

A single crystal X-ray diffraction study of the compound confirmed the stoichiometry inferred from analytical and spectroscopic data. Details of the structure determination and crystal data are summarized in Table 1. Selected interatomic distances and angles are presented in Table 2.

The analysis has shown that the complex forms discrete molecules composed of two formula units related by a centre of symmetry (Fig. 1). The packing of the molecules in the unit cell is displayed in Fig. 2. There are no specific contacts between the dimers, and no extra interstitial hydrocarbon—a common phenomenon in Group 13 arene crystal chemistry—could be detected.

The molecular structure of the title compound is very similar to that of the $[(C_6H_6)_2Ga(GaX_4)]_2$ units in the two crystalline phases $[(C_6H_6)_2Ga(GaX_4)]_2\cdot(C_6H_6)_3$ with X = Cl, Br.[2,3] Apart from the absence of an interstitial hydrocarbon, the main variation stems from the fact that two different arenes are present at each metal(I) centre. The structure thus features two heteroleptic bent-sandwich moieties with interplane angles of 58°, a value typical for this class of compounds.[1]

The most important structural detail is the finding that the metal-to-arene distances are significantly different at each unit, with the durene ring much closer to the metal than the toluene ring (2.642 vs 3.039 Å!). This result is in contrast to expectations on steric grounds (with durene as the more bulky ligand as compared to toluene), and must imply that durene is much more tightly bonded than toluene for electronic reasons.

A simplified molecular orbital description of bonding[1,12] proposes a charge transfer from the arene to the metal, which should be enhanced by electron-donating substituents like methyl groups. This would allow durene to overrule toluene as a donor ligand, especially since its site symmetry is more favourable than that of the toluene competitor (C_{2v} as compared to C_s for durene and toluene, respectively). Along with the differences in metal-to-ring distances, the positioning of the gallium(I)

Table 2. Selected bond distances (Å) and angles (°) in the compound $\{[(\eta^6\text{-}1,2,4,5\text{-}C_6H_2Me_4)(\eta^6\text{-}C_6H_5Me)Ga]GaCl_4\}_2$

Ga(1)—Cl(1)	2.173(1)	Ga(2)—Cl(1)	3.259(1)
Ga(1)—Cl(2)	2.162(1)	Ga(2)—Cl(2)	3.109(1)
Ga(1)—Cl(3)	2.160(2)	Ga(2)—Cl(3*)	3.370(2)
Ga(1)—Cl(4)	2.148(2)	Ga(2)—Cl(1*)	3.991(2)
Ga(2)—$E(1)_{tmbz}$	2.642	Ga(1)—Ga(2)	3.952(5)
Ga(2)—$E(2)_{tol}$	3.039	Ga(2)—Ga(2*)	6.194(6)
Ga(2)—C(11)	2.971(4)	Ga(2)—C(21)	3.339(5)
Ga(2)—C(12)	2.965(4)	Ga(2)—C(22)	3.216(5)
Ga(2)—C(13)	2.976(4)	Ga(2)—C(23)	3.210(5)
Ga(2)—C(14)	3.022(4)	Ga(2)—C(24)	3.331(6)
Ga(2)—C(15)	3.016(4)	Ga(2)—C(25)	3.445(6)
Ga(2)—C(16)	2.980(4)	Ga(2)—C(26)	3.444(6)
Cl(1)—Ga(1)—Cl(2)	107.0(1)	Cl(2)—Ga(2)—Cl(3*)	131.83(1)
Cl(1)—Ga(1)—Cl(3)	109.1(1)	Cl(1)—Ga(2)—E(1)	109.32
Cl(1)—Ga(1)—Cl(4)	111.3(1)	Cl(1)—Ga(2)—E(2)	143.81
Cl(2)—Ga(1)—Cl(3)	110.7(1)	Cl(2)—Ga(2)—E(1)	109.32
Cl(2)—Ga(1)—Cl(4)	109.2(1)	Cl(2)—Ga(2)—E(2)	94.47
Cl(3)—Ga(1)—Cl(4)	109.5(1)	Cl(3*)—Ga(2)—E(1)	104.47
Cl(1)—Ga(2)—Cl(2)	66.33(1)	Cl(3*)—Ga(2)—E(2)	98.43
Cl(1)—Ga(2)—Cl(3*)	76.46(1)	E(1)—Ga(2)—E(2)	118.67

Interarene angle 58.0.
E: centres of the arenes.

centre above each ring is also not the same, as can be shown by the angles between the normals to the planes and the line connecting the arene centres with the metal (1.3 and 6.7°, respectively). Durene is closer to true η^6-bonding than toluene. It remains an intriguing observation, however, that the benzene molecules in the $(C_6H_6)_2Ga^+GaX_4^-$ complexes show non-equivalent bonding to the metal as judged from significant differences in metal–arene distances in both phases (X = Cl, Br).[2,3] There is no obvious explanation for this deviation from an equivalent interaction, though distortion of the highest

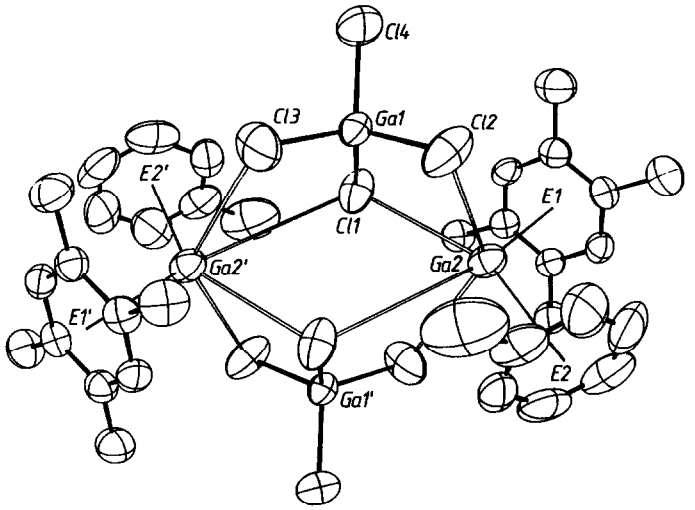

Fig. 1. Molecular structure and atomic numbering of the title compound (ORTEP, 50% probability; the atoms are related by a centre of symmetry).

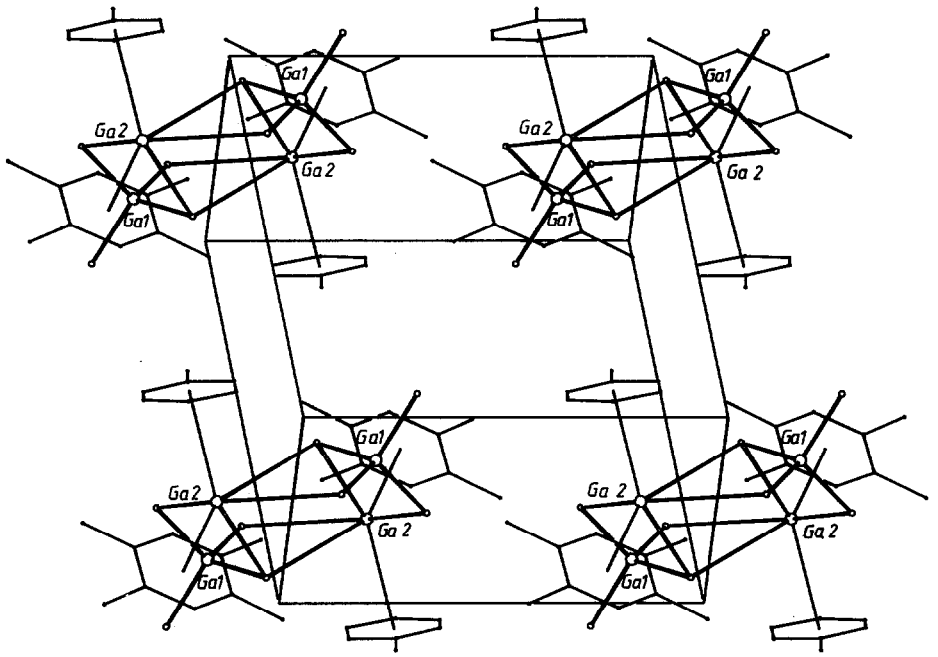

Fig. 2. Molecular packing of the molecules in the unit cell of the title compound (**1**).

symmetry has been shown to be associated with a gain in energy in various related and unrelated species.[13] The complexity of the present systems has discouraged us to produce any more detailed analyses.

The tetramethylbenzene–gallium(I) distance in the title compound (**1**) is the shortest found in bis (arene)gallium(I) complexes, and the toluene–gallium(I) distance is shorter than that in the mixed (toluene)(hexaethylbenzene)gallium(I) complex. These relations show the strengthening influence of an increase in methyl substitution for the *ipso*-ring bonding on one hand, and the weakening effect for the bonding of neighbouring arene ligands on the other. Relatively long C_6H_5Me–Ga^I and C_6Et_6–Ga^I distances (2.960/3.145 Å) in the mixed C_6H_5Me/C_6Et_6 complex appear to be of steric origin,[8] however. 2:1 complexes of gallium(I) with penta- or hexamethylbenzene have not yet been observed, probably due to severe steric interactions of the methyl substituents in a bent-sandwich structure.

The two Ga^+ centres of the dimers are bridged by two $GaCl_4^-$ tetrahedra through contacts with all but one of the chlorine atoms at each anion (Fig. 1). Three of these contacts, the distances Cl(2)—Ga(2) (3.109(1) Å), Cl(1)—Ga(2) (3.259(1) Å) and Cl(3)—Ga(2*) (3.370(2) Å) are much shorter than the fourth one, Cl(1)—Ga(2) = 3.991(2) Å, which originates from a bridgehead position of Cl(1). Taking into account only the short contacts, the structure is based on an eight-membered ring with the sequence of atoms Ga(2)—Cl(2)—Ga(1)—Cl(3)—Ga(2*)—Cl(2*)—Ga(1*)—Cl(3*). This pattern is not only present in the bis(benzene)gallium(I) complexes,[2,3] but also in a bis(arene) complex of tin(II) reported recently[14] from this laboratory.

As expected, the $GaCl_4^-$ tetrahedra in the title complex are distorted with minor deviations of the Cl—Ga(1)—Cl angles from the tetrahedral norm, and with a variation of the Ga(1)—Cl distances within narrow limits (Table 2). The non-bridging chlorine atom Cl(4) has the shortest distance to Ga(1) (2.148(2) Å), while Cl(1) with its bridgehead function has the largest (2.173(1) Å).

With Cl(1) considered as a ligand to Ga(2) and Ga(2*), the environment of Ga^+ can be described as distorted octahedral (trigonal-antiprismatic), as indicated by an almost parallel orientation of the planes Cl(1)—Cl(2)—E(1)(centre of durene) and Cl(1*)—Cl(3*)—E(2)(centre of toluene).

EXPERIMENTAL

General

All experiments were carried out under an atmosphere of pure dry nitrogen. Glassware, as well as solvents and reagents, were treated accordingly. Gallium metal was received from Preussag AG and converted to $Ga[GaCl_4]$ by following literature procedures.[15]

(η^6 - 1,2,4,5 - *Tetramethylbenzene*)(η^6 - *toluene*) *gallium*(I) *tetrachlorogallate*(III)

Gallium(I) tetrachlorogallate(III) (1.88 g, 6.68 mmol) and durene (0.9 g, 6.68 mmol) were dissolved in 20 cm^3 of toluene and heated under reflux for 1 h. On slow cooling to 0°C crystallization occurred after a few days. The mother liquor was decanted and the colourless crystalline product dried in a stream of dry nitrogen. Yield 2.58 g (76%), m.p. 5°C.

^{1}H NMR (C_6D_6): δ = 2.20, s, 3H (*Me*Ph); 2.30, s, 12H (C_6H_2*Me*$_4$); 6.9, m, 5H (Me*Ph*); 7.05, s, 2H (C_6*H*$_2$Me$_4$). ^{71}Ga NMR (C_6D_6): δ = −680 ppm rel. $Ga(NO_3)_3$ in aqueous HNO_3, s. $C_{17}H_{22}Ga_2Cl_4$ (507.62): Found: C, 39.7; H, 4.1. Calc. C, 40.2; H, 4.3%.

(η^6 - 1,2,4,5 - *Tetramethylbenzene*)*gallium*(I) *tetrachlorogallate*(III)

A solution of the same components in toluene at higher concentrations (1.40 mol dm^{-3}) yielded a microcrystalline precipitate on cooling to 0°C in *ca* 80% yield (m.p. 15–16°C). $C_{10}H_{14}Ga_2Cl_4$ (415.48): Found: C, 27.2; H, 3.15. Calc. C, 28.9; H, 3.4.

Structure determination of $\{[(\eta^6\text{-}1,2,4,5\text{-}C_6H_2Me_4)(\eta^6\text{-}C_6H_5CH_3)Ga]GaCl_4\}_2$

A suitable crystal was sealed in a capillary under argon at −60°C and mounted on a CAD-4 diffractometer (Mo-K_α radiation, graphite monochromator, λ = 0.71069 Å). Crystal data and details of the structure determination are summarized in Table 1. The integrated intensities of the reflections were corrected for Lorentz polarization and empirically for absorption effects (relative transmission 0.76–1.00; $(\sin\vartheta/\lambda)_{max}$ = 0.616 $Å^{-1}$, *hkl*: 14, ±14, ±14; ϑ–2ϑ scan, $\Delta\omega = 0.8 + 0.35\tan\vartheta$). The structure was solved by direct methods (SHELXS-86). Thirteen out of a total of 22 hydrogen atoms could be located in difference Fourier maps, the remainder were calculated at idealized positions. In the refinement with anisotropic displacement parameters the hydrogen atoms were included in constant positions (U_{iso} = 0.05 $Å^2$). The maxima of the residual electron density and the relatively large displacement parameters of the toluene carbon atoms suggested a minor disorder of this molecule, which was too small, however, to justify treatment using a split model. A similar situation was encountered in the structure of $[(\eta^6\text{-}C_6Et_6)(\eta^6\text{-}C_6H_5Me)Ga]Cl_4$.[12] Further crystal structure data have been deposited.*

Acknowledgements—This work was generously supported by Deutsche Forschungsgemeinschaft (Leibniz-Programm) and by Fonds der Chemischen Industrie. Mr J. Riede is thanked for producing the crystallographic data set.

REFERENCES

1. H. Schmidbaur, *Angew. Chem.* 1985, **97**, 893; *Angew. Chem. Int. Edn Engl.* 1985, **24**, 893 (Review).
2. H. Schmidbaur, U. Thewalt and T. Zafiropoulos, *Organometallics* 1983, **2**, 1550.
3. M. Usón-Finkenzeller, W. Bublak, B. Huber and G. Müller, *Z. Naturfor.* 1986, **41B**, 346.
4. H. Schmidbaur, U. Thewalt and T. Zafiropoulos, *Chem. Ber.* 1984, **117**, 381; *Angew. Chem.* 1984, **96**, 60; *Angew. Chem. Int. Edn Engl.* 1984, **23**, 76: U. Thewalt, T. Zafiropoulos and H. Schmidbaur, *Z. Naturfor.* 1984, **39B**, 1642; H. Schmidbaur, T. Zafiropoulos, W. Bublak, P. Burkert and F. H. Köhler, *Z. Naturfor.* 1986, **41A**, 315; J. Ebenhöch, G. Müller, J. Riede and H. Schmidbaur, *Angew. Chem.* 1984, **96**, 367; *Angew. Chem. Int. Edn Engl.* 1984, **23**, 386.
5. J. Beck and J. Strähle, *Z. Naturfor.* 1986, **41B**, 1381.
6. S. H. Strausz, M. D. Noirot and O. P. Anderson, *Inorg. Chem.* 1986, **25**, 3850.
7. W. Frank, J. Weber and E. Fuchs, *Angew. Chem.* 1987, **99**, 68; *Angew. Chem. Int. Edn Engl.* 1987, **26**, 74.
8. H. Schmidbaur, W. Bublak, B. Huber and G. Müller, *Organometallics* 1986, **5**, 1647; *Helv. Chim. Acta* 1986, **69**, 1742.
9. H. Schmidbaur, W. Bublak, B. Huber and G. Müller, *Z. Naturfor.* 1987, **42B**, 147; H. Schmidbaur, W. Bublak, B. Huber, J. Huber and G. Müller, *Chem. Ber.* 1989, **122**, 265.
10. H. Schmidbaur, W. Bublak, B. Huber and G. Müller, *Angew. Chem.* 1987, **99**, 248; *Angew. Chem. Int. Edn. Engl.* 1987, **26**, 234; A. Schier, J. M. Wallis, G. Müller and H. Schmidbaur, *Angew. Chem.* 1986, **98**, 742; *Angew. Chem. Int. Edn Engl.* 1987, **25**, 757; H. Schmidbaur, R. Nowak, A. Schier, J. M. Wallis, B. Huber and G. Müller, *Chem. Ber.* 1987, **120**, 1829; H. Schmidbaur, R. Hager, B. Huber and G. Müller, *Angew. Chem.* 1987, **99**, 354; *Angew. Chem. Int. Edn Engl.* 1987, **26**, 338.
11. H. Schmidbaur, R. Nowak, B. Huber and G. Müller, *Z. Naturfor.* 1988, **43B**, 1447.
12. M. S. Weininger, P. F. Rodesiler and E. L. Amma, *Inorg. Chem.* 1979, **18**, 751 and preceding papers.
13. We thank Professor Dr P. Hofmann, TU München, for pointing this out in helpful discussions.
14. H. Schmidbaur, T. Probst, B. Huber, O. Steigelmann and G. Müller, *Organometallics* 1989, **8**, 1567.
15. R. C. Carlston, E. Griswold and J. Kleinberg, *J. Am. Chem. Soc.* 1958, **80**, 1532.

* Fachinformationszentrum karlsruhe GmbH, D-7514 Eggenstein-LeopoldShafen 2, F.R.G. Inquiries should be accompanied by the depository number CSD-54092, the names of the authors, and the full literature citation.

Polyhedron Vol. 9, No. 2/3, pp. 289–300, 1990
Printed in Great Britain

0277-5387/90 $3.00+.00
© 1990 Pergamon Press plc

MULTINUCLEAR NMR STUDIES OF THE REACTIONS OF $(Me_3Al)_2$ WITH Me_2AsNMe_2, $MeAs(NMe_2)_2$ AND $As(NMe_2)_3$

L. K. KRANNICH,* C. L. WATKINS and D. K. SRIVASTAVA

Department of Chemistry, University of Alabama at Birmingham, Birmingham, AL 35294, U.S.A.

Abstract—The reactions of $(Me_3Al)_2$ with Me_2AsNMe_2, $MeAs(NMe_2)_2$ and $As(NMe_2)_3$ were studied as a function of time at room temperature and over the temperature range of −95 to 24°C by using ^1H and ^{13}C NMR spectroscopy. At −95°C, all the aminoarsines form the respective mono Al—N bonded adducts. In addition, $MeAs(NMe_2)_2$ and $As(NMe_2)_3$ form bis Al—N bonded adducts and $As(NMe_2)_3$ forms an Al—As bonded adduct. The bis adducts readily decompose and the Al—As bonded adduct dissociates at low temperature. All the mono Al—N bonded adducts decompose by a pathway that transfers a methyl group from the aluminium to the arsenic atom, cleaves the As—N bond, and yields the next higher methyl homologue in the arsine series [$MeAs(NMe_2)_2$, Me_2AsNMe_2 or Me_3As]. The bis Al—N bonded adducts decompose to the next higher methyl homologue in the mono adduct series [$MeAs(NMe_2)NMe_2 \cdot AlMe_3$ or $Me_2AsNMe_2 \cdot AlMe_3$]. The other product in both cases is the unstable Me_2AlNMe_2, which dimerizes or undergoes further reaction with excess $(Me_3Al)_2$ or aminoarsine. The role of numerous competing side reactions and adduct/aminoarsine exchange equilibria in affecting the rate of adduct decomposition, overall rate of formation of the final product arsine, and final product distribution was established for each aminoarsine/$(Me_3Al)_2$ system. The initial stoichiometry of the reaction greatly influences the relative importance of the various reactions that occur in solution. Only when the moles of available Me_3Al molecules equal those of Lewis base nitrogen sites, do the reactions proceed in a straightforward manner to give Me_3As and $(Me_2AlNMe_2)_2$. The results from the NMR studies were used to design a new, high yield synthetic route to Me_3As.

Organoaluminium chemistry has been extensively reviewed due to its importance in catalysis and chemical synthesis,[1–4] as well as in more recent applications for the preparation of semiconducting[5–7] and ceramic materials.[8] The physical and chemical properties of the trialkylaluminium species, $(R_3Al)_2$, in addition to their reactions with compounds containing Group 15 elements have been reported.[1,2,4] With primary and secondary amines, simple R_3Al–amine 1:1 adducts form. Upon heating, these yield Al—N bonded cyclic dimers and oligomers.[4,9–17] The 1:1 addition product of Me_3Al and Me_2NH, for example, forms the cyclic dimer, $(Me_2AlNMe_2)_2$, at 120°C with the elimination of methane.[18,19] The structure of the dimer has been confirmed by IR,[20] X-ray[21] and NQR[22] studies. Stable 1:1 adducts between R_3Al and tertiary amines have also been well characterized.[1,2,18,22–25] The reactions with bidentate nitrogen-containing ligands, such as substituted hydrazines[26,27] and diamines,[1,2,28–30] as well as multidentate open-chain and cyclic amines,[31–34] lead to Al—N bonded adducts, which in certain cases have been proposed to form five- and six-coordinate aluminium.

Several 1:1 adducts of R_3Al (R = Me, Et) with tertiary organophosphines have also been characterized.[1,2,4,5,18,22,24,25,35–40] Interestingly, $(Me_3Al)_2$ and $(Et_3Al)_2$ react with secondary organophosphines and arsines in some instances to form cyclic dimers, as expected from the analogous secondary amine reactions, but in other cases trimeric species are formed.[18,19,35,41,42] Me_3Al and Et_3Al adducts with diphosphines,[5,43–45] bis(diphenylphosphino)methane[46,47] and polyphosphines[5,48] have been reported. However, only a few Me_3Al

* Author to whom correspondence should be addressed.

adducts of tertiary arsines[22,49] and diarsines[44] are known.

Limited information is available concerning the reactions of aluminium alkyls with molecules containing adjacent, competing, heteroatom Lewis base sites, such as bisphosphinoamines,[43,50–52] aminophosphines,[43] hydrazinophosphines[53] and aminoarsines. $(Et_3Al)_2$ reacts with $(Ph_2P)_2NR$ (R = Me, Et, Pr^n, Bu^n) to give Al—P bonded 1 : 1 adducts, regardless of the reaction stoichiometry.[43,50] The NMR data suggest that bonding involves pentacoordinate aluminium. When the bulkiness of R is increased (R = PhCHMe, Ph CH_2, Me_2N), no reaction occurs with $(Et_3Al)_2$.[43,50] The reaction of $(R_3Al)_2$ (R = Me, Et) with $(Ph_2P)_2NH$ results in ethane evolution and the formation of a dimeric product, $[R_2AlN(PPh_2)_2]_2$.[52] X-ray data for the methyl derivative indicate a six-membered AlNOAlNP ring in a twist-conformation.[52] Such hydrocarbon elimination results typically when Lewis bases that contain an N—H bond react with aluminium alkyls.

With Ph_2PNHPr^i, $(Et_3Al)_2$ reacts with ethane evolution to yield the trimeric species $[Ph_2P(Et_2Al)NPr^i]_3$.[43] In contrast, with the more bulky Bu^t moiety, (Ph_2PNHBu^t) yields the isolable 1 : 1 adduct. Upon heating, this adduct eliminates ethane to give the monomeric $Ph_2P(AlEt_2)NBu^t$.[43] NMR data suggest that the reaction of Me_2PNMe_2 with $(Et_3Al)_2$ yields a mixture of the Al—P and Al—N bonded 1 : 1 adducts with the Al—N bonded adduct being favoured thermodynamically.[43] However, a simple molecular addition product of Et_3Al and Ph_2PNEt_2 is not obtained.[43] For the hydrazinophosphines, $P(MeNNMe)_3P$ and $PhP(MeNNMe)_2PPh$, triethylaluminium gives only the 2 : 1 Al—P bonded adducts where each phosphorus atom is bound to a Et_3Al group.[53]

To our knowledge, no reactions of $(R_3Al)_2$ with aminoarsines have been reported, although the reaction of $(Me_3Al)_2$ with the As—N bond containing arsa(III)azene, ArNH—As=NAr (Ar = $C_6H_2Bu^t_3$-2,4,6), has been reported.[54] The reaction proceeds with As—N bond cleavage and the formation of $Me_2AlNHAr$ and uncharacterized arsenic-containing species.

In view of this, we were interested in establishing Me_3Al bonding site preference in multiple Lewis base site compounds that contain the As—N bond, determining the nature and relative stability of any resulting adducts, and elucidating subsequent decomposition pathways that lead to the thermodynamically stable products. Thus, we have undertaken a systematic ^1H and ^{13}C NMR study of the interaction of $(Me_3Al)_2$ with the following series of aminoarsines: Me_2AsNMe_2, MeAs $(NMe_2)_2$ and $As(NMe_2)_3$, as a function of temperature and reaction stoichiometry. The course of each reaction was followed by the disappearance of reactant peaks and the appearance of new peaks assignable to reaction products. Independent reactions were carried out to establish proposed reaction pathways. A new synthetic route to the high yield synthesis of Me_3As has resulted from these investigations.

EXPERIMENTAL

Standard high vacuum-line techniques and a Vacuum Atmospheres Model HE-43-Dri lab equipped with a Model HE-493 Dri-Train were used for storing and handling of all compounds. Me_2NH (Matheson Gas Products), $(Me_3Al)_2$ (Ethyl Corporation) and $AsCl_3$ (Alfa Products) were used as obtained. Diethyl ether was dried over sodium and distilled before use. Benzene-d_6, toluene-d_8 and Me_4Si were purchased from Aldrich Chemical Company and stored over molecular sieves. Me_2AsCl (106°C)[55] and $MeAsCl_2$ (61–63°C/50 mm Hg)[56] were synthesized by previously reported methods. Me_2AsNMe_2, $MeAs(NMe_2)_2$ and $As(NMe_2)_3$ were synthesized by the aminolysis of the appropriate chloroarsine or $AsCl_3$.[57] All the arsines were distilled on a spinning band column prior to use and their purity was checked by ^1H and ^{13}C NMR spectroscopy (see ^1H and ^{13}C NMR spectral data). $(Me_2AlNMe_2)_2$[18] was independently synthesized to confirm its existence in the studied reaction system (see ^1H and ^{13}C NMR spectral data).

^1H and ^{13}C NMR spectra were recorded on a Nicolet 300 MHz multinuclear FT NMR spectrometer operating at 300.1 and 75.4 MHz, respectively. The chemical shifts were measured with respect to Me_4Si as an internal reference. Table 1 contains the ^1H and ^{13}C NMR spectral data of the Al—N and Al—As adducts observed in the various reaction systems. All reaction systems were studied in NMR tubes that were not acid-washed to minimize the occurrence of acid-catalysed exchange processes. The reaction mixtures were protected from exposure to light. The room-temperature studies were conducted in NMR tubes (10 mm, Pyrex) equipped with screw tops containing a PTFE insert to exclude moisture and air over long periods of time. All variable-temperature studies were carried out in NMR tubes (10 mm, Pyrex) purchased from Wilmad that were equipped with the J. Young VNMR valves. These were attached to the vacuum-line through a specially designed side-arm septum adapter that permitted addition of the aminoarsine reactant solution with a hypodermic syringe.

Table 1. ^1H and ^{13}C NMR data of compounds I–VI

Compound	δ_C (ppm) Me_2N	MeAs	Me_3Al	δ_H (ppm) Me_2N	MeAs	Me_3Al	T (°C)
I	40.90	10.53	−8.07(bd)	1.93	0.62	−0.54	24
	40.21	9.61	−7.64	1.62	0.30	−0.31	−90
II	45.93	13.23	−7.74	2.33	0.61	−0.27	−90
	42.45			1.95			
	39.10			1.91			
	38.88			1.69			
III	44.47	14.85	−7.18	1.91	0.94	−0.42	−95
	40.76			1.66			
IV	40.16		−6.47	2.18		−0.23	−95
V	43.49		−7.87	2.07		−0.42	−95
	41.69			1.93			
VI	42.00		−7.87	2.31		−0.42	−95
	41.69			2.01			
				1.95			

Reactions of $(Me_3Al)_2$ *with* Me_2AsNMe_2, MeAs$(NMe_2)_2$ *and* As$(NMe_2)_3$

The reactions of $(Me_3Al)_2$ with various stoichiometric ratios of Me_2AsNMe_2, MeAs$(NMe_2)_2$ and As$(NMe_2)_3$ were carried out in benzene-d_6 and toluene-d_8 using the following procedures. In the room-temperature studies, the appropriate amount of the respective aminoarsine was weighed into the screw-topped NMR tube and benzene-d_6 was added to give 2 cm^3 of solution. The correct stoichiometric amount of $(Me_3Al)_2$ was weighed into a 1 cm^3 volumetric flask and 1 cm^3 of benzene-d_6 solution was prepared. Using a disposable pipette, the $(Me_3Al)_2$ solution was added rapidly to the aminoarsine solution to achieve thorough mixing of the solutions. These reactions were very exothermic. Each reaction system was then monitored by ^1H and ^{13}C NMR spectroscopy as a function of time.

In the variable-temperature studies, the appropriate amount of $(Me_3Al)_2$ was weighed into the J. Young NMR tube and toluene-d_8 was added to give 2 cm^3 of solution. The correct stoichiometric amount of the aminoarsine was weighed into a 1 cm^3 volumetric flask and toluene-d_8 was added to give a 1 cm^3 solution. The aminoarsine solution was loaded into a hypodermic syringe, which was sealed by inserting the needle into a rubber stopper. After the NMR tube was cooled to −110°C (ethanol–liquid nitrogen slush) up to 2 cm below the VNMR valve and degassed, the space in the working manifold of the vacuum line and the adapter was brought to atmospheric pressure using prepurified nitrogen. The aminoarsine solution was then injected into the adapter space above the VNMR valve. The septum was sealed with stopcock grease and the VNMR valve was opened to allow a trickle of the aminoarsine solution to run down the inside wall of the NMR tube and be cooled to −110°C prior to coming into contact with the $(Me_3Al)_2$ solution. After the addition was complete, the valve was closed, the tube was agitated gently at −110°C, and the tube was inserted within 10 min into the precooled (−95°C) probe of the NMR spectrometer. The reaction was then monitored at the selected 5 or 10°C temperature intervals by ^1H and ^{13}C NMR spectroscopy as a function of time.

Reactions of $Me_2AsNMe_2 \cdot AlMe_3$ *with* MeAs$(NMe_2)_2$ *and* As$(NMe_2)_3$

The reactions of $Me_2AsNMe_2 \cdot AlMe_3$ (I) with MeAs$(NMe_2)_2$ and As$(NMe_2)_3$ in 1 : 1 mmol ratios were carried out in benzene-d_6 at room temperature using the following procedure. The appropriate amount of Me_2AsNMe_2 was weighed into a screw-topped NMR tube and benzene-d_6 was added to give 1 cm^3 of solution. The correct stoichiometric amount of $(Me_3Al)_2$ was weighed into a 1 cm^3 volumetric flask and a 1 cm^3 benzene-d_6 solution was prepared. The $(Me_3Al)_2$ was added slowly to the aminoarsine solution and the ^1H and ^{13}C NMR spectra were obtained on the mixture to establish that the reaction had gone to completion to form I. The appropriate amount of MeAs$(NMe_2)_2$ or

$As(NMe_2)_3$ was weighed into a 1 cm^3 volumetric flask and a 1 cm^3 benzene-d_6 solution was prepared. This solution was then added to the solution of **I**. The reactions were then monitored with time using ^1H and ^{13}C NMR spectroscopy.

Competition studies of $(Me_3Al)_2$ *with* Me_2AsNMe_2, $MeAs(NMe_2)_2$ *and* $As(NMe_2)_3$ *mixtures*

The competition reactions of 1 and 2 mmol of $(Me_3Al)_2$ for the Lewis base sites in a 1 : 1 : 1 mixture of Me_2AsNMe_2, $MeAs(NMe_2)_2$ and $As(NMe_2)_3$ were carried out in benzene-d_6 at room temperature and at −95°C in toluene-d_8 using the following procedures. 1 mmol each of Me_2AsNMe_2, $MeAs(NMe_2)_2$ and $As(NMe_2)_3$ were weighed into a screw-topped NMR tube and benzene-d_6 was added to give 2 cm^3 of solution. The correct stoichiometric amount of $(Me_3Al)_2$ was weighed into a 1 cm^3 volumetric flask and a 1 cm^3 benzene-d_6 solution was prepared. The $(Me_3Al)_2$ was added to the aminoarsine solution. In the low temperature study, the analogous aminoarsine mixture in toluene-d_8 was added to a VNMR valve NMR tube. After degassing the solution at −110°C, the 1 cm^3 toluene-d_8 solution of $(Me_3Al)_2$ was introduced slowly by using the previously described procedure. The reactions were then monitored using ^1H and ^{13}C NMR spectroscopy.

Synthesis of Me_3As

$As(NMe_2)_3$ (0.048 mol) was added to a 100 cm^3 three-necked round-bottom flask equipped with a condenser, nitrogen by-pass adapter, magnetic stirrer and dropping funnel containing 0.072 mol of $(Me_3Al)_2$. After cooling the reaction flask to 0°C, the $(Me_3Al)_2$ was added dropwise to the $As(NMe_2)_3$ over a 1 h period with constant stirring. Solid formed during the addition. After the addition was complete, the reaction mixture was warmed to room temperature and stirred for 6 h. Distillation of the reaction mixture using a 140°C oil bath gave an 84% yield of Me_3As (52°C/760 mm Hg). The purity was checked by ^1H and ^{13}C NMR spectroscopy.

The following is a list of NMR spectral data (values in ppm) determined independently in our laboratory at room temperature in benzene-d_6 solution (concentrations are approximately 0.2 M) on synthesized compounds that were identified in the reaction mixtures. The NMR data for the Al—N and Al—As bonded adducts are given in Table 1.

^1H *NMR spectral data*

Me_3As: 0.76 (MeAs). Me_2AsNMe_2: 0.82 (MeAs) and 2.43 (MeN). $MeAs(NMe_2)_2$: 0.96 (MeAs) and 2.63 (MeN). $As(NMe_2)_3$: 2.59 (MeN). $Me_3As \cdot AlMe_3$: −0.36 (MeAl) and 0.60 (MeAs). $Me_2AlNMe_2 \cdot AlMe_3$: −0.49 (MeAl) and 2.05 (MeN). $(Me_2AlNMe_2)_2$:[58,59] −0.64 (MeAl) and 2.08 (MeN).

^{13}C *NMR spectral data*

Me_3As: 11.22 (MeAs). Me_2AsNMe_2: 9.93 (MeAs) and 41.91 (MeN). $MeAs(NMe_2)_2$: 12.39 (MeAs) and 42.76 (MeN). $As(NMe_2)_3$: 39.72 (MeN). $Me_3As \cdot AlMe_3$: −8.41 (MeAl) and 6.41 (MeAs). $Me_2AlNMe_2 \cdot AlMe_3$: −8.06 (MeAl, bd) and 40.17 (MeN). $(Me_2AlNMe_2)_2$:[59] −11.7 (MeAl, vbd) and 41.49 (MeN).

RESULTS AND DISCUSSION

Reaction of $(Me_3Al)_2$ *with* Me_2AsNMe_2

The ^1H and ^{13}C NMR spectra of the room-temperature reactions of $(Me_3Al)_2$ with Me_2AsNMe_2 in 0.5:1, 1:1, 2:1 and 3:1 mmol Me_3Al–Me_2AsNMe_2 mixtures indicated immediate formation of a 1 : 1 adduct **I**. In the 0.5 : 1 case, peaks assignable to Me_3As, unreacted Me_2AsNMe_2 and $MeAlNMe_2$ moiety containing species (δ_H values at 2.21, 2.19 and −0.40 ppm; δ_C at 38.92 ppm) are observed. Spectral line broadening of the Me_2N and Me_2As moiety peaks suggest exchange averaging involving Me_2AsNMe_2 and **I**. In the 2 : 1 and 3 : 1 reaction systems, peaks assignable to trace amounts of $Me_3As \cdot AlMe_3$ and $Me_2AlNMe_2 \cdot AlMe_3$, along with those for unreacted $(Me_3Al)_2$, are observed.

When a solution of the 1 : 1 system stands at room temperature, **I** slowly decomposes to yield Me_3As and $(Me_2AlNMe_2)_2$. Complete adduct decomposition occurs within 1 week. In the 0.5 : 1 system, as **I** undergoes decomposition to produce Me_3As and the $MeAlNMe_2$ moiety containing species, the line widths of the Me_2N and Me_2As moiety peaks narrow, the peak positions gradually shift toward those of Me_2AsNMe_2, and the peak intensities for **I** decrease as those for Me_3As and the $MeAlNMe_2$ species increase. After 1 week, decomposition is complete with the final products being Me_3As, unreacted Me_2AsNMe_2 and the $MeAlNMe_2$ containing species.

However, in the 2 : 1 and 3 : 1 systems, decomposition is slower (about 60% decomposition within 1 month). The spectra indicate that $Me_3As \cdot AlMe_3$ and $Me_2AlNMe_2 \cdot AlMe_3$ are the initial decomposition products, but with time, $Me_2AlNMe_2 \cdot AlMe_3$ decomposes to $(Me_2AlNMe_2)_2$ and $(Me_3Al)_2$. After three months, the product composition in the respective systems is: [2 : 1 system]—41%

$Me_3As \cdot AlMe_3$, 26% $Me_2AlNMe_2 \cdot AlMe_3$, 5% $(Me_2AlNMe_2)_2$, 28% **I**; [3:1 system]—43% $Me_3As \cdot AlMe_3$, 36% $Me_2AlNMe_2 \cdot AlMe_3$, 9% **I**, 12% $(Me_2Al)_2$.

A variable-temperature study of a 1:1 mmol Me_3Al—Me_2AsNMe_2 ratio sample indicates that **I** is formed in 90% yield at −95°C with reaction being complete by −60°C. No further significant changes in the spectra occur upon heating to room temperature. Thereafter, **I** slowly decomposes to Me_3As and $(Me_2AlNMe_2)_2$ and the results are identical to those of the room temperature 1:1 study. Variable-temperature studies on 2:1 and 3:1 mol ratio systems indicate exclusive formation of **I** at −95°C.

In each case, the NMR spectral and product composition data suggest that $(Me_3Al)_2$ readily reacts with Me_2AsNMe_2 to form an Al—N bonded adduct, **I** [eq. (1)]. This is consistent with the known bonding affinities of $(Me_3Al)_2$ towards Group 15 containing bases ($Me_3N > Me_3P > Me_3As$)[49] and MeN proton chemical shift changes due to complex formation with alanes in benzene solution.[24] Regardless of the stoichiometry used, there was no spectral evidence for the formation of Al—As or Al—As—N—Al bonded adducts. Although **I** subsequently decomposes, the specific decomposition pathway is very dependent upon the reaction stoichiometry. When the moles of the available Lewis acid, Me_3Al, equal those of available Lewis base nitrogen sites (1:1 system), **I** is the sole product. Decomposition then proceeds in a straightforward manner to yield Me_3As [eq. (2)] and $(Me_2AlNMe_2)_2$. The latter probably arises via the initial generation of Me_2AlNMe_2 [eq. (2)], which readily undergoes bisamino bridge dimerization [eq. (3)]. Since peaks could not be assigned to the Me_2AlNMe_2 monomer in the NMR spectra, we assume that it is quite unstable relative to dimerization under the reaction conditions.[18]

The results from the 0.5:1, 2:1 and 3:1 mol ratio studies are readily explained in terms of competing side reactions and exchange equilibria that involve either Me_2AsNMe_2 or $(Me_3Al)_2$. In the presence of excess Me_2AsNMe_2 (0.5:1 mmol system), **I** exchange averages with Me_2AsNMe_2. This process continues throughout the temperature range until **I** has decomposed. Such exchange averaging has been previously noted in aluminium alkyl adducts of bases, when the Lewis base is in excess.[1,2,24,25] Compound **I** decomposes according to eq. (2). Instead of dimerizing, Me_2AlNMe_2 preferentially reacts with the excess Me_2AsNMe_2 to produce additional Me_3As, and the $MeAlNMe_2$ moiety containing species. We propose that this species is the $MeAl(NMe_2)_2$[58] dimer. This assignment is based upon the fact that the observed δ_H and δ_C peaks are in the region expected for the $MeAlNMe_2$ group,[59] the δ_H peaks at 2.21 and 2.19 ppm are in a 1:1 area ratio, as expected for the bis-amino bridged dimer; and the δ_H at −0.40 is associated with a terminal AlMe.[58] We have, however, been unsuccessful in preparing and isolating this species. We postulate the Me_2AlNMe_2 forms an unstable, Al—N bonded intermediate adduct, $Me_2AsNMe_2 \cdot Me_2AlNMe_2$ [eq. (4)], which decomposes to Me_3As and $MeAl(NMe_2)_2$ [eq. (5)]. $MeAl(NMe_2)_2$ is expected to undergo bis-amino bridge dimerization [eq. (6)] to $[MeAl(NMe_2)_2]_2$, similar to Me_2AlNMe_2, H_2NAlMe_2, $Al(NMe_2)_3$, $Me_2AlNHNMe_2$ and $Me_2AlNMeNMe_2$.[9,12,27,58-61]

In the presence of excess $(Me_3Al)_2$ (2:1 and 3:1 mmol systems), the Me_2AlNMe_2, which forms from the decomposition of **I** [eq. (2)], does not dimerize, but preferentially reacts with the excess $(Me_3Al)_2$ to give $Me_2AlNMe_2 \cdot AlMe_3$ [eq. (7)]. This result is consistent with those obtained by Schram *et al.*[61] in the reactions of $B_2(NMe_2)_4$ with large excesses of $(Me_3Al)_2$. Also in the presence of excess $(Me_3Al)_2$, Me_3As forms $Me_3As \cdot AlMe_3$[49] [eq. (8)]. $Me_2AlNMe_2 \cdot AlMe_3$ then decomposes to $(Me_2AlNMe_2)_2$ and $(Me_3Al)_2$ [eq. (9)][61] as $(Me_3Al)_2$ is consumed with time. Although $Me_2AlNMe_2 \cdot AlMe_3$ is unstable at room temperature,[61] it is stabilized by the presence of excess $(Me_3Al)_2$ in solution; thereby retarding its decomposition.

The following equations summarize the reactions that are unique for the indicated mmol ratio systems:

Me_3Al/Me_2AsNMe_2; 1:1 mmol ratio:

$$Me_2AsNMe_2 + Me_3Al \longrightarrow Me_2AsNMe_2 \cdot AlMe_3 \quad (1)$$

$$Me_2AsNMe_2 \cdot AlMe_3 \longrightarrow Me_3As + Me_2AlNMe_2 \quad (2)$$

$$2Me_2AlNMe_2 \longrightarrow (Me_2AlNMe_2)_2; \quad (3)$$

Me_3Al/Me_2AsNMe_2; 0.5:1 mmol ratio:

$$Me_2AlNMe_2 + Me_2AsNMe_2 \longrightarrow Me_2AsNMe_2 \cdot Me_2AlNMe_2 \quad (4)$$

$$Me_2AsNMe_2 \cdot Me_2AlNMe_2 \longrightarrow Me_3As + MeAl(NMe_2)_2 \quad (5)$$

$$2MeAl(NMe_2)_2 \longrightarrow [MeAl(NMe_2)_2]_2; \quad (6)$$

Me_3Al/Me_2AsNMe_2; 2:1 and 3:1 mmol ratios:

$$Me_2AlNMe_2 + Me_3Al \longrightarrow Me_2AlNMe_2 \cdot AlMe_3 \quad (7)$$

$$Me_3As + Me_3Al \longrightarrow Me_3As \cdot AlMe_3 \quad (8)$$

$$Me_2AlNMe_2 \cdot AlMe_3 \longrightarrow (Me_2AlNMe_2)_2 + (Me_3Al)_2. \quad (9)$$

Reaction of $(Me_3Al)_2$ *with* $MeAs(NMe_2)_2$

The ^1H and ^{13}C NMR spectra of the room-temperature reactions of $(Me_3Al)_2$ with $MeAs(NMe_2)_2$ in 0.5:1, 1:1, 1:0.5, 2:1 and 3:1 mmol Me_3Al–$MeAs(NMe_2)_2$ ratios indicate the immediate formation of **I** amongst other products. The most straightforward results occur in the 2:1 system where the moles of available Lewis acid Me_3Al molecules equal those of available Lewis base $MeAs(NMe_2)_2$ nitrogen sites, and competing side reactions and exchange equilibria are minimal. Here, the initial producs are **I** and $(Me_2AlNMe_2)_2$. Over a period of 1 week, **I** decomposes completely to Me_3As and $(Me_2AlNMe_2)_2$.

In the 0.5:1 and 1:1 systems, where the available nitrogen base sites are in stoichiometric excess relative to the Me_3Al molecules, the initial NMR spectra of the reaction solutions contain peaks assignable to **I**, Me_2AsNMe_2, $MeAs(NMe_2)_2$, $(Me_2AlNMe_2)_2$ and the mono Al—N adduct, $MeAs(NMe_2)NMe_2 \cdot AlMe_3$ (**II**). Additional peaks suggest the presence of a trace amount of the postulated $[MeAl(NMe_2)_2]_2$, as in the 0.5:1 mmol Me_3Al/Me_2AsNMe_2 system. Considerable line-width broadening in the ^1H NMR spectra and shifts in δ_H and δ_C position assignments for the peaks associated with the Me_2N, Me_2As and MeAs moieties suggest exchange averaging that involves the Me_2AsNMe_2/**I** and $MeAs(NMe_2)_2$/**II** systems. Intensity data suggest that the 0.5:1 system contains more $MeAs(NMe_2)_2$ and **II** relative to Me_2AsNMe_2 and **I** than does the 1:1 system. With time, spectral line-width narrowing occurs with the concomitant shifts in the exchange averaged δ_H and δ_C values toward the assignments for $MeAs(NMe_2)_2$ and Me_2AsNMe_2. This is also accompanied by increases in the intensities of the $(Me_2AlNMe_2)_2$ and Me_2AsNMe_2 peaks and decreases in the intensities of the **II** and $MeAs(NMe_2)_2$ peaks. After 1 month, the reactions are almost complete with the respective product compositions being: [0.5:1 system] = 47% $MeAs(NMe_2)_2$, 37% Me_2AsNMe_2, 16% $(Me_2AlNMe_2)_2$; [1:1 system] = 3% $MeAs(NMe_2)_2$, 58% Me_2AsNMe_2, 5% **I**, 33% $(Me_2AlNMe_2)_2$. There is no evidence for the formation of Me_3As in either system.

In the 3:1 system, the NMR spectra indicate the presence of **I**, $(Me_2AlNMe_2)_2$, $Me_2AlNMe_2 \cdot AlMe_3$ and unreacted $(Me_3Al)_2$. With time, decomposition of **I** produces $Me_3As \cdot AlMe_3$ and $Me_2AlNMe_2 \cdot AlMe_3$ with the concomitant consumption of $(Me_3Al)_2$. After $Me_2AlNMe_2 \cdot AlMe_3$ no longer forms, it dissociates to yield $(Me_2AlNMe_2)_2$. After 3 months, the product composition is 36% $Me_3As \cdot AlMe_3$, 33% $(Me_2AlNMe_2)_2$, 19% $Me_2AlNMe_2 \cdot AlMe_3$ and 12% $Me_2AsNMe_2 \cdot AlMe_3$.

Variable-temperature, multinuclear NMR studies for 0.5:1, 1:1, 1:0.5, 2:1 and 3:1 mmol Me_3Al–$MeAs(NMe_2)_2$ ratios were carried out to elucidate the reaction pathway to **I**, determine concentration effects and identify possible low-temperature stable adducts of $MeAs(NMe_2)_2$. In a 2:1 system, there is exclusive formation of **II** at −95°C with unreacted $MeAs(NMe_2)_2$ and $(Me_3Al)_2$ remaining. With increasing temperature, more **II** forms and ^1H spectral line-width broadening and shifts in δ_H and δ_C position assignments for the Me_2N moieties suggest $MeAs(NMe_2)_2$/**II** exchange averaging. By −80°C, decomposition of **II** begins to give **I** and $Me_2AlNMe_2 \cdot AlMe_3$. This continues, with the consumption of $(Me_3Al)_2$, as the temperature is increased. Beginning at −60°C, $(Me_2AlNMe_2)_2$ forms and $Me_2AlNMe_2 \cdot AlMe_3$ is consumed as **II** decomposes to **I**. This process continues with increasing temperature until at room temperature the solution contains predominantly **I** and $(Me_2AlNMe_2)_2$ with some $MeAs(NMe_2)_2$, **II** and $Me_2AlNMe_2 \cdot AlMe_3$. Overnight, the conversion to **I** and $(Me_2AlNMe_2)_2$ is almost complete. The product composition is then similar to that of the 2:1 room-temperature system.

The analogous 1:0.5 mmol system, which represents a lower concentration system still having a 2:1 mol ratio of reactants, gives different low temperature results. At −95°C, there is a 5% yield of **II** and a 90% yield of the bis-adduct, $MeAs(NMe_2 \cdot AlMe_3)_2$ (**III**), along with some remaining unreacted $MeAs(NMe_2)_2$ and $(Me_3Al)_2$. With time (2 h) at −95°C, the spectra indicate extensive decomposition of **III** with the formation of **I** and $Me_2AlNMe_2 \cdot AlMe_3$. The decomposition of **III** goes to completion within 1 h at −90°C. ^1H spectral line-width broadening and chemical shift (δ_H and δ_C) positions suggest that $MeAs(NMe_2)_2$ and **II** exchange average. Beginning at −60°C and continuing up to room temperature, $Me_2AlNMe_2 \cdot AlMe_3$ dissociates to form $(Me_2AlNMe_2)_2$. At room temperature, **II** decomposes to **I** and $(Me_2AlNMe_2)_2$ while $MeAs(NMe_2)_2$ is consumed. The composition of the product mixture, at this point, is the same as that of the 2:1 variable-temperature study.

The 0.5:1 mmol system at −95°C gives a mixture of **I**, **II**, **III**, $(Me_2AlNMe_2)_2$, Me_2AsNMe_2 and unreacted $MeAs(NMe_2)_2$. Compounds **III**, **II** and **I** are

in approximately a 5:5:1 mol ratio, respectively. Decomposition of **III** continues with time and goes to completion at −90°C. At −70°C, ^{1}H line-width broadening suggests exchange averaging between $MeAs(NMe_2)_2$ and **II**. Decomposition of **II** begins at −60°C with formation of $(Me_2AlNMe_2)_2$ and Me_2AsNMe_2, which exchange averages with **I**. The product composition at room temperature is that observed in the room-temperature 0.5:1 system.

At −90°C, a 1:1 mmol system contains $MeAs(NMe_2)_2$, $(Me_3Al)_2$ and an equimolar mixture of **II** and **III**. A trace of **I** and Me_2AsNMe_2 are also observed. (In a separate 2:2 mmol system experiment, **II** is exclusively formed at −95°C.) By −80°C, **III** completely decomposes to **I** and $Me_2AlNMe_2 \cdot AlMe_3$. Exchange averaging that involves the Me_2AsNMe_2/**I** and $MeAs(NMe_2)_2$/**II** systems continues as long as Me_2AsNMe_2 and $MeAs(NMe_2)_2$ are present with **I** and **II**. Decomposition of **II** at −70°C gives **I** and $Me_2AlNMe_2 \cdot AlMe_3$ as $(Me_3Al)_2$ is consumed. By −60°C, very little $(Me_3Al)_2$ remains and $(Me_2AlNMe_2)_2$ forms as $Me_2AlNMe_2 \cdot AlMe_3$ dissociates and **II** continues to decompose. At −20°C, the peaks associated with $MeAs(NMe_2)_2$ and $Me_2AlNMe_2 \cdot AlMe_3$ decrease as those associated with **I** and $(Me_2AlNMe_2)_2$ increase. At room temperature, the product composition is similar to that of the 1:1 room-temperature study. Exchange averaging continues with a shift in composition towards $MeAs(NMe_2)_2$ and Me_2AsNMe_2.

In the 3:1 mmol variable-temperature study, only about a 10% yield of **II** results at −95°C. No bis-adduct, **III**, forms. At −90°C, the reaction goes to completion to give exclusively **II**. Compound **II** begins to decompose at −80°C to form Me_2AsNMe_2 (**I**) and $Me_2AlNMe_2 \cdot AlMe_3$ and continues until room temperature. Compounds **I** and Me_2AsNMe_2 exchange average until −60°C, when all the Me_2AsNMe_2 is converted to **I**. The product composition at room temperature is analogous to that in the 3:1 mmol room-temperature system.

Analysis of the room-temperature and variable-temperature data for the various stoichiometric ratio systems suggests that $MeAs(NMe_2)_2$ preferentially forms the mono adduct, **II**, [eq. (10)] at higher $(Me_3Al)_2$ concentrations (2:2, 2:1 and 3:1 mmol ratios) and the bis-adduct, **III**, [eq. (11)] at lower $(Me_3Al)_2$ concentrations (0.5:1, 1:0.5 and 1:1 mmol systems). These concentration effects imply that adduct formation proceeds via the reaction of $MeAs(NMe_2)_2$ with Me_3Al, whose concentration is determined by the $(Me_3Al)_2/Me_3Al$ equilibrium distribution in solution. At lower temperatures and higher alane concentration, the $(Me_3Al)_2/Me_3Al$ equilibrium indicates only slight dissociation to Me_3Al.[62] Thus, the resulting low Me_3Al concentration should favour the formation of the monoadduct, **II**, over that of **III**. Although we tend to prefer this pathway, this is insufficient data to eliminate a reaction mechanism that involves the direct interaction of $MeAs(NMe_2)_2$ with $(Me_3Al)_2$.

In those cases where the bis-adduct, **III**, is observed (0.5:1, 1:0.5 and 1:1 mmol systems), it is quite unstable and readily decomposes at or below −90°C into **I** and Me_2AlNMe_2 [eq. (12)]. The presence of **I**, Me_2AsNMe_2 and $(Me_2AlNMe_2)_2$ at −95°C in the 0.5:1 system suggests that **III** formed and had already decomposed slightly prior to spectral data acquisition.

The NMR spectral and decomposition product data suggest that **II** and **III** are Al—N bonded adducts. The magnitudes and directions of shifts in δ_H and δ_C for the Me_2N and Me_2As groups upon adduct formation are consistent with those observed in the formation of **I**.

In all cases, the mono adduct, **II**, exchange averages with $MeAs(NMe_2)_2$ and/or decomposes to Me_2AsNMe_2 and Me_2AlNMe_2 [eq. (13)]. Decomposition begins typically at −80°C and continues up to room temperature. When the amount of $(Me_3Al)_2$ is low (0.5:1 system), Me_2AlNMe_2 dimerizes [eq. (3)]. Me_2AsNMe_2 exchange averages with **I** formed from the decomposition of **III**. When there are appreciable amounts of $(Me_3Al)_2$ (1:0.5, 1:1, 2:1 and 3:1 systems), Me_2AlNMe_2 reacts to give $Me_2AlNMe_2 \cdot AlMe_2$ [eq. (7)] and Me_2AsNMe_2 forms **I** [eq. (1)]. As the amount of $(Me_3Al)_2$ is depleted through side reactions [eqs (1) and (7)], $Me_2AlNMe_2 \cdot AlMe_3$ dissociates to Me_3Al and Me_2AlNMe_2 [eq. (9)], which dimerizes [eq. (3)]. This dissociation begins around −60°C and continues up to room temperature.

In those systems containing appreciable amounts of $MeAs(NMe_2)_2$ in the presence of **I**, two important competition reactions occur to influence the final product composition. The first [eq. (14)] is the reaction of $MeAs(NMe_2)_2$ and **I** to generate Me_2AsNMe_2 and **II**, which then decomposes according to eq. (13). This process continues until all the $MeAs(NMe_2)_2$ and **I** are consumed to give the final thermodynamically-stable products, Me_2AsNMe_2 and $(Me_2AlNMe_2)_2$. The $MeAs(NMe_2)_2$/**I** reaction has been carried out independently and shown to be more facile than the decomposition of **I**. Thus, it is very important in establishing the final distributions of Me_2AsNMe_2, $MeAs(NMe_2)_2$ and $(Me_2AlNMe_2)_2$ in the 0.5:1 and 1:1 systems where **I** does not decompose to Me_3As at room temperature. Undoubtedly, eq. (14) is also important as a competition reaction at those temperatures

in the 0.5 : 1, 1 : 0.5 and 2 : 1 systems where MeAs$(NMe_2)_2$ and **I** are present. In the 1 : 0.5 and 2 : 1 systems, a second competition reaction plays a significant role in regenerating **I** [eq. (15)]. Here Me_2AsNMe_2 competes effectively for the bound Me_3Al in $Me_2AlNMe_2 \cdot AlMe_3$ [eq. (15)]. After all the MeAs$(NMe_2)_2$ and $Me_2AlNMe_2 \cdot AlMe_3$ are consumed, **I** then slowly decomposes to give Me_3As and $(Me_2AlNMe_2)_2$ [eq. (2)]. Equation (14) does not play a role in the 3 : 1 system, since all the MeAs$(NMe_2)_2$ is consumed by $-90°C$. The presence of a species that we propose is $[MeAl(NMe_2)_2]_2$ in the 0.5 : 1 and 1 : 1 cases suggests that a possible third, but much less important, competition reaction occurs. This involves the reaction of Me_2AlNMe_2 with MeAs$(NMe_2)_2$ [eq. (16)]. The route to $[MeAl(NMe_2)_2]_2$ does not involve Me_2AsNMe_2 [eqs (4) and (5)], since Me_3As is not observed in these systems.

The following reactions are unique to the Me_3Al/MeAs$(NMe_2)_2$ reaction systems:

$$MeAs(NMe_2)_2 + Me_3Al \longrightarrow MeAs(NMe_2)NMe_2 \cdot AlMe_3 \quad (10)$$

$$MeAs(NMe_2)_2 + 2Me_3Al \longrightarrow MeAs(NMe_2 \cdot AlMe_3)_2 \quad (11)$$

$$MeAs(NMe_2 \cdot AlMe_3)_2 \longrightarrow Me_2AsNMe_2 \cdot AlMe_3 + Me_2AlNMe_2 \quad (12)$$

$$MeAs(NMe_2)NMe_2 \cdot AlMe_3 \longrightarrow Me_2AsNMe_2 + Me_2AlNMe_2 \quad (13)$$

$$MeAs(NMe_2)_2 + Me_2AsNMe_2 \cdot AlMe_3 \longrightarrow MeAs(NMe_2)NMe_2 \cdot AlMe_3 + Me_2AsNMe_2 \quad (14)$$

$$Me_2AsNMe_2 + Me_2AlNMe_2 \cdot AlMe_3 \longrightarrow Me_2AsNMe_2 \cdot AlMe_3 + Me_2AlNMe_2 \quad (15)$$

$$2Me_2AlNMe_2 + 2MeAs(NMe_2)_2 \longrightarrow 2Me_2AsNMe_2 + [MeAl(NMe_2)_2]_2 \quad (16)$$

Reaction of $(Me_3Al)_2$ *with* $As(NMe_2)_3$

The ^1H and ^{13}C NMR spectra of the room-temperature reactions of $(Me_3Al)_2$ with $As(NMe_2)_3$ in 1 : 1, 2 : 1, 3 : 1 and 4 : 1 mmol Me_3Al–$As(NMe_2)_3$ ratios indicate the immediate formation of **I** and $(Me_2AlNMe_2)_2$ in all cases. The 1 : 1 and 2 : 1 systems also contain unreacted $As(NMe_2)_3$, as well as exchange averaging of Me_2AsNMe_2 and **I**. In the 4 : 1 case, all the $As(NMe_2)_3$ is consumed and $Me_2AlNMe_2 \cdot AlMe_3$, $Me_3As \cdot AlMe_3$ and Me_3As are also present. ^1H spectral line-width broadening and the δ_H and δ_C peak positions suggest that $Me_3As \cdot AlMe_3$ and Me_3As exchange average. The most straightforward reaction occurs as expected in the 3 : 1 ratio system. Here, **I** decomposes completely with time to yield Me_3As and $(Me_2AlNMe_2)_2$ as the sole reaction products.

In the 1 : 1 case, decomposition of **I** and consumption of $As(NMe_2)_3$ proceeds with time to give a mixture containing Me_2AsNMe_2, MeAs$(NMe_2)_2$, $As(NMe_2)_3$ and $(Me_2AlNMe_2)_2$. For the 2 : 1 system, decomposition is very slow and after 3 months the solution contains **I**, Me_2AsNMe_2 and As$(NMe_2)_3$, with Me_2AsNMe_2/**I** exchange averaging. When excess $(Me_3Al)_2$ is used (4 : 1 system), **I** decomposes and $Me_2AlNMe_2 \cdot AlMe_3$ dissociates within 2 days to give a solution containing $(Me_2AlNMe_2)_2$, Me_3As and $Me_3As \cdot AlMe_3$.

Variable-temperature, multinuclear NMR studies for 1 : 1, 1 : 0.33 and 3 : 1 Me_3Al–$As(NMe_2)_3$ ratios were carried out to elucidate the reaction pathway to **I** and determine concentration effects upon adduct formation. In the 3 : 1 system, there is exclusive formation of the Al—As adduct $(Me_2N)_3As \cdot AlMe_3$ (**IV**), in about 10% yield at $-95°C$. By $-90°C$, the amount of **IV** has greatly increased and a mono Al—N adduct, $(Me_2N)_2AsNMe_2 \cdot AlMe_3$ (**V**), and a bis Al—N adduct, $Me_2NAs(NMe_2 \cdot AlMe_3)_2$ (**VI**), form. The mol ratio of **IV** : **V** : **VI** is 3.5 : 3.3 : 1. The magnitudes of the δ_C changes for the Me_2N groups upon complexation are significantly larger for the formation of **V** (3.08 ppm) and **VI** (4.57 ppm) than for the Al—As bonded adduct, **IV** (0.36 ppm). At $-85°C$, **IV** begins to dissociate with the concomitant formation of more **V** and **VI** in a 1 : 1 mol ratio. This process continues up to $-40°C$. From -80 to $-60°C$, ^1H spectral line-width broadening and δ_H and δ_C peak positions suggest exchange averaging involving $As(NMe_2)_3$, **V** and **VI**. From -70 to $-60°C$, **V** and **VI** decompose to **II**, **III**, $Me_2AlNMe_2 \cdot AlMe_3$ and MeAs$(NMe_2)_2$. Spectral data suggest that **VI** decomposes faster than **V**. Compound **I** also forms as the temperature increases. Above $-60°C$, **II** and **III** decompose with the formation of **I** and Me_2AsNMe_2. ^1H spectral line-width broadening and δ_H and δ_C peak positions suggest that MeAs$(NMe_2)_2$, **II** and **III** exchange average. Decomposition of **III** is complete by $-50°C$, while that of **II** is complete by 0°C. At $-40°C$, peaks associated with $Me_2AlNMe_2 \cdot AlMe_3$ begin to decrease in intensity and peaks assigned to $(Me_2AlNMe_2)_2$ appear. Above $-40°C$, the Me_2AsNMe_2/**I** exchange averaging indicates increasing conversion of Me_2AsNMe_2 to **I**. The room-temperature product composition is analogous to that in the 3 : 1 mmol room-temperature system. The 1 : 0.33 mmol system gives results analogous to those in the 3 : 1 system. The only sig-

nificant difference is the formation of a mixture of **IV**, **V** and **VI** at −95°C.

The 1 : 1 mmol system at −95°C yields a mixture of **IV**, **V** and **VI** in a 0.6 : 1 : 1 mol ratio with unreacted $As(NMe_2)_3$ and $(Me_3Al)_2$. More **V** and **VI** form in a 1 : 1 mol ratio with increasing temperature. Above −80°C, decomposition of **V** and **VI** gives a mixture of **I**, **II**, **III**, $MeAs(NMe_2)_2$, Me_2AsNMe_2 and $Me_2AlNMe_2 \cdot AlMe_3$, with exchange averaging of the Me_2AsNMe_2/**I** and $MeAs(NMe_2)_2$/**II** systems. Dissociation of **IV** begins and is complete by −60°C. At −40°C, $As(NMe_2)_3$ and $Me_2AlNMe_2 \cdot AlMe_3$ are being consumed with increased formation of **I**, $MeAs(NMe_2)_2$ and $(Me_2AlNMe_2)_2$. By room temperature, the solution contains the product composition of the 1 : 1 room-temperature study—only **I**, Me_2AsNMe_2, $(Me_2AlNMe_2)_2$ and unreacted $As(NMe_2)_3$.

Analysis of the room- and variable-temperature NMR spectral data for the various stoichiometric ratio systems suggests that $As(NMe_2)_3$ forms an Al—As bonded adduct, **IV**, and the mono, **V**, and bis, **VI**, Al—N bonded adducts [eqs (17)–(19)]. Analogous adducts form in the reaction of $BH_3 \cdot THF$ with $As(NMe_2)_3$.[63] The Al—As adduct is unstable relative to dissociation [eq. (20)] at low temperatures (> −85°C). At a slightly higher temperature (−70°C), **V** and **VI** decompose. The $As(NMe_2)_3/(Me_3Al)_2$ reaction systems are complicated by the occurrence of not only the decomposition of **V** and **VI**, but the simultaneous participation of many of the competing reactions and exchange equilibria observed in the MeAs $(NMe_2)_2/(Me_3Al)_2$ and $Me_2AsNMe_2/(Me_3Al)_2$ reactions.

By analogy to the decomposition pathways of **II** and **III** and considering the species observed at −70 and −60°C, we postulate that **V** and **VI** decompose according to eqs (21) and (22). The Me_2AlNMe_2, **II**, and $MeAs(NMe_2)_2$ formed can then react with available $(Me_3Al)_2$ to give $Me_2AlNMe_2 \cdot AlMe_3$ [eq. (7)], **III** [eq. (11)] and additional **II** [eq. (10)]. At a slightly higher temperature (−60°C), **II** and **III** begin to decompose to Me_2AsNMe_2, **I** and Me_2AlNMe_2 [eqs (12) and (13)]. Exchange averaging again occurs between Me_2AsNMe_2 and **I**, and $MeAs(NMe_2)_2$ and **II**. In addition to the reaction of $MeAs(NMe_2)_2$ with **I** [eq. (14)], $As(NMe_2)_3$ can also react with **I** [eq. (23)] to provide an alternate route to Me_2AsNMe_2. This reaction [eq. (23)], which is very slow, has been confirmed independently. $As(NMe_2)_3$ competes for the Me_3Al bound in **I** to yield Me_2AsNMe_2 and **V**, which then decomposes to $MeAs(NMe_2)_2$ [eq. (21)]. $MeAs(NMe_2)_2$ now reacts with **I** [eq. (14)] to give **II**, which decomposes to Me_2AsNMe_2 [eq. (13)]. The overall reaction [eq. (23)] is much slower than the rate of decomposition of **I**. Thus, in the 1 : 1 and 2 : 1 systems, the final product composition contains Me_3As in addition to Me_2AsNMe_2 and $(Me_2AlNMe_2)_2$. Since, in the 3 : 1 case, the additional available $(Me_3Al)_2$ converts all the Me_2AsNMe_2 to **I**, only Me_3As and $(Me_2AlNMe_2)_2$ are obtained. In the 4 : 1 system, the amount of $(Me_3Al)_2$ in stoichiometric excess reacts with an equimolar amount of Me_3As [eq. (8)] to give a final product composition containing Me_3As, $Me_3As \cdot AlMe_3$ and $(Me_2AlNMe_2)_2$.

The following reactions are unique to the $(Me_3Al)_2/As(NMe_2)_3$ reaction systems:

$$As(NMe_2)_3 + Me_3Al \longrightarrow (Me_2N)_3As \cdot AlMe_3 \quad (17)$$

$$As(NMe_2)_3 + Me_3Al \longrightarrow (Me_2N)_2AsNMe_2 \cdot AlMe_3 \quad (18)$$

$$As(NMe_2)_3 + 2Me_3Al \longrightarrow Me_2NAs(NMe_2 \cdot AlMe_3)_2 \quad (19)$$

$$(Me_2N)_3As \cdot AlMe_3 \longrightarrow As(NMe_2)_3 + AlMe_3 \quad (20)$$

$$(Me_2N)_2AsNMe_2 \cdot AlMe_3 \longrightarrow MeAs(NMe_2)_2 + Me_2AlNMe_2 \quad (21)$$

$$Me_2NAs(NMe_2 \cdot AlMe_3)_2 \longrightarrow MeAs(NMe_2)NMe_2 \cdot AlMe_3 + Me_2AlNMe_2 \quad (22)$$

$$As(NMe_2)_3 + 2Me_2AsNMe_2 \cdot AlMe_3 \longrightarrow 3Me_2AsNMe_2 + (Me_2AlNMe_2)_2. \quad (23)$$

Reactions of **I** *with* $MeAs(NMe_2)_2$ *and* $As(NMe_2)_3$

The ^1H and ^{13}C NMR spectra of the room-temperature reaction of **I** with $MeAs(NMe_2)_2$ indicate that a 68% conversion of **I** to Me_2AsNMe_2 and of $MeAs(NMe_2)_2$ to **II** occurs rapidly upon mixing. ^1H spectral line-width broadening and the δ_H and δ_C peak positions suggest that the Me_2AsNMe_2/**I** and $MeAs(NMe_2)_2$/**II** systems are exchange averaging. Within 2 days, there is an 81% conversion to Me_2AsNMe_2. The reaction goes to completion in 16 days to give Me_2AsNMe_2, $(Me_2AlNMe_2)_2$ and a trace of Me_3As. The presence of only a trace of Me_3As suggests that the rates of the competition reaction [eq. (14)] and the decomposition of **II** [eq. (13)] are much greater than that of the decomposition of **I** [eq. (2)]. The stabilizing of **I** through exchange averaging may be an important factor. Thus, the reaction of **I** with $MeAs(NMe_2)_2$ is important in determining the final product distribution

and the overall rate of reaction in the reactions of $(Me_3Al)_2$ with $MeAs(NMe_2)_2$ and $As(NMe_2)_3$, and in the $Me_2AsNMe_2/MeAs(NMe_2)_2/As(NMe_2)_3$ competition reactions.

The NMR spectral data for the reaction of **I** with $As(NMe_2)_3$ indicate approximately a 10% conversion of **I** to Me_2AsNMe_2 and the presence of $MeAs(NMe_2)_2$ and **II** within 2 h of mixing. Exchange averaging that involves the Me_2AsNMe_2/**I** and $MeAs(NMe_2)_2$/**II** systems is observed. The $MeAs(NMe_2)_2$ is rapidly consumed and peaks assigned to $[MeAl(NMe_2)_2]_2$ and Me_3As appear. After 2 days, a 90% conversion to Me_2AsNMe_2 has occurred with further formation of $[MeAl(NMe_2)_2]_2$ and Me_3As, and the appearance of peaks associated with uncharacterized Me_2N moiety containing species. With time, the intensities of peaks assigned to Me_2AsNMe_2 decrease while that associated with Me_3As increases. After 1 month, the reaction mixture contains Me_3As, Me_2AsNMe_2, $MeAs(NMe_2)_2$. $[MeAl(NMe_2)_2]_2$, $(Me_2AlNMe_2)_2$ and considerable unreacted As $(NMe_2)_3$. These data suggest that the reaction of **I** with $As(NMe_2)_3$ is initially slow. At room temperature, the Me_3Al adduct(s) of $As(NMe_2)_3$ are unstable and decompose to $MeAs(NMe_2)_2$, **II** and Me_2AlNMe_2 [eqs (21) and (22)]. The $MeAs(NMe_2)_2$ reacts with **I** [eq. (14)] to give **II** and Me_2AsNMe_2. The Me_2AlNMe_2 that also forms from the decomposition of **II** [eq. (13)] probably reacts with the large amount of available $As(NMe_2)_3$ to give $MeAs(NMe_2)_2$ and $[MeAl(NMe_2)_2]_2$ [eq. (24)]. This would be analogous to the Me_2AlNMe_2/$MeAs(NMe_2)_2$ reaction [eq. (16)], where $[MeAl(NMe_2)_2]_2$ was detected only when there was a large amount of $MeAs(NMe_2)_2$ present in solution. It can also react with Me_2AsNMe_2 [eqs (4) and (5)] and $MeAs(NMe_2)_2$ [eq. (16)]. The following reaction is unique to the $I/As(NMe_2)_3$ reaction system:

$$2Me_2AlNMe_2 + 2As(NMe_2)_3 \longrightarrow 2MeAs(NMe_2)_2 + [MeAl(NMe_2)_2]_2. \quad (24)$$

Because this reaction is very slow, it does not play a significant role in the variable temperature $As(NMe_2)_3/(Me_3Al)_2$ reactions nor in the $Me_2AsNMe_2/MeAs(NMe_2)_2/As(NMe_2)_3/(Me_3Al)_2$ competition reactions.

Competition studies of $(Me_3Al)_2$ *with* Me_2AsNMe_2, $MeAs(NMe_2)_2$ *and* $As(NMe_2)_3$ *mixtures*

At −95°C, the NMR spectra of the 1:1:1:1 and 1:1:1:2 mmol Me_2AsNMe_2–$MeAs(NMe_2)_2$–$As(NMe_2)_3$–$AlMe_3$ mixtures indicate the presence of **I**, **II**, **III**, Me_2AsNMe_2, $MeAs(NMe_2)_2$ and $As(NMe_2)_3$. There is no spectral evidence for any reaction of $(Me_3Al)_2$ with $As(NMe_2)_3$. Integration data for both systems suggest that Me_2AsNMe_2 and $MeAs(NMe_2)_2$ react in a 1:1 mol ratio and that approximately 15% of **III** decomposes [eq. (12)]. In the 1:1:1:1 system, equal amounts of **II** and **III** form; in the 1:1:1:2 system, **II** and **III** form in a 1.5:1 mol ratio, respectively. Upon increasing the temperature, further decomposition of **III** occurs. At room temperature, the spectra suggest that Me_2AsNMe_2 is exchanging with **I**, $MeAs(NMe_2)_2$ is exchanging with **II**, and $(Me_2AlNMe_2)_2$ and $As(NMe_2)_3$ are present. After 1 week, new peaks are observed for Me_3As and $[MeAl(NMe_2)_2]_2$ and peaks associated with **I** and **II** are absent in the spectra of the 1:1:1:1 system. The final composition indicates a 1:2:3 mol ratio of Me_3As, $MeAs(NMe_2)_2$ and Me_2AsNMe_2, respectively. In the 1:1:1:2 system, only traces of Me_3As and $MeAs(NMe_2)_2$ are present after 1 week. Me_2AsNMe_2 is the arsenic-containing product from the reaction. In both cases, significant amounts of $As(NMe_2)_3$ remain.

These data suggest that $(Me_3Al)_2$ preferentially reacts with Me_2AsNMe_2 and $MeAs(NMe_2)_2$ as compared with $As(NMe_2)_3$. After the initial formation of **I**, **II** and **III**, these adducts decompose [eqs (2), (12) and (13)]. Since the $(Me_3Al)_2$ is stoichiometrically deficient relative to available nitrogen base sites, all the previously described exchange and competing reactions [eqs (3)–(6), (14), (16) and (24)] for such systems can occur with time and influence the final product composition.

CONCLUSIONS

The results of these studies establish the mode of reaction of $(Me_3Al)_2$ with Me_2AsNMe_2, $MeAs(NMe_2)_2$ and $As(NMe_2)_3$, and the role of competing reactions and exchange equilibria in determining the final product distributions. In all the variable-temperature studies, we have been able to establish the formation of initial Me_3Al adducts at −95°C and to determine their subsequent decomposition pathways. All the aminoarsines form the expected mono Al—N bonded adducts, i.e. **I**, **II** and **V**, with the following order of thermal stability: **I** > **II** > **V**. $MeAs(NMe_2)_2$ and $As(NMe_2)_3$ also form bis Al—N bonded adducts, i.e. **III** and **VI**. These readily decompose at low temperature. The only observed Al—As bonded adduct, **IV**, occurs with $As(NMe_2)_3$ and it dissociates at low temperature. Thus, the nitrogen Lewis base site in the aminoarsines is the preferred bonding site for the Me_3Al Lewis acid.

These results are in contrast to those obtained for the Et_3Al adducts of the bisphosphinoamines and Me_2PNMe_2.[43] For these cases, Al—P bonded 1:1 addition compounds form. However, Me_2PNMe_2, which is the phosphorus analogue of Me_2AsNMe_2, also gives an Al—N bonded adduct. It is apparently more thermodynamically stable than the Al—P bonded adduct.[43]

All the Al—N bonded adducts decompose by a pathway that involves cleavage of the As—N bond and transfer of a methyl group from the aluminium to the arsenic. Whether this proceeds through a four-centred intermediate with simultaneous bond cleavage and formation of a concerted mechanism that involves interaction of the aminoarsine and Me_3Al molecules in an appropriate low energy conformation could not be determined from our study. In each case, the decomposition of a mono adduct yields the next higher methyl homologue in the arsine series [$MeAs(NMe_2)_2$, Me_2AsNMe_2 or Me_3As] and the postulated unstable Me_2AlNMe_2. Decomposition of a bis adduct yields the next higher methyl homologue in the mono adduct series (**I** or **II**) and unstable Me_2AlNMe_2.

Since $(Me_3Al)_2$ is usually in excess at low temperatures, Me_2AlNMe_2 forms $Me_2AlNMe_2 \cdot AlMe_3$, which eventually dissociates and then provides an alternative source of Me_3Al when the $(Me_3Al)_2$ is consumed. When the amount of $(Me_3Al)_2$ is low, either through the initial reaction stoichiometry or further reaction, Me_2AlNMe_2 dimerizes to $(Me_2AlNMe_2)_2$. If the aminoarsine is in stoichiometric excess, we propose the attack of Me_2AlNMe_2 at the arsine amino-nitrogen base site to give a very facile route to the next higher methyl homologue in the arsine series and $(Me_2AlNMe_2)_2$. The relative importance of these side reactions was demonstrated by carrying out the aminoarsine/$(Me_3Al)_2$ reactions in varying stoichiometric ratios. In large excesses of the aminoarsines, the Me_2AlNMe_2 can further react to give $[MeAl(NMe_2)_2]_2$ and the next higher methyl homologue in the arsine series. These results further support the general conclusion that the Al—N bond is more stable than the Al—C bond.[9,12]

In all the studied reaction systems, the Al—N bonded adducts exchange average with their respective parent aminoarsines. This exchange averaging slows dow the rate of adduct decomposition, influences the overall rate of formation of the final product arsine, and affects the final product distribution when other facile competing side-reactions can occur.

The reactions of $(Me_3Al)_2$ with $As(NMe_2)_3$ and $MeAs(NMe_2)_2$ are further complicated by the simultaneous presence of Me_2AsNMe_2, $MeAs(NMe_2)_2$ and $As(NMe_2)_3$, and the mono- and bis-adducts that can enter into separate exchange averaging, decomposition and competing side-reactions. These are all described by eqs (1)–(24). The initial stoichiometry of the reaction greatly influences the relative importance of the various reactions, which ultimately affect the rate of formation and final distribution of products. Only in those systems where the moles of available Me_3Al molecules equal those of Lewis base nitrogen sites, are the overall reactions straightforward and the influence of competing side-reactions minimized. Then the final products are always Me_3As and $(Me_2AlNMe_2)_2$.

We have been successful in adapting the results from these reactions of $(Me_3Al)_2$ with aminoarsines to a new, high-yield synthetic route to Me_3As. By carrying out the neat reaction at 0°C with slow addition of $(Me_3Al)_2$ followed by heating and distillation of the mixture at 140°C, the competing side reactions are driven rapidly to completion and pure Me_3As is obtained in an 84% yield (see Experimental). This is a higher yield route to Me_3As that eliminates the need for a complexing agent for removal of Me_3As from the reaction solution.[64]

Based upon these results, we are also adapting these reactions to the synthesis of mixed tertiary arsines and other symmetric tertiary arsines. Research is also underway on other $R'_nAs(NR_2)_{3-n}$ ($n = 0$–2) arsines to establish the influence of the nature of R and R′ on the binding of Me_3Al. Preliminary work has also established that Me_3Ga reacts in an analogous manner with the aminoarsines. This work is being pursued to establish the nature of the adducts formed and the subsequent decomposition pathways.

REFERENCES

1. J. J. Eisch, in *Comprehensive Organometallic Chemistry* (Edited by G. Wilkinson, F. G. A. Stone and E. W. Abel), Vol. 1, p. 555. Pergamon Press, Oxford (1982).
2. T. Mole and E. A. Jeffery, *Organoaluminum Compounds*. Elsevier, Amsterdam (1972).
3. A. McKillop, J. D. Smith and I. J. Worrall, *Organometallic Compounds of Aluminum, Gallium, Indium and Thallium*. Chapman and Hall, London (1985).
4. G. E. Coates, M. L. H. Green and K. Wade, *Organometallic Compounds*, 3rd edn, Vol. 1. Methuen, London (1967).
5. D. C. Bradley, H. Chudzynska, M. M. Faktor, D. M. Frigo, M. B. Hursthouse, B. Hussain and L. M. Smith, *Polyhedron* 1988, **7**, 1289.
6. H. M. Manasevit and W. I. Simpson, *J. Electrochem. Soc.* 1969, **116**, 1725; *J. Electrochem. Soc.* 1973, **120**, 135.

7. R. H. Moss, *J. Cryst. Growth* 1984, **68**, 78.
8. L. V. Interrante, G. A. Sigel, M. Garbauskas, C. Hejna and G. A. Slack, *Inorg. Chem.* 1989, **28**, 252.
9. A. W. Laubengayer, J. D. Smith and G. G. Ehrlich, *J. Am. Chem. Soc.* 1961, **83**, 542.
10. K. J. Alford, K. Gosling and J. D. Smith, *J. Chem. Soc., Dalton Trans.* 1972, 2203.
11. M. Cohen, J. K. Gilbert and J. D. Smith, *J. Chem. Soc.* 1965, 1092.
12. J. K. Gilbert and J. D. Smith, *J. Chem. Soc. A* 1968, 233.
13. K. Gosling, J. D. Smith and D. H. W. Wharmby, *J. Chem. Soc. A* 1969, 1738.
14. P. B. Hitchcock, J. D. Smith and K. M. Thomas, *J. Chem. Soc., Dalton Trans.* 1976, 1433.
15. G. M. McLaughlin, G. A. Sim and J. D. Smith, *J. Chem. Soc., Dalton Trans.* 1972, 2197.
16. S. Amirkhalili, P. B. Hitchcock and J. D. Smith, *J. Chem. Soc., Dalton Trans.* 1979, 1206.
17. S. Amirkhalili, P. B. Hitchcock, A. D. Jenkins, J. Z. Nyathi and J. D. Smith, *J. Chem. Soc., Dalton Trans.* 1981, 377.
18. N. Davidson and H. C. Brown, *J. Am. Chem. Soc.* 1942, **64**, 316.
19. G. E. Coates and J. Graham, *J. Chem. Soc.* 1963, 233.
20. O. T. Beachley, G. E. Coates and G. Kohnstam, *J. Chem. Soc.* 1965, 3248.
21. H. Hess, A. Hinderer and S. Steinhauser, *Z. Anorg. Allg. Chem.* 1970, **377**, 1.
22. M. J. S. Dewar, D. B. Patterson and W. I. Simpson, *J. Chem. Soc., Dalton Trans.* 1973, 2381.
23. G. A. Anderson, F. R. Forgaard and A. Haaland, *J. Chem. Soc., Chem. Commun* 1971, 480.
24. J. W. Akitt, *Annu. Rep. NMR Spectrosc.* 1972, **5A**, 466.
25. J. W. Akitt, *Prog. Nucl. Magn. Reson. Spectrosc.* 1989, **21**, 1.
26. D. F. Clemens, W. S. Brey Jr and H. H. Sisler, *Inorg. Chem.* 1963, **2**, 1251.
27. N. R. Fetter and B. Bartocha, *Can. J. Chem.* 1961, **39**, 2001.
28. K. H. Thiele, H. K. Müller and W. Brüser, *Z. Anorg. Allg. Chem.* 1966, **345**, 194.
29. O. T. Beachley Jr and K. C. Racette, *Inorg. Chem.* 1975, **14**, 2534.
30. O. T. Beachley Jr and K. C. Racette, *Inorg. Chem.* 1976, **15**, 2110.
31. G. H. Robinson and S. A. Sangokoya, *J. Am. Chem. Soc.* 1987, **109**, 6852.
32. G. H. Robinson, S. A. Sangokoya, F. Moise and W. T. Pennington, *Organometallics* 1988, **7**, 1887.
33. G. H. Robinson, M. F. Self, S. A. Sangokoya and W. T. Pennington, *J. Am. Chem. Soc.* 1989, **111**, 1520.
34. G. H. Robinson, A. D. Rae, C. F. Campana and S. K. Byram, *Organometallics* 1987, **6**, 1227.
35. B. M. Cohen, A. R. Cullingworth and J. D. Smith, *J. Chem. Soc. A* 1969, 2193.
36. T. R. Durkin and E. P. Schram, *Inorg. Chem.* 1972, **11**, 1054.
37. A. R. Barron, *J. Chem. Soc., Dalton Trans.* 1988, 3047.
38. C. H. Henrickson, D. Duffy and D. P. Eyman, *Inorg. Chem.* 1968, **7**, 1047.
39. A. Almenningen, L. Fernholt and A. Haaland, *J. Organomet. Chem.* 1978, **145**, 109.
40. D. A. Wierda and A. R. Barron, *Polyhedron* 1989, **8**, 831.
41. O. T. Beachley and G. E. Coates, *J. Chem. Soc.* 1965, 3241.
42. K. Issleib and H. J. Deyling, *Z. Naturfor.* 1962, **17B**, 198.
43. D. F. Clemens, H. H. Sisler and W. S. Brey Jr, *Inorg. Chem.* 1966, **5**, 527.
44. K. J. Ewing, A. D. Berry and R. A. DeMarco, Abstracts of Papers, 193rd ACS National Meeting of the American Chemical Society, Denver, CO, 5–10 April 1987; *Inorg.* 73.
45. K. Issleib and F. Krech, *Z. Anorg. Allg. Chem.* 1964, **328**, 21.
46. H. Schmidbaur, S. Lauteschläger and G. Müller, *J. Organomet. Chem.* 1985, **281**, 25.
47. T. Kagawa and H. Hashimoto, *Bull. Chem. Soc. Jpn* 1972, **45**, 1739.
48. H. Karsch, A. Appelt, J. Riede and G. Müller, *Organometallics* 1987, **6**, 316.
49. C. A. Smith and M. G. H. Wallbridge, *J. Chem. Soc. A.* 1970, 2675.
50. D. F. Clemens, R. B. Smith Jr and J. G. Dickinson, *Can. J. Chem.* 1973, **51**, 3187.
51. D. Giurgiu, L. Roman, I. Popescu and A. Ciobanu, *Rev. Roum. Chim.* 1971, **16**, 1217.
52. H. Schmidbaur, S. Lauteschläger and B. Milewski-Mahrla, *Chem. Ber.* 1983, **116**, 1403.
53. S. F. Spangenberg and H. H. Sisler, *Inorg. Chem.* 1969, **8**, 1004.
54. P. B. Hitchcock, H. A. Jasim, M. F. Lappert and H. D. Williams, *J. Chem. Soc., Chem. Commun.* 1986, 1634.
55. W. Steinkopf and W. Mieg, *Chem. Ber.* 1920, **53**, 1013.
56. W. M. Dehn and B. B. Wilcox, *Am. Chem. J.* 1906, **35**, 1.
57. K. Moedritzer, *Chem. Ber.* 1959, **92**, 2637.
58. H. Vahrenkampf and H. Nöth, *J. Organomet. Chem.* 1968, **12**, 281.
59. B. A. Amero and E. P. Schram, *Inorg. Chem.* 1976, **15**, 2842.
60. M. Cesari and S. Cucinella, in *The Chemistry of Inorganic Homo- and Heterocycles* (Edited by I. Haiduc and D. B. Sowerby), Vol. 1, p. 167. Academic Press, London (1987).
61. E. P. Schram, R. E. Hall and J. D. Glore, *J. Am. Chem. Soc.* 1969, **91**, 6643.
62. M. B. Smith, *J. Organomet. Chem.* 1972, **46**, 31.
63. L. K. Krannich, C. L. Watkins, D. Srivastava and R. K. Kanjolia, Abstracts of Papers, The Third Chemical Congress of North America, Toronto, Canada, 5–10 June, 1988; *Inorg.* 596.
64. L. Fournier and J. G. Riess, *Synth. Inorg. Met.-Org. Chem.* 1972, **2**, 53.

Polyhedron Vol. 9, No. 2/3, pp. 301–308, 1990
Printed in Great Britain

0277–5387/90 $3.00+.00
© 1990 Pergamon Press plc

EXCHANGE REACTIONS BETWEEN DIALKYLZIRCONOCENE AND ALKYLALUMINIUM COMPOUNDS

A. R. SIEDLE,* R. A. NEWMARK, W. M. LAMANNA and J. N. SCHROEPFER

3M Corporate Research Laboratories, St. Paul, MN 55144, U.S.A.

Abstract—The dimethylmetallocenes $Cp_2Zr(^{13}CH_3)_2$, $(Me_5Cp)_2Zr(^{13}CH_3)_2$, $(indenyl)_2Zr(^{13}CH_3)_2$, $Me_2Si(C_5H_4)_2Zr(^{13}CH_3)_2$ and $Cp_2Hf(^{13}CH_3)_2$ undergo degenerate methyl exchange with the methyl-acceptor materials Me_6Al_2, $(MeAlO)_x$ and MeAl(2,6-di-t-butyl-4-methylphenoxy)$_2$. Free energies, enthalpies and entropies of activation for these processes have been obtained in two solvents by ^{13}C NMR. Increased steric hindrance at zirconium increases the free energy of activation. There appears not to be a correlation with electronic effects as assessed by gas phase appearance potentials for the $(P-CH_3)^+$ ions.

The role of cationic, coordinatively unsaturated zirconium(IV) compounds, as the active species in the catalytic polymerization of ethylene, has recently received considerable attention.[1,2] The cation $Cp_2ZrCH_3^+$ is of special interest. In fluid solution, it may be generated by oxidation or protonation of Cp_2ZrMe_2 but it has been characterized only in solvated form, for example, as $Cp_2ZrMe(S)^+$ (S = CH_3CN or THF).[1a] In the gas phase, successive detachment of methyl groups occurs upon electron impact ionization to afford Cp_2ZrMe^+ and Cp_2Zr^+.[3] It is open to question whether Cp_2ZrMe^+ is stable in solution in the absence of coordinating solvents and if it is, whether it might not exhibit an agnostic Zr—H—CH_2 interaction involving the α-hydrogen on the methyl group.[4] Previously, we reported that Cp_2ZrMe_2 readily exchanges methyl groups with Me_6Al_2 and that it reacts with $(Me_2AlEt)_2$ in neat Me_6Al_2 to form $Cp_2Zr(\mu\text{-}CH_3)(\mu\text{-}1,2\text{-}CH_2CH_2)AlMe_2$.[5] We surmise that methyl exchange may proceed via an ionic intermediate as shown conceptually (i.e. complexation by solvent or by Al_2Me_6 is neglected) in eq. (1):

$$Cp_2ZrMe_2 + Me_3Al \rightleftharpoons Cp_2ZrMe^+AlMe_4^- . \quad (1)$$

This equilibrium lies far to the left. In principle, eq. (1) is generally applicable to any Lewis acid capable of (formally) accepting a CH_3^- group. In order to gain further understanding of the interaction of Cp_2ZrMe_2 with such Lewis acids, we have undertaken a study of methyl exchange reactions with dimethylzirconocene and related compounds with a series of methylaluminium reagents.

RESULTS AND DISCUSSION

Rates of methyl exchange in the systems reported here were studied in two ways; $Cp_2Zr(^{13}CH_3)_2$ was combined with the methylaluminium compound in toluene and diminution of the Zr—CH_3 signal was followed as a function of time by ^{13}C NMR spectroscopy. In some cases, equilibrium was reached in too short a time (< 5 min) for this technique to be useful. In these situations, rates usually could be obtained by total line-shape analysis of the Zr—CH_3 resonance which was exchange-broadened. The methylaluminium compounds were used in large excess, typically 10–20 fold (cf. Experimental), so that kinetics of the exchange reactions are pseudo-first order with respect to the zirconium compound. Toluene was selected as the least interactive solvent capable of producing requisite concentrations of the reactants notwithstanding that it may weakly solvate three-coordinate aluminium(III) (*vide infra*). In the context of eq. (1), we refer to Cp_2ZrMe_2 and its congeners as methyl *donors*, and to Me_3Al and its congeners as methyl *acceptors*. This allows one to view methyl transfer processes in the framework of more generalized acid–base chemistry. The reactions studied are fully reversible and, in the kinetic experiments, no new products are detectable by NMR.

The aluminium-containing methyl acceptors employed in this work are Me_6Al_2, $MeAl(BHT)_2$

* Author to whom correspondence should be addressed.

(BHT = 2,6-di-t-butyl-4-methylphenoxy) and $(MeAlO)_x$. The first of these, Me_6Al_2, exists primarily as a methyl-bridged dimer. Nevertheless, the energetics of bridge–terminal methyl exchange in the dimer are quite solvent-dependent, differing significantly even between cyclopentane and toluene. It is thought that toluene may behave as a π-base toward $AlMe_3$ and thus lead to higher steady-state concentrations of solvated monomer.[6] We believe that it is with monomeric, i.e. solvated, Me_3Al that methyl exchange occurs and that the presence of three-coordinate aluminium is necessary for this reaction (*vide infra*). For this reason, we refer below to Me_3Al and express aluminium concentrations in terms of this monomer. Methylaluminoxane, $(MeAlO)_x$, is a substance produced by the controlled hydrolysis of Me_6Al_2. It is difficult to purify and characterize. Even today, its nature remains an enigma; it is not established whether it is a single substance or whether it has a static or a dynamic structure. However, acting with Cp_2ZrMe_2, it is a powerful if not unique, co-catalyst for the polymerization of ethylene.[7] Its inclusion in this study is warranted on technological grounds alone. Methylaluminoxane represents a special case of methyl acceptor molecules in two regards. First, its reaction with Cp_2ZrMe_2 in toluene leads to slow phase separation; a denser, orange layer contains all the $(MeAlO)_x$. A kinetic study in such a heterogeneous system is fraught with difficulty. Of the compounds studied, only Cp_2HfMe_2 remained homogeneous in toluene in the presence of $(MeAlO)_x$. Methyl exchange chemistry involving $(MeAlO)_x$ was, therefore, examined in dichloromethane. This choice of solvent limits the accessible temperature range so that only free energy data are available (*vide supra* and Experimental). Second, $(MeAlO)_x$ (unlike other organoaluminium compounds studied) and Cp_2ZrMe_2 undergo a *non*-equilibrium reaction that is much slower than the methyl exchange chemistry and which, therefore, does not affect the kinetic results. This reaction is still under investigation and will be described in detail elsewhere. Midway between Me_3Al and $(MeAlO)_x$ is $MeAl(BHT)_2$. The steric effects of the BHT groups prevent dimerization and this compound has been shown to be monomeric by X-ray crystallography (in the solid state)[8] and ^{27}Al NMR spectroscopy (in solution).[9] It is an uncommon and unambiguous example of a material containing three-coordinate aluminium for which reason it has been studied here. We consider, notwithstanding the ability of aryloxy groups to π-backbond, that it may be a heuristically useful model for $(MeAlO)_x$ for it features a MeAl moiety bonded to two oxygen atoms.

The dimethylmetallocene compounds employed include $Cp_2Zr(^{13}CH_3)_2$, $(Me_5Cp)_2Zr(^{13}CH_3)_2$, $(indenyl)_2Zr(^{13}CH_3)_2$, $Me_2Si(C_5H_4)_2Zr(^{13}CH_3)_2$, $(Me_3SiCp)_2Zr(^{13}CH_3)_2$ and $Cp_2Hf(^{13}CH_3)_2$. Using dimethylzirconocene as a reference point, the pentamethylcyclopentadienyl analogue is expected to be considerably more sterically hindered. Also, X-ray photoelectron spectroscopic studies indicate that the metal centre is much more electron-rich in this compound, perhaps approaching zirconium(III).[10] The η^5-indenyl ligand *can*, optionally, "slip" or move laterally so that C_9H_7 becomes a four-electron donor but in a $\leqslant$16-electron system, it is more probable that the η^5 structure is more stable and that the annelated benzo ring will be electron-withdrawing.[11] On the basis of a curious shielding of the C_1 (*ipso*) carbon atom in $Me_2Si(C_5H_4)_2ZrCl_2$ (this shielding is also seen in the $ZrMe_2$ analogue) as well as cyclic voltammetry results, it was concluded that the bridging Me_2Si group is electron-withdrawing.[12] Chemical and structural studies on $[Me_2Si(Me_4C_5)_2ThH_2]_2$ indicate that Me_2Si ring chelation significantly opens the thorium coordination sphere and is associated with enhanced reactivity of Th—H and Th—C σ bonds lying in the equatorial girdle.[13] Thus, the structural modifications to Cp_2ZrMe_2 available in the series under study here can alter relative reactivity through either steric or electronic effects. We shall argue below that the former is more important. It is difficult to predict with confidence the relative reactivity of Cp_2ZrMe_2 and Cp_2HfMe_2 towards a methyl acceptor. It has been noted that the metal–carbon σ bonds in the latter are short[14] and perhaps, therefore, more stable than in the zirconium analogue.

The free energies, enthalpies and entropies of activation of reversible methyl exchange between these materials and Me_3Al (*vide supra*) and $MeAl(BHT)_2$ in toluene are shown in Table 1. All of the reactions exhibit large, negative entropies of activation. This indicates that the transition state has a substantial loss of translational and rotational freedom, consistent with the bimolecular nature of the reaction.

The trends in free energies of activation reveal several correlations between reactivity and structure. First, the relative order of strength of methyl acceptors decreases in the order $(MeAlO)_x > Me_3Al > MeAl(BHT)_2$. This is in agreement with the expectation that two adjacent, electronegative oxygen atoms will increase Lewis acidity, and with the finding that, based on ^1H NMR chemical shifts and changes in ν_{CN} in benzonitrile complexes, that $(Me_2Al)_2O$ is a stronger Lewis acid than Me_3Al.[15] The alkoxide derivative MeAl

Table 1. Free energies,[a] enthalpies and entropies of activation of methyl exchange in toluene[b]

Methyl donor	Methyl acceptor Me_6Al_2	Methyl acceptor $MeAl(BHT)_2$
Cp_2ZrMe_2	$\Delta G^{\ddagger}$ 16.7 $\Delta H^{\ddagger}$ 11 $\Delta S^{\ddagger}$ −21	$\Delta G^{\ddagger}$ 22.4 $\Delta H^{\ddagger}$ 5 $\Delta S^{\ddagger}$ −59
$(Me_5Cp)_2ZrMe_2$	$\Delta G^{\ddagger}$ 22.3 $\Delta H^{\ddagger}$ 9 $\Delta S^{\ddagger}$ −46	No exchange $\leqslant$80°C
$Me_2Si(C_5H_4)_2ZrMe_2$	$\Delta G^{\ddagger}$ 14.3 $\Delta H^{\ddagger}$ 8 $\Delta S^{\ddagger}$ −22	$\Delta G^{\ddagger}$ 21.5 at 22°C
$(indenyl)_2ZrMe_2$	[c]	$\Delta G^{\ddagger}$ 27.7 at 81°C
$(Me_3SiCp)_2ZrMe_2$	No exchange $\leqslant$81°	$\Delta G^{\ddagger}$ 27.7 at 81°C
Cp_2HfMe_2	$\Delta G^{\ddagger}$ 20.4 $\Delta H^{\ddagger}$ 12 $\Delta S^{\ddagger}$ −30	No exchange

[a] At 22°C.
[b] Free energies and enthalpies in kcal mol^{-1}, entropies in cal K^{-1} mol^{-1}.
[c] Too slow for DNMR, too fast for kinetics; $\Delta G^{\ddagger}$ = 17–19 kcal mol^{-1} at 22°C.

$(BHT)_2$ is especially interesting. $\Delta S^{\ddagger}$ for methyl exchange is unusually large, −59 e.u., but $\Delta H^{\ddagger}$, 5 kcal mol^{-1}, is quite small. We interpret these data as meaning that a large fraction of the free energy of activation goes towards twisting the 2,6-di-t-butyl-4-methylphenoxy groups so that the peripheral alkyl groups do not, as the transition state is approached, block access to aluminium. This aluminium atom, being three-coordinate, is expected to be a powerful Lewis acid and accordingly, the activation enthalpy for transfer of a methyl group to it should be, and is, very low.

Again using free energies of activation to illustrate trends, methyl donor strength decreases in the order $Me_2Si(C_5H_4)_2ZrMe_2$ > $(indenyl)_2ZrMe_2$ > Cp_2HfMe_2 > $(Me_5Cp)_2ZrMe_2$.

Free energies of activation at 22°C for methyl exchange between some dimethylmetallocenes and $(MeAlO)_x$ in dichloromethane are shown in Table 2. In contrast to data for Me_3Al in toluene, they are very similar, ranging from 13 to 15 kcal mol^{-1}. We interpret this as a levelling effect; that is, the tendency of a very strong Lewis acid to make all bases appear to be of equal strength. This phenomenon has been long recognized in proton donors and acceptors.[16]

With a weak methyl acceptor, solvent effects are manifest. It would be expected that going from toluene to the more polar solvent dichloromethane should accelerate methyl transfer between Cp_2ZrMe_2 and $MeAl(BHT)_2$ if the transition state involved appreciable charge separation; otherwise, the solvent change should have minimal effect. In fact, the exchange rate in CH_2Cl_2 is immeasurably slow. We suggest that this striking change is due to weak complexation between $MeAl(BHT)_2$ and the lone electron pairs on chlorine in CH_2Cl_2. Organometallic complexes containing halocarbon donors are now well known.[17] Solvent effects exhibited by the stronger methyl acceptor $(MeAlO)_x$ are much less pronounced. For Cp_2HfMe_2, $\Delta G^{\ddagger}$ at 22°C is 15.3 kcal mol^{-1} ($\Delta H^{\ddagger}$ = 7 kcal mol^{-1}, $\Delta S^{\ddagger}$ = −29 e.u.) in toluene and 15.4 kcal mol^{-1} in dichloromethane.

Table 2. Free energies of activation for methyl exchange with $(MeAlO)_x$ in dichloromethane at 22°C

Compound	$\Delta G^{\ddagger}$ (kcal mol^{-1})
Cp_2ZrMe_2	13.9
$(Me_5Cp)_2ZrMe_2$	13.4
$(indenyl)_2ZrMe_2$	13.8
$Me_2Si(C_5H_4)_2ZrMe_2$	13.0
Cp_2HfMe_2	15.4
$(Me_3SiCp)_2ZrMe_2$	Irreversible reaction

In order to help estimate the relative roles of steric and electronic effects in these methyl exchange processes, we have measured the gas phase appearance potentials for ions formed by loss of CH_3^- from dimethylmetallocenes as illustrated in eq. (2):

$$Cp_2ZrMe_2 \rightarrow Cp_2ZrMe^+ + CH_3^-. \quad (2)$$

This was carried out in a mass spectrometric experiment by plotting the integral of the $(P-CH_3)^+$ ion as a function of ionizing voltage and extrapolating the linear portion of the curve to zero intensity, at which point the intercept is the appearance potential. The reaction in eq. (2) can be viewed as proceeding in several steps. These are (1) homolytic cleavage of a Zr—CH_3 bond, (2) ionization of the resulting $Cp_2ZrCH_3^{\cdot}$ radical and (3) electron capture by $CH_3^{\cdot}$. If it is assumed that, in the group of structurally similar compounds studied, the Zr—CH_3 bond dissociation energies are essentially constant, then trends in these appearance potentials reflect relative stabilities of the $(P-CH_3)^+$ ion, that is, the ability of a Cp_2ZrR group to support a positive charge. Typical data for $Me_2Si(C_5H_4)_2ZrMe_2$ are shown in Fig. 1 and appearance potentials are collected in Table 3. Their estimated uncertainties are ± 0.15 eV. In the zirconium compounds, there is no apparent correlation between appearance potentials for $(P-CH_3)^+$ and free energies of activation for methyl exchange. $(Me_5Cp)_2ZrMe_2$ should, because of the electron-releasing effect of the 10 ring-methyl groups, form a more stable $(P-CH_3)^+$ ion than Cp_2ZrMe_2,[10] and this ion does have, accordingly, a 0.5 eV lower appearance potential. But in fact, $(Me_5Cp)_2ZrMe_2$ undergoes methyl exchange with both Me_3Al and $MeAl(BHT)_2$ more slowly than does Cp_2ZrMe_2. As noted above, $(Me_5Cp)_2ZrMe_2$ is sterically more hindered than Cp_2ZrMe_2 and $Me_2Si(C_5H_4)_2ZrMe_2$ less so, and this is reflected in values of $\Delta G^{\ddagger}$ for methyl exchange. Conspicuous is $(Me_3SiCp)_2ZrMe^+$ which has a quite low appearance potential, yet $(Me_3SiCp)_2ZrMe_2$, which contains two large, bulky trimethylsilyl groups, has a large $\Delta G^{\ddagger}$ for exchange with $MeAl(BHT)_2$. This raises the question of whether this ion might not be stabilized in the gas phase by intramolecular Zr—H—C agnostic interactions. We believe that the major determinant of methyl donor ability of a dimethyl zirconium metallocene is comprised of steric effects. The hafnium compound Cp_2HfMe_2 forms a $(P-CH_3)^+$ ion with a lower appearance potential than any of the zirconium compounds studied, except $(Me_3SiCp)_2ZrMe_2$, yet it exchanges more slowly. This may be associated with a higher Hf—CH_3 bond energy noted above. In qualitative agreement with this, we find that the asymmetrical and symmetrical M—CH_3 stretching frequencies in Cp_2MMe_2 are 462 and 422 cm^{-1}, respectively (M = Zr); and 470 and 441 cm^{-1} (M = Hf), cf. Table 3.

Table 3. Gas phase appearance potentials for $(P—CH_3)^+$ ions and metal–carbon stretching frequencies

Compound (precursor)	$\nu_{M—C}$ (as) (cm^{-1})	$\nu_{M—C}$ (s) (cm^{-1})	E_{app} (eV)
Cp_2ZrMe_2	462	422	8.5 ± 0.15
$(Me_5Cp)_2ZrMe_2$	458	427	8.0
$Me_2Si(C_5H_4)_2ZrMe_2$	458	Not resolved	8.1
$(indenyl)_2ZrMe_2$	464	439	8.1
$(Me_3SiCp)_2ZrMe_2$	462	Not resolved	6.9
Cp_2HfMe_2	470	441	6.9

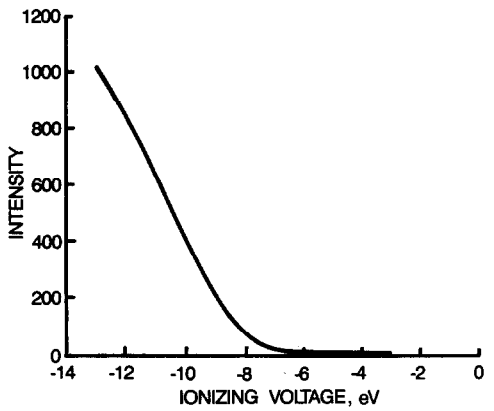

Fig. 1. Plot of integrated ion current of $(P-^{13}CH_3)^+$ from $(^{12}CH_3)_2Si(C_5H_4)_2Zr(^{13}CH_3)_2$ vs ionizing voltage.

What chemical and structural features of aluminium are needed to observe rapid methyl exchange? The issue of reactivity and solvation of Me_6Al_2 has been mentioned above. Aluminium compounds in which four-coordination is maintained by strong bridge bonds, e.g. $(Et_2AlOEt)_2$ and $\{[N(CH_2CH_2O)_3]Al_2Me_3\}_2$[19] are unreactive toward Cp_2ZrMe_2. In contrast, methyl exchange does occur in compounds in which aluminium participates in weak bridge bonds, e.g. $(Me_2AlCl)_2$ (Cp_2ZrCl_2 is produced) or where dissociation of an ancillary ligand is possible, e.g. $Me_2Al(BHT)\cdot PMe_3$.[8] We therefore suggest that three-coordinate aluminium acts as a methyl acceptor with Cp_2ZrMe_2 and its analogues.

Another way of assessing electronic effects, one that leads to the same general conclusions, is X-ray photoelectron spectroscopy (XPS).[10] Here, chloro- rather than methylzirconocenes were studied because the former are less volatile and less susceptible to air oxidation. We consider it probable that zirconium core levels in the two types of

compounds would parallel one another. The Zr($3d_{5/2}$, $3d_{3/2}$) binding energies in Cp_2ZrCl_2, $Me_2Si(C_5H_4)_2ZrCl_2$ and $(Me_3SiCp)_2ZrCl_2$ are 182.0, 184.4; 182.7, 185.1; and 181.8, 184.1 ± 0.1 eV, respectively. This is consistent with the NMR data which indicate that introduction of a Me_2Si bridge into Cp_2ZrCl_2 reduces electron density at the metal centre.[12] The electron-releasing effect of the Me_3Si group as assessed by XPS is almost insignificant. The Cl($2p_{3/2}$) binding energies in the same series of compounds, 199.0, 199.7 and 198.5 eV, parallel the zirconium core energies. Again, if electronic effects contributed significantly to activation energies for methyl exchange, it would be difficult to explain why $(Me_3SiCp)_2ZrMe_2$ exchanges as slowly as it does.

We have also investigated by NMR the reactions of Cp_2ZrMe_2 with other, potential, Group III acceptor compounds. No alkyl exchange is observed with Me_3Ga or Et_3B. Reasoning that substitution of alkyl by alkoxy on boron might increase methyl acceptor strength, Et_2BOMe was examined, but another reaction, methyl–methoxy exchange, eq. (3), supervenes. It is calculated to be exothermic by 44 kcal mol^{-1}.[18]

$$Cp_2ZrMe_2 + 2Et_2BOMe \rightarrow Cp_2Zr(OMe)_2 + 2Et_2BMe. \quad (3)$$

The product Et_2BMe may be recognized by its ^{11}B chemical shift, 86 ppm;[20] $Cp_2Zr(OMe)_2$[21] has $\delta^{13}C$ 61.3, 111.9 and $\delta^{91}Zr$ −447 ppm ($w/2$ 6500 Hz at 55°C). In neat Et_2BOMe, the kinetics of the above reaction are pseudo first-order in Cp_2ZrMe_2 and $k = 1.5 \times 10^{-4}$ min^{-1} at 22°C; $\Delta H^{\ddagger} = 15$ kcal mol^{-1} and $\Delta S^{\ddagger} = -33$ e.u. This exchange reaction involves as an intermediate $Cp_2Zr(OMe)Me$ which can be recognized by its NMR spectra: δ^1H 5.77, 3.65 (OMe), 0.23 (Zr—CH_3); $\delta^{13}C$ 111.9, 63.3 (OMe), 19.0 (Zr—Me); $\delta^{91}Zr$ −127 ($w/2$ 2500 Hz). Cleavage of B—O bonds by Cp_2ZrMe_2 appears to be a general reaction and also occurs with $(C_8H_{14}B)_2O$, $(MeBO)_3$ and $(CF_3SO_3)_3B$. It emerges that $Cp_2Zr(OMe)_2$ undergoes facile exchange of methoxy groups with Et_2BOMe. In neat Et_2BOMe, i.e. under pseudo-first order conditions, thermodynamic parameters determined by ^{13}C DNMR spectroscopy are $\Delta H^{\ddagger} = 7$ kcal mol^{-1} and $\Delta S^{\ddagger} = -21$ e.u.

Dimethylzirconium and -hafnium metallocenes are thus seen to undergo facile exchange of alkyl groups with methylaluminium reagents.[22] This exchange is general in that other (for example ethylaluminium) compounds may be used, but in this case the products are unstable because Cp_2ZrR_2, in which the R group has β-hydrogens, undergoes β-elimination to form olefin and numinous zirconium hydrides. A survey of the kinetics of degenerate methyl exchange reactions indicates that steric effects are important determinants of the free energy of activation relative to electronic effects. We suggest that, according to Hammond's postulate, the transition states in the endothermic equilibrium reactions of the type depicted in eq. (1) lie close along the reaction coordinate to the products. If we assume that a linear free energy relationship of the Brönsted type obtains (a reasonable postulate given the deliberately narrow structural range of the compounds studied), then the activation parameters for methyl exchange can provide insight into the effects of modification of the metallocene ligand set, as well as the choice of Lewis acid, on the position of the equilibrium depicted in eq. (1). This in turn may reflect the relative amounts of catalytically active metallocene cations formed in these systems.

EXPERIMENTAL

^1H, ^{11}B, ^{13}C and ^{91}Zr NMR spectra were recorded on a Varian XL-400 instrument, with a ^1H/multinuclear switchable probe, whose ^1H operating frequency is 400 MHz. External neat $BF_3 \cdot OEt_2$, $(CH_3)_4Si$ in $CDCl_3$ and 1 M Cp_2ZrBr_2 in THF were used as references with positive shifts being to lower field. Appearance potential measurements were made using a Nicolet model 2000 Fourier transform mass spectrometer and associated software. In some cases [$(Me_5Cp)_2ZrMe_2$, $Me_2Si(C_5H_4)_2ZrMe_2$] the Zr—$^{13}CH_3$ derivatives were used to ensure that ions actually derived from the loss of the Zr—Me group were observed. Integrals of the ^{90}Zr isotopomers were measured. Because no significant ion current at 1 mass unit lower was seen, one can be confident that the ions observed were not due to loss of $^{12}CH_3$ from the ^{91}Zr isotopomer. In the case of $(Me_5Cp)_2ZrMe_2$, the $(P-2CH_3)^+$ ion cluster appears to contain ions from loss of ring-methyl groups.

X-ray photoelectron spectra were obtained on a Surface Science Laboratories SSX-100-1 instrument using monochromatic Al-$K_{\alpha_{1,2}}$ radiation. For high resolution spectra, the concentric hemispherical analyser was operated at 25 eV pass energy. The binding energy scale is such that the Au($4f_{7/2}$) photoelectron line occurs at 83.96 ± 0.1 eV and the difference between the Cu($2p_{3/2}$) and 3s photoelectron lines is 810.0 ± 0.1 eV. The C(1s) spectra showed only one component and, for charge referencing purposes, it is assigned an energy of 285.0 eV.[23]

The solvents toluene and 1,2-dimethoxyethane,

and dichloromethane were distilled under nitrogen from Na–K alloy and CaH_2, respectively. Reactants were weighed in a nitrogen-filled dry-box and combined with the solvent in NMR tubes fitted with re-sealable Teflon Young valves (Brunfeldt Co., Bartlesville, Oklahoma). Temperatures were calibrated by substitution of methanol for the analytical sample and the temperature was determined from the data of van Geet.[24] In experiments with $MeAl(BHT)_2$ in toluene-d_8, the [Al]:[Zr] ratio used (10:1), is limited by the solubility of the aluminium reagent. The metallocene concentrations were 0.08 M. In experiments with Me_3Al, 0.5 cm^3 2 M Me_3Al in toluene, 0.1 cm^3 C_6D_6 (to provide a ^2H lock signal) and 0.05 mmol of the metallocene were combined. Thus, [Al]:[Zr] was 20:1 with [Zr] = 0.083. For work with $(MeAlO)_x$, [Al]:[Zr] was 15:1 with [Zr] = 0.11. Kinetic runs in CH_2Cl_2 utilized 0.5 cm^3 of this solvent plus 0.1 cm^3 C_6D_6 or 0.03 cm^3 toluene. ^{13}C DNMR spectra were obtained using a 5–10 s acquisition time (for maximum possible resolution), Waltz-modulated ^1H decoupling and the optimum pulse width for maximum signal:noise. The linewidth of (internal) toluene was taken as the natural linewidth due to field inhomogeneity. [Zr—CH_3] and [Al—CH_3] were determined by weighing the reactants. Slow methyl exchange was followed by recording ^{13}C spectra as a function of time with kinetics being measured directly from integrated spectra. Relaxation times and nuclear Overhauser enhancements (nOe) were measured on equilibrated samples. Single scan spectra were obtained with continuous low-power Waltz decoupling because the nOe was necessary for adequate signal:noise. The nOe corrections were not significant. For Cp_2ZrMe_2 and $(Me_5Cp)_2ZrMe_2$, the Zr—CH_3 nOe decreases from 2.9 at 22°C to 2.5 at 81°C. For $AlMe_3$, it decreases from 2.5 at 22°C to 1.9 at 70°C and from 2.6 to 2.5 over the same temperature range for $MeAl(BHT)_2$.

IR spectra were obtained on *ca* 1 M solutions of the organometallic compound in $CHCl_3$ (vacuum transferred from P_2O_5) on a Beckman 983 spectrometer. A 0.017 mm pathlength cell having KBr windows was employed. Assignment of M—CH_3 symmetric and asymmetric stretching bands was made by use of the M—$^{13}CH_3$ and M—CD_3 isotopomers.

$MeAl(BHT)_2$,[8] Et_2BOMe[25] and $(MeAlO)_x$[7a] were prepared by literature methods. In the synthesis of the latter, $MgCl_2 \cdot 6H_2O$ was used as the water-carrier. Residual Me_6Al_2 was removed at $\leqslant 40°C$ at $< 5 \times 10^{-6}$ mm. Cp_2ZrCl_2, $(Me_5Cp)_2ZrCl_2$, $Me_2Si(C_5H_4)_2ZrCl_2$[12] and $(indenyl)_2ZrCl_2$ were converted using the method of Samuel and Rausch[26] to the corresponding $Zr(^{13}CH_3)_2$ derivatives employing $^{13}CH_3Li$. We used an improved synthesis of $(C_9H_7)_2ZrCl_2$, described below.

Indenyllithium was prepared by the addition of 44 cm^3 2.5 M n-BuLi in hexane to 12.8 g redistilled indene in 100 cm^3 toluene at −78°C. The reaction mixture was stirred overnight as the cooling bath warmed up. The product was collected on a Schlenk filter, washed with hexane and vacuum dried. Yield 12.3 g (99%).

A mixture of 5.5 g C_9H_7Li (50 mmol), 5.8 g (25 mmol) $ZrCl_4$ and 100 cm^3 toluene was stirred for 2 h at room temperature and for 70 h at 90°C. This was then cooled to room temperature and filtered. The solids were *rapidly* washed with two 25 cm^3 portions of absolute ethanol, then with hexane and vacuum dried. Yield: 4.2 g (58%). It is important that the ethanol washing, which removes LiCl, is done rapidly, for otherwise the product dissolves and hydrolyses. $(C_9H_7)_2ZrCl_2$ in wet CH_3CN produces a quantitative yield of indene (^1H NMR analysis). Thus, $(C_9H_7)_2ZrCl_2$ *is* stable in organic solvents provided that they are dry.[27] (The method described in ref. 27 failed in our hands.)

$Me_2Si(C_5H_4)_2ZrMe_2$

$^{13}CH_3Li$ was prepared in diethyl ether under Ar from 2 g (14 mmol) $^{13}CH_3I$ and excess Li wire (1% Na). Ether was removed by pumping in a high vacuum line. Toluene (50 cm^3) and 1.74 g $Me_2Si(C_5H_4)_2ZrCl_2$ (5 mmol) were added. The reaction mixture was stirred for 24 h at room temperature then filtered. The filtrate was evaporated and the residue sublimed (100°C/10^{-3} mm) onto a 20°C probe. The yield of resublimed product was 0.72 g (47%). Yields using diethyl ether solvent were inferior. This is due to cleavage of the Me_2Si bridge, because when the reaction is quenched with Me_3SiCl, $(Me_3SiCp)_2ZrMe_2$ is also formed.

$(Me_3SiCp)_2ZrCl_2$[28]

Me_3SiCl (purified by fractional distillation on a vacuum line to remove HCl) (6.54 g, 60 mmol) in 20 cm^3 THF was added slowly to 60 mmol NaCp in 90 cm^3 THF at −78°C. The reaction mixture was warmed to room temperature then recooled to −78°C. n-BuLi (24 cm^3 2.5 M in hexane) was added dropwise. After stirring for 30 min at room temperature, the temperature was reduced to 0°C and $ZrCl_4$ (7 g, 30 mmol) in 40 cm^3 1,2-dimethoxyethane added dropwise. After stirring overnight, solvents were removed *in vacuo*. The residue was extracted with hexane in a Soxhlet apparatus. The extracts were concentrated to 50 cm^3 and filtered to give 9.2 g crude product. Recrystallization from boiling

methylcyclohexane yielded 6.2 g (48%) pure product. Found: C, 43.7; H, 5.9. Calc. C, 44.0; H, 6.0%. Mass spectrum (11 eV): 436 (P^+), 421 ($P-Cl^+$).

New NMR data for zirconium metallocenes are listed below: $Me_2Si(C_5H_4)_2ZrMe_2$: ^1H: 0.17 ($SiCH_3$), 0.14 ($ZrCH_3$), 5.39 (m), 6.65 (m). ^{13}C: 120.9, 112.5 (Cp), 101.3 (C_{ipso}), 30.0 (Zr—CH_3), −5.30 (Si—CH_3). ^{91}Zr: 440 ($w/2$ 8100 Hz) (toluene-d_8). $(C_9H_7)_2ZrCl_2$: ^{13}C: 127.3 ($C_{3a,7a}$), 126.7, 125.6 ($C_{4,6}$), 122.2 (C_2), 104.4 ($C_{1,3}$) (CD_2Cl_2). $(C_9H_7)_2ZrMe_2$: ^{13}C: 125.1 ($C_{4,7}$), 124.5 ($C_{5,6}$), 124.2 ($C_{3a,7a}$), 115.0 (C_2), 100.0 ($C_{1,3}$), 35.8 ($ZrCH_3$). ^{91}Zr: 500 ($w/2$ 2500 Hz) (toluene-d_8). $(Me_3SiCp)_2ZrCl_2$: ^1H: 6.39, 5.94 (Cp), 0.32 ($SiCH_3$). ^{13}C: 126.3 (C_{ipso}), 126.0, 115.3 (Cp), 0.06 ($SiCH_3$). ^{91}Zr: −85 ($w/2 \cdot 1300$ Hz) (C_6D_6). $(Me_3SiCp)_2ZrMe_2$: ^1H: 6.07, 5.93 (Cp), 0.18 ($SiCH_3$), −0.16 ($ZrCH_3$). ^{13}C: 119.3 (C_{ipso}), 118.2, 113.5 (Cp), 31.0 ($ZrCH_3$), 0.36 ($SiCH_3$). ^{91}Zr: 420 ($w/2$ 3600 Hz) (toluene-d_8).

Acknowledgements—We are grateful to members of the 3M Analytical and Properties Research Laboratory for physical data, John Babin for the IR spectra, Dr G. A. Korba for the XPS data and to Dr G. V. D. Tiers for helpful discussions.

REFERENCES

1. (a) R. F. Jordan, *J. Chem. Ed.* 1988, **65**, 295; (b) R. F. Jordan, C. S. Bajgur, R. Willett and B. Scott, *J. Am. Chem. Soc.* 1986, **108**, 7410; (c) R. F. Jordan, R. E. LaPointe, C. S. Bajgur, S. F. Echols and R. Willett, *J. Am. Chem. Soc.* 1987, **109**, 4111; (d) R. F. Jordan and S. F. Echols, *Inorg. Chem.* 1987, **26**, 383; (e) R. F. Jordan, C. S. Bajgur, W. E. Dasher and A. L. Rheingold, *Organometallics* 1987, **6**, 1041; (f) R. F. Jordan, W. E. Dasher and S. F. Echols, *J. Am. Chem. Soc.* 1986, **108**, 1718; (g) A. R. Siedle, R. A. Newmark and W. B. Gleason, submitted for publication.
2. P. G. Gassman and M. R. Callstrom, *J. Am. Chem. Soc.* 1987, **109**, 7875.
3. C. S. Christ and D. E. Richardson, *J. Am. Chem. Soc.* 1988, **110**, 4038.
4. (a) M. Brookhart, M. L. H. Green and L.-L. Wong, *Prog. Inorg. Chem.* 1988, **36**, 1; (b) cf. $(Me_5Cp)_2ScR$: M. E. Thompson, S. M. Baxler, A. Bulls, B. J. Burger, M. C. Nolan, B. D. Santarsiero, W. P. Shafer and J. E. Bercaw, *J. Am. Chem. Soc.* 1987, **109**, 203.
5. A. R. Siedle and R. A. Newmark, submitted.
6. J. J. Eisch, *Comprehensive Organometallic Chemistry* (Edited by G. Wilkinson, F. G. A. Stone and E. W. Abel), Vol. 1, p. 593. Pergamon Press, New York (1982).
7. (a) W. Kaminsky and H. Hahnsen, U.S. Pat. 4,544,762; (b) W. Kaminsky and M. Miri, *J. Polym. Sci. Polym. Chem. Ed.* 1985, **23**, 2151; (c) W. Kaminsky, K. Kulper, H.-H. Brintzinger and F. R. W. P. Wild, *Angew. Chem. Int. Ed.* 1985, **24**, 507; (d) H. Sinn and W. Kaminsky, *Angew. Chem. Int. Ed.* 1985, **19**, 390.
8. M. D. Healey, D. A. Wierda and A. R. Barron, *Organometallics* 1988, **7**, 2543.
9. A. R. Siedle and R. A. Newmark, manuscript in preparation.
10. P. G. Gassman, D. W. Macomber and J. W. Hershberger, *Organometallics* 1983, **2**, 1470.
11. (a) This is supported by the much greater reactivity of $(C_9H_7)_2ZrCl_2$ towards water (but not aqueous HCl) than Cp_2ZrCl_2; (b) J. W. Faller, R. H. Crabtree and A. H. Habib, *Organometallics* 1985, **4**, 929; (c) J. L. Atwood, W. E. Hunter, D. C. Hrncir, E. Samuel, H. Alt and M. D. Rausch, *Inorg. Chem.* 1975, **14**, 1757.
12. C. S. Bajgur, W. R. Tikkanen and J. L. Peterson, *Inorg. Chem.* 1985, **24**, 2539.
13. C. M. Fendrick, L. D. Schertz, V. W. Day and T. J. Marks, *Organometallics* 1988, **7**, 1828.
14. W. E. Hunter, D. C. Hrncir, R. V. Bynum, R. A. Pentilla and J. L. Atwood, *Organometallics* 1983, **2**, 750.
15. S. Pasynkiewicz, M. Boleslawski and A. Sadowik, *J. Organomet. Chem.* 1976, **113**, 303.
16. J. Hine, *Physical Organic Chemistry*, p. 48. McGraw-Hill, New York (1956).
17. (a) R. J. Kulawiec and R. H. Crabtree, *Organometallics* 1988, **7**, 1891 and refs cited therein; (b) T. D. Newbound, M. R. Colsman, M. M. Miller, G. P. Wulfsberg, O. P. Anderson and S. H. Strauss, *J. Am. Chem. Soc.* 1989, **111**, 3762; (c) An extreme example is the reaction of CH_2Cl_2 with SbF_5 which produces $[(ClCH_2)_2\text{-}\mu\text{-}Cl][Sb_2F_{10}Cl]$. G. A. Olah, A. Wu and O. Farooq, *J. Org. Chem.* 1989, **54**, 1463.
18. Calculated using the following bond dissociation energies (kcal mol^{-1}): B—CH_3 = 132 [E. L. Muetterties, *The Chemistry of Boron and Its Compounds*, p. 13. Wiley, New York]; B—OCH_3 = 118 [D. C. Bradley, R. C. Mehrotra and D. P. Gaur, *Metal Alkoxides*, p. 54. Academic Press, New York (1978); Zr—CH_3 = 74 and Zr—OCH_3 = 132 [M. F. Lappert, D. S. Patil and J. B. Pedley, *J. Chem. Soc., Chem. Commun.* 1975, 830].
19. M. D. Healy and A. R. Barron, *J. Am. Chem. Soc.* 1989, **111**, 398.
20. E. J. Stampf and J. Odom, *J. Organomet. Chem.* 1977, **131**, 171.
21. D. R. Gray and C. H. Brubaker Jr, *Inorg. Chem.* 1971, **10**, 2143.
22. Simple exchange of alkyl groups between zirconium and aluminium has apparently not been reported. Exchange of Zr—Cl and Al—C_2H_5 is known, cf. H. Sinn and G. Opperman, *Angew. Chem. Int. Ed.* 1966, **5**, 962 and W. Kaminsky and H.-J. Vollmer, *Ann. Chem.* 1975, 438. In contrast, benzyl exchange has been reported not to occur on the NMR time scale in the *red* 1:1 complex of $(PhCH_2)_4Zr$ and $(PhCH_2)_3Al$: U. Zucchini, E. Albizzati and U. Giannini, *J. Organomet. Chem.* 1971, **26**, 357.

23. A. R. Siedle, R. A. Newmark, G. A. Korba, L. H. Pignolet and P. D. Boyle, *Inorg. Chem.* 1988, **27**, 1593.
24. A. L. van Geet, *Analyt. Chem.* 1971, **43**, 679.
25. W. Fenzel and R. Koster, *Inorg. Synth.* 1983, **22**, 190.
26. E. Samuel and M. D. Rausch, *J. Am. Chem. Soc.* 1973, **95**, 6263.
27. E. Samuel, *J. Organomet. Chem.* 1965, **4**, 156.
28. M. F. Lappert, C. J. Pickett, P. I. Riley and P. I. W. Yarrow, *J. Chem. Soc., Dalton Trans.* 1981, 805.

Polyhedron Vol. 9, No. 2/3, pp. 309–312, 1990
Printed in Great Britain

0277–5387/90 $3.00 + .00
© 1990 Pergamon Press plc

REDUCTION OF SUGARS WITH ALUMINIUM ALKYLS. PREPARATION AND STRUCTURE OF $[AlCl_2(NC_5H_5)(OEt)]_2(\mu\text{-}O)(\mu\text{-}AlCl\cdot 2NC_5H_5)$

C. MITCHELL MEANS, SIMON G. BOTT and JERRY L. ATWOOD*

Department of Chemistry, University of Alabama, Tuscaloosa, AL 35487–0336, U.S.A.

Abstract—Reaction of ethylaluminium dichloride with glucose in a 10% pyridine solution in toluene leads to the unique compound $[AlCl_2(NC_5H_5)(OEt)]_2(\mu\text{-}O)(\mu\text{-}AlCl\cdot 2NC_5H_5)$, formed through "fermentation" of the sugar and exchange reactions of the aluminium species. This product, which contains two five- and one six-coordinate aluminium, crystallizes in the monoclinic space group $C2/c$ with $a = 16.253(8)$, $b = 11.832(5)$, $c = 16.94(2)$ Å, $\beta = 94.35(9)°$. Full-matrix least-squares refinement using 1640 reflections led to $R = 0.051$. The Al—O bond lengths range from 1.782(2) to 1.891(3) Å, the Al—N lengths from 2.094(4) to 2.132(4) Å and the Al—Cl lengths from 2.188(3) to 2.240(3) Å.

Aluminium alkyls have long been used in the reduction of both organic and inorganic species.[1] However, presumably because of solubility problems, their interaction with sugars has not been extensively investigated.[2] As part of a general programme on the generation of chiral aluminium-containing species with special aromatic solution properties,[3] we have begun a detailed study of the reaction of a range of aluminium alkyls and aluminium alkyl halides with sugars. We report here the unexpected result of the reaction of ethylaluminium chloride ($EtAlCl_2$) with glucose in a toluene solution to which a small amount of pyridine was added.

EXPERIMENTAL

Synthesis of $[AlCl_2(NC_5H_5)(OEt)]_2(\mu\text{-}O)(\mu\text{-}AlCl\cdot 2NC_5H_5)$

$EtAlCl_2$ (0.06 mol) was added to a slurry of $C_6H_{12}O_6$ (0.01 mol) in 100 cm^3 of a 10% pyridine/toluene mixture. This was carried out in a screw-top tube, which was heated to 100°C for 2 days. Colourless crystals of the title compound were obtained in *ca* 10% yield.

X-ray structure determination of $[AlCl_2(NC_5H_5)(OEt)]_2(\mu\text{-}O)(\mu\text{-}AlCl\cdot 2NC_5H_5)$

A single, colourless crystal was mounted in a thin-walled glass capillary. Final lattice parameters as determined from the least-squares refinement of $(\sin\theta/\lambda)^2$ values for 24 reflections ($2\theta > 25°$) accurately centred on an Enraf–Nonius CAD-4 diffractometer are given in Table 1. Data were collected by the θ–2θ scan technique described previously.[4] A summary of data collection and structure solution parameters is also given in Table 1. The intensities were corrected for Lorentz and polarization effects, but not for absorption. Calculations were carried out using the SHELX system of computer programs.[5] Neutral atom scattering factors were taken from ref. 6 and the scattering for the aluminium and chlorine atoms was corrected for the real and imaginary components of anomalous dispersion.[6]

Structure solution was accomplished initially by application of the direct methods program MULTAN,[7] which revealed the positions of most of the non-hydrogen atoms. Difference Fourier maps phased upon these atoms readily afforded the positions of the remaining atoms. Treatment of all atoms with anisotropic thermal parameters enabled the location of all the hydrogen atoms from a further difference map. These were constrained to "ride" upon the appropriate carbon atom. Further refinement converged at reliability values of $R = \Sigma(|F_o| - |F_c|)/\Sigma(F_o) = 0.051$ and $R_w = \{\Sigma w(|F_o| - |F_c|)^2/\Sigma w(F_o)^2\}^{1/2} = 0.051$. A final difference Fourier showed no feature greater than 0.2 e/Å^3. The weighting scheme was based upon unit weights and no systematic variation of $w(|F_o| - |F_c|)$ vs $|F_o|$ or $\sin(\theta/\lambda)$ was noted. Further structural details have been deposited.

* Author to whom correspondence should be addressed.

Table 1. Crystal data for $[AlCl_2(NC_5H_5)(OEt)]_2(\mu\text{-}O)(\mu\text{-}AlCl\cdot 2NC_5H_5)$

Compound	$C_{24}H_{30}Cl_5N_4O_3Al_3$
Molecular weight	680.77
Space group	*C*2/*c*
Cell constants:	
a (Å)	16.253(8)
b (Å)	11.832(5)
c (Å)	16.94(2)
β (°)	94.35(9)
Cell volume (Å^3)	3249
Molecules per unit cell	4
ρ (calc) (g cm^{-3})	1.40
μ (cm^{-1})	5.63
Radiation	Mo-K_α (graphite-monochromated)
Crystal dimensions (mm)	$0.52\times0.43\times0.38$
Scan width (°)	$0.8+0.2\tan\theta$
Standard reflections	200, 020, 002
Crystal decay	< 1%
Reflections measured	2232
2θ range (°)	2–44
Observed reflections [$I > 2.5\sigma(I)$]	1640
Number of least-squares parameters	178
Goodness-of-fit	1.77
R	0.051
R_w	0.051

DISCUSSION

From the Experimental it is clear that the reaction of glucose with $EtAlCl_2$ in the presence of pyridine affords the title compound. The sequence of reactions which accomplishes this is not understood. However, it is interesting to view the product as the result of reaction (1):

$$2EtAlCl_2 + Et_2AlCl + 2EtOH + H_2O + 4NC_5H_5 \longrightarrow 4C_2H_6 + [AlCl_2(NC_5H_5)(OEt)]_2(\mu\text{-}O)(\mu\text{-}AlCl\cdot 2NC_5H_5). \quad (1)$$

The presence of species such as Et_2AlCl in $EtAlCl_2$ is well known,[8] and the reduction of glucose to ethanol and water is simply the fermentation process. Thus, the above reaction serves to indicate that the components of the title compound could be generated from the reactants. We are currently attempting to generate $[AlCl_2(NC_5H_5)(OEt)]_2(\mu\text{-}O)(\mu\text{-}AlCl\cdot 2NC_5H_5)$ directly as in reaction (1).

The structure, shown in Fig. 1, lies on a crystallographically-imposed two-fold rotation axis and contains a planar $(Al—O)_3$ ring in which two four-membered $(Al—O)_2$ rings share an Al—O bond. To our knowledge, this is the first example of this aluminium–oxygen framework. Important bond lengths and angles are given in Table 2.

The coordination of Al(1) is distorted octahedral with the major deviation being the O(2)—Al(1)—O(2)′ angle of 155.7(1)° imposed by the Al(2)—O(2) coordination. The two *trans*-pyridine rings are tilted slightly in the direction of Cl(1) [N(1)—Al(1)—N(1)′ angle, 173.5(1)°], presumably due to C(1)—H···O(ring) contacts. The Al(1)—Cl(1) bond distance, 2.240(3) Å, is long for a terminal Al—Cl bond (cf. the Al—Cl distances in the seven-coordinate $[AlCl_2\cdot$benzo-15-Crown-5$]^+$ cation are 2.197(7) and 2.202(5) Å[9]) presumably due to the strong *trans*-influence of the μ-oxo ligand. Indeed, the value in the title compound is near the short end of the range of Al—Cl(bridging) lengths in the six-coordinate aluminium atom of $(Me_2AlCl)_2(Al\cdot C_{10}H_{20}N_4)(AlMe_2)$.[10] The Al(1)—O(1) distance of 1.890(5) Å falls in the range found by Healy and Barron for six-coordinate aluminium, 1.837(8) and 1.982(9) Å,[11] and the Al(1)—N(1) length, 2.132(4) Å, is longer than those of 1.952(3) and 1.981(3) Å in the above-mentioned cyclam complex.[10]

The coordination of Al(2) is slightly distorted trigonal bipyramidal. The largest deviation is the 167.3(2)° N(2)—Al(2)—O(2) angle which is produced by the constraint of the bond between Al(1) and O(2). The Al(2)—O(2) distance of 1.891(3) Å is well within the normal range of Al—O lengths,[12] whereas the Al(2)—O(1) (1.782(2) Å) distance is at

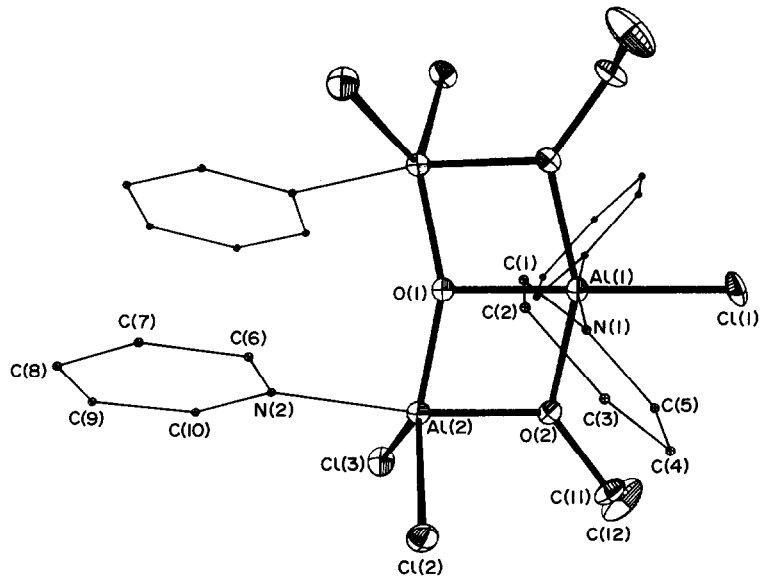

Fig. 1. Molecular structure of $[AlCl_2(NC_5H_5)(OEt)]_2(\mu\text{-}O)(\mu\text{-}AlCl\cdot 2NC_5H_5)$. Pyridine rings are shown as points and hydrogen atoms are omitted for clarity.

Table 2. Selected bond lengths (Å) and angles (°) for $[AlCl_2(NC_5H_5)(OEt)]_2(\mu\text{-}O)(\mu\text{-}AlCl\cdot 2NC_5H_5)$

Bond lengths			
Al(1)—Cl(1)	2.240(3)	Al(1)—O(1)	1.890(5)
Al(1)—O(2)	1.866(3)	Al(1)—N(1)	2.132(4)
Al(2)—Cl(2)	2.198(2)	Al(2)—Cl(3)	2.188(3)
Al(2)—O(1)	1.782(2)	Al(2)—O(2)	1.891(3)
Al(2)—N(2)	2.094(4)		
Bond angles			
Cl(1)—Al(1)—O(1)	180	Cl(1)—Al(1)—O(2)	102.2(1)
Cl(1)—Al(1)—N(1)	86.7(1)	O(1)—Al(1)—O(2)	77.9(1)
O(1)—Al(1)—N(1)	93.3(1)	O(2)—Al(1)—O(2)′	155.7(1)
O(2)—Al(1)—N(1)	90.0(1)	N(1)—Al(1)—N(1)′	173.5(1)
Cl(2)—Al(2)—Cl(3)	111.82(9)	Cl(2)—Al(2)—O(1)	130.32(9)
Cl(2)—Al(2)—O(2)	93.5(1)	Cl(2)—Al(2)—N(2)	85.8(1)
Cl(3)—Al(2)—O(1)	117.85(9)	Cl(3)—Al(2)—O(2)	98.4(1)
Cl(3)—Al(2)—N(2)	93.7(1)	O(1)—Al(2)—O(2)	79.9(2)
O(1)—Al(2)—N(2)	90.9(2)	O(2)—Al(2)—N(2)	167.3(2)
Al(1)—O(1)—Al(2)	101.1(1)	Al(2)—O(1)—Al(2)′	157.7(2)
Al(1)—O(2)—Al(2)	98.1(2)		

the short end of the range (cf. 1.679(2) Å in (μ-oxo)bisphthalocyaninatoaluminium(III) in which there is substantial multiple bond character[13]). The Al—O lengths can be profitably compared with that of 1.772(4) Å for four-coordinate aluminium and 2.174(4) Å for five-coordinate aluminium found by Robinson *et al.*[14] The Al(2)—N(2) distance, 2.094(4) Å, is at the long end of the range for four-coordinate aluminium[15] and may be compared to 2.055(2) and 2.135(2) Å in $(AlMe)(C_8H_{19}N_4)(AlMe_2)$[16] and 1.976(9) and 2.04(1) Å in $(AlMe)_2(C_8H_{20}N_6)(AlMe_2)_2$.[17] Thus, while coordination number is an important consideration in determining bond length, there are other important factors which are discussed in detail elsewhere.[18]

Further work examining both this reaction and those of aluminium species with other carbohydrates is in progress.

REFERENCES

1. T. Mole and E. A. Jeffrey, *Organoaluminium Compounds*. Elsevier, Amsterdam (1972).

2. A. Liptak and Z. Szurmani, *Magy. Kém. Lap.* 1987, **41**, 220.
3. J. L. Atwood, in *Inclusion Compounds* (Edited by J. L. Atwood, J. E. D. Davies and D. D. MacNicol), Vol. 1, Chap. 9. Academic Press, New York (1984).
4. J. Holton, M. F. Lappert, D. G. H. Ballard, R. Pearce, J. L. Atwood and W. E. Hunter, *J. Chem. Soc., Dalton Trans.* 1979, 45.
5. G. M. Sheldrick, SHELX, a system of computer programs for X-ray Structure Determination (1976).
6. *International Tables for X-ray Crystallography*, Vol. IV. Kynoch Press, Birmingham (1974).
7. G. Germain, P. Main and M. M. Woolfson, *Acta Cryst.* 1971, **A27**, 368.
8. G. H. Robinson and S. A. Sangokoya, *Organometallics* 1988, **7**, 1453.
9. S. G. Bott, H. Elgemal and J. L. Atwood, *J. Am. Chem. Soc.* 1985, **107**, 1796.
10. G. H. Robinson, M. R. Self, S. A. Sangokoya and W. T. Pennington, *J. Am. Chem. Soc.* 1989, **111**, 1520.
11. M. D. Healy and A. R. Barron, *J. Am. Chem. Soc.* 1989, **111**, 398.
12. M. J. Zaworotko, C. R. Kerr and J. L. Atwood, *Organometallics* 1985, **4**, 238.
13. K. Wynne, *Inorg. Chem.* 1985, **24**, 1339.
14. G. H. Robinson, B. Lee, W. T. Pennington and S. A. Sangokoya, *J. Am. Chem. Soc.* 1988, **110**, 6260.
15. G. H. Robinson, E. S. Appel, S. A. Sangokoya, H. Zhang and J. L. Atwood, *J. Coord. Chem.* 1988, **17A**, 373; G. H. Robinson, F. Moise, W. T. Pennington and S. A. Sangokoya, *J. Cryst. Spectrosc. Res.* 1988, **18**, 387; G. H. Robinson, H. Zhang and J. L. Atwood, *J. Organomet. Chem.* 1987, **331**, 153.
16. G. H. Robinson, S. A. Sangokoya, F. Moise and W. T. Pennington, *Organometallics* 1988, **7**, 1887.
17. G. H. Robinson and S. A. Sangokoya, *J. Am. Chem. Soc.* 1987, **109**, 6852.
18. S. G. Bott and J. L. Atwood, *J. Coord. Chem., Sect. B*, submitted for publication.

Polyhedron Vol. 9, No. 2/3, pp. 313–318, 1990
Printed in Great Britain

0277–5387/90 $3.00+.00
© 1990 Pergamon Press plc

REACTION OF TRIMETHYLALUMINIUM WITH SULPHUR DERIVATIVES OF BIS(DIPHENYLPHOSPHINO)METHANE AND BIS(DIPHENYLPHOSPHINO)ETHANE. SYNTHESIS AND MOLECULAR STRUCTURE OF $[Al(CH_3)_2][(C_6H_5)_2P(S)CHP(S)(C_6H_5)_2][Al(CH_3)_3]$ AND $[Al(CH_3)_3]_2[(C_6H_5)_2P(S)CH_2CH_2P(S)(C_6H_5)_2]$

MARK F. SELF, BAOSHENG LEE, SAMUEL A. SANGOKOYA,*
WILLIAM T. PENNINGTON and GREGORY H. ROBINSON†

Department of Chemistry, Clemson University, Clemson, SC 29634-1905, U.S.A.

Abstract—Reaction of trimethylaluminium with bis(diphenylthiophosphinoyl)methane and bis(diphenylthiophosphinoyl)ethane affords the crystalline compounds $[Al(CH_3)_2][(C_6H_5)_2P(S)CHP(S)(C_6H_5)_2][Al(CH_3)_3]$ (**I**) and $[Al(CH_3)_3]_2[(C_6H_5)_2P(S)CH_2CH_2P(S)(C_6H_5)_2]$ (**II**), respectively. Compound **I** crystallizes in the monoclinic space group $P2_1/n$ (No. 14) with unit cell parameters $a = 18.126(2)$, $b = 9.569(2)$, $c = 19.394(3)$ Å, $\beta = 110.20(1)°$, $V = 3156.7(7)$ Å^3, and $\rho = 1.21$ g cm^{-3} for $Z = 4$. Least-squares refinement based on 2891 observed reflections $[I > 3\sigma(I)]$ converged at $R = 0.040$, $R_w = 0.051$. Compound **II** crystallizes in the triclinic space group $P\bar{1}$ (No. 2) with unit cell parameters $a = 12.076(3)$, $b = 13.148(3)$, $c = 13.114(3)$ Å, $\alpha = 98.32(2)$, $\beta = 100.55(2)$, $\gamma = 116.41(2)°$, $V = 1772.1(7)$ Å^3, and $\rho = 1.14$ g cm^{-3} for $Z = 2$. Least-squares refinement based on 3012 observed reflections $[I > 3\sigma(I)]$ converged at $R = 0.049$, $R_w = 0.056$. Compound **I** results from a unique condensation reaction in which one of the central methylene C—H bonds was cleaved in addition to one Al—CH_3 bond, resulting in an unusual Al—P—S—C four-membered ring. The length of the hydrocarbon chain in bidentate phosphine ligands appears to play an important role in their reactivity with organoaluminium species, as reaction of bis(diphenylthiophosphinoyl)ethane with trimethylaluminium did not facilitate condensation, but resulted in an addition compound, **II**. These results demonstrate a comparatively greater acidity of the hydrocarbon chain hydrogen atoms of bis(diphenylthiophosphinoyl)methane relative to bis(diphenylthiophosphinoyl)ethane.

The ability of bidentate phosphine ligands to facilitate unique behaviour in bimetallic systems has recently generated considerable activity in organo-transition metal chemistry.[1–5] The organo-main group chemistry in general, and organoaluminium chemistry in particular, of bidentate phosphine ligands has not developed in parallel with that of the transition metals. Although the bidentate phosphine ligand bis(diphenylphosphino)methane has been shown to play a role in a few organoaluminium catalytic systems,[6–8] the organoaluminium chemistry of the sulphur derivatives of bis(diphenylphosphino)methane and bis(diphenylphosphino)ethane remains largely unexplored. Herein we report the synthesis and molecular structure of $[Al(CH_3)_2][(C_6H_5)_2P(S)CHP(S)(C_6H_5)_2][Al(CH_3)_3]$ (**I**) and $[Al(CH_3)_3]_2[(C_6H_5)_2P(S)CH_2CH_2P(S)(C_6H_5)_2]$ (**II**). Both compounds were isolated from reaction of trimethylaluminium with bis(diphenylthiophosphinoyl)methane and bis(diphenylthiophosphinoyl)ethane, respectively. Compound **I** is interesting in that it results from a unique condensation reaction in which one of the central methylene C—H bonds and one Al—CH_3 bond were cleaved resulting in an Al—S—P—C four-membered ring. The length of the hydrocarbon chain in bidentate phosphine ligands appears to affect such reactivity, in that condensation was not observed in compound **II** as only the addition product was isolated.

* Present address: Ethyl Corporation, Ethyl Technical Center, Baton Rouge, LA 70820, U.S.A.

† Author to whom correspondence should be addressed.

EXPERIMENTAL

Synthesis

Standard Schlenk techniques were employed in conjunction with an inert atmosphere dry box (Vacuum Atmospheres HE-43 DriLab). Trimethylaluminium, generously donated by the Ethyl Corporation, was used as received. Both phosphine ligands were prepared in our laboratory. Single crystal X-ray data were collected on a Nicolet R3m/V diffractometer. ^{1}H NMR data were recorded on a JEOL-FX90Q NMR spectrometer. Solid state ^{31}P NMR were recorded on an IBM 200 MHz spectrometer. Solvents were purified and degassed in the usual manner.

(1) $[Al(CH_3)_2][(C_6H_5)_2P(S)CHP(S)(C_6H_5)_2][Al(CH_3)_3]$ (I)

Inside the dry box a reaction vessel was charged with bis(diphenylthiophosphinoyl)methane (0.50 g, 1.1 mmol) and heptane (15 cm^3). Trimethylaluminium (0.25 cm^3, 2.2 mmol) was slowly added to the white suspension. Reaction was immediate and quite vigorous resulting in a clear colourless solution. The reaction vessel was subsequently removed from the dry box and heated in an oil bath (120°C) for 24 h. Upon cooling to room temperature, a multitude of colourless, rectangular, extremely air-sensitive crystals formed (80% based on the phosphine ligand). M.p. = 162–163°C. ^{1}H NMR ($CDCl_3$, $Si(CH_4)$ external reference): δ −0.65 (s, 15H, $Al(CH_3)_2/Al(CH_3)_3$); 1.93 (s, 1H, P—C*H*—P), 7.51 (m, 20H, C_6H_5). ^{31}P {^{1}H} NMR ($CDCl_3$, H_3PO_4 external reference): δ 34.2 (s). ^{31}P NMR (solid state) (Na_2HPO_4 external standard): δ 25.03 (s, $P(S)Al(CH_3)_2$); 36.01 (s, $P(S)Al(CH_3)_3$).

(2) $[Al(CH_3)_3]_2[(C_6H_5)_2P(S)CH_2CH_2P(S)(C_6H_5)_2]$ (II)

A reaction vessel was charged with trimethylaluminium (0.20 cm^3, 2.2 mmol), bis(diphenylthiosphosphinoyl)ethane (0.5 g, 1.1 mmol) and a toluene–heptane mixture (15 cm^3 : 15 cm^3) inside the dry box. The reaction tube was removed from the dry box and heated in an oil bath (120°C) for 24 h. Upon cooling to 0°C, a multitude of small, colourless, rectangular, air-sensitive, X-ray quality crystals resulted in quantitative yield (based on the phosphine ligand). M.p. = 133–135°C. ^{1}H NMR ($CDCl_3$): δ −0.92 (s, 18H, $Al(CH_3)_3$), 2.77 (d, 4H, P—(CH_2)$_2$—P, J_{P-CH} = 2.2 Hz), 7.59 (m, 20H, C_6H_5). ^{31}P {^{1}H} NMR ($CDCl_3$): δ 45.13 (s, 2P, P(S)).

X-ray structural solution and refinement for $[Al(CH_3)_2][(C_6H_5)_2P(S)CHP(S)(C_6H_5)_2][Al(CH_3)_3]$ (I)

A colourless parallelepiped crystal of **I** was mounted in a thin-walled glass capillary under an inert atmosphere of argon. Cell constants and an orientation matrix for data collection, obtained from a least-squares refinement of the setting angles of 42 carefully centred reflections in the range $25.29 < 2\theta < 37.13°$, corresponded to a monoclinic cell. The space group was determined to be $P2_1/n$ (No. 14). The structure was solved by direct methods using SHELXTL PLUS.[9] Non-hydrogen atoms were refined anisotropically and hydrogen atoms were refined isotropically. The weighting scheme was based on counting statistics and included a factor ($p = 0.0005$) to downweight the intense reflections. The maximum and minimum peaks on the final difference map corresponded to 0.20 and −0.19 e$^-$ Å^{-3}, respectively. Refinement converged at $R = 0.040$, $R_w = 0.051$. Relevant crystallographic data is given in Table 1. The X-ray crystal structure of **I** is given in Fig. 1.

X-ray structural solution and refinement for $[Al(CH_3)_3]_2[(C_6H_5)_2P(S)CH_2CH_2P(S)(C_6H_5)_2]$ (II)

A single crystalline sample of **II** was prepared for X-ray examination in the same manner as employed for **I**. Cell constants and an orientation matrix for data collection, obtained from a least-squares refinement of the setting angles of 35 carefully centred reflections in the range $24.48 < 2\theta < 34.60°$, afforded a triclinic cell. The compound crystallized in the triclinic $P\bar{1}$ (No. 2), with two molecules per unit cell. The asymmetric unit consists of two half-molecules situated about inversion centres at ($x = 0.5$, $y = 1.0$, $z = 0.5$) and ($x = 0.5$, $y = 1.0$, $z = 0.0$), respectively. The main difference in the conformation of the two unique molecules involves the orientation of the phenyl rings, as defined by the dihedral angles between their planes, 90.1° for molecule 1 and 84.8° for molecule 2. No uncharacteristically short intermolecular contacts or unusual packing interactions were observed. The structure was solved by direct methods using SHELXTL PLUS.[9] Non-hydrogen atoms were refined using anisotropic thermal parameters. Hydrogen atoms were located by standard difference Fourier techniques, and were included in the structure factor calculation at idealized positions (d_{C-H} = 0.96 Å). An isotropic group thermal parameter [U_{iso} = 0.124(4)] was refined for the hydrogen atoms. The final cycle of full-matrix least-squares refinement, based on 3012 observed reflections [$I > 3\sigma I$)], converged at $R = 0.049$,

Table 1. Crystallographic data for $[Al(CH_3)_2][(C_6H_5)_2P(S)CHP(S)(C_6H_5)_2][Al(CH_3)_3]$ (I) and $[Al(CH_3)_3]_2[(C_6H_5)_2P(S)CH_2CH_2P(S)(C_6H_5)_2]$ (II)

	(I)	(II)
Formula	$Al_2P_2S_2C_{30}H_{36}$	$Al_2P_2S_2C_{32}H_{42}$
Formula weight	576.68	606.76
Crystal system	Monoclinic	Triclinic
Space group	$P2_1/n$	$P\bar{1}$
a (Å)	18.126(2)	12.076(3)
b (Å)	9.569(2)	13.148(3)
c (Å)	19.394(3)	13.114(3)
α (°)		98.32(2)
β (°)	110.20(1)	100.55(2)
γ (°)		116.41(2)
Volume (Å^3)	3156.7(7)	1772.1(7)
Z	4	2
ρ	1.21	1.14
μ (cm^{-1})	3.33	3.00
Diffractometer	Nicolet $R3m/V$	
λ(Mo-K_α) (Å)	0.71073	
Temperature (°C)	21	
2θ limits (°)	3.50–45.0	
Reflections measured	4608 (4155 unique)	4892 (4648 unique)
Reflections observed	2891	3012
G.O.F.	1.20	1.24
R	0.040	0.049
R_w	0.051	0.056

$R_w = 0.056$. The maximum and minimum peaks on the final difference map corresponded to 0.27 and -0.22 e$^-$ Å^{-3}, respectively. A summary of crystallographic data is given in Table 1. The X-ray crystal structure of **II** is given in Fig. 2.

RESULTS AND DISCUSSION

This laboratory has long had an interest in the organoaluminium chemistry of oxygen-,[10–12] sulphur-[13–15] and nitrogen-based multidentate ligands.[16–25] These studies revealed a particularly rich and varied chemistry often involving condensation reactions which resulted in novel organoaluminium cage compounds. The fact that an examination of the organoaluminium chemistry of multidentate phosphorus ligands is a natural extension of this work, coupled with the relative paucity of studies concerning organoaluminium–bidentate phosphine systems, prompted us to initiate a probe into this chemistry.

The initial study from this laboratory regarding the organoaluminium chemistry of bidentate phosphine ligands concerned the 2:1 (AlR_3–ligand) addition product $[Al(CH_3)_3]_2[(C_6H_5)_2PCH_2P(C_6H_5)_2]$ isolated from reaction of trimethylaluminium with bis(diphenylphosphino)methane.[26] As the organoaluminium chemistry of the chalcogen derivatives of bidentate phosphine ligands is largely unexplored, our attention shifted to the oxygen and sulphur derivatives of these ligands. Our next study concerned the di-oxygen analogue of bis(diphenylphosphino)methane, bis(diphenylphosphinoyl)methane. A particularly significant point about bis(diphenylphosphinoyl)methane is the fact that the presence of an oxygen atom on each of the two phosphorus atoms serves to sufficiently increase the acidity of the central methylene CH_2 hydrogen atoms so as to undergo Al—R/C—H condensation upon reaction with trimethylaluminium, thus resulting in the unusual organoaluminium product $[Al(CH_3)][(C_6H_5)_2P(O)CP(O)(C_6H_5)_2]_2[Al(CH_3)_2]_2$.[27] We have also recently reported the triethylaluminium–bis(diphenylphosphinoyl)methane condensation product.[28] The isolation of the trimethylaluminium and triethylaluminium condensation products of bis(diphenylphosphinoyl)methane raised two questions: (1) Would the dithio derivatives of bidentate phosphine ligands react in a similar fashion towards organoaluminium species? (2) Does the length of the hydrocarbon chain in the bidentate phosphine ligands affect the reactivity of these systems? The

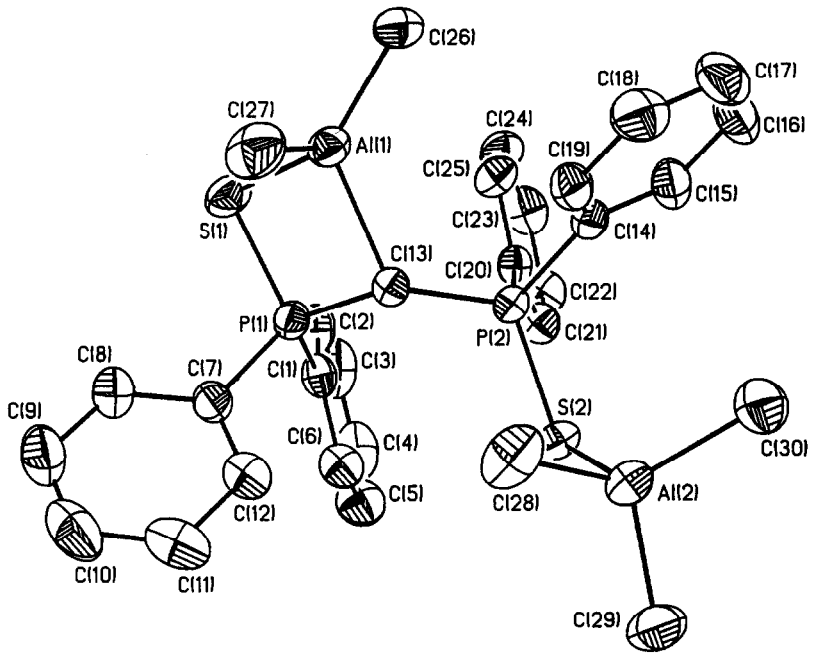

Fig. 1. A view of the $[Al(CH_3)_2][(C_6H_5)_2P(S)CHP(S)(C_6H_5)_2][Al(CH_3)_3]$ (**I**) molecule showing the atom labelling scheme. Thermal ellipsoids show 35% probability levels; hydrogen atoms have been omitted. Selected bond distances (Å) and angles (°):

S(1)—P(1)	2.009(2)	P(2)—C(20)	1.805(4)
S(1)—Al(1)	2.388(2)	P(1)—C(13)	1.788(4)
S(2)—P(2)	2.004(2)	P(2)—C(13)	1.791(4)
S(2)—Al(2)	2.460(2)	Al(1)—C(13)	2.097(4)
P(1)—C(1)	1.803(4)	Al(1)—C(26)	1.943(6)
P(1)—C(7)	1.810(4)	Al(1)—C(27)	1.949(6)
P(1)—S(1)—Al(1)	78.8(1)	S(1)—Al(1)—C(13)	82.8(1)
P(2)—S(2)—Al(2)	108.7(1)	P(1)—C(13)—P(2)	121.3(2)
S(1)—P(1)—C(1)	110.8(2)	P(2)—C(13)—Al(1)	124.0(2)
S(1)—P(1)—C(7)	111.0(2)	P(1)—C(13)—Al(1)	92.2(2)
C(1)—P(1)—C(7)	106.8(2)	C(14)—P(2)—C(20)	105.5(2)
S(1)—P(1)—C(13)	103.0(2)	S(2)—P(2)—C(13)	114.0(1)

present study was undertaken to address these points.

Reaction of trimethylaluminium with bis(diphenylthiophosphinoyl)methane results in $[Al(CH_3)_2][(C_6H_5)_2P(S)CHP(S)(C_6H_5)_2][Al(CH_3)_3]$ (**I**). The X-ray crystal structure of **I** is given in Fig. 1. The first point of note concerning **I** is the presence of two different types of organoaluminium species: one trimethylaluminium and one dimethylaluminium fragment. Indeed, **I** results from a condensation reaction in which one of the central methylene hydrogen atoms and one of the Al—CH_3 bonds were cleaved resulting in an Al—S—P—C four-membered ring. This suggests, qualitatively, that the central methylene hydrogen atoms of the dithio derivatives are not as acidic as those of the di-oxygen derivatives. The aluminium–central methylene carbon [Al(1)—C(13)] bond distance at 2.097(4) Å is somewhat longer than the aluminium–carbon bond in the dimethylaluminium fragment (1.943(6) and 1.949(6) Å for Al(1)—C(26) and Al(1)—C(27), respectively). The Al(1)—S(1) bond distance is 2.388(2) Å, while the Al(2)—S(2) bond is 2.460(2) Å. The P—C—P bond angle in **I** is worthy of note. The P—C—P bond angle in **I** of 121.3(2)° is somewhat distorted from the value of 118.3(2)° obtained for the uncomplexed ligand.[29]

Compound **II** (Fig. 2), isolated from reaction of trimethylaluminium with bis(diphenylthiosphosphinoyl)ethane, represents the first report of an organoaluminium – bis(diphenylthiophosphinoyl) ethane complex. In marked contrast to **I**, condensation did not occur in **II** as only the 2:1 addition compound was isolated. It appears that the length of the hydrocarbon bridge in bidentate phosphine ligands plays a role with respect to

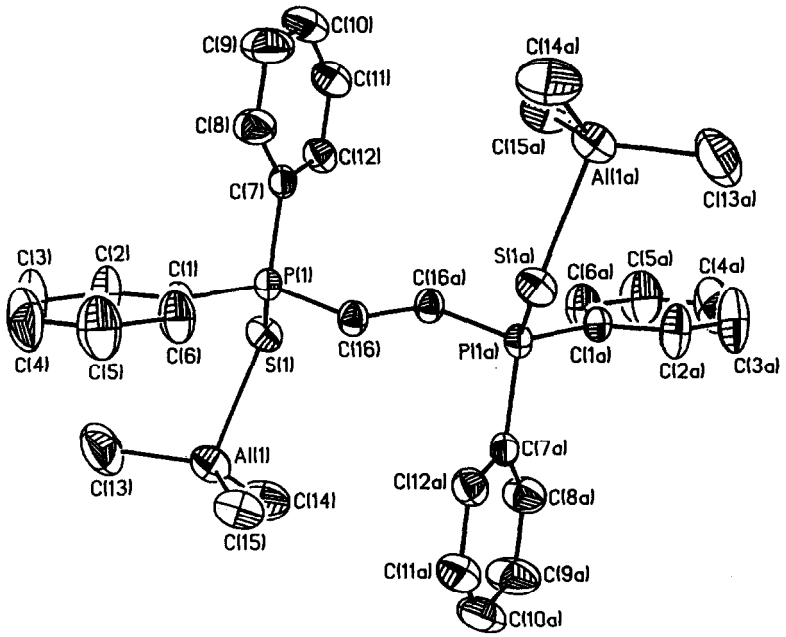

Fig. 2. A view of the $[Al(CH_3)_3]_2[(C_6H_5)_2P(S)CH_2CH_2P(S)(C_6H_5)_2]$ (**II**) molecule showing the atom labelling scheme. Thermal ellipsoids show 35% probability levels; hydrogen atoms have been omitted. Selected bond distances (Å) and angles (°):

S(1)—P(1)	1.989(2)	C(16)—C(16a)	1.530(9)
S(1)—Al(1)	2.506(3)	Al(1)—C(13)	1.965(7)
P(1)—C(1)	1.799(5)	Al(1)—C(14)	1.959(7)
P(1)—C(7)	1.807(5)	Al(1)—C(15)	1.962(7)
P(1)—C(16)	1.818(4)		
P(1)—S(1)—Al(1)	108.4(1)	C(1)—P(1)—C(7)	108.2(2)
S(1)—P(1)—C(1)	114.2(2)	S(1)—P(1)—C(16)	112.2(1)
S(1)—P(1)—C(7)	110.1(2)	P(1)—C(16)—C(16a)	111.0(4)

C—H/Al—R bond cleavage, in that condensation appears to be disfavoured if the length of the hydrocarbon bridge exceeds one $—CH_2—$ fragment. The Al—S bond distances in both **I** and **II** are comparable to other reported values.[13–15]

The trialkyls of the Group III (13) metals, as well as their adducts with various amines and phosphines, have been employed for the Metal–Organic Chemical Vapour Deposition (MOCVD) of III–V materials.[30,32] An interesting alternative method to the practice of employing volatile Group III (13) adducts in MOCVD processes[33–36] has recently been reported wherein metal alkyl adducts with relatively involatile bases, such as multidentate phosphine ligands, having weak donor–acceptor bonds, have been examined.[37] As M—S (M = Al, Ga, In; S = sulphur) interactions are generally rather weak, the organo-main group chemistry of thio derivatives of multidentate phosphine ligands resulting in complexes like **I** and **II** may offer unique possibilities in such processes.

Acknowledgement—We are grateful to the National Science Foundation for support of this work to G.H.R. (RII-8520554).

Supplementary material available: a summary of data collection and refinement, tables of bond distances and angles, and tables of fractional coordinates, in addition to a listing of observed and calculated structure factors have been deposited with the Cambridge Crystallographic Data Centre. Complete structural information is available from the Editor.

REFERENCES

1. N. Van Order Jr, W. E. Geiger, T. E. Bitterwolf and A. L. Rheingold, *J. Am. Chem. Soc.* 1987, **109**, 5680.
2. M. O. Albers, D. C. Liles, D. J. Robinson and E. Singleton, *Organometallics* 1987, **6**, 2179.
3. B. Delavaux, B. Chaudret, F. Dahan and R. Poilblanc, *Organometallics* 1985, **4**, 935.
4. B. Chaudret, F. Dahan and S. Saba, *Organometallics* 1985, **4**, 1490.

5. J. A. Iggo, D. P. Markham, B. L. Shaw and M. Thornton-Pett, *J. Chem. Soc., Chem. Commun.* 1985, 432.
6. H. Schmidbaur, S. Lauteschläger and G. Müller, *J. Organomet. Chem.* 1985, **281**, 25.
7. T. Kagawa and H. Hasimoto, *Bull. Chem. Soc. Jpn* 1972, **45**, 1739.
8. T. Kagawa, Y. Inoue and H. Hashimoto, *Bull. Chem. Soc. Jpn* 1970, **43**, 1250.
9. G. M. Sheldrick, SHELXTL PLUS, Crystallographic Computing System, Revision 5.1. Nicolet Instruments Division, Madison, Wisconsin (1986).
10. J. L. Atwood, H. Elgamal, G. H. Robinson, S. G. Bott, J. A. Weeks and W. E. Hunter, *J. Incl. Phenom.* 1984, **2**, 367.
11. G. H. Robinson, S. G. Bott, H. Elgamal, W. E. Hunter and J. L. Atwood, *J. Incl. Phenom.* 1985, **3**, 65.
12. G. H. Robinson, W. E. Hunter, S. G. Bott and J. L. Atwood, *J. Organomet. Chem.* 1987, **326**, 9.
13. G. H. Robinson, H. Zhang and J. L. Atwood, *Organometallics* 1987, **6**, 887.
14. G. H. Robinson and S. A. Sangokoya, *J. Am. Chem. Soc.* 1988, **110**, 1494.
15. S. A. Sangokoya, B. Lee, W. T. Pennington and G. H. Robinson, *J. Coord. Chem.* 1989, **19**, 331.
16. G. H. Robinson and S. A. Sangokoya, *J. Am. Chem. Soc.* 1987, **109**, 6852.
17. G. H. Robinson, A. D. Rae, C. F. Campana and S. K. Byram, *Organometallics* 1987, **6**, 1227.
18. G. H. Robinson, E. S. Appel, S. A. Sangokoya, H. Zhang and J. L. Atwood, *J. Coord. Chem.* 1988, **17**, 373.
19. G. H. Robinson and S. A. Sangokoya, *Organometallics* 1988, **7**, 1453.
20. G. H. Robinson, S. A. Sangokoya, F. Moise and W. T. Pennington, *Organometallics* 1988, **7**, 1887.
21. G. H. Robinson, F. Moise, W. T. Pennington and S. A. Sangokoya, *J. Cryst. Spectrosc. Res.* 1988, **18**, 387.
22. G. H. Robinson and S. A. Sangokoya, *Polyhedron* 1988, **7**, 2727.
23. G. H. Robinson, B. Lee, W. T. Pennington and S. A. Sangokoya, *J. Am. Chem. Soc.* 1988, **110**, 6260.
24. G. H. Robinson, M. F. Self, S. A. Sangokoya and W. T. Pennington, *J. Am. Chem. Soc.* 1989, **111**, 1520.
25. G. H. Robinson, F. Moise, W. T. Pennington and S. S. Sangokoya, *Polyhedron* 1989, **8**, 1279.
26. G. H. Robinson, M. F. Self, S. A. Sangokoya and W. T. Pennington, *J. Cryst. Spectrosc. Res.* 1988, **18**, 285.
27. G. H. Robinson, B. Lee, W. T. Pennington and S. A. Sangokoya, *J. Am. Chem. Soc.* 1988, **110**, 6260.
28. B. Lee, S. A. Sangokoya, W. T. Pennington and Gregory H. Robinson, *J. Coord. Chem.*, in press.
29. M. F. Self, W. T. Pennington and G. H. Robinson, unpublished results.
30. H. M. Manasevit and W. I. Simpson, *J. Electrochem. Soc.* 1969, **116**, 1725.
31. H. M. Manasevit and W. I. Simpson, *J. Electrochem. Soc.* 1973, **120**, 135.
32. R. H. Moss, *J. Cryst. Growth* 1984, **68**, 78.
33. G. E. Coates, *J. Chem. Soc.* 1951, 2003.
34. G. E. Coates and R. G. Hayter, *J. Chem. Soc.* 1953, 2519.
35. G. E. Coates and R. A. Whitcombe, *J. Chem. Soc.* 1956, 3351.
36. D. C. Bradley, H. Dawes, D. M. Frigo, M. B. Hursthouse and B. Hussain, *J. Organomet. Chem.* 1987, **325**, 55.
37. D. C. Bradley, H. Chudzynska, M. M. Faktor, D. M. Frigo, M. B. Hursthouse, B. Hussain and L. M. Smith, *Polyhedron* 1988, **7**, 1289.

Polyhedron Vol. 9, No. 2/3, pp. 319–327, 1990
Printed in Great Britain

0277–5387/90 $3.00+.00
© 1990 Pergamon Press plc

PREPARATION AND CHEMISTRY OF $Me_3SiCH_2AsH_2$; PREPARATION OF $[Me_3SiCH_2(H)AsGaPh_2]_3$, A TRIMERIC MONO(ARSINO)GALLANE CONTAINING A HYDROGEN BONDED TO ARSENIC. ISOLATION AND X-RAY CRYSTAL STRUCTURE OF $(Me_3SiCH_2As)_5$

RICHARD L. WELLS,* CHONG-YUN KWAG, ANDREW P. PURDY, ANDREW T. McPHAIL and COLIN G. PITT

Department of Chemistry, Paul M. Gross Chemical Laboratory, Duke University, Durham, NC 27706, U.S.A.

Abstract—Reduction of $Me_3SiCH_2AsCl_2$ (**I**) with $LiAlH_4$ at −78°C afforded $Me_3SiCH_2AsH_2$ (**II**) and reaction of **II** with Ph_3Ga produced $[Me_3SiCH_2(H)AsGaPh_2]_3$ (**III**) which was characterized by partial elemental analysis (C and H), ^1H NMR spectroscopy and a cryoscopic molecular weight determination. Based on ^1H NMR data, $[Me_3SiCH_2(H)AsGaMe_2]_3$ (**IV**) was produced by the reaction of **II** with Me_3Ga; however, only H_2, Me_4Si, $(Me_3SiCH_2As)_5$ (**VI**) and unreacted $(Me_3SiCH_2)_3Ga$ were identified after allowing the latter to react with **II**. Reaction of 2 equiv. of Me_3SiCl with a mixture of **II** and *n*-BuLi (1:2 mole ratio) afforded $Me_3SiCH_2As(SiMe_3)_2$ (**V**). The monosilylated arsine was not isolated when 1 equiv. of Me_3SiCl was allowed to react with combined **II** and *n*-BuLi (1:1 mole ratio); rather, a mixture of **II** and **V** resulted. Attempted preparations of $(Me_3SiCH_2AsGaPh)_n$ are described. The ring compound, **VI**, was prepared by reaction of **I** with a mixture of Me_3SiCl and Mg in THF. The molecular structure of this cycloarsane was determined by single-crystal X-ray diffraction methods. Pale yellow crystals of **VI** belong to the monoclinic system with four molecules occupying the general positions of space group $P2_1/c(C_{2h}^5)$ with cell constants: $a = 9.952(1)$, $b = 30.245(9)$, $c = 13.000(3)$ Å, $\beta = 91.69(1)°$, $V = 3911.3$ Å^3, $Z = 4$.

In recent years, after a hiatus of approximately two decades,[1] there has been a considerable amount of activity in the area of gallium–arsenic chemistry,[2] some of which was prompted by the search for new gallium arsenide precusors. As a result, a number of new and interesting compounds have been prepared and characterized. To date, however, the literature contains no reports regarding the isolation and characterization of monomeric or oligomeric compounds of the type $[R(H)AsGaR'_2]_n$ and $(RAsGaR')_n$. As described by Beachley and Coates, the reactions of $MeAsH_2$ and $PhAsH_2$ with Me_3Ga gave only polymers,[1b] whereas we found that the reaction of $PhAsH_2$ with $(Me_3SiCH_2)Ga$ gave a complex mixture of products from which $(PhAs)_6$ and the novel cluster $[(PhAsH)(R_2Ga)(PhAs)_6(RGa)_4]$ ($R = Me_3SiCH_2$) were isolated.[2a]

Here we report the preparation of **I** and its conversion to **II**. Also, the reaction of **II** with Ph_3Ga to prepare **III**, as well as some other reactions, including its conversion to **V** are described. In addition, attempts to prepare $(Me_3SiCH_2AsGaPh)_n$ are reported. Furthermore, we found that an attempted preparation of **V** from **II** resulted in the formation of the cycloarsane **VI**, the crystal structure of which is described herein.

EXPERIMENTAL

General information

All manipulations and reactions were carried out either in Schlenk apparatus, I^2R glove bags or a Vacuum/Atmospheres HE-43 Dri Lab under an inert atmosphere (argon or nitrogen), or on a vacuum line. Quantities of volatile products were measured on a vacuum line. Deionized water was degassed prior to use. All organic solvents were distilled from sodium benzophenone ketyl under nitro-

* Author to whom correspondence should be addressed.

gen. $AsCl_3$, perfluorohexane, Me_3SiCH_2Cl and Et_2NH were purchased from Strem Chemicals Inc., Specialty Chemicals, Petrarch Systems Inc. and EM Science, respectively. $LiAlH_4$, *n*-BuLi and Me_3Ga were obtained from Alfa Products Inc. All commercially available reagents were not further purified. The concentration of the *n*-BuLi was determined each time before use by titration[3] with *sec*-BuOH in C_6H_6 using 1,10-phenanthroline as the indicator. Me_3SiCH_2MgCl was prepared in 97% yield by a slight modification (i.e. baking the I_2 initiator and Mg metal turnings with a flame) of the literature method.[4] $(Et_2N)_2AsCl$,[5] $PhGaCl_2$,[6] Ph_2GaCl,[7] Ph_3Ga[8] and $(Me_3SiCH_2)_3Ga$[9] were also prepared by literature methods. ^1H NMR spectra were recorded on either an IBM NR–80 (80 MHz) or a Varian XL-300 (299.943 MHz) spectrometer, the latter being used to obtain variable temperature spectra. ^{13}C NMR spectra were obtained on either a JEOL FX-90Q spectrometer at 22.5 MHz or a Varian XL-300 spectrometer at 75.429 MHz. All spectra were referenced to TMS using the residual protons or the carbons of the deuterated solvents as the chemical shift reference; for ^1H, C_6D_5H δ 7.15, $C_6D_5CD_2H$ δ 2.09; for $^{13}C\{^1H\}$, C_6D_6 δ 128.0, $C_6D_5CD_3$ δ 20.4. All NMR tubes were flame-sealed under vacuum. A Normag 2029 apparatus was used to determine the molecular weight of **III** (cryoscopically in cyclohexane). All m.p. measurements were performed by using a Buchi 510 apparatus and flame-sealed capillaries. Elemental analyses were performed by E+R Microanalytical Laboratory, Inc., Corona, New York.

Syntheses

$Me_3SiCH_2AsCl_2$ (**I**). Me_3SiCH_2MgCl (249 cm^3, 0.398 mol) was added dropwise with stirring to an Et_2O (300 cm^3) solution of $(Et_2N)_2AsCl$ (99.6 g, 0.391 mol) at −78°C. An exothermic reaction occurred as the Grignard reagent was added dropwise. After stirring for 8 h at RT, the reaction mixture was hydrolysed with a large excess of conc. HCl and the organic layer was separated and combined with a hexane/Et_2O extract of the acid layer. Removal of solvents gave a yellow liquid (77.8 g) which was vacuum distilled to yield pure $Me_3SiCH_2AsCl_2$ as a colourless liquid (73.5 g, 81% yield, b.p. 30°C/0.1–0.2 torr). Calc. for $C_4H_{11}AsCl_2Si$: C, 20.62; H, 4.76; Cl, 30.43. Found: C, 20.67; H, 4.70; Cl, 30.26%. ^1H NMR (C_6D_6, 80.06 MHz): δ −0.070 (s, CH_3), 1.5 (s, CH_2).

$Me_3SiCH_2AsH_2$ (**II**). To a stirred suspension of $LiAlH_4$ (6.68 g, 0.176 mol) in Et_2O (250 cm^3) at −78°C was added, dropwise, a solution of **I** (20.5 g, 0.0880 mol) in Et_2O (50 cm^3). After the addition was complete, the mixture was hydrolysed with a large excess of deionized water at 0°C. A white solid [presumably $Al(OH)_3$ and LiOH] was separated from the mixture by filtration and washed with Et_2O. Addition of $MgSO_4$ to the separated organic layer, followed by filtration and removal of the solvent from the filtrate, afforded a yellow liquid which was vacuum distilled (30–40°C/20–50 torr) to give impure **II** as a colourless liquid. Purification was achieved by trap-to-trap fractionation, with pure **II** (6.81 g, 47.2% yield) being retained in a trap at −63°C. Calc. for $C_4H_{13}AsSi$: C, 29.27; H, 7.98. Found: C, 29.56, 29.41; H, 8.03, 7.92%. ^1H NMR (C_6D_6, 299.944 MHz): δ −0.021 (s, CH_3), 0.301 $^3J_{HH}$ = 7.44 Hz (t, CH_2), 2.054 (t, AsH_2). $^{13}C\{^1H\}$ NMR (C_6D_6, 75.429 MHz): δ −5.425 (CH_2), −1.246 (CH_3).

Treatment of **I** with $LiAlH_4$ at RT afforded **II** in lower yield (25%) as well as some **VI**.

$[Me_3SiCH_2(H)AsGaPh_2]_3$ (**III**). 1. Compound **II** (1.78 g, 10.8 mmol) and Ph_3Ga (3.26 g, 10.8 mmol) were combined in benzene (25 cm^3) and, after stirring the mixture overnight at 55–57°C, the solvent was stripped off, leaving a colourless sticky residue. Volatiles were then removed *in vacuo* over a 4 day period to yield **III** as a less sticky material. Attempts to crystallize the product from C_6H_{14} or a mixture of ligroin and C_6F_{14} were unsuccessful. Melting point measurement: the colourless **III** became mobile at 57–59°C and it started to change to light yellow at 68°C; it became a transparent liquid at 75–77°C. Calc. for $C_{48}H_{66}As_3Si_3Ga_3$: C, 49.65; H, 5.73. Found: C, 51.00, 51.05; H, 5.75, 5.77%. Mol. wt (0.303 g in 13.97 g of cyclohexane): Calc. 1161. Found: 1172±23%. ^1H NMR (C_6D_6, 299.944 MHz): δ −0.329, −0.332, −0.359 (3 s, CH_3), 0.768, 0.818, 0.882 $^3J_{HH}$ = 5.86, 5.88, 5.76 Hz (3 d, CH_2), 2.334, 2.451, 2.600 (3 t, AsH), 7.2–7.4 and 7.7–7.9 (m, Ph).

Reaction of Ph_3Ga (0.550 g, 1.83 mmol) with an excess of **II** (0.324 g, 1.97 mmol) yielded the same sticky product, with all Ph_3Ga being consumed. Drying the product under high vacuum for 5 days afforded colourless sticky **III** (0.708 g, 100% yield; ^1H NMR spectrum same as that of an authentic sample).

2. Slow addition of *n*-BuLi (1.56 cm^3, 2.34 mmol) to a stirred THF solution of **II** (0.384 g, 2.34 mmol) which was cooled in a −78°C bath resulted in a slightly yellow solution. [Note: Treatment of **II** with *n*-BuLi in various solvents (hexane, ligroin, and THF) at RT and even at 0°C, resulted in a complex reaction mixture.] After stirring for 3 h, Ph_2GaCl (0.607 g, 2.34 mmol) was added by means of a side-

arm dumper to the vessel. The bath was removed after stirring for another 3 h and the mixture was stirred for 1 h at RT, yielding a white solid (presumably LiCl). The mixture was filtered and washed with C_6H_6. Removal of solvents *in vacuo* from the filtrate afforded a yellow solid. The ^1H NMR spectrum of the latter revealed that **III** and an adduct of the gallium reactant (presumably $Ph_2GaCl \cdot THF$) were present. Recrystallization of the yellow solid from hexane or a mixture of ligroin and THF provided light yellow crystals of the adduct.

$[Me_3SiCH_2(H)AsGaMe_2]_3$ (**IV**). Me_3Ga (3.42 mmol), measured on a vacuum line, was condensed into a reaction vessel containing a pentane solution of **II** (0.551 g, 3.36 mmol) at −196°C. The mixture was warmed to RT and stirred for 39 h. The evolved CH_4 (3.26 mmol) was measured and volatiles were removed *in vacuo* leaving a mixture of a colourless liquid and a very small amount of a solid. A second experiment using Me_3Ga (1.80 mmol) with an excess of **II** (0.307 g, 1.87 mmol) gave a colourless mixture of a liquid and solid (0.400 g, 84.6% yield) and CH_4 (1.45 mmol). The ^1H NMR spectra of both mixtures showed the same type of coupling pattern as that observed in the spectrum of **III**. ^1H NMR (C_6D_6, 299.944 MHz): δ 0.047 (s, Me_3Si); 0.206, 0.247, 0.294 (3 s, Me_2Ga); 0.785, 0.805, 0.823 $^3J_{HH}$ = 5.80 Hz (3 overlapping d, CH_2As); 1.697, 1.748, 1.790 (3 overlapping t, AsH).

Reaction of **II** *with* $(Me_3SiCH_2)_3Ga$. Compound **II** (0.25 g, 1.5 mmol) and $(Me_3SiCH_2)_3Ga$ (0.05 g, 1.5 mmol) were transferred into a 50 cm^3 bulb equipped with a Teflon stopcock and a magnetic stir bar. The bulb was attached to a vacuum line, cooled to −196°C and degassed. Stirring the mixture for a day at RT, followed by heating and stirring for 2 days at 51–63°C, gave a yellow liquid, H_2 (1.2 mmol, 80% yield) and Me_4Si (0.21 mmol, 14% yield). After the liquid was transferred into a 50 cm^3 flask to which a solution of the remaining liquid and pentane used for rinsing the bulb was added, a few small particles [presumably unreacted $(Me_3SiCH_2)_3Ga$] were removed by filtration. Removal of the pentane *in vacuo* from the filtrate afforded a yellow liquid, the ^1H NMR spectrum of which revealed that **VI** and $(Me_3SiCH_2)_3Ga$ were present. The liquid residue was mixed with ligroin and perfluorohexane and stored at −15°C. A few months later, a crystal was isolated; its ^1H NMR spectrum showed a broad hump and many lines between δ 1.8 and −0.5.

$Me_3SiCH_2As(SiMe_3)_2$ (**V**). To a stirred THF solution of **II** (1.171 g, 7.13 mmol) at −78°C was slowly added *n*-BuLi (4.74 cm^3, 14.26 mmol). After stirring for 3 h, Me_3SiCl (1.8 cm^3, 14.28 mmol) was introduced into the mixture which turned colourless immediately after the addition. After stirring for another 3 h, the mixture was warmed to RT and stirred for 2 h. A white solid (presumably LiCl) was removed by filtration and washed with benzene. Volatiles were removed from the filtrate and the liquid residue was distilled *in vacuo* to give **V** as a colourless liquid (1.82 g, 83% yield, b.p. 52–53°C/0.1–0.2 torr). Calc. for $C_{10}H_{29}AsSi_3$: C, 38.93; H, 9.47. Found: C, 38.72, 38.95; H, 9.55, 9.62%. ^1H NMR (C_6D_6, 299.944 MHz): δ 0.177 (s, Me_3SiC), 0.254 (s, Me_3SiAs), 0.559 (s, CH_2). $^{13}C\{^1H\}$ NMR (C_6D_6, 75.429 MHz): δ −5.690 (s, CH_2), −0.322 (s, Me_3SiC), 1.415 (s, Me_3SiAs).

Attempted preparation of $Me_3SiCH_2As(H)SiMe_3$. *n*-BuLi (1.42 cm^3, 4.14 mmol) was added to a THF solution of **II** (0.680 g, 4.14 mmol) which was cooled with a −78°C bath. After stirring for 3 h, Me_3SiCl (0.52 cm^3, 4.14 mmol) was added to the mixture. The bath was removed and the mixture was stirred for 3 h. A white solid (presumably LiCl) was separated by filtration and removal of solvents from the filtrate gave a liquid mixture of **II** and **V** (based on a ^1H NMR spectrum). Removal *in vacuo* of **II** from the mixture gave **V** (0.777 g, 61% yield).

When this reaction was repeated at RT, **VI**, $(Me_3Si)_3As$ and an unidentified black precipitate were formed.

Attempted preparation of $(Me_3SiCH_2AsGaPh)_n$. 1. Heating **III** at 55–62°C for 2 days in a Dri Lab produced a light yellow solid which on further heating at 76–82°C for 2 days turned more yellow. The ^1H NMR spectrum of the yellow solid revealed that the coupling pattern of the trimer was collapsed and a hump appeared at δ 0.5 to −0.5. Heating the yellow solid at 90–100°C for another 2 days left the colour unchanged and a similar ^1H NMR spectrum was obtained (three peaks at δ 3.106, 0.188, 0.128; two humps at δ 1.0 to 0.8 (small), 0.5 to −0.5 (larger, broad), and a shoulder at δ 2.4–1.0). Melting point measurement: the yellow solid turned brownish at 170°C, red at 190°C and became a liquid at 210–225°C. Calc. for $C_{10}H_{16}SiAsGa$: C, 38.87; H, 5.22. Found: C, 40.44, 40.30; H, 5.41, 5.35%.

2. *n*-BuLi (0.88 cm^3, 2.67 mmol) was added with stirring to an Et_2O solution of **II** (0.219 g, 1.34 mmol) in a reaction vessel which was immersed in a dry ice/acetone bath. After stirring for 1 h, $PhGaCl_2$ (0.292 g, 1.34 mmol) was added to the mixture by means of a side-arm dumper. The bath was removed 1 h later and the precipitation of a white solid (presumably LiCl) was observed. The white solid (0.10 g, 88% yield) was removed by filtration and removal *in vacuo* of solvents from the filtrate gave a light yellow sticky residue. The ^1H NMR spectrum of the residue was relatively simple showing

one peak at δ −0.024 and two broad humps between δ 2.0 and −0.5.

3. (a) A toluene solution of **V** (0.309 g, 1.00 mmol) was combined with a toluene solution of $PhGaCl_2$ (0.218 g, 1 mmol) at −15°C. After 18 h at −15°C, followed by stirring for 27 h at RT, 1.36 equiv. of Me_3SiCl were formed. Heating for 13 h at 66°C increased the amount of Me_3SiCl formed to 1.68 equiv. and afforded a colourless sticky residue. Attempts to crystallize the product from hexane or ligroin were unsuccessful. The ^1H NMR spectrum of the residue was similar to that of the material obtained when **III** was decomposed at 80°C (2 peaks at δ 2.104 and 0.294; 3 humps at δ 3.4 to 3.0, 2.0 to 1.0, and 0.5 to −0.5).

(b) After 12 h at −15°C, a mixture similar to that described in (a) was stirred for 4 days at RT and 1.53 equiv. of Me_3SiCl resulted. Alternating the reaction temperature between RT and −15°C four times in 12 days, with removal of Me_3SiCl after each period, increased the total amount of Me_3SiCl formed to 1.79 equiv. Removal of volatiles *in vacuo* afforded an off-white sticky residue. The ^1H NMR spectrum of the residue showed two peaks at δ 0.254 and 0.176, three humps at δ 2.3–1.1, 1.1–0.8, 0.5 to −0.5 and a small peak at δ 0.559.

$(Me_3SiCH_2As)_5$ (**VI**). Compound **I** (15.0 g, 0.0644 mol) was slowly added to a THF solution of Me_3SiCl (120 cm^3) and Mg turnings (3.14 g, 0.129 mol). The resulting mixture was refluxed for 1 h and then stirred at RT for an additional 8 h. Removal of volatiles *in vacuo* gave a mixture of an off-white solid and a yellow liquid which was filtered and washed with pentane. Removal of solvents from the filtrate afforded crude **VI** as a yellow liquid. Some of the diarsine $[(Me_3SiCH_2)_2As]_2$[2b] was produced during the attempted purification (distillation at 100–120°C/0.1–0.2 torr) of the crude product; but after a week at RT, pale yellow crystals of **VI** formed in the yellow distillate. The crystals (3.28 g, 31.4%; m.p. 47–48°C) were removed mechanically from the liquid. Calc. for $C_{20}H_{55}As_5Si_5$: C, 29.63; H, 6.84. Found: C, 29.61; H, 6.67%. ^1H NMR (C_6D_6, 299.944 MHz): δ 0.185, 0.213, 0.219 (3 s, CH_3), 1.602 (s, CH_2), 1.515 and 1.738 $^2J_{HH}$ = 13.63 Hz, 1.538 and 1.687 $^2J_{HH}$ = 13.55 Hz (2 AB patterns, CH_2). $^{13}C\{^1H\}$ NMR (C_6D_6, 75.429 MHz): δ 0.079, 0.266, 0.349 (3 s, CH_3), 8.145, 10.240, 12.736 (3 s, CH_2). The ^1H NMR spectrum of the remaining liquid showed the presence of the diarsine and **VI** (36 : 64%, based on integral ratios). Total yield of **VI**: 5.53 g, 53%.

X-ray crystal structure determination

$(Me_3SiCH_2As)_5$ (**VI**). All measurements were performed on an Enraf–Nonius CAD-4 diffractometer (Cu-K_α radiation, λ = 1.5418 Å; incident-beam graphite monochromator; ω–2θ scans, θ_{max} = 67°). Unit-cell parameters were derived from the diffractometer setting angles for 25 reflections ($40° < \theta < 55°$) widely separated in reciprocal space. Lorentz, polarization and empirical absorption corrections were applied to the data. The crystal structure was solved by direct methods. Approximate positions for the non-hydrogen atoms were obtained from an *E*-map. Hydrogen atoms were included at their calculated positions in the final rounds of full-matrix least-squares refinement of non-hydrogen atom positional and anisotropic temperature factor parameters. Crystallographic calculations were performed on PDP11/44 and Micro Vax II computers by use of the Enraf–Nonius Structure Determination Package incorporating the direct methods program MULTAN11/82. Neutral atom scattering factors used in the structure-factor calculations were taken from *International Tables for X-Ray Crystallography*, Vol. IV, The Kynoch Press, Birmingham, U.K. (1974). In the full-matrix least-squares iterations, $\Sigma w\Delta^2$ [$w = 1/\sigma^2(|F_o|)$, $\Delta = (|F_o| - |F_c|)$] was minimized. Further details of data collection and refinement are in Table 1. Bond lengths, bond angles and torsion angles are listed in Table 2. Supplementary material: atomic coordinates, thermal parameters, bond lengths and angles and crystal data have been deposited with the Cambridge Crystallographic Data Centre.

RESULTS AND DISCUSSION

Syntheses and reactions

Reduction of **I**, which was prepared according to eqs (1)–(3), with $LiAlH_4$ in Et_2O at −78°C afforded **II** [eq. (4)]. In contrast, the reduction at RT resulted in a significantly lower yield of **II**, as well as some of the cycloarsane, **VI**.

$$4Et_2NH + AsCl_3 \longrightarrow (Et_2N)_2AsCl + 2Et_2NH\cdot HCl \quad (1)$$

$$(Et_2N)_2AsCl + Me_3SiCH_2MgCl \longrightarrow (Et_2N)_2AsCH_2SiMe_3 + MgCl_2 \quad (2)$$

$$(Et_2N)_2AsCH_2SiMe_3 + 4HCl \longrightarrow \underset{\mathbf{I}}{Me_3SiCH_2AsCl_2} + 2Et_2NH\cdot HCl \quad (3)$$

$$2Me_3SiCH_2AsCl_2 + LiAlH_4 \longrightarrow \underset{\mathbf{II}}{2Me_3SiCH_2AsH_2} + LiCl + AlCl_3. \quad (4)$$

Table 1. Crystallographic data and summary of data collection and refinement[a] for $(Me_3SiCH_2As)_5$ (VI)

Formula	$C_{20}H_{55}As_5Si_5$
Formula weight	810.70
Crystal system	Monoclinic
Space group	$P2_1/c(C_{2h}^5)$
Conditions	$0k0$, $k = 2n$; $h0l$, $l = 2n$
Crystal dimensions (mm)	$0.20 \times 0.30 \times 0.30$
Crystal colour and habit	Pale yellow prisms
Temperature (K)	298
a (Å)	9.952(1)
b (Å)	30.245(9)
c (Å)	13.000(3)
β (°)	91.69(1)
Z	4
V (Å^3)	3911.3
$d_{calc.}$ (g cm^{-3})	1.377
Linear absorption coefficient (cm^{-1})	65.5
Scan speed (° min^{-1})	Variable
Scan width (°)	$1.20+0.14\tan\theta$
Max θ (°)	67
Background	25% additional scan at each end of scan
Range of transmission factors	0.48–1.00
Octants	$+h$, $+k$, $\pm l$
Number of variables	272
Data : variable ratio	13.8
Check reflections	$(14\bar{2})$, $(1\bar{4}2)$
Decay of standards	< 1%
Number of reflections collected	7226
R(merge)	0.033 on I, 0.024 on $\|F_o\|$
Number of unique data	6919
Number of data used in refinement	3744 [$I > 3.0\sigma(I)$]
$R(F)$[a]	0.037
$R_w(F)$	0.049
Weighting scheme (ω)	$1/\sigma^2(\|F_o\|)$
ESD of an observation of unit weight	1.22
Largest Δ/σ	0.06
Largest feature of final diff map (e Å^{-3})	0.53
Location of feature	1.4 Å from As(3) and As(4)

[a] $R = \Sigma\,||F_o|-|F_c||/\Sigma\,|F_o|$ and $R_w = [\Sigma\, w(|F_o|-|F_c|)^2/\Sigma\, w|F_o|^2]^{1/2}$ with weighting scheme as listed above.

Table 2. Bond lengths (Å), bond angles (°) and torsion angles (°), with ESD's in parentheses, for $(Me_3SiCH_2As)_5$ (VI)

(a) Bond lengths

As(1)—As(2)	2.428(1)	Si(2)—C(22)	1.847(13)
As(1)—As(5)	2.443(1)	Si(2)—C(23)	1.867(13)
As(1)—C(11)	1.992(6)	Si(2)—C(24)	1.866(12)
As(2)—As(3)	2.424(1)	Si(3)—C(31)	1.870(6)
As(2)—C(21)	1.987(7)	Si(3)—C(32)	1.871(10)
As(3)—As(4)	2.443(1)	Si(3)—C(33)	1.857(10)
As(3)—C(31)	2.014(7)	Si(3)—C(34)	1.865(11)
As(4)—As(5)	2.446(1)	Si(4)—C(41)	1.861(9)
As(4)—C(41)	1.978(8)	Si(4)—C(42)	1.855(10)
As(5)—C(51)	1.995(7)	Si(4)—C(43)	1.840(13)
Si(1)—C(11)	1.861(7)	Si(4)—C(44)	1.853(11)

Table 2—*continued*

Si(1)—C(12)	1.847(11)	Si(5)—C(51)	1.889(8)
Si(1)—C(13)	1.849(11)	Si(5)—C(52)	1.865(12)
Si(1)—C(14)	1.876(10)	Si(5)—C(53)	1.873(11)
Si(2)—C(21)	1.867(8)	Si(5)—C(54)	1.864(12)

(b) Bond angles

As(2)—As(1)—As(5)	99.05(4)	C(22)—Si(2)—C(24)	109.1(6)
As(2)—As(1)—C(11)	97.2(2)	C(23)—Si(2)—C(24)	105.8(5)
As(5)—As(1)—C(11)	99.4(2)	C(31)—Si(3)—C(32)	111.6(4)
As(1)—As(2)—As(3)	96.46(4)	C(31)—Si(3)—C(33)	110.3(4)
As(1)—As(2)—C(21)	104.3(2)	C(31)—Si(3)—C(34)	106.4(4)
As(3)—As(2)—C(21)	101.2(2)	C(32)—Si(3)—C(33)	107.3(5)
As(2)—As(3)—As(4)	105.24(4)	C(32)—Si(3)—C(34)	109.7(5)
As(2)—As(3)—C(31)	94.3(2)	C(33)—Si(3)—C(34)	111.6(5)
As(4)—As(3)—C(31)	98.6(2)	C(41)—Si(4)—C(42)	111.2(4)
As(3)—As(4)—As(5)	104.59(4)	C(41)—Si(4)—C(43)	108.6(5)
As(3)—As(4)—C(41)	96.9(2)	C(41)—Si(4)—C(44)	108.7(5)
As(5)—As(4)—C(41)	96.9(3)	C(42)—Si(4)—C(43)	108.8(5)
As(1)—As(5)—As(4)	98.29(4)	C(42)—Si(4)—C(44)	108.9(5)
As(1)—As(5)—C(51)	96.8(2)	C(43)—Si(4)—C(44)	110.7(5)
As(4)—As(5)—C(51)	95.9(2)	C(51)—Si(5)—C(52)	109.6(4)
C(11)—Si(1)—C(12)	110.7(5)	C(51)—Si(5)—C(53)	107.1(4)
C(11)—Si(1)—C(13)	110.4(4)	C(51)—Si(5)—C(54)	111.9(4)
C(11)—Si(1)—C(14)	107.1(4)	C(52)—Si(5)—C(53)	109.0(6)
C(12)—Si(1)—C(13)	109.2(5)	C(52)—Si(5)—C(54)	110.2(5)
C(12)—Si(1)—C(14)	108.7(5)	C(53)—Si(5)—C(54)	109.1(5)
C(13)—Si(1)—C(14)	110.8(5)	As(1)—C(11)—Si(1)	116.1(3)
C(21)—Si(2)—C(22)	109.1(5)	As(2)—C(21)—Si(2)	115.3(4)
C(21)—Si(2)—C(23)	112.3(4)	As(3)—C(31)—Si(3)	114.0(4)
C(21)—Si(2)—C(24)	111.3(4)	As(4)—C(41)—Si(4)	116.6(5)
C(22)—Si(2)—C(23)	109.0(8)	As(5)—C(51)—Si(5)	112.3(3)

(c) Torsion angles[a]

As(5)—As(1)—As(2)—As(3)	57.91(4)	As(3)—As(4)—As(5)—C(51)	126.8(2)
As(5)—As(1)—As(2)—C(21)	−45.4(2)	C(41)—As(4)—As(5)—As(1)	128.1(2)
C(11)—As(1)—As(2)—As(3)	158.7(2)	C(41)—As(4)—As(5)—C(51)	−134.1(3)
C(11)—As(1)—As(2)—C(21)	55.4(3)	As(3)—As(4)—C(41)—Si(4)	−92.7(4)
As(2)—As(1)—As(5)—As(4)	−54.46(4)	As(5)—As(4)—C(41)—Si(4)	161.6(4)
As(2)—As(1)—As(5)—C(51)	−151.4(2)	As(1)—As(5)—C(51)—Si(5)	−169.3(3)
C(11)—As(1)—As(5)—As(4)	−153.4(2)	As(4)—As(5)—C(51)—Si(5)	91.6(3)
C(11)—As(1)—As(5)—C(51)	109.7(3)	C(12)—Si(1)—C(11)—As(1)	79.3(5)
As(2)—As(1)—C(11)—Si(1)	174.3(4)	C(13)—Si(1)—C(11)—As(1)	−41.8(6)
As(5)—As(1)—C(11)—Si(1)	−85.3(4)	C(14)—Si(1)—C(11)—As(1)	−162.4(5)
As(1)—As(2)—As(3)—As(4)	−38.89(4)	C(22)—Si(2)—C(21)—As(2)	150.0(7)
As(1)—As(2)—As(3)—C(31)	61.2(2)	C(23)—Si(2)—C(21)—As(2)	29.0(7)
C(21)—As(2)—As(3)—As(4)	67.1(2)	C(24)—Si(2)—C(21)—As(2)	−89.5(6)
C(21)—As(2)—As(3)—C(31)	167.2(3)	C(32)—Si(3)—C(31)—As(3)	70.0(6)
As(1)—As(2)—C(21)—Si(2)	178.3(3)	C(33)—Si(3)—C(31)—As(3)	−49.2(5)
As(3)—As(2)—C(21)—Si(2)	78.6(4)	C(34)—Si(3)—C(31)—As(3)	−170.4(5)
As(2)—As(3)—As(4)—As(5)	6.16(5)	C(42)—Si(4)—C(41)—As(4)	45.8(6)
As(2)—As(3)—As(4)—C(41)	−92.9(3)	C(43)—Si(4)—C(41)—As(4)	165.5(5)
C(31)—As(3)—As(4)—As(5)	−90.7(2)	C(44)—Si(4)—C(41)—As(4)	−74.1(6)
C(31)—As(3)—As(4)—C(41)	170.3(3)	C(52)—Si(5)—C(51)—As(5)	58.5(5)
As(2)—As(3)—C(31)—Si(3)	160.3(3)	C(53)—Si(5)—C(51)—As(5)	176.5(4)
As(4)—As(3)—C(31)—Si(3)	−93.6(3)	C(54)—Si(5)—C(51)—As(5)	−64.0(5)
As(3)—As(4)—As(5)—As(1)	29.05(4)		

[a] The torsion angle A—B—C—D is defined as positive if, when viewed along the B—C bond, atom A must be rotated clockwise to eclipse atom D.

The reaction of primary arsine **II** with Ph_3Ga in benzene proceeded slowly at RT; however, the cleavage of a single Ga—C bond occurred quantitatively at 55–57°C, yielding benzene and **III**. This trimer was isolated as a colourless sticky material and it did not eliminate benzene at RT. Monitoring of a sample of the reaction mixture between 43 and 80°C by ^1H NMR spectroscopy revealed that the decomposition of the single cleavage product started at 58–60°C and was completed at 80°C. Efforts to crystallize **III** were not successful but it could be characterized on the basis of molecular weight, ^1H NMR and analytical data. It is interesting to note that, whereas **III** is a trimer, $[(Me_3SiCH_2)_2AsGaPh_2]_2$ is a dimer.[2c] The ^1H NMR spectrum of **III** shows that two diastereoisomers exist depending on the disposition of As—H groups, i.e. axially or equatorially oriented on the $(Ga—As)_3$ ring. One isomer has three equivalent As—H protons, whereas the other has two equivalent As—H protons which are non-equivalent to the third As—H proton. It has been demonstrated by selective decoupling experiments that three different coupling patterns between the CH_2 protons and the As—H protons take place. In addition, reaction of $Me_3SiCH_2(H)AsLi$ with Ph_2GaCl afforded a yellow solid which, on the basis of its ^1H NMR spectrum, contains **III**; however, recrystallization of the yellow solid did not yield **III**.

Reaction of **II** with Me_3Ga in pentane at RT also gave a single cleavage product which was isolated as a colourless liquid containing a small amount of solid that slowly melted/dissolved at RT. On the basis of its ^1H NMR spectrum, we believe this product is $[Me_3SiCH_2(H)AsGaMe_2]_3$ (**IV**). The spectrum shows the same coupling pattern as that exhibited in the spectrum of **III**, but three peaks for the Me_3Si protons are merged into one peak. The four peaks at δ 0.774, 0.795, 0.814 and 0.832 can be explained by the overlapping of three doublets. Also, the three triplets for the As—H protons are partially overlapped. After storing this single cleavage product at −15°C for 9 weeks, it was observed that one of the three peaks in the NMR spectrum for the Me_2Ga protons was split into a doublet and another one appeared to have some splitting. Also, two additional doublets and one singlet appeared in the methylene region, while one more multiplet appeared up-field adjacent to the three As—H triplets. These observations imply that the trimer **IV** underwent the loss of CH_4.

Only H_2, Me_4Si, **VI** and unreacted $(Me_3SiCH_2)_3Ga$ were identified after allowing the latter to react with **II**. These results compare, in part, with those obtained by us in some related earlier work using the same tri(alkyl)gallane. Thus, with $PhAsH_2$, the products were H_2, Me_4Si, $(PhAs)_6$ and the cluster $[(PhAsH)(R_2Ga)(PhAs)_6(RGa)_4]$ ($R = Me_3SiCH_2$);[2a] with Ph_2AsH, the products were H_2, Me_4Si, $(Ph_2As)_2$ and impure $[Ph_2AsGa(CH_2SiMe_3)_2]_n$.[2b] On the other hand no side products were observed in the preparation of $[(Me_3SiCH_2)_2AsGaPh_2]_2$ from the reaction of $(Me_3SiCH_2)_2AsH$ with Ph_3Ga.[2c]

In a one-pot synthesis, **V** was obtained in a high yield from **II** via dilithiation followed by silylation at −78°C. In contrast, efforts to isolate the monosilylated arsine, $Me_3SiCH_2As(H)SiMe_3$, were unsuccessful. Thus, using a procedure similar to that used to prepare **V**, afforded only **II** and **V**. It is reasonable to assume that, in fact, monosilylated **II** was formed at low temperature but on warming to RT it underwent disproportionation. When the entire procedure was repeated at RT, **VI**, $(Me_3Si)_3As$ and an unidentified black precipitate were formed.

Three approaches were utilized in attempts to prepare and isolate an oligomer of the type $(RAs GaR')_n$. First, compound **III** was slowly heated in an effort to eliminate 1 mole equiv. of benzene. A ^1H NMR spectrum of a sample of **III** which had been heated for 2 days at 55–62°C revealed that the elimination had started to occur, but **III** was still the predominant species. On subsequent heating for 2 days at 76–82°C, a yellow solid formed and its ^1H NMR spectrum contained broad peaks indicative of a polymer or mixture of oligomers/polymers. Although a completely "satisfactory elemental analysis" (C and H) was not obtained, the data strongly support a formulation of $(Me_3SiCH_2As GaPh)_n$ for the yellow solid. Second, the reaction of $Me_3SiCH_2AsLi_2$ (prepared *in situ*) with $PhGaCl_2$, was investigated. There was also evidence in this case for the desired reaction product(s), but none was isolated in "pure" form. Third, dechlorosilylation reactions between **V** and $PhGaCl_2$ were carried out. In one experiment, a total of 1.68 equiv. of Me_3SiCl were evolved, leaving a colourless sticky residue. Attempts to crystallize the latter were unsuccessful; however, its ^1H NMR spectrum compares favourably to that obtained for the 80°C decomposition product of **III**.

In an effort to prepare **V** by an alternate and more direct method, the reaction of **I** with a mixture of Me_3SiCl and Mg in THF was carried out. No evidence for the desired product **V** was obtained; rather, the reaction afforded **VI**. This result conforms with the report that the reaction of *t*-$BuAsCl_2$ with Mg in THF or Et_2O yields $(t\text{-BuAs})_5$, in addition to $(t\text{-BuAs})_4$ and *t*-Bu_6As_8.[10] On the other hand, *t*-$BuP(SiMe_3)_2$ has been synthesized in high yield by the reaction of Me_3SiCl with Mg and *t*-

$BuPCl_2$.[11] In the purification of **VI** by distillation *in vacuo*, a small amount of the diarsine $[(Me_3SiCH_2)_2As]_2$ was formed and a mixture of the two products was obtained as a yellow liquid. After 1 week, **VI** crystallized from the liquid at RT and single crystals suitable for an X-ray diffraction study were obtained.

Crystal structure of $(Me_3SiCH_2As)_5$ (VI)

An ORTEP drawing of **VI** is shown in Fig. 1. Crystallographic data and a summary of data collection and refinement are presented in Table 1, bond lengths, bond angles and torsion angles are in Table 2 and a comparison of corresponding lengths and angles in **VI** and $(MeAs)_5$[12] is provided in Table 3. The As—As bond lengths are not all equal, As(1)—As(2) ≃ As(2)—As(3) < As(3)—As(4) ≃ As(4)—As(5) ≃ As(5)—As(1) and their mean at 2.437 Å is slightly longer than that of 2.428 Å in $(MeAs)_5$ as is the mean As—C distance at 1.99 Å in **VI** *vs* 1.96 Å in $(MeAs)_5$ Endocyclic torsion angles are related by an approximate C_s-symmetry axis passing through As(1) and the mid-point of the As(3)—As(4) bond, and thus the ring has an envelope-like conformation although it is clearly twisted somewhat as reflected in the distinctly non-zero value of 6.2° for the As(2)—As(3)—As(4)—As(5) torsion angle. As reflected in the values of corresponding torsion angles for **VI** and $(MeAs)_5$ (Table 3), the five-membered rings have similar conformations in both compounds.

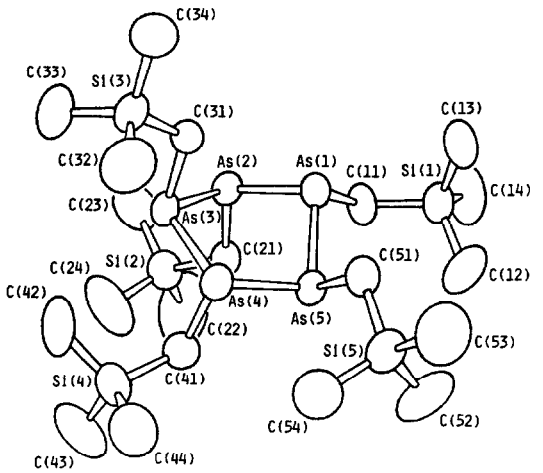

Fig. 1. ORTEP drawing of $(Me_3SiCH_2As)_5$ (**VI**); hydrogen atoms are omitted for clarity.

NMR spectra of $(Me_3SiCH_2As)_5$ (VI)

If the solid-state structure were to persist in solution, the ^1H NMR spectrum of **VI** would be ex-

Table 3. Comparison of bond lengths (Å) and angles (°) in $(MeAs)_5$[a] and $(MeSiCH_2As)_5$ (**VI**)

	$(MeAs)_5$	$(Me_3SiCH_2As)_5$
Bond lengths		
As(1)—As(2)	2.422(5)	2.428(1)
As(1)—As(5)	2.441(5)	2.443(1)
As(2)—As(3)	2.419(5)	2.424(1)
As(3)—As(4)	2.429(4)	2.443(1)
As(4)—As(5)	2.430(5)	2.446(1)
Bond angles		
As(2)—As(1)—As(5)	100.4(2)	99.05(4)
As(1)—As(2)—As(3)	97.5(2)	96.46(4)
As(2)—As(3)—As(4)	105.4(2)	105.24(4)
As(3)—As(4)—As(5)	105.4(2)	104.59(4)
As(1)—As(5)—As(4)	100.0(2)	98.29(4)
Torsion angles		
As(5)—As(1)—As(2)—As(3)	54.6(2)	57.91(4)
As(1)—As(2)—As(3)—As(4)	−38.8(2)	−38.89(4)
As(2)—As(3)—As(4)—As(5)	9.1(2)	6.16(5)
As(3)—As(4)—As(5)—As(1)	24.4(2)	29.05(4)
As(4)—As(5)—As(1)—As(2)	−49.4(2)	−54.46(4)

[a] The bond length and bond angle values for $(MeAs)_5$ were calculated using positional parameters contained in ref. 12.

pected to be very complex; however, it was found to be quite non-complex. It consisted of three singlets (intensity ratio 2:1:2)[13] [δ 0.185, 0.213 and 0.219 (CH_3)], two distinct AB patterns [δ 1.515 and 1.738, $^2J_{HH}$ = 13.63 Hz (CH_2); δ 1.538 and 1.687, $^2J_{HH}$ = 13.55 Hz (CH_2)]. The $^{13}C\{^1H\}$ NMR spectrum of **VI** shows three singlets each for CH_3 and CH_2 carbons, proving that three types of Me_3SiCH_2 groups are present. In the presence of a symmetry-generating torsional (restricted pseudorotational) motion proposed by Rheingold,[14] the symmetrical intermediate of **VI** would give exactly the same resonances as shown in the ^1H NMR spectrum which was obtained. The steric restrictions imposed by bulky Me_3SiCH_2 groups have a dampening effect on pseudorotation[15] of the ring puckering. As a result, a limited pseudorotation responsible for a time-averaged plane of symmetry takes place. According to Rheingold, there are four possible inversional isomers for the five-membered ring in $(ClCH_2As)_5$.[14] Interestingly, compound **VI** in the solid state has the conformation which corresponds to that isomer with the lowest internal energy.

Acknowledgements—We thank the Office of Naval Research and the Duke University Research Council for financial support.

REFERENCES

1. (a) G. E. Coates and J. Graham, *J. Chem. Soc.* 1963, 233; (b) O. T. Beachley and G. E. Coates, *J. Chem. Soc.* 1965, 3241.
2. For example see the following: (a) R. L. Wells, A. P. Purdy, A. T. McPhail and C. G. Pitt, *J. Chem. Soc., Chem. Commun.* 1986, 487; (b) C. G. Pitt, A. P. Purdy, K. T. Higa and R. L. Wells, *Organometallics* 1986, **5**, 1266; (c) R. L. Wells, A. P. Purdy, A. T. McPhail and C. G. Pitt, *J. Organomet. Chem.* 1986, **308**, 281; (d) C. G. Pitt, K. T. Higa, A. T. McPhail and R. L. Wells, *Inorg. Chem.* 1986, **25**, 2483; (e) A. P. Purdy, R. L. Wells, A. T. McPhail and C. G. Pitt, *Organometallics* 1987, **6**, 2099; (f) R. L. Wells, C. G. Pitt, A. T. McPhail, A. P. Purdy, S. Shafieezad and R. B. Hallock, *Chemy Mater.* 1989, **1**, 4; (g) R. L. Wells, W. K. Holley, S. Shafieezad, A. T. McPhail and C. G. Pitt, *Phosph. Sulfur Silicon* 1989, **41**, 15; (h) A. M. Arif, B. L. Benac, A. H. Cowley, R. Geerts, R. A. Jones, K. B. Kidd, J. M. Power and S. T. Schwab, *J. Chem. Soc., Chem. Commun.* 1986, 1543; (i) A. H. Cowley, B. L. Benac, J. G. Ekerdt, R. A. Jones, K. B. Kidd, J. Y. Lee and J. E. Miller, *J. Am. Chem. Soc.* 1988, **110**, 6248; (j) E. K. Byrne, L. Parkanyi and K. H. Theopold, *Science* 1988, **241**, 333.
3. S. C. Watson and J. F. Eastham, *J. Organomet. Chem.* 1967, **9**, 165.
4. F. C. Whitmore and L. H. Sommer, *J. Am. Chem. Soc.* 1946, **68**, 481.
5. C. F. McBrearty, K. Irgolic and R. A. Zingaro, *J. Organomet. Chem.* 1968, **12**, 377.
6. P. G. Perkins and M. E. Twentyman, *J. Chem. Soc.* 1965, 1038.
7. S. B. Miller and T. B. Brill, *J. Organomet. Chem.* 1979, **166**, 293.
8. H. Gilman and R. G. Jones, *J. Am. Chem. Soc.* 1940, **62**, 980.
9. O. T. Beachley and R. G. Simmons, *Inorg. Chem.* 1980, **19**, 1021.
10. M. Baudler and P. Bachmann, *Z. Anorg. Allg. Chem.* 1982, **485**, 129.
11. H. Schumann and L. Roesch, *Chem. Ber.* 1974, **107**, 854.
12. J. H. Burns and J. Waser, *J. Am. Chem. Soc.* 1957, **79**, 859.
13. E. J. Wells, R. C. Ferguson, J. G. Hallet and L. K. Peterson, *Can. J. Chem.* 1968, **46**, 2733.
14. A. L. Rheingold, *J. Organomet. Chem.* 1975, **102**, 445.
15. P. S. Elms, S. Middleton and B. O. West, *Aust. J. Chem.* 1970, **23**, 1559.

Polyhedron Vol. 9, No. 2/3, pp. 329–333, 1990
Printed in Great Britain

0277–5387/90 $3.00+.00
© 1990 Pergamon Press plc

A PHOSPHOLYL COMPLEX OF INDIUM

TREVOR DOUGLAS and KLAUS H. THEOPOLD*

Department of Chemistry, Baker Laboratory, Cornell University, Ithaca, NY 14853, U.S.A.

and

BRIAN S. HAGGERTY and ARNOLD L. RHEINGOLD*

Department of Chemistry and Biochemistry, University of Delaware, Newark, DE 19716, U.S.A.

Abstract—Reaction of InCl with the phospholyl anion, K(18-crown-6)$^+$[PC_4Me_4]$^-$, yielded the indium(III) ate complex K(18-crown-6)$^+$[$(Me_4C_4P)_2InCl_2$]$^-$. Its structure was determined by X-ray diffraction.

Recent interest in the organometallic chemistry of the group 13 elements aluminium, gallium and indium has been fuelled in part by the use of simple alkyls of these elements in the chemical vapour deposition (CVD) of III–V semiconductors (e.g. gallium arsenide, indium phosphide, etc.).[1] Thin films of indium phosphide, for example, are currently grown epitaxially by the high-temperature reaction of $InMe_3$ with PH_3.[2] We are exploring the potential of precursors which contain both of the elements of the desired semiconductor in the same molecule.[3] Herein we report the synthesis and characterization of an indium compound containing phosphorus ligands.

The CVD process requires volatile compounds. In designing synthetic targets we were thus attracted to cyclopentadienyl derivatives of indium(I), which have appreciable vapour pressures.[4] We reasoned, that substitution of a phosphorus atom for a carbon of the cyclopentadienyl ring (see Scheme 1) might yield a volatile molecule containing both indium and phosphorus which might also feature a fragmentation pathway with a low activation barrier and relatively unreactive products. The latter would seem to provide a solution to the persistent problem of carbon incorporation into the growing semiconductor film.[5]

RESULTS AND DISCUSSION

We have recently described convenient syntheses of the phospholyl anion salts $M^+[PC_4Me_4]^-$.[6] Addition of 1.0 equivalent of InCl to a toluene solution of the potassium salt, K(18-crown-6)$^+$[PC_4Me_4]$^-$, yielded a dark precipitate and a colourless solution. Filtration, evaporation of solvent and recrystallization from THF gave colourless crystals of a new material. Based on the spectroscopic and analytical data it was assigned the formula K(18-crown-6)$^+$[$(Me_4C_4P)_2InCl_2$]$^-$ (**1**), an ate complex of indium(III). Complex **1** was isolated in 24% yield based on InCl.

The crystal structure of **1** has been determined by X-ray diffraction and the result is shown in Fig. 1.† Interatomic distances and angles are listed in Tables 1 and 2, respectively. The coordination environment of indium in the complex anion is a distorted tetrahedron consisting of the two phosphorus atoms of η^1-phospholyl ligands and two chlorides. The angles about indium range between 98.7(1)° (between the chloride ligands) to 131.2(1)° (between the bulky phospholyl groups). The indium–phosphorus bond distances of 2.481(3) and 2.491(3) Å closely approximate the sum of the covalent radii of the two elements (In, 1.44 Å; P, 1.06 Å). However, they are significantly shorter than the corresponding distances in comparable molecules. Phosphido-bridged dimers of the type $[R_2In(\mu_2\text{-}PR'_2)]_2$ feature In—P distances in the range 2.59–2.66 Å,[7] while monomeric molecules exhibit slightly shorter bonds, i.e. 2.588(14), 2.574(11) and 2.613(12) Å in the neutral $In(P^tBu_2)_3$[7b] and 2.585(2), 2.576(2),

* Authors to whom correspondence should be addressed.

† Supplementary material available: Atomic coordinates have been deposited with the Director, Cambridge Crystallographic Centre.

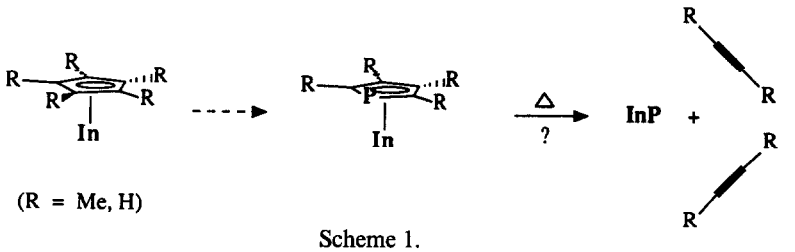

(R = Me, H)

Scheme 1.

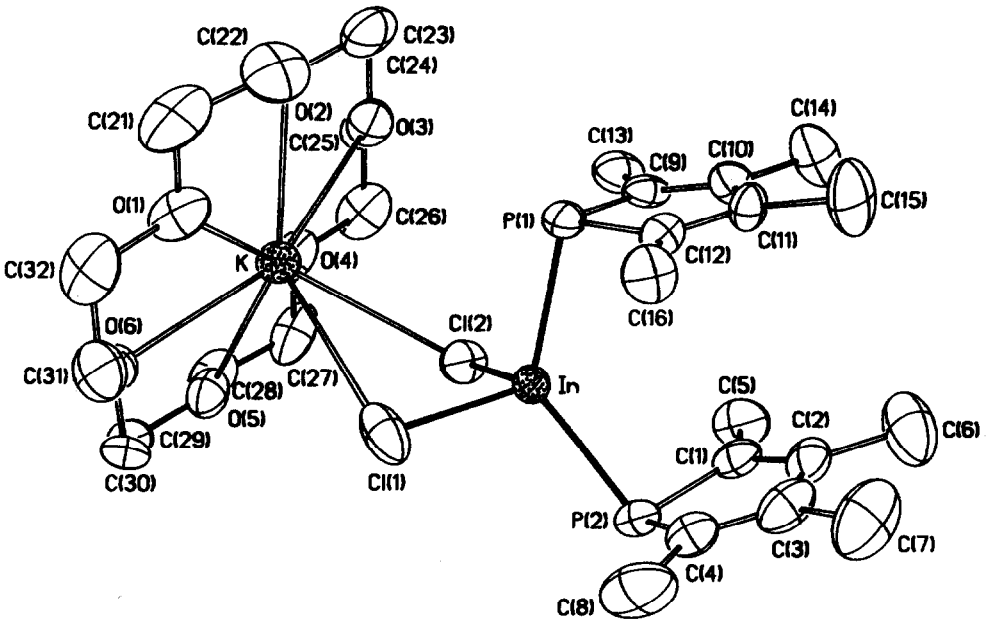

Fig. 1. The molecular structure of $K(18\text{-crown-6})^+[(Me_4C_4P)_2InCl_2]^-$ (**1**) in the crystal.

Table 1. Bond lengths (Å)

In—Cl(1)	2.427(4)	In—Cl(2)	2.441(3)
In—P(1)	2.491(3)	In—P(2)	2.481(3)
In—K	4.258(2)	Cl(1)—K	3.817(4)
Cl(2)—K	3.243(4)	K—O(1)	2.800(8)
K—O(2)	2.874(8)	K—O(3)	2.877(6)
K—O(4)	2.821(8)	K—O(5)	2.789(8)
K—O(6)	2.907(7)	P(1)—C(12)	1.761(10)
P(1)—C(9)	1.793(11)	P(2)—C(4)	1.776(11)
P(2)—C(1)	1.772(12)	C(1)—C(5)	1.466(17)
C(1)—C(2)	1.359(16)	C(2)—C(6)	1.523(18)
C(2)—C(3)	1.426(19)	C(3)—C(7)	1.533(20)
C(3)—C(4)	1.318(16)	C(9)—C(10)	1.322(15)
C(4)—C(8)	1.511(15)	C(10)—C(11)	1.430(15)
C(9)—C(13)	1.495(15)	C(11)—C(12)	1.358(14)
C(10)—C(14)	1.508(16)	C(12)—C(16)	1.513(15)
C(11)—C(15)	1.515(16)		

Table 2. Bond angles (°)

Cl(1)—In—Cl(2)	98.7(1)	Cl(1)—In—P(1)	103.8(1)
Cl(2)—In—P(1)	104.6(1)	Cl(1)—In—P(2)	109.9(1)
Cl(2)—In—P(2)	103.9(1)	P(1)—In—P(2)	131.2(1)
Cl(1)—In—K	62.8(1)	Cl(2)—In—K	49.2(1)
P(1)—In—K	81.6(1)	P(2)—In—K	145.5(1)
In—Cl(1)—K	82.8(1)	In—Cl(2)—K	96.0(1)
In—K—Cl(2)	34.7(1)	Cl(1)—K—Cl(2)	62.5(1)
In—P(1)—C(9)	98.8(3)	In—P(1)—C(12)	101.7(3)
C(9)—P(1)—C(12)	90.9(5)	In—P(2)—C(1)	99.9(4)
In—P(2)—C(4)	98.8(4)	C(1)—P(2)—C(4)	90.6(5)
P(2)—C(1)—C(2)	108.9(9)	P(2)—C(1)—C(5)	123.9(9)
C(2)—C(1)—C(5)	127.0(11)	C(1)—C(2)—C(3)	115.2(11)
C(1)—C(2)—C(6)	123.7(12)	C(3)—C(2)—C(6)	121.0(11)
C(2)—C(3)—C(4)	113.0(11)	C(2)—C(3)—C(7)	122.9(11)
C(4)—C(3)—C(7)	124.0(12)	P(2)—C(4)—C(3)	111.6(9)
P(2)—C(4)—C(8)	121.7(9)	C(3)—C(4)—C(8)	126.2(11)
P(1)—C(9)—C(10)	109.3(8)	P(1)—C(9)—C(13)	124.4(8)
C(10)—C(9)—C(13)	126.0(10)	C(9)—C(10)—C(11)	115.9(10)
C(9)—C(10)—C(14)	124.3(10)	C(11)—C(10)—C(14)	119.8(10)
C(10)—C(11)—C(12)	112.7(9)	C(10)—C(11)—C(15)	123.4(10)
C(12)—C(11)—C(15)	123.8(10)	P(1)—C(12)—C(11)	110.6(8)
P(1)—C(12)—C(16)	123.5(8)	C(11)—C(12)—C(16)	125.9(9)

2.586(2) and 2.556(2) Å in the ate complex $Li(THF)_4[In(PPh_2)_4]$.[8] The latter values probably reflect the steric bulk of the respective phosphide ligands.

η^1-Coordination of the phospholyl moiety to metals is rare.[9] However, in this case it parallels the bonding of the all carbon analogue; i.e. the pentamethylcyclopentadienyl ligand binds to indium(III) in a η^1-fashion also.[10] The bond distances within the heterocycles are very similar to the ones found in the structurally characterized benzylphosphole[11] and unlike those of the delocalized phospholyl anion found in $Li(TMEDA)^+[PC_4Me_4]^-$.[6] The small difference in electronegativity between indium and phosphorus (In, 1.7; P, 2.1) also points to the covalent nature of the In—P bonds in **1**. The phosphorus atoms assume trigonal pyramidal configurations, the sum of the bond angles about them being 291.4° for P(1) and 289.3° for P(2). Their lone pairs are apparently not interacting with the indium, making the phospholyl groups formally one-electron donors.

The In—Cl bond length [In—Cl(1), 2.427(4) Å; In—Cl(2), 2.441(3) Å] are typical for this element combination (sum of covalent radii = 2.43 Å) and similar to the distances reported for the $[MeInCl_3]^-$ ion (In—Cl_{av}, 2.40 Å).[12] One of the chloride ligands [Cl(2)] is interacting weakly with the potassium cation, the distance of 3.244(4) Å being only slightly longer than the sum of the ionic radii (K^+, 1.33 Å; 1.81 Å). The coordination sphere of the potassium is completed by the six oxygen atoms of the crown ether. The bond distances and angles found for this part of the molecule are normal [see for example the structure of $K(18\text{-crown-6})^+SCN^-$].[13]

Complex **1** is obviously the result of a disproportionation reaction (see Scheme 2). The desired indium(I) derivative $(Me_4C_4P)In$, while probably formed initially, may be unstable under the reaction conditions. Beachley *et al.* have found that $(\eta^5\text{-}C_5Me_5)In$ decomposes in donor solvents (THF, pyridine), yielding products consistent with a ligand induced disproportionation.[14] It is possible that free crown ether has a similar effect upon $(Me_4C_4P)In$. In an attempt to eliminate any donor molecules, we have combined InCl with $[LiPC_4Me_4]_n$ in toluene. This reaction yielded an off-white precipitate and a yellow solution, from which a yellow powder precipitated upon standing. This material did not contain chloride and the IR spectrum of the solid as a KBr pellet exhibited bands characteristic of the phospholyl group. The yellow powder was almost completely insoluble in nonpolar organic solvents; however, a very dilute solution in C_6D_6 exhibited resonances consistent with a coordinated phospholyl moiety [1.84 (s), 2.40, (d, J_{PH} = 11 Hz)]. Addition of THF to the yellow solid initially gave a yellow solution, followed by the formation of a black precipitate (indium metal?) and 1,1′-biphospholyl (**2**).[6] Similarly, an attempted sublimation yielded a grey residue and a white sublimate of 1,1′-biphospholyl. Based on these obser-

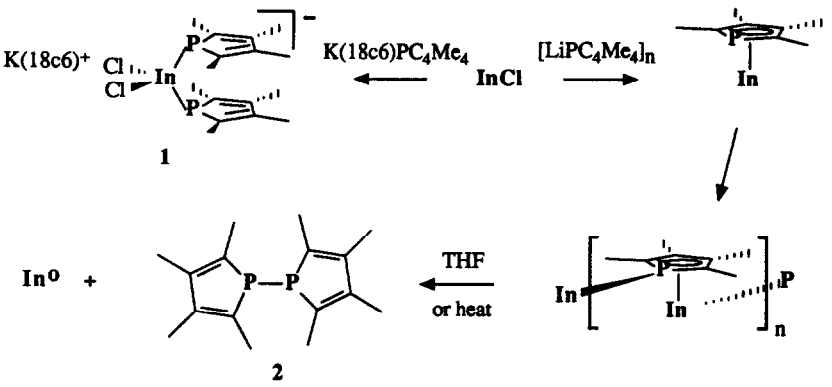

Scheme 2.

vations, we believe that $(Me_4C_4P)In$ is indeed formed. However, in non-polar solvents it apparently polymerizes, while donor solvents or heating lead to its decomposition.

EXPERIMENTAL

All manipulations involving air-sensitive organometallic compounds were carried out in a Vacuum Atmospheres inert-atmosphere box under N_2 or on a Schlenk line using Ar or N_2. Solvents were distilled under N_2 from purple benzophenone ketyl. NMR: Bruker WM 300 spectrometer (300 MHz for ^1H, 75.47 MHz for ^{13}C and 121.49 MHz for ^{31}P). Shifts are reported in ppm downfield of TMS (for ^1H and ^{13}C) using the solvent resonances as reference and relative to an external PCl_3 reference at 219 ppm for ^{31}P. IR: Mattson Alpha Centauri FT–IR. InCl and 18-crown-6 (Aldrich) were used as received.

Potassium(18 - *crown* - 6)*bis*(*chloro*)*bis*(η^1 - 2,3,4,5 - *tetramethylphospholyl*)*indate*(I) (**1**)

To a toluene solution of K(18-crown-6)PC_4Me_4 (451 mg, 1.0 mmol) was added InCl (150 mg, 1.0 mmol) and the reaction mixture was stirred at ambient temperature for 1 h. The dark precipitate was filtered off, the solvent evaporated under vacuum, and the residue recrystallized from THF at −30°C (185 mg, 24% yield). ^1H NMR (CD_2Cl_2): 3.65 (s, 24 H), 2.07 (d, 12 H, J_{PH} = 10.4 Hz), 1.91 (s, 12 H); ^{31}P NMR (CD_2Cl_2): −19.16 (s); ^{13}C NMR (CD_2Cl_2): 140.61 (s), 133.09 (d, J_{PC} = 15.1 Hz), 70.75 (s), 14.38 (d, J_{PC} = 31 Hz), 14.18 (s). IR (KBr): 2897 (vs), 2788 (m), 1974 (m), 1471 (s), 1453 (s), 1351 (vs), 1284 (s), 1120 (vs), 962 (vs), 837 (s), 804 (w), 553 (w), 530 (m), 513 (m) cm^{-1}. Found: C, 43.91; H, 5.72. Calc. for $C_{28}H_{48}Cl_2InKO_6P_2$: C, 43.82; H, 6.26%.

Table 3. Crystallographic data for **1**

Crystal parameters	
Formula	$C_{28}H_{48}Cl_2InKO_6P_2$
Space group	$P2_12_12_1$
Crystal system	Orthorhombic
a (Å)	10.467(2)[a]
b (Å)	13.773(3)
c (Å)	25.840(6)
V (Å^3)	3725.4(25)
Z	4
Crystal dimensions (mm)	0.10 × 0.28 × 0.48
Crystal colour	Colourless
D(calc) (g cm^{-3})	1.197
μ(Mo-K_α) (cm^{-1})	10.0
Temperature (°C)	23
T(max)/T(min)	1.13
Data collection	
Diffractometer	Nicolet R3m
Monochromator	Graphite
Scan technique	Wyckoff
Radiation	Mo-K_α
2θ scan range (°)	$4 \leqslant 2\theta \leqslant 45$
Data collected	$\pm h, +k, +l$
Scan speed (° min^{-1})	var., 6–20
Reflections collected	5184
Independent reflections	4819
R(merg) (%)	4.1
Independent reflections observed	3390
Standard reflections	3 std/197 reflns
Variation in standards	< 2%
Refinement	
$R(F)$	0.0504
RwF	0.0574
Δ/σ (max)	0.09
$\Delta(\rho)$ (e/Å^{-3})	0.82
GOF	1.107
N_o/N_v	9.23

[a] Unit cell parameters from the least-squares best fit of the angular settings of 25 reflections ($21° \leqslant 2\theta \leqslant 26°$).

X-ray structure determination of **1**

Crystallographic data are summarized in Table 3. A colourless specimen mounted in a glass capillary was found to belong to the orthorhombic crystal system. Systematic absences in the reflection data uniquely determined the space group as $P2_12_12_1$. No correction for absorption was required. The structure was solved by direct methods and refined with anisotropic thermal parameters for all non-hydrogen atoms. Hydrogen atoms were treated as idealized contributions ($d_{CH} = 0.96$ Å). All software is contained in the SHELXTL library, version 5.1 (G. Sheldrick, Nicolet XRD, Madison, WI).

Acknowledgements—This research was supported by grants from AKZO Corporate Research America Inc. and the New York State Science and Technology Foundation.

REFERENCES

1. (a) A. H. Cowley and R. A. Jones, *Angew. Chem.* 1989, **101**, 1235; (b) M. R. Leys, *Chemtronics* 1987, **2**, 155.
2. (a) G. B. Stringfellow, *Semiconductors and Semimetals* (Edited by T. S. Tsang), Vol. 22, Pt A, p. 209. Academic Press, New York (1985); (b) M. J. Ludowise, *J. Appl. Phys.* 1985, **58**, R31.
3. (a) E. K. Byrne, L. Parkanyi and K. H. Theopold, *Science* 1988, **241**, 332; (b) E. K. Byrne, T. Douglas and K. H. Theopold, *Mater. Res. Soc. Symp. Proc.* 1989, **131**, 59.
4. E. G. A. Staring and G. J. B. M. Meekes, *J. Am. Chem. Soc.* 1989, **111**, 7648 and refs therein.
5. (a) R. M. Lum, J. K. Klingert, D. W. Kisker, S. M. Abys and F. A. Stevie, *J. Cryst. Growth* 1988, **93**, 120; (b) O. Aina, M. Mattingly, S. Steinhauser, R. Mariella Jr and A. Melas, *J. Cryst. Growth* 1988, **92**, 215; (c) A. D. Reed, S. S. Bose and G. E. Stillman, *Appl. Phys. Lett.* 1989, **54**, 1262.
6. T. Douglas and K. H. Theopold, *Angew. Chem.* 1989, **101**, 1394.
7. (a) O. T. Beachley Jr, J. P. Kopasz, H. Zhang, W. E. Hunter and J. L. Atwood, *J. Organomet. Chem.* 1987, **325**, 69; (b) N. W. Alcock, I. A. Degnan, M. G. H. Wallbridge, H. R. Powell, M. McPartlin and G. M. Sheldrick, *J. Organomet. Chem.* 1989, **361**, C33; (c) K. A. Aitchison, J. D. J. Backer-Dirks, D. C. Bradley, M. M. Faktor, D. M. Frigo, M. B. Hursthouse, B. Hussain and R. L. Short, *J. Organomet. Chem.* 1989, **366**, 11.
8. C. J. Carrano, A. H. Cowley, D. M. Giolando, R. A. Jones, C. M. Nunn and J. M. Power, *Inorg. Chem.* 1988, **27**, 2709.
9. (a) F. Mathey, J. Fischer and J. H. Nelson, *Struct. Bond.* 1983, **55**, 153; (b) E. Abel and C. Towers, *J. Chem. Soc., Dalton Trans.* 1979, 814.
10. T. Douglas and K. H. Theopold, manuscript in preparation on the synthesis and reactions of $[Cp^*(Cl)In—P(SiMe_3)_2]_2$; see ref. 3b for a picture.
11. P. Coggon and A. T. McPhail, *J. Chem. Soc., Dalton Trans.* 1973, 1888.
12. H. J. Guder, W. Schwartz, J. Weidlein, H. J. Widler and H. D. Hausen, *Z. Naturf.* 1976, **31B**, 1185.
13. P. Seiler, M. Dobler and J. D. Dunitz, *Acta Cryst.* 1974, **B30**, 2744.
14. O. T. Beachley Jr, R. Blom, M. R. Churchill, K. Faegri Jr, J. C. Fettinger, J. C. Pazik and L. Victoriano, *Organometallics* 1989, **8**, 346.

Polyhedron Vol. 9, No. 2/3, pp. 335–342, 1990
Printed in Great Britain

0277–5387/90 $3.00+.00
© 1990 Pergamon Press plc

THE CHEMISTRY OF DIPHENYLPHOSPHINE ADDUCTS OF TRIS(NEOPENTYL) AND TRIS(TRIMETHYLSILYLMETHYL)GALLIUM AND -INDIUM INCLUDING THE CRYSTAL AND MOLECULAR STRUCTURE OF $(Me_3CCH_2)_3Ga \cdot P(H)Ph_2$

MICHAEL A. BANKS, O. T. BEACHLEY, Jr* and JOHN D. MALONEY

Department of Chemistry, State University of New York at Buffalo, Buffalo, NY 14214, U.S.A.

and

ROBIN D. ROGERS*

Department of Chemistry, Northern Illinois University, DeKalb, IL 60114, U.S.A.

Abstract—The adducts $(Me_3CCH_2)_3Ga \cdot P(H)Ph_2$ and $(Me_3SiCH_2)_3Ga \cdot P(H)Ph_2$ have been prepared as crystalline solids at room temperature and characterized by cryoscopic molecular weight measurements in benzene solution and ^1H NMR, ^{31}P NMR and IR spectroscopic data. The molecular weight studies demonstrate that both adducts are extensively dissociated in solution and that $Ga(CH_2CMe_3)_3$ is a stronger Lewis acid than $Ga(CH_2SiMe_3)_3$. An X-ray structural study defined the nature of $(Me_3CCH_2)_3Ga \cdot P(H)Ph_2$ in the solid state. The colourless crystal contains two discrete molecules in each unit cell. The compound crystallizes in the triclinic space group $P\bar{1}$ with unit cell dimensions of $a = 9.564(8)$, $b = 12.208(5)$, $c = 12.946(9)$ Å, $\alpha = 100.00(5)$, $\beta = 100.41(8)$, $\gamma = 102.97(7)°$ and $D_{calc} = 1.10$ g cm^{-3}. The adduct has a relatively long Ga—P distance of 2.683(5) Å and the α-carbon atoms of the substituents on gallium and phosphorus are essentially but not perfectly eclipsed. The syntheses of $(Me_3CCH_2)_3In \cdot P(H)Ph_2$ and $(Me_3SiCH_2)_3In \cdot P(H)Ph_2$ were attempted but room temperature elimination reactions, which produced CMe_4 and $SiMe_4$, respectively, and the appropriate organoindium phosphides, precluded the isolation of adducts. Simple kinetic studies revealed that $In(CH_2CMe_3)_3 - P(H)Ph_2$ eliminated CMe_4 at 17°C significantly faster than $In(CH_2SiMe_3)_3 - P(H)Ph_2$ produced $SiMe_4$.

The compound semiconductors GaAs and InP have spurred a renewed interest in the chemistry of gallium and indium. Much of the characteristic chemistry of these group 13 elements can be related to the ability of the metal atom to accept an electron pair. Thus, organo-gallium and -indium compounds react with Lewis bases to form adducts. If the Lewis base has an acidic proton, an elimination reaction can occur typically at elevated temperatures to produce compounds of the type R_2MER_2. Thus, it is logical that compounds of the type MR_3,[1] $R_3M \cdot ER_3$[2] and R_2MER_2[3] have been used as precursors for making the compound semiconductors.

A review of the literature[4] suggests that all of the physical measurements of thermodynamic parameters related to stabilities of adducts and of the structural studies of homoleptic organo-gallium and -indium compounds with phosphorus and arsenic bases have involved $GaMe_3$ or $InMe_3$. The enthalpies of dissociation of $Me_3Ga \cdot L$ and $Me_3In \cdot L$ (L = PMe_3 and $AsMe_3$) were measured by vapour pressure techniques.[5] Even though ^1H NMR studies[6] have been used to relate the ΔH_{diss} of $Et_3Ga \cdot PMe_3$ to $Me_3Ga \cdot PMe_3$, no quantitative studies have verified the early predictions. It is regrettable but no quantitative studies permit comparisons of the effects of different organic substituents on the Lewis acidities of organo-gallium and -indium compounds to a common Lewis base.

* Authors to whom correspondence should be addressed.

There is also a surprising lack of structural information on adducts of gallium or indium. Only the adducts $Me_3M \cdot P(Ph)_2C_2H_4(Ph_2)P \cdot MMe_3$ (M = Ga, In),[7,8] $Me_2ClGa \cdot P(Ph)_2CH_2P(Ph)_2$[9] and $Cl_3Ga \cdot PMe_3$[10] have been the subject of X-ray structural studies, whereas $Me_3Ga \cdot NMe_3$[11] and $Me_3Ga \cdot PMe_3$[11] have been investigated by electron diffraction techniques.

In this paper, we report the synthesis and characterization of two gallium–phosphorus adducts, $(Me_3CCH_2)_3Ga \cdot P(H)Ph_2$ and $(Me_3SiCH_2)_3Ga \cdot P(H)Ph_2$, and the attempted synthesis of $(Me_3CCH_2)_3In \cdot P(H)Ph_2$ and $(Me_3SiCH_2)_3In \cdot P(H)Ph_2$. The indium-containing adducts were not sufficiently stable at room temperature to permit characterization due to the occurrence of elimination reactions. It is noteworthy that the X-ray structural study of $(Me_3CCH_2)_3Ga \cdot P(H)Ph_2$ provides the first structure of an adduct of a heavier group 13 element with a Lewis base which incorporates an acidic hydrogen. Cryoscopic molecular weight studies of $(Me_3CCH_2)_3Ga \cdot P(H)Ph_2$ and $(Me_3SiCH_2)_3Ga \cdot P(H)Ph_2$ permit calculations of the per cent dissociation of the adducts and, in turn, of the equilibrium constants for dissociation of the adducts. Thus, the effects of the neopentyl and trimethylsilylmethyl substituents on the Lewis acidities of the organo-gallium compounds have been evaluated quantitatively.

EXPERIMENTAL

All compounds described in this investigation were extremely sensitive to oxygen and moisture and were manipulated in a standard vacuum line or in a purified argon atmosphere. The gallium and indium alkyls, $Ga(CH_2CMe_3)_2$,[12] $Ga(CH_2SiMe_3)_3$,[13] $In(CH_2CMe_3)_3$[14] and $In(CH_2SiMe_3)_3$[15] were prepared and purified by literature methods. Diphenylphosphine was purchased from Strem Chemicals Inc. and purified by vacuum distillation. Solvents were dried by conventional procedures. Elemental analyses were performed by Schwarzkopf Microanalytical Laboratory, Woodside, New York. IR spectra of Nujol mulls between CsI plates were recorded by means of a Perkin–Elmer 683 spectrometer. Absorption intensities are reported with the abbreviations vs (very strong), s (strong), m (medium), w (weak) and sh (shoulder). The ^1H NMR spectra were recorded at 90 or 300 MHz by using either a Varian EM-390 or a Varian Gemini-300 spectrometer, respectively. Proton chemical shifts are reported in δ units (ppm) and are referenced to $SiMe_4$ as δ 0.00 and benzene as δ 7.13. The ^{31}P NMR spectra were recorded at 36.23 or 161.90 MHz by using either a JEOL FX-90Q or a Varian VXR-400 spectrometer, respectively. Phosphorus chemical shifts are reported relative to 85% H_3PO_4 as δ 0.00 ppm. Negative values are assigned for shifts upfield of H_3PO_4. All samples for NMR spectra were contained in sealed NMR tubes. Melting points were observed in sealed capillaries. Molecular weights were measured cryoscopically in benzene by using an instrument similar to that described by Shriver and Drezdzon.[16]

Synthesis of the tris(neopentyl)gallium(III) *diphenylphosphine adduct*, $(Me_3CCH_2)_3Ga \cdot P(H)Ph_2$

A 100 cm^3 Schlenk flask was charged with 0.377 g (1.33 mmol) of $Ga(CH_2CMe_3)_3$ in the glove box. A tared screw-cap vial was used to weigh 0.248 g (1.33 mmol) of $HPPh_2$. Anhydrous pentane was used to assure quantitative transfer of the $HPPh_2$ to the reaction flask. The tared- screw-cap vial was rinsed five times with aliquots of pentane (4 cm^3 each time). The flask was fitted with an adapter, cooled to −196°C and evacuated on the vacuum line. The resulting mixture was stirred for 10 min at ambient temperature and the pentane was then removed by vacuum distillation to leave 0.591 g of a colourless crystalline solid [1.26 mmol, 94.7% yield based on $Ga(CH_2CMe_3)_3$] of $(Me_3CCH_2)_3Ga \cdot P(H)Ph_2$. Crystals suitable for an X-ray crystallographic study of $(Me_3CCH_2)_3Ga \cdot P(H)Ph_2$ were obtained by allowing a melted sample of the compound to slowly flow down the wall of a Pyrex tube.

$(Me_3CCH_2)_3Ga \cdot P(H)Ph_2$. Melting point: 33.0–34.0°C. ^1H NMR (C_6D_6, δ): 0.0689 m: 1.04 (s, —CH_2—), 1.10 (s, —CMe_3), 5.20 (d, J_{PH} = 232 Hz, H—P), 6.99–7.40 (m, Ph); 0.138 m: 1.06 (s, —CH_2—), 1.12 (s, —CMe_3), 5.22 (d, J_{PH} = 241 Hz, H—P), 6.99–7.40 (m, Ph). ^{31}P NMR (C_6D_6, δ): 0.0689 m: −37.8 (d, J_{PH} = 232 Hz); 0.138 m: −36.5 (doublet of pentets, J_{PH} = 241 Hz, $^3J_{PCCH}$ = 8 Hz). Cryoscopic molecular weight (calculated molality, observed molality, α or per cent dissociation, K) (see Results and Discussion): 0.05223, 0.0828, 58.5%, 0.0431; 0.04632, 0.0732, 58.1%, 0.0372; 0.04154, 0.0668, 60.8%, 0.0392; 0.03284, 0.0532, 62.0%, 0.0446. Found: C, 65.77, 66.76; H, 9.42, 9.13. Calc.: C, 69.08; H, 9.47. (see Results and Discussion). IR (Nujol mull, cm^{-1}): 3075 (w), 3058 (w), 2730 (vw), 2710 (vw), 2328 (vw), 2318 (vw), 2280 (vw), 1968 (vw), 1955 (vw), 1870 (vw), 1803 (vw), 1585 (vw), 1570 (vw), 1567 (vw), 1552 (vw), 1545 (vw), 1432 (s), 1358 (vs), 1325 (vw), 1295 (vw), 1268 (vw), 1222 (s), 1160 (vw), 1155 (vw), 1130 (w), 1102 (w), 1065 (w), 1032 (w), 1020 (w), 997 (w), 960 (w), 925 (vw), 915 (vw), 908 (vw), 885 (m), 840 (vw), 805 (w), 738 (s), 721 (vs), 689 (vs),

670 (w, sh), 612 (vw, sh), 599 (m), 500 (m), 458 (w, sh), 450 (w), 425 (w), 412 (w), 380 (w), 285 (w), 282 (w), 270 (w).

Synthesis of the tris[(trimethylsilyl)methyl]gallium(III) *diphenylphosphine adduct*, $(Me_3SiCH_2)_3Ga \cdot P(H)Ph_2$

A 100 cm^3 round-bottom flask equipped with a 15 mm Solv-Seal joint was charged with 0.390 g (1.18 mmol) of $Ga(CH_2SiMe_3)_3$. A tared screw-cap vial charged with 0.220 g (1.18 mmol) of $HPPh_2$. The $HPPh_2$ was transferred quantitatively to the round-bottom flask by multiple washings with anhydrous pentane (20 cm^3). The flask was fitted with an adapter and evacuated. The reaction mixture was stirred for 15 min and the pentane was removed by vacuum distillation. A colourless, crystalline solid (0.514 g, 0.992 mmol, 84.4% of $(Me_3SiCH_2)_3Ga \cdot P(H)Ph_2$) was isolated.

$(Me_3SiCH_2)_3Ga \cdot P(H)Ph_2$. Melting point: 23.5–24.2°C. ^1H NMR (C_6D_6, δ): 0.0689 m: 0.05 (s, $-CH_2-$), 0.12 (s, $-CMe_3$), 5.21 (d, $J_{PH} = 232$ Hz, H—P), 6.98–7.37 (m, Ph); 0.138 m: 0.03 (s, $-CH_2-$), 0.13 (s, $-CMe_3$), 5.23 (d, $J_{PH} = 240$ Hz, H—P), 6.98–7.37 (m, Ph). ^{31}P NMR (C_6D_6, δ) 0.0689 m: −38.4 (d, $J_{PH} = 232$ Hz); 0.138 m: −37.7 (doublet of pentets, $J_{PH} = 240$ Hz, $^3J_{PCCH} = 8$ Hz). Cryoscopic molecular weight (calculated molality, observed molality, α or per cent dissociation, K) (see Results and Discussion): 0.0492, 0.0794, 61.5%, 0.0482; 0.0376, 0.0629, 67.4%, 0.0523; 0.0375, 0.0628, 67.5%, 0.0525; 0.0314, 0.0541, 72.1%, 0.0586; 0.0312, 0.0519, 65.4%, 0.0408. IR (Nujol mull, cm^{-1}): 3076 (w), 3058 (w), 3020 (w), 3005 (w), 2948 (s), 2895 (m), 2860 (m), 2685 (vw), 2475 (vw, br), 2340 (vw), 2325 (vw), 2285 (vw), 1970 (vw), 1950 (vw), 1928 (vw), 1875 (vw, br), 1850 (vw, br), 1805 (vw), 1584 (vw), 1571 (w), 1468 (m), 1433 (m), 1390 (w), 1350 (w), 1325 (w), 1292 (w), 1251 (s), 1240 (vs), 1180 (w), 1155 (vw), 1102 (w), 1065 (w), 1024 (w), 990 (m, br), 955 (m, sh), 920 (w, sh), 885 (m), 848 (vs), 822 (vs), 749 (vs), 739 (s, sh), 720 (vs), 678 (s), 610 (m), 594 (w), 568 (w), 548 (w), 520 (m), 506 (m), 448 (w), 429 (w), 412 (vw), 286 (vw), 256 (vw), 238 (w), 223 (w).

Reaction of $Ga(CH_2SiMe_3)_3$ *with* $HPPh_2$, *an NMR scale reaction*

An NMR tube was charged with an aliquot of a solution containing 0.105 g (0.318 mmol) of $Ga(CH_2SiMe_3)_3$ and 0.0593 g (0.318 mmol) of $HPPh_2$ in 5 cm^3 of benzene. The NMR tube was flame-sealed with a torch, then both ^1H and $^{31}P\{^1H\}$ NMR spectra were recorded. ^1H NMR (0.07 m, C_6H_6, δ): 0.08 (s, 6 H, $-CH_2-$), 0.15 (s, 27 H, $-CMe_3$), 4.93 (one line of the doublet for H—P). ^{31}P NMR (C_6H_6, δ): −39.3 (doublet, $J_{PH} = 240$ Hz).

Attempted synthesis of the tris(neopentyl)indium(III) *diphenylphosphine adduct*, $(Me_3CCH_2)_3In \cdot P(H)Ph_2$

A 100 cm^3 round-bottom flask was charged with 0.357 g (1.09 mmol) of $In(CH_2CMe_3)_3$, 0.203 g (1.09 mmol) of $HPPh^2$ and 10 cm^3 of pentane. The flask was evacuated and the mixture was stirred for 30 min at ambient temperature. Pentane was removed by vacuum distillation and 0.484 g of a colourless solid was isolated. The ^{31}P NMR spectra indicated that both the adduct $(Me_3CCH_2)_3In \cdot P(H)Ph_2$ and compound $(Me_3CCH_2)_2InPPh_2$[17] were present.

Mixture of $(Me_3CCH_2)_3In \cdot P(H)Ph_2$ *and* $(Me_3CCH_2)_2InPPh_2$. Melting point: partial melting at 48.2–48.8°C, followed by melting with decomposition of solid particles at 150–155°C. ^{31}P NMR (C_6H_6, δ): −31.1 (s, 1.4, $(Me_3CCH_2)_2InPPh_2$), −40.0 (doublet of pentets, 2.6, $J_{PH} = 260$ Hz, $(Me_3CCH_2)_3In \cdot P(H)Ph_2$), −50.6 (s, 1.0, $[(Me_3CCH_2)_2InPPh_2]_2$).

Rates of elimination studies for $(Me_3CCH_2)_3In \cdot P(H)Ph_2$

Equimolar amounts of $In(CH_2CMe_3)_3$ (0.346 g, 1.05 mmol) and $HPPh_2$ (0.197 g, 1.05 mmol) were combined in 0.963 g of benzene by using the procedure described for the preparation of $(Me_3CCH_2)_3Ga \cdot P(H)Ph_2$. After the reagents were thoroughly mixed, an aliquot of the 1.09 m (0.96 M) solution was transferred to an NMR tube. The tube was flame-sealed and the ^{31}P NMR spectra were recorded. The intensities of the lines for $(Me_3CCH_2)_2InPPh_2$,[17] $[(Me_3CCH_2)_2InPPh_2]_2$[17] and $(Me_3CCH_2)_3In \cdot P(H)Ph_2$ and/or free $HPPh_2$ were used to calculate the extent of reaction at a variety of times after mixing. Time, extent of reaction (17°C): 19 h 35 min, 0.221; 41 h, 0.325; 65 h, 0.436; 90 h 15 min, 0.543; 115 h, 0.831; 138 h, 0.948; 161 h 30 min, 0.971; 185 h 30 min, 0.988.

Rate of elimination studies for $(Me_3SiCH_2)_3In \cdot P(H)Ph_2$

A benzene solution of $In(CH_2SiMe_3)_3$ (0.397 g, 1.06 mmol, 1.09 m, 0.96 M) and $HPPh_2$ (0.197 g, 1.06 mmol, 1.09 m, 0.96 M) was prepared as described previously. The intensities of the lines for $(Me_3SiCH_2)_2InPPh_2$,[17] $[(Me_3SiCH_2)_2InPPh_2]_2$[17]

and $(Me_3SiCH_2)_3In \cdot P(H)Ph_2$ and/or $HPPh_2$ were used to calculate the extent of reaction. Time, extent of reaction (17°C): 19h 35 min, 0.0942; 45 h 20 min, 0.257; 67 h 45 min, 0.269; 91 h 25 min, 0.325 185 h 30 min, 0.501; 209 h 35 min, 0.537.

X-ray data collection, structure determination and refinement for $(Me_3CCH_2)_3Ga \cdot P(H)Ph_2$

A transparent single crystal of $(Me_3CCH_2)_3Ga \cdot P(H)Ph_2$ was mounted in a thin-walled glass capillary under argon and transferred to the goniometer. The space group was determined to be either the centric $P\bar{1}$ or acentric $P1$. Statistical tests indicated that the space group was centric and the subsequent solution and successful refinement of the structure in the space group $P\bar{1}$ confirmed this. A summary of data collection parameters is given in Table 1.

The geometrically constrained hydrogen atoms were placed in calculated positions 0.95 Å away from the bonded carbon atom and allowed to ride on that atom with B fixed at 5.5 Å^2. Due to the relatively high thermal motion, the methyl and phosphorus hydrogen atoms were not included in the final refinement. Refinement of the non-hydrogen atoms with anisotropic temperature factors led to final values of $R = 0.102$ and $R_w = 0.114$. The low melting point is consistent with the observed high thermal motion in the 20°C data collected. Resolvable static disorder was not evident.

Table 1. Crystal data and summary of intensity data collection and structure refinement

Compound	$(Me_3CCH_2)_3Ga \cdot P(H)Ph_2$
Colour/shape	Colourless/parallelipiped
Formula weight	469.34
Space group	$P\bar{1}$
Temperature (°C)	20
Cell constants[a]	
a (Å)	9.564(8)
b (Å)	12.208(5)
c (Å)	12.946(9)
α (°)	100.00(5)
β (°)	100.41(8)
γ (°)	102.97(7)
Cell volume (Å^3)	1412
Formula units/unit cell	2
D_{calc} (g cm^{-3})	1.10
μ_{calc} (cm^{-1})	9.88
Diffractometer/scan	Enraf–Nonius CAD-4/θ–2θ
Range of relative transmission factors (%)	44–100
Radiation, graphite monochromator	Mo-K_α ($\lambda = 0.71073$)
Maximum crystal dimensions (mm)	$0.15 \times 0.30 \times 0.35$
Scan width	$0.80 + 0.35 \tan\theta$
Standard reflections	400; 050; 008
Decay of standards (%)	± 3.5
Reflections measured	4369
2θ range (°)	$2 \leqslant 2\theta \leqslant 48$
Range of h, k, l	$+10$, ± 13, ± 14
Reflections observed [$F_o \geqslant 5\sigma(F_o)$][b]	2433
Computer programs[c]	SHELX[18]
Structure solution	Heavy-atom techniques
Number of parameters varied	262
Weights	Unit
Goodness-of-fit	2.51
$R = \Sigma \|\|F_o\| - \|F_c\|\| / \Sigma \|F_o\|$	0.102
R_w	0.114
Largest feature in final difference map	1.0 Å^{-3} near gallium

[a] Least-squares refinement of $[(\sin\theta)/\lambda]^2$ values for 20 reflections $\theta > 20°$.

[b] Corrections: Lorentz-polarization and absorption (empirical, psi scan).

[c] Neutral scattering factors and anomalous dispersion corrections from ref. 19.

RESULTS AND DISCUSSION

Tris(neopentyl)gallium(III) reacts with diphenylphosphine to form the adduct, $(Me_3CCH_2)_3Ga \cdot P(H)Ph_2$, a colourless, crystalline compound with a relatively low melting point of 33.0–34.0°C. The structure of this compound as determined by an X-ray structural study and the labelling of the atoms is presented in Figs 1 and 2. Bond distances and bond angles are collected in Tables 2, 3 and 4. The low melting point of this compound was manifested in high thermal motion and relatively poor crystal quality. No resolvable disorder was observed and the rather large thermal parameters resulted in high standard deviations in bond lengths. Even so, this structure is significant because it is the first of an adduct of a heavier group 13 element compound with a group 15 Lewis base having an acidic proton.

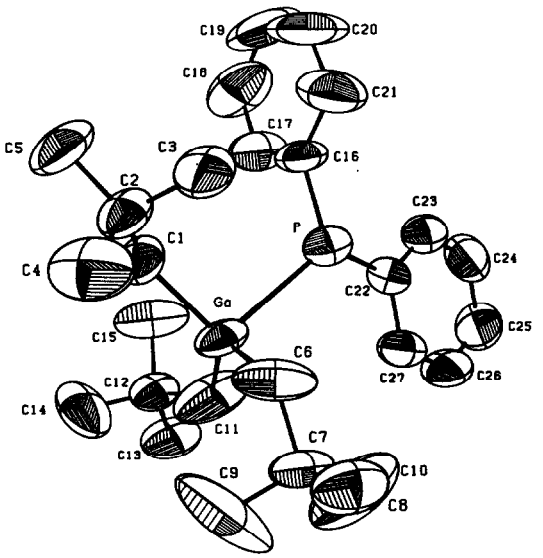

Fig. 1. Labelling of atoms in $(Me_3CCH_2)_3Ga \cdot P(H)Ph_2$. ORTEP diagram with thermal ellipsoids at the 50% probability level.

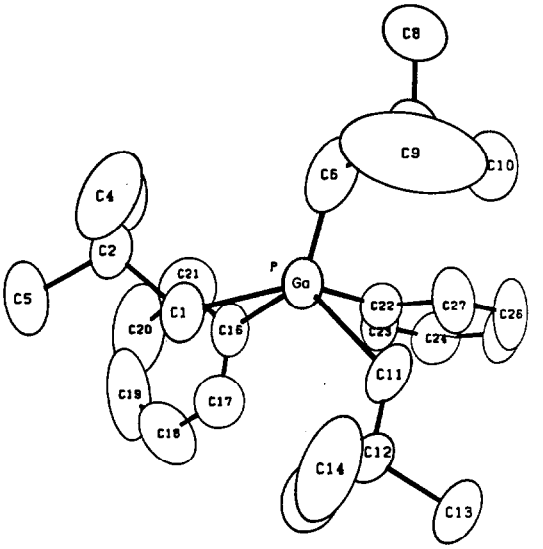

Fig. 2. Projection of $(Me_3CCH_2)_3Ga \cdot P(H)Ph_2$ down the Ga—P bond.

Table 2. Interatomic distances (Å) for $(Me_3CCH_2)_3Ga \cdot P(H)Ph_2$

(A) Gallium–phosphorus distance					
Ga—P	2.683(5)				
(B) Gallium–carbon distances					
Ga—C(1)	2.01(1)				
Ga—C(6)	1.87(2)				
Ga—C(11)	2.04(1)				
(C) Phosphorus–carbon distances					
P—C(16)	1.83(1)				
P—C(22)	1.79(2)				
(D) Neopentyl carbon–carbon distances					
C(1)—C(2)	1.52(2)	C(6)—C(7)	1.60(2)	C(11)—C(12)	1.45(2)
C(2)—C(3)	1.56(2)	C(7)—C(8)	1.50(2)	C(12)—C(13)	1.60(2)
C(2)—C(4)	1.51(2)	C(7)—C(9)	1.49(3)	C(12)—C(14)	1.51(2)
C(2)—C(5)	1.56(2)	C(7)—C(10)	1.58(3)	C(12)—C(15)	1.56(2)
(E) Phenyl carbon–carbon distances					
C(16)—C(17)	1.36(2)	C(22)—C(23)	1.36(2)		
C(16)—C(21)	1.43(2)	C(22)—C(27)	1.43(2)		
C(17)—C(18)	1.38(2)	C(23)—C(24)	1.37(2)		
C(18)—C(19)	1.33(4)	C(24)—C(25)	1.40(2)		
C(19)—C(20)	1.30(5)	C(25)—C(26)	1.34(2)		
C(20)—C(21)	1.41(3)	C(26)—C(27)	1.37(2)		

Table 3. Angles (°) for $(Me_3CCH_2)_3Ga \cdot P(H)Ph_2$

(A)	Angles around the gallium atom			
	P—Ga—C(1)	98.0(5)	C(1)—Ga—C(6)	117.3(7)
	P—Ga—C(6)	96.4(7)	C(1)—Ga—C(11)	117.0(7)
	P—Ga—C(11)	100.0(7)	C(6)—Ga—C(11)	119.8(7)
(B)	Angles around the phosphorus atom			
	Ga—P—C(16)	119.0(5)		
	Ga—P—C(22)	121.7(5)		
	C(16)—P—C(22)	103.4(7)		
(C)	Gallium–carbon–carbon angles			
	Ga—C(1)—C(2)	124(1)		
	Ga—C(6)—C(7)	131(1)		
	Ga—C(11)—C(12)	125(1)		
(D)	Phosphorus–carbon–carbon angles			
	P—C(16)—C(17)	122(1)	P—C(22)—C(23)	126(1)
	P—C(16)—C(21)	118(1)	P—C(22)—C(27)	119(1)
(E)	Neopentyl carbon–carbon–carbon angles			
	C(1)—C(2)—C(3)	110(1)	C(11)—C(12)—C(13)	108(1)
	C(1)—C(2)—C(4)	111(1)	C(11)—C(12)—C(14)	115(2)
	C(3)—C(2)—C(4)	110(2)	C(13)—C(12)—C(14)	110(1)
	C(1)—C(2)—C(5)	108(1)	C(11)—C(12)—C(15)	109(2)
	C(3)—C(2)—C(5)	110(1)	C(13)—C(12)—C(15)	106(1)
	C(4)—C(2)—C(5)	109(2)	C(14)—C(12)—C(15)	108(2)
	C(6)—C(7)—C(8)	115(1)		
	C(6)—C(7)—C(9)	103(2)		
	C(8)—C(7)—C(9)	110(2)		
	C(6)—C(7)—C(10)	107(2)		
	C(8)—C(7)—C(10)	108(2)		
	C(9)—C(7)—C(10)	112(2)		
(F)	Phenyl carbon–carbon–carbon angles			
	C(17)—C(16)—C(21)	120(2)	C(23)—C(22)—C(27)	115(1)
	C(16)—C(17)—C(18)	122(2)	C(22)—C(23)—C(24)	124(1)
	C(17)—C(18)—C(19)	119(3)	C(23)—C(24)—C(25)	120(2)
	C(18)—C(19)—C(20)	120(3)	C(24)—C(25)—C(26)	116(2)
	C(19)—C(20)—C(21)	127(3)	C(25)—C(26)—C(27)	125(2)
	C(16)—C(21)—C(20)	113(2)	C(22)—C(27)—c(26)	120(2)

Table 4. Torsion angles (°) for $(Me_3CCH_2)_3Ga \cdot P(H)Ph_2$

C(1)—Ga—P—C(16)	−19.2
C(1)—Ga—P—C(22)	−150.0
C(6)—Ga—P—C(16)	−138.0
C(6)—Ga—P—C(22)	91.2
C(11)—Ga—P—C(16)	100.1
C(11)—Ga—P—C(22)	−30.7

The most striking structural feature of $(Me_3CCH_2)_3Ga \cdot P(H)Ph_2$ is the extremely long Ga—P distance of 2.683(5) Å. Other addition compounds exhibit shorter Ga—P distances of 2.353(2) Å for $Cl_3Ga \cdot PMe_3$,[10] 2.52(2) Å for $Me_3Ga \cdot PMe_3$[11] (electron diffraction studies), 2.535(2) Å for $Me_2ClGa \cdot P(Ph)_2CH_2P(Ph)_2$[9] and 2.563(3)[7] or 2.54(4) Å[8] for $Me_3Ga \cdot P(Ph)_2C_2H_4(Ph)_2P \cdot GaMe_3$ (two structural studies of the same compound). The long gallium–phosphorus distance suggests that $(Me_3CCH_2)_3Ga \cdot P(H)Ph_2$ is a relatively weak adduct.

The second feature of interest in this structure relates to the observation that the α-carbon atoms of the substituents on gallium and phosphorus are essentially but not perfectly eclipsed. Thus, this observation suggests that the long gallium–phosphorus distance is probably not related to extreme steric stress. The other adduct with an eclipsed conformation, $Cl_3Ga \cdot PMe_3$,[10] has the shortest of the known Ga—P bond distances. In contrast, $Me_3Ga \cdot P(Ph)_2C_2H_4(Ph)_2P \cdot GaMe_3$[8,9] is staggered. Both the gallium and phosphorus centres

have rather distorted tetrahedral coordination environments. The C—Ga—C angles [117.0(7)–119.8(7)°] are typically greater than the normal tetrahedral values but not much smaller than the angle predicted for the uncoordinated trigonal planar monomeric Lewis acid. The C—P—C bond angle [103.4(7)°] is less than the typical tetrahedral angle. In turn, the average P—Ga—C angle of 98(1)° is less than tetrahedral, whereas the average Ga—P—C angle of 120(4)° is greater than tetrahedral. Although the hydrogen bonded to phosphorus was not located, the phosphorus atom is 0.48 Å above the plane defined by Ga, C(16) and C(22). The two phenyl substituents are nearly perpendicular to each other, the dihedral angle between the planes defined by the aryl atoms is 85°. The neopentyl groups arrange themselves in propellar fashion around the Ga—P bond vector.

The elemental analyses of $(Me_3CCH_2)_3Ga \cdot P(H)Ph_2$ for carbon and hydrogen were investigated but non-reproducible results were obtained. The observed per cent carbon was low (69.08, calc.; 65.77, 66.76 found) whereas the observed per cent hydrogen was within the range considered acceptable (9.47, calc.; 9.42, 9.13 found). These results suggest that the sample did not quantitatively decompose during analysis. Alternatively, the observation that the per cent carbon is low might suggest that the sample was deficient in $HPPh_2$. Diphenylphosphine has a higher per cent carbon (77.40) than $Ga(CH_2CMe_3)_3$ (63.61 or the adduct (69.08). A deficiency in $HPPh_2$ would be inconsistent with the observation that $HPPh_2$ is significantly less volatile than $Ga(CH_2CMe_3)_3$. If the sample was not $(Me_3CCH_2)_3Ga \cdot P(H)Ph_2$ because one component was lost during isolation and purification, the more volatile component should have been lost and the experimental per cent carbon should have been higher than that calculated for the adduct. The existence of a crystalline solid at room temperature with a sharp melting point (33.0–34.0°C) and the results of the X-ray structural study support the existence of a pure compound. Since non-reproducible analyses were obtained for $(Me_3CCH_2)_3Ga \cdot P(H)Ph_2$, the related compound $(Me_3SiCH_2)_3Ga \cdot P(H)Ph_2$ was not analysed. It is noteworthy that other adducts of group 13 organometallic compounds have exhibited low elemental analyses for carbon.[7,20]

Crysoscopic molecular weight studies of dilute benzene solutions of $(Me_3CCH_2)_3Ga \cdot P(H)Ph_2$ and $(Me_3SiCH_2)_3Ga \cdot P(H)Ph_2$ suggest that these adducts are significantly dissociated in solution. Tris(neopentyl)gallium–diphenylphosphine is less dissociated than the corresponding tris(trimethylsilylmethyl)gallium–diphenylphosphine adduct. The calculated (based on adduct) and the observed molalities of the solutions permit calculations of an apparent equilibrium constant for dissociation:

$$R_3Ga \cdot P(H)Ph_2 \overset{K}{\rightleftharpoons} R_3Ga + P(H)Ph_2.$$

Thus, $(Me_3CCH_2)_3Ga \cdot P(H)Ph_2$ had an average constant of 0.0410 m (0.0360 M) whereas $(Me_3SiCH_2)_3Ga \cdot P(H)Ph_2$ was 0.0505 m (0.0443 M). These results are consistent with the earlier suggestion[12,14,21] that the neopentyl group has either stronger electron-withdrawing or weaker electron-donating properties, but larger steric effects than the corresponding trimethylsilylmethyl substituent. Apparently, the electron-withdrawing properties of the neopentyl group is the more important factor as $Ga(CH_2CMe_3)_3$ is observed to be the stronger Lewis acid.

The ^{31}P NMR spectra of solutions of $(Me_3CCH_2)_3Ga \cdot P(H)Ph_2$ and $(Me_3SiCH_2)_3Ga \cdot P(H)Ph_2$ support the hypothesis of equilibria between the adduct and the free acid and base, as well as the conclusion that $Ga(CH_2CMe_3)_3$ is the stronger Lewis acid. As the concentrations of the adduct systems increase, the chemical shifts of the ^{31}P NMR lines move to higher field and away from the chemical shift of the line for free $P(H)Ph_2$. Similarly, $^1J_{PH}$ increases as the concentrations of the adduct systems increase. It is noteworthy that $\Delta\delta$ $[R_3Ga \cdot P(H)Ph_2 - P(H)Ph_2]$ is greater for $R = CH_2CMe_3$ (2.6 ppm), the stronger Lewis acid according to molecular weight studies, than for $R = CH_2SiMe_3$ (2.0 ppm). At the higher concentrations (0.138 m) $\Delta\delta$ increases to 3.9 ppm ($R = CH_2CMe_3$) and 2.7 ppm ($R = CH_2SiMe_3$). These studies clearly demonstrate that all investigations of Lewis acidities of group 13 compounds and/or Lewis basicities of phosphines by ^{31}P NMR spectroscopy must include concentration dependencies of the spectra.

An attempt was also made to synthesize and fully characterize the neopentyl- and trimethylsilylmethyl-indium adducts of diphenylphosphine. However, the occurrence of elimination reactions at room temperature to form R_2InPPh_2 and RH precluded the isolation of pure adducts. The ^{31}P NMR spectra clearly revealed the presence of R_2InPPh_2,[17] $[R_2InPPh_2]_2$[17] and $HPPh_2$, either free or as the adduct. The intensities of the lines related to the products of the elimation reaction, R_2InPPh_2 and $[R_2InPPh_2]_2$, increased with time, whereas the line related to $HPPh_2$ decreased. When a solution at 17°C, which was 1.09 m in both $In(CH_2CMe_3)_3$ and $HPPh_2$, was followed in a time dependent study, the elimination reaction was 54.3% complete after

90.2 h from the time of combining the reagents in benzene. In contrast, a 1.09 m solution of $In(CH_2SiMe_3)_3$ and $HPPh_2$ was 53.7% complete after 209.5 h. Thus, $In(CH_2CMe_3)_3-P(H)Ph_2$ undergoes the elimination reaction at a significantly faster rate than does $In(CH_2SiMe_3)_3-P(H)Ph_2$. If the rate law which is appropriate for the $AlMe_2H-N(Me)(Ph)H$ system[22] is applicable to these organoindium–phosphine systems, then the rate constant for the elimination reaction and the equilibrium constant for the formation of the adduct will influence the rate of reaction. If the equilibrium constants in the two indium–phosphorus systems are of similar magnitude to that observed for the related gallium–phosphorus systems, then the dominant factor to influence the rate of elimination will be the rate constant for reaction. The rate constant should be influenced by the charge on the α-carbon atom of the substituents bound to indium. The more strongly electron-withdrawing neopentyl substituted derivative would, in turn, be expected to have the faster rate of elimination, as observed. Kinetic studies for these indium–phosphorus systems will be the subject of a future publication.

Acknowledgements—This work was supported in part by the Office of Naval Research. The National Science Foundation, Chemical Instrumentation Program, provided funds used to purchase the diffractometer (Northern Illinois University) and the Varian Gemini-300 NMR Spectrometer (State University of New York at Buffalo), whereas the Department of Education provided funds used to purchase the Varian VXR-400 NMR spectrometer for ^{31}P NMR spectra (State University of New York at Buffalo).

REFERENCES

1. H. M. Manasevit and W. I. Simpson, *J. Electrochem. Soc.* 1969, **116**, 1725; 1973, **120**, 135.
2. R. H. Moss, *J. Cryst. Growth* 1984, **68**, 78.
3. A. H. Cowley, B. L. Benac, J. G. Ekerdt, R. A. Jones, K. B. Kidd, J. Y. Lee and J. E. Miller, *J. Am. Chem. Soc.* 1988, **110**, 6248.
4. D. G. Tuck in, *Comprehensive Organometallic Chemistry* (Edited By G. Wilkinson, F. G. A. Stone and E. W. Abel), Vol. 1, Chap. 7, p. 703. Pergamon Press, Oxford (1982).
5. (a) G. E. Coates, *J. Chem. Soc.* 1951, 2003; (b) G. E. Coates and R. A. Whitcombe, *J. Chem. Soc.* 1956, 3351.
6. A. Lieb, M. T. Emerson and J. P. Oliver, *Inorg. Chem.* 1965, **4**, 1825.
7. D. C. Bradley, H. Chudzynska, M. M. Faktor, D. M. Frigo, M. B. Hursthouse, B. Hussain and L. M. Smith, *Polyhedron* 1988, **7**, 1289.
8. A. Boardman, R. W. H. Small and I. J. Worrall, *Inorg. Chim. Acta* 1986, **119**, 213.
9. H. Schmidbaur, S. Lauteschlager and G. Muller, *J. Organomet. Chem.* 1985, **281**, 25.
10. J. C. Carter, G. Jugie, R. Enjalbert and J. Galy, *Inorg. Chem.* 1978, **17**, 1248.
11. L. M. Golubinskaya, A. V. Golubinskii, V. S. Mastryukov, L. V. Vilkov and V. I. Bregadze, *J. Organomet. Chem.* 1976, **117**, C4.
12. O. T. Beachley Jr and J. C. Pazik, *Organometallics* 1988, **7**, 1516.
13. O. T. Beachley Jr and R. G. Simmons, *Inorg. Chem.* 1980, **19**, 1021.
14. O. T. Beachley Jr, E. F. Spiegel, J. P. Kopasz and R. D. Rogers, *Organometallics* 1989, **8**, 1915.
15. O. T. Beachley Jr and R. N. Rusinko, *Inorg. Chem.* 1979, **18**, 1966.
16. D. F. Shriver and M. A. Drezdzon, *The Manipulation of Air-sensitive Compounds*, p. 38. John Wiley, New York (1986).
17. O. T. Beachley Jr, J. P. Kopasz, H. Zhang, W. E. Hunter and J. L. Atwood, *J. Organomet. Chem.* 1987, **325**, 69.
18. G. M. Sheldrick, SHELX, A system of computer programs for X-ray structure determination as locally modified (1976).
19. *International Tables for X-ray Crystallography*, Vol. IV, pp. 72, 99, 149. Kynoch Press, Birmingham, U.K. (1972).
20. L. V. Interrante, G. A. Sigel, M. Garbauskas, C. Hejna and G. A. Slack, *Inorg. Chem.* 1989, **28**, 252.
21. O. T. Beachley Jr and L. Victoriano, *Organometallics* 1988, **7**, 63.
22. O. T. Beachley Jr and C. Tessier-Youngs, *Inorg. Chem.* 1979, **18**, 3188.

Polyhedron Vol. 9, No. 2/3, pp. 343–351, 1990
Printed in Great Britain

0277–5387/90 $3.00+.00
Pergamon Press plc

ADDUCTS OF TRIMETHYLGALLIUM AND PERDEUTERIOTRIMETHYLGALLIUM WITH AMINE LIGANDS AND SOME DIMETHYLGALLIUM ORGANYL PNICTIDES (N, P, As). X-RAY CRYSTAL STRUCTURES OF $[Me_3Ga \cdot NH(C_6H_{11})_2]$ and $[Me_3Ga \cdot \overline{NH(CHMe)(CH_2)_3CHMe}]$

DONALD C. BRADLEY,* HELEN M. DAWES, MICHAEL B. HURSTHOUSE,* LESLEY M. SMITH and MARK THORNTON-PETT

Department of Chemistry, Queen Mary College, Mile End Road, London E1 4NS, U.K.

Abstract—The adducts $Me_3Ga \cdot L$ [where $L = NH(C_6H_{11})_2$ (**1**), $\overline{NHCHMe(CH_2)_3CHMe}$ (**2**), $N(CH_2CH_2)_3CH$ (**3**) and $0.5\ N(CH_2CH_2)_3N$ (**4**)] have been prepared by displacement of either (a) ether from $Me_3Ga \cdot Et_2O$ or (b) diphos from $(Me_3Ga)_2 \cdot$diphos (diphos = bisdiphenyl phosphino ethane) and the X-ray crystal structures of **1** and **2** determined. $(CD_3)_3Ga$ and the adducts $(CD_3)_3Ga \cdot L$ [$L = NMe_3$, $NH(C_6H_{11})_2$, $\overline{NHCHMe(CH_2)_3CHMe}$ and $N(CH_2CH_2)_3CH$], were similarly prepared from $[(CD_3)_3Ga]_2 \cdot$diphos. The covalently bonded dimethylgallium organyl pnictides $(Me_2GaL')_n$ [$L' = NPr^i_2$, $\overline{NCHMe(CH_2)_3CHMe}$, PMe_2 and $AsMe_2$] were prepared by reactions of either (c) Me_2GaCl and LiL' or (d) $Me_3Ga \cdot Et_2O$ and HL'. All compounds were characterized by elemental analyses, IR, NMR and mass spectroscopy. The Ga geometry in both **1** and **2** is distorted tetrahedral.

As part of our programme of synthesizing and characterizing a range of volatile precursors for the deposition of III–V semiconductors by Metallo-organic Chemical Vapour Deposition (MOCVD) we have prepared a number of new adducts of trimethylgallium, $Me_3Ga \cdot L$, and some covalently bound dimethylgallium organyl pnictides, $(Me_2GaL')_n$. The extensive literature on these compounds has recently been reviewed[1–3] showing the upsurge in activity in this field following the pioneering work of Manasevit *et al.*[4,5] who demonstrated the feasibility of depositing GaAs from the reaction of Me_3Ga and AsH_3.

We have been exploring the scope for pacifying the exceptional air-sensitivity of trimethylgallium by coordinating various Lewis bases without incurring the penalty of the loss in volatility which may result.[6]

RESULTS AND DISCUSSION

The nitrogen base adducts **1**, **2**, **3** and **4** have been obtained as sublimable white solids (Table 1) by either or both of the following reactions:

$$Me_3Ga \cdot Et_2O + L \longrightarrow Me_3Ga \cdot L + Et_2O \quad (1)$$

$$(Me_3Ga)_2 \cdot \text{diphos} + 2L \longrightarrow 2Me_3Ga \cdot L + \text{diphos}. \quad (2)$$

The details of the synthesis and characterization of the diphos adduct have already been published.[7] The perdeuteriotrimethylgallium·diphos adduct (**9**) was also prepared in this work and converted to the new adducts $[(CD_3)_3Ga \cdot NMe_3]$ (**5**), $[(CD_3)_3Ga \cdot NH(C_6H_{11})_2]$ (**6**), $[(CD_3)_3Ga \cdot \overline{NHCHMe(CH_2)_3CHMe}]$ (**7**) and $[(CD_3)_3Ga \cdot N(CH_2CH_2)_3CH]$ (**8**), which were required for deuterium labelled reactions. In addition the new dimethylgallium organyl pnictides $(Me_2GaNPr^i_2)_2$ (**10**) and $[Me_2Ga\overline{NHCHMe(CH_2)_3CHMe}]_2$ (**11**) and the known compounds $(Me_2GaPMe_2)_3$ (**12**) and $(Me_2GaAsMe_2)_3$ (**13**) were prepared by the following reactions:

$$Me_2GaCl + LiL' \longrightarrow (Me_2GaL')_2 + LiCl \quad (3)$$

$$Me_3Ga \cdot Et_2O + HL' \longrightarrow (Me_2GaL')_3 + Et_2O + CH_4. \quad (4)$$

* Authors to whom correspondence should be addressed.

Table 1.

Compound	Melting point (°C)	Volatility[a] (°C mm Hg)	δ, ^{1}H NMR[b]	Analyses[c] C	H	N
1 [$Me_3Ga \cdot NH(C_6H_{11})_2$]	78–79	40–60/0.01	0.12	60.0 (60.8)	10.6 (10.9)	4.7 (4.7)
2 [$Me_3Ga \cdot \overline{NHCHMe_2(CH_2)_3CHMe}$][d]	49–50	30.0/0.01	0.00	51.6 (52.7)	10.3 (10.6)	6.3 (6.1)
3 [$Me_3Ga \cdot N(CH_2CH_2)_3CH$]	113	70–90/0.02	−0.10	50.1 (53.1)	9.2 (9.8)	6.1 (6.2)
4 [$Me_3Ga \cdot N(CH_2CH_2)_3N \cdot GaMe_3$][e]	96.5	25/0.02	−0.35	41.6 (42.2)	8.6 (8.8)	8.1 (8.2)
5 [$(CD_3)_3Ga \cdot NMe_3$]	96.5	25/0.02	—	39.3 (39.4)	10.2[f] (10.5)	7.5 (7.6)
6 [$(CD_3)_3Ga \cdot NH(C_6H_{11})_2$]	79.5	40–60/0.03	—	58.5 (59.0)	10.5[f] (10.9)	4.6 (4.6)
7 [$(CD_3)_3Ga \cdot NHCHMe(CH_2)_3CHMe$]	50	25/0.02	—	49.1 (50.7)	10.0[f] (10.6)	5.9 (5.9)
8 [$(CD_3)_3Ga \cdot N(CH_2CH_2)_3CH$]	113	60–80/0.02	—	50.8 (51.1)	9.4[f] (9.9)	6.1 (6.0)
9 [$(CD_3)_3Ga \cdot PPh_2CH_2CH_2(Ph)_2P \cdot Ga(CD_3)_3$]	—	[h]	—	59.3 (59.5)	6.6[f] (6.9)	9.4[g] (9.6)[g]
10 [$Me_2Ga \cdot NPr^i_2$]$_2$	124	90/0.03	0.30	46.9 (48.0)	9.7 (10.1)	6.8 (7.0)
11 [$Me_2Ga \cdot \overline{NCHMe(CH_2)_3CHMe}$]$_2$	132	118–125/0.02	0.10	50.8 (51.0)	9.6 (9.5)	6.6 (6.6)

[a] Sublimation temperature.
[b] δ CH_3–Ga ppm (C_6D_6 solvent).
[c] Required values in parentheses.
[d] Found: Ga, 31.6. Required: Ga, 30.5%.
[e] M.p. >180°C (sublimation temperature at 760 mm Hg).
[f] "H" analyses are the weighted sum of hydrogen and deuterium (%).
[g] % P.
[h] $(CD_3)_3$ Ga evolved at >85°C/0.01 mm Hg.

All of the adducts, **1–8**, were volatile white solids which could be sublimed unchanged. It is noteworthy that compounds **1**, **2**, **6** and **7**, which have NH groups, did not eliminate methane. There was no significant difference in melting point or volatility between the Me_3Ga and $(CD_3)_3Ga$ derivatives.

Apart from the expected differences in the C—H and C—D stretching frequencies (2950–2840 cm^{-1} and 2089–2014 cm^{-1}, respectively) there were no discernible differences in the characteristic Ga—CH_3/Ga—CD_3 stretches (*ca* 521, 570 cm^{-1}), rocking modes (*ca* 612, 727, 759 cm^{-1}) or deformation modes (*ca* 163 cm^{-1}).

In the ^{1}H NMR spectra, the CH_3—Ga protons give resonances slightly to lower field in the secondary amine adducts (**1** and **2**) than in the tertiary amine complexes (**3** and **4**). However, it is notoriously difficult to relate these chemical shifts to bonding parameters in these molecules.

It is interesting to note that the bifunctional ditertiary amine, 1,4-diazabicyclo[2.2.2]octane (dabco) forms a stable 2:1 complex [$Me_3Ga \cdot N(CH_2CH_2)_3N \cdot GaMe_3$] (**4**) which sublimed unchanged at 60–80°C/0.03 mm Hg and which did not melt but sublimed (179–180°C) under normal atmospheric pressure of nitrogen. There was no detectable parent molecular ions in its mass spectrum but significant concentrations of Me_2Ga^+, $MeGa^+$ and Ga^+ ions. The formation of the 2:1 complex by Me_3Ga is in marked contrast to trimethylindium which forms an insoluble 1:1 compound [$Me_3In \cdot N(CH_2CH_2)_3N$] which is an infinite linear polymer with five-coordinated (trigonal bipyramidal) indium.[8] We could find no evidence for gallium forming an analogous compound and it

appears that the smaller gallium atom cannot expand its coordination to five with this ligand. The indium compound contained very long (weak) In—N bonds and could be sublimed *in vacuo*.

Turning now to the dimethylgallium organyl amides, **10** and **11**, which were obtained from Me_2GaCl and the lithio derivatives of the ligands [eq. (3)], these compounds appeared to be dimeric according to the fragment ions in their mass spectra. Although the parent molecular ions of the dimers could not be detected there were significant concentrations of the species $(dimer - Me_2Ga)^+$ and $(dimer - L' - Me)^+$. The latter species contained the peaks appropriate to the three isotopic species $^{71}Ga_2$, $^{71}Ga^{69}Ga$ and $^{69}Ga_2$.

Not surprisingly these dimers were less volatile than the mononuclear trimethylgallium adducts (Table 1) but they could be sublimed *in vacuo*. These compounds have potential as precursors for MOMBE (or very low pressure MOCVD) and we have demonstrated that the aluminium complex $(Me_2AlNPr^i_2)_2$ can be used as a precursor for the deposition of AlN.[9]

With regard to the dimethylgallium organyl pnictides **12** and **13** we have found, using ^1H NMR, a significant difference in the fluxionality of the six-membered rings of these trimeric compounds. Even at room temperature ($C_6D_5CD_3$) compound **12** shows two singlets for equatorial and axial methyl groups on gallium and two doublets ($^2J_{HP} = 3$ Hz) for the equatorial and axial methyl groups on the phosphorus atoms. In the arsenic derivative, **13**, only two singlets were observed (δ −0.10, CH_3—Ga; 0.90, CH_3—As) from room temperature down to −70°C in $C_6D_5CD_3$, although the gallium methyls moved to lower field (δ 0.07) and the arsenic methyls moved to higher field (δ 0.84) as the temperature was lowered. Beachley and Coates[10] had previously shown this NMR behaviour of **13** at 60 MHz and we have confirmed it using much higher field equipment (250 MHz). Compound **13** is a white solid which can be sublimed at 100–110°C (0.02 mm Hg) and it gives a rich mass spectrum showing the trimeric molecular ion (with all isotopic species corresponding to $^{71}Ga_3$, $^{71}Ga_2^{69}Ga$, $^{71}Ga^{69}Ga_2$ and $^{69}Ga_3$) in low abundance and also $(trimer - methyl)^+$ species showing that the integrity of the six-membered ring is maintained in the vapour. The fragmentation pattern showed several interesting species such as $(trimer - AsMe_2)^+$, $(trimer - Me_2Ga - 2Me)^+$, $(dimer - Me)^+$, $(dimer - AsMe_2)^+$, $(dimer - AsMe_2 - Me)^+$ and major peaks for $As_2Me_4^+$, $As_2Me_3^+$ and Me_2Ga^+.

Table 2. Selected bond lengths (Å) and angles (deg) for **1**

Bond lengths			
N(1)—Ga(1)	2.151(6)	C(1)—Ga(1)	1.969(8)
C(2)—Ga(1)	1.964(9)	C(3)—Ga(1)	1.983(8)
C(11)—N(1)	1.518(9)	C(21)—N(1)	1.494(8)
C(12)—C(11)	1.506(10)	C(16)—C(11)	1.498(9)
C(13)—C(12)	1.519(11)	C(14)—C(13)	1.491(10)
C(15)—C(14)	1.471(11)	C(16)—C(15)	1.521(11)
C(22)—C(21)	1.504(10)	C(26)—C(21)	1.522(10)
C(23)—C(22)	1.511(11)	C(24)—C(23)	1.511(11)
C(25)—C(24)	1.508(11)	C(26)—C(25)	1.525(11)
Bond angles			
C(1)—Ga(1)—N(1)	97.1(3)	C(2)—Ga(1)—N(1)	105.8(3)
C(2)—Ga(1)—C(1)	111.8(4)	C(3)—Ga(1)—N(1)	108.0(3)
C(3)—Ga(1)—C(1)	116.1(4)	C(3)—Ga(1)—C(2)	115.7(5)
C(11)—N(1)—Ga(1)	110.1(4)	C(11)—N(1)—H(1)	100.8(26)
C(21)—N(1)—Ga(1)	123.1(5)	C(21)—N(1)—H(1)	107.4(21)
C(21)—N(1)—C(11)	115.4(5)	C(12)—C(11)—N(1)	112.2(6)
C(16)—C(11)—N(1)	113.1(6)	C(16)—C(11)—C(12)	112.7(6)
C(13)—C(12)—C(11)	112.0(6)	C(14)—C(13)—C(12)	112.0(7)
C(15)—C(14)—C(13)	112.3(7)	C(16)—C(15)—C(14)	113.7(7)
C(15)—C(16)—C(11)	110.1(6)	C(22)—C(21)—N(1)	111.8(6)
C(26)—C(21)—N(1)	112.1(6)	C(26)—C(21)—C(22)	111.4(6)
C(23)—C(22)—C(21)	113.0(7)	C(24)—C(23)—C(22)	112.3(7)
C(25)—C(24)—C(23)	111.9(7)	C(26)—C(25)—C(24)	111.4(7)
C(25)—C(26)—C(21)	111.5(6)		

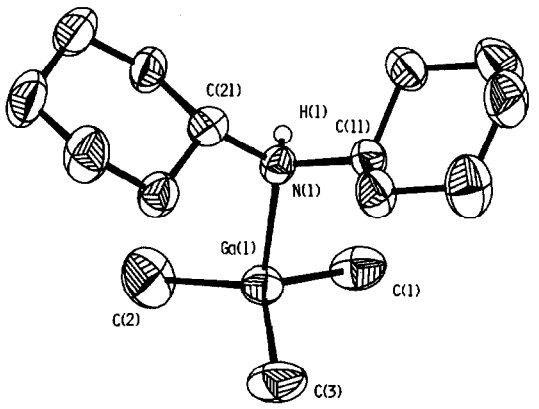

Fig. 1.

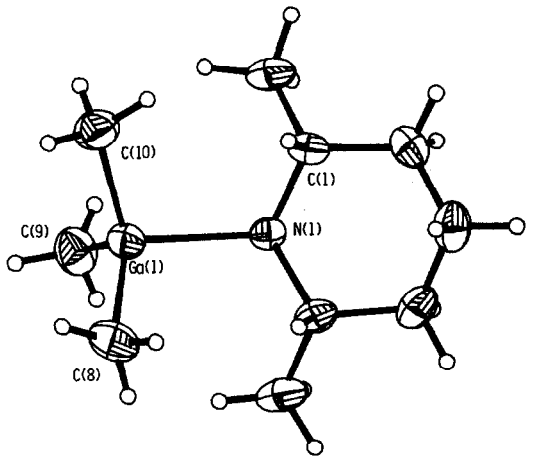

Fig. 2.

X-ray crystal structures

The structure of **1** is shown in Fig. 1; selected bond lengths and angles are in Table 2. The structure of **2** is shown in Fig. 2; selected bond lengths and angles are in Table 3.

In both adducts the geometry at Ga is distorted tetrahedral but there are some interesting similarities and differences between the two structures. In compound **1** the configuration about the Ga—N bond is staggered but in compound **2** it is eclipsed. The latter structure presumably results from minimization of methyl–methyl interactions between the $GaMe_3$ unit and the 2,6-methyls on the piperidine.

The distortions in the Ga coordinations are quite marked. In each case the GaC_3 pyramid is slightly unsymmetrical with angles varying between 111.8–116.1° for **1** and 108.1–119.8° for **2**, whilst the N—Ga—C angles vary between 97.1–108.0° for **1** and 99.9–106.7° for **2**. These deformations are likely to arise from packing and steric effects, and demonstrate considerable deformability in the Ga—amine bonding. The Ga—N bond length also shows flexibility, the values in **1** and **2** differing by ~0.05 Å (cf. the Ga—C range for both compounds 1.964–1.989 Å).

EXPERIMENTAL

All operations were carried *in vacuo* or under an atmosphere of specially dried oxygen-free nitrogen

Table 3. Selected bond lengths (Å) and angles (deg) for **2**

Bond lengths			
N(1)—Ga(1)	2.199(5)	C(8)—Ga(1)	1.986(6)
C(9)—Ga(1)	1.976(7)	C(10)—Ga(1)	1.989(6)
C(1)—N(1)	1.497(5)	C(6)—N(1)	1.492(5)
C(2)—C(1)	1.515(7)	C(3)—C(1)	1.512(7)
C(4)—C(3)	1.504(8)	C(5)—C(4)	1.489(7)
C(6)—C(5)	1.524(7)	C(7)—C(6)	1.510(7)
Bond angles			
C(8)—Ga(1)—N(1)	105.3(2)	C(9)—Ga(1)—N(1)	99.9(3)
C(10)—Ga(1)—N(1)	106.7(3)	C(9)—Ga(1)—C(8)	119.8(3)
C(10)—Ga(1)—C(8)	108.1(3)	C(10)—Ga(1)—C(9)	115.4(3)
C(1)—N(1)—Ga(1)	111.8(3)	C(6)—N(1)—Ga(1)	111.3(3)
C(6)—N(1)—C(1)	115.7(3)	C(2)—C(1)—N(1)	109.0(4)
C(3)—C(1)—N(1)	113.8(4)	C(3)—C(1)—C(2)	110.0(4)
C(4)—C(3)—C(1)	113.0(4)	C(5)—C(4)—C(3)	108.2(4)
C(6)—C(5)—C(4)	112.6(4)	C(5)—C(6)—N(1)	113.1(4)
C(7)—C(6)—N(1)	109.6(4)	C(7)—C(6)—C(5)	111.4(4)

using Schlenk type glass apparatus and a glove box.

Solvents were dried using the sodium ketyl of benzophenone and were freshly distilled prior to use. Melting points were determined in soda glass capillaries sealed under nitrogen using an electrothermal apparatus.

Analyses for C, H, N, P and Cl were obtained from the Microanalytical Laboratory of University College, London. For the deuteriated compounds the "H"% quoted is the weighted sum of the hydrogen and deuterium percentages since combustion gave rise to a mixture of H_2O, HDO and D_2O which was detected as "H_2O". Gallium analyses were determined either gravimetrically as the oxinate or by complexometric titration against Na_2EDTA using "gallocyanine" as indicator.[11]

Gallium trichloride was purchased from Johnson–Matthey Chemicals Ltd and was sublimed before use. Methyl lithium (solution in Et_2O low in halide) was purchased from Alfa Chemicals and *n*-butyl lithium (in hexane) was obtained from Aldrich Chemicals and standardized by titration using the Gilman technique.[12] CD_3I was purchased from Goss Chemicals Ltd, and the organic ligands from Strem Chemicals Inc. and Aldrich Chemicals Ltd. Dimethylarsine was prepared using Feltham and Silverthorn's method.[13] The sample of $(Me_2GaPMe_2)_3$ was donated by Dr Dario M. Frigo. $(Me_3Ga)_2$·diphos was prepared as previously described.[7]

IR spectra were measured as Nujol mulls and CsI windows using Perkin–Elmer 225 or 577 spectrophotometers over the range 4000–200 cm^{-1}. NMR spectra were obtained using Bruker WP80, WM250 or WH400 FT spectrometers using deuteriated solvents. Chemical shifts were measured internally against the trace undeuteriated solvent peaks and referenced against TMS.

Mass spectra were obtained using an AEI MS 902 spectrometer and gallium containing species were identified by the isotopic pattern for ^{71}Ga and ^{69}Ga.

Preparation of trimethyl(dicyclohexylamine)gallium (**1**)

(a) *From* $Me_3Ga \cdot Et_2O$ *and* $HN(C_6H_{11})_2$. Methyl lithium (26.6 cm^3 of a 1.67 M solution in Et_2O) was added dropwise to a stirred solution of $GaCl_3$ (2.6 g, 14.8 mmol) in diethyl ether (100 cm^3) at 0°C. After warming to room temperature and filtering to remove LiCl, hexane (100 cm^3) was added and the solution cooled to −20°C. Dicyclohexylamine (3.5 cm^3, 17.6 mmol) was added with stirring via a syringe and the mixture was allowed to stand overnight at room temperature. On evaporating off the ether under reduced pressure, the solution was concentrated and white crystals (3.0 g, 10 mmol, 68% based on $GaCl_3$) of **1** were obtained which sublimed at 40–60°C/0.01 mm Hg (m.p. 78–79°C).

(b) *From* $(Me_3Ga)_2 \cdot$ *diphos and* $HN(C_6H_{11})_2$. $(Me_3Ga)_2$·diphos (3.12 g, 5 mmol) was heated to 85–110°C under reduced pressure (0.02 mm Hg) and the Me_3Ga thus liberated was condensed onto $HN(C_6H_{11})_2$ (1.6 cm^3, 8 mmol) dissolved in pentane (15 cm^3) at −196°C. After warming to room temperature overnight the pentane was evaporated *in vacuo* leaving a white crystalline solid (2.13 g, 7.2 mmol, 88% yield based on the amine) which sublimed at 40–50°C/0.02 mm Hg (m.p. 78.0–78.5°C).

IR spectra: 3250m, 1365w sh, 1350w sh, 1340w, 1320w, 1310w, 1280w, 1260m, 1220m, 1190s br, 1170m sh, 1165w, 1155w, 1120m, 1080m, 1065m br, 980m, 945s, 898s, 850m, 845m, 800m, 730vs br, 655m br, 620w, 540vs, 520m, 460w, 415w cm^{-1}. ^1H NMR (C_6D_6): δ 0.12(9H, s, Me_3Ga), 0.25 (1H, s, NH), 1.08–1.95(20H, m, CH_2), 2.53–2.85(2H, m, NCH_2). Mass spectra (only major peaks quoted): *m/z* 282(9%, parent ion − Me, ^{71}Ga), 280(13%, parent ion − Me, ^{69}Ga), 182(17%, $(C_6H_{11})_2NH_2$), 181(100%, $(C_6H_{11})_2NH$), 138(57%, $C_9H_{16}N$), 116(3%, $Me_3{}^{71}Ga$), 114(3%, $Me_3{}^{69}Ga$), 101(41%, $Me_2{}^{71}Ga$), 99(65%, $Me_2{}^{69}Ga$).

Preparation of trimethyl(2,6-dimethylpiperidine)gallium (**2**)

(a) *From* Ma_3Ga, Et_2O *and* 2,6-*dimethylpiperidine*. Methyl lithium (20.2 cm^3 of a 1.1 M solution in Et_2O, 22 mmol) was added dropwise to a stirred solution of $GaCl_3$ (1.3 g, 7.4 mmol) in diethyl ether (50 cm^3) at 0°C. After several hours standing at room temperature and filtration to remove LiCl, 2,6-dimethylpiperidine (1.0 cm^3, 7.4 mmol) was added via a syringe at 0°C and allowed to attain room temperature. Removal of ether *in vacuo* left an oily liquid which was extracted with pentane (20 cm^3) from which **2** crystallized (1.05 g, 46 mmol, 62% yield). The white crystals sublimed at 30°C/0.01 mm Hg (m.p. 49.5–50°C).

(b) *From* $(Me_3Ga)_2 \cdot$ *diphos and* 2,6-*dimethylpiperidine*. $(Me_3Ga)_2$·diphos (2.48 g, 3.9 mmol) was heated at 85–110°C *in vacuo* for 2 h and the Me_3Ga liberated was condensed onto a solution of 2,6-dimethylpiperidine (0.83 cm^3, 6.1 mmol) in pentane (15 cm^3) at −196°C. After standing overnight at room temperature the pentane was evaporated *in vacuo* leaving a white solid (1.1 g, 4.8 mmol, 79% based on amine) which sublimed at 25–35°C/0.02 mm Hg (m.p. 49–50°C).

IR spectra: 3255m sh, 1318w sh, 1280w sh, 1220w sh, 1195s br, 1175s br, 1108m br, 1064m sh, 1009m

br, 980m br, 954m br, 918w sh, 870m sh, 835vw sh, 790w sh, 730s vbr, 665m vbr, 570w sh, 550s br, 532s br, 510m sh, 330w br, cm^{-1}. ^1H NMR (C_6D_6): δ 0.0(9H, s, Me_3Ga), 0.95(6H, d, $J = 8$ Hz, $CHCH_3$), 2.2–2.6(3H, m, $NH+CHCH_3$), 0.4–1.4(6H, m, $CH_2CH_2CH_2$). Mass spectra (major peaks): *m/z*, 113(30%, ligand), 112(14%, ligand−H), 101(59%, $Me_2{}^{71}Ga$), 99(89%, $Me_2{}^{69}Ga$), 97(100%, ligand−CH_4), 71(17%, ^{71}Ga), 70(25%, C_5H_{10}), 69(26%, ^{69}Ga).

Preparation of trimethyl(1-azabicyclo[2.2.2]octane) gallium (**3**)

This was prepared as for **1** (method b) from $Me_3Ga \cdot$ diphos (3.15 g, 50 mmol) and quinuclidine (0.9 g, 8.1 mmol) giving **3** as white crystals (1.15 g, 5.9 mmol, 63% based on ligand) which sublimed at 70–90°C/0.02 mm Hg (m.p. 112.7–113.5°C).

IR spectra: 1350w, 1335m, 1315m, 1265w sh, 1260s, 1200m sh, 1190m, 1180m, 1160w, 1080s br, 1045s br, 1020s br, 980m, 865w br, 826m, 800vs br, 730m br, 660w, 635w, 580m, 540s, 515m, 400w br, 325w, 305w cm^{-1}. ^1H NMR (C_6D_6): δ −0.1(9H, s, Me_3Ga), 0.8–1.0 [7H, m, $CH(CH_2CH_2)_3N$], 2.3–2.6(6H, t, $J = 6$Hz, NCH_2). Mass spectra (major peaks): *m/z* 212(41%, ^{71}Ga parent ion−Me), 210*(62%, ^{69}Ga parent ion−Me), 111(41%, ligand), 110(20%, ligand−H), 101(66%, $Me_2{}^{71}Ga$), 99(100%, $Me_2{}^{69}Ga$), 71(22%, ^{71}Ga), 69(36%, ^{69}Ga).

Preparation of hexamethyl(1,4-diazabicyclo[2.2.2] octane)digallium (**4**)

Methyl lithium (36 cm^3 of a 1.83 M solution in Et_2O, 65.9 mmol) was added dropwise to a stirred solution of $GaCl_3$ (3.9 g, 22 mmol) in diethyl ether (80 cm^3) at 0°C. After removal of LiCl by filtration, 1,4-diazabicyclo[2.2.2]octane (2.47 g, 22 mmol) was added to the filtrate at −70°C. Ether was removed *in vacuo* and the product recrystallized from pentane (50 cm^3) giving white crystals (1.9 g, 7.0 mmol, 64% based on $GaCl_3$) which sublimed at 60–80°C/0.03 mm Hg or at 179–180°C under atmospheric N_2.

IR spectra: 1450s, 1370w sh, 1320s, 1260w, 1190vs, 1180s, 1175m, 1080w sh, 1055s, 1010s, 924m, 838s, 800s, 755s sh, 710s br, 540vs, 512m, 420w cm^{-1}. ^1H NMR (C_6D_6): δ −0.35(18H, s, Me_3Ga), 1.98(12H, s, CH_2CH_2). Mass spectra (major peaks): *m/z* 112(18%, ligand), 101(69%, $Me_2{}^{71}Ga$), 99(100%, $Me_2{}^{69}Ga$), 86(7%, $Me^{71}Ga$), 84(11%, $Me^{69}Ga$), 71(25%, ^{71}Ga), 69(34%, ^{69}Ga).

Preparation of tri(methyl-d_3)(trimethylamine) gallium (**5**)

NMe_3 (0.83 g, 14 mmol) was condensed onto $[(CD_3)_3Ga]_2 \cdot$ diphos (5.45 g, 8 mmol) at −196°C. As the reaction mixture warmed to room temperature, a white solid appeared to coat the diphos adduct **9** and it sublimed at 25°C/0.02 mm Hg as product **5** (1.86 g, 10 mmol, 63% based on **9**, m.p. 96.5–97°C).

IR spectra: 3000s, 2780s, 2700w, 2680w, 2310w sh, 2180s br, 2090s br, 2060m sh, 1815w, 1520w sh, 1470s br, 1440s br, 1245s, 1218s, 1095s, 1000vs br, 920s br, 815s br, 570vs br, 480vs br cm^{-1}. Mass spectra (major peaks): **5** gave no gallium containing species (similar behaviour to $Me_3Ga \cdot NMe_3$), the dominant fragment ion was at *m/z* 44(100%, NMe_2).

Preparation of tri(methyl-d_3)(dicyclohexylamine) gallium (**6**)

This was prepared as for **1** (method b) from **9** (2.56 g, 4 mmol) and $HN(C_6H_{11})_2$ (1.3 cm^3, 6 mmol) which gave white crystals of **6** (1.48 g, 4.8 mmol, 80% based on ligand) which sublimed at 40–60°C/0.03 mm Hg (m.p. 79.5–80°C).

IR spectra: 3240m, 2660w, 2220m, 2210m, 2100w, 1350m sh, 1330w, 1320w, 1310w, 1295w, 1265w, 1260m, 1215w, 1170w, 1110m br, 1080m, 1060m, 1015s br, 975m, 930s br, 890m, 850m, 840m, 798s, 710w br, 560vs br, 498s br, 465w, 410w, 335w cm^{-1}. Mass spectra (major peaks): *m/z* 181 (20%, ligand), 107(26%, $(CD_3)_2{}^{71}Ga$), 105(39%, $(CD_3)_2{}^{69}Ga$), 71(8%, ^{71}Ga), 69(12%, ^{69}Ga).

Preparation of tri(methyl-d_3)(2,6-dimethylpiperidine)gallium (**7**)

This was prepared as for **2** (method b) from **9** (3.49 g, 5.4 mmol) and 2,6-dimethyl piperidine (1.64 cm^3, 12 mmol) which gave white crystals of **7** (2.25 g, 9.5 mmol, 88% based on **9**) which sublimed at 25°C/0.02 mm Hg (m.p. 49.5–51°C).

IR spectra: 3240m, 2200m, 2100m, 1450s, 1440m, 1420w, 1365m, 1310w, 1275w, 1255w, 1210m, 1170s, 1130m, 1105s, 1060m, 1005s, 980m, 950m sh, 925s, 855s, 785m, 660m br, 565vs br, 530s, 500s, 480s, 460m, 320w cm^{-1}.

* Accurate mass = 210.0773; calc. 210.0763.

Preparation of tri(methyl-d_3)(1-azabicyclo[2.2.2]octane)gallium (**8**)

This was prepared as for **1** (method b) from **9** (3.98 g, 6.2 mmol) and quinuclidine (1.10 g, 9.9 mmol) giving white crystals of **8** (2.10 g, 8.9 mmol, 91% based on ligand) which sublimed at 70°C/0.02 mm Hg (m.p. 113–113.5°C).

IR spectra: 2198s, 2096s, 1472w, 1365m, 1360w, 1345m, 1330m, 1312s, 1262m, 1255s br, 1198s, 1158w, 1090m br, 1042vs, 1015s br, 995s, 980vs, 960m, 920vs br, 880w, 825s, 805s, 790s, 632m, 570vs br, 500vs br, 490s sh, 464m, 390w br cm^{-1}. Mass spectra (major peaks): *m/z* 218(10%, parent ion $^{71}Ga-CD_3$), 216(13%, parent ion $^{69}Ga-CD_3$, 111(37%, ligand), 107(65%, $(CD_3)_2{}^{71}Ga$], 105(100%, $(CD_3)_2{}^{69}Ga$), 89(7%, $CD_3{}^{71}Ga$), 87(11%, $CD_3{}^{69}Ga$), 71(23%, ^{71}Ga), 69(34%, ^{69}Ga).

Preparation of hexa(methyl-d_3)-μ-[1,2-bis(diphenylphosphino)ethane]digallium (**9**)

A solution of CD_3I (53 cm^3, 833 mmol) in diethyl ether (100 cm^3) was added dropwise to a stirred suspension of magnesium turnings (20.3 g, 833 mmol) in ether (200 cm^3) at 0°C, at a rate to maintain a gentle reflux. The solution was refluxed for another hour and then added to a stirred (magnetically) solution of $GaCl_3$ (43 g, 244 mmol) in ether (300 cm^3) at 0°C. The solution was kept at room temperature overnight and then the solvent and $(CD_3)_3Ga \cdot Et_2O$ separated by fractional distillation. The $(CD_3)_3Ga \cdot Et_2O$ (44.9 g, 227 mmol, 93% based on $GaCl_3$) was added via a transfer tube to a solution of diphos (47.9 g, 120 mmol) in benzene (200 cm^3). The remaining ether was distilled off and the solution concentrated to *ca* 150 cm^3. $[(CD_3)_3Ga]_2 \cdot$ diphos (**9**) was deposited as large white crystals which were recrystallized (54.5 g, 74% based on $GaCl_3$, m.p. 163–163.5°C).

IR spectra: 2200w, 2100w, 1580w, 1480m, 1430vs, 1418m, 1305w, 1280w, 1255m br, 1180w, 1165m, 1095s br, 1080m sh, 1020m br, 1010m sh, 995m, 920m, 795m br, 745vs, 720vs, 692vs, 680w, 570m br, 505s, 490m, 480m, 460m, 450m, 330w cm^{-1}. Mass spectrum showed peaks corresponding to $(CD_3)_3Ga$ (major peaks): *m/z* 107(80%, $(CD_3)_2{}^{71}Ga$), 105(100%, $(CD_3)_2{}^{69}Ga$), 89(10%, $CD_3{}^{71}Ga$), 87(13%, $CD_6{}^{69}Ga$), 71(29%, ^{71}Ga), 69(42%, ^{69}Ga).

Preparation of bis-μ-(diisopropylamido)tetramethyldigallium (**10**)

$LiNPr^i_2$ (8 mmol, prepared from $HNPr^i_2$ and Bu^nLi) in Et_2O (20 cm^3) was added to a stirred solution of Me_2GaCl (13.0 cm^3 of a 0.63 M solution in hexane, 8 mmol) in Et_2O (20 cm^3) at 0°C and a white solid was precipitated. After stirring for 1 h at room temperature the product was extracted with ether (100 cm^3) and the extract evaporated *in vacuo* to remove the ether. The white solid product (contaminated with $LiNPr^i_2$) was purified by sublimation *in vacuo* (90°C/0.03 mm Hg, 0.83 g, 4.2 mmol, 52% yield, m.p. 123.5–124.5°C). The product $(Me_2Ga\ NPr^i_2)_2$ (**10**) was unstable and decomposed over a period of *ca* one month.

IR spectra: 2850s, 1450s br, 1380s, 1300m, 1255m, 1200s, 1160s br, 1130s, 1030m br, 955m, 910m, 830m, 790m, 740s br, 670m br, 630m, 545m, 525m, 425w, 370w cm^{-1}. ^1H NMR spectrum (C_6D_6): δ 0.3(12H, s, Me_2Ga), 1.18 (24H, d, $J = 8$ Hz, Pr^i methyls), 3.58(4, q, $J = 8$ Hz, Pr^i methines). Mass spectra (major peaks): *m/z* 302(7%, dimer $(^{71}Ga_2)-Me_2{}^{71}Ga$), 299(14%, dimer $(^{71}Ga{}^{69}Ga)-Me_2{}^{71}Ga$), 287(6%, dimer $(^{71}Ga_2)-NPr^i_2-Me$), 285(9%, dimer $(^{71}Ga, {}^{69}Ga)-NPr^i_2-Me$), 283(10%, dimer $(^{69}Ga_2)-NPr^i_2-Me$), 186(11%, $Me_2{}^{71}GaNPr^i_2-Me$), 184(17%, $Me_2{}^{69}GaNPr^i_2-Me$), 101(33%, $Me_2{}^{71}Ga$), 99(49%, $Me_2{}^{69}Ga$), 86(5%, $Me^{71}Ga$), 84(6%, $Me^{69}Ga$), 71(11%, ^{71}Ga), 69(18%, ^{69}Ga), 58(15%, $NHPr^i$), 44(100%, CH_2CMe_2).

Preparation of bis-μ-(2,6-dimethylpiperido)tetramethyldigallium (**11**)

The lithio derivative of 2,6-dimethylpiperidine (8 mmol, prepared from the ligand and Bu^nLi) in diethyl ether (20 cm^3) was added to a stirred solution of Me_2GaCl (13.0 cm^3 of 0.63 M solution in hexane, 8 mmol) in Et_2O (30 cm^3) at 0°C. The green amide solution became colourless and some white solid was deposited and the system was stirred at room temperature for 1 h. The product was extracted with Et_2O (40 cm^3) which was filtered through celite and concentrated to *ca* 20 cm^3 and white crystals were deposited and were sublimed at 118–125°C/0.02 mm Hg, m.p. 131.5–132.5°C.

IR spectra: 1460s, 1355m, 1350m, 1314m, 1300m, 1250m, 1184w, 1140s, 1120s, 1110s, 1020m, 990m, 975m, 840s, 815w, 740s br, 670m br, 632m, 542m, 525m, 424w, 370w cm^{-1}. ^1H NMR spectrum (C_6D_6): δ 0.1 (12H, s, Me_2Ga), 0.8–1.6 (12H, m, CH_2), 1.2(12H, d, $J = 8$ Hz, $CHCH_3$), 3.40(4H, m, $CHMe$). Mass spectra (major peaks): *m/z* 325(8%, dimer $(^{71}Ga_2)-Me_2{}^{71}Ga$), 323(12%, dimer $(^{71}Ga{}^{69}Ga)-Me_2{}^{71}Ga$), 299(7%, dimer $(^{71}Ga_2)-$ligand$-$Me), 297(10%, dimer $(^{71}Ga{}^{69}Ga)-$ligand$-$Me), 295(11%, dimer $(^{69}Ga_2)-$ligand$-$Me), 198(12%, monomer $(^{71}Ga)-$Me),

196(15%, monomer (^{69}Ga)−Me), 113(89%, protonated ligand), 112(64%, ligand), 101(34%, $Me_2{}^{71}Ga$), 99(48%, $Me_2{}^{69}Ga$), 86(10%, $Me^{71}Ga$), 84(12%, $Me^{69}Ga$).

Preparation of tris-μ-(dimethylarsenido)hexamethyltrigallium

A solution of Me_2AsH (2.4 g, 24 mmol) in toluene (80 cm^3) was added to a stirred solution of $Me_3Ga \cdot Et_2O$ (4.6 g, 24 mmol, prepared from MeLi and $GaCl_3$ in Et_2O) in toluene (80 cm^3). Warming to 70°C caused effervescence which lasted *ca* 1 h and the solution was maintained at 70°C for a further 2 h. Toluene and ether were removed under reduced pressure at room temperature and the resulting white solid was sublimed at 100–110°C/0.02 mm Hg (17 mmol, m.p. 198°C dec., 77% yield based on $Me_3Ga \cdot Et_2O$). Found: C, 22.5; H, 5.6. $C_{12}H_{36}As_3Ga_3$ requires: C, 23.5; H, 5.9%.

IR spectra: 1422m, 1262w, 1249w, 1191m, 902s, 867s, 750s, 725vs, 593m, 579m, 562s, 524s, 253w cm^{-1}. ^1H NMR spectrum (80 MHz, C_6D_6): δ 0.25(18H, s, Me_2Ga), 0.75(18H, s, Me_2As). At 250 MHz ($C_6D_5CD_3$) at various temperatures: 30°C (δ −0.10 Me_2Ga, 0.90 Me_2As), −60°C (0.02 Me_2Ga, 0.86 Me_2As), −70°C (0.7 Me_2Ga, 0.84 Me_2As). Mass spectra (major peaks): *m/z* 618(190, trimer $^{71}Ga^{69}Ga_2$), 612(2%, trimer $^{69}Ga_3$), 603(2%, trimer ($^{71}Ga_3$)−Me), 601(9%, trimer ($^{71}Ga_2{}^{69}Ga$)−Me), 599(16%, trimer ($^{71}Ga^{69}Ga_2$)−Me), 597(8%, trimer ($^{69}Ga_3$)−Me), 513(5%, trimer ($^{71}Ga_3$)−Me_2As), 511(21%, trimer ($^{71}Ga_2{}^{69}Ga$)−Me_2As), 509(29%, trimer ($^{71}Ga^{69}Ga_2$)−Me_2As), 507(15%, trimer ($^{69}Ga_3$)−Me_2As), 487(3%, trimer ($^{71}Ga_3$)−$Me_2{}^{71}Ga$−2Me), 485(7%, trimer ($^{71}Ga_2{}^{69}Ga$)−$Me_2{}^{7}Ga$−2Me), 483(5%, trimer ($^{71}Ga^{69}Ga_2$)−$Me_2{}^{71}Ga$−2Me), 397(dimer ($^{71}Ga_2$)−Me), 395(12%, dimer ($^{71}Ga^{69}Ga$)−Me), 393(9%, dimer ($^{69}Ga_2$)−Me), 307(10%, dimer ($^{71}Ga_2$)−Me_2As), 305(28%, dimer ($^{71}Ga^{69}Ga$)−Me_2As), 303(21%, dimer ($^{69}Ga_2$)−Me_2As), 210(47%, Me_4As_2), 195(34%, Me_3As_2), 191(18%, $^{71}GaAsMe_3$), 189(28%, $^{69}GaAsMe_3$), 180(13%, Me_2As_2), 105(27%, Me_2As), 101(64%, $Me_2{}^{71}Ga$), 99(100%, $Me_2{}^{69}Ga$), 90(34%, MeAS), 86(4%, $Me^{71}Ga$), 84(7%, $Me^{69}Ga$), 71(44%, ^{71}Ga), 69(68%, ^{69}Ga).

X-ray crystallography

X-ray measurements for both compounds were made on crystals sealed under argon in thin walled glass capillaries using an Enraf–Nonius CAD 4 diffractometer operating in the ω–2θ scan mode with graphite monochromated Mo-K_α radiation

Table 4. Crystal data and details of intensity data collection and structure refinement

Compound	**1**	**2**
Formula	$C_{15}H_{32}NGa$	$C_{10}H_{24}NGa$
Molecular weight	296.21	228.03
Crystal system	Monoclinic	Monoclinic
a (Å)	18.995(3)	7.274(3)
b (Å)	13.557(2)	11.468(2)
c (Å)	6.666(2)	15.221(2)
β (deg)	91.19(2)	96.84(2)
V (Å^3)	1716.1	1260.7
Space group	$P2_1/a$	$P2_1/c$
Z	4	4
D_c(g cm^{-1})	1.16	1.20
μ(cm^{-1})	15.2	20.7
F(000)	640	488
Theta range (deg)	1.5–25.0	1.5–30.0
Number of data measured	3418	4100
Number unique	3005	3669
Number observed	1763	1655
Cut-off	$I > 1.5\sigma(I)$	$I > 2.0\sigma(I)$
Number of parameters	194	194
Weight parameter, g^a	0.0006	0.0001
R	0.063	0.031
R_w	0.063	0.030

[a] Weights = $[\sigma^2(F_o)+gF_o^2]^{-1}$.

($\lambda = 0.71069$ Å) following previously detailed procedures.[14] The structures were solved via the heavy atom method and refined by full-matrix least-squares. Non-hydrogen atoms were assigned anisotropic displacement factor coefficients, hydrogens isotropic. For **1** all hydrogens but the amine hydrogen were included in idealized positions and refined as parts of rigid groups; the amine hydrogen was located experimentally and freely refined. For **2** all hydrogens were freely refined except for those on methyl C(8), which were idealized to obtain stable refinement.

Crystal data and details of intensity measurement and refinement are given in Table 4.

Acknowledgements—We thank the Ministry of Defence (D.C.V.D.), through the sponsorship of R.S.R.E. (Malvern), for financial support (L.M.S.) and also SERC. We are indebted to Mr Greg Coumbarides for obtaining 80 and 250 MHz ^{1}H NMR spectra and to Dr G. E. Hawkes for 400 MHz ^{1}H NMR using the University of London Intercollegiate Research facility at Queen Mary College. Finally we thank Mr Peter Cook for his skill and perseverance in obtaining mass spectra on air-sensitive compounds.

REFERENCES

1. *Gmelin Handbook of Inorganic Chemistry, Ga—Organogallium Compounds, Part 1.* Springer, Berlin (1987).
2. I. J. Worrall and J. D. Smith, *Dictionary of Organometallic Compounds*, Vol. 1. Chapman and Hall, London (1984).
3. D. G. Tuck, *Comprehensive Organometallic Chemistry*, Vol. 1. Pergamon Press, Oxford (1982).
4. H. M. Manasevit and W. I. Simpson, *J. Electrochem. Soc.* 1969, **116**, 1725.
5. H. M. Manasevit and W. I. Simpson, *J. Electrochem. Soc.* 1973, **120**, 135.
6. Lesley M. Smith, PhD thesis, University of London (1986).
7. D. C. Bradley, Halina Chudzynska, M. M. Faktor, D. M. Frigo, M. B. Hursthouse, B. Hussain and L. M. Smith, *Polyhedron* 1988, **7**, 1289.
8. D. C. Bradley, H. Dawes, D. M. Frigo, M. B. Hursthouse and B. Hussain, *J. Organomet. Chem.* 1987, **325**, 55.
9. D. C. Bradley, D. M. Frigo and E. A. D. White, *Forming aluminium nitride films.* UK Patent Applications, 8804707 and 8805524.
10. O. T. Beachley and G. Coates, *J. Chem. Soc.* 1965, 3241.
11. A. N. Dymor and A. P. Savostin, *Analytical Chemistry of Gallium.* Ann Arbor, London (1970).
12. H. Gilman and J. W. Morton, *Organic Reactions*, Vol. 8. Wiley, New York (1954).
13. R. D. Feltham and W. Silverthorn, *Inorg. Synth.* 1967, **10**, 159.
14. R. A. Jones, M. B. Hursthouse, K. M. A. Malik and G. Wilkinson, *J. Am. Chem. Soc.* 1979, **101**, 4128.

Polyhedron Vol. 9, No. 2/3, pp. 353–360, 1990
Printed in Great Britain

0277–5387/90 $3.00+.00
Pergamon Press plc

NOVEL INTRAMOLECULARLY STABILIZED ORGANOGALLIUM AND ORGANOINDIUM COMPOUNDS AND THEIR USE IN MOVPE

HERBERT SCHUMANN,* UWE HARTMANN and WILFRIED WASSERMANN

Institut für Anorganische und Analytische Chemie, Technische Universität Berlin, D-1000 Berlin 12, F.R.G.

Abstract—Novel organogallium and organoindium compounds containing the intramolecularly stabilizing dimethylaminopropyl, diethylaminopropyl or dimethylaminobutyl ligand have been synthesized for use in MOVPE. Syntheses and NMR investigations of the moderately air-stable compounds are reported. Using those compounds, GaAs and InP semiconductor layers of good quality could be grown in initial experiments.

III–V semiconductor layers of GaAs and InP for use in optoelectronic devices can be grown by the technique of MOVPE (Metal Organic Vapour Phase Epitaxy). Currently, trimethylgallium (TMG) and trimethylindium (TMI) are used as group III sources in combination with AsH_3 and PH_3 as group V sources.[1,2] However, both TMG and TMI are pyrophoric and extremely sensitive to oxygen and moisture because of their coordinative unsaturation. Formation of Lewis base adducts with NMe_3, PMe_3 and $AsMe_3$ greatly enhances the stability of TMG and TMI. Unfortunately, these adducts are solids at room temperature, thus allowing their use only in apparatus with heated gas lines in order to avoid condensation.

We describe the use of organic ligands containing a terminal Lewis basic group, like dimethylaminopropyl,[3] which allows intramolecular coordination to gallium or indium via a five- or six-membered ring formation. The vapour pressure of the new compounds is high enough for the use in MOVPE without additional heating of the source. Thus, new moderately air-stable precursors for the production of III–V semiconductor layers are now available.

RESULTS AND DISCUSSION

The reaction of dimethylgallium chloride, diethylgallium chloride, di-n-propylgallium chloride, the newly prepared di-iso-propylgallium chloride (**1**), diphenylgallium chloride and the corresponding diorganoindium chlorides, including the new di-iso-propylindium chloride (**2**), with dimethylaminopropyllithium in pentane, first at 0°C, then 12 h at room temperature results in the formation of intramolecular coordinatively saturated triorganogallium and triorganoindium compounds, which are isolated in high yields as liquids or very low melting solids, eqs (1) and (2):

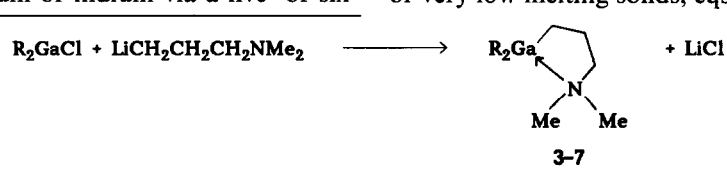

3–7

R = CH_3 (**3**), C_2H_5 (**4**), C_3H_7 (**5**), i-C_3H_7 (**6**), C_6H_5 (**7**) (1)

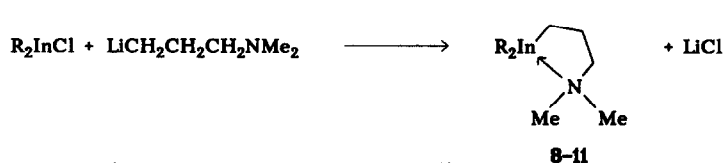

8–11

R = CH_3 (**8**), C_2H_5 (**9**), C_3H_7 (**10**), i-C_3H_7 (**11**) (2)

The use of diethylaminopropyllithium results in the formation of the corresponding diorgano (diethylaminopropyl)derivatives of gallium and indium, eq. (3):

* Author to whom correspondence should be addressed.

$$R_2MCl + LiCH_2CH_2CH_2NEt_2 \longrightarrow$$

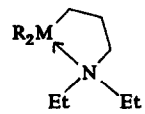

$$+ LiCl$$

12–16

$$M = Ga,\ R = CH_3\ (\mathbf{12});\ M = In,\ R = CH_3\ (\mathbf{13}),\ C_2H_5\ (\mathbf{14}),\ C_3H_7\ (\mathbf{15}),\ i\text{-}C_3H_7\ (\mathbf{16}) \quad (3)$$

These new compounds show almost no decomposition in air. They are readily soluble in organic solvents like ether, benzene or hexane. Slow decomposition occurs in contact with water or alcohol. Cryoscopic molecular weight determinations in benzene for (3-dimethylaminopropyl)dimethylgallium[4] and (3-dimethylaminopropyl)dimethylindium reveal the monomeric constitution in solution. This clearly indicates that the compounds are stabilized intramolecularly via a five-membered ring conformation and not by dimerization.

(3-Dimethylaminopropyl)dimethylindium shows a higher vapour pressure compared to tetrameric TMI, which is commonly used as an indium source in MOVPE.[5,6] The vapour pressures of **3** and **8** in comparison to some compounds commonly used in MOVPE are shown in Table 1.

Six-membered rings formed by this type of intramolecular coordination were expected to be even more stable against oxygen and moisture because of reduced ring strain. An example for this type of compound is (4-dimethylaminobutyl)dimethylgallium (**18**), which is synthesized via hydrogallation[12] of dimethylaminobutene-3[13] with dichlorogallane, followed by methylation with methyllithium, eqs (4) and (5):

$$Cl_2GaH + CH_2{=}CHCH_2CH_2NMe_2 \longrightarrow \underset{\mathbf{17}}{Cl_2Ga(CH_2)_4NMe_2} \quad (4)$$

$$\underset{\mathbf{17}}{Cl_2Ga(CH_2)_4NMe_2} + 2\,MeLi \longrightarrow \underset{\mathbf{18}}{Me_2Ga(CH_2)_4NMe_2} + 2\,LiCl. \quad (5)$$

In comparison to (3-dimethylaminopropyl) dimethylgallium, a solid, this compound has similar physical properties, yet it is a liquid at room temperature.

Triorganogallium- or indium derivatives containing two 3-dimethylaminopropyl or 3-diethylaminopropyl ligands should show an even higher stability against moisture and air because of the possible formation of five-coordinated gallium and indium compounds. This structural feature has been shown already for organoindium compounds with dimethylaminobenzyl[14] or 2,6-bis(diethylaminomethylene)phenyl[15] ligands. Methylgallium dichloride reacts with 2 equivalents of 3-dimethylaminopropyllithium yielding bis(3-dimethylaminopropyl)methylgallium (**19**). Bis(3-alkylaminopropyl)methylindium derivatives were obtained by the reaction of indium trichloride with 2 equivalents of 3-alkylaminopropyllithium to give the bis(3-alkylaminopropyl)indium chlorides (**20**, **21**), which were converted to the corresponding bis(3-alkylaminopropyl)methylindium derivatives (**22**, **23**) by reaction with methyllithium, eqs (6)–(8):

$$CH_3GaCl_2 + 2\,Me_2N(CH_2)_3Li \longrightarrow \underset{\mathbf{19}}{CH_3Ga[(CH_2)_3NMe_2]_2} + 2\,LiCl \quad (6)$$

$$InCl_3 + 2\,R_2N(CH_2)_3Li \longrightarrow \underset{\mathbf{20,21}}{ClIn[(CH_2)_3NR_2]_2} + 2\,LiCl \quad (7)$$

$$ClIn[(CH_2)_3NR_2]_2 + MeLi \longrightarrow \underset{\mathbf{22,23}}{CH_3In[(CH_2)_3NR_2]_2} + LiCl \quad (8)$$

$$R = CH_3\ (\mathbf{20}, \mathbf{22}),\ C_2H_5\ (\mathbf{21}, \mathbf{23}).$$

The NMR spectra of the new compounds, almost all recorded in C_6D_6, show the expected results. The intensity of signals caused by carbon atoms directly bound to a metal atom is diminished to about 20% as compared to other carbon atoms. This is due to the spin of 3/2 and 9/2 of the gallium and indium atom, respectively.[16] Moreover, those carbon signals are broadened and show peak widths up to 10 Hz as compared to normally about 2 Hz. The intramolecular stabilization of **3**–**16** by formation of five- or six-membered ring systems was also confirmed by variable-temperature ^1H NMR studies as is shown for 3-dimethylaminopropyldi-i-propylgallium (**6**) (Fig. 1).

Two sets of doublets were observed at room temperature for the two i-propyl groups present in **6**. At the coalescence temperature of 56°C, only one broad doublet was detected indicating splitting of the internal coordination and causing a free rotation of the 3-dimethylaminopropyl ligand around the metal–carbon bond. Furthermore, the signal of the $(CH_3)_2N$ group is shifted to lower field with increasing temperature. This is most likely due to a break-up of the metal–nitrogen coordination. Spectroscopic evidence for intramolecular coordination was also obtained from NMR investi-

Table 1. Vapour pressure of organogallium and organoindium compounds used as gallium or indium sources in MOVPE

Compound	Temperature (°C) 20	50	75
$Me_2Ga(CH_2)_3NMe_2$	40 [Pa]	230 [Pa]	1050 [Pa]
$Me_3Ga \cdot NMe_3$[7]	2.4 [Pa]	12.1 [Pa]	37.8 [Pa]
Me_3Ga[8]	178 [Pa]	615 [Pa]	1432 [Pa]
$Me_2In(CH_2)_3NMe_2$[9]	~30 [Pa]	—	~500 [Pa]
$Me_3In \cdot NMe_3$[10]	1.2 [Pa]	8.1 [Pa]	28.7 [Pa]
Me_3In[11]	4.9 [Pa]	31.3 [Pa]	89.9 [Pa]

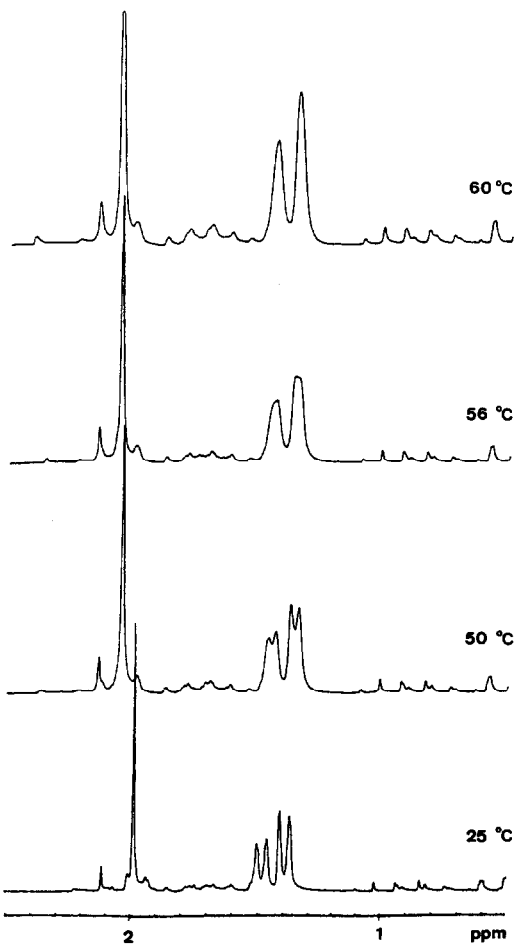

Fig. 1.

gations using the potentially five-coordinated bis(3-dimethylaminopropyl)methylgallium and -indium compounds **19** and **22**. In those compounds either a tetrahedral coordination around the metal centre (one of the ligands is bound, the other rotates freely) or a trigonal-bipyramidal coordination (both ligands are coordinating) is possible. The presence of just one signal for the protons in the $(CH_3)_2N$ moiety in the spectra of **19** and **22**, even at low temperature, clearly indicates that both dimethylamino groups are coordinated to the metal atom.

(3-Dimethylaminopropyl)dimethylindium (**8**) was tested as an indium source for InP layers in MOVPE.[9] Layers of InP were grown at a bubbler temperature of 30°C and a growth temperature of nearly 600°C. The growth rate was 1.2 μm h^{-1}. Hall measurements gave electron mobilities of μ_{77K} = 49,900 $cm^2\ V^{-1}\ s^{-1}$ and carrier concentrations of $n = 3.3 \times 10^{14}\ cm^{-3}$. The layers were of good quality as confirmed by photoluminescence measurements. Zinc was shown to be the main residual acceptor impurity. Further investigations using the other new compounds as precursors for GaAs and InP layers are in progress.[17]

EXPERIMENTAL

All reactions were carried out under the exclusion of oxygen and moisture in an atmosphere of argon using Schlenk tube techniques. Solvents were dried over $LiAlH_4$ or Na/benzophenone and distilled prior to use. The NMR spectra were recorded on a Bruker WH 270 at 270 MHz (^1H NMR) or at 67.93 MHz (^{13}C NMR). For carbon, hydrogen and nitrogen analyses a Perkin–Elmer elemental analyser 240 C was used, and for the determination of the gallium and indium contents a Perkin–Elmer 2380 atomic absorption spectrophotometer was employed. Mass spectra were recorded on a Varian MAT 311 A mass spectrometer. Molecular weights were measured by cryoscopy in benzene solutions, and vapour pressures were determined by the entrainment method.[18]

The starting materials used for the syntheses of the novel compounds were prepared according to literature procedures. The required triorganometal compounds were obtained either by alkylation of the metal trihalides with triorganoaluminium compounds[19] (Me_3Ga, Et_3Ga) or by Grignard reactions (n-Pr_3Ga, i-Pr_3Ga,[20] Et_3In, n-Pr_3In, i-Pr_3In).[21]

Triphenylgallium was made by reaction of diphenylmercury with gallium metal.[22] The corresponding diorganometal chlorides were prepared by redistribution reactions of the triorganometal compounds with the metal trichlorides.[23,24] Dimethylindium chloride could be obtained directly from indium trichloride and methyllithium.[25] The lithium reagents used were synthesized from the corresponding chlorides and lithium powder.[3]

Di-i-propylgallium chloride (**1**)

2.5 g (9.2 mmol) tri-*i*-propylgallium etherate were added via syringe to 0.8 g (4.6 mmol) gallium trichloride. The mixture was heated at 90°C for 5 h. The ether was removed *in vacuo*, and **1** remained as a colourless liquid. Yield: 2.5 g (95%). Found: C, 37.8; H, 7.4. Calc. for $C_6H_{14}ClGa$: C, 37.7; H, 7.4%. ^1H NMR (C_6D_6): δ 1.32–1.36 ppm (m). $^{13}C\{^1H\}$ NMR (C_6D_6): δ 19.8 (CH_3), 21.0 ppm (CH).

Di-i-propylindium chloride (**2**)

3.0 g (12.4 mmol) tri-*i*-propylindium were added via syringe to 1.4 g (6.2 mmol) of indium trichloride. 30 cm^3 pentane were added, and the mixture was refluxed for 30 min. After decanting, the residue was refluxed with 50 cm^3 of benzene. Upon cooling, **2** was obtained as a colourless solid. M.p. 204°C. Yield: 4.2 g (95%). Found: C, 30.8; H, 6.1; In, 48.0. Calc. for $C_6H_{14}ClIn$: C, 30.5; H, 6.0; In, 48.6%. ^1H NMR (C_6D_6): δ 1.04 (m, CH_3CHIn), 1.55 ppm (d, CH_3CHIn). $^{13}C\{^1H\}$ NMR (C_6D_6): δ 22.0 (CH_3CHIn), 22.6 ppm (CH_3CHIn).

(3-*Dimethylaminopropyl*)*dimethylgallium* (**3**)

A solution of 12 g (89.0 mmol) dimethylgallium chloride in 80 cm^3 pentane was added to a stirred suspension of 8.3 g (89.0 mmol) 3-dimethylaminopropyllithium in 50 cm^3 pentane at 0°C. After stirring for 12 h at room temperature, the solution was decanted from lithium chloride, the solvent removed *in vacuo*, and the residue distilled under reduced pressure. Compound **3** was obtained as a colourless liquid, which slowly solidified. B.p. 65°C/10 hPa. M.p. 49°C. Yield: 11.8 g (71%). Found: C, 45.2; H, 9.7; N, 7.8; Ga, 37.2. Calc. for $C_7H_{18}GaN$: C, 45.2; H, 9.8; N, 7.5; Ga, 37.5%. ^1H NMR (C_6D_6): δ −0.16 (s, CH_3Ga), 0.57 (t, CH_2Ga), 1.70 (tt, CH_2), 1.86 (s, CH_3N), 1.98 ppm (t, CH_2N). $^{13}C\{^1H\}$ NMR (C_6D_6): δ −6.2 (CH_3Ga), 9.3 (CH_2Ga), 24.4 (CH_2), 45.9 (CH_3N), 64.0 ppm (CH_2N). MS (70 eV): *m/e* (rel. intensity, %) 170/172* (100) [M $-CH_3$], 58 (55) [$Me_2N^+CH_2$], 84 (50) [$Me_2N^+CHCHCH_2$], 86 (14) [$Me_2N^+(CH_2)_3$], 69/71* (10) [Ga^+], 99/101* (8) [Me_2Ga^+], 44 (6) [$C_2H_6N^+$]; *isotope pattern clearly visible. Mol. wt (cryosc./benzene) Found: 178. Calc. for $C_7H_{18}GaN$: 185.95.

(3-*Dimethylaminopropyl*)*diethylgallium* (**4**)

In analogy to the synthesis of **3**, the reaction between 2.8 g (17.1 mmol) diethylgallium chloride and 1.7 g (18.3 mmol) 3-dimethylaminopropyllithium yielded **4** as a colourless liquid. B.p. 75°C/0.5 hPa. Yield: 2.4 g (65%). Found: C, 50.5; H, 10.5; N, 6.8; Ga, 31.9. Calc. for $C_9H_{22}GaN$: C, 50.5; H, 10.4; N, 6.6; Ga 32.6%. ^1H NMR (C_6D_6): δ 0.37 (q, CH_3CH_2Ga), 0.40 (t, CH_2Ga), 1.35 (t, CH_3CH_2Ga), 1.75 (m, CH_2), 1.97 (s, CH_3N), 2.08 ppm (t, CH_2N). $^{13}C\{^1H\}$ NMR (C_6D_6): δ 3.6 (CH_3CH_2Ga), 5.2 (CH_2Ga), 11.3 (CH_3CH_2Ga), 24.5 (CH_2), 45.9 (CH_3N), 64.5 ppm (CH_2N). MS (70 eV): *m/e* (rel. intensity, %) 184/186* (100) [M $-C_2H_5$], 156/158* (75) [$M^+ - C_2H_5$, $-C_2H_4$], 58 (70) [$Me_2N^+CH_2$], 69/71* (62) [Ga^+], 84 (28) [$Me_2N^+CHCHCH_2$], 86 (26) [$Me_2N^+(CH_2)_3$], 44 (18) [$C_2H_6N^+$]; *isotope pattern clearly visible.

(3-*Dimethylaminopropyl*)*di*-n-*propylgallium* (**5**)

In analogy to the synthesis of **3**, the reaction between 2.26 g (11.8 mmol) di-*n*-propylgallium chloride and 1.2 g (13.0 mmol) 3-dimethylaminopropyllithium yielded **5** as a colourless liquid. B.p. 98°C/0.01 hPa. Yield: 1.8 g (63%). Found: C, 54.4; H, 10.3; N, 6.5; Ga, 28.0. Calc. for $C_{11}H_{26}GaN$: C, 54.6; H, 10.8; N, 5.8; Ga, 28.8%. ^1H NMR (C_6D_6): δ 0.45 (m, $CH_3CH_2CH_2GaCH_2$), 1.17 (t, $CH_3CH_2CH_2Ga$), 1.72 (m, CH_2), 1.98 (s, CH_3N), 2.08 ppm (t, CH_2N). $^{13}C\{^1H\}$ NMR (C_6D_6): δ 6.6 (CH_2Ga), 15.9 ($CH_3CH_2CH_2Ga$), 20.5 ($CH_3CH_2CH_2Ga$), 21.2 (CH_2), 24.5 ($CH_3CH_2CH_2Ga$), 46.1 (CH_3N), 64.6 ppm (CH_2N). MS (70 eV): *m/e* (rel. intensity, %) 198/200* (100) [M $-C_3H_7$], 58 (80) [$Me_2N^+CH_2$], 156/158* (78) [$M^+ - C_3H_7$, $-C_3H_6$], 69/71* (70) [Ga^+], 84 (33) [$Me_2N^+CHCHCH_2$], 86 (32) [$Me_2N^+(CH_2)_3$], 42 (22) [$C_2H_4N^+$], 44 (15) [$C_2H_6N^+$]; *isotope pattern clearly visible.

(3-*Dimethylaminopropyl*)*di*-i-*propylgallium* (**6**)

In analogy to the synthesis of **3**, the reaction between 4.6 g (24.0 mmol) di-*i*-propylgallium chloride and 2.46 g (26.4 mmol) 3-dimethylaminopropyllithium yielded **6** as a colourless liquid. B.p. 86°C/0.01 hPa. Yield: 3.36 g (58%). Found: C, 54.3;

H, 10.4; N, 6.2; Ga, 28.1. Calc. for $C_{11}H_{26}GaN$: C, 54.6; H, 10.8; N, 5.8; Ga, 28.8%. ^{1}H NMR (C_6D_6): δ 0.48 (t, CH_2Ga), 0.82 (sept, CHGa), 1.39 (d) and 1.43 (d, [CH_3]$_2$CH), 1.68 (tt, CH_2), 1.98 (s, CH_3N), 2.01 ppm (t, CH_2N). ^{13}C{^{1}H} NMR (C_6D_6): δ 3.2 (*C*H_2Ga), 14.0 (*C*HGa); 22.4 and 22.5 ([*C*H_3]$_2$CH), 24.2 (*C*H_2), 46.1 (*C*H_3N), 64.8 ppm (*C*H_2N). MS (70 eV): *m/e* (rel. intensity, %) 198/200* (100) [M $-C_3H_7$], 58 (72) [$Me_2N^+CH_2$], 156/158* (55) [$M^+ - C_3H_7$, $-C_3H_6$], 86 (38) [$Me_2N^+(CH_2)_3$], 84 (35) [$Me_2N^+CHCHCH_2$], 69/71* (33) [Ga^+], 42 (16) [$C_2H_4N^+$], 44 (15) [$C_2H_6N^+$]; *isotope pattern clearly visible.

(3-*Dimethylaminopropyl*)*diphenylgallium* (**7**)

In analogy to the synthesis of **3**, the reaction between 4.8 g (18.6 mmol) diphenylgallium chloride and 1.9 g (20.4 mmol) 3-dimethylaminopropyllithium yielded **7** as a colourless solid after crystallization from hexane. M.p. 137°C. Yield: 4.38 g (76%). Found: C, 65.2; H, 7.1; N, 4.9; Ga, 22.1. Calc. for $C_{17}H_{22}GaN$: C, 65.9; H, 7.2; N, 4.5; Ga, 22.5%. ^{1}H NMR (C_6D_6): δ 0.54 (t, CH_2Ga), 1.68 (m, CH_2), 1.83 (s, CH_3N), 1.96 (t, CH_2N), 7.28–7.96 ppm (m, phenyl). ^{13}C{^{1}H} NMR (C_6D_6): δ 10.1 (*C*H_2Ga), 24.6 (*C*H_2), 45.3 (*C*H_3N), 64.5 (*C*H_2N), 125.7, 127.7, 137.1, 143.3 ppm (phenyl).

(3-*Dimethylaminopropyl*)*dimethylindium* (**8**)

In analogy to the synthesis of **3**, the reaction of 9.8 g (54.3 mmol) dimethylindium chloride and 5.06 g (54.3 mmol) 3-dimethylaminopropyllithium yielded **8** as a colourless liquid. B.p. 57°C/5 hPa. M.p. 12°C. Yield: 8.3 g (67%). Found: C, 36.4; H, 8.1; N, 6.3; In, 49.0. Calc. for $C_7H_{18}InN$: C, 36.4; H, 7.9; N, 6.1; In, 49.7%. ^{1}H NMR (C_6D_6): δ -0.28 (s, CH_3In), 0.57 (t, CH_2In), 1.75 (tt, CH_2), 1.88 (s, CH_3N), 1.93 ppm (t, CH_2N). ^{13}C{^{1}H} NMR (C_6D_6): δ -7.5 (*C*H_3In), 10.7 (*C*H_2In), 25.9 (*C*H_2), 46.3 (*C*H_3N), 64.8 ppm (*C*H_2N). MS (70 eV): *m/e* (rel. intensity, %) 58 (100) [$C_3H_8N^+$], 216 (84) [M $-CH_3$], 86 (43) [$Me_2N^+(CH_2)_3$], 115 (31) [In^+], 84 (16) [$Me_2N^+CHCHCH_2$], 42 (15) [$C_2H_4N^+$], 145 (11) [Me_2In^+], 44 (9) [$C_2H_6N^+$], 201 (6) [M -2 CH_3], 130 (2) [$MeIn^+$]. Mol. wt (cryosc./benzene) Found: 247. Calc. for $C_7H_{18}InN$: 231.05.

(3-*Dimethylaminopropyl*)*diethylindium* (**9**)

In analogy to the synthesis of **3**, the reaction of 7.9 g (37.9 mmol) diethylindium chloride and 3.53 g (37.9 mmol) 3-dimethylaminopropyllithium yielded **9** as a colourless liquid. B.p. 80°C/3 hPa. Yield: 6.1 g (62%). Found: C, 41.9; H, 8.5; N, 5.7; In, 44.0. Calc. for $C_9H_{22}InN$: C, 41.7; H, 8.6; N, 5.4; In, 44.3%. ^{1}H NMR (C_6D_6): δ 0.50 (q, CH_3CH_2In), 0.57 (t, CH_2In), 1.41 (t, CH_3CH$_2$In), 1.78 (tt, CH_2), 1.91 (s, CH_3N), 1.93 ppm (t, CH_2N). ^{13}C{^{1}H} NMR (C_6D_6): δ 5.3 (CH_3CH_2In), 7.8 (*C*H_2In), 13.2 (*C*H_3CH$_2$In), 26.2 (*C*H_2), 46.3 (*C*H_3N), 65.3 ppm (*C*H_2N).

(3-*Dimethylaminopropyl*)*di*-n-*propylindium* (**10**)

In analogy to the synthesis of **3**, the reaction of 13.0 g (55.0 mmol) di-*n*-propylindium chloride and 5.19 g (55.0 mmol) 3-dimethylaminopropyllithium yielded **10** as a colourless liquid. B.p. 62°C/0.05 hPa. Yield: 8.2 g (52%). Found: C, 45.7; H, 9.4; N, 5.1; In, 40.5. Calc. for $C_{11}H_{26}InN$: C, 46.0; H, 9.1; N, 4.9; In, 40.0%. ^{1}H NMR (C_6D_6): δ 0.66 (t, CH_2In), 0.73 (t, CH_3CH_2CH_2In), 1.18 (t, CH_3 CH_2CH_2In), 1.62 (m, CH_3CH_2CH_2In), 1.84 (tt, CH_2), 1.94 (s, CH_3N), 1.98 ppm (t, CH_2N). ^{13}C{^{1}H} NMR (C_6D_6): δ 9.2 (*C*H_2In), 17.9 (CH_3CH_2 *C*H_2In), 20.8 (*C*$H_3CH_2CH_2$In), 22.6 (CH_3*C*H_2 CH_2In), 26.1 (*C*H_2), 46.3 (*C*H_3N), 65.1 ppm (*C*H_2N).

(3-*Dimethylaminopropyl*)*di*-i-*propylindium* (**11**)

In analogy to the synthesis of **3**, the reaction of 1.2 g (5.1 mmol) di-*i*-propylindium chloride and 0.47 g (5.1 mmol) 3-dimethylaminopropyllithium yielded **11** as a colourless liquid. B.p. 54°C/0.2 hPa. Yield: 0.8 g (55%). Found: C, 46.2; H, 9.0; N, 4.6; In, 39.8. Calc. for $C_{11}H_{26}InN$: C, 46.0; H, 9.1; N, 4.9; In, 40.0%. ^{1}H NMR (C_6D_6): δ 0.68 (t, CH_2In), 1.12 (sept, C*H*In), 1.62 (d, CH_3CHIn), 1.81 (tt, CH_2), 1.93 (s, CH_3N), 2.02 ppm (t, CH_2N). ^{13}C{^{1}H} NMR (C_6D_6): δ 6.4 (*C*H_2In), 18.9 (CH_3*C*HIn), 24.4 (*C*H_2CHIn), 25.9 (*C*H_2), 46.3 (*C*H_3N), 65.2 ppm (*C*H_2N).

(3-*Diethylaminopropyl*)*dimethylgallium* (**12**)

In analogy to the synthesis of **3**, the reaction of 4.0 g (30 mmol) dimethylgallium chloride and 3.6 g (30 mmol) 3-diethylaminopropyllithium yielded **12** as a colourless solid after sublimation at 45°C onto a 15°C cold finger at 0.01 hPa. M.p. 56°C. B.p. 227°C. Yield: 4.5 g (70%). Found: C, 50.7; H, 10.0; N, 6.7; Ga, 32.2. Calc. for $C_9H_{22}GaN$: C, 50.5; H, 10.4; N, 6.6; Ga, 32.6%. ^{1}H NMR (C_6D_6): δ -0.05 (s, CH_3Ga), 0.60 (t, CH_2Ga), 0.63 (t, CH_3CH$_2$N), 1.81 (tt, CH_2), 2.09 (t, CH_2N), 2.43 ppm (q, CH_3CH_2N). ^{13}C{^{1}H} NMR (C_6D_6): δ -5.6 (*C*H_3Ga), 7.8 (*C*H_3CH_2N), 8.1 (*C*H_2Ga), 23.4 (*C*H_2), 43.7 (CH_3*C*H_2N), 56.6 ppm (*C*H_2N).

MS (70 eV): *m/e* (rel. intensity, %) 198/200* (100) [M $-CH_3$], 86 (91) [$Et_2N^+CH_2$], 112 (37) [$Et_2N^+CHCHCH_2$], 99/101* (15) [Me_2Ga^+], 69/71* (15) [Ga^+]; *isotope pattern clearly visible.

(3-*Diethylaminopropyl*)*dimethylindium* (**13**)

In analogy to the synthesis of **3**, the reaction of 4.0 g (22.2 mmol) dimethylindium chloride and 2.69 g (22.2 mmol) 3-diethylaminopropyllithium yielded **13** as a colourless liquid, which slowly solidified. B.p. 101°C/5 hPa. Yield: 3.9 g (68%). Found: C, 41.8; H, 8.6; N, 5.8; In, 43.7. Calc. for $C_9H_{22}InN$: C, 41.7; H, 8.6; N, 5.4; In, 44.3%. ^{1}H NMR (C_6D_6): δ −0.27 (s, CH_3In), 0.50 (t, CH_2In), 0.62 (t, CH_3CH_2N), 1.73 (CH_2), 2.04 (t, CH_2N), 2.29 ppm (q, CH_3CH_2N). $^{13}C\{^1H\}$ NMR (C_6D_6): −7.3 (CH_3In), 8.4 (CH_3CH_2N), 9.3 (CH_2In), 25.0 (CH_2), 44.4 (CH_3CH_2N), 57.5 ppm (CH_2N). MS (70 eV): *m/e* (rel. intensity, %) 244 (100) [M $-CH_3$], 86 (84) [$Et_2N^+CH_2$], 114 (62) [$Et_2N^+(CH_2)_3$], 112 (52) [$Et_2N^+CHCHCH_2$], 115 (43) [In^+], 58 (21) [$C_3H_8N^+$], 145 (17) [Me_2In^+], 56 (16) [$C_3H_6N^+$], 98 (14) [$C_6H_{12}N^+$], 42 (12) [$C_2H_4N^+$], 44 (5) [$C_2H_6N^+$], 130 (4) [MeIn$^+$].

(3-*Diethylaminopropyl*)*diethylindium* (**14**)

In analogy to the synthesis of **3**, the reaction of 3.70 g (17.8 mmol) diethylindium chloride and 2.16 g (17.8 mmol) 3-diethylaminopropyllithium yielded **14** as a colourless liquid. B.p. 85°C/0.3 hPa. Yield: 3.5 g (68%). Found: C, 45.8; H, 9.1; N, 4.7; In, 40.7. Calc. for $C_{11}H_{26}InN$: C, 46.0; H, 9.1; N, 4.9; In, 40.0%. ^{1}H NMR (C_6D_6): δ 0.57 (q, CH_3CH_2In), 0.58 (t, CH_3CH_2N), 0.73 (t, CH_2In), 1.47 (t, CH_3CH_2In), 1.73 (tt, CH_2), 2.01 (t, CH_2N), 2.28 ppm (q, CH_3CH_2N). $^{13}C\{^1H\}$ NMR (C_6D_6): δ 5.7 (CH_2In), 6.3 (CH_3CH_2In), 8.5 (CH_3CH_2N), 13.3 (CH_3CH_2In), 25.2 (CH_2), 44.4 (CH_3CH_2N), 57.9 ppm (CH_2N).

(3-*Diethylaminopropyl*)*di*-n-*propylindium* (**15**)

In analogy to the synthesis of **3**, the reaction of 3.1 g (13.1 mmol) di-*n*-propylindium chloride and 1.59 g (13.1 mmol) 3-diethylaminopropyllithium yielded **15** as a colourless liquid. B.p. 88°C/0.03 hPa. Yield: 2.1 g (51%). Found: C, 49.1; H, 9.7; N, 4.6; In, 36.8. Calc. for $C_{13}H_{30}InN$: C, 49.5; H, 9.6; N, 4.4; In, 36.4%. ^{1}H NMR (C_6D_6): δ 0.53 (t, $CH_3CH_2CH_2$In), 0.63 (t, CH_3CH_2N), 0.65 (t, CH_2In), 1.10 (t, $CH_3CH_2CH_2$In), 1.77 (m, $CH_3CH_2CH_2$In), 1.80 (tt, CH_2), 2.06 (t, CH_2N), 2.32 ppm (q, CH_3CH_2N). $^{13}C\{^1H\}$ NMR (C_6D_6): δ 7.7 (CH_2In), 8.5 (CH_3CH_2N), 18.0 ($CH_3CH_2CH_2$In), 20.9 ($CH_3CH_2CH_2$In), 22.7 ($CH_3CH_2CH_2$In), 25.1 (CH_2), 44.4 (CH_3CH_2N), 57.9 ppm (CH_2N).

(3-*Diethylaminopropyl*)*di*-i-*propylindium* (**16**)

In analogy to the synthesis of **3**, the reaction of 1.4 g (5.9 mmol) di-*i*-propylindium chloride and 0.72 g (5.9 mmol) diethylaminopropyllithium yielded **16** as a colourless liquid. B.p. 81°C/0.3 hPa. Yield: 0.9 g (53%). Found: C, 49.6; H, 9.5; N, 4.6; In, 36.7. Calc. for $C_{13}H_{30}InN$: C, 49.5; H, 9.6; N, 4.4; In, 36.4%. ^{1}H NMR (C_6D_6): δ 0.58 (t, CH_3CH_2N), 0.59 (t, CH_2In), 1.04 (m, CH_3CHIn), 1.56 (d, CH_3CHIn), 1.75 (tt, CH_2), 2.00 (t, CH_2N), 2.36 ppm (q, CH_3CH_2N). $^{13}C\{^1H\}$ NMR (C_6D_6): δ 4.9 (CH_2In), 8.6 (CH_3CH_2N), 19.4 (CH_3CHIn), 24.8 (CH_3CHIn), 25.1 (CH_2), 44.3 (CH_3CH_2N), 57.9 ppm (CH_2N).

(4-*Diethylaminobutyl*)*gallium dichloride* (**17**)

Dichlorogallane, freshly prepared from 5.2 g (29.5 mmol) gallium trichloride and 2.4 g (32.7 mmol) trimethylsilane, was suspended at −20°C in 50 cm^3 pentane. 2.9 g (29.5 mmol) dimethylaminobutene-3 in 10 cm^3 pentane were added dropwise. The reaction mixture was stirred at this temperature for 1 h and then for 1 h at room temperature. Removal of the solvent *in vacuo* yielded **17** as a colourless oil. Yield: 3.9 g (55%). Found: C, 29.6; H, 5.6; N, 6.0. Calc. for $C_6H_{14}Cl_2Ga$: C, 29.9, H, 5.9; N, 5.8%. ^{1}H NMR (D_8-THF): δ 0.72 (CH_2Ga), 1.27–1.68 (m, CH_2CH_2), 1.92 (s, CH_3N), 2.04 ppm (t, CH_2N). $^{13}C\{^1H\}$ NMR (D_8-THF): δ 2.0 (CH_2Ga), 22.2 (CH_2CH_2Ga), 27.1 (CH_2CH_2N), 45.4 (CH_3N), 62.3 ppm (CH_2N).

(4-*Dimethylaminobutyl*)*dimethylgallium* (**18**)

16.2 cm^3 (29.2 mmol) of a methyllithium solution in ether (1.8 mol dm^{-3}) were added to a stirred solution of 3.5 g (14.6 mmol) (4-dimethylaminobutyl)gallium dichloride in 10 cm^3 ether at 0°C. After stirring for 12 h at room temperature, the solution was decanted. Distillation yielded **18** as a colourless liquid. B.p. 80°C/10 hPa. Yield: 1.4 g (56%). Found: C, 48.0; H, 10.0; N, 7.1. Calc. for $C_8H_{20}GaN$: C, 48.1; H, 10.1; N, 7.0%. ^{1}H NMR (C_6D_6): δ −0.05 (s, CH_3Ga), 0.54 (t, CH_2Ga), 1.19–1.66 (m, CH_2CH_2), 1.93 (s, CH_3N), 2.08 ppm (t, CH_2N). $^{13}C\{^1H\}$ NMR (C_6D_6): δ −5.9 (CH_3Ga), 9.0 (CH_2Ga), 21.2 (CH_2CH_2Ga), 28.1 (CH_2CH_2N), 45.5 (CH_3N), 63.3 ppm (CH_2N). MS (70 eV): *m/e* (rel. intensity,

%) 184/186* (100) [M $-CH_3$], 58 (60) [$Me_2N^+CH_2$], 100 (56) [$Me_2N^+C_4H_8$], 98 (15) [$Me_2N^+C_4H_6$], 69/71* (7) [Ga^+], 99/101* (5) [Me_2Ga^+], 44 (5) [$C_2H_6N^+$]; *isotope pattern clearly visible.

Bis(3-dimethylaminopropyl)methylgallium (**19**)

A solution of 4 g (25.7 mmol) methylgallium dichloride in 20 cm^3 benzene was added dropwise to a stirred suspension of 5 g (53.7 mmol) 3-dimethylaminopropyllithium in 40 cm^3 pentane. The reaction mixture was stirred for 1 h at room temperature and the refluxed for a further 6 h. Filtration and removal of the solvent *in vacuo* left a residue, which was sublimed at 40°C onto a 15°C cold finger at 0.01 hPa to yield **19** as a colourless solid. M.p. 52°C. Yield: 4.5 g (68%). Found: C, 50.8; H, 10.0; N, 10.5. Calc. for $C_{11}H_{27}GaN_2$: C, 51.4; H, 10.6; N, 10.9%. ^{1}H NMR ($CD_3C_6D_5$): δ −0.26 (s, CH_3Ga), 0.49 (t, CH_2Ga), 1.79 (tt, CH_2), 2.04 (CH_3N), 2.13 ppm (t, CH_2N). $^{13}C\{^1H\}$ NMR ($CD_3C_6D_5$): δ −7.1 (CH_3Ga), 9.8 (CH_2Ga), 24.7 (CH_2), 46.0 (CH_3N), 63.6 ppm (CH_2N).

Bis(3-dimethylaminopropyl)indium chloride (**20**)

A solution of 16.8 g (180.8 mmol) 3-dimethylaminopropyllithium in 300 cm^3 ether was added dropwise to a stirred suspension of indium trichloride in 300 cm^3 ether at 0°C. After stirring for 24 h, the reaction mixture was filtered. Cooling at −30°C yielded **20** as colourless crystals, which were washed with cold pentane and dried *in vacuo*. M.p. 92°C. Yield: 19.2 g (66%). Found: C, 37.0; H, 7.5; N, 8.5; In, 35.4. Calc. for $C_{10}H_{24}ClInN_2$: C, 37.2; H, 7.5; N, 8.7; In, 35.6%. ^{1}H NMR (C_6D_6): δ 0.62 (t, CH_2In), 1.71 (tt, CH_2), 1.95 (s, CH_3N), 2.08 ppm (t, CH_2N). $^{13}C\{^1H\}$ NMR (C_6D_6): δ 9.4 (CH_2In), 23.7 (CH_2), 45.3 (CH_3N), 61.8 ppm (CH_2N). MS (70 eV): *m/e* (rel. intensity, %) 58 (100) [$C_3H_8N^+$], 86 (85) [$Me_2N^+(CH_2)_3$], 287 (40) [M^+-Cl], 115 (35) [In^+], 42 (35) [$C_2H_4N^+$], 244 (34) [$M^+ -Cl-C_4H_{10}N$], 236 (32) [$M^+ -C_5H_{12}$], 44 (17) [$C_2H_6N^+$], 264 (16) [$M^+ -C_3H_8N^+$], 114 (14) [$C_7H_{16}N^+$].

Bis(3-diethylaminopropyl)indium chloride (**21**)

In analogy to the synthesis of **20**, the reaction of 17.5 g 3-diethylaminopropyllithium and 16.0 g (72.3 mmol) indium trichloride yielded **21** as colourless crystals. M.p. 94°C. Yield: 14.6 g (53%). Found: C, 44.1; H, 8.7; N, 7.9; In, 30.2. Calc. for $C_{14}H_{32}ClInN_2$: C, 44.4; H, 8.5; N, 7.4; In, 30.3%. ^{1}H NMR (C_6D_6): δ 0.59 (t, CH_2In), 0.78 (t, CH_3CH_2N), 1.75 (tt, CH_2), 2.20 (t, CH_2N), 2.47 ppm (q, CH_3CH_2N). $^{13}C\{^1H\}$ NMR (C_6D_6): δ 8.4 (CH_3CH_2N), 12.3 (CH_2In), 23.2 (CH_2), 43.9 (CH_3CH_2N), 55.4 ppm (CH_2N).

Bis(3-dimethylaminopropyl)methylindium (**22**)

20.7 cm^3 (31.0 mmol) of a methyllithium solution in ether (1.55 mol dm^{-3}) were added dropwise to a stirred solution of 10.0 g (31.0 mmol) bis(3-dimethylaminopropyl)indium chloride in 100 cm^3 diethyl ether. After stirring for 12 h, the ether was removed *in vacuo*. 100 cm^3 hexane were added, the mixture was filtered and the solvent removed. Distillation yielded **22** as a colourless liquid. B.p. 57°C/0.1 hPa. Yield: 5.6 g (60%). Found: C, 43.9; H, 9.0; N, 9.4; In, 38.1. Calc. for $C_{11}H_{27}InN_2$: C, 43.7; H, 9.0; N, 9.3; In, 38.0%. ^{1}H NMR ($CD_3C_6D_5$): δ −0.24 (s, CH_3In), 0.54 (t, CH_2In), 1.91 (tt, CH_2), 2.00 (s, CH_3N), 2.10 ppm (t, CH_2N). $^{13}C\{^1H\}$ NMR ($CD_3C_6D_5$): δ −7.6 (CH_3In), 10.7 (CH_2In), 25.9 (CH_2), 46.1 (CH_3N), 64.6 ppm (CH_2N).

Bis(3-diethylaminopropyl)methylindium (**23**)

In analogy to the synthesis of **22**, the reaction of 17.0 cm^3 (26.4 mmol) methyllithium solution and 10.0 g (26.4 mmol) bis(diethylaminopropyl)indium chloride yielded **23** as a colourless liquid. B.p. 52°C/0.03 hPa. Yield: 5.3 g (56%). Found: C, 50.1; H, 9.9; N, 7.6; In, 32.3. Calc. for $C_{15}H_{35}InN_2$: C, 50.3; H, 9.9; N, 7.8; In, 32.1%. ^{1}H NMR (C_6D_6): δ −0.23 (s, CH_3In), 0.54 (t, CH_2In), 0.59 (t, CH_3CH_2N), 1.74 (tt, CH_2), 2.02 (t, CH_2N), 2.27 ppm (q, CH_3CH_2N). $^{13}C\{^1H\}$ NMR (C_6D_6): δ −7.3 (CH_3In), 8.3 (CH_3CH_2N), 9.1 (CH_2In), 25.0 (CH_2), 44.3 (CH_3CH_2N), 57.5 ppm (CH_2N). MS (70 eV): *m/e* (rel. intensity, %) 244 (100) [$M^+ -CH_3-Et_2N^+$], 86 (84) [$Et_2N^+CH_2$], 114 (41) [$Et_2N^+(CH_2)_3$], 112 (32) [$Et_2N^+CHCHCH_2$], 115 (29) [In^+], 58 (14) [$C_3H_8N^+$], 145 (11) [Me_2In^+], 56 (9) [$C_3H_6N^+$], 42 (7) [$C_2H_4N^+$].

Acknowledgements—This work was supported by E. Merck, Darmstadt and the Bundesminister für Forschung und Technologie, F.R.G., under contract No. 415-7291-NT-2717 E3. We are grateful to A. Molassioti, M. Moser, A. Stapor and F. Scholz of the University Stuttgart for MOVPE experiments.

REFERENCES

1. M. J. Ludowise, *J. Appl. Phys.* 1985, **58**, R31.
2. M. R. Leys, *Chemtronics* 1987, **2**, 155.

3. K.-H. Thiele, E. Langguth and G. E. Müller, *Z. Anorg. Allg. Chem.* 1980, **462**, 152.
4. H. Schumann, U. Hartmann, A. Dietrich and J. Pickardt, *Angew. Chem.* 1988, **100**, 1119; *Angew. Chem. Int. Edn Engl.* 1988, **27**, 1077.
5. J. P. Mullin, S. J. C. Irvine, R. H. Moss, P. N. Robson and D. R. Wright (Eds), *Proc. 2nd Int. Conf. Metalorg. Vapor Epitaxy*, Sheffield (1984); *J. Cryst. Growth* 1984, **68**, 1.
6. G. B. Springfield (Ed), *Proc. 3rd Int. Conf. Metalorg. Vapor Phase Epitaxy*, Universal City, California (1986); *J. Cryst. Growth* 1986, **77**, 1.
7. G. Wiberg, T. Johannsen and O. Stecher, *Z. Anorg. Allg. Chem.* 1943, **251**, 114.
8. L. H. Long and J. F. Sackman, *Trans. Faraday Soc.* 1958, **54**, 1797.
9. A. Molassioti, M. Moser, A. Stapor, F. Scholz, M. Hostalek and L. Pohl, *Appl. Phys. Lett.* 1989, **54**, 857.
10. G. E. Coates and R. A. Whitcombe, *J. Chem. Soc.* 1956, 3351.
11. L. M. Dennis, R. W. Work and E. G. Rochow, *J. Am. Chem. Soc.* 1934, **56**, 1047.
12. H. Schmidbaur and H. F. Klein, *Chem. Ber.* 1967, **100**, 1129; *Angew. Chem.* 1966, **78**, 306.
13. G. M. Robinson and R. Robinson, *J. Chem. Soc.* 1923, **123**, 532.
14. J. T. B. H. Jastrzebski, G. van Koten, D. G. Tuck, H. A. Meinema and J. G. Noltes, *Organometallics* 1982, **1**, 1492.
15. H. Schumann, W. Wassermann and A. Dietrich, *J. Organomet. Chem.* 1989, **365**, 11.
16. J. W. Emsley, J. Feeney and L. H. Sutcliffe, *High Resolution Magnetic Resonance Spectroscopy*, Vol. II. Pergamon Press, Oxford (1966).
17. M. Hostalek, L. Pohl, A. Brauers, P. Balk, V. Frese, H. Hardtdegen, R. Hövel, G. K. Regel, A. Molassioti, M. Moser, F. Scholz, H. Schumann, U. Hartmann and W. Wassermann, MRS meeting, San Diego (1989).
18. R. Brdička, *Grundlagen der Physikalischen Chemie*, 15. Aufl., VEB. Dt. Verl. d. Wissensch., Berlin (1982).
19. D. F. Gaines, J. Borlin and E. P. Fody, *Inorg. Synth.* 1979, **15**, 203.
20. J. P. Oliver and L. G. Stevens, *J. Inorg. Nucl. Chem.* 1962, **24**, 953.
21. F. Runge, W. Zimmermann and I. Pfeiffer, *Z. Anorg. Allg. Chem.* 1951, **267**, 39.
22. J. J. Eisch and R. B. King, *Organometallic Synth.* 1981, **2**, 148.
23. J. J. Eisch, *J. Am. Chem. Soc.* 1962, **84**, 3836.
24. J. J. Eisch and R. B. King, *Organometallic Synth.* 1981, **2**, 150.
25. H. C. Clark and A. L. Pickard, *J. Organomet. Chem.* 1967, **8**, 427.

Polyhedron Vol. 9, No. 2/3, pp. 361–366, 1990
Printed in Great Britain

0277–5387/90 $3.00+.00
© 1990 Pergamon Press plc

OXYGEN- OR SULPHUR-CONTAINING ORGANOINDIUM COMPOUNDS FOR PRECURSORS OF INDIUM OXIDE AND SULPHIDE THIN FILMS

RYOKI NOMURA,* SATORU FUJII, KOUICHI KANAYA and HARUO MATSUDA

Department of Applied Chemistry, Faculty of Engineering, Osaka University, Yamada-Oka, Suita, Osaka 565, Japan

Abstract—Dibutylindium carboxylates and butylindium thiolates are prominent precursors for the preparation of indium oxide and sulphide thin layers via a solution pyrolysis process. Their application has been enlarged to include the preparation of ternary compound thin films, taking advantage of the formation of binuclear complexes with organotin oxides or copper(II) dithiocarbamate complexes. Thus, addition of $Bu^n_2In(OCOEt)$ to Bu^n_2SnO gave the mixed stannoxane $Bu^n(EtCOO)In—O—SnBu^n_3$ (**I**). While, $Bu^i_2InSPr^n$ and $Cu(S_2CNBu^n_2)_2$ afforded similar bimetallic complexes $Bu^i_2In(SPr^n)Cu(S_2CNBu^n_2)$ (**VI**). Solution pyrolysis of **I** and **VI** gave uniform indium–tin oxide and copper–indium sulphide thin films, respectively. The course of thermal decomposition of **I** and **VI** was also investigated.

Although an increasing interest has been shown in the utilization of organometallics as precursors in the fabrication of several compound semiconductor materials,[1] only limited numbers of metal alkyls such as trimethylgallium and trimethylindium, etc., are practically employable.[1–3] Recently, more sophisticated organometallic precursors than these single metal alkyls have been developed and introduced in order to prepare thin films of binary or ternary compounds, via the OMCVD process, avoiding "premature reaction"; for example, trialkylindium phosphine adducts[4,5] and, more advanced, dialkylphosphinodialkylindium derivatives[6,7] were exploitable for the preparation of InP epitaxial layers. It should be emphasized that these binuclear organometallic precursors already contain all the necessary elements to construct the target compounds. This is the most characteristic feature of such one-source systems. Further, they possess the large advantage of diminishing undesired reactions during the film deposition. However, few attempts have been made on the application of the one-source systems for the preparation of compounds other than some group III pnictides such as InP, etc. Thus, conventional inorganic and metallorganics precursors such as indium salts, alkoxides and acetylacetonates are predominantly utilized in the preparation of the oxide or chalcogenide derivatives of indium.[8–10]

The success of binuclear organometallics in the fabrication of the pnictide thin films stimulated our studies on the utilization of organoindium compounds for preparation of oxide or chalcogenide materials. In this paper, we describe the effectiveness of organoindium precursors in the preparation of III/VI semiconductor thin films. In addition, the reaction of organoindium compounds such as dibutylindium propionate, $Bu^n_2In(OCOEt)$, or butylindium propylthiolates, $(Bu^i_{3-x}In(SPr^n)_x$, $x = 1$ or 2), with dibutyltin oxide or copper dithiocarbamate complexes, respectively, are also reported.

EXPERIMENTAL

General

^1H and ^{13}C NMR, and IR spectra were recorded on a Hitachi R90H FT spectrometer and on a Hitachi 260–30 spectrophotometer, respectively. Mass spectra were obtained by the use of a JEOL JMS–DX303 (Faculty of Engineering, Osaka University). Molecularity was measured by a VPO method using a Corona 117 type vapour pressure osmometer, and TG/DTA measurements were made using a SEIKO TG/DTA 20 type thermal

* Author to whom correspondence should be addressed.

analyser. All reactions were carried out under a dry N_2 atmosphere.

Materials

Dibutylindium propionate was prepared directly from tributylindium with propionic acid in an ether solution.[11,12] Dibutylindium thiolates and butylindium dithiolates were synthesized from the reaction of tributylindium with the corresponding alkane thiols in 1 : 1 and 1 : 2 molar ratios, respectively.[13] Copper dithiocarbamate complexes were prepared by direct condensation of copper(II) oxide with dithiocarbamic acids as reported previously.[14-17]

*Reaction of di-*n*-butylindium propionate with di-*n*-butyltin oxide*

To a suspension of di-*n*-butyltin oxide (5 mmol) in *p*-xylene (20 cm^3), di-*n*-butylindium propionate (5 mmol) was added slowly with stirring at 0°C, then the mixture was heated under reflux for 3.5 h. After evaporation of *p*-xylene, $Bu^n(EtCOO)In—O—SnBu^n_3$ (**I**) was obtained at room temperature as a gummy solid and further purified by distillation *in vacuo*.

Reaction of diisobutylindium n*-propylthiolate with copper*(II) *bis(di-*n*-butyldithiocarbamate)*

Into a solution of copper bis(di-*n*-butyldithiocarbamate) (5 mmol) in *p*-xylene (20 cm^3), diisobutylindium *n*-propylthiolate (5 mmol) was added dropwise at 0°C and the resulting solution was stirred at room temperature. After stirring for 6 h, the resulting yellowish-brown viscous oils were chromatographed on a silica gel column by eluting with chloroform. The binuclear complex **VI** was obtained in a quantitative yield.

RESULTS AND DISCUSSION

Organoindium carboxylates for indium oxide thin films

It is well known that indium oxide and tin-doped indium oxide (ITO) have a wide range of applications as transparent conductors in planar display panels and solar cell windows, etc.[8] Solution pyrolysis is one of the most facile processes suitable for preparation of large areas of thin films and patterned layers. The merits of such a process in contrast to some physical processes and spray pyrolysis, are less highlighted, because of a lack of adequate precursors. An introduction of the fully organometallic precursor systems, however, would compensate for such a defect and their use could give high quality ITO films under milder conditions than those of the existing precursor systems.[12]

Highly conductive and transparent ITO films ($\rho \fallingdotseq 10^{-3}$ Ω cm, $T_v > 90\%$) have been prepared as follows: (1) dissolve dibutylindium carboxylates and dibutyltin oxide (5 wt% with respect to dibutylindium carboxylate employed) in *p*-xylene, (2) coat the resulting *p*-xylene solution onto a substrate such as borosilicate glass or quartz, (3) heat the coated substrate at 100°C for 40 min, then (4) pyrolyse the organometallics on the substrate at 450°C for 1 h to form uniform oxide layers. We expected that the formation of inorganic In—O—Sn networks should be preceded by the formation of organometallic In—O—Sn linkages as indicated in Scheme 1.

A model reaction using equimolar amounts of dibutylindium propionate and dibutyltin oxide in *p*-xylene was carried out. It was found that these two organometallics readily coupled together to form a novel mixed stannoxane (**I**),* associated with a butyl migration from indium to tin as shown in Scheme 2. One should compare this addition with the telomerization of dibutyltin oxide with di-

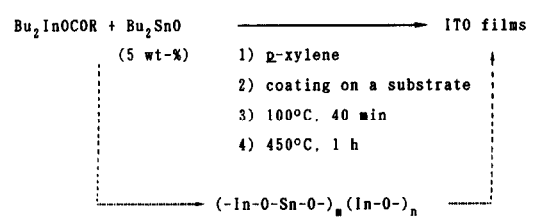

Scheme 1.

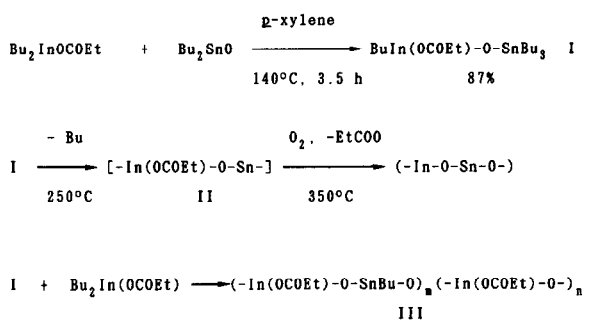

Scheme 2.

* Selective spectral data: **I**, softening point 55°C. IR (cm^{-1}, KRS-5): ν(COOIn) 1560s, ν(In—O—Sn) 650. ^1H NMR (90 MHz, $CDCl_3$): δ 0.91t (12H, CH_3), 0.9–2.0m (27H), 2.31q (2H, CH_2COO). ^{13}C NMR {1H} (22.6 MHz, $CDCl_3$): δ 10.1q (CH_3CH_2—), 13.7q (δ-CH_3), 16.3t (α-CH_2), 27.1t (γ-CH_2), 27.9t (β-CH_2), 29.3t (CH_3CH_2—), 184.0s (*C*OO). Found: C, 42.10; H, 7.54; In, 20.22; Sn, 21.09, mol. wt (VPO, benzene) 550. Calc. for $C_{19}H_{41}InO_3Sn$: C, 41.41; H, 7.50; In, 20.84; Sn, 21.54%, mol. wt 551.1.

Table 1. Increase of the molecularity of **I** and **III** in benzene on standing under moist air[a]

Day	I		III	
	M_n	n^b	M_n	n^b
0	549	1	860	2.9
1	1960	3.6		
2	2310	4.2	2350	7.8
3	2770	5.0		
5			3930	13.0

[a] Molecular weights were measured by VPO at 35°C.

[b] Mean degree of oligomerization, n, calculated on the basis of **I** and $Bu_2In(OCOEt)$ as a monomeric unit, respectively.

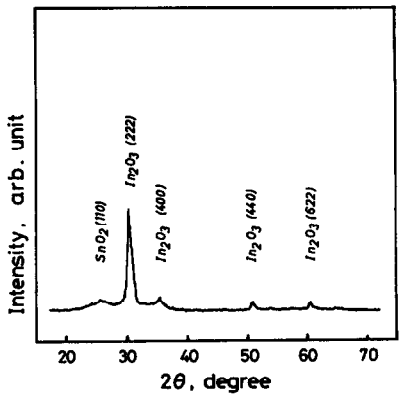

Fig. 1. XRD patterns of the pyrolysate of copolymer **III** at 400°C for 1 h under air.

butyltin halides and with the formation of the mixed metallastannoxanes, in which it can be seen that electronegative groups generally migrated onto tin nuclei.[18] Similar migrations of alkyl groups from indium centres were reported for the reactions of trimethylindium with trimethylstibine sulphide[19] and of triethylindium with thiobenzophenone.[20] The investigations of the coupling reactions of other dibutylindium derivatives and tributylindium with several organotin oxides other than dibutyltin oxide is now in progress and the detailed aspects of the reactions will be published elsewhere.

Bimetallic stannoxane **I** was formed as a gummy solid. In addition, **I** is only moderately air-sensitive and can be stored unchanged for months under an inert atmosphere. Compound **I** gradually solidified to give a wet gel[21] after contact with moist air for several days and immediately formed gels when an equimolar amount of water was added to a solution of **I**. The increase of molecularity of **I** on standing under moist air is displayed in Table 1. The gelation was considered to result from the formation of copolymer **II**. The bimetallic μ-oxo compound **I** also reacted with 9 equivalents of $Bu_2InOCOEt$ in the presence of *ca* 100 ppm of water and gave copolymer **III**, as illustrated in Scheme 2. During the course of the copolymerization, a quantitative evolution of butane was detected by GLC analysis.

Stepwise weight loss curves associated with the two exothermic peaks (265 and 348°C) were observed in TG/DTA analysis of **I**, and the composition of the pyrolysates at 265, 350 and 400°C are summarized in Table 2. Thus, **I** was converted into indium–tin oxide on heating by releasing the butyl moieties bound to the metal centres (~265°C) and carboxylates (~350°C) in this order, as shown in Scheme 2. Further, pyrolysis of the copolymer **III** at 400°C gave indium–tin oxide (ITO) powders as shown in Fig. 1.

Organoindium thiolates for indium sulphide thin films

We can prepare both di-*n*-butylindium isopropylthiolate (**IV**) and *n*-butylindium bis(isopropylthiolate) (**V**) by changing the mole ratios

Table 2. Analytical data of pyrolysates of **I**[a]

Temperature (°C)	Yields of pyrolysates (%)	Found (%)				ν(C—H)	ν(COO)
		C	H	In	Sn		
r.t.	—	42.4	7.5	20.2	21.1	2870bd	1550s, 1400s
265[b]	58	11.4	1.8	34.9	36.9	2860vw	1540s, 1400s
350[c]	51	2.0	0.9	43.3	43.4	—	1500w, 1400w
400[c]	50	—	—	43.4	44.0	—	—

[a] 0.500 g of specimen in a porcelain crucible were heated at the prescribed temperatures for 1 h under N_2.

[b] **II**, calc. for $(C_3H_5InO_3Sn)_n$: C, 11.2; H, 1.6; In, 35.6; Sn, 36.8% and yield, 58.6%.

[c] 0.5 In_2O_3–SnO_2, calc. yield, 52.5%.

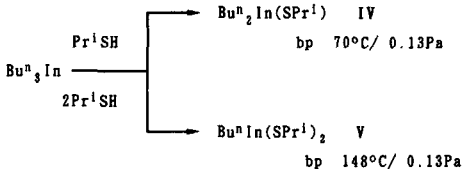

Scheme 3.

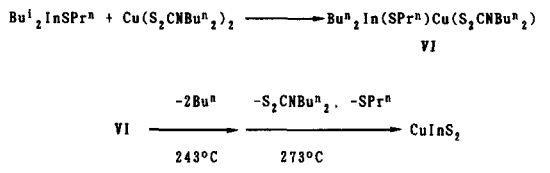

Scheme 4.

of the starting tributylindium and thiols[13,22] as shown in Scheme 3. These two butylindium thiolates are liquids at room temperature and are distillable under reduced pressure, which is a desirable property for their application as precursors of semiconductor materials via chemical procedures e.g. OMCVD.[23] Further, **IV** and **V** are only moderately air-sensitive and exist as monomers in aprotic solvents such as benzene or chloroform at room temperature.[13] Pyrolysis of **IV** under an Ar atmosphere below 300°C, afforded orthorhombic InS powders, in contrast, that of **V** gave tetragonal In_2S_3 powders at *ca* 300°C.[23]

The indium sulphides, InS and In_2S_3, possess medium band gap energies, 2.44[24] and 2.07 eV,[25] respectively, and are promising materials for optoelectronics and photovoltaics.[26,27] Solution pyrolysis of **IV** gave InS thin films at 250°C under Ar, but gave transparent and conducting In_2O_3 films at above 300°C.[27] Thus, InS films obtained from the pyrolysis of $Bu^n_2InSPr^n$ should be fairly oxidizable and deposited InS was easily converted into In_2O_3 films even by trace amounts of oxygen contained in Ar (99.9% purity). Further, indium oxide films occurring at 375°C showed high transparency and low resistivity ($T_v > 90\%$, and $\rho \fallingdotseq 10^{-3}\ \Omega$ cm).

Preparation of $CuInS_2$ *thin films via solution pyrolysis of* $Bu^i_2InSPr^n$—$Cu(S_2CNBu^n_2)_2$ *systems*

Indium sulphide, InS, is also employed as a component of binary sulphides, especially $CuInS_2$ which is one of the best suited materials for photovoltaics.[28,29] Thus, we attempted to prepare $CuInS_2$ thin films using dibutylindium thiolates. It was found that solution pyrolysis of the $Bu^i_2InSPr^n$—$Cu(S_2CNBu^n_2)_2$ system at 350°C successfully gave stoichiometric $CuInS_2$ thin films.[17] We tentatively assumed that initial formation of a binary complex between two organometallic sources affected the stoichiometry and homogeneity of the final pyrolysates.

Reaction of copper(II) dibutyldithiocarbamate with dibutylindium propylthiolate gave a novel bimetallic complex $Bu^i_2In(SPr^n)Cu(S_2CNBu^n_2)$ (**VI**), as shown in Scheme 4. Analytical and spectral data* were consistent with the formula but we could not determine the identity of the bridge between the copper and indium nuclei. It is interesting that reduction of the copper(II) species occurred during the coupling. The reduction was confirmed by disappearance of the black colour, characteristic of copper(II) dithiocarbamates,[16] and by significant line-sharpening observed in ^1H and ^{13}C NMR spectra, indicating the reduction of paramagnetic copper(II) to copper(I) species. Further, lower $\delta(^{13}CH_2N)$ at 55.8 indicated the formation of copper(I) dithiocarbamate.[30] Although molecularity measurements showed that **VI** existed as a monomer in solution, a set of peaks assignable to the trimer of **VI** could be detected at around $m/z = 1721$ in FAB MS.

Thermal decomposition of **VI** was observed by TG/DTA and the compositions of pyrolysates were estimated by microanalysis and XRD. The results obtained are summarized in Tables 3 and 4. As can be seen in Table 3, **VI** decomposed with the appearance of exothermic and endothermic peaks, which appeared at lower temperatures than those of the parent compounds, and gave $CuInS_2$ in quantitative yield. Analysis of the pyrolysates suggested that two butyl groups bonded to indium were released below 250°C which coincided with the exothermic peak, and the dithiocarbamate and thiolate moieties were successively released at 300°C which agreed with the endothermic peak.

SUMMARY

Based on the model reactions, it is concluded that solution pyrolysis of $Bu_2InOCOEt$—Bu_2SnO and

* Selective spectral data: **VI**, yellowish-brown oil. IR (cm^{-1}, KRS-5): ν(C—N) 1480. ^1H NMR (90 MHz, $CDCl_3$): δ 0.95t (6H, CH_3, Bu^n), 1.00d (12H, CH_3, Bu^i), 1.03t (3H, CH_3, Pr^n), 1.0–2.2m (14H, CH_2), 2.26m (1H, CH), 2.70t (2H, $SCH2$), 3.94t (2H, NCH_2). ^{13}C NMR {1H} (22.6 MHz, $CDCl_3$): δ 13.1q (CH_3, Pr^n), 13.7q (CH_3, Bu^n), 20.1t (CH_2CH_3), 22.5t (SCH_2CH_2), 26.9t (In—CH_2), 27.6q (CH_3, Bu^i), 28.9t (NCH_2CH_2), 32.6d, 41.2t (SCH_2), 55.8t (NCH_2), 203.6s (S_2CN). Found: C, 43.1; H, 7.9; Cu, 11.1; In, 19.5; N, 2.5; S, 16.0, mol. wt (VPO, benzene) 568.5. Calc. for $C_{20}H_{43}CuInNS_3$: C, 42.0; H, 7.6; Cu, 11.1; In, 20.1; N, 2.5; S, 16.8%, mol. wt 572.1.

Table 3. Thermal analysis data of **VI**[a]

Compounds	DTA (°C) *exo*(*endo*)	TG Weight loss (%) Initial	Final	Product
$Bu^i_2InSPr^n$	266	123	329	InS
$Cu(S_2CNBu^n_2)_2$	(289)	264	358	Cu_2S
VI	243(273)	64	323	$CuInS_2$

[a] Measured on a SEIKO TG/DTA 20 under N_2, 10°C min^{-1}.

Table 4. Compositions of pyrolysates of **VI** under Ar

Temperature (°C)	Found (%)[a] C	H	Cu	In	N	S	Crystal structure[b]
r.t.	43.1	7.9	11.0	19.5	2.5	16.0	
250[c]	31.6	5.7	13.3	25.6	3.3	21.5	
280[d]	5.8	0.7	24.3	43.4	0.3	25.4	$CuInS_2$
350[d]	0.9	—	26.6	46.4	—	27.1	$CuInS_2$

Pyrolysis conditions. Ar atmosphere, the specimens were held at the prescribed temperature for 1.5 h.

[a] Contents of Cu, In and S were determined by X-ray fluorescence analysis.

[b] Determined by consultation with JCPDS No. 32–339 (charcopylite).

[c] **VI** $-2Bu^n$, Calc. for $C_{12}H_{25}CuInNS_3$: C, 31.5; H, 5.5; Cu, 13.1; In, 25.1; N, 3.1; S, 7.0%.

[d] Calc. for $CuInS_2$: Cu, 26.2; In, 47.3; S, 26.4%.

Bu_2InSPr—$Cu(S_2CNBu_2)_2$ proceeded via formation of **I** and **VI** as key intermediates to give homogeneous ternary compound layers of indium–tin oxide and copper–indium sulphide, respectively.

Acknowledgement—Part of this work was financially supported by a Grant-in-Aid for scientific research No. 01750784, Ministry of Education, Science and Culture.

REFERENCES

1. R. J. M. Griffths, *Chem. Ind.* (*Lond.*) 1985, 247.
2. H. M. Manasevit, *Appl. Phys. Lett.* 1968, **12**, 156.
3. H. M. Manasevit and W. I. Simpson, *J. Electrochem. Soc.* 1969, **116**, 1725.
4. R. H. Moss, *J. Cryst. Growth* 1984, **68**, 78.
5. D. C. Bradley, H. Dowes, D. H. Frigo, M. B. Hursthouse and B. Hussain, *J. Organomet. Chem.* 1987, **325**, 55.
6. D. C. Bradley, M. M. Faktor, D. M. Frigo and L. M. Smith, *J. Cryst. Growth* 1988, **92**, 37.
7. D. C. Bradley, M. M. Faktor and D. M. Frigo, *J. Cryst. Growth* 1988, **89**, 227.
8. K. L. Chopra, S. Major and D. K. Pandya, *Thin Solid Films* 1983, **102**, 1.
9. W.-T. Kim and C.-D. Kim, *J. Appl. Phys.* 1986, **60**, 2631.
10. S. Belgacem, M. Dachraoui, J. Kessler and J. Vedel, *Thin Solid Films* 1988, **167**, 217.
11. H. C. Clark and A. L. Pickard, *J. Organomet. Chem.* 1967, **8**, 427.
12. R. Nomura, S.-J. Inazawa, H. Matsuda and S. Saeki, *Polyhedron* 1987, **6**, 507.
13. R. Nomura, S.-J. Inazawa, K. Kanaya and H. Matsuda, *Polyhedron* 1989, **8**, 763.
14. R. Nomura, A. Takabe and H. Matsuda, *Polyhedron* 1987, **6**, 411.
15. R. Nomura, S. Fujii, A. Takabe and H. Matsuda, *Polyhderon* 1989, **8**, 1891.
16. R. Nomura, K. Kanaya and H. Matsuda, *Ind. Engng Chem. Res.* 1989, **28**, 877.
17. R. Nomura, K. Kanaya and H. Matsuda, *Chem. Lett.* 1988, 1849.
18. T. Maeda, G. Yoshida and R. Okawara, *J. Organomet. Chem.* 1972, **44**, 237.
19. A. G. Davies and P. G. Harrison, *J. Organomet. Chem.* 1967, **10**, P31 and P33.
20. H. Tada, K. Yasuda and R. Okawara, *Inorg. Nucl. Chem. Lett.* 1967, **3**, 315.
21. S. Sakka, K. Kamiya and Y. Yoko, *Inorganic and Organometallic Polymers* (Edited by M. Zedlin,

K. J. Wynne and H. R. Allcock), Chap. 28. American Chemical Society, Washington DC (1988).
22. D. G. Tuck, *Comprehensive Organometallic Chemistry* (Edited by G. Wilkinson, F. G. A. Stone and E. W. Abel), Vol. 1, pp. 694–701 and 712–719. Pergamon Press, Oxford (1982).
23. R. Nomura, S.-J. Inazawa, K. Kanaya and H. Matsuda, *Appl. Organomet. Chem.* 1989, **3**, 195.
24. T. Nishino and Y. Hamakawa, *Jpn J. Appl. Phys.* 1977, **16**, 1291.
25. R. S. Becker, T. Zheng, J. Elton and M. Saeki, *Sol. Energy Mater.* 1986, **13**, 97.
26. W.-T. Kim and C.-D. Kim, *J. Appl. Phys.* 1986, **60**, 2631.
27. R. Nomura, K. Kanaya, A. Moritake and H. Matsuda, *Thin Solid Films* 1988, **167**, L27.
28. L. L. Kazmeriski, M. S. Ayyagari and G. A. Sauborn, *J. Appl. Phys.* 1975, **46**, 4865.
29. Y. Mirouski, R. Tenne, D. Cahen, G. Sawatzky and M. Polark, *J. Electrochem. Soc.* 1985, **132**, 1070.
30. H. L. M. Van Gaal, J. W. Diesveld, F. W. Pijpers and J. G. M. Van der Linden, *Inorg. Chem.* 1979, **18**, 3251.

Polyhedron Vol. 9, No. 2/3, pp. 367–370, 1990
Printed in Great Britain

0277–5387/90 $3.00+.00
© 1990 Pergamon Press plc

FORMATION OF ALKOXY-DERIVED $NbAlO_4$

OSAMU YAMAGUCHI* and MASAKAZU SHIRAI

Department of Applied Chemistry, Faculty of Engineering, Doshisha University, Kyoto 602, Japan

Abstract—In the system Nb_2O_5–Al_2O_3, δ-Nb_2O_5 (hexagonal) solid solutions crystallize at low temperatures (with up to 50 mol% Al_2O_3) from amorphous materials prepared by the simultaneous hydrolysis of niobium and aluminium alkoxides. The lattice parameter a is relatively constant regardless of composition, whereas parameter c decreases linearly with increasing Al_2O_3. The δ- to γ-Nb_2O_5 (orthorhombic) phase transformation occurs at $\approx$ 640 to $\approx$ 700°C. The solid solution containing 50 mol% Al_2O_3 transforms to $NbAlO_4$ (monoclinic) at 800–860°C.

Niobium pentoxide, Nb_2O_5, exists in many polymorphic modifications: α-, α'-, β-, γ-, δ-, ε-, ζ-, η-, N- and R-phases.[1,2] The exact relationships of the polymorphs are still uncertain because of the lack of suitable crystals needed to properly characterize the phases. However, it has been concluded that α-Nb_2O_5 (monoclinic) is stable and all other forms transform to it at $\approx$ 1100°C regardless of the preparation method. Little attention has been paid to the formation of solid solutions in the system Nb_2O_5–Al_2O_3. Goldschmidt[3] reported that Nb_2O_5 took up to $\approx$ 15 mol% Al_2O_3 into solution, resulting in a slight distortion of the Nb_2O_5 lattice. On the other hand, Layden[4] suggested that little or no solid solution of Al_2O_3 in Nb_2O_5 occurred. Niobium aluminate, $NbAlO_4$,[3–12] is one of the compounds in this system. Four preparation methods were used: a solid-state reaction,[3,6,7,10,12] a fusion technique,[3,12] oxidation of a compound metal[7] and a co-precipitation method.[10] We now report, here, the formation of $NbAlO_4$ at low temperatures by the transformation of a Nb_2O_5 solid solution containing 50 mol% Al_2O_3 from an amorphous material prepared by the simultaneous hydrolysis of niobium and aluminium alkoxides.

EXPERIMENTAL

Niobium isopropoxide, $Nb(OC_3H_7)_5$ (99.999% pure), was used as received. Aluminium isopropoxide, $Al(OC_3H_7)_3$, was synthesized by heating aluminium metal (> 99.9% pure) in an excess of analytical-grade 2-propanol with mercury(II) chloride (10^{-4} mol/mol of metal) as a catalyst for 10 h at 82°C.[13] The mixed alkoxides of the various compositions were heated under reflux for 10 h and then hydrolysed by adding conductivity water at room temperature. The temperature was slowly increased to 75°C while the resulting suspensions were stirred. The hydrolysis products were separated from the suspensions by filtration, washed 10 times with hot water, and dried at 100°C under reduced pressure. The powders obtained are termed "starting powders". Their average particle size, determined by electron microscopy, was $\approx$ 30 nm for A and $\approx$ 90 nm for B–F.

Differential thermal analysis (DTA) was conducted in air at a rate of 10°C min^{-1}; α-alumina was used as the reference. The starting powders and specimens, obtained from the DTA studies and then quenched, were examined by X-ray diffraction (XRD) using Ni-filtered Cu-K_α radiation. Interplanar spacings were measured with the aid of an internal standard of silicon, and unit cell values were determined by a least-squares refinement. IR spectroscopy was performed on a dispersion in potassium bromide using the pressed-disc technique.

RESULTS AND DISCUSSION

Differential thermal analysis

Figure 1 shows the DTA curves for powders A, C and F; they reveal sharp exotherms resulting from the crystallization of δ-Nb_2O_5 (δ-Nb_2O_5 solid solution), although the peaks decreased successively in height from A to F. The crystallization temperature of each starting powder is listed in Table 1.

* Author to whom correspondence should be addressed.

Table 1. Chemical composition of starting powders, and temperatures of crystallization and transformation

Starting powder	Composition mol% Nb_2O_5–Al_2O_3	Crystallization temperature (°C)	Transformation temperature (°C)
A	100 : 0	560–585	640–700[a]
B	90 : 10	645–675	800–830
C	80 : 20	690–730	790–830
D	70 : 30	705–755	790–830
E	60 : 40	725–780	790–845
F	50 : 50	745–800	800–860

[a] Determined by X-ray analysis.

As can be seen from the data, with increasing Al_2O_3 the crystallization was shifted to higher temperatures and increased in the peak temperature range. Although no peak for A was observed at higher temperatures, other starting powders showed the second exothermic peaks (Fig. 1). Contrary to the peaks of crystallization, they increased in height from B to F. As will be described, the second peaks were confirmed to result from the transformation of δ-Nb_2O_5 solid solutions into $NbAlO_4$. The transformation temperature is shown in Table 1.

X-ray analysis

XRD analysis showed that all starting powders were amorphous. No significant change in structure was observed up to the temperatures of the first exothermic peaks. When the starting powders were heated at temperatures above the first exothermic peaks, the specimens gave the XRD pattern of the only δ-Nb_2O_5 phase; these results suggest that δ-Nb_2O_5 solid solutions were formed up to 50 mol% Al_2O_3.* Metastable δ-Nb_2O_5 was first found in the commercial sample by Frevel and Rinn.[14] Later this modification was prepared by heating or hydrothermal treatment of amorphous Nb_2O_5[1,15] and by oxidation of NbO_2 or Nb metal.[16–18] The X-ray data for δ-Nb_2O_5 prepared from A by heating for 2 h at 585°C were in agreement with those reported.[1,14,17,18] The diffraction lines were indexed as a hexagonal unit cell with $a = 0.3604$ and $c = 0.3923$ nm. Compositional changes result in a significant variation in the cell dimensions. Figure 2 shows the variation of lattice parameters of the δ-Nb_2O_5 phases obtained from each starting powder. The lattice parameter a was relatively constant regardless of composition, whereas parameter c decreased linearly with increasing Al_2O_3.

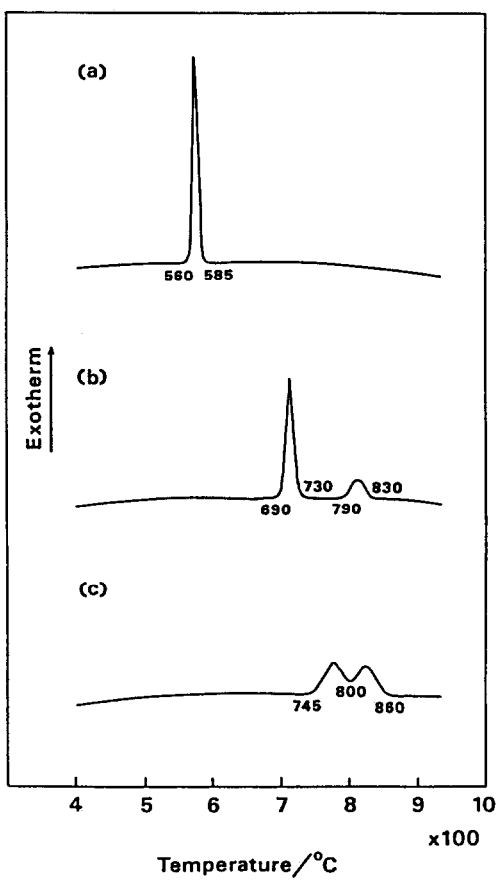

Fig. 1. Differential thermal analysis curves for (a) A, (b) C and (c) F. Sample weight 45 mg.

The δ- to γ-Nb_2O_5 phase transformation in A occurred at ≈ 640°C, although no peak was detected in the DTA; only γ-Nb_2O_5 was present above 700°C. The δ-Nb_2O_5 phases from other start-

*In the Al_2O_3-rich region, although the starting powder prepared in 55 mol% Al_2O_3 was amorphous, α-Al_2O_3 was observed when it was heated above 1200°C. Above 60 mol% Al_2O_3, boehmite AlO(OH) was present in the starting powder.

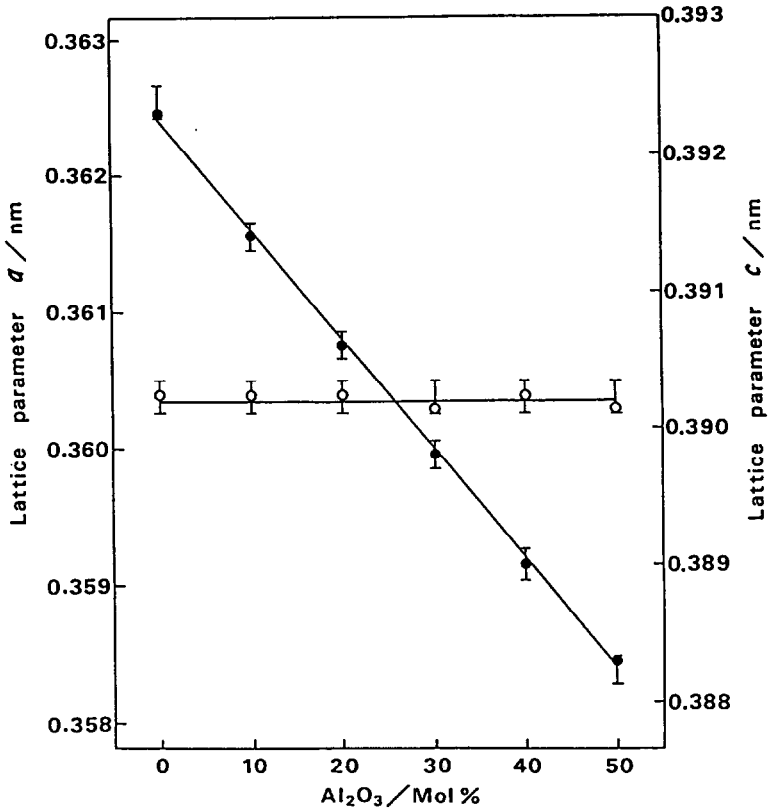

Fig. 2. Lattice parameters (○) a and (●) c for the δ-Nb_2O_5 phase as a function of composition.

ing powders were observed up to the temperatures of the second exothermic peaks. When B–E were heated at temperatures above the second exothermic peaks, the specimens were mixtures of $NbAlO_4$ and γ-Nb_2O_5. The specimen gave an XRD pattern characteristic of $NbAlO_4$. These indicate that the solid solutions were transformed into $NbAlO_4$. The X-ray data for $NbAlO_4$ are presented in Table 2. On the crystal structure of $NbAlO_4$, Whiston and Smith,[12] and Pedersen[8] determined it as a monoclinic unit cell by the use of single crystals, while Burdese and Borlera[9] indexed on the basis of an orthorhombic unit cell from the powder diffraction data. The compound in the present study was classified into the monoclinic system with $a = 1.2174$, $b = 0.3708$, $c = 0.6476$ nm and $\beta = 107.50°$. The dimensions of the monoclinic unit cell determined were in agreement with the parameters reported.[8,12] Thus $NbAlO_4$ could be easily prepared at low temperatures by transformation of the δ-Nb_2O_5 solid solution formed from alkoxides in the mole ratio $Nb^{5+} : Al^{3+} = 1 : 1$.

Infrared spectrum

Three absorption bands in pure δ-Nb_2O_5 obtained from A were present at 850, 800 and 560

Table 2. X-ray diffraction data for $NbAlO_4$[a]

d_{obs} (nm)	d_{calc} (nm)	I/I_0	hkl
0.620	0.618	10	001
0.581	0.581	5	200
0.507	0.506	20	$\bar{2}01$
0.371	0.371	25	201, 010
0.355	0.353	100	110
0.322	0.324	5	$\bar{1}02$
0.309	0.309	55	002
0.2995	0.2997	30	$\bar{4}01$
0.2900	0.2903	25	400
0.2677	0.2677	50	310
0.2529	0.2528	15	$\bar{4}02$
0.2444	0.2439	20	202
0.2367	0.2367	5	401
0.2289	0.2289	10	311
0.2228	0.2226	10	112
0.2157	0.2155	5	$\bar{2}03$
0.2059	0.2059	25	003
0.2029	0.2029	20	$\bar{6}01$
0.1968	0.1968	10	510
0.1930	0.1930	5	103
0.1893	0.1893	5	$\bar{5}12$
0.1863	0.1863	50	$\bar{2}13$
0.1831	0.1831	10	120

[a] Monoclinic; $a = 1.2174$, $b = 0.3708$, $c = 0.6476$ nm, $\beta = 107.50°$.

cm^{-1}, agreeing with the spectral data of α-Nb_2O_5.[19] In the spectra of δ-Nb_2O_5 solid solutions, the intensity of the bands decreased with increasing Al_2O_3. On the other hand, the spectrum of $NbAlO_4$ showed the absorption bands at 975, 835, 725, 555 and 505 cm^{-1}. No spectral data for $NbAlO_4$ have been reported; however, the spectrum is very similar to that of $TaAlO_4$[20] in which the bands are located at 984, 840, 750, 562 and 505 cm^{-1}. According to the data of Povarennykh,[20] $TaAlO_4$ contains octahedral TaO_6 groups and the strong band at ≈ 980 cm^{-1} is a characteristic frequency. Accordingly, it must be suggested that $NbAlO_4$ contains octahedral NbO_6 groups in the structure.

REFERENCES

1. R. Moser, *Mineralog. Petrogr. Mitt.* 1965, **45**, 35.
2. H. Schafer, R. Gruehn and F. Schulte, *Angew. Chem. Int. Edn Engl.* 1966, **5**, 40.
3. H. J. Goldschmidt, *Metallurgia* 1960, **62**, 241.
4. G. K. Layden, *J. Am. Ceram. Soc.* 1963, **46**, 506.
5. E. J. Felten, *J. Less-Common Met.* 1965, **9**, 206.
6. C. Keller, *Z. Anorg. Allg. Chem.* 1962, **318**, 89.
7. E. K. Meuller and B. J. Nicholson, *J. Am. Ceram. Soc.* 1962, **45**, 250.
8. B. F. Pedersen, *Acta Chem. Scand.* 1962, **16**, 421.
9. A. Burdese and M. L. Borlera, *Ric. Sic. Rend. Sez.* 1964, **A7**, 434.
10. N. A. Godina, E. N. Isuprova and E. K. Keller, *Izv. Akad. Nauk. SSSR, Neorg. Mater.* 1970, **6**, 1465.
11. N. A. Toropov, I. F. Fedrov, I. F. Andreev and R. M. Kasparyan, *Izv. Akad. Nauk SSSR, Neorg. Mater.* 1971, **7**, 643.
12. C. D. Whiston and A. J. Smith, *Acta Cryst.* 1978, **B34**, 1454.
13. O. Yamaguchi, K. Sugiura, A. Mitsui and K. Shimizu, *J. Am. Ceram. Soc.* 1985, **68**, C44.
14. L. K. Frevel and H. W. Rinn, *Analyt. Chem.* 1955, **27**, 1329.
15. F. Holtzberg, A. Reisman, M. Berry and M. Berkenblit, *J. Am. Chem. Soc.* 1957, **79**, 2039.
16. H. Nowotny, F. Benesovaky, E. Rudy and A. Witmann, *Mh. Chem.* 1960, **91**, 975.
17. N. Terao, *Jpn J. Appl. Phys.* 1963, **2**, 156.
18. T. Mukaibo, M. Kanno and M. Yamawaki, *J. Nucl. Sci. Technol.* 1965, **2**, 516.
19. R. A. Nyquist and R. O. Kagel, *Infrared Spectra of Inorganic Compounds.* Academic Press, New York (1971).
20. A. S. Povarennykh, *Mineral. Zh.* 1981, **3**, 14.

Polyhedron Vol. 9, No. 2/3, pp. 371–376, 1990
Printed in Great Britain

0277–5387/90 $3.00+.00
© 1990 Pergamon Press plc

COORDINATION STRUCTURE OF THE ALUMINIUM ATOMS OF POLY(METHYLALOXANE), POLY(ISOPROPOXYLALOXANE) AND POLY[(ACYLOXY)ALOXANE]

Y. KIMURA,* S. TANIMOTO, H. YAMANE and T. KITAO

Department of Polymer Science and Engineering, Kyoto Institute of Technology, Matsugasaki, Kyoto 606, Japan

Abstract—Poly(methylaloxane) (**1**), prepared by hydrolytic polymerization of trimethylaluminium (TMA), was reacted with isopropanol (IP) to obtain poly(isopropoxylaloxane) (**2**). This was further reacted with propionic acid (PA) to prepare poly[(propionyloxy)aloxane] (**3**), with various ratios of PA ligands. By gasmetry of the methane produced in the reaction, as well as by the ^{1}H NMR spectroscopy of the products, both **1** and **2** were found to contain less reactive terminal Al—Me and Al—OH groups. For **3**, the unit structure and molecular weight were controlled by the PA/TMA ratio reacted. The ^{27}Al NMR spectra of these products revealed that the coordination states of the aluminium atoms are different, depending on the O/Al atomic ratio in the products. In the case of **1**, which has a low O/Al ratio, the aluminium atoms are penta-coordinated, while in **2** and **3** hexa-coordination is involved. Based on these data the structures of poly(aloxanes) (**1–3**) are discussed.

Poly[(acyloxy)aloxane], consisting of an Al—O backbone and acyloxy pendants, has been utilized as the preceramics for alumina.[1–3] It is readily prepared by substitution of the side groups of the poly(alkylaloxane) which is the product of hydrolytic polycondensation of trialkylaluminium [eq. (1)]:

$$R_3Al \xrightarrow{H_2O} \underset{\displaystyle R}{\underset{|}{(Al}}\text{—}O)_n \xrightarrow{R'COOH} \underset{\displaystyle OCOR'}{\underset{|}{(Al}}\text{—}O)_n. \quad (1)$$

However, the structure of poly[(acyloxy)aloxane], as well as that of poly(alkylaloxane), is known to be very complex because of their intermolecular aggregation and has not yet been clarified completely. Recently,[2] we found that the coordination of their aluminium atoms could be changed by variation of the ligands. For example, the poly[(acyloxy)aloxane] with an appropriate amount of carboxylic acid ligand has a hexa-coordinate aluminium by chelation of both carboxylato and carboxyl ligands. In the present study, **1** was prepared by hydrolytic polymerization of trimethylaluminium (TMA) and was then converted to **2** and further to **3** by the substitution reactions of the side groups [eq. (2)]. For these three poly(aloxanes) the structural changes were studied in detail, especially by the application of ^{27}Al NMR spectroscopy.

$$Me_3Al \xrightarrow{H_2O} \underset{\displaystyle \mathbf{1}}{\underset{|}{(Al}}\text{—}O)_n \xrightarrow{i\text{-}PrOH} \underset{\displaystyle \mathbf{2}}{\underset{|}{(Al}}\text{—}O)_n$$

$$\xrightarrow{EtCOOH} \left[\begin{array}{c} (HOCOEt)_z \\ | \\ \text{—Al—O—} \\ | \\ OCOEt \end{array}\right]_n \quad (2)$$

3 $(0 < z < 1)$.

EXPERIMENTAL

Materials

TMA was provided by Toso–Akzo Chemical Corp. (Tokyo, Japan) and was used without further purification. Tetrahydrofuran (THF) and 1,4-dioxane (DOX) were distilled over sodium metal under a nitrogen atmosphere. Isopropanol (IP) and propionic acid (PA) were supplied from Tokyo Kasei

* Author to whom correspondence should be addressed.

Kogyo, Ltd (Tokyo, Japan), and were purified by distillation.

Measurements

^{27}Al NMR spectra were measured at 20.7 MHz on a Varian FT-80 spectrometer. The chemical shift of the signals was recorded relative to an external standard: deuterated hexa-aqua-aluminium chloride $[Al(D_2O)_6]Cl_3$ in D_2O (50 wt%) at pD 1. ^{1}H NMR spectra were measured at 200 MHz on a Varian XL–200 spectrometer with tetramethylsilane as the external standard. IR spectra were measured by a JASCO IRA–1 spectrometer. Dilute solution viscosity was measured with a Ubbelohde type viscometer at 30°C for solutions (0.4 g dl^{-1}) of the polymer in a mixture of 1:1 (w/w) phenol (PhOH): 1,1,2,2-tetrachloroethane (TCE). Molecular weights were determined cryoscopically[4] with DOX as the solvent.

Poly(methylaloxane) (**1**)

All of the following reactions were carried out under an argon atmosphere. A solution of 0.56 g of water in 12.0 cm^3 of THF was added to a stirred solution of 2.24 g (31 mmol) of TMA at −40°C over a period of 1 h. The methane gas produced was collected for volumetry in one side of a U-tube containing glycerol as the liquid seal. The levels of the glycerol in both sides of the U-tube were balanced as the gas was introduced to determine the gas volume. After the addition was over, the solution was stirred at room temperature for 0.5 h to complete the reaction. The total amount of methane gas obtained was *ca* 1270 cm^3 (57 mmol). The solvent was then removed *in vacuo* to isolate the white powdery product (yield: ~ 2 g).

Poly(isopropoxylaloxane) (**2**)

The solution finally obtained in the above experiment was cooled to 0°C and the solution of 1.86 g (31 mmol) of IP in 2.0 cm^3 of THF was added dropwise over a period of 1 h. Methane gas of *ca* 700 cm^3 (*ca* 31 mmol) in volume evolved from the system. After the addition was over, the solution was stirred at 60°C for 1 h. The solvent was then removed *in vacuo* to isolate the white powdery products.

Poly[(propionyloxy)aloxane] (**3**)

Into the solution finally obtained in the above experiment, a THF solution containing a predetermined amount of PA (50 wt%) was added dropwise at room temperature. In the first stage of the addition a small amount of methane gas was produced. As PA was added further, the gas evolution ceased, and the solution gradually became viscous. When the PA ratio was over 0.7 relative to TMA a gel was formed. The gel turned to sol again at a PA/TMA ratio of around 2.0. After standing overnight at room temperature, the reaction system was poured into an excess amount of *n*-hexane to precipitate out the polymeric products, which were filtered and dried *in vacuo*.

RESULTS AND DISCUSSION

Primary structure of poly(aloxanes)

It is known that poly(aloxanes) are prepared by hydrolytic polycondensation of organoaluminium compounds.[4–9] In these reactions a stepwise hydrolysis and condensation mechanism has been considered as indicated in Scheme 1. However, the product obtained is usually an oligomer with a degree of polymerization less than 50, or a cross-linked polymer with poorer solubility.[4] We reinvestigated the hydrolysis of TMA with an equimolar amount of H_2O in THF at −40°C. The total amount of methane produced during the reaction was 1.84 mol relative to TMA, a little lower than the theoretical value of 2.0 obtained by assuming the complete condensation. The molecular weight of the condensate **1** was determined to be *ca* 570–650 by cryoscopy, which corresponds to *ca* 10 in degree of polymerization. Figure 1(a) shows the ^{1}H NMR spectrum of **1** in C_6D_6. The signals at δ −0.2 and 0.4 ppm were assigned to the pendent methyl and terminal hydroxy groups, respectively. From

$$AlMe_3 + H_2O \longrightarrow Me_2Al{-}OH + MeH \quad (3)$$

$$Me_2AlOH + Me_2AlOH \longrightarrow Me_2Al{-}O{-}Al(Me)OH + MeH \quad (4)$$

$$Me_2Al{-}O{-}Al(Me)OH + (n-2)Me_2AlOH \longrightarrow Me\text{-}(\text{-}Al(Me)\text{-}O\text{-})_n\text{-}OH + (n-2)MeH \quad (5)$$

Scheme 1.

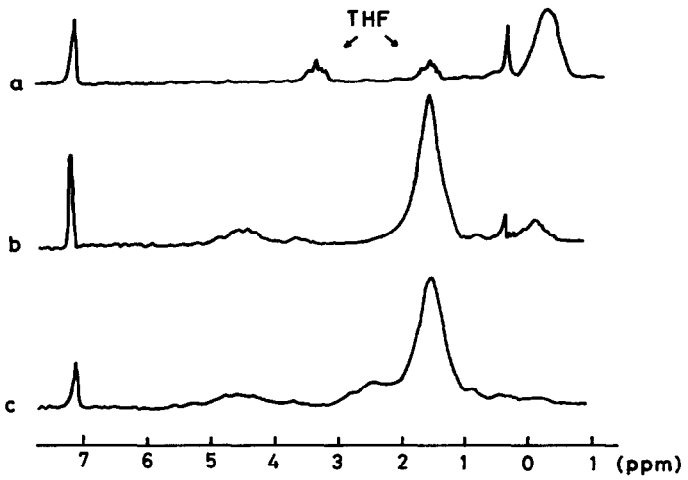

Fig. 1. ^{1}H NMR spectra of (a) **1**, (b) **2** (run 1) and (c) **3** with a PA/TMA ratio of 0.25 (run 2) in C_6D_6.

the integral ratio of these signals the degree of polymerization was calculated as 15, which is not so far from that determined by cryoscopy. These findings suggested that the condensation of the hydroxy groups and aluminium–methyl groups was incomplete, and that **1** comprises not only hydroxy groups, but also methyl groups in the terminals. The THF signals observed in the spectrum indicated that the complexation of THF and **1** is very strong.

In the second step, **1** was reacted with an equimolar amount of IP relative to TMA to obtain **2**. During the reaction almost one equivalent mol of methane gas was produced. The viscosity of the system, however, was not increased. Figure 1(b) shows the ^{1}H NMR spectrum of the product **2** in C_6D_6. Besides the signals of the isopropoxy group at δ 1.5 and 4.5 ppm, the signals at δ −0.2 and 0.5 ppm, which are ascribed to the Al—Me and Al—OH groups, respectively, were still noted. These peaks were found to appear even if an excess amount of IP was reacted with **1**. It is therefore assumed that **2** has both inactive methyl and hydroxyl groups in the chain terminals. Unfortunately, the molecular weight of **2** could not be determined by cryoscopy because of its poor solubility in DOX. Judging from its solution viscosity (see Table 1), **2** was considered to be an oligomer with a similar degree of polymerization to **1**.

In the third step **2** was reacted with various ratios of PA relative to TMA to substitute the side groups from isopropoxyl to propionyloxyl. On addition of the first portion of PA, evolution of a small amount of methane was observed. Its amount was *ca* 0.1 mol relative to TMA, which was slightly lower than the estimated value (0.16 mol relative to TMA) for the Al—Me remaining in **2**, perhaps due to experimental error. When the molar ratio (x) of PA relative to TMA was over 0.7, the system formed a gel state. The gel was re-solubilized to a viscous sol, as the PA/TMA ratio rose above 2.0. Table 1 shows the yield and the solution viscosity of the isolated product **3** as a function of the PA/TMA ratio. As the substitution reaction proceeded, the amount of the product increased because all reacted PA was taken up by the product. The solution viscosity also increased with increasing PA/TMA ratio. Figure

Table 1. Preparation of poly[(propanoyloxy)aloxane] (**3**) by sequential reaction[a] of TMA with H_2O, IP and PA in THF

Run	PA/TMA ratio	Yield (g)[b]	Yield (%)[c]	Ligand ratio[d] [IP]/[PA]	η_{sp}/C[e]
1	0	2.81	89	100:0	0.05
2	0.25	3.02	92		0.07
3	0.50	3.30	98	74:50	0.16
4	0.75	3.56	102		0.19
5	1.00	3.95	110	30:100	0.25
6	1.25	4.40	106		0.72
7	1.50	4.82	102	15:100	2.52
8	1.75	5.21	98		2.95
9	2.00	5.48	93	0:100	2.52

[a] [TMA] = [H_2O] = [IP] = 31 mmol.
[b] After reprecipitation.
[c] Based on the ideal unit structures (see text).
[d] Determined by the ^{1}H NMR spectra.
[e] At 0.4 g dl^{-1} in PhOH/TCE (50:50, v/v) at 30°C.

1(c) shows the ^{1}H NMR spectrum of **3** with $x = 0.2$ in C_6D_6. The methylene signal of the propanoyl group showed up around δ 2.5 ppm, and the signals at δ −0.2 ppm became negligibly small. It was therefore noted that both the terminal and isopropoxy groups were replaced by propionyloxy groups.

As we reported previously,[1] the poly[(acyloxy)aloxanes] (**3**) occurring as PA ratios below 1.0 should consist of both isopropoxylaloxane (I) and (propionyloxy)aloxane (P) units in a ratio corresponding to the feed ratio of PA. Similarly, the polymers occurring at PA ratios above 1.0 should comprise the PA-coordinated (propionyloxy)aloxane (PP) units and P units. With these assumed and with the presence of the terminal groups neglected, the theoretical yield of the product could be estimated for each run. On this estimated value the net yield was calculated, and is

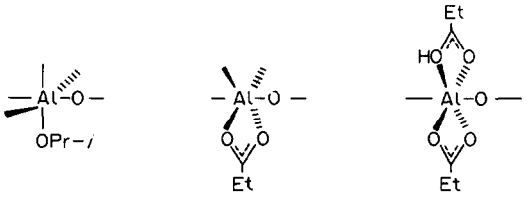

shown in per cent in Table 1. As noted in runs 4–7 the yields exceeded 100%. This was ascribed to the incorporation of IP in the products even after the purification. Since the products with the higher PA/TMA ratios were insoluble in most organic solvents, their ^{1}H NMR spectra were measured in D_2O. The signals due to the isopropoxyl were shown at δ 1.3 (d, $J_H = 6$ Hz, CH_3, 6H) and 4.1 ppm (m, CH, 1H) in relatively larger intensities, together with the propionyl signals at δ 1.1 (t, $J_H = 6$ Hz, CH_3, 3H) and 2.3 ppm (q, CH_2, 2H). Although partial hydrolysis of their molecular chain had occurred in D_2O, the ratios of the isopropoxyl to propionyloxyl could be determined from these spectra, which are also shown in Table 1. With an increasing PA ratio in feed, the IP ligand ratio in the products decreased and became zero at the PA ratio of 2.0 where only PP units are involved. Therefore, it was supported that a considerable amount of IP was incorporated in the product as the ligands. In the present case the IP-coordinated

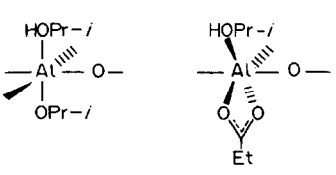

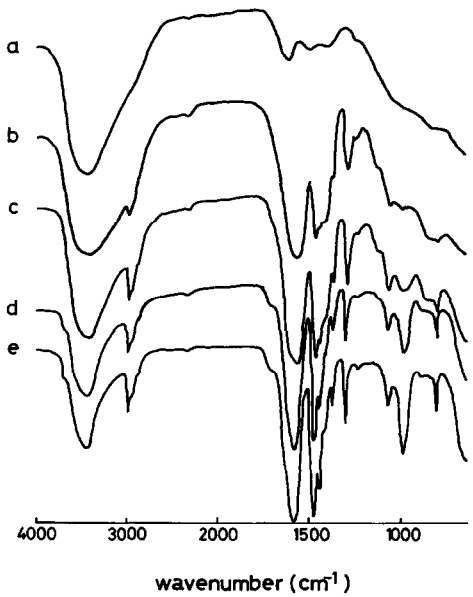

Fig. 2. IR spectra of (a) **2** and **3** with PA ratios of (b) 0.5, (c) 1.0, (d) 1.5 and (e) 2.0.

units like I′ and P′ are thought to be formed by the coordination of IP with aluminium atoms. As the PA/TMA ratio increased from 1.0 to 2.0, the units with two chelate ligands (PP) were formed and the IP ligands were eliminated.

Figure 2 shows the IR spectra of the products of runs 1, 3, 5, 7 and 9. The absorptions at 1570 and 1460 cm^{-1} are ascribed to the carboxylate groups. Even at a PA/TMA ratio higher than 1.0 only the carboxylate absorptions were detected, without any absorption of carboxylic acid noted. This is more support for the PA coordination with the aluminium atom in the PP unit. As the PA ratio increased, the absorption at 980 cm^{-1} due to ν_{Al-O} increased and the broad absorption at 3400 cm^{-1} due to Al—OH decreased. This suggests that the poly(aloxane) chain extended with an increasing PA ligand ratio. This is compatible with the increase of the solution viscosity shown in Table 1. The chain extension at higher PA/TMA ratios is considered to be allowed because intermolecular aggregation was dissociated by the coordination of PA with aluminium atoms and the chain terminals are freed to react with each other.

Coordination states of the aluminium atoms

It was indicated in the above section that the poly(aloxanes) (**1**–**3**) with a lower ratio of PA ligands, have tight chain aggregation. This aggregation may be ascribed to the sharing of the ligand by more than two aluminium atoms whose coor-

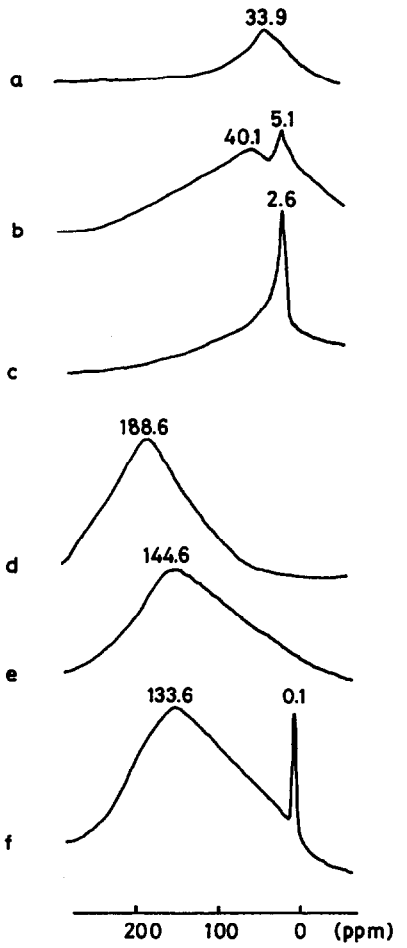

Fig. 3. ^{27}Al NMR spectra of (a) **1**, (b) **2** and (c) **3** with the PA ratio of 1.0 and their TMA complexes of (d) **1**, (e) **2** and (f) **3**.

dination sites are unfilled. Therefore, knowledge of the coordination states of the aluminium atoms should be essential information for the structure analysis of those polymers. Figure 3 shows the typical ^{27}Al NMR spectra of **1**, **2** and **3** ($x = 1.0$) in THF/C_6D_6 (50:50, v/v). The spectrum of **1** consisted of a broad signal centred at δ 33.9 ppm, indicating the coordination state of the aluminium atoms to be penta-coordinate.[10–13] Since the aluminium atom of one unit of **1** is bonded with two oxygen atoms in the main chain and with one methyl side group, at least two other sites should be filled by other ligands. They may be inactive terminal hydroxy groups and the methyl groups which are known to occur in bridge formations as below (see Structures M and M′). The solvent THF

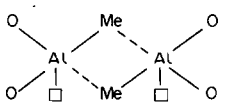

(M)

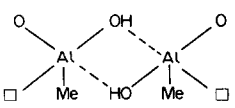

(M′)

and the oxygen atom of the main chain are also available for the coordination. So, the steric structure of **1** should be three-dimensional and possibly takes on various forms of coordination structure, as was discussed by Lasserre and Derouault[4] based on their IR data. This may be one reason for the various catalytic activities of **1** which acts as the cationic initiator and as the co-catalyst of Kaminsky catalysts.[14]

The ^{27}Al NMR of **2** showed two signals centred at δ 40.1 and 5.1 ppm. The broad low-field signal is ascribed to the penta-coordinated aluminium atoms, while the relatively sharp upfield signal is ascribed to the hexa-coordinated ones. Therefore, the aggregation state of **2** is intrinsically similar to that of **1**, except that the isopropoxy groups having higher coordination ability than Al—Me are able to be used as the ligands, so as to form the more stable hexa-coordination states.

The ^{27}Al NMR of **3** with a PA/TMA ratio of 1.0, in return, showed a relatively sharp signal at δ 2.6 ppm, and most of the aluminium atoms of **3** are thought to be in a hexa-coordinate state. In this case four of the six coordination sites of the aluminium atoms are filled with two main chain oxygen atoms and a bidentate carboxylate ligand as shown in the P unit. Therefore, the vacant sites are filled with the eliminated IP and by mutual coordination of ligands. At higher PA/TMA ratios, the vacant sites are filled by the coordination of the carboxylic acid ligand to form the PP units. The signal of its ^{27}Al NMR spectrum, centred at δ 0 ppm, became broader and broader with an increasing PA ratio and finally undetectable at a PA/TMA ratio of 2.0.

When the products **1–3** were reacted with TMA, their signals shifted to lower fields as shown in Fig. 3(d)–(f). It is therefore known that the penta- and hexa-coordination states of their aluminium atoms had turned to tetra-coordinated ones. In the presence of TMA, many of the oxygen atoms of **1–3** which were effective ligands for aluminium atoms are complexed with TMA, and the aluminium atoms in the system turn to the tetra-coordination states, as shown in M″, I″ and P″. The hydroxy groups especially, are blocked by reaction with

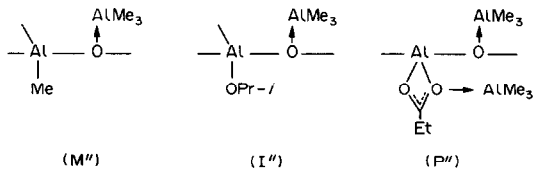

(M″) (I″) (P″)

TMA. Thus, the coordination geometry of the aluminium atoms, either tetra-, penta-, or hexa-coordinated, seems to be determined by the O/Al atomic ratio in the system. In the case of **3**, a sharp signal

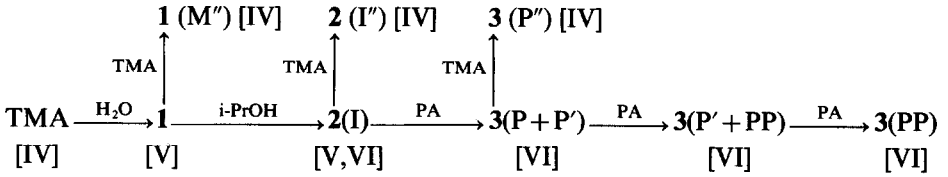

Scheme 2. (The Roman numerals indicate the coordination states.)

was shown at δ 0.1 ppm together with a broad peak at δ 134 ppm. The former should be assigned to the reaction products of TMA and IP or some unknown by-products occurring by the reaction of carbonyl groups and TMA. These results suggest that how the coordination sites of the aluminium atoms are filled is responsible for the aggregation structure of poly(aloxanes).

CONCLUSIONS

Scheme 2 shows the structural changes of the products on the basis of the above analyses. Poly(methylaloxane) **1** obtained by hydrolytic polymerization is an oligomer, consisting of the penta-coordinated aluminium atoms, with OH groups in the terminals. Poly(isopropoxylaloxane) **2** is also an oligomer, having both penta- and hexa-coordinated units, with OH and Me terminals. On the other hand, poly[(propionyloxy)aloxane] **3** consists of hexa-coordinate aluminium atoms, having the carboxylate ligand. When the PA/TMA ratio was above 1.0 the aluminium atoms are coordinated with carboxyl groups to form the units with the double chelate ligands. In the case of **1**, **2** and **3**, with relatively low PA ligand ratios, the oligomeric molecular chains are cross-linked tightly through ligand–aluminium atom coordination. The aggregation was released at high PA ratios, so that inter-oligomer condensation was allowed to give the high molecular weight product **3**. If **1**, **2** and **3**, with lower PA ligand ratios, are reacted with TMA, the coordination states of their aluminium atoms turn to tetra-coordination states because of the coordination of TMA with the oxygen ligands.

REFERENCES

1. Y. Kimura, A. Nishimura, T. Shimooka and I. Taniguchi, *Makromol. Chem., Rapid Commun.* 1985, **6**, 247.
2. Y. Kimura, S. Sugaya, T. Ichimura and I. Taniguchi, *Macromolecules* 1987, **20**, 2329.
3. Y. Kimura, M. Furukawa, H. Yamane and T. Kitao, *Macromolecules* 1989, **22**, 79.
4. S. Lesserre and J. Derouault, *Nouv. J. Chim.* 1983, **7**, 659.
5. S. Alan, J. Kenneth and A. W. Laubengayer, *J. Am. Chem. Soc.* 1968, **5**, 3173.
6. M. Boleslawski, S. Pasynkiewicz, A. Kunicki and J. Serwatowski, *J. Organomet. Chem.* 1976, **116**, 285.
7. A. Wolinska, *J. Organomet. Chem.* 1982, **234**, 1.
8. W. Boesklawski and J. Serwatowski, *J. Organomet. Chem.* 1983, **254**, 159.
9. W. Boesklawski and J. Serwatowski, *J. Organomet. Chem.* 1983, **255**, 269.
10. M. Haraguchi and S. Fujiwara, *J. Phys. Chem.* 1969, **73**, 3467.
11. D. Muller, W. Gessner, H. J. Behrens and G. Scheler, *Chem. Phys. Lett.* 1981, **79**, 59.
12. H. J. Bestmann and R. Schoebert, *Angew. Chem. Int. Edn Engl.* 1983, **22**, 780.
13. A. D. Toy, T. D. Smith and J. R. Pilbrow, *Aust. J. Chem.* 1937, **26**, 1889.
14. W. Kaminsky, J. Kopf, H. Sinn and H. J. Vollmer, *Angew. Chem. Int. Edn Engl.* 1976, **15**, 629.

Polyhedron Vol. 9, No. 2/3, pp. 377–386, 1990
Printed in Great Britain

0277–5387/90 $3.00+.00
© 1990 Pergamon Press plc

GALLIUM AND INDIUM DIHALIDES: A CLASSIC STRUCTURAL PROBLEM

DENNIS G. TUCK

Department of Chemistry and Biochemistry, University of Windsor, Windsor, Ontario N9B 3P4, Canada

CONTENTS

1. INTRODUCTION 377
2. BINARY M^{II} COMPOUNDS 377
3. DERIVATIVES OF MX_2 COMPOUNDS 378
4. THE PROPERTIES OF THE M—M BONDS 379
5. INTRAMOLECULAR HALIDE TRANSFER 382
6. MONONUCLEAR DERIVATIVES OF M^{2+} IONS 383
7. M^{II} SPECIES AS REACTION INTERMEDIATES 384
REFERENCES 385

1. INTRODUCTION

A "Symposium-in-Print" on the chemistry of aluminium, gallium and indium is an opportunity to discuss one of the interesting problems which arises in any discussion of the low oxidation states of these elements, namely, the structure of the dihalides. By way of a starting point, it would be generally accepted that the synthetic and structural chemistry of the +III oxidation state of all three elements has now been developed to a high level of sophistication in both the inorganic and organometallic fields, although this should not conceal the fact that many of the experimental problems still present fascinating challenges. Both the possible lower oxidation states, +I and +II, are known, although the extent of the published information varies considerably from one element to another. It is well established that thallium(I) compounds are the dominant feature for this element in both the solid state and in aqueous solution, whereas much less is known about indium(I) species, and gallium(I) compounds are few in number. For aluminium and boron, there is little evidence to date of a significant M(I) chemistry.

The situation with the +II state is rather different. Boron dihalides are well known, but the aluminium analogues are not, while a small number of gallium, indium and thallium compounds have been prepared and investigated. The present paper, therefore, reviews the known structural and reaction chemistry of these species in the cases of gallium and indium, attempts to understand why some of the lacunae in this area exist, suggests a rationalization of the experimental data, and identifies some matters on which future research might prove fruitful. The treatment is not intended as a definitive review of the literature and relies heavily on earlier review articles[1–5] as sources of background information.

2. BINARY M^{II} COMPOUNDS

Little is known about the dihalides of aluminium, presumably because the large (estimated) negative enthalpy change in the process[1]

$$AlX_2(s) \longrightarrow \frac{1}{3}Al(s) + \frac{2}{3}AlX_3(s)$$

($\Delta H \sim -225$ kJ mol^{-1}) has prevented any detailed study of these substances. The dihalides of gallium can be made by heating equimolar quantities of GaX_3 and Ga metal (X = Cl, Br, I), or by halogenation of the metal, directly or by using mercury halides. Similarly, InX_2 compounds (X = Br, I) can be prepared by halogenation of the metal, by reduction of InX_3 by the metal in the liquid or solution state, or by the reaction between InX and InX_3. The study of phase diagrams has helped to some extent in the elucidation of the various lower halides of indium and in addition to InX_2, a variety of compounds such as In_2Cl_3, In_4X_7 (X = Cl, Br) and In_7Br_9 have been reported; there is serious doubt about the existence of $InCl_2$ as a pure substance.[5] Some, if not all, of these latter compounds clearly involve mixed oxidation state structures, as do the InX_2 species (see below), but we shall not consider them further in this discussion.

The solid-state structure of these dihalides of the Group III elements is one of the classical problems of main group chemistry. The conventional starting point for any discussion is that a M^{2+} ion of such an element must be paramagnetic and since the MX_2 compounds are without exception diamagnetic, one must postulate dimeric structures, either containing an M—M bond ($X_2M—MX_2$), or in the form of the mixed oxidation state ionic species $M^+[MX_4]^-$. The gallium compounds are all of this latter type for X = Cl, Br and I, on the basis of X-ray and spectroscopic data,[2] while for indium, InI_2 has been shown to be so by X-ray crystallography,[5,6,7] and the Raman spectrum of $InBr_2$ confirms the presence of the $InBr_4^-$ anion.[8] The only dihalide about which any structural question remains is $InCl_2$, but as indicated above the existence of this substance is in some doubt. Indium dicyanide is also reported to be $In[In(CN)_4]$, again from the vibrational spectrum.[9]

3. DERIVATIVES OF MX_2 COMPOUNDS

Both gallium and indium dihalides are now known to form a number of neutral and anionic halide derivatives for which M—M bonding has been established beyond question by crystallographic or spectroscopic methods. The most useful diagnostic tool, apart from a complete structural analysis, is Raman spectroscopy, which under favourable conditions can be used to identify both M—X and M—M vibrations; ν(Ga—Ga) decreases[10] from 235 cm^{-1} in $Ga_2Cl_6^{2-}$ to 122 cm^{-1} in $Ga_2I_6^{2-}$, and ν(In—In) modes have been assigned in the 150–120 cm^{-1} region.[11] Force constants have been reported for the M—M and M—X vibrations.

Hexahalogenogallate(II) anions have been identified as the intermediates in the reaction between the metal and aqueous HX, but a more convenient preparative route involves the direct electrochemical oxidation of a metal anode in aqueous or non-aqueous solutions of HX.[12] All three $Ga_2X_6^{2-}$ anions (X = Cl, Br, I) are known, with Me_4N^+, i-Pr_4N^+ or Ph_3PH^+ cations and the structures have been established by X-ray crystallography.[13–15] The $Ga_2X_6^{2-}$ anions are ethane-like molecules, with staggered configurations and the M—M bonds distances are approx. 2.4 Å (see Table 1 for actual values), with a significant lengthening in the order Cl < Br < I. The stretching force constant for the Ga—Ga bond also shows a significant softening in the same order.[10] Neutral M—M bonded derivatives of Ga_2X_4 can be prepared by simple methods which essentially involve the addition of N, P, As, O or S-donors to GaX_2 in benzene, in which these latter compounds are readily soluble. The identification of the Ga—Ga bond by Raman spectroscopy lead to the formulation of these species as $Ga_2X_4L_2$, or $X_2(L)GaGa(L)X_2$, and in the case of $Ga_2X_4(diox)_2$ (X = Cl, Br; diox = 1,4-dioxane) and $Ga_2Br_4(py)_2$, four-coordination at the metal and the presence of an M—M bond were confirmed by X-ray crystallography.[4,17–19]

The situation with indium(II) derivatives is rather similar. Neutral adducts of In_2X_4 can be prepared, either by direct reaction of a N- or P-donor ligand with In_2X_4,[21] or by reaction between InX and InX_3 in the presence of the donor (not for X = Cl),[22] and the structure of $In_2Br_3I \cdot 2tmen$ involves M—M bonding between five-coordinate indium atoms.[20] The anions $In_2X_6^{2-}$ have been prepared by treating InX_2 in solution with n-Bu_4NX, and the vibrational spectra confirm the $[X_3InInX_3]^{2-}$ structure in the solid state.[11] Anions containing Ga—In bonds have also been prepared and stabilized as the salts $(n\text{-}Bu_4N)_2[X_3InGaX_3]$ (X = Cl, Br).[23]

No analogous Al—Al bonded species appear to have been reported, but the compounds $Me_6Al_4B(NMe_2)_3$ and $Me_3Al_3(NMe_2)_3$, prepared by the reduction of Me_3Al by $(Me_4N)_4B_2$, have

Table 1. M—M bond distances and stretching force constants for M_2X_4 derivatives

Compound	r(M—M) (Å)	f_R (10^2 N m^{-1})[a]	Reference
B_2F_4(c)	1.67	—	16
B_2Cl_4(g)	1.74(5)	—	16
B_2Cl_4(c)	1.75(5)	—	16
B_2Br_4(g)	1.69	—	16
$Ga_2Cl_4 \cdot 2$diox	2.406(1)	—	17
$Ga_2Br_4 \cdot 2$diox	2.395(6)	—	18
$Ga_2Br_4 \cdot 2$py	2.421(3)	—	19
$(Me_4N)_2Ga_2Cl_6$	2.39	—	13
$(i\text{-}Pr_4N)_2Ga_2Br_6$	2.42	—	14
$(Ph_3PH)_2Ga_2Cl_6$	2.407(1)	1.275	15
$(Ph_3PH)_2Ga_2Br_6$	2.410(2)	0.92	15
$(Ph_3PH)_2Ga_2I_6$	2.414(5)	0.57	15
$In_2Br_3I \cdot 2$tmed	2.775(2)	—	20
$(n\text{-}Bu_4N)_2In_2Cl_6$	—	0.63(8)	11
$(n\text{-}Bu_4N)_2In_2Br_6$	—	0.69(6)	11
$(n\text{-}Bu_4N)_2In_2I_6$	—	0.24(1)	11

[a] See references for the details of these calculations; cross-comparisons between results for different metals may not be valid.

been formulated as[24,25]

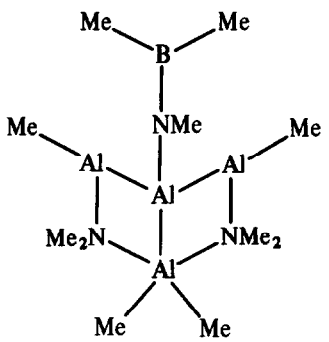

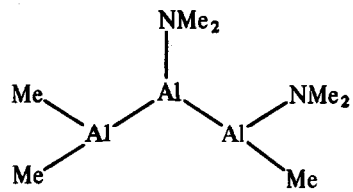

The absence of simple dinuclear derivatives of Al_2^{4+} contrasts sharply with the behaviour of gallium and indium, and of boron, since there is an extensive chemistry based on B_2X_4 compounds (X = F, Cl, Br, NMe_2, OMe, OH) and their derivatives, which include both neutral adducts (e.g. $B_2Cl_4 \cdot 2Me_3N$) and anionic species (e.g. $B_2Cl_6^{2-}$).[16]

In the light of this information on the complex derivatives of the binary dihalides, the structures reported for various lower chalcogenides of gallium and indium are interesting. The crystalline compounds GaS, GaSe and GaTe all apparently involve species in which Ga—Ga bonding is significant, with Ga—Ga distances in the range 2.4–2.5 Å, and similarly, In—In distances in the order of 2.75 Å have been reported for In_6S_7 and In_6Se_7, in which formally In_2^{4+} units are present. These compounds might well prove to be useful starting materials for the synthesis of compounds containing M—M bonds.[4,5,12]

4. THE PROPERTIES OF THE M—M BONDS

The structural data presented thus far show that the binary halides of gallium and indium form ionic structures $M^+[MX_4^-]$ in the solid state, but that reaction with either neutral or anionic donor ligands invariably gives rise to derivatives of M—M bonded species. In trying to arrive at the reasons for this behaviour, it is important to consider the properties of the M—M bonds of gallium and

Table 2. Spectroscopic properties of M_2(g) molecules[a]

M	Ground state	r(M—M) (Å)	D(kJ mol^{-1})
B	$^3\Sigma_g^-$	1.589	280±39
Al	$^3\Sigma_g^-$	2.466	198
Ga	—	—	134±21
In	$^3\Sigma_g^-$	—	85±14
Tl	—	—	<88

[a] Data from ref. 26.

indium, and to a lesser extent of the other elements of this group. A useful starting point is the spectroscopic information on M_2 molecules in the gas phase, given in Table 2. Although many important details are lacking, a number of useful conclusions do emerge. The ground state triplet identified for B_2, Al_2 and In_2 corresponds to the simple MO bonding scheme (e.g.) $(\sigma_g 2s)^2(\sigma_u^* 2s)^2(\pi_u 2p)^2$. The bond dissociation energies, D, decrease monotonically down the group and although the uncertainties in the values are substantial, there can be little doubt that M_2 molecules are all reasonably stable against dissociation into the atoms in the gas phase. There is unfortunately an absence of results on D(M—M) in M_2X_4 compounds, with the exceptions of B_2F_4 and B_2Cl_4, for which D is 303 and 330 kJ mol^{-1}, respectively.[16] These values are only slightly higher than D for B_2 itself (280 kJ mol^{-1}) and if this correspondence were to extend to other M_2X_4 species, one would conclude that M—M bonding in M_2X_4 molecules and their derivatives will be weak but certainly not negligible. A further similarity between the B—B bond in B_2 and that in B_2X_4 lies in the bond length, which shows an increase of 0.1–0.2 Å in the dihalide relative to B_2. There are two obvious factors which could explain both the weak bonding and the effect of the atomic number (Z) on the bond strength. Firstly, the atomic orbital overlap terms presumably become smaller as Z increases and secondly, the decreasing electronegativity of the elements implies an increasing Coulombic repulsion between the constituent atoms. We shall return to this latter point below.

The caveat that obviously applies to such arguments is that all the values have been derived for the gas phase, where little inorganic chemistry is actually studied. We can gain some idea of the other factors involved by considering the overall thermodynamics of the processes, acknowledging from the outset that the lack of bond dissociation energies will prevent any definitive quantitative analysis. The component parts of the enthalpy changes in

$$X_2MMX_2 \xrightarrow{(1)} MX + MX_3 \xrightarrow{(2)} M^+MX_4^-$$

can be broken down into two arguments, the first of which is;

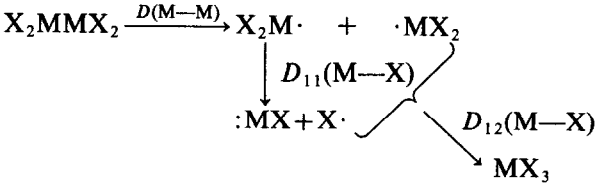

The bond energies D(M—M) for gallium and indium in M_2X_4 are presumably 150–100 kJ mol^{-1} (c.f. Table 2). The energies for removing a halogen atom from MX_2 to form MX (D_{11}) and for adding the same atom to MX_2, giving MX_3 (D_{12}), should be similar to each other, so that $D_{11}-D_{12} \approx 0$. Finally, if M_2X_4 has the same planar D_{2h} stereochemistry as B_2X_4,[16] there should be no significant rearrangement of energy terms in the formation of either MX or MX_3. At a conservative estimate, the overall ΔH for the disproportionation of X_2MMX_2 in the gas phase can

be taken as being in the order of $+200$ kJ mol^{-1}.

The remaining step is the formation of the ions by

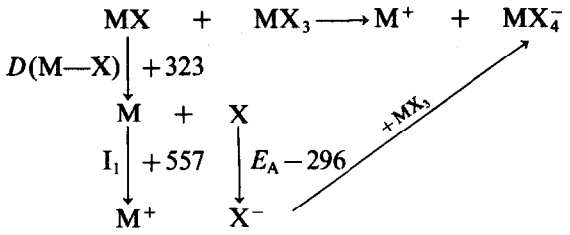

and here some of the terms are known, as exemplified in the cycle for M = In, X = I, but again the uncertainties constitute a major difficulty. The energy for the formation of the $X_3M—X^-$ bond and for the subsequent rearrangement from C_{3v} to T_d symmetry, should contribute large negative enthalpy terms (see Table 3) and a reasonable conclusion is that ΔH for eq. (2) does not exceed $+100$ kJ. The very tentative conclusion then is that ΔH for the gas phase process

$$X_2MMX_2 \longrightarrow M^+ + MX_4^- \tag{3}$$

is of the order of $+300$ kJ. The difference between this value and that for the analogous solid state process

$$M_2X_4(c) \longrightarrow M^+[MX_4]^-(c) \tag{4}$$

lies in $\Delta H_{sub}[M_2X_4(c)]$ and U, the lattice energy for the ionic solid $M^+[MX_4]^-$. If $-[U+\Delta H_{sub}] > 300$ kJ, then eq. (4) will lie to the right, ignoring any entropy factors, which will in any case presumably favour the formation of the ionic species. The calculated lattice energy[28] for $Ga[GaCl_4]$ is 547 kJ mol^{-1}, and similar values are found for $Cs[AlCl_4]$ (486 kJ mol^{-1}) and $Cs[GaCl_4]$ (495 kJ mol^{-1}), so that there is every reason to conclude that in the solid state, $M[MX_4]$ will indeed be the stable form of the gallium and indium dihalides.

This highly simplified argument has the virtue of emphasizing that the lattice energy, together with the various M—X bond energies, affect the direction of eq. (4) to a much greater extent than does the dissociation energy of the weak M—M bond. The identification of the ionic structure for M = Ga and X = Cl, Br or I, and for M = In and X = Br or I, appears to give some credence to the above argument and the apparent absence of $In^+[InCl_4]^-$ from the list (see above) may be a consequence of the magnitude of the D(In—Cl) terms in that particular system. Table 3 shows the variations in some of the terms used in the above argument.

Table 3. Metal–halogen bond dissociation energies and related data (in kJ mol^{-1})[a]

System	D(MX)	$\bar{D}$(MX$_3$)	D(X$^-$—MX$_3$)	$E_{reorg.}$[b]
Al F	660	614	—	—
Cl	489	426	210	134
Br	435	360	—	117
I	364	284	—	79
Ga F	585	—	—	—
Cl	477	280	180	—
Br	418	301	—	—
I	334	—	—	—
In F	514	—	—	—
Cl	435	—	—	—
Br	385	288	—	—
I	322	—	—	—

[a] Data from refs 1 and 27.

[b] $C_{3v} \rightarrow T_d$.

5. INTRAMOLECULAR HALIDE TRANSFER

The above arguments give a credible rationale for the existence of "MX_2" as the ionic $M[MX_4]$ mixed oxidation state species in the solid state. The only known authenticated derivatives of this same structural type are those compounds $[InL][InX_4]$ (L = 18-crown-6, cyclam; X = Cl, Br, I) in which the ligands were deliberately chosen to stabilize the In^+ cation. What additional factors beyond those just discussed must be considered to explain the apparently complete dominance of M—M bonded structures in the derivatives of M_2X_4 with neutral or anionic ligands? One arises immediately from the Coulombic repulsion in the M—M bond, namely, that by adding negative charge to the metal atoms the process of ligation would be expected to stabilize the M—M bond and hence affect the balance of the terms in the thermodynamic arguments. Furthermore, equations such as eq. (4) now become

$$M_2X_2L_2 \rightarrow [ML][MX_4L], \tag{5}$$

and eq. (1) must be rewritten as

$$M_2X_4L_2 \rightarrow MX \cdot L + MX_3 \cdot L \tag{6}$$

with a new set of enthalpies of complexation, themselves dependent upon ligand, halide and coordination number, to be considered. In sum, it is safe to conclude that the M—M bond dissociation energy is certainly not the single most important factor involved.

A different type of argument can now be considered. There are two investigations which bear upon the mechanism of halide transfer processes such as eq. (6). The first involved the study of the equilibria

$$In_2X_6^{2-} \rightleftharpoons InX_2^- + InX_4^- \tag{7}$$

in non-aqueous media by ^{115}In NMR spectroscopy[29] and showed that K lies in the order I > Br > Cl. The second approach[30] concentrated upon the inverse, namely the reaction

$$InX + InY_3 \longrightarrow X(Y)InInX_2, \tag{8}$$

which corresponds formally to the oxidative insertion of In^I into the In^{III}—Y bond of the trihalide. A number of similar oxidation reactions are known,[31] including

$$In + \begin{cases} Ph_2S_2 \longrightarrow XIn(SPh)_2 \\ Ph_3SnX \longrightarrow Ph_3SnInX_2 \\ RI \longrightarrow RIn(X)I, \end{cases}$$

and in all these cases one can write a scheme which allows for electron counting,

e.g.

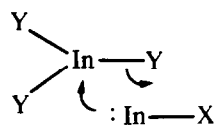

but which does nothing to explain the detailed electron transfer processes (see below). Equally relevant to the present discussion is that the intermediate

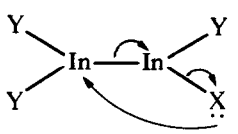

can be used to explain both oxidative addition and its reverse, the reductive elimination process of eq. (1). The second important role of donor ligands on the metal is that coordinative saturation must minimize, and in the ultimate case, prevent the halide transfer process which is an essential accompaniment to the disproportionation (or reductive elimination).

It follows that coordination at the metal centres in M_2X_4 must favour stabilization, both thermodynamically and kinetically. The coordinative saturation argument suggests that Ga_2X_4 species should be more readily stabilized than the In_2X_4 analogues, since gallium typically forms

complexes of lower coordination number than indium. The stabilization of M_2X_4 as $M_2X_6^{2-}$ anions is also interesting in this context, since one would again predict a higher stability against disproportionation for $Ga_2X_6^{2-}$ than for $In_2X_6^{2-}$, for the reason just stated and it has been reported[12] that $Ga_2X_6^{2-}$ anions do not disproportionate in solution, unlike their indium analogues. Furthermore, lattice energy effects should serve to stabilize salts in the solid state even if the anions are of marginal stability in terms of disproportionation in solution, and the salts of $In_2X_6^{2-}$ follow this pattern of behaviour. Finally, these arguments suggest that the preparation of stable M—M bonded derivatives of gallium and indium is likely to be achieved most easily by using ligands which are good donors and poor leaving groups. Steric bulk will also obviously help in preventing ligand transfer. The results obtained to date, including the recent preparation of $[M(O_2C_6X_4)phen]_2$ (M = Ga, In; $O_2C_6X_4$ = substituted *o*-diolate; X = Cl, Br) confirm these conclusions.[32] The topic of organometallic derivatives is beyond the scope of the present discussion (cf. ref. 12) except to note that the recent[33] preparation and characterization of the uncomplexed In—In bonded molecule $In_2[CH_3(SiMe_3)_2]_4$, for which r(In—In) = 2.828(1)Å, underlines the above conclusions.

It is interesting and helpful to look at the chemistry of the M—M bonded molecules of tin. Firstly, the bond dissociation energy of Sn_2 in the gas phase is 192 kJ mol^{-1}, while in the R_6Sn_2 species (R = Me, Ph) the corresponding values are 265 ± 15 kJ mol^{-1}, so that the parallel arguments for Ga—Ga etc. receive some justification. Secondly, while the organotin species are stable, the inorganic compounds Sn_2X_6 (X = H, Cl) are unstable, and Sn_2Cl_6 disproportionates above -65°C to give $SnCl_2 + SnCl_4$, although the acetato compound is more stable. As in Group III, the M—M bonded inorganic germanium compounds are apparently more stable than their heavier analogues.[34]

6. MONONUCLEAR DERIVATIVES OF M^{2+} IONS

As noted earlier, there are no authenticated instances of stable mononuclear compounds of M^{2+} ions for M = Al, Ga or In, and it is worth considering the reasons for this situation, other than the issue of dimerization. The absence of bond energy data is again a handicap, but it is possible to arrive at one useful conclusion from the ionization and other spectroscopic data given in Table 4, and by treating the M—X bonds as being purely ionic. The thermodynamics of forming MX_2 or MX_3 in the gas phase involve the sequences

$$\left.\begin{array}{l} M(g) \rightarrow M^{2+}(g) \\ X_2(g) \rightarrow 2X(g) \rightarrow 2X^-(g) \end{array}\right\} \rightarrow MX_2(g)$$

and

$$\left.\begin{array}{l} M(g) \rightarrow M^{2+}(g) \rightarrow M^{3+}(g) \\ \tfrac{3}{2}X_2(g) \rightarrow 3X(g) \rightarrow 3X^-(g) \end{array}\right\} \rightarrow MX_3(g),$$

Table 4. Ionization energies (I_n) and related data for elemental Al, Ga, In and the halogens (in eV)

Element	I_1	I_2	I_1+I_2	I_3	$I_1+I_2+I_3$	$ns^1 \rightarrow np^1$ for $M^{2+}(g)$
Al	5.98	18.82	24.80	28.44	53.24	6.70
Ga	6.00	20.51	26.51	30.70	57.21	8.19
In	5.79	18.86	24.65	28.03	52.68	7.36

Element	Bond dissociation energy D	Electron affinity E_A	$-(D-2E_A)$	$-(\frac{3}{2}D-3E_A)$
F	1.65	3.45	5.25	13.28
Cl	2.51	3.61	4.71	10.37
Br	2.00	3.37	4.74	11.22
I	1.57	3.06	4.55	12.00

Table 5. Total energies for the formation of ionic components of $MX_2(g)$ and $MX_3(g)$

System		$M^{2+}+2X^-$	$M^{3+}+3X^-$
Al	F	19.6	40.0
	Cl	20.1	42.9
	Br	20.1	42.0
	I	20.3	41.2
Ga	F	21.3	43.9
	Cl	21.8	46.8
	Br	21.8	46.0
	I	22.0	45.2
In	F	19.4	39.4
	Cl	19.9	42.3
	Br	19.9	41.5
	I	20.1	40.7

and the various atomic terms can be easily evaluated and compared. The energy differences between the formation of $[M^{2+}+2X^-]$, and of $[M^{3+}+3X^-]$, are surprisingly constant for the three elements, with the average values for X = Cl, Br or I being 21.9 eV for Al, 24.2 eV for Ga and 21.1 eV for In, and it may be relevant that the largest energy differences found for gallium, the element for which M^{II} compounds are apparently most easily prepared. For MX_2 to be stable in the gas phase, $\bar{D}(M^+—X^-)$ must be *ca* 11 eV, since the total energy input to form the $M^{2+}+2X^-$ ions is of the order of 19–22 eV (Table 5). By the same token, $\bar{D}(M—X)$ for MX_3 should be *ca* 14 eV for Al, 15 eV for Ga, and 14 eV for In.

The actual $\bar{D}$ values for a number of MX_3 molecules are given in Table 3 and are substantially lower than the values required by this ionic argument. The most important conclusion to be drawn is that there is no reason to conclude that the non-existence of MX_2 molecules arises from an inaccessible set of atomic states, or from the lack of thermodynamically stable M—X bonds. The absence of simple derivatives of M^{2+} in the solid state must therefore come down to lattice energy effects which promote disproportionation (see above), and/or to the reactivity inherent in the unpaired electron, which as Table 4 shows, can be promoted in the gaseous ion into a *p*-orbital at the cost of 600–800 kJ mol^{-1}.

This raises the possibility of the preparation of a kinetically stable monomeric M^{II} compound. In the light of the arguments developed here, any such compound would require bulky ligands to hinder dimerization and should be covalent in order to minimize lattice effects. The ligands should transfer minimum electron density to the metal, since this would tend to constrict whichever orbital contains the unpaired electron and thereby reduce the tendency to dimerize or to react with electrophilic reagents. Such requirements should not be beyond experimental reach.

7. M^{II} SPECIES AS REACTION INTERMEDIATES

We have recently studied some reactions in which good evidence has been obtained for indium(II) species as intermediates and the general conclusions are relevant to the present discussion. The reaction of In^IX (X = Cl, Br, I) with tetrahalogeno-*o*-quinones (*o*-$O_2C_6X_4$; X = Cl, Br) in non-aqueous media yields derivatives of $XIn(O_2C_6X_4)$, in which indium is in the +III state and the ligand is the *o*-diolate.[35] These conclusions depend on spectroscopic (especially ^{13}C NMR) and crystallographic studies. There are clear indications of paramagnetic species as intermediates, but these systems are much less suitable for study than are those involving InX and *o*-$O_2C_6H_2Bu^t_2$ or phenanthrene-9,10-quinone, for which electron spin resonance spectroscopy has demonstrated unequivocally that semiquinone radicals are involved in these processes.[36] The details of the argument have been given elsewhere, but can be summarized in Scheme 1. Strong oxidants, aided by electron pair donors, yield the indium(III)-*o*-diolato derivative, but with milder oxidants the final solution

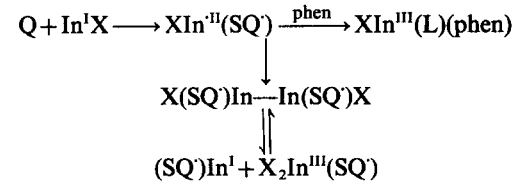

Q = *o*-quinone; $SQ^{\cdot -}$ = *o*-semiquinonate anion; L = *o*-diolato anion; phen = 1,10-phenanthroline.

Scheme 1.

contains both In^{I} and In^{III} species, which have quite different and identifiable coupling constants for the unpaired electron. The ESR results have been supported by the independent preparation and study of $(SQ^{\cdot})In^{I}$ and $(SQ^{\cdot})InX_2$ compounds of $o\text{-}O_2C_6H_2Bu^{t}_2$, including a crystallographic investigation of $(SQ^{\cdot})InBr_2 \cdot (\gamma\text{-picoline})_2$ which confirmed the presence of the semiquinone form of the ligand.[36,37] These results are in good agreement with the arguments presented in the present paper, in that the one-electron oxidation of InX can and does occur and the resultant indium(II) complex is thermodynamically stable, but dimerizes rapidly to an In—In bonded molecule which undergoes intramolecular halide transfer as a means of disproportionation.

The identification of one-electron transfer in these reactions with *ortho-* (and *para-*) quinones and in others involving low oxidation state main group compounds such as tin[38,39] raises the question of the generality of such processes, as opposed to the two-electron transfer generally assumed to occur with these molecules. It should be emphasized that detailed mechanistic evidence is often lacking for this latter premise, since it is generally the stoichiometry alone (e.g. $InX + X_2 \rightarrow InX_3$) which provides the basis for the assumed mechanism. One critical experimental factor is that the oxidizing agents themselves generally imply a two-electron stoichiometry (e.g. $X_2 \rightarrow 2X^{-}$) and only when one-electron oxidants are used is the M^{II} state identified. There is clearly considerable scope for developments in this field and for other developments in the area of the low oxidation states of these elements.

REFERENCES

1. K. Wade and A. J. Banister, in *Comprehensive Inorganic Chemistry* (Edited by A. F. Trotmen-Dickenson), Ch. 12. Pergamon Press, Oxford (1973).
2. N. N. Greenwood, *Adv. Inorg. Radiochem.* 1963, **5**, 91.
3. A. J. Carty and D. G. Tuck, *Prog. Inorg. Chem.* 1975, **19**, 245.
4. M. J. Taylor, in *Comprehensive Coordination Chemistry* (Edited by G. Wilkinson, R. D. Gillard and J. A. McCleverty), Ch. 25.1. Pergamon Press, Oxford (1987).
5. D. G. Tuck, in *Comprehensive Coordination Chemistry* (Edited by G. Wilkinson, R. D. Gillard and J. A. McCleverty), Ch. 25.2. Pergamon Press, Oxford (1987).
6. H. P. Beck, *Z. Naturf.* 1984, **398**, 310.
7. M. A. Khan and D. G. Tuck, *Inorg. Chim. Acta* 1985, **97**, 73.
8. J. G. Contreras, J. S. Poland and D. G. Tuck, *J. Chem. Soc., Dalton Trans.* 1973, 922.
9. P. L. Goggin and I. J. McColm, *J. Less-Common Met.* 1966, **11**, 292.
10. C. A. Evans, K. H. Tan, S. P. Tapper and M. J. Taylor, *J. Chem. Soc., Dalton Trans.* 1973, 988.
11. B. H. Freeland, J. L. Hencher, D. G. Tuck and J. G. Contreras, *Inorg. Chem.* 1976, **15**, 2144.
12. M. J. Taylor, *Metal-to-metal Bonded States of the Main Group Elements*, Ch. 3. Academic Press, New York (1975).
13. K. L. Brown and D. Hall, *J. Chem. Soc., Dalton Trans.* 1973, 1843.
14. H. J. Cumming, D. Hall and C. E. Wright, *Cryst. Struct. Commun.* 1974, **3**, 107.
15. M. A. Khan, M. J. Taylor, D. G. Tuck and D. A. Rogers, *J. Cryst. Spectr. Res.* 1986, **16**, 895.
16. N. N. Greenwood and B. S. Thomas, in *Comprehensive Inorganic Chemistry* (Edited by A. F. Trotman-Dickenson), Ch. 10. Pergamon Press, Oxford (1973).
17. J. C. Beamish, R. W. H. Small and I. J. Worrall, *Inorg. Chem.* 1979, **18**, 220.
18. R. W. H. Small and I. J. Worrall, *Acta Cryst.* 1982, **B38**, 250.
19. R. W. H. Small and I. J. Worrall, *Acta Cryst.* 1982, **B38**, 86.
20. M. A. Khan, C. Peppe and D. G. Tuck, *Can. J. Chem.* 1984, **62**, 601.
21. I. Sinclair and I. J. Worrall, *Can. J. Chem.* 1982, **60**, 695.
22. M. J. Taylor, D. G. Tuck and L. Victoriano, *Can. J. Chem.* 1982, **60**, 691.
23. I. Sinclair and I. J. Worrall, *Inorg. Nucl. Chem. Lett.* 1981, **17**, 279.

24. E. P. Schram, *Inorg. Chem.* 1966, **5**, 1291.
25. E. P. Schram, R. E. Hall and J. D. Glore, *J. Am. Chem. Soc.* 1969, **91**, 6643.
26. S. N. Suchard and J. E. Melzer (Eds), *Spectroscopic Data.* Plenum Press, London (1976).
27. N. N. Greenwood and K. Wade, in *Friedel-Crafts and Related Reactions* (Edited by G. A. Olah), Vol. 1, p. 606. Interscience, New York (1963).
28. H. D. B. Jenkins, *Inorg. Chem.* 1976, **15**, 241.
29. B. R. McGarvey, C. O. Trudell, D. G. Tuck and L. Victoriano, *Inorg. Chem.* 1980, **19**, 3432.
30. C. Peppe and D. G. Tuck, *Can. J. Chem.* 1984, **62**, 2798.
31. C. Peppe and D. G. Tuck, *Can. J. Chem.* 1984, **61**, 2793.
32. T. A. Annan and D. G. Tuck, *Can. J. Chem.*, in press.
33. W. Uhl, M. Layh and W. Hiller, *J. Organomet. Chem.* 1989, **368**, 139.
34. M. J. Taylor, *Metal-to-metal Bonded States of the Main Group Elements*, Ch. 4. Academic Press, New York (1975).
35. T. A. Annan and D. G. Tuck, *Can. J. Chem.* 1988, **66**, 2935.
36. T. A. Annan, R. K. Chadha, P. Doan, D. H. McConville, B. R. McGarvey, A. Ozarowski and D. G. Tuck, unpublished results.
37. T. A. Annan, D. H. McConville, B. R. McGarvey, A. Ozarowski and D. G. Tuck, *Inorg. Chem.* 1989, **28**, 1644.
38. T. A. Annan, R. K. Chadha, D. G. Tuck and K. D. Watson, *Can. J. Chem.* 1987, **65**, 2670.
39. T. A. Annan, R. K. Chadha, B. R. McGarvey, A. Ozarowski and D. G. Tuck, *J. Chem. Soc., Dalton Trans.* 1988, 2539.

Polyhedron Vol. 9, No. 2/3, pp. 387–408, 1990
Printed in Great Britain

0277–5387/90 $3.00+.00
Pergamon Press plc

A NEW STAGE IN THE DEVELOPMENT OF TRANSITION METAL ALUMOHYDRIDES

B. M. BULYCHEV

Department of Chemistry, Moscow State University, 119899 Moscow, U.S.S.R.

CONTENTS

1. INTRODUCTION 387

2. STRUCTURAL CHEMISTRY OF TRANSITION METAL ALUMOHYDRIDES . . 387
2.1. Dinuclear transition metal alumohydrides 392
2.2. Tetranuclear transition metal alumohydrides 393
2.3. Trinuclear transition metal alumohydrides 397
2.4. Polynuclear transition metal alumohydrides 400

3. CATALYTIC PROPERTIES OF TRANSITION METAL ALUMOHYDRIDES . . . 402

REFERENCES 406

1. INTRODUCTION

Structural features of transition metal alumohydrides evaluated by X-ray structural analysis are summarized and discussed. The role of these compounds in the catalysis of homogeneous hydrogenation and isomerization of hexene-1 is also considered.

2. STRUCTURAL CHEMISTRY OF TRANSITION METAL ALUMOHYDRIDES

More than 40 years have passed since the first publication of the synthesis of a novel type of coordination compound—alkali metal alumohydrides.[1] These have had a considerable impact on various branches of modern chemistry including both synthetic routines and the theory of chemical bonding. As reagents, alkali metal alumohydrides have found various applications not only in inorganic chemistry as a main source of hydrogen in the preparation of many molecular and ionic metal hydrides, but also in organic chemistry as a powerful and selective reducing agent. Accordingly, the considerable practical and scientific significance of these compounds stimulated intensive studies in the field of aluminium hydrides, the highest research activity being in the mid-sixties. One of the fundamental results obtained was the evidence for the ionic nature of all alumohydrides of alkali and rare earth metals as well as of "onium" cations both in solution and the crystalline state.[2–5] Even in lithium alumohydride, the most "covalent" compound in this series, the tetrahedral anion AlH_4^- has an almost ideal structure ($r_{Al-H} = 1.55 \pm 0.03$ Å, $\angle_{HAlH} = 109.5°$).[2] Interatomic distances, Li—H, in $LiAlH_4$ being in the range 1.84–2.16 Å are comparable with those in ionic lithium hydride (2.04 Å[6]), providing further evidence for the ionic structure of the former compound. Taking into account the structural data, the splitting of the F_2 stretching frequency in the IR spectrum of $LiAlH_4$ may be rationalized in terms of the crystal-field effect, the symmetry of which decreases in the series Cs–Li,[3] rather than in terms of the "self-symmetry" of the anion[7] on assumption of the covalent Li—H—Al bridging mode.

Alumohydride cations are solvated in aprotic donor solvents. As a result, the effective radii increases leading to the formation of contact or separated ion-pairs.[8,9] Elimination of the crystal-field effect eliminates the degeneracy, and spectra of all alumohydrides contain two (IR) or four (Raman) bands which are allowed for an ideal T_d tetrahedron of AlH_4. As a rule, rare earth

alumohydrides crystallize as ionic solvates $L_nM^{2+}(AlH_4)_2^-$ and the L—M bond strength decreases in the series Mg → Ba. The alkali metal solvates $L_nM^+AlH_4^-$,[9-12] where L = Et_2O, THF, etc., decompose on crystallization (Na, K, Rb, Cs) or on mild heating (Li).[6] Whereas ionic solvates, $MAlH_4$, with the macrocyclic polyether (15-crown-5) are rather stable and soluble even in aromatic solvents.[13] To this end, there is only ionic bonding between the metals in non-transition metal alumohydrides and onium cations, and all the data available provide no hope for discovering novel structural types.

In marked contrast with the impressive achievements in the chemistry of non-transition metal complexes, progress in the chemistry of transition metal alumohydrides (TMA) has not been as evident. This was the time of preliminary search. During the fifties, sixties and seventies, the publications were rare and were mostly descriptive (see the references cited in 14). The slow progress in this field was probably due to unclear perspectives in the utilization of TMA, their low stability and the absence of physico-chemical methods for structural analysis. The only method for structural determinations was IR spectroscopy. There are many examples in chemistry, however, when erroneous conclusions have been made on the basis of only one type of structural information. Such a conclusion concerning the ionic structure of TMA has been made on the basis of the Al—H stretching frequencies in the region 1600–1850 cm^{-1}, i.e. in the region typical of non-transition metal alumohydrides. This rationalization seems to be very strange now since even in the sixties it was known that the compounds closely related to alumohydrides, i.e. transition metal borohydrides, form molecular complexes $L_mMH_{3-n}BH_{1+n}$ with bridging hydrogens (see ref. 15). Despite this, until the late seventies (and in some cases until now) there has been a point of view that TMA obtained by exchanging the corresponding chlorides with $M'AlH_4$ in aprotic solvents (δ-donors) appear to be salt-like hydrides with ionic structure. This early stage, the stage of creation and preliminary studies, may be termed *synthetic*.

The ligands which stabilize TMA came into use in the mid-seventies. This stimulated studies under ambient conditions and posed the question of possible applications of TMA. This work manifested a *structural* stage in the chemistry of TMA, and was associated with the direct structural investigations of the compounds obtained. The crucial point in the isolation of TMA was the utilization of two different ligands, i.e. a π-donor cyclopentadienyl (C_5H_5 = Cp) ligand and σ-donor phosphines and phosphites. Table 1 shows both the composition and some typical structural characteristics of TMA evaluated by X-ray crystallography. There is also a large body of data obtained by spectral means (NMR, IR, ESR) which will be used in the present review as illustrations to structural works.

Experimental evidence reveals that despite the different nature of cyclopentadienyl and phosphine ligands the general features of complex formation, structural types and the bonding between metal heteroatoms, as well as some chemical and physico-chemical properties of TMA are very similar. This provides confidence to assume that in all other cases when the synthesis of TMA is carried out in common σ-donor solvents (Et_2O, THF, DME, etc.) the reactivity patterns and the structure of the products formed will not differ markedly from the complexes with cyclopentadienyl and phosphine ligands considered below.

There are three main types of reactions leading to TMA, mixed hydridoalkyl transition metal complexes or halohydride transition metal complexes. These are various exchange reactions, eqs (1)–(3):

$$2(Me_3P)_4OsCl_2 + 4LiAlH_4 \xrightarrow{THF} [(Me_3P)_3HOs(AlH_4)]_2 + 2AlH_3 \cdot L + 2LiCl \quad (1)$$

$$(Cp_2TiCl)_2 + 2M'AlH_4 \xrightarrow{L} 2Cp_2TiAlH_4 \cdot L + 2M'Cl \quad (2)$$

$$Cp_2TiBH_4 + LiAlH_4 \xrightarrow{L} Cp_2TiAlH_4 \cdot L + 2LiCl, \quad (3)$$

exchange redox reactions, eqs (4) and (5)

$$Cp_2NbCl_2 + 2LiAlH_4 \xrightarrow{L} Cp_2NbAlH_4 \cdot L + AlH_3 \cdot L + \tfrac{1}{2}H_2 + 2LiCl \quad (4)$$

$$Cp_2TiCl_2 + AlH_3 \xrightarrow{L} Cp_2TiH_2AlCl_2 \cdot L + \tfrac{1}{2}H_2, \quad (5)$$

and addition reactions, eqs (6) and (7), in which metal halide or alkyl halide behaves as a pseudobase

$$(Cp_2TiX)_2 + AlH_{3-n}X_n \cdot L \xrightarrow{L} Cp_2TiH_2AlH_{1-n}Cl_{n+1} \cdot L \quad (6)$$

$$Cp_2WH_2 + AlR_3 \xrightarrow{ArH} Cp_2WH_2AlR_3. \quad (7)$$

In some cases the addition and exchange reactions may be accompanied by redox processes, eq. (8):

$$(Me_2PhP)_2ReH_7 + AlR_3 \xrightarrow{ArH} (Me_2PhP)_2H_4ReH_2AlR_2 + RH. \quad (8)$$

Solvents play an important role in all reactions and their successful choice often guarantees isolation of products as monocrystals suitable for structural determinations. In particular, the interaction between Cp_3UBH_4 and $LiAlH_4$ to yield Cp_3UAlH_4 occurs in ether, while in THF the product undergoes decomposition with hydrogen evolution.[46] In contrast, reaction (1) can be carried out in THF but not in ether.[47] It should be pointed out, however, that oxygen-containing solvents and especially THF appear to be very "fine" ones for reactions of metal hydrides, since the latter can undergo ready solvolysis to afford the corresponding alkoxides. This phenomenon has already been mentioned in the literature in connection with the investigation of homonuclear aluminium hydrides (see, for example, ref. 48), although this observation was not supported by structural data. In the case of TMA, the complexes $[(Me_3P)_3H_3W(AlH_3OBu)]_2$[26] and $[Cp_2TiH_2Al(H)OMe]_2$[25] were isolated from THF and DME solutions (and then characterized by X-ray crystallography) as a result of decomposition of solvent molecules.

The literature also contains many examples of the formation of TMA as intermediates or unstable products, the decomposition of which provides homonuclear transition metal hydrides.[49-51,52]

Preliminary information about the presence of terminal Al—H bonds in TMA is available from IR spectral data. It should be remembered, however, that the known Dautel–Zeil rule which links the Al—H stretching frequency in molecular complexes and the coordination number of aluminium in TMA[52] does not hold. In particular, the wavenumbers of $AlH_3 \cdot L \cdot L'$ complexes, the coordination number of aluminium in which is five, occupy the range 1670–1750 cm^{-1},[53] while for the majority of TMA complexes having the same coordination number they are higher than 1750 cm^{-1}, i.e. as typical of the compounds with a coordination number of four. The assignment of bridging M—H—Al bonds in TMA becomes a rather reliable method when deuterium labelled species are used, since, as a rule, the corresponding bands do not overlap with those from the organic portions of the molecules. The bands due to the bridging μ_2-H ligands are seen at 1200–1650 cm^{-1}, while those due to the μ_3-H ligands are observed at 950–1200 cm^{-1}. Different types of M—H bond can also be observed by NMR, which usually provides more reliable information {as in the case of $[(Me_3P)_3H_3WH_2AlH_2]_2$} compared with IR data. Various applications of NMR to TMA are discussed in detail elsewhere.[52] It should be pointed out that because of the specific magnetic properties of the aluminium nucleus and because of the technical problems involved with the preparation of solutions of required quality, the use of NMR for analysis of TMA is strongly limited. Paramagnetic TMA can be investigated but in some cases is not successful using ESR. For example, it was concluded on the basis of ESR data that hydride and alkyl complexes of aluminium and titanocene afford heterometallic compounds with 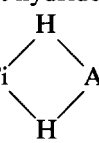 bridges.[54] Until now ESR was the main diagnostic tool for investigation of solutions of these compounds.[55]

Unfortunately, neither of the spectral methods aimed at M—H bridges gives a true structural picture without making assumptions. Therefore application of diffraction structural methods involving monocrystals is necessary for further progress in the chemistry of TMA, since it is the case that even with a vivid imagination one cannot design the structures which are in fact realized.

The structures of TMA disclosed by X-ray crystallography show that they are all molecular compounds. In general, TMA can be classified according to the number of metal nuclei in a molecule, starting from the simplest dinuclear species to the more complex polynuclear complexes.

Table 1. Composition and main bond distances (in Å) in TMA according to X-ray structural data

Compound	M—Al	M—H	Al—H	Al—X	M—M	Al—E	M—L	References
			Dinuclear complexes					
$(Cp_2TiH_2AlH_2)_2 \cdot Me_2NCH_2CH_2NMe_2$ **(I)**	2.79	1.61	1.68, 1.80	1.55		2.11	2.04[a]	16
$Cp_2LuHAlH_3 \cdot NEt_3$ **(II)**	3.23	1.81	1.81	1.52	3.64	2.13	2.30[a]	17
$Cp_2TiH_2AlCl_2 \cdot OEt_3$ **(III)**	2.75	1.89	1.73	2.16		1.97		18
$Cp_2WH_2AlMe_3$ **(IV)**	3.11	1.70, 1.22	2.04					19
$(MePh_2P)_2H_4ReH_2AlMe_2$ **(V)**	2.51	1.70	1.79, 2.0	1.33, 1.57			2.39	20
$(MePh_2P)_3HReH_3AlMe_2$ **(VI)**	2.50	1.54	1.76, 1.93, 2.1	1.58			2.37	20
$(Me_3P)_3H_2WH_3AlCl_2 \cdot NMe_3$ **(VII)**	2.50	1.68[av]	1.68, 1.91, 1.81	2.20		2.07	2.43	21
			Tetranuclear complexes					
$[(C_5Me_5)_2TiH_2AlH_2]_2$ **(VIII)**	2.75	1.89	1.67	1.51			2.08[a]	22
$[(dmpe)_2MnH_2AlH_2]_2$ **(IX)**		1.62	1.81				2.21	23
$[(dmpe)_2TaH_2Al(OC_2H_4OMe)_2]_2$ **(X)**	2.73						2.52	24
$[Cp_2TiH_2Al(H)OMe]_2$ **(XI)**	2.78					1.87	2.02	25
$[(Me_3P)_3H_3WH_2Al(H)OBu^n]_2$ **(XII)**	2.66					1.84	2.42	26
$[(Me_3P)_3H_3WH_2Al(Cl)NCHEt]_2$ **(XIII)**	2.62			2.21		1.94	2.42	21
$[Cp_2TiH_2Al(H)OEt]_2$ **(XIV)**								27
$[Cp_2TiH_2Al(H)NEt_2]_2$ **(XV)**								27
$(Cp_2YH)_2(AlH_3 \cdot THF)_2$ **(XVI)**	3.24	2.2	1.6	1.5	3.75	1.97	2.36[a]	28
$(Cp_2YH)_2(AlH_3 \cdot NEt_3)_2$ **(XVII)**	3.31	2.2	1.8		3.70	2.13		29
$(Cp_2LuH)_2(AlH_3 \cdot NEt_3)_2$ **(XVIII)**								17
$(Cp_2YAlH_4)_2 \cdot OEt_2$ **(XIX)**	3.20, 3.57	2.2	1.6	1.5	4.38	1.94		30

$(Cp_2YCl)_2(AlH_3 \cdot NEt_3)_2$ (XX)	3.62	2.1	1.8	1.5	4.38	2.04	2.37[a]	30
$[(C_5H_5)(C_5H_4)TiHAlEt_2]_2$ (XXI)	2.79	1.8	1.8		3.11			31
$[(C_5H_4)TiHAlEt_2]_2(C_{10}H_8)$ (XXII)	2.82		1.7		2.91			42
			Trinuclear complexes					
$[(Me_3P)_3H_3W]_2AlH_5$ (XXIII)	2.69	1.77	1.80–2.02	1.65			2.42	33
$[(C_5Me_5)_2Ti]_2AlH_5$ (XXIV)	2.77, 2.83						2.07[a]	22
$(Cp_2Y)_2AlH_4Cl \cdot NEt_3$ (XXV)	3.24	2.1, 2.4	1.6, 1.8	1.5, 1.4	3.95	2.09	2.36[a]	34
$[(Cp_2Y)_2AlH_4Cl \cdot OEt_2]_n$ (XXVI)	3.64, 3.91	2.3	1.4, 1.6	1.5	4.35	1.89	2.36[a]	35
$(Cp_2Ti)_2AlH_4Cl$ (XXVII)	2.77	1.8, 1.9	1.4, 1.7	2.18			2.02[a]	36
$(Cp_2Ti)_2AlH_4BH_4$ (XXVIII)	2.79	1.6, 1.9	1.7, 1.8	2.27 (Al—B)			2.03[a]	37
$(Cp_2Ti)_2AlH_4Me$ (XXIX)	2.82	1.7, 1.8	1.5, 1.7	1.94			2.03[a]	38
$[(C_5H_5)Ti]_2H(AlH_2Et_2)(C_{10}H_8)$ (XXX)		1.7, 1.8	1.7		3.31			32
$[Cp_2Zr(C,O\text{-}\eta^2OCR)]_2(HAlEt_2)$ (XXXI)	3.84, 3.57	2.02	1.7	1.95	4.26	1.79		39
$[Cp_2Zr(C,O\text{-}\eta^2OCR)]_2(H)(AlEt_2)$ (XXXII)		2.01		1.96	3.98	1.81		39
			Polynuclear complexes					
$[Cp_2TiH_2Al(H)(C_5H_4)TiCpH]_2$ (XXXIII)	2.78	1.8–2.0	1.6–1.8		3.72		2.01,[a] 2.04[a]	38, 40, 41
$[(Bu^t_2C_5H_3)LuHAlH_4 \cdot AlH_3 \cdot OEt_2]_4$ (XXXIV)	2.89–3.27			1.84–2.01	3.34		2.57[a]	42
$\{[(C_5Me_5)(C_5Me_4\overline{CH_2})TiH_2\overline{Al}]_2O\}_2$ (XXXV)	2.74, 2.85	1.6–1.8	1.7–1.8			1.75, 1.85		43
$[(C_5H_5)(C_5H_4)MoH]_2Al_3(CH_3)_5$ (XXXVI)	2.66–3.00			2.03	4.76		1.96[a]	44

Terminal X = H, Cl, Alk; bridging and terminal E = O, N; L is any ligand except hydride bound to the transition metal.

[a] The distance from the mid-point of the Cp-ring.

2.1. Dinuclear transition metal alumohydrides

Dinuclear TMA with a purely hydridic environment around the aluminium atoms are probably formed in solution in all exchange reactions of transition metal halides with alkali metal alumohydrides under carefully controlled conditions. On crystallization, however, the products may undergo either dimerization liberating solvent molecules, or decomposition producing hydrogen to afford polynuclear conglomerates or homonuclear hydrides.

Because of the low stability of the dinuclear complexes with a hydridic environment, the structures of only two such compounds are presently available. The first compound is formed at the expense of stabilization of the alumohydride molecule by a bidentate base (TMEDA) and its formula is $[Cp_2TiH_2AlH_2]_2 \cdot TMEDA$ (I).[16] The titanium and aluminium atoms are bonded through the double, strongly asymmetric Ti—H_2—Al bridge. The polyhedron around aluminium is a trigonal

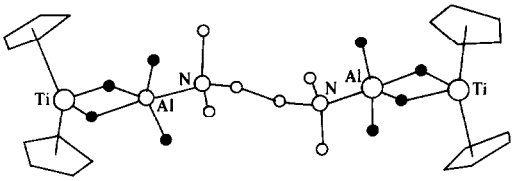

(I)

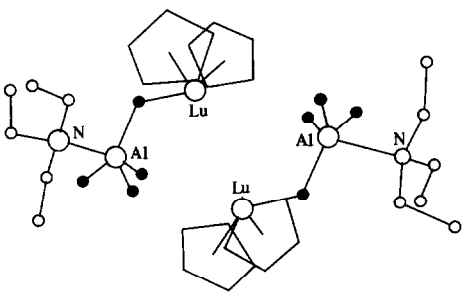

(II)

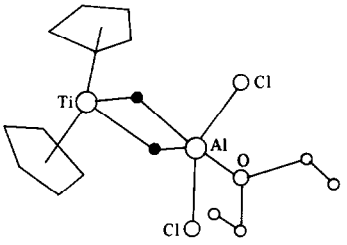

(III)

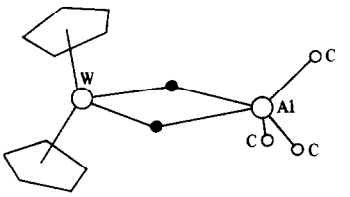

(IV)

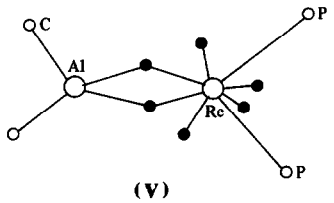

(V)

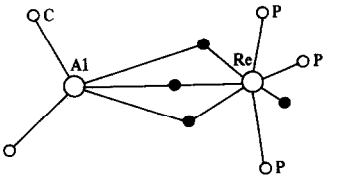

(VI)

bipyramid with nitrogen and a bridging hydrogen in the axial positions. The second complex, $Cp_2LuHAlH_2 \cdot NEt_3$ (II), is a unique example of the lutetium and aluminium bonding through a single Lu—H—Al bridge,[17] although the coordination polyhedron around aluminium is the same as in I. This compound, however, is produced by the homolytic cleavage of the Lu 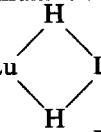 Lu fragment in the tetranuclear complex $(Cp_2LuH)_2(AlH_3 \cdot NEt_3)_2$ under the action of high-energy X-rays, eq. (9):

$$(Cp_2LuH)_2(AlH_3 \cdot NEt_3)_2 \xrightarrow{h\nu} 2Cp_2LuHAlH_3 \cdot NEt_3. \quad (9)$$

Substitution of halo or alkyl ligands for terminal hydrides leads to some stabilization of dinuclear complexes. These compounds are generally obtained by addition reactions. The complexes Cp_2Ti $H_2AlCl_2 \cdot OEt_2$ **(III)** and $Cp_2WH_2AlMe_2$ **(IV)** can be prepared by reacting the corresponding transition metal species, $(Cp_2TiCl)_2$, and Cp_2WH_2 with $AlH_3 \cdot L$[18] and $(AlMe_3)_2$,[19] respectively. As in **I**, the metal heteroatoms in complexes **III** and **IV** are bonded via the double M—H_2—Al bridge, suggesting an intramolecular rearrangement with chlorine migration from titanium to aluminium during the formation of **III**. It should be emphasized that the migration of chloro, alkyl and other ligands from titanium to aluminium and vice versa plays an important role in titanocene chemistry and in some cases the process is a key factor for understanding the high reactivity of these species in the hydrogenation and isomerization of alkenes.[36–38]

In $(Me_3P)_3H_4ReH_2AlMe_2$ **(V)**[20] the aluminium atom has a rare tetrahedral environment with a double Re—H_2—Al bridge, although also known is the related compound $(Ph_2MeP)_3HReH_3AlMe_2$ **(VI)**[20] where aluminium is five-coordinated and its bonding with rhenium occurs through a triple Re—H_3—Al bridge. An example of octahedral coordination at aluminium is seen in $(Me_3P)_3H_3WH_2AlCl_2 \cdot NMe_3$ **(VII)**, obtained by treating $[(Me_3P)_3H_3WH_2Al(H)H]_2$ with $HCl \cdot NMe_3$.[21] It should be pointed out that due to the short M—Al contacts in complexes **III** and **V–VII** (Table 1), close to or even less than the corresponding covalent radii, a true bonding mode in these compounds may be more complex than that described in terms of the multi-centred model. This may be true for TMA in which multi-centred bonding is realized together with the short M—Al contacts providing direct metal–metal interactions. The latter is also possible when a transition metal in a complex has either unshared pairs of electrons or one electron (d^1–d^4 bases). In complexes where this condition does not hold, for example, in all rare earth alumohydrides (d^0 bases), the M—Al distances are always much greater than the sum of the covalent radii ($r_{Lu—Al} = 3.23$ Å in **II**[17]).

2.2. *Tetranuclear transition metal alumohydrides*

As was mentioned in the previous section, dinuclear TMA with a purely hydridic environment around aluminium are rather unstable and undergo various transformations on crystallization. Dimerization is accompanied by desolvation (dissociation of a coordinated solvent molecule or other aluminium bound organic ligand) and formation of the Al—H_2—Al fragment. The existence of the latter among other hydridic aluminium compounds caused prolonged debates between the supporters of the bridging association of trialkylaminealkanes ($AlH_3 \cdot L$) via 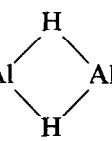 Al bridges[56,57] and the supporters of dipole–dipole interactions.[58] The question, however, remained unresolved due to the lack of conclusive evidence from both sides involved. In addition, the observation of 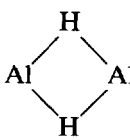 Al bridges in TMA does not support the conclusions made in refs 56 and 57, since this may reflect a change in the electronic properties of these particular heterometallic compounds, but not for homonuclear ones.

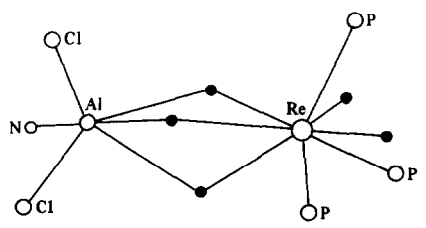

(VII)

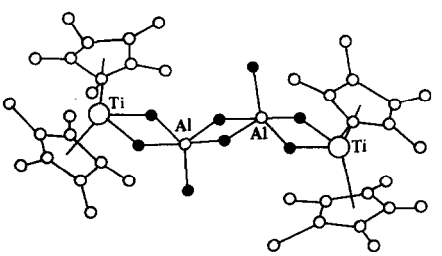

(VIII)

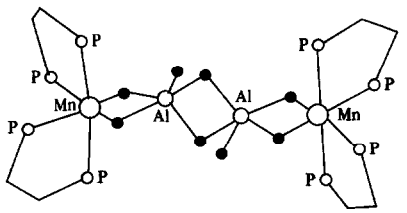

(IX)

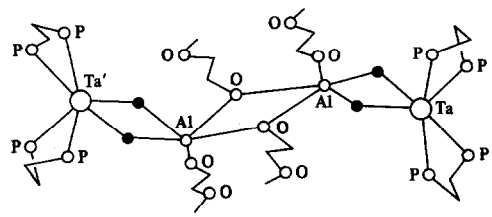

(X)

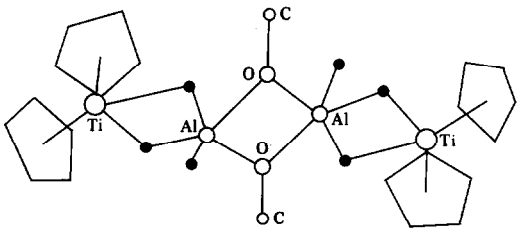

(XI)

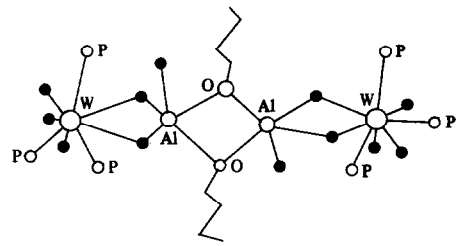

(XII)

Desolvation and dimerization of dinuclear compounds can probably be realized when a transition metal in the species is coordinated with a strong donor ligand which is able to increase the electron density at the metal to greater than the critical value. In particular, coordination of permethylcyclopentadiene instead of the usual cyclopentadiene is equivalent to a decrease in the charge at the metal by one unit.[59] In fact, permethylated titanocene alumohydride is crystallized as the non-solvated dimer $[(C_5Me_5)_2TiH_2Al(H)H]_2$ **(VIII)** with two different hydrogen bridges, namely Ti—H_2—Al, and Al—H_2—Al.[22] Similar structural types are realized in the complex with Bis(dimethylphosphino)ethane $[(dmpe)_2MnH_2Al(H)H]_2$ **(IX)**.[23] In both cases the coordination around aluminium is a strongly distorted trigonal bipyramid.

A crucial role of the ligand on the transition metal in the chemistry of heterometallic hydridic complexes (and apparently not only of hydridic) is illustrated by the compounds $(C_5H_5)_2TaH_3$ $ZnCl_2 \cdot THF$ and $[(C_5H_4Bu^t)_2TaH_3ZnCl_2]_2$.[60] Both are crystallized from THF, but the former as a monomer and the latter as a non-solvated dimer containing a 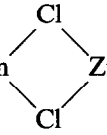 fragment.

Phosphines so strongly stabilize some valent states of transition metals that the reactions of $MCl_4(PMe_3)_x$ (M = Mo, W) with $LiAlH_4$ occur without reduction of the transition metals in refluxing THF and afford dimeric species $[(PMe_3)_3H_3MH_2Al(H)H]_2$, eq. (10):[33]

$$2MCl_4(PMe_3)_3 + 8LiAlH_4 \xrightarrow{L} [(PMe_3)_3H_3MH_2AlH_2]_2 + 6AlH_3 \cdot L + 8LiCl. \qquad (10)$$

The reduction takes place in a large excess of $LiAlH_4$ and is better in Li_3AlH_6,[61] but even in this case the last chloride is not substituted by hydride and the compound formed has the formula $[(PMe_3)_4ClMH_2AlH_2]_2$.

Fully substituted alumohydrides of divalent Cr, Mo, W,[61] Ru and Os[47] are prepared from the corresponding divalent chlorides and $LiAlH_4$, eq. (11):

$$2MCl_2(PR_3)_4 + 4LiAlH_4 \xrightarrow{L} [(PR_3)_4HMH_2AlH_2]_2 + 3AlH_3 \cdot L + 4LiCl. \qquad (11)$$

Additionally, an exchange reaction between $(dmpe)_2FeCl_2$ and $LiAlH_4$ affords a very unstable alumohydride which on decomposition gives $(dmpe)_2FeH_2$.[52]

The present literature contains more examples of structural studies on dinuclear complexes, the dimerization of which involves oxygen and nitrogen heteroatoms. The process can occur both with and without a change in the composition of dinuclear complexes. The former is observed in the

case of $[(dmpe)_2TaH_2Al(OC_2H_4OMe)_2]_2$ (**X**), with bridging and terminal alkoxides, obtained from $(dmpe)_2TaCl_2$ and $LiAlH_2(OC_2H_4OMe)_2$.[24] The latter is typical of the complexes formed either by the cleavage of the organic ligand coordinated to aluminium or by the attack of organic proton donors. For example, the synthesis of some dinuclear TMA in DME, THF or nitrile media occurs with the cleavage of solvent molecules, departure of one hydride and formation of the compounds with alumoxane fragments—$[Cp_2TiH_2Al(H)OMe]_2$ (**XI**),[25] $[(Me_3P)_3H_3WH_2Al(H)OBu]_2$ (**XII**),[26] or with imine—$[(Me_3P)_3H_3WH_2Al(Cl)NCHEt]_2$ (**XIII**)[21] fragments (hydride coordinates were not determined). Similar compounds $[Cp_2TiH_2Al(H)OEt]_2$ (**XIV**) and $[Cp_2TiH_2Al(H)NEt_2]_2$ (**XV**) can be obtained from $Cp_2TiH_2AlH_2 \cdot OEt_2$ by reacting with ethanol[27] or diethylamine,[27] respectively, in ether at a Cp_2TiAlH_4HR ratio of 1 : 0.25.

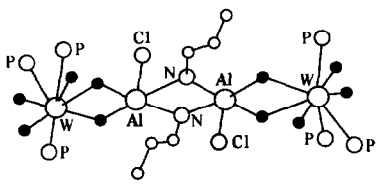

XIII

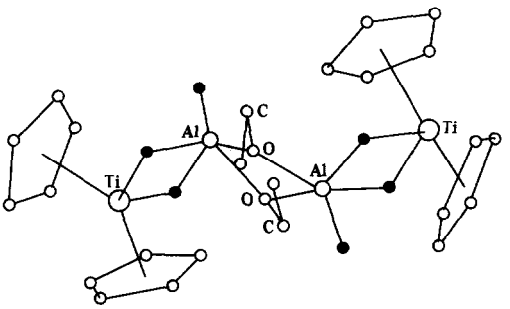

XIV

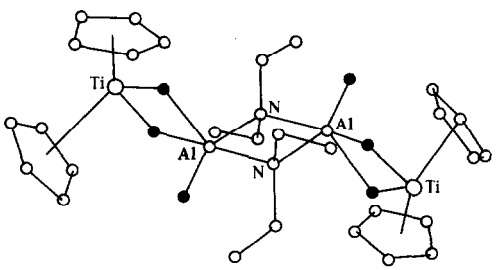

XV

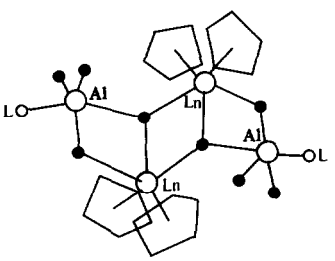

(**XVI**) Ln = Y; L = THF; (**XVII**) Ln = Y; L = NEt_3
(**XVIII**) Ln = Lu; L = NEt_3

Dimerization of sandwich rare earth alumohydride complexes takes place in a rather peculiar way. The typical feature of these compounds is the fragment Ln—μ_3-X_2—Ln, in which the X atom (H,Cl) is three-coordinated and bound to three metal atoms. This structural difference of hydridic rare earth metals compared with other non-transition metal complexes is, apparently, a result of a symmetry change of three frontal (valent) molecular orbitals a_1, b_2 and $2a_1$ located in the bisector plane of the wedge-like sandwich Cp_2M.[62]

The composition and structure of hydridic rare earth complexes formed from Cp^*_2LuCl and $MAlH_4$ strongly depend on the molar ratio of reagents used, solvent donicity and the nature of the cyclopentadienyl ligand. The reaction between Cp_2LnCl and $LiAlH_4$ at Ln : Al = 1 : 1 in THF or an equimolar amount of NEt_3 affords the compounds of practically identical composition $(Cp_2LnH)_2(AlH_3 \cdot L)$ (Ln = Y, L = THF (**XVI**);[28] Ln = Y, L = NEt_3 (**XVIII**)[17]) and structure. All metal atoms and hydrides are located in the plane of a wedge-like sandwich. The lanthanide atom makes up the 18-electron shell by coordinating the third hydrogen atom. As above, the aluminium atom in **XV–XVII** has trigonal bipyramidal coordination with axial oxygen and nitrogen atoms. The unique behaviour of the lutetium complex **XVIII** which decomposes under high-energy X-rays along the diagonal of the

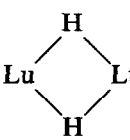

fragment to afford monomer **II** of greater density (the volume

decreases by 15%) without loss of monocrystalline properties of the sample (there are two monomeric molecules of complex **II** in the diagram) should be noted.[17] Other examples having similar behaviour, to our knowledge, are unknown. The transition described in ref. 63 is characterized by only a 2–3% volume decrease.

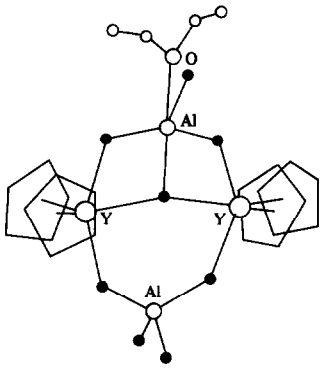

(XIX)

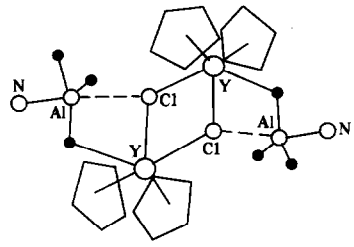

(XX)

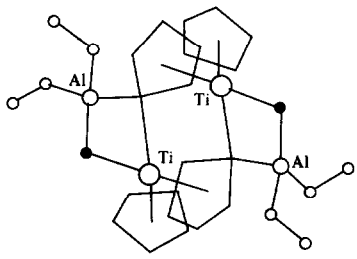

(XXI)

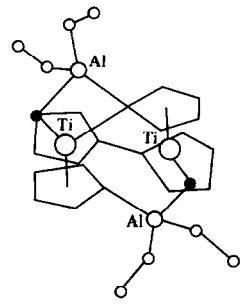

(XXII)

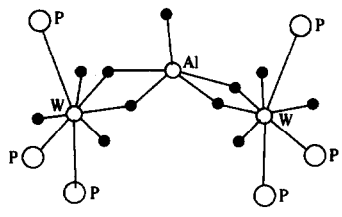

(XXIII)

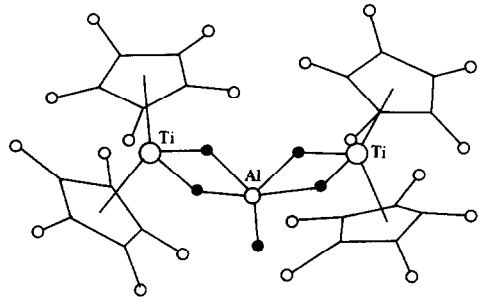

(XXIV)

The reaction of $(Cp_2YCl)_2$ with $LiAlH_4$ in ether at a Y:Al ratio of 1:1 also leads to the tetranuclear complex $(Cp_2YAlH_4)_2 \cdot OEt_2$ (**XIX**). This contains two different aluminium centres, namely the trigonal bipyramid AlH_4O and trigonal pyramid AlH_4.[29] It seems likely that this compound arises from partial desolvation of the "normal" dimer $(Cp_2YH)_2(AlH_3 \cdot OEt_2)_2$ which is built in the same way as **XVI–XVIII**.

Introduction of two bulky donor t-butyl groups markedly changes the course of the reaction between Cp^*_2LnCl and $LiAlH_4$. Interaction of $(Bu^t_2C_5H_3)_2LuCl$ with $LiAlH_4$ in ether leads to at least three products: $[(Bu^t_2C_5H_3)_2LuHAlH_3 \cdot OEt_2]_4$, $(Bu^t_2C_5H_3)LuCl_2Li \cdot L$ and $[(Bu^t_2C_5H_3)_2LuH]_2$.[42,50] The formation of these species is a result of the exchange reaction giving unstable $(Bu^t_2C_5H_3)_2LuAlH_4 \cdot nOEt_2$. Its decomposition proceeds with loss of both the fragments containing aluminium hydride and one $Bu^t_2C_5H_3$ ligand.

In contrast to the reaction of $(Cp_2TiCl)_2$ with $AlH_3 \cdot L$, the reaction of $(Cp_2YCl)_2$ with $AlH_3 \cdot L$ (L = THF, NEt_3) affords the tetranuclear species $(Cp_2YCl)_2(AlH_3 \cdot L)_2$ (L = NEt_3) (**XX**)[30] which may be considered as an adduct of two alane molecules to yttricene chloride. The coordination sphere of aluminium in **XX** is a trigonal bipyramid achieved by formation of a weak "secondary" Al—Cl bond (3.01 Å).

Hydridoalkyl titanocene complexes are different from the majority of compounds considered. These are very unstable and in solution or even under uncontrolled conditions decompose liberating alkane and hydrogen to form structures with σ–π bonded cyclopentadienyl rings. For example, interaction of Cp_2TiX (X = Cl, Ph) with $AlEt_3$ provides $[(C_5H_5)(C_5H_4)TiHAlEt_2]_2$ (**XXI**), where titanium and aluminium are σ-bound to the cyclopentadienyl ligand of the second titanium atom.[31] It is assumed that the structurally related compound is formed from $[(C_5H_5)(C_5H_4)NbH]_2$ and $AlEt_3$.[64]

High-temperature thermolysis of titanocene hydridoalkyl complexes obtained from the so-called "stable titanocene" $(CpTiH)_2(C_{10}H_8)$ and $AlEt_3$ leads to several products, one of which is the fulvalene derivative $[(C_5H_4)TiHAlEt_2]_2(C_{10}H_8)$ (**XXII**). Other structural characteristics of this compound are very similar to those of **XXI**.[32] The formation of these compounds, from our point of view, perfectly illustrates the extreme lability of the Ziegler systems used as catalysts in alkene polymerization. The tetranuclear fulvalene alumohydride $(CpNbAlH_4)_2(C_{10}H_8)$ was also postulated to account for the reaction between $[CpNb]_2(H)Cl(C_{10}H_8)$ and $LiAlH_4$.[65]

2.3. *Trinuclear transition metal alumohydrides*

Dinuclear and tetranuclear TMA and especially hydrido alkyl alumohydrides are rather unstable and when dissolved they spontaneously, or in the presence of strong bases such as TMEDA, decompose to afford trinuclear M : Al = 2 : 1 complexes together with alanes $AlH_3 \cdot L$, eq. (12).

$$2L_nMH_2AlH_2 + L' \longrightarrow L_nMH_2Al(H)H_2ML_n + AlH_3 \cdot L' \qquad (12)$$

Titanium and tungsten compounds obtained in this way have a practically identical arrangement of the M_2AlH_5 fragment: $[(Me_3P)_3H_3W]_2AlH_5$ (**XXIII**)[33] and $[(C_5Me_5)_2Ti]_2AlH_5$ (**XXIV**).[22] In these species aluminium has common although strongly distorted trigonal-bipyramidal coordination, but the complexes may be rationalized as adducts of a Lewis acid (AlH_3) with two base molecules L_nMH.

Mixed hydridochloro trinuclear sandwich transition metal complexes are available either from the exchange reactions of the corresponding dimeric chlorides with $M'AlH_4$ at M : Al = 2 : 1 and the addition reactions of alanes with two L_nMX molecules, or by decomposing several dinuclear hydridochlorides, for example $Cp_2TiH_2Al(H)Cl$. In particular, substitution of AlH_4^- for one bridging chloride of $(Cp_2YCl)_2$, which takes place in the presence of an equimolar amount of NEt_3, leads to the trinuclear cyclic complex $(Cp_2Y)_2AlH_4ClNEt_3$ (**XXVI**) where μ_2-chloride co-exists with μ_2- and μ_3-hydrogens.[34] Surprisingly, the geometry of the central nucleus of **XXVI** comprised of three metals and one chloride is very similar to that of $(Cp_2ErH)_3Cl^-$.[66] Complex **XXV** can even be prepared by

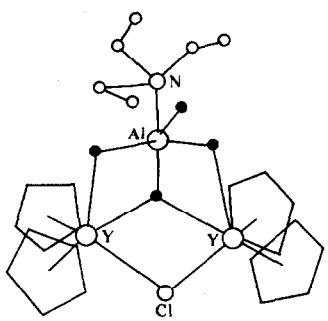

(**XXV**)

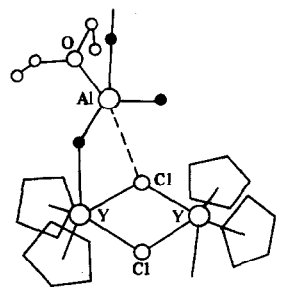

(**XXVI**)

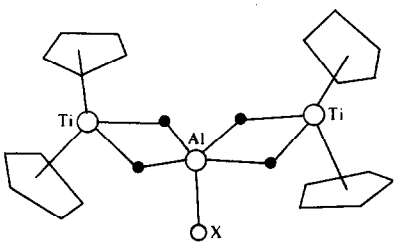

(**XXVII**) X = Cl; (**XXIX**) X = CH_3

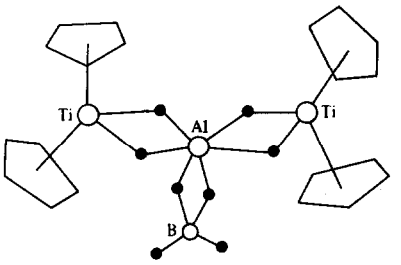

(**XXVIII**)

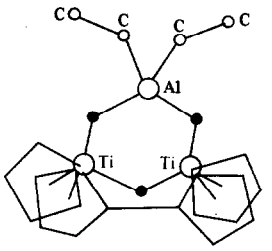

(**XXX**)

the addition of $AlH_3 \cdot NEt_3$, eq. (13):

$$(Cp_2YCl)_2 + 2AlH_3 \cdot NEt_3 \longrightarrow (Cp_2Y)_2AlH_4Cl \cdot NEt_3 + AlH_2Cl \cdot NEt_3. \quad (13)$$

The analogous reaction with $AlH_3 \cdot THF$ gives, probably, the trinuclear linear complex $Cp_2Y(THF)H_2Al(Cl)H_2(THF)YCp_2$,[34] while the same reaction in ether affords polymeric $[(Cp_2YCl)_2AlH_3 \cdot OEt_2]_n$ (**XXVI**),[35] in which three metals are also localized in one structural unit. Trigonal bipyramid geometry around aluminium in **XXVI**, as in **XX**, is accomplished by the "secondary" Al—Cl bond.

The synthesis of hydridochloro titanocene complexes is in principal identical to that of the yttricene complexes. In this case, however, all possible reactions in ether [eqs (14)–(16)] lead to the same non-solvated product $(Cp_2Ti)_2AlH_4Cl$ (**XXVII**).[36]

$$(Cp_2TiCl)_2 + LiAlH_4 \xrightarrow{Et_2O} \mathbf{XXVII} + LiCl \quad (14)$$

$$(Cp_2TiCl)_2 + 2AlH_3OEt_2 \xrightarrow{Et_2O} \mathbf{XXVII} + AlH_2Cl \cdot OEt_2 \quad (15)$$

$$2Cp_2TiH_2Al(H)Cl \xrightarrow{Et_2O} \mathbf{XXVII} + AlH_2Cl \cdot OEt_2. \quad (16)$$

Addition of alkenes or rather strong bases (NR_3) to a solution of **XXVII** induces the cleavage of the trinuclear complex yielding $(\alpha\text{-CpTiCl})_2$ and $Cp_2TiH_2AlH_2 \cdot L$.[36,37] The degree of decomposition is greater in the presence of PPh_3. One of the products formed is the fulvalene chloro derivative $(C_{10}H_8)(C_5H_5TiCl)_2$.

The terminal chloride in **XXVII** favours the introduction of other substituents. For example, the trinuclear complex $(Cp_2Ti)_2AlH_4BH_4$ (**XXVIII**) with a hydridic octahedron around aluminium is obtained either by reactions (17) and (18), or by decomposing the very unstable species $Cp_2TiH_2Al(H)_n(BH_4)_{2-n}$ ($n = 0, 1$), eq. (19):[37]

$$(Cp_2Ti)_2AlH_4Cl + LiBH_4 \xrightarrow{L} (Cp_2Ti)_2AlH_4BH_4 + 2LiCl \quad (17)$$

$$2[Cp_2TiH_2Al(H)Cl] + 2LiBH_4 \xrightarrow{L} (Cp_2Ti)_2AlH_4BH_4 + 2LiCl + AlH_2BH_4 \cdot L \quad (18)$$

$$2[Cp_2TiH_2Al(BH_4)_2] \xrightarrow{L} (Cp_2Ti)_2AlH_4BH_4 + Al(BH_4)_3 \cdot L. \quad (19)$$

Complex **XXVIII** is unprecedently stable compared with other titanium alumohydrides. All the metals in this complex are bonded by double hydrogen bridges and the complex may be treated as a heterometallic derivative of aluminium borohydride.

Substitution of a methyl group for chloride occurs in a more complex manner. Direct reaction of **XXVIII** with LiMe affords a hexanuclear complex[38] (its structure is considered below) rather than the expected trinuclear one. The complex $(Cp_2Ti)_2AlH_4CH_3$ (**XXIX**) was prepared by decomposing the unstable tetranuclear alkyl complex, the product of reaction of **XXV** with $LiAlMe_4$, eq. (2):

$$(Cp_2Ti)_2AlH_4Cl + LiAlMe_4 \xrightarrow{L} \{(Cp_2Ti)_2AlH_4(AlMe_4)\} + LiCl$$
$$\longrightarrow (Cp_2Ti)_2AlH_4Me + AlMe_3 \cdot L. \quad (20)$$

In this compound, which is in fact similar to **XXVII** and **XXVIII**, the coordination number of trigonal bipyramidal aluminium is five. It seems likely that a change of coordination polyhedron, the coordination number staying the same, is due to donor properties of the methyl group. This is also supported by very high catalytic activity of **XXIX** in the homogeneous hydrogenation of alkenes.[38]

By reactions similar to eq. (17), trinuclear species $(Cp_2Ti)_2AlH_4X$ (X = OR, NR_2, Ph, R) have been prepared and characterized by IR, ESR and analytical data.[41]

As in the above section, the fulvalene hydridoalkyl complex $[(C_5H_5)TiH](H_2AlEt_2)(C_{10}H_8)$ (**XXX**)[32] occupies a separate position. It is obtained from $(CpTiH)_2(C_{10}H_8)$ and $AlEt_3$ at room temperature. Therefore, compound **XXII** is the product of decomposition of **XXX**, whereas the majority of other trinuclear species, on the contrary, are derived from di- or tetranuclear complexes.

The unsymmetrical trinuclear zirconium–aluminium μ-ketene complex $[Cp_2Zr(C,O\text{-}\eta^2\text{-}OCR)]_2(\mu\text{-}HAlEt_2)$ (**XXXI**), obtained from $[Cp_2Zr(C,O\text{-}\eta^2\text{-}OCR)]_2$ and $AlEt_2H$, is also an example of an organometallic hydride.[39] When thermolysed in toluene, **XXXI** isomerizes into the symmetric trinuclear complex $[Cp_2Zr(C,O\text{-}\eta^2\text{-}OCR)]_2(\mu\text{-}H)(\mu\text{-}AlEt_2)$ (**XXXII**).[36]

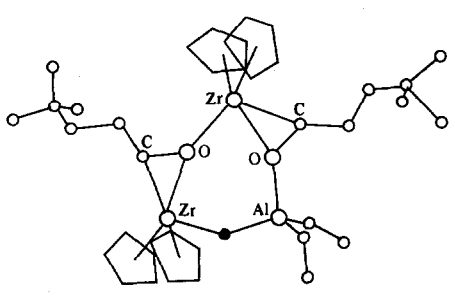

(XXXI)

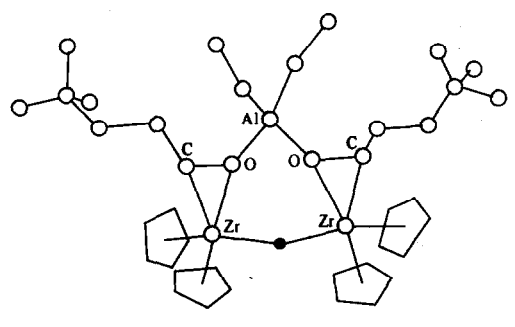

(XXXII)

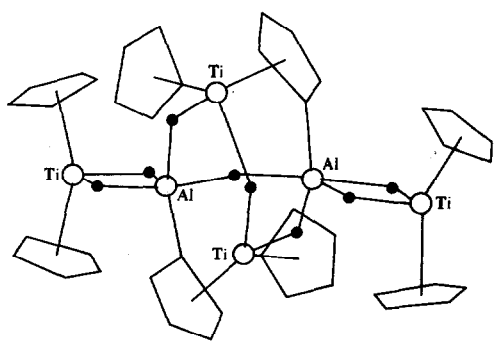

(XXXIII)

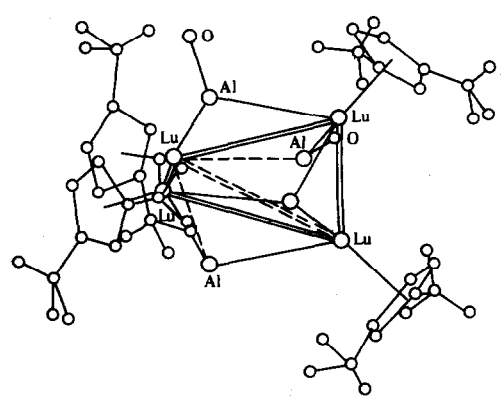

(XXXIV)

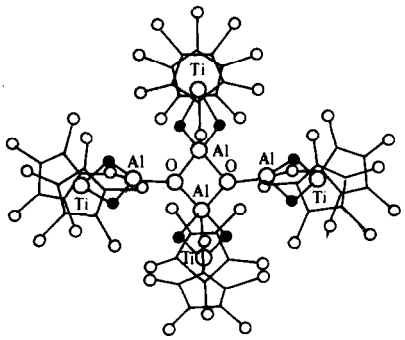

(XXXV)

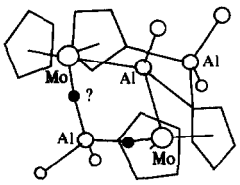

(XXXVI)

2.4. *Polynuclear transition metal alumohydrides*

Polynuclear TMA with more than four metals in a molecule are formed on decomposition of metal complexes of lower nuclearity. One of them, the hexanuclear compound $[Cp_2TiH_2AlH(C_5H_4)TiCpH]_2$ **(XXXIII)**, was recovered from a toluene solution of binuclear $Cp_2TiH_2AlH_2 \cdot L$ in the presence of TMEDA, 1,4-dioxane or water (in the latter case no more than 0.5 M H_2O per 1 M $Cp_2TiH_2AlH_2$), eq. (21):[40]

$$4Cp_2TiH_2AlH_2 \cdot L \longrightarrow [Cp_2TiH_2Al(H)(C_5H_4)TiCpH]_2 + 2AlH_3 \cdot L + 2H_2. \quad (21)$$

An easier route to the compound, although with other crystalline modifications, involves decomposition of trinuclear $(Cp_2Ti)_2AlH_4X$ (X = Me, Ph,[38] NR_2).[41] As seen from the diagram, the structure of **XXXIII** accumulates all types of M—H and L—M bonds considered above. The metal core is reminiscent of the spread wings of a seagull which are tied up at five-coordinated aluminium atoms by the Al—H—Al bridge. It is assumed that decomposition of dinuclear complexes occurs via trinuclear hydrides $(Cp_2^*Ti)_2AlH_5$, followed by rearrangement into the intermediate $\{Cp_2Ti^{III}AlH_4Ti^{II}Cp_2\}$ which contains bi- and trivalent titanium.[38,40] If Cp = C_5Me_5, only the first step of decomposition takes place and $[(C_5Me_5)_2Ti]_2AlH_5$ **(XXIV)** is isolated from solution.[22] If Cp = C_5H_5, the process always goes to completion. The formation of **XXXIII** from $(Cp_2Ti)_2AlH_4X$ is accounted for by equilibrium (22)[38] which affords unstable organometallic derivatives of titanium(III) such as Cp_2TiR, Cp_2TiPh and Cp_2TiNR_2:

$$(Cp_2Ti)_2AlH_4X \rightleftharpoons Cp_2TiAlH_4 + Cp_2TiX \quad (22)$$

Decomposition of the latter promotes the formation of the mixed-valent titanium intermediate and, correspondingly, of **XXXIII**. Since **XXXIII** is the final product of decomposition of practically all known titanocene alumohydrides [except of $(Cp_2Ti)_2AlH_4BH_4$[37]], it could be assumed that **XXXIII** is kinetically the most stable compound formed in the systems Cp_2TiCl_2–$LiAlH_4(AlH_3)$—L and $(Cp_2TiCl)_2$—$LiAlH_4(AlH_3)$—L.

Decomposition of $[Cp_2^*LuAlH_4 \cdot OEt_2]_2$ with two bulky t-butyl substituents in the Cp-rings occurs in its own original way. Together with the mononuclear dimer $[(Bu^t_2C_5H_3)_2LuH]_2$, the octanuclear complex $[(Bu^t_2C_5H_3)LuHAlH_4AlH_3 \cdot OEt_2]_4$ **(XXXIV)** with one di-t-butylcyclopentadienyl ring was isolated from solution.[42] Unfortunately, hydrogen coordinates in **XXXIV** were not determined, but there is strong IR evidence for the presence of bridging and terminal hydrogen atoms. It is also obvious that the formation of **XXXIV** requires not only the loss of one Cp* ring but a considerable rearrangement of the whole skeleton of the starting molecule.

As was mentioned above, the controlled hydrolysis of the dinuclear titanocene alumohydride affords **XXXIII**, whereas hydrolysis of the permethyltitanocene alumohydride [eq. (23)] gives the beautiful octanuclear cluster $\{[(C_5Me_5)(C_5Me_4\overline{CH_2})\overline{TiH_2}\overline{Al}]_2O\}_2$**(XXXV)** with a C—Al σ-bond.[43]

$$2[(C_5Me_5)_2TiH_2AlH_2]_2 + 2H_2O \longrightarrow \mathbf{XXXII} + 8H_2. \quad (23)$$

Besides the alumoxane AlO_2Al fragment, complex **XXXV** contains two coordination polyhedrons around aluminium, namely trigonal bipyramid and trigonal pyramid. The formation of **XXXV**

shows also that the methyl protons of the cyclopentadienyl rings are not as inert as is usually assumed and under certain conditions may undergo substitution reactions.

Metallocene hydrides Cp_2MH_{3-n} (M = Ta, Nb, Mo, W, Re; n = 0–2) of groups **V–VII** react with alanes and haloalanes to form unstable compounds of unknown composition. Their stability decreases in the series Ta ≪ Mo < Re.[68,69] In turn, Cp_2MH_{3-n} complexes react with AlR_3 to afford compounds which are quite stable under ambient conditions and are probably dinuclear species.[64,70] In solution, on heating they, however, eliminate hydrogen and in the case of Cp_2MoH_2 and $AlMe_3$ the pentanuclear complex $C_{25}H_{35}Al_3Mo_2$ (**XXXVI**) is produced at 80°C, while the heptanuclear complex $C_{26}H_{34}Al_4Mo_2$ is formed in refluxing toluene.[44,45] Hydrogen atoms were not localized in these compounds but their presence in **XXXVI** is supported by IR data and the complex stoichiometry. Tridentate cyclopentadienyl ligands in **XXXIII** and **XXXVI** bind molybdenum and two aluminium atoms (coordination numbers four and five) through a π-bond and a four-centred σ-bond, respectively. Although $C_{25}H_{35}Al_2W_2$ is not isostructural with **XXXVI**, its composition is probably similar to the molybdenum analogue.[71]

Concluding the consideration of structural data of TMA, two generalizations can be made. At present TMA of all groups, except for iron, uranium and actinoid subgroups, have been isolated and structurally characterized. The lack of structural data on transuranium alumohydrides seems to be temporary since the synthesis of Cp_3UAlH_4 has been already reported.[46] Concerning heterometallic hydrides of iron, more powerful stabilizing ligands compared with phosphines are probably needed. In any case, however, despite the generally accepted view of the ease of rupture of the Al—H bonds by transition metal salts, this bond appeared to be rather stable in the complexes considered. At the same time TMA themselves, if added even in catalytic amounts to solutions of aluminium hydride, decompose the latter. This suggests the existence of an intermediate coordination of TMA by monomeric molecules of a simple hydride providing activation of Al—H bonds. Such species were registered in the systems Cp_2TiCl_2–$LiAlH_4$, $CpTiCl_3$–$LiAlH_4$[72] and $MAlH_4$–AlH_4–crown (M = Li, Na).[73]

The second remark concerns a phenomenological description of the formation of TMA and their structures. In all cases considered the formation of TMA may be accounted for in terms of acid–base interactions, in which a transition metal with its ligand environment behaves as a Lewis base sometimes containing two basic centres, i.e. nucleophilic hydridic hydrogens or alkyl groups and/or unshared pairs of *d*-electrons, the aluminium-containing fragment being a Lewis acid. In addition to its own ligands, aluminium can coordinate one or two organometallic ligands of the Cp_2MX type as, for example, seen in complexes **IV–VI** and in all trinuclear complexes; organometallic and hydridic ligands as seen in the tetranuclear complexes **VIII** and **IX**; or organometallic and terminal or bridging organic ligands as observed in complexes **I**, **II**, **X–XX**, **XXV**, etc. Despite such diversity, the binding between metal heteroatoms of TMA both in the solid (X-ray and IR data) and in solution (NMR and ESR data) occurs through the single or double μ_2-bridges or the triple μ_3-bridge. Therefore, all the compounds considered refer to covalent alanes, $AlXX'X'' \cdot L$ or $L \cdot AlXX'X'' \cdot L'$ derived from aluminium hydride rather than to alumohydrides (tetrahydroaluminates) with discrete AlH_4^- anions which comprise ionic structures. Since in neither case, solid or solution, was the formation of AlH_4^- detected, one may conclude that ionic structures with complete charge separation are not typical of TMA and all the so-called "salt-like alumohydrides" are also covalent transition metal species which are solvated by alanes. The only difference between the compounds from **I** to **XXXVI** is that because of a weaker stabilizing effect of the "common" ligands (Et_2O, THF, etc.) they are unstable and undergo ready decomposition liberating hydrogen, binary transition metal hydrides and aluminium metal. Accordingly, the term "transition metal alumohydrides" may only exist as a term of trivial nomenclature. These considerations rule out the structural models of $Cp_2Zr(H)AlH_4$[74] and Cp_3UAlH_4[46] according to which the compounds were treated as polymers with a bidentate or ionic AlH_4 moiety. The spectral data reported may be naturally interpreted in terms of the four-centred model involving the 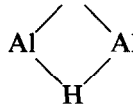 fragment or M—H_2—Al bridges between metal heteroatoms.

It is clear now that the stabilization of TMA is due to an increase in electron density at the transition metal nuclei which is achieved by coordination of donor ligands. In addition to the

evidence presented above there is an additional observation supporting this point of view. Permethyltitanocene alumohydrides are stable in air for 20–40 min, while complexes with "common" cyclopentadienyl ligands are oxidized within seconds under these conditions. It is the controlled selection of ligands with different electronic and stereochemical properties which seems to be most promising for further progress in the synthetic and structural chemistry of TMA. Another breakthrough in TMA chemistry is associated with practical utilization of these compounds. It is unlikely that the compounds can compete with alkali metal alumohydrides as synthetic reagents. Instead, they find reasonable applications in catalysis, and from this point of view detailed structural studies of TMA become extremely important since only such studies provide the relationship between the substance composition and its catalytic activity. Some results of this approach for the investigation of catalytic properties of TMA are presented below.

3. CATALYTIC PROPERTIES OF TRANSITION METAL ALUMOHYDRIDES

Studies of catalytic properties of TMA which are characterized by direct structural methods are presently limited to the sandwich complexes, rare earth and yttrium derivatives. In addition to their stabilizing function, the cyclopentadienyl ligands are involved in the rigid fixation of the three molecular orbitals (MOs) of the Cp_2M moiety ($1a_1$, b_2 and $2a_1$) in the plane of the wedge-like sandwich which are involved in binding other ligands. This structural feature is responsible for the wide variation in acidic properties of transition metal atoms (from d^0 to d^4 configurations with 14-, 15-, 16-, 17- and 18-electron environments), although the general structural type is the same.

As discussed above, all sandwich, rare earth and yttrium alumohydrides are d^0 18e species. Therefore, taking into account the general postulates of metal complex catalysis, these compounds, if not modified, can hardly display catalytic activity in transformations of alkenes. In fact, reactions of rare earth alumohydrides with linear and cyclic alkenes under a variety of conditions (e.g. in hydrogen atmosphere) are stoichiometric and result in formation of hydrido alkyl complexes, eq. (24):

$$(CpLnH)_2(AlH_3 \cdot L)_2 + 2RCH{=}CH_2 \longrightarrow (Cp_2LnH)_2(AlHR_2)_2 + 2L. \qquad (24)$$

Alkenes undergo insertion into terminal Al—H bonds liberating a ligand and preserving bridging hydrogens as confirmed by IR data.[75] Better reactivity of terminal Al—H bonds compared with bridging ones is nicely illustrated by the reaction of $Cp_2^*TiH_2AlH_2$ with water,[43] alcohols and secondary amines.[27] Evidently, reaction (24) begins with π-coordination of the alkene by aluminium. This leads to the labilization of the Al—L bond, elimination of L and then to insertion of alkene into the Al—H bond. Although π-coordination of unsaturated hydrocarbons to non-transition metals caused some doubt before recent experimental evidence.[76]

Interaction of 17-electron $Cp_2TiH_2AlH_2 \cdot OEt_2$ with isomerization resistant cyclohexene also occurs as a stoichiometric reaction and, according to ESR, IR and GLC data, affords non-solvated $Cp_2TiH_2Al(H)C_6H_{15}$ with the unchanged fragment 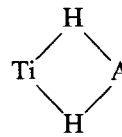 [77] Also, the reaction between $Cp_2TiH_2AlH_2 \cdot OEt_2$ and linear hexene-1 is catalytic and results in isomerization of the latter.[77] As seen from Table 2, the rate of isomerization at the dinuclear complex has a clear-cut tendency to decrease as the number of terminal hydrogen atoms decreases, as the steric bulk of ligands increases (at linked Cp-ligands, for example), and as the donor ability of ligands or substituents increases also. As in the previous case, the first step of catalysis is undoubtedly associated with the formation of the hydroalkyl complex. The rate of isomerization by the mixed hydroalkyl complex $Cp_2TiH_2Al(C_7H_{15})_2$ obtained by reaction (25) ($L = OEt_2$) is practically indistinguishable from that by $Cp_2TiH_2AlH_2 \cdot OEt_2$:

$$Cp_2TiH_2AlCl_2 \cdot L + 2C_7H_{15}MgBr \xrightarrow{L} Cp_2TiH_2Al(C_7H_{15})_2 + MgClBr. \qquad (25)$$

In the presence of NR_3 or THF the insertion does not occur. This is suggested by identical ESR spectra for the treated complex and for those treated by alkene titanocene alumohydride.

Table 2. The rates of isomerization and hydrogenation of hexene-1 catalysed by titanocene alumohydrides

Compound	$W\left(\frac{\text{mol } C_6H_{12}}{\text{g.a.Ti} \cdot \text{min}}\right)$	$W\left(\frac{\text{mol } H_2}{\text{g.a.Ti} \cdot \text{min}}\right)$
$Cp_2TiH_2AlH_2 \cdot OEt_2$	20	0
$Cp_2TiH_2AlH_2 \cdot NEt_3$	0	0
$Cp_2TiH_2AlH(Cl) \cdot OEt_2$	6	80
$Cp_2TiH_2AlCl_2 \cdot OEt_2$	0	0
$CH_2(C_5H_4)_2TiH_2AlH_2 \cdot OEt_2$	0	0
$(CH_2)_2(C_5H_4)_2TiH_2AlH_2 \cdot OEt_2$	0.03	0
$(CH_2)_3(C_5H_4)_2TiH_2AlH_2 \cdot OEt_2$	0.4	0
$(MeC_5H_4)_2TiH_2AlH_2 \cdot OEt_2$	14	0
$(Me_5C_5)_2TiH_2AlH_2 \cdot OEt_2$	0	0
$(Cp_2Ti)_2AlH_4Cl$	4.2	125
$(Cp_2Ti)_2AlH_4Me$	11.8	185
$(Cp_2Ti)_2AlH_4Bu$	9.0	180
$(Cp_2Ti)_2AlH_4O^iPr$	8.0	240
$(Cp_2Ti)_2AlH_4OBu$	6.9	325
$(Cp_2Ti)_2AlH_4NEt_2$	6.7	265
$(Cp_2Ti)_2AlH_4Ph$	7.3	90
$(Cp_2Ti)_2AlH_4BH_4$	6.5	10
$[(C_5H_4Me)_2Ti]_2AlH_4Cl$	11.6	250
$[(C_5H_4Me)_2Ti]_2AlH_4Me$	12.3	195
$[(C_5H_4Me)_2Ti]_2AlH_4Bu$	12.5	195
$[(C_5H_4Me)_2Ti]_2AlH_4OBu$	7.2	330
$[(C_5H_4Me)_2Ti]_2AlH_4NEt_2$	10.0	300
$[(C_5H_4Me)_2Ti]_2AlH_4Ph$	12.0	92
$[(C_5H_4Me)_2Ti]_2AlH_4BH_4$	8.8	10
$[(C_5Me_5)_2Ti]_2AlH_4Cl$	[a]	80
$[(C_5H_4Bu^t)_2Ti]_2AlH_4Cl$	[a]	55
$[(C_5H_4Bu^t)_2Ti]_2AlH_4OBu$	[a]	60
$(Cp_2Ti)_2AlH_4Cl(NEt_3)$	0	0

[a] Not determined.

Additionally the system shows no catalytic activity.[77] The hydroalkyl complex obtained by reaction (25) is also not active in the presence of these ligands.

The rationalization of subsequent steps of the catalytic reaction is less straightforward. Taking into account literature data[78,79] one can propose four different active sites able to carry out the migration of double bonds. These are the hydroalkyl complex itself (**A**) generated during the first step of the process and the products of either partial (**B**) or complete (**C,D**) dissociation ("classical" centres), see Scheme 1. The possibility of ligand drift from titanium to aluminium has received considerable evidence.[18,36,80] Therefore, the formation of a $15e^-$ centre **D**, as well as **C**, is also probable. In contrast, the centre of type **B** with a bridging alkyl group should be extremely unstable in donor solvents and, therefore, is not considered here.

Dissociation of dinuclear titanocene alumohydrides in aromatic solvents in the presence of dienes to form unstable titanocene hydrides has been postulated, since without this assumption one could not account for the various rearrangements leading to the fulvalene structures.[81] Nevertheless, for the catalytic isomerization of hexene-1 in ether, one should reject all "classical" centres for reasons which could not be neglected, although they do not directly support the mechanism chosen. The major reason is that dinuclear titanocene alumohydrides do not catalyse hydrogenation,

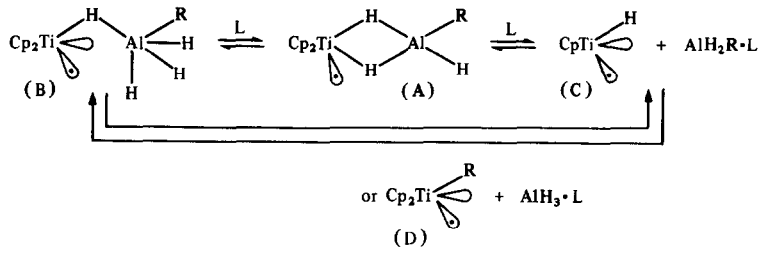

Scheme 1.

although it is known that mononuclear titanocene and rare earth hydrides, which may be formed on dissociation of dinuclear molecules, are the effective catalysts.[82,83] Thus, catalysis should occur if the mononuclear centres **B**, **C** and **D** (Scheme 1) are formed. Moreover, $[(Bu^t_2C_5H_3)_2LuH]_2$, which is the catalyst of hexene-1 isomerization (40–50 mol H_2/g.a.Ti·min), does not isomerize it. Furthermore, an alkyl group in the dinuclear hydrido alkyl complex is directly involved in isomerization. In particular, the products of the reaction between $Cp_2TiH_2Al(C_7H_{15})_2$ and hexene-1 contain hexene-2. Therefore, the active site of type **A**, in which both metals are equal partners, seems to be more probable. The corresponding mechanism of isomerization is shown in Scheme 2. It is assumed that alkene is coordinated with aluminium during the catalytic act, but it is the isomerization that proceeds in the coordination sphere of titanium.[77]

Despite the fact that there are neither terminal hydrogens or good leaving ligands in trinuclear alumohydrides of the type $Cp^*_2TiH_2Al(X)H_2TiCp^*_2$, these species are rather active in the isomerization of olefins (Table 2).[41] However, taking into account their ability to decompose in the presence of alkenes and bases according to eq. (22),[38] the catalysis by trinuclear complexes may be rationalized by the method carried out for dinuclear titanocene alumohydrides. The data in Table 2 show that the specific rate of isomerization of hexene-1 by $Cp_2TiH_2Al(X)H_2TiCp_2$, which is close to 10 mol C_6H_{12}/g.a. Ti·min, is similar to that by $Cp_2TiH_2AlH_2 \cdot OEt$, corrected in accordance with the stoichiometry of reaction (22). Lower values of W for some complexes may be associated with a decrease in the rate of reaction (22), while higher values of W may be associated with the catalytic activity of Cp_2TiX formed in this reaction. However, taking into account the significant uncertainty in determining W, the rate differences observed do not allow more specific conclusions to be made.

As has already been mentioned, all dinuclear titanocene alumohydrides except for $Cp_2TiH_2Al(H)(Cl) \cdot OEt_2$ are inactive in alkene hydrogenation. Since $Cp_2TiH_2Al(H)(Cl) \cdot OEt_2$ dissociates in solution to give $Cp_2TiH_2Al(Cl)H_2TiCp_2$ [eq. (16)],[36] it can be assumed that only the trinuclear clusters $Cp_2TiH_2Al(X)H_2TiCp_2$ catalyse hydrogenation.[41,85] The rates of hydrogenation of hexene-1

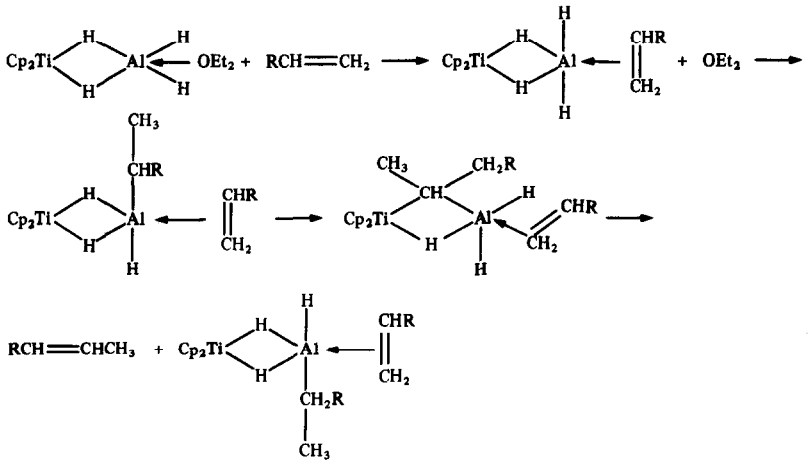

Scheme 2.

in the presence of these compounds are much higher than those when the Cp_2TiCl_2–AlR_3 system is used,[78,79] and as seen from Table 2 depends on the nature of the X substituents and cyclopentadienyl rings. In particular, substitution of alkyl groups for chloride in $Cp_2TiH_2Al(Cl)H_2TiCp_2$ increases the reaction rate by a factor of nearly 1.5. Greater effects are achieved on introducing OR and NR_2 functions into the coordination sphere of aluminium. The introduction of one methyl group into the Cp ring brings about the same result. Hence, in contrast to the catalysts of isomerization, the activity of catalysts of hydrogenation increases with increasing electron density at the metal centres. A relative change of the electron density at titanium may be characterized by the value of the H—Ti—H bond angle, which becomes lower as the population of an a_1 orbital increases.[86] For the structurally characterized complexes the angle decreases in the series X = BH_4 (73°) > Cl (63.5°) > Me (60°), and inversely the specific rate of hexene-1 hydrogenation varies (Table 2).

Introduction of bulky tert-butyl groups into cyclopentadienyl rings decreases the rate of hydrogenation on one hand and levels off the activity of complexes with high and moderate reactivity, on the other. The same effect is observed in sterically hindered permethyl cyclopentadienyl complexes and also in complexes which contain sterically demanding X substituents, such as OiPr, NR_2 and Ph.

Since all the metal centres in the trinuclear complexes are coordinately saturated, the compounds are probably not the true catalysts of hydrogenation but rather their precursors. ESR data suggest the equilibria in solutions of $Cp_2^*TiH_2Al(X)H_2TiCp_2^*$ involving less stable species.[85] In particular, under the action of cyclohexene, THF or tertiary amines on trinuclear compounds, the crystallization of $[\alpha\text{-}Cp_2TiCl]_2$ occurs while the mother liquor contains paramagnetic species which from the ESR spectra correspond to the individual compounds $Cp_2TiH_2AlH_2 \cdot L$ or $Cp_2TiH_2Al(H)C_6H_{13}$.[38]

Apparently, the formation of the latter two involves the mixed bridged intermediate 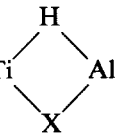

(Scheme 3) which further dissociates along the α-diagonal. (The formation of 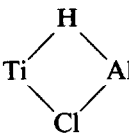 hetero-

metallic species was previously observed by ESR in the system Cp_2TiCl_2–$AlEt_3$.[87]) It is this process which accounts for the catalytic activity of trinuclear complexes in isomerization reactions. Since neither of the compounds formed in this way catalyses the hydrogenation, it may be assumed that when both alkene and hydrogen are present another pathway of dissociation of the

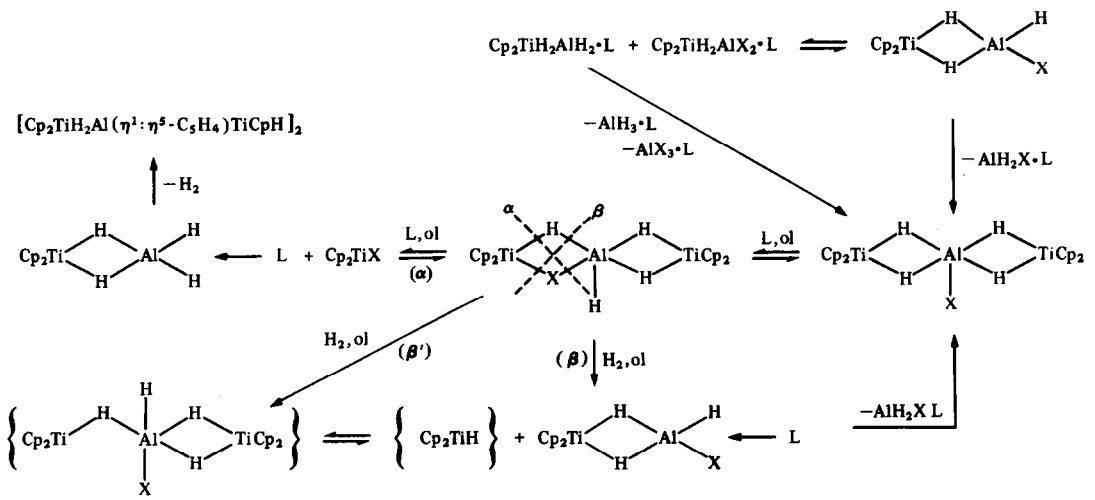

Scheme 3.

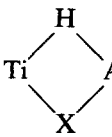

fragment is realized, for example, via the β-diagonal, providing monomeric titanocene hydrides. Unfortunately, all attempts to register such species by ESR after treating the latter with phosphines (PR_3 or PPh_3) in the way described above for alkyl systems based on Cp_2TiCl_2[82] were not successful. This is probably due to the partial bridge cleavage in the

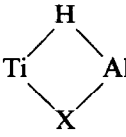

fragment and the association of Cp_2TiH with dinuclear complex **B** (second "classical" centre, Scheme 1) which has the same structure as the 14-electron complex $Cp_2LuHAlH_4 \cdot NEt_3$.[17] Indirect evidence in favour of the formation of intermediate titanocene hydrides is the isolation, in high yield, of the structurally characterized fulvalene complex, $(\eta^1:\eta^5\text{-}C_5H_4\text{-}\eta^1:\eta^5\text{-}C_5H_4)Ti_2Cl_2Cp_2$, which has been formed in the system $Cp_2TiH_2Al(Cl)H_2TiCp_2$–hex-1-ene–H_2–PPh_3.

The dissociation of trinuclear compounds along the α- and β-diagonals should be apparently facilitated by the presence of donor groups which destabilize the bridging bonds. This is nicely illustrated when acceptor chlorine atoms in **XXVII** are substituted by donor methyl or alkoxide groups, thus increasing the catalytic activity by a factor of 2–3. The role of steric factors in catalysis is also apparent: bulky X groups prevent the formation of

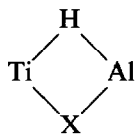

bridges, whereas bulky substituents on cyclopentadienyl rings prevent coordination and further transformations of alkenes.

To this end, the experimental data concerning catalytic activity of di- and trinuclear aluminium and titanocene hydride complexes in homogeneous isomerization and hydrogenation of alkenes are best accounted for in terms of the dimetallic mechanism. Although, aluminium behaves as an equal partner in isomerization, the centre is truly dimetallic, it is a part of the well-known monometallic centre in hydrogenation, and its role is the creation of such ligand environments which on simultaneous reaction with alkenes and hydrogen provides partial or complete dissociation of the bridging hydrogens.

In conclusion, the following remarks can be made. The catalytic mechanisms involving di- and trimetallic aluminium and titanocene hydrides in homogeneous isomerization and hydrogenation of alkenes should not pretend to represent "true mechanisms". In tandem with the experimental data, they allow the prediction of a proportion of the catalytic properties of certain compounds. Questions about the true mechanisms are still open, but, obviously, it cannot be solved without finding out the relationship between the structure of the catalyst and its catalytic activity. In turn, it requires the necessary evaluation of the structures of the compounds used as homogeneous catalysts by direct structural methods. Of course, the complete preservation of all structural elements during the catalysis is an exception rather than a rule. Nevertheless, straightforward structural data create the basis for interpretation of spectral information obtained during the catalysis. From our point of view, the virtue of such an approach is well illustrated by the example of catalysis by aluminium and titanocene hydrides. Due to the high catalytic activity of the latter or their precursors there is hope for discovering the catalytic properties of other TMA. Obviously, further development of the catalytic chemistry of these compounds is associated with the expansion of the direction of research of the catalytic reactions, among which the most important are alkene and alkyne polymerization, and with structural modification of complexes by a variation of the ligand environment of both metal centres.

REFERENCES

1. A. E. Finholt, A. C. Bond and H. I. Schlesinger, *J. Am. Chem. Soc.* 1947, **69**, 1199.
2. N. Sclar and B. Post, *Inorg. Chem.* 1967, **6**, 669.
3. K. N. Semenenko, A. P. Chavgun, V. B. Polyakova, A. L. Dorosinsky and A. A. Plakhty, *Zh. Neorg. Khim.* 1970, **15**, 2890.
4. J. W. Lauher, D. Dougherty and P. J. Herley, *Acta Cryst.* 1979, **B35**, 1454.

5. B. M. Bulychev, V. K. Belsky and A. V. Golubeva, *Zh. Neorg. Khim.* 1983, **28**, 2694.
6. A. F. Zhigach and D. S. Stasinevich, *Khimia Hidridov, L.* 1969.
7. T. G. Adiks, V. V: Gavrilenko, L. I. Zakharkin and L. A. Ignat'eva, *Zh. Prikl. Spectrosc.* 1967, **6**, 806.
8. E. C. Ashby, F. R. Dobbs and H. P. Hopkins, *J. Am. Chem. Soc.* 1973, **95**, 2823.
9. A. E. Shirk and D. F. Shriver, *J. Am. Chem. Soc.* 1973, **95**, 5904.
10. K. N. Semenenko, B. M. Bulychev and K. B. Bitsoev, *Vest. Mosk. Gos. Univ., Ser. Khim.* 1974, 185.
11. E. C. Ashby, R. D. Schwartz and B. D. James, *Inorg. Chem.* 1970, **9**, 325.
12. B. M. Bulychev, V. K. Belsky, A. V. Golubeva and P. A. Storozhenko, *Zh. Neorg. Khim.* 1983, **28**, 1131.
13. P. A. Storozhenko, L. V. Ivakina and B. M. Bulychev, *Zh. Neorg. Khim.* 1988, **33**, 254.
14. G. L. Soloveichik and B. M. Bulychev, *Usp. Khim.* 1983, **52**, 72.
15. T. J. Marks and J. R. Kolb, *Chem. Rev.* 1977, **77**, 263.
16. E. B. Lobkovskii, G. L. Soloveichik, A. I. Sizov and B. M. Bulychev, *J. Organomet. Chem.* 1984, **265**, 167.
17. S. A. Knjashansky, B. M. Bulychev, V. K. Belsky and G. L. Soloveichik, *J. Organomet. Chem.* 1987, **327**, 173.
18. E. B. Lobkovskii, G. L. Soloveichik, B. M. Bulychev, R. G. Gerr and Yu. T. Struchkov, *J. Organomet. Chem.* 1984, **270**, 45.
19. J. W. Bruno, J. C. Huffman and K. G. Coulton, *J. Am. Chem. Soc.* 1984, **106**, 444.
20. W. Skupinski, J. C. Huffman, J. W. Bruno and K. G. Coulton, *J. Am. Chem. Soc.* 1984, **106**, 8128.
21. A. R. Barron, G. Wilkinson, M. Motevalli and M. B. Hursthouse, *J. Chem. Soc., Dalton Trans.* 1987, 837.
22. V. K. Belsky, A. I. Sizov, B. M. Bulychev and G. J. Soloveichik, *J. Organomet. Chem.* 1985, **280**, 67.
23. C. G. Howard, G. S. Girolami, G. Wilkinson, M. Thornton-Pett and M. B. Hursthouse, *J. Chem. Soc., Dalton Trans.* 1985, 921.
24. T. J. McNeese, S. S. Wreford and B. M. Foxman, *J. Chem. Soc., Chem. Commun.* 1978, 500.
25. V. K. Belsky, A. I. Sizov, B. M. Bulychev and G. L. Soloveichik, *Koord. Khim.* 1985, **11**, 1003.
26. A. R. Barron, D. Lyons, G. Wilkinson, M. Motevalli and M. B. Hursthouse, *J. Chem. Soc., Dalton Trans.* 1986, 275.
27. V. K. Belsky, A. I. Sizov, T. Yu. Sokolova, B. M. Bulychev and G. L. Soloveichik, *Metalloorg. Khim.*, in press.
28. V. K. Belskii, A. B. Erofeev, B. M. Bulychev and G. L. Soloveichik, *J. Organomet. Chem.* 1984, **268**, 107.
29. V. K. Belskii, A. B. Erofeev, B. M. Bulychev and G. L. Soloveichik, *J. Organomet. Chem.* 1984, **265**, 123.
30. E. B. Lobkovski, G. L. Soloveichik, B. M. Bulychev, A. B. Erofeev, A. J. Gusev and N. I. Kirillova, *J. Organomet. Chem.* 1983, **254**, 167.
31. F. N. Tebbe and L. J. Guggenberger, *J. Chem. Soc., Chem. Commun.* 1973, 227.
32. F. N. Tebbe and L. J. Guggenberger, *J. Am. Chem. Soc.* 1973, **95**, 7870.
33. A. R. Barron, M. Motevalli, M. B. Hursthouse and G. Wilkinson, *J. Chem. Soc., Chem. Commun.* 1985, 664.
34. A. B. Erofeev, B. M. Bulychev, V. K. Belskii and G. L. Soloveichik, *J. Organomet. Chem.* 1987, **335**, 189.
35. E. B. Lobkovskii, G. L. Soloveichik, B. M. Bulychev, A. B. Erofeev and V. K. Belskii, *J. Organomet. Chem.* 1982, **235**, 151.
36. A. I. Sizov, I. V. Molodnitskaj, B. M. Bulychev, E. V. Evdokimova, G. L. Soloveichik, A. I. Gusev, E. B. Chuklanova and V. I. Andrianov, *J. Organomet. Chem.* 1987, **335**, 323.
37. A. I. Sizov, I. V. Molodnitskaj, B. M. Bulychev, G. L. Soloveichik and V. K. Belskii, *J. Organomet. Chem.* 1988, **344**, 185.
38. A. I. Sizov, I. V. Molodnitskaj, B. M. Bulychev, V. K. Belskii and G. L. Soloveichik, *J. Organomet. Chem.* 1988, **344**, 293.
39. R. M. Waymouth, B. D. Sautarsiero, R. J. Coots, M. J. Brounikowski and R. H. Grubbs, *J. Am. Chem. Soc.* 1986, **108**, 1427.
40. E. B. Lobkovskii, G. L. Soloveichik, A. I. Sizov and B. M. Bulychev, *J. Organomet. Chem.* 1985, **280**, 53.
41. A. I. Sizov, I. V. Molodnitskaya, B. M. Bulychev, V. K. Belskii, E. V. Evdokimova and G. L. Soloveichik, *Metalloorg. Khim.*, in press.
42. E. B. Lobkoskii, A. N. Chekhlov, C. Ya. Knyazhansky, B. M. Bulychev and G. L. Soloveichik, *Metalloorg. Khim.*, in press.
43. E. B. Lobkovskii, A. I. Sizov, B. M. Bulychev, I. V. Sokolova and G. L. Soloveichik, *J. Organomet. Chem.* 1987, **319**, 69.
44. R. A. Forder and K. Prout, *Acta Cryst.* 1974, **B30**, 2312.
45. S. J. Pettig, A. Storr, B. S. Thomas and J. Troffer, *Acta Cryst.* 1974, **B30**, 666.
46. F. Ossola, N. Brianese, N. Porchia, G. Rosseto and P. Zanella, *J. Organomet. Chem.* 1986, **310**, C1.
47. A. R. Barron and G. Wilkinson, *J. Chem. Soc., Dalton Trans.* 1986, 287.
48. D. C. Ayres and R. Sewdays, *J. Chem. Soc.* 1971, C44.

49. M. Antberg, L. Dahlenburg, K.-M. Frosin and N. Hock, *Chem. Ber.* 1988, **121**, 859.
50. C. Ya. Knyazhansky, V. K. Belskii, B. M. Bulychev and G. L. Soloveichik, *Metalloorg. Khim.*, in press.
51. H. Marquet-Ellis and G. Folcher, *J. Organomet. Chem.* 1977, **131**, 247.
52. A. R. Barron and G. Wilkinson, *Polyhedron* 1986, **5**, 1897.
53. R. Dautel and W. Zeil, *Z. Electrochem.* 1960, **64**, 1234.
54. A. E. Shilov, A. K. Zefirova and N. N. Tikhomirova, *Zh. Fiz. Khim.* 1959, **33**, 2113.
55. V. V. Saraev and F. K. Shmidt, *Electronic Paramagnetic Resonance of Metal Complex Catalysts* (in Russian). Irkutsk, Gosuniversitet (1985).
56. J. K. Buff and M. F. Howthorne, *J. Am. Chem. Soc.* 1960, **82**, 2141.
57. D. C. Hendricker and C. W. Heitch, *J. Phys. Chem.* 1967, **71**, 2683.
58. G. S. Schomburg and E. G. Hoffman, *Z. Electrochem.* 1957, **71**, 2683.
59. F. G. Bordell and M. J. Bausch, *J. Am. Chem. Soc.* 1983, **105**, 6188.
60. T. M. Arkhireeva, B. M. Bulychev, T. A. Sokolova, G. L. Soloveichik, V. K. Belskii and G. N. Boiko, *Inorg. Chim. Acta* 1988, **141**, 221.
61. A. R. Barron, J. E. Salt and G. Wilkinson, *J. Chem. Soc., Dalton Trans.* 1986, 1329.
62. J. Ortiz and R. Hoffman, *Inorg. Chem.* 1985, **24**, 2095.
63. H. Nakanish, W. Jones, J. M. Thomas, M. B. Hursthouse and M. Motevalli, *J. Chem. Soc., Chem. Commun.* 1980, 611.
64. F. N. Tebbe, *J. Am. Chem. Soc.* 1973, **95**, 5412.
65. D. A. Lemenovskii, I. F. Urazovskii, I. E. Nifant'ev and E. G. Perevalova, *J. Organomet. Chem.* 1985, **292**, 217.
66. W. J. Evans, J. H. Meadows and A. L. Wayda, *J. Am. Chem. Soc.* 1982, **104**, 2015.
67. V. K. Belskii, I. V. Sokolova, B. M. Bulychev and A. I. Sizov, *Zh. Strukt. Khim.* 1987, **28**, 187.
68. A. V. Aripovsky and B. M. Bulychev, *Zh. Neorg. Khim.* 1984, **25**, 2191.
69. V. M. Ischenko, G. L. Soloveichik, B. M. Bulychev and T. A. Sokolova, *Zh. Neorg. Khim.* 1984, **29**, 119.
70. M. L. H. Green, L. Pratt and G. Wilkinson, *J. Chem. Soc.* 1958, 3916.
71. R. A. Forder, M. L. H. Green, R. E. McKensie, J. C. Pland and K. Prout, *J. Chem. Soc., Chem. Commun.* 1973, 426.
72. B. M. Bulychev, S. E. Tokareva, G. L. Soloveichik and E. V. Evdokimova, *J. Organomet. Chem.* 1979, **179**, 263.
73. V. V. Gavrilenko, L. A. Chekulaeva, V. A. Antonovich and L. I. Zakharkin, *Izv. AN SSSR, Ser. Khim.* 1987, 969.
74. P. C. Wailes and H. Weigold, *J. Organomet. Chem.* 1970, **24**, 406.
75. S. Ya. Knyazhansky, B. M. Bulychev and G. L. Soloveichik, *Metalloorg. Khim.*, in press.
76. P. Jutzi, *Adv. Organomet. Chem.* 1986, **26**, 217.
77. B. M. Bulychev, E. V. Evdokimova, A. I. Sizov and G. L. Soloveichik, *J. Organomet. Chem.* 1982, **239**, 313.
78. D. V. Sokolsky and N. F. Noskova, *Katalizatory Tipa Ziegler-Natta V Reaktsii Hydrirovania.* Alma-Ata (1977).
79. G. Henrici-Olive and S. Olive, *Coordination and Catalysis.* New York (1977).
80. B. M. Bulychev, A. L. Kostenko, G. L. Soloveichik and V. B. Polyakova, *Transition Met. Chem.* 1981, **6**, 240.
81. K. Mach, H. Antropiusova and V. Hanus, *Transition Met. Chem.* 1985, **10**, 302.
82. F. K. Schmidt, *Kataliz Kompleksami Metallov Pervogo Perekhodnogo Ryada Reaktsii Hydrirovania i Dimerizatsii.* Irkutsk, Gosuniversitet (1986).
83. T. J. Marks, *Pat. USA 4716257.*
84. B. M. Bulychev, G. L. Soloveichik, V. K. Belskii and A. I. Sizov, *Metalloorg. Khim.* 1989, **2**, 92.
85. E. V. Evdokimova, G. L. Soloveichik and B. M. Bulychev, *Kinet. Katal.* 1981, **22**, 170.
86. L. M. Enhelhardt, W. P. Leung, C. L. Raston and A. H. White, *J. Chem. Soc., Chem. Commun.* 1983, 386.
87. A. K. Zefirov, N. N. Tikhomirova and A. E. Shilov, *Dokl. AN SSSR* 1960, **132**, 1082.

Polyhedron Vol. 9, No. 2/3, pp. 409–427, 1990
Printed in Great Britain

0277-5387/90 $3.00+.00
Pergamon Press plc

STRUCTURES AND DYNAMIC PROPERTIES OF ALUMINIUM–GROUP 16 DERIVATIVES

JOHN P. OLIVER* and RAJESH KUMAR

Department of Chemistry, Wayne State University, Detroit, MI 48202, U.S.A.

CONTENTS

1. INTRODUCTION 409

2. THREE-COORDINATE ALUMINIUM DERIVATIVES 410

3. $R_3Al \cdot ER'_2$ ADDITION COMPOUNDS 411

4. BRIDGED DERIVATIVES 414

5. THIOLATES 419

6. FIVE-COORDINATE ALUMINIUM DERIVATIVES 421

7. SIX-COORDINATE ORGANOALUMINIUM COMPOUNDS 424

REFERENCES 426

1. INTRODUCTION

The chemistry of organoaluminium compounds which contain either a group 15 or 16 element has been under investigation for many years. The earlier work has been extensively reviewed by Mole and Jeffery,[1] Eisch,[2] Bradley,[3] and Oliver.[4,5] A very extensive discussion of exchange processes, including those of the group 13 elements has been presented by Matteson.[6] The group 15 containing derivatives of aluminium and the heavier group 13 metals have come under intensive investigation for the past several years because of the interest in 13–15 semiconductor material. The 13–16 compounds, on the other hand, have received only modest attention. The recent recognition that the 13–16 compounds may serve as precursors for ceramic materials, as models for aluminium oxide catalysts, and in applications for regio- and stereoselective organic synthesis has led to a renewed interest in the synthesis and characterization of these derivatives.

This short review is not intended to be comprehensive, but will emphasize the structures and exchange reactions of these derivatives. We hope to outline some of the past observations and provide new information based on our recent work, much of which has not yet appeared in the literature. With these data in hand, we will then discuss some of the future directions anticipated for work on 13–16 compounds.

There are several general classes of derivatives to be discussed: (1) three-coordinate species; (2) simple four-coordinate $R_3Al \cdot ER'_2$ addition compounds; (3) bridged four-coordinate derivatives of the general form $[R_2Al(-\mu-ER')]_2$; (4) compounds containing five-coordinate aluminium; and (5) compounds with six-coordinate aluminium. Further, under each of these broad classifications, both structural studies and exchange processes will be discussed.

* Author to whom correspondence should be addressed.

2. THREE-COORDINATE ALUMINIUM DERIVATIVES

The formation of electron deficient three-coordinate organoaluminium compounds has been invoked in many cases to account for the reactivity of these derivatives. Until recently, the only structural data for the three-coordinate derivatives was that obtained by Haaland and co-workers for Me_3Al in the gas phase.[7] Recent studies have shown that species can be stabilized in this configuration by the use of suitable bulky ligands such as mesityl,[8] BHT (2,6-di-*t*-butyl-4-methylphenoxide),[9] or bis(trimethylsilyl)amide.[10] Two of the known structures are depicted below. In the trimesityl derivative no secondary interaction with the ligands should occur. Thus, providing suitable ligands are available, addition compounds should form. This is the case with both THF and 4-picoline forming stable addition compounds.

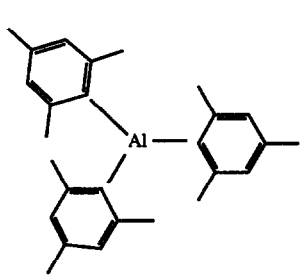

I

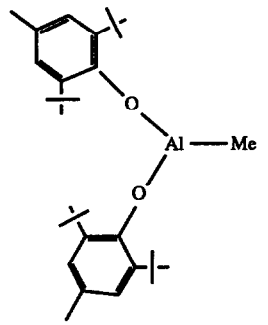

II

The structures of these three-coordinate derivatives show some distortion with a support for modest steric interference between the base and the mesityl group. With the BHT and bis(trimethylsilyl)amide derivative, delocalization of electron density from the oxygen (nitrogen) might be expected. The extent of the delocalization will depend on several factors, including the separation of the atoms, the relative energies of the orbitals involved in bond formation, and the orientation of the orbitals. These mesomeric effects in the alkoxide, as illustrated in **III**, should be reflected in

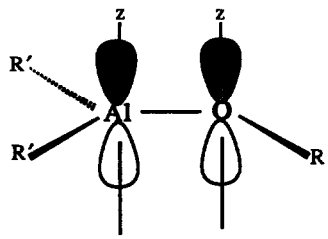

III

two ways; first, the Al—O bond should decrease in length as the electron delocalization increases, and second, the formation of addition compounds should become less favourable with the increasing electron delocalization.

Several structures of BHT derivatives have appeared in the literature. In the $MeAl(BHT)_2$ monomer, the Al—O bond distance is short in comparison with other Al—O distances which supports the proposed interaction between the π-electrons on the oxygen and the vacant *p*-orbital of aluminium (compare data in Tables 1 and 2). It should be noted, however, that aluminium BHT derivatives readily form addition compounds in which the aluminium has become four-coordinate, precluding the back donation of electron density from the oxygen to the aluminium. Furthermore, the Al—O bond distance increases only slightly with addition compound formation and remains less than that observed in many Al—O bonded compounds. Both the ease of formation of the addition compounds and the limited increase in the Al—O bond distance on adduct formation are indicative of limited back donation.

Only one significant NMR study has been reported which involves these compounds.[9] In this study it was demonstrated that there is an equilibrium between *mono* and *di* BHT species in solution.

This equilibrium is depicted in eq. (1) with all four species in the equilibrium mixture observed:

$$Al_2R_6 + RAl(BHT)_2 \rightleftharpoons R_2AlBHT + R_5Al_2BHT. \quad (1)$$

Further, it was noted that the simple alkylaluminium dimers such as Al_2Me_6 undergo very fast exchange with the R_2AlBHT derivative, but that exchange is relatively slow on the NMR time scale for the $RAl(BHT)_2$ species. It appears that this may be accounted for in terms of the ease of bridge formation with the BHT containing compound. With only one BHT group present, alkyl bridged dimers can form, providing a path for exchange, but with two BHT moieties present, formation of the bridged intermediate becomes far more difficult and slows the exchange process. Additional studies in this area seem warranted because of the interest in the use of these species in catalytic processes and for stereo-controlled synthesis. A better understanding, both of the structures and of the reaction mechanisms of these sterically hindered derivatives, is required in order to establish the role played by the bulky ligands in these systems.

The third class of three-coordinate aluminium compounds is that containing a direct Al—Al bond. Only one compound of this type, shown in **IV**, has been characterized by X-ray crystallography.[11] Other Al—Al bonded compounds have been described which are stabilized with bulky ligands.[12]

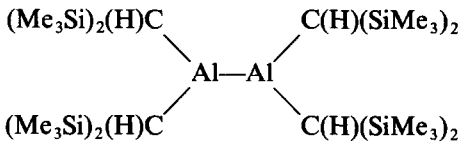

IV

The formation of these species once again illustrates the ability of sterically demanding ligands to stabilize highly reactive species.

Studies on three-coordinate compounds in the future will go in at least two directions, the exploration of alkoxides, and perhaps other species containing group 15 or 16 elements bound to the aluminium atom, for use in catalysts and materials precursors and, second, the study of compounds containing Al—Al bonds to explore the chemistry of this metal–metal bond.

3. $R_3Al \cdot ER'_2$ ADDITION COMPOUNDS

The $R_3Al \cdot ER'_2$ addition compounds can be represented by the generalized structure shown in **V**. The Al—E bond is best described in terms of a simple donor–acceptor bond with the aluminium

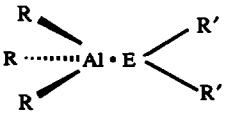

V

atom seving as the Lewis acid site and E serving as the Lewis base. The chemistry of these complexes is best represented in terms of the simple dissociative process shown in eq. (2). The reactivity of these compounds is associated with the free trialkylaluminium derivative formed and is therefore determined by the ease of dissociation of the complex.

$$R_3Al \cdot ER'_2 \rightleftharpoons R_3Al + ER'_2 \quad (2)$$

The structures, the stability of the addition compounds, and their dissociation/exchange have been studied. The most significant factor is the nature of E, with the stability of the compounds formed following the order N > P ≥ O > S > Se > Te based on the reaction of the methyl derivatives, Me_nE, with trimethylaluminium. This order may be altered when other ligands are present, either on the aluminium or on the Lewis base. Thus, the energy for the formation of the adduct $Me_3Al \cdot$ Base falls from approximately 100 to 50 kJ mol^{-1} on going from Me_2O to Bu_2O.[2] Similar qualitative observations have been made for a number of derivatives but only limited quantitative data are available. These have been summarized in refs 1 and 2.

The structures of a variety of simple adducts have been determined and are listed in Table 2 for the ether derivatives and in Table 3 for the sulphur complexes. No structures for selenium compounds

Table 1. Bond distances and angles in three-coordinate organoaluminium compounds

Compound	Al—C (Å)	Al—O (Å)	Al—N (Å)	Al—Al (Å)	C—Al—C (°)	C—Al—O (°)	O—Al—O (°)	Reference
Mes_3Al	1.995	—	—	—	120	—	—	8
Me_3Al	1.957	—	—	—	120	—	—	7
$MeAl(BHT)_2$	1.927	1.686	—	—	—	123.7	111.9	9
$Al[N(SiMe_3)_2]_3$	—	—	1.78	—	—	—	120 (N—Al—N)	10
$Al_2(C(H)(SiMe_3)_2)_4$	1.982	—	—	2.660	116.7	116.1–127.1 (Al—Al—C)	—	11

BHT = 2,6-di(*t*-butyl)-4-methylphenoxide.

Table 2. Selected average bond distances and angles in monomeric four-coordinate organoaluminium compounds containing oxygen donor ligands

Compound	Al—O (Å)	Al—C (Å)	C—Al—C (°)	C—Al—O (°)	Reference
$Mes_3Al \cdot THF$	1.969	2.017	116.2	101.5	*a*
$Mes_2(Et)Al \cdot THF$	1.934	2.003	114.9	—	*b*
	—	—	120.8 (Mes—Al—Mes)		
$Mes_2(Cl)Al \cdot THF$	1.890	1.992	124.8	105.6	*b*
$Me_3Al \cdot OMe_2$ (gas)	2.014	1.976	117.8	98.7	*c*
$Me_3Al \cdot \overline{OCH_2CH_2CH_2}$ (gas)	2.03	1.965	117.7	98.8	*d*
$(o\text{-Tol})_3Al \cdot OEt_2$	1.928	1.990	114.4	103.8	*e*
$(PhCH_2)_3Al \cdot OEt_2$	1.901	1.986	113.0	105.6	*f*
$Et_2AlBHT \cdot MeC_6H_4CO_2Me$	1.749	1.964	116.4	115.7	*g*
	1.887 (ester)	—	—	101.8	
$Ph_2[(Me_3Si)_3Si]Al \cdot THF$	1.927	1.985	114.8	103.2	*h*
$[Cl_3Al]_2 \cdot [\{Ph_2P(O)\}_2CH_2]$	1.956	—	—	—	*i*
$[Me_3Al]_2 \cdot p$-dioxane	2.02	1.96	116.6	100.8	*j*

$[\{(Me_3Al)_2\}\{dibenzo\text{-}18\text{-}crown\text{-}6\}]$	1.967	1.960	115.5	102.4	[k]
$[\{(AlMe_2)_4\}\{15\text{-}crown\text{-}5\}]$	2.005	1.93	115.9	101.8	[k]
	2.005	1.95	116.2	101.4	—
$Me_2AlBHT \cdot PMe_3$	1.736	1.970	111.7	117.5	[l]
$[\{Me_3NH\}\{Me(Cl)_2AlBHT\}]$	1.713	1.995	—	117.2	[l]
$Al(OSiPh_3)_2(Acac)$	1.796, 1.690	—	—	—	[m]
$K[Me_2Al(OPh)_2]$	1.800	1.968	119.4	108.7	[n]
$[K \cdot dibenzo\text{-}18\text{-}crown\text{-}6][Al_2Me_6OPh]$	1.89	2.01	112.1	108.9	[n]
$[(AlMe_3)_2\{N,O\text{-}(MeN{=}C(Ph)C{-}(Ph){=}O\}]$	1.983	1.954	115.4	101.5	[o]
$[(Al_2Me_5)\{(t\text{-}Bu)N{=}CHC(Me)_2O\}]$	1.868	1.951	115.1	108.7	[o]
$[Me_2AlOC(Ph){=}N(Ph)] \cdot ONMe_3$	1.770/1.826	1.962	117.3	108.1	[p]

BHT = 2,6-di(*t*-butyl)-4-methylphenoxide.

[a] Reference 13.

[b] Reference 14.

[c] A. Haaland, S. Samdal, O. Stokkeland and J. Weidlein, *J. Organomet. Chem.* 1977, **134**, 165.

[d] L. Fernholt, A. Haaland, M. Hargittai, R. Seip and J. Weidlein, *Acta Chem. Scand.* 1981, **A35**, 529.

[e] M. Barber, D. Liptak and J. P. Oliver, *Organometallics* 1982, **1**, 1307.

[f] A. F. M. Rahman, K. F. Siddiqui and J. P. Oliver, *J. Organomet. Chem.* 1987, **319**, 161.

[g] Reference 9.

[h] M. L. Sierra, V. S. J. de Mel and J. P. Oliver, *Organometallics* 1989, **8**, 2312.

[i] S. A. Sangokoya, B. Lee, M. F. Self, W. T. Pennington and G. H. Robinson, *Polyhedron* 1989, **8**, 1497.

[j] J. L. Atwood and G. D. Stucky, *J. Am. Chem. Soc.* 1967, **89**, 5362.

[k] J. L. Atwood, D. C. Hrncir, R. Shakir, M. S. Dalton, R. D. Priester and R. D. Rogers, *Organometallics* 1982, **1**, 1021.

[l] M. D. Healy, D. A. Wierda and A. R. Barron, *Organometallics* 1988, **7**, 2543.

[m] M. F. Garbauskas, J. H. Wengrovius, R. C. Going and J. S. Kasper, *Acta Cryst.* 1984, **C40**, 1536.

[n] M. J. Zaworotko, C. R. Kerr and J. L. Atwood, *Organometallics* 1985, **4**, 238.

[o] M. R. P. van Vliet, G. van Koten, M. A. Rotteveel, M. Schrap, K. Vrieze, B. Kojić-Prodić, A. L. Spek and A. J. M. Duisenberg, *Organometallics* 1986, **5**, 1389.

[p] Y. Kai, N. Yasuoka, N. Kasai and M. Kakudo, *Bull. Chem. Soc. Jpn* 1972, **45**, 3388.

Table 3. Selected bond distances in organoaluminium thioether derivatives

Compound	Al—S (Å)	Al—C (Å)	C—Al—C (°)	S—Al—C (°)	Reference
$(Me_3Al)(12)aneS_4$	2.718(3)	1.949 (av)	119.8	88.7–98.6	[a]
$(Me_3Al)_4(14)aneS_4$	2.522	1.954(6)	—	—	[b]
$(Me_3Al)_4(12)aneS_4$	2.515	1.948	117.0	99.9	[c]
$Me_3Al \cdot SMe_2$ (gas phase)	2.55	1.985	118.9	98.8	[d]

[a] G. H. Robinson and S. A. Sangokoya, *J. Am. Chem. Soc.* 1988, **110**, 1494.
[b] G. H. Robinson, H. Zhang and J. L. Atwood, *Organometallics* 1987, **6**, 887.
[c] S. A. Sangokoya, B. Lee, W. T. Pennington and G. H. Robinson, *J. Coord. Chem.* 1989, **19**, 331.
[d] L. Fernholt, A. Haaland, M. Hargittai, R. Seip and J. Weidlein, *Acta Chem. Scand.* 1981, **A35**, 529.

have been reported at this time. Careful examination of the data presented in Table 2 shows that the average Al—O bond distance observed in these derivatives is approximately 1.95 Å. There appears to be some modest bond shortening when a halogen is present, while slightly longer bonds are observed when two R_3Al units are bound to a polyether. There is a small but significant decrease in both the Al—O and Al—C bond lengths in the limited series of compounds $Mes_3Al \cdot THF$,[13] $Mes_2(Et)Al \cdot THF$[14] and $Mes_2(Cl)Al \cdot THF$.[14] This decrease in bond length can be attributed to two factors, a decrease in steric hinderance on substitution of a smaller group for the mesityl moiety and substitution of a better electron-withdrawing group for the mesityl unit which leads to a further decrease in bond length. When an alkoxide is present, substantial bond shortening is observed with bond distances in the range of 1.7–1.8 Å.

Another measure of the stability of these complexes is afforded by study of the exchange of ether with the addition compound. The exchange appears to go through a rate-determining dissociation step when excess aluminium alkyl is present or even when only the addition compound is in solution. This mechanism has been discussed extensively elsewhere.[4,6] In the presence of excess base, a bimolecular mechanism may become dominant as illustrated in eq. (3). Unfortunately, only very limited information is available from this type of study and even this is complicated by the additional reaction of R_3Al to form dimeric molecules, Al_2R_6.

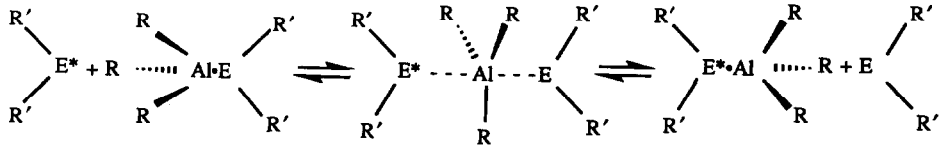

(3)

For the sulphur derivatives substantially less information is available. The structures are listed in Table 3. The Al—S bond distance observed in two addition compounds is 2.52 and 2.72 Å. Additional information needs to be obtained to provide a basis for comparison with adduct stability and to establish a better base for these systems. No quantitative exchange studies have been carried out on the thioether derivative, but exchange has been reported to be fast on the NMR time scale in keeping with the lower dissociation energy for these compounds.

Further examination of the simple addition compounds will be relatively limited. Structures of the complexes are well established, especially for the oxygen derivatives. Some studies on hindered complexes of the heavier group 16 derivatives and on complexes with unusual ligands could be justified. Further studies on exchange processes are also warranted to better establish the kinetic parameters for exchange, both in the presence of excess alkylaluminium and with excess base present. The major interest in these derivatives is likely to be in their use as precursors to other materials, especially where volatile, easily decomposed materials can be prepared.

4. BRIDGED DERIVATIVES

The reaction of an aluminium alkyl with an alcohol or thiol leads to the formation of an aluminium alkoxide or thiolate with alkane elimination as indicated in eq. (4):

$$nR_3Al + nR'EH \rightarrow (R_2AlER')_n + nRH. \quad (4)$$

The degree of aggregation, n, is dependent on the nature of E and on the groups R and R′.

The derivatives are typically dimeric for simple alkoxides as shown in **VI**, although $(Me_2AlOMe)_3$ forms a six-membered ring in a chair conformation[15] and higher aggregates with $n = 4$ have been reported in solution.[1,2] As noted in the previous section, monomers are formed when R or R′ becomes sufficiently bulky.

The Al_2O_2 ring system is normally planar, with this plane perpendicular to the plane described by the four R groups and the two aluminium atoms. Some modest deviations from this have been observed in sterically hindered species where the ring is distorted from the planar geometry. The bond distances and angles in selected four-coordinate derivatives containing aluminium–oxygen bonds are given in Table 4.

The stability of the Al—O—Al bridge is quite high with values for the Al—O—Al bond energy

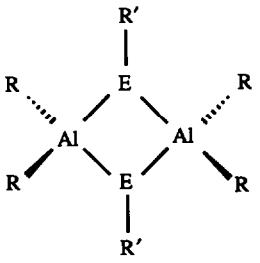

VI

typically in the range of 80–150 kJ mol^{-1}, thus making it difficult to disrupt this bond. Earlier studies established a lower limit of 131.5 kJ mol^{-1} for the Al—O—Al bridge bond in $[Al(O\text{-}i\text{-}Pr)_3]_4$,[16] which is in mid-range for these bridge bond energy. The stability of these bonds inhibits the interchange between bridge and terminal sites. Further, in the monomer–dimer equilibrium shown in eq. (5), the dimer is predominant in most cases. Formation of a larger ring system is not

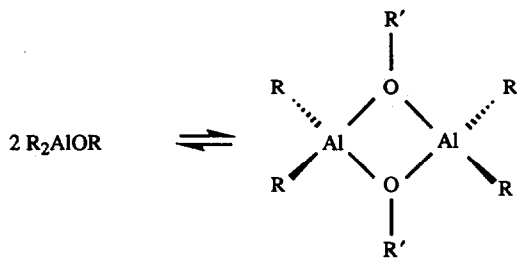

(5)

common since little additional energy of stabilization is gained, and the entropy change for the formation of larger aggregates is unfavourable. The reactions of alkoxides are typically dependent on the dimer concentration, and the compounds tend to be far less reactive than those of more readily dissociated species. Another manifestation of the strength of the alkoxide bridge is shown by the difficulty in disruption of the bridge by a base. Thus, the equilibrium for the reaction shown in eq. (6) typically lies far to the left with the alkoxide bridged dimer favoured. This indicates that

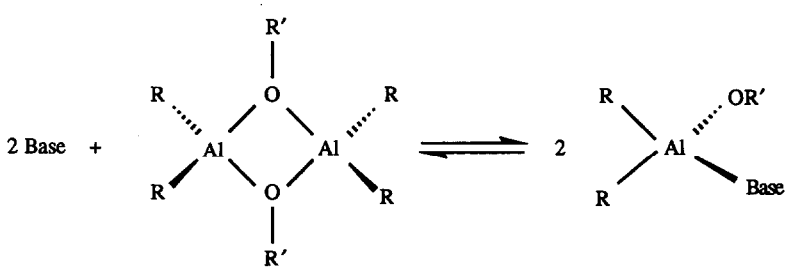

(6)

the alkoxide oxygen bound to the aluminium atom serves as a stronger Lewis base than the ether molecule. An alternative way to view this is that the energy provided from the formation of two $R_2(R'O)Al \cdot$ Base molecules is less than that derived from the formation of two Al—O—Al bridge bonds. Again, it should be noted that the entropy change is favourable for the last process as well.

An interesting feature that is readily observed because of the stability of the Al—O—Al bridge is the formation of *syn* and *anti* conformers. Both forms have been observed in the solid state and

Table 4. Selected bond distances and angles in dimeric four-coordinate organoaluminium alkoxides

Compound	Al—O (Å)	Al—C (Å)	Al—Al (Å)	C—Al—C (°)	O—Al—O (°)	Al—O—Al (°)	Reference
$[Me_2Al(l\text{-borneolate})]_2$	1.837	1.949	2.779	122.3	82.0	99.4	[a]
$[Me_2Al(l\text{-mentholate})]_2$	1.841	1.963	2.807	118.7	80.6	98.0	[a]
$[Me_2Al(2\text{-allyl-6-}MeC_6H_3O)]_2$	1.858	1.946	2.866	115.4	79.1	100.9	[b]
$[Et_2Al(2\text{-allyl-6-}MeC_6H_3O)]_2$	1.862	1.951	2.865	117.0	79.3	100.7	[c]
$[Me_2Al(O\text{-}t\text{Bu})]_2$ (gas)	1.864	1.962	2.82	121.7	81.9	98.1	[d]
$[AsMe_4]_2[Me_2AlOAlMe_3]_2$	1.79	—	—	—	—	96.0	[e]
$[Al_2(OSiMe_3)_4(Acac)_2]$	1.788	—	—	—	86.8	97.4	[f]
$[Me_2AlOMe]_3$ (gas phase)	1.851	1.957	—	117.3	103.2	125.8	[g]

[a] Reference 20.

[b] Reference 17.

[c] M. Barber, V. S. J. de Mel, R. Kumar and J. P. Oliver, unpublished results.

[d] A. Haaland and O. Stokkeland, *J. Organomet. Chem.* 1975, **94**, 345.

[e] J. L. Atwood and M. J. Zaworotko, *J. Chem. Soc., Chem. Commun.* 1983, 302.

[f] J. H. Wengrovius, M. F. Garbauskas, E. A. Williams, R. C. Going, P. E. Donahue and J. F. Smith, *J. Am. Chem. Soc.* 1986, **108**, 982. Note that there are four sets of Al—O distances: Al—$OSiMe_3$ terminal, 1.700 Å; Al—$OSiMe_3$ bridge to four-coordinate aluminium, 1.788 Å; Al—$OSiMe_3$ bridge to six-coordinate aluminium, 1.948 Å; and Al—O (Acac), 1.879 Å.

[g] Reference 15.

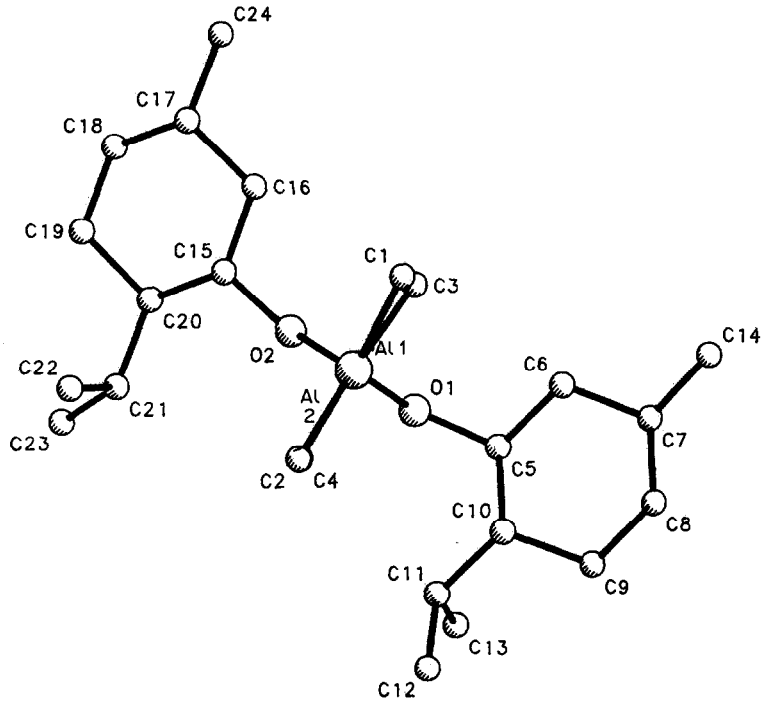

Fig. 1. A PLUTO diagram of tetramethyl-bis(μ-*l*-mentholato)dialuminium showing the *syn* configuration.

are illustrated by the *l*-menthol and *l*-borneol derivatives shown in Figs 1 and 2. The observation of these two conformations raises the question of their behaviour in solution. Recent variable-temperature NMR studies on a series of 2-methyl-6-allylphenoxide derivatives of aluminium clearly establish the presence of both *syn* and *anti* conformations in solution.[17,18] Further, the relative populations of the *syn* and *anti* forms are temperature dependent, giving a measure of the difference in energy of the two conformers. This is illustrated in Fig. 3 which shows the temperature dependent ^{1}H NMR spectrum of tetraethyl-bis(μ-2-allyl-6-methylphenoxy)dialuminium. The difference in populations of the two forms depicted in eq. (7) is very small with a ratio of 1 : 1.1 at −30°C and 1 : 1 at −75°C for the dimethylaluminium derivative. This shows the minor effects of the substituent groups both on the phenoxide and on the aluminium. One anticipates that, as the asymmetry of the substituents and their bulk increases, larger deviations will be observed. Studies are presently underway in our laboratory to assess some of these factors in more detail by examination of a number of related systems where the substituent on the aluminium has been modified.

A further point to be made is that *syn* and *anti* conformations interconvert through rotation of the bridging group without apparent disruption of the Al—O—Al bridge bond. The rotational

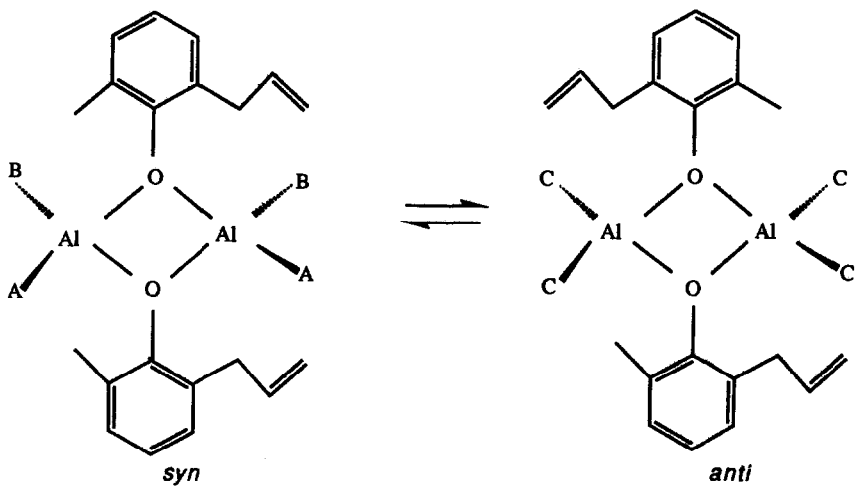

(7)

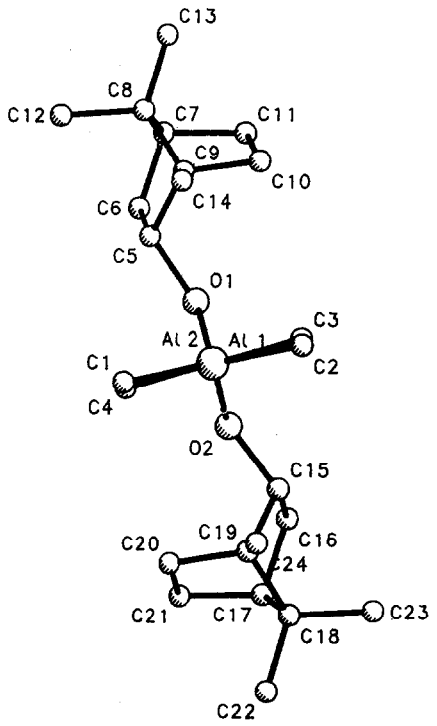

Fig. 2. A PLUTO diagram of the tetramethyl-bis(μ-*l*-borneolato)dialuminium showing the *anti* configuration.

barrier is in the range of 30–50 kJ mol^{-1},[18] which is clearly less than the energy required for disruption of the bridge bond, but of the same order of magnitude as reported for rotation of the bridging groups in tricyclopropylaluminium.[19] Further examination of the *l*-menthol and *l*-borneol derivatives cited earlier provides additional information on these systems. The ^{1}H NMR spectrum of the *l*-menthol derivatives shows the influences of the optically active centre on the terminal alkyl groups giving rise to diastereotopic protons. Variable-temperature NMR studies show that the chemical shifts of the various groups are temperature dependent, but also indicate that over the

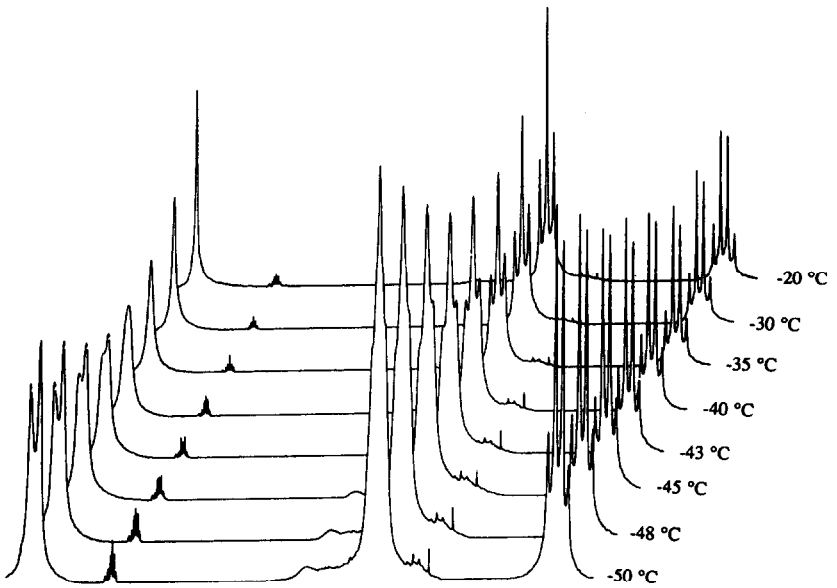

Fig. 3. Variable-temperature ^{1}H NMR spectra of tetraethyl-bis(μ-2-allyl-6-methylphenoxy) dialuminium. The region shown is for the 6-methyl group and the ethyl groups attached to aluminium.

temperature range studied, the protons remain diastereotopic. In contrast, the ^{1}H NMR spectrum of the *l*-borneol derivatives shows no effect from the optically active centre even as the temperature is decreased to −75°C. At the same time, no evidence for stable *syn* and *anti* conformers in these systems is indicated. The interpretation of these results is discussed in detail elsewhere,[20] but they appear to arise from two facts. First, the optically active centre in *l*-borneol is at a substantial distance from the alkyl groups attached to the aluminium and, second, the *l*-borneol group has a low barrier to rotation about the Al—O—Al bridge and O—C bonds, giving rise to rapid rotation on the NMR time scale even at low temperature. The *l*-menthol derivative is in close proximity to the alkyl groups attached to the aluminium, thus permitting interaction with the optically active centre in this moiety causing the protons on the alkyl groups to become diastereotopic. Rotation about the O—C and Al—O—Al bridge bond remains rapid on the NMR time scale, however, so *syn* and *anti* forms could not be observed.

5. THIOLATES

The chemistry of binary thiolato derivatives of aluminium compounds has not received significant attention. Structures of only three simple derivatives have been reported: the solid-state structure of $(Me_2AlSMe)_n$;[21] its structure in the gas phase where it is a dimer;[22] and the recently characterized $(Me_2AlSC_6F_5)_2$.[23]

There are three interesting features of these systems which should be commented upon. First, the Al—S—Al bridge bond distances range from 2.35 to 2.41 Å and are much shorter than the Al—S bond lengths observed for the adducts. The bond lengths and angles for all compounds containing direct aluminium to sulphur bonds are listed in Table 5. Second, the Al—S—Al bridge bonds are substantially weaker than the Al—O—Al bridge bonds. Thus, they can be readily cleaved or disrupted by ethers and amines as indicated in eq. (8). For example, the aluminium thiolate may react with aldehydes or esters via eq. (8) to yield the simple adduct followed by a rearrangement to yield the dialkylaluminium thioalkoxide shown in eq. (9).[23] One also should anticipate that monomer–dimer equilibria should be observed in these systems with monomers favoured with increasing size of the organic substituents. This has not been tested. Third, the Al_2S_2 ring system is puckered or butterfly shaped with the angle between the two planes described by Al—S(1)—Al and Al—S(2)—Al atoms near 150°. This deviation from planarity is substantial and clearly results from the substitution of sulphur for oxygen in the bridging site.

Table 5. Average bond distances in selected organoaluminium derivatives

Compound	Al—S (Å)	Al—C (Å)	Al—N (Å)	Reference
$(Me_2AlSMe)_n$	2.348(2)	1.944(7)	—	[a]
$(Me_2AlSMe)_2$ (gas phase)	2.370	1.945	—	[b]
$K(Me_3AlSCNAlMe_3)$	2.489(2)	1.971 (av)	1.951(5)	[c]
$(Al\textit{i}\text{-}Bu)_2[(C_6H_5)_2P(S)CP]^-$				
$(C_6H_5)_2(S)_2][Al\textit{i}\text{-}Bu_2]_2$	2.304	—	2.458 (AlP)	[d]
$Al_4I_4(SCH_3)_4S_2$	2.18 Å	—	—	[e]
	2.30 Å	—	—	
$Me_2Al(\mu\text{-}PyS)_2AlMe_2$	2.338(3)	1.981(6) (Al1—C)	1.993(4)	[f]
	—	1.965(5) (Al2—C)	—	
$[Me_2AlSC_6F_5]_2$	2.408	1.944	—	[g]

[a] Reference 21.
[b] Reference 22.
[c] R. Shakir, M. J. Zaworotko and J. L. Atwood, *J. Organomet. Chem.* 1979, **171**, 9.
[d] G. H. Robinson, M. F. Self, W. T. Pennington and S. A. Sangokoya, *Organometallics* 1988, **7**, 2424.
[e] A. Boardman, R. W. H. Small and I. J. Worrall, *Inorg. Chim. Acta*, 1986, **120**, L23.
[f] Reference 24.
[g] Reference 23.

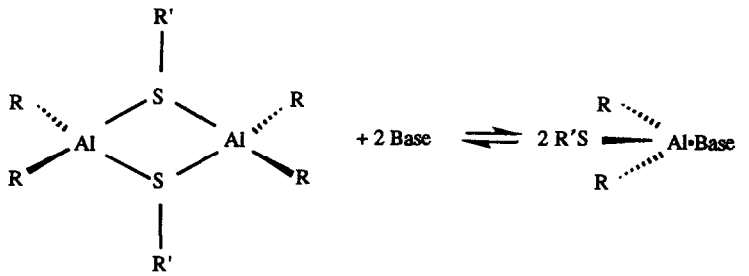

(8)

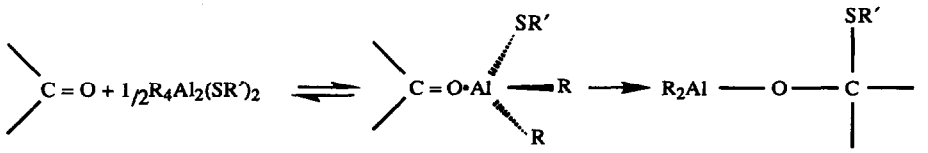

(9)

In addition to the simple derivatives discussed above, recent studies in our laboratory have shown that reaction of 2-thiopyridine with alkylaluminium compounds yield the dimeric molecule shown in **VII**.[24] The central core of this compound contains an $Al_2S_2C_2N_2$ ring with the bridging

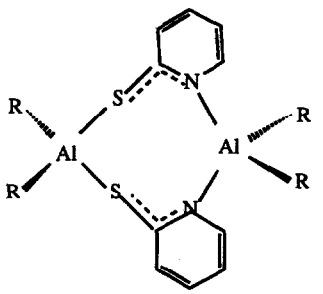

VII

2-thiolatopyridine ligand arranged in an unexpected head-to-head fashion. Further, variable-temperature NMR studies have established that the 2-thiopyridine ligand is fluxional on the NMR time scale. This exchange appears to involve some type of bridge reorganization with probable involvement of either the five-coordinate complexes shown in **VIII** or the uncoordinated dimer shown in **IX**, although other isomers may be participants in the rearrangement. These results show the wide

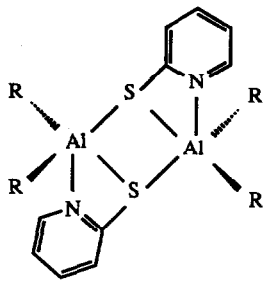

VIII

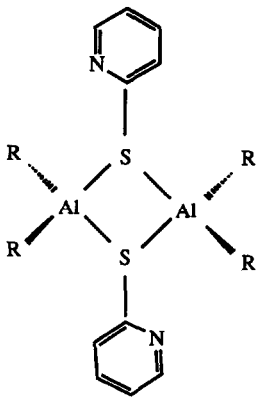

IX

range of possible structures for thiol derivatives of aluminium and of systems containing mixed ligands.

Additional studies on the simple bridged species will continue with interest in the effects of bridging groups on the reactivity of the bridged dimeric molecules, especially for use in asymmetric synthesis, and on the factors which control the conformations and barriers to exchange. Studies involving the heavier group 16 species will also become a focus of attention because of the renewed interest in formation of new materials for semiconductors and other applications.

6. FIVE-COORDINATE ALUMINIUM DERIVATIVES

Five-coordinate aluminium derivatives have been proposed for a number of years, and structural evidence for species of this type has been reported by a number of groups with the compounds listed in Table 6. These compounds have two general structures, the first of which involves the coordination of the metal centre by several donor ligands from nitrogen-containing macrocycles[25–27] or crown ethers[28] as illustrated in **X** and **XI**. Other systems, which may be represented by the square pyramidal structure depicted in **X**, have been reported, and in one case the complex contains both four- and five-coordinate aluminium atoms.[27]

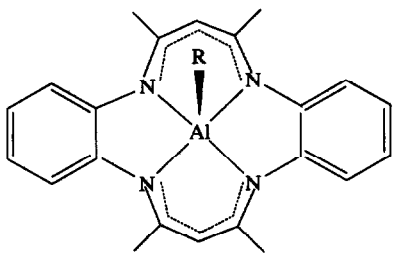

X

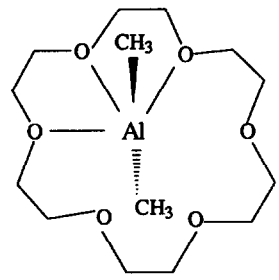

XI

The crown ether complexes show additional complexity with high coordination in the case of the 15-crown-5 complex which has the AlR_2 unit trapped in the central region with five oxygen atoms surrounding it in addition to the two methyl groups.[28]

Both the nitrogen and oxygen macrocyclic and polydentate acyclic ligands offer the potential for the formation of a variety of new complexes with unusual coordination around the aluminium. Little is known about the reactivity of these complexes, but it is anticipated that substantial differences between the reactivity of these complex species and other organoaluminium compounds will be observed. Further, introduction of other hetero-atoms can lead to additional changes in structure and reactivity. Thus, there is a new area of chemistry to explore on the organoaluminium complexes formed with macrocyclic and polydentate acyclic ligands. Studies on the ease of exchange and reactivity of these species seem very promising in terms of new reagents which may offer methods for control of the reaction path.

At this writing, several such complexes have already been described by Goedken,[25] by Robinson *et al.*,[26,27] and by Atwood *et al.*[28] These represent the majority of simple cationic organoaluminium derivatives. Further exploration of their chemistry appears to be very promising since they provide relatively stable cationic aluminium species with active alkyl groups which may be used in reactions.

The second class of five-coordinate compounds has been studied by several groups including our own and is best represented by structures of the type shown in **XII**. Examples have been reported

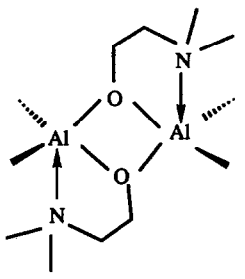

XII

in which the bridging site is occupied by either oxygen or nitrogen. Similarly, the secondary coordination illustrated in **XII** could be occupied in principle by any Lewis base. In practice, only nitrogen and oxygen have been observed to form stable complexes of this type, but it seems likely that sulphur and phosphorus will also be found to participate in structures of this type under suitable conditions.

Table 6. Average bond distances and angles in selected five-coordinate organoaluminium compounds containing nitrogen and oxygen donor ligands

Compound	Al—O (Å)	Al—C (Å)	Al—N (Å)	C—Al—C (°)	O—Al—O (°)	Al—O—Al (°)	Reference
$[Me_2Al(l\text{-ephdrinato})]_2$	1.905	1.994	2.193	118.5	74.8	104.0	[a]
$[Me_2AlPCH_2C_4H_7O\text{-}2]_2$	1.851/2.221	1.940/2.024	—	123.7	74.8	—	[b]
$[Et_2Al(isolucinoato)]_2$	1.92	2.02	2.199	117.8	76.8	102.9	[c]
$[Et_2Al(8\text{-quinolinoato})]_2$	1.932	1.958	2.131	122.5	72.6	107.4	[d]
$[(2\text{-methyl-8-quinolinolato})_2Al]_2O$	1.677 (μ-O)	—	2.085	—	120.1	178.0	[e]
	1.813	—	—	—	—	—	
$[AlMe][C_8H_{19}N_4][AlMe_2]$	—	—	1.826/1.987/2.135/2.055	—	—	—	[f]
$[AlMe]_2[C_8H_{20}N_6][AlMe_2]_2$	—	1.962	2.01	—	—	—	[g]
$[EtAlC_{22}H_{22}N_4]$	—	1.976	1.967	—	—	—	[h]
$[i\text{-}Bu_2AlOCH_2\text{-}2\text{-}C_5H_4N]_2$	1.894	1.994	—	119.1	74.1	105.9	[i]
$[Me_2AlO(CH_2)_2(OMe)]_2$	1.827	1.951	—	120.8	76.3	103.7	[j]
	2.269	—	—	—	158.3	—	
$[Me_2AlO(O)MeCHPhNPhC]_2$	1.921	1.964	—	119.4	73.3	105.3	[k]
	2.045 (adduct)	—	—	—	—	—	
$[AlMe_2[18]\text{-Crown-}6][AlCl_2Me_2]$	1.929/2.181/2.435	1.927 (cation)	—	140.6	—	—	[l]
	2.308	2.029	—	—	—	—	
$[MeAl][Ph_2P(O)CP(O)Ph_2]_2[AlMe_2]_2$	1.772	1.981	—	119.5	163.2	—	[m]
	2.174	1.994	—	—	—	—	
$[(Me_2Al)\{OC(Ph)=N(Ph)CH(Me)O\}]_2$	1.963	1.877	—	116.3	106.8	—	[n]

[a] M. L. Sierra, V. S. J. de Mel and J. P. Oliver, *Organometallics* 1989, **8**, 2486.
[b] M. L. Sierra, V. S. J. de Mel and J. P. Oliver, unpublished results.
[c] Reference 29.
[d] S. T. Dzugan and V. L. Goedken, *Inorg. Chim. Acta* 1988, **54**, 169.
[e] Y. Kushi and Q. Fernando, *J. Am. Chem. Soc.* 1970, **92**, 91.
[f] Reference 27.
[g] Reference 26.
[h] Reference 25.
[i] M. R. P. van Vliet, P. Buysingh, G. van Koten, K. Vrieze, B. Kojić-Prodić and A. L. Spek, *Organometallics* 1985, **4**, 1701.
[j] T. Benn, A. Rufińska, H. Lehmkuhl, E. Janssen and C. Krüger, *Angew. Chem. Int. Ed. Engl.* 1983, **22**, 779.
[k] Y. Kai, N. Yasuoka, N. Kasai and M. Kakudo, *Bull. Chem. Soc. Jpn* 1972, **45**, 3397.
[l] Reference 28.
[m] G. H. Robinson, B. Lee, W. T. Pennington and S. A. Sangokoya, *J. Am. Chem. Soc.* 1988, **110**, 6260.
[n] Y. Kai, N. Yasuoka, N. Kasai and M. Kakudo, *Bull. Chem. Soc. Jpn* 1972, **45**, 3397.

These complexes afford a variety of interesting features to explore. Among these are the potential for rearrangement from five- to four-coordinate complexes. This is illustrated by eq. (10) in which

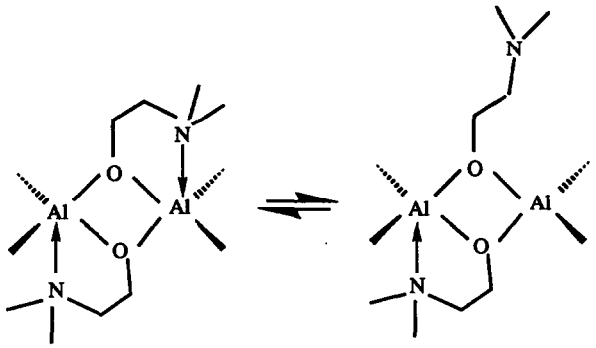

(10)

the second coordination site has undergone dissociation. This can be easily observed in the variable-temperature NMR spectra of complexes of this type. In the five-coordinate species the protons in the CH_2 units connecting the two coordination sites become diastereotopic giving rise to complex NMR spectra. On dissociation full rotation becomes possible, and this non-equivalence of the CH_2 groups disappears. This is shown qualitatively in Fig. 4 in which the methyl region of the ^1H NMR spectrum of tetramethyl-bis(μ-1*R*,2*S*)(−)-λ-(1-methylaminoethyl)benzylalkoxide dialuminium is shown as a function of temperature.[29] A detailed examination of a number of systems showing this type of behaviour is underway in our laboratory, but sufficient data have already been obtained to provide some insight into these systems.[30] We have found that the ease of dissociation is a function of the substituents on the nitrogen and on the aluminium centres, and the activation energies range from approximately 40 to 100 kJ mol^{-1} for the systems studied in our laboratory. Further, the energy of activation for the exchange is directly related to the heat of formation of the five-coordinate aluminium and provides a measure of the steric interactions between the substituent groups on the

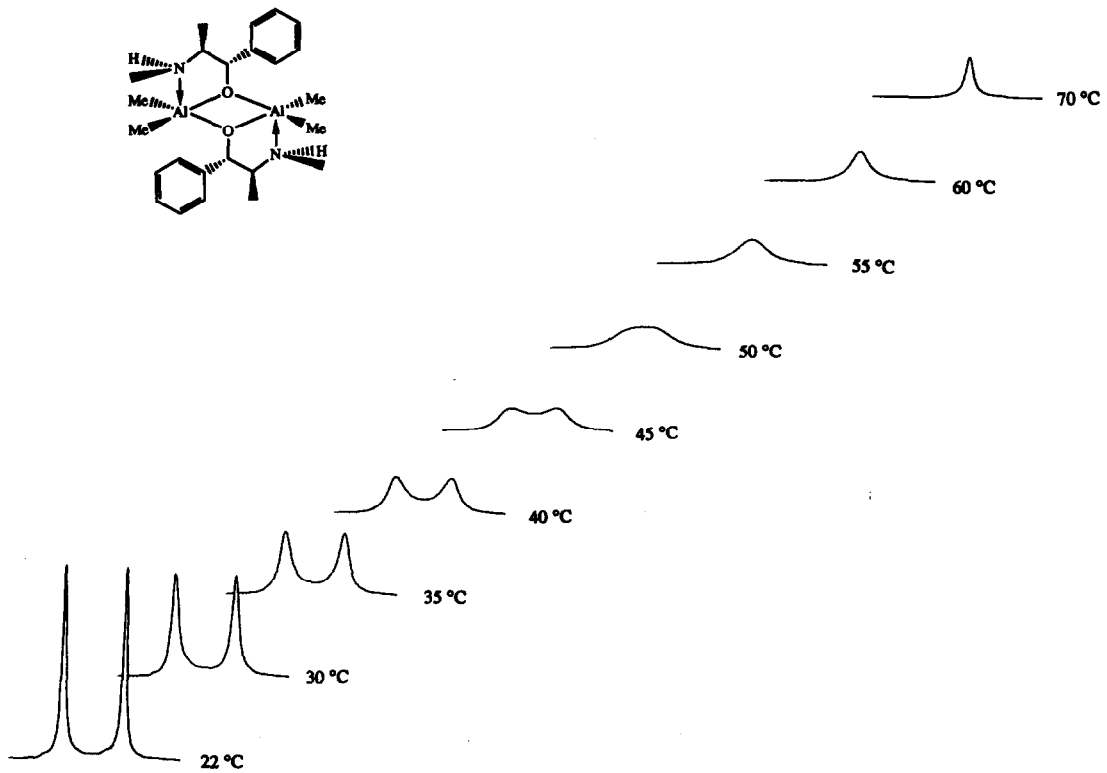

Fig. 4. A variable-temperature ^1H NMR spectrum of the Al–Me region of tetramethyl-bis(μ-1*R*,2*S*)-(−)-λ-(1-methylaminoethyl)benzylalkoxide dialuminium.

aluminium and on the coordination centre. Thus, it appears that the order of coordination is O > N > S, with the steric interactions playing an important role to reduce the activation energy when nitrogen is present. In fact, in our efforts to obtain other five-coordinate species containing a thiol ether, we have observed other classes of reactions occurring as noted in the section on six-coordinate complexes.

An additional feature of the five-coordinate aluminium complexes is that one may readily introduce optically active centres in the bridging ligands at the same time one causes the aluminium atom to become an optically active centre. Thus, both the ligand and the aluminium centre may be optically active. This feature makes use of these reagents in stereospecific synthesis particularly attractive. Further work is needed to establish the use of these complexes as reagents. At the same time, detailed studies of a number of these systems should provide substantial information on the reaction paths and make it possible to design specific reagents for reduction and/or alkyl transfer reagents.

7. SIX-COORDINATE ORGANOALUMINIUM COMPOUNDS

Until quite recently, the few six-coordinate aluminium derivatives known contained only bonds between the metal and electronegative atoms such as oxygen or nitrogen. Recently, however, several more complex species have been characterized which contain aluminium atoms bound to alkyl or silyl groups in addition to a central metal surrounded only by the electronegative groups. In two instances derivatives containing a carbon atom directly bonded to the six-coordinate aluminium atom have been observed. These derivatives, along with a number of those described earlier are listed in Table 7.

In all cases the six-coordinate aluminium atom is in an octahedral or pseudo-octahedral environment as shown in **XIII** surrounded by oxygen, nitrogen or carbon atoms from the ligands.

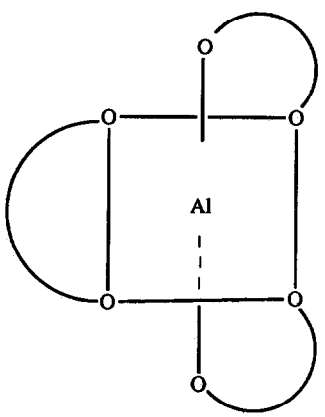

XIII

In the initial studies, the ligands were typically bidentate with two oxygen or nitrogen coordination sites. Complexes of this type remain of interest because of their potential use in biological systems,[31-33] but do not contain metal–carbon bonds. The second class of six-coordinate derivatives is made up of systems which contain aluminium in two different environments. These systems commonly have a central six-coordinate aluminium surrounded by three AlR_4^- groups which can be thought of as bidentate chelating ligands. This class of compounds has been illustrated by several of the species listed in Table 7 and was unexpectedly obtained.

Recently our research group has been exploring the reaction of bidentate ligands with R_3Al. The reaction of 2-thiophenemethanol and of furfuryl alcohol with R_3Al eliminates RH and presumably R_2AlOR'. The latter product then goes through a rearrangement process yielding the tetrameric complex with both four- and six-coordinate aluminium atoms shown in Fig. 5.[34] Compounds with similar structures have been obtained by other research groups using silylaluminium derivatives reacted with ammonia.[35] When tetrahydrofurfuryl is used rather than furfuryl, the reaction originally anticipated, i.e. the formation of a dimeric bridged molecule, occurred.[34] This suggests that the energy differences between the complex species observed for the furfuryl alcohol and

Table 7. Selected average bond distances (Å) and angles (°) in some six-coordinate organoaluminium and related derivatives

Compound	Al—O (Å)	Al—C (Å)	Al—N (Å)	Al—S (Å)	E—Al—E (°) (bite)	E—Al—E (°) (*trans*)	Reference
$(Tropolonato)_3Al$	1.888	—	—	—	83	171	[a]
$(Maltolato)_3Al$	1.904	—	—	—	90	—	[b]
$(Isomaltolato)_3Al$	1.889	—	—	—	94	176	[c]
$(dpp)_3Al \cdot 12H_2O$	1.908	—	—	—	84	172	[d]
$\{[Me_2Al]_3[\mu\text{-}2\text{-}(OCH_2)SC_4H_3]_6Al\}$	1.873	1.968	—	—	86	—	[e]
$[MeAl(PhNNNPh)_2 2,5\text{-}Me_2Py]$	—	1.999	2.071	—	—	153	[f]
$\{[MeAl][Me_2Al][(OCH_2CH_2)_3N]\}_2$	1.905	1.990	2.058	—	75	166	[g]
$\{[(OCH_2CH_2)_3N]Al\}_4$	1.855	—	2.069	—	75	166	[h]
$[(Me_3Si)_2Al(NH_2)_2]_3Al$	—	—	1.962	—	83	174	[i]
$Al(1\text{-}Et\text{-}3\text{-}OH\text{-}2\text{-}Me\text{-}4\text{-}Pyridone)_3$	1.912	—	—	—	84	173	[j]
$Al(S_2CNMe_2)_3$	—	—	—	2.395	75	164	[k]

dppH = 2-methyl-3-hydroxy-4-pyridinone.

[a] Reference 37.

[b] M. M. Finnegan, S. J. Rettig and C. Orvig, *J. Am. Chem. Soc.* 1986, **108**, 5033.

[c] Reference 31.

[d] Reference 32.

[e] Reference 34.

[f] Reference 38.

[g] Reference 39.

[h] V. E. Shklover, Y. T. Struchkov, M. G. Voronkov, Z. A. Ovchinnikova and V. P. Baryshok, *Dokl. Akad. Nauk. SSSR* 1984, **277**, 1185.

[i] Reference 35.

[j] Reference 33.

[k] Reference 36.

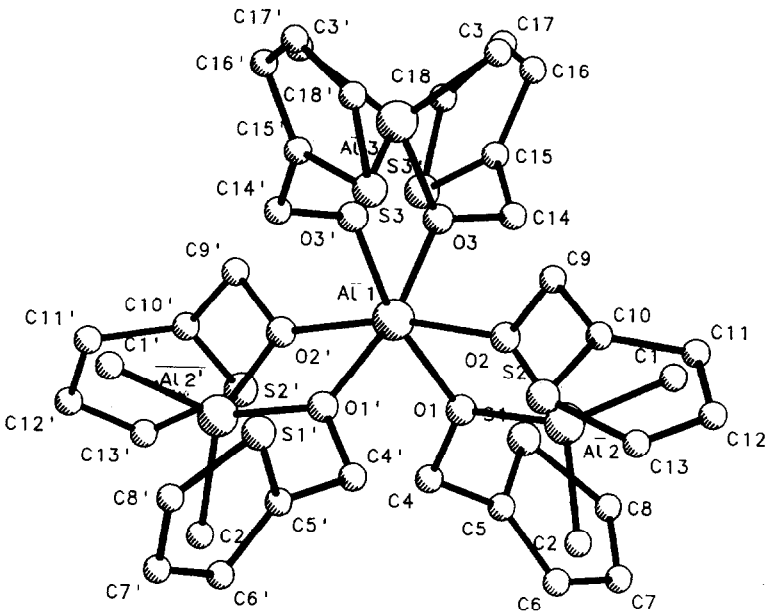

Fig. 5. A PLUTO diagram of $[(Me_2Al)_3(\mu\text{-}OCH_2C_4H_3S)_6Al]$.

2-thiophenemethanol and the tetrahydrofurfuryl alcohol are quite small. In the $(Et_2Al)_3(\mu\text{-}OCH_2C_4H_3S)_6Al$ derivative, the methylene protons are diastereotopic.[30] Variable-temperature NMR studies have established that exchange does not occur on the NMR time scale below 75°C, indicating that the complex does not undergo dissociation under these conditions. This is surprising in view of the rapid rearrangement observed for tris(tropolonato)aluminium(III) by Mutterties and Guggenberger some years ago.[37] It implies that the "bidentate" group $R_2Al(\mu\text{-}OR)_2$ forms stable bridges with the central aluminium atom, similar to those observed for other stable bidentate chelating groups.

Two other interesting compounds have been recently reported by Barron and co-workers.[38,39] The first is a relatively simple six-coordinate derivative with a methyl group directly attached to the aluminium atom which has five nitrogen atoms coordinated to fill out the coordination sphere, and the other is a tetramer which contains two types of aluminium centres, one bound to a single methyl group with four oxygen atoms and a nitrogen atom completing the coordination while the other aluminium is bound to two methyl groups and two oxygen atoms, giving a four-coordinate centre. Preparation of these systems indicates that other new and unusual products may be obtained and shows that even the limited effort that has gone into investigation of the higher coordinate organoaluminium compounds has been very fruitful.

Exploration of these higher coordinate organoaluminium derivatives seems likely to yield exciting new developments in several directions. First, the work of Rettig points out the potential use of some of the more stable compounds in biological systems. Second, the group of derivatives with aluminium in several coordination sites indicates the possibility of forming systems in which two or more metals are bound in close proximity to one another. This may allow for a more rational development of catalysts. Third, the formation of six-coordinate aluminium with direct carbon–aluminium bonds opens a whole new area to study.

REFERENCES

1. T. Mole and E. A. Jeffrey, *Organoaluminium Compounds*. Elsevier, Amsterdam (1972).
2. J. J. Eisch in *Comprehensive Organometallic Chemistry* (Edited by G. Wilkinson, F. G. A. Stone and E. W. Abel), Vol. 1, Ch. 6, pp. 555–683. Pergamon Press, Oxford (1982).
3. D. C. Bradley, *Adv. Inorg. Radio Chem.* 1972, **15**, 259; D. C. Bradley, R. C. Mehrotra and D. P. Gear, *Metal Alkoxides*. Academic Press, New York (1978).
4. J. P. Oliver, *Adv. Organomet. Chem.* 1970, **8**, 167.
5. J. P. Oliver, *Adv. Organomet. Chem.* 1977, **15**, 235.

6. D. S. Matteson, *Organometallic Reaction Mechanisms*. Academic Press, New York (1974).
7. A. Almenningen, S. Halvorsen and A. Haaland, *Acta Chem. Scand.* 1971, **25**, 1937.
8. J. J. Jerius, J. M. Hahn, A. F. M. M. Rahman, O. Mols, W. H. Ilsley and J. P. Oliver, *Organometallics* 1986, **5**, 1812.
9. A. P. Shreve, R. Mulhaupt, W. Fultz, J. Calabrese, W. Robbins and S. D. Ittel, *Organometallics* 1988, **7**, 409.
10. G. M. Sheldrick and W. S. Sheldrick, *J. Chem. Soc. A* 1969, 2279.
11. W. Uhl, *Z. Naturfor.* 1988, **43b**, 1113.
12. M. A. Miller and E. P. Schram, *Organometallics* 1985, **4**, 1362.
13. V. S. J. de Mel and J. P. Oliver, *Organometallics* 1989, **8**, 827.
14. J. Kampf, M. Lalama and J. P. Oliver, unpublished results.
15. D. A. Drew, A. Haaland and J. Weidlein, *Z. Anorg. Allg. Chem.* 1973, **398**, 241.
16. J. W. Wilson, *J. Chem. Soc. A*, 1971, 981.
17. R. Kumar, M. L. Sierra, V. S. J. de Mel and J. P. Oliver, *Organometallics* in press.
18. M. Barber, R. Kumar and J. P. Oliver, unpublished results.
19. D. A. Sanders, P. A. Scherr and J. P. Oliver, *Inorg. Chem.* 1976, **15**, 861; J. W. Moore, D. A. Sanders, P. A. Scherr, M. D. Glick and J. P. Oliver, *J. Am. Chem. Soc.* 1971, **93**, 1035.
20. M. L. Sierra, R. Kumar, V. S. J. de Mel and J. P. Oliver, *Organometallics* in press.
21. D. J. Brauer and G. D. Stucky, *J. Am. Chem. Soc.* 1969, **91**, 5462.
22. A. Haaland, O. Stokkeland and J. Weidlein, *J. Organomet. Chem.* 1975, **94**, 353.
23. R. Kumar and J. P. Oliver, unpublished results; V. S. J. de Mel, R. Kumar and J. P. Oliver, *Organometallics* in press.
24. R. Kumar, V. S. J. de Mel and J. P. Oliver, *Organometallics* 1989, **8**, 2488.
25. V. L. Goedken, H. Ito and T. Ito, *J. Chem. Soc., Chem. Commun.* 1984, 1453.
26. G. H. Robinson and S. A. Sangokoya, *J. Am. Chem. Soc.* 1987, **109**, 6852.
27. G. H. Robinson, S. A. Sangokoya, F. Moise and W. T. Pennington, *Organometallics* 1988, **7**, 1887.
28. S. G. Bott, A. Alvanipour, S. D. Morley, D. A. Atwood, C. M. Means, A. W. Coleman and J. L. Atwood, *Agnew. Chem. Int. Ed. Engl.* 1987, **26**, 485.
29. M. L. Sierra, V. S. J. de Mel and J. P. Oliver, unpublished results.
30. M. Barber, V. S. J. de Mel, R. Kumar, M. L. Sierra and J. P. Oliver, unpublished results.
31. T. G. Lutz, D. J. Clevette, S. J. Rettig and C. Orvig, *Inorg. Chem.* 1989, **28**, 715.
32. W. O. Nelson, T. B. Karpishin, S. J. Rettig and C. Orvig, *Inorg. Chem.* 1988, **27**, 1045.
33. W. O. Nelson, S. J. Rettig and C. Orvig, *Inorg. Chem.* 1989, **28**, 3153.
34. R. Kumar, V. S. J. de Mel, M. L. Sierra and J. P. Oliver, unpublished results.
35. J. F. Janik, E. N. Duesler and R. T. Paine, *Inorg. Chem.* 1988, **27**, 4335.
36. H. Nöth and P. Konrad, *Chem. Ber.* 1983, **116**, 3552.
37. E. L. Mutterties and L. J. Guggenberger, *J. Am. Chem. Soc.* 1972, **94**, 8046.
38. J. T. Leman and A. R. Barron, *Organometallics* 1989, **8**, 1828.
39. M. D. Healy and A. R. Barron, *J. Am. Chem. Soc.* 1989, **111**, 398.

Polyhedron Vol. 9, No. 2/3, pp. 429–453, 1990
Printed in Great Britain

0277–5387/90 $3.00+.00
© 1990 Pergamon Press plc

ALUMOXANES: SYNTHESIS, STRUCTURES, COMPLEXES AND REACTIONS

S. PASYNKIEWICZ

Faculty of Chemistry, Warsaw Technical University, Warsaw, Poland

CONTENTS

INTRODUCTION 429

SYNTHESIS 430
Reactions with water 430
Reactions with oxygen-containing compounds 431

STRUCTURE 431

REACTION MECHANISMS OF ORGANOALUMINIUM COMPOUNDS WITH WATER 438
R_3Al+H_2O, 2:1 system 438
R_3Al+H_2O, 1:1 system 441

COMPLEXES OF ALUMOXANES WITH ELECTRON DONORS 444

REACTIONS OF ALUMOXANES WITH ELECTRON DONORS 446
Ethers 446
Acetylacetone 447
Ketones 448
Amines 449
Nitriles 450

APPLICATION OF ALUMOXANES 451

REFERENCES 451

INTRODUCTION

By alumoxanes we understand species containing an oxygen bridge binding two aluminium atoms, Al—O—Al. Alkoxyaluminium compounds, R_2AlOR, having an oligomeric structure in which the aluminium atoms are bonded by the alkoxy group oxygen bridge Al—O(R)—Al will not be included in this paper. Any alkyl, aryl, halide alkoxy or other group can, however, be the pendent ligand bonded to the aluminium atoms.

Alumoxanes, obtained from the reactions of organoaluminium compounds and water, were extensively studied in the 1960s as active catalysts in the polymerization of propylene oxide, monosubstituted epoxides, acetaldehyde, butadiene, propylene, isobutylene, etc. Renewed interest in alumoxanes has arisen in the 1980s, mainly resulting from the works of Kaminsky. He applied methyl alumoxanes as components of highly active catalysts for the polymerization of ethylene and propylene.

Alumoxanes easily undergo association yielding di-, tri-, tetra- and oligoalumoxanes. They also easily undergo disproportionation reactions at elevated temperatures, or when one of the disproportionation components is removed from the reaction medium by precipitation or distillation

under reduced pressure. These properties of alumoxanes make the preparation of a respective alumoxane in a crystalline form and the determination of its crystal structure difficult. It is not surprising, therefore, that the experimental data and proposed structure of alumoxanes differ and depend on the synthetic conditions, isolation methods, solvents used and many other factors. Discussion concerning the structure of alumoxanes recalls the controversies surrounding the structure of Grignard reagents which lasted for many years, before it was established that the Schlenk equilibrium depends on many factors.

The catalytic properties of alumoxanes result from the simultaneous presence of acidic and basic centres in an alumoxane molecule. The fact that the catalytically active centres may be separated from each other by any distance probably plays a considerable role.

Alumoxanes are intermediates in the hydrolysis of organoaluminium compounds to aluminium hydroxides. Materials of a high thermal or mechanical resistance can be obtained by converting alumoxanes to a suitable form, e.g. a fibre, and then hydrolysing or thermally decomposing them.

Taking the above into account it seems timely to review the preparation methods, structure, complexes and reactions of alumoxanes.

SYNTHESIS

Two main methods of synthesis of alumoxanes are known. The first method includes the reactions of organoaluminium compounds with water and the second one includes the reactions of organoaluminium compounds with species containing reactive oxygen.

Reactions with water

Organoaluminium compounds react violently with water yielding only decomposition products:

$$R_3Al + 3H_2O \longrightarrow Al(OH)_3 + 3RH. \quad (1)$$

A number of methods were applied to decrease the hydrolysis rate and to stop the hydrolysis at a required stage. Saegusa *et al.*[1] added a precise amount of water to a stirred solution of triethylaluminium in hexane containing diisopropyl ether. The reduction product was further stirred for an additional 3 h at 0°C. Saegusa proposed that triethylaluminium reacts with a controlled amount of water as follows:

$$(C_2H_5)_3Al + H_2O \longrightarrow (C_2H_5)_2AlOH + C_2H_6 \quad (2)$$

$$(C_2H_5)_2AlOH + (C_2H_5)_3Al \longrightarrow (C_2H_5)_2AlOAl(C_2H_5)_2 + C_2H_6 \quad (3)$$

$$(C_2H_5)_2AlOAl(C_2H_5)_2 + H_2O \longrightarrow (C_2H_5)_2AlOAl(C_2H_5)OH + C_2H_6. \quad (4)$$

Ishida obtained alumoxanes in a similar manner,[2] while Longiave and Castelli[3] described the synthesis of tetraethylalumoxane and diethyldichloroalumoxane as follows. A benzene solution (10%) of $(C_2H_5)_2AlCl$ was added dropwise to a saturated solution of water in benzene (0.4 g dm^{-3}). The compounds obtained were isolated by distilling off the solvent. Sakharovskaya *et al.*[4] hydrolysed the organoaluminium compound, cooled to −40°C, with a mixture of nitrogen and a small amount of water vapour for 18 h. The unreacted organoaluminium compound was then distilled off. A modified method consisted of carrying out the above reaction in an etheral medium.[5] The method we have developed[6] consisted of the introduction of wet toluene vapours (b.p. of azeotrope, 84°C) into a toluene solution of the organoaluminium compound cooled to −78°C. The condensed vapours introduced to the vigorously stirred, cooled solution of the organoaluminium compound caused the slow hydrolysis reaction. Storr *et al.*[7] have developed a method for treating water with an organoaluminium compound which enables the reaction to proceed very slowly and minimizes the risk of precipitation of highly polymeric material from the reaction sphere. The hydrolysis was carried out under high vacuum and at low temperatures. Water vapour was introduced very slowly into the organoaluminium compound solution at 5°C. This method permitted Storr to carry out the reaction in such a way to avoid the formation of higher oligomers.

Razuvaev *et al.*[8] described the now widely used method of alumoxane synthesis. The reactions of organoaluminium compounds with water of copper sulphate pentahydrate were carried out in

aromatic hydrocarbons as the medium. The reaction proceeded according to eq. (5):

$$8AlR_3 + CuSO_4 \cdot 5H_2O \longrightarrow 4 \begin{matrix} \diagdown \\ Al—O—Al \\ \diagup \end{matrix} + CuSO_4 \cdot H_2O + 8RH. \quad (5)$$

Reactions with oxygen-containing oxygen compounds

Ziegler[9,10] first mentioned the formation of tetraethylalumoxane in the reaction of triethylaluminium with carbon dioxide:

$$3Et_3Al + CO_2 \longrightarrow Et_2AlOAlEt_2 + Et_3COAlEt_2. \quad (6)$$

An alumoxane was not, however, isolated in this reaction. Zakharkin *et al.*[11] obtained tetraisobutylalumoxane by reaction (7):

$$RCONR_2 + 2i\text{-}Bu_2AlH \longrightarrow i\text{-}Bu_2AlOAl\text{-}i\text{-}Bu_2 + RCH_2NR_2, \quad (7)$$

while Mole *et al.*[12] used carboxylic acids in the reaction with Me_3Al:

$$MeCO_2H \xrightarrow{Me_3Al} MeCO_2AlMe_2 \xrightarrow{Me_3Al} Me_2AlOAlMe_2 + Me_2CO. \quad (8)$$

We found[13] that reactions of alkylaluminium compounds, $Me_x(OMe)AlCl_{2-x}$ (where $x = 0$–2), with Me_yAlCl_{3-y} ($y = 1$–3) and Et_3Al lead to the formation of alumoxanes with the evolution of alkanes and methyl chloride.

Another method of alumoxane synthesis, without using water, consists of using the oxygen atom bonded to the metal. By treating PbO with an organoaluminium compound a corresponding alumoxane[14] can be obtained from reaction (9):

$$2R_3Al + PbO \longrightarrow R_2AlOAlR_2 + R_2Pb. \quad (9)$$

A similar reaction takes place with alkylaluminium chlorides.[15] By treating the post-reaction mixture with an excess of diethyl ether the trimethylchloroalumoxane ether complex was obtained:

$$4PbO + 8Me_2AlCl \longrightarrow \text{post-reaction mixture} \xrightarrow{Et_2O} 4Me_3ClAl_2O \cdot OEt_2 + Me_4Pb + 2PbCl_2 + Pb. \quad (10)$$

Araki and co-workers [16,17] disclosed a method for preparing alkali metal dialuminates (R_2AlOM) by equimolar reactions of trialkylaluminium and alkali metal hydroxide. Equimolar condensation of R_2AlOLi with R_2AlCl, in toluene at $-20°C$, proceeded without formation of gaseous products, eq. (11):

$$R_2AlOLi + R_2AlCl \longrightarrow R_2AlOAlR_2 + LiCl \quad (11)$$

(R = Me, Et, *i*-Bu).

An interesting method of alumoxane synthesis was reported by Serwatowski.[18] Tetraethylalumoxane is formed in good yield from the reaction of tetraorganodiboroxane with triethylaluminium, eq. (12):

$$R_4B_2O + 2Et_3Al \xrightarrow[\text{toluene}]{20°C} Et_4Al_2O + 2R_2BEt \quad (12)$$

(R_2 = Et_2, 1,5-cyclooctadienyl).

The alumoxane formed was isolated and studied by means of molecular weight and ^{27}Al and ^{17}O NMR.

The methods described above are those most often applied to alumoxane synthesis.

STRUCTURE

Only a few alumoxane structures, determined by single-crystal X-ray investigations, are known. Alumoxanes of a determined structure usually contain bulky ligands or are ionic.

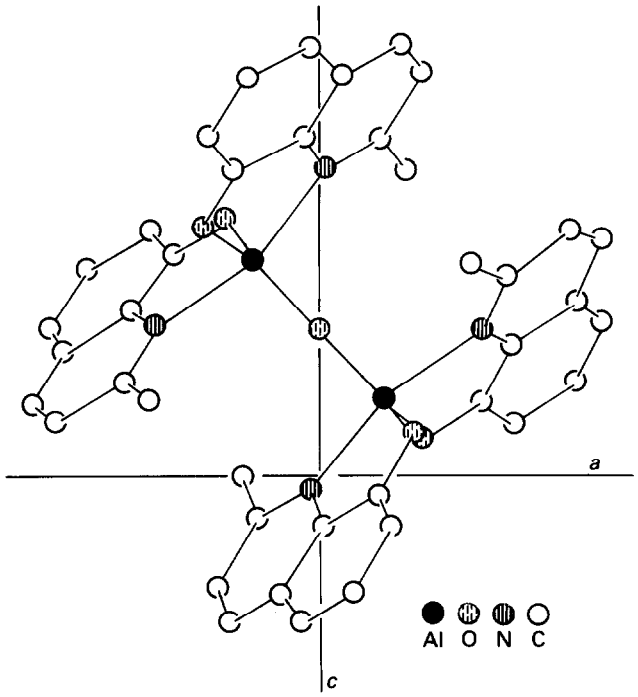

Fig. 1. Structure of μ-oxo-di[bis(2-methyl-8-quinolinato)]aluminium.

Kushi and Fernando[19] have synthesized a complex formed by the reaction of aluminium chloride and 2-methyl-8-quinolinol in a non-aqueous medium. The complex was found, by X-ray investigation, to be μ-oxo-di[bis(2-methyl-8-quinolinolato)]aluminium, containing two penta-coordinated aluminium atoms. The structure consists of discrete molecules of $Al_2O(C_{10}H_8NO)_4$ as shown in Fig. 1. Each of the two aluminium atoms is coordinated to two molecules of 2-methyl-8-quinolinol which act as a bidentate ligand. The two aluminium atoms in the molecule are also connected by an oxo-bridge and it is therefore an alumoxane. The coordination around each of the aluminium atoms is trigonal bipyramidal; the three oxygen atoms and the aluminium atoms are in a plane and the two nitrogen atoms occupy the apical positions (Fig. 2). The stability of the complex, at room temperature on exposure to air and X-rays, was unexpectedly high. The bond angle, Al—O—Al, is 180°. This angle, which is unusual for alumoxanes, is probably caused by the bulky groups, which, when mutually repulsing, straighten the Al—O—Al bond which normally exhibits an angle smaller than 180°.

An interesting alumoxane, occurring as a dimer, was obtained by Bulychev *et al.*[20] $\{[(C_5Me_5)Ti(C_5Me_4CH_2)H_2Al]_2O\}_2 \cdot 2C_6H_6$ has been obtained by treating $(C_5Me_5)_2TiCl$ with $LiAlH_4$ in a 2 : 1 mole ratio. The composition and structure of this compound was identified by X-ray structural

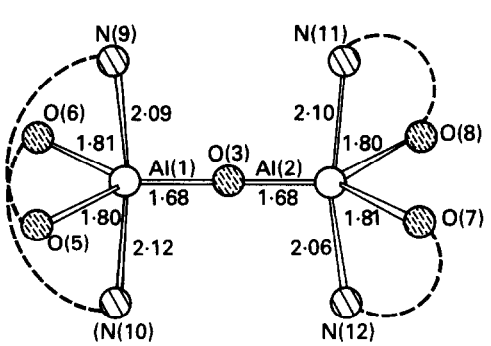

Fig. 2. Arrangement of oxygen and nitrogen atoms around aluminium atoms in $Al_2O(C_{10}H_8NO)_4$.

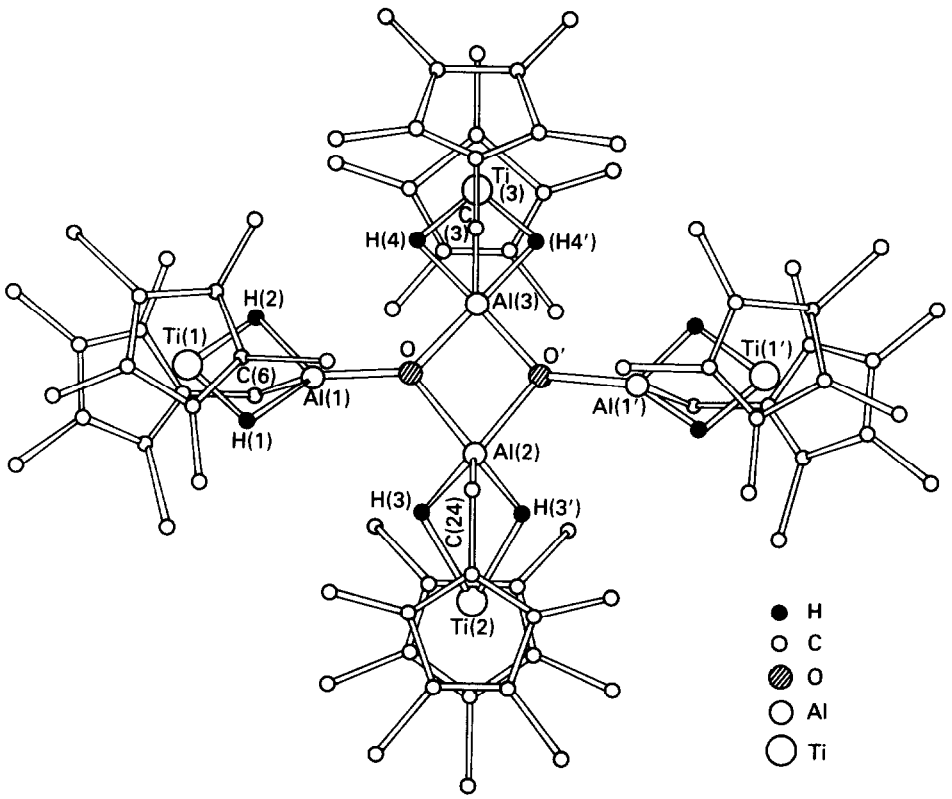

Fig. 3. Molecular structure of the complex $\{[(\eta^5\text{-}C_5Me_5)(\eta^5\text{-}C_5Me_4CH_2)Ti(\mu_2\text{-}H)_2Al]_2\text{-}\mu_3\text{-}O\}_2 \cdot 2C_6H_6$.

analysis. The presence of oxygen atoms in the molecule is, as the authors suggest, most likely to be caused by the partial hydrolysis of the reaction products by traces of water.

The crystal structure of the complex is a sandwich of $\{[(C_5Me_5)Ti(C_5Me_4CH_2)H_2Al]_2O\}_2$ molecules and two crystallographically independent benzene molecules (Fig. 3). All aluminium atoms in the molecule are arranged in pairs with coordination numbers of four and five. The molecule has a typical structure postulated for an alumoxane dimer of $i\text{-}Bu_4Al_2O$.[21] Obviously, the molecule

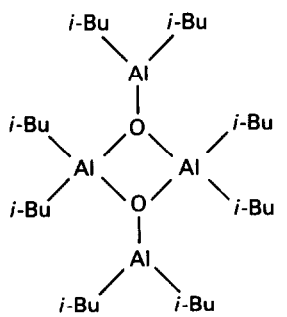

shown in Fig. 3 consists of aluminium atoms with coordination numbers four and five, instead of those with coordination numbers three and four. This causes a stabilization of the molecule obtained by Bulychev.

A typical system for alumoxanes containing three aluminium atoms bonded via μ_3-oxygen bridges occurs in the $[Al_7O_6Me_{16}]^-$ anion obtained by Atwood *et al.*[22] If KO_2 and $AlMe_3$ in a 1 : 2 molar ratio are placed in refluxing benzene, large, colourless crystals are deposited on the walls of the flask. X-ray diffraction studies have shown the product to be $K[Al_7O_6Me_{16}] \cdot C_6H_6$. The structure of this anion is shown in Fig. 4. The anion essentially consists of an open Al_2O_6 ring capped by a

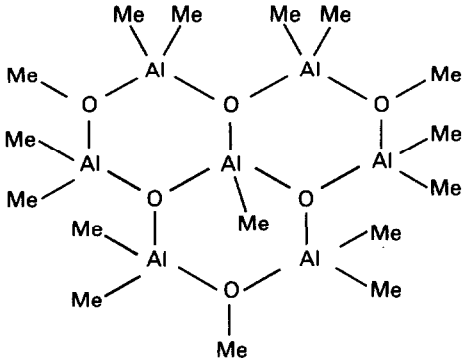

Fig. 4. Structure of the anion of $K[Al_7O_6Me_{16}]\cdot C_6H_6$.

seventh aluminium atom which is bonded to three alternate oxygen atoms in the ring. The six ring aluminium atoms are each bonded to two terminal methyl groups, while the unique aluminium atom is attached to only one methyl group. Each oxygen atom is three-coordinate. The ones on the exterior (not bonded to the unique aluminium atom) bridge two aluminium atoms and are also each bonded to one methyl group, while the interior three oxygen atoms each bridge three aluminium atoms; which is a typical system for alumoxane.[5] Both types of oxygen atom exhibit bond angles as expected for sp^2-hybridization. The angles at the oxygen atoms range from 117 to 123°. The bond angles at the aluminium atoms of the Al_6O_6 unit are near the tetrahedral value, except for the O—Al—O interior angles which range from 97 to 90°. The O—Al—O values, for the unique aluminium atom, 106–108°, are close to those predicted for sp^3-hybridization.

Atwood *et al.*[23] have also obtained the novel alumoxane anion $[Me_2AlOAlMe_3]_2^{2-}$. This result is significant for a better understanding of the structure, stability and oligomerization tendency of the alumoxanes. Trimethylaluminium methylates the cacodylate anion, $[AsMe_2O_2]^-$, with formation of $[AsMe_4]_2[Me_2AlOAlMe_3]_2$, and an X-ray crystal structure has shown the alumoxane anion to consist of a planar Al_2O_2 ring with $AlMe_3$ molecules coordinated to the oxygen atoms (Fig. 5).

The stability of the anion in comparison with the dimeric form of tetramethylalumoxane is much greater since in the anion both aluminium atoms are four-coordinate, and in the tetramethylalumoxane dimer two atoms are three-coordinate and coordinatively unsaturated. The formation of a 3c–2e bond by one of the methyl groups not only causes an increase of the aluminium coordination number to four, but also facilitates the abstraction of a Me_3Al molecule and $Me_3Al_2O_2$, which subsequently oligomerizes (Scheme 1).

The structure of the $[Me_2AlOAlMe_3]_2^{2-}$ anion resembles those of the trimethylchloroalumoxane–diethyl ether[24] and methylchloroalumoxane–diethyl ether[25] complexes (Fig. 6).

The formation of the etheral complex causes an increase in the coordination number of the exterior of two aluminium atoms and stabilizes the alumoxane molecule, as in the $[Me_2AlO Me_3]_2^{2-}$ anion. Despite many papers concerning the synthesis and structural studies of alumoxanes,

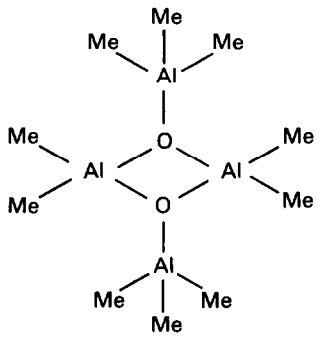

Fig. 5. Crystal structure of the alumoxane anion.

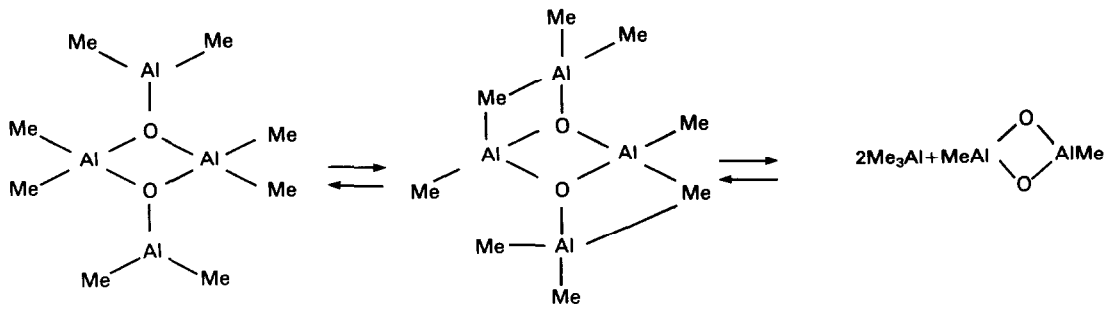

Scheme 1.

the number of structures determined by X-ray investigations is small. This is caused by the ease of disproportionation and association reactions of monomeric alumoxanes.

Storr *et al.*[7] first proposed a trimeric structure for $(Et_2Al)_2O$, on the basis of molecular weight determination.

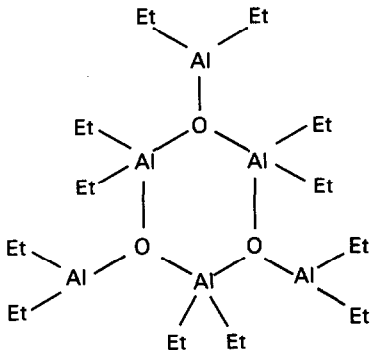

Then Araki and co-workers[16] found that molecular weight determination indicated $(Et_2Al)_2O$ to be on average a tetrameric aggregate, at a given concentration. Proton magnetic resonance and cryoscopic studies lead us to propose the structure shown in Fig. 7 for $(Et_2Al)_2O$.[26] In this structure each aluminium atom has a coordination number of four. Independence of the character of the spectra on the concentration of alumoxane in toluene solution (2–20 wt%), indicates that the bridging ethyl groups occur inside the trimer. Further ^{17}O and ^{27}Al NMR studies carried out by Serwatowski[18] confirmed the structure shown in Fig. 7. A narrow signal at 59 ppm occurs in the ^{17}O NMR spectrum, characteristic of the signals for a three-coordinated oxygen atom and typical for a symmetrical structure. A single signal is observed at 156 ppm in the ^{27}Al NMR spectrum corresponding to the four-coordinated aluminium atom.[27] No signals corresponding to the three-

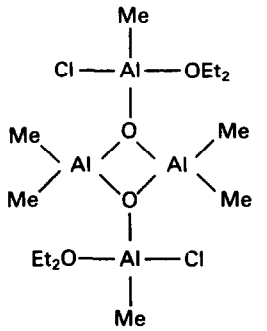

Fig. 6. Structure of methylchloroalumoxane–diethyl complex.

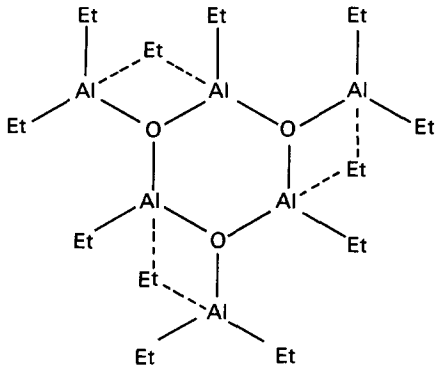

Fig. 7. Proposed structure for the $(Et_2Al)_2O$ trimer.

coordinated aluminium atom are present. The failure in establishing a method of synthesis of $(Et_2Al)_2O$ so as to obtain it in a crystalline form, meant that various structures were assigned to tetraethylalumoxane,[28-30] not always based on comprehensive and exhaustive studies.

Siergiejczyk and Synoradzki[31] have found by means of gel permeation chromatography that raw tetraethylalumoxane consists of ethyloligoalumoxanes (**I**), a tetraethylalumoxane trimer (**II**) and triethylaluminium (**III**). The mass ratio of phases **I/II/III** was 15:65:20. The first phase consisted of a mixture of ethyloligoalumoxanes of average molecular weight, *ca* 1670, the second corresponded to that of trimeric tetraethylalumoxane (Found: 562; Calc. for Et_4Al_2O: 186) and the third phase was triethylaluminium, mol. wt 228. Almost all the triethylaluminium could be distilled off from the raw tetraethylalumoxane at room temperature in high vacuum, and no change in the position of equilibrium was observed. However, after heating pure tetraethylalumoxane up to 80°C for 2 h, small amounts of ethyloligoalumoxane and triethylaluminium appeared. The investigations carried out showed that the trimer of tetraethylalumoxane is stable at room temperature, and at elevated temperatures an equilibrium is established between the trimer and the oligomer and triethylaluminium, eq. (13):

$$(Et_4Al_2O)_3 \rightleftharpoons 3Et_3Al + (EtAlO)_3. \tag{13}$$

Storr *et al.*[7] and Araki and co-workers[16] showed that a compound of the type $R_2AlOAlR_2$ disproportionates readily into AlR_3 and polymeric $(RAlO)_n$ substances on heating under reduced pressure and slowly on storage at room temperature.

An interesting structure of alumoxane has been proposed for $Me_2Br_2Al_2O$.[32] A viscous yellow liquid was obtained from reaction (14) carried out in boiling toluene; after filtering off lead bromide and removal of toluene, white cubic-like crystals appeared. The association degree of $n = 3.86$ was determined by means of cryoscopic measurements [MW = 1002 in benzene (2%)]:

$$2MeAlBr_2 + PbO \xrightarrow[\text{Toluene}]{110°C} Me_2Br_2Al_2O + PbBr_2. \tag{14}$$

The proposed structure of the alumoxane tetramer is shown in Fig. 8. The results of spectroscopic (IR and ^1H NMR) studies are in agreement with the proposed structure. The structure presented in Fig. 8 consists of two $(Me_2Br_2Al_2O)_2$ dimers linked via bromide bridges. The terminal aluminium atoms have the coordination number four and are bonded by a stable bromide bridge:

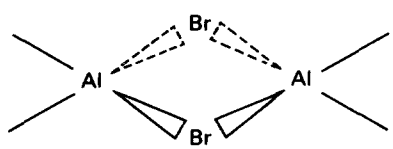

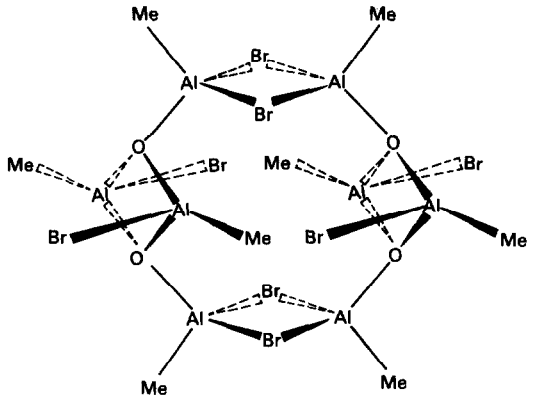

Fig. 8. The hypothetical molecular structure of the crystalline dimethyldibromodialumoxane tetramer.

A similar structure to the one above was proposed for triisobutyldichloroalumoxane.[33] The crystalline alumoxane in *ca* 20% yield was obtained from reaction (15):

$$3(i\text{-Bu})_2AlCl + 2H_2O \xrightarrow[\text{Toluene}]{-78°C} (i\text{-Bu})_3Cl_2Al_3O_2 + \text{side products.} \quad (15)$$

The results of elemental analysis, molecular weight determination and spectroscopic measurements confirm the proposed structure (Fig. 9). In this case the monomer contains three aluminium atoms connected via two oxygen atoms:

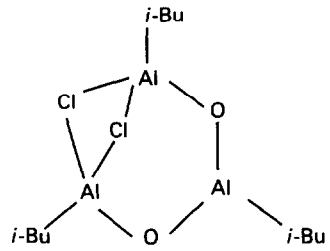

The presence of the three-coordinated aluminium atom and the two-coordinated oxygen atom causes the association of the monomer to trimerize.

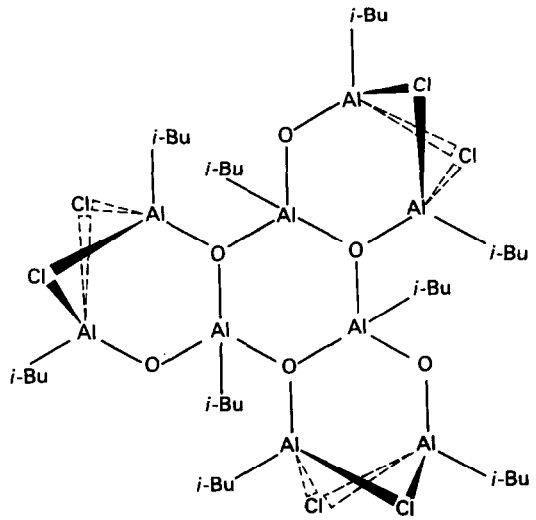

Fig. 9. The hypothetical molecular structure of the crystalline triisobutyldichlorooligoalumoxane trimer.

REACTION MECHANISMS OF ORGANOALUMINIUM COMPOUNDS WITH WATER

A basic synthetic method for alumoxanes sys is the reaction of organoaluminium compounds with water. The homogeneity of the synthesized alumoxane depends on the hydrolysis procedure. The milder the reaction conditions (lower temperature, low reactant concentration, vigorous stirring, long reaction time, presence of a solvent decreasing the reactivity of the organoaluminium compound) the more homogeneous will the alumoxane be and thus there will be less side products such as higher oligomers and even aluminium hydroxide. Many difficulties which cannot easily be avoided are encountered while carrying out the reaction. The type of alumoxane formed depends on the method of hydrolysis. The organoaluminium compound/water molar ratio has a great effect on the hydrolysis product formed. This is presented in a simplified way in Scheme 2.

Sakharovskaya *et al.*[4] have proposed a two-step reaction course in which the dialkylaluminium hydroxide is the relevant intermediate, eqs (16) and (17):

$$R_3Al + H_2O \longrightarrow R_2AlOH + RH \tag{16}$$

$$R_2AlOH + R_3Al \longrightarrow R_2AlOAlR_2 + RH. \tag{17}$$

Amdurski *et al.*[34] have postulated on the basis of the stoichiometry and kinetics of the Et_3Al hydrolysis reaction (1 : 1) the presence of a hydroxyl group in the final product. Such a possibility was confirmed by radioisotopic investigation of the Et_3Al/T_2O system.[35] Ueyama *et al.*[16] have even observed the weak resonance signal of the hydroxyl group protons ($\tau = 6$ ppm) in the ^1H NMR spectrum of the products of the reaction of *i*-Bu_3Al with water (2 : 1). We have also observed in the IR and ^1H NMR spectra dimethylaluminium hydroxide as an intermediate product of Me_3Al hydrolysis in dimethoxyethane.[36] Petrova *et al.*[37,38] have limited their investigations to the analysis of complex formation of Et_2AlCl and $EtAlCl_2$ with water. The hydrolysis of R_3Al (R = CH_3, C_2H_5, *i*-C_6H_9) at 1 : 1 and 2 : 1 mol ratios was studied by ^1H NMR spectroscopy in the temperature range -70–$0°C$.[39] A multi-step reactions course was found: in the first step a 1 : 1 complex of R_3Al with water is formed. This complex undergoes intramolecular elimination of alkane to produce dialkylaluminium hydroxide, R_2AlOH. In the next step R_2AlOH forms stable auto-associates (in 1 : 1 system) or reacts with the excess of R_3Al to give alumoxane.

On the basis of literature data and our studies, the mechanisms of R_3Al and water reactions at 2 : 1 and 1 : 1 mole ratios can be presented as follows.

$R_3Al + H_2O$, 2 : 1 *system*

In the first reaction step a water molecule attacks the $[R_3Al]_2$ dimer forming complex **I** (Scheme 3). At $-72°C$ and in diethyl ether medium, complex **I** can be observed by ^1H NMR.[39] At higher temperatures it undergoes reaction yielding **II** and RH. Dialkylaluminium hydroxide forms an intramolecular complex with R_3Al via carbon and oxygen bridges. Complex **II** is quite stable and reacts with the evolution of RH only at *ca* 0°C. The $[R_3Al]_2$ dimer reacts more readily with water than complex **II**. The reactivity of the R groups is lower in **II** due to the basicity of the oxygen atoms. Thus it can be assumed that the formation of complex **II** is the dominating reaction until the water is used up (Al/H_2O mole ratio = 2 : 1).

At *ca* 0°C complex **II** undergoes reaction yielding RH. An intramolecular reaction is the most probable one (Scheme 3). A number of reactions of **II** [eq. (18)] and of all of the intermediate and

$$\underset{2:1}{2R_3Al + H_2O} \longrightarrow R_2Al{-}O{-}AlR_2 + 2RH$$

$$\underset{1:1}{R_3Al + H_2O} \longrightarrow [RAlO] + 2RH$$

$$\underset{1:3}{R_3Al + 3H_2O} \longrightarrow Al(OH)_3 + 3RH$$

Scheme 2.

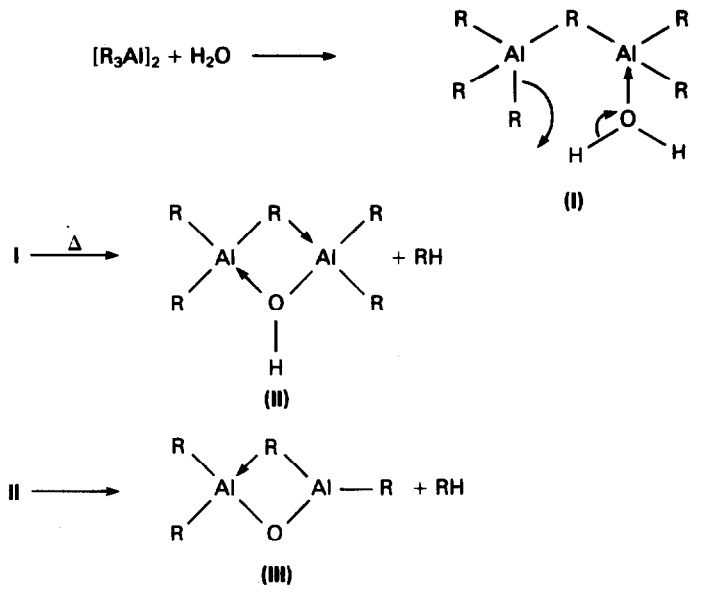

Scheme 3.

final products [eqs (19) and (20)] with water can take place:

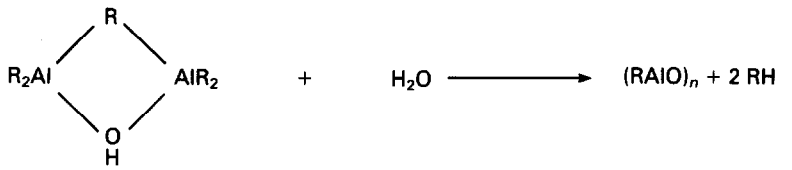

(18)

$$R_2AlOAlR_2 + H_2O \longrightarrow (RAlO)_n + 2RH \quad (19)$$

$$(RAlO)_n + H_2O \longrightarrow (HOAlO)_n + RH. \quad (20)$$

Nearly all of the intermediate and final products of the hydrolysis of organoaluminium compounds may also react with trialkylaluminium, eq. (21), yielding tetraalkylalumoxane:

$$(RAlO)_n + nR_3Al \rightleftharpoons (R_2AlOAlR_2)_n. \quad (21)$$

An equilibrium, dependent on many parameters, is probably established. In the case when a highly associated oligomer $(RAlO)_n$ is formed, the shift of the equilibrium of reaction (21) to the right is a very slow process. Further hydrolysed products, such as $Al(OH)_3$ or Al_2O_3, practically do not react with R_3Al.

Compound **III** easily forms associates due to the acidic, three-coordinated aluminium atom and basic, two-coordinated oxygen atom. The smallest ring strain and steric hindrance occur for the trimer of **III** forming structure **IV** (Scheme 4).

In compound **IV** the aluminium and oxygen atoms are four- and three-coordinated, respectively, so this compound is structurally stable. Due to strain occurring in the carbon bridge, its cleavage does not require much energy and proceeds easily. Depending on the position of cleavage of the Al—C—Al bridge, compounds **V** or **VI** can be formed from complex **IV** (Scheme 4).

No bridge strains appear in **V**, but three aluminium atoms in the ring are three-coordinated and can easily form complexes. A similar situation occurs in the case of structure **VI**, but here three terminal aluminium atoms are three-coordinated.

From the above it appears that mutual transformations of structures **IV**, **V** and **VI** proceed easily at or below room temperature. A number of signals with small differences in chemical shifts, occur in the ^1H NMR spectrum. A considerable decrease of temperature causes a retardation of

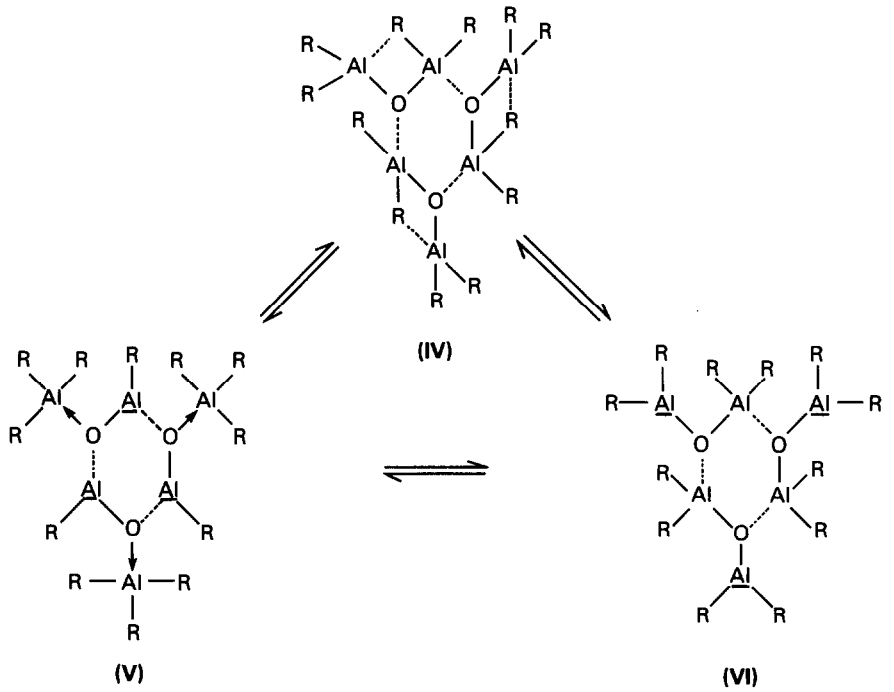

Scheme 4.

these mutual transformations, but still all three structures are present. This has a decisive effect on the ^{1}H NMR spectrum pattern, which still consists of many signals from different protons.

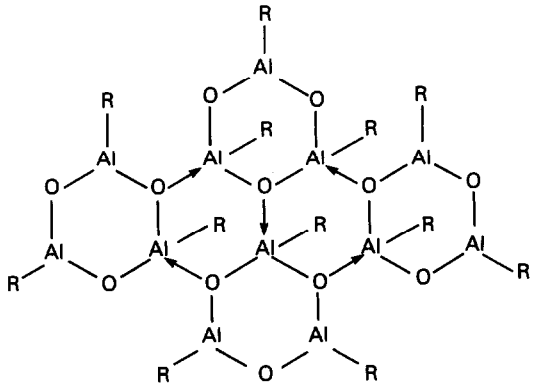

Structure **V** can be treated as a six-membered system consisting of three [RAlO] monomeric units and three R_3Al molecules coordinated via the bridging oxygen atoms. Thus, there exists a possibility of R_3Al abstraction under the influence of temperature, high vacuum or a respective electron donor (Scheme 5). Alumoxane (**VII**) associates immediately, since it has three-coordinated aluminium atoms and two-coordinated oxygen atoms. Structure **VIII** is the most probable structure for the $[RAlO]_n$ associate, in which all the aluminium and oxygen atoms are four- and three-coordinated, respectively. It should be noted that the six-membered Al_3O_3 rings are not planar. Structure **VIII** can be extended and does not exhibit strain. It is formed from four cyclic $[RAlO]_3$ monomeric units forming six six-membered rings. In general, the reaction product has the formula $[RAlO]_n$.

It is obvious that the two-coordinated oxygen atoms are still capable of coordinating R_3Al

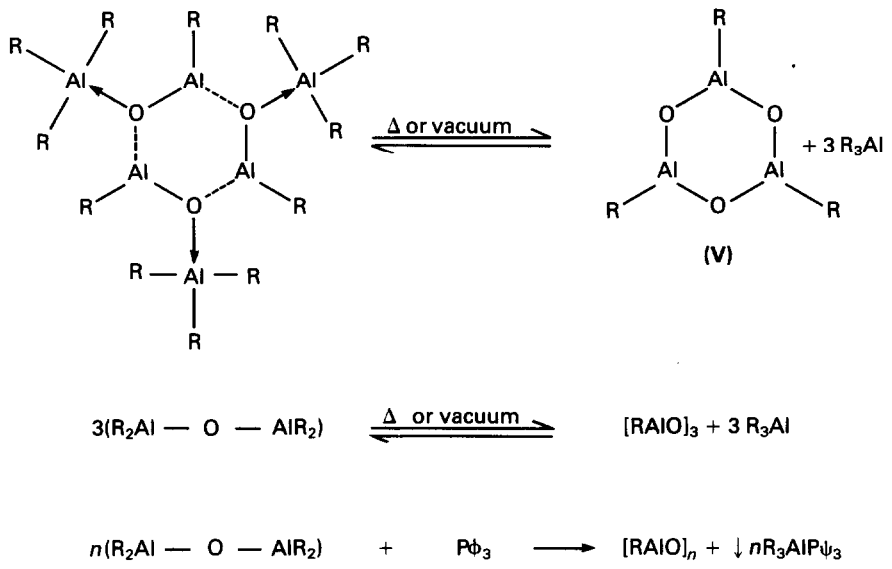

Scheme 5.

molecules. By treating **VIII** with an equimolar amount of trialkylaluminium ($RAlO/R_3Al = 1:1$), the equilibrium of reaction (21) shifts to the right:

$$[RAlO]_{3n} + 3n\,R_3Al \rightleftharpoons n(R_4Al_2O)_3. \tag{21}$$

The decomposition of alumoxane with the liberation of trialkylaluminium, as well as the facility of the reverse reaction, eq. (21), indicate a comparable acidity of the aluminium atoms in R_3Al and RAlO. The Al—O—Al bridging oxygen is the base with which these Lewis acids react. Its basicity for different bridging systems can be assumed to be constant.

The equilibrium of reaction (21) is shifted to the right because R_3Al is a stronger Lewis acid than $[RAlO]_n$. When removing trialkylaluminium from the reaction medium $(RAlO)_n$ is formed as the final product. This can be achieved by the distillation of R_3Al at elevated temperatures or under reduced pressure, or by precipitating it in the form of a complex with PPh_3 (Scheme 5). Attack of the aluminium atom of R_3Al on the ring oxygen atom can be assumed as the probable reaction mechanism of **VIII** with trialkylaluminium. Further cleavage of the O—Al bond in the bridge and formation of a new Al—O bond with trialkylaluminium takes place. Consecutive formation and cleavage of Al—O bonds does not require high energy and is kinetically controlled. The equilibrium described by eq. (21) results from these reactions.

As can be seen from the above, the complexity of alumoxane structures, as a result of the reaction presented in Scheme 4, become still more complicated due to the equilibrium presented by eq. (21). This is the main reason precluding the preparation of methyl, ethyl or butyl alumoxane in crystalline froms or their isolation by distillation.

$R_3Al + H_2O$, 1 : 1 *system*

The first step of the reaction proceeds according to Scheme 6. Further reactions proceed, in which the next water molecule reacts with **II** (Scheme 6) and **III** yielding **IX**, **X**, respectively. Both **IX** and **X** undergo further reactions at higher temperatures [eqs (22) and (23)]:

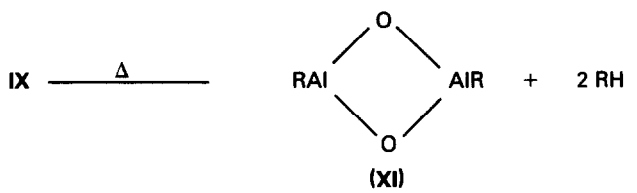

(22)

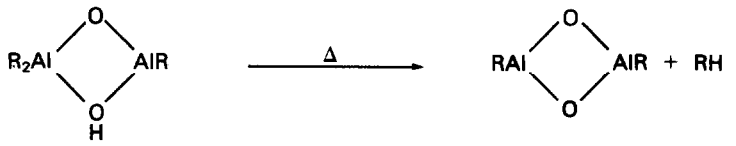

(X) (XI) (23)

Compound **XI** undergoes association since it has two aluminium and two oxygen atoms, three- and two-coordinated, respectively (Scheme 7).

Compound **X** can also undergo association since it has one three-coordinated aluminium atom and one two-coordinated oxygen atom. A structure analogous to **IV** can be formed in which the OH group oxygen atom bridges the terminal aluminium atom and the ring aluminium atom (**XII**).

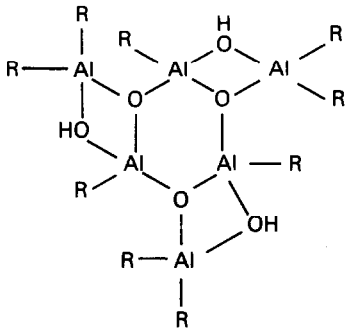

(XII)

The reactivity of the OH groups is considerably decreased in compound **XII** because the aluminium and oxygen atoms are coordinatively saturated. This is the reason why a number of OH groups do not react easily and remain in the products of hydrolysis of R_3Al. Structure **XII** is more stable than **IV** since the stability of the oxygen bridges is higher than that of the carbon bridges. The association of **XI** can proceed in many ways (Scheme 8).

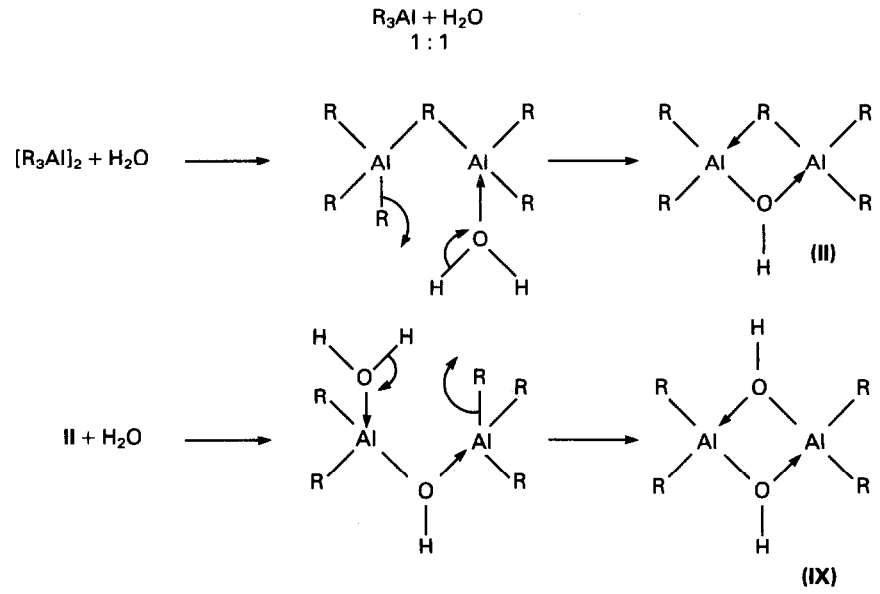

Scheme 6.

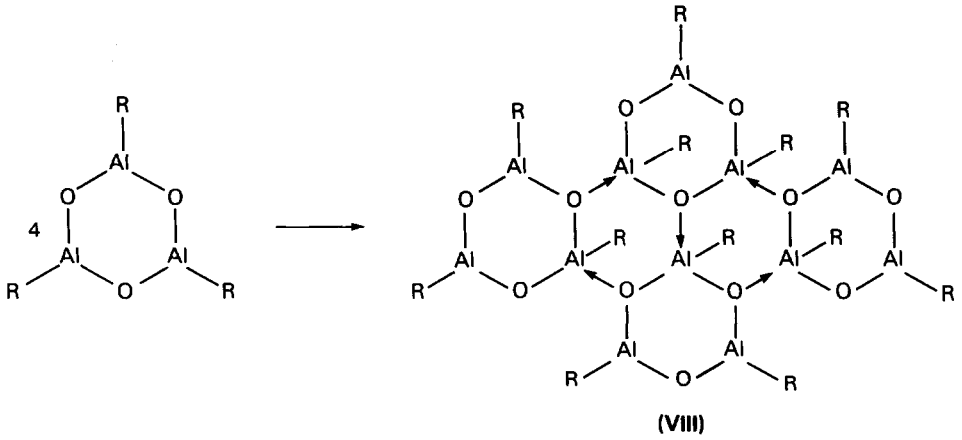

(VIII)

$4(RAlO)_3 \longrightarrow [RAlO]_{12}$

found : n = 10–12

Scheme 7.

The associate which is formed without cleavage of the bridge has aluminium and oxygen atoms coordinatively saturated with the exception of terminal atoms, thus stabilizing the associate. Strain in the four-membered bridges acts against the stability of the associates. This strain may be the reason for the cleavage of internal Al—O bonds and for the formation of a more stable six-membered system (Scheme 8). Internal three-coordinated aluminium atoms and two-coordinated oxygen atoms occur in this associate. This may be the driving force for further association to compound **VIII**.

Assuming that compounds formed in the reaction of R_3Al with water have a chain structure with a variable number of [RAlO] units, then the chains formed will immediately react giving the structure shown in Scheme 8. Formed associates with $[RAlO]_n$ can undergo reactions with R_3Al yielding alumoxane, **IV**. These are reversible reactions and can be presented by eq. (21).

For ethyl alumoxanes at room temperature and under normal pressure, the equilibrium of reaction (21) is shifted further to the right compared with that of the methyl alumoxane.

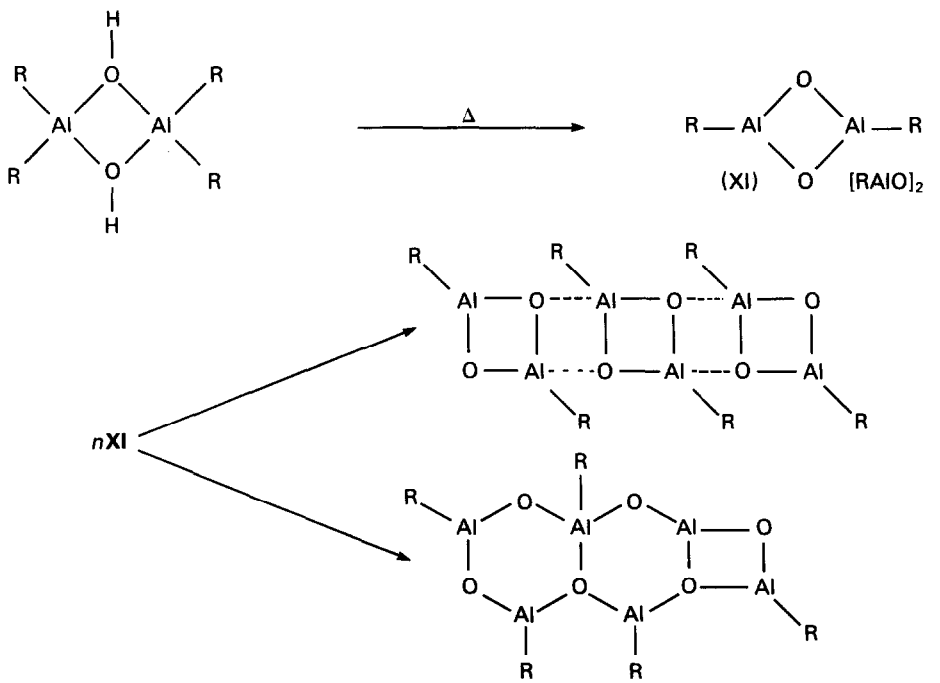

Scheme 8.

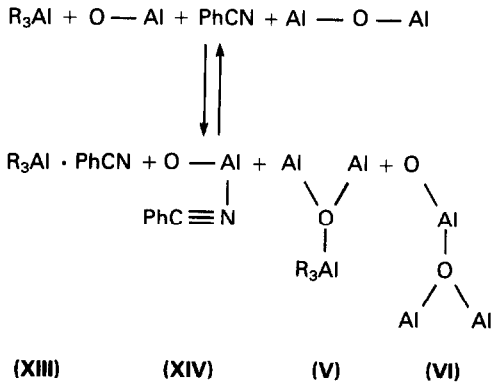

Scheme 9.

COMPLEXES OF ALUMOXANES WITH ELECTRON DONORS

The reactions of alumoxanes with bases are of a complex character. Two Lewis acids and two bases are present in the reaction medium, which are denoted as A and A′, B and B′, respectively. These can react with each other forming donor–acceptor complexes and the reaction may be represented by eq. (24):

$$A+A'+B+B' \rightleftharpoons AB+A'B+AB'+A'B'. \qquad (24)$$

If the aluminium atom of R_3Al is denoted as A, and that of O—Al—O alumoxane as A′, the nitrogen in PhCN as B and the Al—O—Al alumoxane oxygen as B′, then eq. (24) can be represented as in Scheme 9. The equilibrium between forms **V** and **VI** has already been presented in Scheme 4.

By considering that from amongst the three possible structures of the alumoxane trimer (**IV**, **V** and **VI**, Scheme 4) benzonitrile can react with **V** and **VI**, then complexes **V′** and **VI′** should be formed (Scheme 10). Both dimeric complexes, **V′** and **VI′**, can, however, dissociate forming the monomeric complex **XIV**.

A nearly monomeric ($n = 1.325$) complex was obtained by Storr *et al.*[7] for $(Et_4Al_2O)_3$ and trimethylamine. Ueyama *et al.*[16] isolated and determined the crystalline monomeric complex of $(Et_4Al_2O)_3$ with 5,6-benzoquinoline and also the complexes $(Et_4Al_2O)_3$ and $(Me_4Al_2O)_3$ with styrene oxide in a crystalline form soluble in benzene. We have isolated a similar monomeric complex from the reaction of $(Et_4Al_2O)_3$ with benzonitrile.[40,41]

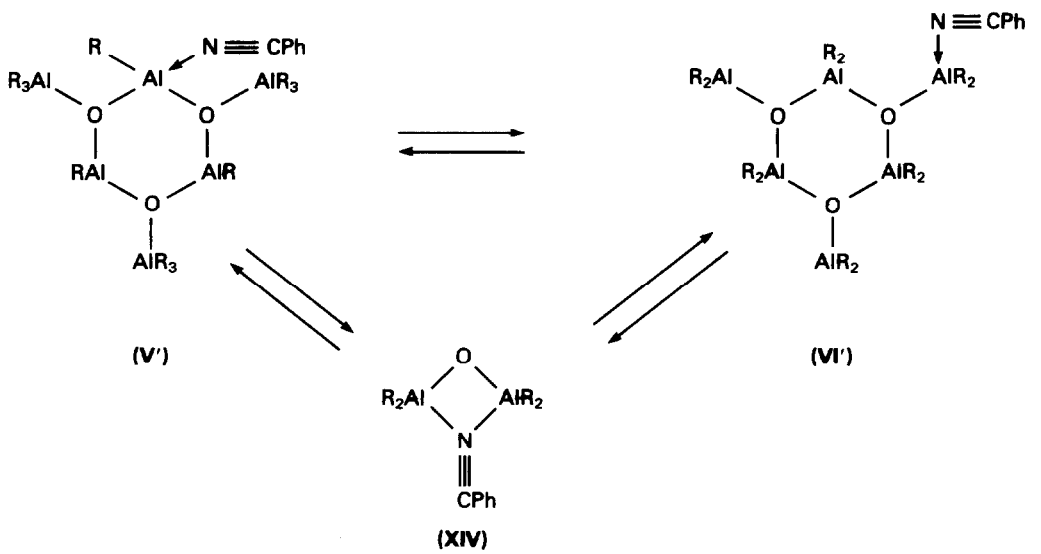

Scheme 10.

A complex of tetramethylalumoxane and N,N,N′,N′-tetramethylethylenediamine (TMEDA) was obtained[42] by the partial hydrolysis of trimethylaluminium, eq. (25):

$$2Me_3Al + H_2O \xrightarrow[-30°C]{TMEDA} Me_4Al_2O \cdot TMEDA + 2CH_4. \quad (25)$$

Pale crystals (m.p. 78–82°C) in 5–10% yield were obtained (RT, high vacuum sublimation). Spectral data, mol. wt and mass spectra of the sublimate correspond to the alumoxane complex, $Me_4Al_2O \cdot TMEDA$. The data obtained prove the existence of the monomeric tetramethylalumoxane–TMEDA complex of structure **XV**.

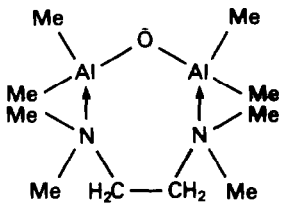

(XV)

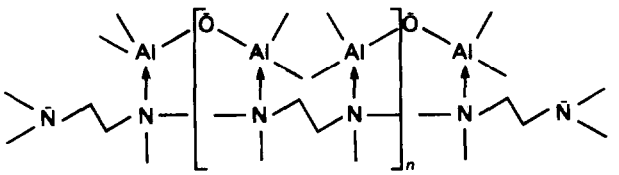

(XVI)

The highly viscous residue of sublimation which is also insoluble in hydrocarbons seems to be of the donor–acceptor type polymers like **XVI**.

The Et_4Al_2O alumoxane reacts with triphenylphosphine and acridine to give mainly $Et_3Al \cdot PPh_3$ and $Et_3Al \cdot$acridine complexes, respectively,[43] which precipitate from the post-reaction mixture upon cooling. The results obtained confirm the existence of the equilibrium presented in Scheme 9. Therefore, complexes of type **XIII** or **XIV** are the reaction products depending on the kind of alumoxane and base used, as well as on the solubility and volatility of complexes formed.

The alumoxanes Et_4Al_2O and Me_4Al_2O form 1 : 1 complexes with primary amines.[43] They are unstable and undergo reaction at *ca* 0°C with the evolution of ethane and methane, respectively. The complexes of deuterated amines are more stable and their association degrees are: for $Et_4Al_2O \cdot PhCH_2ND_2$ ($n = 1.20$) and for $Me_4Al_2O \cdot PhCH_2ND_2$ ($n = 2.23$).

The tertiary amines[41] N,N-dimethylaniline (NMe_2Ph) and benzylidene-*n*-butylamine (PhHC=N—*n*-Bu) form equimolar complexes with Et_4Al_2O. The *i*-Bu_4Al_2O alumoxane, however, does not form a complex with NMe_2Ph, probably due to steric hindrance.

Complexes of alumoxanes with ethers have been described in the literature. Ueyama *et al.*[16] described the crystalline complex of Me_4Al_2O with anisole having a melting point of −16°C and decomposing during distillation with the formation of $Me_3Al \cdot PhOMe$. The alumoxane Et_4Al_2O yields a complex with THF, which during vacuum distillation affords $Et_3Al \cdot THF$.

The $Me_4Al_2O \cdot OEt_2$ complex was obtained by Sadownik[44] in the form of a viscous liquid whose mol. wt was near to that of the dimer. Complexes of Me_4Al_2O with dimethoxymethane and dimethoxyethane have also been described.[44] Both complexes are viscous liquids of the association degree $n \approx 2$.

Structure **XVII** has been proposed for $Me_4Al_2O \cdot Et_2O$, analagous to $Me_2Cl_2Al_2O \cdot Et_2O$.[25]

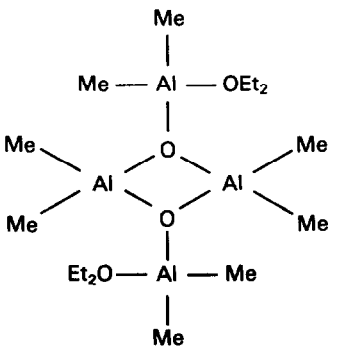

(XVII)

All the aluminium and oxygen atoms in the dimer are four- and three-coordinated, respectively, and hence the dimer should be stable.

A decrease in the tendency to form internal associates is observed for chlorine derivatives of alumoxanes. For Me_3ClAl_2O complexes with ethyl ether[24] the monomer slowly undergoes transformation to the dimer, and after 60 h the degree of association, n, equals 1.45.

This can be explained in two ways. Either by the dynamic coordination of etheral oxygen to both aluminium atoms in the alumoxane, thus stabilizing of the monomeric form, or by the formation

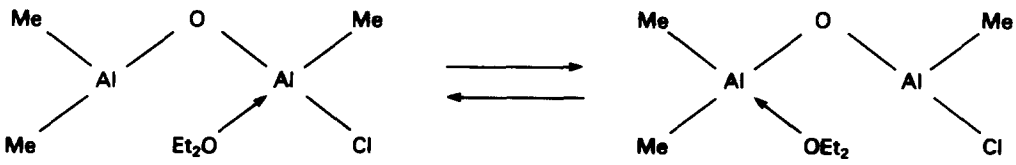

of a quite stable bridge via the chlorine atom, thus coordinative saturation of both aluminium atoms in the alumoxane monomer is attained. Dimerization or association is difficult but possible for both these structures. $Me_2Cl_2Al_2O$ forms a complex with diethyl ether, the association degree of which

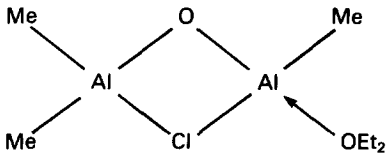

is $n = 1.89$. The $Me_3ClAl_2O \cdot O(CH_2CH_2Cl)_2$ complex is less associated ($n = 1.64$).[44] Complexes of methylchloroalumoxanes with dimethoxymethane are unstable and decompose at *ca* 0°C.[44]

Diethyldichloroalumoxane was obtained by Storr *et al.*,[7] who found that its association degree is $n = 4.9$. $Et_2Cl_2Al_2O$ and trimethylamine form a 1 : 1 complex as a viscous liquid, which is stable up to 150–200°C. The mol. wt of the complex was not determined.

Methylchloroalumoxanes form complexes with benzonitrile with variable reactant mole ratios.[45] Tetrachloroalumoxane forms a complex with benzonitrile having a nearly 1 : 2 ratio; $Me_2Cl_2Al_2O$ with an excess of benzonitrile forms both complexes with the alumoxane/benzonitrile mole ratios of 1 : 1 and 1 : 2. However, Me_3ClAl_2O forms a nearly 1 : 1 complex. The various mole ratios of these complexes can be explained by the increased acidity of the aluminium atoms in the chloroalumoxanes. The complexes of chloroalumoxanes with benzonitrile are, therefore, mixtures of complexes in equilibrium with the substrates. The formation and dissociation of alumoxane complexes is shown in eq. (26):

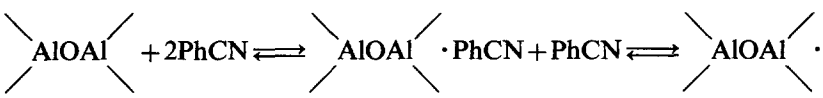

(26)

REACTIONS OF ALUMOXANES WITH ELECTRON DONORS

Ethers

Tetramethylalumoxane,[44] obtained from the reaction of trimethylaluminium with water in a dimethoxymethane (DMM) medium, reacts with DMM at *ca* 75°C. Methyl ether and traces of methane result from reaction (27):

$$Me_4Al_2O \cdot (MeO)_2CH_2 \xrightarrow{75°C} Me_3(MeO)Al_2O + MeOEt. \qquad (27)$$

No ethane was found in the reaction products. This indicates the cleavage of the CH_2—O bond and not the CH_3—O bond in DMM. The formation of the $CH_3OCH_2^+$ carbocation is easier than

the CH_3^+ carbocation, due to its stabilization.[46,47] The reaction course is presented in eq. (28):

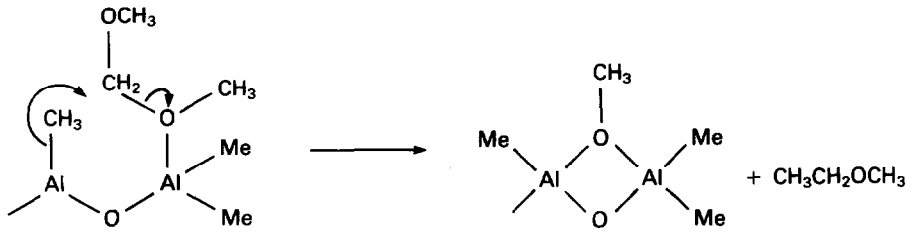

(28)

It can also be assumed that $(Me_4Al_2O \cdot DMM)_2$ decomposes forming the monomeric $Me_3Al \cdot DMM$ complex and $[RAlO]_n$. This complex undergoes reaction yielding methylethyl ether and the methoxyaluminium derivative, eq. (29):

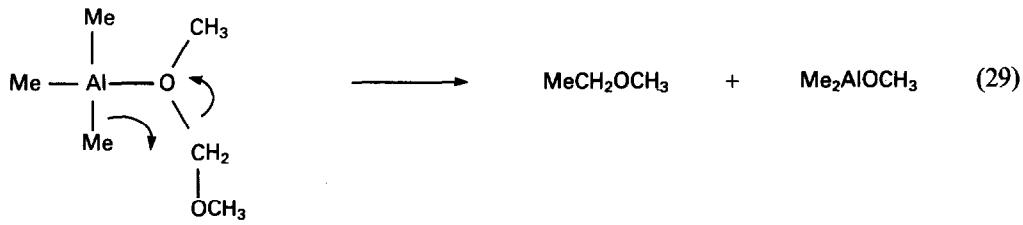

(29)

The reaction of the alumoxane with diethyl ether is more probable than that of monomeric trimethylaluminium with diethyl ether because it proceeds more easily in a six-membered system than in a four-membered one.[46,47]

Methylchloroalumoxanes react with DMM much more easily than Me_4Al_2O. For $Me_3ClAl_2O \cdot DMM$ the reaction proceeds at $-10°C$, and for $Me_2Cl_2Al_2O \cdot DMM$ at $-20°C$. Chloroalumoxanes are more reactive than the corresponding methylaluminium chlorides. $Me_2AlCl \cdot DMM$ and $MeAlCl_2 \cdot DMM$ react with complexed DMM at 50 and 10°C. This confirms the conclusion that a favourable six-membered system is formed in alumoxanes, compared with the less favourable four-membered system in methylaluminium chlorides.

Methylchloromethyl ether decomposes further yielding methyl chloride and formic aldehyde, eq. (30):

$$ClCH_2OCH_3 \longrightarrow CH_3Cl + HCHO. \tag{30}$$

Therefore, methylethyl ether and methyl chloride are the main reaction products. The aldehyde reacts further in the reaction medium.

Acetylacetone

Tetraalkylalumoxanes,[48] R_4Al_2O (where R = Me, Et, *i*-Bu), react easily with acetylacetone (acac) in a diethyl ether or 1,2-dimethoxyethane (DME) medium, eq. (31):

$$R_4Al_2O \cdot DME + acacH \xrightarrow[DME]{-70°C} R_3(acac)Al_2O + RH. \tag{31}$$

$Me_3(acac)Al_2O$ is stable in solution up to 0°C. Above 0°C it slowly decomposes forming aluminium triacetylacetonate and $(MeAlO)_n$, eq. (32):

$$3\,Me_3(acac)Al_2O \xrightarrow[DME]{0°C} Al(acac)_3 + [MeAlO]_3 \cdot 2AlMe_3. \tag{32}$$

$Et_3(acac)Al_2O$ and $i\text{-}Bu_3(acac)Al$, obtained by the same method, are more stable than the methyl derivative and slowly disproportionate at room temperature. These are colourless, viscous liquids, very soluble in ethers, benzene, toluene, etc. $Et_3(acac)Al_2O$ is a dimer to a great extent: mol. wt: 460. Calc. for the dimer: 512.

The reactions of R_4Al_2O with acetyloacetone for the 1:2 and 1:4 mole ratios proceed at low temperatures, from −70 to −40°C. No products of the $R_2(acac)_2Al_2O$ or $(acac)_4Al_2O$ type were isolated from the reaction mixtures. They appear to undergo disproportionation forming aluminium triacetylacetonate and $[RAlO]_n$, eq. (33):

$$Me_2(acac)_2Al_2O \xrightarrow{-15°C} Al(acac)_3 + \text{oligomers.} \tag{33}$$

$(acac)_4Al_2O$ decomposes at low temperature during formation. Aluminium triacetylacetonate and aluminium oxide are the final decomposition products, eq. (34):

$$3\,(acac)_4Al_2O \longrightarrow 4\,(acac)_3Al + Al_2O_3. \tag{34}$$

The stability of alumoxane acetylacetonates increases in the following order for various alkyl substituents, R: $Me_3(acac)Al_2O < Et_3(acac)Al_2O < i\text{-}Bu_3(acac)Al_2O$, and decreases in the following order depending on the number of acac groups bonded to aluminium: $R_3(acac)Al_2O > R_2(acac)_2Al_2O \gg (acac)_4Al_2O$.

Ketones

The reactions of methylalumoxanes, $Me_nCl_{4-n}Al_2O$ ($n = 4, 3, 2$), with 4-*t*-butylcyclohexanone in the presence of diethyl ether have been studied.[49]

It was found that alumoxane alkylate ketones react in a similar manner to alkylaluminiums. The reaction yield decreases with an increase in the number of chlorine atoms bonded to the aluminium atom, in agreement with the previously found reactivity of organoaluminium compounds.[50] The reaction yield with alumoxane does not depend on the reactant mole ratios, unlike for organoaluminium compounds. This can be explained by the formation of a six-membered system irrespective of the reactant mole ratio, eq. (35):

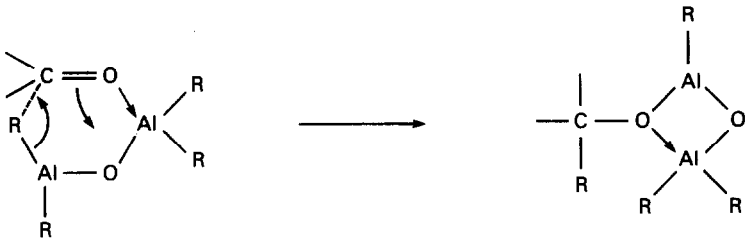

(35)

A mixture of an equatorial and axial alcohol is formed upon hydrolysis, with considerable predominance of the axial form (*ca* 65%), eq. (36):

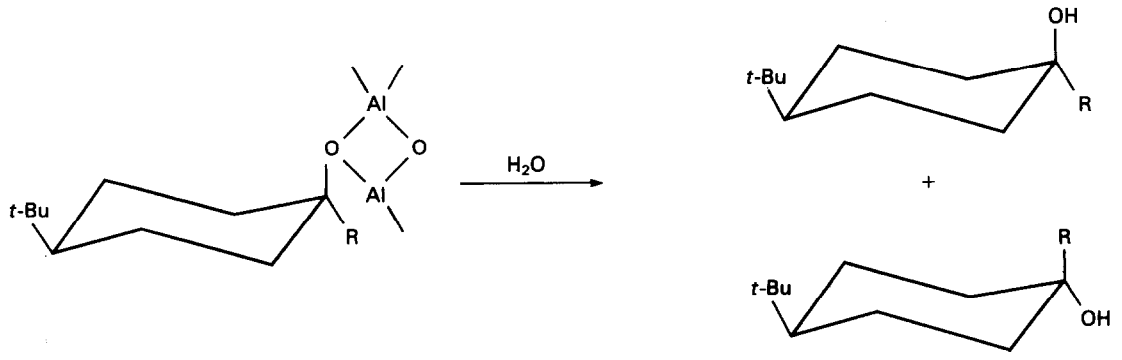

(36)

The lack of a relationship between the reaction yield and reactant mole ratios confirms that the reaction proceeds between the alumoxane and the ketone, and not with an organoaluminium compound abstracted from the alumoxane.

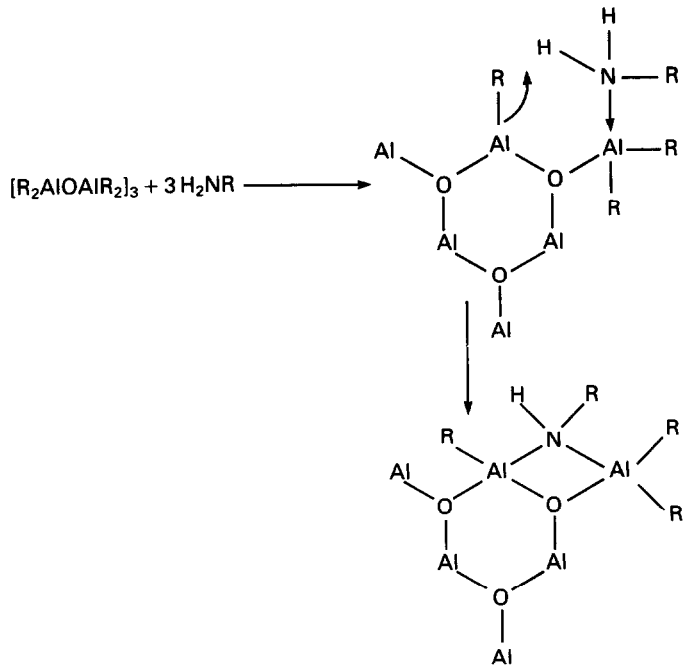

Scheme 11.

Amines

Tetraethylalumoxane and diethyldichloroalumoxane form complexes with trimethylamine.[7] These complexes are thermally stable and do not decompose up to 170°C.

The reactions of Et_4Al_2O and Me_4Al_2O with methylamine and benzylamine have been studied.[51] The complexes react at 40–80°C forming a corresponding hydrocarbon and an alumoxane with nitrogen substituted at aluminium, eq. (37):

$$Et_4Al_2O + PhCH_2NH_2 \longrightarrow Et_4Al_2O \cdot PhCH_2NH_2 \xrightarrow{>60°C} Et_2AlOAl(Et)NHCH_2Ph + C_2H_6. \quad (37)$$

Spectroscopic studies and molecular weight determinations indicate that triethylaminoalumoxane is a trimer and has a cyclic structure (**XVIII**). Alumoxane can react as a monomer or as a trimer yielding the same product (Scheme 11).

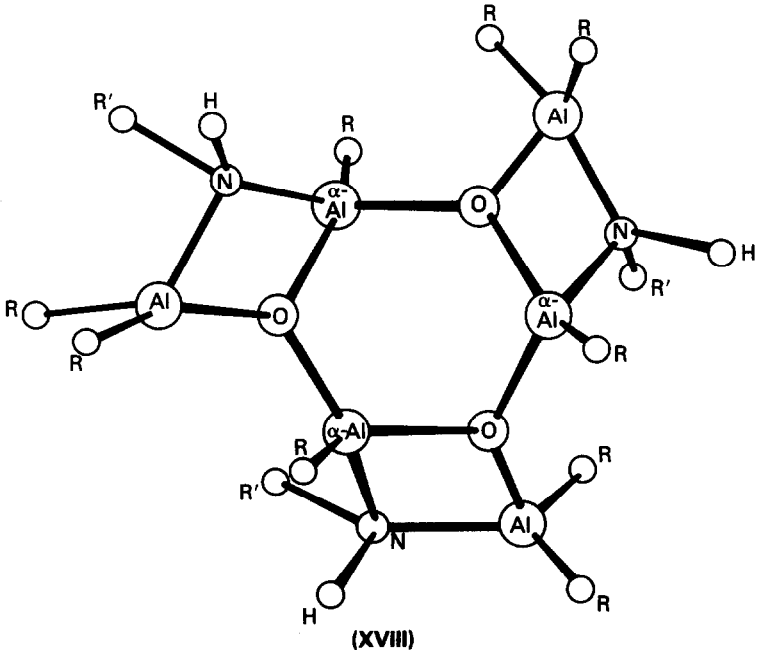

(XVIII)

All the aluminium and oxygen coordination sites are saturated in the trimeric product **XVIII**. The nitrogen bridge between two aluminium atoms is stable enough not to undergo cleavage under the influence of benzonitrile. Therefore, benzonitrile does not form a complex with any of the aluminium atoms in trialkylaminoalumoxane.

Nitriles

The reactions of Me_4Al_2O and Et_4Al_2O with benzonitrile have been studied.[52] Methylalumoxane reacts with benzonitrile at 80°C producing acetophenone, similar to trimethylaluminium.[53,54]

After heating at 120°C for 12 h $Me_4Al_2O \cdot PhCN$ yields, upon hydrolysis, acetophenone (24%) and unreacted benzonitrile (70%), eq. (38):

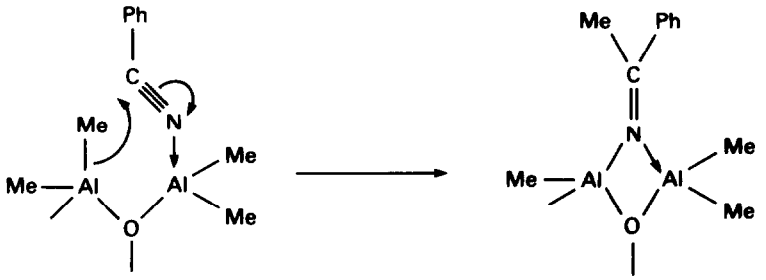

(38)

Ethylalumoxane reacts with benzonitrile in a different way to methylalumoxane, with the formation of a number of products. Nitrogen derivatives (66%) are formed in addition to small amounts of ketone and aldehyde (5%); mostly 1,3,5-triphenyl-2,4-diaza-1-aminoheptadiene-1,4 (40%). The alkylation of benzonitrile by ethylalumoxane probably proceeds in a similar manner to that for methylalumoxane, eq. (39):

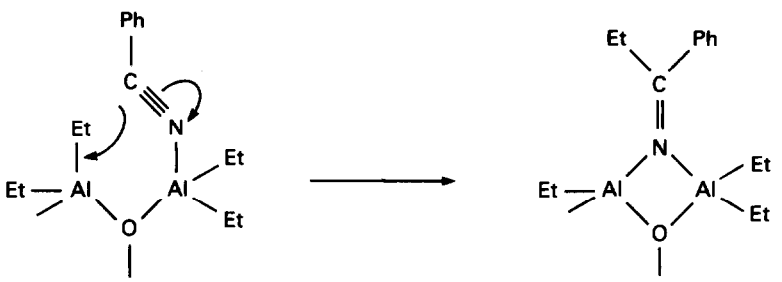

(39)

The alumoxane formed can react further, hydrogenating the nitrile carbon, eq. (40):

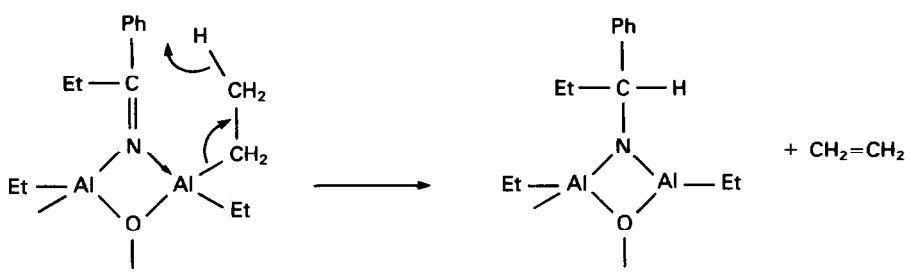

(40)

Benzonitrile, present in the reaction medium, undergoes insertion into the N—Al bond of the product formed, as a result of the decomposition of the $Et_4Al_2O \cdot PhCN$ complex, eq. (41):

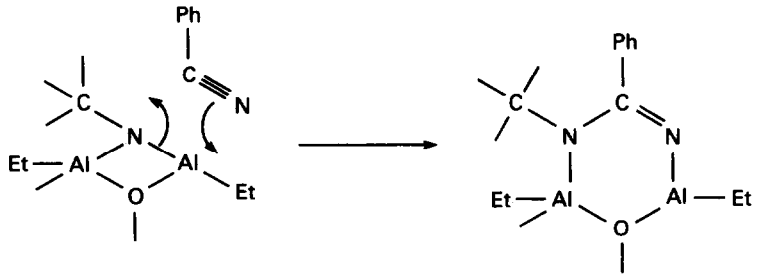

(41)

The insertion of benzonitrile into the N—Al bond may be repeated several times affording a mixture of products, in which 5-methyl-2,4,6-triphenylpyrimidine and 1,3,5-triphenyl-2,4-diaza-1-aminoheptadiene-1,4 [eq. (42)] are present:

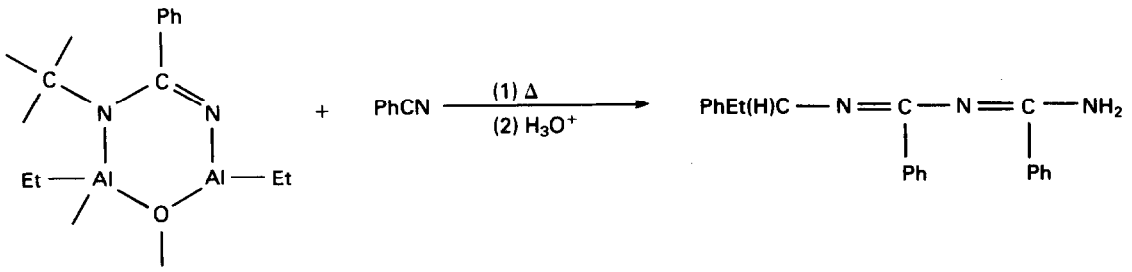

(42)

Similar insertion reactions of benzonitrile into N—Al bonds for organoaluminium compounds proceed only for strong acids, e.g. CH_3AlCl_2.[55] This indicates the role played by the Al—O—Al system in reactions of nitriles with alumoxanes.

APPLICATION OF ALUMOXANES

As it has already been mentioned, alumoxanes have been applied as catalysts for polymerization of propylene oxides,[56] monosubstituted epoxides,[57] acetaldehyde,[1,2] butadiene,[3] propylene and isobutene,[58] epichlorohydrin,[17] etc.

Recently alumoxanes, and especially methylalumoxane, have found a wider and wider application as components of catalysts for olefin polymerization.[59–67]

Zambelli and co-workers[68] have recently succeeded in preparing highly syndiotactic polystyrene in the presence of catalytic systems consisting of tetrabenzyltitanium and methylalumoxane. Catellani *et al.*[69] have used catalytic systems with $Ti(OBu)_4$ and alumoxanes as cocatalysts for the synthesis of polyacetylene films, which have interesting mechanical properties and improved air stability.

Despite many attempts of using alumoxanes as components of highly active soluble catalysts, the role of alumoxane in the catalysts' formation has not been yet fully understood, and further studies are required.

REFERENCES

1. T. Saegusa, Y. Fuji, H. Fuji and J. Furukawa, *Makromolek. Chem.* 1962, **55**, 232.
2. S. I. Ishida, *J. Polym. Sci.* 1962, **62**, 1.
3. C. Longiave and R. Castelli, *J. Polym. Sci.* 1963, **C-4**, 387.
4. G. B. Sakharovskaya, N. N. Korneev, A. F. Popov, E. J. Larikov and A. F. Zhigach, *Zh. Obshch. Khim.* 1964, **34**, 3435.
5. G. B. Sakharovskaya, N. N. Korneev, A. F. Popov, Yu. V. Kissin, S. M. Mezhkovskii and E. Kristalnyi, *Zh. Obshch. Khim.* 1969. **39**, 788.
6. J. Serwatowski, Doctoral thesis, Warsaw Technical University (1978).
7. A. Storr, K. Jones and A. W. Laubengayer, *J. Am. Chem. Soc.* 1968, **90**, 3173.
8. G. A. Razuvaev, Yu. A. Sangalov, Yu. Ya. Nel'kenbaum and K. S. Minsker, *Izv. Akad. Nauk SSSR, Ser. Khim.* 1975, 2547.

9. K. Ziegler, *Angew. Chem.* 1956, **68**, 721.
10. K. Ziegler, F. Krupp, K. Weyer and W. Larbig, *Ann.* 1960, **629**, 251.
11. L. J. Zakharkin and I. M. Khorlina, *Izv. Akad. Nauk SSSR, Ser. Khim.* 1959, 2146.
12. D. W. Harney, A. Meisters and T. Mole, *Aust. J. Chem.* 1974, **27**, 1639.
13. W. Kosinska, A. Kunicki, M. Boleslawski and S. Pasynkiewicz, *J. Organomet. Chem.* 1978, **161**, 289.
14. M. Boleslawski and S. Pasynkiewicz, *J. Organomet. Chem.* 1972, **43**, 81.
15. M. Boleslawski, S. Pasynkiewicz, K. Jaworski and A. Sadownik, *J. Organomet. Chem.* 1975, **97**, 15.
16. N. Ueyama, T. Araki and H. Tani, *Inorg. Chem.* 1973, **12**, 2218.
17. T. Araki, T. Aoyagi, N. Uyeama, T. Aoyama and H. Tani, *J. Polym. Sci.* 1973, **11**, 699.
18. J. Serwatowski, *Synthesis and Some Chemical Reactions of Tetraalkyldiboroxanes.* Wydawnictwa Politechniki Warszawskiej (1989).
19. Y. Kushi and Q. Fernando, *J. Chem. Soc., Chem. Commun.* 1969, 555.
20. E. B. Lobkovskii, A. I. Sizov, B. M. Bulychev, I. V. Sokolova and G. L. Soloveichik, *J. Organomet. Chem.* 1987, **319**, 69.
21. M. Boleslawski and J. Serwatowski, *J. Organomet. Chem.* 1983, **254**, 159.
22. J. L. Atwood, D. C. Hrncir, R. D. Priester and R. D. Rogers, *Organometallics* 1983, **2**, 985.
23. J. L. Atwood and M. J. Zaworotko, *J. Chem. Soc., Chem. Commun.* 1983, 302.
24. M. Boleslawski, S. Pasynkiewicz, K. Jaworski and A. Sadownik, *J. Organomet. Chem.* 1975, **97**, 15.
25. M. Boleslawski, S. Pasynkiewicz, A. Minorska and W. Hryniow, *J. Organomet. Chem.* 1974, **65**, 165.
26. M. Boleslawski, S. Pasynkiewicz, A. Kunicki and J. Serwatowski, *J. Organomet. Chem.* 1976, **116**, 285.
27. R. Benn, E. Janssen, H. Lehmkuhl and A. Rufinska, *J. Organomet. Chem.* 1987, **333**, 155.
28. A. Wolinska, *J. Organomet. Chem.* 1982, **234**, 1.
29. S. L. Gershkohen, I. V. Chaplina, I. L. Poletaeva, A. V. Kisin, V. M. Nosova and N. N. Korneev, *Zh. Obshch. Khim.* 1984, **54**, 2714.
30. P. N. Korneev, S. L. Gershkohen, I. V. Chaplina and A. V. Kisin, *Zh. Obshch. Khim.* 1985, **55**, 978.
31. L. Siergiejczyk and L. Synoradzki, *J. Organomet. Chem.* 1986, **311**, 253.
32. L. Siergiejczyk, M. Boleslawski and L. Synoradzki, *Polimery-Tworzywa Wielkoczasteczkowe* 1986, 397.
33. L. Siergiejczyk and M. Boleslawski, *Polimery-Tworzywa Wielkoczasteczkowe* 1986, 395.
34. S. Amdurski, C. Eden and H. Feihfeld, *Inorg. Chem.* 1961, **23**, 133.
35. T. Ueshima, T. Fujii, T. Saegusa and J. Furukawa, *Makromolek. Chem.* 1960, **38**, 58.
36. S. Pasynkiewicz, A. Sadownik and A. Kunicki, *J. Organomet. Chem.* 1977, **124**, 265.
37. D. W. Petrova, N. N. Rzevskaya, N. W. Shcherbakova, J. J. Nelkenbaum, J. A. Sangalov and K. S. Minskier, *Zh. Obshch. Khim.* 1977, **48**, 1985.
38. D. W. Petrova, N. N. Rzevskaya, N. W. Shcherbakova, J. A. Sangalov and K. S. Minskier, *Izv. Akad. Nauk SSSR, Ser. Khim.* 1978, **6**, 1373.
39. M. Boleslawski and J. Serwatowski, *J. Organomet. Chem.* 1983, **255**, 269.
40. A. Kunicki, J. Serwatowski, S. Pasynkiewicz and M. Boleslawski, *J. Organomet. Chem.* 1977, **128**, 21.
41. M. Boleslawski, J. Serwatowski and S. Pasynkiewicz, *J. Organomet. Chem.* 1978, **161**, 279.
42. A. Sadownik, S. Pasynkiewicz, M. Boleslawski and H. Szachnowska, *J. Organomet. Chem.* 1978, **152**, C49.
43. S. Pasynkiewicz and A. Piotrowski, unpublished data.
44. A. Sadownik, Praca doktorska, Warszawa (1977).
45. S. Pasynkiewicz, M. Boleslsawski and A. Sadownik, *J. Organomet. Chem.* 1976, **113**, 303.
46. S. Pasynkiewicz, *Pure Appl. Chem.* 1972, **30**, 509.
47. K. Starowieyski and S. Pasynkiewicz, *J. Organomet. Chem.* 1969, **19**, 249.
48. A. Pietrzykowski, S. Pasynkiewicz and A. Wolinska, *J. Organomet. Chem.* 1980, **201**, 89.
49. A. Sadownik, S. Pasynkiewicz and A. Kunicki, *J. Organomet. Chem.* 1977, **141**, 275.
50. S. Pasynkiewicz and W. Arabas, *Roczn. Chem.* 1965, **39**, 1393.
51. A. Piotrowski, A. Kunicki and S. Pasynkiewicz, *J. Organomet. Chem.* 1980, **186**, 185.
52. A. Piotrowski, A. Kunicki and S. Pasynkiewicz, *J. Organomet. Chem.* 1980, **201**, 105.
53. S. Pasynkiewicz and W. Kuran, *Roczn. Chem.* 1965, **39**, 979.
54. S. Pasynkiewicz and W. Kuran, *Roczn. Chem.* 1965, **39**, 1199.
55. W. Kuran, S. Pasynkiewicz and J. Serzysko, *J. Organomet. Chem.* 1971, **32** 299.
56. R. O. Colclough, *J. Polym. Sci.* 1959, **34**, 178; R. O. Colcough, *J. Polym. Sci.* 1960, **48**, 273.
57. E. J. Vandenberg. *J. Polym. Sci.* 1960, **47**, 486.
58. G. B. Sakharovskaya, *Zh. Obshch. Khim.* 1969, **39**, 788.
59. H. Sinn, W. Kaminsky, H. J. Vollmer and R. Woldt, *Angew. Chem.* 1980, **92**, 396.
60. H. Sinn and W. Kaminsky, *Adv. Organomet. Chem.* 1980, **18**, 99.
61. W. Kaminsky, *Makromolek. Chem., Rapid Commun.* 1983, **4**, 417.
62. W. Kaminskuy, K. Kulper and S. Niedoba, *Makromolek. Chem., Makromolek. Symp.* 1986, **3**, 377.
63. W. Kaminsky and H. Luker, *Makromolek. Chem., Rapid Commun.* 1984, **5**, 225.

64. W. Kaminsky, *Coordination Chemistry and Catalysis, Proc. 11th Summer School*, p. 212. World Scientific, Singapore (1988).
65. J. C. W. Chien and B. P. Wang, *J. Polym. Sci., Polym. Chem. Ed.* 1988, **26**, 3089.
66. J. C. W. Chien and A. Razavi, *J. Polym. Sci., Polym. Chem. Ed.* 1988, **26**, 2369.
67. D. T. Mallin, M. D. Rausch and J. C. W. Chien, *Polym. Bull.* 1988, **20**, 421.
68. C. Pellecchia, P. Longo, A. Grassi, P. Ammendola and A. Zambelli, *Makromolek. Chem., Rapid Commun.* 1987, **8**, 277.
69. M. Catellani, S. Destri, A. Bolognesi and E. Albizzati, *Makromolek. Chem.* 1986, **187**, 1345.

Polyhedron Vol. 9, No. 4, pp. 455–474, 1990
Printed in Great Britain

0277–5387/90 $3.00+.00
Pergamon Press plc

POLYHEDRON REPORT NUMBER 30

ELECTROCHEMICAL STUDIES ON IRON, RUTHENIUM AND OSMIUM CARBONYL CLUSTERS

SIMON R. DRAKE

University Chemical Laboratory, Lensfield Road, Cambridge CB2 1EW, U.K.

CONTENTS

1. INTRODUCTION 455

2. ONE-ELECTRON TRANSFER PROCESSES 456
   2.1. Reversible electrochemical processes 456
   2.2. The redox chemistry of trinuclear metal carbonyl clusters of Fe, Ru or Os 457
   2.3. Nucleophilic substitution in clusters 457
   2.4. Irreversible one-electron transfer reactions 459

3. MULTI-ELECTRON TRANSFER PROCESSES 460
   3.1. The mechanism of electrochemical metal–metal bond cleavage 460
   3.2. Structural change induced by electron transfer 461
   3.3. Oxidative addition in clusters 463
   3.4. Heteronuclear metal clusters 465
   3.5. Clusters containing interstitial main group atoms 466
   3.6. The electrochemical preparation of clusters 469

4. CONCLUSIONS 471

ACKNOWLEDGEMENTS 471

1. INTRODUCTION

The area of cluster electrochemistry has been the subject of but four reviews in the last 7 years.[1–4] Since these reviews were published considerable progress has been made in the now burgeoning area of cluster electrochemistry. The aim of this report is to summarize some of the important results obtained in the electrochemistry of the iron-triad carbonyl clusters, and to point out potential future trends.

Transition metal carbonyl clusters have been shown to behave as electron "sinks",[5,6] stabilizing reversible one-electron transfer reactions and hence a range of oxidation states.[7] In addition to this, unsaturated coordination sites on a cluster may enhance the reactivity of these species. Hence for the chemist, there are several fundamentally important reasons for investigating these molecular compounds, e.g. multiple oxidation states and unsaturated coordination sites.

It has previously been shown that the highest occupied molecular orbital (HOMO) is usually a σ-bonding MO of metal–metal bonding character, and the lowest unoccupied molecular orbital (LUMO) is a MO of metal–metal antibonding character.[5] As a result of this, it has been found that clusters are subject to fragmentation by electrochemical oxidation or reduction, with consequent metal–metal bond cleavage, leading to metal carbonyl fragments of lower nuclearity.[8,9] It has been shown by us[10] and others,[11] that the metal core cohesion may be reinforced towards fragmentation by chelation, capping by donor ligands or interstitial heteroatoms (C, H, N, P, As, O, S, etc.) bonded to the metal framework.[12] These examples provide information on the effects of ligands on the electrochemistry of clusters.

A variety of clusters undergo multiple one-electron redox steps, including $[FeCpS]_4$ and $[FeCp(CO)]_4$,[13,14] and several examples of multi-electron reactions, involving structural changes have been reported.[15] Many of these electron-transfer reactions take place according to an ECE mechanism. Where two-electron reduction steps are considered to occur, formally the mechanism has been interpreted to occur via stepwise one-electron transfers, in which the product of the first electron transfer is unstable, and may rearrange and is in turn further reduced.[6,16,17] When a multi-electron reduction occurs, the cluster is often degraded, leading to fragments of lower nuclearity.[18]

The activation of clusters induced by electron-transfer processes are important routes for finding new processes or alternatively improving earlier synthesis.[19,20] Electron induced nucleophilic substitution (via the Na/Ph_2CO technique)[19,20] in metal carbonyl clusters is an efficient and rapid method for the synthesis of cluster derivatives. A considerable number of results in this area have appeared over the last 6 years, with a growing interest in the elucidation of the mechanism of electron-transfer catalysed reactions involving paramagnetic intermediates. Related studies concerning the activation of iron-triad carbonyl cluster anions have been reported, via a process of oxidative addition.[21] Both of the above studies are directly connected with those using redox reagents, photochemistry, or sonochemistry in homogeneous redox catalysis.

The relationship between the structure and electrochemical activity in transition metal carbonyl clusters is discussed herein. Electrochemical redox reactions in clusters may be divided broadly into two main areas, which correspond to sections 2 and 3 of this report.

In the first section, it is noted that the vast majority of clusters undergo reversible one-electron transfer reactions (either oxidation or reduction). Generally these compounds have "closed" structures or contain ligands or heteroatoms able to stabilize the different oxidation states electrochemically generated. Examples of such clusters include the sulphur capped clusters with Fe_3S_2 cores and their derivatives, the nitrogen capped cluster $[Ru_3(CO)_9(\mu_3\text{-}NAr)_2]$,[22] tetrahedral ruthenium clusters and cubane-like clusters. Clusters of both low and high nuclearity have also been shown to be subject to stepwise one-electron transfers, and may consequently be considered as "sinks" and "sources" of electrons. Radical anions have been found to be considerably more reactive than the parent species towards nucleophilic substitution, which are often very unreactive, or only react under extreme thermal or photochemical conditions.

A considerable number of one-step multi-electron transfer reactions have been reported in the literature. These clusters may be either "open" or "closed", with the possibility of a variety of electrochemical pathways being available, leading to either cluster fragmentation or a stabilization via reinforcement by heteroatoms. The oxidized forms of a series of iron-triad carbonyl cluster dianions, were found to be more reactive towards nucleophiles than the starting materials. Thus, electron-induced oxidative addition of presumably unsaturated highly reactive materials, is a novel and extremely efficient method for the synthesis of new compounds.[21,23] Clusters with heterometallic cores are also subject to multi-electron processes which can be related again to the electrochemistry of metal–metal bonded carbonyl clusters.[24] The mechanism of a single two-electron transfer including structural changes has also been extensively studied.

2. ONE-ELECTRON TRANSFER PROCESSES

2.1. *Reversible electrochemical processes*

It has frequently been concluded that the observation of a reversible electron-transfer reaction by using techniques such as cyclic voltametry, that there is little overall change in structure between the electrochemical reactant and the product. It has recently been shown by Geiger,[3] that the observation of a reversible electrochemical wave implies that any structural change accompanying the electron transfer is chemically reversible and rapid with respect to the time scale of the electrochemical experiment.

The currents used in a cyclic voltammetry experiment may be determined by the Nernst equation and mass transport at potentials close to $E^{\ominus}$, but predominantly by the latter (i.e. convection or diffusion controlled) at relatively high potentials (e.g. very negative of $E^{\ominus}$, for a reduction). Consider the electrode processes in which it is recognized that either the oxidized or reduced form of a redox couple is in equilibrium with another compound, considering them to be initially non-redox active:

$$Ox_1 + ne^- \rightleftharpoons Red_1 \rightleftharpoons Red_2 \quad (1)$$

$$Ox_2 \rightleftharpoons Ox_1 + ne^- \rightleftharpoons Red_1. \quad (2)$$

These are the well-known CE and EC mechanisms, in which the symbol E designates a heterogeneous electron-transfer step, and C is a chemical reaction (generally taking place in solution, e.g. homogeneous). Equations (1) and (2) are mirror images, in that the CE process of eq. (2) for Ox_1 becomes an EC process when looked at from the viewpoint of the oxidation of Red_1. Hence some components of their theoretical treatments will be identical; and thus if the coupled chemical reactions and electron transfer are both rapid, a Nernstian process is observed.

Two types of equilibria are generally best considered, either intermolecular or intramolecular reactions. This area of electrochemistry has been covered in great detail by Geiger in an excellent review.[3]

In the following literature survey, it may be seen that there is a considerable number of unambiguous examples of four component (ECEC) schemes and also a number of quasi-reversible processes having well-defined structural changes between the reactants and products. These reactions provide a fascinating insight into the relationship between oxidation state and structure of the clusters under study.

2.2. *The redox chemistry of trinuclear metal carbonyl clusters of* Fe, Ru *or* Os

The clusters $[Fe_3(CO)_{12-n}L_n]$ ($n = 0$–3; L = PPh_3, $P(OMe)_3$ or $P(OPh)_3$) all undergo a chemically reversible one-electron reduction step, leading to radical anions of the type, $[Fe_3(CO)_{12-n}L_n]^{-\cdot}$.[25] These species were extensively investigated by variable-temperature ESR spectroscopy.[26] Further reduction of these radical species to the dianions $[Fe_3(CO)_{12-n}L_n]^{2-}$ occurred readily, and these species rapidly disintegrated, as shown below:

$$[Fe_3(CO)_{12-n}L_n] + e^- \overset{195\,K}{\rightleftharpoons} [Fe_3(CO)_{12-n}L_n]^{-\cdot}$$

$$[Fe_3(CO)_{12-n}L_n]^{-\cdot} + e^- \overset{195\,K}{\rightleftharpoons} [Fe_3(CO)_{12-n}L_n]^{2-} \xrightarrow{Fast} \text{Products.}$$

For one of this series of clusters, $[Fe_3(CO)_9\{P(OMe)_3\}_3]$, a one-electron reversible oxidation leads to the cationic species $[Fe_3(CO)_9\{P(OMe)_3\}_3]^+$. Presumably in this case, the replacement of three carbonyl groups by three $P(OMe)_3$ ligands results in a sufficient increase in electron density on the iron atoms to raise the energy of the highest occupied level to a point where oxidation can occur within the potential range of the solvent. The related heterometallic species $[Fe_2Ru(CO)_{12}]$ and $[FeRu_2(CO)_{12}]$ were also both readily reduced *in situ* in an ESR spectrometer cavity to produce the radical anions $[Fe_2Ru(CO)_{12}]^{-\cdot}$ and $[FeRu_2(CO)_{12}]^{-\cdot}$. These species are all active in nucleophilic substitution and electron-induced reactions.[27] It has also recently been shown by theoretical calculations that the additional electron of the radical anion occupies an antibonding orbital centred on the metallic core.[28–30]

The sulphido-capped cluster radical anion $[FeCo_2(\mu_3\text{-}S)(CO)_9]^{-\cdot}$ has a very long half-life, although the unpaired electron density is unequally distributed over the metallic cluster core.[28] A related series of clusters $[RPCoMM'(CO)_9]$ (R = Me, Ph; M = Fe; M′ = Mo, Ni) has been investigated by electrochemical and spectroscopic measurements.[31] It has been noticed that the incorporation of another metal into the trinuclear cobalt framework induces kinetic instability into the resulting radical anions, and the behaviour of these clusters has been further correlated with a mixture of steric and electronic effects of the heterometal atom and the capping groups.[31]

Thus clusters which were Lewis base derivatives exhibited one-electron reversible oxidation at fast scan rates and/or at low temperatures. In the heteronuclear clusters discussed here, the electrochemical behaviour of most mixed-metal systems was extremely complex, thereby making cyclic voltammetry data very difficult to analyse.

2.3. *Nucleophilic substitution in clusters*

The process of single electron-transfer is commonly regarded as a highly important pathway in the fields of organic chemistry, biochemistry and inorganic chemistry,[32,33] and the reactivity of the electrochemically generated radical species is a field of considerable and current interest, with much

controversy surrounding the use of radical probes and traps.[34] Classically, metal carbonyl clusters were activated only under extreme thermal conditions in their reactions with simple donor ligands. The conditions employed often resulted in polysubstitution or substantial transformation of the ligand after complexation to the metal cluster. In recent years, Lewis and co-workers have devised elegant low temperature synthesis of substituted clusters via the trimethyl amine N-oxide approach.[35] Photochemistry, redox reagents and sonochemistry have all been successfully applied to enhance the reactivity of metal carbonyl clusters in substitution reactions.[20]

As previously mentioned, the thermal reaction of ligand substitution often produces a vast range of substituted products in low yield; whereas the electron-induced nucleophilic substitution reaction is a more convenient route for the synthesis of a single product at a controlled potential. It has also been noted that the carbonyl groups around the cluster may be replaced stepwise by more basic ligands. For instance, the electron-induced replacement of carbonyl groups by $\{P(OMe)_3\}$ ligands in the tri-iron cluster $[Fe_3S_2(C_3H_2S_2)]$ has been found to proceed in a stepwise manner, leading to the new compounds, $[Fe_3S_2(C_3H_2S_2)\{P(OMe)_3\}_n]$ ($n = 1$, 2 or 3) in high yield according to the reaction sequence below.[36,37]

The addition of catalytic amounts of sodium diphenylketyl in THF to a mixture of the cluster and stoichiometric amounts of Lewis base, generates the radicals *in situ*, hence this technique may replace the electrode in the electron-induced reaction. The thermal reactions of $[H_4Ru_4(CO)_{12}]$ and $[Ru_3(CO)_{12}]$ with Lewis bases, L, give all possible derivatives $[H_4Ru_4(CO)_{12-n}L_n]$ ($n = 1$–4) and predominantly the trisubstituted complex $[Ru_3(CO)_9L_3]$, whereas stoichiometric products are obtained by the addition of catalytic amounts of diphenylketyl.[19,20] The range of new Lewis base complexes prepared numbers over 80 by this technique, and includes, tertiary phosphines and phosphites, chelating phosphines, arsines and stibines. The reactions were found to have a degree of specificity, and up to four ligands could be introduced into a cluster. This technique was also extended to $[M_3(CO)_{12}]$ (M = Fe or Os) and $[H_4Os_4(CO)_{12}]$, giving improved yields of the primary substitution products.

The mechanism proposed for these reactions is essentially one of electron-transfer chain-catalysed reactions; as an example eqs (1)–(3) give the chain reaction for $[Ru_3(CO)_{12}]$:

$$[Ru_3(CO)_{12}] + Ph_2CO^{-\cdot} \longrightarrow [Ru_3(CO)_{12}]^{-\cdot} + Ph_2CO \quad (1)$$

$$[Ru_3(CO)_{12}]^{-\cdot} + L \longrightarrow [Ru_3(CO)_{11}L]^{-\cdot} + CO \quad (2)$$

$$[Ru_3(CO)_{11}L]^{-\cdot} + [Ru_3(CO)_{12}] \longrightarrow [Ru_3(CO)_{11}L] + [Ru_3(CO)_{12}]^{-\cdot}. \quad (3)$$

The reactive species is considered to be the radical anion $[Ru_3(CO)_{12}]^{-\cdot}$, where the excess electron density is in a Ru—Ru (σ^*) antibonding orbital, which leads to a weakened bond. The cleavage of a Ru—Ru metal bond gives a 17-electron centre which readily undergoes attack by a ligand, L, and elimination of CO [eq. (2)]; and reformation of the Ru—Ru metal bond gives $[Ru_3(CO)_{11}L]^{-\cdot}$ which rapidly transfers an electron to $[Ru_3(CO)_{12}]$ to continue the catalytic cycle [eq. (3)].

Electron-induced substitution has also been found to occur in the bicapped cluster $[Ru_3(CO)_9(\mu_3\text{-NAr})_2]$, with isocyanides at an axial site, and with PR_3 at an equatorial site.[22] The radical anion of the bicapped tri-iron cluster $[Fe_3(\mu_3\text{-PPh})_2(CO)_9]^{-\cdot}$ undergoes rapid ligand substitution by CO replacement with various phosphine ligands.[38,39] Two isomeric forms of the tri-iron radical anion have been described,[39] and it is considered that the opening of the μ_3-PPh capping ligand to μ_2-coordination plays a role in the mechanism of ligand substitution, and in the reaction of the dianion formed.

The formally unsaturated clusters $[Os_4(CO)_{12}(AuPR_3)_2]$ ($PR_3 = PEt_3$, PPh_3, $PMePh_2$) undergo two reversible one-electron reductions to the radical monoanion $[Os_4(CO)_{12}(AuPR_3)_2]^{-\cdot}$ and finally the dianion $[Os_4(CO)_{12}(AuPR_3)_2]^{2-}$.[24] The existence of the radical anion was confirmed by low-temperature ESR spectroscopy at 4.2 K. The reduction could also be achieved chemically by the use of Na–Hg amalgam.[41]

A related cluster, $[Os_3(CO)_{10}(AuPPh_3)_2]$, has been studied in MeCN and it was shown that this cluster undergoes a quasi-reversible one-electron reduction at -1.31 V and a second one-electron irreversible reduction at -1.58 V (vs Ag/AgCl). On cooling to -20°C, the first reduction to the radical anion $[Os_3(CO)_{10}(AuPPh_3)_2]^{-\cdot}$ becomes reversible.[40]

The increased reactivity of anionic cluster carbonyls has recently been used in the catalytic

reduction of terminally unactivated alkenes. In the reaction sequence, the first step is loss of CO,[41] which represents the first example of a catalytic reaction that proceeds under mild enough conditions that the cluster integrity remains intact in the cycle.

2.4. *Irreversible one-electron transfer reactions*

The electrochemical generation of short lived radical anions often leads to ireversible one-electron transfers on the cyclic voltammetry time scale. An early report of the preparation of metal carbonyl cluster radical anions, $[M_3(CO)_{12}]^{-\cdot}$ (M = Fe, Ru, or Os), prepared via alkali metal reduction in THF, appears to be at variance with later results.[42] For instance the redox properties of the series of clusters $[M_3(CO)_{12}]$ (M = Ru or Os) have been extensively studied.[19,20,29,43] The latest study[44] has confirmed the generality of an overall two-electron ECE process for $[M_3(CO)_{12}]$ (M = Ru or Os) and $[M_3(CO)_{12-n}(PPh_3)_n]$ in all solvents, which probably involves a metal–metal bond cleavage step. Concomitant with reduction of the $M_3(CO)_x$ unit one finds solvent dependent, CO dissociative and ligand dissociative pathways as well as nucleophilic attack on a coordinated CO group.

Trends in the redox chemistry of the initially formed $[M_3(CO)_{12}]^{-\cdot}$ (M = Ru or Os) are summarized in Scheme 1 below, (where * represents an "opened" structure). In step A, conproportionation is only important for $[Fe_3(CO)_{12}]$, and it is only with this cluster that the $[M_3(CO)_{12}]^{-\cdot}$ radical anion has been characterized.[26,45] The thermodynamic driving force for conproportionation is probably the instability of a triangulo $[Fe_3(CO)_{12}]^{2-}$ complex. Pathway B decreases in importance from iron through to osmium which may simply be due to steric factors; also, solvent effects on this pathway are expected. The increasing thermodynamic strength of the metal–metal bond down a group is reflected in the absence of pathway E (other than M = iron) and the increasing rate for pathway C from iron through to osmium.

Reports of irreversible electrode processes but efficient electron-transfer chain (ETC)-catalysed reactions for $[Ru_3(CO)_{12}]$ contradicted the view that suitable substrates are those that exhibit chemically reversible redox behaviour. It is clear that the important criteria are relative, rather than absolute, rates of nucleophilic substitution and alternative pathways involving the key radical anions. ETC-catalysed reactions with $[Fe_3(CO)_{12}]$ are fast and efficient because of the high $[M_3(CO)_{12}]^{-\cdot}$ concentration through pathway A; the low yields are due to fragmentation reactions E, while pathway C reduces the available $[M_3(CO)_{12}]^{-\cdot}$ (M = Ru or Os) with consequential lower ETC efficiency.

Thus the reduction step has been shown to include a two-electron exchange and ring opening to yield $[Ru_3(CO)_{12}]^{2-}$, which then undergoes CO loss followed by ring closure to give the $[Ru_3(CO)_{11}]^{2-}$ anion. The intermediates in the scheme are the linear $[Ru_3(CO)_{12}]^{-\cdot}$ and the triangulo-anions $[Ru_3(CO)_{12}]^{-\cdot}$ and $[Ru_3(CO)_{11}]^{-\cdot}$. Selective and apparently fast nucleophilic substitution with $[Ru_3(CO)_{12}]$ via K/Ph_2CO has possibly been shown to be due to the intermediacy of $[\eta^1\text{-}C(O)(X)Ru_3(CO)_{11}]^{2-}$ species as well as an ETC-catalysed reaction. These trends in the electrochemical mechanisms correlate well with those attendant upon photochemical initiation.

The hydrido-anion $[HRu_3(CO)_{11}]^-$ undergoes a chemically irreversible but diffusion controlled first oxidation, and a further irreversible oxidation at higher potential. The first oxidation process becomes more reversible as the temperature is decreased and at fast scan rates, yielding a radical anion.[44]

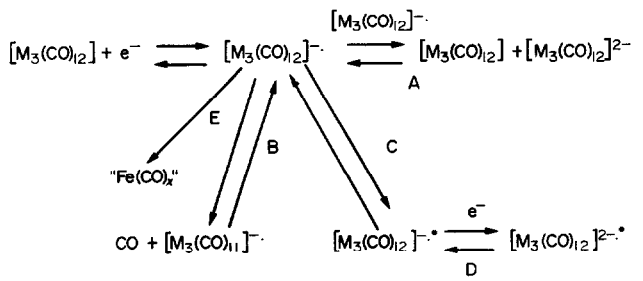

Scheme 1. The redox chemistry of $[M_3(CO)_{12}]$.

The triangulo-anionic cluster $[HRu_3(CO)_{10}(SiEt_3)_2]^-$ has been extensively studied by a variety of physical measurements, including electrochemical techniques.[46] The reaction was monitored *in situ* by cyclic voltammetry. The one-electron oxidation of the anion leads to the neutral cluster $[HRu_3(CO)_{10}(SiEt_3)_2]$ which has an extremely short lifetime.

The unsaturated clusters $[Os_4(CO)_{12}(AuPR_3)_2]$ ($PR_3 = PEt_3$, PPh_3 or PMe_2Ph) undergo two irreversible one-electron oxidation steps at $-40°C$.[24]

The linear tri-iron cluster $[Fe_3(CO)_7\{\alpha\text{-}C_6H_4(S)(N_2)\}]$ undergoes a single one-electron reduction to produce the radical anion $[Fe_3(CO)_7\{\alpha\text{-}C_6H_4(S)(N_2)\}]^{-\cdot}$, which decomposes at temperatures greater than $-10°C$ by an ECE mechanism. A single one-electron oxidation produces the radical cation $[Fe_3(CO)_7\{\alpha\text{-}C_6H_4(S)(N_2)\}]^{+\cdot}$, which is also unstable, decomposing completely at room temperature by an EC mechanism.[47]

3. MULTI-ELECTRON TRANSFER PROCESSES

3.1. *The mechanism of electrochemical metal–metal bond cleavage*

While most metal carbonyl clusters undergo one-electron redox steps, a considerable number of clusters also exhibit two-electron waves that involve structural changes, which are often extremely difficult to characterize. For a single two-electron reduction process to occur, it is necessary for the addition of the second electron to be at a potential more negative than the first. As the first electron "enters" a σ-antibonding molecular orbital of metal–metal bond character, the metal bond order is decreased, and the energy of the lowest unoccupied molecular orbital is lowered. This ensures that the second reduction is thermodynamically more favoured than the first. Cluster reduction or oxidation is in principle a useful approach to study structure and or redox relationships.

In view of their obvious importance, structural studies of redox-related pairs of clusters are still not widespread, which is possibly due to the difficulties involved in the isolation and full characterization of the usually reactive anions obtained in redox processes. A variety of examples involving dielectronic processes has appeared in the literature, and will be discussed here.

The complex $[Fe_2(CO)_6(PPh_2)_2]$ is a non-planar species, which shows in its cyclic voltammogram a single two-electron reduction to the dianion $[Fe_2(CO)_6(PPh_2)_2]^{2-}$.[48] The crystal structure of this compound showed the Fe_2P_2 core to be planar, with the Fe—Fe bond now being non-bonding. Hence the two-electron reduction causes cleavage of a metal–metal bond rather than loss of CO. The presence of the bridging diphenylphosphine ligands ensures that no fragmentation occurs, but the reduced species has a different geometry. The mechanism of electrochemical metal–metal bond cleavage in other related complexes without bridging ligands has also been investigated.[49,50]

In a related series of trimetal carbonyl clusters $[M_3(CO)_{12}]$ (M = Fe, Ru or Os) an alternative mechanism for chemical substitution of the carbonyl ligands by more basic ligands has been demonstrated.[51] The key step was the heterolytic cleavage of a metal–metal bond in the trimer unit, as shown in Scheme 2 below.

The hexanuclear osmium cluster $[Os_6(CO)_{18}]^{2-}$ has an octahedral structure, as predicted for an 86-electron cluster. Cyclic voltammetry studies show that the neutral complex and dianion are interrelated by a quasi-reversible two-electron couple. The ΔE_p values were found to follow closely the predictions of slow charge-transfer kinetics as the scan rate is increased, and the resulting change

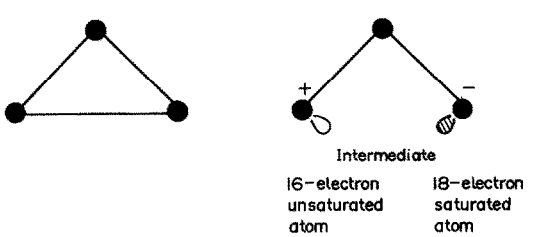

Scheme 2. A mechanism for chemical substitution of the carbonyl ligands by more basic ligands in $[M_3(CO)_{12}]$ (M = Fe, Ru, or Os).

in cathodic peak potential is consistent with a two component scheme (as shown below):[17]

$$Ox_1 + ne^- \rightleftharpoons Red_2.$$

It was concluded that, on the time scale of the cyclic voltammetry experiment, the neutral bicapped tetrahedron $[Os_6(CO)_{18}]$ and the dianionic octahedron $[Os_6(CO)_{18}]^{2-}$ appear to be interconverting directly in the electron-transfer step.

This mechanism may also apply to clusters of higher nuclearity discussed elsewhere in this review, e.g. $[Os_7(CO)_{21}]$.

3.2. *Structural change induced by electron transfer*

A series of organotriruthenium clusters, namely, $[HRu_3(CO)_9(\mu_3\text{-allenyl})]$, $[HRu_3(CO)_9(\mu_3\text{-allyl})]$ and $[HRu_3(CO)_9(\mu_3\text{-akynyl})]$, have been studied by cyclic voltammetry techniques at mercury and platinum microelectrodes.[52] A correlation between the resulting electrode potentials and both ^{13}C NMR and $\nu(CO)$ frequencies were presented. The lifetimes of all the radicals generated (e.g. $[HRu_3(CO)_9(\mu_3\text{-allenyl})]^{\cdot}$) were qualitatively longer on the electrochemical timescale than that of $[Ru_3(CO)_{12}]$, indicating that the capping organic chains favour the retention of the cluster framework on reduction. The products isolated from controlled potential electrolysis at negative potentials were found to yield dimeric complexes (e.g. $[Ru_2(CO)_6(C_6H_8)]$) which may possibly have resulted from the work-up procedures.

The tetranuclear cluster $[H_3Os_4(CO)_{12}]^-$ is irreversibly oxidized in MeCN ($E_p = 0.44$ V vs $Ag/AgNO_3$), and bulk electrolysis at this potential provides the cationic cluster $[H_3Os_4(CO)_{12}(NCMe)_2]^+$ in high yield. The cation was the first example of an osmium cluster with an unsupported butterfly structure; it was also prepared via an independent chemical route, involving chemical oxidation of $[H_3Os_4(CO)_{12}]^-$ in MeCN using $[NO]BF_4$.[53,54]

The irreversible reduction of the cation $[H_3Os_4(CO)_{12}(NCMe)_2]^+$ in MeCN ($E_p = -1.69$ V vs $Ag/AgNO_3$) leads to the regeneration of $[H_3Os_4(CO)_{12}]^-$, hence the two clusters are related by a chemically reversible electron-transfer reaction:

$$[H_3Os_4(CO)_{12}]^- + MeCN \rightleftharpoons [H_3Os_4(CO)_{12}(NCMe)_2]^+ + 2e^-.$$

The tetrahydrido clusters $[H_4Ru_4(CO)_{12}]$ and $[H_4Os_4(CO)_{12}]$ appear to be non-redox active complexes in CH_2Cl_2 and THF, with the latter cluster being nearly insoluble in both solvents.[55]

The chemistry of pentanuclear clusters has recently been extensively studied.[56,57] The cluster $[Os_5(CO)_{16}]$ and its corresponding dianion $[Os_5(CO)_{15}]^{2-}$ have related trigonal bipyramidal structures, as shown in Fig. 1.[58]

The dianion $[Os_5(CO)_{15}]^{2-}$ was found to undergo ready chemical or electrochemical oxidation to yield a radical anion $[Os_5(CO)_{15}]^{\cdot-}$ via a reversible one-electron oxidation process ($E_p = +0.08$ V). A second irreversible oxidation was also shown to occur ($E_p = +0.47$ V vs Ag/AgCl) and associated with this one-electron oxidation step was a consequent reduction. Oxidation of the dianion $[Os_5(CO)_{15}]^{2-}$ under a CO atmosphere yields the neutral cluster $[Os_5(CO)_{16}]$ in high yield. The corresponding reduction of $[Os_5(CO)_{16}]$ ($E_p = -0.65$ V) is an irreversible two-electron reduction process, and yields the dianion in high yield with loss of a carbonyl ligand.

In the oxidation of the hexanuclear octahedral ruthenium cluster $[Ru_6(CO)_{18}]^{2-}$,[59] an overall two-electron process is involved, which is chemically irreversible under normal conditions ($E_p = -0.35$ V). However, this process was shown to become chemically reversible in dilute CH_2Cl_2 solutions at 293 K providing water and oxygen are removed from the system. Even so it was

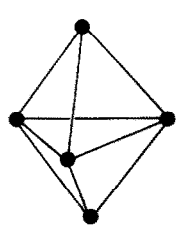

Fig. 1. The metal framework core of $[Os_5(CO)_{15}]^{2-}$.

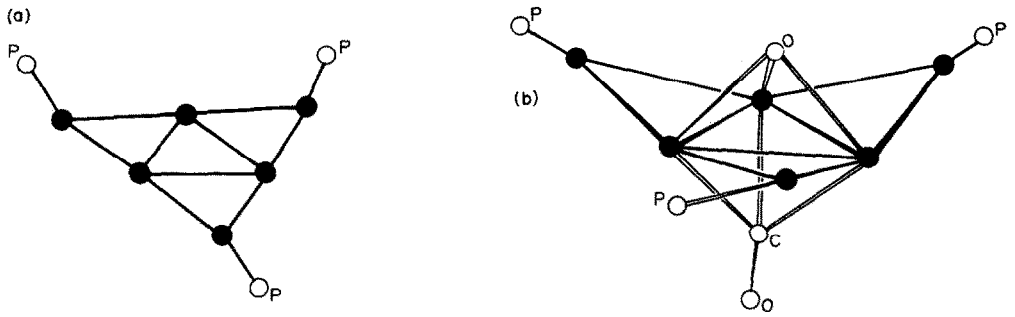

Fig. 2. The metal and phosphorus framework cores of (a) $[Os_6(CO)_{18}\{P(OMe)_3\}_3]$ and (b) $[Os_6(\mu_3\text{-}O)(CO)_{14}(\mu_3\text{-}CO)(PPh_3)_3]$.

considered that the half-life of "$[Ru_6(CO)_{18}]$" on the electrochemical timescale is less than 10^{-3} s and it seemed unlikely that it could be isolated. A simultaneous two-electron transfer is unlikely, but no paramagnetic intermediates were detected by ESR at low temperatures.[44]

A related hexanuclear osmium cluster $[Os_6(CO)_{18}]$ and its related dianion $[Os_6(CO)_{18}]^{2-}$ are notable since the structural change from the bicapped tetrahedron of $[Os_6(CO)_{18}]$ to the octahedron of $[Os_6(CO)_{18}]^{2-}$ is exactly that predicted by polyhedral skeletal electron-pair theory.[60]

The reduction of $[Os_6(CO)_{18}]$ with iodide ion proceeds by an inner-sphere process involving pre-reductive association. The electrochemical reduction involves a single, chemically reversible two-electron transfer at 0.0 V. The large peak splittings observed in the cyclic voltammograms of $[Os_6(CO)_{18}]$ at Hg, Pt or Au electrodes, are due to slow charge-transfer kinetics for the reduction process. The slowness of the electron-transfer may arise from the accompanying structural re-arrangement.[17]

The hexanuclear osmium rafts have a rich redox chemistry. Using polagraphic and cyclic voltammetry, a series of 14 compounds in the series, $[Os_6(CO)_{21-x}L_x]$ (L = $P(OMe)_3$, $P(OPh)_3$, MeCN and x = 1–4) were studied, as illustrated in Fig. 2(a).[61] In general, the compounds undergo two quasi-reversible one-electron transfer steps, to finally yield dianionic clusters. It was observed that as the number of ligands L increases, then the reduction potentials are shifted to more negative values. This was taken to be indicative of an increase in energy of the LUMO caused by inductive effects due to the donor ligands.

The observation that these raft compounds may be readily reduced to the corresponding dianions provides experimental confirmation of Mingos' theoretical calculations; which predicted the existence of such a low-lying unfilled molecular orbital in the hexanuclear raft systems.[63]

The related complexes $[Os_6(\mu_3\text{-}O)(CO)_{18-x}L_x]$ [see Fig. 2(b)] were also studied by cyclic voltammetry, and all the species studied (where L = PPh_3; x = 0–3) were shown to undergo a quasi-reversible two-electron oxidation. Additionally, as the phosphine substitution increases in this oxide species, the reduction becomes less reversible. If we assume that an empty low-lying orbital of a_2' symmetry is still present in the oxide compounds, then the steric constraints of the capping oxygen oppose the effect of addition of two electrons into the antibonding orbitals of the inner triangle, hence a less stable system is produced.[62,64]

The heptanuclear cluster $[Os_7(CO)_{21}]$ has a structure comprising of a monocapped octahedron,[65] as shown in Fig. 3, and it may be readily chemically reduced to the related dianionic species $[Os_7(CO)_{20}]^{2-}$.

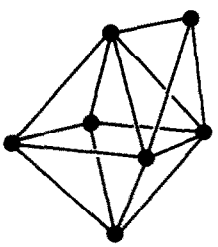

Fig. 3. The metal core geometry of the heptanuclear cluster $[Os_7(CO)_{21}]$.

The electrochemical reduction of $[Os_7(CO)_{21}]$ at a platinum electrode involves a single, chemically irreversible two-electron transfer at -0.10 V to yield the related dianion $[Os_7(CO)_{20}]^{2-}$.[66] Very complex electrochemical behaviour is observed at a hanging drop mercury electrode, possibly indicative of "non-innocent" electrode behaviour.

3.3. *Oxidative addition in clusters*

The relationship between the structure and redox state of a molecule has an impact on a wide variety of chemical, physical and biological phenomena. There is a need for more studies on the interconversion of structurally characterized pairs of clusters. This need arises in part from the difficulty of determining structures of reduction or oxidation products, which are generally quite reactive. Additionally, structural changes are often minor in chemically reversible redox couples. Thus there is increasing interest in redox processes involving more drastic, yet reversible, molecular changes during charge-transfer reactions.[3]

The approach employed in studying controlled synthesis in osmium and ruthenium carbonyl cluster chemistry has been the utilization of stable intermediates that allow the displacement of ligand groups under mild conditions. The ready preparation of $[M_3(CO)_{11}NCMe]$ and $[M_3(CO)_{10}(NCMe)_2]$ (M = Ru or Os) by trimethylamine *n*-oxide oxidation of the carbonyl groups in acetonitrile has led to an extensive chemistry of these trinuclear clusters.[35] More recently this approach has been extended to $[H_4Os_4(CO)_{12}]$, $[Os_5(CO)_{16}]$ and $[Os_6(CO)_{18}]$ clusters.[35] Our attempts to extend this technique to iron, ruthenium and osmium cluster anions have so far proved unsuccessful, possibly because the trimethylamine *n*-oxide mediated reactions go via an anionic intermediate, involving nucleophilic attack of trimethylamine *n*-oxide at a metal carbonyl.[67]

Recent studies[6] on the redox chemistry of the deca-osmium carbido cluster $[Os_{10}C(CO)_{24}]^{2}$ have shown that it has a diverse electrochemistry. This observation prompted us to investigate a series of iron, ruthenium and osmium anionic clusters, namely, $[Fe_5C(CO)_{14}]^{2-}$, $[Ru_3(CO)_{11}]^{2-}$, $[Ru_5C(CO)_{14}]^{2-}$, $[Ru_6C(CO)_{16}]^{2-}$, $[Os_5(CO)_{15}]^{2-}$, $[Os_5C(CO)_{14}]^{2-}$, $[Os_7(CO)_{20}]^{2-}$ and $[Os_{10}C(CO)_{24}]^{2-}$. An alternative technique to activate iron, ruthenium and osmium clusters by the use of either electrochemical or chemical oxidative addition is discussed here.

Previous studies by Bruce *et al.* demonstrated the use of electrochemically stimulated substitution reactions of trinuclear ruthenium clusters,[20] and prompted us initially to investigate the hexanuclear ruthenium carbido cluster $[Ru_6C(CO)_{16}]^{2-}$.[23]

The dianionic cluster $[Ru_6C(CO)_{16}]^{2-}$ (as illustrated in Fig. 4) shows an irreversible two-electron oxidation wave in dichloromethane at $E_p = +0.48$ V (vs Ag/AgCl), and associated with this wave is the consequent reduction at $E_p = -0.47$ V, i.e. the reduction wave of the oxidized product. Ferrocene was used as a one-electron standard, since it is known to be oxidized reversibly to a stable monocation. Quantitative oxidation of $[Ru_6C(CO)_{16}]^{2-}$ at a platinum gauze electrode in CH_2Cl_2 under a steady stream of carbon monoxide, yields the desired product $[Ru_6C(CO)_{17}]$ in near quantitative yield as the oxidative addition product. Oxidation at a platinum gauze at $+0.50$ V consumed 1.9 ± 0.2 electrons as the solution changed from orange to red. Cyclic voltammograms after bulk electrolysis were the reverse of those prior to electrolysis. Reduction of this solution of $[Ru_6C(CO)_{17}]$ at -0.50 V consumed 1.9 ± 0.2 electrons and re-established the original cyclic voltammogram of $[Ru_6C(CO)_{16}]^{2-}$.

Likewise, the neutral cluster $[Ru_6C(CO)_{17}]$ (see also Fig. 4) shows an irreversible two-electron reduction at $E_p = -0.46$ V vs Ag/AgCl, and also associated with this reduction step is an oxidation wave at $E_p = +0.45$ V, i.e. the oxidation wave of the reduced product $[Ru_6C(CO)_{16}]^{2-}$. The reduction of this cluster to the dianion at a platinum gauze electrode in CH_2Cl_2 under a constant

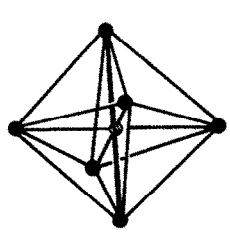

Fig. 4. The ruthenium carbide cores of $[Ru_6C(CO)_{16}]^{2-}$ and $[Ru_6C(CO)_{17}]$.

stream of argon gas occurs in quantitative yield. No paramagnetic species could be detected by ESR during the formation of the dianion. On the same electrochemical scale the $Fe(Cp)_2/[Fe(Cp)_2]BF_4$ couple is +0.54 eV.[6] These simple experiments demonstrate that the wave observed at −0.46 V is due to a two-electron process resulting in the formation of $[Ru_6C(CO)_{16}]^{2-}$, which can be anodically oxidized back to the starting material. These results are consistent with the previously established stability of both the neutral and dianionic forms of the hexanuclear ruthenium cluster.

Treatment of $[Ru_6C(CO)_{16}]^{2-}$ with Lewis base donor ligands such as CO, $P(OMe)_3$, PPh_3, PPh_2Me, dppm, RCCR′ or C_5Me_5H, in the presence of two equivalents of the oxidant $[Fe(CP)_2]BF_4$, results in the formation of a series of new substituted compounds in excellent yield. These derivatives may also be prepared by controlled potential electrolysis at +0.50 V in the presence of the required ligand using a platinum electrode in CH_2Cl_2, followed by chromatographic separation of the products.

Thus an alternative method of synthesis using either chemical (with a suitably matched oxidant—see Table 1) or electrochemical oxidation of iron, osmium or ruthenium cluster dianions in the presence of the ligand is possible at room temperature.

Table 1 summarizes (all oxidations were found to be irreversible) electrochemical data for the clusters examined, with E_p oxidation being the second oxidation wave (for Ru_6 and Os_7 clusters only a single two-electron irreversible oxidation wave is observed) and E_p reduction being the reduction wave of the oxidized cluster. The chemical oxidation routes were generally preferred to the electrochemical oxidation as preparative methods, since isolation of the products from electrochemical solutions is complicated by the presence of an excess of base electrolyte.

The dianions $[Os_7(CO)_{20}]^{2-}$ and $[Os_{10}C(CO)_{24}]^{2-}$ were found to be less reactive than the smaller iron, osmium and ruthenium anionic clusters. This could possibly be due to the increasing carbonyl saturation of the cluster surface. However, the lower temperature used results in moderate yields of several new compounds.

The redox reactions described above appear to be general for systems satisfying the following requirements:

(i) The oxidation potential of the cluster anion is between −0.5 to +1.5 V vs Ag/AgCl.
(ii) The reduction potential of the oxidant is higher than the oxidation potential of the cluster to ensure that the redox reaction may occur.
(iii) The oxidant does not react with the cluster anion, i.e. it acts as an "innocent" oxidant.
(iv) The metal carbonyl cluster bears at least a dinegative charge.

The mechanism proposed for these reactions is essentially one of electron transfer between the cluster anion and the oxidant. As an example, for $[Ru_6C(CO)_{16}]^{2-}$ the reactive species is presumably the electron-deficient cluster "$[Ru_6C(CO)_{16}]$" (containing a vacant coordination site) which may

Table 1.

Cluster	E_p(Oxidation) (V)[a,b]	E_p(Reduction) (V)[a,c]	Oxidant
$[PPN]_2[Fe_5C(CO)_{14}]$	+0.60	−0.60[68]	$AgBF_4$
$[PPN]_2[Ru_3(CO)_{11}]$	+0.22	−0.20[43]	$[C_7H_7]BF_4$
$[PPN]_2[Ru_5C(CO)_{14}]$	+0.15	−1.78	Ph_3CBF_4 or $[C_7H_7]BF_4$
$[PPN]_2[Ru_6C(CO)_{16}]$	+0.48	−0.47	$Fe(Cp)_2BF_4/FeCl_3$
$[PPN]_2[Os_5(CO)_{15}]$	+0.47	−0.65	$Fe(Cp)_2BF_4/FeCl_3$
$[PPN]_2[Os_5C(CO)_{14}]$	+0.35	−1.50	$Fe(Cp)_2BF_4$
$[PPN]_2[Os_7(CO)_{20}]$	+0.41	−0.10	$Fe(Cp)_2BF_4/FeCl_3$
$[PPN]_2[Os_{10}C(CO)_{24}]$	+1.11	−1.30	$AgBF_4$

[a] Recorded at a Ag/AgCl reference electrode in CH_2Cl_2, all solutions used for electrochemical experiments were 0.1 M in electrolyte (tetrabutylammonium tetrafluoroborate). All potentials are uncorrected for solution resistance and junction potentials. Typical scan rates were 100 or 200 mV s^{-1}.

[b] Controlled potential electrolysis performed using a platinum basket electrode.

[c] E_p(reduction) is the reduction wave of the oxidized cluster.

lose or gain more carbonyl ligands as necessary:

$$[Ru_6C(CO)_{16}]^{2-} + Fe(Cp)_2^+ \longrightarrow \text{"}[Ru_6C(CO)_{16}]\text{"} + Fe(Cp)_2 \quad (1)$$

$$\text{"}[Ru_6C(CO)_{16}]\text{"} + L \longrightarrow [Ru_6C(CO)_{16}L] \quad (2)$$

$$\text{"}[Ru_6C(CO)_{16}]\text{"} + L{-}L \longrightarrow \text{"}[Ru_6C(CO)_{16}L{-}L]\text{" etc.} \quad (3)$$

$$\text{"}[Ru_6C(CO)_{16}L{-}L]\text{"} \longrightarrow [Ru_6C(CO)_{15}L{-}L] + CO. \quad (4)$$

(where L is a two-electron donor and L—L is a four-electron donor).

Thus rapid, and large, stoichiometric preparations in non-polar solvents may be performed using simple chemical redox reagents. It is now possible to tune a redox reagent to a potential slightly higher than that of the redox potential of the reaction. The metal cyclopentadienyl cations $[Fe(C_5R_5)_2]^+$ (R = H, Me, Et, etc.) readily spring to mind, with a wide range of electrochemical potentials, and are easily removed at the end of the reaction and most importantly act as "innocent" oxidants. Tropyllium ($C_7H_7^+$) and trityl (Ph_3C^+) salts have also found limited application, but both are known to cause further complications in that they can both act as "non-innocent" oxidants, either by reacting with the cluster to form an adduct, e.g. $[Ru_6C(CO)_{14}(C_{14}H_{14})]$,[69] or by hydride abstraction in the case of the trityl cation.

A wide variety of other cationic redox reagents are still largely unexplored territory or conversely, widely misunderstood! Salts of Ag^+ have been used for a long time as oxidants because of their strong oxidizing power, but caution is necessary in their use, since their relative oxidizing power is strongly solvent dependent, and because they are well known to react with the cluster being studied.

Nitrogen cations of the type $[N(C_6H_4Br\text{-}p)_3]^+PF_6^-$ and $[N_2C_6H_4NO_2\text{-}p]^+PF_6^-$ are also readily obtained, and are powerful oxidizing agents (E_p = +1.32 and +0.48 V vs Ag/AgCl in CH_2Cl_2),[70] and nitrosonium salts $[NO]^+BF_4^-$ are also good oxidants, but it has also been observed that they can react with the cluster, rather than oxidize it.

Thus for anionic metal carbonyl clusters where the above conditions are favourable, the fast reaction time and mild reaction conditions should readily facilitate a vast expansion in their chemistry.

3.4. *Heteronuclear metal clusters*

The role of solvent donicity has been shown to be of some considerable importance in the stabilization of reduced and oxidized cluster species. Results obtained for the $[RuCo_3(CO)_{12}]^-$ complex in donor solvents such as DMF or DMSO show that the anion undergoes two one-electron reduction steps;[71] while in the poorer donor solvent, 1,2-dichloroethane, a single two-electron wave is obtained. Hence it is possible to separate a single two-electron wave into two one-electron waves by careful choice of the solvent.[72]

A number of formally unsaturated heteronuclear clusters containing metals of group 1b have been characterized.[73–75] These clusters contain fewer electrons than is formally required by the effective atomic number rule if the metal–metal bonds are considered as localized two-centre two-electron interactions. For the clusters $[HOs_3(CO)_{10}AuPPh_3]$ and $[Os_3(CO)_{10}(AuPEt_3)_2]$,[75] there is a close analogy with the hydrido carbonyl complex $[H_2Os_3(CO)_{10}]$,[76] which contains two electrons fewer than the 48 electrons required for three two-centre two-electron bonds. In these compounds the supposed "unsaturation" is considered to be localized in the Os—Os "double" bond, which is itself doubly-bridged by two one-electron donor groups, either hydrides or $AuPR_3$ groups. A similar explanation has been offered for the anion $[(HOs_3(CO)_{10})_2Au]^-$ (as shown in Fig. 5), where the gold

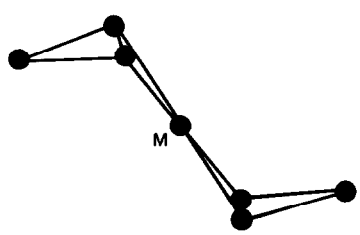

Fig. 5. The metal framework geometries of $[(HOs_3(CO)_{10})_2M]^-$ (M = Au, Ag or Tl).

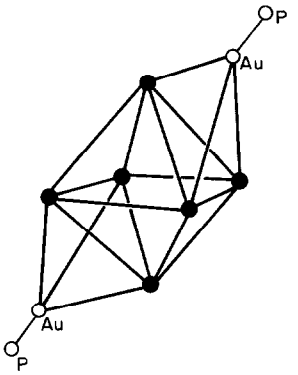

Fig. 6. The metal core structure of $[Os_6(CO)_{18}(AuPMe_3)_2]$.

atom links the two Os_3 units via bonding across two short Os—Os bonds.[74] In view of this "unsaturation" it should be readily possible to add electron pairs either chemically or electrochemically without causing cluster breakdown.

For the monoanion $[(HOs_3(CO)_{10})_2Ag]^-$ (see Fig. 5),[77] the cyclic voltammogram in MeCN at 293 K shows a single irreversible reduction step ($E_p = -1.35$ V). On cooling the solution to 268 K the reduced species is stabilized, and two quasi-reversible reduction steps ($E_p = -1.29$ and -1.38 V) are observed, leading to the corresponding di- and trianionic species, respectively. These results indicate that the anion can accept an electron pair without fragmentation occurring.

The related mixed-metal bow-tie complex $[AsPh_4][(HOs_3(CO)_{10})_2Tl]$ (as illustrated in Fig. 5), has also been studied by cyclic voltammetry. This thallium containing compound was investigated in CH_2Cl_2, and at 293 K, a single irreversible reduction step is observed at $E_p = -1.07$ V. For this species a quasi-reversible oxidation was observed at $E_p = +0.39$ V leading to the neutral cluster.[78]

The heterometal gold derivative $[PPN][(HOs_3(CO)_{10})_2Au]$ was similarly studied. Surprisingly at 293 K this cluster has two reduction steps, the first is reversible ($E_p = -1.19$ V) and the second is a quasi-reversible reduction ($E_p = -1.41$ V) leading to the trianion species $[(HOs_3(CO)_{10})_2Au]^-$. While above +0.6 V degradative oxidation waves are observed, resulting in cluster decomposition.[79]

For the digold cluster $[Os_6(CO)_{18}(AuPMe_3)_2]$ (see Fig. 6) the cyclic voltammogram in CH_2Cl_2 at 293 K, showed an irreversible one-electron oxidation at $E_p = +0.61$ V, which led to cluster decomposition, rather than the hoped for isolation of a radical cation.[66,80]

Finally the giant planar cluster $[Os_9Hg_3(CO)_{33}]$ was investigated exhaustively via cyclic voltammetry, and no redox chemistry was observed.[81]

3.5. *Clusters containing interstitial main group atoms*

Changes in structure accompanying electrochemical oxidation or reduction of clusters have been reviewed recently.[46] A wide variety of compounds were discussed, including triangular, cubane, octahedral and larger clusters. There is an increasing interest in redox processes involving more drastic, yet reversible, molecular transfer reactions.[82]

The presence of heteroatoms (C, H, N, P, As, S) in metal carbonyl clusters may be responsible for some of their unusual electrochemical behaviour and stabilization of a wide range of oxidation states.

The ruthenium cluster $[Ru_4C(CO)_{13}]$ has a butterfly geometry, with the carbide atom attached to all four ruthenium atoms (see Fig. 7). It shows a reversible one-electron oxidation step at +0.63

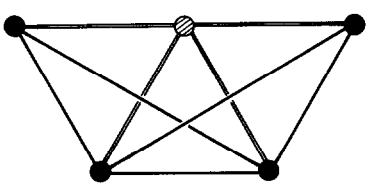

Fig. 7. The Ru_4C geometry adopted by $[Ru_4C(CO)_{13}]$.

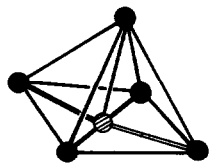

Fig. 8. The core geometry of the M_5E clusters (E = C or N) $[M_5C(CO)_{15}]$, $[M_5C(CO)_{14}]^{2-}$ and $[M_5N(CO)_{14}]^{-}$ (where M = Fe, Ru, or Os).

V (vs Ag/AgCl) to yield the cationic cluster $[Ru_4C(CO)_{13}]^+$, which may also be prepared via Ag^+ oxidation of the parent compound. Surprisingly no readily discernible reduction waves could be interpreted, apart from those leading to probable cluster decomposition.[83]

In the clusters $[M_5C(CO)_{15}]$ (M = Fe, Ru and Os), the carbido atom sits at the bottom of the square-based pyramid (see Fig. 8). It is formally considered to donate four electrons to the cluster framework, and thereby "hold" the cluster together.

The cluster $[Fe_5C(CO)_{15}]$ has recently been shown to be reduced to the dianion $[Fe_5C(CO)_{14}]^{2-}$ in a single quasi-reversible two-electron reduction step, followed by the loss of one carbonyl ligand.[68] The chemical and electrochemical reduction of $[M_5C(CO)_{15}]$ (M = Ru or Os) likewise proceeds via a two-electron reduction to yield the corresponding dianions $[M_5C(CO)_{14}]^{2-}$ (as shown in Fig. 8) with structures identical to that of the iron analogue.[84] All three pentanuclear carbido clusters $[M_5C(CO)_{14}]^{2-}$ have recently been activated via the oxidative addition technique, to produce the parent cluster $[M_5C(CO)_{15}]$.[21] Thus yielding three more pairs of interconvertible structurally characterized clusters, which may be further studied.

The related nitrido anionic clusters $[M_5N(CO)_{14}]^-$ (M = Fe or Ru) (see Fig. 8), have also been investigated by electrochemical techniques; they undergo an irreversible one-electron oxidation (for iron only), and an irreversible two-electron reduction step to the trianion $[M_5N(CO)_{14}]^{3-}$.[68,85] This difference in electrochemical behaviour on changing the heteroatom may possibly be ascribed to the difference in overall anionic charge between the two series of clusters:

$$\text{"}[Fe_5N(CO)_{14}]\text{"} \longleftarrow [M_5N(CO)_{14}]^- + 2e^- \longrightarrow [M_5N(CO)_{14}]^{3-}.$$

For hexanuclear clusters, the dianion $[PPN]_2[Fe_6C(CO)_{16}]$ has an octahedral structure (see Fig. 9), and undergoes two irreversible oxidation steps. Controlled potential electrolysis at the second oxidation step leads to the known pentanuclear cluster $[Fe_5C(CO)_{15}]$ by cluster fragmentation (see below). This is consistent with previous observations[86] that the chemical oxidation of $[Fe_6C(CO)_{16}]^{2-}$ generates the neutral cluster $[Fe_5C(CO)_{15}]$:

$$[Fe_6C(CO)_{16}]^{2-} \longrightarrow \text{"}[Fe_6C(CO)_{16}]\text{"} + 2e^- \longrightarrow [Fe_5C(CO)_{15}] + \text{other products.}$$

This cluster also shows an irreversible reduction step, initially forming the tetraanionic species $[Fe_6C(CO)_{16}]^{4-}$, which rapidly fragments to yield the dianion $[Fe_5C(CO)_{14}]^{2-}$.[18]

The dianionic cluster $[Ru_6C(CO)_{16}]^{2-}$ has an octahedral geometry, with the carbide at the centre. This cluster has an irreversible two-electron oxidation, and associated with this is a consequent reduction at $E_p = -0.47$ V, i.e. the reduction wave of the oxidized product. Quantitative oxidation of $[Ru_6C(CO)_{16}]^{2-}$ at a platinum gauze electrode in CH_2Cl_2 under a steady stream of CO, gives the desired product $[Ru_6C(CO)_{17}]$ in near quantitative yield as the oxidative addition product.

In a similar manner, the neutral cluster $[Ru_6C(CO)_{17}]$ shows an irreversible two-electron

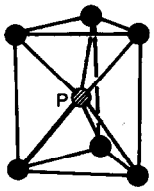

Fig. 9. The Os_6P framework of $[PPh_3Me][Os_6P(CO)_{18}]$.

reduction. Also associated with this reduction step is an oxidation wave at $E_p = +0.45$ V, i.e. the oxidation wave of the reduced product $[Ru_6C(CO)_{16}]^{2-}$. These redox processes have yielded another pair of interconvertible structurally characterized complexes.[21,23]

The substituted ruthenium cluster $[Ru_6C(CO)_{14}(\eta^6\text{-}C_6H_3Me_3)]$ shows a two-electron reduction step in CH_2Cl_2 at $E_p = -0.84$ V (vs Ag/AgCl) to yield the dianion $[Ru_6C(CO)_{13}(\eta^6\text{-}C_6H_3Me_3)]^{2-}$. Associated with this reduction is the oxidation wave of the reduced product at -0.07 V. These results are in accord with the chemical reduction of $[Ru_6C(CO)_{14}(\eta^6\text{-}C_6H_3Me_3)]$ with Na_2CO_3/MeOH to yield the dianionic species $[Ru_6C(CO)_{13}(\eta^6\text{-}C_6H_3Me_3)]^{2-}$.[87]

The related nitrido complex $[PPN][Ru_6N(CO)_{16}]$ has recently been shown to consist of an octahedron of ruthenium atoms, with the nitride at the centre.[85] The cyclic voltammogram of this cluster shows one irreversible two-electron reduction step, and potential electrolysis at the required potential yields the trianionic cluster $[Ru_6N(CO)_{16}]^{3-}$.[85]

Recent elegant studies in this laboratory have yielded the first encapsulated phosphorus cluster of the iron-triad, namely $[PPh_3Me][Os_6P(CO)_{18}]$, which has a trigonal prismatic geometry, as illustrated in Fig. 9.[88] Electrochemical investigations on this cluster revealed the presence of a quasi-reversible two-electron reduction ($E_p = -1.24$ V) to yield the trianionic complex $[Os_6P(CO)_{18}]^{3-}$.

Oxidized and reduced states of large metal carbonyl clusters are of increasing interest. This is due in part to their higher reactivity and also, as mentioned earlier, to the possible analogy between the binding of ligands to a metal cluster and the binding of ligands to a metal surface. The chemistry and reactivity of high nuclearity osmium clusters has been extensively reported, but little information on the redox chemistry of these species is available. However, of the larger clusters that have been studied by electrochemical techniques it has been reported that the addition or removal of electrons is often associated with changes in structure. Well-defined examples include $[FeCpS]_4$ and $[FeCp(CO)]_4$ which both show several reversible one-electron steps, each associated with a small change in the structure of the cluster.[13,14] For osmium carbonyl clusters evidence is accumulating, which suggests that the stronger Os—Os bonds lead to higher activation energies for structural changes generating electrochemically irreversible features in the cyclic voltammogram.[6,17]

The decanuclear ruthenium cluster $[PPN]_2[Ru_{10}(C)_2(CO)_{24}]$ has a structure comprising two Ru_6 octahedra joined by one common edge, as shown in Fig. 10(a).[89] This dianionic cluster undergoes three quasi-reversible one-electron reduction–oxidation steps, as shown by cyclic voltammetry; two cathodic one-electron reductions yield the paramagnetic species $[Ru_{10}(C)_2(CO)_{24}]^{3-}$ and the diamagnetic cluster $[Ru_{10}(C)_2(CO)_{24}]^{4-}$. The dianionic species also shows one quasi-irreversible oxidation wave to the radical anion $[Ru_{10}(C)_2(CO)_{24}]^{-\cdot}$. Thus four oxidation states $-1/-2/-3/-4$ of this cluster may be reached and stabilized.[90]

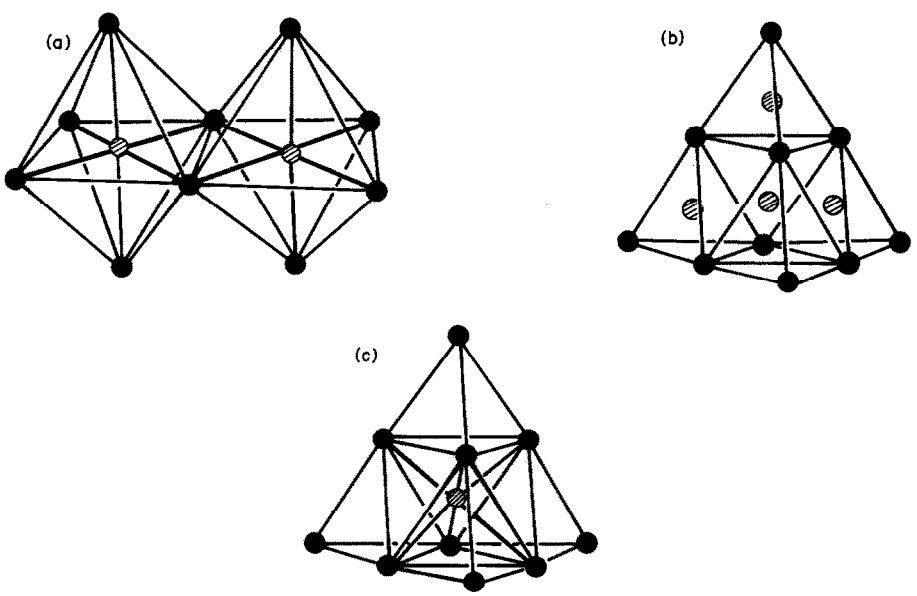

Fig. 10. The metal-heteroatom cores of (a) $[PPN]_2[Ru_{10}(C)_2(CO)_{24}]$, (b) $[PPN]_2[H_4Os_{10}(CO)_{24}]$ and (c) $[PPN]_2[Os_{10}C(CO)_{24}]$.

Two other related decanuclear clusters have been extensively studied, namely the complexes $[PPN]_2[H_4Os_{10}(CO)_{24}]$ and $[PPN]_2[Os_{10}C(CO)_{24}]$. These two compounds have related tetracapped octahedral structures, with the main group heteroatoms in interstitial sites as shown [see Figs 10(b) and (c)].[91,92] The latter cluster has been investigated more extensively, possibly because its mode of preparation is a little more straightforward. Both of these dianionic decanuclear osmium clusters were found to undergo ready chemical or electrochemical oxidation to yield a radical anion $[Os_{10}X(CO)_{24}]^{-\cdot}$ (X = H_4 or C) via a reversible one-electron oxidation process.[93,94] A second irreversible oxidation was also shown to occur for both clusters, and associated with this one-electron oxidation step was a consequent reduction.

The dianionic cluster $[PPN]_2[Os_{10}C(CO)_{24}]$ was oxidized at a hanging drop mercury electrode with "non-innocent" behaviour by the electrode occurring. The resultant cyclic voltammograms showed two quasi-reversible oxidations, indicating that a new species had been generated on the mercury surface.[16] Mercury is known to interact strongly with many organometallic complexes,[95,96] and to speed up the kinetics of some electrochemical reactions.[95] It is possible that a similar interaction in this case may lead to the incorporation of mercury into an oxidized form of $[Os_{10}C(CO)_{24}]^{2-}$. Evidence for the strong interaction between this cluster and a mercury electrode were also found in the reductive electrochemistry.[16]

This dianonic complex was readily reduced in THF or CH_2Cl_2 at a platinum electrode (see Fig. 11(a), wave A in the cyclic voltammogram), by two electrons (in a chemically reversible reduction) to yield the tetraanionic species $[Os_{10}C(CO)_{24}]^{4-}$. This reduction was studied at a variety of electrodes and in different media and was found to be associated with an oxidation at more positive potentials (wave C). When a solution of $[Os_{10}C(CO)_{24}]^{2-}$ is cooled [see Fig. 11(b)–(d)] the two-electron wave (wave A) is split into a quasi-reversible one-electron process (wave A) and an irreversible wave (wave A′) which moved to a more negative potential as the temperature is reduced. The broad wave was linked to the oxidative feature (wave C) and demonstrated that the structural change occurs on the addition of the second electron to $[Os_{10}C(CO)_{24}]^{2-}$, as illustrated in Scheme 3. The quasi-reversible electrochemical process was associated with the formation of the trianion $[Os_{10}C(CO)_{24}]^{3-}$, which could be independently synthesized by the slow chemical reduction of $[PPN]_2[Os_{10}C(CO)_{24}]$.

The above study demonstrated that the electrochemical reduction of $[Os_{10}C(CO)_{24}]^{2-}$ occurs in two chemically reversible steps. The addition of the first electron is fast and reversible while the addition of the second is kinetically slow because of a small change in structure of the cluster during this step. The surprising result is that such a minor change in structure is associated with such a substantial peak separation between the reduction and oxidation waves of this second reduction step.

It should be noted that $[Os_{10}C(CO)_{24}]^{2-}$ is the only osmium cluster to date and one of few clusters of any type to have been characterized in five oxidation states. The sequence $[Os_{10}C(CO)_{24}]^{0/-1/-2/-3/-4}$ contains three diamagnetic species and two radical species. The impressive range of redox states for this cluster (Scheme 3) testifies to the great stability of the "$[Os_{10}C(CO)_{24}]$" core, and also the ability of this decanuclear cluster to act as an electron reservoir.

3.6. *The electrochemical preparation of clusters*

There are now a wide variety of clusters that have been prepared using this technique, of which the following are but a choice selection. The cluster $[PPh_4][Fe_3(CO)_9(\mu_3\text{-}CCH_3)(\mu_3\text{-}CO)]$ undergoes

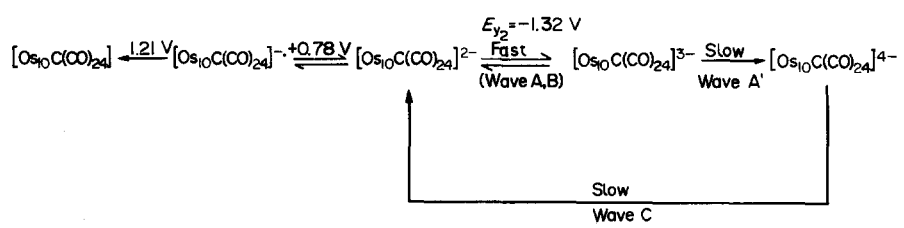

Scheme 3. The electrochemical interconversion of $[PPN]_2[Os_{10}C(CO)_{24}]$ to its other related redox states.

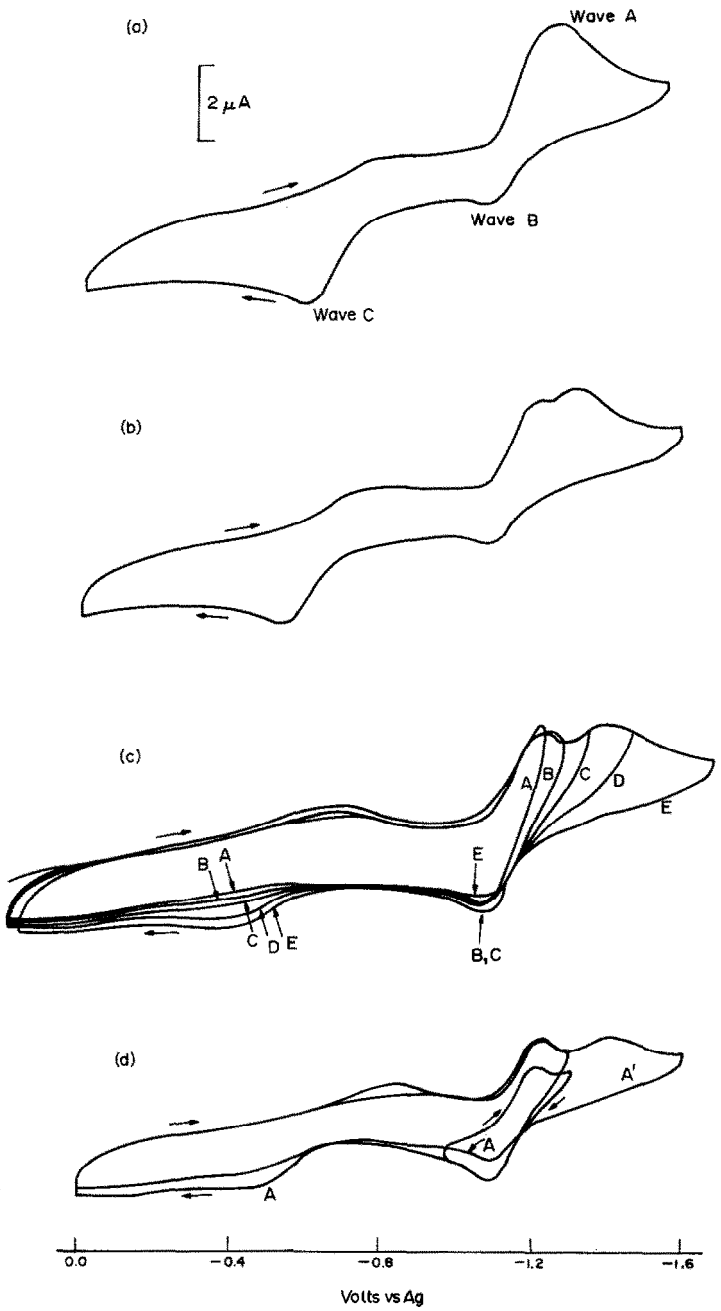

Fig. 11. The cyclic voltammogram of $[PPN]_2[Os_{10}C(CO)_{24}]$ in THF–0.1 M TBAF, showing the effect of temperature on the shape of wave A: (a) −5°C, (b) −25°C, (c) −35°C with a range of switching potentials, (d) −50°C. All scan rates are 100 mV s^{-1}, and the voltammograms are recorded against a silver wire pseudo-reference.

a one-electron reduction leading to an unstable paramagnetic dianion $[Fe_3(CO)_{10}(\mu_3\text{-}CCH_3)]^{2-}$; this complex regenerates the starting material on exposure to air. While treatment of the electrochemically generated complex $[Fe_3(CO)_{10}(\mu_3\text{-}CCH_3)]^{2-}$ with MeOH yields the cluster anion $[Fe_3(CO)_9(\mu_3\text{-}CCCH_3)]^-$.[97]

Tetranuclear clusters with four triply-bridging ligands have a cubane-like structure and show rich electrochemistry, often undergoing multiple reversible electron-transfer reactions. The complex $[Cp_4Fe_4(\mu\text{-}CO)_4]$ is oxidized in four reversible one-electron steps from the neutral complex through to a tetracation.[4] This complex may thus be viewed as an "electron sponge". Structural data is

limited to the neutral and monocationic complexes. An increase in metal–metal bond length is observed as the cluster goes from a slightly distorted tetrahedral to a tetragonal geometry.[98]

Oxidative addition reactions offer a rapid and convenient route for the synthesis of new compounds or modified clusters. For example, the alkyne substituted cluster $[Ru_6C(CO)_{15}(RCCR')]$ is formed via reaction of $[Ru_6C(CO)_{16}]^{2-}$ with $Fe(Cp)_2BF_4$ in the presence of the appropriate alkyne.[21]

4. CONCLUSIONS

A great number of electrochemical investigations into a wide variety of iron-triad clusters have been discussed in this review. In particular, high nuclearity clusters have finally been studied in some detail. A variety of clusters were shown to undergo multiple one-electron oxidation and reductions, the mechanisms of which have been extensively probed.

It has been shown that a host of transition metal carbonyl clusters of the iron-triad undergo reversible one-electron reactions. These species may be considered as "sinks" for electrons. The major problem being in their isolation, since electrochemically generated radicals are often unstable and/or air-sensitive. However, recent advances in techniques of electrocrystallization,[99] now make it possible to crystallize unstable species electrochemically. The added possibility of stabilizing or alternatively bridging clusters with charge-transfer cation–anions (TCNQ or TTF etc.) may also be pursued. Although it seems likely that by adding these species to the electrochemical cell, the resulting crystals may show unusual conducting properties and in different crystal packing to the parent compound.

The synthesis and chemistry of clusters with organic fragments attached is now well developed,[100] and it seems timely for detailed electrochemical investigations into their redox properties. The use of dichelating ligands ligand is well precedented, with the use of chelating phosphine ligands, e.g. dppm; but very little work has appeared on the corresponding dialkyne bridged clusters, e.g. the use of long chain acetylenes (or possibly polyacetylene) to link clusters and then to study their electrochemical properties.

These developments could, if successful, be applied to doping clusters into polymeric supports and their subsequent use as electrode materials in their own right. Microelectrodes are slowly finding application in electrochemistry,[101] and it seems possible that for clusters which are stable to air and moisture and have a known set of potentials which they may be oxidized at or conversely reduced at could be used as electrodes.[102]

The use of variable temperature cyclic voltammetry is still in its infancy, but the few papers which report the use of this technique, show its great potential for a deeper understanding and knowledge of electrochemical processes. This technique coupled with variable temperature ESR and optical studies would allow a more precise evaluation of electrochemically generated complexes, and also the evaluation of the onset of band-like properties in these complexes.[103]

The observation of an electrochemical–chemical–electrochemical reaction, in which the chemical step involves a structural change in the cluster, has been discussed. The cluster geometry changes induced by electron-transfer are now being actively investigated. Although a study of a series of clusters containing different heteroatoms (e.g. C, H, P, N, or S; or alternatively Fe, Ru and Os)[104] has not yet been properly undertaken; or more pertinently how does the value of E_p reduction/oxidation change with increasing size of the cluster?

The behaviour of heterometal carbonyl clusters is still very poorly understood. This may possibly be because their electrochemical behaviour is more complex than their corresponding homonuclear clusters, and cluster decomposition or fragmentation is more often the norm.

In conclusion, the field of cluster metal carbonyl electrochemistry is a one of growing interest, with many novel applications now becoming possible in the areas of electrosynthesis, the isolation of paramagnetic species and in electrocatalysis.

Acknowledgements—I am grateful to St John's College Cambridge for the award of a research fellowship and to Professor Lord Lewis for encouragement and advice.

REFERENCES

1. P. Lemoine, *Coord. Chem.* 1982, **47**, 56.
2. P. Lemoine, *Coord. Chem.* 1988, **83**, 169.

3. W. E. Geiger, *Progress in Inorganic Chemistry* (Edited by S. J. Lippard) Vol. 33, p. 275. John Wiley, New York (1985).
4. Cyclic voltammetry data in Ref. 14 was misinterpreted, so what was considered to be a reversible reduction, was in fact the first oxidation wave of the neutral compound. W. E. Geiger and N. G. Connelly, *Adv. Organomet. Chem.* 1985, **24**, 114.
5. J. W. Lauher, *J. Am. Chem. Soc.* 1979, **101**, 2604.
6. S. R. Drake, M. H. Barley, B. F. G. Johnson and J. Lewis, *J. Chem. Soc., Chem. Commun.* 1987, 1657.
7. See ref. 2, in particular refs 7–14.
8. C. U. Pittman, M. G. Richmond, M. Absi-Halibi, H. Vahrenkamp, F. Richter and H. Beurich, *Angew. Chem. Int. Edn Engl.* 1982, **21**, 786.
9. M. G. Richmond, C. U. Pittman and M. Absi-Halibi, *J. Molec. Catal.* 1984, **22**, 367.
10. S. R. Drake, B. F. G. Johnson and J. Lewis, *J. Chem. Soc., Dalton Trans.* 1987, 1051.
11. A. Darchen, C. Mahe and H. Patin, *J. Chem. Soc., Chem. Commun.* 1982, 243.
12. J. Jeffrey, PhD thesis, University of Cambridge (1985).
13. T. Toan, B. K. Teo, J. A. Ferguson, T. J. Meyer and L. F. J. Dahl, *J. Am. Chem. Soc.* 1977, **99**, 408.
14. J. A. Ferguson and T. J. Meyer, *J. Chem. Soc., Chem. Commun.* 1971, 623.
15. J. G. M. van der Linden, M. L. H. Paulissen and J. E. J. Schmitz, *J. Am. Chem. Soc.* 1983, **105**, 1903.
16. S. R. Drake, M. H. Barley, B. F. G. Johnson and J. Lewis, *Organometallics* 1988, **7**, 806.
17. B. Tulyathan and W. E. Geiger, *J. Am. Chem. Soc.* 1985, **107**, 5960.
18. J. Rimmelin, P. Lemoine, M. Gross, R. Mathieu and D. De Montauzon, *J. Organomet. Chem.* 1986, **309**, 355.
19. M. I. Bruce, J. G. Matisons and B. K. Nicholson, *J. Organomet. Chem.* 1983, **247**, 321.
20. M. I. Bruce, D. C. Kehoe, J. G. Matisons, B. K. Nicholson, P. H. Reiger and M. L. Williams, *J. Chem. Soc., Chem. Commun.* 1982, 442.
21. S. R. Drake, B. F. G. Johnson and J. Lewis, *J. Chem. Soc., Chem. Commun.* 1988, 1033.
22. M. I. Bruce, M. G. Humphrey, O. S. Shawkataly, M. R. Snow and E. R. T. Tiekink, *J. Organomet. Chem.* 1986, **315**, C51.
23. S. R. Drake, B. F. G. Johnson and J. Lewis, *J. Chem. Soc., Dalton Trans.* 1989, 243.
24. C. H. Hay, B. F. G. Johnson, J. Lewis, R. C. S. McQueen, P. R. Raithby, R. M. Sorrell and M. J. Taylor, *Organometallics* 1985, **4**, 202.
25. A. M. Bond, P. A. Dawson, B. M. Peake, B. H. Robinson and J. Simpson, *Inorg. Chem.* 1977, **16**, 2199.
26. P. A. Dawson, B. M. Peake, B. H. Robinson and J. Simpson, *Inorg. Chem.* 1980, **19**, 465.
27. C. M. Arewgoda, B. H. Robinson and J. Simpson, *J. Am. Chem. Soc.* 1983, **105**, 1893.
28. B. M. Peake, P. H. Reiger, B. H. Robinson and J. Simpson, *Inorg. Chem.* 1981, **20**, 2540.
29. C. M. Arewgoda, B. H. Robinson and J. Simpson, *J. Am. Chem. Soc.* 1983, **105**, 1893.
30. A. M. Bond, P. A. Dawson, B. M. Peake, P. H. Reiger, B. H. Robinson and J. Simpson, *Inorg. Chem.* 1979, **18**, 1413.
31. P. N. Lindsay, B. M. Peake, B. H. Robinson, J. Simpson, U. Honrath, H. Z. Vahrenkamp and A. M. Bond, *Organometallics* 1984, **3**, 413.
32. M. Chanon and M. L. Tobe, *Angew. Chem. Int. Edn Engl.* 1982, **21**, 1.
33. A. Benoit, A. Darche, J. Y. Le Marouille, C. Mahe and H. Patin, *Organometallics* 1983, **2**, 555.
34. E. C. Ashby, T. Pham and A. A. Madjabadi, *J. Org. Chem.* 1988, **53**, 6156.
35. G. A. Foulds, B. F. G. Johnson and J. Lewis, *J. Organomet. Chem.* 1985, **296**, 147 and refs therein.
36. A. Darchen, C. Mahe and H. Patin, *J. Chem. Soc., Chem. Commun.* 1982, 243.
37. A. Darchen, C. Mahe and H. Patin, *Nouv. J. Chim.* 1982, **6**, 539.
38. H. H. Ohst and J. K. Kochi, *Inorg. Chem.* 1986, **25**, 2066.
39. H. H. Ohst and J. K. Kochi, *J. Am. Chem. Soc.* 1986, **108**, 2897.
40. R. Sorrell, PhD thesis, University of Cambridge (1985).
41. J. L. Zuffa, M. L. Blohm and W. L. Gladfelter, *J. Am. Chem. Soc.* 1986, **108**, 1884.
42. B. M. Peake, B. H. Robinson, J. Simpson and D. Watson, *J. Chem. Soc., Chem. Commun.* 1974, 945.
43. J. E. Cyr, J. A. De Gray, D. K. Gosser, E. S. Lee and P. H. Rieger, *Organometallics* 1985, **4**, 950.
44. A. J. Downard, B. H. Robinson, J. Simpson and A. M. Bond, *J. Organomet. Chem.* 1987, **320**, 363.
45. J. L. Graff, R. D. Sanner and M. S. Wrighton, *J. Am. Chem. Soc.* 1979, **101**, 273; D. R. Tyler, M. Altobelli and H. B. Gray, *J. Am. Chem. Soc.* 1980, **102**, 3022.
46. H. P. Klein, U. Thewalt, G. Herrmann, G. Suss-Fink and C. Moinet, *J. Organomet. Chem.* 1986, **286**, 225.
47. J. R. Fish, T. Malinski, A. J. Mayr and K. H. Pannell, *Inorg. Chim. Acta* 1988, **150**, 249.
48. J. P. Collman, R. K. Rothrock, R. G. Finke, E. J. Moore and F. Rose-Munch, *Inorg. Chem.* 1982, **21**, 146.
49. K. M. Kadish, D. A. Lacombe and J. E. Anderson, *Inorg. Chem.* 1986, **25**, 2074.
50. K. M. Kadish, D. A. Lacombe and J. E. Anderson, *Inorg. Chem.* 1986, **25**, 2246.

51. B. F. G. Johnson, *Inorg. Chim. Acta* 1986, **115**, L39.
52. P. Zanello, S. Aime and D. Osella, *Organometallics* 1984, **3**, 1374.
53. B. F. G. Johnson, J. Lewis, W. J. H. Nelson, J. Puga, P. R. Raithby, M. Schroder and K. H. Whitmire, *J. Chem. Soc., Chem. Commun.* 1982, 610.
54. B. F. G. Johnson, J. Lewis, W. J. H. Nelson, J. Puga, P. R. Raithby and K. H. Whitmire, *J. Chem. Soc., Dalton Trans.* 1983, 1339.
55. S. R. Drake, T. Coston and J. Lewis, unpublished results.
56. R. Khattar, PhD thesis, University of Cambridge (1987).
57. M. Rosales, PhD thesis, University of Cambrige (1983).
58. C. R. Eady, B. F. G. Johnson, J. Lewis, B. E. Reichert, K. T. Schropp and G. M. Sheldrick, *J. Chem. Soc., Chem. Commun.* 1977, 385; G. R. John, B. F. G. Johnson and J. Lewis, *J. Organomet. Chem.* 1979, **169**, C9.
59. P. F. Jackson, B. F. G. Johnson, J. Lewis, M. McPartlin and W. J. H. Nelson, *J. Chem. Soc., Chem. Commun.* 1979, 735.
60. K. Wade, *Adv. Inorg. Chem. Radiochem.* 1976, **18**, 1.
61. R. J. Goudsmit, J. G. Jeffrey, B. F. G. Johnson, J. Lewis, R. C. S. McQueen, A. J. Sanders and J.-C. Liu, *J. Chem. Soc., Chem. Commun.* 1986, 24.
62. J. G. Jeffrey, PhD thesis, University of Cambridge (1985).
63. D. M. P. Mingos and D. G. Evans, *Organometallics* 1983, **2**, 35.
64. R. J. Goudsmit, B. F. G. Johnson, J. Lewis, P. R. Raithby and K. H. Whitmire, *J. Chem. Soc., Chem. Commun.* 1983, 246.
65. C. R. Eady, B. F. G. Johnson, J. Lewis, R. Mason, P. B. Hitchcock and K. Thomas, *J. Chem. Soc., Chem. Commun.* 1977, 385.
66. M. D. Vargas, PhD thesis, University of Cambridge (1984).
67. B. F. G. Johnson, J. Lewis and D. A. Pippard, *J. Chem. Soc., Dalton Trans.* 1981, 407.
68. A. Gourdon and Y. Jeanin, *J. Organomet. Chem.* 1985, **290**, 199.
69. G. B. Ansell and J. S. Bradley, *Acta Cryst.* 1980, **36**, 1939.
70. F. A. Bell, A. Ledwith and D. C. Sherrington, *J. Chem. Soc., Chem. Commun.* 1969, 2719; *J. Chem. Soc., Dalton Trans.* 1984, 2713.
71. V. Gutmann, *Electrochim. Acta* 1976, **21**, 661.
72. P. Lemoine, PhD thesis, University Loius Pasteur, Strasbourg (1987).
73. B. F. G. Johnson, D. A. Kaner, J. Lewis and P. R. Raithby, *J. Organomet. Chem.* 1981, **215**, C33.
74. B. F. G. Johnson, D. A. Kaner, J. Lewis and P. R. Raithby, *J. Chem. Soc., Chem. Commun.* 1981, 753.
75. K. Burgess, B. F. G. Johnson, D. A. Kaner, J. Lewis, P. R. Raithby and S. N. A. B. Syed-Mustaffa, *J. Chem. Soc., Chem. Commun.* 1983, 445.
76. R. W. Broach and J. M. Williams, *Inorg. Chem.* 1979, **18**, 314.
77. M. Fajardo, M. P. Gomez-Sal, H. D. Holden, B. F. G. Johnson, J. Lewis, R. C. S. McQueen and P. R. Raithby, *J. Organomet. Chem.* 1984, **267**, C25.
78. D. A. Kaner, R. C. S. McQueen, B. F. G. Johnson and J. Lewis, unpublished results.
79. D. A. Kaner, PhD thesis, University of Cambridge (1984).
80. R. C. S. McQueen, M. D. Vargas, B. F. G. Johnson and J. Lewis, unpublished results, see also ref. 65.
81. M. Fajardo, H. D. Holden, B. F. G. Johnson, J. Lewis and P. R. Raithby, *J. Chem. Soc., Chem. Commun.* 1984, 24.
82. D. H. Evans and K. M. O'Connell, *Electroanalytical Chemistry* (Edited by A. J. Bard). Marcel Dekker, New York (1988).
83. S. R. Drake, A. J. Edwards and J. Lewis, unpublished results.
84. B. F. G. Johnson, J. Lewis, W. J. H. Nelson, J. N. Nicholls, J. Puga, P. R. Raithby, M. J. Rosales, M. Schroder and M. D. Vargas, *J. Chem. Soc., Dalton Trans.* 1983, 2447.
85. A. Moule, PhD thesis, University of Cambridge (1989).
86. V. G. Albano, D. Braga, P. Chini, G. Chiani and S. Martinengo, *J. Chem. Soc., Dalton Trans.* 1982, 645.
87. S. R. Drake, M. H. Barley and J. Lewis, unpublished results; M. P. Gomez-Sal, B. F. G. Johnson, J. Lewis, P. R. Raithby and A. H. Wright, *J. Chem. Soc., Chem. Commun.* 1985, 1682.
88. S. B. Colbran, F. J. Lahoz, P. R. Raithby, J. Lewis, B. F. G. Johnson and C. J. Cardin, *J. Chem. Soc., Dalton Trans.* 1988, 173.
89. C. M. T. Hatward, J. R. Shapley, M. R. Churchill, C. Buens and A. L. Rheingold, *J. Am. Chem. Soc.* 1982, **104**, 7347.
90. S. R. Drake and J. Lewis, unpublished results.
91. B. F. G. Johnson, J. Lewis, W. J. H. Nelson, M. D. Vargas, D. Braga and M. McPartlin, *J. Chem. Soc., Chem. Commun.* 1983, 241.
92. P. F. Jackson, B. F. G. Johnson, J. Lewis, M. McPartlin and W. J. H. Nelson, *J. Chem. Soc., Chem. Commun.* 1980, 224.

93. S. R. Drake, B. F. G. Johnson, J. Lewis and R. C. S. McQueen, *J. Organomet. Chem.* 1987, **325**, C31.
94. S. R. Drake, B. F. G. Johnson, J. Lewis and R. C. S. McQueen, *J. Chem. Soc., Dalton Trans.* 1987, 1051.
95. A. Albruati, A. Moor, P. S. Pregosin and L. M. Venanzi, *J. Am. Chem. Soc.* 1977, **104**, 7672.
96. S. B. Colbran, PhD thesis, University of Otago, New Zealand (1983).
97. D. De Montauzon and R. Mathieu, *J. Organomet. Chem.* 1983, **252**, C83.
98. T.-Toan, W. P. Fehlhammer and L. F. Dahl, *J. Am. Chem. Soc.* 1972, **104**, 3409.
99. A. Penicaud, P. Batail, C. Perrin, C. Coulon, S. S. P. Parkin and J. B. Torrance, *J. Chem. Soc., Chem. Commun.* 1987, 330.
100. P. R. Raithby and M. J. Rosales, *Adv. Inorg. Chem. Radiochem.* 1986, **29**, 169.
101. C. D. Baer, C. A. Camaioni-Neto, D. A. Sweigart, A. M. Bond, T. F. Mann and G. A. Tondreau, *Coord. Chem. Rev.* 1989, **93**, 1.
102. J.-C. Moutet and C. J. Pickett, *J. Chem. Soc., Chem. Commun.* 1989, 188.
103. J. A. Baumann, S. T. Wilson, D. J. Salmon, P. L. Hood and T. J. Meyer, *J. Am. Chem. Soc.* 1979, **101**, 2916.
104. J. N. Nicholls, *Polyhedron* 1984, **3**, 1307.

Polyhedron Vol. 9, No. 4, pp. 475–477, 1990
Printed in Great Britain

0277–5387/90 $3.00+.00
© 1990 Pergamon Press plc

THE NEW TRIAZA MACROCYCLIC COMPLEX OF YTTRIUM

WANDA RADECKA-PARYZEK† and EMILIA LUKS

Faculty of Chemistry, Adam Mickiewicz University, 60–780 Poznań, Poland

(*Received* 19 *July* 1989; *accepted* 8 *August* 1989)

Abstract—The new triaza macrocyclic ligand complex of formula $[YL^1(NO_3)_3]\cdot 3H_2O$, where L^1 is Me_2bzopyo[10]tetraeneN_3, has been prepared by template condensation of 2,6-diacetylpyridine with *m*-phenylenediamine in the presence of a yttrium salt. In the absence of the yttrium ion as a template agent, only the open-chain compound L^2 with partially uncondensed carbonyl and amine groups was formed. The IR, UV–vis, ^{1}H NMR and MS data along with elemental and thermogravimetric analysis were used to characterize the compounds obtained in this work.

Until the late 1970's there have been relatively few reports of complexes containing tridentate macrocyclic ligands when compared with the large number of papers involving tetradentate macrocycles.[1]

Recently, very interesting reviews have appeared covering the literature dealing with the coordination chemistry of the tridentate macrocycles.[2,3] However, the coordinating ability of triaza macrocyclic ligands towards the rare earth elements has received little attention. The investigations have been limited to potential application of lanthanide triazacyclononane complexes as water soluble axially symmetric shift reagents.[4–6]

As a continuation of our studies on the effectiveness of metal ions of varying radius and electron configuration in the synthesis of macrocyclic compounds we have previously reported the first example of the template action of the yttrium ion in the synthesis of a tetradentate NNNN-donor macrocycle.[7]

In this paper, the template synthesis and characterization of the new 10-membered triaza macrocyclic complex of yttrium nitrate is described.

EXPERIMENTAL

The hydrated yttrium nitrate was prepared from Y_2O_3 in the manner described previously.[7]

Preparation of the yttrium macrocyclic complex of L^1

To a solution of $Y(NO_3)_3\cdot 6H_2O$ (0.1 mmol) in methanol (10 cm^3), 2,6-diacetylpyridine (0.1 mmol) in methanol (10 cm^3) and *m*-phenylenediamine (0.1 mmol) in methanol (10 cm^3) were added dropwise with stirring. The reaction was carried out for 8 h. Removal of the solvent left a yellow oily solid which, on washing with ether, gave a yellow powder. This was dried *in vacuo*. Found: C, 32.4; H, 3.4; N, 14.9. Calc. for $YC_{15}H_{19}N_6O_{12}$: C, 32.0; H, 3.4; N, 14.9%.

Preparation of the compound L^2

The reaction of 2,6-diacetylpyridine (0.1 mmol) with *m*-phenylenediamine (0.1 mmol) in methanol (20 cm^3) was carried out in the absence of the yttrium salt for 24 h. Solvent was then removed and the residue washed with ether. Recrystallization from ethanol gave yellow crystals. Found: C, 70.9; H, 5.9; N, 16.7. Calc. for $C_{15}H_{15}N_3O$: C, 71.1; H, 6.0; N, 16.6%.

Measurements

IR spectra were recorded using CsI pellets in the range 4000–200 cm^{-1} on a Perkin–Elmer 580 spectrophotometer. Electronic absorption spectra were measured on a Beckman 25 spectrophotometer. ^{1}H NMR spectra were run on a Varian EM–360 60 MHz spectrometer for solutions in DMSO-d_6 using TMS as internal standard. Mass spectra were obtained on a JEOL–JMS mass spectrometer. Thermogravimetric measurements were performed using the Derivatograph OD–102, MOM.

† Author to whom correspondence should be addressed.

RESULTS AND DISCUSSION

Condensation of 2,6-diacetylpyridine with *m*-phenylenediamine with the use of $Y(NO_3)_3 \cdot 6H_2O$ as a template agent gave the new 10-membered triaza macrocyclic complex of stoichiometry $[YL^1(NO_3)_3] \cdot 3H_2O$, where L^1 is Me_2bzopyo[10] tetraeneN_3 ligand. The complex was identified by spectral data (IR, UV–vis, ^{1}H NMR, MS) and thermal and elemental analysis.

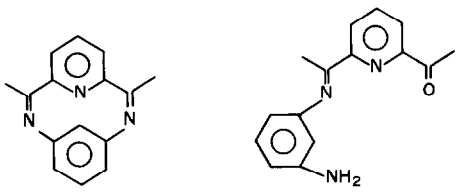

L^1 L^2

The IR spectrum of this complex shows significant bands at 1630, 1605 and 1450 cm^{-1}, which may be assigned to C=N stretching modes and two high energy pyridine vibrations. The low energy pyridine bands observed at 625 and 440 cm^{-1} suggest coordination of pyridine.[8] Absence of bands characteristic of carbonyl and amine groups confirms the formation of the macrocyclic compound. A broad diffuse band of strong intensity in the 3500–3100 cm^{-1} region may be assigned to an O—H stretching vibration for lattice water. The absorption characteristic of coordinated water does not appear. The thermogravimetric analysis confirms this observation, indicating the loss of three water molecules at 45–75°C.

The IR spectrum of this complex gives valuable information on the type of nitrate binding. The separation of two combination bands in the 1700–1800 cm^{-1} region is about 35 cm^{-1}. The two strong bands associated with the asymmetric stretch appear at 1480 and 1310 cm^{-1}. The magnitude of the separation, which is proportional to the strength of the yttrium–oxygen bond, along with absorption at 818 cm^{-1} gives evidence for chelating bidentate behaviour of the nitrate groups in this complex.[9,10]

The electronic spectrum of the yttrium complex of L^1 for a solution in methanol exhibits an absorption band at 226 nm with a shoulder at 280 nm attributable to the $\pi \rightarrow \pi^*$ transitions of the coordinated macrocycle.[11]

The ^{1}H NMR spectrum of this complex shows the pyridine ring protons at δ 8.1–8.5, the benzene ring protons at δ 6.4–6.8 and the methyl protons at δ 2.3 and 2.6. The integrated relative intensities of the above signals are in the ratio 3:4:6, respectively, consistent with the proposed formulation of the complex.

Further evidence for the formulation of the macrocyclic complex comes from the mass spectrum. The highest fragment with 100% relative intensity is observed at *m/z* 235 and corresponds to the molecular weight of the uncoordinated macrocycle.

Attempts to obtain a free macrocycle in the reaction of the 2,6-diacetylpyridine with *m*-phenylenediamine without using the yttrium nitrate as a template agent were unsuccessful and resulted in the formation of the acyclic compound L^2. This product was identified by IR, UV–vis, ^{1}H NMR and MS as well as elemental analysis.

The band characteristic of the C=N stretching mode is observed in the IR spectrum of this compound at 1620 cm^{-1}, indicating the partial condensation reaction. An important feature is the occurrence of the strong band at 1695 cm^{-1} assigned to the C=O stretching vibration and the bands at 3350 and 3210 characteristic of antisymmetric and symmetric stretching modes of the NH_2 group. The electronic spectrum of L^2 in methanol consists of two bands at 220 and 275 nm.

The ^{1}H NMR spectrum shows pyridine protons at δ 8.0–8.4, the benzene protons at δ 6.3–7.1 and methyl protons at δ 2.3 and 2.7, with integrated intensities in the ratio 3:4:6, respectively. The parent ion in the mass spectrum of L^1 observed at *m/z* 253 corresponds to the formula $C_{15}H_{15}N_3O$.

Treatment of the yttrium nitrate with L^2 in methanol for 10 h leads to isolation of the product, which turns out to be the yttrium complex of L^1.

This finding appears to be in accordance with the general observation, that for the majority of macrocyclic compounds, the use of a metal ion to direct the steric course of the condensation process, which ultimately ends with ring closure, remains the best way of preparation.

On the basis of spectral and analytical data along with the molecular model analysis it seems reasonable to tentatively assign the coordination number of nine for the yttrium ion in this complex. The metal ion is presumably coordinated to the three nitrogen donor atoms of the 10-membered macrocycle and to the six oxygen atoms of the three bidentate nitrate groups. Reference to the known structure of nine-coordinate yttrium complexes allows us to predict the tricapped trigonal prism geometry for this new complex with the tridentate macrocycle occupying the triangular face.[12]

It may be possible to obtain the lanthanide complexes of this triaza macrocyclic with the sandwich structure and we are pursuing that line of investigation.

Acknowledgement—Financial support from the Polish Academy of Sciences (Project CPBP No. 01.12.4.18) is gratefully acknowledged.

REFERENCES

1. G. A. Melson, *Coordination Chemistry of Macrocyclic Compounds*. Plenum Press, New York (1979).
2. P. Chaudhuri and K. Wieghardt, *Prog. Inorg. Chem.* 1987, **35**, 329.
3. R. Bhula, P. Osvath and D. C. Weatherburn, *Coord. Chem. Rev.* 1988, **91**, 89.
4. J. F. Desreux, *Inorg. Chem.* 1980, **19**, 1319.
5. C. C. Bryden, C. N. Reilley and J. F. Desreux, *Analyt. Chem.* 1981, **53**, 1418.
6. C. F. G. C. Geraldes, M. C. Alpoim, M. P. M. Marques, A. D. Sherry and M. Singh, *Inorg. Chem.* 1985, **24**, 3876.
7. W. Radecka-Paryzek, *Polyhedron* 1989, **8**, 1217 and refs therein.
8. N. S. Gill, R. H. Nuttal and D. E. Scaife, *J. Inorg. Nucl. Chem.* 1961, **18**, 79.
9. J.-C. G. Bünzli, G. A. Leonard, D. Plancherel and G. Hapuis, *Helv. Chim. Acta* 1986, **60**, 288.
10. W. Radecka-Paryzek and E. Jankowska, *Inorg. Chim. Acta* 1987, **134**, 179; W. Radecka-Paryzek, E. Jankowska and E. Luks, *Polyhedron* 1988, **7**, 439.
11. M. G. B. Drew, A. H. Othman, S. G. McFall, P. D. A. McIlroy and S. M. Nelson, *J. Chem. Soc., Dalton Trans.* 1977, 1173.
12. R. D. Rogers and E. J. Voss, *J. Coord. Chem.* 1988, **16**, 405.

Polyhedron Vol. 9, No. 4, pp. 479–485, 1990
Printed in Great Britain

0277–5387/90 $3.00+.00
© 1990 Pergamon Press plc

STUDIES ON ORGANOLANTHANIDE COMPLEXES—XXIV.* SYNTHESES OF 1,1′-(XYLYLENE)BIS-η^5-CYCLOPENTADIENYL RARE EARTH CHLORIDES

CHANGTAO QIAN,† XIURAN WANG,‡ YUQIN LI and CHANGQING YE

Shanghai Institute of Organic Chemistry, Academia Sinica, 345 Lingling Lu, 200032 Shanghai, China

(*Received* 1 *August* 1989; *accepted* 15 *August* 1989)

Abstract—THF-solvated 1,1′-(xylylene)bis-cyclopentadienyl rare earth chlorides [$C_5H_4CH_2C_6H_4CH_2C_5H_4$]LnCl·THF (Ln = La, Pr, Nd, Dy, Y, Er and Yb), were synthesized by using 1,1′-(*m*-xylylene)bis-cyclopentadiene and 1,1′-(*p*-xylylene)bis-cyclopentadiene as ligands. Disproportionation of early lanthanocene chlorides (Ln = La, Pr, Nd) is thus successfully prevented and stable early lanthanocene chlorides are obtained. Their structures were verified by elemental analyses, IR, ^{1}H NMR, MS and XPS spectroscopy; they are possibly dimeric. The solubility of these complexes in aromatic hydrocarbons is lower than the corresponding 1,1′-(trimethylene)bis-cyclopentadienyl lanthanide chlorides.

Recently, the syntheses of early organolanthanide complexes has attracted much attention. In order to stabilize the bis-cyclopentadienyl early lanthanide chlorides and to prevent their disproportionation, bulky pentamethylcyclopentadienyl,[1–6] bis-(trimethylsilyl)cyclopentadienyl[6,7] and hexamethylindenyl[9] have been used as ligands. Another way is to use bridged cyclopentadienyl as the ligand. Previously, we have reported that the stabilization of early organolanthanide complexes has been achieved by using 1,1′-(trimethylene)bis-cyclopentadienyl[10,11] and 1,1′-(3-oxapentamethylene) bis-cyclopentadienyl as ligands. Marks *et al.*[13] succeeded in stabilizing early lanthanocene chlorides by generating an anionic complex. The THF-solvated mid- or late-organolanthanide chlorides can be isolated using 1,1′-(pentamethylene)bis-cyclopentadienyl as ligand. Unfortunately, under similar conditions, we did not succeed in obtaining the early lanthanocene chloride with this chelating ligand.[14] We found by ^{1}H NMR that the flexibility of the pentamethylene chain is more than that of 1,1′-trimethylene ones; put in another way, the mobility of bridged cyclopentadienyl is larger. In order to increase the rigidity of the pentamethylene chain, a benzene ring was introduced into the chain and, therefore, we studied the syntheses of early lanthanocene chlorides using 1,1′-(*m*-xylylene)bis-cyclopentadienyl and 1,1′-(*p*-xylylene)bis-cyclopentadienyl as ligands. At the same time we have attempted to improve the solubility of lanthanocene chlorides in aromatic hydrocarbons by using a ligand containing a benzene ring. It is very important to study their reactivity. Herein, we would like to report the syntheses and identification of nine new THF-solvated 1,1′-(xylylene)bis-cyclopentadienyl rare earth chlorides.

RESULTS AND DISCUSSION

The preparation of 1,1′-(xylylene)bis-cyclopentadienyl disodium salt/THF solution is similar to the methods reported in the literature.[11,12,15] It could be stored for over 1 month with the exclusion of moisture and oxygen. Anhydrous lanthanide chlorides, $LnCl_3$, reacted with disodium salt/THF solution in THF at −50°C to give complexes **1–6**,

* For part XXIII, see ref. 25.

† Author to whom correspondence should be addressed.

‡ Permanent address: Laboratory of Organic Chemistry, Anhui Normal University, China.

which are shown in eq. (1):

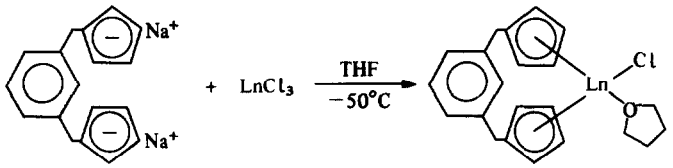

(1)

Ln = La (**1**), Nd (**2**), Dy (**3**), Er (**4**), Y (**5**), Yb (**6**).

We have succeeded in synthesizing the early lanthanum and neodymium chlorides, thus confirming that the rigidity of a pentacarbon chain which contains a benzene ring is much greater than that of a pentamethylene chain. Considering the coordination effect, this ligand not only matches the early lanthanide ions with a larger ionic radii but also matches the later lanthanide ions with a smaller ionic radii. However, using 1,1′-(*p*-xylylene)biscyclopentadienyl as a ligand, only the chlorides of early lanthanides having larger ionic radii were isolated, the later lanthanide chlorides were not obtained under similar reaction conditions. The reaction is shown in eq. (2):

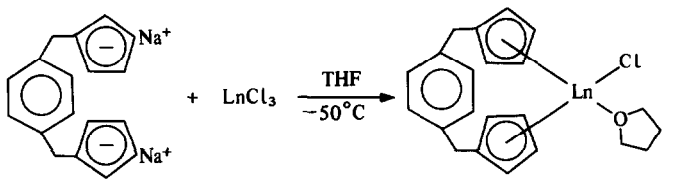

(2)

Ln = La (**7**), Pr (**8**), Nd (**9**).

The IR spectra of complexes **1–9** were measured from 4000 to 50 cm^{-1}. The spectral features are very similar. The complexes exhibit four to six characteristic absorption peaks in the low frequency, 50–500 cm^{-1} region. The data of absorption peaks are listed in Table 1. The strong absorption peak at about 250–260 cm^{-1} was assigned to a characteristic absorption of a π-bonded cyclopentadienyl group to Ln metal.[16] It is noticeable that the characteristic absorption of the π-bond in complex **5** is shifted to 290 cm^{-1}, which is in agreement with those of Cp_2YCl, $(CH_3C_5H_4)_2YCl$, $[C_5H_4(CH_2)_3C_5H_4]YBu^t \cdot THF$ and $(C_5H_4CH_2CH_2OCH_2CH_2C_5H_4)YCl$ reported in our previous work.[12] It is probably caused by a difference between yttrium and lanthanide metals. The characteristic absorption peaks of coordinated tetrahydrofuran appear at 890 and 1046 cm^{-1}. Four characteristic cyclopentadienyl absorptions at 760–780, 1012, 1440 and 3080 cm^{-1} are apparently present. The characteristic absorptions of *m*-xylylene are evidently different from *p*-xylylene. The characteristic absorption peaks of *m*-xylylene appear at 720 and 1585 cm^{-1}, respectively, all absorption peaks at 720, 1458, 1585, 1603 and 3060 cm^{-1} were contributed by *m*-xylylene. Whereas *p*-xylylene exhibits four characteristic absorption peaks at about 805, 1500–1510, 1600–1610 and 3040 cm^{-1}. Therefore, the cyclopentadienyl, benzene ring and coordinated THF in complexes are evidently present.

Table 1. IR data of complexes in the low frequency region (50–500 cm^{-1})[a]

2(Nd)	4(Er)	5(Y)	6(Yb)	7(La)	8(Pr)	9(Nd)
	120m	120m	117m			
216s	203s	193m	202m	208s	208s	212s
	238s	235s	225vs			
250m	262vs	290vs	250vs	250s	250s	250m
388m	367m	372s	365s	388w	408s	390m
436w	435m	410s	433m	450w	463m	465m

[a] w: weak; m: medium; s: strong; vs: very strong.

The ^1H NMR spectra of complexes **1** and **7** were measured using perdeuterotetrahydrofuran as solvent and the results are similar. For example in complex **1** protons of the benzene ring appear at δ 6.85; cyclopentadienyl at δ 6.03 and 5.80; THF at δ 3.45 and 1.62; and CH_2 at δ 2.75 and 2.62. ^1H NMR of the organic ligand obtained via hydrolysis of complex **7** was also recorded. The chemical shift of the benzene ring is at δ 7.05; cyclopentadienyl at δ 6.45 becoming a single peak; THF at δ 3.60 and 1.80; and CH_2 becoming a single peak at δ 2.87 from two multiple peaks of the corresponding complex. The four protons of the ring-bridged cyclopentadienyl exhibit a characteristic AA′BB′ pattern which is two groups of multiple peaks. Martin *et*

al.[17] assigned the resonance peak of the cyclopentadienyl β-proton at high field. The four hydrogens at positions 6 and 10 exhibit two groups of

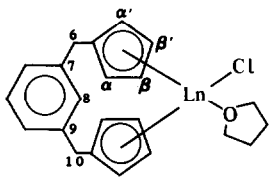

equal proton peaks, which indicates that the electrons of the benzene ring partly transfer to the metal. Therefore, these hydrogens are not homomagnetic.

Smith *et al.*[18] found that in the case of ring-bridged bis-cyclopentadienyl titanium dichlorides, increasing the length of the methylene chain [—$(CH_2)_n$—; $n = 1$–3], decreases the $\Delta\delta$ values between α and β of cyclopentadienyl. Owing to the increasing chain length, β-protons are closer to the central metal than α-protons.

The $\Delta\delta$ values for different ring-bridged lanthanocene chlorides are compared and the data are listed in Table 2.

From Table 2 we found that (1) by increasing the chain length, the angle between the two rings and the torsional ring mobility of cyclopentadienyl increases, therefore, the $\Delta\delta$ values between the α- and β-protons evidently decreases and (2) the type of chain effects a change in $\Delta\delta$. When a chain containing oxygen is introduced to the bridged bis-cyclopentadienyl ligand, because of the formation of an intramolecular coordination bond, the mobility of the ring decreases. Moreover, the $\Delta\delta$ value obviously increases compared with the complexes with the same chain length. In the case of the chain containing the benzene ring, the rigidity of the chain is strengthened; this results in $\Delta\delta$ increasing. In conclusion, the ring proton splitting degree is related to the chain length and different kinds of chain.

The mass spectra of 1,1′-(trimethylene)bis-cyclopentadienyl lanthanide chlorides did not show the parent molecular ion and gave only some fragments.[11] However, the complete mass spectra of 1,1′-(3-oxa-pentamethylene)bis-cyclopentadienyl lanthanide chlorides were obtained.[12] The mass spectra of the title complexes are between 1,1′-(trimethylene)bis-cyclopentadienyl and 1,1′-(3-oxa-pentamethylene)bis-cyclopentadienyl lanthanide chlorides. Complexes **1** and **2** gave the complete mass spectra which exhibited the monomeric parent molecular ion $[M]^+$ and related fragments. Mass spectra data of complex **2** are listed in Table 3. It is different from the mass spectra of 1,1′-(3-oxa-pentamethylene)bis-cyclopentadienyl lanthanide chlorides in that the relative intensity of $[M—Cl]^+$ is very weak and the relative intensity of $[C_5H_6]^+$ is very strong. Therefore, it is similar to the mass spectra of $(CH_3C_5H_4)_2LnCl$ and Cp_2LnCl in that the cyclopentadienyl is first cleaved.[22] Moreover, in the mass spectra of **1**, **2**, **5**, **7** and **9**, related fragments including m/z being larger than the monomeric fragment $[M]^+$ and being equal to 72 or 73, all appear. These indicate that they are THF-solvated dimers.

In general, the organolanthanide complexes are able to coordinate with a Lewis base because of their coordination unsaturation and the oxyphilicity of the metal in these complexes. In our previous work, Cp_2LnCl and $[C_5H_4(CH_2)_3C_5H_4]$

Table 2. Correlation of the bridged chain with ring-proton splitting

Number	Complexes	n	Angle between two rings	$\Delta\delta$	Reference
1.	$(CH_2)_n(C_5H_4)_2LaCl$	3		0.17	10
2.	$(CH_2)_n(C_5H_4)_2LaC(CH_3)_3 \cdot THF$	3		0.16	20, 21
3.	m-$C_6H_4(CH_2)_2(C_5H_4)_2LaCl \cdot THF$	5		0.23	This work
4.	p-$C_6H_4(CH_2)_2(C_5H_4)_2LaCl \cdot THF$	6		0.20	This work
5.	$(CH_2)_n(C_5H_4)_2LuCl \cdot THF$	3		0.40	19
6.	$(CH_2)_n(C_5H_4)_2LuCl \cdot THF$	5		0.07	19
7.	$(CH_2)_2O(CH_2)_2(C_5H_4)_2LuCl$	4+0		0.09	19
8.	$(CH_2)_n(C_5H_4)_2YCl \cdot THF$	5		0.07	14
9.	$(CH_2)_2O(CH_2)_2(C_5H_4)_2YCl$	4+0		0.14	19
10.	m-$C_6H_4(CH_2)_2(C_5H_4)_2YCl \cdot THF$	5		0.22	This work
11.	$(CH_2)_n(C_5H_4)_2TiCl_2$	1	121	1.37	19
12.	$(CH_2)_n(C_5H_4)_2TiCl_2$	2	128	0.82	19
13.	$(CH_2)_n(C_5H_4)_2TiCl_2$	3	133	0.04	19

Table 3. Mass spectra data for 1,1′-(*m*-xylylene)bis-cyclopentadienyl neodymium chloride (**2**) at 70 eV[a]

m/z	Relative intensity	Assignment
616	1.09	> $[M]^+$
481	2.27	$[M]^+ = [C_6H_4(CH_2)_2(C_5H_4)_2]NdCl \cdot THF$
480	3.99	$[M-1]^+$
446	1.03	$[M-Cl]^+$
374	36.25	$[M-Cl-THF]^+$
311	2.06	$[CH_3C_6H_4CH_2C_5H_4Nd]^+$
296	2.07	$[C_6H_4CH_2C_5H_4Nd]^+$
272	37.87	$[(C_5H_5)_2Nd]^+$
234	8.48	$[C_5H_5CH_2C_5H_4CH_2C_5H_5]^+$
207	4.15	$[C_5H_5Nd]^+$
170	52.92	$[CH_3C_6H_4CH_2C_5H_5]^+$
155	23.96	$[C_5H_5CH_2C_6H_4]^+$
142	4.35	$[Nd]^+$
105	36.51	$[CH_3C_6H_4CH_2]^+$
91	6.96	$[C_6H_4CH_3]^+$
77	3.84	$[C_6H_5]^+$
73	31.42	$[C_4H_8O+1]^+$
66	100.00	$[C_5H_6]^+$
65	39.04	$[C_5H_5]^+$
42	35.02	$[C_3H_6]^+$

[a] Mass number is based upon ^{142}Nd, ^{35}Cl, ^{12}C and ^{1}H.

LnCl·THF coordinate with α,α′-bipyridine affording bipyridine complexes[11,23] and the lone pair of electrons on the oxygen atom in $[C_5H_4CH_2CH_2OCH_2CH_2C_5H_4]LnCl$ are partly transferred to the rare earth metal centre forming an intramolecular coordination bond.[12] Although the title complexes do not contain a heteroatom rich in electrons there is an electron-rich benzene ring. XPS of complexes **3**–**6** were measured and the results are listed in Table 4. We found that the binding energies of the rare earth metal atoms all decrease and that those of Cl_{2p} are unchanged compared with those in the corresponding bis-cyclopentadienyl rare earth chlorides. This is probably caused by the electrons in the benzene ring in this complexes partly shifting to the rare earth metal.

Table 4. Binding energy data (eV) for complexes and Cp_2LnCl

Complex	$Ln_{3d5/2}$ Binding energy	ΔE[a]
3	154.4	−0.9
Cp_2DyCl	155.3	
4	170.5	−0.5
Cp_2ErCl	171.0	
5	159.4	−0.4
Cp_2YCl	159.8	
6	186.7[b]	−0.4
Cp_2YbCl	187.1[b]	

[a] E = B.E.($Ln_{3d5/2}$) − B.E.[Ln(Cp_2LnCl)].
[b] Yb_{4d}.

The solubility of complex **4** (Ln = Er) was measured in a variety of organic solvents, showing that the solubility decreases in the order: THF > $CHCl_3$ > $(C_2H_5)_2O$ > C_6H_6 > $CH_3(CH_2)_4CH_3$. The solubility of complex **4** in benzene is evidently not improved compared with the corresponding 1,1′-(trimethylene)bis-cyclopentadienyl erbium chloride complex.

EXPERIMENTAL

All operations were carried out under purified argon by use of Schlenk techniques or in a glovebox. Tetrahydrofuran was refluxed and distilled, either over finely divided $LiAlH_4$ or over blue sodium benzophenone under argon immediately before use. Anhydrous lanthanide chlorides were prepared from the hydrates by the published procedure.[16] α,α′-Dibromo-*m*-xylene and α,α′-dibromo-*p*-xylene were obtained by the method of Atkinson and Thorpe.[24]

Thermal decomposition temperatures were deter-

mined in sealed argon-filled capillaries and were uncorrected. IR spectra were recorded on a Perkin–Elmer 983 and a Digilab FTS-20/E Fourier transform IR spectrometers with Nujol and Fluorolube mulls and were examined between disc-shaped CsI crystals; the mulls were prepared in an argon-filled glovebox. Mass spectra were recorded on a Finnigan 4021 spectrometer; recorded at EI, T = 50–300°C, EM = 1.3 KV. ^{1}H NMR spectra were obtained on a EM 360L (60 MHz) spectrometer referenced to external Me_4Si in THF-d_8. THF-d_8 (E. Merck for NMR spectroscopy) was dried over Na/K alloy and was degassed by freeze–thaw cycles on a vacuum line. X-ray photoelectron spectra were recorded on a Np-1 spectrometer equipped with a Mg-K_α X-ray source.

Analyses of rare earth metal complexes were accomplished using a direct complexometric titration procedure with disodium EDTA.[16] Carbon and hydrogen analyses were performed by the combustion method in an aluminium tube.

Disodium 1,1′-(xylylene)bis-cyclopentadienide, $C_6H_4(CH_2)_2(C_5H_4Na)_2$

C_5H_5Na (45.2 mmol) was prepared in the usual manner from cyclopentadiene and sodium sand in 50 cm^3 of THF at room temperature. The solution of C_5H_5Na was added to α,α′-dibromoxylene (5.7 g, 21.6 mmol) in 50 cm^3 of THF at 0–50°C and the mixture stirred for 2 h. The mixture was centrifuged and the precipitate separated from the solution. The red solution thus obtained was allowed to react again with an excess of sodium hydride (3.95 g, 163.8 mmol) in 140 cm^3 of THF at 30°C for about 2.5 h. The concentration of this solution was 0.1106 M by titration with standard hydrochloric acid. The 1,1′-(xylylene)bis-cyclopentadienyldisodium/THF solution was stored under argon for use as an intermediate.

1,1′-(m-*Xylylene)bis-cyclopentadienyl lanthanum chloride · THF* (**1**)

A THF solution of an equivalent of 1,1′-(*m*-xylylene)bis-cyclopentadienyl disodium was added slowly to anhydrous $LaCl_3$ (1.26 g, 5.14 mmol) in 30 cm^3 of THF at −50°C. The reaction mixture was stirred for 2 h at −45 to −50°C, then allowed to warm up to room temperature and stirred overnight. The Schlenk flask was centrifuged, the precipitate separated from solution, and the THF solution reduced in volume to about 10 cm^3. Addition of 30 cm^3 of *n*-hexane gave a white solid product which was dried *in vacuo* to give a white solid, 1.10 g. Yield 50%; melting point 170–175°C (decomposed). Found: La, 29.6; Cl, 6.9. Calc. for $C_{22}H_{24}OClLa$: La, 29.0; Cl, 7.4%. MS: *m/z* (relative intensity) and fragment: 570 $[M]^+$; 407(1.97), $[M-THF+1]^+$; 234(45.40), $[C_5H_4CH_2C_6H_4CH_2C_5H_5+1]^+$; 205(5.24), $[LaC_5H_5+1]^+$; 169(41.11), $[CH_2C_6H_4CH_2C_5H_5]^+$; 155(57.09), $[C_5H_4CH_2C_6H_4+1]^+$; 91(11.19), $[CH_2C_6H_4+1]^+$; 77(2.02), $[C_6H_4+1]^+$; 73(1.53), $[C_4H_8O+1]^+$; 66(100.00), $[C_5H_5+1]^+$; 65(40.06), $[C_5H_5]^+$; 42(3.92), $[C_3H_6]^+$. IR (cm^{-1}): 665m, 720s, 770vs, 805m, 870m, 890m, 1015m, 1040m, 1485m, 1585m, 1604s, 2890s, 2960s, 3020m, 3050m. ^{1}H NMR (δ, THF-d_8, TMS): 6.85 (m, C_6H_4); 6.03, 5.80 (m, $2C_5H_4$); 3.45, 1.62 (m, C_4H_8O); 2.75, 2.62 (m, $2CH_2$).

1,1′-(m-*Xylylene)bis-cyclopentadienyl neodymium chloride · THF* (**2**)

The procedure followed was similar to that for **1**. A pale purple solid (**2**) was obtained, yield 40%; decomposition temperature 180–186°C. Found: C, 53.3; H, 5.1; Nd, 30.6; Cl, 7.7. Calc. for $C_{22}H_{24}OClNd$: C, 54.6; H, 5.0; Nd, 29.8; Cl, 7.3%. IR (cm^{-1}): 216s, 250m, 388m, 436w, 758s, 775vs, 860w, 1012s, 1030s, 1078m, 1484m, 1580w, 1604s, 2880s, 2950s, 3040m, 3080s. The MS data is listed in Table 3.

1,1′-(m-*Xylylene)bis-cyclopentadienyl dysprosium chloride · THF* (**3**)

The procedure followed was similar to that for **1**. A pale yellow solid (**3**) was obtained, yield 45%; decomposition temperature 174–178°C. Found: C, 53.3; H, 5.1; Dy, 32.8; Cl, 7.5. Calc. for $C_{22}H_{24}OClDy$: C,52.6; H, 4.8; Dy, 32.3; Cl, 7.1%. IR (cm^{-1}): 721s, 773vs, 890m, 1012m, 1045s, 1450m, 1458vs, 1587m, 1603s, 2850s, 2953s, 3057m. MS: *m/z* (relative intensity) and fragment: 234(1.83), $[C_5H_5CH_2C_6H_4CH_2C_5H_5]^+$; 169(2.02), $[CH_2C_6H_4CH_2C_5H_5]^+$; 155(2.01), $[C_5H_5CH_2C_6H_4]^+$; 91(1.75), $[CH_2C_6H_4+1]^+$; 72(38.35), $[C_4H_8O]^+$; 66(6.19), $[C_5H_6]^+$; 65(3.57), $[C_5H_5]^+$; 57(23.25), $[C_4H_8+1]^+$; 42(100.00), $[C_3H_6]^+$.

1,1′-(m-*Xylylene)bis-cyclopentadienyl erbium chloride · THF* (**4**)

The procedure followed was similar to that for **1**. An orange-red solid (**4**) was obtained, yield 61%; melting point 87–91°C. Found: C, 52.1; H, 5.1; Er, 33.4; Cl, 7.1. Calc. for $C_{22}H_{24}OClEr$: C, 52.1; H, 4.8; Er, 33.0; Cl, 7.0%. MS: *m/z* (relative intensity) and fragment: 234(8.41), $[C_5H_5CH_2C_6H_4CH_2C_5H_5]^+$; 169(6.25), $[CH_2C_6H_4CH_2C_5H_5]^+$; 155(11.96), $[C_5H_5CH_2C_6H_4]^+$; 154(6.10), $[C_5H_4CH_2C_6H_4]^+$;

105(3.88), $[CH_2C_6H_4CH_2+1]^+$; 91(5.52), $[CH_2C_6H_4+1]^+$; 77(9.29), $[C_6H_4+1]^+$; 72(27.92), $[C_4H_8O]^+$; 66(40.71), $[C_5H_6]^+$; 65(15.16), $[C_5H_5]^+$; 57(14.53), $[C_4H_8+1]^+$; 42(100.00), $[C_3H_6]^+$. IR (cm^{-1}): 120m, 203s, 238s, 262vs, 367m, 435m, 722s, 774vs, 890m, 1013m, 1046s, 1445m, 1461vs, 1586m, 1604s, 2850s, 3060m.

1,1′-(m-*Xylylene*)*bis-cyclopentadienyl yttrium chloride · THF* (5)

The procedure followed was similar to that for **1**. A pale yellow solid (**5**) was obtained, yield 50%; decomposition temperature 172–176°C. Found: C, 61.3; H, 6.1; Y, 20.0; Cl, 7.7. Calc. for $C_{22}H_{24}OClY$: C, 61.6; H, 5.8; Y, 20.7; Cl, 8.3%. MS: *m/z* (relative intensity) and fragment: 468 $[M]^+$; 234(37.77), $[C_5H_5CH_2C_6H_4CH_2C_5H_5]^+$; 169(24.06), $[CH_2C_6H_4CH_2C_5H_5]^+$; 155(45.60), $[C_5H_5CH_2C_6H_4]^+$; 154(21.89), $[C_5H_4CH_2C_6H_4]^+$; 105(2.80), $[CH_2C_6H_4CH_2+1]^+$; 91(13.23), $[CH_2C_6H_4+1]^+$; 77(20.99), $[C_6H_4+1]^+$; 72(27.47), $[C_4H_8O]^+$; 66(21.40), $[C_5H_6]^+$; 65(18.47), $[C_5H_5]^+$; 57(15.73), $[C_4H_8+1]^+$; 42(100.0), $[C_3H_6]^+$. IR (cm^{-1}): 120(m,sh), 193m, 235s, 290s, 372s, 410s, 722s, 781vs, 890m, 1014m, 1047s, 1430m, 1440vs, 1585m, 1603s, 2895s, 2950s, 3060m. ^1H NMR (δ, THF-d_8, TMS): 6.9 (m, C_6H_4), 6.00, 5.78 (m, $2C_5H_4$), 3.50, 1.70 (m, C_4H_8O), 2.80, 2.70 (m, $2CH_2$).

1,1′-(m-*Xylylene*)*bis-cyclopentadienyl ytterbium chloride · THF* (6)

The procedure followed was similar to that for **1**. An orange-yellow solid was obtained, yield 79%; decomposition temperature 168–174°C. Found: C, 51.3; H, 4.9; Yb, 33.3; Cl, 7.4. Calc. for $C_{22}H_{24}OClYb$: C, 51.5; H, 4.8; Yb, 33.7; Cl, 6.9%. MS: *m/z* (relative intensity) and fragment: 234(88.75), $[C_5H_5CH_2C_6H_4CH_2C_5H_5]^+$; 219(2.48), $[C_5H_4CH_2C_6H_5C_5H_5]^+$; 169(52.01), $[CH_2C_6H_4CH_2C_5H_5]^+$; 155(94.65), $[C_5H_5CH_2C_6H_4]^+$; 105(8.57), $[CH_2C_6H_4CH_2+1]^+$; 91(27.84), $[CH_2C_6H_4+1]^+$; 77(42.90), $[C_6H_4+1]^+$; 72(38.29), $[C_4H_8O]^+$; 66(35.34), $[C_5H_6]^+$; 65(28.92), $[C_5H_5]^+$; 57(18.94), $[C_4H_8+1]^+$; 42(100.00), $[C_3H_6]^+$: IR (cm^{-1}): 117m, 202m, 225vs, 250vs, 365s, 433m, 721s, 778vs, 889m, 1014m, 1046s, 1450m, 1462s, 1586m, 1603s, 2858s, 2930s, 3053m.

1,1′-(p-*Xylylene*)*bis-cyclopentadienyl lanthanum chloride · THF* (7)

The procedure followed was similar to that for **1** except using disodium 1,1′-(*p*-xylylene)bis-cyclopentadienide instead of disodium 1,1′-(*m*-xylylene)bis-cyclopentadienide. A white solid product was obtained, yield 50%; decomposition temperature 160–165°C. Found: La, 29.6; Cl, 6.7. Calc. for $C_{22}H_{24}OClLa$: La, 29.0; Cl, 7.4%. MS: *m/z* (relative intensity) and fragment: 672 $[M]^+$; 234(7.59), $[C_5H_4CH_2C_6H_4CH_2C_5H_5+1]^+$; 205(0.13), $[C_5H_5La+1]^+$; 170(2.08), $[CH_2C_6H_4CH_2C_5H_5+1]^+$; 169, $[CH_2C_6H_4CH_2C_5H_5]^+$; 155(3.97), $[C_5H_5CH_2C_6H_4]^+$; 139(0.05), $[La]^+$; 105(1.47), $[CH_2C_6H_4CH_2+1]^+$; 91(3.13), $[CH_2C_6H_4+1]^+$; 77(0.36), $[C_6H_4+1]^+$; 71(54.55), $[C_4H_8O-1]^+$; 66(38.09), $[C_5H_6]^+$; 65(19.37), $[C_5H_5]^+$; 57(3.4), $[C_4H_8+1]^+$; 42(100.00), $[C_3H_6]^+$. IR (cm^{-1}): 208s, 250s, 388w, 450w, 770s, 805s, 890m, 1014s, 1045m, 1430s, 1508s, 1600m, 2880s, 2950s, 3040m, 3080m. ^1H NMR (δ, THF-d_8, TMS): 6.83 (m, C_6H_4), 5.97, 5.77 (m, $2C_5H_4$), 3.40, 1.54 (m, C_4H_8O), 2.70, 2.52 (m, $2CH_2$).

1,1′-(p-*Xylylene*)*bis-cyclopentadienyl preseodymium chloride · THF* (8)

The procedure followed was similar to that for **7**. A pale yellow product was obtained, yield 35%; decomposition temperature 186–190°C. Found: Pr, 29.4; Cl, 8.0. Calc. for $C_{22}H_{24}OClPr$: Pr, 29.3; Cl, 7.4%. MS: *m/z* (relative intensity) and fragment: 234(5.18), $[C_5H_4CH_2C_6H_4CH_2C_5H_5+1]^+$; 205(0.19), $[C_5H_4Pr]^+$; 170(2.22), $[CH_2C_6H_4C_5H_5+1]^+$; 169(5.58), $[CH_2C_6H_4CH_2C_5H_5]^+$; 155(3.26), $[C_5H_4CH_2C_6H_4]^+$; 141(0.84), $[Pr]^+$; 105(2.61), $[CH_2C_6H_4CH_2+1]^+$; 91(3.56), $[CH_2C_6H_4+1]^+$; 77(2.20), $[C_6H_4+1]^+$; 72(32.98), $[C_4H_8O]^+$; 66(81.08), $[C_5H_6]^+$; 65(38.55), $[C_5H_5]^+$; 57(1.82), $[C_4H_8+1]^+$; 42(100.00), $[C_3H_6]^+$. IR (cm^{-1}): 208s, 250s, 408s, 463m, 760s, 800m, 884m, 1012s, 1040s, 1420s, 1500s, 1604s, 2860s, 2940m, 3030m, 3070m.

1,1′-(p-*Xylylene*)*bis-cyclopentadienyl neodymium chloride · THF* (9)

The procedure followed was similar to that for **7**. A purple-blue solid (**9**) was obtained, yield 49%; decomposition temperature 195–199°C. Found: Nd, 29.4; Cl, 7.0. Calc. for $C_{22}H_{24}OClNd$: Nd, 29.8; Cl, 7.3%. MS: *m/z* (relative intensity) and fragment: 570(0.20), $[M]^+$; 234(16.68), $[C_5H_4CH_2C_6H_4CH_2C_5H_5+1]^+$; 207(0.51), $[C_5H_5Nd]^+$; 170(6.89), $[CH_2C_6H_4CH_2C_5H_5+1]^+$; 169(25.30), $[CH_2C_6H_4CH_2C_5H_5]^+$; 155(8.49), $[C_5H_5CH_2C_6H_4]^+$; 154(3.42), $[C_5H_4CH_2C_6H_4]^+$; 142(0.52), $[Nd]^+$; 105(2.05), $[CH_2C_6H_4CH_2+1]^+$; 91(5.43), $[CH_2C_6H_4+1]^+$; 77(0.66), $[C_6H_4+1]^+$; 72(33.88), $[C_4H_8O]^+$; 66(100.00), $[C_5H_6]^+$; 65(53.40), $[C_5H_5]^+$; 42(72.12), $[C_3H_6]^+$. IR (cm^{-1}): 212s, 250m,

390m, 465m, 770s, 804s, 890m, 1015s, 1045s, 1430m, 1510s, 1610m, 2880s, 2950s, 3040s, 3080m.

Acknowledgements—The authors wish to express their cordial thanks to the National Natural Science Foundation of China and Academia Sinica for their financial support.

REFERENCES

1. A. L. Wayda and W. J. Evans, *Inorg. Chem.* 1980, **19**, 2190.
2. T. D. Tilley and R. A. Andersen, *Inorg. Chem.* 1981, **20**, 3267.
3. Q. Shen and P. Zhou, *Kexue Tong Bao* 1985, **30**, 319.
4. G. Jeske, H. Lauke, H. Mauermann, P. N. Swepston, H. Schumann and T. J. Marks, *J. Am. Chem. Soc.* 1985, **107**, 8091.
5. Q. Shen, H. Tian, Z. Sum and R. Shi, *Youji Huaxue* 1985, 241.
6. M. D. Rausch and K. J. Morlarty, *Organometallics* 1986, **5**, 1281.
7. M. F. Lappert, A. Singh, J. L. Atwood and W. E. Hunter, *J. Chem. Soc., Chem. Commun.* 1981, 1190.
8. M. F. Lappert, A. Singh, J. L. Atwood and W. E. Hunter, *J. Chem. Soc., Chem. Commun.* 1981, 1191.
9. M. Tsutsui, L. Chen, D. E. Bergbreiter and T. K. Miyamoto, *J. Am. Chem. Soc.* 1982, **104**, 855.
10. J. John and M. Tsutsui, *J. Coord. Chem.* 1980, **10**, 177.
11. C. Qian, C. Ye, H. Lu, Y. Li and Y. Huang, *J. Organomet. Chem.* 1984, **263**, 333.
12. C. Qian, Z. Xie and Y. Huang, *J. Organomet. Chem.* 1987, **323**, 285.
13. G. Jeske, L. E. Schock, P. N. Swepston, H. Schumann and T. J. Marks, *J. Am. Chem. Soc.* 1985, **107**, 8103.
14. C. Qian, Z. Xie and Y. Huang, *Inorg. Chim. Acta* 1987, **139**, 195.
15. T. S. Dory and J. J. Zuckerman, *J. Organomet. Chem.* 1984, **264**, 295.
16. C. Qian, C. Ye, H. Lu, Y. Li, J. Zhou, Y. Ge and M. Tsutsui, *J. Organomet. Chem.* 1983, **247**, 161.
17. H. A. Martin, M. Y. Gorkom and R. O. Jongh, *J. Organomet. Chem.* 1972, **36**, 93.
18. J. A. Smith, J. V. Seyerl, C. Huttner and H. H. Brintzinger, *J. Organomet. Chem.* 1979, **173**, 175.
19. C. Chen, X. Zhong, C. Qian, Z. Xie and Y. Huang, *Youji Huaxue* 1988, 235.
20. X. You, W. Wu, C. Li, C. Li and Ç. Qian, *Acta Phys. Chim. Sin.* 1987, **3**, 430.
21. C. Qian, C. Ye and Y. Li, *J. Organomet. Chem.* 1986, **302**, 171.
22. G. Fu, Y. Xu, Z. Xie and C. Qian, *Acta Chim. Sin., Engl. Edn* 1989, 431.
23. C. Qian, B. Yao, S. Huang, C. Ye, Y. Li, H. Lu and Y. Huang, *Synth. React. Inorg. Met.-Org. Chem.* 1984, **14**, 663.
24. E. F. J. Atkinson and J. F. Thorpe, *J. Chem. Soc., Dalton Trans.* 1907, **91**, 1696.
25. C. Qian and Y. Gu, *J. Organomet. Chem.*, submitted.

Polyhedron Vol. 9, No. 4, pp. 487–489, 1990
Printed in Great Britain

0277-5387/90 $3.00+.00
© 1990 Pergamon Press plc

EPOXIDATION OF OLEFINS USING A CrO_3/TBHP SYSTEM

D. D. AGARWAL,* SAVITA SRIVASTAVA and POONAM CHADHA

School of Studies in Chemistry, Jiwaji University, Gwalior–474011, M.P. India

(*Received* 28 *April* 1989; *accepted* 31 *August* 1989)

Abstract—The epoxidation of cyclohexene using CrO_3/TBHP gave cyclohexene oxide, cyclohexenol and cyclohexenone in the ratio 3 : 1 : 40. The nature of the solvent affects the yield of the product. Pyridine, imidazole, NaH_2PO_4 and surfactants were found to have negative effects on the yield of epoxide while sodium bicarbonate increases the yield of the epoxide. The relative rate of epoxidation of cyclic olefins was norbornene > cycloheptene > cyclooctene > cyclopentene > cyclohexene.

The catalytic functionalization of hydrocarbons is of chemical and biochemical significance.[1] Within such functionalization epoxidation of olefins using a metal catalysed system poses a synthetic and theoretical challenge.[2] Recently porphyrin and non-porphyrin metal catalysts[3–12] using iodosylbenzene, hypochlorite, tert-butylhydroperoxide, sodium periodate, sodium ascorbate/O_2, etc., have been studied. Studies with chromium(III) complexes using iodosylbenzene gave epoxide, and chromium(V) is the active oxidizing species.[2] But chromium(IV) with TBHP has been found to give only the hydroperoxide of cyclohexene.[13] CrO_2Cl_2 and $CrO_2(NO_3)_2$ have been studied as stoichiometric reagents for epoxidation.[14] In continuation of our studies[15,16] on the epoxidation of olefins, we extended our studies to a CrO_3/TBHP system which has recently been used for the oxidation of alcohols.[17] The system has been studied in detail and a possible mechanism suggested.

EXPERIMENTAL

Materials

Cyclopentene, cyclohexene, cyclooctene, cycloheptene and norbornene were commercial samples from Aldrich. Tert-butylhydroperoxide (70%) was purchased from Aldrich and dried by a literature procedure.[18] All the olefins were purified[19] from sodium hydride before use and stored at −30°C. All the standard samples of olefins were prepared[20,21] using *m*-chloroperbenzoic acid. Sodium bicarbonate, sodium dihydrogen phosphate, pyridine, imidazole, sodium lauryl sulphate, Triton X–100 and cetyltrimethylammonium bromide were obtained from Aldrich, Glaxo and Loba chemical laboratories.

Procedure for catalytic epoxidation

A typical procedure for carrying out the catalytic epoxidation of cyclohexene is heating cyclohexene (20 mmol), benzene (10 cm^3), CrO_3 (0.02 mmol) and tert-butylhydroperoxide (2.0 mmol) at 80°C under a nitrogen atmosphere for 4 h with continuous stirring. After 4 h the contents were worked-up by adding sodium sulphite to destroy tert-butylhydroperoxide and then extracted with ether, followed by drying with anhydrous magnesium sulphate. The samples were analysed by gas chromatography (GC) using an XE–60 column at 120°C. The retention times were 3.46 min (epoxide), 6.5 min (cyclohexenol) and 10.44 min (cyclohexenone).

In a separate experiment, epoxidation of cyclohexene was carried out using CH_2Cl_2 as the solvent in place of benzene, but using the same compositions and conditions as stated above. Also, in another experiment, epoxidation of cyclohexene using 70% TBHP was studied. The effect of various additives, *viz.* pyridine, imidazole, NaH_2PO_4, $NaHCO_3$, sodium lauryl sulphate, Triton X–100 and cetyltrimethylammonium bromide, on the epoxidation of cyclohexene was studied by adding 100 mg of additive to the epoxidation system.

The competitive epoxidation of cyclic olefins, *viz.* cyclopentene, cyclohexene, cycloheptene, cyclo-

* Author to whom correspondence should be addressed.

octene and norbornene, was carried out by heating CrO_3 (0.04 mmol), cyclohexene (20 mmol), other cyclic olefins (20 mmol), tert-butylhydroperoxide (4.0 mmol), dodecane (0.1 cm^3) at 80°C under nitrogen for 4 h. The products were analysed by GC.

RESULTS AND DISCUSSION

The epoxidation of cyclohexene using a CrO_3/TBHP system in benzene shows the formation of three products: cyclohexene oxide, cyclohexenol and cyclohexenone in a 3:1:40 ratio, but when the epoxidation was carried out in dichloromethane instead of benzene the yield of cyclohexenol was higher and the yield of cyclohexenone lower. The selectivity of epoxide was 16%. The epoxidation when 70% TBHP was used showed that selectivity of epoxide was 20% and the yield of cyclohexenone was 0.059 mmol compared to 0.016 mmol for cyclohexenol. These results show that the medium for epoxidation has an effect on the selectivity of epoxide. The fact that commercial TBHP, which is as good an epoxidizing agent as water, has no detrimental effect on epoxidation is contrary to an inhibitory effect found in molybdenum catalysed reactions.[1] The formation of cyclohexenol and cyclohexenone shows that a free radical pathway[1] is operative. The reaction of CrO_3 with cyclohexene in the absence of TBHP did not give any product and neither did the reaction between cyclohexene and TBHP in the absence of CrO_3. The secondary alcohol was found to oxidize to ketone under these conditions. When the kinetics of the cyclohexene epoxidation were studied (Fig. 1) it was observed that in the first 10 min the formation of cyclohexenol is greater than that of cyclohexenone, but as the reaction continues the ratio of cyclohexenone: cyclohexenol increases; this suggests that the cyclohexenol being formed in the reaction is being oxidized to cyclohexenone.

The results of the effects of the additives pyridine, imidazole, NaH_2PO_4 and $NaHCO_3$ on the epoxidation of cyclohexenene are incorporated in Table 1. This shows that pyridine, imidazole and NaH_2PO_4 have negative effects on the yield of epoxide, while the addition of $NaHCO_3$ increases the yield of the epoxide. This behaviour of CrO_3 is in contrast to that observed with OMo(TPP)OMe/TBHP[7] and OTi(TPP)/TBHP[7] systems which lower the yield of epoxide.

The effect of surfactant shows that sodium lauryl sulphate and Triton X–100 decrease the yield of all three products, but the addition of cetyltrimethylammonium bromide gave high selectivity for cyclohexenol, thus showing that it retards the oxidation of cyclohexenol to cyclohexenone.

The competitive epoxidation of cycloolefins shows the reactivity order: norbornene (6.3) > cycloheptene (4.0) > cyclooctene (3.2) > cyclopentene (2.4) > cyclohexene (1.0). The higher rates of epoxidation observed with norbornene, cyclooctene and cycloheptene compared with cyclohexene show that the olefin is not coordinated to the metal centre during the rate-determining step.[13,15] The observed results shows that torsional strain and

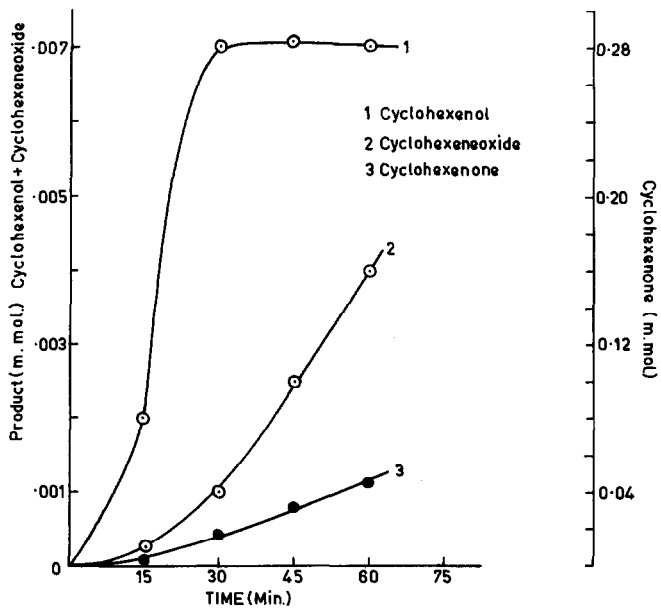

Fig. 1. Cyclohexene epoxidation using the CrO_3/TBHP system.

Table 1. Epoxidation of cyclohexene in the presence of different additives

Additive	Product ratio (mmol) (a)	(b)	(c)	Turnover number of CrO_3
NO	0.021	0.007	0.281	15.0
Pyridine	Nil	0.008	0.05	3.0
Imidazole	Nil	Traces	Traces	0.0
NaH_2PO_4	0.012	0.0008	0.184	10.0
$NaHCO_3$	0.032	0.0005	0.131	8.0
Sodium lauryl sulphate	0.013	0.0004	0.110	6.0
Triton X–100	Nil	0.0005	0.0004	—
Cetyltrimethylammonium bromide	Nil	0.023	0.047	3.5

bond angle strain play an important role in determining the relative reactivity of cyclic olefins.[15]

As far as the mechanism of epoxidation is concerned, the CrO_3 reacts with tert-butylhydroperoxide resulting in the development of a deep orange–red colour which can be attributed to a peroxo–metal intermediate:

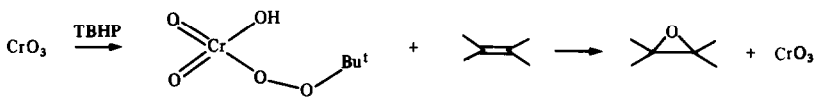

(1)

A similar kind of species has been reported in the OTi(TPP)/TBHP[7] and OMo(TPP)OMe/TBHP[7] systems which are responsible for epoxidation. This species has also recently been reported to oxidize alcohols;[17] it transfers oxygen to the olefin resulting in the formation of epoxide. The formation of allylic oxidation products, cyclohexenone and cyclohexenol, has also been reported by Groves *et al.*[22] in the Cr^{III}(TPP)Cl/PhIO system (96%). In the present system too, the cyclohexenone is obtained as a major product. Thus it shows that this system can be used as an effective reagent for the oxidation of alkenes.

REFERENCES

1. R. A. Sheldon and J. K. Kochi, *Metal Catalysed Oxidation of Organic Compounds*, Academic Press, New York (1981).
2. E. G. Samsel, K. Srinivasan and J. K. Kochi, *J. Am. Chem. Soc.* 1985, **107**, 7606.
3. J. T. Groves and T. E. Nemo, *J. Am. Chem. Soc.* 1983, **105**, 6243.
4. J. R. Lindsay Smith and P. R. Sleath, *J. Chem. Soc. Perkin Trans. II* 1983, 1165.
5. B. Meunier, E. Guilmet, M. De Carvalho and R. Poilblanc, *J. Am. Chem. Soc.* 1984, **106**, 6668.
6. B. Meunier, M. De Carvalho, O. Bartolini and M. Momenteau, *Inorg. Chem.* 1988, **27**, 161.
7. H. J. Ledon and F. Varescon, *Inorg. Chem.* 1984, **23**, 2735.
8. P. N. Balsubramanian, A. Sinha and T. C. Bruice, *J. Am. Chem. Soc.* 1987, **109**, 1456.
9. D. Mansuay, M. Fontecave and J. F. Bartoli, *J. Chem. Soc., Chem. Commun.* 1983, 253.
10. J. T. Groves and M. K. Stern, *J. Am. Chem. Soc.* 1987, **109**, 3812.
11. K. Srinivasan, P. Michaud and J. K. Kochi, *J. Am. Chem. Soc.* 1986, **108**, 2309.
12. M. Faraj and C. L. Hill, *J. Chem. Soc., Chem. Commun.* 1987, 1487.
13. F. Varescon, Thesis, L'Universite Claude Bernard, Lyon, France (1982).
14. N. Miyaura and J. K. Kochi, *J. Am. Chem. Soc.* 1983, **105**, 2368.
15. D. D. Agarwal, *J. Molec. Catal.* 1988, **44**, 65.
16. D. D. Agarwal and Savita Srivastava, *Polyhedron* 1988, **7**, 2569.
17. J. Muzart, *Tetrahedron Lett.* 1987, **28**, 2133.
18. K. B. Sharpless and T. R. Verhoeven, *Aldrichim. Acta* 1979, **12**, 63.
19. D. D. Perrin, W. L. Armarego and D. R. Perrin, *Purification of Laboratory Chemicals*, Pergamon Press, New York (1980).
20. D. Swern (Ed.), *Organic Peroxides*, Vol. II, Wiley-Interscience (1971).
21. D. Swern, *J. Am. Chem. Soc.* 1947, **69**, 1692.
22. J. T. Groves, W. J. Kruper, T. E. Nemo and R. S. Myers, *J. Molec. Catal.* 1980, **7**, 169.

Polyhedron Vol. 9, No. 4, pp. 491–494, 1990
Printed in Great Britain

0277–5387/90 $3.00+.00
© 1990 Pergamon Press plc

SYNTHESIS AND CRYSTAL STRUCTURE OF 10-COORDINATE $[Th(C_5H_5NO)_6(NO_3)_2](NO_3)_2$ (C_5H_5NO = 2-(1H)-PYRIDONE)

DAVID M. L. GOODGAME,* SALLY NEWNHAM, CAROLINE A. O'MAHONEY and DAVID J. WILLIAMS*

Chemistry Department, Imperial College of Science, Technology and Medicine, London SW7 2AY, U.K.

(*Received* 1 *August* 1989; *accepted* 31 *August* 1989)

Abstract—Attempts to prepare polynuclear, heterometallic Cu^{II}/Th^{IV} complexes with 2-pyridone (= L) bridges, analogous to those formed by Cu^{II}/Dy^{III} and Cu^{II}/Gd^{III} gave instead $[ThL_6(NO_3)_2](NO_3)_2$, which has been characterized by X-ray diffraction. The Th atom is 10-coordinate with two bidentate nitrates and the six pyridone oxygen atoms forming a distorted bicapped square antiprism.

We recently described[1] some heterometallic hexanuclear compounds containing unusual $Cu_4^{II}M_2^{III}$ arrays, where M^{III} = Dy or Gd. These green complexes were obtained by the reaction of copper(II) hydroxide, 2-pyridone, and Dy (or Gd) nitrate in methanol. The use of other lanthanide(III) nitrates has also given green materials, full characterization of which has been hindered by poor crystal quality. However, use of the same synthetic method with the tetravalent metal ion Th^{IV} gave a quite different reaction, in which colourless crystals of stoichiometry $Th(C_5H_5NO)_6(NO_3)_4$ (**1**) were formed. We report here the structure of this compound.

EXPERIMENTAL

Preparation

Reaction of copper hydroxide (1 mmol), 2-pyridone (6 mmol) and hydrated thorium nitrate (2 mmol) in refluxing methanol (100 cm^3) gave a blue solution from which colourless needles formed. Found: C, 33.6; H, 2.7; N, 13.0. Calc. for $Th(C_5H_5NO)_6(NO_3)_4$: C, 34.3; H, 2.9; N, 13.3%.

X-ray study

Crystals of **1** form as colourless needles. The crystal data are: $C_{30}H_{30}N_{10}O_{18}Th$, M_r = 1050.7, monoclinic, a = 19.749(6), b = 9.802(4), c = 20.339(6) Å, β = 100.77(2)°, V = 3868 $Å^3$, space group $C2/c$, Z = 4 (the molecule is disposed about a two-fold axis), D_c = 1.80 g cm^{-3}, Cu radiation, λ = 1.54178 Å, μ(Cu-K_α) = 132 cm^{-1}, $F(000)$ = 2040. Data were measured on a Nicolet R3m diffractometer with Cu-K_α radiation (graphite monochromator) using ω-scans.

A crystal of dimensions 0.10 × 0.10 × 0.27 mm was used. 1997 independent reflections ($2\theta \leqslant 116°$) were measured, of which 1958 had $|F_o| > 3\sigma(|F_o|)$ and were considered observed. The data were corrected for Lorentz and polarization factors; a numerical absorption correction (face-indexed crystal) was applied; maximum and minimum transmission factors 0.401 and 0.174.

The structure was solved by the heavy atom method. The non-hydrogen atoms were refined anisotropically. The protons on N(2), N(9) and N(16) were located from a ΔF map and refined isotropically subject to a distance constraint of 0.98 Å. The positions of the remaining hydrogen atoms were idealized, C—H = 0.98 Å, assigned isotropic thermal parameters, $U(H) = 1.2U_{eq}(C)$ and allowed to ride on their parent carbon atoms. Refinement was by block-cascade full-matrix least-squares to R = 0.034, R_w = 0.033 [$w^{-1} = \sigma^2(F) + 0.00050F^2$]. The maximum and minimum residual electron densities in the final ΔF map were 1.95 and −1.95 e $Å^{-3}$, respectively. The mean and maximum shift/error in the final refinement were 0.003 and 0.015, respectively. Computations were carried out on an Eclipse S140 computer using the SHELXTL pro-

* Authors to whom correspondence should be addressed.

Table 1. Bond lengths (Å) and angles (°) for (1) with ESDs in parentheses

Th—O(1)	2.365(4)	Th—O(7)	2.413(5)
Th—O(14)	2.413(4)	Th—O(21)	2.686(5)
Th—O(23)	2.610(5)	Th—O(1′)	2.365(4)
Th—O(7′)	2.413(5)	Th—O(14′)	2.413(4)
Th—O(21′)	2.686(5)	Th—O(23′)	2.610(5)
O(1)—Th—O(7)	82.3(1)	O(1)—Th—O(14)	71.6(2)
O(7)—Th—O(14)	70.9(2)	O(1)—Th—O(21)	128.5(2)
O(7)—Th—O(21)	107.0(2)	O(14)—Th—O(21)	64.9(2)
O(1)—Th—O(23)	141.8(1)	O(7)—Th—O(23)	67.9(2)
O(14)—Th—O(23)	76.3(2)	O(21)—Th—O(23)	47.6(1)
O(1)—Th—O(1′)	78.2(2)	O(7)—Th—O(1′)	146.0(2)
O(14)—Th—O(1′)	76.6(1)	O(21)—Th—O(1′)	66.3(2)
O(23)—Th—O(1′)	114.0(1)	O(1)—Th—O(7′)	146.0(2)
O(7)—Th—O(7′)	126.8(2)	O(14)—Th—O(7′)	130.0(2)
O(21)—Th—O(7′)	65.2(2)	O(23)—Th—O(7′)	71.9(2)
O(1)—Th—O(14′)	76.6(1)	O(7)—Th—O(14′)	130.0(2)
O(14)—Th—O(14′)	138.7(2)	O(21)—Th—O(14′)	121.6(1)
O(23)—Th—O(14′)	141.1(1)	O(1)—Th—O(21′)	66.3(2)
O(7)—Th—O(21′)	65.2(2)	O(14)—Th—O(21′)	121.6(1)
O(21)—Th—O(21′)	163.6(2)	O(23)—Th—O(21′)	117.1(1)
O(1)—Th—O(23′)	114.0(1)	O(7)—Th—O(23′)	71.9(2)
O(14)—Th—O(23′)	141.1(1)	O(21)—Th—O(23′)	117.1(1)
O(23)—Th—O(23′)	79.7(2)		

gram system.[2] Selected bond lengths and angles are listed in Table 1.

RESULTS AND DISCUSSION

The X-ray structural analysis shows that the Th atom in **1** is coordinated to 10 oxygen atoms (Fig. 1). Four of these are from two bidentate nitrates and the remaining six are from the 2-pyridone ligands. The Th—O(nitrate) bonds [2.610(5) and 2.686(5) Å] are distinctly longer than the Th—O bonds to the pyridone ligands [2.365(4)–2.413(5) Å]. A similar difference has been observed in other Th complexes containing combinations of bidentate nitrates and organic oxygen donor ligands in the coordination sphere.[3,4]

The coordination polyhedron about the Th atom

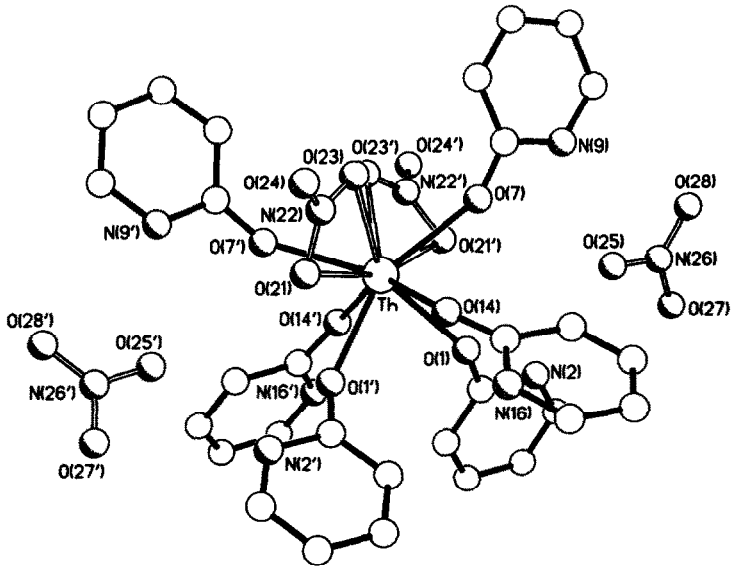

Fig. 1. The molecular structure of $[Th(C_5H_5NO)_6(NO_3)_2](NO_3)_2$, showing the crystallographic numbering scheme.

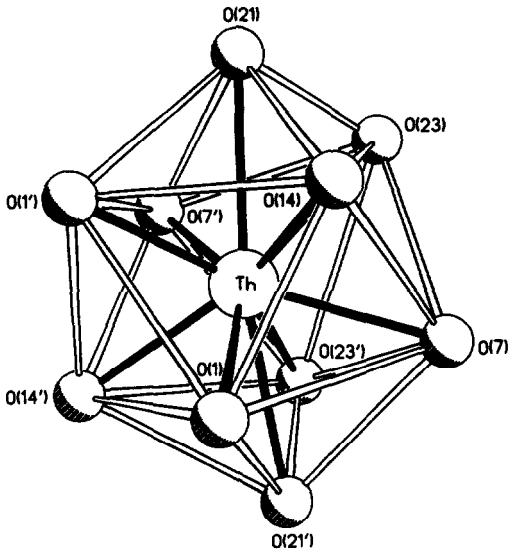

Fig. 2. The distorted bicapped square antiprismatic coordination geometry about Th. The non-bonded O···O distances are in the range 2.14 Å (nitrate)–3.14 Å for O(1)···O(7) (pyridone).

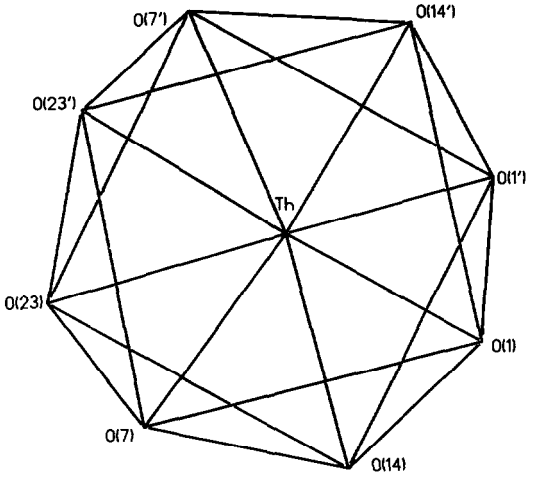

Fig. 3. Plan view of the Th coordination showing the degree of square antiprismatic register.

is best described as a distorted bicapped square antiprism (Fig. 2), one plane of which comprises O(1), O(14′), O(23′) and O(7) capped by O(21′); the other comprising O(1′), O(14), O(23) and O(7′) capped by O(21). The maximum distortion from planarity of each of these planes is 0.17 Å. The two planes are almost parallel, being inclined by only *ca* 4°. The Th and apical O atoms lie 1.18 and 1.46 Å, respectively, from these planes. The two planes deviate from idealized mutual square antiprismatic register by *ca* 5° (Fig. 3). The O(21)—Th—O(21′) angle is 163.6(2)° [cf. 171.4° for the corresponding angle in $Hg_2Th(C_4H_6NO)_4(NO_3)_4$ (**2**)[4] and 174.7° for that in $K_4[Th(C_2O_4)_4]\cdot 4H_2O$ (**3**)[5]].

As both the capping oxygen atoms, O(21) and O(21′), are provided by bidentate nitrate groups there is a significant reduction in one of the pyramid edge angles [O(21)—Th—O(23) 47.6(1)°] whilst the others [64.9(1)–66.3(2)°, mean 65.5°] are more normal (cf. 62–66°, mean 64.0°, in the oxalato complex, **3**[5]). The small coordination "bite" of the bidentate nitrates does not appear to influence the other angles subtended at the Th atom. The square edge angles are 71.9(2)–82.3(1)°, mean 76.8° (cf. 71.6–91.0°, mean 78.9°, in **3**). The equatorial edge angles are 67.9–79.7°, mean 72.3° (cf. 63.6–75.8°, mean 68.1°, in **3**).

The other two nitrate groups are present as non-coordinated ions which are linked by H-bonding to the NH groups of the pyridones. These H-bonds are of two types. In one, the nitrate oxygen atom, O(25), serves to bridge adjacent pyridone ligands [N(2) and N(9)] within the same coordination sphere.* The other pyridone ligand links intermolecularly to O(27) via N(16).*

As compound **1** resulted from attempts to make a Th/Cu polynuclear complex related to the Ln compounds $Cu_4Ln_2L_8(LH)_4(OH)_2(NO_3)_4(H_2O)_2$ (**4**, Ln = Dy, Gd; LH = 2-pyridone)[1] it is pertinent to compare the Th environment in **1** with the Ln environment in **4**. Although the Ln atoms in **4** are only nine-coordinate, they also contain six oxygen bonded pyridone ligands (the rest of the coordination sphere comprises one bidentate nitrate and a water molecule). An important difference is that in **4**, four of the pyridone ligands are deprotonated and it is the oxygen atoms of those pyridones which serve to link each Ln ion to two copper(II) ions. In **1** none of the pyridones bonded to Th is deprotonated and a mononuclear compound results. The compounds of type **4** were obtained by using copper(II) hydroxide and more forcing deprotonation conditions may be more conducive to the formation of pyridone bridged Th/Cu compounds.

Acknowledgement—We thank the SERC for funds for the diffractometer and for a Research Studentship (to C.A.O'M).

* N(2)···O(25) = 2.85, H(2)···O(25) = 1.87 Å, N(2)—H(2)···O(25) angle = 176°, N(9)···O(25) = 2.81, H(9)···O(25) = 1.84 Å, N(9)—H(9)···O(25) angle = 171°, N(16)···O(27′) = 2.88, H(16)···O(27′) = 1.97 Å, N(16)—H(16)···O(27′) angle = 153°.

REFERENCES

1. D. M. L. Goodgame, D. J. Williams and R. E. P. Winpenny, *Polyhedron* 1989, **8**, 1531.
2. G. M. Sheldrick, SHELXTL. An Integrated System for Solving, Refining and Displaying Crystal Structures from Diffraction Data, Revision 4.1. University of Gottingen, F.R.G. (1983).
3. A. Bino and R. Chayat, *Inorg. Chim. Acta* 1987, **129**, 273.
4. D. M. L. Goodgame, D. J. Williams and R. E. P. Winpenny, *Polyhedron* 1988, **7**, 1807.
5. M. N. Akhtar and A. J. Smith, *Acta Cryst.* 1975, **31B**, 1361.

Polyhedron Vol. 9, No. 4, pp. 495–500, 1990
Printed in Great Britain

0277–5387/90 $3.00+.00
© 1990 Pergamon Press plc

HYBRID TELLURIDE LIGANDS—TELLUROAMINES 1-(NMe_2)-2-(TeAr)-4-MeC_6H_3 (Ar = C_6H_5, 4-$MeOC_6H_4$ OR 4-$EtOC_6H_4$): SYNTHESIS AND COMPLEXATION WITH PALLADIUM(II) AND PLATINUM(II)

AJAI K. SINGH, VINOD SRIVASTAVA and B. L. KHANDELWAL*

Department of Chemistry, Indian Institute of Technology, New Delhi–110 016, India

(*Received* 12 *June* 1989; *accepted* 5 *September* 1989)

Abstract—The aniline derivative 1-(NMe_2)-4-MeC_6H_4 on *ortho*-mercuration followed by reaction with $ArTeCl_3$ (Ar = C_6H_5, 4-$MeOC_6H_4$ or 4-$EtOC_6H_4$) gives 1-(NMe_2)-2-($ArTeCl_2$)-4-MeC_6H_3 which on reduction with sodium metabisulphite gives hybrid telluride ligands—telluroamines (**1–3**). These newly synthesized asymmetric tellurides were characterized by elemental analysis, typical reaction with MeI, IR, ^1H and ^{13}C NMR spectra, molecular weight and conductance measurements. The (Te, N) ligands react with Na_2MCl_4/K_2MCl_4 (M = Pt or Pd) resulting in $MCl_2 \cdot L$ (L = telluroamines) type complexes. These complexes are monomeric, non-electrolyte and diamagnetic, indicating a square-planar arrangement of ligands around the metal, which is supported by electronic spectra. ^1H NMR data in conjunction with IR spectra suggest that these telluroamines behave as bidentate ligands in the present complexes.

A lot of interest has been developing in the ligand chemistry of tellurium[1–4] for the last one and a half decades but very few hybrid bidentate or polydentate ligands[5–6] containing the element are known and explored for their complexation behaviour. We were interested in synthesizing potentially bidentate ligands containing both Te and donor atoms such as N or O for two reasons. First, these donor atoms may strongly ligate with the hard metals of the first and second transition series and consequently generate a system in which the forced interaction (if any) of Te with such metals can be investigated. Second, they can favourably influence catalytic activity of Pt group metallic centres (e.g. for hydrogenation) if incorporated into their coordination sphere. This is expected on the basis of the larger size of Te due to which the formation and reaction of intermediates may be facilitated in comparison to complexes containing donors like (P, N) or (P, O). Thus asymmetric tellurides **1–3** have been prepared by mercuration of N,N-dimethyl-*p*-toluidine followed by transmetallation with suitable aryltellurium(IV) chloride in good yield. Their complexation with Pd^{II} and Pt^{II} has been investigated. The synthesis and spectra of these new (Te, N) donors and their complexes are the subject of the present paper.

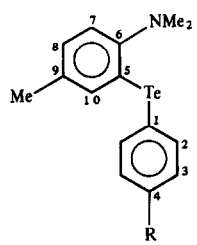

R	
H	**1**
OMe	**2**
OEt	**3**

EXPERIMENTAL

Published methods[7] were used to synthesize $C_6H_5TeCl_3$, 4-$MeOC_6H_4TeCl_3$ and 4-$EtOC_6H_4$ $TeCl_3$. The chloride, mercury and tellurium were estimated by standard methods.[8] The C, H and N analyses were carried out with a Perkin–Elmer elemental analyser 240C. ^1H and $^{13}C\{^1H\}$ NMR spectra were recorded on a JEOL FX 100 FT–NMR spectrometer, at 99.55 and 25 MHz, respectively. IR spectra (of Nujol mulls between

* Author to whom correspondence should be addressed.

CsI windows or KBr/CsI discs) in the range 4000–200 cm^{-1} were recorded on a Nicolet 5DX FT-IR spectrometer. Electronic spectra in $CHCl_3$ were recorded on a Hitachi 330 UV–vis spectrophotometer. The conductivity measurements were made on *ca* 1 mM solutions in acetonitrile with a Pye conductivity bridge. The molecular weights were determined in chloroform for 5–20 m solutions with a Knauer vapour pressure osmometer.

Procedure for mercuration[9]

N,N-Dimethyl-*p*-toluidine (Riedal) (0.1 mol) was dissolved in 50 cm^3 methanol and mixed with a solution of mercuric acetate (0.1 mol) made in 200 cm^3 methanol. The mixture was heated on a water bath at 60–70°C for 0.5 h after adding 2 cm^3 of glacial acetic acid to avoid the formation of HgO. Sodium chloride (0.1 mol), dissolved in a minimum amount of water, was added to this mixture. The white precipitate thus formed was filtered, washed with water, dried and extracted with chloroform. The extract was concentrated to crystallize 1-(NMe_2)-2-(HgCl)-4-MeC_6H_3 as white needles. Yield 50%, m.p. 165–167°C. Found: Hg, 53.8; Cl, 9.2; Calc: Hg, 54.2; Cl, 9.6%. NMR (^1H, $CDCl_3$, 25°C): δ, 2.29 (s, 3H, Me), 2.71 (s, 6H, NMe_2), 7.06–7.25 (m, 3H, phenyl).

Procedure for transmetallation with aryltellurium(IV) chloride

Mercurated aniline (10 mmol) was refluxed with equimolar amounts of $C_6H_5TeCl_3$, 4-$MeOC_6H_4TeCl_3$ or 4-$EtOC_6H_4TeCl_3$ in 60 cm^3 of chloroform for 6 h. The solution was cooled and the precipitated $HgCl_2$ was filtered off. On concentrating the filtrate the pale yellow/yellowish brown $ArAr'TeCl_2$ type derivative crystallized, which was filtered off, washed with 5–10 cm^3 of cold methanol and recrystallized from a benzene–chloroform (30:70) mixture. The yield, melting point, results of elemental analysis, characteristic IR bands, ^1H and $^{13}C\{^1H\}$ NMR data are given below.

4: Yield, 80%; m.p. 175–177°C. Found: C; 43.1; H, 3.9; N, 3.4; Te, 30.9; Cl, 17.2. Calc. for $C_{15}H_{17}NCl_2Te$: C, 43.9; H, 4.1; N, 3.4; Te, 31.1; Cl, 17.3%. IR(cm^{-1}): 1301m [ν(N—C(Ar))]; 1242s [ν(N—C(Me))]; 290m, 260s [ν(Te—Cl)]; 275m, 248m [ν(Te—C)]. NMR (^1H, $CDCl_3$, 25°C): δ, 2.26 (s, 3H, Me); 2.92 (s, 6H, NMe_2); 7.18–7.96 (m, 8H, phenyl); ($^{13}C\{^1H\}$, $CDCl_3$, 25°C): δ, 21.2 (Me); 46.5 (NMe_2); 139.2 (C_1); 133.9 (C_2); 129.6 (C_3); 131.1 (C_4); 143.9 (C_5); 149.9 (C_6); 123 (C_7); 128.9 (C_8); 112.1 (C_9); 135.3 (C_{10}).

5: Yield, 85%; m.p. 219–221°C. Found: C, 45.2; H, 5.0; N, 3.4; Te, 28.9; Cl, 15.5. Calc. for $C_{16}H_{19}NOCl_2Te$: C, 43.7; H, 4.3; N, 3.2; Te, 29.0; Cl, 16.1%. IR(cm^{-1}): 1305s [ν(N—C(Ar))]; 1263s [ν(N—C(Me))]; 300m, 280s [ν(Te—Cl)]; 265m, 250m [ν(Te—C)]. NMR (^1H, $CDCl_3$, 25°C): δ, 2.27 (s, 3H, Me); 2.91 (s, 6H, NMe_2); 3.90 (s, 3H, OMe); 7.08–8.29 (m, 7H, phenyl); ($^{13}C\{^1H\}$, $CDCl_3$, 25°C): δ, 21.2 (Me); 46.6 (NMe_2); 55.5 (OMe); 123.0 (C_1); 133.9 (C_2); 115.5 (C_3); 161.0 (C_4); 129.0 (C_7); 137.0 (C_8); 139.0 (C_{10}); C_5, C_6, C_9 not observed.

6: Yield, 83%; m.p. 193–195°C. Found: C, 43.9; H, 4.2; N, 3.2; Te, 27.8; Cl, 15.1. Calc. for $C_{17}H_{21}NOCl_2Te$: C, 45.0; H, 4.6; N, 3.1; Te, 28.1; Cl, 15.6%. IR (cm^{-1}): 1306s [ν(N—C(Ar))]; 1263s [ν(N—C(Me))]; 290w, 280m [ν(Te—Cl)]; 260s, 245m [ν(Te—C)]. NMR (^1H, $CDCl_3$, 25°C): δ, 1.40–1.60 (t, 3H, CH_3 of OEt); 2.26 (s, 3H, Me); 2.91 (s, 6H, NMe_2); 4.02–4.23 (q, 2H, CH_2 of OEt); 7.06–8.33 (m, 7H, phenyl); ($^{13}C\{^1H\}$, $CDCl_3$, 25°C): δ, 21.1 (Me); 46.4 (NMe_2); 14.5 (CH_3 of OEt); 63.6 (CH_2 of OEt); 119.8 (C_1); 133.8 (C_2); 115.7 (C_3); 161.19 (C_4); 143.9 (C_5); 149.9 (C_6); 122.9 (C_7); 128.7 (C_8); 139.1 (C_9); 136.8 (C_{10}).

Reduction of **4–6**

The aqueous suspension of **4–6** was stirred with a five-fold molar excess of sodium metabisulphite dissolved in water for 2 h at 50°C. Compound **4** yielded a dense liquid which was separated, washed with water and extracted with hexane. The hexane was removed *in vacuo* to give a yellow oil. Compounds **5** and **6** yielded pale yellow solids which were filtered, washed with water, dried and extracted with petroleum ether (40–60°C) or hexane. The extract on concentration gave a pale yellow crystalline solid, which was filtered and dried *in vacuo*. The yield, melting point, results of elemental analysis, IR, ^1H and ^{13}C NMR data are given below.

1: Yield, 85%. Found: Te, 36.8; Calc. for $C_{15}H_{17}NTe$: Te, 37.7%. IR(cm^{-1}): 1267s [ν(N—C(Ar))]; 1206s [ν(N—C(Me))]; 275m, 250m [ν(Te—C)]. NMR (^1H, $CDCl_3$, 25°C): δ, 2.10 (s, 3H, Me); 2.68 (s, 6H, NMe_2); 6.66–7.96 (m, 8H, phenyl); ($^{13}C\{^1H\}$, $CDCl_3$, 25°C): δ, 20.8 (Me); 45.6 (NMe_2); 114.2 (C_1); 141.3 (C_2); 129.2; (C_3); 127.9 (C_4); 136.4 (C_5); 151.1 (C_6); 128.2 (C_7); 131.9 (C_8); 122.2 (C_9); 120.2 (C_{10}).

2: Yield, 87%; m.p. 73–75°C. Found: C, 53.2; H, 5.4; N, 4.1; Te, 34.1. Calc. for $C_{16}H_{19}NOTe$: C, 52.1; H, 5.1; N, 3.8; Te, 34.6%. IR(cm^{-1}): 1280s [ν(N—C(Ar))]; 1240s [ν(N—C(Me))]; 290m, 260w [ν(Te—C)]. NMR (^1H, $CDCl_3$, 25°C): δ, 2.12

(s, 3H, Me); 2.68 (s, 6H, NMe_2); 3.84 (s, 3H, OMe); 6.60–7.80 (m, 7H, phenyl); ($^{13}C\{^1H\}$, $CDCl_3$, 25°C): δ, 20.9 (Me); 45.6 (NMe_2); 55.0 (OMe); 103.5 (C_1); 143.1 (C_2); 115.4 (C_3); 159.9 (C_4); 136.4 (C_5); 151.2 (C_6); 127.8 (C_7); 131.9 (C_8); 122.5 (C_9); 120.2 (C_{10}).

3: Yield, 90%; m.p. 98–100°C. Found: C, 54.2; H, 5.9; N, 4.1; Te, 32.8. Calc. for $C_{17}H_{21}NOTe$: C, 53.3; H, 5.5; N, 3.7; Te, 33.3%. IR(cm^{-1}): 1276m [ν(C—N(Ar))]; 1242s [ν(C—N(Me))]; 300m, 262w [ν(Te—C)]. NMR (^1H, $CDCl_3$, 25°C): δ, 1.36–1.50 (t, 3H, CH_3 of OEt); 2.11 (s, 3H, Me); 2.68 (s, 6H, NMe_2); 3.96–4.17 (q, 2H, CH_2 of OEt); 6.62–7.80 (m, 7H, phenyl); ($^{13}C\{^1H\}$, $CDCl_3$, 25°C): δ, 20.7 (Me), 45.5 (NMe_2); 14.7 (CH_3 of OEt); 63.1 (CH_2 of OEt); 103.3 (C_1); 143.0 (C_2); 115.9 (C_3); 159.3 (C_4); 136.3 (C_5); 151.1 (C_6); 127.7 (C_7); 131.8 (C_8); 122.4 (C_9); 120.1 (C_{10}).

Synthesis of platinum(II) *and palladium*(II) *complexes of* (Te, N) *donors* (**1–3**)

Sodium tetrachloropalladate (0.147 g, 0.5 mmol) or potassium tetrachloroplatinate (0.20 g, 0.5 mmol) was dissolved in 5 cm^3 of water. The solution of $\simeq$ 0.5 mmol ligand **1–3** in 10 cm^3 of acetone was added dropwise with stirring at room temperature. The mixture was further stirred for 2–3 h. The resulting orange (palladium) or pale yellow (platinum) coloured precipitate was filtered, washed with water and dried *in vacuo*. It was recrystallized from a chloroform–hexane (90:10) mixture. The yield, melting point, results of elemental analysis, IR and ^1H NMR data are recorded below.

$PdCl_2$·**1**: Yield, 80%; m.p. 185–190°C (dec.). Found: C, 33.6; H, 3.5; N, 2.6. Calc. for $C_{15}H_{17}NTe \cdot PdCl_2$: C, 34.9; H, 3.3; N, 2.7%. Mol. wt, Found: 480–535; calc.: 516. IR(cm^{-1}): 1242s [ν(N—C(Ar))]; 1180s [ν(N—C(Me))]; 255m, 245m [ν(Te—C)]; 320bm, 287bm [ν(Pd—Cl)]. NMR (^1H, $CDCl_3$, 25°C): δ, 2.41 (s, 3H, Me); 3.37 (s, 3H, NMe); 3.50 (s, 3H, NMe); 7.15–7.78 (m, 8H, phenyl).

$PdCl_2$·**2**: Yield, 85%; m.p. 180–183°C (dec.). Found: C, 34.9; H, 3.1; N, 2.5. Calc. for $C_{16}H_{19}NOTe \cdot PdCl_2$: C, 35.2; H, 3.5; N, 2.6%. Mol. wt, Found: 500–564; calc.: 546. IR(cm^{-1}): 1252s [ν(N—C(Ar))]; 1180m [ν(N—C(Me))]; 280m, 240m [ν(Te—C)]; 325bm, 290bm [ν(Pd—Cl)]. NMR (^1H, $CDCl_3$, 25°C): δ, 2.39 (s, 3H, Me); 3.41 (s, 3H, NMe); 3.49 (s, 3H, NMe); 3.80 (s, 3H, OMe); 6.86–7.76 (m, 7H, phenyl).

$PdCl_2$·**3**: Yield, 82%; m.p. 182–185°C (dec.). Found: C, 36.1; H, 3.6; N, 2.4. Calc. for $C_{17}H_{21}NOTe \cdot PdCl_2$: C, 36.4; H, 3.7; N, 2.5%. Mol. wt, Found: 530–580; calc.: 560. IR(cm^{-1}): 1251s [ν(C—N(Ar))]; 1180m [ν(N—C(Me))]; 280w, 245m [ν(Te—C)]; 325bm, 289bm [ν(Pd—Cl)]. NMR (^1H, $CDCl_3$, 25°C): δ, 2.38 (s, 3H, Me); 3.39 (s, 3H, NMe); 3.46 (s, 3H, NMe); 3.98–4.13 (q, 2H, CH_2 of OEt); 1.35–1.43 (t, 3H, CH_3 of OEt); 6.83–7.76 (m, 7H, phenyl).

$PtCl_2$·**1**: Yield, 82%; m.p. 195–200°C (dec.). Found: C, 28.9; H, 2.7; N, 2.4. Calc. for $C_{15}H_{17}NTe \cdot PtCl_2$: C, 29.8; H, 2.8; N, 2.3%. Mol. wt, Found: 585–620; calc.: 604.6. IR(cm^{-1}): 1267wb [ν(N—C(Ar))]; 1177m [ν(N—C(Me))]; 266w, 248m [ν(Te—C)]; 321s, 303s [ν(Pt—Cl)]. NMR (^1H, $CDCl_3$, 25°C): δ, 2.40 (s, 3H, Me); 3.61 (s (with side bands), 3H, NMe, $^3J(^{195}Pt—H)$, 26 Hz); 3.65 (s (with side bands), 3H, NMe, $^3J(^{195}Pt—H)$, 26 Hz); 7.35–7.93 (m, 8H, phenyl).

$PtCl_2$·**2**: Yield, 87%; m.p. 187–190°C (dec.). Found: C, 29.7; H, 2.8; N, 2.4. Calc. for $C_{16}H_{19}NOTe \cdot PtCl_2$: C, 30.2; H, 3.0; N, 2.2%. Mol. wt, Found: 615–645; calc.: 634.6. IR(cm^{-1}): 1252m [ν(N—C(Ar))]; 1180s [ν(N—C(Me))]; 252m, 248w [ν(Te—C)]; 333bm, 290bm [ν(Pt—Cl)]. NMR (^1H, $CDCl_3$, 25°C): δ, 2.38 (s, 3H, Me); 3.79 (s, 3H, OMe); 3.64 (unresolved doublet with side bands, 6H, NMe_2, $^3J(^{195}Pt—H)$, 28.1 Hz); 6.84–7.91 (m, 7H, phenyl).

$PtCl_2$·**3**: Yield, 85%; m.p. 190–195°C (dec.). Found: C, 30.3; H, 3.0; N, 2.3. Calc. for $C_{17}H_{21}NOTe \cdot PtCl_2$: C, 31.4; H, 3.2; N, 2.2%. Mol. wt, Found: 630–670; Calc. 648.6. IR(cm^{-1}): 1251s [ν(N—C(Ar))]; 1172m [ν(N—C(Me))]; 245m, 267m [ν(Te—C)]; 326s, 300m [ν(Pt—Cl)]. NMR (^1H, $CDCl_3$, 25°C): δ, 2.38 (s, 3H, Me); 1.31–1.45 (t, CH_3 of OEt); 3.91–4.12 (q, 2H, CH_2 of OEt); 3.63 (s (with side bands), 6H, NMe_2, $^3J(^{195}Pt—H)$, 26.1 Hz); 6.81–7.88 (m, 7H, phenyl).

RESULTS AND DISCUSSION

The number of asymmetric tellurides known[1–4] at present is a lot less than the symmetric ones. Telluroamines **1–3** belonging to this rare class have been synthesized by following the sequence of reactions given in Scheme 1.

Telluroamines **1–3** and their respective dichlorides, **4–6**, are fairly soluble in non-polar organic solvents. Like other tellurides and diaryltellurium(IV) chlorides, they all behave in solution as non-electrolytes. ^1H NMR spectra of **1–3** and their respective dichlorides are as expected for such compounds. The NMe_2 protons undergo a small upfield ($\simeq$ 0.1–0.2 ppm) shift on *ortho*-mercuration of the dimethylaniline derivative. In the ^1H NMR spectra of *ortho*-tellurated anilines **4–6**, however, the NMe_2 protons appear at a position almost identical to that of the parent aniline. Prob-

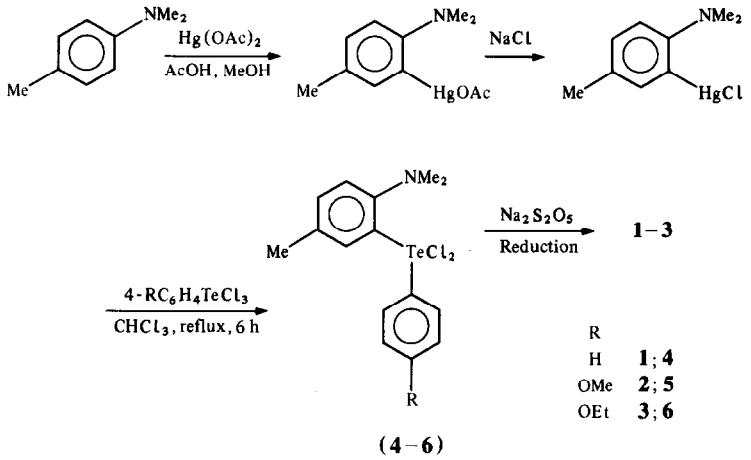

Scheme 1.

ably, the substitution of an aryl proton *ortho* to NMe_2 with HgCl group increases the electron density at nitrogen which seems to marginally shield the NMe_2 protons. The Te in the dichlorides **4–6** being more electronegative than mercury fails in affecting these protons. On reduction of **4–6** into tellurides **1–3**, respectively, the NMe_2 protons are again shielded ($\simeq$ 0.2 ppm). This may be due to a decrease in electronegativity of Te and strength of Te···N interaction, which otherwise seems to be very weak in nature. $^{13}C\{^1H\}$ NMR spectra of **1–3** and their dichlorides are characteristic of them.[10] The shielding of NMe_2 carbons on the reduction of dichlorides, **4–6** to **1–3** supports ^1H NMR spectra. IR spectra of **1–3** have two ν(Te—C) bands around 260 and 295 cm^{-1} as expected for such compounds.[11] Two bands occur for C—N stretching also; the one around 1280 cm^{-1} seems to originate from N—C(aryl) and the other between 1200–1250 cm^{-1} from N—C(methyl) bond. Methyl iodide reacts with asymmetric tellurides **1–3** according to eq. (1) which is typical of telluride characteristics:

$$\text{ArAr'Te} + \text{MeI} \xrightarrow[\text{overnight}]{\text{RT}} \text{ArAr'MeTeI} \quad (1)$$

(Yield = 90%).

Complexation of **1–3** *with platinum*(II) *and palladium*(II)

The tetrachloroplatinate or palladate reacts with telluroamine ligands **1–3** according to eq. (2):

$$[MCl_4]^{2-} + L \xrightarrow[\text{RT, } \simeq 3\text{h.}]{\text{aq. acetone}} MCl_2 \cdot L + 2Cl^- \quad (2)$$

(M = Pt or Pd; L = **1–3**).

The resulting Pt and Pd complexes were fairly soluble in chloroform, dichloromethane and acetonitrile, and were found to be diamagnetic. The specific conductance of their solutions in acetonitrile ($\simeq$ 1 mmol range) has been found to be almost equal to that of the pure solvent. This observation in conjunction with molecular weights suggests that the Pd and Pt complexes are monomeric and non-electrolytes. The comparison of IR spectra of the ligands with those of complexes exhibits that the ν[N—C(Me)] vibrations shift to lower frequency by 30–50 cm^{-1}, indicating the coordination of Pd or Pt with NMe_2. The red shift also occurs in ν[N—C(Ar)] vibrations but of 10–15 cm^{-1} only, concurring with the hypothesis of coordination. The two ν(Te—C) bands appear at 10–30 cm^{-1} lower frequency in the Pd and Pt complexes. The presence of two broad peaks around 330 and 290 cm^{-1}, assignable to M—Cl vibrations, indicates that two M—Cl bonds in the complexes are in a *cis*-conformation of a square-planar arrangement of the ligands around the metal atoms,[12] if presumed in view of magnetic properties, molecular weights and molar conductance values. The electronic spectra of these Pd and Pt complexes exhibit three bands around 25, 30 and 42 kK and 25, 38 and 42 kK, respectively. The first band in both the complexes seems to arise from $^1A_{1g} \rightarrow {}^1B_{1g}$ transitions, further supporting the square-planar arrangement of ligands around Pt and Pd. On comparison with the electronic spectra of the ligands (bands at *ca* 35.7 and 41.7 kK) it appears that second and third bands of each of these complexes probably originate from intraligand transitions.

In the ^1H NMR spectra of Pd–telluroamine complexes the NMe_2 protons have been found deshielded ($\simeq$ 0.7–0.8 ppm) in comparison to the free ligand, suggesting that the NMe_2 group coordinates

with Pd as inferred by IR data. Moreover, the two methyl signals separated by 0.07–0.13 ppm appeared, indicating the non-equivalence of two methyl groups after involvement of nitrogen in coordination. The proton *ortho* to the tellurium in the aniline ring of **1–3** on chelation has been found to be significantly deshielded ($\simeq$ 0.5 ppm). The other ring protons also appear at a lower field (0.10–0.15 ppm). In the Pt complexes, also, the ligands seem to chelate through N and Te. The coordination through N is supported by the appearance of NMe_2 protons down field by $\simeq$ 1 ppm, in comparison to the free ligand. However, the NMe_2 signals in the spectra of Pt complexes have some interesting features. In the spectrum of $PtCl_2 \cdot$ **1** it appears as two peaks of equal intensity at 3.61 and 3.65 ppm with side bands due to $^3J(^{195}Pt—H)$ couplings (Fig. 1), whereas an unresolved doublet at 3.64 ppm is observed for these protons in the spectrum of $PtCl_2 \cdot$ **2**, with a side band of a similar type. The other side band probably merges with the methoxy signal as indicated by the enhanced intensity of the latter. In the $PtCl_2 \cdot$ **3** complex, the NMe_2 signal appears as a singlet but with the expected side bands. The coupling constant $^3J(^{195}Pt—H)$ in these complexes was between 28 and 26 Hz, concurring with the earlier reports.[14,16] The aniline ring proton *ortho* to Te was also found deshielded by $\simeq$ 1 ppm. The large deshielding in Pt complexes indicates that **1–3** ligate more strongly with Pt in comparison to Pd.

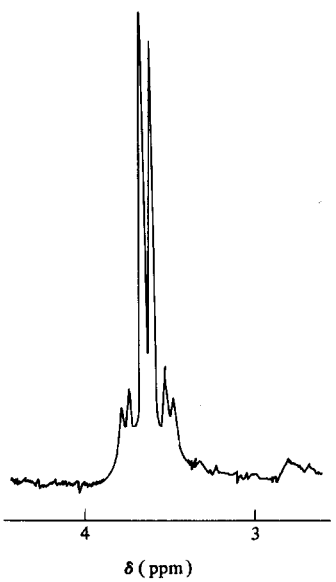

Fig. 1. ^1H NMR spectrum of $PtCl_2 \cdot$ **1** showing $^3J[^{195}Pt—H(NMe_2)]$ coupling.

The two methyl signals for the NMe_2 group probably originate because the inversion of the pyramidal Te in these complexes is slow at the temperature of NMR measurement in the five-membered chelate ring rigid structure **7**. The aryl

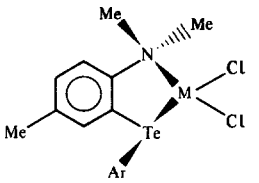

M = Pt or Pd
Ar = C_6H_5, 4-$MeOC_6H_4$ or 4-$EtOC_6H_4$

(**7**)

groups attached to Te thus result in the different magnetic environments for the two methyl groups fixed sterically above and below the five-membered ring because there is no possibility of inversion at the four-coordinate ring nitrogen atom. For the NMe_2 group coordinated to Pt and Pd, such behaviour has been reported[13–16] earlier in a few cases.

CONCLUSION

The dimethyl aniline derivative on *ortho*-mercuration followed by transmetallation with $ArTeCl_3$ and reduction of the resulting $ArAr'TeCl_2$ type derivatives with sodium metabisulphite give interesting (Te, N) donors which behave as bidentate neutral ligands with Pt^{II} and Pd^{II}.

Acknowledgement—The authors thank CSIR (India) for the financial support of this work.

REFERENCES

1. H. J. Gysling, *Coord. Chem. Rev.* 1982, **42**, 133.
2. H. J. Gysling, *Proceedings of the Fourth International Conference on the Organic Chemistry of Selenium and Tellurium* (Edited by F. J. Berry and W. R. McWhinnie), p. 32. The University of Aston, Birmingham (1983).
3. H. J. Gysling, *The Chemistry of Organic Selenium and Tellurium Compounds* (Edited by S. Patai and Z. Rappoport), Ch. 18, p. 815. John Wiley, New York (1986).
4. F. J. Berry, *Comprehensive Coordination Chemistry* (Edited by G. Wilkinson, R. D. Gillard and J. A. McCleverty), Ch. 17, p. 668. Pergamon Press, Oxford (1987).
5. H. J. Gysling and H. R. Luss, *Organometallics* 1984, **3**, 596.
6. N. Al-Salim, T. A. Hamor and W. R. McWhinnie, *J. Chem. Soc., Chem. Commun.* 1986, 453.
7. K. J. Irgolic and R. A. Zingaro, *Organomet. React.* 1971, **2**, 117.

8. F. H. Kruse, R. E. Sanftner and J. F. Suttle, *Analyt. Chem.* 1953, **25**, 500; A. I. Vogel, *A Text Book of Quantitative Inorganic Analysis*, 4th edn. Longmans, London (1978).
9. L. G. Makarova and A. N. Nesmeyanov, *The Organic Chemistry of Mercury Compounds*, Vol. 4 in *Methods of Elemento Organic Chemistry* (Edited by A. N. Nesmeyanov and K. A. Kocheshkov), Ch. 5, p. 94. North-Holland, Amsterdam (1967).
10. R. K. Chadha and J. M. Miller, *J. Chem. Soc., Dalton Trans.* 1982, 117.
11. W. R. McWhinnie and M. G. Patel, *J. Chem. Soc., Dalton Trans.* 1972, 199.
12. K. Nakamoto, *Infrared and Raman Spectra of Inorganic and Coordination Compounds*, 3rd Edn. John Wiley, New York (1978).
13. M. O. Okoroafor, L. H. Shen, R. V. Honeychuck and Carl H. Brubaker Jr, *Organometallics* 1988, **7**, 1297.
14. A. C. Cope and E. C. Friedrich, *J. Am. Chem. Soc.* 1968, **90**, 909.
15. G. Longoni, P. Fantucci, P. Chini and F. Canziami, *J. Organomet. Chem.* 1972, **39**, 413.
16. G. van Koten, K. Timmer, J. G. Noltes and A. L. Spek, *J. Chem. Soc., Chem. Commun.* 1978, 250.

Polyhedron Vol. 9, No. 4, pp. 501–503, 1990
Printed in Great Britain

0277–5387/90 $3.00+.00
© 1990 Pergamon Press plc

COMPLEXATION EQUILIBRIA BETWEEN CADMIUM(II) AND 4-(4′-METHYL-2′-THIAZOLYLAZO)-2-METHYL-RESORCINOL. A SPECTROPHOTOMETRIC STUDY

Mª J. SÁNCHEZ, B. SANTANA, F. JIMÉNEZ and F. GARCÍA MONTELONGO*

Department of Analytical Chemistry, University of La Laguna, E–38204 La Laguna, Spain

(*Received* 12 *June* 1989; *accepted* 5 *September* 1989)

Abstract—The complexation equilibria between Cd^{II} and 4-(4′-methyl-2′-thiazolylazo)-2-methyl-resorcinol have been spectrophotometrically studied in an ethanol–water medium (50:50, v/v) at $I = 0.25$ M ($NaClO_4$) and species $CdHR_2$ ($\log\beta_{112} = 20.38 \pm 0.09$) and CdH_2R_2 ($\log\beta_{122} = 27.00 \pm 0.09$) are established by a numerical calculation method.

Heteroazo compounds have been widely used as chromogenic reagents for several metal ions but only in recent times have the equilibria involved been studied.[1,2] The ligand 4-(4′-methyl-2′-thiazolylazo)-2-methyl-resorcinol, MTAMR, has been previously synthesized and complexation equilibria with V^{V}, Zn^{II} and Cu^{II} studied.[3–6] The kinetics of the ligand-substitution reaction of the Zn–MTAMR complex by DCTA has also been studied.[7]

In this paper the acid–base equilibria of MTAMR and its complexation equilibria with Cd^{II} in an ethanol–water medium (50:50, v/v) at $I = 0.25$ M $NaClO_4$ are reported. Graphical and numerical calculation methods are used to establish the nature of the species in solution and to calculate the stability constants which have not previously been reported in the literature.

EXPERIMENTAL

Absorption measurements were performed on a Perkin–Elmer 550S recording spectrophotometer provided with 1 cm matched quartz cells. A Radiometer PHM64 digital pHmeter with glass–calomel combination electrode, calibrated by the Gran method,[8] was used for pH measurements. Measurements were performed at 25±0.1°C. Calculations were carried out on a Digital VAX/VMS 11/780 (V.4.8) computer.

A 10^{-3} M solution of MTAMR in absolute ethanol, standard 10^{-2} M $Cd(ClO_4)_2$ (prepared from the nitrate by perchloric acid treatment and standardized complexometrically), analytical reagent grade chemicals and deionized water were used throughout with no further purification.

RESULTS AND DISCUSSION

Acid–base behaviour of MTAMR

To study the acid–base behaviour of MTAMR in ethanol–water medium (50:50, v/v) at $I = 0.25$ M $NaClO_4$, a method of graphical analysis of the absorbance–pH curves was first used.[9] Values calculated for pK_{ax} together with the optical characteristics of each species are listed in Table 1. The experimental data were further refined using the LETAGROP–SPEFO numerical calculation method.[10] The results obtained are included in Table 1 along with the pK_{ax} values previously determined in methanol–water medium (50:50, v/v).[4]

Complexation equilibria in the Cd^{II}–MTAMR system

Cd^{II} and MTAMR react to give violet coloured species in solutions of pH 4. The absorption spectra at pH 8.5 of solutions with several $C_{Cd}:C_R$ ratios show the presence of an absorption maximum at 520 nm for $C_{Cd}:C_R \geqslant 10$ and an absorption maximum at 550 nm for solutions with $C_{Cd}:C_R = 0.1$, Fig. 1, which may indicate the presence of at least two complex species in solution. However, the stoichiometry as established by the continuous variation and mole ratio methods shows only the presence of 1:2 Cd:R complex species in solution. Thus, taking into account the formation

* Author to whom correspondence should be addressed.

Table 1. Optical characteristics and pK_a values of MTAMR in ethanol–water medium (50 : 50, v/v) at $I = 0.25$ M $NaClO_4$

Species	pK_A graphical	pK_A numerical	ε (dm^3 mol^{-1} cm^{-1}) numerical at λ = 450 nm	490 nm	520 nm	pK_a[a]
H_3R^+	0.89	0.85±0.22	18,530±234	15,027±723	24,500±135	1.21
H_2R	5.70	5.63±0.15	17,042±825	11,920±255	13,750±200	6.49
HR^-	10.12	10.03±0.10	27,201±100	29,489±206	25,625±175	11.07
R^{2-}			20,500±125	19,033±310	30,000±250	

[a] In methanol–water medium (50 : 50, v/v) at $I = 0.25$ M $NaClO_4$, graphical method (4).

pH range, the most probable mechanism of complex formation will be:

$$Cd^{2+} + 2H_2R \rightleftarrows CdH_2R_2 + 2H^+;$$

K_{122} being the equilibrium constant. To check the validity of this equilibrium, the method of graphical analysis of the absorbance–pH dependences of Hnilickova and Sommer[9] was first used, from which the presence of species CdH_2R_2 results and two protons are split off during complexation and $\log \beta_{122} = 26.18$ was calculated as the mean value for the stability constant. Next, the experimental data were analysed by application of the LETAGROP–SPEFO program[10] using the species and β_{122} value obtained by the graphical method as starting values. The species model was then modified by introducing new species in order to ascertain which one of the proposed models would fit the experimental data with a minimum sum of squares of residuals, U, and of standard deviation, $\sigma(A)$. Using the values obtained for the minimal U and $\sigma(A)$ it can be seen from Table 2 that the model including the species CdH_2R_2 and $CdHR_2$ fits the experimental data best. Calculations for other models assuming the formation of hydroxo-complexes, mixed ligand complexes and/or polynuclear species in addition to the CdH_2R_2 and $CdHR_2$ species, did not converge. Calculated values for the stability constants and molar absorptivities of these complex species are included in Table 2.

When compared with the cadmium complexes of TAR[9] and TAMR[11] the Cd^{II}–MTAMR species are the most stable and show higher molar absorptivities.

Table 2. Results from the numerical analysis for some species models in the system Cd^{II}–MTAMR

Species model	U	$\sigma(A)$	$\log \beta_{pqr} \pm 3$ SD ($\log \beta_{pqr}$)	$\varepsilon_{pqr}^{520} \pm 3$ SD (ε)
CdH_2R_2	3.7×10^{-2}	0.02	27.25 Max. 27.45	
CdR_2			13.58 Max. 13.87	
$CdHR_2$	9.2×10^{-3}	0.04	20.92 Max. 21.19	
CdR_2			11.83 Max. 12.70	
$CdHR_2$	1.6×10^{-2}	0.02	20.28±0.26	67,500±700
$CdHR$			13.21 Max. 13.60	
CdH_2R_2			27.21±0.19	24,000±350
$CdHR_2$	7.7×10^{-3}	0.012	20.42±0.21	78,000±846
$CdHR$			8.07 Max. 12.62	
CdH_2R_2			27.06±0.09	15,270±115
$CdHR_2$	6.5×10^{-3}	0.01	20.29±0.11	62,000±500
CdR_2			11.82 Max. 12.09	
CdH_2R_2	3.8×10^{-3}	0.009	27.00±0.09	39,520±346
$CdHR_2$			20.38±0.09	72,678±333

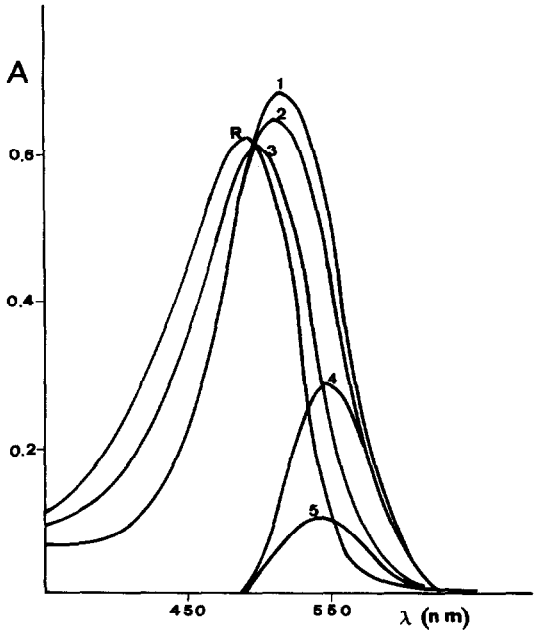

Fig. 1. Absorption spectra of the system Cd^{II}–MTAMR at pH 8.5 for some $C_{Cd}:C_R$ ratios. $C_R = 2\times10^{-5}$ M, C_{Cd} = (1) 8×10^{-4} M, (2) 2×10^{-4} M, (3) 2×10^{-5} M; $C_{Cd} = 2\times10^{-5}$ M, C_R = (5) 1×10^{-4} M; (R) reagent alone.

Acknowledgement—The authors wish to acknowledge the financial support of this work by CAICYT (Spain) grant No. 4133/79.

REFERENCES

1. S. Shibata, in *Chelates in Analytical Chemistry* (Edited by H. Flaschka and A. J. Barnard Jr), Vol. 4, p. 1. Dekker, New York (1972).
2. H. R. Hovind, *Analyst* 1975, **100**, 1196.
3. F. García Montelongo, J. J. Arias and F. Jiménez, *Microchem. J.* 1980, **25**, 410.
4. J. J. Arias, F. Jiménez and F. García Montelongo, *An. Quim.* 1980, **76B**, 452.
5. F. García Montelongo, J. J. Arias and F. Jiménez, *Analusis* 1981, **9**, 400.
6. J. J. Arias, F. Jiménez, S. Suárez and F. Garcia Montelongo, *Quim. Anal.* 1984, **3**, 193.
7. J. J. Arias, F. Jiménez and F. Garcia Montelongo, *Microchem. J.* 1981, **26**, 354.
8. G. Gran, *Analyst* 1952, **77**, 661.
9. M. Hnilickova and L. Sommer, *Talanta* 1966, **13**, 667.
10. L. G. Sillén and B. Warnqvist, *Ark. Kemi* 1968, **31**, 377.
11. A. Afonso, V. González and F. García Montelongo, *An. Quim.* 1984, **80B**, 93.

Polyhedron Vol. 9, No. 4, pp. 505–510, 1990
Printed in Great Britain

0277–5387/90 $3.00+.00
© 1990 Pergamon Press plc

COMPUTER MODELS OF BIOFLUIDS—AN EXPERIMENTAL VERIFICATION

GRAHAM E. JACKSON* and M. SINGH

Department of Chemistry, University of Cape Town, Rondebosch 7700, South Africa

(*Received* 6 *April* 1989; *accepted after revision* 7 *September* 1989)

Abstract—Ultrafiltration of blood serum has been used as a test of the computer model ECCLES. Both coordinating polyaminocarboxylate ligands and anti-inflammatory drugs used in the treatment of rheumatoid arthritis have been evaluated. For the polyaminocarboxylates the computer model is able, to a large extent, to explain the experimental results for copper(II), calcium(II) and zinc(II). However, for the anti-inflammatory drugs, the model fails to predict the observed mobilization of copper(II) and zinc(II). In this case it is postulated that the metal ions are released via an allosteric mechanism.

In recent years computer models have been developed which attempt to mirror the various metal-ion equilibria occurring in biofluids.[1–4] These models, which are based on thermodynamic considerations, have been used in discussions of therapeutic chelating agents.[5] Indeed, the ability of these models to screen promising chelating agents and to explain the failure of existing chelating agents is very impressive. However, animal tests have shown that computer model predictions are not always correct. There are many reasons for these failures. Certainly the small size of the earlier models was a contributing factor. The development of the model by May *et al.*[4] overcame this size limitation. Jones[6] has proposed an alternative model for the selection of therapeutic chelating agents in which he emphasized the importance of rate processes. The majority of these rate processes, such as rate of absorption of the chelating agent, excretion and metabolism of the chelating agent, transport of the chelating agent into cellular compartments and excretion and reabsorption of chelate complexes, are all *in vivo* processes. Attempts have been made[7] to include some of these factors into a computer model. However, to date, no direct experimental verification of these complex biomodels has been attempted. In this paper we have devised an *in vitro* test of the thermodynamic model of blood plasma, ECCLES.[4] Ultrafiltration of pooled human blood serum has been carried out and the experimental results correlated with those predicted by the computer model.

EXPERIMENTAL

Human blood serum was obtained from the Western Province Blood Transfusion Service. Drugs involved in this study were kindly donated by pharmaceutical companies and used without further purification. These drugs were prednisolone, piroxicam and mefanamic acid (Warner Lambert), aspirin (May and Baker), indomethacin (Beecham Pharmaceuticals), tiaprofenic acid (Russel Laboratories) and D-penicillamine (Lilly Laboratories, U.S.A.).

Ultrafiltration was carried out using a low cost ultrafiltration apparatus designed in our laboratory. Centrifugal pressure at 3000 r.p.m. (~900 g) allowed a filtration rate of 1×10^{-2} cm^3 min^{-1} through YMT (Amicon) membranes to be achieved. Varying concentrations of drug/ligand were added to 10 cm^3 aliquots of pooled human serum at pH 7.5. The pH was measured before and after the experiment and found not to vary by more than 0.07 pH units. The solutions were incubated at 37°C for 15 min to allow the system to come to equilibrium and then ultrafiltered. Each titration was repeated four times. The ultrafiltrates (~0.1 cm^3) were collected and immediately analysed for copper, zinc and calcium by atomic absorption spectrometry. Calcium was measured using a N_2O/C_2H_2 flame at 422.7 nm. A 100-fold excess of lanthanum nitrate was added to each of the ultra-

* Author to whom correspondence should be addressed.

filtrate samples, so as to suppress ionization of the analyte. Zinc was measured at 213.9 nm using a very lean (oxidizing) air/C_2H_2 flame. Copper was measured by atomic absorption on a Perkin–Elmer 5000 atomic absorption spectrophotometer (graphite furnace) coupled to a HGA 500 programmer.

The presence of protein in the filtrate was monitored using Coomassic Brilliant Blue G-250.[8]

A 5-cell spectrum equilibrium dialysis apparatus together with Spectrapor membranes were used for equilibrium dialysis experiments. The membranes were boiled in 2% EDTA and 5% $NaHCO_3$, followed by copious rinsing and boiling for 3×1 h in double-distilled deionized water. This treatment removed all contaminating metal ions and nucleases from the dialysis membranes. Finally, the membranes were soaked for 15 min in 0.1 M N-ethylmorpholine HCl buffer. After charging, the dialysis cells were allowed to rotate at 5 r.p.m. for 24 h at 37°C.

Theoretical predictions of the mobilization of metal ions in blood plasma by chelating agents and drugs were obtained using the ECCLES program and data base.[4] In the cases of the drugs, where equilibrium constants were not available, they were estimated from analogous model compounds in the literature[9] and, where necessary, adjusted to 37°C and an ionic strength of 0.15.

RESULTS AND DISCUSSION

It is generally believed that ultrafiltration gives only approximate results and that only small amounts of filtrate should be removed so as not to disturb the initial equilibrium. This belief has recently been shown to be unfounded.[10,11]

If we consider a system involving the metal/protein equilibrium

$$M + P \rightleftharpoons MP,$$

the conditional equilibrium constant is given by,

$$K = [MP]/[M][P]$$

and $T_P = [MP]+[P]$ and $T_M = [MP]+[M]$, where T_M and T_P are the total concentration of metal and protein, respectively.

Upon rearrangement we get:

$$K = \frac{T_M - [M]}{[M](T_P - T_M + [M])}.$$

Considering the situation before (i) and after (o) removal of a small amount (dV) of ultrafiltrate we can write,

$$T_P^i = T_P^o V/(V - dV) \quad \text{and}$$

$$T_M^i = VT_M^o - dV[M^o]/(V - dV),$$

where V is the initial volume.

Substituting into the equilibrium expression we get:

$$K^o = (T_M^o - [M^o])/[M^o](T_P^o - T_M^o + [M^o])$$

and

$$K^i = \frac{T_M^o V - dV[M^o] - [M^i](V - dV)}{[M^i]\{T_P^o V - VT_M^o + dV[M^o] + [M^i](V - dV)\}}.$$

But the equilibrium constant before and after ultrafiltration must be the same and hence the two expressions are equivalent. This condition is satisfied if $[M^o] = [M^i]$, a result which is independent of dV. Clearly then the free metal concentration is independent of the percent ultrafiltration. However, if a substantial volume of solution is removed, changes in ionic strength etc. could occur which would modify the conditional equilibrium constant.

Table 1 lists the results for an example of the above calculation. From these results it is clear that while the total concentrations of protein and metal increase, the free metal concentration remains constant. We have checked this result experimentally

Table 1. Species concentrations calculated for the equilibrium $M + P \rightleftharpoons MP$ following the removal of dV cm^3 of solution by ultrafiltration. Initial total metal (T_M) = total protein (T_L) = 0.1 mM, conditional equilibrium constant $K = 10^3$ and initial volume = 2 cm^3

dV	$T_M \times 10^4$	$T_L \times 10^4$	$[MP] \times 10^6$	$[P] \times 10^5$	$[M] \times 10^5$
0	1.0	1.0	8.39	9.16	9.16
0.2	1.004	1.053	8.83	9.64	9.16
0.4	1.015	1.176	9.87	1.08	9.16
0.6	1.028	1.333	1.12	1.22	9.16
0.8	1.045	1.538	1.29	1.41	9.16
1.0	1.069	1.818	1.53	1.67	9.16

Table 2. Effect of volume change during ultrafiltration of the system 6×10^{-4} M HSA and 6×10^{-4} M $CuCl_2$ in 0.1 M N-ethylmorpholine HCl

Volume of ultrafiltrate (10^{-3} cm^3)	% Volume filtered	$[Cu^{II}]_{free} \times 10^5$ M
92	4.6	5.6
176	8.8	5.5
242	12.1	5.8
348	21.0	5.4

(Table 2) by analysing successive aliquots of filtrate for the Cu–HSA system. Similar results have been found for other systems.[12] In addition we have compared our ultrafiltration technique with the more established technique of equilibrium dialysis. While the results for equilibrium dialysis (Fig. 1) are consistently lower than the results for ultrafiltration, there is good agreement between the two methods. Subsequent experiments have shown that the discrepancy between the two methods is a result of metal-ion binding to the dialysis membrane.

Figure 2(a) shows the calculated copper(II) PMI curves for four chelating agents in blood plasma. The order of ability of these agents to mobilize copper(II) at pH 7.5 and 37°C is calculated to be:

TRIEN > EDDA > DTPA > EDTA.

Apart from structural considerations, the mobilizing order can be rationalized by taking into account the binding of zinc(II) and calcium(II) by these ligands. The computer model, ECCLES, predicts that both TRIEN and EDDA are unable to mobilize calcium(II) (see Fig. 4), and that TRIEN is a weaker mobilizer of zinc(II) than DTPA and EDTA [see Fig. 3(a)]. Therefore, the high mobilization of copper(II) by TRIEN is a consequence of its limited calcium(II) and zinc(II) complex formation and hence, most of the TRIEN in blood plasma is available for copper(II) mobilization. It must be remembered that the concentration of calcium(II) and zinc(II) in blood plasma, is several orders of magnitude higher than that of copper(II).

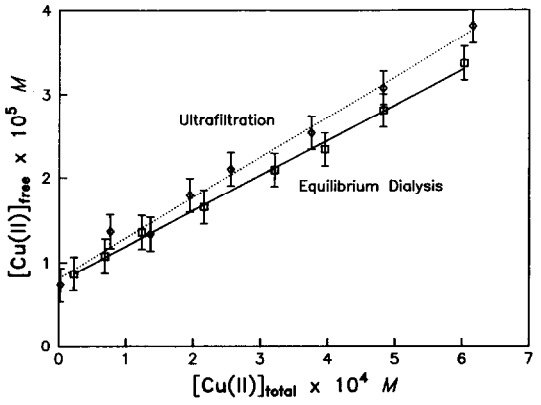

Fig. 1. Comparison of ultrafiltration and equilibrium dialysis study of copper(II) binding to HSA in 0.1 M N-ethylmorpholine HCl at pH 7.5 and 37°C.

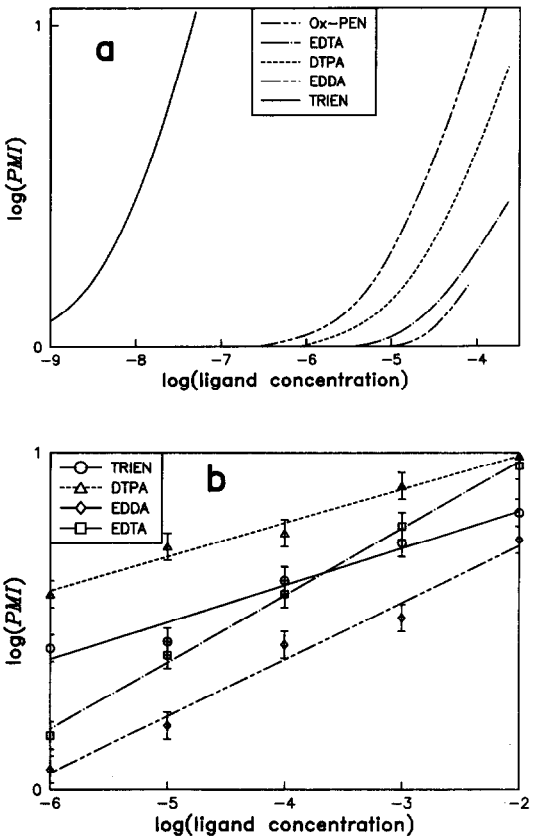

Fig. 2. (a) Calculated and (b) experimental copper(II) PMI curves for chelating ligands in pooled human blood serum.

Similarly, although EDDA forms weaker copper(II) complexes than DTPA and EDTA, it has a greater ability to mobilize copper(II). Hence, the powerful copper(II) binding abilities of EDTA and DTPA are suppressed in plasma by competition with zinc and calcium. The higher mobilization of copper(II) by DTPA rather than EDTA is expected as DTPA forms more stable copper(II) complexes than EDTA.

Figure 2(b) shows the experimental copper(II) PMI curves for the same four chelating agents in human blood serum under physiological conditions of pH and temperature. From a comparison of Figs 2(a) and (b) it is evident that there are a number of discrepancies between the experimental and theoretical results. Firstly, the order of ability of the chelating agents to mobilize copper(II) in serum

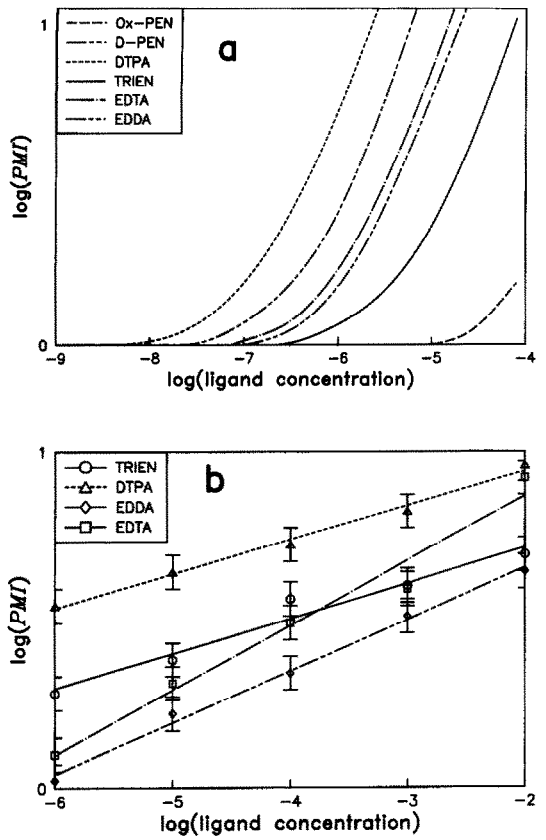

Fig. 3. (a) Calculated and (b) experimental zinc(II) PMI curves for chelating ligands in pooled human blood serum.

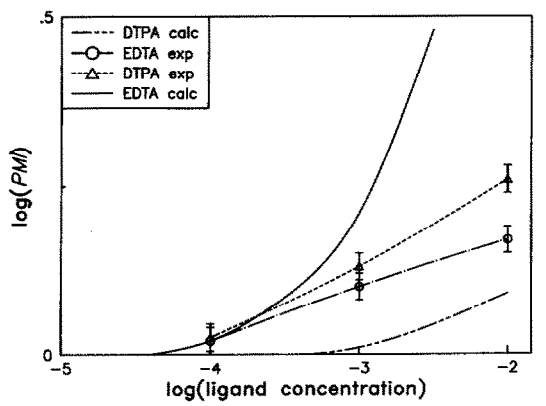

Fig. 4. Calculated and experimental PMI curves for calcium(II).

is now found to be:

DTPA > TRIEN > EDTA > EDDA.

Secondly, the shape of the experimental PMI curves are distinctly different from the theoretical curves. At first sight there appears to be no correlation between the experimental and theoretical results. However, a careful examination of the data shows that, with the exception of TRIEN, the amount of copper(II) mobilized by the polyaminopolycarboxylic acids is similar to the amount of copper(II) predicted to be mobilized by ECCLES, i.e. copper(II) starts to be mobilized at a ligand concentration of between 10^{-5} and 10^{-6} M. In both the theoretical and experimental plots, above a threshold value of PMI = 0.2, the curves are linear, but the theoretical curves are much steeper than the experimental curves. Thus, the model is partially correct in that it predicts the right order of magnitude for the PMI values, but fails to predict the finer details of mobilization.

Calculated zinc(II) PMI curves for chelating agents in blood plasma are shown in Fig. 3(a). The order of ability of these chelating agents to mobilize zinc(II) from serum albumin at pH 7.5 and 37°C is calculated to be:

DTPA > EDDA > EDTA > TRIEN.

The experimental results confirm the computer predictions, in that the chelating agents are found to mobilize zinc(II) in blood serum, but once again there are discrepancies between the theoretical and experimental results [Fig. 3(b)] with respect to the relative order in which these agents mobilize zinc(II), as well as the shapes of the PMI curves. Experimentally the order in which zinc(II) is found to be mobilized in blood serum is the same as that found for copper(II).

At the same time that the zinc(II) and copper(II) mobilizing ability of these ligands was monitored, the calcium(II) mobilization was also determined. In the absence of any administered chelating agent the computer model predicts a citrate species distribution of 58 mM calcium citrate, 32 mM magnesium citrate and 31 mM citrate. This is in good agreement with measured values of 38, 44 and 39 mM, respectively.[13] In the presence of the chelating agent, with the exception of EDTA and DTPA, none of the ligands studied is predicted to be able to mobilize calcium(II). Experimentally this prediction is confirmed in that only DTPA and EDTA are found to increase the amount of ultrafilterable calcium(II) in blood serum (Fig. 4). The experimental results are well supported by the fact that DTPA and EDTA are known to form very stable complexes with "hard" metal ions in blood serum.[14] This property of the chelating agents has been exploited in their use as antidotes for heavy metal poisoning.[15] DTPA is also the most effective known chelating agent for the removal of internally deposited transuranium elements in humans.[16] The chelating agents are invariably administered as the calcium(II) complex so as to prevent calcium

depletion in the body. Experimentally, DTPA is found to be more efficient in mobilizing calcium(II) than EDTA. This is to be expected as DTPA is a higher homologue of EDTA and the stability constant for the calcium DTPA complex is higher than the corresponding EDTA complex.[9]

In a second series of experiments, theoretical and experimental PMI curves were generated for several drugs which are currently used in the treatment of rheumatoid arthritis. From the results (Figs 5 and 6) it is clear that these drugs are capable of mobilizing endogenous copper and zinc. These results are supported by the findings of Fiabane and Williams,[17] who reported that non-steroidal anti-inflammatory drugs (NSAIDs) are capable of releasing copper ions from serum albumin. The order of ability of the various drugs to mobilize copper(II) in blood serum is found to be:

D-penicillamine > aspirin > mefanamic acid > indomethacin > piroxicam > tiaprofenic acid > prednisolone.

By comparison with Fig. 2(b) the NSAIDs are found to be approximately equivalent to EDDA, with respect to copper(II) mobilization, while D-penicillamine is equivalent to EDTA. Contrary to these findings, the computer model predicts that these drugs would be incapable of mobilizing copper(II) in blood plasma. Of course D-penicillamine, because of its tendency to undergo reductive chelation with copper(II), could not be included in the computer model for copper(II). If instead oxidized penicillamine is used in the calculation then a weak mobilization of copper(II) is seen [Fig. 2(a)]. Even this is much lower than the observed increase in ultrafiltrable copper.

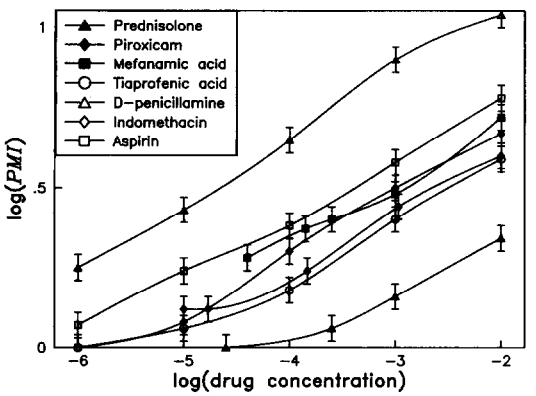

Fig. 5. Experimental copper(II) PMI curves for anti-inflammatory drugs in pooled human blood serum.

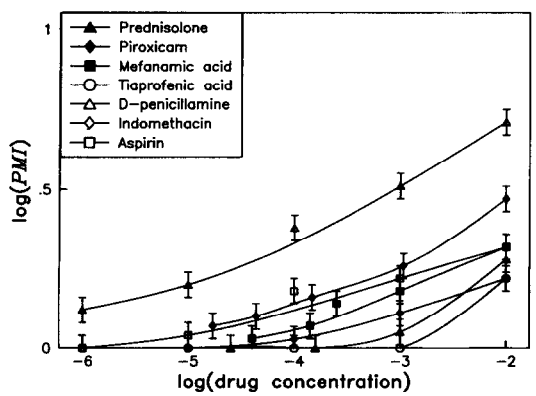

Fig. 6. Experimental zinc(II) PMI curves for anti-inflammatory drugs in pooled human blood serum.

Experimental PMI curves for zinc(II) with anti-inflammatory drugs are shown in Fig. 6. The order of ability of these drugs to mobilize zinc(II) under physiological conditions is found to be:

D-penicillamine > aspirin > piroxicam > mefanamic acid > indomethacin > prednisolone > tiaprofenic acid.

D-Penicillamine exhibits a similar zinc(II) mobilizing ability to EDDA. Clinically, D-penicillamine has been shown to increase zinc excretion.[18] The NSAIDs and prednisolone are found to be much weaker mobilizers of zinc(II) than the polyaminocarboxylates. It is interesting to note that, with the exception of piroxicam and prednisolone, the order in which these drugs mobilize zinc(II) is remarkably similar to the order in which copper(II) is mobilized in blood serum. Computer simulation of these drugs shows that only D-penicillamine increases the low molecular weight fraction of zinc(II) in blood plasma.

CONCLUSION

Comparison between experimental and theoretical results has shown that the computer model, ECCLES, with a few notable exceptions, is surprisingly good at calculating metal-ion mobilization in blood plasma. The model is able to, within an order of magnitude, predict the ligand concentration at which mobilization begins, and predict the observed linear dependence of PMI upon ligand concentration. On the other hand, the computer model fails to simulate some of the finer details of metal-ion mobilization. Notably the model calculates a much higher ligand concentration dependence than is actually seen. This is a consequence of the assumption that the free metal-ion concentration is perfectly buffered by the protein–metal interactions. While this assumption may be valid for small increases in the concentration of low molecular weight metal species, as more and more mobilization occurs the buffer capacity of the

protein will be exceeded. Also the model does not take into consideration ligand binding by protein or the binding of low molecular weight complexes to protein. In addition we have shown that not all metal–protein interactions can be described by simple equilibria and that as metal ions are removed from the protein, it may become progressively more difficult to remove the remaining metal ions bound to the protein.[19] These three factors would explain why the limiting slopes of the experimental PMI curves are less than the slopes of the theoretical PMI curves.

Serum albumin is known to be a versatile carrier protein, not solely for copper ions, but also for long chain fatty acids and for smaller molecules. In addition, Brown's structural elucidation of serum albumin,[20,21] suggests that serum albumin binds to drug molecules of the type used in our studies.[17] If this binding is not taken into account in the computer model, then an overestimation of the amount of metal ion mobilized would occur.

A further point to note has been raised by Duffield *et al.*,[22] who showed that the current knowledge concerning the interaction of polyaminopolycarboxylic acids with metal ions, under biological conditions, is imperfect, mainly due to the interaction of the background electrolyte. Since the computer model relies on thermodynamic data any error in this data will affect the accuracy of the model.

Finally, the ECCLES computer model of blood plasma is a model of the complex coordination equilibria occurring in blood plasma. It is possible that metal ions are removed from protein by means other than chelation. The ultrafiltration studies of the NSAIDs and prednisolone, which complex metal ions only weakly, showed that these agents are capable of mobilizing copper(II) and zinc(II) in blood serum. Fiabane and Williams[17] have observed the same phenomenon with aspirin and have postulated that in this case the release of copper(II) from serum albumin is via an allosteric mechanism.

In conclusion, while there are some notable differences between the experimental and calculated results for blood plasma, the computer model is surprisingly good at explaining observed physical phenomena.

REFERENCES

1. J. Schubert, *Fed. Proc.*, **20**, *Suppl.*, 1961, **10**, 220.
2. R. R. Agarwal and D. D. Perin, *Agents Actions* 1976, **15**, 667.
3. S. H. Laurie, O. H. Prime and B. Sarkar, *Can. J. Chem.* 1979, **57**, 1411.
4. P. M. May, P. W. Linder and D. R. Williams, *J. Chem. Soc., Dalton Trans.* 1977, 588.
5. G. E. Jackson, P. M. May and D. R. Williams, *J. Inorg. Nucl. Chem.* 1978, **40**, 1227.
6. M. M. Jones, *Inorg. Chim. Acta* 1985, **107**, 235.
7. M. M. Jones and P. M. May, *Inorg. Chim. Acta* 1987, **138**, 67.
8. M. M. Bradford, *Analyt. Biochem.* 1976, **72**, 242.
9. A. E. Martell and R. E. Smith, *Critical Stability Constants*. Plenum Press, New York (1974).
10. J. Buffle and C. Staub, *Analyt. Chem.* 1984, **56**, 2837.
11. J. Sophianopoulos, S. Durham, A. Sophianopoulos, H. Ragsdale and W. Crapper, *Arch. Biochem. Biophys.* 1978, **187**, 132.
12. R. Judd and A. Pesco, *Clin. Chem.* 1982, **28**, 1726.
13. M. Walser, *J. Clin. Invest.* 1961, **40**, 723.
14. R. Pribel, *Analytical Applications of EDTA and Related Compounds*. Pergamon Press, Oxford (1972).
15. N. Rubin, S. Gignac, S. P. Bessman and E. L. Belkamp, *Science* 1953, **117**, 659.
16. A. Katsh, *Diagnosis and Treatment of Incorporated Radionuclides*, p. 295. International Atomic Energy Agency, Vienna (1976).
17. A. M. Fiabane and D. R. Williams, *J. Inorg. Nucl. Chem.* 1978, **40**, 1209.
18. M. M. Jones, *Metal Ions in Biological Systems* (Edited by H. Segal), Vol. 16. Marcel Dekker, New York (1974).
19. M. Singh, MSc thesis, University of Cape Town (1989).
20. J. R. Brown, *Fed. Proc.* 1974, **33**, 1389.
21. J. R. Brown, *Fed. Proc.* 1975, **34**, 591.
22. J. P. Duffield, P. M. May and D. R. Williams, *J. Inorg. Biochem.* 1984, **20**, 199.

Polyhedron Vol. 9, No. 4, pp. 511–516, 1990
Printed in Great Britain

0277–5387/90 $3.00+.00
© 1990 Pergamon Press plc

CATION-EXCHANGE AND SPECTROPHOTOMETRIC STUDY OF COPPER(II)–CYCLOPOLYPHOSPHATE COMPLEXES

GENICHIRO KURA*

Department of Chemistry, Fukuoka University of Education, Akama, Munakata, Fukuoka 811-41, Japan

and

HIROHIKO WAKI

Department of Chemistry, Faculty of Science, Kyushu University, Hakozaki 6-10-1, Higashiku, Fukuoka 812, Japan

(*Received* 20 *June* 1989; *accepted* 7 *September* 1989)

Abstract—The stability constants of copper(II)–cyclopolyphosphate complexes were determined by the spectrophotometric and cation-exchange methods. For cyclohexa- and cyclo-octaphosphate complexes, the stability constants by the above two methods did not agree. The stability constants determined by spectrophotometry were somewhat lower and depended on the wavelength measured. The definition of a constant molar absorption coefficient for the complex formed contains various problems.

Cyclopolyphosphate ions presented as $P_nO_{3n}^{n-}$ are known[1] as very interesting materials which have high negative charges on their relatively compact molecules from the viewpoint of electrolyte solution chemistry.

We have been investigating various properties of these phosphates and have reported some results about the interactions between the phosphate anions and various cations by various methods.[2–6] In our previous paper,[5] we determined the stability constants of the cyclopolyphosphate complexes with cerium(III) ion by both ion-exchange and spectrophotometric methods. The two methods gave different stability constants for the same complex. The difference between the stability constants for the cyclohexa- and cyclo-octaphosphate complexes were remarkable. The stability constants determined by the spectrophotometric method were lower for all cases. A satisfactory explanation of the above experimental results has not yet been obtained.

In this paper, complex formation between copper(II) ion and cyclopolyphosphate ions was investigated by cation-exchange and spectrophotometric methods. The stability constants of the copper(II)–cyclopolyphosphate ion complexes have already been determined by the potentiometric method using an ion-selective electrode.[6] We have compared the stability constants determined by the three different methods for the same complexes and have discussed the observed difference.

For the copper(II)–cyclotri- and cyclotetraphosphate complexes, the stability constants determined by the three methods agreed well with each other. For the copper(II)–cyclohexa- and cyclo-octaphosphate complexes, the coincidence between the values obtained by the potentiometric and cation-exchange methods was satisfactory. However, the stability constants determined by the spectrophotometric method depended on the wavelength at which the stability was determined. Even the highest value obtained at 230 nm was somewhat lower than those determined by cation-exchange or potentiometric method. We do not know the details of the wavelength dependence of the stability constants by spectrophotometry, however, the origin of the difficulty is supposed to arise from the assumption that the various types of complexes (e.g. inner- and outer-sphere types) formed have an identical molar absorption coefficient.

* Author to whom correspondence should be addressed.

The stability constants obtained by both cation-exchange and potentiometric methods for the copper(II)–cyclopolyphosphate complexes increase linearly with the anion charge.[6] We have concluded that complex formation is due to the electrostatic force between the copper(II) ion and cyclopolyphosphate anion. The light absorption of the complex in the UV might be considered to be due to the charge-transfer. The wavelengths of maximal absorption are shifted to longer ones as the anionic charge on the ligands increases.

In this paper the cyclopolyphosphates are abbreviated as P_{nm}, where n is the polymerization degree.

EXPERIMENTAL

The absorption spectra and quantitative absorbance were measured at about 25°C with a Hitachi-228A spectrophotometer by the use of 1 cm quartz cells. The distribution ratio of the copper(II) ion on the cation-exchanger was determined by measuring the copper concentration with a Hitachi 180-80 atomic absorption spectrophotometer. Copper(II) perchlorate as a copper(II) source was prepared from copper(II) carbonate hydroxide and perchloric acid. The standard solution of copper(II) was determined by complexometric titration with EDTA. Sodium cyclopolyphosphates were prepared by the usual methods and their purity was checked by liquid chromatography.[7] As a supporting electrolyte to keep the ionic strength constant in each experiment, sodium perchlorate was used. As a cation-exchange resin, BIO-RAD AG 50W X-8, 100–200 mesh was used. The other chemicals used in this study were reagent grade and commercially available. The distribution ratio of copper(II) between the resin and solution phase was measured by the usual batch equilibrium method.

RESULTS AND DISCUSSION

The stability constants of copper(II)–cyclopolyphosphate complexes can be estimated from the distribution ratio of copper(II) between the cation-exchange resin and solution phase[8] which contained copper(II) ion and excess ligands. Under these conditions, the possibility of more than two copper(II) ions combining with one ligand ion can be ignored, while that of more than two ligand anions binding to one copper(II) ion must be considered. However, the possibility of the formation of higher complexes in which more than three ligands bind seemed to be low since the anionic complex must bind to the multi-valent anionic ligand. Therefore the formation of 1:1 and 1:2 (copper(II)–cyclopolyphosphate ratio) complexes was considered.

Since the complexes thus formed which have an anionic charge are not absorbed on the cation-exchanger, the distribution ratio, D, of copper(II) on the cation-exchange resin can be presented as

$$D = \frac{[Cu^{2+}]_r}{[Cu^{2+}]+[CuP]+[CuP_2]}, \quad (1)$$

where $[Cu^{2+}]_r$ is the concentration of the copper(II) ion in the exchanger phase and $[Cu^{2+}]$, [CuP] and $[CuP_2]$ denote the concentration of the free copper(II) ion, the 1:1 complex and the 1:2 complex in the solution phase, respectively. Equation (1) can be rewritten as

$$D = \frac{[Cu^{2+}]_r/[Cu^{2+}]}{1+[CuP]/[Cu^{2+}]+[CuP_2]/[Cu^{2+}]}.$$

This equation is finally presented as

$$\frac{1}{D}\frac{[Cu^{2+}]_r}{[Cu^{2+}]} - 1 = \beta_1[P]+\beta_2[P]^2. \quad (2)$$

The distribution ratio of the free copper(II) ion, $[Cu^{2+}]_r/[Cu^{2+}]$ depends only on the concentration of sodium ion added as the supporting electrolyte, and can be easily determined by the separate experiments. In the equations, the charges of the complexes are omitted and P denotes the cyclopolyphosphate ion.

The stability constants are defined as

$$Cu^{2+} + P \rightleftarrows CuP \quad \beta_1 = \frac{[CuP]}{[Cu^{2+}][P]} \quad (3)$$

$$Cu^{2+} + 2P \rightleftarrows CuP_2 \quad \beta_2 = \frac{[CuP_2]}{[Cu^{2+}][P]^2}. \quad (4)$$

From the variation of the distribution ratio with the quantity of excess ligands added, the stability constants, β_1 and β_2, can be determined by the use of eq. (2). In eq. (2), the concentration of the free ligands, [P], is not known if the stability constants are not found. In this study, as a first approximation, the formation of only 1:1 complex was assumed and the free ligand concentration is equal to the total ligand concentration. Thus, from the linear relation between $1/D([Cu^{2+}]_r/[Cu^{2+}])-1$ and $[P]_t$, the first approximate value of β_1 was obtained. From this stability constant, the approximate value of the free ligand concentration can be calculated. Next, $1/D([Cu^{2+}]_r/[Cu^{2+}])-1$ and [P] thus calculated were newly plotted and a new stability constant was obtained. This procedure was repeated until the true stability constant was obtained. The final plots are shown in Fig. 1. Except for the Cu^{2+}–$P_3O_9^{3-}$ complex, the linear plots of

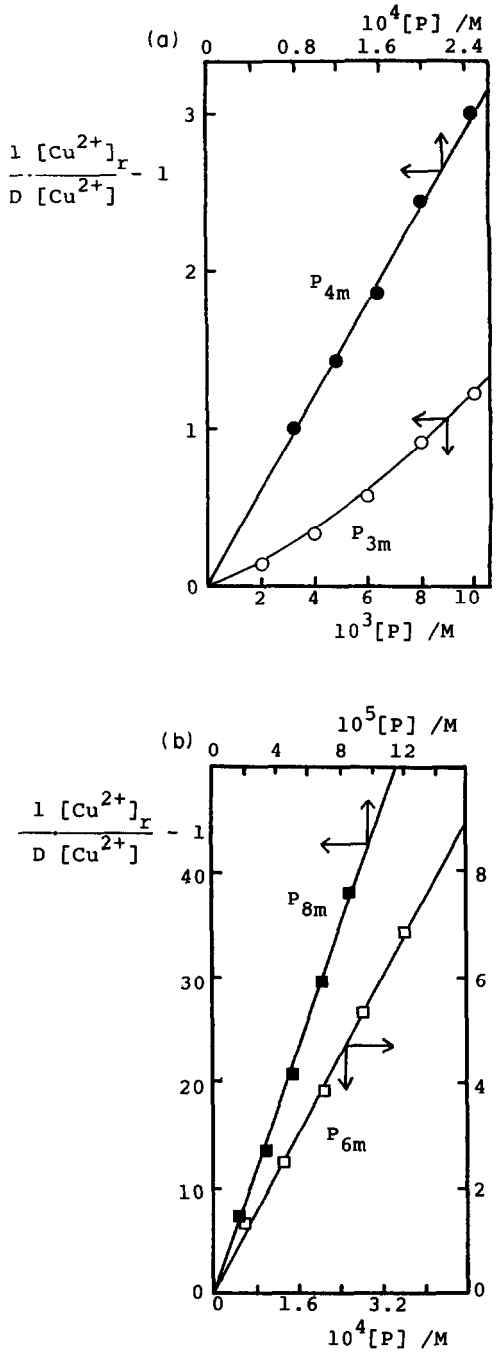

Fig. 1. Determination of the stability constants by the cation-exchange method.

$1/D([Cu^{2+}]_r/[Cu^{2+}])-1$ vs [P] were obtained, and the approximation of the formation of only the 1 : 1 complex is reasonable. For the Cu^{2+}–$P_3O_9^{3-}$ system, a linear relation was not obtained. This suggested the presence of higher complexes in which more than two ligand anions combine with one copper(II) ion. We have assumed formation of the 1 : 1 and 1 : 2 complexes in this case, and β_1 and β_2 are simultaneously determined from the following equation using the successive approximations mentioned above:

$$((1/D)\cdot([Cu^{2+}]_r/[Cu^{2+}])-1)[P] = \beta_1+\beta_2[P]. \quad (5)$$

The stability constants at each ionic strength thus obtained are summarized in Table 1. The reason for the formation of the 1 : 2 complex, $Cu(P_3O_9)_2^{4-}$, only in the case of Cu^{2+}–$P_3O_9^{3-}$ system is speculated as follows. The negative charge of the 1 : 1 complex is low and the electrostatic repulsion between the complex and the secondary ligand to bond is relatively small compared with other cases. Furthermore, steric hindrance between the first ligand and second ligand approaching each other to form a complex is minimal since cyclo-triphosphate is a relatively compact molecule.

It was observed that the UV spectrum of the copper(II) ion was markedly affected by the addition of cyclopolyphosphate anions. The aquo ion of copper(II) also absorbs UV light and a marked increase in absorption occurred by the addition of the ligands. We have estimated the stability constants of the complexes by analysing the increase in absorbance.[9–11] The values of absorbance at 230 nm, measured experimentally, on changing the ligand concentration at a constant copper(II) ion concentration are shown in Table 2. It was assumed that the complex formed has a constant molar absorption coefficient at a measured wavelength. For Cu^{2+}–$P_4O_{12}^{4-}$, Cu^{2+}–$P_6O_{18}^{6-}$, Cu^{2+}–$P_8O_{24}^{8-}$ systems, the formation of only a 1 : 1 complex was reasonably assumed from the results by the cation-exchange method described above. The absorbance (Abs) can be represented as

$$Abs = \varepsilon_0[Cu^{2+}]+\varepsilon_1[CuP], \quad (6)$$

where ε_0 and ε_1 are molar absorption coefficient of free copper(II) ion and the complex, respectively. The stability constant of the 1 : 1 complex is defined as β_1 and the apparent molar absorption coefficient of copper(II) ion, ε_{app}, is written as in eq. (7):

$$\varepsilon_{app} = \frac{Abs}{[Cu^{2+}]_t}, \quad (7)$$

Table 1. Stability constants determined by the cation-exchange method at 25°C; P_{3m}, P_{4m}: $I = 0.3$; P_{6m}, P_{8m}: $I = 0.15$

	P_{3m}	P_{4m}	P_{6m}	P_{8m}
$\log\beta_1$	1.8	2.8	4.3	5.6
$\log\beta_2$	3.6			

Table 2. Spectrophotometric data at 230 nm

		$P_{4m'}$ $[Cu^{2+}]_t = 2.1\times10^{-3}$ M, $I = 0.3$					
$[P]_t$/M	0	2×10^{-3}	4×10^{-3}	6×10^{-3}	8×10^{-3}	1.0×10^{-2}	1.4×10^{-2}
Abs.	0.5477	1.2938	1.7052	1.9290	2.0618	2.1480	2.2731
		$P_{6m'}$ $[Cu^{2+}]_t = 5.0\times10^{-4}$ M, $I = 0.15$					
$[P]_t$/M	0	2×10^{-4}	4×10^{-4}	8×10^{-4}	1.2×10^{-3}	1.6×10^{-3}	2.4×10^{-3}
Abs.	0.1348	0.3832	0.5641	0.7210	0.7640	0.7794	0.8037
		$P_{8m'}$ $[Cu^{2+}]_t = 4.0\times10^{-4}$ M, $I = 0.15$					
$[P]_t$/M	0	1×10^{-4}	2×10^{-4}	4×10^{-4}	6×10^{-4}	8×10^{-4}	1.0×10^{-3}
Abs.	0.1041	0.3738	0.6339	1.0795	1.1402	1.1587	1.1591

where $[Cu^{2+}]_t$ is the total concentration of copper(II). Substituting β_1 and ε_{app} in eq. (6) yields the following equation:

$$\frac{[P]}{\varepsilon_{app}-\varepsilon_0} = \frac{[P]}{\varepsilon_1-\varepsilon_0} + \frac{1}{\beta_1(\varepsilon_1-\varepsilon_0)}, \qquad (8)$$

where [P] is the concentration of free ligands which is not known if the stability constants are not determined. Initially, $[P]_t$ was substituted in eq. (8) instead of [P] and plotting $[P]_t/(\varepsilon_{app}-\varepsilon_0)$ vs $[P]_t$ yielded the first approximate values of β_1 and ε_1. Next, from these stability constants, the free ligand concentration was calculated, then $[P]/(\varepsilon_{app}-\varepsilon_0)$ vs [P] was re-plotted and new β_1 and ε_1 values were calculated. The above procedure was successively repeated until constant values of β_1 and ε_1 were obtained. As an example, the final plot of $[P]/(\varepsilon_{app}-\varepsilon_0)$ vs [P] for the Cu^{2+}–$P_4O_{12}^{4-}$ system is shown in Fig. 2. The data follow a good straight line. The stability constants and ε_1 obtained at the wavelengths 230, 240 and 250 nm are shown in Table 3. For the Cu^{2+}–$P_3O_9^{3-}$ system, the above treatment was difficult since the 1:2 complex was evidently formed. Then from the stability constants, β_1 and β_2, determined by the cation-exchange method, the concentrations of CuP, CuP_2 were calculated and using the data in Table 2 and eq. (9), the molar absorption coefficients for the 1:1 and 1:2 complexes, ε_1 and ε_2, were calculated by the least-squares method:

$$\text{Abs} = \varepsilon_0[Cu^{2+}]+\varepsilon_1[CuP]+\varepsilon_2[CuP_2]. \qquad (9)$$

At 230 nm, ε_1 and ε_2 were 523 and 724, respectively.

Except for the Cu^{2+}–$P_3O_9^{3-}$ system in which a 1:2 complex was formed, absorbance at the same wavelength approaches a constant value when excess ligand is added to copper(II) ions. The results for the Cu^{2+}–$P_8O_{24}^{8-}$ system are shown in Fig. 3. This constancy can be explained by the 1:1 complex formation of all the copper(II) ions in the solution.

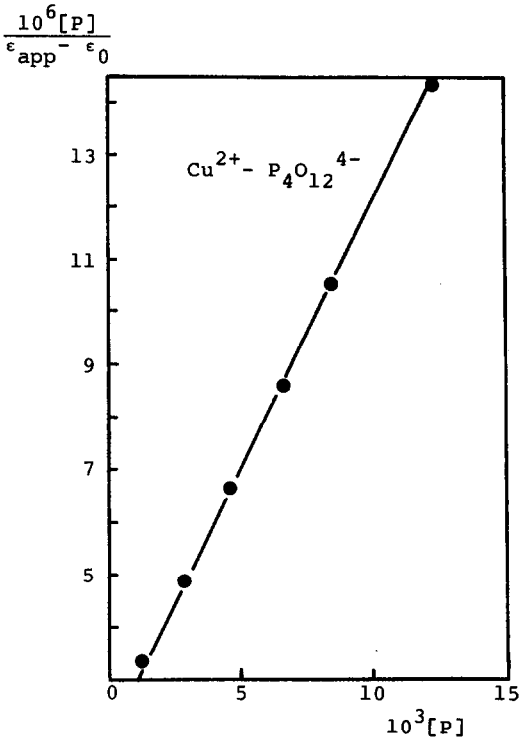

Fig. 2. Spectrophotometric determination of the stability constant for the Cu^{2+}–$P_4O_{12}^{4-}$ system.

Table 3. Stability constants and molar absorption coefficients at 230, 240 and 250 nm

		P_{4m}	P_{6m}	P_{8m}
230 nm	$\log\beta_1$	2.66	4.19	5.44
	ε_1	1230	1670	2940
240 nm	$\log\beta_1$	2.59	4.09	5.27
	ε_1	547	944	2340
250 nm	$\log\beta_1$	2.57	4.01	5.13
	ε_1	183	420	1270

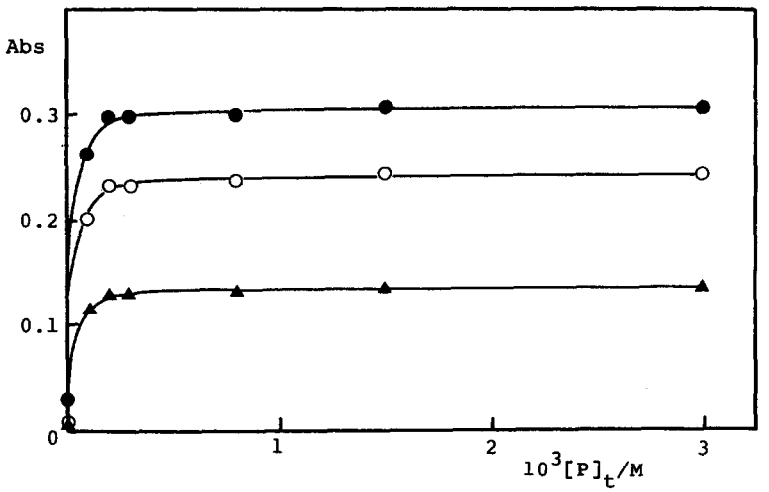

Fig. 3. Absorbance for the Cu^{2+}–$P_8O_{24}^{8-}$ system as a function of total ligand concentration at constant $[Cu^{2+}]_t$. ▲, 250 nm; ○, 240 nm; ●, 230 nm.

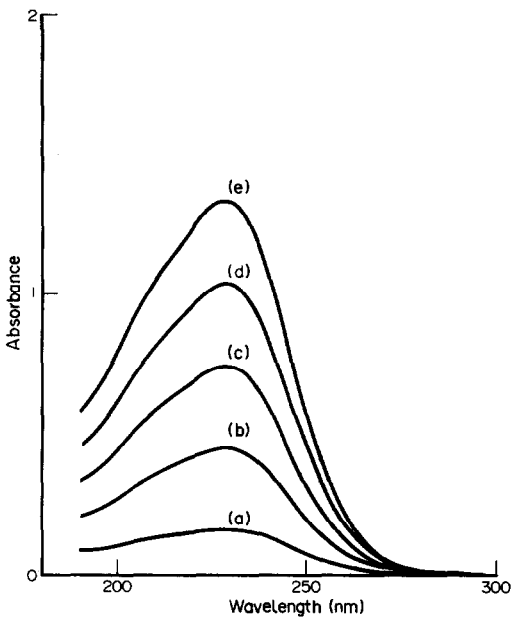

Fig. 4. Absorption spectra for the $CuP_8O_{24}^{6-}$ complex. $[P]_t = 1 \times 10^{-3}$ M; $[Cu^{2+}]_t$: (a) 5×10^{-5} M; (b) 1.5×10^{-4} M; (c) 2.5×10^{-4} M; (d) 3.5×10^{-4} M; (e) 4.5×10^{-4} M.

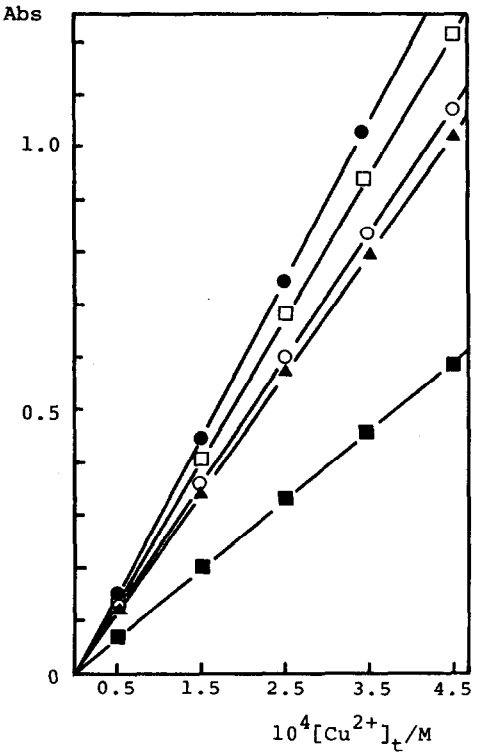

Fig. 5. Variation of absorbance with $[Cu^{2+}]_t$ for the Cu^{2+}–$P_8O_{24}^{8-}$ system with excess ligand. ■, 250 nm; ▲, 240 nm; ○, 230 nm; □, 220 nm; ●, 210 nm.

The absorption spectra for the Cu^{2+}–$P_8O_{24}^{8-}$ system shown in Fig. 4, where the concentration of copper(II) ion was varied in the presence of excess and constant ligand anions. These spectra contain only the 1:1 complex. At wavelengths from 210 to 250 nm, the relationship between absorbance and total copper(II) ion concentration is shown in Fig. 5 for the Cu^{2+}–$P_8O_{24}^{8-}$ system. At all the wavelengths, good straight lines through the origin were obtained. The slope of the line is expected to be identical to the molar absorption coefficient, ε_1, of the $CuP_8O_{24}^{6-}$ complex. The ε_1 value from the slope at 230 nm was 2940 and is consistent with that obtained by the equilibrium method using eq. (8). The ε_1 values for the $CuP_4O_{12}^{2-}$ and $CuP_6O_{18}^{4-}$ complexes, determined by the above same method, agreed with the respective values in Table 3.

For the Cu^{2+}–$P_3O_9^{3-}$ system, a linear relation-

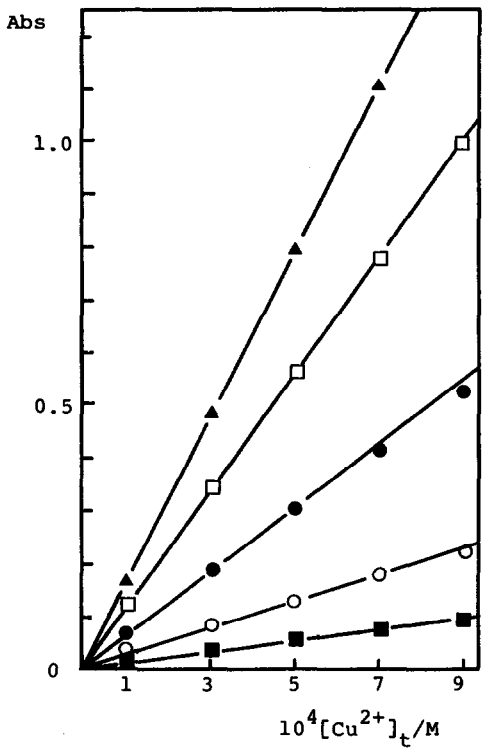

Fig. 6. Variation of absorbance with $[Cu^{2+}]_t$ for the Cu^{2+}–$P_3O_9^{3-}$ system with excess ligand. ■, 250 nm; ○, 240 nm; ●, 230 nm; □, 220 nm; ▲, 210 nm.

ship, as shown in Fig. 6, was observed when the copper(II) ion concentration was varied in the presence of excess ligand. Since both $CuP_3O_9^-$ and $Cu(P_3O_9)_2^{4-}$ form under these conditions, ε_1 and ε_2 could not be directly determined from the slopes. The slopes obtained from the results in Fig. 6 were not in agreement with the ε_1 and ε_2 values calculated by using β_1 and β_2 in the cation-exchange method. For the Cu^{2+}–$P_3O_9^{3-}$ system, the following equations can be derived.

$$\frac{[CuP]}{[Cu^{2+}]} = \beta_1[P]$$

$$\frac{[CuP_2]}{[CuP]} = \frac{\beta_2}{\beta_1}[P]$$

$$[Cu^{2+}]+[CuP]+[CuP_2] = [Cu^{2+}]_t.$$

Substituting the values of $[Cu^{2+}]$, $[CuP]$ and $[CuP_2]$ calculated from the above three equations into eq. (9) yields the following equation:

$$\text{Abs} = \frac{\varepsilon_0+\varepsilon_1\beta_1[P]+\varepsilon_2\beta_2[P]^2}{1+\beta_1[P]+\beta_2[P]^2}[Cu^{2+}]_t. \quad (10)$$

If the ligand added is in large excess compared with the copper(II) ion and the free ligand concentration is assumed to be constant, the absorbance should increase linearly with the total copper(II) ion concentration through the origin. The slope calculated from eq. (10) was 20% lower than that experimentally determined from Fig. 6. This difference may arise from the assumption that the free ligand concentration is constant.

Any differences between the stability constants for the Cu^{2+}–$P_nO_{3n}^{n-}$ complexes determined by the cation-exchange method and potentiometry are not observed. However, the values determined even at 230 nm by the spectrophotometric method in Table 3 are somewhat lower than those by the above two methods. For the previous Ce^{3+}–$P_nO_{3n}^{n-}$ systems, the stability constants obtained by spectrophotometry were lower than those determined by the ion-exchange method. We have no clear explanations about the incomprehensible difference in the stability constants. Perhaps the difference may originate from the assumption that the complex formed has a constant molar absorption coefficient at a constant wavelength. In the case studied here, the formation of various types of complexes, e.g. inner-sphere and outer-sphere complexes, is known. In outer-sphere complexes, a contact ion-pair and solvent separated ion-pairs are included. We must define different molar absorption coefficients for the respective different types of complexes when applying the spectrophotometric method to the analysis of complex formations of systems such as copper(II)–cyclopolyphosphate.

REFERENCES

1. J. R. van Wazer, *Phosphorus and Its Compounds.* Interscience, New York (1958).
2. G. Kura and S. Ohashi, *J. Inorg. Nucl. Chem.* 1972, **34**, 3899.
3. G. Kura, S. Kura and S. Ohashi, *J. Inorg. Nucl. Chem.* 1974, **36**, 1605.
4. G. Kura and S. Ohashi, *J. Inorg. Nucl. Chem.* 1976, **38**, 1151.
5. M. Koganemaru, H. Waki, S. Ohashi and G. Kura, *J. Inorg. Nucl. Chem.* 1979, **41**, 1457.
6. G. Kura, *Polyhedron* 1986, **5**, 2097.
7. G. Kura, *J. Chromatogr.* 1988, **447**, 91.
8. F. J. C. Rossotti and H. Rossotti, *The Determination of Stability Constants.* McGraw-Hill, New York (1961).
9. H. McConnell and N. Davidson, *J. Am. Chem. Soc.* 1950, **72**, 3164.
10. T. W. Newton and G. M. Arcand, *J. Am. Chem. Soc.* 1953, **75**, 2449.
11. Z. Libus, *Inorg. Chem.* 1973, **12**, 2972.

Polyhedron Vol. 9, No. 4, pp. 517–525, 1990
Printed in Great Britain

0277–5387/90 $3.00+.00
© 1990 Pergamon Press plc

^{29}Si MASNMR INVESTIGATIONS OF THE THERMOCHEMISTRY OF LAPONITE AND HECTORITE

ARVIND-PAL S. MANDAIR, PAUL J. MICHAEL and WILLIAM R. McWHINNIE*

Department of Chemical Engineering and Applied Chemistry, Aston University, Aston Triangle, Birmingham B4 7ET, U.K.

(*Received* 21 *August* 1989; *accepted* 7 *September* 1989)

Abstract—^{29}Si MASNMR spectra were used (together with some ^{23}Na MASNMR spectra and XRD and IR measurements) to monitor the thermolysis of laponite–RD and hectorite. For laponite, even at 400°C, some breakdown of the silicate (Q^3) lattice is observed although this is reversible on rehydration. Lithium ions migrate from trioctahedral positions at 600°C and by 800°C irreversible breakdown to polymorphs of enstatite occurs. At 1300°C *ortho*- and *clino*-enstatite co-exists with a glassy phase. The thermal behaviour of hectorite is broadly similar. ^{23}Na MASNMR spectra reveal that the location of sodium ions in rehydrated specimens, particularly for laponite heated to 400 and 600°C, may be very "solution"-like. The exchange-doping of hectorite with paramagnetic ions such as Cu^{2+}, Ni^{2+}, Mn^{2+} was explored; the loading level beyond which resolution of the silicon spectra is lost was defined in terms of gramme magnetic susceptibilities. The combined use of ^{29}Si MASNMR and ESR to monitor the thermolysis to 1200°C of a sample of hectorite with a Cu^{2+} loading of 10.5 mg g^{-1} clay is illustrated.

Non-invasive resonance spectroscopies are proving powerful techniques for the study of non- or poorly-crystalline materials and also of the reactions that such materials undergo. For example, greater insight into the dehydroxylation of kaolinite has recently been obtained[1,2] by the application of ^{29}Si and ^{27}Al MASNMR spectroscopy. Although, in broad terms the thermal decomposition of kaolinite was well understood from more classical investigations notably those of Brindly and Nakahira,[3,4] the application of the NMR technique has produced a more detailed understanding particularly of the transition to the metakaolinite phase.[2] We have recently demonstrated that ^{57}Fe Mössbauer spectroscopy is also sensitive to the phase changes that accompany the thermal decomposition of clay minerals such as montmorillonite and illite.[5]

Our interest in the thermal decomposition of clay minerals relates to our use of resonance spectroscopies to examine the chemical changes that occur in the formation of ceramic glazes. This objective is more readily accomplished if a reasonable understanding of the thermochemistry of the individual glaze components is available, at least up to the firing temperature of 1300°C. In this paper we turn our attention to two species which are attractive for NMR study due to an extremely low paramagnetic content: the synthetic lithium magnesium clay, laponite, and the naturally occurring counterpart, hectorite (obtained from Hector, California). Our objective was to investigate how accurately the ^{29}Si MASNMR spectra mirror the various stages of thermal decomposition of the clay, and we carried out the NMR studies in parallel with XRD and IR investigations. Further, since both laponite and hectorite have significant ion exchange capacities, the opportunity existed to exchange varying quantities of ESR active ions such as Cu^{2+} onto the clay and thereby (a) explore the influence of the paramagnetic ion on the resolution of the ^{29}Si MASNMR spectra, and (b) attempt to use ESR spectroscopy to obtain information on the fate of the interlamellar ions on decomposition of the clay mineral (we also report preliminary ^{23}Na MASNMR data on laponite).

* Author to whom correspondence should be addressed.

EXPERIMENTAL

Materials

Laponite–RD was obtained from Laporte Industries Ltd and was in the sodium form. Hectorite was a natural specimen obtained from Hector, California. The ideal composition is $Na_{0.33}[(Mg_{2.67}Li_{0.33})Si_4O_{10}(OH)_2]$, the actual composition determined by XRF analysis is in Table 1. The XRD trace was typical of hectorite with $d(001) = 12.83$ Å, but evidence of a small calcite impurity was seen; this was removed on treatment with dilute acetic acid. Although 0.18% Fe_2O_3 was detected, this did not interfere with the resolution of the ^{29}Si MASNMR spectra.

Methodology

Samples of laponite–RD (5 g) were placed in a porcelain crucible and fired in a carbolite furnace for 3 h at constant temperatures of 200, 400, 600, 800 and 1300°C. Fired samples were removed from the furnace, covered, and cooled overnight in a desiccator. The 200, 400, 600 and 800°C samples were divided into two parts; following grinding one part was retained for analysis and the other was immersed in distilled water for 1 h. Excess water was decanted off and the samples were air-dried for 1 week. The rehydrated samples were then analysed. Samples of hectorite were treated similarly, but no rehydration experiments were attempted.

Samples of hectorite were exchanged with Cu^{2+}, Ni^{2+}, Mn^{2+}, Co^{2+} and Zn^{2+} by treating the clay with solutions of the appropriate metal chloride. The amount of cation taken up by the clay was determined from atomic absorption measurements of cation concentration of the supernatant liquid following exchange. Table 2 lists the cation-exchanged hectorites considered. Each specimen was then heated to 1200°C following the procedure detailed above (1200°C rather than 1300°C was selected in these instances to avoid instances of glass formation).

Physical measurements

MASNMR spectra were obtained with a Bruker AC(E) 300 MHz spectrometer. The "magic angle" was set with KBr and Delrin rotor spinning rates were 5 kHz. Frequencies were 59.580 MHz (^{29}Si) and 79.392 MHz (^{23}Na). Some ^{29}Si MASNMR spectra were obtained at the University of Durham using Varian VH 300 MHz and Bruker CPX 200 spectrometers. (We thank the SERC for time allocation and M. B. Say, Dr D. Apperly and Dr R. Young for their help and hospitality.) ESR spectra were recorded with a JEOL PE-1X spectrometer; g values were recorded using a manganese(II) standard. IR spectra were recorded for KBr discs with a Perkin–Elmer 1710 FTIR instrument. XRD data were obtained with a Philips X-ray diffractometer using Co-K_α radiation with a typical scan speed of 1° 2θ min^{-1}. The d-spacings of the various phases

Table 1. X-ray fluorescence analysis of hectorite

Oxide	Wt %
Fe_2O_3	0.18
MnO	0.00
TiO_2	0.04
CaO	0.42
K_2O	0.04
P_4O_{10}	0.01
SiO_2	60.78
Al_2O_3	0.15
MgO	28.50
Na_2O	1.96
SO_3	0.02
Li_2O^a	1.22
H_2O^b	4.70
H_2O^c	3.20
Total	101.22

The data represent the mean of results for two samples.
[a] Not analysed; ref. 6 value used.
[b] H_2O lost at 400°C.
[c] H_2O lost at 1100°C (i.e. "structural" water).

Table 2. Exchanged cation loading of hectorite prior to treatment at 1200°C

Cation (as chloride)	pH of exchange solution (molarity)	Cation loading of clay (mg g^{-1})
Cu^{2+}	5.3 (0.100 M)	17.2
	5.5 (0.075 M)	19.3
	5.6 (0.050 M)	18.4
	5.9 (0.025 M)	11.2
	6.2 (0.010 M)	10.5
Ni^{2+}	6.7 (0.100 M)	17.1
	6.6 (0.075 M)	16.9
	6.8 (0.050 M)	16.3
	7.2 (0.025 M)	11.9
	7.5 (0.010 M)	9.8
Mn^{2+}	6.5 (0.100 M)	17.6
	7.2 (0.010 M)	9.1
Co^{2+}	5.9 (0.100 M)	16.9
	6.6 (0.010 M)	9.7
Zn^{2+}	5.9 (0.100 M)	18.7

present were calculated from 2θ values using standard Co-K_α charts.[7]

RESULTS

The ^{29}Si MASNMR parameters for the heated laponite samples (together with data for rehydrated samples) are shown in Table 3. The data are interpreted in terms of the number of SiO_4 tetrahedra linked to a central SiO_4 tetrahedron via bridging oxygen atoms, thus Q^3 denotes an SiO_4 group with one terminal oxygen and three forming common vertices with three other SiO_4 tetrahedra.[8] Some ^{23}Na MASNMR data for dehydrated and rehydrated laponite constitute Table 4. Figure 1 shows a well resolved spectrum of laponite and Fig. 2 shows the changes in spectra that occur on heating laponite. Figure 3 shows the ^{23}Na spectra of the de- and rehydrated samples. Figure 4 illustrates the spectral changes (^{29}Si) which occur on heating hectorite.

Varying quantities of divalent paramagnetic ions were exchanged onto hectorite (Table 2). One objective was to see to what extent the resolution in the ^{29}Si MASNMR spectra would tolerate the paramagnetic presence; Table 5 summarizes our observations. These observations have been quantified by Dr P. A. Gillespie[9] in terms of the simple gramme susceptibility of the specimen, thus:

$\chi_g < 1.4 \times 10^{-6}$ cgs units g^{-1}
—signal always obtained;

χ_g 1.4–2.2×10^{-6} cgs units g^{-1}
—signal may or may not be obtained;

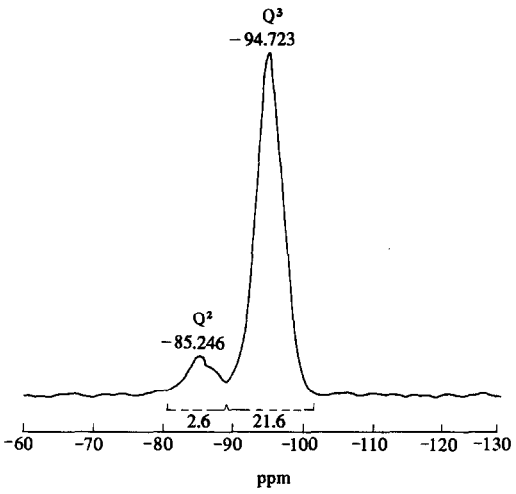

Fig. 1. ^{29}Si MASNMR spectrum of laponite–RD.

$\chi_g > 2.2 \times 10^{-6}$ cgs units g^{-1}
—signal never obtained.

Figure 5 shows the effect of exchanged ions on samples of hectorite heated to 1200°C and Fig. 6 illustrates the ESR spectrum of hectorite with a copper(II) loading of 10.5 mg g^{-1} heated to 1200°C.

DISCUSSION

Laponite–RD

Laponite is a synthetic trioctahedral clay related to the naturally occurring hectorite but free from

Table 3. ^{29}Si MASNMR data for laponite–RD (dehydrated and rehydrated)

Laponite (temperature)	Dehydration (δ ppm)[a]		Rehydration (δ ppm)[a]	
	Q^2	Q^3	Q^2	Q^3
Room temperature	−84.1(9)[b]	−93.6(91)[b]		
200°C	−85.9(9)	−95.9(91)	−85.3(8)	−94.9(92)
400°C	−81.8(16) −85.3(33)	−90.8(41)	−85.3(8)	−94.9(92)
600°C		−97.7	−88.5 −85.6 [b]	−98.0(90)
800°C	−81.0(41) −83.5(59)		−80.8(40) −83.3(60)	
1300°C	−80.9(20) −83.5(30) −85.1(41)	−96(9)		

[a] Relative to tetramethylsilane.
[b] Relative intensity (%).

Table 4. ^{23}Na MASNMR data for laponite–RD (dehydrated and rehydrated)

	δ (^{23}Na) (ppm)[a]	$\Gamma_{1/2}$ (Hz)[b]
Laponite–RD	−15.3	1200
Heated to 200°C	−18.9	2100
Heated to 400°C	−18.9	2100
Heated to 600°C	−19.5	2300
Heated to 800°C	−17.5	2200
200°C—rehydrated	−19.4	5800
400°C—rehydrated	−8.8	1050
600°C—rehydrated	−9.6	1050
800°C—rehydrated	−13.7	1950

[a] Relative to NaBr (apparent chemical shifts).
[b] Full width at half-height.

the extraneous elements which are normally present in samples of that mineral (see Table 1). The clay used was in the sodium-exchanged form. The ^{29}Si MASNMR spectrum of laponite (Fig. 1) shows two

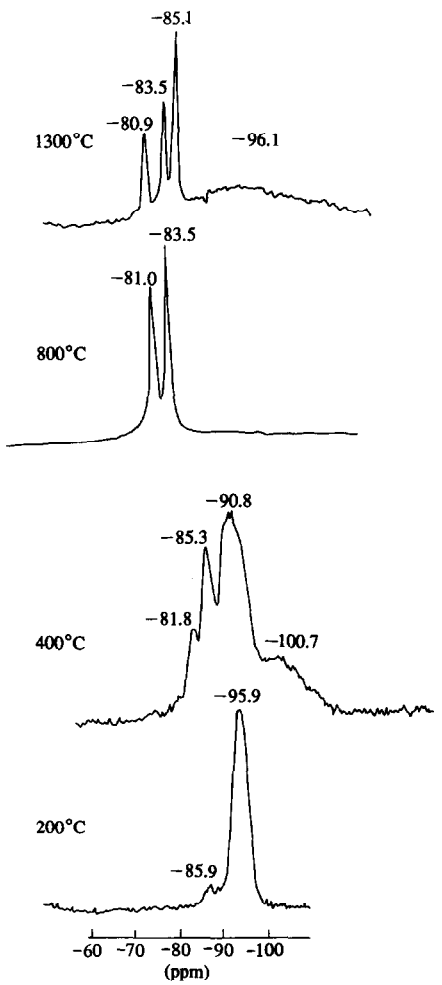

Fig. 2. ^{29}Si MASNMR spectra of laponite–RD heated to the indicated temperatures.

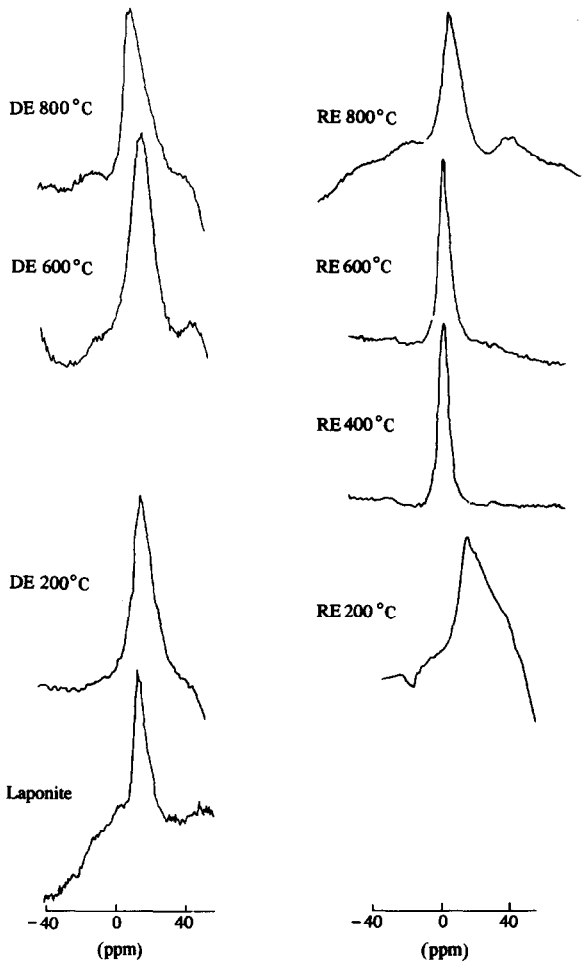

Fig. 3. ^{23}Na MASNMR spectra of dehydrated and rehydrated laponite–RD.

resonances in the intensity ratio 1 : 10. The more intense band at −93.6 ppm arises from Q^3 silicons and may be compared with the resonances reported for hectorite at −95.3 ppm for a sample containing 0.09 aluminium atoms per 10 oxygen atoms,[10] or −94.2 ppm for a sample containing no tetrahedral aluminium, but with a small quantity of Fe^{2+} substituting for Mg^{2+} in the trioctahedral layer.[11] The influence of other ions in the tetrahedral layer (Al) or the octahedral layer (Fe^{2+}) is then to increase the shielding at silicon. In a sense, the parent substance of laponite is talc which shows a Q^3 resonance at −98 ppm; thus the substitution of Mg^{2+} by Li^+ (together with the influence of fluoride) leads to a deshielding of the silicon atoms in the tetrahedral layer. It has been argued[11] that, in trioctahedral minerals, the replacement of one cation with another of lower electronegativity will cause a deshielding of the layer silicon atoms; given that, on the Pauling scale, the electronegativities of magnesium and lithium are 1.2 and 1.0, respectively,

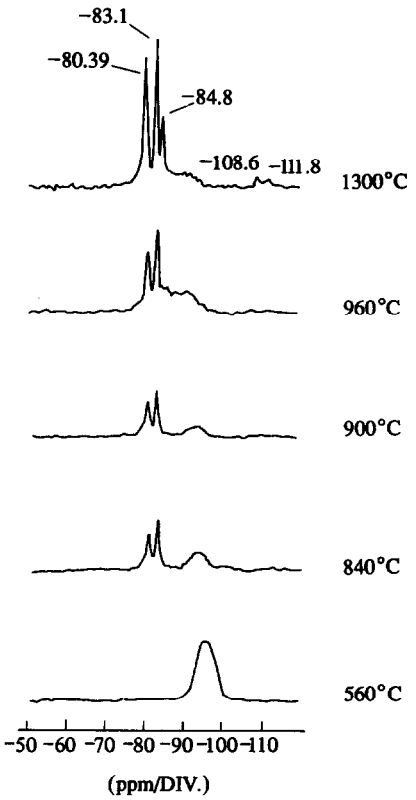

Fig. 4. ^{29}Si MASNMR spectra of hectorite heated to the indicated temperatures.

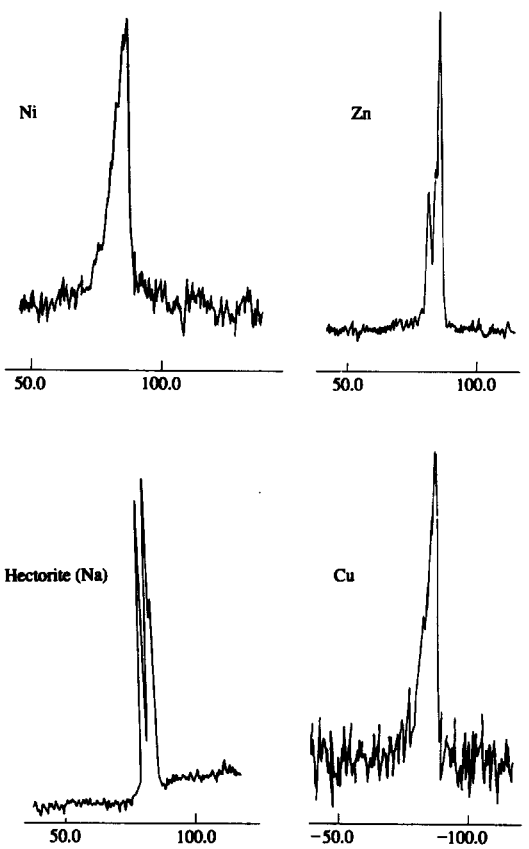

Fig. 5. ^{29}Si MASNMR of ion-exchanged hectorite (Ni^{2+}, Cu^{2+}, Zn^{2+}) heated to 1200°C (see Table 5).

then the observed deshielding from talc to laponite is consistent with that view, i.e. the deshielding can be attributed to slightly more covalent Li—O than Mg—O bonds.

A weak Q^2 resonance is seen at -84.9 ppm and we attribute this to Q^2 sites which must occur at the silicate sheet edges. Indeed, we suggest that an average sheet size can be calculated from the NMR data. If the starting point is a single siloxane ring, $(SiO_3)_6^{12-}$ and other rings are then condensed concentrically, it can be shown that the ratio of edge (Q^2) to sheet (Q^2) silicon sites becomes 1 : 10 when a total of 271 condensed rings are present.

The changes in the ^{29}Si MASNMR spectra which occur on heating the clay to temperatures of 200, 400, 600, 800 and 1300°C are illustrated in Fig. 2 and tabulated in Table 3. XRD data suggest that there is significant loss of crystallinity at 400°C but, by contrast, those samples fired to 800 and 1300°C give evidence of well-developed crystalline phases.

Table 5. Hectorite exchanged with divalent metal ions—some observations on the quality of ^{29}Si MASNMR spectra

Sample (all heated to 1200°C)	χ_g (cgs units $g^{-1} \times 10^6$)	Cation loading (mg g^{-1})	^{29}Si spectrum
Hectorite	—	—	Good[a]
Hectorite/Mn^{2+}	3.209	9.1	No signal
Hectorite/Co^{2+}	1.998	9.7	No signal
Hectorite/Ni^{2+}	—	17.1	Broad[a]
Hectorite/Cu^{2+}	—	19.3	Broad
Hectorite/Cu^{2+}	2.100	11.2	Poor[a]
Hectorite/Zn^{2+}	—	18.7	Good[a]

[a] See Fig. 5 for illustration of the spectra.

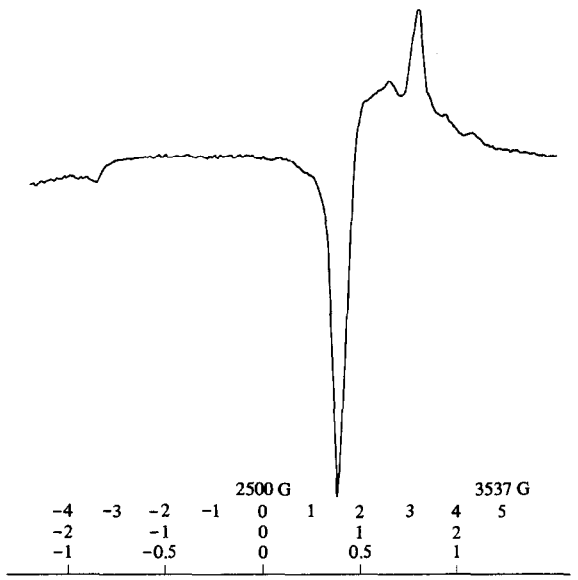

Fig. 6. ESR spectrum of copper(II)-exchanged hectorite (10.5 mg g^{-1}) heated to 1200°C.

Trioctahedral magnesium-containing minerals are expected to give enstatite ($MgSiO_3$), a pyroxene mineral, on topotactic reaction at 800°C, and indeed clear XRD evidence for this is obtained for laponite heated to this temperature. Enstatite exists in four polymorphic forms, see Scheme 1.[12] The orthorhombic form has two crystallographically distinct silicon sites, the monoclinic form one site. The XRD trace for the sample of laponite fired to 1300°C does in fact contain extra reflections which are consistent with the presence of low *clino*-enstatite, which is quite consistent with Scheme 1.

The IR data provide further confirmation of the formation of enstatite polymorphs at 800 and 1300°C. Thus, for *ortho*-enstatite, diagnostic bands have been reported by Gadsden[13] and Saksena[14] at 1056–1070 cm^{-1}, 1010–1020 cm^{-1} and 928–942 cm^{-1}. We observe bands at 1079 cm^{-1} (s, br), 1012 cm^{-1} and 932 cm^{-1} for the sample fired to 800°C. In addition to those bands, the sample fired to 1300°C also contains bands at 1152 cm^{-1} (sh), 900 cm^{-1} (s), 737, 725 cm^{-1} and 684 cm^{-1} (w). These may be compared with diagnositic bands for *clino*-enstatite:[13,14] 1160 cm^{-1} (sh), 899 (s), 737, 724 cm^{-1} and 683 cm^{-1} (w).

The ^{29}Si MASNMR data may now be discussed. On heating laponite to 200°C the silicon resonances become more negative and line widths increase by 150 Hz. Similar effects have been observed for the onset of dehydroxylation for kaolinite and sepiolite and, in those cases, have been attributed to loss of hydrogen bonding between the basal oxygen atoms and surface hydroxyl groups of the next layer. It is possible to invoke a similar explanation, although in this case the loss of interlayer water would be the critical factor. We attempted to rehydrate the sample (see Experimental and Table 3) and indeed the Q^3 resonance does undergo a positive shift of 1 ppm; however, it does not recover the value for laponite nor does the Q^2 resonance show any sensitivity to the rehydration attempts. The specimen heated to 400°C gives a poor XRD trace indicating loss of crystallinity; this is reflected also in large line widths for the silicon spectra (> 1000 Hz); however, the spectra are well enough resolved to reveal that even at this temperature major structural breakdown is beginning, interestingly, however, this is reversible since rehydration generates a specimen with a ^{29}Si MASNMR spectrum indistinguishable from that of the rehydrated 200°C specimen. Hence the initial stages of the loss of structural water are accompanied by some breakdown of the Q^3 structure. The specimen heated to 600°C is in some respects the most peculiar in the set. The Q^2 resonance was not resolved but a relatively sharp ($\Gamma_{1/2}$ < 50 Hz) Q^3 resonance is seen at −97.7 ppm; rehydration gives a specimen with two Q^2 sites and a Q^3 resonance similar to that for talc. We suggest that the lithium ions have become labile and been removed from their "structural" octahedral sites to edge sites and that this is reflected in the shielding of the silicon Q^3 sites. By 800°C new crystalline phases are present and we assign the −81.4 and 83.5 ppm resonances to orthorhombic *ortho*-enstatite, the two signals arising from the two crys-

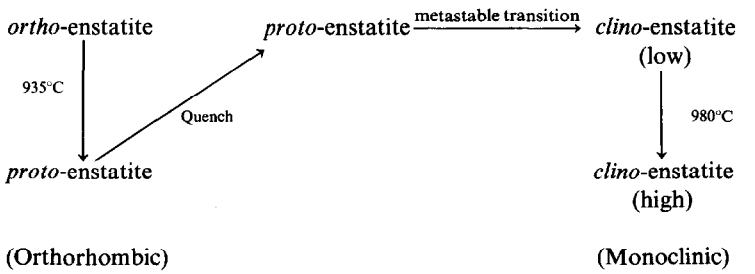

Scheme 1.

tallographically distinct silicon sites.[12] The intensity ratio for the two resonances, 2 : 3, is in good agreement with data reported by Lippmaa *et al.*[15] and Oldfield *et al.*[16] Not surprisingly, the spectrum proved insensitive to attempts to rehydrate; the region of irreversible structural breakdown having been reached. Heating laponite to 1300°C gave a specimen in which the presence of *ortho*-enstatite was detected (−80.9, −83.5 ppm), together with a new resonance at −85.1 ppm. We assign this new resonance to *clino*-enstatite, for which good IR and XRD evidence is available. Inspection of Scheme 1 suggests that it arose via *proto*-enstatite which was quenched and then underwent a metastable transition to low *clino*-enstatite.

Inspection of Fig. 2 shows that the three well-resolved enstatite resonances are superimposed on a very broad resonance which spans the Q^2, Q^3 and Q^4 regions, and is centred at approximately −96 ppm. We propose that this arises from a glassy phase based on a mixture of lithium and sodium silicates.

The conclusions from XRD, IR and ^{29}Si NMR data are summarized in Scheme 2.

^{23}Na *MASNMR data*

The ^{29}Si NMR data enabled the fate of the silicate network to be monitored as laponite underwent thermal decomposition. We report in this section some preliminary results on attempts to monitor the fate of the exchanged ions, in this instance, sodium. ^{23}Na is a quadrupolar nucleus ($I = 3/2$) with a substantial quadrupole moment. Although magic-angle spinning is expected to average first-order quadrupole effects to zero, this is not true for second-order effects. Inspection of Fig. 3 indicates that the majority of the spectra show clear signs of quadrupole broadening. Thus it must be recognized that the peak maxima in Table 4 (the apparent chemical shifts) are not the isotropic chemical shifts.

Laponite in the sodium form has sodium ions associated with a monolayer of water [$d(001) = 12.5$ Å], thus the ^{23}Na MASNMR spectrum of the clay may be taken as characteristic of the ions in that environment. The changes that occur on heating are such as to increase the second-order quadrupole line broadening thus implying, quite reasonably, that the environment of Na^+ in the dehydroxylated clay is of lower symmetry. It was the rehydrated samples that produced the more interesting results. Even for the 800°C specimen the peak maximum was sensitive to the water treatment but the resonance remained broad. The rehydrated 400 and 600°C specimens gave relatively sharp spectra ($\Gamma_{1/2} \simeq 1$ kHz) and the change in apparent chemical shift is sufficiently great to suggest a real change in shielding. It is, however, the sharpness of the spectra that is the most striking aspect—this, coupled with the more positive centre shift, suggests

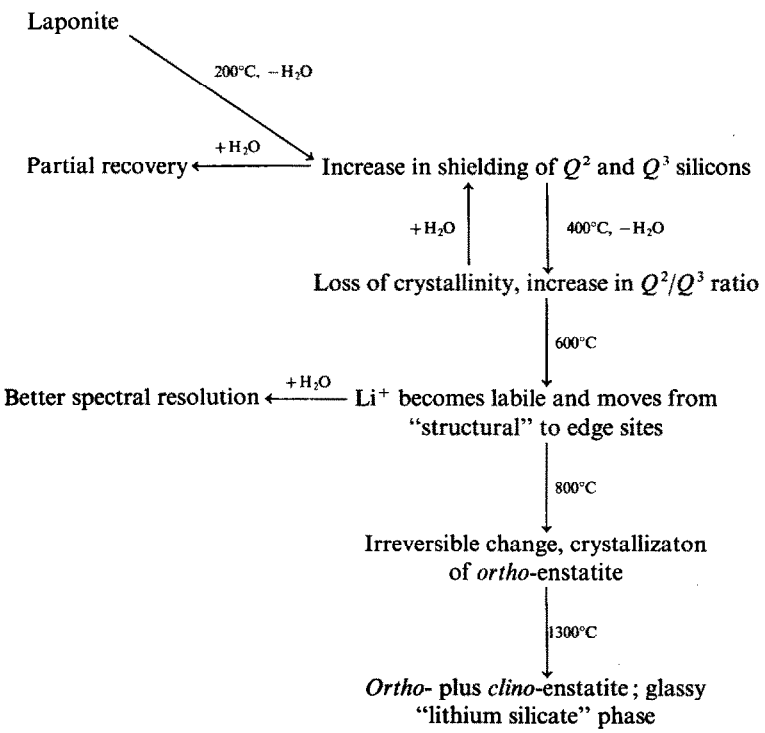

Scheme 2.

that the ions might even experience a more "solution"-like environment in which some motional narrowing of the line may be possible; similar phenomena have been observed for a sodium-exchanged Y-zeolite (Si/Al = 2.36).[17] The ^{29}Si studies suggested that, on rehydration, the samples heated to 200°C and 400°C became virtually indistinguishable; however the ^{23}Na MASNMR spectra of the two samples are clearly very different—thus the rehydration mechanism of the 400°C sample which leads to a decrease in the Q^2/Q^3 silicon ratio, leads to a very different solution-type environment for the sodium ions compared to that which these ions experience in the rehydrated 200°C specimen. In the latter specimen, quadrupole effects are greater than for any other spectrum in the series, implying that the sodium ions are constrained to an environment (or environments) of low symmetry with little motional freedom.

In one sense this preliminary ^{23}Na NMR study has raised more questions than it has answered. It has, however, highlighted the necessity to consider the fate of the exchanged ions as well as the structural ions if a complete picture of the thermal behaviour of clay minerals is to emerge. We address this question again in the following section.

Hectorite

Some ^{29}Si MASNMR spectra illustrating the changes which occur on heating a natural sample of hectorite (Table 1) are shown in Fig. 4. It is clear that very similar behaviour to that discussed in detail for laponite is observed, although there are some differences worthy of comment. The breakdown of the Q^3 lattice occurs at a higher temperature for hectorite, e.g. compare the 400°C spectrum for laponite in Fig. 2 with the 580°C spectrum for hectorite in Fig. 4. At 1300°C, the *clino*-enstatite phase is less prominent than is the case for laponite (however, that may be a function of the extraneous ions in hectorite, *vide infra*); also the glassy phase is less obvious, indeed there is evidence of the presence of two Q^4 crystalline phases. The resonance at −108.6 ppm may be assigned to cristobalite,[18,19] an expected product. The assignment of the −111.8 ppm resonance is less obvious, but tentatively β_2 tridymite is proposed.[19]

Partially ion-exchanged hectorites

It is clear from the above sections that a complete picture of the thermolysis of smectite clays will only emerge if the fate of exchanged as well as of structural ions can be monitored. A possible experimental approach is to exchange the clay either completely or partially with an ion which may be suitable for study by either NMR (e.g. ^{23}Na) or another resonance spectroscopy such as Mössbauer[20] or ESR. In this work we opted for ESR spectroscopy, but first addressed the question as to what paramagnetic loading of hectorite would be possible before resolution of the ^{29}Si MASNMR spectra was totally lost. The data in Tables 3 and 5 summarize the experiments and observations and, with the assistance of Dr P. A. Gillespie of the University of Durham, it was found that the data could be best quantified in terms of the gramme susceptibility of the specimen (see Results). Provided, therefore, that the constraints on the value of χ_g were observed, it was possible to obtain both ^{29}Si MASNMR data and copper(II) ESR data on the same sample. Thus the ^{29}Si NMR spectrum of the Cu^{2+}-exchanged hectorite heated to 1200°C, illustrated in Fig. 5, is the same specimen for which the ESR spectrum is given in Fig. 6.

XRD examination of the partially-exchanged hectorites heated to 1200°C does *not* reveal new phases which are directly attributable to the dipositive ions, thus it is likely that the ion isomorphically substitutes, probably for magnesium, in existing silicate phases. It would appear that the presence of these ions increases the proportion of *clino*-enstatite in the fired product as shown in Fig. 5 where, even for the Cu^{2+}- and Ni^{2+}-exchanged specimens, the resolution of the −84.8 ppm resonance is sufficiently good to illustrate this point.

The ESR spectrum of the partially exchanged Cu^{2+}–hectorite is typical of copper(II) in a rhombic environment;[21] g values are 2.005 (A = 154 Hz), 2.197 and 2.335. The observation of the lowest g value close to the free electron value is indicative of a d_{z^2} ground state for the copper(II) ion which, in the present case, could arise from a rhombic distortion superimposed on a compressed tetragonal environment. This observation is consistent with copper(II) being located in the enstatite structure.

CONCLUSIONS

The paper illustrates the value of solid-state NMR spectroscopy for following the thermolysis of mineral species. Not only can the fate of the silicate network be determined, but information on the behaviour of the interlayer ions may also be obtained as illustrated by a recent study of Na^+ and Li^+ montmorillonites;[22] of particular interest are the results of our rehydration experiments which indicate that the environment of the interlayer cation following rehydration may be very different to that prior to water loss.

Acknowledgements—P.M. thanks the SERC and ASM, Aston University, for studentships. We thank Dr P. A. Gillespie for help and discussion.

REFERENCES

1. T. Watanabe, H. Shimizu, K. Nagasawa, A. Masuda and H. Saito, *Clay Miner.* 1987, **22**, 37.
2. J. F. Lambert, W. S. Millman and J. J. Fripiat, *J. Am. Chem. Soc.* 1989, **111**, 3517.
3. G. W. Brindley and M. Nakahira, *Mineral. Mag.* 1958, **31**, 781.
4. G. W. Brindley and M. Nakahira, *J. Am. Ceram. Soc.* 1959, **42**, 311.
5. P. J. Michael and W. R. McWhinnie, *Polyhedron* 1989, **8**, 2709.
6. R. E. Grim, *Clay Mineralogy*. McGraw-Hill, New York (1953).
7. G. W. Brindley and G. Brown, in *Crystal Structure of Clay Minerals and Their X-Ray Identification*. Mineralogical Society, Monograph No. 5 (1951).
8. G. Englehardt, D. Zeigan, H. Janake, D. Hoebbel and W. Wicher, *Z. Anorg. Allg. Chem.* 1975, **418**, 17.
9. P. A. Gillespie, personal communication to P.J.M. and W.R.M.
10. R. A. Kinsey, R. J. Kirkpatrick, J. Hower, K. A. Smith and E. Oldfield, *Am. Miner.* 1985, **70**, 537.
11. C. A. Weiss, S. P. Altaner and R. J. Kirkpatrick, *Am. Miner.* 1987, **72**, 935.
12. W. A. Deer, R. A. Howie and J. Zussman, *Single Chain Silicates*, Vol. 2A, 2nd edn. Longman Group, London (1978).
13. J. A. Gadsden, *Infrared Spectra of Minerals and Related Inorganic Compounds*. Butterworths, London (1975).
14. B. D. Saksena, *Trans. Faraday Soc.* 1961, **57**, 242.
15. E. Lippmaa, M. Magi, A. Samoson, G. Englehardt and A. R. Grimmer, *J. Am. Chem. Soc.* 1980, **102**, 4889.
16. E. Oldfield and N. James, *J. Am. Chem. Soc.* 1985, **107**, 6769.
17. W. D. Basler, *Z. Naturfor.* 1980, **35A**, 645.
18. J. B. Murdoch, J. F. Stebbins and I. S. E. Carmichael, *Am. Miner.* 1985, **70**, 332.
19. J. V. Smith and C. S. Blackwell, *Nature* 1983, **303**, 223.
20. N. Davson and W. R. McWhinnie, *Inorg. Chim. Acta* 1989, **162**, 257.
21. B. J. Hathaway and D. E. Billing, *Coord. Chem. Rev.* 1970, **5**, 143.
22. V. Luca, C. M. Cardile and R. H. Meinhold, *Clay Miner.* 1989, **24**, 115.

Polyhedron Vol. 9, No. 4, pp. 527–534, 1990
Printed in Great Britain

0277-5387/90 $3.00+.00
© 1990 Pergamon Press plc

MONOMETALLIC, HOMO- AND HETEROBIMETALLIC COMPLEXES BASED ON REDOX ACTIVE TRIS(3,5-DIMETHYLPYRAZOLYL)BORATO–MOLYBDENUM AND –TUNGSTEN NITROSYLS—I. *META* SUBSTITUENT EFFECTS ON THE REDUCTION POTENTIALS OF MONOMETALLIC ARYLAMIDE COMPLEXES

SITHY S. SALAM, CARL J. LOVELY, ALISTAIR G. R. POOLE, CHRISTOPHER J. JONES* and JON A. McCLEVERTY

Department of Chemistry, University of Birmingham, PO Box 363, Birmingham B15 2TT, U.K.

(*Received* 22 *August* 1989 ; *accepted* 7 *September* 1989)

Abstract—The complexes [Mo(NO)LCl(NHC$_6$H$_4$-3-Z)] (L = HB(3,5-Me$_2$C$_3$N$_2$H)$_3$; Z = F, Cl, Br, Me, OMe, CF$_3$, NO$_2$), [W(NO)L(NHC$_6$H$_4$-3-Z)] (Z = F, Cl, Br, Me, OMe, COMe, CF$_3$, NO$_2$) and [W(NO)L(NHC$_6$H$_4$-3-CF$_3$)$_2$] have been synthesized and characterized by spectroscopic methods. All of the monoarylamide complexes undergo one-electron reduction processes at potentials which vary according to the nature of Z. A linear correlation was found between the reduction potentials within each of the two series and the Hammett *meta* substituent parameters, σ_m, for Z. The respective reaction constants, ρ_m, and intercepts, E_f^0, are for [Mo(NO)LCl(NHC$_6$H$_4$-3-Z)], ρ_m = 5.50 (0.39), E_f^0 = −0.848 (0.009) V and for [W(NO)L(NHC$_6$H$_4$-3-Z)], ρ_m = 4.75 (0.50), E_f^0 = −1.291 (0.011) V.

An extensive chemistry has been developed for complexes containing the {M(NO)L}$^{2+}$ (M = Mo or W, L = hydrotris(3,5-dimethylpyrazol-1-yl)borate) moiety[1] in which a formally 16-electron metal centre is present. A wide variety of monometallic derivatives of general formula [M(NO)LXY] (M = Mo and X = Cl, I or Y; M = W and X = Cl or Y; Y = aryloxide, thiophenoxide or arylamide) has been prepared. These species are all redox active undergoing a one-electron reduction process at potentials which are strongly dependent upon the nature of M, X and Y.[2] EPR measurements on the molybdenum complexes indicate that the electron is largely localized in a metal-centred orbital in the reduced species.[3,4] The {Mo(NO)L}$^{2+}$ redox centre has now been incorporated into a variety of larger molecules which are of considerable current interest because of their novel physical properties. Thus homobimetallic species, in which the two metal centres may be present in different oxidation states, have been prepared.[5–8] The extent of interaction between the two metal centres has been shown by electrochemical studies to be highly sensitive to the nature of the bridging ligand linking the metal centres. Redox responsive compounds containing the {Mo(NO)L} centre incorporated into a cyclic polyether have been synthesized and the reduction potentials of these species have been shown to respond to the binding of cationic substrates.[9,10] More recently, the {Mo(NO)L} moiety has been attached as a peripheral substituent in tetraphenylporphyrin derivatives. The presence of the redox centre causes fluorescence quenching of the porphyrin.[11] Finally, materials which exhibit substantial second-order non-linear optical properties have been obtained by linking {Mo(NO)LCl} to a ferrocenyl substituent via a polarizable diazadiaryl bridge.[12]

Electrochemical measurements are often useful in providing a more quantitative basis for understanding the properties of the new materials described above. In order to more fully interpret the results of such electrochemical studies, it is necessary to define the way in which the reduction potential of the metal-based redox centre changes with variations in ligand substituents. The sen-

* Author to whom correspondence should be addressed.

sitivity of transition metal redox centres to variations in ligand substituents is now well established in a number of examples,[13–16] including metallocene derivatives,[17,18] metal isonitrile derivatives[19–21] and substituted aryldiazenido complexes of molybdenum.[22] We have previously established that a linear correlation exists between the reduction potentials of [M(NO)LX(NHC$_6$H$_4$-4-Z)] [M = Mo and X = I or Cl; M = W and X = Cl) and the Hammett substituent parameters, σ_p, for the substituent Z.[23] We now report the results of a similar study of [M(NO)LCl(NHC$_6$H$_4$-3-Z)] involving *meta*-substituted arylamide ligands.

EXPERIMENTAL

All reagents were used as supplied. [Mo(NO){HB(3,5-Me$_2$C$_3$N$_2$H)$_3$}Cl$_2$] and [W(NO){HB(3,5-Me$_2$C$_3$N$_2$H)$_3$}Cl$_2$] were prepared according to previously described methods.[24] Solvents used as reaction media were dried according to standard methods and freed of oxygen before use. All reactions were carried out under nitrogen but purification procedures were carried out in air. Activated alumina UGI (100 mesh) or silica gel 60 (70–230 mesh) were used as the stationary phase for column chromatography. Elemental analyses were carried out by the Microanalytical Laboratory, University of Birmingham.

IR spectra were recorded using a PE 297 spectrometer with samples as KBr discs. 270 MHz ^{1}H NMR spectra were obtained from solutions in $CDCl_3$ using a Jeol GX 270 spectrometer. Mass spectra were recorded using a Kratos MS80 spectrometer and cyclic voltammetric measurements were made using a PAR 174A polarograph. Solutions in MeCN were *ca* 10^{-3} mol dm^{-3} in complex and 0.2 mol dm^{-3} in [Bu^{n}N]BF$_4$ as base electrolyte. A Pt bead test electrode was used with an SCE reference electrode. Potentials are quoted relative to the SCE and under these conditions E_f for the oxidation of ferrocene was found to be 0.42 V with ΔE_p in the range 60–120 mV. No compensation for internal cell resistance was made.

[Mo(NO){HB(3,5-Me$_2$C$_3$N$_2$H)$_3$}Cl(NHC$_6$H$_4$-3-F)]

A mixture of [Mo(NO){HB(3,5-Me$_2$C$_3$N$_2$H)$_3$}Cl$_2$] (0.5 g, 1.0 mmol) and 3-fluoroaniline (0.24 g, 2.2 mmol) in dichloromethane (50 cm^3) was stirred at room temperature for 6 days. After this time the mixture was filtered and the solvent removed from the filtrate under reduced pressure. The resulting dark brown solid was purified by column chromatography on alumina using 3:7 *n*-hexane–dichloromethane as the eluant and collecting the major dark brown fraction. Further purification of this material could be effected by recrystallization from dichloromethane–hexane mixtures to give the black crystalline product (0.23 g, 41%). Found: C, 41.6; H, 4.5; N, 18.2. $C_{21}H_{27}N_8BOFClMo \cdot 0.5\ CH_2Cl_2$ requires: C, 42.2; H, 4.6; N, 18.3%.

Spectroscopic data. ^{1}H NMR (δ_{TMS} ppm):* amide NH 12.44 (1 b); aryl protons 7.35 (1 m), 7.22 (2 m), 6.89 (1 m); CH_2Cl_2 5.25 (1 s); pyrazolyl-4-H 5.87 (2 s), 5.81 (1 s); pyrazolyl-3- and 5-Me 2.67 (3 s), 2.42 (3 s), 2.38 (3 s), 2.37 (6 s), 2.03 (3 s). IR: ν_{NO} = 1655, ν_{NH} = 3300 cm^{-1}. *Mass spectra*: m/z = 570, 540, 444. *Electrochemical data*:† E_f = −0.735 V, ΔE_p = 90 mV.

[Mo(NO){HB(3,5-Me$_2$C$_3$N$_2$H)$_3$}Cl(NHC$_6$H$_4$-3-Cl)]

This compound was prepared according to the procedure for [Mo(NO){HB(3,5-Me$_2$C$_3$N$_2$H)$_3$}Cl(NHC$_6$H$_4$-3-F)] using 3-chloroaniline (0.27 g, 2.1 mmol) in place of 3-fluoroaniline and a reaction time of 3 days. Chromatography on alumina was carried out using dichloromethane as the eluant. A brown product was obtained (0.21 g, 37%). Found: C, 43.0; H, 4.6; N, 19.0. $C_{21}H_{27}N_8BOCl_2Mo$ requires: C, 43.1; H, 4.6; N, 19.2%.

Spectroscopic data. ^{1}H NMR (δ_{TMS} ppm): amide NH 12.38 (1 b); aryl protons 7.46 (1 d, $^3J_{HH}$ = 9 Hz), 7.39 (1 s), 7.36 (1 dd, $^3J_{HH}$ = 8 and 9 Hz), 7.15 (1 d, $^3J_{HH}$ = 8 Hz); pyrazolyl-4-H 5.87 (2 s), 5.81 (1 s); pyrazolyl-3- and 5-Me 2.67 (3 s), 2.42 (3 s), 2.38 (3 s), 2.37 (6 s), 2.02 (3 s). IR: ν_{NO} = 1660, ν_{NH} = 3240 cm^{-1}. *Mass spectra*: m/z = 586, 556, 460. *Electrochemical data*: E_f = −0.720 V, ΔE_p = 140 mV.

[Mo(NO){HB(3,5-Me$_2$C$_3$N$_2$H)$_3$}Cl(NHC$_6$H$_4$-3-Br)]

This compound was prepared according to the procedure for [Mo(NO){HB(3,5-Me$_2$C$_3$N$_2$H)$_3$}Cl(NHC$_6$H$_4$-3-F)] using 3-bromoaniline (0.35 g, 2.0 mmol) in place of 3-fluoroaniline. Chromatography on alumina was carried out using dichloromethane as the eluant. A dark brown product was obtained (0.21 g, 37%). Found: C, 39.9; H, 4.6; N, 17.5.

* Relative area and multiplicity given in parentheses; s = singlet, d = doublet, t = triplet, m = multiplet with couplings not fully resolved, b = broad.

† Electrochemical data, E_f = formal electrode potential for reduction, ΔE_p = separation between cathodic and anodic peak potentials of cyclic voltammogram.

$C_{21}H_{27}N_8BOClBrMo$ requires: C, 40.1; H, 4.3; N, 17.8%.

Spectroscopic data. ^{1}H NMR (δ_{TMS} ppm): amide NH 12.36 (1 b); aryl protons 7.52 (2 m), 7.30 (2 m); pyrazolyl-4-H 5.87 (2 s), 5.81 (1 s); pyrazolyl-3- and 5-Me 2.67 (3 s), 2.42 (3 s), 2.38 (3 s), 2.36 (6 s), 2.02 (3 s). IR: ν_{NO} = 1655, ν_{NH} = 3245 cm^{-1}. *Mass spectra*: *m/z* = 630, 600, 504. *Electrochemical data*: E_f = −0.710 V, ΔE_p = 80 mV.

[Mo(NO){HB(3,5-$Me_2C_3N_2H)_3$}Cl(NHC_6H_4-3-Me)]

This compound was prepared according to the procedure for [Mo(NO){HB(3,5-$Me_2C_3N_2H)_3$}Cl(NHC_6H_4-3-F)] using 3-methylaniline (0.23 g, 2.1 mmol) in place of 3-fluoroaniline and a reaction time of 2 days. A dark brown product was obtained (0.52 g, 91%). Found: C, 47.1; H, 5.4; N, 20.6. $C_{22}H_{30}N_8BOClMo$ requires: C, 46.8; H, 5.3; N, 19.8%.

Spectroscopic data. ^{1}H NMR (δ_{TMS} ppm): amide NH 12.69 (1 b); aryl protons 7.33 (1 s), 7.26 (2 m), 7.00 (1 d, $^3J_{HH}$ = 7 Hz); pyrazolyl-4-H 5.87 (2 s), 5.79 (1 s); pyrazolyl-3- and 5-Me 2.69 (3 s), 2.42 (3 s), 2.38 (3 s), 2.37 (6 s), 2.01 (3 s), aryl Me 2.41 (3 s). IR: ν_{NO} = 1650, ν_{NH} = 3270 cm^{-1}. *Mass spectra*: *m/z* = 566, 536, 440. *Electrochemical data*: E_f = −0.875 V, ΔE_p = 60 mV.

[Mo(NO){HB(3,5-$Me_2C_3N_2H)_3$}Cl(NHC_6H_4-3-OMe)]

This compound was prepared according to the procedure for [Mo(NO){HB(3,5-$Me_2C_3N_2H)_3$}Cl(NHC_6H_4-3-F)] using 3-methoxyaniline (0.26 g, 2.1 mmol) in place of 3-fluoroaniline and a reaction time of 4 days. Chromatography on alumina was carried out using 2:8 *n*-hexane–dichloromethane as the eluant. A red–brown product was obtained (0.25 g, 43%). Found: C, 45.4; H, 5.4; N, 19.2. $C_{22}H_{30}N_8BO_2ClMo$ requires: C, 45.5; H, 5.2; N, 19.3%.

Spectroscopic data. ^{1}H NMR (δ_{TMS} ppm): amide NH 12.64 (1 b); aryl protons 7.33 (1 s), 7.25 (1 m), 6.77 (2 m); pyrazolyl-4-H 5.88 (1 s), 5.87 (1 s), 5.79 (1 s); aryl OMe 3.94 (3 s); pyrazolyl-3- and 5-Me protons 2.69 (3 s), 2.42 (3 s), 2.39 (3 s), 2.38 (3 s), 2.37 (3 s), 2.02 (3 s). IR: ν_{NO} = 1640, ν_{NH} = 3240 cm^{-1}. *Mass spectra*: *m/z* = 582, 552, 456. *Electrochemical data*: E_f = −0.825 V, ΔE_p = 70 mV.

[Mo(NO){HB(3,5-$Me_2C_3N_2H)_3$}Cl(NHC_6H_4-3-CF_3)]

This compound was prepared according to the procedure for [Mo(NO){HB(3,5-$Me_2C_3N_2H)_3$}Cl(NHC_6H_4-3-F)] using 3-(trifluoromethyl)aniline (0.34 g, 2.1 mmol) in place of 3-fluoroaniline and a reaction time of 4 days. Chromatography on alumina was carried out using 2:8 *n*-hexane–dichloromethane as the eluant. A brown product was obtained (0.16 g, 27%). Found: C, 42.6; H, 4.6; N, 18.2. $C_{22}H_{27}N_8BOF_3ClMo$ requires: C, 42.7; H, 4.4; N, 18.1%.

Spectroscopic data. ^{1}H NMR (δ_{TMS} ppm): amide NH 12.43 (1 b); aryl protons 7.85 (1 d $^3J_{HH}$ = 8 Hz), 7.57 (1 t $^3J_{HH}$ = 8 Hz), 7.50 (1 s), 7.43 (1 d $^3J_{HH}$ = 8 Hz); pyrazolyl-4-H 5.88 (2 s), 5.82 (1 s); pyrazolyl-3- and 5-Me 2.67 (3 s), 2.42 (3 s), 2.38 (3 s), 2.37 (6 s), 1.98 (3 s). IR: ν_{NO} = 1650, ν_{NH} = 3245, ν_{CF} = 1120 cm^{-1}. *Mass spectra*: *m/z* = 620, 590, 494. *Electrochemical data*: E_f = −0.710 V, ΔE_p = 140 mV.

[Mo(NO){HB(3,5-$Me_2C_3N_2H)_3$}Cl(NHC_6H_4-3-NO_2)]

This compound was prepared according to the procedure for [Mo(NO){HB(3,5-$Me_2C_3N_2H)_3$}Cl(NHC_6H_4-3-F)] using 3-nitroaniline (0.27 g, 2.1 mmol) in place of 3-fluoroaniline and a reaction time of 8 days under reflux. Chromatography on silica gel was carried out using 3:7 *n*-hexane–dichloromethane as the eluant. A green product was obtained (0.29 g, 48%). Found: C, 42.5; H, 4.5; N, 20.7. $C_{21}H_{27}N_9BO_3ClMo$ requires: C, 42.3; H, 4.6; N, 21.2%.

Spectroscopic data. ^{1}H NMR (δ_{TMS} ppm): amide NH 12.26 (1 b); aryl protons 8.05 (3 m), 7.63 (1 t $^3J_{HH}$ = 8 Hz); pyrazolyl-4-H 5.89 (2 s), 5.81 (1 s); pyrazolyl-3- and 5-Me protons 2.69 (3 s), 2.43 (3 s), 2.40 (3 s), 2.38 (3 s), 2.37 (6 s), 1.99 (3 s). IR: ν_{NO} = 1665, ν_{NH} = 3280, ν_{NO_2} = 1.540 cm^{-1}. *Mass spectra*: *m/z* = 597, 567, 471. *Electrochemical data*: E_f = −0.620 V, ΔE_p = 80 mV.

[W(NO){HB(3,5-$Me_2C_3N_2H)_3$}Cl(NHC_6H_4-3-F)]

A mixture of [W(NO){HB(3,5-$Me_2C_3N_2H)_3$}Cl_2] (0.29 g, 0.5 mmol) and 3-fluoroaniline (0.15 cm^3, 1.6 mmol) was stirred under reflux in toluene (50 cm^3) for 24 h. The reaction mixture was cooled and filtered and the filtrate evaporated to dryness under reduced pressure. The resulting brown solid was redissolved in the minimum of dichloromethane and the product slowly precipitated by dropwise addition of *n*-hexane to the solution. The brown crystalline solid produced was collected by filtration, washed with a little *n*-pentane and dried *in vacuo* (0.13 g, 40%). Found: C, 36.3; H, 4.1; N, 15.8. $C_{21}H_{27}N_9BOFClW \cdot 0.5\ CH_2Cl_2$ requires: C, 36.9; H, 4.0; N, 16.0%.

Spectroscopic data. ^{1}H NMR (δ_{TMS} ppm): amide NH 10.59 (1 b); aryl protons 7.33 (1 m), 7.14 (2 m), 6.77 (1 m, $^3J_{HH}$ = 8 Hz); pyrazolyl-4-H 5.94 (1 s), 5.88 (1 s), 5.84 (1 s); CH_2Cl_2 5.25 (1 s); pyrazolyl-3- and 5-Me 2.71 (3 s), 2.44 (3 s), 2.42 (3 s), 2.37 (3 s), 2.36 (3 s), 2.15 (3 s). IR: ν_{NO} = 1625, ν_{NH} = 3310 cm^{-1}. *Mass spectra*: *m/z* = 656, 572, 542. *Electrochemical data*: E_f = −1.185 V, ΔE_p = 75 mV.

[W(NO){HB(3,5-$Me_2C_3N_2H)_3$}Cl(NHC$_6H_4$-3-Cl)]

A mixture of [W(NO){HB(3,5-$Me_2C_3N_2H)_3$}Cl_2] (0.58 g, 1.0 mmol) and 3-chloroaniline (0.30 cm^3, 2.8 mmol) was stirred under reflux in toluene (75 cm^3) for 24 h. The reaction mixture was cooled and filtered and the filtrate evaporated to dryness under reduced pressure. The resulting brown solid was purified by column chromatography on silica gel using 1 : 1 dichloromethane–hexane as the eluant and collecting the major brown fraction. The material obtained was then recrystallized from dichloromethane–*n*-hexane mixtures to give the brown crystalline product, which was washed with a little *n*-pentane and dried *in vacuo* (0.30 g, 45%). Found: C, 37.7; H, 4.0; N, 16.6. $C_{21}H_{27}N_8BOCl_2W$ requires: C, 37.5; H, 4.0; N, 16.7%.

Spectroscopic data. ^{1}H NMR (δ_{TMS} ppm): amide NH 10.54 (1 b); aryl protons 7.41 (1 d, $^3J_{HH}$ = 8 Hz), 7.33 (1 t, $^3J_{HH}$ = 8 Hz), 7.27 (1 m), 7.05 (1 d, $^3J_{HH}$ = 8 Hz); pyrazolyl-4-H 5.94 (1 s), 5.88 (1 s), 5.84 (1 s); pyrazolyl-3- and 5-Me 2.71 (3 s), 2.43 (3 s), 2.42 (3 s), 2.37 (3 s), 2.36 (3 s), 2.15 (3 s). IR: ν_{NO} = 1630, ν_{NH} = 3255 cm^{-1}. *Mass spectra*: *m/z* = 674. *Electrochemical data*: E_f = −1.200 V, ΔE_p = 80 mV.

[W(NO){HB(3,5-$Me_2C_3N_2H)_3$}Cl(NHC$_6H_4$-3-Br)]

This compound was prepared according to the procedure for [W(NO){HB(3,5-$Me_2C_3N_2H)_3$}Cl(NHC$_6H_4$-3-Cl)] using 3-bromoaniline (0.3 cm^3, 2.7 mmol), in place of 3-chloroaniline, in toluene (50 cm^3). A red–brown product was obtained (0.40 g, 56%). Found: C, 35.3; H, 3.8; N, 15.3. $C_{21}H_{27}N_8BOClBrMo$ requires: C, 35.1; H, 3.8; N, 15.6%.

Spectroscopic data. ^{1}H NMR (δ_{TMS} ppm): amide NH 10.52 (1 b); aryl protons 7.49 (1 d, $^3J_{HH}$ = 8 Hz), 7.39 (1 m), 7.28 (1 t, $^3J_{HH}$ = 8 Hz), 7.19 (1 d, $^3J_{HH}$ = 8 Hz); pyrazolyl-4-H 5.94 (1 s), 5.88 (1 s), 5.84 (1 s); pyrazolyl-3- and 5-Me 2.71 (3 s), 2.43 (3 s), 2.42 (3 s), 2.37 (3 s), 2.35 (3 s), 2.15 (3 s). IR: ν_{NO} = 1625, ν_{NH} = 3295 cm^{-1}. *Mass spectra*: *m/z* = 718, 622, 592. *Electrochemical data*: E_f = −1.175 V, ΔE_p = 80 mV.

[W(NO){HB(3,5-$Me_2C_3N_2H)_3$}Cl(NHC$_6H_4$-3-Me)]

This compound was prepared according to the procedure for [W(NO){HB(3,5-$Me_2C_3N_2H)_3$}Cl(NHC$_6H_4$-3-Cl)] using [W(NO){HB(3,5-$Me_2C_3N_2H)_3$}Cl_2] (0.87 g, 1.5 mmol) and with 3-methylaniline (0.3 cm^3, 2.7 mmol) in place of 3-chloroaniline and a reaction time of 18 h. A red–brown product was obtained (0.35 g, 36%). Found: C, 40.3; H, 4.5; N, 17.2. $C_{22}H_{30}N_8BOClW$ requires: C, 40.5; H, 4.6; N, 17.2%.

Spectroscopic data. ^{1}H NMR (δ_{TMS} ppm): amide NH 10.79 (1 b); aryl protons 7.27 (1 t, $^3J_{HH}$ = 8 Hz), 7.24 (1 s), 7.18 (1 d, $^3J_{HH}$ = 8 Hz), 6.89 (1 d, $^3J_{HH}$ = 8 Hz); pyrazolyl-4-H 5.93 (1 s), 5.88 (1 s), 5.84 (1 s); aryl-3-Me with pyrazolyl-3- and 5-Me 2.73 (3 s), 2.45 (3 s), 2.42 (3 s), 2.38 (3 s), 2.36 (3 s), 2.35 (3 s), 2.14 (3 s). IR: ν_{NO} = 1645, ν_{NH} = 3295 cm^{-1}. *Mass spectra*: *m/z* = 652, 556, 526. *Electrochemical data*: E_f = −1.325 V, ΔE_p = 70 mV.

[W(NO){HB(3,5 - $Me_2C_3N_2H)_3$}Cl(NHC$_6H_4$ - 3 - OMe)]

This compound was prepared according to the procedure for [W(NO){HB(3,5-$Me_2C_3N_2H)_3$}Cl(NHC$_6H_4$-3-F)] using [W(NO){HB(3,5-$Me_2C_3N_2H)_3$}Cl_2] (0.58 g, 1.0 mmol) in toluene (75 cm^3) and with 3-methoxyaniline (0.3 cm^3, 2.7 mmol) in place of 3-fluoroaniline and a reaction time of 18 h. A red–brown product was obtained (0.33 g, 49%). Found: C, 39.6; H, 4.2; N, 16.9. $C_{22}H_{30}N_8BO_2ClW$ requires: C, 39.5; H, 4.5; N, 16.8%.

Spectroscopic data. ^{1}H NMR (recorded in CD_2Cl_2, δ_{TMS} ppm): amide NH 10.76 (1 b); aryl protons 7.28 (1 t, $^3J_{HH}$ = 8 Hz), 7.23 (1 m), 7.72 (1 m), 7.64 (1 m); pyrazolyl-4-H 5.94 (1 s), 5.88 (1 s), 5.82 (1 s); aryl-3-OMe 3.94 (3 s); pyrazolyl-3- and 5-Me 2.72 (3 s), 2.45 (3 s), 2.42 (3 s), 2.37 (3 s), 2.36 (3 s), 2.15 (3 s). IR: ν_{NO} = 1625, ν_{NH} = 3255 cm^{-1}. *Mass spectra*: *m/z* = 668, 572, 542. *Electrochemical data*: E_f = −1.280 V, ΔE_p = 70 mV.

[W(NO){HB(3,5 - $Me_2C_3N_2H)_3$}Cl(NHC$_6H_4$ - 3 - CF_3)]

A mixture of [W(NO){HB(3,5-$Me_2C_3N_2H)_3$}Cl_2] (0.5 g, 0.86 mmol) and 3-(trifluoromethyl) aniline (0.28 g, 1.7 mmol) was stirred under reflux in toluene (50 cm^3) for 2 days. Sodium hydride (*ca* 100 mg) was then added and the reaction mixture heated under reflux for a further 8 days. The reaction mixture was cooled and filtered and the filtrate evaporated to dryness under reduced pressure. The resulting brown solid was purified by column chromatography on successive columns

of silica gel then alumina using 3:7 *n*-hexane–dichloromethane as the eluant and collecting the major brown fraction in each case. The material obtained was then recrystallized from dichloromethane–*n*-hexane mixtures to give the brown crystalline product (0.04 g, 6%). Found: C, 37.9; H, 3.7; N, 15.4. $C_{22}H_{27}N_8BOF_3ClW$ requires: C, 37.4; H, 3.9; N, 15.9%.

Spectroscopic data. IR: ν_{NO} = 1630, ν_{NH} = 3265, ν_{CF} = 1120 cm^{-1}. *Mass spectra*: m/z = 704, 611. *Electrochemical data*: E_f = −1.135 V, ΔE_p = 150 mV.

[W(NO){HB(3,5-$Me_2C_3N_2H)_3$}Cl(NHC_6H_4-3-COMe)]

This compound was prepared according to the procedure for [W(NO){HB(3,5-$Me_2C_3N_2H)_3$}Cl(NHC_6H_4-3-Cl)] using 3-acetylaniline (0.4 g, 3.0 mmol) in place of 3-chloroaniline in toluene (50 cm^3). Chromatography on silica gel was performed using 3:7 *n*-hexane–dichloromethane as eluant. A brown product was obtained (0.27 g, 40%). Found: C, 40.9; H, 4.5; N, 16.2. $C_{23}H_{30}N_8BO_2ClW$ requires: C, 40.6; H, 4.4; N, 16.5%.

Spectroscopic data. ^{1}H NMR (δ_{TMS} ppm): amide NH 10.72 (1 b); aryl protons 7.98 (1 s), 7.70 (1 d, $^3J_{HH}$ = 8 Hz), 7.62 (1 d, $^3J_{HH}$ = 8 Hz), 7.49 (1 t, $^3J_{HH}$ = 8 Hz); pyrazolyl-4-H 5.95 (1 s), 5.89 (1 s), 5.83 (1 s); aryl-3-COMe with pyrazolyl-3- and 5-Me 2.72 (3 s), 2.71 (3 s), 2.45 (3 s), 2.43 (3 s), 2.37 (3 s), 2.36 (3 s), 2.10 (3 s). IR: ν_{NO} = 1620, ν_{NH} = 3275 cm^{-1}. *Mass spectra*: m/z = 680, 584, 554. *Electrochemical data*: E_f = −1.200 V, ΔE_p = 70 mV.

[W(NO){HB(3,5-$Me_2C_3N_2H)_3$}Cl(NHC_6H_4-3-NO_2)]

This compound was prepared according to the procedure for [W(NO){HB(3,5-$Me_2C_3N_2H)_3$}Cl(NHC_6H_4-3-Cl)] using 3-nitroaniline (0.35 g, 2.5 mmol) in place of 3-chloroaniline in toluene (50 cm^3). Unreacted 3-nitroaniline was removed from the crude reaction product by sublimation *in vacuo* prior to purification. A red–brown product was obtained (0.16 g, 25%). Found: C, 37.8; H, 3.8; N, 17.7. $C_{21}H_{27}N_9BO_3Mo$ requires: C, 37.6; H, 4.2; N, 18.2%.

Spectroscopic data. ^{1}H NMR (δ_{TMS} ppm): amide NH 10.49 (1 b); aryl protons 8.04 (1 d, $^3J_{HH}$ = 8 Hz), 7.93 (1 d, $^3J_{HH}$ = 8 Hz), 7.91 (1 s), 7.60 (1 t, $^3J_{HH}$ = 8 Hz); pyrazolyl-4-H 5.96 (1 s), 5.90 (1 s), 5.86 (1 s), pyrazolyl-3- and 5-Me 2.71 (3 s), 2.43 (6 s), 2.38 (3 s), 2.37 (3 s), 2.12 (3 s). IR: ν_{NO} = 1645, ν_{NH} = 3290, ν_{NO_2} = 1.540 cm^{-1}. *Mass spectra*: m/z = 683, 587, 557. *Electrochemical data*: E_f = −1.130, −1.440 V.

[W(NO){HB(3,5-$Me_2C_3N_2H)_3$}(NHC_6H_4-3-$CF_3)_2$]

A mixture of [W(NO){HB(3,5-$Me_2C_3N_2H)_3$}Cl_2] (0.5 g, 0.86 mmol), 3-(trifluoromethyl)aniline (0.28 g, 1.7 mmol) and sodium hydride (*ca* 100 mg) was stirred under reflux in toluene (50 cm^3) for 2.5 days. The reaction mixture was cooled and filtered and the filtrate evaporated to dryness under reduced pressure. The resulting brown solid was purified by column chromatography on alumina using 3:7 *n*-hexane–dichloromethane as the eluant and collecting the major scarlet fraction. The material obtained was then recrystallized from dichloromethane–*n*-hexane mixtures to give the scarlet crystalline product (0.16 g, 25%). Found: C, 42.2; H, 3.7; N, 15.1. $C_{29}H_{32}N_9BOF_6W$ requires: C, 41.9; H, 3.9; N, 15.2%.

Spectroscopic data. ^{1}H NMR (δ_{TMS} ppm): amide NH 8.37 (2 b); aryl protons 7.68 (2 d, $^3J_{HH}$ = 8 Hz), 7.39 (2 t, $^3J_{HH}$ = 8 Hz), 7.31 (2 s), 7.04 (1 d, $^3J_{HH}$ = 8 Hz); pyrazolyl-4-H 6.04 (1 s), 5.80 (2 s); pyrazolyl-3- and 5-Me 2.48 (3 s), 2.40 (3 s), 2.35 (6 s), 2.30 (6 s). IR: ν_{NO} = 1615, ν_{NH} = 3260, ν_{CF} = 1120 cm^{-1}. *Mass spectra*: m/z = 799, 734, 702.

DISCUSSION

Synthetic studies

The new complexes were synthesized according to previously established procedures.[1] Generally 2 molar equivalents of arylamine, $ArNH_2$, were reacted with 1 molar equivalent of [M(NO)LCl_2], acording to eq. (1):

$$[M(NO)LCl_2] + 2ArNH_2 \Rightarrow [M(NO)LCl(NHAr)] + ArNH_3Cl. \quad (1)$$

The second equivalent of amine being present to consume the HCl liberated during the reaction. Under these reaction conditions there was no evidence for the formation of bis-amide complexes. However, the reaction between [W(NO)LCl_2] and $H_2NC_6H_4$-3-CF_3 proved to be very slow and NaH was added to stimulate the reaction. Only a very low yield of the monoamide complex [W(NO)LCl(NHC_6H_4-3-CF_3)] could be obtained, therefore this material was characterized by IR and elemental analysis measurements only. The primary product of the reaction in the presence of sodium hydride proved to be the bis-amide complex [W(NO)LCl(NHC_6H_4-3-$CF_3)_2$]. This finding is unusual since in a previous study we were unable to prepare

bis-arylamide derivatives of the $\{W(NO)L\}^{2+}$ moiety.[25] However, such species could be obtained from reactions involving 2-aminopyridine[26] and it seems that the outcome of reactions between $[W(NO)LCl_2]$ and aryl amines is surprisingly sensitive to the nature of the aryl group.

The new complexes all exhibited ν_{BH} at *ca* 2550 cm^{-1} in their IR spectra, in addition to other bands attributable to the presence of the ligand L. The values observed for ν_{NO} were in accord with expectations, in that molybdenum monoarylamide derivatives typically have ν_{NO} in the range 1645–1665 cm^{-1}, while their tungsten analogues exhibit somewhat lower NO stretching frequencies. The IR spectra also contained ν_{NH} in the range 3260–3320 cm^{-1} due to the amide moiety, in addition to other bands attributable to the presence of the substituted aryl group.

The ^1H NMR spectra of the monosubstituted complexes $[M(NO)LCl(NHC_6H_4\text{-}3\text{-}Z)]$ exhibit signals consistent with the presence of the 1,3-disubstituted aryl group in the region 6.5–7.5 ppm. In addition, the molybdenum amide complexes exhibit a broad signal at *ca* 12.5 ppm due to the amide proton. In the case of the tungsten derivatives this resonance is shifted to *ca* 10.5 ppm. In the bis-amide complex, $[W(NO)LCl(NHC_6H_4\text{-}3\text{-}CF_3)_2]$, the amide protons were observed at 8.37 ppm. The pyrazolyl 4-H protons are observed in the range 5.5–6.0 ppm and, in the molybdenum complexes, often appear as two signals of relative area 2:1 despite the absence of a plane of symmetry in the molecule. However, the observation of at least five pyrazolyl–methyl resonances in the region 1.9–2.8 ppm establishes unequivocally that the monoamide derivatives have been obtained. In the case of $[W(NO)LCl(NHC_6H_4\text{-}3\text{-}CF_3)_2]$ the pyraxolyl-4-H and methyl signals appear as singlets of relative area 1:2:3:3:6:6 in accord with the presence of a plane of symmetry as required for a bis-amide derivative.

The mass spectra of all of the new complexes contained polyisotopic ion envelopes at the expected m/z values for the molecular ion. In addition, the mass spectra of the molybdenum complexes exhibited ions in the m/z range expected for $[M-(NO)]^+$ and for $[M-\{(NO)+(Me_2C_3N_2H)\}]^+$. In contrast, the tungsten complexes exhibited ions attributable to $[M-(Me_2C_3N_2H)]^+$ due to the loss of dimethylpyrazole rather than nitric oxide, in addition to $[M-\{(NO)+(Me_2C_3N_2H)\}]^+$.

Electrochemical studies

It is now well established that complexes of the type $[M(NO)LCl(NHC_6H_4Z)]$ undergo a one-electron reduction process at potentials which are sensitive to the nature of the aryl substituent Z.[6,7] The reduction potentials of the *meta*-substituted arylamide complexes in acetonitrile solution were determined by cyclic voltammetry. In accord with expectations[6,7] the molybdenum complexes have formal reduction potentials, E_f, in the region of -0.8 V, while the tungsten complexes have E_f values which are *ca* 450 mV more cathodic. Plots of $i_p v^{-1/2}$ (i_p = peak current and v = scan rate) against v for the reduction wave are linear over the scan rate range 100–500 mV, indicating that the electron transfer process is reversible. Deviations of the shape parameter ΔE_p (the separation between the cathodic and anodic peak potentials) from the ideal value of 59 mV are thus primarily ascribed to uncompensated cell resistance. With the exception of $[W(NO)LCl(NHC_6H_4\text{-}3\text{-}NO_2)]$, the reduction processes are judged to be chemically reversible since the ratio of anodic to cathodic peak currents is close to one. In the case of $[W(NO)LCl(NHC_6H_4\text{-}3\text{-}NO_2)]$ the first wave with a cathodic peak potential $E_{pc} = -1.13$ V gives an anodic peak current substantially less than for the cathodic process. In addition a second irreversible wave is observed at -1.44 V. On the basis of previous results[7] we assign the first wave to the reduction of the tungsten centre. The second wave may be associated with the reduction of the nitro group thus giving rise to the irreversible behaviour. In the data analysis described below the value $E_{pc} - 30$ mV $= -1.1$ V is used as an approximation for the E_f of $[W(NO)LCl(NHC_6H_4\text{-}3\text{-}NO_2)]$. Removal of this point from the data set produces no significant change in the outcome of the calculations, hence it has been retained in the data analysis.

A linear regression analysis of the formal reduction potentials, $E_f^z(Mo)$, for the molybdenum complexes against the appropriate values of the Hammett *meta*-substituent parameter, σ_m, for Z was carried out. The data used, and the best fit line obtained, are presented in Fig. 1. The regression gave a correlation coefficient $r = 0.9858$ indicative of a good correlation between E_f^z and σ_m. At the intercept with $\sigma_m = 0$ the value of E_f is given by $E_f^0(Mo) = -0.848(0.009)$, standard errors being given in parentheses. The slope, $S(Mo)$, of the line is 326(23) mV giving a reaction constant, $\rho_m(Mo)$, 5.50(0.39) according to eq. (2):

$$E_f^z - E_f^0 = \rho_m \sigma_m (2.303RT/F), \qquad (2)$$

where R, T and F have their usual meaning. The value of $E_f^0(Mo)$ agrees, within experimental error, with that of $-0.833(0.011)$ obtained[7] for $[Mo(NO)LCl(NHC_6H_4\text{-}4\text{-}Z)]$. However, the reaction constant is somewhat reduced compared to that

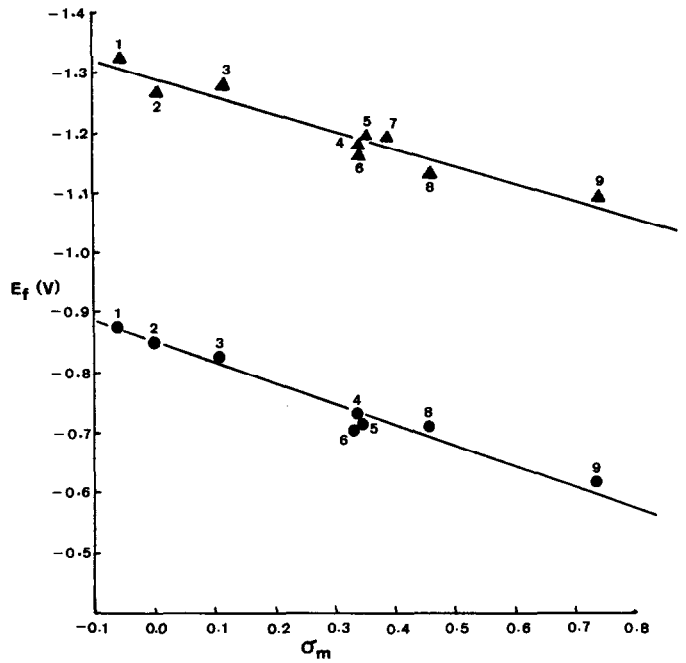

Fig. 1. Plots of E_f against σ_m for [Mo(NO)L(NHC$_6$H$_4$-3-Z)] (●) and [W(NO)L(NHC$_6$H$_4$-3-Z)] (▲) for Z = Me (**1**), H (**2**), OMe (**3**), F (**4**), Cl (**5**), Br (**6**), COMe (**7**), CF_3 (**8**) and NO_2 (**9**). The lines shown are for $E_f = -0.848 + 0.326\ \sigma_m$ (●) and $E_f = -1.291 + 0.281\ \sigma_m$ (▲).

of ρ_p(Mo) = 6.68(0.47) obtained for the *para*-substituted arylamide complexes; although the errors on these figures preclude definitive comment. A dual parameter analysis was also carried out using the inductive and resonance substituent parameters σ_I and σ_R.[27] This analysis gave a χ^2 statistic of -4.64×10^{-4} for six degrees of freedom, compared with -2.03×10^{-3} for the linear regression. Thus the dual parameter model gave a better fit to the data than the linear model but the errors of *ca* ± 10 mV in the measurement of E_f suggest that this finding may have no physical significance. The value of E_f^0(Mo) obtained from the dual parameter model was $-0.851(0.006)$, in good agreement with that obtained from the linear model. The reaction constants, ρ_I and ρ_R, for the respective inductive and resonance parameters according to eq. (3) were ρ_I(Mo) = 5.62(0.21) and ρ_R(Mo) = 2.01(0.21). The value of ρ_R being 36% that of ρ_I, close to the normal value of 40%

$$E_f^z - E_f^0 = (\rho_I \sigma_I + \rho_R \sigma_R)(2.303RT/F) \qquad (3)$$

for *meta*-substituent effects.[27] Unlike the case for [Mo(NO)LCl(NHC$_6$H$_4$-4-Z)], where σ_I and σ_{R-} gave a better fit to the E_f data than σ_I and σ_R, use of the σ_{R-} parameter in place of σ_R gave a substantially poorer model for the E_f data.

A similar analysis of the E_f data obtained from the tungsten complexes was carried out and the best fit line and data are shown in Fig. 1. In this case the linear regression gave a slightly reduced correlation coefficient of 0.9636. The value of E_f^0(W) is $-1.291(0.011)$ V which agrees, within experimental error, with the value of $-1.301(0.011)$ obtained from [W(NO)LCl(NHC$_6$H$_4$-4-Z)].[7] The slope of the best fit line is S(W) = 281(30) mV, giving a reaction constant of ρ_m(W) = 4.75(0.50) according to eq. (2). As with the molybdenum complexes this is smaller than that of ρ_p(W) = 6.44(0.57) obtained for [W(NO)LCl(NHC$_6$H$_4$-4-Z)].[7] The dual parameter analysis provided a better model for the E_f data with a χ^2 statistic of -1.84×10^{-3} for seven degrees of freedom, compared to -2.46×10^{-3} for the linear regression. However, taking into account the errors, this finding may have no physical significance. The value of E_f^0(W) from the dual parameter model is $-1.287(0.012)$ V, in good agreement with that obtained from the linear model. The values of ρ_I(W) and ρ_R(W) are, respectively, 4.72(0.50) and 2.06(0.43). The value of ρ_R is 44% that of ρ_I and, as with the molybdenum complexes, this is close to the normal value of 40%.[27] Also in accord with the findings for molybdenum, a dual parameter model using σ_{R-} in place of σ_R gave a substantially poorer description of the E_f(W) data. The differences between the values of E_f^0(W) and E_f^0(Mo) obtained, respectively, from the linear and dual parameter models are 443 and 436 mV, in good agreement

with the previously determined value of 429 mV for [M(NO)LCl(NHC$_6$H$_4$-4-Z)].[7]

In conclusion, the results presented here show that the reduction potentials of the *meta*-substituted arylamide complexes [M(NO)LCl(NHC$_6$H$_4$-3-Z)] (M = Mo or W) may be satisfactorily correlated with the Hammett *meta*-substituent constant, σ_m, using a simple linear model. The reaction constants for the molybdenum and tungsten series are consistently smaller than for the *para*-substituted systems [M(NO)LCl(NHC$_6$H$_4$-4-Z)], but the errors on these values preclude any quantitative conclusions. The dual parameter model shows that the substituent effects on E_f conform to the normal pattern. Thus, in the *para*-substituted systems, the value of the reaction constant ρ_R is approximately equal to that of ρ_I.[7] However, in the *meta*-substituted systems the value of ρ_R is only *ca* 40% that of ρ_I. The data presented here, and in previous papers,[6,7] provide a basis for using E_f data to evaluate the effects on the $\{M(NO)LCl\}^+$ moiety of other groups linked through arylamide bridging ligands. Substituent effects on E_f are also apparent in substituted phenoxide complexes of the type [M(NO)LCl(OC$_6$H$_4$Z)], although the reaction constants appear to be smaller than for the arylamide derivatives.[28]

Acknowledgements—We are grateful to Mr T. Green for technical assistance and to the British Council for a Commonwealth Scholarship (to S.S.S.).

REFERENCES

1. J. A. McCleverty, *Chem. Soc. Rev.* 1983, **12**, 331.
2. N. AlObaidi, D. Clague, M. Chaudhury, C. J. Jones, J. A. McCleverty, J. C. Pearson and S. S. Salam, *J. Chem. Soc., Dalton Trans.* 1987, 1733.
3. T. N. Briggs, C. J. Jones, J. A. McCleverty, B. D. Neaves, N. ElMurr and H. Colquhoun, *J. Chem. Soc., Dalton Trans.* 1985, 1249.
4. N. AlObaidi, A. J. Edwards, C. J. Jones, J. A. McCleverty, B. D. Neaves, F. E. Mabbs and D. Collison, *J. Chem. Soc., Dalton Trans.* 1989, 127.
5. S. M. Charsley, C. J. Jones, J. A. McCleverty, B. D. Neaves, S. J. Reynolds and G. Denti, *J. Chem. Soc., Dalton Trans.* 1988, 293.
6. S. M. Charsley, C. J. Jones, J. A. McCleverty, B. D. Neaves and S. J. Reynolds, *J. Chem. Soc., Dalton Trans.* 1988, 301.
7. S. M. Charsley, C. J. Jones, J. A. McCleverty, B. D. Neaves and S. J. Reynolds, *Transition Met. Chem.* 1986, **11**, 329.
8. N. AlObaidi, T. A. Hamor, C. J. Jones, J. A. McCleverty and K. Paxton, *J. Chem. Soc., Dalton Trans.* 1987, 2653.
9. N. AlObaidi, P. D. Beer, J. P. Bright, C. J. Jones, J. A. McCleverty and S. S. Salam, *J. Chem. Soc., Chem. Commun.* 1986, 239.
10. P. D. Beer, C. J. Jones, J. A. McCleverty and S. S. Salam, *J. Incl. Phenom.* 1987, **5**, 521.
11. S. Kurek, N. M. Rowley, P. D. Beer, C. J. Jones and J. A. McCleverty, manuscript in preparation.
12. B. J. Coe, C. J. Jones, J. A. McCleverty, D. Bloor, P. V. Kolinsky and R. J. Jones, *J. Chem. Soc., Chem. Commun.* 1989, 1485.
13. C. V. Senoff, *Coord. Chem. Rev.* 1980, **32**, 111.
14. W. Hussain, G. J. Leigh, H. M. Ali, C. J. Pickett and D. A. Rankin, *J. Chem. Soc., Dalton Trans.* 1984, 1703.
15. B. V. DePamphilis, B. A. Averill, T. Herskovitz, L. Que Jr and R. H. Holm, *J. Am. Chem. Soc.* 1974, **96**, 4159.
16. W. L. Bowden, W. F. Little, T. J. Meyer and D. Salmon, *J. Am. Chem. Soc.* 1975, **97**, 6897.
17. K. I. Klabunde, *Ann. N.Y. Acad. Sci.* 1977, **295**, 83.
18. A. N. Nesmeyanov, L. I. Denisovich, S. P. Gubin, N. I. Vol'kenau, E. I. Sirotkina and I. N. Belesova, *J. Organomet. Chem.* 1969, **20**, 169.
19. G. J. Essenmacher and P. M. Treichel, *Inorg. Chem.* 1977, **16**, 800.
20. P. M. Treichel and H. J. Mueh, *Inorg. Chem.* 1977, **16**, 800.
21. J. Chatt, E. M. Elson, A. J. L. Pombiero, R. L. Richards and G. H. D. Royston, *J. Chem. Soc., Dalton Trans.* 1978, 165.
22. G. Butler, J. Chatt, G. J. Leigh and C. J. Pickett, *J. Chem. Soc., Dalton Trans.* 1979, 113.
23. S. M. Charsley, C. J. Jones, J. A. McCleverty, B. D. Neaves and S. J. Reynolds, *Transition Met. Chem.* 1986, **11**, 329.
24. J. A. McCleverty, D. Seddon, N. A. Bailey and N. W. Walker, *J. Chem. Soc., Dalton Trans.* 1976, 898.
25. N. AlObaidi, T. A. Hamor, C. J. Jones, J. A. McCleverty and K. Paxton, *J. Chem. Soc., Dalton Trans.* 1986, 1525.
26. N. AlObaidi, T. A. Hamor, C. J. Jones, J. A. McCleverty and K. Paxton, *J. Chem. Soc., Dalton Trans.* 1987, 1063.
27. M. Charlton, *Prog. Phys. Org. Chem.* 1981, **13**, 119.
28. R. P. Sidebotham, C. J. Jones and J. A. McCleverty, unpublished results.

Polyhedron Vol. 9, No. 4, pp. 535–539, 1990
Printed in Great Britain

0277–5387/90 $3.00+.00
© 1990 Pergamon Press plc

SYNTHESIS, PROPERTIES AND X-RAY CRYSTAL STRUCTURES OF COPPER(II) AND NICKEL(II) THIOCYANATE COMPLEXES WITH ETHANOLAMINE: A NEW STRUCTURE FOR AN AMINOALKOXIDE CLUSTER

MICHAEL B. HURSTHOUSE,* KEITH J. IZOD, M. A. MAZID and PETER THORNTON*

Department of Chemistry, Queen Mary and Westfield College, Mile End Road, London E1 4NS, U.K.

(*Received* 25 *August* 1989; *accepted* 7 *September* 1989)

Abstract—The new antiferromagnetic polymer $[Cu(NH_2C_2H_4O)(NCS)]_\infty$ has been prepared and shown by X-ray crystallography to contain a new polymeric linkage of pairs of copper(II) atoms linked alternately by two oxygen bridges and one weaker thiocyanate bridge. Electronic, ESR and IR spectra and temperature-variable magnetochemical data are described. $[Ni(NH_2C_2H_4OH)_2(NCS)_2]$ is fully characterized by its magnetism, electronic and IR spectra and crystal structure as a centrosymmetric octahedral monomer with nitrogen-coordinated thiocyanates.

When reviewing[1] structures of complexes with the formula $[Cu\{R_2N(CH_2)_nO\}X]$ (R = alkyl; $n = 2$, 3; X = halide, pseudohalide) Haase and co-workers recognized three general types of structure. These were (a) dimers with two oxygen bridges; (b) cubane tetramers, also with oxygen bridges; and (c) polymers, which were dimers of the (a) type linked by two X bridges. Despite many compounds having been found with different alkyl groups, R, and numbers of methylene linkages, n, there are no reports of structures and physical studies on the unalkylated alkoxide $H_2N(CH_2)_nO$ complexes. We report here the preparation, structure, magnetic properties, electronic, ESR and IR spectra of $[Cu(H_2NC_2H_4O)(NCS)]_\infty$, which we find has a new form of interdimer bridging for this type of compound. We have also studied the corresponding nickel(II) system and report the characterization of $[Ni(NH_2C_2H_4OH)_2(NCS)_2]$, which has only been partly characterized previously.[2]

RESULTS AND DISCUSSION

$[Cu(NH_2C_2H_4O)(NCS)]$

This compound is prepared by the addition of methanolic KNCS (1 mol) to a methanolic solution of $[Cu(H_2O)(O_2CCH_3)_4]$ (1 mol) and $NH_2C_2H_4OH$ (2 mol), using a procedure[3] which is successful for complexes with N-substituted aminoalcohols. An analogous azide complex was also prepared; its properties are rather different and it will be described elsewhere. Attempts to prepare NCO^- and $NCSe^-$ complexes failed. The IR spectrum of the NCS^- complex shows bands for NH_2 and NCS moieties but no OH vibrations, in keeping with the formulation as an alkoxide rather than alcohol complex. The NCS symmetric stretching mode at 803 cm^{-1} is consistent with bridging coordination.[4] This indicates a dimeric structure (I) with S—Cu interactions making a polymeric arrangement of type (c) described by Haase and co-workers,[1] but it is also consistent with non-bridging thiocyanate coordinating through the nitrogen atom only.

The diffuse reflectance electronic spectrum shows a broad absorption centred at 14,700 cm^{-1}, typical of copper(II) in many geometries, and a shoulder at 26,300 cm^{-1} on the stronger ultraviolet ligand absorption. This shoulder has been attributed[3] to O—Cu charge-transfer in bridging aminoalkoxo complexes. In solution, in DMSO, these absorptions are found at 15,000 cm^{-1} ($\varepsilon = 514$ cm^{-1} dm^3 mol^{-1}) and 26,300 cm^{-1} ($\varepsilon = 1550$), suggesting some change in structure in solution but with retention of oxygen bridging. The X-band ESR spectrum

* Authors to whom correspondence should be addressed.

Table 1. Magnetochemical data for $[Cu(NH_2C_2H_4O)(NCS)]_2$

Temperature (K)	$\chi/10^{-3}$	μ (μ_B)
90.3	1.294	0.97
104.1	1.487	1.11
117.8	1.535	1.20
131.4	1.520	1.26
144.9	1.511	1.32
162.8	1.455	1.37
180.8	1.398	1.42
198.9	1.328	1.45
212.3	1.280	1.48
230.1	1.215	1.50
247.8	1.174	1.53
265.7	1.106	1.53
283.7	1.051	1.55

of the solid complex consists of a very weak $\Delta M_s = 1$ signal at $g = 2.05$ with a much weaker $\Delta M_s = 2$ signal at $g \sim 4.0$, which indicates the presence of the expected antiferromagnetic copper–copper spin interaction in a dimer structure.

Details of the antiferromagnetism are given by magnetic susceptibility measurements down to 70 K (Table 1) where the magnetic moment is seen to fall from its room temperature value of 1.55 μ_B and the susceptibility is seen to achieve its maximum value near 120 K. The data can be fitted to the Bleaney–Bowers treatment[5] for an antiferromagnetic $S = 1/2$ dimer, showing good agreement with parameters of $g = 2.05$ (from the ESR data), $J = -42$ cm^{-1} and $N_\alpha = 60 \times 10^{-6}$ emu mol^{-1}. This shows that the principal path for antiferromagnetism is through the bridging oxygen atoms and that the thiocyanate bridges between dimers have an insignificant role in spin coupling. An alternative interpretation in which the thiocyanate bridges provide the principal route for antiferromagnetism is unlikely in view of the propensity of alkoxide bridges for generating strong antiferromagnetism in copper(II) dimers.[6] Indeed, polymerized dimers of type **I** are commonly more

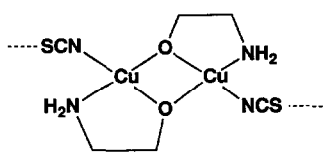

I

antiferromagnetic than our complex, even with chloride interdimer bridges, less effective exchange propagators than our thiocyanates.

To confirm our assignment we undertook an X-ray crystal structure determination. This reveals the dimeric structure we anticipated and shows interdimer bonding through thiocyanate bridges, but these bridging units are more interesting than we expected. Instead of configuration **II** in which two

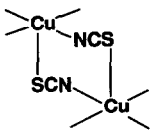

II

thiocyanate ligands linked neighbouring dimers, as found in $[Cu(R_2NC_2H_4O)(NCS)]_\infty$ (R = Me,[7] Et,[8] Pr[9]), polymerization is much more elaborate, each dimer being linked to four other dimers by single NCS bridges (Fig. 1).

The dimer units are centrosymmetric and the copper coordination is best described as distorted tetragonal pyramidal (4+1). Important bond lengths and angles are listed in Table 2. The Cu—O and Cu—N distances are all much shorter than the weaker axial Cu—S interaction of 2.872(5) Å. The bond lengths are generally similar to those in the previously reported $[Cu(R_2NC_2H_4O)(NCS)]$ complexes[7-9] despite the difference in interdimer linkage. The Cu—Cu separation of 2.974(4) Å is also typical of this kind of structure and shows that the antiferromagnetic exchange interaction between the copper atoms must be transmitted through the ligands.

$[Ni(NH_2C_2H_4OH)_2(NCS)_2]$

The previous report[2] of this compound describes briefly, without analytical data, the preparation,

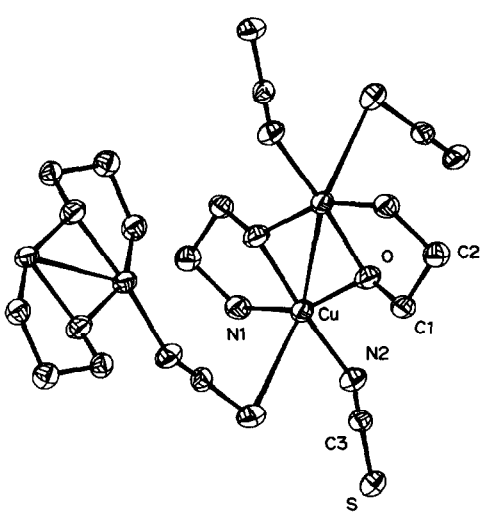

Fig. 1. Structure of $[Cu_2(NH_2C_2H_4O)_2(NCS)_2]_\infty$.

Table 2. Bond lengths and angles for $[Cu_2(NH_2C_2H_4O)_2(NCS)_2]$

Bond lengths (Å)			
Cu—S	2.872(5)	Cu—N(1)	1.983(6)
Cu—O	1.942(5)	Cu—N(2)	1.976(6)
Cu—Cu	2.974(4)		
Bond angles (°)			
O—Cu—S	101.9(2)	N(1)—Cu—S	100.1(2)
N(1)—Cu—O	156.2(2)	N(2)—Cu—S	81.8(2)
N(2)—Cu—O	98.9(3)	N(2)—Cu—N(1)	93.4(3)
C(3)—S—Cu	102.2(3)	C(1)—O—Cu	131.0(3)
C(2)—C(1)—O	107.0(5)		

electronic spectra and room temperature magnetic moment. Our method of preparation is slightly different; we used the addition of ethanolic $NH_2C_2H_4OH$ to ethanolic $Ni(NCS)_2$, prepared *in situ* by mixing ethanolic solutions of $[Ni(H_2O)_6](NO_3)_2$ and KNCS and filtering precipitated $KNO_3 \cdot NH_2$ and OH stretching modes occur at 3330, 3260, 3200 and 3160 cm^{-1}, the strong antisymmetric NCS mode occurs at 2085 cm^{-1} and the symmetric mode at 773 cm^{-1}. The diffuse reflectance electronic spectrum shows the expected transitions for a tetragonally-distorted octahedral complex from the $^3B_{1g}$ ground state to ^3E_g (10,800), $^3B_{2g}$ (11,900), ^3E_g (15,600 sh), $^3A_{2g}$ (17,200) and $^3T_{1g}$(P) (27,500 cm^{-1}). The room temperature magnetic moment is 3.23 μ_B; this value is constant down to 90.4 K and the value of θ of 5 K indicates no antiferromagnetism. These data are generally similar to those in ref. 2 but are different in detail and show the complex has octahedral coordination for nickel, probably with N-bonding for thiocyanate.[4]

We have also confirmed these conclusions by a crystal structure determination. The nickel atom occupies a crystallographic centre of symmetry. Important bond lengths and angles are listed in Table 3 and the structure is illustrated in Fig. 2. The chelating aminoethanol gives a bite angle of 81.7(2)° at nickel, but the other bond lengths and angles are all normal values for this type of complex and require no further comment.

EXPERIMENTAL

Physical measurements were made using magnetic[10] and spectroscopic[11] equipment already described.

$[Cu(NH_2C_2H_4O)(NCS)]$

A methanolic solution of KNCS (1.94 g, 0.02 mol) was added to a hot solution of $NH_2C_2H_4OH$ (2.44 g, 0.04 mol) and $[Cu_2(H_2O)_2(O_2CCH_3)_4]$ (4.0 g, 0.01 mol) in methanol (60 cm^3). Slow cooling over 3 days gave dark green crystals of the product, which was filtered, washed with ethanol and air-dried. The compound could not be recrystallized. Yield 1.8 g, 50%. Found: C, 19.8; H, 3.3; N, 15.2; S, 17.0. $C_3H_6CuN_2OS$ requires C, 19.8; H, 3.35; N, 15.4; S, 17.6%.

Table 3. Bond lengths and angles for $[Ni(NH_2C_2H_4OH)_2(NCS)_2]$

Bond lengths (Å)			
Ni—N(1)	2.065(5)	Ni—O	2.096(4)
Ni—N(2)	2.081(5)	C(3)—S	1.639(5)
C(3)—N(2)	1.149(5)	C(1)—O	1.440(6)
C(2)—N(1)	1.492(6)	C(1)—C(2)	1.467(7)
Bond angles (°)			
O—Ni—N(2)	89.5(2)	N(1)—Ni—N(2)	90.7(2)
N(1)—Ni—O	81.7(2)	C(3)—N(2)—Ni	159.4(3)
N(2)—C(3)—S	179.1(3)	C(1)—O—Ni	108.0(3)
C(2)—N(1)—Ni	108.2(3)	C(2)—C(1)—O	107.6(5)
C(1)—C(2)—N(1)	110.3(5)		

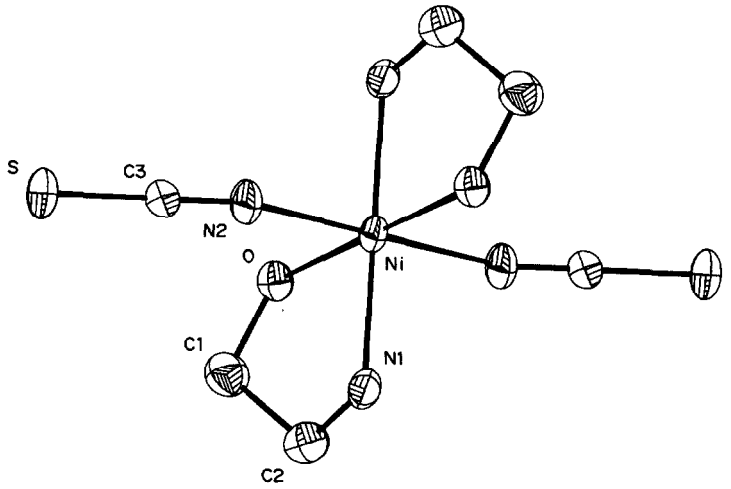

Fig. 2. Structure of $[Ni(NH_2C_2H_4OH)_2(NCS)_2]$.

$[Ni(NH_2C_2H_4OH)_2(NCS)_2]$

Hot ethanolic solutions of $[Ni(H_2O)_6](NO_3)_2$ (2.9 g, 25 cm^3, 0.01 mol) and KNCS (3.88 g, 150 cm^3, 0.04 mol) were mixed, the precipitated KNO_3 filtered and the filtrate concentrated to half volume. A solution of $NH_2C_2H_4OH$ (1.22 g, 0.02 mol) in ethanol (10 cm^3) was added and the solution left to stand. After 3 days dark blue clusters of the product were filtered, washed with ethanol and air-dried. Yield 1.04 g, 43%. Found: C, 24.2; H, 4.75; N, 19.1; S. 19.6. $C_6H_{14}N_4NiO_2S_2$ requires C, 24.3; H, 4.75; N, 18.9; S, 21.6%.

X-ray crystallography

Unit cell parameters and intensity data were obtained at 294 K using a CAD4 diffractometer,

Table 4. Crystal data, details of intensity measurements and structure refinement

Compound	$[Cu(NH_2C_2H_4O)(NCS)]$	$[Ni(NH_2C_2H_4OH)_2(NCS)_2]$
Stoichiometry	$C_3H_6CuN_2OS$	$C_6H_{14}N_4NiO_2S_2$
Molecular weight	181.71	297.02
Crystal system	Monoclinic	Monoclinic
a (Å)	7.564(1)	8.518(2)
b (Å)	8.910(1)	9.707(4)
c (Å)	9.390(2)	7.539(5)
α (°)	90	90
β (°)	105.60(1)	97.14(3)
γ (°)	90	90
Volume (Å^3)	609.53	618.52
Space group	$P2_1/c$	$P2_1/c$
Z	4	2
D_c (g cm^{-3})	1.98	1.60
Radiation	Mo–K_α, $\lambda = 0.71069$	Mo–K_α, $\lambda = 0.71069$
μ (cm^{-1})	38.195	33.74
$F(000)$	364	308
θ min/max	1.50, 25.0	1.50, 25.0
Temperature (K)	219	219
Total data measured	1285	1314
Total data unique	1201	1093
Total data used [$F > 3\sigma(F)$]	1002	941
Number of parameters	80	77
Weighting scheme parameter g in $\omega = 1/\sigma^2(F)+gF_0^2$	0.0005	0.000731
Final R	0.040	0.044
Final R_G	0.054	0.059

operating in the θ–2θ mode with graphite-monochromated Mo-K_α radiation. The structures were solved by the application of routine heavy-atom methods and refined by full-matrix least-squares techniques. In the refinement cycles all non-hydrogen atoms were refined anisotropically; hydrogen atoms were inserted in idealized positions and constrained to ride on the atoms to which they were bonded at a distance of 1.08 Å. The weighting scheme $\omega = 1/[\sigma^2(F_o)+g(F_o)^2]$ was used in each case, with the parameter g determined in the refinement process so as to give flat analyses of variance with $\sin\theta$ and F_o/F_{max}. Experimental details are summarized in Table 4.

Acknowledgements—We thank D. J. Ironmonger for technical assistance in magnetochemistry, the University of London for providing magnetochemical equipment and SERC for providing crystallographic equipment, and Buckinghamshire County Council for a maintenance grant to K.J.I.

REFERENCES

1. L. Walz, H. Paulus and W. Haase, *J. Chem. Soc., Dalton Trans.* 1985, 913.
2. M. S. Masoud, *J. Inorg. Nucl. Chem.* 1977, **39**, 413.
3. Y. Nishida and S. Kida, *J. Inorg. Nucl. Chem.* 1976, **38**, 451.
4. A. H. Norbury, *Adv. Inorg. Chem. Radiochem.* 1975, **17**, 232.
5. B. Bleaney and K. D. Bowers, *Proc. R. Soc. Lond.* 1952, **A214**, 451.
6. B. Piggott, M. B. Hursthouse, P. Thornton and N. P. C. Walker, *Polyhedron* 1988, **7**, 323.
7. W. Haase, R. Mergehenn and W. Krell, *Z. Naturfor.* 1976, **31B**, 85.
8. A. Pajunen and K. Smolander, *Finn. Chem. Lett.* 1974, 99.
9. M. Mikuriya, Y. Nishida, S. Kida, T. Mechi and I. Meda, *Acta Cryst.* 1977, **B33**, 538.
10. M. A. Laffey and P. Thornton, *J. Chem. Soc., Dalton Trans.* 1982, 313.
11. O. D. Sloan and P. Thornton, *Inorg. Chim. Acta* 1986, **120**, 173.

Polyhedron Vol. 9, No. 4, pp. 541–544, 1990
Printed in Great Britain

0277–5387/90 $3.00+.00
© 1990 Pergamon Press plc

THE X-RAY CRYSTAL STRUCTURES OF THE CADMIUM COMPLEXES OF PYRIDINE-1-THIOL AND MERCAPTOBENZOTHIAZOLE, $[Cd(C_5H_4NS)_2]_n$ AND $[Cd(C_7H_4N_2S_2)_2]_n$: TWO UNUSUAL VOLATILE POLYMERIC COMPLEXES

MICHAEL B. HURSTHOUSE,* OMAR F. Z. KHAN, MUHAMMED MAZID, MAJID MOTEVALLI and PAUL O'BRIEN*

Department of Chemistry, Queen Mary and Westfield College, Mile End Road, London E1 4NS, U.K.

(*Received* 27 *July* 1989; *accepted* 12 *September* 1989)

Abstract—The structures of the 2:1 complexes formed by pyridine-1-thiol (**I**) and mercaptobenzothiazole (**II**) with cadmium(II) are polymeric but both sublime at reduced pressure and decompose cleanly to CdS in air. Both structures contain approximately octahedrally-coordinated cadmium atoms (CdN_2S_4) and involve bridging and chelating modes for the ligand.

There is considerable current interest in the structures adopted by thiolate complexes of the main group elements.[1,2] In this context we report the X-ray crystal structures of the title complexes; the mercaptobenzothiazolato complex has been previously reported,[3,4] but no equivocal structural information is available, and the pyridine thiolato complex is a new compound. In addition, both of the compounds can be sublimed; the surprising volatility of these materials may mean that they are of interest for MOCVD, MOMBE and related crystal growth processes.

RESULTS AND DISCUSSION

In the pyridine-1-thiolato complex, coordination at each cadmium is close to octahedral (N_2S_4) with two different ligand coordination modes; one approximately parallel and the other perpendicular to the polymer chain, Fig. 1. The ligand perpendicular to the chain chelates one cadmium with Cd(1)—S(1) 2.81 Å and Cd(1)—N(2) 2.34 Å (bite angle 60.80°) and bridges to the adjacent cadmium Cd(1′)—S(1) 2.65 Å. The second ligand, approximately parallel to the chain, also chelates Cd(1) with Cd(1)—S(2) 3.04 Å and Cd(1)—N(1) 2.34 Å (bite angle 57.10°), and bridges to the adjacent cadmium in the opposite direction along the chain to the first ligand Cd(1″)—S(2) 2.54 Å. The two nitrogens on Cd(1) are *cis*. The compound is hence a genuine inorganic polymer with the shorter Cd—S

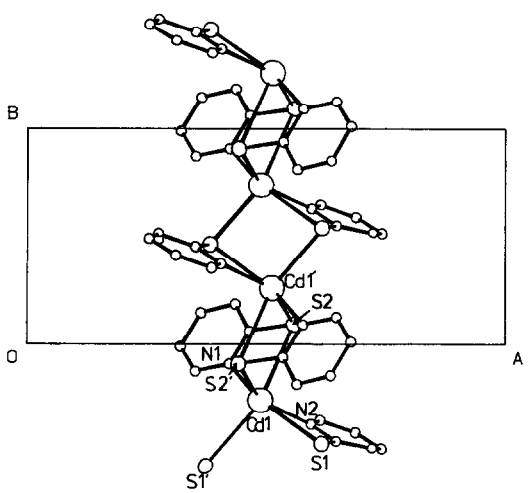

Fig. 1. A short section of the polymeric chain in the pyridine thiolatato complex, viewed down *c*; selected bond lengths (Å) and angles (°) are as follows: Cd(1)—S(1) 2.809(4), Cd(1)—S(1′) 2.649(4), Cd(1)—S(2) 3.038(4), Cd(1)—S(2′) 2.543(5), Cd(1)—N(1) 2.342(4), Cd(1)—N(2) 2.343(4), S(1′)—Cd(1)—S(2′) 103.4(3), S(1′)—Cd(1)—N(1) 93.57, S(2′)—Cd(1)—N(1) 101.6(3), S(1′)—Cd(1)—N(2) 100.06(3), N(2)—Cd(1)—S(1) 60.6(2), N(1)—Cd(1)—S(2) 57.2(2).

* Authors to whom correspondence should be addressed.

distances forming the chain. The four proximal sulphurs are within the sum of the van der Waals' radii[5] (3.4 Å). The shorter distances are similar to those found in other thiolate complexes of cadmium[1,6] (2.5–2.7 Å) and the Cd—N distances are typical of those found in relevant coordination complexes of cadmium[7] (2.27–2.36 Å). The bonding modes of mercaptopyridine have recently been surveyed,[8] the doubly bridging, five-electron, mode of bonding has only been unequivocally characterized in one other case,[8] the complex $[(pyS)_2CO_6Re_2]$, and there are no other complexes showing this kind of polymeric network developed in this structure.

The structure of the mercaptothiopyrazolato complex is similar, with the short ligand-to-metal contacts (Cd—N and Cd—S) to different cadmium atoms. Again, a polymeric structure is developed but in this case the ligands take up a helical pattern, Fig. 2. The two nitrogens are coordinated *cis* to each approximately octahedral cadmium atom (2.28 and 2.33 Å), the exocyclic sulphur atoms of each of the ligands coordinate with short Cd—S distances (2.55 and 2.60 Å) to adjacent cadmium atoms in opposite directions along the polymer chain. The distances from the first cadmium (3.06 and 3.12 Å) are within the sum of the van der Waals' radii[5] for cadmium and sulphur (3.4 Å). The two additional Cd—S contacts are unusually long, the cadmium atoms are separated by 3.77 Å, well outside the sum of the van der Waals' radii (3.2 Å). The mode of ligation is very different from the chelate mode shown in the anionic tris complex with cadmium(II),[4] Cd—S 2.66 Å and Cd—N 2.47 Å, with a bite angle of 62°

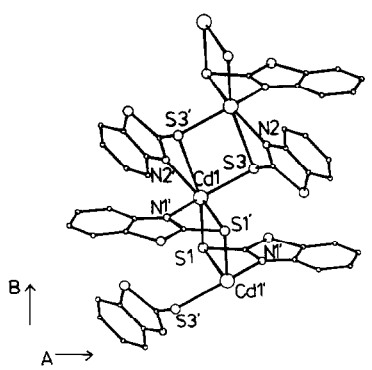

Fig. 2. A short section of a polymeric chain in the mercaptopyrazolato complex, viewed down *c*; selected bond lengths (Å) and angles (°) are as follows: Cd(1)—S(1) 2.606(4), Cd(1)—S(1′) 3.061(5), Cd(1)—S(3) 2.547(4), Cd(1)—S(3′) 3.129(4), Cd(1)—N(1′) 2.283(4), Cd(1)—N(2′) 2.328(3), S(1)—Cd(1)—S(1′) 96.8(3), S(1)—Cd(1)—N(1) 98.2(3), S(1′)—Cd(1)—N(1′) 57.7(3), S(1)—Cd(1)—S(3) 102.3(4).

and strict C_3 symmetry (distorted from trigonal prismatic toward octahedral by 25.8°).

The two structures presented are remarkably similar in terms of both coordination mode and symmetry. Both structures are based on extended networks of $—Cd_2S_2—$ four-membered rings.

Further characterization of the compounds has been carried out by a range of spectroscopic techniques. Solid-state NMR spectra have been impossible to obtain for compound **I**, the explanation for this lies in the long relaxation time for protons (*ca* 31 s) in this rigid complex which makes MAS/CP experiments difficult. The mercaptobenzothiazolato complex (**II**) gave excellent solid-state NMR spectra for both ^{13}C and ^{113}Cd. The ^{113}Cd chemical shift of the crude powdered complex showed that there were two cadmium sites characterized by chemical shifts of 340.1 and 329.3 ppm. The crystalline material gave a single peak at 325 ppm, as would be expected from the crystal structure. Possible explanations for the two sites observed include, the system is dimorphic or that the microcrystalline powder as initially obtained contains a relatively large number of terminal or chain-bridging cadmium atoms with a different chemical shift from that found for a cadmium centre within the polymer. In either case the environment of the cadmium in both sites is similar and consistent with the coordination geometry observed in the structure of the crystalline material (CdN_2S_4). Earlier workers may have studied a mixture of phases by IR spectroscopy[3] and ^{113}Cd NMR is clearly a powerful technique for detecting different cadmium centres in such compounds.

Mass spectra (electron impact) were recorded for both complexes. The spectrum of the pyridine-1-thiolato complex (**I**) showed a highest mass peak for the molecular ion of the 2:1 complex (m/z = 335.9 ^{115}Cd, 25%), with adjacent peaks for all the other common isotopes of cadmium. The mercaptobenzothiazole complex (**II**) gave a small clear peak for the molecular ion of the bis complex (m/z = 445 ^{113}Cd), with satellite peaks for the other isotopes of cadmium; this may indicate that the bis complex is a significant vapour phase species, however, other peaks trailing off to higher mass were seen. Thermogravimetric analysis of the complexes in a stream of air (Stanton–Redcroft TG750, 10°C min^{-1}, air 10 cm^3 min^{-1}) gave rise to cadmium sulphide (as a mixture of hexagonal and cubic phases). The yield was close to that theoretically required 43.3% (**I**) 230–500°C and 32.5% (**II**) 250–500°C, although the volatility of CdS made precise measurements difficult. These complexes are further examples of cadmium thiolates decomposing cleanly to CdS.[9]

Table 1. Crystal data

$(C_{20}H_{16}N_4S_4Cd_2)_n$: $M_w = 665.42$ (for the monomer), space group $C2/c$, $a = 17.464(2)$, $b = 7.323(1)$, $c = 18.981(2)$ Å, $V = 2270.45$ Å^3, $\beta = 110.72(1)°$, $D_c = 1.95$ g cm^{-3}, $Z = 4$, μ(Mo-K_α) = 22.36 cm^{-1}.
$R = 0.0295$, $w = 1/(\sigma^2(F_o)+0.000033(F_o)^2)$, $R_g = 0.0289$, for 2796 of 3308 reflections with $F_o > 3\sigma(F_o)$.

$(C_{28}H_{16}N_4S_8Cd_2)_n$: $M_w = 761.52$ (for the monomer), space group $C2/c$, $a = 19.452(3)$, $b = 7.203(1)$, $c = 23.962(3)$ Å, $V = 3142.75$ Å^3, $\beta = 110.60(2)°$, $D_c = 1.60$ g cm^{-3}, $Z = 4$, μ(Mo-K_α) = 15.95 cm^{-1}.
$R = 0.024$, $w = 1/(\sigma^2(F_o)+0.000706(F_o)^2)$, $R_g = 0.037$, for 2211 of 2640 reflections with $F_o > 3\sigma(F_o)$.

The atomic coordinates for the two structures reported in this communication are available from The Director of the Cambridge Crystallographic Centre, University Chemical Laboratory, Lensfield Road, Cambridge CB2 1EW, U.K. Any request for information should be accompanied by the full literature citation for this communication.

EXPERIMENTAL

Materials and methods

IR spectra were taken as either Nujol mulls or KBr discs (1%, 200 mg) between 4000 and 400 cm^{-1} using a Matteson Polaris FTIR, and solid-state NMR spectra were recorded with a Brüker MSL-300 instrument (equivalent proton frequency 300 MHz). ^{113}Cd shifts are in ppm relative to an external $Cd(ClO_4)_2$ reference. Mass spectra were recorded by electron bombardment using an AEI MS902.

Preparation of the complexes

The compounds both immediately precipitated on the stoichiometric reaction of an ethanolic solution of the ligand with an aqueous solution of cadmium acetate (room temperature 10^{-2}–10^{-3} mol dm^{-3} in cadmium). The use of cadmium acetate avoids the co-precipitation of basic complexes, a problem noted in earlier studies of **II**.[4] Single crystals were obtained by slow recrystallization of the crude complexes from hot pyridine (**I**) or dimethylformamide (**II**), both compounds could also be purified by sublimation (160°C and 0.01 torr); specimens large enough for diffraction studies could not be obtained by this method. The complexes, both before and after recrystallization, had satisfactory microanalyses (C,H,N,S) for the 2:1 ligand-to-metal stoichiometry.

Crystallography

All measurements were made on samples mounted in glass capillaries using a CAD4 diffractometer operating in the ω–2θ scan mode with graphite monochromated Mo-K_α radiation ($\lambda = 0.70169$ Å) as previously described.[10] The structures were solved via standard heavy-atom procedures and refined using full-matrix least-squares methods[11] with scattering factors calculated using data from ref. 12. All non-hydrogen atoms were refined with anisotropic displacement factors; many hydrogen atoms were identified in difference maps and included with geometric constraints, whilst the remainder were included in geometrically required positions. Details of the crystal data and intensity measurements are given in Table 1.

Acknowledgements—We thank the SERC and Polaron Equipment Ltd for a CASE Award to O.F.Z.K. and the SERC for support of crystallography at Queen Mary and Westfield College. Solid-state NMR spectra were recorded by Dr C. J. Groombridge of the ULIRS solid-state NMR service of the University of London, whom we thank for his enthusiastic help.

REFERENCES

1. (a) I. G. Dance, R. G. Garbutt and D. C. Craig, *Inorg. Chem.* 1987, **26**, 3732; (b) I. G. Dance, R. G. Garbutt, D. C. Craig and M. L. Scrudder, *Inorg. Chem.* 1987, **26**, 4057.
2. I. G. Dance, *Polyhedron* 1986, **5**, 1037.
3. I. P. Khullar and U. Agarwal, *Can. J. Chem.* 1975, **53**, 1165.
4. J. A. McCleverty, S. Gill, R. S. Kowalski, N. A. Bailey, H. Adams, K. W. Lumbard and M. A. Murphy, *J. Chem. Soc., Dalton Trans.* 1982, 493.
5. J. E. Huheey, *Inorganic Chemistry*, 3rd edn, p. 259. Harper International, New York (1983).
6. S. J. Black, F. W. B. Einstein, P. C. Hayes, R. Kuma and D. J. Tuck, *Inorg. Chem.* 1986, **25**, 4181.
7. O. F. Z. Khan, D. M. Frigo, P. O'Brien, A. Howes and M. B. Hursthouse, *J. Organomet. Chem.* 1987, **334**, C27.
8. For a review of the coordination modes of pyridine-2-thiol see, A. J. Deeming, M. Karim, P. A. Bates and M. B. Hursthouse, *Polyhedron* 1988, **7**, 1401.

9. K. Osakada and T. Yamamoto, *J. Chem. Soc., Chem. Commun.* 1987, 1117.
10. R. A. Jones, M. B. Hursthouse, K. M. Malik and G. Wilkinson, *J. Am. Chem. Soc.* 1979, **101**, 4128.
11. G. M. Sheldrick, SHELX 76, Program for crystal structure determination, University of Cambridge (1976).
12. *International Tables for X-Ray Crystallography*, Vol. 4. Kynoch Press, Birmingham.

Polyhedron Vol. 9, No. 4, pp. 545–551, 1990
Printed in Great Britain

0277–5387/90 $3.00+.00
© 1990 Pergamon Press plc

REACTIONS OF COORDINATED DINITROGEN—XXII.* SYNTHESIS, CHARACTERIZATION AND REACTIONS OF HYDRAZIDO(2−) COMPLEXES OF MOLYBDENUM. CRYSTAL STRUCTURES OF TWO HYDRAZIDO(2−) COMPLEXES

T. ADRIAN GEORGE,† LENORE M. KOCZON and ROBERT C. TISDALE

Department of Chemistry, University of Nebraska, Lincoln, NE 68588-0304, U.S.A.

and

KASSU GEBREYES, LIDUN MA,‡ SHADID N. SHAIKH and JON ZUBIETA†

Department of Chemistry, State University of New York at Albany, Albany, NY 12222, U.S.A.

(*Received* 28 *April* 1989; *accepted* 12 *September* 1989)

Abstract—The reactions of anhydrous HX (X = Br, Cl) with *trans*-$Mo(N_2)_2$(triphos)(PPh_3) (**1**) where triphos = $PhP(CH_2CH_2PPh_2)_2$, yield $[MoX(NNH_2)$(triphos)$(PPh_3)]X$ as a mixture of isomers: **1A(X)** and **1B(X)**. In solution, PPh_3 dissociates rapidly from the **B** isomer. Addition of PPh_3 to a mixture of **1A(X)** and **1B(X)** enabled the separation of the isomers by fractional crystallization. Addition of PPh_2Me to a mixture of **1A(X)** and **1B(X)** led to the isolation of **1A(X)** and $[MoX(NNH_2)$(triphos)$(PPh_2Me)]X$ [**2B(X)**]. Amber **1A(Cl)** crystallizes with one molecule of toluene in the monoclinic space group $P2_1$ with $a = 13.714(2)$, $b = 13.924(2)$, $c = 14.279(3)$ Å, $\beta = 102.44(1)°$, and $Z = 2$. Olive-green **2B(Cl)** crystallizes with two molecules of solvation; one each of pentane and toluene, in the triclinic space group $P\bar{1}$ with $a = 12.922(2)$, $b = 13.552(3)$, $c = 18.067(4)$ Å, $\alpha = 106.04(1)$, $\beta = 107.65(1)$, $\gamma = 97.22(1)°$, and $Z = 2$. Loss of PPh_3 from **1B(X)** is proposed to be due to steric factors. Yields of ammonia and hydrazine formed from all the nitrogen hydride complexes are summarized.

The reduction of N_2 to ammonia occurs where mono-[1,2] and bis-N_2[3–6] complexes of molybdenum and bis-N_2 complexes of tungsten[3,4] are treated with strong acids. The only nitrogen hydride species to have been definitively characterized for molybdenum in these reactions contain the hydrazido(2−), NNH_2, ligand.[7] Although a number of complexes containing an N_2H_2 fragment[8] have been structurally characterized,[9] it is only the hydrazido(2−) ligand, *which is so far unique to molybdenum and tungsten*, that has been shown to react further to yield ammonia. Studies of the reaction of *trans*-$Mo(N_2)_2$(triphos)(PPh_3) (**1**)[10] with strong acids have led to (i) establishment of the stoichiometry of the reaction with HBr in THF to yield ammonia [eq. (1)][5,11]

$$\mathbf{1} \xrightarrow[\text{THF}]{\text{HBr}} NH_4Br + \tfrac{1}{2}N_2 + MoBr_3(\text{triphos}) + PPh_3 \qquad (1)$$

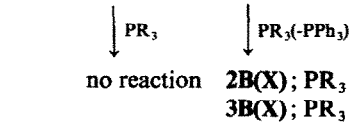

Scheme 1.

* For part XXI, see ref. 1.

† Authors to whom correspondence should be addressed.

‡ Permanent address: Center of Analysis and Measurement, Fudan University, Shanghai, P.R.C.

and (ii) recognition of nitrogenase-like behaviour,[12] namely the hydrazine-forming property of nitrogenase, in these systems.[5] The reactions of **1** with HX (X = Br, Cl) yield a pair of isomeric hydrazido(2−) complexes, $[MoX(NNH_2)(triphos)(PPh_3)]X$ [**1A(X)**] and [**1B(X)**]. Triphenylphosphine dissociates readily at room temperature from **1B(X)**, a key step in the reaction that produces ammonia, and can be replaced by PPh_2Me or PMe_2Ph, but not from **1A(X)**; see Scheme 1.[13] Full details are given of the crystal structures of $[MoCl(NNH_2)(triphos)(PPh_3)]Cl$ [**1A(Cl)**] and $[MoCl(NNH_2)(triphos)(PPh_2Me)]Cl$ [**2B(Cl)**] which have been communicated previously.[14]

RESULTS AND DISCUSSION

Formation of hydrazido(2−) complexes

Reactions of **1** with HX (X = Br, Cl) resulted in the loss of 1 mol of N_2 and rapid formation of a pair of isomeric hydrazido(2−) complexes (Scheme 1). In solution at room temperature with acid present, PPh_3 dissociated from the **B** isomer and within *ca* 0.5 h the ^{31}P NMR spectrum revealed resonances due to only the **A** isomer and PPh_3 (Scheme 1). No resonances due to the triphos-containing residue from **B** were observed. In THF solution a gold coloured solid began to form slowly following the loss of PPh_3. Precipitation was complete within *ca* 1 h.

Separation and isolation of **1A(X)** and **1B(X)** were affected by adding PPh_3 to a mixture of **1A(X)** and **1B(X)** in THF or toluene solution in the absence of acid. **1A(X)** precipitated first and reduction of the volume of solution resulted in precipitation of **1B(X)**. PPh_3 was added to maintain the equilibrium [eq. (2)] in favour of **1B(X)** in solution. Addition of PPh_2Me to a mixture of **1A(X)** and **1B(X)** in toluene solution in the absence of acid

$$\mathbf{1B(X)} \rightleftharpoons PPh_3 + \{[Mo(NNH_2)(triphos)]X\} \quad (2)$$

resulted in the formation of crystals of **1A(X)** and after reduction of the volume of solution crystals of $[MoX(NNH_2)(triphos)(PPh_2Me)]X$ [**2B(X)**] formed. Complex **2B(X)**, formed by displacement of PPh_3 in **1B(X)** by PPh_2Me, has the same ^{31}P NMR spectrum as **2B(X)** made by the reaction of *trans*-$Mo(N_2)_2(triphos)(PPh_2Me)$ (**2**) with HX, which afforded a mixture of **2A(X)** and **2B(X)**.[5]

Description of structures

The structures of the molecular cations of **1A(Cl)** and **2B(Cl)** are illustrated in Figs 1 and 2. Crystal data are given in Table 1 and relevant bond lengths and angles in Table 2.

Both complex cations display similar pseudo-octahedral coordination environments about the molybdenum atom, with the four phosphorus atoms defining the equatorial plane about molybdenum, while the chloride donor and N(1) of the end-on bonded hydrazido(2−) ligand occupy axial positions. In either case, the Mo—N(1) distance is short and the N(1)—N(2) distance is intermediate between calculated single and double bond

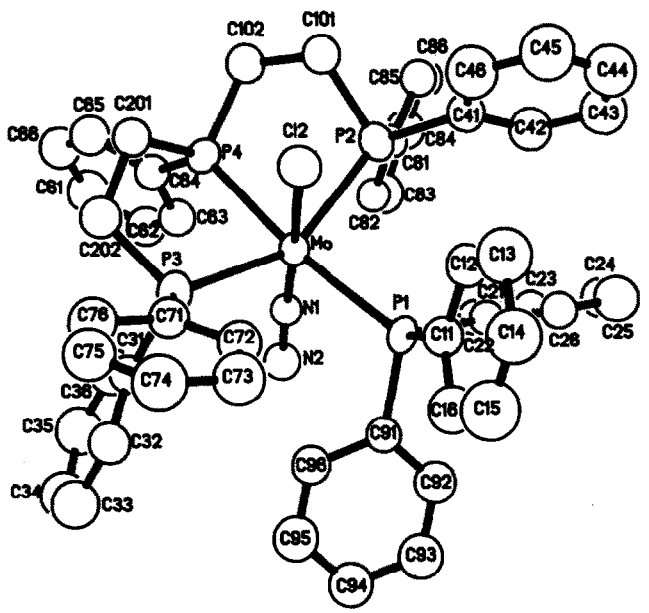

Fig. 1. Perspective view of the structure of the cation *syn*-$[MoCl(NNH_2)(triphos)(PPh_3)]^+$ of **1A(Cl)**.

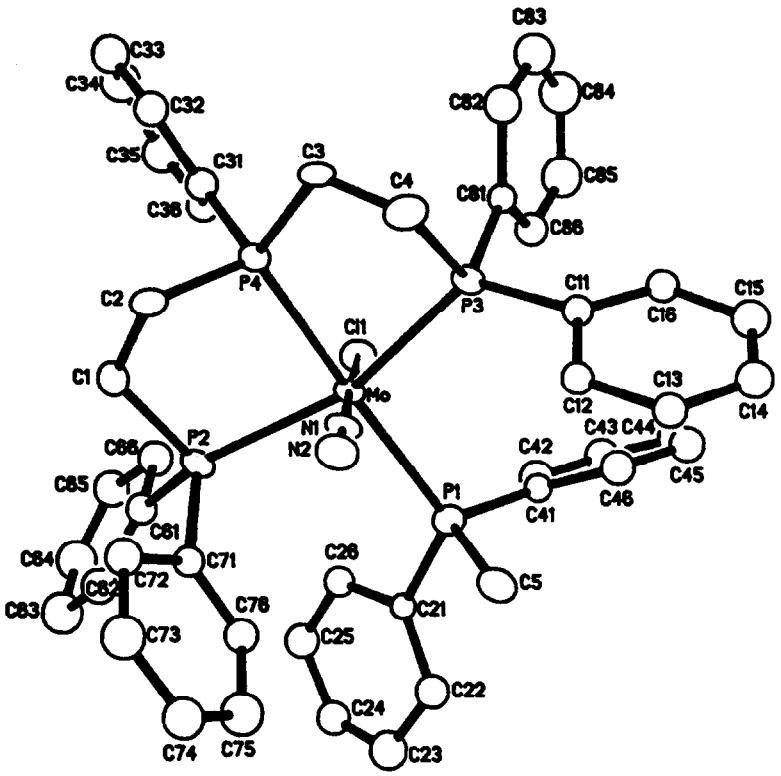

Fig. 2. Perspective view of the structure of the cation *anti*-$[MoCl(NNH_2)(triphos)(PPh_2Me)]^+$ of **2B(Cl)**.

distances, indicating a high degree of delocalization and significant multiple bond character throughout the Mo—N(1)—N(2) moiety; in fact very similar to other structurally characterized molybdenum hydrazido(2−) complexes.[15] The NNH_2 hydrogen atoms were located but not refined. Their positions and that of the chloride counterions, to which hydrogen bonding is indicated in the IR spectra, are shown in Fig. 3.

The occurrence of isomers arises because of the configuration at P(4), the central phosphorus atom of triphos. Thus in **1** (see Fig. 4) the two N_2 ligands are in different environments. One N_2 is on the same side of the P_4 plane as the Ph group (*syn*) on P(4),

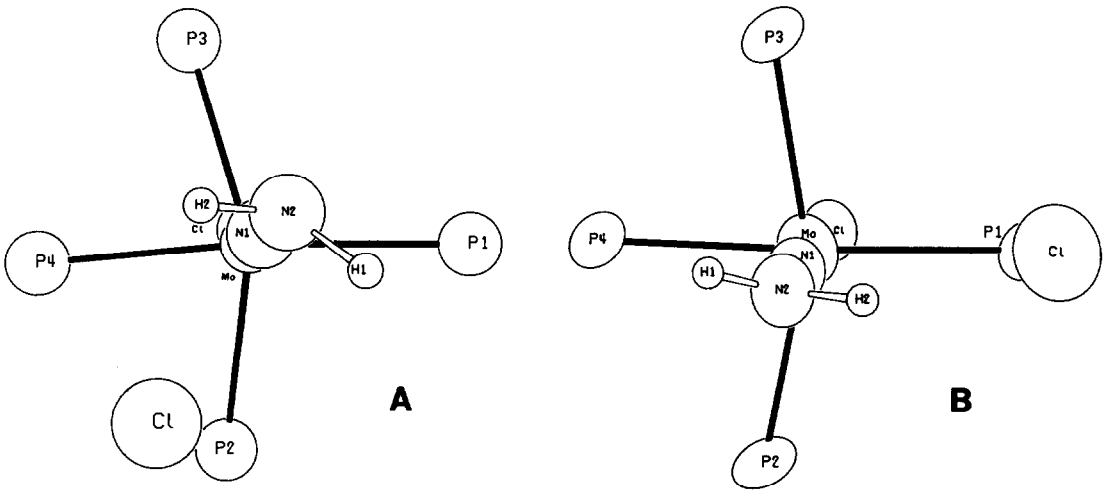

Fig. 3. Position of hydrazido(2−) protons relative to chloride counterions: **A** is **1A(Cl)** and **B** is **2B(Cl)**.

Table 1. Crystallographic data for $[MoCl(NNH_2)(triphos)(PPh_3)]Cl \cdot CH_3C_6H_5$ **[1A(Cl)]** and $[MoCl(NNH_2)(triphos)(PPh_2Me)]Cl \cdot CH_3C_6H_5 \cdot C_5H_{12}$ **[2B(Cl)]**

	1A(Cl)	**2B(Cl)**
Chemical formula	$MoC_{59}H_{58}Cl_2N_2P_4$	$MoC_{59}H_{68}Cl_2N_2P_4$
Formula weight	1085.86	1095.9
Crystal system	Monoclinic	Triclinic
Space group	$P2_1$	$P\bar{1}$
a (Å)	13.714 (2)	12.922(2)
b (Å)	13.924(2)	13.552(3)
c (Å)	14.279(3)	18.067(4)
α (°)		106.04(1)
β (°)	102.44(1)	107.65(1)
γ (°)		97.22(1)
V (Å^3)	2662.6(11)	2820.7(14)
Z	2	2
λ (Å)	Mo-K_α(0.71069)	
ρ_{calc} (g cm^{-3})	1.24	1.29
Crystal size (mm)	0.24 × 0.20 × 0.18	0.16 × 0.25 × 0.18
μ (cm^{-1})	4.92	4.70
Diffractometer	Nicolet R3m	
Temperature (°C)	23	
Scan mode	θ–2θ	
θ range (°)	2–45	
Reflections collected	3595	7281
Reflections used	2437	2672
Criteria	$I_o \geqslant 3\sigma(I_o)$	
R^a	0.0689	0.0851
$R_w{}^b$	0.0795	0.0833
Quality-of-fit indicator^c	1.606	1.759

$^a R = \Sigma[|F_o| - |F_c|/\Sigma|F_o|]$.
$^b R_w = [\Sigma w(|F_o| - |F_c|)^2/\Sigma w|F_o|^2]^{1/2}$; $w = 1/[\sigma^2(F_o) + g(F_o)^2]$, $g = 0.001$.
^{c} Quality-of-fit $= [\Sigma w(|F_o| - |F_c|)^2/(N_{obs}\text{-}N_{parameters})]^{1/2}$.

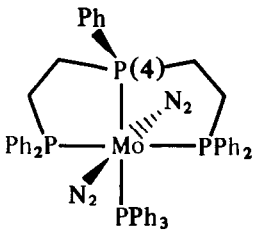

Fig. 4. Proposed structure of *trans*-$[Mo(N_2)_2(triphos)(PPh_3)]$ showing inequivalent N_2 ligands due to orientation of the Ph group on P(4). See ref. 16.

whereas the other N_2 is on the opposite side of the plane *anti* to the Ph group. In the crystal structure of a related complex, *trans*-$Mo(N_2)_2[PhP(CH_2CH_2PPh_2)_2]$, the two Mo—N distances are different; 1.998(4) and 2.018(4) Å.[16] The particular hydrazido(2−) complex formed will depend upon which N_2 ligand is protonated. Protonation of N_2 *syn* to the Ph group yields the **A** (*syn*) isomer, whereas protonation of the other N_2 affords the **B** (*anti*) isomer. The results from experiments indicate that formation of the **B** isomer is favoured, 2:1. The observation of isomers resulting from the orientation of the Ph group on the central phosphorus atom has been reported for an iridium and ruthenium complex containing $PhP(CH_2CH_2CH_2PR_2)_2$, where R = Ph and c-C_6H_{11}.[17]

An important geometrical feature that was revealed in the crystal structure but not reported previously[14] is the position of the molybdenum atom relative to the P_4 plane. Thus, in both **1A(Cl)** and **2B(Cl)** molybdenum sits above the P_4 plane on the same side as five Ph groups that create a pocket. These displacements are 0.28 and 0.08 Å respectively (see Table 3). Below the plane there are three Ph groups in **1A(Cl)** and in **2B(Cl)** the Me and two Ph groups. The net result is that in **1A(Cl)** the hydrazido(2−) group is on the same side of the P_4 plane as Mo with Cl below the plane. When these two ligands change places, as observed in **2B(Cl)**, the hydrazido(2−) ligand is below the plane and

Table 2. Selected bond lengths (Å) and bond angles (°) for [MoCl(NNH$_2$)(triphos)(PPh$_3$)]Cl·CH$_3$C$_6$H$_5$ [**1A(Cl)**] and [MoCl(NNH$_2$)(triphos)(PPh$_2$Me)]Cl·CH$_3$C$_6$H$_5$·C$_5$H$_{12}$ [**2B(Cl)**]

	1A(Cl)	**2B(Cl)**
Mo—N(1)	1.694(12)	1.778(18)
Mo—P(1)	2.556(4)	2.552(7)
Mo—P(2)	2.564(4)	2.513(7)
Mo—P(3)	2.506(4)	2.497(7)
Mo—P(4)	2.475(4)	2.475(4)
Mo—Cl(2)	2.503(4)	2.479(7)
N(1)—N(2)	1.34(2)	1.31(2)
N(2)···Cl(1)	3.15	3.12
HA[N(2)]···Cl(1)	2.68	2.78
P(1)—Mo—P(2)	95.9(1)	101.7(2)
P(1)—Mo—P(3)	106.3(1)	99.1(2)
P(1)—Mo—P(4)	172.9(1)	176.7(3)
P(1)—Mo—N(1)	85.8(4)	94.0(6)
P(1)—Mo—Cl	91.4(1)	83.3(2)
P(2)—Mo—P(3)	148.2(1)	157.0(2)
P(2)—Mo—P(4)	77.7(1)	80.6(2)
P(2)—Mo—N(1)	108.7(4)	82.2(6)
P(2)—Mo—Cl	79.1(1)	96.8(2)
P(3)—Mo—P(4)	78.5(1)	79.1(2)
P(3)—Mo—N(1)	95.6(4)	86.7(6)
P(3)—Mo—Cl	77.9(1)	95.3(2)
P(4)—Mo—N(1)	99.1(4)	88.7(6)
P(4)—Mo—Cl	84.4(1)	94.1(2)
N(1)—Mo—Cl	171.9(4)	176.9(6)
Mo—N(1)—N(2)	172.2(11)	178.1(15)

on the *opposite side to* Mo. Frequently, metal ions are displaced from an equatorial plane, particularly towards a strongly π-bonding ligand[15a,18] In **2B(Cl)** the π-bonding ligand is on the opposite side of the plane. N(1) is 1.95 Å out of the P$_4$ plane in **1A(Cl)**, whilst in **2B(Cl)** N(1) is only 1.69 Å out of the plane on the other side and therefore much closer to atoms about Mo. Molybdenum is probably displaced from the plane for two reasons: (i) because of the acute P(2)—Mo—P(4) and P(3)—Mo—P(4) angles ($\leqslant 81°$) and (ii) to minimize steric interactions between the five Ph groups.

The one significant difference in the chemical behaviour of **1A(Cl)** and **1B(Cl)** that we have observed is the relative rate of loss of PPh$_3$. In the absence of acid **1A(Cl)** does not dissociate PPh$_3$ in solution at room temperature, whereas **1B(Cl)** does. Unfortunately, while we could isolate **1B(Cl)** we were unable to obtain suitable crystals for a structure study. However, we were able to displace PPh$_3$ with PPh$_2$Me to form **2B(Cl)** and obtain suitable crystals. The PPh$_2$Me ligand has a choice of four coordination orientations depending upon the positions of the Me and two Ph groups relative to triphos. It is notable that the two Ph groups occupy positions above the plane just like PPh$_3$ in **1A(Cl)**. The Me group is *syn* to NNH$_2$. This geometric arrangement which arises both from the ligand exchange reaction [**1B(Cl)** + PPh$_2$Me → **2B(Cl)** + PPh$_3$] and direct protonation of **2** [**2** + HCl (excess) → **2A(Cl)** + **2B(Cl)**] suggests that the Me rather than the Ph group occupies the *syn* position in the **B** isomer for steric reasons. The closest non-bonding distance to N(1) is with P(2) at 2.873 Å. However, a simple calculation using trigonometry to determine nearest-neighbour interactions when a phenyl group is present instead of the methyl group in **2B(Cl)** places an *ortho* hydrogen within 1.7 Å of N(2) when the phenyl ring and Mo—N(1)—N(2) atoms are coplanar. Therefore, we propose that PPh$_3$ is labile in the **1B** isomers because of steric interactions between the hydrazido(2−) ligand and the Ph group of PPh$_3$.

Reactions of hydrazido(2−) complexes to form ammonia and hydrazine

Previously we reported yields of N$_2$, ammonia and hydrazine from the reactions of **1** and mixtures of **A** and **B** isomers with acid.[5] More recently we have been able to separate **A** and **B** and study them individually in reactions with acids (HBr, HCl, CF$_3$COOH and CF$_3$SO$_3$H), in various solvents (THF, benzene, toluene, CH$_2$Cl$_2$, MeOH and CF$_3$COOH), and at different temperatures. The general observations made previously and conclusions drawn hold true for this work.

Table 3. Mean least-square plane calculation for **1A(Cl)** and **2B(Cl)**

1A(Cl): Plane through P(1), P(2), P(3), P(4)	**2B(Cl)**: Plane through P(1), P(2), P(3), P(4)
$10.817x + 8.548y - 2.862z = 3.758$	$3.448x - 6.586y + 14.479z = 1.238$
Mo: −0.28 Å out of plane	Mo: +0.08 Å out of plane
N(1): −1.948 Å out of plane	N(1): −1.69 Å out of plane
Mo displaced towards N(1)	Mo displaced towards Cl

EXPERIMENTAL

General procedures

All preparations and reactions were carried out under a N_2 atmosphere or *in vacuo*. Compounds were handled in a water- and oxygen-free environment which was provided by use of Schlenk equipment, glovebags, and a Vacuum Atmospheres Corp. drybox. Specific procedures for carrying out acid reactions with **1** and quantitative determination of yields of N_2, ammonia and hydrazine have been reported elsewhere.[5]

Elemental analyses were performed by Galbraith Laboratories Inc., Knoxville, Tennessee.

Instrumentation

IR spectra (4000–250 cm^{-1}) were recorded on a Perkin–Elmer 283 spectrophotometer. Solid samples were run as KBr pellets. ^1H NMR spectra were recorded using a Nicolet NMC 360 spectrometer operating at 361.06 MHz. ^{31}P NMR spectra were run either on a Nicolet 360 (146.17 MHz) or Varian XL-200 (80.984 MHz) spectrometer. All spectra were recorded at ambient temperature. All chemical shifts are reported in ppm relative to Me_4Si (^1H) or 85% H_3PO_4 (^{31}P), with positive values being to low field. Phosphorus atom designations are as follows: $PhP_a(CH_2CH_2P_bPh_2)_2$, P_xR_3. No $^2J_{P_aP_b}$ was observed in these complexes. Similar observations have been noted for other complexes of molybdenum containing *mer*-triphos.[5,14,19]

Reagents and materials

Details have been given elsewhere.[5] The following complexes were prepared by published procedures: *trans*-$Mo(N_2)_2$(triphos)(PR_3), where PR_3 = PPh_3 and PPh_2Me, **1A(Cl)**, **3B(Cl)**, and mixtures of **1A(X)** and **1B(X)**.[5]

[$MoBr(NNH_2)$(*triphos*)(PPh_3)]Br [**1A(Br)**] *and* [**1B(Br)**]

To a mixture of **1A(Br)** and **1B(Br)** prepared from **1** (0.25 g, 0.25 mmol) was added PPh_3 (0.13 g, 0.5 mmol). THF (8 cm^3) was condensed (−196°C) onto the solid and the reaction mixture warmed to room temperature with swirling. The clear solution was allowed to stand (1 h) undisturbed. A brown solid was filtered off and washed with THF (10 cm^3) and pentane (10 cm^3) and dried *in vacuo*. The yield of **1A(Br)** was 33% (0.09 g, 0.08 mmol). ^{31}P NMR (CH_2Cl_2): δ 90.5 (d, 1, $^2J_{P_aP_x}$ = 146.2 Hz, P_a), 54.1 (d, 2, $^2J_{P_bP_x}$ = 16.7 Hz, P_b), 31.5 (dt, 1, P_x). ^1H NMR (CD_2Cl_2): δ 0.76 (t, CH_2, THF), 2.5 (br, PCH_2), 3.6 (t, CH_2, THF), 6.5–7.5 (m, Ph), 8.4 (br, NH_2: disappeared upon addition of D_2O).

The filtrate from the above reaction was transferred to a Schlenk tube, cooled to −196°C and evacuated. After the solution had frozen, pentane (20–30 cm^3) was added via cannula. The tube was warmed to −78°C and left undisturbed (24 h). The green solid which precipitated was filtered off, washed with pentane (10 cm^3) and dried *in vacuo*. The yield of **1B(Br)** was 65% (0.18 g, 0.16 mmol). ^{31}P NMR (THF): δ 72.75 (d, 1, $^2J_{P_aP_x}$ = 163.25 Hz, P_a), 34.55 (d, 2, $^2J_{P_bP_x}$ = 17.48 Hz, P_b), 7.96 (dt, 1, P_x). ^1H NMR (CD_2Cl_2): δ 2.5 (br, PCH_2), 6.5–7.7 (m, Ph).

[$MoCl(NNH_2)$(*triphos*)(PPh_3)]Cl [**1A(Cl)**] *and* [**1B(Cl)**]

To a mixture of **1A(Cl)** and **1B(Cl)** prepared from **1** (0.22 g, 0.22 mmol) was added PPh_3 (0.12 g, 0.45 mmol). THF (6 cm^3) was condensed in at −196°C and the reaction mixture warmed to room temperature with swirling. The clear solution was allowed to stand (18 h) undisturbed. The resulting brown solid was filtered off, washed with THF (10 cm^3) and pentane (10 cm^3) and dried *in vacuo* to afford **1A(Cl)** (18%, 0.04 g, 0.04 mmol).

Crystals of **1A(Cl)**, analytically pure and suitable for X-ray diffraction studies, were prepared by the addition of PPh_2Me in toluene rather than PPh_3 in THF.[5] The presence of a toluene of crystallization was inadvertently omitted from the original report of the structure.[14]

A sample of **1B(Cl)** was obtained in 33% yield by treating the filtrate from the above reaction as per the isolation of **1B(Br)** described above. **1B(Cl)**: ^{31}P NMR (THF): δ 84.4 (d, 1, $^2J_{P_aP_x}$ = 170.17 Hz, P_a), 37.9 (d, 2, $^2J_{P_bP_x}$ = 16.17 Hz, P_b), 32.8 (dt, 1, P_x).

[$MoBr(NNH_2)$(*triphos*)(PPh_2Me)]Br [**2B(Br)**]

To a mixture of **1A(Br)** and **1B(Br)** prepared from **1** (405 mg, 0.40 mmol) was added toluene (40 cm^3) and the suspension was filtered. To the dark greenish-amber filtrate was added dropwise PPh_2Me (0.15 cm^3, 4 equiv.). Amber microcrystals of **1A(Br)** formed almost immediately and were collected by filtration, washed with toluene and pentane. Further solid formed from the filtrate (2.5 h) and was collected as described above. The ^{31}P NMR spectrum indicated that this solid was a mixture of **1A(Br)** and **2B(Br)**. The volume of the green filtrate was reduced by *ca* 25% *in vacuo*. Lime-green microcrystals began to form and were collected

(15 h) to yield 103 mg (0.01 mmol, 24%) of **2B(Br)**. ^{31}P NMR (CD_2Cl_2): δ 67.17 (d, 1, $^2J_{P_aP_x}$ = 162.4 Hz, P_a), 32.50 (d, 2, $^2J_{P_bP_x}$ = 18.5 Hz, P_b), 3.42 (dt, 1, P_x).

[MoCl(NNH$_2$)(*triphos*)(PPh$_2$Me)]Cl [**2B(Cl)**]

Toluene (17 cm^3) was added to a mixture of **1A(Cl)** and **1B(Cl)**, prepared from **1** (298 mg, 0.30 mmol), and the suspension filtered. To the filtrate was added PPh$_2$Me (0.25 cm^3, 6 equiv.). After 15 h, **1A(Cl)** (54 mg) was removed by filtration as described in the previous experiment. The filtrate was allowed to stand for 15 h, after which time olive-green "layered" rectangular prisms of **2B(Cl)** (58 mg, 0.06 mmol, 20%) were isolated, washed with pentane and dried *in vacuo*. These crystals were suitable for an X-ray diffraction study. Found: C, 62.23; H, 5.54; N, 2.11. Calc. for $C_{47}H_{48}Cl_2MoN_2P_4 \cdot 0.5C_7H_8$: C, 62.04; H, 5.36; N, 2.87%. ^{31}P NMR (CD_2Cl_2): δ 68.97 (d, 1, $^2J_{P_aP_x}$ = 169.1 Hz, P_a), 35.52 (d, 2, $^2J_{P_bP_x}$ = 18.4 Hz, P_b), 7.32 (dt, 1, P_x). IR: ν(NH) 3205 (w), 2708 (sbr) cm^{-1}.

X-ray crystallography

Full details of the crystallographic methodologies may be found in ref. 20. Crystallographic data are given in Table 1. Molybdenum atom positions were located in a three-dimensional sharpened Patterson map; all non-hydrogen atoms were located on subsequent difference Fourier maps. Hydrogen atoms were included as fixed contributors in the final refinement cycles. Data were corrected for background, attenuators, Lorentz and polarization effects.

Since **1A(Cl)** crystallized in the non-centric space group $P2_1$, it was necessary to refine the alternative enantiomorph. Although the two structures presented no statistically significant differences in the final metrical parameters, the reported structure is that associated with the slightly lower value of R_w.

Acknowledgements—This work was supported by the National Science Foundation through Grants CHE83-05478 and INT-8420371. Additional support was received from the University of Nebraska Research Council.

REFERENCES

1. T. A. George and R. C. Tisdale, *Inorg. Chem.* 1988, **27**, 2909.
2. T. A. George and R. C. Tisdale, *J. Am. Chem. Soc.* 1985, **107**, 5157.
3. J. Chatt, A. J. Pearman and R. L. Richards, *J. Chem. Soc., Dalton Trans.* 1977, 1852.
4. T. Takahashi, Y. Mizobe, M. Sato, Y. Uchida and M. Hidai, *J. Am. Chem. Soc.* 1980, **102**, 7461.
5. J. A. Baumann, G. E. Bossard, T. A. George, D. B. Howell, L. M. Koczon, R. K. Lester and C. M. Noddings, *Inorg. Chem.* 1985, **24**, 3568.
6. N. J. Lazarowych, R. H. Morris and J. M. Ressner, *Inorg. Chem.* 1986, **25**, 3926.
7. (a) J. Chatt, A. J. Pearman and R. L. Richards, *J. Chem. Soc., Dalton Trans*, 1978, 1766; (b) S. N. Anderson, M. E. Fakley, R. L. Richards and J. Chatt, *J. Chem. Soc., Dalton Trans.* 1981, 1973.
8. R. A. Henderson, G. J. Leigh and C. J. Pickett, *Adv. Inorg. Chem. Radiochem.* 1983, **27**, 197.
9. (a) [{Cr(CO)$_5$}$_2$N$_2$H$_2$]; G. Huttner, W. Gartzke and K. Allington, *Angew. Chem. Int. Edn Engl.* 1974, **13**, 822; (b) [{W(η^5-C$_5$Me$_4$Bu^t)(CCMe$_3$)I$_2$}$_2$N$_2$H$_2$]; M. R. Churchill, L. Yong-Ji, K. H. Theopold and R. R. Schrock, *Organometallics* 1984, **3**, 109; (c) [W(NPh)Me$_3$]$_2$(μ-η^1, η^1-NH$_2$NH$_2$)(μ-η^2, η^2-NHNH); L. Blum, I. D. Williams and R. R. Schrock, *J. Am. Chem. Soc.* 1984, **106**, 8316.
10. T. A. George and R. A. Kovar, *Inorg. Chem.* 1981, **20**, 285.
11. J. A. Baumann and T. A. George, *J. Am. Chem. Soc.* 1980, **102**, 6153.
12. T. A. George and L. M. Koczon, *J. Am. Chem. Soc.* 1983, **105**, 6334.
13. G. E. Bossard, T. A. George, D. B. Howell, L. M. Koczon and R. K. Lester, *Inorg. Chem.* 1983, **22**, 1968.
14. K. Gebreyes, T. A. George, L. M. Koczon, R. C. Tisdale and J. Zubieta, *Inorg. Chem.* 1986, **25**, 407.
15. (a) [MoF(NNH$_2$)(dppe)$_2$]BF$_4$: M. Hidai, T. Kodama, M. Sato, M. Harakawa and Y. Uchida, *Inorg. Chem.* 1976, **15**, 2694; (b) [Mo(NNH$_2$)(quin)(PMe$_2$Ph)$_3$]X, where quin = quinolin-9-olate; X = Br or I: I. R. Hanson and D. L. Hughes, *J. Chem. Soc., Dalton Trans.* 1981, 390.
16. B. Pietsch and L. Dahlenburg, *Acta Cryst.* 1986, **C42**, 995.
17. (a) J. B. Letts, T. J. Mazanec and D. W. Meek, *J. Am. Chem. Soc.* 1982, **104**, 3898; (b) C. Yang, S. M. Socol, D. W. Kountz, D. W. Meek and R. Glaser, *Inorg. Chim. Acta* 1986, **114**, 119.
18. (a) W. P. Griffith, *Coord. Chem. Rev.* 1972, **8**, 369; (b) W. A. Nugent and B. L. Haymore, *Coord. Chem. Rev.* 1980, **31**, 123; (c) M. Sato, T. Kodama, M. Hidai and Y. Uchida, *J. Organomet. Chem.* 1978, **152**, 239; (d) E. M. Shutorovich, Yu. A. Buslaev and Yu. V. Kokunov, *Zh. Struckt. Khim.* 1972, **13**, 111.
19. M. C. Davies and T. A. George, *J. Organomet. Chem.* 1982, **224**, C25.
20. A. Bruce, J. L. Corbin, P. L. Dahlstrom, J. R. Hyde, M. Minelli, E. I. Stiefel, J. T. Spence and J. Zubieta, *Inorg. Chem.* 1982, **21**, 917.

Polyhedron Vol. 9, No. 4, pp. 553–555, 1990
Printed in Great Britain

0277–5387/90 $3.00+.00
© 1990 Pergamon Press plc

PHOSPHORUS–CARBON NUCLEAR MAGNETIC COUPLING CONSTANTS IN PHOSPHORUS(III) CYANIDES

BRUCE W. TATTERSHALL

Department of Chemistry, The University, Newcastle upon Tyne NE1 7RU, U.K.

(*Received* 21 *August* 1989; *accepted* 18 *September* 1989)

Abstract—Coupling constants $|^1J(^{31}P-^{13}C)|$ have been found to have unexpectedly large values, 60.2, 102.5 and 152.4 Hz, for $P(CN)_3$, $P(CN)_2Cl$ and $P(CN)Cl_2$, respectively, in MeCN. Significantly different values were found for solutions in 1-iodopropane. Secondary isotope shifts $^1\Delta^{31}P(^{13/12}C)$ and ^{13}C chemical shifts are also reported.

Values of $^1J(^{31}P-^{13}C)$ nuclear magnetic coupling constants in simple phosphorus(III) cyanides were required for comparison with that in a phosphorus–sulphur cage compound, α-$P_4S_3(CN)_2$.[1] The compounds $P(CN)_2Cl$ and $P(CN)Cl_2$ were made in solution with $P(CN)_3$ and PCl_3 in either MeCN or Pr^nI by Dillon *et al.*,[2] but they were identified only by rationalization of their observed ^{31}P chemical shifts by empirical interpolation methods. The ^{31}P NMR spectra were obtained for mixtures of the solutions with solid silver salts in unspun tubes, so only chemical shift information could be obtained. I have now approximately repeated this work, but with filtration of the solutions (obtained by reaction of PCl_3 with AgCN) to allow high resolution ^{31}P and ^{13}C (natural abundance) NMR spectra to be measured, and hence $^{31}P-^{13}C$ coupling constants to be obtained. The sequence of coupling constants found confirmed the original assignment of ^{31}P chemical shifts by Dillon *et al.*, and hence has established more firmly the identity of the compounds. ^{13}C chemical shifts could be assigned because of observation of similar splittings of doublets in the ^{13}C spectra, as in the ^{13}C satellite doublets in the ^{31}P spectra.

EXPERIMENTAL

All operations were carried out under nitrogen by Schlenk methods. Appropriate care was exercised in handling Pr^nI and solutions containing cyanides. PCl_3 (BDH) was used as received. AgCN (BDH) was dried by heating to 70°C under vacuum for > 5 h. MeCN was distilled from CaH_2, and Pr^nI (Aldrich) was dried over $MgSO_4$, before use. NMR spectra were measured in 10-mm diameter tubes using a Bruker WM300WB spectrometer, operating at 121.5 MHz for ^{31}P and 75.47 MHz for ^{13}C. A $(CD_3)_2CO$ capillary was used for locking. ^{31}P chemical shifts, obtained by substitution experiments using the same capillary and frequency offset, are reported relative to H_3PO_4–H_2O. ^{13}C shifts are reported relative to TMS in the external $(CD_3)_2CO$.

Typical procedure

AgCN (1.95 g, 14.6 mmol) was dried in a Schlenk tube, then suspended in MeCN (10 cm^3) and stirred rapidly while PCl_3 (0.6 cm^3, 6.9 mmol) was added slowly by pipette. Stirring was continued at 20°C for 24 h, then the mixture was filtered and the filtrate sampled for NMR.

RESULTS AND DISCUSSION

Preparation of compounds

The ^{31}P NMR spectrum of the solution of $P(CN)_nCl_{3-n}$ ($n = 0$–3) in MeCN (see Experimental), accumulated between 1 and 17 h after filtration, showed PCl_3 (37.0% of total P), $P(CN)Cl_2$ (3.9%), $P(CN)_2Cl$ (4.1%) and $P(CN)_3$ (37.1%), an unknown product with singlet absorption at −98.24 ppm (8.2%), and several unidentified more minor products. The product distribution resembled that reported by Dillon *et al.* "shortly after preparation",[2] but while they found that "by the following day" their mixture (still in the presence of silver salts) had undergone a redistribution reaction to produce more $P(CN)Cl_2$ and $P(CN)_2Cl$, in what was believed to be a state of equilibrium, I have found that the filtered solution showed prac-

tically the same low concentrations (3.5 and 3.9%, respectively) of $P(CN)Cl_2$ and $P(CN)_2Cl$ in a second accumulation of the spectrum started 48 h after the first. [$P(CN)_3$ now represented 32.9% of the phosphorus content, and PCl_3 42.5%.] Since it is hard to believe that the relative concentrations now reported could have been those of thermodynamic equilibrium, it is probable that the rates of redistribution reactions were negligible at room temperature, and that the measured concentrations of cyanide-containing products reflected the relative rates at which these products originally left the surface of the silver salt particles.

Broadening of the ^{31}P NMR peaks by scalar coupling relaxation by quadrupolar chlorine nuclei was as expected in the order $PCl_3 > P(CN)Cl_2 > P(CN)_2Cl$, and this broadening, together with low concentration and low natural abundance of the ^{13}C isotopomer, made it impossible to distinguish the satellite ^{31}P NMR spectrum of $P(^{13}CN)Cl_2$ from noise, although a small doublet was tentatively assigned to this compound in the corresponding ^{13}C NMR spectrum, where the complication of an overlying main spectrum was absent. In order to confirm this assignment, by observation of the satellite doublet in the ^{31}P NMR spectrum, a higher concentration of $P(CN)Cl_2$ was required. Consequently, the preparative reaction was repeated, but with Pr^nI instead of MeCN as solvent, since this was reported to yield $P(CN)Cl_2$ rather than $P(CN)_3$ as the initial product.[2] In order to observe this, the reaction mixture was filtered after stirring for only 100 min after addition of the PCl_3, and a 16 h ^{31}P NMR accumulation was started immediately. The spectrum showed 93.9% of total phosphorus remaining as PCl_3, but already the concentration of $P(CN)_3$ (3.0%) exceeded that of $P(CN)Cl_2$ (0.3%). Clearly the use of MeCN as solvent favoured the production of $P(CN)_3$, but use of Pr^nI was not a good way of making $P(CN)Cl_2$ instead. The solution was reunited with the precipitate of silver salts, and stirred at 20°C for a further 4 days. Concentrations were now PCl_3 (75.8%), $P(CN)Cl_2$ (7.1%), $P(CN)_2Cl$ (4.5%) and $P(CN)_3$ (6.6%), along with other minor products. These concentrations allowed satellite doublets to be found in the ^{31}P NMR spectrum for all three cyano compounds. The ^{13}C NMR spectrum of $P(CN)Cl_2$ was now clearly distinguishable from noise, but surprisingly that of $P(CN)_2Cl$ could not be found in this case.

Chemical shifts

^{31}P chemical shifts of the cyano compounds in MeCN were different from those in Pr^nI (Table 1) by much more than the appropriate magnetic susceptibility corrections. Dillon *et al.* proposed that this reflected specific interactions between MeCN and these solutes, but that only $P(CN)_3$ was "markedly affected".[2] The present, more detailed data showed the following trends (Table 1): (a) the decrement in shift on replacing Cl by CN was in each case less for solution in Pr^nI than in MeCN; (b) these differences in decrements accumulated so that while PCl_3 absorbed to higher frequency in MeCN than in Pr^nI, $P(CN)_3$ absorbed 8.11 ppm to lower frequency in MeCN than in Pr^nI; and (c) the decrement between $P(CN)_2Cl$ and $P(CN)_3$ was for both solvents much less than the other decrements.

The ^{13}C chemical shifts (Table 1) formed a regular series. There was little change in shift in going from solution in MeCN to solution in Pr^nI, though the decrement in chemical shift between $P(CN)Cl_2$ and $P(CN)_3$ was slightly less (9.10 ppm) in solution in MeCN than in Pr^nI (10.73 ppm).

Table 1. Chemical shifts and chemical shift differences (ppm) for $P(CN)_nCl_{3-n}$ ($n = 0$–3)

	^{31}P chemical shifts					^{13}C chemical shifts	
	In solution in MeCN		In solution in Pr^nI		Difference	Solution	Solution
Compound	Shifts	Differences	Shifts	Differences	$\delta(MeCN)-\delta(Pr^nI)$	in MeCN	in Pr^nI
PCl_3	220.63		218.81		1.82		
		126.83		125.98			
$P(CN)Cl_2$	93.80		92.83		0.97	119.64	116.93
		128.26		125.01			
$P(CN)_2Cl$	−34.46		−32.18		−2.28	115.29	[a]
		103.37		97.54			
$P(CN)_3$	−137.83		−129.72		−8.11	110.54	106.20

[a] Not observed.

Coupling constants

The relatively wide range of ^{31}P NMR chemical shifts for the mixtures, the broadening of the ^{31}P NMR peaks by scalar coupling relaxation by chlorine, and the difficulties inherent in observing satellite spectra, made the accuracy of ^{31}P–^{13}C coupling constants obtained from the ^{31}P spectra considerably less than of those obtained from the ^{13}C spectra. Consequently, except for the case of $P(CN)_2Cl$ in Pr^nI, the values presented in Table 2 are from the ^{13}C spectra, and comparison with those from the ^{31}P spectra was used to confirm the ^{13}C shift assignments.

Absolute values of the $^1J(^{31}P–^{13}C)$ coupling constants (Table 2) increased strongly as cyanide ligands were replaced by the more electronegative chloride. This trend was consistent with, but more extreme than, increases in $^1J(^{31}P–^{15}N)$ in going from $P(^{15}NCS)_3$ to $P(^{15}NCS)_2Cl$,[1] or from $P(^{15}NMe_2)(^{14}NMe_2)_2$ to $P(^{15}NMe_2)Cl_2$,[3] and with the algebraic decrease in $^1J(^{31}P–^{13}C)$ in going from $P(^{13}CH_3)(^{12}CH_3)_2$ (−13.6 Hz) to $P(^{13}CH_3)Cl_2$ (−45 Hz).[4] Most reported $^1J(^{31}P–^{13}C)$ couplings for three-coordinate phosphorus compounds are for alkyl derivatives, and values differ little from that for Me_3P, except in cases of ring strain or steric crowding (typical range 0 to −40 Hz).[5] Orbital involvement in P—C bonding in phosphorus(III) cyanides will clearly be very different from that in alkyl derivatives, but some similarity in size of $^1J(^{31}P–^{13}C)$ might have been expected between phosphorus(III) cyanides and corresponding acetylides. However, $^1J_{PC}$ has been reported as +8.8 Hz for $(MeC{\equiv}C)_3P$, moving to relatively small negative values with substitution of more electronegative groups [as in e.g. $(MeC{\equiv}C)P(OEt)_2$ (−39.1 Hz) or $(HC{\equiv}C)P(OEt)_2$ (−50.0 Hz)].[6] It is very probable that the numerically larger coupling constants reported here are negative.

Changes of chemical shift with solvent, such as those reported here, are common and could reflect only a comparatively weak solute–solvent interaction. However, $^1J_{PC}$ was also strongly affected by solvent (Table 2), the couplings for solution in MeCN being consistently 5–7 Hz numerically larger than for solution in Pr^nI. This was a stronger pointer to specific interaction between MeCN and the phosphorus(III) cyanides. If numerically increased coupling constants here reflected stronger P—C bonds, then these would have been consistent with the favouring of the formation of P—CN bonds by the use of MeCN as a solvent.

Table 2. Coupling constants $|^1J(^{31}P–^{13}C)|$ (Hz) for $P(CN)_nCl_{3-n}$ (n = 1–3)

Compound	In solution in MeCN	In solution in Pr^nI	Difference $\|J(MeCN)-J(Pr^nI)\|$
$P(CN)Cl_2$	152.4	145.7	6.7
$P(CN)_2Cl$	102.5	96.9	5.6
$P(CN)_3$	60.2	55.1	5.1

Secondary isotope shifts

Isotope shifts $^1\Delta^{31}P(^{13/12}C)$, for solution in Pr^nI, increased numerically slowly in the sequence $P(CN)_3 < P(CN)_2Cl < P(CN)Cl_2$ (−0.043, −0.049 and −0.053 ppm, respectively), probably corresponding to increasing bond strengths as the series of $^1J_{PC}$ coupling constants did for these compounds. In contrast to the couplings, for the two cases measured [$P(CN)_3$ and $P(CN)_2Cl$], the secondary isotope shifts in solution in MeCN were not significantly different from those in Pr^nI.

Acknowledgements—Miss C. J. Dodds is thanked for her contribution during an undergraduate product, and Dr M. N. S. Hill for obtaining the NMR spectra.

REFERENCES

1. B. W. Tattershall, *J. Chem. Soc., Chem. Commun.* 1989, 216; *J. Chem. Soc., Dalton Trans.*, in press.
2. K. B. Dillon, M. G. Craveirinha Dillon and T. C. Waddington, *J. Inorg. Nucl. Chem.* 1976, **38**, 1149.
3. J.-P. Gouesnard, J. Dorie and G. J. Martin, *Can. J. Chem.* 1980, **58**, 1295.
4. J. P. Albrand and D. Gagnaire, *Chem. Commun.* 1970, 874.
5. L. D. Quin, in *Phosphorus-31 NMR Spectroscopy in Stereochemical Analysis* (Edited by J. G. Verkade and L. D. Quin). VCH, Deerfield Beach, Florida (1987).
6. R.-M. Lequan, M.-J. Pouet and M.-P. Simonnin, *Org. Magn. Reson.* 1975, **7**, 392.

Polyhedron Vol. 9, No. 4, pp. 557–563, 1990
Printed in Great Britain

0277–5387/90 $3.00+.00
© 1990 Pergamon Press plc

STUDIES ON TETRAMETALLIC COMPLEXES OF FERROCENE

P. P. SINGH* and N. B. SINGH

Chemistry Department, Bareilly College, Bareilly—243001, India

(*Received* 13 *April* 1989; *accepted* 12 *September* 1989)

Abstract—Tetrametallic complexes having four different metals, mercury, iron, M and M′ (M = Ni^{II}, Co^{II}, Cu^{II}, Zn^{II} and Mn^{II}; M′ = Co^{II} and Ni^{II}) have been prepared by reacting $Fe(C_5H_4HgSCN)_2M(NCS)_2$ with M′(salen) [salen = $(C_6H_4CH{=}NCH_2O)_2$]. All the complexes have been characterized by elemental analyses, molar conductance, magnetic moment, IR and electronic spectral studies. The studies indicate that the geometry around M in the complexes is octahedral. Additional support for the proposed structure has been provided by softness parameters.

In this paper studies on a new class of complexes containing four different metals are presented, for the first time.

EXPERIMENTAL

Reagent grade solvents were purified before use. $M(NCS)_2$ (M = Ni^{II}, Co^{II}, Cu^{II}, Zn^{II} and Mn^{II}) were prepared by reacting their respective nitrates with KNCS in ethanol. Co(salen) and Ni(salen) were prepared and recrystallized by the method described elsewhere.[1] $Fe(C_5H_4HgSCN)_2M(NCS)_2$ and the tetrametallic complexes [$Fe(C_5H_4HgSCN)_2M(NCS)_2M'(C_6H_4CH{=}NCH_2O)_2$] were prepared as given below.

Preparation of $Fe(C_5H_4HgSCN)_2M(NCS)_2$ (M = Ni^{II}, Co^{II}, Cu^{II}, Zn^{II} *and* Mn^{II})

To a solution of 18.4 g (0.1 mol) of ferrocene in dry benzene, a homogeneous suspension of 32.8 g (0.1 mol) of mercuric acetate in methanol was slowly added with stirring. A dark brown solution was obtained, to which a water solution of 9.7 g (0.1 mol) of KSCN was added and stirred. An orange precipitate was formed, which was separated. This precipitate was subjected to Soxhlet extraction using 1,2-dichloroethane as solvent, several times until the extract became colourless. The residue was FMBT, which was purified by dissolving in DMSO, followed by addition of water. FBMT was dissolved in a small quantity of DMSO and diluted to 100 cm^3 with acetone. To this solution an acetone solution of an equimolar quantity of $M(NCS)_2$ was added and stirred for 24 h. A precipitate which appeared in each case was filtered, washed with ethanol and dried *in vacuo*. The compounds were recrystallized from an acetone–ethanol mixture.

Preparation of tetrametallic complexes [$Fe(C_5H_4HgSCN)_2M(NCS)_2M'(C_6H_4CH{=}NCH_2O)_2$] (M = Ni^{II}, Co^{II}, Cu^{II}, Zn^{II} *and* Mn^{II}; M′ = Co^{II} *and* Ni^{II})

$Fe(C_5H_4HgSCN)_2M(NCS)_2$ (1 mmol) was dissolved in 10 cm^3 of DMSO and diluted to 100 cm^3 with 1,2-dichloroethane. An equimolar quantity of $M'(C_6H_4CH{=}NCH_2O)_2$ was dissolved in the same solvent. The two solutions were mixed and stirred for 36 h at room temperature. In each case a precipitate appeared which was filtered, washed with petroleum ether and dried *in vacuo*. The compound was recrystallized by dissolving in DMSO, followed by the addition of water.

Analyses of the complexes

The compounds were analysed for cobalt as anthranilate, nickel as dimethylglyoximate, sulphur as sulphate and mercury as sulphide. Nitrogen was estimated by semi-micro Kjeldahl's method. Analytical results along with melting points are presented in Table 1.

* Author to whom correspondence should be addressed.

Table 1. Analytical data of the complexes

Complexes	Colour	Melting point[a]	% S Calc.	% S Found
Lewis acids				
1. $Fe(C_5H_4HgSCN)_2Ni(NCS)_2$	Yellowish-green	240	14.6	14.3
2. $Fe(C_5H_4HgSCN)_2Cu(NCS)_2$	Light green	150	14.5	14.2
3. $Fe(C_5H_4HgSCN)_2Zn(NCS)_2$	Dirty white	175	14.5	14.3
4. $Fe(C_5H_4HgSCN)_2Mn(NCS)_2$	Grey	165	14.7	14.5
5. $Fe(C_5H_4HgSCN)_2Co(NCS)_2$	Blue	230	14.6	14.2
Adducts				
6. $Fe(C_5H_4HgSCN)_2Ni(NCS)_2Co(C_6H_4CH{=}NCH_2O)_2$	Olive green	130	10.7	10.4
7. $Fe(C_5H_4HgSCN)_2Cu(NCS)_2Co(C_6H_4CH{=}NCH_2O)_2$	Cabinet olive	138	10.6	10.2
8. $Fe(C_5H_4HgSCN)_2Zn(NCS)_2Co(C_6H_4CH{=}NCH_2O)_2$	Green	150	10.6	10.5
9. $Fe(C_5H_4HgSCN)_2Mn(NCS)_2Co(C_6H_4CH{=}NCH_2O)_2$	Brown	135	10.7	10.5
10. $Fe(C_5H_4HgSCN)_2Co(NCS)_2Co(C_6H_4CH{=}NCH_2O)_2$	Brown	145	10.7	10.1
11. $Fe(C_5H_4HgSCN)_2Co(NCS)_2Ni(C_6H_4CH{=}NCH_2O)_2$	Golden brown	189	10.7	10.4
12. $Fe(C_5H_4HgSCN)_2Cu(NCS)_2Ni(C_6H_4CH{=}NCH_2O)_2$	Olive green	186	10.6	10.6
13. $Fe(C_5H_4HgSCN)_2Zn(NCS)_2Ni(C_6H_4CH{=}NCH_2O)_2$	Golden brown	156	10.6	10.3
14. $Fe(C_5H_4HgSCN)_2Mn(NCS)_2Ni(C_6H_4CH{=}NCH_2O)_2$	Olive green	204	10.7	10.6
15. $Fe(C_5H_4HgSCN)_2Ni(NCS)_2Ni(C_6H_4CH{=}NCH_2O)_2$	Olive green	180	10.7	10.3

[a] All the complexes are decomposed.

Physical measurements

The molar conductance of the complexes were measured in DMSO using a Toshniwal conductivity bridge type CL01/02A. The magnetic susceptibility measurements were carried out at room temperature by Gouy's method using $CoHg(SCN)_4$ as standard. The diamagnetic corrections were made using Pascal's constants. IR spectra of the compounds were recorded as Nujol mulls on a Pye Unicam SP-3-300 spectrophotometer in the range 4000–200 cm^{-1}. Electronic spectra in the range 200–999 nm were recorded on a Pye Unicam SP-5-500 spectrophotometer.

RESULTS AND DISCUSSION

M′(salen)[M′ = Ni^{II} *and* Co^{II}; salen = $(C_6H_4CH{=}NCH_2O)_2$]

These compounds are reported to act as bidentate ligands through oxygen atoms towards transition and non-transition metals.[2-4] The coordination geometry around M′ in M′(salen) is square-planar[4] as shown in Fig. 1. The Co(salen) has one unpaired electron and the magnetic moment value is 2.10 BM whereas the Ni(salen) is diamagnetic. The IR spectral band at 1536 cm^{-1} in M′(salen) has been assigned to C—O bond stretching[5] and the frequency of this absorption is expected to increase, when it is involved in coordination. The IR spectral bands at 1380 and 1340 cm^{-1} are assigned to the imino group in M′(salen). The electronic spectral bands of Co(salen) are present at 18,750 and 10,240 cm^{-1} and are assigned to $^2A_{1g} \rightarrow {}^2E_g$ and $^2A_{1g} \rightarrow {}^2B_{2g}$ transitions, respectively.

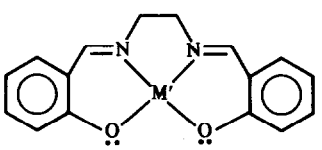

(M′ = Ni^{II} and Co^{II})

Fig. 1.

$Fe(C_5H_4HgSCN)_2M(NCS)_2$ (M = Ni^{II}, Co^{II}, Cu^{II}, Zn^{II} *and* Mn^{II})

These compounds are reported to act as Lewis acids.[6-8] The IR spectra, magnetic moment values, molar conductance and electronic spectral data are presented in Table 2, which indicate that the geometry[8-11] around M is tetrahedral when M is Co^{II}, Mn^{II} and Zn^{II}, and octahedral when Cu^{II} or Ni^{II}, through axial bonding as shown in Fig. 2(a) and (b), respectively.

Table 1 (*continued*)

% Hg		% Cu/Zn/Mn		% N		% Ni		% Co		Molar conductance
Calc.	Found	Calc.	Found	Calc.	Found	Calc.	Found	Calc.	Found	($cm^2 \Omega mol^{-1}$)
45.7	45.6	—	—	6.4	6.2	6.6	6.5	—	—	70.34
45.4	45.0	7.1	7.2	6.4	6.3	—	—	—	—	30.58
45.3	44.0	7.4	7.1	6.3	6.1	—	—	—	—	48.38
46.0	44.1	6.2	6.0	6.4	6.2	—	—	—	—	48.02
45.7	44.0	—	—	6.4	6.2	—	—	6.6	6.5	58.62
33.4	32.8	—	—	7.0	6.7	4.9	4.6	4.9	4.7	52.50
33.3	32.0	5.3	5.1	7.0	6.6	—	—	4.9	4.6	42.00
33.2	32.1	5.4	5.1	7.0	6.7	—	—	4.9	4.6	73.50
33.5	32.9	4.6	4.4	7.0	6.9	—	—	4.9	4.8	80.00
33.4	32.5	—	—	7.0	6.7	—	—	9.8	9.5	60.28
33.4	33.0	—	—	7.0	6.8	4.9	4.7	4.9	4.8	60.00
33.3	31.7	5.3	4.9	7.0	6.3	4.9	4.7	—	—	50.00
33.2	32.4	5.4	5.2	7.0	6.8	4.9	4.7	—	—	65.00
33.5	31.3	4.6	4.3	7.0	6.9	4.9	4.8	—	—	68.06
33.4	32.0	—	—	7.0	6.3	9.8	9.7	—	—	65.50

Tetrametallic complexes $Fe(C_5H_4HgSCN)_2M(NCS)_2$ $M'(C_6H_4CH{=}NCH_2O)_2$ (M = Ni^{II}, Co^{II}, Cu^{II}, Zn^{II} *and* Mn^{II}; M′ = Co^{II} *and* Ni^{II})

The coordination number of M in $Fe(C_5H_4HgSCN)_2M(NCS)_2$, where M is Co^{II}, Zn^{II} and Mn^{II}, is four against the maximum of six. Due to this unsaturation at M, they have been referred to as Lewis acids. When M is Ni^{II} or Cu^{II} the six coordination has been achieved through weak axial bonding which can easily be replaced by ligands. Accordingly, both types of compounds have the potentiality of behaving as an acceptor, and reacting with ligands. Ni(salen) and Co(salen) act as bidentate ligands. On reaction with these acceptors they form adducts of the general formula $Fe(C_5H_4HgSCN)_2M(NCS)_2M'(C_6H_4CH{=}NCH_2O)_2$, which have four different metals and are the first of their types.

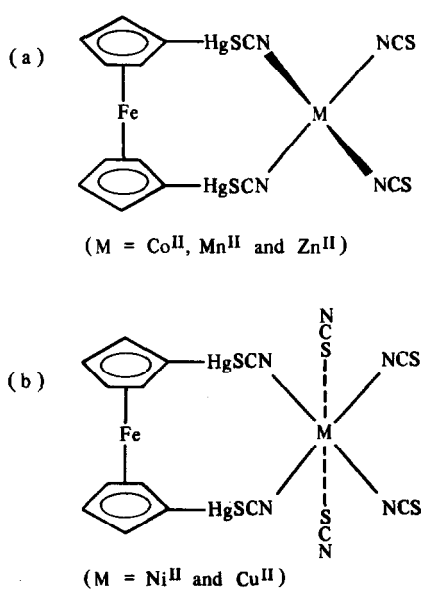

Fig. 2.

A change in the phenolic C—O stretching mode in the 1500–1600 cm^{-1} region can be used to indicate coordination through the oxygen of M′(salen). A comparison of the IR spectra of Co(salen) and Ni(salen) with the spectra of adducts show that there is a positive shift in the bands assigned to phenolic C—O stretching (Table 2). The positive shift in phenolic C—O stretching indicates coordination of M′(salen) through the oxygen atom to M of $Fe(C_5H_4HgSCN)_2M(NCS)_2$. The other possible site of coordination is the imino group of M′(salen). The bands at 1380 and 1340 cm^{-1} assigned to the imino group remain unaltered.

The position of IR bands diagnostic of thio-

Table 2. IR spectral and electronic spectral bands with parameters

Complexes	IR spectral bands (cm^{-1}) ν (C—N)	ν (C—S)	δ (NCS)	δ M(NCS)
Ligand				
1. Co(salen)	—	—	—	—
2. Ni(salen)	—	—	—	—
Lewis acids				
3. $Fe(C_5H_4HgSCN)_2Mn(NCS)_2$	2180(s) 2110(w)	750(w) 720(s)	460(m) 450(s)	315(m) 285(s)
4. $Fe(C_5H_4HgSCN)_2Co(NCS)_2$	2190(s) 2120(s)	790(s) 760(w)	480(sh) 460(s)	320(s) 295(s)
5. $Fe(C_5H_4HgSCN)_2Ni(NCS)_2$	2117(w) 2100(s)	780(s) 760(s)	470(s) 450(s)	260(s) 240(sh)
6. $Fe(C_5H_4HgSCN)_2Cu(NCS)_2$	2180(s) 2100(m)	760(s) 740(s)	480(w) 440(s)	265(s) 245(m)
7. $Fe(C_5H_4HgSCN)_2Zn(NCS)_2$	2160(sh) 2100(s)	770(m) 740(s)	470(s) 450(s)	325(s) 280(m)
Adducts				
8. $Fe(C_5H_4HgSCN)_2Ni(NCS)_2Co(C_6H_4CH{=}NCH_2O)_2$	2160(s) 2100(w)	755(s) 720(s)	490(s) 470(sh)	275(s) 265(s)
9. $Fe(C_5H_4HgSCN)_2Cu(NCS)_2Co(C_6H_4CH{=}NCH_2O)_2$	2170(s) 2110(s)	760(s) 750(sh)	490(s) 440(sh)	280(s) 265(s)
10. $Fe(C_5H_4HgSCN)_2Zn(NCS)_2Co(C_6H_4CH{=}NCH_2O)_2$	2160(s) 2100(sh)	760(s) 720(s)	470(s) 445(s)	275(s) 260(s)
11. $Fe(C_5H_4HgSCN)_2Mn(NCS)_2Co(C_6H_4CH{=}NCH_2O)_2$	2150(s) 2090(s)	750(s) 720(w)	465(s) 440(w)	275(s) 260(m)
12. $Fe(C_5H_4HgSCN)_2Co(NCS)_2Co(C_6H_4CH{=}NCH_2O)_2$	2160(s) 2130(s)	750(s) 720(s)	460(s) 440(s)	290(s) 230(m)
13. $Fe(C_5H_4HgSCN)_2Ni(NCS)_2Ni(C_6H_4CH{=}NCH_2O)_2$	2170(s) 2110(s)	770(s) 750(s)	480(s) 440(m)	260(m) 250(s)
14. $Fe(C_5H_4HgSCN)_2Co(NCS)_2Ni(C_6H_4CH{=}NCH_2O)_2$	2180(s) 2150(s)	770(s) 730(s)	460(s) 445(s)	290(m) 260(m)
15. $Fe(C_5H_4HgSCN)_2Cu(NCS)_2Ni(C_6H_4CH{=}NCH_2O)_2$	2190(s) 2130(s)	760(s) 740(s)	465(s) 440(s)	260(m) 235(m)
16. $Fe(C_5H_4HgSCN)_2Zn(NCS)_2Ni(C_6H_4CH{=}NCH_2O)_2$	2175(s) 2110(s)	770(s) 720(s)	480(s) 450(s)	250(s) 230(m)

s = strong, m = medium, sh = shoulder, w = weak.

Bands at 18,750 and 10,240 cm^{-1} in the electronic spectra are assigned to ν_3 and ν_2 in Co(salen) and are also observed in the corresponding adducts.

cyanate regions have also been examined, to see the effect of coordination through the oxygen atom of M′(salen) to M of $Fe(C_5H_4HgSCN)_2M(NCS)_2$. The coordination of M′(salen) will change the geometry of Co^{II}, Mn^{II} and Zn^{II} from tetrahedral in the Lewis acids to octahedral in the adducts. The change will affect the positions of IR spectral bands and also the electronic spectral parameters. The positions of the δ (M—NCS) bands, where M is Co^{II}, Zn^{II} and Mn^{II}, is changed from 280–325 to 230–290 cm^{-1}. This negative shift is on account of a change in the tetrahedral geometry around M in the Lewis acids to octahedral[9–11] in the adducts. Such a change is not observed when M is Ni^{II} or Cu^{II}, because the geometry around M remains octahedral both in the Lewis acids and the adducts. The IR

Table 2 (*continued*)

IR spectral bands (cm^{-1})		Electronic spectral bands (cm^{-1}) and parameters						
ν (C—O)	ν (imino group)	ν_3	ν_2	ν_1	Dq (cm^{-1})	B'	β	μ_{eff} (BM)
1540(s) 1520(m)	1380(s) 1340(s)	18,750	10,240	—	610	712	0.69	2.10
1535(s) 1525(s)	1380(s) 1340(w)	—	—	—	—	—	—	—
—	—	—	—	—	—	—	—	6.40
—	—	15,400	6100	—	401	631	0.61	4.24
—	—	27,290	16,650	10,400	906	906	0.87	3.07
—	—	—	—	—	—	—	—	1.92
—	—	—	—	—	—	—	—	—
1555(s) 1535(m)	1380(s) 1340(w)	24,250	16,380	10,640	945	685	0.67	5.57
1550(m) 1540(s)	1380(s) 1340(s)	—	—	—	—	—	—	3.87
1560(s) 1540(s)	1380(w) 1340(s)	—	—	—	—	—	—	2.05
1550(s) 1535(s)	1380(s) 1380(m)	—	—	—	—	—	—	7.95
1560(s) 1535(m)	1380(m) 1340(s)	22,220	15,150	—	881	729	0.70	6.70
1550(s) 1540(s)	1380(s) 1340(m)	25,640	16,250	10,400	1040	712	0.69	3.25
1550(s) 1540(s)	1380(m) 1340(s)	21,740	15,150	—	716	861	0.88	4.87
1550(s) 1535(w)	1380(s) 1340(m)	—	—	—	—	—	—	2.36
1555(s) 1540(w)	1380(s) 1340(s)	—	—	—	—	—	—	—

spectra of adducts (Table 2) show that there is no significant change in the positions of the ν(C—N), ν(C—S) and δ(NCS) bands. This shows that the bridging nature of thiocyanate in the Lewis acids is retained in the adducts.

The electronic spectral data of the Lewis acids and the adducts, where M is Co^{II} and Ni^{II}, are presented in Table 2. Adducts where M is Co^{II} show the presence of two bands in the region 21,740–22,220 and 15,150 cm^{-1}, which are assigned to $^4A_{2g} \rightarrow {}^4T_{2g}$ (F) (ν_3) and $^4A_{2g} \rightarrow {}^4T_{1g}$ (P) (ν_2) transitions, respectively. In the Lewis acids of Co^{II}, two intense bands were present in the region 15,400 and 6100 cm^{-1} assigned to $^4A_2 \rightarrow {}^4T_2$ (F) (ν_3) and $^4A_2 \rightarrow {}^4T_1$ (P) (ν_2) transitions, respectively. This shows that the positions of the electronic spectral bands have changed from the tetrahedral to octahedral region. Accordingly, spectral parameters Dq, β and B' have also changed. The adducts where M is Ni^{II} show the presence of three bands in the region 24,250–25,640, 16,250–16,380 and 10,400–10,640 cm^{-1} which are assigned to $^3A_{2g} \rightarrow {}^3T_{1g}$ (P)

Table 3. $\Delta E^{\ddagger}_{nm(\text{eff})}$ derived from $E^{\ddagger}_{n(\text{eff})}$ of M in $Fe(C_5H_4HgSCN)_2M(NCS)_2$ and the oxygen centre of Ni(salen) and Co(salen) in the formation of adducts

Complexes	$E^{\ddagger}_{n(\text{eff})}$ of M in Lewis acid	$E^{\ddagger}_{n(\text{eff})}$ of L at oxygen	$\Delta E^{\ddagger}_{nm(\text{eff})}$
1. $Fe(C_5H_4HgSCN)_2Ni(NCS)_2Co(C_6H_4CH{=}NCH_2O)_2$	−2.28	−20.38	18.10
2. $Fe(C_5H_4HgSCN)_2Zn(NCS)_2Co(C_6H_4CH{=}NCH_2O)_2$	−4.11	−20.38	16.27
3. $Fe(C_5H_4HgSCN)_2Mn(NCS)_2Co(C_6H_4CH{=}NCH_2O)_2$	−8.90	−20.38	11.48
4. $Fe(C_5H_4HgSCN)_2Co(NCS)_2Co(C_6H_4CH{=}NCH_2O)_2$	−2.83	−20.38	17.55
5. $Fe(C_5H_4HgSCN)_2Ni(NCS)_2Ni(C_6H_4CH{=}NCH_2O)_2$	−2.28	−20.40	18.12
6. $Fe(C_5H_4HgSCN)_2Co(NCS)_2Ni(C_6H_4CH{=}NCH_2O)_2$	−2.83	−20.40	17.57
7. $Fe(C_5H_5HgSCN)_2Zn(NCS)_2Ni(C_6H_4CH{=}NCH_2O)_2$	−4.11	−20.40	16.29
8. $Fe(C_5H_4HgSCN)_2Mn(NCS)_2Ni(C_6H_4CH{=}NCH_2O)_2$	−8.90	−20.40	11.50

L = $Co(C_6H_4CH{=}NCH_2O)_2Co$(salen) and $Ni(C_6H_4CH{=}NCH_2O)_2Ni$(salen).

(ν_3), $^3A_{2g} \rightarrow {}^3T_{1g}(F)$ (ν_2) and $^3A_{2g} \rightarrow {}^3T_{2g}(F)$ (ν_1) transitions, respectively. In the Lewis acid of Ni^{II} these bands were contained in the regions 27,790, 16,650 and 10,400 cm^{-1}. This shows that the electronic spectral bands and spectral parameters (Dq, β and B') in adducts are changed slightly but are in the octahedral region, indicating octahedral geometry around M in Lewis acids and adducts also.

The magnetic moment value of $Fe(C_5H_4HgSCN)_2Ni(NCS)_2$ is 3.07 BM and that of the Ni(salen) adduct is 3.25 BM. Since the two values are very similar, it can be inferred that the diamagnetic nature of Ni(salen) is not disturbed and it does not contribute to the magnetic moment value of the adduct. The cobalt analogue, however, causes an increase in the magnetic moment value to 6.70 BM, which is the sum of the magnetic moment values of the Lewis acid and of the Co(salen). Thus the magnetic moment value of $Fe(C_5H_4HgSCN)_2M(NCS)_2Ni(C_6H_4CH{=}NCH_2O)_2$ is entirely due to paramagnetism of M, because $Ni(C_6H_4CH{=}NCH_2O)_2$ does not contribute on account of its diamagnetic character. The magnetic moment values of M in $Fe(C_5H_4HgSCN)_2M(NCS)_2Co(C_6H_4CH{=}NCH_2O)_2$ are raised because $Co(C_6H_4CH{=}NCH_2O)_2$ contributes to the magnetic moment in the range of 2.1–2.8 BM.[12] All the adducts are non-conducting in nature. On the basis of these results the structure shown in Fig. 3 is proposed for the adducts.

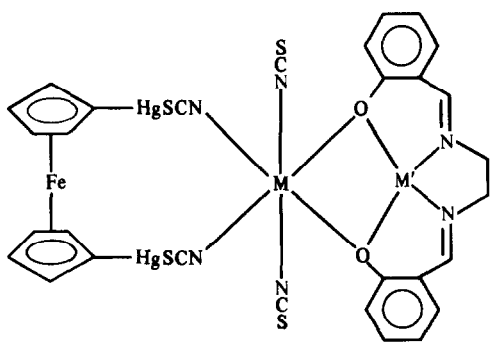

(M = Ni^{II}, Co^{II}, Cu^{II}, Zn^{II} and Mn^{II}; M' = Co^{II}, Ni^{II})

Fig. 3.

Quantitative softness parameters

The effective softness values of metal and base ions have been denoted by $E^{\ddagger}_{n(\text{eff})}$ and $E^{\ddagger}_{m(\text{eff})}$, respectively and the difference between the two by $\Delta E^{\ddagger}_{nm(\text{eff})}$. These values have been derived by adopting the procedure described elsewhere.[13] The $\Delta E^{\ddagger}_{nm(\text{eff})}$ between $E^{\ddagger}_{n(\text{eff})}$ of M in $Fe(C_5H_4HgSCN)_2M(NCS)_2$ and $E^{\ddagger}_{m(\text{eff})}$ at oxygen in Ni(salen) and Co(salen) have been derived, and are presented in Table 3. The $\Delta E^{\ddagger}_{nm(\text{eff})}$ values of Ni(salen) adducts are higher than Co(salen) adducts, indicating that Ni(salen) forms more stable M—L bonds than Co(salen). $\Delta E^{\ddagger}_{nm(\text{eff})}$ values are highest when M is Ni^{II} and lowest when M is Mn^{II}. This indicates that nickel forms more stable bonds with these ligands than manganese, and the sequence is as follows: nickel > cobalt > zinc > manganese.

Acknowledgement—The authors are grateful to the CSIR, New Delhi for financial assistance.

REFERENCES

1. R. H. Bailes and M. Calvin, *J. Am. Chem. Soc.* 1947, **69**, 1880.
2. C. Floriani, F. Calderazzo and L. Randaccio, *J. Chem. Soc., Chem. Commun.* 1973, 384.
3. N. Bresciani-Pahor, M. Calligaris, P. Delise, G. Nardini, L. Randaccio, E. Zotti, G. Franchinetti and C. Floriani, *J. Chem. Soc., Dalton Trans.* 1976, 2310.

4. L. G. Armstrong, H. P. Lip, L. F. Lindoy, M. McPartlin and P. A. Tasker, *J. Chem. Soc., Dalton Trans.* 1977, 1771.
5. G. E. Batley and D. P. Graddon, *Austral. J. Chem.* 1967, **20**, 877.
6. P. P. Singh and Divya Singh, *Synth. React. Inorg. Met.-Org. Chem.* 1985, **15**, 1219.
7. P. P. Singh and Divya Singh, *Ind. J. Chem.* 1986, **25A**, 620.
8. P. P. Singh and D. S. Gupta, *Polyhedron* 1986, **5**, 1941.
9. R. J. H. Clark and C. S. Williams, *Spectrochim. Acta* 1966, **22**, 1081.
10. D. Forster and D. M. L. Goodgame, *Inorg. Chem.* 1965, **4**, 715.
11. R. Makhija, L. Pazdernika and R. Rivest, *Can. J. Chem.* 1973, **51**, 2987.
12. R. L. Dutta and A. Syamal, *Elements of Magnetochemistry*. S. Chand, New Delhi (1982).
13. P. P. Singh, S. K. Srivastava and A. K. Srivastava, *J. Inorg. Nucl. Chem.* 1980, **42**, 521.

Polyhedron Vol. 9, No. 4, pp. 565–571, 1990
Printed in Great Britain

0277–5387/90 $3.00+.00
© 1990 Pergamon Press plc

REACTIONS OF THE A-FRAME-LIKE MONOCARBONYL COMPLEXES $Re_2(\mu\text{-}X)(\mu\text{-dppm})_2X_3(CO)$ (X = Cl OR Br; dppm = $Ph_2PCH_2PPh_2$) WITH TRIMETHYLPHOSPHINE AND TRIALKYLPHOSPHITE LIGANDS. THE STRUCTURAL CHARACTERIZATION OF $[Re_2(\mu\text{-}Cl)(\mu\text{-}CO)(\mu\text{-dppm})_2Cl_2(PMe_3)_2]Cl$

JU-SHENG QI, PHILLIP E. FANWICK and RICHARD A. WALTON*

Department of Chemistry, Purdue University, West Lafayette, IN 47907, U.S.A.

(*Received* 15 *June* 1989; *accepted* 11 *September* 1989)

Abstract—The 1 : 1 carbonyl adduct $Re_2Cl_4(dppm)_2(CO)$ reacts with PMe_3 in CH_2Cl_2 at room temperature to afford the green diamagnetic complex $[Re_2Cl_3(dppm)_2(CO)(PMe_3)_2]Cl$. When similar reactions are carried out in the presence of $NaBPh_4$ or $TlPF_6$, with THF or CH_2Cl_2 as the reaction solvents, respectively, the salts $[Re_2Cl_3(dppm)_2(CO)(PMe_3)_2]X$ (X = BPh_4 or PF_6) are produced. Similar procedures have been used to prepare the bromo-derivative $[Re_2Br_3(dppm)_2(CO)(PMe_3)_2]PF_6$, and the phosphite complexes $\{Re_2Cl_3(dppm)_2(CO)[P(OR)_3]_2\}PF_6$ (R = Me or Et). IR spectroscopy shows that the CO ligand is bridging the two metal centres (ν(CO) *ca* 1635 cm^{-1} for the PMe_3 complexes and *ca* 1680 cm^{-1} for the $P(OR)_3$ derivatives). This conclusion has been confirmed by a crystal structure determination on $[Re_2Cl_3(dppm)_2(CO)(PMe_3)_2]Cl \cdot 1/2CH_2Cl_2$. The crystallographic data are as follows: triclinic space group $P\bar{1}$, $a = 13.261(1)$, $b = 19.246(2)$, $c = 11.860(2)$ Å, $\alpha = 97.57(1)$, $\beta = 98.98(1)$, $\gamma = 79.08(1)°$, $V = 2919(1)$ $Å^3$ and $Z = 2$. The structure was refined to $R = 0.043$ ($R_w = 0.056$) for 5949 data with $I > 3.0\sigma(I)$. The dirhenium cation has the structure of an edge-shared bioctahedron with virtual C_{2v} symmetry. There is a *trans* disposition of bridging dppm ligands. The equatorial plane contains a bridging carbonyl and a bridging chloride ligand. The three chloride ligands are in an all-*cis* arrangement to one another on one side of this plane; the two PMe_3 ligands are *cis* to the μ-CO ligand. The Re—Re distance is 2.602(1) Å.

The monocarbonyl complexes of stoichiometry $Re_2X_4(dppm)_2(CO)$ (**1**; X = Cl or Br; dppm = $Ph_2PCH_2PPh_2$),[1,2] which are formed upon treating the triply bonded dirhenium(II) complexes

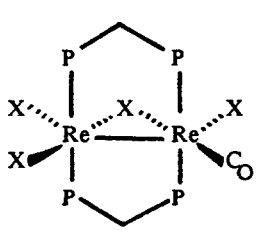

1

$Re_2X_4(dppm)_2$[3,4] with CO, react with additional equivalents of the π-acceptor CO ligand to form, sequentially, $Re_2(\mu\text{-}X)(\mu\text{-}CO)(\mu\text{-dppm})_2X_3(CO)$ (**2**)[1] and $[Re_2(\mu\text{-}X)(\mu\text{-}CO)(\mu\text{-dppm})_2X_2(CO)_2]^+$ (**3**),[5] species in which a metal–metal bonded dimetal unit is preserved. In a recent study,[6] in which the dicarbonyl complexes **2** were reacted with PMe_3 and $P(OR)_3$ ligands (R = Me or Et) in the presence of $TlPF_6$, the "phosphine-rich" species $[Re_2(\mu\text{-}X)(\mu\text{-}CO)(\mu\text{-dppm})_2X_2(CO)(L)]PF_6$ (L = PMe_3, $P(OMe)_3$ or $P(OEt)_3$) were isolated. These complexes were found to contain a semi-bridging CO ligand, a bonding mode which is probably a consequence of the charge disparity that is introduced in these unsymmetric species because of the disparate donor/acceptor properties associated with the terminal CO and PR_3 (or $P(OR)_3$) ligands.

In the present report, we describe the reactions of **1** (**a**, X = Cl; **b**, X = Br) with PMe_3, $P(OMe)_3$

*Author to whom correspondence should be addressed.

and $P(OEt)_3$ to give salts of the $[Re_2X_3(dppm)_2(CO)(L)_2]^+$ cations, in which the metal–metal bonded dirhenium unit is retained. The properties of these complexes are described, including a report on the X-ray crystal structure of the chloride salt $[Re_2Cl_3(dppm)_2(CO)(PMe_3)_2]Cl$.

EXPERIMENTAL

Starting materials

The monocarbonyl complexes $Re_2X_4(dppm)_2(CO)$ (X = Cl or Br) were prepared from the reactions of $Re_2X_4(dppm)_2$ with CO according to the established procedure.[1,2] Carbon monoxide (99.9%) was purchased from Matheson Gas Products. The tertiary phosphine and phosphite ligands were obtained from Strem Chemicals and Aldrich Chemical Co., respectively. Solvents used in the preparation of the complexes were of commercial grade and were thoroughly deoxygenated prior to use.

Reaction procedures

All reactions were performed under an atmosphere of dry dinitrogen.

(a) *Synthesis of* $[Re_2Cl_3(dppm)_2(CO)(PMe_3)_2]Cl$. A mixture of **1a** (0.047 g, 0.036 mmol) and PMe_3 (0.010 cm^3, 0.10 mmol) in dichloromethane (10 cm^3) was stirred at room temperature for 48 h. The green precipitate that resulted was filtered off, washed with a diethyl ether–methanol mixture (10:1, 10 cm^3), then with diethyl ether (25 cm^3), and finally dried *in vacuo*, yield 0.019 g (36%). Found: C, 46.7; H, 4.5. Calc. for $C_{57}H_{62}Cl_4OP_6Re_2$: C, 46.8; H, 4.3%.

(b) *Synthesis of* $[Re_2Cl_3(dppm)_2(CO)(PMe_3)_2]BPh_4$. A mixture of **1a** (0.079 g, 0.060 mmol), $NaBPh_4$ (0.021 g, 0.060 mmol) and 2 equiv. of PMe_3 (0.012 cm^3, 0.120 mmol) in THF (15 cm^3) was stirred at room temperature for 48 h. The colour of the reaction mixture changed from amber to green. The resulting green mixture was filtered to remove the white precipitate of NaCl. The filtrate was evaporated to dryness and the residue was extracted with 10 cm^3 of dichloromethane. The extract was filtered and the product isolated as green crystals by allowing cyclohexane vapour to diffuse into the solution contained within a closed system; yield 0.03 g (29%). Found: C, 56.1; H, 5.4. Calc. for $C_{81}H_{82}BCl_3OP_6Re_2$: C, 55.7; H, 4.7%.

(c) *Synthesis of* $[Re_2X_3(dppm)_2(CO)(PMe_3)_2]PF_6$ (X = Cl *or* Br). (i) X = Cl: A mixture comprising **1a** (0.019 g, 0.083 mmol), $TlPF_6$ (0.029 g, 0.083 mmol), and *ca* 3.6 equiv. of PMe_3 (0.03 cm^3, 0.295 mmol) in dichloromethane (10 cm^3) was stirred at room temperature for 48 h. The resulting green reaction mixture was filtered to remove the precipitated TlCl and the filtrate evaporated to dryness. The residue was extracted with a small volume of dichloromethane and filtered. The filtrate was transferred to a test tube that was, in turn, placed inside another tube of larger diameter that contained 10 cm^3 of hexane. The larger tube was capped under N_2(g) with a septum. The slow diffusion of hexane vapour into the dichloromethane solutions of the complex was allowed to take place. After 2 weeks, the green crystals that had formed on the side and at the bottom of the inner tube were collected, then washed with a 10 cm^3 portion of a diethyl ether–dichloromethane mixture (10:1) followed by 5 cm^3 of diethyl ether, and finally dried *in vacuo*; yield 0.068 g (52%). Found: C, 43.4; H, 4.2. Calc. for $C_{57}H_{62}Cl_3F_6OP_7Re_2$: C, 43.5; H, 4.0%.

(ii) X = Br: This complex was prepared from **1b** with the use of a procedure similar to that described in section c(i); yield, 52%. Found: C, 40.3; H, 4.0. Calc. for $C_{57}H_{62}Br_3F_6OP_7Re_2$: C, 40.1; H, 3.7%.

(d) *Synthesis of complexes of the type* $\{Re_2Cl_3(dppm)_2(CO)[P(OR)_3]_2\}PF_6$. These complexes were prepared, in the case of R = Me or Et, by the reaction of **1a** with the appropriate phosphite ligand with the use of a procedure very similar to that described in c(i). In all instances, the products were obtained as green crystals or powders.

(i) R = Me: Yield, 26%. Found: C, 40.6; H, 3.8. Calc. for $C_{57}H_{62}Cl_3F_6O_7P_7Re_2$: C, 41.0; H, 3.8%.

(ii) R = Et: Yield, 24%. Found: C, 42.4; H, 4.1. Calc. for $C_{63}H_{74}Cl_3F_6O_7P_7Re_2$: C, 43.2; H, 4.3.%.

Preparation of single crystals of $[Re_2Cl_3(dppm)_2(CO)(PMe_3)_2]Cl \cdot 1/2CH_2Cl_2$. A solution of PMe_3 (2 equiv.) in 5 cm^3 of CH_2Cl_2 was carefully layered over a similar solution containing **1a** (1 equiv.). This mixture was sealed under a N_2(g) atmosphere; diffusion of the solutions resulted in a colour change from amber to green. When the solvent was allowed to slowly evaporate from this mixture, suitable crystals of the title complex were obtained.

X-ray crystallographic studies

The structure of $[Re_2Cl_3(dppm)_2(CO)(PMe_3)_2]Cl \cdot 1/2CH_2Cl_2$ was determined with the use of general procedures that are described elsewhere.[7] A summary of the crystallographic data is given in Table 1. The cell constants are based on 25 reflections with $21° < \theta < 23°$. Three standard reflections were measured after every 5000 s of beam time during data collection. There was no systematic variations in intensity. Calculations were performed

Table 1. Crystal data and data collection parameters for $[Re_2Cl_3(dppm)_2(CO)(PMe_3)_2]Cl \cdot 1/2CH_2Cl_2$[a]

Formula	$Re_2Cl_5P_6OC_{57.5}H_{63}$
Formula weight	1505.65
Space group	$P\bar{1}$ (No. 2)
a (Å)	13.261(1)
b (Å)	19.246(2)
c (Å)	11.860(2)
α (°)	97.57(1)
β (°)	98.98(1)
γ (°)	79.08(1)
V (Å^3)	2919(1)
Z	2
d_{calc} (g cm^{-3})	1.713
Crystal dimensions (nm)	$0.30 \times 0.26 \times 0.13$
Temperature (°C)	20
Radiation (wavelength)	Mo-K_α (0.70930 Å)
Monochromator	Graphite
Linear absorption coefficient (cm^{-1})	46.49
Absorption correction applied	Empirical[b]
Transmission factors: min, max	0.71, 1.00
Diffractometer	Enraf–Nonius CAD4
Scan method	ω–2θ
h, k. l, limits	0–14, −20–20, −12–12
2θ range (°)	4.00–45.00
Scan width (°)	$0.78 + 0.35 \tan\theta$
Take-off angle (°)	1.90
Programs used	Enraf–Nonius SDP
$F(000)$	1476.0
p-Factor used in weighting	0.040
Data collected	7635
Unique data	7635
Data with $I > 3.0\sigma(I)$	5949
Number of variables	640
Largest shift/ESD in final cycle	0.05
R[c]	0.043
R_w[d]	0.056
Goodness-of-fit[e]	1.535

[a] Number in parentheses following certain data are ESDs occuring in the least significant digit.

[b] N. Walker and D. Stuart, *Acta Cryst.* 1983, **A39**, 158.

[c] $R = \Sigma \| F_o | - | F_c \| / \Sigma | F_o |$.

[d] $R_w = [\Sigma w(|F_o| - |F_c|)^2 / \Sigma w |F_o|^2]^{1/2}$; $w = 1/\sigma^2(F_o)$.

[e] Goodness-of-fit $= [\Sigma w(|F_o| - |F_c|)^2 / (N_{obs} - N_{parameters})]^{1/2}$.

on a MicroVAX II computer using the Enraf–Nonius structure determination package.

The crystal selected for the structure determination belongs to the triclinic space group $P\bar{1}$ with $Z = 2$. As a check on crystal quality, omega scans of several intense reflections were measured; the width at half-height was 0.78° with a take-off angle of 1.9°, indicating relatively poor crystal quality. The structure was solved by the use of the Patterson heavy-atom method, which revealed the positions of the rhenium atoms in the asymmetric unit. The remaining atoms were located in succeeding difference Fourier syntheses. Refinement of the outer-sphere chloride anion [Cl(1000)] proceeded satisfactorily. Lorentz and polarization corrections were applied to the data. An empirical absorption correction was applied,[8] the linear absorption coefficient being 46.49 cm^{-1}. No corrections for extinction were applied. The structure was refined in full-matrix least-squares where the function minimized was $\Sigma w(|F_o| - |F_c|)^2$, where w is the weighting factor defined as $w = 1/\sigma^2(F_o)$.

During the course of the refinement, it became apparent that residual electron density at non-

Table 2. Selected bond distances (Å) and angles (°) for $[Re_2Cl_3(dppm)_2(CO)(PMe_3)_2]Cl \cdot 1/2CH_2Cl_2$[a]

Distances			
Re(1)—Re(2)	2.6021(6)	Re(2)—Cl(2)	2.418(3)
Re(1)—Cl(1)	2.420(3)	Re(2)—Cl(B)	2.450(2)
Re(1)—Cl(B)	2.462(2)	Re(2)—P(21)	2.481(3)
Re(1)—P(11)	2.473(3)	Re(2)—P(22)	2.475(3)
Re(1)—P(12)	2.486(3)	Re(2)—P(23)	2.427(3)
Re(1)—P(13)	2.434(3)	Re(2)—C(1)	2.00(1)
Re(1)—C(1)	2.02(1)	O(1)—C(1)	1.20(1)
Angles			
Re(2)—Re(1)—Cl(1)	147.24(7)	Cl(B)—Re(1)—P(13)	177.3(1)
Re(2)—Re(1)—Cl(B)	57.80(6)	Cl(B)—Re(1)—C(1)	107.2(3)
Re(2)—Re(1)—P(11)	94.51(7)	P(11)—Re(1)—P(12)	165.84(9)
Re(2)—Re(1)—P(12)	95.31(7)	P(11)—Re(1)—P(13)	91.5(1)
Re(2)—Re(1)—P(13)	124.68(7)	P(11)—Re(1)—C(1)	96.2(4)
Re(2)—Re(1)—C(1)	49.5(3)	P(12)—Re(1)—P(13)	91.2(1)
Cl(1)—Re(1)—Cl(B)	89.46(9)	P(12)—Re(1)—C(1)	97.9(4)
Cl(1)—Re(1)—P(11)	84.2(1)	P(13)—Re(1)—C(1)	75.2(3)
Cl(1)—Re(1)—P(12)	82.0(1)	Re(1)—Cl(B)—Re(2)	63.97(6)
Cl(1)—Re(1)—P(13)	88.1(1)	Re(1)—C(1)—Re(2)	80.6(4)
Cl(1)—Re(1)—C(1)	163.3(3)	Re(1)—C(1)—O(1)	138(1)
Cl(B)—Re(1)—P(11)	87.10(9)	Re(2)—C(1)—O(1)	141(1)
Cl(B)—Re(1)—P(12)	89.52(9)		

[a] Numbers in parentheses are ESDs in the least significant digits.

bonding distances to the dirhenium cation and Cl^- anion could be satisfactorily modelled as lattice dichloromethane. This was located on a general position, and it refined to a site of half occupancy, the carbon and chlorine atoms having satisfactory thermal parameters. Accordingly, the unit cell contains one molecule of CH_2Cl_2 for the pair of $[Re_2Cl_3(dppm)_2(CO)(PMe_3)_2]Cl$ molecules that are present. Hydrogens were not included in the refinement. With the exception of the lattice CH_2Cl_2 molecules, all non-hydrogen atoms were refined anisotropically; corrections for anomalous scattering were applied to all atoms so refined.[9]

Further details concerning the data set and the structure solution and refinement may be obtained from Dr P. E. Fanwick. Table 2 lists important bond distances and angles.*

Physical measurements

IR spectra were recorded as Nujol mulls between KBr plates on an IBM Instruments IR/32 Fourier transform spectrometer or a Perkin–Elmer Model 1420 spectrophotometer. Electrochemical measurements were carried out on dichloromethane solutions that contained 0.1 M tetra-*n*-butylammonium hexafluorophosphate (TBAH) as supporting electrolyte. $E_{1/2}$ values, determined as $(E_{p,a}+E_{p,c})/2$, were referenced to the silver/silver chloride (Ag/AgCl) electrode at room temperature and are uncorrected for junction potentials. Under our experimental conditions $E_{1/2} = +0.47$ V vs Ag/AgCl for the ferrocenium/ferrocene couple. Voltammetric experiments were performed with a Bioanalytical Systems Inc. Model CV-1A instrument in conjunction with a Hewlett–Packard Model 7035 B *x–y* recorder. Conductivity measurements were performed on 1×10^{-3} M acetone solutions of the complexes on an Industrial Instruments Inc. Model RC-16B2 conductivity bridge. $^{31}P\{^1H\}$ NMR spectra were recorded on a Varian XL-200 spectrometer operated at 80.98 MHz with the use of an internal deuterium lock and 85% H_3PO_4 as an external standard. ^1H NMR spectra were obtained on a Varian XL-200 spectrometer. Resonances were referenced internally to the residual protons in the incompletely deuterated solvent.

Analytical procedures

Elemental microanalyses were performed by Dr H. D. Lee of the Purdue University Microanalytical Laboratory.

* Atomic positional and thermal parameters and full listings of bond lengths and angles have been deposited with the Editor and with the Director, Cambridge Crystallographic Data Centre.

RESULTS AND DISCUSSION

(a) *Reactions of* $Re_2X_4(dppm)_2(CO)$ (1) *with* PMe_3, $P(OMe)_3$ *and* $P(OEt)_3$

The complex $Re_2Cl_4(dppm)_2(CO)$ (**1a**) reacts with PMe_3 in CH_2Cl_2 at room temperature to afford the green diamagnetic complex $[Re_2Cl_3(dppm)_2(CO)(PMe_3)_2]Cl$ in isolated yields of *ca* 40%. This complex dissolves in acetone ($c_m = 1.0 \times 10^{-3}$ M) to give a solution that has a conductivity ($\Lambda_m = 101\ \Omega^{-1}\ cm^2\ mol^{-1}$) characteristic of a 1:1 electrolyte.[10] When similar reactions are carried out in the presence of $NaBPh_4$ or $TlPF_6$, with THF or CH_2Cl_2 as the reaction solvents, respectively, the analogous salts $[Re_2Cl_3(dppm)_2(CO)(PMe_3)_2]X$ (X = BPh_4 or PF_6) are produced. The hexafluorophosphate salt dissolved in DMF to give a solution with properties characteristic of a 1:1 electrolyte,[10] with $\Lambda_m = 89\ \Omega^{-1}\ cm^2\ mol^{-1}$ for $c_m = 1.0 \times 10^{-3}$ M. Similar procedures have been used to prepare the diamagnetic bromo-derivative $[Re_2Br_3(dppm)_2(CO)(PMe_3)_2]PF_6$, as well as the analogous phosphite complexes $\{Re_2Cl_3(dppm)_2(CO)[P(OR)_3]_2\}PF_6$ (R = Me or Et).

The complexes mentioned above have very similar IR spectra (Nujol mulls) which show a single ν(CO) mode at frequencies characteristic of a bridging carbonyl ligand (Table 3). The electrochemical properties of these complexes, as measured by the cyclic voltammetric (CV) technique are strikingly similar. Solutions of these complexes in 0.1 M TBAH/CH_2Cl_2 show three well-defined electrochemical processes, one of which corresponds to a one-electron oxidation of the bulk complex while the other two processes are one-electron reductions. Compared to the related CV properties of the dicarbonyl complexes $[Re_2X_3(dppm)_2(CO)_2(L)]PF_6$ (X = Cl or Br; L = PMe_3, $P(OMe)_3$ or $P(OEt)_3$),[6] the monocarbonyl derivatives reported in the present work have their redox processes shifted by 0.4–0.5 V to more negative potentials. This reflects the relative electron-richness of the metal centres in the monocarbonyl complexes as a result of replacing a CO ligand (in $[Re_2X_3(dppm)_2(CO)_2(L)]PF_6$) by the better σ-donor PMe_3 and $P(OR)_3$ ligands.

In the case of $[Re_2Cl_3(dppm)_2(CO)[P(OEt)_3]_2PF_6$, we observed that the formation of the carbonyl-bridged form is favoured by the use of a fairly large excess of $P(OEt)_3$ (i.e. a stoichiometric ratio for **1a**–$P(OEt)_3$ of *ca* 1:6). The formation of this species is preceded by the generation of an intermediate that is characterized by a terminal CO ligand (ν(CO) at 1870(s) cm^{-1}) and quite different CV properties from those presented in Table 3 for the carbonyl-bridged form (i.e. $E_{1/2}(ox) = +1.42$ V, $E_{1/2}(ox) = +0.80$ V, $E_{1/2}(red) = -0.32$ V and $E_{1/2}(red) = -1.42$ V vs Ag/AgCl). This could be the 1:1 complex $\{Re_2Cl_3(dppm)_2(CO)[P(OEt)_3]\}PF_6$, or a structural variation of the 1:2 complex in which there is no bridging CO ligand.

The complexes $[Re_2Cl_3(dppm)_2(CO)(PMe_3)_2]PF_6$ and $\{Re_2Cl_3(dppm)_2(CO)[P(OMe)_3]_2\}PF_6$ gave good quality ^1H and ^{31}P NMR spectra that are representative of this group of complexes as a whole. The ^1H NMR spectrum of $[Re_2Cl_3(dppm)_2(CO)(PMe_3)_2]PF_6$ in CD_2Cl_2 shows a

Table 3. IR spectra and electrochemical properties of salts of the $[Re_2X_3(dppm)_2(CO)(L)_2]^+$ cations (X = Cl or Br; L = PMe_3, $P(OMe)_3$ or $P(OEt)_3$)

Complex	IR (cm^{-1})[a]	CV half-wave potentials (V)[b]		
	ν(CO)	$E_{1/2}$(ox)	$E_{1/2}$(red)(1)	$E_{1/2}$(red)(2)
$[Re_2Cl_3(dppm)_2(CO)(PMe_3)_2]Cl$	1637 s	+1.03(110)	−0.47(140)	−1.47(140)
$[Re_2Cl_3(dppm)_2(CO)(PMe_3)_2]BPh_4$	1630 s	+1.02(100)[c]	−0.48(90)	−1.49(110)
$[Re_2Cl_3(dppm)_2(CO)(PMe_3)_2]PF_6$	1638 s	+1.03(130)	−0.49(130)	−1.50(150)
$[Re_2Br_3(dppm)_2(CO)(PMe_3)_2]PF_6$	1635 s	+1.04(120)	−0.43(140)	−1.44(150)
$\{Re_2Cl_3(dppm)_2(CO)[P(OMe)_3]_2\}PF_6$	1683 s	+1.04(130)	−0.44(120)	−1.40(150)
$\{Re_2Cl_3(dppm)_2(CO)[P(OEt)_3]_2\}PF_6$	1680 m	+1.06(140)	−0.50(120)	[d]

[a] Recorded as Nujol mulls. The hexafluorophosphate salts show a characteristic intense ν(P—F) mode between 837 and 842 cm^{-1}.

[b] Measured in 0.1 M TBAH/CH_2Cl_2 and referenced to the Ag/AgCl electrode, with scan rate (ν) of 200 mV s^{-1} at a Pt-bead electrode. Numbers in parentheses are the $E_{p,a} - E_{p,c}$ values.

[c] An additional irreversible oxidation at $E_{p,a} = +0.92$ V is associated with the BPh_4^- anion; for $NaBPh_4$ this process is at $E_{p,a} = +0.86$ V.

[d] This process overlaps with one that arises from another species which is present in the solution (see text).

resonance at δ +1.24 due to the PMe_3 ligands, an $ABM_2X_2X'_2$ pattern centred about δ +3.8 (with individual multiplets at $\delta \simeq +4.3$ and $\simeq +3.3$) that arises from the bridgehead —CH_2— resonances of the dppm ligands, as well as several well-resolved phenyl resonances located between δ +7.9 and +6.8. The $^{31}P\{^1H\}$ NMR spectrum (recorded in CD_2Cl_2) exhibits multiplets at δ −33.2 and −57.8 (relative intensity 2:1; $J_{P-P} \simeq 6.5$ Hz) that are assigned to the dppm and PMe_3 phosphorus ligand atoms, respectively. The downfield resonance shows three resolved components, while that at δ −57.8 shows at least five components. The NMR spectrum of the trimethylphosphite complex (recorded in $(CD_3)_2CO$) is very similar to the aforementioned spectrum of its PMe_3 analogue. For example, the methyl resonance of the $P(OMe)_3$ ligands is a doublet at δ +3.34, while the —CH_2— resonance of the dppm ligands is centred at about δ +4.6 (multiplets at $\delta \simeq +5.02$ and $\simeq +4.18$) and appears as an $ABM_2X_2X'_2$ pattern. In the $^{31}P\{^1H\}$ NMR spectrum (in $(CD_3)_2CO$), multiplets at δ +62.5 and −23.8 (relative intensity ratio 1:2) are due to the $P(OMe)_3$ and dppm ligands, respectively.

(b) *Crystal structure of* $[Re_2Cl_3(dppm)_2(CO)(PMe_3)_2]Cl$

The structure of the crystallographically unique dirhenium cation, as present in the crystals of $[Re_2Cl_3(dppm)_2(CO)(PMe_3)_2]Cl \cdot 1/2CH_2Cl_2$, is that of an edge-shared bioctahedron. An ORTEP representation of the structure of the monocation is shown in Fig. 1 and gives the full atomic numbering scheme. There is no crystallographically imposed symmetry for the asymmetric unit. The important structural parameters are listed in Table 2. The bridging dppm ligands are in a *trans* disposition to one another, and the bridgehead methylene carbon atoms of this ligand fold over on the side of the cation that contains a bridging carbonyl ligand and two PMe_3 ligands. The three chloride ligands (one in a bridging disposition, the other two present in terminal Re—Cl bonds) are in an all-*cis* arrangement to one another. The virtual symmetry of the cation is C_{2v}.

The Re—Re distance is 2.602(1) Å, a value which is very similar to the values reported previously for structurally related dirhenium complexes that contain edge-shared bioctahedral geometries, e.g. 2.582(1) Å in $[Re_2Cl_3(dppm)_2(CO)_3]PF_6$[5] and 2.593(1) Å in $[Re_2Cl_3(dppm)_2(CO)_2(PMe_3)]PF_6$.[6] The structural parameters associated with the $[Re_2(\mu\text{-}Cl)Cl_2(\mu\text{-}dppm)_2]$ moiety are also very similar to those reported for related complexes.[5,6,11] Small differences between the chemically equivalent sets of Re—P and Re—Cl distances do not appear to be statistically significant (within 3σ).

The CO ligand symmetrically bridges the two metal centres. The Re—C distances are within ex-

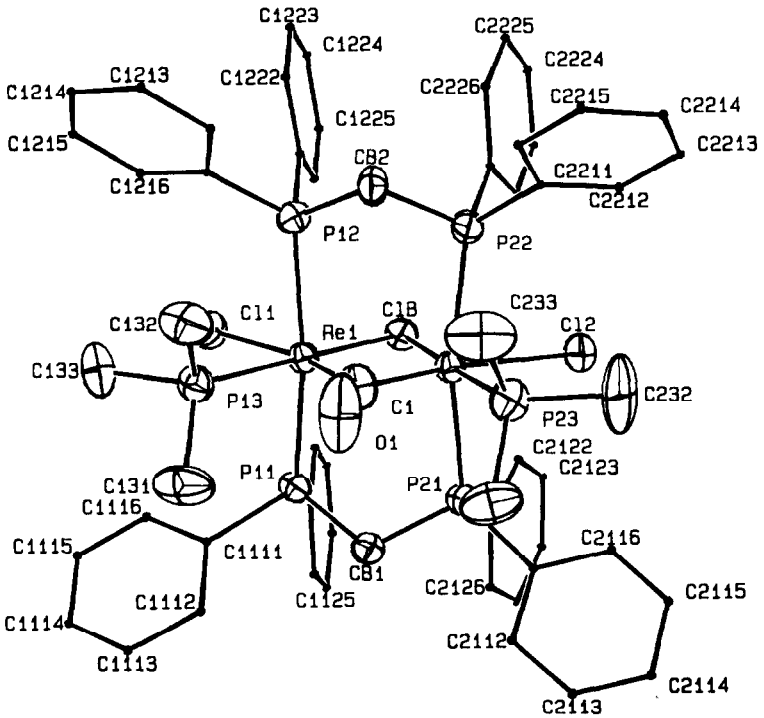

Fig. 1. ORTEP representation of the structure of the $[Re_2Cl_3(dppm)_2(CO)(PMe_3)_2]^+$ cation showing the atomic numbering scheme. The thermal ellipsoids are drawn at the 50% probability level.

perimental error the same (Re(1)—C(1) = 2.02(1) Å and Re(2)—C(1) = 2.00(1) Å), and are much longer than the Re—C bond distance of 1.90(1) Å associated with the terminal Re—CO unit in $[Re_2Cl_3(dppm)_2(CO)_2(PMe_3)]PF_6$.[6] The latter complex also contains an *unsymmetrical* CO ligand bridge whose Re—C distances are 1.96(1) and 2.16(1) Å; the Re—C distances for $[Re_2Cl_3(dppm)_2(CO)(PMe_3)_2]Cl$ are intermediate between these. The Re—P distances involving the PMe_3 ligands are essentially the same (Re(1)—P(13) = 2.434(3) Å and Re(2)—P(23) = 2.427(3) Å) and are, in turn, shorter than those associated with the dppm ligands which are in the range 2.473(3)—2.486(3) Å. These differences may largely reflect the stronger σ-donor characteristics of the more basic PMe_3 ligand (compared to dppm).

CONCLUDING REMARKS

This work shows that the sort of charge disparity that exists in the dirhenium(II) complexes of the type $[Re_2(\mu\text{-}X)(\mu\text{-}CO)(\mu\text{-}dppm)_2X_2(CO)(L)]PF_6$ (X = Cl or Br; L = PMe_3, $P(OMe)_3$ and $P(OEt)_3$), and which leads to an unsymmetrical structure (including a semibridging CO ligand),[6] is no longer present in the analogous series of complexes in which the terminal CO ligand has been replaced by PMe_3 or $P(OR)_3$. The dirhenium cations $[Re_2(\mu\text{-}X)(\mu\text{-}CO)(\mu\text{-}dppm)_2X_2(PMe_3)_2]^+$ contain a symmetrically bridging CO ligand and a symmetric disposition of dppm, PMe_3 and terminal halide ligands. Based upon the similarity of the Re—Re distances in these two groups of complexes, it seems reasonable to conclude that the electronic structures of the dirhenium cores are the same.

Acknowledgements—Support from the National Science Foundation, through Grant No. CHE88-07444 to R.A.W., and Grant No. CHE86-15556 for the purchase of the MicroVAX II computer and diffractometer, is gratefully acknowledged. We also acknowledge the National Institute of Health (Grant No. RR-01077) and the National Science Foundation (Grant No. 87-14258) for funds for the purchase of the NMR spectrometers.

REFERENCES

1. F. A. Cotton, L. M. Daniels, K. R. Dunbar, L. R. Falvello, S. M. Tetrick and R. A. Walton, *J. Am. Chem. Soc.* 1985, 107, 3524.
2. F. A. Cotton, K. R. Dunbar, A. C. Price, W. Schwotzer and R. A. Walton, *J. Am. Chem. Soc.* 1986, **108**, 4843.
3. J. R. Ebner, D. R. Tyler and R. A. Walton, *Inorg. Chem.* 1976, **15**, 833.
4. T. J. Barder, F. A. Cotton, K. R. Dunbar, G. L. Powell, W. Schwotzer and R. A. Walton, *Inorg. Chem.* 1985, **24**, 2550.
5. P. E. Fanwick, A. C. Price and R. A. Walton, *Inorg. Chem.* 1987, **26**, 3920.
6. J.-S. Qi, P. E. Fanwick and R. A. Walton, *Inorg. Chem.*, accepted for publication.
7. P. E. Fanwick, W. S. Harwood and R. A. Walton, *Inorg. Chim. Acta* 1986, **122**, 7.
8. N. Walker and D. Stuart. *Acta Cryst.* 1983, **A39**, 158.
9. (a) D. T. Cromer, *International Tables for X-ray Crystallography*, Vol. IV, Table 2.3.1. Kynoch Press, Birmingham, U.K. (1974); (b) For the scattering factors used in the structure solution see: D. T. Cromer and J. T. Waber, *International Tables for X-ray Crystallography*, Vol. IV, Table 2.2B. Kynoch Press, Birmingham U.K. (1974).
10. W. J. Geary, *Coord. Chem. Rev.* 1971, **7**, 81.
11. F. A. Cotton, K. R. Dunbar, L. R. Falvello and R. A. Walton, *Inorg. Chem.* 1985, **24**, 4180.

Polyhedron Vol. 9, No. 4, pp. 573–580, 1990
Printed in Great Britain

0277–5387/90 $3.00+.00
© 1990 Pergamon Press plc

STUDIES DIRECTED TOWARDS THE ISOLATION AND CHARACTERIZATION OF THE PARAMAGNETIC CATIONS $[Re_2X_4(LL)_2]^+$ (X = Cl OR Br; LL = $Ph_2PCH_2PPh_2$, $Ph_2AsCH_2AsPh_2$ OR $Ph_2PNHPPh_2$), AND THE CRYSTAL STRUCTURE OF $Re_2Cl_4(Ph_2PNHPPh_2)_2 \cdot (CH_3)_2CO$

MICHAEL T. COSTELLO, DANIEL R. DERRINGER, PHILLIP E. FANWICK, ANDREW C. PRICE, MARIA I. RIVERA,† ELIZABETH SCHEIBER,‡ EDWARD W. SIUREK III‡ and RICHARD A. WALTON§

Department of Chemistry, Purdue University, West Lafayette, IN 47907, U.S.A.

(*Received* 10 *July* 1989; *accepted* 11 *September* 1989)

Abstract—The synthesis of the triply bonded dirhenium(II) complexes $Re_2X_4(dpam)_2$ (X = Cl or Br; dpam = $Ph_2AsCH_2AsPh_2$) has been accomplished through the reactions of $Re_2(O_2CCH_3)_2X_4(H_2O)_2$ with dpam in hot methanol. Solutions of these complexes, and of $Re_2X_4(dppm)_2$ (X = Cl or Br; dppm = $Ph_2PCH_2PPh_2$) and $Re_2Cl_4(dppa)_2$ (dppa = $Ph_2PNHPPh_2$), in n-Bu_4NPF_6/CH_2Cl_2 have been oxidized electrochemically (at *ca* +0.5 V vs Ag/AgCl) to generate solutions of the paramagnetic, ESR-active monocations. The salts $[Re_2X_4(dppm)_2]PF_6$ have been prepared by the reaction of $Re_2X_4(dppm)_2$ with $[(\eta^5\text{-}C_5H_5)_2Fe]PF_6$ in acetone. Cyclic voltammetric data for solutions of all these complexes in 0.1 M n-Bu_4NPF_6/CH_2Cl_2 are reported. The crystal structure of $Re_2Cl_4(dppa)_2 \cdot (CH_3)_2CO$ has been determined and shown to resemble that of $Re_2Cl_4(dppm)_2$. The crystallographic data are as follows: monoclinic space group $P2_1/n$, $a = 11.382(2)$, $b = 23.273(5)$, $c = 19.212(3)$ Å, $\beta = 92.429(8)°$, $V = 5084(3)$ Å^3 and $Z = 4$. The structure was refined to $R = 0.031$ ($R_w = 0.036$) for 4490 data with $I > 3.0\sigma(I)$. The complex has a Re—Re bond distance of 2.2417(5) Å, and contains intramolecular dppa ligand bridges. A staggered rotational geometry is characterized by average Cl—Re—Re—Cl and P—Re—Re—P torsional angles of 51.7[2] and 41.8[5]°, respectively.

The triply bonded dirhenium(II) complexes $Re_2X_4(PR_3)_4$ (X = Cl, Br or I; PR_3 = monodentate phosphine) are readily converted to salts of their mono- and dicationic species $[Re_2X_4(PR_3)_4]PF_6$ and $[Re_2X_4(PR_3)_4](PF_6)_2$ that possess Re—Re bond orders of 3.5 and 4, respectively, with associated ground-state electronic configurations of $\sigma^2\pi^4\delta^2\delta^{*1}$ and $\sigma^2\pi^4\delta^2$.[1–4] The complexes $Re_2X_4(\mu\text{-}LL)_2$, where LL represents an intramolecular bridging ligand such as $Ph_2PCH_2CH_2PPh_2$ (dppe) that has a $-(CH_2)_2-$ unit linking the donor atoms of the ligands LL, have also been oxidized in this fashion and salts of the corresponding cations can be isolated in certain circumstances.[5,6]

Although $Re_2Cl_4(dppm)_2$ (dppm = $Ph_2PCH_2PPh_2$) has been oxidized to $Re_2Cl_5(dppm)_2$ and subsequently to $Re_2Cl_6(dppm)_2$, by controlled potential electrolysis in the presence of chloride ion,[7] the simple monocation $[Re_2Cl_4(dppm)_2]^+$ has never been isolated, in spite of the accessibility of two sequential one-electron oxidations as shown by electrochemical measurements on this complex.[7] The same is true for other complexes of dirhenium(II) in which there is a *single* bridgehead group linking the two phosphorus atoms of the bidentate phosphine ligand.[7]

In view of the importance of $Re_2Cl_4(dppm)_2$ and related complexes as synthetic precursors to a wide range of dirhenium complexes,[8,9] we have examined the redox chemistry of such complexes with a view

† Participant in the 1987 Purdue–MARC Summer Research Program.

‡ Undergraduate research participant.

§ Author to whom correspondence should be addressed.

to generating and characterizing their oxidized derivatives. In the present report we describe (1) the syntheses of the new complexes $Re_2X_4(dpam)_2$ (X = Cl or Br; dpam = $Ph_2AsCH_2AsPh_2$), (2) the electrochemical and chemical oxidations of these complexes and of $Re_2X_4(dppm)_2$ (X = Cl, Br or I) and $Re_2Cl_4(dppa)_2$ (dppa = $Ph_2PNHPPh_2$), and (3) the crystal structure of $Re_2Cl_4(dppa)_2 \cdot (CH_3)_2CO$.

EXPERIMENTAL

Starting materials

The complexes $Re_2(O_2CCH_3)_2X_4(H_2O)_2$ (X = Cl, Br or I),[10] $Re_2Cl_4(dppa)_2$,[11] $Re_2X_4(dppm)_2$[12] and ferrocenium hexafluorophosphate $[(\eta^5\text{-}C_5H_5)_2Fe]PF_6$,[13] were prepared according to the reported methods. Bis(diphenylarsino)methane (abbreviated dpam) was purchased from Pressure Chemicals and was used without further purification. Solvents used in the preparation of the complexes were of commercial grade and were thoroughly deoxygenated with dinitrogen prior to use.

Reactions procedures

All reactions were performed under an atmosphere of dry dinitrogen.

(a) *Preparation of* $Re_2X_4(dpam)_2$. (i) $Re_2Cl_4(dpam)_2$: A mixture of $Re_2(O_2CCH_3)_2Cl_4(H_2O)_2$ (0.20 g, 0.24 mmol) and 4 equiv. of dpam (0.45 g, 0.96 mmol) in methanol (20 cm^3) was refluxed for 24 h. The resulting purple–brown precipitate was filtered hot and washed with 3×15 cm^3 portions of hot methanol. Recrystallization from dichloromethane–methanol at 0°C gave the product as a purple powder; yield, 0.045 g (10%). Found: C, 39.8; H, 2.9. Calc. for $C_{50}H_{44}Cl_4As_4Re_2$: C, 41.2; H, 3.0%. This sample probably contains some dichloromethane of crystallization, thereby accounting for the slightly low carbon and hydrogen elemental microanalyses.

(ii) $Re_2Br_4(dpam)_2$: The preparation of this complex was carried out in exactly the same manner as that described in section a(i); yield, 40%. Found: C, 35.7; H, 2.7; Br, 19.8. Calc. for $C_{50}H_{44}Br_4As_4Re_2$: C, 36.7; H, 2.7; Br, 19.5%.

(b) *Oxidation of* $Re_2X_4(dppm)_2$ *with* $[(\eta^5\text{-}C_5H_5)_2Fe]PF_6$. (i) $[Re_2Cl_4(dppm)_2]PF_6$: A quantity of $Re_2Cl_4(dppm)_2$ (0.20 g, 0.16 mmol) was allowed to react with 1 equiv. of $[(\eta^5\text{-}C_5H_5)_2Fe]PF_6$ (0.052 g, 0.16 mmol) in acetone (15 cm^3) for 5 min at room temperature. The resulting green–brown solution was filtered into a large excess of diethyl ether ($\simeq$ 100 cm^3) to yield a green precipitate. This was filtered off, washed with diethyl ether and dried *in vacuo*; yield, 0.19 g (85%). Found: C, 41.9; H, 3.3. Calc. for $C_{50}H_{44}Cl_4F_6P_5Re_2$: C, 42.1; H, 3.1%.

(ii) $[Re_2Br_4(dppm)_2]PF_6$: The preparation of this complex was carried out in exactly the same manner as that described in section b(i); yield, 70%. Found: C, 37.9; H, 3.0. Calc. for $C_{50}H_{44}Br_4F_6P_5Re_2$: C, 37.4; H, 2.8%.

(c) *Bulk electrolysis of* $Re_2X_4(dppm)_2$, $Re_2Cl_4(dppa)_2$ *and* $Re_2Br_4(dpam)_2$. Approximately 0.02 g quantities of these compounds were dissolved in 0.1 M *n*-Bu_4NPF_6–CH_2Cl_2 (20 cm^3) contained in an H-cell. Exhaustive electrolysis was performed on these solutions at *ca* +0.50 V for approximately 15 min at room temperature. Cyclic voltammograms were recorded and found to be essentially the same as those for their neutral precursors except that the processes at $E_{1/2} \simeq +0.3$ V (vs Ag/AgCl) now corresponded to reductions of the bulk complexes, thereby confirming that a one-electron oxidation had taken place.

Preparation of single crystals of $Re_2Cl_4(dppa)_2 \cdot (CH_3)_2CO$

Crystals were grown by diffusion of heptane vapour into a toluene solution of the complex that also contained a small amount of acetone.

X-ray crystallographic studies

The structure of $Re_2Cl_4(dppa)_2 \cdot (CH_3)_2CO$ was determined with the use of general procedures that are described elsewhere.[14] A summary of the crystallographic data is given in Table 1. The cell constants are based on 25 reflections with $20° < \theta < 23°$. Three standard reflections were measured after every 5000 s of beam time during data collection. There was no systemmatic variations in intensity. Calculations were performed on a Micro VAX II computer using the Enraf–Nonius structure determination package.

The crystal selected for the structure determination belonged to the monoclinic space group $P2_1/n$ with $Z = 4$. As a check on crystal quality, omega scans of several intense reflections were measured; the width at half-height was 0.70° with a take-off angle of 2.4° indicating relatively poor crystal quality. The structure was solved by the use of the Patterson heavy-atom method, which revealed the positions of the rhenium atoms in the asymmetric unit. The remaining atoms were located in succeeding difference Fourier syntheses. Lorentz and polarization corrections were applied to the data. An empirical absorption correction was

Table 1. Crystal data and data collection parameters for $Re_2Cl_4(dppa)_2 \cdot (CH_3)_2CO$[a]

Formula	$Re_2Cl_4P_4ON_2C_{51}H_{48}$
Formula weight	1343.07
Space group	$P2_1/n$ (No. 14)
a (Å)	11.382(2)
b (Å)	23.273(5)
c (Å)	19.212(3)
β (°)	92.479(8)
V (Å^3)	5084(3)
Z	4
d_{calc} (g cm^{-3})	1.755
Crystal dimensions (mm)	$0.26 \times 0.22 \times 0.14$
Temperature (°C)	20
Radiation (wavelength)	Mo-K_α (0.71073 Å)
Monochromator	Graphite
Linear absorption coefficient (cm^{-1})	51.97
Absorption correction applied	Empirical[b]
Transmission factors: min, max	0.69, 1.00
Diffractometer	Enraf–Nonius CAD4
Scan method	ω–2θ
h, k, l limits	−12–12, 0–25, 0–20
2θ range (°)	4.00–45.00
Scan width (°)	$0.70 + 0.35 \tan\theta$
Take-off angle (°)	2.40
Programs used	Enraf–Nonius SDP
$F(000)$	2616.0
p-Factor used in weighting	0.040
Data collected	6835
Unique data	6835
Data with $I > 3.0\sigma(I)$	4490
Number of variables	557
Largest shift/ESD in final cycle	0.00
R[c]	0.031
R_w[d]	0.036
Goodness-of-fit[e]	0.937

[a] Number in parentheses following certain data are ESDs occurring in the least significant digit.

[b] N. Walker and D. Stuart, *Acta Cryst.* 1983, **A39**, 158.

[c] $R = \Sigma ||F_o| - |F_c|| / \Sigma |F_o|$.

[d] $R_w = [\Sigma w(|F_o| - |F_c|)^2 / \Sigma w|F_o|^2]^{1/2}$; $w = 1/\sigma^2(F_o)$.

[e] Goodness-of-fit $= [\Sigma w(|F_o| - |F_c|)^2 / (N_{obs} - N_{parameters})]^{1/2}$.

applied,[15] the linear absorption coefficient being 51.97 cm^{-1}. No corrections for extinction were applied. The structure was refined in full-matrix least-squares where the function minimized was $\Sigma w(|F_o| - |F_c|)^2$; w is the weighting factor defined as $w = 1/\sigma^2(F_o)$.

During the course of the refinement, it became apparent that residual electron density at a fairly close contact to the bridgehead NH group of one of the dppa ligands could be satisfactorily modelled as lattice acetone. This was located on a general position, and it refined to a site of full occupancy, the carbon and oxygen atoms having satisfactory thermal parameters. Accordingly, the unit cell contains one molecule of acetone for each dirhenium molecule. Positions for the hydrogen atoms of the dppa ligands and the lattice acetone were calculated by assuming idealized geometry and a C—H bond distance of 0.95 Å. We also assumed that the value of B(H), i.e. the isotropic equivalent thermal parameter for the hydrogen atoms, was equal to $1.3[B_{eqv}(C)]$ at the time of the inclusion of this parameter in the refinement procedure. While these hydrogen atoms were used in the calculation of F_o, they were not included in the least-squares refinement. With the exception of the lattice acetone molecules, all non-hydrogen atoms were refined anisotropically; corrections for anomalous scattering

Table 2. Selected bond distances (Å) and angles (°) for $Re_2Cl_4(dppa)_2 \cdot (CH_3)_2CO$[a]

Distances			
Re(1)—Re(2)	2.2417(5)	Re(2)—P(21)	2.413(3)
Re(1)—Cl(11)	2.353(3)	Re(2)—P(22)	2.422(3)
Re(1)—Cl(12)	2.357(3)	P(11)—N(1)	1.683(8)
Re(1)—P(11)	2.450(3)	P(12)—N(2)	1.702(8)
Re(1)—P(12)	2.428(3)	P(21)—N(1)	1.679(8)
Re(2)—Cl(21)	2.352(2)	P(22)—N(2)	1.684(8)
Re(2)—Cl(22)	2.362(3)		
Angles			
Re(2)—Re(1)—Cl(11)	117.93(7)	Re(1)—Re(2)—P(22)	93.05(6)
Re(2)—Re(1)—Cl(12)	119.26(8)	Cl(21)—Re(2)—Cl(22)	128.0(1)
Re(2)—Re(1)—P(11)	90.31(6)	Cl(21)—Re(2)—P(21)	86.68(9)
Re(2)—Re(1)—P(12)	89.55(6)	Cl(21)—Re(2)—P(22)	91.92(9)
Cl(11)—Re(1)—Cl(12)	122.8(1)	Cl(22)—Re(2)—P(21)	92.52(9)
Cl(11)—Re(1)—P(11)	95.43(9)	Cl(22)—Re(2)—P(22)	85.08(9)
Cl(11)—Re(1)—P(12)	84.46(9)	P(21)—Re(2)—P(22)	175.63(9)
Cl(12)—Re(1)—P(11)	84.46(9)	Re(1)—P(11)—N(1)	105.4(3)
Cl(12)—Re(1)—P(12)	95.77(9)	Re(1)—P(12)—N(2)	107.0(3)
P(11)—Re(1)—P(12)	179.88(9)	Re(2)—P(21)—N(1)	106.6(3)
Re(1)—Re(2)—Cl(21)	114.80(7)	Re(2)—P(22)—N(2)	105.7(3)
Re(1)—Re(2)—Cl(22)	117.23(7)	P(11)—N(1)—P(21)	119.1(5)
Re(1)—Re(2)—P(21)	91.29(6)	P(12)—N(2)—P(22)	118.6(5)

[a] Numbers in parentheses are ESDs in the least significant digits.

were applied to all atoms so refined.[16] The largest peak in the final difference Fourier map was 0.83 e $Å^{-3}$.

Further details concerning the data set and the structure solution and refinement may be obtained from Dr P. E. Fanwick. Table 2 lists important bond distances and angles.†

Physical measurements

IR spectra were recorded as Nujol mulls between KBr plates on an IBM Instruments IR/32 Fourier transform spectrometer or a Perkin–Elmer Model 1420 spectrophotometer. Electrochemical measurements were carried out on dichloromethane solutions that contained 0.1 M tetra-*n*-butylammonium hexafluorophosphate (*n*-Bu_4NPF_6 or TBAH) as supporting electrolyte. $E_{1/2}$ values, determined as $(E_{p,a}+E_{p,c})/2$, were referenced to the silver/silver chloride (Ag/AgCl) electrode at room temperature and are uncorrected for junction potentials. Under our experimental conditions, $E_{1/2} = +0.47$ vs Ag/AgCl for the ferrocenium/ferrocene couple. Voltammetric experiments were performed with a Bioanalytical Systems Inc. Model CV-1A instrument in conjunction with a Hewlett–Packard Model 7035 B *x-y* recorder. Conductivity measurements were performed on 1×10^{-3} M methanol solutions of the complexes on an Industrial Instruments Inc. Model RC-16B2 conductivity bridge. $^{31}P\{^1H\}$ NMR spectra were recorded on a Varian XL-200 spectrometer operated at 80.98 MHz with the use of an internal deuterium lock and 85% H_3PO_4 as an external standard. ^1H NMR spectra were obtained on a Varian XL-200 spectrometer. Resonances were referenced internally to the residual protons in the incompletely deuterated solvent.

Analytical procedures

Elemental microanalyses were performed by Dr H. D. Lee of the Purdue University Microanalytical Laboratory.

RESULTS AND DISCUSSION

(a) *Preparation and characterization of* $Re_2X_4(dpam)_2$

The bidentate arsine ligands 1,2-bis(diphenylphosphino)ethane (dpae; $Ph_2AsCH_2CH_2AsPh_2$) and 1-diphenylphosphino-2-diphenylarsinoethane

† Atomic positional and thermal parameters and full listings of bond lengths and angles have been deposited with the Editor and with the Director, Cambridge Crystallographic Data Centre.

(arphos; $Ph_2PCH_2CH_2AsPh_2$) have been shown to react with $(n\text{-}Bu_4N)_2Re_2Cl_8$ to yield $Re_2Cl_6(dpae)_2$ and $Re_2Cl_4(arphos)_2$, respectively.[17] However, with the use of similar reaction conditions to these, we have been unable to synthesize the corresponding derivatives with 1,2-bis(diphenylarsino) methane (dpam; $Ph_2AsCH_2AsPh_2$). The synthetic approach we successfully employed followed the one we have recently developed for the preparation of $Re_2X_4(dppm)_2$,[12] i.e. the reactions of the bis (acetate) complexes $Re_2(O_2CCH_3)_2X_4(H_2O)_2$ with an excess of dpam in hot methanol. The chloride derivative was produced in only a 10% yield. The use of different reaction solvents, and also $Re_2Cl_6(P\text{-}n\text{-}Bu_3)_2$ or $Re_2Cl_4(PEt_3)_4$ in place of $Re_2(O_2CCH_3)_2Cl_4(H_2O)_2$, failed to generate any identifiable products. Despite this rather low preparative yield for $Re_2Cl_4(dpam)_2$, satisfactory elemental microanalyses and cyclic voltammetric (CV) data were obtained for this complex. Two reversible one-electron oxidations, at $E_{1/2} = +0.32$ V and +0.84 V vs Ag/AgCl, were observed; these redox potentials are very close to those obtained for $Re_2Cl_4(dppm)_2$ as shown in Table 3. The bromide derivative $Re_2Br_4(dpam)_2$ was obtained in a much higher yield (*ca* 40%) than its chloride analogue. Its CV properties and electronic absorption spectrum are very similar to those for $Re_2Br_4(dppm)_2$ (Table 3). Accordingly, it may be concluded that $Re_2X_4(dpam)_2$ and $Re_2X_4(dppm)_2$ are structurally and electronically closely related.

The NMR spectral properties for $Re_2X_4(dppm)_2$ (X = Cl, Br or I) and $Re_2Br_4(dpam)_2$ are also listed in Table 3, and show a close similarity to one another. Note that electrochemical and spectroscopic data for $Re_2Br_4(dppm)_2$ and $Re_2I_4(dppm)_2$ are reported here for the first time. A comparison is also made with the corresponding data for $Re_2Cl_4(dppa)_2$.

(b) *Preparation and characterization of* $[Re_2X_4(dppm)_2]PF_6$

Nitrosonium hexafluorophosphate ($NOPF_6$) has been successfully used to oxidize dirhenium(II) complexes that contain monodentate and bidentate phosphines. Examples include $[Re_2Cl_4(PEt_3)_4]PF_6$,[18] $[Re_2Cl_4(PMe_2Ph)_4]PF_6$,[2] $[Re_2Cl_4(PMe_2Ph)_4](PF_6)_2$,[2] $[Re_2Cl_4(dppe)_2]PF_6$[5] and $[Re_2Cl_4(arphos)_2]PF_6$,[5] all of which can be prepared from their neutral precursors. However, acetone or THF solutions of $Re_2Cl_4(dppm)_2$ react readily with $NOPF_6$ to give unidentifiable products that may contain the nitrosyl ligand but which were not the desired oxi-

Table 3. Electrochemical and spectroscopic data for $Re_2X_4(LL)_2$ (X = Cl, Br or I; LL = dppm, dppa or dpam) and for $[Re_2X_4(dppm)_2]^+$ (X = Cl or Br)

Complex	CV half-wave potentials, V[a]		Electronic absorbance spectra	^1H NMR (δ)[c]	$^{31}P\{^1H\}$ NMR (δ)[e]
	$E_{1/2}(2)$	$E_{1/2}(1)$	λ (nm) (ε)[b]	—CH_2—[d]	
$Re_2Cl_4(dppm)_2$	+0.87(ox)[f]	+0.29(ox)[f]	680 sh, 510(500), 420 sh[g]	+5.21 p[g]	−3.30 s[g]
$Re_2Br_4(dppm)_2$	+0.94(ox)	+0.34(ox)	600 sh, 545(800), 450(780)	+5.39 p	−5.44 s
$Re_2I_4(dppm)_2$	+0.95(ox)	+0.34(ox)	614(950)	+5.63 p[h]	+8.54 s
$Re_2Cl_4(dppa)_2$	+0.94(ox)	+0.40(ox)[i]	635(40), 510(500), 440sh[g]		
$Re_2Cl_4(dpam)_2$	+0.84(ox)	+0.32(ox)	[j]	[j]	
$Re_2Br_4(dpam)_2$	+0.92(ox)	+0.37(ox)	680 sh, 540(830), 425 sh	+4.97 s	
$[Re_2Cl_4(dppm)_2]PF_6$	+0.88(ox)	+0.30(red)	1520(540), 670(1900), 520 sh, 445(2300)	[k]	
$[Re_2Br_4(dppm)_2]PF_6$	+0.92(ox)	+0.33(red)	1545(600), 695(860), 460(2350)	[k]	

[a] Versus Ag/AgCl. Recorded on solutions in 0.1 M TBAH/CH_2Cl_2 by the use of a Pt-bead electrode. Data obtained at a scan rate of 200 mV s^{-1}. For each couple, the value of ΔE_p (i.e. $E_{p,a} - E_{p,c}$) falls in the range 110–140 mV.

[b] Measured in dichloromethane; molar extinction coefficients (ε) are given in parentheses.

[c] Spectra recorded in CD_2Cl_2 unless otherwise stated.

[d] The —CH_2— resonance of the dppm or dpam ligands; p = pentet, s = singlet.

[e] Spectra recorded in CD_2Cl_2; s = singlet.

[f] Data similar to that reported in ref. 7.

[g] Data taken from ref. 7.

[h] Spectrum recorded in $CDCl_3$.

[i] Data similar to that reported in ref. 11.

[j] Not measured.

[k] Paramagnetic complex.

dized product. By resorting to the milder oxidant ferrocenium hexafluorophosphate, $[(\eta^5\text{-}C_5H_5)_2Fe]PF_6$, we have found that this reagent cleanly oxidizes acetone solutions of $Re_2X_4(dppm)_2$ to $[Re_2X_4(dppm)_2]PF_6$ (X = Cl or Br). A similar strategy in the case of $Re_2Cl_4(dppa)_2$ and $Re_2Br_4(dpam)_2$ (acetone or dichloromethane as solvents) failed to give pure products, even when low reaction temperatures were employed. The monocations are apparently very unstable and prone to decomposition under these reaction conditions, although they can be generated electrochemically (*vide infra*).

Conductivity measurements on methanol solutions of $[Re_2X_4(dppm)_2]PF_6$ ($c_m \simeq 1 \times 10^{-3}$ M) show them to be 1:1 electrolytes ($\Lambda_m \simeq 105\ \Omega^{-1}\ cm^2\ mol^{-1}$).[19] Also, the IR spectra of these complexes confirm the presence of the PF_6^- anion (ν(P—F) at $\simeq 840\ cm^{-1}$). The electrochemical properties of these salts (Table 3) resemble those of $Re_2X_4(dppm)_2$; the only difference being that the process at $E_{1/2} \simeq +0.3$ V (vs Ag/AgCl) now corresponds to a reduction of the bulk complex. Their electronic absorption spectra (Table 3) show a broad absorption at $\simeq 1500$ nm in the near-IR region. This band appears to be typical of species that contain a $\sigma^2\pi^4\delta^2\delta^{*1}$ electronic configuration[18,20] and may be assigned to a $\delta \rightarrow \delta^*$ transition. This is further evidence that the Re_2^{5+} moiety is present in these oxidized species.

Magnetic moments of dichloromethane solutions of these monocations (determined by the Evans method[21]) were found to be 1.5 ($\pm$0.1) BM at room temperature. X-band ESR spectra of frozen dichloromethane solutions (−160°C) also confirm the paramagnetism of these complexes. Complex patterns showing a considerable amount of hyperfine structure were observed. The spectra are centred at 2750 G ($g \simeq 2.35$) for the chloride and 2700 G ($g \simeq 2.40$) for the bromide derivative, and have a spectral width of approximately 3500 G.

(c) *Electrochemical generation of* $[Re_2X_4(dppm)_2]^+$ (X = Cl *or* Br), $[Re_2Cl_4(dppa)_2]^+$ *and* $[Re_2Br_4(dpam)_2]^+$

Bulk electrolyses of purple solutions of $Re_2X_4(dppm)_2$ (X = Cl or Br), $Re_2Cl_4(dppa)_2$ and $Re_2Br_4(dpam)_2$ in n-Bu_4NPF_6–CH_2Cl_2 generated solutions of the paramagnetic monocations that are green–brown in colour, except for $[Re_2Cl_4(dppa)_2]^+$ which is red. In all instances, CV measurements confirmed that oxidation had proceeded with little evidence for decomposition. In view of the reversibility of the couple at *ca* +0.3 V (Table 3), it is apparent that the oxidations proceed with retention of the staggered rotational geometry that is characteristic of the structurally characterized derivatives $Re_2Cl_4(dppm)_2$[22] and $Re_2Cl_4(dppa)_2$ (*vide infra*).

The X-band ESR spectra of these solutions, recorded at −160°C (Fig. 1), verified the paramagnetism of these species. The spectrum of $[Re_2Cl_4(dppa)_2]^+$ (not shown) is similar to that of the other derivatives; in all instances, the spectra are centred at *ca* 3000 G (i.e. $g \simeq 2.16$) with a spectral width of *ca* 3500 G. As can be seen in Fig. 1, the spectra are very similar and, in spite of the poorer resolution of the spectrum of $[Re_2Br_4(dppm)_2]^+$, it is apparent that the hyperfine structure must primarily be associated with the rhenium nuclei; an eleven-line pattern is expected for coupling to two rhenium nuclei with $I = 5/2$. There is little evidence for coupling to phosphorus or halogen nuclei in these spectra. Further confirmation that these signals are due to the monocations was shown by cycling between the oxidized and neutral species

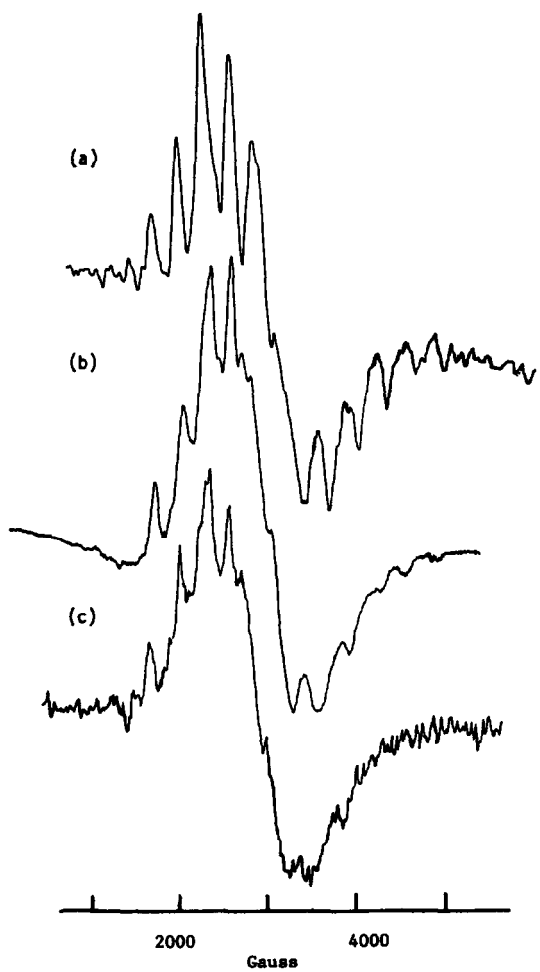

Fig. 1. The X-band ESR spectra, in frozen dichloromethane solutions at −160°C, for (a) $[Re_2Br_4(dpam)_2]^+$, (b) $[Re_2Cl_4(dppm)_2]^+$ and (c) $[Re_2Br_4(dppm)_2]^+$. All species were generated electrochemically.

and monitoring the growth and disappearance of the spectra.

(d) *Structural considerations*

At the outset, we had hoped to obtain crystals of one or more derivatives of the type $[Re_2X_4(LL)_2]PF_6$ (LL = dppm, dppa or dpam) in order to confirm that they did indeed possess a structure similar to that of $Re_2Cl_4(dppm)_2$.[22] Unfortunately, all attempts to grow such crystals led to the decomposition of the complexes. However, during the course of this aspect of our work we obtained crystals of $Re_2Cl_4(dppa)_2 \cdot (CH_3)_2CO$ and took the opportunity to determine its structure and compare it to $Re_2Cl_4(dppm)_2$.[22]

The structure of the dirhenium complex $Re_2Cl_4(dppa)_2$, as present in the crystals of $Re_2Cl_4(dppa)_2 \cdot (CH_3)_2CO$, is that of a multiply bonded M_2L_8 complex.[3] An ORTEP representation of the structure is shown in Fig. 2 and gives the full atomic numbering scheme. There is no crystallographically imposed symmetry for the asymmetric unit. The important structural parameters are listed in Table 2. While the bridging dppa ligands are in a *trans* disposition to one another, the molecule assumes an overall staggered rotational geometry. This geometry can best be defined in terms of the averages of the torsional angles Cl(11)—Re(1)—Re(2)—Cl(21) and Cl(12)—Re(1)—Re(2)—Cl(22), and P(11)—Re(1)—Re(2)—P(21) and P(12)—Re(1)—Re(2)—P(22), which are 51.7[2] and 41.8[5]°, respectively. These can be compared with average Cl—Re—Re—Cl and P—Re—Re—P angles of 56[1] and 47[1]°, respectively, in the structure of $Re_2Cl_4(dppm)_2$.[22]

The Re—Re distance of 2.2417(5) Å is similar to that of 2.234(3) Å in the structure of $Re_2Cl_4(dppm)_2$.[22] Very close similarities are also seen between the sets of Re—Cl and Re—P distances and the corresponding angles of these two structures. The compounds have essentially identical average Re—P and Re—Cl distances; these are 2.43[2] and 2.356[5] Å for the dppa derivative and 2.45[3] and 2.360[11] Å for the analogous dppm complex.

One molecule of acetone per formula unit of $Re_2Cl_4(dppa)_2$ was found in the unit cell. The oxygen atom of the acetone molecule was found to be 3.12(1) Å away from N(1) of the dirhenium complex. This represents, at best, a very weak hydrogen-bonding interaction. Typical lengths of N—H···O hydrogen bonds fall in the range 2.81–3.04 Å.[23] Recently, Usón *et al.*[24] have reported a case of a diplatinum(I)–dppa complex that

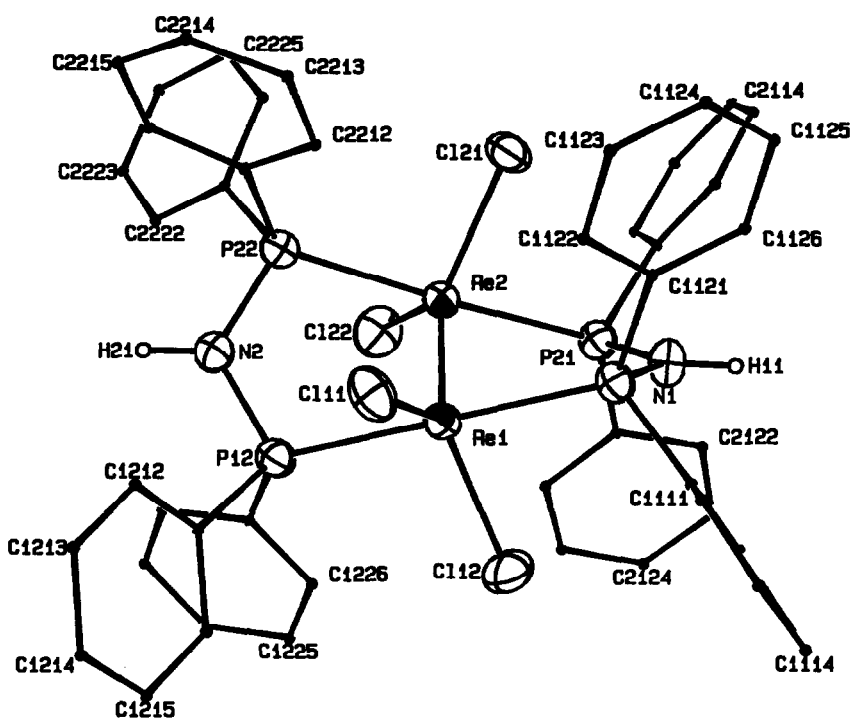

Fig. 2. ORTEP representation of the structure of the complex $Re_2Cl_4(dppa)_2$ showing the atomic numbering scheme. The thermal ellipsoids are drawn at the 50% probability level. The molecule of lattice acetone is not shown.

exhibits $(CH_3)_2CO\cdots H—N$ hydrogen-bonding; the $N—H\cdots O$ distance (for $Pd_2Cl_2(\mu\text{-dppa})_2\cdot(CH_3)_2CO$) was determined to be 2.915(7) Å. To our knowledge, there are only five other reports describing the structures of dimetal complexes that contain bridging dppa ligands. These are the aforementioned diplatinum complex,[24] the dirhenium(II) complexes *cis*-$Re_2(O_2CCH_3)_2Cl_2(\mu\text{-dppa})_2$ and *cis*-$[Re_2(O_2CCH_3)_2Cl_2(\mu\text{-dppa})_2]PF_6$,[11] $Au_2Cl_2(C_6F_5)_2(\mu\text{-dppa})$[25] and $Rh_2(\mu\text{-CO})(\mu\text{-Cl})(\mu\text{-dppa})_2(CO)_2$;[26] several of these contain solvent of crystallization hydrogen-bonded to the N—H group of dppa.

Acknowledgements—Support from the National Science Foundation, through Grant No. CHE88-07444 to R.A.W., and Grant No. CHE86-15556 for the purchase of the Micro VAX II computer and diffractometer, is gratefully acknowledged. We also acknowledge the National Institute of Health (Grant No. RR-01077) and the National Science Foundation (Grant No. 87-14258) for funds for the purchase of the NMR spectrometers.

REFERENCES

1. P. Brant, D. J. Salmon and R. A. Walton, *J. Am. Chem. Soc.* 1978, **100**, 4424.
2. F. A. Cotton, K. R. Dunbar, L. R. Falvello, M. Tomas and R. A. Walton, *J. Am. Chem. Soc.* 1983, **105**, 4950.
3. F. A. Cotton and R. A. Walton, *Multiple Bonds Between Metal Atoms*. John Wiley, New York (1982).
4. F. A. Cotton and R. A. Walton, *Struct. Bonding (Berlin)* 1985, **62**, 1.
5. P. Brant, H. D. Glicksman, D. J. Salmon and R. A. Walton, *Inorg. Chem.* 1978, **17**, 3203.
6. I. F. Fraser and R. D. Peacock, *J. Chem. Soc., Chem. Commun.* 1985, 1727.
7. T. J. Barder, F. A. Cotton, D. Lewis, W. Schwotzer, S. M. Tetrick and R. A. Walton, *J. Am. Chem. Soc.* 1984, **106**, 2882.
8. A. C. Price and R. A. Walton, *Polyhedron* 1987, **6**, 729, and refs cited therein.
9. R. A. Walton, *Polyhedron* 1989, **8**, 1689, and refs cited therein.
10. A. R. Chakravarty, F. A. Cotton, A. R. Cutler and R. A. Walton, *Inorg. Chem.* 1986, **25**, 3619, and refs cited therein.
11. D. R. Derringer, P. E. Fanwick, J. Moran and R. A. Walton, *Inorg. Chem.* 1989, **28**, 1384.
12. A. R. Cutler, D. R. Derringer, P. E. Fanwick and R. A. Walton, *J. Am. Chem. Soc.* 1988, **110**, 5024.
13. D. N. Hendrickson, Y. S. Sohn and H. B. Gray, *Inorg. Chem.* 1971, **10**, 1559.
14. P. E. Fanwick, W. S. Harwood and R. A. Walton, *Inorg. Chim. Acta* 1986, **122**, 7.
15. N. Walker and D. Stuart, *Acta Cryst.* 1983, **A39**, 158.
16. (a) D. T. Cromer, *International Tables for X-ray Crystallography*, Vol. IV, Table 2.3.1. Kynoch Press, Birmingham, U.K. (1974); (b) For the scattering factors used in the structure solution see: D. T. Cromer and J. T. Waber, *International Tables for X-ray Crystallography*, Vol. IV, Table 3.3B. Kynoch Press, Birmingham, U.K. (1974).
17. J. R. Ebner, D. R. Tyler and R. A. Walton, *Inorg. Chem.* 1976, **15**, 833.
18. P. Brant, D. J. Salmon and R. A. Walton, *J. Am. Chem. Soc.* 1978, **100**, 4424.
19. W. J. Geary, *Coord. Chem. Rev.* 1971, **7**, 81.
20. F. A. Cotton, P. E. Fanwick, L. D. Gage, B. Kalbacher and D. S. Martin, *J. Am. Chem. Soc.* 1977, **99**, 5642.
21. D. F. Evans, *J. Chem. Soc.* 1959, 2003.
22. T. J. Barder, F. A. Cotton, K. R. Dunbar, G. L. Powell, W. Schwotzer and R. A. Walton, *Inorg. Chem.* 1985, **24**, 2550.
23. N. N. Greenwood and A. Earnshaw, *Chemistry of the Elements*, p. 65. Pergamon Press, Oxford (1984).
24. R. Usón, J. Fornies, R. Navarro, M. Tomas, C. Fortuno, J. I. Cebollada and A. J. Welch, *Polyhedron* 1989, **8**, 1045.
25. R. Usón, A. Laguna, M. Laguna, M. N. Fraile, P. G. Jones and G. M. Sheldrick, *J. Chem. Soc., Dalton Trans.* 1986, 291.
26. G. Liehr, G. Szuesanyi and J. Ellermann, *J. Organomet. Chem.* 1984, **265**, 95.

Polyhedron Vol. 9, No. 4, pp. 581–587, 1990
Printed in Great Britain

0277–5387/90 $3.00+.00
© 1990 Pergamon Press plc

ELECTRON PARAMAGNETIC RESONANCE STUDIES OF THE 19-ELECTRON COMPLEXES, $(\eta^5\text{-}C_5H_5)NiL_2$ (L = PR_3, $P(OR)_3$)

ANNA BECALSKA, JEFF D. DEBAD, HALEH K. SANATI and ROSS H. HILL*

Department of Chemistry, Simon Fraser University, Burnaby, B.C. Canada, V5A 1S6

(*Received* 12 *April* 1989; *accepted* 11 *September* 1989)

Abstract—Photolysis of $(\eta^5\text{-}C_5H_5)Ni(R)PPh_3$ (R = Me, Et) in air-free benzene leads to the production of the stable radical $(\eta^5\text{-}C_5H_5)Ni(PPh_3)_2$. In the presence of free ligands, L (L = PPh_3, $P(p\text{-}FPh)_3$, $P(p\text{-}MeOPh)_3$, $P(n\text{-}Bu)_3$, $P(OEt)_3$, $P(OPh)_3$, $P(OMe)_3$, dppe/2, bipy/2, C_2Ph_2 and HCCPh), photolysis of $(\eta^5\text{-}C_5H_5)Ni(R)PPh_3$ leads to the production of $(\eta^5\text{-}C_5H_5)Ni(L)_2$. The ESR spectra of several derivatives of the radical, $(\eta^5\text{-}C_5H_5)NiL_2$, have been analysed and the variation of the *sp* hybridization of the phosphorus donor atom determined.

Herein we report the results of our study of the photochemistry of $C_5H_5Ni(R)PPh_3$ (R = Me, Et). We previously studied the photochemistry of $(\eta^5\text{-}C_5H_5)Co(PPh_3)Me_2$ and found that photolysis in air-free benzene led to the production of the stable cobalt radical $(\eta^5\text{-}C_5H_5)Co(PPh_3)Me$.[1] Literature describing both the photolysis and thermolysis of the nickel complexes indicated that the production of nickel radicals in the photochemistry of $(\eta^5\text{-}C_5H_5)Ni(R)PPh_3$ may be observable under the right conditions.

The photolysis of $(\eta^5\text{-}C_5H_5)Ni(Me)PPh_3$ was reported by Emad and Rausch[2] to lead to the production of methyl radicals, whereas the same authors reported $(\eta^5\text{-}C_5H_5)Ni(Et)PPh_3$ when irradiated produced ethylene and ethane in a near 1:1 ratio. In both cases the presumed organometallic intermediate would be $(\eta^5\text{-}C_5H_5)NiPPh_3$. The thermolysis of these complexes was reported by Thomson and Baird[3] to lead to Ni—CH_3 bond homolysis for the methyl derivatives and β-hydride elimination from the ethyl derivative. The indication here is that once again, at least in the thermolysis of the methyl derivative, $(\eta^5\text{-}C_5H_5)NiPPh_3$ should be produced. In neither of these reports were the identities of the nickel-containing products determined.

Barefield *et al.* reported[4] that reaction of nickelocene with NiL_4 led to the production of radicals of the general formula $(\eta^5\text{-}C_5H_5)NiL_2$. The paper also contained evidence suggestive of $(\eta^5\text{-}C_5H_5)NiL$ being an intermediate in the equilibrium between $(\eta^5\text{-}C_5H_5)_2Ni$ and NiL_4 with $(\eta^5\text{-}C_5H_5)NiL_2$. Considering the reported result of either photolysis or thermolysis of $(\eta^5\text{-}C_5H_5)Ni(R)PPh_3$ it seemed reasonable that in the presence of a suitable two-electron donor either thermolysis or photolysis of $(\eta^5\text{-}C_5H_5)Ni(R)PPh_3$ should produce these radicals.

Initial results indicated that the nickel radicals could be prepared via photolysis of the alkyl complexes. The ESR indicated a large variation of isotropic hyperfine coupling constants in this system. In order to investigate if this was a result of a change in the orbital content of the singly occupied molecular orbital (SOMO) we prepared a variety of complexes and studied their anisotropic ESR spectra.

RESULTS

Characterization of the products

Photolysis ($\lambda > 413$ nm) of $(\eta^5\text{-}C_5H_5)Ni(Me)PPh_3$ in degassed benzene solutions containing PPh_3 was monitored by ^1H NMR spectroscopy. Due to the production of radicals, spectra were obtained with relaxation delays of 60 s. Use of a long relaxation delay ensures that the changes in the relaxation times due to the presence of radicals had only minimal effects on the integrals of the signals allowing the use of NMR to monitor the extent of reaction. Irradiation resulted in loss of ^1H NMR signals associated with substrate and the

*Author to whom correspondence should be addressed.

appearance of weak NMR signals due to methane, ethane and other unidentified products. The use of cyclopentane as an internal standard allowed calculation of the extent of reaction by measuring the remaining intensity in the NMR due to the starting complex. When the reaction was complete the NMR was obtained over a wider sweep width using short acquisition times and pulse angles of 30°, allowing observation of the NMR signals due to the paramagnetic products.

The absorptions due to the cyclopentadienyl protons from $(\eta^5\text{-}C_5H_5)_2Ni$ (−255.3 ppm) and $(\eta^5\text{-}C_5H_4Me)_2Ni$ (−247.5 ppm) were observed.[5] The approximate ratio of methylated to unmethylated cyclopentadienyl in the nickelocenes was 1 : 1.3. Although this region did not confirm the existence of the mixed derivative, $(\eta^5\text{-}C_5H_4Me)(\eta^5\text{-}C_5H_5)Ni$, examination of the methyl group resonances indicated that the mixed derivative was also formed. In this region, absorptions at 208 ppm and 209 ppm were observed. In addition to the signals due to the nickelocene derivatives, signals due to phosphine-substituted derivatives were also observed.

The new absorption at −265 ppm was found to be consistent with the known complex, $(\eta^5\text{-}C_5H_5)Ni(PPh_3)_2$, by comparison with a sample prepared by independent synthesis via a known thermal route.[4,6] We assign the new peaks at −262 and 218.5 ppm to the complex $(\eta^5\text{-}C_5H_4Me)Ni(PPh_3)_2$. In the case of these derivatives the ratio of methylated to unmethylated cyclopentadienyl was found to be 1 : 1.

The ESR spectrum of the sample was obtained after photolysis when the NMR resonance due to the methyl group of $(\eta^5\text{-}C_5H_5)Ni(Me)PPh_3$ was no longer discernible in the baseline. The ESR showed a triplet centred at $g = 2.060$ with hyperfine, $a = 111$ G, due to coupling with two phosphorus nuclei. This ESR signal is characteristic of the known complex, $(\eta^5\text{-}C_5H_5)Ni(PPh_3)_2$, however, as it is the only signal observed in these solutions, it must also be degenerate with the signal from $(\eta^5\text{-}C_5H_4Me)Ni(PPh_3)_2$. In order to confirm the assignment a sample of $(\eta^5\text{-}C_5H_5)Ni(PPh_3)_2$ was prepared by a published procedure[4,6] and its ESR signal was found to be identical with that of our product.

In order to measure the yield of the radical, $(\eta^5\text{-}C_5H_4R)Ni(PPh_3)_2$ (R = H, Me), the integral of the ESR signal was compared with that of degassed standard solutions of $Ti(acac)_3$. This gave a yield of 9% for the production of $(\eta^5\text{-}C_5H_4R)Ni(PPh_3)_2$. In the absence of excess PPh_3 this yield dropped to ~ 0.3%. The low yield is presumably a result of the instability of the radical product under these conditions.

Similar results were obtained upon photolysis of the ethyl derivative, $(\eta^5\text{-}C_5H_5)Ni(Et)PPh_3$. In this case the nickelocene products were a mixture of nickelocene and its ring-substituted ethyl derivatives.[5] Ring protons were found to resonate at −256 and −248 ppm, respectively, and the α-protons of the ethyl group were seen at 208.6 ppm. The ratio of $(\eta^5\text{-}C_5H_4Et)$ to $(\eta^5\text{-}C_5H_5)$ was 1 : 1.8 in the nickelocene products. Unfortunately, direct detection of $(\eta^5\text{-}C_5H_4Et)Ni(\eta^5\text{-}C_5H_5)$ was not possible. Presumably the signals due to the mixed derivative are degenerate with the signals of the two symmetrical nickelocenes. The signals due to both $(\eta^5\text{-}C_5H_5)Ni(PPh_3)_2$ and $(\eta^5\text{-}C_5H_4Et)Ni(PPh_3)_2$ were also observed. Resonance due to ring protons was observed at −263 ppm and the α-protons of the ethyl group were seen at 217 ppm. Weak NMR signals due to ethane and ethylene were also observed.

The spectroscopic yields of the 19-electron radical, $(\eta^5\text{-}C_5H_4R)Ni(PPh_3)_2$ (R = H, Et), were determined by comparison of the ESR signal with the signal produced by stock $Ti(acac)_3$ solutions. The yields were approximately the same as observed for the previous system accounting for 6% of the original nickel. Once again in the absence of free PPh_3 the yield dropped to ~ 0.5%.

The yields in each case represent maximum yields based on total organometallic complex. If the spectroscopic yields are calculated using the integration in the NMR to determine the amount of $(\eta^5\text{-}C_5H_5)Ni(Me)PPh_3$ lost, the calculated yield is ~ 20% in the early stages of the reaction (this is not true in the absence of free PPh_3 where the yield calculated by this method is only ~ 8%). The apparent low yields are due, in part, to the photosensitivity of the compounds. Solutions containing $(\eta^5\text{-}C_5H_5)Ni(PPh_3)_2$, stored at room temperature in the dark, are stable for at least 1 year; however, photolysis leads to loss of the ESR signal over the course of days. The initial reaction in the presence of excess ligand is given by eq. (1):

$$(\eta^5\text{-}C_5H_5)Ni(R)PPh_3 \xrightarrow[h\nu]{PPh_3} (\eta^5\text{-}C_5H_5)Ni(PPh_3)_2 + R^{\cdot} \quad (1)$$

Several derivatives were obtained by photolysis of either $(\eta^5\text{-}C_5H_5)Ni(R)PPh_3$ (R = Me or Et) in benzene solutions containing free phosphines or phosphites. Photolysis ($\lambda > 413$ nm) of the methyl derivative in the presence of 5 equivalents of free phosphine or phosphite led to the production of the disubstituted derivatives $(\eta^5\text{-}C_5H_5)NiL_2$, [L = P(*p*-FPh)$_3$, P(*p*-MeOPh)$_3$, P(*n*-Bu)$_3$, P(OMe)$_3$, P(OEt)$_3$, P(OPh)$_3$, dppe/2 (dppe = bis-diphenylphosphinoethane)]. The phosphine-con-

taining compounds all showed ^{31}P hyperfine coupling due to the presence of two equivalent phosphorus donors. The ESR signals from the phosphite derivatives were split into a doublet of doublets, indicating that the two phosphites are not equivalent. This inequivalence has been noted previously.[4] In each case the products were established not to be mixed phosphine/phosphite derivatives by comparison of the ESR obtained with the ESR produced when the free ligand was mixed with nickelocene in benzene. The ESR spectra of each of the derivatives were also obtained at $-120°C$. Figure 1 shows the room-temperature and low-temperature ESR spectra due to $(\eta^5\text{-}C_5H_5)Ni(P(OEt)_3)_2$. The ESR parameters for these complexes are given in Table 1. The yields for the various phosphine and phosphite derivatives were also measured and varied from less than 1–11% (see Experimental).

Degassed NMR samples containing $(\eta^5\text{-}C_5H_5)Ni(R)PPh_3$ [R = Me, Et, and 2,2′-bipyridyl (bipy)] in benzene were also prepared and photolysed. During the course of the reaction the samples turned from the green colour of $(\eta^5\text{-}C_5H_5)Ni(Me)PPh_3$ to blue. The reaction was monitored by NMR which indicated the loss of intensity due to substrate and the production of free phosphine, ethane and methane. No peaks attributable to a new metal cyclopentadienyl group were observed. We were unable to obtain the NMR for the radical products. The ESR spectrum of the reaction mixture was obtained and a single peak, $g = 2.084$, showing no hyperfine coupling, was observed. We identify this peak as due to the known complex $(\eta^5\text{-}C_5H_5)Ni(bipy)$. Comparison of the anisotropic ESR obtained in toluene glass, where nitrogen hyperfine is observed,[4] of our product with that independently synthesized via the known thermal route[4,6] confirmed the identity of the product as $(\eta^5\text{-}C_5H_5)Ni(bipy)$. The chemical yield of the nickel radical was estimated by comparison of the integral of its ESR signal with that of stock solutions of $Ti(acac)_3$ and found to be 80%. The photochemical reaction of $(\eta^5\text{-}C_5H_5)Ni(Me)PPh_3$ with bipy must involve methyl radical cleavage and bipy substitution for phosphine. The overall reaction is given as eq. (2):

$$(\eta^5\text{-}C_5H_5)Ni(R)PPh_3 \xrightarrow[h\nu]{bipy} (\eta^5\text{-}C_5H_5)Ni(bipy) + R^{\cdot} + PPh_3. \quad (2)$$

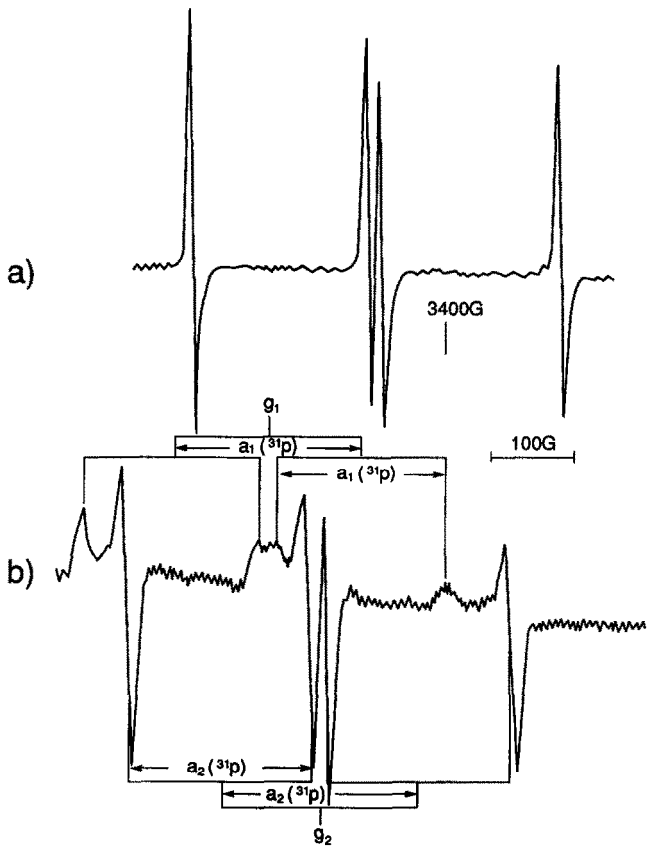

Fig. 1. The room temperature (a) and frozen solution (b) ESR spectra of $(\eta^5\text{-}C_5H_5)Ni(P(OEt)_3)_2$.

Table 1. ESR parameters for the complexes $(\eta^5\text{-}C_5H_5)NiL_2$

L	g	a, MHz (G)	g_1	g_2	g_3	a_1,[a] MHz	a_2, MHz (G)	a_3, MHz
$P(p\text{-}FC_6H_4)_3$	2.057	320 (112)	2.102	2.042	2.026	268 (94)	343 (120)	346 (122)
$P(p\text{-}OMeC_6H_4)_3$	2.065	317 (110)	2.120	2.038	2.021	270 (93)	337 (118)	342 (121)
$P(C_6H_5)_3$	2.060	320 (111)	2.182	2.039	2.022	305 (100)	334 (117)	339 (120)
$P(n\text{-}Bu)_3$	2.063	360 (124)	2.121	2.038	2.024	297 (100)	393 (138)	391 (138)
dppe	2.040	360 (126)	2.073	2.050	2.014	345 (119)	367 (128)	389 (138)
$P(OMe)_3$	2.041	576 (196, 207)	2.088	2.030		546/602 (187/206)	574/625 (202/220)	
$P(OEt)_3$	2.046	573 (200)	2.090	2.029		550/590 (188/202)	567/616 (200/217)	
$P(OPh)_3$	2.037	627 (212/228)	2.059	2.014		657/599 (228/208)	677/617 (219/240)	

[a] For molecules of rhombic symmetry, a_1 is calculated from the known isotropic hyperfine.

In the presence of diphenylacetylene, irradiation of $(\eta^5\text{-}C_5H_5)Ni(R)PPh_3$ leads to a similar result. The major radical product is characterized by its room-temperature ESR spectrum which shows a simple singlet $g = 2.090$. This product is assigned as $(\eta^5\text{-}C_5H_5)Ni(C_2Ph_2)_2$. The maximum yield observed for this product was 1%. In addition to this a doublet was also observed at $g = 2.028$, characterized by a phosphorus hyperfine of 120 G. This we assign as due to the mixed phosphine acetylene adduct, $(\eta^5\text{-}C_5H_5)NiPPh_3(C_2Ph_2)$. The yield of the mixed radical in this system was found to be 0.1%. Over a period of time the mixed phosphine diphenylacetylene adduct was found to convert to the bis-diphenylacetylene radical.

Similar results were obtained when photolysis was carried out in solutions containing phenylacetylene. Once again signals due to both a disubstituted adduct, $(\eta^5\text{-}C_5H_5)Ni(HCCPh)_2$, $g = 1.992$, and a monosubstituted adduct, $(\eta^5\text{-}C_5H_5)NiPPh_3(HCCPh)$, $g = 2.016$, $a = 80$ G, were observed. Once again, only low yields, $\sim 0.1\%$, were obtainable for either derivative. Unfortunately in neither case was the mixed adduct sufficiently concentrated to obtain the anisotropic ESR parameters.

Photolysis in the presence of $AsPh_3$ was also done and the ESR of the resultant solutions obtained. The product was primarily the bis-phosphine adduct. The ESR spectrum did however indicate that the production of $(\eta^5\text{-}C_5H_5)NiPPh_3AsPh_3$ had also occurred, albeit to a much lesser extent ($< 1/8$). The mixed phosphine arsine derivative was characterized by $g = 2.071$ and the observation of hyperfine to both ^{71}As, 150 G, and ^{31}P, 95 G. As the signals due to the mixed arsine phosphine derivative were always less intense than those due to the bis-phosphine complex we were unable to obtain its anisotropic ESR spectrum.

DISCUSSION

The photochemically initiated reactions of $(\eta^5\text{-}C_5H_5)Ni(Me)PPh_3$ and $(\eta^5\text{-}C_5H_5)Ni(Et)PPh_3$ were studied earlier by Emad and Rausch[2] and the thermal reaction by Thomson and Baird.[3] However, in neither of these studies were the metal-containing products identified. Herein we have found the products of both thermal and photochemical decomposition of $(\eta^5\text{-}C_5H_5)Ni(R)PPh_3$ (R = Me, Et) to consist of the nickel(I) species, $(\eta^5\text{-}C_5H_5)NiL_2$ (in the absence of added ligand or in the presence of PPh_3, L = PPh_3; in the presence of bipy, L_2 = bipy), eq. (3). The complexes where L = PPh_3, L_2 = bipy, are known and can be synthesized by reactions of L with nickelocene:[4,6]

$$(\eta^5\text{-}C_5H_5)Ni(R)PPh_3 \xrightarrow[h\nu]{L} (\eta^5\text{-}C_5H_5)NiL_2 + R^{\cdot} + PPh_3. \quad (3)$$

At longer photolysis times nickelocene and its ring-substituted derivatives are formed. The complexes, $(\eta^5\text{-}C_5H_5)NiL_2$, have previously been reported to be unstable towards disproportionation to nickelocene and NiL_4.[7] The net reaction is hence

given by eq. (4):

$$(\eta^5\text{-}C_5H_5)Ni(R)PPh_3 \xrightarrow[h\nu]{PPh_3} (\eta^5\text{-}C_5H_4R')Ni(PPh_3)_2 + (\eta^5\text{-}C_5H_4R')_2Ni + Ni(PPh_3)_4 + HR$$

R = Me, R′ = H and Me; R = Et, R′ = H and Et. (4)

Each of the nickel(I) complexes is best described as having a 19-electron configuration with an η^5-cyclopentadienyl ring.[8] An alternative formulation, a 17-electron system with an η^3-cyclopentadienyl ring, is considered less likely based on the following considerations. The crystal structure of the bipyridine derivative, $(\eta^5\text{-}C_5H_5)Ni(bipy)$, has been reported and establishes that the C_5H_5 ligand is pentahapto in this derivative.[4] Since the anisotropic shifts in the bipy complex ($g_1 = 2.184$, $g_2 = 2.080$, $g_3 = 2.033$ G) are in the range of those found for the phosphine substituted complexes (Table 1), the electronic structures are also expected to be similar. In addition it has been demonstrated that association of a ligand and a 17-electron complex to form a 19-electron complex is generally facile.[9] Here we find no evidence for formation of 19-electron complexes of the formula $(\eta^3\text{-}C_5H_5)NiL_3$ even for the smaller ligands such as $P(OMe)_3$. This lack of formation of $(\eta^3\text{-}C_5H_5)NiL_3$, even at low temperatures, is most consistent with a pentahapto arrangement for the C_5H_5 moiety.

It should also be noted that a variety of 19-electron complexes containing the $(\eta^5\text{-}C_5H_5)$ ligand have been structurally characterized.[8] We are aware of no example of a 17-electron complex with an $(\eta^3\text{-}C_5H_5)$ group. There is precedent for the existence of the related η^3-indenyl group.[8,9] Given the above factors, the most reasonable formulation of these complexes is as 19-electron complexes with $(\eta^5\text{-}C_5H_5)$ ligands.

The stabilities of the radicals are surprising. The bipy substituted radical is indefinitely stable. It should be noted, however, that significant disproportionation to nickelocene and $Ni(PR_3)_4$ does occur and the phosphite radicals are particularly unstable, undergoing complete decomposition over several hours. The phosphine radicals were much more stable. Solutions containing $(\eta^5\text{-}C_5H_5)Ni(PPh_3)_2$ were stored at room temperature in sealed tubes with no noticeable decomposition for periods of 1 year. The unsymmetrical derivative, $(\eta^5\text{-}C_5H_5)Ni(PPh_3)(C_2Ph_2)$, is less stable and reacts thermally to produce the $(\eta^5\text{-}C_5H_5)Ni(C_2Ph_2)_2$ derivative in the presence of excess diphenylacetylene. Solutions of $(\eta^5\text{-}C_5H_5)Ni(C_2Ph_2)_2$ are stable for periods of greater than 1 year when stored at 4°C.

In each derivative no evidence was found in the ESR spectra for an effect due to the methylation (or ethylation) of the $(\eta^5\text{-}C_5H_5)$ ring. This was determined by thermal synthesis of each (non-mixed) derivative from nickelocene and free ligand. The ESR in each case was identical to that found from the photochemical preparations.

The ESR spectra of the phosphine derivatives show hyperfine coupling to the phosphine, both in the isotropic and anisotropic spectra. For the alkyl and aryl phosphines a simple triplet, due to hyperfine coupling to two ^{31}P nuclei, is observed in the isotropic ESR. The anisotropic spectra, in frozen benzene or toluene, of the phosphine complexes display rhombic symmetry. In each of these cases overlap between the high-field components of g_1 and absorptions due to g_2 and g_3 made the direct assignment of a_1 difficult. Since the isotropic and anisotropic hyperfine constants are related, we have calculated values of a_1 for use in the analysis. The extent of phosphorus *s*-orbital contribution to the SOMO has been assessed by the standard method[10] using the atomic values of Morton and Preston.[11] The contribution for the triaryl phosphines is ~ 2.4%, whereas dppe and $P(n\text{-}Bu)_3$ are both slightly higher at 2.7%. The phosphorus *p*-orbital contribution to the SOMO, determined from the anisotropic spectra, is ~ 8% in these derivatives, with both dppe and $P(n\text{-}Bu)_3$ being somewhat higher.

Phosphite complexes display apparent axial symmetry in their ESR spectra. The two phosphorus donor atoms are inequivalent as evidenced by the appearance of a doublet of doublets in both the isotropic and anisotropic ESR, Fig. 1. The spectra were analysed as above but using the individual constants, giving rise to the individual contribution of each phosphite donor of a given compound. The analysis was carried out on the related hyperfines, giving the phosphorus *s*- and *p*-orbital contribution to the SOMO from each of the individual phosphites. In each case the contribution to the SOMO from the phosphorus *s*-orbital was ~ 4.5%. The phosphorus *p*-orbital contribution was similarly in the region of 4%.

The results are summarized in Table 2. We can see that in each case the total contribution to the SOMO from *s*-phosphorus and *p*-orbitals remains approximately 9% for both the phosphites and the aryl phosphines. The only variation that is significant is that of the trialkyl phosphine which is slightly higher at ~ 12%. However, the relative *s* and *p* contributions vary considerably. For the alkyl and aryl phosphines the phosphorus donor orbital is composed of approximately 25% *s* character. For the phosphites the *s* contribution is increased to ~ 50%. This is the expected result as more elec-

Table 2. Calculated contributions of *s*- and *p*-orbitals on phosphorus to the SOMO

L	*s*(%)	*p*(%)	*s*+*p*(%)	*s*/(*s*+*p*)
P(*p*-FC_6H_4)$_3$	2.4	7.1	9.5	25
P(*p*-$OMeC_6H_4$)$_3$	2.4	6.8	9.2	26
P(C_6H_5)$_3$	2.4	5.2	7.6	31
P(*n*-Bu)$_3$	2.7	9.0	11.7	23
dppe	2.7	7.9	10.6	34
P(OMe)$_3$	4.2	5.2	9.4	45
	4.6	4.1	8.7	53
P(OEt)$_3$	4.2	3.2	7.5	56
	4.5	4.6	9.1	49
P(OPh)$_3$	4.5	3.3	7.8	58
	5.0	3.8	8.8	56

tronegative substituents on the phosphorus should cause an increase in the amount of phosphorus *s* character in the donor orbital. This result indicates that the variation in isotropic hyperfine constants observed, the phosphites being much larger than the phosphines, is the result of changes in hybridization at the phosphorus and not a result of varying content of donor orbital participation in the SOMO. Similar findings have been reported earlier in studies of monophosphine adducts of cobalt.[12,13] The relative hybridization found there is in agreement with our results.

The phosphites are interesting in that the two donors in each bis-phosphite complex are inequivalent. The contribution to the SOMO is 9.4 and 8.7%, respectively, for each P(OMe)$_3$ in (η^5-C_5H_5)Ni(P(OMe)$_3$)$_2$. In (η^5-C_5H_5)Ni(P(OEt)$_3$)$_2$ a similar result is obtained, the contribution to the SOMO by each P(OEt)$_3$ differing by 1.6%. The two triphenylphosphite ligands in (η^5-C_5H_5)Ni(P(OPh)$_3$)$_2$ show that the total contribution to the SOMO from the two donor atoms differs by $\sim$ 1%. The average difference in participation in the SOMO from phosphorus atomic orbitals is $\sim$ 1% in these compounds. Surprisingly, the hybridization also is significantly different in the two inequivalent phosphites for both of the trialkyl phosphites. For the trimethylphosphite the donor orbital of one phosphite is $\sim$ 45% *s* whereas the other is $\sim$ 53% *s*. The triethyl derivative shows similar variation in that the *s* character varies from 49 to 56%. Only in the triphenylphosphite is the hybridization near constant with the donor orbitals comprised of 58 and 56% *s* character.

This inequivalence, only observed for the phosphites, may be a result of the greater *s* character in the donor orbital. The higher *s* content in the donor orbital is expected to result in a shorter P—Ni bond. This in turn would lead to more steric interaction between the phosphites and the metal centre. It may be as a result of this steric interaction that the phosphites are inequivalent. Of the inequivalent phosphites, the one having more *s* character makes a smaller contribution to the SOMO than the phosphite with less *s* character. One might expect that a higher *s* contribution to the donor orbital would lead to shorter bond lengths and hence a greater contribution to the SOMO. The dominant effect, however, appears to be the greater extension into space of the *p*-orbital causing greater overlap of the resultant donor orbital with the metal *d*-orbital.

CONCLUSIONS

Photolysis of (η^5-C_5H_5)Ni(R)PPh$_3$ (R = Me, Et) in air-free benzene solution leads to the production of (η^5-C_5H_5)Ni(PPh$_3$)$_2$. If irradiated in the presence of a variety of ligands, L, the corresponding complexes (η^5-C_5H_5)NiL$_2$ may be produced.

Various phosphine derivatives have been prepared by this method and both the isotropic and anisotropic ESR spectra obtained. Analysis of the nuclear hyperfine data indicates that the SOMO in all the various phosphorus ligand derivatives contains a $\sim$ 20% contribution from the phosphorus donor orbital. The variation in the observed isotropic hyperfine is due not to the amount of donor orbital character in the SOMO but to differing degrees of *sp*-hybridization in the PR$_3$ donor orbital. The *s*-orbital content of the phosphite donor orbital is much higher than in the phosphines giving a higher isotropic ^{31}P hyperfine.

EXPERIMENTAL

Triphenylphosphine was obtained from BDH and recrystallized from hexane prior to use. The ligands P(*p*-OMePh)$_3$ and P(OMe)$_3$ were obtained from Strem Chemical and Eastman Kodak, respectively. All other ligands were obtained from Aldrich Chemical. The complexes (η^5-C_5H_5)Ni(Et)PPh$_3$, (η^5-C_5H_5)Ni(Me)PPh$_3$ and Ti(acac)$_3$ were synthesized by published procedures.[2,14,15] Benzene was distilled from sodium prior to use.

^{1}H NMR spectra were obtained using Bruker SY100 or WM400 spectrometers. Chemical shifts are reported relative to TMS. UV–vis spectra were measured with a Cary 17 spectrophotometer. ESR data were collected with a Varian E4 equipped with an E-257 variable temperature accessory.

Photolysis of $(\eta^5\text{-}C_5H_5)Ni(Me)PPh_3$

A sample of $(\eta^5\text{-}C_5H_5)Ni(Me)PPh_3$ (0.0030 g) in d_6-benzene (1.0 cm^3) was degassed and flame sealed into a 5 mm NMR tube. The sample was then photolysed with the filtered (5 cm H_2O in Pyrex and bandpass $\lambda > 413$ nm) output of a 150 W xenon lamp. The sample was cooled by immersion in an H_2O bath at $\sim 6°C$ during photolysis. The reaction was monitored by both NMR and ESR. Similar experiments were conducted in the presence of PR_3, (R = *n*-Bu, Ph, *p*-OMePh, *p*–FPh, OMe, OEt, OPh, dppm, dppe, C_2Ph_2, HCCPh and bipy). Spectroscopic yields were calculated by comparison of the double integral of the ESR signal, obtained as a first derivative, with that of stock solutions of $Ti(acac)_3$ of known concentration. In the absence of added ligand the spectroscopic yield of $(\eta^5\text{-}C_5H_5)Ni(PPh_3)_2$ was 0.3%. In experiments where ligands were added the yields were: $P(n\text{-}Bu)_3$, $\sim 0.1\%$; PPh_3, 9%; $P(p\text{-}OMePh)_3$, 6%; $P(p\text{-}FPh)_3$, 11%; $P(OMe)_3$, 0.3%; $P(OEt)_3$, 1%; $P(OPh)_3$, 0.5%; dppm, 0.1%; dppe, 8%; C_2Ph_2, 1%; HCCPh, 0.3%; bipy, 80%. Similar experiments were conducted with $(\eta^5\text{-}C_5H_5)Ni(Et)PPh_3$.

Acknowledgements—We thank the Natural Sciences and Engineering Research Council of Canada and President's Research Grant (Simon Fraser University) for financial support. H.K.S. acknowledges the British Columbia Government for support through a Challenge '87 award.

REFERENCES

1. A. Becalska and R. H. Hill, *J. Am. Chem. Soc.* 1989, **111**, 4346.
2. A. Emad and M. D. Rausch, *J. Organomet. Chem.* 1980, **191**, 313.
3. J. Thomson and M. C. Baird, *Can. J. Chem.* 1970, **48**, 3444.
4. E. K. Barefield, D. A. Krost, D. S. Edwards, D. G. Van Derveer, R. L. Trytko, S. P. O'Rear and A. N. Williamson, *J. Am. Chem. Soc.* 1981, **103**, 6219.
5. F. M. Kohler, *J. Organomet. Chem.* 1976, **110**, 235; M. F. Rettig and R. S. Drago, *J. Am. Chem. Soc.* 1969, **91**, 1361.
6. E. Uhlig and H. Walther, *Z. Chem.* 1971, **11**, 23.
7. See ref. 4 and also relevant information is contained in, H. Werner, H. Harder and E. Deckelmann, *Helv. Chim. Acta* 1969, **52**, 1081, where the proposed intermediate is clearly $(\eta^5\text{-}C_5H_5)Ni(L)_2$.
8. Although the evidence indicates a pentahapto C_5H_5 ligand we use the 19-electron terminology only in the formal sense. It should be noted that a substantial part of the electron density is presumably on the C_5H_5 ring, hence the metal would in reality have less than 19 electrons. For a more complete discussion of this point see D. Astruc, *Chem. Rev.* 1988, **88**, 1189.
9. M. C. Baird, *Chem. Rev.* 1988, **88**, 1217.
10. (a) M. C. R. Symons, *Electron-spin Resonance Spectroscopy*. Halsted, New York (1978); (b) P. B. Ayscough, *Electron Spin Resonance in Chemistry*. Methuen, London (1967).
11. J. R. Morton and K. F. J. Preston, *Mag. Reson.* 1978, **30**, 577.
12. B. B. Wayland and M. E. Abd-Elmageed, *J. Am. Chem. Soc.* 1974, **96**, 4809.
13. B. B. Wayland, M. E. Abd-Elmageed and L. F. Mehne, *Inorg. Chem.* 1975, **14**, 1456.
14. M. D. Rausch, Y. F. Chang and H. B. Gordon, *Inorg. Chem.* 1969, **8**, 1355.
15. G. Y.-S. Lo and C. H. Brubaker, *J. Inorg. Nucl. Chem.* 1972, **34**, 2375.

Polyhedron Vol. 9, No. 4, pp. 589–595, 1990
Printed in Great Britain

0277-5387/90 $3.00+.00
© 1990 Pergamon Press plc

SELENIUM CHLORIDE AND BROMIDE EQUILIBRIA IN APROTIC SOLVENTS; A ^{77}Se NMR STUDY

MARC LAMOUREUX and JOHN MILNE*

Department of Chemistry, University of Ottawa, Ottawa, Ontario, Canada, K1N 6N5

(*Received* 26 *June* 1989; *accepted* 18 *September* 1989)

Abstract—The ^{77}Se NMR spectra of solutions with stoichiometries near those for SeX_2 and Se_2X_2 (X = Br, Cl) formation in aprotic solvents of varying basicity have been recorded. Chemical shifts for $SeCl_4$, SeX_2, Se_2X_2, Se_3X_2 and Se_4X_2 are reported. The constants for the equilibria,

$$2SeBr_2 \rightleftharpoons Se_2Br_2 + Br_2$$

$$3SeCl_2 \rightleftharpoons SeCl_4 + Se_2Cl_2$$

$$2Se_2X_2 \rightleftharpoons SeX_2 + Se_3X_2$$

$$3Se_2X_2 \rightleftharpoons 2SeX_2 + Se_4X_2$$

have been determined in various solvents from NMR spectra and chemical analysis. The position of the equilibria is very sensitive to solvent donor strength, with the selenium halide of stronger Lewis acidity favoured in the more basic solvent. Selenium bromide chloride, Se_2BrCl, has been shown to exist in equilibrium with Se_2Br_2 and Se_2Cl_2 in dichloromethane.

The oxidation state +2 is uncommon for selenium and none of the dihalides are known as pure compounds. The presence of selenium dichloride and dibromide in solution in non-aqueous solvents[1,2] and in the gas phase[3,4] has been demonstrated. It has recently been shown that pure liquid diselenium dichloride and dibromide disproportionate to a small extent and contain equilibrium concentrations of the selenium dihalide and polyselenium dihalides.[5] Selenium(II) is known in chloro- and bromoselenate(II) compounds[6] where it is apparently stabilized by halo coordination. Selenium(II) has been shown to be in equilibrium with selenium(IV) and Se_2X_2 in aqueous HCl and HBr also.[7,8] Stabilization by solvent coordination may also occur and have an important influence on the selenium dihalide concentration in solution. This present study was carried out, to determine the influence of solvent on the equilibrium distribution of selenium, diselenium and polyselenium dichlorides and dibromides in solution.

Few ^{77}Se NMR studies of inorganic selenium compounds have been made[9] and this study relies principally on this technique.

EXPERIMENTAL

Elemental selenium (99.999, Aldrich) was used directly. Selenium tetrachloride was prepared from chlorine and selenium.[10] Bromine (Fisher reagent) was distilled from phosphorus pentoxide before use. Dimethylformamide (DMF) (Fisher certified) and pyridine (py) (BDH assured) were dried over, and distilled from Dreirite. Carbon tetrachloride (Fisher certified), dichloromethane (Fisher certified) and acetonitrile (BDH assured) were dried over and distilled from phosphorus pentoxide. Solutions of the desired stoichiometry were made up by weight from selenium and $SeCl_4$ or selenium and Br_2 and the solvent, using a balance accurate to ± 2 mg. In a typical experiment 82 mg of selenium were combined with 228 mg of $SeCl_4$ in 3.993 g of acetonitrile to yield a solution of $SeCl_x$ composition with $x = 2.00 \pm 0.003$, where $c(SeCl_2) = 0.41 \pm 0.01$ M. The solution volume was considered to be that of the solvent alone. All solutions were made up in a dry box. In several cases

* Author to whom correspondence should be addressed.

an initial precipitate of red selenium was produced, which dissolved to yield clear yellow–brown coloured solutions.

Analyses for chloride and selenium were carried out, respectively, by Volhard and gravimetric methods.[11] For the pyridine mixture of 2:1 Cl/Se mole ratio, containing the insoluble $SeCl_4$ adduct (see below), dilution in aqueous acid (1 in 10) resulted in disproportionation to elemental selenium and selenate(IV). After gravimetric analysis for the precipitated selenium, the supernatant was analysed for chloride.

The bis(pyridine) adduct of $SeCl_4$, $SeCl_4 \cdot 2py$, was prepared by shaking $SeCl_4$ and dry pyridine (1:50 mol ratio) together for 12 h and filtering out the yellow product in a dry atmosphere. The product was very difficult to filter and free of solvent. Found: Se, 36.3; Cl, 20.0. Calc.: Se, 37.4; Cl, 20.8%.

Raman spectra were recorded using equipment described earlier.[2] ^{77}Se NMR spectra were recorded in 10 mm tubes, using a Varian FT300 spectrometer operating at 57.28 MHz. All shifts are reported with respect to the reference shift of saturated aqueous selenous acid solution at 20°C. The chemical shifts were determined by sample replacement and are accurate to ± 0.7 ppm. The shift of saturated selenous acid is at 1282 ppm with respect to dimethyl selenium.[12]

RESULTS AND DISCUSSION

Selenium chlorides

Selenium tetrachloride exhibits a broad range of solubility in aprotic solvents. Saturation molarities at 20($\pm$1)°C have been determined for several solvents and these are CCl_4: insoluble; CH_2Cl_2: 1.36×10^{-3}; CH_3CN: 2.05×10^{-2}; py: 5.82×10^{-2}; DMF: >1.15. The solubility increases with the donor strength of the solvent, reflecting the Lewis acidic nature of $SeCl_4$. In the case of CCl_4, CH_2Cl_2 and CH_3CN, the insoluble phase is pure $SeCl_4$ as shown by the Raman spectrum, which has characteristic strong bands at 387, 340 and 97 cm^{-1}.[13] However, in the case of pyridine the insoluble phase is a yellow adduct, $SeCl_4 \cdot 2py$, with Raman bands at 119 (6), 149 (7), 247 (9) and 279 (10) cm^{-1} (intensities in parentheses). In CH_2Cl_2 and CH_3CN solutions, even at such low concentrations, Raman bands corresponding to $SeCl_4$ species are observed,[2,14] but the ^{77}Se NMR signal could only be observed for the DMF solution, as given in Table 1 (solution No. 1). The signal observed at 153.7 ppm, which is 25 ppm to low field of that reported by Birchall *et al.*[9] for $SeCl_4$ in DMF, is broad (width at half-height = 3.4 ppm). The earlier measurement was carried out with a saturated solution, using broad-line techniques, which may account for the difference between the two results. Because of low solubility and signal breadth, the $SeCl_4$ shift could not be detected in CH_2Cl_2, CH_3CN and py. $SeCl_4$, which is known to be monomeric in CH_3CN,[15] is expected to give a broad NMR signal due to coupling to the 4 Cl's ($I = 3/2$ for both ^{35}Cl and ^{37}Cl), which will be quadrupole relaxed, and due to intramolecular chlorine exchange via a Berry mechanism. Intermolecular exchange may also occur. Similar processes causing broadening will occur with $SeCl_4$ in other solvents.

When elemental selenium is added to a saturated solution of $SeCl_4$ in CH_3CN, CH_2Cl_2 or CCl_4, there is reaction to give lower selenium chlorides:

$$SeCl_4 + Se \rightleftharpoons 2SeCl_2 \quad (1)$$

$$SeCl_4 + 3Se \rightleftharpoons 2Se_2Cl_2. \quad (2)$$

After sufficient selenium has been added all of the $SeCl_4$ reacts and the solution becomes saturated with respect to elemental selenium. The Raman spectra[14] of the Se/$SeCl_4$ solutions saturated with $SeCl_4$ exhibit peaks characteristic of $SeCl_2$ (417, 397 and 164 cm^{-1})[2] and those, saturated with selenium, peaks characteristic of Se_2Cl_2 (373 and 131 cm^{-1}).[2] The ^{77}Se NMR spectra of Se/$SeCl_4$ solutions saturated with $SeCl_4$, consist of two signals as given in Table 2 (solutions Nos 2, 4, 6). The weaker signal to highest field has a chemical shift corresponding to that of Se_2Cl_2[5,9] and that at lowest field arises from $SeCl_2$.[5] The chemical shifts of these two compounds in Se_2Cl_2 as solvent[5] are given for comparison (No. 9). The UV–vis spectra of CH_3CN solutions of 2:1 Cl/Se stoichiometry have been interpreted in terms of the equilibrium,

$$3SeCl_2 \overset{K(SeCl_2)}{\rightleftharpoons} Se_2Cl_2 + SeCl_4. \quad (3)$$

The ^{77}Se NMR spectra of the solutions in CH_3CN and CH_2Cl_2 may be interpreted similarly. The equilibrium constant at 20($\pm$1)°C may be calculated from the saturation concentration for $SeCl_4$ in each solvent, the ratio of the concentrations of Se_2Cl_2 and $SeCl_2$ calculated from NMR signal intensities and from the stoichiometric concentration of elemental selenium dissolved, c_{Se} (Table 1), which is related to the Se_2Cl_2 and $SeCl_2$ concentrations by,

$$c_{Se} = \frac{[SeCl_2]}{2} + \frac{3[Se_2Cl_2]}{2}. \quad (4)$$

The calculated values of $K(SeCl_2)$ are given in Table 2. The ^{77}Se NMR signals for pyridine were too weak for observation but chemical analysis for

Table 1. ^{77}Se NMR chemical shifts (ppm)[a] of selenium chlorides, bromides and bromide chloride

Solvent	Number	Stoichiometry	Selenium chlorides						
			$SeCl_4$	$SeCl_2$	Se_2Cl_2	Se_3Cl_2		Se_4Cl_2	
						β	α	α	β
DMF	1	1.15 M $SeCl_4$	153.7	—	—	—		—	
CH_3CN	2	c_{Se} = 0.20 M; $SeCl_4$ saturated	—	470.5 (117)	8.3 (14)	—		—	
	3	c_{SeCl_4} = 0.97 M; Se saturated	—	464.2 (32)	5.1 (1520)	11.0 (7),	−3.3 (12)	—	
CH_2Cl_2	4	c_{Se} = 0.25 M; $SeCl_4$ saturated	—	459.7 (103.4)	−23.1 (47.1)	—		—	
	5	c_{SeCl_4} = 0.14 M; Se saturated	—	458.1 (16.5)	−23.8 (1170)	−10.3 (3.9),	−30.6 (4.4)	−356.5 (1.5),	−374.9 (2.1)
CCl_4	6	c_{Se} = 0.10 M; $SeCl_4$ saturated	—	445.5 (63.5)	−47.1 (37.5)	—		—	
	7	c_{SeCl_4} = 0.20 M; Se saturated	—	444.4	−47.5	—		—	
	8	c_{SeCl_4} = 2.2 M; Se saturated	—	438.2 (11.4)	−30.4 (3114)	−23.2 (7.6),	−39.2 (11.0)	−353 (2.4), −373 (7.1),	−391 (2.7)
Se_2Cl_2[b]	9	Liquid Se_2Cl_2 containing 3.34 weight % Se	—	425.4 (6.6)	−9.74 (736)	−10.3 (12)		−365.5 (14)	

Solvent	Number	Stoichiometry	Selenium bromides					
			$SeBr_2$	Se_2Br_2	Se_3Br_2		Se_4Br_2	
					α	β	α	β
CH_3CN	10	$c_{Se_2Br_2}$ = 1.23 M	—	−110.3	—		—	
	11	c_{SeBr_2} = 2.34 M	195.0 (168)	−108.0 (40.2)	—		—	
	12	$c_{\text{"}SeBr_4\text{"}}$ = 1.11 M	194.7 (144)	−110.5 (trace, broad)	—		—	
CH_2Cl_2[c]	13	$c_{Se_2Br_2}$ = 1.02 M c_{Se} = 0.34 M	173.9 (15.6)	−132.5 (2020)	−150.4 (28),	−168.2(14)	−372.0 (10),	−381.8 (10)
Se_2Br_2[b]	14	Liquid Se_2Br_2	164.4 (4)	−110.9 (163)	−132.2 (5),	−143.9(2)	−360.7 (1),	−372.7 (2)

Solvent	Number	Stoichiometry	Diselenium bromide chloride			
			Se_2Cl_2	Se_2Br_2	Se_2BrCl	
CH_2Cl_2	15	$c_{Se_2Cl_2}$ = 1.6 M $c_{Se_2Br_2}$ = 1.5 M	−22.1 (64)	−128.5 (50.5)	−13.6 (50.5)	−137.5 (48)
Se_2Cl_2/Se_2Br_2	16	0.92 : 1.00 : 0.21 mol ratio $Se_2Br_2/Se_2Cl_2/Se$	−9.11 (152)	−110.9 (164)	−12.7 (166)	−115.1 (140)

[a] Chemical shifts are measured from saturated aqueous H_2SeO_3 at 20°C; relative signal intensities are given in parentheses (peak areas are given except in the case of solution No. 5 where peak heights are given).

[b] From Ref. 5.

[c] An additional signal was observed at −133.2(24).

Table 2. Disproportionation equilibria for $SeCl_2$ and Se_2Cl_2 at 20(±1)°C in aprotic solvents

Solvent	Donor number	Dielectric constant (25°C)	$K(SeCl_2)^a$ ($dm^3\ mol^{-1}$)	$K(Se_2Cl_2)^b$	$K'(Se_2Cl_2)^c$
CCl_4	0	2.24	0	2.9×10^{-5}	8.4×10^{-8}
CH_2Cl_2	0	9.08	3.7×10^{-3}	1.3×10^{-4}	1.2×10^{-6}
Se_2Cl_2[d]	—	—	—	4×10^{-4}	3×10^{-6}
CH_3CN	14.3	36.7	0.024	5.4×10^{-4}	—
py	33.1	12.3	663	—	—

[a] Equilibrium (3).
[b] Equilibrium (5).
[c] Equilibrium (6).
[d] Reference 5.

selenium and chlorine in the supernatant over $SeCl_4\cdot 2py$ to which elemental selenium had been added ($c_{Se} = 0.204$ M) gave $[SeCl_2] = 0.0090$ M and $[Se_2Cl_2] = 0.0083$ M. The equilibrium constant, $K(SeCl_2)$, in pyridine, is given in Table 2. The value of $K(SeCl_2)$ for the CCl_4 solution is also given in Table 2 for comparison.

Solutions of $SeCl_4$ saturated with Se give the ^{77}Se NMR spectra shown in Fig. 1 and listed in Table 1 (Nos 3, 5, 7 and 8). In these solutions the low field shift due to $SeCl_2$ is now much weaker in intensity than that due to Se_2Cl_2. However, in addition to these peaks, there are several peaks to higher field, which may be assigned to Se_nCl_2 species ($n = 3, 4$). These signals have also been observed in solutions of selenium in Se_2Cl_2[5] and there is Raman spectroscopic evidence for Se_nCl_2 species in Se/Se_2Cl_2 mixtures.[5,17] The strongest ^{77}Se signals, and the only ones observed in this work, will arise from Se_nCl_2 species with one ^{77}Se in the chain. For Se_3Cl_2 ($ClSe^{\alpha}Se^{\beta}Se^{\alpha}Cl$), two chemical shifts, from α- and β-selenium atoms, of relative intensity 2 : 1, respectively, are expected. For Se_4Cl_2 ($ClSe^{\alpha}Se^{\beta}Se^{\beta}Se^{\alpha}Cl$), two chemical shifts of equal intensity are expected. The two weak chemical shifts which bracket the Se_2Cl_2 shift may be assigned to Se_3Cl_2 on the basis of their 2 : 1 intensity ratio with the α-selenium shift lying to high field of the Se_2Cl_2 shift in all cases. The chemical shifts of Se_3Cl_2 lie close to that of Se_2Cl_2 in pure Se_2Cl_2 also[5] and these shifts have been listed in Table 1 for comparison. The chemical shifts for Se_4Cl_2 lie to high field of those of Se_3Cl_2.[5] These are not observed for CH_3CN solutions but for CH_2Cl_2, a pair of weak signals of equal intensity at −356.5 and −374.9 ppm are observed. The lowest field signal of these two, while of the same intensity as that at −374.9 ppm, is the broader of the two and is therefore assigned to the α-selenium, which is expected to be broader due to greater coupling to the spin 3/2 chlorine nuclei, which undergo quadrupole relaxation.

In CCl_4, three signals, −353.0, −372.7 and −391.0 ppm are observed in the Se_4Cl_2 region of the spectrum. The low intensity of these signals precludes a definite interpretation, but it is not possible to assign the peaks in terms of the overlapping spectra of Se_4Cl_2 and Se_5Cl_2 (three signals of 2 : 2 : 1 relative intensity). The spectra of Se_4Br_2 in liquid Se_2Br_2, containing dissolved selenium, has a similar appearance and that of Se_4Cl_2 in liquid Se_2Cl_2 consists of a single broad peak.[5] The spectrum in CCl_4 may be accounted for by the presence of the chain form of Se_4Cl_2 and some other isomer, or higher homologue, undergoing rapid intramolecular exchange.

As in the case of pure Se_2Cl_2,[5] disproportionation equilibria of the type,

$$2Se_2Cl_2 \overset{K(Se_2Cl_2)}{\rightleftharpoons} SeCl_2 + Se_3Cl_2 \qquad (5)$$

$$3Se_2Cl_2 \overset{K'(Se_2Cl_2)}{\rightleftharpoons} 2SeCl_2 + Se_4Cl_2 \qquad (6)$$

take place in these solutions. From the relative intensities of the signals, $K(Se_2Cl_2)$ and $K'(Se_2Cl_2)$ may be determined and these are given in Table 2 along with the equilibrium constants determined for liquid Se_2Cl_2.[5]

Selenium bromides

Selenium tetrabromide is known as a crystalline solid but in the gas phase or when dissolved in

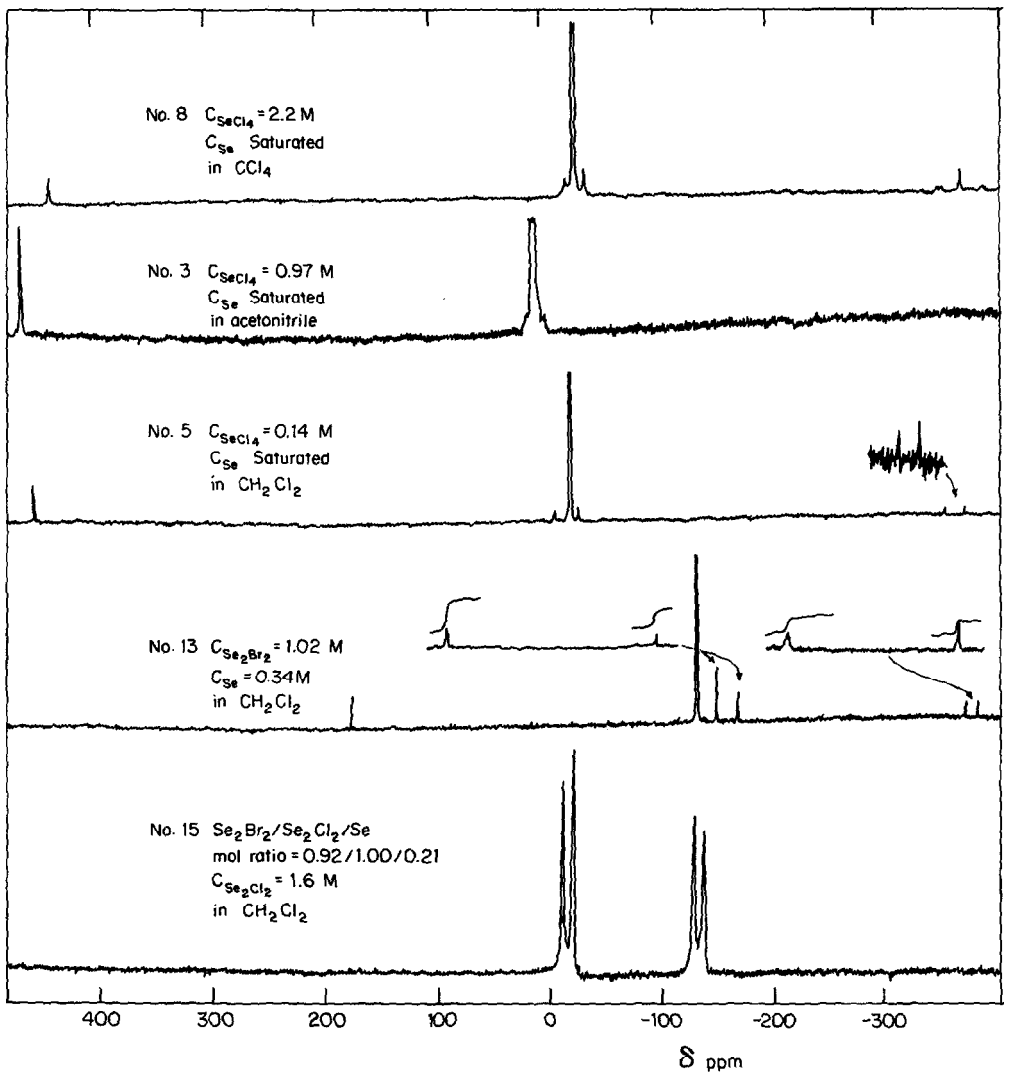

Fig. 1. ^{77}Se NMR spectra of solutions of selenium chlorides, bromides and bromide chlorides in aprotic solvents.

aprotic solvents at 25°C, it dissociates according to,

$$SeBr_4 \rightleftharpoons SeBr_2 + Br_2. \quad (7)$$

The $SeBr_2$ dissociates further to Se_2Br_2:[1,2,18]

$$2SeBr_2 \overset{K(SeBr_2)}{\rightleftharpoons} Se_2Br_2 + Br_2. \quad (8)$$

The chemical shifts for selenium bromide solutions are given in Table 1. The spectrum of a solution with a 1 : 4 atomic ratio of Se/Br (No. 12) in CH_3CN consists of a strong signal at 194.7 ppm and a very weak signal at −110.5 ppm, which is near to the reported shift for pure Se_2Br_2[5,9] and Se_2Br_2 in CH_3CN. The strong, low field signal is assigned to $SeBr_2$. For a solution in acetonitrile of 1 : 2 Se/Br atomic ratio (No. 11), the same two chemical shifts are observed but the Se_2Br_2 signal has become stronger, compared to that of $SeBr_2$, reflecting a shift of equilibrium (8) to the right due to a decrease in Br_2 concentration. The equilibrium constant, $K(SeBr_2)$, for equilibrium (8) was determined from the signal intensities of solution No. 11 and this is given in Table 3. There is excellent agreement between the value calculated here and that for the CH_3CN solution determined from UV–vis spectrophotometry.[2] The spectrum of a solution of Se_2Br_2 in acetonitrile (No. 10) had only one signal. No signals for Se_3Br_2 of Se_4Br_2 were observed due to the small number of transients collected.

The ^{77}Se NMR spectrum of a solution of a 1.17 : 1.00 Se/Br atomic ratio in CH_2Cl_2 is shown in Fig. 1 and the chemical shifts and intensities are given in Table 1 (No. 13). In addition to signals for $SeBr_2$ and Se_2Br_2, at 173.9 and −132.5 ppm, respectively, there are two sets of two signals each to high field of the Se_2Br_2 signal, which may be

Table 3. Disproportionation equilibria for $SeBr_2$ and Se_2Br_2 at 20(±1)°C in aprotic solvents

Solvent	Donor number	Dielectric constant (25°C)	$K(SeBr_2)^a$	$K(Se_2Br_2)^b$	$K'(Se_2Br_2)^c$
CCl_4	0	2.24	0.0252[d]	—	—
CH_2CL_2	0	9.08	—	2.2×10^{-4}	1.2×10^{-6}
CH_3CN	14.3	36.7	0.14 0.014[e]	—	—
Se_2Br_2	—	—	—	1.1×10^{-3}	1.7×10^{-6}

[a] Equilibrium (8).
[b] Equilibrium (9).
[c] Equilibrium (10).
[d] Reference 1.
[e] Spectrophotometric determination.[2]

clearly assigned to Se_3Br_2 and Se_4Br_2 on the basis of their relative intensities. The assignment of the α- and β-selenium signals for Se_3Br_2 is readily made on the basis of signal intensity and width at half-height and, for Se_4Br_2 on the basis of width at half-height alone. There is an additional weak signal at −133.2 ppm, which may be due to an isotope shift in Se_2Br_2, although the shift is large compared to that observed in other compounds.[19] The signals are all assigned in Table 1. The spectra show that the diseleniumdibromide disproportionates in CH_2Cl_2 in an analogous manner to diselenium dichloride:

$$2Se_2Br_2 \overset{K(Se_2Br_2)}{\rightleftharpoons} SeBr_2 + Se_3Br_2 \qquad (9)$$

$$3Se_2Br_2 \overset{K'(Se_2Br_2)}{\rightleftharpoons} 2SeBr_2 + Se_4Br_2. \qquad (10)$$

From the signal intensities of solution No. 13, $K(Se_2Br_2)$ and $K'(Se_2Br_2)$ have been determined and these are listed in Table 3 along with analogous constants for disproportionation in pure Se_2Br_2.[5]

Diselenium bromide chloride

The ^{77}Se NMR spectrum of a 0.92:1.00:0.21 $Se_2Br_2/Se_2Cl_2/Se$ mol ratio mixture dissolved in CH_2Cl_2 is shown in Fig. 1 and the chemical shifts are listed in Table 1. Four signals are observed corresponding to the chemical shifts of pure Se_2Cl_2 and Se_2Br_2 in CH_2Cl_2 at −22.1 and −128.5 ppm, respectively, and, to ^{77}Se α to chlorine and bromine in Se_2BrCl, respectively, at −13.6 and −137.5 ppm. No signals were observed for any triselenium compound in this routine spectrum. The spectrum shows that the following equilibrium is established,

$$Se_2Br_2 + Se_2Cl_2 \overset{K_d}{\rightleftharpoons} 2Se_2BrCl. \qquad (11)$$

This equilibrium occurs in mixtures of liquid Se_2Cl_2 and Se_2Br_2 also.[5] The equilibrium constant, K_d, calculated from the intensities listed in Table 1, is 3.0.

CONCLUSIONS

For the selenium dihalide compounds in general, the chemical shifts for ^{77}Se move to higher field with increasing chain length. For the dialkyl polyselenides, the change in shift is in the opposite sense.[19] Since chlorine and bromine are more electronegative than selenium while carbon is of equivalent or lower electronegativity,[20] it appears that these trends are due to changing shielding effects arising from greater withdrawal of electrons from the selenium by chlorine and bromine than by carbon. The chemical shift of $SeCl_4$ in DMF lies to high field of that of $SeCl_2$, which is in the opposite direction of that expected on the basis of electron shielding. Birchall *et al.*[9] have noted that ^{77}Se resonance of selenium(VI) compounds lies in general to high field of those of the selenium(IV) compounds.

The change in chemical shift with changing solvent is much greater than that which can be accounted for by bulk susceptibility changes and must arise from solute–solvent interactions. For each of the Se_nX_2 species (n = 1, 2, 3) in aprotic solvents at comparable concentrations, the shift is to low field with increasing solvent donor strength.

Tables 2 and 3 list the values of the various disproportionation constants, $K(SeX_2)$, $K(Se_2X_2)$ and $K'(Se_2X_2)$, determined for selenium bromides and chlorides, as well as the dielectric constants and donor numbers for the different solvents.[21] In all cases, except for $K(SeBr_2)$, the disproportionation

is favoured by greater solvent donor strength. The dielectric constant appears to play a less important role as shown by a comparison of the CH_3CN and pyridine values for $K(SeCl_2)$ in Table 2. This is expected for these equilibria where no ions are involved. The Lewis acidity of the selenium halides is expected to follow the order,

$$SeX_4 > SeX_2 > Se_2X_2. \quad (12)$$

Thus, in pyridine, the Lewis acid base adduct formation is so favourable for $SeCl_4$ that, in spite of the weak interaction of Se_2Cl_2 with pyridine, $SeCl_2$ disproportionates extensively. Similarly, the relatively strong Lewis acidities of $SeCl_2$ and $SeBr_2$ favour the disproportionation of Se_2Cl_2 and Se_2Br_2 in more strongly donating solvents. Ultimately one of the disproportionation products is elemental selenium, which is insoluble in the solvents studied. The addition of Cl^- or Br^- to their respective selenium halides will promote disproportionation of the lower halides in some cases as well:[6]

$$Se_2Cl_2 + Cl^- \underset{CH_3CN}{\rightleftharpoons} Se^0 + SeCl_3^- \quad (13)$$

$$2SeCl_3^- \underset{\substack{Et_4NSeCl_3 \\ solid}}{\rightleftharpoons} SeCl_6^{2-} + Se^0. \quad (14)$$

In the vapour phase where there is no Lewis acid–base stabilization, $SeCl_2$ disproportionates to a very small extent.[16] No doubt in CCl_4, $K(SeCl_2)$ has a small value also and not, as shown in Table 2, zero, which is a result of the immeasurably small solubility of $SeCl_4$ in this solvent.

Selenium dibromide dissociates to Se_2Br_2 and Br_2, according to eq. (8). The dissociation constant in CCl_4[1] is greater than that in CH_3CN (Table 3). This may also be accounted for by the strong solvent–$SeBr_2$ interaction in the stronger donor solvent, CH_3CN. Apparently the Lewis acid–base interaction of the solvent with either of the two products of dissociation is weaker than that with $SeBr_2$. The Br^- ion acts to stabilize selenium(II) as well,[6] and halo coordination even permits the stabilization of bromoselenate(IV) anions,[22] while $SeBr_4$ is unstable.

The previous ^{77}Se NMR study by Birchall *et al.*[9] concluded that no Se_2BrCl was formed in a mixture of Se_2Cl_2 and Se_2Br_2. Recently it has been shown, however, that Se_2BrCl is formed.[5] The present study shows that Se_2BrCl is also formed in CH_2Cl_2. The equilibrium constants for Se_2BrCl formation, eq. (11), are both 3.0 in the two media, indicating that a small change in the polarity of the solvent has little effect on equilibrium (11).

Acknowledgement—Raj Kapoor is thanked for recording the NMR spectra.

REFERENCES

1. N. W. Tideswell and J. D. McCullough, *J. Am. Chem. Soc.* 1956, **78**, 3026.
2. J. Milne, *Polyhedron* 1985, **4**, 65.
3. G. A. Ozin and A. Van der Voet, *J. Chem. Soc. D* 1970, 896.
4. D. M. Yost and J. B. Hatcher, *J. Am. Chem. Soc.* 1931, **53**, 2549.
5. M. Lamoureux and J. Milne, *Can. J. Chem.* 1989, **67**, 1936.
6. J. B. Milne, *Polyhedron* 1987, **6**, 849.
7. M. Mahadevan and J. Milne, *Inorg. Chem.* 1983, **22**, 1648.
8. J. Milne, *Can. J. Chem.* 1989, **69**, 1056.
9. T. Birchall, R. J. Gillespie and S. L. Vekris, *Can. J. Chem.* 1965, **43**, 1672.
10. H. G. Novak and J. F. Suttle, *Inorganic Synthesis*, Vol. V, p. 125. McGraw-Hill, New York (1957).
11. A. I. Vogel, *Quantitative Inorganic Analysis*, 3rd ed, p. 508. Longmans, Green and Co., New York (1961).
12. R. K. Harris and B. Mann, *NMR and the Periodic Table*, p. 403. Academic Press, New York (1979).
13. H. Gerding, *Rec. Trav. Chim.* 1956, **75**, 589.
14. Unpublished results.
15. N. Katsaros and J. W. George, *Inorg. Chim. Acta* 1969, **3**, 165.
16. W. Wehrli, *Helv. Phys. Acta* 1936, **9**, 637.
17. S. V. Volkov, Z. A. Fokina, V. F. Lapko, V. E. Pogrelov and G. I. Salivon, *Ukr. Khim. Zh.* 1982, **48**, 899.
18. N. Katsaros and J. W. George, *Inorg. Chem.* 1969, **8**, 759.
19. H. Eggert, O. Nielsen and L. Henriksen, *J. Am. Chem. Soc.* 1986, **108**, 1725.
20. J. E. Huheey, *Inorganic Chemistry*, 3rd Edn, p. 146. Harper and Row, New York (1983).
21. V. Gutmann, *Chimia* 1977, **31**, 1.
22. J. Milne and P. Lahaie, *Inorg. Chem.* 1985, **24**, 80; P. Lahaie, MSc thesis, University of Ottawa, Canada (1981).

Polyhedron Vol. 9, No. 4, pp. 597–601, 1990
Printed in Great Britain

0277–5387/90 $3.00+.00
© 1990 Pergamon Press plc

MERCURY AND METHYLMERCURY COMPLEXES OF THE 1-BUTYL AND 1-HEXADECYL ESTERS OF L-CYSTEINE AND 2,3-DIMERCAPTOSUCCINIC ACID

KEITH WILLE, JUSTIN K. MORAN and D. MAX ROUNDHILL*

Department of Chemistry, Tulane University, New Orleans, LA 70118, U.S.A.

(*Received* 5 *July* 1989 ; *accepted* 12 *September* 1989)

Abstract—The 1-butyl and 1-hexadecyl esters of l-cysteine have been synthesized from l-cysteine hydrochloride and the corresponding alcohol. These compounds [$HSCH_2CH(NH_3)CO_2R$]Cl (R = 1-C_4H_9, 1-$C_{16}H_{33}$) complex to methylmercury via the thiolate sulphur. The complexes [$CH_3HgSCH_2CH(NH_3)CO_2R$]Cl show bands in the IR spectrum in the 300–350 cm^{-1} region due to ν(Hg—S), and in the 500–550 cm^{-1} region due to ν(Hg—C). The ethyl, 1-butyl and 1-hexadecyl esters of 2,3-dimercaptosuccinic acid have been synthesized. Complexation with mercuric ion yields polymers $(CH(SHg)CO_2R)_n$, and complexation with methylmercury gives bimetallic complexes $(CH(SHgCH_3)CO_2R)_2$. The partition coefficients between 1-octanol and water for the complexes $CH_3HgSCH_2CH(NH_2)CO_2R$ have been measured, and the values compared with that of the analogous cysteine complex $CH_3HgSCH_2CH(NH_2)CO_2H$.

The toxicity of methylmercury compounds and their ability to cross the blood–brain barrier are well known phenomena.[1] The presence of these compounds in nature continues to be a persistent problem because of their tendency to be biosynthesized and accumulated by marine organisms.[2] Ingestion of these compounds by humans results in the occurrence of neurological and other medical problems. These toxic effects are further aggravated by the fact that methylmercury compounds are only slowly expelled by the body.[3] The most commonly used therapeutic agents for ingested heavy metals are thiols. These compounds are being effective agents because the mercuric ion forms complexes of high stability by coordination via the thiolate moiety.[4]

The ability of methylmercury complexes to pass through the blood–brain barrier is a consequence of both their small size and of their lipophilicity. We have, therefore, prepared ester derivatives of l-cysteine with both short (1-C_4H_9) and long (1-$C_{16}H_{33}$) chain alkyl substituents,[5] and we have prepared the complexes of these ligands with methylmercury. The lipophilicity of these methylmercury complexes has then been compared with that of the methylmercury complex of cysteine itself.

EXPERIMENTAL

Methylmercuric acetate was purchased from Morton Thiokol Inc. L-Cysteine hydrochloride was purchased from Aldrich and stored under refrigeration. 2,3-Dimercaptosuccinic acid was synthesized by the literature procedure.[6] 1-Butanol was purchased from Mallinkrodt, and 1-hexadecyl alcohol from Aldrich. IR spectra were measured on a Mattson Cygnus 100 spectrometer. Mid-range spectra were measured with the sample coated on sodium chloride plate as a Nujol mull; in the far IR range the sample was coated on a polyethylene sheet as a vaseline mull. ^1H NMR spectra were measured in $CDCl_3$ (ligands) or d^6-DMSO (methylmercury complexes) solvent. Mercury analysis was carried out on a Beckman Spectrospan 5 direct current plasma spectrometer. Conductivity measurements were obtained with an Industrial Instruments Inc. conductivity bridge (model RC 16B2). Dimethyl sulphoxide (Mallinkrodt) was used as solvent in a cell containing platinized electrodes (cell constant

* Author to whom correspondence should be addressed.

0.417). Microanalyses were performed by Galbraith Laboratories, Knoxville, Tennessee.

1-Butyl-1-cysteine hydrochloride: [$HSCH_2CH(NH_3)CO_2C_4H_9$-1]Cl

1-Cysteine hydrochloride (3.000 g, 20 mmol) and 1-butanol (15.000 g, 200 mmol) were mixed and heated under reflux in a stream of hydrogen chloride for 2 h according to published procedures.[7] The clear solution was allowed to cool, and any excess 1-butanol was removed on a rotary evaporator at 50°C. The resulting solution was cooled to 0°C to give a white precipitate. This precipitate was filtered and washed several times with diethyl ether. Yield 1.240 g (35%), m.p. 88–89°C. Found: C, 39.3; H, 7.70; N, 6.48; S, 15.4. Calc. for $C_7H_{16}ClNO_2S$: C, 39.3; H, 7.55; N, 6.55; S, 15.0%.

1-Hexadecyl-1-cysteine hydrochloride: [$HSCH_2CH(NH_3)CO_2C_{16}H_{33}$-1]Cl

1-Cysteine hydrochloride (1.000 g, 6.4 mmol) and 1-hexadeconal (8.500 g, 35 mmol) were mixed and heated gently under reflux in a stream of hydrogen chloride for 2 h. The clear solution was allowed to cool and solidify, and any excess 1-hexadecanol was removed by dissolution in benzene. The solid product was washed with acetone and collected by filtration. Yield 1.590 g (65%), m.p. 81–82°C. Found: C, 59.6; H, 10.8; N, 3.66; S, 9.11. Calc. for $C_{19}H_{40}ClNO_2S$: C, 59.7; H, 10.6; N, 3.67; S, 8.39%.

Diethyl-2,3-dimercaptosuccinate: $(CH(SH)CO_2C_2H_5)_2$

Dimercaptosuccinic acid (0.360 g, 1.98 mmol), ethanol (10 cm^3) and sulphuric acid (0.5 cm^3) were refluxed under nitrogen for 5 h. The solution was allowed to cool to room temperature, and anhydrous magnesium sulphate added. The solution was filtered, and the solvent evaporated to give the compound as colourless crystals which were washed with brine. Yield 0.240 g (51%). Found: C, 39.5; H, 5.68; S, 26.9. Calc. for $C_8H_{14}O_4S_2$: C, 40.3; H, 5.92; S, 26.9%.

Dibutyl-2,3-dimercaptosuccinate: $(CH(SH)CO_2C_4H_9$-$1)_2$

This compound was prepared by an analogous procedure to the diethyl ester using dimercaptosuccinic acid (0.390 g, 2.16 mmol) and 1-butanol (10 cm^3). Yield 0.290 g (45%). Found: C, 48.9; H, 7.35; S, 21.7. Calc. for $C_{12}H_{22}O_4S_2$: C, 49.0; H, 7.53; S, 21.8%.

Diecetyl-2,3-dimercaptosuccinate: $(CH(SH)CO_2C_{16}H_{33}$-$1)_2$

Dimercaptosuccinic acid (0.470 g, 2.59 mmol), cetyl alcohol (1.870 g, 7.66 mmol) and hydrochloric acid (0.5 cm^3) were refluxed under nitrogen until all of the dimercaptosuccinic acid had dissolved. The solution was allowed to cool to room temperature, when the reaction mixture solidified. The solid was dissolved in benzene, and magnesium sulphate added. The solution was filtered and the benzene solvent removed on a rotary evaporator. The solid residue was stirred with ethanol to remove excess cetyl alcohol, then filtered. The crude solid product was recrystallized from chloroform solution by the addition of ethanol. Yield 0.780 g (48%). Found: C, 68.8; H, 11.4; S, 10.2. Calc. for $C_{36}H_{70}O_4S_2$: C, 68.5; H, 11.2; S, 10.2%.

1-Butyl-1-cysteinato methylmercury hydrochloride: [$CH_3HgSCH_2CH(NH_3)CO_2C_4H_9$-1]Cl

Methylmercury acetate (0.155 g, 0.57 mmol) and 1-butyl-1-cysteine hydrochloride (0.100 g, 0.57 mmol) were dissolved in dichloromethane (8 cm^3) and the solution stirred for 5 h. The white precipitate which formed was collected by filtration and washed with dichloromethane. Yield 0.145 g (60%), m.p. 142–144°C. Found: C, 22.5; H, 4.23; N, 3.26; S, 8.22. Calc. for $C_8H_{18}HgNO_2S$: C, 22.4; H, 4.23; N, 3.26; S, 7.49%.

1-Hexadecyl-1-cysteinato methylmercury hydrochloride: [$CH_3HgSCH_2CH(NH_3)CO_2C_{16}H_{33}$-1]Cl·$H_2O$

Methylmercuric acetate (0.072 g, 0.26 mmol) and 1-hexadecyl-1-cysteine hydrochloride (0.100 g, 0.26 mmol) were dissolved in dichloromethane (8 cm^3), and the solution stirred for 5 h. The white precipitate which formed was collected by filtration, and washed with dichloromethane. Yield 0.101 g (65%), m.p. 117–119°C. Found: C, 39.5; H, 7.07; N, 2.58. Calc. for $C_{20}H_{43}ClNO_3HgS$: C, 39.1; H, 7.06; N, 2.28%.

Diethyl-2,3-dimercaptosuccinato mercury: $(CH(SHg)CO_2C_2H_5)_n$

A solution of diethyl-2,3-dimercaptosuccinate (0.079 g, 0.33 mmol) in nitrogen saturated methanol

($3\ cm^3$) was added to a stirred solution of mercuric chloride (0.089 g, 0.33 mmol) in nitrogen saturated methanol ($7\ cm^3$). A white precipitate formed immediately. After 3 h the solution was filtered and the precipitate washed with methanol. Yield 0.780 g (54%). Found: C, 21.9; H, 2.75; S, 15.0. Calc. for $C_8H_{12}HgO_4S_2$: C, 22.0; H, 2.77; S, 14.7%.

Dibutyl-2,3-dimercaptosuccinato mercury: $(CH(SHg)CO_2C_4H_9\text{-}1)_n$

A solution of dibutyl-2,3-dimercaptosuccinate (0.129 g, 0.439 mmol) in acetonitrile ($3\ cm^3$) was added to a stirred solution of mercuric chloride (0.119 g, 0.441 mmol) in acetonitrile ($6\ cm^3$). After 24 h the white precipitate was filtered and washed with acetonitrile. Yield 0.087 g (40%). Found: C, 27.5; H, 3.87; S, 12.6. Calc. for $C_{12}H_{26}HgO_4S_2$: C, 29.2; H, 4.09; S, 13.0%.

Dicetyl-2,3-dimercaptosuccinato mercury: $(CH(SHg)CO_2C_{26}H_{33}\text{-}1)_n$

A solution of dicetyl-2,3-dimercaptosuccinate (0.237 g, 0.375 mmol) in benzene ($3\ cm^3$) was added to a stirred solution of mercuric chloride (0.102 g, 0.377 mmol) in benzene ($8\ cm^3$). The white precipitate which formed was filtered and washed with benzene. Yield 0.118 g (38%). Found: C, 52.1; H, 8.47; S, 7.97. Calc. for $C_{36}H_{68}HgO_4S_2$: C, 52.1; H, 8.26; S, 7.73%.

Diethyl-2,3-dimercaptosuccinato methylmercury: $(CH(SHgCH_3)CO_2C_2H_5)_2$

A solution of methylmercuric acetate (0.113 g, 0.414 mmol) in water ($4\ cm^3$) was added to a stirring solution of diethyl-2,3-dimercaptosuccinate (0.099 g, 0.414 mmol) in water ($10\ cm^3$). A white precipitate formed immediately. This precipitate was filtered and washed with water. Yield 0.062 g (45%). Found: C, 18.6; H, 2.78. Calc. for $C_{10}H_{18}O_4Hg_2S_2$: C, 18.0; H, 2.72%.

Dibutyl-2,3-dimercaptosuccinato methylmercury: $(CH(SHgCH_3)CO_2C_4H_9\text{-}1)_2$

A solution of dibutyl-2,2-dimercaptosuccinate (0.129 g, 0.439 mmol) was added to a stirred solution of methylmercuric acetate (0.119 g, 0.435 mmol) in acetonitrile ($6\ cm^3$). The solution was stirred for 24 h, filtered and washed with acetonitrile. Yield 0.067 g (42%). Found: C, 22.4; H, 3.81. Calc. for $C_{14}H_{26}Hg_2O_4S_2$: C, 23.2; H, 3.62%.

RESULTS AND DISCUSSION

Cysteine esters

The 1-butyl and 1-hexadecyl esters of l-cysteine were prepared by standard esterification procedures from the alcohols in the presence of hydrogen chloride [eq. (1)]. The product esters were collected as solids, and their purity confirmed by both melting point and by microanalysis. Both compounds react with methylmercuric acetate in a 1 : 1 stoichiometric ratio to to form a colourless complex. The same complexes are obtained when a 2 : 1 ratio of ligand–methylmercuric acetate is used. Complexation occurs to mercury via the thiolato anion of the cysteinyl ester [eq. (2)]. This complexation is verified by loss of the IR band due to ν(SH), and its replacement by an IR band due to ν(HgS) at 323 cm^{-1} (R = 1-C_4H_9) and at 322 cm^{-1} (R = 1-$C_{16}H_{33}$). The frequencies of these bands closely correlate with that found at 325 cm^{-1} for the thiolate bonded complex formed between cysteine and methylmercury.[7] The methyl group is not displaced from mercury in these complexes as evidenced by the presence of IR bands at 541 cm^{-1} (R = 1-C_4H_9) and 538 cm^{-1} (R = 1-$C_{16}H_{33}$), along with a methyl resonance in the ^1H NMR spectrum at δ 0.6 for the methyl group bonded to mercury. By comparison, the analogous complex with cysteine shows ν(Hg—S) at 538 cm^{-1} (Table 1).

$$[HSCH_2CH(NH_3)CO_2H]Cl + ROH \longrightarrow [HSCH_2CH(NH_3)CO_2R]Cl + H_2O \quad (1)$$

(R = 1-C_4H_9, 1-$C_{16}H_{33}$)

$$CH_3HgOAc + [HSCH_2CH(NH_3)CO_2R]Cl \longrightarrow [CH_3HgSCH_2CH(NH_3)CO_2R]Cl + HOAc \quad (2)$$

Table 1. Characteristic IR bands (cm^{-1}) for the ligands and methylmercury complexes of $[H_3NCH_2CH(SH)CO_2R]Cl$

R = 1-C_4H_9		R = 1-$C_{16}H_{33}$		
Ligand	Complex	Ligand	Complex	Assignment
3371	3425	3472	—	$\nu(NH_3)$
2465	—	2469	—	ν(SH)
1746	1745	1748	1749	ν(CO)
1579	1579	1593	1586	$\delta(NH_3)_{asym}$
1507	1507	1505	1503	$\delta(NH_3)_{sym}$
1208	1203	1208	1203	ν(COC)
—	541	—	538	ν(Hg—C)
—	323	—	322	ν(Hg—S)

Table 2. Conductivity data for $[CH_3HgS(CO_2R)CHCH_2NH_3]Cl$ in DMSO solvent

Concentration (mM)	Molar conductivity (Ω^{-1} cm^2 mol^{-1})
R = 1-C_4H_9	
1.0	27.5
0.7	33.4
0.5	32.5
0.25	38.3
R = 1-$C_{16}H_{33}$	
1.0	29.2
0.7	32.2
0.5	34.2
0.25	40.0
0.1	43.8

Table 3. Characteristic IR bands (cm^{-1}) for 2,3-dimercaptosuccinate esters and their mercury and methylmercury complexes

	ν(SH)	ν(CO)	ν(COC)	ν(HgS)
$CH(SH)CO_2R$				
R = C_2H_5	2532	1719	1202	—
R = 1-C_4H_9	2548	1718	1217	—
R = 1-$C_{16}H_{33}$	2554	1718	1216	—
$(CH(SHg)CO_2R)_n$				
R = C_2H_5	—	1704	1183	378
R = 1-C_4H_9	—	1705	1151	378
R = 1-$C_{16}H_{33}$	—	1716	1151	374
$(CH(SHgCH_3)CO_2R)_2$				
R = C_2H_5	—	1703	1150	361
R = 1-C_4H_9	—	1706	1151	346

The complexes $[CH_3HgSCH_2CH(NH_3)CO_2R]Cl$ (R = 1-C_4H_9, 1-$C_{16}H_{33}$) are isolated as their hydrochloride salts. These stoichiometries are confirmed by analytical and conductivity data, the salts having the molar conductivity of a 1 : 1 electrolyte in dimethyl sulphoxide solvent (Table 2).[8] The complexes are only very slightly soluble in water, but solutions can be prepared in aqueous potassium hydroxide. Solutions of each complex, along with the complex synthesized from free cysteine, in aqueous potassium hydroxide (pH 12) have been shaken with 1-octanol and the partition coefficient between the solvent layers measured for each.[9] The complexes with R = H, 1-C_4H_9 are insoluble in 1-octanol, but the complex with R = 1-$C_{16}H_{33}$ has a 9:1 distribution coefficient between 1-octanol and water. the lipophilicity of the 1-hexadecyl complex, as measured by this parameter, is therefore greater than that of the analogous complexes with cysteine itself, or with the 1-butyl ester.

2,3-Dimercaptosuccinic acid esters

Two of the more commonly used therapeutic agents for heavy metal toxicity are compounds which are chelating dithiols. These compounds are dimercaprol and 2,3-dimercaptosuccinic acid.[10–12] We have prepared both short and long chain aliphatic esters of 2,2-dimercaptosuccinic acid. The ethyl, 1-butyl and 1-hexadecyl esters have been prepared by standard esterification procedures in acidic medium [eq. (3)]. The compounds shows IR bands due to both ν(SH) and ν(CO) (Table 3). In addition to resonances due to the ester functionalities, the compounds show resonances in the ^{1}H NMR spectra due to both the SH and the backbone CH groups. These resonances each show a six-line multiplicity pattern centre around δ 2.3 (SH) and 3.6 (CH) and the spectral lines can be fitted to an AA′XX′ spectrum. This multiplicity is therefore not a consequence of the two hydrogens being bonded to diastereotopic carbons. Furthermore, solutions of the compounds in D_2O/OD^- show a single resonance in the C—H region.

The compounds $(CH(SH)CO_2R)_2$ (R = Et, 1-C_4H_9, 1-$C_{16}H_{33}$) react with methylmercuric acetate and mercuric chloride to form thiolate-coordinated complexes. The complexes have the respective stoichiometries $(CH(SHgCH_3)CO_2R)_2$ and $(CH(SHg)CO_2R)_n$ [eqs (4) and (5)]. All of the complexes exhibit poor solubility in organic solvents, and all are insoluble in 1-octanol. We have, therefore, been unsuccessful in increasing the lipophilicity of the mercury complexes of 2,3-dimercaptosuccinic acid by esterification of the carboxylic acid functionality with either short or long chain alkyl functional groups.

$$HO_2CCH(SH)CH(SH)CO_2H + 2ROH \longrightarrow RO_2CCH(SH)CH(SH)CO_2R + 2H_2O \quad (3)$$

(R = C_2H_5, 1-C_4H_9, 1-$C_{16}H_{33}$)

$$2\,CH_3HgOAc + [CH(SH)CO_2R]_2 \longrightarrow$$

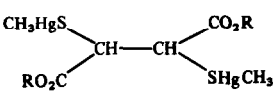

$$+ 2\,HOAc \quad (4)$$

$$n\,HgCl_2 + n[CH(SH)CO_2R] \longrightarrow$$

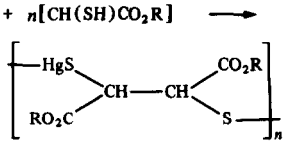

$$+ 2n\,HCl \quad (5)$$

REFERENCES

1. P. J. Craig, in *Organometallic Compounds in the Environment* (Edited by P. J. Craig), Chap. 2. John Wiley, New York (1986).
2. J. W. Huckabee, J. W. Elwood and S. G. Hildebrand, in *The Biogeochemistry of Mercury in the Environment* (Edited by J. O. Nrinagu), pp. 207–302. Elsevier, North Holland Biomedical Press, Amsterdam (1980).
3. T. Norseth and T. W. Clarkson, *Arch. Environ. Health* 1970, **21**, 717.
4. J. S. Thayer, *Organometallic Chemistry*, Chap. 12. VCH, New York (1987).
5. M. M. Joullie, M. Laurre, G. Maillard, P. Muller and R. Zoui, *Fr. Patent* 1,241,102; *Chem. Abstr.* 25782f (1961).
6. M. Gerecke, E. A. H. Friedheim and A. Bross, *Helv. Chim. Acta* 1961, **44**, 953.
7. N. J. Taylor, Y. S. Wong, P. C. Chieh and A. J. Carty, *J. Chem. Soc., Dalton Trans.* 1975, 438.
8. W. J. Geary, *Coord. Chem. Rev.* 1971, **7**, 81.
9. A. J. Carty, P. W. Moors and G. B. Deacon, *J. Inorg. Biochem.* 1984, **22**, 65.
10. N. W. Alcock, P. A. Lampe and P. Moore, *J. Chem. Soc., Dalton Trans.* 1980, 1471.
11. A. J. Canty and R. Kishimoto, *Inorg. Chim. Acta* 1977, **24**, 109.
12. A. P. Arnold, A. J. Canty, P. W. Moors and G. B. Deacon, *J. Inorg. Biochem.* 1983, **19**, 319.

Polyhedron Vol. 9, No. 4, pp. 603–610, 1990
Printed in Great Britain

0277–5387/90 $3.00+.00
© 1990 Pergamon Press plc

ORGANOIMIDO COMPLEXES OF TUNGSTEN(IV) CONTAINING π-ACCEPTOR LIGANDS

ALASTAIR J. NIELSON* and DAVID C. WARE

Department of Chemistry, University of Auckland, Private Bag, Auckland, New Zealand

(*Received* 19 *July* 1989; *accepted* 18 *September* 1989)

Abstract—Reaction of PhC≡CPh with $[WCl_2(NR)(PMe_3)_3]$ gives the *cis*-dichloro-*trans*-phosphine complexes $[WCl_2(NR)(PhC{\equiv}CPh)(PMe_3)_2]$ [R = Ph (**1**), R = $CHMe_2$ (**3**)] in which the π-acceptor acetylene ligand lies *cis* to the imido function. For **1** ν(C≡C) is at 1760 cm^{-1} and for **3**, 1740 cm^{-1}. $Me_3SiC{\equiv}CSiMe_3$ and PhC≡CPh do not replace phosphine ligands from $[WCl_2(NPh)(PMe_3)_3]$ or $[WCl_2(NPh)(PMePh_2)_3]$. Reaction of PhC≡CPh with $[WCl_2(NPh)(PMe_2Ph)_3]$ gives $[WCl_2(NPh)(PhC{\equiv}CPh)(PMe_2Ph)_2]$ (**2**). Alkyl substituted acetylenes do not react cleanly with $[WCl_2(NPh)(PMe_3)_3]$ but HC≡CH gives $[WCl_2(NPh)(HC{\equiv}CH)(PMe_3)_2]$ (**4**). Reaction of PhC≡CH with $[WCl_2(NR)(PMe_3)_3]$ gives $[WCl_2(NR)(PhC{\equiv}CH)(PMe_3)_2]$ [R = Ph (**5**), R = $CHMe_2$ (**6**)]. The phenylacetylene ligand gives rise to asymmetry in **5** and **6** leading to AB system $^{31}P\{^1H\}$ NMR spectra. Different values of ^1J(PW) for the two phosphine ligands in both complexes indicate small differences in W—P bonding. The acetylenic protons and carbons in the ^1H and $^{13}C\{^1H\}$ NMR spectra of the phenylacetylene complexes couple differently to the two phosphines. For **5** ^3J(HP) *cis* and *trans* = 5.90 and 17.26 Hz, ^2J(C[H]P) *cis* and *trans* = 5.29 and 21.99 Hz and ^2J(C[Ph]P) *cis* and *trans* = 4.88 and 15.63 Hz. The $^{13}C\{^1H\}$ NMR acetylenic carbon resonance positions in complexes **1**, **3**, **5** and **6** suggest that an isopropylimido ligand is a better π-donor than a phenylimido ligand, allowing more metal–acetylene π-back donation. Reduction of $[WCl_3(NPh)(PMe_3)_2]$ with Na/Hg amalgam under CO gives $[WCl_2(NPh)(C{\equiv}O)(PMe_3)_2]$ (**7**) for which ν(C≡O) at 1925 cm^{-1} indicates considerable π-backbonding.

High valence state complexes which contain both a strong π-donor and a π-acceptor ligand constitute an emerging area of study in early transition metal chemistry. These complexes presently form a basis for studies involving the interaction of multiple bonded organic compounds with high valent metal species in various catalytic processes.[1] Although strong π-donation is normally associated with high valent complexes and π-acceptor ligands with metals in low valency states, there are nevertheless examples known which contain both ligand types. These complexes which mostly contain the terminal oxo ligand and have the d^2 electron configuration include $[Mo(O)(alkyne)(S_2CNR_2)_2]$,[2,3] $[W(O)Cl_2(L)(PMePh_2)_2]$ (L = $CH_2{=}CH_2$, $CH_2{=}CHMe$, $CH_2{=}CH{-}CH{=}CH_2$, C≡O, Me_3CNC),[4] $[W(O)Cp(C_6H_5)(PhC{\equiv}CPh)]$,[5] $[W(O)Cp(HC{\equiv}CH)R]$ (R = Me, COMe),[6] and $[W(S)(PhC{\equiv}CPh)(S_2CNMe_2)_2]$.[7] Several organoimido complexes (M≡NR)[8] are also known including $[W(NR)(L)(S_2CNR_2)_2]$ (L = $MeO_2CC{\equiv}CCO_2Me$,[9] C≡O[10]), $[ReCl_3(NPh)(C{\equiv}O)(PPh_3)]$,[11] $[TaCl_2(NPh)(CH_2{=}CHR)(PMe_3)_2]$ (R = Me, Ph)[12] and $[W_2Cl_4(\mu{=}N{-}N{=})(PhC{\equiv}CPh)_2(MeOCH_2CH_2OMe)_2]$.[13] As part of our continuing studies of organoimido chemistry[14] we have prepared complexes containing acetylene or carbon monoxide ligands in conjunction with an organoimido function. In particular, the scope of the reaction of $[WCl_2(NR)(P)_3]$ complexes (R = phenyl, alkyl; P = phosphine) with various acetylene ligands and the NMR spectra of the resulting complexes has been studied. A preliminary report of this work has appeared.[15]

RESULTS AND DISCUSSION

When $[WCl_2(NPh)(PMe_3)_3]$[16] was refluxed in benzene with dimethyl acetylenedicarboxylate, a

* Author to whom correspondence should be addressed.

brown intractable material formed for which spectral data indicated decomposition of the acetylene component. However, with diphenylacetylene, one phosphine ligand was replaced giving rise to $[WCl_2(NPh)(PhC{\equiv}CPh)(PMe_3)_2]$ (**1**) which, in contrast to $[WCl_2(NPh)(PMe_3)_3]$, is air stable. The IR spectrum showed $\nu(C{\equiv}C)$ for the diphenylacetylene ligand as a weak absorption at 1760 cm^{-1} and $\nu_{sym}(W{-}N{-}C)$ for the phenylimido ligand at 1350 cm^{-1}[17] (Table 1). W—Cl stretches at 268 and 245 cm^{-1} indicated a *cis* orientation of the two chloro ligands.[18] The presence of virtually coupled triplets for the PMe_3 ligands in both the ^1H and $^{13}C\{^1H\}$ NMR spectra[19] and a singlet with associated tungsten-183 sidebands in the $^{31}P\{^1H\}$ NMR spectrum, indicated equivalent *trans* phosphines (Table 2). Based on this *cis*-dichloro-*trans*-phosphine geometry the diphenylacetylene ligand in the complex lies *cis* to the imido function [Structure (a)].

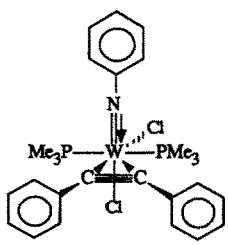

(a)

Symmetry inherent in complex **1** and the bonding modes of the imido and acetylene ligands are apparent from the $^{13}C\{^1H\}$ NMR spectrum. The acetylenic carbons appear as a ^{31}P-coupled triplet with associated ^{183}W satellites ($^1J(CW) = 28.52$ Hz) and are shifted 66 ppm downfield compared with the free ligand. While the *ipso*-carbon of the aromatic ring is somewhat broadened by poorly resolved coupling to ^{31}P, the *ortho*-carbons and *ipso*-carbon of the phenylimido ligand aromatic ring appear as well-defined triplets ($^4J(CP)_{ortho} = 1.89$ Hz and $^3J(CP)_{ipso} = 2.36$ Hz). Only the *ipso*-carbon shows coupling to ^{183}W ($^2J(CW) = 36.29$ Hz). The position of the phenylimido ligand *ipso*-carbon (154.76 ppm) indicates the imido ligand acts as a four-electron donor to the central tungsten atom.[20] Thus for the complex to attain an 18-electron configuration the acetylene ligand must represent a two-electron donor. This formalism is evident from the position of the acetylenic carbon resonance (155.77 ppm) which is similar to that shown by two-electron donor diphenylacetylene complexes of molybdenum and tungsten.[21]

An X-ray crystal structure determination of $[WCl_2(NPh)(PhC{\equiv}CPh)(PMe_3)_2]$ (**1**)[15] has confirmed the *cis*-dichloro-*trans*-phosphine geometry about the tungsten centre as well as the *cis* orientation of the phenylimido and diphenylacetylene ligands. The $W{-}N{-}C_{imido}$ bond angle of

Table 1. Physical data

Complex	Melting point (°C)[a]	Analytical data[b] C	H	N	IR data (cm^{-1})[c] $\nu(C{\equiv}C)$	$\nu_{sym}(W{-}N{-}C)$	$\nu(W{-}Cl)$ (*cis*)
$[WCl_2(NPh)(PhC{\equiv}CPh)(PMe_3)_2]$ (**1**)	168	46.6 (46.2)	5.3 (4.9)	2.2 (2.1)	1760	1350	268, 245
$[WCl_2(NPh)(PhC{\equiv}CPh)(PMe_2Ph)_2]$ (**2**)	154–156	54.1 (54.0)	4.9 (4.7)	2.0 (1.8)	1760	1345	260, 235
$[WCl_2(NCHMe_2)(PhC{\equiv}CPh)(PMe_3)_2]$ (**3**)	160d	42.7 (43.1)	5.6 (5.5)	2.1 (2.2)	1740	1275	270, 245
$[WCl_2(NPh)(HC{\equiv}CH)(PMe_3)_2]$ (**4**)	113–115d	32.4 (32.7)	4.9 (4.8)	2.6 (2.6)	1632	1348	275, 240
$[WCl_2(NPh)(PhC{\equiv}CH)(PMe_3)_2]$ (**5**)	147	40.4 (40.0)	5.1 (4.9)	2.2 (2.3)	1731	1354	271, 230
$[WCl_2(NCHMe_2)(PhC{\equiv}CH)(PMe_3)_2]$ (**6**)[d]	123–125	37.3 (37.3)	5.8 (5.6)	2.5 (2.4)	1730	1300	265, 220
$[WCl_2(NPh)(C{\equiv}O)(PMe_3)_2]$ (**7**)	159	30.2 (29.7)	4.4 (4.4)	2.5 (2.7)	[e]	1345	300, 260

[a] d = decomposition point.
[b] Calculated figures in parentheses.
[c] Spectra obtained in Nujol mulls between caesium iodide plates.
[d] Contains $1/6C_6H_6$ solvent molecules. Supported by ^1H NMR spectrum.
[e] $\nu(C{\equiv}O)$ 1925 cm^{-1}.

176.3(1.5)° and the W—N_{imido} bond length of 1.770(14) Å supports the assignment of the phenylimido ligand as a four-electron donor, while the W—$C_{acetylene}$ and C≡C bond lengths (2.128(20), 2.123(21) and 1.26(2) Å, respectively) are consistent with a two-electron donor diphenylacetylene ligand. This indicates that the +4 oxidation state prevails in the complex, which would make available two *d*-electrons for π-backbonding to the acetylene. The +4 oxidation state is thought to be present in $[WCl_4(PhC{\equiv}CPh)]$.[22] The structure of **1** contrasts with that of $[Mo(N\text{-}p\text{-tolyl})(MeO_2CC{\equiv}CCO_2Me)(S_2CNEt_2)_2]$ where the acetylene ligand competes with the imido ligand in contributing π-electron density to the metal.

Coordination of the acetylene ligand *cis* to the strongly π-donating imido function rather than *trans* [Structure (b)] is also found in the related

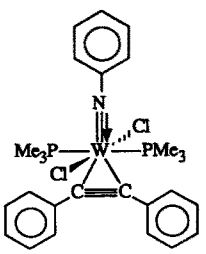

(b)

oxoacetylene complexes of tungsten and is the configuration expected on simple MO grounds. The electronic influence of the imido group forces the metal non-bonding *d*-electrons to lie in the d_{xy}-orbital where they are only available to π-backbond with the unsaturated ligand if it is in the *cis* position.[23]

The position of ν(C≡C) in the complex (1760 cm^{-1}) suggests considerable backbonding to the acetylene takes place. It is significantly lower than in the molybdenum oxo complexes $[Mo(O)(PhC{\equiv}CPh)(S_2CNR_2)_2]$ (R = Et, Me, ν(C≡C) 1870–1790 cm^{-1})[2,3] for which dissociation of the alkyne ligand readily occurs. It is only slightly higher than for the tungsten complex $[W(S)(PhC{\equiv}CPh)(S_2CNEt_2)_2]$ (ν(C≡C) 1745 cm^{-1}) where the ^1H NMR spectrum suggests alkyne rotation is appreciable only at 100°C in *p*-xylene solution (activation energy 18 kcal mol^{-1}).[7] The barrier to alkyne rotation in complex **1** is expected to be similarly large as the π-backbonding component would be lost when the ligand rotates 90°.

Bis(trimethylsilyl)acetylene does not replace a phosphine ligand from $[WCl_2(NPh)(PMe_3)_3]$ and diphenylacetylene fails to react with $[WCl_2(NPh)(PMePh_2)_3]$ suggesting that steric effects are important in the reaction. Diphenylacetylene does, however, react with $[WCl_2(NPh)(PMe_2Ph)_3]$ under reflux in benzene to give $[WCl_2(NPh)(PhC{\equiv}CPh)(PMe_2Ph)_2]$ (**2**). The green complex is again air stable and spectral data indicate the *cis*-dichloro-*trans*-phosphine geometry of complex **1** (ν(W—Cl) 260 and 235 cm^{-1}; ^1H and $^{13}C\{^1H\}$ NMR spectrum: two virtually coupled PMe_3 triplets; $^{31}P\{^1H\}$ NMR spectrum: one singlet) and a similar degree of π-back donation to the acetylene ligand (ν(C≡C) 1760 cm^{-1}). In the $^{13}C\{^1H\}$ NMR spectrum the *ipso*- and *ortho*-carbons of the phosphine aromatic ring appear as ^{31}P-coupled triplets as do the acetylenic carbon resonances and the *ipso*-carbon of the phenylimido ligand aromatic ring.

$[WCl_2(NCHMe_2)(PhC{\equiv}CPh)(PMe_3)_2]$ (**3**) was prepared for spectral comparison with the phenylimido analogue (**1**). In the IR spectrum ν(C≡C) occurs at 1740 cm^{-1} which is 20 cm^{-1} lower than complex **1** and may represent a slight increase in π-backbonding to the acetylene. The IR and NMR spectral features indicate the usual *cis*-dichloro-*trans*-phosphine geometry. No asymmetry is present in the complex so the isopropylimido ligand methyl groups are a single doublet in the ^1H NMR spectrum. In the $^{13}C\{^1H\}$ NMR spectrum the methyl carbons and the CH carbon appear as triplets, the latter showing coupling to ^{183}W ($^2J(CW) = 30.97$ Hz). The acetylenic carbons appear as a ^{31}P-coupled triplet lying slightly upfield to those in complex **1** (151.41 cf. 155.77 ppm) which also suggests a small increase in π-backbonding.[24]

Alkyl substituted acetylenes (e.g. $CH_3CH_2C{\equiv}CCH_2CH_3$, $CH_3CH_2CH_2C{\equiv}CCH_3$) do not react cleanly with $[WCl_2(NPh)(PMe_3)_3]$ but $[WCl_2(NPh)(HC{\equiv}CH)(PMe_3)_2]$ (**4**) forms when acetylene gas is used. Spectral data indicate the usual *cis*-dichloro-*trans*-phosphine geometry and ν(C≡C) in the IR spectrum is at 1632 cm^{-1} (cf. 1974 cm^{-1} for free acetylene). Features of the ^1H NMR spectrum are the ^{31}P-coupled triplet for the acetylenic protons ($^3J(HP) = 3.26$ Hz) and the deceptively simple phenylimido aromatic ring pattern. The *ortho*-protons appear as a doublet lying upfield of the other resonances and the *meta*- and *para*-protons are triplets both of which approximate the A part of an AX_2 system.[25]

Reaction of phenylacetylene with $[WCl_2(NPh)(PMe_3)_3]$ gives rise to $[WCl_2(NPh)(PhC{\equiv}CH)(PMe_3)_2]$ (**5**) which has the usual *cis*-dichloro-*trans*-phosphine geometry. However, coordination of this unsymmetrical acetylene leads to asymmetry in the complex which is reflected in the NMR spectra of the phosphine ligands. The ^1H, $^{13}C\{^1H\}$ and $^{31}P\{^1H\}$ NMR spectra each show two doublets suggesting *cis*-phosphines but on the basis of the large P—P coupling constant ($^2J(PP) = 164.31$ Hz)

Table 2. NMR spectral data

Complex	^{31}P NMR[a] δ (ppm)	^{1}J(PW) (Hz)	^{1}H NMR[a,b]	^{13}C NMR[a,b,c]
$[WCl_2(NPh)(PhC{\equiv}CPh)(PMe_3)_2]$ (**1**)	−15.23	216.5	1.51 [t (^{2}J(HP) 4.68 Hz), 18H, $2PMe_3$]; 7.12–7.20 [m, aromatic Hs]; 7.23–7.36 [m, aromatic Hs]	14.54 [t (^{1}J(CP) 15.23 Hz), *trans*-PMe_3]; 125.13 [t (^{4}J(CP) 1.89 Hz), *ortho*-Cs, imido]; 126.63 [*para*-C, acet]; 127.36 [*para*-C, imido]; 127.42 [*ortho*-Cs, acet]; 128.24 [*meta*-Cs, acet]; 128.64 [*meta*-Cs, imido]; 143.52 [*ipso*-C, acet]; 154.76 [t (^{3}J(CP) 2.36 Hz, ^{2}J(CW) 36.29 Hz), *ipso*-C, imido]; 155.77 [t (^{2}J(CP) 11.56 Hz, ^{1}J(CW) 28.52 Hz), C≡C]
$[WCl_2(NPh)(PhC{\equiv}CPh)(PMe_2Ph)_2]$ (**2**)	−6.62	218.0	1.60–2.15 [2t (^{2}J(HP) 4.62 and 4.50 Hz), 12H, $2PMe_2$]; 6.60–7.31 [m, 25H, aromatic Hs]	11.61 and 15.88 [2t (^{1}J(CP) 15.83 and 16.33 Hz), *trans*-PMe_3]; 126.02 [*ortho*-Cs, imido]; 126.28 [*para*-Cs, acet]; 127.67 [*para*-C, imido]; 127.71 [*ortho*-Cs, acet]; 127.76 [*meta*-Cs, phosphine]; 127.89 [*meta*-Cs, acet]; 128.31 [*meta*-Cs, imido]; 129.14 [*para*-Cs, phosphine]; 130.70 [t (^{2}J(CP) 4.57 Hz), *ortho*-Cs, phosphine]; 134.78 [t, (^{1}J(CP), 20.65 Hz), *ipso*-Cs, phosphine]; 141.76 [*ipso*-C, acet]; 155.13 [prt, *ipso*-C, imido]; 156.38 [t (^{2}J(CP) 11.46 Hz), C≡C]
$[WCl_2(NCHMe_2)(PhC{\equiv}CPh)(PMe_3)_2]$ (**3**)	−15.55	220.4	1.15 [d (^{3}J(HP) 6.30 Hz), 6H, 2Me]; 1.54 [t (^{2}J(HP) 4.60 Hz), 18H, $2PMe_3$]; 3.82–4.25 [sept, 1H, CH]; 7.20–7.65 [m, 10H, aromatic Hs]	15.49 [t (^{1}J(CP) 15.20 Hz), *trans*-PMe_3]; 23.51 [t (^{4}J(CP) 1.63 Hz), Me_2]; 64.32 [t (^{3}J(CP) 1.35 Hz, ^{2}J(CW) 30.97 Hz), CH]; 126.22 [*para*-C]; 127.20 [*ortho*-Cs]; 128.14 [*meta*-Cs]; 144.17 [*ipso*-C]; 151.41 [t (^{2}J(CP) 11.84 Hz, ^{1}J(CW) 28.57 Hz), C≡C]
$[WCl_2(NPh)(HC{\equiv}CH)(PMe_3)_2]$ (**4**)	−15.82	217.1	1.80 [t (^{2}J(HP) 4.53 Hz), 18H, $2PMe_3$]; 6.89–6.94 [m, 2H, *ortho*-Hs]; 7.05–7.11 [m, 1H, *para*-H]; 7.13–7.19 [m, 2H, *meta*-Hs]; 9.30 [t (^{3}J(HP) 3.26 Hz), 2H, HC≡CH]	14.22 [t (^{1}J(CP) 15.66 Hz), *trans*-PMe_3]; 124.97 [t (^{4}J(CP) 1.91 Hz), *ortho*-Cs]; 127.04 [*para*-C]; 128.36 [*meta*-Cs]; 138.52 [t (^{2}J(CP) 12.08 Hz, ^{1}J(CW) 27.26 Hz), C≡C]; 154.28 [t (^{3}J(CP) 2.26 Hz), *ipso*-C]

$[WCl_2(NPh)(PhC{\equiv}CH)(PMe_3)_2]$ (5)[d]	−13.30 −17.72	209.6 222.7	1.47 and 1.83 [2d (^2J(HP) 9.77 and 9.87 Hz), 18H, $2PMe_3$]; 7.03 [d (^3J(HH) 7.51 Hz), *ortho*-Hs, imido]; 7.13 [t (^3J(HH) 7.37 Hz), *para*-H, imido]; 7.19–7.25 [m, 3H, *meta*-, *para*-Hs, acet]; 7.28 [dd (^3J(HH) 6.81 Hz, ^4J(HH) 1.39 Hz), *ortho*-Hs, acet]; 7.38 [t (^3J(HH) 7.60 Hz), meta-Hs, imido]; 9.91 [dd, (^3J(HP)*cis* 5.90 Hz, ^3J(HP) *trans* 17.26 Hz), 1H, acet]	14.29 and 14.30 [2d (^1J(CP) 31.82 and 29.06 Hz), *trans*-PMe_3]; 125.32 [t (^4J(CP) 1.87 Hz), *ortho*-Cs, imido]; 126.83 [*para*-C, acet]; 126.94 [*ortho*-Cs, acet]; 127.32 [*para*-C, imido]; 128.42 [*ortho*-Cs, acet]; 128.75 [*ortho*-Cs, imido]; 140.22 [dd (^2J(CP)*cis* 5.29 Hz, ^2J(CP)*trans* 21.99 Hz, ^1J(CW) 23.11 Hz), ≡CH]; 144.58 [t (^3J(CP) 3.35 Hz), *ipso*-C, acet]; 152.80 [dd (^2J(CP)*cis* 4.88 Hz, ^2J(CP)*trans* 15.63, ^1J(CW) 31.26 Hz), PhC≡]; 154.72 [t (^3J(CP) 2.32 Hz, ^2J(CW) 36.47 Hz), *ipso*-C, imido]
$[WCl_2(NCHMe_2)(PhC{\equiv}CH)(PMe_3)_2]$ (6)[e]	−13.49 −17.87	214.5 228.5	1.04 and 1.06 [2d (^3J(HH) 6.48 Hz), 6H, 2Me]; 1.50 and 1.87 [2d (^2J(HP) 9.67 and 9.77 Hz), 18H, $2PMe_3$]; 3.82 [sept (^3J(HH) 6.04 Hz), 1H, CH]; 7.13–7.25 [m, 3H, *meta*-, *para*-Hs]; 7.29–7.38 [m, 2H, *ortho*-Hs]; 9.55 [dd (^3J(HP)*cis* 5.97 Hz, ^3J(HP)*trans* 16.60 Hz), 1H, CH]	14.24 and 14.32 [2d (^1J(CP) 31.16 and 29.38), *trans*-PMe_3]; 21.95 and 22.22 [2s, 2Me]; 63.05 [s, ^2J(CW) 30.86 Hz), CH]; 125.43 [*para*-C]; 125.69 [*ortho*-Cs]; 127.18 [*meta*-Cs], 135.33 [dd (^2J(CP)*cis* 5.45 Hz, ^2J(CP)*trans* 22.10 Hz, ^1J(CW) 23.12 Hz), ≡CH]; 143.55 [t (^3J(CP) 3.07 Hz), *ipso*-C]; 148.54 [dd (^2J(CP)*cis* 5.04 Hz; ^2J(CP)trans 15.71 Hz, ^1J(CW) 31.27 Hz), PhC≡]
$[WCl_2(NPh)(C{\equiv}O)(PMe_3)_2]$ (7)	−20.74	228.0	1.61 [t (^2J(HP) 4.16 Hz), 18H, $2PMe_3$]; 6.97–7.03 [dd (^3J(HH) 8.01 Hz, ^4J(HH) 1.39 Hz), 2H, *ortho*-Hs]; 7.11–7.20 [m, 3H, *meta*-, *para*-Hs]	14.35 [t (^1J(CP) 14.79 Hz), *trans*-PMe_3]; 124.15 [t (^4J(CP) 1.53 Hz), *ortho*-Cs]; 125.57 [*para*-C]; 127.92 [*meta*-Cs]; 153.69 [t (^3J(CP) 1.77 Hz), *ipso*-C]; 237.19 [t (^2J(CP) 4.78 Hz), CO]

[a] Spectra obtained in $CDCl_3$.

[b] d = doublet, dd = doublet of doublets, m = multiplet, prt = poorly resolved triplet, s = singlet, sept = septet, t = triplet.

[c] Aromatic ring resonances assigned by spectral comparisons of complexes; *meta*-Cs based on δ128.5, *para*-Cs from relative peak height, *ortho*-Cs as triplets for phenylimido ligands, otherwise tentative.

[d] ^2J(PP) = 164.31 Hz.

[e] ^2J(PP) = 156.45 Hz.

the phosphines are *trans*,[26] with the doublets arising from non-equivalent PMe_3 ligands.* The ^1H and $^{13}C\{^1H\}$ NMR spectra of the PMe_3 ligands show virtual coupling and the $^{31}P\{^1H\}$ NMR spectrum represents an AB system which has been simulated.[28] The two phosphines show different ^{31}P–^{183}W couplings ($^1J(PW) = 209.6$ and 222.7 Hz) suggesting small differences in the W—P bonding modes.[27,29]

Asymmetry present in the complex has a marked effect on the appearance of the acetylenic carbons and proton in the NMR spectra. The CH proton in the ^1H NMR spectrum is a doublet of doublets showing different coupling to the phosphines which lie *cis* and *trans* to it ($^3J(HP)_{cis} = 5.90$ Hz, $^3J(HP)_{trans} = 17.26$ Hz).

Variable-temperature studies to 80°C (353 K) show no change in the spectrum ruling out fluxional processes such as rotation or dissociation. Simulation shows that the doublet of doublets is the X part of an AMX system while the coupling pattern is confirmed in the proton coupled ^{31}P NMR spectrum. Each line of the phosphine doublet of doublet AB system splits further with the lower field portion ($\delta = -13.30$ ppm) showing $^3J(HP)$ of 17.26 Hz while for the higher field portion, $^3J(HP)$ is 5.90 Hz. Simulation shows the expected 20-line spectrum consisting of 10 doublet sets.

The acetylenic CH carbon in the $^{13}C\{^1H\}$ NMR spectrum appears as a doublet of doublets for which $^2J(CP)_{cis}$ is 5.29 Hz and $^2J(CP)_{trans}$ is 21.99 Hz, and the phenyl substituted acetylenic carbon is also a doublet of doublets with $^2J(CP)_{cis}$ 4.88 Hz and $^2J(CP)_{trans}$ 15.63 Hz. Simulation of these carbon–phosphorus coupled spectra show they are AMX systems. The two acetylenic carbons exhibit different C—W coupling constants ($^1J(C[H]W) = 23.11$ Hz, $^1J(C[Ph]W) = 31.26$ Hz) which is consistent with the two different carbons being non-equivalent. Of the remaining ^{31}P-coupled carbon resonances in the spectrum, the phenylimido *ortho*- and *ipso*-carbons and the phenylacetylene *ipso*-carbons all appear as triplets.

$[WCl_2(NCHMe_2)(PhC{\equiv}CH)(PMe_3)_2]$ (**6**) was prepared for spectral comparison with phenylimido complex **5**. The isopropylimido ligand methyl groups of this *cis*-dichloro-*trans*-phosphine complex appear in the ^1H NMR spectrum as two doublets which arise due to asymmetry present in the molecule. Similar to the phenylimido complex **5**, the acetylenic proton for **6** is a doublet of doublets in the ^1H NMR spectrum ($^3J(HP)_{cis} = 5.97$ Hz, $^3J(HP)_{trans} = 16.60$ Hz), the acetylenic carbons in the $^{13}C\{^1H\}$ NMR spectrum are doublet of doublets and the phenylacetylene *ipso*-carbon is a triplet. However, the positions of the acetylenic carbon resonances in **5** and **6** are different (i.e. for **5** and **6**, CH at 140.22 and 135.33 ppm, respectively, CPh at 152.80 and 148.54 ppm, respectively) which suggests a small increase in π-backbonding in **6**.[24] This feature was also found for complexes **2** and **1** and indicates that the isopropylimido ligand is a slightly better π-donor than the phenylimido ligand.

The $^{31}P\{^1H\}$ NMR spectrum AB systems are similar in both complexes, but $^2J(PP)$ for **6** is smaller (156.45 Hz cf. 164.31 Hz for **5**). The $^1J(PW)$ values of 214.5 and 228.5 Hz for **6** again suggest small differences in the W—P bonding modes.[27,29]

Carbon monoxide also replaces one phosphine ligand from $[WCl_2(NPh)(PMe_3)_3]$ under reflux in benzene, but a cleaner reaction occurs when $[WCl_3(NPh)(PMe_3)_2]$ is reduced in the presence of C≡O with one equivalent of Na/Hg amalgam. This reductive process does not give the previously described acetylene complexes cleanly but does give good yields of olefin–imido complexes.[27]

$[WCl_2(NPh)(C{\equiv}O)(PMe_3)_2]$ (**7**) is a purple, air-stable solid for which IR and NMR spectral data show the same *cis*-dichloro-*trans*-phosphine geometry exhibited by the acetylene complexes which places the C≡O ligand *cis* to the imido function. $\nu(C{\equiv}O)$ lies at 1925 cm^{-1} in the IR spectrum indicating significant backbonding to C≡O.[30] In comparison, $\nu(C{\equiv}O)$ is found at 2006 cm^{-1} for $[WCl_2(O)(C{\equiv}O)(PMePh_2)_2]$,[4] 2040 cm^{-1} for $[ReCl_3(NPh)(C{\equiv}O)(PPh_3)]$,[11] and 1912 cm^{-1} for $[W(NPh)(S_2CNEt_2)_2(C{\equiv}O)]$.[10] In the $^{13}C\{^1H\}$ NMR spectrum the phenylimido ligand *ipso*- and *ortho*-carbons show the normal triplet as does the C≡O carbon ($^2J(CP) = 4.78$ Hz).

EXPERIMENTAL

$[WCl_2(NPh)(PMe_3)_3]$, $[WCl_2(NPh)(PMe_2Ph)_3]$ and $[WCl_2(NCHMe_2)(PMe_3)_3]$ were prepared by Na/Hg amalgam reduction of $[WCl_4(NPh)]_2$ or $[WCl_4(NCHMe_2)]_2$ in the presence of the appropriate phosphine, and $[WCl_3(NPh)(PMe_3)_2]$ by reaction of $[WCl_4(NPh)]_2$ with PMe_3 in THF.[16] Commercial acetylene and carbon monoxide were used as supplied. Petroleum ether (b.p. 40–60°C) and benzene were distilled from sodium wire. All distillations and bench-top manipulations were carried out under N_2 treated to remove oxygen and water.[31] IR spectra were recorded on a Perkin–Elmer 597 spectrometer and ^1H NMR (400 MHz),

* The $^2J(PP)$ coupling constant value is similar to that found for $[WCl_2(NPh)(Me_2C{=}CH_2)(PMe_3)_2]$ which shows an AB pattern in the $^{31}P\{^1H\}$ NMR spectrum for *trans*-orientated PMe_3 ligands, confirmed by an X-ray crystal structure.[27]

$^{13}C\{^1H\}$ NMR (100.6 MHz) and $^{31}P\{^1H\}$ NMR (162 MHz) spectra on a Bruker AM400 spectrometer. Analytical data were obtained by Professor A. D. Campbel and his associates, University of Otago, New Zealand. Melting points were determined in sealed tubes under N_2 on an electrothermal melting point apparatus and are uncorrected.

Dichloro(diphenylacetylene)phenylimidobis(trimethylphosphine)tungsten(IV) (**1**)

Diphenylacetylene (0.5 g, 2.8 mmol) in benzene (30 cm^3) was added to dichloro(phenylimido) tris(trimethylphosphine)tungsten(IV) (1.0 g, 1.74 mmol) in benzene (80 cm^3) and the mixture was refluxed for 20 h. The solution was filtered and the solvent removed to give a yellow gum which solidified on washing with petroleum ether (50 cm^3). Crude yield, 1.0 g (85%). An analytically pure sample was obtained by extracting the crude product with petroleum ether (5 × 100 cm^3), combining the extracts, and reducing the volume to give the complex as yellow crystals (0.35 g).

IR (Nujol) 1760bm, 1578m, 1570m, 1555w, 1460s, 1400m, 1330s, 1292m, 1271s, 1140w, 1085w, 1055m, 1010m, 995w, 975m, 935vs, 904m, 878w, 845m, 836m, 768s, 757s, 750s, 740m, 727s, 690s, 678s, 672m, 620w, 611w, 583w, 564m, 554m, 538w, 527w, 480w, 458w, 395w, 373w, 345w, 258m, 255s, 230s and 215m cm^{-1}.

Dichlorobis(dimethylphenylphosphine)diphenylacetylene(phenylimido)tungsten(IV) (**2**)

Diphenylacetylene (0.25 g, 1.4 mmol) and dichlorotris (dimethylphenylphosphine) phenylimidotungsten (IV) (0.9 g, 1.2 mmol) were refluxed in benzene (30 cm^3) for 16 h. The solution was filtered, the solvent removed and the residue washed with petroleum ether (100 cm^3). Crude yield, 0.8 g (84%). Concentration of the petroleum ether extracts (5 × 100 cm^3) gave the complex as yellow crystals (0.2 g).

IR (Nujol) 1760w, 1590w, 1564w, 1345m, 1294w, 1272w, 1255w, 1134w, 1100w, 1060w, 1018w, 988w, 944m, 922s, 910s, 904s, 864w, 845w, 830w, 795w, 775m, 760s, 742s, 718m, 690m, 680s, 670m, 684s, 585w, 570m, 560m, 544w, 525w, 484m, 455w, 415w, 378w, 335w, 260m and 235m cm^{-1}.

Dichloro(diphenylacetylene)isopropylimidobis(trimethylphosphine)tungsten(IV) (**3**)

Diphenylacetylene (0.2 g, 1.1 mmol) and dichloro (isopropylimido) tris (trimethylphosphine) tungsten (IV) (0.4 g, 0.74 mmol) were refluxed in benzene (80 cm^3) for 18 h. The solution was filtered, the volume reduced to *ca* 15 cm^3 and petroleum ether (100 cm^3) added. On standing, colourless crystals of the complex were formed. Yield, 0.36 g (76%).

IR (Nujol) 1740bw, 1595w, 1480m, 1420m, 1378m, 1300m, 1275s, 1155w, 1110w, 1068w, 1024w, 950s, 865m, 785s, 778m, 755s, 722s, 705s, 680w, 632w, 584m, 565w, 558w, 510m, 475w, 458w, 410w, 270s and 245s cm^{-1}.

Acetylenedichlorophenylimidobis(trimethylphosphine)tungsten(IV) (**4**)

Dichloro (phenylimido) tris (trimethylphosphine) tungsten(IV) (0.7 g, 1.2 mmol) was refluxed in benzene (80 cm^3) for 16 h under an acetylene atmosphere (balloon). The solution was filtered while hot, and the volume reduced to *ca* 40 cm^3 keeping the solution hot. On standing, yellow microcrystals of the product separated (0.4 g) which were filtered off and washed with petroleum ether (50 cm^3). Addition of petroleum ether (50 cm^3) to the filtrate gave a further crop of yellow microcrystals (0.2 g). Total yield, 94%.

IR (Nujol) 1632w, 1582w, 1482s, 1462s, 1423m, 1348s, 1305w, 1294m, 1288m, 1282m, 1173w, 1256w, 1074w, 1028w, 1008w, 996m, 988m, 955vs, 868m, 860m, 777m, 768s, 750m, 745s, 725w, 700s, 683w, 675w, 630w, 625w, 560w, 538w, 496w, 398w, 355w, 285m, 275s and 240s cm^{-1}.

Dichloro(phenylacetylene)phenylimidobis(trimethylphosphine)tungsten(IV) (**5**)

Phenylacetylene (0.16 g, 1.6 mmol) in benzene (30 cm^3) was added to dichloro(phenylimido) tris(trimethylphosphine)tungsten(IV) (0.8 g, 1.4 mmol) in benzene (80 cm^3) and the mixture was refluxed for 18 h. The solution was filtered and the solvent removed to give a gum which solidified on standing under petroleum ether (100 cm^3). Crude yield, 0.74 g (88%). Combination of petroleum ether extracts (3 × 100 cm^3) and reduction of the volume gave the complex as yellow crystals (0.3 g).

IR (Nujol) 1731bw, 1595w, 1580w, 1462m, 1415s, 1354s, 1308w, 1285m, 1162w, 1071m, 1028m, 990m, 950vs, 857m, 784s, 770s, 745s, 730w, 710s, 700s, 682w, 635w, 628w, 565w, 552w, 538w, 528w, 515w, 398w, 353w, 271s, 248m, 230s and 208m cm^{-1}.

Dichloro(isopropylimido)phenylacetylenebis(trimethylphosphine)tungsten(IV) (**6**)

Dichloro(isopropylimido)tris(trimethylphosphine) tungsten(IV) (0.9 g, 1.7 mmol) and phenylacetyl-

ene (0.2 g, 2.0 mmol) in benzene (100 cm^3) were refluxed for 16 h. The solution was filtered, the volume reduced to *ca* 25 cm^3 and petroleum ether (100 cm^3) added, giving the complex as a yellow non-crystalline solid which was filtered off, washed with petroleum ether (30 cm^3) and dried *in vacuo*. Yield, 0.53 g (55%).

IR (Nujol) 1730m, 1590w, 1475s, 1412s, 1350m, 1300m, 1268s, 1165w, 1145w, 1110w, 1068w, 1020w, 950vs, 858m, 800w, 760s, 750s, 735s, 704s, 675m, 630m, 618w, 565w, 520w, 345w, 265s and 220m cm^{-1}.

Carbonyldichloro (phenylimido) bis (trimethylphosphine)tungsten(IV) (7)

Trichloro(phenylimido)bis(trimethylphosphine) tungsten(V) (1.0 g, 1.9 mmol) in benzene (100 cm^3) was reduced with Na/Hg amalgam (50 mg Na, 2.2 mmol; 40 g Hg) under carbon monoxide (20 p.s.i.) for 5 h. The solution was filtered and the solvent removed to give a purple–brown crystalline solid which was extracted with warm petroleum ether (5×200 cm^3). The combined extracts were filtered and the solvent reduced to *ca* 5 cm^3 giving the complex as a purple crystalline solid. Yield, 0.7 g (70%).

IR (Nujol) 1925s, 1464s, 1418s, 1345s, 1305m, 1284s, 1160w, 1070w, 1025w, 945s, 860m, 855m, 775s, 742s, 695s, 670m, 570m, 558m, 460w, 380w, 340w, 305s and 260s cm^{-1}.

REFERENCES

1. W. A. Nugent and J. M. Mayer, *Metal–Ligand Multiple Bonds*. Wiley Interscience, New York (1988).
2. E. A. Maatta and R. A. D. Wentworth, *Inorg. Chem.* 1979, **18**, 524.
3. W. E. Newton, J. W. McDonald, J. L. Corbin, L. Ricard and R. Weiss, *Inorg. Chem.* 1980, **19**, 1997.
4. F.-M. Su, C. Cooper, S. J. Geib, A. L. Rheingold and J. M. Mayer, *J. Am. Chem. Soc.* 1986, **108**, 3545.
5. N. G. Bokiy, Yu. V. Gatilov, Yu. T. Struchkov and N. A. Ustynyuk, *J. Organomet. Chem.* 1973, **54**, 213.
6. H. G. Alt and H. I. Hayen, *J. Organomet. Chem.* 1986, **316**, 105.
7. J. R. Morrow, T. L. Tonker and J. L. Templeton, *Organometallics* 1985, **4**, 745.
8. W. A. Nugent and B. L. Haymore, *Coord. Chem. Rev.* 1980, **31**, 123.
9. D. D. Devore, E. A. Maatta and F. Takusagawa, *Inorg. Chim. Acta* 1986, **112**, 87.
10. G. L. Hillhouse and B. L. Haymore, *J. Organomet. Chem.* 1978, **162**, C23.
11. G. La Monica and S. Cenini, *Inorg. Chim. Acta* 1978, **29**, 183; *J. Chem. Soc., Dalton Trans.* 1980, 1145.
12. S. M. Rocklage and R. R. Schrock, *J. Am. Chem. Soc.* 1982, **104**, 3077.
13. M. R. Churchill, Y.-J. Li, K. H. Theopold and R. R. Schrock, *Inorg. Chem.* 1984, **23**, 4472.
14. A. J. Nielson, *Chem. N.Z.* 1988, **52**, 131.
15. G. R. Clark, A. J. Nielson, C. E. F. Rickard and D. C. Ware, *J. Chem. Soc., Chem. Commun.* 1989, 343.
16. D. C. Bradley, M. B. Hursthouse, K. M. A. Malik, A. J. Nielson and R. L. Short, *J. Chem. Soc., Dalton Trans.* 1983, 2651; A. J. Nielson, *Inorg. Synth.* 1986, **24**, 193.
17. W. P. Griffith, A. J. Nielson and M. J. Taylor, *J. Chem. Soc., Dalton Trans.* 1988, 647.
18. K. Nakamoto, *Infrared and Raman Spectra of Inorganic and Coordination Compounds*, 4th edn, p. 327. John Wiley, New York (1986).
19. D. A. Redfield, J. H. Nelson and L. W. Cory, *Inorg. Nucl. Chem. Lett.* 1974, **10**, 727.
20. B. R. Ashcroft, A. J. Nielson, D. C. Bradley, R. J. Errington, M. B. Hursthouse and R. L. Short, *J. Chem. Soc., Dalton Trans.* 1987, 2059.
21. J. L. Templeton and B. C. Ward, *J. Am. Chem. Soc.* 1980, **102**, 3288.
22. E. C. Walborsky, D. E. Wigley, E. Roland, J. C. Dewar and R. R. Schrock, *Inorg. Chem.* 1987, **26**, 1615.
23. W. A. Nugent and J. M. Mayer, *Metal–Ligand Multiple Bonds*, p. 33. Wiley Interscience, New York (1988).
24. C. A. Tolman, A. D. English and L. E. Manzer, *Inorg. Chem.* 1975, **14**, 2353.
25. A. J. Nielson, J. M. Waters and D. C. Bradley, *Polyhedron* 1985, **4**, 285.
26. J. G. Verkade, *Coord. Chem. Rev.* 1972/73, **9**, 1.
27. G. R. Clark, A. J. Nielson, C. E. F. Rickard and D. C. Ware, *J. Chem. Soc., Dalton Trans.*, in press.
28. A. J. Nielson and D. C. Ware, unpublished work.
29. F. A. Cotton and G. N. Mott, *J. Am. Chem. Soc.* 1982, **104**, 5978; P. S. Pregosin and R. W. Kunz, *NMR, Basic Principles and Progress* (Edited by P. Diehl, E. Fluck and R. Kosfield), Vol. 16, p. 25. Springer, Berlin (1979).
30. K. Nakamoto, *Infrared and Raman Spectra of Inorganic and Coordination Compounds*, 4th edn, p. 291. John Wiley, New York (1986).
31. A. J. Nielson, *Chem. N.Z.* 1985, **49**, 11.

Polyhedron Vol. 9, No. 4, pp. 611–613, 1990
Printed in Great Britain

0277–5387/90 $3.00+.00
© 1990 Pergamon Press plc

COMMUNICATION

PREPARATION AND X-RAY CRYSTAL STRUCTURES OF VOLATILE COPPER(II) ALKOXIDES

SUBHASH C. GOEL, KEITH S. KRAMER, MICHAEL Y. CHIANG and WILLIAM E. BUHRO*

Department of Chemistry, Washington University, St. Louis, MO 63130, U.S.A.

(*Received* 27 *July* 1989; *accepted* 12 *September* 1989)

Abstract—Volatile amino–alkoxide complexes $Cu[OCH_2CH_2NMe_2]_2$ (**1**), $Cu[OCHMeCH_2NMe_2]_2$ (**2**) and $Cu[OCH_2CH_2NMeCH_2CH_2NMe_2]_2$ (**3**) have been prepared. X-ray crystal structures reveal a mononuclear, square-planar geometry for **2**, and a mononuclear, distorted, square-pyramidal geometry for **3**. Thermal decomposition (25–300°C) of **1** gives a mixture of copper, CuO and Cu_2O whereas thermal decomposition of **2** gives copper.

Efforts to prepare films of cuprate oxide superconductors by metal–organic chemical vapour deposition have used β-diketonate complexes as the volatile metal-containing sources.[1–6] These precursors require decomposition in the presence of O_2,[2–5] H_2O,[6] or both,[1] to successfully deposit oxides. Since alkoxide complexes of some metals, such as yttrium(III),[7] zirconium(IV)[8,9] and hafnium(IV),[9] pyrolyse cleanly to the corresponding oxides, alkoxides may provide a general, *direct* vapour-deposition route to metal oxides when suitably volatile derivatives can be identified.[10] Thus, we began to investigate means of volatilizing copper(II) alkoxides, which are typically non-volatile, insoluble solids,[11] for testing as cupric oxide (CuO) sources. The first volatile example, $Cu[OCH_2CH_2NEt_2]_2$, was recently obtained elsewhere, although structural characterization and pyrolysis behaviour were not addressed.[12] We now describe three volatile copper(II) amino–alkoxides and preliminary studies of their thermal decomposition. To our knowledge, this work provides the first X-ray crystal structures of mononuclear copper(II) alkoxides.

We initially attempted to prepare mononuclear ether–alkoxide complexes of type **I** or **II** (see below). However, $Cu[OCH_2CH_2OMe]_2$ was a non-volatile, insoluble solid, and $Cu[OCH_2CH_2OCH_2CH_2OMe]_2$ was a non-volatile, soluble oligomer; in the latter case ^1H NMR established the presence of dangling ligands.[13] Replacement of ether-type oxygens with more basic NMe units resulted in chelated structures of types **III** and **IV** (see below).

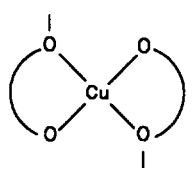

I

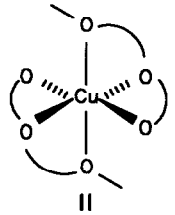

II

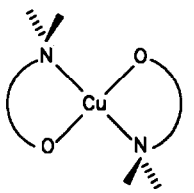

III

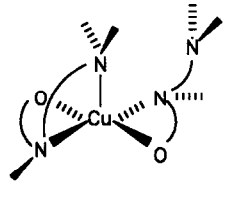

IV

The new compounds $Cu[OCH_2CH_2NMe_2]_2$ (**1**), $Cu[OCHMeCH_2NMe_2]_2$ (**2**) and $Cu[OCH_2CH_2NMeCH_2CH_2NMe_2]_2$ (**3**) were prepared by the alcohol-exchange procedure of Mehrotra and

* Author to whom correspondence should be addressed.

co-workers [see eq. (1)].[11] Green–blue **1*** and purple **2*** were isolated by sublimation in 71 and 75% yields, respectively. Purple, low-melting **3*** was obtained in a total yield of 83% by crystallization from hexane (66%) and distillation of the mother liquor (23%). Although alkoxide complexes of the later transition elements are typically unstable with respect to β-H elimination,[14] the copper(II) alkoxides reported here, and some others,[11,12] have good thermal stability; each of **1–3** is sublimed or distilled in $\geqslant$ *ca* 85% recovery between 60–110°C at 10^{-4} torr. The magnetic moments* of **1–3** indicate they are monomeric in solution.

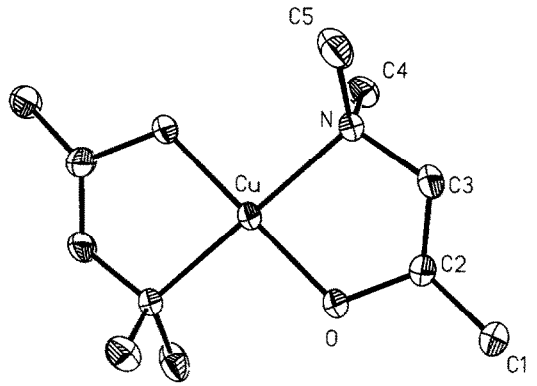

Fig. 1. Structure of $Cu[OCHMeCH_2NMe_2]_2$ (**2**). Selected distances (Å): Cu—O, 1.865(3); Cu—N, 2.052(3). Hydrogen atoms were omitted for clarity.

$$Cu(OMe)_2 + 2ROH \longrightarrow Cu(OR)_2 + 2MeOH \quad (1)$$

R = $CH_2CH_2NMe_2$, **1**
$CHMeCH_2NMe_2$, **2**
$CH_2CH_2NMeCH_2CH_2NMe_2$, **3**.

Crystals of **2** and **3** suitable for X-ray structure determinations were obtained from hexane.† The *trans*, square-planar structure of **2** is shown in Fig. 1, and the distorted square-pyramidal structure of **3** is shown in Fig. 2. The latter geometry results

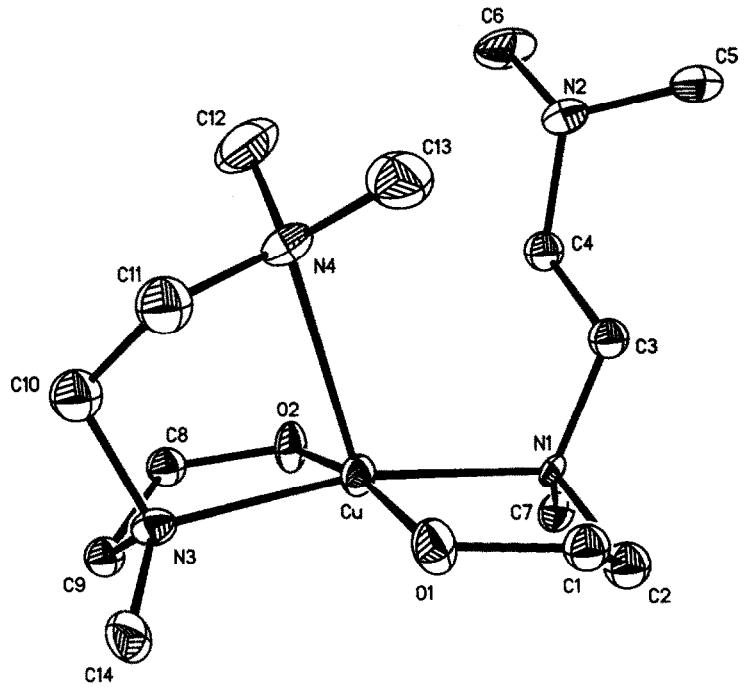

Fig. 2. Structure of $Cu[OCH_2CH_2NMeCH_2CH_2NMe_2]_2$ (**3**). Selected distances (Å): Cu—O(1), 1.892(17); Cu—O(2), 1.887(13); Cu—N(1), 2.113(14); Cu—N(3), 2.102(14); Cu—N(4), 2.598(12). Hydrogen atoms were omitted for clarity.

* *Physical data:* Satisfactory elemental analyses were obtained for **1–3** (C, H, Cu, N). **1**: m.p. 184–185°C dec; sublimed 80°C/10^{-4} torr; μ_{eff} (0.06 M in toluene) 1.82(7) BM. **2**: m.p. 134–135°C dec; sublimed 60°C/10^{-4} torr; μ_{eff} (0.06 M in toluene) 1.76(5) BM. **3**: m.p. 49–51°C; b.p. 110–112°C/10^{-4} torr; μ_{eff} (0.05 M in toluene) 1.81(3) BM.

† Atomic positional parameters have been deposited with the Director, Cambridge Crystallographic Centre. Crystal data at ambient temperature: for **2**: space group $P2_1/c$, $a = 5.643(3)$, $b = 10.357(4)$, $c = 11.723(5)$ Å, $\beta = 92.49(5)°$, $D_c = 1.299$ g cm^{-3}, $Z = 2$, final residuals were $R = 0.0407$ and $R_w = 0.0428$. **3**: space group Cc, $a = 16.405(12)$, $b = 10.192(6)$, $c = 12.038(10)$ Å, $\beta = 113.60(7)°$, $D_c = 1.275$ g cm^{-3}, $Z = 4$, final residuals were $R = 0.0578$ and $R_w = 0.0737$.

from one of the $OCH_2CH_2NMeCH_2CH_2NMe_2$ ligands of **3** coordinating in a tridentate fashion, and the other in a bidentate fashion, leaving a terminal NMe_2 group dangling. The axial Cu—N(4) separation of 2.60(1) Å in **3** is considerably longer than the basal Cu—N distances of 2.11(1) Å (av.); these values are typical of the Jahn–Teller-distorted, five- and six-coordinate complexes of copper(II).[15,16] The copper atom sits 0.21 Å above the least-squares basal plane [O(1), O(2), N(1), N(2)], and the Cu—N(4) vector forms a *ca* 72° angle with it. The Cu—O distances of 1.89(2) Å (av.) in **3** are in the short end of the range of corresponding distances (1.89(1)–1.95(1) Å) in a series of alkoxide-bridged, dinuclear copper(II) complexes.[17–20] The Cu—O distances of 1.865(3) Å in **2** and 1.81(1)–1.88(1) Å in a copper(I) alkoxide, $[Cu(\mu\text{-O-}t\text{-Bu})]_4$,[21] are comparable to **3**.

We next sought to establish whether the more volatile compounds **1** and **2** would serve as cupric oxide precursors. In rare mechanistic studies of metal–alkoxide decomposition, Bradley and Faktor determined that $Zr(OR)_4$ compounds pyrolysed to ZrO_2 more readily at atmospheric pressure than at reduced pressure.[8,22] Consequently, we carried out pyrolysis of solid **2** at ambient pressure under a N_2 stream (25–300°C, 2 h), and obtained copper metal as the only phase detected by X-ray powder diffraction. In related work, Jeffries and Girolami recently reported the vapour deposition of metallic copper using $[Cu(\mu\text{-O-}t\text{-Bu})]_4$ as the volatile source.[23] However, pyrolysis of **1** under the same conditions employed for **2** led to a mixture of copper metal, CuO and Cu_2O in a 48 : 33 : 19 ratio, respectively. Thus, the course of thermal decomposition is ligand dependent. Efforts to design a useful CuO precursor through suitable ligand modifications are in progress. The high volatility of **2** suggests it may be a useful source for copper deposition.

Acknowledgements—We thank Washington University and the Petroleum Research Fund (Grant No. 20412-G3), administered by the ACS, for support, and Laura D. Borowy for technical assistance. Washington University's X-Ray Crystallography Facility was funded by the NSF Chemical Instrumentation Program (Grant CHE-8811456).

REFERENCES

1. A. D. Berry, D. K. Gaskill, R. T. Holm, E. J. Cukauskas, R. Kaplan and R. L. Henry, *Appl. Phys. Lett.* 1988, **52**, 1743.
2. H. Abe, T. Tsuruoka and T. Nakamori, *Jap. J. Appl. Phys.* 1988, **27**, L1473.
3. H. Yamane, H. Masumoto, T. Hirai, H. Iwasaki, K. Watanabe, N. Kobayashi, Y. Muto and H. Kurosawa, *Appl. Phys. Lett.* 1988, **53**, 1548.
4. K. Shinohara, F. Munakata and M. Yamanaka, *Jap. J. Appl. Phys.* 1988, **27**, L1683.
5. A. D. Berry, R. T. Holm, E. J. Cukauskas, M. Fatemi, D. K. Gaskill, R. Kaplan and W. B. Fox, *J. Cryst. Growth* 1988, **92**, 344.
6. J. Zhao, K.-H. Dahmen, H. O. Marcy, L. M. Tonge, T. J. Marks, B. W. Wessels and C. R. Kannewurf, *Appl. Phys. Lett.* 1988, **53**, 1750.
7. K. S. Mazdiyasni, C. T. Lynch and J. S. Smith, *Inorg. Chem.* 1966, **5**, 342.
8. D. C. Bradley and M. M. Faktor, *Trans. Faraday Soc.* 1959, **55**, 2117.
9. K. S. Mazdiyasni, C. T. Lynch and J. S. Smith, *J. Am. Ceram. Soc.* 1965, **48**, 372.
10. K. S. Mazdiyasni, C. T. Lynch and J. S. Smith, *J. Am. Ceram. Soc.* 1966, **49**, 286.
11. J. V. Singh, B. P. Baranwal and R. C. Mehrotra, *Z. Anorg. Allg. Chem.* 1981, **477**, 235.
12. H. S. Horowitz, S. J. McLain, A. W. Sleight, J. D. Druliner, P. L. Gai, M. J. VanKavelaar, J. L. Wagner, B. D. Biggs and S. J. Poon, *Science* 1989, **243**, 66.
13. S. C. Goel, K. S. Kramer, P. C. Gibbons and W. E. Buhro, *Inorg. Chem.* 1989, **28**, 3619.
14. H. E. Bryndza and W. Tam, *Chem. Rev.* 1988, **88**, 1163.
15. A. A. G. Tomlinson and B. J. Hathaway, *J. Chem. Soc. A* 1968, 1685.
16. T. Distler and P. A. Vaughan, *Inorg. Chem.* 1967, **6**, 126.
17. R. Mergehenn, L. Merz and W. Haase, *Z. Nat. B* 1975, **30b**, 14.
18. L. Merz and W. Haase, *Acta Cryst.* 1978, **B34**, 2128.
19. M. Mikuriya, H. Okawa and S. Kida, *Inorg. Chim. Acta* 1980, **42**, 233.
20. N. Matsumoto, S. Kida and I. Ueda, *J. Coord. Chem.* 1979, **9**, 133.
21. T. Greiser and E. Weiss, *Chem. Ber.* 1976, **109**, 3142.
22. D. C. Bradley and M. M. Faktor, *J. Appl. Chem.* 1959, **9**, 435.
23. P. M. Jeffries and G. S. Girolami, *Chem. Mater.* 1989, **1**, 8.

Polyhedron Vol. 9, No. 4, pp. 615–618, 1990
Printed in Great Britain

0277–5387/90 $3.00+.00
© 1990 Pergamon Press plc

COMMUNICATION

INCOMPLETE COORDINATION TO RHENIUM(V) BY A FACULTATIVE QUINQUEDENTATE LIGAND. THE X-RAY CRYSTAL STRUCTURE OF [ReO(OMe){2′-(NC_4H_3-2-CH=N$(CH_2)_3$NMe$(CH_2)_3$CH=N—)C_4H_3NH}]PF_6

HILARY J. BANBERY, FERIDA S. McQUILLAN, THOMAS A. HAMOR,* CHRISTOPHER J. JONES* and JON A. McCLEVERTY

Department of Chemistry, University of Birmingham, PO Box 363, Birmingham B15 2TT, U.K.

(*Received* 26 *September* 1989; *accepted* 12 *October* 1989)

Abstract—The reaction between $Bu_4N[ReOCl_4(H_2O)]$ and the Schiff base ligand $\{HNC_4H_3$-2-CH=N$(CH_2)_3\}_2$NMe in methanol affords the cationic complex [ReO(OMe){2′-(NC_4H_3-2-CH=N$(CH_2)_3$NMe$(CH_2)_3$CH=N—)C_4H_3NH}]PF_6. An X-ray diffraction study of this complex reveals a six coordinate, nearly octahedral rhenium(V) centre coordinated to only four nitrogen donor atoms from the quinquedentate ligand. One terminal pyrrolyl group remains protonated and uncoordinated. The remaining two coordination sites are occupied by the mutually *trans* oxo and methoxide ligands.

Reports of rhenium complexes containing facultative ligands with more than four potential donor atoms are rare.[1] Mazzi and co-workers have reported the complexes $[ReO(N(R)\{(CH_2)_nN$=CH—C_6H_4-2-$O\}_2)]^z$ (R = nothing, $n = 2$ and $z = 0$; R = Me, $n = 3$ and $z = +1$) and have determined the molecular structure of the technetium counterpart of the former, $[TcO(N\{(CH_2)_2N$=CHC_6H_4-2-$O\}_2)]$.[2] More recently we have found that not all potential donor atoms in a facultative ligand may bind to the ReO^{3+} core in rhenium(V) complexes.[3,4] In the complex [ReO(OEt)$\{OC_6H_4$-2-CH=$N(CH_2)_2\}_2$S] the thioether sulphur of the potentially quinquedentate ligand remains uncoordinated,[3] while in [ReO(Cl)$\{OC_6H_4$-2-CH=$N(CH_2)_2$ $OCH_2\}_2$] it is the two ether oxygen atoms of the sexidentate ligand which do not coordinate.[4] Thus, in both of these cases the ligands function as quadridentate although they have the capacity to coordinate further. Wilkinson and co-workers have noted this phenomenon previously[5] but did not present crystallographic data.

In the examples cited above, the finding that the thioether sulphur or ether oxygen donor atoms in polydentate facultative ligands do not bind to the rhenium may not be too surprising. The binding capacities of these non-coordinated atoms would be expected to be rather weak compared to an alkoxide or halide ligand. Certainly when two phenoxide and three nitrogen donors are present in $N(R)\{(CH_2)_nN$=CH—C_6H_4-2-$O\}_2$, five-coordination is achieved.[2] We have now examined the reactions between $[ReOCl_4(H_2O)]^-$ and the potentially quinquedentate ligands $\{HNC_4H_3$-2-CH=N$(CH_2)_2\}_2$NH and $\{HNC_4H_3$-2-CH=N$(CH_2)_3\}_2$NMe which contain terminal pyrrolyl coordinating groups and offer five nitrogen donor sites.

The ligands $\{HNC_4H_3$-2-CH=N$(CH_2)_2\}_2$NH and $\{HNC_4H_3$-2-CH=N$(CH_2)_3\}_2$NMe were prepared by condensation of 2-formylpyrrole with $\{H_2N(CH_2)_2\}_2$NH or $\{H_2N(CH_2)_3\}_2$NMe, respectively. They have been characterized by spectroscopic methods and by elemental analyses. The former ligand reacts with $Bu_4N[ReOCl_4(H_2O)]$ in methanol to produce a red–brown solution. Treatment of this solution with KNCS affords an orange–brown solid, the IR spectrum of which con-

* Authors to whom correspondence should be addressed.

tains bands attributable to $\nu_{C\equiv N}$ and $\nu_{Re=O}$. In addition, a band is observed at 2050 cm^{-1} attributable[6] to N-bound thiocyanate. The ^1H NMR spectrum of the complex is consistent with the presence of a plane of symmetry in the molecule and contains no pyrrolyl-NH signals. The complex is a non-conductor in MeCN solution and the elemental analysis is in accord with the formulation $[ReO(NCS)\{NC_4H_3\text{-}2\text{-}CH{=}N(CH_2)_2\}_2NH]$. A structure consistent with these findings would contain a six-coordinate rhenium centre with the N-bound NCS ligand *trans* to the rhenyl oxo-group. The quinquedentate ligand would occupy the remaining "equatorial" sites with the central —NH— donor group remaining non-coordinated as illustrated in Fig. 1(a).

Treatment of the reaction solution with the non-coordinating anions PF_6^- or ClO_4^- affords species which exhibit appropriate solution conductivities for 1 : 1 electrolytes. It is possible that the central —NH— group of the quinquedentate ligand is bound *trans* to the rhenyl oxo-group in these compounds as illustrated in Fig. 1(b). However, their NMR spectra, in CD_3CN solution, are very similar to that of $[ReO(NCS)\{NC_4H_3\text{-}2\text{-}CH{=}N(CH_2)_2\}_2NH]$. It seems likely, therefore, that a neutral ligand such as MeCN or OH_2 is bound *trans* to the oxo-group in place of NCS^-. Further studies are in progress to establish unequivocally the structure of the cationic complex in these compounds.

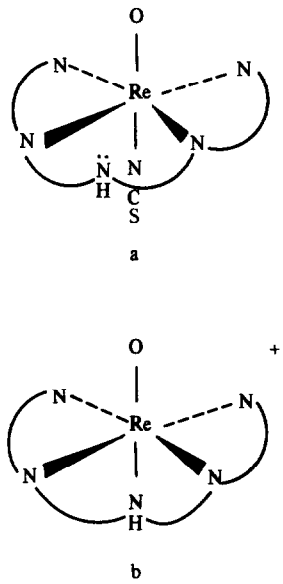

Fig. 1. Schematic representations of possible structures for: (a) $[ReO(NCS)\{NC_4H_3\text{-}2\text{-}CH{=}N(CH_2)_2\}_2NH]$; (b) $[ReO\{HNC_4H_3\text{-}2\text{-}CH{=}N(CH_2)_2\}_2NH]^+$.

The ligand $\{HNC_4H_3\text{-}2\text{-}CH{=}N(CH_2)_3\}_2NMe$ also reacts with $Bu_4N[ReOCl_4(H_2O)]$ in methanol to produce a red–brown solution. However, in this case, treatment with NH_4PF_6 affords a complex with a ^1H NMR spectrum which indicates the absence of a plane of symmetry in the molecule and the presence of a pyrrolyl NH proton. Crystals of this compound which were suitable for an X-ray diffraction study could be obtained, allowing the structure of the complex to be determined. The structure* of the complex cation is illustrated[10] in Fig. 2, which also shows the crystallographic atom numbering scheme used. The ligand and methoxy group bind to the ReO^{3+} core to produce a distorted octahedral geometry, involving three chelate rings, one five-membered and two six-membered. The oxo-group lies *trans* to the oxygen of the methoxy group, similar to previous observations in related complexes,[3,4] and four sequential nitrogen atoms occupy the equatorial sites, producing the *trans*(1, 6) octahedral isomer. One pyrrolyl nitrogen is *trans* to the amine nitrogen and the two imine nitrogen atoms, N(2) and N(4), are mutually *trans*. The remaining pyrrolyl nitrogen is protonated and uncoordinated. The maximum angular distortion from ideal octahedral geometry occurs in the angle N(1)—Re—N(2), 77.7°, which involves the five-membered chelate ring. There are three types of Re—N distances corresponding to the three different bonding geometries at nitrogen. The shortest is that involving the pyrrolic nitrogen at 2.059(10) Å. Next longest are those to imine nitrogens, 2.097(9)

*Crystals of $[ReC_{18}H_{27}N_5O_2][PF_6]$, $M_r = 676.6$ are monoclinic, space group $P2_1/n$, $a = 10.828(2)$, $b = 18.564(2)$, $c = 11.897(2)$ Å, $\beta = 105.47(7)°$, with $Z = 4$, $\mu(Mo\text{-}K_\alpha) = 57.1\ cm^{-1}$. A crystal with dimensions $0.5 \times 0.1 \times 0.2$ mm was mounted on an Enraf–Nonius CAD-4 diffractometer; cell dimensions and intensities were measured by ω–2θ scans with graphite-monochromated Mo-K_α radiation. 3521 unique reflections were scanned within $2 < \theta < 25°$. Three standard reflections measured every 2 h showed no significant alteration in intensity. Lorentz and polarization corrections were applied and 2820 structure amplitudes with $F > 5\sigma(F)$ were considered observed and used in the analysis. The structure was determined[7] by Patterson and Fourier methods and refined[8] by least-squares using anisotropic thermal parameters for the heavier atoms. Hydrogen atoms were placed in calculated positions. An empirical absorption correction was applied to the data using DIFABS.[9] The weighting scheme used was $w = 1/[\sigma_2(F) + 0.00035F^2]$, and the refinement converged to $R = 0.036$, $R' = 0.062$. The residual electron density in a final difference map was within ± 1.1 e $Å^{-3}$.

Atomic coordinates, bond lengths and angles and thermal parameters have been deposited at the Cambridge Crystallographic Data Centre. See Deposition of Crystallographic Data on p. ii.

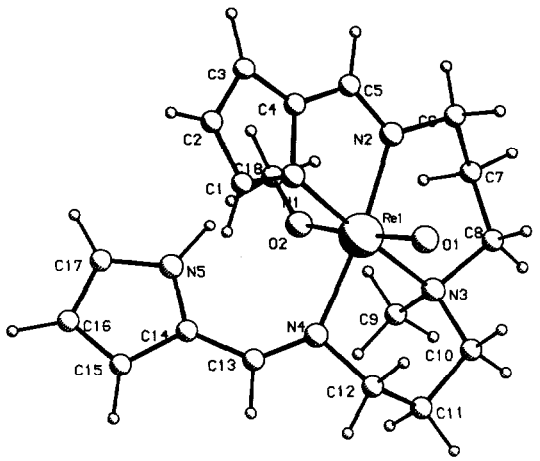

Fig. 2. A view of the complex cation, $[ReO(OMe)\{2'-(NC_4H_3-2-CH{=}N(CH_2)_3NMe(CH_2)_3CH{=}N-)-C_4H_3NH\}]^+$ showing the atom numbering. Selected distances (Å) and angles (°):

Re—O(1)	1.679(7)	Re—O(2)	1.875(6)
Re—N(1)	2.059(10)	Re—N(2)	2.097(9)
Re—N(3)	2.221(8)	Re—N(4)	2.136(9)

O(1)—Re—O(2)	171.8(4)
O(1)—Re—N(2)	90.3(4)
O(1)—Re—N(4)	96.1(4)
N(2)—Re—N(3)	96.2(4)
O(1)—Re—O(2)	171.8(4)
N(2)—Re—N(4)	172.7(3)
O(1)—Re—N(1)	95.6(4)
O(1)—Re—N(3)	88.4(4)
N(1)—Re—N(2)	77.7(4)
N(3)—Re—N(4)	87.5(3)
N(1)—Re—N(3)	172.8(4)

and 2.136(9) Å, for N(2) and N(4), respectively. The longest Re—N distance is the amine nitrogen bond, 2.221(8) Å. The imine nitrogens and the coordinated pyrrole nitrogen are planar, sum of angles; N(2) 360.0, N(4) 359.8, N(1) 359.9°, while the amine nitrogen atom has approximately tetrahedral geometry, angles at N(3) ranging from 103.6(8) to 112.1(7)°.

The angles at N(1), coordinated to rhenium, and N(5), which is bonded to a hydrogen atom, are significantly different; C(4)—N(1)—C(1), 105.6(11)° and C(17)—N(5)—C(14), 110.0(11)°, indicating the difference in bonding at these atoms. A search of the Cambridge Structural Database[11] during August 1989, revealed examples of 18 compounds containing pyrrole coordinated to a metal atom and 131 compounds containing a free pyrrole ring. Calculations showed that the angle C—N—C had a mean value of 105.9(3)° and range from 103.6 to 107.9°, when coordinated to a metal atom, whereas a mean of 109.6(3)° and range from 101.7 to 118.1° was found for the pyrrolyl nitrogen bonded to a hydrogen. These values correlate well with those for this compound.

The Re=O distance of 1.679(7) Å is similar to those reported previously,[4] while the Re—OMe distance, 1.875(6) Å, is shorter than for an alkoxy ligand in the related complex $[ReO(OEt)\{OC_6H_4-2-CH{=}N(CH_2)_2\}_2S]$,[3] in which Re—OEt is 1.947(5) Å. A mutually *trans* arrangement of a rhenyl oxo-atom and another singly-bonded oxygen atom, appears to be favoured in structures of this type.[3,4]

There is a possible intramolecular hydrogen bond interaction between H(N5) and the methoxy oxygen atom; N(5)···O(2) 1.91 Å. There are no short interactions with the PF_6^- counterion.

This structure contrasts with the previously reported examples where not all potential donor atoms in a ligand bind to the metal, in that a terminal rather than an internal ligand donor atom fails to coordinate. Furthermore, it is a nitrogen atom rather than the less basic ether oxygen or thioether sulphur atoms which does not bind. The results obtained by Mazzi and co-workers indicate that with the ligands $N(R)\{(CH_2)_nN{=}CHC_6H_4-2-OH\}_2$ (R = H, n = 2; R = Me, n = 3) changing the internal chelate ring size from five- to six-membered does not preclude binding by all five donor atoms to the ReO^{3+} core. However, in the examples described here the use of quinquedentate ligands forming five- rather than six-membered terminal chelate rings, and having pyrrolyl rather than salicylyl terminal groups, leads to non-coordination of a potential donor atom. It is worthy of note that with first row *d*-block metal ions both quadridentate N(4)[12,13] and sexidentate N(6)[14] ligands can bind to metal ions through all of their nitrogen atoms as exemplified by $[Ni\{NC_4H_3-2-CH{=}N(CH_2)-\}_2(X)]$ (X = nothing or CH_2) and $[Fe\{NC_4H_3-2-CH{=}N(CH_2)_2NHCH_2\}_2]PF_6$.

Acknowledgements—We are grateful to the SERC and Amersham International plc for their support (to H.J.B. and F.S.McQ.).

REFERENCES

1. G. Bandoli, U. Mazzi, A. Moresco, M. Nicolini, F. Refosco and F. Tisato, in *Technetium in Chemistry and Nuclear Medicine 2* (Edited by M. Nicolini, G. Bandoli and U. Mazzi). Raven Press, New York (1986).
2. F. Refosco, F. Tisato, U. Mazzi, G. Bandoli and M. Nicolini, *J. Chem. Soc., Dalton Trans* 1988, 611.
3. H. J. Banbery, F. McQuillan, T. A. Hamor, C. J. Jones and J. A. McCleverty, *Polyhedron* 1989, **8**, 559.
4. H. J. Banbery, F. McQuillan, T. A. Hamor, C. J.

Jones and J. A. McCleverty, *J. Chem. Soc., Dalton Trans.* 1989, 1405.
5. A. R. Middleton, A. F. Masters and G. Wilkinson, *J. Chem. Soc., Dalton Trans.* 1979, 542.
6. K. Nakamoto, *Infrared and Raman Spectra of Inorganic and Coordination Compounds*, 3rd edn. Wiley Interscience, New York (1978).
7. G. M. Sheldrick, SHELXS-86, Program for the solution of crystal structure. University of Gottingen, F.R.G. (1987).
8. SHELX-76, Program for crystal structure determination. University of Cambridge, U.K. (1978).
9. N. Walker and D. Stuart, *Acta Cryst.* 1983, **A39**, 158.
10. W. D. S. Motherwell and W. Clegg, PLUTO 78, Program for plotting molecular and crystal structures. University of Cambridge, U.K. (1978).
11. F. H. Allen, S. Bellard, M. D. Brice, B. A. Cartwright, A. Doubleday, H. Higgs, T. Hummelink, B. G. Hummelink-Peters, O. Kennard, W. D. S. Motherwell, J. R. Rodgers and D. G. Watson, *Acta Cryst.* 1979, **B35**, 2331.
12. J. H. Weber, *Inorg. Chem.* 1967, **6**, 258.
13. C. J. Jones and J. A. McCleverty, *J. Chem. Soc. A* 1971, 1052.
14. A. S. Rothin, H. J. Banbery, F. J. Berry, T. A. Hamor, C. J. Jones and J. A. McCleverty, *Polyhedron* 1989, **8**, 491.

Polyhedron Vol. 9, No. 4, pp. 619–621, 1990
Printed in Great Britain

0277–5387/90 $3.00+.00
© 1990 Pergamon Press plc

COMMUNICATION

STERICALLY-INDUCED REARRANGEMENTS OF THE TRIPODAL LIGAND $HB(Pr^iMeC_3N_2H)_3$ IN SOME MOLYBDENUM MONONITROSYL DERIVATIVES

MERCEDES CANO and JOSE V. HERAS

Departamento de Quimica Inorganica, Facultad Quimicas, Universidad Complutense, Madrid 28040, Spain

and

CHRISTOPHER J. JONES* and JON A. McCLEVERTY

Department of Chemistry, University of Birmingham, PO Box 363, Birmingham B15 2TT, U.K.

and

SWIATOSLAW TROFIMENKO

Du Pont Electronics Department, Experimental Station 336/38, E.I. du Pont de Nemours and Company, Wilmington, DE 19898, U.S.A.

(*Received* 25 *October* 1989; *accepted* 2 *November* 1989)

Abstract—The new complexes $[Mo(NO)\{HB(Pr^iMeC_3N_2H)_3\}XY]$ (X = Y = CO, I, OMe, OEt; X = I and Y = OMe, OEt, OPr^i, OBu^t, OCH_2SiMe_3, OPh, OC_6H_4-4-Me, NHPh or NHC_6H_4-4-Me) have been synthesized. In the cases where X = I, or where X = Y = CO or I, these compounds were isolated as a mixture of at least two isomers. However, ^1H NMR studies show that the complexes with X = I and Y = OPr^i, OBu^t, NHPh, NHC_6H_4-4-Me undergo rearrangement reactions at elevated temperature to give selectively a single isomer. These reactions involve 1,2-boratropic shifts of the substituted pyrazolyl moieties and appear to be promoted by the more bulky of the co-ligands X and Y.

Since they were first described[1,2] the tripodal hydrotrispyrazol-1-ylborate ligand and its derivative hydrotris(3,5-dimethylpyrazol-1-yl)borate have made important contributions to transition metal chemistry in the development of both coordination compounds[3–5] and organometallic species.[6,7] Much of this work has exploited the analogy between these ligands and the cyclopentadienide ligand and its derivatives. However, there are significant electronic[8] and steric[5] differences between these two types of ligand. Furthermore, the trispyrazolylborate derivates may be functionalized in the 3-position so as to create structured cavities which may enforce unusual coordination geometries on metal ions.[3,9] The possibility also exists of using polar substituents in the 3-position to promote reactions of, or enter into reactions with, co-ligands coordinated to a metal ion incorporated in the cavity created by the tripodal ligand. In the longer term such species may lead to more elaborate models of metalloenzymes[10,11] or offer novel catalytic systems. However, in the shorter term it is necessary to develop the synthesis and chemistry of complexes containing more simply functionalized

* Author to whom correspondence should be addressed.

trispyrazolylborate ligands. As a part of this endeavour we have been studying the synthesis and derivative chemistry of the complex [Mo(NO)$(CO)_2${HB(Pr^{i}Mepz)$_3$}] (where pz = C_3N_2H) and present here a preliminary account of our initial findings.

A sample of [Mo(NO)$(CO)_2${HB(Pr^{i}Mepz)$_3$}] was prepared from $Mo(CO)_6$ and HB(3,5-Pr^{i}Mepz)$_3^-$ using a procedure similar to that used to prepare [Mo(NO)$(CO)_2${HB(3,5-Me_2pz)$_3$}].[12] The ^{1}H NMR spectrum of this compound indicated that two principal isomers were present. In fact six isomers are possible based on the distribution of three methyl and three isopropyl groups among the 3- and 5-positions on the pyrazolyl rings of the tripodal ligand, but it is likely that those with the isopropyl groups predominantly occupying the 3-positions will be preferred.[13]

Again, following the precedent[12] provided by the synthesis of [Mo(NO){HB(3,5-Me_2pz)$_3$}I_2], the reaction of [Mo(NO)$(CO)_2${HB(Pr^{i}Mepz)$_3$}] with iodine produced [Mo(NO){HB(Pr^{i}Mepz)$_3$}I_2].* This compound was initially obtained as a mixture of isomers as indicated by the ^{1}H NMR spectral data. However, after heating at 70°C for 40 h *in vacuo* in the solid state it was found that conversion to a single isomer had occurred. The ^{1}H NMR spectrum of this material contained signals of relative area 1 : 2 at δ_{TMS} = 6.16 and 5.86 attributable to the pyrazolyl-4-H protons. The pyrazolyl methyl protons appeared as singlets of relative area 3 : 6 at δ_{TMS} = 2.57 and 2.29, while the isopropyl methyl signals gave rise to three doublets of relative area 6 : 6 : 6 at δ_{TMS} = 1.30, 1.05 and 0.98 ($^3J_{HH}$ = 7 Hz). In the absence of structural data it is not possible to unambiguously define the distribution of the isopropyl groups in this complex. However, in terms of minimizing steric interactions[13] the most likely structure would place the isopropyl group on the pyrazolyl ring between the two bulky iodide ligands in the 5-position near to the BH group. The other two isopropyl groups would then occupy the 3-positions on the pyrazolyl rings lying between the iodide and nitrosyl ligands as shown in Fig. 1. The only other structure consistent with the NMR data would reverse these positions and place two isopropyl substituents near to the BH group which would not be in accord with the precedents reported so far for this type of complex.[9,13] The rearrangement to produce a single isomer involves a 1,2-

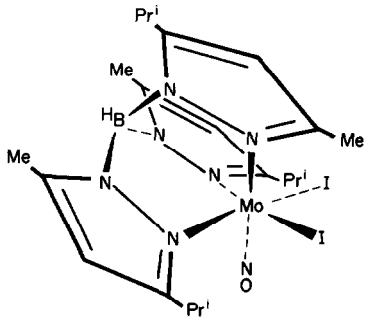

Fig. 1. The proposed structure of [Mo(NO){HB(Pr^{i}Mepz)$_3$}I_2].

borotropic shift of one or more methylisopropylpyrazolyl groups in the ligand. Such rearrangements have been observed previously[13] in cobalt(II) complexes of the ligands HB(3-Pr^{i}Hpz$_2$)$_3$ and HB(3,4-Pr^{i}Brpz)$_3$.

Since the reactions of [Mo(NO){HB(3,5-Me_2pz)$_3$}I_2] with alcohols or organoamines have been found to afford air-stable alkoxide or organoamide derivatives, we were interested in establishing whether a similar derivative chemistry could be developed from [Mo(NO){HB(Pr^{i}Mepz)$_3$}I_2]. Unlike HB(3-Bu^{t}Hpz$_2$)$_3$, HB(3,5-Pr^{i}Hpz$_2$)$_3$ does not enforce tetrahedral coordination geometries on coordinated first row *d*-block metal ions. However, it is apparent that steric interactions occur between the isopropyl groups on the opposing ligands in octahedral cobalt(II) complexes of HB(3-Pr^{i}Hpz)$_3$. This results in a rearrangement to form [Co{HB(3-Pr^{i}Hpz$_2$)$_2$(5-Pr^{i}Hpz$_2$)}$_2$] which is the isomer actually isolated.[13] A similar situation arises with [Mo(NO){HB(Pr^{i}Mepz)$_3$}I_2] in that pseudo-octahedral coordination at the molybdenum atom is tolerated but a facile thermal rearrangement occurs to reduce steric congestion near the large iodide ligands. Replacing iodide by smaller alkoxide ligands such as OMe or OEt might be expected to reduce steric interactions somewhat, while larger alkoxide ligands such as OPr^i or OBu^t might be expected to increase steric congestion.

The reaction between the isomeric mixture of [Mo(NO){HB(Pr^{i}Mepz)$_3$}I_2] and methanol proceeds smoothly over a period of 2 h under reflux. The reaction product was found to be primarily [Mo(NO){HB(Pr^{i}Mepz)$_3$}I(OMe)] contaminated with some [Mo(NO){HB(Pr^{i}Mepz)$_3$}$(OMe)_2$] which could be separated by column chromatography. The ^{1}H NMR spectrum of [Mo(NO){HB(Pr^{i}Mepz)$_3$}I(OMe)] indicated that a mixture of isomers was present and attempts to produce a single isomer by heating the material were unsuccessful. A similar situation was found for the

* The new complexes were characterized by elemental analyses and by IR, mass and ^{1}H NMR (270 MHz) spectroscopy. Some of the compounds could only be obtained as mixtures of isomers as detailed in the discussion.

reaction with EtOH. However, when Pr^iOH or Bu^tOH were used to produce the monoalkoxides $[Mo(NO)\{HB(Pr^iMepz)_3\}I(OR)]$ ($R = Pr^i$, Bu^t) the isomer mixtures which formed initially could be rearranged to a single isomer by heating. Thus the ^1H NMR spectrum of $[Mo(NO)\{HB(Pr^iMepz)_3\}I(OPr^i)]$, for example, contained three resonances of relative area one attributable to the pyrazolyl-4-H protons, three resonances of relative area three attributable to the pyrazolyl methyl protons and eight doublets of relative area three attributable to the isopropyl methyl protons. The effect of placing the sterically bulky group one atom removed from the oxygen was investigated by using the alcohol Me_3SiCH_2OH. In this case a mixture of isomers was obtained which, like the methoxide or ethoxide derivatives, could not be converted to a single isomer on heating.

The reactions between the mixed isomers of $[Mo(NO)\{HB(Pr^iMepz)_3\}I_2]$ and $PhNH_2$ or $4\text{-}MeC_6H_4NH_2$ also afforded products which were mixtures of isomers, but in these cases single isomers were obtained after heating to 70°C for 40 h as revealed by NMR spectral studies. However, the reactions with PhOH and $4\text{-}MeC_6H_4OH$ afforded isomer mixtures which could not be converted to a single isomer by heating. This may reflect the lower steric demands of the oxygen atom as compared to the NH donor group.

The bis-alkoxide complexes $[Mo(NO)\{HB(Pr^iMepz)_3\}(OR)_2]$ (R = Me, Et) could be prepared by the reactions of the respective monoalkoxide mixed isomers with an excess of ROH in the presence of AgOAc. In these cases single isomers were obtained directly. These gave NMR spectra consistent with the presence of a plane of symmetry in the molecule and which contained no additional signals attributable to other isomers.

In conclusion we have found that, with the sterically less demanding ligands, the monoalkoxide complexes $[Mo(NO)\{HB(Pr^iMepz)_3\}I(OR)]$ (R = Me, OEt, CH_2SiMe_3) are isolated as isomeric mixtures which do not rearrange to a single isomer on heating to 70°C for 40 h. In contrast, the more bulky alkoxide ligands OPr^i and OBu^t afford complexes which can be rearranged to single isomers. However, the incorporation of two OMe or OEt ligands in the bis-alkoxide derivatives does lead to the formation of single isomers. There is a difference in behaviour between the aryloxo and arylamido ligands which may reflect steric effects associated with the sizes of the oxygen versus NH donor groups. These systems thus provide novel examples where subtle changes in co-ligand size appear to have a pronounced effect on the relative stability of different isomeric arrangements within the $HB(Pr^iMepz)_3$ ligand. In order to obtain a fully detailed picture of the structural arrangements in these complexes it is necessary to carry out X-ray structural studies of representative compounds. Attempts to obtain suitable crystals and to carry out such studies are in progress.

Acknowledgement—We are grateful to the MEC of Spain, D-4 programme, for support (to M.C.).

REFERENCES

1. (a) S. Trofimenko, *J. Am. Chem. Soc.* 1966, **88**, 1842; (b) S. Trofimenko, *J. Am. Chem. Soc.* 1967, **89**, 3170; (c) S. Trofimenko, *J. Am. Chem. Soc.* 1967, **89**, 6288; (d) S. Trofimenko, *Inorg. Chem.* 1970, **9**, 2493; (e) S. Trofimenko, *Prog. Inorg. Chem.* 1986, **34**, 115; (f) S. Trofimenko, *Chem. Rev.* 1972, **72**, 497.
2. K. Niedenzu and S. Trofimenko, *Top. Curr. Chem.* 1986, **131**, 1.
3. J. A. McCleverty, *Chem. Soc. Rev.* 1982, **12**, 331.
4. G. Ferguson, B. L. Ruhl, F. J. Lalor and M. E. Deane, *J. Organomet. Chem.* 1985, **282**, 75.
5. M. A. J. Moss, C. J. Jones and A. J. Edwards, *J. Chem. Soc., Dalton Trans.* 1989, 1393.
6. C. K. Ghosh and W. A. G. Graham, *J. Am. Chem. Soc.* 1987, **109**, 4726.
7. C. K. Ghosh and W. A. G. Graham, *J. Am. Chem. Soc.* 1989, **111**, 375.
8. N. D. Curtis, K. B. Shiu, W. M. Buller and J. C. Huffmann, *J. Am. Chem. Soc.* 1986, **108**, 3335.
9. S. Trofimenko, J. C. Calabrese and J. S. Thompson, *Inorg. Chem.* 1987, **26**, 1507.
10. W. E. Cleland, K. M. Barnhart, K. Yamanouchi, D. Collison, F. E. Mabbs, R. B. Ortega and J. H. Enemark, *Inorg. Chem.* 1987, **26**, 1017.
11. W. H. Armstrong, A. Spool, G. C. Papaefthymiou, R. B. Frankel and S. J. Lippard, *J. Am. Chem. Soc.* 1984, **106**, 3653.
12. S. J. Reynolds, C. F. Smith, C. J. Jones, J. A. McCleverty, D. C. Blower and J. L. Templeton, *Inorg. Synth.* 1985, **23**, 4.
13. S. Trofimenko, J. C. Calabrese, P. J. Domaille and J. S. Thompson, *Inorg. Chem.* 1989, **28**, 1091.

Polyhedron Vol. 9, No. 4, pp. 623–626, 1990
Printed in Great Britain

0277-5387/90 $3.00+.00
Pergamon Press plc

COMMUNICATION

SYNTHESIS AND STRUCTURES OF TWO ISOMERS OF $[Re_3Ru(S)(C_5H_4N)(C_5H_4NS)_2(CO)_{11}]$ WHICH DIFFER IN THE DISTRIBUTION OF PYRIDINE-2-THIONATO LIGANDS BETWEEN DOUBLY- AND TRIPLY-BRIDGING POSITIONS

ANTONY J. DEEMING,* MANZURUL KARIM and NICHOLAS I. POWELL

Department of Chemistry, University College London, 20 Gordon Street, London WC1H 0AJ, U.K.

and

KENNETH I. HARDCASTLE

Department of Chemistry, California State University Northridge, Northridge, CA 91330, U.S.A.

(*Received* 17 *October* 1989; *accepted* 13 *November* 1989)

Abstract—The pyridine-2-thionato (pyS) bridged compound $[Re_2(pyS)_2(CO)_6]$ reacts with $[Ru_3(CO)_{12}]$ to give various tetranuclear compounds built from $Re(pyS)(CO)_3$ and $Ru(CO)_x$ ($x = 2$, 3 or 4) units: $[ReRu_3(S)(C_5H_4N)(CO)_{14}]$, $[Re_2Ru_2(S)(C_5H_4N)(pyS)(CO)_{13}]$, and $[Re_3Ru(S)(C_5H_4N)(pyS)_2(CO)_{11}]$ as two isomers. X-ray structures of these isomers show that one contains two doubly-bridging pyS ligands and the other one doubly- and one triply-bridging pyS ligands.

The heteroatoms of the pyridine-2-thionato radical (pyS) have potentially seven non-bonding electrons for metal–ligand bonding and by bridging it can make use of three or five of these. However, oxidative addition with C—S bond cleavage would give the strongly bridging sulphur and 2-pyridyl groups which together could donate as many as nine electrons. This high capacity for supplying electrons for metal–ligand bonding and hence to facilitate the aggregation of metal centres is encountered in a reaction we have observed between $[Re_2(pyS)_2(CO)_6]$ and $[Ru_3(CO)_{12}]$.

$[Re_2(CO)_{10}]$ reacts with pyridine-2-thione (pySH) to give high yields of the rhenium dimer $[Re_2(pyS)_2(CO)_6]$ (**1**).[1] Slow scrambling of **1** at room temperature with the 6-methyl substituted analogue $[Re_2(MepyS)_2(CO)_6]$ give an equilibrium involving $[Re_2(pyS)(MepyS)(CO)_6]$ and we argued for the intermediacy of the mononuclear species $[Re(pyS)(CO)_3]$, which may be trapped by various neutral ligands L to give $[Re(pyS)(CO)_3L]$ (L = MeCN, PMe_2Ph etc).[1] Believing that this 16-electron intermediate might react with simple metal carbonyl compounds with electron donation to rhenium and simultaneously from sulphur, we treated **1** with $[Ru_3(CO)_{12}]$ in refluxing *m*-xylene (30 min) to give four products separable by TLC on silica: $[ReRu_3(S)(C_5H_4N)(CO)_{14}]$ (**2**) (32%), $[Re_2Ru_2(S)(C_5H_4N)(pyS)(CO)_{13}]$ (**3**) (31%), and two isomers of $[Re_3Ru(S)(C_5H_4N)(pyS)_2(CO)_{11}]$ (**4**) (9%) and (**5**) (9%). Each compound has been

* Author to whom correspondence should be addressed.

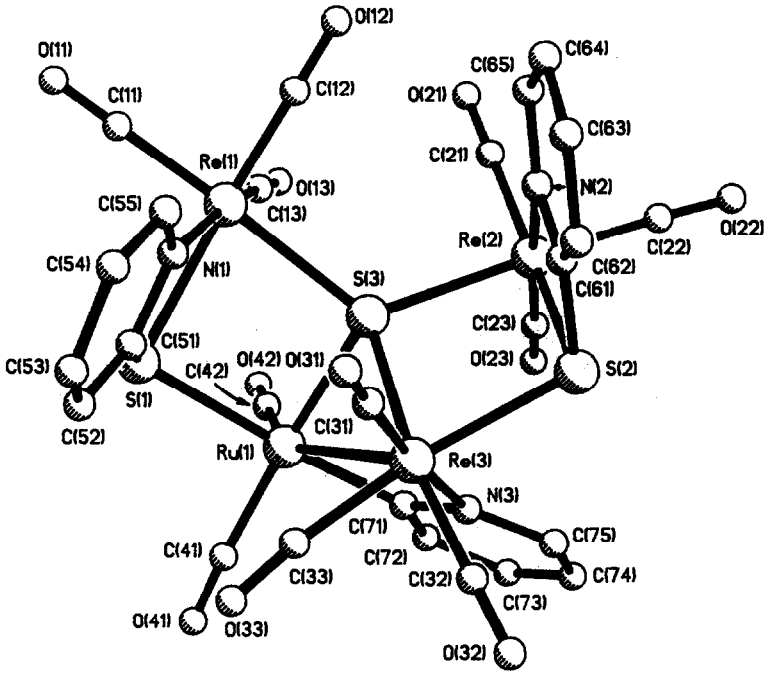

Fig. 1. Molecular structure of $[Re_3Ru(S)(C_5H_4N)(pyS)_2(CO)_{11}]$ (**4**).

Ru(1)—Re(3)	2.902(1)	Re(2)—S(2)	2.576(3)
Ru(1)—S(1)	2.525(4)	Re(2)—S(3)	2.537(3)
Ru(1)—S(3)	2.410(3)	Re(2)—N(2)	2.17(1)
Ru(1)—C(71)	2.03(1)	Re(3)—S(2)	2.500(3)
Re(1)—S(1)	2.545(3)	Re(3)—S(3)	2.480(3)
Re(1)—S(3)	2.532(3)	Re(3)—N(3)	2.19(1) Å
Re(1)—N(1)	2.160(9)		

Ru(1)—S(3)—Re(1)	95.8(1)	Re(1)—S(3)—Re(2)	121.3(1)
Ru(1)—S(3)—Re(2)	131.1(1)	Re(1)—S(3)—Re(3)	132.4(1)
Ru(1)—S(3)—Re(3)	72.8(1)	Re(2)—S(3)—Re(3)	98.4(1)°

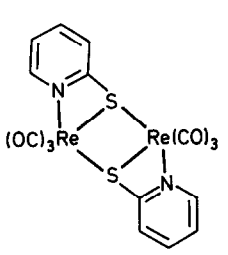

1

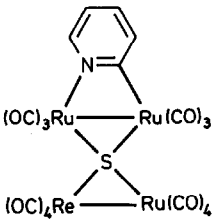

2

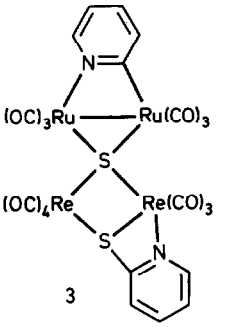

3

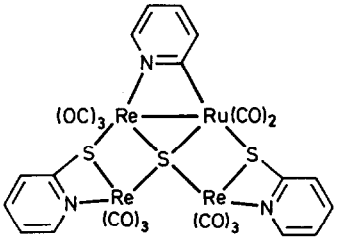

4

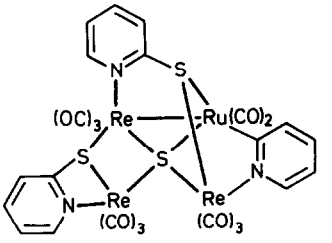

5

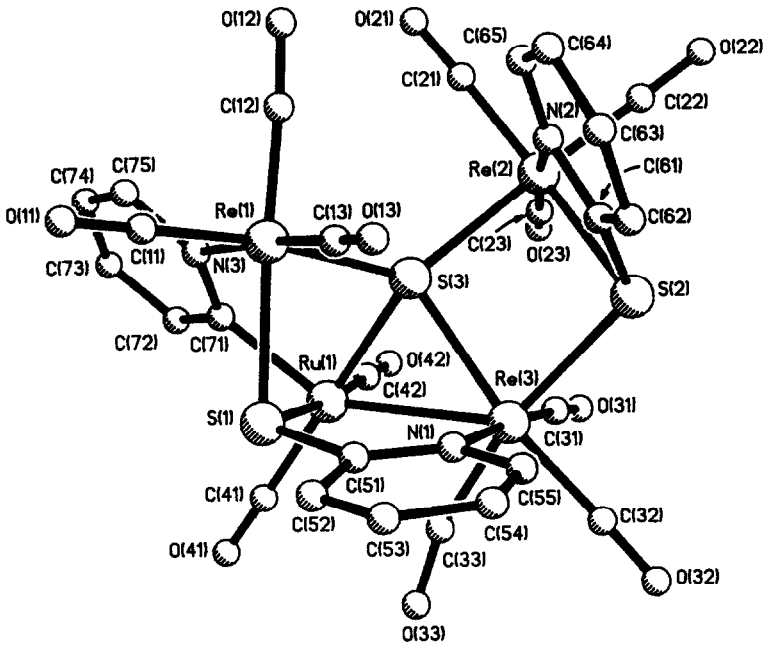

Fig. 2. Molecular structure of $[Re_3Ru(S)(C_5H_4N)(pyS)_2(CO)_{11}]$ (**5**).

Ru(1)—Re(3)	2.884(1)	Re(2)—S(2)	2.610(4)
Ru(1)—S(1)	2.443(4)	Re(2)—S(3)	2.507(3)
Ru(1)—S(3)	2.384(3)	Re(2)—N(2)	2.15(1)
Ru(1)—C(71)	2.05(1)	Re(3)—S(2)	2.528(3)
Re(1)—S(1)	2.517(3)	Re(3)—S(3)	2.490(3)
Re(1)—S(3)	2.502(3)	Re(3)—N(1)	2.22(1) Å
Re(1)—N(3)	2.19(1)		

Ru(1)—S(3)—Re(1)	89.4(1)	Re(1)—S(3)—Re(2)	126.8(1)
Ru(1)—S(3)—Re(2)	139.5(1)	Re(1)—S(3)—Re(3)	123.2(1)
Ru(1)—S(3)—Re(3)	72.5(1)	Re(2)—S(3)—Re(3)	96.6(1)°

characterized by elemental analysis,* by IR and ^{1}H NMR spectra, and by a single-crystal X-ray structure determination.

Flattened representations of **2**–**5** are shown. Each is made up of one, two, or three Re(pyS)(CO)$_3$ units coupled with three, two, or one Ru(CO)$_x$ (x = 2, 3 or 4) units, respectively, and each is electron-precise

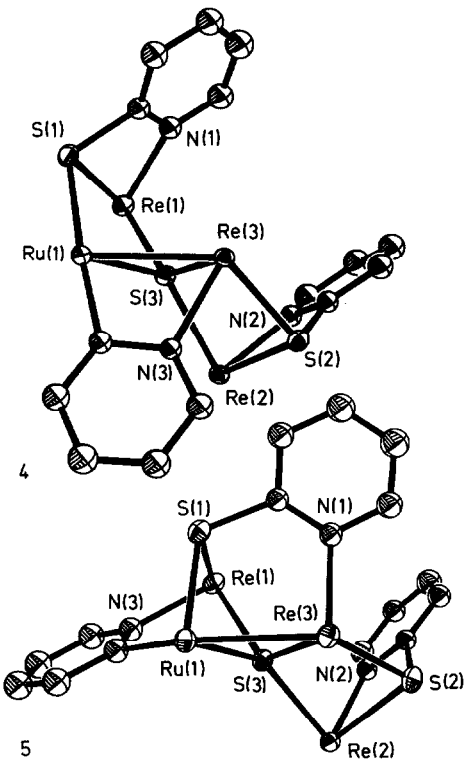

Fig. 3. Comparison of the skeletons of isomers **4** and **5**.

* *Key spectroscopic data*: IR ν(CO) (cm^{-1}) (cyclo-C_6H_{12}): compound **2**, 2112w, 2079s, 2075m, 2046s, 2050vs, 2041w, 2033m, 2015m, 2004s, 2000m, 1993w, 1977m, 1971m, 1947m, 1942m; compound **3**, 2102m, 2076vs, 2046vs, 2027vs, 2011sh, 2006vs, 1994s, 1985m, 1927m, 1954s, 1932s, 1923s; compound **4**, 2146w, 2046vs, 2037w, 2030w, 2021s, 2001s, 1958s, 1918m, 1891m; compound **5**, 2062m, 2030s, 2018sh, 2015vs, 2020m, 1957m, 1934s, 1929m, 1913s, 1904m, 1890w. ^{1}H NMR: compound **2** (CD_2Cl_2) δ 7.85, 7.84 (H^6), 7.35, 7.36 (H^4), 7.25, 7.23 (H^3), 6.95, 6.95 (H^5) (two isomers in solution); compound **3** ($CDCl_3$) δ 8.57, 8.51, 7.80, 7.63 (H^6), 7.59, 7.55, 6.78, 6.76 (H^5), 7.95, 7.95, 7.15, 7.11 (H^4), 7.26, 7.26, 7.22, 7.01 (H^3) (two isomers in solution); compound **4** (CD_2Cl_2) δ 8.89, 8.24, 7.88 (H^6), 7.49, 7.14, 7.05 (H^5), 7.91, 7.64, 7.46 (H^4), 7.58, 7.26, 7.15 (H^3); compound **5** (CD_2Cl_2) δ 8.89, 8.86, 8.51 (H^6), 7.34, 7.11, 6.69 (H^5), 7.62, 7.59, 7.41 (H^4), 7.80, 7.73, 7.16 (H^3).

with two metal–metal bonds in **2** and one each in **3** to **5**. Compounds **4** and **5** are isomers of an interesting and novel type; their X-ray structures (Figs 1 and 2)† are presented here but the structures of **2** and **3** will be reported elsewhere. Each isomer contains the fragments of a pyS ligand formed by C—S bond cleavage: a central four-coordinate sulphur atom linking four metal atoms and a 2-pyridyl ligand bridging a rhenium and a ruthenium atom. The two intact pyS ligands act as five-electron donors. In total the three pyS ligands contribute 19 electrons and with a Re—Ru bond in each (2.902(1) and 2.884(1) Å in **4** and **5**, respectively) and the valence electron count of 70 leads to saturation in each. The isomers differ in the arrangement of the 2-pyridyl and pyS ligands. In **4** the 2-pyridyl ligand bridges a metal–metal bonded edge but in **5** it bridges a non-bonded edge. But the main difference, however, between the isomers is that both pyS ligands are doubly-bridging in **4** as in the parent compound **1**, while in **5** one pyS is doubly-bridging but the other triply-bridges Ru(1), Re(1) and Re(3). Triply-bridging pyS ligands have been found previously. For examples see refs 2 to 4. In spite of these overall geometric differences the metal atoms in each isomer have very similar coordination spheres. Specifying the metal-bonded atoms, both isomers have *fac*-$Re(CO)_3S_2N$ for Re(1) and Re(2), *fac*-$Re(CO)_3NS_2Ru$ for Re(3), and $Ru(CO)_2S_2CRe$ for Ru(1). Figure 3 shows how the cages relate in spite of their overall different shapes and how the μ_4-S atoms are similarly distorted from a tetrahedral geometry. Compound **4** is in principle simply converted into **5** by coordinating N(1) to Re(3) and N(3) to Re(1) instead of the other way round. However, even at high temperatures this conversion does not occur and instead other products are obtained which we are investigating.

These results show that the pyS in mono- or dinuclear complexes can add oxidatively to give strongly bound cages with S and C_5H_4N ligands. Another example is the reaction of $[Ru(pyS)_2(CO)_2]$ with $[Ru_3(CO)_{12}]$ to give $[Ru_5(\mu_4\text{-}S)_2(\mu\text{-}C_5H_4N)_2(CO)_{11}]$ containing a Ru_5S_2 pentagonal bipyramid.[5] We believe this could be a general route from mono- or dinuclear compounds to robust cage compounds.

Acknowledgements—We thank the Association of Commonwealth Universities and the SERC for research studentships (to M.K. and N.I.P., respectively), the SERC and NSF for diffractometer grants, NATO for support for our collaboration, and Johnson–Matthey plc for a loan of ruthenium salts.

REFERENCES

1. A. J. Deeming, M. Karim, P. A. Bates and M. B. Hursthouse, *Polyhedron* 1988, **7**, 1401.
2. L. A. Oro, M. A. Ciriano, F. Viguri, A. Tiripicchio, M. Tiropicchio-Camellini and F. J. Lahoz, *Nouv. J. Chim.* 1986, **10**, 75.
3. A. J. Deeming, M. N. Meah, P. A. Bates and M. B. Hursthouse, *J. Chem. Soc., Dalton Trans.* 1988, 235.
4. A. J. Deeming, M. N. Meah, P. A. Bates and M. B. Hursthouse, *J. Chem. Soc., Dalton Trans.* 1988, 2193.
5. A. J. Deeming, M. Karim and K. I. Hardcastle, unpublished results.

† *Crystal data*: Compound **4**: $[Re_3Ru(S)(C_5H_4N)(pyS)(CO)_{11}]\cdot 0.5CH_2Cl_2$, orange crystal, $C_{26.5}H_{13}ClN_3O_{11}Re_3RuS_3$, $M = 1340.71$, monoclinic, $P2_1/c$, $a = 10.400(1)$, $b = 17.163(4)$, $c = 20.887(6)$ Å, $\beta = 104.32(2)°$, $U = 3613(1)$ Å^3, $Z = 4$, Mo-K_α radiation, $\lambda = 0.71073$ Å, μ(Mo-K_α) = 108.6 cm^{-1}, $F(000) = 2460$. Final R and R_w values 0.0461 and 0.0441 for 5165 absorption-corrected data [$5 \leqslant 2\theta \leqslant 50°$] with $F_o \geqslant 3\sigma(F_o)$.

Compound **5**: $[Re_3Ru(S)(C_5H_4N)(pyS)_2(CO)_{11}]$, yellow crystal, $C_{26}H_{12}N_3O_{11}Re_3RuS_3$, $M = 1298.26$, monoclinic, $P2_1/n$, $a = 10.732(2)$, $b = 16.818(2)$, $c = 18.038(3)$ Å, $\beta = 96.36(1)°$, $U = 3236(1)$ Å^3, $Z = 4$, Mo-K_α radiation, $\lambda = 0.71073$ Å, μ(Mo-K_α) = 120.4 cm^{-1}, $F(000) = 2376$. Final R and R_w values 0.0521 and 0.0523 for 4684 absorption-corrected data [$5 \leqslant 2\theta \leqslant 50°$] with $F_o \geqslant 3\sigma(F_o)$.

Both compounds: Nicolet R3V/m diffractometer, direct methods, all non-hydrogen atoms except in the C_5H_4N rings and CH_2Cl_2 molecules in **4** anisotropic, no hydrogen atoms in the models. The CH_2Cl_2 molecules in **4** did not refine well, with the best model having $0.5CH_2Cl_2$ per complex disordered over three positions.

Atomic coordinates, bond lengths and angles, and thermal parameters have been deposited with the Editor. Coordinates have also been deposited with the Cambridge Crystallographic Data Centre, University Chemical Laboratory, Lensfield Road, Cambridge CB2 1EW, U.K.

Polyhedron Vol. 9, No. 4, p. 627, 1990
Pergamon Press plc. Printed in Great Britain

BOOK REVIEW

Gmelin Handbuch der Anorganischen Chemie : Fe—Organoiron Compounds. Part B13—Mononuclear Compounds 13; 1988 xi+274pp.; ISBN 3-540-93577-0, price not stated.
Part B14—Mononuclear Compounds 14; 1989 xi+239pp.; ISBN 3-540-93578-9; price not stated.
Part B15—Mononuclear Compounds 15; 1989 xii+409pp.; ISBN 3-540-93579-7; price not stated.
Springer; Berlin, Heidelberg, New York, Tokyo.

The "Gmelin" treatment of organoiron compounds falls into three series; series A deals with ferrocene derivatives, series B with mononuclear organoiron compounds, and series C with compounds containing two or more iron atoms.

Earlier volumes in series B, up to B10, covered the compounds with ligands bound via 1–4 carbon atoms; B11 and B12 began the consideration of compounds of C_5 ligands, continued in the three latest volumes.

Volume B13 continues the compounds $(C_5H_5)Fe(CO)_2R$, where R is a substituted alkyl, alkenyl, alkynyl, aryl, or other carbocyclic group. As usual in the Gmelin approach, compounds are considered systematically, with quick-reference tables. Taking $(C_5H_5)Fe(CO)_2COCH_3$ as an example of the utility of the book, one can ascertain from one table its appearance; melting point; IR, UV, Mössbauer, ^1H and ^{13}C NMR spectra, as well as the yields from four alternative preparative methods. One can find out much more about this compound from the five pages of text dedicated to it, including details of its reactions and solubility, as well as critical comment on the spectroscopic data. This approach is particularly useful in view of the propensity of some research workers to omit "basic" information like colour, solubility and melting points of compounds, and is especially useful to researchers wishing to repeat the preparations of "known" compounds. Similarly, when an X-ray structure is available, a diagram giving important bond lengths and angles is provided, as for the fluxional $(\eta^5\text{-}C_5H_5)Fe(CO)_2(\eta'\text{-}C_5H_5)$, discussed in some five pages of text.

Volume B14 completes coverage of the $(C_5H_5)Fe(CO)_2R$ compounds, before passing to the related species with substituted cyclopentadienyls, ending up with anionic and cationic species. The volume contains an empirical formula index for both volumes B13 and B14.

Volume B15 starts by covering compounds of the type $(L_5Fe(CO)_3)^+$. The prototype $[(C_5H_5)Fe(CO)_3]^+$, synthesized by oxidation of $[(C_5H_5)Fe(CO)_2]_2$, has an interesting and well-defined "tripod" structure. Other ligands like C_6H_6 and C_7H_9 form related compounds in which only five of the ring carbon atoms are bound to iron. This very thorough treatment consumes some 260 pages of the volume followed by consideration of those compounds with thiocarbonyl and isocyanide groups. The volume has its own empirical formula index.

For all three volumes, literature coverage is complete to at least the end of 1986, but in fact there are many additional references up to 1988, so that these volumes represent extremely up to date treatment of the primary literature.

"Gmelin" is undoubtedly the first choice as a means of rapid access to *all* the published data on a particular compound or family of compounds. The intelligibility of the distilled data within its pages is excellent, helped by the lucidity of the tabulated material. They are, as always, highly recommended.

SIMON COTTON
Stanground School
Peterborough
Cambridgeshire PE7 3BY, U.K.

Polyhedron Vol. 9, No. 5, pp. 629–638, 1990
Printed in Great Britain

0277–5387/90 $3.00+.00
© 1990 Pergamon Press plc

COMPLEXES OF VITAMIN B_6—XXI.* THE AFFINITY OF THE BINARY COMPLEXES OF THE 2,2′-BIPYRIDYL COPPER(II) SYSTEM TO THE VITAMIN B_6 COMPOUNDS

NADIA M. SHUAIB,† M. S. EL-EZABY† and R. GHODSIAN

Chemistry Department, Faculty of Science, Kuwait University, P.O. Box 5969, 13060 Safat, Kuwait

(*Received* 26 *June* 1989; *accepted* 31 *August* 1989)

Abstract—The interaction of the vitamin B_6 (VB_6) compounds, pyridoxol (P), pyridoxal (PL) and pyridoxamine (PM), with the binary species 2,2′-bipyridyl (BP) of copper(II) has been studied potentiometrically and polarographically at an ionic strength of 0.15 M Cl^-. The potentiometric data at 37°C were assessed by the SUPERQUAD program. The results indicated that BP enhances ternary complex formation with vitamin B_6 compounds, especially with P and PL. The differential pulse polarographic technique further confirmed the formation of ternary species, especially at pHs greater than 5.5. The ternary complex enhancement was discussed in terms of log K_1 (log β_{111i} − log β_{1010} − log β_{011i}) and log K_2 (2 log β_{111i} − log β_{2010} − log β_{0211i}).

VB_6 compounds, P, PL and PM, Fig. 1(a), form various complexes with Cu^{II} of varied stabilities. The order of stability of Cu^{II} with the three ligands for the 1:1 (VB_6–Cu^{II}) species is as follows: CuPM ≫ CuPL > CuP.[1–3] Ternary complexes involving the binary complexes of Cu^{II}–PM with other potential ligands have been investigated.[4–9] Ternary stability enhancement has been shown to occur in these systems. However, ternary systems involving PL and P are rare, although the isolation of a ternary complex involving P, BP[10] and Cu^{II} has been recently reported. On the other hand, BP, Fig. 1(a), forms stable complexes with Cu^{II} in aqueous solution.[11] Ternary complexes involving BP as one of the ligands and other secondary ligands have been the subject of many reports in the last two decades.[12,13] The presence of BP in the Cu^{II} inner sphere usually enhances ternary complex formation.[12] This concept has been tested in this work, especially that the binary complexes of Cu^{II} with PL and P are weak.

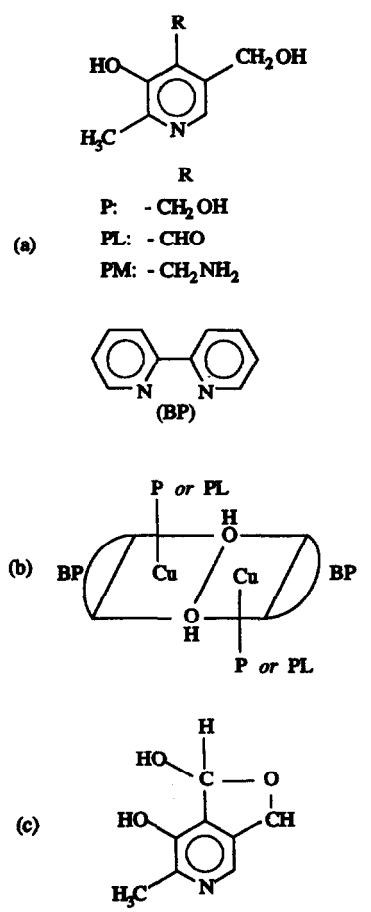

Fig. 1. Structural formulae.

EXPERIMENTAL

Materials

Pyridoxol hydrochloride (P·HCl), pyridoxal hydrochloride (PL·HCl) and pyridoxamine dihydro-

* For Part XX, see ref. 9.

† Authors to whom correspondence should be addressed.

chloride (PM·2HCl) (Merck, > 99%) were analytically pure and used without further purification. Stock solutions of P, PL and PM were 0.10 M. BP (Fluka >99%) was used without further purification. The stock solution of BP was 0.10 M in 0.20 M HCl. The ligands stock solutions were kept in the dark at 4°C to avoid any possible photodecomposition. A stock solution of $CuCl_2$ ($\simeq$0.202 M) was prepared and its concentration was checked by EDTA complexometric titration as previously reported.[2] KCl was used to keep the ionic strength of solutions constant at 0.15 M. Carbonate-free KOH titrant (0.0967 M) was used in the titrations.

Measurements

The potentiometric titrations were carried out as previously reported[3] using an Orion Research Ionalyser type 901 in the pH mode. The ion meter was provided with Orion glass (91–01) and calomel (90–05–00) electrodes. It was calibrated before use with two buffers; Merck buffer at pH 6.96 and Radiometer buffer at pH 4.03. The titrant was delivered by the Radiometer autoburette type ABU12 accurate to ± 0.001 cm^3. The titrations were carried out in a thermostated cell at 37°C under the surge of purified nitrogen. The analytical concentration of the ligands (T_{PM}, T_{PL}, T_P) and the metal (T_{Cu}) were $(1.0–3.0) \times 10^{-3}$ M and that for BP (T_{BP}) was $(1.0–4.0) \times 10^{-3}$ M.

Differential pulse polarograms (DPP) were obtained using Metrohm polarocord 156 provided with a three electrode arrangement, dropping mercury indicator electrode, saturated calomel reference electrode and counter platinum-wire electrode. The settings of the polarographs were as follows: the voltage range was either 0.0 to -0.5 or -0.8 to -1.8 V, the pulse amplitude was -40 mV, the drop time was 1 s, the recorder speed was 0.5 mm s^{-1}. The pH range used was $\simeq$2.00–11.20.

The solution was deoxygenated by passing pure humidified nitrogen through before taking the polarograms. The ionic strength was 0.15 M Cl^-. For the binary system the BP concentration was identical to that of the metal ion, whereas in the case of ternary systems, the BP and Cu^{II} concentrations were 1.0×10^{-3} M and that of PM, PL and P were 2.0×10^{-3} M. The polarograms were taken at room temperature (23 ± 1)°C.

Calculations

The formation constants of the binary species of Cu^{II}–BP and the ternary species of Cu^{II}–BP–L (where L = P or PL or PM) system were determined using the SUPERQUAD program.[14] The procedures used to select the correct equilibrium models were similar to those reported previously.[15] In addition, allowance has been made for errors in pH and titrant volume in the range 0.001–0.005 of a pH unit and volume (cm^3). In most cases, the final equilibrium model was not changed except that sigma decreases drastically as the preselected errors increase. The distribution diagrams of the binary and ternary systems as a function of pH were made by using the SPECN program.[16]

RESULTS AND DISCUSSION

pH-metric study

Table 1 depicts the protonation constants of the ligands used in this work together with the formation constants of their Cu^{II} binary complexes. It is worth mentioning that the binary complex formation of Cu^{II}–P and Cu^{II}–PL cannot be easily studied at a wide pH range as in the Cu^{II}–BP and Cu^{II}–PM systems due to the early precipitation of hydrolysed products. However, the addition of BP stabilizes these systems against precipitation up until a pH of $\sim$10.5. It seems that the electron-withdrawing property of BP enhances ternary complex formation with the vitamin B_6 compounds. Although this is true, it is also dependent on the basicity as well as the denticity of the second incoming ligand. The ternary formation constants are shown in Table 2. The larger values of the formation constant of the 1 : 1 : 1 : 0 and 1 : 1 : 1 : 1 species of BP–PM–Cu^{II}–H than those of BP–P (or PL)–Cu^{II} systems indicate a different mode of ligation of the vitamin B_6 compounds to the BP–Cu^{II} system. One should expect that chelation takes place in the BP–PM–Cu^{II} system rather easier than in the other two systems where monodentate ligation of P or PL to the BP–Cu^{II} system is more favourable. The proton in the 1 : 1 : 1 : 1 species is likely to be located on the pyridinic nitrogen of the vitamin B_6 compounds. The order of basicity of this moiety is still the same as in the free ligand, i.e. PM > P > PL, as shown by the protonation constant of the 1 : 1 : 1 : 0 species (= 7.3, 6.6, 5.9 for PM, P and PL containing ternary systems). However, the monodenticity of PM is shown by the occurrence of 2 : 2 : 1 : i (i = 1, 2, 3 or 4) species if it is assumed that BP will remain unprotonated in the ternary complex formation. Moreover, these species emphasize the hexacoordination nature of Cu^{II}. In addition, the strong chelation property of PM over PL and P overcomes the formation of dimerized ternary species, 2 : 2 : 2 : -2 encountered in the BP–P (or PL)–Cu^{II} systems, Fig. 1(b).

It is interesting to notice that the species exhibited

Table 1. The protonation constants of the ligands used in this work together with their binary formation constants with copper(II). l, p, q, and s are stoichiometric coefficients for $BP_lL_pCu_qH_s$ (L stands for P, PL or PM); $I = 0.15$ M Cl^- and $T = 37°C$

System	Stoichiometry l	p	q	s	Log β ($\pm\sigma$) this work	Reported log β
BP–H	1	0	0	1	4.37 (0.002)	4.49[b]
P–H	0	1	0	1	8.80 (0.003)	
	0	1	0	2	13.67 (0.004)	
PL–H	0	1	0	1	8.45 (0.006)	8.70[c]
	0	1	0	2	12.62 (0.009)	12.90[c]
PM–H	0	1	0	1		10.41,[d] 10.57[c]
	0	1	0	2		18.56,[d] 18.79[c]
	0	1	0	3		22.06,[d] 22.41[c]
BP–Cu^{II}	1	0	1	0		8.00[a]
	2	0	1	0	13.07 (0.02)	13.60[a]
	1	0	1	−1	0.87 (0.04)	
	2	0	2	−2	5.16 (0.02)	
P–Cu^{II}[e]	0	1	1	1		11.60
	0	2	1	2		18.41
PL–Cu^{II}[f]	0	1	1	0		3.51
	0	2	1	0		7.00
PM–Cu^{II}[d]	0	1	1	0		10.81
	0	1	1	1		17.23
	0	1	1	2		21.34
	0	2	1	0		17.47
	0	2	1	1		25.46
	0	2	1	2		32.54
	0	2	1	3		38.91

[a] SUPERQUAD values.
[b] G. Anderegg, *Helv. Chim. Acta* 1963, **46**, 2397; $I = 0.1$ M, $T = 25°C$.
[c] M. S. El-Ezaby and F. R. El-Eziri, *J. Inorg. Nucl. Chem.* 1977, **38**, 1901; $I = 0.5$ M, $T = 25°C$.
[d] M. S. El-Ezaby, M. Rashad and N. M. Moussa, *Polyhedron* 1983, **2**, 245; $I = 0.15$ M, $T = 37°C$.
[e] M. S. El-Ezaby and N. Gayed, *J. Inorg. Nucl. Chem.* 1975, **37**, 1065; $I = 0.5$ M, $T = 25°C$.
[f] E. L. Leussing and N. Huq, *Anal. Chem.* 1966, **38**, 1388; $I = 0.10$ M, $T = 25°C$.

by the BP–P (or PL)–Cu^{II} systems are almost the same with their formation constants close in value. In other words, the presence of the formyl or alcoholic groups in the *ortho* position to the phenoxy group has no effect on the ligation of the P or PL to BP–Cu^{II} binary complexes (if the phenoxy group is assumed to be the ligation site). This finding is true since the formyl group in PL is also thought to add intramolecularly to the alcoholic group to form a hemiacetal,[17] in a wide pH range, Fig. 1(c).

The extent of ternary complex enhancement over binary complex formation for the 1:1:1:0 and 1:1:1:1 may be recognized if one examines the following equilibrium reactions:

$$CuBP + CuPH_i \rightleftharpoons CuBPPH_i + Cu;$$
$$K_1 = \beta_{111i}/\beta_{1010}\beta_{011i} \quad (1)$$
$$Cu(BP)_2 + CuP_2H_i \rightleftharpoons 2CuBPPH_i;$$
$$K_2 = \beta^2_{111i}/\beta_{2010}\beta_{021i} \quad (2)$$

(where $i = 0$, 1 or 2). The charges have been omitted for clarity. Table 3 depicts the values of log K_1 and log K_2 whenever enough information is obtained. Statistically, log K_1 should have a value of −0.6, values markedly greater than this indicate a stabilization of the ternary complex. Actually, positive

Table 2. The ternary formation constants for the system BP–L–Cu^{II}–H (L stands for P, PL or PM)

System	Stoichiometry l	p	q	s	Log β^* ($\pm\sigma$) this work	Remarks S; Xi^2; n;[a] pH range
BP–P–Cu^{II}	1	1	1	0	12.26 (0.07)	1.36; 45; 606; 2.11–8.76
	1	1	1	1	18.84 (0.02)	
	1	2	1	0	16.40 (0.03)	
	1	2	1	1	23.83 (0.05)	
	2	1	1	0	16.29 (0.03)	
	2	2	2	−2	12.07 (0.04)	
BP–PL–Cu^{II}–H	1	1	1	0	12.53 (0.02)	0.97; 72; 465; 2.39–8.57
1st model	1	1	1	1	18.44 (0.05)	
	1	2	1	0	16.03 (0.03)	
	1	2	1	1	22.86 (0.12)	
	2	1	1	0	16.16 (0.03)	
	2	2	2	−2	12.46 (0.04)	
2nd model	1	1	1	0	12.41 (0.02)	1.24; 69; 606; 2.39–8.57
	1	1	1	1	18.01 (0.1)	
	2	1	1	0	16.36 (0.02)	
	1	2	1	0	15.82 (0.03)	
	2	2	2	−2	12.15 (0.04)	
BP–PM–Cu^{II}–H	1	1	1	0	17.27 (0.02)	1.29; 19; 472; 2.07–8.9
	1	1	1	1	24.57 (0.01)	
	2	2	1	1	34.68 (0.1)	
	2	2	1	2	42.21 (0.08)	
	2	2	1	3	49.80 (0.08)	
	2	2	1	4	55.69 (0.04)	

[a] S = sigma in measurements; Xi^2 = Chi square; n = number of titration points.

values mean that the second ligand prefers to bond to the binary complex rather than to the solvated metal ion. On the other hand, values greater than 0.6 for log K_2 suggests the stabilization of the ternary complexes. The value of log K_2 is dependent on the stabilities of the bis complexes and since these bis complexes are not intermediates in the formation of the ternary complexes, the value of log K_2 may not reflect the stability of the mixed complex. However, log K_2 tends to be less dependent than log K_1 on differences in the charges of the ligands involved in the ternary metal complex formation.[18] It seems that ternary enhancement of the 1:1:1:0 species is favoured more by the systems BP–P–Cu^{II} and BP–PL–Cu^{II} than BP–PM–Cu^{II}, as it is shown by the positive values of log K_1 (the system containing P is assumed to behave similar to that containing PL) for the former systems and the negative value of log K_1 for the latter system. However, the disproportionation of the bis binary complexes to form the 1:1:1:0 species is favoured by all of the three systems exemplified by the positive values of log K_2. On the other hand, the ternary enhancement of the 1:1:1:1 species is not favoured in the reaction of the three systems indicated by their negative values of log K_1. However, disproportionation reaction is favoured for all the three systems as shown by the positive values of log K_2.

The ternary enhancement of species other than 1:1:1:0 and 1:1:1:1 may be similarly explained except that the statistical values of log K_i of various equilibrium reactions will be different from log K_1 and log K_2 depending on the geometry of the formed ternary complexes. It is interesting to notice that the ternary species 2:2:1:i (i = 1, 2, 3 or 4) of the PM containing system is not the product of the disproportionation of the binary species 2:0:1:0 and 0:2:1:i (i = 1, 2, 3 or 4) since their log K's have negative values, but rather by the disproportionation of 2:0:1:0 and 0:2:1:0 species, Table 3. Figure 2(a), (b) and (c) shows the distribution diagrams of the various species for the three systems as a function of pH.

Polarographic study

Binary systems. The DPP of a $CuCl_2$ solution at pH ~3.0 shows two cathodic peaks at E_{max} (the potential at maximum differential faradic current

Table 3. Summary of log K_1 and log K_2 for the equilibrium reactions (1) and (2) and other log K_i values

Stoichiometry				Log K_i	BP–P–Cu^{II}	BP–PM–Cu^{II}	BP–PL–Cu^{II}
1	1	1	0	log K_1		1.02	−1.54
1	1	1	0	log K_2		5.00	4.00
1	1	1	1	log K_1	−0.76		−0.66
1	1	1	1	log K_2	6.20		3.54
1	2	1	0	log K_3		+1.03	
				log K_4		+4.00	
1	2	1	1	log K_5	−2.58		
				log K_6	+0.36		
2	1	1	0	log K_7		−0.41	
				log K_8		−0.39	
2	2	2	−2	log K_9		−0.09	
				log K_{10}		+3.33	
2	2	1	1	log K_{11}			4.15

K_3, K_4, K_5, K_6, K_7, K_8, K_9, K_{10} and K_{11} are for the following equilibrium reactions:
$CuBP + Cu(PL)_2 \rightleftharpoons CuBP(PL)_2 + Cu$; $K_3 = \beta_{1210}/\beta_{1010}\beta_{0210}$
$Cu(BP)_2 + Cu(PL)_2 \rightleftharpoons CuBP(PL)_2 + CuBP$; $K_4 = \beta_{1010}\beta_{1210}/\beta_{2010}\beta_{0210}$
$CuBP + CuP_2H_2 \rightleftharpoons CuBPP_2H + Cu + H$; $K_5 = \beta_{1211}/\beta_{1010}\beta_{0212}$
$Cu(BP)_2 + CuP_2H_2 \rightleftharpoons CuBPP_2H + CuBP + H$; $K_6 = \beta_{1211}\beta_{1010}/\beta_{2010}\beta_{0212}$
$Cu(BP)_2 + CuPL \rightleftharpoons Cu(BP)_2PL + Cu$; $K_7 = \beta_{2110}/\beta_{2010}\beta_{0110}$
$Cu(BP)_2 + Cu(PL)_2 \rightleftharpoons Cu(BP)_2PL + CuPL$; $K_8 = \beta_{2110}\beta_{0110}/\beta_{2010}\beta_{0210}$
$Cu_2(BP)_2(OH)_2 + Cu(PL)_2 \rightleftharpoons Cu_2(BP)_2(PL)_2(OH)_2 + Cu$; $K_9 = \beta_{222-2}/\beta_{202-2}\beta_{0210}$
$2CuBPOH + 2CuPL \rightleftharpoons Cu_2(BP)_2(PL)_2(OH)_2 + 2Cu$; $K_{10} = \beta_{222-2}/\beta^2_{101\ \ 1}\beta^2_{0110}$
$Cu(BP)_2 + Cu(PM)_2 + H \rightleftharpoons Cu(BP)_2(PM)_2H + Cu$; $K_{11} = \beta_{2211}/\beta_{2010}\beta_{0211}$
(charges have been omitted for clarity).

(δ_i) of −64 and −220 mV and one anodic at −348 mV, Fig. 3(a). No appreciable change has been found in these peaks until the precipitating pH is reached. The cathodic peaks have been previously rationalized,[19] using direct current polarography, as being due to the stepwise reduction of Cu^{2+} to Cu as a result of the formation of the more stable chloro complex of Cu^{I}. The anodic peak was also interpreted as due to the further oxidation of the cuprous complex to the cupric state.

On the addition of an equimolar concentration of BP to the $CuCl_2$ solution, considerable changes were observed in the DPP in the potential range of 0.0 to −400 mV, Fig. 3(b). The experimental conditions used imposed the formation of the 1 : 1 species and possibly their hydroxy species in the pH range 2.0–11.0. The DPP of the 1 : 1 (Cu^{II}–BP) solution shows two overlapping cathodic peaks in the pH range 2.7–3.4. The differential faradic current (δ_i) decreases as the pH increases. A new cathodic peak arises above pH 3.4. The E_{max} of the peak shifts regularly to a lower potential as the pH increases up until pH ~5.0 with constant δ_i. The peak stays constant in E_{max} and δ_i over a wide pH range (5.0–11.0). Furthermore, the peak at $E_{max} \sim -80$ mV in the pH range 2.7–3.4 shifts suddenly at pH ≃ 6.8 with an increase in δ_i as the pH increases, Fig. 3(b). Figure 4(a) shows the effect of pH on this peak. If one refers to the distribution diagram of Cu^{II}–BP system, Fig. 5, it may be concluded that the first two overlapping peaks mainly correspond to the reduction properties of the chloro species of the $CuBP^{2+}$ complex with some traces of the chloro species of Cu^{2+}. The anodic peak of $CuCl_2$ vanished in the Cu^{II}–BP–Cl system due to the stabilization effect of BP on the Cu^{II} oxidation state, Table 1. However, BP also stabilizes the Cu^{I} oxidation state.[20] One should obtain two anodic peaks, each corresponding to a single electron reduction step. This may explain the presence of two peaks in the DPP in the pH range 2.7–5.0; one at an E_{max} of −80 mV and the other at $E_{max} \simeq -300$ mV. The change in the peak E_{max} from −80 to −184 mV may be attributed to the reduction of the 1 : 1 : −1 and 2 : 2 : −2 (BP–Cu^{II}–OH) species formed at pH ~6.6. The shift in the last peak as the pH increases above 9.4 may correspond to the formation of other species showing slight different reduction properties. The half-height width ($W_{1/2}$)[21] of the peaks at −80, −184 and −220 mV amounts

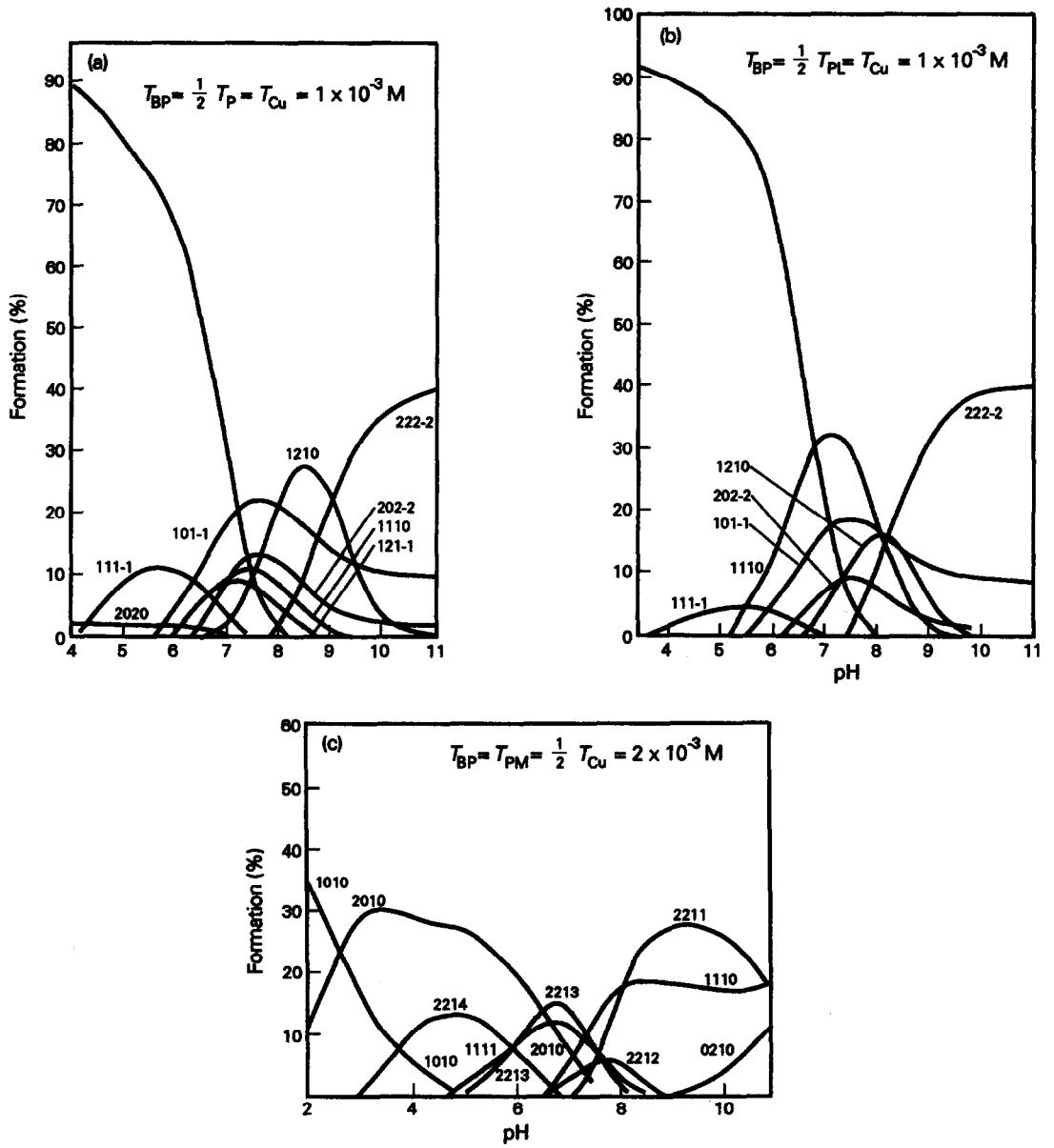

Fig. 2. Distribution diagram of the various species as function of pH. (a) BP–P–Cu^{II}; (b) BP–PL–Cu^{II}; (c) BP–PM–Cu^{II}.

to ~ -84 mV indicating a single electron reduction process.

The DPP's of the P or PL–Cu^{II} system are similar in pattern when the composition ratio of 2 : 1 has been used with one cathodic and one anodic peak, Fig. 3(a), in the pH range 3.0–5.0. At pH's greater than 5 the anodic peak is lost. The cathodic peak has $W_{1/2} \simeq -96$ mV, possibly indicating a single electron step. The DPP's are not affected greatly by variation in the type of the species which may be encountered in solution. This finding emphasizes the weak ligation properties of P and PL to Cu^{II}. On the other hand, the differential pulse polarography of the PM–Cu^{II} system is different from the P or PL–Cu^{II} systems under identical experimental conditions. In the pH range 3.0–4.0 DPP is similar to that of the P or PL–Cu^{II} system exhibiting two peaks, one is cathodic and the other is anodic with approximately the same E_{max}. The anodic peak shifts to more negative potentials as the pH increases from 4.0 to 5.0. However, at pH's greater than 4 the anodic peak is lost and a new cathodic peak appears, Fig. 3(c), which shifts regularly toward more negative potential as the pH increases from 4.0 to 9.0. At pH's above 5.0, a new cathodic peak appears which also shifts regularly to lower potential as the pH increases from 5.0 to 11.0. The first cathodic peak gradually vanishes as the pH

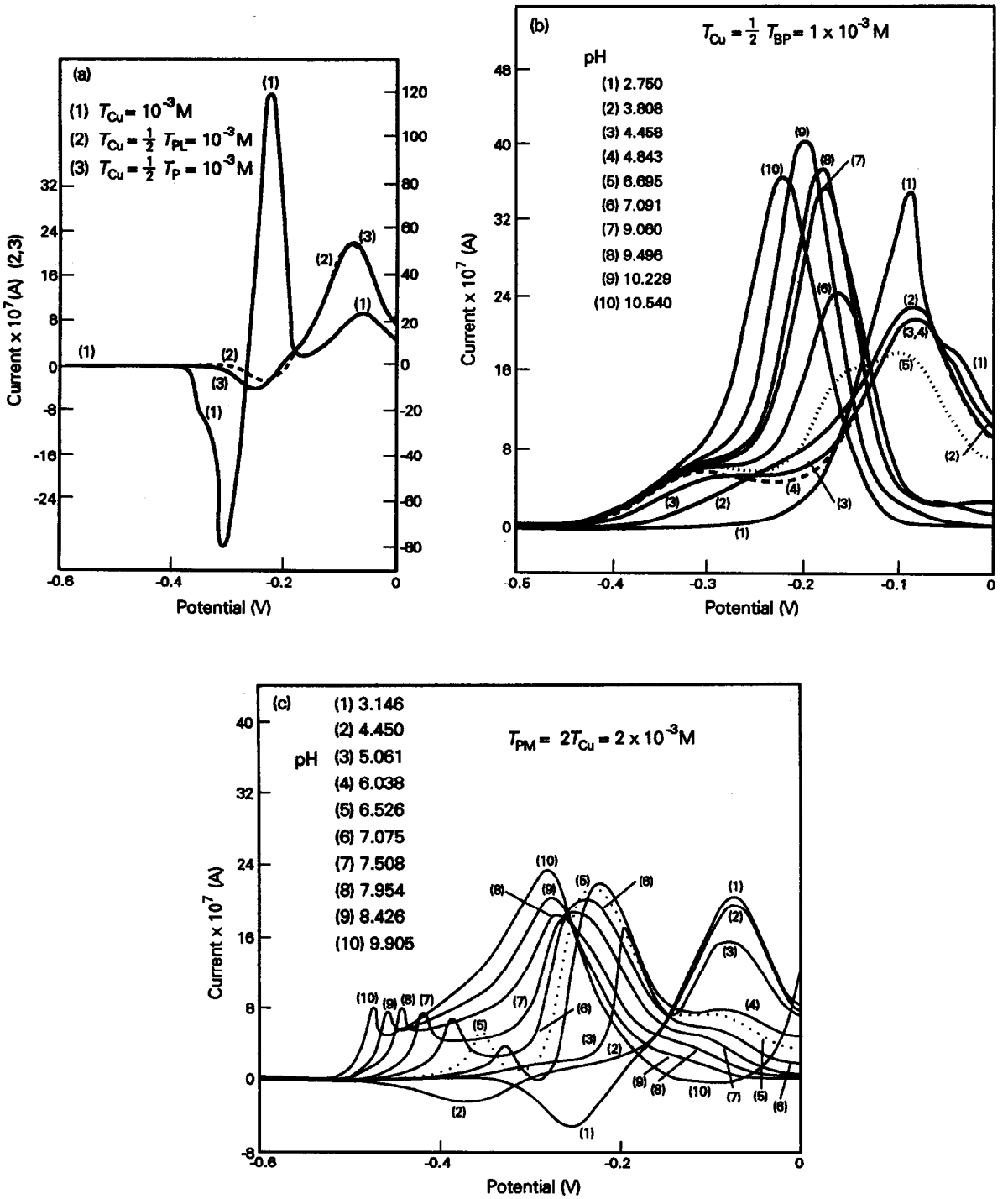

Fig. 3. (a) DPP of $CuCl_2$ solution, Cu^{II}–P and Cu^{II}–PL systems at different pH. (b) DPP of Cu^{II}–BP at various pH. (c) DPP of Cu^{II}–PM at various pH.

increases from 4.0 to 11.0. The first cathodic peak may explain the reduction property of the 1 : 1 : *i* species (*i* = 0, 1 or 2) (PM–Cu^{II}–*i*H) in the pH range 3.0–4.0. However, the 1 : 1 : *i* species (PM–Cu^{I}–*i*H) may be oxidized further to the Cu^{II} species as in the $CuCl_2$ system. The second and third cathodic peaks may correspond to the reduction property of the 2 : 1 : *i* (*i* = 0, 1, 2 or 3) species in the pH range 5.0–11.0. Figure 4(b) shows the effect of pH on the E_{max} of the second and third cathodic peaks. However, the third peak may be due to the reduction of hydrolysed products not detected by potentiometric methods.

Ternary systems. The differential pulse polar-

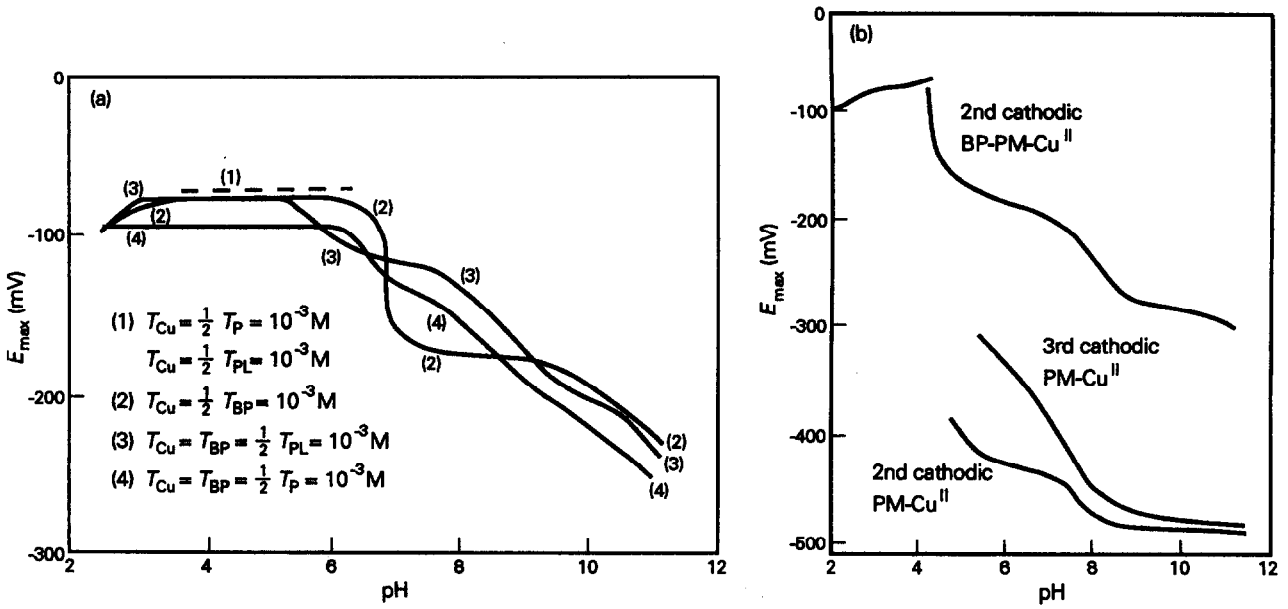

Fig. 4. (a) The DPP E_{max} of BP–Cu^{II}, P–Cu^{II}, PL–Cu^{II}, BP–P–Cu^{II} and BP–PL–Cu^{II} systems. (b) The DPP E_{max} of PM–Cu^{II} and BP–PM–Cu^{II} systems as function of pH.

ography of BP–P or PL or PM–Cu^{II} systems has been taken in the potential range of 0.00 to −2.00 V, Fig. 6(a), (b) and (c). Although the range from 0.9 to −2.00 V was informative and interesting, the presence of the reduction peaks of the ligands complicated the results. The DPP's of the BP–P or PL–Cu^{II} systems are alike except that the E_{max} for the BP–P–Cu^{II} system shifts to more negative potential than the BP–PL–Cu^{II} system, Fig. 4(a). Both systems show different behaviour of E_{max} as a function of pH from the parent binary systems, especially in the pH range 6–11. Figure 4(a) indicates the formation of ternary species of different redox properties. At least two ternary species may be recognized in this pH range. The degree of negativity of E_{max} reflects, somewhat, the stability of the ternary

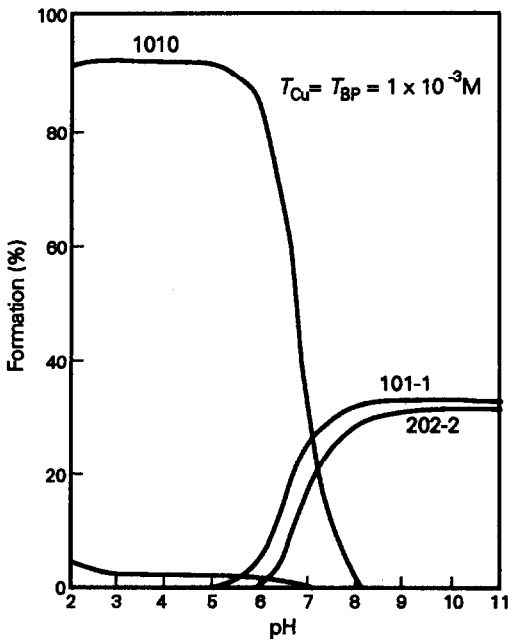

Fig. 5. The distribution diagram of BP–Cu^{II} species as function of pH.

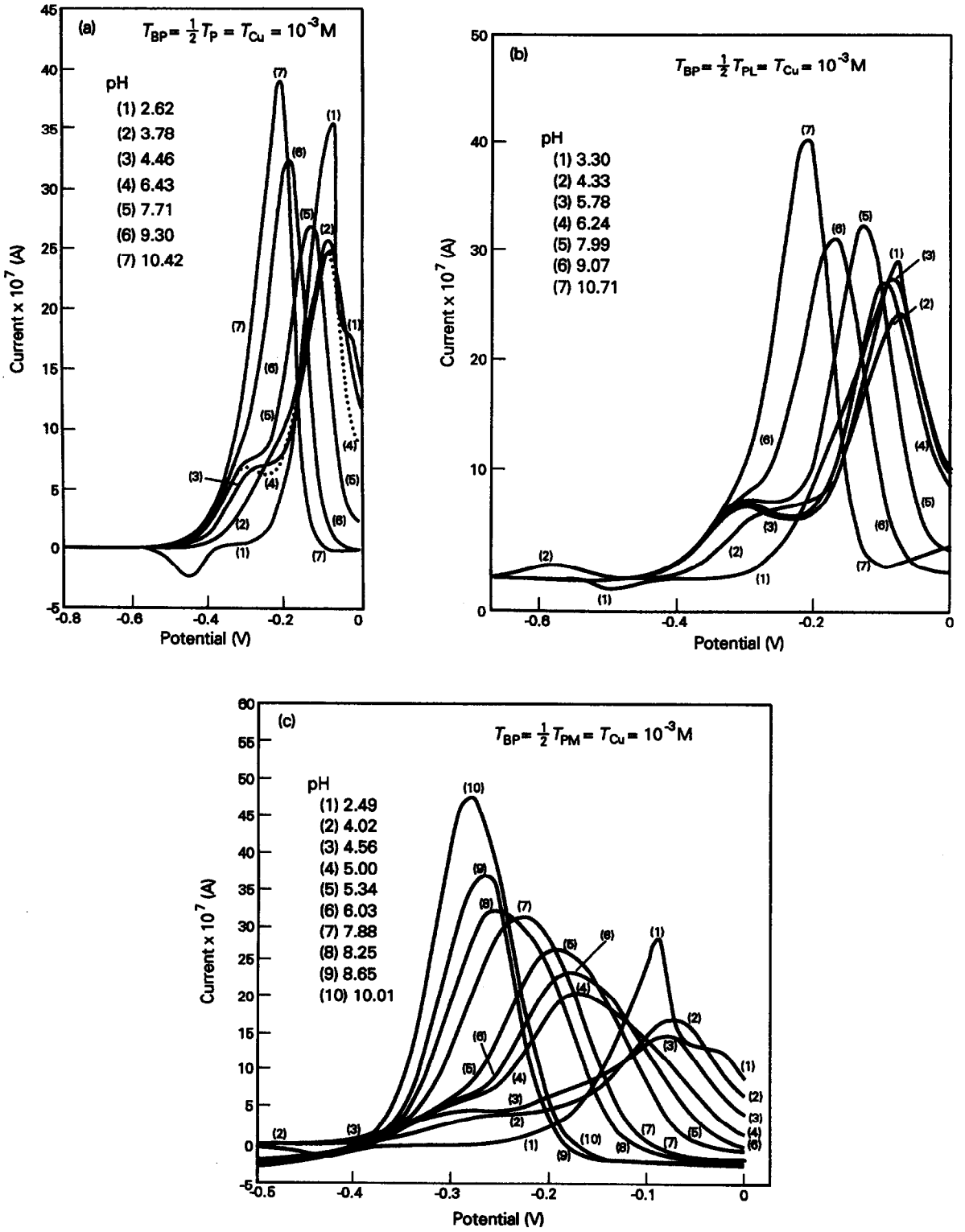

Fig. 6. The DPP of the ternary systems as function of pH. (a) BP–P–Cu^{II}; (b) BP–PL–Cu^{II}; (c) BP–PM–Cu^{II}.

species or the extent of σ and π bonding between the ligands and the metal, being slightly larger in the case of the BP–P–Cu^{II} system.

The DPP of BP–PM–Cu^{II} is different from the former ternary systems and parent binary systems, BP–Cu^{II}, P or PL–Cu^{II} and is characterized by a more negative E_{max}, Fig. 4(b). However, the ternary system still has a less negative E_{max} than that of the binary system PM–Cu^{II}, Fig. 4(b). This may be due to the loss of coplanarity of the ternary complex, assumed to be experienced by the bis complex of PM ($0:2:1:i$), with reduction of electron density on the Cu^{II}, accompanied by facile reduction.

Acknowledgements—The authors would like to thank Kuwait University for the provision of research grant No. SC036 and KFAS for research grant No. 86–07–09. The authors would also like to thank Miss Omniya Al-Hussaini for taking part in the experimental work.

REFERENCES

1. M. S. El-Ezaby and N. Gayed, *J. Inorg. Nucl. Chem.* 1975, **37**, 1065.
2. M. S. El-Ezaby, M. Rashad and N. Moussa, *Polyhedron* 1983, **2**, 245.
3. D. L. Leussing and N. Huq, *Anal. Chem.* 1966, **38**, 1388.
4. H. M. Marafie, M. S. El-Ezaby, B. A. Abd El-Nabey and N. Kitaneh, *Trans. Metal Chem.* 1982, **7**, 227.
5. M. S. El-Ezaby and F. M. Al-Sogair, *Polyhedron* 1982, **1**, 791.
6. N. Al-Awadi, M. S. El-Ezaby and H. M. Abu-Soud, *Inorg. Chim. Acta* 1982, **67**, 131.
7. H. M. Marafie, M. S. El-Ezaby and A. S. Shawalli, *Polyhedron* 1983, **2**, 775.
8. H. M. Marafie, M. S. El-Ezaby, M. Rashad and N. M. Moussa, *Polyhedron* 1984, **3**, 78.
9. H. M. Marafie, M. S. El-Ezaby and S. Fareed, *J. Inorg. Biochem.*, in press.
10. S. P. Sudhakaran Rao, K. I. Varughese and H. Manohar, *Inorg. Chem.* 1986, **25**, 734.
11. G. Anderegg, *Helv. Chim. Acta* 1963, **46**, 2397.
12. R. Griesser and H. Sigel, *Inorg. Chem.* 1971, **10**, 2229.
13. M. Otto, H. Zwanziger and G. Werner, *Inorg. Chim. Acta* 1983, **70**, 41.
14. P. Gans, A. Sabatini and A. Vacca, *J. Chem. Soc., Dalton Trans.* 1985, 1195.
15. M. S. El-Ezaby, N. M. Shuaib, H. M. Marafie and M. M. Hassan, *J. Inorg. Biochem.* 1988, **33**, 161.
16. D. J. Leggett, private communication.
17. E. E. Snell, *Vitam. Horm.* 1958, **16**, 77.
18. H. Sigel, *Angew. Chem.* 1975, **14**, 394.
19. I. M. Kolthoff and J. J. Lingane, *Polarography*, Vol. II. Interscience Publishers, New York (1952).
20. D. D. Perrin, *Stability Constants of Metal-ion Complexes*, Part B: organic ligands. IUPAC, Pergamon Press Inc., New York (1979).
21. A. J. Bard and L. R. Faulkner, *Electrochemical Methods*. John Wiley, New York (1980).

Polyhedron Vol. 9, No. 5, pp. 639–644, 1990
Printed in Great Britain

0277–5387/90 $3.00+.00
© 1990 Pergamon Press plc

OPTICALLY ACTIVE TRANSITION METAL COMPOUNDS, CHIRAL AT THE METAL CENTRE. SYNTHESIS AND STEREOCHEMICAL STUDIES OF THE CHIRAL CYCLOPENTADIENYL IRON COMPLEXES $[Fe(\eta^5\text{-}C_5H_5)\{(S)\text{-Prolophos}\}(CO)]PF_6$*

E. CESAROTTI,† M. GRASSI and L. PRATI

Università di Milano, Dipartimento di Chimica Inorganica e Metallorganica, Via Venezian 21, 20133 Milano, Italy

(*Received* 31 *March* 1989; *accepted* 18 *September* 1989)

Abstract—The reaction between $[Fe(\eta^5\text{-}C_5H_5)(CO)_2Cl]$ and {(S)-Prolophos}, a chiral chelating ligand without a C_2 axis, yields $[Fe(\eta^5\text{-}C_5H_5)\{(S)\text{-Prolophos}\}(CO)]Cl$ spontaneously and quantitatively; the chelation of the ligand forms a pair of diastereoisomers differing only in the iron configuration. Reprecipitation with NH_4PF_6 leads to $[Fe(\eta^5\text{-}C_5H_5)\{(S)\text{-Prolophos}\}(CO)]PF_6$ with 83% diastereoisomeric excess (d.e. %) at the iron chiral centre. One recrystallization is sufficient to give the optically pure iron complex whose absolute configuration has been tentatively assigned as *S*. $[Fe(\eta^5\text{-}C_5H_5)\{(S)\text{-Prolophos}\}(CO)]PF_6$ on UV irradiation in THF splits off the CO ligand to give the highly reactive complex $[Fe(\eta^5\text{-}C_5H_5)\{(S)\text{-Prolophos}\}(THF)]PF_6$; the iron(tetrahydrofuran) complex regenerates the title compound with an overall retention of configuration upon treatment with carbon monoxide.

Optically active organometallic compounds in which the transition element is the centre of chirality have been available since 1969;[1] most of them are cyclopentadienyl and carbonyl complexes optically stable at the metal centre in the solid state. As far as the behaviour in solution is concerned the compounds can be divided into two groups: those which are configurationally stable at the metal centre and those which are configurationally labile, racemizing or epimerizing with respect to the metal atom prior to any reaction. To the former class of compounds belong optically active iron complexes which have been shown to exert powerful stereocontrol in a wide variety of stoichiometric reactions of attached ligands.[2,3] A general application in the strategy of synthesis of optically active molecules requires, however, that the chiral auxiliary organometallic complex should be in an optically pure form. The synthesis of chiral organometallic compounds usually proceeds with very low or even without stereocontrol at the metal centre; this implies that the availability of reasonable amounts of chiral, not racemic, organometallic compounds is still related to classical, long, tedious and sometimes unsuccessful methods to separate the antipodes.

We describe here the synthesis of cyclopentadienyl carbonyl iron complexes of potential utility in which the centre of chirality, the metal, is generated with a high stereoselectivity (d.e. $\geqslant$ 80%) in high chemical yield. A simple recrystallization leads to one optically pure antipode. UV irradiation splits off the carbonyl generating a highly reactive species.

EXPERIMENTAL

General procedures

Solvents were distilled under an inert atmosphere and stored under nitrogen. Elementary analyses were performed by the Microanalytical Laboratory

* {(S) - Prolophos} = (S) - N - diphenylphosphino - 2-(diphenylphosphinoxymethyl)pyrrolidine.

† Author to whom correspondence should be addressed.

of the Dipartimento di Chimica Organica e Industriale, University of Milan. ^1H and ^{31}P NMR were recorded on Varian XL200 and Bruker NS80 spectrometers, whereas circular dichroism (CD) were recorded on a Jobin–Yvon Dichrographe III instrument using CH_2Cl_2 as a solvent and with concentrations of 0.4–0.5 g dm^{-3}. FAB^+ mass spectra were recorded on a VG-7070 Eq mass spectrometer; M^+ is the peak in the parent multiplet which arises from the most abundant iron isotope.

$[Fe(\eta^5\text{-}C_5H_5)(CO)_2Cl]$ and {(S)-Prolophos}[4] were prepared according to previously published methods.

Preparation of $[Fe(\eta^5\text{-}C_5H_5)\{(S)\text{-Prolophos}\}(CO)]PF_6$

3.33 g of $[Fe(\eta^5\text{-}C_5H_5)(CO)_2Cl]$ (15.5 mmol) and 9.6 g of {(S)-Prolophos} (20.5 mmol) were thoroughly mixed in a flask under nitrogen followed by the slow addition of 5 cm^3 of THF. The addition gave rise to an immediate and violent reaction and generated a sticky light brown mass which was dissolved in CH_2Cl_2–MtOH 1 : 1 (30 cm^3) and treated with 2.82 g of solid NH_4PF_6 (17.3 mmol). The suspension was then passed through a short column of Florisil to remove NH_4Cl and the solution was evaporated to dryness giving 10 g of yellow microcrystalline $[Fe(\eta^5\text{-}C_5H_5)\{(S)\text{-Prolophos}\}(CO)]PF_6$ as a 9.2:0.8 mixture of epimers at the iron atom. The diastereoisomeric mixture was dissolved in boiling MtOH (150 cm^3) under nitrogen, and upon standing at 4°C for 24 h the racemic mixture precipitated. The solution was filtered and evaporated giving 6.9 g of optically pure $[CD(-)_{319}Fe(\eta^5\text{-}C_5H_5)\{(S)\text{-Prolophos}\}(CO)]PF_6$; 58% yield based on $[Fe(\eta^5\text{-}C_5H_5)(CO)_2Cl]$. Found: C, 54.6; H, 4.5; N, 1.9. Calc. for $C_{35}H_{34}F_6NO_2P_3Fe$: C, 55.1; H, 4.5; N, 1.8%. M^+(FAB) 618. IR, 1969 cm^{-1}.

Preparation of $[Fe(\eta^5\text{-}C_5H_5)\{(S)\text{-Prolophos}\}(THF)]PF_6$

500 mg of $[CD(-)_{319}Fe(\eta^5\text{-}C_5H_5)\{(S)\text{-Prolophos}\}(CO)]PF_6$, dissolved in THF (200 cm^3), were placed in a Pyrex Schlenk vessel, degassed with argon for 15 min and irradiated with a Phillips high-pressure Mercury 125-W lamp until the carbonyl band disappeared (6 h). The solution was then evaporated to give a brown residue which was washed with petroleum ether and dried again; the yield is almost quantitative. Found: C, 54.9; H, 5.1; N, 1.6. Calc. for $C_{38}H_{42}F_6NO_2P_3Fe$: C, 56.5; H, 5.2; N, 1.7%. (FAB) $M^+(-THF)$ 590.

RESULTS AND DISCUSSION

In the cyclopentadienyl iron complex $[Fe(\eta^5\text{-}C_5H_5)(CO)_2Cl]$ the two carbonyls are in an enantiomeric relationship; the substitution of one CO with a ligand L gives two enantiomers differing only in the configuration at the metal (Fig. 1, reaction 1). The same result can be obtained when both carbonyls are replaced with a chelating ligand lacking a C_2 axis (Fig. 1, reaction 2).

If the chelating ligand, together with the absence of a C_2 axis, has one or more chiral but not racemic centres, the substitution gives rise to a couple of diastereoisomers which may be resolved into pure enantiomers (with respect to the metal atom).

{(S)-Prolophos}, because it is easily obtainable from the natural (S)-Prolinol in high yield,[4] has a centre of chirality and lacks a C_2 axis. {(S)-Prolophos} reacts immediately and quantitatively with $[Fe(\eta^5\text{-}C_5H_5)(CO)_2Cl]$ (Fig. 2, reaction i) expelling the chloride ion and one carbonyl to give $[Fe(\eta^5\text{-}C_5H_5)\{(S)\text{-Prolophos}\}(CO)]Cl$ as a pale yellow amorphous compound. The treatment of the chloro iron complex with NH_4PF_6 gives the yellow cyclopentadienyl iron complex $[Fe(\eta^5\text{-}C_5H_5)\{(S)\text{-Prolophos}\}(CO)]PF_6$, as a mixture of diastereoisomers **3** and **3′** which differ only in the chirality of the metal atom (Fig. 2, reaction ii).

The complexity of the ligand makes the ^1H NMR spectrum of the mixture rather complicated and not diagnostic for the stereochemistry of the reaction; by contrast the ^{31}P NMR spectrum is extremely useful in determining the stereoselectivity. The ^{31}P NMR spectrum of the ligand {(S)-Prolophos} shows two singlets at δ 113.7 and 46.7 ppm ($CDCl_3$, H_3PO_4 internal standard) assigned, respectively, to the phosphito and aminophosphine groups.[5] Upon coordination the two signals are shifted downfield to around δ 170 ppm for PO and δ 110 ppm for PN. The ^{31}P NMR of the diastereoisomeric mixture, **3**

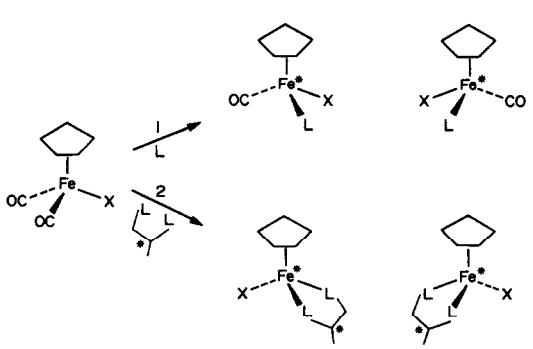

Fig. 1.

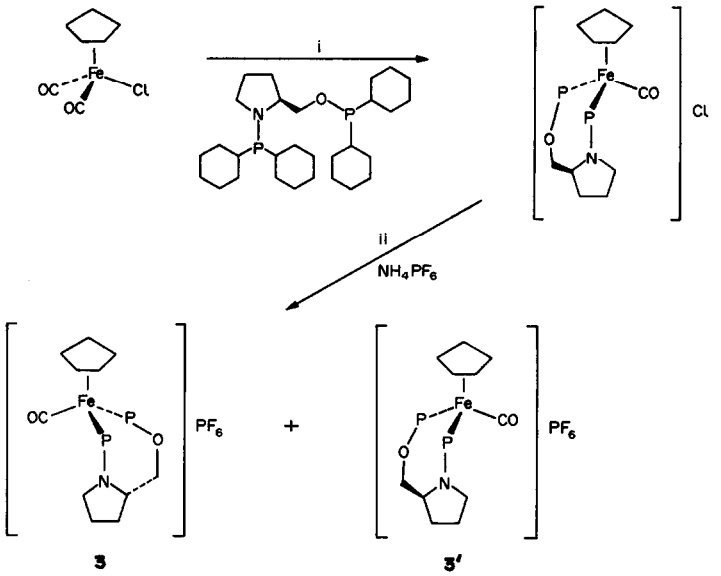

Fig. 2.

and 3', shows only two major doublets at δ 168.2 and 109.6 ppm (J_{PO-PN}, 78.2 Hz) and two doublets of lower intensity at δ 177.2 and 119.0 ppm (J_{PO-PN}, 68.4 Hz) in a 9.2:0.8 ratio, thus indicating that the reaction is chemically quantitative and proceeds with a high diastereoselectivity, close to 83% d.e. (Fig. 3).

A simple recrystallization from methanol gives the more abundant diastereoisomer optically pure; ^{31}P NMR shows the almost complete absence of the two doublets at δ 177.2 and 119.0 ppm. The chemical yield is close to 60% (based on the [Fe(η^5-C_5H_5)$(CO)_2$Cl] loaded). The assignment of the configuration of the metal, usually performed by X-ray crystallographic determination, is not possible as the optically pure diastereoisomer has always been

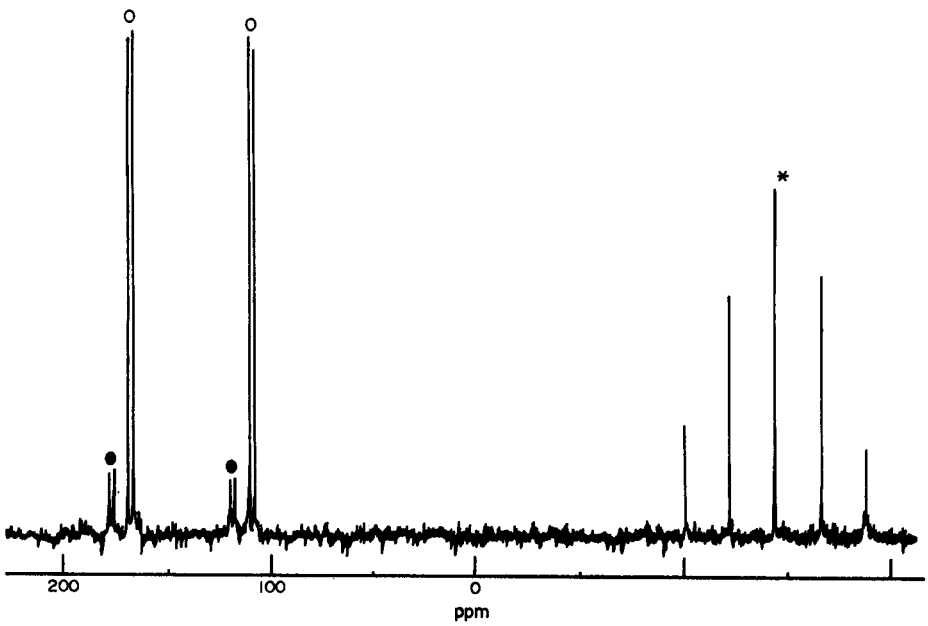

Fig. 3. ^{31}P NMR spectrum of diastereoisomeric [Fe(η^5-C_5H_5){(S)-Prolophos}(CO)]PF_6; the open circles represent the major diastereoisomer, the solid circles the minor one, the asterisk indicates the counter ion PF_6^-.

obtained as disordered microcrystals; however, we think it is possible to infer the configuration at the metal by correlation of the CD spectra to those of known compounds.

CD spectra of the pure diastereoisomer and of the racemic mixture are recorded in solution and in the solid state (KBr pellets). To normalize the data with respect to both concentration and the optical path, the spectra in Fig. 4(a) and (b) are plotted as $\Delta A/A$(415 nm) where A(415 nm) is the UV absorbance of the solution and of the KBr pellet at 415 nm; a clear analogy between the sign and relative intensities is evident for both the pure diastereoisomer and for the racemic mixture. While the chiral ligand does not show any CD active transition between 300 and 500 nm, the optically pure [Fe(η^5-C_5H_5){(S)-Prolophos}(CO)]PF_6 shows two negative maxima of the same sign and intensity, respectively, at 319 and 415 nm [Fig. 4(a)]. The racemic mixture shows only one negative CD maximum at 415 nm [Fig. 4(b)].

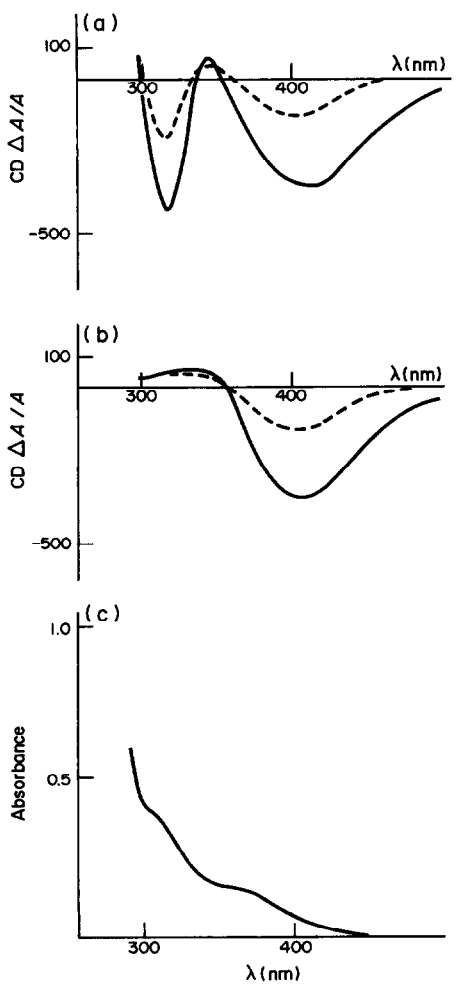

Fig. 4. (a) CD spectra of the optically pure [Fe(η^5-C_5H_5){(S)-Prolophos}(CO)]PF_6 complex in solution (continuous line) and in the solid state (dashed line). (b) CD spectra of the racemic [Fe(η^5-C_5H_5){(S)-Prolophos}(CO)]PF_6 complex in solution (continuous line) and in the solid state (dashed line). (c) UV spectra of the [Fe(η^5-C_5H_5){(S)-Prolophos}(CO)]PF_6 complex in solution.

The complexes [Pd{(S)-Prolophos}Cl_2],[6] [Pt{(S)-Prolophos}Cl_2],[6] [Rh{(S)-Prolophos}(COD)]$^+$ BF_4^- [5] show the same negative CD absorption in the 400–450 nm region. In these complexes the only element of dissymmetry is the chiral centre on the ligand; therefore, by analogy with the negative transitions mentioned above it is possible to assign the 415 nm negative band in the pure diastereoisomer, as well as in the racemic mixture, to a transition mainly due to the chelated diphosphine, its negative band arising from the particular conformation of the metal–{(S)-Prolophos} chelated ring. The transition at 319 nm is very intense in the optically pure [Fe(η^5-C_5H_5){(S)-Prolophos}(CO)]PF_6 whilst almost absent in the racemic mixture. Assignments of the bands in the spectra of pseudo-tetrahedral molecules appear to be very uncertain, but these transitions are thought to be a mixture of *d–d* and metal-to-cyclopentadienyl ligand charge-transfer types.[7] If one accepts that the transition at 319 nm is essentially a Fe–C_5H_5 charge-transfer, it seems logical that this transition should be CD active and intense in the optically pure [Fe(η^5-C_5H_5){(S)-Prolophos}(CO)]PF_6, but almost absent in the racemic mixture because it reflects the intrinsic chirality of the metal atom. This implies that such a transition can be considered diagnostic to assign the absolute configuration in cyclopentadienyl–iron complexes, as it is for cyclopentadienyl–ruthenium compounds.[8]

The X-ray crystallographic determination of the structure of the complexes [(η^5-C_5H_5)Ru{(S)-Prolophos}Cl],[8] [Rh{(S)-Prolophos}(COD)]BF_4,[5] [(η^3-C_4H_7)Pd{(S)-Prolophos}]PF_6[9] and [Pt{(S)-Prolophos}Cl_2][6] clearly shows that the conformation of the chelating ligand in the solid state is almost the same whatever the metal and the formula of the complex. This is almost certainly due to the presence of the rigid five-membered pyrrolidine ring fused with the seven-membered ring, generated by chelation.

In [Fe(η^5-C_5H_5){(S)-Prolophos}(CO)]PF_6, independent of the conformation of the chelating ligand in solution, the comparison between the spectra in solution with that in the solid state supports not only that one conformation prevails but also that the conformations are the same; we can conclude, therefore, that it is very probable, even if not proved, that the conformation of the chiral ligand

in the optically pure [Fe(η^5-C_5H_5){(S)-Prolophos}(CO)]PF_6 is the same as that found in the complexes mentioned above.

As an example, Fig. 5 shows the conformation of the chelating ligand determined from the X-ray structures of known complexes with {(S)-Prolophos} and from CPK models. The upper and lower faces of the plane defined by P(O)—M—P(N) atoms are diastereotopic and present a rather general feature: the P(O)—M—P(N) plane bisects the PPh_2—P(O) arm of the ligand disposing the phenyl groups under and above the plane by approximately the same angle; contrary to this, the phenyl rings of the PPh_2—P(N) plane assume an axial and equatorial disposition with the axial phenyl group pointing away from the metal. This implies that in the [Fe(η^5-C_5H_5){(S)-Prolophos}(CO)]PF_6 complex the bulky cyclopentadienyl group may be better located in the upper cavity and the CO group in the lower one. Assuming, operationally that η-$^5C_5H_5$ is a single group, it is possible to refer to [Fe(η^5-C_5H_5){(S)-Prolophos}(CO)]PF_6 as a pseudo-tetrahedral complex and extend to it the Cahn–Ingold–Prelog notation, the priority sequence being: η^5-C_5H_5 > PO > PN > CO.

^{31}P NMR spectroscopy, a defined conformation of the chelating ligand based on a comparison of the CD spectra in solid and in solution with those of different compounds of known structure and the inspection of CPK models led us to conclude that the more probable configuration of the iron atom in the major diastereoisomer **3** is *S*

The configurational stability of [Fe(η^5-C_5H_5){(S)-Prolophos}(CO)]PF_6 is reflected in its lack of reactivity; if the aim is to make available a chiral and stable organometallic reagent, it is necessary to overcome this inertness by transforming the cyclopentadienyl iron complex into a more reactive compound.

Irradiation of optically pure [Fe(η^5-C_5H_5){(S)-Prolophos}(CO)]PF_6 (**3**) in THF leads quantitatively to the replacement of the CO ligand by a tetrahydrofuran molecule. The reaction is rather slow but is easily monitored by IR spectroscopy. The [Fe(η^5-C_5H_5){(S)-Prolophos}(THF)]PF_6 complex has been fully characterized. Elemental analyses and FAB$^+$ MS gave satisfactory results, and ^{1}H NMR clearly shows the coordination of one THF.

^{31}P NMR recorded at room temperature does not give any signal, but on decreasing the temperature to −50°C a complicated pattern of at least five broad triplets appears. Bubbling CO into a solution of [Fe(η^5-C_5H_5){(S)-Prolophos}(THF)]PF_6 immediately and quantitatively regenerates the [Fe(η^5-C_5H_5){(S)-Prolophos}(CO)]PF_6 complex as a mixture of **3** and **3′**; ^{31}P NMR indicates a 62% diastereoisomeric excess, the major diastereoisomer being that obtained in the synthesis of **3** and **3′** from [Fe(η^5-C_5H_5)$(CO)_2$Cl] and {(S)-Prolophos} [two doublets at δ 168.2 and 109.6 ppm ($J_{PO—PN}$, 78.2 Hz) and two doublets at δ 177.2 and 119.0 ppm ($J_{PO—PN}$, 68.4 Hz; 8:2 ratio)].

It is undeniable that the activation process of [Fe(η^5-C_5H_5){(S)-Prolophos}(CO)]$^+$ by photocatalysed expulsion of the CO ligand proceeds with a certain loss of steric control, but it appears proven that the entire sequence

$$[CpFe(L—L)(CO)]^+ \xrightarrow{h\nu/THF}$$

$$[CpFe(L—L)(THF)]^+ \xrightarrow{+CO} [CpFe(L—L)(CO)]^+$$

proceeds with partial retention of configuration at the metal atom. Surprisingly when the racemic mixture of [Fe(η^5-C_5H_5){(S)-Prolophos}(CO)]PF_6 is subjected to the same procedure, irradiation in THF followed by CO addition, the final product [Fe(η^5-C_5H_5){(S)-Prolophos}(CO)]PF_6 is regenerated with a 42% diastereoisomeric excess, also in this case the major diastereoisomer (two doublets at δ 168.2 and 109.6 ppm ($J_{PO—PN}$, 78.2 Hz; 7:3 ratio) is that obtained in the direct synthesis of the title compound.

Scheme 1 summarizes the results: the expulsion of the CO ligand gives rise to the 16-electron diastereoisomeric species **4** and **4′** (*vide infra*), which are in fast equilibrium between themselves and the THF-containing complexes **5** and **5′**. This fast exchange is evidenced by the broad signals in the low temperature ^{31}P NMR. The incoming ligand (CO in the present case) reacts rapidly with the coordinatively unsaturated species **4** and **4′** and regenerates **3** and **3′**.

The assumption that the 16-electron complexes **4** and **4′** could exist as a couple of diastereoisomers is suggested by theoretical studies of the dynamic

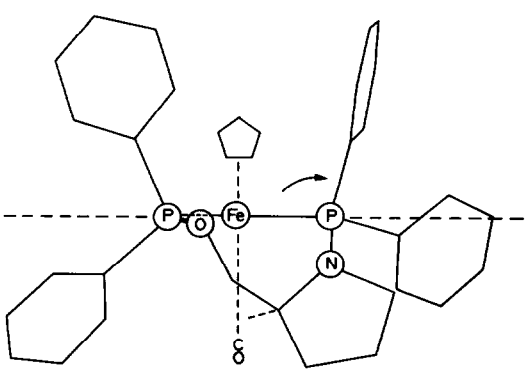

Fig. 5.

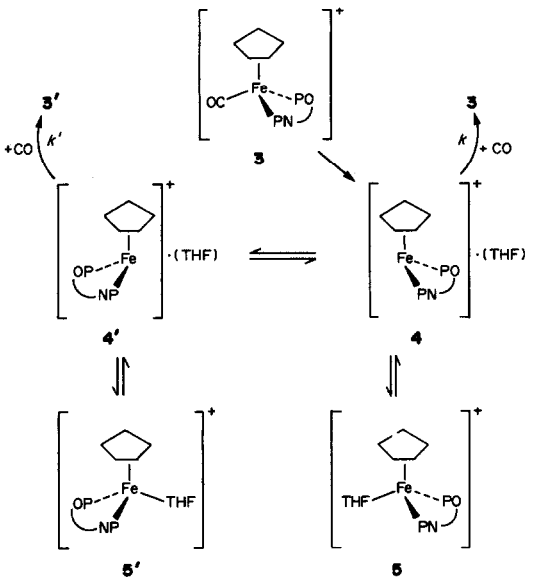

Scheme 1.

behaviour of the 16-electron intermediates $CpML_1L_2$, which concluded that such intermediates can retain a "pyramidal" geometry instead of a "planar" one and may indeed be configurationally stable depending upon the metal and the nature of the ligands L_1 and L_2.[10]

In the present work it is still a matter of speculation if the observed stereoselectivities in the exchange reaction depend on thermodynamic or kinetic effects, i.e. different equilibrium concentrations between **4** and **4'** or a different rate of reaction of **4** and **4'** with the incoming ligand.

Work is currently in progress to elucidate this latter question, as well as studying the reaction with other ligands, particularly with prochiral olefins.

Acknowledgements—Financial support from "Centro CNR per la Sintesi e la Struttura dei Metalli di Transizione nei bassi Stati di Ossidazione" is greatefully acknowledged. We wish to thank Dr A. Pasini for helpful discussions.

REFERENCES

1. H. Brunner, *Accts Chem. Res.* 1979, **12**, 250; S. G. Davies, I. M. Dordor Hedgecock, K. H. Sutton and M. Whittaker, *J. Am. Chem. Soc.* 1987, **109**, 5711.
2. S. G. Davies, I. M. Dordor Hedgecock, K. H. Sutton and J. C. Walker, *Tetrahedron* 1986, **42**, 5123; L. S. Liebeskind, M. E. Welker and R. W. Fengl, *J. Am. Chem. Soc.* 1986, **108**, 6328.
3. H. Brunner, B. Hammer, M. Brookhart, D. Timmers, J. R. Tucher, G. D. Williams and G. R. Husk, *J. Am. Chem. Soc.* 1983, **105**, 6721.
4. E. Cesarotti, A. Chiesa and G. D'Alfonso, *Tetrahedron Lett.* 1982, **23**, 2995.
5. E. Cesarotti, A. Chiesa, G. Ciana and A. Sironi, *J. Organomet. Chem.* 1983, **251**, 79.
6. Unpublished results, manuscript in preparation.
7. C. K. Chou, D. L. Miles, R. Bau and T. C. Flood, *J. Am. Chem. Soc.* 1978, **100**, 7271 and refs therein.
8. E. Cesarotti, L. Prati, A. Sironi, G. Ciani and C. White, *J. Chem. Soc., Dalton Trans.* 1987, 1149.
9. E. Cesarotti, L. Prati, M. Grassi and F. Demartin, *J. Organomet. Chem.* 1989, **370**, 407.
10. P. Hofmann, *Angew. Chem. Int. Edn Engl.* 1977, **16**, 1536.

Polyhedron Vol. 9, No. 5, pp. 645–651, 1990
Printed in Great Britain

0277-5387/90 $3.00+.00
© 1990 Pergamon Press plc

APPLICATION OF THE MOLYBDENUM(IV) HYDRIDE COMPLEXES IN CYCLOHEXANE SOLUTIONS TO THE RADIATION-CATALYTIC REDUCTION OF MOLECULAR NITROGEN

J. O. DZIĘGIELEWSKI*

Department of Inorganic and Radiation Chemistry, Institute of Chemistry, Silesian University, Katowice, Szkolna 9 Street, Poland

and

R. GRZYBEK

Department of Chemistry, Institute of Chemistry, Silesian University, Katowice, Poland

(*Received* 14 *February* 1989; *accepted* 18 *September* 1989)

Abstract—The two molybdenum(IV) hydride complexes $[MoH_4(dppe)_2]$ [dppe = $(C_6H_5)_2PCH_2CH_2P(C_6H_5)_2$] and $[MoH_4(dtpe)_2]$ [dtpe = $(o\text{-}CH_3C_6H_4)_2PCH_2CH_2P(o\text{-}CH_3C_6H_4)_2$] were applied in a process of radiation-catalytic reduction of molecular nitrogen. The yields of ammonia and hydrazine were determined for different concentrations of these complexes in cyclohexane solutions. The mechanism of the reduction of molecular nitrogen by γ-radiation is suggested. It has also been discovered that the $[MoH_4(LL)_2]$ complexes are useful in the process of radiation-catalytic fixation and reduction of nitrogen.

In a previous paper[1] we described a new route to the reduction of molecular nitrogen using the $[MoOCl(dppe)_2]Cl$ complex by γ-radiation. In this paper, intermediate and final products of reduction of N_2 were defined and the mechanism of this process was put forward. In another paper[2] the radiation yields of ammonia in the process, when the gaseous N_2 was passed through the irradiated solutions, were determined. The determined yields of the reduction of N_2[2] ($G_{(NH_4)_2SO_4} = 348$ molecules per 100 eV in a solution of $[MoOCl(dppe)_2]Cl$ of concentration 10^{-1} mol dm^{-3}) supports the conclusion that the process of fixation and reduction of N_2 appears to be a chain reaction. However, the fixation and reduction of N_2 using the $[MoOCl(dppe)_2]Cl$ complex proceeds by a multistep reaction:

(1) reduction of the molybdenum(IV) complex to molybdenum(0);
(2) modification of the coordination sphere and formation of the dinitrogen complex;
(3) reduction of the coordinated nitrogen into hydrazide, hydrazine and finally ammonia;
(4) oxidation of molybdenum(0) to molybdenum(IV) with replacement of the initial coordination sphere.

The purpose of this work is to simplify this process using the molybdenum(IV) hydride complexes $[MoH_4(dppe)_2]$ and $[MoH_4(dtpe)_2]$ instead of $[MoOCl(dppe)_2]Cl$. We used dtpe in order to obtain a complex which is more soluble in cyclohexane. It is well known that in solutions of certain transition metal complexes the following equilibrium occurs: $[MH_4L_4]+N_2 \rightleftharpoons [M(N_2)_2L_4]+2H_2$.[3,4] The complex $[MoH_4(dppe)_2]$ was obtained as a result of passing gaseous H_2 through a $[Mo(N_2)_2(dppe)_2]$ solution.[5] The $[Mo(N_2)_2(dppe)_2]$ complex was obtained in a similar way from the $[MoH_4(dppe)_2]$ solution which was irradiated with UV while simultaneously passing gaseous N_2 through the solution.[6] Therefore, it is expected that under γ-radiation either nitrogen will much more effectively displace hydrogen ions from the coordination sphere or N_2 molecules will fill the released coor-

* Author to whom correspondence should be addressed.

dination places in the process of molybdenum(IV) reduction. Thus, the process of N_2 fixation and reduction can be simplified. It was assumed that application of the molybdenum(IV) hydride complex would lead to higher H_4N_2 and H_3N yields. Some hydride metal complexes were used earlier by Japanese scientists[7] for reduction of coordinated nitrogen. The complexes that they successfully applied either contained positive or negative charges on the hydrogen atoms. Thus, it can be expected that H^- ions will reduce the Mo=N—NH^+ moieties (and others) under γ-radiation. Consequently, the hydrogen atoms generated by γ-radiation from H^- ions will reduce coordinated nitrogen. Cyclohexane was used as a solvent because hydride complexes are soluble in it without decomposition and, moreover, cyclohexane gives a considerably high yield of hydrogen atoms and e_s^-, necessary for the reduction of the molybdenum(IV) atoms, and cations which are the H^+ ion donors for the Mo—N=N moiety.

EXPERIMENTAL

Dppe was synthesized by the standard method from lithium phosphide and 1,2-dichloroethane. Dtpe was synthesized by the same method from lithium phoshide using $P(o\text{-}CH_3C_6H_4)_3$[8] instead of triphenylphosphine. The complexes $[MoH_4(dppe)_2]$, $[MoH_4(dtpe)_2]$, and $[Mo(N_2)_2(dppe)_2]$ were synthesized in a one-step reaction by reducing the $MoCl_5$ solution in tetrahydrofuran with sodium in the presence of proper phosphine under a H_2 or N_2 atmosphere, respectively.[9] $[Mo(dtpe)_2]$ was obtained by heating the hydride complex under reduced pressure to 80°C until the ν_{Mo-H} vibration disappeared. Other reagents (POCH Gliwice) were purified when necessary, and all solvents were saturated with hydrogen or nitrogen, respectively, before use. The $[MoH_4(dppe)_2]$ complex was dissolved in acidified methanol (H_2SO_4 concentration, 5×10^{-2} mol dm^{-3}). Solutions made in this way were then irradiated by the γ-radiation source "Issledovatiel" (stationary ^{60}Co γ-radiation source) with simultaneous saturation with gaseous, deoxygenated N_2 (dose rate in conversion to methanol was calculated as 4.5×10^{15} eV cm^{-3} s^{-1}). The cyclohexane solutions of the molybdenum(IV) hydride complexes and $[Mo(dtpe)_2]$ were continuously saturated with a 1 : 3 mixture of nitrogen and hydrogen during the irradiation, or with nitrogen only in other experiments. The dose rate was the same as in the case of irradiation in the methanol solutions. The dose rate was calculated on the basis of a Fricke dosimeter. In order to keep the concentration of molybdenum complexes and H_2SO_4 constant the gases were passed through washers filled with methanol or cyclohexane, respectively, before introduction into the irradiated solutions. The generated H_4N_2 and H_3N were absorbed in aqueous solutions of 5×10^{-2} mol dm^{-3} H_2SO_4. Hydrazine was estimated spectrometrically using *p*-dimethylaminobenzaldehyde[10,11] and ammonia was determined by the indophenol test.[12,13]

In the solid phase radiolysis experiment samples of $[Mo(N_2)_2(dppe)_2]$ (0.2 g) and $[MoH_4(dppe)_2]$ (0.2 g) were placed in glass tubes and then the air was pumped out and replaced with hydrogen (nitrogen complex) or hydrogen mixed with nitrogen (hydride complexes). Next, the tubes were placed into the γ-radiation field. The gaseous products of reactions were estimated using a WMS-2 mass spectrometer operating at an ionization energy of 100 eV.

RESULTS AND DISCUSSION

In order to determine the importance of H^- ions in the radiation-catalytic process of reduction of N_2, the yields of H_4N_2 and H_3N were determined either in cyclohexane or methanol solutions of the molybdenum(IV) hydride complexes. The typical curve shapes of dependence of numbers of H_4N_2 molecules on dose for different molybdenum(IV) hydride complex concentrations are shown in Fig. 1.

Similar shapes were also obtained for $N_2H_6SO_4$

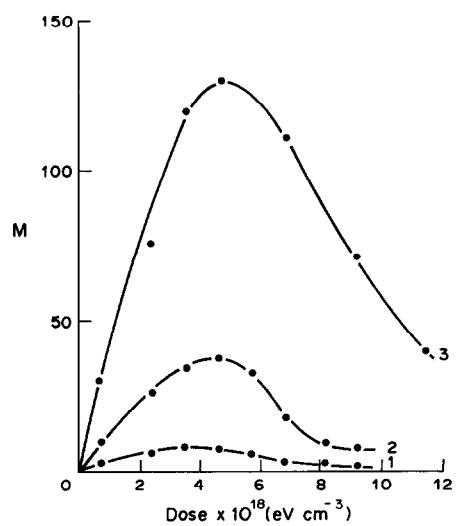

Fig. 1. Dependence of numbers of H_4N_2 molecules on dose for different molybdenum(IV) hydride complex concentrations in cyclohexane: (1) $c = 5\times10^{-4}$ mol dm^{-3} $[MoH_4(dppe)_2]$; (2) $c = 10^{-3}$ mol dm^{-3} $[MoH_4(dppe)_2]$; (3) $c = 10^{-2}$ mol dm^{-3} $[MoH_4(dtpe)_2]$. M—number of H_4N_2 molecules $\times10^{15}$ for (1) and (2) and $\times10^{16}$ for (3).

Table 1. Radiation yields of H_4N_2 for different molybdenum(IV) hydride complex concentrations in either cyclohexane or methanol solutions

Cyclohexane solutions saturated with N_2 and H_2		Methanol solutions acidified with H_2SO_4 [$c = 5\times10^{-2}$ mol dm^{-3}], saturated with N_2	
Concentration of the Mo^{IV} hydride complex (mol dm^{-3})	Number of H_4N_2 molecules per 100 eV	Concentrations of the Mo^{IV} hydride complex (mol dm^{-3})	Number of H_4N_2 molecules per 100 eV
5×10^{-4}	4.3	10^{-3}	0.47
10^{-3}	15.0	2×10^{-3}	0.86
10^{-2}	37.5	4×10^{-3}	1.4

in $CH_3OH_2^+$. Radiation yields of H_4N_2 and $N_2H_6SO_4$ are presented in Table 1.

It can be seen that removing H^- ions from the coordination sphere of molybdenum(IV) leads to yields of $N_2H_6SO_4$ which are typical for the $[MoOCl(dppe)_2]Cl$ complex.[1] Application of the molybdenum(IV) hydride complex gives much higher H_4N_2 yields. Generation of hydrazine was also evidenced in the radiolysis of the solid $[MoH_4(dppe)_2]$ and $[Mo(N_2)_2(dppe)_2]$ in an atmosphere of N_2 or a mixture of N_2 and H_2. Mass spectra of hydrazine and the gaseous products from the radiolysis of solid $[MoH_4(dppe)_2]$ and $[Mo(N_2)_2(dppe)_2]$ irradiated in an atmosphere of N_2 or a mixture of N_2 and H_2 are presented in Table 2.

The mass spectra of the gaseous products from radiolysis of $[MoH_4(dppe)_2]$ are very similar to the spectrum of hydrazine. In the tubes in which $[MoH_4(dppe)_2]$ was under a N_2 atmosphere, much less hydrazine was observed than in those which were filled with a mixture of H_2 and N_2. This is due to the fact that there was much less of the released hydrogen and hydrogen atoms consequently from the hydride complex. It can also be seen (see Table 2) that coordinated nitrogen was reduced by hydrogen atoms and molecular ions H_2^+ (their yields in gaseous H_2 are, respectively, $G_H = 17.6$[14] and $G_{H_2^+} = 2.75$[15]). The shapes of the curves in Fig. 1 suggest that the process of conversion of H_4N_2 into H_3N takes place. The mechanism of hydrogenation of hydrazine was explained earlier.[1] Dependence of the numbers of H_3N molecules on dose for different molybdenum(IV) hydride complex concentrations is shown in Fig. 2.

There is an induction period in these curves which is connected with the generation of a bis-dinitrogen complex and its subsequent reduction to H_4N_2 and

Table 2. The mass spectra of H_4N_2 and the gaseous products from the irradiation of the solid $[MoH_4(dppe)_2]$ and $[Mo(N_2)_2(dppe)_2]$ complexes

			Relative intensity		
			$[MoH_4(dppe)_2]$, dose 2.58×10^{19} eV g^{-1}		$[Mo(N_2)_2(dppe)_2]$ dose 1.1×10^{19} eV g^{-1}
m/e	Assignment	H_4N_2	(N_2 atmosphere)	(N_2+H_2 atmosphere)	(H_2 atmosphere)
14	$^{14}N^+$	4.92	30	20	11
15	$^{14}NH^+$	8.05	0.5 ^{15}N	1.4	7.69
16	$^{14}NH_2^+$	29.2	1.4	10	8.97
17	$^{14}NH_3^+$	26.1	0.5	1.4	7.69
27	?	0.30	—	—	2.56
28	$^{14}N_2^+$	21.4	100	100	100
29	$^{14}N_2H^+$	40.1	18 ^{14}N–^{15}N	18 ^{14}N–^{15}N	6.0
30	$^{14}N_2H_2^+$	31.3	—	6	7.56
31	$^{14}N_2H_3^+$	47.3	—	10	8.97
32	$^{14}N_2H_4^+$	100	1.8	50	73.08
33	$^{15}N^{14}NH_4^+$	0.87	—	—	—

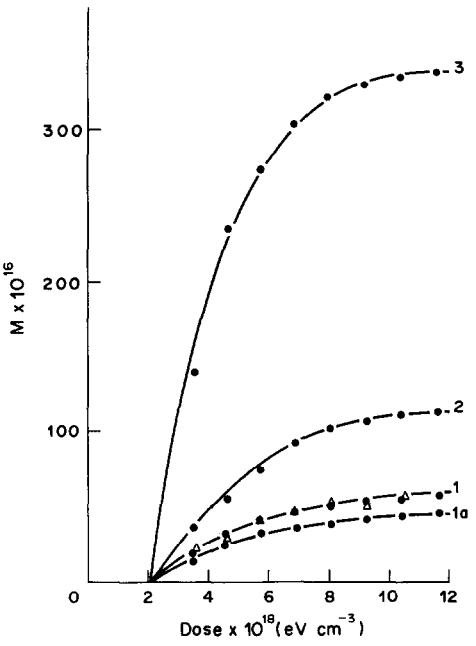

Fig. 2. Dependence of numbers of H_3N molecules on dose for different molybdenum(IV) hydride complex concentrations: (1) $c = 10^{-3}$ mol dm^{-3}, ● $[MoH_4(dppe)_2]$ saturated with the mixture of N_2 and H_2, △ $[MoH_4(dtpe)_2]$ saturated with the mixture of N_2 and H_2; (1a) $c = 10^{-3}$ mol dm^{-3} $[MoH_4(dppe)_2]$ saturated with N_2 only; (2) $c = 5 \times 10^{-3}$ mol dm^{-3} $[MoH_4(dtpe)_2]$ saturated with the mixture of N_2 and H_2; (3) $c = 10^{-2}$ mol dm^{-3} $[MoH_4(dtpe)_2]$ saturated with the mixture of N_2 and H_2.

finally to H_3N. In acidified solutions the induction period is longer and the yields of NH_4^+ are lower (see Table 3). Yields of H_3N and NH_4^+ ions are listed in Table 3.

From the data given in Fig. 2 and Table 3 it can be seen that from the molybdenum(IV) hydride complex solutions saturated with a mixture of N_2 and H_2 the yields of ammonia obtained are independent of the kind of ligated phosphine. Yields of NH_4^+ ions are much lower than yields of H_3N (see Table 3). Comparison of the yields of H_3N ($[MoH_4(dtpe)_2]$ complex dissolved in cyclohexane, $c = 10^{-2}$ mol dm^{-3}) at the same dose rate with the yields of NH_4^+ ions ($[MoOCl(dppe)_2]Cl$ dissolved in acidified methanol, $c = 10^{-2}$ mol dm^{-3}, $G_{NH_4^+} = 25$ ions per 100 eV[2]) shows that the former complex is about 5.2 times more effective than the latter. By considering the overall yield, $G_{H_4N_2} + G_{H_3N} = 168.5$ molecules per 100 eV (see Tables 1 and 3), it can be concluded that the molar ratio of nitrogen reduction products to the molybdenum(IV) hydride complex (the dose rate, as in ref 1, being approx. 3.17×10^{17} eV cm^{-3} s^{-1}) after 1 min of irradiation is about: $([H_3N] + [H_4N_2])/[MoH_4(dtpe)_2] \cong 6.7$. At a dose rate of 4.5×10^{15} eV cm^{-3} s^{-1} this ratio is about 7.8×10^{-2}. In order to define the way in which the dinitrogen complex is being formed (either as a result of displacement of H^- ions for N_2 or by placing N_2 into the released coordination places), the yields of H_3N were stated in cyclohexane solutions of the $[Mo(dtpe)_2]$ complex saturated with N_2 or with a mixture of N_2 and H_2. Results of this experiment are presented in Figs 3 and 4 and in Table 4.

By making a comparison between Figs 2 and 3 and Fig. 4 the same induction period can be noticed but the yields of H_3N are different. It supports the hypothesis that the dinitrogen complex is formed by a process which places N_2 into the free coordination positions (formed by the release of H^- ions). If N_2 displaced H^- ions in the coordination sphere, induction periods in this experiment should be longer. The similar induction periods (see Figs 2, 3 and 4) also suggest that $[Mo(N_2)_2(dtpe)_2]$ is converted into $[MoH_4(dtpe)_2]$ by H_2 generated by γ-radiation in C_6H_{12} or by H_2 supplied to the system. The different yields of H_3N (see Figs 2, 3 and 4) are due to the different overall concentrations of the

Table 3. Radiation yields of H_3N and NH_4^+ ions for different molybdenum(IV) hydride complex concentrations in cyclohexane solutions saturated with the mixture of N_2 and H_2 1:3 and in acidified methanol solutions of the $[MoH_4(dppe)_2]$ (concentrations of $H_2SO_4 = 5 \times 10^{-2}$ mol dm^{-3})

Cyclohexane solutions		Methanol solutions	
Concentration of the Mo^{IV} hydride complex (mol dm^{-3})	Number of H_3N molecules per 100 eV	Concentration of the Mo^{IV} hydride complex (mol dm^{-3})	Number of NH_4^+ ions per 100 eV
10^{-3}	16.0	10^{-3}	2.2
10^{-3}[a]	11.6	2×10^{-3}	3.9
5×10^{-3}	29.0	4×10^{-3}	8.0
10^{-2}	131.0		

[a] Solution saturated with N_2 only.

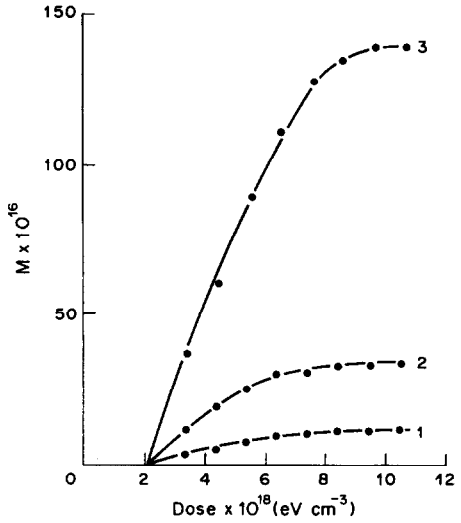

Fig. 3. Dependence of numbers of H_3N molecules on dose for different $[Mo(dtpe)_2]$ complex concentrations in cyclohexane saturated with N_2: (1) $c = 2.5 \times 10^{-3}$ mol dm^{-3}; (2) $c = 5 \times 10^{-3}$ mol dm^{-3}; (3) $c = 10^{-2}$ mol dm^{-3}.

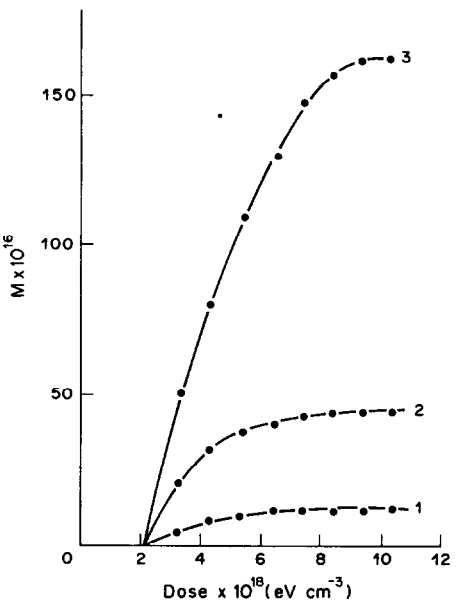

Fig. 4. Dependence of numbers of H_3N molecules on dose for different $[Mo(dtpe)_2]$ complex concentrations in cyclohexane saturated with the mixture of N_2 and H_2: (1) $c = 2.5 \times 10^{-3}$ mol dm^{-3}; (2) $c = 5 \times 10^{-3}$ mol dm^{-3}; (3) $c = 10^{-2}$ mol dm^{-3}.

dinitrogen complex in the systems. H^- ions are also presumed to take part in the reduction of coordinated nitrogen (see Tables 3, 4 and Figs 2, 3, 4). Although supplying gaseous H_2 into the irradiated system makes the generation of H atoms and H_2^+ ions more effective, this effect cannot be considered as the only reason responsible for the increase of H_3N molecules in the solutions saturated with a mixture of N_2 and H_2, compared with the solutions saturated with N_2 only. Such a great difference between the yields of H_3N in $[MoH_4(dtpe)_2]$ and $[Mo(dtpe)_2]$ solutions also suggests that H^- ions react with the coordinated nitrogen. In the previous paper[1] it was shown that the yields of H_4N_2 and H_3N are independent to a high degree of the H^+ ions concentration. There are a lot fewer H^+ ions in the $[Mo(dtpe)_2]$ solutions (and fewer H^- ions) than in the solutions of $[MoH_4(dtpe)_2]$. A high yield such as $G_{H_4N_2} + G_{H_3N} = 168.5$ cannot be explained as a result of reduction of the coordinated nitrogen with H_2^+ and $C_6H_{12}^+$ ions and hydrogen atoms (their overall yield is about 30 ions and hydrogen atoms per 100 eV). It seems to be obvious, therefore, that in the system $[MoH_4(LL)_2]$–C_6H_{12} nitrogen is reduced by H_2 in a catalytic process. By considering the charge allocation on the coordinated nitrogen (especially the negative charge on N_β in $Mo—N_\alpha—N_\beta$) the protonation of N_β appears to be the first step in the reduction. Protons are transferred from H_2^+ and $C_6H_{12}^+$ cations ($G_{C_6H_{12}^+} = 5.3$[16]). Another source of protons is the hydrogen atoms which are converted to H^+ ions in the process of the molybdenum(IV) reduction. Free or bound protons are promoted to the acceptors in a very short time according to the tunnel mechanism.[17] Intramolecular proton promotion has been observed earlier.[19–21] Protons from $C_6H_{12}^+$ are promoted to

Table 4. Radiation yields of H_3N in cyclohexane solutions of the $[Mo(dtpe)_2]$ complex saturated with N_2 or with the mixture of N_2 and H_2 (1 : 3)

Concentration of the $[Mo(dtpe)_2]$ complex (mol dm^{-3})	Number of H_3N molecules per 100 eV in solutions saturated with N_2	Number of H_3N molecules per 100 eV in solutions saturated with the mixture of N_2 and H_2 (1 : 3)
2.5×10^{-3}	3.9	6.0
5×10^{-3}	8.6	17.5
10^{-2}	28.0	55.2

the acceptors in a process which is not controlled by diffusion (e.g. the rate constant of the reaction $C_6H_{12}^+ + H_3N \rightarrow NH_4^+ + C_6H_{11}$ is very high, $K_f = 2.4 \times 10^{11}$ dm^{-3} mol^{-1} s^{-1} [21]). The dinitrogen complex, starting from the moment when its concentration is high enough (see Tables 3 and 4), successfully competes for protons along with the molybdenum(IV) hydride complex (H^- ions are also the proton acceptors which converts them into hydrogen atoms). Dinitrogen as a ligand is easier to reach than the H^- ions (because of the symmetry and the distance from the central atom), which makes the reaction of the $[Mo(N_2)_2(dppe)_2]$ complex with protons more probable. The supply of gaseous hydrogen into the irradiated system allows the H^- ion concentration (in the molybdenum(IV) complex solution) to be kept at a level high enough to maintain their ability to react with a Mo=N—NH$^+$ moiety forming the Mo=N—MH$_2$ moiety (or others, or their conversion into hydrogen atoms). Thus, the H^- ions in this way protect the central atom from oxidation to the higher oxidation state. Support for this comes from Tables 3 and 4. Based on the data given in ref. 7, it cannot be excluded that H^- ions react directly with the Mo—N≡N moiety. Generation of $[MoH_4(dtpe)_2]$ as a result of irradiation of the cyclohexane solution of $[Mo(dtpe)_2]$ saturated with a mixture of N_2 and H_2 was evidenced when a substance with characteristic ν_{Mo-H} vibrations at *ca* 1750 and 1809 cm^{-1} was separated from this solution. From the four possible Mo—H vibrations (two B_2 and two E) associated with the $[MoH_4(LL)_2]$ complexes with D_{2d} symmetry, the two δ_{Mo-H} vibrations (*ca* 770 and 636 cm^{-1}) are obscured by phenyl vibrations. The other vibrations in the 400–3000 cm^{-1} range are identical to those from the non-irradiated molybdenum(IV) complex (with dppe). When the $[MoH_4(dtpe)]$ complex was irradiated without saturation with N_2 the ν_{Mo-H} vibrations vanished whilst the other vibrations were left unchanged. Based either on the data gathered in the tables and figures and on the discussion above or on the data from ref. 1, the following mechanism for the radiation-catalytic reduction of N_2 using the molybdenum(IV) hydride complexes can be suggested:

$$C_6H_{12} \rightsquigarrow C_6H_{12}^+, e_s^-, H, M^*, H_2 \quad (1)$$

$$H_2 \rightsquigarrow H_2^+, e^-, H, M^* \quad (1a)$$

$[MoH_4(dtpe)_2]$

$$\begin{array}{l} \xrightarrow[2e_s^-]{2H} [Mo(dtpe)_2] + 2H_2 + 2H^- \\ \xrightarrow[(2H_2^+)]{M^*} [Mo(dtpe)_2] + 2H_2 + M + 2H^- + 2H \end{array} \quad (2)$$

$$[Mo(dtpe)_2] + 2N_2 \longrightarrow [Mo(N_2)_2(dtpe)_2] \quad (3)$$

$$[Mo(N_2)_2(dtpe)_2] \xrightarrow[(C_6H_{12}^+)]{H^+} \left[\begin{array}{c} Mo(dtpe)_2 \\ \| \\ N—NH^+ \end{array}\right] + N_2 + (C_6H_{11}) \quad (4)$$

$$\left[\begin{array}{c} Mo(dtpe)_2 \\ \| \\ N—NH^+ \end{array}\right] \xrightarrow{H^-(H)} \left[\begin{array}{c} Mo(dtpe)_2 \\ \| \\ N—NH_2 \end{array}\right] \quad (5)$$

$$\left[\begin{array}{c} Mo(dtpe)_2 \\ \| \\ N—NH_2 \end{array}\right] \xrightarrow[(H)]{H^+} \left[\begin{array}{c} Mo(dtpe)_2 \\ | \\ HN—NH_2 \end{array}\right]^+ \xrightarrow{H^-} \left[\begin{array}{c} Mo(dtpe)_2 \\ | \\ H_2N—NH_2 \end{array}\right] \quad (6)$$

$$\left[\begin{array}{c} Mo(dtpe)_2 \\ | \\ H_2N—NH_2 \end{array}\right] \xrightarrow[C_6H_{12}^+]{H^+} 2H_3N + [Mo(dtpe)_2]^{2+} + C_6H_{11} \quad (7)$$

$$[Mo(dtpe)_2]^{2+} \xrightarrow[2N_2]{2H} [Mo(N_2)_2(dtpe)_2] + 2H^+ \quad (8)$$

$$[Mo(N_2)_2(dtpe)_2] + 2H_2 \longrightarrow [MoH_4(dtpe)_2] + 2N_2. \quad (9)$$

REFERENCES

1. J. O. Dzięgielewski, *Polyhedron* 1989, **8**, 1463.
2. J. O. Dzięgielewski and R. Grzybek, *J. Radioanal. Nucl. Chem.* 1989, **132**, 28.
3. A. Sacco and M. Rossi, *Inorg. Chim. Acta* 1968, **2**, 127.
4. A. D. Allen, R. O. Harris, B. R. Loescher, J. R. Stevens and R. N. Whiteley, *Chem. Rev.* 1973, **73**, 11.
5. L. J. Archer and T. A. George, *Inorg. Chem.* 1979, **18**, 2079.
6. R. Pierantozzi and G. L. Geoffrey, *Inorg. Chem.* 1980, **19**, 1821.
7. M. Hidai, T. Takahashi, J. Yokotake and Y. Uchida, *Chem. Lett.* 1980, 645.
8. G. Wittig, H. D. Weigmann and M. Schlosser, *Chem. Ber.* 1961, **94**, 676.
9. L. J. Archer, T. A. George and M. E. Noble, *J. Chem. Ed.* 1981, **53**, 727.
10. M. Pares and A. Retit, *Bull. Soc. Chim. Fr.* 1947, 122.
11. G. V. Watt, J. D. Chisp, *Analyt. Chem.* 1952, **24**, 2006.
12. W. T. Bolleter, C. J. Bushmann and P. W. Tidwell, *Analyt. Chem.* 1961, **33**, 592.
13. C. J. Pickett, K. S. Ryder and J. Talarmin, *J. Chem. Soc., Dalton Trans.* 1986, 1453.
14. O. J. Nielsen, *Risö Rep.* N 480, 1984, 126.

15. V. B. Nesterenko, A. A. Gvozdev and N. N. Doroshkevich, *Radiat. Phys. and Chem.* 1980, **21**, 345.
16. J. P. Suwalski and N. Getoff, *Radiat. Phys. Chem.* 1981, **17**, 279.
17. S. J. Rsad and J. H. Fendler, *J. Chem. Phys.* 1970, **52**, 5395.
18. J. O. Dzięgielewski, *Tetrahedron* 1986, **42**, 109.
19. J. O. Dzięgielewski, E. Kalecińska, B. Jeżowska-Trzebiatowska, J. Kaleciński and J. Nawojska, *Nukleonika* 1978, **23**, 209.
20. J. O. Dzięgielewski and K. Filipek, *J. Radioanal. Nucl. Chem. Lett.* 1988, **128**, 109.
21. J. Kroch, *Wybrane Zagadnienia Chemii Radiacyjnej*, p. 424. PWN, Warszawa (1984).

Polyhedron Vol. 9, No. 5, pp. 653–657, 1990
Printed in Great Britain

0277-5387/90 $3.00+.00
© 1990 Pergamon Press plc

SYNTHESIS OF ORGANOTIN COMPLEXES WITH LIGANDS OF BIOLOGICAL SIGNIFICANCE

F. L. LEE and E. G. GABE

Chemistry Division, NRC, Ottawa K1A 0R6, Canada

L. E. KHOO

Universiti Sains Malaysia, Penang, Malaysia

G. ENG

University of the District of Columbia, Washington D.C. 20008, U.S.A.

and

F. E. SMITH*

Chemistry Department, Laurentian University, Sudbury, Ontario, Canada

(*Received* 7 *August* 1989; *accepted* 18 *September* 1989)

Abstract—A series of new 1:1 complexes of formula $Ph_3SnCl \cdot L$ for a range of ligands L, where L_1 = 2-$HOC_6H_4CH{=}NCH_2CO_2Et$, L_2 = 2-$HOC_6H_4C(CH_3){=}NCH_2CO_2Et$, L_3 = $2HOC_6H_4CH{=}NCH(CH_3)CO_2Me$ and L_4 = 2-$HOC_{10}H_6CH{=}NCH_2CO_2Et$, have been prepared and characterized. A full X-ray crystal structure analysis of the compound chlorotriphenyl(ethyl N-salicylideneglycinate)tin(IV) ($Ph_3SnCl \cdot L_1$) has been performed. The crystals are monoclinic, space group $P2_1/n$, $a = 8.191(4)$, $b = 18.575(5)$, $c = 17.983(7)$ Å, $\beta = 101.41(4)°$, $V = 2682.1(18)$ Å^3, $Z = 4$, $D_{calc} = 1.455$ Mg m^{-3}, $\mu = 1.08$ mm^{-1}, final $R = 4.3\%$ for 1174 unique observed reflections. It was found that the ligand behaves as a unidentate and binds to the tin via the phenolic oxygen atom. The complexes have a five-coordinated trigonal bipyramidal geometry with the phenyl groups taking up the equatorial position around the tin atom.

There have been several reports recently concerning the Schiff base complexes of organotin(IV) halides and pseudo-halides, and involving the coordination of the ligands in either their deprotonated or neutral forms.[1–5] We now wish to report the synthesis and characterization of a series of new complexes of general formula $Ph_3SnCl \cdot L$ with a range of biologically-significant Schiff bases in their neutral forms, and the results of an X-ray structural investigation for one of the complexes, $Ph_3SnCl \cdot L$ (L = L_1). The various α-amino acid derivatives used as ligands are shown overleaf.

* Author to whom correspondence should be addressed.

EXPERIMENTAL

Triphenyltin chloride was purchased from Alfa Inorganics and used without further purification.

Either glycine ethyl ester hydrochloride or alanine methyl ester hydrochloride, in ether, were neutralized by bubbling gaseous ammonia through the stirred solution. The ammonium chloride was filtered off and the neutral α-amino acid ester in ether was used immediately for condensation with either salicylaldehyde or 2-hydroxynaphthaldehyde. After refluxing the mixture for about 1 h, the ether was evaporated and petroleum ether (60–80°C) was added. The mixture was cooled in the refrigerator

$2\text{-}HOC_6H_4CH{=}NCH_2CO_2Et$ L_1

$2\text{-}HOC_6H_4C(CH_3){=}NCH_2CO_2Et$ L_2

$2\text{-}HOC_6H_4CH{=}NCH(CH_3)CO_2Me$ L_3

$2\text{-}HOC_{10}H_6CH{=}NCH_2CO_2Et$ L_4

and the ligands produced were filtered off and recrystallized with ether–petroleum ether (1 : 1). Melting point and analytical data for the ligands are given in Table 1.

The complexes were prepared by refluxing the calculated amount of ligand and triphenyltin chloride in petroleum ether. The complexes crystallized out when the solutions were cooled in the refrigerator overnight. They were filtered off and recrystallized from petroleum ether or ether–petroleum ether (1 : 1). Melting point and analytical data are summarized in Table 2.

Conductance measurements in nitrobenzene were made at room temperature using a Phillips PW 9501 conductivity bridge with a cell constant of 0.71. Molar conductances of the complexes are recorded in Table 2.

The IR spectra of the ligands and complexes were recorded in the region 4000–600 cm^{-1} with a Beckmann Acculab "4" instrument either as neat liquid films or Nujol mulls between NaCl plates or as KBr pellets. For the 600–200 cm^{-1} region, the Beckmann IR4250 spectrophotometer was used.

PMR spectra were obtained using a Perkin–Elmer R12B spectrometer with deuterochloroform as solvent.

Tin was estimated as SnO_2. Microanalyses were carried out by the Chemistry Department, National University of Singapore, Singapore.

Crystal data

Monoclinic, space group $P21/n$, $a = 8.191(4)$, $b = 18.575(5)$, $c = 17.983(7)$ Å, $\beta = 101.41(4)°$, $V = 2682.1(18)$ $Å^3$, $Z = 4$, $D_{calc} = 1.455$ Mg m^{-3}, $\mu = 1.08$ mm^{-1}.

Intensity data

Intensity data were collected with a Nonius diffractometer from a $0.1 \times 0.3 \times 0.3$ mm crystal to 2θ max = 44.8°, using the θ–2θ scan mode and

Table 1. Analytical, melting point and IR data for the ligands

Ligand	Melting point (°C)	Elemental analysis (%) Found (calc.) C	H	N	IR (cm^{-1}) ν(C=N)
L_1	35–36		[a]		1610
L_2	76–77	65.0(65.1)	6.9(6.8)	6.6(6.3)	1620
L_3	39–40	63.5(63.7)	6.3(6.3)	6.6(6.8)	1615
L_4	100–102	69.9(70.0)	5.7(5.9)	5.6(5.4)	1620

[a] Ligand L_1 is not stable at room temperature.

Table 2. Analytical, conductivity, melting point and IR data for the complexes

Complex L	λ[a]	Melting point (°C)	Elemental analysis (%) Found (calc.) C	H	N	Sn	IR (cm^{-1}) ν(C=N)	ν(Sn—Cl)
L_1	2.20	104–106	58.8(58.8)	4.7(4.8)	1.7(2.4)	19.3(20.0)	1630	235
L_2	2.40	107–108	59.2(59.4)	4.8(4.9)	2.3(2.3)	19.7(19.6)	1645	240
L_3	2.50	73–74	58.2(58.8)	4.6(4.7)	2.2(2.4)	20.9(20.0)	1640	230
L_4	1.45	135–137	61.6(61.7)	4.7(4.7)	2.4(2.2)	18.4(18.5)	1645	230

[a] λ, is molar conductance (Ω^{-1} cm^2 mol^{-1}).

graphite monochromatized Mo-K_α radiation. A total of 11822 reflections were measured including 3465 which were unique, of which 1174 were considered significant, with $I_{net} > 2.5\sigma$ (I_{net}). No correction was made for absorption [I(Mo-K_α) = 0.70932 Å].

Structure solution and refinement

The structure was solved by Patterson and heavy-atom methods and refined with full-matrix least-squares. All non-hydrogen atoms were refined anisotropically. The hydrogen atoms were calculated and were not refined. The final residuals are $R_F = 0.043$ and $R_w = 0.036$ for the significant reflections and $R_F = 0.063$ and $R_w = 0.036$ for all reflections. In the final D-map, the deepest hole showed a density of $-0.690e/Å^3$ and the highest peak, a density of $0.680e/Å^3$. Weights based on counting statistics were used throughout. All calculations were performed with the NRCVAX system of programs.[6] Literature values[7] were used for the scattering factors.*

RESULTS AND DISCUSSION

Regardless of the proportions of ligand and triphenyltin compound used, the complexes all recrystallized with 1 : 1 stoichiometry. Like the ligands, they were all yellow in colour, thermally stable with sharply defined melting points and were found to be soluble in the common organic solvents. Microanalytical and conductance data for the complexes are presented in Table 2. The observed molar conductances in nitrobenzene were in the range 1.4–2.5 Ω^{-1} cm^2 mol^{-1}, indicating that the compounds were non-electrolytes and in each instance, the chloride group is bound to the tin atom. (Molar conductances expected for 1 : 1 or 1 : 2 electrolytes in nitrobenzene are 25–35 and 44–60 Ω^{-1} cm^2 mol^{-1}, respectively.[8])

Comparison of the integrated intensities of the ligand and organotin protons confirms the 1 : 1 stoichiometry of the complexes. The sharp singlet assigned to the azomethine proton of all the ligands ($\delta \sim 8.5$ ppm) was found to be unchanged on coordination, indicating that the nitrogen atom is not coordinated to the metal. On the other hand, the peak due to the phenolic proton for each ligand molecule ($\delta \sim 13$ ppm) was significantly broadened on complex formation. As the ring formed by the intramolecular hydrogen bond of the Schiff base ligand is retained but distorted in the complexes,[9] coordination through oxygen will result in a weakening of the O—H bond, and a strengthening of the C=N---H hydrogen bond, which in turn leads to the observed broadening of the peak due to the phenolic proton. Similar observations have been reported for the dialkytin dichloride complexes of N-arylsalicylideneimines,[10] and of N,N′-bis(salicylaldehyde)ethylenediimine.[11]

The IR evidence (Table 2) also suggests that the ligands are behaving as monodentates via the phenolic oxygen atoms. This is based on the stretching vibration of the phenolic O—H which is lowered and broadened, the Sn—Cl stretching mode which is shifted downfield by some 100 cm^{-1} from its value in triphenyltin chloride,[12] as well as the shift to higher frequency (*ca* 20 cm^{-1}) of the C=N stretching vibration for the triphenyltin complexes. Similar shifts in the C=N stretching frequency for ligands of this type have been found to indicate coordination to the tin atom by oxygen.[9,13] This has been confirmed by the X-ray structural analysis of the complex of triphenyltin chloride with N-4′-methylphenyl-2-hydroxynaphthylideneimine.[5]

In the present instance, the structural implications of the experimental findings outlined above are again confirmed by the X-ray results. A full X-ray crystal structure analysis of the compound chlorotriphenyl(ethyl - N - salicylideneglycinate)tin (IV) ($Ph_3SnCl \cdot L_1$) has been performed. This complex has a trigonal bipyramidal structure, with the three phenyl groups occupying the equatorial positions around the tin atom, while the oxygen atom of the ligand and the chlorine occupy the axial positions.

The structure of the complex and the atomic numbering scheme are shown in Fig. 1. Table 3 lists selected bond distances and angles. The Cl—Sn—O angle is 173.76(13)°, similar to that (173.0(1)°) in the 1,10-phenanthroline complex of triphenyltin chloride.[14] The average Sn—C(Ph) distance of 2.136(8) Å is almost the same as that reported for the picolinic acid complex of triphenyltin chloride (2.135(5) Å)[15] and within the range of Sn—C(Ph) distances (2.105–2.16 Å) reported in the literature.[12,16] The C—C bond lengths in the phenyl groups are all normal. The Sn—Cl bond length of 2.5138(24) Å is similar to that found in the picolinic acid complex (2.515 Å)[15] and within the range (2.32–2.58 Å) of Sn—Cl distances found in other chloro complexes.[12,16] The Sn—O distance of 2.310(5) Å is comparable to that (2.280(4) Å) in the

* Atomic coordinates, thermal parameters, full lists of bond lengths and angles and lists of F_o/F_c values have been deposited as supplementary data with the Editor, from whom copies are available on request. Atomic coordinates have also been deposited with the Cambridge Crystallographic Data Centre.

Table 3. Bond lengths (Å) and angles (°)

Sn—Cl	2.5138(24)	N—C(8)	1.454(10)
Sn—O(1)	2.310(5)	C(1)—C(2)	1.406(12)
Sn—C(1A)	2.102(8)	C(1)—C(6)	1.418(11)
Sn—C(1B)	2.162(8)	C(2)—C(3)	1.345(14)
Sn—C(1C)	2.143(7)	C(3)—C(4)	1.385(15)
O(1)—C(1)	1.309(10)	C(4)—C(5)	1.365(14)
O(2)—C(9)	1.343(12)	C(5)—C(6)	1.391(12)
O(2)—C(10)	1.476(13)	C(6)—C(7)	1.420(11)
O(3)—C(9)	1.179(13)	C(8)—C(9)	1.497(13)
N—C(7)	1.303(11)	C(10)—C(11)	1.355(17)

Cl—Sn—O(1)	173.76(13)	C(4)—C(5)—C(6)	122.2(8)
Cl—Sn—C(1A)	92.6(3)	C(1)—C(6)—C(5)	118.4(7)
Cl—Sn—C(1B)	94.20(23)	C(1)—C(6)—C(7)	122.8(7)
Cl—Sn—C(1C)	92.64(22)	C(5)—C(6)—C(7)	118.8(7)
O(1)—Sn—C(1A)	88.5(3)	N—C(7)—C(6)	122.3(7)
O(1)—Sn—C(1B)	90.2(3)	N—C(8)—C(9)	111.8(7)
O(1)—Sn—C(1C)	81.49(25)	O(2)—C(9)—O(3)	124.1(9)
C(1A)—Sn—C(1B)	125.6(3)	O(2)—C(9)—C(8)	109.5(8)
C(1A)—Sn—C(1C)	119.6(3)	O(3)—C(9)—C(8)	126.4(9)
C(1B)—Sn—C(1C)	113.9(3)	O(2)—C(10)—C(11)	117.5(9)
Sn—O(1)—C(1)	133.5(5)	Sn—C(1A)—C(2A)	121.3(7)
C(9)—O(2)—C(10)	119.5(8)	Sn—C(1A)—C(6A)	122.2(6)
C(7)—N—C(8)	121.1(6)	C(2A)—C(1A)—C(6A)	116.4(8)
O(1)—C(1)—C(2)	122.2(7)	Sn—C(1B)—C(2B)	121.4(6)
O(1)—C(1)—C(6)	119.3(7)	Sn—C(1B)—C(6B)	121.0(6)
C(2)—C(1)—C(6)	118.5(8)	C(2B)—C(1B)—C(6B)	117.6(7)
C(1)—C(2)—C(3)	120.5(8)	Sn—C(1C)—C(2C)	120.9(6)
C(2)—C(3)—C(4)	122.1(8)	Sn—C(1C)—C(6C)	120.8(6)
C(3)—C(4)—C(5)	118.4(8)	C(2C)—C(1C)—C(6C)	118.4(7)

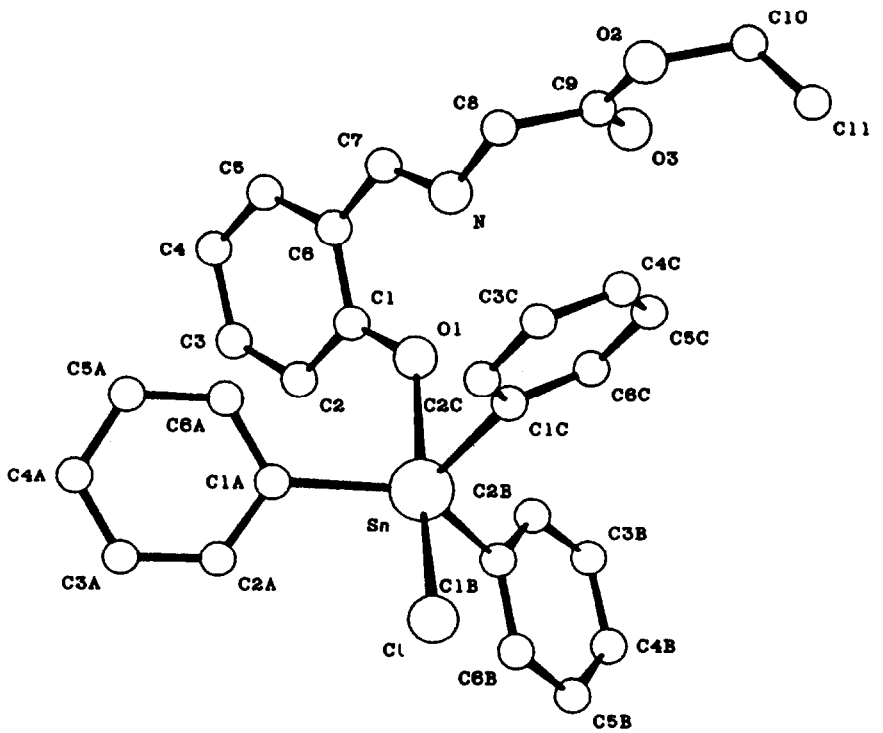

Fig. 1. Molecular configuration and atomic numbering scheme.

complex of triphenyltin isothiocyanate with N-4′-methylphenyl-2-hydroxynaphthylideneimine.[4]

In view of the similarities in PMR, IR and conductivity data, and in the light of the identical stoichiometries shown by the complexes reported here, they are all assigned trigonal bipyramidal structures analogous to that found for $Ph_3SnCl \cdot L_1$.

Acknowledgements—Financial support from the Laurentian University Research Fund (LURF), Universiti Sains Malaysia (R & D) and Datuk Keremat Smelting Holdings is gratefully acknowledged.

REFERENCES

1. R. C. Mehrotra, G. Srivastava and B. S. Saraswat, *Reviews of Silicon, Germanium Tin and Lead Compounds*, 1982, **16**, 171.
2. L. Pellerito, R. Cefalu, A. Silvistri, F. DiBianca, R. Barbieri, H. J. Haupt, H. Preut and F. Huber, *J. Organomet. Chem.* 1974, **78**, 101.
3. T. N. Srivastava, A. K. S. Chauhan and P. C. Kamboj, *J. Ind. Chem. Soc.* 1983, **60**, 625.
4. L. E. Khoo, J. P. Charland, E. J. Gabe and F. E. Smith, *Inorg. Chim. Acta* 1987, **128**, 139.
5. J. P. Charland, F. L. Lee, E. J. Gabe, L. E. Khoo and F. E. Smith, *Inorg. Chim. Acta* 1987, **130**, 55.
6. E. J. Gabe, F. L. Lee and Y. Le Page, *Int. Un. Cryst. Summer School on Crystallographic Computing*, Mulheim, F.R.G. (1985).
7. *International Tables for X-Ray Crystallography*, 2nd edn, Vol. 4. Kynoch Press, Birmingham (1974).
8. J. A. Walmsley and S. Y. Tyree, *Inorg. Chem.* 1963, **2**, 312.
9. B. S. Sarawat, G. Srivatava and R. C. Mehrotra, *J. Organomet. Chem.* 1979, **164**, 153.
10. L. E. Khoo and F. E. Smith, *Polyhedron* 1982, **1**, 213.
11. K. Kawakami, M. Miya-uchi and T. Tanaka, *J. Inorg. Nucl. Chem.* 1971, **33**, 3773.
12. R. C. Poller, *The Chemistry of Organotin Compounds*, p. 227. Logos Press, London (1970).
13. B. S. Sarawat, G. Srivastav and R. C. Mehrota, *Inorg. Chim. Acta* 1979, **36**, 289.
14. E. J. Gabe, F. L. Lee and F. E. Smith, *Inorg. Chim. Acta* 1984, **90**, L11.
15. L. Prasad, E. J. Gabe and F. E. Smith, *Acta Cryst.* 1982, **B38**, 1325.
16. P. G. Harrison, T. J. King and J. A. Richards, *J. Chem. Soc., Dalton Trans.* 1974, 1723.

Polyhedron Vol. 9, No. 5, pp. 659–664, 1990
Printed in Great Britain

0277–5387/90 $3.00+.00
© 1990 Pergamon Press plc

ABSORPTION, LUMINESCENCE, IR AND RAMAN SPECTROSCOPY OF A NOVEL POLYNUCLEAR NEODYMIUM COMPOUND: $Nd_2(OH)_3(ClO_4)_3 \cdot 5H_2O$

E. HUSKOWSKA and J. LEGENDZIEWICZ*

Institute of Chemistry, University of Wrocław, 14 Joliot-Curie, 50-383 Wrocław, Poland

and

J. HANUZA

Institute for Low Temperature and Structure Research, Polish Academy of Sciences, Wrocław P.O. Box 937, Poland

(*Received* 7 *August* 1989; *accepted* 19 *September* 1989)

Abstract—The novel polynuclear compound $Nd_2(OH)_3(ClO_4)_3 \cdot 5H_2O$ was characterized by different spectroscopic methods. IR and Raman spectra in the 50–4000 cm^{-1} region were measured. The stretching ν(Nd—O) and bending δ(O—Nd—O), as well as ClO_4^- vibrations, are discussed in relation to the crystal structure. Absorption spectra along the crystallographic *c*-axis of a single crystal were recorded at room and liquid helium temperatures. The effect of ion-pair interaction was stated. Oscillator strengths, values and τ_λ parameters were calculated on the basis of Judd theory and compared with those for the aquo-ion. Laser-excited luminescence spectra at low temperatures were measured, and Stark components were determined and energy diagrams for $^4I_{9/2}$ and $^4I_{11/2}$ levels were proposed.

It has been proved that perchlorate ions do not enter the first coordination sphere of lanthanide ions in water solutions even at high concentrations.[1–4] Also, solid perchlorates of formula $M(ClO_4)_3 \cdot 6H_2O$ contain metal ions octahedrally coordinated by water molecules.[5] However, we obtained recently in our laboratory single crystals of $Nd_2(OH)_3(ClO_4) \cdot 5H_2O$ from water solution.

The results of X-ray diffraction studies to be published elsewhere[6] show that neodymium ions are eight-coordinated and perchlorate ions are strongly involved in coordination, acting as bridging bidentate and tridentate units. The IR, Raman and electron spectroscopy studies were undertaken to give the full characterization of this novel compound and to explain how perchlorate coordination can influence its spectroscopic properties.

* Author to whom correspondence should be addressed.

EXPERIMENTAL

Sample preparation

The preparation of the title compound is described elsewhere.[6] Crystals for all spectroscopic studies were controlled by X-ray diffraction methods.

IR and Raman spectra

IR spectra in the range 50–4000 cm^{-1} were recorded on a Perkin–Elmer 180 grating spectrophotometer. The solid samples were mulled in Nujol and placed between CsBr (middle-IR) or polyethylene plates (far-IR).

Raman spectra in the range 50–1400 cm^{-1} were measured on a Jeol IRS-S1 spectrophotometer equipped with a Coherent Radiation CRS argon ion laser (488 line). Measurements in the 1400–4000

cm^{-1} range were impossible due to the excitation of Nd^{3+} luminescence.

Electronic spectra

Absorption spectra of a single crystal of $Nd_2(OH)_3(ClO_4)_3 \cdot 5H_2O$ along the *c*-direction and of the Nd^{3+} aquo-ion were recorded on a Cary–Varian spectrophotometer over the range 11000–31250 cm^{-1} at room temperature and at 4.5 K. Stark components were determined at 4.5 K; absorption spectra taken at room temperature were used for intensity analysis of the *f–f* transitions. Oscillator strength values for the electronic transitions were calculated throughout the measured spectral range by the graphical integration method. These experimental values were used to calculate the τ_λ parameters from the Judd relation.[7] The calculation procedure is described in ref. 8. Fluorescence spectra were measured at 50 and 5 K; Nd^{3+} ions were excited by means of an argon laser ILA 120 (C. Zeiss Jena) with 488 and 514 nm lines and recorded on a grating double GDM monochromator with an EMI 9684 B type S1 cooled photomultiplier.

RESULTS AND DISCUSSION

IR and Raman data

The IR and Raman spectra of the complex are shown in Fig. 1. The wavenumbers of bands observed, their relative intensities and tentative assignments are presented in Table 1.

The IR and Raman vibrational patterns of the sample studied are very complex due to the structural complexity of this compound arising from the interactions of four molecules in the low symmetry unit cell as well as from alternative roles played by the perchlorate ligands. The crystal structure of the title compound is described by the monoclinic unit cell of the $C2/c = C_{2h}^6$ symmetry and $Z = 4$. Therefore 152 atoms in the unit cell should be taken into account in the vibrational analysis based on the factor group approximation. Such an approach leads to the 456 unit cell modes subdivided into three acoustic and 453 optic modes. In the site group approximation the number of optic modes is reduced to 57 which is very close to the summary number of bands observed in IR and Raman spectra. Therefore, the qualitative discussion of these spectra can be carried out based on the site group approach and ascent in symmetry method.

The central atom in the Nd^{3+} coordination polyhedron is surrounded by eight oxygen atoms. Four of them belong to four different perchlorate ligands and the remaining four oxygens correspond to the hydroxy- and/or aquo-ligands with their statistical distribution to compensate the ion charge. Both oxygen sets form distorted tetrahedrons around the Nd^{3+} cation and together create a strongly distorted dodecahedron. The ascent in symmetry method allows us to describe this figure by D_{2d} symmetry in which the eight ligands are divided into two non-equivalent sets of four in each set. The vibrations of the NdO_8 polyhedron are described by 21 normal modes which for D_{2d} symmetry are divided in the following form:

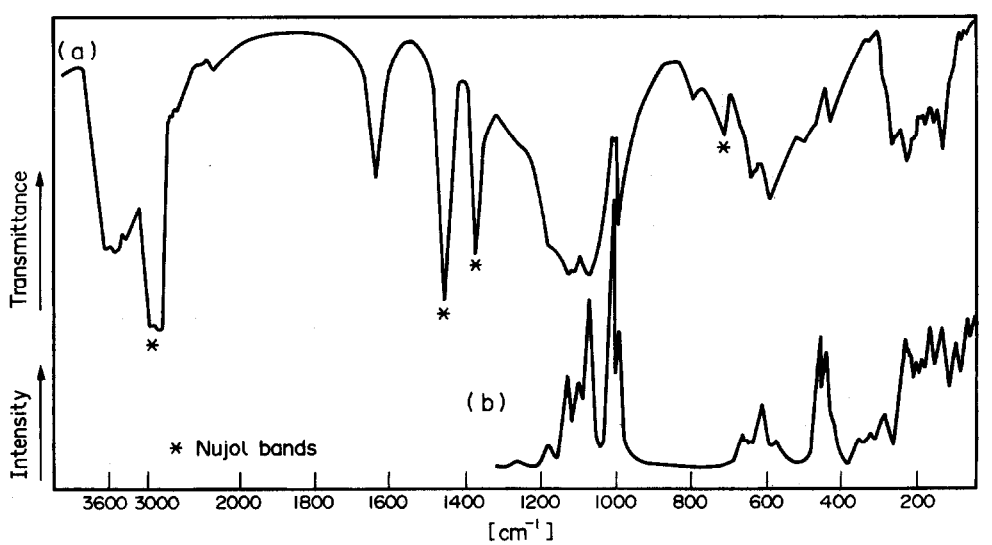

Fig. 1. Vibrational spectra of $Nd_2(OH)_3(ClO_4) \cdot 5H_2O$ in the range 50–4000 cm^{-1}: (a) IR, (b) Raman.

Table 1. IR and Raman data for the title compound

IR (cm^{-1})	Raman (cm^{-1})	Assignment	IR (cm^{-1})	Raman (cm^{-1})	Assignment
3460 s		ν(OH)	500 m		$\omega(H_2O)$
3350 s		$\nu(H_2O)$	475 sh	465(44)	$\rho(OClO_n)$
3240 s		$\nu(H_2O)$	436 w	445(40)	δ(OClO)
1640 s		δ(HOH)		420 sh	$\tau(O_2ClO_2)$
1250 sh	1270(4)		330 vw	357(9)	
1180 vs	1178(10)		290 sh	327(12)	
1130 vs	1130(33)	$\nu_{as}(Cl—O_n)$	269 m	290(17)	ν(NdO)
1120 vs	1102(29)		254 sh	235(38)	
1040 sh	1060 sh	δ(NdOH)	230 m	227 sh	
1080 vs	1070(60)		216 sh	221 sh	
1008 sh	1012(100)	$\nu_s(ClO_n)$	192 w	203(30)	
998 s	998(48)		181 w	185(31)	
800 w		$\rho(H_2O)$	159 w	170(42)	
670 sh	660(9)	$\delta_{as}(ClO_n)$	133 m	160 sh	δ(ONdO)
642 m	650 sh	$\delta_s(ClO_n)$	128 sh	137(44)	
630 sh	640 sh	$\rho(ClO_n)$	114 sh	110 sh	
625 sh	610(18)		94 vw	104(35)	
598 s	578(9)	$\delta_s(ClO_n)$	83 vw	77(46)	

ν—stretching, δ—bending, ρ—rocking, τ—twisting, ω—wagging.

$$\Gamma_{D_{2d}} = 4A_1(RS)+A_2(ia)+2B_1(RS) +4B_2(RS,IR)+5E(RS,IR).$$

Among them four ν(NdO) stretching and five bending frequencies are active in the IR spectrum. The number of Raman active bands is equal to six for stretching and nine for bending frequencies. Since the Nd^{3+} ion occupies the C_1 site, all IR and Raman modes became active in both spectra. Therefore, the multiplets composed of six and nine bands are expected to exist both in IR and Raman spectra corresponding to stretching and bending modes, respectively. This is in accordance with the experimental results. The bands observed in the FIR region at 330, 290, 269, 254, 230, 216 cm^{-1} and in the Raman spectrum at 357, 327, 290, 235, 227, 221 cm^{-1} should be assigned to the stretching ν(NdO) vibrations. Respective bending δ(ONdO) vibrations were detected at 192, 181, 159, 133, 128, 114, 94, 83 cm^{-1} in the IR spectrum and at 203, 185, 170, 160, 137, 110, 104, 77 cm^{-1} in the Raman spectrum. The broad range of energies for these vibrations arises from the distinct variation of the Nd—O distances, which vary between 2.549 and 2.374 Å.[6]

The internal vibrations of the hydroxo- and aquo-ligands appear at the standard frequency regions: ν(OH), 3460; $\nu(H_2O)$, 3350, 3240; δ(HOH), 1640; δ(NdOH), 1000–1200 (partially obscured by $\nu(ClO_4)$ vibrations), $\rho(H_2O)$, 800 and $\omega(H_2O)$, 500 cm^{-1}. The energetic position of these vibrations supports the X ray-structural data[6] which shows that the positive charge excess of the Nd—ClO_4 framework is neutralized by the hydroxyl groups.

The perchlorate ions usually have no tendency to enter the inner-sphere of the Ln^{3+} cations. Praseodymium glutamate perchlorate hydrate, described recently,[9] and the complex under investigation are the only examples grown from water solutions where ClO_4^- groups were found to be directly coordinated to the lanthanide ion. In the title compound perchlorate ligands play a double role as the bridging tridentate and bridging bidentate units. The Cl—O distances are 1.501, 1.461, 1.469, 1.454 Å for Cl(1) and 1.471, 1.472 Å for Cl(2), respectively.[6] The ascent in symmetry method allows us to decribe the vibrations of the perchlorate ligands based on C_{2v} (bidentate) and C_1 (tridentate) point groups. The correlation schemes between the $T_d \rightarrow C_{3v} \rightarrow C_{2v} \rightarrow C_1$ symmetries describe these vibrations as follows:

$$\nu_1: A_1 \rightarrow A_1 \rightarrow A_1 \rightarrow A;$$

$$\nu_2: E \rightarrow E \rightarrow A_1+A_2 \rightarrow 2A;$$

$$\nu_3 \text{ and } \nu_4: F_2 \rightarrow A_1+E \rightarrow A_1+B_1+B_2 \rightarrow 3A.$$

According to refs 10 and 11 the following groups of bands are expected to be active depending on the

symmetry and frequency range:

	900–1300	600–700	400–500 cm^{-1}
C_{3v}	3 (IR,RS)	2 (IR,RS)	1 (IR,RS)
C_{2v}	4 (IR,RS)	3 (IR,RS)	1 (IR,RS)+1(RS)
C_1	4 (IR,RS)	3 (IR,RS)	2 (IR,RS)

Some accidental reduction of this number may appear since the Cl(2) atom of our sample occupies the special C_1 site position and all Cl—O distances are very close to each other. We obtained good agreement between the observed and literature data[12-16] for the last two frequency ranges. However, some discrepancies are observed in the 900–1300 cm^{-1} range where the band positions are significantly shifted in relation to those of other authors[12-16] and there are no IR or Raman lines in the 900–980 cm^{-1} region. The stretching vibration of ClO_2 in bidentate perchlorate is considerably shifted from the standard energy ($\sim$ 930 cm^{-1}). This is not surprising because for known lanthanide compounds only the chelating perchlorates were observed and not the bridging ones, as in our case. The presence of the tribonding bridging perchlorate in lanthanide compounds has not been reported, so we cannot compare our results with any others.

Absorption and luminescence results

The results of crystal studies revealed that in the title compound the perchlorate ions are involved in coordination. It is interesting how this is reflected in the intensity of the *f–f* transitions, especially the hypersensitive one, and in the splitting of levels, and how much these properties differ from those of the aquo-ion.

The absorption spectra of the $Nd_2(OH)_3(ClO_4)_3 \cdot 5H_2O$ single crystal are shown in Fig. 2. The oscillator strength values for the bands observed in its spectra and those of the aquo-ion are listed in Table 2. The band intensities of all the *f–f* transitions are similar, but the intensity of the hypersensitive transition is somewhat higher. Thus

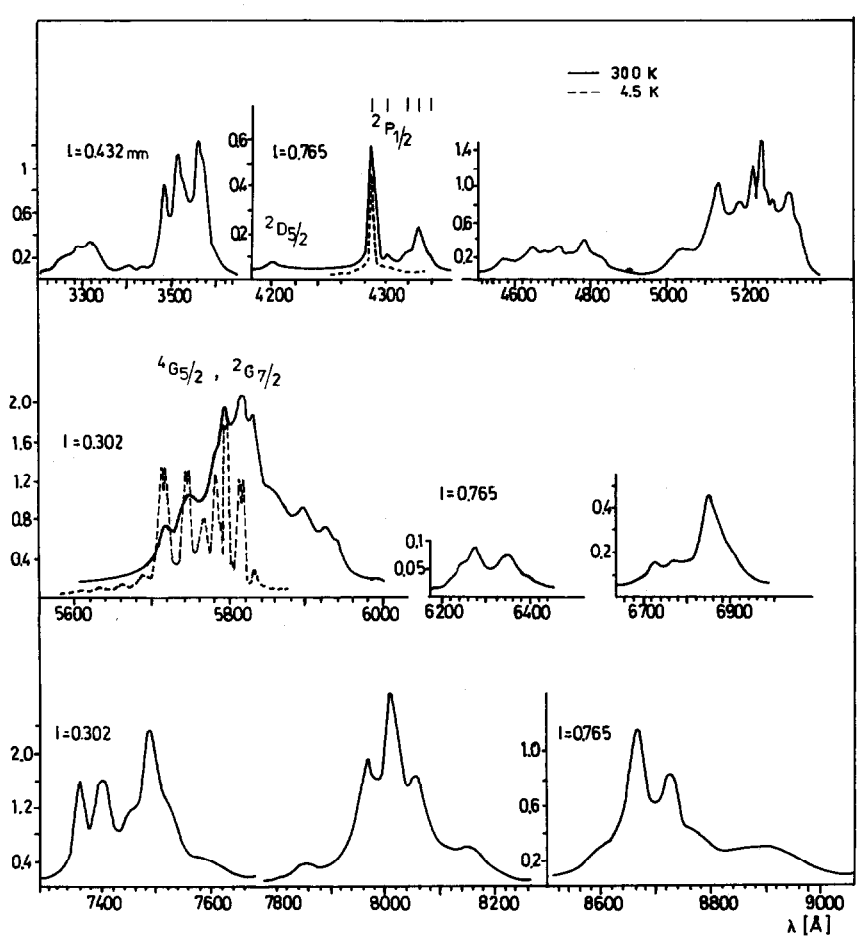

Fig. 2. Absorption spectra of the $Nd_2(OH)_3(ClO_4)_3 \cdot 5H_2O$ single crystal at room and liquid helium temperatures.

Table 2. Oscillator strength values of *f–f* transitions for the $Nd_2(OH)_3(ClO_4)_3 \cdot 5H_2O$ single crystal (I) and for the Nd^{3+} aquo-ion (II)

Spectral region (Å)	$S'L'J'$	P_{exp}I ($\times 10^8$)	P_{exp}II ($\times 10^8$)
8460–9120	$^4F_{3/2}$	195.4	214.2
7720–8400	$^4F_{5/2}$, $^2H_{9/2}$	896.5	852.0
7140–7720	$^4F_{7/2}$, $^4S_{3/2}$	885.2	885.4
6540–7100	$^4F_{9/2}$	68.3	53.3
6160–6540	$^2H_{11/2}$	18.7	16.9
5560–6100	$^4G_{5/2}$, $^2G_{7/2}$	1104.4	967.9
4940–5440	$^2K_{13/2}$, $^4G_{7/2}$, $^4G_{9/2}$	635.9	688.5
4460–4940	$^2K_{15/2}$, $^2G_{9/2}$, $(^2D,^2F)_{3/2}$, $^4G_{11/2}$	215.7	191.2
4130–4400	$^2P_{1/2}$, $^2D_{5/2}$	42.17	39.6
3385–3700	$^4D_{3/2}$, $^4D_{5/2}$, $^2I_{11/2}$, $^4D_{1/2}$, $^2L_{15/2}$	891.7	906.8
3200–3385	$^2I_{13/2}$, $^4D_{7/2}$, $^2L_{17/2}$	223.3	195.7

I: $\tau_2 = (2.96 \pm 0.54) \times 10^{-9}$; $\tau_4 = (4.86 \pm 0.49) \times 10^{-9}$; $\tau_6 = (10.58 \pm 0.71) \times 10^{-9}$.
II: $\tau_2 = (2.02 \pm 0.60) \times 10^{-9}$; $\tau_4 = (4.98 \pm 0.55) \times 10^{-9}$; $\tau_6 = (10.36 \pm 0.78) \times 10^{-9}$.

when in a solution, the same form as in the solid state will be present in a small amount, the intensity of the hypersensitive transition would not change significantly.

The existence of this species can explain the results of Breen and Horrocks[3] and Tanaka and Yamashita[4] on the decay time measurements of lanthanide perchlorate solutions. These authors suggested that in solutions with a high excess of ClO_4^-, higher coordination numbers of the aquo-ions are forced to occur, leading to more effective non-radiative de-excitation. If the perchlorate bridges of the Ln—O—Cl—O—Ln type are formed, the energy would be transferred and the decay time would be shorter even when the coordination number of the lanthanide ions remains unchanged. It could be added as a comment, that our compound was obtained at the concentrations Nd ≈ 2 M and ClO_4 ≈ 6 M, and the coordination of Nd^{3+} was eight, i.e. lower than usually accepted for the aquo-ion.[17]

The formula of the compound suggests at least two different environments for the Nd^{3+} ions because of the odd number of OH^- and H_2O. The

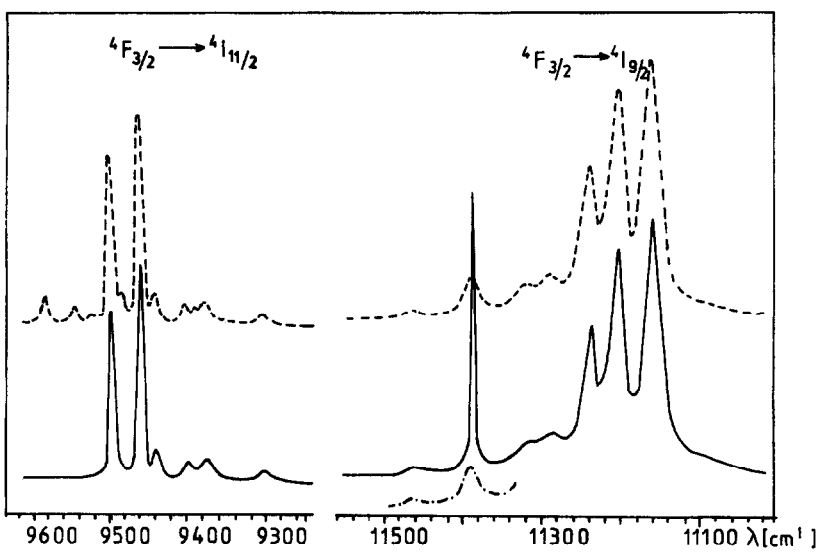

Fig. 3. Fluorescence spectra of $Nd_2(OH)_3(ClO_4)_3 \cdot 5H_2O$ at 5 and 50 K (—, $T = 5$ K, $\lambda_{exc} = 488$ nm; – – –, $T = 50$ K, $\lambda_{exc} = 488$ nm; – · – · –, $T = 5$ K, $\lambda_{exc} = 514$ nm).

crystallographic data, however, suggest the equivalence of all the Nd^{3+} ions. The absorption spectra (at helium temperature) confirm this supposition. The band corresponding to the $^4I_{9/2} \rightarrow {}^2P_{1/2}$ transition is a singlet. The observed equivalence of the neodymium ions from the crystal structure and spectroscopy is due to the migration of the proton. For the $^4I_{9/2} \rightarrow {}^4G_{5/2}, {}^2G_{7/2}$ band, however, we observed more components than follows from group theory for one structural position. The neodymium atoms are bonded by O—Cl—O bridges and the distance between them is equal to 5.13 Å. This is short enough to make the ion-pair interaction possible. As a consequence we observe a doublet structure of the bands of the hypersensitive transition. Moreover, the vibronic components[18] are observed at the higher energies of this transition (Fig. 2). The detailed analysis of all components observed in the whole spectral region will be given in a following paper.

The luminescence spectra of the $^4F_{3/2} \rightarrow {}^4I_{9/2}$ and $^4F_{3/2} \rightarrow {}^4I_{11/2}$ transitions, at low temperatures, are shown in Fig. 3. At 5 K, five and six components should be expected for these two transitions respectively. However, in the region of $^4F_{3/2} \rightarrow {}^4I_{9/2}$ we observed some additional lines. Since it was found from the absorption spectra that the separation of the two sub-levels of the $^4F_{3/2}$ term is almost equal to the energy of the first Stark component of the ground state, the strong line observed at 11200 cm^{-1} can be probably related to the resonance effect. Another reason for the discrepancy between the theoretical and the observed number of components could be either the ion-pair effect or the vibronic transitions. Furthermore, the intensity of the line at 11,387 cm^{-1} is very sensitive to the energy of excitation at 5 K.

The Stark components of $^4I_{9/2} \rightarrow {}^2P_{1/2}$ and $^4I_{9/2} \rightarrow {}^4F_{3/2}$ transitions, together with the transitions in the luminescence spectrum at 5 K, were used to determine the energy level diagrams (Table 3). Splitting of the ground and first excited states is equivalent to 303 and 196 cm^{-1}, respectively.

Table 3. Energy level diagrams for the ground and first excited states of the Nd^{3+} ion

	Observed fluorescence Series I (cm^{-1})	Observed fluorescence Series II (cm^{-1})	Positions of level (cm^{-1})
	11552	11467	
	11472	11387	80
$^4I_{9/2}$	11375	11290	177
	11323	11238	229
	11249	11164	303
	9584	9498	1968
	9545	9460	2007
$^4I_{11/2}$	9520	9440	2029
	9483	9400	2068
	9454	9371	2098
	9387	9303	2165

Splitting of $^4F_{3/2} = 84$ cm^{-1}.

Acknowledgement—This work supported by the Polish Academy of Sciences.

REFERENCES

1. L. Niinistö and M. Leskelä, *Handbook on the Physics and Chemistry of Rare Earths* (Edited by K. A. Gschneider Jr and L. Eyring), Vol. 9, pp. 91–321. North Holland, Amsterdam (1987).
2. F. H. Spedding, M. A. Mohs, J. L. Derer and A. Habenschuss, *J. Chem. Engng Data* 1977, **22**, 142.
3. P. J. Breen and W. De W. Horrocks Jr, *Inorg. Chem.* 1983, **22**, 536.
4. F. Tanaka and S. Yamashita, *Inorg. Chem.* 1984, **23**, 2044.
5. J. Glaser and G. Johansson, *Acta Chem. Scand.* 1981, **35A**, 639.
6. I. Csöregh, E. Huskowska, A. Ertan, J. Legendziewicz and P. Kierkegaard, *Acta Chem. Scand. Ser. A*, to be published.
7. B. R. Judd, *Phys. Rev.* 1962, **127**, 750.
8. J. Legendziewicz, E. Huskowska, A. Waśkowska and Gy. Argay, *Inorg. Chim. Acta* 1984, **92**, 151.
9. I. Csöregh, P. Kierkegaard, J. Legendziewicz and E. Huskowska, *Acta Chem. Scand.* 1987, **41A**, 453.
10. J. Hathaway and A. E. Underhill, *J. Chem. Soc.* 1961, 3091.
11. M. R. Rosenthal, *J. Chem. Educ.* 1973, **50**, 331.
12. M. Ciampolini, C. Mealli and N. Nardi, *J. Chem. Soc., Dalton Trans.* 1980, 376.
13. M. Ciampolini, N. Nardi, R. Cini, S. Mangani and P. Orioli, *J. Chem. Soc., Dalton Trans.* 1979, 1983.
14. M. Ciampolini, P. Dapporto and N. Nardi, *J. Chem. Soc., Chem. Commun.* 1979, 974.
15. J.-C. G. Bünzli and C. Mabillard, *Inorg. Chem.* 1986, **25**, 2750.
16. R. P. Scholer and A. E. Merbach, *Inorg. Chim. Acta* 1975, **15**, 15.
17. A. Habenschuss and F. H. Spedding, *J. Chem. Phys.* 1979, **70**, 3758.
18. P. Caro, O. K. Moune, E. Antic-Fidancev and M. Lemaitre-Blaise, *J. Less Common Met.* 1985, **112**, 153.

Polyhedron Vol. 9, No. 5, pp. 665–668, 1990
Printed in Great Britain

0277–5387/90 $3.00+.00
© 1990 Pergamon Press plc

EQUILIBRIUM CONSTANTS OF METAL AMINO ACID COMPLEXES

F. REY, J. M. ANTELO, F. ARCE* and F. J. PENEDO

Departamento de Química Física, Universidad, 15706 Santiago de Compostela, Spain

(*Received* 15 *June* 1989; *accepted* 21 *September* 1989)

Abstract—The complexation equilibria of the amino acids L-serine and L-leucine with the ions Mg^{2+}, Ca^{2+}, Co^{2+}, Ni^{2+}, Cu^{2+}, Zn^{2+}, Cd^{2+} and Pb^{2+} have been studied at 298 K and ionic strength $I = 0.1$ M in various ethanol–water media. The complexes found and their equilibrium constants are discussed in terms of the acid–base characteristics of the amino acids and the properties of the cations.

The properties of metal ions in solutions containing potential ligands, such as nitrogen-bearing compounds, depend to a large extent on the formation of complexes, calculation of whose distribution requires knowledge of their stability constants. Previous studies of complexes between amino acids and divalent cations have been rather sketchy and carried out under very different conditions,[1–8] which hinders meaningful comparison of the reported stability constants and stoichiometries. On the other hand, the stability of these kind of complexes is sensitive to the solvent composition.[9,10] This article describes an investigation of the formation of complexes between the divalent cations Mg^{2+}, Ca^{2+}, Co^{2+}, Ni^{2+}, Cu^{2+}, Zn^{2+}, Cd^{2+} and Pb^{2+} and the amino acids L-serine and L-leucine. The solvents considered were water and two water–ethanol mixtures.

EXPERIMENTAL

All reagents were Merck p.a. products. The amino acids were purified by standard procedures and their purity checked by gas chromatography.[11] Solutions of the metal ions were prepared from their nitrates except for Zn^{2+}, for which the chloride was used, and their concentrations were determined by titration against EDTA.[2]

Potentiometric titrations were performed in a 250 cm^3 cell thermostatted at 298.0 ± 0.1 K by a HAAKE D3 thermostat. Nitrogen purified by Fieser solutions and passed through the same solvent as used in the cell was bubbled through the cell solution to provide both stirring and an inert atmosphere. The EMF was measured, as indicated by Bates,[13] using a Crison Digilab 517 pH-meter accurate to ± 0.1 mV equipped with an Ingold electrode.

Amino acid–metal solutions of ionic strength $I = 0.1$ M (controlled with KNO_3) were made up in three solvents (water and water–ethanol with 10 and 25% of ethanol by weight) and titrated against solutions of NaOH in the same solvent at the same ionic strength up to an EMF corresponding to pH = 9. All titrations were performed at least twice, and the replicate values of EMF always agreed to within 0.1 mV. The initial concentrations of the various substances used are listed in Table 1 (solutions with different metal–ligand ratios were studied, the concentrations of metal ions and amino acids always being the same for the eight cations).

Protonation and stability constants were calculated by using the program MINIQUAD 75.[14]

RESULTS AND DISCUSSION

Table 2 lists the values obtained for the protonation constants of L-serine and L-leucine, and the stability constants of their complexes with the metal ions studied. The protonation constants of LH stoichiometries correspond to the proton's binding to the amino group of the most basic form of the ligand. L-Serine is less basic than L-leucine, i.e. its protonation constants are smaller, because

* Author to whom correspondence should be addressed.

Table 1. Initial concentrations of solutions of the metal–amino acid complexes

System	[Amino acid] (M)	[Metal] (M)	pH range
Ser–H	$1.06 \cdot 10^{-3}$–$6.37 \cdot 10^{-4}$		2.25–9.12
Leu–H	$1.02 \cdot 10^{-3}$–$6.11 \cdot 10^{-4}$		2.30–9.16
Ser–M	$1.00 \cdot 10^{-3}$–$6.00 \cdot 10^{-4}$	$1.24 \cdot 10^{-4}$–$4.41 \cdot 10^{-5}$	6.64–9.10
Leu–M	$1.02 \cdot 10^{-3}$–$6.11 \cdot 10^{-4}$	$1.24 \cdot 10^{-4}$–$4.41 \cdot 10^{-5}$	6.60–9.01

Table 2. Stability constants of the metal–amino acid complex system. p, q and r refer to the $M_pL_qH_r$ species

				Ethanol (% w/w)		
				0	10	25
System	p	q	r	$\log \beta_{pqr}$	$\log \beta_{pqr}$	$\log \beta_{pqr}$
Ser–H	0	1	1	9.25±0.01	9.27±0.01	9.29±0.01
	0	1	2	11.14±0.02	11.89±0.01	12.05±0.01
Ser–Mg	1	1	0	3.37±0.01	3.63±0.02	3.88±0.03
Ser–Ca	1	1	0	3.59±0.07	3.67±0.05	3.93±0.04
	1	1	−1	−5.25±0.05	−5.11±0.04	−5.13±0.03
Ser–Co	1	1	0	4.40±0.01	4.58±0.03	4.78±0.04
	1	2	0	7.58±0.02	8.32±0.02	9.23±0.03
Ser–Ni	1	1	0	5.19±0.02	5.57±0.04	5.81±0.06
	1	2	0	8.40±0.05	9.07±0.06	10.07±0.08
Ser–Cu	1	1	0	8.08±0.03	8.38±0.07	8.77±0.09
	1	2	0	13.31±0.06	14.25±0.08	15.31±0.06
Ser–Zn	1	1	0	4.47±0.02	4.72±0.01	5.24±0.02
	1	2	0	8.66±0.02	8.79±0.01	9.56±0.02
Ser–Cd	1	1	0	3.95±0.01	4.06±0.02	4.22±0.05
	1	2	0	7.08±0.05	7.75±0.02	8.73±0.02
Ser–Pb	1	1	0	4.66±0.05	4.89±0.01	5.25±0.02
	1	1	−1	−3.53±0.03	−3.57±0.01	−3.53±0.02
Leu–H	0	1	1	9.89±0.01	9.90±0.01	9.91±0.01
	0	1	2	12.12±0.01	12.64±0.01	12.90±0.01
Leu–Mg	1	1	0	3.69±0.02	3.94±0.05	4.21±0.04
Leu–Ca	1	1	0	3.96±0.04	4.07±0.09	4.25±0.05
	1	1	−1	−5.09±0.03	−5.1±0.1	−5.04±0.08
Leu–Co	1	1	0	4.52±0.03	4.68±0.04	4.99±0.03
	1	2	0	8.35±0.03	9.03±0.02	9.50±0.02
Leu–Ni	1	1	0	5.33±0.02	5.68±0.02	6.10±0.01
	1	2	0	8.71±0.05	9.86±0.02	10.84±0.01
Leu–Cu	1	1	0	8.34±0.04	8.62±0.05	9.31±0.04
	1	2	0	14.48±0.07	15.17±0.08	15.93±0.03
Leu–Zn	1	1	0	4.73±0.03	4.94±0.03	5.43±0.02
	1	2	0	9.30±0.01	9.58±0.02	10.15±0.01
Leu–Cd	1	1	0	4.30±0.04	4.39±0.04	4.62±0.04
	1	2	0	8.44±0.03	8.73±0.02	9.24±0.02
Leu–Pb	1	1	0	5.07±0.05	5.21±0.02	5.36±0.02
	1	1	−1	−3.64±0.04	−3.63±0.02	−3.54±0.02

of the electron-withdrawing effect of the neighbouring OH group.

The stoichiometries and stability constants of the complexes formed were determined by trying various possible composition models for the system ($ML+ML_2$, $ML+ML_2+MLH_{-1}$, $ML+ML_2+ML_3$) and using the program MINIQUAD 75 to identify that which, according to χ^2, r factor and sum of squares parameters, best fitted the experimental data. The absence of polynuclear species was shown by an individual analysis of each of the experimental curves obtained for the various concentrations of metal ion and amino acid, since the same stoichiometric indices and stability constants were obtained in all cases. It may be concluded that the only complexes present were those listed in Table 2.

All of the systems studied, except for those involving Mg^{2+}, Ca^{2+} and Pb^{2+}, were found to contain only complexes of the forms ML and ML_2, which agrees with other published findings. The detection of just a single amino acid–magnesium complex may be attributed to the instability of high-order complexes in the working conditions of this study. Moreover, in systems involving Ca^{2+} and Pb^{2+}, MLH_{-1} complexes were formed by the loss of a proton from the ML complexes.

The fact that the L-leucine complexes had greater stability constants than the corresponding complexes between the same metal ion and L-serine may be attributed to L-leucine being the more basic of the two amino acids. That the Ca^{2+} complexes are more stable than Mg^{2+} ones is explicable in terms of the smaller hydration energy of the Ca^{2+} ion,[14] since the formation of ion–ligand bonds requires that ion–solvent bonds are broken first.

The order of stability found for the complexes of the other divalent ions studied ($Cd^{2+} < Co^{2+} < Zn^{2+} < Pb^{2+} < Ni^{2+} < Cu^{2+}$) coincides with that observed for almost all amino acid ligands. Figure 1 shows that $\log\beta_1$ and $\log\beta_2$ increase from Co^{2+} to Ni^{2+} as predicted by ligand field theory, and then drop to Zn^{2+} and Cd^{2+}. The classic sharp maximum for Cu^{2+} is due to the stabilizing contribution of the Jahn–Teller effect, and the ratio $\log\beta_1$ (Ni^{2+})/$\log\beta_1$ (Cu^{2+}) agrees with the value observed in complexes with a wide range of other amino acids.[6] Figure 1 also shows that the variation of $\log\beta_2$ is greater than that of $\log\beta_1$, i.e. the binding of the second ligand is more sensitive to the nature of the metal ion.

The results listed in Table 2 show that the presence of ethanol in the solvent brings about an increase in the stability of the complexes. This confirms that the formation of a metal ion complex in solution is dependent on the competition of ethanol and water for coordination sites around cations.[15,16]

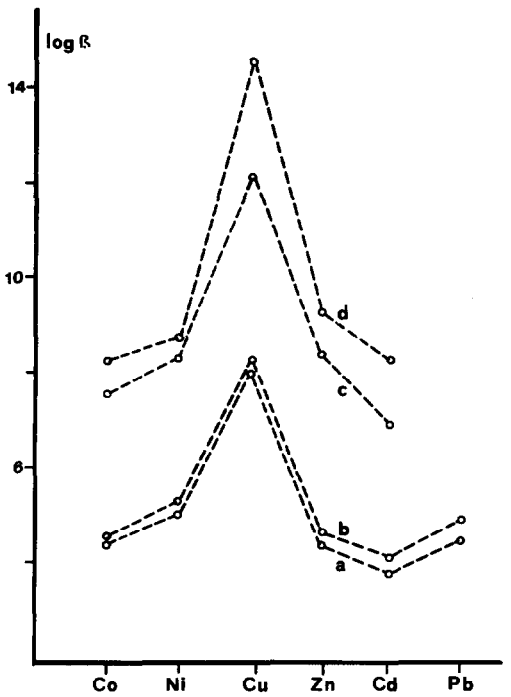

Fig. 1. Variation of stability constants of some divalent metal complexes: (a) $\log\beta_1$ L-serine; (b) $\log\beta_1$ L-leucine; (c) $\log\beta_2$ L-serine; (d) $\log\beta_2$ L-leucine.

REFERENCES

1. L. G. Sillén and A. E. Martell, *Stability Constants of Metal–Ion Complexes*, Special Publications 17 and 25. Chemical Society, London (1964) and (1971).
2. R. M. Smith and A. E. Martell, *Critical Stability Constants*, Vols 1–5. Plenum Press, New York (1974), (1975), (1976), (1977) and (1982).
3. H. Irving and R. J. P. Williams, *J. Chem. Soc.* 1953, 3192.
4. M. L. S. Simoes Gonçalves and M. M. Correia dos Santos, *J. Electroanal. Chem.* 1984, **163**, 357; 1985, **187**, 333.
5. A. Cole, C. Furnival, Z. X. Huang, D. C. Jones, P. M. May, G. S. Smith, J. Whitaker and D. R. Williams, *Inorg. Chim. Acta* 1985, **108**, 165.
6. R. M. Smith, R. J. Moteikakis and A. E. Martell, *Inorg. Chim. Acta* 1985, **103**, 73.
7. J. M. Pingarron, I. del Barrio and L. M. Polo, *Anal. Quim.* 1984, **40B**, 141.
8. D. D. Perrin, *Stability Constants of Metal–Ion Complexes. Part B. Organic Ligands*, IUPAC Chemical Data Series, No. 22. Pergamon Press, Oxford (1977).
9. P. K. Migal and G. F. Serova, *Russ. J. Inorg. Chem.* 1965, **10**, 1366.
10. B. Kirson and L. Barsily, *Bull. Soc. Chim. Fr.* 1959, 1226.

11. S. L. McKenzie and D. Tenaschuk, *J. Chromatogr.* 1979, **171**, 195.
12. F. Bermejo and A. Prieto, *Aplicaciones Analíticas del AEDT y Análogos*. Serv. Publ. Univ., Santiago de Compostela (1960).
13. R. G. Bates, *Crit. Rev. Anal. Chem.* 1981, **10**, 247.
14. P. Gans, A. Sabbatini and A. Vacca, *Inorg. Chim. Acta* 1976, **18**, 237.
15. Y. I. Tur'yan and N. I. Bondarenko, *Zh. Neorg. Khim.* 1959, **4**, 2970.
16. J. M. Antelo, F. Arce, F. Rey and A. Varela, *Bull. Soc. Chim. Fr.* 1987, 435.

Polyhedron Vol. 9, No. 5, pp. 669–679, 1990
Printed in Great Britain

0277–5387/90 $3.00+.00
© 1990 Pergamon Press plc

REDUCTION OF TUNGSTEN COMPLEXES WITH PRIMARY PHOSPHINES AND LITHIUM DIALKYL PHOSPHIDES. X-RAY CRYSTAL STRUCTURES OF $[(Cp^*WCl_2)_2 \cdot (t\text{-}Bu_2PPt\text{-}Bu_2)_2]$, $[(Cp^*WCl_4)(H_2PPh)]$, $[\{(PhN)WCl_2(PMe_3)_2\}_2(\mu\text{-}N_2)]$ and *trans*-$WCl_4(H_2Pt\text{-}Bu)_2$ ($Cp^* = \eta^5\text{-}C_5Me_5$)

C. JEFF HARLAN, RICHARD A. JONES,† STEFAN U. KOSCHMIEDER and CHRISTINE M. NUNN

Department of Chemistry, The University of Texas at Austin, Austin, TX 78712, U.S.A.

(*Received* 30 *June* 1989 ; *accepted* 21 *September* 1989)

Abstract—The reduction of several high oxidation state tungsten halide complexes by lithium organophosphides and primary phosphines is described. Reaction of Cp^*WCl_4 ($Cp^* = \eta 5\text{-}C_5Me_5$) with $t\text{-}Bu_2PLi$ (4 equiv.) results in reduction of the metal and coupling of $t\text{-}Bu_2P$ units to form a mixture of $[Cp^*WCl_2]_2$ and $t\text{-}Bu_2PPt\text{-}Bu_2$ which co-crystallize as $[(Cp^*WCl_2)_2 \cdot (t\text{-}Bu_2PPt\text{-}Bu_2)_2]$ (**1**). There are no close intermolecular contacts between the tungsten(III) chloride-bridged dimer $(Cp^*WCl_2)_2$ and $(t\text{-}Bu_2PPt\text{-}Bu_2)$ in the solid state. In the crystal structure of **1** the diphosphine exists in the *gauche* conformation found in other structurally characterized diphosphines. The $(Cp^*WCl_2)_2$ dimer has all four chloride ligands in bridging positions. Reaction of $[Cp^*WCl_4]_2$ with 2 equiv. of Ph(H)PLi forms the monomeric phosphine adduct $(Cp^*WCl_4)(H_2PPh)]$ (**2**) in 50% yield. The reaction of WCl_6 with excess $t\text{-}BuPH_2$ in dichloromethane gives *trans*-$WCl_4(H_2Pt\text{-}Bu)_2$ (**3**). Reaction of $[(PhN)Cl_3W(PMe_3)_2]$ with $t\text{-}Bu_2PLi$ (2 equiv.) under nitrogen leads to reduction and formation of the $\mu\text{-}N_2$ bridged W(IV) dimer $[\{(PhN)WCl_2(PMe_3)_2\}_2(\mu\text{-}N_2)]$ (**4**) in which the W—N—N—W core is virtually linear. Crystal data for **1**: $C_{52}H_{102}P_4Cl_4W_2$, $M = 1360.8$, monoclinic, $P2_1/n$ (No. 14), $a = 8.309(9)$, $b = 24.50(1)$, $c = 15.117(8)$ Å, $\beta = 95.98(1)°$, $U = 3060.5$ Å^3, $Z = 2$, $R = 0.0385$, $R_w = 0.0474$. Crystal data for **2**: $C_{16}H_{21}PCl_4W$, $M = 569.98$, monoclinic, $P2_1/c$ (No. 14), $a = 8.776(9)$, $b = 16.310(6)$, $c = 16.580(1)$ Å, $\beta = 101.21(6)°$, $U = 2327.8$ Å^3, $Z = 4$, $R = 0.046$, $R_w = 0.069$. Crystal data for **3**: $C_8H_{20}P_2Cl_4W$, M = 503.85, monoclinic, $C2$ (No. 5), $a = 11.136(5)$, $b = 8.218(7)$, $c = 9.832(8)$ Å, $\beta = 93.20(6)°$, $U = 898.29$ Å^3, $Z = 1$, $R = 0.0330$, $R_w = 0.0369$. Crystal data for **4**: $C_{24}H_{46}P_4Cl_4N_4W_2$, $M = 1024.07$, monoclinic, $P2_1/c$ (No. 14), $a = 15.702(2)$, $b = 12.580(2)$, $c = 19.416(4)$ Å, $\beta = 94.41(1)°$, $U = 3823.9$ Å^3, $Z = 4$, $R = 0.043$, $R_w = 0.051$.

The reduction of high valent tungsten halide compounds has been the focus of much research.[1–5] This interest stems in part from the prospect of activating dinitrogen and finding a catalytic cycle by which nitrogen may be functionalized and then released to yield industrially important chemicals.[6] Low valent tungsten and molybdenum complexes have been shown to be effective binding agents for the ligation of molecular nitrogen and, in some cases, the stoichiometric conversion of N_2 to hydrazine or ammonia.[7–10] Traditional reducing reagents such as Na, Mg, Zn are most commonly employed to effect stoichiometric reductions of transition metal centres, however, a number of alternative routes, such as pyridine and tertiary phosphines, have been used in tungsten and molybdenum chemistry.[3–11] In this paper we describe the reactions of a number of high valent tungsten (W^V, W^{VI}) chloride complexes with primary phosphines and lithium di-

† Author to whom correspondence should be addressed.

organophosphides as reducing agents to give lower oxidation state (W^{III} and W^{IV}) products.

As part of our studies of sterically demanding phosphido (R_2P^-) and arsenido (R_2As^-) complexes of the transition metals[1,2] we recently turned our attention to the group 6 metal tungsten for which relatively few phosphido complexes are known. One general route to phosphido complexes which works well for both early and late transition metals is salt elimination reactions involving alkali metal phosphides, e.g.

$$LiPR_2 + L_yMX \rightarrow L_yMPR_2 + LiX$$

L_y = other ligands, M = transition metal, X = halide.

We therefore investigated the reactions of several high oxidation state tungsten complexes with lithium phosphides with the aim of synthesizing some new phosphido complexes. Reduction of the tungsten occurred with the $LiPR_2$ reagents acting as reducing agents. We were, however, able to isolate and characterize a number of interesting new complexes from these reactions. Thus reaction of Cp^*WCl_4 with t-Bu_2PLi produces a mixture of $[Cp^*WCl_2]_2$ and [t-Bu_2PPt-Bu_2] (1 : 2) (**1**) in which the tungsten(III) dimer $[Cp^*W(\mu\text{-}Cl)_2]_2$ and [t-Bu_2PPt-Bu_2] co-crystallize. There are no close intermolecular contacts between the two molecules in the solid state and the structural characterization of both moieties is of interest. In contrast, a similar reaction of Cp^*WCl_4 with Ph(H)PLi simply produced the phosphine adduct $[(Cp^*WCl_4)(H_2PPh)]$ (**2**) in low yield. This may be a result of disproportionation of Ph(H)PLi into Li_2PPh and H_2PPh. The reaction of t-$BuPH_2$ with WCl_6 in dichloromethane results in the formation of *trans*-$WCl_4(H_2Pt\text{-}Bu)_2$ (**3**). The reduction of tungsten(VI) in this case is effected by the primary phosphine t-$BuPH_2$. Finally the phenylimido tungsten(V) complex $[(PhN)WCl_3(PMe_3)_2]$ reacts with t-Bu_2PLi under a nitrogen atmosphere to give the linear dinitrogen bridged complex $[\{(PhN)WCl_2(PMe_3)_2\}_2(\mu\text{-}N_2)]$ (**4**). The new compounds **1**–**4** have been characterized spectroscopically and their solid-state structures have been determined by X-ray crystallography. The reactions and new compounds are shown in Scheme 1.

RESULTS AND DISCUSSION

Reaction of $[Cp^*WCl_4]_2$ *with* LiPt-Bu_2: $[(Cp^*WCl_2)_2 \cdot (t\text{-}Bu_2PPt\text{-}Bu_2)_2]$ (**1**)

The compound $[Cp^*WCl_4]_2$ was first reported by Schrock and co-workers and has been used for the synthesis of alkyl and hydrido derivatives which are

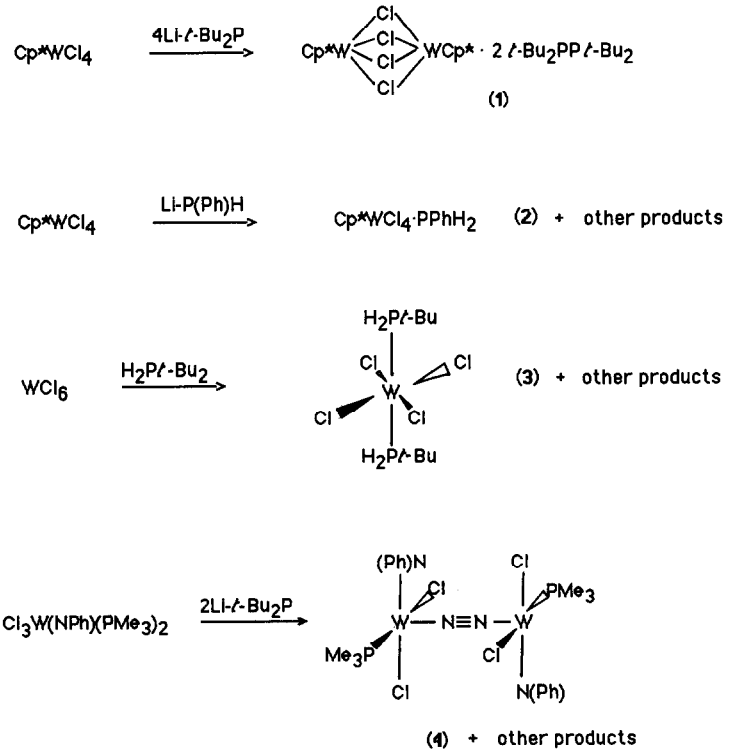

Scheme 1.

relevant to catalytic CO reduction.[14,15] We initially hoped to synthesize sterically hindered phosphido derivatives of tungsten *via* reactions of $[Cp^*WCl_4]_2$ and other compounds with alkali metal phosphido species. However, these appear to be too powerful reducing reagents and give only reduced tungsten complexes.

Thus reaction of $[Cp^*WCl_4]_2$ with four equivalents of LiP*t*-Bu_2 in THF produces the tungsten(III) product $[Cp^*WCl_2]_2$ as a green microcrystalline solid. If the supernatant liquid remaining from the initial crystallization is concentrated further and cooled (−20°C), brown X-ray quality crystals of formula $[(Cp^*WCl_2)_2 \cdot (t\text{-}Bu_2PPt\text{-}Bu_2)_2]$ (**1**) may be isolated. A single crystal X-ray analysis showed this to be a mixture of co-crystallized $[Cp^*WCl_2]_2$ and $[t\text{-}Bu_2PPt\text{-}Bu_2]$. The origin of the coupled *t*-Bu_2P units is presumably from the reduction of $[Cp^*WCl_4]_2$ to $[Cp^*WCl_2]_2$ and LiCl [eq. (1)]. Of relevance here is the reduction of $MoCl_3$ by LiP*t*-Bu_2 to yield the homoleptic phosphido complex $[Mo(\mu\text{-}t\text{-}Bu_2P)(t\text{-}Bu_2P)]_2$. This reaction also produces $[t\text{-}Bu_2PPt\text{-}Bu_2]$.[16]

$$[Cp^*WCl_4]_2 + 4LiPt\text{-}Bu_2 \rightarrow [Cp^*WCl_2]_2 + 4LiCl + 2[t\text{-}Bu_2PPt\text{-}Bu_2] \quad (1)$$

The ^1H NMR spectrum for **1** shows resonances for both moieties. The protons of the Cp* ligand appear as a singlet (δ 2.4 ppm) and the *t*-Bu protons of the diphosphine appear as a 1 : 2 : 1 triplet (δ 1.35 ppm, $J_{P\text{—}H(apparent)} = 19$ Hz). The ^{31}P NMR shows a singlet at 39.94 ppm which is close to the literature value for free $[t\text{-}Bu_2PPt\text{-}Bu_2]$ ($\delta = 37.40$ ppm).[17]

X-ray structure of **1**

An ORTEP view of the tungsten moiety is shown in Fig. 1 and a ball and stick representation of the diphosphine, down the P—P axis, in Fig. 2. A view of the crystal packing arrangement in the unit cell is shown in Fig. 3. Data collection and crystal structure parameters are given in Table 1 and key bond lengths and angles are in Table 2. There are no close intermolecular contacts between the diphosphine and the tungsten dimer in the solid state. Compound **1** crystallizes in the monoclinic space group $P2_1/n$ with two molecules of $[Cp^*WCl_2]_2$ and four molecules of $[t\text{-}Bu_2PPt\text{-}Bu_2]$ in the unit cell. The

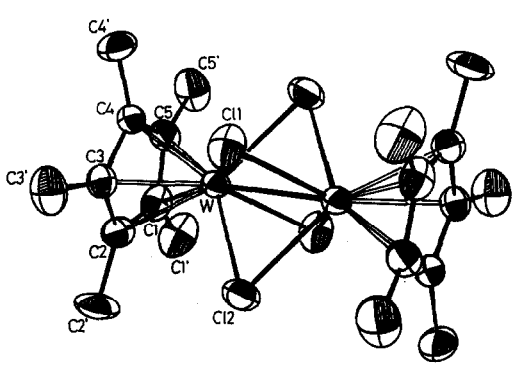

Fig. 1. ORTEP view of the $[Cp^*WCl_2]_2$ part of **1**.

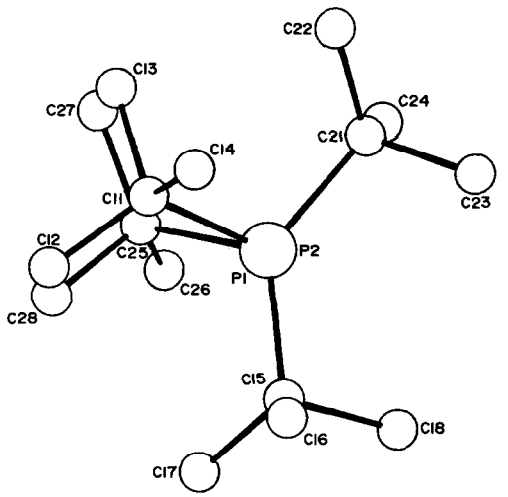

Fig. 2. Ball and stick view of the $[t\text{-}Bu_2PPt\text{-}Bu_2]$ part of **1** viewed down the P—P axis.

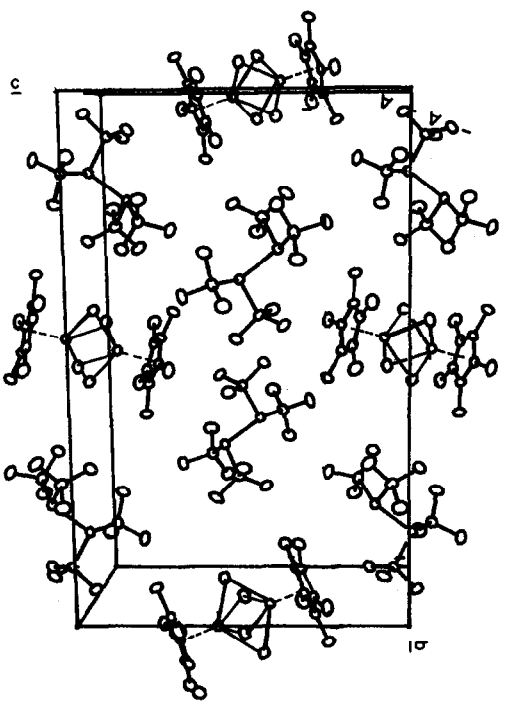

Fig. 3. View of the unit cell of **1**.

Table 1. Crystal structure parameters for **1–4**

	1	**2**	**3**	**4**
Description of crystal				
Colour	Brown	Green	Red	Black
Habit	Prism	Prism	Irregular	Prism
Maximum crystal dimensions (mm)	0.3 × 0.15 × 0.5	0.30 × 0.25 × 0.45	0.15 × 0.20 × 0.25	0.15 × 0.20 × 0.25
Unit cell				
Crystal system	Monoclinic	Monoclinic	Monoclinic	Monoclinic
Space group	$P2_1/n$ (No. 14)	$P2_1/c$ (No. 14)	$C2$ (No. 5)	$P2_1/c$ (No. 14)
Unit cell parameters:				
a (Å)	8.309(2)	8.776(2)	11.136(2)	15.702(2)
b (Å)	24.495(4)	16.310(3)	8.218(2)	12.580(2)
c (Å)	15.117(3)	16.580 (4)	9.832(3)	19.416(4)
β (°)	95.979(2)	101.21(2)	93.196(2)	94.41(1)
U (Å^3)	3060.5	2327.8	898.29	3823.8
Z	2	4	1	4
Formula	$C_{52}H_{102}P_4Cl_4W_2$	$C_{16}H_{21}PCl_4W$	$C_8H_{20}P_2Cl_4W$	$C_{24}H_{46}P_4N_4Cl_4W_2$
Molecular weight (g mol^{-1})	1360.80	569.98	503.86	1024.07
Calculated density (g cm^{-3})	1.477	1.626	0.93	1.779
μ-calc. (cm^{-1})	41.47	55.97	36.61	66.11
Data collection				
Radiation (Å)	Mo–K_α (0.71073)	Mo–K_α (0.71073)	Mo–K_α (0.71073)	Mo–K_α (0.71073)
Scan technique	θ–2θ	θ–2θ	θ–2θ	θ–2θ
Scan width (°)	1.0 + 0.35 (tan θ)	0.8 + 0.35 (tan θ)	0.8 + 0.35 (tan θ)	0.9 + 0.35 (tan θ)
Range of indices	(0, 9) (0, 29) (−18, 18)	(0, 10) (0, 19) (−19, 19)	(0, 12) (0, 9) (−11, 11)	(0, 17) (0, 14) (−22, 22)
2θ range (°)	3.0–50.0	3.0–50.0	3.0–50.0	3.0–48.0
Number of reflections measured	5908	4552	898	6553
Standard reflections				
Intensity	(3, 15, −1) (0, 16, −3)	(1, 5, 10) (0, 11, 3)	(6, 0, 2) (5, 3, 1)	(3, 0, −12) (5, 2, 10)
Orientation	Not used	(6, 2, −5) (6, 0, −6)	(6, 2, 1) (6, 2, 0)	(4, 6, 7) (4, 7, 4)
Decay of standards	−1.5%	−1%	−10.4%	−6.4%
Minimum % transmission	54.62	56.04	43.64	68.46
Maximum % transmission	99.89	99.74	99.56	99.83
Average % transmission	79.53	83.94	75.37	81.02
Agreement factor for averaged reflections intensity	0.011	0.026	0.019	0.063
Structure determination				
Number of reflections used [$I > 3\sigma(I)$]	4000	2740	828	2612
Number of parameters varied	280	199	82	343
Data/parameter ratio	14.286	13.769	10.098	7.615
Shift-to-error ratio	0.001	0.023	3.670	0.028
ESD of an observation of unit weight	6.0812	7.7556	3.8023	2.7228
R	0.038	0.046	0.033	0.043
R_w	0.047	0.069	0.037	0.051

$R = \Sigma(|F_o| - |F_c|)/\Sigma|F_o|$.
$R_w = [\Sigma\omega(|F_o| - |F_c|)^2/\Sigma\omega(|F_o|)^2]^{1/2}$.

Table 2. Selected bond lengths (Å) and angles (°) for **1**

Lengths (Å)			
W—W	2.626(1)	W—C(5)	2.238(9)
W—Cl(1)	2.482(3)	P(1)—P(2)	2.233(3)
W—Cl(2)	2.482(3)	P(1)—C(11)	1.93(1)
W—C(1)	2.35(1)	P(1)—C(15)	1.92(1)
W—C(2)	2.335(9)	P(2)—C(21)	1.92(1)
W—C(3)	2.209(9)	P(2)—C(25)	1.92(1)
W—C(4)	2.162(8)		
Angles (°)			
W—W—Cl(1)	58.31(6)	Cl(1)—W—C(1)	90.3(2)
W—W—Cl(2)	58.03(6)	Cl(1)—W—C(2)	110.5(2)
W—W—C(1)	148.4(2)	Cl(1)—W—C(3)	148.1(2)
W—W—C(2)	148.3(2)	Cl(1)—W—C(4)	141.4(3)
W—W—C(3)	145.7(2)	Cl(1)—W—C(5)	103.6(2)
W—W—C(4)	146.2(2)	Cl(1)—W—Cl(2)	73.64(9)
W—W—C(5)	146.9(2)	Cl(2)—W—Cl(2)′	116.15(9)
Cl(1)—W—Cl(1)	116.27(9)	W—Cl(1)—W′	63.73(6)
Cl(1)—W—Cl(2)	73.90(8)	W—Cl(2)—W′	63.85(6)
P(1)—C(11)—C(12)	117.7(8)	Cl(2)—W—C(1)	120.5(3)
P(1)—C(11)—C(13)	106.9(7)	Cl(2)—W—C(2)	152.4(3)
P(1)—C(11)—C(14)	104.6(7)	Cl(2)—W—C(3)	132.5(2)
P(1)—C(15)—C(16)	108.7(7)	Cl(2)—W—C(4)	96.7(2)
P(1)—C(15)—C(17)	116.2(7)	Cl(2)—W—C(5)	91.6(3)
P(1)—C(15)—C(18)	105.2(7)		
P(2)—C(21)—C(22)	115.4(7)	(P2)—P(1)—C(15)	100.1(3)
P(2)—C(21)—C(23)	104.9(7)	C(11)—P(1)—C(15)	109.6(5)
P(2)—C(21)—C(24)	109.0(7)	P(1)—P(2)—C(21)	99.4(3)
P(2)—C(25)—C(26)	104.8(7)	P(1)—P(2)—C(25)	121.6(4)
P(2)—C(25)—C(27)	119.1(7)	C(21)—P(2)—C(25)	108.7(5)
P(2)—C(25)—C(28)	107.0(8)		

Numbers in parentheses are the ESDs in the least significant digits.

tungsten moiety exists as a dimer in the solid state with all four chlorine atoms occupying bridging positions across a W—W single bond (2.626(1) Å), each tungsten atom thus achieves an 18-electron count. Dimeric structures containing one bridging chloride per metal atom have been proposed for $[Cp^*WCl_4]_2$[13] and $[CpMoCl_4]_2$.[18a] The five-coordinate tungsten atoms have a square-pyramidal coordination geometry if the ring centroids of the Cp* ligands are taken as the apexes of the respective pyramids. There is a crystallographically imposed centre of inversion in the molecule and the C_5Me_5 rings adopt a staggered configuration. The molecule is essentially isostructural with $[Mo(\eta^5\text{-}C_5H_4i\text{-}Pr)(\mu\text{-}Cl)_2]_2$[18b] and the group 5 tantalum species $[Ta(\eta^5\text{-}C_5Me_5)(\mu\text{-}Br)_2]_2$.[18c]

The *t*-Bu_2P units of the diphosphine molecule adopt the semi-eclipsed form also found in $[Cy_2PPCy_2]$.[19] This structural type has also been observed in other P_2X_2 species (X = H, halide) and is thought to be a manifestation of the *gauche* effect.[20] The torsion angle about the eclipsed *t*-Bu_2P units is slightly greater than that found in $[Cy_2PPCy_2]$ (for $[t\text{-}Bu_2PPt\text{-}Bu_2]$; 13.5°, for $[Cy_2PPCy_2]$; 5.5°).[19] The C(25)—P(2)—P(1) angle [121.6(4)°] is also wider than the corresponding bond angle in $[Cy_2PPCy_2]$ [108.0(3) and 107.4(3)°]. Both differences may be ascribed to the greater steric demands of *t*-butyl groups relative to cyclohexyl groups. The P—P distance of 2.233(3) Å is within normal bonding distances for P—P bonded molecules.[21] While the average of the P—C bond lengths $[(P—C)_{av}]$ in $[t\text{-}Bu_2PPt\text{-}Bu_2]$ is slightly longer than that found for the cyclohexyl derivative or the tetramer $[t\text{-}BuP]_4$, there are no unusual distortions and this slight lengthening may again be attributed to the greater steric influences of the *t*-butyl groups (for $[t\text{-}Bu_2PPt\text{-}Bu_2]$; P—$C_{av}$ = 1.92 Å, for $[Cy_2PPCy_2]$; P—C_{av} = 1.88 Å, for $[Pt\text{-}Bu]_4$; P—C_{av} = 1.89 Å).[22]

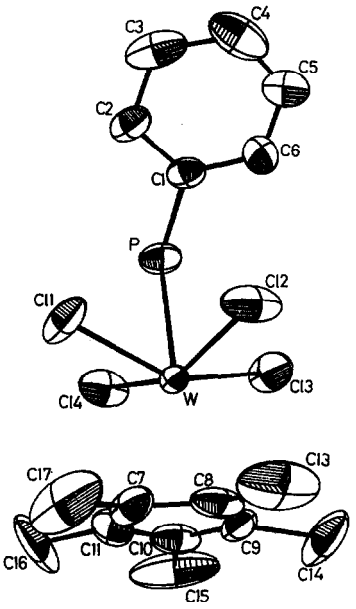

Fig. 4. ORTEP view of **2** showing atom numbering scheme.

Reaction of LiPPh(H) *with* $[Cp^*WCl_4]_2$; *synthesis of* $[(Cp^*WCl_4)(H_2PPh)]$ (**2**)

The reaction between LiPPh(H) and $[Cp^*WCl_4]_2$ led to the formation of the 17-electron species $[(Cp^*WCl_4)(H_2PPh)]$ (**2**). Dark brown hydrocarbon soluble crystals of **2** are stable for short periods in air. Paramagnetic behaviour is observed in the solution state ($\mu_{eff} = 0.6$ BM, Evans' method, 23°C, toluene). The source of H_2PPh is presumably from abstraction of a proton from the solvent (THF) or from a disproportionation of LiPHPh. The analogous trimethylphosphine adduct $[Cp^*WCl_4(PMe_3)]$ has been described but no crystal structure has been reported.[14] The paramagnetic product shows only broad resonances in the ^1H and ^{31}P NMR spectra.

X-ray structure of **2**

Crystals of **2** may be crystallized from toluene (−20°C) and an ORTEP view of the molecule is

Table 3. Selected bond lengths (Å) and angles (°) for **2**

		Lengths (Å)	
W—Cl(1)	2.412(7)	W—C(11)	2.38(2)
W—Cl(2)	2.376(7)	P—C(1)	1.80(2)
W—Cl(3)	2.369(6)	W—C(8)	2.40(2)
W—Cl(4)	2.399(6)	W—C(9)	2.40(2)
W—P	2.569(5)	W—C(10)	2.37(2)
W—C(7)	2.40(2)		
		Angles (°)	
Cl(1)—W—Cl(2)	86.9(3)	Cl(2)—W—C(9)	96.6(5)
Cl(1)—W—Cl(3)	149.0(2)	Cl(2)—W—C(10)	128.7(6)
Cl(1)—W—Cl(4)	85.7(2)	Cl(2)—W—C(11)	129.3(6)
Cl(1)—W—P	73.0(2)	Cl(3)—W—Cl(4)	86.6(3)
Cl(1)—W—C(7)	76.9(6)	Cl(3)—W—P	76.1(2)
Cl(1)—W—C(8)	103.8(6)	Cl(3)—W—C(7)	133.8(6)
Cl(1)—W—C(9)	133.0(5)	Cl(3)—W—C(8)	103.2(6)
Cl(1)—W—C(10)	119.8(6)	Cl(3)—W—C(9)	77.6(5)
Cl(1)—W—C(11)	86.5(6)	Cl(3)—W—C(10)	83.3(6)
Cl(2)—W—Cl(3)	84.6(3)	Cl(3)—W—C(11)	121.5(6)
Cl(2)—W—Cl(4)	149.3(2)	Cl(4)—W—P	70.8(2)
Cl(2)—W—P	78.5(2)	Cl(4)—W—C(7)	109.2(6)
Cl(2)—W—C(7)	98.0(6)	Cl(4)—W—C(8)	133.3(6)
Cl(2)—W—C(8)	77.4(6)	Cl(4)—W—C(9)	110.2(5)
Cl(4)—W—C(10)	80.3(5)	P—W—C(10)	147.7(5)
Cl(4)—W—C(11)	79.9(6)	P—W—C(11)	145.0(6)
P—W—C(7)	149.9(6)	W—P—C(1)	122.9(6)
P—W—C(8)	155.9(6)	P—C(1)—C(2)	117(2)
P—W—C(9)	153.6(5)	P—C(1)—C(6)	119(2)

Numbers in parentheses are the ESDs in the least significant digits.

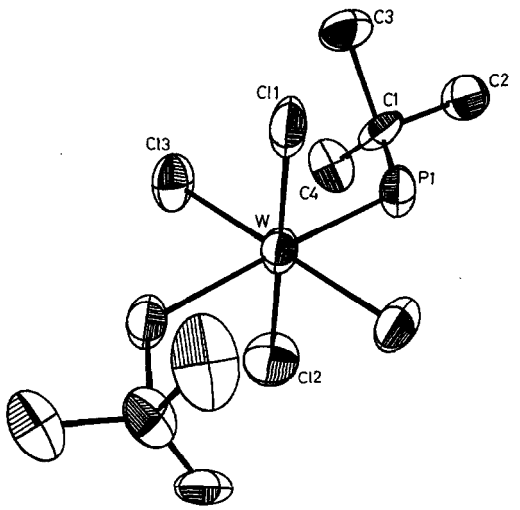

Fig. 5. ORTEP view of **3** showing atom numbering scheme.

shown as Fig. 4. Key bond lengths and angles are given in Table 3. Compound **2** crystallizes in the monoclinic space group $P2_1/c$ with four molecules in the unit cell. The molecule exists as a monomer in the solid state. The molecular geometry may be described as distorted octahedral with the chlorine atoms lying in the equatorial plane. The W—P separation of 2.568(5) Å is clearly indicative of a dative interaction. The hydrogen atoms of the H_2PPh ligand were not located in the X-ray structure, however a ν(P—H) stretch at 2300 cm^{-1} in the IR spectrum confirms their presence. There is a slight but interesting distortion in the W—Cl bond lengths. The chlorine atoms lying underneath the phenyl substituent of the coordinated phosphine have slightly shorter W—Cl bonds [W—Cl(2) = 2.376(7) Å, W—Cl(3) = 2.369(6) Å] than the remaining chloride ligands [W—Cl(1) = 2.412(7), W—Cl(4) = 2.399(6) Å]. This may be a reflection of steric compression exerted on the chloride ligands by the bulky Cp* ligand and the phenyl substituent of the phosphorus ligand. Presumably the steric congestion about the tungsten atom in **2** makes it impossible for two monomers to couple and achieve an electron count of 18 *via* a dimeric structure.

Reaction of WCl_6 *with* t-$BuPH_2$: *synthesis of* trans-$WCl_4(H_2Pt\text{-}Bu)_2$ **(3)**

The reduction of tungsten hexachloride to form WCl_4L_2 derivatives is well known.[10,23,24] This class of molecule has seen broad use as a starting material in the preparation of many tungsten compounds.[4,5,7,11,25–28] To our knowledge no analogous complexes featuring primary phosphines have so far been reported.

Excess t-$BuPH_2$ reacts with WCl_6 in dichloromethane to give a red solution from which the crystalline compound *trans*-$WCl_4(H_2Pt\text{-}Bu)_2$ **(3)** may be obtained in high yield. The compound is paramagnetic in solution (μ_{eff} = 3.11 BM, Evans' method, 23°C, toluene), as is found for other WX_4L_2 complexes,[29] and shows two ν(P—H) stretches in the Raman spectrum 2352, 2369 cm^{-1}). The IR spectrum contains no corresponding absorp-

Table 4. Selected bond lengths (Å) and angles (°) for **3**

		Lengths (Å)	
W—Cl(1)	2.34(1)	W—Cl(3)	2.343(2)
W—Cl(1)	2.34(1)	W—P(1)	2.540(2)
W—Cl(2)	2.301(8)	W—P(1)	2.540(2)
W—Cl(2)	2.301(8)	P(1)—C(1)	1.851(8)
W—Cl(3)	2.343(2)	P(1)—C(4)	2.57(2)
		Angles (°)	
Cl(1)—W—Cl(2)	180.00(0)	Cl(2)—W—Cl(3)	90.5(4)
Cl(1)—W—Cl(3)	89.5(4)	P(1)—W—P(1)	178.3(8)
Cl(1)—W—P(1)	90.8(4)	W—P(1)—C(1)	125.0(3)
Cl(2)—W—Cl(3)	90.5(4)	W—P(1)—C(4)	106.3(5)
Cl(2)—W—P(1)	89.2(4)	P(1)—C(1)—C(2)	104.6(7)
Cl(3)—W—Cl(3′)	179.0(8)	P(1)—C(1)—C(3)	106(2)
Cl(3)—W—P(1)	96.58(6)	P(1)—C(1)—C(4)	109(2)
Cl(3)—W—P(1)	83.44(6)		

Numbers in parentheses are the ESDs in the least significant digits.

tions consistent with the *trans* configuration and a centre of symmetry.

X-ray structure of **3**

An ORTEP of **3** is shown in Fig. 5. Crystal structure parameters and key bond lengths and angles are given in Tables 1 and 4, respectively. The compound crystallizes in the monoclinic space group $C2$ (No. 5) with a single molecule in the unit cell. The molecular geometry is pseudo-octahedral and the molecule has a crystallographically imposed two-fold axis of symmetry passing through the Cl(1)—W—Cl(2) vector. The four chlorine atoms are essentially planar and lie in equatorial positions. The two phosphine ligands are *trans* [W—P(1) = 2.540(2) Å]. The steric influence of the *t*-butyl substituents on the phosphorus ligand is reflected in the Cl(3)—W—P(1) angle of 96.58(6)° and the Cl(3)′—W—P(1) angle of 83.44(6)°, the other chloride ligands lie essentially orthogonal to the P—W—P vector.

The structure of **3** may be compared to other structurally characterized tungsten(IV) species. A recent structural analysis of $WCl_4(PPh_3)_2$ also shows *trans*-phosphines coordinated at the apexes of an octahedral tungsten centre.[30] The average of the W—Cl distances (2.33 Å) is the same for both molecules. The W—P bond in **3** [2.540(2) Å] is slightly shorter than that for the triphenylphosphine analogue [W—P = 2.629(6) Å] due to the greater steric influence of the triphenylphosphine ligand. On going to the tris-substituted complex $WCl_4(PMe_3)_3$ the W—Cl bond distances increase by an averge of 0.1 Å, however, the W—P distance (2.55 Å) is still close to that found for **3**.[24]

Reduction of $(PhN)WCl_4(PMe_3)_2$ *with* $LiPt\text{-}Bu_2$: *synthesis of* $[\{(PhN)WCl_2(PMe_3)_2\}_2(\mu\text{-}N_2)]$ (**4**)

The imido ligand $[RN]^{2-}$ has recently seen a renewal of interest due to its ability to bind in a linear or bent fashion as a four- or two-electron donor, respectively.[9] Imido ligands may also bridge two metal centres as four-electron donor ligands. This electronic versatility is often used to create a flexible coordination environment around a metal centre so that certain aspects of its reactivity may be explored. Recent work by Nielson and co-workers has focussed on the synthesis and characterization of a number of high oxidation state organoimidotungsten complexes,[31–34] however, the reaction chemistry of these organoimidotungsten complexes with main group substrates has not received much attention.

From the reaction of $[(PhN)WCl_4(PMe_3)_2]$ and $t\text{-}Bu_2PLi$ we were able to isolate and structurally characterize the $\mu\text{-}N_2$ complex $[\{(PhN)WCl_2(PMe_3)_2\}_2(\mu\text{-}N_2)]$ (**4**). While the fate of the $t\text{-}Bu_2P$ units in this reaction is not known it is likely that coupling occurs to yield the diphosphine species as happens in the reaction of $[Cp^*WCl_4]_2$ with $LiPt\text{-}Bu_2$ (see above). Earlier work using Na/Hg as a reductant in the presence of PMe_3 resulted in the isolation of the monomeric octahedral complex $[W(NPh)Cl_2(PMe_3)_3]$.[33]

X-ray structure of **4**

An ORTEP view of **4** may be seen in Fig. 6. Crystal structure parameters and key bond lengths and angles are given in Tables 1 and 5, respectively. The compound crystallizes in the monoclinic space group $P2_1/c$ (No. 14) with four molecules in the unit cell. The molecular geometry of the tungsten atoms is distorted octahedral with the phosphine ligands at the apexes of the octahedron. The two $[(PMe_3)_2(NPh)WCl_2]$ units are twisted essentially 90° with respect to each other so that steric interactions between pairs of trimethylphosphine ligands is minimized. The dinitrogen ligand is end-on bonded to both tungsten centres with W—N—N angles almost linear [W(1)—N(3)—N(4) = 178(2)°, W(2)—N(4)—N(3) = 173(2)°] as commonly found for bridging N_2 species.[35] W—N and N—N bond lengths [W(1)—N(3) = 1.9(2), W(2)—N(4) = 1.90(2) and N(3)—N(4) = 1.19 Å] favour dative coordination of the N_2 ligand over the recently characterized bis-imido bonding mode $[\mu\text{-}N_2]^{4-}$.[36] The phenyl imido groups are bonded in an almost linear fashion [W—N—C = 167(1)°,

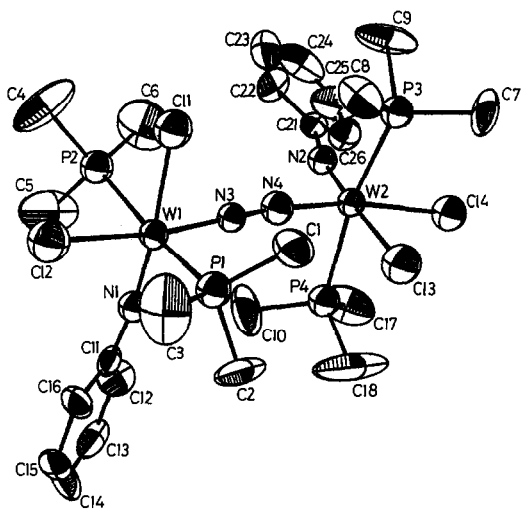

Fig. 6. ORTEP view of **4** showing atom numbering scheme.

Table 5. Selected bond lengths (Å) and angles (°) for **4**

Lengths (Å)			
W(1)—Cl(1)	2.470(6)	W(2)—P(3)	2.518(6)
W(1)—Cl(2)	2.464(6)	W(2)—P(4)	2.515(6)
W(1)—P(1)	2.519(6)	W(2)—N(2)	1.78(2)
W(1)—P(2)	2.507(6)	W(2)—N(4)	1.90(2)
W(1)—N(1)	1.74(2)	N(1)—C(11)	1.37(3)
W(1)—N(3)	1.91(2)	N(2)—C(21)	1.42(3)
W(2)—Cl(3)	2.490(6)	N(3)—N(4)	1.19(2)
W(2)—Cl(4)	2.460(6)		
Angles (°)			
Cl(1)—W(1)—Cl(2)	84.9(2)	N(1)—W(1)—N(3)	100.1(7)
Cl(1)—W(1)—P(1)	84.5(2)	Cl(3)—W(2)—Cl(4)	84.5(2)
Cl(1)—W(1)—P(2)	84.4(2)	Cl(3)—W(2)—P(3)	81.9(2)
Cl(1)—W(1)—N(1)	173.2(5)	Cl(3)—W(2)—P(4)	87.4(2)
Cl(1)—W(1)—N(3)	86.5(5)	Cl(3)—W(2)—N(2)	175.9(5)
Cl(2)—W(1)—P(1)	88.9(2)	Cl(3)—W(2)—N(4)	84.7(5)
Cl(2)—W(1)—P(2)	86.1(2)	Cl(4)—W(2)—P(3)	88.1(2)
Cl(2)—W(1)—N(1)	88.5(5)	Cl(4)—W(2)—P(4)	86.9(2)
Cl(2)—W(1)—N(3)	171.4(5)	Cl(4)—W(2)—N(2)	93.7(6)
P(1)—W(1)—P(2)	168.2(2)	Cl(4)—W(2)—N(4)	168.5(5)
P(1)—W(1)—N(1)	93.7(6)	P(3)—W(2)—P(4)	168.5(2)
P(1)—W(1)—N(3)	90.9(5)	P(3)—W(2)—N(2)	94.4(5)
P(2)—W(1)—N(1)	96.8(6)	P(3)—W(2)—N(4)	94.3(5)
P(2)—W(1)—N(3)	92.5(5)	P(4)—W(2)—N(2)	96.2(5)
P(4)—W(2)—N(4)	88.7(5)	N(2)—C(21)—C(22)	114(2)
N(2)—W(2)—N(4)	97.4(8)	N(2)—C(21)—C(26)	118(2)
C(10)—P(4)—C(18)	105(2)	W(1)—N(3)—N(4)	178(2)
C(17)—P(4)—C(18)	101(2)	W(2)—N(4)—N(3)	173(2)
N(1)—C(11)—C(12)	121(2)	W(1)—N(1)—C(11)	167(1)
N(1)—C(11)—C(16)	117(2)	W(2)—N(1)—C(21)	167(1)

Numbers in parentheses are the ESDs in the least significant digits.

W—N = 1.74(2) Å] suggesting some participation of the nitrogen lone pair in multiple bonding.[37] If the phenyl imido ligands are counted as four-electron donors each tungsten atom attains an electron count of 18. The average W—Cl and average W—P bond lengths ($W—Cl_{av}$ = 2.47 Å, $W—P_{av}$ = 2.51 Å) may be compared with those found in $[W(NPh)Cl_2(PMe_3)_3]$ ($W—Cl_{av}$ = 2.52 Å, $W—P_{av}$ = 2.48 Å).[33]

EXPERIMENTAL

All compounds were prepared under dry nitrogen using standard vacuum-line techniques. Toluene was distilled from sodium metal under nitrogen before use. Hexane and THF were distilled from sodium benzophenone ketyl under nitrogen. $[Cp^*WCl_4]_2$[14] and $[(PhN)WCl_3(PMe_3)_2]$[30] were prepared by the literature methods. Instruments: IR: Perkin–Elmer 1330; NMR (^1H and ^{31}P): GE 300 IR spectra were recorded as KBr disks. NMR spectra were recorded in C_6D_6 at ambient temperature and are referenced to Me_4Si (δ 0.0, ^1H) and 85% H_3PO_4(aq.) (δ 0.0, ^{31}P).

Synthesis of **1**

A suspension of $[Cp^*WCl_4]_2$ (0.34 g, 0.37 mmol) in THF (40 cm^3) was cooled to −78°C. The rapid injection of four equivalents of $LiPt\text{-}Bu_2$ (6.53 cm^3 of a 0.226 M solution) led to a colour change from orange to green to red. The reaction mixture was allowed to warm to room temperature then stirred for an additional 4 h. Removal of solvent *in vacuo* left a green–burgundy residue which was extracted into toluene (2 × 30 cm^3), concentrated (20 cm^3) and cooled (−20°C) to yield X-ray quality crystals of **1**, yield = 0.059 g, 35%. M.p. 237–245°C (dec). IR: 2960 s, 2930 s, 2858 s, 1463 s, 1378 s, 1363 s, 1260 m, 1165 m, 1448 w, 1028 m, 804 m (cm^{-1}). ^1H NMR: δ 2.4 (s, *Me*), δ 1.35 (dd, *t-Bu*). ^{31}P NMR: δ 39.94 (s).

Synthesis of **2**

A suspension of $[Cp^*WCl_4]_2$ (0.43 g, 0.47 mmol) in THF (30 cm^3) was cooled to −78°C, 5.4 cm^3 of 0.19 M LiHPPh/THF was then added dropwise via syringe. The solution turned light green over a period of 5 min then changed to an opaque suspension. The reaction mixture was allowed to stir overnight at room temperature then dried *in vacuo* and extracted with toluene (2×35 cm^3). Cooling of the extract to −20°C gave dark crystals of **3** in low yield. IR (Nujol mull): 1460 s, 1370 s, 1108 w, 1077 w, 1023 w, 922 w, 888 s, 738 s, 730 s, 688 m (cm^{-1}).

Synthesis of **3**

An excess of mono-*t*-butylphosphine (3 cm^3 H_2Pt-Bu) was added to solution of WCl_6 (3 g, 7.58 mmol) in dichloromethane (40 cm^3) at −78°C. The reaction mixture was allowed to warm to room temperature and stirred (12 h). The resulting purple solution was extracted with CH_2Cl_2 (3×20 cm^3). The extract was then concentrated and cooled (−20°C) for 24 h to yield bright red crystals of **1**, yield 2.5 g, 65%. M.p. 120–126°C (dec). IR: 2880 s br, 1640 s, 1568 s, 1459 m, 1440 m, 1374 w, 1354 w, 1310 s, 1254 m, 1195 m, 1153 w, 1088 m, 1050 w, 1067 w, 976 m, 721 w, 690 w, 625 w, 590 w, 523 m, 485 w (cm^{-1}).

Synthesis of **4**

A solution of $Cl_3W(NPh)(PMe_3)_2$ (0.25 g, 0.47 mmol) in THF (30 cm^3) was cooled to −78°C, LiPt-Bu_2 (1.42 cm^3 of a 0.33 M THF solution) was quickly added, whereupon the solution turned dark green after several minutes. After stirring overnight at room temperature the solution became deep burgundy. The reaction mixture was dried *in vacuo* and extracted with toluene (2×30 cm^3). The extract was concentrated (25 cm^3) and cooled to −20°C to yield dark red crystals of **4**, yield 0.117 g, 50%. IR (Nujol mull): 1460 s, 1370 m, 1335 m, 1275 w, 945 s (cm^{-1}).

† P is used in the calculation of $\sigma(I)$ to downweight intense reflections in the least-squares refinement. The function minimized was $\Sigma\omega(|F_o|-|F_c|)^2$, where $\omega = 4(F_o)^2/[\Sigma(F_o)^2]^2$, where $[\Sigma(F_o)^2]^2 = [S^2(C+R^2B)+\{P(|F_o|)^2\}^2]/(L_p)^2$, where S is the scan rate, C is the total integrated peak count, R is the ratio of scan time to background count and L_p is the Lorentz polarization factor.

X-ray experimental for **1–4**

Crystals of **1–4** were sealed in thin-walled glass capillaries under nitrogen. Details of crystal data and a summary of intensity data and collection parameters for all four compounds are given in Table 1. Data were collected on an Enraf–Nonius CAD-4 diffractometer at 23 ± 1°C using graphite monochromated Mo-K_α radiation. All calculations were performed on a Microvax-II computer using the Enraf–Nonius software package "SDP-PLUS".[38] For each structure the data were corrected for Lorentz and polarization effects. The structures were solved by direct methods (MULTAN)[39] or Patterson methods, and successive cycles of difference Fourier maps followed by least-squares refinement. Scattering factors were taken from ref. 40.

For compound **1**. Unit cell parameters were obtained by centering 25 reflections having 2θ values between 28 and 31°. The monoclinic space group $P2_1/n$ (No. 14) was uniquely determined by the systematic absences $0k0$, $k = 2n+1$, $h0l$, $h+l = 2n+1$. The structure was solved using direct methods (MULTAN). Hydrogen atoms were not located but their contributions were included in the final refinements. Data with intensities less than $3\sigma(I)$ and $(\sin\sigma)/\lambda$ less than 0.10 were excluded, and a non-Poisson contribution weighting scheme with an experimental instability factor of P set at 0.08 was used in the final stages of refinement.† The maximum peak in the final difference Fourier map has a height of 2.12 $eÅ^{-3}$ and was located 1.088 Å from tungsten and 1.467 Å from Cl(1).

For compound **2**. The X-ray crystallography for **2** was similar to that of **1** with the following specific details. The 2θ range for unit cell parameters was 28–30°. The structure was solved using Patterson methods. A non-Poisson contribution weighting scheme with $P = 0.07$. Hydrogen atoms were not located. The highest peak in the final difference Fourier map was 1.8 $eÅ^{-3}$.

For compound **3**. The X-ray crystallography for **3** was similar to that of **1** with the following specific details. The 2θ range for unit cell parameters 24–26°. The structure was solved using Patterson methods. A non-Poisson contribution weighting scheme with $P = 0.06$. Hydrogen atoms were not located. The highest peak in the final difference Fourier map had a height of 1.084 $eÅ^{-3}$ and was located 1.03 Å from tungsten.

For compound **4**. The X-ray crystallography for **4** was similar to that of **1** with the following specific details. 2θ range for unit cell parameters 25–28°. The structure was solved using direct methods (MULTAN). A non-Poisson contribution weight-

ing scheme with $P = 0.04$. Hydrogen atoms were not located. The highest peak in the final difference Fourier map had a height of 0.87 eÅ^{-3} and was located close to N(2).†

Acknowledgements—We thank the Robert A. Welch Foundation (F-816) and the National Science Foundation (CHE-8818984) for support. R.A.J. thanks the Alfred P. Sloan Foundation for a fellowship (1985–1989). We also thank Mr Scott S. Perry who recorded the Raman spectrum of *trans*-$WCl_4(H_2Pt\text{-}Bu)_2$.

REFERENCES

1. T. Godemeyer, A. Berg, H.-D. Gross, U. Muller and K. Dehnicke, *Z. Naturf.* 1985, **40B**, 999.
2. J. C. Bryan, S. J. Geib, A. L. Rheingold and J. M. Mayer, *J. Am. Chem. Soc.* 1987, **109**, 2826.
3. V. C. Gibson, G. E. Graimann, P. M. Hare, M. L. H. Green, J. A. Bandy, P. D. Grebenik and K. Prout, *J. Chem. Soc., Dalton Trans.* 1985, 2025.
4. R. R. Schrock, L. G. Sturgeoff and P. R. Sharp, *Inorg. Chem.* 1983, **22**, 2801.
5. P. R. Sharp, *Organometallics* 1984, **3**, 1217.
6. A. K. Rappé, *J. Am. Chem. Soc.* 1986, **25**, 4686.
7. S. Anderson, R. L. Richards and D. L. Hughes, *J. Chem. Soc., Dalton Trans.* 1986, 245; M. Y. Mohammed and C. J. Pickett, *J. Chem. Soc., Chem. Commun.* 1988, 1119.
8. A. George and M. E. Noble, *Inorg. Chem.* 1978, **17**, 1678.
9. W. A. Nugent, *Coord. Chem. Rev.* 1980, **31**, 123.
10. A. V. Butcher, J. Chatt, G. J. Leigh and P. L. Richards, *J. Chem. Soc., Dalton Trans.* 1972, 313.
11. B. Bell, J. Chatt and G. J. Leigh, *J. Chem. Soc., Dalton Trans.* 1972, 2492.
12. See for example, A. M. Arif, A. J. Bard, D. J. Chandler, R. A. Jones and R. D. Moulton, *J. Am. Chem. Soc.* 1988, **110**, 5714; R. A. Jones, S. U. Koschmieder and C. M. Nunn, *Inorg. Chem.* 1988, **27**, 4524; A. M. Arif, T. A. Bright, R. A. Jones and C. M. Nunn, *J. Am. Chem. Soc.* 1988, **110**, 6894 and refs therein.
13. S. J. Holmes and R. R. Schrock, *Organometallics* 1983, **2**, 1463.
14. R. C. Murray, L. Blum, A. H. Liu and R. R. Schrock, *Organometallics* 1985, **4**, 953.
15. J. Okuda, R. C. Murray, J. C. Dewar and R. R. Schrock, *Organometallics* 1986, **5**, 1681.
16. W. E. Buhro, M. H. Chisholm, K. Folting and J. C. Huffman, *Inorg. Chem.* 1987, **26**, 3087.
17. S. Aime, R. K. Harris, E. M. McVicker and M. Fild, *J. Chem. Soc., Chem. Commun.* 1975, 426.
18. (a) M. Cousins and M. L. H. Green, *J. Chem. Soc. A* 1969, 16; (b) M. L. H. Green, A. Izquierdo, J. J. Martin-Polo, V. S. B. Mtetwa and K. Prout, *J. Chem. Soc., Chem. Commun.* 1983, 538; (c) C. Ting, N. C. Baeziger and L. Messerle, *J. Chem. Soc., Chem. Commun.* 1988, 1133.
19. V. R. Richter, J. Kaiser, J. Sieler, H. Hartung and C. Peter, *Acta Cryst.* 1977, **B33**, 1887.
20. S. G. Baxter, A. H. Cowley, R. E. Davis and P. E. Riley, *J. Am. Chem. Soc.* 1981, **103**, 1699.
21. A. H. Cowley, *Compounds Containing Phosphorus–Phosphorus Bonds*, p. 6. Dowden, Hutchinson and Ross, Stroudsburg (1973).
22. W. Weigand, A. W. Cordes and P. N. Swepston, *Acta Cryst.* 1981, **B37**, 1631.
23. A. V. Butcher, J. Chatt, G. J. Leigh and P. L. Richards, *J. Chem. Soc., Dalton Trans.* 1972, 1064.
24. E. Carmona, L. Sanchez, M. L. Poveda, R. A. Jones and J. G. Hefner, *Polyhedron* 1983, **2**, 797.
25. A. R. Barron, J. E. Salt, G. Wilkinson, M. Motevalli and M. B. Hursthouse, *Polyhedron* 1986, **5**, 1833.
26. E. Carmona, J. M. Marin, M. L. Poveda, L. Sanchez, R. D. Rogers and J. L. Atwood, *J. Chem. Soc., Dalton Trans.* 1983, 1003.
27. J. R. Moss and B. L. Shaw, *J. Chem. Soc., Dalton Trans.* 1972, 1910.
28. D. G. Blight and D. L. Kepert, *J. Chem. Soc. A* 1968, 534.
29. M. A. Schaefer-King and R. E. McCarley, *Inorg. Chem.* 1973, **12**, 1972.
30. M. G. B. Drew, E. M. Page and D. A. Rice, *J. Chem. Soc., Dalton Trans.* 1983, 61.
31. A. J. Nielson, J. M. Waters and D. C. Bradley, *Polyhedron* 1984, **2**, 1985.
32. D. C. Bradley, M. B. Hursthouse, K. M. A. Malik and A. J. Nielson, *J. Chem. Soc., Chem. Commun.* 1981, 103.
33. D. C. Bradley, M. B. Hursthouse, K. M. A. Malik, A. J. Nielson and R. L. Short, *J. Chem. Soc. Dalton Trans.* 1983, 2651.
34. B. R. Ashcroft, D. C. Bradley, G. R. Clark, R. J. Errington, A. J. Nielson and C. E. F. Rickard, *J. Chem. Soc., Chem. Commun.* 1987, 170.
35. F. A. Cotton and G. Wilkinson, *Advanced Inorganic Chemistry*, 5th edn, p. 86. Wiley, New York (1980).
36. M. R. Churchill and Y.-J. Li, *J. Organomet. Chem.* 1986, **301**, 49; M. R. Churchill, Y.-J. Li, K. H. Theopold and R. R. Shrock, *Inorg. Chem.* 1984, **23**, 4472.
37. B. R. Ashcroft, G. R. Clark, A. J. Nielson and C. E. F. Rickard, *Polyhedron* 1985, **5**, 2081.
38. B. A. Frenz and Associates, College Station, TX 77840, U.S.A.
39. G. Germain, P. Main and W. W. Wolfson, *Acta Cryst.* 1971, **A27**, 368.
40. *International Tables for X-ray Crystallography*, Vol. 4. Kynoch Press, Birmingham, U.K. (1974).

† Tables of atomic positional and thermal parameters and observed and calculated structure factors for **1–4** have been deposited as supplementary material with the Editor, from whom copies are available on request. Atomic coordinates have also been submitted to the Cambridge Crystallographic Data Centre.

Polyhedron Vol. 9, No. 5, pp. 681–685, 1990
Printed in Great Britain

0277–5387/90 $3.00+.00
© 1990 Pergamon Press plc

CRYSTALLOGRAPHICALLY DETERMINED Se---O AND P---O INTERACTIONS IN TRIS(2,4-DIMETHOXYPHENYL) PHOSPHINE SELENIDE AND THE 2,4,6-TRIMETHOXY ANALOGUE. CORRELATIONS OF P—Se BOND LENGTHS WITH ^{77}Se NMR DATA

DAVID W. ALLEN,* NORMAN A. BELL, LORRAINE A. MARCH and IAN W. NOWELL†

Department of Chemistry, Sheffield City Polytechnic, Pond Street, Sheffield S1 1WB, U.K.

(*Received* 20 *July* 1989; *accepted* 21 *September* 1989)

Abstract—(2,4-Dimethoxyphenyl)$_3$PSe crystallizes in the monoclinic space group $P2_1/n$ with four molecules in the unit cell having dimensions of $a = 9.0660(1)$, $b = 17.2102(3)$, $c = 17.2475(3)$ Å, $\beta = 98.3(2)°$ and refined to $R = 5.2\%$ for 1258 observed reflections. (2,4,6-Trimethoxyphenyl)$_3$PSe is orthorhombic, space group $P2_12_12_1$ with four molecules in the unit cell $a = 18.2983(5)$, $b = 12.3716(1)$, $c = 12.4696(1)$ Å and refined to $R = 6.4\%$ for 1229 observed diffractometer data. In both cases the rings are orientated so that weak P---O interactions take place between one of the *o*-methoxy groups and phosphorus. Similar interactions between selenium and oxygen are also found. These interactions may account for the significant deshielding of the selenium atom in these compounds compared with related triarylphosphine selenides as shown by ^{77}Se NMR data.

In earlier publications, we have reported studies of the donor properties of heteroaryl- and substituted arylphosphines towards selenium, as indicated by the magnitude of the one-bond coupling constants $^1J(^{77}Se–^{31}P)$ of a series of phosphine selenides,[1] and also recently, by studies of the ^{77}Se chemical shifts for these molecules.[2] It has been shown that the coupling constants increase as the groups attached to phosphorus become more electron-withdrawing, indicating an increased *s*-character for the phosphorus orbital involved in bonding to selenium, in accordance with Bent's rule.[3] Consequently, for electron-withdrawing substituents, the phosphorus–selenium bond would be expected to be shorter than in related molecules bearing less electron-withdrawing groups. Support for this view has been gained from X-ray studies of the phosphine selenides (**1**)[4] and (**2**),[2] in which the phosphorus–selenium bonds show significant shortening compared with that in triphenylphosphine selenide. Our recent studies[2] of ^{77}Se chemical shifts also revealed

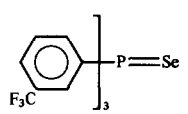

(**1**)

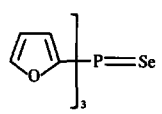

(**2**)

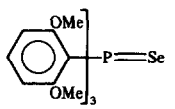

(**3**)

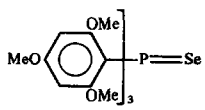

(**4**)

that in **2** the selenium atom is shielded by 86 ppm compared with that in triphenylphosphine selenide, the X-ray study also revealing that each of the three oxygen atoms is arranged about the selenium at an average distance of 3.577 Å. In contrast, it was found that introduction of *ortho* substituents into phenylphosphine selenides causes a deshielding of the selenium. In particular, in **3** and **4**, the selenium is deshielded by, respectively, 222 and 240 ppm compared with that in triphenylphosphine selenide; the coupling constants $^1J(^{77}Se–^{31}P)$ are also reduced, in keeping with the anticipated electron-donating properties of the substituents. In order

* Author to whom correspondence should be addressed.
† Present address: Robert Gordon's Institute of Technology, Queen's Road, Aberdeen AB9 2PG, Scotland, U.K.

to seek further understanding of the influence of substituents on the selenium shielding and the length of the phosphorus–selenium bond, we have carried out full X-ray studies of **3** and **4**, and now report key aspects of their structures and also draw attention to a possible correlation between phosphorus–selenium bond length and selenium shielding in a number of phosphine selenides.

EXPERIMENTAL

The compounds tris(2,6-dimethoxyphenyl) phosphine selenide (**3**) and tris(2,4,6-trimethoxyphenyl)phosphine selenide (**4**) were prepared as described previously[2] from the corresponding phosphine and selenium and recrystallized from ethanol. Crystals of **3** and **4** were mounted with one axis coincident with the ω-axis of a Stoe Stadi 2 two-circle diffractometer. Data were corrected for Lorentz and polarization effects but absorption corrections were not applied. Details of the crystal data and X-ray data collection are listed in Table 1.

Structure determination and refinement

The selenium coordinates were determined from three-dimensional Patterson maps. The remaining non-hydrogen atoms were located from successive difference Fourier maps. The structure was refined by full-matrix least-squares techniques with all non-hydrogen atoms being assigned anisotropic temperature factors. The hydrogen atoms were included in ideal positions (C—H, 1.08 Å) and given isotropic temperature factors [**3**, 0.102(22) and 0.139(19) Å^2, **4**, 0.036(27) and 0.141(30) Å^2] for the ring and methyl hydrogens, respectively. Complex neutral atom scattering factors[5] were employed throughout the refinements and a non-unit weighting scheme (Table 1) was adopted for both structures. Selected bond distances are listed in Table 2, and selected bond angles in Table 3. Full atomic parameters, thermal parameters, bond lengths and bond angles have been deposited at the Cambridge Crystallographic Data Centre (CCDC). All calculations were performed with an IBM4341 computer using the SHELX computing package.[6]

Table 1. Crystal data and details of data collection

		Compound **3**	Compound **4**
Crystal data			
M_r		526.9	611.2
Crystal system		Monoclinic	Orthorhombic
Crystal size (mm)		0.220 × 0.100 × 0.100	0.200 × 0.100 × 0.150
a (Å)		9.0660(1)	18.2983(5)
b (Å)		17.2102(3)	12.3716(1)
c (Å)		17.2475(3)	12.4696(1)
β (°)		98.3(2)	—
U (Å^3)		2663	2823
D_m (g cm^{-3})		1.29	1.47
D_c (g cm^{-3})		1.31	1.46
Z		4	4
F(000)		1176	1264
μ(Mo-K_α) (cm^{-1})		14.40	13.66
Space group		$P2_1/n$	$P2_12_12_1$
Collection of intensity data			
Mounting axis		a	c
Reflections collected		2299	2281
Number of observed reflections[a]		1258	1229
$I/\sigma(I)$		3	3
Final R value		0.052	0.064
Final R' value		0.048	0.063
Weighting scheme[b]	a	1.6281	1.7967
	b	0.000506	0.001105

[a] Those reflections having $I/\sigma(I)$ greater than the indicated value were considered to be observed.

[b] For the weighting scheme $w = a/(\sigma^2(F_o) + b(F_o)^2)$, values of a and b are as shown.

Table 2. Selected bond distances (Å) (ESDs in parentheses)

	3	4
P—Se	2.135(3)	2.119(5)
P—C(11)	1.84(1)	1.82(2)
P—C(21)	1.84(1)	1.86(1)
P—C(31)	1.85(1)	1.80(2)
P—O(11)	3.089	2.838
P—O(12)	2.873	3.168
P—O(21)	2.864	2.858
P—O(22)	3.093	3.071
P—O(31)	3.154	2.935
P—O(32)	2.819	2.996
Se—O(11)	[a]	3.311
Se—O(12)	3.254	[a]
Se—O(21)	[a]	[a]
Se—O(22)	3.083	3.046
Se—O(31)	[a]	3.453
Se—O(32)	3.191	[a]
Se—O(4)	3.338	

[a] Value not determined but is > 3.7 Å.

Table 3. Selected bond angles (°) (ESDs in parentheses)

	3	4
Se—P—C(11)	106.2(4)	116.3(5)
Se—P—C(21)	117.0(4)	118.5(6)
Se—P—C(31)	110.0(4)	103.6(6)
C(11)—P—C(21)	110.5(6)	97.8(7)
C(21)—P—C(31)	102.1(5)	112.0(7)
C(11)—P—C(31)	111.0(5)	108.7(7)
P—C(11)—C(12)	125(1)	116(1)
P—C(11)—C(16)	116(1)	127(1)
C(11)—C(12)—O(11)	119(1)	116(1)
C(11)—C(16)—O(12)	117(1)	119(2)
P—C(21)—C(22)	118(1)	120(1)
P—C(21)—C(26)	125(1)	123(1)
C(21)—C(22)—O(21)	114(1)	113(1)
C(21)—C(26)—O(22)	118(1)	116(1)
P—C(31)—C(32)	128(1)	119(1)
P—C(31)—C(36)	115(1)	125(1)
C(31)—C(32)—O(31)	115(1)	116(1)
C(31)—O(36)—O(32)	117(1)	114(1)

DISCUSSION

Both **3** and **4** are distorted tetrahedral monomers (Figs 1 and 2) with angles about phosphorus ranging from 102.1(5) to 117.0(4)° for **3** and from 97.8(7) to 118.5(6)° for **4**. The average Se—P—C angles are 111.1(4)° for **3** and 112.8(6)° for **4**, and average C—P—C angles 107.9(6)° for **3** and 106.2(7)° for **4**, all very close to the tetrahedral bond angle.

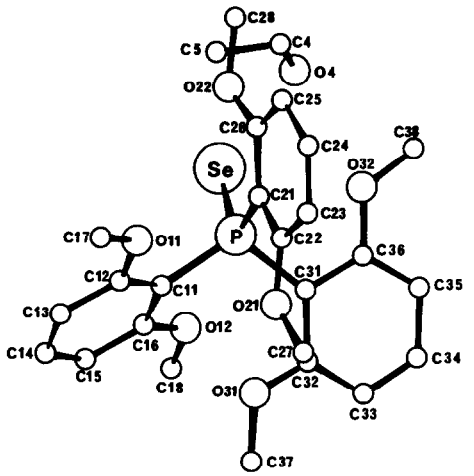

Fig. 1. Structure and atom labelling for tris(2,6-dimethoxyphenyl)phosphine selenide (H atoms omitted for clarity).

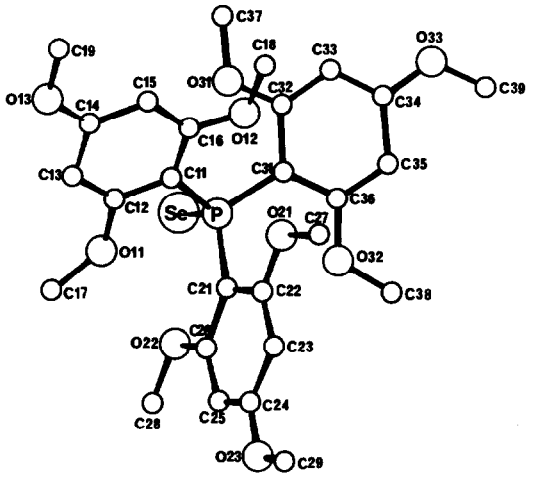

Fig. 2. Structure and atom labelling for tris(2,4,6-trimethoxyphenyl)phosphine selenide (H atoms omitted for clarity).

In both compounds the rings are tilted so that, except for ring 3 in **4** where both P---O distances are very similar (2.935, 2.996 Å), one of the two oxygen atoms of the *o*-methoxy groups in each ring lies within the sum of the van der Waals' radii for phosphorus and oxygen (3.35 Å), whereas the other P---O distances are greater than 3.7 Å (Table 2). Thus phosphorus is enclosed in a cage of three carbon and one selenium atoms, with further weak bonding to three oxygen atoms in **3** and four in **4**. The tilting of the rings also results in both smaller P—C—C angles associated with the shorter P---O distances together with correspondingly smaller C—C—O angles, except in ring 3 for both compounds. However, in both cases, the larger

Table 4. Comparison of: P---O, Se---O distances, P—C—C and C—C—O angles for R_3PSe [R = 2,6-$(MeO)_2C_6H_3$, (**3**); 2,4,6-$(MeO)_3C_6H_2$, (**4**)]

	Compound **3** Ring			Compound **4** Ring		
	1	2	3	1	2	3
P---O (Å)	2.873	2.864	2.819	2.838	2.858	2.935
	3.089	3.093	3.154	3.168	3.071	2.996
P—C—C (°)	116(1)	118(1)	115(1)	116(1)	120(1)	119(1)
	125(1)	125(1)	128(1)	127(1)	123(1)	125(1)
C—C—O (°)	117(1)	114(1)	117(1)	116(1)	113(1)	116(1)
	119(1)	118(1)	115(1)	119(2)	116(1)	114(1)
Se---O (Å)	3.254	3.083	3.191	3.311	3.046	3.453

C—C—O angles in ring 3 are compensated by much smaller P—C—C angles, thus enabling oxygen to be involved in a weak interaction with phosphorus (Table 4).

A related interaction between the oxygen of the *o*-methoxyphenyl substituent and phosphorus in the phosphonium salt (5), resulting in a P---O distance of 2.88 Å, has been reported by McEwen and co-workers[7] and attributed to a specific O_{2p}–P_{3d} overlap. However, in a recent related study of the chemistry of *o*-dimethylaminophenylphosphonium salts, Cairns and McEwen[8] have pointed out that it is more appropriate to discuss such interactions from the point of view of hypervalent bonding to phosphorus rather than to a specific 3*d* orbital involvement. If, in the above phosphine selenides, the oxygen atoms are involved in specific hypervalent interactions with the partially positive phosphorus atom (considering the phosphine selenide as a resonance hybrid of the two principal contributing canonical forms, **6** and **7**), then one might expect that this would also influence the extent to which the phosphorus atom is able to become involved in back-donation via $P_{3d\pi}$–$Se_{p\pi}$ overlap with selenium, and result in a lengthening of the phosphorus–selenium bond. In this connection, it is of interest that the phosphorus–selenium distances in **3** and **4** (2.135(3) and 2.119(5) Å, respectively) are longer than that in triphenylphosphine selenide (2.106(1) Å) (although, because of the errors associated with the phosphorus–selenium distance in **4**, the latter increase in length is not *crystallographically significant*).

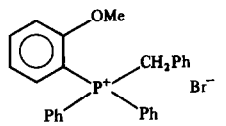

(5)

(6) (7)

In both compounds, there are also weak interactions between selenium and one of the oxygen atoms of the *o*-methoxy groups in each ring, resulting in an average Se---O distance in **3** of 3.176 Å and in **4** of 3.266 Å, compared with the sum of the van der Waals' radii for selenium and oxygen of 3.40 Å. As expected, there are no intermolecular interactions involving the methoxy groups in either compound. The *o*-methoxy–selenium interaction noted above may therefore be a factor in explaining the marked deshielding of the selenium observed in our earlier ^{77}Se NMR studies.

The bonding around selenium in **3** is further extended by a weak interaction with a molecule of solvent ethanol (Se---O, 3.338 Å).

A consideration of the data in Table 5 for a range of triarylphosphine selenides reveals a possible correlation between phosphorus–selenium bond length and the NMR shielding of the selenium atoms. The shorter the bond, the greater is the shielding of the selenium. As the bond length increases, the selenium becomes less shielded, but clearly the very marked deshielding observed in compounds **3** and **4** is due to the interactions with nearby oxygen atoms as revealed in the present study.

It is of interest that a recent structural study of the formally two-coordinate copper(I) complexes (**8**) has also revealed a significant interaction

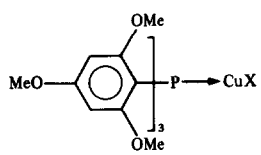

(8) X = Cl or Br

between one *o*-methoxy oxygen and the copper, which results in a distortion of the expected linear geometry at copper.[9]

Table 5. P—Se bond distances, $^1J(^{31}P-^{77}Se)$ coupling constants and ^{77}Se chemical shifts for R_3PSe

R	P—Se (Å)	$J(^{31}P-^{77}Se)$ (Hz)	$\delta(^{77}Se)$ (ppm)
o-MeC_6H_4	2.116(5)[a]	708[b]	−204[c]
m-MeC_6H_4	2.109(5)[d]	726[b]	
C_6H_5	2.106(1)[e]	732[f]	−268[c]
m-$CF_3C_6H_4$	2.094(2)[c]	766[f]	−268[c]
2-Furyl	2.094[g]	793[f]	−354[c]
5-Phenyldibenzophosphole	2.098(3)[h]	747[i]	−364.7[i]
2,6-$(MeO)_2C_6H_3$	2.135(3)	717	−46.2[c]
2,4,6-$(MeO)_3C_6H_2$	2.119(5)	703	−28.4[c]

[a] T. S. Cameron and E. Dahlen, *J. Chem. Soc., Perkin Trans. 2* 1975, 1737.
[b] R. P. Pinnell, C. A. Megerle, S. L. Manatt and P. A. Kroon, *J. Am. Chem. Soc.* 1973, **95**, 977.
[c] Reference 4.
[d] T. S. Cameron, K. D. Howlet and K. Miller, *Acta Cryst.* 1978, **B34**, 1639.
[e] P. W. Codding and K. A. Kerr, *Acta Cryst.* 1979, **B35**, 1261.
[f] Reference 1.
[g] Reference 2.
[h] E. C. Alyea, G. Ferguson, J. Malito and B. L. Ruhl, *Acta Cryst.* 1986, **C42**, 882.
[i] D. W. Allen and B. F. Taylor, *J. Chem. Res. (S)* 1986, 392.

REFERENCES

1. D. W. Allen and B. F. Taylor, *J. Chem. Soc., Dalton Trans.* 1982, 51.
2. D. W. Allen, I. W. Nowell and B. F. Taylor, *J. Chem. Soc., Dalton Trans.* 1985, 2505.
3. H. A. Bent, *Chem. Rev.* 1961, **61**, 275.
4. D. W. Allen, L. A. March and I. W. Nowell, *J. Chem. Soc., Dalton Trans.* 1984, 483.
5. *International Tables for X-ray Crystallography*, Vol. 4. Kynoch Press, Birmingham (1974).
6. G. M. Sheldrick, SHELX, program for crystal structure determination. University of Cambridge (1976).
7. J. S. Wood, R. J. Wilkholm and W. E. McEwen, *Phosphorus Sulfur* 1977, **3**, 163.
8. S. M. Cairns and W. E. McEwen, *J. Org. Chem.* 1987, **52**, 4829.
9. G. A. Bowmaker, J. D. Cotton, P. C. Healy, J. D. Kildea, S. B. Silong, B. W. Skelton and A. H. White, *Inorg. Chem.* 1989, **28**, 1462.

Polyhedron Vol. 9, No. 5, pp. 687–691, 1990
Printed in Great Britain

0277–5387/90 $3.00+.00
© 1990 Pergamon Press plc

THE SYNTHESIS, ELECROCHEMISTRY AND THERMAL BEHAVIOUR OF SOME MOLYBDENUM MONONITROSYL COMPLEXES INCORPORATING LONG CHAIN ALKYL SUBSTITUENTS

BENJAMIN J. COE, CHRISTOPHER J. JONES* and JON A. McCLEVERTY

Department of Chemistry, University of Birmingham, PO Box 363, Birmingham B15 2TT, U.K.

and

DUNCAN W. BRUCE

Department of Chemistry, University of Sheffield, Sheffield S3 7HF, U.K.

(*Received* 25 *August* 1989; *accepted* 21 *September* 1989)

Abstract—The new mononitrosyl complexes $[Mo(NO)LI(OC_6H_4CO_2C_{12}H_{25})]$, $[Mo(NO)LCl(OC_6H_4CO_2C_{12}H_{25})]$, $[Mo(NO)L(OC_6H_4CO_2C_{12}H_{25})_2]$, $[Mo(NO)LI(NHC_6H_4C_{10}H_{21})]$, $[Mo(NO)LCl(NHC_6H_4C_{10}H_{21})]$ and $[Mo(NO)L(NHC_6H_4C_{10}H_{21})_2]$ [L = $HB(3,5\text{-}Me_2C_3N_2H)_3$] have been synthesized and characterized by spectroscopic methods. All undergo one-electron reduction processes at potentials ranging from −0.18 to −1.40 V (SCE). These new compounds have been examined by differential scanning calorimetry. Although these compounds have reduced melting points compared to compounds lacking long alkyl chain substituents, 44°C in the case of the bis-phenoxide derivative, none exhibits liquid crystalline behaviour.

There is considerable current interest in the synthesis of redox-active transition metal complexes which form liquid crystal mesophases.[1–5] Such materials are usually coloured and may undergo electron-transfer processes which lead to a significant change in their optical and magnetic properties. The molybdenum mononitrosyl derivatives [Mo(NO)LXY] (L = hydrotris(3,5-dimethylpyrazol-1-yl)borate, X = Cl, I or Y and Y = phenoxide or arylamide)[6] are redox active,[7,8] strongly coloured and can, in certain cases, exhibit non-linear optical properties.[9] In order to discover whether the incorporation of long chain alkyl substituents into complexes of this type might reduce their melting points and produce materials which exhibit ordering phenomena in the liquid phase, we have synthesized derivatives containing anilide or phenolate ligands carrying long chain alkyl substituents in the 4-position of the aryl ring. Differential scanning calorimetry (DSC) and polarizing hot-stage microscopy studies have been used to establish whether liquid crystalline mesophases are formed by these new compounds.

EXPERIMENTAL

All reagents were used as supplied. $[Mo(NO)\{HB(3,5\text{-}Me_2C_3N_2H)_3\}I_2]$ and $[Mo(NO)\{HB(3,5\text{-}Me_2C_3N_2H)_3\}Cl_2]$ were prepared according to previously described methods.[10,11] Solvents used as reaction media were dried according to standard methods and freed of oxygen before use. Silica gel 60 (70–230 mesh) was used as the stationary phase for column chromatography with dichloromethane as eluent. All reactions were carried out under nitrogen but purification procedures were carried out in air. Elemental analyses were carried out by the Microanalytical Laboratory, University of Birmingham.

* Author to whom correspondence should be addressed.

IR spectra were recorded using a PE 297 spectrometer with samples as KBr discs. 270 MHz ^{1}H NMR spectra were obtained from solutions in $CDCl_3$ using a Jeol GX 270 spectrometer. Cyclic voltammetric measurements were made using a PAR 174A polarograph. Solutions in CH_2Cl_2 were *ca* 10^{-3} mol dm^{-3} in complex and 0.2 mol dm^{-3} in $[Bu^n_4N]BF_4$ as base electrolyte. A Pt–bead test electrode was used with a scan rate of 200 mV s^{-1}. An SCE reference electrode was used with ferrocene as an internal standard. Potentials are quoted relative to the SCE and under these conditions E_f for the oxidation of ferrocene was found to be 0.58 V. DSC measurements were carried out using a Perkin–Elmer DSC7 instrument with samples (typically 1.4–3 mg) being hermetically sealed in 10 μl aluminium pans. In all cases heating and cooling rates of 10 K min^{-1} were used. The microscopy studies were carried out using a CZ Scientific Labpol system equipped with a Link-Am PR600 controller and TH600 hot-stage. Heating rates were 10 K min^{-1} unless otherwise stated.

$[Mo(NO)\{HB(3,5\text{-}Me_2C_3N_2H)_3\}I(OC_6H_4CO_2C_{12}H_{25})]$

A solution of $[Mo(NO)\{HB(3,5\text{-}Me_2C_3N_2H)_3\}I_2]$ (0.5 g, 0.74 mmol), *n*-dodecyl-4-hydroxybenzoate (0.5 g, 1.63 mmol) and hexamine (0.05 g, 0.36 mmol) was stirred under reflux in toluene (50 cm^3) for 5 h. The reaction mixture was cooled and filtered, and the filtrate evaporated to dryness under reduced pressure. The resulting brown solid was purified by column chromatography using dichloromethane as the eluant. The major brown fraction was collected and afforded the red–brown product after evaporation. Further purification could be effected by recrystallization from CH_2Cl_2–hexane mixtures (0.35 g, 55%). *Spectroscopic data.* ^{1}H NMR (δ_{TMS} ppm):* aryl protons, 8.07 (2 d $^3J_{HH}$ = 11 Hz), 7.46 (2 d $^3J_{HH}$ = 11 Hz); pyrazolyl-4-H protons, 5.91 (1 s), 5.86 (1 s), 5.85 (1 s); pyrazolyl-3- and 5-Me protons, 2.53 (3 s), 2.45 (3 s), 2.40 (3 s), 2.37 (3 s), 2.28 (3 s), 1.97 (3 s); aliphatic protons, 4.30 (2 t $^3J_{HH}$ = 6.5 Hz), 1.76–0.85 (23 bm); IR: ν_{NO} = 1683, ν_{CO} = 1715 cm^{-1}. UV–vis λ_{max} (nm) (ε, mol^{-1} dm^3 cm^{-1}): 450 (10,500), 324 (5600). M.p. 105–109°C. Found: C, 47.6; H, 6.2; N, 11.4. $C_{34}H_{51}N_7BMoO_4I$ requires: C, 47.7; H, 6.0; N, 11.5%. *Electrochemical data.*† E_f = −0.18 V, ΔE_p = 125 mV, ΔE_p(Fc) = 160 mV.

$[Mo(NO)\{HB(3,5\text{-}Me_2C_3N_2H)_3\}Cl(OC_6H_4CO_2C_{12}H_{25})]$

This compound was prepared in an identical manner to its iodide-containing counterpart using $[Mo(NO)\{HB(3,5\text{-}Me_2C_3N_2H)_3\}Cl_2]$ (0.5 g, 1.0 mmol) instead of $[Mo(NO)\{HB(3,5\text{-}Me_2C_3N_2H)_3\}I_2]$. A golden brown solid was obtained (0.59 g, 77%). *Spectroscopic data.* ^{1}H NMR (δ_{TMS} ppm): aryl protons, 8.11 (2 d $^3J_{HH}$ = 8 Hz), 7.34 (2 d $^3J_{HH}$ = 8 Hz); pyrazolyl-4-H protons, 5.93 (1 s), 5.92 (1 s), 5.77 (1 s); pyrazolyl-3- and 5-Me protons, 2.56 (3 s), 2.43 (3 s), 2.41 (3 s), 2.39 (3 s), 2.17 (3 s), 2.05 (3 s); aliphatic protons, 4.31 (2 t $^3J_{HH}$ = 6.5 Hz), 1.78–0.85 (23 bm); IR: ν_{NO} = 1690, ν_{CO} = 1710 cm^{-1}. UV–vis λ_{max}(nm) (ε, mol^{-1} dm^3 cm^{-1}): 450 (7200), 312 (8400). M.p. 102–107°C. Found: C, 53.2; H, 6.7; N, 12.7. $C_{34}H_{51}N_7BMoO_4Cl$ requires: C, 53.5; H, 6.7; N, 12.8%. *Electrochemical data.* E_f = −0.20 V, ΔE_p = 115 mV, ΔE_p(Fc) = 125 mV.

$[Mo(NO)\{HB(3,5\text{-}Me_2C_3N_2H)_3\{(OC_6H_4CO_2C_{12}H_{25})_2]$

This compound was prepared from $[Mo(NO)\{HB(3,5\text{-}Me_2C_3N_2H)_3\}I_2]$ (0.5 g, 0.74 mmol) and *n*-dodecyl-4-hydroxybenzoate (1.0 g, 3.26 mmol) using the procedure described for $[Mo(NO)\{HB(3,5\text{-}Me_2C_3N_2H)_3\}I(OC_6H_4CO_2C_{12}H_{25})]$ except that triethylamine (1.5 cm^3, 11 mmol) was used in place of hexamine. A pale brown solid was obtained (0.57 g, 75%). *Spectroscopic data.* ^{1}H NMR (δ_{TMS} ppm): aryl protons, 8.00 (4 d $^3J_{HH}$ = 9 Hz), 7.02 (4 d $^3J_{HH}$ = 9 Hz); pyrazolyl-4-H protons, 5.89 (2 s), 5.70 (1 s); pyrazolyl-3- and 5-Me protons, 2.43 (6 s), 2.41 (3 s), 2.21 (6 s), 1.95 (3 s); aliphatic protons, 4.31 (4 t $^3J_{HH}$ = 6.5 Hz), 1.79–0.85 (46 bm); IR: ν_{NO} = 1665, ν_{CO} = 1710 cm^{-1}. UV–vis λ_{max}(nm) (ε, mol^{-1} dm^3 cm^{-1}): 407 (5700). M.p. 41–44°C. Found: C, 61.4; H, 8.0; N, 9.0. $C_{53}H_{80}N_7BMoO_7$ requires: C, 61.6; H, 7.8; N, 9.5%. *Electrochemical data.* E_f = −0.44 V, ΔE_p = 145 mV, ΔE_p(Fc) = 140 mV.

$[Mo(NO)\{HB(3,5\text{-}Me_2C_3N_2H)_3\}I(NHC_6H_4C_{10}H_{21})]$

This compound was prepared in similar manner to $[Mo(NO)\{HB(3,5\text{-}Me_2C_3N_2H)_3\}I(OC_6H_4CO_2$

* Relative area and multiplicity given in parentheses; s = singlet, d = doublet, t = triplet, m = multiplet with unresolved coupling, b = broad, throughout.

† E_f = formal electrode potential for reduction, ΔE_p = separation between cathodic and anodic peak potentials of cyclic voltammogram, ΔE_p(Fc) = value of ΔE_p for ferrocene present as internal standard. No compensation was made for internal resistance in the cell, throughout.

$C_{12}H_{25}$)] using 4-decyl aniline (0.25 g, 1.07 mmol) in place of *n*-dodecyl-4-hydroxybenzoate, and triethylamine (1.5 cm^3, 11 mmol) in place of hexamine. A dark brown solid was obtained (0.49 g, 85%). *Spectroscopic data.* ^1H NMR (δ_{TMS} ppm): amide proton, 13.20 (1 b); aryl protons, 7.54 (2 d $^3J_{HH}$ = 8 Hz), 7.19 (2 d $^3J_{HH}$ = 8 Hz); pyrazolyl-4-H protons, 5.92 (1 s), 5.85 (1 s), 5.76 (1 s); pyrazolyl-3- and 5-Me protons, 2.71 (3 s), 2.47 (3 s), 2.46 (3 s), 2.37 (6 s), 1.98 (3 s); aliphatic protons, 1.63–0.86 (21 bm); IR: ν_{NO} = 1658, ν_{NH} = 3280 cm^{-1}. UV–vis λ_{max}(nm) (ε, mol^{-1} dm^3 cm^{-1}): 468 (13,900), 400 (7000). M.p. 110°C (dec). Found: C, 48.0; H, 6.3; N, 14.6. $C_{31}H_{48}N_8BMoOI$ requires: C, 47.6; H, 6.2; N, 14.3%. *Electrochemical data.* E_f = −0.83 V, ΔE_p = 110 mV, ΔE_p(Fc) = 125 mV.

[Mo(NO){HB(3,5 - $Me_2C_3N_2H)_3$}Cl($NHC_6H_4C_{10}H_{21}$)]

This compound was prepared in an identical manner to its iodide-containing counterpart using [Mo(NO){HB(3,5-$Me_2C_3N_2H)_3$}Cl_2], (0.5 g, 1.0 mmol) instead of [Mo(NO){HB(3,5-$Me_2C_3N_2H)_3$}I_2], 4-decylaniline (0.35 g, 1.50 mmol) and triethylamine (1.5 cm^3, 11 mmol). A red–brown solid was obtained (0.38 g, 55%). *Spectroscopic data.* ^1H NMR (δ_{TMS} ppm): amide proton, 12.73 (1 b); aryl protons, 7.40 (2 d $^3J_{HH}$ = 8 Hz), 7.22 (2 d $^3J_{HH}$ = 8 Hz); pyrazolyl-4-H protons, 5.86 (2 s), 5.78 (1 s); pyrazolyl-3- and 5-Me protons, 2.69 (3 s), 2.42 (3 s), 2.38 (3 s), 2.37 (3 s), 2.36 (3 s), 2.01 (3 s); aliphatic protons, 1.63–0.86 (21 bm); IR: ν_{NO} = 1655, ν_{NH} = 3260 cm^{-1}. UV–vis λ_{max} (nm) (ε, mol^{-1} dm^3 cm^{-1}): 446 (14,800), 292 (5100). M.p. 105°C (dec). Found: C, 54.0; H, 7.0; N, 16.3. $C_{31}H_{48}N_8BMoOCl$ requires: C, 53.9; H, 7.0; N, 16.2%. *Electrochemical data.* E_f = −0.87 V, ΔE_p = 115 mV, ΔE_p(Fc) = 115 mV.

[Mo(NO){HB(3,5 - $Me_2C_3N_2H)_3$}[$NHC_6H_4C_{10}H_{21})_2$]

Sodium (0.1 g, 4.35 mmol) was heated under reflux in dry THF (35 cm^3) for 30 min. Naphthalene (0.1 g, 0.78 mmol) was then added and the mixture stirred for 1 h under reflux during which time the solution became dark green. The mixture was then filtered under nitrogen, to remove excess sodium, and 4-decylaniline (0.1 g, 0.43 mmol) was added to the filtrate. After stirring the resulting solution for 30 min at room temperature, [Mo(NO){HB(3,5-$Me_2C_3N_2H)_3$}I($NHC_6H_4C_{10}H_{21}$)] (0.1 g, 0.13 mmol) was added and the mixture stirred for a further 2.5 h. The final dark green mixture was filtered in air to give a dark purple filtrate from which the solvent was removed under reduced pressure. The product was purified by column chromatography using CH_2Cl_2 as eluant, the major purple fraction being collected. Further purification was effected by recrystallization from *n*-pentane (0.11 g, 57%). *Spectroscopic data.* ^1H NMR (δ_{TMS} ppm): amide protons, 8.78 (2 b); aryl protons, 7.19 (4 d $^3J_{HH}$ = 8 Hz), 7.04 (4 d $^3J_{HH}$ = 8 Hz); pyrazolyl-4-H protons, 5.94 (1 s), 5.72 (2 s); pyrazolyl-3- and 5-Me protons, 2.47 (3 s), 2.34 (9 s), 2.24 (6 s); aliphatic protons, 1.54–0.86 (42+12 from pentane bm); IR: ν_{NO} = 1631, ν_{NH} = 3320 cm^{-1}. UV–vis λ_{max}(nm) (ε, mol^{-1} dm^3 cm^{-1}): 549 (12,600), 369 (11,400). Found: C, 64.8; H, 8.5; N, 12.5. $C_{47}H_{74}N_9BMoO \cdot C_5H_{12}$ requires: C, 65.1; H, 9.0; N, 13.1%. *Electrochemical data.* E_f = −1.40 V, ΔE_p = 200 mV, ΔE_p(Fc) = 95 mV.

DISCUSSION

Synthetic studies

The new complexes were synthesized according to established procedures. In the case of the phenoxide derivatives hexamine was used to selectively induce mono-substitution of iodide in [Mo(NO)LI_2] and triethylamine to induce bis-substitution.[11] In forming the bis-arylamide derivative more forcing conditions involving sodium naphthalenide were used to substitute the remaining iodide in [Mo(NO)LI($NHC_6H_4C_{10}H_{21}$)].[12] In the remaining cases, triethylamine was used to consume the HI or HCl liberated in the halide substitution reactions.

All of the new complexes exhibit ν_{BH} at *ca* 2550 cm^{-1} in their IR spectra. In addition, the phenoxide derivatives exhibit ν_{CO} at 1710–1715 cm^{-1} attributable to the carboxylate moiety, while the arylamide derivatives exhibit ν_{NH} at 3260–3320 cm^{-1} due to the amide moiety. It has been found that ν_{NO} in complexes of this type is highly sensitive to the nature of the co-ligands attached to the {Mo(NO)L} moiety. Thus values of *ca* 1680, 1660, 1660 and 1635 cm^{-1} are observed, respectively, for mono-phenoxide, bis-phenoxide, mono-arylamide and bis-arylamide complexes.[6,12] All of the new compounds exhibit ν_{NO} at frequencies in accord with their formulations.

The ^1H NMR spectra of the mono-substituted complexes [Mo(NO)LXY] (X = I or Cl; Y = $OC_6H_4CO_2C_{12}H_{25}$ or $NHC_6H_4C_{10}H_{21}$) exhibit signals attributable to the presence of the aryl and alkyl groups in Y. In addition, the amide complexes exhibit a broad signal at *ca* 13 ppm due to the amide proton. The bis-substituted complexes similarly

contain signals due to the phenoxide or aryl amide ligands but with twice the relative area found for their mono-substituted counterparts. The amide protons in $[Mo(NO)L(NHC_6H_4C_{10}H_{21})_2]$ are substantially shifted from their position in the spectrum of the mono-substituted complex to 8.78 ppm. The signals from the three pyrazolyl-4-H and six methyl protons in the ligand, L, are indicative of the molecular symmetry. In the absence of overlap nine resonances in the area ratio 1 : 1 : 1 : 3 : 3 : 3 : 3 : 3 : 3 should be present for mono-substituted derivatives, whilst the bis-substituted derivatives exhibit signals in the area 1 : 2 : 3 : 3 : 6 : 6. The area ratios observed for the new complexes are in all cases in accord with their formulations. The bis-arylamide complex $[Mo(NO)L(NHC_6H_4C_{10}H_{21})_2]$ could only be isolated in solvated form and both the ^1H NMR and analytical data are consistent with the presence of one mole of pentane in the compound. All attempts to remove this by heating *in vacuo* have failed.

Electrochemical studies

The electrochemical properties of the complexes have been determined by cyclic voltammetry and are in accord with expectations. Previous work has shown that the reduction potentials of the complexes [Mo(NO)LXY] are highly sensitive to the nature of X and Y. Thus for X = halide and Y = phenoxide a reduction potential of *ca* −0.4 V might be expected compared to *ca* −0.8 V for X = halide Y = arylamide.[7] However, the presence of substituents on the aryl ring also has a significant effect on the reduction potentials.[8,13] Thus the ester function on the phenoxide ligand would be expected to give rise to more anodic potentials, whilst the alkyl substituent on the amide ligand should give slightly more cathodic potentials. The observed potentials of −0.18 (X = I, Y = $OC_6H_4CO_2C_{12}H_{25}$), −0.20 (X = Cl, Y = $OC_6H_4CO_2C_{12}H_{25}$), −0.83 (X = I, Y = $NHC_6H_4C_{10}H_{21}$) and −0.87 V (X = Cl, Y = $NHC_6H_4C_{10}H_{21}$) are entirely consistent with this expectation. Similarly, the reduction potentials of bis-phenoxide and bis-arylamide derivatives would be expected to be *ca* −0.8 and −1.3 V, modified by the presence of the substituents on the aryl rings. The observed potentials of −0.44 (X = Y = $OC_6H_4CO_2C_{12}H_{25}$) and −1.40 V (X = Y = $HNC_6H_4C_{10}H_{21}$) are consistent with this expectation. On the basis of the cathodic to anodic peak current ratios these reduction processes appear chemically reversible when the phenoxide ligand is present, but they are not fully reversible in the complexes containing the arylamide ligand.

Thermal studies

Typical melting points for complexes of the type described here, and which contain phenoxide or arylamide ligands with methyl substituents, are in excess of 200°C {e.g. 210–215°C for [Mo(NO)LCl(OC_6H_4-4-Me)] and 250–255°C for [Mo(NO)LCl(NHC_6H_4-4-Me)]}. As expected, the incorporation of the long alkyl chain substituents leads to a marked reduction in the melting points of these materials. In the case of $[Mo(NO)L(OC_6H_4CO_2C_{12}H_{25})_2]$ the melting point is as low as 41–44°C. In order to assess whether these materials exhibit any liquid crystalline behaviour, the complexes were examined by polarizing hot-stage microscopy and DSC.

When viewed under the polarizing microscope $[Mo(NO)LI(OC_6H_4CO_2C_{12}H_{25})]$ showed no changes until the material melted at 106°C. This process appeared to be accompanied by some decomposition. Cooling the freshly melted sample at 10 K min^{-1} failed to show any birefringent textures. The DSC trace revealed two fairly well-resolved endothermic events with a combined enthalpy of 47.9 J g^{-1}. The former had T_{ON} = 107°C (ΔH = 46.6 J g^{-1}) while the latter, which peaked at about 124.5°C, accounted for 1.3 J g^{-1}. Nothing corresponding with this second event could be observed by microscopy and its origin is thus unclear.

In the case of $[Mo(NO)LCl(OC_6H_4CO_2C_{12}H_{25})]$ a melting event was observed at 100°C which corresponded with an endothermic event in the DSC trace with T_{ON} = 104°C (ΔH = 31.13 J g^{-1}). Another event was observed at 122°C and involved a darkening of the sample. This corresponded with an *exothermic* event in the DSC trace with ΔH = −3.95 J g^{-1}. Although the sample appeared birefringent on melting at 100°C, this turned out to be unmelted crystallites in an isotropic environment and so again, no mesomorphic behaviour was observed.

The bis-phenoxide derivative $[Mo(NO)L(OC_6H_4CO_2C_{12}H_{25})_2]$ melted at 43°C corresponding with two poorly resolved events in the DSC trace having T_{ON} = 42.5°C (ΔH = 33.6 J g^{-1}) and T_{peak} = 46°C (ΔH = 20.3 J g^{-1}). Cooling the resulting fluid to −40°C revealed nothing in either the microscopy or the DSC study.

Heating the arylamide derivative, $[Mo(NO)LI(NHC_6H_4C_{10}H_{21})]$, at 10 K min^{-1} revealed the onset of melting at 186.7°C, a possible second event at 189.7°C and finally clearing at 190.5°C. Despite the birefringent appearance of the material between the highest and lowest temperatures this is not a liquid crystalline phase, as evidenced by the melting

of solid crystallites into an isotropic background at the clearing point. On heating the DSC showed two fairly well-resolved events with $T_{ON} = 175°C$ ($\Delta H = 19$ J g^{-1}) and $T_{peak} = 186°C$ ($\Delta H = 18.5$ J g^{-1}), while on cooling the trace was featureless. This suggests that the first event may be a transition between two crystalline modifications while the second is associated with melting, apparently without decomposition. Although the sample solidifies at around 136°C on cooling under the microscope, no thermal evidence of solidification was observed by DSC.

The related complex, [Mo(NO)LCl($NHC_6H_4C_{10}H_{21}$)], melted into an isotropic fluid over a broad range at about 110°C. The DSC study revealed a broad endothermic event with $T_{ON} = 92.6°C$ ($\Delta H = 27$ J g^{-1}). No other events were observed on cooling. The bis-arylamide complex [Mo(NO)L($NHC_6H_4C_{10}H_{21}$)$_2$] could not be freed of solvent and this material became more fluid on heating to 64°C before turning black and decomposing at 74°C. There was no evidence for any liquid crystalline behaviour.

Two of the arylamido complexes melt at higher temperatures than their aryloxo counterparts. This might reflect the presence of opportunities for hydrogen bonding in the amido systems (which appears[14] to greatly increase the melting points of other mesogenic systems) which are not present in the aryloxo systems. However, structural studies have shown that the amide proton is sterically protected to some extent by the bulky ligand L as well as by the aryl groups.[6,15–17] Another feature which emerges from the results is that the replacement of the chloride co-ligand by iodide in the mono-aryloxo complexes appears to have little effect. In contrast, this change produces almost a 100°C increase in melting point for the mono-arylamido systems.

In conclusion, it may be noted that the incorporation of long chain alkyl substituents can be a successful strategy for reducing the melting points of these trispyrazolylborate complexes containing the redox active {Mo(NO)L} moiety. However, the use of co-ligands containing only one aryl ring produces insufficient structural anisotropy to stabilize liquid crystalline mesophases; this may be attributed, in part at least, to the steric bulk of the trispyrazolylborate ligand, L. Work is in progress to assess the effect of using co-ligands of much higher structural anisotropy including hydroxybiphenyl and hydroxystilbene. One final point which may be noted is that the aryloxo complexes appear more suitable when seeking redox active liquid crystalline complexes. Not only are their reduction potentials more accessible than those of their arylamido counterparts, but they also appear to show superior thermal properties.

Acknowledgements—We are grateful to Mr T. Green for technical assistance, to the Royal Society (D.W.B.) and the SERC (B.J.C.) for support. The calorimeter and microscope were purchased with the aid of grants from the SERC, the University of Sheffield and the European Community (Twinning Grant No. ST2J-0387-C).

REFERENCES

1. C. Piechocki and J. Simon, *Nouv. J. Chim.* 1985, **9**, 159.
2. U. T. Mueller-Westerhoff, A. Nazzal, R. J. Cox and A.-M. Giroud, *J. Chem. Soc., Chem. Commun.* 1980, 497.
3. M. Veber, R. Fugnitto and H. Strzeleka, *Mol. Cryst. Liq. Cryst.* 1983, **96**, 221.
4. K. Ohta, A. Takagi, H. Muroki, I. Yamamoto and K. Matsuzaki, *Mol. Cryst. Liq. Cryst.* 1987, **147**, 15.
5. M. Khan, J. Bhatt, B. M. Fung, K. M. Nicholas and E. Wachtel, *Liq. Cryst.* 1989, **5**, 285.
6. J. A. McCleverty, *Chem. Soc. Rev.* 1983, **12**, 331.
7. N. AlObaidi, D. Clague, M. Chaudhury, C. J. Jones, J. A. McCleverty, J. C. Pearson and S. S. Salam, *J. Chem. Soc., Dalton Trans.* 1987, 1733.
8. N. AlObaidi, S. M. Charsley, W. Hussain, C. J. Jones, J. A. McCleverty, B. D. Neaves and S. J. Reynolds, *Transition Met. Chem.* 1987, **12**, 143.
9. B. J. Coe, C. J. Jones, J. A. McCleverty, D. Bloor, P. V. Kolinsky and R. J. Jones, *J. Chem. Soc., Chem. Commun.* 1989, 1485.
10. S. J. Reynolds, C. F. Smith, C. J. Jones, J. A. McCleverty, D. C. Bower and J. L. Templeton, *Inorg. Synth.* 1985, **23**, 4.
11. J. A. McCleverty, D. Seddon, N. A. Bailey and N. W. Walker, *J. Chem. Soc., Dalton Trans.* 1976, 898.
12. N. AlObaidi, T. A. Hamor, C. J. Jones, J. A. McCleverty and K. Paxton, *J. Chem. Soc., Dalton Trans.* 1986, 1525.
13. R. P. Sidebotham, C. J. Jones and J. A. McCleverty, unpublished results.
14. D. W. Bruce and J. Leadbetter, unpublished observations.
15. J. A. McCleverty, G. Denti, S. J. Reynolds, A. S. Drane, N. ElMurr, A. E. Rac, N. A. Bailey, H. Adams and J. M. Smith, *J. Chem. Soc., Dalton Trans.* 1983, 81.
16. N. AlObaidi, T. A. Hamor, C. J. Jones, J. A. McCleverty and K. Paxton, *J. Chem. Soc., Dalton Trans.* 1987, 1063.
17. N. AlObaidi, T. A. Hamor, C. J. Jones, J. A. McCleverty, K. Paxton, A. J. Howes and M. B. Hursthouse, *Polyhedron* 1988, **7**, 1931.

Polyhedron Vol. 9, No. 5, pp. 693–696, 1990
Printed in Great Britain

0277–5387/90 $3.00+.00
© 1990 Pergamon Press plc

THE SYNTHESES AND ELECTROCHEMISTRY OF BIMETALLIC COMPLEXES CONTAINING MOLYBDENUM MONONITROSYL REDOX CENTRES LINKED BY SATURATED-α,ω-DIAMIDO BRIDGING LIGANDS

NAJAT J. AlOBAIDI

Department of Chemistry, College of Science, AlMustansiriyah University, Baghdad, Iraq

and

CHRISTOPHER J. JONES* and JON A. McCLEVERTY

Department of Chemistry, University of Birmingham, PO Box 363, Birmingham B15 2TT, U.K.

(*Received* 31 *August* 1989; *accepted* 21 *September* 1989)

Abstract—The bimetallic complexes $[\{Mo(NO)\{HB(3,5\text{-}Me_2C_3N_2H)_3\}Cl\}_2(NHCH_2)_2Z)]$ (Z = nothing, CH_2 or $\{CH_2OCH_2\}_2$), have been synthesized and characterized by spectroscopic methods. The reduction potentials of these compounds were determined by cyclic voltammetry. Although the complexes exhibit irreversible reduction behaviour, their first reduction poentials occur at increasingly more anodic potentials as the size of the α,ω-diamido-bridging ligand is decreased; the values being E_{pc} (V, SCE) = −1.46 (Z = $\{CH_2OCH_2\}_2$, −1.38 (Z = CH_2) and −1.19 (Z = nothing).

The synthesis and electrochemistry of complexes of general formula [Mo(NO)LX(YR)] (L = $HB(3,5\text{-}Me_2C_3N_2H)_3$; X = I or Cl; Y = O, S or NH and R = alkyl or aryl) have been extensively studied in recent years.[1–4] A topic of particular interest has been the way in which the molybdenum mononitrosyl redox centres in bimetallic complexes of the type [Mo(NO)LCl—BL—Mo(NO)LCl] (BL is a bridging ligand) influence one another. Cyclic voltammetric studies have shown that the metal based redox centres do influence one another, as manifest in their electrochemical properties, to an extent which depends upon the nature of BL. Thus when BL is $—NHC_6H_4CH_2CH_2C_6H_4NH—$, a single broadened two-electron reduction wave is observed corresponding with the near simultaneous reduction of both redox centres.[5] However, when BL is $—NHC_6H_4NH—$, two quite separate one-electron reduction processes are observed with the difference between the potentials being 850 mV for mutually *para* —NH— substituents and 450 mV for mutually *meta* —NH— substituents.[6,7] Evidence for a strong interaction between the redox centres is also found with the saturated cyclohexa-1,4-diazyl bridging ligand $—N(CH_2CH_2)_2N—$.[8] As a continuation of these studies we were interested to determine the extent of interaction between {Mo(NO)} redox centres bridged by the single saturated aliphatic chain bridges $—NH(CH_2)_nNH—$ (n = 2, 3). However, because of the tendency for primary alkyl amide derivatives [Mo(NO)LX(NHR)] to exhibit irreversible electrochemistry, we were not optimistic that useful information could be obtained from such systems. Despite this expectation we have synthesized $[\{Mo(NO)LCl\}_2(NHCH_2)_2Z)]$ (Z = nothing, CH_2 or $\{CH_2OCH_2\}_2$) for the sake of completeness and have investigated their electrochemistry.

EXPERIMENTAL

All reagents were used as supplied. $[Mo(NO)\{HB(3,5\text{-}Me_2C_3N_2H)_3\}Cl_2]$ was prepared according to a previously described method.[9] Silica gel 60 (70–

* Author to whom correspondence should be addressed.

230 mesh) was used as the stationary phase for column chromatography unless otherwise stated. All reactions were carried out under nitrogen but purification procedures were carried out in air. Elemental analyses were carried out by the Microanalytical Laboratory, University of Birmingham.

IR spectra were recorded using a PE 297 spectrometer. ^{1}H NMR spectra were obtained using Varian XL100 (100 MHz) or Jeol GX 270 (270 MHz) at the University of Birmingham or a Bruker WH400 (400 MHz) instruments at the SERC high field NMR service, University of Warwick. Cyclic voltammetric and other electrochemical measurements were made using a Hitek PPR 1 waveform generator and DT 2101 potentiostat or a PAR 174A polarograph. Solutions were *ca* 10^{-3} mol dm^{-3} in a complex and 0.2 mol dm^{-3} in [Bu^{n}N]BF_4 as base electrolyte. A Pt-bead test electrode was used with an SCE reference electrode. Under these conditions the formal electrode potential, E_f, for the Fc/Fc$^+$ couple was found to be at 0.56 V with the cathodic and anodic peak potential separation, $\Delta E_p = 120$ mV. The number of electrons associated with electrode processes was estimated by comparison with [Mo(NO)LCl_2].

[{Mo(NO)LCl(NHCH$_2$—)}$_2$]

A solution containing [Mo(NO)LCl_2] (1.0 g, 2.2 mmol) and 1,2-diaminoethane (0.06 g, 1.0 mmol) in dichloromethane (60 cm^3) was heated under reflux for 3 days in the presence of NaH (0.2 g). The reaction mixture was then filtered and the solvent removed from the filtrate *in vacuo*. The crude product was purified by column chromatography on silica gel using 1% (v/v) tetrahydrofuran in dichloromethane as the eluant, the major orange band being collected. Further purification could be effected by recrystallization from dichloromethane–*n*-hexane mixtures to give an orange solid (0.2 g, 20%). *Spectroscopic data.* 270 MHz ^{1}H NMR $CDCl_3$ (δ_{TMS} ppm):* amide NH 12.20 (2 b); pyrazolyl-4-H 5.87 (2 s), 5.84 (2 s), 5.83 (2 s); NCH_2 CH_2N protons 5.45 (2 m), 4.92 (2 m); pyrazolyl-3- and 5-Me 2.57 (6 s), 2.51 (6 s), 2.38 (6 s), 2.36 (12 s), 2.32 (6 s). IR: $\nu_{NO} = 1655$, $\nu_{NH} = 3290$ cm^{-1}. Found: C, 39.4; H, 5.1; N, 23.0. $C_{32}H_{50}N_{16}B_2O_2Cl_2Mo_2$ requires: C, 39.4; H, 5.1; N, 23.0%.

[{Mo(NO)LCl(NHCH$_2$)}$_2$CH$_2$]

A solution containing [Mo(NO)LCl_2] (2.0 g, 4.4 mmol) and 1,3-diaminopropane (0.15 g, 2.0 mmol) in dichloromethane (60 cm^3) was heated under reflux for 5 days in the presence of NaH (0.2 g). The reaction mixture was then filtered and the solvent removed from the filtrate *in vacuo*. The crude product was purified by column chromatography on silica gel using dichloromethane as the eluant, the major orange band being collected. Further purification could be effected by recrystallization from dichloromethane–*n*-hexane mixtures to give an orange solid (0.6 g, 30%). *Spectroscopic data.* 400 MHz ^{1}H NMR $CDCl_3$ (δ_{TMS} ppm): amide NH 12.54 (1 dd, $^3J_{HH} = 7$ and 10 Hz), 12.31 (1 dd, $^3J_{HH} = 7$ and 10 Hz); pyrazolyl-4-H 5.86 (1 s), 5.84 (1 s), 5.83 (2 s), 5.81 (1 s), 5.80 (1 s); NCH_2 protons 5.42 (2 m), 4.66 (2 m); pyrazolyl-3- and 5-Me 2.59 (3 s), 2.58 (6 s), 2.47 (3 s), 2.44 (3 s), 2.40 (3 s), 2.39 (3 s), 2.38 (3 s), 2.36 (6 s), 2.33 (6 s). IR: $\nu_{NO} = 1655$, $\nu_{NH} = 3230$ and 3290 cm^{-1}. Found: H, 40.0; H, 5.3; N, 21.4. $C_{33}H_{52}N_{16}B_2O_2Cl_2Mo_2$ requires: C, 39.5; H, 5.2; N, 22.3%.

[{Mo(NO)LClNHCH$_2$CH$_2$OCH$_2$—}$_2$]

A solution containing [Mo(NO)LCl_2] (1.0 g, 2.2 mmol) and 1,8-diamino-3,6-dioxaoctane (0.15 g, 1.0 mmol) in dichloromethane (100 cm^3) containing NEt_3 (0.2 cm^3) was heated under reflux for 24 h. The reaction mixture was then filtered and the solvent removed from the filtrate *in vacuo*. The crude product was purified by column chromatography on silica gel using 2% (v/v) tetrahydrofuran in dichloromethane as the eluant, the major red–orange band being collected. Further purification could be effected by recrystallization from dichloromethane–*n*-hexane mixtures to give a red–orange solid (0.41 g, 35%). *Spectroscopic data.* 100 MHz ^{1}H NMR $CDCl_3$ (δ_{TMS} ppm): amide NH 12.52 (2 b); pyrazolyl-4-H 5.80 (5 s), 5.71 (1 s); NCH_2 protons 5.25 (2 m), 4.60 (2 m); N—C—CH_2O protons 3.75 (4 m); OCH_2CH_2O protons 3.56 (4 s); pyrazolyl-3- and 5-Me 2.59 (6 s), 2.48 (3 s), 2.45 (3 s), 2.38 (s 18), 2.33 (6 s). IR: $\nu_{NO} = 1655$, $\nu_{NH} = 3300$ cm^{-1}. Found: C, 41.8; H, 5.9; N, 19.6. $C_{36}H_{58}N_{16}B_2O_4Cl_2Mo_2 \cdot \frac{1}{2}C_6H_{14}$ requires: C, 42.3; H, 5.9; N, 20.3%.

DISCUSSION

The new complexes were prepared following established methods[1,10] in which [Mo(NO)LCl_2] was reacted with the appropriate diamine in the presence of NEt_3 or NaH to consume the HCl liberated during the reaction. All of the compounds exhibited ν_{BH} at 2550 cm^{-1} along with other bands attributable to the presence of the ligand L. The values observed for ν_{NO} were in accord with the

* NMR data relative area and multiplicity given in parentheses; s = singlet, d = doublet, t = triplet, m = multiplet with unresolved couplings, throughout.

formulation of the complexes as monoalkylamide derivatives, and ν_{NH} was observed at *ca* 3300 cm^{-1}. In the case of [{Mo(NO)LCl(NHCH$_2$—)}$_2$] and {Mo(NO)LClNHCH$_2$CH$_2$OCH$_2$—}$_2$] only one NH stretching band was observed but in the case of [{Mo(NO)LCl(NHCH$_2$)}$_2$CH$_2$] two were observed in accord with the ^{1}H NMR results.

The 270 MHz ^{1}H NMR spectrum of [{Mo(NO)L(NHCH$_2$—)}$_2$] was in accord with a structure having a centre of symmetry as found[8] in [{Mo(NO)LCl}$_2${N(CH$_2$CH$_2$)$_2$N}]. This would arise from the {Mo(NO)LClNH—} groups being present in an antiperiplanar configuration with respect to the bridging —CH$_2$CH$_2$— moiety. As in [{Mo(NO)LCl}$_2${N(CH$_2$CH$_2$)$_2$N}] it would appear that the two chiral metal centres are bound sufficiently closely for the diastereoisomer containing two metal centres of opposite chirality to be preferred. Thus the pyrazolyl-4-H protons appeared as three signals, each of relative area two, whilst the pyrazolyl-3 and 5-methyl protons appeared as five signals of relative area 6:6:6:12:6. As required, these findings are consistent with the absence of a plane of symmetry through the {Mo(NO)L} moiety. The diamide —CH$_2$— protons appeared as two unresolved multiplets each of relative area two corresponding with the two diastereotopic sites on the α-carbon. The two-bond and three-bond couplings to CH protons and the three-bond coupling to the adjacent NH proton were not resolved at 270 MHz so that broadened signals were observed. These signals were shifted to low field as a result of their proximity to the formally 16-electron {Mo(NO)}$^{3+}$ core as is now well established.

The odd number of carbon atoms in the central bridge of [{Mo(NO)LCl(NHCH$_2$)}$_2$CH$_2$] precludes the formation of a centrosymmetric molecule and this is reflected in the ^{1}H NMR spectrum which was obtained at 400 MHz. This contains two signals attributable to the NH protons, each appearing as a doublet of doublets as a result of coupling to the two diastereotopic α-protons of the diamido group. The α-protons themselves appear as two complex multiplets as a result of the combination of two-bond coupling to the adjacent diastereotopic CH proton and the three-bond couplings to the NH and central β-CH$_2$ protons. The signal from the central β-CH$_2$ protons lies under the signals from the pyrazolyl-3 and 5-methyl protons and is obscured. The pyrazolyl-4-H protons appeared as five signals in the area ratio 1:1:2:1:1, whilst the pyrazolyl-3 and 5-methyl protons appeared as nine signals of relative area 3:6:3:3:3:3:3:6:6.

The ^{1}H NMR spectrum of [{Mo(NO)LClNHCH$_2$CH$_2$OCH$_2$—}$_2$] was obtained at 100 MHz and contains a single, broad signal attributable to the NH protons. The N—CH$_2$— protons again appear as two unresolved multiplets in the region δ 5.1–4.7 ppm, whilst the N—C—CH$_2$O protons appear as a broad unresolved multiplet just to the low field side of the OCH$_2$CH$_2$O protons which appear as a singlet. The pyrazolyl-4-H protons appeared as two signals of relative area 5:1, whilst the pyrazolyl-3 and 5-methyl protons appeared as five signals of relative area 6:3:3:18:6.

The complexes derived from diaminoethane and diaminopropane did not exhibit high mass ions in their mass spectra. However, in the case of [{Mo(NO)LClNHCH$_2$CH$_2$OCH$_2$—}$_2$], isotope envelopes based around $m/z = 932$ and 904 were observed. These may be attributed to the fragment ions {M−(Me$_2$C$_3$N$_2$H+NO)}$^+$ and {M−(Me$_2$C$_3$N$_2$H+2NO)}$^+$.

As expected, the new complexes exhibited only irreversible processes in their cyclic voltammograms. All exhibited irreversible oxidation processes, these being at +1.88 V in the cases of [{Mo(NO)LClNHCH$_2$}$_2$Z] (Z = nothing or CH$_2$) and at +1.68 V in the case of [{Mo(NO)LClNHCH$_2$CH$_2$OCH$_2$—}$_2$]. The reduction processes of [{Mo(NO)LClNHCH$_2$}$_2$Z] were of the greatest interest in view of our previous findings. Each of the three complexes exhibited a reduction process in the region −1.0 to −1.5 V, but in each case these had i_{pa}/i_{pc} values of approximately 0.5 indicating their chemically irreversible nature. The shape parameters, ΔE_p, were also substantially larger than that of the ferrocene reference (120 mV), being in the range 230–440 mV. Despite the irreversible nature of these processes the E_{pc} values do exhibit a trend in accord with our previous findings and indicative of a varying degree of interaction between the metal centres. Thus in [{Mo(NO)LClNHCH$_2$CH$_2$OCH$_2$—}$_2$], where the metal atoms are well separated and may be presumed to have essentially no interaction, a value of $E_{pc} = -1.46$ V was obtained for the only observable reduction process. In the case of [{Mo(NO)LClNHCH$_2$}$_2$CH$_2$] a one-electron reduction was observed at −1.38 V [{Mo(NO)LClNHCH$_2$}$_2$Z], with a second irreversible two-electron process at −2.0 V. A further anodic shift in the first reduction potential was observed in going to [{Mo(NO)LClNHCH$_2$—}$_2$], where $E_{pc} = -1.19$ V, and no second reduction process was observed. These findings are in accord with the second electron-withdrawing {Mo(NO)} centre facilitating reduction of the first as the distance between them is reduced by shortening the aliphatic chain linking the {Mo(NO)LClNH} moieties.

The irreversible character of the reduction

processes precludes any detailed comment. However, the anodic shift of 80 mV in going from [{Mo(NO)LClNHCH$_2$CH$_2$OCH$_2$—}$_2$] to [{Mo(NO)LClNHCH$_2$}$_2$CH$_2$], with a three-carbon atom bridge, compares favourably with the previously determined[5,7] shift of 70 mV in going from [{Mo(NO)LClNHC$_6$H$_4$-4-CH$_2$CH$_2$C$_6$H$_4$-4′-NHMo(NO)LCl] to [1,3-{Mo(NO)LClNH}$_2$C$_6$H$_4$], which also contains a three-carbon atom bridge. Similarly the anodic shift of 270 mV in going from [{Mo(NO)LClNHCH$_2$CH$_2$OCH$_2$—}$_2$] to [{Mo(NO)LClNHCH$_2$—}$_2$], with a two-carbon atom bridge, may be compared with the shift of 280 mV found[8] on going from [Mo(NO)LCl(NC$_4$H$_8$)] to [{Mo(NO)LCl}$_2${N(CH$_2$CH$_2$)$_2$N}], which also contains saturated two-carbon atom bridges. Thus the results described here establish that the effects observed in other bimetallic systems are also present in these compounds containing a bridging single aliphatic chain. Furthermore, the magnitude of the anodic shift in the first reduction potential is sensitive to the length of the chain just as it is to the relative position of disubstitution when aryl bridges are present.[2–5]

Acknowledgement—We are grateful to Mr T. Green for experimental assistance.

REFERENCES

1. J. A. McCleverty, *Chem. Soc. Rev.* 1983, **12**, 331.
2. N. AlObaidi, M. Chaudhury, D. Clague, J. C. Pearson, C. J. Jones, J. A. McCleverty and S. S. Salam, *J. Chem. Soc., Dalton Trans.* 1987, 1733.
3. N. AlObaidi, S. M. Charsley, W. Hussain, C. J. Jones, J. A. McCleverty, B. D. Neaves and S. J. Reynolds, *Transition Metal Chem.* 1987, **12**, 143.
4. C. J. Jones, J. A. McCleverty, B. D. Neaves, S. J. Reynolds, H. Adams, N. A. Bailey and G. Denti, *J. Chem. Soc., Dalton Trans.* 1986, 733.
5. S. M. Charsley, C. J. Jones, J. A. McCleverty, B. D. Neaves and S. J. Reynolds, *J. Chem. Soc., Dalton Trans.* 1988, 301.
6. S. M. Charsley, C. J. Jones, J. A. McCleverty, B. D. Neaves, S. J. Reynolds and G. Denti, *J. Chem. Soc., Dalton Trans.* 198, 293.
7. S. M. Charsley, C. J. Jones and J. A. McCleverty, *Transition Met. Chem.* 1986, **11**, 329.
8. N. AlObaidi, T. A. Hamor, C. J. Jones, J. A. McCleverty and K. Paxton, *J. Chem. Soc., Dalton Trans.* 1987, 2653.
9. J. A. McCleverty, D. Seddon, N. A. Bailey and N. W. Walker, *J. Chem. Soc., Dalton Trans.* 1976, 898.
10. N. AlObaidi, T. A. Hamor, C. J. Jones, J. A. McCleverty and K. Paxton, *J. Chem. Soc., Dalton Trans.* 1986, 1525.

Polyhedron Vol. 9, No. 5, pp. 697–702, 1990
Printed in Great Britain

0277–5387/90 $3.00+.00
© 1990 Pergamon Press plc

HETEROLEPTIC POLYPYRAZOLYLBORATE DERIVATIVES OF THE LANTHANIDE IONS. BIDENTATE LIGAND EXCHANGE REACTIONS OF $[Ln\{HB(C_3N_2H_3)_3\}_2(\beta\text{-DIKETONATE})]$ (Ln = Ce, La, Sm, Eu, Yb, Lu)

MICHAEL A. J. MOSS and CHRISTOPHER J. JONES*

Department of Chemistry, University of Birmingham, PO Box 363, Birmingham B15 2TT, U.K.

(*Received* 21 *August* 1989; *accepted* 9 *October* 1989)

Abstract—The complexes $[LnL_2X]$ [$L = HB(C_3N_2H_3)_3$, X = PhC(O)CHC(Me)O and Ln = Y, La, Ce, Pr, Nd, Sm, Eu, Tb, Ho, Er, Yb, Lu or X = PhC(O)CHC(Ph)O and Ln = Y, La, Ce, Sm, Eu, Tb, Yb, Lu] have been prepared. In selected cases the intermolecular ligand exchange reactions involving the β-diketonate ligand have been studied by ^1H NMR methods. For the sets of complexes $[YbL_2X]$ [X = OC(Ph)CHC(Ph)O or OC(Me)CHC(Me)O] with $[LuL_2X]$ and $[LaL_2X]$ with $[CeL_2X]$, ligand exchange was found to be slow on the ^1H NMR time scale. A time-resolved study of the exchange of β-diketonate ligands between $[SmL_2X]$ and $[EuL_2X]$ gave results which were in accord with a model involving two opposing bimolecular reactions.

Previously we have found that, unlike their homoleptic counterparts $[LnL_3]$ [Ln = lanthanide or Y and L = hydrotris(pyrazolyl)borate] which exhibit rigid structures in solution on the ^1H NMR time scale,[1] the heteroleptic complexes $[LnL_2(acac)]$ [Ln = lanthanide ion, acac = OC(Me)CHC(Me)O] are dynamic.[2,3] These latter compounds exhibit intramolecular ligand reorganization reactions which are rapid on the NMR time scale at room temperature. Similar observations have been made by Takats and co-workers in studies of $[LnL_2(dik)]$ (Ln = Yb, Lu and dik = 3-trifluoroacetyl-D-camphoryl or 2,2,6,6-tetramethyl-3,5-heptanedionyl).[4] We have also found that complexes of the type $[LnL_2X]$ (X^- = β-diketonate) exhibit intermolecular ligand exchange reactions which are slow compared to the intramolecular processes. Such intermolecular exchange processes are of fundamental importance, since they provide a mechanism for the disproportionation of heteroleptic complexes. In particular, heteroleptic organolanthanides such as $[LnL_2R(Sol)]$ (R = hydrocarbyl and Sol = solvent or nothing) may be prone to disproportionation to form $[LnL_3]$ and solvated lanthanide ions if rapid ligand exchange reactions can occur. We report here an investigation of intermolecular co-ligand–ligand exchange in heteroleptic complexes containing the $\{LnL_2\}^+$ moiety.

A previous ligand exchange study involving mixed solutions of $[AsPh_4][Y(tfac)_4]$ and $[AsPh_4][Y(hfac)_4]$ [tfac = OC(CF$_3$)CHC(Me)O and hfac = OC(CF$_3$)CHC(CF$_3$)O] has been reported by Cotton *et al.*[5] The experiments were carried out at −40°C in a NMR spectrometer and five compounds were found in the resulting solution, *viz.* $[Y(hfac)_4]^-$, $[Y(hfac)_3(tfac)]^-$, $[Y(hfac)_2(tfac)_2]^-$, $[Y(hfac)(tfac)_3]^-$ and $[Y(tfac)_4]^-$, the three mixed-ligand complexes being formed by intermolecular exchange. At −40°C eight separate methine proton signals were observed, one for the methine proton of hfac in each of the four molecules in which it occurs and one for the methine proton of tfac in each of the four molecules in which it occurs. In this case coalescence of the methine resonances to give a single resonance for hfac and another for tfac was observed at +40°C.

In order to observe ligand exchange processes in the $[LnL_2X]$ system, chemically equivalent but spectroscopically different ligands are required. The polypyrazolylborate ligands are not easy to modify

* Author to whom correspondence should be addressed.

chemically and, in any event chemical modification leads to profound changes in reactivity. Consequently our initial studies have utilized different β-diketonate co-ligands, and to this end the new complexes [LnL_2X] were prepared where X = PhC(O)CHC(Me)O (bzac) or PhC(O)CHC(Ph)O (dbzm).

SYNTHETIC STUDIES

The complexes [LnL_2X] where X = bzac, Ln = Y, La, Ce, Pr, Nd, Sm, Eu, Tb, Ho, Er, Yb, Lu and where X = dbzm, Ln = Y, La, Ce, Sm, Eu, Tb, Yb, Lu, were prepared using similar procedures to those used in the preparation of [LnL_2(acac)].[3,6] The new complexes are air- and moisture-stable and are soluble in polar organic solvents. They were characterized by IR, ^{1}H NMR and mass spectrometric measurements and by elemental analyses.* The IR spectra of the complexes [LnL_2(bzac)] are superimposable for different Ln in the set, as are the spectra of the complexes [LnL_2(dbzm)]. All of the spectra contain ν_{BH} at 2450–2460 cm^{-1} and $\nu_{C=O}$ at 1600 cm^{-1}, along with characteristic bands attributable to the phenyl and polypyrazolylborate moieties. The [LnL_2(bzac)] and [LnL_2(dbzm)] complexes are volatile and have similar mass spectra to their acac-containing analogues, consisting of a molecular ion of the correct isotopic pattern, and fragment ions including [LnL_2]$^+$ and [LnLpz]$^+$.

The ^{1}H NMR spectra of the [LnL_2(bzac)] and [LnL_2(dbzm)] derivatives presented in Table 1 are similar to those of the related [LnL_2(acac)] complexes containing the same metal.[3,6] All nine complexes containing the three diamagnetic ions (Ln = Y, La, Lu) have very similar pyrazolyl proton chemical shifts, i.e. $\delta_{TMS} = 7.66(\pm 0.02)$, $7.10(\pm 0.05)$ and $5.98(\pm 0.03)$ ppm with $^3J_{HH} = 2$ Hz. The complexes of the paramagnetic ions exhibit pyrazolyl proton resonances which are singlets. The pyrazolyl and methyl proton resonances appear at the same chemical shifts in the spectra of both the acac and the bzac complexes. However, in the spectrum of the bzac complex the methyl resonance integrates for three rather than six protons in accord with the complex formula. The spectra of complexes containing holmium and erbium could not be phased or integrated with sufficient accuracy for unequivocal assignment.

* Supplementary data available. Tables of elemental analyses and kinetic data have been deposited with the Editor.

LIGAND EXCHANGE STUDIES

The ligand exchange process was observed at 20°C by mixing two equimolar $CDCl_3$ solutions, one containing a complex of a paramagnetic ion and the other a complex of a neighbouring diamagnetic ion of similar ionic radius. The 270 MHz ^{1}H NMR spectrum of the mixture was then recorded. Three different mixtures were studied. These contained [YbL_3] and [LuL_2(acac)], [YbL_2(bzac)] and [LuL_2(acac)] and [CeL_2(acac)] and [LaL_2(bzac)]. In each case the spectrum obtained contained signals attributable to four compounds arising, respectively, from the following equilibria:

$$[YbL_3] + [LuL_2(acac)] \rightleftharpoons [YbL_2(acac)] + [LuL_3] \quad (1)$$

$$[YbL_2(bzac)] + [LuL_2(acac)] \rightleftharpoons [YbL_2(acac)] + [LuL_2(bzac)] \quad (2)$$

$$[CeL_2(acac)] + [LaL_2(bzac)] \rightleftharpoons [CeL_2(bzac)] + [LaL_2(acac)]. \quad (3)$$

Monitoring the spectra as a function of time revealed that intermolecular exchange had proceeded to completion during the time required to prepare the sample and acquire the ^{1}H NMR spectrum (*ca* 10 min). In all three reactions there was approximately the same concentration of all four complexes in solution at equilibrium. Therefore the equilibrium constants appear to be close to unity. These qualitative observations indicate that, for [LnL_2X], bidentate ligand exchange processes occur within a period of minutes at room temperature and are slow on the NMR time scale at 270 MHz.

In order to determine whether intermolecular ligand exchange might become fast on the ^{1}H NMR time scale at elevated temperatures trichlorobenzene was used as a solvent. A mixture of [SmL_2(acac)] and [YL_2(acac)] exhibits two methyl resonances, one at 2.00 ppm due to the acac coordinated to yttrium and one at 2.80 ppm due to the acac coordinated to samarium. In trichlorobenzene no broadening of these methyl resonances was observed at 200°C in the ^{1}H NMR spectra recorded at 270 MHz, eq. (4):

$$[SmL_2(acac')] + [YL_2(acac)] \rightleftharpoons [SmL_2(acac)] + [YL_2(acac')]. \quad (4)$$

Thus, even at this temperature, β-diketonate exchange appears to be slow on the ^{1}H NMR time scale. This finding contrasts with the observation of fast ligand exchange at +40°C for $[Y(tfac)_4]^-$/$[Y(hfac)_4]^-$ mixtures using a 60 MHz spectrom-

Table 1. ^{1}H NMR data as δ_{TMS} (ppm) for complexes [LnL_2X] where X = (a) (bzac) and (b) (dbzm)[a]

Ln	MHz	Pyrazolyl resonances			C—H	Co-ligand resonances Me	Ph	Ph	Ph
(a) Benzoylacetonate complexes									
		Int = 6	Int = 6	Int = 6	Int = 1	Int = 3	Int = 2	Int = 2	Int = 1
Y	60	7.65d	7.05d	5.95m	6.31s	2.09s	7.9m	7.4m	
La	60	7.67d	7.18d	6.00m	6.32s	2.12s	7.9m	7.4m	
Ce	270	9.06s	6.20s	2.82s	26.0s	7.99s	9.27s	7.60s	7.96s
Pr	270	10.2s	6.70s	5.56s	49.2s	17.8s	17.1s	10.1s	
Nd	270	9.57s	7.31s	5.48s	23.1s	7.60s	10.6d	8.13s	8.34t
Sm	270	8.35d	5.85s	4.64s	9.84s	2.91s	7.57d	7.23t	7.36t
Eu	60	8.30s	4.05d	3.60m	−7.35s	−2.15s	5.2m	6.4m	
Tb	270	6.9d	−3.4s	−70.7s	346s	107s	36.9s	16.6s	17.8s
Yb	270	13.4s	7.86s	5.79s	−47.3s	−21.0s	3.1s	−5.8s	3.8t
Lu	400	7.65d	7.05d	5.97m	6.32s	2.10s	7.86m	7.4m	
(b) Dibenzoylmethide complexes									
		Int = 6	Int = 6	Int = 6	Int = 1		Int = 4	Int = 4	Int = 2
Y	100	7.65d	7.10d	5.95m	7.06s	—	7.9m	7.4m	
La	60	7.65d	7.20d	5.98m	7.05s	—	8.0m	7.4m	
Ce	270	9.16s	6.23s	2.85s	26.5s	—	9.08s	7.66s	7.96t
Sm	270	8.42d	5.86s	4.53	10.66s	—	7.59d	7.25t	7.38t
Eu	60	8.70d	3.85d	3.55m	−6.40s	—	5.7m	6.7m	
Tb[b]	270	9.2s	−2.9s	−72.2s	338	—	29.7s	14.4s	16.1s
Yb	270	16.9s	6.54s	5.79m	−47.8s	—	3.3d	−4.6s	4.0t
Lu[b]	400	7.7d	7.1d	6.0m	7.1s	—	8.0m	7.5m	

[a] Spectra run in $CDCl_3$; s = singlet, d = doublet, t = triplet, m = multiplet, Int denotes the area of the signal.
[b] Spectrum run in CD_2Cl_2.

eter.[5] Even allowing for the difference in field strength between the two experiments, exchange of the β-diketonate ligand is much slower in complexes of the type [LnL_2(acac)] than in [$Y(tfac)_4$]$^-$. This is perhaps not surprising since the steric bulk of the L^- ligands in [LnL_2X], and the presence of only one β-diketonate ligand X, will result in a much smaller fraction of molecular collisions leading to co-ligand exchange.

The co-ligand exchange reaction was found to be very slow at −50°C and could be followed using ^{1}H NMR spectroscopy at sub-ambient temperatures. Time resolved studies were carried out by mixing $CDCl_3$ solutions of [SmL_2(acac)] and [EuL_2(bzac)] at *ca* −50°C, then warming the mixture to a constant −20°C and monitoring the changing composition of the mixture according to eq. (5) as revealed

$$[SmL_2(acac)] + [EuL_2(bzac)] \underset{k_{5'}\ (-20°C)}{\overset{k_5}{\rightleftharpoons}} [SmL_2(bzac)] + [EuL_2(acac)] \quad (5)$$

by the ^{1}H NMR spectrum. Similarly the reverse reaction between [SmL_2(bzac)] and [EuL_2(acac)] according to eq. (6) was studied at −10°C. Under these conditions it was found that equilibration

$$[SmL_2(bzac)] + [EuL_2(acac)] \underset{k_6\ (-10°C)}{\overset{k_{6'}}{\rightleftharpoons}} [SmL_2(acac)] + [EuL_2(bzac)] \quad (6)$$

was essentially complete after 2–5 h. The results obtained indicate the presence of slightly larger concentrations of the complexes with the sterically larger ligand (bzac) coordinated to the larger lanthanide (Sm), and the smaller ligand (acac) coordinated to the smaller lanthanide (Eu), as compared to the other reaction products. Thus the equilibrium constant for the reaction is not exactly unity. In the case of the reaction as written in eq. (5) the final concentrations of the products lead to an equilibrium constant of 1.31. The final equilibrium concentrations for the reaction as written in eq. (6) gave an equilibrium constant of 0.774, the reciprocal of which is 1.29.

Table 2. Data from the syntheses of the complexes $[Ln\{HBpz_3\}_2X]$ where X = (a) (bzac) and (b) (dbzm)

Ln	Amount of $LnCl_3 \cdot 6H_2O$	Crude Yield g(%)	Recrystallized Yield g(%)	Melting point (°C)	Colour
(a) Benzoylacetonate complexes					
Y	0.30	0.61(90)	0.50(74)	232–234	Colourless
La	0.35	0.64(88)	0.45(62)	225–227	Colourless
Ce	0.35	0.68(94)	0.39(54)	202–203	Orange
Pr	0.36	0.64(88)	0.50(67)	208–210	Green
Nd	0.36	0.63(86)	0.49(67)	212–213	Purple
Sm	0.36	0.65(88)	0.53(72)	215–216	Yellow
Eu	0.37	0.63(85)	0.50(68)	225–226	Yellow
Tb	0.37	0.67(90)	0.52(70)	229–231	Colourless
Ho	0.38	0.68(90)	0.50(67)	221–223	Yellow
Er	0.38	0.72(95)	0.51(68)	215–217	Pink
Yb	0.39	0.74(97)	0.53(70)	236–237	Yellow
Lu	0.39	0.74(97)	0.55(72)	235–237	Colourless
(b) Dibenzoylmethide complexes					
Y	0.30	0.70(95)	0.51(69)	285–290	Yellow
La	0.35	0.56(71)	0.41(52)	282–284	Yellow
Ce	0.35	0.68(86)	0.52(66)	265–267	Red
Sm	0.36	0.78(98)	0.60(75)	280–281	Yellow
Eu	0.37	0.67(84)	0.54(67)	280–285	Yellow
Tb	0.37	0.63(78)	0.52(64)	291–295	Yellow
Yb	0.39	0.78(95)	0.53(64)	289–291	Yellow
Lu	0.39	0.82(100)	0.56(68)	285–286	Yellow

Assuming that these reactions can be described as "opposing second-order reactions", and assuming that the same initial concentration of the two starting materials is used, the integrated rate equation (7) can be derived:[7]

$$\ln\{[a-x(1-K^{-1/2})]/[a-x(1+K^{-1/2})]\} = I = 2aK^{-1/2}kt, \quad (7)$$

where a is the initial concentration of one of the starting materials, x is the concentration of one of the products at time t, K is the equilibrium constant and k is the rate of the forward reaction. A plot of the left-hand side of eq. (7), *viz.* I, vs time (t) should give a straight line of slope $2aK^{-1/2}k$ if the mechanism of the two opposing second-order reactions is correct.

The ^1H NMR spectra of the reaction mixtures used are complicated, but in the region between −3 and −4 ppm, the two methyl resonances of acac and bzac coordinated to europium are well separated. Thus these two resonances can be integrated accurately and the relative concentrations of $[EuL_2(acac)]$ and $[EuL_2(bzac)]$ can be calculated. Graphs of the function I against t are linear as shown in Fig. 1 with correlation coefficients of 0.9993 and 0.9975 for the plots from reactions (5) and (6), respectively. The slopes of these plots are $(1.76\pm0.02)\times10^{-4}$ and $(6.2\pm0.1)\times10^{-4}$ s^{-1}, respectively. These values give a forward rate constant for reaction (5) at −20°C (k_5) of $(2.5\pm0.1)\times10^{-3}$ $dm^3\,mol^{-1}\,s^{-1}$ and a forward rate constant for reaction (6) at −10°C ($k_{6'}$) of $(8.8\pm0.4)\times10^{-3}$ $dm^3\,mol^{-1}\,s^{-1}$. The errors of 5% in these rate constants are estimated on the basis of the uncertainty in the concentration since the errors in both the slopes and equilibrium constants are less than 2%. The kinetic data calculated from these two experiments for the reaction as written in eq. (5) can be summarized as follows: $K = 1.30\pm0.01$; $k_5 = (2.5\pm0.1)\times10^{-3}$ $dm^3\,mol^{-1}\,s^{-1}$ and $k_{5'} = (1.9\pm0.1)\times10^{-3}$ $dm^3\,mol^{-1}\,s^{-1}$ at −20°C; $k_6 = (11.4\pm0.6)\times10^{-3}$ $dm^3\,mol^{-1}\,s^{-1}$ and $k_{6'} = (8.8\pm0.4)\times10^{-3}$ $dm^3\,mol^{-1}\,s^{-1}$ at −10°C.

The reaction described by eq. (6) was observed to have essentially reached completion in 2 h at −10°C and so at 20°C it would reach completion in approximately 5 min. In view of this dynamic character the resistance of these heteroleptic complexes to disproportionation is remarkable. It would appear to indicate a thermodynamic preference for the heteroleptic ligand set in $[LnL_2(\beta$-

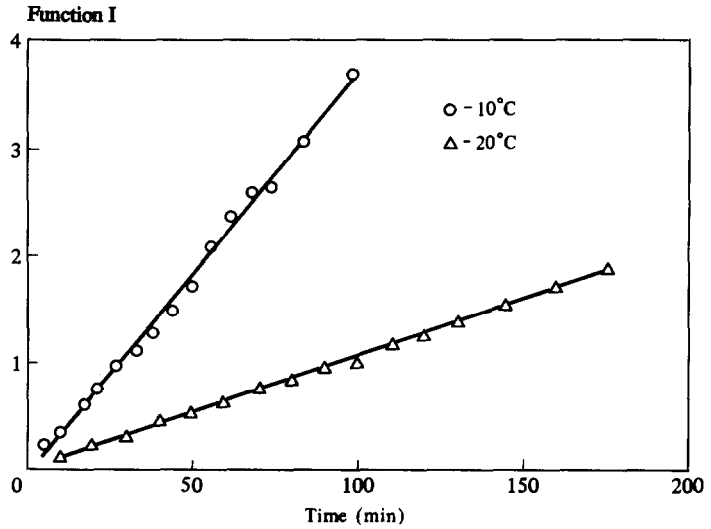

Fig. 1. Plots showing the magnitude of function *I* as defined in eq. (7) against time for experiments (5) (−20°C) and (6) (−10°C). The graph plotting program was TELL-A-GRAF.[10]

diketonate)] as compared to a mixture of [LnL_3] and solvated [Ln(β-diketonate)$_3$] or [Ln(β-diketonate)$_4$]$^-$.

EXPERIMENTAL

Synthetic studies

Potassium hydrotris(pyrazol-1-yl)borate was prepared by the literature method.[8] Hydrated lanthanide trichlorides were obtained from Ventron GMBH and acetylacetone, benzoylacetone and dibenzoylmethane were obtained from Aldrich Chemicals Ltd, they were used without further purification. Water was distilled before use. ^{1}H NMR spectra were recorded using Perkin–Elmer R12B (60 MHz), Varian XL 100 (100 MHz) or JEOL JNM GX270 (270 MHz) spectrometers. Deuterated NMR solvents were obtained from Aldrich Chemicals Ltd, and chemical shifts are reported with tetramethylsilane as internal reference at 293 K. IR spectra were recorded using potassium bromide pellets and a Perkin–Elmer 297 spectrometer. Mass spectra were obtained using a Kratos MS80RF mass spectrometer, ions being produced by electron impact.

Benzoylacetonatobis{hydrotris(pyrazol-1-yl)borato} yttrium(III)

K{$HBpz_3$) (0.5 g, 2 mmol), benzoylacetone (0.16 g, 1 mmol), ethanol (20 cm^3) and 0.1 mol dm^{-3} aqueous KOH (10 cm^3) were mixed and the resulting solution added to a stirred solution of $YCl_3 \cdot 6H_2O$ (0.30 g, 1 mmol) in water (5 cm^3). Stirring was continued for 1 h, after which time the white amorphous precipitate produced was collected by filtration (0.61 g, 90%). Recrystallization from CH_2Cl_2–hexane gave white crystals (0.50 g, 74%), m.p. = 232–234°C.

Dibenzoylmethidobis{hydrotris(pyrazol-1-yl)borato} yttrium(III)

This complex was prepared by the same method as the benzoylacetonate complex using dibenzoylmethane (0.22 g, 1 mmol).

The corresponding complexes [Ln{$HBpz_3$}$_2$X] (X = (bzac), Ln = La, Ce, Pr, Nd, Sm, Eu, Tb, Ho, Er, Yb and Lu; and X = (dbzm), Ln = La, Ce, Sm, Eu, Tb, Yb and Lu) were prepared similarly. Details of the amounts of lanthanide starting material used, and of the yields, melting points and colours of the products are given in Table 2.

Ligand exchange experiments

All ligand exchange experiments were carried out using a JEOL JNM GX270 NMR spectrometer. Experiments (1)–(6) relate, respectively, to the reactions shown in eqs (1)–(6). In experiment (4) 1,2,4-trichlorobenzene was used as the solvent, in all other experiments $CDCl_3$ was used. [YbL_3] was prepared by a published method,[9] and other lanthanide complexes were prepared according to previously described methods.[3,5]

Experiment (1). [YbL_3] (40.6 mg, 0.05 mmol) and [LuL_2(acac)] (35.0 mg, 0.05 mmol) were dissolved

in $CDCl_3$ (0.5 cm^3) and an NMR spectrum obtained within 15 min at room temperature (20°C). This spectrum contained the resonances for four previously characterized complexes: $[LnL_3]$ and $[LnL_2(acac)]$, where Ln = Yb and Lu.

Experiment (2). $[YbL_2(bzac)]$ (38.0 mg, 0.05 mmol) and $[LuL_2(acac)]$ (35.0 mg, 0.05 mmol) were treated as in experiment (1), the resulting spectrum again contained resonances for four complexes: $[LnL_2(bzac)]$ and $[LnL_2(acac)]$, where Ln = Yb and Lu.

Experiment (3). $[LaL_2(bzac)]$ (36.3 mg, 0.05 mmol) and $[CeL_2(acac)]$ (33.3 mg, 0.05 mmol) were treated as in experiment (1), the resulting spectrum again contained resonances for four complexes: $[LnL_2(bzac)]$ and $[LnL_2(acac)]$, where Ln = Yb and Lu.

Experiment (4). $[YL_2(acac)]$ (18.4 mg, 0.03 mmol) and $[SmL_2(acac)]$ (20.2 mg, 0.03 mmol) were dissolved in 1,2,4-trichlorobenzene (b.p. = 215°C) and spectra acquired at high temperatures up to a maximum of 200°C, no broadening of the signals was observed.

Experiment (5). A solution of $[SmL_2(acac)]$ (16.8 mg, 0.0249 mmol) in $CDCl_3$ (0.40 cm^3) was placed in a 5 mm NMR tube and cooled to between −60 and −50°C. To this was added a similarly cooled solution of $[EuL_2(bzac)]$ (18.4 mg, 0.0249 mmol) in $CDCl_3$. The mixture was stirred vigorously with a narrow, flat ended glass rod. The NMR spectrometer probe was pre-cooled to −60°C. The cold well-mixed solution was inserted into the spectrometer and warmed to −20°C then held at this temperature. The first spectrum was acquired as quickly as possible and spectra were recorded subsequently at intervals of 10 min. Only the region between −3 and −4 ppm was integrated and printed since this region contains the methyl resonances of acac and bzac attached to europium. Integrations were converted to a ratio of reactant, $[EuL_2(bzac)]$, to product, $[EuL_2(acac)]$.

Experiment (6). The procedure used in experiment (5) was repeated using $[SmL_2(bzac)]$ (18.2 mg, 0.0247 mmol) and $[EuL_2(acac)]$ (16.7 mg, 0.0247 mmol). The equilibration was observed at −10°C in this case, readings being taken at intervals of 5–7 min.

Acknowledgements—The authors are grateful to Professor W. J. Evans and Drs S. Kurek and C. F. Wells for helpful discussions, to Mr P. P. Clayton and Mr T. R. Desson for technical assistance, to the SERC and BP Chemicals, Hull for support (to M.A.J.M.) and to NATO for the provision of travel grant 175/84.

REFERENCES

1. M. V. R. Stainer and J. Takats, *J. Am. Chem. Soc.* 1983, **105**, 410.
2. M. A. J. Moss and C. J. Jones, Abstracts of the XXIV International Conference on Coordination Chemistry, *Chimica Chronika*, Association of Greek Chemists (1986) A7-488.
3. M. A. J. Moss, C. J. Jones and A. J. Edwards, *Polyhedron* 1988, **7**, 79.
4. W. D. Moffat, M. V. R. Stainer and J. Takats, *Inorg. Chim. Acta* 1987, **139**, 75.
5. F. A. Cotton, P. Legzdins and S. J. Lippard, *J. Chem. Phys.* 1966, **45**, 3461.
6. M. A. J. Moss, C. J. Jones and A. J. Edwards, *J. Chem. Soc., Dalton Trans.* 1989, 1393.
7. E. A. Moelwyn-Hughes, *Physical Chemistry*, p. 1125. Pergamon Press, Oxford (1961).
8. S. Trofimenko, *Inorg. Synth.* 1970, **12**, 99.
9. K. W. Bagnall, A. C. Tempest, J. Takats and A. P. Masino, *Inorg. Nucl. Chem. Lett.* 1976, **12**, 555.
10. TELL-A-GRAF, ISSCO (Integrated Software Systems Corporation), San Diego, California (1984).

Polyhedron Vol. 9, No. 5, pp. 703–711, 1990
Printed in Great Britain

0277–5387/90 $3.00+.00
© 1990 Pergamon Press plc

AN NMR STUDY OF THE FLUXIONALITY OF GROUP VI METAL PENTACARBONYL COMPLEXES OF 1,3-DITHIOLANES

EDWARD W. ABEL, KEITH G. ORRELL,* KHURSHID B. QURESHI and VLADIMIR ŠIK

Department of Chemistry, University of Exeter, Exeter EX4 4QD, U.K.

(*Received* 12 *June* 1989; *accepted* 25 *September* 1989)

Abstract—The complexes $[M(CO)_5(\overline{SC_2H_4SC}RR')]$ (M = Cr, Mo or W, R = R′ = H; M = Cr or W, R = R′ = Me, R = H, R′ = Me, Bu^t or Ph) have been synthesized and characterized. Their solution stereodynamics were examined by ^{1}H NMR spectroscopy. Pyramidal inversion of the metal-coordinated sulphur atoms occurs rapidly at ambient temperatures ($\Delta G^{\ddagger}$ (298 K) = 40–44 kJ mol^{-1}). An appreciably slower 1,3-metal–sulphur shift is also evident at temperatures where sulphur inversion is rapid on the proton NMR timescale. For the ligand complexes (R = R′ = H, Me) this shift is purely intramolecular in nature ($\Delta G^{\ddagger}$ (298 K) values ~ 78 kJ mol^{-1}), in contrast to the 2-mono-substituted ligand complexes (R = H, R′ = Me, Bu^t, Ph) where it is accompanied by a dissociation process.

Group VI metal pentacarbonyl complexes with chalcogen ligands are widely known and their solution structures have been rigorously examined by NMR methods.[1] Much of this previous work has been centred around $M(CO)_5$ complexes of cyclic polythioethers such as $\overline{SCH_2SCH_2SCH_2}$,[2,3] $\overline{SCHMeSCHMeSCHMe}$[2–4] and $\overline{SCH_2SCH_2SCH_2SCH_2}$,[5] where in addition to facile pyramidal sulphur inversion and ligand ring reversals, slower 1,3-metal–sulphur shifts occur. Because of the alternating —C—S—C—S— ligand backbone, the $M(CO)_5$ moiety is able to commute freely around these six-membered rings. In five-membered rings, however, this is not possible, as for example in the case of the ligand complexes $[M(CO)_5(\overline{Me_2CCH_2EECH_2})]$ (E = S, Se) where the commutation is restricted to the two adjacent E atoms.[6] Fluxional 1,3-metal shifts restricted to three bonds might be expected to occur in $M(CO)_5$ complexes of the five-membered rings $\overline{SC_2H_4SPPh}$, $\overline{SC_2H_4SP(O)Ph}$ and $\overline{SC_2H_4SP(S)Ph}$, but NMR investigations up to 150°C produced no evidence for such fluxionality, possibly due to the donor in these ligands being the phosphorus, oxygen or exocyclic sulphur atoms rather than the endocyclic sulphur.[7] The 1,3-dithiolanes, $\overline{SC_2H_4SCRR'}$ (R = H, R′ = H, alkyl, aryl), however, can only coordinate via their endocyclic sulphur atoms and so these ligands have been chosen for identifying any 1,3-shifts that might be occurring in five-membered cyclic polythioethers of $M(CO)_5$.

These ligands have recently been shown to form stable palladium(II) and platinum(II) complexes, viz. *trans*-$[MCl_2(\overline{SC_2H_4SCRR'})]$ (R = R′ = H, Me; R = H, R′ = Me, Bu^t, Ph), in which 1,3-metal–sulphur shifts do indeed occur in most cases, usually accompanying pyramidal sulphur inversion or ligand dissociation/recombination.[8,9] This present work therefore serves both to examine the influence of the metal on the fluxional nature of the M → S bond in five-membered ligand ring complexes and also to compare the effect of ligand ring size on 1,3-metallotropic shifts. To this end the following complexes have been synthesized, viz. $[M(CO)_5(\overline{SC_2H_4SCRR'})]$ (M = Cr, Mo, W, R = R′ = H; M = Cr, W, R = R′ = Me, R = H, R′ = Me, Bu^t or Ph), and we report herein their solution structures as evidenced by dynamic ^{1}H NMR spectroscopy.

EXPERIMENTAL

Materials and preparations

Ligands. The preparations of the ligands 1,3-dithiolane, 2-alkyl-1,3-dithiolanes, 2-phenyl-1,3-dithiolane and 2,2-dimethyl-1,3-dithiolane were

* Author to whom correspondence should be addressed.

based on the original method of Gibson.[10] Full details are given in our earlier papers.[8,9]

Metal pentacarbonyl complexes. These were all prepared by reacting the appropriate ligand with $[M(CO)_5THF]$ (M = Cr, Mo, W; THF = tetrahydrofuran). The latter was prepared by UV irradiation of a solution of $[M(CO)_6]$ (0.5 g) in THF (130 cm^3) in an immersion reaction vessel and a 450 W Hanovia medium pressure Hg lamp. The solution was deoxygenated and purged with nitrogen before being irradiated for 12 h to produce a yellow solution of $[W(CO)_5THF]$, or for 40 h to produce a deep orange solution of $[Cr(CO)_5THF]$, or for 88 h to produce a yellow solution of $[Mo(CO)_5THF]$. The irradiated solution was slowly filtered into a Schlenk tube containing a stirred, ice-cold solution of the ligand (1 molar equivalent) dissolved in dichloromethane (20 cm^3). The reaction mixture was stirred for 3 h whilst being allowed to warm up to room temperature. The solvent was removed and the residue dissolved in dichloromethane–petroleum spirit (1 : 1) (20 cm^3) and chromatographed with grade II alumina. The chromatogram was developed using dichloromethane–petroleum spirit (40–60°C) (1 : 1) at room temperature, the product being eluted as a yellow band. The solvents were removed from the yellow fraction under reduced pressure and the yellow complex dried *in vacuo*. Analytical data for the complexes are given in Table 1. The complexes $[M(CO)_5(\overline{SC_2H_4SCHPh})]$ (M = Cr, W) remained as oils and were not isolated as analytically pure crystalline products.

NMR spectra

All spectra were obtained using a Bruker AM250 FT spectrometer operating at 250.1 MHz (^1H). All complexes were examined as solutions in either dichloromethane-d_2 (low temperatures) or 1,1,2,2-tetrachloroethane–nitrobenzene-d_5 mixtures (high temperatures). Proton shifts were measured relative to Me_4Si (internal). Sample temperature variation was achieved by a standard variable-temperature unit, calibrated to read temperatures accurate to at least ± 1°C. Band shape analyses employed the authors' version of the DNMR program of Kleier and Binsch.[11]

IR spectra

The IR-active carbonyl stretching modes of these complexes were measured using a Perkin–Elmer Model 398 spectrophotometer. The complexes were examined as solutions in hexane and data are given in Table 2, where the assignments of the three fundamental stretching modes ($2A_1 + E$) are based on an assumed C_{4v} point group. In most cases an additional band in the region 1975–1990 cm^{-1} was also observed due to the presence of a trace of $M(CO)_6$ in the hexane solutions.

RESULTS

$[M(CO)_5(\overline{SC_2H_4SCH_2})]$ (M = Cr, Mo, W)

Room temperature ^1H NMR spectra of these complexes consisted of a singlet for the —SCH_2S—

Table 1. Physical data for the complexes $[M(CO)_5(\overline{SC_2H_4SCRR'})]$

Complex[a]	Melting point (°C)	Yield (%)[b]	Found C(%)	Found H(%)	Calculated C(%)	Calculated H(%)
$[W(CO)_5(\overline{SC_2H_4SCH_2})]$	35	33.0	23.0	1.7	23.3	1.4
$[Cr(CO)_5(\overline{SC_2H_4SCH_2})]$	35	12.0	31.0	1.2	32.2	2.0
$[Mo(CO)_5(\overline{SC_2H_4SCH_2})]$	22	33.0	28.6	1.5	28.0	1.7
$[W(CO)_5(\overline{SC_2H_4SC(H)Me})]$	105	4.0	22.7	1.2	24.3	1.8
$[Cr(CO)_5(\overline{SC_2H_4SC(H)Me})]$	100[c]	26.0	33.0	1.7	34.6	2.5
$[W(CO)_5(\overline{SC_2H_4SCMe_2})]$	40	50.0	26.2	2.2	26.2	2.2
$[Cr(CO)_5(\overline{SC_2H_4SCMe_2})]$	105[c]	51.0	34.3	2.0	36.8	3.0
$[W(CO)_5(\overline{SC_2H_4SC(H)Bu^t})]$	48	46.0	29.5	2.9	29.6	2.9
$[Cr(CO)_5(\overline{SC_2H_4SC(H)Bu^t})]$	45	85.0	40.7	4.0	40.6	3.9
$[W(CO)_5(\overline{SC_2H_4SC(H)Ph})]$	[d]	52.8	[e]	[e]	33.2	1.9
$[Cr(CO)_5(\overline{SC_2H_4SC(H)Ph})]$	[d]	62.6	[e]	[e]	44.9	2.6

[a] All are yellow in colour.
[b] All yields are quoted relative to the $M(CO)_6$ utilized.
[c] Decomposed.
[d] Yellow oils.
[e] Not determined.

Table 2. IR data[a] for complexes $[M(CO)_5(\overline{SC_2H_4SCRR'})]$

Complex			Metal–carbonyl stretching wavenumbers ν(CO) (cm^{-1})		
M	R	R′	A_1	E	A_1
W	H	H	2070 m	1940 m	1935 m
Cr	H	H	2060 s	1940 m	1935 s
Mo	H	H	2080 s	1950 w	1945 m
W	H	Me	2070 s	1935 s	1915 w
Cr	H	Me	2070 s	1950 w	1940 m
W	Me	Me	2075 s	1940 m	1935 m
Cr	Me	Me	2060 s	1940 m	1935 m
W	H	Bu^t	2070 s	1935 s	1920 w
Cr	H	Bu^t	2070 s	1950 m	1940 s
W	H	Ph	2070 s	1945 w	1940 m
Cr	H	Ph	2070 s	1950 m	1940 m

[a] In *n*-hexane solutions.
m = medium, s = strong, w = weak.

protons and a symmetrical second order AA′BB′ type pattern for the —SCH_2CH_2S— protons. Chemical shift data are given in Table 3. Such a spectral pattern is indicative of rapid inversion of the coordinated sulphur atom which renders the two —SCH_2S— protons isochronous and also removes distinction between the geminal proton pairs of the —SCH_2CH_2S— grouping. This is depicted in Fig. 1, where the two structures represent an enantiomeric pair, with the proton averaging being AB⇌BA and CDEF⇌DCFE. The correctness of this interpretation was confirmed by low-temperature measurements, since on cooling to *ca* −70°C the —SCH_2S— signal split into an AB quartet ($\Delta\nu$ = 129 Hz, $^2J_{AB}$ = 10.4 Hz, for M = W and $\Delta\nu$ = 123 Hz, $^2J_{AB}$ = 10.4 Hz for M = Mo), and the —SCH_2CH_2S— signals became more complex, indicative of four different chemical shifts C,

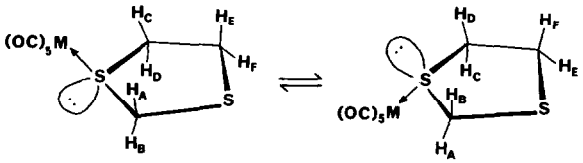

Fig. 1. Enantiomerism in $[M(CO)_5(\overline{SC_2H_4SCH_2})]$ complexes as a result of pyramidal inversion of the coordinated sulphur. The labels A–F on the ring protons refer to the environments, not the identities of the protons.

Table 3. ^{1}H NMR chemical shifts (δ)[a] for $[(\overline{SC_2H_4SCRR'})]$ and $[M(CO)_5(\overline{SC_2H_4SCRR'})]$

Ligand	Temperature (°C)	—SC*R*R′S—	—SCR*R*′S—	—SC_2H_4S—
$\overline{SC_2H_4SCH_2}$	22	3.9	3.9	3.22
$\overline{SC_2H_4SC}$(H)Me	21	4.60	1.59	3.30, 3.20[b]
$\overline{SC_2H_4SCMe_2}$	20	1.80	1.80	3.42
$\overline{SC_2H_4SC}$(H)Bu^t	−80	4.51	1.01	3.16, 3.15[b]
$\overline{SC_2H_4SC}$(H)Ph	21	5.63	7.42	3.49, 3.33[b]

Complex	Temperature (°C)	—SC*R*R′S	—SCR*R*′S—	$MSCH_2$—[b]	—SCH_2CH_2[b]
$[W(CO)_5(\overline{SC_2H_4SCH_2})]$	30	4.10	4.10	3.43	3.29
$[Cr(CO)_5(\overline{SC_2H_4SCH_2})]$	20	3.92	3.92	3.30	3.28
$[Mo(CO)_5(\overline{SC_2H_4SCH_2})]$	20	4.00	4.00	3.43	3.33
$[W(CO)_5(\overline{SC_2H_4SC}$(H)Me)]	30	4.38	1.78	3.83	3.58
$[Cr(CO)_5(\overline{SC_2H_4SC}$(H)Me)]	20	4.07	1.75	3.66	3.32
$[W(CO)_5(\overline{SC_2H_4SCMe_2})]$	30	1.80	1.80	3.68	3.48
$[Cr(CO)_5(\overline{SC_2H_4SCMe_2})]$	20	1.78	1.78	3.73	3.73
$[W(CO)_5(\overline{SC_2H_4SC}$(H)Bu^t)]	25	4.51	1.09	3.51	3.30
$[Cr(CO)_5(\overline{SC_2H_4SC}$(H)Bu^t)]	20	4.27	1.06	3.38	3.08
$[W(CO)_5(\overline{SC_2H_4SC}$(H)Ph)]	22	5.48	7.40	3.88	3.60
$[Cr(CO)_5(\overline{SC_2H_4SC}$(H)Ph)]	20	5.33	7.44	3.78	3.65

[a] Relative to Me_4Si; solvent CD_2Cl_2.
[b] Chemical shifts for all AA′BB′ and ABCD spin systems have only been approximately measured.

D, E and F. In the case of the chromium complex, the band shape changes were less clearly defined, probably as a result of accidental near equality of the geminal methylene shifts and the somewhat lower purity of the sample.

Accurate expanded spectra of the $-SCH_2S-$ signals of the molybdenum and tungsten complexes were recorded over the temperature range -25 to *ca* $-90°C$ and the band shapes were computed as exchanging $AB \rightleftharpoons BA$ systems. Good fits of experimental and computed spectra were obtained as shown in Fig. 2 for the complex $[W(CO)_5(\overline{SC_2H_4SCH_2})]$.

Examination of the ^1H NMR spectra of $[W(CO)_5(\overline{SC_2H_4SCH_2})]$ above room temperature revealed further changes in the band shapes due to the $-SCH_2CH_2S-$ protons (Fig. 3). The two methylene multiplets commenced to broaden and proceed towards coalescence at *ca* 115°C as the temperature was raised. However, above *ca* 80°C decomposition became significant but spectra for band shape analysis were acquired up to 105°C (Fig.

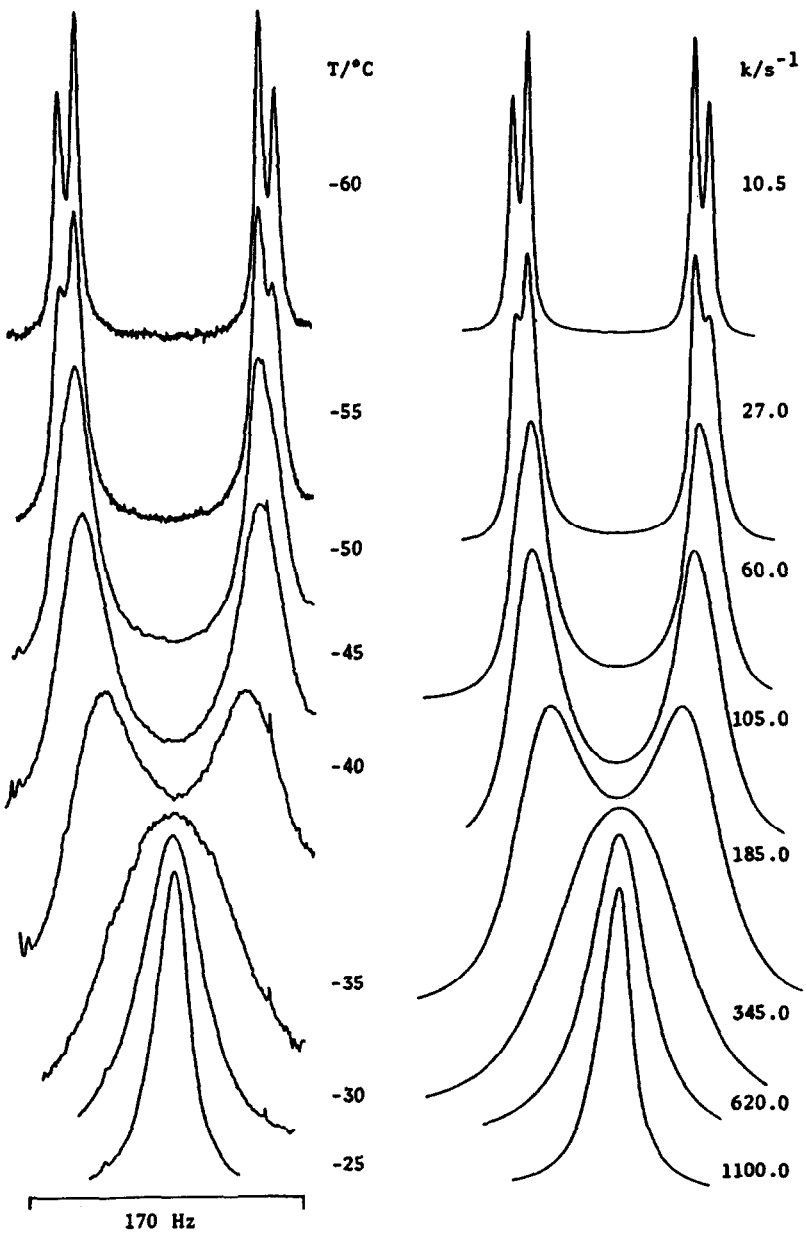

Fig. 2. Variable temperature 250 MHz ^1H NMR spectra of $[W(CO)_5(\overline{SC_2H_4SCH_2})]$ showing the $-SCH_2S-$ region, with the computer synthesized spectra alongside.

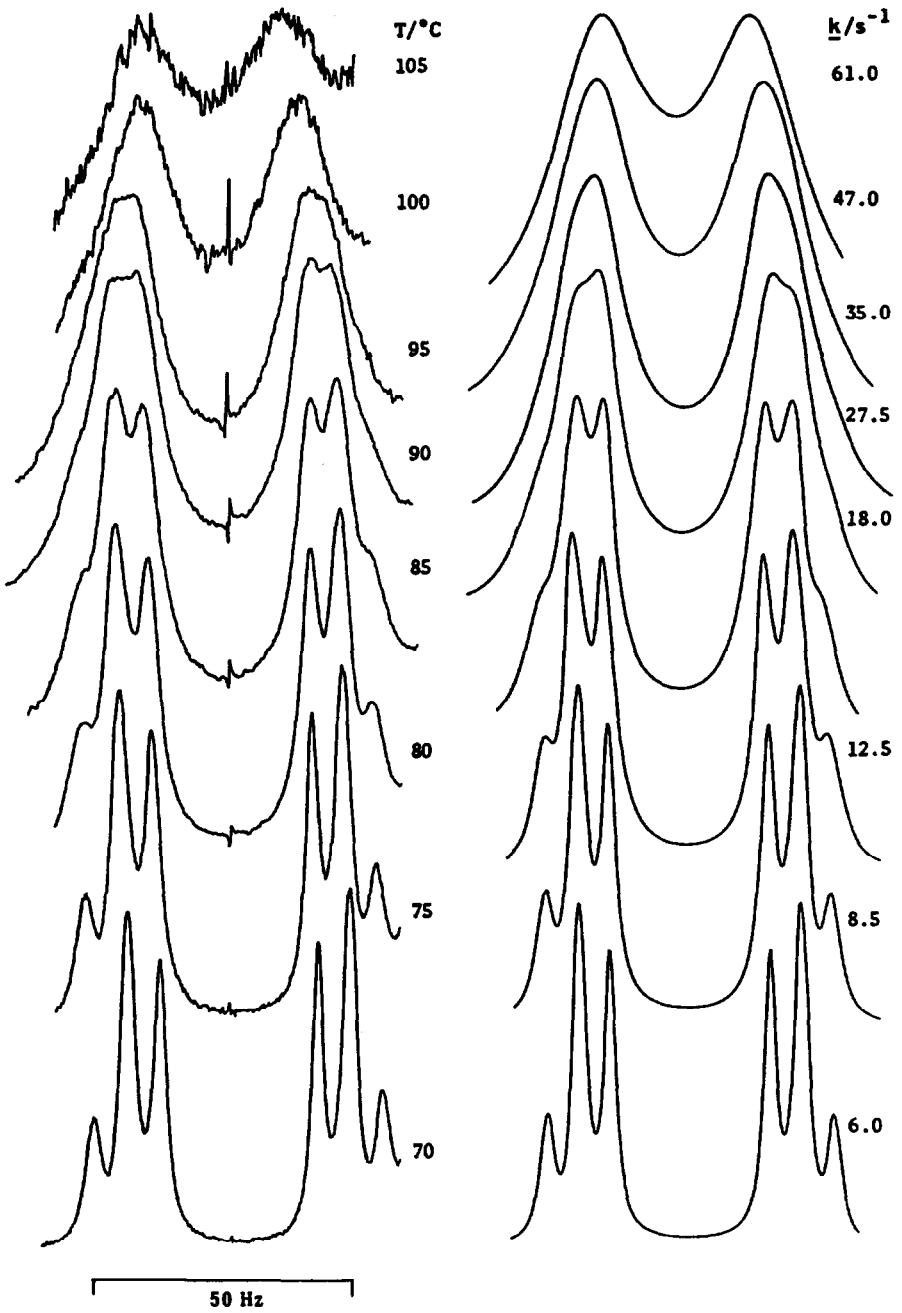

Fig. 3. Variable temperature 250 MHz ^{1}H NMR spectra of $[W(CO)_5(\overline{SC_2H_4SCH_2})]$ showing the $—SCH_2CH_2S—$ region and the effects of the 1,3-shift. Theoretical spectra are shown alongside.

3). Spectra up to *ca* 80°C were fully temperature reversible and clearly indicative of an intramolecular 1,3-shift fluxion which caused averaging of the two ring methylene environments. The kinetics of this process were computed on the basis of an exchanging AA′BB′ ⇌ BB′AA′ spin system where the chemical shifts A, B represent inversion-averaged values ⟨CD⟩ and ⟨EF⟩, respectively. The static parameters used in these calculations are given in Table 4 and the results of the band shape analysis are shown in Fig. 3.

Attempts to repeat these experiments with the chromium complex were unsuccessful due to the production of paramagnetic species, and in the case of the molybdenum complex, because of the very small chemical shift difference $(\nu_A - \nu_B)$, of the adjacent methylene protons.

$[M(CO)_5(\overline{SC_2H_4SCMe_2})]$ (M = Cr, W)

Low and high temperature NMR studies were performed only on the tungsten complex of 2,2-

Table 4. Static ^{1}H NMR parameters used for calculating energy barriers for the 1,3-metal shift

Complex	Temperature (°C)	ν_A (Hz)[a]	ν_B (Hz)[b]	$^2J_{AA'}$ (Hz)	$^2J_{BB'}$ (Hz)	$^2J_{AB'}$ (Hz)[c]	$^2J_{AB}$ (Hz)[d]	T_2^* (s)
$[W(CO)_5(\overline{SC_2H_4SCH_2})]$	70	823.0	864.0	−6.1	−6.2	12.3	~0	6.0
$[W(CO)_5(\overline{SC_2H_4SCMe_2})]$	50	865.0	911.0	−6.9	−7.0	13.9	~0	2.0

[a] $\nu_A = \nu_{A'}$.
[b] $\nu_B = \nu_{B'}$.
[c] $^2J_{AB'} = {}^2J_{A'B}$(*trans* vicinal coupling).
[d] $^2J_{AB} = {}^2J_{A'B'}$(*cis* vicinal coupling).

dimethyl-1,3-dithiolane, as the chromium complex was far less stable in solution particularly at ambient temperatures and above. Even in the case of the tungsten complex the band shape changes were less well defined than in the unsubstituted 1,3-dithiolane complexes due to close similarities of chemical shifts. For instance, the geminal C-methyls were only just resolved at < 70°C on a 400 MHz spectrum, whereas the ring methylene signals consisted of an exchange-broadened ABCD type spectrum with three of the shifts very similar. The line widths of the signals were at a maximum at *ca* −70°C (203 K) from which approximate values of the rate constant and $\Delta G^{\ddagger}$ parameter for the pyramidal inversion process at this temperature could be deduced.

At above-ambient temperatures and AA′BB′ system of the —SCH_2CH_2S— protons again broadened due to the onset of the 1,3-shift process and band shape fittings were carried out in an analogous way to that used for the 1,3-dithiolane complexes (See Table 4 for the static parameters used).

$[M(CO)_5(\overline{SC_2H_4SCHR})]$ (M = Cr, W; R = Me, Bu^t, Ph)

In 2-substituted 1,3-dithiolane complexes, the coordinated sulphur is a chiral centre and pyramidal inversion produces a distinct diastereomer (Fig. 4) rather than a mirror-image enantiomer as

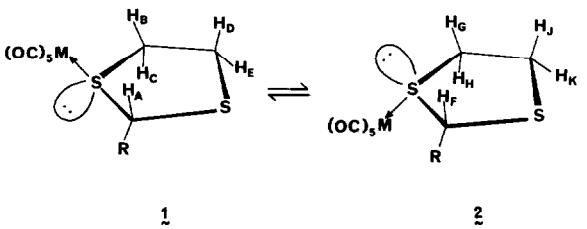

1 2

Fig. 4. Diastereomerism in $[M(CO)_5(\overline{SC_2H_4SCHR})]$ complexes as a result of pyramidal inversion of the coordinated sulphur. Structure 1 is the thermodynamically favoured species.

in the case of the unsubstituted 1,3-dithiolanes (Fig. 1). All the ring proton environments in both species are different and thus complex absorption patterns due to these protons are expected.

$[M(CO)_5(\overline{SC_2H_4SCHMe})]$ (M = Cr, W)

At room temperature the ^{1}H NMR spectra of both complexes comprise a methyl 1 : 1 doublet, a methine 1 : 3 : 3 : 1 quartet and a complex symmetrical AA′BB′ type pattern for the ring methylenes (Table 3). On cooling to *ca* −100°C in CD_2Cl_2 solvent, the methylene region changed to a very complex pattern of lines associated with the strongly coupled four-spin systems of each invertomer (Fig. 4). At this limiting low temperature the methyl proton absorption consisted of two doublets in an intensity ratio 63 : 37% for the tungsten complex. The more intense signal was attributed to the *trans* invertomer, i.e. the structure with $M(CO)_5$ *trans* to the ring methyl. The *cis–trans* distinction became less clear on raising the temperature somewhat and the coalescence temperature of the methyl signals was at *ca* −80°C from which an approximate value of $\Delta G^{\ddagger}$ (193 K) was calculated from the Eyring equation.

Warming the complexes to ambient temperatures was expected to change the two ABCD type patterns of the —SC_2H_4S— protons to a single ABCD spectrum, due to rapid inversion of the coordinated sulphur. However, the observed outcome of this temperature elevation was an AA′BB′ pattern of lines. Such a change can only be accommodated by assuming the onset of pyramidal sulphur inversion *and/or* 1,3-metal–sulphur commutation. Such an interpretation implies a considerable lowering of the energy barrier for the 1,3-metal shift process compared to the unsubstituted and 2,2-disubstituted 1,3-dithiolane complexes. An analogous observation was recorded for the 1,3-shifts of the complexes $[M(CO)_5(\overline{SCHMeSCHMeSCHMe})]$ (M = Cr, W)[2-4] compared to the unsubstituted trithian ligand complexes $[M(CO)_5$

($\overline{SCH_2SCH_2SCH_2}$)].[2,3] In that work it was suggested that steric factors confined the ring methyls to equatorial positions and the $M(CO)_5$ to an axial position with respect to the six-membered ring, with the other possible conformational structures unfavoured and undetected by NMR. For the fixed axial $M(CO)_5$ moiety the other sulphur lone pairs were ideally positioned to facilitate a 1,3-metal shift. In contrast, in the unsubstituted $M(CO)_5$–trithian complexes, rapid sulphur inversion and ring reversal alters the relative positioning of $M(CO)_5$ and the sulphur lone pairs and reduces the probability of the 1,3-shift. In the present [$M(CO)_5$ ($\overline{SC_2H_4SCHMe}$)] complexes similar arguments appear valid. In other words, the $M(CO)_5$ moiety adopts a *trans* relationship with respect to the ring methyl and comparable amounts of energy are required to invert the configuration of the coordinated sulphur and to produce a 1,3-metal–sulphur shift without inversion of configuration. The two dynamic processes therefore cannot be separated. The pyramidal inversion process is assumed to proceed via the trigonal planar intermediate,[12] whereas the 1,3-shift must involve a weakly bound pseudo-seven-coordinate metal intermediate which can be most readily envisaged if the five-membered ring adopts a half-chair puckered configuration[13–15] (Fig. 5), although the classical envelope structure or some intermediate between these two extreme forms is almost equally probable.[16] This dual fluxional process is rapid at room temperature for both the chromium and tungsten complexes. Both complexes tended to dissociate at temperatures above *ca* 30°C as evidenced by a colour change from yellow to green and the appearance of free ligand signals in the spectra.

In contrast, in the complexes of $\overline{SC_2H_4SCH_2}$ and $\overline{SC_2H_4SCMe_2}$, where the pyramidal inversion process does *not* produce distinct diastereomers but simply chemical enantiomers, the inversion process proceeds readily, and the 1,3-shifts only occur with relative difficulty at temperatures where the inversion process is rapid, causing the other sulphur lone pair to be less favourably positioned than in the mono-substituted ligand complexes

[$M(CO)_5$($\overline{SC_2H_4SCHR}$)] (M = Cr, W; R = Bu^t, Ph)

These complexes exhibited similar variable-temperature NMR spectral features to the 2-methyl 1,3-dithiolane complexes. The significant difference was that because of the greater steric factors associated with Bu^t and Ph groups compared to Me, only a single solution species was detected at low temperatures. This is confidently attributed to the structure with the $M(CO)_5$ group *trans* to the ring substituent. Since only one invertomer species is thermodynamically favoured, the sulphur inversion process cannot be monitored. The variable-temperature spectra imply that any tendency of the coordinated sulphur atom to invert its configuration leads to a 1,3-shift (via the pseudo-seven-coordinate intermediate, Fig. 5) and/or ligand dissociation.

DISCUSSION

The results of the NMR band shape and coalescence temperature measurements are collected in Table 5. Most of the data refer to tungsten complexes which were most thermally stable in solution. Despite the somewhat limited amount of data certain clear points of discussion arise.

Firstly, for the unsubstituted and symmetrical 2,2-disubstituted 1,3-dithiolanes, sulphur inversion and 1,3-metal shifts are quite separate, uncorrelated processes, $\Delta G^{\ddagger}$ (298 K) values being in the region of 40–44 and 78 kJ mol^{-1}, respectively. Secondly, in the case of 2-substituted 1,3-dithiolane complexes, the steric constraints of the 2-substituent favour the 1,3-shift mechanism and cause

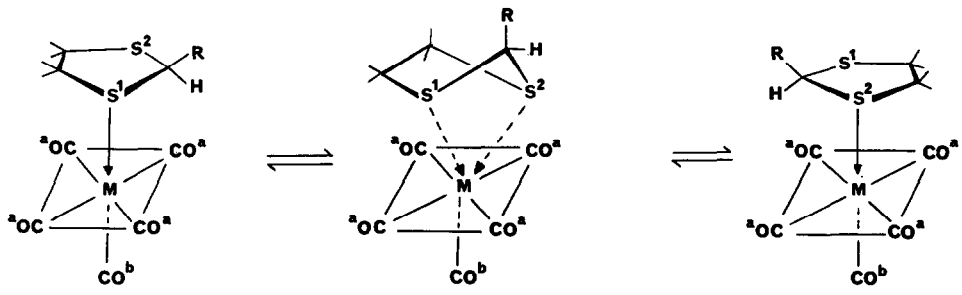

Fig. 5. The proposed mechanism of the 1,3-metal shift fluxion in [$M(CO)_5$($\overline{SC_2H_4SCHR}$)] complexes via the pseudo-seven-coordinate metal intermediate. The carbonyls are labelled to indicate the stereochemical rigidity of the $M(CO)_5$ moiety.

Table 5. Eyring activation parameters for fluxional processes in $[M(CO)_5(\overline{SC_2H_4SCRR'})]$ complexes

Complex	Process	$\Delta H^{\ddagger}$ (kJ mol^{-1})	$\Delta S^{\ddagger}$ (J K^{-1} mol^{-1})	$\Delta G^{\ddagger}$(298 K) (kJ mol^{-1})	Reference
$[W(CO)_5(\overline{SC_2H_4SCH_2})]$	S inversion	54.8±1.3	36±6	44.1±0.4	This work
$[W(CO)_5(\overline{SC_2H_4SCH_2})]$	1,3-shift	69.8±1.7	−23±5	78.0±0.3	This work
$[Mo(CO)_5(\overline{SC_2H_4SCH_2})]$	S inversion	42.5±0.9	4±4	41.2±0.4	This work
$[W(CO)_5(\overline{SC_2H_4SCMe_2})]$	S inversion			~ 40.2[a] (203 K)	This work
$[W(CO)_5(\overline{SC_2H_4SCMe_2})]$	1,3-shift	82.6±3.4	16±10	77.8±0.5	This work
$[W(CO)_5(\overline{SC_2H_4SCHMe})]$	S inversion 1,3-shift/dissociation			~ 40.5[a] (193 K)	This work
$[W(CO)_5(\overline{SCH_2SCH_2SCH_2})]$	S inversion	52.5±0.7	1.8±2.8	53.0±0.1	2
	1,3-shift	78.4±1.6	0.8±4.6	78.3±0.3	3
$[W(CO)_5(\overline{SCH_2SCH_2SCH_2SCH_2})]$	S inversion	39.0±1.7	−8±9	41.3±1.0	5
	1,3-shift	84.7±3.1	3±9	83.5±0.6	5
$[W(CO)_5(\overline{SCHMeSCHMeSCHMe})]$	1,3-shift	70.7±3.7	7±12	68.47±0.02	2
$[W(CO)_5(MeSeCH_2SeMe)]$	1,3-shift			85.8±0.5[b]	17

[a] Coalescence temperature value.

[b] Value for W ← Se shift. No data available for W ← S.

this fluxion to be indistinguishable in NMR terms from the sulphur inversion process. An analogous lowering of the activation energies of 1,3-metal shifts was observed in the six-membered trithian complexes $[W(CO)_5(\overline{SCH_2SCH_2SCH_2})]$ and $[W(CO)_5(\overline{SCHMeSCHMeSCHMe})]$ (Table 5). Thirdly, the significantly lower sulphur inversion energy for the molybdenum complex compared to the tungsten complex is in line with more extensive data[1] which reflect combined metal electronegativity and $(p\text{–}d)\pi$ ligand–metal interactions. In this present work we were unable to measure a sulphur inversion energy for $[Cr(CO)_5(\overline{SC_2H_4SCH_2})]$ due to solution decomposition, but a $\Delta G^{\ddagger}$ value of 44.5 ± 1.5 kJ mol^{-1} has recently been reported elsewhere.[18] This value, however, is of questionable accuracy as it is based on a simplified DNMR analysis of a solution which, the authors claim, consists of both mono- and bis-$Cr(CO)_5$ complexes of 1,3-dithiolane plus free ligand. Nevertheless, the lower limit of this value would bring it in line with the expected trend in inversion energies, namely Mo < Cr < W. Fourthly, no clear dependence of ligand ring size on the inversion energy is apparent in this series of $W(CO)_5$ complexes. This is in contrast to the series $[MX_2\{\overline{S(CH_2)_n}\}_2]$ ($M = Pd^{II}$, Pt^{II}, $n = 3$–5)[19] where a decrease in ring size constrains access to the planar transition state and thus increases the activation energy of sulphur inversion. In the present work the $\Delta G^{\ddagger}$ (298 K) value for $[W(CO)_5\overline{SC_2H_4SCH_2}]$ is anomalously low, but this may simply indicate that comparisons between ligands with different numbers of heterocyclic atoms are not valid. In contrast, the 1,3-shift energies *do* appear to show a clear dependence on ring size, the order being, five-membered < six-membered < eight-membered < open chain. This reflects the previously noted[3,5] dependence on ligand flexibility, although it should be noted that the difference in shift energies between five- and six-membered rings is very slight (Table 5).

A further point of interest in these fluxional complexes concerns the nature of the $W(CO)_5$ moiety, particularly during the 1,3-shifts. This has already been investigated in the cases of the complexes $[W(CO)_5L]$ (L = $MeSCH_2SMe$, $\overline{SCHMeSCHMeSCHMe}$ and $\overline{SC_2H_4SCMe_2}$) by two-dimensional exchange NMR spectroscopy (2D-EXSY).[20] No carbonyl scrambling was noted either in the absence or presence of 1,3-shifts, implying a remarkable stability of the square pyramidal geometry of $W(CO)_5$. Clearly this moiety remains bonded to the ligand in some formal sense throughout the metal shift process (Fig. 5). No evidence for a highly fluxional "naked" $W(CO)_5$ moiety[21] is available and the 1,3-shift can be envisaged as simply a lateral movement of a rigid $W(CO)_5$ moiety.

REFERENCES

1. E. W. Abel, S. K. Bhargava and K. G. Orrell, *Prog. Inorg. Chem.* 1984, **32**, 1.
2. E. W. Abel, M. Booth, K. G. Orrell and G. M. Pring, *J. Chem. Soc., Dalton Trans.* 1981, 1944.
3. E. W. Abel, G. D. King, K. G. Orrell, G. M. Pring and V. Šik, *Polyhedron* 1983, **2**, 1117.
4. W. A. Schenk and M. Schmidt, *Z. Anorg. Allg. Chem.* 1975, **416**, 311.
5. E. W. Abel, G. D. King, K. G. Orrell and V. Šik, *Polyhedron* 1983, **2**, 1363.
6. E. W. Abel, P. K. Mittal, K. G. Orrell and V. Šik, *J. Chem. Soc., Dalton Trans.* 1985, 1569.
7. K. M. Higgins, PhD Thesis, University of Exeter (1984).
8. E. W. Abel, K. G. Orrell, K. B. Qureshi and V. Šik, *Polyhedron* 1988, **7**, 1321.
9. E. W. Abel, K. G. Orrell, K. B. Qureshi and V. Šik, *Polyhedron* 1988, **7**, 1329.
10. D. T. Gibson, *J. Chem. Soc.* 1930, 13.
11. D. A. Kleier and G. Binsch, *DNMR3 Program 165. Quantum Chemistry Program Exchange.* Indiana University (1970).
12. J. B. Lambert, *Top. Stereochem.* 1971, **6**, 19.
13. K. S. Pitzer and W. E. Donath, *J. Am. Chem. Soc.* 1959, **81**, 3213.
14. F. V. Brutcher, Jr., T. Roberts, S. J. Barr and N. Pearson, *J. Am. Chem. Soc.* 1959, **81**, 4915.
15. F. V. Brutcher Jr and W. Bauer, *J. Am. Chem. Soc.* 1962, **84**, 2233.
16. L. A. Sternson, D. A. Coviello and R. S. Egan, *J. Am. Chem. Soc.* 1971, **93**, 6529.
17. E. W. Abel, T. E. MacKenzie, K. G. Orrell and V. Šik, *Polyhedron* 1987, **6**, 1785.
18. A. Gryff-Keller and P. Szczecinski, *Spectroscopy (Ottawa)* 1988, **6**, 41.
19. E. W. Abel, M. Booth and K. G. Orrell, *J. Chem. Soc., Dalton Trans.* 1979, 1994.
20. E. W. Abel, I. Moss, K. G. Orrell, K. B. Qureshi, V. Šik and D. Stephenson, *J. Chem. Soc., Dalton Trans.* 1988, 1489.
21. J. P. Jesson and P. Meakin, *J. Am. Chem. Soc.* 1973, **95**, 1344.

Polyhedron Vol. 9, No. 5, pp. 713–718, 1990
Printed in Great Britain

0277–5387/90 $3.00+.00
© 1990 Pergamon Press plc

COPPER(II) COMPLEXES WITH 1-(2-CARBAMYLETHYL)-2-ALKYLIMIDAZOLES

M. CLARA R. M. P. BASTO and ADÉLIO A. S. C. MACHADO*

Department of Chemistry, Faculty of Science, University of Oporto,
P 4000 Oporto, Portugal

(*Received* 19 *July* 1989; *accepted* 22 *September* 1989)

Abstract—Complexes of copper(II) and 1-(2-carbamylethyl)-2-alkylimidazoles have been studied. The following have been synthesized and characterized by spectral (vis–UV, IR and EPR) and variable temperature magnetic data: $CuX_2(CIm)_4$ (X = ClO_4, Cl, Br, NCS) and $CuX_2(CMIm)_4 \cdot H_2O$ (X = Cl, Br), tetragonally distorted hexa-coordinated; $CuX_2(CIm)_2$ (X = Cl, Br), square distorted tetra-coordinated or bridged with higher coordination number; and $CuCl_2(CEIm)_2$, whose geometry was not unequivocally characterized.

Complexes of imidazole and derivatives have been thoroughly investigated and are important, for instance, as biochemical, analytical, industrial and anticancer reagents.[1–7] In a project in progress in this department, we have been investigating complexes of 1-(2-carbamylethyl)-2-alkylimidazoles (alkyl = R) both in the solid state[8] and in solution.[9,10] These imidazole derivatives include two

R = H	CIm
R = CH_3	CMIm
R = C_2H_5	CEIm

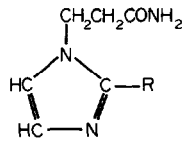

important coordinating groups in bioinorganic chemistry, imidazole and amide, and three potential coordinating positions: the unsaturated nitrogen atom of the heterocyclic ring and the oxygen and nitrogen atoms of the amide group (however, the literature suggests that the last only coordinates when the amide group is deprotonated[11]). To study the coordinating abilities of these ligands we have tried the preparation of a large variety of their complexes with metals of the first transition series and have studied properties of the synthesized complexes. In the present paper, the study of compounds obtained from the ligands and copper(II) halides or pseudo-halides is reported.

* Author to whom correspondence should be addressed.

EXPERIMENTAL

Chemicals

CIm was prepared according to Dowbenko *et al.*[5] (m.p. 141–144°C; ref. 5 143–145°C). Analysis: Found (Calc.): C, 51.6 (51.8); N, 30.4 (30.2); H, 6.5 (6.5)%. CMIm and CEIm were synthesized by a similar procedure from acrylamide and the corresponding 2-alkylimidazole. Yields: CMIm, 53%; CEIm, 30%. M.p. CMIm, 162–166°C; CEIm, 120–122°C. Analysis: Found (Calc.): CMIm, C, 54.7 (54.9); N, 27.4 (27.4); H, 7.2 (7.2). CEIm, C, 57.5 (57.5); N, 25.3 (25.1); H, 8.0 (7.8)%.

Commercial copper(II) salts were used without further purification. Copper(II) thiocyanate was obtained in methanol from copper(II) perchlorate and potassium thiocyanate.

Synthesis and analysis of the complexes

The complexes were obtained by the following general procedure. A solution of the copper(II) salt in methanol, dehydrated with 2,2′-dimethoxypropane, was added to a solution of the organic ligand in methanol. When no precipitate was obtained, the solution was concentrated by slow evaporation (IR lamp). The solids were filtered off and dried *in vacuo* (over P_4O_{10}). Some of the compounds are hygroscopic.

In the preparation of $CuBr_2(CIm)_2$ and

Table 1. Analytical data and some properties of the compounds

Compound	Colour	Melting point (°C)	Analysis (%): Found (Calc.)				
			Cu	C	N	H	Anion
$Cu(ClO_4)_2(CIm)_4$	Violet	139–141	7.7 (7.8)	35.3 (35.2)	20.0 (20.5)	4.8 (4.4)	—
$CuCl_2(CIm)_4$	Violet	174–176	9.1 (9.2)	41.5 (41.7)	24.6 (24.3)	5.2 (5.2)	10.2 (10.3)
$CuBr_2(CIm)_4$	Violet	173–175	8.2 (8.2)	36.8 (37.0)	21.2 (21.6)	4.6 (4.6)	20.4 (20.5)
$Cu(NCS)_2(CIm)_4$	Blue	122–124	8.6 (8.6)	42.2 (42.4)	26.4 (26.6)	4.8 (4.9)	—
$CuCl_2(CIm)_2$	Oil blue	176–178	15.2 (15.4)	34.8 (34.9)	20.6 (20.4)	4.4 (4.4)	17.1 (17.2)
$CuBr_2(CIm)_2$	Green	177–179	12.4 (12.7)	28.9 (28.7)	17.0 (16.8)	3.6 (3.6)	31.1 (31.9)
$CuCl_2(CMIm)_4 \cdot H_2O$	Blue	130–132	8.2 (8.3)	43.8 (44.0)	21.7 (22.0)	5.8 (6.1)	9.1 (9.3)
$CuBr_2(CMIm)_4 \cdot H_2O$	Blue	132–134	7.5 (7.4)	40.6 (39.4)	19.7 (19.7)	5.5 (5.4)	18.7 (18.7)
$CuCl_2(CEIm)_2$	Brick	151–152	13.8 (13.6)	41.9 (41.0)	18.0 (17.9)	5.7 (5.6)	14.9 (15.1)

$CuCl_2(CEIm)_2$, brown oily products (a dark brown solid in the preparation of $CuBr_2(CMIm)_4 \cdot H_2O$) were obtained immediately after mixing the ligand and salt solutions. These were filtered off and discarded. The complexes precipitated upon leaving the mother solution at room temperature.

Carbon, nitrogen and hydrogen microanalysis were performed by the Microanalytical Unit of the Chemistry Department, Surrey University. The copper contents of the complexes were determined by titration with EDTA and the halogen contents by potentiometric titration with silver(I) nitrate, with ion-selective electrodes as indicator electrodes. Analytical results are presented in Table 1.

Physical measurements

The following equipment was used: Pye–Unicam SP700C spectrophotometer for electronic spectra of solid compounds (30–4.5 × 10^3 cm^{-1}) and a Varian–Cary 17DX spectrophotometer for spectra of solutions (30–8.0 × 10^3 cm^{-1}); Perkin–Elmer 457 spectrophotometer for IR spectra (KBr pellets, 4000–250 cm^{-1}); Newport Instruments Gouy balance for magnetic susceptibility determinations in the range from liquid nitrogen to room temperature ($Hg[Co(NCS)_4]$ was used as calibrating agent;[12] molar susceptibilities were corrected for diamagnetism by using Pascal's constants and for temperature independent paramagnetism, TIP = 0.75 mm^3 mol^{-1}[13]); Bruker ER200tt spectrophotometer for X-band EPR spectra (operated at ~9 GHz and 100 kHz field modulation); Metrohm E518 conductivity meter for measurements on methanolic solutions of the complexes (at 25°C).

RESULTS AND DISCUSSION

Synthesis

The colours, melting points and analytical data for the complexes are tabulated in Table 1.

Only bis- and tetrakis-complexes have been obtained. Attempts to prepare hexakis-complexes were unsuccessful, even with anions of very low coordinating tendency like perchlorate. This is not unexpected because copper(II) hexakis-complexes with N-coordinating ligands are rare.[14] Although a hexakis(imidazole)copper(II) nitrate has been reported,[15] no 1:6 copper(II) compounds with N-alkyl-substituted imidazoles[16,17] appear to be described in the literature.

Attempts to prepare copper(II) compounds with iodide and CIm were unsuccessful. Normally, copper(II) is reduced to copper(I) by iodide, but imidazole and N-methylimidazole stabilize the +2

oxidation state.[18,19] In the present case, grey–blue products were obtained from copper(II) and CIm, but their composition was slightly different from that expected for a 1:4 compound and we were unable to purify them. In contrast, unlike the results observed with imidazole or N-alkylimidazoles,[17,20] a thiocyanate copper(II) compound with CIm could be isolated.

Spectral properties of CuX_2L_4 *compounds*

The electronic spectra (Table 2) for $CuX_2L_4 \cdot xH_2O$ compounds are characterized by one broad *d–d* band in the visible region (16–18 × 10^3 cm^{-1}), with a more or less pronounced shoulder on the lower energy side [except for $Cu(NCS)_2(CIm)_4$], whose position is difficult to assign. These spectra are consistent with tetragonal environments for the copper(II) ion, the observed broad bands being assigned, assuming D_{4h} symmetry, to $^2B_{1g} \rightarrow {}^2B_{2g}, {}^2E_g$. Maxima are in the usually observed region for copper(II) compounds with nitrogen donor atoms and weakly coordinated anions[14] and, for the CIm compounds, are in the order $ClO_4^- > Br^- > Cl^- > NCS^-$, expected from decreasing distortion from octahedral symmetry as the anion coordinating power increases. The lower frequencies of band maxima for $CuX_2(CMIm)_4 \cdot H_2O$ are very probably due to the existence of a steric effect of the 2-methyl group (organic ligands being coordinated by the pyridine nitrogen atom of the imidazolic ring).

EPR data also support the tetragonal symmetry and nitrogen ligand coordination. Except for $Cu(NCS)_2(CIm)_4$, the EPR spectra for the powdered compounds, at room and liquid nitrogen temperatures, are all similar (Fig. 1), of axial type with $g_\parallel > g_\perp$, characteristic of monomeric tetragonal copper(II) complexes with a $d_{x^2-y^2}$ ground state. Partially resolved hyperfine structure due to copper is observed in the parallel signal and observed g values are in the ranges usually found for tetragonally distorted copper(II) compounds with four monodentate nitrogen donor ligands and weakly coordinated anions ($g_\parallel = 2.20$–2.30 and $g_\perp = 2.04$–2.09[21]). $Cu(NCS)_2(CIm)_4$ yields a pseudo-isotropic

Table 2. Electronic spectra, EPR data and magnetic moments of the compounds

Compound		Electronic spectra	EPR data						μ^b
		$\nu(\varepsilon)$ 10^3 cm^{-1} (M^{-1} cm^{-1})	T^a (K)	$g_\parallel$	$g_\perp$ or g_m		$A_\parallel$ (10^4 cm^{-1})	A_N	(BM)
$Cu(ClO_4)_2(CIm)_4$	Solid	17.9	293	2.24	2.05		199		1.98
	Solution	15.9 (60)	77	2.25	2.05		194	14	
$CuCl_2(CIm)_4$	Solid	17.4	293	2.25	2.05		194		1.90
	Solution	15.4 (68)	77	2.26	2.06		195	14	
$CuBr_2(CIm)_4$	Solid	17.6	293	2.25	2.05		194		1.85
$Cu(NCS)_2(CIm)_4$	Solid	16.5 26.3 (sh)[c]	293		2.06				1.82
	Solution	15.2 (88)	77	2.26	2.05		190	14	
$CuCl_2(CIm)_2$	Solid	15.5	293	2.23	2.06	2.03			1.82
			77	2.24	2.07	2.03			
$CuBr_2(CIm)_2$	Solid	15.8[c]	293		2.12				1.83
$CuCl_2(CMIm)_4 \cdot H_2O$	Solid	16.4	293	2.26	2.06		185		1.81
			77	2.25	2.05		189		
	Solution	15.9 (68)	77	2.24	2.06		193	14	
$CuBr_2(CMIm)_4 \cdot H_2O$	Solid	15.9	293	2.25	2.06		194		2.12[d]
			77	2.26	2.06		195		
	Solution	16.1 (78)							
$CuCl_2(CEIm)_2$	Solid	21.7 (sh) 28.7[c]	293		2.13				1.91
			77	2.34	2.17	2.07			
	Solution	14.4 (53)							

[a] When not indicated, EPR parameters at 77 K for powdered compounds are equal to the parameters at 293 K.
[b] At 300 K.
[c] Nujol mull.
[d] Slightly magnetic field dependent.

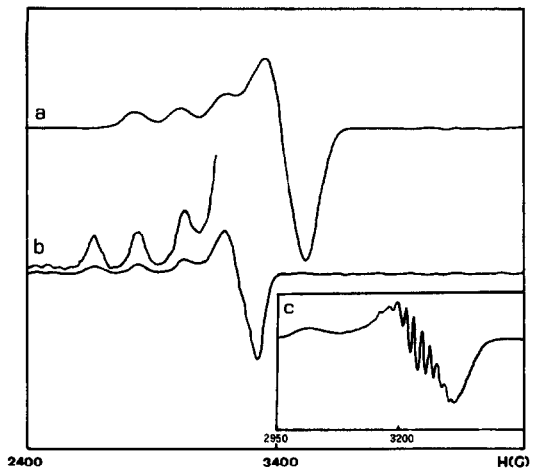

Fig. 1. EPR spectra of: (a) $CuBr_2(CIm)_4$, powder, at 293 K; (b) $CuCl_2(CIm)_4$, in methanol, at 77 K; (c) $CuCl_2(CIm)_4$, in methanol, at 77 K in the $g_\perp$ region.

spectrum, with one unsymmetrical band, probably due to large line widths with respect to the difference between $g_\parallel$ and $g_\perp$ values and the A value.

For tetragonally distorted octahedral copper(II) compounds, the value of $A_\parallel$ decreases and the $g_\parallel$ value increases when the strength of the axial ligands increases.[21] Present results for complexes with CIm are compatible with this order, from the compound with perchlorate to the two halide compounds. However, the observed differences are very small and may be not significant when compared to the experimental error.

The electronic spectra and electrical conductance data in methanol ($\sim 10^{-3}$ M) indicate that the compounds undergo some structural change in this solvent (anion substitution by solvent molecules). Observed molar conductance values are in the range usually found for 1:1 electrolytes ($CuCl_2(CIm)_4$, 114 S cm^2 mol^{-1}; $Cu(NCS)_2(CIm)_4$, 85.0 S cm^2 mol^{-1}) or even 1:2 electrolytes ($CuBr_2(CMIm)_4 \cdot H_2O$, 166 S cm^2 mol^{-1}).

The axial EPR spectra obtained in frozen solutions show (Fig. 1) superhyperfine structure, in the $g_\perp$ region, which indicates coordination of the organic ligands by nitrogen atoms. For complexes with CIm, $A_\parallel$ and $g_\parallel$ values (Table 2) are close to those obtained for powdered compounds, therefore, the interaction with the solvent seems to be unimportant.

Owing to the large number of bands due to the organic ligands and the limited range of the instrument used, IR spectra provided limited information. For $Cu(NCS)_2(CIm)_4$, the only band safely assigned is a band at 2065 cm^{-1} (C—N stretching of the nitrogen coordinated thiocyanate). Bands at 838 (CS stretching), 475 and 467 cm^{-1} (NCS bending) are tentatively assigned by comparison with spectra for $CuX_2(CIm)_4$.

Spectral properties of CuX_2L_2 *compounds*

Band maxima in the spectra of the two $CuX_2(CIm)_2$ compounds (at $15–16 \times 10^3$ cm^{-1}) and the very different spectrum for $CuCl_2(CEIm)_2$ (one shoulder at about 21.7×10^3 cm^{-1} and no visible or near-IR absorption band until 12.5×10^3 cm^{-1}) provide no unequivocal information about the ligand arrangements around copper(II). For $CuX_2(CIm)_2$ compounds, maxima positions are compatible with distorted octahedral geometries, which would imply polymeric structures, but distorted square geometries cannot be excluded. The spectrum of $CuCl_2(CEIm)_2$ is compatible with a pseudo-tetrahedral structure, but a dimeric pentacoordinated copper(II) compound might also be possible.

IR spectra for the CuX_2L_2 compounds, exhibit two well-resolved bands in the region 1550–1700 cm^{-1} with small displacements relative to the corresponding bands of the free ligand, but this alone cannot be taken as evidence of coordination by the amide group.[22,23]

EPR spectra for powdered CuX_2L_2 compounds are all different (Table 2). $CuCl_2(CIm)_2$ shows a three g value spectrum of the rhombic type, without resolved hyperfine splittings. This spectrum indicates a low symmetry environment around copper(II) and the absence of extensive exchange coupling. The X-band EPR spectrum of $CuBr_2(CIm)_2$ is isotropic, showing one broad band.

At room temperature, $CuCl_2(CEIm)_2$ exhibits a very broad EPR spectrum. The spectrum obtained at liquid nitrogen temperature yields three g values in the high field region ($\Delta M_S = \pm 1$) and shows a very weak-intensity feature at the $\Delta M_S = \pm 2$ region, but without any other signals. Therefore it is not characteristic of a dimeric copper(II) compound. In a rhombic type spectrum, the high value for g_1 could point to a distorted tetrahedral stereochemistry.

Magnetic properties

Magnetic results for $CuCl_2(CEIm)_2$ (Table 3) show that the molar magnetic susceptibility depends on temperature accordingly to the Curie–Weiss law. Magnetic moments do not depend on the temperature as expected for an orbitally non-degenerated ground state of a magnetically diluted compound. Therefore, magnetic data provide no

Table 3. Magnetic data for some of the compounds

Compound	T/K	μ (BM) 299.7	251.1	206.3	176.5	156.4	127.2	97.2	Curie–Weiss law[a] $10^5 C$ (m^3 mol^{-1} K)	θ	g
$CuCl_2(CIm)_4$		1.90	1.91	1.90	—	1.89	1.91	1.90	0.5708	−0.6	2.20
$CuBr_2(CIm)_4$		1.85	1.85	1.85	—	1.84	1.88	1.87	0.5319	2	2.13
$CuCl_2(CIm)_2$		1.82	1.84	1.84	—	1.84	1.85	1.85	0.5236	3	2.11
$CuBr_2(CIm)_2$		1.83	1.84	1.86	1.86	1.85	1.86	1.87	0.5260	4	2.11
$CuCl_2(CMIm)_4 \cdot H_2O$		1.81	1.83	1.83	1.83	1.83	1.85	1.85	0.5208	2	2.10
$CuCl_2(CEIm)_2$		1.91	1.93	1.93	1.93	1.93	1.94	1.93	0.5767	2	2.21

[a] Values of C and θ were obtained by least-squares adjustment of magnetic susceptibility data to the Curie–Weiss law, $\chi = C/(T-\theta)$. Values of the correlation coefficients were always greater than 0.9999 except for $CuCl_2(CMIm)_4 \cdot H_2O$ ($r = 0.9998$).

useful new elements for assignment of stereochemistry to the compound, since the low value for θ suggests no significant magnetic interaction between neighbouring metal ions and no reasonable results were obtained by fitting the magnetic data to the equation derived by van Santen *et al.*[24] (with $J' = 0$ and the g value obtained from the Curie–Weiss law) for dimeric copper(II) compounds. In conclusion, the spectral and the magnetic data neither clearly support a dimeric structure nor exclude the possibility of a monomeric distorted tetrahedral copper(II) compound.

Room temperature magnetic moments for all the compounds (Table 2) are above the spin-only value for a single copper(II) ion. The variable temperature date in the range 90–300 K for some of the $CuX_2L_4 \cdot xH_2O$ compounds (Table 3) show that their magnetic moments do not vary significantly with temperature as would be expected for monomeric tetragonally distorted octahedral copper(II) compounds, and their molar magnetic susceptibilities obey the Curie–Weiss law with very low θ values. Data for polycrystalline samples of $CuX_2(CIm)_2$ compounds show that magnetic moments increase slightly when the temperature decreases, but the positive Weiss constants are very small. Intramolecular magnetic interaction could be present if these compounds were polymeric with bridged halides, but these experimental results show no clear evidence of exchange interaction in the accessible temperature range (additional measurements at lower temperatures may clarify this point).

CONCLUSIONS

The copper(II) compounds with 1-(2-carbamylethyl)-2-alkylimidazoles and halides or thiocyanate, which we were able to synthesize, show two different stoichiometries, $CuX_2L_4 \cdot xH_2O$ and CuX_2L_2. Magnetic and spectral data obtained for the first type of compounds show that they have tetragonally distorted geometries with the organic ligands coordinated by the pyridine nitrogen of the imidazolic group. For $CuX_2(CIm)_2$ complexes, although not confirmed, a polymeric structure with bridged copper(II) ions cannot be ruled out. The properties measured for $CuCl_2(CEIm)_2$ allow no unequivocal conclusion about its stereochemistry.

Acknowledgements—We thank M. F. Vasconcelos for preliminary work on some of the CIm complexes. Financial support by INIC (Lisbon) to Research Line nr 4 of CIQ(UP) is gratefully acknowledged.

REFERENCES

1. R. J. Sundberg and R. B. Martin, *Chem. Rev.* 1974, **74**, 471.
2. J. A. Welleman, F. B. Hulsbergen, J. Verbiest and J. Reedijk, *J. Inorg. Nucl. Chem.* 1978, **40**, 143.
3. T. Yoshimura and T. Ozaki, *Bull. Chem. Soc.* 1979, **52**, 2268.
4. D. P. Drolet, D. M. Manuta, A. J. Lees, A. D. Katnani and G. J. Coyle, *Inorg. Chim. Acta* 1988, **146**, 173.
5. R. Dowbenko, C. C. Anderson and W. H. Chang, *Ind. Engng Chem. Prod. Res. Develop* 1971, **10**, 344.
6. A. J. Canty and E. A. Stevens, *Inorg. Chim. Acta* 1981, **55**, L57.
7. H. Tamura, H. Imai, J. Kuwahara and Y. Sugiura, *J. Am. Chem. Soc.* 1987, **109**, 6870.
8. M. C. R. M. P. Basto, Doctoral Thesis, Faculty of Science of Oporto, Oporto (1984).
9. M. T. S. D. Vasconcelos, Doctoral Thesis, Faculty of Science of Oporto, Oporto (1983).

10. M. T. S. D. Vasconcelos and A. A. S. C. Machado, *Talanta* 1987, **34**, 525.
11. T. A. Kabanos and J. M. Tsangaris, *J. Coord. Chem.* 1984, **13**, 89.
12. J.-C. G. Bünzli, *Inorg. Chim. Acta* 1979, **36**, L413.
13. E. Maarschall, A. Batterman, S. Veta and A. Miedema, *Physica* 1969, **41**, 473.
14. J. Reedijk, J. C. A. Windhorst, N. H. M. Van Ham and W. L. Groeneveld, *Recl. Trav. Chim.* 1971, **111**, 234.
15. D. L. McFadden, A. T. McPhail, C. D. Garner and F. E. Mabbs, *J. Chem. Soc., Dalton Trans.* 1975, 263.
16. CH. Krushna, C. Mohapatra and K. C. Dash, *J. Inorg. Nucl. Chem.* 1977, **39**, 1253.
17. J. Reedijk, *Recl. Trav. Chim.* 1971, **90**, 1249.
18. F. Akhtar, D. M. L. Goodgame, M. Goodgame, G. W. Rayner-Canham and A. C. Skapski, *J. Chem. Soc., Chem. Commun.* 1968, 1389.
19. D. M. L. Goodgame, M. Goodgame and G. W. Rayner-Canham, *Nature* 1969, **222**, 866.
20. M. Massacesi and G. Ponticelli, *J. Inorg. Nucl. Chem.* 1974, **36**, 2209.
21. J. Reedijk, *Transition Met. Chem.* 1981, **6**, 195.
22. J. Reedijk, *Inorg. Chim. Acta* 1971, **5**, 687.
23. M. Nonoyama, S. Tomita and K. Yamasaki, *Inorg. Chim. Acta* 1975, **12**, 33.
24. J. A. van Santen, A. J. van Duyneveldt and R. L. Carlin, *Inorg. Chem.* 1980, **19**, 2152.

Polyhedron Vol. 9, No. 5, pp. 719–726, 1990
Printed in Great Britain

0277–5387/90 $3.00+.00
© 1990 Pergamon Press plc

PENTANUCLEAR OXOALKOXIDE CLUSTERS OF SCANDIUM, YTTRIUM, INDIUM AND YTTERBIUM, X-RAY CRYSTAL STRUCTURES OF $[M_5(\mu_5\text{-}O)(\mu_3\text{-}OPr^i)_4(\mu_2\text{-}OPr^i)_4(OPr^i)_5]$ (M = In, Yb)

D. C. BRADLEY,* HALINA CHUDZYNSKA, D. M. FRIGO, M. E. HAMMOND, M. B. HURSTHOUSE* and M. A. MAZID

Department of Chemistry, Queen Mary and Westfield College, Mile End Road, London E1 4NS, U.K.

(*Received* 31 *July* 1989; *accepted* 25 *September* 1989)

Abstract—Attempts to prepare the metal tri-isopropoxides $M(OPr^i)_3$ (M = Sc, Y, In, Yb) by various methods always produced the pentanuclear oxoalkoxide clusters $[M_5(\mu_5\text{-}O)(\mu_3\text{-}OPr^i)_4(\mu_2\text{-}OPr^i)_4(OPr^i)_5]$ as the stable products. X-ray single crystal diffraction showed (M = In, Yb) the presence of the μ_5-oxygen atom bonded in a square pyramidal configuration to five metal atoms which had terminal isopropoxo groups *trans* to the oxo atom. The μ_3- and μ_2-isopropoxo groups contribute to the distorted octahedral coordination of each metal atom. The scandium, yttrium and ytterbium clusters could be sublimed *in vacuo* and gave mass spectra containing pentanuclear cluster ions. The ^1H NMR spectra for each compound was consistent with the X-ray crystal structure and variable-temperature studies showed fluxionality in the indium complex.

In recent years there has been a resurgence of interest in the application of metal alkoxides as precursors for the deposition of pure metal oxides using either sol–gel or MOCVD techniques.[1] The metal oxides and heterometal oxides are currently of considerable importance in the electronics, ceramics, glass and optical industries.

The alkoxides of yttrium,[2] indium[3] and ytterbium[4] have been known for some time whilst those of scandium[5,6] have received less attention. In attempting to prepare indium tri-isopropoxide from the reaction of indium trichloride with the requisite amount of sodium isopropoxide we obtained a crystalline product which surprisingly had the analysis corresponding to the novel pentanuclear oxoalkoxide $In_5O(OPr^i)_{13}$. Further work established that analogous compounds were given by scandium, yttrium and ytterbium and this was reported in a preliminary communication[7] which included the single crystal X-ray structure of the indium compound. We now report full details of our work including the single crystal X-ray structure of $Yb_5O(OPr^i)_{13}$. Quite independently the yttrium analogue $Y_5O(OPr^i)_{13}$ was discovered and fully characterized jointly by Professor Liliane Hubert-Pfalzgraf at Nice and Professor K. Caulton at Bloomington and their co-workers.[8]

RESULTS AND DISCUSSION

All attempts to prepare the tri-isopropoxides $M(OPr^i)_3$ (M = AC, Y, In, Yb) by a variety of methods resulted in the isolation of the pentanuclear species $M_5O(OPr^i)_{13}$ which were characterized by elemental analyses, NMR spectra, IR spectra and in some cases mass spectra (Sc, Y, Yb) and single crystal X-ray structures (In, Yb). Our results on the yttrium compound are in agreement with the independent work of Hubert-Pfalzgraf and co-workers.[8]

Preparation of $M_5O(OPr^i)_{13}$ (M = Sc, Y, In, Yb)

It was realized that our initial preparation of $In_5O(OPr^i)_{13}$ may have been caused by hydrolysis but repeated preparations using exceptional precautions to exclude water always resulted in the formation of the pentanuclear oxoalkoxide. The indium compound was prepared by reaction of

* Authors to whom correspondence should be addressed.

anhydrous $InCl_3$ with $NaOPr^i$ in a 1 : 3 molar ratio in a benzene–isopropanol mixed solvent. To check whether the isopropanol was implicated in the formation of the oxo species a reaction was carried out in benzene with sodium isopropoxide powder, from which all isopropanol had been removed, but the product was still $In_5O(OPr^i)_{13}$. The yields of $In_5O(OPr^i)_{13}$ were always less than 50% and the precipitated NaCl was heavily contaminated with some insoluble indium compound. When heated to 145°C/10^{-2} mm Hg this "NaCl" gave an off-white sublimate and the volatile products were isopropanol and acetone. This off-white indium-containing sublimate was extraordinarily air-sensitive rendering it practically impossible to characterize. However, an ^1H NMR spectrum (C_6D_6, 80 MHz) was obtained with signals at δ 1.50 (6 H, d, CH_3) and 4.67 (1H, CH) corresponding to a single isopropoxide species in contrast to the complex spectrum of $In_5O(OPr^i)_{13}$. The off-white sublimate contained no chloride and on heating to 130°C/10^{-2} mm Hg gave a small amount of sublimate but the major part decomposed to metallic indium. A solution of the sublimate in toluene at room temperature decomposed to indium within a few hours but was stable for several days at −20°C, during which colourless crystals were deposited. The behaviour of this compound suggests that it may be indium monoisopropoxide which would be expected to have a cubane tetrameric structure $(InOPr^i)_4$ analogous to the thallium(I) alkoxides.[9] In fact, further heating of the original precipitated "NaCl" to 230°C/10^{-2} mm Hg gave a red sublimate of InCl. When the pentanuclear oxo cluster $In_5O(OPr^i)_{13}$ was heated to 80°C/10^{-2} mm Hg some acetone and isopropanol were released but no indium compound was sublimed up to 170°C.

Treatment of anhydrous $ScCl_3$ with $NaOPr^i$ (1 : 3 molar ratio) in isopropanol gave, after removal of sodium chloride and solvent, a white solid which sublimed at 220–280°C/10^{-2} mm Hg accompanied by a more volatile liquid. The sublimate which contained no sodium gave a complex ^1H NMR spectrum, but after recrystallization from isopropanol gave a spectrum consistent with $Sc_5O(OPr^i)_{13}$. The volatile liquid was shown by ^1H NMR to be almost entirely isopropanol contaminated with a scandium species (peaks in the mass spectrum at *m/z*, 355, 281, 207 in addition to OPr^i, 59 and Sc, 45).

In another experiment freshly sublimed $Sc\{N(SiMe_3)_2\}_3$, obtained from the reaction of $ScCl_3$ and $LiN(SiMe_3)_2$,[10] suspended in a benzene–pentane mixture was treated with excess isopropanol under reflux. On cooling, a high yield of $Sc_5O(OPr^i)_{13}$ crystallized out and sublimed at 220–280°C/10^{-2} mm Hg.

The analogous pentanuclear clusters $M_5O(OPr^i)_{13}$ (M = Y, Yb) were obtained from the reaction of the respective metal with isopropanol catalysed by $HgCl_2$, although it had been reported previously that this method gave the metal tri-isopropoxides.[3] Indeed, both compounds could be sublimed at *ca* 220°C/10^{-2} mm Hg which is similar to the sublimation temperatures (Y, 200–210°C/0.1 mm Hg; Yb, 190–200°C/0.2 mm Hg) reported for the "tri-isopropoxides". Addition of excess isopropanol to $Y\{N(SiMe_3)_2\}_3$ at room temperature followed by removal of excess alcohol and $HN(SiMe_3)_2$ *in vacuo* left a solid which gave a ^1H NMR spectrum which was complex and different from that of $Y_5O(OPr^i)_{13}$. It remained unchanged in isopropanol solution for several days at room temperature but upon heating under reflux for 1 h it was converted into the pentanuclear oxoalkoxide. This suggests that $Y(OPr^i)_3$ is thermally unstable and is converted in boiling isopropanol to $Y_5O(OPr^i)_{13}$. It is noteworthy that Hubert-Pfalzgraf and co-workers[8] found that $Y_5O(OPr^i)_{13}$ did not react with aluminium tri-isopropoxide whereas their initial product of the reaction of yttrium and Pr^iOH did react to give the heterometal alkoxide $YAl_3(OPr^i)_{12}$.

It is significant that in spite of exceptional precautions to prevent hydrolysis we have isolated $M_5O(OPr^i)_{13}$ as the thermally stable species and not the previously reported metal tri-isopropoxides. The analytical data presented in Table 1 show that the two types of compound can be distinguished on the basis of their elemental analyses. The comparison of the IR data in Table 2 of $M_5O(OPr^i)_{13}$ and "$M(OPr^i)_3$" compounds shows striking similarities between them. This was also noted for $Y_5O(OPr^i)_{13}$ by Hubert-Pfalzgraf and co-workers.[8] The mechanism of the breakdown of the tri-isopropoxides to give the pentanuclear oxoalkoxides has not yet been elucidated because the presence of isopropanol renders it diffult to identify other volatile products such as propene or di-isopropyl ether. Elimination of alkene is facile for metal tertiary alkoxides[12] but we have found that yttrium tritertiary alkoxides can be prepared under similar conditions of reaction and can be sublimed unchanged.[13] It appears therefore that elimination of di-isopropyl ether may account for the presence of the oxo atom in the pentanuclear clusters:

$$5M(OPr^i)_3 \longrightarrow M_5O(OPr^i)_{13} + Pr^i_2O.$$

Mass spectra of $M_5O(OPr^i)_{13}$

The scandium, yttrium and ytterbium complexes all gave positive ions containing the pentanuclear

Table 1. Analytical and spectroscopic data for the compounds

Compound	Analysis (%)[a,b] M	OPr^i	Accurate mass[c] Species	m/z	^{1}H NMR (δ ppm)[d] CH	CH_3
$Sc_5O(OPr^i)_{13}$	22.5 (22.3) [20.2]	75.6 (76.1) [79.8]	$[P-OPr^i]^+$	949.371 (949.371)	4.40–4.65[e]	1.70, 1.54, 1.41, 1.37[f] (4:4:4:1)
$Y_5O(OPr^i)_{13}$	36.0 (36.2) [33.4]	62.5 (62.5) [66.6]	$[P-OPr^i]^+$	1169.118 (1169.121)	4.35–4.70[e]	1.65, 1.48, 1.40, 1.36[f] (4:4:4:1)
$In_5O(OPr^i)_{13}$	42.9 (42.3) [39.4]	56.6 (56.6) [60.4]	Not obtained		4.57[g]	1.63, 1.49[f] (8:5)
$Yb_5O(OPr^i)_{13}$	52.5 (52.5) [49.4]	47.5 (46.6) [50.6]	$[P-3(OPr^i)]^+$	1476.188 (1476.186)[h]	191, 111, −46, +134[i] (4:4:1:4)	97, 61, 1, −70[i] (4:4:1:4)

[a] Calculated values for oxo cluster in parentheses.
[b] Calculated values for $M(OPr^i)_3$ in brackets.
[c] $P = M_5O(OPr^i)_{13}$ calculated in parentheses.
[d] Obtained in C_6D_6 except for Yb compound in $C_6D_5CD_3$; relative integrations in parentheses.
[e] Cluster of septets, J 6 Hz.
[f] Doublets, J 6 Hz.
[g] Broad septet, J 6 Hz.
[h] Calculated with ^{174}Yb isotope.
[i] Broad signals.

cluster (Table 1) but the indium complex was thermally unstable and gave no mass spectrum. For scandium, $[P-OPr^i]^+$ (where $P = M_5O(OPr^i)_{13}$; M = Sc) was the most abundant metal-containing species, whereas for yttrium the highest mass peak was $[P-Me]^+$ but the $[P-OPr^i]^+$ peak was considerably more abundant. For ytterbium, the highest mass peak corresponded to $[P-3(OPr^i)]^+$. In each case the fragmentation pattern was complex and attention was focussed on those peaks closest to the parent molecular ion P^+. The fact that numerous peaks near the parent ion were observed emphasizes the stability of the $M_5(\mu_5\text{-}O)O_{13}$ cluster.

NMR spectra of $M_5O(OPr^i)_{13}$

The ^{1}H NMR chemical shifts are presented in Table 1. The room temperature spectra of the scandium and yttrium clusters in C_6D_6 at 250 MHz were in agreement with the requirements of the single crystal X-ray structures found for $M_5O(OPr^i)_{13}$ (M = In and Yb, which are discussed later), namely four sharp doublets and associated septets in the ratio 4:4:4:1. The scandium compound in $C_6D_5CD_3$ gave a similar spectrum which was unchanged on heating to 90°C, thus showing that the alkoxo ligands were non-fluxional on the NMR timescale and even the terminal groups remained resolved in the 4:1 ratio (basal–apical). On some occasions the spectrum of the yttrium compound at room temperature (C_6D_6) was collapsed into one resolved peak and two broad peaks in the ratio 4:4:5 possibly due to exchange caused by the presence of a trace of isopropanol. In $C_6D_5CD_3$, the 4:4:5 spectrum was always observed and it remained unchanged up to 80°C showing that the μ_3- and μ_2-isopropoxides remained distinguishable from the terminal groups which had collapsed into one signal.

The paramagnetic ytterbium compound at 30°C gave four broad signals between δ +97 and −70 in approximately a 4:4:1:4 ratio due to the methyl groups, and four corresponding peaks for the methine protons between δ +191 and −134. On changing the temperature all of the peaks change in chemical shift due to the paramagnetism but the overall spectrum is unchanged. Thus at 90°C the spectrum covers the range δ +144 to −101. Whilst at −60°C the highest field signal is at δ −169.5 and the lowest field signal is beyond the range of the instrument (i.e. $> \delta$ +200).

By contrast, the ^{1}H NMR spectrum of the indium complex at room temperature showed only two ligand environments in the ratio 8:5. The minor doublet at higher field remained unchanged down to −80°C ($C_6D_5CD_3$, 400 MHz), whereas the major

Table 2. Comparison between IR bands below 1375 cm^{-1} for the oxo clusters and literature values for $M(OPr^i)_3$ (M = Y, Yb)

$Sc_5O(OPr^i)_{13}$	$Y_5O(OPr^i)_{13}$	$Y(OPr^i)_3$[a]	$In_5O(OPr^i)_{13}$	$Yb_5O(OPr^i)_{13}$	$Yb(OPr^i)_3$[a]
1368s	1366s	1363sh	1371s	1368s	1365sh
1356s	1355s	1354m	1359m	1353s	1356s
1342m	1338s	1336m	1342m br	1335m	1337s
1254w	1260w	—	1263w	1257w	—
1173vs	1170vs br	1168vs	1164m	1169vs br	1172vs
1158s sh	—	—	—	—	—
1130vs	1124vs br	1123s	1126vs	1123vs br	1123s
1015vs	1007vs	1005vs	988s	1006vs	1010vs
980s	975s sh	974s	—	—	—
970s	970s br	—	970 m sh	971s	976s
960s	952s sh	950s	952s	950s	953s
868w	—	—	—	—	—
842m	831s	835m	832m	835m sh	839m
832m		830m			833m
—	—	822m	—	826m	825m
780w	830w sh	—	805w sh	799w	—
—	—	—	730m	—	—
720w	721w	—	720m	719w	—
—	—	—	570s br	—	—
559vs br	533s	532s	554s br	530vs	534s
515vs br	512s sh	—	502s br	498s br	497m
489m	496s	493s	—	486s sh	—
461m sh	—	—	—	—	—
450m	452s	450s	455m br	445s	447m
416m	421m	418m	—	414m	416m
—	399s br	393s	401vs br	391s	393m
350m br	343w sh	[b]	—	—	[b]
330m br	332w br	[b]	—	328w br	[b]
296m br	292w br	[b]	305w br	299w	[b]
279m sh	—	[b]	—	—	[b]
245w br	259m br	[b]	240m br	252w	[b]

[a] From ref. 11.

[b] Beyond reported range.

doublet collapsed at *ca* −30°C (250 MHz) but gave two broad equal peaks at −60°C straddling the minor doublet. This behaviour demonstrated a greater lability of the isopropoxide groups in the indium cluster. Thus the μ_2- and μ_3-ligands were exchanging rapidly above −30°C (ΔG 43–49 kJ mol^{-1}) whilst the terminal ligands were inseparable down to −80°C. This suggests either that the terminal basal–apical exchange is much more facile than μ_2–μ_3 bridging exchange or, more likely, that the chemical shifts of the basal and apical terminal ligands are very close in value.

X-ray crystal structures of $[In_5O(OPr^i)_{13}]$ *and* $[Yb_5O(OPr^i)_{13}]$

We have already reported the molecular structure of $[In_5(\mu_5\text{-}O)(\mu_3\text{-}OPr^i)_4(\mu_2\text{-}OPr^i)_4(OPr^i)_5]$ which was determined by single crystal X-ray diffraction.[7] We have now found that the ytterbium analogue $[Yb_5(\mu_5\text{-}O)(\mu_3\text{-}OPr^i)_4(\mu_2\text{-}OPr^i)_4(OPr^i)_5]$ is isostructural with the same M_5O_{14} cluster framework. Whilst our work was in progress Hubert–Pfalzgraf and Caulton and their co-workers[8] independently determined the crystal structure of $[Y_5(\mu_5\text{-}O)(\mu_3\text{-}OPr^i)_4(\mu_2\text{-}OPr^i)_4(OPr^i)_5]$ and this compound is isostructural with the indium and ytterbium clusters. The structural unit M_5O_{14} is shown in Fig. 1 and the more important bond distances and bond angles are listed in Table 3. In essence, the structure contains a μ_5-oxygen bonded to five metal atoms in a square pyramidal configuration with four μ_2-isopropoxy groups bridging the four basal metal atoms. The four μ_3-isopropoxy groups occupy the triangular faces of the square pyramid. Each metal has one terminal isopropoxy group completing a

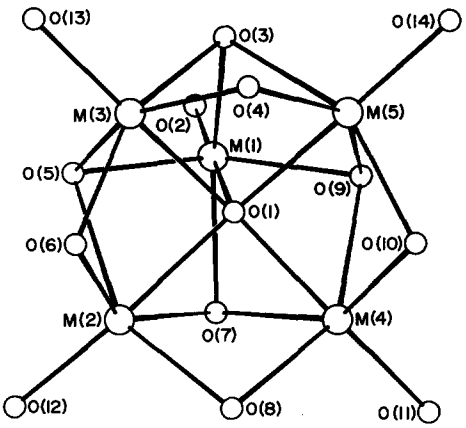

Fig. 1. The metal–oxygen core in $[M_5O(\mu_3\text{-}OPr^i)_4(\mu_2\text{-}OPr^i)_4(OPr^i)_5]$.

distorted octahedral coordination. It is interesting to note that the first example of a structurally characterized cluster molecular containing a μ_5-oxo atom was the organoyttrium methoxo compound $[Y_5(\mu_5\text{-}O)(\mu_3\text{-}OMe)_4(\mu_2\text{-}OMe)_4(C_5H_5)_5]$ reported by Evans and Sollberger.[14] In this case the terminal alkoxo groups have been replaced by η^5-Cp ligands. This reinforces our view that the $[M_5(\mu_5\text{-}O)(\mu_3\text{-}OR)_4(\mu_2\text{-}OR)_4]$ framework (M_5O_9) possesses special stability and must be the driving force for the breakdown of the tri-isopropoxides of scandium, yttrium, indium and ytterbium. Presumably the more stable tritertiary alkoxides[13] cannot attain the M_5O_4 cluster grouping because of steric hindrance and the metals are compelled to adopt a lower coordination number (except Y which gives trinuclear t-butoxide).

The metal–metal distances basal–basal and basal–apical are, respectively, 3.16 and 3.26 Å for indium and 3.26 and 3.38 Å for ytterbium and thus, as expected, there is no evidence for metal–metal bonding within these cluster molecules. The four basal metal atoms are virtually in a square with the μ_5-oxygen atoms slightly above this plane, e.g. 0.16 Å (In) and 0.19 Å (Yb). The apical metal atoms are closer to the μ_5-oxygen (2.21 Å In—O; 2.28 ÅYb—O) than the basal metal atoms (average 2.24 Å, In—O; 2.31 Å, Yb—O). The shortest M—O bonds involve the terminal isopropoxo groups with average bond lengths of 1.96 (In) and 2.00 Å (Yb). The μ_2-isopropoxo groups are symmetrically bonded to the basal metal atoms with average M—O bond lengths of 2.14 (In) and 2.19 Å (Yb). The μ_3-isopropoxy groups have shorter apical M—O bond lengths [average 2.22 (In) and 2.28 Å (Yb)] than the basal M—O bond lengths [average 2.34 (In) and 2.39 Å (Yb)]. The mean bond angles about the μ_5-oxygen are the same for each compound with the mean apical metal–oxygen–basal metal angles of 94.2 ± 0.6 (In) and $94.6\pm0.4°$ (Yb), reflecting the slight displacement of the μ_5-oxygen above the plane of the four basal metals. The angles subtended by the μ_5-oxygen and the basal metals are *cis*: 89.7 ± 0.7 (In) and $89.6\pm0.5°$ (Yb) and *trans*: 171.5 ± 1.1 (In) and $170.7\pm0.9°$ (Yb).

Hubart-Pfalzgraf and co-workers[8] have discussed the structure of $Y_5O(OPr^i)_{13}$ in relation to other cluster alkoxides of yttrium, viz. $[Y_3(OBu^t)_8Cl(THF)_2]$ and $[Y_4O(OBu^t)_{10}Cl_2]^{2-}$ isolated by Evans *et al.*[15] from reactions involving YCl_3 with $LiOBu^t$ or $NaOBu^t$, respectively. The formation of an octahedral configuration for yttrium was considered to be a driving force for the formation of the $Y_5O(OPr^i)_{13}$ structure with the interesting suggestion that the ultimate structure could be the anion $[Y_6O(\mu_2\text{-}OR)_{12}(OR)_6]^{2-}$ containing a μ_6-O octahedrally coordinated to six equivalent metal atoms. It is possible that the sodium salt of such a species is precipitated with NaCl in the reaction between MCl_3 and NaOR. In this respect it is also relevant to note that Andersen *et al.*[16] had earlier reported the neodymium complex chloride isopropoxide $[Nd_6(\mu_6\text{-}Cl)(\mu_3\text{-}OPr^i)_2(\mu_2\text{-}OPr^i)_9(OPr^i)_6]$ which contains a μ_6-Cl at the centre of a trigonal prismatic cluster of neodymium atoms.

EXPERIMENTAL

All operations were performed under an atmosphere of purified nitrogen using Schlenk-style apparatus and a glove box. Solvents were distilled from sodium benzophenone under nitrogen, and isopropanol was initially heated under reflux with CaO (preheated to 700°C) for several hours. Then a small quantity of dried benzene was added and the azeotropes (benzene–isopropanol–water, if still present, then benzene–isopropanol) were removed by fractional distillation; the remaining isopropanol was distilled onto activated 3 Å molecular sieves prior to use. Anhydrous $ScCl_3$ was prepared from the reaction of Sc_2O_3 with concentrated HCl followed by removal of H_2O/HCl *in vacuo*, then heating under reflux for 7 days with $SOCl_2$ (freshly distilled from linseed oil) and finally $SOCl_2$ was removed by distillation *in vacuo*. Anhydrous $InCl_3$ was obtained from commercial sources and heated *in vacuo* for several hours prior to use. Yttrium and ytterbium powder (40 mesh, 99.9%), sodium metal (lumps), and Bu^nLi (solution in hexane), were obtained from commercial sources. Hexamethyldisilazane was prepared by a literature route from reacting Me_3SiCl with ammonia.[11]

^1H NMR spectra were obtained using Bruker WP80 FT, WM250 FT and WH400 FT spec-

Table 3. Selected bond lengths (Å) and angles (°) for $M_5O(OPr^i)_{13}$ (M = In, Yb)

	In	Yb	Category
M(1)—O(1)	2.208(8)	2.285(23)	M_5O core
M(2)—O(1)	2.260(8)	2.339(24)	
M(3)—O(1)	2.242(9)	2.311(24)	
M(4)—O(1)	2.220(9)	2.300(24)	
M(5)—O(1)	2.235(8)	2.301(24)	
M(1)—O(2)	1.957(15)	2.003(24)	Terminal M—O
M(2)—O(12)	1.988(16)	2.026(29)	
M(3)—O(13)	1.984(16)	1.991(33)	
M(4)—O(11)	1.984(15)	2.015(32)	
M(5)—O(14)	1.982(15)	1.981(29)	
M(2)—O(6)	2.140(11)	2.192(29)	Basal M—μ_2-O
M(3)—O(6)	2.154(10)	2.181(25)	
M(3)—O(4)	2.162(11)	2.219(35)	
M(5)—O(4)	2.135(11)	2.177(29)	
M(5)—O(10)	2.147(11)	2.173(31)	
M(4)—O(10)	2.126(11)	2.183(30)	
M(4)—O(8)	2.147(10)	2.171(28)	
M(2)—O(8)	2.123(11)	2.229(34)	
M(1)—O(3)	2.219(10)	2.306(26)	Basal M—μ_3-O
M(1)—O(5)	2.204(10)	2.262(29)	
M(1)—O(9)	2.222(10)	2.305(27)	
M(2)—O(5)	2.326(9)	2.397(24)	
M(3)—O(5)	2.340(10)	2.285(3)	
M(3)—O(3)	2.318(9)	2.371(25)	
M(5)—O(3)	2.327(9)	2.379(27)	
M(5)—O(9)	2.297(10)	2.370(27)	
M(4)—O(9)	2.382(10)	2.368(25)	
M(4)—O(7)	2.330(10)	2.390(27)	
M(2)—O(7)	2.361(10)	2.371(24)	
M(1)—O(1)—M(2)	93.6(3)	93.9(9)	
M(1)—O(1)—M(3)	94.4(3)	94.7(9)	
M(1)—O(1)—M(4)	95.0(4)	95.2(9)	
M(1)—O(1)—M(5)	94.2(3)	94.7(8)	
M(2)—O(1)—M(3)	88.9(3)	88.9(8)	
M(3)—O(1)—M(5)	89.7(3)	90.0(9)	
M(5)—O(1)—M(4)	90.4(3)	90.3(9)	
M(4)—O(1)—M(2)	89.7(3)	89.3(9)	
M(2)—O(1)—M(5)	172.2(3)	171.4(10)	
M(3)—O(1)—M(4)	170.5(3)	170.1(10)	

trometers; chemical shifts are quoted relative to tetramethylsilane, although calibration was made from the solvent signals from incomplete deuteration. IR spectra were recorded as Nujol mulls between CsI plates in the range 4000–200 cm^{-1} using a Perkin–Elmer 577 spectrophotometer, and mass spectra using a Kratos MS50 TC spectrometer. Metals were analysed gravimetrically as the oxide M_2O_3 by hydrolysis of a sample in a platinum crucible followed by heating in air to 650°C for In and 750°C for the others (for Y and Yb this was followed by heating in a roaring bunsen flame). The isopropoxide analyses were by the method of Bradley *et al.*[17]

(1) $Sc_5O(OPr^i)_{13}$

(a) Sodium (5.0 g, 0.22 mol) was added to isopropanol (250 cm^3) and heated under reflux for 2 h, after which dissolution of metal was complete. This was cooled to room temperature whereupon a solution of anhydrous $ScCl_3$ (11 g, 73 mmol) in

isopropanol (250 cm^3) was added. The mixture was heated under reflux for a further 2 h and then stirred at room temperature for 60 h. The white precipitate was filtered off and the solvent was removed *in vacuo* to leave a white residue. This was heated to 220°C/10^{-2} mm Hg whereupon sublimation began to occur, but was slow, and was therefore continued at up to 280°C/10^{-2} mm Hg; a more volatile liquid was also obtained in a trap held at −196°C (see Results and Discussion). The sublimate was recrystallized from isopropanol to give white needle *crystals* of $Sc_5O(OPr^i)_{13}$ (m.p. > 320°C, 2.5 g, 17% based upon $ScCl_3$). Further washing of the precipitate with isopropanol enhanced the yield slightly.

(b) The $(Me_3Si)_2NH$ (34.6 cm^3, 164 mmol) was cautiously added to Bu^nLi (53 cm^3 of 3.15 M solution, 0.17 mol) and then solvent was removed *in vacuo*. The residue was dissolved in tetrahydrofuran (100 cm^3) and to this a solution of $ScCl_3$ (8.4 g, 56 mmol) in tetrahydrofuran (100 cm^3) was added dropwise. After stirring at room temperature overnight the solvent was removed *in vacuo* and the residue was triturated with pentane (200 cm^3) and any undissolved solid was filtered off. The trituration, etc., was repeated with fresh pentane (200 cm^3) and the two filtrates were combined, concentrated *in vacuo* and held at −25°C, whereupon white crystals of $Sc[N(SiMe_3)_2]_3$ were obtained. These were sublimed at 110°/10^{-2} mm Hg (20.0 g, 69% based upon $ScCl_3$). A sample of the sublimate (8.5 g, 16 mmol) was suspended in benzene (250 cm^3) and isopropanol was added (20 cm^3, ~ fivefold excess), whereupon all the solid dissolved. The contents were heated under reflux for 1 h, then allowed to cool to room temperature, at which point solvents were removed *in vacuo* to leave a white residue. The residue was recrystallized from isopropanol to give white *crystals* of $Sc_5O(OPr^i)_{13}$ (2.1 g, 65% based upon $Sc[N(SiMe_3)_2]_3$).

(2) $Y_5O(OPr^i)_{13}$

To yttrium powder (25 g, 0.28 mol) were added a few small crystals of $HgCl_2$ followed by isopropanol (400 cm^3, large excess), and the contents were heated under reflux for 60 h. By this time most of the metal had dissolved but a small quantity of black solid remained, which was filtered off and discarded. Solvent was removed from the filtrate and a sample of the residue (6 g) was recrystallized from isopropanol to give white *crystals* of $Y_5O(OPr^i)_{13}$ (4.9 g, 7% yield based upon Y). The bulk of the residue was sublimed at 220°C/10^{-2} mm Hg, although presumably some decomposition also occurred since much non-volatile residue remained (sublimed yield of $Y_5O(OPr^i)_{13}$ was 22.2 g, 32% based upon Y). The combined yield of 39% would presumably have been much higher if the whole sample had been recrystallized.

(3) $In_5O(OPr^i)_{13}$

Sodium (34.7 g, 1.48 mol) was added to a mixture of isopropanol (200 cm^3, large excess) and benzene (800 cm^3) and the contents heated under reflux overnight, after which the metal had dissolved. To this was added a solution of $InCl_3$ (106 g, 0.48 mol) in isopropanol (500 cm^3) and the contents were heated under reflux for 2 h, after which they were cooled to room temperature and the white precipitate filtered off. Further extraction from the precipitate was attempted with isopropanol (200 cm^3), and the filtrates were combined and concentrated *in vacuo*, whereupon colourless *crystals* of $In_5O(OPr^i)_{13}$ were obtained (62 g, 48% based upon $InCl_3$). The compound began to turn yellow when heated to 160°C under an atmosphere of nitrogen.

(4) $Yb_5O(OPr^i)_{13}$

To ytterbium powder (10.2 g, 59 mmol) were added a few small crystals of $HgCl_2$ followed by isopropanol (250 cm^3, large excess), and the contents were heated under reflux for 24 h. The residual black solid was filtered off and solvent was removed from the filtrate *in vacuo*. The white residue was sublimed at 215°C/10^{-2} mm Hg as white *crystals* of $Yb_5O(OPr^i)_{13}$ (17.8 g, 86% based upon Yb). M.p. > 300°C.

X-ray crystallography

Crystals of the indium and ytterbium clusters used for the X-ray work were sealed under nitrogen in thin-walled glass capillaries. All crystallographic measurements were performed at 293 K using a Nonius CAD4 diffractometer and graphite-monochromated Mo-K_α radiation (λ = 0.71069 Å), following previously detailed procedures.[18] The structures were solved by direct methods and refined by full-matrix least-squares analysis. For the indium compound all included atoms were refined anisotropically, but due to large thermal motion in the isopropyl groups, C—O and C—C distances were fixed at 1.40 and 1.50 Å, respectively. These distances were also fixed for the ytterbium compound, but in addition all carbon atoms were refined isotropically. No hydrogens were included for either compound.

Details of the crystal data, data collection and refinement are given in Table 4. Computer pro-

Table 4. Crystal data, details of intensity measurements and structure refinement

Molecular formula	$C_{39}H_{91}O_{14}In_5$	$C_{39}H_{91}O_{14}Yb_5$
Molecular weight	1358.12	1649.12
Crystal system	Monoclinic	Monoclinic
a (Å)	12.665(2)	12.878(4)
b (Å)	21.305(2)	21.621(4)
c (Å)	20.910(6)	21.377(3)
α (°)	90.0	90.0
β (°)	90.70(2)	91.38(2)
γ (°)	90.0	90.0
V (Å^3)	5641.7	5950.39
Space group	$P2_1/n$	$P2_1/n$
Z	4	4
D_c (g cm^{-3})	1.60	1.84
μ (cm^{-3})	20.32	78.05
$F(000)$	2728	3148
h, k, l, range	$\pm 13, 23, 23$	$\pm 15, 25, 25$
Total number of reflections	8323	11084
Number of unique reflections	7828	10471
Number of reflections used; $[F > 3\sigma(F)]$	4680	4164
Number of parameters	525	328
Weighting scheme parameter g in $w = 1/[\sigma^2(F)+gF_o^2]$	0.003486	0.002529
Final R	0.057	0.071
Final R_w	0.080	0.091

grams and sources of scattering factor were as previously described.[18]

Acknowledgements—We thank the SERC for financial support. We are indebted to Mr Peter Cook for obtaining the mass spectra and to Mr Greg. Coumbarides and Mr Peter Haycock for obtaining the NMR spectra at 250 and 400 MHz (University of London Intercollegiate Research Service), respectively.

REFERENCES

1. D. C. Bradley, *Chem. Rev.* 1989, **89**, 1317; see also L. A. Ryabora, *Curr. Top. Mater. Sci.* 1981, **7**, 587; B. J. J. Zelinski and D. R. Uhlmann, *J. Phys. Chem. Sol.* 1984, **45**, 1069.
2. K. S. Mazdyasni, C. T. Lynch and J. S. Smith, *Inorg. Chem.* 1966, **5**, 342.
3. S. Chatterjee, S. R. Bindal and R. C. Mehrotra, *J. Ind. Chem. Soc.* 1976, **53**, 867.
4. U. D. Tripathi, J. M. Batwara and R. C. Mehrotra, *J. Chem. Soc. A* 1967, 991.
5. V. H. Funk and B. Köhler, *Z. Anorg. Allg. Chem.* 1963, **325**, 68.
6. V. A. Schreider, E. P. Turevskaya, N. I. Koslova and N. Y. Turova, *Inorg. Chem. Acta* 1981, **53**, L73.
7. D. C. Bradley, H. Chudzynska, D. M. Frigo, M. B. Hursthouse and M. A. Mazid, *J. Chem. Soc., Chem. Commun.* 1988, 1258.
8. O. Poncelet, W. J. Sartain, L. G. Hubert-Pfalzgraf, K. Folting and K. G. Caulton, *Inorg. Chem.* 1989, **28**, 263.
9. D. C. Bradley, R. C. Mehrotra and D. P. Gaur, *Metal Alkoxides*. Academic Press, London (1978).
10. E. C. Alyea, D. C. Bradley and R. G. Copperthwaite, *J. Chem. Soc., Dalton Trans.* 1972, 1580.
11. R. C. Osthoff and S. W. Kantor, *Inorg. Synth.* 1957, 55.
12. D. C. Bradley and M. M. Faktor, *J. Appl. Chem.* 1959, **9**, 5425; *Trans. Faraday Soc.* 1959, **55**, 2117.
13. D. C. Bradley and H. Chudzynska, Poster presentation at Int. Coord. Chem. Conf., Gold Coast, Brisbane, Australia (July 1989).
14. W. J. Evans and M. S. Sollberger, *J. Am. Chem. Soc.* 1986, **108**, 6095.
15. W. J. Evans, M. S. Sollberger and T. P. Hanusa, *J. Am. Chem. Soc.* 1988, **110**, 1841.
16. R. A. Andersen, D. H. Templeton and A. Zalkin, *Inorg. Chem.* 1978, **17**, 1962.
17. D. C. Bradley, F. M. Abd-El Halim and W. Wardlaw, *J. Chem. Soc.* 1950, 3450.
18. R. A. Jones, M. B. Hursthouse, K. M. A. Malik and G. Wilkinson, *J. Am. Chem. Soc.* 1979, **101**, 4128.

Polyhedron Vol. 9, No. 5, pp. 727–738, 1990
Printed in Great Britain

0277–5387/90 $3.00+.00
© 1990 Pergamon Press plc

PROTON-INDUCED COUPLING OF A TERT-BUTYLISOCYANIDE WITH A DIETHYLAMINOCARBYNE TO YIELD AN ALKYNE LIGAND AT A SINGLE TUNGSTEN CENTRE

A. C. FILIPPOU

Anorganisch-chemisches Institut der Technischen Universität München, Lichtenbergstr. 4, D-8046 Garching, F.R.G.

(*Received* 24 *July* 1989; *accepted* 27 *September* 1989)

Abstract—The tert-butylisocyanide substituted diethylaminocarbyne complex $I(CO)_2(t\text{-}BuNC)_2W{\equiv}CNEt_2$ (**1**) reacts with one equivalent of HI in CH_2Cl_2 at room temperature to yield a mixture of complexes $(I)_2(CO)_2(t\text{-}BuNC)W[\eta^2\text{-}(t\text{-}Bu)HN\text{-}C{\equiv}C\text{-}NEt_2]$ (**2**), major product, and $(I)_2(CO)(t\text{-}BuNC)_2W[\eta^2\text{-}(t\text{-}Bu)HN\text{-}C{\equiv}C\text{-}NEt_2]$ (**3**), minor product, separable by column chromatography on silica. The exclusive preparation of compound **3** can be achieved by treating $I(CO)(t\text{-}BuNC)_3W{\equiv}CNEt_2$ (**4**) with one equivalent of HI in CH_2Cl_2 at room temperature. Complexes **2** and **3** contain a 4e-donor alkyne ligand resulting from the proton-induced coupling of one tert-butylisocyanide with the diethylaminocarbyne ligand at a single tungsten centre. Both complexes react with t-BuNC in refluxing CH_2Cl_2 to give quantitatively the cationic alkyne complex $[I(CO)(t\text{-}BuNC)_3W[\eta^2\text{-}(t\text{-}Bu)HN\text{-}C{\equiv}C\text{-}NEt_2]]^+I^-$ (**5**). Thermal decarbonylation of this complex in toluene in the presence of t-BuNC at 90°C leads to the carbonyl-free alkyne complex $[I(t\text{-}BuNC)_4W[\eta^2\text{-}(t\text{-}Bu)HN\text{-}C{\equiv}C\text{-}NEt_2]]^+I^-$ (**6**). The ionic nature of **5** and **6** has been confirmed by comparison of their conductivity data in 1,2-dichloroethane with $NR_4^+X^-$ salts (R = alkyl; X = PF_6, Br, I). The composition and structure of the alkyne complexes **2**, **3**, **5** and **6** have been determined by total elemental analyses, IR, ^1H NMR and ^{13}C NMR spectroscopies and mass spectrometry. The spectroscopic results indicate a substantial bond delocalization and a hindered rotation of the diethylamino-group in the alkyne ligand. The barrier to this rotation is calculated to be *ca* 13.9–15.3 kcal mol^{-1} for compounds **2**, **3**, **5** and **6**.

Since the discovery of the first compounds containing a metal–carbon triple bond in 1973 by E. O. Fischer and co-workers,[1] considerable progress has been made in the field of transition metal carbyne complexes as shown by the large number of review articles[2–7] and a monograph,[8] which have appeared in the last 14 years. Carbyne complexes are divided into two classes. Class (a) contains compounds of low-valent metals known as Fischer-type carbyne complexes. In these complexes, the electron-rich metal centre is stabilized by good π-acceptor ligands such as CO, e.g. *trans*-$X(CO)_4M{\equiv}CR$ (X = halogen; M = Cr, Mo, W; R = alkyl, aryl).[9] Class (b) includes complexes of high-valent metals known as Schrock-type alkylidyne (carbyne) complexes. In these compounds, the electron-deficient metal is bonded to good π-donors, such as halogen, alkoxy or imido ligands, e.g. $X_3(dme)W{\equiv}C^tBu$ (X = halogen; dme = 1,2-dimethoxyethane).[10–13]

In this context, low-valent complexes containing a diethylamino-group in the carbyne moiety, e.g. $X(CO)_{4-n}L_nW{\equiv}CNEt_2$ (X = halogen; L = 2e-donor ligand; n = 1–4)[14–17] and $(\eta^5\text{-}C_5R_5)(CO)_2W{\equiv}CNEt_2$ (R = H, Me),[18–20] are very attractive because striking differences are observed in the reactivity of these complexes and that of analogous aryl- or alkylcarbyne complexes. Thus, $I(CO)_2L_2W{\equiv}CNEt_2$ (L = PMe_3, MeNC, t-BuNC, $P(OMe)_3$; L_2 = 2.2′-bipy, *o*-phen) and $(\eta^5\text{-}C_5R_5)(CO)_2W{\equiv}CNEt_2$ (R = H, Me) react with I_2 to yield, by partial oxidative decarbonylation, the seven-coordinated, carbonyl-containing compounds $I_3(CO)L_2W{\equiv}CNEt_2$ and $(\eta^5\text{-}C_5R_5)(CO)(I)_2W{\equiv}CNEt_2$, respectively.[19–25] These complexes

are unique because they combine features of both Fischer-type carbyne complexes, such as π-acceptor CO ligands, and Schrock-type alkylidyne complexes, i.e. a high-valent metal centre. In comparison, *trans*-$Br(CO)_4W{\equiv}CR$ (R = Me, CH_2CMe_3, Ph) react with Br_2 in dme to yield the octahedral coordinated, carbonyl-free, Schrock-type alkylidyne complexes $Br_3(dme)W{\equiv}CR$.[26]

Different products are also obtained from the reactions of diethylamino- and aryl- or alkylcarbyne complexes with nucleophiles, e.g. *trans*-$I(CO)_4W{\equiv}CNEt_2$ reacts with PMe_3 by CO elimination to give the mono- or disubstituted carbyne complexes $I(CO)_3(PMe_3)W{\equiv}CNEt_2$ or *cis,trans*-$I(CO)_2(PMe_3)_2W{\equiv}CNEt_2$.[21] However, the reaction of *trans*-$Br(CO)_4W{\equiv}CPh$ with PMe_3 results in addition of the nucleophile to the carbyne-carbon and formation of the ylide complexes $Br(CO)_3(PMe_3)W[C(PMe_3)Ph]$ and $Br(CO)_2(PMe_3)_2W[C(PMe_3)Ph]$.[27]

Nucleophiles induce a carbyne–carbonyl coupling in substituted aryl- or alkylcarbyne complexes to yield η^1- or η^2-ketenyl complexes. Representative examples of this pathway are the reactions of $Cp(CO)_2W{\equiv}CR$ (R = Ph, *p*-C_6H_4Me) with PMe_3 to $Cp(CO)(PMe_3)W[\eta^2\text{-}C(CO)R]$ or $Cp(CO)(PMe_3)_2W[\eta^1\text{-}C(CO)R]$,[28,29] $Br(CO)_2L_2W{\equiv}CR$ (L_2 = 2.2′-bipy, *o*-phen; R = Ph, Me) with KCN to $K[(CN)_2(CO)L_2W(\eta^2\text{-}C(CO)R)]$,[30,31] $[(CO)_2(dppe)W{\equiv}CCH_2Ph]BF_4$ with NaS_2CNMe_2 to $(\eta^2\text{-}Me_2NCS_2)(CO)(dppe)W[\eta^2\text{-}C(CO)CH_2Ph]$[32] and $Cl(CO)_2(py)_2W{\equiv}CPh$ with NaS_2CNEt_2 to $Na[(\eta^2\text{-}Et_2NCS_2)_2(CO)W(\eta^2\text{-}C(CO)Ph)]$.[33] In comparison, a nucleophile-induced carbonylation of the carbyne ligand has not been observed so far for the reactions of substituted diethylaminocarbyne complexes.[34–38]

Reactions of low-valent, substituted aryl- or alkylcarbyne complexes with electrophiles have also been extensively investigated. The electrophile can attack either the carbyne-carbon or the metal centre. Illustrative examples of the former to give carbene complexes are the protonations of $Cl(CO)(PPh_3)_2Os{\equiv}CR$ (R = *p*-C_6H_4Me), $Cp(CO)_2W{\equiv}CR$ (R = Me, *p*-C_6H_4Me) and $Cl(CO)(PMe_3)_3W{\equiv}CR$ (R = C_6H_5, *p*-C_6H_4Me) with HX (X = Cl, I) to $(Cl)_2(CO)(PPh_3)_2Os[C(H)R]$,[39] $Cp(I)(CO)_2W[C(H)R]$[40] and $(Cl)_2(CO)(PMe_3)_2W[C(H)R]$, respectively.[41] Protonation of the metal centre yields hydrido carbyne complexes shown by the reactions of $Cl(PMe_3)_4W{\equiv}CH$, $Cl(dmpe)_2W{\equiv}CR$ (R = H, ^{t}Bu) and $Br(PMe_3)_4W{\equiv}CPh$ with HX (X = Cl, Br) to $(Cl)_2(H)(PMe_3)_3W{\equiv}CH$, $[Cl(H)(dmpe)_2W{\equiv}CR]Cl$[42] and $(Br)_2(H)(PMe_3)_3W{\equiv}CPh$, respectively.[41] In a few cases, electrophile-induced carbon–carbon coupling reactions involving the carbyne ligand are observed, as in the transformation of $Cp(CO)_2W{\equiv}CR$ (R = Me, *p*-C_6H_4Me) by HBF_4 to the dinuclear, alkyne-bridged complex $[Cp_2(CO)_4(\mu\text{-}H)(\mu\text{-}RC{\equiv}CR)W_2]BF_4$[40,43] or by HCl to the η^2-acyl complex $Cp(Cl)_2(CO)W[\eta^2\text{-}C(O)CH_2R]$,[44] and in the carbonylation of $Cl(PMe_3)_4W{\equiv}CH$ in the presence of $AlCl_3$ to the alkyne complex $Cl(CO)(PMe_3)_3W[\eta^2\text{-}HC{\equiv}COAlCl_3]$.[45,46] In comparison, studies involving reactions of low-valent diethylaminocarbyne complexes with electrophiles are limited to a few examples, e.g. the protonation of $Cp(CO)_2W{\equiv}CNEt_2$ with HCl to give the carbene complex $Cp(Cl)(CO)_2W[C(H)NEt_2]$,[47] the addition of CO_2 across the metal–carbon triple bond in $[(CO)_4Mo(\mu\text{-}PPh_2)_2W(CO)_2(CNEt_2)]^-$[34] and the substitution reactions of $I(CO)_nL_{4-n}W{\equiv}CNEt_2$ (n = 1, 2; L = PMe_3, t-BuNC) with MeOTf to give $(OTf)(CO)_nL_{4-n}W{\equiv}CNEt_2$.[48]

We have, therefore, been interested in the reactivity of electron-rich carbyne complexes towards electrophiles and developed synthetic routes to highly-substituted and carbonyl-free phenyl- and diethylaminocarbyne complexes.[16,17,21,23,49] We studied firstly the reactions of $X(CO)_n(t\text{-}BuNC)_{4-n}W{\equiv}CPh$ (X = Br, I; n = 0, 1) with HX (X = Br, I), found a clean proton-induced coupling reaction of one tert-butylisocyanide with the phenylcarbyne ligand at tungsten to yield an alkyne complex, and then demonstrated the effect of CO ligands on the reaction pathway.[50] These results are important in the context of the reductive coupling of two alkylisocyanide ligands to give a bis(amino)acetylene ligand in seven-coordinated isocyanide complexes of molybdenum and tungsten, reported by Lippard and co-workers.[51–53] They assume for this reaction the intermediate formation of an isocyanide substituted carbyne complex.[54] For rhenium, they have isolated such a carbyne isocyanide complex, but have failed to demonstrate coupling of the two ligands.[55]

In this paper we describe the proton-induced isocyanide–carbyne coupling reaction in diethylaminocarbyne complexes of tungsten. A preliminary report of this work has already been published.[56]

RESULTS AND DISCUSSION

The bis(tert-butylisocyanide) substituted diethylaminocarbyne complex **1** reacts with HI (generated from NEt_4I and $HBF_4 \cdot Et_2O$) to yield a mixture of the alkyne complexes $(I)_2(CO)_2(t\text{-}BuNC)W[\eta^2\text{-}(t\text{-}Bu)HN\text{-}C{\equiv}C\text{-}NEt_2]$ (**2**) and $(I)_2(CO)(t\text{-}BuNC)_2W[\eta^2\text{-}(t\text{-}Bu)HN\text{-}C{\equiv}C\text{-}NEt_2]$ (**3**) (Scheme 1).

Complex **2**, the major product, is separated from

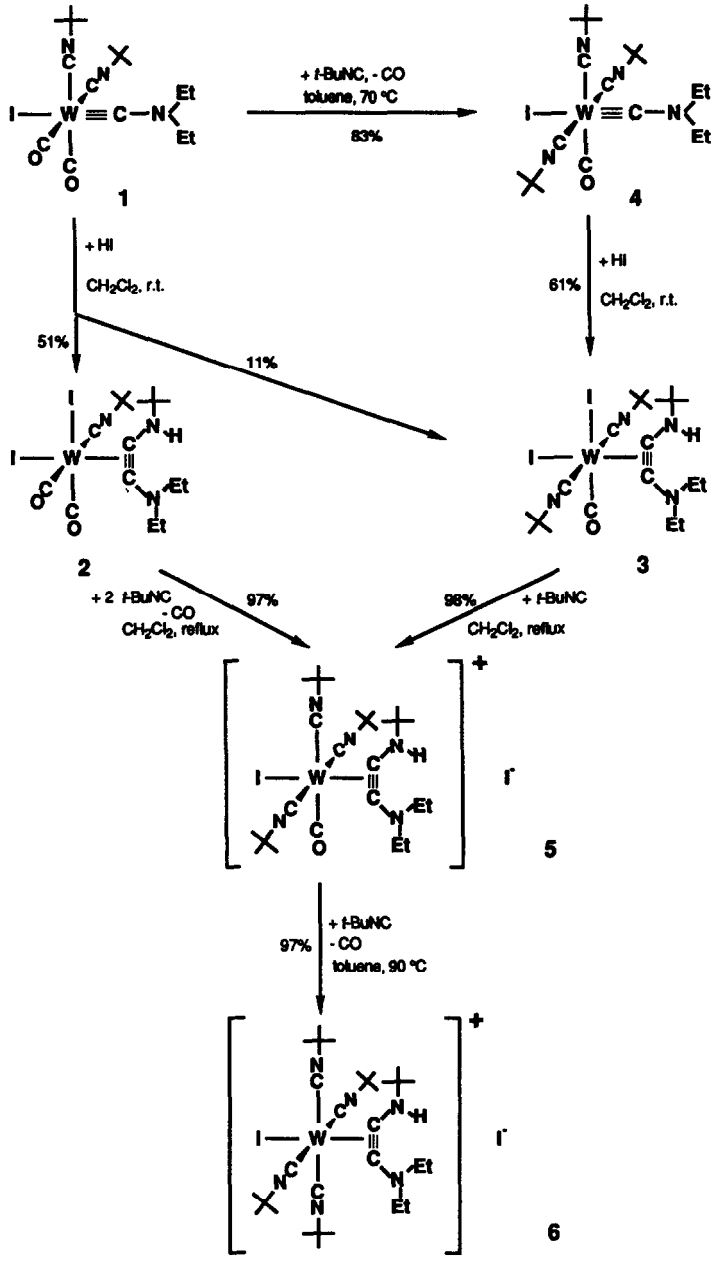

Scheme 1. Synthesis and reactions of the coupling products **2**, **3**, **5** and **6**.

complex **3**, the minor product, by column chromatography on silica gel at 0°C and is isolated as a red, microcrystalline solid in 51% yield. Complex **3**, a purple microcrystalline solid, is obtained in 11% yield. Complexes **2** and **3** are soluble in CH_2Cl_2, Et_2O and toluene, but insoluble in *n*-pentane. They decompose in a sealed capillary at 95 and 128°C, respectively. Complex **3** can be prepared from **1** following a two-step route. The first step involves the transformation of **1** into the tris(tert-butylisocyanide) substituted carbyne complex **4**. Complex **4** reacts then with HI to form exclusively **3**, which is isolated after purification by column chromatography on silica gel in 61% yield (Scheme 1).

The reaction time for formation of the coupling products with HI is appreciably shorter for **4** than for **1**. This result suggests that an increase in electron density at the tungsten centre accelerates the isocyanide–carbyne coupling reaction.

The reaction of **2** with t-BuNC in refluxing CH_2Cl_2 results in elimination of one CO and one

iodide ligand from the coordination sphere and quantitative formation of the cationic complex **5** (Scheme 1). Complex **5**, which can also be prepared from **3** and t-BuNC in refluxing CH_2Cl_2, reacts further with t-BuNC in toluene at a higher temperature (90°C) to produce quantitatively the carbonyl-free, cationic complex **6** (Scheme 1). Complexes **5** and **6** are isolated as red and purple, microcrystalline solids, respectively, which are very soluble in CH_2Cl_2, sparingly soluble in toluene, but insoluble in Et_2O and *n*-pentane. Complex **6** decomposes in a sealed capillary at 160°C.

Attempts to prepare the neutral, carbonyl-free analogue of **2** or **3** $(I)_2$(t-BuNC)$_3$W[η^2-(t-Bu)HN-C≡C-NEt$_2$] by thermal decarbonylation of **5** in toluene at 90°C have so far failed. The only product isolated is **6** along with decomposition products.[57]

The coupling products **2**, **3**, **5** and **6** are best considered as isocyanide-substituted complexes containing a 4e-donor (tert-butylamino)diethylaminoacetylene ligand. The reality of 4e donation of the alkyne ligand to tungsten is indicated for these complexes by the spectroscopic data (cf. for example ^{13}C NMR spectra, Table 4) and substantiated by their lack of chemical reactivity. They are not only thermally stable, crystalline solids, but also decompose slowly in the presence of atmospheric water and oxygen. These properties are not consistent with a 16e tungsten(II) formulation for complexes **2**, **3**, **5** and **6** counting the alkyne ligand as 2e-donor.[58] The consideration of **2**, **3**, **5** and **6** as complexes containing a 4e-donor alkyne ligand is also supported by the close similarity to the structurally characterized complexes [X(t-BuNC)$_4$M[η^2-(t-Bu)HN-C≡C-NH(t-Bu)]]Y (X = Cl, Br, I, CN; M = Mo, W; Y = Cl, I, BF_4, PF_6) containing a 4e-donor bis(tert-butylamino)acetylene ligand.[52,59] These complexes have been previously prepared by reductive coupling of two isocyanide ligands in the seven-coordinated complexes of the general formula [M(t-BuNC)$_6$X]$^+$ (M = Mo, W) and [Mo(t-BuNC)$_7$]$^{2+}$.[51,53]

The diethylaminocarbyne complexes, **1** and **4**, do not react with NEt_4I. The presence of a proton source (in this case HBF_4) is necessary to initiate the isocyanide–carbyne coupling reaction. We suggest, therefore, that the first step in the reaction sequence, leading from the carbyne complex to the coupling product, involves protonation of the carbyne complex.

Figure 1 illustrates one possible reaction mechanism for this proton promoted carbon–carbon coupling reaction. The initial step involves proton attack on the isocyanide nitrogen to form a cationic bis(aminocarbyne) intermediate (**A**).

This transformation of an isocyanide to an aminocarbyne ligand upon protonation has been previously observed in isocyanide complexes of electron-rich metals, e.g. in the reaction of *trans*-Mo(MeNC)$_2$(dppe)$_2$ with one or two equivalents of $HBF_4 \cdot Et_2O$ to give the cationic aminocarbyne complex *trans*-[(MeNC)(dppe)$_2$W≡CNHMe]BF_4 and the dicationic bis(aminocarbyne) complex *trans*-[(dppe)$_2$Mo(≡CNHMe)$_2$]$(BF_4)_2$, respectively,[60–62] or in the reaction of *trans*-ReCl(RNC)(dppe)$_2$ (R = H, Me, t-Bu) with $HBF_4 \cdot Et_2O$ to yield the cationic aminocarbyne complexes *trans*-[Cl(dppe)$_2$Re≡CNHR]BF_4.[63,64]

The second step (Fig. 1) involves coupling of the two carbynes to a bis(amino)alkyne ligand, a reaction which is possibly promoted by the nucleophile I^-. A similar carbyne–carbyne ligand coupling reaction at a single tungsten centre has previously been proposed to account for formation of the alkyne complex $(Br)_2(CO)(PPh_3)_2W[\eta^2$-CH$_3$-C≡C-C$_6H_5$] from the anionic carbyne complex Li[Br(CO)$_2$(PPh$_3$)(η^1-CH$_3$CO)W≡CC$_6$H$_5$], oxalylbromide and PPh_3,[65] and is in agreement with theoretical predictions on carbyne–carbyne coupling in bis(carbyne) complexes by Hoffmann *et al.*[66]

Other reaction pathways for the proton-promoted isocyanide–carbyne coupling involving proton attack at the carbyne-carbon or at the metal centre to give carbene or hydrido carbyne intermediates should also be considered since the formation of such products has been previously observed in protonation reactions of substituted, low-valent carbyne complexes.[39–42] Currently,

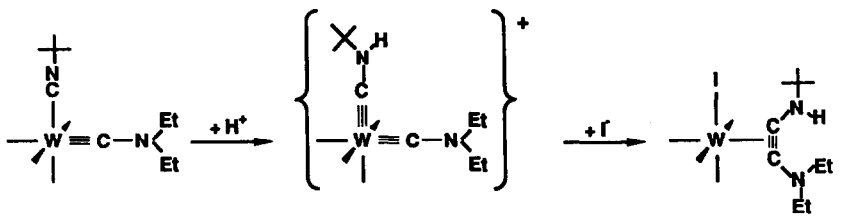

Fig. 1. Possible mechanism for the proton-promoted isocyanide–carbyne coupling reaction.

experimental work is underway in an attempt to trap intermediates to distinguish between the possible pathways for the coupling reaction.

The solution IR spectra of **2**, **3**, **5** and **6** in CH_2Cl_2 show characteristic absorptions for the stretching vibrations of the coordinated tert-butylisocyanide and carbonyl ligands (Table 1). The relative position of these ligands in the coordination sphere is indicated by the number and relative intensity of the ν(C≡N^{t}Bu) and ν(C≡O) absorption bands. Thus, two bands of almost equal intensity are observed for the *cis*-oriented carbonyl ligands in **2** and one band for the two *trans*-positioned tert-butylisocyanide ligands in **3**, resulting, respectively, from the symmetric A_1 and antisymmetric B_1 CO stretching mode in **2** and the A_2 isocyanide stretching mode in **3**.[67] The *trans*-orientation of the four tert-butylisocyanide ligands in **6** gives rise to a strong absorption at 2125 cm^{-1} and a weak, higher energy band at 2175 cm^{-1}, which can be assigned, respectively, to the E and A_1 isocyanide stretching modes.[68]

A shift of the ν(C≡N^{t}Bu) absorptions to lower frequency is observed when the IR data of **2** with **3** or **5** with **6** are compared. This shift can be attributed to an increase in the electron density at the metal and the simultaneous strengthening of the metal–isocyanide back-bonding resulting from substitution of one carbonyl (better π-acceptor) in **2** and **5** by one isocyanide ligand (poorer π-acceptor) in **3** and **6**.[68]

Two IR bands characterize the presence of the (tert-butylamino)diethylaminoacetylene ligand in the coupling products. A ν(N—H) absorption band ~3330 cm^{-1} (complexes **2** and **3**) and ~3230 cm^{-1} (complexes **5** and **6**) (Nujol mull) and another absorption band ~1630 cm^{-1} (CH_2Cl_2 solution), which can be assigned to a ν(C=N) stretching vibration. Similar absorption bands ~1600–1700 cm^{-1} have been previously reported for complexes containing amino-substituted alkyne ligands and have also been assigned to a ν(C=N) and not to a ν(C=C) stretching vibration of the coordinated alkyne ligand (Table 1).[50,51,53] This assignment is supported by the fact that a ν(C≡C) stretching vibration has so far not been observed for alkyl- or aryl-substituted alkyne ligands acting as 4e-donors in d^4 metal complexes.[69,70]

Several resonance forms can be used to describe the metal–alkyne bond in the coupling products **2**, **3**, **5** and **6** and are depicted in Fig. 2. The mesomeric formulas **A**–**D** represent the alkyne ligand acting as a 4e-donor. The complexes **2**, **3**, **5** and **6** thus achieve a closed shell configuration. The fairly high-frequency of the ν(C=N) stretching vibration in **2**, **3**, **5** and **6**, which is comparable with that in immonium cations $(R_2C{=}NR_2)^+$ [ν(C=N): 1640–1690 cm^{-1}],[71] is consistent with a strong contribution of the canonical forms **B**, **C** and **D** to the structure. Its value is, however, lower than for the analogous (tert-butylamino)phenylacetylene complexes $(Br)_2(CO)(t\text{-BuNC})_2W[\eta^2\text{-}(t\text{-Bu})HN\text{-}C{\equiv}C\text{-}C_6H_5]$ and $[I(t\text{-BuNC})_4W[\eta^2\text{-}(t\text{-Bu})HN\text{-}C{\equiv}C\text{-}C_6H_5]]^+PF_6$ (Table 1). Similarly, the ν(C≡N^{t}Bu) and ν(C≡O) stretching vibrations of **3** and **6** are observed at lower frequency than for the analogous (tert-butylamino)phenylacetylene complexes (Table 1), indicating the stronger donor properties of the (tert-butylamino)diethylaminoacetylene ligand.

Variable temperature NMR studies indicate fluxional behaviour for complexes **2**, **3**, **5** and **6**. The fluxionality is best explained by rotation of the diethylamino-group around the C_{alkyne}—N bond in

Table 1. ν(N—H), ν(C≡N^{t}Bu), ν(C≡O) and ν(C=N) stretching vibrations (in cm^{-1}) of the alkyne complexes **2**, **3**, **5** and **6** and of related compounds

Complex	ν(N—H)[a]	ν(C≡N^{t}Bu)[b]	ν(C≡O)[b]	ν(C=N)[b]
$(I)_2(CO)_2(t\text{-BuNC})W[(t\text{-Bu})HN\text{-}C{\equiv}C\text{-}NEt_2]$ (**2**)	3334 w	2188 m	2028 s; 1948 s	1635 m
$(I)_2(CO)(t\text{-BuNC})_2W[(t\text{-Bu})HN\text{-}C{\equiv}C\text{-}NEt_2]$ (**3**)	3331 w	2151 s	1921 s	1625 m
$[I(CO)(t\text{-BuNC})_3W[(t\text{-Bu})HN\text{-}C{\equiv}C\text{-}NEt_2]]^+I^-$ (**5**)	3232 w, br	2186 w, 2152 s	1984 m	1635 m
$[I(t\text{-BuNC})_4W[(t\text{-Bu})HN\text{-}C{\equiv}C\text{-}NEt_2]]^+I^-$ (**6**)	3223 w, br	2175 w, 2125 vs	—	1629 w
$(Br)_2(CO)(t\text{-BuNC})_2W[(t\text{-Bu})HN\text{-}C{\equiv}C\text{-}C_6H_5]$[50]	3397 w[c]	2195 w, 2165 s	1970 s	1680 m
$[I(t\text{-BuNC})_4W[(t\text{-Bu})HN\text{-}C{\equiv}C\text{-}C_6H_5]]^+PF_6^-$[50]	3386 w[c]	2194 w, 2151 vs	—	1670 w
$[I(t\text{-BuNC})_4W[(t\text{-Bu})HN\text{-}C{\equiv}C\text{-}NH(t\text{-Bu})]]^+I^-$[53]	3185 m[c]	2175 m, 2120 s 2065 sh[c]	—	1590 m[c]

[a] In Nujol.
[b] In CH_2Cl_2.
[c] In KBr.

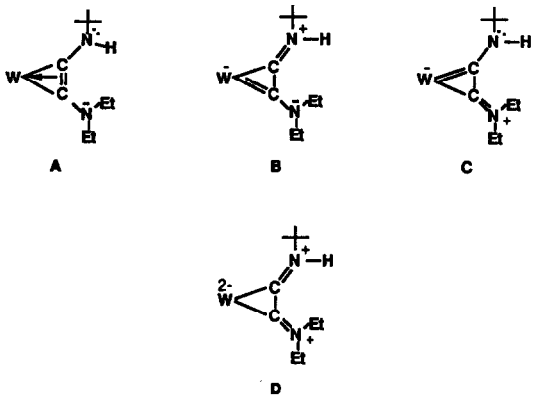

Fig. 2. Resonance forms for the metal–alkyne bond in the coupling products **2**, **3**, **5** and **6**.

the alkyne ligand. Thus, the low temperature limit spectra show two distinct triplets indicating different environments for the methyl protons of the diethylamino-group (Table 2). Two different signals are also observed for the methylene groups. In complexes **3**, **5** and **6** the protons of each methylene group are homotopic and give rise to a quartet. In comparison, complex **2** contains diastereotopic protons in both methylene groups. Therefore a signal of four partially overlapping quartets results for each methylene group (Table 2), which can be assigned to an ABX_3 spin system.

The two distinct signals for the methyl groups broaden upon heating the samples and then collapse to one signal at the coalescence temperature (Table 3). The signals of the methylene protons exhibit similar behaviour as the temperature is raised. The high temperature limit spectra of complexes **3** and **6** have been recorded in CD_2Cl_2 using sealed NMR tubes ($T > 40°C$) and exhibit only one triplet for the methyl and one quartet for the methylene protons indicating an averaged environment for the ethyl groups. The activation barrier for rotation of the diethylamino-group, $\Delta G^{\dagger}(T_c)$, was calculated from the Eyring equation after the Gutowsky–Holm equation was employed to obtain k_{ex} at the coalescence temperature (methyl protons) (Table 3).[72,73]

The signals for the tert-butylisocyanide ligands and the tert-butylamino-group in the alkyne ligand are independent of this dynamic process indicating

Table 2. ^1H NMR spectroscopic data of **2**, **3**, **5** and **6** in CD_2Cl_2; chemical shifts (in δ) relative to the solvent ($CDHCl_2$, $\delta = 5.32$ ppm); relative intensities and multiplicities in parentheses, coupling constants in Hz

Complex	NCH_2CH_3	$(CH_3)_3CNC$	$(CH_3)_3CNH$	NCH_2CH_3	$(CH_3)_3CNH$	Temperature (°C)
2	1.16 (3, t) $^3J(HH) = 7.3$; 1.35 (3, t) $^3J(HH) = 7.3$	1.54 (9, s)	1.55 (9, s)	3.48 (1, dq) $^2J(H_AH_B) = 14.5$ $^3J(H_AH_X) = 7.3$; 3.54 (1, dq) $^2J(H_AH_B) = 14.5$ $^3J(H_BH_X) = 7.3$; 3.83 (1, dq) $^2J(H'_AH'_B) = 14.0$ $^3J(H'_AH'_X) = 7.3$; 4.10 (1, dq) $^2J(H'_AH'_B) = 14.0$ $^3J(H'_BH'_X) = 7.3$	7.40 (1, s)	−30
3	1.12 (3, t) $^3J(HH) = 7.3$; 1.33 (3, t) $^3J(HH) = 7.3$	1.51 (18, s)	1.52 (9, s)	3.44 (2, q) $^3J(HH) = 7.3$; 3.90 (2, q) $^3J(HH) = 7.3$	7.24 (1, s)	−40
5	1.13 (3, t) $^3J(HH) = 7.3$; 1.32 (3, t) $^3J(HH) = 7.3$	1.46 (18, s); 1.48 (9, s)	1.58 (9, s)	3.72 (2, q) $^3J(HH) = 7.3$; 3.81 (2, q) $^3J(HH) = 7.3$	8.08 (1, s)	−20
6	1.11 (3, t) $^3J(HH) = 7.3$; 1.31 (3, t) $^3J(HH) = 7.3$	1.45 (36, s)	1.51 (9, s)	3.47 (2, q) $^3J(HH) = 7.3$; 3.80 (2, q) $^3J(HH) = 7.3$	7.25 (1, s)	−30

Table 3. Rotational activation barriers, $\Delta G^{\dagger}(T_c)$ and coalescence temperatures, T_c, (270 MHz) of complexes **2**, **3**, **5** and **6**

Complex	T_c (K)	$\Delta G^{\dagger}(T_c)$ (kcal mol^{-1})
2	303	14.9
3	278	13.6
5	313	15.3
6	283	13.9

that rotation of the diethylamino-group causes the observed fluxionality. Thus, in the temperature range −80 to +40°C only one singlet is observed for the tert-butyl protons of the two and four, *trans*-oriented isocyanide ligands in **3** and **6**. In **5**, two singlets with a 2 : 1 intensity ratio indicate the *meridional* arrangement of the three tert-butylisocyanide ligands. Moreover, two singlets with a relative ratio of 1 : 9 are observed for all complexes and are assigned, respectively, to the N—H proton and the tert-butyl protons of the alkyne ligand.

Assuming a near coplanarity of the diethylamino-, the tert-butylamino-group and the alkyne-carbon atoms, two isomers (**A** and **B**, Fig. 3) may be expected for complexes **2**, **3**, **5** and **6**, which differ in the relative orientation of the tert-butylamino- and the diethylamino-group in the alkyne ligand. However, ^{1}H NMR spectra show the presence of only one isomer even at low temperature where interconversion of the two possible isomers due to rotation of the tert-butylamino-group around the C_{alkyne}—N bond can be excluded (cf. rotation of the diethylamino-group).

X-ray structures of the related complexes [X(t-BuNC)$_4$Mo[η^2-(t-Bu)HN-C≡C-NH(t-Bu)]]Y (X = Br, I, CN; Y = I, PF_6, BPh_4)[51–53,59] containing a bis(tert-butylamino)acetylene ligand show the presence of only one (isomer **A**) of the three possible isomers depicted in Fig. 4. The molybdenum atom, the halogen ligand, X, and the NCCN atoms of the alkyne ligand are coplanar in the observed isomer **A** (Fig. 4). However, the protons bonded to the nitrogen atoms are distorted out of the plane to diminish the H ··· H steric repulsion that would result if the tert-butylamino-groups were rigidly coplanar with the NCCN fragment.[59] Therefore, the sterically more crowded isomers **B** and **C** are not observed (Fig. 4).

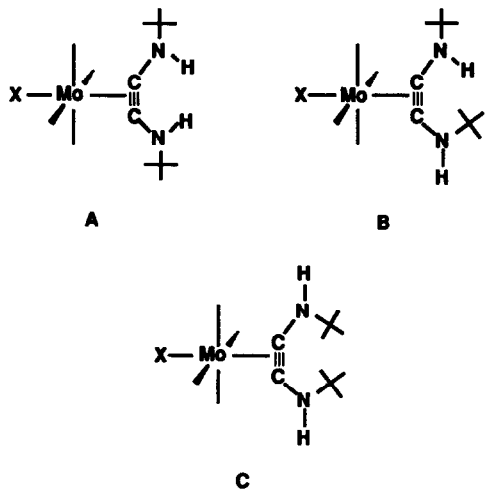

Fig. 4. Three possible isomers for complexes containing a bis(tert-butylamino)acetylene ligand.

Similarly, steric factors have also been used to explain the presence of only isomer **A** (Fig. 5) in the complexes [X(t-BuNC)$_4$W[η^2-(t-Bu)HN-C≡C-C_6H_5]]$^+PF_6^-$ (X = Cl, Br, I) containing a (tert-butylamino)phenylacetylene ligand.[50] In accordance with these data we suggest that in complexes **2**, **3**, **5** and **6** isomer **A** (Fig. 3) is thermodynamically favoured because of steric reasons.

The ^{13}C NMR data of compounds **2**, **3**, **5** and **6** are summarized in Table 4. ^{13}C NMR spectra of the complexes **2**, **3**, **5** and **6** have been recorded below the coalescence temperature. Therefore all complexes exhibit two resonances for the methylene- and two resonances for the methyl-carbon atoms of the inequivalent ethyl groups (Table 4).

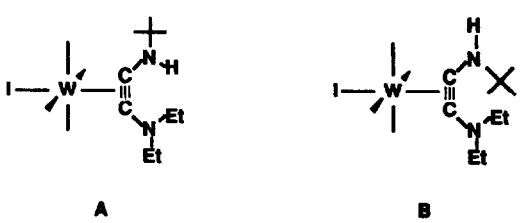

Fig. 3. Two possible isomers for complexes **2**, **3**, **5** and **6** resulting from the relative orientation of the amino-groups in the alkyne ligand.

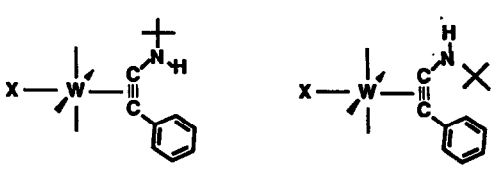

Fig. 5. Two possible isomers for complexes containing a tert(butylamino)phenylacetylene ligand.

Table 4. ^{13}C NMR spectra of **2**, **3**, **5** and **6** in CD_2Cl_2; chemical shifts (in δ) relative to CD_2Cl_2 ($\delta = 53.8$ ppm)

Complex	NCH_2CH_3	Me_3CNC	Me_3CNH	NCH_2CH_3	Me_3CNH	Me_3CNC	Me_3CNC	C≡C	CO	Temperature (°C)
2	13.9; 14.8	29.4	30.2	47.0; 51.7	55.6	58.2	140.0	174.9; 182.1	204.6; 206.3	−30
3	14.6; 15.0	29.7	30.5	46.8; 51.1	54.9	57.8	148.0	180.1; 186.9	216.5	−20
5	14.2; 14.8	29.7;[a] 29.8[b]	30.3	47.8; 50.4	56.4	58.0;[b] 58.2[a]	139.2;[b] 141.3[a]	176.7; 182.6	206.7	−20
6	14.7; 15.0	30.0	30.5	46.3; 49.8	55.0	57.5	148.3	177.5; 183.8	—	−30

[a] Signal for the mutually *trans*-oriented isocyanide ligands.
[b] Signal for the isocyanide ligand with a *trans*-orientation relative to CO.

Two distinct environments are observed for the *cis*-coordinated carbonyl ligands in **2** and the *meridional* arranged isocyanide ligands in **5**. However, the two isocyanide ligands in **3** and the four isocyanide ligands in **6** are *trans*-arranged and therefore chemical shift equivalent. All these results are consistent with a *trans*-orientation of one iodide to the alkyne ligand in the pseudo-octahedral coordinated complexes **2**, **3**, **5** and **6**.

The chemical shift of the alkyne-carbon atoms bound to a metal have been correlated with the extent of donation from the filled alkyne π-orbital to a vacant metal $d\pi$-orbital indicating the electron-donor properties of the alkyne ligand.[74] ^{13}C resonances nearly 200 ppm downfield from Me_4Si are observed for the alkyne carbons in complexes, where the alkyne ligand is acting as a 4e-donor. Their position is ~80 ppm downfield of that observed for alkyne ligands acting as 2e-donors.[69,74–76] A comparison of these results with the ^{13}C resonances observed for the alkyne ligand carbons in **2**, **3**, **5** and **6** (174.9–186.9 ppm, Table 4) and in the structurally related complexes [I(t-BuNC)$_4$W[η^2-(t-Bu)HN-C≡C-NH(t-Bu)]]I (δ_C = 181.5 ppm, $CDCl_3$ solution, RT)[53] and [I(t-BuNC)$_4$W[η^2-(t-Bu)HN-C≡C-C$_6$H$_5$]]PF_6 (δ_C = 193.6 and 206.1 ppm, CD_2Cl_2 solution, RT)[50] suggests a 4e-donation from the alkyne ligand to the metal centre in **2**, **3**, **5** and **6**.

The isocyanide carbons in **2**, **3**, **5** and **6** appear as broad singlets in the range 140–149 ppm because of the quadrupol relaxation of nitrogen. Therefore a ^{13}C–^{14}N coupling cannot be resolved. Comparing the data of **2** with **3** and **5** with **6**, a downfield shift for the isocyanide-carbon resonances is observed. This can be explained by the stronger metal–isocyanide backbonding in **3** than **2** and in **6** than **5** and is consistent with the trend found for the chemical shift of isocyanide carbons in other tungsten complexes.[16,17,22,24,77,78] A similar relationship has been observed in tungsten carbonyl complexes between the strength of the metal carbonyl backbonding and the chemical shift of carbonyl carbons[79] and is apparent in the CO resonances of **2** and **3** (Table 4).

The mass spectral data of **2**, **3**, **5** and **6** are collected in Table 5. The neutral complexes **2** and **3**, under EI conditions, reveal characteristic fragmentation patterns of complexes containing CO and t-BuNC ligands. Loss of CO and t-BuNC, or elimination of isobutene ($Me_2C{=}CH_2$) from the t-BuNC ligand and the tert-butylamino substituent in the alkyne ligand is observed.[16,17,24,25,49,50,77]

Using the SIMS method for the ionic complexes **5** and **6** the parent cations [I(CO)(t-BuNC)$_3$W[η^2-(t-Bu)HN-C≡C-NEt$_2$]]$^+$ (K^+: m/z = 756) and

Table 5. Mass spectra of complexes **2**, **3**, **5** and **6**

Complex	*m/z* (relative ^{184}W isotope)	Assignment
2	689	$[M-2CO]^+$
	633	$[M-2CO-Me_2C{=}CH_2]^+$
	606	$[M-2CO-{}^tBuNC]^+$
	577	$[M-2CO-2Me_2C{=}CH_2]^+$
3	800	M^+
	772	$[M-CO]^+$
	689	$[M-CO-{}^tBuNC]^+$
	633	$[M-CO-{}^tBuNC-Me_2C{=}CH_2]^+$
	606	$[M-CO-2{}^tBuNC]^+$
	577	$[M-CO-{}^tBuNC-2Me_2C{=}CH_2]^+$
5	756	K^+
	728	$[K-CO]^+$
	645	$[K-CO-{}^tBuNC]^+$
	562	$[K-CO-2{}^tBuNC]^+$
	506	$[K-CO-2{}^tBuNC-Me_2C{=}CH_2]^+$
	450	$[K-CO-2{}^tBuNC-2Me_2C{=}CH_2]^+$
6	811	K^+
	728	$[K-{}^tBuNC]^+$
	645	$[K-2{}^tBuNC]^+$
	562	$[K-3{}^tBuNC]^+$
	506	$[K-3{}^tBuNC-Me_2C{=}CH_2]^+$
	450	$[K-3{}^tBuNC-2Me_2C{=}CH_2]^+$

$[I(t\text{-}BuNC)_4W[\eta^2\text{-}(t\text{-}Bu)HN\text{-}C{\equiv}C\text{-}NEt_2]]^+$ (K^+: $m/z = 811$) are observed, respectively, and confirm their ionic composition. The fragmentation patterns of **5** and **6** are the same as that of **2** and **3**. The equivalent conductance, Λ, of 1,2-dichloroethane solutions of **5** and **6** (**5**: $c = 4.8 \times 10^{-4}$ mol dm^{-3}, $T = 19.8°C$, $\Lambda = 35\ \Omega^{-1}\ cm^2\ mol^{-1}$; **6**: $c = 5.3 \times 10^{-4}$ mol dm^{-3}, $T = 19.8°C$, $\Lambda = 40\ \Omega^{-1}\ cm^2\ mol^{-1}$) has been calculated from the ratio of the measured specific conductivity and the equivalent concentration.[80] It has comparable values with the equivalent conductance of $NR_4^+X^-$ salts (R = ^{n}Bu, ^{n}Pr; X = Br, I, PF_6) and other ionic tungsten complexes in 1,2-dichloroethane.[22–24,77,81,82]

CONCLUSION

We have discovered a new reaction path for low-valent, tert-butylisocyanide-substituted tungsten diethylaminocarbyne complexes involving a proton-induced carbon–carbon coupling reaction of one isocyanide with the carbyne ligand to yield an amino-substituted alkyne ligand, and have shown that an increase of the electron density accelerates the isocyanide–carbyne coupling reaction at the tungsten centre. We have further demonstrated that the presence of one or two CO ligands in the coordination sphere of tungsten does not strongly affect the course of the reaction, i.e. formation of the coupling products. In comparison, tert-butylisocyanide-substituted phenylcarbyne complexes have also been previously shown to undergo a proton-induced isocyanide–carbyne coupling reaction, which, however, is dramatically influenced by the presence of even one CO ligand in the coordination sphere.[50] This proton-induced isocyanide–carbyne coupling reaction represents an important step in the recently proposed mechanism by Lippard and co-workers for reductive coupling of two alkylisocyanide ligands at one molybdenum or tungsten centre involving isocyanide-substituted aminocarbyne intermediates.[54] For rhenium they have isolated such a carbyne isocyanide complex but have failed to achieve coupling of the two ligands.[55] The close structural relationship between the coupling products **2**, **3**, **5** and **6** containing a 4e-donor (tert-butylamino)diethylaminoacetylene ligand and the previously reported products from reductive coupling of two tert-butylisocyanide ligands containing a bis(tert-butylamino)acetylene ligand[51–53,59] provides further support for Lippard's mechanistic proposal for the reductive coupling of two isocyanide ligands.

Current experiments are underway to elucidate

the mechanism for the proton-induced isocyanide–carbyne coupling reaction. We have suggested an attractive mechanism involving bis(aminocarbyne) intermediates and have briefly mentioned alternative pathways involving the intermediate formation of isocyanide-substituted carbene or hydrido carbyne complexes. These mechanistic suggestions are based upon known reactivity patterns of low-valent isocyanide and carbyne complexes towards electrophiles.[39–42,47,60–64]

EXPERIMENTAL

$I(CO)_2(t\text{-}BuNC)_2W{\equiv}CNEt_2$ (**1**) and $I(CO)(t\text{-}BuNC)_3W{\equiv}CNEt_2$ (**4**) were synthesized as described previously.[16,22] t-BuNC was prepared according to the literature,[83] distilled and stored under nitrogen. All other reagents were commercially available. All operations were carried out under a nitrogen atmosphere using Schlenk tube techniques. The solvents were dried and purified by standard methods (*n*-pentane, toluene, Et_2O over sodium wire; CH_2Cl_2 over P_4O_{10} and Na/Pb alloy) followed by distillation under an atmosphere of nitrogen. All column chromatography was performed by using silica gel (Merck, 0.063–0.02 mm, activity 1, dried *in vacuo* and stored under nitrogen) as the stationary phase and a thermostated column of 45 cm length and 1.5 cm diameter. Elemental analyses were determined by the Microanalytical Laboratory of this department. IR spectra were obtained with a Nicolet DX 5 FT spectrophotometer. NMR spectra were measured with Jeol GX 270 and GX 400 FT instruments and mass spectra with a Varian MAT CH7 spectrometer using EI conditions for complexes **2** and **3** and the SIMS method for complexes **5** and **6**. Conductance measurements were carried out as described elsewhere.[22,23,77,81,82]

(1) $(I)_2(CO)_2(t\text{-}BuNC)W[\eta^2\text{-}(t\text{-}Bu)HN\text{-}C{\equiv}C\text{-}NEt_2]$ (2)

To a yellow solution of **1** (360 mg, 0.58 mmol) in CH_2Cl_2 (60 cm^3) was added first NEt_4I (160 mg, 0.62 mmol) as a solid and then dropwise at $-30°C$ a solution of $HBF_4 \cdot Et_2O$ (0.080 cm^3, 0.58 mmol) in CH_2Cl_2 (10 cm^3). The reaction mixture was slowly warmed to room temperature. After 24 h the solvent was removed *in vacuo* and the oily red residue dissolved in CH_2Cl_2 and purified by column chromatography on silica gel at 0°C. Elution with Et_2O–pentane (3 : 1) afforded a purple band, from which complex **3** was isolated as a purple, microcrystalline solid after crystallization from Et_2O–pentane (50 mg, 11% relative to **1**). Complex **3** was identified by comparison of its IR and NMR spectra with that of an authentic sample [prepared as described under (2)].

Further elution with Et_2O gave a red band, which afforded complex **2** as a red, microcrystalline solid after evaporation of the solvent and crystallization from Et_2O–pentane (220 mg, 51% relative to **1**). (Found: C, 27.8; H, 3.9; I, 33.3; N, 5.5; O, 4.3; W, 24.6. $C_{17}H_{29}I_2N_3O_2W$ (745.09) requires: C, 27.4; H, 3.9; I, 34.1; N, 5.6; O, 4.3; W, 24.7%.)

(2) $(I)_2(CO)(t\text{-}BuNC)_2W[\eta^2\text{-}(t\text{-}Bu)HN\text{-}C{\equiv}C\text{-}NEt_2]$ (3)

To a mixture of **4** (240 mg, 0.36 mmol) and NEt_4I (95 mg, 0.37 mmol) was added first CH_2Cl_2 (60 cm^3) and then dropwise at $-30°C$ a solution of $HBF_4 \cdot Et_2O$ (0.048 cm^3, 0.35 mmol) in CH_2Cl_2 (10 cm^3). The colour of the reaction mixture turned from yellow first to orange and then, upon warming to room temperature, to red. After 1 h the solvent was evaporated *in vacuo*, the residue was dissolved in CH_2Cl_2 and purified by column chromatography on silica gel at 0°C. Elution with Et_2O–pentane (3 : 1) gave a purple band, which yielded complex **3** as a purple, microcrystalline solid after evaporation of the solvent and crystallization from Et_2O–pentane (175 mg, 61% relative to **4**). (Found: C, 31.7; H, 4.6; I, 31.2; N, 6.9; O, 2.1; W, 21.9. $C_{21}H_{38}I_2N_4OW$ (800.22) requires: C, 31.5; H, 4.8; I, 31.7; N, 7.0; O, 2.0; W, 23.0%.)

(3) $[I(CO)(t\text{-}BuNC)_3W[\eta^2\text{-}(t\text{-}Bu)HN\text{-}C{\equiv}C\text{-}NEt_2]]^+ I^-$ (5) *from* **2** *and* t-BuNC

A solution of **2** (200 mg, 0.27 mmol) and t-BuNC (0.050 cm^3, 0.44 mmol) in CH_2Cl_2 (50 cm^3) was refluxed for 5 h. Evaporation of the solvent *in vacuo* and crystallization of the residue from CH_2Cl_2–Et_2O yielded complex **5** as a red, microcrystalline solid (230 mg, 97% relative to **2**). (Found: C, 35.6; H, 5.6; I, 28.4; N, 8.1; O, 2.0; W, 20.1. $C_{26}H_{47}I_2N_5OW$ (883.35) requires: C, 35.3; H, 5.4; I, 28.7; N, 7.9; O, 1.8; W, 20.8%.)

(4) $[I(CO)(t\text{-}BuNC)_3W[\eta^2\text{-}(t\text{-}Bu)HN\text{-}C{\equiv}C\text{-}NEt_2]]^+ I^-$ (5) *from* **3** *and* t-BuNC

A solution of **3** (120 mg, 0.15 mmol) and t-BuNC (0.02 cm^3, 0.18 mmol) in CH_2Cl_2 (30 cm^3) was refluxed for 3 h. The resulting red solution was worked up as described under (3) and complex **5** isolated as a red, microcrystalline solid (130 mg, 98% relative to **3**). Complex **5** was characterized spectroscopically.

$[I(t\text{-}BuNC)_4W[\eta^2\text{-}(t\text{-}Bu)HN\text{-}C{\equiv}C\text{-}NEt_2]]^+ I^-$ (**6**)

A solution of **5** (300 mg, 0.34 mmol) and t-BuNC (0.045 cm^3, 0.4 mmol) in toluene (30 cm^3) was heated at 90°C for 4 h. The solution was reduced in volume and an Et_2O–pentane mixture was added. The almost colourless supernatant solution was removed and the purple microcrystalline solid dried *in vacuo* (310 mg, 97% relative to **5**). (Found: C, 38.6; H, 6.3; I, 26.2; N, 8.9; W, 20.1. $C_{30}H_{56}I_2N_6W$ (938.47) requires C, 38.4; H, 6.0; I, 27.0; N, 9.0; W, 19.6%.)

Acknowledgements—I would like to thank Professor E. O. Fischer for introducing me to this research area, the Bavarian Ministry of Culture for financial support, Professor W. A. Herrmann for providing institute facilities and encouraging this work, Dr M. R. Cook for discussion, M. Barth, L. Eidel and U. Graf for elemental analyses and Professor H. G. Alt for assistance with mass spectrometry.

REFERENCES

1. E. O. Fischer, G. Kreis, C. G. Kreiter, J. Müller, G. Huttner and H. Lorenz, *Angew. Chem.* 1973, **85**, 618; *Angew. Chem. Int. Edn Engl.* 1973, **12**, 564.
2. E. O. Fischer and U. Schubert, *J. Organomet. Chem.* 1975, **100**, 59.
3. E. O. Fischer, *Adv. Organomet. Chem.* 1976, **14**, 1.
4. E. O. Fischer, U. Schubert and H. Fischer, *Pure Appl. Chem.* 1978, **50**, 857.
5. F. G. A. Stone, *Angew. Chem.* 1984, **96**, 85; *Angew. Chem. Int. Edn Engl.* 1984, **23**, 89.
6. W. R. Roper, *J. Organomet. Chem.* 1986, **300**, 167.
7. H. P. Kim and R. J. Angelici, *Adv. Organomet. Chem.* 1987, **27**, 51.
8. H. Fischer, P. Hofmann, F. R. Kreißl, R. R. Schrock, U. Schubert and K. Weiss, *Carbyne Complexes*. VCH Verlagsgesellschaft, Weinheim (1988).
9. E. O. Fischer, Nobel prize lecture (11 December 1973), Stockholm, *Angew. Chem.* 1974, **86**, 651.
10. J. D. Fellmann, G. A. Rupprecht, C. D. Wood and R. R. Schrock, *J. Am. Chem. Soc.* 1978, **100**, 5964.
11. J. H. Wengrovius, J. Sancho and R. R. Schrock, *J. Am. Chem. Soc.* 1981, **103**, 3932.
12. R. R. Schrock, D. N. Clark, J. Sancho, J. H. Wengrovius, S. M. Rocklage and S. F. Pedersen, *Organometallics* 1982, **1**, 1645.
13. D. S. Edwards, L. V. Biondi, J. W. Ziller, M. R. Churchill and R. R. Schrock, *Organometallics* 1983, **2**, 1505.
14. E. O. Fischer, G. Kreis, F. R. Kreißl, W. Kalbfus and E. Winkler, *J. Organomet. Chem.* 1974, **65**, C53.
15. E. O. Fischer, W. Kleine, G. Kreis and F. R. Kreißl, *Chem. Ber.* 1978, **111**, 3542.
16. A. C. Filippou and E. O. Fischer, *J. Organomet. Chem.* 1988, **352**, 141.
17. A. C. Filippou and E. O. Fischer, *J. Organomet. Chem.* 1989, **365**, 317.
18. E. O. Fischer, T. L. Lindner, G. Huttner, P. Friedrich, F. R. Kreißl and J. O. Besenhard, *Chem. Ber.* 1977, **110**, 3397.
19. A. C. Filippou and E. O. Fischer, *J. Organomet. Chem.* 1988, **341**, C35.
20. A. C. Filippou and E. O. Fischer, *J. Organomet. Chem.* 1988, **349**, 367.
21. A. C. Filippou, E. O. Fischer and J. Okuda, *J. Organomet. Chem.* 1988, **339**, 309.
22. A. C. Filippou, E. O. Fischer and R. Paciello, *J. Organomet. Chem.* 1988, **347**, 127.
23. A. C. Filippou, E. O. Fischer and H. G. Alt, *J. Organomet. Chem.* 1988, **344**, 215.
24. A. C. Filippou, *Polyhedron* 1989, **8**, 1285.
25. A. C. Filippou and E. O. Fischer, *J. Organomet. Chem.*, in press.
26. A. Mayr and G. A. McDermott, *J. Am. Chem. Soc.* 1986, **108**, 548.
27. E. O. Fischer, A. Ruhs and F. R. Kreißl, *Chem. Ber.* 1977, **110**, 805.
28. F. R. Kreißl, P. Friedrich and G. Huttner, *Angew. Chem.* 1977, **89**, 110; *Angew. Chem. Int. Edn Engl.* 1977, **16**, 102.
29. F. R. Kreißl, K. Eberl and W. Uedelhoven, *Chem. Ber.* 1977, **110**, 3782.
30. E. O. Fischer, A. C. Filippou, H. G. Alt and K. Ackermann, *J. Organomet. Chem.* 1983, **254**, C21.
31. E. O. Fischer, A. C. Filippou and H. G. Alt, *J. Organomet. Chem.* 1984, **276**, 377.
32. K. R. Birdwhistell, T. L. Tonker and J. L. Templeton, *J. Am. Chem. Soc.* 1985, **107**, 4474.
33. A. Mayr, G. A. McDermott, A. M. Dorries, A. K. Holder, W. C. Fultz and A. L. Rheingold, *J. Am. Chem. Soc.* 1986, **108**, 310.
34. E. O. Fischer, A. C. Filippou, H. G. Alt and U. Thewalt, *Angew. Chem.* 1985, **97**, 215; *Angew. Chem. Int. Ed. Engl.* 1985, **24**, 203.
35. E. O. Fischer, A. C. Filippou and H. G. Alt, *J. Organomet. Chem.* 1985, **296**, 69.
36. A. C. Filippou, E. O. Fischer, K. Öfele and H. G. Alt, *J. Organomet. Chem.* 1986, **308**, 11.
37. A. C. Filippou and E. O. Fischer, *J. Organomet. Chem.* 1987, **330**, C1.
38. A. C. Filippou, E. O. Fischer, H. G. Alt and U. Thewalt, *J. Organomet. Chem.* 1987, **326**, 59.
39. G. R. Clark, K. Marsden, W. R. Roper and L. J. Wright, *J. Am. Chem. Soc.* 1980, **102**, 6570.
40. J. A. K. Howard, J. C. Jeffery, J. C. V. Laurie, I. Moore, F. G. A. Stone and A. Stringer, *Inorg. Chim. Acta* 1985, **100**, 23.
41. A. Mayr, M. F. Asaro, M. A. Kjelsberg, K. S. Lee and D. V. Engen, *Organometallics* 1987, **6**, 432.
42. S. J. Holmes, D. N. Clark, H. W. Turner and R. R. Schrock, *J. Am. Chem. Soc.* 1982, **104**, 6322.
43. J. C. Jeffery, J. C. V. Laurie, I. Moore and F. G. A. Stone, *J. Organomet. Chem.* 1983, **258**, C37.
44. F. R. Kreißl, W. J. Sieber, M. Wolfgruber and J. Riede, *Angew. Chem.* 1984, **96**, 618; *Angew. Chem. Int. Edn Engl.* 1984, **23**, 640.
45. M. R. Churchill, H. J. Wasserman, S. J. Holmes and R. R. Schrock, *Organometallics* 1982, **1**, 766.

46. S. J. Holmes, R. R. Schrock, M. R. Churchill and H. J. Wasserman, *Organometallics* 1984, **3**, 476.
47. F. R. Kreißl, W. J. Sieber and M. Wolfgruber, *J. Organomet. Chem.* 1984, **270**, C45.
48. A. C. Filippou and E. O. Fischer, *J. Organomet. Chem.* 1988, **352**, 149.
49. A. C. Filippou and E. O. Fischer, *J. Organomet. Chem.*, submitted for publication.
50. A. C. Filippou and W. Grünleitner, *Z. Naturfor. B* 1989, **446**, 1023.
51. C. T. Lam, P. W. R. Corfield and S. J. Lippard, *J. Am. Chem. Soc.* 1977, **99**, 617.
52. J. C. Dewan, C. M. Giandomenico and S. J. Lippard, *Inorg. Chem.* 1981, **20**, 4069.
53. C. M. Giandomenico, C. T. Lam and S. J. Lippard, *J. Am. Chem. Soc.* 1982, **104**, 1263.
54. R. N. Vrtis, C. P. Rao, S. Warner and S. J. Lippard, *J. Am. Chem. Soc.* 1988, **110**, 2669.
55. S. Warner and S. J. Lippard, *Organometallics* 1989, **8**, 228.
56. A. C. Filippou, *Advances in Metal Carbene Chemistry* (Edited by U. Schubert). Kluwer Academic Publishers, Dordrecht (1989).
57. A. C. Filippou, unpublished results.
58. W. Beck and K. Schloter, *Z. Naturfor.* 1978, **33b**, 1214.
59. P. W. R. Corfield, L. M. Baltusis and S. J. Lippard, *Inorg. Chem.* 1981, **20**, 922.
60. J. Chatt, A. J. L. Pombeiro and R. L. Richards, *J. Chem. Soc., Dalton Trans.* 1979, 1585.
61. J. Chatt, A. J. L. Pombeiro and R. L. Richards, *J. Chem. Soc., Dalton Trans.* 1980, 492.
62. A. J. L. Pombeiro and R. L. Richards, *Transition Met. Chem.* 1980, **5**, 55.
63. A. J. L. Pombeiro, M. F. N. N. Carvalho, P. B. Hitchcock and R. L. Richards, *J. Chem. Soc., Dalton Trans.* 1981, 1629.
64. A. J. L. Pombeiro, D. L. Hughes, C. J. Pickett and R. L. Richards, *J. Chem. Soc., Chem. Commun.* 1986, 246.
65. G. A. McDermott and A. Mayr, *J. Am. Chem. Soc.* 1987, **109**, 580.
66. R. Hoffmann, C. N. Wilker and O. Eisenstein, *J. Am. Chem. Soc.* 1982, **104**, 632.
67. F. A. Cotton and C. S. Kraihanzel, *J. Am. Chem. Soc.* 1962, **84**, 4432.
68. F. A. Cotton and F. Zingales, *J. Am. Chem. Soc.* 1961, **83**, 351.
69. L. Ricard, R. Weiss, W. E. Newton, G. J. J. Chen and J. W. McDonald, *J. Am. Chem. Soc.* 1978, **100**, 1318.
70. J. R. Morrow, T. L. Tonker and J. Templeton, *J. Am. Chem. Soc.* 1985, **107**, 6956.
71. G. Sandorfy, *The Chemistry of the Carbon–Nitrogen Double Bond* (Edited by S. Patai). Interscience, London (1970).
72. H. S. Gutowsky and C. H. Holm, *J. Chem. Phys.* 1956, **25**, 1228.
73. H. Kessler, *Angew. Chem.* 1970, **82**, 237; *Angew. Chem. Int. Edn Engl.* 1970, **9**, 219.
74. J. L. Templeton and B. C. Ward, *J. Am. Chem. Soc.* 1980, **102**, 3288.
75. B. C. Ward and J. L. Templeton, *J. Am. Chem. Soc.* 1980, **102**, 1532.
76. P. B. Winston, S. J. N. Burgmayer and J. L. Templeton, *Organometallics* 1983, **2**, 167.
77. A. C. Filippou and W. Grünleitner, *Z. Naturfor.* 1989, **44b**, 666.
78. D. L. Cronin, J. R. Wilkinson and L. J. Todd, *J. Magn. Res.* 1975, **17**, 353.
79. L. J. Todd and J. R. Wilkinson, *J. Organomet. Chem.* 1974, **77**, 1.
80. J. J. Lingane, *Electroanalytical Chemistry* 2nd edn. Interscience, New York (1958).
81. A. C. Filippou, E. O. Fischer and H. G. Alt, *J. Organomet. Chem.* 1988, **340**, 331.
82. A. C. Filippou, E. O. Fischer and H. G. Alt, *Z. Naturfor.* 1988, **43b**, 654.
83. J. Casanova, N. D. Werner and R. E. Schuster, *J. Org. Chem.* 1966, **31**, 3473.

Polyhedron Vol. 9, No. 5, pp. 739–741, 1990
Printed in Great Britain

0277–5387/90 $3.00+.00
© 1990 Pergamon Press plc

THE STRUCTURE OF A COPPER(I)–SCHIFF BASE COMPLEX $[CuN(CH_2CH_2N{=}CH{-}C_6H_5)_3]^+[BPh_4]^-$

ELMER C. ALYEA,* GEORGE FERGUSON,* MICHAEL C. JENNINGS and ZHENG XU

Department of Chemistry and Biochemistry, University of Guelph, Guelph, Ontario, Canada N1G 2W1

(*Received* 6 *June* 1989; *accepted* 27 *September* 1989)

Abstract—A crystal structure analysis of $[CuN(CH_2CH_2N{=}CH{-}C_6H_5)_3]^+[BPh_4]^-$ reveals that the complex has approximate three-fold symmetry in the solid state with the copper(I) atom having trigonal-pyramidal geometry. Principal dimensions are Cu—N (apical) 2.232(2), Cu—N(equatorial) 2.004, 2.006 and 2.019(2) Å, N(ap)—Cu—N(eq) 83.7–84.6(1)°. The Cu···H distances to the *ortho*-phenyl hydrogen atoms are too long to be considered agostic. The ^{1}H NMR spectrum is consistent with a similar structure for the copper(I) cation complex in solution.

The structural chemistry of copper(I) and copper(II) complexes of various tripodal ligands has been discussed by Zubieta *et al.*[1] A recent review[2] has also described the X-ray analyses of several divalent transition metal complexes of the potentially heptadentate Schiff base ligand tris-[(4-pyridyl)-3-aza-3-butenyl]amine, $N\{CH_2CH_2N{=}CH(C_5H_4N)\}_3$, abbreviated as py_3tren; other abbreviations are: tren = $N\{CH_2CH_2NH_2\}_3$, $S_3tren = N\{CH_2CH_2N{=}CH(C_4H_3S)\}_3$ and $Ph_3tren = N\{CH_2CH_2N{=}CH(C_6H_5)\}_3$. Our laboratories have undertaken the spectroscopic and structural characterization of copper complexes of new Schiff base ligands derived from tris(2-aminoethyl)amine (tren), and the tripodal nature of the Schiff base ligand, S_3tren, has been reported.[3] This paper describes the coordination geometry of a copper(I) complex of another tren derivative, tris[4-phenyl-3-aza-3-butenyl]amine (Ph_3tren).

The copper(I) complex $[Cu(Ph_3tren)][BPh_4]$ was obtained by adding an excess of $NaBPh_4$ to a stirred acetone solution of $Cu(OAc)_2 \cdot 2H_2O$ and Ph_3tren. $[Cu(S_3tren)][BPh_4]$ can be isolated in an analogous fashion using the preformed Schiff base ligand S_3tren. A series of copper(II) salts, $Cu(S_3tren)X_2$, has been isolated by the reaction of CuX_2 (X = Cl, Br, N_3, NCS, ClO_4) with S_3tren; similar reactions with Ph_3tren are under study.[4]

The structure of $[Cu(Ph_3tren)][BPh_4]$ has been determined crystallographically (Fig. 1).† The geometry about the copper(I) centre is a distorted trigonal pyramid comprised of four nitrogen donor atoms. The Cu—N distances to the equatorial nitrogens [N(1), N(2), N(3)] are 2.019(2), 2.006(2) and 2.004(2) Å, respectively, while the N(1)—Cu—N(2), N(2)—Cu—N(3) and N(1)—Cu—N(3) angles are 112.3(1), 127.8(1) and 116.7(1)°, respectively. The copper atom sits 0.208(1) Å above the plane of the equatorial azomethine nitrogen atoms, while the apical tertiary amine atom (N) lies 2.024(2) Å below that plane; the Cu—N distance is 2.232(2) Å and the

* Authors to whom correspondence should be addressed.

† Crystal data for $C_{51}H_{50}CuN_4B$, $M_r = 793.3$, monoclinic, space group $P2_1/n$, $a = 12.078(4)$, $b = 17.669(2)$, $c = 19.913(3)$ Å, $\beta = 94.32(2)°$, $V = 4238(3)$ Å^3, $Z = 4$, $D_c = 1.24$ g cm^{-3}, $\mu = 5.5$ cm^{-1}, $F(000) = 1672$, Mo-K_α radiation ($\lambda = 0.71073$ Å), $T = 21°C$. 9658 reflections were measured on a CAD4 diffractometer ($2\theta_{max} = 54°$), 9234 were unique and 4277 had $I > 3\sigma(I)$. Lorentz, polarization and Gaussian absorption corrections were applied. The structure was solved using the heavy-atom method. Refinement (with weights derived from the counting statistics) by full-matrix least-squares calculations (with all hydrogen atoms allowed for but not refined) converged with $R = 0.036$ and $wR = 0.042$ for the 4277 observed reflections. An extinction correction was also refined. The final cycle of refinement had 515 variables and maximum shift/error ratio of 0.02. A final difference map had no chemically significant features. Full details of the analysis are available from the Cambridge Crystallographic Data Centre or from the authors.

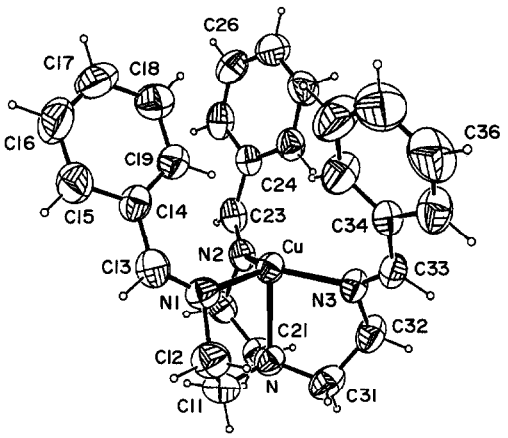

Fig. 1. A view of the $[CuN(CH_2CH_2N{=}CH{-}C_6H_5)_3]^+$ cation with the crystallographic numbering scheme; ellipsoids are at the 50% level.

N—Cu—N(1), N—Cu—N(2) and N—Cu—N(3) angles are 83.9(1), 84.6(1) and 83.7(1)°, respectively. These structural parameters are similar to those reported by Zubieta *et al.*[1] for $[Cu(pmas)]^+$, where pmas is the tripodal ligand $N(CH_2py)(CH_2CH_2SR)_2$: Cu—N(ap) = 2.158(8), Cu—N(py) = 2.035(10) Å, and copper is 0.077 Å from the equatorial plane.

A feature of the cation geometry is the conformation adopted by the complex in the solid state as shown in Fig. 1. The cation has approximate three-fold symmetry and three *ortho*-hydrogen atoms complete a distorted trigonal antiprism around the copper centre, with Cu···H distances 2.55, 2.62 and 2.71 Å, too long to be considered agostic. To accommodate this conformation there is substantial angle opening in the Cu—Nx = Cx3—Cx4—Cx9 (x = 1–3) portion of the molecule (details in Table 1). The Cu—Nx = Cx3 angles have a mean value of 136.6(2)° and the mean Nx = Cx3—Cx4 angle is 125.8(3)°. There are no untoward intermolecular contacts and presumably the conformation adopted in the crystal structure serves to minimize intramolecular and crystal packing forces. This bonding situation is somewhat similar to that exhibited by the pyramidal lithium atom in $[Li(\mu\text{-OAr-2,6-Ph}_2)_3Sn]$, wherein the Li···H distance to one of the *ortho*-hydrogen atoms of one of the aryloxide side-chain phenyl groups was found to be 2.695(9) Å. The authors[5] considered the possibility that very weak agostic interactions to three *ortho*-CH bonds stabilized the electron-deficient lithium atoms. Such two-electron three-centre bonds, represented by C—H→M, have been shown to be widespread in organometallic chemistry[6] and are proposed as precursor species in the skeletal rearrangement of hydrocarbons on metals.[7] A relevant example of an M···H interaction that only arises because of ligand geometry was described by Deeming *et al.*[8] Their X-ray analysis of square-planar $PdCl_2$(mpq), where mpq is (8-methyl-2-quinolylmethyl)di-t-butylphosphine, showed that distortions occurred which drastically reduced the 8Me···Pd and 8Me···Cl interactions. Similarly, the Cu···H dis-

Table 1. Molecular dimensions

Bond lengths (Å)			
Cu—N	2.232(2)	N(2)—C(23)	1.274(4)
Cu—N(1)	2.019(2)	N(3)—C(32)	1.475(4)
Cu—N(2)	2.006(2)	N(3)—C(33)	1.272(4)
Cu—N(3)	2.004(2)	C(11)—C(12)	1.513(5)
N—C(11)	1.466(4)	C(13)—C(14)	1.455(4)
N—C(21)	1.459(4)	C(21)—C(22)	1.510(5)
N—C(31)	1.459(4)	C(23)—C(24)	1.458(4)
N(1)—C(12)	1.473(4)	C(31)—C(32)	1.509(5)
N(1)—C(13)	1.270(4)	C(33)—C(34)	1.450(4)
N(2)—C(22)	1.475(4)		

Bond angles (°)			
Cu—N(1)—C(13)	137.1(2)	C(13)—C(14)—C(19)	123.7(3)
C(12)—N(1)—C(13)	116.4(3)	N(2)—C(23)—C(24)	125.5(3)
Cu—N(2)—C(23)	135.3(2)	C(23)—C(24)—C(25)	118.5(3)
C(22)—N(2)—C(23)	115.9(2)	C(23)—C(24)—C(29)	122.6(3)
Cu—N(3)—C(33)	137.3(2)	N(3)—C(33)—C(34)	125.8(3)
C(32)—N(3)—C(33)	115.8(2)	C(33)—C(34)—C(35)	118.7(3)
N(1)—C(13)—C(14)	126.2(3)	C(33)—C(34)—C(39)	123.0(3)
C(13)—C(14)—C(15)	118.0(3)		

Table 2. ^{1}H NMR data for the ligand and the copper complex

Compound	δ (ppm)[a] and J (Hz)
Ph_3tren[b]	8.08 (H_a), 7.49 (H_o, d, J = 8.0), 7.39 (H_p, t, J = 7.3), 7.34 (H_m, t, J = 7.6), 3.68 (H_b, t, J = 6.1), 2.93 (H_c, t, J = 6.3)
$[Cu(Ph_3tren)][BPh_4]$[c]	8.68 (H_a), 8.17 (H_o, d, J = 8.0), 7.45 (H_p, t, J = 7.3), 7.34 (H, phenyl, m), 6.95 (H_m, t, J = 7.6), 6.92 (H, phenyl, t, J = 7.4), 6.77 (H, phenyl, t, J = 7.2), 4.03 (H_b, t, J = 5.3), 3.29 (H_c, t, J = 5.6)

[a] d = doublet, t = triplet, m = multiplet.
[b] $CDCl_3$ solution.
[c] $(CD_3)_2CO$ solution.

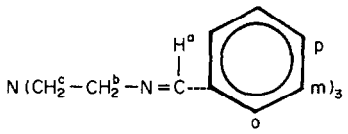

tances in the $[Cu(Ph_3tren)]^+$ cation appear to be influenced by intramolecular forces rather than an agostic interaction. In uncomplexed S_3tren[3], the corresponding C—N=C and N=C—C angles are close to the ideal undistorted value and lie in the ranges 117.7(3)–118.5(3) and 121.9(3)–123.1(3)°, respectively. The tetraphenylborate anion has the usual tetrahedral geometry with B—C 1.634–1.651(4), mean 1.644 Å. Other dimensions in the cation and anion are in accord with anticipated values.

The ^{1}H NMR spectrum of the complex, compared with that of the free ligand (Table 2), clearly shows coordination of all four nitrogen donor atoms by the downfield shift of resonances due to adjacent protons. The shift is most marked for the azomethine protons [(H_a), 0.60 ppm] but still significant (0.35 ppm) for the bridging ethylene protons (H_b, H_c). Resonances due to the phenyl ring protons are also shifted considerably, especially for the *ortho*-protons [(H_o) 0.68 ppm]. These shifts are attributable to electronic effects due to conjugation with the C=N linkage rather than a consequence of any interaction of *ortho*-hydrogen atoms with the copper atom; it is noteworthy that the *ortho*-hydrogen atoms on each ring remain equivalent in the complex, i.e. each phenyl ring undergoes free rotation, at least in solution.

Acknowledgement—We thank NSERC Canada for Operating and Infrastructure Grants (E.C.A. and G.F.), and for a CIDA award (Z.X.).

REFERENCES

1. J. Zubieta, K. D. Karlin and J. C. Hayes, in *Copper Coordination Chemistry: Biochemical and Inorganic Perspectives* (Edited by K. D. Karlin and J. Zubieta), p. 97. Adenine Press, New York (1983).
2. R. M. Kirchner, C. Mealli, M. Bailey, N. Howe, L. P. Torre, L. J. Wilson, L. C. Andrews, N. J. Rose and E. C. Lingafelter, *Coord. Chem. Rev.* 1987, **77**, 89.
3. E. C. Alyea, S. Liu, B. Li, Z. Xu and X. You, *Acta Cryst.* 1989, **C45**, 1566.
4. E. C. Alyea, B. Li and Z. Xu (1989), unpublished work.
5. G. D. Smith, P. E. Fanwick and I. P. Rothwell, *Inorg. Chem.* 1989, **28**, 618.
6. M. Brookhart and M. L. H. Green, *J. Organomet. Chem.* 1983, **250**, 395.
7. F. Garin and G. Maire, *Accts Chem. Res.* 1989, **22**, 100.
8. A. J. Deeming, I. P. Rothwell, M. B. Hursthouse and K. M. A. Malik, *J. Chem. Soc., Dalton Trans.* 1974, 1980.

Polyhedron Vol. 9, No. 5, pp. 743–750, 1990
Printed in Great Britain

0277–5387/90 $3.00+.00
© 1990 Pergamon Press plc

REACTIVITY OF COMPLEXES OF THE TYPE $Re_2X_4(LL)_2$ TOWARDS BIS(TRIPHENYLPHOSPHINE)IMINIUM CARBOXYLATES. A CONVENIENT, NON-REDOX SYNTHETIC ROUTE TO *CIS* AND *TRANS* ISOMERS OF $Re_2(O_2CR)_2X_2(LL)_2$ (R = CH_3, C_2H_5, C_6H_5 or 4-C_5H_4N; X = Cl or Br; LL = $Ph_2PCH_2PPh_2$ or $Ph_2AsCH_2AsPh_2$)

DANIEL R. DERRINGER, EUPHEMIE A. BUCK, SYLVIA M. V. ESJORNSON, PHILLIP E. FANWICK and RICHARD A. WALTON*

Department of Chemistry, Purdue University, West Lafayette, IN 47907, U.S.A.

(*Received* 10 *July* 1989; *accepted* 27 *September* 1989)

Abstract—The clean conversion of the complexes $Re_2X_4(LL)_2$ [X = Cl when LL = $Ph_2PCH_2PPh_2$ (dppm) and X = Br when $Ph_2AsCH_2AsPh_2$ (dpam)] to pure *trans*-$Re_2(O_2CR)_2X_2(LL)_2$ occurs when these complexes are reacted with $[(Ph_3P)_2N]O_2CR$ (R = CH_3, C_2H_5, C_6H_4 or 4-C_5H_4N) in CH_2Cl_2 at room temperature. When these same reactions are carried out in refluxing ethanol, the related *cis* isomers are formed when R = CH_3 or C_2H_5; in the case of $Re_2(O_2CC_6H_5)_2Cl_2(dppm)_2$ a mixture of *cis* and *trans* isomers is produced, whereas for $Re_2(O_2C\text{-}4\text{-}py)_2Cl_2(dppm)_2$ (4-py = 4-C_5H_4N) the *trans* isomer is again produced. When *trans*-$Re_2(O_2CR)_2Cl_2(dppm)_2$ (R = CH_3 or C_2H_5) are heated in ethanol for *ca* 3 h, isomerization to *cis*-$Re_2(O_2CR)_2Cl_2(dppm)_2$ takes place. The structure of *trans*-$Re_2(O_2CCH_3)_2Cl_2(dppm)_2$ was established by X-ray crystallography. The crystallographic data for $Re_2(O_2CCH_3)_2Cl_2(dppm)_2 \cdot C_7H_8 \cdot 2H_2O$ are as follows: monoclinic space group $C2/c$, $a = 22.247(7)$, $b = 19.257(7)$, $c = 14.358(4)$ Å, $\beta = 94.73(2)°$, $V = 6129(6)$ Å^3 and $Z = 4$. The structure was refined to $R = 0.042$ ($R_w = 0.056$) for 3110 data with $I > 3.0\sigma(I)$. The molecule contains *trans* dispositions of bridging acetate and dppm ligands. The Cl—Re—Re—Cl unit approaches linearity, with Re—Re—Cl angles of 175.76(6)°. The Re—Re distance of 2.2763(7) Å is consistent with the presence of a Re—Re triple bond.

In an earlier study[1] we showed that the dirhenium(III) complexes $Re_2(\mu\text{-}O_2CR)_4X_2$ (R = CH_3, C_2H_5, or C_6H_5; X = Cl or Br) react with the diphosphine ligand $Ph_2PCH_2PPh_2$ (abbreviated dppm) in refluxing alcohol (methanol or ethanol) to give *cis* and *trans* isomers of the dirhenium(II) complexes $Re_2(\mu\text{-}O_2CR)_2X_2(\mu\text{-}dppm)_2$. The *cis* isomers were obtained conveniently and in moderately high yield when the reactions were carried out for several days with stoichiometric ratios of reactants (dppm: $Re_2(O_2CR)_4X_2$) of *ca* 6:1. Shorter reaction times (1 day or less) and smaller stoichiometric ratios (*ca* 4:1) favoured the formation of the *trans* isomers, but in no instance were we able to isolate the pure *trans* form; these were always present as components of *cis–trans* mixtures. The aforementioned results are important for two reasons. Firstly, the complexes represent the first examples of isomeric metal–metal bonded systems in which the two bridging diphosphine ligands are in *cis* and *trans* arrangements to one another. Secondly, unlike the α- and β-isomeric forms of $Re_2Br_4(depe)_2$ (depe = $Et_2PCH_2CH_2PEt_2$),[2] $Re_2X_4(dppee)_2$ (X = Cl or Br; dppee = $Ph_2PCH{=}CHPPh_2$)[2,3] and $Re_2X_4(dppe)_2$ (X = Cl or Br; dppe = $Ph_2PCH_2CH_2PPh_2$),[3,4] which contain chelating (α) or bridging (β) forms of the bidentate phosphine ligands, the $Re_2(\mu\text{-}O_2CR)_2X_2(\mu\text{-}dppm)_2$ complexes exhibit relatively large differences (*ca* +0.5 V) in

* Author to whom correspondence should be addressed.

the values of the half-wave potentials for the Re_2^{5+}/Re_2^{4+} and Re_2^{6+}/Re_2^{5+} couples.

In order to study these systems in greater detail, we set out to find a more convenient synthetic route to the *trans* isomers. In so doing, we discovered that the dirhenium(II) complexes $Re_2X_4(LL)_2$, where X = Cl or Br and LL = dppm[5] or dpam ($Ph_2AsCH_2AsPh_2$),[6] within which the bridging ligands are already *trans* to one another,[7] react rapidly with the carboxylate salts $[PPN]O_2CR$ ($PPN^+ = (Ph_3P)_2N^+$; R = CH_3, C_2H_5, C_6H_5 or 4-py) in dichloromethane at room temperature to give *trans*-$Re_2(O_2CR)_2X_2(LL)_2$. These same reagents react to give *cis*-$Re_2(O_2CR)_2X_2(LL)_2$ when the reactions are carried out in refluxing ethanol. In addition to describing these synthetic details, we also report the full structural characterization of *trans*-$Re_2(O_2CCH_3)_2Cl_2(dppm)_2$.

EXPERIMENTAL

Starting materials

The complexes *trans*-$[Re_2(O_2CC_6H_5)_2Br_2(dppm)_2]Br$,[1] $Re_2Cl_4(dppm)_2$[1] and $Re_2Br_4(dpam)_2$[6] were prepared as described previously. Cobaltocene, bis(triphenylphosphine)iminium chloride and the reaction solvents were obtained from commercial sources and were used as received.

Reaction procedures

Syntheses were performed under an atmosphere of dry nitrogen under the overpressure provided by a mineral oil manometer. Solvents were thoroughly deoxygenated prior to use.

(A) *Synthesis of* $[PPN]O_2CR$ (R = CH_3, C_2H_5, C_6H_5 *or* 4-py)

Except for a slight modification in the work-up procedure, the acetate salt was prepared as described in the literature.[8] The other derivatives were prepared and worked up by the use of a similar procedure, the general description of which is as follows. A quantity (1 g) of [PPN]Cl was dissolved in a minimum volume of warm water (60–80°C). A warm concentrated solution of NaO_2CR (usually containing 5–10 g of the salt) was added to the chloride solution with constant stirring. The mixture was cooled to 0°C in an ice-water bath. The precipitate was filtered off, washed with copious amounts of diethyl ether, and dried *in vacuo*. The salt was recrystallized from acetone–diethyl ether. We note that these carboxylate salts are sometimes contaminated with small amounts of [PPN]Cl, but since [PPN]Cl is itself a by-product in the reactions of $Re_2X_4(LL)_2$ with $[PPN]O_2CR$ (*vide infra*), this did not present a problem.

These salts were characterized by IR and NMR spectroscopy. The $[PPN]^+$ cations exhibit bands in their IR spectra at 800 (w), 995 (m), 1113 (s), 1260 (s), 1440 (s) and 1485 (m) cm^{-1}. These values are in accord with those (803, 995, 1115, 1250, 1440 and 1490 cm^{-1}) reported previously.[8] The carboxylate anions display characteristic ν(COO) stretching vibrations in the region 1550–1660 cm^{-1}. Their ^1H NMR spectra (in CD_2Cl_2) display resonances for the phenyl protons of the $[PPN]^+$ cation between δ +7.8 and +7.4. The acetate salt shows a singlet at δ +1.81 for the methyl protons, while the propionate salt exhibits resonances at δ +2.05 (q, —CH_2—) and δ +1.01 (t, —CH_3). Resonances for the phenyl protons of the benzoate anion appear in the region δ +8.2 to +7.2, and the isonicotinate anion exhibits resonances in the region δ +8.5 to +7.4. The ^{31}P NMR spectrum of the $[PPN]^+$ cation (in CD_2Cl_2) displays a singlet at δ +21.6.

(B) *Synthesis of* trans-$Re_2(O_2CR)_2X_2(LL)_2$ (R = CH_3, C_2H_5, C_6H_5 *or* 4-py; X = Cl *or* Br; LL = dppm *or* dpam)

With one exception, these compounds were prepared by application of the following general procedure. Dichloromethane (5 cm^3) was added to a mixture of $Re_2X_4(LL)_2$ (*ca* 0.10 g) and $[PPN]O_2CR$ (2 equiv). The orange solution was stirred at room temperature for 5 min, the solvent was then evaporated under reduced pressure, and the orange residue washed with 2-propanol and dried *in vacuo*. Samples were recrystallized from dichloromethane–diethyl ether. Details relating to the product yield, and the elemental microanalyses for each derivative are given in (a)–(f).

(a) trans-$Re_2(O_2CCH_3)_2Cl_2(dppm)_2$. Yield, 68%. Found: C, 46.6; H, 3.8. Calc. for $C_{55}H_{52}Cl_4O_4P_4Re_2$ (i.e. *trans*-$Re_2(O_2CCH_3)_2Cl_2(dppm)_2 \cdot CH_2Cl_2$): C, 46.7; H, 3.7%.

(b) trans-$Re_2(O_2CC_2H_5)_2Cl_2(dppm)_2$. Yield, 72%. Found: C, 49.5; H, 4.4. Calc. for $C_{56}H_{54}Cl_2O_4P_4Re_2$: C, 49.5; H, 4.0%.

(c) trans-$Re_2(O_2CC_6H_5)_2Cl_2(dppm)_2$. Yield, 90%. Found: C, 52.3; H, 4.4. Calc. for $C_{64}H_{54}Cl_2O_4P_4Re_2$: C, 52.9; H, 3.7%.

(d) trans-$Re_2(O_2C\text{-}4\text{-}py)_2Cl_2(dppm)_2$. Yield, 74%. Found: C, 51.6; H, 4.1. Calc. for $C_{62}H_{52}Cl_2N_2O_4P_4Re_2$: C, 51.1; H, 3.6%.

(e) trans-$Re_2(O_2CCH_3)_2Br_2(dpam)_2$. Yield, 69%. Found: C, 38.0; H, 3.2. Calc. for $C_{56}H_{54}As_4Br_2$

$Cl_4O_4Re_2$ (i.e. *trans*-$Re_2(O_2CCH_3)_2Br_2(dpam)_2 \cdot 2CH_2Cl_2$): C, 38.1; H, 3.1%.

(f) trans-$Re_2(O_2CC_6H_5)_2Br_2(dpam)_2$. Yield, 67%. Found: C, 41.4; H, 3.0. Calc. for $C_{66}H_{58}As_4Br_2Cl_4O_4Re_2$ (i.e. *trans*-$Re_2(O_2CC_6H_5)_2Br_2(dpam)_2 \cdot 2CH_2Cl_2$): C, 42.0; H, 3.1%.

(g) trans-$Re_2(O_2CC_6H_5)_2Br_2(dppm)_2$. A mixture containing *trans*-$[Re_2(O_2CC_6H_5)_2Br_2(dppm)_2]Br$[1] (0.100 g, 0.062 mmol) and cobaltocene (0.021 g, 0.11 mmol) in acetone (15 cm^3) was stirred at room temperature for 1 h. The red–brown product was filtered off and washed with acetone. The compound was recrystallized from dichloromethane–diethyl ether; yield 0.070 g (74%). Found: C, 49.0; H, 3.8. Calc. for $C_{64}H_{54}Br_2O_4P_4Re_2$: C, 49.8; H, 3.5%.

(C) *Synthesis of* cis-$Re_2(O_2CR)_2X_2(LL)_2$ (R = CH_3, C_2H_5 *or* C_6H_5; X = Cl *or* Br; LL = dppm *or* dpam)

These compounds were prepared through the use of the following general procedure. A suspension of $Re_2X_4(LL)_2$ (*ca* 0.10 g) and $[PPN]O_2CR$ (2 equiv) in ethanol was refluxed for 3 h. The product was filtered off, washed with ethanol and diethyl ether, and dried *in vacuo*.

Note: Attempts to prepare *cis*-$Re_2(O_2C\text{-}4\text{-}py)_2Cl_2(dppm)_2$ with the use of this procedure gave only the *trans* isomer; yield, 63%.

(a) cis-$Re_2(O_2CCH_3)_2Cl_2(dppm)_2$. Yield, 48%. The identity of this compound was confirmed by comparison of its electrochemical properties with those of an authentic sample.[1]

(b) cis-$Re_2(O_2CC_2H_5)_2Cl_2(dppm)_2$. Yield, 33%. The identity of this compound was confirmed by comparison of its electrochemical properties with those of an authentic sample.[1]

(c) cis-$Re_2(O_2CC_6H_5)_2Cl_2(dppm)_2$. Yield, 67%. A cyclic voltammogram of this material revealed that it contained *ca* 60% of the *cis* isomer and *ca* 40% of the *trans* isomer. The components of this mixture were identified by comparison of their electrochemical properties with those of authentic samples.[1]

(d) cis-$Re_2(O_2CCH_3)_2Br_2(dpam)_2$. Yield, 61%. Found: C, 40.7; H, 3.5. Calc. for $C_{54}H_{50}As_4Br_2O_4Re_2$: C, 40.7; H, 3.2%.

(e) cis-$Re_2(O_2CC_6H_5)_2Br_2(dpam)_2$. Yield, 49%. A cyclic voltammogram of this material revealed that it contained *ca* 85% of the *cis* isomer and *ca* 15% of the *trans* isomer. A pure sample of the *cis* isomer was obtained upon the slow addition of diethyl ether to a dichloromethane solution of the mixture. Found: C, 43.5; H, 2.9. Calc. for $C_{65}H_{56}As_4Cl_2Br_2O_4Re_2$ (i.e. *cis*-$Re_2(O_2CC_6H_5)_2Br_2(dpam)_2 \cdot CH_2Cl_2$): C, 43.3; H, 3.1%.

(D) *Reactions of* cis- *and* trans-$Re_2(O_2CR)_2Cl_2(dppm)_2$ *with an excess of* $[PPN]O_2CR'$ (R = CH_3 *or* C_2H_5; R′ = CH_3 *or* C_2H_5)

(a) cis-$Re_2(O_2CCH_3)_2Cl_2(dppm)_2$ *with* $[PPN]O_2CC_2H_5$. A suspension of *cis*-$Re_2(O_2CCH_3)_2Cl_2(dppm)_2$ (0.100 g, 0.075 mmol) and $[PPN]O_2CC_2H_5$ (0.44 g, 0.72 mmol) in ethanol (20 cm^3) was refluxed for 3 h. The product was collected by filtration, washed with ethanol and diethyl ether, and dried *in vacuo*; yield, 0.047 g. ^1H and $^{31}P\{^1H\}$ NMR spectroscopy revealed that the product was a mixture of *cis*-$Re_2(O_2CC_2H_5)_2Cl_2(dppm)_2$, *cis*-$Re_2(O_2CCH_3)_2Cl_2(dppm)_2$ and, probably, *cis*-$Re_2(O_2CCH_3)(O_2CC_2H_5)Cl_2(dppm)_2$; a pure sample of the mixed-carboxylate species has not yet been isolated.

(b) cis-$Re_2(O_2CC_2H_5)_2Cl_2(dppm)_2$ *with* $[PPN]O_2CCH_3$. This reaction was carried out with the use of a procedure analogous to the one reported in D(a); yield, 0.073 g. NMR spectroscopy revealed that this product contained the same mixture of *cis* isomers as that found in D(a).

(c) trans-$Re_2(O_2CCH_3)_2Cl_2(dppm)_2$ *with* $[PPN]O_2CC_2H_5$. A mixture of *trans*-$Re_2(O_2CCH_3)_2Cl_2(dppm)_2$ (0.056 g, 0.042 mmol) and $[PPN]O_2CC_2H_5$ (0.260 g, 0.425 mmol) was combined with ethanol (10 cm^3) and heated to reflux. After 3 h, the product was collected, washed with ethanol and diethyl ether, and dried *in vacuo*; yield, 0.028 g. ^1H NMR spectroscopy revealed that this product was a mixture of *cis* isomers and that *cis*-$Re_2(O_2CC_2H_5)_2Cl_2(dppm)_2$ was the major component.

(d) trans-$Re_2(O_2CC_2H_5)_2Cl_2(dppm)_2$ *with* $[PPN]O_2CCH_3$. A mixture containing *trans*-$Re_2(O_2CC_2H_5)_2Cl_2(dppm)_2$ (0.100 g, 0.073 mmol) and $[PPN]O_2CCH_3$ (0.44 g, 0.74 mmol) in ethanol (20 cm^3) was refluxed for 3 h. The product was collected, washed with ethanol and diethyl ether, and dried; yield, 0.041 g. ^1H NMR spectroscopy again revealed that the product was a mixture of these same *cis* isomers; in this case *cis*-$Re_2(O_2CCH_3)_2Cl_2(dppm)_2$ was the major component.

(E) *Thermolysis of* trans-$Re_2(O_2CR)_2Cl_2(dppm)_2$ *in ethanol*

(a) R = CH_3. A suspension of *trans*-$Re_2(O_2CCH_3)_2Cl_2(dppm)_2$ (0.040 g) in ethanol (10 cm^3) was refluxed for 3 h. The product was filtered off, washed with ethanol and diethyl ether, and dried. The product was shown by cyclic voltammetry to be

cis-$Re_2(O_2CCH_3)_2Cl_2(dppm)_2$; yield 0.022 g (55%).

(b) R = C_2H_5. A mixture of *trans*-$Re_2(O_2CC_2H_5)_2Cl_2(dppm)_2$ (0.045 g) and ethanol (10 cm^3) was refluxed for 3 h. The product was collected by filtration, washed with ethanol and diethyl ether, and dried. The product was shown by cyclic voltammetry to be *cis*-$Re_2(O_2CC_2H_5)_2Cl_2(dppm)_2$; yield, 0.022 g (49%).

Preparation of single crystals for a structure determination

Maroon, rhomboidal crystals of *trans*-$Re_2(O_2CCH_3)_2Cl_2(dppm)_2$, which were suitable for X-ray crystallographic studies, were grown by slow diffusion of toluene vapour into a dichloromethane solution of the complex. The crystals proved to be of composition $Re_2(O_2CCH_3)_2Cl_2(dppm)_2 \cdot C_7H_8 \cdot 2H_2O$.

X-ray crystallography

The structure of a crystal of composition *trans*-$Re_2(O_2CCH_3)_2Cl_2(dppm)_2 \cdot C_7H_8 \cdot 2H_2O$ was determined with the use of general procedures that are described elsewhere.[9] A summary of the crystallographic data is given in Table 1. The cell constants are based on 25 reflections with $20 < \theta < 23°$. Three standard reflections were measured after every 5000 s of beam time during data collection. There were no systematic variations in intensity. Calculations were performed on a microVAX II computer using the Enraf–Nonius structure determination package.

The crystal selected for the structure determination belongs to the monoclinic space group $C2/c$ with $Z = 4$. As a check on crystal quality, omega scans of several intense reflections were measured; the width at half-height was 0.89° with a take-off angle of 2.2°, indicating relatively poor crystal quality. The position of the crystallographically unique rhenium atom was determined from a three-dimensional Patterson map with the molecule residing on an inversion centre. The remaining atoms were located in succeeding difference Fourier syntheses. Lorentz and polarization corrections were applied to the data. An empirical absorption correction was applied,[10] the linear absorption coefficient being 42.36 cm^{-1}. No corrections for extinction were applied. The structure was refined in full-matrix least-squares where the function minimized was $\Sigma w(|F_o| - |F_c|)^2$, where w is the weighting factor defined as $w = 1/\sigma^2(F_o)$.

During the course of the refinement, it became apparent that residual electron density at non-bonding distances to the dirhenium complex could be satisfactorily modelled as lattice toluene and water molecules. The toluene molecule was located on a special position. It was disordered about a two-fold axis in such a way that the methyl group could not be refined. The four crystallographically unique carbon atoms of the phenyl ring [C(901)—C(904)] refined with relatively large thermal parameters, implying high thermal motion for the lattice toluene molecule. The crystallographically unique water molecule was present at a general position and refined satisfactorily. Accordingly, the unit cell contains one molecule of

Table 1. Crystal data and data collection parameters for *trans*-$Re_2(O_2CCH_3)_2Cl_2(dppm)_2 \cdot C_7H_8 \cdot 2H_2O$[a]

Formula	$Re_2Cl_2P_4O_6C_{61}H_{62}$
Formula weight	1458.37
Space group	$C2/c$ (No. 15)
a (Å)	22.247(7)
b (Å)	19.257(7)
c (Å)	14.358(4)
β (°)	94.73(2)
V (Å^3)	6129(6)
Z	4
d_{calc} (g cm^{-3})	1.580
Crystal dimensions (nm)	0.63 × 0.38 × 0.31
Temperature (°C)	20
Radiation (wavelength)	Mo-K_α (0.71073 Å)
Monochromator	Graphite
Linear absorption coefficient (cm^{-1})	42.36
Absorption correction applied	Empirical[b]
Transmission factors: min, max	0.65, 1.00
Diffractometer	Enraf–Nonius CAD4
Scan method	ω–2θ
h, k, l limits	0–23, 0–20, −15–15
2θ range (°)	4.00–45.00
Scan width (°)	$0.89 + 0.35 \tan\theta$
Take-off angle (°)	2.20
Programs used	Enraf–Nonius SDP
$F(000)$	2880.0
p-Factor used in weighting	0.070
Data collected	4153
Unique data	4153
Data with $I > 3.0\sigma(I)$	3110
Number of variables	314
Largest shift/ESD in final cycle	0.17
R[c]	0.042
R_w[d]	0.056
Goodness-of-fit[e]	1.157

[a] Numbers in parentheses following certain data are ESDs occurring in the least significant digit.

[b] N. Walker and D. Stuart, *Acta Cryst.* 1983, **A39**, 158.

[c] $R = \Sigma||F_o| - |F_c||/\Sigma|F_o|$.

[d] $R_w = [\Sigma w(|F_o| - |F_c|)^2/\Sigma w|F_o|^2]^{1/2}$; $w = 1/\sigma^2(F_o)$.

[e] Goodness-of-fit = $[\Sigma w(|F_o| - |F_c|)^2/(N_{obs} - N_{parameters})]^{1/2}$.

Table 2. Selected bond distances (Å) and angles (°) for *trans*-$Re_2(O_2CCH_3)_2Cl_2(dppm)_2 \cdot C_7H_8 \cdot 2H_2O$[a]

Distances			
Re—Re	2.2763(7)	P(1)—C(B)	1.83(1)
Re—Cl	2.571(3)	P(2)—C(B)	1.84(1)
Re—P(1)	2.449(2)	O(1)—C(1)	1.29(1)
Re—P(2)	2.442(2)	O(2)—C(1)	1.27(1)
Re—O(1)	2.072(6)	C(1)—C(3)	1.50(2)
Re—O(2)	2.115(6)		
Angles			
Re—Re—Cl	175.79(6)	P(2)—Re—O(1)	85.2(2)
Re—Re—P(1)	98.19(6)	P(2)—Re—O(2)	96.1(2)
Re—Re—P(2)	98.93(6)	O(1)—Re—O(2)	178.3(2)
Re—Re—O(1)	90.7(2)	Re—P(1)—C(B)	109.8(3)
Re—Re—O(2)	88.0(2)	Re—P(2)—C(B)	111.1(4)
Cl—Re—P(1)	83.99(8)	Re—O(1)—C(1)	118.9(6)
Cl—Re—P(2)	79.41(9)	Re—O(2)—C(1)	120.0(6)
Cl—Re—O(1)	93.0(2)	O(1)—C(1)—O(2)	121.8(9)
Cl—Re—O(2)	88.3(2)	O(1)—C(1)—C(3)	117(1)
P(1)—Re—P(2)	161.37(8)	O(2)—C(1)—C(3)	121.7(9)
P(1)—Re—O(1)	87.3(2)	P(1)—C(B)—P(2)	110.9(5)
P(1)—Re—O(2)	91.8(2)		

[a] Numbers in parentheses are ESDs in the least significant digits.

disordered toluene and two molecules of water for each *trans*-$Re_2(O_2CCH_3)_2Cl_2(dppm)_2$ molecule. Hydrogens were not included in the refinement. With the exception of the lattice toluene and water molecules, all non-hydrogen atoms were refined anisotropically; corrections for anomalous scattering were applied to all atoms so refined.[11]

Further details concerning the data set and the structure solution and refinement may be obtained from Dr P. E. Fanwick. Table 2 lists important bond distances and angles.*

Physical measurements. Perkin–Elmer 1420 and 1800 spectrophotometers were used to record the IR spectra of compounds as mineral oil (Nujol) mulls supported on KBr plates in the region 4800–400 cm^{-1}. Electrochemical measurements were carried out by the use of a Bioanalytical Systems Inc. Model CV-1A instrument on dichloromethane solutions that contained 0.1 M tetra-*n*-butylammonium hexafluorophosphate (TBAH) as the supporting electrolyte. A Pt-bead working electrode and a Pt-wire auxiliary electrode were used. $E_{1/2}$ values, determined as $(E_{p,a}+E_{p,c})/2$, were referenced to the silver/silver chloride (Ag/AgCl) electrode at room temperature and are uncorrected for junction potentials. Under our experimental conditions, the ferrocenium/ferrocene couple is at $E_{1/2} = +0.47$ V vs Ag/AgCl. ^1H and $^{31}P\{^1H\}$ NMR spectra were recorded on a Varian XL-200 spectrometer. Proton resonances were referenced internally to the residual protons in the incompletely deuteriated solvent. Phosphorus resonances were referenced externally to 85% H_3PO_4.

Elemental microanalyses were performed by Dr H. D. Lee of Purdue University Microanalytical Laboratory.

RESULTS AND DISCUSSION

(A) *Synthesis of* cis- *and* trans-$Re_2(O_2CR)_2X_2(LL)_2$

The heterogeneous-phase reactions between $Re_2X_4(LL)_2$ (X = Cl or Br; LL = dppm or dpam) and $[PPN]O_2CR$ (R = CH_3, C_2H_5, C_6H_5 or 4-py) in refluxing ethanol afford *cis*-$Re_2(O_2CR)_2X_2(LL)_2$, except in the case of $Re_2(O_2CC_6H_5)_2Cl_2(dppm)_2$ (where a mixture of the *cis* and *trans* isomers is produced) and $Re_2(O_2C\text{-}4\text{-}py)_2Cl_2(dppm)_2$ (where only the *trans* isomer is produced). That *cis*-$Re_2(O_2CR)_2X_2(LL)_2$ is the major product in these reactions is not surprising in the light of our earlier observation that $Re_2X_4(dppm)_2$ (X = Cl or Br) reacts with lithium acetate in refluxing methanol to give *cis*-$Re_2(O_2CCH_3)_2X_2(dppm)_2$.[1] The fact that we see only the *trans* isomer, or a mixture of the *cis*

* Atomic positional and thermal parameters and full listings of bond lengths and angles have been deposited with the Editor and with the Director, Cambridge Crystallographic Data Centre.

and *trans* isomers, in the cases involving aryl carboxylates, is also consistent with the earlier observation that the benzoate derivatives of *trans*-$Re_2(O_2CR)_2X_2(dppm)_2$ (X = Cl, Br) are more stable and more resistant to isomerization (to the corresponding *cis* isomers) than are the corresponding alkyl carboxylate complexes.

When $Re_2X_4(LL)_2$ and $[PPN]O_2CR$ are combined in dichloromethane at room temperature *trans*-$Re_2(O_2CR)_2X_2(LL)_2$ is produced. This is an important result, because this reaction represents the best and most reliable synthetic route to the *trans* isomers. Note that in the work-up of the *trans* isomers care must be taken to exclude oxygen from the system. If not, a purple material is formed whose identity has not yet been fully determined.

We have also shown that *trans*-$[Re_2(O_2CC_6H_5)_2Br_2(dppm)_2]Br$[1] is reduced by cobaltocene to give *trans*-$Re_2(O_2CC_6H_5)_2Br_2(dppm)_2$, with no evidence for isomerization to the *cis* isomer.

(B) *Carboxylate exchange and thermolysis reactions*

Samples of *cis*- and *trans*-$Re_2(O_2CR)_2Cl_2(dppm)_2$ (R = CH_3 or C_2H_5) were reacted with an excess (10 equiv) of $[PPN]O_2CR'$ (R′ = CH_3 or C_2H_5) in refluxing ethanol for 3 h. The reactions involving *cis*-$Re_2(O_2CR)_2Cl_2(dppm)_2$ afford mixtures of *cis*-$Re_2(O_2CR)_2Cl_2(dppm)_2$, *cis*-$Re_2(O_2CR')_2Cl_2(dppm)_2$ and possibly a small amount of *cis*-$Re_2(O_2CR)(O_2CR')Cl_2(dppm)_2$, although a pure sample of the latter species has not been isolated.* A similar distribution of products is obtained in each case. The reactions of *trans*-$Re_2(O_2CR)_2Cl_2(dppm)_2$ with $[PPN]O_2CR'$ also afford a mixture of *cis* isomers, of which the major component is *cis*-$Re_2(O_2CR')_2Cl_2(dppm)_2$. The importance of these results is two-fold: (1) the *cis* isomers undergo carboxylate exchange but do not convert to the *trans* isomers, and (2) the *trans* isomers react with carboxylate ion to give mixtures that contain only the *cis* isomers, the major component of which is the *cis* isomer that contains the alien carboxylate.

When samples of *trans*-$Re_2(O_2CR)_2Cl_2(dppm)_2$ (R = CH_3 or C_2H_5) are heated in refluxing ethanol for 3 h, the corresponding *cis* isomeric form is produced. This result is consistent with our earlier conclusion that the *cis* isomers are the thermodynamically favoured form.[1]

(C) *Spectroscopic and electrochemical properties*

The identities of the newly prepared dpam and isonicotinate derivatives are based upon the close similarity of their electrochemical and NMR spectral properties to those of previously characterized derivatives of this type.[1] The ^1H NMR spectrum of *cis*-$Re_2(O_2CCH_3)_2Cl_2(dppm)_2$, recorded in CD_2Cl_2, displays resonances for the phenyl protons in the range δ +7.6 to +6.8. The methyl protons of the acetate ligand appear as a singlet at δ + 2.31. The dppm bridgehead methylene protons (—CH_AH_M—) show up as doublets of triplets at δ_A +6.34 and δ_M +4.89. The splitting pattern arises from geminal coupling between H_A and H_M, and further coupling between these protons and two equivalent phosphorus nuclei ($I = 1/2$), with $J(H_A—H_M) \simeq 12$ Hz, $J(H_A—P) \simeq 10$ Hz and $J(H_M—P) \simeq 12$ Hz. The ^1H NMR spectrum of *cis*-$Re_2(O_2CCH_3)_2Br_2(dpam)_2$ (in CD_2Cl_2) is qualitatively similar to that for *cis*-$Re_2(O_2CCH_3)_2Cl_2(dppm)_2$ in that it shows only phenyl resonances (δ +7.7 to +6.9), bridgehead methylene resonances (δ_M +5.76, δ_A +4.51), and a methyl resonance (δ +2.24). However, it differs in that the methylene resonances now appear as doublets with $J(H_A—H_M) \simeq 12$ Hz. The ^1H NMR spectrum of *trans*-$Re_2(O_2C\text{-}4\text{-}py)_2Cl_2(dppm)_2$ (in CD_2Cl_2) shows an unresolved multiplet at δ +5.07, which we assign to the four equivalent bridgehead methylene protons of dppm. The remainder of the spectrum shows the phenyl proton resonances in the range δ +8.7 to +7.1. A doublet at δ +8.70 (with 5.2 Hz splitting) most likely corresponds to the protons *ortho* to nitrogen in the isonicotinate ligands. The $[PPN]^+$ salt of the isonicotinate anion shows a similar doublet centred at δ +8.49 with 5.6 Hz splitting. The $^{31}P\{^1H\}$ NMR spectrum of this particular *trans* species displays a singlet at δ +3.67.

Cyclic voltammetric (CV) data for solutions of these complexes in 0.1 M TBAH/CH_2Cl_2 are listed in Table 3 (all potentials are vs Ag/AgCl). CVs of the new dpam and isonicotinate derivatives resemble quite closely those for the other derivatives, in that they exhibit two reversible one-electron oxidations. However, there is one notable difference, namely, the redox potentials for *trans*-$Re_2(O_2C\text{-}4\text{-}py)_2Cl_2(dppm)_2$ are approximately 0.2 V more positive than the corresponding values for the other *trans* derivatives.

* The identity of the components of these mixtures was established by ^1H and $^{31}P\{^1H\}$ spectroscopy. The ^1H NMR spectral data are reported in section (c) for *cis*-$Re_2(O_2CCH_3)_2Cl_2(dppm)_2$ and in ref. 1 for *cis*-$Re_2(O_2CC_2H_5)_2Cl_2(dppm)_2$. The $^{31}P\{^1H\}$ NMR spectra (in CD_2Cl_2) for these two complexes appear as singlets (δ −10.13 for the acetate, δ −10.18 for the propionate).

Table 3. Cyclic voltammetric data[a] for complexes of the type *cis*- and *trans*-$Re_2(O_2CR)_2X_2(LL)_2$

	Complex			CV half-wave potentials (V)[b]		
	R	X	LL	$E_{1/2}$(ox)(2)	$E_{1/2}$(ox)(1)	Reference
cis	CH_3	Cl	dppm	+1.34(110)	+0.28(100)	1
	C_2H_5	Cl	dppm	+1.38(120)	+0.30(140)	1
	C_6H_5	Cl	dppm	+1.34(120)	+0.29(120)	1
	CH_3	Br	dpam	+1.38(110)	+0.28(110)	[c]
	C_6H_5	Br	dpam	+1.31(120)	+0.20(110)	[c]
trans	CH_3	Cl	dppm	+0.93(110)	−0.27(110)	1
	C_2H_5	Cl	dppm	+0.93(100)	−0.29(110)	1
	C_6H_5	Cl	dppm	+1.00(110)	−0.25(110)	1
	4-py	Cl	dppm	+1.17(110)	−0.08(110)	[c]
	C_6H_5	Br	dppm	+1.00(100)	−0.22(100)	1
	CH_3	Br	dpam	+1.01(120)	−0.24(110)	[c]
	C_6H_5	Br	dpam	+1.03(120)	−0.25(120)	[c]

[a] Versus Ag/AgCl. Recorded on solutions in 0.1 M TBAH/CH_2Cl_2 by the use of a Pt-bead electrode. Data obtained at $v = 200$ mV s^{-1}. Under our experimental conditions $E_{1/2}$ for the ferrocenium/ferrocene couple is +0.47 V vs Ag/AgCl.

[b] Numbers in parentheses are ΔE_p values (i.e. $E_{p,a} - E_{p,c}$).

[c] Present study.

(D) *X-ray structure results*

The molecular structure of *trans*-$Re_2(O_2CCH_3)_2Cl_2(dppm)_2 \cdot C_7H_8 \cdot 2H_2O$ has been determined by X-ray crystallography. Important bond distances and angles are listed in Table 2. An ORTEP representation of the structure is shown in Fig. 1.

This structure determination is important because it allows us to compare key distances in *trans*-$Re_2(O_2CCH_3)_2Cl_2(dppm)_2$ (**1**) with those for the previously characterized salt *trans*-$[Re_2(O_2CCH_3)_2Cl_2(dppm)_2]PF_6$ (**2**)[1] and the neutral *cis*-$Re_2(O_2CCH_3)_2(dppm)_2$ (**3**).[1] The average Re—P distance is 2.446[4] in **1** and 2.478[1] Å in **2**.* This bond lengthening is statistically significant[12] and presumably reflects a decrease in Re → P π-bonding in going from the neutral to the cationic species. A similar lengthening has been observed in the cases involving $Re_2Cl_4(PMe_2Ph)_4$ and $[Re_2Cl_4(PMe_2Ph)_4]PF_6$,[13] and *cis*-$Re_2(O_2CCH_3)_2Cl_2(dppa)_2$ and *cis*-$[Re_2(O_2CCH_3)_2Cl_2(dppa)_2]PF_6$ (dppa = $Ph_2PNHPPh_2$).[14] The average Re—Cl distance in **1** is 2.571(3) and in **2** it is 2.532(2) Å. These distances are also statistically different and represent a bond shortening from **1** to **2**. This trend can be attributed to contraction of the metal valence orbitals and/or, the increased electrostatic attraction as the metal core charge increases. The average Re—O distances in **1** and **2** are 2.09[2] and 2.06[1] Å, respectively, and are not statistically different. Neither are the Re—Re distances, which are 2.2763(7) for **1** and 2.2748(6) Å for **2**.

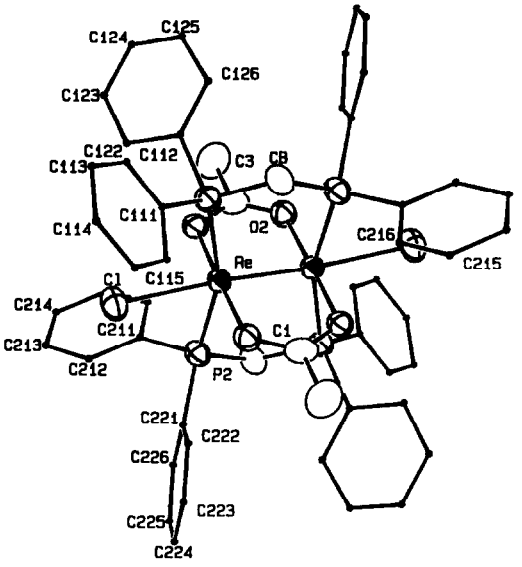

Fig. 1. ORTEP representation of the structure of *trans*-$Re_2(O_2CCH_3)_2Cl_2(dppm)_2$ showing the atomic numbering scheme. The labelled atoms are related to the unlabelled ones by an inversion centre. The thermal ellipsoids are drawn at the 50% probability level.

* The estimated deviation in brackets is calculated as $[\ ] = [\Sigma_n \Delta_i^2/n(n-1)]^{1/2}$, in which Δ_i is the deviation of the ith of n values from the arithmetic mean of the set.

Only two distances change significantly in going from **1** to **3**; these are Re—Re and Re—P. The Re—Re distance in **3** (2.3151(7) Å) is longer than that in **1** (2.2763(7) Å), while the average Re—P distances follow the opposite order (2.446[4] for **1** and 2.396[6] Å for **3**). The conformational demands associated with the two fused five-membered rings P—C—P—Re—Re—P—C—P in these *trans* and *cis* isomers may dictate that the Re—Re and Re—P distances differ between **1** and **3** in this manner.

Acknowledgements—We thank the National Science Foundation (Grant No. CHE88–07444) and the Purdue Research Foundation (for a David Ross Fellowship to D.R.D.) for support of this work, and the National Institutes of Health (Grant No. RR-01077) and the National Science Foundation (Grant No. 8714258) for funds for the purchase of the NMR spectrometers.

REFERENCES

1. A. R. Cutler, D. R. Derringer, P. E. Fanwick and R. A. Walton, *J. Am. Chem. Soc.* 1988, **110**, 5024.
2. L. B. Anderson, M. Bakir and R. A. Walton, *Polyhedron* 1987, **6**, 1483.
3. M. Bakir, F. A. Cotton, L. R. Falvello, K. Vidyasagar and R. A. Walton, *Inorg. Chem.* 1988, **27**, 2460.
4. P. Brant, H. D. Glicksman, D. J. Salmon and R. A. Walton, *Inorg. Chem.* 1978, **17**, 3203.
5. J. R. Ebner, D. R. Tyler and R. A. Walton, *Inorg. Chem.* 1976, **15**, 833.
6. A. C. Price, PhD thesis, Purdue University (1987).
7. T. J. Barder, F. A. Cotton, K. R. Dunbar, G. L. Powell, W. Schwotzer and R. A. Walton, *Inorg. Chem.* 1985, **24**, 2550.
8. A. Martinsen and J. Songstad, *Acta Chem. Scand.* 1977, **A31**, 645.
9. P. E. Fanwick, W. S. Harwood and R. A. Walton, *Inorg. Chim. Acta* 1986, **122**, 7.
10. N. Walker and D. Stuart, *Acta Cryst.* 1983, **A39**, 158.
11. D. T. Cromer, *International Tables for X-ray Crystallography*, Vol. IV, Table 2.3.1. Kynoch Press, Birmingham, U.K. (1974); (b) For the scattering factors used in the structure solution see: D. T. Cromer and J. T. Waber, Table 2.2B of above.
12. We use 3σ as our criterion for statistical significance; cf. J. P. Glusker and K. N. Trueblood, *Crystal Structure Analysis*, p. 163. Oxford University Press, New York (1985).
13. F. A. Cotton, K. R. Dunbar, L. R. Falvello, M. Tomas and R. A. Walton, *J. Am. Chem. Soc.* 1983, **105**, 4950.
14. D. R. Derringer, P. E. Fanwick, J. Moran and R. A. Walton, *Inorg. Chem.* 1989, **28**, 1384.

Polyhedron Vol. 9, No. 5, pp. 751–756, 1990
Printed in Great Britain

0277–5387/90 $3.00+.00
© 1990 Pergamon Press plc

MIXED-LIGAND IMIDAZOLE COMPLEXES OF ORGANOLANTHANIDES

A. L. WAYDA,*† M. L. KAPLAN* and A. M. LYONS

AT & T Bell Laboratories, Murray Hill, NJ 07974, U.S.A.

and

R. D. ROGERS*

Department of Chemistry, Northern Illinois University, De Kalb, IL 60115, U.S.A.

(*Received* 26 *May* 1989; *accepted* 29 *September* 1989)

Abstract—Heptacoordinate trivalent lanthanide complexes containing mixed ligands were prepared and characterized. These complexes were of general structure $M(THD)_3$–IM. In this formula M represents the lanthanide +3 ions of europium, holmium, praseodymium, dysprosium, ytterbium and gadolinium. THD stands for 2,2,6,6-tetramethyl-3,5-heptanedionato and IM for imidazole. The IR spectra of these materials were compared and we have demonstrated that the C—H stretching frequency of the imidazole moiety exhibits a monotonic decrease as a function of increasing size of the lanthanide +3 ion. The N—H stretching frequency for imidazole shows a similar trend, except that the point for the europium occurs at a position quite far above that of the other compounds. These results suggest that the bond strength between the lanthanide ion and the imidazole is sensitive to the radius of the ion and that the chemical reactivity of the imidazole may be influenced by this effect. The crystal and molecular structures of $Eu(THD)_3$–IM have been determined. The following cell constants were found: $a = 19.40(1)$, $b = 10.243(5)$, $c = 21.76(1)$ Å, $\beta = 108.70(5)°$ and $Z = 4$. The space group is $P2_1/n$. The europium ion is seven-coordinate with bonding to the six carbonyl groups of the three THD units and to one of the imidazole nitrogens, thereby forming a capped trigonal prism. Preliminary X-ray data from other members of the series indicate that all are isotructural with the europium compound.

Large chemical shifts are induced in the NMR spectra of certain compounds in the presence of complexes of lanthanide ions with large ligands. The first example of this effect used the dipyridinate of tris(2,2,6,6-tetramethyl-3,5-heptanedionato) europium, $[Eu(THD)_3(PY)_2]$, with cholesterol.[1] Following this landmark paper, a wide variety of other systems were discovered and shown to exhibit similar behaviour.[2] The origin of this dramatic effect has been attributed both to through-space dipolar pseudo-contact interactions[3] and through-bond Fermi contact interactions.[4,5] It is now generally believed that the former are exclusively or nearly exclusively responsible for the observed shifts.[2]

The purpose of the present work is to study the structural differences responsible for the chemical and spectroscopic behaviour of related compounds in a series of organolanthanide shift reagents in the form of their stable seven-coordinate complexes with the nitrogen base, imidazole. In particular, we were interested in the way in which complexation of the imidazole to the shift reagent could modify its chemical reactivity in epoxy resin cure reactions. The series we chose to work with are the $M(THD)_3$–IM chelates. A paper on the preparation of these compounds has been published although the

* Authors to whom correspondence should be addressed.
† Present address: Morgan & Finnegan, New York, U.S.A.

authors reported only minimal details of the characterization.[6] As part of our present effort, we have examined the X-ray crystal structure of one of the examples of this family of compounds together with the IR spectra of all of these materials. From this information we are able to know, in detail, the precise molecular structure of the complexes and thereby infer relative reactivity relationships.

In addition, we have correlated spectroscopic properties of the complexes with the size of the lanthanide +3 ion. Specifically, we have obtained a measure of the strength of bonding of the imidazole to the metal by use of IR spectroscopy. In related work, we have shown that the reactivity of these different complexes, in an epoxy curing reaction, depends on lanthanide size in the same way that the specroscopic properties do.[7]

EXPERIMENTAL

Preparation of materials

The lanthanide–imidazole complexes were all prepared by the same general route. The following procedure for the europium compound can be utilized for each of the congeners.

A solution of tris(2,2,6,6-tetramethyl-3,5-heptanedionato)europium, [Eu(THD)$_3$] (25.0 g, 0.0356 mol), was prepared in hot methanol (300 cm^3). To this hot, filtered solution was added a solution of imidazole (2.42 g, 0.0356 mol) in hot methanol (100 cm^3). The mixture was boiled for approximately 10 min, and then transferred to a rotary evaporator where the solvent was removed. The crude product was recrystallized from 1,2-dichloroethane (500 cm^3). Yield: 20.9 g (76%). The analytical data and melting points for each of the mixed-ligand complexes are given in Table 1.

Each of the materials was examined by differential scanning calorimetry (DSC) and exhibited a single sharp endothermic peak at the melting point without any evidence of decomposition up to 300°C. The instrument used was a Perkin–Elmer Model 4 Differential Scanning Calorimeter. Standard conditions for the DSC analyses were: heating rate 20° min^{-1}; temperature range, 30–280 or 30–300°C; sample size, 1–5 mg.

Mass spectroscopy was performed on a Hewlett–Packard Model 5985 B instrument. A heated solid sample probe was used to insert the samples into the ionization region.

IR spectra were obtained on a Nicolet MX-1 Fourier Transform Spectrometer in the range from 4000 to 400 cm^{-1}. Samples were prepared as pressed KBr pellets (approximately 1 mg of complex per 100 mg of KBr). Spectra of the M(THD)$_3$–IM complexes are essentially equivalent. Several new absorption lines appear in these complexes and these are summarized in Table 2 together with specific frequencies of the new lines in the europium complex and their comparison with the absorptions in uncomplexed imidazole.

Table 1. Melting point and analytical data for M(THD)$_3$–IM complexes

M^{3+}	Ionic radius (pm)[a]	Melting point (°C)	Element	Calculated	Found
Yb	86.8	198	C	54.7	53.4
			H	7.8	7.1
			N	3.5	3.4
			Yb	21.9	21.9
Ho	90.1	208	C	55.2	54.5
			H	7.8	7.6
			N	3.6	3.7
			Ho	21.1	21.8
Dy	91.2	203	C	55.4	55.0
			H	7.9	7.9
			N	3.6	3.6
			Dy	20.8	21.4
Gd	93.8	206	C	55.8	55.3
			H	7.9	7.9
			N	3.6	3.5
			Gd	20.3	20.9
Eu	94.7	206	C	56.2	55.8
			H	8.0	8.2
			N	3.6	3.7
			Eu	19.7	19.2
Pr	99.0	193	C	57.0	56.5
			H	8.1	8.1
			N	3.7	4.0
			Pr	18.6	18.9

[a] N. N. Greenwood and A. Earnshaw, *Chemistry of the Elements*, p. 1430. Pergamon Press, New York (1984).

Single crystal X-ray structure determinations were performed on some of these compounds. The experimental details are as follows: A transparent single crystal of Eu(THD)$_3$–IM was mounted on a pin and transferred to the goniometer. From the systematic absences the space group was determined to be the centric $P2_1/n$ type. The data collection and refinement parameters are summarized in Table 3.

Very small crystals of marginal quality resulted in an observed/scanned ratio of 0.40. In addition, obvious disorder and high thermal motion complicated the solution and refinement process. Never-

Table 2. IR absorptions of lanthanide–imidazole complexes

$Eu(THD)_3$–IM	Range for lanthanides	Imidazole	Assignment[8,9]
3350	3294–3360	2800	N—H stretch
3140	3137–3150	3112, 3102	C—H stretch
1434	1430–1435	1448	Ring stretch
1324	1323–1325	1322, 1328	Ring stretch
1064	1064	1055	In-plane C—H bend
918	917–918	924	Out-of-plane C—H bend
848	847–850	842	Out-of-plane C—H bend
750	749–751	738	Out-of-plane C—H bend
656	655–657	660	Ring deformation
613	612–614	621	Ring deformation

theless, the structure was solved as completely as possible (Fig. 1). Disorder was resolvable only for the atoms C(12), C(13), C(14) and C(34), C(35) and C(36). The former exhibited a 0.65/0.35 disorder [C(12)—C(14) and C(12)′—C(14)′] and the latter a 0.50/0.50 disorder [C(34)—C(36) and C(34)′—C(36)′]. No other resolvable disorder was observed. Due to the poor data-to-parameter ratio

Table 3. Data collection and structure refinement parameters

Compound	$EuC_{36}H_{61}N_2O_6$
Formula weight	769.8
Space group	$P2_1/n$
Temperature (°C)	20
a (Å)	19.40(1)
b (Å)	10.243(5)
c (Å)	21.76(1)
β (°)	108.70(5)
Z	4
D_{calc} (g cm^{-3})	1.25
μ_{calc} (cm^{-1})	14.7
Diffractometer/scan	Enraf–Nonius CAD-4/θ–2θ
Range of relative transmission factors (%)	40/100
Radiation, graphite monochromator	Mo-K_α (λ = 0.71073)
Maximum crystal dimensions (mm)	0.10 × 0.15 × 0.20
Scan width	$0.80+0.35\tan\theta$
Standard reflections	600; 020; 004
Decay of standards (%)	±2
Reflections measured	7673
2θ range (°)	$2 \leqslant 2\theta \leqslant 50$
Range of h, k, l	+22, +12, ±25
Reflections observed[a] [$F_o \geqslant 5\sigma(F_o)$]	3060
Computer programs[b,c]	SHELX
Structure solution	Heavy-atom techniques
Number of parameters varied	221
Weights	$[\sigma(F_o)^2]^{-1}$
G-O-F	2.40
$R = \Sigma \|\|F_o\|-\|F_c\|\|/\Sigma\|F_o\|$	0.097
R_w	0.113
Largest feature in final difference map	2.0 e$^-$ Å^{-3} near Eu

[a] Corrections: Lorentz-polarization and absorption (empirical, psi scan).

[b] G. M. Sheldrick, SHELX, a system of computer programs for X-ray structure determinations as locally modified (1976).

[c] Neutral scattering factors and anomalous dispersion corrections from: *International Tables for X-ray Crystallography*. Kynoch Press, Birmingham, U.K.

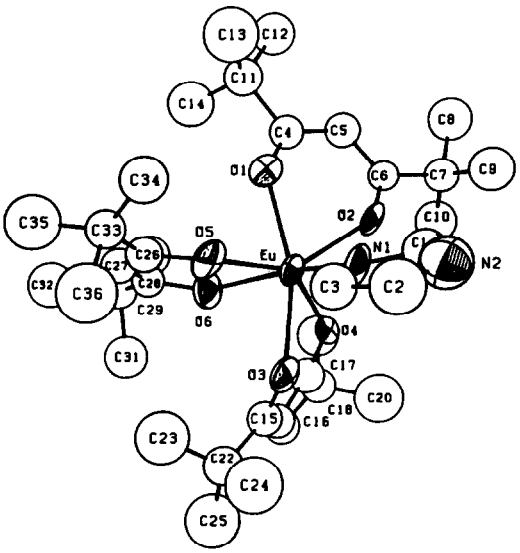

Fig. 1. Molecular structure of $Eu(THD)_3$–IM.

no attempt was made to refine the carbon atoms anisotropically or to locate hydrogen atoms. Refinement of the europium, oxygen and coordinated nitrogen atoms with anisotropic temperature factors led to final values of $R = 0.097$ and $R_w = 0.113$. Selected bond distances and bond angles in $EuC_{36}H_{61}N_2O_6$ are given in Table 4.

Crystals of M = Pr, Gd, Dy, Ho and Yb were examined and preliminary unit cell data were obtained. These cells, their symmetries and space group extinctions match those observed for M = Eu. The best of these, M = Yb, gave $a = 19.355(8)$, $b = 10.225(2)$, $c = 21.765(8)$ Å, $\beta = 108.85(4)°$: with a calculated density of 1.29 g cm^{-3}. A preliminary data set on $Yb(THD)_3$–IM confirmed that it is indeed isostructural with $Eu(THD)_3$–IM.

RESULTS AND DISCUSSION

The preparation of the mixed-ligand complexes is straightforward. It simply requires that the $M(THD)_3$ complex be dissolved with an equimolar amount of imidazole in methanol. Removal of the solvent yields the new complex. In all cases, the crude yields are quantitative and this product can be used as is for most purposes. If purification is necessary it is accomplished by recrystallization from 1,2-dichloroethane with about 70–80% recovery. The melting points we report (Table 1) are between 5 to 14°C higher than those in the literature.[6] Also, the elemental analyses indicate a higher state of purity than those given in the literature.

In our attempts to characterize these materials we undertook a variety of spectroscopic measurements. One of the first approaches was to look at the mass spectrum of these complexes. Using the solid sample insert, and heating from 30 to 300°C

Table 4. Selected bond distances (Å) and bond angles (°) in $Eu(THD)_3$–IM[a]

Atoms	Distance	Atoms	Distance
Eu—O(1)	2.35(2)	Eu—O(2)	2.29(1)
Eu—O(3)	2.38(2)	Eu—O(4)	2.33(2)
Eu—O(5)	2.30(2)	Eu—O(6)	2.31(2)
Eu—N(1)	2.53(3)		

Atoms	Angle	Atoms	Angle
O(1)—Eu—O(2)	69.6(6)	O(1)—Eu—O(3)	160.2(5)
O(2)—Eu—O(3)	129.9(6)	O(1)—Eu—O(4)	122.3(7)
O(2)—Eu—O(4)	77.1(6)	O(3)—Eu—O(4)	71.3(6)
O(1)—Eu—O(5)	79.8(6)	O(2)—Eu—O(5)	140.4(7)
O(3)—Eu—O(5)	81.3(6)	O(4)—Eu—O(5)	142.1(6)
O(1)—Eu—O(6)	83.9(7)	O(2)—Eu—O(6)	124.2(6)
O(3)—Eu—O(6)	85.7(7)	O(4)—Eu—O(6)	77.6(6)
O(5)—Eu—O(6)	74.7(6)	O(1)—Eu—N(1)	103.4(8)
O(2)—Eu—N(1)	82.0(7)	O(3)—Eu—N(1)	79.1(8)
O(4)—Eu—N(1)	117.1(7)	O(5)—Eu—N(1)	81.4(6)
O(6)—Eu—N(1)	153.4(6)		

[a] Atomic coordinates have been submitted to the Cambridge Crystallographic Data Centre.

we found no evidence of the molecular ion for the intact complex. The mass peak corresponding to the $M(THD)_3$ substance was found in each case. This result is puzzling since DSC of these compounds exhibits a single sharp endothermic peak at the melting point with no evidence of decomposition even up to nearly 300°C. Apparently, the combination of the high temperature required to vaporize the complexes and the high vacuum in the ionization chamber of the mass spectrometer result in dissociation of the complex and loss of the imidazole portion.

A comparison of the Fourier Transform IR spectra of the $M(THD)_3$ complexes before adding imidazole shows that they are basically very similar, with only small shifts observed for most peaks. When the imidazole complex is prepared several new IR bands appear. Their assignments are given in Table 2 and are based on the spectroscopy of imidazole.[8,9] The largest shift was observed for the N—H stretching frequency of the imidazole and was found to be approximately 500 cm^{-1} from the value in the free ligand. This shift places the N—H frequency close to that for gaseous imidazole[9] (3518 cm^{-1}), and indicates greatly reduced hydrogen bonding in the complexes as compared to that in uncomplexed imidazole.

We noted that there was a small, but perceptible, difference in the measured frequencies of the IR absorption bands for the different lanthanide metal complexes. We surmised that the compounds in the series would be essentially identical in structure except for the effects due to the changing size of the central metal ion. When the N—H absorption frequency and the C—H absorption frequency for the imidazoles in the various complexes were plotted as a function of the size of the lanthanide +3 ion we obtained the results shown in Figs 2 and 3. In the former the monotonic relationship of stretching frequency with ion size is apparent. There is one

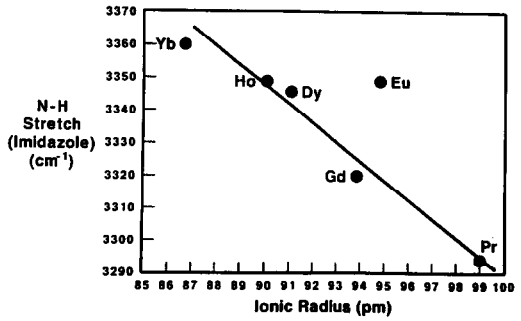

Fig. 2. IR N—H stretching frequencies of imidazole in $M(THD)_3$–IM complexes as a function of the ionic radius of the lanthanide.

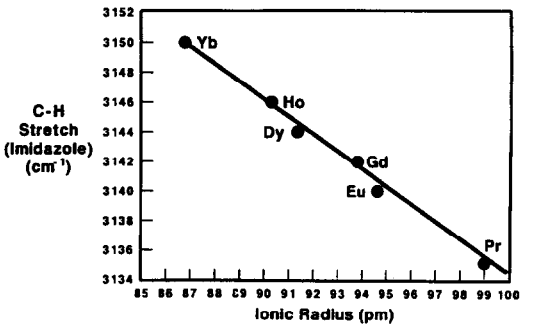

Fig. 3. IR C—H stretching frequencies of imidazole in $M(THD)_3$–IM complexes as a function of the ionic radius of the lanthanide.

exception in this plot. The stretching frequency for the europium compound is higher than it would be for its normal position on the graph. Although we have no adequate explanation for this apparent anomaly, we speculate that the N—Eu bond strength may be influenced by the unusual oxidation–reduction properties of europium. Among the lanthanide metals studied here, europium has the lowest reduction potential, at least 0.3 V lower than the others.[10] This lower reduction potential probably arises from the easy accessibility of the +2 state of europium. The variation of the C—H stretching frequency is monotonic through all compounds tested (Fig. 3).

The variation in the imidazole stretching frequencies in the complexes arises from the variation in the strengths of the metal–nitrogen bonds. The sensitivity of N—H stretching frequencies to cation radius has been previously reported for transition metal complexes of imidazole.[11] The magnitude of this effect will be directly proportional to the electrostatic attraction between the lone pair electrons on the imidazole imino nitrogen and the metal ion. Larger ions result in weaker interactions which appear at lower frequencies in the IR. As we stated above, the anomalous behaviour of the N—H stretching frequency of imidazole in the europium complex is probably attributable to the unusual oxidation states of the europium ion and the manner in which they form bonds with imidazole.

Other shifts observed in the positions of the imidazole bands upon complexation (Table 2) are consistent with shifts observed for imidazole complexes with transition metal (+2) salts.[11] Most absorption bands due to the THD anion are shifted in the order of 0–2 cm^{-1} after complexation. Larger shifts (*ca* 5 cm^{-1}) are observed for the bands associated with the conjugated O=C—C=C—O system[12] in the range 1500–1600 cm^{-1}. The metal–oxygen bond length appears to be unchanged by complexation

as evidenced by the constancy of the absorption bands at 602 and 474 cm^{-1}.[13]

Because of the intriguing chemical possibilities across the lanthanide series using mixed ligands it is important to know the details of the structure of at least one of these compounds. When we recrystallized these $M(THD)_3$–IM materials from 1,2-dichloroethane, crystals were obtained which appeared to the naked eye as being of good enough quality for single crystal X-ray determinations. However, when we attempted to do diffraction studies it was plain that crystal quality was borderline and high R values were obtained, $R = 0.097$ and $R_w = 0.113$.

The structure of the europium compound was solved, however, and the molecular structure is shown in Fig. 1. The europium atom is seven-coordinate with bonding to the six carbonyl units of the β-diketone groups and to one of the nitrogens in the imidazole ring. The five atoms in each of the oxygen-containing rings, O—C—C—C—O are quite planar, and define the least-squares planes in this chelate, and have average deviations from the planes of 0.011, 0.020 and 0.009 Å, respectively. The average Eu—O bond length is 2.33(3) Å (Table 4) which is very similar to the value of 2.35 Å found for the dipyridyl adduct of $Eu(THD)_3$[14] and the value of 2.36 Å found for the bis(dimethylformamide) adduct of $Eu(THD)_3$.[15] The Eu—N bond distance is 2.53(3) Å, which is somewhat shorter than the 2.65 Å found in the dipyridyl adduct[14] but identical to the bond length found for Lu—N in the 3-methylpyridine complex of $Lu(THD)_3$.[16] The long Eu—N bond length in the dipyridyl complex of $Eu(THD)_3$ may be due to the extreme crowding necessitated by the eight-fold coordination around europium. In the present compound, the steric strain is apparently relieved because of the seven-coordinate geometry. The large differences in ionic size of the lanthanides may also play an important role in the bond lengths and bond angles which are observed. A complete study of analogous compounds across the lanthanide series is necessary to elucidate the effect of ionic size. Fortunately, this series of compounds is isostructural for M = Pr–Yb and this will allow a detailed examination of the effect of ionic size on structure when suitable single crystals can be obtained.

CONCLUSIONS

We have prepared and characterized a series of mixed-ligand complexes of the general formula, $M(THD)_3$–IM, where M represents any of the group of lanthanide ions, europium, praseodymium, dysprosium, holmium, gadolinium and ytterbium. The complexes were prepared by mixing solutions of $M(THD)_3$ and imidazole and then removing the solvent. In the IR spectra of these compounds we observed that both the C—H and N—H stretching frequencies of the imidazole group are sensitive to the size of the lanthanide ion. Both bands show a monotonic decrease in frequency as the ionic radii increase.

The single crystal X-ray structure of $Eu(THD)_3$–IM was determined. It is pure seven-coordinate, with six Eu—O bonds and one Eu—N bond, and is best described as being a capped trigonal prism. The three oxygen chelate rings are planar, and bond lengths and bond angles are similar to those found in related compounds. Continued research to obtain quality single crystals for these compounds and thus accurate structural details across this isostructural series is warranted.

Acknowledgements—We thank E. A. Chandross, T. W. Weidman and D. W. Dahringer for constructive comments on this manuscript and A. M. Mujsce for the mass spectral analyses.

REFERENCES

1. C. C. Hinckley, *J. Am. Chem. Soc.* 1969, **91**, 5160.
2. W. DeW. Horrocks Jr and James P. Sipe III, *J. Am. Chem. Soc.* 1971, **93**, 6800 and refs therein.
3. W. DeW. Horrocks Jr, *Inorg. Chem.* 1970, **9**, 690.
4. G. H. Wahl Jr and M. R. Peterson Jr, *J. Chem. Soc., Chem. Commun.* 1970, 422.
5. P. V. Demarco, T. K. Elzey, R. B. Lewis and E. Wenkert, *J. Am. Chem. Soc.* 1970, **92**, 5734.
6. M. Sayeed and N. Ahmad, *J. Inorg. Nucl. Chem.* 1981, **43**, 3197.
7. M. L. Kaplan, A. L. Wayda and A. M. Lyons, *J. Polym. Sci. Polym. Chem. Ed.*, in press (1990).
8. M. Cordes de N. D. and J. L. Walter, *Spectrochim. Acta* 1968, **24A**, 237.
9. A. M. Bellocq, C. Perchard, A. Novak and M-L. Josien, *J. Chim. Phys.* 1965, 1334.
10. F. A. Cotton and G. Wilkinson, *Advanced Inorganic Chemistry*, 4th edn, p. 982. John Wiley, New York (1980).
11. J. Reedijk, *Recl. Trav. Chim. Pays-Bas* 1969, **88**, 1451.
12. K. Nakamoto, *Infrared and Raman Spectra of Inorganic and Coordination Compounds*, 3rd edn, p. 249. Wiley Interscience, New York (1978).
13. J. B. Hodgson, G. C. Percy and D. A. Thornton, *Transition Met. Chem.* 1978, **3**, 302.
14. R. E. Cramer and K. Seff, *J. Chem. Soc., Chem. Commun.* 1972, 400.
15. J. A. Cunningham and R. E. Sievers, *Inorg. Chem.* 1980, **19**, 595.
16. S. J. Schuchart Wasson, D. E. Sands and W. F. Wagner, *Inorg. Chem.* 1973, **12**, 187.

Polyhedron Vol. 9, No. 5, pp. 757–761, 1990
Printed in Great Britain

0277–5387/90 $3.00+.00
© 1990 Pergamon Press plc

η^3-2-METHYLALLYL PHOSPHINE COMPLEXES OF NICKEL(II)

ERNESTO CARMONA,† PILAR PALMA and MANUEL L. POVEDA

Departamento de Química Inorgánica-Instituto de Ciencia de Materiales, Universidad de Sevilla-CSIC, Apartado 553, 41071-Sevilla, Spain

(*Received* 15 *September* 1989; *accepted* 16 *October* 1989)

Abstract—The reaction of $[Ni(cod)_2]$ (cod = 1,5-cyclooctadiene) with $2\text{-}MeC_3H_4Cl$ (2-methylallyl chloride), in the presence of different phosphine ligands, has been investigated. PMe_3 furnishes the 16-electron allyl species $[Ni(\eta^3\text{-}2\text{-}MeC_3H_4)Cl(PMe_3)]$ (**1**), while dmpe (dmpe = $Me_2PCH_2CH_2PMe_2$) provides an 18-electron, five-coordinate complex, $[Ni(\eta^3\text{-}2\text{-}MeC_3H_4)Cl(dmpe)]$ (**2**). By contrast, the diphosphines $Ph_2PCH_2PPh_2$ (dppm) and $Me_2PCH_2PMe_2$ (dmpm) form the binuclear complexes $[[Ni(\eta^3\text{-}2\text{-}MeC_3H_4)Cl]_2(\mu\text{-}R_2PCH_2PR_2)]$ (R = Ph, **3**; Me, **4**) containing bridging phosphine ligands. Alkylation of the chloride complex **1** with various Grignard reagents, Mg(R)Cl, allows the isolation of the alkyl–allyl derivatives $[Ni(\eta^3\text{-}2\text{-}MeC_3H_4)R(PMe_3)]$ (R = CH_2SiMe_3, **5**; CH_2CMe_3, **6**; $CH_2C_6H_4$-*o*-Me, **7**). The new compounds have been characterized by analytical and spectroscopic techniques (IR, ^1H, ^{13}C and ^{31}P NMR).

Allyl nickel compounds are key intermediates in a number of catalytic reactions, and have been widely used for the synthesis of complex organic molecules.[1,2] A large number of nickel derivatives containing allyl ligands have been characterized.[3] Many of these compounds contain also a halide, alkyl or aryl group, and in some cases further stabilization is provided by the presence of a donor ligand.[3] As a continuation of previous studies on the chemistry of allyl complexes of nickel,[4] we have now prepared some η^3-2-methylallyl compounds containing mono- and bidentate phosphine ligands. Their synthesis and characterization are the subject of this paper. Analytical and selected ^1H NMR data for the new compounds are reported in the Experimental; ^{13}C and ^{31}P NMR data are collected in Table 1.

RESULTS AND DISCUSSION

(a) 2-*Methylallyl phosphine halide complexes*

The 2-methylallyl halide compounds have been synthesized by a route commonly used for the preparation of this type of compounds, namely by oxidative addition of 2-methylallyl chloride to $[Ni(cod)_2]$ (cod = 1,5-cyclooctadiene), in the presence of the phosphine ligand.[3]

Addition of 1 equiv of $2\text{-}MeC_3H_4Cl$ to a cold (−40°C), stirred suspension of $[Ni(cod)_2]$ in Et_2O, in the presence of 1 equiv of PMe_3, produces no apparent reaction, but upon warming at room temperature, the suspended solid is taken up into the solution which then becomes red in colour. When the reaction is complete [eq. (1)], red–orange needles of $[Ni(\eta^3\text{-}2\text{-}MeC_3H_4)Cl(PMe_3)]$ (**1**) can be isolated in high yields. Compound **1** is an air-sensitive solid,

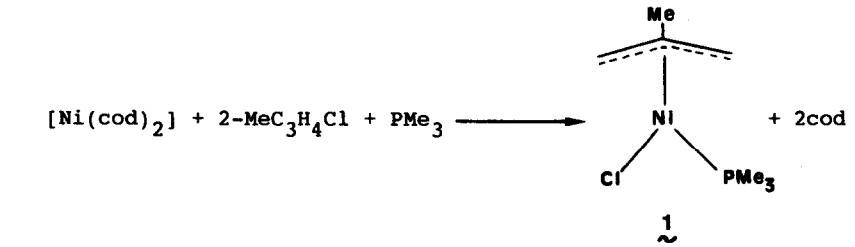

(1)

† Author to whom correspondence should be addressed.

Table 1. Selected NMR data for the new complexes

	$^{13}C\{^1H\}$					
		Allylic ligand				
Compound	P—Me	Me	CH_2	C—Me	Others	$^{31}P\{^1H\}$
1[a]	13.4d (26.7)	23.1s	46.9d (6.0) 70.2d (22.8)	121.8s		−12.7s
2[a]	13.8pst (12.5) 14.6pst (12.6)	24.1s	59.3pst (10.1)	119.1s	28.4pst (P—CH_2, 23.6)	39.0s
3		22.5s	62.5brs	111.3s	26.8brs (P—CH_2), 128.2, 129.1, 133.1, 136.1 (brs, aromatics)	1.86brs
4[b]	19.2brs	18.8s	64.6brs	107.3s	20.3brs (P—CH_2)	−0.5s
5	16.3d (24.8)	24.0s	55.3d (5.1) 58.2d (25.8)	119.5s	−10.3d (CH_2Si, 11.0), 4.0s ($SiMe_3$)	−7.5s
6	16.4d (24.3)	23.8s	55.3s 58.0d (25.1)	119.8s	22.3d (CH_2CMe_3, 12.9), 34.6s (CMe_3), 35.9s (CMe_3)	−8.4s
7	15.2d (24.9)	24.0s	52.2d (4.8) 67.6d (22.9)	122.5s	15.6d (CH_2Ar, 10.2), 21.3s ($MeAr$), 120.1, 125.4, 126.3, 129.2 (s, CH arom), 131.3s (C_{Ar}—Me), 157.5d (C_{Ar}, 5.9)	−9.0s

Coupling constants (Hz) in parentheses. In C_6D_6 unless otherwise indicated. pst = pseudotriplet.
[a] In CD_2Cl_2 at −80°C.
[b] In CD_2Cl_2, RT.

readily soluble in common, non-polar, organic solvents. It is fluxional in solution as evidenced by the appearance of broad, unresolved NMR features in its NMR spectra. The $^{13}C\{^1H\}$ room temperature spectrum shows two rather broad signals at *ca* 65.0 and 41.6 ppm, that can be assigned to the terminal carbon atoms of the allyl ligand.[5] Upon cooling at −70°C (CD_2Cl_2) they convert into two doublets as a result of coupling to the ^{31}P nuclei. This is in accord with the rigid structure shown for this complex in eq. (1). The values of the ^{31}P–^{13}C coupling constants are 23 and 6 Hz for the signals at 65.0 and 41.6 ppm, respectively. Thus, the former is ascribed to the methylene allylic carbon *trans* to the PMe_3 ligand, while the latter corresponds to the other terminal carbon atom. The *meso*-carbon provides a singlet at 119.5 ppm, that remains unchanged with temperature. Above room temperature, the signals at 65.0 and 41.6 ppm further broaden and begin to coalesce. At 65°C only a broad hump is observed at an average chemical shift, and the decomposition of the sample at higher temperatures prevents attainment of the fast-exchange limit. All other resonances, including those associated with the PMe_3 ligand, remain sharp in this temperature range (−70 to +65°C). The fluxional processes responsible for the temperature dependence of the NMR spectra of allyl compounds have been studied in detail.[3,5–7] Since, on the other hand, very limited data are available for compound **1**, this problem has not been investigated any further.

The chelating phosphine dmpe reacts similarly and provides high yields (*ca* 85%) of the five-coordinated species [Ni(η^3-2-MeC_3H_4)Cl(dmpe)] (**2**), as shown in eq. (2). The proposed structure for **2** is in accord with analytical and spectroscopic data, and it is similar to that found by X-ray studies for the analogous complex [Ni(η^3-2-MeC_3H_4)Br(dppe)][8] (dppe = $Ph_2PCH_2CH_2PPh_2$). Com-

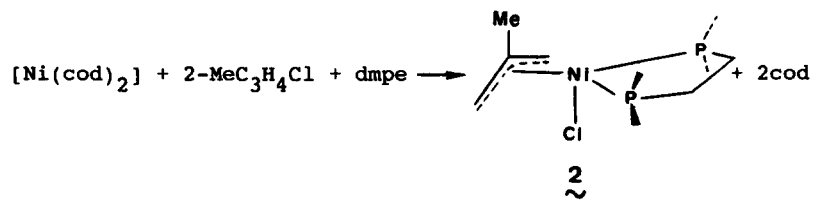

2

(2)

pound **2** is also fluxional and the available low temperature NMR data indicate the above structure is maintained in solution. Thus, in the slow-exchange limit the terminal allylic carbons are equivalent and produce a virtual triplet at 59.3 ppm ($J_{CP_{app}} \simeq 10$ Hz), as a result of their coupling to two chemically equivalent phosphorus nuclei, i.e. a deceptively simple AXX′ spin system. Interestingly, and again in agreement with the proposed structure, the methyl groups of the diphosphine ligand appear at −85°C as two multiplets that collapse into a virtual triplet at room temperature. The remaining carbon resonances, as well as the ^{31}P resonance characteristic of **2** (see Table 1) show no variation with temperature. ^1H NMR studies indicate that the *syn*- and *anti*-protons of the allyl moiety become equivalent in the fast-exchange limit. These observations can be explained in terms of a rapid exchange between the two degenerate ground structures, **A** and **B** shown below, by means of one or more

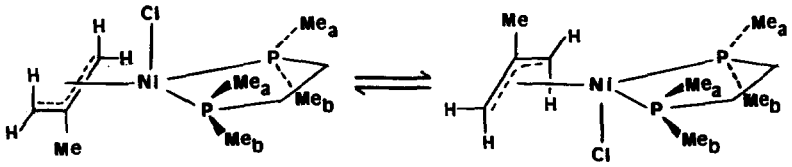

A **B**

thermally accessible pathways. A simple mechanistic route that would account for the above changes involves the formation of a four-coordinate, $^1\eta$-allyl intermediate, such as species **C** shown below.

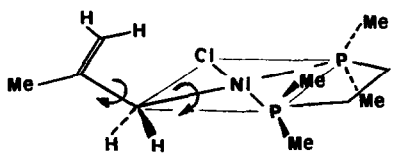

C

We have attempted the synthesis of compounds related to **2** by using other bidentate phosphines such as dppm and dmpm. These, however, display different behaviour. For instance, addition of equimolar amounts of dppm to a 1:1 mixture of $[Ni(cod)_2]$ and 2-MeC_3H_4Cl, provides a dark red species of analytical composition "$Ni(2\text{-}MeC_3H_4)Cl(dppm)_{0.5}$", which seems to be a binuclear species, whose formation takes place as depicted in eq. (3):

$$2[Ni(cod)_2] + 2\,2\text{-}MeC_3H_4Cl + P{-}P \longrightarrow [Ni_2(\eta^3\text{-}2\text{-}MeC_3H_4)_2Cl_2(P{-}P)] \quad (3)$$

(P—P = dppm, **3**; dmpm, **4**).

A similar reaction using dmpm as the phosphine ligand yields the related complex **4**. Compound **3** exhibits a complex behaviour in solution. The $^{13}C\{^1H\}$ NMR spectrum recorded at 20°C (C_6D_6) shows equivalence of the allyl ligands, the terminal allylic carbons giving rise to a slightly broad singlet centred at 64.6 ppm. We have been unable to attain the slow-exchange spectrum for this complex. On the other hand, the $^{31}P\{^1H\}$ spectrum, recorded at −80°C, consists of several broad resonances that suggest that this compound exists as a mixture of different isomeric species. At room temperature these are in an equilibrium that is fast with respect to the NMR time scale. A definite structural proposal cannot obviously be made with the data available.

The analogous dmpm derivative **4** is sparingly soluble in non-polar organic solvents, although it dissolves readily in acetone and other polar solvents. Attempts to obtain crystalline samples of this material from different solvent mixtures have proved unsuccessful, although the available analytical data are in reasonable agreement with the proposed formulation (see Experimental). The $^{13}C\{^1H\}$ and $^{31}P\{^1H\}$ spectra display relatively simple features that remain essentially unchanged with temperature and provide no useful information with regards to the structure of this complex.

(b) 2-*Methylallyl phosphine alkyl complexes*

Some new alkyl–allyl complexes of nickel(II) have been synthesized by the general reaction route outlined in eq. (4), i.e. by alkylation of the chloride derivative **1** with the corresponding Grignard reagent. The new compounds are extremely soluble in all common organic solvents tested. This has prevented us to induce their crystallization even from very concentrated solutions, but they have been isolated as spectroscopically pure oils, with NMR and other properties fully in accord with the proposed formulation. The trimethylsilylmethyl derivative **5** gives rise to two ^{13}C doublets at 55.3 ($^2J_{CP}$ = 5 Hz) and 58.2 ppm ($^2J_{CP}$ = 25 Hz), that can be readily assigned to the two different methylene carbons of the allyl ligand (*cis* and *trans* to the PMe_3 ligand, respectively). The *meso*-carbon

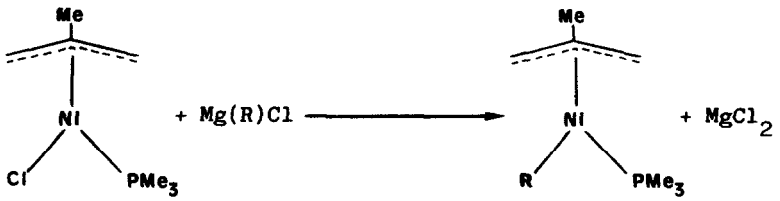

(4)

R= CH_2SiMe_3, 5; CH_2CMe_3, 6

appears at *ca* 119 ppm and exhibits no coupling to the ^{31}P nuclei. On the other hand, the nickel-bound carbon atom of the alkyl group appears also as a doublet as a result of its coupling to the ^{31}P nucleus. The low value of 11 Hz found for this coupling constant is clearly indicative of a *cis* distribution of the alkyl and phosphine ligands. Finally, the non-planarity of the molecules of **5** (and **6**) is clearly manifested by the diastereotopicity of the Ni—CH_2R protons in the ^1H NMR spectra.

We have shown recently[4] that the halide Me-*o*-$C_6H_4CH_2Cl$ oxidatively adds to [Ni(cod)$_2$], in the presence of trimethylphosphine, with formation of an equilibrium mixture of the η^1- and η^3-pseudoallylic complexes [Ni(η^1-$CH_2C_6H_4$-*o*-Me)Cl(PMe_3)$_2$] and [Ni(η^3-$CH_2C_6H_4$-*o*-Me)Cl(PMe_3)], respectively [eq. (5)]:

$$[Ni(cod)_2] + ClCH_2C_6H_4\text{-}o\text{-}Me \xrightarrow{PMe_3} [Ni(\eta^1\text{-}CH_2C_6H_4\text{-}o\text{-}Me)Cl(PMe_3)_2] + [Ni(\eta^3\text{-}CH_2C_6H_4\text{-}o\text{-}Me)Cl(PMe_3)] \quad (5)$$

The η^3-allyl complex can be readily prepared by carrying out the above reaction in the presence of equimolar quantities of PMe_3. The facility with which the *o*-methylbencyl group yields η^3-pseudoallylic structures and the fact that compounds of the type [Ni(η^3-allyl)$_2$(PR_3)] are known,[3] prompted us to attempt the synthesis of a mixed allylic complex by reaction of **1** with Mg($CH_2C_6H_4$-*o*-Me)Cl. This interest was further enhanced by the knowledge from the literature that attempts to prepare mixed bis(π-allyl) complexes of nickel, [Ni(η^3-allyl)(η^3-allyl*)], lead[3] to the disproportionation products, i.e. [Ni(η^3-allyl)$_2$] and [Ni(η^3-allyl*)$_2$]. With this aim in mind, the reaction of complex **1** and Mg($CH_2C_6H_4$-*o*-Me)Cl was undertaken. However, as shown in eq. (6), the resulting compound was not the desired mixed bis(allyl), but rather an alkyl–allyl complex **7**, analogous to **5** and **6**. Formation of **7** as an η^1-*o*-methylbencyl species follows from spectroscopic data. They are collected in Table 1 (^{13}C and ^{31}P) and in the Experimental (^1H) and require no further comment.

EXPERIMENTAL

Microanalyses were by Pascher Microanalytical Laboratory, Remagen (F.R.G.), and the Microanalytical Service of the University of Seville. The spectroscopic instruments used were Perkin–Elmer models 557 and 684 for IR spectra and Varian XL-200 for ^1H, ^{13}C and ^{31}P NMR spectra. All preparations and other operations were carried out under oxygen-free nitrogen, following conventional Schlenk techniques. Solvents were dried and degassed before use. [Ni(cod)$_2$] and PMe_3 were prepared according to literature methods.[9,10]

Synthesis of [Ni(η^3-2-MeC_3H_4)Cl(PMe_3)] (**1**)

To a stirred suspension of [Ni(cod)$_2$] (0.82 g, *ca* 3 mmol) in 40 cm^3 of diethyl ether, cooled to −40°C, 0.3 cm^3 of PMe_3 (3 mmol) and 3 cm^3 of a 1 M solution of 2-MeC_3H_4Cl in Et_2O (3 mmol) were added. The reaction mixture was warmed and stirred at room temperature until all the starting material had dissolved (2 h), when a red solution was obtained. The solvent was removed under vacuum, the residue extracted with Et_2O and filtered. Concentration of the resulting solution and cooling at −30°C provided compound **1** as red–orange needles in 85% yield. Found: C, 36.7; H, 7.0. Calc. for $C_7H_{16}PClNi$: C, 37.3; H, 7.1%. ^1H NMR (C_6D_6, 200 MHz): δ 0.92 (d, $^2J_{HP}$ = 8.8 Hz, PMe_3), 1.73 (s, C—Me), 1.38, 1.96, 2.88 and 3.80 (brs, CH_2).

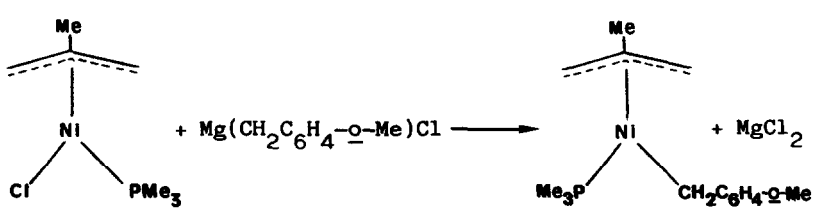

(6)

7

Following a similar procedure the following complexes were prepared: [Ni(η^3-2-MeC_3H_4)Cl(dmpe)] (**2**), orange needles from Et_2O, 85% yield. Found: C, 40.0; H, 7.6. Calc. for $C_{10}H_{23}P_2ClNi$: C, 40.1; H, 7.7%. ^1H NMR (C_6D_6, 200 MHz, 70°C): δ 1.15 (d, $^2J_{HP}$ = 9.6 Hz, P—Me), 1.33 (d, $^2J_{HP}$ = 14.8 Hz, P—CH_2), 1.41 (s, C—Me), 3.23 (brs, allylic CH_2). [$Ni_2(\eta^3$-2-$MeC_3H_4)_2(\mu$-dppm)] (**3**), dark red crystals from Et_2O, 75% yield. Found: C, 58.5; H, 5.9. Calc. for $C_{33}H_{36}P_2Cl_2Ni_2$: C, 58.0; H, 5.3%. ^1H NMR (C_6D_6, 200 MHz, 70°C): δ 1.77 (brs, P—CH_2), 3.05 (s, C—Me), 2.60, 3.45 (brs, allylic CH_2), 6.8–7.7 (m, Ph).

When dmpm is used as the complexing ligand, compound **4** precipitates out of the reaction mixture. After 2 h of stirring at room temperature, the resulting suspension was filtered off and the yellow solid residue washed with Et_2O. Found: C, 34.8; H, 7.1. Calc. for $C_{13}H_{28}P_2Cl_2Ni_2$: C, 35.9; H, 6.4%. ^1H NMR (CD_2Cl_2, 200 MHz): δ 1.5 (brs, P—Me); 1.75 (s, C—Me), 2.70 (brs, P—CH_2), 2.76, 3.43 (brs, allylic CH_2).

Preparation of [Ni(η^3-2-MeC_3H_4)CH_2SiMe_3(PMe_3)] (**5**)

4.1 cm^3 of a 0.8 N solution of Mg(CH_2SiMe_3)Cl in diethyl ether (*ca* 3.5 equiv) were added to a cold (−40°C) solution of complex **1** (0.8 g, 3.5 mmol) in Et_2O (40 cm^3). The colour of the reaction mixture gradually changed from red to yellow and the stirring was continued for 1 h at room temperature. The solvent was then stripped off under reduced pressure and the residue extracted with 25 cm^3 of petroleum ether and centrifuged. Evaporation to dryness gave an oily residue that was shown to be spectroscopically pure **5**. ^1H NMR (C_6D_6, 200 MHz): δ −0.39 (dd, H_A, CH_2Si, $^2J_{AB}$ = 10.5, $^3J_{AP}$ = 13.9 Hz), −0.16 (t, H_B, CH_2Si, $^3J_{BP}$ = 10.4 Hz), 0.08 (s, $SiMe_3$), 1.00 (d, $^2J_{HP}$ = 7.8 Hz, PMe_3), 1.58, (s, C—Me), 1.40, 2.08, 2.36 and 3.03 (H_1, H_2, H_3 and H_4 allylic protons, respectively, d, d, dd and t, $^3J_{H_1P}$ = 2.6, $^3J_{H_2P}$ = 5.9, $^3J_{H_3P}$ = 5.4, $^3J_{H_4P}$ = 4.9, $^2J_{H_AH_B}$ = 3.5 Hz).

The corresponding reactions of **1** with Mg(CH_2CMe_3)Cl and Mg($CH_2C_6H_4$-*o*-Me)Cl, were carried out using a similar procedure, and allowed the isolation of [Ni(η^3-2-MeC_3H_4)CH_2CMe_3(PMe_3)] (**6**) and [Ni(η^3-2-MeC_3H_4)($CH_2C_6H_4$-*o*-Me)(PMe_3)] (**7**) in the form of pure highly soluble oils. (**6**): ^1H NMR (C_6D_6, 200 MHz): δ 0.71 (d, $^2J_{HP}$ = 6.9 Hz, PMe_3), 0.94 (s, CMe_3), 0.81, 1.06 (brs, CH_2CMe_3), 1.33 (s, C—Me), 1.12, 1.95, 2.05 and 3.08 (brs, allylic protons). (**7**): ^1H NMR (C_6D_6, 200 MHz): δ 0.85 (d, $^2J_{HP}$ = 7.8 Hz, PMe_3), 1.33 (d, $^3J_{HP}$ = 2.6 Hz, CH_2Ar), 1.50 (s, C—Me), 2.28 (s, Ar—*Me*), 1.84–2.25 (m, allylic protons), 6.8–7.2 (m, aromatic protons).

Acknowledgement—We thank the Dirección General de Política Científica for financial support.

REFERENCES

1. G. Wilke, *Angew. Chem. Int. Edn Engl.* 1988, **27**, 185.
2. P. S. Braterman, *Reactions of Coordinated Ligands* (Edited by P. S. Braterman). Plenum Press, New York (1986).
3. (a) P. W. Jolly, *Comprehensive Organometallic Chemistry* (Edited by G. Wilkinson, F. G. A. Stone and E. W. Abel), Vol. 6. Pergamon Press, Oxford (1982); (b) P. W. Jolly and G. Wilke, *The Organic Chemistry of Nickel* (Edited by P. M. Maitlis, F. G. A. Stone and R. West), Col. 1. Academic Press, London (1974).
4. (a) E. Carmona, J. M. Marín, M. Paneque and M. L. Poveda, *Organometallics* 1987, **6**, 1757; (b) E. Carmona, M. Paneque and M. L. Poveda, *Polyhedron* 1989, **8**, 285.
5. (a) P. W. Jolly and R. Mynott, *Adv. Organomet. Chem.* 1981, **19**, 257; (b) B. E. Mann and B. F. Taylor, ^{13}C *NMR Data for Organometallic Compounds*. Academic Press, London (1981).
6. K. Vrieze, *Dynamic Nuclear Magnetic Resonance Spectroscopy* (Edited by L. M. Jackman and F. A. Cotton). Academic Press, London (1975).
7. B. Henc, P. W. Jolly, R. Salz, G. Wilke, R. Benn, E. G. Hoffman, R. Mynott, G. Schroth, K. Seevogel, J. C. Sekutowski and C. Krüger, *J. Organomet. Chem.* 1980, **191**, 425; 1980, **191**, 449.
8. T. S. Cameron and C. K. Prout, *Acta Cryst.* 1972, **28B**, 2021.
9. F. Guerrieri and G. Salermo, *J. Organomet. Chem.* 1976, **114**, 339.
10. W. Wolfsberger and H. Schmidbaur, *Synth. React. Inorg. Met.-Org. Chem.* 1974, **4**, 149.

Polyhedron Vol. 9, No. 5, pp. 763–768, 1990
Printed in Great Britain

0277–5387/90 $3.00 + .00
© 1990 Pergamon Press plc

SYNTHESIS AND STRUCTURE OF A MONONUCLEAR ZINC(II) COMPLEX OF 2-(DIMETHYLAMINO)ETHANETHIOL

I. CASALS and P. GONZÁLEZ-DUARTE*

Departament de Química, Universitat Autònoma de Barcelona, 08193 Bellaterra, Barcelona, Spain

and

C. LÓPEZ and X. SOLANS

Departament de Cristal·lografia i Mineralogia, Universitat de Barcelona, c/Martí i Franquès, s/n, 08028 Barcelona, Spain

(*Received* 31 *July* 1989; *accepted* 16 *October* 1989)

Abstract—The preparation of $[Zn\{SCH_2CH_2N(CH_3)_2\}_2]$ by electrochemical oxidation of zinc and simultaneous reduction of 2-(dimethylamino)ethanethiol disulphide in an acetonitrile solution containing triethylamine is described. The compound crystallizes in the orthorhombic space group $P2_12_12_1$ with $a = 22.010(5)$, $b = 11.313(3)$ and $c = 10.170(3)$ Å. The structure consists of two crystallographically independent neutral monomeric units, which are optical isomers. Each zinc atom is bonded to two nitrogen and two sulphur atoms yielding a distorted tetrahedral coordination geometry. The chelating behaviour of the ligand is also evidenced in the IR and ^1H and ^{13}C NMR spectra.

The X-ray crystal structure of metal complexes of *v*-mercaptoamines has shown that the chelating ability of this family of ligands is a function of the flexibility of the carbon chain linking nitrogen and sulphur donor atoms and also of the metal character. Thus, while 3-amino-1-propanethiol has always behaved as a chelating ligand,[1–3] 3-dimethylamino-1-propanethiol[4–6] and aliphatic cyclic *v*-mercaptoamines[7–9] have preferred coordination via the thiolate group exclusively. The only known examples where 3-dimethylamino-1-propanethiol,[10] 4-mercapto-1-methylpiperidine,[11] 2-(mercaptoethyl)-1-methylpiperidine,[12] 3-(mercaptomethyl)-1-methylpiperidine[13] and 3-(mercaptomethyl)piperidine[10,14] behave as bidentate chelating ligands are restricted to palladium(II) and platinum(II) complexes. Up to now, metal atoms belonging to the first transition series have never yielded chelates. In order to assess the stereochemical constraints imposed by the N-methyl substituted amine function in mercaptoamine ligands, a zinc derivative of 2-(dimethylamino)ethanethiol has been prepared by direct electrochemical synthesis. The crystal and molecular structure of the $[Zn\{SCH_2CH_2N(CH_3)_2\}_2]$ complex together with the corresponding IR, ^1H and ^{13}C NMR spectra are described in this paper. To our knowledge no complex of the previous ligand with group 12† metals has yet been reported.

EXPERIMENTAL

2-(Dimethylamino)ethanethiol disulphide was obtained from 2-(dimethylamino)ethanethiol by adding an equimolecular amount of NaOH to an aqueous solution of 2-(dimethylamino)ethanethiol hydrochloride (purchased from Fluka) and then distilling the mixture under the open atmosphere. Acetonitrile and methanol were stored over molecular sieves before use. The rest of the reagents were research grade and were not further purified.

Preparation of $[Zn\{SCH_2CH_2N(CH_3)_2\}_2]$

A zinc foil (60 × 15 × 0.2 mm) and a platinum wire (10 × 0.5 mm diameter) were placed on the

* Author to whom correspondence should be addressed.
† Refers to the 18-group format of the Periodic Table.

longest opposite faces of a glass cell (75 × 60 × 30 mm) as anode and cathode, respectively. A solution consisting of 2 cm^3 (8.78 mmol) of 2-(dimethylamino)ethanethiol disulphide, 6 cm^3 (43 mmol) of NEt_3 and 0.023 g (0.1 mmol) of Et_4NClO_4 in 50 cm^3 of acetonitrile was added to the cell, which was sealed by means of the corresponding glass lid. A constant voltage of 20 V was applied to the electrodes for 24 h, meanwhile the current intensity varied from the initial 20 mA to the final 5 mA. Then, to the filtered solution, 20 cm^3 of dry diethyl ether were added. This new solution was extracted successively 10 times with 20 cm^3-portions of *n*-hexane. The combined extracts of *n*-hexane were evaporated *in vacuo* down to 5 cm^3 and then the solution was left under a slow stream of nitrogen until a crystalline white solid appeared, which was filtered and dried *in vacuo*. (Found: C, 35.3; N, 10.1; S, 23.3; Zn, 24.2. $C_8H_{20}N_2S_2Zn$ requires C, 35.1; N, 10.2; S, 23.4; Zn, 23.9%.)

This compound is soluble in methanol, ethanol, acetone, diethyl ether, acetonitrile and dichloromethane and slightly soluble in *n*-hexane. It decomposes in water and also in either acid or basic aqueous solutions.

Suitable crystals for X-ray diffraction were obtained by slow evaporation of anhydrous methanolic solutions of the title compound by means of a controlled stream of nitrogen. Analogous attempts with other solvents already mentioned always led to poor quality crystals.

Analyses

Microanalyses were performed by one of the authors (I.C.) with a Carlo Erba NA-1500 analyser. The zinc content was determined by complexometric titration with EDTA.

Physical measurements

IR spectra were recorded from 4000 to 400 cm^{-1} in KBr or between NaCl plates on a Perkin–Elmer 1710 spectrophotometer. The far-IR spectrum of the solid complex was recorded as Nujol mull supported between polythene plates using a Perkin–Elmer 983 apparatus.

^1H and $^{13}C\{^1H\}$ NMR spectra were recorded on a Bruker AM-400 in CD_3OD (99.6%) solutions.

Crystallography

Crystal data. $[C_8H_{20}N_2S_2Zn]$, $M = 273.76$, orthorhombic, $a = 22.010(5)$, $b = 11.313(3)$, $c = 10.170(3)$ Å, $V = 2532(2)$ $Å^3$, $Z = 8$, $D_c = 1.436$ g cm^{-3}, $F(000) = 1152$, space group $P2_12_12_1$, $\lambda(\text{Mo-}K_\alpha) = 0.71069$ Å, $\mu(\text{Mo-}K_\alpha) = 22.69$ cm^{-1}, room temperature.

A prismatic white crystal (0.1 × 0.1 × 0.2 mm) was selected and mounted on a Philips PW-1100 four circle diffractometer. Unit-cell parameters were determined from automatic centring of 15 reflections ($4 \leqslant \theta \leqslant 12°$) and least-squares refinement on setting angles. Intensities were collected with graphite monochromatized Mo-K_α radiation, using the ω-scan technique, scan width 0.8°, scan speed 0.03° s^{-1}. 1734 reflections were measured in the range $2 \leqslant \theta \leqslant 25°$; 1050 of which were assumed as observed, applying the condition $I \geqslant 2.5\sigma(I)$. Three reflections were measured every 2 h as orientation and intensity control, no significant intensity decay was observed. Lorentz-polarization but not absorption corrections were made.

Solution and refinement. The structure was solved by direct methods, using the MULTAN system of computer programs[15] and refined by full-matrix least-squares using the SHELX76 computer program.[16] The function minimized was $\Sigma w(|F_o| - |F_c|)^2$, where $w = (\sigma^2(F_o) + 0.037|F_o|^2)^{-1}$, *f*. *f'* and *f''* were taken from the *International Tables of X-ray Crystallography*.[17] The positions of hydrogen atoms were computed and refined with an overall isotropic temperature factor, using a riding model. The final *R* factor was 0.053 ($wR = 0.057$) for all observed reflections.* Maximum shift/ESD = −0.2 in *Z* of N8(B), maximum and minimum peaks in final difference synthesis were 0.4 and −0.4 e $Å^{-3}$, respectively.

RESULTS AND DISCUSSION

Synthesis

The anodic oxidation of zinc and the simultaneous cathodic reduction of 2-(dimethylamino) ethanethiol disulphide is a direct route for obtaining a very pure zinc chelate of formula $[Zn\{SCH_2CH_2N(CH_3)_2\}_2]$. The same procedure using either the thiol or the corresponding disulphide as starting materials has already been reported for the synthesis of neutral $[M^{II}(SR)_2]$ compounds (M = Zn, Cd, Hg), for which a polymeric structure has been proposed,[18] and also for the syn-

* Atomic coordinates, thermal parameters, full lists of bond lengths and angles and lists of F_o/F_c values have been deposited as supplementary data with the Editor, from whom copies are available on request. Atomic coordinates have also been deposited with the Cambridge Crystallographic Data Centre.

thesis of the anionic cluster $[Zn_4(SPh)_{10}]^{2-}$ whose structure consists of discrete tetrahedra of zinc atoms with four terminal and six bridging thiolate ligands. Despite that, the formula of the complex reported in this work is compatible with a polymeric structure, the ability of the ligand to behave as a chelate has caused formation of discrete mononuclear species, in agreement with the high solubility of $[Zn\{SCH_2CH_2N(CH_3)_2\}_2]$ in common organic solvents. The main difference in the synthesis of this complex and those mentioned above is that in our case the electrochemical reaction has never attained a 90% yield as has been reported for the other complexes. Even though the amount of pure complex recovered is a function of the number of extractions, its solubility in *n*-hexane accounts for the low yield. On the other hand, evaporation of the acetonitrile–ethereal solution has always led to a yellow solid whose elemental analyses and IR spectrum indicated that it corresponded to a slightly impure zinc complex.

Description of the structure of $[Zn\{SCH_2CH_2N(CH_3)_2\}_2]$

The title compound crystallizes in orthorhombic space group $P2_12_12_1$ and contains discrete neutral monomeric units exclusively. The most relevant metrical parameters for the two crystallographically independent molecules, denoted as **A** and **B**, are given in Table 1. The X-ray analysis shows that **A** and **B** differ slightly in bond distances and angles. Molecules **A** and **B** together with the atom numbering scheme are displayed in Fig. 1. In each unit the zinc atom is coordinated to two ligand molecules by means of the nitrogen and sulphur donor atoms. Thus, both aminothiolate ligands give rise to a five-membered chelate ring. The chelate groups are non-planar. The coordination geometry around zinc is that of a flattened tetrahedron as evidenced by the bite angle of the ligands, which is close to 90°C and by the S(1)—Zn—S(2) and N(3)—Zn—N(8) angles, which are about 141 and 116°, respectively (Table 1). The degree of distortion from tetrahedral geometry can also be measured by the dihedral angle determined by the planes defined by S(1), Zn, S(2) and N(3), Zn, N(8) atoms, which is 77.5 and 78.7° for molecules A and B, respectively. Similar distortions from tetrahedral geometry have been reported for ZnN_2S_2 units and five-membered S,N-chelate rings. By comparing $[Zn\{SCH_2CH_2N(CH_3)_2\}_2]$ with $[Zn\{SC(CH_3)_2CH_2NH_2\}_2]$[20] and $[Zn_2LCl_2]_2$ (L = $^-SCH_2CH_2N(CH_3)CH_2CH_2N(CH_3)CH_2CH_2S^-$),[21] Table 2, it is possible to conclude that: (a) Zn—S and Zn—N bond distances are comparable in the three complexes and agree well with other literature values;[22–24] (b) the bite angle of the ligands, S—Zn—N, and that formed by adjacent donor atoms of different ligands, S—Zn—N′, depend very little on the ligand nature and (c) the geometrical constraints of the $^-SCH_2CH_2N(CH_3)CH_2CH_2N(CH_3)CH_2CH_2S^-$ ligand account for the great S—Zn—S′ and small N—Zn—N′ angles; meanwhile the methyl groups in $^-SC(CH_3)_2CH_2NH_2$ and $^-SCH_2CH_2N(CH_3)_2$ cause the previous angles to vary in the opposite

Table 1. Bond distances (Å) and angles (°) with ESDs in parentheses for $[Zn\{SCH_2CH_2N(CH_3)_2\}_2]$

	Molecule A	Molecule B
(a) Bond lengths		
S(1)—Zn	2.270(7)	2.253(8)
S(2)—Zn	2.274(7)	2.270(8)
N(3)—Zn	2.137(17)	2.158(21)
N(8)—Zn	2.095(20)	2.156(21)
C(1)—S(1)	1.864(26)	1.829(25)
C(6)—S(2)	1.851(23)	1.798(28)
C(2)—C(1)	1.450(36)	1.587(35)
N(3)—C(2)	1.459(28)	1.508(29)
C(4)—N(3)	1.500(27)	1.451(27)
C(5)—N(3)	1.457(25)	1.481(23)
C(7)—C(6)	1.517(33)	1.521(28)
N(8)—C(7)	1.507(28)	1.487(28)
C(9)—N(8)	1.485(27)	1.473(27)
C(10)—N(8)	1.437(27)	1.513(25)
(b) Bond angles		
S(2)—Zn—S(1)	142.3(4)	141.1(3)
N(3)—Zn—S(1)	90.0(6)	91.8(6)
N(3)—Zn—S(2)	110.2(6)	109.2(6)
N(8)—Zn—S(1)	110.0(6)	109.9(6)
N(8)—Zn—S(2)	89.6(6)	90.7(6)
N(8)—Zn—N(3)	116.6(7)	115.5(8)
C(1)—S(1)—Zn	95.5(8)	94.9(8)
C(6)—S(2)—Zn	95.6(9)	96.6(7)
C(2)—C(1)—S(1)	114.1(19)	112.9(15)
N(3)—C(2)—C(1)	115.9(22)	107.8(21)
C(2)—N(3)—Zn	107.4(17)	104.3(14)
C(4)—N(3)—Zn	113.7(15)	115.7(17)
C(4)—N(3)—C(2)	113.9(20)	105.9(19)
C(5)—N(3)—Zn	106.4(14)	106.9(13)
C(5)—N(3)—C(2)	108.6(22)	110.9(21)
C(5)—N(3)—C(4)	106.5(18)	112.9(20)
C(7)—C(6)—S(2)	115.1(18)	114.3(17)
N(8)—C(7)—C(6)	108.5(20)	114.6(21)
C(7)—N(8)—Zn	108.9(17)	104.0(14)
C(9)—N(8)—Zn	115.5(14)	115.7(15)
C(9)—N(8)—C(7)	107.4(19)	112.2(18)
C(10)—N(8)—Zn	108.5(15)	102.7(14)
C(10)—N(8)—C(7)	111.2(18)	113.4(20)
C(10)—N(8)—C(9)	105.3(20)	108.6(20)

Table 2. Comparison of the most relevant metrical parameters (Å, °) for zinc(II) complexes containing ZnN_2S_2 units and five-membered S,N-chelate rings

	$[Zn\{SC(CH_3)_2CH_2NH_2\}_2]$[20]	$[Zn_2LCl_2]_2$[a,21]	$[Zn\{SCH_2CH_2N(CH_3)_2\}_2]$[b] Molecule **A**	Molecule **B**
Zn—S	2.297(4)	2.356(4), 2.343(4)	2.270(7), 2.274(7)	2.253(8), 2.270(8)
Zn—N	2.06(1)	2.079(11), 2.103(11)	2.137(17), 2.095(20)	2.158(21), 2.156(21)
S—Zn—N	91.5(3)	91.6(3), 91.8(3)	90.0(6), 89.6(6)	91.8(6), 90.7(6)
S—Zn—N′	108.9(3)	110.8(3), 112.4(4)	110.0(6), 110.2(6)	109.9(6), 109.2(6)
S—Zn—S′	137.1(2)	148.1(2)	142.3(4)	141.1(3)
N—Zn—N′	122.8(6)	87.0(4)	116.6(7)	115.5(8)
Dihedral angle between planes defined by S—Zn—S′ and N—Zn—N′ atoms	79.5(3)	75.2(3)	77.5	78.7

[a] L = $^-SCH_2CH_2N(CH_3)CH_2CH_2N(CH_3)CH_2CH_2S^-$.
[b] This work.

sense as would be expected based on their steric requirements only.

The structure of the $^-SCH_2CH_2N(CH_3)_2$ ligand itself shows no unusual features and compares well with the $^-SC(CH_3)_2CH_2NH_2$ ligand in tetrahedral zinc(II)[20] and cobalt(II)[25] complexes.

The closest distance between two molecules is 3.8 Å which denotes that no chemical forces act between them. The unit cell contains eight molecules, four of each optical isomer of the title compound. The absence of an inversion centre or a plane of symmetry in the molecule accounts for the existence of two enantiomeric forms, Δ and Λ,[26] and consequently for the two crystallographically independent units, **A** and **B**, respectively.

IR data

The comparison of the IR spectrum of the crystalline $[Zn\{SCH_2CH_2N(CH_3)_2\}_2]$ complex with that of $HSCH_2CH_2N(CH_3)_2$ and the corresponding halohydrates leads to the same conclusions as those drawn from aliphatic ν-mercaptoamine ligands.[11,27] Thus, also in the present case, the 3000–2500 cm^{-1} region indicates unambiguously the ligand behaviour, as displayed in Fig. 2. Meanwhile, free $HSCH_2CH_2N(CH_3)_2$ shows two strong and resolved bands at 2945 and 2780 cm^{-1}, assigned to $\nu(CH_2)$ and $\nu(CH_3—\bar{N})$, respectively, the chelating $^-SCH_2CH_2N(CH_3)_2$ anion only shows one, also strong and resolved, and centred at *ca* 2900 cm^{-1}.

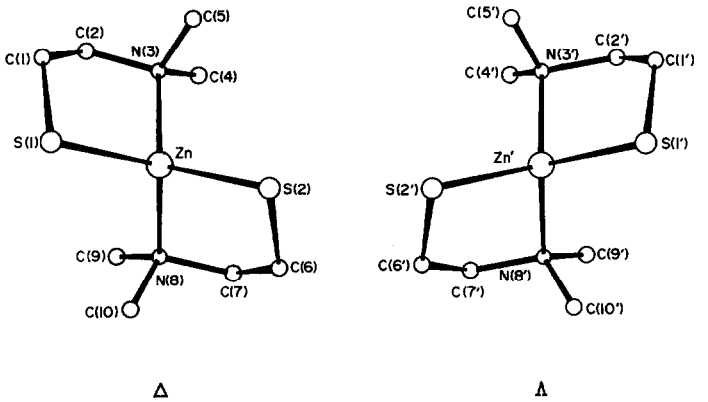

Δ Λ

Fig. 1. View of the two crystallographically independent molecules, **A** and **B**, in $[Zn\{SCH_2CH_2N(CH_3)_2\}_2]$, which correspond to Δ and Λ enantiomorphic forms, respectively. The atom numbering scheme is also shown.

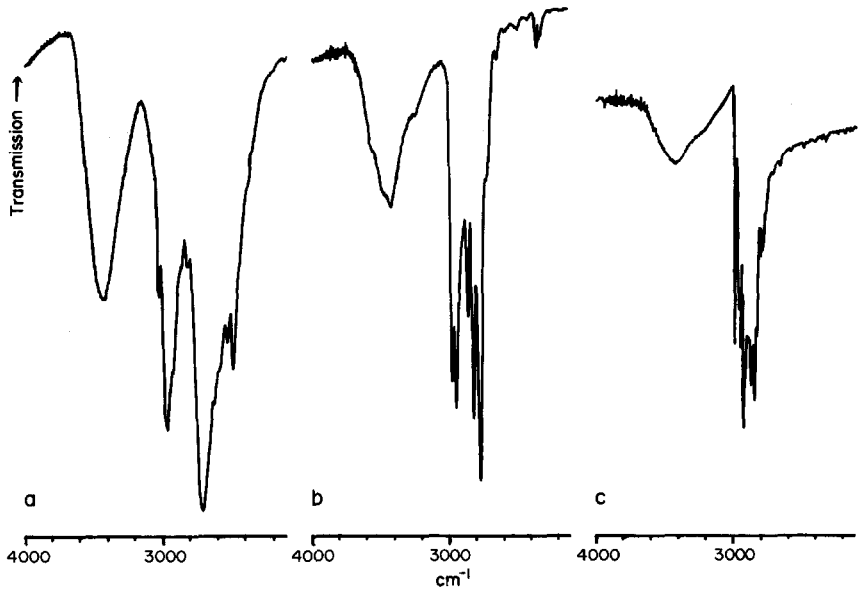

Fig. 2. The 4000–2200 cm^{-1} region of the IR spectra of (a) $HSCH_2CH_2N(CH_3)_2 \cdot HBr$, (b) $HSCH_2CH_2N(CH_3)_2$ and (c) $[Zn\{SCH_2CH_2N(CH_3)_2\}_2]$.

Based on the behaviour of *v*-mercaptoamine ligands[11,26] the IR spectrum of complexes where 2-(dimethylamino)ethanethiol is in the anionic form and coordinating through the sulphur atom exclusively should be practically identical to that of the free ligand. In the case of the halohydrates, which is comparable to complexes where the aminothiol is in the zwitterionic form and thus coordinating through the sulphur atom exclusively, $^-SCH_2CH_2\overset{+}{N}H(CH_3)_2$, the band at 2945 cm^{-1} remains, but a new very broad band centred at *ca* 2700 cm^{-1} is also present. This one can be assigned to ν(N—H) according to previous reports.[27] The far-IR spectrum (400–50 cm^{-1}) of $[Zn\{SCH_2CH_2N(CH_3)_2\}_2]$ shows bands at 377(s), 335(s), 299(m), 270(w), 232(s), 212(m), 169(w), 116(s), 92(m) and 76(m). The corresponding intensities are given in parentheses.

^1H *and* ^{13}C NMR *data*

Peaks observed in the ^1H and ^{13}C, ^1H-decoupled NMR spectra of solutions of $(CH_3)_2NCH_2CH_2SSCH_2CH_2N(CH_3)_2$ and $[Zn\{SCH_2CH_2N(CH_3)_2\}_2]$ are given in Table 3, together with the corresponding assignments, which have been made based on reported information on aliphatic *v*-mercaptoamine complexes.[11,12,28] By comparing the ^1H NMR spectra of the zinc complex with that of the free disulphide it is observed that in the complexed ligand, the singlet corresponding to the methyl groups shifts 0.16 ppm to lower fields which

Table 3. ^1H and $^{13}C\{^1H\}$ NMR spectra of 2-(dimethylamino)ethanethiol disulphide and bis[2-(dimethylamino)ethanethiolato-N,S]zinc(II) in CD_3OD solution

	^1H NMR[a]		$^{13}C\{^1H\}$ NMR	
	δ (ppm, Me_4Si)	assignment	δ (ppm, Me_4Si)	assignment
$[(CH_3)_2NCH_2CH_2S]_2$	2.65(t)	—CH_2—	36.78	S—CH_2
	2.84(t)	—CH_2—	59.78	N—CH_2
	2.27(s)	$(CH_3)_2N$	45.38	$(CH_3)_2N$
$[Zn\{SCH_2CH_2N(CH_3)_2\}_2]$	2.63(t)	—CH_2—	24.60	S—CH_2
	2.72(t)	—CH_2—	64.66	N—CH_2
	2.43(s)	$(CH_3)_2N$	45.91	$(CH_3)_2N$

[a] (s) and (t) denote singlet and triplet, respectively.

is consistent with its chelating behaviour. However, this shift is smaller than that found for palladium(II)[11,12] and platinum(II)[11] complexes of *v*-mercaptoamines, thus indicating that the metal nature plays an important role on the referred displacement.

The main features of the ^{13}C NMR spectra of the above compounds complete the information obtained from the ^{1}H NMR spectra. Thus, the chemical shifts of the peaks assigned to $C(H_2—S)$ and $C(H_2—N)$ differ significantly from the free disulphide to the chelated aminothiolate ligand, while that corresponding to the methyl groups is practically unaffected by metal coordination. The structure found for $[Zn\{SCH_2CH_2N(CH_3)_2\}_2]$ (Fig. 1) may account for these data, as it clearly shows that the aliphatic chain linking nitrogen and sulphur donor atoms becomes rigid by metal chelation, meanwhile the exo-oriented methyl groups are much less affected by coordination.

Acknowledgement—We thank the Comisión de Investigación Científica y Técnica (Grant PB87-0188) of Spain for financial support.

REFERENCES

1. H. Barrera, J. Suades, M. C. Perucaud and J. L. Briansó, *Polyhedron* 1984, **3**, 839.
2. J. Suades, X. Solans, M. Font-Altaba and M. Aguiló, *Inorg. Chim. Acta* 1985, **99**, 1.
3. J. Suades, X. Solans and M. Font-Altaba, *Polyhedron* 1984, **3**, 1227.
4. M. Capdevila, P. González-Duarte, J. Sola, F. H. Cano, C. Foces-Foces and M. Martínez-Ripoll, *Polyhedron* 1989, **8**, 1253.
5. P. González-Duarte, J. Sola, J. Vives and X. Solans, *J. Chem. Soc., Chem. Commun.* 1987, 1641.
6. M. Capdevila, P. González-Duarte, F. H. Cano, C. Foces-Foces and M. Martínez-Ripoll, *J. Chem. Soc., Dalton Trans.*, in press.
7. W. Gaete, J. Ros, X. Solans, M. Font-Altaba and J. L. Briansó, *Inorg. Chem.* 1984, **23**, 39.
8. W. Gaete, J. Ros, R. Yáñez, X. Solans, C. Miravitlles and M. Aguiló, *Inorg. Chim. Acta* 1986, **119**, 55.
9. W. Gaete, J. Ros, R. Yáñez, X. Solans and M. Font-Altaba, *J. Organomet. Chem.* 1986, **316**, 169.
10. X. Solans, M. Font-Altaba, J. L. Briansó, J. Sola, J. Suades and H. Barrera, *Acta Cryst.* 1983, **C39**, 1653.
11. J. A. Ayllón, P. González-Duarte, C. Miravitlles and E. Molins, submitted for publication.
12. H. Barrera, J. M. Viñas, M. Font-Altaba and X. Solans, *Polyhedron* 1985, **4**, 2027.
13. P. González-Duarte, M. Mas, J. Sola and R. Yáñez, Communication EUCHEM. CONF. in *Inorg. Chem.*, Dourdan, France (5–9 April 1988).
14. J. Sola and R. Yáñez, *J. Chem. Soc., Dalton Trans.* 1986, 2021.
15. P. Main, S. E. Fiske, S. L. Hull, L. Lessinger, C. Germain, J. P. Declerq and M. M. Woolfson, MULTAN 84. A system of computer programs for crystal structure determination from X-ray diffraction data. Universities of York (U.K.) and Louvain (Belgium) (1984).
16. G. M. Sheldrick, SHELX76. A program for crystal structure determination. University of Cambridge, U.K. (1976).
17. *International Tables for X-ray Crystallography*. Kynoch Press, Birmingham (1974).
18. F. F. Said and D. G. Tuck, *Inorg. Chim. Acta* 1982, **59**, 1.
19. K. L. Hencher, M. A. Khan, F. F. Said and D. G. Tuck, *Polyhedron* 1985, **4**, 1263.
20. B. Cohen, D. Mastropaolo, J. A. Potenza and H. J. Schugar, *Acta Cryst.* 1978, **B34**, 2859.
21. W. J. Hu, D. Barton and S. J. Lippard, *J. Am. Chem. Soc.* 1973, **95**, 1170.
22. L. F. Lindoy, D. H. Busch and V. Goedken, *J. Chem. Soc., Chem. Commun.* 1972, 683.
23. B. Kaptein, L. Wang-Griffin, G. Barf and R. M. Kellog, *J. Chem. Soc., Chem. Commun.* 1987, 1457.
24. A. Mawby and H. M. N. H. Irving, *J. Inorg. Nucl. Chem.* 1972, **34**, 109.
25. D. Mastropaolo, J. A. Thich, J. A. Potenza and H. J. Schugar, *J. Am. Chem. Soc.* 1977, **99**, 424.
26. R. E. Ernst, M. J. O'Connor and R. H. Holm, *J. Am. Chem. Soc.* 1967, **89**, 6104.
27. H. Barrera, J. C. Bayón, J. Suades, C. Germain and J. P. Declerq, *Polyhedron* 1984, **3**, 969.
28. H. Barrera, J. Sola and J. M. Viñas, *J. Chem. Res. (S)* 1985, 270.

Polyhedron Vol. 9, No. 5, pp. 769–771, 1990
Printed in Great Britain

0277–5387/90 $3.00+.00
© 1990 Pergamon Press plc

COMMUNICATION

MOLECULAR STRUCTURE OF $\{[Ag_{13}(\mu\text{-}SC_5H_9NHMe)_{16}]^{13+}\}_n$, A NOVEL ONE-DIMENSIONAL NON-MOLECULAR SILVER–THIOLATE

ISIDRE CASALS, PILAR GONZÁLEZ-DUARTE,* JOAN SOLA and JOSEP VIVES

Departament de Química, Universitat Autònoma de Barcelona, Bellaterra, 08193 Barcelona, Spain

and

MERCÈ FONT-BARDIA and XAVIER SOLANS

Departament de Cristal·lografia i Mineralogia, Universitat de Barcelona, Martí i Franquès s/n, 08028 Barcelona, Spain

(*Received* 14 *September* 1989; *accepted* 4 *October* 1989)

Abstract—The polymeric structure of the $\{[Ag_{13}(\mu\text{-}SC_5H_9NHMe)_{16}]^{13+}\}_n$ cation contains $Ag_{10}S_{16}$ units linked by three silver atoms. Each unit consists of a central $Ag_6(\mu\text{-}SR)_6$ core and two $Ag_4(\mu\text{-}SR)_4$ rings, and comprises digonal, trigonal and tetrahedral silver and doubly- and triply-bridging sulphur atoms.

Despite the fact that copper and silver thiolates have been known for many years, their molecular structures are still of considerable interest.[1] Recent reports indicate that the difficulties encountered in obtaining X-ray quality crystals can be overcome either by reacting metal tertiary alkanethiolates, such as $[M(SBu^t)]_\infty$, with triphenylphosphine,[2] or by using sterically hindered (triorganosilyl) methanethioles, $(RR'R''Si)_nCH_{3-n}SH$, as ligands.[3] However, up until now only two non-molecular silver(I) thiolates, $[AgSCMeEt_2]_n$[4] and $[Ag_4\{SCH_2(SiMe_3)\}_3(OCH_3)]_n$,[3] have been characterized structurally. The introduction of the amine function as a solubilizing group in thiol ligands has to be considered as an alternative method for obtaining crystalline silver(I) thiolate complexes. Thus, solution equilibria studies with several aliphatic γ-mercaptoamines in aqueous media have shown that in a wide pH-range they behave as simple thiolate ligands,[5] and they have also led to the structural chacterization of the cation $\{Ag_5[\mu_2\text{-}S\text{-}(CH_2)_3\text{-}NHMe_2]_3[\mu_2\text{-}S\text{-}(CH_2)_3\text{-}NMe_2]_3\}^{2+}$, the first thiolate complex with trigonal bipyramido-M_5-trigonal prismo-S_6 polyhedral stereochemistry.[6]

We report here the synthesis and structure of the polymeric $\{[Ag_{13}(S\text{-}C_5H_9NHMe)_{16}]^{13+}\}_n$ cation (**1**). When a six-fold excess of 4-mercapto-1-methylpiperidine is added to a solution of $AgNO_3$ in water containing $NaClO_4$ (2.3 M), and after the pH is adjusted to 8.5 with $HClO_4$, pale yellow crystals are obtained, whose formula correspond to the perchlorate of **1**. The structure was determined by X-

* Author to whom correspondence should be addressed.

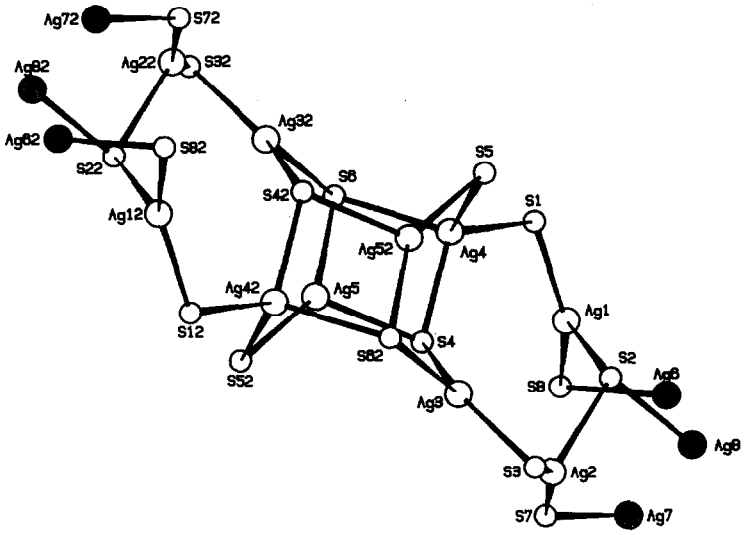

Fig. 1. Skeleton of the $Ag_{10}(\mu\text{-}SR)_{16}$ unit with the atom numbering (all labels ending with 2 mean positions $-x, 2-y, 1-z$). Shaded atoms have an occupancy factor of 0.5. All ligand atoms, except for sulphur have been omitted for the sake of clarity.

ray crystallography.* The anodic oxidation of silver in a $NaNO_3$ saturated acetonitrile solution containing 4-mercapto-1-methylpiperidium nitrate and triphenylphosphine in a 1 : 2 molar ratio, and after diffusion of ether, leads to pale yellow crystals corresponding to the nitrate of **1**. In this case the X-ray crystal structure determination could not be completed because of too much disorder, but the molecular structure very much resembles that of the perchlorate as far as the heavy atoms are concerned. Both the perchlorate and nitrate of **1** are hydrated compounds. However, neither elemental analysis nor crystal structure determination have allowed us to establish unambiguously the degree of hydration.

The $\{[Ag_{13}(\mu\text{-}SC_5H_9NHMe)_{16}]^{13+}\}_n$ cation, as shown schematically in Fig. 1, consists of a central core of Ag_6S_6 atoms from which two eight-membered cycles of alternating silver and sulphur atoms emerge. The Ag_6S_6 core can be described as four fused $Ag_3(\mu\text{-}SR)_3$ cycles, each in a boat conformation, containing two tetrahedral [Ag(4), Ag(42)] and four trigonal-planar [Ag(3), Ag(5), Ag(32),

* Crystal data. $C_{96}H_{208}Ag_{13}Cl_{13}N_{16}O_{52}S_{16}$, triclinic, space group $P\bar{1}$, $a = 21.129(4)$, $b = 20.383(4)$, $c = 15.172(3)$ Å, $\alpha = 121.59(3)$, $\beta = 114.53(4)$, $\gamma = 96.21(3)°$, $Z = 1$, $2\theta_{max} = 50°$, crystal dimensions $0.05 \times 0.05 \times 0.2$ mm. 9492 measured reflections including 4083 observed reflections with $I \geqslant 2.5\sigma(I)$ were collected using a Philips PW-1100 four cycle diffractometer, Mo-K_α radiation, graphite monochromator, ω-scan technique, scan width 0.8°, scan speed 0.03° s^{-1}, 288 K. No absorption corrections were made. The silver and sulphur atoms were located with the MULTAN system of computer programs. The Fourier synthesis of MULTAN revealed three positions, Ag(6), Ag(7) and Ag(8), with an intermediate electronic number between silver and sulphur. Three isotropic refinement cycles confirmed that these three peaks correspond to three silver atoms, with an occupancy factor of 0.5. Carbon, nitrogen and several chlorine atoms were located from a DIRDIF. Subsequent isotropic refinements and difference synthesis revealed the position of more chlorine and oxygen atoms of the perchlorate ions or water molecules. This process was terminated when difference synthesis did not reveal more atoms clearly. At this point 11 ClO_4^- ions (Cl(6) has an occupancy factor of 0.5) and six H_2O (confirmed by hydrogen bonding with nitrogen atoms) had been located as well as two positions [O(w4) and O(w5)] which could be assigned either to H_2O molecules or two chlorine atoms with an occupancy factor of 0.5. The neutrality of the crystal requires two additional ClO_4^- ions which have not been located. We suspect they are in a disordered position. The structure was refined anisotropically by using the SHELX76 computer program. The function minimized was $\Sigma w(|F_o|-|F_c|)^2$, where $w = (\sigma^2(F_o) + 0.076|F_o|^2)^{-1}$. The final R factor with the located atoms was 0.093 ($R_w = 0.096$) for all observed reflections. Number of refined parameters = 938. Max. shift/ESD = 0.4 in U_{12} of O(33). Maximum and minimum peaks in a final difference synthesis were 1.7 and -0.8 e $Å^{-3}$, respectively.

Atomic coordinates, bond lengths and angles and thermal parameters have been deposited at the Cambridge Crystallographic Data Centre (see p. ii at front).

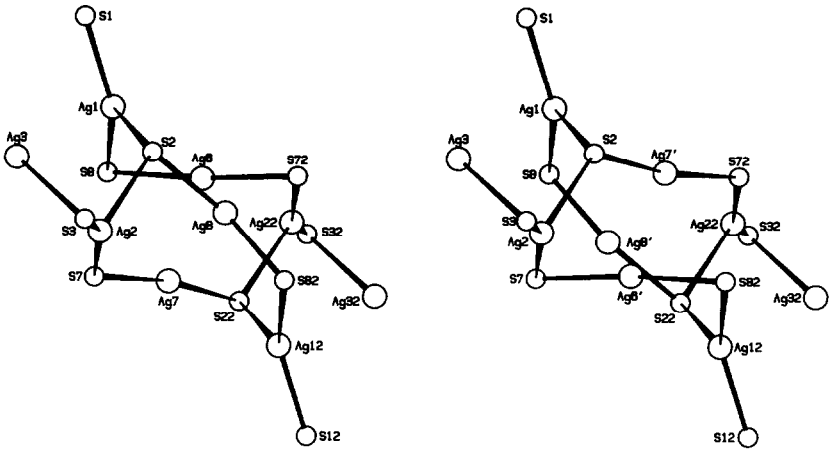

Fig. 2. The two alternative connections for the $Ag_{10}(\mu\text{-}SR)_{16}$ units (symmetry code $' = -x, 1-y, -z$).

Ag(52)] silver atoms and four triply-bridging [S(4), S(6), S(42), S(62)] and two doubly-bridging [S(5), S(52)] sulphur atoms. Ag(3), Ag(4) and S(4), and their symmetry related Ag(32), Ag(42) and S(42), belong simultaneously to a $Ag_4(\mu\text{-}SR)_4$ cycle, respectively, all but the Ag(4) atoms having trigonal-planar coordination. Considering the $Ag_4(\mu\text{-}SR)_4$ rings and ignoring Ag(6), Ag(7) and Ag(8), three sulphur atoms [S(1), S(2), S(3)] are doubly-bridging and two [S(8), S(7)] are terminal. Because of the inversion centre in the Ag_6S_6 core the same applies to the symmetry related sulphur atoms.

The $Ag_6(\mu\text{-}SR)_6$ core and the two $Ag_4(\mu\text{-}SR)_4$ rings just described constitute the unit that repeats in the one-dimensional non-molecular structure. Three disordered and digonally coordinated silver atoms [Ag(6), Ag(7), Ag(8)] are responsible for linking these $Ag_{10}S_{16}$ units, thus accounting for the empirical formula of the $[Ag_{13}(\mu\text{-}SR)_{16}]^{13+}$ cation. The two different ways that the Ag(6), Ag(7), Ag(8) atoms link the $Ag_{10}S_{16}$ units are illustrated in Fig. 2. With either of the two possibilities, sulphur [S(2), S(7), S(8) and their symmetry related] and silver atoms are at normal Ag—S bonding distances. The sulphur atoms describe a distorted octahedron, Fig. 3, where of the three silver atoms, one is in an equatorial and two are in axial edges. By including the disordered silver atoms the previously called terminal sulphur atoms [S(7), S(8)] now become doubly-bridging and the already doubly-bridging sulphur [S(2)] becomes triply-bridging in the crystallographic $Ag_{13}S_{16}$ unit.

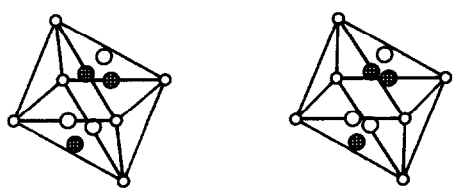

Fig. 3. Stereoview of the S_6-octahedron at the junction of two $Ag_{10}(\mu\text{-}SR)_{16}$ units showing the localization of the three disordered silver atoms (open and marked circles identify both sets).

Mean values of Ag—S bonding distances are as follows: Ag^{dig}—S, 2.40(8) Å; Ag^{trig}—S, 2.50(7) Å; Ag^{tetr}—S, 2.61(9) Å. There is very good agreement with literature values.[1-3] The shortest Ag—Ag distance is 3.00 Å [Ag(6)—Ag(8)], which precludes metal–metal interactions.[2] More details about this structure will be reported in the future.

Acknowledgement—This work was supported by the Comisión de Investigación Científica y Técnica (Grant PB87-0188) of Spain.

REFERENCES

1. I. G. Dance, *Polyhedron* 1988, **7**, 2205.
2. I. G. Dance, L. J. Fitzpatrick, D. C. Craig and M. L. Scudder, *Inorg. Chem.* 1989, **28**, 1853.
3. K. Tang, M. Aslam, E. Bloch, T. Nicholson and J. Zubieta, *Inorg. Chem.* 1987, **26**, 1488.
4. I. G. Dance, L. J. Fitzpatrick, A. D. Rae and M. L. Scudder, *Inorg. Chem.* 1983, **22**, 3785.
5. P. González-Duarte and J. Vives, *J. Chem. Soc., Dalton Trans.* 1990, in press (two articles).
6. P. González-Duarte, J. Sola, J. Vives and X. Solans, *J. Chem. Soc., Chem. Commun.* 1987, 1641.

Polyhedron Vol. 9, No. 5, pp. 773–776, 1990
Printed in Great Britain

0277–5387/90 $3.00+.00
© 1990 Pergamon Press plc

COMMUNICATION

THE FIRST EVIDENCE FOR REDUCTIVE COUPLING OF TRANSITION METAL SUBSTITUTED HALOGERMANES

G. BARSUASKAS, D. LEI, M. J. HAMPDEN-SMITH* and E. N. DUESLER

Department of Chemistry and Center for Micro-Engineered Ceramics,
University of New Mexico, Albuquerque, NM 87131, U.S.A.

(*Received* 25 *September* 1989; *accepted* 24 *October* 1989)

Abstract—The reduction of 1-(cyclopentadienylirondicarbonyl)-1-bromo-3,4-dimethylgermacyclopent-3-ene (**1**) with lithium metal results in practically quantitative yield of the coupled product (**2**). The formation of a Ge—Ge bond was confirmed by a single crystal X-ray diffraction study. The lithium reduction of **3**, $Br_2Ge[Fe(CO)_2Cp]_2$, results in the formation of the first examples of homoleptic transition metal substituted polygermanes.

The synthesis of small ring cyclopolysilanes and -germanes remained elusive for many years, even though the Wurtz coupling method of preparation for larger cyclopolysilanes was discovered early in the century.[1] However, the realization that the nature of both the organic substituents and the reducing agent are of vital importance ultimately led to the successful synthesis of trisilacyclopropanes,[2,3] disilenes,[4] trigermacyclopropanes[5] and digermenes[6] from R_2EX_2 (E = Si; Ge) species. Lithium naphthalenide has been widely employed as a reducing agent, and sterically demanding substituents, such as 2,6-dimethylphenyl, adamantyl and tert-butyl, have resulted in isolation of surprisingly inert species, such as $Si_3(tert\text{-}Bu)_6$, which is reportedly air stable when heated close to its melting point (180°C).[3] In some cases, heavy carbene analogues have been invoked as the reactive intermediates formed during reductive coupling;[3,7] in other cases, a radical mechanism is more likely. Very recently, the reduction of organo–group 14 trichlorides,[8] or their equivalents, such as $RX_2E—EX_2R$,[9,10] have been studied, and a number of fascinating new polyhedral oligomers have been characterized.

As part of our studies of the chemistry of transition metal–germanium bonds,[11] we are interested in determining whether the germanium–halide bond is susceptible to reductive coupling in the presence of transition metal substituents at germanium, with the ultimate goal of preparing homoleptic transition metal substituted polygermanes. Oligosilanes and -germanes with transition metal substituents have been previously prepared, but generally by salt elimination reactions.[12] We now report our initial findings on the reductive coupling of transition metal substituted halogermanes.

As a starting point, we have examined the reduction of a simple transition metal substituted diorganohalogermane, 1-(cyclopentadienylirondicarbonyl) - 1 - bromo - 3,4 - dimethylgermacyclopent-3-ene (**1**),† with 0.5 equiv. of lithium metal. The reaction proceeded virtually quantitatively according to eq. (1) to produce, after work-up, a crystalline species with spectroscopic and ana-

* Author to whom correspondence should be addressed.

† Complex **1** was prepared by the reaction of 1,1-dibromo-3,4-dimethylgermacyclopent-3-ene with one equivalent of $Na[Fe(CO)_2Cp]$, as described elsewhere (see ref. 11).

lytical data consistent with the formation of the coupled product, **2**.*

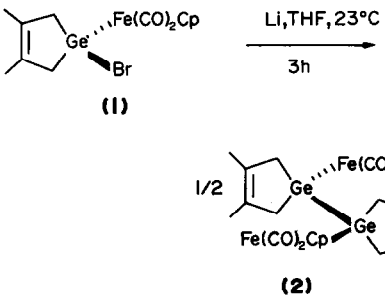

(1)

To provide unambiguous evidence for the formation of the Ge—Ge bond, a single crystal X-ray diffraction study was performed.† The molecular structure of **2** is shown in Fig. 1, together with the appropriate bond lengths and angles. The molecule possesses C_i point group symmetry and adopts a staggered conformation about the Ge—Ge bond in which the two sterically demanding —$Fe(CO)_2Cp$

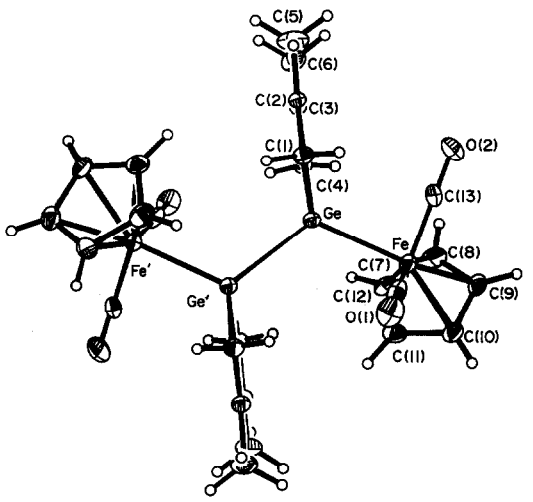

Fig. 1. 25% thermal ellipsoid plot showing the molecular structure of **2**.

Relevant bond distances (Å):

Ge—Ge'	2.448(1)	Fe—C(12)	1.740(6)
Ge—Fe	2.416(1)	Fe—C(13)	1.741(6)
Ge—C(1)	1.986(s)	Fe—Cp	2.093(6)
Ge—C(4)	1.983(1)		(av.)

Relevant bond angles (°):

Ge'—Ge—Fe	115.7(1)
C(1)—Ge—C(4)	91.6(2)
C(4)—Ge—Fe	110.8(2)
C(4)—Ge—Ge'	112.0(2)
C(1)—Ge—Fe	113.1(2)
C(1)—Ge—Ge'	111.1(2)

substituents are *anti* with a slightly enlarged Ge—Ge'—Fe' angle of 115.7(1)°. The Ge—Ge' distance of 2.448(1) Å and the Fe—Ge distances of 2.416(1) Å are in the ranges expected.‡ The germacyclopent-3-ene ring is almost planar, in contrast to 1,1-ditransition metal substituted germacyclopent-3-enes we have structurally characterized previously.[13] Other features of the structure in the present context are unremarkable.

Having demonstrated that the —$Fe(CO)_2Cp$ substituent is inert to the conditions of reductive coupling of Ge—Ge bonds, $[Cp(CO)_2Fe]_2GeBr_2$ (**3**) was reacted with lithium according to eq. (2):

$$[Cp(CO)_2Fe]_2GeBr_2 + Li \xrightarrow{THF,\ 17\ h,\ 23°C} \underset{(3)}{} \quad 1/n\{Ge[Fe(CO)_2Cp]_2\}_n + 2LiBr \quad (2)$$
$$(4)$$

Upon addition of lithium, the pale orange THF solution of **3** became deep red–brown, and the for-

*300 mg of **1** (0.73 mmol) and 3.0 mg (0.5 equivalent) of lithium foil were placed in a 50 cm^3 Schlenk flask under dry nitrogen and 5 cm^3 of THF added. After stirring for 3 h, the initial pale orange solution had become a deep orange–red colour. The THF was removed *in vacuo*, and the dark residue thus obtained was extracted with two 10 cm^3 portions of toluene and filtered. The volume of the solvent was reduced by three-quarters and the solution cooled to −30°C. After 2 days, pale yellow crystals had formed that were isolated by filtration, washed with cold toluene and dried *in vacuo*. Yield of **2**, 200 mg (0.3 mmol), 82.2% yield. Found: C, 47.3; H, 4.4; N, 0.1. Calc: for $C_{13}H_{15}O_2GeFe$: C, 47.0; H, 4.6%. ^1H NMR (250 MHz, C_6D_6, 20°) $\delta = 2.32$, d, $J_{H-H} = 15.7$ Hz, 2H, CH_2; $\delta = 2.09$, d, 2H, CH_2; $\delta = 1.87$, s, 6H, CH_3; $\delta = 4.23$, s, 5H, C_5H_5. $^{13}C\{^1H\}$ NMR (62.9 MHz, C_6D_6, 20°C) $\delta = 19.8$, CH_3; $\delta = 33.8$, CH_2; $\delta = 82.8$, C_5H_5; $\delta = 132.1$, C—Me; $\delta = 215.9$, CO.

† Crystal structure data for **2**: monoclinic, space group $P2_1/n$, $a = 10.340(2)$, $b = 7.0124(12)$, $c = 18.295(4)$ Å, $\beta = 95.99(2)°$, $V = 1319.3(5)$ Å^3, $Q_{calc} = 1.670$ g cm^{-3}, $Z = 4$, 1943 unique reflections collected from $2\theta = 2.0$ to 50.0° with $F_o > 3.0\sigma(F)$. Nicolet R3M/V diffractometer, Mo-K_α radiation, $\gamma = 0.71073$ Å, $T = 20°C$. Solution by direct methods using SHELXTL PLUS (Microvax II) refined by full-matrix least-squares, $R_w = 3.64\%$. Further details are available as Supplementary Material. Atomic positional parameters have been deposited with the Director, Cambridge Crystallographic Centre.

‡ D(Ge—Ge) in $(Ph_2Ge)_n$ are $n = 4$, 2.465 Å; $n = 5$, 2.453 Å; $n = 6$, 2.460 Å; L. Ross and M. Drager, *J. Organomet. Chem.* 1980, **199**, 195; D(Fe—Ge) in $Cl_2Ge[Fe(CO)_2Cp]_2$ is 2.357(4) Å, M. A. Bush and P. Woodward, *J. Chem. Soc. A* 1967, 1833.

mation of a colourless precipitate was observed. After work-up, ^{1}H NMR spectroscopy indicated that there was no starting material present and that four new cyclopentadienyl resonances had been produced in the approximate ratio 1:2:4:12.* Elemental analysis of this mixture of products is consistent with the empirical formula: {Ge[Fe $(CO)_2Cp]_2$} (**4**).† Repeating the lithium reduction using solutions of **3** with different concentrations and using sodium naphthalenide as the reducing agent resulted in formation of the same ^{1}H NMR cyclopentadienyl resonances, but in different ratios. We therefore conclude that each resonance corresponds to a single reaction product: $\{Ge(Fe(CO)_2Cp]_2\}_n$.

When the reduction of eq. (2) is carried out in the presence of a large (> 10-fold) excess of 2,3-dimethylbutadiene, eq. (3), 1,1-bis(cyclopentadienylirondicarbonyl) - 3,4 - dimethylgermacyclopent-3-ene (**5**) was isolated in high yield,‡ in addition to oligomers $\{Ge[Fe(CO)_2Cp]_2\}_n$ (**4**) identical to those formed according to the reaction of eq. (2).

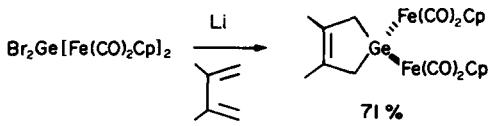

(3) (5)

$$+ \{Ge[Fe(CO)_2Cp]_2\}_n \quad (3)$$

(4)

The identity of **5** was confirmed by comparison of its spectroscopic and physical data with those of an authentic sample prepared by independent synthesis.§ No evidence for any other trapping products was obtained. At this stage, we are unable to determine whether the "$Ge[Fe(CO)_2Cp]_2$" moiety generated by the lithium reduction of **3** and trapped by 2,3-dimethylbutadiene is derived from a free transition metal substituted germylene [eq. (4)], or formed via interception of a radical pathway, such as eq. (5):

$$[Cp(CO)_2Fe]_2GeBr_2 \xrightarrow{Li} \text{"}[Cp(CO)_2Fe]_2Ge\text{:"} \longrightarrow \text{oligomerization} \quad (4)$$

$$Br_2Ge[Fe(CO)_2Cp]_2 \underset{-LiBr}{\overset{+Li^\cdot}{\rightleftharpoons}} [Cp(CO)_2Fe]Ge(Li)(Br) \Longrightarrow \text{oligomerization.} \quad (5)$$

In conclusion, this work provides the first evidence that halogermanes can be reductively coupled in the presence of transition metal substituents in high yield and that the —$Fe(CO)_2Cp$ moiety is innocent to the reaction conditions. Further studies concerning the chromatographic separation of the mixture of oligomers, **4**, and determination of their ring size by cryoscopic molecular weight determination in benzene solution are in progress.

Acknowledgements—We thank the NSF for an NMR instrumentation grant, Dr Dan Doughty for helpful discussions, the Sandia-University Research Program for support and Eva Quesnell for technical assistance. G.B. thanks NSF for support on the Research Experience for Undergraduates Program.

REFERENCES

1. F. S. Kipping, *Proc. Chem. Soc.* 1911, **27**, 143.
2. S. Masamune, Y. Hanzawa, S. Murakami, T. Bally and J. Blount, *J. Am. Chem. Soc.* 1982, **104**, 1150.
3. A. Schaefer, M. Weidenbrich, K. Peters and H. G.

*0.5 g of **3** were placed in a 200 cm^3 Schlenk flask under nitrogen, together with 12 mg of lithium foil. 20 cm^3 of THF was added and the mixture stirred for 20 h. During this time, the solution changed colour from pale orange to deep red–brown. The THF was removed *in vacuo*, and the dark residue was extracted with 2 × 20 cm^3 of benzene. The benzene was removed *in vacuo* to give a dark red–brown oil. ^{1}H NMR data (250 MHz, C_6D_6, 20°C): 4.57 ppm (12H), 4.56 (1H), 4.51 (2H), 4.24 (4H). Authentic **3** exhibits a single cyclopentadienyl resonance at 4.29 ppm and did not coincide with any of the peaks above when added to the NMR tube.

† Elemental analysis: Found: C, 39.4; H, 2.2; N, 0.00. Calc. for $C_{14}H_{10}O_4Fe_2Ge$: C, 39.3; H, 2.3%.

‡ To a mixture of **3** (500 mg, 0.85 mmol) and Li (24 mg) was added a mixture of 20 cm^3 of THF and 1 cm^3 of 2,3-dimethylbutadiene. After stirring for 20 h, the volatile components were removed *in vacuo* and the red–brown residue was extracted with 3 × 10 cm^3 of toluene. The volatile components were removed *in vacuo* and the residue extracted with 30 cm^3 of *n*-pentane. The volume of the solution was reduced to about 5 cm^3 *in vacuo* and placed at −30°C. After 16 h, 310 mg (0.61 mmol) of crystalline **5** was recovered (71.7% yield): oligomers, **4**, were obtained from the toluene soluble fraction.

§ ^{1}H NMR data for **5** (250 MHz, C_6D_6, 20°C): δ = 4.31, s, 5H, C_5H_5; δ = 2.43 ppm, q, 2H, J_{H-H} = 1 Hz, CH_2; δ = 1.92, t, 3H, CH_3. ^{13}C NMR (62.9 MHz, C_6D_6, 20°C): δ = 19.5, CH_3; δ = 41.9, CH_2; δ = 83.8, C_5H_5; δ = 131.9, *C*—Me; δ = 216.7, *C*O. Identical to a sample of **5** prepared from the reaction of 1,1-dibromo-3,4-dimethylgermacyclopent-3-ene and two equivalents of $Na[Fe(CO)_2Cp]$, see ref. 11.

von Schnering, *Angew. Chem. Int. Edn Engl.* 1984, **23**, 302.
4. R. West, *Science* 1984, **225**, 4667.
5. S. Masamune and Y. Hanzawa, *J. Am. Chem. Soc.* 1982, **104**, 6136.
6. J. Park, S. A. Batcheller and S. Masamune, *J. Organomet. Chem.* 1989, **367**, 39.
7. P. Boudjouk, U. Samaraweera, R. Sorriyakumaran, J. Chrusciel and K. Anderson, *Angew. Chem. Int. Edn Engl.* 1988, **27**, 1355.
8. A. Sekiguchi, C. Kabuto and H. Sakurai, *Angew. Chem. Int. Ed. Engl.* 1989, **28**, 55.
9. M. Weidenbrich, F.-T. Grimm, S. Pohl and W. Saak, *Angew. Chem. Int. Edn Engl.* 1989, **28**, 198.
10. Y. Kabe, M. Kuroda, Y. Honda, O. Yammashita, T. Kawase and S. Masamune, *Angew. Chem. Int. Edn Engl.* 1988, **27**, 1725.
11. D. Lei, M. J. Hampden-Smith, *J. Chem. Soc., Chem. Commun.* 1989, 1211.
12. See for example K. H. Pannell, J. M. Rozell and C. Hernandez, *J. Am. Chem. Soc.* 1989, **111**, 4482, and refs therein.
13. D. Lei, M. J. Hampden-Smith, J. C. Huffman and E. N. Duesler, *Inorg. Chem.*, in press.

Polyhedron Vol. 9, No. 5, pp. 777–779, 1990
Printed in Great Britain

0277–5387/90 $3.00+.00
© 1990 Pergamon Press plc

COMMUNICATION

SYNTHESIS AND CRYSTAL STRUCTURE DETERMINATION OF TETRAPHENYLARSONIUM *p*-BROMOPHENYLTHIOCHROMATE

WALDEMAR MAZUREK

Materials Research Laboratories, Defence Science and Technology Organisation, P.O. Box 50, Ascot Vale, Victoria 3032, Australia

and

GARY D. FALLON, PETER J. NICHOLS and BRUCE O. WEST*

Department of Chemistry, Monash University, Clayton, Victoria 3168, Australia

(*Received* 20 *October* 1989; *accepted* 13 *November* 1989)

Abstract—The initial step in the reaction of $[Cr_2O_7]^{2-}$ with *p*-bromothiophenol in dimethylformamide is the formation of the chromium(VI)–thioester $[p\text{-}BrC_6H_4SCrO_3]^-$, which has been isolated as the $[Ph_4As]^+$ salt and its structure determined by a single crystal X-ray diffraction study, thus confirming the proposed first step in the mechanism for the overall oxidation of thiophenols by dichromate.

In aqueous solution thiols are considered to react rapidly with chromate ions forming "thioesters" ($[RSCr^{VI}O_3]^-$) which then participate in the overall reduction of chromium(VI) to chromium(III) as the thiol is oxidized to a disulphide.[1,2] The orange thioesters are transient species, however, and have only been detected by visible spectroscopy[1,2] (characteristic absorptions at *ca* 420–440 nm), while more recently the chromium(VI)–glutathione thioester has been characterized by ^1H and ^{13}C NMR spectroscopy.[3] Less is known about the subsequent redox chemistry of the systems although the production of a chromium(V) intermediate in the chromate oxidation of glutathione[4] indicates a possible initial step as: $[RSCr^{VI}O_3]^- \rightarrow$ "Cr^{V}" + $RS^{\bullet}$.

While studying the kinetics of dichromate oxidations of thiols in organic solvents we have observed that the addition of an excess of thiol to $Na_2Cr_2O_7$ in dimethylformamide (DMF) results in the formation of species characterized by visible absorptions in the region of 420 nm with extinction coefficients, ε, of *ca* 2000 $mol^{-1}\ dm^3\ cm^{-1}$. This is similar to the behaviour observed in aqueous solution, and these species have been similarly assigned as chromium thioesters.

The subsequent decomposition of such species occurs notably more slowly in DMF than in aqueous solution and this has encouraged our attempts to isolate the products. The addition of a precipitate such as ether to DMF solutions of sodium or ammonium dichromate and various thiols gave only small amounts of paramagnetic material. However when *p*-bromothiophenol was the reductant and $[Ph_4As]^+$ ions were present in the system the addition of ether resulted in the isolation of the compound $[Ph_4As][p\text{-}BrC_6H_4SCrO_3]$.† It was recrystallized from DMF/ether to remove traces of paramagnetic material to yield a diamagnetic compound having $\lambda_{max} = 414$ nm; ε [per Cr] = 2440 $mol^{-1}\ dm^3\ cm^{-1}$ in DMF, the same spectral characteristics as had been obtained when $p\text{-}BrC_6H_4SH$ was initially added to a DMF solution of $Na_2Cr_2O_7$.

* Author to whom correspondence should be addressed.

† Microanalytical data, Found: C, 53.6; H, 3.5; Br, 12.0; S, 4.6. Calc. for $C_{30}H_{24}AsBrCrO_3S$: C, 53.7; H, 3.6; Br, 11.9; S, 4.8%.

The IR spectrum of the salt contains strong bands at 946 and 890 cm^{-1}, which by analogy with $KCrO_3Cl$ correspond to $\nu(Cr—O)_{asym}$ and $\nu(Cr—O)_{sym}$, respectively.[5] Other absorptions around this region indicate the presence of *p*-Br C_6H_4S (1008 and 818 cm^{-1}) and $[Ph_4As]^+$ (977, 741 and 689 cm^{-1}). The absence of bands around 770 cm^{-1} indicate the loss of the μ-oxo bond.[6]

Similar salts have also been isolated with $[(Ph_3P)_2N]^+$ cations and the thioesters derived from thiophenol and its *p*-Br and *p*-NO_2 derivatives.

A crystal structure determination has been made of $[Ph_4As][p\text{-}BrC_6H_4SCrO_3]$ which has confirmed the chromium(VI) thioester assignment.* Figure 1 shows the atomic labelling scheme used and appropriate bond lengths and angles are listed. The structure represents the first example of a chromium(VI)–sulphur compound to have been characterized as well as the first chromium(VI)–thioester compound.

The Cr—O bond lengths are somewhat shorter than the mean bond distance for many chromate anions (1.646(25) Å) and closer to the mean non-bridging Cr—O distances reported for dichromates (1.615(18) Å) and trichromates (1.598(10) Å).[8] The opening of the O—Cr—O angles beyond the tetrahedral value is presumably a result of the incorporation of the large sulphur atom bonded to chromium with a Cr—S bond distance of 2.263(7) Å. This results in an approximate C_{3v} symmetry for the four bond group connected to chromium(VI). The shortening of three Cr—O distances below that of the chromate anion as the fourth chromium–ligand bond lengthens has been noted in the case of a series of polychromates.[8] In two alkali metal $[CrO_3Cl]^-$ compounds the Cr—O lengths are comparable with those in the thioester (1.601–1.613).[9]

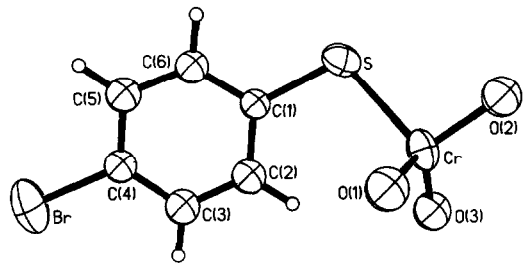

Fig. 1. ORTEP drawing of the $[p\text{-}BrC_6H_4SCrO_3]^-$ anion structure (standard deviations are given in parentheses)

Cr—O(1)	1.609(12)	Cr—O(3)	1.621(12)
Cr—O(2)	1.607(11)	Cr—S	2.263(7) Å

O(1)—Cr—O(2)	114.1(6)
O(2)—Cr—O(3)	112.9(6)
O(1)—Cr—O(3)	112.9(7)
O(1)—Cr—S	107.5(5)
S—C(1)—C(2)	123.1(14)
Cr—S—C(1)	105.1(6)°.

We are currently studying the kinetics of formation and decomposition of such chromium(VI)–thioesters in DMF solution. Whilst they eventually decompose to give chromium(III) and disulphides there is evidence for further transient intermediates and the use of non-aqueous solvents may allow isolation of these species.

Acknowledgements—This work was supported in part by contract No. CDS 12/87 with the Materials Research Laboratory, Australian Defence Science and Technology Organization (B.O.W., P.J.N.) and by an Australian Research Committee grant (B.O.W.).

*Crystal data (Nicolet R3m/V diffractometer): $C_{30}H_{24}AsBrCrO_3S$, $M = 671.4$, orthorhombic, space group $Pna2_1$, $a = 19.650(8)$, $b = 9.388(4)$, $c = 15.436(4)$ Å, $V = 2848(2)$ Å^3, $D_{calc} = 1.57$, $D_m = 1.55(2)$ g cm^{-3}, $Z = 4$, $F(000) = 1344$, $\mu = 30.0$ cm^{-1} (Mo-K_α, $\lambda = 0.71073$ Å, graphite monochromator, $3.5 < 2\theta < 50°$, ω scan range 1.30°), $T = 20(1)$°C, cryst. $0.23 \times 0.08 \times 0.08$ mm, max/min transmission coefficients 0.988/0.955, 2871 data collected ($+h$, $+k$, $+l$) having 1127 independent observed [$F \geq 6\sigma(F)$] reflections.

Cell parameters were derived by least-squares calculations from angular settings of 25 reflections in the range between $6 < 2\theta < 17°$. The structure was solved by Patterson methods with full-matrix least-squares refinement[7] employing anisotropic thermal parameters for As, Br, Cr and S and isotropic thermal parameters for all other atoms (fixed isotropic thermal parameter for hydrogen of 0.080 Å^2, positioned in geometrically idealized positions: C—H 0.96 Å), reducing R to 0.053 and R_w to 0.037 at convergence for $R_w = (\Sigma w(||F_o| - |F_c||)^2/\Sigma w|F_o|^2)^{1/2}$ and $w = [\sigma^2(F_o)]^{-1}$.

Supplementary material available from the Editor: Tables of atomic coordinates, thermal parameters, bond lengths and angles. Coordinates have also been deposited with the Cambridge Crystallographic Data Centre.

REFERENCES

1. P. H. Connett and K. E. Wetterhahn, *Struct. Bond.* 1983, **54**, 93.
2. P. H. Connett and K. E. Wetterhahn, *J. Am. Chem. Soc.* 1986, **108**, 1842.
3. S. L. Bauer and K. E. Wetterhahn, *Inorganic Section of the Third Chemical Congress of North America*, Toronto, Canada, Abstract 472 (June 1988).
4. (a) P. O'Brien, J. Barrett and F. Swanson, *Inorg. Chim. Acta* 1985, **108**, L19; (b) D. M. L. Goodgame and A. M. Joy, *J. Inorg. Biochem.* 1986, **26**, 219.
5. H. Stammreich, O. Sala and K. Kawai, *Spectrochim. Acta* 1961, **17**, 226.

6. H. Stammreich, D. Bassi, O. Sala and H. Siebert, *Spectrochim. Acta* 1958, **13**, 192.
7. G. M. Sheldrick, SHELXTL PLUS, Revision 3.4, Siemens Analytical X-Ray Instruments, Inc., Madison, Wisconsin, U.S.A. (1988).
8. M. R. Pressprich, R. D. Willett, R. D. Poshusta, S. C. Saunders, H. B. Davis and G. L. Gard, *Inorg. Chem.* 1988, **27**, 260.
9. J. J. Foster and M. Sterns, *J. Cryst. Molec. Struct.* 1974, **4**, 149.

Polyhedron Vol. 9, No. 5, p. 781, 1990
Pergamon Press plc. Printed in Great Britain

ADDENDUM

Photoacoustic calorimetry studies of ligand-exchange of aliphatic amines with $Cr(CO)_6$: steric effects and hydrogen bonding. T. J. Burkey (*Polyhedron*, Vol. 8, No. 22, pp. 2681–2687, 1989).

The Author wishes to add the following Acknowledgements to the above paper:

The Donors of the Petroleum Research Fund, administered by the American Chemical Society, and a MSU Faculty Grant are gratefully acknowledged for the partial support of this research.

Polyhedron Vol. 9, No. 6, pp. 783–787, 1990
Printed in Great Britain

0277–5387/90 $3.00+.00
© 1990 Pergamon Press plc

SYNTHESIS, CHARACTERIZATION AND STRUCTURE OF CARBOXYLATE DERIVATIVES OF BIS(METHYLCYCLOPENTADIENYL)TITANIUM(IV)

ZHOU YAOKUN* and WANG ZHIQIANG

Department of Chemistry, Lanzhou University, Lanzhou, P.R.C.

and

WANG XIN and ZHU YING

Center of Analyses and Research, Lanzhou University, Lanzhou, P.R.C.

(*Received* 15 *March* 1989; *accepted* 31 *August* 1989)

Abstract—Seventeen bis-carboxylate derivatives of bis(methylcyclopentadienyl)titanium have been prepared by the reaction of bis(methylcyclopentadienyl)titanium dichloride with the appropriate sodium salts of substituted benzoates. They have been characterized by elemental analysis, IR and ^{1}H NMR. When treated with electrophilic reagents such as $SOCl_2$, CH_3COCl and HX, $(CH_3C_5H_4)_2TiX_2$ were obtained. The crystal and molecular structure of bis(methylcyclopentadienyl)bis(*o*-methylbenzoate)titanium has been determined by X-ray diffraction. The compound crystallizes in the monoclinic group $P2_1/c$ with four molecules in a cell having $a = 8.098(3)$, $b = 28.747(4)$, $c = 10.374(3)$ Å, $\beta = 95.48(2)°$. The molecules have a distorted tetrahedral structure in which the titanium atom is attached to two η^5-$CH_3C_5H_4$ groups and two monodentate *o*-methylbenzoate ligands (Ti—C, 2.323–2.409 Å; Ti—O, 1.979(3) and 1.961(3) Å; O—Ti—O, 90.5(3)°; (cent-$CH_3C_5H_4$)—Ti—(cent-$CH_3C_5H_4$), 130.1(3)°.

The synthesis, characterization and structure of the complexes $(C_5H_5)_2Ti(O_2CR)_2$ (R = alkyl and aryl) have been reported.[1–4] On account of the biological activity of the complexes, this work has attracted the interest of many researchers.[5–6] One study on $(CH_3C_5H_4)_2Ti(O_2CR)_2$ has been reported, but the structure of this type of complex is still of interest.[1] We report here the synthesis of 17 new complexes of $(CH_3C_5H_4)_2Ti(O_2CR)_2$ (R = aryl) and discuss the IR spectra and ^{1}H NMR of these new complexes. The structure of bis(methylcyclopentadienyl)titanium bis(*o*-methylbenzoate) has been determined by X-ray diffraction and its molecular structure is discussed in detail.

* Author to whom correspondence should be addressed.

EXPERIMENTAL

All reagents were obtained commercially and were not purified before use. Benzene and petroleum ether were dried using sodium/benzophenone. Anhydrous sodium salts of substituted benzoic acids were prepared by reaction of substituted benzoic acids with sodium ethoxide, and were dried. $(CH_3C_5H_4)_2TiCl_2$ was prepared according to the literature method.[8]

Melting points were determined using a Kofler instrument, but the temperature was not calibrated. ^{1}H NMR spectra were recorded with a Bruker FT-80A spectrometer, using $CDCl_3$ as solvent. The chemical shifts were reported in ppm relative to $Si(CH_3)_4$. IR spectra were recorded with an FT-5DX spectrophotometer (in KBr pellets) in the 4000–400 cm^{-1} range. The titanium analyses were

Table 1. Physical and analytical data of the $Cp'_2Ti(O_2CC_6H_4X)_2$ complexes[a]

Number	X	Colour	Melting point (°C)	Yield	Elemental analyses, Found (Calc.) C	H	Ti	N
1	*o*-F	Orange–red	118–119	45	64.3 (64.5)	4.6 (4.5)	9.5 (9.9)	
2	*m*-F	Orange–red	125–126	50	64.3 (64.5)	4.7 (4.5)	9.8 (9.9)	
3	*p*-F	Orange–red	142–143	56	64.4 (64.5)	4.6 (4.5)	9.9 (9.9)	
4	*o*-Br	Orange–red	148–150	85	51.6 (51.5)	3.6 (3.6)	7.9 (7.9)	
5	*m*-Br	Orange–red	86–88	44	51.1 (51.5)	3.6 (3.6)	8.1 (7.9)	
6	*p*-Br	Orange–red	144–145	65	51.5 (51.5)	3.4 (3.6)	8.2 (7.9)	
7	*o*-NO_2	Orange–red	171–172	71	57.6 (58.0)	4.1 (4.1)	9.2 (8.9)	5.6 (5.2)
8	*m*-NO_2	Orange–red	158–160	82	58.6 (58.0)	4.1 (4.1)	8.7 (8.9)	4.8 (5.2)
9	*p*-NO_2	Orange	188–190	62	57.5 (58.0)	4.0 (4.1)	9.1 (8.9)	5.0 (5.2)
10	*o*-CH_3	Orange–red	99–100	51	70.1 (70.6)	5.8 (5.9)	10.1 (10.1)	
11	*m*-CH_3	Orange–red	126–127	48	70.0 (70.6)	5.9 (5.9)	9.8 (10.1)	
12	*p*-CH_3	Orange–red	168–169	63	70.4 (70.6)	6.0 (5.9)	9.8 (10.1)	
13	*p*-Cl	Orange–red	163–164	60	60.2 (60.3)	4.2 (4.3)	9.1 (9.3)	
14	*o*-I	Orange	179–180	57	45.0 (44.6)	3.2 (3.1)	6.9 (6.7)	
15	*p*-I	Orange	130–131	68	44.7 (44.6)	3.3 (3.1)	6.9 (6.7)	
16	*p*-OCH_3	Orange	146–148	75	65.7 (66.1)	5.3 (5.5)	9.7 (9.4)	
17	*p*-CN	Orange–red	194–196	84	67.2 (67.5)	4.3 (4.4)	9.8 (9.6)	5.6 (5.6)

[a] $Cp' = \eta^5$-methylcyclopentadienyl.

determined gravimetrically as TiO_2. Carbon, hydrogen and nitrogen contents of the complexes were carried out with a 1106-elemental analysis instrument.

Preparation of $(CH_3C_5H_4)_2Ti(O_2CC_6H_4X)_2$

$(CH_3C_5H_4)_2TiCl_2$ (2 mmol) and an excess of the anhydrous sodium salt of the substituted benzoic acid were added to 50 cm^3 of dry benzene and stirred for 12 h at 30°C. The colour of the reactant liquid changed from deep red to orange–red. The precipitated salt was removed by filtration and the filtrate was concentrated under reduced pressure until the remaining liquid was about 10 cm^3. Petroleum ether was added, the solution refrigerated at 0°C overnight, and a crystalline product was obtained. The crystals were washed with petroleum ether. Physical data and elemental analyses of the complexes are listed in Table 1. Complexes **4** and **8** were selected to react with CH_3COCl, $SOCl_2$ and HX (X = Cl, Br, I), respectively, in THF at room temperature. The products $(CH_3C_5H_4)_2TiX_2$ (X = Cl, Br, I) were characterized by ^1H NMR and their melting points.

Structure determination of complex **10**

An orange–red single crystal of complex **10** was obtained by recrystallization from benzene–*n*-hexane (1 : 1). The diffraction experiment was performed on a CAD4 diffractometer with graphite-monochromated Cu-K_α radiation ($\lambda = 1.5418$ Å). A total of 3007 reflections were collected in the range $3 < 2\theta < 110°$, and there were 2176 reflections with $I > 3\sigma(I)$. The crystal data are summarized in Table 2. The structure was solved by direct and Fourier methods, and refined by full-matrix least-squares techniques with the anisotropic temperature factor for non-hydrogen atoms. Hydrogen atoms in calculated positions with isotropic thermal parameters were included in final structure factor calculations. Final $R = 0.055$ and $R_w = 0.058$; all calculations were performed on a PDP11/44 computer with the SDP program package.

Table 2. Crystallographic parameters

Formula	$C_{28}H_{28}O_4Ti$
Crystal system,	Monoclinic
Space group	$P2_1/n$
a (Å)	8.098(2)
b (Å)	28.747(4)
c (Å)	10.474(3)
β (°)	95.84(2)
V (Å^3)	2402.4 (7)
Z	4
Absorption coefficient (cm^{-1})	32.7
D_c (g cm^{-3})	1.317
R (%)	5.5
R_w (%)	5.8
F (000)	1000

RESULTS AND DISCUSSION

The new complexes of $(CH_3C_5H_4)_2Ti(O_2CC_6H_4X)_2$ were synthesized by the reaction of $(CH_3C_5H_4)_2TiCl_2$ with $XC_6H_4CO_2Na$. This method is easy and simple. Complexes **1–17** are stable to dry air at room temperature and have regular melting points. They are soluble in polar organic solvents such as C_6H_6, $CHCl_3$, CH_2Cl_2, CH_3COCH_3, etc., but insoluble in petroleum ether and water.

The molecular structure of complex **10**

An ORTEP drawing of complex **10** is given in Fig. 1. Atoms of the two η^5-methylcyclopentadienyl and two *o*-methylbenzoate ligands are distinguished by a literal subscript. Bond distances and angles in the coordination group are listed in Table 3.

The molecules of complex **10** have a bent metallocene structure in which the titanium atom is attached to two monodentate *o*-methylbenzoate ligands and two η^5-$CH_3C_5H_4$ groups. The centroids of the $CH_3C_5H_4$ and the coordinated oxygen atoms define a distorted tetrahedron with the cent-$CH_3C_5H_4$—Ti—cent-$CH_3C_5H_4$ angle being 130.1° and the O_{2A}—Ti—O_{2B} angle being 90.5°; these figures should be compared with data for the known compound $(C_5H_5)_2Ti(O_2CC_6H_5)_2$ (137.7 and 91.4°).[1] Because C_{6C} and C_{6D} are on the same side and the non-bonded contacts of C_{3C}—C_{3D} (2.93 Å) and C_{4C}—C_{4D} (2.95 Å); C_{2C}—C_{2D} (4.05 Å) and C_{5C}—C_{5D} (4.12 Å) are similar, the two η^5-$CH_3C_5H_4$ rings are eclipsed. The conformation of complex

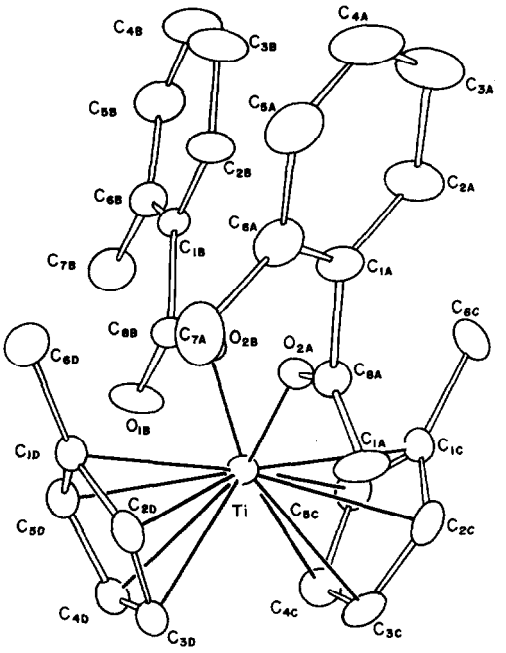

Fig. 1.

10 is also different from $(C_5H_5)_2Ti(O_2CC_6H_5)$[1] but similar to $(CH_3C_5H_4)_2TiCl_2$.[9] The Ti—C distances and the distances from the titanium atom to the centroids of the CH—C—H rings (2.075 Å) are in excellent agreement with the corresponding distances in the other $(CH_3C_5H_4)_2Ti$ structure.[9]

There is considerable crowding in the TiO_2C_{10} coordination group as evidenced by the conformation (eclipsed conformation including methyl groups). Due to crowding, the Ti—O bond lengths (1.979 and 1.961 Å) are relatively longer than the Ti—O bonds in $(C_5H_5)_2Ti(O_2CC_6H_5)_2$ (1.992 and

Table 3. Some important bond distances and bond angles for complex **10**

Bond distances (Å)			
Ti—O_{2A}	1.979(3)	Ti—O_{2B}	1.961(3)
Ti—C_{1D}	2.400(4)	Ti—C_{1C}	2.407(4)
Ti—C_{2D}	2.388(4)	Ti—C_{2C}	2.378(5)
Ti—C_{3D}	2.352(5)	Ti—C_{3C}	2.332(5)
Ti—C_{4D}	2.337(5)	Ti—C_{4C}	2.348(5)
Ti—C_{5D}	2.380(5)	Ti—C_{5C}	2.400(4)
Ti—cent-CP_D	2.057(1)		
Ti—cent-CP_C	2.055(1)		
O_{1A}—C_{8A}	1.216(5)	O_{1B}—C_{8B}	1.214(5)
O_{2A}—C_{8A}	1.281(5)	O_{2B}—C_{8B}	1.295(5)
Bond angles (°)			
O_{2A}—Ti—O_{2B}	90.5(1)	O_{1B}—C_{8B}—O_{2B}	124.0(4)
cent-CP_C—Ti—CP_D	130.1(3)	O_{1A}—C_{8A}—C_{1A}	120.0(4)
Ti—O_{2A}—C_{8A}	138.6(4)	O_{1B}—C_{8B}—C_{1B}	121.6(4)
Ti—O_{2B}—C_{8B}	137.9(7)	O_{2A}—C_{8A}—C_{1A}	114.5(4)
O_{1A}—C_{8A}—O_{2A}	125.6(4)	O_{2B}—C_{8B}—C_{1B}	114.5(4)

1.930 Å). Fay and co-workers have reported a large Ti—O—C angle and a relatively short Ti—O bond length in the $(C_5H_5)_2Ti(O_2CC_6H_5)_2$ complex, which is formally a 16-electron complex if only Ti—O σ-bonding is considered, achieving an effective 18-electron configuration via Ti—O π-bonding. On comparing the Ti—O—C angles of complex **10** (138.6 and 137.9°) and $(C_5H_5)_2Ti(O_2CC_6H_5)_2$ (148.6 and 147.9°), it is seen that the Ti—O—C angle of complex **10** is less by 10°. Thus, complex **10** may be formally a 16-electron complex because of the smaller Ti—O—C angle and the longer Ti—O bond distance.

IR spectra

The important IR frequencies are given in Table 4. Some characteristic absorptions of the methylcyclopendienyl ring appeared. The C—H stretching frequency at 3090–3114 cm^{-1} is indicative of the methylcyclopentadienyl ring. The frequency at 1370–1415 cm^{-1} is due to the C—C stretching of π-bonding in the methylcyclopentadienyl ring. δ(C—H) in the methylcyclopentadienyl ring is at 1013–1059 cm^{-1} and changes in the order F > Cl > Br > I (the halogen is in the *p*-position of the phenyl ring).

Strong bands are observed at 1626–1650 cm^{-1} and 1295–1345 cm^{-1}, which are characteristic absorptions of the (COO) group. The difference ($\Delta\nu$) between ν_{asym}(COO) and ν_{sym}(COO) is about 290 cm^{-1}. Chandra *et al.*[7] reported the IR spectra of $(CH_3C_5H_4)_2Ti(O_2CC_6H_5)_2$. They suggested that in this compound the ligand is bidentate as in $Cp_2Ti(O_2CR)$ complexes.[10] Fay[1] pointed out that this result may be wrong and our experimental results are also different to those of Chandra. The large difference, $\Delta\nu$ (*ca* 290 cm^{-1}), is indicative that the ligand is monodentate. This result is consistent with the analogous complexes $(C_5H_5)_2Ti(O_2CC_6H_4X)_2$.[2] Our X-ray structure determination of complex **10** further confirms this result.

As indicated in Table 4, some characteristic absorptions of the substituted phenyl ring appeared. The data for complexes **1–17** compare well with the analogous complexes, $(C_5H_5)_2Ti(O_2CC_6H_4X)_2$.[2]

^{1}H *NMR spectra*

Chemical shifts for the protons (δ scale) of complexes **1–17** are given in Table 5. The spectra consist of one sharp peak due to the methyl on the methylcyclopentadienyl ring. The protons of the two methylcyclopentadienyl rings give two groups of asymmetric triplet peaks, the standard AB system. This result is consistent with that for the analogous complexes of $(CH_3C_5H_4)_2Ti^{IV}$.

For complexes **3**, **13** and **6** (*p*-F, *p*-Cl, *p*-Br, respectively, on the phenyl ring), the chemical shift of the methylcyclopentadienyl ring decreases in the order F, Cl, Br. This is very similar to the changes which occur in the compounds $(C_5H_5)_2Ti(p\text{-}XC_6H_4)_2$ (X = F, Cl, Br)[11] and opposite to those

Table 4. IR data for complexes **1–17** (cm^{-1})

Number	O—C—O asym	O—C—O sym		CP′($CH_3C_5H_4$)				C_6H_{6-n} (n = 1)						Ti—O
1	1633s	1339s	294	3096m		1054w	3048w		1483m	1452m	857s	756s	586m	
2	1631s	1341s	290	3114m	1376m	1054w	3064w	1585s	1482w	1441m	847s	762s	582m	
3	1636s	1338s	298	3100m	1408m	1030w	3064w	1601s	1502m	1458m	853s	771s	529m	
4	1600s	1345s	255	3103m	1372w	1037m	3064w	1522m	1475w	1430w	851s	740s	581m	
5	1630s	1332s	298	3103m	1374w	1040w	3063m	1565s	1501w	1419m	848s	751s	573s	
6	1630s	1339s	291	3089m	1392w	1013w	3061w	1589m	1502w	1454w	854s	762s	569s	
7	1650s	1344s	306	3107m	1415w	1030w	3091w	1573w	1504m	1456w	840s	778m	602m	
8	1641s	1338s	303	3093m	1413w	1031w	3069w	1577w	1502w	1444w	840s	716s	581m	
9	1641s	1336s	305	3107m	1403w	1016w	3097w	1601s	1553w	1456w	850s	719s	589m	
10	1626s	1337s	289	3106m	1388w	1054w	2967w	1597m	1502w	1454w	853s	739s	583m	
11	1626s	1328s	298	3107m	1378w	1059w		1584m	1502w	1483w	842s	751s	608s	
12	1629s	1338s	291	3109m	1373w	1023w	3021w	1573m	1503w	1453w	853s	758s	577s	
13	1626s	1334s	292	3100m	1367m	1015w	3008w	1573m	1502w	1455w	853s	766s	570s	
14	1633s	1341s	292	3075w	1396w	1013m	3075w	1581m	1499w	1456w	849s	744s	581m	
15	1631s	1334s	297	3100w	1385m	1006m	3084w	1582m	1503w	1452w	832s	757s	569s	
16	1635s	1296s	339	3093w	1379w	1031w		1607s	1509m	1456w	850s	777s	619m	
17	1628s	1342s	286	3107m	1377m	1020m		1564m	1501m	1459w	865s	774s	578s	

s = strong; m = medium; w = weak.

Table 5. ^{1}H NMR data for complexes **1–17** (ppm)

Number	CH_3	$-C_5H_4-$	C_6H_4	Other
1	2.06s	6.32–6.59m	7.07–8.01m	
2	2.06s	6.34–6.62m	7.29–7.91m	
3	2.08s	6.34–6.60m	6.98–8.14m	
4	2.12s	6.44–6.60m	7.17–7.77m	
5	2.06s	6.32–6.65m	7.35–8.27m	
6	2.05s	6.22–6.53m	7.39–7.87q	
7	2.12s	6.36–6.61m	7.42–7.85m	
8	2.10s	6.37–6.71m	7.58–8.87m	
9	2.07s	6.32–6.67m	8.23s	
10	2.07s	6.30–6.60m	7.14–7.91m	2.64s
11	2.06s	6.32–6.60m	7.25–7.70m	2.40s
12	2.05s	6.31–6.58m	7.20–8.03m	2.43s
13	2.07s	6.27–6.66m	7.30–8.00q	
14	2.06s	6.32–6.60m	6.94–7.99m	
15	2.03s	6.32–6.60m	7.77s	
16	2.06s	6.22–6.49m	7.07–7.98q	3.60s
17	2.06s	6.30–6.66m	7.66–8.19q	

s = single; m = multiple; q = quadruple.

which occur in $(CH_3C_5H_4)_2Ti(OC_6H_4X)_2$ compounds.[12] The reason may be that the Ti—O bond in the complexes has little double bond character, therefore, the ^{1}H NMR spectra indicate that the complexes are more like the phenyltitanocenes than the aryloxytitanocenes. Another characterization in the ^{1}H NMR different from the appropriate aryloxytitanocenes was also observed. The chemical shift of the protons on the methylcyclopentadienyl ring in the carboxylate complexes is lower than the analogous chloride and much lower than the analogous aryloxy complexes.

REFERENCES

1. D. M. Hoffman, N. D. Chester and R. C. Fay, *Organometallics* 1983, **2**, 48.
2. Dang Yi, Zhang Yohong and Shi Shujiang, *Synth. React. Inorg. Met.-Org. Chem.* 1987, 374.
3. P. C. Wailes, R. S. P. Coutts and H. Weigold, *Organometallic Chemistry of Titanium, Zirconium and Hafnium*, p. 66. Academic Press, London (1974).
4. D. Michael, *Organometallic Compounds*, Vol. I, p. 29. Springer, New York (1966).
5. S. C. Dixii, R. Sharan and R. N. Kapoor, *Inorg. Chim. Acta.* 1988, **145**, 39.
6. D. R. Cardin and A. Roy, *Inorg. Chim. Acta.* 1985, **107**, L33.
7. K. Chandra, R. K. Sharama, B. S. Garg and R. P. Singh, *J. Inorg. Nucl. Chem.* 1980, **42**, 187.
8. L. T. Reynolds and G. Wilkinson, *J. Inorg. Nucl. Chem.* 1959, **9**, 86.
9. J. L. Petersen and L. F. Dahl, *J. Am. Chem. Soc.* 1975, **97**, 6422.
10. R. S. P. Coutts and P. C. Wailes, *Aust. J. Chem.* 1976, **20**, 1579.
11. H. C. Beachell and S. A. Butter, *Inorg. Chem.* 1965, **4**, 1133.
12. Shen Shoushan and Liu Yiying, *Huaxue Xue Bao* 1982, **40**, 913.

Polyhedron Vol. 9, No. 6, pp. 789–793, 1990
Printed in Great Britain

0277–5387/90 $3.00+.00
© 1990 Pergamon Press plc

POTENTIOMETRIC AND ^{13}C NMR STUDY OF THE INTERACTION BETWEEN BORIC ACID AND PYROGALLOL (1,2,3-TRIHYDROXYBENZENE)

GUIDO CRISPONI* and VALERIA NURCHI

Dipartimento di Chimica e Tecnologie Inorganiche e Metallorganiche, via Ospedale 72, 09124 Cagliari, Italy

and

MARIA LUISA GANADU and GIUSEPPE LUBINU

Dipartimento di Chimica, via Vienna 2, 07100 Sassari, Italy

(*Received* 31 *August* 1989; *accepted* 9 *October* 1989)

Abstract—The boric acid–pyrogallol system has been studied in aqueous solution by means of potentiometric methods. Evidence is given for two adducts of 1 : 1 and 1 : 2 stoichiometry. An analysis of ^{13}C NMR spectra of the 1 : 2 adduct is presented.

In this paper we present the characterization of the boric acid–pyrogallol system by potentiometric and ^{13}C NMR methods. This study is part of general research on the interactions between buffer systems and the medium in which they act; in fact in many cases the importance of these interactions is neglected, even though they can completely distort the results of the systems studied. For example, borate buffer is often used in the study of the enzyme polyphenoloxidase (PPO),[1] but it inhibits the reaction because all substrates of the reactions catalysed by PPO, i.e. L-Dopa, catechol, pyrogallol, chlorogenic, caffeic and gallic acid, strongly interact at pH 8.5 with the buffer itself.

The reaction of boric acid with diols has been extensively studied both for analytical purposes[2–4] (boric acid is transformed into a relatively strong acid by addition of an organic compound containing two or more hydroxy groups and, therefore, can be easily titrated with a strong base) and for structural studies[5,6] (boric acid, interacting only with compounds with two hydroxy groups in the *cis* position or two phenoxy groups in the *ortho* position, distinguishes between *cis*- and *trans*-dihydroxy compounds and between *ortho* and *meta* or *para* compounds).

The existence of only a 1 : 1 complex, or both 1 : 1 and 1 : 2 complexes in such systems has been examined by different authors.[7–9] In this study we have attempted to characterize reliably the boric acid–pyrogallol system by potentiometric and NMR methods.

EXPERIMENTAL

NMR studies

^{13}C NMR spectra were determined in D_2O solution with a CFT-20 Varian Spectrometer at a probe temperature of *ca* 37°C, under an argon atmosphere. Chemical shifts are expressed in ppm relative to internal TMS. Typical Fourier transform conditions under which the ^{13}C results were obtained are as follows: spectral width 6000 Hz, data points 8 K, pulse repetition times 0.8–4.0 s, number of accumulated transients 10,000–40,000.

Potentiometric studies

The titrations were performed on a pH M 84 Radiometer pH meter, equipped with a Dosimat 655 Metrohm automatic titrator, at an ionic strength of 0.1 M (KNO_3) and at 25°C. The standard potential of the electrode and the slope was determined daily by titrations of chloridic acid with

* Author to whom correspondence should be addressed.

NaOH, at an ionic strength of 0.1 M (KNO_3). All titrations using pyrogallol were made under a nitrogen atmosphere to prevent decomposition. The boric acid and pyrogallol concentrations used in the various titrations were in the range 0.003–0.018 M and their ratio varied from 2 : 1 to 1 : 6.

Calculations

Potentiometric data for the electrode standardization were analysed by the Magec program.[10] The ionization constants of boric acid and pyrogallol, and the formation constants of their adducts were calculated by the PSEQUAD program,[11] which we slightly modified to present a graphic display of experimental and calculated data.

The calculations were performed on a PS II/50 IBM personal computer.

Materials

Boric acid, pyrogallol, isopropanol and *sec*-butanol were purchased from Fluka; D_2O and NaOD from Merck.

RESULTS AND DISCUSSION

The potentiometric titrations of H_3BO_3, pyrogallol and of their mixtures in different ratios allow the evaluation of the ionization constants of the two reagents (reported in Table 1) and the proposal of the equilibria:

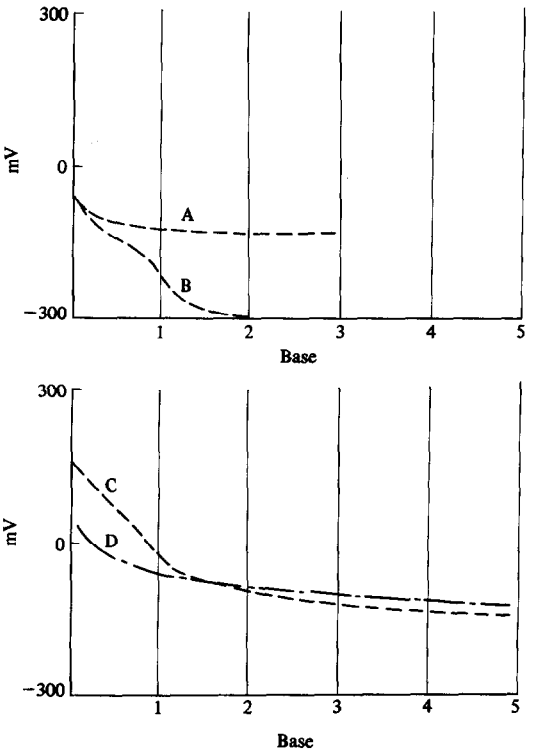

Fig. 1. The titration curves (EMF vs the ratio [base added]/[total pyrogallol] for curve A or [base added]/[total boric acid] for curves B, C and D) are reported for pure pyrogallol 0.003 M (curve A), pure boric acid 0.003 M (curve B) and for the mixtures boric acid 0.022 M–pyrogallol 0.066 M (curve C) and boric acid 0.0033 M–pyrogallol 0.0099 M (curve D).

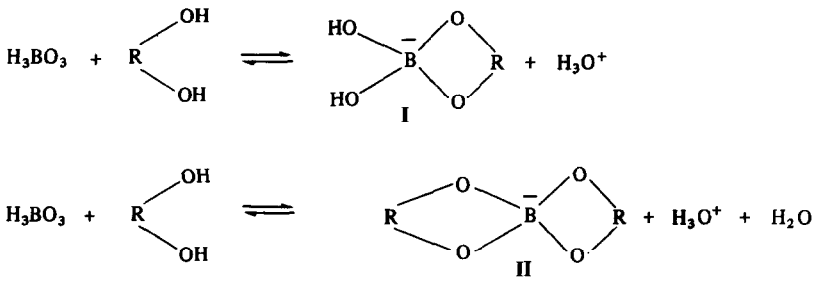

(1)

The relative formation constants are also reported in Table 1 and are in good agreement with those of Antikainen and Katila.[12] Some differences between our results and the literature values[13] for the boric acid ionization constant are noteworthy.

Table 1. pK values for the ionization of boric acid and pyrogallol, and log of formation constants for the reactions in Scheme 1

	K_1	K_2
Boric acid	9.07±0.03	—
Pyrogallol	8.83±0.03	10.81±0.04
Adducts	−6.4±0.01	−2.8±0.1

The titration curves of the mixtures were tentatively fitted with a simple 1 : 1 complexation model, but the fit was significantly poorer than that obtained with the scheme above.

The mixture of boric acid and isopropanol or *sec*-butanol were also examined under the same conditions; their titration curves do not show any significant difference to those of free boric acid. This was expected on the basis of the behaviour of boric acid with simple alcohols, but is also permits the exclusion of medium effects for alcohol concentration on H_3BO_3 titration.

The titration curves in Fig. 1 and the distribution functions in Fig. 2 require some comments:

(1) the titration graphs of the pure compounds,

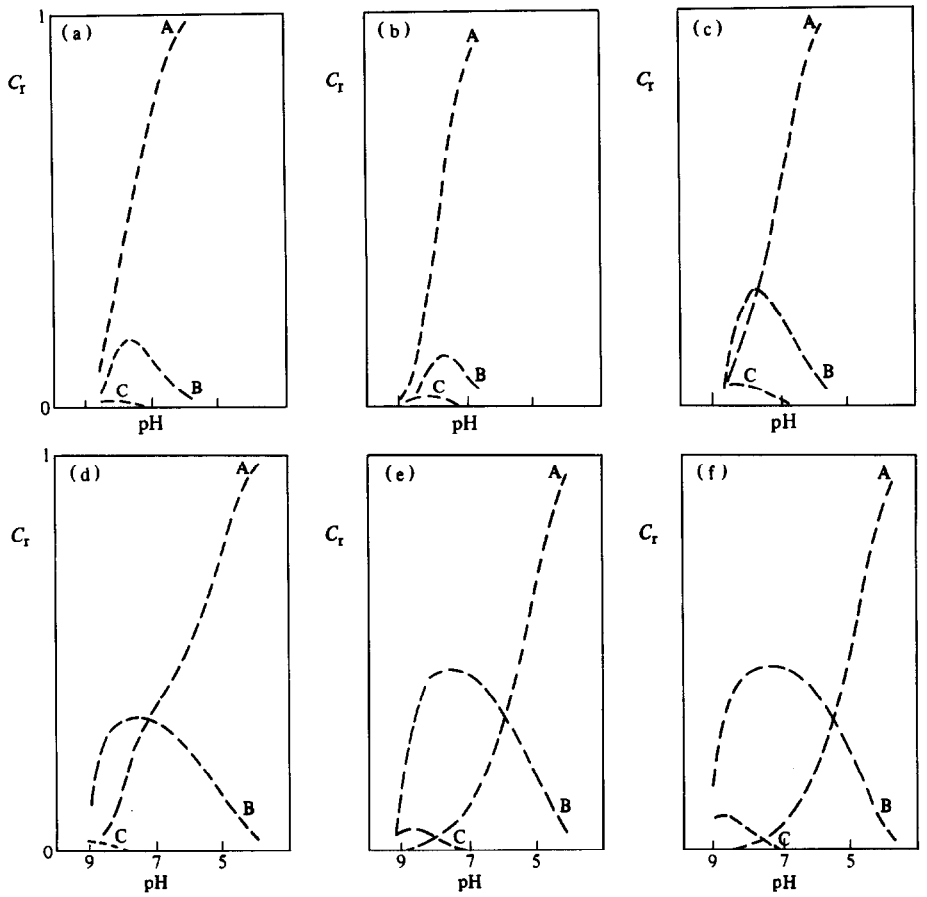

Fig. 2. The ratios [free pyrogallol]/[total pyrogallol] (curves A), [1:2 complex]/[total pyrogallol] (curves B) and [1:1 complex]/[total pyrogallol] (curves C) are reported as a function of pH, calculated with the equilibrium constants reported in Table 1, for the solutions: (a) Boric acid (B.A.) 0.0033 M, pyrogallol (Pyr) 0.0099 M; (b) B.A. 0.0033 M, Pyr 0.0033 M; (c) B.A. 0.013 M, Pyr 0.0066 M; (d) B.A. 0.022 M, Pyr 0.066 M; (e) B.A. 0.066 M, Pyr 0.066 M; (f) B.A. 0.13 M, Pyr 0.066 M.

having similar pK_1 values, look very different because of the second ionization constant of pyrogallol;

(2) opposite to the behaviour with other diols, the addition of pyrogallol eliminates the inflection in the boric acid curve rather than emphasize it. This is ascribed to two reasons:

   (a) the interaction of boric acid with pyrogallol is weaker than with other diols;

   (b) pyrogallol exhibits an acid behaviour which is different from the other diols, and this leads to a flattening of the titration curve when an excess of pyrogallol is titrated. The formation of adducts with pyrogallol, therefore, cannot be exploited for the analytical determination of boric acid. The complexes, as can be clearly seen from the distribution curves in Fig. 2, have a sensible weight at pH values above 5.

In particular, the 1:2 complex, whose existence has been significantly demonstrated by the potentiometric analysis, exists alone at a concentration of 0.07 mol dm^{-3} and pH 7.5. A study by ^{13}C NMR spectroscopy has therefore been possible.

The ^{13}C NMR spectrum of the pure pyrogallol, shown in Fig. 3(a), exhibits four peaks: from off-resonance experiments the two bands at 146.61 and 133.57 ppm were attributed to the three quaternary carbon atoms C(1), C(2) and C(3); in particular, from symmetry considerations, the more intense band at 146.61 to C(1) and C(3) carbon atoms, and that at 133.57 to C(2). By analogous considerations the band at 121.67 can be attributed to C(5) and that at 109.69 to the two equivalent C(6) and C(4) carbon atoms.

By addition of boric acid, in the reported amounts, six new narrow peaks appear well distinct from the four of pure pyrogallol [see Fig. 3(b) and Table 2]. These peaks can be attributed to the complexed form (II) of pyrogallol, in slow exchange with the free form, at the probe temperature of

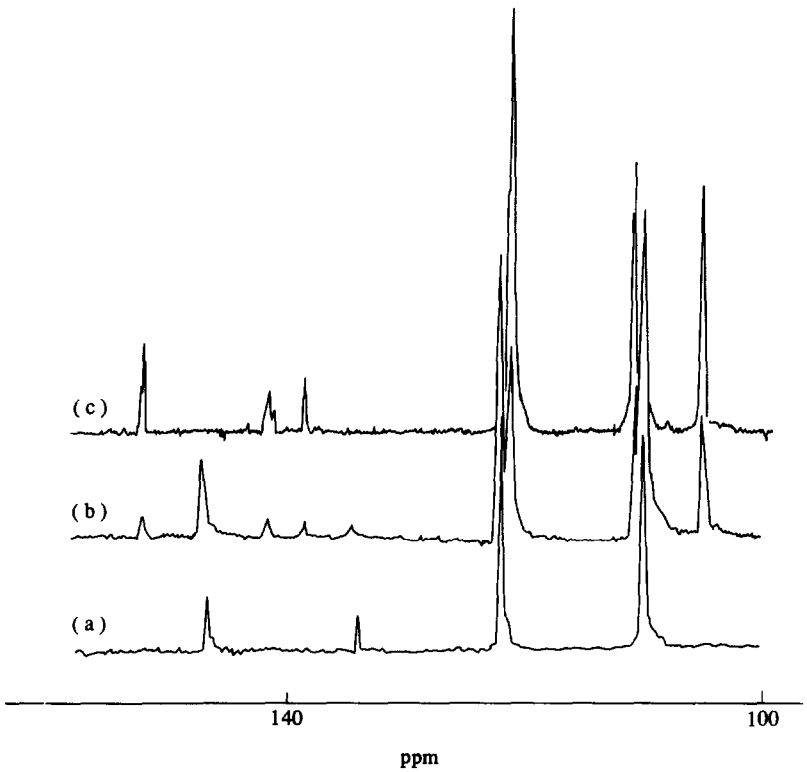

Fig. 3. ^{13}C NMR spectra of pyrogallol from aqueous solutions at pH 7 of (a) pure pyrogallol 0.07 M, (b) pyrogallol 0.07 M–boric acid 0.02 M and (c) pyrogallol 0.07 M–boric acid 0.14 M.

37°C. Their assignment can be made on the basis of shielding effects for the complexation with boric acid; it can, in fact, bind only to two hydroxy groups in the *ortho* position, according to the structure:

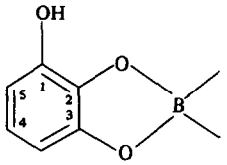

The peaks at 151.77 and 138.06 ppm can therefore be attributed to the C(3) and C(2) atoms, for the high-field shifts of 5.16 and 4.49 ppm from the bands of the free pyrogallol; these shifts have been assigned to a deshielding effect caused by binding with boric acid. The C(1) and C(4) atoms, which are one bond apart from C(2) and C(3), exhibit a downfield shift of −5.52 and −5.21 ppm from the peaks of pure pyrogallol, according to the values of transmission of substituent effects along an aromatic molecule.[14]

C(5) and C(6) show a low shift of −0.89 and 0.63 ppm, respectively. The slight high-field shift of C(6), opposite to the expected downfield shift of C(5), can be tentatively explained in terms of resonance effects with the neighbouring OH group on the C(1) atom. These values are in a very good agreement with those reported by Pasdeloup and Brisson[9] for the analogous 1 : 2 complex of boric acid with cat-

Table 2. ^{13}C chemical shifts (in ppm downfield from TMS) of the species present in the solution of boric acid and pyrogallol at pD 7.5

	C(1), C(3)		C(2)	C(5)	C(4), C(6)	
Free pyrogallol	146.41		133.57	121.67	109.69	
	C(3)	C(1)	C(2)	C(5)	C(6)	C(4)
1 : 2 Complex	151.77	141.09	138.06	120.78	110.32	104.48
$\Delta\delta$	+5.36	−5.32	+4.49	−0.89	+0.63	−5.21

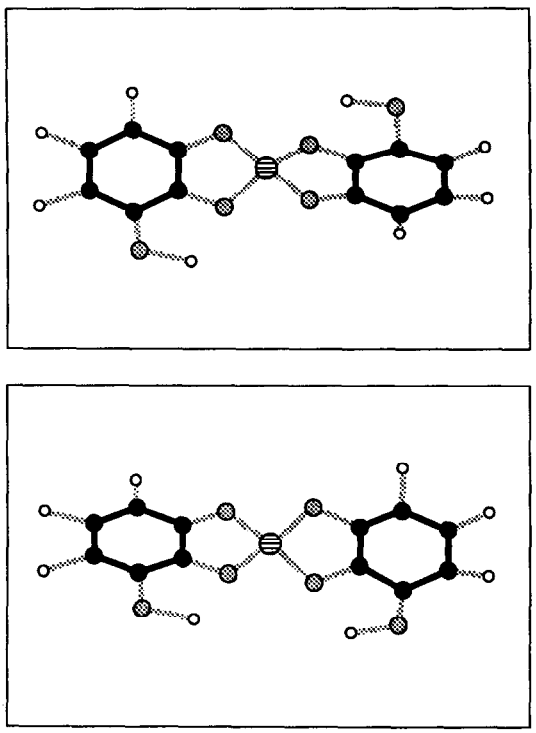

Fig. 4. The enantiomers of the 1 : 2 complex, showing the two possible relative positions of the —OH groups.

echol, and the shifts of C(2) and C(3) agree with the statement[15] that all C—OH carbon atoms are shifted about 6 ppm downfield in the carbohydrate residues of nucleosides. At higher boric acid concentrations the spectrum of pure pyrogallol completely disappears.

At the concentrations used, also with an excess of boric acid, we were not able to detect the resonance of 1 : 1 adducts, but this could also be expected on the basis of the distribution curves.

The spectra of the 1 : 2 complex indicate that the boron forms equivalent bonds with the two pyrogallol moieties in the adduct. In fact no splitting of the signals is observed which implies symmetry of the molecule. The enantiomers of the adduct, recognized as centrally chiral, are shown in Fig. 4, where the two-fold axis of symmetry contains a chiral centre of stereoisomery.[16]

Acknowledgement—This work has been supported by M.P.I.

REFERENCES

1. G. G. Pinna, personal communication.
2. *Mellor's Comprehensive Treatise on Inorganic and Theoretical Chemistry*, Supplement, Vol. V—Boron, Part A—Boron–Oxygen Compounds. Longmans, London (1980).
3. N. H. Greenwood and A. Earnshaw, *Chemistry of the Elements*. Pergamon Press, Oxford (1984).
4. I. M. Kolthoff, E. B. Sandell, E. J. Meehan and S. Bruckenstein, *Quantitative Chemical Analysis*. Macmillan, New York (1973).
5. W. G. Henderson, M. J. Howe, G. R. Kennedy and E. F. Mooney, *Carbohydrate Res.* 1973, **28**, 1.
6. G. R. Kennedy and M. J. How, *Carbohydrate Res.* 1973, **28**, 13.
7. R. Pizer and L. Babcock, *Inorg. Chem.* 1977, **16**, 1677.
8. G. L. Roy, A. L. Laferriere and J. O. Edwards, *J. Inorg. Nucl. Chem.* 1957, **4**, 106.
9. M. Pasdeloup and C. Brisson, *Org. Magn. Res.* 1981, **16**, 167.
10. P. M. May, D. R. Williams, P. V. Linder and R. G. Torrington, *Talanta* 1982, **29f**, 249.
11. L. Zekany and I. Nagypal, *Computational Methods for the Determination of Formation Constants* (Edited by D. J. Leggett), Chap. 11. Plenum Press, New York (1985).
12. P. J. Antikainen and R. Katila, *Suomen Kemistilehti B* 1971, **44**, 256.
13. E. Hogfeldt, *Stability Constants of Metal-Ion Complexes, Part A Compiled for IUPAC*, Pergamon Press, Oxford (1982); D. D. Perrin, *Stability Constants of Metal-Ion Complexes, Part B*. Pergamon Press, Oxford (1979).
14. F. W. Wehrly and T. Wirthlin, *Interpretation of Carbon-13 NMR Spectra*. Heyden, London (1976).
15. E. Breitmaier and W. Voelter, *^{13}C-NMR Spectroscopy*, Vol. 5, p. 269. Verlag Chemie, Weinheim (1978).
16. B. Testa, *Principles of Organic Stereochemistry* (Edited by P. Gassman). Marcel Dekker, New York (1979).

Polyhedron Vol. 9, No. 6, pp. 795–799, 1990
Printed in Great Britain

0277–5387/90 $3.00+.00
© 1990 Pergamon Press plc

SYNTHESIS AND IR SPECTRAL STUDIES OF SOME LANTHANIDE NITRATE COMPLEXES WITH 4-BENZOYL-3-METHYL-1-PHENYLPYRAZOL-5-ONE

SAM KUNCHANDY and P. INDRASENAN*

Department of Chemistry, University of Kerala, Trivandrum 695 034, India

(*Received* 22 *March* 1989; *accepted* 18 *October* 1989)

Abstract—Nine complexes of lanthanide nitrates with 4-benzoyl-3-methyl-1-phenylpyrazol-5-one (BMPP) having the general formula $[Ln(BMPP)_2(NO_3)_3]$ (where Ln = La, Pr, Nd, Sm, Eu, Gd, Tb, Dy and Y) have been synthesized and their IR spectra obtained. In these complexes BMPP acts as a bidentate ligand coordinating through the oxygen of both the carbonyl groups and the nitrate ion acts as a unidentate ligand coordinating through one of the oxygen atoms with the lanthanide ion.

4-Benzoyl-3-methyl-1-phenylpyrazol-5-one forms stable complexes with some transition metals and lanthanides in which BMPP acts as a monobasic bidentate ligand in which both the carbonyl groups (ring and side chain) are participating in coordination.[1,2] As part of our programme for the synthesis and characterization of solid lanthanide complexes,[3–8] we presently report on the isolation and IR spectral studies of nine lanthanide nitrates, in which BMPP acts as a neutral bidentate rather than monobasic bidentate ligand.

EXPERIMENTAL

Reagents

The nitrates of La^{III}, Pr^{III}, Nd^{III}, Sm^{III}, Eu^{III}, Gd^{III}, Tb^{III}, Dy^{III} and Y^{III} were prepared from the respective oxides (99.9% pure) as reported earlier.[5] BMPP was prepared by a modified Jenson method,[2,9] in which ethanol was used as solvent rather than dioxane, and 2 N hydrochloric acid, which had been cooled in ice, was used for neutralization to give a better yield. The crude sample of BMPP was recrystallized from 95% ethanol. The purity of the sample was checked by elemental analysis, IR spectral, TLC and melting point data.

Preparation and analysis of complexes

Lanthanide nitrates (2 mmol) and BMPP (4.1 mmol) were dissolved separately in minimum amounts of hot ethanol and these solutions were mixed together and kept under reflux on a water bath for 2 h. The reaction mixture was then concentrated to obtain a viscous mass, which was stirred vigorously with hot benzene to separate the complex. The complex was collected by removal of the benzene layer and was washed repeatedly with hot benzene to remove excess ligand. All the complexes so isolated were dried *in vacuo* over phosphorus(V) oxide.

The lanthanide contents of the complexes were determined by the oxalate–oxide method.[10] Microanalyses for carbon, hydrogen and nitrogen were performed by the microanalytical unit of the Regional Sophisticated Instrumentation Centre (Central Drug Research Institute, Lucknow, India).

Physical measurements

Molar conductivities of the complexes in acetonitrile and nitrobenzene ($\sim 10^{-3}$ M solutions) were measured at room temperature ($28 \pm 2°C$) using an ELICO type MB2T conductivity unit with dip type cell (Type CC-03) containing platinum electrodes (cell constant = 1.40 cm^{-1}). Magnetic susceptibilities of the complexes were measured at room temperature by the Gouy method using mercury(II) tetrathiocyanatocobaltate(II) as the calibrant. The IR spectra of the ligand and complexes were recorded on a double-beam Perkin–Elmer 397 IR spectrophotometer in the range 4000–400 cm^{-1} using the KBr disc technique. Molecular weights of

* Author to whom correspondence should be addressed.

Table 1. Analytical, magnetic, molecular weight and conductivity data of lanthanide nitrate complexes of BMPP (calculated values in parentheses)

Complex	Colour	Metal (%)	Carbon (%)	Hydrogen (%)	Nitrogen (%)	μ_{eff}[a] (BM)	Molecular weight	Molar conductivity[b]	
								In acetonitrile	In nitrobenzene
$[La(BMPP)_2(NO_3)_3]$	White	15.7 (15.8)	46.1 (46.3)	3.1 (3.2)	11.0 (11.1)	0.00 (0.00)	920 (881)	48.32	6.24
$[Pr(BMPP)_2(NO_3)_3]$	Greenish yellow	15.8 (16.0)	46.1 (46.2)	3.2 (3.2)	10.9 (11.1)	3.52 (3.58)	922 (881)	45.71	6.51
$[Nd(BMPP)_2(NO_3)_3]$	Pale violet	16.1 (16.3)	46.0 (46.0)	3.1 (3.2)	10.9 (11.1)	3.56 (3.62)	930 (886)	46.80	6.74
$[Sm(BMPP)_2(NO_3)_3]$	White	16.6 (16.9)	45.5 (45.7)	3.0 (3.1)	10.9 (11.0)	1.66 (1.65)	941 (892)	47.20	5.97
$[Eu(BMPP)_2(NO_3)_3]$	White	16.9 (17.0)	45.5 (45.6)	3.1 (3.1)	10.9 (11.0)	3.37 (3.40)	950 (894)	46.50	6.91
$[Gd(BMPP)_2(NO_3)_3]$	White	17.3 (17.5)	45.4 (45.4)	3.1 (3.1)	10.8 (10.9)	7.82 (7.97)	960 (899)	45.92	7.48
$[Tb(BMPP)_2(NO_3)_3]$	White	17.5 (17.6)	45.1 (45.3)	3.1 (3.1)	10.8 (10.9)	9.72 (9.70)	941 (901)	48.89	7.33
$[Dy(BMPP)_2(NO_3)_3]$	White	17.9 (18.0)	45.0 (45.1)	3.1 (3.1)	10.8 (10.8)	10.70 (10.61)	961 (904)	47.50	6.41
$[Y(BMPP)_2(NO_3)_3]$	Yellow	10.8 (10.7)	49.2 (49.1)	3.3 (3.4)	11.7 (11.8)	0.00 (0.00)	863 (831)	46.82	5.43

[a] Calculated using the Van Vleck formula.
[b] Ω^{-1} cm^2; the concentration $\sim 10^{-3}$ M.

the complexes ($\sim 10^{-4}$ M solutions) were determined by the cryoscopic method in nitrobenzene.[11]

RESULTS AND DISCUSSION

All the complexes are non-hygroscopic solids with varying colours (Table 1), which are soluble in polar solvents such as acetone, acetonitrile, ethanol, methanol and nitrobenzene and insoluble in solvents of low polarity such as benzene, carbon tetrachloride, chloroform and diethyl ether. The elemental analysis, magnetic susceptibility, molecular weight and molar conductivity data of the complexes are presented in Table 1. All of these complexes show non-electrolytic behaviour in nitrobenzene and acetonitrile.[12] The lanthanum and yttrium complexes are diamagnetic while all the other complexes are paramagnetic, as expected. The measured magnetic moments (Table 1) are in good agreement with the theoretical values calculated from the Van Vleck formula.[13] These observations suggest that the present series of complexes can be formulated as $[Ln(BMPP)_2(NO_3)_3]$, where Ln = La, Pr, Nd, Sm, Eu, Gd, Tb, Dy and Y.

IR spectra

The important IR spectral bands of the ligand and complexes are presented in Table 2. The observed IR spectral bands of the ligand and lanthanum complex with their tentative assignments are given in Table 3.

The IR spectrum of BMPP exhibits a broad band with a peak maximum at 2550 cm^{-1}, which is attributed to strongly hydrogen bonded ν(OH). The very strong band at 1630 cm^{-1}, observed in the spectrum of BMPP, is due to a stretching vibration of the intramolecular hydrogen bonded side chain carbonyl group. Absence of any stretching band corresponding to the ring carbonyl group in the spectrum of the ligand indicates that the enol form (II) is stabilized in the free ligand as shown in Fig. 1.

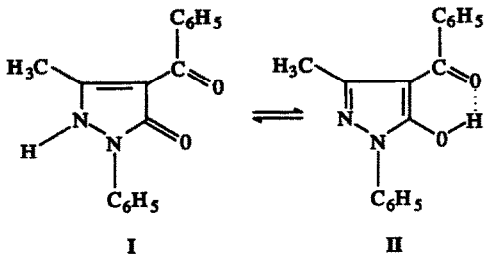

Fig. 1. Keto (I) and enol (II) forms of BMPP.

In the spectra of the complexes the band corresponding to ν(OH) is absent. Instead, a new band is observed at 3160 cm^{-1} in these spectra, assignable to ν(NH), which has no parallel band in the spectrum of the ligand. This shows that the keto form (I) of the ligand is coordinated to the lanthanide ion in the complexes. This is also supported by the appearance of two very strong bands, one at 1620 cm^{-1} and another at 1650 cm^{-1} in the spectra of the complexes, which are attributed to the stretching vibrations of the ring carbonyl and side chain carbonyl groups, respectively. The relative positions of ν(C=O) (ring) and ν(C=O) (side chain) suggest that both the carbonyl groups are coordinated to the metal ion. The apparent lowering of the side carbonyl stretching frequency of the free ligand (1630 cm^{-1}) is due to very strong intramolecular hydrogen bonding by way of forming a six-membered ring as shown in Fig. 1. The observed positions of the ν(C=O) (ring) and ν(C=O) (side chain) modes in the spectra of the complexes (1620 and 1650 cm^{-1}) may be attributed to vibrational

Table 2. Important IR spectral bands of BMPP and its lanthanide nitrate complexes

Complex	ν(OH)	ν(NH)	ν(C=O) (ring)	ν(C=O) (side chain)	$\nu_1(NO_3)$	$\nu_2(NO_3)$	$\nu_4(NO_3)$	ν(M—O)
BMPP	2550 s,br	—	—	1630 vs	—	—	—	—
$[La(BMPP)_2(NO_3)_3]$	—	3160 m	1620 vs	1650 vs	1430 vs	1025 s	1300 m	408 w
$[Pr(BMPP)_2(NO_3)_3]$	—	3140 m	1625 vs	1655 vs	1430 vs	1025 s	1300 m	410 w
$[Nd(BMPP)_2(NO_3)_3]$	—	3140 m	1620 vs	1650 vs	1430 vs	1025 s	1300 m	410 w
$[Sm(BMPP)_2(NO_3)_3]$	—	3140 m	1625 vs	1650 vs	1430 vs	1025 s	1300 m	410 w
$[Eu(BMPP)_2(NO_3)_3]$	—	3140 m	1625 vs	1650 vs	1430 vs	1025 s	1300 m	410 w
$[Gd(BMPP)_2(NO_3)_3]$	—	3140 m	1625 vs	1650 vs	1430 vs	1025 s	1305 m	405 w
$[Tb(BMPP)_2(NO_3)_3]$	—	3130 m	1620 vs	1650 vs	1420 vs	1015 s	1305 m	410 w
$[Dy(BMPP)_2(NO_3)_3]$	—	3140 m	1625 vs	1650 vs	1430 vs	1020 s	1300 m	410 w
$[Y(BMPP)_2(NO_3)_3]$	—	3140 m	1620 vs	1640 vs	1430 vs	1025 s	1310 m	408 w

Abbreviations: vs = very strong; s = strong; m = medium; w = weak; br = broad.

Table 3. Observed IR spectral bands of BMPP and its lanthanum complex

BMPP	$[La(BMPP)_2(NO_3)_3]$	Tentative assignment
—	3160 m	ν(N—H)
3060 w	3060 w	ν(C—H) (aryl)
2880 w	2900 w	ν(C—H) (saturated)
2550 s,br	—	ν(O—H···O) (hydrogen bonded)
1635 vs	1645 vs	ν(C=O) (side chain)
—	1620 vs	ν(C=O···H) (hydrogen bonded) ν(C=O) (ring)
1590 s	1590 sh	ν(C=N)
1570 m	1565 s	ν(C—C) (phenyl)
1520 s	1520 sh	ν(C—C—C) (chelate ring) as pyrazole ring stretch
1490 s 1470 sh	1490 s 1480 sh	ν_s(C—C—C) (chelate ring)
1450 w	1450 s	Phenyl ring + methyl
—	1430 vs	$\nu_1(NO_3)$
1390 s	1375 vs	$\nu_1(CH_3)$
1340 s	1340 s	Pyrazole ring stretch
1310 m	—	ν(C—O) (phenolic)
—	1300 vs	$\nu_4(NO_3)$
1220 w	1210 m	C—H in-plane bending
1190 m	1170 m	ν(C—N)
1170 w	1160 m	ν(C—N)
1100 w	1130 w	ν(C=O + C—C)
1070 w	1070 m	Phenyl ring stretch + ν(CH)
—	1025 s	$\nu_2(NO_3)$
990 w	990 w	CH_3 rocking
940 w 930 s	940 sh 930 s	ν(C—C_6H_5—)
830 sh 820 sh	835 s	β(C—C—C)
800 w	800 w	ν(CH)
750 s	760 s	Monosubstituted benzene
725 m	730 s	ν(CH)
700 s 680 m	700 s 685	Chelating ring deformation
665 m	660 m	δ(C=O) (in-plane)
610 s	610 s	δ(C=O) (out-of-plane)
540 w	540 m	δ(C—H) (out of plane) of phenyl ring
490 w	490 m	δ(C—H) (out-of-plane) of pyrazole ring
—	410 w	ν(M—O) (carbonyl)

Abbreviations: vs = very strong; s = strong; m = medium; w = weak; br = broad; sh = shoulder.

coupling effects. These observations suggest that the free ligand exists in the enol form (**II**) and the coordinated ligand exists in the keto form (**I**). The presence of ν(NH) in the spectra of the complexes shows that BMPP acts as a neutral ligand rather than a monobasic one, in disagreement with the observation made by Okafor.[2] The present observation on the coordination of BMPP towards lanthanides is confirmed by the presence of three nitrate ions in all the complexes (Table 1).

The spectra of the complexes contain four additional bands at 1430, 1300, 1025 and 410 cm^{-1}, which are not present in the spectrum of the ligand. Of these, the first three are assigned to ν_1, ν_4, and ν_2 modes, respectively, of the coordinated nitrate ion. In fact the ν_1 and ν_4 modes of the nitrate

ion are the two split bands of the ν_3 mode of the uncoordinated nitrate ion. The magnitude of splitting of ν_1 and ν_4 is in the order of 130 cm^{-1}. This type of splitting and comparison with recent papers on similar complexes, which have been characterized by X-ray analysis, suggest that the nitrate ions are coordinated unidentately to the lanthanide ions in the present complexes.[14–16] The fourth additional band at 410 cm^{-1} is assigned to stretching vibrations of the Ln—O bond formed out of coordination through the carbonyl groups.

Based on the above discussion and observations, it is concluded that BMPP acts as a neutral bidentate ligand coordinating through both the carbonyl groups, and the nitrate ion acts as a unidentate ligand coordinating through one of the three oxygen atoms with the lanthanide ion. Hence the lanthanide ion has a coordination number of seven in the present complexes.

Acknowledgement—The authors are grateful to the University Grants Commission (New Delhi, India) for awarding a Teacher fellowship to one of them (S.K.).

REFERENCES

1. C. Brecher, A. Lempicki and H. Samuelson, *J. Chem. Phys.* 1964, **41**, 279.
2. E. C. Okafor, *J. Inorg. Nucl. Chem.* 1980, **42**, 1155.
3. V. Giri and P. Indrasenan, *Polyhedron* 1983, **2**, 573.
4. P. K. Radhakrishnan, P. Indrasenan and C. G. R. Nair, *Polyhedron* 1984, **3**, 67.
5. H. Jayasankar and P. Indrasenan, *J. Less-Common Met.* 1987, **132**, 43.
6. H. Jayasankar and P. Indrasenan, *Ind. J. Chem.* 1987, **26A**, 964.
7. H. Jayasankar and P. Indrasenan, *Ind. J. Chem.* 1988, **27A**, 362.
8. H. Jayasankar and P. Indrasenan, *Ind. J. Chem.* 1988, **27A**, 545.
9. B. S. Jenson, *Acta Chem. Scand.* 1959, **13**, 1668.
10. I. M. Kolthoff and P. S. Elving, *Treatise on Analytical Chemistry*, Part II, Vol. 8. Interscience, New York (1963).
11. W. G. Palmer, *Experimental Physical Chemistry*. The University Press, Cambridge (1954).
12. W. J. Geary, *Coord. Chem. Rev.* 1971, **7**, 81.
13. J. H. Van Vleck and N. Frank, *Phys. Rev.* 1929, **34**, 1494.
14. N. F. Curtis and Y. M. Curtis, *Inorg. Chem.* 1965, **4**, 804.
15. M. Mohan, J. P. Tandon and N. S. Gupta, *Inorg. Chim. Acta* 1986, **111**, 187.
16. G. S. Conary, A. A. Russel, R. T. Paine, J. H. Hall and R. R. Ryan, *Inorg. Chem.* 1988, **27**, 3242.

Polyhedron Vol. 9, No. 6, pp. 801–804, 1990
Printed in Great Britain

0277–5387/90 $3.00+.00
© 1990 Pergamon Press plc

MONO- AND DINUCLEAR PHOSPHINE COORDINATED 1,4-BIS(DIPHENYLPHOSPHINO)ETHYNE SEVEN-COORDINATE COMPLEXES OF MOLYBDENUM(II) AND TUNGSTEN(II)

PAUL K. BAKER* and ELAINE M. ARMSTRONG

Department of Chemistry, University College of North Wales, Bangor, Gwynedd LL57 2UW, U.K.

(*Received* 6 *May* 1989; *accepted* 18 *October* 1989)

Abstract—Equimolar quantities of the seven-coordinate compounds $[MI_2(CO)_3(NCMe)_2]$ (M = Mo and W) and $Ph_2PC{\equiv}CPPh_2$ react in CH_2Cl_2 at room temperature to afford the $Ph_2PC{\equiv}CPPh_2$ phosphine coordinated bridged complexes $[M_2I_4(CO)_6(\mu\text{-}Ph_2PC{\equiv}CPPh_2)_2]$ in good yield. Reaction of $[MI_2(CO)_3(NCMe)_2]$ with two equivalents of $Ph_2PC{\equiv}CPPh_2$ in CH_2Cl_2 at room temperature gives the mononuclear compounds $[MI_2(CO)_3(Ph_2PC{\equiv}CPPh_2)_2]$. ^{31}P NMR studies show the $Ph_2PC{\equiv}CPPh_2$ ligand in $[MI_2(CO)_3(Ph_2PC{\equiv}CPPh_2)_2]$ to have monodentate phosphine coordination.

In the past the ligand $Ph_2PC{\equiv}CPPh_2$ has been shown to coordinate via the phosphorus atoms to transition metal centres.[1–14] However, in 1970 Ward and Templeton[15] reported the synthesis of the alkyne coordinated 1,4-bis(diphenylphosphino) ethyne complex $[W(CO)(S_2CNEt_2)_2(\eta^2\text{-}Ph_2PC{\equiv}CPPh_2)]$. Very recently, Went and co-workers[16] have studied the chemistry of $[W(CO)(S_2CNEt_2)_2(\eta^2\text{-}Ph_2PC{\equiv}CPPh_2)]$, and interestingly found it could coordinate by either bridging a cobalt–cobalt bond in $[(S_2CNEt_2)_2(CO)W(\mu\text{-}Ph_2PC{\equiv}CPPh_2)Co_2(\mu\text{-}CO)_2(CO)_4]$, or as a bidentate phosphine to molybdenum in $[(S_2CNEt_2)_2(CO)W(\mu\text{-}Ph_2PC{\equiv}CPPh_2)Mo(CO)_4]$.

In recent years we have been studying the reactions of the highly versatile seven-coordinate compounds $[MI_2(CO)_3(NCMe)_2]$ (M = Mo and W).[17] These compounds are prepared by reacting the zero-valent six-coordinate complexes $[M(CO)_3(NCMe)_3]$ *in situ* with one equivalent of iodine at 0°C to give $[MI_2(CO)_3(NCMe)_2]$ in quantitative yield.[17] For example, the complexes $[MI_2(CO)_3(NCMe)_2]$ react either with two equivalents of monodentate ligands (PPh_3, $AsPh_3$ or $SbPh_3$) (L)[18] or one equivalent of bidentate phosphines (L_2)[19] to give the substituted products $[MI_2(CO)_3L_2]$. The complexes $[MI_2(CO)_3(NCMe)_2]$ also react with either one equivalent of alkyne, RC_2R' (M = Mo and W; R = R′ = Me, Ph and CH_2Cl; R = Ph, R′ = Me and CH_2OH; R = Me, R′ = PhS and *p*-MeC_6H_4S) to afford the iodo-bridged complexes $[M(\mu\text{-}I)I(CO)(NCMe)(\eta^2\text{-}RC_2R')]_2$[20] or with two equivalents of RC_2R' (M = Mo and W; R = R′ = Me or Ph; R = Me, R′ = Ph; for M = W only, R = R′ = Me, CH_2Cl and *p*-MeC_6H_4; R = Ph, R′ = CH_2OH) to give the mononuclear bisalkyne complexes $[MI_2(CO)(NCMe)(\eta^2\text{-}RC_2R')_2]$ and the iodo-bridged molybdenum compound $[Mo(\mu\text{-}I)I(CO)(\eta^2\text{-}MeC_2Me)_2]_2$.[21] In view of this work the ligand $Ph_2PC{\equiv}CPPh_2$ could coordinate to molybdenum or tungsten in $[MI_2(CO)_3(NCMe)_2]$ via either the phosphorus atoms or the alkyne group. In this paper we describe the reactions of $[MI_2(CO)_3(NCMe)_2]$ with $Ph_2PC{\equiv}CPPh_2$.

EXPERIMENTAL

All reactions described in this paper were carried out under an atmosphere of nitrogen using standard Schlenk-line techniques. CH_2Cl_2 was dried and distilled before use. The seven-coordinate compounds $[MI_2(CO)_3(NCMe)_2]$ (M = Mo and W) were prepared by the published method.[17] All chemicals used were purchased from commercial sources.

Elemental analyses (C, H and N) were determined using a Carlo Erba Elemental Analyser MOD 1106 (using helium as a carrier gas). IR spectra were recorded on a Perkin–Elmer 197 IR spectrophotometer. ^{13}C and ^{31}P NMR spectra were recorded on a Bruker WH-400 NMR spec-

* Author to whom correspondence should be addressed.

Table 1. Physical and analytical[a] data for the complexes $[M_2I_4(CO)_6(\mu\text{-}Ph_2PC{\equiv}CPPh_2)_2]$ and $[MI_2(CO)_3(Ph_2PC{\equiv}CPPh_2)_2]$

Complex	Colour	Yield (%)	C (%)	H (%)
$[Mo_2I_4(CO)_6(\mu\text{-}Ph_2PC{\equiv}CPPh_2)_2]$ (**1**)	Orange	37	42.3 (42.1)	3.0 (2.4)
$[W_2I_4(CO)_6(\mu\text{-}Ph_2PC{\equiv}CPPh_2)_2]$ (**2**)	Yellow/orange	37	38.2 (38.0)	2.5 (2.2)
$[MoI_2(CO)_3(Ph_2PC{\equiv}CPPh_2)_2]$ (**3**)	Orange	38	54.6 (54.0)	3.2 (3.3)
$[WI_2(CO)_3(Ph_2PC{\equiv}CPPh_2)_2]$ (**4**)	Yellow	61	51.0 (50.4)	3.2 (3.1)

[a] Calculated values in parentheses.

trometer at the University of Warwick (^{13}C NMR spectra were calibrated against tetramethylsilane; ^{31}P NMR spectra were calibrated against 85% H_3PO_4). Molecular weights of $[M_2I_4(CO)_6(\mu\text{-}Ph_2PC{\equiv}CPPh_2)_2]$ (**1** and **2**) were determined by Rast's method,[22] with camphor as the solvent.

$[Mo_2I_4(CO)_6(\mu\text{-}Ph_2PC{\equiv}CPPh_2)_2]$ (1)

To a stirred solution of $[MoI_2(CO)_3(NCMe)_2]$ (0.2501 g, 0.388 mmol) in CH_2Cl_2 (15 cm^3), under a stream of nitrogen, was added $Ph_2PC{\equiv}CPPh_2$ (0.1530 g, 0.388 mmol). After 3 min, filtration, followed by removal of the solvent *in vacuo* gave orange crystals of $[Mo_2I_4(CO)_6(\mu\text{-}Ph_2PC{\equiv}CPPh_2)_2]$ (**1**), which were recrystallized from CH_2Cl_2, yield of pure product = 0.17 g, 37%. Molecular weight for $C_{58}H_{20}I_4Mo_2O_6P_4$: Found: 1519. Calc: 1656.

In a similar reaction, $[WI_2(CO)_3(NCMe)_2]$ and an equimolar quantity of $Ph_2PC{\equiv}CPPh_2$ gave $[W_2I_4(CO)_6(\mu\text{-}Ph_2PC{\equiv}CPPh_2)_2]$ (**2**). Molecular weight for $C_{58}H_{20}I_4O_6P_4W_2$: Found: 1956. Calc: 1832.

$[MoI_2(CO)_3(Ph_2PC{\equiv}CPPh_2)_2]$ (3)

To a stirred solution of $[MoI_2(CO)_3(NCMe)_2]$ (0.1000 g, 0.194 mmol) in CH_2Cl_2 (15 cm^3), under a stream of nitrogen, was added $Ph_2PC{\equiv}CPPh_2$ (0.1529 g, 0.388 mmol). After 10 min, filtration, followed by removal of the solvent *in vacuo* gave orange crystals of $[MoI_2(CO)_3(Ph_2PC{\equiv}CPPh_2)_2]$ (**3**), which were recrystallized from CH_2Cl_2, yield of pure product = 0.09 g, 38%.

In a similar reaction, $[WI_2(CO)_3(NCMe)_2]$ with two equivalents of $Ph_2PC{\equiv}CPPh_2$ gave $[WI_2(CO)_3(Ph_2PC{\equiv}CPPh_2)_2]$ (**4**).

RESULTS AND DISCUSSION

The seven-coordinate bisacetonitrile complexes $[MI_2(CO)_3(NCMe)_2]$ (M = Mo and W) react in CH_2Cl_2 at room temperature with an equimolar amount of $Ph_2PC{\equiv}CPPh_2$ to eventually give the seven-coordinate phosphine-bridged dimeric compounds $[M_2I_4(CO)_6(\mu\text{-}Ph_2PC{\equiv}CPPh_2)_2]$ (**1** and **2**). However, reaction of $[MI_2(CO)_3(NCMe)_2]$ with two equivalents of $Ph_2PC{\equiv}CPPh_2$ in CH_2Cl_2 at room temperature gave the monomeric seven-coordinate compounds $[MI_2(CO)_3(Ph_2PC{\equiv}CPPh_2)_2]$ (**3** and **4**). The new complexes (**1**–**4**) were fully characterized by elemental analysis (C, H and N) (Table 1), IR (Table 2), ^{13}C and ^{31}P NMR spectroscopy (Tables 3 and 4). The complexes are stable in the solid state when stored under nitrogen, and are soluble in chlorinated solvents such as CH_2Cl_2 and $CHCl_3$.

The reactions of $[MI_2(CO)_3(NCMe)_2]$ with $Ph_2PC{\equiv}CPPh_2$ in a 1:1 ratio should initially give the monoacetonitrile compounds $[MI_2(CO)_3(NCMe)(Ph_2PC{\equiv}CPPh_2)]$. Complexes of the type $[MI_2(CO)_3(NCMe)L]$ [L = PPh_3, PPh_2Cy, $AsPh_3$, $SbPh_3$ and $P(OPh)_3$] have been isolated and fully characterized from reactions of $[MI_2(CO)_3(NCMe)_2]$ with an equimolar quantity of L.[23] The

Table 2. IR data[a] for the complexes $[M_2I_4(CO)_6(\mu\text{-}Ph_2PC{\equiv}PPh_2)_2]$ and $[MI_2(CO)_3(Ph_2PC{\equiv}CPPh_2)_2]$

Complex	ν(C≡O) (cm^{-1})
1	2025 (m), 1960 (vs), 1930 (sh), 1860 (s)
2	2015 (m), 1945 (s), 1915 (s)
3	1965 (s), 1930 (m), 1865 (s)
4	2015 (m), 1945 (s), 1915 (m)

[a] Spectra run as $CHCl_3$ films between NaCl plates.

Table 3. ^{13}C NMR data[a,b] for the complexes $[M_2I_4(CO)_6(\mu\text{-}Ph_2PC{\equiv}CPPh_2)_2]$ and $[MI_2(CO)_3(Ph_2PC{\equiv}CPPh_2)_2]$

Complex	^{13}C (δ ppm)
1[a]	206.65 (s, $C{\equiv}O$); 132.82–128.66 (bm, Ph); 86.70 (s, $C{\equiv}C$)
2[a]	207.90 (s, $C{\equiv}O$); 134.31–127.97 (bm, Ph); 106.01 (s, $C{\equiv}C$)
3[a]	208.88 (s, $C{\equiv}O$); 135.94–128.39 (bm, Ph); 107.19 (s, $C{\equiv}C$)
4[b]	229.13, 210.01, 208.16, 206.56 (s, $C{\equiv}O$); 135.82–128.18 (bm, Ph); 111.60–98.31 (9 resonances, $C{\equiv}C$)

[a] Spectra recorded in CD_2Cl_2 (+26°C).
[b] Spectrum recorded in CD_2Cl_2 (−90°C).
All spectra were referenced to Me_4Si.

Table 4. ^{31}P NMR data[a] for the complexes $[M_2I_4(CO)_6(\mu\text{-}Ph_2PC{\equiv}CPPh_2)_2]$ and $[MI_2(CO)_3(Ph_2PC{\equiv}CPPh_2)_2]$

Complex	^{31}P (δ ppm)
1	+9.94; +1.61
2	+9.91; +1.94
3	+8.44; −32.51
4	+7.18; −33.15

[a] Spectra recorded in CD_2Cl_2 (+26°C) and referenced to 85% H_3PO_4.

steric constraints of the ligand $Ph_2PC{\equiv}CPPh_2$ do not allow easy coordination in a bidentate manner to a transition metal centre, compared to a more flexible bidentate phosphine such as $Ph_2P(CH_2)_2PPh_2$ which reacts with an equimolar amount of $[MI_2(CO)_3(NCMe)_2]$ to give $[MI_2(CO)_3\{Ph_2P(CH_2)_2PPh_2\}]$.[19] The monoacetonitrile complexes $[MI_2(CO)_3(NCMe)(Ph_2PC{\equiv}CPPh_2)]$ rapidly dimerize to give the phosphine-bridged dimeric complexes $[M_2I_4(CO)_6(\mu\text{-}Ph_2PC{\equiv}CPPh_2)_2]$ (**1** and **2**). The dimeric nature of **1** and **2** was confirmed by molecular weight measurements by Rast's method[22] (see Experimental). ^{31}P NMR studies (Table 4) show that all four phosphine atoms in each of **1** and **2** are coordinated to the metal (the phosphine resonance in the ^{31}P NMR spectrum of uncoordinated $Ph_2PC{\equiv}CPPh_2$ in $CDCl_3$ at 25°C is −31.19 ppm relative to 85% H_3PO_4).

The reactions of $[MI_2(CO)_3(NCMe)_2]$ (M = Mo or W) with $Ph_2PC{\equiv}CPPh_2$ in a 2:1 molar ratio afford the bismonodentate coordinated phosphine complexes $[MI_2(CO)_3(Ph_2PC{\equiv}CPPh_2)_2]$. The ^{31}P NMR spectra (Table 4) of **3** and **4** showed resonances due to the coordinated phosphine atoms at δ = +8.44 and +7.18 ppm and due to the uncoordinated phosphine atoms at δ = −32.51 and −33.15 ppm, respectively (uncoordinated $Ph_2PC{\equiv}CPPh_2$ has a single ^{31}P resonance at δ = −31.19 ppm). This evidence confirms that the ligand $Ph_2PC{\equiv}CPPh_2$ is coordinated via one of its phosphorus atoms in **3** and **4**.

The structures of both the dimeric and monomeric complexes are likely to have capped octahedral geometries, since the structure of the dimer $[W(\mu\text{-}Br)Br(CO)_4]_2$[24] and a number of monomeric seven-coordinate complexes of the type $[MX_2(CO)_3L_2]$[25–32] have been determined by X-ray crystallography and shown to have capped octahedral geometry. The IR spectral properties [ν(C≡O)] (Table 2) of **3** and **4** are similar to other seven-coordinate complexes which have been shown to have capped octahedral geometry. Further evidence to support the proposed capped octahedral structures comes from measuring the low temperature (−70°C, CD_2Cl_2) ^{13}C NMR spectrum of **4**. The spectrum shows a carbonyl resonance at very low field (229.13 ppm) (Table 3), which is likely to be due to a carbonyl ligand in the unique capping position from some work of Colton and Kevekordes[33] on the low temperature ^{13}C NMR spectra on related seven-coordinate complexes. However, the existence of four carbonyl resonances suggests there are several isomers in solution. One

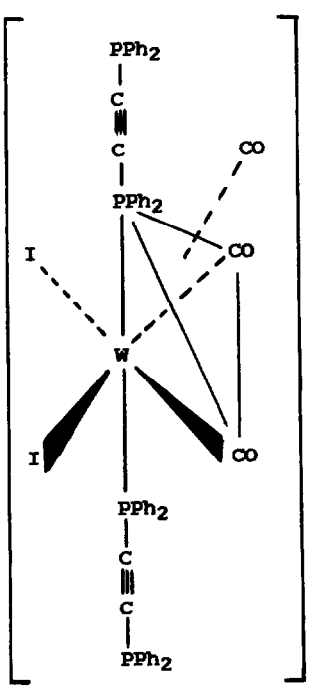

Fig. 1. One possible isomer of $[WI_2(CO)_3(Ph_2PC{\equiv}CPPh_2)_2]$.

likely isomer of **4** is shown in Fig. 1, i.e. with *trans*-phosphine ligands and a carbonyl ligand in the unique capping position. Unfortunately we were unable to grow suitable single crystals for X-ray crystallography of **1–4**.

In conclusion, although the complexes $[MI_2(CO)_3(NCMe)_2]$ have been shown to react with phosphine donor ligands[18,19] and alkynes,[20,21] the reactions of $[MI_2(CO)_3(NCMe)_2]$ with the mixed phosphine/alkyne ligand $Ph_2PC{\equiv}CPPh_2$ give complexes with either one or both phosphine atoms attached to the metal.

Acknowledgements—We wish to thank Dr O. W. Howarth for running the ^{13}C and ^{31}P NMR spectra of complexes **1–4** at the University of Warwick and we thank the SERC for support.

REFERENCES

1. A. J. Carty and A. Efraty, *J. Chem. Soc., Chem. Commun.* 1968, 1559.
2. A. J. Carty and A. Efraty, *Can J. Chem.* 1968, **46**, 1598.
3. A. J. Carty and A. Efraty, *Can. J. Chem.* 1969, **47**, 2573.
4. A. J. Carty and A. Efraty, *Inorg. Chem.* 1969, **8**, 543.
5. R. B. King, L. W. Houk and P. N. Kapoor, *Inorg. Chem.* 1969, **8**, 1792.
6. R. B. King and A. Efraty, *Inorg. Chem.* 1969, **8**, 2374.
7. A. D. Westland, *Can. J. Chem.* 1969, **47**, 4135.
8. A. J. Carty, A. Efraty, T. W. Ng and T. Birchall, *Inorg. Chem.* 1970, **9**, 1263.
9. K. S. Wheelock, J. H. Nelson and H. B. Jonassen, *Inorg. Chim. Acta* 1970, **4**, 399.
10. G. R. Eaton and R. H. Holm, *Inorg. Chem.* 1971, **10**, 805.
11. B. P. Sullivan, D. J. Salmon and T. J. Meyer, *Inorg. Chem.* 1978, **17**, 3334.
12. H. C. Bechthold and D. Rehder, *J. Organomet. Chem.* 1979, **172**, 331.
13. C. M. Bollinger and T. B. Rauchfuss, *Inorg. Chem.* 1982, **21**, 3947.
14. J.-C. Daran, E. Cabrera, M. I. Bruce and M. L. Williams, *J. Organomet. Chem.* 1987, **319**, 239.
15. B. C. Ward and J. L. Templeton, *J. Am. Chem. Soc.* 1980, **102**, 1532.
16. T. M. Nickel, S. Y. W. Yau and M. J. Went, *J. Chem. Soc., Chem. Commun.* 1989, 775.
17. P. K. Baker, S. G. Fraser and E. M. Keys, *J. Organomet. Chem.* 1986, **309**, 319.
18. P. K. Baker and S. G. Fraser, *Inorg. Chim. Acta* 1986, **116**, L1.
19. P. K. Baker and S. G. Fraser, *Inorg. Chim. Acta* 1987, **130**, 61.
20. E. M. Armstrong, P. K. Baker and S. G. Fraser, *J. Chem. Res. (S)* 1988, 52; *J. Chem. Res. (M)* 1988, 0410.
21. E. M. Armstrong, P. K. Baker and M. G. B. Drew, *Organometallics* 1988, **7**, 319.
22. F. G. Mann and B. C. Saunders, *Practical Organic Chemistry*, pp. 342–344. Longmans Green, London (1954).
23. P. K. Baker and S. G. Fraser, *Transition Met. Chem.* 1987, **12**, 560.
24. F. A. Cotton, L. R. Falvello and J. H. Meadows, *Inorg. Chem.* 1985, **24**, 514.
25. A. Mawby and G. E. Pringle, *J. Inorg. Nucl. Chem.* 1972, **34**, 517.
26. M. G. B. Drew, *J. Chem. Soc., Dalton Trans.* 1972, 1329.
27. M. G. B. Drew, A. W. Johans and A. P. Wolters, *J. Chem. Soc., Chem. Commun.* 1971, 819.
28. M. G. B. Drew, *J. Chem. Soc., Dalton Trans.* 1972, 626.
29. M. G. B. Drew and J. D. Wilkins, *J. Chem. Soc., Dalton Trans.* 1977, 194.
30. M. G. B. Drew and C. J. Rix, *J. Organomet. Chem.* 1975, **102**, 467.
31. M. G. B. Drew and A. P. Wolters, *Acta Cryst.* 1977, **B33**, 205.
32. M. G. B. Drew and J. D. Wilkins, *J. Chem. Soc., Dalton Trans.* 1977, 557.
33. R. Colton and J. Kevekordes, *Aust. J. Chem.* 1982, **35**, 895.

Polyhedron Vol. 9, No. 6, pp. 805–811, 1990
Printed in Great Britain

0277–5387/90 $3.00+.00
Pergamon Press plc

ESR AND OTHER SPECTRAL STUDIES ON COPPER(II) COMPLEXES WITH 2,3-DISUBSTITUTED QUINAZOLINE-(3H)-4-ONES

B. PRABHAKAR and P. LINGAIAH*

Department of Chemistry, Kakatiya University, Warangal, Andhra Pradesh, India

and

K. LAXMA REDDY

Department of Chemistry, Regional Engineering College, Warangal 506 004, India

(*Received* 24 *May* 1989; *accepted* 18 *October* 1989)

Abstract—A number of copper(II) complexes of some tridentate O—N—O donors and bidentate O—O and O—N donors in the form of 2,3-disubstituted quinazolin-(3H)-4-ones have been synthesized and characterized based on analytical, conductivity, magnetic, IR, electronic and ESR spectral data. The reaction between copper(II) acetate and tridentate O—N—O donor ligands such as 2-(R)-3-(X)-substituted quinazoline-(3H)-4-ones, where R = methyl/phenyl and X = 2′-hydroxyphenylamino (MHBQ/PHBQ), yielded neutral complexes of the type $Cu(O—N—O)_2$. The bidentate O—O or O—N donor ligands like 2-(R)-3-(X)-substituted quinazoline-(3H)-4-ones, where R = methyl/phenyl and X = carboxymethyl (MCMQ/PCMQ), furylamino (MFQ/PFQ), acetamino (MAQ/PAQ), uramino (MUQ/PUQ) and thiouramino (MTUQ/PTUQ), yielded neutral complexes of the type $Cu(O—O)_2$ or $Cu(O—N)_2(CH_3COO)_2$. The IR spectral data of the metal complexes indicate that the ligands like MHBQ and PHBQ act as uninegative tridentate, MCMQ and PCMQ act as uninegative bidentate and MFQ, PFQ, MAQ, PAQ, MUQ, PUQ, MTUQ and PTUQ act as neutral bidentate ligands. The reflectance spectral studies of these complexes indicate that they contain square-planar or tetragonal geometry around copper(II).

Quinazolones contain both an oxygen on the ring and a nitrogen and oxygen on the substituent at the three-position (Structure I) as donor centres in the proper orientation to chelate with the metal ion. The chelating tendency of these compounds is not very well documented except for a few publications involving similar ligands.[1–4] Spectral studies of copper(II) complexes are of great interest because their ground states orbitally degenerate in regular geometries and non-degenerate in distorted geometries, since an orbitally degenerate configuration is susceptible to a Jahn–Teller distortion. As a result, the ESR studies of copper(II) complexes yield valuable information regarding the nature of bonding between the metal ion and donor atom. Basically, the interpretation of the ESR spectrum of an isolated transition metal ion yields values for two types of parameter: (1) the spectroscopic splitting constants (g-values) which describe the frequencies between the different electron spin states and (2) the hyperfine coupling constants (A) which give a measure of electron spin–nuclear spin interactions. These parameters are affected by the presence of ligands around the central metal ion. In order to discover the nature of the interaction of these ligands with the copper(II) ion, the present study was undertaken. In this paper, complexes of copper(II) with 2-(R)-3-(X)-substituted quinazolin-(3H)-4-ones, where R = methyl/phenyl and X = carboxymethyl (MCMQ/PCMQ), 2′-hydroxy benzylamino (MHBQ/PHBQ), furylamino (MFQ/PFQ), acetamino (MAQ/PAQ), uramino (MUQ/PUQ) and thiouramino (MTUQ/PTUQ), are discussed.

* Author to whom correspondence should be addressed.

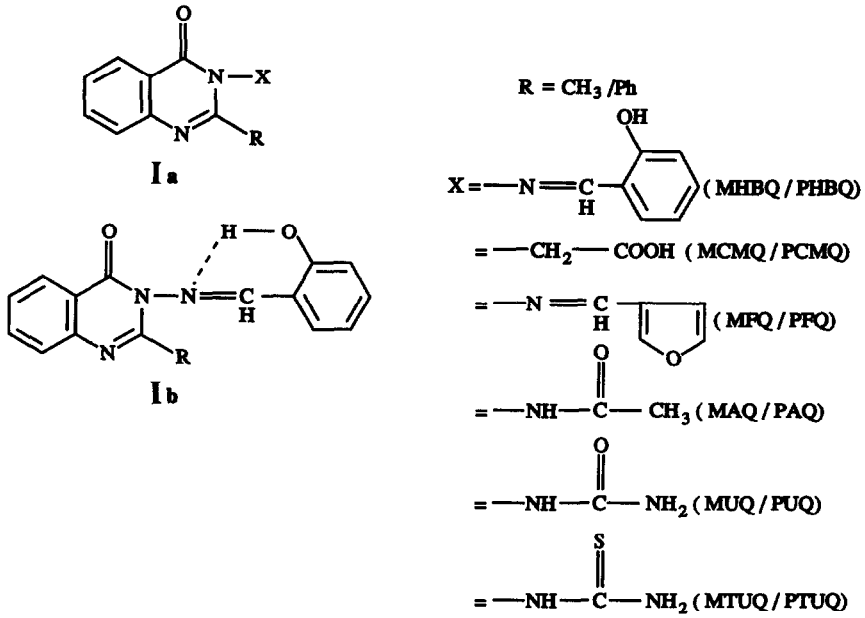

Structure **Ia** and **b**. Structures of the ligands.

EXPERIMENTAL

All the chemicals used were of AR grade. The ligands were prepared by literature methods.[5,6] The purity of these compounds was checked by TLC and melting point determinations.

Preparation of complexes

Copper acetate solution (1 mmol) in acetone was added dropwise to a solution (3 mmol) in acetone with constant stirring. The reaction mixture was refluxed on a water bath for 60–120 min and cooled. The solid thus obtained was filtered and washed several times with water and acetone until the washings were free from excess ligands. These complexes were finally dried *in vacuo* over fused calcium chloride. All the copper(II) complexes are crystalline powders, light or dark green in colour. They are stable to room temperature, non-hygroscopic and insoluble in common organic solvents like methanol, ethanol, acetone and CCl_4, but appreciably soluble in DMF and DMSO.

Physical measurements

The analytical data (C, H, N) for the ligands and their metal complexes were obtained from the Microanalytical Laboratory, Calcutta University, Calcutta, India. The metal content of the complexes after heating to decomposition temperatures was determined using standard procedures. Molar conductivities of the complexes in DMF were measured using a Digisun digital conductivity meter, Model-DI-909 with a Philips dip-type conductivity cell. The magnetic measurements of the complexes in the solid state were made on a Gouy balance at room temperature using $Hg[Co(SCN)_4]$ as calibrant. Diamagnetic corrections were applied using Pascal's constants. The TGA and DTA curves of the complexes were recorded on a Leeds and Nathrup DTA unit (U.S.A.), using calcined alumina as reference material. The experiments were carried out in an atmosphere of static air using Pt/Rh thermocouples, and the rate of heating was maintained at 6°C min^{-1}. The IR spectra of the ligands and their complexes in Nujol and KBr, in the range 4000–200 cm^{-1}, were recorded on a Perkin–Elmer IR spectrophotometer, Model-283. The UV and visible spectra of the complexes in DMF were recorded on a Shimadzu multipurpose recording spectrometer, Model MPS-5000. The reflectance spectra of the complexes were measured on a Perkin–Elmer Lambda-15 spectrophotometer. The ESR spectra of the complexes in solid state and in DMF solutions at liquid nitrogen temperature were recorded on a Varian E-4, X-band spectrometer.

RESULTS AND DISCUSSION

The analytical and physical data for the complexes are listed in Table 1. On the basis of analytical data the metal complexes are found to have 1:2 (metal–ligand) stoichiometry and some complexes are also associated with two acetate molecules. The molar conductance values of the complexes in DMF at 10^{-3} M concentrations are low (10–20 Ω^{-1} cm^2

Table 1. Analytical and thermal data of copper(II) complexes

Sl. No.	Complex	Found (Calc.) % Cu	C	N	H	S	Molar conductance (Ω^{-1} cm^2 mol^{-1})	Decomposition temperature (°C)
1	$[Cu(MCMQ)_2]$	12.7 (12.7	52.8 52.8	11.2 11.2	4.0 4.0)	—	17	300
2	$[Cu(PCMQ)_2]$	10.2 (10.2	61.6 61.5	9.0 8.9	3.8 3.8)	—	20	305
3	$[Cu(MHBQ)_2]$	10.2 (9.9	62.9 61.0	13.6 13.1	3.8 3.2)	—	15	340
4	$[Cu(PHBQ)_2]$	8.5 (8.1	67.8 67.0	11.3 10.9	3.8 3.1)	—	10	335
5	$[Cu(MFQ)_2(CH_3COO)_2]$	9.1 (9.1	55.9 55.8	12.2 12.2	4.1 4.0)	—	10	320
6	$[Cu(PFQ)_2(CH_3COO)_2]$	7.8 (7.7	62.1 62.1	10.3 10.3	3.9 3.9)	—	17	310
7	$[Cu(MAQ)_2(CH_3COO)_2]$	10.3 (10.2	50.7 50.5	13.6 13.6	4.5 4.5)	—	16	310
8	$[Cu(PAQ)_2(CH_3COO)_2]$	8.6 (8.5	58.4 58.4	11.3 11.3	4.3 4.3)	—	12	315
9	$[Cu(MUQ)_2(CH_3COO)_2]$	10.2 (10.2	46.7 46.6	18.1 18.1	4.2 4.2)	—	18	320
10	$[Cu(PUQ)_2(CH_3COO)_2]$	8.5 (8.4	55.1 55.0	15.1 15.1	4.0 4.0)	—	12	328
11	$[Cu(MTUQ)_2(CH_3COO)_2]$	9.7 (9.7	44.4 44.3	17.2 17.2	4.0 4.0)	9.9 (9.8)	13	318
12	$[Cu(PTUQ)_2(CH_3COO)_2]$	8.9 (8.8	57.5 57.4	15.8 15.7	4.2 4.2)	9.0 (9.0)	11	330

mol^{-1}) suggesting that they are non-electrolytes.[7]

Decomposition temperatures of the complexes, determined from their thermograms, are given in Table 1. The complexes are thermally stable up until 200°C and are not hydrated. This fact is further confirmed by their DTA curves which do not give endothermic peaks in the 150–200°C region. The sharp decomposition associated with the loss of ligand starts above 230°C. The final products of decomposition above 600°C in all the complexes correspond to metallic oxide. The decomposition temperatures of the complexes are a measure of their thermal stability. The ligands under study form complexes of varying stability in the order MCMQ < PCMQ < PFQ ≃ MAQ < PAQ < MTUQ < MFQ ≃ MUQ < PUQ < PTUQ < PHBQ < MHBQ.

Despite the large amount of work on thermogravimetry, considerable difficulties still exist in rationalizing the increase or decrease in thermal stability of complexes with different ligands. The literature contains various explanations of the relative order of thermal stability of the complexes. For example, thermal stability is said to increase with an increase in π-electron delocalization, the size of the molecule and also the nature of the rings formed.[8] The relative order of stability observed for the present complexes may be accounted for by such factors.

Important IR absorption frequencies of ligands and their complexes, along with their assignments, are listed in Table 2. A strong band corresponding to ν(C=O) of the quinazolone ring at 1700 cm^{-1} is shifted to lower wavenumbers by 40–50 cm^{-1} in the IR spectra of all the complexes, indicating that the carbonyl oxygen is invariably coordinated to copper(II).[9] The bands due to ν(OH) observed in the spectra of MHBQ, PHBQ,[10] MCMQ and PCMQ[11] disappeared completely in the spectra of their complexes confirming the coordination of these ligands by deprotonation. The band at 1640 cm^{-1} due to ν(C=N) of quinazolone remains unaltered in the spectra of complexes, whereas the band at 1600 cm^{-1} due to the benzylamino/furylamino group undergoes a lower shift of 40–50 cm^{-1}, suggesting coordination through this nitrogen.[12]

The ν(N—H) frequency observed at 3300 cm^{-1} in MAQ, PAQ, MUQ, PUQ, MTUQ and PTUQ has shifted to a lower region ($\Delta\nu$ = 50 cm^{-1}) in the

Table 2. Infrared spectral data (cm^{-1}) and their assignment of copper(II) complexes

Complex	ν(C=O)	ν(N—H)	ν(O—H)/NH_2	ν(C=N)	ν(Cu—O)	ν(Cu—N)
1	1650	—	—	1635	450, 430	—
	(1700)		(2500)[a]	(1640)		
2	1635	—	—	1640	430, 420	—
	(1690)		(2500)[a]	(1640)		
3	1640	—	—	1570	400, 450	500
	(1680)		(3150)	(1610)		
4	1640	—	—	1570	410, 440	500
	(1690)		(3200)	(1610)		
5	1650	—	—	1560	420	470
	(1700)			(1610)		
6	1650	—	—	1560	420	490
	(1700)			(1600)		
7	1660	3260	—	1640	440, 420	460
	(1680)	(3300)		(1640)		
8	1655	3240	—	1635	430, 420	460
	(1690)	(3300)		(1640)		
9	1640	3230	3390[b]	1630	435	500
	(1690)	(3280)	(3400)	(1630)		
10	1640	3260	3390[b]	1630	435	490
	(1700)	(3310)	(3400)	(1630)		
11[c]	1635	3280	3390[b]	1640	430	490
	(1690)	(3320)	(3390)	(1640)		
12[c]	1640	3270	3390[b]	1635	440	480
	(1700)	(3320)	(3390)	(1640)		

Values presented in parentheses are of the free ligand bands.

[a] OH of carboxyl group.

[b] Stretching frequency of NH_2 group.

[c] (C=S) of thiouramino group observed at 860 cm^{-1} in MTUQ and PTUQ and at 850 cm^{-1} in their complexes.

complexes, indicating the involvement of the imino-nitrogen in coordination,[13] whereas the bands due to ν(NH_2)[14] (MUQ, PUQ, MTUQ and PTUQ), ν(C=O) (MAQ, PAQ, MUQ and PUQ)[5] and ν(C=S) (MTUQ and PTUQ)[15] at 3400, 1660 and 860 cm^{-1}, respectively, remain unchanged in the complexes, indicating the non-participation of the N/O/S of these groups in coordination. The presence of acetate ion in the coordination sphere in some complexes is also confirmed from their IR data.[16] The mode of coordination is further supported by the appearance of ν(Cu—O) and ν(Cu—N) bands around 400 and 500 cm^{-1}, respectively.[17,18]

The electronic spectral data along with the assignments are presented in Table 3. All the ligands exhibit strong bands around 35,000 and 32,000 cm^{-1} which may be assigned to $\pi^* \leftarrow \pi$ and $\pi^* \leftarrow n$ transitions, respectively. The reflectance spectra of all the copper(II) complexes, except those complexes of MCMQ and PCMQ, exhibit one broad band around 16,000 cm^{-1}, and complexes **3**, **4**, **6** and **7** also show one shoulder around 13,000 cm^{-1}. Due to the Jahn–Teller effect, tetragonal copper(II) complexes involve three transitions, *viz.* $^2B_{2g} \leftarrow {}^2B_{1g}$, $^2E_g \leftarrow {}^2B_{1g}$ and $^2A_{1g} \leftarrow {}^2B_{1g}$, but bands due to these transitions usually overlap to give a broad absorption band. Based on earlier reports, the present complexes are tentatively assigned tetragonal geometry.[19–21] However, the copper(II) complexes of MCMQ and PCMQ display two bands around 15,000 and 20,000 cm^{-1} which may be due to $^2B_{2g} \leftarrow {}^2B_{1g}$ and $^2E_g \leftarrow {}^2B_{1g}$ transitions and are also tentatively assigned square-planar geometry.[22]

All the copper(II) complexes are paramagnetic and possess magnetic moment values equivalent to one unpaired electron. The value is found to be less than 1.9 BM indicating the complexes have tetragonal or square-planar arrangements around the copper(II) ion.[23] But the excess over the spin-only value of 1.73 BM observed (Table 3) in these complexes might be due to spin-orbit coupling.

The ESR spectra of the copper(II) complexes of MFQ and PFQ at liquid nitrogen temperature in

Table 3. Magnetic and electronic spectral data of copper(II) complexes

Complex	μ_{eff} (BM)	Electronic spectral bands	(cm^{-1})
1	1.82	15,000, 20,000	31,000, 35,000
2	1.82	15,500, 21,000	31,000, 34,000
3	1.82	13,200, 16,000, 31,000	34,000
4	1.83	13,100, 16,000, 32,000	35,000
5	1.82	16,500,[a] 30,000	34,000
6	1.81	13,000, 16,500, 31,000	34,500
7	1.83	13,150, 16,500, 31,000	33,000
8	1.82	16,000,[a] 30,000	34,000
9	1.82	15,800,[a] 29,000	34,000
10	1.81	15,900,[a] 30,000	35,000
11	1.81	16,000,[a] 31,000	36,000
12	1.82	16,200,[a] 31,000	35,000

[a]Broad band indicating overlapping of different transitions.

the solid state and in solutions are given in Figs 1 and 2. The ESR spectral and bonding parameters are listed in Table 4.

The ESR spectra of all the copper(II) complexes in the solid state at liquid nitrogen temperature show two peaks, one of intense absorption at high field and the other of less intensity at low field. From these peaks $g_{\parallel}$ and $G_{\perp}$ have been calculated. However, the ESR spectra of all the copper(II) complexes in solution at liquid nitrogen temperature exhibit a set of four well-resolved peaks in the low field region and intense unresolved peaks in the high field region.

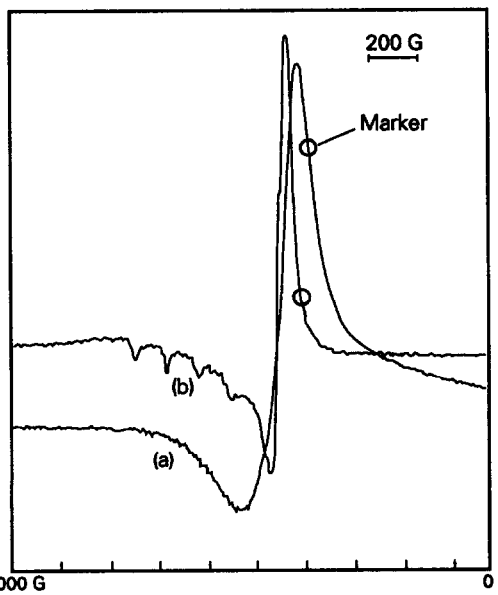

Fig. 1. ESR spectra of copper(II) MFQ complexes at liquid nitrogen temperature: (a) in the solid state; (b) in solution.

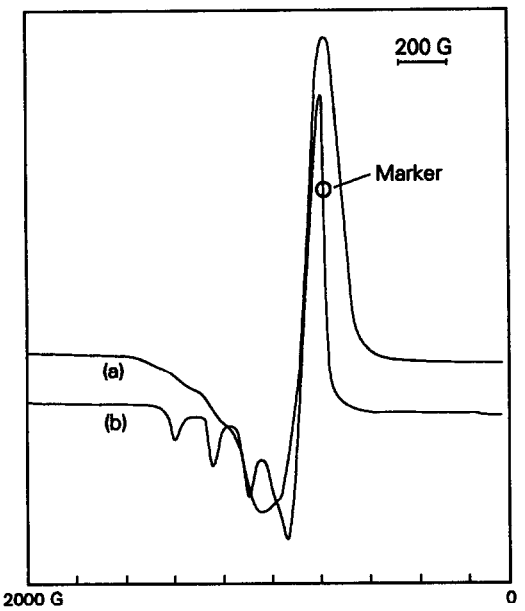

Fig. 2. ESR spectra of copper(II) PFQ complexes at liquid nitrogen temperature: (a) in the solid state; (b) in solution.

The $g_{\parallel}$ and $g_{\perp}$ values have been calculated using Kneubuhl's method.[24] $A_{\parallel}$ and $A_{\perp}$ values were calculated by using one third of the line widths at half maximum and A_0 as 1/3 $(A_{\parallel}+2A_{\perp})$ and g_0 as 1/3 $(g_{\parallel}+2g_{\perp})$.[25] No bands corresponding to Ms = ± 2 transitions were observed in the spectra, ruling out any Cu—Cu interaction.

The g tensor values of copper(II) complexes can be used to derive the ground state.[26] In elongated octahedral (tetragonal) and square-planar complexes, the unpaired electron lies in the $d_{x^2-y^2}$ orbitals giving $^2B_{1g}$ as the ground state with $g_{\parallel} > g_{\perp}$.

Table 4. ESR spectral data of copper(II) complexes

Complex	Spectral parameter					
	$g_{\parallel}$	$g_{\perp}$	g_0	$A_{\parallel} \times 10^4$ (cm^{-1})	$A_{\perp} \times 10^4$ (cm^{-1})	$A_0 \times 10^4$ (cm^{-1})
1	2.14	2.03	2.06	—	—	—
2	2.13	2.03	2.06	—	—	—
3	2.24	2.06	2.12	—	—	—
4	2.23	2.05	2.11	—	—	—
5	2.20	2.05	2.10	173	74	107
6	2.18	2.04	2.08	142	68	92
7	2.23	2.05	2.11	—	—	—
8	2.22	2.04	2.10	—	—	—
9	2.20	2.05	2.10	167	87	113
10	2.21	2.05	2.10	173	56	95
11	2.20	2.05	2.10	143	99	113
12	2.21	2.05	2.10	173	80	111

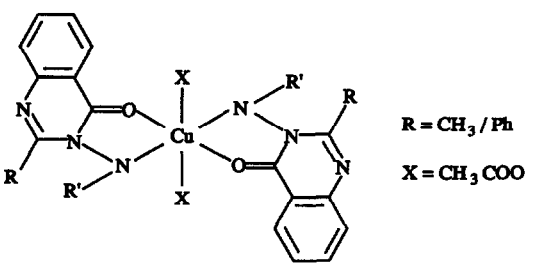

IIa

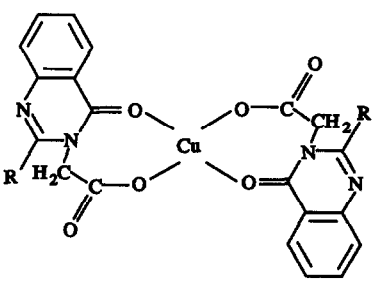

IIb

Structure **IIa**: Copper(II) complexes of the (O—N) donor ligands; **IIb**: copper(II) complexes of the (O—O) donor ligands.

In a compressed octahedron, on the other hand, the unpaired electron lies in the d_{z^2} orbital giving $^2A_{1g}$ as the ground state with $g_{\perp} > g_{\parallel}$. From the observed values it is evident that the unpaired electron lies predominantly in the $d_{x^2-y^2}$ orbital. The complexes also show anisotropic ESR spectra with $g_{\parallel} > g_{\perp}$ characteristic of tetragonal or square-planar geometry. Recalling the complexes with the $d_{x^2-y^2}$ ground state, strong interactions along the z axis are accompanied by an increase in the value of $g_{\parallel}$. Strong axial bonding leads to an increase in the length of the bond in the X–Y plane, which results in a decrease of both in-plane covalency and the energy of the $d_{x^2-y^2}$ transition.[27] Both these effects tend to increase the values of $g_{\parallel}$.

$g_{\parallel}$ is the most sensitive function for indicating the covalency, being 2.3 or more for ionic compounds and less than 2.3 for covalent compounds.[28] It is clear from Table 4 that the value of $g_{\parallel}$ obtained is less than 2.3 indicating covalent character of the metal–ligand bond.

Based on the foregoing data all the copper(II) complexes are assigned to the tetragonal or square-planar geometry and are shown in structures **IIa** and **b**.

Acknowledgements—The authors thank the Head, IIT, Bombay, for providing facilities for recording ESR spectra. One of us (B.P.) is grateful to CSIR, New Delhi, for the award of a SRF.

REFERENCES

1. K. Laxma Reddy, P. Lingaiah and K. Veera Reddy, *Polyhedron* 1986, **5**, 1519.
2. K. Laxma Reddy, S. SriHari and P. Lingaiah, *Ind. J. Chem.* 1985, **24A**, 318.
3. B. Prabhakar, K. Laxma Reddy and P. Lingaiah, *Ind. J. Chem.* 1988, **27A**, 217.
4. B. Prabhakar, K. Laxma Reddy and P. Lingaiah, *Proc. Ind. Acad. Sci.* 1989, **101**, 121.
5. R. Soliman and F. S. G. Soliman, *Synthesis* 1979, 803.
6. Ch. Ravishankar, Studies on synthesis, biological and pharmacological evaluation of some 6,8-dibro-

moquinazoline-(3H)-one derivatives, PhD thesis, Kakatiya University, Warangal (1984).
7. W. J. Geary, *Coord. Chem. Rev.* 1971, **7**, 81.
8. V. Ravinder, S. J. Swamy, S. SriHari and P. Longaiah, *Transition Met. Chem.* 1984, **9**, 106 and refs therein.
9. R. Sahai, R. S. Agarwal and S. S. Kushwaha, *J. Ind. Chem. Soc.* 1982, **7**, 853.
10. A. Sammour, A. F. M. Fammy and M. Mohmoud, *Ind. J. Chem.* 1973, **13**, 272.
11. B. Singh, V. Banerjee, B. V. Agarwala and K. D. Arun, *J. Ind. Chem. Soc.* 1980, **57**, 365.
12. C. P. Prabhakaran and C. C. Patel, *J. Inorg. Nucl. Chem.* 1972, **12**, 3485.
13. S. K. Sengupta, S. K. Sahni and R. N. Kapoor, *Ind. J. Chem.* 1981, **20A**, 692.
14. R. C. Agarwal, R. Bala and R. L. Prasad, *Ind. J. Chem.* 1983, **22A**, 568.
15. K. Mukkanti and R. P. Singh, *Proc. Ind. Acad. Sci.* 1988, **100**, 21.
16. K. Nakamoto, *Infrared and Raman Spectra of Inorganic and Coordination Compounds*, p. 229. John Wiley, New York (1978).
17. D. M. Adams, *Metal–Ligand and Related Vibrations.* Arnold, London (1967).
18. G. T. Behnke and K. Nakamoto, *Inorg. Chem.* 1967, **6**, 443.
19. Y. Nishida and S. Kida, *Coord. Chem. Rev.* 1979, **27**, 275.
20. D. Sutton, *Electronic Spectra of Transition Metal Complexes*, p. 148. McGraw-Hill, New York (1968).
21. A. B. P. Lever, *Inorganic Electronic Spectroscopy.* Elsevier, New York (1968).
22. B. C. Werden, E. Billing and H. B. Gray, *Inorg. Chem.* 1966, **5**, 78.
23. B. N. Figgis, *Introduction to Ligand Field Theory*, 1st edn, p. 265. Wiley Eastern Ltd, New Delhi (1966).
24. F. K. Kneubuhl, *J. Chem. Phys.* 1960, **33**, 1074.
25. H. M. McConnel, *J. Chem. Phys.* 1956, **25**, 709.
26. C. J. Baul Hausen, *Introduction to Ligand Field Theory*, p. 134. McGraw-Hill, New York (1962).
27. D. N. Smith, *J. Chem. Soc. A* 1970, 3108.
28. D. Kivelson and R. Neiman, *J. Chem. Phys.* 1961, **35**, 149.

Polyhedron Vol. 9, No. 6, pp. 813–823, 1990
Printed in Great Britain

0277–5387/90 $3.00+.00
© 1990 Pergamon Press plc

NUCLEAR MAGNETIC RESONANCE STUDIES OF SILICON(IV) COMPLEXES IN AQUEOUS SOLUTION—I. TRIS-CATECHOLATO COMPLEXES

DENNIS F. EVANS,* JONATHAN PARR and ERIC N. COKER

Inorganic Chemistry Laboratories, Imperial College, London SW7 2AY, U.K.

(*Received* 26 *September* 1989; *accepted* 18 *October* 1989)

Abstract—Quantitative data for the reaction $3LH_2 + Si(OH)_4 \rightleftharpoons SiL_3^{2-} + 4H_2O$ in aqueous solution have been obtained by ^1H and ^{29}Si NMR spectroscopy, where LH_2 = catechol, 4,5-dichlorocatechol, 4-nitrocatechol or 3,4-dinitrocatechol. By a suitable choice of LH_2 it is possible to obtain stable solutions of tris-catecholato complexes of silicon(IV), in the presence of $Si(OH)_4$, at pH values ranging from alkaline to as low as 4.1. When LH_2 = 2,3-dihydroxybenzaldehyde or tiron, meridional and facial isomers have been characterized. Mixed complexes containing catechol and 4-nitrocatechol or catechol and 4,5-dichlorocatechol have also been studied. Information has been obtained about the rate of Si—O bond breaking from the ^1H NMR spectra of the tris-complex derived from gallic acid.

There has been considerable interest recently in the biochemistry of silicon.[1] It has been known for many years that organisms such as diatoms and siliceous sponges utilize dissolved silica to produce elaborate structures of amorphous silica, and there is now considerable evidence that active transport of silicon is involved.[2] Since 1972 it has also been realized that silicon is an essential element participating in the normal metabolism of higher animals.[3] However, the mechanism of silicon transport in living organisms is largely unknown, although it seems likely that silicon(IV) complexes will be involved. Silica is quite soluble in aqueous solutions of strong alkalis, and a large number of polysilicate species have been characterized by ^{29}Si NMR spectroscopy.[4] This elegant work is, however, not relevant to the biochemistry of silicon since the polysilicate species are only stable at high pH values. Apart from hydrofluoric acid and the well-known SiF_6^{2-} ion[5] only two classes of ligands have been reliably reported to react to give silicon(IV) complexes from silica in water. In 1931, Rosenheim *et al.*[6] prepared the tris-catecholato silicon(IV) anion by heating freshly prepared "silicic acid" with aqueous alkaline solutions of catechol, followed by crystallization. Subsequently, Muetterties and Wright[7] showed that silicic acid reacted with tropolone in aqueous acid to give the tris-tropolonato silicon(IV) cation. Although stable in acid solution, this cation is rapidly hydrolysed at neutral pH. In the present work, ^1H and ^{29}Si NMR spectroscopy have been used to determine quantitatively the reaction between silica and various catechols in aqueous solution, and also to obtain more detailed information about the species present in solution.

EXPERIMENTAL

Materials

Catechol ($catH_2$) was purified by sublimation, and 4-chlorocatechol[8,9] (4-$ClcatH_2$), 4,5-dichlorocatechol[9] (4,5-Cl_2catH_2), 3,4-dinitrocatechol[10] [3,4-$(NO_2)_2catH_2$] and 4,5-dinitrocatechol[11] [4,5-$(NO_2)_2catH_2$] were prepared by literature methods. The remaining catechols were pure commercial samples. Catechol-d_6 was prepared by heating $catH_2$ (2 g) in D_2O (10 cm^3) with 1 cm^3 of 20% DCl in D_2O in a sealed ampoule under argon at 110°C for 24 h. The solution was taken to dryness *in vacuo*, and the procedure repeated once. The ^1H NMR in D_2O indicated an isotopic purity for the aromatic protons of > 98%. Silicic acid (for chromatography) was obtained from Fluka.

Preparation of solid tris-catecholato complexes

All preparations were carried out under argon until the point of precipitation of the complex.

* Author to whom correspondence should be addressed.

$(Et_3NH)_2[Si(cat)_3]$ (cf. ref. 12). To a stirred solution of $catH_2$ (3.99 g, 36.2 mmol) in ethanol (25 cm^3), triethylamine (3.4 cm^3, 24.5 mmol) was added, followed by $Si(OEt)_4$ (2.7 cm^3, 12.1 mmol). After 20 min, the white precipitate was filtered, washed with ethanol, then diethyl ether and dried *in vacuo*. Yield: 2.16 g, 32%. Found: C, 64.1; H, 7.9; N, 5.0. $(Et_3NH)_2[Si(cat)_3]$ requires: C, 64.7; H, 7.9; N, 5.0%. The corresponding complexes derived from 4-$ClcatH_2$, 4,5-Cl_2catH_2 and 4-NO_2catH_2 were prepared in a similar manner and gave satisfactory analyses.

$K_2[Si(cat)_3]\cdot xH_2O$. The following procedure was found to be more convenient than that used by Rosenheim *et al.*[6]

To $catH_2$ (5.00 g, 45.4 mmol) in ethanol (20 cm^3), a solution of potassium (1.21 g, 31.1 mmol) in ethanol (20 cm^3) was added. The fine white precipitate formed initially, disappeared on warming to *ca* 50°C and $Si(OEt)_4$ (3.38 cm^3, 18.5 mmol) was added. The reaction mixture was warmed for a further 30 min and then cooled to 0°C. The white precipitate was filtered off, washed with ethanol, then diethyl ether and dried *in vacuo* at 70°C to constant weight. Yield: 5.1 g, 64%. Found: C, 50.9; H, 2.9. $K_2[Si(cat)_3]$ requires: C, 50.2; H, 2.8%. Mass spectra (FAB^+) $m/z = 431$, as $K_2[Si(cat)_3]H^+$. Analyses for carbon and hydrogen, and the loss in weight on heating to 110°C *in vacuo* indicate that samples dried at room temperature contained slightly variable amounts of H_2O, with x being in the range 2–4. (Rosenheim *et al.*[6] report $x = 12H_2O$ for complexes prepared in H_2O.) The potassium salts of the tris-catecholato complexes derived from 4-NO_2catH_2, 4,5-$(NO_2)_2catH_2$, 3,4-$(NO_2)_2catH_2$ and 4,5-Cl_2catH_2 were prepared in a similar manner, and satisfactory analyses were obtained. They were found to be more water soluble than their triethylammonium counterparts.

With 1,2-dihydroxybenzaldehyde (3-$CHOcatH_2$) and 3,4-dihydroxybenzaldehyde (4-$CHOcatH_2$) the extreme insolubility of both K[3-CHOcatH] and K[4-CHOcatH] led to incomplete conversion to the $[Si(3\text{-}CHOcat)_3]^{2-}$ and $[Si(4\text{-}CHOcat)_3]^{2-}$ complexes. Accordingly, the tetramethylammonium salts were prepared, the method of preparation being as for $K_2[Si(cat)_3]$, using a stoichiometric amount of tetramethylammonium hydroxide in place of the potassium ethoxide. Found: C, 60.6; H, 6.9; N, 4.4. $(N(Me)_4)_2[Si(3\text{-}CHOcat)_3]$ requires: C, 59.6; H, 6.2; N, 4.4%.

Equilibrium studies

A solution of the catechol was sealed in a fused silica ampoule under argon with an excess of silicic acid, in a 0.2 M buffer solution. Acetate buffer was used for pH 4.0–5.0; thereafter, 2-(N-morpholino)ethanesulphonic acid (5.1–6.5); piperazine-NN′-bis-2-ethanesulphonic acid (6.6–7.5); N-2-hydroxyethylpiperazine-N′-2-ethanesulphonic acid (7.6–8.0); N-2-hydroxyethylpiperazine-N′-3-propanesulphonic acid (8.1–8.6). The ampoules were shaken for 8 weeks in a water bath at 25.0°C. After an ampoule was opened, the contents were centrifuged, and following a measurement of pH, an aliquot of the supernatant fluid was rapidly taken to dryness.[13] The residue was redissolved in D_2O, and the ^1H NMR recorded before any change in the equilibrium could occur. With 3,4-$(NO_2)_2catH_2$, the ^{29}Si NMR spectrum of the formed tris-complex was measured directly on the aqueous solution after centrifugation, in a 10 mm tube, using a 5 mm insert tube containing D_2O for the lock signal. 3-(Trimethylsilyl)-1-propanesulphonate was used as an internal intensity standard. For the hydrolysis experiments, buffered solutions of $K_2[Si(cat)_3]$ or $K_2[Si(4\text{-}NO_2cat)_3]$ were kept at 25.0°C for 8 weeks in sealed silica ampoules under argon. The solutions remained clear, because of the small size of the silica particles formed. For a 0.05 M solution of $K_2[Si(cat)_3]$ at pH 8.4, which had been allowed to hydrolyse extensively (2 weeks), it was shown, using laser diffraction techniques, that the majority of the particles formed had diameters of 35 ± 3 nm. This is sufficiently large to exclude any appreciable increase in the equilibrium solubility of the silica.[3]

Physical measurements

For NMR measurements of the pure and the mixed tris-complexes, the potassium, triethylammonium or tetramethylammonium salts were used either dissolved directly in D_2O, or if pH control was required, in aqueous buffers, which were then rapidly evaporated, and the residue redissolved in D_2O. Where pH values are quoted for solutions in D_2O, they refer to the pH of the aqueous solution before evaporation and redissolution in D_2O. Reported pD values refer to the observed pD of the solution in D_2O. A number of the triethylammonium salts were only sparingly soluble in water, and in these cases, the solid was stirred with a little water and an excess of Dowex 50-X8 ion exchange resin in the Na^+ form. Solid complexes were not isolated with 4,5-dihydroxybenzene-1,3-disulphonate (tiron) or 3,4,5-trihydroxybenzoic (gallic) acid. Solutions of the tris-complexes were prepared by adding a slight excess of $Si(OEt)_4$ to a buffered solution of the ligand in water, which was then stirred for 18 h. For the determinations of the solubility of silica, silicic acid was shaken, in

polypropylene tubes under argon, with buffer solutions for 8 weeks, at 25.0°C. The dissolved silica was determined colourimetrically, using ammonium molybdate and 4-amino-3-hydroxy-1-naphthalene-sulphonic acid.[14]

^1H NMR spectra were recorded on Bruker WM250 (250 MHz), Jeol GSX270 (270 MHz) and Bruker WM500 (500 MHz) spectrometers. ^{29}Si NMR spectra and ^{13}C NMR spectra were recorded on Bruker WM250 and Jeol FX90Q spectrometers. The relaxation reagent, Na[Cr(dtpa)], which has been used for ^{13}C NMR in aqueous solution,[15] was added (0.08 M) to overcome the problems associated with the long relaxation times and the negative magnetic moment of the ^{29}Si nucleus. Line shape calculations for the gallic acid system were made using a program kindly provided by Dr H. S. Rzepa. Measurements in the slow exchange region showed that $\delta\nu$ varied with temperature, and accordingly extrapolated values of $\delta\nu$ were used in the calculations. Mass spectra were recorded on a Micromass VG 7070E spectrometer in the FAB^+ mode, with the sample suspended in a water–glycerol matrix. Photon correlation spectroscopy for the determination of particle size was carried out using a He/Ne laser and a standard 96 channel Malvern correlator. Raman spectra were recorded using a Spex Ramalog V instrument (488 nm, 150 mW).

IR spectra were measured using a Perkin–Elmer 1720 FT spectrometer.

RESULTS AND DISCUSSION

The solubility of amorphous silica in water has been determined by several groups of workers[2] and is found to be only slightly dependent on pH in the range 1–*ca* 8.5, and equal to *ca* 2×10^{-3} M. The silica is thought to be present as monomeric $Si(OH)_4$.[3] For aqueous solutions containing silica and a catechol, we therefore have equilibrium (1), with an equilibrium constant given by eq. (2):

$$3LH_2 + Si(OH)_4 \rightleftharpoons SiL_3^{2-} + 4H_2O + 2H^+ \quad (1)$$

$$\frac{[SiL_3^{2-}][H^+]^2}{[LH_2]^3[Si(OH)_4]} = K. \quad (2)$$

If excess solid silica is present, then to a reasonable approximation, over the pH range 1–*ca* 8.5,

$$\frac{[SiL_3^{2-}][H^+]^2}{[LH_2]^3} = K' \quad (3)$$

where K' is *ca* 2×10^{-3} K.

We also have the ionization of the catechol [eqs (4) and (5)]:

$$LH_2 \rightleftharpoons LH^- + H^+ = K_1 \quad (4)$$

$$[LH_2] = [LH_2]_{tot}\cdot\frac{[H^+]}{[H^+]+K_1}, \quad (5)$$

where $[LH_2]_{tot}$ = total free catechol, i.e. $[LH_2]+[LH^-]$, if the second ionization constant can be neglected; this is reasonable when $pH < pK_2 - 2$.

Substituting in eq. (3),

$$\frac{[SiL_3^{2-}]([H^+]+K_1)^3}{[LH_2]_{tot}^3[H^+]} = K' \quad (6)$$

or

$$\frac{[SiL_3^{2-}]}{[LH_2]_{tot}} = \frac{K'[H^+]}{([H^+]+K_1)^3}. \quad (7)$$

The left-hand side of eq. (7) is a measure of the extent of formation of the tris-complex, and will have a maximum when

$$pH = pK_1 + 0.301$$

corresponding to the equation

$$2LH^- + LH_2 + Si(OH)_4 \rightleftharpoons SiL_3^{2-} + 4H_2O.$$

For any catechol, this gives the optimum pH, and suggests that to obtain reasonable equilibrium concentrations of the tris-complex at neutral or slightly acid pH, a catechol with an electron-withdrawing group(s) and a consequent value of pk_1 of < 7 might be suitable. Values of pk_1 (and some pk_2 values) are given in Table 1.

Figure 1 shows the ^1H NMR spectrum of a solution obtained from silicic acid and $catH_2$ (initial concentration 0.15 M) at pH 8.35. The $catH_2$ gives a characteristic AA'BB' pattern, while for $[Si(cat)_3]^{2-}$, δ_A and δ_B are almost the same. Chemical exchange between free and complexed $catH_2$ is therefore slow on an NMR time scale, and this was true for all the catechols studied except 4,5-$(NO_2)_2catH_2$. By integration it is possible to obtain the relative values for the concentration of $catH_2$

Table 1. Values of pK_1 and pK_2 for some catechols in water at 25°C

Catechol	pK_1	pK_2
$catH_2$	9.27[a]	*ca* 13[a]
4,5-Cl_2catH_2	7.46[b]	—
4-NO_2catH_2	6.69[a]	10.57[a]
3,4-$(NO_2)_2catH_2$	4.39[c]	8.27[c]

[a] A. E. Martell and R. E. Smith, *Critical Stability Constants*, Vol. 3. Plenum Press, New York (1977).

[b] This work.

[c] D. H. Rosenblatt, J. Epstein and M. Levitch, *J. Am. Chem. Soc.* 1953, **75**, 3277.

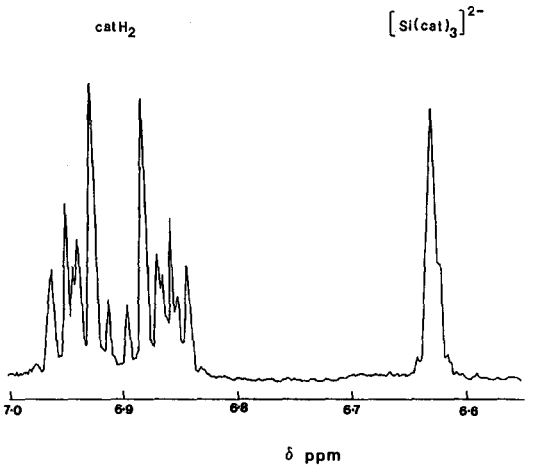

Fig. 1. ^{1}H NMR spectrum (270 MHz, D_2O) of a mixture of $[Si(cat)_3]^{2-}$ and $catH_2$ prepared from silicic acid and $catH_2$ at pH 8.35.

and $[Si(cat)_3]^{2-}$, and from a knowledge of the initial concentration of the $catH_2$, or the tris-complex in the hydrolysis experiments, their absolute magnitudes. Values of K' can then be calculated from eq. (6). For 3,4-$(NO_2)_2catH_2$, at room temperature the tris-complex gave an extremely broad proton resonance, almost lost in the baseline, presumably due to an intermediate rate of fluxionality. Accordingly, the concentration of the tris-complex formed was found from ^{29}Si NMR spectroscopy. The equilibrium data obtained are presented in Table 2, together with the calculated values of K'. Attempts were made to shorten the time taken for equilibration by using $Si(OEt)_4$ (which hydrolyses to form SiO_2) in place of silicic acid. However, after 36 h stirring at 25°C, the amounts of $[Si(cat)_3]^{2-}$ formed were considerably greater (by a factor of *ca* 4) than those obtained in the same pH range (8.0–8.5) for both the formation and decomposition experiments, giving much larger apparent values for K'. This is presumably because the hydrolysis of $Si(OEt)_4$ produces very small particles of SiO_2 which will have a higher free energy and solubility than bulk SiO_2.[3] The solubility of the silicic acid used was found to be 1.78×10^{-3} M at pH 7.41 and 1.91×10^{-3} M at pH 8.35, in good agreement with literature values.[3] An average value of 1.85×10^{-3} was used to calculate the approximate values of the true equilibrium constant K given in the table. The results of the hydrolysis and formation equilibria for both $catH_2$ and 4-NO_2catH_2 indicate that true equilibria have been reached. For any one catechol, there is a scatter in the values of K and K' observed. In addition, for $catH_2$ itself, a possible increase in K and K' with pH may be due to an increase in the solubility of silica in the more alkaline solutions.[3] Nevertheless, the experimental results are reasonably consistent with eqs (6) and (7). As expected, K values increase in the sequence

$$catH_2 < 4,5\text{-}Cl_2catH_2 < 4\text{-}NO_2catH_2 < 3,4\text{-}(NO_2)_2catH_2,$$

which also corresponds to the decrease in pK_1 and pK_2 for the free catechols. It is certainly clear that by an appropriate choice of catechol, stable aqueous solutions of tris-catecholato complexes of silicon(IV) can be obtained in the presence of dissolved silica at pH values ranging from alkaline to as low as 4.1. There have been two previous attempts to obtain values of K for tris-catecholato complexes of silicon(IV) in aqueous solution. Bartels[16] carried out base titrations of a number of catechols in the presence of silicic acid. The concentration of silicic acid was taken as being the total amount added, equivalent to 6.67×10^{-3} M, which considerably exceeds the equilibrium solubility of silica (*ca* 2×10^{-3}). It is also not clear whether true equilibria were obtained during the titrations. It is therefore not surprising that he reported values of K for $catH_2$ (1.3×10^{-11}) and 4-NO_2catH_2 (7.4×10^{-6}) which differ considerably from our values (3.8×10^{-13} and 1.8×10^{-8}, respectively). Baumann[17] used the molybdate reaction to obtain the concentration of "molybdate active silicic acid" in aqueous solutions containing $catH_2$ and excess silicic acid. He derived a value for K of 4.8×10^{-12}, which is still considerably greater than that reported here.

Pichet and Benoit[18] using UV spectrophotometry, have reported values of K for the formation in aqueous solution of a number of tris-catecholato complexes of germanium(IV), which exist in a similar equilibrium to that found for silicon(IV). They also observed a correlation between an increase in K and a decrease in pK_1 and pK_2 for the free catechol. The values of K are much larger, however, which reflects the greater stability of the germanium(IV) complexes.

Facial and meridional isomers

When the catechol is asymmetrically substituted, and the two oxygens become non-equivalent in the dianion, there is the possibility of meridional and facial isomerism in the corresponding tris-catecholato silicon(IV) complex. In the facial isomer, the ligands are equivalent but in the meridional isomer they are all different. The meridional–facial isomer ratio expected on a purely statistical basis is 3 : 1. Figure 2 shows the ^{1}H NMR spectrum of the $[Si(3\text{-}CHOcat)_3]^{2-}$ anion in D_2O. Four peaks of

Table 2. Equilibrium data for the reactions $3LH_2+SiO_2$ in water at 25°C[a]

pH	Ratio c/f[b]	K'	
$catH_2$: Formation equilibria			
8.09	0.080	4.4×10^{-16}	
8.35	0.179	6.4×10^{-16}	
8.53	0.298	7.4×10^{-16}	
		$K'_{av}=6.1\times10^{-16}$	$K_{av}=3.3\times10^{-13}$
$catH_2$: Hydrolysis equilibria			
8.05	0.083	5.6×10^{-16}	
8.31	0.179	6.5×10^{-16}	
8.71	0.298	1.1×10^{-15}	
		$K'_{av}=7.7\times10^{-16}$	$K_{av}=4.2\times10^{-13}$
			K_{mean}[c] $=3.8\times10^{-13}$
4,5-Cl_2catH_2: Formation equilibria			
6.70	0.379	5.1×10^{-12}	
7.23	0.827	6.8×10^{-12}	
		$K'_{av}=6.0\times10^{-12}$	$K_{av}=3.2\times10^{-9}$
4-NO_2catH_2: Formation equilibria[d]			
5.89	0.101	2.1×10^{-11}	
6.23	0.324	4.7×10^{-11}	
7.08	0.418	2.7×10^{-11}	
7.10	0.460	3.6×10^{-11}	
		$K'_{av}=3.9\times10^{-11}$	$K_{av}=2.1\times10^{-8}$
4-NO_2catH_2: Hydrolysis equilibria[d]			
5.87	0.081	2.1×10^{-11}	
5.94	0.184	1.6×10^{-11}	
7.14	0.459	3.6×10^{-11}	
7.15	0.429	4.1×10^{-11}	
		$K'_{av}=2.9\times10^{-11}$	$K_{av}=1.6\times10^{-8}$
			$K_{mean}=1.8\times10^{-8}$
3,4-$(NO_2)_2catH_2$: Formation equilibria			
pH	Final concentration $[Si(3,4\text{-}(NO_2)_2cat)_3]^{2-}$ (M)	K'	
4.05	3.1×10^{-2}	8.4×10^{-8}	
4.39	4.3×10^{-2}	1.2×10^{-7}	
		$K'_{av}=1.0\times10^{-7}$	$K_{av}=5.4\times10^{-5}$

[a] The initial concentration of the catechols was 0.15 M (0.05 M for the tris-catecholato complexes in the hydrolysis experiments), except for 3,4-$(NO_2)_2catH_2$ (0.3 M).

[b] The value is for $[L_{complexed}]/[L_{free}]$, i.e. $[SiL_3]^{2-}/3[L_{free}]$, where $[L_{free}]$ is the total concentration of the free catechol.

[c] K_{mean} is the mean of the values of K found from hydrolysis and formation reactions, assuming $[Si(OH)_4]=1.83\times10^{-3}$.

[d] Based on the H_6 resonances.

equal intensity are observed for the aldehydic protons, showing the presence of meridional and facial isomers in the statistical ratio, within experimental error. The aromatic resonances are more complex, but for H_6 four overlapping sets of double doublets can be discerned (Fig. 2). The distinction between H_4 and H_6 was made on the basis of a difference NOE experiment, with the aldehydic resonances being irradiated.

In Fig. 3 the ^1H NMR spectrum of the tris-complex derived from tiron and silicic acid is shown. The H_6 resonance consists of three doublets of equal

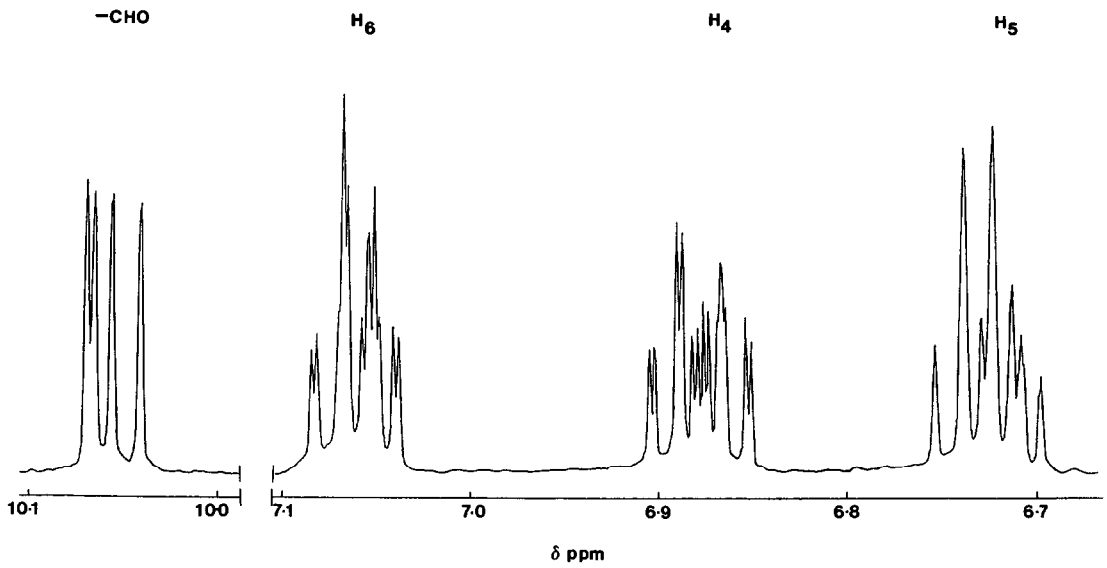

Fig. 2. ^{1}H NMR spectrum (500 MHz, D_2O) of the $[Si(3\text{-}CHOcat)_3]^{2-}$ anion.

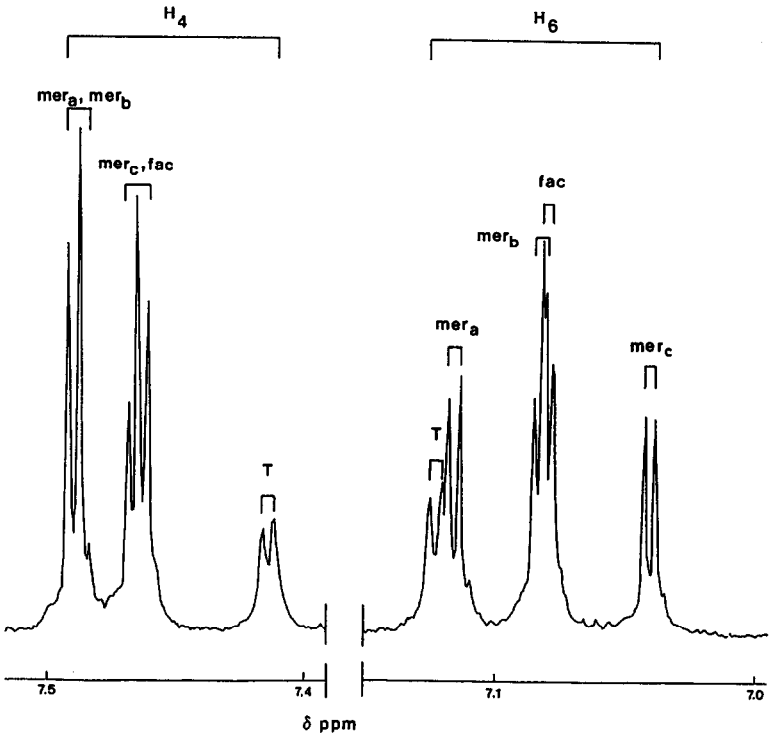

Fig. 3. ^{1}H NMR spectrum (500 MHz, D_2O) of the tris-complex derived from tiron; T = free tiron.

intensity, together with one of greater intensity, which can be assigned to the facial isomer. The meridional–facial ratio is $2.3 \pm 0.2 : 1$. The difference from the statistical value may be due to steric effects associated with the bulky sulphonate groups. The detailed assignment given in Fig. 3 is based on a 2D COSY experiment (500 MHz).

Facial and meridional isomers would also be expected for the tris-complexes derived from 4-substituted catechols. The ^{1}H NMR spectra of $[Si(4\text{-}CHOcat)_3]^{2-}$ and $[Si(4\text{-}NO_2cat)_3]^{2-}$ suggested that meridional and facial isomers were present, but only very limited resolution could be achieved. With $[Si(4\text{-}NO_2cat)_3]^{2-}$, the H_3 resonances comprised two overlapping sets of doublets of equal intensity. Measurements at both 250 and 500 MHz showed

that a chemical shift was involved and not an abnormally large *para*-{^{1}H–^{1}H} coupling. For the free ligand, H_6 consisted of one doublet only. It seems likely that in both complexes two of the meridional resonances and one facial and one meridional resonance have almost identical chemical shifts. The ^{1}H NMR spectra of $[Si(4\text{-}CHOcat)_3]^{2-}$ and $[Si(3\text{-}MeOcat)_3]^{2-}$ also showed no clear resolution of the resonances from the facial and meridional isomers. The presence of a strongly anisotropic group in the 3-position of the catechol ring may therefore be necessary to obtain adequate resolution of the meridional and facial isomers in the ^{1}H NMR spectra.

The ^{1}H resonances of $[Si(3\text{-}CHOcat)_3]^{2-}$ began to broaden at *ca* 50°C, with appreciable broadening at *ca* 80°C, while for $[Si(tiron)_3]^{2-}$, broadening begins at *ca* 40°C with partial collapse at *ca* 70°C. These changes indicate the onset of fluxionality since the resonances of the free ligand remain sharp throughout. Although $[Si(3\text{-}CHOcat)_3]^{2-}$ is rigid on an NMR time scale at room temperature, it is probably fluxional in the time taken to obtain the NMR spectrum since it is unlikely that the solid tetramethylammonium salt used contains the isomers in almost the exact statistical ratio.

Mixed complexes

When freshly prepared 0.1 M solutions of $K_2[Si(cat)_3]$ and $K_2[Si(4\text{-}NO_2cat)_3]$ in D_2O at pH 8.0 were mixed at room temperature, the ^{1}H NMR spectrum measured immediately consisted of a superposition of those of the two complexes. After *ca* 60 min, resonances characteristic of the mixed complexes began to appear, and equilibrium was reached after *ca* 14 h. Ligand exchange was found to be faster at the lower pH of 7.0. For mixed solutions of $(Et_3NH)_2[Si(cat)_3]$ and $(Et_3NH)_2[Si(4\text{-}NO_2cat)_3]$ in dimethyl sulphoxide-d_6 no such complexes could be detected after 24 h, suggesting that in water ligand exchange involves as a first step H^+ attack on a Si—O bond.

Two series of mixed complexes were studied in detail, those formed from $[Si(cat)_3]^{2-}$ and $[Si(4\text{-}NO_2cat)_3]^{2-}$ and those from $[Si(catd_4)_3]^{2-}$ and $[Si(4,5\text{-}Cl_2cat)_3]^{2-}$. The former system is one with both a symmetrical and an asymmetrical catechol, the latter has two symmetrical catechols. $K_2[Si(catd_4)_3]$ was used to obtain the ^{1}H NMR spectra of the mixed complexes involving 4,5-Cl_2catH_2 to avoid interference caused by the resonances of free $catH_2$ formed by hydrolysis during equilibration. The mixed complexes expected are illustrated in Figs 4 and 6, and the observed ^{1}H and ^{29}Si NMR spectra are shown in Figs 5 and 7. For the $[Si(catd_4)_3]^{2-}$ and $[Si(4,5\text{-}Cl_2cat)_3]^{2-}$ systems, the different species can be distinguished in both the ^{1}H NMR and ^{29}Si NMR spectra. The assignment given in Fig. 5 was confirmed by studying a solution prepared from a different initial molar ratio of the pure tris-complexes (1 : 2). As expected, two ^{1}H resonances of equal intensity are observed for the $[Sicatd_4(4,5\text{-}Cl_2cat)_2]^{2-}$ anion. Because of the appreciable hydrolysis that occurred during equilibration, it was not possible to obtain accurate data concerning the position of the equilibrium, although it seems to be close to the statistical value. Three geometrical isomers are expected for the $[Sicat(4\text{-}NO_2cat)_2]^{2-}$ anion (Fig. 6). In the asymmetrical isomer (which has twice the statistical weight of the others) the two 4-NO_2cat ligands are not equivalent. Accordingly, the H_3 resonance for the mixed species should comprise four doublets. Only three are actually observed, with two overlapping to give an apparent triplet. It seems likely that the strong, slightly broad high-field doublet comprises two highly overlapped doublets. The ^{29}Si NMR spectrum (Fig. 7) distinguishes between complexes of different formula, but not between the $[Sicat(4\text{-}NO_2cat)_2]^{2-}$ isomers.

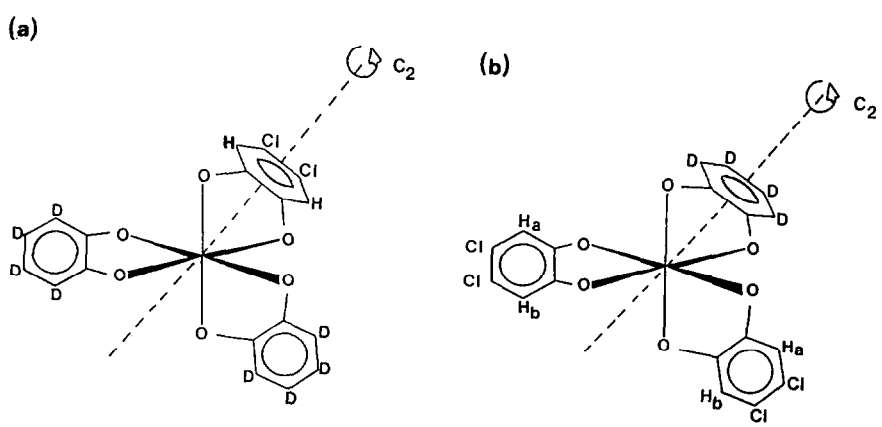

Fig. 4. The structures of (a) $[Si(catd_4)_24,5\text{-}Cl_2cat]^{2-}$ and (b) $[Sicatd_4(4,5\text{-}Cl_2cat)_2]^{2-}$.

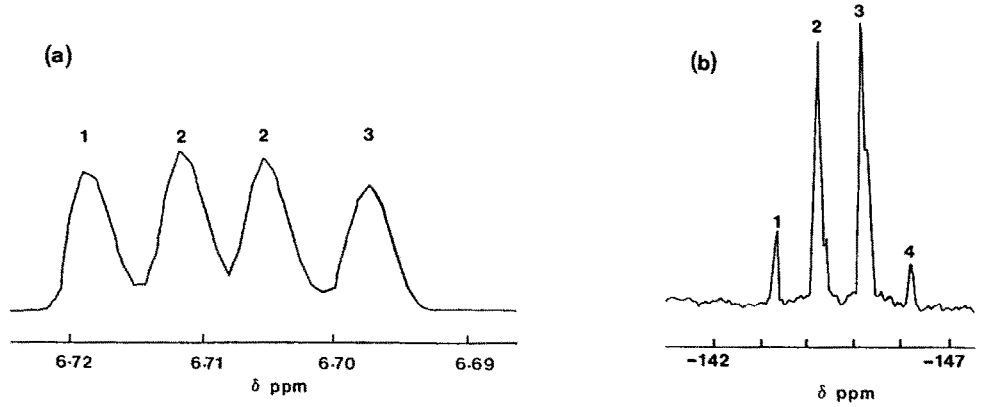

Fig. 5. (a) ^{1}H NMR spectrum (270 MHz, D_2O) of an equilibrated solution initially 0.1 M in both $[Si(catd_4)_3]^{2-}$ and $[Si(4,5\text{-}Cl_2cat)_3]^{2-}$ at pH 7.4; (b) ^{29}Si NMR spectrum (49.69 MHz, H_2O) of a similar solution. 1 = $[Si(4,5\text{-}Cl_2cat)_3]^{2-}$, 2 = $[Sicatd_4(4,5\text{-}Cl_2cat)_2]^{2-}$, 3 = $[Si(catd_4)_2 4,5\text{-}Cl_2cat]^{2-}$, 4 = $[Si(catd_4)_3]^{2-}$.

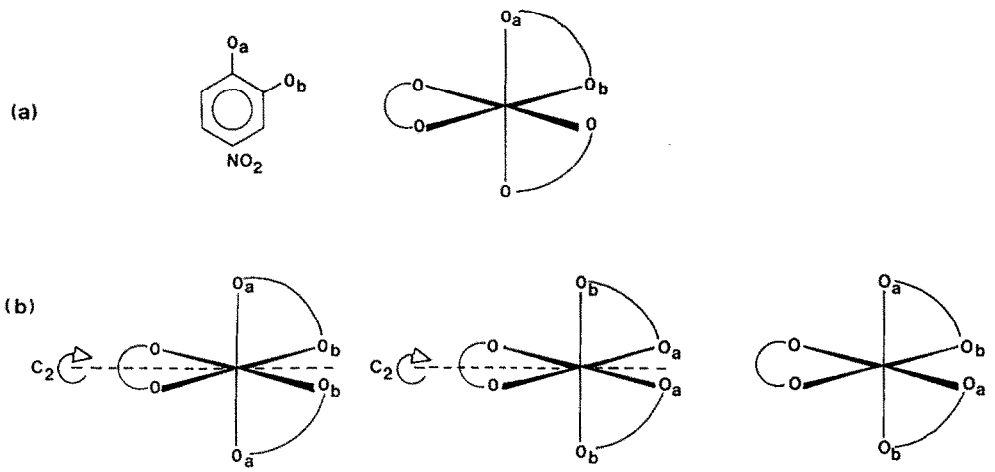

Fig. 6. The structures of (a) $[Si(cat)_2 4\text{-}NO_2cat]^{2-}$ and (b) the three isomers of $[Sicat(4\text{-}NO_2cat)_2]^{2-}$.

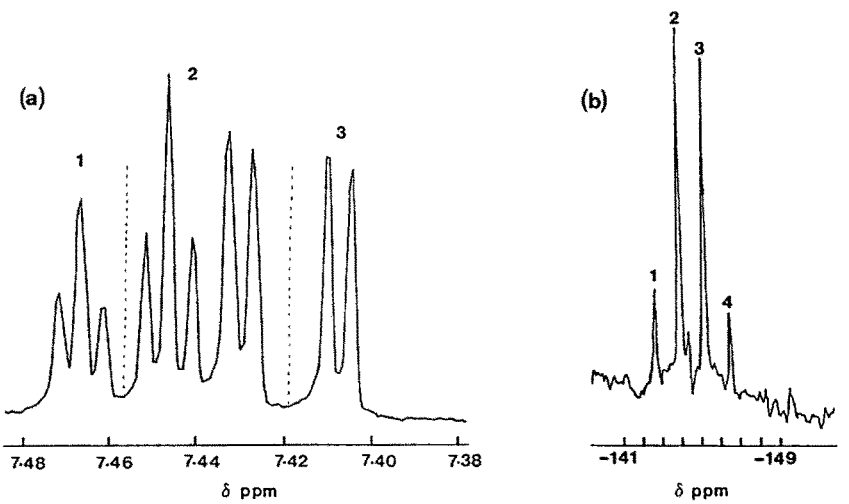

Fig. 7. (a) ^{1}H NMR spectrum (500 MHz, D_2O) of an equilibrated solution initially 0.1 M in both $[Si(cat)_3]^{2-}$ and $[Si(4\text{-}NO_2cat)_3]^{2-}$ at pH 8.1; (b) ^{29}Si NMR (46.96 MHz, H_2O) of a similar solution. 1 = $[Si(4\text{-}NO_2cat)_3]^{2-}$, 2 = $[Sicat(4\text{-}NO_2cat)_2]^{2-}$, 3 = $[Si(cat)_2 4\text{-}NO_2cat]^{2-}$, 4 = $[Si(cat)_3]^{2-}$.

The $[Si(gallate)_3]^{5-}$ *complex*

In this work qualitative information has been obtained from ^1H NMR spectra concerning the rates of a number of processes, i.e. the exchange between free and complexed ligand, the interchange between different ligands and the "scrambling" of meridional and facial isomers. ^1H NMR spectra of the tris-complex derived from gallic acid provides quantitative rate data for another process, the breaking of one Si—O bond to give a five-coordinate complex, which is a plausible first step in these other reactions. If bond breaking in the tris-complex is slow on the NMR time scale then two separate resonances are expected (H_A and H_B in Fig. 8). Fast bond breaking, with concomitant fast proton transfer, will result in a single resonance only. Figure 8 shows the ^1H NMR spectra of the tris-complex in D_2O as a function of temperature, together with the calculated mean lifetimes, τ. The free ligand resonance remains sharp throughout, showing that intermolecular exchange does not contribute appreciably to the observed collapse of the H_A and H_B resonances. The rate of bond breaking is dependent upon the pD of the solution. At a pD of 8.4 (25°C) the mean lifetime, τ, was 0.014 s at 85°C, compared with an interpolated value of 0.008 s at the same temperature and a pD of 7.8. It therefore seems likely that bond breaking is assisted by H^+ attack on one of the Si—O bonds, although the situation is complicated by a probable change in species with pD, arising from the ionization of the free phenolic-OD group. At low temperature and high pH, some additional structure in the H_A and H_B resonances was observed, presumably arising from the presence of meridional and facial isomers. In the corresponding germanium(IV) complex,[19] where bond breaking is slow, this structure is more clearly resolved.

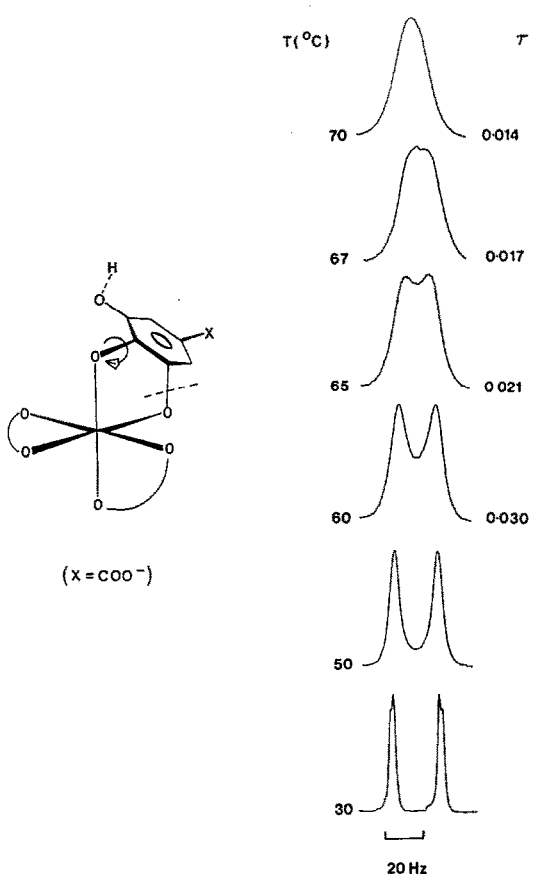

Fig. 8. ^1H NMR spectra (250 MHz, D_2O, pD at 25°C = 7.8) of $[Si(gallate)_3]^{5-}$ at various temperatures, together with the calculated values of the mean lifetimes, τ, for the interchange of H_A and H_B.

^{29}Si and ^{13}C NMR spectra

The ^{29}Si chemical shifts observed for the tris-catecholato complexes are given in Table 3. Cella *et al.*[20] showed that in organic solvents six-coordinate complexes of silicon give much more negative values of δ than do complexes in which the silicon is bound to four oxygens only. For $(Et_3NH)_2[Si(cat)_3]$ in dimethyl sulphoxide-d_6 they report a value for δ of -139.3, in reasonable agreement with our result of -140.3 for $K_2[Si(cat)_3]$ in dimethyl sulphoxide. The more negative value of δ for an aqueous solution (-146.3) presumably arises from solvent effects, possibly due, in part, to hydrogen-bonding from the water to the oxygens in the tris-complex. The main factor affecting the chemical shifts in Table 3 seems to be the electron density on the

Table 3. ^{29}Si chemical shifts for tris-catecholato complexes in H_2O

Catechol	δ (ppm, relative to $(Si(CH_3)_4)$
cat	-146.3 (-140.3)[a]
4-Mecat	-146.0 (-140.5)[a]
4-CNcat	-145.5 (-138.0)[a]
4-Clcat	-144.8
4-CHOcat	-144.2
4,5-Cl_2cat	-143.4
3-CHOcat	-142.6
4-NO_2cat	-142.4
tiron	-142.0
4,5-$(NO_2)_2$cat	-139.3
$(cat)_2$4,5-$(Cl)_2$cat	-145.3
cat(4,5$(Cl)_2$cat)$_2$	-144.4
$(cat)_2$4-NO_2cat	-145.1
cat(4-NO_2cat)$_2$	-143.8

[a] In $(CH_3)_2SO$ with 0.08 M $Cr(acac)_3$.

oxygens, with electron-withdrawing groups leading to deshielding of the ^{29}Si nucleus. For the 4- and 4,5-substituted catechols there is a reasonable correlation between δ and $\Sigma\sigma$, where $\Sigma\sigma$ is the sum of the Hammett σ_m and σ_p values for the substituent, calculated with respect to the oxygens. There are two anomalies, $[Si(4\text{-}Mecat)_3]^{2-}$, where δ is less negative in water (though not in $(CH_3)_2SO$) than that for $[Si(cat)_3]^{2-}$, and $[Si(4\text{-}CNcat)_3]^{2-}$, for which a less negative value would be expected. As with $[Si(4\text{-}Mecat)_3]^{2-}$, the δ value of $[Si(4\text{-}CNcat)_3]^{2-}$ in $(CH_3)_2SO$ is closer to that expected from the relevant Hammett σ values, suggesting that these anomalous results in water may also be largely associated with solvent effects. Quite good additivity of the ^{29}Si chemical shifts is observed in the mixed complexes (Table 3, Figs 5 and 7). The ^{13}C NMR spectrum of the $[Si(cat)_3]^{2-}$ anion in H_2O shows resonances at 152.1 ($C^{1,2}$), 120.4 ($C^{4,5}$) and 113.4 ppm ($C^{3,6}$), compared to 147.7, 123.1 and 118.9 ppm, respectively, for $catH_2$. Griffith *et al.*[21] have reported the ^{13}C NMR spectra of catecholato complexes of molybdenum, tungsten and some platinum metals, which show similar but more marked deshielding of $C^{1,2}$ on coordination of the $catH_2$. For $[Si(4\text{-}NO_2cat)_3]^{2-}$ in H_2O, the ^{13}C resonances were at 169.4 (C^1), 151.6 (C^2), 135.8 (C^4), 124.1 ($C^{3(5)}$), 118.9 ($C^{5(3)}$) and 111.4 ppm (C^6). All ^{13}C resonances were measured relative to internal (trimethylsilyl)propane sulphonate.

Table 4. Raman and IR data for $K_2[Si(cat)_3]$. Raman spectra were recorded on the solid (1) and on a saturated aqueous solution (2). (Relative intensity compared to largest peak in parentheses)

Raman (cm^{-1}) (1)	Raman (cm^{-1}) (2)	IR (cm^{-1}) (KBr pellet)
1591 (3)	1593 (2)	1674 (m,b)
1507 (1)	1504 (1)	1618 (m,b)
1484 (1)	1493 (1)	1592 (s)
1455 (1)	1458 (1)	1495 (s)
1354 (2)	1357 (3)	1490 (s)
1274 (1)	1283 (1)	1456 (w)
1149 (2)	1157 (2)	1350 (m)
1053 (1)	1041 (1)	1255 (s)
1020 (5)	1020 (8)	1101 (m)
882 (1)	875 (1)	1019 (m)
827 (10)	830 (10)	885 (w)
808 (2)	818 (1)	872 (m)
750 (1)	773 (1)	817 (s)
678 (2)	685 (2)	758 (s)
640 (1)	645 (1)	742 (m)
587 (1)	592 (1)	693 (s,b)
524 (1)	519 (1)	599 (w)
454 (1)	452 (1)	521 (m,b)
247 (4)	250 (4)	455 (w)
		434 (w)

Vibrational spectra of the $[Si(cat)_3]^{2-}$ *ion*

The ^1H NMR spectra reported for the meridional and facial isomers, the mixed complexes, and the complexes derived from gallic acid prove that in these cases silicon is octahedrally coordinated in solution. Further evidence for the parent $[Si(cat)_3]^{2-}$ ion is provided by the almost identical Raman spectra of $K_2[Si(cat)_3]$ in the solid state and in aqueous solution (Table 4). The X-ray crystal structure of $(Cu^{II}(en)_2)[Si(cat)_3]$ has been reported[22] and shows that silicon is surrounded by six oxygens, with O—Si—O bond angles close to 90° (88.3 to 94.4°). Table 4 also gives the IR data for solid $K_2[Si(cat)_3]$. The IR and Raman spectra of $K_2[Si(catd_4)_3]$ were also measured, and indicated that the vibrations were highly "mixed". Accordingly, no assignments of the bands in Table 4 are attempted.

Acknowledgements—We thank Mr R. N. Sheppard for the 500 MHz NMR spectra, Mr J. N. Bilton for the mass spectra, and Dr D. Young for the laser diffraction data. One of us (J.P.) thanks the SERC for a grant.

REFERENCES

1. R. J. P. Williams (Ed.), *Silicon Biochemistry*, Ciba Foundation Symposium 121. John Wiley, New York (1986).
2. D. Werner, *The Biology of Diatoms*. Blackwell Scientific, Oxford (1977); F. W. Harrison and R. R. Cowxen (Eds), *Aspects of Sponge Biology*. Academic Press, New York (1976).
3. R. K. Iler, *The Chemistry of Silica*. John Wiley, New York (1979).
4. R. K. Harris, C. T. G. Knight and W. E. Hull, *Soluble Silicates* (Edited by J. S. Falcone), ACS Symp. Ser. 1982, **194**, 79; C. T. G. Knight, *J. Chem. Soc., Dalton Trans* 1988, 1457.
5. J. Priestly, *Experiments and Observations on Different Kinds of Air*, Birmingham, 1790, **2**, 399; P. A. W. Dean and D. F. Evans, *J. Chem. Soc. A* 1967, 698.
6. A. Rosenheim, B. Raibman and G. Schendel, *Z. Anorg. Allg. Chem.* 1931, **196**, 160.
7. E. L. Muetterties and C. M. Wright, *J. Am. Chem. Soc.* 1964, **86**, 160.
8. Y. Murakami and M. Tokunaga, *Bull. Chem. Soc. Jpn* 1964, **37**, 1562.
9. R. Willstätter and H. E. Muller, *Berichte* 1911, **44**, 2182.
10. D. H. Rosenblatt, J. Epstein and M. Levitch, *J. Am. Chem. Soc.* 1953, **75**, 3277.
11. J. Elrich and M. T. Bogert, *J. Org. Chem.* 1947, **12**, 522.
12. C. L. Frye, *J. Am. Chem. Soc.* 1964, **86**, 3170.

13. D. F. Evans and D. A. Jakubovic, *Polyhedron* 1988, **7**, 1881.
14. I. M. Kolthoff and P. J. Elving, *Treatise on Analytical Chemistry*, Part 2, Vol. II. John Wiley, New York (1962).
15. T. J. Wenzel, M. E. Ashley and R. E. Seivers, *Analyt. Chem.* 1982, **54**, 615.
16. H. Bartels, *Helv. Chim. Acta* 1964, **47**, 615.
17. H. Baumann, *Bietr. Silikose Forch. Sonderb.* 1960, **5**, 11.
18. P. Pichet and R. L. Benoit, *Inorg. Chem.* 1967, **6**, 1505.
19. D. F. Evans and J. Parr, unpublished results.
20. J. A. Cella, J. D. Cargioli and E. A. Williams, *J. Organomet. Chem.* 1980, **186**, 13.
21. W. P. Griffith, C. A. Pumphrey and T-A. Rainey, *J. Chem. Soc., Dalton Trans.* 1986, 1125.
22. Von D. Sackerer and G. Nagorsen, *Z. Anorg. Allg. Chem.* 1977, **437**, 188.

Polyhedron Vol. 9, No. 6, pp. 825–830, 1990
Printed in Great Britain

0277–5387/90 $3.00+.00
© 1990 Pergamon Press plc

COPPER(II) AND NICKEL(II) COMPLEXES OF DIASTEREOMERIC SEGMENTS OF THYMOPOIETIN

I. SÓVÁGÓ*

Department of Inorganic and Analytical Chemistry, L. Kossuth University, 4010-Debrecen, Hungary

and

B. RADOMSKA

Institute of Chemistry, University of Wrocław, 50-383 Wrocław, Poland

and

I. SCHÖN and O. NYÉKI

Chemical Works of Gedeon Richter Ltd, H-1475 P.O. Box 27, Budapest, Hungary

(*Received* 28 *May* 1989; *accepted* 18 *October* 1989)

Abstract—Copper(II) and nickel(II) complexes of tri- and tetrapeptide segments of thymopoietin—ArgLysAspVal (TP4), ArgLysAsp (TP3, LLL, LLD, LDL, DLL) and ArgLys-(Arg)Asp (ETP3)—were studied by potentiometric spectrophotometric, CD and EPR methods. The coordination of terminal amino, two deprotonated amide nitrogens and the β-carboxylate of the aspartic acid residue was proved in all cases. Significant stereoselectivity was not observed in the copper complexes of diastereomeric tripeptides.

Thymopoietin, a 49 amino acid polypeptide, is a hormone of the thymus which influences the differentiation of various cells. The synthetic pentapeptide segment—Arg–Lys–Asp–Val–Tyr (TP5)—was reported to correspond to a biologically-active site of the parent thymopoietin molecule.[1]

Concerning the coordination chemistry of TP5, its various transition metal and lanthanide complexes have so far been studied.[2–4] It was found that TP5 forms stable 1 : 1 complexes with copper(II) in which coordination takes place via the terminal-amino, two deprotonated amide nitrogens and the β-carboxylate group of the aspartic acid residue. On the basis of this result it was stated that during complex formation TP5 acts as a tripeptide, and the aspartic acid present in the third position in the peptide chain is able to hinder the coordination of the fourth and fifth amino acid residues. The same effect of the aspartyl moiety was found in the copper(II) complexes of other peptides containing aspartic acid,[5] while the coordination of four nitrogens (NH_2 and 3 N^-) is characteristic of tetraglycine.[6]

Carbon terminally shortened segments of TP5—ArgLysAspVal, TP4 and ArgLysAsp, TP3—eliciting remarkable immunostimulating effects, are under clinical studies.[7] Taking into account the governing role of the aspartyl residue during complex formation it is worthwhile studying the transition metal complexes of TP4 and TP3 and their diastereomers. This is also supported by literature values, because a significant stereoselectivity can be observed in the copper(II) complexes of diastereomeric dipeptides.[8–10] Namely, $CuAH_{-1}$ complexes of (LL)-dipeptides are more stable than the complexes of (LD)-dipeptides. The difference in stability largely depends on the side-chain disposition, and it is explained by hydrophobic interactions between the side chains. Similar studies for the diastereomeric tripeptides have not been published yet.

In this paper we present the results of potentiometric and spectrophotometric studies for the

* Author to whom correspondence should be addressed.

copper(II) and nickel(II) complexes of TP4 (LLLL), TP3 (LLL, DLL, LDL, LLD) and ETP3 containing arginyl residues both at the α- and ε-amino groups of lysine, Arg–Lys(Arg)–Asp.

EXPERIMENTAL

The acetate forms of the peptides—Arg–Lys–Asp–Val (TP4, LLLL), Arg–Lys–Asp (TP3 LLL, DLL, LDL, LLD) and Arg–Lys(Arg)–Asp (TP3, LL(L)L)—were synthesized by usual methods. Details of the synthesis will be published elsewhere.

In the pH-metric studies, the ligand concentration varied between 1 and 4×10^{-3} mol dm^{-3}, while the metal ion to ligand ratios ranged from 2:1 to 1:3. The 5 cm^3 samples were titrated with carbonate-free potassium hydroxide, and argon was bubbled through the samples to ensure the absence of carbon dioxide and for stirring the solutions. All pH-metric studies were carried out at 298 K and at a constant ionic strength of 0.2 mol dm^{-3} (KCl). The pH measured was converted to [H$^+$]-ion concentration by the method of Irving *et al.*[11] Measurements were made with a Radiometer pHM84 pH-meter with GK2421C combined electrodes and an ABU80 autoburette. Stability constants defined by the following equation (charges are omitted and "A" denotes the fully deprotonated forms of TP3, TP4 and ETP3)

$$pM + qA + rH \rightleftharpoons M_pA_qH_r$$

$$\beta_{pqr} = \frac{[M_pA_qH_r]}{[M]^p[A]^q[H]^r}$$

were calculated with a general computational program (PSEQUAD) which was published earlier.[12]

Absorption spectra were recorded on a Beckman Acta MIV spectrophotometer and the concentrations were similar to those used in the potentiometric measurements. Circular dichroism (CD) spectra were measured on an automatic spectropolarimeter JASCO-J-20 in the 200–740 nm region, in equimolar solutions. All CD spectra are expressed in terms of $\Delta\varepsilon/(\varepsilon_l - \varepsilon_r)$. EPR spectra of the solution in a glycol–water mixture were taken on a JEOL JES-ME-3X spectrometer at liquid nitrogen temperature and at 9.15 GHz.

RESULTS AND DISCUSSION

The ligands investigated in this study can be classified into two categories. TP4, TP3 and ETP3, containing only L-amino acids, represent one type of ligand, and their protonation constants are summarized in Table 1.

Table 1. Protonation constants of TP3, TP4 and ETP3. $I = 0.2$ mol dm^{-3} (KCl); $T = 298$ K

	TP4	TP3	ETP3
pK_1	10.48±0.03	10.49±0.03	7.84±0.03
pK_2	7.34±0.02	7.44±0.02	7.13±0.03
pK_3	3.89±0.06	4.20±0.05	4.03±0.05
pK_4	3.04±0.05	2.77±0.05	2.67±0.05

It can be seen from Table 1 that all peptides have four dissociable protons in the measurable pH-range. pK_3 and pK_4 belong to the β-carboxylate and C-terminal carboxylate groups of the peptides, respectively. Data reveal that pK_3 and pK_4 values of TP3 and ETP3 are almost the same, but the difference between these values is smaller for TP4, because of the longer distances of the carboxylate groups in the molecule. Deprotonation of the terminal (arginyl) amino group (pK_2) and the side-chain lysyl ε-amino group (pK_1) are well separated in TP4 and TP3. The pK values obtained are similar to each other (and to those of TP5[2]), suggesting that the length of the peptide chain does not significantly influence the deprotonation processes of the amino groups. Both amino groups of the lysyl residue are in amide linkage in ETP3, therefore the ligand can be characterized by two "terminal (arginyl) amino" groups. Deprotonation of these ammonium groups takes place simultaneously, and their difference does not significantly exceed the statistical value (0.6 log unit). The average of pK_1 and pK_2 corresponds well with the deprotonation of the arginyl amino group (pK_2) in TP3 or TP4, supporting the independent deprotonation of the ammonium groups in ETP3.

Stability constants of the copper(II) and nickel(II) complexes of TP4, TP3 and ETP3 are collected in Table 2, while the concentration distribution of the complexes formed in the copper(II)–TP3 system are depicted in Fig. 1.

From Table 2 it can be seen that the same species are present in TP3 and TP4 systems, suggesting the same type of coordination for both ligands. $[CuAH_2]^{2+}$ and $[CuAH]^+$ are present in low concentration in acidic solution where the coordination takes place via the terminal amino and neighbouring carbonyl groups, similar to other oligopeptides.[6] $[CuAH_{-1}]^-$ is the main species between pH 5 and 10, which means that TP3 and TP4 act as tripeptides. Namely, both ligands are coordinated via the terminal amino, two deprotonated amide nitrogens and the β-carboxylate group of aspartic acid, while the ε-amino group of the lysyl residue remains protonated in the $[CuAH_{-1}]^-$ species. Consequently the real composition is

Table 2. Stability constants of the copper(II) and nickel(II) complexes of TP4, TP3 and ETP3. $I = 0.2$ mol dm^{-3} (KCl); $T = 298$ K

	TP4		TP3		ETP3
	Cu^{II}	Ni^{II}	Cu^{II}	Ni^{II}	Cu^{II}
$[MAH_2]^{2+}$	19.65±0.10	—	20.46±9.10	—	18.10±0.10
$[MAH]^{+}$	15.27±0.07	13.20±0.10	16.02±0.06	13.17±0.10	13.74±0.05
$[MAH_{-1}]^{-}$	5.95±0.04	0.38±0.08	5.59±0.04	−0.69±0.08	3.01±0.05
$[MAH_{-2}]^{2-}$	−4.40±0.05	−9.65±0.08	−4.29±0.04	−10.66±0.07	−3.85±0.05
[MA]	—	—	—	—	8.20±0.06
$[M_2AH_{-2}]$	—	—	—	—	0.88±0.10
$[M_2AH_{-3}]^{-}$	—	—	—	—	−5.66±0.12
pK'	4.66	6.41	5.22	6.93	5.37
pK^{Lys}	10.35	10.03	9.88	9.97	—

$[CuAH_{-1}]^{-} = [Cu(HAH_{-2})]^{-}$. This type of coordination is supported by the spectrophotometric results: the absorption band of $[CuAH_{-1}]^{-}$ appears at $\lambda = 542$ nm for both peptides with $\varepsilon = 159$ and 165 dm^3 mol^{-1} cm^{-1} for TP3 and TP4, respectively. It corresponds to the coordination of three nitrogens, and is in a good agreement with the absorption spectra of copper(II)–TP5 where the same tripeptide-like coordination was proved.

In basic solution $[CuAH_{-1}]^{-}$ is deprotonated and corresponding pK^{Lys} values are close to the pK value of the ε-amino group of the lysyl residues. There is no change in the absorption spectra in that pH-range, supporting the fact that the lysyl side chain of thymopoietin oligopeptide segments does not take part in coordination. CD and EPR measurements provide more unambiguous proof for the existence of the suggested binding mode, as is demonstrated in Table 3.

It can also be seen from Table 2 that complex formation processes of copper(II) and nickel(II) are very similar to each other. Standard deviations of stability constants of nickel(II) complexes are, however, significantly larger because the formation of square-planar diamagnetic complexes is quite slow (especially for the tetrapeptide). The existence of $[NiAH_2]^{2+}$ species can be excluded because of the higher pH-range of complex formation. Deprotonation of the amide groups takes place in a cooperative manner again, which results in the high concentration of $[NiAH_{-1}]^{-} = [Ni(HAH_{-2})]^{-}$.

Deprotonation of the amide group, therefore, can be characterized by an average pK value (pK') given

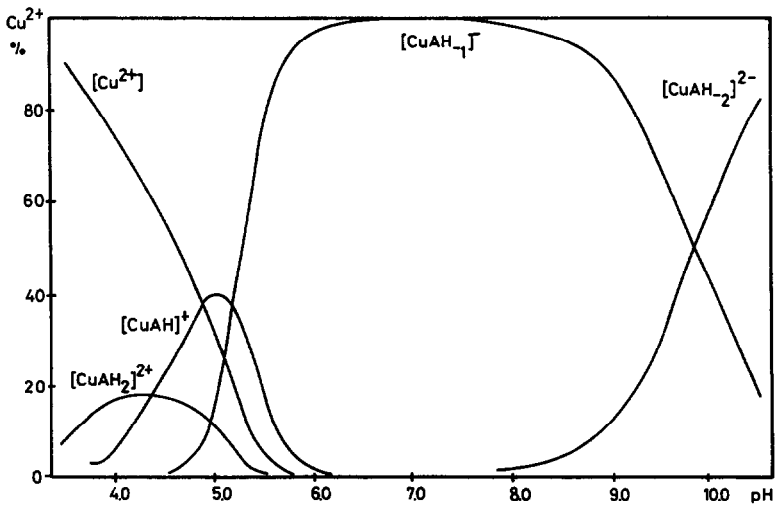

Fig. 1. Concentration distribution of the complexes formed in the copper(II)–TP3 system; $C_{Cu^{2+}} = 1.1 \times 10^{-3}$, $C_{TP3} = 2.9 \times 10^{-3}$ mol dm^{-3}.

Table 3. CD and EPR parameters for the copper(II) and nickel(II) complexes of TP3(LLL)

System	pH	Species	CD λ_{max} (nm)		CD Assignment	EPR A_{II}[G]	EPR g_{II}
Cu^{II}–TP3 (LLL)	4.4	$CuAH$	720	−0.046	*d–d*(IN)	120	2.400
	7.2	$CuAH_{-1}$	554	−0.99	*d–d*(3N)	202	2.199[a]
			302	+0.90	$N^- \rightarrow Cu^{II}$		
			265	−1.4	$NH_2 \rightarrow Cu^{II}$		
	10.5	$CuAH_{-1}$	555	−0.98	*d–d*	201	2.201[a]
			302	+0.98	$N^- \rightarrow Cu^{II}$		
			265	−1.5	$NH_2 \rightarrow Cu^{II}$		
Ni^{II}–TP3 (LLL)	7.3 au.	$NiAH_{-1}$	485	−0.38	*d–d*		
			255	+0.48	$N^- \rightarrow Ni^{II}$		
	10.5	$NiAH_{-1}$	485	−0.62	*d–d*		
			255	+0.73	$N^- \rightarrow Ni^{II}$		

[a] Seven superhyperfine lines were observed.

by the equation:

$$[Cu(HA)]^+ \rightleftharpoons [Cu(HAH_{-2})]^- + 2[H^+].$$

The data in Table 2 reveal that amide coordination is more favoured in copper(II) complexes ($\sim$ 1.7 log unit), similar to other peptide complexes. Comparing the pK' values of TP4 and TP3, it can be stated that TP4 forms the more stable complexes both with copper(II) and nickel(II) ($\sim$ 0.5 log unit).

ETP3–Arg–Lys(Arg)–Asp (Structure I) can be regarded as a "doubled" peptide molecule, at least from the coordination chemical viewpoint.

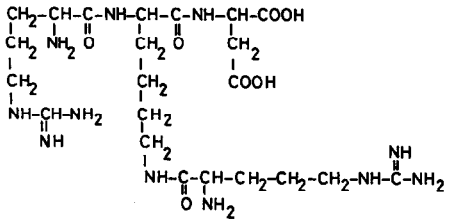

Structure I.

The molecule has the same donor groups as TP3 on one side, but another set of donor atoms is also present with the participation of the peptide bond at the ε-amino group of lysine. Consequently, complex formation processes of ETP3 are much more complicated than those of TP3, and species distribution largely depends on the metal ion to ligand ratios. Figures 2 and 3 show the concentration distribution of the complexes formed in the copper(II)–ETP3 system at 1:2 and 2:1 metal ion to ligand ratios, respectively.

It can be seen from Fig. 2 that in the presence of excess ligand the same species are formed both in copper(II)–TP3 and copper(II)–ETP3 systems. Namely, a stable coordination occurs via the tripeptide part of the ETP3 molecule and the lysyl residue behaves like an independent side chain. Of course, the ratio of $[CuAH_{-1}]^-$ and $[CuAH_{-2}]^{2-}$ is different for the two ligands because the pK of the terminal amino group in ETP3 is much smaller than the pK value of the ε-amino group in TP3. Spectrophotometric results also support the 3N-coordination because spectral parameters above pH 7 (at 1:2 ratio) are almost the same as for copper(II)–TP3 (λ_{max} = 540 nm, ε_{max} = 160 dm^3 mol^{-1} cm^{-1}). Deprotonation of two amide groups takes place simultaneously, and pK' is in a good agreement with TP3.

Figure 3 shows that the peptide bond at the lysyl locus can also be a binding site in the presence of excess copper(II) ion. Formation of $[Cu_2AH_{-2}]$ can be represented by the equation:

$$[CuAH_{-2}]^{2-} + [Cu^{2+}] \rightleftharpoons [Cu_2AH_{-2}].$$

The equilibrium constant for this process is $\log K = 4.73$ which corresponds well to a glycineamide-type coordination with the participation of the amino and carbonyl groups.[13] The amide bond at the ε-amino group deprotonates above pH 6–7 which leads to the formation of $[Cu_2AH_{-3}]^-$. Spectroscopic results also support the existence of two different copper(II) ions around pH $\sim$ 6, because an absorption band can be observed at λ = 540 nm (from the tripeptide coordination) and a shoulder appears between λ = 650 and 700 nm

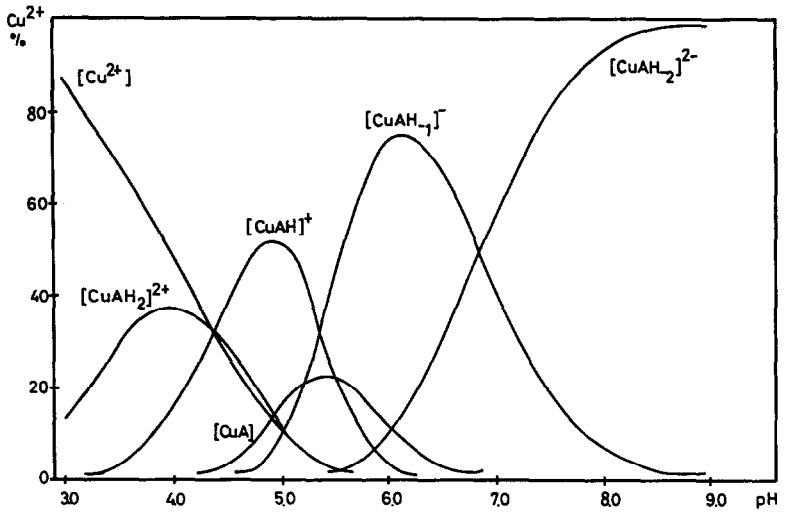

Fig. 2. Concentration distribution of the complexes formed in the copper(II)–ETP3 system; $C_{Cu^{2+}} = 1.04 \times 10^{-3}$, $C_{ETP3} = 2 \times 10^{-3}$ mol dm^{-3}.

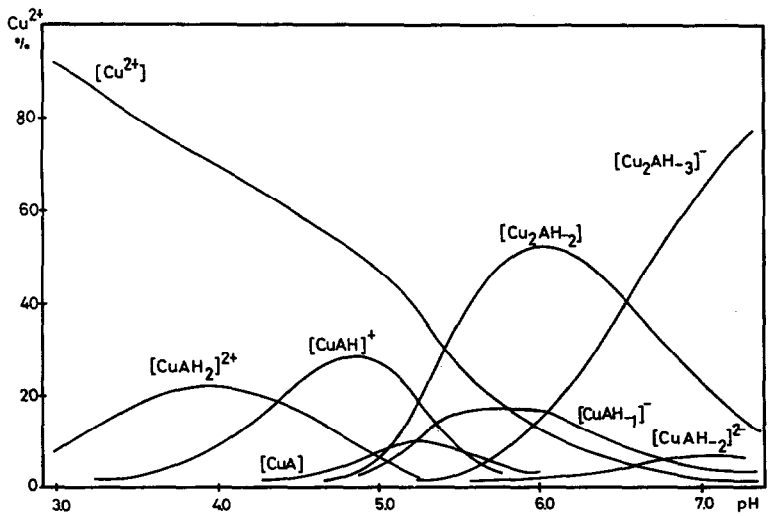

Fig. 3. Concentration distribution of the complexes formed in the copper(II)–ETP3 system; $C_{Cu^{2+}} = 2.45 \times 10^{-3}$, $C_{ETP3} = 1.34 \times 10^{-3}$ mol dm^{-3}.

which is characteristic of glycineamide coordination. Precipitation occurs above pH 7.5 because the bound lysyl peptide is not able to compete with the hydrolysis of excess metal ions. To summarize the results obtained for the complexes of copper(II)–ETP3, it can be stated that the tripeptide-like coordination is the governing factor during complex formation, while the peptide linkage at the ε-amino group represents a weak binding site for metal ions.

Derivatives of TP3 containing one amino acid in the D-configuration (DLL, LDL, LLD) represent the second type of ligands studied in this work. A literature survey shows that pK values of diastereomeric dipeptides differ from each other.[8] Namely, the terminal ammonium is less acidic and the carboxylic group is more acidic in the (LD)-dipeptides than in the pure (LL)-form. In the copper(II) complexes it results in the enhanced stability of [$CuAH_{-1}$] formed with (LL)-dipeptides. Data show that the stability increase is related to intramolecular interaction of the hydrophobic side chains of the dipeptides.[9-10]

Stability constants of the proton and copper(II) complexes of four different diastereomers of TP3 are summarized in Table 4. The data in Table 4 reveal that significant differences can not be observed in the pK values of various diastereomers of TP3. It is probably due to the long distance between the terminal groups in the tri-

Table 4. pK values and stability constants of the copper(II) complexes and the various optically active forms of TP3. $I = 0.2$ mol dm^{-3} (KCl); $T = 298$ K

	LLL	DLL	LDL	LLD
pK_1	10.49	10.29	10.45	10.55
pK_2	7.44	7.50	7.39	7.42
pK_3	4.20	4.20	4.07	4.12
pK_4	2.77	2.76	2.78	2.71
$[CuAH_2]^{2+}$	20.46	19.58	20.57	20.65
$[CuAH]^{+}$	16.02	15.45	16.17	16.10
$[CuAH_{-1}]^{-}$	5.59	5.06	5.54	5.65
$[CuAH_{-2}]^{2-}$	−4.29	−4.73	−4.38	−4.51
pK'	5.22	5.20	5.32	5.23
pK^{Lys}	9.88	9.79	9.92	10.16

Standard deviations are the same as for TP3(LLL) in Tables 1 and 2.

peptide and the lack of hydrophobic side chains in the molecules. A decrease in the pK value of TP3 (DLL) exceeds the error limit, which probably can be explained by the modification of hydrogen bonds in the (DLL)-form. The pK values of β-carboxylate of aspartic acid show two sets of pK_3. p$K_3 \sim 4.20$ is characteristic for LLL- and DLL-forms, and p$K_3 \sim$ 4.10 for LDL- and LLD-tripeptides. These results correspond well with data obtained for diastereomeric dipeptides, but the extent of the differences is much smaller in this case.

Concerning the complex formation with the copper(II) ion, the existence of the same species can be detected for all diastereomers and the equilibrium data show the same trend as was observed with the pK values. (There is a small difference in the concentration of protonated complexes in the copper(II)–TP3(DLL) system, but they are minor species, and the equilibrium constant can not be easily calculated because of the acetate content of the ligands; pK for acetate is 4.55.) Absorption spectra of various copper(II) complexes exclude the structural differences between the various $[CuAH_{-1}]^{-}$ complexes of TP3 derivatives. Namely, $\lambda_{max} = 542, 540, 542, 540$ nm, and $\varepsilon = 159, 150, 152, 158$ dm^3 mol^{-1} cm^{-1} were obtained for the LLL-, DLL-, LDL- and LLD-forms of TP3, respectively. The lack of stereoselectivity can probably be explained by the presence of hydrophilic side chains and by the existence of a stable tripeptide-like coordination mode. As was mentioned above, deprotonation of two amide groups takes place simultaneously, resulting in the formation of three fused chelate rings. The existence of this fused chelate structure is the governing factor during complex formation with tripeptides, and non-coordinated side chains have only minor effects on the thermodynamic stability. Of course, this conclusion can not be generalized for all metal ions and for other diastereomeric tripeptides, and further investigations are necessary to elucidate the role of side chains during complex formation with various tripeptides.

REFERENCES

1. G. Goldstein, M. P. Scheid, E. A. Bape, D. H. Schesinger and J. Van Wauwe, *Science* 1979, **204**, 1309.
2. J. B. Vaughn, R. L. Stephens, R. E. Lenkinski, N. R. Krishna, G. A. Heavner and G. Goldstein, *Biochim. Biophys. Acta* 1981, **671**, 50.
3. I. Sóvágó, T. Kiss and A. Gergely, *Inorg. Chim. Acta* 1984, **93**, L53.
4. M. Wéber, I. Horváth and L. Burger, *Inorg. Chim. Acta* 1985, **108**, L21.
5. B. Decock-Le Reverend, A. Lebriki, C. Livera and L. D. Pettit, *Inorg. Chim. Acta* 1986, **124**, L19.
6. H. Sigel and R. B. Martin, *Chem. Rev.* 1982, **82**, 385.
7. L. Kisfaludy, G. Nyéki, I. Schön, L. Dénes, J. Ember, L. Szporny, Gy. Hajós and B. Szende, *Hoppe-Seyler's Z. Physiol. Chem.* 1983, **364**, 933.
8. L. D. Pettit and R. J. W. Hefford, Stereoselectivity in the metal complexes of amino acids and dipeptides, in *Metal Ions in Biological Systems* (Edited by H. Sigel), Vol. 9, Chap. 6. Marcel Dekker, New York (1979).
9. R. P. Bonomo, R. Cali, V. Cucinotta, G. Impellizeri and E. Rizzarelli, *Inorg. Chem.* 1986, **25**, 1641.
10. R. P. Bonomo, G. Maccorone, E. Rizzarelli and M. Vidali, *Inorg. Chem.* 1987, **26**, 2893.
11. H. M. Irving, M. H. Miles and L. D. Pettit, *Anal. Chim. Acta* 1967, **38**, 479.
12. L. Zékány and I. Nagypál, in *Computational Methods for the Determination of Stability Constants* (Edited by D. Leggett). Plenum Press, New York (1985).
13. I. Sóvágó, B. Harman, A. Gergely and B. Radomska, *J. Chem. Soc., Dalton Trans.* 1986, 235.

Polyhedron Vol. 9, No. 6, pp. 831–837, 1990
Printed in Great Britain

0277–5387/90 $3.00+.00
Pergamon Press plc

CADMIUM ION INTERACTION WITH SULPHUR CONTAINING AMINO ACID AND PEPTIDE LIGANDS

H. KOZŁOWSKI* and J. URBAŃSKA

Institute of Chemistry, University of Wrocław, 14, F.Joliot-Curie str., 50-383 Wrocław, Poland

and

I. SÓVÁGÓ, K. VARNAGY and A. KISS

Institute of Chemistry, University of Debrecen, 4010 Debrecen, Hungary

and

J. SPYCHAŁA

Department of Basic Medical Sciences, Medical Academy of Wrocław, 14, J.Kochanowskiego str., 51-601 Wrocław, Poland

and

K. CHERIFI

Laboratoire de Chimie Macromoleculaire, Unite Associee au CNRS, Université des Sciences et Techniques de Lille, 59655 Villeneuve d'Ascq, France

(*Received* 11 *August* 1989; *accepted* 20 *October* 1989)

Abstract—Cadmium complexes of 15 ligands containing sulphur donors in various environments were studied by potentiometric and polarographic methods. Thiol donors were the most effective in cadmium binding in the order of (S,N,O) > (S,N) > (S,O,O) > (S,O) donor sets. Thioamide groups also enhance the stability of the complexes formed, while the disulphide group is ineffective in the presence of amino acid or peptide binding sites.

Thioneins, which are thought to detoxify heavy metals incorporated in biological systems,[1–4] are low molecular weight proteins rich in cysteine residues (one third of the amino acid content). Cysteine residues are very effective ligands for many heavy metal ions, especially the very toxic cadmium ion. Recently two cadmium binding oligopeptides were found in the fission yeast.[5–9] These peptides (cadystins) are also rich in cysteine residues and they can be induced in the fission yeast by several heavy metals, such as copper(II), zinc(II), lead(II), cobalt(II) and mercury(II).[10] The greatest yield from the synthesis of cadystins is, however, induced by cadmium ions. It was intriguing to find that plants are also able to synthesize peptides called phytochelatins, which have the same sequence as cadystins.[11–13] The general structure of this set of peptides is (γ-Glu–Cys)$_n$–Gly (n = 2–8, for cadystins n = 2 and 3).[14,15] It seems likely that all these peptides are synthesized from glutathione or its precursor, γ-Glu–Cys, in a sequential manner.[12,16] Thus, the oligopeptide chelating agents differ in origin from thioneins (primary gene products), though both products may be important in detoxification and homeostasis of heavy metal ions. The

* Author to whom correspondence should be addressed.

molecular biology of metal tolerances of plants in which phytochelatins are involved was discussed recently by Tomsett and Thurman.[17]

The presence of thiol groups significantly changes the binding ability of a peptide molecule as compared to non-cysteine peptides. The available data do not allow us to conclude about the general features of the thiol moiety in peptide ligands, but it is already accepted that its powerful coordination ability is critical for the ligands protecting living organisms against heavy metal ions. Cadmium complexes of simple thiol-containing ligands have already been extensively studied and the data obtained reveal that this metal ion can form very stable chelates with the (S,O) or (S,N) donor sets involved. The formation of the oligonuclear species involving sulphur bridges seems to be a characteristic feature for the thiol-containing systems.[18–20] Not much data on the cadmium interaction with the cysteine-containing peptides including glutathione is available.[21,22] Hence, to be able to conclude more precisely about the stability and structure of the systems containing metal ion–sulphur bonds we have performed potentiometric and polarographic studies on the cadmium complexes with 15 ligands containing different sulphur donors, including thiol, disulphide and thioamide moieties.

EXPERIMENTAL

Polarographic meausurements (d.c.) were performed on a Radelkis OH-105 polarograph using a dropping mercury electrode with a capillary output of 2.61 mg s^{-1} and a drop time of 3.4 s. The saturated calomel electrode was used as a reference electrode. The cadmium ion concentration was equal to 5×10^{-5} or 1×10^{-4} mol dm^{-3}. The ligand concentrations varied from 2×10^{-5} to 5×10^{-4} mol dm^{-3} for L-cysteine (Cys) and from 5×10^{-4} to 2×10^{-2} mol dm^{-3} for D-penicillamine (D-Pen). A constant ionic strength of 0.15 or 3.0 mol dm^{-3} was maintained by means of sodium perchlorate. The measurements were performed at pH 5.5 for Cys and pH 6.5 and 10.5 for D-Pen. The different conditions used for the solutions containing Cys and Pen derived from the fact that cadmium complexes with Cys precipitated very easily. Differential pulse polarographic (DPP) measurements on a hanging mercury drop electrode (HMDE) were carried out on a PA-4 polarographic analyser (Prague). The three electrode system comprised an HMDE, a platinum counter electrode and a saturated calomel electrode. A scan rate of 20 mV s^{-1}, pulse amplitude of 50 mV and potential range from 0 to −1.2 V were applied. Deoxygenated solutions with ionic strength 0.2 M (KNO_3) were measured at 25°C. The stability constants from the polarographic data were estimated from the Ilkovic equation or by the Lingane method.[23] Potentiometric measurements were performed on a Radiometer pHM84 pH-meter with a GK2421C combined electrode and an ABU 80 automatic burette. In the pH-metric studies the ligand concentration varied between 0.001 and 0.01 mol dm^{-3} while the metal ion-to-ligand ratios ranged from 1:1 to 1:5. Nitrogen was bubbled through the samples (10 cm^3) to ensure the absence of oxygen and carbon dioxide and to mix the solutions during titrations with carbonate-free KOH. All titrations were carried out at 25°C and at constant ionic strength (0.2 mol dm^{-3} of KNO_3). The proton concentration calculations from the measured pH and other details of the pH-metric procedure have been described previously.[24] Stability constants, defined by the following equations:

$$pM + qA + rH \rightleftarrows M_pA_qH_r$$

$$\beta_{pqr} = \frac{[M_pA_qH_r]}{[M]^p[A]^q[H]^r}$$

were calculated with PSEQUAD, a general computational program.[25]

RESULTS AND DISCUSSION

The protonation constants of the studied ligands are collected in Table 1. Deprotonation of the carboxylic group ($pK \sim 2$–3.5) is well separated from the other proton dissociations of thiol and/or ammonium groups. The deprotonation of both the latter groups takes place simultaneously and the real acidity of these functions can be characterized by the microconstants, as was shown earlier.[22] The ligands containing disulphide bridges or a thioamide group, which are presented in the lower part of Table 1, may only dissociate protons from the carboxylate and ammonium groups as indicated.

The calculated stability constants of cadmium complexes are given in Table 2. For the cadmium–cysteine system only one species could be detected (by d.c. polarography) because of precipitation. The ligands containing the thiol group, i.e. L-cysteine (Cys), L-cysteine-methylester (CysOMe), N-acetyl-L-cysteine (N-Ac-Cys), D-penicillamine (D-Pen), N-acetyl-D-penicillamine (N-Ac-D-Pen), mercaptopropionylglycine (MPGly), mercapto-succinic acid (MSA), dipeptides Cys–Gly, Ala–Cys and tripeptide Ala–Ala–Cys, form considerably stronger complexes with cadmium ions than the other ligands presented in Table 2. The first four ligands collected in this table form three monomeric species MA, MA_2 and MA_3. Among them, CysOMe is most effectively bound to the metal ion. All these ligands

Table 1. Proton dissociation constants of the ligands studied; $I = 0.2$ mol dm^{-3} (KNO_3), $T = 298$ K

Ligand	pK_1	pK_2	pK_3	pK_4	pK_5	pK_6
Cys–OMe	6.53(3) (NH_3)[a]	8.93(4) (SH)[a]				
N-Ac-D-Pen	3.26(3) (COOH)	10.02(4) (SH)				
N-Ac–Cys	3.03(3) (COOH)	9.51(3) (SH)				
M-P–Gly	3.43(2) (COOH)	8.31(1) (SH)				
D-Pen	1.90(5) (COOH)	7.96(3) (NH_3)[a]	10.66(4) (SH)[a]			
MSA	3.11(3) (COOH)	4.58(3) (COOH)	10.36(3) (SH)			
Cys–Gly	3.17(4) (COOH)	6.89(3) (NH_3)[a]	9.23(3) (SH)			
Ala–Cys	2.88(4) (COOH)	7.96(3) (NH_3)[a]	9.53(3) (SH)[a]			
Ala–Ala–Cys	3.23(3) (COOH)	7.97(3) (NH_3)[a]	9.72(3) (SH)[a]			
Oxidized glutathione	1.80(7) (COOH)	2.37(5) (COOH)	3.16(4) (COOH)	3.81(4) (COOH)	8.83(3) (NH_3^+)	9.53(3) (NH_3^+)
Cys–Gly–disulphide	2.68(4) (COOH)	3.40(3) (COOH)	6.31(2) (NH_3)	7.26(2) (NH_3)		
Gly–NH_2	7.99(2) (NH_3)					
Mett–NHMe	7.29(2) (NH_3)					
Met–NHMe	7.35(2) (NH_3)					
Alat–Ala–OMe	7.84(2) (NH_3)					

[a] Macroconstants do not correspond precisely to proton dissociation of the NH_3 or SH group, respectively (see ref. 22). Standard deviations are in parentheses.

have only two potential binding sites for cadmium ions, i.e. (S,N) in CysOMe and (S,O) in the other three molecules. The stability constants of these complexes suggest that the (S,N) donor set is distinctly more effective in the binding of cadmium ions than the (S,O) set. This conclusion is also supported by the data obtained for the di- and tripeptide ligands. Since the cadmium ion is not able to deprotonate and bind an amide nitrogen,[22] all three peptides, Cys–Gly, Ala–Cys and Ala–Ala–Cys, also act as the bidentate ligands. Due to the steric effects only one or two species (and their protonated forms) can be detected for these ligands using potentiometric titrations. Again the Cys–Gly ligand which can bind the metal ion using the (S,N) donor set forms more stable complexes than those bound via (S,O) donors (Table 2). Three of the other thiol ligands, D-Pen, Cys and MSA, form the MA species which are even more stable than those just discussed. All these ligands are potentially tridentate and the involvement of three donors makes the equimolar species very stable. The (S,N,O) binding mode which is possible for Cys and D-Pen ligands is more effective than the (S,O,O) coordination which occurs for the MSA ligand (Table 2). The distinct difference in the stability of the MA_2 complexes of the D-Pen and MSA ligands indicates the considerable intermolecular interactions between ligand molecules. The high values of $\log(K_1/K_2)$ clearly support this conclusion (Table 2). The precipitation of the Cd–Cys complexes does not allow evaluation of the stability of the MA_2 species for cysteine. Another characteristic feature of the studied thiol ligands excluding peptides is formation of the oligomeric species which dominate in solution at lower pH (Fig. 1, Table 2). Only in the case of CysOMe is the dimeric species formed, while for the other ligands the trimeric complex gives the best fit in the calculations performed.

In order to obtain more firm evidence that the models assumed for the potentiometric data calculations are realistic, the polarographic techniques were also applied. The stability constants of the respective species which were evaluated from the polarographic data are presented in Table 2 and are in very good agreement with those obtained from the potentiometric titrations. More important evidence was needed to support oligomer formation in the system studied. The DPP reduction peaks of the metal ion in the Cd–CysOMe system are shown in Fig. 2. A similar reduction pattern of the cadmium complexes was obtained for all other systems. Figure 2 indicates that at around pH 5–6 there are two distinct peaks for cadmium reduction simultaneously present. They appear at considerably different potentials than the free metal ion reduction

Table 2. Stability constants of cadmium(II) complexes; $I = 0.2$ mol dm^{-3} (KNO_3), $T = 298$ K[a]

Ligand	Species									
	MA	MA_2	MA_3	MAH	$M(AH)_2$	MA_2H	MA_2H_{-1}	M_2A_3	M_3A_4	$\log K_1/K_2$
Cys–OMe [S,N]	8.51(3) (8.41)[b]	16.41(4) (16.46)[b]	19.28(8) (19.6)[b]	—	—	—	—	29.52(5)	—	0.61
N-Ac–D–Pen [S,O]	7.53(3)	14.11(5)	17.44(8)	—	—	—	—	—	35.99(5)	0.55
N-Ac–Cys [S,O]	7.05(3)	13.49(4)	17.41(7)	—	—	—	—	—	35.53(5)	—
M–P–Gly [S,O]	6.83(3)	12.78(3)	16.70(8)	—	—	—	—	—	33.01(8)	0.88
D-Pen [S,N,O]	11.53(2) (11.92)[b] (11.59)[c]	19.64(5) (19.30)[b] (19.30)[c]	—	—	—	—	—	—	50.22(8)	3.42
Cys [S,N,O]	(12.5)[d]	—	—	—	—	—	—	—	—	—
MSA [S,O,O]	10.05(2) (9.61)[b]	13.51(10) (13.92)[b]	—	—	—	—	—	—	41.59(8)	6.59
Cys–Gly [S,N]	9.84(9)	17.36(12)	—	—	—	—	—	—	—	2.32
Ala–Cys [S,O]	—	13.71(5)	—	15.30(5)	30.28(2)	22.40(5)	2.88(10)	—	—	0.32
Ala–Ala–Cys [S,O]	—	14.06(3)	—	15.42(2)	30.08(5)	22.34(5)	3.45(10)	—	—	0.76
Oxidized glutathione $[N,O]_n$	6.18(5)	—	—	13.43(8)	—	—	—	—	—	—
Cys–Gly–disulphide [N,O]	3.14(6)	—	—	9.87(6)	—	—	—	—	—	—
Gly–NH_2 [N,O]	2.65(5)	4.88(7)	—	—	—	—	—	—	—	0.42
Mett–NHMe [N,CS]	3.99(3)	—	—	—	—	—	—	—	—	—
Met–NHMe [N,O]	2.29(8)	—	—	—	—	—	—	—	—	—
Alat–Ala–OMe [N,CS]	3.49(5)	6.79(7)	—	—	—	—	—	—	—	0.19

[a] Stability constants obtained from polarographic data are given in parentheses. The involved donors are indicated in square brackets.
[b] DPP Method, 0.2 M KNO_3.
[c] d.c. Method, 0.15 M $NaClO_4$.
[d] d.c. Method, 3 M $NaClO_4$.

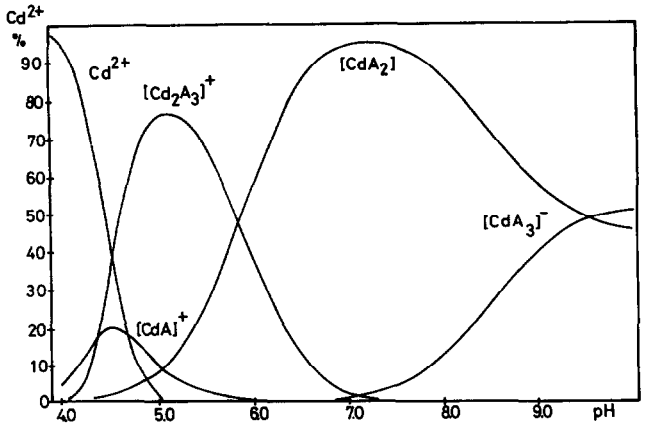

Fig. 1. Concentration distribution of the complexes formed in the Cd–CysOMe system as a function of pH; $c_{Cd} = 1 \times 10^{-3}$ mol dm^{-3}, $c_A = 5 \times 10^{-3}$ mol dm^{-3}.

peak and their relative heights depend on the pH and ligand-to-metal ratios. The interesting variation of these two peaks was observed when the solution studied was diluted with 0.2 M KNO_3 and the pH was kept constant. These changes are presented for the Cd–MSA system in Fig. 3. The 20-fold dilution of the solution leads to the almost complete disappearance of the major peak. The remaining peak indicates that all cadmium ions transfer into one species in diluted solution, which corresponds well with an equimolar complex. The stability constant calculated for this species is in

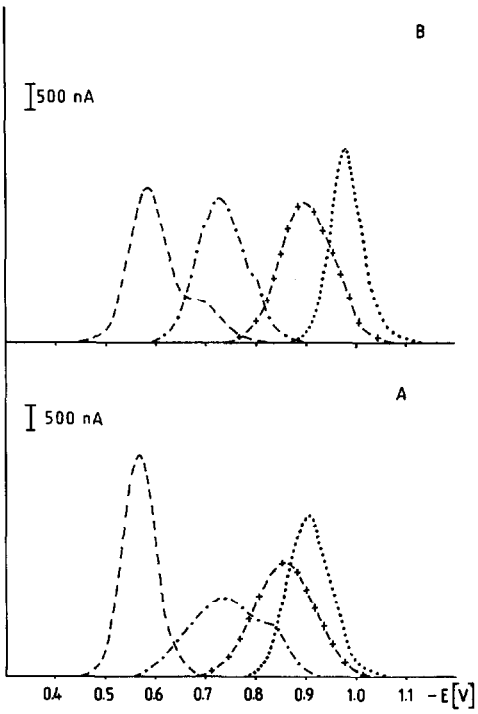

Fig. 2. pH dependence of DPP reduction peak of the cadmium ion for the Cd–CysOMe system, for 1:5 (A) and 1:25 (B) metal-to-ligand ratios; $c_{Cd} = 8 \times 10^{-4}$ M; pH = 3.3 (———); pH = 5.4 (— · — · —); pH = 7.4 (—+—); pH = 12.1 (· · · ·).

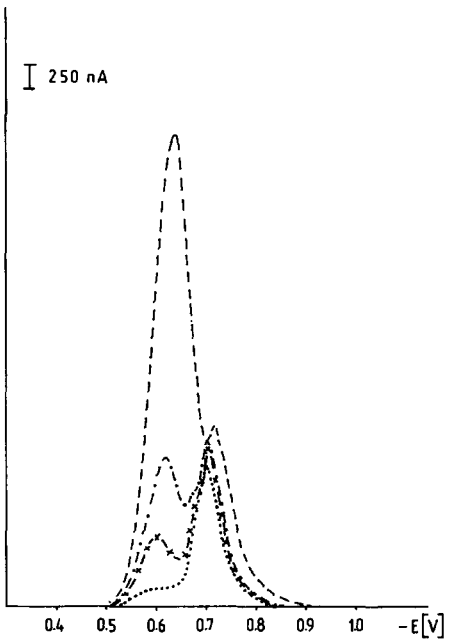

Fig. 3. Dependence of the DPP reduction peak of the cadmium ion of two complexes (M_3A_4, MA) for the Cd–MSA system on dilution with 0.2 M KNO_3. To 10 cm^3 of solution [Cd] = 8×10^{-4} M, [A] = 4×10^{-3} M in 0.2 M KNO_3 (pH = 5.3). 0.2 M KNO_3 was added as follows: 0 cm^3 (———); 35 cm^3 (— · — · —); 70 cm^3 (—+—); 160 cm^3 (· · · ·).

good agreement with the value obtained from potentiometric data (Table 2). According to the potentiometric data calculations the two peaks discussed above could correspond to the MA and oligomeric species. Thus, the dilution presented in Fig. 3 destabilizes the oligomeric complex, as was also found for the strong complexes of silver(I) with thioether amino acids.[26]

The stability of the cadmium complexes with ligands containing a sulphur donor involved in disulphide bridges are much lower than those obtained for the thiol ligands. Comparison of the stability of MA species of Cys–Gly (S,N) coordination and Cys–Gly–disulphide indicates that involvement of the (S,N) donor set in the cadmium ion binding is unlikely in the latter ligand. The (S,N) coordination mode leads to formation of species which are more than six orders more stable than that created by chelation via the (N,O) donor set available in Cys–Gly–disulphide[27] (Table 2).

The thioamide sulphur was shown to be very effective in the binding of copper(II) and nickel(II) ions by several amino acid or peptide derivatives.[28,29] The (NH_2,CS) coordination leads to formation of species which are two or even four orders more stable than the corresponding species with (NH_2,CO) chelation. A comparison of the stability of the MA complexes of, for example, methionine-N-methylamide (Met–NHMe) and of its thioamide analogue clearly indicates that also in the case of cadmium ions, binding of thioamide sulphur stabilizes the complex formed (1.7 log units, Table 2). The distinct stabilization is also observed for complexes of Alat–AlaOMe, containing thioamide as a peptide bond, when compared, for example, with the glycineamide or MetNHMe.

CONCLUSIONS

The sulphur donor is a basic binding site for cadmium ions even in simple ligands containing the thiol group. The presence of such a group leads to formation of very stable complexes, having stability constants several orders higher than respective complexes without a sulphur donor. The thiol donors of the cysteine (or D-Pen) residue are the most effective, although the thioamide sulphur may also stabilize the complexes formed. The (S,N) donor set is a more effective donor set than the (S,O) chelation. The disulphide group seems to be quite ineffective as a potential binding site for cadmium ions, at least in the presence of amino acid moieties. The other characteristic feature of sulphur donation in cadmium complexes is the formation of oligomeric structures as was already found in the case of, for example, nickel(II) complexes.[18–20,22]

Acknowledgements—This work was supported by the Polish Ministry of National Education (Project RP.II.13.1.5) and the Hungarian Academy of Sciences (Project OTKA 240/86).

REFERENCES

1. B. L. Vallee, in *Metallothionein* (Edited by J. H. R. Kägi and M. Nordberg), p. 19. Birkhäuser, Basel (1979).
2. A. Hata, H. Tsunoo, H. Nakajima and M. Kimura, *Toxicol. Lett.* 1978, **2**, 45.
3. H. Tsunoo, K. Kino, H. Nakajima, A. Hata, I-Y. Huang and A. Yoshida, *J. Biol. Chem.* 1978, **253**, 4172.
4. M. M. Kissling and J. H. R. Kägi, in *Metallothionein* (Edited by J. H. R. Kägi and M. Nordberg), p. 145. Birkhäuser, Basel (1979).
5. A. Murasugi, C. Wada and Y. Hayashi, *J. Biochem.* 1981, **90**, 1561.
6. A. Murasugi, C. Wada and Y. Hayashi, *Biochem. Biophys. Res. Commun.* 1981, **103**, 1021.
7. N. Kondo, M. Isobe, K. Imai and T. Goto, *Tetrahedron Lett.* 1983, **24**, 925.
8. A. Murasugi, C. Wada and Y. Hayashi, *J. Biochem.* 1983, **93**, 661.
9. A. Murasugi, C. W. Nakagawa and Y. Hayashi, *J. Biochem.* 1984, **96**, 137.
10. Y. Hayashi, C. W. Nakagawa and A. Murasugi, *Environ. Health Perspect.* 1986, **65**, 13.
11. E. Grill, E.-L. Winnacker and M. H. Zenk, *Science* 1985, **230**, 674.
12. E. Grill, E.-L. Winnacker and M. H. Zenk, *Proc. Natl. Acad. Sci. USA* 1987, **84**, 439.
13. K. C. Taylor, L. G. Albrigo and C. D. Chase, *J. Am. Soc. Hort. Sci.* 1988, **113**, 407.
14. E. Grill, E.-L. Winnacker and M. H. Zenk, *FEBS Lett.* 1986, **197**, 115.
15. N. Kondo, M. Isobe, K. Imai and T. Goto, *Agric. Biol. Chem.* 1985, **49**, 71.
16. Y. Hayashi, C. W. Nakagawa, D. Uyakul, K. Imai, M. Isobe and T. Goto, *Biochem. Cell Biol.* 1988, **66**, 288.
17. A. B. Tomsett and D. A. Thurman, *Plant Cell Environ.* 1988, **11**, 383.
18. I. Sóvágó, K. Varnagy and A. Bényei, *Magyar Kémiai Folyóirat* 1986, **92**, 114.
19. A. Ardeef and D. L. Kearney, *J. Am. Chem. Soc.* 1984, **104**, 7212.
20. W. Tremel, M. Kriege, B. Krebs and G. Henkel, *Inorg. Chem.* 1988, **27**, 3886.
21. A. H. Corrie, M. D. Walker and D. R. Williams, *J. Chem. Soc., Dalton Trans.* 1976, 1012.
22. K. Cherifi, B. Decock-Le-Reverend, K. Varnagy, T. Kiss, I. Sóvágó, C. Loucheux and H. Kozłowski, *J. Inorg. Biochem.*, in press.
23. J. J. Lingane, *Chem. Rev.* 1941, **29**, 1.
24. A. Gergely and I. Nagypál, *J. Chem. Soc., Dalton Trans.* 1977, 1104.
25. L. Zékány and I. Nagypál, in *Computational Methods*

for the Determination of Stability Constants (Edited by D. Leggett). Plenum Press, New York (1985).
26. L. D. Pettitt, K. F. Siddiqui, H. Kozłowski and T. Kowalik, *Inorg. Chim. Acta* 1981, **55**, 87.
27. K. Varnagy, I. Sóvágó and H. Kozłowski, *Inorg. Chim. Acta* 1988, **151**, 117.
28. T. Kowalik, H. Kozłowski, I. Sóvágó, K. Varnagy, G. Kupryszewski and K. Rolka, *J. Chem. Soc., Dalton Trans.* 1987, 1.
29. K. Varnagy, H. Kozłowski, I. Sóvágó, T. Kowalik-Jankowska, M. Kruszyński and J. Zboińska, *J. Inorg. Biochem.* 1988, **34**, 83.

Polyhedron Vol. 9, No. 6, pp. 839–845, 1990
Printed in Great Britain

0277–5387/90 $3.00+.00
© 1990 Pergamon Press plc

SYNTHESIS AND STRUCTURE OF SOME ASYMMETRIC ARYLOXIDE DERIVATIVES OF ZIRCONIUM(IV): X-RAY CRYSTAL STRUCTURES OF $Cp_2Zr(OAr\text{-}2,4Me_2,6cyMe)(CH_2Ph)$ AND $Cp_2Zr(OAr\text{-}2Me,6Bu^t)(\eta^2\text{-}Bu^tNCCH_2Ph)$, WHERE OAr-2,4Me$_2$,6cyMe = 2,4-DIMETHYL,6-(α-METHYLCYCLOHEXYL)PHENOXIDE AND OAr-2Me,6Bu^t = 2-METHYL,6-TERT-BUTYLPHENOXIDE

BRYAN D. STEFFEY, NHAN TRUONG, DIEGO E. CHEBI, JUDITH L. KERSCHNER, PHILLIP E. FANWICK and IAN P. ROTHWELL*

Department of Chemistry, Purdue University, West Lafayette, IN 47907, U.S.A.

(*Received* 7 *September* 1989; *accepted* 20 *October* 1989)

Abstract—Reaction of all asymmetric phenols 2-methyl,6-tert-butylphenol (HOAr-2Me,6Bu^t) and 2,4-dimethyl,6-(α-methylcyclohexyl)phenol (HOAr-2,4Me$_2$,6cyMe) with $Cp_2Zr(CH_2Ph)_2$ at 120°C in toluene leads to the slow formation of the mono-substituted derivatives $Cp_2Zr(OAr\text{-}2Me,6Bu^t)(CH_2Ph)$ (**1**) and $Cp_2Zr(OAr\text{-}2,4Me_2,6cyMe)(CH_2Ph)$ (**2**) along with one equivalent of toluene. A single crystal X-ray diffraction analysis of **2** confirmed the stoichiometry and shows the carbon and oxygen atoms of the benzyl and aryloxide ligands occupying positions about the zirconium atom typical of $Cp_2Zr(X)(Y)$ type compounds. The large Zr—O—Ar angle of 165.3(5)° results in the aryloxide occupying a "wedge-like" space within the coordination sphere. This wedge is oriented within the plane which bisects the metallocene unit, i.e. almost coplanar with the ZrCO plane, and is oriented so that the bulky α-methylcyclohexyl group lies next to the benzyl ligand. The reaction of **1** with Bu^{t}NC also takes place very slowly leading to the η^2-iminoacyl compound $Cp_2Zr(OAr\text{-}2Me,6Bu^t)(\eta^2\text{-}Bu^tNCCH_2Ph)$ (**3**). Despite the steric demands of the bulky aryloxide ligand, the spectroscopic and structural data on **3** show the iminoacyl to be η^2-bonded to zirconium, Zr—N = 2.244(4) Å, Zr—C = 2.208(5) Å. In the solid state the 18-electron compound **3** has the η^2-iminoacyl group lying along the plane bisecting the metallocene unit. Crystal data at 20°C for $ZrOC_{34}H_{42}$ (**2**): $a = 10.201(1)$, $b = 14.372(3)$, $c = 20.365(3)$ Å, $\beta = 95.210(9)°$, $Z = 4$, $d_{calc} = 1.287$ g cm^{-3} in space group $P2_1/n$; for $ZrONC_{33}H_{41}$ (**3**): $a = 9.708(1)$, $b = 10.698(1)$, $c = 27.829(3)$ Å, $Z = 4$, $d_{calc} = 1.284$ g cm^{-3} in space group $P2_12_12_1$.

The demonstrated ability of high valent early *d*-block, lanthanide and actinide metal compounds to inter- and intramolecularly activate carbon–hydrogen bonds has led to numerous synthetic, mechanistic and theoretical studies.[1–6] During our studies of early transition metal aryloxide chemistry we have demonstrated the sometimes facile cyclometallation of 2,6-di-tert-butylphenoxide (OAr-2,6Bu$^t_2$) and 2,6-diphenylphenoxide (OAr-2,6Ph$_2$) ligands at d^0-metal centres, especially in the presence of alkyl leaving groups.[7] Due to the thermal robustness and excellent NMR characteristics of the metallocene unit, Cp_2M, we have argued that cyclometallation of aryloxide ligands in a system such as $Cp_2M(OAr)(R)$ (M = Ti, Zr, Hf) would allow valuable mechanistic studies to be obtained. The cyclometallation of bis(trimethylsilyl)amido ligands in related metallocene systems has been reported by Bradley and Andersen and co-workers.[8,9] In this paper we wish to report on the synthesis and remarkable thermal stability of just such a series of alkyl, aryloxide compounds of zirconium. As aryloxide ligands we have chosen 2-methyl,6-tert-butylphenoxide (OAr-2Me,6Bu^t) and 2,4-dimethyl,6-(α-methylcyclohexyl)phenoxide

* Author to whom correspondence should be addressed.

$Cp_2Zr(CH_2Ph)_2$ $\xrightarrow{+HOAr}$ $Cp_2Zr(OAr)(CH_2Ph) + PhCH_3$

(1) OAr = 2-Methyl, 6-tert-butylphenoxide

(2) OAr = 2,4-Dimethyl,6(α-methylcyclohexyl) phenoxide

(1) + t-BuNC $\longrightarrow$ $Cp_2Zr(OAr)(\eta^2\text{-}Bu^tNCCH_2Ph)$

(3)

Scheme 1.

(OAr-2,4Me_2,6cyMe) for study. While both of these ligands offer the potential for formation of either five- or six-membered metallacycle rings, the α-methylcyclohexyl substituent of OAr-2,4Me_2,6cy Me also offers both primary and secondary sp^3-CH bonds for activation.

RESULTS AND DISCUSSION

The bis(benzyl) compound $Cp_2Zr(CH_2Ph)_2$[10] fails to react with HOAr-2Me,6Bu^t or HOAr-2,4Me_2,6cyMe in hydrocarbon solvents at ambient temperatures. However, at 120°C in toluene solution, substitution occurs via a protonolysis reaction to yield the mono-alkyl compounds **1** and **2** in excellent yields (Scheme 1). The NMR spectroscopic properties of orange **1** and **2** are very similar, the most striking feature besides the Cp and aryloxide resonances being the characteristic chemical shift of the carbon atom of the remaining Zr—CH_2Ph bond in the ^{13}C NMR spectrum at δ 53.1 and 51.0 ppm, respectively.

A single crystal X-ray diffraction analysis of **2** was undertaken not only to characterize the coordination environment but also to determine the conformation adopted by the aryloxide ligand and in particular the α-methylcyclohexyl substituent. It can be seen (Fig. 1) that the central $Cp_2Zr(O)(C)$ coordination environment appears unexceptional. The Zr—O distance of 1.981(6) Å (Table 1) is comparable to that reported by Lappert and coworkers[11] for $Cp_2Zr(OAr\text{-}2,6Bu^t_2)Cl$, 1.98(2) Å, but is slightly longer than the values of 1.903(4) and 1.936(4) Å reported for the aryloxide ligands in Zr $(OAr\text{-}2,6Bu^t_2)(OAr\text{-}2,6Bu^t_2\text{-}4OMe)(CH_2Ph)_2$.[12] The Zr—C(benzyl) distance of 2.321(9) Å also ap-

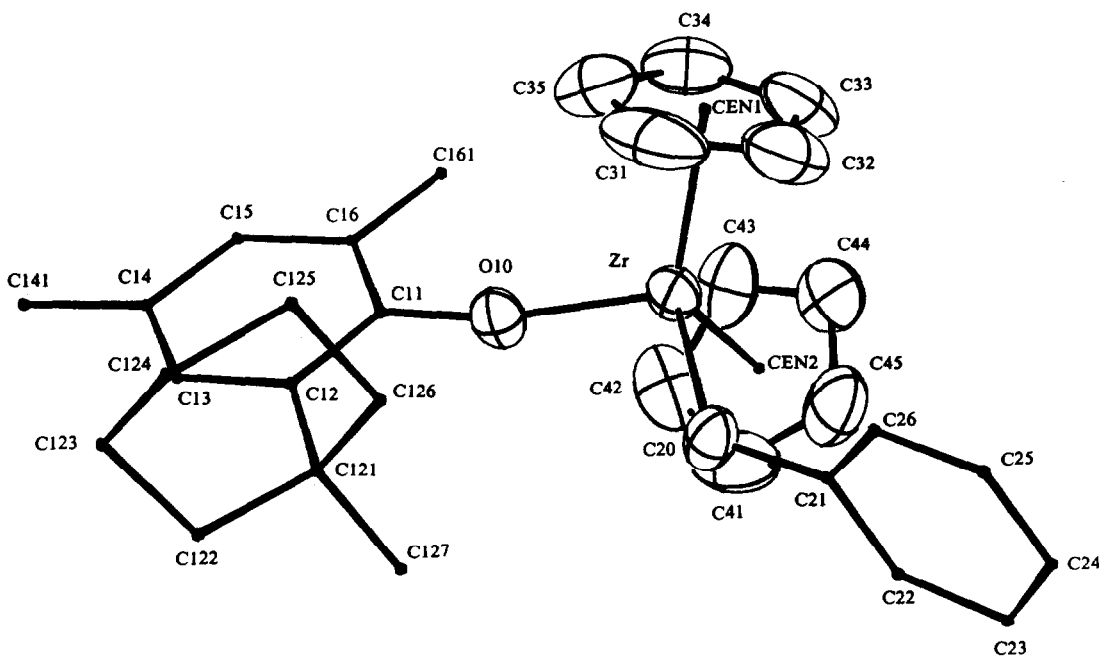

Fig. 1. ORTEP view of $Cp_2Zr(OAr\text{-}2,4Me_2,6cyMe)(CH_2Ph)$ (**2**).

Table 1. Selected bond distances (Å) and angles (°) for $Cp_2Zr(OAr\text{-}2,4Me_2,6cyMe)(CH_2Ph)$ (**2**)

Zr—O(10)	1.981(6)	Zr—C(20)	2.321(9)
Zr—C(31)	2.56(1)	Zr—C(32)	2.55(1)
Zr—C(33)	2.51(1)	Zr—C(34)	2.53(1)
Zr—C(35)	2.53(1)	Zr—C(41)	2.50(1)
Zr—C(42)	2.51(1)	Zr—C(43)	2.49(1)
Zr—C(44)	2.52(1)	Zr—C(45)	2.52(1)
O(10)—Zr—C(20)	95.9(3)	Zr—O(10)—C(11)	165.3(5)

pears typical for $Cp_2M(R)(X)$ compounds and can be compared with a value of 2.330(5) Å in $Cp'_2Zr(CH_2C_6Me_5)(Cl)$ ($Cp' = C_5H_4SiMe_3$).[11] However, these distances are slightly shorter than those in $Zr(OAr\text{-}2,6Bu^t_2)(CH_2Ph)_3$, 2.26–2.29(1) Å, and $Zr(OAr\text{-}2,6Bu^t_2)(OAr\text{-}2,6Bu^t\text{-}4OMe)(CH_2Ph)_2$, 2.243(9) and 2.272(8) Å. The large Zr—O—Ar angle of 165.3(5)° is typical of high-valent early *d*-block metal derivatives of these ligands and results in the aryloxide group occupying what can be thought of as a wedge within the coordination sphere.[13] It can be seen (Fig. 1) that this wedge, defined essentially by the plane of the central phenoxy ring, is lying so as to bisect the metallocene unit, i.e. approximately coplanar with the ZrOC plane. A very similar arrangement of the aryloxide ligands in $Cp_2Zr(OAr\text{-}2,6Bu^t_2)Cl$ and $Cp_2Zr(OAr\text{-}2,6Bu^t_2)(NMe_2)$ is observed.[11] However, the asymmetric *ortho*-substitution within the OAr-2Me,6cy Me ligand means that two different conformers can be imagined, either with the smaller methyl or the bulky α-methylcyclohexyl group adjacent to the Zr—CH_2Ph bond. From Figs 1 and 2 it can be seen that compound **2** prefers to orientate itself with the α-methylcyclohexyl group next to the benzyl ligand. Presumably this conformation is sterically favoured over a situation where the bulky group is pushed between the cyclopentadienyl ligands.

The alkyl compound **1** will react with Bu^tNC to produce an η^2-iminoacyl derivative (**3**), although the reaction is very slow, requiring heating in toluene for several hours (Scheme 1). In the ^{13}C NMR spectrum of **3** the η^2-binding of the iminoacyl group is strongly implicated by the chemical shift of the $Zr(Bu^tNCCH_2Ph)$ carbon atom at δ 236.4 ppm, which lies very close to the region reported for other zirconocene η^2-iminoacyl compounds.[14] A single crystal X-ray diffraction analysis of **3** confirmed the η^2-binding of the iminoacyl group (Fig. 3; Table 2) despite the presence of the sterically demanding aryloxide ancillary ligand. As for other structurally characterized η^2-acyl and η^2-iminoacyl compounds of stoichiometry $Cp_2M(\eta^2\text{-}RCX)(Y)$ (M = Ti, Zr, Hf; X = O, NR')[14] the iminoacyl unit in **3** lies along the equatorial girdle of the metallocene unit. In this case the nitrogen atom lies proximal to the aryloxide oxygen atom. An identical conform-

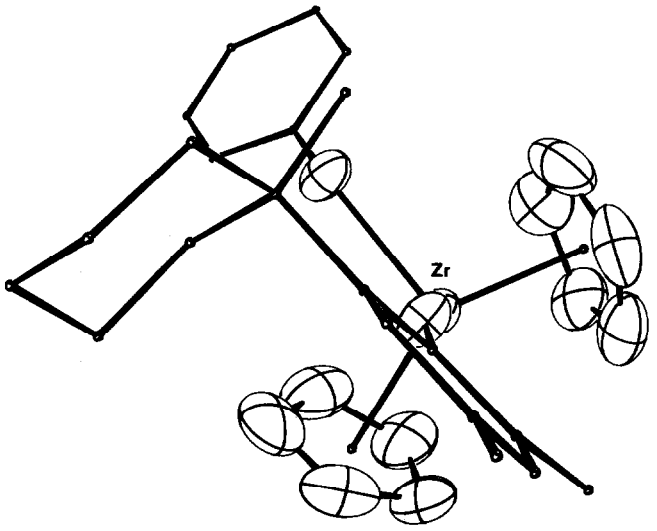

Fig. 2. ORTEP view of **2** highlighting the conformation of the α-methylcyclohexyl substituent.

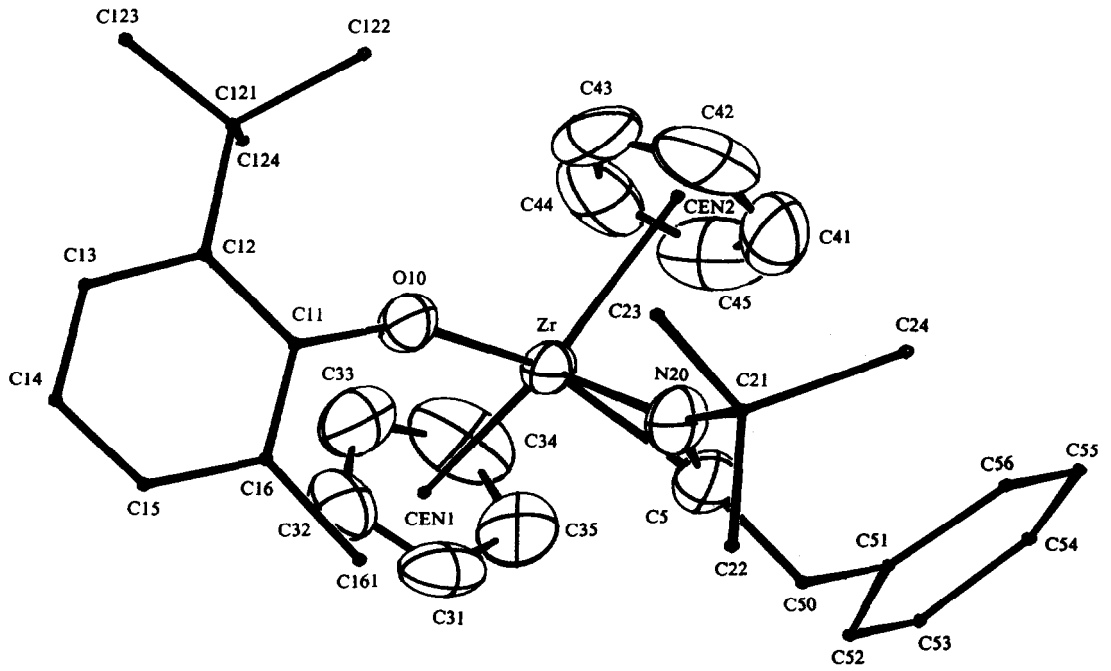

Fig. 3. ORTEP view of $Cp_2Zr(OAr\text{-}2Me,6Bu^t)(\eta^2\text{-}Bu^tNCCH_2Ph)$ (**3**).

Table 2. Selected bond distances (Å) and angles (°) for $Cp_2Zr(OAr\text{-}2Me,6Bu^t)(\eta^2\text{-}Bu^tNCCH_2Ph)$ (**3**)

Zr—O(10)	2.079(3)	Zr—N(20)	2.244(4)
Zr—C(5)	2.208(5)	C(5)—N(20)	1.263(7)
Zr—C(31)	2.520(6)	Zr—C(32)	2.576(6)
Zr—C(33)	2.576(6)	Zr—C(34)	2.599(7)
Zr—C(35)	2.554(6)	Zr—C(41)	2.551(7)
Zr—Cl(42)	2.577(6)	Zr—C(43)	2.551(6)
Zr—C(44)	2.547(5)	Zr—C(45)	2.547(6)
O(10)—Zr—N(20)	86.4(1)	O(10)—Zr—C(5)	115.8(2)
N(20)—Zr—C(5)	32.9(2)	Zr—O(10)—C(11)	154.8(3)

ation is found in the compounds $Cp_2Zr(\eta^2\text{-}MeNCCHPh_2)(Me)$[11] and $Cp_2Hf[\eta^2\text{-}xyNCCH(Ph)(py)](Cl)$ (xy = 2,6-dimethylphenyl).[15] However, the sterically demanding aryloxide ligand does appear to have an impact on the bonding of the iminoacyl group to the metal centre. One measure of the degree of η^2-binding of iminoacyl groups is to consider a parameter Δ, defined as d(M—N)−d(M—C).[14] In compound **3** the Zr—N distance of 2.244(4) Å is longer than the Zr—C distance of 2.208(5) Å yielding a value for Δ of +0.036 Å. In contrast, a value of −0.037 Å is found for $Cp_2Zr(\eta^2\text{-}MeNCCHPh_2)(Me)$, i.e. where the Zr—N distance of 2.210(4) Å is *shorter* than the Zr—C distance of 2.247(5) Å.[11] Similarly, in the compound $Cp_2Hf[\eta^2\text{-}xyNCCH(Ph)(py)](Cl)$ the Hf—N distance is shorter than the Hf—C distance to yield a Δ value of −0.016 Å.[15] A survey of other zirconium and hafnium η^2-iminoacyl compounds, including those containing aryloxide ancillary ligands show that in all cases the M—N distance is shorter than the M—C distance to yield negative values of Δ.[14] We ascribe the elongation of the Zr—N bond in **3** to the extremely crowded coordination sphere. However, it is also possible that a weakening of the Zr—N bond is a consequence of the π-donor properties of the aryloxide ligand in this formally 18-electron compound. The steric congestion in this compound is also indicated by the twisting of the plane of the aryloxide ligand out of the equatorial girdle of the metallocene unit (Fig. 3).

A final point of interest concerning these compounds arises from the conformation adopted by the α-methylcyclohexyl group in **2** (Figs 1 and 2). In the majority of compounds containing 2,6-di-

tert-butylphenoxide ligation the CMe_3 groups are oriented so as to maximize the distance between the metal and the methyl groups. Hence conformation **A** shown in the diagram is typically adopted. However, in a few cases one of the tert-butyl groups is found to be oriented so that a unique methyl group points directly towards the metal centre (conformation **B**).[16] It can be seen that for compound **2** a conformation similar to **A** is adopted so that ZrHC

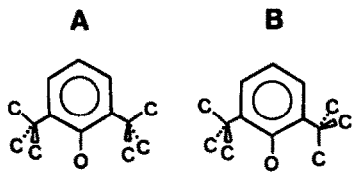

contacts are minimized. The cyclohexyl group does not have the effect of forcing the methyl group towards the metal. However, due to the presence of the cyclohexyl group it can be seen that a static solution structure identical to that found in the solid state would result in non-equivalent Cp ligands and a diastereotopic Zr—CH_2Ph group. The ^{1}H NMR spectrum of **2** at ambient temperatures shows sharp singlets for both the C_5H_5 and CH_2Ph protons. On cooling toluene-d_8 solutions of **2** to −65°C only negligible broadening of these signals is observed in the ^{1}H NMR spectrum. Hence it appears that there must exist a very low barrier to rotation of the α-methylcyclohexyl group in **2** such that an effective plane of symmetry is generated through the molecule in solution.

EXPERIMENTAL

The HOAr-2,4Me_2,6cyMe ligand was prepared by treating 2,4-dimethylphenol with an excess of 1-methylcyclohexene in the presence of a catalytic amount of H_2SO_4.[17] Purification was achieved after work-up by fractional distillation. The compound $Cp_2Zr(CH_2Ph)_2$ was prepared by published procedures,[10] while 2-methyl,6-tert-butylphenol and Bu^{t}NC were obtained commercially. The methods employed for the manipulation of the air- and moisture-sensitive products have been described previously.[12,13]

Cp_2Zr(OAr-2Me,6Bu^t)(CH_2Ph) (**1**)

To a solution of $Cp_2Zr(CH_2Ph)_2$ (0.68 g, 1.7 mmol) in toluene (25 cm^3) was added HOAr-2Me,6Bu^t (0.33 g, 2.0 mmol). The mixture was heated at 100°C in a sealed flask for 4 h. Removal of the solvent under vacuum yielded a sticky solid which was taken up in a minimum amount of hot toluene. Slow cooling of the solution yielded the product as yellow crystals in 55% yield. Found: C, 70.1; H, 7.1. Calc. for $ZrC_{28}H_{32}O$: C, 70.7; H, 6.8%. ^{1}H NMR (C_6D_6, 30°C): δ 2.58 (s, Zr—CH_2); 1.28 (s, *Bu^t*); 1.99 (s, CH_3); 5.77 (s, C_5H_5); 6.8–7.8 (m, aromatics). ^{13}C NMR (C_6D_6, 30°C): δ 53.0 (Zr—CH_2); 112.5 (C_5H_5); 29.9 (2-CH_3); 34.1 (CMe_3); 18.9 (CMe_3).

Cp_2Zr(OAr-2,4Me_2,6cyMe)(CH_2Ph) (**2**)

A mixture of $Cp_2Zr(CH_2Ph)_2$ (1.9 g, mmol) and HOAr-2,4Me_2,6cyMe (1.0 g, mmol) in toluene (15 cm^3) was heated at 120°C in a sealed flask for 4 h. The resulting clear solution was cooled, diluted with hexane (15 cm^3) and placed in a freezer at −15°C, whereupon large yellow crystals of product were obtained. Found: C, 73.8; H, 7.4. Calc. for $ZrC_{35.5}H_{42}O$: C, 74.0; H, 7.3%. The compound crystallizes with 1/2 toluene per zirconium. ^{1}H NMR (C_6D_6, 30°C): δ 2.58 (s, Zr—CH_2); 5.69 (s, C_5H_5); 1.32 (s, α-CH_3); 1.98 (s), 2.24 (s, 2,4Me_2); 1.3–2.0 (series of multiplets, cyclohexyl protons). ^{13}C NMR (C_6D_6, 30°C): δ 50.9 (Zr—CH_2); 110.9 (C_5H_5); 17.5, 19.0, 21.2, 25.0, 35.8, 36.0 (2,4Me_2 and α-methylcyclohexyl).

Cp_2Zr(OAr-2Me,6Bu^t)(η^2-Bu^{t}NCCH_2Ph) (**3**)

To a solution of **1** (0.81 g, 1.7 mmol) in toluene (25 cm^3) was added Bu^{t}NC (1 g, excess). The mixture was heated at 100°C in a sealed flask for 6 h. Removal of solvent and excess Bu^{t}NC *in vacuo* yielded **3** as a crude solid. Crystals suitable for X-ray diffraction studies were obtained by slow cooling of a saturated, hot (100°C) toluene solution. Found: C, 71.4; H, 7.5; N, 2.4. Calc. for $ZrC_{33}H_{41}NO$: C, 70.9; H, 7.4; N, 2.5%. ^{1}H NMR (C_6D_6, 30°C): δ 3.63 (s, CH_2Ph); 1.09 (s, CN*Bu^t*); 2.03 (s, 2*Me*); 1.62 (s, 6*Bu^t*). ^{13}C NMR (C_6D_6, 30°C): δ 236.4 (Bu^{t}N*C*CH_2Ph).

X-ray crystallography

Crystal data and data collection parameters are collected in Table 3. A suitable crystal of each of the two compounds was mounted in a glass capillary in a random orientation. Cell constants were obtained from least-squares refinement using the scattering angles of 25 reflections as measured by the computer-controlled diagonal slit method of centring. Systematic absences and subsequent least-squares refinement indicated the space group $P2_1/n$ for **2** and $P2_12_12_1$ for **3**. The data were collected to a maximum 2θ of 45° in both cases using the ω–2θ

Table 3. Crystal data and data collection parameters

	2	3
Formula	$ZrOC_{35.5}H_{42}$	$ZrONC_{33}H_{41}$
f_w	575.95	558.92
Space group	$P2_1/n$	$P2_12_12_1$
a (Å)	10.201(1)	9.708(1)
b (Å)	14.372(3)	10.698(1)
c (Å)	20.365(3)	27.829(3)
β (°)	95.210(9)	90
V (Å^3)	2973(1)	2890.1(9)
Z	4	4
d_{calc} (g cm^{-3})	1.287	1.284
Crystal dimensions (mm)	0.39 × 0.30 × 0.28	0.63 × 0.54 × 0.41
Temperature (°C)	20	19
Radiation (wavelength)	Mo-K_α (0.71073 Å)	Mo-K_α (0.71073 Å)
Monochromator	Graphite	Graphite
Linear absorbance coefficient (cm^{-1})	3.90	3.97
Absorption correction applied	Empirical[a]	None
Diffractometer	Enraf–Nonius CAD4	Enraf–Nonius CAD4
Scan method	ω–2θ	ω–2θ
h, k, l limits:	−10 to 10 0 to 15 0 to 21	0 to 10 0 to 11 0 to 29
2θ range (°)	4.00–45.00	4.00–45.00
Scan width (°)	0.49 + 0.35 tan (θ)	0.80 + 0.35 tan (θ)
Take-off angle (°)	2.80	1.80
Programs used	Enraf–Nonius SDP	Enraf–Nonius SDP
F(000)	1200.0	1176.0
ρ-Factor used in weighting	0.040	0.040
Data collected	4044	2202
Unique data	4044	2202
Data with $I > 3.0\sigma(I)$	2179	1926
Number of variables	319	325
Largest shift/ESD in final cycle	0.05	0.01
R	0.065	0.030
R_w	0.088	0.040
Goodness of fit	1.906	1.430

[a] N. Walker and D. Stuart, *Acta Cryst.* 1983, **A39**, 158.

scan technique. Moving crystal, moving counter background counts were made by scanning an additional 25% above and below the scan width. The counter aperture was adjusted as a function of θ. For intense reflections an attenuator (factor 12.9) was automatically inserted in front of the detector. As a check on crystal and electronic stability three standard reflections were measured every 2000 s of beam time. In the case of **2** some decay was observed and an empirical correction was applied. No decay was observed for **3**.

The structures were solved by using the Patterson heavy-atom method to reveal the position of the zirconium atoms. The remaining heavy atoms were then located in succeeding Fourier syntheses. Hydrogen atoms were located and added to the structures but were not refined. In the case of **3** choice of the alternate enantiomorph yielded $R = 0.03097$, $R_w = 0.04116$ and goodness of fit = 1.460.*

Acknowledgement—We thank the National Science Foundation (Grant CHE-8612063) for support of this research.

* *Supplementary material available*: Listings of fractional coordinates, anisotopic thermal parameters, full bond distances and angles and a listing of observed and calculated structure factor amplitudes for **2** and **3**.

REFERENCES

1. I. P. Rothwell, in *Activation and Functionalization of Alkanes* (Edited by C. L. Hill). John Wiley, New York (1989).

2. (a) Pl. L. Watson and G. W. Parshall, *Accts Chem. Res.* 1985, **18**, 51 and refs therein; (b) H. Rabaa, J.-Y. Saillord and R. Hoffman, *J. Am. Chem. Soc.* 1986, **108**, 4327 and refs therein.
3. M. E. Thompson, S. M. Baxter, A. R. Bulls, B. J. Burger, M. C. Nolan, B. D. Santarsiero, W. R. Schaefer and J. E. Bercaw, *J. Am. Chem. Soc.* 1987, **109**, 203.
4. J. W. Bruno, G. M. Smith, T. J. Marks, C. K. Fair, A. J. Schultz and J. M. Williams, *J. Am. Chem. Soc.* 1986, **108**, 40.
5. W. J. Evans, L. R. Chamberlain, T. A. Ulibarri and J. W. Ziller, *J. Am. Chem. Soc.* 1988, **110**, 6423.
6. (a) P. J. Walsh, F. J. Hollander and R. G. Bergman, *J. Am. Chem. Soc.* 1988, **110**, 8729; (b) C. C. Cummins, S. M. Baxter and P. T. Wolczanski, *J. Am. Chem. Soc.* 1988, **110**, 8731; (c) S. L. Buchwald and R. B. Neilson, *J. Am. Chem. Soc.* 1988, **110**, 3171.
7. I. P. Rothwell, *Accts Chem. Res.* 1988, **21**, 153.
8. C. R. Bennett and D. C. Bradley, *J. Chem. Soc., Chem. Commun.* 1974, 29.
9. S. J. Simpson and R. A. Andersen, *Inorg. Chem.* 1981, **20**, 3627.
10. F. G. Fanchinett, G. Fochi and C. Floriani, *J. Chem. Soc., Dalton Trans.* 1977, 1946.
11. A. Antinolo, G. S. Bristow, G. K. Campbell, A. W. Duff, P. B. Hitchcock, R. A. Kamandin, M. F. Lappert, R. J. Norton, N. Sarudeen, D. J. W. Winterborn, J. L. Atwood, W. E. Hunter and H. Zhang, *Polyhedron* 1989, **8**, 1601.
12. S. L. Latesky, A. K. McMullen, I. P. Rothwell and J. C. Huffman, *Organometallics* 1985, **4**, 902.
13. S. L. Latesky, A. K. McMullen, J. Keddington, I. P. Rothwell and J. C. Huffman, *Inorg. Chem.* 1985, **24**, 995.
14. L. D. Durfee and I. P. Rothwell, *Chem. Rev.* 1988, **88**, 1059.
15. D. E. Chebi and I. P. Rothwell, *Polyhedron*, in press.
16. P. E. Fanwick, A. E. Ogilvy and I. P. Rothwell, *Organometallics* 1987, **6**, 73.
17. N. I. Shvikin and E. A. Viktonova, *Russ. Chem. Rev.* 1960, **29**, 560.

Polyhedron Vol. 9, No. 6, pp. 847–849, 1990
Printed in Great Britain

0277–5387/90 $3.00+.00
© 1990 Pergamon Press plc

CHARGE-TRANSFER COMPLEXES OF 5,6-DIMETHYL-1,3-DIHYDRO-2-TELLURAINDENE WITH QUINONES

ALI Z. AL-RUBAIE* and EMAN A. AL-MASOUDI

Department of Chemistry, College of Science, University of Basrah, Basrah, Iraq

(*Received* 26 *April* 1989; *accepted* 20 *October* 1989)

Abstract—The new 5,6-dimethyl-1,3-dihydro-2-telluraindene was used as a donor to form 1:1 donor–acceptor complexes with *p*-benzoquinone, 1,4-naphthaquinone and 2,3-dimethylanthraquinone, respectively. Solid conductivity, UV–vis, IR, ^{1}H NMR, ESR and mass spectral data are discussed, and it is concluded that the degree of charge-transfer is small. The $[C_{10}H_{12}Te]^+[C_{10}H_6O_2]^-$ complex shows evidence of semiconducting properties.

Recently there has been considerable interest in the studies on the charge-transfer complexes of organotellurium compounds with 7,7,8,8-tetracyano-*p*-quinodimethane (TCNQ)[1–4] and chloranil.[3,5]

However, there is no reference in the literature, as far as we aware, concerning the preparation and characterization of charge-transfer complexes with *p*-benzoquinone, 1,4-naphthaquinone or 2,3-dimethylanthraquinone.

The aim of the present work is to synthesize new charge-transfer complexes with 5,6-dimethyl-1,3-dihydro-2-telluraindene, and to clarify the ability of the new cyclic telluride to act as an electron-donor in the reaction with quinones. Physical studies of the new complexes are reported.

EXPERIMENTAL

(a) *Synthesis*

5,6-Dimethyl-1,3-dihydro-2-telluraindene. Sodium borohydride was added to a boiling ethanolic solution of $C_{10}H_{12}TeI_2$[6] (3.0 g) until the orange colour had disappeared. The solution was filtered, then poured into 500 cm^3 of water and extracted with ether (3 × 100 cm^3). The combined ether extracts were dried over $CaCl_2$ and concentrated to dryness on a rotatory evaporator. The yellow plates of 5,6-dimethyl-1,3-dihydro-2-telluraindene which melted at 90–92°C were recrystallized from petroleum ether (60:80). Found: C, 46.0; H 4.6. Calc. for $C_{10}H_{12}Te$: C, 46.2; H, 4.7%.

Synthesis of charge-transfer complexes. All complexes were prepared by the reaction of $C_{10}H_{12}Te$ with the corresponding quinone. The general preparation route is ilustrated by the following example:

Complex of p-*benzoquinone with* 5,6-*dimethyl*-1,3-*dihydro*-2-*telluraindene.* A mixture of 2.16 g (0.02 mol) of *p*-benzoquinone and 5.19 g (0.02 mol) of 5,6-dimethyl-1,3-dihydro-2-telluraindene in dry dichloromethane (50 cm^3) was heated to reflux for 3 h. A small quantity of black–brown crystals was deposited from this reaction on cooling. The precipitate was washed with a small amount of dichloromethane and recrystallized from ethanol, m.p. 100–102°C.

Table 1 lists the 1:1 charge-transfer complexes synthesized, together with their analytical data.

(b) *Physical measurements*

Analytical measurements for C and H were carried out by the Analytical Service Unit, Fakultät für Chemie, Universität Konstaz, F.R.G.: tellurium was determined volumetrically.[7] IR spectra were recorded with KBr discs in the range 4000–200 cm^{-1} on a Beckman TM spectrophotometer. UV–vis spectra were obtained with Pye–Unicam SP3-300S. ^{1}H NMR spectra were recorded on a Bruker WM-250 at 250 Hz using TMS as internal reference. ESR spectra were obtained at room temperature with a Varian E-109 spectrometer. Mass spectral data were determined at 70 eV with a MAT 1125 Finnigan mass spectrometer instrument.

* Author to whom correspondence should be addressed.

Table 1. Analytical and physical data for the new complexes

	Compound	Colour	Melting point (°C)	Analysis[a] (%) C(%)	H(%)
(I)	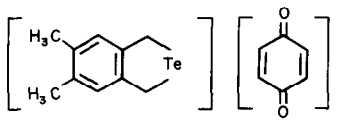	Black–brown	100–102	51.8 (52.2)	4.6 (4.4)
(II)	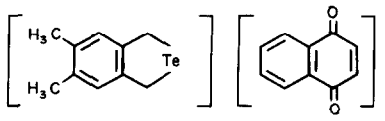	Brown	60–62	54.0 (54.5)	4.4 (4.3)
(III)	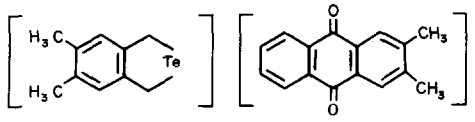	Yellow	72–74	[b]	[b]

[a] Calculated values are given in parentheses.
[b] Te: Found: 25.3; calc.: 25.7%.

Conductivity measurements. A sample of the $[C_{10}H_{12}Te]^{+}[C_{10}H_6O_2]^{-}$ complex was compressed into a disc of 12 mm diameter and 0.8 mm thickness. Two nickel electrodes were deposited on the disc by evaporation using a special apparatus *in vacuo* (10^{-7} torr). Copper wires were attached by silver paint. The sample was studied over a temperature range of 292–362 K.

RESULTS AND DISCUSSION

The reaction of $C_{10}H_{12}Te$ with quinones (i.e. *p*-benzoquinone, 1,4-naphthaquinone and 2,3-dimethylanthraquinone) in dichloromethane gave complexes of 1 : 1 stoichiometry (Table 1). The changes in their colour from black–brown to yellow, as the number of benzene rings increased, may be attributed to the distribution of the free electron over the benzene rings.

IR spectra of the complexes are compared with the spectra of the components alone; the spectra of the complexes are quite similar to the superposition of the spectra of the components. There are slight shifts in frequency and some alterations in the intensity, which reflect the molecular association. The degree of charge-transfer of the complexes could be monitored by examination of ν(CO) for quinones, similar to ν(CN) in TCNQ complexes.[8] The slight changes in the C=O frequencies may imply a small degree of charge-transfer (Table 2). We particularly

Table 2. Electronic, IR and ESR spectral data for the CT complexes

Compound	λ_{max}[a] (nm)	ν(CO)[b] (cm^{-1})	*g*-Factor (∓0.0009)
$[C_{10}H_{12}Te]^{+}[C_6H_4O_2]^{-}$	242(11,350), 272(7420), 282(5950), 314(2790), 340(1490)	1660	2.0030
$[C_{10}H_{12}Te]^{+}[C_{10}H_6O_2]^{-}$	238(26,900), 244(27,600), 258(20,650), 276(5800), 282(29,500), 336(4400)	1660	2.0029
$[C_{10}H_{12}Te]^{+}[C_{16}H_{12}O_2]^{-}$	242(17,020), 258(17,960), 266(16,960), 282(7730), 328(1580)	1670	2.0029

[a] $CHCl_3$ solution. Molar extinction values (M^{-1} cm^{-1}) are given in parentheses.
[b] $C_{10}H_{12}Te$ gives $\nu(CH_2)$ at 2928 cm^{-1} and ν(Te—C) at 518 cm^{-1}.

noted shifts of $+15\ cm^{-1}$ for $\nu(CH_2)$ which seems reasonable for the more positive tellurium atom.[9]

The electronic spectra of the complexes (I, II and III) show complexity. This is due to the overlapping between charge-transfer, n–π^* and π–π^* transitions. New bands at 314 (I), 276 (II) and 282 (III) nm are also observed (Table 2).

^1H NMR and mass spectra of the complexes are quite similar to the total signals of the components. The ^1H NMR spectra showed downfield signals at 8.64 (I), 10.38 (II) and 9.19 (III) ppm due to the hydroxyl group. This implies that the complexes are dissociated in solution and that hydroquinones were formed due to the presence of H_2O and using DMSO-d_6 as solvent.

Strong, and in general sharp, ESR signals for the solid complexes (I, II and III) were detected. The g-value of the ESR absorption by the unpaired electron for the complexes are close to the free electron value.[10,11] This indicates that each signal arises from unpaired electron density on the quinones (Table 2). It was not possible to observe a resonance from the tellurium cationic radical. This may be a consequence of a large spin–orbital coupling constant leading to increased line width,[12] or it could imply a diamagnetic ground state achieved by dimerization of the radical cations.[3,13]

The powder of complex II was pressed at 11 tons into a disc, and then the conductivity was measured at various temperatures within the range 292–362 K by a direct method. The variation of the resistivity with temperature was found to obey the usual behaviour of an intrinsic semiconductor[14] (see Fig. 1). The activation energy (E_a) was obtained from a plot of $\ln \rho$ against $1/T$ and found to be 0.56 eV.

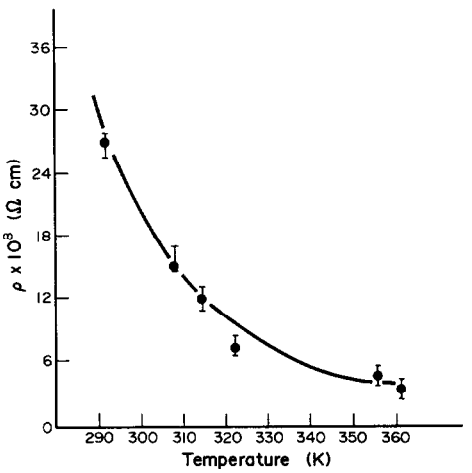

Fig. 1. The relation between specific resistivity (ρ) and temperature.

Acknowledgements—The authors thank Professor Pfleiderer, Professor Brozenjki and Dr N. A. Al-Masoudi, Fakultät für Chemie, Universität Konstanz, F.R.G., for providing C and H analysis, ^1H NMR and mass spectral data. We are grateful to Dr M. T. Mohammod, Department of Physics, for providing the facilities for conductivity measurements, and to Dr A. H. Al-Mawalli for obtaining the ESR spectra.

REFERENCES

1. (a) H. B. Singh, P. K. Khanna and S. K. Kumar, *J. Organomet. Chem.* 1988, **338**, 1; (b) K. Y. Abid and W. R. McWhinnie, *J. Organomet. Chem.* 1987, **330**, 337.
2. (a) M. R. Bryce, *Aldrichim. Acta* 1985, **18**, 73; (b) D. P. Rainville, R. A. Zingaro and J. P. Ferraris, *Can. J. Chem.* 1980, **58**, 1133.
3. H. B. Singh, W. R. McWhinnie, R. F. Ziolo and C. H. Jones, *J. Chem. Soc., Dalton Trans.* 1984, 1267.
4. (a) K. Lestrup, D. Talham, A. Bloch, T. Poehler and D. Cowan, *J. Chem. Soc., Chem. Commun.* 1982, 336; (b) F. Wudl and E. Aharon-Shalom, *J. Am. Chem. Soc.* 1982, **104**, 1154.
5. C. A. Heller, R. A. Zingaro and E. A. Meyer, *Can. J. Chem.* 1974, **52**, 3814.
6. L. Z. Yousif, MSc thesis, University of Basrah, Iraq (1988).
7. F. H. Kruse, R. W. Sanftner and J. F. Suttle, *Analyt. Chem.* 1953, **25**, 500.
8. J. S. Chappell, A. N. Bloch, W. A. Bryden, M. Maxfield, T. O. Poehler and D. O. Cowan, *J. Am. Chem. Soc.* 1981, **103**, 2442.
9. H. B. Singh, W. R. McWhinnie, T. A. Hamor and R. H. Jones, *J. Chem. Soc., Dalton Trans.* 1984, 23.
10. A. Z. Al-Rubaie, PhD thesis, University of Aston, Birmingham (1982).
11. D. N. Stamires and J. Turkevich, *J. Am. Chem. Soc.* 1963, **85**, 2557.
12. H. Bock, G. Brahler, D. Dauplaise and J. Meinwald, *Chem. Ber.* 1981, **114**, 2622.
13. G. Cauquis and M. M. Mey, *Bull. Soc. Chim. Fr.* 1973, 2912.
14. B. A. Bolto, *Organic Semiconducting Polymers* (Edited by J. E. Katon). Marcel Dekker, New York (1968).

Polyhedron Vol. 9, No. 6, pp. 851–857, 1990
Printed in Great Britain

0277–5387/90 $3.00+.00
© 1990 Pergamon Press plc

SYNTHESIS AND LIGAND CHEMISTRY OF BIS[(2-ARYLTELLURO)ETHYL]AMINE AND BIS[(2-ARYLTELLURO)ETHYL]METHYLAMINE—NOVEL (Te, N, Te) DONORS

AJAI K. SINGH,* VINOD SRIVASTAVA and B. L. KHANDELWAL

Department of Chemistry, Indian Institute of Technology, New Delhi—110 016, India

(*Received* 19 *July* 1989; *accepted* 20 *October* 1989)

Abstract—New tridentate ligands, bis[(2-aryltelluro)ethyl]amine (**1** and **2**) and bis[(2-aryltelluro)ethyl]methylamine (**3** and **4**) (aryl = 4-$MeOC_6H_4$ or 4-$EtOC_6H_4$) were synthesized by the reaction of sodium aryltellurolate with bis(2-chloroethyl)amine and bis(2-chloroethyl)methylamine, respectively, and characterized by molecular weight measurements, elemental analyses, IR, ^1H and $^{13}C\{^1H\}$ NMR spectra. Complexes of the type $MCl_2 \cdot L$ (L = **1** or **2**; M = Hg, Pd or Pt) were synthesized by reacting the ligand with $HgCl_2$, $(C_6H_5CN)_2PdCl_2$ and K_2PtCl_4. Mercury complexes were found to be non-ionic and monomeric. ^1H and $^{13}C\{^1H\}$ NMR spectra suggest that the ligands in these complexes coordinate only through two tellurium atoms. Palladium and platinum complexes of **1** and **2** were found to be diamagnetic, monomeric and non-ionic in nitrobenzene. However, they exhibit conductance in acetonitrile and methanol due to solvolysis. ^1H and $^{13}C\{^1H\}$ (recorded for **1** only) NMR spectra suggest that **1** and **2** act as a tridentate ligand in palladium and platinum complexes. On considering their electronic and IR spectral data in conjunction with the various properties, a square pyramidal structure with two chlorine atoms *trans* to each other seems to be most plausible for palladium/platinum complexes.

Bidentate or polydentate hybrid telluride ligands are somewhat rare.[1–3] We have reported recently[4] novel (Te, N) ligands, *viz.* 1-(NMe_2)-2-(TeAr)-4-MeC_6H_3 (Ar = C_6H_5, 4-$MeOC_6H_4$, or 4-$EtOC_6H_4$), and their complexation with palladium(II) and platinum(II). They also behave as unidentate ligands (coordinating through tellurium only) in mercury(II) complexes.[5] In continuation of our studies on the syntheses and ligation of (Te, N) donors we have synthesized bis[(2-aryltelluro)ethyl]amine and bis[(2-aryltelluro)ethyl]methylamine (**1–4**). It was thought worthwhile to explore their complexation with metal ions in detail because their phosphorus analogues have been found to give interesting structures[6] and induce catalytic activities[7] in platinum metal complexes. In the present paper the syntheses of **1–4** and the ligational behaviour of **1** and **2** with mercury(II), palladium(II) and platinum(II) are reported.

* Author to whom correspondence should be addressed.

EXPERIMENTAL

Published methods were used to synthesize the ditellurides, $(4\text{-}MeOC_6H_4)_2Te_2$ and $(4\text{-}EtOC_6H_4)_2Te_2$,[8] bis(2-chloroethyl)amine and bis(2-chloroethyl)methylamine.[9] Chloride, mercury and tellurium were estimated by standard methods.[10] The C, H and N analyses were carried out with a Perkin–Elmer elemental analyser 240C. ^1H and $^{13}C\{^1H\}$ NMR spectra in $CDCl_3$ were recorded at 25°C on a JEOL FX100 FT-NMR spectrometer at 99.55 and 25 MHz, respectively. IR spectra (Nujol mulls between CsI windows or CsI/KBr discs) in the range 4000–200 cm^{-1} were recorded on a Nicolet 5DX FT-IR spectrometer. Electronic spectra in chloroform were recorded on a Hitachi 300 UV–vis spectrometer. The conductivity measurements were made on *ca* 1 mM solutions in acetonitrile, methanol and nitrobenzene with a Metrohm 660 conductometer. The molecular weights were determined in chloroform solution (~ 10 mmolal) with a Knauer vapour pressure osmometer.

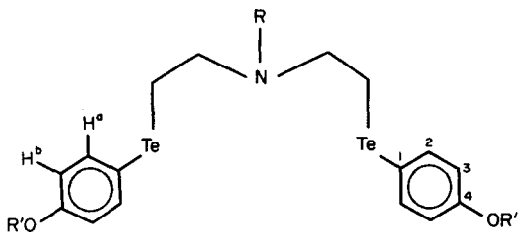

R'	R	
Me	H	(1)
Et	H	(2)
Me	Me	(3)
Et	Me	(4)

Synthesis of bis[(2-aryltelluro)ethyl]amine and bis[(2-aryltelluro)ethyl]methylamine

Diaryl ditelluride (2.5 mmol) was refluxed in ethanol (30 cm^3) under a nitrogen atmosphere. Sodium borohydride (0.2 g in 2 cm^3 of 1 M NaOH) was added to it dropwise until the refluxing solution became colourless. Bis(2-chloroethyl)amine or bis(2-chloroethyl)methylamine (2.5 mmol) dissolved in ethanol (10 cm^3) was added dropwise to this refluxing solution of sodium aryl tellurolate with vigorous stirring. The resulting pale yellow mixture was further refluxed for 1 h, cooled to room temperature and poured into 200 cm^3 of water. The ligand (**1–4**) was extracted into chloroform (200 cm^3) from this aqueous mixture. The extract was washed with water, dried over anhydrous sodium sulphate and concentrated to ~5 cm^3 under vacuum. The precipitated pale yellow–white crystalline solid was recrystallized from a chloroform–hexane (70 : 30) mixture to give the white crystalline ligand (**1–4**). The yield, melting point, molecular weight, results of elemental analyses, characteristic IR bands, ^1H and $^{13}C\{^1H\}$ NMR data for **1–4** are given below.

Ligand **1**. Yield 75%; m.p. 78°C. Analysis: Found: C, 39.5; H, 4.1; N, 2.5; Te, 46.6. Calc. for $C_{18}H_{23}NO_2Te_2$: C, 40.0; H, 4.3; N, 2.6; Te, 47.2%. Mol. wt: Found: 522.8; Calc.: 540.2. IR (cm^{-1}): 1180m [ν(C—N)]; 3261m [ν(N—H)]; 268mb, 297mb [ν(Te—C(Ar))]. NMR [^1H]: δ, 1.65 (bs, 1H, NH); 2.92 (bs, 8H, NCH_2CH_2Te); 3.78 (s, 6H, OMe); 6.69–6.78 (d, 4H, H^b of phenyl ring *-m* to Te); 7.62–7.71 (d, 4H, H^a of phenyl ring *-o* to Te); [$^{13}C\{^1H\}$]: δ, 10.5 ($TeCH_2$); 49.5 (NCH_2); 55.1 (OMe); 100.4 (C_1); 115.0 (C_3); 140.8 (C_2); 159.6 (C_4).

Ligand **2**. Yield 80%; m.p. 85°C. Analysis: Found: C, 41.7; H, 4.1; N, 2.4; Te, 43.8. Calc. for $C_{20}H_{27}NO_2Te_2$: C, 42.2; H, 4.8; N, 2.5; Te, 44.9%. Mol. wt: Found: 547.0; Calc.: 568.2. IR (cm^{-1}): 1180m [ν(C—N)]; 3261bm [ν(N—H)]; 270mb, 315mb [ν(Te—C(Ar))]. NMR [^1H]: δ, 1.65 (bs, 1H, NH); 2.83 (bs, 8H, NCH_2CH_2Te); 3.80–4.10 (q, 4H, OCH_2); 1.32–1.46 (t, 6H, CH_3); 6.67–6.76 (d, 4H, H^b of phenyl ring); 7.58–7.66 (d, 4H, H^a of phenyl ring); [$^{13}C\{^1H\}$]: δ, 10.4 ($TeCH_2$); 14.7 (CH_3); 49.5 (NCH_2); 63.2 (OCH_2); 100.1 (C_1); 115.5 (C_3); 140.8 (C_2); 158.9 (C_4).

Ligand **3**. Yield 85%; m.p. 58°C. Analysis: Found: C, 40.2; H, 4.2; N, 2.7; Te, 45.7. Calc. for $C_{19}H_{25}NO_2Te_2$: C, 41.1; H, 4.5; N, 2.5; Te, 46.1%. Mol. wt: Found: 530.5; Calc.: 554.2. IR (cm^{-1}): 1180m [ν(C—N)]; 280m, 245m [ν(Te—C(Ar))]. NMR [^1H]: δ, 2.23 (s, 3H, NMe); 3.77 (s, 6H, OMe); 2.78–2.84 (unresolved triplet, 4H, $TeCH_2$); 2.91–2.97 (unresolved triplet, 4H, NCH_2); 6.69–6.78 (d, 4H, H^b of phenyl ring); 7.61–7.69 (d, 4H, H^a of phenyl ring); [$^{13}C\{^1H\}$]: δ, 8.6 ($TeCH_2$); 40.9 (NMe); 55.0 (OMe); 58.0 (NCH_2); 101.3 (C_1); 114.9 (C_3); 140.4 (C_2); 159.3 (C_4).

Ligand **4**. Yield 87%; m.p. 62°C. Analysis: Found: C, 42.5; H, 4.7; N, 2.3; Te, 42.6. Calc. for $C_{21}H_{29}NO_2Te_2$: C, 43.3; H, 5.0; N, 2.4; Te, 43.8%. Mol. wt: Found: 562.4; Calc.: 582.2. IR (cm^{-1}): 1180m [ν(C—N)]; 250w, 280m [ν(Te—C(Ar))]. NMR [^1H]: δ, 2.23 (s, 3H, NMe); 2.78–2.84 (unresolved triplet, 4H, $TeCH_2$); 2.91–2.98 (unresolved triplet, 4H, NCH_2); 1.32–1.46 (t, 6H, CH_3); 3.89–4.10 (q, 4H, OCH_2); 7.60–7.69 (d, 4H, H^a of phenyl ring); 6.81–6.90 (d, 4H, H^b of phenyl ring); [$^{13}C\{^1H\}$]: δ, 8.13 ($TeCH_2$); 14.7 (CH_3); 41.0 (NMe); 58.2 (NCH_2); 63.3 (OCH_2); 101.1 (C_1); 115.6 (C_3); 140.5 (C_2); 158.9 (C_4).

Synthesis of mercury complexes (**5** *and* **6**)

To a solution of $HgCl_2$ (0.3 mmol) in acetone (5 cm^3) was added the solution of the ligand (**1, 2**) (0.3 mmol) in acetone (5 cm^3) with stirring at room temperature. Hexane was added to precipitate the complex (**5** or **6**) as a pale yellow solid which was filtered, washed with acetone (2 cm^3) and dried *in vacuo*. These complexes are soluble in $CHCl_3$, CH_2Cl_2 and CH_3CN. The physical and spectral data are recorded below.

$HgCl_2 \cdot$ **1** (**5**). Yield 67%; m.p. 70°C. Analysis: Found: C, 26.6; H, 2.8; N, 1.7; Cl, 8.7; Te, 31.4; Hg, 24.7. Calc. for $C_{18}H_{23}NO_2Te_2 \cdot HgCl_2$: C, 26.0; H, 2.7; N, 1.7; Cl, 8.1; Te, 30.5; Hg, 24.1%. Mol. wt: Found: 830.8; Calc.: 811.7. IR (cm^{-1}): 1180m [ν(C—N)]; 250m, 290w [ν(Te—C(Ar))]; 3261bw [ν(N—H)]; 325wb (ν(Hg—Cl)]. NMR [^1H]:

δ, 3.76 (s, 6H, OMe); 3.12 (bs, 4H, $TeCH_2$); 3.40 (bs, 4H, NCH_2); 1.67 (bs, 1H, NH); 7.79–7.87 (d, 4H, H^a of phenyl ring); 6.78–6.87 (d, 4H, H^b of phenyl ring); [$^{13}C\{^1H\}$]: δ, 24.8 ($TeCH_2$); 46.1 (NCH_2); 55.2 (OMe); 103.2 (C_1); 115.8 (C_3); 139.6 (C_2); 161.0 (C_4).

$HgCl_2 \cdot$ **2** (**6**). Yield 63%; m.p. 80°C. Analysis: Found: C, 28.5; H, 3.2; N, 1.7; Cl, 8.5; Te, 30.4; Hg, 23.9. Calc. for $C_{20}H_{27}NO_2Te_2 \cdot HgCl_2$: C, 27.7; H, 3.2; N, 1.6; Cl, 7.9; Te, 29.4; Hg, 23.0%. Mol. wt: Found: 855.0; Calc.: 839.7. IR (cm^{-1}): 1180m [ν(C—N)]; 3282bw [ν(N—H)]; 265m, 290w [ν(Te—C(Ar))]; 315m [ν(Hg—Cl)]. NMR [^1H]: δ, 2.00 (bs, 1H, NH); 3.14 (bs, 4H, $TeCH_2$); 3.37 (bs, 4H, NCH_2); 1.30–1.43 (t, 6H, CH_3); 3.84–3.98 (q, 4H, OCH_2); 7.73–7.82 (d, 4H, H^a of phenyl ring); 6.73–6.82 (d, 4H, H^b of phenyl ring); [$^{13}C\{^1H\}$]: δ, 14.6 (CH_3); 24.5 ($TeCH_2$); 46.2 (NCH_2); 63.4 (OCH_2); 103.1 (C_1); 116.3 (C_3); 139.5 (C_2); 160.3 (C_4).

Synthesis of palladium complexes (**7** *and* **8**)

Bis(benzonitrile)palladium dichloride (0.5 mmol) dissolved in chloroform (20 cm^3) was stirred at room temperature with **1** or **2** (0.5 mmol) (added as solid) for 2 h. The resulting orange–yellow solution was mixed with hexane (50 cm^3) with stirring. The orange coloured precipitate of the complex (**7** or **8**) was filtered, washed with hexane, dried *in vacuo* and recrystallized from a chloroform–hexane (75:25) mixture. These complexes are soluble in a wide range of polar organic solvents, *vis.* CH_2Cl_2, $CHCl_3$, CH_3CN, MeOH, EtOH, DMF and DMSO, as well as in H_2O. The physical and spectral data for **7** and **8** are recorded below.

$PdCl_2 \cdot$ **1** (**7**). Yield 75%; m.p. 125°C. Analysis: Found: C, 30.6; H, 3.4; N, 1.8. Calc. for $C_{18}H_{23}NO_2Te_2 \cdot PdCl_2$: C, 30.1; H, 3.2; N, 2.0%. Mol. wt: Found: 698.2; Calc.: 717.6. IR (cm^{-1}): 3028.8 [ν(N—H)]; 1112m [ν(C—N)]; 270w, 240w [ν(Te—C(Ar))]; 320bw [ν(Pd—Cl)]. NMR [^1H]: δ, 3.83 (s, 6H, OMe); 5.39 (bs, 1H, NH); 2.60–3.70 (broad unresolved multiplet, 8H, NCH_2CH_2Te); 6.90–6.98 (d, 4H, H^b of phenyl ring); 7.97–8.06 (unresolved doublet, 4H, H^a of phenyl ring); [$^{13}C\{^1H\}$]: δ, 16.1 ($TeCH_2$); 55.4 (OMe); 59.1 (NCH_2); 105.6 (C_1); 116.2 (C_3); 138.6 (C_2); 161.6 (C_4).

$PdCl_2 \cdot$ **2** (**8**). Yield 80%; m.p. 155°C. Analysis: Found: C, 31.3; H, 4.1; N, 1.7. Calc. for $C_{20}H_{27}NO_2Te_2 \cdot PdCl_2$: C, 32.2; H, 4.2; N, 1.9%. Mol. wt: Found: 730.4; Calc.: 754.6. IR (cm^{-1}): 3071bw [ν(N—H)]; 1112m [ν(C—N)]; 275w, 243w [ν(Te—C(Ar))]; 320bw [ν(Pd—Cl)]. NMR [^1H]: δ, 5.39 (bs, 1H, NH); 3.95–4.15 (q, 4H, OCH_2); 1.36–1.50 (t, 6H, CH_3); 2.67–3.75 (broad unresolved multiplet, 8H, NCH_2CH_2Te); 7.95–8.01 (unresolved doublet, 4H, H^a of phenyl ring); 6.88–6.96 (d, 4H, H^b of phenyl ring).

Synthesis of platinum complexes (**9** *and* **10**)

To a solution of K_2PtCl_4 (0.5 mmol) in water (15 cm^3) was added **1** or **2** (0.5 mmol) in acetone (10 cm^3). The resulting solution was stirred for 3 h at room temperature and poured into water (100 cm^3). From an aqueous mixture the complex (**9** or **10**) was extracted into chloroform (150 cm^3). The chloroform extract was dried over anhydrous sodium sulphate and the solvent was reduced under vacuum to ~ 5 cm^3. The platinum complex **9** or **10** crystallized as pale yellow crystals on keeping the concentrated solution for 4–5 h at room temperature. They were recrystallized from a chloroform–hexane (80:20 mixture). In CH_2Cl_2, $CHCl_3$, CH_3CN, MeOH, EtOH, DMF and DMSO the platinum complexes are fairly soluble and sparingly in H_2O. The analytical and spectral data for these complexes are given below.

$PtCl_2 \cdot$ **1** (**9**). Yield 80%; m.p. 75°C. Analysis: Found: C, 25.8; H, 2.4; N, 1.7. Calc. for $C_{18}H_{23}NO_2Te_2 \cdot PtCl_2$: C, 26.8; H, 2.9; N, 1.8%. Mol. wt: Found: 830.4; Calc.: 806.3. IR (cm^{-1}): 1110w [ν(C—N)]; 270m, 245m [ν(Te—C(Ar))]; 325m [ν(Pt—Cl)]; 2965.5bw [ν(N—H)]. NMR [^1H]: δ, 3.84 (s, 6H, OMe); 4.93 (bs, 1H, NH); 2.34–3.66 (broad unresolved multiplet, 8H, NCH_2CH_2Te); 6.88–9.97 (d, 4H, H^b of phenyl ring); 7.88–7.96 (d, 4H, H^a of phenyl ring).

$PtCl_2 \cdot$ **2** (**10**). Yield 95%; m.p. 105°C. Analysis: Found: C, 27.6; H, 3.0; N, 1.4. Calc. for $C_{20}H_{27}NO_2Te_2 \cdot PtCl_2$: C, 28.7; H, 3.2; N, 1.7%. Mol. wt: Found: 856.4; Calc.: 834.3. IR (cm^{-1}): 1100m [ν(C—N)]; 285w, 250w [ν(Te—C(Ar))]; 330bm [ν(Pt—Cl)]; 2944.4bw [ν(N—H)]. NMR [^1H]: δ, 4.96 (bs, 1H, NH); 2.26–3.61 (broad unresolved multiplet, 8H, NCH_2CH_2Te); 3.95–4.15 (q, 4H, OCH_2); 1.34–1.48 (t, 6H, CH_3); 6.86–6.95 (d, 4H, H^b of phenyl ring); 7.98–8.15 (bd, 4H, H^a of phenyl ring).

The $^{13}C\{^1H\}$ NMR spectra of **8**, **9** and **10** could not be recorded due to an inadequate solubility problem.

RESULTS AND DISCUSSION

The ligands, bis[(2-aryltelluro)ethyl]amine and bis[(2-aryltelluro)ethyl]methylamine were synthesized by the reactions given in eqs (1)–(3):

$$RN(C_2H_4OH)_2 \xrightarrow[CHCl_3/Reflux]{SOCl_2} RN(C_2H_4Cl)_2 \cdot HCl \xrightarrow{10\%\ NaOH} RN(C_2H_4Cl)_2 \quad (1)$$

$$(4\text{-}R'OC_6H_4)_2Te_2 \xrightarrow[NaOH/N_2\,atm.]{NaBH_4/EtOH} 4\text{-}R'OC_6H_4TeNa \quad (2)$$

$$4\text{-}R'OC_6H_4TeNa + RN(C_2H_4Cl)_2 \xrightarrow[N_2\,atm.,\,1\,h]{EtOH/Reflux} RN(C_2H_4TeC_6H_4\text{-}4\text{-}OR')_2 \quad (3)$$

(1–4)

(R = H or Me; R′ = Me or Et).

The ligands, **1–4**, are white crystalline solids with low melting points. They are more soluble in $CHCl_3$, CH_2Cl_2 and Me_2CO than in MeOH and EtOH. Like other tellurides they also behave as non-electrolytes in solution. ^{1}H NMR spectra of **1–4** exhibit some interesting features. In the spectra of **1** and **2** a broad resonance at 1.65 ppm attributable to the NH group appears, whereas ligands **3** and **4** show a sharp singlet at 2.23 ppm due to the NMe group, concurring with earlier reported values.[11] In **1** and **2** the protons of the "NCH_2 CH_2Te" bridge appear as a broad singlet at 2.92 and 2.83 ppm, respectively [Fig. 1(a)], contrary to the expected triplets for the $TeCH_2$ and NCH_2 protons. But in the spectra of **3** and **4** these CH_2 protons give two partly resolved triplets [Fig. 1(b)], centred at 2.94 and 2.81 ppm for the NCH_2 and $TeCH_2$ groups, respectively. The appearance of a broad singlet for the protons of the "NCH_2CH_2Te" bridge may be explained by considering the ^{1}H NMR spectrum of diethanolamine (precursor of these ligands) in which the NCH_2 and OCH_2 appear as triplets centred at 2.80 and 3.69 ppm, respectively. When oxygen is replaced by a less electronegative tellurium, the protons of the CH_2 group attached to it experience shielding and their signal probably merges with the NCH_2 signal, thereby giving a broad singlet. In **3** and **4** the protons of the NCH_2 group are shielded with respect to the similar protons of **1** and **2** due to the presence of the methyl group on nitrogen and, therefore, partly resolved signals [Fig. 1(b)] for the NCH_2 and $TeCH_2$ groups were observed. The ^{1}H NMR spectra of **1–4** were also recorded in CF_3COOD in which the ligands may exist as $D(R)N(C_2H_4TeAr)_2^+$. The "NCH_2 CH_2Te" bridge in this medium has two magnetically non-equivalent groups of CH_2 protons, i.e. $CH_2(N)$ and $CH_2(Te)$, thereby showing the expected coupling of these protons in the spectra [Fig. 1(c)]. The merging of two CH_2 signals may be partly as a result of the weak N → Te interaction

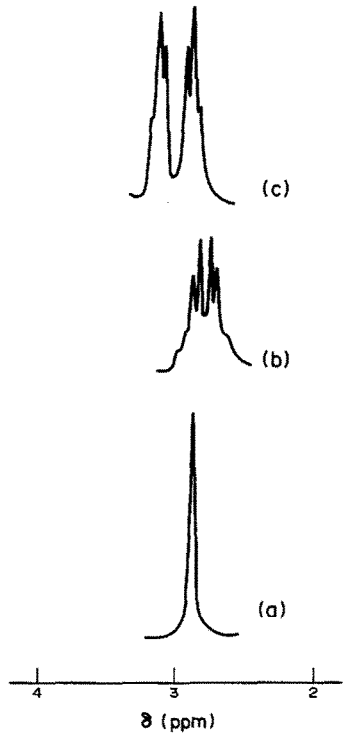

Fig. 1.

which is possible in ligands **1–4**. In acid solution such an interaction breaks down resulting in the expected ^{1}H NMR spectrum for the methylene groups. Moreover, the two tellurium atoms seem to be involved in a dynamic process fast enough on the ^{1}H NMR time scale, in which they interact alternatively with the nitrogen, otherwise protons of the CH_2 groups would have become magnetically non-equivalent, resulting in a complex ^{1}H NMR spectrum. The ring protons H^a and H^b appear as doublets, as expected for a 1,4-substituted phenyl ring. The $^{13}C\{^1H\}$ NMR spectra of **1–4** have been found to be in agreement with ^{1}H NMR spectra as the $CH_2(Te)$ resonances appear between 8 and 10.5 ppm in **1–4**, consistent with the earlier reported values,[12] supporting the shielding of carbon linked to tellurium. The carbon of $CH_2(N)$ in the spectra of these ligands appears between 50 and 58 ppm as reported for such carbons.[11] The carbons of the *p*-ethoxyphenyl and *p*-methoxyphenyl groups linked to tellurium also exhibit signals in agreement with the reported values for such moieties.[13] The two *ν*[Te—C(Ar)] vibrations in the IR spectra of **1–4** at 280–315 and 250–270 cm^{-1} are consistent with the earlier reports on tellurides.[14]

Complexation of **1** *and* **2** *with mercury*(II), *palladium*(II) *and platinum*(II)

The ligands **1** and **2** form complexes with bivalent mercury, palladium and platinum according to eqs

(4)–(6):

$$L + HgCl_2 \xrightarrow[r.t.]{acetone} HgCl_2 \cdot L \quad (5, 6) \qquad (4)$$

$$L + (C_6H_5CN)_2PdCl_2 \xrightarrow[r.t., 2\,h]{CHCl_3} [PdCl_2 \cdot L] \quad (7, 8) \qquad (5)$$

$$L + K_2PtCl_4 \xrightarrow[r.t., 3\,h]{aq.\text{-}acetone} [PtCl_2 \cdot L] \quad (9, 10) \qquad (6)$$

(L = **1** or **2**).

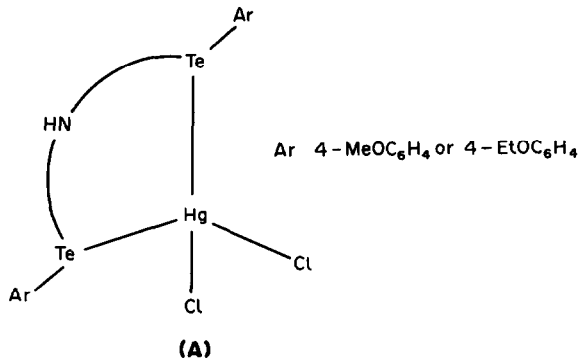

(A)

Molecular weights of mercury complexes indicate that they are monomeric. Their molar conductance values in acetonitrile indicate that they are non-ionic in nature. In the IR spectra of **5** and **6**, two ν[Te—C(Ar)] bands have been found at lower frequency ($\sim$ 15–30 cm^{-1}) in comparison to the similar bands of **1** and **2**. On coordination, ν(C—N) remains unaffected and the shift of ν(N—H) is too insignificant to conclude coordination of the NH group. Thus, probably two tellurium atoms are the only ligating site of **1** and **2** in the mercury complexes. The ^1H NMR spectra of **5** and **6** have two broad singlets due to NCH_2 and $TeCH_2$. This suggests that on coordination, these protons (almost similar in **1** and **2**) become magnetically non-equivalent and therefore appear as two broad singlets. The signal of the NH protons does not show any change in **5** and **6** when compared with that of free ligand, indicating the presence of an uncoordinated NH group in the mercury complexes. The H^a protons of the phenyl ring undergo a greater downfield shift ($\sim$ 0.15 ppm) than the H^b protons ($\sim$ 0.10 ppm). In the $^{13}C\{^1H\}$ NMR spectra of these mercury complexes, carbon signals of CH_2(Te) and C_1(Te) were found to be deshielded by $\sim$ 14.3 and $\sim$ 3.0 ppm, respectively, with respect to the corresponding signals of the free ligands. However, the carbon signal of CH_2(N) appears around 3.5 ppm upfield relative to the free ligand, which supports the possibility of a weak N $\rightarrow$ Te interaction in **1** and **2**. If these spectral observations are considered together they indicate that **1** and **2** probably coordinate with mercury through their two tellurium atoms. On consideration of the spectral data in conjunction with molecular weight and molar conductance values, it is reasonable to presume that structure **A** is most plausible for **5** and **6**.

The molar conductances of the solutions of **7–10** in acetonitrile ($\sim$ 1 mM) were found in the range 30–40 Ω^{-1} cm^2 mol^{-1}. These values are lower than those expected for a 1 : 1 electrolyte.[15] The conductances (Λ_M = $\sim$ 100 Ω^{-1} cm^2 mol^{-1}) of **7–10** in methanol ($\sim$ 0.1 mM solution) are very close to that of a 1 : 1 electrolyte and decrease on increasing the concentration (Λ_M for 1 mM solution is $\sim$ 60 Ω^{-1} cm^2 mol^{-1}). In nitrobenzene the conductance is very low (Λ_M = $\sim$ 4 Ω^{-1} cm^2 mol^{-1} at 1 mM concentration) compared to the value expected for a 1 : 1 electrolyte and does not change much on dilution (Λ_M = $\sim$ 10 Ω^{-1} cm^2 mol^{-1} at 0.1 mM concentration). These observations suggest that conductance probably arises from solvolysis of $MCl_2 \cdot$ **1/2** (M = Pt or Pd), and to assume that these complexes are non-ionic is reasonable. Molecular weights of these complexes (**7–10**) in chloroform favour their monomeric and non-ionic nature. In the IR spectra of **7** and **8**, the ν(Te—C) consists of two bands with a red shift of the order of 27–35 cm^{-1}. The ν(C—N) and ν(N—H) are also red shifted by an order of $\sim$ 70 and $\sim$ 200 cm^{-1}, respectively, in comparison to the free ligand, which suggests that **1** and **2** coordinate with palladium through the nitrogen and tellurium atoms. A broad peak at 320 cm^{-1} in the IR spectra of **7** and **8** may be assigned to the ν(Pd—Cl) vibrations.[6,16] The assignment of ν(Pd—Cl) was confirmed by examining the IR spectra of $PdBr_2 \cdot$ **1/2** prepared by the metathetical reaction of $PdCl_2 \cdot$ **1/2** with KBr. The band assigned to ν(Pd—Cl) was absent in the spectra of $PdBr_2 \cdot$ **1/2**. In the ^1H NMR spectra of **7** and **8**, the NH signal was observed $\sim$ 4.7 ppm downfield from its position in the spectra of the free ligand, indicating strong coordination of the NH group with palladium. The H^a protons of the phenyl ring were found to be more deshielded (0.35 ppm) than the H^B protons (0.20 ppm), on formation of palladium complexes. Only the $^{13}C\{^1H\}$ NMR spectrum of **7** could be recorded due to the low solubility of the other complexes. Complex **7** displays carbon signals for the CH_2(Te) and CH_2(N) groups at 5.6 and 9.5 ppm downfield, respectively, relative to the free ligand. The signal of C_1(Te) also moves 5.2 ppm downfield on coordination. On considering the information derived from the IR and NMR spectra together, it appears that in palladium complexes (**7** and **8**) the ligands most probably coordinate through the nitrogen and two tellurium atoms. The

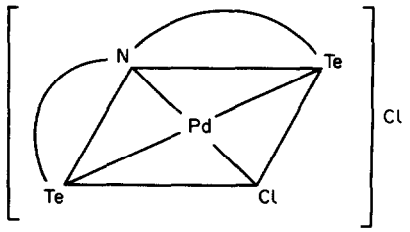

(B)

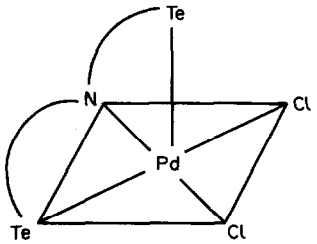

(C)

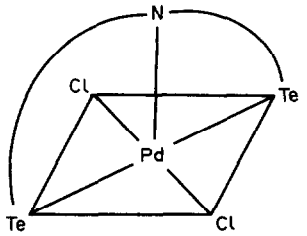

(D)

electronic spectra of the palladium complexes which are found to be diamagnetic have three bands at 33.3, 29.4 and 23.8 kK. The first band probably originates from intra-ligand transitions (the electronic spectra of **1** and **2** show only one band at 41.6 kK). The second and third bands suggest that palladium complexes have either square-planar or pyramidal geometry. The bands may be assigned to $^1A_{1g} \rightarrow {}^1E_g$ and $^1A_{1g} \rightarrow {}^1B_{1g}$ transitions.[17] In view of the non-ionic nature of the palladium complexes, the square-planar ionic structure **B** is ruled out. Of the two structures **C** and **D**, the value of ν(Pd—Cl) being somewhat lower than expected for a Cl *trans* to N, favours the *trans* structure **D**.[16] The trigonal bipyramidal geometry around palladium does not seem possible due to steric reasons also.

The IR spectra of **9** and **10** show two ν(Te—C) bands which are red shifted by the order of 20–30 cm^{-1}. The ν(C—N) and ν(N—H) are also red shifted by the order of ~ 70 and ~ 300 cm^{-1}, respectively. The ν(Pt—Cl) bond appears[6,16] around 330 cm^{-1} in the spectra of **9** and **10**, which is supported by the IR spectrum of $PtBr_2 \cdot$ **1/2** (prepared by metathesis) as for the palladium complexes. In the ^{1}H NMR spectra of the platinum complexes (**9** and **10**) the "NCH_2CH_2Te" bridge protons appear as a broad unresolved multiplet compared to a broad singlet for the free ligands, indicating a strong involvement of the nitrogen and both the tellurium atoms of **1** and **2** in coordination to platinum. The signal for H^a protons also undergoes a downfield shift, 0.26 and 0.44 ppm for **9** and **10**, respectively. Similarly, H^b protons undergo a downfield shift of the order 0.20 ppm in **9** as well as in **10**. These trends in the "shifts" indicate that in platinum complexes **1** and **2** probably also coordinate through the nitrogen and two tellurium atoms. The electronic spectra of diamagnetic **9** and **10** show only one band at 29.8 kK which indicates that the platinum complexes are either square-planar or pyramidal. The band may be due to an $^1A_{1g} \rightarrow {}^1E_g$ transition.[17] On considering the above mentioned spectral data and the fact that the conductance behaviour of platinum complexes **9** and **10** is similar to that of palladium complexes, and that they are monomeric, it seems reasonable to presume that the platinum complexes also have a square-pyramidal structure **D** as proposed for palladium complexes (**7** and **8**).

Preliminary investigations have revealed that the palladium complexes (**7** and **8**) have good activity for the homogeneous catalytic hydrogenation of simple olefins, e.g. cyclohexene, which is like the palladium complexes of (P, N, P) ligands.[6]

Acknowledgement—Financial support from CSIR (India) for this work is gratefully acknowledged.

REFERENCES

1. H. J. Gysling and H. R. Luss, *Organometallics* 1984, **3**, 596.
2. N. I. Al-Salim, T. A. Hamor and W. R. McWhinnie, *J. Chem. Soc., Chem. Commun.* 1986, 453; T. Kemmitt and W. Levason, *Organometallics* 1989, **8**, 1303.
3. H. J. Gysling, *The Chemistry of Organic Selenium and Tellurium Compounds* (Edited by S. Patai and Z. Rappoport), Ch. 18, p. 815. John Wiley, New York (1986).
4. A. K. Singh, V. Srivastava and B. L. Khandelwal, *Polyhedron* 1990, **9**, 495.

5. A. K. Singh, V. Srivastava and B. L. Khandelwal, *Polyhedron*, communicated.
6. M. M. Taqui Khan and E. Rama Rao, *Polyhedron* 1987, **6**, 1727.
7. M. M. Taqui Khan, B. T. Khan and S. Begum, *J. Molec. Catal.* 1988, **45**, 305.
8. K. J. Irgolic and R. A. Zingaro, *Organomet. React.* 1971, **2**, 117.
9. J. P. Mason and D. J. Gosch, *J. Am. Chem. Soc.* 1938, **60**, 2816.
10. F. H. Kruse, R. E. Sanftner and J. F. Suttle, *Analyt. Chem.* 1953, **25**, 500; A. I. Vogel, *A Text Book of Quantitative Inorganic Analysis*, 3rd edn. Longmans, London (1961).
11. R. M. Silverstein and G. C. Bassler, *Spectrometric Identification of Organic Compounds*, 4th edn. John Wiley, New York (1980).
12. E. G. Hope, T. Kemmitt and W. Levason, *Organometallics* 1988, **7**, 78.
13. R. K. Chadha and J. M. Miller, *J. Chem. Soc., Dalton Trans.* 1982, 117.
14. W. R. McWhinnie and M. G. Patel, *J. Chem. Soc., Dalton Trans.* 1972, 199.
15. W. J. Geary, *Coord. Chem. Rev.* 1971, **7**, 81.
16. K. Nakamoto, *Infrared and Raman Spectra of Inorganic and Coordination Compounds*, 4th edn, pp. 199, 324. John Wiley, New York (1986).
17. A. B. P. Lever, *Inorganic Electronic Spectroscopy*, p. 524. Elsevier, Amsterdam (1984).

Polyhedron Vol. 9, No. 6, pp. 859–862, 1990
Printed in Great Britain

0277–5387/90 $3.00+.00
© 1990 Pergamon Press plc

SYNTHESIS AND CHARACTERIZATION OF LANTHANIDE MORPHOLINE-4-CARBODITHIOATE COMPLEXES

TANG NING, GAN XINMIN, ZHU HAILIANG and TAN MINYU*

Department of Chemistry, Lanzhou University, Lanzhou, P.R.C.

(*Received* 3 *August* 1989; *accepted* 20 *October* 1989)

Abstract—The lanthanide morpholine-4-carbodithioate complexes with the general formula $(MorphH_2)[Ln(MorphCS_2)_4]\cdot H_2O$ (Morph = morpholino, Ln = La, Pr, Nd, Sm, Eu and Gd) have been prepared using anhydrous lanthanide chloride and morpholinium morpholine-4-carbodithioate as reactants. These new complexes were characterized by chemical analyses, IR spectra, electronic spectra, conductivity measurements and TG–DTA techniques. In all the complexes the carbodithioate ligands show bidentate behaviour.

Many complexes of carbodithioates with *d*- and *p*-block metal ions have been investigated,[1–4] while the corresponding type complexes of *f*-block metal ions have been reported much less. According to the "hard and soft" acids and bases rule, carbodithioates are not considered as ligands which prefer to bind to lanthanide ions to form complexes. However recent research has shown that under certain conditions the formation of lanthanide carbodithioate complexes is possible, and most of these complexes are relatively stable and some of them have bacteriostatsis and optical rotation properties.[5–7] Therefore, systematic studies on lanthanide complexes coordinated with organic ligands containing sulphur atoms have important theoretical and practical significance. As an extension of our previous research into the ion-association type complexes of lanthanides with diethyldithiocarbamate,[8] we have recently synthesized the solid complexes of lanthanides with morpholine-4-carbodithioate, and investigated the composition and properties of the new complexes.

EXPERIMENTAL

Preparation of anhydrous lanthanide chlorides

Anhydrous lanthanide chlorides were prepared by a literature method[9] with sulphinyl chloride as the dehydrating agent.

Preparation of the ligand

Morpholinium morpholine-4-carbodithioate ($[\overline{CH_2CH_2OCH_2CH_2NH_2}]\cdot[\overline{CH_2CH_2OCH_2CH_2NCS_2}]$) was obtained according to the literature[10] by the reaction of morpholine and carbon disulphide (molar ratio 2 : 1) in carbon tetrachloride medium. The product was purified by sublimation and then verified by elemental analysis, IR and ^1H NMR spectroscopy.

Preparation of the complexes

Anhydrous lanthanide chloride (0.1 mmol) and the ligand (0.4 mmol) were dissolved in 20 cm^3 of absolute ethanol. After being stirred for 24 h at room temperature the solution was allowed to evaporate spontaneously to dryness. The residual solid obtained was dissolved in 20 cm^3 of anhydrous acetonitrile and then the solution was filtered. To the filtrate was added 100 cm^3 of anhydrous ethyl ether with stirring so that that complex precipitated. The product was isolated by filtration, washed with anhydrous ethyl ether and dried *in vacuo* over P_4O_{10} for 1 week. The complete synthesis of the complexes was carried out in a glove box containing dry nitrogen gas.

Analyses

The metal ion was determined by EDTA titration using xylenol-orange as indicator. Carbon, nitrogen

* Author to whom correspondence should be addressed.

and hydrogen were determined using a Carlo Erba 1106 elemental analyser.

IR measurements

The IR spectra were recorded in the 4000–200 cm^{-1} region using KBr pellets and a 170 SX FTIR spectrometer.

Electronic spectra

The electronic spectra were recorded with a Shimadzu UV-240 spectrophotometer in acetonitrile solution in the 190–400 nm range.

Thermal analyses

Thermal analyses (TG and DTA) were performed on a Dupont 1090 thermobalance. The heating rate was $10^{\circ}C\ min^{-1}$.

Conductivity measurements

These measurements were carried out with a DDS-11A type conductivity bridge for freshly prepared solutions in acetonitrile at 25°C.

RESULTS AND DISCUSSION

Composition of the complexes

The analytical data for the newly synthesized complexes listed in Table 1 indicate that there is one morpholinium ion, one lanthanide ion, four morpholine-4-carbodithioate groups and one water molecule in each of the complex molecules.

IR spectra

The most important IR peaks of the ligand morpholinium salt and the complexes are reported in Table 2.

The presence of a single, strong band due to a ν(CSS) mode in the range 998–1005 cm^{-1} in the spectra of the complexes is strongly indicative of bidentate behaviour of the dithio ligand in the complexes;[3,4] otherwise a doublet is expected in the $1000 \pm 70\ cm^{-1}$ region for the case of monodentate coordination.[11,12] Analysis of the position of the ν(C···N) mode, in the range 1462–1469 cm^{-1}, gives further confirmation of the above suggested behaviour: this band, in fact, undergoes a blue shift in all the complexes, while for unidentate coordination this stretching mode would be shifted towards lower wavenumbers or would remain unchanged at the value of the free carbodithioate sodium salt.[13]

In the far-IR region, the bands of the ligand appear unchanged in the spectra of the complexes; in addition, new bands, absent in the spectra of the starting materials, are present in the 331–358 cm^{-1} range, which may be assigned as the ν(M—S) stretching frequency.[3,14]

In all the IR spectra of the complexes, medium and weak bands are present near 3400 cm^{-1} and in the 1630–1638 cm^{-1} range, respectively, which are clearly due to ν(OH) and δ(HOH), respectively. The absence of the vibrational modes activated by coordination to the metal (wagging, twisting and rocking)

Table 1. Analytical data

Compound[a]	%N Found (Calc.)	%C Found (Calc.)	%H Found (Calc.)	%M Found (Calc.)
$MorphH_2[La(MorphCS_2)_4]\cdot H_2O$	8.0 (7.8)	31.9 (32.2)	5.1 (5.0)	15.6 (15.5)
$MorphH_2[Pr(MorphCS_2)_4]\cdot H_2O$	7.8 (7.8)	32.0 (32.1)	5.1 (4.9)	15.8 (15.7)
$MorphH_2[Nd(MorphCS_2)_4]\cdot H_2O$	8.2 (7.8)	31.8 (32.0)	5.1 (4.9)	16.1 (16.0)
$MorphH_2[Sm(MorphCS_2)_4]\cdot H_2O$	7.8 (7.7)	31.2 (31.8)	5.1 (4.9)	16.7 (16.6)
$MorphH_2[Eu(MorphCS_2)_4]\cdot H_2O$	7.8 (7.7)	31.5 (31.8)	5.0 (4.9)	16.8 (16.8)
$MorphH_2[Gd(MorphCS_2)_4]\cdot H_2O$	7.8 (7.7)	31.6 (31.6)	5.1 (4.9)	17.6 (17.2)

[a] Morph = morpholino ($\overline{CH_2CH_2OCH_2CH_2N}$—).

Table 2. Most important IR bands (cm^{-1})

Compound	ν(CSS)	ν(C···N)	ν(M—S)	ν(O—H) and ν(N—H)	δ(HOH)
$MorphH_2(MorphCS_2)$	984s	1448s		3388w	
$MorphH_2[La(MorphCS_2)_4]\cdot H_2O$	998s	1462s	358w	3388m	1630w
$MorphH_2[Pr(MorphCS_2)_4]\cdot H_2O$	998s	1469s	349w	3402m	1630w
$MorphH_2[Nd(MorphCS_2)_4]\cdot H_2O$	998s	1469s	346w	3409m	1631w
$MorphH_2[Sm(MorphCS_2)_4]\cdot H_2O$	1005s	1462s	331w	3374m	1631w
$MorphH_2[Eu(MorphCS_2)_4]\cdot H_2O$	1005s	1462s	335w	3367m	1638w
$MorphH_2[Gd(MorphCS_2)_4]\cdot H_2O$	1005s	1462s	332w	3367m	1638w

suggests that coordinated water is not present and these results are confirmed by the thermogravimetric studies (see below).

Electronic spectra

The electronic spectra are given in Table 3. All the complexes show three absorption bands due to the chromophore group NCS_2[15] (these absorptions are labelled as Band I, Band II and Band III).

Band I is assigned to an intramolecular charge transfer in the ligand, i.e. a $\pi \rightarrow \pi^*$ transition located mainly in the N···C···S group.[16,17] Band II is attributed to a $\pi \rightarrow \pi^*$ transition of the S···C···S group.[18] This band does not undergo splitting and this fact clearly indicates the equivalence of the C···S bands in the complexes. Band III is a low intensity band assigned to an $n \rightarrow \pi^*$ transition, i.e. a transition of an electron of the lone pair on the sulphur atom to an antibonding π-orbital.[19] It can be seen from Table 3 that Bands II and III, but not Band I, undergo a considerable violet shift upon complexation. This change can be attributed to the formation of M—S bonds and the deviation of the electron cloud around the sulphur atoms, the electron donors, towards the lanthanide ions, which decreases the π–π and p–π conjugate effects in the chromophore group and increases the energy needed for the π–π^* and n–π^* transitions. This results in the absorption bands shifting towards shorter wavelengths.

Thermal analyses

Thermal analysis studies were performed by means of TG and DTA techniques.

The processes of thermal decomposition for all the complexes are almost the same. After the loss of one water molecule in the 27–70°C range, the complexes decompose very rapidly between 126 and 270°C. Then continuous weight loss is detected up to 850°C. At this temperature Ln_2O_3 (Pr_6O_{11} for the praseodymium complex) is formed.

Solubility and molar conductance

All the complexes are hardly soluble in ethyl ether and cyclohexane, but are soluble in methanol, ethanol, acetone and tetrahydrofuran, and are readily soluble in acetonitrile and methylene dichloride. The molar conductance values of the complexes measured in acetonitrile at 25°C lie in the range

Table 3. The electronic spectra (nm)

Compound	Band I	Band II	Band III
$MorphH_2(MorphCS_2)$	211	284	309
$MorphH_2[La(MorphCS_2)_4]\cdot H_2O$	211	274	301
$MorphH_2[Pr(MorphCS_2)_4]\cdot H_2O$	210	272	296
$MorphH_2[Nd(MorphCS_2)_4]\cdot H_2O$	211	271	299
$MorphH_2[Sm(MorphCS_2)_4]\cdot H_2O$	209	269	298
$MorphH_2[Eu(MorphCS_2)_4]\cdot H_2O$	209	268	298
$MorphH_2[Gd(MorphCS_2)_4]\cdot H_2O$	210	268	296

124.4–128.3 Ω^{-1} cm^2 mol^{-1}, which indicates that all the complexes are 1 : 1 electrolytes and that each of the complex molecules dissociates as one cation and one anion in solution.[20]

From the above discussion it can be concluded that the new complexes reported in this paper are ion-association types of coordination compounds. In each of the complexes four carbodithioate groups, acting as uninegative bidentate ligands, are coordinated to a lanthanide ion through eight sulphur atoms to form a complex anion and the morpholinium cation lies outside of the coordination shell. This coordination state was also found in other types of lanthanide carbodithioate complexes.[7,21]

REFERENCES

1. G. E. Manoussakis and C. A. Tsipis, *J. Inorg. Nucl. Chem.* 1973, **35**, 743.
2. G. Marcotrigiano, G. C. Pellacani and C. Preti, *J. Inorg. Nucl. Chem.* 1974, **36**, 3709.
3. C. Preti, G. Tosi and P. Zannini, *J. Molec. Struct.* 1980, **65**, 283.
4. R. C. Aggarwal, R. Bala and R. L. Prasad, *Spectrochim. Acta* 1986, **42A**, 725.
5. S. P. Mital, S. K. Sharma, R. V. Singh and J. P. Tandon, *Curr. Sci.* 1981, **50**, 483.
6. P. Biscarini, *Inorg. Chim. Acta* 1983, **74**, 65.
7. Huang Jinshun, Lin Shanhuo, Wang Manfang, Zhang Qianer and Lu Jiaxi, *J. Inorg. Chem. Chin.* 1987, **3**, 1.
8. Tang Ning, Zhu Hailiang, Tan Minyu, Gan Xinmin and Wang Xin, *Acta Chim. Sin.*, in press.
9. A. R. Pray, *Inorganic Syntheses*, Vol. 5, p. 153. McGraw-Hill, New York (1957).
10. J. S. Fritz and S. A. Sutton, *Analyt. Chem.* 1956, **28**, 1301.
11. F. Bonati and R. Ugo, *J. Organomet. Chem.* 1967, **10**, 257.
12. T. N. Srivastava and V. Kumar, *J. Organomet. Chem.* 1976, **107**, 55.
13. C. O'Connor, J. D. Gilbert and G. Wilkinson, *J. Chem. Soc. A* 1969, 84.
14. D. Perry and R. A. Geanangel, *Inorg. Chim. Acta* 1975, **13**, 185.
15. C. K. Jorgensen, *Inorganic Complexes*. Academic Press, London (1963).
16. C. K. Jorgensen, *J. Inorg. Nucl. Chem.* 1962, **24**, 1571.
17. F. Takami, S. Wakahara and T. Maeda, *Tetrahedron Lett.* 1971, 2645.
18. M. J. Janssen, *Recl. Trav. Chim.* 1960, **79**, 1066.
19. M. J. Janssen, *Recl. Trav. Chim.* 1960, **79**, 454.
20. W. J. Geary, *Coord. Chem. Rev.* 1971, **7**, 81.
21. Tian Yongchi, Zhao Fengyun, Liu Juzheng and Liang Yingqiu, *J. Struct. Chem.* 1985, **4**, 115.

Polyhedron Vol. 9, No. 6, pp. 863–874, 1990
Printed in Great Britain

0277–5387/90 $3.00+.00
© 1990 Pergamon Press plc

PREPARATION AND STRUCTURAL PROPERTIES OF MONONUCLEAR AND BINUCLEAR RUTHENIUM(II) CYCLOPENTADIENYL COMPLEXES WITH 4-CYANOPYRIDINE AND 4-CYANOPYRIDINE 1-OXIDE

A. MISHRA, K. MISHRA* and U. C. AGARWALA†

Department of Chemistry, Indian Institute of Technology, Kanpur—208016, India

(*Received* 16 *August* 1989; *accepted* 20 *October* 1989)

Abstract—Reactions of $[Ru(\eta^5\text{-}C_5H_5)L_2Cl]$ (L = PPh_3 or $AsPh_3$, L_2 = $Ph_2PCH_2CH_2PPh_2$ or $Ph_2PCH_2PPh_2$) have been carried out with 4-cyanopyridine and 4-cyanopyridine 1-oxide in the presence of suitable anions (PF_6^- or BPh_4^-). The reaction products were found to be cationic mono- and binuclear complexes which have been characterized by elemental analyses, spectroscopic (IR, UV–vis and NMR) and electrochemical studies. Conductivity measurements have also been carried out to confirm the charges on these cationic species.

In extending our studies related to the properties of $[Ru(\eta\text{-}C_5H_5)(EPh_3)_2Cl]$ (E = P, As or Sb) we became interested in the interaction of these molecules with 4-cyanopyridine and its corresponding oxide. Although several detailed reports concerning the complexes of these ligands with metal ions have been published,[1–13] our primary interest in undertaking such a study was (a) to ascertain the relative donor capabilities of these ligands, (b) to examine the nature of the ruthenium(II) orbitals' (d^6) interaction with the low-lying vacant ligand orbitals while the set of "spectator" ligands are also donors, and (c) to investigate the possibility of the formation of cyclopentadienyl-containing ruthenium(II) bi- and/or polynuclear-bridged complexes.

This paper describes the characterized products of the reactions of 4-cyanopyridine and 4-cyanopyridine 1-oxide with $[Ru(\eta^5\text{-}C_5H_5)(EPh_3)_2Cl]$ and $[Ru(\eta^5\text{-}C_5H_5)(L—L)Cl]$ (E = P or As; L—L = dppe or dppm). Their structural properties have been discussed and the influence of the asymmetric nature of these ligands on the structure of the complexes has been assessed.

EXPERIMENTAL

Pure chemicals and dry solvents[14] were used in the reactions. $[Ru(\eta^5\text{-}C_5H_5)Cl(EPh_3)_2]$ and $[Ru(\eta^5\text{-}C_5H_5)(L—L)Cl]$ (E = P or As; L—L = dppe or dppm) were prepared by literature methods.[15–18] 4-Cyanopyridine and 4-cyanopyridine 1-oxide (Aldrich) were purified prior to their use by recrystallization from 95% ethanol. HPLC grade deaerated acetonitrile (distilled over $KMnO_4$ and P_2O_5) for spectral and electrochemical measurements and spectroscopic grade solvents for the study of solvatochromism and conductivity measurements were used.

Analytical, spectral and conductivity data of the products were obtained as described elsewhere.[16] The electronic and ^{13}C NMR spectra of the complexes were recorded on a Shimadzu UV 190 and a JEOL FT-90 spectrophotometer, respectively. Cyclic voltammetry experiments were carried out on a MPI model MP-1042 cyclic voltameter.

Preparation of complexes

Reactions of $[Ru(\eta^5\text{-}C_5H_5)L_2Cl]$ (L = PPh_3 or $AsPh_3$; L_2 = dppe or dppm) with 4-cyanopyridine and 4-cyanopyridine 1-oxide.

(a) *Preparation of the complexes* $[Ru(\eta^5\text{-}C_5H_5)L_2(4\text{-}CNpy)]X$ *and* $[Ru(\eta^5\text{-}C_5H_5)L_2(4\text{-}CNpyo)]X$ (L = PPh_3 *or* $AsPh_3$; L_2 = dppe *or* dppm; X^- = Cl^-, PF_6^- *or* BPh_4^-). In a typical reaction, addition of 4-cyanopyridine (0.57 mmol) or 4-cyanopyridine 1-oxide (0.33 mmol) to a suspension of $[Ru(\eta^5\text{-}C_5H_5)L_2Cl]$ (0.13 mmol) in methanol (50 cm^3), followed by heating under reflux (Table 1), yielded a yellow coloured solution. This was

*Present address: Defence Materials & Stores Research & Development Establishment, P.B. No. 320, Kanpur, India.

†Author to whom correspondence should be addressed.

Table 1. (a) Preparation, analytical data and physical properties of the complexes

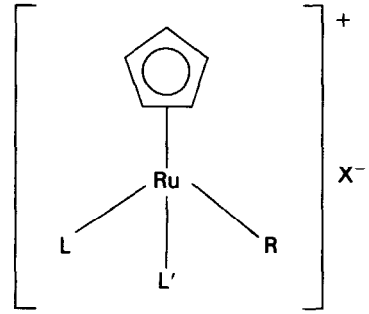

Compound number	Ligand L	Ligand L'	Ligand R	Anion X	Time (h)	Colour (m.p./°C)	Found(calc) (%) C	H	N	IR band (CN), cm^{-1}	^1H NMR (C_5H_5), ppm	^{13}C NMR (C_5H_5), ppm
1	P	P	4-CNpy	Cl	6	Tan (105)	68.2 (67.9)	4.41 (4.69)	3.1 (3.37)	2240	4.6(s)	83.0, 84.5
2	P	P	4-CNpy	BPh_4	—	Brown (150)	75.8 (76.5)	5.2 (5.3)	2.7 (2.5)	2248	4.58(s)	83.2, 84.5
3	P	P	4-CNpy	PF_6	—	Reddish-brown (158–160)	59.3 (60.1)	4.3 (4.15)	2.4 (3.0)	2245	4.6(s)	83.59, 84.9
4	A	A	4-CNpy	Cl	8	Tan (94)	62.1 (61.4)	4.6 (4.2)	2.9 (3.0)	2243	4.62(s)	83.0, 84.6
5	A	A	4-CNpy	BPh_4	—	Brown (155)	70.7 (70.9)	5.1 (4.9)	2.4 (2.3)	2243	4.58(s)	83.6, 84.6
6	A	A	4-CNpy	PF_6	—	Reddish-brown (164–166)	53.8 (54.9)	4.0 (3.8)	3.1 (2.7)	2245	4.6(s)	83.2, 84.0
7	A	P	4-CNpy	Cl	6	Tan (100)	64.9 (64.5)	4.9 (4.5)	2.9 (3.2)	2242	4.6(s)	83.4, 84.8
8	A	P	4-CNpy	BPh_4	—	Brown (153)	74.0 (73.6)	5.5 (5.1)	2.8 (2.4)	2243	4.64(s)	83.0, 84.2
9	A	P	4-CNpy	PF_6	—	Reddish-brown (160)	56.9 (57.4)	4.3 (3.9)	2.2 (2.8)	2242	4.6(s)	83.5, 84.5
10	dppe		4-CNpy	Cl	10	Yellow (130)	62.8 (63.1)	4.8 (4.7)	3.89 (3.97)	2243	4.98(s)	81.0, 82.5
11	dppe		4-CNpy	BPh_4	—	Brown (164)	74.8 (74.2)	5.7 (5.4)	3.1 (2.8)	2245	4.8(s)	81.0, 82.4

12	dppe		4-CNpy	PF_6	—	Yellowish-brown (165)	53.9 (54.6)	4.06 (4.05)	3.1 (3.4)	2244	4.92(s)	81.4, 82.6
13	dppm		4-CNpy	Cl	12	Yellow (135)	63.1 (62.6)	4.2 (4.5)	3.9 (4.1)	2245	4.9(s)	81.0, 81.9
14	dppm		4-CNpy	BPh_4	—	Brown (158)	54.8 (54.0)	3.9 (3.8)	3.2 (3.5)	2243	4.9(s)	81.5, 82.9
15	dppm		4-CNpy	PF_6	—	Yellowish-brown (160)	74.6 (73.9)	5.4 (5.24)	2.6 (2.9)	2242	4.86(s)	81.5, 82.5
16	P	P	4-CNpyO	Cl	5	Yellow (120)	66.8 (66.6)	3.94 (4.6)	3.8 (3.3)	2238, 1295	4.6(s)	84.0(s)
17	P	P	4-CNpyO	BPh_4	—	Yellow (140)	74.8 (75.4)	5.59 (5.2)	2.78 (2.48)	2240, 1298	4.6(s)	84.3(s)
18	P	P	4-CNpyO	PF_6	—	Yellow (148)	58.8 (59.0)	4.3 (4.1)	2.7 (2.93)	2238, 1290	4.65(s)	83.9(s)
19	A	P	4-CNpyO	Cl	5	Yellow (115–120)	63.8	4.5	3.7	2237, 1310	4.6(s)	83.3(s)
20	A	P	4-CNpyO	BPh_4	—	Yellow (130)	73.0 (72.6)	5.3 (5.0)	2.5 (2.38)	2240, 1300	4.5(s)	84.0
21	A	P	4-CNpyO	PF_6	—	Yellow (145)	56.9 (56.4)	3.3 (3.9)	2.5 (2.8)	2238, 1295	4.6(s)	84.5
22	A	A	4-CNpyO	Cl	5	Yellow (125)	61.0 (60.3)	4.4 (4.2)	3.1 (2.9)	2240, 1300	4.7(s)	83.5(s)
23	A	A	4-CNpyO	BPh_4	—	Yellow (128)	69.3 (70.0)	5.2 (4.8)	2.5 (2.3)	2236, 1305	4.68(s)	83.8(s)
24	A	A	4-CNpyO	PF_6	—	Yellow (143)	54.5 (54.0)	4.2 (3.7)	3.2 (2.7)	2237, 1298	4.6(s)	84.0(s)
25	dppe		4-CNpyO	Cl	6	Yellow (125–130)	62.1 (61.6)	4.9 (4.6)	4.2 (3.8)	2236, 1305	4.9(s)	83.17(s)
26	dppe		4-CNpyO	BPh_4	—	Yellow (152)	73.4 (72.9)	5.5 (5.3)	3.0 (2.8)	2238, 1298	4.96(s)	83.2(s)
27	dppe		4-CNpyO	PF_6	—	Yellow (150)	54.0 (53.5)	4.3 (3.9)	3.6 (3.3)	2239, 1305	4.92(s)	83.4(s)
28	dppm		4-CNpyO	Cl	6	Yellow (132)	61.8 (61.2)	4.9 (4.4)	4.2 (3.9)	2242, 1295	4.9(s)	83.0(s)
29	dppm		4-CNpyO	BPh_4	—	Yellow (148)	72.2 (72.6)	5.6 (5.2)	3.0 (2.8)	2238, 1300	4.84(s)	83.6(s)
30	dppm		4-CNpyO	PF_6	—	Yellow (145)	53.8 (53.0)	4.2 (3.8)	3.8 (3.4)	2239, 1305	4.86(s)	83.2(s)

Table 1. (b) Analytical data and physical properties of the complexes

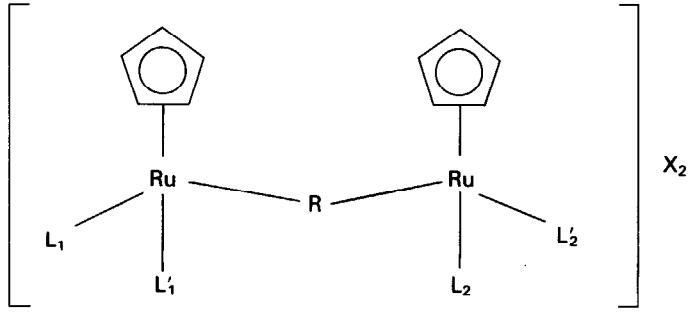

Compound number	Ligands L_1	L'_1	L_2	L'_2	R	X^- anion	Colour (m.p./°C)	Found(calc) (%) C	H	N	IR band (CN), cm^{-1}	^1H NMR (C_5H_5), ppm	^{13}C NMR (C_5H_5), ppm
31	P	P	P	P	4-CP	BPh_4	Maroon 160 dec	76.2 (76.9)	5.4 (5.37)	1.2 (1.3)	2238	4.3, 4.75	83.0, 84.5
32	P	P	P	P	4-CP	PF_6	Orangish-brown (165–170)	60.2 (59.5)	4.4 (4.17)	1.62 (1.57)	2236	4.3, 4.8	83.2, 84.4
33	P	P	A	A	4-CP	BPh_4	Maroon (158)	74.6 (73.8)	5.5 (5.2)	1.6 (1.26)	2237	4.2, 4.7	83.3, 84.8
34	P	P	A	A	4-CP	PF_6	Orangish-brown (168)	56.9 (56.7)	4.2 (3.9)	1.8 (1.5)	2236	4.28, 4.7	83.5, 84.5
35	A	P	A	P	4-CP	PF_6	Brown (165)	57.0 (56.7)	4.3 (3.9)	1.7 (1.5)	2235	4.3, 4.8	83.0, 84.4
36	A	A	A	A	4-CP	BPh_4	Maroon (155)	70.7 (71.0)	4.3 (4.9)	1.53 (1.2)	2235	4.3, 4.68	82.9, 84.0
37	A	A	A	A	4-CP	PF_6	Orangish-brown (168–170)	54.7 (54.1)	4.1 (3.8)	1.7 (1.4)	2237	4.4, 4.8	83.0, 84.5

38	dppe		P	P	4-CP	BPh_4	Maroon (142–145)	75.2 (75.7)	5.5 (5.3)	1.6 (1.4)	2238	4.34, 4.7	81.9, 82.6
39	dppe		A	A	4-CP	BPh_4	Maroon (140)	72.9 (72.5)	5.8 (5.2)	1.6 (1.3)	2240	4.4, 4.74	82.0, 82.9
40	dppe		dppe		4-CP	BPh_4	Maroon (148)	71.1 (71.6)	5.7 (5.3)	1.8 (1.4)	2238	4.4, 4.69	81.3, 82.7
41	dppm		P	P	4-CP	BPh_4	Maroon (145)	74.5 (75.6)	5.4 (5.34)	1.28 (1.4)	2237	4.3, 4.7	81.3, 82.2
42	dppm		A	A	4-CP	BPh_4	Brown (138)	72.9 (72.5)	5.8 (5.2)	1.6 (1.3)	2240	4.4, 4.6	80.8, 82.7
43	dppm		dppm		4-CP	PF_6	Brown (135–140)	51.2 (50.6)	4.2 (3.7)	2.3 (1.8)	2238	4.3, 4.5	81.2, 82.5
44	P	P	P	P	4-CNpyO	BPh_4	Yellowish-brown (148)	76.9 (76.3)	5.7 (5.3)	1.6 (1.3)	2230, 1294	4.7(s)br	83.4, 84.2
45	P	P	P	P	4-CNpyO	PF_6	Yellow (130–132)	58.3 (58.9)	4.6 (4.1)	1.8 (1.56)	2232, 1295	4.62(s)br	83.9, 84.5
46	A	P	A	P	4-CNpyO	PF_6	Yellow (142)	56.8 (56.2)	4.4 (3.9)	1.9 (1.5)	2230, 1290	4.7(s)br	83.4, 84.2
47	A	A	A	A	4-CMpyO	PF_6	Yellowish-brown (145)	54.0 (53.7)	3.9 (3.7)	1.78 (1.4)	2234, 1295	4.68(s)br	84.0, 84.8
48	P	P	A	A	4-CNpyO	PF_6	Yellowish-brown (145–148)	56.8 (56.2)	4.3 (3.9)	1.8 (1.5)	2236, 1292	4.7(s)br	83.8, 84.6
49	dppe		dppe		4-CNpyO	PF_6	Yellow (155)	45.9 (45.2)	3.9 (3.4)	2.4 (1.8)	2232, 1290	4.9(s)br	81.9, 82.3
50	dppm		dppm		4-CNpyO	PF_6	Yellowish-brown (152)	44.9 (44.5)	3.8 (3.2)	2.2 (1.9)	2234, 1295	4.86(s)	82.0, 83.6

P = PPh_3; A = $AsPh_3$; dppe = 1,2 bis-diphenylphosphinoethane; dppm = 1,2 bis-diphenylphosphinomethane; 4-CNpy = 4-cyanopyridine; 4-CNpyO = 4-cyanopyridineoxide.

filtered, evaporated to dryness under reduced pressure and the residue was extracted with dichloromethane. Addition of about 50 cm^3 of petroleum ether to the extract yielded a microcrystalline product. This was separated by centrifugation, washed several times with petroleum ether and dried *in vacuo*. The chloro complex thus obtained, was purified by neutral alumina column chromatography (25 cm). The complex was dissolved in methanol (10 cm^3) and passed through the column, and the major band was eluted with a 1 : 1 mixture of methanol and acetone. The resulting solution was evaporated to dryness and the residue was extracted with dichloromethane. From the extract the complex was precipitated by petroleum ether. It was separated by centrifugation, washed several times with petroleum ether and dried *in vacuo*. The complex was analysed as $[Ru(\eta^5\text{-}C_5H_5)L_2(4\text{-}CNpy)]Cl$ (yield, *ca* 40%) or $[Ru(\eta^5\text{-}C_5H_5)L_2(4\text{-}CNpyo)]Cl$ (yield, *ca* 50%).

The corresponding tetraphenylborate and hexafluorophosphate salts of the monomeric cyanopyridine and cyanopyridine 1-oxide complexes were obtained by precipitating the complexes by adding $NaBPh_4$ (0.06 mmol) and NH_4PF_6 (0.12 mmol), respectively, to a solution of the chloro complexes in 20 cm^3 of methanol, followed by brief stirring for about 20 min. These were filtered, and washed several times with methanol and ether. The compounds were purified by dissolving in 5 cm^3 of dichloromethane and eluting on a neutral alumina column (25 cm) with a 1 : 1 mixture of CH_2Cl_2 and acetone. The eluant was dried *in vacuo*, the residue was extracted with CH_2Cl_2 and from the extract the complex was precipitated with petroleum ether. The precipitates after washing and drying were analysed as $[Ru(\eta^5\text{-}C_5H_5)L_2(4\text{-}CNpy)]X$ (yield, *ca* 40%) and $[Ru(\eta^5\text{-}C_5H_5)L_2(4\text{-}CNpyo)]X$ (yield, *ca* 45%) (X = BPh_4^- or PF_6^-).

(b) *Preparation of the dimeric complexes* $[(\eta^5\text{-}C_5H_5)L_2Ru\text{-}4CNpy\text{-}RuL'_2(\eta^5\text{-}C_5H_5)]X_2$ *and* $[(\eta^5\text{-}C_5H_5)L_2Ru4CNpyoRuL'_2(\eta^5\text{-}C_5H_5)]X_2$ (L,L′ = PPh_3 *or* $AsPh_3$; L_2,L'_2 = dppe *or* dppm; X = BPh_4^- *or* PF_6^-). A typical reaction procedure is as follows. $[Ru(\eta^5\text{-}C_5H_5)ClL_2]$ (0.13 mmol) was added to a 50 cm^3 methanolic solution of $[Ru(\eta^5\text{-}C_5H_5)L'_2(4\text{-}CNpy)]Cl$ (0.13 mmol) or $[Ru(\eta^5\text{-}C_5H_5)L'_2(4CNpyo)]Cl$ (0.13 mmol). The resulting mixture was stirred overnight, whereupon the starting complex $[Ru(\eta^5\text{-}C_5H_5)L_2Cl]$ gradually dissolved. The resulting solution was filtered and $NaBPh_4$ (0.12 mmol) was added to the filtrate, followed by stirring for a brief period. The precipitated complex was separated by centrifugation, washed with methanol and purified chromatographically on a neutral alumina column.

The corresponding hexafluorophosphate salt of the binuclear complex was obtained by adding NH_4PF_6 (0.12 mmol) in place of $NaBPh_4$, followed by stirring the solution for 0.5 h. The solution was evaporated to dryness under reduced pressure. The residue was dissolved in CH_2Cl_2 and the PF_6^- complex was precipitated by the addition of petroleum ether to the extract. BPh_4 or PF_6 salts of binuclear cyanopyridine or cyanopyridine 1-oxide were dissolved in about 5–10 cm^3 of CH_2Cl_2 and passed through a neutral alumina column for purification. The major band was eluted with a 1 : 1 mixture of CH_2Cl_2 and acetone. The eluant was evaporated to dryness and the complex was obtained by extracting the residue with CH_2Cl_2 and precipitating with petroleum ether. It was centrifuged, washed several times with petroleum ether and dried *in vacuo*. It was then analysed for $[(\eta^5\text{-}C_5H_5)L_2Ru\text{-}4CNpy\text{-}RuL'_2(\eta^5\text{-}C_5H_5)]X_2$ (yield, *ca* 35%) or $[(\eta^5\text{-}C_5H_5)L_2Ru4CNpyoRuL'_2(\eta^5\text{-}C_5H_5)]X_2$ (yield, *ca* 30%) (X = BPh_4^- or PF_6^-).

RESULTS AND DISCUSSION

Reactions of $[Ru(\eta^5\text{-}C_5H_5)L_2Cl]$ (L = PPh_3 or $AsPh_3$; L_2 = dppe or dppm) with 4-cyanopyridine in the presence of suitable anions (PF_6^- or BPh_4^-) yield reddish-brown mononuclear and maroon-coloured binuclear complexes, and with 4-cyanopyridine-1-oxide, bright yellow mononuclear and yellowish-brown binuclear cationic complexes. Microanalytical data suggest the formulae given in Table 1. They are non-hygroscopic, readily soluble in chloroform, dichloromethane, acetone, acetonitrile, benzene and other organic solvents, but insoluble in light petroleum and diethyl ether. The chloride salts are readily soluble, while those of PF_6^- or BPh_4^- are only slightly soluble in methanol. All the complexes become adsorbed in the cationic ion-exchanger suggesting their cationic nature.

Conductivity measurements

The elecrolyte behaviour of the complexes was determined by their conductivity measurements in nitromethane using the Feltham and Hayter procedure.[19] From the measured values of the equivalent conductance (λ_e) in the concentration range of 10^{-2}–10^{-4} equiv dm^{-3}, λ_0 was determined by extrapolating the straight lines [Fig. 1(b)] and subsequently values of $(\lambda_0 - \lambda_e)$ [Fig. 1(a)] were plotted as a function of $\sqrt{c}$.[20–22] The respective slopes of the mono- (216) and binuclear (420) complexes of the straight lines for the 4-cyanopyridine complexes compared very well with those of the Feltham's values for 1 : 1 and 1 : 2 species in nitromethane.[23,24]

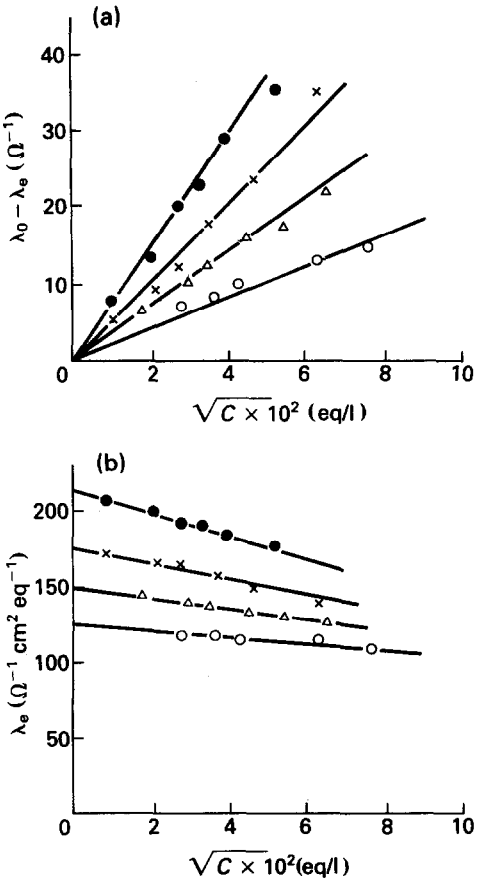

Fig. 1. (a) Plots of $\lambda_0 - \lambda_e$ vs $\sqrt{c}$; (b) plots of λ_e vs $\sqrt{c}$ for the complexes: ○ $[(\eta^5\text{-}C_5H_5)Ru(4\text{-}CNpy)(PPh_3)_2]PF_6$; × $[(\eta^5\text{-}C_5H_5)_2Ru_2(\mu\text{-}4\text{-}CNpy)(PPh_3)_4](PF_6)_2$; △ $[(\eta^5\text{-}C_5H_5)Ru(4\text{-}CNpyO)(PPh_3)_2]PF_6$; ● $[(\eta^5\text{-}C_5H_5)_2Ru_2(\mu\text{-}4\text{-}CNpyO)(PPh_3)_4](PF_6)_2$.

The corresponding slopes (358 and 728) for 4-cyanopyridine 1-oxide complexes, though a little high, also fall well within the range reported by them for 1 : 1 and 1 : 2 electrolytes.

IR spectra

The shifts in the positions of ν(CN) and the pyridine ring vibrations have been used to elucidate the site of coordination of the cyanopyridines. Coordination through the nitrogen of the nitrile group should result in an increase in ν(CN), while coordination through the pyridine nitrogen should lead to characteristic shifts in the positions of pyridine ring vibrations without much change in the position of ν(CN).

The IR spectra of all mononuclear complexes of cyanopyridine and its oxide exhibited bands of $\nu(C{\equiv}N)$ around 2240 cm^{-1} (Table 1) (ν(CN) for free ligand = 2243 cm^{-1}). Thus suggesting that the linkage of ruthenium is through the aromatic nitrogen of 4-cyanopyridine and through oxygen of the NO group of 4-cyanopyridine 1-oxide, in keeping with earlier observations.[7,11–13,25–28] An insignificant shift (± 3 cm^{-1}) in the positions of ν(CN) is not unexpected and could arise from both resonance and electronic effects (π-backbonding) due to bonding with the metal ion centre. Further support of ruthenium bonding to the aromatic nitrogen of cyanopyridine complexes comes from the blue shifts in the positions of $\nu(C{\cdots}C)$ and $\nu(C{\cdots}N)$ of cyanopyridines in the region 1400–1600 cm^{-1}.[5,7,28]

In monomeric, 4-cyanopyridine 1-oxide complexes the oxygen atom of the N-oxide group having partial negative charge coordinates to the ruthenium(II) nucleus. The contributing resonance structure of 4-cyanopyridine 1-oxide may be shown by a dipolar representation indicating charge separation and the polar character of the N—O bond, where the oxygen atom is regarded as an addition to the molecule of 4-cyanopyridine. The NO stretching vibration in the complexes appeared at higher frequency relative to that in the free 4-cyanopyridine 1-oxide (1280 cm^{-1}) (Table 1). Bands due to ν(NO) in monomeric complexes appeared around 1305 cm^{-1}. The blue shift indicated its coordination to the metal centre. In dimeric complexes in which the uncoordinated CN group of the monomeric complexes coordinates to another ruthenium centre, a decrease in the position of ν(CN) (2232 cm^{-1}) relative to that in the free ligand was observed.[29] The reason for this expected decrease could be attributed to the metal ($d\pi$) → ligand π^*-backbonding.

^{1}H NMR spectra

In the ^{1}H NMR spectra of monomeric 4-CNPy and 4-CNPy 1-oxide complexes with $PPh_3/AsPh_3$ as co-ligands, η^5-C_5H_5 protons appeared as a singlet around δ 4.6, whereas in complexes containing dppe or dppm, they occurred around δ 4.9 (Table 1). The downfield shift of η^5-C_5H_5 protons relative to the starting complexes (δ 4.1 in $PPh_3/AsPh_3$; δ 4.5 in dppe/dppm) may result from the change of electron density on ruthenium due to backbonding from metal to 4-CNPy, and more so because of the presence of a strong electron-withdrawing —CN group substituted in the para-position of the pyridine ring. The electron-withdrawing, as well as the conjugative ability of the —CN, pulls the electron density away from the pyridine nucleus towards itself, which affects the electron deficiency on the ruthenium metal. It may consequently lead to a pull of more electrons from C_5H_5 towards the ruthenium centre resulting in deshielding of the C_5H_5 protons.

In binuclear cyanopyridine cationic complexes, η^5-C_5H_5 protons resonate around δ 4.3 and 4.75 as two separate peaks, suggesting a difference in the local electron density on the protons of the two η^5-C_5H_5 molecules present in the binuclear complexes. This could arise because of the difference in the nature of M—L bonding of two ruthenium centres. In complexes of 4-cyanopyridine 1-oxide, the signal for C_5H_5 protons appeared as a broad singlet around δ 4.7 (Table 1). Since the difference in the positions of two signals in binuclear complexes should be sensitive to the nature of L, it is therefore possible that the two resonances in the 4-cyanopyridine 1-oxide complexes should appear in very similar positions, resulting in signal broadening. Furthermore, the signals from binuclear complexes appeared at higher field with respect to those from mononuclear complexes. This behaviour can be anticipated if one considers the fact that the two ruthenium(II) ions in a binuclear complex compete to donate the electron density to 4-cyanopyridine (or 4-cyanopyridine 1-oxide) through π-backbonding both from the cyano nitrogen and the aromatic nitrogen (or through the oxygen of the N → O moiety). This competition would result in the net reduction of the π-bonding effect on the C_5H_5 protons (Structure 1) in binuclear complexes compared to that in mononuclear ones. The signals for the α-protons of the pyridine were observed towards higher field (δ 8.3–8.5) in both mono- and binuclear complexes of 4-cyanopyridine and 4-cyanopyridine 1-oxide relative to ones reported for the free 4-cyanopyridine ligand (δ 9.05).[30–32] This upfield shift is ascribed to the "paramagnetic" anisotropy of ruthenium(II) arising due to temperature independent paramagnetism, as expected of the metal centre.[30] The difference in the signal positions of the cyanopyridine and cyanopyridine 1-oxide complexes may perhaps be caused by the variation in the "paramagnetic" anisotropic effect. It also suggests that a degree of $d\pi$–$p\pi$ backbonding influences the chemical shifts of the hydrogens. The β-protons in the majority of these complexes exhibited shifts towards higher field (δ 7.0–7.9). Since this region was found to be dominated by broad multiplets of aromatic phenyl protons of PPh_3, $AsPh_3$, dppe or dppm co-ligands, the pyridine protons, signals could not be distinguished from them. The experimental observations of upfield shifts of these protons, could again be explained by the higher "shielding" effect caused by the enhanced, stronger π-backbonding from the ruthenium(II) to cyanopyridine group.

^{13}C *NMR*

The ^{13}C NMR spectra of these complexes also support the conclusions drawn from ^1H NMR. The η^5-C_5H_5 carbons in the mononuclear 4-cyanopyridine 1-oxide complexes appeared as a singlet (δ 84.0), towards the downfield side relative to the C_5H_5 carbons (δ 81.5) in the starting complexes. In binuclear complexes with PPh_3/$AsPh_3$ as co-ligands, the spectra exhibited two signals around δ83.0 and 84.5 and in those with dppe/dppm as co-ligands, around δ 81.0 and 82.5. The phenyl carbons in all these complexes exhibited sharp multiplets in the expected region for aromatic carbon (*ca* δ 128–137). The cyanide carbon (—CN) underwent a downfield shift both in mono- and binuclear complexes (δ 119.6, sharp singlet in the mononuclear and δ 121.5 in the binuclear complexes) compared

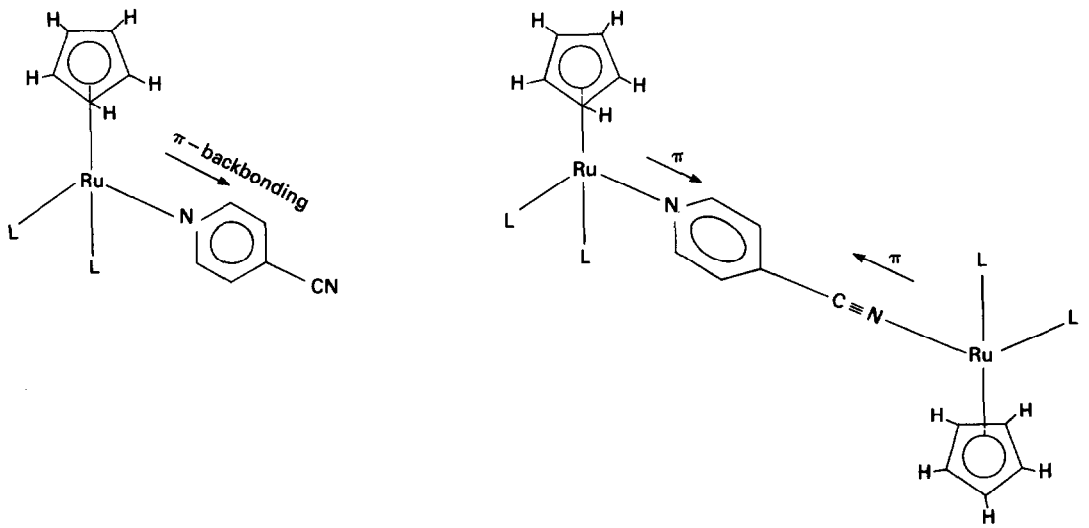

Structure 1.

to the value in the free ligand (δ 117.6). This downfield shift indicated deshielding of the carbon atoms on coordination to the metal atom. Coordination of 4-cyanopyridine or 4-cyanopyridine 1-oxide resulted in an upfield shift of the pyridine ring carbons (δ 145 and 140) relative to the free ligand (δ 150.5). Though the signals arising from the β- and γ-carbons could not be distinguished from the phenyl carbons in all the complexes, in a few complexes signals due to the γ-carbon appeared in the upfield region with respect to the ones found in 4-cyanopyridine ($\beta = 127$; $\gamma = 121.4$) or 4-cyanopyridine 1-oxide. The shielding of all the carbon atoms on coordination is not unexpected because factors like polarization of the N—C bond due to σ-bonding at the pyridine nitrogen, metal-centred anisotropic diamagnetic currects and increased electron density due to π-bonding will provide net shielding contributions to the carbon atoms of the pyridine ring.

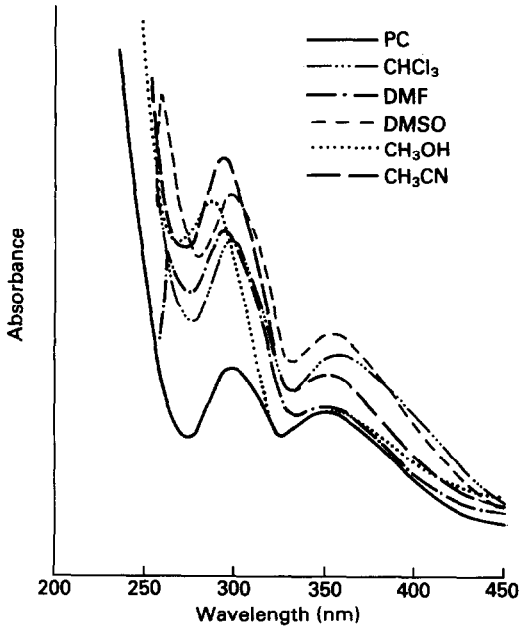

Fig. 2. Electronic absorption spectra of the complex $[(\eta^5\text{-}C_5H_5)_2Ru_2(\mu\text{-}4\text{-}CNpyO)(PPh_3)_4](PF_6)_2$.

^{31}P *NMR*

^{31}P NMR of the 4-cyanopyridine and 4-cyanopyridine 1-oxide complexes exhibited a single sharp signal around δ 41.5 and 41.9, respectively, for the PPh_3 phosphorus. Similarly, in dppe complexes a single, sharp peak appeared at δ 80.4 for the diphos phosphorus. The deshielding of phosphorus may be caused by relatively less donation of electrons from metal to phosphorus through backbonding. This suggests that the degree of $d\pi$–$p\pi$ backbonding influences the chemical shift of the phosphorus atoms and there exists a competition of the π-electrons between the 4-cyanopyridine or 4-cyanopyridine 1-oxide and other ligands supporting the ^1H and ^{13}C NMR spectral conclusions.

Electronic absorption spectra

The low spin d^6 configuration of both the mono- and binuclear series of complexes provides filled orbitals of proper symmetry on ruthenium(II) which interact with the relatively low-energy unoccupied π^*-orbitals on the pyridine ring of 4-cyanopyridine or 4-cyanopyridine 1-oxide ligands. One should, therefore, expect a band attributable to a MLCT transition ($t_{2g} \rightarrow \pi^*$) in the complexes. Furthermore the energy of these transitions should vary with the nature of the ligand acting as a π-acceptor. The presence of an electron-withdrawing substituent, like a —CN group, in the 4-position of the pyridine and pyridine 1-oxide should decrease the energy of the transition, causing a red shift in the MLCT maximum as well as greater ground state delocalization of the $d\pi$-electron density onto the ligand (π-backbonding), while the electron-donating group on the pyridine ring should increase the transition energy.[34,35] The electronic bands and their assignments for 4-cyanopyridine complexes in various solvents are shown in Table 2. A band around 450 nm has been assigned to a MLCT transition ($t_{2g}Ru^{II} \rightarrow \pi^*$-ligand of 4-cyanopyridine or 4-cyanopyridine 1-oxide). The λ_{max} and the ε_{max} values correlated very well with those of the pyridine bound 4-cyanopyridine complexes of ruthenium(II) and iron(II) in the literature.[5–7] The bonding of ruthenium(II) to the aromatic nitrogen is supported by the fact that the 485 nm band in our complexes appeared at lower energies compared to that in $[(\eta^5\text{-}C_5H_5)Ru(PPh_3)(Py)Cl]$ (465 nm) because of the electron-withdrawing property of the CN group.[34–36] Further support for the bonding is provided by the fact that aromatic nitrogen bonded complexes always absorb at a longer wavelength compared to the nitrile bound complexes.

In the spectra of the binuclear cationic complexes of 4-cyanopyridine there is a slight shift of λ_{max} towards higher frequencies in a few solvents (Table 2). In some solvents λ_{max} remains unaltered. (A slight decrease was also observed in the position of λ_{max} in one or two solvents with respect to the mononuclear cationic 4-cyanopyridine complexes.) This "anomalous" behaviour could be explained on the basis of the asymmetrical nature of the bridging ligand π-backbonding from ruthenium(II)[a] to the pyridine ring must raise the energy of the π^*-orbitals of the nitrile end of the 4-cyanopyridine, while the π-backbonding from the ruthenium(II)[b] to the NC

Table 2. Electronic spectral data of the complexes in various solvents

Solvents	Complexes λ_{max} (nm), log ε A	B	C	D
Acetone	470, 3.671	465, 3.702	—	—
Acetonitrile	460, 3.528	455, 3.790	291.6, 3.934	295, 4.439
Chloroform	—	—	297, 3.819	299, 4.568
Dichloromethane	483, 3.722	450, 3.826	297, 3.849	296, 4.322
Dimethylformamide	490, 3.584	480, 3.728	295, 3.778	297, 4.356
Dimethylsulphoxide	—	—	299, 3.753	295, 4.322
Isopropyl alcohol	—	—	287.5, 3.856	289, 4.505
Methanol	465, 3.184	470, 4.041	289, 4.021	287, 4.492
Nitromethane	430, 3.586	420, 3.465	—	—
Propylene carbonate	475, 3.676	475, 3.856	294, 3.762	298, 4.137

A = $[(\eta^5\text{-}C_5H_5)Ru(4\text{-}CNpy)(PPh_3)_2]BPh_4$; B = $[(\eta^5\text{-}C_5H_5)_2Ru_2(\mu\text{-}4\text{-}CNpy)(PPh_3)_4](BPh_4)_2$; C = $[(\eta^5\text{-}C_5H_5)Ru(4\text{-}CNpyO)(PPh_3)_2]Cl$; D = $[(\eta^5\text{-}C_5H_5)_2Ru_2(\mu\text{-}4\text{-}CNpyO)(PPh_3)_4](PF_6)_2$.

group should also raise the energy of the pyridine π^*-orbitals. Because the energy of the MLCT transition is related to that of the LUMO of the ligand, the increase in energy of the π^*-orbital by both electron transfers from the metal centres should result in the shift of the MLCT bands towards higher frequencies with respect to mononuclear complexes.

The MLCT absorptions exhibited a solvatochromic effect. Various parameters, for example, donor number (DN), the Reichardt Dimroth parameter (ET), $1/D_{op}-1/D_s$, E^*_{MLCT}, etc. have been defined[37–40] and correlated with the absorption energies of MLCT transitions. Figures 3 and 4 display these representative plots. They all show an excellent linear correlation between the variation of the MLCT band positions with the solvent polarity. The donor number plots have negative slopes suggesting a decrease in the energy of the transition as the donor property of the solvent increases and the intercepts give the energy of the transition when the compound is dissolved in dichloroethane. Further, a linear relationship is expected between the MLCT band positions and χ_{outer}, assuming the applicability of the Hush model[41–43] in these systems. Accordingly, the energy of the MLCT band which ought to be related to the Frank Condon term (χ_{inner}) and the solvent reorientation properties (χ_{outer}) by the equation $E_{op} = \chi_{inner}+\chi_{outer}+E'_{op}$, should show linearity with χ_{outer}. The χ_{outer} value can be calculated using the relationship $\chi_{outer} = (\Delta e)^2(1/2a_1+1/2a_2-1/r)(1/D_{op}-1/D_s)$, where Δe is charge transferred, D_{op} and D_s are the optic and static dielectric constants of the medium, a_1, a_2 and r, radii of the electron donor, acceptor and distance separating them. Figure 4(b) shows the plot of

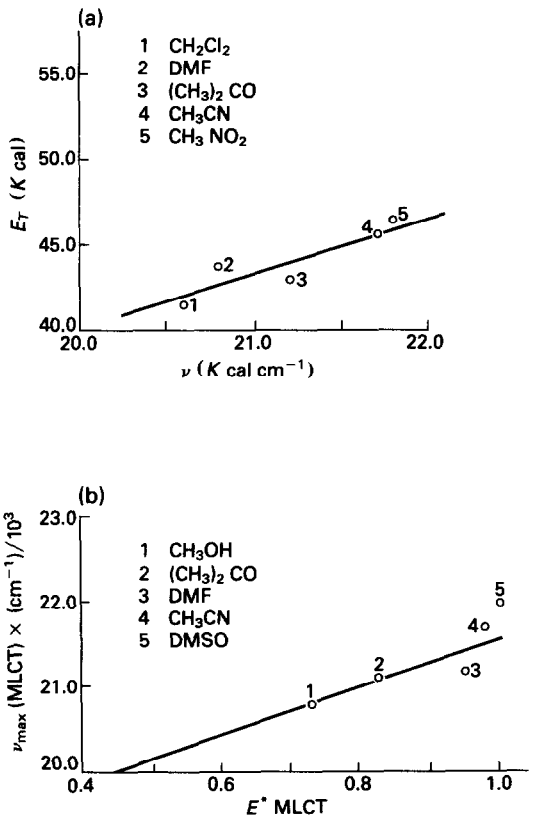

Fig. 3. (a) Plot of E_T vs MLCT for $[(\eta^5\text{-}C_5H_5)_2Ru_2(\mu\text{-}4\text{-}CNpy)(PPh_3)_4](BPh_4)_2$; (b) plot of MLCT vs E^* MLCT for $[(\eta^5\text{-}C_5H_5)_2Ru_2(\mu\text{-}4\text{-}CNpy)(PPh_3)_4](BPh_4)_2$.

E_{MLCT} vs $(1/D_{op}-1/D_s)$ for one representative compound. This shows a somewhat satisfactory relationship for both mono- and binuclear 4-cyanopyridine complexes. The generally observed shift to higher energy of the MLCT transition in solvents

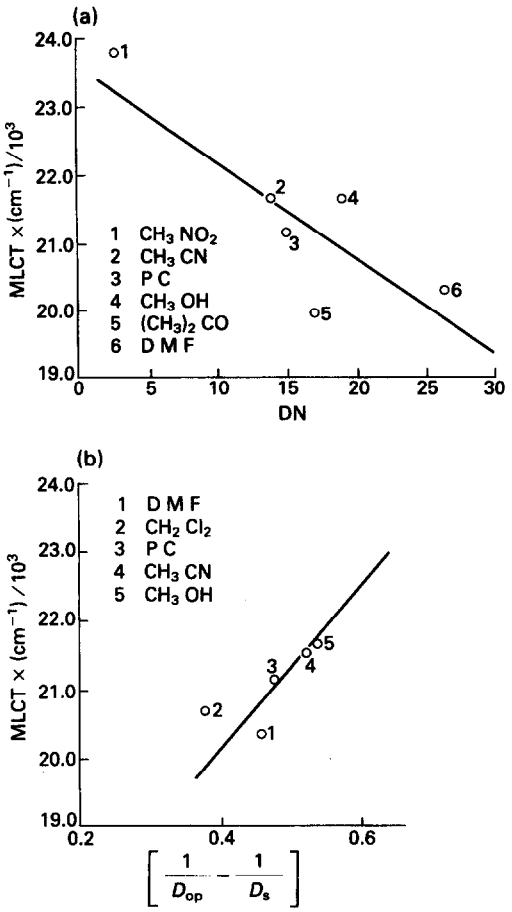

Fig. 4. (a) Plot of MLCT vs DN for $[(\eta^5\text{-}C_5H_5)Ru(4\text{-}CNpy)(PPh_3)_2]BPh_4$; (b) plot of MLCT vs $[1/D_{op} - 1/D_s]$ for $[(\eta^5\text{-}C_5H_5)Ru(4\text{-}CNpy)(PPh_3)_2]BPh_4$.

of high polarity has been attributed to the ground state stabilization or the excited state destabilization of non-centrosymmetric complexes in more polar solvents. Furthermore, strong solvatochromism is expected when the dissolved complex is ionic/polar.

The mononuclear and binuclear cationic complexes of 4-cyanopyridine also exhibited broad, medium intensity bands centred around 360 and 350 nm, respectively. These bands are assigned to the metal-to-ligand charge-transfer transition from ruthenium(II) to the antibonding C_5H_5 orbitals. The possibility of these bands arising from other MLCT transitions may be ruled out since the likelihood of transitions appearing from ruthenium(II) to either EPh_3 (E = P, As) or dppe/dppm in the near UV region is obscured. The intraligand $\pi \rightarrow \pi^*$ transitions in 4-cyanopyridine lie in the region < 300 nm (*ca* 250–256 nm). These bands did not show any solvatochromic effect in the 4-cyanopyridine complexes, indicating no change in the dipole moments of the molecule in the ground and excited states.

In mono- and binuclear 4-cyanopyridine 1-oxide complexes there appeared to be a very weak band in the visible region, 400–500 nm, assigned to a metal-to-ligand charge-transfer band. Since this band is very weak and it appears to be masked by the tail of the 350 nm band, no solvatochromic effect could be studied. A band in the region (340–370 nm) was found to be very slightly solvent sensitive, showing a small solvatochromic effect. These bands have been assigned to either a n–π^* transition where one of the p-electrons is excited from the non-bonding orbital of the oxygen atom to an antibonding π^*-orbital or to the MLCT (Ru^{II}) to antibonding C_5H_5 orbitals. Very strong absorption bands appeared in the UV region < 300 nm (Fig. 2) (λ_{max} varies within the range 280–300 nm depending on the solvent used) in the spectra of both the mono- and the binuclear 4-cyanopyridine 1-oxide complexes. These strong bands due to a $\pi \rightarrow \pi^*$ charge-transfer in the pyridine oxide ring, were found to be the most striking feature in these complexes,[44,45] and are very sensitive to the nature of the solvents used. This suggested a strong interaction between the NO group and the π-electrons of the ring. These transitions also showed a distinct blue shift in going from non-polar to polar solvents. In —OH group-containing polar solvents like methanol or isopropyl alcohol there is an average shift of 10–15 nm in λ_{max} towards the higher energy side (Table 2). There hypsochromic shifts could be explained on the basis of stabilization of the ground state by hydrogen bonding between the pyridine 1-oxide ring and methanol or isopropyl alcohol.

Table 3. Values for ruthenium(II) 4-cyanopyridine and ruthenium(II) 4-cyanopyridine-1-oxide complexes vs SSCE at 22+2°C in acetonitrile

Complexes	Process	$E_{1/2}$ (V)
$[(\eta^5\text{-}C_5H_5)Ru(4\text{-}CNpy)(PPh_3)_2]Cl$	$Ru^{III/II}$	0.52, 1.24
$[(\eta^5\text{-}C_5H_5)_2Ru_2(\mu\text{-}4\text{-}CNpy)(PPh_3)_4](BPh_4)_2$	$Ru^{III/II}$	0.26, 0.96
$[(\eta^5\text{-}C_5H_5)Ru(4\text{-}CNpy)(PPh_3)_2]Cl$	$Ru^{III/II}$	0.8, 1.16
$[(\eta^5\text{-}C_5H_5)_2Ru_2(\mu\text{-}4\text{-}CNpyO)(PPh_3)_4](PF_6)_2$	$Ru^{III/II}$	0.36, 1.12

Cyclic voltammograms were recorded at 0.2 V s^{-1} in acetonitrile and the values of $E_{1/2}$ (vs SSCE) for the different processes are shown in Table 3, including the corresponding values for related mono- and binuclear species. Both the metal- and ligand-centred redox processes were found to be chemically irreversible. For monodentate 4-cyanopyridine complexes the Ru^{III}/Ru^{II} potential falls in the range consistent with pyridine nitrogen coordination. The C_5H_5- and PPh_3-centred redox processes were also observed,[46] $E_{1/2} = 0.59$ V, in addition to the 4-cyanopyridine-centred redox process.

Acknowledgement—Thanks are due to CSIR, New Delhi, for the award of a Senior Research Fellowship to one of the authors (A.M.).

REFERENCES

1. N. E. Katz, C. Creutz and N. Sutin, *Inorg. Chem.* 1988, **27**, 1687.
2. E. H. Cutin and N. E. Katz, *Polyhedron* 1987, **6**, 159.
3. H. E. Toma and J. M. Malin, *Inorg. Chem.* 1973, **12**, 1039.
4. R. E. Clarke and P. C. Ford, *Inorg. Chem.* 1970, **9**, 227.
5. R. E. Clarke and P. C. Ford, *Inorg. Chem.* 1970, **9**, 495.
6. A. P. Szecsy, S. S. Miller and A. Haim, *Inorg. Chim. Acta* 1978, **28**, 189.
7. N. G. del V. Moreno, N. E. Katz, J. A. Olabe and P. J. Aymonino, *Inorg. Chim. Acta* 1979, **35**, 183.
8. J. E. Figard, J. V. Paukstelis, E. F. Byrne and J. D. Peterson, *J. Am. Chem. Soc.* 1977, **99**, 8417.
9. K. J. Moore, L. Lee, G. A. Mabbott and J. D. Peterson, *Inorg. Chem.* 1983, **22**, 1108.
10. P. D. Kaplan and M. Orchin, *Inorg. Chem.* 1967, **6**, 1096.
11. D. W. Herlocker, R. S. Drago and V. I. Meek, *Inorg. Chem.* 1966, **5**, 2009.
12. A. R. Brause, M. Rycheok and M. Orchin, *J. Am. Chem. Soc.* 1967, **89**, 6500.
13. P. T. T. Wong and D. G. Brewer, *Can. J. Chem.* 1968, **46**, 131.
14. A. I. Vogel, *A Text Book of Quantitative Inorganic Analysis*, 3rd edn. Longmans, London (1951).
15. M. I. Bruce and N. J. Windsor, *Aust. J. Chem.* 1977, **30**, 1601.
16. K. M. Rao, L. Mishra and U. C. Agarwala, *Polyhedron* 1986, **5**, 791.
17. K. M. Rao, L. Mishra and U. C. Agarwala, *Ind. J. Chem.* 1987, **27A**, 755.
18. G. S. Ashby, M. I. Bruce, I. B. Tomkins and R. C. Wallis, *Aust. J. Chem.* 1979, **32**, 1003.
19. R. D. Feltham and R. G. Hayter, *J. Chem. Soc.* 1964, 4587.
20. R. G. Hayter, *J. Am. Chem. Soc.* 1962, **84**, 3046; R. G. Hayter and F. S. Humiec, *Inorg. Chem.* 1963, **2**, 306.
21. R. D. Feltham, *Inorg. Chem.* 1964, **3**, 1038.
22. J. Chatt and R. C. Hayter, *J. Chem. Soc.* 1961, 896.
23. A. Davison, D. V. Howe and E. T. Shawl, *Inorg. Chem.* 1967, **6**, 458.
24. F. A. Cotton, W. R. Robinson, R. A. Walton and R. Whyman, *Inorg. Chem.* 1967, **6**, 931.
25. J. A. Olabe and P. J. Aymonino, *J. Inorg. Nucl. Chem.* 1976, **38**, 225.
26. F. Farha Jr and R. I. Iwamoto, *Inorg. Chem.* 1965, **4**, 844.
27. R. A. Walton, *J. Inorg. Nucl. Chem.* 1966, **28**, 2229.
28. I. S. Ahuja and R. Singh, *J. Inorg. Nucl. Chem.* 1974, **36**, 1505.
29. A. R. Katritzky and J. N. Gardner, *J. Chem. Soc.* 1958, 2192.
30. J. M. Malin, C. F. Schmidt and H. E. Toma, *Inorg. Chem.* 1975, **14**, 2924.
31. A. R. Katritzky and J. M. Lagowski, *J. Chem. Soc.* 1961, **43**.
32. D. K. Lavallee, M. D. Baughman and M. P. Phillips, *J. Am. Chem. Soc.* 1977, **99**, 718.
33. J. E. Figard, J. V. Paukstelis, E. F. Byrne and J. D. Peterson, *J. Am. Chem. Soc.* 1977, **99**, 8417.
34. P. Ford, De F. P. Rudd, R. Gaunder and H. Taube, *J. Am. Chem. Soc.* 1968, **90**, 1187.
35. C. R. Johnson and R. E. Shepherd, *Inorg. Chem.* 1983, **22**, 2439.
36. R. F. N. Ashok, M. Gupta, K. S. Arulsamy and U. C. Agarwala, *Inorg. Chim. Acta.* 1984, **273**, 361.
37. D. M. Manuta and A. J. Lees, *Inorg. Chem.* 1983, **22**, 3825.
38. V. Gutmann, *The Donor–Acceptor Approach to Molecular Interactions*. Plenum Press, New York (1980).
39. C. Reichardt, *Angew. Chem. Int. Ed. Engl.* 1965, **4**, 29.
40. C. Reichardt, *Angew. Chem. Int. Ed. Engl.* 1979, **18**, 98 and refs therein.
41. N. S. Hush, *Prog. Inorg. Chem.* 1967, **8**, 391.
42. A. B. P. Lever, *Inorganic Electronic Spectroscopy*, 2nd edn. Elsevier, Amsterdam (1984).
43. J. C. Curtis, B. P. Sullivan and T. J. Meyer, *Inorg. Chem.* 1983, **22**, 224.
44. S. Ghersetti, G. Maccagnani, A. Mangini and F. Montanari, *J. Heterocyclic Chem.* 1969, **6**, 859.
45. M. Ito and N. Hata, *Bull. Chem. Soc. Jpn* 1955, **28**, 260.
46. J. Amarasekera, T. B. Rauchfuss and S. R. Wilson, *Inorg. Chem.* 1987, **26**, 3328.

Polyhedron Vol. 9, No. 6, pp. 875–879, 1990
Printed in Great Britain

0277–5387/90 $3.00+.00
© 1990 Pergamon Press plc

SYNTHESIS AND REACTIVITIES OF LANTHANIDE–YLIDIC COMPLEXES

WAI-KWOK WONG,* HUA CHEN and FONG-LUNG CHOW

Department of Applied Biology and Chemical Technology, Hong Kong Polytechnic, Hung Hom, Kowloon, Hong Kong

(*Received* 12 *September* 1989; *accepted* 24 *October* 1989)

Abstract—The reaction of $[Li(Et_2O)_2][Cp'_2MCl_2]$ ($Cp' = C_5Me_5$; M = Nd, Sm) with 1 equivalent of $Li(CH_2)(CH_2)PRR'$ (**a**, R = Me, R′ = Ph; **b**, R = R′ = Ph; **c**, R = R′ = Me; **d**, R = R′ = *t*-Bu) produces $Cp'_2M[(CH_2)(CH_2)PPR'] \cdot (LiCl)_2$ (**I**, M = Sm; **II**, M = Nd) in moderate yield. Variable-temperature ^1H NMR studies on $Cp'_2M[(CH_2)(CH_2)P(Me)R] \cdot (LiCl)_2$ (M = Nd, Sm; R = Me, Ph) show that the methyl protons on the phosphorus of the chelating ylide undergo rapid exchange with the bridging methylene protons even at −40°C. A mechanism which is based on a series of metal–carbon bond breaking, rotation and recombination processes has been proposed for the fluxional behaviour. The ylidic complexes react with hydrogen (1 atm) at ambient temperature producing C_5Me_5H and the corresponding phosphonium salts, $[RR'PMe_2]Cl$. ^1H NMR studies on the reactivity of **Ia** towards hydrogen and acid review that the metal–carbon bond formed between the lanthanide metal and the chelating phosphorus ylide is more stable than that formed between the lanthanide metal and the pentamethylcyclopentadienyl ring.

Phosphorus ylides have been shown to possess an extensive coordination chemistry with main group and transition metal atoms and to form metal–carbon σ-bonds of unusual stability.[1] Gilje and coworkers have extended the ylidic chemistry to actinide metals and have synthesized a series of phosphorus ylidic organouranium complexes.[2] Although σ-alkyl organolanthanide complexes have been studied extensively recently, only a few ylidic organolanthanide complexes have been reported.[3] In this paper, we describe the preparation, solution dynamics and reactivities of a series of phosphorus ylidic organolanthanide complexes, $Cp'_2M[(CH_2)(CH_2)PRR'] \cdot (LiCl)_2$, ($Cp' = C_5Me_5$; M = Sm, Nd).

RESULTS AND DISCUSSION

Preparation of chelating phosphorus ylidic organolanthanide complexes

The interaction of $[Li(Et_2O)_2][Cp'_2MCl_2]$ (M = Nd, Sm; $Cp' = C_5Me_5$) with 1 equivalent of $Li(CH_2)(CH_2)PRR'$ in an ether–THF or toluene solution at −78°C gives the corresponding chelating phosphorus ylidic organolanthanide complexes in moderate yield, as shown in eq. (1):

$$[Li(Et_2O)_2][Cp'_2MCl_2] + Li(CH_2)(CH_2)PRR' \xrightarrow[-78°C]{Et_2O\text{–}THF \text{ or toluene}} Cp'_2M[(CH_2)(CH_2)PRR'] \cdot (LiCl)_2 \quad (1)$$

Ia-d or **IIa–b**

I, M = Sm; **II**, M = Nd

a, R = Me, R′ = Ph; **b**, R = R′ = Ph;

c, R = R′ = Me; **d**, R = R′ = *t*-Bu.

Invariably, the organolanthanide complexes always co-crystallize with lithium chloride. The novel organolanthanide complexes are characterized by elemental analyses, NMR and IR spectroscopies. These complexes are insoluble in saturated hydrocarbons, sparingly soluble in toluene and ether, very soluble in THF, and extremely air- and moisture-sensitive. The physical and spectroscopic data are given in Tables 1 and 2.

Both the neodymium- and samarium–ylidic complexes show strong absorption and emission in the visible region. Details of the photochemistry of

* Author to whom correspondence should be addressed.

Table 1. Physical properties and IR data of $Cp'_2M[(CH_2)(CH_2)PRR']\cdot(LiCl)_2$

M	R	R′	Melting point (°C)	Colour	ν (cm^{-1}) (Nujol)
Sm	Me	Ph	196–198	Yellow	3057m, 2724m, 2269w, 1975w, 1583m, 1414m, 1344m, 1317m, 1300m, 1190w, 1162m, 1132m, 1113m, 1072w, 1024w, 997w, 961s, 874s, 801w, 773m, 749s, 726m, 690s, 663w, 621w, 588w, 477m.
	Ph	Ph	226–228	Yellow	3056m, 2725m, 2193w, 1586m, 1437s, 1348m, 1316m, 1299m, 1152m, 1117s, 1023m, 998m, 968s, 933s, 882m, 802w, 782m, 749s, 739s, 715m, 688s, 620w, 594w, 489m, 472m, 445m.
	Me	Me	210 dec.	Yellow	2727m, 2305w, 2250w, 2213w, 2110w, 2080w, 1300s, 1108w, 1061m, 1022m, 983s, 801w, 780m, 723w, 621w, 586w.
	t-Bu	*t*-Bu	220 dec.	Yellow	2724m, 2332w, 1739w, 1418s, 1400s, 1317w, 1305m, 1260m, 1198m, 1090m, 1061m, 1018m, 951s, 939m, 920s, 861m, 814m, 802m, 773m, 732m, 695w, 623w, 590w.
Nd	Me	Ph	191–193	Blue	3054m, 2723m, 2280w, 1969w, 1585m, 1420m, 1345m, 1315w, 1298m, 1163w, 1132m, 1115m, 1077w, 1023w, 1000w, 967s, 888m, 844w, 801w, 776m, 744s, 726m, 688s, 620w, 585w, 475m.
	Ph	Ph	209–210	Blue	3055m, 2725m, 2282w, 1958w, 1827w, 1586m, 1441s, 1348w, 1316w, 1299m, 1193w, 1151m, 1117s, 1070m, 1024m, 997w, 967s, 932s, 882s, 852w, 802w, 792m, 749s, 737s, 715m, 690s, 621w, 597w, 489m, 473m, 446m.

Table 2. ^1H and $^{31}P\{^1H\}$ NMR data of $Cp'_2M[(CH_2)(CH_2)PRR']\cdot(LiCl)_2$

M	R	R′	^1H[a]	Assignment	^{31}P[b]	Assignment
Sm	Me	Ph	1.37s(30) 2.08d(7) 7.55m(5)	$C_5(CH_3)_3$ PCH_2, PCH_3; J_{P-CH} = 14.0 Hz C_6H_5	19.5s	$(CH_2)(CH_2)P$(Me)(Ph)
	Ph	Ph	1.39s(30) 2.51d(4) 7.60m(10)	$C_5(CH_3)_5$ PCH_2; J_{P-CH} = 13.5 Hz C_6H_5	18.7s	$(CH_2)(CH_2)P(Ph)_2$
	Me	Me	1.35s(30) 1.79d(10)	$C_5(CH_3)_5$ PCH_2, PCH_3; J_{P-CH} = 14.0 Hz	20.2s	$(CH_2)(CH_2)P(Me)_2$
	t-Bu	*t*-Bu	1.31d(18) 1.37s(30) 1.72d(4)	$PC(CH_3)_3$; J_{P-CH} = 15.7 Hz $C_5(CH_3)_5$ PCH_2; J_{P-CH} = 12.2 Hz	44.8s	$(CH_2)(CH_2)P(t\text{-Bu})_2$
Nd	Me	Ph	−3.55m(7) 4.36m(2) 6.28m(2) 6.80m(1) 8.46br,s(30)	PCH_2, PCH_3 C_6H_5 $C_5(CH_3)_5$	15.1s	$(CH_2)(CH_2)P$(Me)(Ph)
	Ph	Ph	−4.52m(4) 4.03m(4) 6.42m(4) 7.01m(2) 8.44br,s(30)	PCH_2 C_6H_5 $C_5(CH_3)_5$	19.2s	$(CH_2)(CH_2)P(Ph)_2$

[a] In $CDCl_3$ at 30°C, referenced to Me_4Si (δ 0.00).
[b] In $CDCl_3$ at 30°C, referenced to external 85% H_3PO_4 (δ 0.0), negative for upfield shift.
Abbreviations: s, singlet; d, doublet; m, multiplet; br, broad.

these phosphorus ylidic organolanthanide complexes will be reported in a separate paper.

^{1}H *NMR studies*

Variable-temperature ^{1}H NMR studies on the chelating phosphorus ylidic organolanthanide complexes review the following:

(i) The chemical shifts of the proton resonances of the novel complexes vary as a function of the temperature. The effect is more pronounced for the neodymium complexes than for the samarium complexes. In the case of the samarium complex, **Ia**, the resonance of the the C_5Me_5 protons shifts from δ 1.60 ppm at -40°C to δ 1.37 ppm at 30°C; whereas the chemical shifts of the methyl, bridging methylenes and phenyl protons remain relatively unchanged over the temperature range -40–30°C. Similar results are also observed for the other samarium complexes, **Ib–d**. In the case of the neodymium complex, **IIa**, the resonance of the C_5Me_5 protons shifts from δ 10.61 ppm at -40°C to δ 8.46 ppm at 30°C, and the resonances of the methyl and bridging methylene protons shift from δ -6.27 ppm at -40°C to δ -3.55 ppm at 30°C. Similar results are also observed for the neodymium complex, **IIb**.

(ii) A facile exchange process takes place between the methyl group and the bridging methylene groups of the phosphorus ylide of $Cp'_2M[(CH_2)(CH_2)P(Me)R]\cdot(LiCl)_2$ (M = Sm, Nd; R = Me, Ph). In $CDCl_3$ at 30°C, the ^{1}H NMR spectrum of **Ia** exhibits a singlet, a doublet and a multiplet of relative intensity 30:7:5 at δ 1.37, 2.08 and 7.55 ppm, respectively. The doublet at δ 2.08 ppm (J = 14.0 Hz) of intensity 7 is assigned to the methyl protons and the bridging methylene protons. The chemical shifts of the methyl protons and the bridging methylene protons of the phosphorus ylide coalesce even at -40°C. Similar results are also observed for **Ic** and **IIa**. For **IIa**, the ^{1}H NMR spectrum in $CDCl_3$ at 30°C exhibits a multiplet centred at δ -3.55 ppm of intensity 7 for the methyl group and the two bridging methylene groups. At -40°C, the resonance shifts to δ -6.27 ppm without any change in intensity. The above observations suggest that the methyl protons undergo a facile exchange with the bridging methylene protons of the phosphorus ylide. The observed fluxional behaviour can be explained by the mechanism shown in Scheme 1, which involves a series of metal–carbon bond-breaking, proton transfer, rotation and recombination processes. A similar mechanism has also been proposed for the fluxional behaviour of the bridging methylene protons of the phosphorus ylide of $Cp'_2M(Cl)[(CH_2)(CH_2)P(Me)(Ph)]$ (M = Th, U).[2]

Reaction with hydrogen

In THF solution, complexes **Ia,b** and **IIa,b** react rapidly with hydrogen (1 atm) at ambient temperature to give C_5Me_5H and the corresponding phosphonium salt, $[Me_2PhPR]Cl$, as the only isolated products. Their identities were confirmed by ^{1}H NMR spectroscopy. Attempts to isolate the organometallic fragments were unsuccessful. ^{1}H NMR studies on the above reaction revealed that the ylidic complexes react rapidly with hydrogen to release C_5Me_5H first, then the phosphonium salt, $[Me_2PhPR]Cl$. For example, the ^{1}H NMR spectrum of **Ia** in $CDCl_3$, after passing hydrogen through it

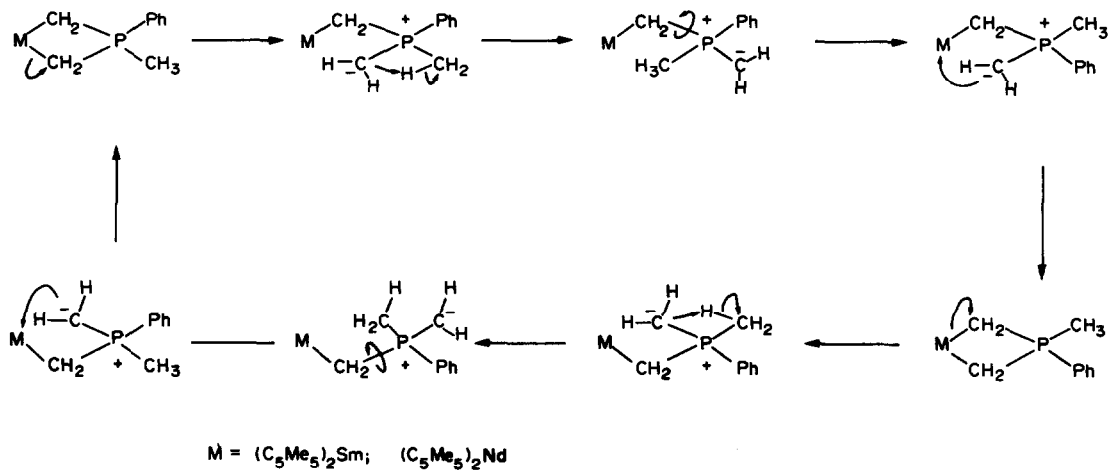

Scheme 1. Exchange mechanism for the fluxional behaviour of **Ia** and **IIa**.

for 1 min at 1 atm, shows that the intensity of the singlet at δ 1.37 ppm, which corresponds to the $C_5Me_5^-$ resonance, of **Ia** decreases with the concomitant appearance of a broad singlet and a doublet (J = 8.1 Hz) of relative intensity 4:1 at δ 1.79 and 0.99 ppm, respectively. The new resonances are indicative of C_5Me_5H. The intensity of the C_5Me_5H resonances increases as the intensity of the C_5Me_5 resonances of **Ia** decreases. Upon complete disappearance of the singlet at δ 1.37 ppm, a new doublet (J = 14.4 Hz) appears at δ 2.59 ppm. The intensity of this doublet increases as the intensity of the doublet (J = 14.0 Hz) at δ 2.08 ppm, which corresponds to the methyl and bridging methylene protons of the chelating phosphorus ylide, decreases. Eventually, the doublet at δ 2.08 ppm disappears completely, then the intensity of the new doublet at δ 2.59 ppm remains relatively constant. The new doublet at δ 2.59 ppm is identical to the methyl resonance of a genuine sample of $[PhPMe_3]Cl$. The results suggest that the metal–carbon bond formed between the lanthanide metal and the phosphorus ylide is stronger and more stable than that formed between the lanthanide metal and the $C_5Me_5^-$ ring.

Reaction with acid

The relative strength of the metal–carbon bonds is further demonstrated by the reaction of **Ia** with trifluoroacetic acid. A ^1H NMR study of the above reaction shows that when **Ia** is treated with a limited amount of CF_3CO_2H, the intensity of the C_5Me_5 resonances of **Ia** at δ 1.37 ppm decreases with the concomitant appearance of C_5Me_5H resonances. The intensity of **Ia** resonances decreases and that of the C_5Me_5H resonances increases as more CF_3CO_2H is added to the sample. After complete disappearance of the resonance at δ 1.37 ppm, further addition of CF_3CO_2H decreases the intensity of the chelating phosphorus ylide resonance at δ 2.08 ppm (doublet, J = 14.0 Hz) with the concomitant appearance of $[PhPMe_3]Cl$ resonances at δ 2.59 ppm (doublet, J = 14.4 Hz). The intensity of the chelating phosphorus ylide resonances decreases and that of the phosphonium salt resonances increases as more CF_3CO_2H is added to the sample. When excess CF_3CO_2H is added to the sample, the only observable resonances are those of C_5Me_5H and $[PhPMe_3]Cl$. The above ^1H NMR study shows that when **Ia** reacts with acid, C_5Me_5H is liberated first, followed by the corresponding phosphonium salt. This further supports the idea that the metal–carbon bond formed between the lanthanide metal and the chelating phosphorus ylide is more stable than that formed between the lanthanide metal and the $C_5Me_5^-$ ring.

EXPERIMENTAL

Microanalyses were performed by Butterworth (U.K.). IR spectra were obtained on a Perkin–Elmer 983 spectrometer; data given in cm^{-1} for Nujol mulls unless otherwise specified. NMR spectra were recorded on a JEOL FX90Q spectrometer. Chemical shifts were referenced to internal deuterated solvents and then recalculated to TMS = 0.0 ppm. ^{31}P NMR spectra were referenced to external 85% H_3PO_4.

All operations were carried out under nitrogen or *in vacuo*. All chemicals used were of reagent grade. Solvents were dried by standard procedures, distilled and deaerated prior to use. Melting points were taken in sealed capillaries and are uncorrected. $Li[(CH_2)(CH_2)PRR']$[4] and $[Li(OEt_2)_2][Cp'_2MCl_2]$[5] were prepared according to literature methods.

Syntheses

$Cp'_2Sm[(CH_2)(CH_2)P(Me)(Ph)]\cdot(LiCl)_2$ (**Ia**). A solution of $[Li(OEt_2)_2][Cp'_2SmCl_2]$ (1.40 g, 2.2 mmol in 20 cm^3 of a 3:1 mixture of Et_2O–THF) was added to a suspension of $Li[(CH_2)(CH_2)P(Me)(Ph)]$ (0.39 g, 2.4 mmol) in 20 cm^3 of Et_2O at −78°C. The orange solution turned yellow. The reaction mixture was allowed to warm slowly to room temperature and stirred for an additional 30 min. The light yellow solution was filtered and the yellow residue was extracted twice with 10 cm^3 of Et_2O and once with 5 cm^3 of THF. The combined filtrate was cooled to −20°C to give yellow crystals which were filtered and dried under high vacuum. Yield: 0.8 g, 55%; m.p. 196–198°C. [Found (required): C, 51.5 (53.0); H, 6.4 (6.5); P, 4.6 (4.7); Cl, 10.2 (10.8)%.]

$Cp'_2Sm[(CH_2)(CH_2)P(Ph)_2]\cdot(LiCl)_2$ (**Ib**). **Ib** was prepared according to the general procedure outlined above for **Ia** using 0.56 g (0.87 mmol) of $[Li(OEt_2)_2][Cp'_2SmCl_2]$ and 0.23 g (1.05 mmol) of $Li[(CH_2)(CH_2)P(Ph)_2]$. Yellow crystals were obtained. Yield: 0.4 g, 64%; m.p. 226–228°C. [Found (required): C, 55.8 (56.8); H, 6.3 (6.2); P, 4.4 (4.3); Cl, 9.0 (9.8)%.]

$Cp'_2Nd[(CH_2)(CH_2)P(Me)(Ph)]\cdot(LiCl)_2$ (**IIa**). **IIa** was prepared according to the general procedure outlined above for **Ia** using 1.37 g (2.3 mmol) of $[Li(OEt_2)_2][Cp'_2NdCl_2]$ and 0.40 g (2.5 mmol) of $Li[(CH_2)(CH_2)P(Me)(Ph)]$. Blue crystals were obtained from the combined blue filtrate. Yield: 0.9 g, 60%; m.p. 191–193°C. [Found (required): C, 52.5 (53.5); H, 6.3 (6.5); P. 4.8 (4.8); Cl, 10.4 (10.9)%.]

$Cp'_2Nd[(CH_2)(CH_2)P(Ph)_2]\cdot(LiCl)_2$ (**IIb**). **IIb** was prepared according to the general procedure outlined above for **Ia** using 2.30 g (3.6 mmol) of $[Li(OEt_2)_2][Cp'_2NdCl_2]$ and 0.82 g (3.7 mmol) of $Li[(CH_2)(CH_2)P(Ph)_2]$. Blue crystals were obtained from the combined blue filtrate. Yield: 1.7 g, 66%; m.p. 209–210°C. [Found (required): C, 56.5 (57.3); H, 6.1 (6.2); P, 4.5 (4.4); Cl, 9.1 (9.9)%.].

$Cp'_2Sm[(CH_2)(CH_2)P(Me)_2]\cdot(LiCl)_2$ (**Ic**) (*one-pot procedure*). A suspension of Cp'Li (0.95 g, 6.7 mmol) and anhydrous $SmCl_3$ (0.81 g, 3.2 mmol) in 60 cm^3 of THF was refluxed overnight. The resultant orange solution of $[Li(THF)_2][Cp'_2SmCl_2]$ was filtered and kept for later use. MeLi (10 cm^3 of a 1.0 M solution in Et_2O, 10 mmol) was added to a suspension of Me_4PI (0.77 g, 3.5 mmol) in 40 cm^3 of Et_2O at room temperature. During the course of the reaction, the suspension turned clear and then gave white precipitates. After stirring at room temperature for 4 h, the solution was filtered and the white precipitates were washed twice with 20 cm^3 of Et_2O to remove LiI and excess MeLi. The white precipitates were then dissolved in 10 cm^3 of THF at −78°C. The $[Li(THF)_2][Cp'_2SmCl_2]$ solution obtained from above was then added to the $Li[(CH_2)(CH_2)P(Me)_2]$ solution at −78°C. The orange solution turned yellow immediately. The solution was allowed to warm to room temperature and stirred for an additional 2 h before it was filtered. The residue was then extracted with 10 cm^3 of THF. The combinated filtrate was evaporated *in vacuo*. The resultant yellow residue was extracted with CH_2Cl_2 (3×10 cm^3). The solution was filtered, concentrated to *ca* 10 cm^3, and cooled to −20°C to give yellow needle crystals which were filtered and dried *in vacuo*. Yield: 1.2 g, 63%; m.p. 210°C (decomposed). [Found (required): C, 48.6 (48.5); H, 7.1 (6.8); P, 4.8 (5.2); Cl, 11.2 (11.9)%.].

$Cp'_2Sm[(CH_2)(CH_2)P(t\text{-}Bu)_2]\cdot(LiCl)_2$ (**Id**). **Id** was prepared according to the general procedure outlined above for **Ic** using 0.69 g (4.9 mmol) of Cp'Li and 0.61 g (2.4 mmol) of $SmCl_3$ to prepare $[Li(THF)_2][Cp'_2SmCl_2]$, and 6 mmol (6 cm^3 of 1.0 M solution in Et_2O) of MeLi and 0.69 g (2.3 mmol) of $[t\text{-}Bu_2PMe_2]I$ to prepare $Li[(CH_2)(CH_2)P(t\text{-}Bu)_2]$. The resultant yellow solution was filtered, evaporated and the residue extracted with a toluene–CH_2Cl_2 mixture (2×20 cm of a 1 : 1 mixture). The filtered extract was concentrated to *ca* 25 cm^3 and cooled to −20°C to give yellow crystals which were filtered and dried *in vacuo*. Yield: 0.8 g, 51%; m.p. 220°C (decomposed). [Found (required): C, 52.5 (53.1); H, 8.0 (7.7); P, 4.2 (4.6); Cl, 9.8 (10.4)%.]

Reaction with hydrogen

Hydrogen gas (1 atm) was bubbled through a solution of **Ia** (0.40 g, 0.6 mmol) in 20 cm^3 of THF at ambient temperature. After passing hydrogen gas for 5 min, the solution turned cloudy and white solids were precipitated out from the solution. Hydrogen gas was continuously bubbled through the solution for a further 25 min. The solution was then allowed to stir for an additional 2 h at ambient temperature. The solution was filtered and the white precipitates were washed twice with 5 cm^3 of THF. The ^1H NMR spectrum of the white precipitates was identical to that of a genuine sample of $[PhPMe_3]Cl$. Yield of $[PhPMe_3]Cl$ was 0.10 g, 88%. The combined filtrate was evaporated and the residue was extracted twice with 10 cm^3 of Et_2O. Upon removal of the solvent from the Et_2O filtrate, a light yellow oil was obtained. The ^1H NMR spectrum of the oil was identical to that of a genuine sample of C_5Me_5H.

^1H NMR studies

(i) **Ia** *with hydrogen*. 20 mg of **Ia** was dissolved in 0.5 cm^3 of $CDCl_3$ at ambient temperature. Hydrogen gas (1 atm) was bubbled through the solution slowly for 1 min. Then the course of the reaction was monitored by ^1H NMR spectroscopy at 5 min intervals for 1 h.

(ii) **Ia** *with* CF_3CO_2H. 20 mg of **Ia** was dissolved in 0.5 cm^3 of $CDCl_3$ at ambient temperature. CF_3CO_2H was then added to the solution via a microsyringe. The course of the reaction was monitored by ^1H NMR spectroscopy after every addition of 1×10^{-3} cm^3 of CF_3CO_2H to the solution. Addition of CF_3CO_2H was continued until there was no further change in the ^1H NMR spectrum upon addition of more CF_3CO_2H.

Acknowledgements—We thank the Croucher Foundation and the Hong Kong Polytechnic for financial support.

REFERENCES

1. H. Schmidbaur, *Accts Chem. Res.* 1975, **8**, 62 and refs therein.
2. R. E. Cramer, S. Roth, F. Edelmann, M. A. Bruck, K. C. Cohn and J. W. Gilje, *Organometallics* 1989, **8**, 1192 and refs therein.
3. (a) H. Schumann and S. Hohmann, *Chem. Z.* 1976, **100**, 336; (b) H. Schumann, I. Albrecht, F. W. Reier and E. Hahn, *Angew. Chem. Int. Ed. Engl.* 1984, **23**, 522.
4. L. E. Manzer, *Inorg. Chem.* 1976, **15**, 2567.
5. T. D. Tilley and R. A. Andersen, *Inorg. Chem.* 1981, **20**, 3267.

Polyhedron Vol. 9, No. 6, pp. 881–890, 1990
Printed in Great Britain

0277–5387/90 $3.00+.00
© 1990 Pergamon Press plc

CHEMISTRY OF MOLYBDENUM WITH HARD–SOFT DONOR LIGANDS—III. OXOMOLYBDENUM(VI) AND *CIS*-DIOXOMOLYBDENUM(VI) MIXED LIGAND COMPLEXES

SANCHITA PUROHIT, ADITYA PRASAD KOLEY and SAKTIPROSAD GHOSH*

Department of Inorganic Chemistry, Indian Association for the Cultivation of Science, Calcutta—700032, India

(*Received* 19 *June* 1989; *accepted* 2 *November* 1989)

Abstract—The syntheses and characterization of a number of oxomolybdenum(VI) and *cis*-dioxomolybdenum(VI) complexes with 4-substituted thiosemicarbazides in the form of 4-phenyl, 4-(*p*-methylphenyl) and 4-(*p*-chlorophenyl)thiosemicarbazide (represented as LH) as the NS donor metal binding substrates are described. The oxomolybdenum(VI) complexes are of the type $MoO(NS)_2X_2$ and $MoO(NS)_2(O—O)$ (where X = Br or SCN and O—O = oxalate or malonate) with a pentagonal bipyramidal geometry. The *cis*-dioxomolybdenum(VI) complexes are mixed chelate complexes, $MoO_2(NS)L'$, where L'H is either a monoprotic NO donor like oxine, 2-methyloxine or a NS donor such as 2-aminobenzenethiol, 2-aminocyclopent-1-ene-1-dithiocarboxylic acid and its methyl ester. The electrochemical behaviour of these complexes along with *cis*-$MoO_2(NS)_2$ and $MoO(NS)_2Cl_2$ complexes are discussed.

Recently there has been much interest in the chemistry of oxo complexes of molybdenum[1–8] with sulphur, nitrogen and/or oxygen donor ligands due to their relevance to the active sites of certain molybdoenzymes. Thus, design and synthesis of oxomolybdenum complexes have currently become a fascinating field of research in the domain of coordination chemistry. As a part of our ongoing research programme in this area we have recently reported[9] the synthesis and characterization of some *cis*-dioxomolybdenum(VI) complexes of the type MoO_2L_2 and seven-coordinated pentagonal bipyramidal oxomolybdenum(VI) complexes, $MoOL_2Cl_2$, where LH is a monoprotic bidentate NS donor ligand in the form of the 4-substituted thiosemicarbazides (**I**). Here, we present the synthesis and characterization of $MoOL_2Br_2$ (LH = 4-phenyl, 4-(*p*-methylphenyl), 4-(*p*-chlorophenyl) thiosemicarbazides) obtained by the reaction of MoO_2L_2 with HBr and the complexes obtained by direct replacement of the halogens (of $MoOL_2X_2$, X = Cl, Br) by thiocyanate, oxalate and malonate. The redox behaviour of MoO_2L_2, $MoOL_2X_2$ (X = Cl, Br, SCN) and $MoOL_2(O—O)$ (O—O = ox, mal) complexes have been studied by cyclic voltammetry.

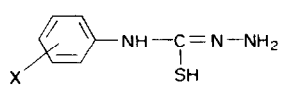

X = H, *p*-CH_3, *p*-Cl

I

Although a number of *cis*-dioxomolybdenum(VI) bis-chelate complexes having NS, NO or SS donor atoms have been studied earlier,[9–14] complexes containing two different bidentate ligands have not been investigated adequately. In the present paper, along with the homochelate complexes we also report the synthesis, characterization and electrochemical properties of a number of *cis*-dioxomolybdenum(VI) heterochelate complexes of the type MoO_2LL', where LH is either a 4-phenyl or 4-(*p*-chlorophenyl)thiosemicarbazide and L'H is either a NO donor ligand like 8-hydroxyquinoline (oxine), 2-methyl-8-hydroxyquinoline (2-Me-oxine) or a NS donor ligand like 2-aminobenzenethiol (abt), 2-aminocyclopent-1-ene-

* Author to whom correspondence should be addressed.

1-dithiocarboxylic acid (acda) and its methyl ester (acdaMe).

EXPERIMENTAL

Molybdenyl acetylacetonate was prepared from ammonium *para*-molybdate (Aldrich Chemicals) by a known[15] method. Analytical reagent grade solvents, distilled and dried by standard methods were used in all cases. All other chemicals were of reagent grade and were employed without further purification. Tetraethylammonium perchlorate (TEAP) was prepared from tetraethylammonium bromide (Fluka AG) using a standard procedure.[16] The ligands 4-phenylthiosemicarbazide (4-PhTSC), 4-(*p*-chlorophenyl)thiosemicarbazide [4-(*p*-Cl)PhTSC] and 4-(*p*-methylphenyl)thiosemicarbazide [4-(*p*-CH_3)PhTSC] were prepared from the corresponding amines using the reported[17] method. The compounds acda[18] and its methyl ester, acdaMe,[19] were prepared following the methods reported earlier.

Synthesis of complexes

$MoOL_2Br_2$ (**2c–e**). To a stirred suspension of MoO_2L_2[9] (1 mmol) in methanol (25 cm^3), concentrated HBr (48%, 0.5 cm^3) was added dropwise over a period of 30 min with constant stirring. The maroon complex slowly dissolved to yield a dark red solution. Stirring was continued for 48 h at room temperature and the volume of the solution was reduced to 10 cm^3 when a dark microcrystalline compound separated out. It was filtered, washed with cold methanol followed by solvent ether and dried *in vacuo*. Yield: 50%.

$MoO(4\text{-PhTSC})_2(SCN)_2 \cdot 2H_2O$ (**3a**). A well stirred solution of 0.258 g (0.5 mmol) of $MoO(4\text{-PhTSC})_2Cl_2$[9] in 25 cm^3 of dry methanol was allowed to react with 0.76 g (1 mmol) of ammonium thiocyanate. The solution turned deep red and was stirred for about 3 h at room temperature. Then the volume of the solution was reduced to about 10 cm^3 when a dark red microcrystalline compound separated out. It was filtered off, washed with ice-cold methanol and dried *in vacuo*. Yield: 40%.

$MoO(4\text{-PhTSC})_2(ox) \cdot 4H_2O$ (**3b**) *and* $MoO(4\text{-PhTSC})_2(mal) \cdot 2H_2O$ (**3c**). These were prepared using the same procedure as above but using oxalic acid and malonic acid, respectively. These complexes were also prepared using $MoO(4\text{-PhTSC})_2Br_2$ as the starting materials.

MoO_2(4-PhTSC) (acda) (**4a**). To a filtered solution of 0.33 g (1 mmol) of $MoO_2(acac)_2$ in 30 cm^3 of dry methanol, a solution of 0.17 g (1 mmol) of 4-PhTSC in 20 cm^3 of dry methanol was added very slowly (over a period of 1 h) with constant stirring at ice-bath temperature when the solution turned deep red. To this solution, 0.16 g (1 mmol) of acda, dissolved in 15 cm^3 of ice-cold methanol, was added over a period of 15 min when a dark microcrystalline compound gradually separated out from the reaction mixture. This was filtered, washed thoroughly with methanol and dried over fused $CaCl_2$ *in vacuo*. Yield: 60%.

MoO_2(4-PhTSC)(acdaMe) (**4c**), MoO_2(4-PhTSC)(abt) (**4e**) *and the corresponding* 4-(*p*-Cl)PhTSC *complexes* (**4b**, **4d** *and* **4f**). These were prepared following the procedure described above. In all cases, dark microcrystalline compounds were obtained in good yield.

MoO_2(4-PhTSC)(oxine) (**4g**). A solution of 0.17 g (1 mmol) of 4-PhTSC in 20 cm^3 of dry methanol was added very slowly to a filtered solution of 0.33 g (1 mmol) of $MoO_2(acac)_2$ in 30 cm^3 of dry methanol with constant stirring at ice-bath temperature. To this solution, 0.16 g (1 mmol) of oxine in 20 cm^3 of dry methanol was added over 0.5 h when a dark maroon microcrystalline compound began to separate out. The stirring was continued for about 4 h at room temperature and the precipitated compound was collected by filtration. It was washed thoroughly with methanol and dried *in vacuo*. Yield: 70%.

MoO_2(4-PhTSC)(2-Me-oxine) (**4i**) *and the corresponding* 4-(*p*-Cl)PhTSC *complexes* (**4h, 4j**). These were prepared in good yield using the same procedure described above.

Physical measurements

Carbon, hydrogen and nitrogen analyses were performed on a Perkin–Elmer 240 C,H,N-analyser. Molybdenum was estimated gravimetrically using oxine as the reagent. The IR spectra were recorded as KBr discs using a Perkin–Elmer 783 spectrophotometer. Electronic spectra of the compounds were recorded on a Pye-Unicam model SP8-150 UV–vis spectrophotometer using spectral grade solvents. Electrical conductance data in solution were obtained on a Philips PR-9500 conductivity bridge fitted with a dip-type cell calibrated with 0.02 M KCl solution. Static susceptibility measurements at room temperature were made with the help of a Princeton Applied Research Vibrating Sample Magnetometer Model 155 using $Hg[Co(SCN)_4]$ as the calibrant. Electrochemical studies were carried out with the help of a PAR Model 370-4 electrochemistry system: 174A polarographic analyser, 175 universal programmer, RE 0089 *X–Y* recorder. All the experiments were carried out under a dry nitrogen atmosphere in a three-electrode con-

figuration. A planar Beckman Model 39273 platinum electrode was used as the working electrode. The results were collected at 298 ± 1 K and are referenced to a saturated calomel electrode (SCE). The reported potentials are uncorrected for junction contribution.

RESULTS AND DISCUSSION

During syntheses of $MoOL_2Br_2$ complexes (**2c–e**) by the reaction of a suspension of MoO_2L_2 in methanol with two equivalents of HBr, the electron-rich oxygen atom undergoes protonation in the first step which is immediately followed by bromide ion inclusion in the metal coordination sphere with simultaneous expansion of coordination number. These are assumed to be two consecutive steps involved in the actual reaction pathway.[20–22] The thiocyanato, oxalato and malonato complexes (**3a–c**) were prepared by the direct replacement of the halide ions from $MoOL_2X_2$ (L = 4-PhTSC, X = Cl, Br). The mixed chelate complexes (**4a–j**) of the type MoO_2LL' have been prepared *in situ* by adding the ligand L'H to a solution of MoO_2(acac)(L) generated in the medium. Thin-layer chromatography (TLC) indicates the presence of a single species in each of these compounds. All the compounds are found to be air-stable.

Results of elemental analysis (Table 1) are in good agreement with the assigned formulations. All the complexes are diamagnetic as expected for the d^0 molybdenum(VI) state. All the oxomolybdenum(VI) complexes (**2c–e**, **3a–c**) are highly soluble in common organic solvents. The com-

Table 1. Analytical data of the complexes

Complex	Found (Calc.) (%)			
	C	H	N	Mo
$MoO(4\text{-PhTSC})_2Br_2$ (**2c**)	28.1 (27.8)	2.6 (2.6)	13.5 (13.9)	15.6 (15.9)
$MoO(4\text{-}(p\text{-}CH_3)\text{PhTSC})_2Br_2$ (**2d**)	30.0 (30.4)	3.0 (3.2)	12.8 (13.3)	15.7 (15.2)
$MoO(4\text{-}(p\text{-Cl})\text{PhTSC})_2Br_2$ (**2e**)	24.1 (24.9)	2.1 (2.1)	12.2 (12.5)	13.9 (14.3)
$MoO(4\text{-PhTSC})_2(SCN)_2\cdot 2H_2O$ (**3a**)	32.4 (32.2)	3.4 (3.3)	18.9 (18.8)	16.8 (16.1)
$MoO(4\text{-PhTSC})_2(ox)\cdot 4H_2O$ (**3b**)	31.4 (31.8)	3.8 (3.9)	13.7 (13.9)	15.0 (15.9)
$MoO(4\text{-PhTSC})_2(mal)\cdot 2H_2O$ (**3c**)	35.2 (35.0)	3.2 (3.1)	14.4 (14.4)	16.7 (16.5)
$MoO_2(4\text{-PhTSC})(acda)$ (**4a**)	34.0 (35.5)	3.7 (3.9)	11.9 (12.4)	20.7 (21.2)
$MoO_2(4\text{-}(p\text{-Cl})\text{PhTSC})(acda)$ (**4b**)	32.5 (32.0)	3.7 (3.5)	11.6 (11.5)	19.2 (19.7)
$MoO_2(4\text{-PhTSC})(acdaMe)$ (**4c**)	36.3 (36.0)	4.4 (4.3)	12.3 (12.0)	20.4 (20.6)
$MoO_2(4\text{-}(p\text{-Cl})\text{PhTSC})(acdaMe)$ (**4d**)	33.4 (33.5)	3.7 (3.8)	11.0 (11.2)	18.9 (19.2)
$MoO_2(4\text{-PhTSC})(abt)$ (**4e**)	36.9 (37.3)	3.7 (3.8)	13.2 (13.4)	22.3 (21.9)
$MoO_2(4\text{-}(p\text{-Cl})\text{PhTSC})(abt)$ (**4f**)	34.5 (34.5)	3.3 (3.3)	12.2 (12.4)	20.9 (21.2)
$MoO_2(4\text{-PhTSC})(oxine)$ (**4g**)	43.7 (43.8)	3.5 (3.6)	12.7 (12.8)	22.1 (21.2)
$MoO_2(4\text{-}(p\text{-Cl})\text{PhTSC})(oxine)$ (**4h**)	40.6 (40.6)	3.1 (3.2)	11.6 (11.8)	20.5 (20.3)
$MoO_2(4\text{-PhTSC})(2\text{-Me-oxine})$ (**4i**)	45.4 (45.3)	3.9 (3.8)	11.6 (11.4)	21.0 (21.2)
$MoO_2(4\text{-}(p\text{-Cl})\text{PhTSC})(2\text{-Me-oxine})$ (**4j**)	41.8 (41.9)	3.4 (3.5)	11.4 (11.5)	19.6 (19.7)

pounds are non-electrolytes in dry acetonitrile. However, it was noted that in a freshly prepared DMF solution of the bromo complexes the conductivity slowly increases, probably due to the partial dissociation[23] of the coordinated bromide ions. It was found that the extent of dissociation of bromide ions is greater than that of the chloride ions in the analogous complexes. Attempts to isolate the solvolysed products yielded dark oils that could not be crystallized. The *cis*-dioxomolybdenum(VI) mixed chelate complexes are highly soluble in DMF and DMSO but are found to have poor solubility in common organic solvents. These are non-electrolytes in DMF.

IR spectra

Analysis of the IR spectra of the complexes indicate that the substituted thiosemicarbazides coordinate exclusively in the enol form via the deprotonated thiol sulphur and the nitrogen atom of the terminal $—NH_2$ group as reported earlier.[9]

In the oxomolybdenum(VI) complexes (**2c–e**, **3a–c**), the strong terminal $\nu(Mo{=}O)$[20,21,24] mode is observed in the region 935–955 cm^{-1}. For the $MoOL_2Br_2$ complexes, the $\nu(Mo—Br)$ bands are observed around 280 cm^{-1}. In the thiocyanato complex, the $\nu(CN)$ vibration is located at 2070 cm^{-1}, indicating that the SCN^- moiety is coordinated to the molybdenum(VI) acceptor centre through the nitrogen atom.[25]

All the *cis*-dioxomolybdenum(VI) heterochelate complexes (**4a–j**) display their characteristic two-band pattern[26,27] in the 900–960 cm^{-1} region. In the acda complexes (**4a**, **b**), the absence of the $\nu(SH)$[18] band of the free ligand (acda) at $\sim$ 2550 cm^{-1} indicates metal–ligand bond formation through the deprotonated thiocarboxylate sulphur. Because of the involvement of the $—NH_2$ group of the free ligand in strong hydrogen bonding, the observed difference in the position of $\nu(NH)$[18] bands in the free ligand and its complexes bonded through the amino group is very small. In the complexes, the $\nu_{as}(CSS)$ stretching of the ligand at 880 cm^{-1} is found to split symmetrically[18] into two bands at 900 and 860 cm^{-1}, respectively and points to unidentate sulphur chelation. Hence, it is expected that in these complexes acda is coordinated to the metal ion through the nitrogen atom of the $—NH_2$ group and the deprotonated thiocarboxylate sulphur. The ligand, acdaMe, is also intramolecularly hydrogen bonded.[28] For this reason, the broad, weak ligand band at 3300 cm^{-1}, assignable to $\nu(NH)$, remains almost unaffected in the complexes (**4c**, **d**). The band due to $\nu(SCH_3)$ in the ligand remains unchanged in the complexes. Two medium intensity bands at 915 and 620 cm^{-1} assignable to $\nu_{as}(CSSCH_3)$ and $\nu_s(CSSCH_3)$, respectively,[28] are slightly shifted ($\sim$ 10 cm^{-1}) to the higher frequency region in these metal chelates. Hence, it may be suggested that in conformity with earlier observations,[28] acdaMe coordinates through the thiocarbonyl sulphur and the deprotonated amino group ($—NH^-$). Disappearance of the ligand (abt) band at 2520 cm^{-1} due to $\nu(SH)$[29] in the IR spectra of the abt complexes (**4e**, **f**) clearly indicates that the ligand coordinates to the metal through the deprotonated thiol sulphur. Shifting of the ligand bands at 3450 and 3355 cm^{-1}, arising due to $\nu_{as}(NH)$ $\nu_s(NH)$,[29] towards lower wave numbers by a margin of $\sim$ 80 cm^{-1} in the complexes points to the involvement of the nitrogen atom of the $—NH_2$ group in coordination. This is corroborated by the fact that the ligand band due to $\delta(NH_2)$ is found to suffer a reduction of 30–40 cm^{-1} in the complexes.

Electronic spectra

For all the complexes the lowest energy band observed in the 450–500 nm region may be assigned to $S(p\pi) \rightarrow Mo(d\pi)$[10,22,30] ligand-to-metal charge-transfer (LMCT) transitions. Other LMCT bands are observed in the region 300–430 nm (Table 2). For the complexes of oxine and 2-Me-oxine (**4g–j**), the bands appearing around 360 and 330 nm may be assigned to the nitrogen-to-molybdenum and oxygen-to-molybdenum charge-transfer transitions,[31] respectively. In the other dioxomolybdenum(VI) complexes it is very difficult to ascertain whether a definite molybdenyl band ($O \rightarrow Mo$ CT) occurs near 330 nm. Even if it is present, this band is probably obscured by the other LMCT bands. For all the complexes, higher energy bands appearing below 300 nm are probably due to internal ligand transitions.

Proposed structures of the complexes

For the seven-coordinated $MoOL_2X_2$ (X = Br, SCN) and $MoOL_2(O—O)$ (O—O = oxalate, malonate) complexes, the most probable structure is a pentagonal bipyramid which has been reported earlier[9,32,33] for the related type of complexes. With one of the two coordinated nitrogen atoms *trans* to the Mo=O bond[9] and the two X groups in *cis* positions,[9] the two possible seven-coordinated pentagonal bipyramid structures are **IIa** and **IIb**. Structures of the $MoOL_2(O—O)$ type complexes can be easily visualized by replacing the two *cis* X ions by an oxalate or malonate moiety.

Structures of the mixed ligand complexes (**4a–j**)

Table 2. Electronic spectral band positions (nm) of the compounds[a]

Compound	λ_{max}/nm (ε/dm^3 mol^{-1} cm^{-1})
2c	495(6040), 410(4831), 370(4993), 265(21,956)
2d	495(5787), 410(4834), 370(4928), 260(21,524)
2e	495(3911), 410(4205), 370(4448), 265(23,043)
3a	513(7284), 438(6169), 320(12,766), 255(21,011)
3b	495(4778), 405(4042), 268(23,923), 260(24,116)
3c	490(8586), 400(5618), 355(6996), 250(18,017)
4a	435(7917), 400(10,000), 325(13,125), 260[b](sh)
4b	440(11,228), 398(16,140), 323(17,192), 260[b](sh)
4c	440(6400), 380(8160), 270[b](sh)
4d	450(8362), 390(10,603), 270[b](sh)
4e	435(6169), 265[b](sh)
4f	435(8060), 265[b](sh)
4g	445(2245), 360(7704), 300(7061), 250[b](sh)
4h	435(5454), 330(9746), 250[b](sh)
4i	435(7108), 360(9262), 310(5516), 250[b](sh)
4j	435(8670), 360(9874), 310(12,185), 250[b](sh)

[a] **2c–e**, **3a–c** in CH_3CN, **4a–j** in DMF.
[b] In CH_2Cl_2.
sh = shoulder.

are easily derived from the octahedral structure **IIc**[9] by replacing one of the two thiosemicarbazide N—S donors by other bidentate chelating ligands like oxine (NO), 2-methyl oxine (NO), 2-aminobenzenethiol (NS), 2-aminocyclopent-1-ene-1-dithiocarboxylic acid (NS) and its methyl ester (NS).

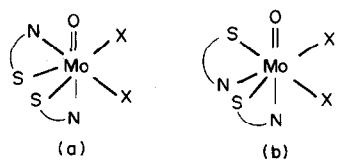

X = Br, SCN

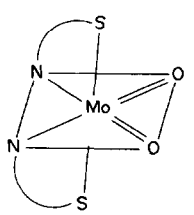

(c)

II

Voltammetric studies

The redox behaviour of some of the MoO_2L_2, $MoOL_2X_2$ (X = Cl, Br, SCN), $MoOL_2$(O—O) (O—O = oxalate, malonate) and MoO_2LL' complexes has been studied using cyclic voltammetry. The results are given in Table 3.

The cyclic voltammogram of MoO_2(4-PhTSC)$_2$ which is typical of all the MoO_2L_2 complexes (**1a–c**) is shown in Fig. 1. For these complexes two irreversible reductive responses are observed near −0.9 and −1.6 V, respectively. On comparing the observed current height at E_{pc}'s with those of the authentic one-electron reductions,[34,35] the first one appears to be a metal-centred one-electron transfer involving the molybdenum(VI) and molybdenum(V) oxidation states:

$$[Mo^{VI}O_2L_2] + e^- \longrightarrow [Mo^{V}O_2L_2]^-.$$

The lack of an anodic response even at high scan rates (500 mV s^{-1}) is evidently due to the instability of the reduced species $[Mo^{V}O_2L_2]^-$.

Electrochemical behaviour of the pentagonal bipyramidal $MoOL_2X_2$ (X = Cl, Br) complexes (**2a–e**) in DMF is complicated but interesting. For these complexes two or more reductive responses are observed (Table 3). All these responses are found to be irreversible which is evidenced by no observable oxidation wave during the reverse anodic scan in the cyclic voltammograms. Irreversible electrochemistry at seven coordinate MoO^{4+} centres results[36] from the fact that the four molybdenum d_{xy} orbital lobes that become singly occupied upon reduction to molybdenum(V) experience unfavourable interactions with the five equatorial bonds

Table 3. Cyclic voltammetry data for the complexes[a] in 0.1 M TEAP at 298 K

Complex	E_{pc}/V (vs SCE)
MoO_2(4-PhTSC)$_2$ (**1a**)	−0.92, −1.61
MoO_2(4-(*p*-CH_3)PhTSC)$_2$ (**1b**)	−0.90, −1.60
MoO_2(4-(*p*-Cl)PhTSC)$_2$ (**1c**)	−0.90, −1.51
MoO(4-PhTSC)$_2Cl_2$ (**2a**)	−0.63, −1.085
MoO(4-(*p*-Cl)PhTSC)$_2Cl_2$ (**2b**)	−0.865, −1.09, −1.85
MoO(4-PhTSC)$_2Br_2$ (**2c**)	−0.57, −0.88, −1.03, −1.45, −1.75
MoO(4-(*p*-CH_3)PhTSC)$_2Br_2$ (**2d**)	−0.60, −0.87, −1.10, −1.51, −1.69
MoO(4-(*p*-Cl)PhTSC)$_2Br_2$ (**2e**)	−0.62, −0.88, −1.15, −1.88
MoO(4-PhTSC)$_2$(SCN)$_2\cdot 2H_2O$ (**3a**)	−0.85, −1.05
MoO(4-PhTSC)$_2$(ox)$\cdot 4H_2O$ (**3b**)	−1.13, −1.85
MoO(4-PhTSC)$_2$(mal)$\cdot 2H_2O$ (**3c**)	−1.11, −1.81
MoO_2(4-PhTSC)(acda) (**4a**)	−0.87, −1.12, −1.72
MoO_2(4-(*p*-Cl)PhTSC)(acda) (**4b**)	−0.83, −1.01, −1.73
MoO_4(4-PhTSC)(abt) (**4e**)	−1.02, −1.72
MoO_2(4-PhTSC)(oxine) (**4g**)	−1.10(−0.94),[b] −1.79(−1.72)[b]
MoO_2(4-(*p*-Cl)PhTSC)(oxine) (**4h**)	−1.15(−0.90),[b] −1.82(−1.75)[b]
MoO_2(4-PhTSC)(2-Me-oxine) (**4i**)	−1.01, −1.20, −1.72, −2.02
MoO_2(4-(*p*-Cl)PhTSC)(2-Me-oxine) (**4j**)	−0.92, −1.02, −1.62, −1.97

[a] Solvent, **4a**, **b**, **e**, **g**–**j** in DMSO and all other in DMF; solute concentration $\sim 10^{-3}$ M; working electrode, platinum; reference electrode, SCE.

[b] Values in parentheses are coupled oxidation peaks observed with complete CVA cycle.

present in the pentagonal bipyramidal geometry and initiate metal–ligand bond cleavage reactions during charge-transfer. It has been observed for all these complexes that on multiple scan reversal the cyclic voltammogram continuously changes with time until a steady state is reached. It is found that, in the bromo complexes, the first reductive response ~ -0.6 V (Table 3) completely disappears in the second cycle, even when the scan is extended up to +0.5 V. But when the potential is scanned in such a manner as to cycle only the first reductive response, this cathodic peak is found to be reproducible on multiple scan reversal between +0.5 and −0.7 V. Also, the first reductive response is always observed with a fresh scan. It has been noticed that the cyclic voltammograms of the steady state are identical for all the $MoOL_2X_2$ (**2a**–**e**) complexes. The final voltammogram consists of two reductive responses at around −0.85 and −1.55 V (Table 3), respectively, both of which are reproducible on multiple scan reversal. Again, the first response at $E_{pc} \sim -0.85$ V is found to be reproducible when the potential is scanned to cover only the first response and also the E_{pc} value for this peak is almost the same in all cases.

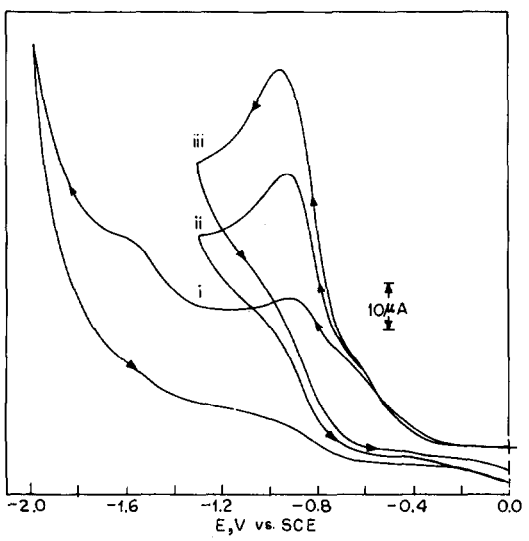

Fig. 1. Cyclic voltammograms for $\sim 1\times10^{-3}$ M MoO_2(4-PhTSC)$_2$ (**1a**) in DMF; scan rates (i) 50, (ii) 100 and (iii) 200 mV s^{-1}.

The course of change of the cyclic voltammogram for MoO(4-(*p*-Cl)PhTSC)$_2Br_2$ is illustrated by Fig. 2. It is noticed that the first reduction wave completely disappears in the second scan, but the current height of the second cathodic peak gradually increases until the steady state is reached. On the other hand, the current height of the third response at around −1.1 V gradually diminishes indicating the decrease in concentration of the species reduced

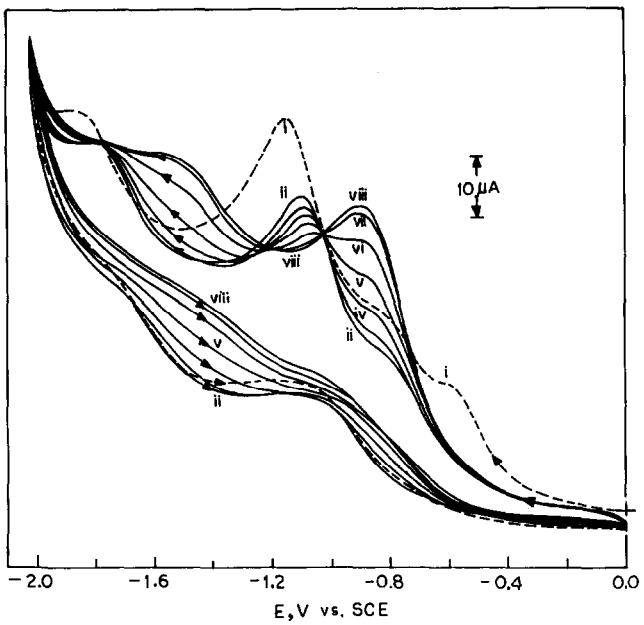

Fig. 2. Cyclic voltammograms for $\sim 1 \times 10^{-3}$ M MoO(4-(*p*-Cl)PhTSC)$_2$Br$_2$ (**2e**) in DMF showing the change with time: (i) initial cathodic scan, (ii) second cycle and (iii) final scan at the steady state.

at this potential and ultimately this response vanishes at the steady state. Also, an anodic shift of the last cathodic wave is observed. The overall process occurring at the electrode may be expressed by the following couples:

is reduced to the corresponding molybdenum(IV) species at ~ -1.1 V, which is ultimately reduced to a molybdenum(III) species with the loss of the remaining halide ion. Thus, the concentration of

$$\begin{array}{ccccc} Mo^{VI}OL_2X_2 & \xrightarrow{+e^-,-X^-} & Mo^{V}OL_2X(DMF) & \xrightarrow{+e^-} & [Mo^{IV}OL_2X(DMF)]^- \\ & & & & \downarrow{\scriptstyle +e^-} \\ [Mo^{VI}OL_2X(DMF)]^+ & \xrightarrow{+e^-} & \uparrow & & \downarrow{\scriptstyle -X^-} \\ [Mo^{VI}OL_2(DMF)_2]^{2+} & \xrightarrow{+2e^-} & Mo^{IV}OL_2(DMF)_2 & \xrightarrow{+e^-} & [Mo^{III}OL_2(DMF)_2]^-. \end{array}$$

It has been confirmed by conductance measurement in DMF that each of the chloro complexes has appreciable conductance ($\Lambda \sim 40\ \Omega^{-1}\ cm^2\ mol^{-1}$), indicating partial dissociation of the chloride ions, while the bromo compounds have conductance values ($\Lambda \sim 100\ \Omega^{-1}\ cm^2\ mol^{-1}$) which lie just above the range of a 1 : 1 electrolyte in DMF. For this reason, all the three possible species $MoOL_2X_2$, $[MoOL_2X(DMF)]^+$ and $[MoOL_2(DMF)_2]^{2+}$ that may be present in the medium, have been taken into active consideration. Here, it is reasonable to guess that the species $[MoOL_2(DMF)_2]^{2+}$, because of its fairly high positive charge, may undergo a facile two-electron reduction at around −0.85 V vs SCE. On the other hand, it is assumed that the halogen-containing species are at first reduced to a molybdenum(V) species, $[MoOL_2X(DMF)]$, which in turn the halide-containing species gradually decreases on multiple scan reversal and finally halogenless species are produced at the steady state when the final species cycles between molybdenum(V), molybdenum(IV) and molybdenum(III) oxidation states. The proposed mechanism, mainly based on the dissociation of the halide ions from the inner coordination sphere of these complexes, receives indirect support from the cyclic voltammetric results (Table 3) of the thiocyanato, oxalato and malonato complexes (**3a–c**), where no change in the cyclic voltammogram (Fig. 3) with time is observed.

Electrochemical behaviour of the MoO_2LL' complexes (**4a–j**) has been examined in deaerated DMSO/0.1 M TEAP within the potential range +0.8 to −2.0 V. Two or more irreversible reductive

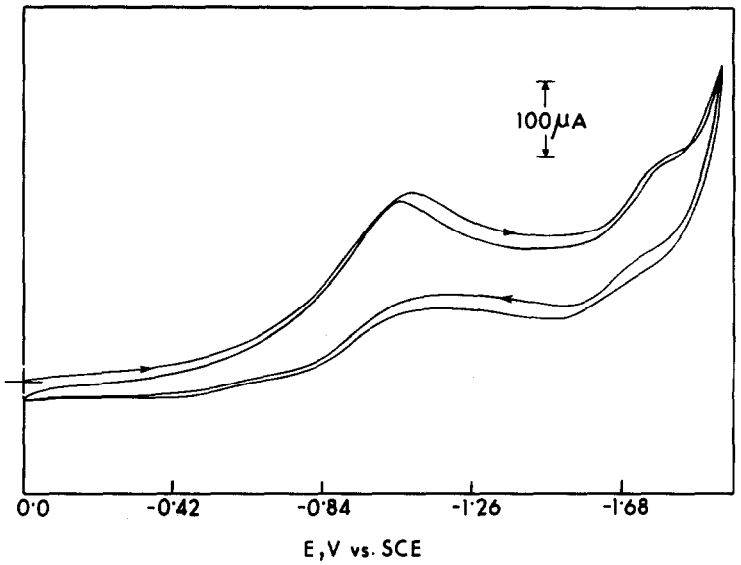

Fig. 3. Cyclic voltammograms for $\sim 1 \times 10^{-3}$ M MoO(4-PhTSC)$_2$(mal)·2H$_2$O (**3c**) in DMF/0.1 M TEAP; scan rate: 50 mV s^{-1}.

responses are observed (Table 3) in the potential range -0.8 to -2.0 V for these complexes [except in the case of oxine compounds (**4g**, **h**)], and that is indicative of either slow electron-transfer kinetics or a chemical process associated with electrochemical reduction. However, on multiple scan reversal the nature of the waves retains their original shapes indicating high reproducibility of the electrode reaction. This suggests that the product of the ECE process, if associated, is not re-oxidized or further reduced in the potential range studied. Electrochemical studies on other *cis*-dioxomolybdenum(VI) complexes have revealed that such complexes[10,23,38,39] generally exhibit irreversible or quasi-reversible behaviour. Spence[13] has shown for a series of molybdenum complexes that molybdenum(V) monomers are not obtainable by electrochemical reduction of the corresponding molybdenum(VI) dioxo complexes. Upon reduction, the dioxomolybdenum(VI) complexes lose an oxo ligand instead of being protonated.[23,40] This oxo loss and subsequent reorganization of the ligand undoubtedly accounts for their irreversible behaviour. A freshly prepared DMSO solution of the complexes (except **4g** and **4h**) exhibits a broad peak/a pair of peaks between -0.8 and -1.1 V (vs SCE). A second broad cathodic peak is observed around -1.72 V for these complexes. At potentials more negative than the second broad peak, another reduction wave, associated with a one- or two-electron transfer process, is observed in the cyclic voltammograms of the 2-Me-oxine compounds (**4i** and **4j**). However, the exact nature of the reduced products cannot be ascertained at this stage due to insufficient data. In this context it may be mentioned here that similar cyclic voltammetric results have been obtained for other *cis*-dioxomolybdenum(VI) complexes.[41,42]

Compared to those of the other MoO_2LL' complexes, the cyclic voltammograms of MoO_2(4-PhTSC)(oxine) (**4g**) and MoO_2(4-(*p*-Cl)PhTSC)(oxine) (**4h**) in DMSO solution are well behaved (Fig. 4) and are highly reproducible. Both compounds undergo two successive reductions near -1.10 and -1.80 V (vs SCE), respectively. These two cathodic peaks produce their corresponding anodic waves near -1.70 and -0.90 V on scan reversal. That the second anodic peak arises only from the first cathodic response and the second couple has no contribution to it, is substantiated by scanning the potential in a manner so as to cycle only the first response. The same current for this second anodic response is obtained irrespective of whether it is scanned taking both the two couples or only the first one. On comparing the current height with that reported[37] for corresponding couples of similar systems, the first step of the reduction process seems to involve one-electron transfer. On multiple scan rates (v = 50, 100 and 200 mV s^{-1}) the overall shape of the voltammograms remains the same. However, the difference in peak potentials increases (peak-to-peak separations, ΔE_p, 160, 180 and 220 mV, respectively) with increasing sweep rate. The difference in peak potentials and the i_{pc}/i_{pa} ratio (which

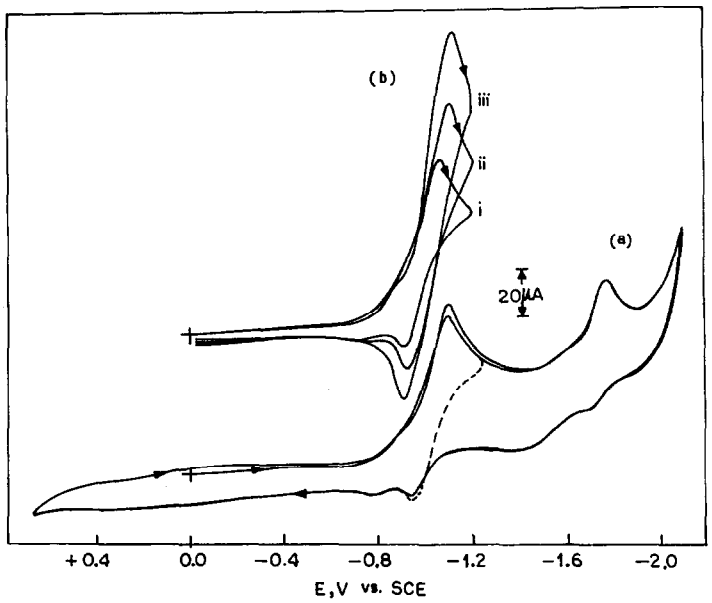

Fig. 4. Cyclic voltammograms for $\sim 1 \times 10^{-3}$ M MoO_2(4-PhTSC)(oxine) (**4g**) in 0.1 M TEAP/DMSO: (a) multiple scan reversal at a scan rate of 50 mV s^{-1}; (b) first cathodic peak at scan rates (i) 50, (ii) 100 and (iii) 200 mV s^{-1}.

deviates slightly from unity) are consistent with a quasi-reversible process characterized by slow electron transfer.[37] The second step involves a complicated process of electron transfer which appears to be irreversible on the cyclic voltammetric time scale. The cathodic peak near −1.80 V has nearly the same current height as that of the cathodic peak of the first couple and this indicates one-electron stoichiometry of this step. The separation between the two peak potentials is 70 mV which refers to a one-electron process. All these results suggest that the dianionic species generated due to reduction is unstable during cyclic voltammetric measurement. The overall electrochemical results for these two complexes can be rationalized as follows.

The compounds (**4g** and **4h**) undergo reduction near −1.10 V forming the corresponding monoanionic molybdenum(V) species. This electrochemically generated molybdenum(V) species is further reduced near −1.80 V to the corresponding dianionic molybdenum(IV) species. The slightly less cathodic current height of this step ($E_{pc} \sim -1.80$ V) compared to the former ($E_{pc} \sim -1.10$ V) is indicative of a chemical reaction that follows the initial one-electron reduction and that prevents a portion of the one-electron reduction product from undergoing a second one-electron reduction step. Again, the observation that the current height of the anodic peak ($E_{pa} \sim -1.70$ V) at which the two-electron reduced product is reoxidized is small, may be explained by the existence of a competing chemical reaction associated with the post electrochemical reaction.

It may be pointed out in this context that major differences are observed in the electrochemical behaviour of MoO_2(oxine)$_2$ and MoO_2(4-PhTSC)(oxine) or MoO_2(4-(*p*-Cl)PhTSC)(oxine). The electrochemistry of the former has been studied[37] in DMSO at a platinum electrode. The reduction of $Mo^{IV}O_2$(oxine)$_2$ occurs in two one-electron steps, with solvent attack of the reduction intermediates and subsequent displacement of the oxinate ligand. The proposal that oxine is a product of $Mo^{VI}O_2$(oxine)$_2$ reduction requires the source of a proton and water present in the solvent (DMSO) has been proposed to be the source of H^+ during the reduction. It has been shown that free oxine is reduced at −1.78 V (vs Ag—AgCl) and the oxinate ion is oxidized at +0.05 V. The absence of any anodic peak around +0.05 V in the cyclic voltammogram of any of the oxine compounds reported in this study indicates that no free oxine is generated during electrolysis. The sharply contrasting behaviour of the above compounds is thus recognized. The reproducibility and reversibility of these electron transfer steps in **4g** or **4h** compared to those in MoO_2(oxine)$_2$ indicates that the presence of 4-substituted thiosemicarbazide ligand within the coordination sphere in place of one of the oxinate ligands, stabilizes the lower valent states.

REFERENCES

1. S. P. Cramer, *Adv. Inorg. Bioinorg. Mech.* 1983, **2**, 259.
2. S. P. Cramer, R. C. Wahl and K. V. Rajagopalan, *J. Am. Chem. Soc.* 1981, **103**, 7721.
3. G. N. George, R. C. Bray and S. P. Cramer, *Biochem. Soc. Trans.* 1986, **14**, 651.
4. R. C. Bray and G. N. George, *Biochem. Soc. Trans.* 1985, **13**, 560.
5. R. C. Bray, S. Gutteridge, D. A. Storter and S. J. Tanner, *Biochem. J.* 1979, **177**, 357.
6. W. E. Newton and S. Otsuka (Eds), *Molybdenum Chem. Biol. Significance* [Proc. Int. Symp.], p. 1979 (1980).
7. E. I. Stiefel, *Prog. Inorg. Chem.* 1977, **22**, 1.
8. M. P. Coughlan (Ed.), *Molybdenum and Molybdenum-containing Enzymes.* Pergamon Press, New York (1980).
9. S. Ghosh and S. Purohit, *Ind. J. Chem.* 1987, **26A**, 131.
10. M. Chaudhury, *J. Chem. Soc., Dalton Trans.* 1984, 115.
11. F. W. Moore and M. L. Larson, *Inorg. Chem.* 1967, **6**, 998.
12. R. N. Jowitt and P. C. H. Mitchell, *J. Chem. Soc. A* 1970, 1702.
13. J. T. Spence, *Coord. Chem. Rev.* 1983, **48**, 59.
14. H. M. Stevens, *Anal. Chim. Acta* 1956, **14**, 126.
15. G. J.-J. Chen, J. W. McDonald and W. E. Newton, *Inorg. Chem.* 1976, **15**, 2612.
16. D. T. Sawyer and J. L. Roberts Jr, *Experimental Electrochemistry for Chemists*, p. 212. John Wiley, New York (1974).
17. A. B. Sen and S. K. Sengupta, *J. Ind. Chem. Soc.* 1982, **39**, 628.
18. K. Nag and D. S. Joardar, *Inorg. Chim. Acta* 1975, **14**, 133.
19. B. Bordas, P. Sohar, G. Matolesy and P. Berencsi, *J. Org. Chem.* 1972, **37**, 1/2.
20. J. Topich and J. T. Lyon, *Inorg. Chem.* 1984, **23**, 3203.
21. E. A. Maata and R. A. D. Wentworth, *Inorg. Chem.* 1979, **18**, 2409.
22. M. Chaudhury, *Inorg. Chem.* 1985, **24**, 3011.
23. R. D. Taylor, J. P. Street, M. Minelli and J. T. Spence, *Inorg. Chem.* 1978, **17**, 3207.
24. J. Dirand, L. Richard and R. Weiss, *J. Chem. Soc., Dalton Trans.* 1976, 278.
25. K. Nakamoto, *Infrared and Raman Spectra of Inorganic and Coordination Compounds*, p. 270. John Wiley, New York (1978).
26. P. C. H. Mitchell, *Quart. Rev.* 1966, **20**, 103.
27. F. W. Moore and M. L. Larson, *Inorg. Chem.* 1967, **6**, 998.
28. D. S. Joardar, PhD Dissertation, Calcutta University (1976).
29. N. B. Colthup, L. H. Daly and S. E. Wiberley, *Introduction to Infrared and Raman Spectroscopy.* Academic Press, New York (1964).
30. M. Chaudhury, *Inorg. Chem.* 1984, **23**, 4434.
31. F. W. Moore and R. E. Rice, *Inorg. Chem.* 1968, **7**, 2511.
32. M. Chaudhury, *Inorg. Chem.* 1985, **24**, 3011.
33. J. R. Dilworth, B. D. Neaves, C. J. Pickett, J. Chatt and J. A. Zubieta, *Inorg. Chem.* 1983, **22**, 3524.
34. P. Bandyopadhyay, P. K. Mascharak and A. Chakravorty, *J. Chem. Soc., Dalton Trans.* 1982, 675.
35. P. Ghosh, P. Bandyopadhyay and A. Chakravorty, *J. Chem. Soc., Dalton Trans.* 1983, 401.
36. J. U. Mondal, F. A. Schultz, T. D. Brennan and W. R. Scheidt, *Inorg. Chem.* 1988, **27**, 3950.
37. C. A. Cliff, G. D. Fallom, B. M. Gatehouse, K. S. Marray and P. J. Newman, *Inorg. Chem.* 1980, **19**, 773.
38. J. T. Spence, M. Minelli and P. Kroneck, *J. Am. Chem. Soc.* 1980, **102**, 4538.
39. L. J. DeHayes, H. C. Faulkner, W. H. Doub Jr and D. T. Sawyer, *Inorg. Chem.* 1975, **14**, 2110.
40. R. Colton and G. G. Rose, *Aust. J. Chem.* 1970, **23**, 1111.
41. A. F. Isbell Jr and D. T. Sawyer, *Inorg. Chem.* 1971, **10**, 2449.
42. J. Topich and J. T. Lyon, *Polyhedron* 1984, **3**, 55.

Polyhedron Vol. 9, No. 6, pp. 891–892, 1990
Printed in Great Britain

0277–5387/90 $3.00+.00
© 1990 Pergamon Press plc

COMMUNICATION

SYNTHESIS OF A CARBORANYL NUCLEOSIDE FOR POTENTIAL USE IN NEUTRON CAPTURE THERAPY OF CANCER

ABUL K. M. ANISUZZAMAN,† FAZLUL ALAM and ALBERT H. SOLOWAY

College of Pharmacy, The Ohio State University, Columbus, Ohio 43210, U.S.A.

(*Received* 5 *October* 1989; *accepted* 8 *December* 1989)

Abstract—The reaction of 2′,3′-O-(dibutylstannylene)uridine (**1**) with 3-bromopropyne yielded 2′,(3′)-O-(3-propynyl)uridine (**2** and **3**). The mixture of **2** and **3** on acetylation followed by chromatographic purification yielded 3′,5′-di-O-acetyl-2′-O-(3-propynyl) uridine (**4**). Reaction of **4** with bis(acetonitrile)decaborane produced 3′,5′-di-O-acetyl-2′-O-(*o*-carboran-1-ylmethyl)uridine (**5**). Deacetylation of **5** gave 2′-O-(*o*-carboran-1-ylmethyl) uridine (**6**), a boronated nucleoside for potential use in neutron capture therapy of cancer.

The concept of boron neutron capture therapy (BNCT) for the treatment of cancer[1] is based on the nuclear reaction between thermal neutrons and boron-10 to yield alpha particles and lithium-7 nuclei:

$$^{10}_{5}B + {}^{1}_{0}n \longrightarrow [^{11}_{5}B] \begin{cases} \longrightarrow {}^{4}_{2}He + {}^{7}_{3}Li + 2.79\ MeV(6\%) \\ \longrightarrow {}^{4}_{2}He + {}^{7}_{3}Li^{*} + 2.31\ MeV(94\%) \end{cases}$$
$$\downarrow$$
$$^{7}_{3}Li + \gamma + 0.48\ MeV.$$

The high linear energy transfer (LET) alpha particles released in this nuclear reaction have a range in tissue of about 10 μm, approximately equal to the diameter of a single cell. Their destructive effect is, therefore, highly localized to boron-loaded tissue. A key requirement of BNCT is the selective delivery of an adequate concentration of boron-10 to tumors (15–30 $\mu g\,^{10}B/g$ tumor).[2] The lack of boron compounds with the requisite biological properties has been a major limitation for the clinical use of BNCT. Boronated analogues of compounds that are known to localize in various tumors (amino acids, thioruracils, chlorpromazine, nucleosides, antibodies, etc.) have been the focus of compound development in this area.[3] The rationale for the synthesis of boron-containing nucleosides is that such structures would be conserved by rapidly proliferating tumor cells and phosphorylated by cellular kinases to mononucleotides. These may persist "locked-in" within the tumor cell or possibly be converted to the active precursors of nucleic acids, the di- and triphosphate forms.

One boronated nucleoside, 5-dihydroxyboryl-2′-deoxyuridine, containing one boron atom linked at the 5-position, was reported[4] in 1985. We have focused on linking the icosahedral *o*-carborane moiety, containing 10 boron atoms, to various purine and pyrimidine nucleosides. This communication describes the first synthesis‡ of a carboranyl nucleoside.

The alkylation of 2′,3′-O-(dibutylstannylene) uridine[5] (**1**) with 3-bromopropyne yielded a mixture, 2′,(3′)-O-(3-propynyl)uridine (**2** and **3**). The mixture was acetylated and chromatographically purified to give 3′,5′-di-O-acetyl-2′-O-(-3-propynyl)uridine (**4**), in 45% overall yield from **1**, and the structure of **4** was confirmed by ^{1}H NMR, mass spectrometry and microanalysis. Reaction[6] of **4** with the bis(acetonitrile)decaborane yielded the

† Author to whom correspondence should be addressed.

‡ After we had submitted the manuscript for publication, Professor Yoshinori Yamamoto of Tohoku University, Japan, personally communicated that his group had succeeded in synthesizing two nucleoside analogues having the *o*-carborane moiety attached to the pyrimidine base.

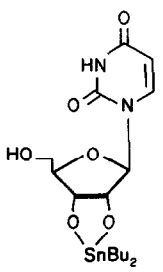

1

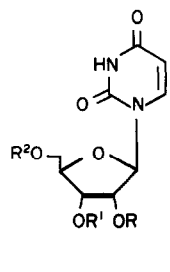

2 R = $-CH_2-C\equiv CH$, R^1, R^2 = H

3 R^1 = $-CH_2-C\equiv CH$, R^1, R^2 = H

4 R = $CH_2-C\equiv CH$, R^1 R^2 = Ac

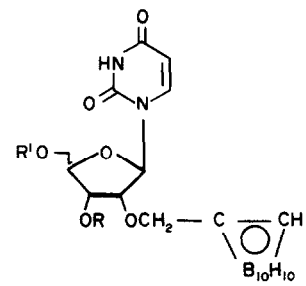

5 R, R^1 = Ac

6 R, R^1 = H

corresponding carborane-containing derivative **5** (50% yield).

Derivative **5** was quantitatively deacetylated by catalytic amounts of sodium methoxide in methanol at 4°C for 20 h; sodium was removed with cation exchange resin and the solution concentrated. Addition of ether yielded crystalline 2′-O-(*o*-carboran-1-ylmethyl)uridine (**6**) as an ether adduct, m.p. 136–137°C, $[\alpha]_{25}^{D}+4.6°$ (cl, MeOH). The IR spectrum exhibits a strong absorption at 2575 cm^{-1}, characteristic of a B—H stretch and the carbonyl absorption at 1695 cm^{-1}. The ^1H NMR spectrum (in CD_3OD, 250 MHz; δ in ppm downfield from TMS, coupling constant in Hz) exhibits the following peaks: 3.67, 3.80 (ABq, H-5′a, H-5′b; $J_{5'a,5'b}$12.3; $J_{4',5'a}$2.7; $J_{4',5'b}$2.3); 4.64 (bs, carborane C—H); 5.60 (d, H-5; $J_{5,6}$8.1); 5.77 (d, H-1′; $J_{1',2'}$2.7); 8.00 (d, H-6). The peaks due to ether in the solvated **6** occur as a triplet at 1.11 and a quartet at 3.42. The mass spectra (FAB) shows the (M^+ + H) peak at *m/z* 401 as part of the carborane isotopic cluster. Elemental analysis ($C_{16}H_{34}O_7N_2B_{10}\cdot 0.8Et_2O$): Found: C, 39.47; H, 7.09; N, 5.89. Calc.: C, 39.71; H, 7.02; N, 6.09%.

The position of the boron cage on the D-ribofuranose moiety in **6** should not interfere with conformational or hydrogen bonding properties of the pyrimidine base. The biological evaluation of **6** is being undertaken and will be reported separately. The described preparative sequence is applicable to the synthesis of a variety of carborane-containing nucleosides of purines and pyrimidines.

Acknowledgements—Support of this research by the National Cancer Institute (P-30-CA 16058-13) and the Department of Energy (DE-AC02-82ERG0040) is gratefully acknowledged.

REFERENCES

1. G. I. Locher, *Am. J. Roentgenol.* 1936, **36**, 1.
2. R. G. Fairchild and V. P. Bond, *Int. J. Radiat. Oncol. Biol. Phys.* 1985, **11**, 831.
3. R. G. Fairchild and V. P. Bond, *Proc. 1st Intl. Symp. NCT*, Brookhaven National Laboratory Reports [BNL-5173], pp. 1–12 (1984).
4. R. F. Schinazi and W. H. Prusoff, *J. Org. Chem.* 1985, **50**, 841.
5. D. Wagner, J. P. H. Verheyden and J. G. Moffatt, *J. Org. Chem.* 1974, **39**, 24.
6. T. L. Heying, J. W. Ager, S. L. Clark, D. J. Mangold, H. L. Goldstein, M. Hillman, R. J. Polak and J. W. Szymansk, *Inorg. Chem.* 1963, **2**, 1089.

Polyhedron Vol. 9, No. 6, pp. 893–895, 1990
Printed in Great Britain

0277–5387/90 $3.00+.00
© 1990 Pergamon Press plc

COMMUNICATION

APPLICATION OF MICROWAVE DIELECTRIC LOSS HEATING EFFECTS FOR THE RAPID AND CONVENIENT SYNTHESIS OF COORDINATION COMPOUNDS

DAVID R. BAGHURST, STEPHEN R. COOPER, DAVID L. GREENE, D. MICHAEL P. MINGOS* and SELENA M. REYNOLDS

Inorganic Chemistry Laboratory, University of Oxford, South Parks Road, Oxford OX1 3QR, U.K.

(*Received* 18 *December* 1989; *accepted* 5 *January* 1990)

Abstract—A wide range of coordination compounds of substitutionally-inert transition metal ions have been rapidly and conveniently synthesized using microwave dielectric loss heating effects. The compounds were synthesized in good yields in a Teflon autoclave, which can sustain temperatures up to 250°C and pressures up to 80 atm. With microwave techniques, reactions requiring 24 h take place in approximately 1 min.

The application of microwave dielectric loss heating effects for accelerating the rates of organic reactions,[1,2] the dissolution of geological samples,[3] organometallic syntheses,[4] intercalation processes[5] and solid-state reactions[6,7] is now well documented. For solution reactions the most dramatic results have been obtained using sealed Teflon containers which can sustain temperatures up to 250°C and pressures up to 80 atm,[8] although alternative methods for refluxing solutions under 1 atm pressure conditions have recently been described.[9] In this communication we describe the application of these techniques to the synthesis of coordination compounds. The synthesis of coordination compounds of substitutionally-inert transition metal ions can frequently be problematical and can lead to long and tedious synthetic procedures. This is particularly true for second- and third-row transition metal complexes which are exceptionally inert in a number of their common oxidation states.

The coordination compounds given in Table 1 represent a range of metals and commonly used ligands, but their syntheses require refluxing conditions for a minimum of 2 h, e.g. $[IrCl_3(9S3)]$, to 1 week for $[RuCl(CO)(bipy)_2]Cl$. Using a sealed Teflon container[8] and a microwave oven operating at 2450 MHz with power levels of 500–650 W, we have found that the coordination compounds listed in Table 1 can be conveniently synthesized in good yields in a matter of minutes. In the reactions 0.2–1.0 g of the metal salts were used with a total reaction volume of *ca* 15 cm^3.

The range of compounds synthesized in this manner, their yields, the reaction mixtures, solvents and reaction times are summarized in Table 1. The work-up procedures for the reactions generally follow those reported in the literature. The dramatic contraction in reaction times is large and parallels that reported previously for organic and organometallic reactions.[1,2,4]

The large decrease in reaction times should not be attributed to specific molecular absorption effects, but rather to macroscopic dielectric loss heating effects associated with the solvents. Water, alcohols and DMF all have high dielectric loss properties and efficiently convert microwave energy into thermal energy.[10] These efficient heating effects rapidly (within a matter of seconds) lead to a "pressure cooker" effect inside the sealed Teflon container due to the volatilities of the solvents. In the case of some of these reactions the formation of gaseous products further increases the pressure build-up. Indeed, in some cases the pressure release mechanism indicated that the pressure was approaching 80 atm before the reaction was complete and it was necessary to allow the reaction

* Author to whom correspondence should be addressed.

Table 1. Examples of coordination compounds synthesized using dielectric loss heating effects

Product[a]	Reaction mixture	Solvent	Reaction time (s)	Yield (%)	Conventional time (h)	Reference
$[Cr(DPM)_3]$	$CrCl_3 \cdot 3H_2O$, urea, dipivalolylmethane	$EtOH/H_2O$	40	71	24	11
$[IrCl(CO)(PPh_3)_2]$	$IrCl_3 \cdot xH_2O$, PPh_3	DMF	45	70	12[b]	12
$[IrCl_3(9S3)]$	$IrCl_3 \cdot xH_2O$, 9S3	MeOH	16	98	2	13
$[PtCl(terpy)]Cl \cdot 3H_2O$	K_2PtCl_4, terpy	H_2O	2×30	47	24–100	15
$[AuCl(terpy)]Cl_2 \cdot 3H_2O$	$HAuCl_4$, terpy	H_2O	2×30	37	24	15
$[RuCl(CO)(bipy)_2]Cl$	$RuCl_3 \cdot xH_2O$, bipy	DMF	3×20	70	168	16
$[Ru(9S3)_2](PF_6)_2$	$RuCl_3 \cdot xH_2O$, 9S3	MeOH	6×25	49	Cannot be synthesized directly	17

[a] DPM = 2,2,6,6-tetramethyl-3,5-heptadionato; 9S3 = 1,4,7-trithiacyclononane; terpy = 2,2′,2″-terpyridine; bipy = 2,2′-dipyridyl.

[b] The reaction product was at times contaminated with $[IrCl_3(CO)(PPh_3)_2]$ which was reduced to $[IrCl(CO)(PPh_3)_2]$ with zinc in DMF.

mixture to cool for 10–15 min before a subsequent exposure to microwaves was made. For example, in Table 1 the entries under reaction time of 2×30 indicate that two exposures of microwaves each of 30 s duration were used.

The synthesis of the crown thioether complex, $[IrCl_3(9S3)]$,[13] which has an octahedral geometry based on the tridentate thioether ligand, required only 16 s to synthesize in virtually quantitative yield. However, the synthesis of this complex is relatively easy using conventional reflux techniques (2 h in MeOH). The synthesis of the related ruthenium complex, $[Ru(9S3)_2](PF_6)_2$, by conventional methods required the prior conversion of $RuCl_3 \cdot xH_2O$ into the labile intermediate $Ru(SO_3CF_3)_3$ or $[Ru(DMSO)_6]^{2+}$.[17] Using the microwave techniques synthesis directly from $RuCl_3 \cdot xH_2O$ required a total of 150 s of microwave exposure (6×25) and gave the product in 49% yield.

The terpyridine complexes of platinum(II) and gold(III) listed in Table 1 have been extensively studied as metallo-intercalation reagents for DNA.[14,15] Both compounds were obtained in good yield using water as the solvent. The synthesis of the gold compound resulted in the formation of small quantities of the complex salt $[Au(terpy)Cl]_2[AuCl_2]_3[AuCl_4]$ which had been previously characterized by Lippard and co-workers.[15]

The heptadionato–chromium complex listed in Table 1 provides an example of a substitutionally-inert first-row transition metal complex which is conveniently made by this technique. It has been widely used as a spin–lattice relaxation reagent in NMR.[11] $[IrCl(CO)(PPh_3)_2]$,[12] Vaska's compound, and $[RuCl(CO)(bipy)_2]Cl$[16] used DMF as the solvent capable of efficiently coupling with the microwaves. In these reactions the DMF also provided the source of the carbonyl ligands.

In summary the application of microwave techniques for the synthesis of coordination compounds has been demonstrated. The technique should open up aspects of the coodination chemistries of second- and third-row transition metals both by facilitating the preparation of known compounds and by providing convenient routes to new compounds.

Acknowledgements—The SERC is thanked for financial support, Johnson Matthey plc for a generous loan of platinum metal salts and Rhode Island College for supporting D.L.G.'s sabbatical leave in Oxford.

REFERENCES

1. R. J. Giguere, T. L. Bray, S. M. Duncan and G. Majetich, *Tetrahedron Lett.* 1986, **27**, 4945; R. Gedye, F. Smith, K. Westaway, H. Ali, L. Baldisera, L. Laberge and J. Rousell, *Tetrahedron Lett.* 1986, **27**, 279.
2. A. B. Alloum, B. Labaid and D. Villemin, *J. Chem. Soc. Chem. Commun.* 1989, 386; E. Gutierrez, A. Loupy, G. Bram and E. Ruiz-Hitzky, *Tetrahedron Lett.* 1989, **30**, 945.
3. L. B. Fischer, *Analyt. Chem.* 1986, **58**, 261.
4. D. R. Baghurst, D. M. P. Mingos and M. J. Watson, *J. Organomet. Chem.* 1989, **368**, C43.
5. K. Chatakondu, M. L. H. Green, S. M. Reynolds and D. M. P. Mingos, *J. Chem. Soc., Chem. Commun.* 1989, 1515.
6. D. R. Baghurst and D. M. P. Mingos, *J. Chem. Soc., Chem. Commun.* 1988, 829.
7. D. R. Baghurst, A. M. Chippindale and D. M. P. Mingos, *Nature* 1988, **332**, 311.
8. Parr Microwave Acid Digestion Bombs available from the Parr Instrument Company, Illinois.

9. D. R. Baghurst and D. M. P. Mingos, *J. Organomet. Chem.*, in press.
10. A. C. Metaxas and R. J. Meredith, *Industrial Microwave Heating*. IEE Power Engineering Series 4, Peter Peregrinus, London (1983).
11. D. Stille and J. R. Doyle, *Inorg. Synth.* 1985, **24**, 183.
12. K. Vrieze, J. P. Collman, C. T. Sears and M. Kubota, *Inorg. Synth.* 1968, **11**, 101.
13. S. R. Cooper and P. J. Blower, unpublished results.
14. E. M. A. Ratilla and N. M. Kostic, *J. Am. Chem. Soc.* 1988, **110**, 4427.
15. L. S. Hollis and S. J. Lippard, *J. Am. Chem. Soc.* 1983, **105**, 4293; M. Howe-Grant and S. J. Lippard, *Inorg. Synth.* 1980, **20**, 101.
16. D. Choudhury, R. F. Jones, G. Smith and D. J. Cole-Hamilton, *J. Chem. Soc., Dalton Trans.* 1982, 1143.
17. S. R. Cooper, S. C. Rawle and T. J. Sewell, *Inorg. Chem.* 1987, **26**, 3769.

Polyhedron Vol. 9, No. 6, p. 897, 1990
Pergamon Press plc. Printed in Great Britain

BOOK REVIEW

Gmelin Handbook of Inorganic Chemistry—8th edn. Organotin Compounds, Part 16. By Herbert Schumann and Ingeborg Schumann. Springer, Berlin, Heidelberg, New York, London, Paris, Tokyo, 1988. ISBN 3-540-93581-9; 290 pp. Hard cover DM 1334,–(R).

This text, the sixteenth in the Gmelin series of handbooks on organotin chemistry, deals exclusively with tetravalent compounds which contain two organyl ligands and two oxygen-bonded groups. It should be noted, however, that compounds of the type $R_2Sn(OR')_2$ or $R_2\overline{Sn—O—R—O}$, in which R is an unsubstituted alkyl of four or fewer carbons, were dealt with in earlier volumes (parts 14 and 15) and have consequently been excluded from this one. On the other hand, compounds in which either the two organyl ligands and/or the two O-bonded ligands, are different have been included.

These distinctions are quite arbitrary in any chemical sense and reflect a compartmentalization strategy based upon editorial convenience. Of course, this presents no problem for collectors of substantial portions of the organotin series, but more selective purchasers are advised to examine carefully the scope of each volume.

After a classified list of general literature sources (which includes sections on analysis, toxicology and uses), the main body of the text begins with compounds containing two identical organyl and either two identical O-bonded groups or a single bidentate one. The compounds described contain the following organyl ligands: unsubstituted alkyls from C_5 to C_{10}, although examples of C_{12}, C_{18} and C_{20}, are also included; cyclohexyl; alkyls substituted with aryl, halogen or oxygen, functional groups, of which the most numerous is benzyl; alkenyls; aryls, most commonly phenyl; and finally cyclic organyls with N, O, or S heteroatoms. The oxygen ligands therewith include alkoxides, β-diketonates, carboxylates and dicarboxylates, as well as those containing the linkage Sn—O—G—, where G is B, Si, N, P, As, O, S or Se.

The next section covers compounds in which the two organyls and/or the two O-bonded ligands, are different, as well as the few known compounds of the type $R—Sn(OR')_2$ or $R—O—Sn—O—R$.

In keeping with other volumes in the Gmelin Inorganic Chemistry series, the data provided are comprehensive and meticulously researched. They include synthetic methods, physical properties, structural details, spectroscopic data, and, of particular importance for organotin compounds, uses.

The general presentation follows the format of previous volumes: a large proportion of data is tabulated whilst the more important compounds are further described in the text. Besides the fairly detailed table of contents, finding a specific compound is facilitated by the empirical formula and ligand formula indexes.

In conclusion, therefore, besides the minor but certainly understandable irritation concerning the scope, this volume is yet another example of the excellence of the Gmelin series.

DARIO M. FRIGO

Billiton Research B.V.
Postbox 40
6800 AA Arnhem
The Netherlands

Polyhedron Vol. 9, No. 6, p. 899, 1990
Pergamon Press plc. Printed in Great Britain

BOOK REVIEW

Gmelin Handbook of Inorganic Chemistry—8th edn. Re—Organorhenium Compounds, Part 1. Edited by A. Slawisch. Springer, Berlin, 1989. ISBN 3-540-93580-0, ISBN 0-387-93580-0 (Eng.), 612 pp., 89 illustrations, DM 2800.

Gmelin Handbook of Inorganic Chemistry—8th edn. Re—Organorhenium Compounds, Part 2. Edited by A. Slawisch. Springer, Berlin, 1989. ISBN 3-540-93587-8, ISBN 0-387-93587-8 (Eng.), 474 pp., 59 illustrations, DM 2135.

These two Gmelin volumes, the first in a series dealing with organorhenium compounds, cover the literature up to the end of 1987. The material is well organized using the "L and "'D notation, where L represent an organic ligand bonded to rhenium by *n*C atoms and D represents a neutral donor donating *m* electrons.

Mononuclear complexes containing CO and/or "L are described in *Part 1* and compounds are divided into classes according to the type and number of ligands. The first section (24 pp.) deals with non-carbonyls containing ^{1}L ligands, starting with homoleptic alkyls and progressing through oxo- and halohydrocarbyl species (including alkylidenes and alkylidynes) to chelating ^{1}L complexes and reflects the recent upsurge in interest in higher oxidation-state organometallics.

The remaining four major sections successively deal with compounds containing from one to four CO groups (27, 55, 230 and 165 pp.). Sub-division of compounds within these sections is according to the number and type of D ligands and heteronuclear compounds are collected together at the end of each section.

In *Part 2*, the first two sections describe compounds with five (215 pp.) and six (30 pp.) CO ligands, and then six sections are allocated to complexes with from one to six isonitrile ligands (75 pp.). ^{2}L (68 pp.), ^{3}L (24 pp.) and ^{4}L (23 pp.) complexes are covered in the remaining sections. It is worth noting that heterometallic fragments bonded to Re via organic bridges are treated as "L ligands.

This compound classification works well and in each section the systematic listing of compound, method of preparation, properties (physical, spectroscopic etc.) and miscellaneous remarks, in tabulated form whereover possible, is easy to follow. The text and tables are clearly arranged, the figures and diagrams are excellent (complete with bond lengths and angles where appropriate), and empirical formula and ligand formula indexes are provided. Consequently, these volumes are easy to use. I particularly like the footnotes giving the location of references on each page.

The high quality of these volumes is very impressive and, although expensive, their availability in English should attract the previously reluctant Gmelin readers.

Department of Chemistry **R. J. ERRINGTON**
University of Newcastle upon Tyne
Newcastle upon Tyne, NE1 7RU, U.K.

Polyhedron Vol. 9, No. 7, pp. 901–906, 1990
Printed in Great Britain

0277-5387/90 $3.00+.00
© 1990 Pergamon Press plc

FLUORIDE COMPLEXES OF ZINC(II) AND CADMIUM(II)

G. T. HEFTER*

School of Mathematical and Physical Sciences, Murdoch University, Murdoch, WA 6150, Australia

and

N. H. TIOH and C. B. CHAN

Chemistry Department, University of Malaya, Kuala Lumpur 59100, Malaysia

(*Received* 28 *September* 1989; *accepted* 24 *October* 1989)

Abstract—The stability constants, $\beta_1[MF^+(aq)]$, for the formation of the monofluoride complexes of zinc(II) and cadmium(II) in aqueous solution have been determined at 25°C and ionic strengths ranging from 0.01 to 3 M ($NaClO_4$) by fluoride ion-selective electrode potentiometry. Despite the difference in size of the zinc(II) and cadmium(II) ions their β_1 values are almost identical. Lack of variation of β_1 at high ionic strengths has been attributed to weak complexing of the metal ions by perchlorate. Measurements with amalgam electrodes at $I = 1$ M ($NaClO_4$) have indicated the existence of a very weak second complex $MF_2^0(aq)$ for both zinc(II) and cadmium(II).

Zinc(II) and cadmium(II) are generally regarded as "borderline" ions in the class A/class B or hard/soft classification systems of Ahrland *et al.*[1] and Pearson.[2] As such, the stability of their halide complexes is of some theoretical interest. On the basis of existing data[3,4] it appears that in aqueous solution zinc(II) ions show class A (hard) behaviour, with overall stability constants (β_n) for the reactions

$$M^{2+} + nX^- \overset{\beta_n}{\rightleftharpoons} MX_n^{2-n} \qquad (1)$$

being in the order $F^- > Cl^- > Br^- > I^-$.[3–5] On the other hand, cadmium(II) shows clear class B character with the overall stability constants of its halide complexes in aqueous solution being $F^- < Cl^- < Br^- < I^-$.[3–5]

However, the differences in the halide stability constants of both ions are not large: a feature often observed for borderline metal ions.[5] Interestingly, closely related lead(II) shows a "mixed" order of $F^- > Cl^- < Br^- < I^-$ in aqueous solution.[5] In non-aqueous solvents such as acetonitrile,[6] DMSO[7,8] and DMF[9] both zinc(II) and cadmium(II) show clear class A behaviour, with halide stability constants $Cl^- > Br^- > I^-$ (the analogous fluoride stability constants have rarely been measured in non-aqueous solvents[5,10]).

Although the zinc(II)– and cadmium(II)–halide systems in aqueous solution have been investigated on many occasions,[3,4] the relatively few studies of the fluoride complexes are not in particularly good agreement and show an uncertain dependence on ionic strength.[10] Since such measurements are also of interest for modelling the behaviour of geological brines,[11,12] seawater[13] and mineral extraction process streams,[14] a thorough study of the fluoride complexes of zinc(II) and cadmium(II) as a function of ionic strength has been undertaken using fluoride ion-selective electrode measurements. Some measurements have also been made with metal amalgam electrodes to look for the possible existence of higher order complexes.

EXPERIMENTAL

Reagents and apparatus

All chemicals used were of reagent grade purity. All solutions were prepared using glass-distilled

* Author to whom correspondence should be addressed.

water and calibrated volumetric glassware. Crude zinc(II) and cadmium(II) perchlorates were prepared by neutralizing the appropriate carbonate or oxide with perchloric acid, followed by removal of water to approximately 50% of the original volume. The crystals so obtained were purified twice by recrystallization from hot water and then vacuum dried (10^{-2} mm Hg) at 110–120°C for at least 24 h. Sodium perchlorate (A.R. grade) was similarly purified. Sodium fluoride (A.R. grade) was purified by the method of Lingane.[15]

Stock solutions of zinc and cadmium perchlorates were standardized against EDTA (BDH Concentrated Volumetric Standard). Stock fluoride solutions were prepared by weight and stored in pre-leached air-tight polyethylene containers. The pH of all solutions was maintained at 5.0–5.5. At this pH the formation of HF and HF_2^-[10] and metal-ion hydroxy species[3,4] may be neglected, as may the OH^- interference with the fluoride ISE.[16]

All measurements were made in a paraffin wax-coated glass cell at 25.00 ± 0.02°C maintained with a circulating thermostat (Haake Model Fe) which was itself cooled by thermostatted (20.0 ± 0.2°C) water.

Free fluoride concentrations were determined by a commercial fluoride ISE (Orion Model 94–09). Zinc and cadmium amalgam electrodes were prepared as described previously.[17,18] All potentials were measured to 0.1 mV with a digital voltmeter (Orion, Models 801A or 901), relative to a Ag/AgCl electrode consisting of a silver wire in contact with solid AgCl.[19] Titrations were performed with a 5 cm^3 Metrohm Mico Hand-burette (Model E457).

The technique of *in situ* calibration and all other details are as described previously.[19] Stability constants reported are the average of at least three and usually more than five independent titrations.

Calculations

(a) *Fluoride electrode measurements.* Assuming that the equilibria in aqueous divalent metal ion–fluoride solutions can be represented as in eq. (1), i.e. there are no "polynuclear" or mixed complexes formed, it is readily shown that if $[M^{2+}]_T \gg [F^-]_T$ (where T denotes the total or analytical concentration):

$$\frac{1}{[M^{2+}]_T}\left\{\frac{[F^-]_T}{[F^-]} - 1\right\} = F_0(X) = \sum_1^n n\beta_n[F^-]^{n-1}, \quad (2)$$

where β_n are the overall concentration stability constants corresponding to the equilibria (1) and $F_0(X)$ is introduced to represent the experimentally-determined left hand side of eq. (2).

(b) *Amalgam electrodes.* Again assuming only the equilibria corresponding to eq. (1) and using the usual mass balance relationships, it can be shown that

$$\frac{1}{[F^-]}\left\{\frac{[M^{2+}]_T}{[M^{2+}]} - 1\right\} = F'_0(X) = \sum_1^n \beta_n[F^-]^n, \quad (3)$$

where $F'_0(X)$ is again introduced for convenience to represent the experimentally determined left hand side of the equation.

If $[F^-]_T \gg [M^{2+}]_T$ then $[F^-] \simeq [F^-]_T$. Alternatively, $[F^-]$ can be obtained iteratively by initially assuming $[F^-] = [F^-]_T$, calculating tentative values of β_n which can then be used to calculate $[F^-]$, etc. Usually two iterations are sufficient to calculate consistent values of β_n and $[F^-]$.[19]

Liquid junction potentials

Cells used for this study may be represented in general terms as

	Reference half cell		Salt bridge		Indicating half cell		
Ag | AgCl	0.1 *I* M ACl 0.9 *I* M AB		*I* M (AB)		*x* M MB_2 *y* M AF (*I* − 3*x* − *y*) M AB		FE or M (Hg)
		E_{j1}		E_{j2}			

(4)

where FE represents the fluoride ISE, M(Hg) a metal amalgam electrode, I ($= 1/2\,\Sigma[i]z_i^2$) the total ionic strength (maintained constant throughout by the addition of a supposedly non-complexing "swamping" electrolyte AB: $NaClO_4$ in the present work) and $E_{j1\text{ and }2}$ are liquid junction potentials (LJPs).

It has been shown[20] that for accurate work LJPs must be taken into consideration even at relatively high ionic strengths. Fortunately, LJPs for the "constant ionic medium" junctions, represented in

cell (4) may be calculated with considerable reliability from the Henderson equation as demonstrated elsewhere.[20] Under typical experimental conditions E_{j1} is essentially constant and may be incorporated into the "standard" cell potential. E_{j2} was calculated for both cell types [i.e. FE or M(Hg)], as described in detail previously.[19,20] The necessary conductivity and transference data for the calculation of E_{j2} were obtained by appropriate interpolation and extrapolation of literature data[21-25] and, in some cases, by direct measurement.[26]

RESULTS AND DISCUSSION

Stability constants at I = 1 M ($NaClO_4$)

Because most of the literature data on metal ion–fluoride complexes have been reported at $I = 1$ M,[5,10] a detailed study at this ionic strength of the zinc(II)– and cadmium(II)–fluoride systems was undertaken using both fluoride and amalgam electrodes. Typical experimental data for the fluoride electrode are presented for the Cd^{II}/F^- system in Table 1. Similar data were obtained for zinc(II) and for both metal ions with the amalgam electrodes. The results obtained at $I = 1$ M are summarized in Table 2.

With the fluoride electrode only the first complex $MF^+(aq)$ is detected, as indicated by the constancy of the $F_0(X)$ values in the right hand column of Table 1 [cf. eq. (2)]. This is not surprising since, in order to maximize the accuracy of the fluoride electrode data,[19] conditions are chosen such that $[M^{2+}] \gg [F^-]$, which means only insignificant amounts of any higher order complexes will be formed.[27] Higher complexes are best detected with

Table 1. Typical potentiometric (fluoride electrode) data for the Cd^{II}/F^- system ($I = 1.00$ M ($NaClO_4$); $T = 25.00$°C)

E^a (mV)	$E_{j2}{}^b$ (mV)	$[F^-]_T{}^c$ (10^4 M)	$[F^-]^{d,e}$ (10^4 M)	$[Cd^+]^e$ (10^2M)	$F_0(X)^{e,f}$
−29.8	0.08	6.219	5.892	1.667	3.32
−28.0	0.12	6.012	5.589	2.302	3.29
−26.2	0.16	5.695	5.138	3.270	3.31
−24.2	0.21	5.410	4.762	4.144	3.28
−20.6	0.29	4.919	4.153	5.651	3.27
−17.5	0.35	4.509	3.609	6.909	3.22
−14.7	0.41	4.162	3.316	7.973	3.20
−8.7	0.52	3.491	2.637	10.03	3.23
−3.9	0.60	3.006	2.194	11.53	3.21
+0.1	0.66	2.639	1.882	12.64	3.18
+3.7	0.71	2.352	1.639	13.52	3.21

Average (11 points): $\beta_1[CdF^+(aq)] = 3.25 \pm 0.05$ dm^3 mol^{-1}.

[a] Observed cell potential.

[b] Calculated from Henderson equation:[20] $E_{j2} = -12.71 \log(1 - 1.829[Cd^{2+}])$.

[c] Total fluoride concentration corrected for background fluoride impurity,[19] data not shown.

[d] Calculated from Nernst equation: $E_{corr} = E^{0\prime} - 59.16 \log[F^-]$, where $E_{corr} = E - E_{j2}$ and $E^{0\prime} = -220.95 \pm 0.03$ mV determined by *in situ* calibration,[19] data not shown.

[e] Calculated iteratively.[19]

[f] Defined in eq. (2).

Table 2. Summary of M^{II}/F^- stability constants at $I = 1.00$ M ($NaClO_4$) and $T = 25.00$°C

Method	$\beta_n[ZnF_n^{2-n}(aq)]$ (M^{-n})		$\beta_n[CdF_n^{2-n}(aq)]$ (M^{-n})	
F^- ISE	β_1 3.5±0.1		β_1 3.2±0.1	
M(Hg)	β_1 3.6±0.2	β_2 3.8±0.5	β_1 3.5±0.1	β_2 3.6±0.1

an M^{2+}-responsive electrode where optimal experimental data are obtained when $[F^-] \gg [M^{2+}]$.

In addition to giving values of $\beta_1[MF^+(aq)]$ in excellent agreement with those obtained via the fluoride electrode, M(Hg)-electrode measurements established the existence of a weak second complex $MF_2^0(aq)$ (Table 2) for both metal ions. $CdF_2^0(aq)$ is reasonably well established, having been observed in a number of previous potentiometric and polarographic studies.[3,4,10] However, $ZnF_2^0(aq)$ has not previously been reported probably because of difficulties associated with polarographic study of zinc(II) systems (see below) and also because no previous zinc amalgam measurements appear to have been undertaken.[3,4,10] The $MF_2^0(aq)$ complexes are extremely weak with an overall stability constant approximately equal to that of the first complex (Table 3). That is, the stepwise constant K_2 ($= \beta_2/\beta_1$) for the process

$$MF^+(aq) + F^-(aq) \rightleftharpoons MF_2^0(aq)$$

is very small. No further complexes for either zinc(II) or cadmium(II) were detected even at $[F^-]/[M^{II}]$ ratios up to 1000, consistent with most other studies.[3,4,10]

The stability constants of metal ion–fluoride complexes in aqueous solution have been shown to correlate well with simple electrostatic quantities such as $[Z/(r_{M^{z+}} + r_{F^-})]$.[5] However, it has been noted[5] that the borderline ions do not conform well with this model, having stability constants that are greater than would be predicted by a simple electrostatic model. A plausible explanation of this behaviour is that the borderline cations have higher *effective* charges than other cations because of the inadequate shielding by their inner *d*-electrons.[5]

Whilst $\beta_1[ZnF^+(aq)]$ is greater than $\beta_1[CdF^+(aq)]$, consistent with simple electrostatics, the difference is much less than might be expected given the considerable difference in their size: $r_{Zn^{2+}} = 74$ pm, $r_{Cd^{2+}} = 97$ pm.[28]

Table 3. Summary of present results for $\beta_1[MF^+(aq)]$ at 25°C using the fluoride ISE

I (M) ($NaClO_4$)	$\beta_1[ZnF^+(aq)]$ (M^{-1})	$\beta_1[CdF^+(aq)]$ (M^{-1})
3.0	3.6±0.1	3.0±0.1
2.0	3.5±0.5	3.6±0.1
1.0	3.5±0.1	3.2±0.1
0.5	3.6±0.2	3.6±0.1
0.2	4.6±0.1	4.6±0.1
0.1	5.2±0.5	4.8±0.4
0.05	6.7±0.1	6.8±0.1
0.02	9.6±1.0	9.6±0.4
0.01	12.0±3.0	11.0±1.0
0[a]	15.9±1.6	15.2±1.5

[a] Extrapolated using eq. (7); see text.

Variation of stability constants with ionic strength

Measurements at ionic strengths other than 1 M were performed only using the fluoride electrode under conditions where $[M^{2+}] > [F^-]$ and so only the first complex $MF^+(aq)$ was detected. The data obtained are summarized in Table 3 and plotted in Figs 1 and 2 along with literature values.[3,10]

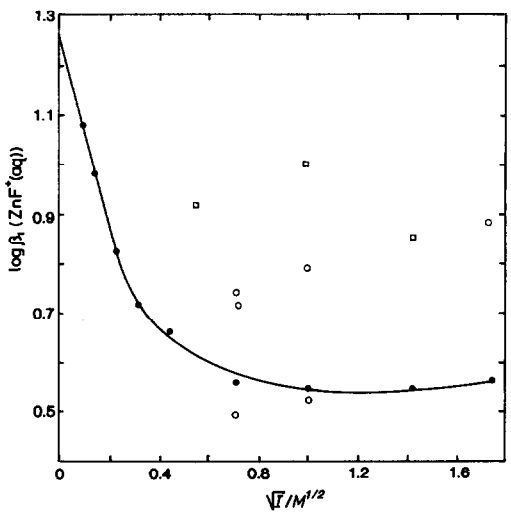

Fig. 1. Comparison of present and literature values for $\log\beta_1[ZnF^+(aq)]$ at 25°C as a function of ionic strength: ●, present results (Table 3); ○, other EMF data; □, polarographic data. Literature values from ref. 10, in $NaClO_4$ or $NaNO_3$ media (see text).

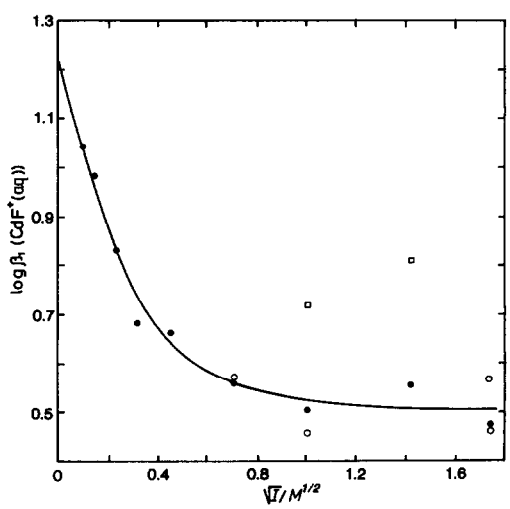

Fig. 2. Comparison of present and literature values for $\log\beta_1[CdF^+(aq)]$ at 25°C as a function of ionic strength. Other details as for Fig. 1.

The present results are the first systematic study of the Zn^{II}/F^- and Cd^{II}/F^- systems as a function of ionic strength.[3,4,10] The Cd^{II}/F^- data are in general in good agreement with previous determinations (Fig. 2). However, the $\beta_1[ZnF^+(aq)]$ results are generally lower than literature values (Fig. 1), although they are in reasonable agreement with previous fluoride electrode studies.[10]

It is apparent from Figs 1 and 2 that most of the higher values for $\beta_1[MF^+(aq)]$ for both zinc(II) and cadmium(II) have been determined polarographically. This technique is generally regarded as somewhat less precise than potentiometry. However, in the absence of complicating factors such as anion adsorption (which should be virtually absent for fluoride systems[29]), polarographic stability constants are usually in good agreement with potentiometric values.[20]

Whilst it is possible to discount the Zn^{II}/F^- data, because of lingering doubts[31] about the reversibility of the polarographic reduction of zinc(II), which would significantly influence the measured β_n values, the cadmium(II) reduction is strictly reversible.[32]

The source of the discrepancy between the polarographic and EMF measurements is not obvious and clearly merits further investigation.

The other remarkable feature of the data in Figs 1 and 2 is the small change in $\beta_1[MF^+(aq)]$ at higher ionic strengths. The stability constants for most equilibria involving ionic species exhibit a characteristic asymmetric U-shaped curve with increasing ionic strength as a result of changing activity coefficients.[19,33,34]

Strictly speaking, the stability constant expression for the formation of the first fluoride complex (eq. (1), $n = 1$) should be written in terms of activities (omitting the aq symbols):[33,34]

$$\beta_1^\theta(MF^+) = \frac{a_{MF^+}}{a_{M^{2+}}a_{F^-}} = \frac{[MF^+]}{[M^{2+}][F^-]} \cdot \frac{\gamma_{MF^+}}{\gamma_{M^{2+}}\gamma_{F^-}}.$$

That is

$$\log \beta_1^\theta = \log \beta_1 + \log\left(\frac{\gamma_{MF^+}}{\gamma_{M^{2+}}\gamma_{F^-}}\right), \qquad (5)$$

where β_1^θ is the "true" or "thermodynamic" constant.

Although activity coefficients for individual ions cannot be measured, their behaviour as a function of ionic strength can be approximated by an appropriate function such as the extended Debye–Huckel, Davies or Pitzer equations.[35] For simplicity the Davies equation[34]

$$\log \gamma_i = -Az_i^2\left(\frac{\sqrt{I}}{1+\sqrt{I}} - 0.3I\right) \qquad (6)$$

will be assumed, where A is the Debye–Huckel constant ($= 0.509$ at 25°C in H_2O).

Combination and rearrangement of eqs (6) and (7) gives

$$\log \beta_1 = \log \beta_1^\theta - 4A\left(\frac{\sqrt{I}}{1+\sqrt{I}} - 0.3I\right), \qquad (7)$$

which accounts for the well-known U-shaped curve: an initial decrease in $\log \beta_1$ at low I, due to the predominance of the first activity coefficient term inside the parentheses, followed by an increase at higher I as the second activity coefficient term becomes dominant. The position of the mimimum in $\log \beta_1$ vs $\sqrt{I}$ curves depends on a number of factors but typically occurs around 0.5–1.0 M.[33–35]

The fact that $\log \beta_1[MF^+(aq)]$ vs $\sqrt{I}$ curves (Figs 1 and 2) do not follow the accepted shape at high ionic strengths indicates that other factors must be taken into consideration. The most likely explanation is competition for the metal ion from the supposedly non-complexing background electrolyte.[36,37] That is, the reaction actually being measured does not correspond to eq. (1) but rather to the competitive equilibrium

$$MClO_4^+(aq) + F^-(aq) \rightleftharpoons MF^+(aq) + ClO_4^-(aq).$$

The effect of such competition is to reduce the dependence of $\log \beta$ on ionic strength at high I values.[36,37]

Although perchlorate is generally regarded as non-complexing in aqueous solution, even a very weak $MClO_4^+$ complex is sufficient to produce the effect seen in Figs 1 and 2.[37] Unfortunately, the data available for the zinc(II)– and cadmium(II)–ClO_4^- systems are rather limited, although at least one conductance study suggests there may be quite strong association.[3] It may also be noted that, unlike most metal ion–fluoride complexes,[37] there does not seem to be much difference between $\beta_n[MF_n^{2-n}(aq)]$ determined in nitrate and perchlorate media.[10] This suggests $\beta_n[M(NO_3)_n^{2-n}(aq)] \simeq \beta_n[M(ClO_4)_n^{2-n}(aq)]$. Since NO_3^- is generally rather more strongly complexing than ClO_4^- this is circumstantial evidence that zinc(II) and cadmium(II) perchlorate complexes are unusually "strong".

Standard state stability constants

The standard state for solutes in solution is arbitrary but is normally taken to be infinite dilution in the solvent.[33] Application of eq. (7) to the low ionic strength $\beta_1[MF^+(aq)]$ data in Table 3 gives $\beta_1^\theta[ZnF^+(aq)] = 15.9 \pm 1.6\ M^{-1}$ and $\beta_1^\theta[CdF^+(aq)] = 15.2 \pm 1.5\ M^{-1}$. The values for $ZnF^+(aq)$ are in good agreement with previous estimates of

13.8 M^{-1} by Cook *et al.* and 18.2 by Connick and Paul.[3,4] No previous estimate of β_1^θ[CdF^+ (aq)] has been made.[3,4,10]

Acknowledgement—The authors thank Dr B. W. Clare of Murdoch University for assistance with the calculations.

REFERENCES

1. S. Ahrland, J. Chatt and N. R. Davies, *Quart. Rev. Chem. Soc.* 1958, **12**, 265.
2. R. G. Pearson, *J. Am. Chem. Soc.* 1963, **85**, 3533.
3. L. G. Sillen and A. E. Martell (Eds), *Stability Constants of Metal-ion Complexes*, Special Publications Nos 17 (1964) and 25 (1971). Chemical Society, London.
4. E. Hoegfeldt (Ed.), *Stability Constants of Metal-ion Complexes*, Part A, Inorganic Ligands. IUPAC Chemical Data Series No. 21. Pergamon Press, Oxford (1982).
5. G. T. Hefter, *Coord. Chem. Rev.* 1974, **12**, 221.
6. R. C. Kapoor and J. Kishan, *Rev. Anal. Chem.* 1981, **5**, 257.
7. R. C. Kapoor, J. Kishan and B. S. Aggarwal, *Rev. Anal. Chem.* 1982, **6**, 241.
8. S. Ahrland, in *The Chemistry of Non-aqueous Solvents* (Edited by J. J. Lagowski), Vol. 5A. Academic Press, New York (1978).
9. R. C. Kapoor and J. Kishan *J. Sci. Ind. Res. (India)* 1982, **41**, 314.
10. A. M. Bond and G. T. Hefter, *Critical Survey of Stability Constants and Related Thermodyamic Data of Fluoride Complexes in Aqueous Solution*. IUPAC Chemical Data Series No. 27. Pergamon Press, Oxford (1980).
11. C. K. Richardson and H. D. Holland, *Geochim. Cosmochim. Acta* 1979, **43**, 1327 and refs cited therein.
12. B. A. Bilal and V. Koss, *Polyhedron* 1982, **1**, 239 and refs cited therein.
13. J. P. Riley and G. Skirrow (Eds.), *Chemical Oceanography*, 2nd edn, Vol. 1. Academic Press, London (1975).
14. See for example, G. Senanayake and D. M. Muir, *Met. Trans. B* 1988, **19**, 37.
15. J. J. Lingane, *Analyt. Chem.* 1967, **39**, 881.
16. M. S. Frant and J. W. Ross, *Science* 1966, **154**, 1553.
17. B. W. Clare, G. T. Hefter and P. Singh, *Austral. J. Chem.* 1990, **43**, 257.
18. A. M. Bond and G. T. Hefter, *J. Electroanal. Chem.* 1976, **68**, 203.
19. G. T. Hefter, *J. Soln. Chem.* 1982, **11**, 45.
20. G. T. Hefter, *Analyt. Chem.* 1982, **54**, 2518.
21. E. M. Kartzmark, *Can. J. Chem.* 1972, **50**, 2845.
22. J. H. Jones, *J. Am. Chem. Soc.* 1945, **67**, 855.
23. M. L. Miller, *J. Phys. Chem.* 1956, **60**, 189.
24. R. Haase, G. Lehnert and H. J. Jansen, *Z. Phys. Chem. Neue Folge* 1964, **42**, 32.
25. A. N. Campbell, G. H. Debus and E. M. Kartzmark, *Can. J. Chem.* 1955, **33**, 1508.
26. C. B. Chan, G. T. Hefter and N. H. Tioh, unpublished observations.
27. A. M. Bond and G. T. Hefter, *Inorg. Chem.* 1970, **9**, 1021.
28. Y. Marcus, *Ion Solvation*. Wiley, New York (1985).
29. J. O. Bockris and A. K. N. Reddy, *Modern Electrochemistry*. Plenum Press, New York (1970).
30. A. M. Bond and G. T. Hefter, *J. Electroanal. Chem.* 1973, **42**, 1.
31. A. M. Bond, *J. Electroanal. Chem.* 1969, **20**, 109.
32. A. M. Bond, *J. Electroanal. Chem.* 1969, **20**, 223.
33. R. A. Robinson and R. H. Stokes, *Electrolyte Solutions*, 2nd edn. Butterworths, London (1959).
34. G. H. Nancollas, *Interactions in Electrolyte Solutions*. Elsevier, Amsterdam (1966).
35. R. M. Pytkowicz (Ed.), *Activity Coefficients in Electrolyte Solutions*. CRC Press, Palm Beach (1979).
36. G. T. Hefter, *J. Soln Chem.* 1984, **13**, 179.
37. G. T. Hefter, C. B. Chan and N. H. Tioh, *Analyt. Chem.* 1984, **56**, 749.

Polyhedron Vol. 9, No. 7, pp. 907–911, 1990
Printed in Great Britain

0277–5387/90 $3.00+.00
© 1990 Pergamon Press plc

REACTION OF $Ru(CO)Cl(RC{=}CHR')(PPh_3)_2$ WITH THE 3,3-DIMETHYLACRYLATE ANION. THE MOLECULAR STRUCTURE OF $Ru(O_2CCH{=}CMe_2)(CO)(C(CO_2Me){=}CH(CO_2Me))(PPh_3)_2$

HASSANE LOUMRHARI and JOSEP ROS*

Departament de Química, Universitat Autónoma de Barcelona, 08193—Bellaterra, Barcelona, Spain

and

M. ROSARIO TORRES and AUREA PERALES

Instituto de Química-Física "Rocasolano" C.S.I.C., Serrano 119, 28006—Madrid, Spain

(*Received* 28 *July* 1989; *accepted* 2 *November* 1989)

Abstract—The unsaturated complexes $Ru(CO)Cl(CR{=}CHR')(PPh_3)_2$ react rapidly with the sodium salt of the anion 3,3-dimethylacrylate. The family of complexes obtained contains the 3,3-dimethylacrylate ligand η^2-coordinated through the carboxylate group. The structure of the complex $Ru(O_2CCH{=}CMe_2)(CO)(C(CO_2Me){=}CH(CO_2Me))(PPh_3)_2$ was determined by X-ray diffraction. The complex is triclinic, space group $P\bar{1}$, with dimensions of the unit cell of $a = 17.401(1)$, $b = 12.633(3)$, $c = 12.054(1)$ Å; $\alpha = 119.092(4)$, $\beta = 72.423(5)$, $\gamma = 109(7)°$ and $D_{calc} = 1.226$ g cm^{-3} for $Z = 2$. The molecule consists of a ruthenium hexacoordinated with two triphenylphosphines in the apical positions and the rest of the ligands in the equatorial plane of a distorted octahedron.

The carboxylate complexes of ruthenium present interesting catalytic activity in reactions of hydrogenation[1] and hydroformylation.[2] In these reactions the ruthenium atom quickly activates the molecule of H_2 forming hydrides which participate in the catalytic cycle. For this reason we are interested in the reactivity of mononuclear hydrides of ruthenium with unsaturated molecules such as acetylenes and the possible application of products in catalysis. In this way, the unsaturated alkenyl complexes obtained from $RuCl(CO)H(PPh_3)_2$ and acetylenes[3] have been reacted with small molecules like CS_2,[4] acetylenes,[5] pyrazoles,[6] CO[7] and carboxylates.[8] The reaction with CS_2 and acetylenes produces a coupling with the alkenyl ligand; with pyrazoles the alkenyl group is transformed to alkynyl; with CO, a η^2-acyl ligand is formed depending on the alkyne.[7] With carboxylates only saturation of the metal occurs by η^2-coordination.[8] A very interesting reaction is the oxidation of the acyl ligand, obtained from the reaction with CO, with methanol giving rise to an alkenecarboxylate group. The exact nature of the ligand was confirmed by the resolution of the crystal structure of the complex $RuCl(CO)(O_2CC(Me){=}CHMe)(PPh_3)_2$. For a better knowledge of this type of complex we initiated a systematic study of the addition of sodium 3,3-dimethylacrylate to the unsaturated complexes $RuCl(CO)(CR{=}CHR')(PPh_3)_2$.

RESULTS AND DISCUSSION

Previously we have studied the reactivity of the 16-electron complexes $RuCl(CO)(CR{=}CHR')(PPh_3)_2$ toward bidentate anionic ligands such as carboxylates.[8] The results with acetate indicated a fast substitution of the monodentate ligand by a chelating carboxylate. In the same fashion, a methanolic solution of the sodium salt of the anion 3,3-dimethylacrylate reacts with the alkenyl complexes of ruthenium dissolved in dichloro-

* Author to whom correspondence should be addressed.

methane and gives rise to complexes whose elemental analyses are in accordance with the presence of two PPh_3 groups, one molecule of CO, an alkenyl group and a 3,3-dimethylacrylate ligand. The isolated products of formula $Ru(O_2CCH{=}CMe_2)(CO)(CR{=}CHR')(PPh_3)_2$ (with R = R′ = H, Me, Ph and CO_2Me; R = H and R′ = CMe_3, $SiMe_3$, Ph, CO_2Me and CO_2Et) are stable to air and soluble in dichloromethane, but insoluble in alcohols and petroleum ether. The complexes are obtained as yellow microcrystals which can be recrystallized from dichloromethane–methanol mixtures forming suitable crystals for X-ray diffraction studies.

The IR spectrum of the sodium salt of the 3,3-dimethylacrylate ligand presents typical carboxylate group absorptions at 1575 and 1412 cm^{-1} with a $\nu(C{=}C)$ band at 1567 cm^{-1}. The IR spectra of complexes show $\nu(OCO)_{asym}$ at 1515–1567 cm^{-1} and $\nu(OCO)_{sym}$ at 1413–1450 cm^{-1}, characteristic of chelated carboxylate ligands.[9] In some synthesized complexes the $\nu(OCO)_{sym}$ band is obscured by the strong absorptions of the triphenylphosphines making their assignment difficult. This situation also occurred in the complex $RuCl(CO)(O_2CC(Me){=}CHMe)(PPh_3)_2$ which obstructed their spectroscopic identification.[7] The $\nu(CO)$ band appears at 1909–1937 cm^{-1} depending on the alkenyl group and the $\nu(C{=}C)$ is located at $\approx$ 1550 cm^{-1} but is also obscured by the carboxylate absorption.[10] There are no important differences between the $\nu(CO)$ bands of the synthesized products and those of the acetate complexes previously quoted, indicating similar electronic effects on the metal centre. The ^1H NMR spectra of the complexes contain signals due to all the coordinated ligands. The acrylic hydrogen appears at $\approx$ 4.4 ppm and the alkenylic protons —CH= are shifted upfield, while the hydrogens of =CHR′ are shifted downfield with respect to the position of the hydrogens of the unsaturated alkenyl complexes $RuCl(CO)(CR{=}CHR')(PPh_3)_2$. The coupling between the protons in the monosubstituted alkenyl ligands, $\approx$ 16 Hz, indicates that the geometry of the organic group is maintained.[3,11]

All analytical and spectroscopic data of the presented products are in accordance with a structure containing the ruthenium atom coordinated to an η^2-carboxylate (3,3-dimethylacrylate), an η^1-alkenyl, CO and two triphenylphosphine ligands: $Ru(O_2CCH{=}CMe_2)(CO)(CR{=}CHR')(PPh_3)_2$. The majority of similar ruthenium complexes obtained at room temperature contain the two phosphines in *trans* positions. For a complete study of this family of products the structure of the complex $Ru(O_2CCH{=}CMe_2)(CO)(C(CO_2Me){=}CH(CO_2Me))(PPh_3)_2$ (**9**) by X-ray diffraction was undertaken.

The structure of complex $Ru(O_2CCH{=}CMe)_2(CO)(C(CO_2Me){=}CH(CO_2Me))(PPh_3)_2$ (**9**)

The molecular structure of the complex is presented in Fig. 1 and consists of discrete molecules linked by van der Waals' forces. Table 1 lists some selected bond distances and angles. In the molecule the ruthenium atom displays a distorted octahedral geometry where the two phosphines are in the axial sites and C(1), O(2), O(3) and C(2) are in the equatorial plane. The angle formed by the two phosphines and the ruthenium [174.82(4)°], the Ru—P(1) [2.389(1) Å] and the Ru—P(2) [2.386(1) Å] distances are comparable to the values found in other complexes.[3] The carboxylate ligand is η^2-bonded to ruthenium with Ru—O(1) and Ru—O(2) distances of 2.239(4) and 2.161(3) Å, respectively. The observed difference in the distances could be attributed to the positions of the carbonyl and alkenyl ligands with different *trans* effects to the oxygens of the carboxylate ligands.[12] The angle O(1)—C(8)—O(3) of 117.96(48)° produces a distortion of the rest of the angles in the equatorial plane, with a O(1)—Ru—O(2) angle of 59.24(13)°. The C(9)—C(10) double bond of the carboxylate has a length of 1.367(11) Å. The C(1)—O(1) distance of 1.164(5) Å is similar to those observed in other carbonyl complexes of ruthenium.[13] The alkenyl ligand contains two methylcarboxylate groups in a *cis* disposition. The Ru—C(2) distance of 2.034(5) Å lies in the observed range of ruthenium–alkenyl bonds.[13] The C(2)—C(3) bond length of 1.341(7) Å has the same value as in other dimethylcarboxylate alkenyl ligands.[13] Of particular note is the spatial disposition of the α-methylcarboxylate group which is turned to minimize the possible interactions with the ligands.

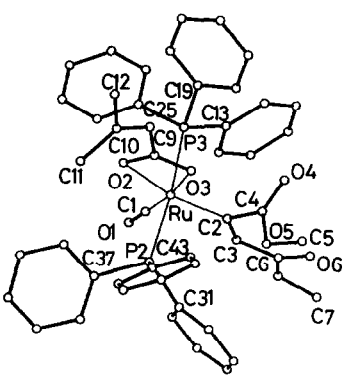

Fig. 1. Molecular structure of complex **9**.

Table 1. Selected bond lengths (Å) and angles (°) for $Ru(O_2CCH{=}CMe_2)(CO)(C(CO_2Me){=}CH(CO_2Me))(PPh_3)_2$ (**9**)

Ru—P(1)	2.389(1)	C(8)—O(2)	1.279(5)
Ru—P(3)	2.386(1)	C(8)—O(3)	1.260(8)
Ru—O(2)	2.239(4)	C(8)—C(9)	1.473(9)
Ru—O(3)	2.161(3)	C(1)—C(4)	1.492(5)
Ru—C(1)	1.808(4)	C(2)—C(3)	1.341(7)
Ru—C(2)	2.034(5)	C(4)—O(4)	1.208(6)
P(2)—C(13)	1.818(6)	C(4)—O(5)	1.337(7)
P(2)—C(19)	1.825(5)	C(6)—O(6)	1.193(6)
P(2)—C(25)	1.830(4)	C(6)—O(7)	1.334(7)
P(3)—C(31)	1.825(5)	C(7)—O(7)	1.436(13)
P(3)—C(37)	1.824(6)	C(5)—O(5)	1.438(7)
P(3)—C(43)	1.828(5)	C(9)—C(10)	1.367(11)
C(1)—O(1)	1.164(5)		

P(2)—Ru—P(3)	174.82(4)	P(3)—Ru—C(1)	89.06(17)
O(3)—Ru—C(1)	170.97(21)	P(3)—Ru—C(2)	91.98(13)
O(2)—Ru—C(2)	158.86(13)	C(13)—P(2)—C(25)	105.34(26)
O(2)—Ru—O(3)	59.24(13)	C(13)—P(2)—C(25)	102.46(23)
P(2)—Ru—O(2)	89.19(11)	C(19)—P(2)—C(25)	103.15(19)
P(2)—Ru—O(3)	92.84(9)	C(31)—P(3)—C(37)	101.93(22)
P(2)—Ru—C(1)	87.92(16)	C(31)—P(3)—C(43)	106.51(20)
P(2)—Ru—C(2)	92.20(13)	C(37)—P(3)—C(43)	102.48(28)
P(3)—Ru—O(2)	88.01(11)	O(2)—C(8)—O(3)	117.96(48)
P(3)—Ru—O(3)	89.48(10)	C(3)—C(2)—C(4)	117.83(46)

EXPERIMENTAL

The elemental analyses of carbon and hydrogen were performed with a Perkin–Elmer 240-B analyser. The IR spectra were recorded on a Perkin–Elmer 1710-FT instrument using KBr discs. The ^1H NMR spectra were recorded on a Bruker AM 400 apparatus in $CDCl_3$ solutions and referenced to $SiMe_4$. All preparations were performed under a nitrogen atmosphere using conventional Schlenk techniques. The complexes of departure: $RuCl(CO)(CR{=}CHR')(PPh_3)_2$ were synthesized by published methods.[3,5]

Synthesis of complexes

To a dichloromethane solution of the complexes, $RuCl(CO)(CR{=}CHR')(PPh_3)_2$, a slight excess of sodium 3,3-dimethylacrylate, dissolved in methanol, was added with stirring. The solution turned green and stirring was continued until the liquid became yellow (30 min). The solution was evaporated *in vacuo* and the residue dissolved in dichloromethane. A white solid was separated by filtration and the yellow product was precipitated with hexane. The crystalline complexes were obtained by crystallization from dichloromethane–methanol mixtures.

Complex **1**: $Ru(O_2CCH{=}CMe_2)(CO)(CH{=}CH_2)(PPh_3)_2$. Found: C, 67.5; H, 5.3. Calc. for $C_{44}H_{40}O_3P_2Ru$: C, 67.80; H, 5.13%. IR: ν(CO) 1916, ν(C=C) 1653, 1560, ν(OCO) 1544, 1444 cm^{-1}. ^1H NMR: δ 1.34 (s, 3H), 1.53 (s, 3H), 4.46 (s, 1H), 4.71 (d, $J = 16$ Hz, 1H), 5.01 (d, $J = 8$ Hz, 1H), 7.2–7.8 (m, Ph+1H) ppm.

Complex **2**: $Ru(O_2CCH{=}CMe_2)(CO)(CH{=}CHCMe_3)(PPh_2)_3$. Found: C, 68.6; H, 5.8. Calc. for $C_{48}H_{48}O_3P_2Ru$: C, 69.00; H, 5.75%. IR: ν(CO) 1920, ν(C=C) 1652, ν(OCO) 1496 cm^{-1}. ^1H NMR: δ 0.33 (s, 9H), 1.30 (s, 3H), 1.44 (s, 3H), 4.41 (s, 1H), 4.96 (d, $J = 16$ Hz, 1H), 6.27 (d, $J = 16$ Hz, 1H), 7.2–7.6 (m, Ph) ppm.

Complex **3**: $Ru(O_2CCH{=}CMe_2)(CO)(CH{=}CHSiMe_3)(PPh_3)_2$. Found: C, 66.9; H, 5.7. Calc. for $C_{47}H_{48}O_3P_2SiRu$: C, 66.29; H, 5.64%. IR: ν(CO) 1921, ν(C=C) 1654, ν(OCO) 1498 cm^{-1}. ^1H NMR: δ −0.5 (s, 9H), 1.31 (s, 3H), 1.46 (s, 1H), 4.46 (s, 1H), 4.58 (d, $J = 16$ Hz, 1H), 5.53 (d, $J = 16$ Hz, 1H), 7.2–7.6 (m, Ph) ppm.

Complex **4**: $Ru(O_2CCH{=}CMe_2)(CO)(CH{=}CHPh)(PPh_3)_2$. Found: C, 70.6; H, 5.1. Calc. for $C_{50}H_{42}O_3P_2Ru$: C, 70.36; H, 4.92%. IR: ν(CO) 1922, ν(C=C) 1652, 1558, ν(OCO) 1496 cm^{-1}. ^1H NMR: δ 1.38 (s, 3H), 1.56 (s, 3H), 4.52 (s, 1H), 5.77 (d, $J = 16$ Hz, 1H), 6.4–7.6 (m, Ph), 7.85 (d, $J = 16$ Hz, 1H) ppm.

Table 2. Crystal data and summary of intensity data collection and structure refinement

Crystal data	
Formula	$C_{48}H_{44}O_7P_2Ru$
Crystal habit	Prismatic, yellow–orange
Crystal size	$0.35 \times 0.30 \times 0.26$ mm
Symmetry	triclinic, $P\bar{1}$
Unit cell dimensions	28 reflections, $10 < 2\theta < 45°$
	$a = 17.401(1)$, $b = 12.633(3)$
	$c = 12.054(1)$ Å; $\alpha = 119.092(4)$
	$\beta = 72.423(5)$, $\gamma = 109(7)°$
D_{calc} (g cm^{-3}), M	1.226, 795.474
Z, $F(000)$, μ (cm^{-1})	2, 1026, 13.061
Experimental data	
Scanning range for θ	$2 < 2\theta < 65°$
Number of reflections:	
Measured	6904
Observed	6298 [$I > 2\sigma(I)$] criterion
Final R and R_w	4.9 and 5.3

Atomic coordinates, thermal parameters, full lists of bond lengths and angles and lists of F_o/F_c values have been deposited as supplementary data with the Editor, from whom copies are available on request. Atomic coordinates have also been deposited with the Cambridge Crystallographic Data Centre.

Complex **5**: $Ru(O_2CCH{=}CMe_2)(CO)(CMe{=}CHMe)(PPh_3)_2$. Found: C, 68.1; H, 5.2. Calc. for $C_{46}H_{44}O_3P_2Ru$: C, 68.42; H, 5.45%. IR: ν(CO) 1909, ν(C=C) 1652, ν(OCO) 1513, 1413 cm^{-1}. ^{1}H NMR: δ 1.03 (d, $J = 4$ Hz, 3H), 1.28 (s, 3H), 1.30 (s, 3H), 1.47 (s, 3H), 4.40 (br, 2H), 7.2–7.7 (m, Ph) ppm.

Complex **6**: $Ru(O_2CCH{=}CMe_2)(CO)(CPh{=}CHPh)(PPh_3)_2$. Found: C, 72.4; H, 5.5. Calc. for $C_{56}H_{48}O_3P_2Ru$: C, 72.20; H, 5.15%. IR: ν(CO) 1920, ν(C=C) 1650, ν(OCO) 1561, 1449 cm^{-1}. ^{1}H NMR: δ 1.28 (s, 3H), 1.53 (s, 3H), 4.31 (s, 1H), 5.84 (s, 1H), 5.9–7.6 (m, Ph) ppm.

Complex **7**: $Ru(O_2CCH{=}CMe_2)(CO)(CH{=}CH(CO_2Me))(PPh_3)_2$. Found: C, 66.2; H, 5.3. Calc. for $C_{46}H_{42}O_5P_2Ru$: C, 65.97; H, 5.02%. IR: ν(CO) 1928, 1671, ν(C=C) 1654, ν(OCO) 1553, 1144 cm^{-1}. ^{1}H NMR: δ 1.33 (s, 3H), 1.56 (s, 3H), 3.36 (s, 3H), 4.27 (s, 1H), 5.45 (d, $J = 16$ Hz, 1H), 7.1–7.7 (m, Ph), 9.60 (d, $J = 16$ Hz, 1H) ppm.

Complex **8**: $Ru(O_2CCH{=}CMe_2)(CO)(CH{=}CH(CO_2Et))(PPh_3)_2$. Found: C, 66.4; H, 5.3. Calc. for $C_{47}H_{44}O_5P_2Ru$: C, 66.29; H, 5.17%. IR: ν(CO) 1924, 1683, ν(C=C) 1652, ν(OCO) 1553, 1138 cm^{-1}. ^{1}H NMR: δ 1.27 (t, $J = 8$ Hz, 3H), 1.53 (s, 3H), 1.76 (s, 3H), 4.02 (q, $J = 8$ Hz, 2H), 4.61 (s, 1H), 5.64 (d, $J = 16$ Hz, 1H), 7.2–7.9 (m, Ph), 9.76 (d, $J = 16$ Hz, 1H) ppm.

Complex **9**: $Ru(O_2CCH{=}CMe_2)(CO)(C(CO_2Me){=}CH(CO_2Me))(PPh_3)_2$. Found: C, 64.3; H, 4.8. Calc. for $C_{48}H_{44}O_7P_2Ru$: C, 64.38; H, 4.91%. IR: ν(CO) 1937, 1705, ν(C=C) 1648, ν(OCO) 1567, 1450, 1209, 1155 cm^{-1}. ^{1}H NMR: δ 1.35 (s, 3H), 1.76 (s, 3H), 3.35 (s, 3H), 3.56 (s, 3H), 4.93 (s, 1H), 4.90 (s, 1H), 7.2–7.7 (m, Ph) ppm.

Structure solution and refinement

The crystal data and a summary of the intensity data collection and structure refinement are given in Table 2. The unit cell dimensions were obtained by least-squares refinement on setting angles of 28 well-centred reflections in the range $10 < 2\theta < 64°$, measured on a diffractometer. Data were collected on a Philips PW 1100 diffractometer using graphite monochromated Cu-K_α radiation and the ω–2θ scan technique.

Two standard reflections were monitored every 90 measurements, no intensity variation was observed. Corrections for Lorentz and polarization effects and absorption[14] were made.

The structure was solved by the heavy-atom method and direct methods. Full-matrix least-squares refinement using F with non-hydrogen atoms anisotropic. The hydrogen atom positions were calculated assuming an idealized geometry

with isotropic thermal parameters equal to those of the atoms to which they are bonded and included in the structure factor calculation. The weighting scheme was chosen so as not to give trends in $\langle \Delta^2 F \rangle$ vs $\langle |F_o| \rangle$ and $\langle \sin\theta/\lambda \rangle$.[15] Scattering factors were taken from the *International Tables of Crystallography*.[16] All calculations were performed with the XRAY76 system,[17] MULTAN,[18] DIFABS[14] and some local programs on a VAX 11/750.

Acknowledgements–We are very grateful to CICYT of Spain for financial support and the Ministère de l'Education Nationale du Maroc for a fellowship (to H.L.).

REFERENCES

1. A Dobson, D. S. Moore and S. D. Robinson, *J. Organomet. Chem.* 1979, **177**, C8; R. A. Sanchez-Delgado, N. Valencia, R. Marquez-Silva, A. Andriollo and M. Medina, *Inorg. Chem.* 1986, **25**, 1106; A. J. Lindsay, G. McDermott and G. Wilkinson, *Polyhedron* 1988, **7**, 1239.
2. J. Jenck, P. Kalck, E. Pinelli, M. Siani and A. Thorez, *J. Chem. Soc., Chem. Commun.* 1988, 1428.
3. M. R. Torres, A. Vegas, A. Santos and J. Ros, *J. Organomet. Chem.* 1986, **306**, 169; M. R. Torres, A. Santos, J. Ros and X. Solans, *Organometallics* 1987, **6**, 1901.
4. M. R. Torres, A. Perales and J. Ros, *Organometallics* 1987, **7**, 1233.
5. M. R. Torres, A. Santos, A. Vegas and J. Ros, *J. Organomet. Chem.* 1987, **326**, 413.
6. M. R. Torres, A. Santos, A. Perales and J. Ros, *J. Organomet. Chem.* 1988, **353**, 221.
7. M. R. Torres, A. Perales, H. Loumrhari and J. Ros, *J. Organomet. Chem.*, submitted for publication.
8. M. R. Torres, A. Perales, H. Loumrhari and J. Ros, *J. Organomet. Chem.*, in press.
9. S. D. Robinson and M. F. Uttley, *J. Chem. Soc., Dalton Trans.* 1973, 1912; G. L. Hillhouse and B. L. Haymore, *Inorg. Chem.* 1986, **26**, 1876; G. D. Deacon and F. Huber, *Inorg. Chim. Acta* 1985, **104**, 41.
10. T. Blackmore, M. I. Bruce and F. G. A. Stone, *J. Chem. Soc., Dalton Trans.* 1974, 106.
11. B. E. Mann, B. L. Shaw and N. I. Tucker, *J. Chem. Soc. A* 1971, 2667.
12. M. K. Holl, G. L. Hillhouse, K. Folting and J. C. Huffman, *Organometallics* 1987, **6**, 1522.
13. A. Romero, A. Santos and A. Vegas, *Organometallics* 1988, **7**, 1988.
14. N. Walker and P. Stuart, *Acta Cryst.* 1983, **A39**, 158.
15. M. Martinez-Ripoll and F. H. Cano, PESOS. A Computer Program for the Automatic Treatment of Weighting Schemes. Instituto Rocasolano C.S.I.C. Madrid.
16. *International Tables for X-ray Crystallography*, Vol. IV. Kynoch Press, Birmingham, U.K. (1974).
17. J. M. Stewart, F. A. Kundell and J. C. Baldwin, The XRAY70 System. Computer Science Center, University of Maryland, College Park (1970).
18. P. Main, S. J. Fiske, S. E. Hull, L. Lessinger, G. Germain, J. P. Leclercq and M. M. Woolfson, MULTAN. A System of Computer Programs for the Automatic Solution of Crystal Structures from X-Ray Diffraction Data. Universities of York (U.K.) and Louvain (Belgium) (1980).

Polyhedron Vol. 9, No. 7, pp. 913–919, 1990
Printed in Great Britain

0277–5387/90 $3.00+.00
© 1990 Pergamon Press plc

ENZYME INHIBITION BY SODIUM NITROPRUSSIDE

ANTHONY R. BUTLER,* ADRIANNE M. CALSY and IAN L. JOHNSON

Department of Chemistry, The University, St Andrews, Fife KY16 9ST, Scotland, U.K.

(*Received* 1 *September* 1989; *accepted* 2 *November* 1989)

Abstract—The enzyme which mediates relaxation of arterial muscle, and thus controls blood pressure, is guanylate cyclase, an enzyme with a thiol group at the active site and others elsewhere and a prosthetic haem group. Reaction of nitroprusside, a potent vasodilator, with other enzymes (papain and GAPDH) possessing a thiol group at an active site leads only slowly to enzyme inhibition by formation of disulphide bonds. Computer graphics show that the significant thiol group is accessible to the bulky nitroprusside. With enzymes containing a haem group (lactoperoxidase and catalase) inhibition by, or reaction with, nitroprusside is much faster. This suggests that the rapid vasodilator action of nitroprusside is due to its reaction with the haem group of guanylate cyclase.

It has been suggested by a number of workers that the hypotensive action of nitroprusside is due to reaction with the thiol groups of the enzyme guanylate cyclase.[1–6] In a previous paper[7] the reactions between nitroprusside and a number of low molecular weight thiols (cysteine, N-acetylcysteine, β-methylcysteine, penicillamine, and N-acetylpenicillamine) with formation of intermolecular S—S bonds, were described. The overall anaerobic reaction is shown, non-stoichiometrically, in Scheme 1. A similar reaction with the thiol groups of guanylate cyclase, with formation of a disulphide bond within the enzyme, is possible. Before attempting to investigate this we thought it would be of value to examine the effect of nitroprusside on other enzymes containing thiol groups at the active site, and which were commercially available, e.g. papain and glyceraldehyde-3-phosphate dehydrogenase.

The enzyme papain (EC 3.4.410) is an example of a proteinase with a catalytic thiol group. It is a simple protein of 212 amino acid residues forming one peptide chain. The active site cysteine (cys-25) is the only thiol residue of papain and the reactive intermediate in acyl transfer reactions is a thiol-acylated enzyme. Crystallographic studies[8,9] of papain have revealed the proximity of cys-25 to his-159 and asp-158 in what may be some kind of catalytic triad.

Glyceraldehyde-3-phosphate dehydrogenase (GAPDH, EC 1.2.1.12) is the enzyme that catalyses the oxidation and phosphorylation of D-glyceraldehyde-3-phosphate to 1,3-diphosphoglycerate. The enzyme consists of a tetramer for four identical subunits. Acetaldehyde has been used as a substrate for GAPDH and a thiol group has been implicated in the mechanism as a ^{14}C-labelled thioester is formed after incubation of ^{14}C-labelled acetaldehyde with GAPDH.[10] The essential thiol (cys-149) is, by virtue of a helical configuration, close to the non-reactive thiol of the active site (cys-153). A histidine residue (his-176), also considered to be important to the catalytic mechanism of GAPDH, lies within hydrogen-bonding distance of the essential thiol. The cysteine content of GAPDH varies from one to five for each subunit but it is the essential thiol (cys-149) that is the most reactive. The other thiol of the active site (cys-153), while not generally reactive,[11] can be

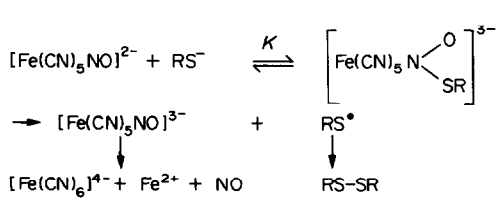

Scheme 1.

* Author to whom correspondence should be addressed.

induced to form a disulphide bond with cys-149, thereby permanently inactivating the enzyme, possibly due to irreversible conformational changes.

A well-established[12] aspect of guanylate cyclase activity is that if it is purified so that the haem content is removed the enzyme no longer responds to nitric oxide, nitroprusside, or S-nitrosocysteine in the absence of exogenous haematin. On the other hand, preformed nitrosohaemoglobin produces a substantial increase in enzyme activity. The reaction of nitroprusside and haemoglobins has been examined and, as an extension to this work,[13] we thought it would be of value to examine the reaction of nitroprusside with two commercially available enzymes which are known to contain haem: peroxidase and catalase.

Peroxidase (EC 1.11.17, hydrogen peroxide oxidoreductase) is a haem-bearing enzyme found in a variety of animal and plant tissues. The source used in this study was cow's milk, i.e. lactoperoxidase. Its structure has not been completely determined but the haem environment is thought to be similar to that of horseradish peroxidase.[14] The lactoperoxidase haem iron is in a crevice of the protein molecule and its sixth coordination site is vacant or occupied by a loosely associated water ligand. The inhibition of lactoperoxidase by cyanide, sulphide and fluoride is attributed to attachment of these ions at the coordination site of the haem iron.[15] Lactoperoxidase has 16 cysteine residues, which are thought to form eight disulphide bridges.

The haem-bearing enzyme catalase (EC 1.11.16, hydrogen peroxide oxidoreductase) is present in nearly all aerobically respiring organisms and protects cells from the toxic effect of hydrogen peroxide by catalysing its decomposition. Catalase, in the presence of hydrogen proxide,[17] can effect oxidation of a variety of compounds, including ethanol. The structure of catalase has been determined[18] and it consists of four identical subunits. The sixth coordination site of the haem is vacant but the accessibility of the haem, in a crevice in the protein molecule, is limited by a channel 30 Å long and 15 Å wide.

RESULTS AND DISCUSSION

Papain activity at pH 7.5 was determined by monitoring the hydrolysis of N-benzoyl-L-arginine ethyl ester (BAEE) according to an established procedure.[19] Also, the inhibition of papain by cyanate, a known[20] inhibitor, was recorded. At similar concentrations nitroprusside inhibited papain only marginally and after a long incubation time. However, at higher concentrations of nitroprusside, inhibition was observed (Fig. 1). The reason for the incubation time will be discussed later. At the same concentration nitroprusside is more effective as an inhibitor than nitrite, and both react with thiol groups. This parallels their effect as vasodilators. On the other hand, even at high concentrations (nitroprusside–enzyme molar ratio of 1000:1) nitroprusside did not inhibit the trypsin catalysed hydrolysis of BAEE. That enzyme is known not to have a thiol group as a key part of the active site.

The structure of papain is known and when it was displayed on a screen by the use of Chem-X it was clear that cys-25 is not embedded within the protein structure. To assess the accessibility of cys-25 to nitroprusside the latter was drawn in the same scale as all the atoms within 10 Å (in $\pm x$, $\pm y$ and $\pm z$ directions) of the cys-25 sulphur atom. These graphics demonstrate that there is no steric impediment to the reaction of nitroprusside with the cys-25 of papain. If the sulphur in the active site of guanylate cyclase is similarly accessible it is possible that its action could be inhibited by reaction with nitroprusside.

Glyceraldehyde-3-phosphate dehydrogenase, unlike papain, does not require activation and its interaction with nitroprusside was more readily examined by ^{13}C NMR and ESR spectroscopy. The activity of GAPDH was determined by monitoring the increase in absorbance at 340 nm due to the reduction of NAD. It was found that a 15–20 min incubation of the enzyme solution with nitroprusside prior to initiation of the reaction by addition of the substrate glyceraldehyde-3-phosphate, resulted in significant inhibition of enzyme

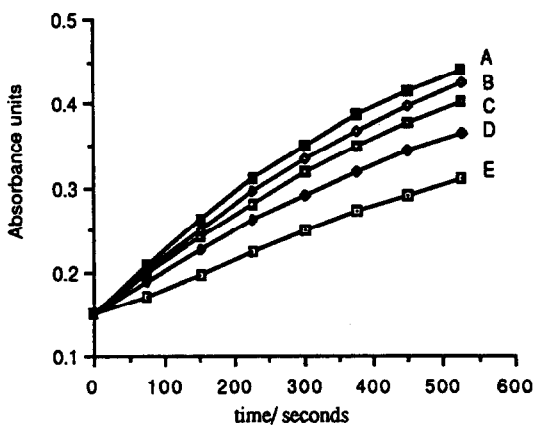

Fig. 1. Hydrolysis of BAEE catalysed by papain in the presence of inhibitors (incubation time, in min, in parentheses): (A) none; (B) 1.5×10^{-4} M nitroprusside (19); (C) 3×10^{-3} M nitrite (23); (D) 3×10^{-3} M nitroprusside (0); (E) 3×10^{-3} M nitroprusside (21). [Papain] = 5.36×10^{-6} M; [BAEE] = 1.24×10^{-3} M.

activity at pH 7.5 (see Fig. 2). The data displayed in Fig. 2 show the general features of the inhibitory effect of nitroprusside. The effects of other vasodilators, nitrite and nitroethane, are also shown; at identical concentrations nitroprusside is more effective. Although not shown, nitroprusside was found to be more effective than nitrate, a known inhibitor of GAPDH.[22] These results provide further evidence that nitroprusside can affect the action of an enzyme containing thiol groups at the active site.

Display of the structure of GAPDH by Chem-X shows that the essential thiol, cys-149, of each subunit is located towards the centre of the enzyme and again not embedded within the protein structure. The accessibility of the active site to nitroprusside was determined by displaying both a window of all atoms within 10 Å (in $\pm x$, $\pm y$ and $\pm z$ directions) of the cys-149 sulphur atom and nitroprusside on the same scale. There is no obvious steric impediment to reaction of nitroprusside at cys-149. The unreactive thiol, cys-153, was also seen, close to cys-149, but clearly remote from the active site.

Not only were we able to show that an enzymatic thiol group can react with nitroprusside but we were able to identify the inorganic product of reaction. The ESR spectra of a degassed solution of nitroprusside added to GAPDH, dissolved in phosphate buffer, were recorded over 1 day. No signal was observed on mixing but after 2 h a strong three-line signal was noted. At the same time the solution, originally clear, became turbid. Five hours later

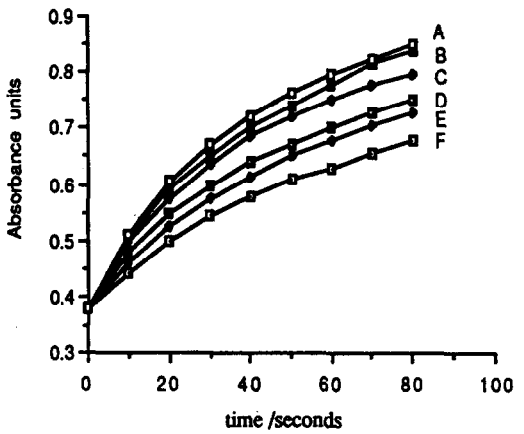

Fig. 2. Late data for the activity of GAPDH due to reduction of NAD in the presence of inhibitors (incubation time, in min, in parentheses): (A) none; (B) 1.66×10^{-2} M nitroethane (20); (C) 1.66×10^{-2} M nitrite (17); (D) 1.66×10^{-3} M nitroprusside (1); (E) 8.3×10^{-3} M nitroprusside (14); (F) 1.66×10^{-2} M nitroprusside (16). [GAPDH] = 2.79×10^{-7} M; [NAD] = 1.50×10^{-3} M.

the signal was unchanged. This three line signal is identical to that observed on reaction of nitroprusside with thiols[7] and corresponds[23] to the species $[Fe(CN)_4NO]^{2-}$.

The ^{13}C NMR spectrum of a solution of ^{13}C-labelled nitroprusside and GAPDH, taken shortly after mixing, showed only the presence of unreacted nitroprusside. However, after several hours turbidity was observed and the spectrum, recorded after filtering and storage under nitrogen, showed a signal at 177.8 ppm corresponding to hexacyanateferrate,[24] as well as the spectrum of unreacted nitroprusside (Fig. 3). Hexacyanoferrate and $[Fe(CN)_4NO]^{2-}$ are known as *in vitro* products of reaction of thiols and nitroprusside, the former the final product and the latter a well-characterized intermediate. Thus, in any attempt to delineate the vasodilator action of nitroprusside via its interaction with guanylate cyclase, it is reasonable to assume that what is known of the reaction of nitroprusside with simple thiols[7] also applies to its reaction with thiol groups within the enzyme.

The turbidity observed in the above experiments suggests denaturation of the enzyme, giving rise to a change in enzyme solubility. It is likely that this arises from formation of disulphide bonds, possibly by reaction of the essential thiol with the adjacent cys-153.[9]

The origin of the apparent time dependence of both papain and GAPDH inhibition by nitroprusside may be due to the formation of intramolecular disulphide bonds. It is known[25] that the first step in the reaction of a thiol, or rather thiolate (RS^-), with nitroprusside is formation of an adduct (Scheme 1). Decomposition of the adduct leads to formation of the short-lived thiyl radical (RS) and possibly the pentacyanonitrosylferrate complex $[Fe(CN)_5NO]^{3-}$. The latter can be oxidized back to nitroprusside by oxygen in the solvent and thus the cycle is repeated. There are other routes by which $[Fe(CN)_5NO]^{3-}$ may decompose and so the cycling does not continue indefinitely.[26] Dimerization of the radical creates the disulphide bond. The rate of disulphide bond formation depends not only upon the rate of dimerization, but also upon the equilibrium constant for adduct formation (K). If, for steric reasons, K is small for thiols within the enzyme, then disulphide bond formation will be slow and significant inhibition of the enzyme occurs only after a long incubation time. This assumes that inhibition is the result of disulphide bond formation.

The activity of lactoperoxidase was measured by the standard assay: oxidation of pyrogallol to purpurogallin by hydrogen peroxide, monitored by the increase in absorbance at 425 nm due to pur-

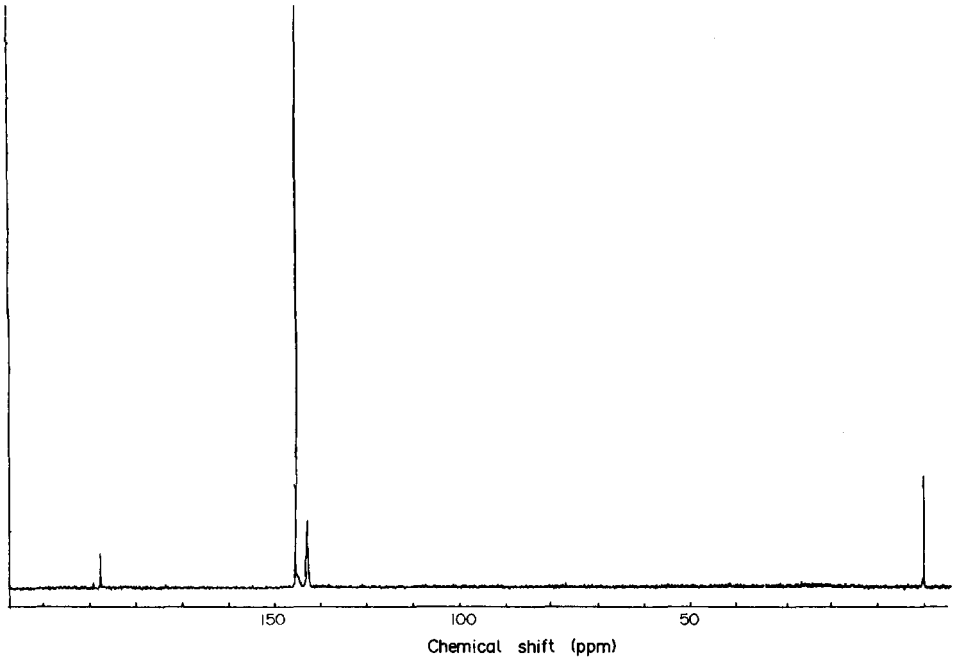

Fig. 3. ^{13}C NMR spectrum after reaction of nitroprusside with GAPDH. [GAPDH] = *ca* 10^{-5} M; [Nitroprusside] = 10^{-3} M.

purogallin formation.[27] Addition of nitroprusside to the enzyme solution, followed by initiation of the reaction with hydrogen peroxide and pyrogallol, led to markedly decelerated purpurogallin formation (Fig. 4). From these data it is clear that nitroprusside is an effective inhibitor for lactoperoxidase but this effect is not dependent on prolonged incubation, as it was with papain and GAPDH.

We could obtain no information on the inhibition of catalase activity because nitroprusside absorbs in the region where disappearance of hydrogen peroxide is monitored (λ_{max} 240 nm). However, spectral changes were observed when catalase and nitroprusside were incubated in phosphate buffer. The resulting spectrum (Fig. 5) corresponded closely to that of a genuine sample of a nitrosyl catalase complex (NO-catalase), prepared from catalase and nitric oxide, and literature values for the absorbance maxima of NO-catalase.[28] The signals due to NO-catalase disappeared over the course of 3 h.

The ESR spectrum of a solution of nitroprusside and catalase was recorded at room temperature and showed a weak three-line signal, identical with that observed on reaction of nitroprusside with simple thiols.[7] There was no signal corresponding to catalase itself or to NO-catalase at room temperature or after cooling the sample to 120 K. Upon warming the sample to room temperature the intensity of the three-line signal was enhanced but the solution in the ESR tube had become turbid, a manifestation of enzyme denaturation. It is known[29] that bovine liver catalase contains eight thiol groups which could have become exposed during warming and reacted with nitroprusside with formation of disulphide bonds. A solution of nitroprusside and catalase at similar concentrations to those of the former

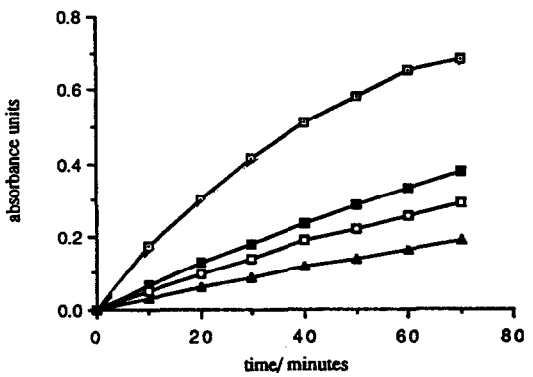

Fig. 4. Formation of purpurogallin catalysed by lactoperoxidase in the presence of inhibitors: (A) none; (B) 1.5×10^{-3} M nitroprusside; (C) 7.6×10^{-3} M nitroprusside; (D) 7.6×10^{-2} M nitroprusside. $[Pyrogallol]_0 = 2.72 \times 10^{-2}$ M; [Lactoperoxidase] = 1.23×10^{-8} M.

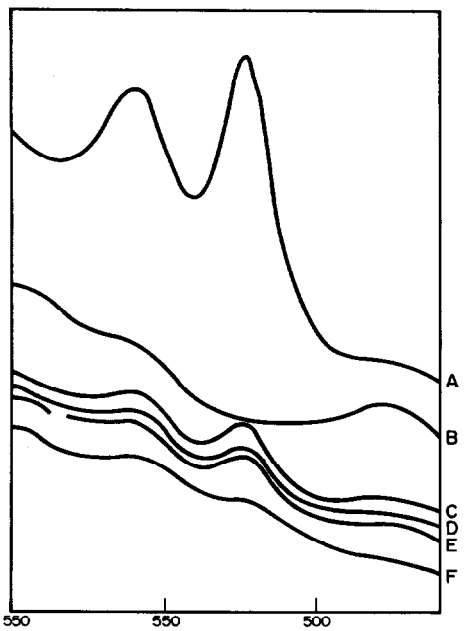

Fig. 5. Spectral changes accompanying the reaction of nitroprusside with catalase: (A) authentic NO-catalase; (B) catalase; (C) spectrum of nitroprusside (5.87×10^{-3} M) and catalase (3.57×10^{-5} M) 5 min after mixing; (D) 20 min after mixing; (E) 30 min after mixing; (F) 3 h after mixing.

experiment but left at room temperature did not become turbid within the same period and the ESR signal remained weak.

The results obtained with lactoperoxidase suggest that inhibition is not due to slow reaction with thiol groups in the enzyme but is consistent with reaction of nitroprusside with haem, possibly a fast electron transfer.[23] The results with catalase present a more complex picture: there is evidence of fast reaction to give NO-catalase and also of reaction with thiols in a much slower process. In view of the rapid vasodilator effect of nitroprusside when used clinically, we tend to favour the former process, i.e. reaction with haem, as the origin of the effective reaction of nitroprusside with guanylate cyclase.

EXPERIMENTAL

Material

Papain, BAEE, dithiothreitol, trypsin (type IX, porcine pancreas), GAPDH (rabbit muscle), NAD (thymol free purified powder), lactoperoxidase (bovine milk, lyophilized powder) and sodium arsenate were obtained from Sigma and used without further purification. DL-Glyceraldehyde-3-phosphate was prepared from the barium salt of DL-glyceraldehyde-3-phosphate diacetal according to the standard procedure.[30] Most other reagents were AnalaR grade. The preparation of ^{13}C-labelled sodium nitroprusside has been described previously.[31] All nitroprusside solutions were protected from light during use. NO-catalase was prepared by a literature method.[32]

Instruments

NMR spectra were recorded on a Brucker AM 300 spectrophotometer. The number of scans was typically 3700 with a pulse width of 2.0 μs and a delay of 1.5 s. For the ESR spectra a Brucker ER 2000 spectrometer was used. UV–vis spectra were recorded on a Pye Unicam SP8 100 spectrophotometer.

Papain assay

Papain activity at 30°C was determined after activation following an established procedure.[19] In a standard experiment papain was eluted from a Sephadex column (G25) with phosphate buffer (pH 7.5, $I = 0.1$ M, containing 10 mM EDTA) following activation of papain (2.5 mg, 60 units) in buffer (0.4 cm^3) with dithiothreitol (2.4 mg) at room temperature for 1 h. The concentration of the enzyme "stock" solution was determined from the absorbance at 278 nm. Temperature-equilibrated stock solution (1 cm^3, 1.34×10^{-5} M) was added to water or inhibitor solution (1 cm^3) and left to incubate. The reaction was initiated by addition of temperature-equilibrated BAEE (0.5 cm^3, 6.2×10^{-3} M) and the change in absorbance at 263 nm, read against a BAEE reference (1.24×10^{-3} M), was recorded.

Trypsin assay

Activity at 30°C was determined by a standard procedure. Nitroprusside (up to 2.7×10^{-4} M) was incubated with trypsin (2.8×10^{-7} M) at 21°C for 20 min in phosphate buffer (pH 7.5, $I = 0.1$ M containing 10 mM EDTA). BAEE (10^{-3} M) was added to initiate the reaction and BAEE hydrolysis was followed as detailed above for the papain assay.

GAPDH assay

The activity of GAPDH at 30°C was determined by monitoring the change in absorbance at 340 nm due to the reduction of NAD. An enzyme "stock"

solution was prepared with GAPDH (105 units, 8.77×10^{-9} mol), NAD (35.8 mg, 4.8×10^{-5} mol) and Na_2HAsO_4 (4.8 cm^3, 1 M) in phosphate buffer (pH 7.32, $I = 0.1$ M containing 10 mM EDTA), total volume 24.8 cm^3. For each experiment, water or a solution of the inhibitor (0.2 cm^3) was added to temperature-equilibrated enzyme "stock" solution (1.9 cm^3) and, following incubation, the reaction was initiated by the addition of temperature-equilibrated glyceraldehyde-3-phosphate solution (0.3 cm^3, 2 mM).

Lactoperoxidase assay

The activity of lactoperoxidase at 18°C was determined by following purpurogallin formation at 425 nm. An enzyme solution was prepared with lactoperoxidase (0.26 units cm^{-3}, 4.07×10^{-8} M) in phosphate buffer (pH 7.0, $I = 0.067$ M). For each experiment, buffer or inhibitor (0.5 cm^3) was added to the temperature-equilibrated enzyme solution (1 cm^3) and buffer (1 cm^3). The reaction was initiated by addition of hydrogen peroxide (0.5 cm^3, 4×10^{-3} M) and pyrogallol (0.3 cm^3, 3×10^{-2} M).

Catalase assay

The activity of catalase at 30°C was determined by following the decrease in absorbance of hydrogen peroxide at 245 nm. An enzyme solution was prepared with catalase (50 units cm^{-3}, 1.96×10^{-8} M) in phosphate buffer (pH 7.00, $I = 0.067$ M). The catalysed decomposition was initiated by addition of hydrogen peroxide (2.9 cm^3, 1.96×10^{-2} M) to the enzyme solution (0.1 cm^3) and buffer or inhibitor (0.1 cm^3, maximum concentration 2×10^{-3} M).

Computer graphics

All atomic parameters and structural data for molecular modelling were obtained from the Daresbury Laboratory Chemical Databank Service. The program Chem-X, developed and distributed by Chemical Design Ltd, Oxford, was used to display and manipulate structures in conjunction with a Tektronics 4107 colour terminal linked to a VAX 11/785 computer.

Acknowledgement—A.M.C. thanks the University of St Andrews for a studentship.

REFERENCES

1. E. H. Ohlstein, K. S. Wood and J. L. Ignarro, *Arch. Biochem. Biophys.* 1982, **218**, 187.
2. L. J. Ignarro, B. K. Barry, D. Y. Gruetter, E. H. Ohlstein, C. A. Gruetter, P. J. Kadowitz and W. H. Baricos, *Biochim. Biophys. Acta* 1981, **673**, 394.
3. L. J. Ignarro, P. J. Kadowitz and W. H. Baricos, *Arch. Biochem. Biophys.* 1981, **208**, 75.
4. H. J. Brandwein, J. A. Lewicki and F. Murad, *J. Biol. Chem.* 1981, **256**, 2958.
5. L. J. Ignarro and C. A. Gruetter, *Biochim. Biophys. Acta* 1980, **631**, 221.
6. J. C. Edwards, B. K. Barry, D. Y. Gruetter, E. H. Ohlstein, W. H. Baricos and L. J. Ignarro, *Biochem. Pharm.* 1981, **30**, 2531.
7. A. R. Butler, A. M. Calsy-Harrison, C. Glidewell and P. E. Sørensen, *Polyhedron* 1988, **7**, 1197.
8. G. Lowe, *Tetrahedron* 1976, **32**, 291.
9. A. N. Glazer and E. L. Smith, in *The Enzymes* (Edited by P. Boyer), Vol. III, pp. 502–546. Academic Press, London (1971).
10. P. C. Jocelyn, *Biochemistry of the* SH *Group*, p. 204. Academic Press, London (1972).
11. J. I. Harris and M. Waters, in *The Enzymes* (Edited by P. Boyer), Vol. XIII, 3rd edn, pp. 1–50. Academic Press, London (1976).
12. P. A. Craven and F. R. DeRubertis, *Biochim. Biophys. Acta* 1983, **745**, 310.
13. A. R. Butler, C. Glidewell, I. L. Johnson and A. S. McIntosh, *Inorg. Chim. Acta* 1987, **138**, 159.
14. T. Shiro and I. Morishima, *Biochemistry* 1986, **25**, 5844.
15. B. C. Saunders, A. G. Holmes-Siedle and B. P. Stark, *Peroxidase*, pp. 8 and 9. Butterworth, London (1964).
16. M. Morrison, W. A. Rombants and W. A. Shroeder, *Hemes and Hemoproteins* (Edited by B. Chance, R. W. Estabrook and T. Yonetani), p. 345. Academic Press, London (1966).
17. G. R. Schonbaum and B. Chance, *The Enzymes* (Edited by P. Boyer), Vol. XIII, 3rd edn, pp. 363–408. Academic Press, London (1976).
18. M. R. N. Murthy, T. J. Reid, A. Sicignano, N. Tanaka and M. G. Rossman, *J. Molec. Biol.* 1981, **152**, 465.
19. J. R. Whitaker and M. L. Bender, *J. Am. Chem. Soc.* 1965, **87**, 2728.
20. L. A. Æ. Sluyterman, *Biochim. Biophys. Acta* 1967, **135**, 439.
21. J. Drenth, J. N. Jansonius, R. Koekoek and B. G. Wolthers, *Advances in Protein Chemistry* (Edited by C. B. Anfinsen, J. T. Edsall and F. M. Richar), Vol. 25, p. 103. Academic Press, London (1971).
22. A. Orsi and W. W. Cleland, *Biochemistry* 1972, **11**, 102.
23. C. Glidewell and I. L. Johnson, *Inorg. Chim. Acta* 1987, **132**, 145.
24. A. R. Butler, C. Glidewell, A. S. McIntosh, D. Reed and I. H. Sadler, *Inorg. Chem.* 1986, **25**, 970.
25. M. D. Johnson and R. G. Wilkins, *Inorg. Chem.* 1984, **23**, 231.
26. P. J. Morando, E. B. Borghi, L. M. de Schteingart and M. A. Blesa, *J. Chem. Soc., Dalton Trans.* 1987, 435.

27. S. M. Siegel and P. Frost, *J. Am. Chem. Soc.* 1960, **82**, 2773.
28. T. Yonetani, H. Yamamoto, J. E. Erman, J. S. Leigh and G. H. Reed, *J. Biol. Chem.* 1972, **247**, 2447.
29. A. Pihl, R. Lange and A. Evang, *Acta Chem. Scand.* 1961, **15**, 1271.
30. G. W. Schwert and Y. Takenaka, *Biochim. Biophys. Acta* 1955, **16**, 570.
31. A. R. Butler, C. Glidewell, J. McGinnis and W. I. K. Bisset, *Clin. Chem.* 1987, **33**, 490.
32. P. A. Craven, F. R. DeRubertis and P. W. Pratt, *J. Biol. Chem.* 1979, **254**, 8213.

Polyhedron Vol. 9, No. 7, pp. 921–929, 1990
Printed in Great Britain

0277–5387/90 $3.00+.00
© 1990 Pergamon Press plc

SELECTION OF ORGANOMETALLICS FOR MOCVD* OF $Hg_{1-x}Cd_xTe$ AND DOPED SEMICONDUCTORS†

G. N. PAIN and G. I. CHRISTIANSZ

Infrared Optoelectronics, Telecom Australia Research Laboratories, 770 Blackburn Road, Clayton, Victoria 3168, Australia

and

R. S. DICKSON,‡ G. B. DEACON, B. O. WEST, K. McGREGOR and R. S. ROWE

Department of Chemistry, Monash University, Clayton, Victoria 3168, Australia

(*Received* 2 *June* 1989; *accepted* 2 *November* 1989)

Abstract—Organometallic feedstocks of cadmium, mercury and tellurium, as well as dopants to create n-type, p-type or diluted magnetic semiconductors, can impose limits on the range of programmable parameters in the MOCVD reactor. The influence of the chosen organometallics on the crystal growth process is critically reviewed.

Binary, ternary and quaternary alloy semiconductors formed from various combinations of elements from groups II and VI of the Periodic Table (or groups 12 and 16 under recent nomenclature) are becoming increasingly important due to their useful electronic, optoelectronic, magneto-optic and piezoelectric properties.[1] MOCVD is an important method of creating II–VI semiconductors in thin films for device applications.[2] In this paper we discuss the benefits and limitations imposed on the MOCVD process and material quality by the currently available organometallics. The recent literature concerning MOCVD of mercury cadmium telluride (MCT), ($Hg_{1-x}Cd_xTe$, $0 \leqslant x \leqslant 1$), n- and p-type extrinsically doped MCT, and zinc or manganese substituted alloys is reviewed. Photo-assisted MOCVD, plasma-enhanced MOCVD and precracking techniques are included. Use of these methods to lower the growth temperature has been intensively studied in order to improve crystalline perfection and control of intentional internal composition gradients which are required in the preparation of heterojunctions. In the case of mercury alloys the equilibrium cation vacancy concentration and the necessary overpressure of mercury during growth can be greatly reduced.[3]

Many interesting patent applications[4–7] concerning growth of MCT by MOCVD contain long lists of possible candidate organometallics, however, experimental MOCVD results have been published for only relatively few compounds. These compounds and some selected possible alternatives are listed in Tables 1–4, together with available data on vapour pressure and thermal stability. Various growth methods which have been employed are indicated in the tables. Conventional growth refers to thermal pyrolysis with hydrogen carrier gas; the substrate is placed on a heated support and this is the only source of energy for cracking the organometallics. A variation of the conventional process is the Interdiffused Multilayer Process (IMP).[6] Photo-assisted growth is generally performed in one of two illumination conditions. Most commonly, the light source impinges directly onto the substrate. Alternatively the light beam is directed through the gas close to and parallel to the substrate. Plasma-enhanced MOCVD and thermal precracking methods also separate the energetic cleavage of the organometallics from the dependence on substrate temperature.

* MOCVD refers to Metal Organic Chemical Vapour Deposition.

† Paper presented at the meeting on "Applied Organometallic Chemistry; An Entry to New Technology", Pokolbian, New South Wales, Australia, 10–12 July 1989.

‡ Author to whom correspondence should be addressed.

Table 1. Zinc, cadmium and mercury organometallics for MOCVD

Organometallic	Vapour pressure[a] (mmHg) (Temperature) [Reference]	Material grown	Substrate temperature (°C)	Growth method [Reference]
Me_2Zn	124 (0°C) [8]	ZnTe	300–400	Precracking (350–450°C) [9]
	$A = 7.802$ $B = 1560$ [8]	ZnTe	410	Conventional [10]
$Me_2Zn(NEt_3)_2$	~ 8 (17.5°C) [11]	ZnS ZnSe	300–450 300–450	Conventional [11]
Me_2Zn(1-4 dioxan)		ZnSe	200–550	Conventional [12]
Et_2Zn	15 (29°C) [8] 3.6 (0°C), 16 (25°C) [13]	Zn	332(onset)	Flow pyrolysis [14]
	$A = 8.280$ $B = 2190$ [8]	ZnTe	350	Conventional [15]
Me_2Cd	$A = 7.764$ $B = 1850$ [8]	Cd	320(onset)	Flow pyrolysis [14]
	$C = 6.717$ $D = 1165$ $E = 198$ [13]	Cd	380(complete)	Flow pyrolysis [3]
		CdTe	310–370	Conventional [16]
	$C = 6.49055$ $D = 1126.36$ $E = 201.7$[17]	CdTe	< 300	Precracking [18]
	16 (20°C) [19]	CdTe		
Me_2Cd(1-4 dioxan)		CdSe CdS		Conventional [20]
Et_2Cd	2 (30°C) [21]	CdTe MCT	300–350 350	Conventional [21] Conventional (IMP) [21]
Me_2Hg	$A = 7.515$ $B = 1750$ [8]	HgTe	165	Photo-assisted (parallel) [22]
		HgTe MCT MCT	325 225 132–146	Conventional [23] Precracking [24] Plasma-enhancement [25]
Et_2Hg		HgTe	275–300	Conventional [5]
$(CH_2{=}CH)_2Hg$		HgTe	165	Photo-assisted (parallel) [22]

[a] A–E are constants in the equations: $\log P = A - B/T$ and $\log P = C - [D/(E+t)]$, where p is the vapour pressure in torr, T is the temperature in Kelvin, and t is the temperature in Celcius.

In compiling Tables 1–4, we found some spread in the values reported for vapour pressures, but more seriously no data were found for some of the compounds used.

Organometallics of zinc, cadmium and mercury (Table 1)

In general, ethyl organometallics are less stable and less volatile than the corresponding methyl compounds. Dimethylzinc could probably be regarded as too volatile and consequently is frequently used diluted in hydrogen. This has the disadvantages of requiring accurate dilution at the manufacturing plant and the possible long-term degradation of dilute mixtures by reaction with residual water and other contaminants in cylinders. For these reasons considerable effort has recently been made to produce adducts which have lower volatility. These have the added advantage of

Organometallic	Vapour pressure (mmHg) (Temperature) [Reference]	Material grown	Substrate temperature (°C)	Grown method [Reference]
Me_2Te	50 (22°C) [19]	Te	500(complete)	Flow pyrolysis [3]
	$A = 7.97$			
	$B = 1865$ [8]	Te	406(onset)	Flow pyrolysis (hydrogen) [14]
		Te	490(onset)	Flow pyrolysis (helium) [14]
		ZnTe	350	Precracking (350–400°C) [26]
		CdZnTe		
		CdTe	200–400	Conventional [27]
Et_2Te	12 (30°C) [28]	Te	351(onset)	Flow pyrolysis [14]
	14 (38°C) [19]			
		CdTe	350	Conventional [7]
	$A = 7.99$			
	$B = 2093$ [8]			
		CdTe	100–150	Photo-assisted (parallel) [29]
	$A = 8.16 \pm 0.2$			
	$B = 2168 \pm 72$ [30].			
		CdTe, HgTe	165	Photo-assisted (parallel) [22]
		CdTe	250	Precracking (670°C) [31]
		CdTe, HgTe	< 300	Precracking (400°C) [18]
		MCT	410	Conventional [7]
		MCT	200–300	Photo-assisted (perpendicular) [32]
		MCT	225	Precracking (400–500°C) [24, 25]
		MCT	132–146	Plasma-enhancement [25]
n-Pr_2Te	2.0 (30°C) [28]	HgTe	390–410	Conventional [28]
i-Pr_2Te	5.6 (30°C) [28]	MCT	350	Conventional (IMP) [16]
t-Bu_2Te	4 (40°C) [28]	HgTe	200	Precracking [33]
		HgTe, CdTe	230	Conventional [34]
$MeTe_2Me$		CdTe	250–500	Conventional [35]
		CdTe	160–250	Photo-assisted (perpendicular) [36]
$(C_4H_6)Te$	0.5 (25°C) [5]	CdTe	250	Conventional [38]
	0.85 (25°C) [37]			
	2.1 (35°C) [37]			
	$A = 12$			
	$B = 3596$			
$(CH_2{=}CHCH_2)TeMe$	1.9 (0°C) [37]	CdTe	290	Conventional [23]
	3.6 (10°C) [37]			
	6.3 (20°C) [37]			
		HgTe	325	Conventional [23]
	$A = 7.718$			
	$B = 2028$ [37]			
$(CH_2{=}CHCH_2)_2Te$		HgTe	180	Conventional [39]

Table 3. Organometallics for n- and p-types

Organometallic	Vapour pressure (mmHg) (Temperature) [Reference]	Material grown	Substrate temperature (°C)	Growth method [Reference]
Me_3In	7.2 (30°C) [8] 1.52 (18.5°C) [40] 1.40 (18°C) [42] 1.80 (25°C) [19] $A = 10.520$ $B = 3014$ [8] $A = 9.2197$ $B = 2535$ [13]	In MCT : In	299(onset) 410	Flow pyrolysis [14, 41] Conventional (IMP) [43]
Et_3In	1.18 (40°C) [19] 1.2 (44°C) [8] 0.24 (18°C) [42]	CdTe : In	420	Conventional [20]
Me_3Sb	30 (0°C) [44] 78 (20°C) [8] $A = 7.7280$ $B = 1709$ [8] $A = 7.7068$ $B = 1697$ [13]	Sb Sb MCT : Sb	412(onset) 800–900 (complete) 410	Flow pyrolysis [14] Vacuum pyrolysis [45] Conventional (IMP) [43]
Et_3Sb	~ 1 (27°C) [45] 17 (75°C) [8]			
Me_3As	238 (20°C) [8] $A = 7.7119$ $B = 1563$ [8] $A = 7.3936$ $B = 1456$ [13]	MCT : As	410	Conventional (IMP) [43]
Et_3As	15.5 (37°C) [8]			
$PhAsH_2$	1.7 (20°C) [46]			
t-$BuAsH_2$	81 (10°C) [37] 96 (10°C) [40] $A = 7.243$ $B = 1509$ [37] $A = 7.500$ $B = 1562.3$ [47]	As As	250–450 425 (50% reaction)	Flow pyrolysis [47] Flow pyrolysis [40]
t-$BuPH_2$	141 (10°C) [37] 286 (23°C) [40]	P	450 (50% reaction)	Flow pyrolysis [40]

reduced prereaction due to steric hindrance when H_2E (E = S, Se and Te) are employed as the group VI reagents. Similar adducts of Me_2Cd are also being developed.[61]

Photo-assisted growth of HgTe[22] using divinyl mercury or Me_2Hg occurs at a much lower temperature (165°C) than thermal growth using Me_2Hg[23] (325°C) or Et_2Hg[5] (275°C). Other possible alternative R_2Hg MOCVD sources have been discussed,[28,34] however, many would likely have considerably lower vapour pressures.

Relatively little work has been reported on alternatives to Me_2Hg. It would seem that use of elemental mercury would be preferable on economic, purity and safety grounds, although there are potential prereaction problems caused by the naked mercury atom.[4]

Tellurium organometallics for MOCVD (Table 2)

Considerably more results have been published concerning alternative tellurium sources (Table 2), probably due to the relatively rich MOCVD chemistry known for this element. The bulk of reports concerning MOCVD of MCT employ Et_2Te which exhibits a relatively high onset cracking tempera-

Table 4. Manganese compounds for MOCVD of magnetic dopants

Organometallic	Vapour pressure (mmHg) (Temperature) [see ref. 48]	Material grown	Substrate temperature (°C)	Growth method [Reference]
$(MeC_5H_4)Mn(CO)_3$	0.051 (20°C) 12 (112°C)	ZnS : Mn	500	Conventional [49–51]
		ZnS : Mn	325–400 (incomplete)	Conventional [49, 52–54]
		ZnS : Mn	300	Precracking (580°C) [55, 56]
		ZnS : Mn	Not specified	Photo-assisted [57]
		ZnSe : Mn	500	Conventional [49, 51]
		CdTe : Mn	410–450	Conventional [57]
$(C_5H_5)_2Mn$	Solid : $A = 10.58$ $B = 3780$	ZnS : Mn	280–350	Low pressure [54]
		ZnSe : Mn	300	Plasma-enhancement [58]
	Liquid : $A = 5.93$ $B = 2615$ Subl. 10^{-4}–10^{-5} mm (100–130°C)			
$(MeC_5H_4)_2Mn$	Subl. 0.5 mm (40°C)	ZnS : Mn	280–350	Low pressure [54]
$MeMn(CO)_5$	3 (28.8°C)	$Cd_{1-x}Mn_xTe$	< 350	Conventional [59]
		$Hg_{1-x}Mn_xTe$	< 350	Precracking [59]
$EtMn(CO)_5$	3.5 (45°C)			[60]

ture. Pyrolysis of this alkyl is autocatalytic[14] and the presence of Me_2Cd reduces the onset temperature for deposition of CdTe by ~ 60°C from the temperature required for growth of HgTe (~ 410°C). Precracking, photo-assistance and plasma-enhancement have all been successfully employed to reduce the growth temperature using Et_2Te. A problem common to all low-temperature techniques is the tendency toward gas-phase nucleation due to the low saturation vapour pressures of tellurium, and MCT. For this reason growth by a surface-selective technique is preferred if significant growth rates are to be achieved. Some branched alkyls are made less stable by the enhanced probability of β-hydrogen elimination as well as reduced activation energy for homolytic radical cleavage due to the more stable radicals.[28] The latter effect is also involved in R_2Te which incorporate ligands offering delocalization of the radical unpaired electron, such as the allyl group. Kinetic simulation studies have shown that heterogeneous decomposition can significantly affect observed cracking temperatures.[62] For photo-assisted growth the liberated ligands should not have significant absorption of the light in order to avoid undesirable side reactions, and the reaction products should have a low sticking probability on the growing crystal surface. Unsaturated products such as butadiene might yield involatile degradation or polymerization products under certain pyrolysis conditions. Long term stability of feedstocks is an important consideration when selecting a source with low cracking temperature, with some commercial sources (e.g. tellurophene, TeC_4H_6) requiring shipment in dry ice.[37]

Good compromise between thermal stability and volatility is offered by Et_2Te and Pr^i_2Te, and both can be used for growth at low temperatures by precracking techniques. The low volatility of some of the other tellurium sources is compensated by enhanced cracking efficiency. Little data are available on carbon incorporation or other possible undesirable effects of using any of the organometallics listed in Table 2.

Organometallics for extrinsic n- and p-type MCT (Table 3)

Although PH_3 and AsH_3 have been employed successfully to dope p-type CdTe and MCT,[63–66] prereaction problems, the low cracking efficiency and necessary extra safety precuations for these compounds have stimulated interest in organometallic dopants. The thermal instability of stibine

would add further difficulties in attempts to use it as a p-type dopant. The very high volatilities of Me_3As and Me_3Sb lead to difficulties in controlling doping levels[43] and their high thermal stabilities would restrict growth of MCT to conventional (410°C) or precracking techniques. The triethyl derivative should be less stable and certainly has a more controllable vapour pressure. Doping of MCT has been reported using Me_3As,[43] however, experience of GaAs growth[40] indicates that substantial carbon incorporation might occur. Other potentially useful arsenic sources with cracking temperatures substantially below that of AsH_3 are listed in Table 3. The volatility of Bu^tAsH_2 and Bu^tPH_2 would necessitate dilution in hydrogen for use as dopants. Recently it has been shown[47] that Bu^tAsH_2 decomposes by the first-order elimination of isobutane, i.e. intramolecular coupling elimination, previously only observed in transition metal systems.

n-Doping of CdTe and MCT using indium alkyls has been reported with the less volatile Et_3In potentially offering better low level doping control and lower growth temperatures. The problems of solid Me_3In delivery have been addressed.[67]

Organometallics of manganese for diluted magnetic semiconductors (*Table* 4)

Methylcyclopentadienyltricarbonylmanganese, $(MeC_5H_4)Mn(CO)_3$, has been used to dope ZnS, ZnSe[49–51,55–58] and CdTe[58] films by the MOCVD process, but a high substrate temperature (500°C) is required for complete cracking. It is possible to grow ZnS–Mn films by MOCVD at substrate temperatures as low as 325°C,[49,50] but at this temperature cracking is incomplete and doping is inefficient. In recent studies,[52,53] a compromise temperature near 400°C has been employed. A number of problems result from the high temperatures required for effective manganese doping. They include poor surface morphology and crystallinity in the deposited film, the promotion of reaction between the II–VI layer and commonly used transparent conducting oxides, hydrogen reduction of the oxides, and enhanced solid-state diffusion rates.[51,55,68]

The problem of the high cracking temperature of $(MeC_5H_4)Mn(CO)_3$ has been partially overcome by thermally precracking the manganese compound at 580°C, or by decomposing it by glow discharge (plasma-enhanced MOCVD). Both techniques allow substantial reduction of the substrate temperature (e.g. to 300°C),[55,56] but each places special requirements on reactor geometry. A further problem with the plasma technique is the liberation of oxygen atoms from the carbonyl complex and the consequent possible incorporation of [O] in the epilayer.

There is yet another problem with $(MeC_5H_4)Mn(CO)_3$. To generate sufficient vapour pressure[49–51] for growth of alloys such as $Cd_{0.7}Mn_{0.3}Te$, it is necessary to keep the bubbler temperature at 120–140°C (probably the high temperature limit for valves used in the stainless steel bubblers). In turn, the tubing, valves and front end of the reactor must also be heated[57] so that there is no condensation in the plumbing on the way to the reactor. Clearly, alternative feedstocks with higher vapour pressure and lower growth temperature are required.

Surprisingly, $(C_5H_5)Mn(CO)_3$ seems not to have been tried as a dopant feedstock. It is an air-stable solid which can be purified[69] by vacuum sublimation at 50°C (0.1 mm). Although little detailed information is available about its mode of thermal decomposition, it is completely decomposed at 280–350°C.

To overcome the problem of oxygen incorporation in the epilayer when $(MeC_5H_4)Mn(CO)_3$ is used in plasma-enhanced MOCVD, dicyclopentadienylmanganese, $(C_5H_5)_2Mn$, has been tried as the manganese source. It was introduced from containers at 75[54] and 140°C,[58] and was decomposed by RF glow discharge at 13.56 MHz. The related compound $(MeC_5H_4)_2Mn$ is more volatile and can be introduced from a bubbler at 5°C.[54]

$(C_5H_5)_2Mn$ may not be the best choice for this work because it is one of the most air-sensitive and least volatile of the $(RC_5H_4)_2Mn$ compounds. Its magnetic properties[70,71] are consistent with a high spin, ionic character $Mn^{2+}(C_5H_5^-)_2$. On heating under nitrogen to 158°C, the brown solid changes to a pale pink solid (phase change?) which melts on further heating to 173°C. Under vacuum (0.1 mm), heating to 100–150°C results in sublimation of the compound.

The alkyl-substituted cyclopentadienyl analogues are more volatile. At room temperature, $(MeC_5H_4)_2Mn$[72] is a low melting solid (m.p. 61–63°C) and the compounds $(RC_5H_4)_2Mn$ (R = Et, Pr^i, Bu^t) are liquids. All can be purified by slow distillation.[71] For example, $(EtC_5H_4)_2Mn$ distils under high vacuum with a bath temperature of only 50–60°C. A detailed study[71] of paramagnetic NMR data for these compounds establishes that low and high spin states are in equilibrium.

Compounds with more highly substituted rings can also be obtained. The pentamethylcyclopentadienyl compound, $(C_5Me_5)_2Mn$,[73] is an example. It has a covalent sandwich structure with

the metal in a low spin state. As the solid, $(C_5Me_5)_2Mn$ is easier to handle than the $(RC_5H_4)_2Mn$ compounds because it is only slowly decomposed in the air. However, its volatility is relatively low, and purification by vacuum sublimation is achieved at 100°C (10^{-5} mm). This detracts from its potential as an MOCVD feedstock.

Other carbonyl-free manganese compounds include dialkyl species, R_2Mn. The simple compounds such as Me_2Mn[74] are rather unstable and some are known to detonate. Moreover, the insolubility of these compounds in organic solvents is consistent with a polymeric composition and their volatility is therefore likely to be low. Higher alkyls including R_2Mn ($R = CH_2CMe_3$ and CH_2SiMe_3) have been more thoroughly characterized.[75] They are dimeric in the solid state, and can be sublimed (e.g. $R = CH_2CMe_3$ at 110°C *in vacuo*). However, these compounds are extremely air sensitive. Stable adducts with N,N,N′,N′-tetramethylethylenediamine (tmed) have been formed,[75] and the 1 : 1 adducts $R_2Mn \cdot tmed$ sublime unchanged at 80°C in vacuum. When the alkyl groups are even bulkier ($R = C(SiMe_3)_3$), monomeric dialkyl compounds MnR_2 are obtained.[76] Further study of the thermal properties of these alkyl–manganese compounds seems warranted.

For low temperature, large area MOCVD growth of doped semiconductors, carbonyl and related derivatives of manganese seem to offer greatest potential as alternative feedstocks. Although it has been suggested[49] that $Mn_2(CO)_{10}$ is not suitable for MOCVD, consideration of its properties[77] indicates that it fulfils many of the requirements. The solid is only slowly decomposed in the air, and it can be kept for very long periods under an inert atmosphere. It is reported to decompose above 110°C to a metallic mirror. The major limitation in its possible use for MOCVD is the relatively low volatility.[48]

A volatile hydrido derivative of manganese carbonyl is known.[78] It is a colourless, malodorous liquid (m.p. −25°C) at room temperature and it rapidly oxidizes in air to regenerate $Mn_2(CO)_{10}$. The parent carbonyl is also formed when the hydride decomposes thermally at about 100°C. It seems probable that this thermal decomposition would be inhibited in a hydrogen atmosphere, and so $HMn(CO)_5$ may be a very good carrier of $Mn_2(CO)_{10}$ under MOCVD conditions. High dopant concentration could be obtained because the vapour pressure of the hydride is 5 mm at room temperature.

The related compounds, $RMn(CO)_5$, are more chemically robust than the hydride, and they display a wide range of volatilities. The methyl derivative $MeMn(CO)_5$ is a volatile solid (m.p. 95°C; vapour pressure at 28.8°C, 3 mm) at room temperature. It is reported[79] to decompose at *ca* 100°C, and we have determined that pyrolysis of the compound in a hydrogen stream does produce a metallic mirror. The ethyl derivative $EtMn(CO)_5$ is a volatile liquid (m.p. −30°C; vapour pressure at 45°C, 3.5 mm) and it is somewhat less thermally stable than the methyl analogue. There is a report in the patent literature[60] covering the suitability of this compound for MOCVD applications. The thermochemical properties of some other $RMn(CO)_5$ compounds have been investigated. The most recent involves the benzyl compound $PhCH_2Mn(CO)_5$ and it establishes[80] that the $Mn\overset{\sigma}{-}R$ bond is more thermally stable than the Mn—CO bonds. We intend to prepare a range of these compounds with different R groups, and to systematically study their thermal properties, including thermal degradation in a hydrogen stream with identification of the products. Recently, we reported[59] growth of $Cd_{1-x}Mn_xTe$ and $Hg_{1-x}Mn_xTe$ using $MeMn(CO)_5$ at low temperatures.

Since manganese is co-deposited with other semiconductor metals in the MOCVD process, there is interest in finding volatile dimetallic complexes in which manganese is bound to mercury, cadmium or tellurium. A number of such compounds are known and two examples are briefly discussed below.

The mercury–manganese compound $Hg[Mn(CO)_5]_2$ is readily prepared,[81] and can be purified by sublimation (100–140°C at 0.1 mm). It decomposes thermally at 155°C, but it is not indicated if total cracking occurs at this temperature. The volatility of this compound is probably too low for convenient use in MOCVD applications.

The direct reaction between manganese carbonyl and dialkyltellurium gives manganese–tellurium species[82] as shown in eq. (1):

$$Mn_2(CO)_{10} + TeR_2 \longrightarrow Mn_2(TeR)_2(CO)_8 \underset{CO}{\rightleftharpoons} 2Mn(TeR)(CO)_5. \quad (1)$$

The monomeric product may be of interest for the controlled formation of MnTe by MOCVD. These and related bimetallic compounds warrant further investigation, particularly since co-metal chemical vapour deposition has been achieved with other mixed-metal compounds. Recent examples include the formation of $FeCo_x$ films from iron–cobalt carbonyl clusters,[83] and of FeTe and $FeTe_2$ from $[(C_5H_5)Fe(CO)(PEt_3)]_2(Te)_n$.[84]

Acknowledgements—We are grateful to Dr T. McAllister for providing a manuscript of his paper (ref. 62). The

permission of the Executive General Manager, Research SRU, Telecom Australia to publish this paper is acknowledged. Partial support was provided under the Generic Technology component of the Industry Research and Development Act 1986, Grant No. 15019.

REFERENCES

1. Proceedings of the Third International Conference on II-VI Compounds II-VI-87, Monterey, CA, U.S.A., July 1987: *J. Cryst. Growth*, Vol. 86 (1988).
2. Proceedings of the Fourth International Conference on Metal Organic Vapor Phase Epitaxy, Hakone, Japan, May 1988: *J. Cryst. Growth*, Vol. 93 (1988).
3. S. J. C. Irvine, J. B. Mullin, J. Giess, J. S. Gough, A. Royle and G. Crimes, *J. Cryst. Growth* 1988, **93**, 732.
4. W. Hoke and L. Specht, *German Pat. DE 3743132A* (21 July 1988).
5. L. S. Lichtmann and J. D. Parsons, *Int. Pat. Applic. PCT/US87/00357* (24 February 1987).
6. S. J. C. Irvine, J. B. Mullin and J. Tunnicliffe, *U.K. Pat. Applic. 8422817* (24 April 1985).
7. S. J. C. Irvine and J. B. Mullin, *U.K. Pat. GB2078695* (18 May 1981).
8. Alfa Catalogue 1986/87.
9. M. Ekawa, Y. Kawakami, T. Taguchi and A. Hiraki, *J. Surface Sci. Soc. Jap.* 1988, **9**, 384.
10. J. T. Mullins, P. A. Clifton, G. J. Russell, A. W. Brinkman and J. Woods, *J. Cryst. Growth* 1988, **93**, 755.
11. P. J. Wright, P. J. Parbrook, B. Cockayne, A. C. Jones, E. D. Orell, K. P. O'Donnell and B. Henderson, *J. Cryst. Growth* 1989, **94**, 441.
12. P. J. Wright, B. Cockayne, A. J. Williams, A. C. Jones and E. D. Orell, *J. Cryst. Growth* 1987, **84**, 552.
13. Strem Chemicals, Inc. Data Sheet.
14. D. A. Jackson Jr, *J. Cryst. Growth* 1988, **87**, 205.
15. H. Shtrikman, A. Raizman, M. Oron and D. Eger, *Mater. Lett.* 1987, **5**, 345.
16. J. Thompson, P. Mackett, L. M. Smith, D. J. Cole-Hamilton and D. V. Shenai-Khatkhate, *J. Cryst. Growth* 1988, **86**, 233.
17. N. A. Lange, *Handbook of Chemistry*, 13th edn, Table 10.8. McGraw-Hill, New York (1985).
18. S. R. Glanvill, M. S. Kwietniak, G. N. Pain, C. J. Rossouw, R. Warminski, L. S. Wielunski and I. J. Wilson, *Phil. Mag. Lett.* 1989, **59**, 17.
19. Toyo Stauffer, Electronic Grade Metal Alkyls Catalogue.
20. P. J. Wright, B. Cockayne, A. C. Jones, E. D. Orrell, P. O'Brien and O. F. Z. Kahn, *J. Cryst. Growth* 1989, **94**, 97.
21. L. M. Smith, J. Thompson, A. C. Jones, P. R. Jacobs and S. A. Rushworth, *J. Cryst. Growth* 1988, **93**, 930.
22. J. E. Jensen, P. D. Brewer, G. L. Olson, L. W. Tutt and J. J. Zinck, *J. Vac. Sci. Technol.* 1988, **A6**, 2808.
23. J. D. Parsons and L. S. Lichtmann, *J. Cryst. Growth* 1988, **86**, 22.
24. C. G. Bethea, B. F. Levine, P.-Y. Lu, L. M. Williams and M. H. Ross, *Appl. Phys. Lett.* 1988, **53**, 1629.
25. P.-Y. Lu, L. M. Williams, C.-H. Wang, S. N. G. Chu and M. H. Ross, *Mater. Res. Soc. Proc.* 1988, **102**, 77.
26. M. Ekawa, Y. Kawakami, T. Taguchi and A. Hiraki, *J. Cryst. Growth* 1988, **93**, 667.
27. P. I. Kuznetsov, L. A. Zhuravlev, I. N. Odin, V. V. Shemet and A. V. Novoselova, *Inorg. Mater. U.S.S.R.* 1982, **18**, 779.
28. W. E. Hoke, P. J. Lemonias and R. Korenstein, *J. Mater. Res.* 1988, **3**, 329 and refs therein.
29. S. Fujii, Y. Fujita and T. Iuchi, *J. Cryst. Growth* 1988, **93**, 750.
30. A. I. Gal', O. V. Kuzmin, E. A. Chemyshev, R. A. Rostunova, E. N. Lebedev and O. S. Sheveleva, Soviet Ministry of the Chemical Industry, NIITEKHIM (Institute of Technico-Economic Research) Series: *Hetero-Organic Compounds and their Use, "The Properties and Synthesis of Lower Alkyl Compounds of Tellurium"*. Moscow (1981).
31. K. Shiina, Y. Tanaka, O. Sugiura, S. Oda and M. Matsumura, *Appl. Phys. Lett.* 1988, **52**, 1306.
32. S. J. C. Irvine, J. B. Mullin, H. Hill, G. T. Brown and S. J. Barnett, *J. Cryst. Growth* 1988, **86**, 188.
33. S. Oda, Y. Tanaka, O. Sugiura and M. Matsumura, *J. Appl. Phys.* 1989, **65**, 1809.
34. W. E. Hoke, *Mater. Res. Soc. Proc.* 1987, **90**, 379.
35. D. W. Kisker, M. L. Steigerwald, T. Y. Kometami and K. S. Jeffers, *Appl. Phys. Lett.* 1987, **50**, 1681.
36. S. J. C. Irvine, H. Hill, O. D. Dosser, J. E. Hails, J. B. Mullin, D. V. Shenai-Khatkhate and D. Cole-Hamilton, *Mater. Lett.* 1988, **7**, 25.
37. American Cyanamid Company, Product Information.
38. L. S. Lichtmann, J. D. Parsons and E.-H. Cirlin, *J. Cryst. Growth* 1988, **86**, 217.
39. R. Korenstein, W. E. Hoke, P. J. Lemonias, K. T. Higa and D. C. Harris, *J. Appl. Phys.* 1987, **62**, 4929.
40. G. B. Stringfellow, *J. Electronic. Mater.* 1988, **17**, 327 and refs therein.
41. C. A. Larsen and G. B. Stringfellow, *J. Cryst. Growth* 1986, **75**, 247.
42. O. Kayser, H. Heinecke, A. Brauers, H. Luth and P. Balk, *Chemtronics* 1988, **3**, 90.
43. J. S. Whiteley, P. Koppel, V. L. Conger and K. E. Owens, *J. Vac. Sci. Technol.* 1988, **A6**, 2804.
44. C. Harrison and E. H. Tompkins, *Inorg. Chem.* 1962, **1**, 951.
45. H. Ito and T. Ishibashi, *Jap. J. Appl. Phys.* 1988, **27**, 1554.
46. A. Brauers, O. Kayser, R. Kall, H. Heinecke, P. Balk and H. Hofmann, *J. Cryst. Growth* 1988, **93**, 7.
47. C. A. Larsen, N. I. Buchan, S. H. Li and G. B. Stringfellow, *J. Cryst. Growth* 1989, **94**, 663.
48. G. I. Christiansz, T. J. Elms, G. N. Pain and R. R. Pierson, *J. Cryst. Growth* 1988, **93**, 589 (see Table 1).
49. P. J. Wright, B. Cockayne, A. F. Cattell, P. J. Dean, A. D. Pitt and G. W. Blackmore, *J. Cryst. Growth* 1982, **59**, 155.

50. A. F. Cattell, B. Cockayne, K. Dexter, J. Kirton and P. Wright, *IEEE Trans. Electron Devices* ED-30, 471 (1983).
51. P. J. Dean, *Phys. Stat. Sol.* 1984, **81**, 625.
52. A. P. C. Jones, D. Y. Watts, A. W. Brinkman, G. J. Russell and J. Woods, *J. Cryst. Growth* 1988, **86**, 880.
53. Z. C. Feng, R. Sudharsanan, S. Perkowitz, A. Erbil, K. T. Pollard and A. Rohatgi, *J. Appl. Phys.* 1988, **64**, 6861.
54. M. Migita, O. Kanehisa, M. Shiiki and H. Yamamoto, *J. Cryst. Growth* 1988, **93**, 686.
55. K. Hirabayashi and H. Kozawaguchi, *Jpn J. Appl. Phys.* 1986, **25**, 711 and L379.
56. K. Hirabayashi, H. Kozawaguchi and B. Tsujiyama, *Kenkyu Jitsuyoka Hokoku* 1987, **36**, 829.
57. A. Nouhi and R. J. Stirn, *Appl. Phys. Lett.* 1987, **51**, 2251.
58. N. Mino, M. Kobayashi, M. Konagai and K. Takahashi, *Jpn J. Appl. Phys.* 1985, **24**, L383; *Jpn J. Appl. Phys.* 1986, **59**, 2216.
59. G. B. Deacon, R. S. Dickson, K. McGregor, R. S. Rowe, B. O. West, G. N. Pain, G. I. Christiansz and M. Kwietniak, *Proc. 3rd Australian Conference on II–VI Semiconductors*, Adelaide, April (1989): to be submitted to *J. Cryst. Growth.*
60. T. Shimobayashi, N. Akamoto and N. Ho, *Japan Pat. JP 61/53194 A2[86/53194].*
61. *Epichem Newsletter* No. 1 (May 1988).
62. T. McAllister, *J. Cryst. Growth*, submitted.
63. P. Capper, P. A. C. Whiffin, B. C. Easton, C. D. Maxey and I. Kenworthy, *Mater. Lett.* 1988, **6**, 365.
64. S. K. Ghandhi, N. R. Tasker and I. B. Bhat, *Appl. Phys. Lett.* 1987, **50**, 900.
65. P. Capper, B. C. Easton, P. A. C. Whiffin and C. B. Maxey, *J. Cryst. Growth* 1986, **79**, 508.
66. S. K. Ghandhi, N. R. Taskar, K. K. Parat, D. Terry and I. B. Bhat, *Appl. Phys. Lett.* 1988, **53**, 1641.
67. B. R. Butler and J. P. Stagg, *J. Cryst. Growth* 1989, **94**, 481.
68. A. M. Glass, R. D. Feldman, D. W. Kisker, P. M. Bridenbaugh and P. M. Markiewich, in: *SPIE, Materials Technologies for IR Detectors* 1986, **659**, 142.
69. A. N. Nesmeyanov, K. N. Anisimov and N. E. Kolobova, *Bull. Acad. Sci. U.S.S.R. (Transl.)* 1964, 2120.
70. G. Wilkinson, F. A. Cotton and J. M. Birmingham, *J. Inorg. Nucl. Chem.* 1956, **2**, 95.
71. N. Hebendanz, T. W. Köhler, G. Müller and J. Reid, *J. Am. Chem. Soc.* 1986, **108**, 3281.
72. L. T. Reynolds and G. Wilkinson, *J. Inorg. Nucl. Chem.* 1959, **9**, 86.
73. J. L. Robbins, N. M. Edelstein, S. R. Cooper and J. C. Smart, *J. Am. Chem. Soc.* 1979, **101**, 3853.
74. C. Beerman and K. Claus, *Angew. Chem.* 1959, **71**, 627.
75. R. A. Andersen, E. Carmona-Guzman, J. F. Gibson and G. Wilkinson, *J. Chem. Soc., Dalton Trans.* 1976, 2204.
76. N. H. Buttrus, C. Eaborn, P. B. Hitchcock, J. D. Smith and A. C. Sullivan, *J. Chem. Soc., Chem. Commun.* 1985, 1380.
77. H. E. Podall, J. H. Dunn and H. Shapiro, *J. Am. Chem. Soc.* 1960, **82**, 1325.
78. W. Hieber and G. Wagner, *Z. Naturf.* 1957, **12b**, 478; *Z. Naturf.* 1958, **13b**, 339.
79. R. D. Closson, J. Kozikowski and T. H. Coffield, *J. Org. Chem.* 1957, **22**, 598.
80. J. A. Martinho-Simoes, J. C. Schultz and J. L. Beauchamp, *Organometallics* 1985, **4**, 1238.
81. W. Hieber and W. Schropp Jr, *Chem. Ber.* 1960, **93**, 455.
82. W. Hieber and T. Kruck, *Chem. Ber.* 1962, **95**, 2027.
83. C. L. Czekaj and G. J. Geoffrey, *Inorg. Chem.* 1988, **27**, 8.
84. M. L. Steigerwald, *Chem. Mater.* 1989, **1**, 52.

Polyhedron Vol. 9, No. 7, pp. 931–937, 1990
Printed in Great Britain

0277–5387/90 $3.00+.00
© 1990 Pergamon Press plc

ALKYL COMPLEXES OF COBALT(II). X-RAY CRYSTAL STRUCTURES OF $(Me_2NCH_2CH_2NMe_2)CoR_2$, R = CH_2SiMe_3, CH_2CMe_3, $[(Me_2NCH_2CH_2NMe_2)Li]_2[Co(CH_2SiMe_3)_4]$ AND $[(Me_2NCH_2CH_2NMe_2)_2Li][CoCl\{CH(SiMe_3)_2\}_2]$

ROBYN S. HAY-MOTHERWELL and GEOFFREY WILKINSON*

Johnson Matthey Laboratory, Chemistry Department, Imperial College, London SW7 2AY, U.K.

and

BILQUIS HUSSAIN and MICHAEL B. HURSTHOUSE*

Chemistry Department, Queen Mary and Westfield College, London E1 4NS, U.K.

(*Received* 27 *October* 1989; *accepted* 2 *November* 1989)

Abstract—The interaction of lithium alkyls in diethyl ether in the presence of tetramethylethylenediamine (TMED, $Me_2NCH_2CH_2NMe_2$) with cobalt(II) chloride has led to the isolation of four complexes whose crystal structures have been determined. The complexes (TMED)CoR_2, R = CH_2SiMe_3 and CH_2CMe_3, have tetrahedral geometry about cobalt; in $[(TMED)Li]_2[Co(CH_2SiMe_3)_4]$ there are CH_2SiMe_3 groups bridging the lithium and cobalt atoms; in the ionic complex $[(TMED)_2Li][CoCl\{CH(SiMe_3)_2\}_2]$ the geometry about cobalt is trigonal planar. Electron paramagnetic resonance spectra of the complexes and of the products of the reaction with oxygen are reported.

Relatively few cobalt(II) alkyl or aryl compounds are known, either neutral with a donor ligand, CoR_2L_2, or anionic $[CoR_n]^{2-}$ (n = 3, 4), and X-ray data is particularly scanty; some often unstable and air-sensitive lithium alkylate or arylate anions with, for example, CH_3, CH_2SiMe_3, 2,4,6-MeC_6H_2, C_6F_5 and C_6Cl_5, are listed;[1a] no X-ray structures are so far reported although some structures of neutral species, viz. $Co(C_6F_5)_2$(η-toluene) and Co(mesityl)$_2(PEt_2Ph)_2$ are known,[1b] the latter being planar on account of steric blocking of two sites by methyl groups [cf. Co_2(mesityl)$_4$ noted below].

In a preliminary note[2] we briefly reported some lithium alkylate anions of manganese(II), cobalt(II) and uranium(IV) and showed[3] that the manganese trimethylsilylmethyl could be oxidized to a green unstable species believed to be $Mn^{IV}(CH_2SiMe_3)_4$ on the basis of EPR spectra. Oxidation of the similar cobalt species by air led, however, only to decomposition. The present studies are made with the hope that cobalt(IV) species could be identified or isolated on oxidation—without success; so far the only cobalt(IV) alkyl is the tetranorbornyl first made by Bower and Tennant[4] and recently studied in great detail.[5] In the latter work, the cobalt(III) anion $[Co(nor)_4]^-$ was isolated as salts of $[Li(THF)_4]^+$, [Na(18-C-6)]$^+$ and Et_4N^+.

After completion of our present study the first neutral homoleptic cobalt(II) species, bis(μ-mesityl)dimesityldicobalt(II), has been reported.[6] It was made from the previously known $[Li(THF)_4][Co(mes)_3]$ and both compounds have been characterized in detail and the crystal structure of $[Co(mes)_2]_2$ determined.

Our initial attempts to isolate crystalline salts from reactions of lithium alkyls with $CoCl_2$ or $CoCl_2$THF in diethyl ether or tetrahydrofuran solutions were unsuccessful, although the alkylate anions were evidently readily formed. Even the subsequent addition of TMED did not yield tractable products. The best procedure for the lithium compounds and (TMED)$Co(CH_2CMe_3)_2$, described in the Experimental, involves addition of excess lith-

* Authors to whom correspondence should be addressed.

ium reagent in Et_2O to $CoCl_2$ and TMED in Et_2O at −78°C—even so, black solids separated and the final yields of products were low, 20–30%. The neutral species (TMED)Co(CH_2SiMe_3)$_2$ was isolated in a similar manner but using less alkylating agent.

Although attempts to oxidize the alkylate anions chemically led to decomposition, the initial reaction with O_2 could be followed by EPR spectra as discussed later. Cyclic voltammetry in THF showed only irreversible oxidation waves. No evidence for any formation of cobalt(IV) species has been found.

X-ray crystal structures

The structures of the complexes (TMED)CoR_2, R = CH_2SiMe_3 (**1**) and R = CH_2CMe_3 (**2**), are very similar, as would be expected. Diagrams of the two molecules are given in Figs 1 and 2, respectively, whilst selected bond lengths and angles are given in Table 1. The geometry at cobalt is best described as distorted tetrahedral since the planes defined by the metal and the two carbons and the metal and two nitrogens interact at angles of 84.1(2)° (**1**) and 82.1(2)° (**2**), i.e. close to 90°. Nevertheless, there are significant bond angle distortions away from the ideal 109.5°; the N—Co—N angles, constrained by the bidentate nature of the TMED ligand are 83–84°, whilst the expanded C—Co—C angles of 122.3(2) (**1**) and 132.3(4)° (**2**) reflect the large, but differing, steric size of the alkyls. Increased steric effects may also account for the slightly greater Co—C and Co—N distances in the neopentyl.

Table 1. Selected bond lengths and angles for compounds **1** and **2**

Bond lengths (Å)	1	2
C(10)—Co(1)	2.025(7)	2.039(6)
C(20)—Co(1)	2.024(7)	
N(1)—Co(1)	2.179(7)	2.213(5)
N(2)—Co(1)	2.170(7)	
Bond angles (°)		
C(20)—Co(1)—C(10)	122.3(3)	132.2(4)
N(1)—Co(1)—C(10)	113.4(3)	112.7(3)
N(1)—Co(1)—C(20)	106.5(3)	
N(2)—Co(1)—C(10)	108.1(3)	
N(2)—Co(1)—C(20)	116.0(3)	
N(2)—Co(1)—N(1)	84.0(3)	83.2(3)
C(1)—N(1)—Co(1)	111.9(6)	103.2(4)

The cobalt coordination in [(TMED)Li]$_2$ [Co(CH_2SiMe_3)$_4$] (**3**) is also distorted tetrahedral with the Me_3SiCH_2 groups bridging lithium and cobalt atoms. A diagram of the molecule is given in Fig. 3, bond lengths and angles in Table 2. Here the angle of intersection of the two C_2Co planes is 88.8(3)°. The distribution of tetrahedral angles is affected mainly by the lithium bridging which gives closed-down C—Co—C angles of 101.3(4) and 101.7(3)°. The open C—Co—C angles are 110.6(4) and 114.4(5)°. The Co—C distances

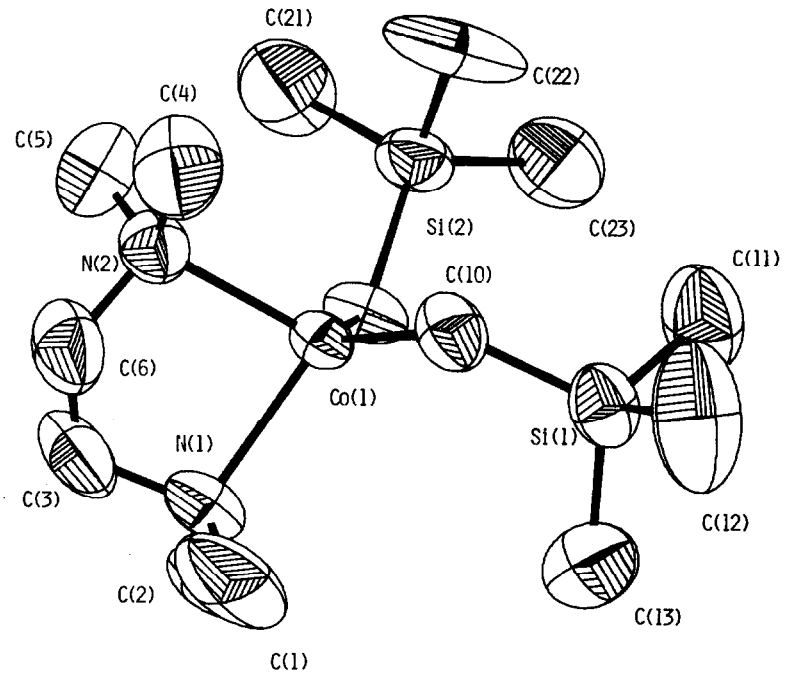

Fig. 1. Structure of (TMED)Co(CH_2SiMe_3)$_2$ (**1**).

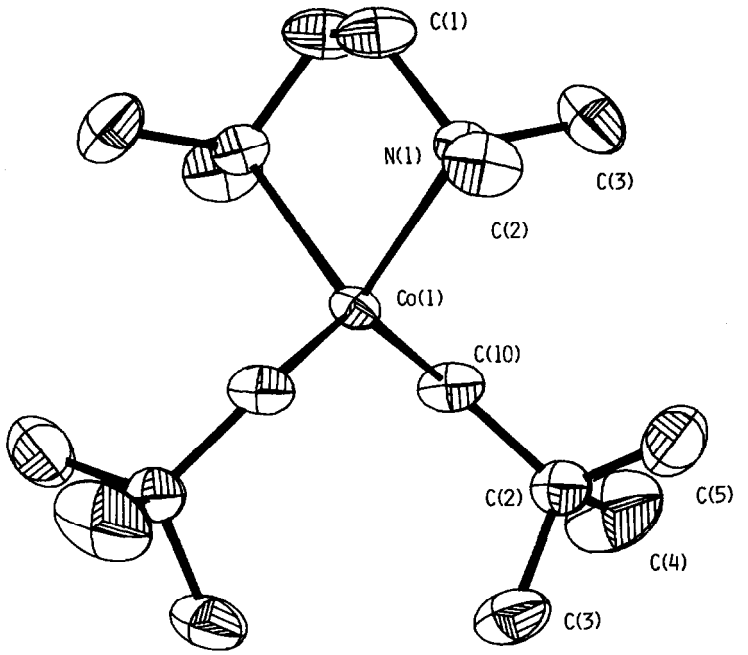

Fig. 2. Structure of (TMED)Co(CH_2CMe_3)$_2$ (**2**).

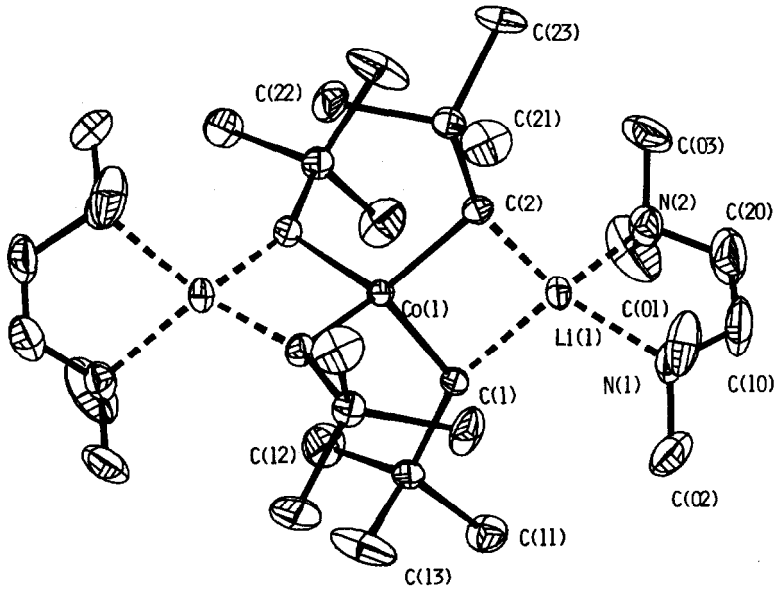

Fig. 3. Structure of [(TMED)Li]$_2$[Co(CH_2SiMe_3)$_4$] (**3**).

are more than 0.1 Å longer than those in the two N_2CoC_2 compounds, possibly affected by the lithium bridging.

For the compound [(TMED)$_2$Li][CoCl{CH(SiMe$_3$)$_2$}$_2$] (**4**) the structure is shown in Fig. 4; bond lengths and angles are in Table 3. The cobalt coordination is trigonal planar (sum of angles = 360.0°) but remarkably, in view of the different ligands, the three angles Cl—Co—C (×2) and C—Co—C are all very close to 120°—119.3(6)–120.8(7)°. A close to planar CoC_3 group has been found[6] in the homoleptic bridged dimer [(mes)Co(μ-mes)]$_2$. Furthermore, there is close similarity to the mononuclear alkoxides and dialkylamides,[7] [Li(THF)$_3$][CoCl(OBu^t$_3$)$_2$], [Li(THF)$_{4.5}$][Co{N(SiMe$_3$)$_2$}(OBu^t$_3$)$_2$] and Li[Co{N(SiMe$_3$)$_2$}(OBu^t$_3$)$_2$], all of which have, however, distorted trigonal planar geometry about cobalt(II). The significant differences in cobalt(II) geometries between the alkyls and the alkoxides and

Table 2. Selected bond lengths and angles for compound **3**

Bond lengths (Å)			
C(1)—Co	2.151(8)	C(2)—Co	2.154(8)
Li(1)—C(1)	2.268(13)	Li(1)—C(2)	2.197(13)
Li(1)—N(1)	2.190(13)	Li(1)—N(2)	2.145(13)
Bond angles (°)			
C(2)—Co—C(1)	101.7(3)	C(1)—Co—C(1B)	110.6(4)
C(1)—Co—C(2B)	114.4(5)	C(1B)—Co—C(2B)	101.3(4)
Li(1)—Co—C(1)	51.8(3)	Li(1)—Co—C(2)	49.9(2)
Si(1)—C(1)—Co	122.7(4)	Li(1)—C(1)—Co	80.0(4)
Li(1)—C(1)—Si(1)	157.1(4)	Si(2)—C(2)—Co	120.5(4)
Li(1)—C(2)—Co	81.5(4)	Li(1)—C(2)—Si(2)	158.0(4)
Li(1)—N(1)—C(10)	102.0(7)	Li(1)—N(1)—C(01)	109.0(7)
Li(1)—N(1)—C(02)	115.9(7)	Li(1)—N(2)—C(20)	102.1(8)
Li(1)—N(2)—C(03)	115.5(7)	Li(1)—N(2)—C(04)	109.7(8)
C(2)—Li(1)—C(1)	96.8(5)	N(1)—Li(1)—C(1)	112.2(6)
N(1)—Li(1)—C(2)	125.9(6)	N(2)—Li(1)—C(1)	126.6(6)
N(2)—Li(1)—C(2)	113.3(6)	N(2)—Li(1)—N(1)	85.2(5)

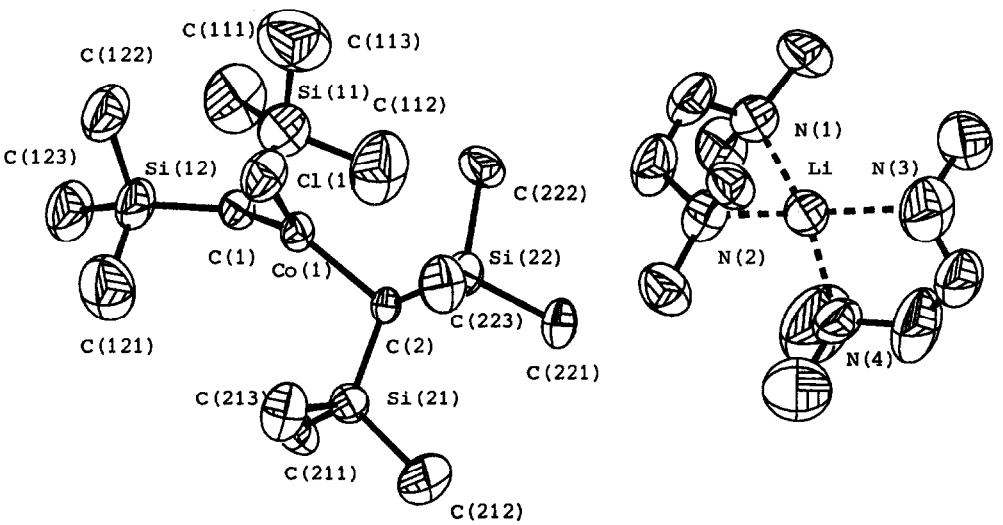

Fig. 4. Structure of $[(TMED)_2Li][CoCl\{CH(SiMe_3)_2\}_2]$ (**4**).

silylamides may well reflect the differing covalent vs ionic character (and therefore stereochemical rigidity) of the metal-to-ligand bonding. Other three-coordinate species are $[Co(NR_2)_2]_2$ (R = $SiMe_3$, Ph) and $Co[N(SiMe_3)_2]_2PPh_3$).

EPR spectra

The X-band EPR spectra of the three tetrahedral cobalt(II) compounds in frozen, degassed toluene at liquid nitrogen temperature (77 K) were typical of such tetrahedral cobalt(II) complexes with large zero-field splittings[8] (Fig. 5). On exposure of solutions to a trace of air followed by rapid freezing, the original cobalt(II) signal was replaced by a signal characteristic of a cobalt(III) dioxygen complex;[9] the colour also changed from blue to brownish. The effective g values for all the dioxygen adducts have $g_z > g_{x,y} \simeq 2.0$ with relatively small A_{iso}^{Co} values, suggesting that the unpaired electron spin density no longer resides on the cobalt metal centre but is delocalized on the dioxygen moiety.[9] The spectrum for $(TMED)Co^{III}(CH_2SiMe_3)_2(O_2)$, Fig. 6, gives the parameters g_x 2.017, g_y 2.067 and g_z 2.341 with ^{59}Co hyperfine constants of 1.49, 1.26 and 6.65×10^{-3} cm^{-1}, respectively. The differences in the EPR spectra of the other dioxygen compounds were very slight. All the species on warming to room temperature decomposed to insoluble brown–black precipitates.

Table 3. Selected bond lengths and angles for compound **4**

Bond lengths (Å)			
Cl(1)—Co(1)	2.261(7)	C(1)—Co(1)	2.042(17)
C(2)—Co(1)	2.029(16)	Si(11)—C(1)	1.849(18)
Si(12)—C(1)	1.843(17)	Si(21)—C(2)	1.857(17)
Si(22)—C(2)	1.843(17)	Li—N(1)	2.121(35)
Li—N(2)	2.198(33)	Li—N(3)	2.164(35)
Li—N(4)	2.153(32)		
Bond angles (°)			
C(1)—Co(1)—Cl(1)	119.9(5)	C(2)—Co(1)—Cl(1)	119.3(6)
C(2)—Co(1)—C(1)	120.7(7)	Si(11)—C(1)—Co(1)	107.9(8)
Si(12)—C(1)—Co(1)	110.2(9)	Si(21)—C(2)—Co(1)	108.9(8)
Si(22)—C(2)—Co(1)	112.0(8)	N(2)—Li—N(1)	86.5(13)
N(3)—Li—N(1)	121.8(15)	N(3)—Li—N(2)	124.4(17)
N(4)—Li—N(1)	127.5(17)	N(4)—Li—N(2)	114.5(15)
N(4)—Li—N(3)	86.5(13)		

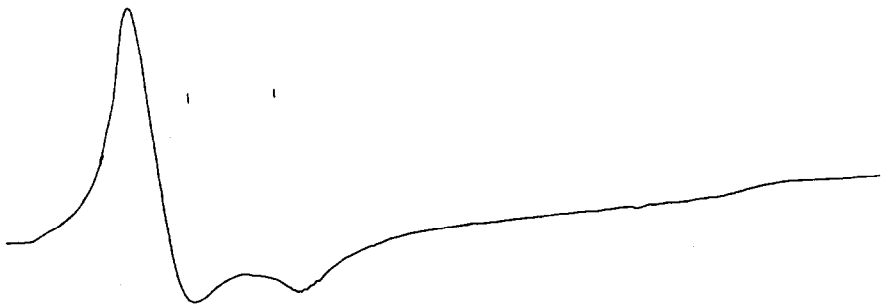

Fig. 5. Typical EPR spectrum of $(TMED)CoR_2$ and $(TMEDLi)_2CoR_4$, R = CH_2SiMe_3 and CH_2CMe_3 at 77 K (scale 100 mT; field increasing to right).

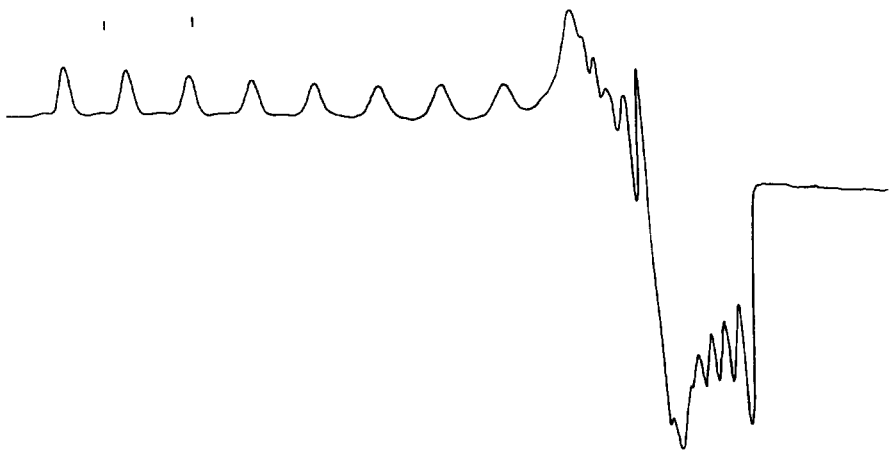

Fig. 6. Typical EPR spectrum of $(TMED)CoR_2$ and $(TMEDLi)_2CoR_4$, R = CH_2SiMe_3 and CH_2CMe_3 after addition of a small amount of oxygen at 77 K (scale 10 mT; field increasing to right).

For the trigonal planar complex $[(TMED)_2Li][CoCl\{CH(SiMe_3)_2\}_2]$ the EPR spectrum was quite different from the others. The spectrum in frozen toluene, Fig. 7, yielded the parameters $g_{\parallel}$ 2.550 and $g_{\perp}$ 2.065. The geometry around the cobalt atom may be approximated to D_{3h}. In this point group, a low spin d^7 ion would be expected to have the configuration $d_{z^2}^2$; $(d_{xz}, d_{yz})^4$; $(d_{x^2-y^2}, d_{xy})^1$ with

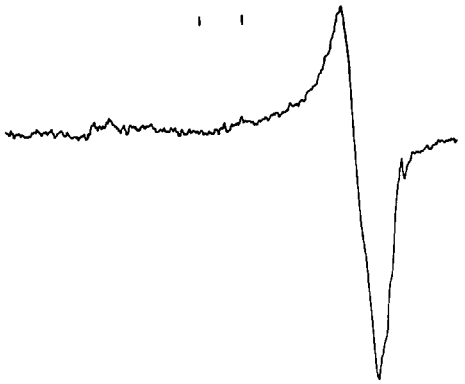

Fig. 7. EPR spectrum of $[(TMED)_2Li][CoCl\{CH(SiMe_3)_2\}]$ at 77 K (scale 10 mT; field increasing to right).

the unpaired electron in a two-fold degenerate E state. However, the relative sharpness of the EPR spectrum indicated a non-degenerate ground state such as might be expected from the more realistic point group of C_{2v}. The observed g values are quite consistent with the d_{xy} ground state, thus predicted if the Co—Cl bond is chosen as the x direction.

On exposure to varying amounts of oxygen the solution became progressively brown giving a decrease in the size of the original EPR signal without showing any new spectrum associated with the cobalt centre.

EXPERIMENTAL

Techniques and instrumentation are similar to those described previously.[10] EPR spectra were obtained at X-band on a Varian E-12 spectrometer. All operations were carried out under N_2 or Ar. Tetramethylethylenediamine was refluxed and distilled over KOH under N_2. Bis(trimethylsilyl)chloromethane was prepared from CH_2Cl_2 and Me_3SiCl;[11] the other halides were from Aldrich. Alkyllithiums were prepared by standard methods from lithium metal and the chlorides in refluxing hexane as for $LiCH_2SiMe_3$;[12] sonification at 50°C using lithium dispersion (2% Na) in a Heat Systems-Ultrasonic Inc. W380 sonicator was also successful. The hexane solution was filtered, evaporated and the residue dissolved in diethyl ether.

(1) $(TMED)Co(CH_2CMe_3)_2$ (2), $[(TMED)Li]_2[Co(CH_2SiMe_3)_4]$ (3) *and* $[(TMED_2Li)][CoCl\{CH(SiMe_3)_2\}_2]$ (4)

For these three complexes the following procedure was used. To a stirred solution of anhydrous $CoCl_2$ (*ca* 0.5 g) and a two-fold excess of TMED in ether at −78°C was added a solution of the alkyllithium in ether (−78°C) in a six-fold excess. The mixture was allowed to warm to room temperature with vigorous stirring. The solution first became red, then green, whilst a black solid deposited. After filtration and evaporation, the residues were dissolved in hexane and blue solutions cooled to −20°C to give blue microcrystalline products in 23% (**1**), 33% (**2**) and 20% (**4**) yields. Recrystallization from hexane gave X-ray quality crystals.

(2) $(TMED)Co(CH_2SiMe_3)_2$ (1)

This was prepared in a manner similar to that described above except that only a four-fold excess of alkyllithium was used and TMED was added to the hexane extract from the reaction of $CoCl_2$ and the alkyllithium. The yield of the crystalline product was 11%.

X-ray crystallography

Crystals of the four compounds were sealed under argon in thin-walled glass capillaries. Following preliminary photographic checks, all subsequent X-ray measurements were made on an Enraf–Nonius CAD4 using the ω–2θ scan mode with graphite monochromated Mo-K_α radiation ($\lambda = 0.71069$ Å) following previously detailed procedures[13] and standard CAD4 software. The structures were solved via the heavy-atom method and refined by full-matrix least-squares. Non-hydrogen atoms were assigned anisotropic displacement factor coefficients in all cases. Hydrogens were included (in idealized positions with group isotropic displacement factor coefficients) only for compounds **1** and **2**. The crystals of compounds **3** and **4** were very weakly diffracting (cf. proportion of observed data in Table 4), probably as a result of poor crystal packing and both molecular and ligand disorder or thermal motion. Thus, the structure modelling and R values for these two are disappointing, although the identity of the complexes and the molecular configurations are clearly established. No attempts were made to establish a detailed disorder model in view of the paucity of the data. Experimental and other details of the structure analyses are given in Table 4.

Sources of scattering factor data and computer programs used are given in ref. 13; all calculations were made on a DEC VAX 11/750 computer. Lists of atomic coordinates, thermal parameters, bond lengths and angles and F_o/F_c values have been deposited as supplementary material with the Editor, from whom copies are available on request.

Table 4. Crystal data and details of intensity measurement and structure refinement

Compound	1	2	3	4
Molecular formula	$C_{14}H_{34}CoN_2Si_2$	$C_{16}H_{38}CoN_2$	$C_{28}H_{76}CoLi_2N_4Si_4$	$[C_{14}H_{38}ClCoSi_4][C_{12}H_{32}LiN_4]$
Molecular weight	345.542	317.414	533.828	652.545
Crystal system	Monoclinic	Monoclinic	Tetragonal	Triclinic
a (Å)	25.545(10)	17.005(3)	11.124	14.569(7)
b (Å)	10.147(3)	9.349(3)	11.124	12.925(4)
c (Å)	17.395(4)	12.738(3)	35.881	12.193(2)
α (°)	90.0	90.0	90.0	71.97(3)
β (°)	100.03	107.43(2)	90.0	84.87(3)
γ (°)	90.0	90.0	90.0	77.57(3)
Volume (Å^3)	4439.963	1932.10	4440.04	2131.43
Space group	C2/c	C2/c	$P4_32_12$	$P\bar{1}$
Z	8	4	4	2
D_c (g cm^{-3})	1.034	1.091	0.799	1.21
μ (cm^{-1})	9.48	5.12	3.30	4.20
$F(000)$	1496	699	1156	1002
h, k, l, range	$0 \rightarrow 30$	$-20 \rightarrow 20$	$0 \rightarrow 13$	$-17 \rightarrow 17$
	$0 \rightarrow 12$	$0 \rightarrow 11$	$0 \rightarrow 13$	$0 \rightarrow 15$
	$-20 \rightarrow 20$	$0 \rightarrow 15$	$0 \rightarrow 42$	$-14 \rightarrow 14$
Total number of reflections	4248	1902	4557	7875
Number of unique reflections	3904	1701	4431	7514
Number of reflections used	1503	1243	2251	1278
Number of parameters	216	165	193	334
Weighting scheme parameter g in $w = 1/[\sigma^2(F)+gF_o^2]$	0.000107	0.00017	0.008	0.000978
Final R	0.0395	0.0420	0.0770	0.1257
Final R_w	0.0348	0.0337	0.0841	0.0943

Atomic coordinates have also been deposited with the Cambridge Crystallographic Data Centre.

Acknowledgements—We thank the SERC for provision of X-ray facilities, Dr J. F. Gibson for discussions on EPR spectra and Dr R. Poli for some preliminary studies.

REFERENCES

1. (a) R. D. W. Kemmitt and D. R. Russell, *Comprehensive Organometallic Chemistry* (Edited by G. Wilkinson, F. G. A. Stone and E. W. Abel), Vol. 5, Sect. 34.3.4, p. 74. Pergamon Press, Oxford (1982); (b) P. G. Owston and J. M. Rowe, *J. Chem. Soc.* 1963, 3411.
2. R. A. Andersen, E. Carmona, K. Mertis, E. Sigurdson and G. Wilkinson, *J. Organomet. Chem.* 1975, **99**, C19.
3. R. A. Andersen, E. Carmona, J. F. Gibson and G. Wilkinson, *J. Chem. Soc., Dalton Trans.* 1976, 2204.
4. B. K. Bower and H. G. Tennant, *J. Am. Chem. Soc.* 1972, **94**, 2572.
5. E. K. Byrne and K. H. Theopald, *J. Am. Chem. Soc.* 1989, **111**, 3887.
6. (a) K. H. Theopold, J. Silvestre, E. K. Byrne and D. S. Richeson, *Organometallics* 1989, **8**, 2001.
7. M. M. Ohmstead, P. P. Power and G. Sigel, *Inorg. Chem.* 1986, **25**, 1027 and refs therein.
8. See K. Dyrek, M. Dyrek and A. Weselucha-Birczyńska, *Polyhedron* 1985, **4**, 169 and refs therein.
9. Y. Sugiura, *J. Am. Chem. Soc.* 1980, **102**, 5216; M. Tirant, T. D. Smith and J. R. Pilbrow, *J. Chem. Soc., Dalton Trans.* 1987, 2341; D. F. Evans and D. Wood, *J. Chem. Soc., Dalton Trans.* 1987, 3099; J. H. Cameron, M. Kojima, B. Korybut-Daszkiewicz, B. K. Coltram, T. J. Meade, N. W. Alcock and D. H. Busch, *Inorg. Chem.* 1987, **26**, 427.
10. A. A. Danopoulos, C. J. Longley, G. Wilkinson, B. Hussain and M. B. Hursthouse, *Polyhedron* 1989, **8**, 2657.
11. A. H. Cowley and R. A. Kemp, *Synth. React. Inorg. Met. Org. Chem.* 1981, **11**, 591.
12. H. L. Lewis and T. L. Brown, *J. Am. Chem. Soc.* 1970, **92**, 4664.
13. R. A. Jones, M. B. Hursthouse, K. M. A. Malik and G. Wilkinson, *J. Am. Chem. Soc.* 1979, **101**, 4128.

Polyhedron Vol. 9, No. 7, pp. 939–942, 1990
Printed in Great Britain

0277–5387/90 $3.00+.00
© 1990 Pergamon Press plc

STUDIES ON LANTHANIDE COMPLEXES WITH PYRONIC LIGANDS—III.* SYNTHESIS AND CHARACTERIZATION OF NOVEL COMPLEXES WITH 4-METHYLESCULETIN

C. BISI CASTELLANI† and O. CARUGO

Dipartimento di Chimica Generale, Università di Pavia, via Taramelli 12, 27100 Pavia, Italy

(*Received* 13 *March* 1989; *accepted* 2 *November* 1989)

Abstract—The novel complexes $Ln(Hmes)Cl_2 \cdot 3H_2O$ (Ln = La, Sm, Eu, Gd, Tb, Dy; Hmes = monodeprotonated 4-methylesculetin) have been synthesized and characterized by elemental and thermogravimetric analysis, and by vibrational and electronic absorption spectra. The ligand, potentially diprotic, is only monodeprotonated. The complexation constants have been determined potentiometrically. Contrary to many other complexes of lanthanides with benzopyrone ligands, the compounds described in this paper do not show metal luminescence promoted by the excited states of the ligand. This behaviour is discussed.

The luminescence of lanthanide cation complexes and its applications are the focus of attention of many researchers.[1] In previous works, we showed that ligands containing the α- or the γ-pyronic rings are able to stimulate the lanthanide ion luminescence.[2] Among the α-pyrone derivatives, the 7-hydroxocoumarins are of relevant interest because of their peculiar electronic structure.[3] The presence of a hydroxy group in the 7-position causes a shift to lower energy of the bands in the electronic absorption spectra, with respect to the parent coumarin. This shift results from mesomeric effects, as shown in Scheme 1.

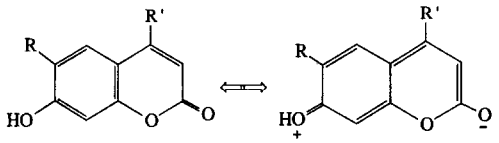

Scheme 1. H_2mes (4-methylesculetin): R = OH, R′ = Me.

The decrease in electronic transition energy may influence the ability of these molecules to transfer their electronic energy to the lanthanide cations. In order to verify if the 7-hydroxocoumarins behave as good chromophores toward lanthanide ions, like other α-pyrone ligands, we used the 4-methylesculetin as ligand and obtained the novel complexes $Ln(Hmes)Cl_2 \cdot 3H_2O$ [Ln = La, Sm, Eu, Gd, Tb, Dy; Hmes = deprotonated form of 4-methylesculetin (referred to as H_2mes in Scheme 1)]. The compounds were characterized by means of elemental and thermogravimetrical analysis, and electronic and vibrational spectroscopy. The formation constants of all the complexes were determined. No increase in lanthanide cation luminescence was observed in any case.

EXPERIMENTAL

Synthesis

6,7-Dihydroxo-4-methyl-2H-1-benzopyran-2-one (4-methylesculetin) was obtained from Aldrich-Chemie. The lanthanide chlorides were prepared as previously described.[4] An ethanolic solution of H_2mes (1 mmol in 40 cm^3) was added to an aqueous solution of the appropriate lanthanide salt (1 mmol in 15 cm^3). On adjusting the pH to 6.2–6.5 with aqueous NaOH, the product separated from the solution as a brown–orange powder. It was centrifugated, washed with ethanol and water, and dried at 1 mm Hg and room temperature for 3 h.

* For the preceding parts see ref. 2.

† Author to whom correspondence should be addressed.

If kept in contact with the solution, it decomposes in a few hours to a dark pitch.

Physicochemical measurements

IR and electronic spectra were recorded, and TGA measurements performed, as previously described.[5] Emission and excitation spectra were obtained with an Aminco-Baumen MPF spectrophotofluorimeter. Proton–ligand and metal–ligand stability constants were determined using the Calvin–Wilson pH-titration technique,[6] in 1:1 ethanol–water. An E366 Metrohm pH-meter, equipped with a Metrohm glass electrode, was used for pH measurements; the concentrations of the various species were in the range 1×10^{-4}–4×10^{-4} M, temperature 28.0 ± 0.1°C, and $I = 0.1$ M $NaClO_4$. The accuracy in the stability constants determination was not very high, because of the precipitation of the complexes, after addition of a small volume of NaOH 0.05 M. The elemental and thermogravimetric analysis and the stability constants are reported in Table 1.

RESULTS AND DISCUSSION

Some complexes of 4-methylesculetin have already been described; in all cases it was found that the metal cation is bonded by H_2mes in its dianionic form.[7] On the contrary, in the complexes synthesized by us the ligand behaves as a monoanion (Hmes). It is known that the OH group in the 7-position is significantly more acidic than the OH group in the 6-position;[3] thus it seems probable that in our complexes the 7-hydroxy group is deprotonated. The proton of the 6-hydroxy group might be stabilized through hydrogen bonding to one or more of the several oxygen atoms available in the complexes.

The water content of the complexes has been verified by TGA, as reported in Table 1; in each compound all the water molecules are lost in a one-step process at relatively low temperature, indicating that they are not coordinatively bonded to the metal. This fact, together with the well known requirement of the lanthanide cations to reach a high coordination number, might indicate a polymeric structure, with a ligand behaving as a bridge. This hypothesis is supported by the insolubility of the complexes in most common solvents (including DMSO). A polymeric structure has often been observed in lanthanide complexes.[8] Attempts to synthesize complexes with a ligand–metal ratio higher than 1:1 have been unsuccessful, even when operating with a large excess of H_2mes.

The electronic spectra of all the complexes in the solid state are very similar, and quite different from that of H_2mes (Fig. 1). In DMSO they are somewhat different from those in the solid state, indicating partial decomposition of the complexes in solution; therefore it seems more appropriate to compare the spectra in the solid state. The two bands at higher energy are shifted from 198 and 236 nm in the ligand, to 220 and 244 nm in the complexes. The main band at lower energy undergoes a larger shift passing from 340 nm in H_2mes

Table 1. Elemental and thermogravimetric analytical data, and stability constants

Compound	% C Found Calc.	% H Found Calc.	% Ln Found Calc.	TGA[a] Found Calc. (for $3H_2O$)	$\log(\beta_1)^b$
$La(Hmes)Cl_2 \cdot 3H_2O$	26.4	3.0	30.4	12.04	4.19 ± 0.04
	26.4	2.9	30.5	11.88	
$Sm(Hmes)Cl_2 \cdot 3H_2O$	25.4	2.9	32.0	11.50	4.92 ± 0.07
	25.7	2.8	32.2	11.59	
$Eu(Hmes)Cl_2 \cdot 3H_2O$	25.6	2.9	32.3	11.77	4.99 ± 0.07
	25.7	2.8	32.5	11.55	
$Gd(Hmes)Cl_2 \cdot 3H_2O$	25.4	2.8	33.3	11.50	4.64 ± 0.06
	25.4	2.8	33.2	11.42	
$Tb(Hmes)Cl_2 \cdot 3H_2O$	25.3	2.7	33.6	11.30	4.99 ± 0.06
	25.3	2.8	33.5	11.38	
$Dy(Hmes)Cl_2 \cdot 3H_2O$	25.2	2.7	33.8	10.66	5.04 ± 0.05
	25.1	2.7	33.9	10.76	

[a] Percent weight loss in the range 54–105°C.

[b] Referred to the reaction: $LnCl_3 + H_2mes = Ln(Hmes)Cl_2 + Cl^- + H^+$.

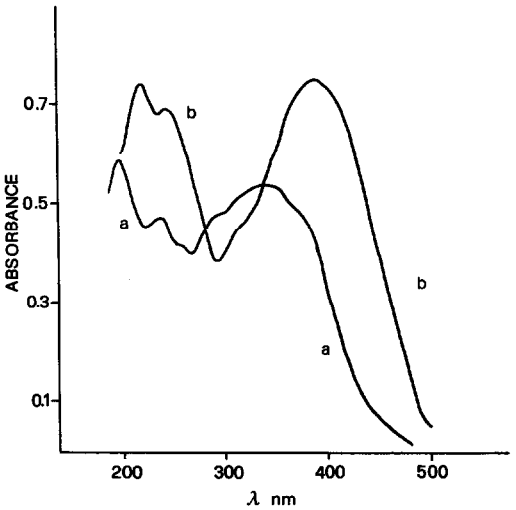

Fig. 1. Solid state absorption spectra of (a) 4-methylesculetin, and (b) $Eu(Hmes)Cl_2 \cdot 3H_2O$.

to 390 nm in the complexes; also its pattern changes noticeably. The decrease in the electronic energy transitions of the complexes with respect to the free ligand could result from an increase of the mesomeric effect (see Scheme 1) after deprotonation and complexation of H_2mes.

This hypothesis is supported by IR spectral data. The H_2mes vibrational spectrum is characterized, in addition to a large ν(OH) band at 3350 cm^{-1}, by a strong signal at 1660 cm^{-1} due to the pyrone ν(C=O) and by two other bands at 1610 and 1560 cm^{-1} assigned to ν(C=C). In the complexes of 4-methylesculetin which have already been described in the literature, the ν(C=O) bond remains unaltered, but the ν(C=C) bonds are very slightly shifted to lower energy (less than 10 cm^{-1}).[7] In the lanthanide complexes described in this work, the pyrone ν(C=O) is located at 1645 cm^{-1} and the ν(C=C) bonds are found at 1575 and 1525 cm^{-1}. These shifts to lower energy with respect to the free H_2mes could indicate that in the complexes the importance of form **II** of the free ligand (see Scheme 1) is increased. However, the IR data might also be indicative of the formation of a coordinative bond between the lanthanide cations and the coumarine carbonyl oxygen atom. Packing effects may also be present.

The formation constants of all the described complexes have been determined, and are reported in Table 1. In order to calculate them, the pK_a of H_2mes was previously determined, and a value of 8.12 ± 0.3 was found. The slight difference from the value (7.90) reported by other authors may be due to different experimental conditions.*[9] The variation of metal–ligand stability constants with increasing atomic number of the cation follows an expected trend.[10] In fact at the Gd level there appears a break, which has often been noted and theoretically studied.[11]

As far as the luminescence is concerned, we recorded the emission spectra of the complexes of 4-methylesculetin with Sm^{III}, Eu^{III}, Tb^{III} and Dy^{III} which are known to be lanthanide cations which can luminesce in the visible region.[12] However, when exciting in the range 300–430 nm, no lanthanide ion luminescence was observed, either in DMSO or in water–methanol (pH 5.5). The ligand fluorescence is reduced to about 70% with respect to the free H_2mes fluorescence. The fact that the metal ions do not luminesce could result from different reasons. For example, we could suppose a very efficient quenching via multiphonon-like processes due to the OH stretching vibrations of water molecules or of the non-deprotonated OH group of the ligand. However, in our opinion, it is more reasonable to suppose that 4-methylesculetin is not effective in transferring energy to luminescent lanthanide cations. In fact, if the metal ion luminescence was quenched by OH stretching vibrations, we should have observed some difference on passing from DMSO to water–methanol as solvent; moreover, some differences had to arise by changing the energy gap between the lowest emitting level and the highest accepting level of the metal; the gaps are 7500, 7800, 12,300 and 14,700 cm^{-1} for Sm^{III}, Dy^{III}, Eu^{III} and Tb^{III}, respectively.[13] Moreover, the brown–orange colour of all the complexes indicates that the first singlet excited state of the ligands is quite low in energy; as a consequence, the first triplet excited state of the ligands, generally involved in the ligand to lanthanide energy transfer,[12] is probably at too low energy to allow an effective energy transfer.

* The experimental conditions are not exhaustively described in ref. 9.

REFERENCES

1. J.-C. Bünzli, *Inorg. Chim. Acta* 1987, **139**, 219; W. deW. Horrocks and A. Albin, *Prog. Inorg. Chem.* 1984, **31**, 1; F. S. Richardson, *Chem. Rev.* 1982, **82**, 541.
2. C. Bisi Castellani, O. Carugo, C. Tomba and A. Gamba Invernizzi, *Inorg. Chem.* 1988, **27**, 3965; C. Bisi Castellani and O. Carugo, *Inorg. Chim. Acta.* 1989, **159**, 157.
3. M. Katyal and H. B. Singh, *Talanta* 1968, **15**, 1043.

4. C. Bisi Castellani, *J. Inorg. Nucl. Chem.* 1970, **32**, 2899.
5. C. Bisi Castellani, O. Carugo, C. Tomba, V. Berbenni and S. Cinquetti, *Inorg. Chim. Acta* 1988, **145**, 157.
6. F. J. C. Rossotti and H. Rossotti, *The Determination of the Stability Constants*. McGraw–Hill, New York (1961).
7. D. Singh and H. B. Singh, *Z. Naturfor.* 1977, **32b**, 438.
8. C. Bisi Castellani and V. Tazzoli, *Acta Cryst.* 1984, **C40**, 1834; C, Bisi Castellani and A. Coda, *Acta Cryst.* 1985, **C41**, 186.
9. B. D. Jain and H. B. Singh, *Ind. J. Chem.* 1963, **1**, 369.
10. L. C. Thompson, in *Handbook of the Physics and Chemistry of Rare Earths* (Edited by K. A. Gschneider and L. Eyring), Vol. 3, p. 45. North–Holland, Amsterdam (1979).
11. V. G. Vokhmin and G. V. Ionova, *Russ. J. Inorg. Chem.* 1987, **32**, 1552; B. F. Dzhurinskii, *Russ. J. Inorg. Chem.* 1980, **25**, 41.
12. A. P. B. Sinha, in *Spectroscopy in Inorganic Chemistry* (Edited by C. N. R. Rao and J. R. Ferraro), p. 255. Academic Press, New York (1971).
13. W. T. Carnall, in *Handbook on the Physics and Chemistry of Rare Earths* (Edited by K. A. Gschneider and L. Eyring), Vol. 3, p. 171. North–Holland, Amsterdam (1979).

Polyhedron Vol. 9, No. 7, pp. 943–948, 1990
Printed in Great Britain

0277–5387/90 $3.00+.00
© 1990 Pergamon Press plc

SYNTHESIS, CHARACTERIZATION AND STRUCTURAL ASPECTS OF DIORGANOTELLURIUM(IV) COMPOUNDS CONTAINING (Te—S) BONDS

T. N. SRIVASTAVA and JAI DEO SINGH

Department of Chemistry, University of Lucknow, Lucknow 226007, India

and

SANJAY KUMAR SRIVASTAVA*

School of Studies in Chemistry, Jiwaji University, Gwalior 474011, India

(*Received* 25 *April* 1989; *accepted* 2 *November* 1989)

Abstract—Diorganotellurium(IV) compounds containing (Te—S) bonds of the general formulae $[R_2Te(S_2POGO)_2]$ [R = Ph or *p*-$MeOC_6H_4$; G = —CH(Me)CH(Me)—, —Me_2C—CMe_2—, —$CH_2C(Me_2)CH_2$—, (Me)$CHCH_2C(Me_2)$—, $CH_2C(Et_2)CH_2$—] have been prepared by the reaction of $R_2Te(OR')_2$ (R′ = Me or Et) and corresponding O,O′-alkylene dithiophosphoric acids or by the reaction of R_2TeCl_2 with $[NH_4S_2POGO]$ in anhydrous toluene. The products have been characterized using analytical and spectroscopic (IR, ^1H, ^{13}C, ^{31}P and ^{125}Te NMR) data. The products are monomeric in nature and their possible structures are discussed.

Although several dithiocarbamates containing the (Te—S) bond are well known,[1–4] the analogous dithiophosphate complexes are scarce.[5,6] This may be due to the instability of the products due to their reduction from Te^{IV} to Te^{II} and the formation of the corresponding disulphides. Recently from this laboratory[7–9] and also by other workers,[10,11] it has been reported that diorganotellurium(IV) bis(O,O′-dialkyl dithiophosphates) $[R_2Te\{S_2P(OR')_2\}_2]$ decompose in low boiling solvents into R_2Te^{II} and the disulphides $[(R'O)_2P(S)SS(S)P(OR')_2]$. In view of the increasing interest in (Te—S) bonded compounds,[11,12] we report the synthesis and characterization of $[R_2Te(S_2POGO)_2]$ compounds where the alcoholic (OR′) unit of $[R_2Te\{S_2P(OR')_2\}_2]$ is replaced by the glycolic unit. The stability of $[R_2Te(S_2POGO)_2]$ in comparison to that of $[R_2Te\{S_2P(OR')_2\}_2]$ derivatives is examined.

RESULTS AND DISCUSSION

The diorganotellurium(IV) bis(O,O′-alkylene dithiophosphates) were synthesized by the reaction of diorganotellurium(IV) alkoxides in anhydrous toluene by refluxing and removing the alcohol azeotropically or by stirring a mixture of diorganotellurium(IV) dihalide and the ammonium salt of the O,O′-dialkylene dithiophosphoric acids in 1:2 molar ratio in toluene. Alternatively they may be prepared by the reaction of R_2TeO and corresponding O,O′-alkylene dithiophosphoric acid in

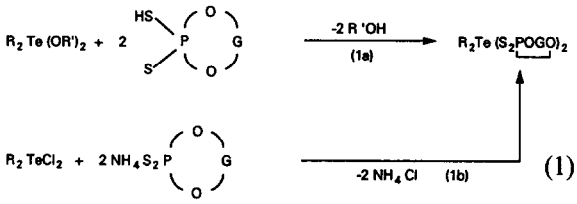

(1)

[R = C_6H_5 or *p*-$MeOC_6H_4$—;
G = —(CH_3)CHCH(CH_3)—,
—$(CH_3)_2$C—C$(CH_3)_2$—,
—$(CH_3)_2CCH_2CHCH_3$—,
—$CH_2C(C_2H_5)_2CH_2$—,
$CH_2C(CH_3)_2CH_2$—].

2,2′-dimethoxypropane. The yield of the products in the latter case is less than that by the former [eq. (1)]. Similar reactions in benzene gave products

* Author to whom correspondence should be addressed.

which were different than those expected and are characterized as $[R_2Te(S_2POGO)]_2O$ or $[\{R_2Te(S_2POGO)\}_2]\cdot H_2O$. All the reactions [eq. (1)] are facile and are completed by stirring the reactant in toluene (30 min) or by refluxing the reactants in toluene (1 h). The products were obtained in greater than 80% yield in each case. The compounds are yellow, crystalline, sharp melting solids, soluble in all common organic solvents such as MeOH, EtOH, Pr^iOH, C_6H_6, CCl_4, $CHCl_3$, CH_2Cl_2, Me_2SO, Me_2CO, MeCN, etc. They are stable towards atmospheric oxygen and moisture. However, they decompose slowly in low boiling organic solvents according to [eq. (2)]:

$$[R_2Te(S_2POGO)_2] \longrightarrow R_2Te + [OGOP(S)S{-}S(S)POGO] \quad (2)$$

They are completely decomposed by keeping them in solution for 24 h or by refluxing them in low boiling solvents such as CH_2Cl_2, CCl_4, $CHCl_3$, etc. for 10–12 h. The decomposition of the products $[R_2Te(S_2POGO)_2]$ is slower than $[R_2Te\{S_2P(OR')_2\}_2]$ in low boiling solvents. This may be due to the presence of the cyclic ring in the former and an open chain alkoxy group in the latter. The cyclic ring makes the molecules stable.

IR spectra

IR spectra of these new compounds have been examined in KBr as discs and in CS_2 solution in the region 4000–400 cm^{-1}, and tentative assignments have been made on the basis of earlier reports.[13,14] The bands present in the regions 1090–970 and 890–760 cm^{-1} are assigned to ν(P)—O—C and νP—O—(C). A strong to medium band in the region 950–910 cm^{-1} is due to rings. A strong band present in the region 685–620 cm^{-1} in O,O-alkylene dithiophosphoric acids assigned to ν(P=S) does not undergo shifts in the compounds reported in the present study. The bands of medium intensity in the region 510–470 cm^{-1} may be attributed to ν(P—S) vibrations. The IR spectra of the products in KBr discs and in CS_2 solution are almost similar and do not yield any significant information about the nature of coordination of the diothiophosphate ligand.

^{1}H NMR spectra

The ^{1}H NMR spectra of the compounds have been recorded in $CDCl_3$ and the data are given in Table 2. The ^{1}H NMR spectra show the characteristic proton resonances of the corresponding

Table 1. Analytical data for $[R_2Te(S_2POGO)_2]$ derivatives

	Compound	Melting point (°C)	Elemental analysis; Found(%) (Calc.) Te	C	H	S
1	$[Ph_2Te\{S_2PO(Me)CHCH(Me)O\}_2]$	117	19.4 (19.7)	36.9 (37.0)	3.8 (4.0)	19.5 (19.7)
2	$[Ph_2Te\{S_2PO(Me_2)CC(Me_2)O\}_2]$	139	18.0 (18.1)	40.5 (40.9)	4.6 (4.8)	18.0 (18.2)
3	$[Ph_2Te\{S_2PO(Me_2)CCH_2CH(Me)O\}_2]$	126	18.0 (18.1)	40.7 (40.9)	4.6 (4.8)	18.0 (18.2)
4	$[Ph_2Te\{S_2POCH_2C(Et_2)CH_2O\}_2]$	155	17.4 (17.4)	42.3 (42.6)	5.1 (5.2)	17.3 (17.5)
5	$[Ph_2Te\{S_2POCH_2C(Me_2)CH_2O\}_2]$	108	18.7 (18.9)	38.9 (39.1)	4.5 (4.4)	18.6 (18.9)
6	$[(p\text{-}MeOC_6H_4)_2Te\{S_2PO(Me)CHCH(Me)O\}_2]$	Viscous	17.8 (18.0)	37.1 (37.3)	4.1 (4.2)	17.8 (18.1)
7	$[(p\text{-}MeOC_6H_4)_2Te\{S_2PO(Me_2)CC(Me_2)O\}_2]$	149	16.6 (16.7)	40.4 (40.8)	4.6 (5.0)	16.6 (16.8)
8	$[(p\text{-}MeOC_6H_4)_2Te\{S_2PO(Me_2)CCH_2CH(Me)O\}_2]$	153	16.4 (16.7)	40.7 (40.8)	4.8 (5.0)	16.7 (16.8)
9	$[(p\text{-}MeOC_6H_4)_2Te\{S_2POCH_2C(Et_2)CH_2O\}_2]$	160d	16.0 (16.1)	42.3 (42.4)	5.1 (5.3)	16.1 (16.2)
10	$[(p\text{-}MeOC_6H_4)_2Te\{S_2POCH_2C(Me_2)CH_2O\}_2]$	137	17.1 (17.3)	39.1 (39.1)	4.5 (4.6)	17.2 (17.4)

alkylene as well as aryl groups. A sharp singlet at δ 3.15–3.7 due to the S—*H* protons of free acids is absent in the spectra of the compounds indicating elimination of "H" of the acid derivatives on compound formation.

^{13}C *NMR spectra*

^{13}C NMR spectra of the representative complexes were recorded and the data are summarized in Table 3. The ^{13}C resonances of the compounds show that the two O,O-alkylene dithiophosphate ligands are equivalent.

^{31}P *NMR spectra*

The ^{31}P chemical shift values depend on the size of the glycol ring. In the case of five-membered rings $[S_2POGO]^-$ [G = —$C(Me_2)C(Me_2)$—, —CH(Me)CH(Me)—] the ^{31}P signals are not very different from those in the free ligands, indicating monodentate coordination of the O,O-alkylene dithiophosphate ligand. In the case of the six-membered glycol rings, G = —$CH(Me)CH_2C(Me_2)$—, —$CH_2C(Me_2)CH_2$—, —$CH_2C(Et_2)CH_2$—, a shift of ~ 10–15 ppm in the ^{31}P signals is observed in comparison to that in the free acids. The downfield chemical shift indicates a chelated structure with bidentate alkylene dithiophosphate groups.[15]

^{125}Te *NMR spectra*

^{125}Te NMR spectra of a few representative compounds have been recorded in C_6H_6 and $CHCl_3$ and are listed in Table 3. Only a single peak was observed. However, at high scans instead of the product signal (^{125}Te chemical shift) another peak was observed at 724.8 ppm in the case of $[(p\text{-}MeOC_6H_4)_2Te(S_2POGO)_2]$ and at 689 ppm in the case of $[Ph_2Te(S_2POGO)_2]$, corresponding to R_2Te (R = p-$MeOC_6H_4$— and Ph) indicating a slow decomposition of the products[16] in solution [$Te^{IV} \rightarrow Te^{II}$].

Structure and bonding

The ^{31}P NMR spectra of the products show that there are two modes of bonding in $[R_2Te(S_2POGO)_2]$ derivatives. Where the glycol unit is five-membered, monodentate bonding of alkylene dithiophosphate ligand is observed, while in the case of six-membered glycol units a bidentate nature of the ligand is indicated.

The change in the bonding may be explained as due to the electron-releasing effect of the alkyl groups in the six-membered ring is more than that in the five-membered ring. Further, the soft nature of the Te^{4+} species and also that of the ligand enables a soft–soft interaction of the metal and ligand atom, the bidentate nature of the ligand more plausible. The unusual behaviour of the two types of ligand (five- and six-membered glycol unit) also seems to be due to stereochemical activity[17] of the lone pair present in the tellurium(IV) species (as observed in many Te—S compounds where the tellurium(IV) lone pair is stereochemically active) or it may be due secondary interactions[18,19] between tellurium and the non-bonded sulphur atom of the ligand.

Thus for $[R_2Te(S_2POGO)_2]$ two possible structures may be suggested for five- and six-membered glycol units of the alkylene dithiophosphate ligands and these are consistent with the reported X-ray crystal structure of R_2TeX_2 derivatives.[12,19]

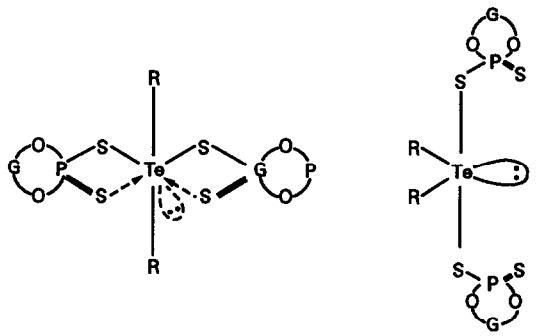

(R = Ph or p-$MeOC_6H_4$)

G = —$CH_2C(Me_2)CH_2$—,
—$CH(Me)CH_2C(Me_2)$—,
—$CH_2C(Et_2)CH_2$—
G = —CH(Me)CH(Me)—,
—$C(Me_2)C(Me_2)$—

Scheme 1.

EXPERIMENTAL

All manipulations were carried out under a dry nitrogen atmosphere. $TeCl_4$ (BDH) was used as such, and Ph_2TeCl_2 (ref. 20) and $(p\text{-}MeOC_6H_4)_2TeCl_2$ (ref. 21) were prepared according to the established procedures. Solvents were purified and dried by standard procedures. Alkylene dithiophosphoric acids, HS_2POGO, and their ammonium salts were prepared by reported methods[22,23] by passing dry ammonia through a benzene solution of the acids. $R_2Te(OR')_2$ (R = Me or Et) were prepared *in situ* by reaction of R_2TeCl_2 with the corresponding sodium or potassium alkoxides in benzene. ^1H, ^{13}C, ^{31}P and ^{125}Te NMR spectra were recorded on a Jeol Fx 90 Q FT NMR spectrometer and other physicochemical studies were made as

Table 2. ^{1}H NMR spectral data for $[R_2Te(S_2POGO)_2]$

Compound	Aryl protons	Alkyl protons
$[Ph_2Te\{S_2PO(Me)CHCH(Me)O\}_2]$	7.87–7.35, m, 10H(C_6H_5—Te)	4.22, m, 4H(OC*H*), 1.67–1.18, d, 12H, d(—CH_3)
$[Ph_2Te\{S_2PO(Me_2)CC(Me_2)O\}_2]$	7.83–7.30, m, 10H(C_6H_5—Te)	1.45, s, 24H(CH_3)
$[Ph_2Te\{S_2PO(Me_2)CCH_2CH(Me)O\}_2]$	7.86–7.30, m, 10H(C_6H_5—Te)	5.10–4.66, m, 2H(OC*H*), 1.89–0.83, m, 22H(CH_2, CH_3)
$[Ph_2Te\{S_2POCH_2C(Et_2)CH_2O\}_2]$	7.83–7.17, m, 10H(C_6H_5—Te)	4.26–3.74, d, 8H(OCH_2), 1.67–1.05, q, 8H(CH_2, CH_3), 1.01–0.57, t, 12H(CH_3)
$[Ph_2Te\{S_2POCH_2C(Me_2)CH_2O\}_2]$	8.05–7.34, m, 10H(C_6H_5—Te)	4.22–3.87, d, 8H(OCH_2), 1.05, s, 12H(CH_3)
$[(p\text{-}MeOC_6H_4)_2Te\{S_2PO(Me)CHCH(Me)O\}_2]$	7.96–7.39, d, 4H(*ortho* protons) (J_{H-H} = 9.0 Hz); 7.04–6.51, d, 4H(*meta* protons) (J_{H-H} = 9 Hz); 3.78, s, 6H(OCH_3)	4.84–4.00, d, 4H(OC*H*), 1.62–1.23, d, 12H(CH_3)
$[(p\text{-}MeOC_6H_4)_2Te\{S_2POCH_2C(Me_2)CH_2O\}_2]$	8.00–7.43, d, 4H(*ortho* protons) (J_{H-H} = 9.0 Hz); 7.08–6.55, d, 4H(*meta* protons) (J_{H-H} = 9.0 Hz), 3.82, s, 6H(OCH_3)	4.00–3.9, d, 8H(OCH_3), 0.99, s, 12H(CH_3)
$[(p\text{-}MeOC_6H_4)_2Te\{S_2POC(Me_2)C(Me_2)O\}_2]$	8.00–7.6, d, 4H(*ortho* protons) (J_{H-H} = 9.0 Hz); 7.08–6.8, d, 4H(*meta* protons) (J_{H-H} = 9.0 Hz); 3.80, s, 6H(OCH_3)	0.96, s, 24H(CH_3)
$[(p\text{-}MeOC_6H_4)_2Te\{S_2POC(Me_2)CH_2CH(Me)O\}_2]$	8.05–7.6, d, 4H(*ortho* protons) (J_{H-H} = 9.0 Hz); 7.08–6.8, d, 4H(*meta* protons) (J_{H-H} = 9.0 Hz) 3.78, s, 6H(OCH_3)	5.14–4.44, m, 2H(OC*H*), 2.1–1.14, m, 22H(CH_2, CH_3)
$[(p\text{-}MeOC_6H_4)_2Te\{S_2POCH_2C(Et_2)CH_2O\}_2]$	8.03–7.68, d, 4H(*ortho* protons) (J_{H-H} = 9.0 Hz); 7.1–6.67, d, 4H(*meta* protons) (J_{H-H} = 9.0 Hz); 3.82, s, 6H(OCH_3)	4.25–3.74, d, 8H(OCH_2), 1.67–1.1, q, 8H(CH_2, CH_3), 1.1–0.51, t, 12H(CH_3)

Table 3. ^{13}C, ^{31}P and ^{125}Te NMR spectral data for $[R_2Te(S_2POGO)_2]$

Compounds	Chemical shift (δ) ppm		
	^{13}C NMR	^{31}P NMR	^{125}Te NMR
$[(p\text{-}MeOC_6H_4)_2Te\{S_2POC(Me_2)C(Me_2)O\}_2]$	122.7(C_1), 138.98(C_2), 115.60(C_3), 160.80(C_4); 55.4(C_5), aryl carbons; 24.90, 24.26 C(CH_3)$_2$; 91.10, 90.70, CMe_2	93.17($CHCl_3$) [92.98($CHCl_3$)][a]	—
$[(p\text{-}MeOC_6H_4)_2Te\{S_2POCH_2C(Me_2)CH_2O\}_2]$	129.48(C_1), 138.15(C_2), 116.81(C_3), 163.02(C_4), 54.34(C_5), aryl carbons; 77.80, 77.42(OCH_2); 22.44(CH_3), 33.65, 33.33 [$C(CH_3)_2$]	92.21(C_6H_6) 91.51(CH_2Cl_2) 112.51(DMSO) [(78.77)$CHCl_3$][a]	884.68(C_6H_6)
$[(p\text{-}MeOC_6H_4)_2Te\{S_2POCMe_2CH_2CHMeO\}_2]$	125.4(C_1), 139.5(C_2), 115.2(C_3), 161.47(C_4), 54.9(C_5), aryl carbons; 86.67, 81.19(C—Me_2); 71.29, 70.96(CH_2), 76.95, 75.11(CH), 21.37, 20.99, 31.07, 30.75, 43.38, 43.05 [C(CH_3)$_2$ and CH_3CH]	88.53($CHCl_3$) 87.48(C_6H_6) [(78.98)(C_6H_6)][a]	886.7(C_6H_6) 877.86(CH_3CN)
$[(p\text{-}MeOC_6H_4)_2Te\{S_2POCHMeCHMeO\}_2]$	121.67(C_1), 139.44(C_2), 115.60(C_3), 161.49(C_4), 55.3(C_5), aryl carbons; 82.67, 81.26, (OCH); 17.55, 17.17(OCHCH_3)	95.53($CHCl_3$) [(95.41)$CHCl_3$][a]	900.70($CHCl_3$)
$[(p\text{-}MeOC_6H_4)_2Te\{S_2POCH_2C(Et_2)CH_2O\}_2]$	—	97.13(C_6H_6) [(77.73)C_6H_6][a]	—
$[Ph_2Te\{S_2POC(Me_2)C(Me_2)O\}_2]$	134.91(C_2), 132.04(C_1), 130.74(C_4), 127.38(C_3); aryl carbons, 24.46, 24.24 (CMe_2), 90.06, 89.17C(Me_2)	93.06($CHCl_3$) 122.05(DMSO)	—
$[Ph_2Te\{S_2POCH_2C(Et_2)CH_2O\}_2]$	—	97.63(C_6H_6)	867.70(C_6H_6)
$[Ph_2Te\{S_2POCH_2C(Me_2)CH_2O\}_2]$	—	92.16(C_6H_6)	881.55(C_6H_6)
$[Ph_2Te\{S_2POCH(Me)CH(Me)O\}_2]$	—	94.48(C_6H_6)	889.66(C_6H_6)
$[Ph_2Te\{S_2POC(Me_2)CH_2CHMe_2O\}_2]$	134.91(C_2), 132.09(C_1), 130.79(C_4), 126.78(C_3), aryl carbons, 86.50, 84.76(C—Me_2); 71.60, 71.10(CH_2), 76.80, 75.60(CH); 21.16, 20.98, 31.17, 30.88, 43.55, 43.17, [C(CH_3)$_2$ and CH_3CH]	89.16($CHCl_3$)	883.19($CHCl_3$)

[a] ^{31}P NMR signals for the free ligands.

described earlier.[7] Some representative reactions are described for the preparation of $[R_2Te(S_2POGO)_2]$.

(a) *Reaction of* $(p\text{-}MeOC_6H_4)_2TeCl_2$ *and* $[NH_4S_2POC(Me_2)C(Me_2)O]$

To a stirring suspension of $[NH_4S_2POC(Me_2)C(Me_2)O]$ (4.58 g, 20 mmol) in toluene (25 cm^3) was added a solution of $(p\text{-}MeOC_6H_4)_2TeCl_2$ (4.12 g, 10 mmol) in toluene (50 cm^3). The reaction mixture was stirred for 1 h. Filtration followed by the distillation of the solvent gave the yellow product which was recrystallized from toluene–*n*-pentane (1 : 5 ratio).

(b) *Reaction of* $R_2Te(OR')_2$ *and* $[HS_2POGO]$

In a representative reaction, a mixture of $Ph_2Te(OC_2H_5)_2$ was prepared by the reaction of sodium (0.46 g, 20 mmol) and Ph_2TeCl_2 (3.52 g, 10 mmol) in ethanol. The solution was filtered to remove NaCl, and to the concentrated viscous mass in toluene (20 cm^3) was added $[HS_2POCH_2C(Me_2)CH_2O]$ (3.96 g, 20 mmol) in toluene (10 cm^3). The reaction mixture was refluxed for 1 h and ethanol was removed azeotropically. The solvent was removed under reduced pressure and dried *in vacuo* giving a yellow viscous mass which was recrystallized from a toluene–pentane (1 : 9 ratio) mixture.

(c) *Reaction of* Ph_2TeO *and* $[HS_2POGO]$

Ph_2TeO (2.97 g, 10 mmol) and $[HS_2POCH_2C(Me_2)CH_2O]$ (3.96 g, 20 mmol) were refluxed together in anhydrous benzene (60 cm^3). The water was removed azeotropically. The yellow product thus obtained was identified as $Ph_2Te(S_2POCH_2C(Me_2)CH_2O)_2O$ after several washings with C_6H_6–pet-ether mixture:

$$2Ph_2TeO + 4[HS_2POCH_2C(Me_2)CH_2O] \longrightarrow [Ph_2Te(S_2POCH_2C(Me_2)CH_2O)]_2O + H_2O + 2[HS_2POCH_2C(Me_2)CH_2O].$$

^{31}P NMR signals at δ 91.98 (C_6H_6). Found (%) (Calc.): C, 48.1 (48.2); H, 4.6 (4.7); S, 14.9 (15.1); Te, 14.9 (15.1%). The products are slightly soluble in common organic solvents. When a similar reaction was carried out in methanol and the solution was filtered and allowed to evaporate slowly, yellow crystals of $[\{Ph_2Te(S_2POCH_2CMe_2CH_2O)\}_2O]_2 H_2O$ were produced. ^{31}P NMR signals at δ 91.87 (C_6H_6). Found (%) (Calc.): C, 41.4 (41.5); H, 4.0 (4.2); S, 13.0 (13.0); Te, 25.6 (26.0%); ^1H NMR spectra ($CDCl_3$): δ 7.96–7.22, *m*, 4OH (C_6H_5—Te); 4.20–3.85, *d*, 16H (OCH_2); 1.02, *s*, 24H (CH_3); H_2O, δ 3.35 (br).

Acknowledgements—Financial support from the CSIR and UGC, New Delhi, for the present work is gratefully acknowledged.

REFERENCES

1. W. R. McWhinnie and J. E. Stuckey, *The Use of Selenium and Tellurium in Rubber Technology*. Selenium & Tellurium Development Corp. Inc. (1983).
2. M. A. K. Ahmed, W. R. McWhinnie and P. Granger, *Polyhedron* 1986, **5**, 859.
3. S. Husebye, in *Proceedings of the Fourth International Conference on the Organic Chemistry of Selenium and Tellurium* (Edited by F. J. Berry and W. R. McWhinnie), pp. 298–369. University of Aston in Birmingham (1983).
4. N. Zumbulyadis and H. J. Glysling, *Inorg. Chem.* 1982, **21**, 564.
5. S. Husebye, *Acta Chem. Scand.* 1965, **19**, 1045.
6. L. S. Refaat, M. K. Maartmann and S. Husebye, *Acta Chem. Scand.* 1984, **38A**, 147.
7. T. N. Srivastava, Jai Deo Singh and Sanjay Kumar Srivastava, *Phosphorus Sulfur* 1989, submitted for publication.
8. T. N. Srivastava, J. D. Singh and S. K. Srivastava, *Synth. React. Inorg. Met. Org. Chem.* 1989, in press.
9. Jai Deo Singh, PhD thesis, Lucknow University, India (1985).
10. D. Dakternieks, R. D. Giacomo, R. W. Gable and B. F. Hoskins, *J. Organomet. Chem.* 1988, **349**, 305.
11. D. Dakternieks, R. D. Giacomo, R. W. Gable and B. F. Hoskins, *J. Am. Chem. Soc.* 1988, **110**, 6541, 6753 and 6762.
12. R. K. Chadha, J. E. Drakes, N. T. McManus, B. A. Quinlan and A. B. Sarkar, *Organometallics* 1987, **6**, 813.
13. R. J. Rao, G. Srivastava, R. C. Mehrotra, B. S. Saraswat and J. Mason, *Polyhedron* 1984, **3**, 485.
14. C. P. Bhasin, G. Srivastava and R. C. Mehrotra, *Inorg. Chim. Acta* 1983, **77**, L131.
15. C. Glidewell, *Inorg. Chim. Acta* 1977, **25**, 159.
16. C. Rodger, N. Sheppard, C. Mcfarlane and W. Mcfarlane, in *NMR and Periodic Table* (Edited by R. V. Harris and B. F. Mann), p. 383. Academic Press, London (1978).
17. S. Esperas, J. W. George, S. Husebye and O. Mikalsen, *Acta Chim. Scand.* 1975, **29A**, 141.
18. N. W. Alcock, *Adv. Inorg. Chem. Radiochem.* 1972, **15**, 1.
19. N. W. Alcock and W. D. Harrison, *J. Chem. Soc., Dalton Trans.* 1984, 869.
20. R. C. Paul, K. K. Bhasin and R. K. Chadha, *J. Inorg. Nucl. Chem.* 1975, **37**, 2337.
21. J. Bergman, *Tetrahedron* 1972, **37**, 3323.
22. G. M. Kosolapoff and L. Maier, *Organic Phosphorus Compounds*, Vol. 7, p. 519. John Wiley, New York (1976).
23. H. P. S. Chauhan, C. P. Bhasin, G. Srivastava and R. C. Mehrotra, *Phosphorus Sulfur* 1983, **15**, 99.

Polyhedron Vol. 9, No. 7, pp. 949–955, 1990
Printed in Great Britain

0277–5387/90 $3.00+.00
© 1990 Pergamon Press plc

SYNTHESIS OF $R_2R'_2C_4B_8H_8$ TETRACARBON CARBORANES FROM (η^6-CYCLOOCTATRIENE)IRON(DICARBAHEXABORANE) COMPLEXES VIA MIXED-LIGAND THERMAL FUSION*

KATHLEEN K. FONDA and RUSSELL N. GRIMES†

Department of Chemistry, University of Virginia, Charlottesville, VA 22901, U.S.A.

(*Received* 1 *September* 1989; *accepted* 6 *November* 1989)

Abstract—Reactions of $(R_2C_2B_4H_4)Fe(\eta^6\text{-}C_8H_{10})$ complexes with $Na^+R'_2C_2B_4H_5^-$ salts ($R = C_2H_5$, $n\text{-}C_4H_9$, $CH_2C_6H_5$; $R' = CH_3$, C_2H_5, $n\text{-}C_4H_9$, $CH_2C_6H_5$) at 150°C in the absence of solvent gave products of the general formula $R_2R'_2C_4B_8H_8$, accompanied in each case by $R_4C_4B_8H_8$ carboranes. ^{11}B, ^1H, and ^{13}C NMR studies of the $R_2R'_2C_4B_8H_8$ clusters indicated that each consists of two isomers consistent with the "open" and "closed" geometries identified in earlier work on $R_4C_4B_8H_8$ clusters, and that the isomer ratios do not change over time in solution at room temperature.

Tetracarbon carboranes of the $R_4C_4B_8H_8$ class were first prepared serendipitously[1] by the low-temperature oxidative fusion of $R_2C_2B_4H_4^{2-}$ ligands in $(R_2C_2B_4H_4)_2MH_x$ complexes ($MH_x = Fe^{II}H_2$ or $Co^{III}H$). Since the original discovery, the ligand fusion reaction has been extensively investigated, as have the chemistry and the unusual cage-fluxionality of the $R_4C_4B_8H_8$ products.[2] The original assumption that the fusion in $(R_2C_2B_4H_4)_2MH_x$ complexes occurred intramolecularly was subsequently demonstrated;[3] for example, oxidation of solutions containing both $(Me_2C_2B_4H_4)_2FeH_2$ and $(Et_2C_2B_4H_4)_2FeH_2$ gave only the homosubstituted species $Me_4C_4B_8H_8$ and $Et_4C_4B_8H_8$, respectively.

Mixed-substituent derivatives of the type $R_2R'_2C_4B_8H_8$ are formed in the simultaneous reaction of $R_2C_2B_4H_5^-$ and $R'_2C_2B_4H_5^-$ ions with $FeCl_2$ followed by air-oxidation.[3] However, such reactions are complicated by the competitive formation of the $R_4C_4B_8H_8$ and $R'_4C_4B_8H_8$ species, which not only lowers the yields of the desired compounds but requires separation of at least three products. In principle, the most efficient approach to the mixed-substituent compounds would entail controlled stepwise addition of dissimilar C_2B_4 carborane units to a metal centre, followed by oxidative fusion to give the desired C_4B_8 product. Since work in this laboratory over several years has demonstrated that $(R_2C_2B_4H_4)Fe(\eta^6\text{-}C_8H_{10})$ complexes readily undergo displacement of the cyclooctatriene ligand by arenes (over $AlCl_3$ in solution, or in thermal reactions) to give $(R_2C_2B_4H_4)Fe$(arene) products,[4] it occurred to us that similar C_8H_{10} displacement might take place at elevated temperatures with small *nido*-carborane ligands. If so, this could provide a controlled route to mixed-ligand $(R_2C_2B_4H_4)FeH_2(R'_2C_2B_4H_4)$ complexes, which in turn could be oxidized to yield the desired $R_2R'_2C_4B_8H_8$ products. An investigation of this approach is the subject of the present report.

RESULTS AND DISCUSSION

Reactions of cyclooctatriene–iron–carborane complexes (1) *with* nido-*dicarbahexaborate*(1−) *salts*

The net process, depicted in Scheme 1, is presumed to involve initial formation of a mixed-ligand bis(carboranyl)iron sandwich (2) as shown, with conversion of the latter species to the observed tetracarbon metallacarborane (3). However, in no case was the proposed intermediate isolated or directly observed. In parallel with previously described arene–$(R_2C_2B_4H_4)Fe(\eta^6\text{-}C_8H_{10})$ thermolyses,[4] all reactions were conducted in glass reactors at 150°C in the absence of solvent; the iron–cyclooctatriene complex is liquid at the reaction

* Based in part on the M.S. thesis of K.K.F., University of Virginia (1988).

† Author to whom correspondence should be addressed.

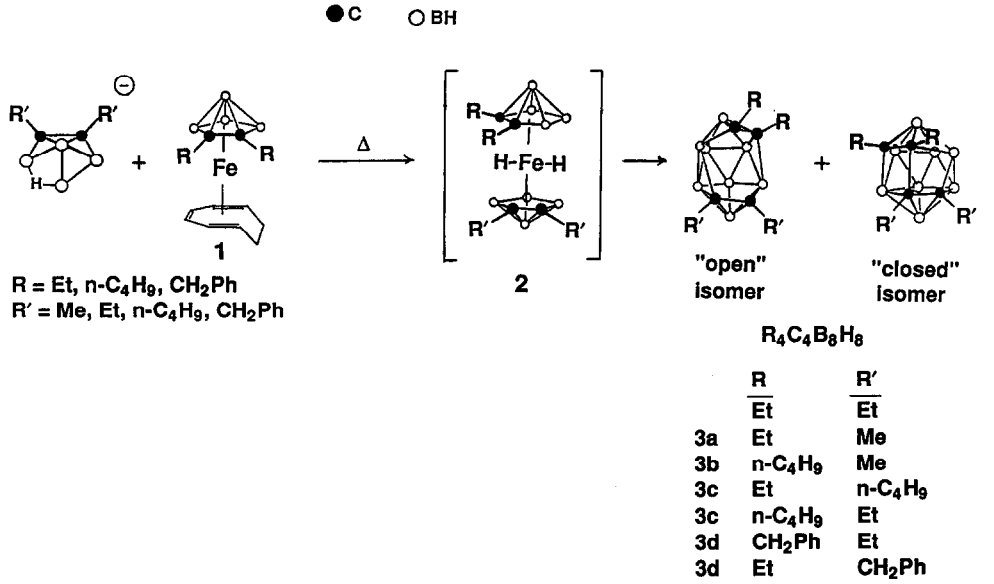

$R_4C_4B_8H_8$

	R	R′
3a	Et	Me
3b	n-C_4H_9	Me
3c	Et	n-C_4H_9
3c	n-C_4H_9	Et
3d	CH_2Ph	Et
3d	Et	CH_2Ph

Scheme 1.

temperature, melting at 88°C. The products were isolated via column and/or plate chromatography in air, and characterized from their ^{11}B, ^{1}H and ^{13}C NMR and mass spectra (see Tables 1–3 and Experimental).

The product yields are presented in Table 4. As can be seen, all reactions examined generated not only the desired mixed-substituent products **3a–d**, but also the corresponding $R_4C_4B_8H_8$ homosubstituted carborane. For comparison, the tetraethyl compound $Et_4C_4B_8H_8$ was prepared by the thermal reaction of $(Et_2C_2B_4H_4)Fe(\eta^6\text{-}C_8H_{10})$ (**1a**) with $Na^+Et_2C_2B_4H_5^-$, which as expected generated a relatively high yield of the target compound (since in this case the main product and by-product are identical). As a control experiment, **1a** was heated alone under conditions identical to the reactions with carborane salts. This afforded $Et_4C_4B_8H_8$ in 33% yield, indicating that thermal decomposition of the reactant complexes **1a–c** may be one source of the $R_4C_4B_8H_8$ by-products listed in Table 4. In another control designed to test the inertness of the reactants to each other at room temperature, **1a** and $Na^+Et_2C_2B_4H_5^-$ in THF solution were stirred for 12 h at room temperature, after which the starting materials were recovered unchanged.

Yields of the isolated heterosubstituted compounds were unfortunately lower than would be required for an efficient synthetic route, probably because of side reactions including decomposition, oligomerization and polymerization of the carborane units occurring at elevated temperature. More efficient experimental arrangements can be envisioned, such as a flow system enabling the trapping of C_4B_8 products as formed. However, the method does provide an apparently general route to heterosubstituted tetracarbadodecaboranes which are accompanied by few soluble side products and hence are easily purified. In a further extension of the synthetic utility of cyclooctatriene displacement, we have recently reported in a collaborative study[5] that reactions of $(R_2C_2B_4H_4)Fe(\eta^6\text{-}C_8H_{10})$ (R = Et, CH_2Ph) with the dihydrodiborole complex $CpCo(Et_2MeHC_3B_2Et_2)$ give novel carborane–dihydrodiborolene triple-decker complexes.

NMR studies

The behaviour of $R_4C_4B_8H_8$ carboranes in solution has been studied in detail by NMR spectroscopy,[1b,6] which revealed that when R = methyl, the solid state consists of one isomer which was shown crystallographically[7] to have a "closed" form (Scheme 1), but when placed in solution a second "open" isomer begins to form and within minutes an equilibrium is established between them. Conversely, when R = ethyl, the solid state is exclusively "open",[6] but in solution the closed isomer is slowly produced until equilibrium is reached. In both cases, evaporation of the solvent causes the compound to revert to its original one-isomer state. In the tetra(*n*-propyl) derivative, both isomeric forms are evidently present even in the solid, but

Table 1. 115.8 MHz ^{11}B FT–NMR data

Compound[a,b]	[B]/[A][c]	δ (J_{BH}, Hz)	Relative areas
$Me_2Et_2C_4B_8H_8$ (**3a**)	1.2		
Isomer A ("closed")		10.68 (160), 9.17 (158), 4.98 (156), −21.94 (143), −26.05 (135), −29.47 (136), −30.65 (117)[d]	1:2:1:1:1:1:1
Isomer B ("open")		−3.49 (126), −11.32 (150), −12.88 (128)	6:1:1
$Me_2(C_4H_9)_2C_4B_8H_8$ (**3b**)	1.0		
Isomer A		10.52 (172), 8.87 (170), 4.69 (159), −22.17 (159), −26.65 (156), −29.53 (170), −31.13 (162)	1:2:1:1:1:1:1
Isomer B		−3.81 (120), −11.64 (160),[d] −13.36 (155)	6:1:1
$Et_2(C_4H_9)_2C_4B_8H_8$ (**3c**)	2.6		
Isomer A		9.90 (152), 6.88 (163), 4.69 (159), −25.39 (157), −29.89 (140)	1:1:1:1
Isomer B		−3.95 (144), −12.98 (145)	6:2
$Et_2(PhCH_2)_2C_4B_8H_8$ (**3d**)	3.5		
Isomer A		10.77 (155), 6.26,[e] −24.42 (127),[d] −25.08 (134),[d] −29.21 (139)	2:2:1:2:2
Isomer B		−3.64 (113), −13.14 (142)	6:2

[a] Shifts relative to $BF_3 \cdot OEt_2$, positive values downfield.
[b] Dichloromethane solution.
[c] Calculated from integrated peak areas.
[d] Estimated from overlapping peaks.
[e] Coupling constant not measurable.

Table 2. 300 MHz ^1H FT–NMR data

Compound	δ[a,b,c]
3a	2.46 m (Et CH_2 [**A**]), 2.30 m (7.5, Et CH_2 [**A**]), 2.06 s (Me), 2.01 s (Me), 1.65 s (Me), 1.56 s (Me), 1.264 t (7.5, Et CH_3 [**A**]), 1.252 t (7.5, Et CH_3 [**A**]), 1.150 t (7.5, Et CH_3 [**B**]), 1.145 q (7.5, Et CH_2 [**B**]), 1.039 q (7.5, Et CH_2 [**B**]), 0.973 t (7.5, Et CH_3 [**B**])
3b	2.365 m (butyl α-CH_2), 2.225 m (butyl α-CH_2), 2.057 s (Me), 1.999 s (Me), 1.97 m (butyl β-CH_2), 1.634 s (Me), 1.537 s (Me), 1.569 m (butyl β-CH_2), 1.433 q (7.2, butyl α-CH_2), 1.389 q (7.2, butyl α-CH_2), 1.341 q (7.2, butyl α-CH_2), 0.977 t (7.2, butyl Me), 0.921 t (7.2, butyl Me)
3c	2.31 m, 1.984 m, 1.63 m, 1.45 m, 1.0–1.3 (overlapping multiplets), 1.140 t (7.2), 0.955 (overlapping multiplets), 0.904 t (7.2)
3d	7.25 m (C_6H_6), 3.885 dd (84.8, 14.4, benzyl CH_2), 3.803 dd (20.1, 14.1, benzyl CH_2), 3.383 dd (23.4, 14.4, benzyl CH_2), 3.196 dd (42.9, 13.8, benzyl CH_2), 2.328 m (7.2, Et CH_2), 2.165 m (7.2, Et CH_2), 2.103 m (7.2, Et CH_2), 1.940 m (7.2, Et CH_2), 1.873 m (7.2, Et CH_2), 1.133 t (7.2, Et CH_2), 0.920 t (7.2, Et CH_2), 0.862 t (7.2, Et CH_2), 0.801 t (7.2, Et CH_2)

[a] $CDCl_3$ solution.
[b] Shifts relative to $(CH_3)_4Si$; coupling constants in Hz and tentative assignments are given in parentheses. Isomer assignments (**A**, **B**) are given where possible. Integrated peak areas in all cases are consistent with the assignments given. Legend: m = multiplet, s = singlet, d = doublet, dd = doublet of doublets, t = triplet, q = quartet.
[c] $B—H_{terminal}$ resonances are broad quartets and mostly obscured by other signals.

Table 3. 75.5 MHz $^{13}C\{^1H\}$ FT–NMR data

Compound	$\delta^{a,b}$
3a	29.73 (Me [**A**]), 29.31 (Et CH_2 [**B**]), 27.24 (Et CH_2 [**A**]), 26.44 (Me [**A**]), 25.71 (Et CH_2 [**B**]), 25.25 (Et CH_2 [**A**]), 19.44 (Me [**B**]), 18.66 (Me [**B**]), 18.48 (Et CH_3 [**A**]), 15.56 (Et CH_3[**A**]), 14.34 (Et CH_3 [**B**]), 12.52 (Et CH_3 [**B**])
3b	36.37 (Me [**A**]), 34.08 (butyl α-CH_2), 33.48 (butyl α-CH_2), 33.25 (butyl α-CH_2), 32.28 (butyl β-CH_2), 31.85 (butyl β-CH_2), 31.70 (butyl β-CH_2), 30.60 (Me [**A**]), 23.49 (Me [**B**]), 23.40 (butyl α-CH_2), 23.27 (butyl α-CH_2), 18.74 (Me [**B**]), 14.37 (butyl CH_3), 14.30 (butyl CH_3), 14.15 (butyl CH_3)
3c	35.95 (butyl α-CH_2), 33.99 (butyl α-CH_2), 32.68 (butyl α-CH_2), 32.44 (butyl β-CH_2), 32.24 (butyl β-CH_2), 31.51 (butyl β-CH_2), 29.32 (Et CH_2 [**B**]), 26.20 (Et CH_2 [**A**]), 26.08 (Et CH_2 [**A**]), 25.73 (Et CH_2 [**B**]), 23.40 (butyl α-CH_2), 23.27 (butyl α-CH_2), 16.18 (Et CH_3 [**A**]), 14.56 (Et CH_3 [**A**]), 14.33 (butyl CH_3), 14.17 (butyl CH_3), 13.87 (butyl CH_3), 13.79 (Et CH_3 [**B**]), 12.55 (Et CH_3 [**B**])
3d	138.88 (benzyl C1 [**A**]), 136.41 (benzyl C1 [**B**]), 130.57 (benzyl C2,C6 [**A**]), 130.14 (benzyl C3,C5 [**A**]), 128.97 (benzyl C2,C6 [**B**]), 128.81 (benzyl C3,C5 [**B**]), 127.58 (benzyl C4 [**A**]), 127.24 (benzyl C4 [**B**]), 42.47 (benzyl CH_2 [**A**]), 39.64 (benzyl CH_2 [**B**]), 28.66 (Et CH_2 [**A**]), 25.50 (Et CH_2 [**A**]), 13.99 (Et CH_3 [**B**]), 12.22 (Et CH_3 [**B**])

[a] $CDCl_3$ solution.

[b] Shifts relative to $(CH_3)_4Si$; tentative assignments are given in parentheses. Isomer assignments (**A**, **B**) are given where possible. Cage carbon resonances were not observed. Legend: m = multiplet, s = singlet, d = doublet, dd = doublet of doublets, t = triplet, q = quartet.

there is some change in the open/closed ratio in solution over a period of hours. When R is still larger, e.g. *n*-butyl, the relative amounts of open and closed forms are fixed; in some cases, such as the tetrabenzyl derivative,[8] only the open-cage isomer is seen. These observations, buttressed by kinetic and thermodynamic studies,[6] have been interpreted as reflecting primarily steric effects of the R substituents.

In light of these earlier observations, the solution behaviour of the mixed-substituent compounds **3a–d** was examined via high-resolution NMR spectroscopy as a function of time. Each species was dissolved in dichloromethane and its ^{11}B FT–NMR spectrum recorded within 1–2 min. In all cases, the spectra revealed peaks characteristic of both the open- and closed-cage forms (Table 1), in contrast to the tetramethyl and tetraethyl derivatives referred to above, but consistent with the earlier observations on the tetrapropyl species.[6] Surprisingly, the spectra exhibited no change over time, even on standing for days. For all derivatives, evaporation of the solution to dryness followed by redissolving gave spectra identical to the original.

As is indicated in Table 1, the ratio of open to closed isomers in **3a–d**, as in other examples studied* tends to increase with increasing size of the R substituents, consistent with stabilization of the open form via intramolecular steric repulsion across the open face. The apparent absence of isomer interconversion in solution in the derivatives examined in this work should be interpreted with caution, particularly since the diethyl–dimethyl compound **3a** would not be expected to differ fundamentally from the tetramethyl and tetraethyl derivatives. It is possible that the lowering of symmetry caused by the presence of dissimilar substituents on the two halves of the C_4B_8 cage interferes with the "open"–"closed" interchange process and prevents its occurrence as solvent is removed; this would account for the failure of **3a** to revert to a single isomer in the solid state, in contrast to $Me_4C_4B_8H_8$ and $Et_4C_4B_8H_8$. While the formation of both cage isomers in all four compounds may take place either during synthesis at elevated temperatures or in solu-

* For comparison, the (open isomer)/(closed isomer) equilibrium values[6] for $Me_4C_4B_8H_8$, $Et_4C_4B_8H_8$, and $(n\text{-}C_3H_7)_4C_4B_8H_8$ are, respectively, 0.56, 2.2 and 1.9.

Table 4. Yields of fusion products

Product	Substituents on starting materials[a] R	R′	$R_2R'_2C_4B_8H_8$[b]	$R_4C_4B_8H_8$[c]
$Et_4C_4B_8H_8$	Et	Et	65	—
3a	Et	Me	37	11
3b	*n*-C_4H_9	Me	14	20
3c	Et	*n*-C_4H_9	12	12
3c	*n*-C_4H_9	Et	20	13[d]
3d	CH_2Ph	Et	17	12[d]
3d	Et	CH_2Ph	8	13

[a] $(R_2C_2B_4H_4)Fe(\eta^6\text{-}C_8H_{10})$ and $Na^+R'_2C_2B_4H_7^-$.
[b] Percent yield based on iron reagent consumed.
[c] Percent yield based on carborane starting reagent.
[d] $Et_4C_4B_8H_8$.

tion during subsequent work-up, the observed open–closed ratios in solution are regarded as equilibrium values since they remain constant over extended periods.

The ^1H and proton-decoupled ^{13}C NMR data on compounds **3a–f** (Tables 2 and 3) further support the characterizations based on ^{11}B spectra as discussed above, and are consistent (as far as can be determined given the complex patterns arising from the organic substituents) with the open–closed isomer ratios which are indicated in the boron NMR data.

EXPERIMENTAL

Materials

n-Hexane and dichloromethane were distilled prior to use and stored over molecular sieves. Tetrahydrofuran (THF) was dried over lithium aluminium hydride and stored over zinc containing titanium tetrachloride as an indicator. Sodium hydride (60% dispersion in mineral oil) and potassium metal were washed three times in dry *n*-hexane prior to each use. Column chromatography was conducted on 70/230 mesh silica gel (EM Science), and preparative-scale plate chromatography was conducted on 250 μm silica gel plates (Merck). *Nido*-2,3-$Et_2C_2B_4H_6$ was prepared by a previously published method,[9] modified in that 3-hexyne and triethylamine were added to the reaction vessel in air and subjected to three cycles of freezing in a liquid nitrogen bath, degassing on the vacuum line and thawing. After addition of B_5H_9 as described earlier,[9] the reactor was stirred for 1 day at 0°C and for 2 days at room temperature, and isolated according to the published procedure. *Nido*-2,3-$Me_2C_2B_4H_6$ was prepared via the literature method[9] except that the B_5H_9 was added over a 10 h period. *Nido*-2,3-(*n*-$C_4H_9)_2C_2B_4H_6$[10] and *nido*-2,3-$(PhCH_2)_2C_2B_4H_6$[4c] were prepared as previously described. $(Et_2C_2B_4H_4)Fe(\eta^6\text{-}C_8H_{10})$[11] (**1a**) and $[(PhCH_2)_2C_2B_4H_4]Fe(\eta^6\text{-}C_8H_{10})$[4c] (**1c**) were synthesized as reported elsewhere.

Instrumentation

^{11}B (115.8 MHz) and ^1H (300 MHz) NMR spectra were acquired on Nicolet NT-360 and GE QE300 spectrometers, respectively. Unit-resolution mass spectra were obtained on a Finnegan MAT 4600 GC/MS spectrometer using perfluorotributylamine (FC43) as a calibration standard. Simulated mass spectra based on natural isotopic abundances were calculated on an AT&T 3B5 computer using the program MASPEC by R. N. Grimes. In all cases, strong parent envelopes were observed, and the calculated and observed unit-resolution spectral patterns were in close agreement.

Synthesis of $[(C_4H_9)_2C_2B_4H_4]Fe(\eta^6\text{-}C_8H_{10})$ (**1b**)

This compound was prepared from Na^+(*n*-$C_4H_9)_2C_2B_4H_5^-$, $FeCl_2$ and cyclooctatetraene by a procedure analogous to that used in the preparation of the C,C′-diethylcarborane homologue[11] and was purified via preparative TLC using 3 : 1 *n*-hexane–dichloromethane eluant and isolated in 13% yield as a red–orange solid, accompanied by a small quantity of $[(C_4H_9)_2C_2B_4H_4]Fe(\eta^6\text{-}C_6H_6)$, identified from its NMR and mass spectra (analogous

iron–benzene by-products have been obtained in previous syntheses of carboranyl iron cyclooctatriene complexes[11a]). ^{11}B NMR at 115.8 MHz (dichloromethane, 25°C, shifts in ppm relative to $BF_3 \cdot OEt_2$, H–B coupling constants in Hz): 9.88 (148), 1B; 4.99 (169), 1B; 2.17 (150), 2B. ^1H NMR at 300 MHz ($CDCl_3$, 25°C, shifts in ppm relative to $SiMe_4$; s = singlet, m = multiplet, q = quartet, t = triplet): 5.37 s (C_6H_6), 2.561 m (α-CH_2), 2.317 m (α-CH_2), 1.575 m (β-CH_2), 1.451 q (γ-CH_2), 0.966 t (CH_3). Mass spectrum: cut-off at m/z 349, corresponding to $^{13}C^{12}C_{17}^{56}Fe^{11}B_4^1H_{32}^+$

Syntheses of $R_2R'_2C_4B_8H_8$ *carboranes*

The procedure followed was the same in all cases; data for specific reactions are given below. In a Pyrex apparatus[12] consisting of upper and lower bulbs separated by a medium-porosity frit and a stopcock, with the upper bulb connected via a Teflon stopcock to an attached tip-tube and the entire apparatus connected to a vacuum line, the $R_2C_2B_4H_6$ reactant was placed in the tip-tube, frozen in liquid nitrogen, and evacuated. An excess of NaH powder was placed together with a stirring bar in the upper bulb, and the iron–cyclooctatriene complex was placed with a stirring bar in the lower bulb. The apparatus was evacuated and the stopcock between the frit and the lower bulb was closed, and 30–40 cm^3 of dry THF was distilled onto the NaH at −196°C. The carborane was added to the NaH–THF mixture via rotation of the tip-tube and the contents were warmed to room temperature and stirred for 1 h, after which the solution of $Na^+R_2C_2B_4H_5^-$ was added through the filter frit to the lower flask containing the iron reagent. The upper flask was rinsed with THF (still *in vacuo*) and the solution added to the lower flask. The lower (reactor) bulb was isolated by closing the stopcock and the bulb was removed from the apparatus and placed in an oil bath at 150°C for *ca* 12 h. After cooling, the flask was opened to the air and the contents were dissolved in dichloromethane and filtered through a few cm of silica gel. The solution was concentrated to a small volume by rotary evaporation and the products purified by preparative layer chromatography. Yields given below are calculated on the basis of the $(R_2C_2B_4H_4)Fe(\eta^6$-$C_8H_{10})$ complex or $Na^+R'_2C_2B_4H_5^-$ consumed, as appropriate.

Reaction of $(Et_2C_2B_4H_4)Fe(\eta^6$-$C_8H_{10})$ *and* $Na^+Et_2C_2B_4H_5^-$

A 0.12 g quantity (0.40 mmol) of the iron reagent and 50 mg (0.41 mmol) of the carborane salt gave 67 mg (0.26 mmol, 65% yield) of $Et_4C_4B_8H_8$, R_f 0.36 in *n*-hexane.

Reaction of $(Et_2C_2B_4H_4)Fe(\eta^6$-$C_8H_{10})$ *and* $Na^+Me_2C_2B_4H_5^-$

A 0.25 g quantity (0.86 mmol) of the iron reagent and 90 mg (0.86 mmol) of the carborane salt gave 74 mg (0.32 mmol, 37%) of $Me_2Et_2C_4B_8H_8$ (**3a**), R_f 0.30 in *n*-hexane, and 12 mg (0.046 mmol, 11%) of $Et_4C_4B_8H_8$, R_f 0.35.

Reaction of $[(C_4H_9)_2C_2B_4H_4]Fe(\eta^6$-$C_8H_{10})$ *and* $Na^+Me_2C_2B_4H_5^-$

A 0.184 g quantity (0.53 mmol) of the iron reagent and 55 mg (0.53 mmol) of the carborane salt gave 20 mg (0.070 mmol, 14%) of $(C_4H_9)_2Me_2C_4B_8H_8$ (**3b**), R_f 0.73 in cyclohexane, and 20 mg (0.054 mmol, 22%) of $(C_4H_9)_4C_4B_8H_8$, R_f 0.64. Also recovered was 15 mg (0.042 mmol, 8%) of the iron complex reagent, R_f 0.17.

Reaction of $(Et_2C_2B_4H_4)Fe(\eta^6$-$C_8H_{10})$ *and* $Na^+(C_4H_9)_2C_2B_4H_5^-$

A 0.32 g quantity (1.1 mmol) of the iron reagent and 21 mg (1.1 mmol) of the carborane salt gave 40 mg (0.13 mmol, 12%) of $(C_4H_9)_2Et_2C_4B_8H_8$ (**3c**), R_f 0.53 in cyclohexane, and 23 mg (0.063 mmol, 12%) of $(C_4H_9)_4C_4B_8H_8$, R_f 0.65. Also recovered was 13 mg (0.044 mmol, 4%) of the iron complex reagent.

Reaction of $[(C_4H_9)_2C_2B_4H_4]Fe(\eta^6$-$C_8H_{10})$ *and* $Na^+Et_2C_2B_4H_5^-$

A 0.134 g quantity (0.39 mmol) of the iron reagent and 53 mg (0.40 mmol) of the carborane salt gave 23 mg (0.073 mmol, 20%) of $(C_4H_9)_2Et_2C_4B_8H_8$ (**3c**, identical with the product of the preceding reaction), and 7 mg (0.026 mmol, 13%) of $Et_4C_4B_8H_8$, R_f 0.48 in cyclohexane. Also recovered was 7 mg (0.02 mmol, 5%) of the iron complex reagent.

Reaction of $(Et_2C_2B_4H_4)Fe(\eta^6$-$C_8H_{10})$ *and* $Na^+(PhCH_2)_2C_2B_4H_5^-$

A 0.219 g quantity (0.75 mmol) of the iron reagent and 0.192 g (0.75 mmol) of the carborane salt gave 21 mg (0.055 mmol. 8%) of $(PhCH_2)_2Et_2C_4B_8H_8$ (**3d**), R_f 0.46 in cyclohexane, and 13 mg (0.050 mmol, 13%) of $Et_4C_4B_8H_8$. Also recovered was 18 mg (0.060 mmol, 8%) of the unreacted iron complex.

Reaction of $[(PhCH_2)_2C_2B_4H_4]Fe(\eta^6\text{-}C_8H_{10})$ *and* $Na^+Et_2C_2B_4H_5^-$

A 0.15 g quantity (0.36 mmol) of the iron reagent and 43 mg (0.33 mmol) of the carborane salt gave 22 mg (0.057 mmol, 17%) of $(PhCH_2)_2Et_2C_4B_8H_8$ (**3d**, identical with the product of the preceding reaction) and 5 mg (0.02 mmol, 12%) of $Et_4C_4B_8H_8$. Also recovered was 9 mg (0.022 mmol, 6%) of the unreacted iron complex.

Acknowledgements—We thank the National Science Foundation for support of this research, and Drs Henry Boyter and James H. Davis Jr for the mass spectra.

REFERENCES

1. (a) W. M. Maxwell, V. R. Miller and R. N. Grimes, *J. Am. Chem. Soc.* 1974, **96**, 7116; (b) W. M. Maxwell, V. R. Miller and R. N. Grimes, *Inorg. Chem.* 1976, **15**, 1343.
2. For a review of this area, see: R. N. Grimes, *Adv. Inorg. Chem. Radiochem.* 1983, **26**, 55 and refs therein.
3. R. B. Maynard and R. N. Grimes, *J. Am. Chem. Soc.* 1982, **104**, 5983.
4. (a) R. G. Swisher, E. Sinn and R. N. Grimes, *Organometallics* 1983, **2**, 506; (b) R. G. Swisher, E. Sinn, R. J. Butcher and R. N. Grimes, *Organometallics* 1985, **4**, 882; (c) J. T. Spencer and R. N. Grimes, *Organometallics* 1987, **6**, 323 and 328 and refs therein.
5. M. D. Attwood, K. K. Fonda, R. N. Grimes, G. Brodt, D. Hu, U. Zenneck and W. Siebert, *Organometallics* 1989, **8**, 1300.
6. T. L. Venable, R. B. Maynard and R. N. Grimes, *J. Am. Chem. Soc.* 1984, **106**, 6187.
7. (a) D. P. Freyberg, R. E. Weiss, E. Sinn and R. N. Grimes, *Inorg. Chem.* 1977, **16**, 1847; (b) R. N. Grimes, W. M. Maxwell, R. B. Maynard and E. Sinn, *Inorg. Chem.* 1980, **19**, 2981.
8. J. T. Spencer, M. R. Pourian, R. J. Butcher, E. Sinn and R. N. Grimes, *Organometallics* 1987, **6**, 335.
9. R. B. Maynard, L. Borodinsky and R. N. Grimes, *Inorg. Synth.* 1983, **22**, 211.
10. H. A. Boyter Jr and R. N. Grimes, *Inorg. Chem.* 1988, **27**, 3075.
11. (a) R. B. Maynard, R. G. Swisher and R. N. Grimes, *Organometallics* 1983, **2**, 500; (b) R. G. Swisher and R. N. Grimes, *Organomet. Synth.* 1986, **3**, 104.
12. A drawing of an identical set-up appears in: H. A. Boyter Jr, R. G. Swisher, E. Sinn and R. N. Grimes, *Inorg. Chem.* 1985, **24**, 3810.

Polyhedron Vol. 9, No. 7, pp. 957–962, 1990
Printed in Great Britain

0277–5387/90 $3.00+.00
© 1990 Pergamon Press plc

STRUCTURE OF SODIUM DINEOPENTYLDIOXORHENIUM(V)

SHIANG CAI, DAVID M. HOFFMAN* and DERK A. WIERDA

Department of Chemistry, Harvard University, 12 Oxford Street, Cambridge, MA 02138, U.S.A.

(*Received* 23 *August* 1989; *accepted* 6 *November* 1989)

Abstract—Sodium dineopentyldioxorhenium(V), $[Na(CH_3CN)][ReO_2(CH_2CMe_3)_2]$, $C_{12}H_{25}NNaO_2Re$, $M_r = 424.53$, triclinic, $P\bar{1}$ (No. 2), $a = 14.209(3)$, $b = 14.631(3)$, $c = 11.144(2)$ Å, $\alpha = 97.80(1)$, $\beta = 104.69(2)$, $\gamma = 64.54(1)°$, $V = 2022.5(7)$ Å^3, $Z = 2$, $D_x = 1.39$ g cm^{-3}, λ(Mo-K_α) = 0.71073 Å, $\mu = 61.04$ cm^{-1}, $F(000) = 796$, $T = 233(1)$ K, final $R = 0699$ for 3216 unique reflections with $F_o > 6\sigma(F_o)$ and 308 variables. There are two independent molecules of $[Na(CH_3CN)][ReO_2(CH_2CMe_3)_2]$ in the asymmetric unit. In the solid state the compound is polymeric having $\{[Na(CH_3CN)][ReO_2(CH_2CMe_3)_2]\}_2$ repeating units. The $\{[Na(CH_3CN)][ReO_2(CH_2CMe_3)_2]\}_2$ units are eight-membered rings of composition $Re_2O_4Na_2$, which are connected via Na—O bonds thereby forming the polymer. The $[ReO_2(CH_2CMe_3)_2]^-$ anions within the repeating units have distorted tetrahedral geometries with open O—Re—O (av. 136°) and closed C—Re—C (av. 83°) angles. The planes defined by O—Re—O and C—Re—C are perpendicular (90.6° and 90.0° for Re(1) and Re(2), respectively). Average Re—O multiple bond and Re—C single bond distances ae 1.72 and 2.11 Å, respectively. A comparison of the structures of related d^0, d^1 and d^2 MO_2R_2 (R = alkyl and aryl) compounds is presented. The structural changes which occur as a function of electron count in these compounds are explained in the context of an earlier MO study.

We recently reported the synthesis and spectroscopic characterization of the lithium, sodium and tetraethylammonium salts of the d^2 $[ReO_2(CH_2CMe_3)_2]^-$ anion, and X-ray structures of the lithium and tetraethylammonium salts.[1] In both of the structurally characterized compounds the anions have severely distorted tetrahedral geometries with open O—Re—O and closed H_2C—Re—CH_2 angles. Herein we report the X-ray structure determination of the sodium salt and compare its structure to the other members of the series and some related compounds.

* Author to whom correspondence should be addressed.

† Lists of atom coordinates, complete bond distances and angles, anisotropic thermal parameters, hydrogen atom parameters and structure factors, as well as a packing diagram, have been deposited with the Editor as supplementary material.

RESULTS AND DISCUSSION

Structure of sodium dineopentyldioxorhenium(V)

The molecular structure and atom-numbering scheme for $[Na(CH_3CN)][ReO_2(CH_2CMe_3)_2]$ are presented in Fig. 1. An extended structure is presented in Fig. 2 in order to clarify the polymeric nature of the compound in the solid state. Selected bond lengths and angles are given in Table 1.† There are two crystallographically independent molecules of $[Na(CH_3CN)][ReO_2(CH_2CMe_3)_2]$ in the asymmetric unit. The two independent $[ReO_2(CH_2CMe_3)_2]^-$ anions differ only by a twist of the neopentyl t-butyl groups; all chemically equivalent distances and angles are equal by the 3σ criterion. A few angles about the two sodium ions, however, do differ by more than 3σ.

As Fig. 2 illustrates, the compound is polymeric in the solid state with $\{[Na(CH_3CN)][ReO_2(CH_2CMe_3)_2]\}_2$ repeating units linked via Na—O

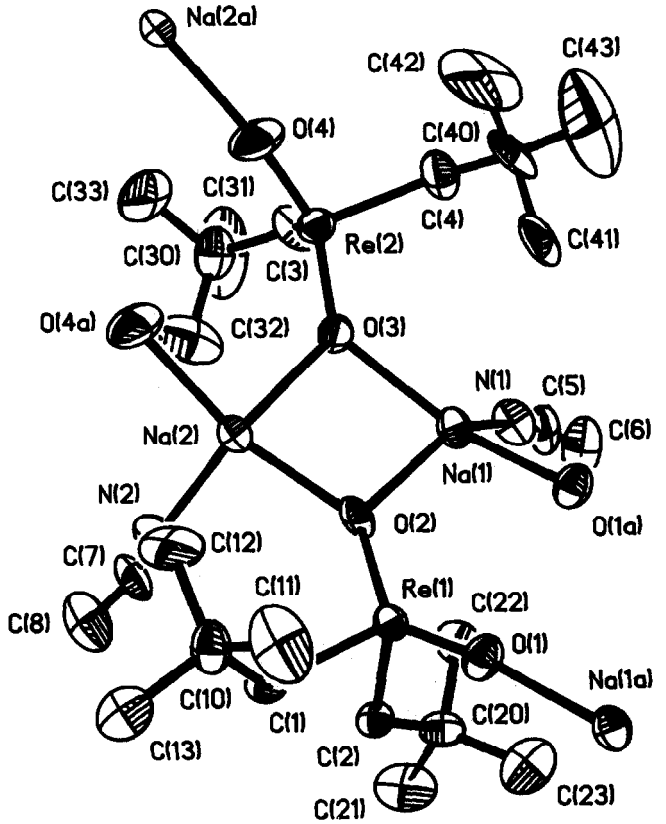

Fig. 1. The molecular structure of $[Na(CH_3CN)][ReO_2(CH_2CMe_3)_2]$, $C_{12}H_{25}NNaO_2Re$ (ORTEP, 30% probability level).

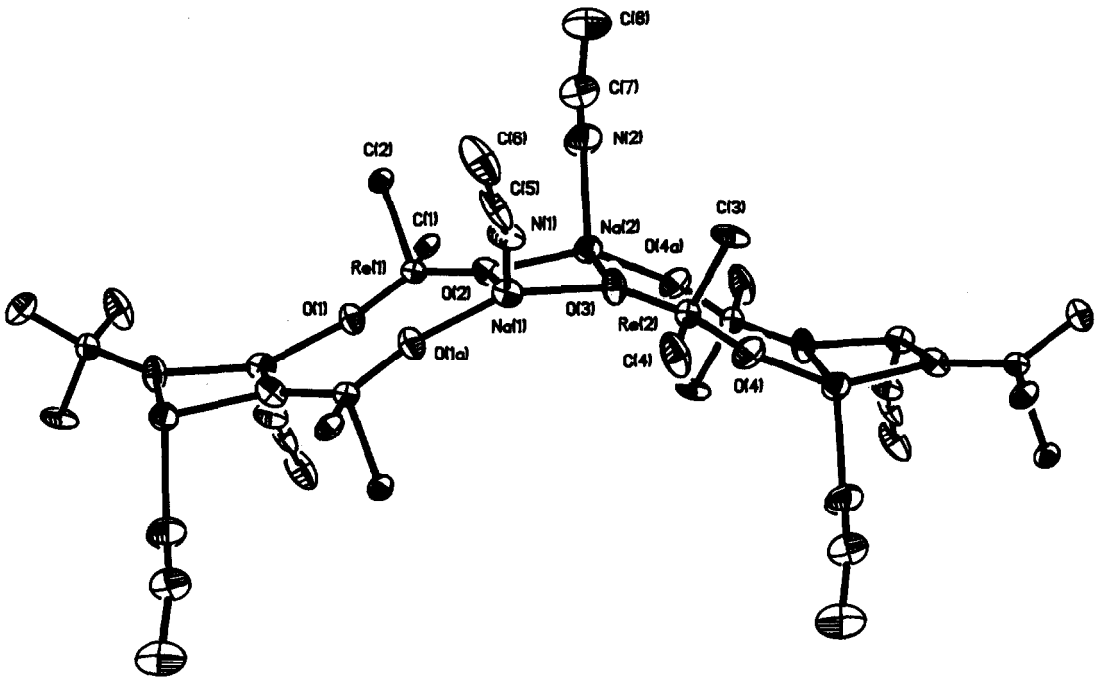

Fig. 2. A different view of the $[Na(CH_3CN)][ReO_2(CH_2CMe_3)_2]$ structure highlighting the $Re_2O_4Na_2$ rings and polymeric nature of the compound (ORTEP, 30% probability level). The t-Bu groups of the neopentyl ligands have been omitted for clarity.

Table 1. Listing of selected bond lengths (Å) and angles (°) for $[Na(CH_3CN)][ReO_2(CH_2CMe_3)_2]$

Re(1)—O(1)	1.711(20)	Re(2)—O(3)	1.716(18)
Re(1)—O(2)	1.765(19)	Re(2)—O(4)	1.683(20)
Re(1)—C(1)	2.102(16)	Re(2)—C(3)	2.087(23)
Re(1)—C(2)	2.110(17)	Re(2)—C(4)	2.136(20)
Na(1)—N(1)	2.412(24)	Na(2)—N(2)	2.485(29)
Na(1)—O(1A)	2.237(23)	Na(2)—O(4A)	2.239(23)
Na(1)—O(2)	2.293(15)	Na(2)—O(3)	2.280(17)
Na(1)—O(3)	2.306(20)	Na(2)—O(2)	2.270(22)
		Na(1)—Na(2)	3.315(11)
O(1)—Re(1)—O(2)	134.4(8)	O(3)—Re(2)—O(4)	137.7(10)
C(1)—Re(1)—C(2)	83.2(6)	C(3)—Re(2)—C(4)	83.4(9)
O(1)—Re(1)—C(1)	107.3(8)	O(3)—Re(2)—C(3)	105.1(9)
O(2)—Re(1)—C(1)	106.7(7)	O(4)—Re(2)—C(3)	105.5(11)
O(1)—Re(1)—C(2)	107.7(8)	O(3)—Re(2)—C(4)	105.8(9)
O(2)—Re(1)—C(2)	105.7(8)	O(4)—Re(2)—C(4)	106.1(10)
Re(1)—C(1)—C(10)	121.8(12)	Re(2)—C(3)—C(30)	122.2(13)
Re(1)—C(2)—C(20)	122.1(11)	Re(2)—C(4)—C(40)	120.2(16)
O(2)—Na(1)—N(1)	138.5(8)	O(3)—Na(2)—N(2)	122.9(9)
N(1)—Na(1)—O(3)	101.4(10)	N(2)—Na(2)—O(2)	102.0(9)
O(2)—Na(1)—O(3)	85.8(6)	O(2)—Na(2)—O(3)	86.9(6)
O(3)—Na(1)—O(1A)	153.5(7)	O(2)—Na(2)—O(4A)	146.3(9)
N(1)—Na(1)—O(1A)	99.2(9)	N(2)—Na(2)—O(4A)	106.5(9)
O(2)—Na(1)—O(1A)	89.8(7)	O(3)—Na(2)—O(4A)	92.3(8)
Re(1)—O(1)—Na(1A)	170.4(10)	Re(2)—O(4)—Na(2A)	169.2(14)
Re(1)—O(2)—Na(1)	123.7(8)	Re(2)—O(3)—Na(2)	127.2(8)
Re(1)—O(2)—Na(2)	142.8(7)	Na(1)—O(3)—Re(2)	138.8(8)
Na(1)—O(2)—Na(2)	93.2(8)	Na(1)—O(3)—Na(2)	92.6(8)

bonds. The $\{[Na(CH_3CN)][ReO_2(CH_2CMe_3)_2]\}_2$ repeating units, which each contain one half of the crystallographically unique atoms, are eight-membered $Re_2O_4Na_2$ rings. The rings are nearly planar with the largest deviation from the least-squares plane being Re (0.2 Å).

An analogous eight-membered ring structure was also found in $[Li(CH_3CN)_2][ReO_2(CH_2CMe_3)_2]$ (**I**).[1] The lithium and sodium structures differ, however, in how the cations fill their four coordination sites and in the number of cations bound to the oxo ligands. In the present structure, each sodium is coordinated to three oxo ligands, one each from two separate (but crystallographically equivalent) $[ReO_2(CH_2CMe_3)_2]^-$ anions that are part of the $Re_2O_4Na_2$ ring and an oxo ligand that is part of an adjacent ring, and a terminal acetonitrile; thus, one oxo ligand from each $[ReO_2(CH_2CMe_3)_2]^-$ anion

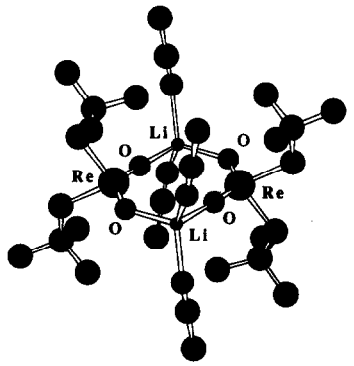

$\{[Li(CH_3CN)_2][ReO_2(CH_2CMe_3)_2]\}_2$

I

Scheme 1.

Table 2. Selected distances (Å) and angles (°) for transition metal MO_2R_2 compounds

Compound	Electron count	M—O	M—C	O—M—O	C—M—C	OMO/CMC[a]	Reference
$[Na(CH_3CN)][ReO_2(CH_2CMe_3)_2]$[b]	d^2						This work
A		1.711(20) 1.765(19)	2.102(16) 2.110(17)	134.4(8)	83.2(6)	90.6	
B		1.716(18) 1.683(20)	2.087(23) 2.136(20)	137.7(10)	83.4(9)	90.0	
$[NEt_4][ReO_2(CH_2CMe_3)_2]$	d^2	1.732(8) 1.733(8)	2.107(12) 2.099(11)	127.5(4)	81.2(5)	92.0	1
$[Li(CH_3CN)_2][ReO_2(CH_2CMe_3)_2]$	d^2	1.749(9) 1.739(8)	2.108(14) 2.106(12)	134.9(4)	83.7(5)	90.5	1
$[ReO_2(CH_2SiMe_3)_2]^-$ fragment in $Re_3O_4(PMe_3)_4(CH_2SiMe_3)_3$	d^2	1.78(1) 1.71(2)	2.13(2) 2.13(2)	132.1(6)	85.5(8)	86.4	2
$OsO_2(mesityl)_2$	d^2	1.700(7) 1.690(7)	2.053(8) 2.047(8)	136.1(3)	96.0(3)	84	3
$OsO_2(2,6\text{-}Me_2C_6H_3)_2$	d^2	1.699(5) 1.688(5)	2.058(6) 2.060(6)	139.1(2)	93.9(3)	84.3	4
$ReO_2(mesityl)_2$[c]	d^1	1.688(5)	2.062(6)	121.5(4)	102.2(3)	88	3
$ReO_2(2,6\text{-}Me_2C_6H_3)_2$	d^1	1.686(7) 1.672(6)	2.065(7) 2.069(7)	121.3(4)	100.4(3)	87.7	4
$MoO_2(mesityl)_2$[c]	d^0	1.699(3)	2.101(3)	109.5(1)	112.5(2)	88.8	5

[a] Angle between the OMO and CMC planes.
[b] A and B designate crystallographically independent molecules.
[c] Crystallographic two-fold axis.

is bound to two cations and the other to only one. The lithium structure, on the other hand, consists of discrete $Re_2O_4Li_2$ eight-membered rings. The four Li^+ ligation sites are occupied by two bridging oxo ligands and two terminal acetonitrile molecules; thus, each oxo ligand is bound to only one lithium cation.

The sodium cation coodination geometry is best described as flattened tetrahedral with the two open angles being O(2)—Na—N(1) and O(3)—Na—O(1a) for Na(1), and O(3)—Na—N(2) and O(2)—Na—O(4a) for Na(2). The six Na—O distances in the structure are equivalent by the 3σ criterion. It is not clear why the sodium cations do not have normal tetahedral geometries. These are, however, two possible interactions, C(41)···Na(1) = 3.11 Å and C(12)···Na(2) = 3.47 Å (cf. to 2.98 Å, the sum of the van der Waals' radius for a CH_3 group and the Na^+ ionic radius), that may be involved in the cation distortions.

The $[ReO_2(CH_2CMe_3)_2]^-$ anions in the sodium salt have distorted tetrahedral geometries with open O—Re—O (av. 136°) and closed C—Re—C (av. 83°) angles. The planes defined by O—Re—O and C—Re—C are perpendicular (90.6° and 90.0° for Re(1) and Re(2), respectively). The Re—O multiple bond and Re—C single bond distances are within 3σ of those observed in $[NEt_4][ReO_2(CH_2CMe_3)_2]$ and $[Li(CH_3CN)_2][ReO_2(CH_2CMe_3)_2]$.

In Table 2 is presented a comparison of M—O and M—C distances, O—M—O and C—M—C angles, and OMO/CMC plane dihedral angles for four-coordinate dioxo–dialkyl and dioxo–diaryl compounds. Most notable is the difference between d^0 MoO_2(mesityl)$_2$ and the d^1 and d^2 compounds.[2-5] The d^0 MoO_2(mesityl)$_2$ complex displays a nearly undistorted tetrahedral geometry,[5] whereas the d^1 and d^2 MO_2R_2 complexes all have open O—M—O and closed C—M—C angles.[1-4] Importantly, the d^1 compounds are less distorted (i.e. are closer to tetrahedral) than the d^2 compounds.

The smooth progression of distortion from a tetrahedral geometry on going from d^0 to d^1 to d^2 is entirely consistent with our earlier extended Hückel theoretical analysis of distorted d^2 $[ReO_2(CH_2CMe_3)_2]^-$.[1] As part of the theoretical analysis we examined both d^0 and d^2 MO_2R_2 complexes. For the d^0 case, the opening or closing of the O—M—O and C—M—C angles from 109° gave a relatively "soft" energy surface; that is, the d^0 MO_2R_2 complex did not show a strong electronic preference for a tetrahedral geometry. On this basis it was predicted that d^0 MO_2R_2 compounds should have geometries with angles close to 109° if the alkyls or aryls were not too sterically demanding.

HOMO
II
Scheme 2.

In contrast to the d^0 case, the theoretical analysis indicated that the distortions in d^2 $[ReO_2(CH_2CMe_3)_2]^-$ are strongly electronically driven and HOMO controlled. The HOMO, which is schematically illustrated in **II**, has primarily *d*-orbital character and is M–O π-antibonding. Orbital **II** and the complex were stabilized by opening the O—Re—O and closing the C—Re—C angles. In both cases the stabilization resulted from a reduction in Re—O π-antibonding. The strong preference of the HOMO in the d^2 compounds for distortion is tempered only by the weaker electronic and steric factors which favour a geometry with angles near 109°.

Because the HOMOs for all of the d^1 and d^2 compounds listed in Table 2 are similar to **II**, the theoretical results discussed above are generally applicable and, in particular, the analysis explains the large structural differences between the d^0 and d^2 compounds. The lesser distortions observed in the d^1 MO_2R_2 compounds are also readily explained: for the d^1 compounds only one electron in the HOMO is stabilized by the distortions whereas in the d^2 compounds, two are stabilized.*

CONCLUSION

The structures of the $[ReO_2(CH_2CMe_3)_2]^-$ anions in $[Na(CH_3CN)][ReO_2(CH_2CMe_3)_2]$ are similar to those in $[NEt_4][ReO_2(CH_2CMe_3)_2]$ and $[Li(CH_3CN)_2][ReO_2(CH_2CMe_3)_2]$. All have distorted tetrahedral geometries with open O—Re—O and C—Re—C angles. Analogous d^1 rhenium aryls, $ReO_2(Ar)_2$, and d^2 osmium aryls, $OsO_2(Ar)_2$, have similarly distorted tetrahedral geometries, but the d^0 complex MoO_2(mesityl)$_2$ is close to a normal tetrahedral geometry. All of the structural variations are readily explained in the context of a previously reported theoretical study.

* See also ref. 3, wherein a related MO based explanation of the structural differences between the d^1 and d^2 compounds is presented.

EXPERIMENTAL

$Na[ReO_2(CH_2CMe_3)]$ was prepared according to our literature method.[1] Dark green crystals were grown by low temperature crystallization from a saturated acetonitrile solution (−20°C; 2 days). The crystals were handled under a nitrogen atmosphere saturated with acetonitrile.

A crystal of dimensions $0.20 \times 0.20 \times 0.40$ mm was mounted on a glass fibre. Lattice parameters were obtained by a least-squares refinement of 24 selected reflections, including 12 Friedel pairs ($20° < 2\theta < 25°$). Collection data: Nicolet R3m/V diffractometer equipped with an LT-1 low-temperature device, graphite-momochromated Mo-K_α radiation; θ–2θ scan mode, scan width (1.8+dispersion)°; range $4° < 2\theta < 45°$; 5741 reflections measured, 5326 unit ($R_{int} = 0.0597$), 3216 observed [$F_o > 6\sigma(F_o)$]. Index range: $-15 \leqslant h \leqslant 14$, $-15 \leqslant k \leqslant 15$, $0 \leqslant l \leqslant 12$. Three intensity control reflections were monitored every 60 reflections of data collection; an average 8% crystal decay was observed. Lorentz-polarization and empirical absorption (ψ-scans) corrections were applied. The structure was solved from Patterson and difference syntheses. An extinction correction was applied.

Non-hydrogen atoms were refined anisotropically by full-matrix least-squares methods. Hydrogen atoms were placed in idealized positions [C—H = 0.96 Å; $U(H) = 1.2U_{eq}(C)$]. The function $w(\Delta F)^2$ was minimized ($w = [\sigma^2(F) + 0.0103F^2]^{-1}$). Final $R = 0.0699$, $wR = 0.0752$, $S = 0.9061$, $\Delta/\sigma(\text{max.}) = 0.014$. The final difference map contained three peaks with heights of 1.58, 1.34 and 1.30 e Å^{-3} located within 0.96 Å of the rhenium atoms. All other peaks were less than 0.99 e Å^{-3}; min. = −1.24 e Å^{-3}. Scattering factors were from the *International Tables for X-ray Crystallography*.[6] Computer programs used: SHELXTL+ programs[7] and PSICOR (public domain).

Acknowledgements—The authors thank the Petroleum Research Fund, administered by the American Chemical Society, for the support of this research, and Professor M. B. Hursthouse for his comments and help in obtaining some of the unpublished data in Table 2.

REFERENCES

1. S. Cai, D. M. Hoffman, D. A. Wierda and H.-G. Woo, *Inorg. Chem.* 1987, **26**, 3693.
2. K. W. Chiu, W.-K. Wong, G. Wilkinson, A. M. R. Galas and M. B. Hursthouse, *Polyhedron* 1982, **1**, 31.
3. P. Stavropoulos, P. G. Edwards, T. Behling, G. Wilkinson, M. Motevalli and M. B. Hursthouse, *J. Chem. Soc., Dalton Trans.* 1987, 169.
4. C. J. Longley, P. D. Savage, G. Wilkinson, B. Hussain and M. B. Hursthouse, *Polyhedron* 1988, **7**, 1079.
5. F. Djafri, R. Lai and M. Pierrot, *Acta Cryst.* 1989, **C45**, 585.
6. *International Tables for X-ray Crystallography*, Vol. IV. Kynoch Press, Birmingham (1974) (Present distributor: Kluwer Academic Publishers, Dordrecht.)
7. G. M. Sheldrick, SHELXTL+. An Integrated System for Solving, Refining and Displaying Crystal Structures from Diffraction Data, Revision 2.22. University of Göttingen, F.R.G. (1987).

Polyhedron Vol. 9, No. 7, pp. 963–968, 1990
Printed in Great Britain

0277–5387/90 $3.00+.00
© 1990 Pergamon Press plc

SOLID STATE STRUCTURE OF THE TANTALUM BIS-ARYL COMPOUNDS $Ta(OAr\text{-}2,6R_2)_3(C_6H_5)_2$ ($R = CH_3$, Pr^i; $OAr\text{-}2,6R_2$ = 2,6-DIALKYLPHENOXIDE): OBSERVATION OF A LACK OF CORRELATION OF M—OAr DISTANCES AND M—O—Ar ANGLES FOR ARYLOXIDE DERIVATIVES OF NIOBIUM(V) AND TANTALUM(V)

BRYAN D. STEFFEY, PHILLIP E. FANWICK and IAN P. ROTHWELL*

Department of Chemistry, Purdue University, West Lafayette, IN 47907, U.S.A.

(*Received* 11 *September* 1989; *accepted* 6 *November* 1989)

Abstract—Treatment of the tantalum dichloride compounds $Ta(OAr\text{-}2,6Me_2)_3Cl_2$ or $Ta(OAr\text{-}2,6Pr^i_2)_3Cl_2$ ($OAr\text{-}2,6Me_2$ = 2,6-dimethylphenoxide; $OAr\text{-}2,6Pr^i_2$ = 2,6-diisopropylphenoxide) with phenyl lithium (2 equiv) leads to the formation of the bis-phenyl compounds $Ta(OAr\text{-}2,6Me_2)_3(C_6H_5)_2$ (**1**) and $Ta(OAr\text{-}2,6Pr^i_2)_3(C_6H_5)_2$ (**2**), respectively, in moderate yields. Single crystal X-ray diffraction analyses of both **1** and **2** show them to be isostructural. In both compounds a trigonal bipyramidal environment about the metal centre is evident with *trans*, axial aryloxide oxygen atoms. Short Ta—O distances in the range of 1.848(5)–1.881(3) Å and almost linear Ta—O—Ar angles are present. The central coordination environments in **1** and **2** are strikingly similar to those found for the bis-cyclometallated compound $Ta(OC_6H_3Ph\text{-}C_6H_4)_2(OAr\text{-}2,6Ph_2)$. Combining the structural data for **1** and **2** with those of other alkyl, aryloxide compounds of niobium(V) and tantalum(V) shows that the M—OAr distances span a narrow range of 1.85–1.95 Å, while the corresponding M—O—OAr angles vary from 135 to 180° with no correlation between the two parameters. Crystal data for $TaO_3C_{36}H_{37}$ (**1**) at 19°C: a = 19.313(3), b = 11.652(1), c = 15.288(1) Å, β = 113.13(1)°, Z = 4, d_{calc} = 1.446 g cm^{-3} in space $C2/c$; for $TaO_3C_{48}H_{61}$ (**2**) at 21°C: a = 11.955(2), b = 19.585(2), c = 19.337(2) Å, β = 103.742(9)°, Z = 4, d_{calc} = 1.309 g cm^{-3} in space group $P2_1/n$.

The last 15 years has seen an explosion of interest in the organometallic chemistry of tantalum.[1] This interest was initially stimulated by the demonstrated ability of this metal to undergo multiple bonding to carbon ligands, generating the first examples of stable metal alkylidene and alkylidyne functionalities.[2] These developments rapidly led to a better mechanistic understanding of the olefin metathesis reaction.[3] Recently, attention has been focussed on the importance of π-donor ligation such as alkoxide and aryloxide groups in promoting such reactivity.[4] Hence, for this and other reasons there has been a recent interest in the structure/reactivity relationship of organometallic compounds of tantalum containing oxygen donor ligation.[5–7] During our studies of the organometallic chemistry of niobium and tantalum surrounded by sterically demanding aryloxide ligation we have recently synthesized two new mixed aryloxide, phenyl compounds of tantalum. We wish to report here on their solid-state structures and comment on the known structural types reported for niobium(V) and tantalum(V) mixed alkyl, aryloxide compounds, focusing particular attention on the metal–aryloxide bonding.

RESULTS AND DISCUSSION

The dichloride compounds $Ta(OAr\text{-}2,6Me_2)_3Cl_2$ and $Ta(OAr\text{-}2,6Pr^i_2)_3Cl_2$ ($OAr\text{-}2,6R_2$ = 2,6-dialkylphenoxide) can be readily obtained in high yields

* Author to whom correspondence should be addressed.

by the treatment of $TaCl_5$ with 3 equiv of either HOAr-2,6Me_2 or LiOAr-2,6Pr^i_2 in hydrocarbon solvents.[6,8] Treatment of either substrate with phenyl lithium in benzene leads to the formation of the corresponding diphenyl compounds Ta(OAr-2,6Me_2)$_3$$Ph_2$ (**1**) and Ta(OAr-2,6Pr^i_2)$_3$$Ph_2$ (**2**) in moderate yields. Exposure of solutions of **1** or **2** to an excess of LiPh causes substitution of aryloxide ligands to take place leading initially to the formation of triphenyl derivatives.[9] Further reaction leads to dark solutions containing decomposition products presumably formed via the unstable, homoleptic [$TaPh_5$].[8] The spectroscopic properties of **1** and **2** are as one would predict. The new Ta—C_6H_5 groups are readily detected in the NMR spectra by the characteristic downfield multiplet in the ^{1}H NMR spectrum of the hydrogen atoms *ortho* to the Ta—C bond and the downfield resonance of the Ta—*C*(*ipso*) carbon atom in the ^{13}C NMR spectrum.[10]

Single crystal X-ray diffraction analyses of **1** and **2** show the molecules to adopt almost identical geometries in the solid state. In the case of the 2,6-dimethylphenoxide complex (**1**) a crystallographically imposed two-fold axis is present (Fig. 1) through the pseudo-trigonal-bipyramidal coordination sphere, so that the unique equatorial aryloxide ligand has a linear Ta—O—Ar bond angle. In both molecules (Figs 1 and 2) the phenyl groups bound to tantalum lie within the equatorial plane. Some selected bond distances and angles are collected in Tables 1 and 2. Compounds **1** and **2** represent new members in a now extensive series of five-coordinate organometallic derivatives of niobium(V) and tantalum(V) containing aryloxide ligation. In Table 3 are collected certain structural data

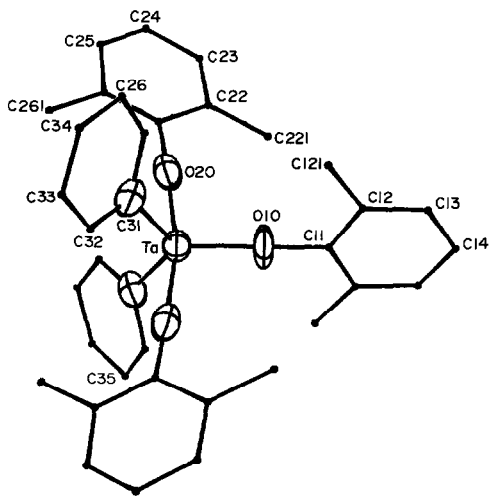

Fig. 1. ORTEP view of Ta(OAr-2,6Me_2)$_3$$Ph_2$ (**1**).

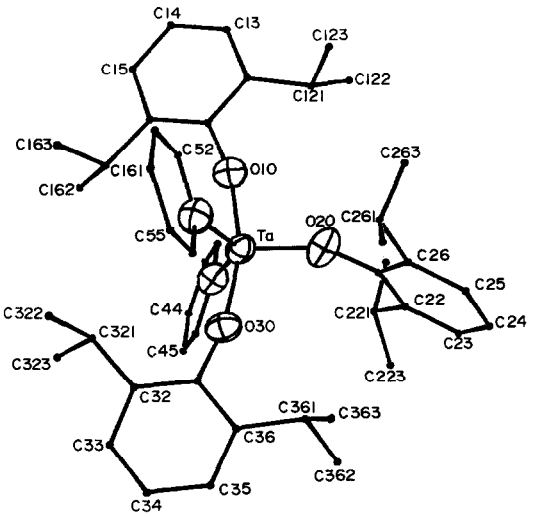

Fig. 2. ORTEP view of Ta(OAr-2,6Pr^i_2)$_3$$Ph_2$ (**2**).

for those compounds that have been the subject of a crystallographic study. For all compounds both the M—C and M—O distances can be seen to lie in a very narrow range of 2.136–2.248 Å and 1.85–1.95 Å, respectively. For the metal–alkyl (aryl) bonds the largest distances are found for the unique methyl groups in Ta(OAr-2,6Bu^t_2)$_2$$Me_3$ and Ta(OAr-2,6Bu^t_2-4OMe)$_2$$Me_3$, where steric pressure from the aryloxide ligands leads to a significant lengthening.[11] Both the M—O and M—C distances appear to be insensitive to whether they are terminal or contained within metallacycle rings formed by aryloxide cyclometallation.

Another interesting feature of the compounds contained in Table 3 concerns the bonding of the aryloxide ligands to the metal centre. All compounds are five-coordinate, formally containing a 10-electron count for the central metal core. The electron deficiency of the metal centre can be relieved by oxygen-*p* to metal-*d* π-bonding, and this argument is normally used to account for the short M—O distances.[16] Consistent with this picture are the results of two studies that show an excellent correlation between Nb—OAr[12] and W—OAr[17] distances and the formal electron count at the metal centre. However, it was also pointed out that the M—O—Ar angle, which theoretically could also be a measure of the amount of π-donation to the metal centre, did not correlate at all with the electron deficiency of the metal.[12,17] This fact is highlighted by the data in Table 3 (Fig. 3) for aryloxide compounds of niobium(V) and tantalum(V). Although the M—OAr distances only vary over the range

Table 1. Selected bond distances (Å) and angles (°) for $Ta(OAr\text{-}2,6Me_2)_3Ph_2$ (1)

Ta—O(10)	1.848(5)	Ta—O(20)	1.879(4)
Ta—C(31)	2.180(6)		
O(10)—Ta—O(20)	96.1(1)	O(10)—Ta—C(31)	115.8(2)
O(20)—Ta—O(20)	167.7(2)	O(20)—Ta—C(31)	87.3(2)
C(31)—Ta—C(31)	128.4(3)	Ta—O(10)—C(11)	180.0(0)
Ta—O(20)—C(21)	175.5(4)		

1.85–1.95 Å, the M—OAr angles vary from 135 to 180°. Furthermore, there is no correlation between the two parameters; i.e. the M—O—Ar angle does not open up as the M—OAr distance falls. Hence, based upon data in this study (Fig. 3) as well as previous studies,[12,17] it can be concluded that the M—O—Ar angle in early *d*-block transition metal aryloxide compounds is an extremely flexible parameter giving little insight into M—OAr bonding.

This situation contrasts markedly with that found for aryloxide derivatives of the Group 14 metals germanium and tin and the later *d*-block transition metals. In these cases terminal M—O—Ar angles appear to be more confined into a narrow range of 120–130°.[18]

EXPERIMENTAL

The chloride compounds $Ta(OAr\text{-}2,6Me_2)_3Cl_2$ and $Ta(OAr\text{-}2,6Pr^i_2)_3Cl_2$ were obtained by published procedures. Phenyl lithium was prepared as a precipitate from a Bu^nLi/C_6H_5Br mixture in hexane/toluene. After washing with hexane the compound was dried and stored in the Dri-Lab prior to use. All solvents were dried by refluxing over sodium benzophenone before being distilled under nitrogen.

$Ta(OAr\text{-}2,6Me_2)_3Ph_2$ (1)

To a yellow solution of $Ta(OAr\text{-}2,6Me_2)_3Cl_2$ (3.0 g, 4.88 mmol) in benzene (75 cm^3) was slowly added LiC_6H_5 (0.82 g, 9.8 mmol) as a powder over a period of 30 min. The resulting dark brown solution was stirred for 3 h, filtered and the filtrate evaporated *in vacuo*. Extraction of the crude product with hexane followed by slow cooling of the solution yielded yellow crystals of the pure product in 35% yield. Found: C, 62.7; H, 5.6. Calc. for $TaC_{36}H_{37}O_3$: C, 61.9; H, 5.3%. ^1H NMR (C_6D_6, 30°C): δ 8.11 (m, *ortho*-C_6H_5), 2.12 (s, OAr-2,6Me_2), 6.8–7.5 (m, aromatic). ^{13}C NMR (C_6D_6, 30°C): δ 192.2 (Ta—*C*), 18.2 (CH_3).

$Ta(OAr\text{-}2,6Pr^i_2)_3Ph_2$ (2)

An essentially identical procedure to that described above only using $Ta(OAr\text{-}2,6Pr^i_2)_3Cl_2$ (0.5 g, 0.78 mmol), benzene (25 cm^3), and LiC_6H_5 (0.16 g, 1.9 mmol) yielded the product as pale crystals from hexane. Found: C, 66.3; H, 6.9. Calc. for $TaC_{48}H_{61}O_3$: C, 66.5; H, 7.1%. ^1H NMR (C_6D_6, 30°C): δ 8.28 (m, *ortho*-C_6H_5), 1.41 (d, $CHMe_2$), 3.41 (m, $CHMe_2$), 6.8–7.5 (m, aromatics). ^{13}C NMR (C_6D_6, 30°C): δ 193.8 (Ta—*C*), 18.2 ($CHMe_2$), 2.43 ($CHMe_2$).

Table 2. Selected bond distances (Å) and angles (°) for $Ta(OAr\text{-}2,6Pr^i_2)_3Ph_2$ (2)

Ta—O(10)	1.881(3)	Ta—O(20)	1.852(3)
Ta—O(30)	1.880(3)	Ta—C(41)	2.206(5)
Ta—C(51)	2.209(5)		
O(10)—Ta—O(20)	97.7(2)	O(10)—Ta—O(20)	161.4(1)
O(10)—Ta—C(41)	86.5(2)	O(10)—Ta—C(51)	86.2(2)
O(20)—Ta—O(30)	101.02(2)	O(20)—Ta—C(41)	112.2(2)
O(20)—Ta—C(51)	111.1(2)	O(30)—Ta—C(41)	86.8(2)
O(30)—Ta—C(51)	86.8(2)	C(41)—Ta—C(51)	136.7(2)
Ta—O(10)—C(11)	165.0(4)	Ta—O(20)—C(21)	152.5(4)
Ta—O(30)—C(31)	166.4(4)		

Table 3. Selected bond distances (Å) and angles (°) for a series of mixed alkyl, aryloxide compounds of Nb, Ta[a]

Compound	M—C	M—O	M—O—Ar	O—M—O	Reference
$Nb(OAr\text{-}2,6Me_2)_5$	—	1.910(2) 1.893(2) 1.890(2) 1.901(2) 1.903(2)	157.0(2) 166.5(2) 144.8(2) 143.8(2) 169.3(2)	176.98(8)	12
$Ta(OAr\text{-}2,6Me_2)_4Me$	2.155(10)	1.899(4)	157.8(3)	[a]	8
$Ta(OAr\text{-}2,6Me_2)_3Ph_2$	2.180(6)	1.879(4) 1.848(5)	175.5(4) 180	167.7(2)	This work
$Ta(OAr\text{-}2,6Pr^i_2)_3Ph_2$	2.206(5) 2.209(5)	1.881(3) 1.880(3) 1.852(3)	165.0(4) 166.4(4) 152.5(4)	161.4(1)	This work
$Ta(OC_6H_3Ph\text{-}C_6H_4)_2(OAr\text{-}2,6Ph_2)$	2.142(4) 2.165(4)	1.905(2) 1.897(2) 1.903(3)	136.8(2) 147.1(3)	168.1(1)	13
$Ta(OC_6H_3Ph\text{-}C_6H_4)(OAr\text{-}2,6Ph_2)_2(Me)$	2.215(5) 2.125(2)	1.909(4) 1.899(4) 1.883(4)	141.4(4) 169.5(4) 146.6(4)	168.9(2)	14
$Ta(OC_6H_3Ph\text{-}C_6H_4)(OAr\text{-}2,6Ph_2)_2(Bu^n)$	2.182(4)c 2.149(4)	1.913(3) 1.890(3) 1.910(3)	136.5(3) 160.7(3) 136.9(3)	164.5(1)	14
$Ta(OC_6H_3\text{-}2,6Bu^t_2)_2Me_3$	2.248(10) 2.136(10) 2.138(10)	1.930(6) 1.945(6)	144.8(5) 155.3(6)	164.1(2)	11
$Ta(OC_6H_2\text{-}2,6Bu^t_2\text{-}4OMe)_2Me_3$	2.219(8) 2.169(8) 2.150(8)	1.925(4)	153.2(3)	167.2(2)	11
$Ta(OAr\text{-}2,6Me_2)_2(CH_2Ph)_3$	2.204(6) 2.204(7) 2.136(7)	1.919(4) 1.887(4)	150.6(4) 158.9(4)	165.5(2)	8
$Nb(OAr\text{-}2,6Ph_2)_2(CH_2Ph\text{-}4Me)_3$	2.181(3) 2.192(4) 2.181(3)	1.917(2) 1.915(2)	167.7(2) 178.1(2)	174.77(9)	15
$Ta(OAr\text{-}2,6Ph_2)_2(CH_2Ph\text{-}4Me)_3$	2.154(4) 2.179(6) 2.161(6)	1.906(4) 1.903(4)	167.1(4) 177.5(4)	174.(2)	15

[a] All compounds adopt an approximately trigonal bipyramidal geometry about the metal centre with *trans*, axial *aryloxide* ligands, except $Ta(OAr\text{-}2,6Me_2)_4Me$ which is square pyramidal.

X-ray crystallography

Crystal data and data collection parameters are collected in Table 4. A suitable crystal of each of the two compounds was mounted in a glass capillary in a random orientation. Cell constants were obtained from least-squares refinement using the scattering angles of 25 reflections as measured by the computer-controlled diagonal slit method of centring. Systematic absences and subsequent least-squares refinement indicated the space group $C2/c$ for **1** and $P2_1/n$ for **2**. The data were collected to a maximum 2θ of 45° in both cases using the ω–2θ scan technique. Moving crystal, moving counter background counts were made by scanning an additional 25% above and below the scan width. The counter aperture was adjusted as a function of θ. For intense reflections an attenuator (factor 12.9) was automatically inserted in front of the detector. As a check on crystal and electronic stability three standard reflections were measured every 2000 s of beam time. In both cases some decay was observed and

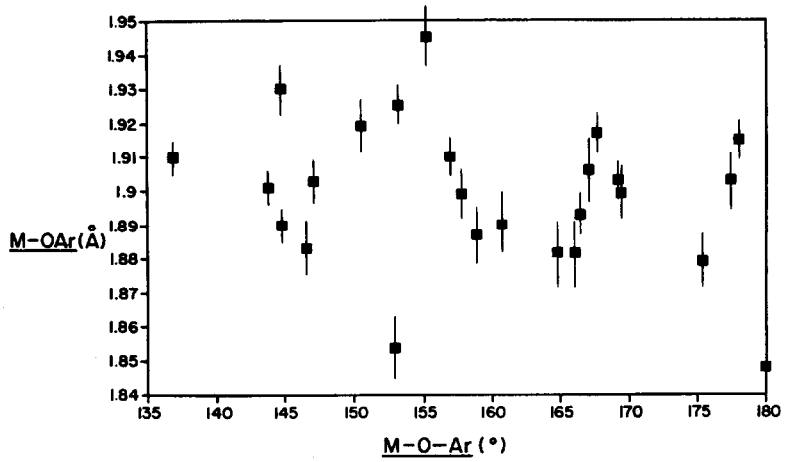

Fig. 3. A plot of M—OAr distance vs M—O—Ar angle for the terminal (i.e. non-metallated) aryloxide ligands contained in the compounds listed in Table 3.

Table 4. Crystal data and data collection parameters

	(1)	(2)
Formula	$TaO_3C_{36}H_{37}$	$TaO_3C_{48}H_{61}$
fw	688.56	866.97
Space group	*C*2/*c*	$P2_1/n$
a (Å)	19.313(3)	11.955(2)
b (Å)	11.652(1)	19.585(2)
c (Å)	15.288(1)	19.337(2)
β (°)	113.13(1)	103.742(9)
V (Å^3)	3163(1)	4397(2)
Z	4	4
d_{calc} (g cm^{-3})	1.446	1.309
Crystal dimensions (mm)	0.50 × 0.43 × 0.38	0.81 × 0.74 × 0.34
Temperature (°C)	19	21
Radiation (wavelength)	Mo-K_α (0.71073 Å)	Mo-K_α (0.71073 Å)
Monochromater	Graphite	Graphite
Linear absorbance coefficient (cm^{-1})	34.63	25.05
Absorption correction applied	Empirical[a]	Empirical[a]
Crystal radius (cm)	0.043	0.063
Diffractometer	Enraf–Nonius CAD4	Enraf–Nonius CAD4
Scan method	ω–2θ	ω–2θ
h, *k*, *l* limits:	0 to 20 0 to 12 −16 to 15	−12 to 12 0 to 21 0 to 20
2θ Range (°)	4.00–45.00	4.00–45.00
Scan width (°)	0.72 + 0.35 tan(θ)	0.62 + 0.35 tan(θ)
Take-off angle (°)	1.80	2.80
Programs used	Enraf–Nonius SDP	Enraf–Nonius SDP
F(000)	1360.0	1184.0
p-Factor used in weighting	0.040	0.040
Data collected	2183	5904
Unique data	2183	5904
Data with $I > 3.0\sigma(I)$	1835	4518
Number of variables	187	469
Largest shift/ESD in final cycle	0.00	0.28
R	0.037	0.032
R_w	0.045	0.043
Goodness-of-fit	1.576	1.517

[a] H. D. Flack, *Acta Cryst.* 1977, **A33**, 890.

an empirical correction was applied. The structures were solved by using the Patterson heavy-atom method to reveal the position of the zirconium atoms. The remaining heavy atoms were then located in succeeding Fourier syntheses. Hydrogen atoms were located and added to the structures but were not refined.

Acknowledgement—We thank the National Science Foundation (Grant CHE-8612063) for support of this research.

Supplementary materials available: Listings of fractional coordinates, anisotropic thermal parameters, full bond distances and angles and a listing of observed and calculated structure factor amplitudes for **1** and **2**.

REFERENCES

1. E. Abel, F. G. A. Stone and G. Wilkinson (Eds), *Comprehensive Organometallic Chemistry*. Pergamon Press, Oxford (1982).
2. R. R. Schrock, in *Reactions of Coordinated Ligands* (Edited by P. S. Braterman). Plenum Press, New York (1986).
3. (a) R. H. Grubbs, Ch. 54 of ref. 1; (b) R. R. Schrock, *J. Organomet. Chem.* 1986, **300**, 96 and refs therein.
4. R. R. Schrock, R. T. DePue, J. Feldman, C. J. Schaverien, J. C. Dewan and A. H. Liu, *J. Am. Chem. Soc.* 1988, **110**, 1423 and refs therein.
5. (a) R. E. Lapointe, P. T. Wolczanski and J. F. Mitchell, *J. Am. Chem. Soc.* 1986, **108**, 6283; (b) T. V. Lubben and P. T. Wolczanski, *J. Am. Chem. Soc.* 1985, **107**, 701; (c) R. E. Lapointe and P. T. Wolczanski, *Organometallics* 1985, **4**, 1810.
6. (a) K. R. Ballard, I. M. Gardiner and D. E. Wigley, *J. Am. Chem. Soc.* 1989, **111**, 2159; (b) M. A. Bruck, A. S. Copenhaver and D. E. Wigley, *J. Am. Chem. Soc.* 1987, **109**, 6525.
7. I. P. Rothwell, *Accts Chem. Res.* 1988, **21**, 153.
8. L. R. Chamberlain, I. P. Rothwell, K. Folting and J. C. Huffman, *J. Chem. Soc., Dalton Trans.* 1987, 155.
9. B. D. Steffey and I. P. Rothwell, unpublished results.
10. L. R. Chamberlain, J. L. Kerschner, A. P. Rothwell, I. P. Rothwell and J. C. Huffman, *J. Am. Chem. Soc.* 1987, **109**, 6471.
11. L. R. Chamberlain, I. P. Rothwell and J. C. Huffman, *J. Am. Chem. Soc.* 1986, **108**, 1502.
12. T. W. Coffindaffer, B. D. Steffey, I. P. Rothwell, K. Folting, J. C. Huffman and W. E. Streib, *J. Am. Chem. Soc.* 1989, **111**, 4742.
13. B. D. Steffey, L. R. Chamberlain, R. W. Chesnut, D. E. Chebi, P. E. Fanwick and I. P. Rothwell, *Organometallics* 1989, **8**, 1419.
14. (a) R. W. Chesnut, B. D. Steffey, I. P. Rothwell and J. C. Huffman, *Polyhedron* 1988, **7**, 753; (b) R. W. Chesnut, J. S. Yu, P. E. Fanwick, I. P. Rothwell and J. C. Huffman, *Polyhedron* in press.
15. J. S. Yu, R. W. Chesnut, P. E. Fanwick and I. P. Rothwell, results to be published.
16. M. H. Chisholm and I. P. Rothwell, in *Comprehensive Coordination Chemistry* (Edited by G. Wilkinson, R. D. Gillard and J. A. McCleverty), Ch. 15.3. Pergamon Press, Oxford (1987).
17. J. L. Kerschner, P. E. Fanwick, I. P. Rothwell and J. C. Huffman, *Inorg. Chem.* 1989, **28**, 780.
18. G. D. Smith, D. E. Chebi and I. P. Rothwell, results to be published.

Polyhedron Vol. 9, No. 7, pp. 969–974, 1990
Printed in Great Britain

0277–5387/90 $3.00+.00
© 1990 Pergamon Press plc

SYNTHESIS AND SOLID STATE STRUCTURE OF SOME 2,6-DIPHENYLPHENOXIDE DERIVATIVES OF RHODIUM(I) AND IRIDIUM(I)

DIEGO E. CHEBI, PHILLIP E. FANWICK and IAN P. ROTHWELL*

Department of Chemistry, Purdue University, West Lafayette, IN 47907, U.S.A.

(*Received* 22 *September* 1989; *accepted* 6 *November* 1989)

Abstract—Treatment of the carbonyl dimer $Rh_2Cl_2(CO)_4$ with 2 equivalents of LiOAr-2,6Ph_2 (OAr-2,6Ph_2 = 2,6-diphenylphenoxide) produces the aryloxide bridged dimer $[(CO)_2Rh(\mu\text{-OAr-2,6}Ph_2)_2Rh(CO)_2]$ (**1**) in excellent yield. Compound **1** shows two, equal intensity carbonyl stretching frequencies at 2090 and 2006 cm^{-1} in the IR spectrum (Nujol mull) consistent with a solid state structure consisting of two edge shared square planes. A single crystal X-ray diffraction analysis of **1** confirmed this formulation showing no evidence for π-bonding by the side chain aryl groups to the 16-electron metal centre. Treatment of the dimer $Ir_2Cl_2(COD)_2$ (COD = 1,5-cyclooctadiene) with LiOAr-2,6Ph_2 yielded a mixture of products. Eventually sparingly soluble crystals of a salt $[(COD)Ir(\eta^5\text{-HOAr-2,6}Ph_2)]^+[(COD)Ir(OAr\text{-2,6}Ph_2)_2]^-$ (**2**) were obtained in very minor yield. The presence of a 2,6-diphenylphenol ligand η^5-bound through the central phenoxy ring to the iridium metal centre was confirmed by a single crystal X-ray diffraction analysis of **2**. The distances Ir—C to the COD ligand in the cation in **2**, 2.10(2)–2.16(2) Å, are slightly shorter than the distances of 2.25(2)–2.35(2) Å to the five carbon atoms of the central phenoxy ring. The *ipso* carbon attached to the hydroxyl group is non-bound. The anion in **2** contains two terminal aryloxide ligands bound approximately *trans* to the two iridium–olefinic bonds of the COD group yielding a structure best described as square planar. Crystal data at 20°C for $Rh_2O_6C_{40}H_{26}$ (**1**): $a = 10.750(2)$, $b = 28.307(5)$, $c = 11.311(2)$ Å, $\beta = 96.21(1)°$, $Z = 4$, $d_{calc} = 1.569$ g cm^{-3} in space group $P2_1/n$; for $Ir_2Cl_6O_3C_{72}H_{58}$ (**2**) $2CHCl_3$: $a = 13.428(2)$, $b = 22.838(3)$, $c = 20.937(2)$ Å, $\beta = 92.775(9)°$, $Z = 4$, $d_{calc} = 1.624$ g cm^{-3} in space group $P2_1/n$.

There has been a dramatic increase in recent years in the study of alkoxide and aryloxide derivatives of the electron-rich later transition elements.[1–4] These studies have focussed not only on the types of compounds available but also upon the reactivity of the M—OR and M—OAr bonds. During our studies of the early *d*-block metal chemistry associated with sterically demanding aryloxide ligation[5] we have identified a range of coordination modes for the ligand 2,6-diphenylphenoxide (OAr-2,6Ph_2).[6,7] Besides simple terminal aryloxide bonding, this ligand may also chelate to the metal centre either via a π-interaction or via metallation of the substituent aryl rings.[6,7] Furthermore, a simple non-chelated η^6-interaction with one of the side chain phenyl rings is seen in the compound $(\eta^6\text{-}C_6H_5\text{-HOAr-Ph})Mo(CO)_3$.[8] In this paper we wish to report our preliminary investigation of the later transition metal derivatives of OAr-2,6Ph_2 ligation, focusing on derivatives of rhodium(I) and iridium(I). Although initially anticipated compounds involving chelation via an η^x-interaction ($x < 6$) with the substituent side chain rings were not observed, a new bonding mode for this ligand involving an iridium–η^5-interaction with the central phenoxy ring has been characterized.

RESULTS AND DISCUSSION

Treatment of the carbonyl dimer $[(CO)_2Rh(\mu\text{-}Cl)_2Rh(CO)_2]$ with LiOAr-2,6Ph_2 (≥ 2 equiv)

* Author to whom correspondence should be addressed.

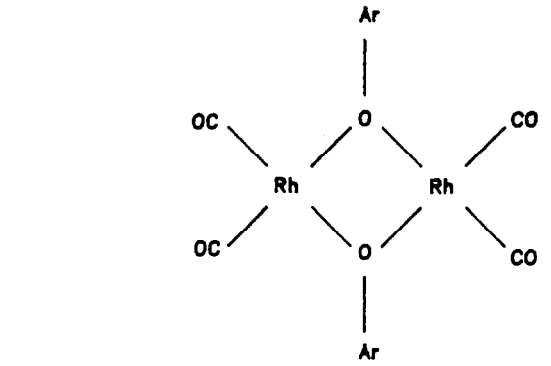

(1)

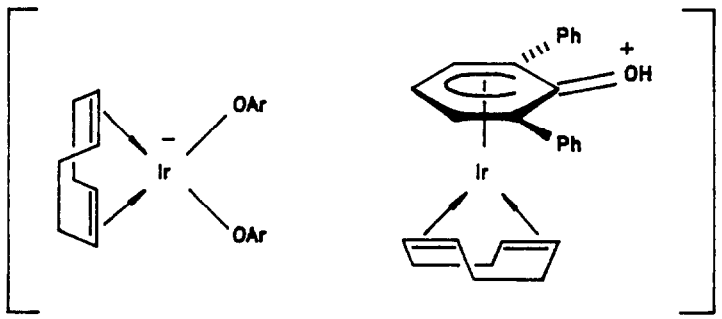

(2)

OAr = 2,6–Diphenylphenoxide

in hydrocarbon solvents leads to the formation of orange solutions of $[(CO)_2Rh(\mu\text{-}OAr\text{-}2,6Ph_2)_2Rh(CO)_2]$ (**1**) (see Diagram). Recrystallization of **1** from toluene solution yields large yellow blocks suitable for X-ray diffraction analysis. The ^1H NMR spectrum of **1** shows a series of multiplets in the δ 6.8–7.5 ppm region characteristic of the OAr-2,6Ph_2 ligand. The absence of any resonances in the ^1H NMR spectrum upfield of the aromatic region indicates the lack of any π-interaction of the rhodium metal centre with the substituent aryl rings.[7,8] In the ^{13}C NMR spectrum the Rh—*C*O carbon atoms are found to resonate at δ 179.4 ppm with a typical $^1J(^{103}Rh\text{–}^{13}C)$ coupling constant of 76 Hz. In the IR spectrum of **1** as a Nujol mull, two equal intensity bands at 2090 and 2006 cm^{-1} are observed. The complexity observed in the carbonyl region of the IR spectrum of $[(CO)_2Rh(\mu\text{-}Cl)_2Rh(CO)_2]$[9] is missing for **1**, consistent with the solid state structure consisting of a planar $C_2Rh(\mu\text{-}O)_2RhC_2$ unit.

A single crystal X-ray diffraction analysis of **1** confirmed this postulate (Fig. 1). Some selected bond distances and angles are collected in Table 1. The aryloxide groups in **1** adopt a bridging mode holding together two square-planar rhodium units. There are no close contacts between the substituent aryl group and the rhodium metal centres. There are no distortions evident in the solid state structure of **1** involving a bending of the two square-planar units about the bridging oxygen atoms. A significant dihedral angle is present in the chloro-bridged dimer $(CO)_2Rh(\mu\text{-}Cl)_2Rh(CO)_2$ about the Cl—Cl vector.[9] Presumably the sterically demanding aryloxide ligands in **1** preclude close packing of the dimeric units in the solid state so that weak electronic interactions between adjacent molecules cannot take place.

In contrast to this straightforward reactivity, the reaction of LiOAr-2,6Ph_2 with the iridium dimer, $[(COD)Ir(\mu\text{-}Cl)_2Ir(COD)]$, leads to a complex mixture of products as indicated by the ^1H NMR spectrum of the reaction mixture. Simple, dimeric, phenoxide and alkoxide bridged compounds of the type $[(COD)Ir(\mu\text{-}OR)_2Ir(COD)]$ have been reported in the literature.[10] The preferred synthetic route to these compounds involves a combination of parent phenol or alcohol with sodium carbonate reacting with the chloro-bridged dimer.[10] In our hands a mixture of $[(COD)Ir(\mu\text{-}Cl)_2Ir(COD)]$/HOAr-2,6$Ph_2$/$Na_2CO_3$ failed to react. The complexity of the reaction mixture formed by the use of LiOAr-2,6Ph_2 may be a consequence of nucleophilic attack taking place by the phenoxide ion on the coor-

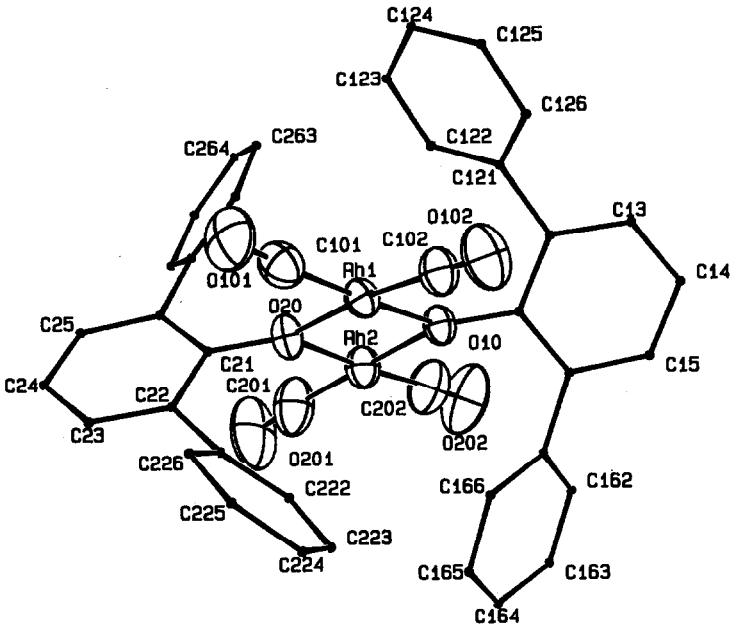

Fig. 1. ORTEP view of $[(CO)_2Rh(\mu\text{-}OAr\text{-}2,6Ph_2)_2Rh(CO)_2]$ (**1**).

dinated COD ligands. This reaction may be competing with a simple exchange process. Repeated attempts at recrystallization of the complex reaction mixture did eventually yield a few crystals of an iridium compound (**2**) from chloroform. A single crystal X-ray diffraction analysis of **2** (Figs 2 and 3) shows the compound to be a salt, with both an iridium-containing cation and anion (see Diagram). Some selected bond distances and angles are collected in Table 2. The anion in **2** can be seen to consist of an iridium(I) metal centre coordinated to a chelating COD molecule and two $OAr\text{-}2,6Ph_2$ ligands. The central coordination sphere in $[(COD)Ir(OAr\text{-}2,6Ph_2)_2]^-$ is best described as a typical square-planar arrangement of the two olefinic parts of the COD and two aryloxide oxygen atoms (Fig. 2). The Ir—O distances of 2.08(1) and 2.09(1) Å in the anion **2** compare favourably with the distance of 2.049(4) Å in the neutral iridium(I) compound *trans*-$Ir(PPh_3)_2(CO)(OPh)$.[11] The cation

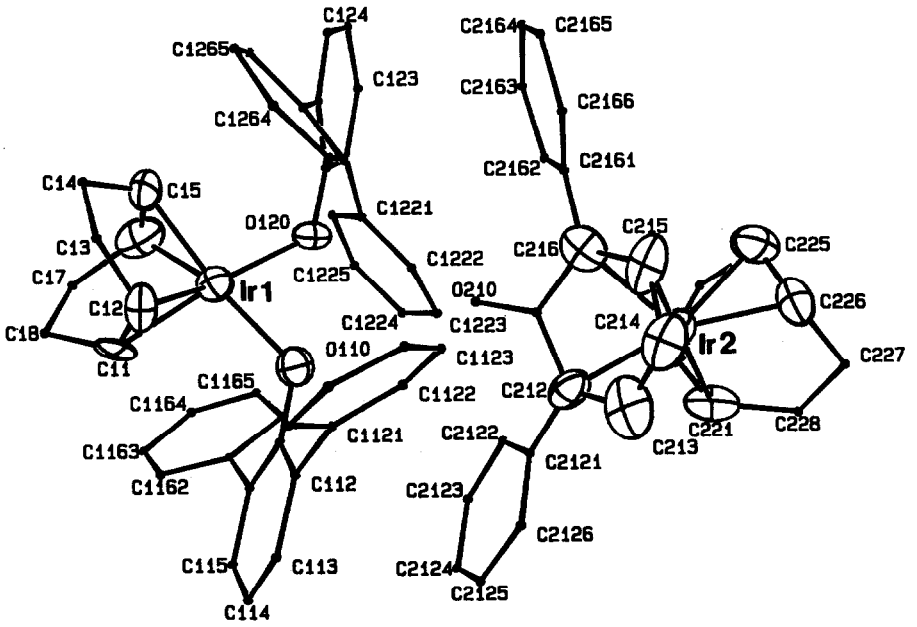

Fig. 2. ORTEP view of the mutual packing of the anion and cation within **2**.

in **2** can be thought of as an $Ir(COD)^+$ unit π-bound to the central phenoxy ring of 2,6-diphenylphenol (presumably generated by partial hydrolysis). The iridium metal centre can be seen to be interacting with the central ring in an η^5-fashion leading to a formal 18-electron count for the metal (Fig. 3). The carbon atom attached to the hydroxide group is bent away leading to a non-bonding distance between it and the metal centre. The π-binding of phenoxide rings to transition metal centres is well established. A considerable number of η^6-phenol and η^6-phenoxide compounds have been reported and structurally characterized.[4,12,13] The compound $[Rh(\eta^5\text{-OAr-2,6Bu}^t_2)(PPh_3)_2]$ was synthesized by Lappert and co-workers and the η^5-cyclohexadienonyl ligand confirmed by a single crystal X-ray diffraction study.[14] In compounds **2** the η^5-HOAr-2,6Ph_2 group can best be described as a protonated η^5-cyclohexadienonyl ligand (see Diagram). Consistent with this picture is the short C—OH distance of 1.26(2) Å compared to values of 1.31(3) and 1.37(2) Å for the O-bound aryloxide ligands contained within the anion.

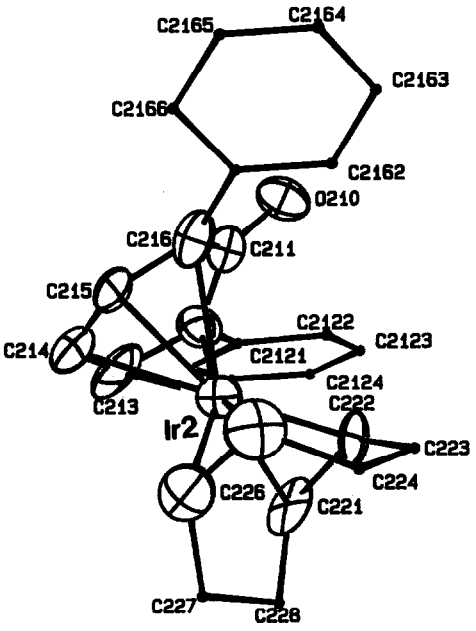

Fig. 3. ORTEP view of the $[(COD)Ir(\eta^5\text{-HOAr-2,6Ph}_2)]^+$ cation in **2**.

Table 1. Selected bond distances (Å) and angles (°) for $[(CO)_2Rh(\mu\text{-OAr-2,6Ph}_2)_2Rh(CO)_2]$ (**1**)

Rh(1)—Rh(2)	3.2696(6)	Rh(1)—O(10)	2.083(3)
Rh(1)—O(20)	2.063(3)	Rh(1)—C(101)	1.820(7)
Rh(1)—C(102)	1.835(7)	Rh(2)—O(10)	2.101(3)
Rh(2)—O(20)	2.067(4)	Rh(2)—C(201)	1.815(8)
Rh(2)—C(202)	1.817(8)		

Rh(1)—O(10)—Rh(2)	102.8(1)	Rh(1)—O(20)—Rh(1)	104.7(1)
O(10)—Rh(1)—O(20)	76.4(1)	O(10)—Rh(2)—O(20)	76.0(1)
C(101)—Rh(1)—C(102)	86.3(3)	C(201)—Rh(2)—C(202)	84.4(3)
Rh(1)—C(101)—O(101)	176.8(6)	Rh(1)—C(102)—O(102)	176.3(5)
Rh(2)—C(201)—O(201)	177.1(8)	Rh(2)—C(202)—O(202)	176.3(6)

Table 2. Selected bond distances (Å) and angles (°) for $[(COD)Ir(\eta^5\text{-HOAr-2,6Ph}_2)]^+[(COD)Ir(OAr\text{-2,6Ph}_2)_2]^-$

$[(COD)Ir(OAr\text{-2,6Ph}_2)_2]^-$

Ir(1)—O(110)	2.08(1)	Ir(1)—C(15)	2.08(2)
Ir(1)—O(120)	2.09(1)	Ir(1)—C(16)	2.09(2)
Ir(1)—C(11)	21.13(2)	O(110)—C(111)	1.37(2)
Ir(1)—C(12)	2.10(2)	O(120)—C(121)	1.31(3)
O(110)—Ir(1)—O(120)	79.5(5)	Ir(1)—O(110)—C(111)	126(1)
		Ir(1)—O(120)—C(121)	131(1)

$[(COD)Ir(\eta^5\text{-HOAr-2,6Ph}_2)]^+$

Ir(2)—C(212)	2.25(2)	Ir(2)—C(221)	2.10(2)
Ir(2)—C(213)	2.30(2)	Ir(2)—C(222)	2.12(2)
Ir(2)—C(214)	2.33(2)	Ir(2)—C(225)	2.16(2)
Ir(2)—C(215)	2.26(2)	Ir(2)—C(226)	2.212(2)
Ir(2)—C(216)	2.35(2)		
C(211)—O(210)	1.26(2)		

EXPERIMENTAL

The reagent lithium 2,6-diphenylphenoxide (LiOAr-2,6-Ph_2) was prepared by treating the commercially obained 2,6-diphenylphenol with one equivalent of n-butyl lithium in hexane. Purification was achieved by successive hexane washes of the white powder. The compounds $[(CO)_2Rh(\mu\text{-Cl})]_2$ and $[(COD)Ir(\mu\text{-Cl})]_2$ were obtained by published procedures.[9,15] The methods employed for the manipulation of the air- and moisture-sensitive products have been described previously.[7]

$[(CO)_2Rh(\mu\text{-OAr-2,6Ph}_2)_2Rh(CO)_2]$ (1)

To a solution of $[(CO)_2Rh(\mu\text{-Cl})]_2$ (0.15 g, 0.39 mmol) in benzene (15 cm^3) was added LiOAr-2,6Ph_2 (0.21 g, 0.82 mmol). The mixture was stirred for 40 min. Removal of solvent under vacuum yielded a pale yellow powder which was taken up in 10 cm^3 of toluene. Slow cooling of the solution in the freezer at −15°C for 12 h yielding the product as large yellow crystals in 60% yield. ^1H NMR (C_6D_6, 30°C): δ 6.7–7.2 (m, aromatics). ^{13}C NMR ($CDCl_3$, 30°C): δ 179.4 (Rh—*C*O), $^1J(^{103}Rh\text{–}^{13}C) = 76$ Hz. IR (Nujol mull): ν(CO) = 2090, 2006 cm^{-1}.

$[(COD)Ir(\eta^5\text{-HOAr-2,6Ph}_2)]^+[(COD)Ir(OAr\text{-}2,6Ph_2)_2]^-$ (2)

A mixture of $[(COD)Ir(\mu\text{-Cl})]_2$ (0.20 g, 0.30 mmol) and LiOAr-2,6Ph_2 (0.16 g, 0.65 mmol) in benzene (15 cm^3) was stirred for 4 h and filtered. The filtrate was evaporated under vacuum, and the resulting solid was washed with hexane and dissolved in chloroform. After cooling the solution for 48 h at −15°C, a few crystals of **2** suitable for X-ray crystallography were obtained.

Table 3. Crystal data and data collection parameters

	(1)	(2)
Formula	$Rh_2O_6C_{40}H_{26}$	$Ir_2Cl_6O_3C_{72}H_{58}$
f_w	808.46	1568.38
Space group	$P2_1/n$ (No. 14)	$P2_1/n$ (No. 14)
a (Å)	10.750(2)	13.428(2)
b (Å)	28.307(5)	22.838(3)
c (Å)	11.311(2)	20.937(2)
β (°)	96.21(1)	92.775(9)
V (Å^3)	3421(2)	6413(2)
Z	4	4
d_{calc} (g cm^{-3})	1.569	1.624
Crystal size (mm)	0.50 × 0.17 × 0.15	0.22 × 0.20 × 0.06
Temperature (°C)	20	20
Radiation	Mo-K_α (0.71073 Å)	Mo-K_α (0.71073 Å)
Monochromator	Graphite	Graphite
Linear absorbance coefficient (cm^{-1})	9.94	44.28
Absorption correction applied	None	Empirical[a]
Scan method	ω–2θ	ω–2θ
h, k, l limits:	0 to 11 0 to 30 −12 to 12	−14 to 14 0 to 24 0 to 22
2θ Range (°)	4.00–45.00	4.00–45.00
Scan width (°)	0.55 + 0.35 tan (θ)	0.40 + 0.35 tan (θ)
Take-off angle (°)	2.20	1.90
Programs used	Enraf–Nonius SDP	Enraf–Nonius SDP
F(000)	1616.0	3080.0
p-Factor used in weighting	0.040	0.040
Data collected	4610	8640
Unique data	4610	8640
Data with $I > 3.0\sigma(I)$	3250	4047
Number of variables	433	721
Largest shift/ESD in final cycle	0.05	0.02
R	0.032	0.067
R_w	0.039	0.075
Goodness-of-fit	1.040	1.424

[a] N. Walker and D. Stuart, *Acta Cryst.* 1983, **A39**, 158.

X-ray crystallography

Crystal data and data collection parameters are collected in Table 3. A suitable crystal of each of the two compounds was mounted in a glass capillary in a random orientation. Cell constants were obtained from least-squares refinement using the scattering angles of 25 reflections as measured by the computer-controlled diagonal slit method of centring. Systematic absences and subsequent least-squares refinement indicated the space group $P2_1/n$ for both **1** and **2**. The data were collected to a maximum 2θ of 45° in both cases using the ω–2θ scan technique. Moving crystal, moving counter background counts were made by scanning an additional 25% above and below of θ. For intense reflections an attenuator (factor 12.1) was automatically inserted in front of the detector. As a check on crystal and electronic stability three standard reflections were measured every 5000 s of beam time. No decay was observed in either case. The structures were solved by using the Patterson heavy-atom method to reveal the position of the rhodium atoms for **1** and iridium atoms for **2**. The remaining heavy atoms were then located in succeeding Fourier syntheses. Hydrogen atoms were located and added to the structures but were not refined.

Acknowledgement—We thank the National Science Foundation (Grant CHE-8612063) for support of this research.

Supplementary material available: Listings of fractional coordinates, anisotropic thermal parameters, full bond distances and angles and a listing of observed and calculated structure factor amplitudes for **1** and **2**.

REFERENCES

1. H. E. Bryndza and W. Tam, *Chem. Rev.* 1988, **88**, 1163 and refs therein.
2. R. C. Mehrotra, S. K. Agarwal and Y. P. Singh, *Coord. Chem. Rev.* 1985, **68**, 101.
3. M. H. Chisholm and I. P. Rothwell, *Comprehensive Coordination Chemistry* (Edited by G. Wilkinson, R. Gillard and J. A. McCleverty), Vol. 2, Ch. 15.3. Pergamon Press, Oxford (1987).
4. S. D. Loren, B. K. Campion, R. H. Heyn, T. D. Tilley, B. E. Bursten and K. W. Luth, *J. Am. Chem. Soc.* 1989, **111**, 4712 and refs therein.
5. I. P. Rothwell, *Accts Chem. Res.* 1988, **21**, 153.
6. J. L. Kerschner, P. E. Fanwick, I. P. Rothwell and J. C. Huffman, *Inorg. Chem.* 1989, **28**, 780.
7. J. L. Kerschner, P. E. Fanwick and I. P. Rothwell, *Organometallics* 1989, **8**, 1431.
8. J. L. Kerschner, E. M. Torres, P. E. Fanwick and I. P. Rothwell, *Organometallics* 1989, **8**, 1424.
9. (a) J. G. Norman and D. J. Gmur, *J. Am. Chem. Soc.* 1977, **99**, 1446; (b) P. W. de Haven and V. L. Goedken, *Inorg. Chem.* 1979, **18**, 827.
10. (a) S. D. Robinson and B. L. Shaw, *J. Chem. Soc.* 1965, 4997; (b) G. Pannetier, P. Fougenoux, R. Bonnair and N. Platzer, *J. Less-Common Met.* 1971, **24**, 83.
11. W. M. Rees, M. R. Churchill, J. C. Feltinger and J. D. Atwood, *Organometallics* 1985, **4**, 2179.
12. J. A. Heppert, T. J. Boyle and F. Takusagaw, *Organometallics* 1989, **8**, 461 and refs therein.
13. (a) R. O. Rosete, D. J. Cole-Hamilton and G. Wilkinson, *J. Chem. Soc., Dalton Trans.* 1979, 1618; (b) M. A. Bennett and T. W. Matheson, *J. Organomet. Chem.* 1979, **175**, 87.
14. B. Cetinkaya, P. B. Hitchcock, M. F. Lappert and S. Torioni, *J. Organomet. Chem.* 1980, **88**, C31.
15. R. H. Crabtree and J. M. Quirk, *Synth. React. Inorg. Met-Org. Chem.* 1982, **12**, 407.

Polyhedron Vol. 9, No. 7, pp. 975–979, 1990
Printed in Great Britain

0277-5387/90 $3.00+.00
Pergamon Press plc

THE CRYSTAL STRUCTURE OF LYSIDINE·$HAu(CN)_2$—A MODEL COMPOUND OF A WEAK-BASE ANION-EXCHANGE RESIN LOADED WITH GOLD CYANIDE

A. H. SCHWELLNUS*

Mintek, Private Bag X3015, Randburg 2125, Republic of South Africa

and

L. DENNER and J. C. A. BOEYENS

Department of Chemistry, University of the Witwatersrand, 1 Jan Smuts Avenue, Johannesburg, 2000, Republic of South Africa

(*Received* 18 *September* 1989; *accepted* 13 *November* 1989)

Abstract—The crystal structure of lysidine·$HAu(CN)_2$ was determined so that the influence of steric hindrance at the active site of weak-base imidazoline resins could be established. These resins, which have alkyl groups attached to the basic nitrogen, have lower basicities, and are also eluted more slowly, than imidazoline resins that have no substituents at the active site. The crystal structure of lysidine·$HAu(CN)_2$ (a model compound for one of the unsubstituted resins) consists of two interpenetrating hydrogen-bonded networks that are perpendicular to each other. The structure suggests that the presence of an alkyl substituent on the basic nitrogen of an imidazoline weak-base resin could hinder the approach of a hydrogen atom and the gold cyanide anion to the basic nitrogen in the functional group, thus lowering the basicity of the amine. However, the crystal structure does not explain the steric effects that have been postulated as causing the rate of elution of disubstituted imidazoline resins to be slower than that of monosubstituted imidazoline resins.

Weak-base anion-exchange resins can be used for the extraction of gold cyanide from cyanide leach liquors. The metal anion can be adsorbed onto the resin owing to the interaction of the negative charge of the anion with the positive charge on the functional group of the resin. A weak-base resin is positively charged only when it is protonated. The basicity of the resin (i.e. the pH value at which it protonates) therefore determines the pH value at which the resin can extract gold cyanide—a resin with a higher basicity can extract gold cyanide at a higher pH value.[1]

The loaded resin can be eluted by contact of the resin with a basic solution. The deprotonation of the resin's functional groups results in the removal of the positive charge on the resin, and hence the means by which gold cyanide is adsorbed. The gold cyanide is washed out of the bed of resin, and the gold metal can be recovered by electrowinning.[2]

Gold cyanide is adsorbed onto the resin by the following mechanism:

$$P{-}NR_2 + H^+ \rightleftharpoons P{-}NR_2H^+ \xrightarrow{Au(CN)_2^-} P{-}NR_2H^+ {}^-Au(CN)_2,$$

where P is the polymer matrix and R is the substituent attached to the basic nitrogen.

The elution of gold cyanide from a resin occurs as follows:

$$P{-}NR_2H^+ {}^-Au(CN)_2 + OH^- \rightleftharpoons P{-}NR_2 + H_2O + Au(CN)_2^-.$$

The basicities of resins that have alkyl groups attached to the basic nitrogen (e.g. DUMEIM and

* Author to whom correspondence should be addressed.

DUETIM) are lower than those of resins with hydrogen atoms as the substituents[3] (e.g. DUIM). This is in contrast to what would be expected from purely inductive effects, and is probably due to an increase in steric hindrance caused by the larger substituent on the basic nitrogen in the resin's functional group:

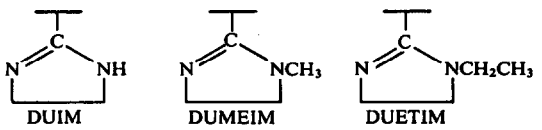

The elution of resins with disubstituted imidazoline functional groups (LYSIDINE, DUMEIM and DUETIM) is also slow in comparison with that of the monosubstituted resins[4] (DUIM and STIM). It was considered that steric hindrance to the approach of hydroxyl anions, which deprotonate the loaded amine groups, could retard the rate of elution:

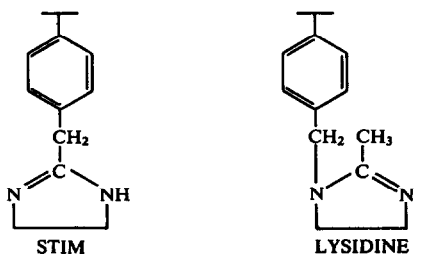

It was considered that the investigation of the orientation of the gold cyanide anion relative to the protonated amine group could provide evidence that would either substantiate or discount the importance of steric effects. Consequently, a crystal of lysidine·$HAu(CN)_2$, a model compound for the resin DUIM, was prepared, and the structure was determined:

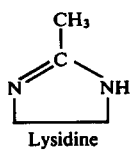

The ion-exchange reaction occurs in an aqueous environment and hence the preferred solvent for the growing of crystals is water. However, since water hydrolyses lysidine,[4] methanol was used as the solvent.

The crystals were grown from two different solutions that contained potassium aurocyanide and lysidine in the molar ratios of 1.0 and 0.5, respectively. An excess of lysidine was used in the second solution because the molar ratio of functional group to gold cyanide in a loaded resin is less than unity (about 0.1).

The crystals grown from the two solutions consisted of needle- and unneedle-like forms, both of which had the same point group symmetry (established from oscillation and Weissenberg photographs). Analyses of the crystals by energy-dispersive spectroscopy (EDS) using a scanning electron microscope showed that they all had a gold cyanide-to-lysidine ratio of unity. The shape of the crystal used for the determination of the crystal structure was therefore not important. However, a needle form was used for the sake of ease of alignment in the instrument.

Lysidine·$HAu(CN)_2$ did not readily crystallize in forms suitable for single-crystal X-ray techniques. Imperfect, twinned and several small crystals were obtained in spite of the long crystallization time allowed. The crystals were also brittle, and broke easily when handled. A different solvent could not be used because potassium aurocyanide is insoluble in other organic solvents that have properties (such as polarity) that are similar to those of the resin phase.

Attempts to crystallize potassium argentocyanide with the lysidine group from methanolic solutions were unsuccessful.

EXPERIMENTAL

The compound $C_4H_9N_2^+ \cdot Au(CN)_2^-$ (M_r = 334.13) was crystallized from a methanolic solution at pH 7. A needle-shaped crystal was used for the determination of the crystal structure. The cell dimensions were determined by the least-squares refinement of 25 high-angle reflections measured on an Enraf–Nonius CAD4 single-crystal diffractometer. The intensity data were measured at room temperature in the range $3 \leqslant \theta \leqslant 30°$ with an incident-beam graphite-crystal monochromator (λ(Mo-K_α) = 0.70169 Å). The total number of reflections recorded was 1941. The cut-off criterion was $F > 4\sigma(F)$. A variable scan speed in the ω–2θ mode was used. The scanning speed, which was adjusted in terms of the intensity during a pre-scan, did not exceed 5.5° min^{-1}, and the time for the measurement of each reflection was not less than 1 min. Data reduction consisted of correction for Lorentz factor, polarization and absorption; μ = 68.88 cm^{-1}.

The structure was solved by the Patterson method, and refined by the full-matrix least-squares method (101 parameters) by means of the SHELX program.[5] Convergence was attained, with a residual of 0.036 after the last cycle of full-matrix least-squares refinement including anisotropic temperature factors for all the non-hydrogen atoms. The hydrogen atoms on the carbon atoms were

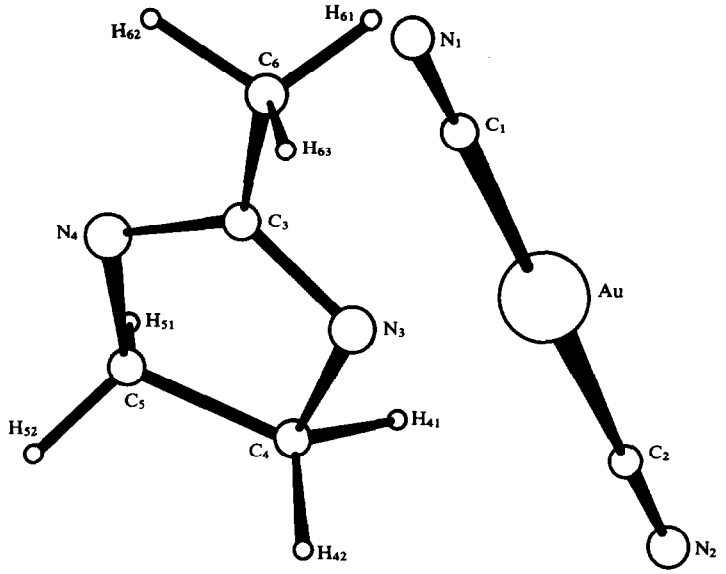

Fig. 1. The asymmetric unit of lysidine·$HAu(CN)_2$.

placed in their calculated positions (d(CH) = 1.08 Å), and were then refined with a common isotropic factor. The hydrogen atoms on the nitrogen atoms were not observed in the difference Fourier synthesis.

The crystal structure of lysidine·$HAu(CN)_2$ is monoclinic, and the space group is $P2_1/c$. This was shown by the systematic absence of reflections in the oscillation and single-crystal data, i.e. $h0l$: $l = 2n$ and $0k0$: $k = 2n$. The unit cell constants are as follows: $a = 10.754(1)$, $b = 13.962(2)$ and $c = 6.324(1)$ Å; $\beta = 109.65(1)°$, $U = 894.23$ Å^3, $Z = 4$, $F(000) = 608$.

RESULTS AND DISCUSSION

The bond lengths and angles involving the atoms (numbered according to Fig. 1) in the asymmetric unit calculated after the last cycle of refinement are listed in Table 1.

The crystal structure consists of two interpenetrating hydrogen-bonded networks. These networks are identical, and are mutually perpendicular. The crystal structure can therefore be described with reference to the structure of one network (Fig. 2), and the orientation of two networks relative to each other. A stereoscopic diagram of the crystal structure is shown in Fig. 3.

In each network, the nitrogen atoms in the gold cyanide are linked, by hydrogen bonds, to two lysidine groups. The gold cyanide anions in the network are parallel to one another. On one side of the gold cyanide anions is a chain of bifurcated hydrogen bonds while, on the other side, a centre of symmetry relates the two lysidine groups to two gold cyanide anions. These four moieties round the centre of symmetry are linked by hydrogen bonds. The rings round the centres of symmetry are perpendicular to the planes formed by the other molecules in the network.

The gold atoms of the two networks are superimposed, possibly because the ionic radii of the gold

Table 1. Bond lengths (Å) and angles (°)

Au—C(1)	2.022(12)	Au—C(2)	2.015(12)
N(1)—C(1)	1.100(14)	N(2)—C(2)	1.112(14)
N(3)—C(4)	1.479(14)	N(4)—C(3)	1.311(13)
C(3)—C(6)	1.47(2)	C(4)—C(5)	1.55(2)
C(1)—Au—C(2)	178.0(5)	Au—C(1)—N(1)	178.7(11)
Au—C(2)—N(2)	178.8(11)	N(4)—C(3)—C(6)	123.0(11)
N(3)—C(4)—C(5)	101.1(9)		

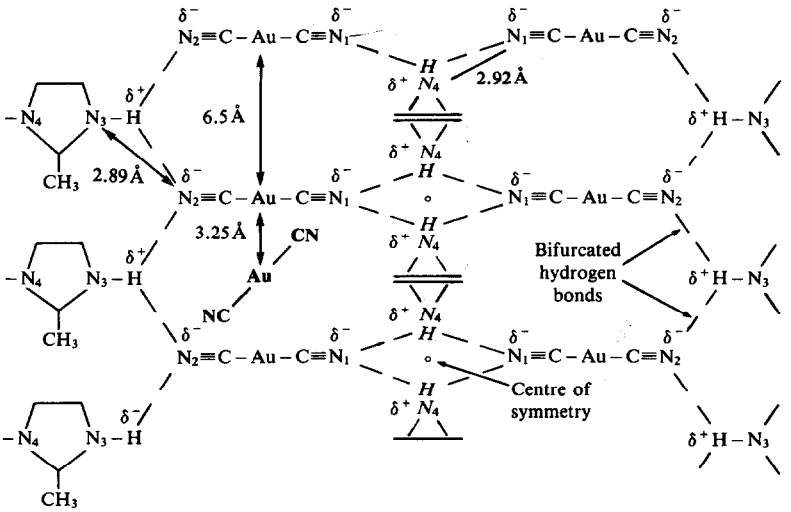

Notes
The structures in normal type are in the plane of the paper
The structures in italic type are perpendicular to the plane of the paper
Bold type indicates a gold-cyanide molecule that is part of the second network. The second network is identical to, but perpendicular to, that represented above

Fig. 2. A schematic diagram of the crystal structure of lysidine · $HAu(CN)_2$.

atoms are the smallest in the structure. The stacking of the planes in the networks can therefore be represented as follows:

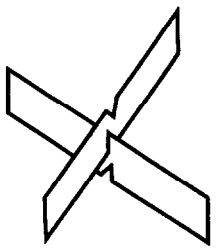

where each network is represented by

The distance between the gold atoms in the two networks is 3.25 Å—almost as short as that of a metal–metal bond. The hydrogen bonds between the lysidine groups and gold cyanide anions are strong, and should consequently be fairly stable. Solvation is probably not essential for stabilization, and, therefore, the absence of methanol molecules in the crystal is not surprising. The hydrogen bonds at the chain of bifurcated bonds and at the centre of symmetry are similar in length, and are therefore almost identical in strength.

CONCLUSIONS

The crystal structure of lysidine · $HAu(CN)_2$ suggests that, as proposed, the presence of an alkyl substituent on the basic nitrogen in the resin's functional group could hinder the approach of a proton and a gold cyanide anion, thus weakening or eliminating the hydrogen bond between the amine and the gold cyanide anion. The positively charged species on the resin would be less stable, and the basicity of the amine could be relatively lowered.

The results of the investigation did not discount or prove the part played by steric effects in the relatively slower rate of elution of disubstituted imidazoline resins compared with that of monosubstituted imidazoline resins. The elution of disubstituted imidazoline resins would, from a consideration of the crystal structure, be expected to proceed more easily than that of monosubstituted imidazoline resins because only one strong hydrogen bond is formed with the gold cyanide anion. The hydrogen bond at the other end of the gold cyanide anion could be weak or totally absent.

Gold cyanide anions could have different orientations with respect to protonated disubstituted imidazoline and monosubstituted imidazoline (i.e. lysidine) groups. Confirmation of the existence of steric effects that would be expected to influence the elution of resins with disubstituted imidazoline

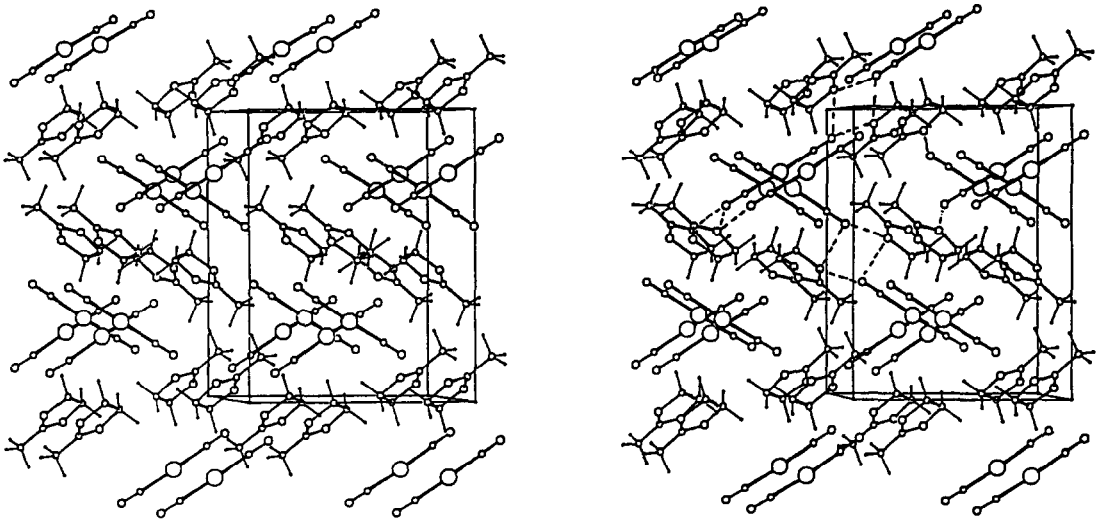

Fig. 3. A stereoscopic diagram of the crystal structure of lysidine · $HAu(CN)_2$.

groups would require the determination of the structure of a crystal grown with benzyllysidine or an alkyllysidine.

Acknowledgement—This paper is published by permission of Mintek.

REFERENCES

1. B. R. Green and A. H. Potgieter, in *Ion Exchange Technology* (Edited by D. Naden and M. Streat), pp. 626–636. Ellis Horwood, Chichester (1984).
2. R. L. Paul, A. O. Filmer and M. J. Nicol, in *Hydrometallurgy—Research, Development and Plant Practice* (Edited by K. Osseo-Asare and J. D. Miller), pp. 689–704. Metallurgical Society of AIME (1982).
3. A. H. Schwellnus and B. R. Green, in *Ion Exchange for Industry* (Edited by M. Streat), pp. 207–218. Ellis Horwood, Chichester (1988).
4. A. H. Schwellnus, Factors influencing the interaction of resins with gold cyanide, MSc thesis, 241 pp. University of the Witwatersrand (1987).
5. G. M. Sheldrick, in *Computing in Crystallography* (Edited by H. Schenk *et al.*), pp. 34–42. Delft University Press, The Netherlands (1978).

Polyhedron Vol. 9, No. 7, pp. 981–986, 1990
Printed in Great Britain

0277–5387/90 $3.00+.00
© 1990 Pergamon Press plc

SYNTHESIS AND CHARACTERIZATION OF COPPER(I) HALIDE COMPLEXES WITH HETEROCYCLIC THIONES AND TRIPHENYLPHOSPHINE AS LIGANDS. THE X-RAY CRYSTAL STRUCTURE OF COPPER(I) 1-METHYL-1,3-IMIDAZOLINE-2-THIONE BIS(TRIPHENYLPHOSPHINE)BROMIDE, [$Cu(PPh_3)_2$(meimtH)Br]

P. KARAGIANNIDIS,* P. ASLANIDIS and S. PAPASTEFANOU

Department of General and Inorganic Chemistry, Aristotle University of Thessaloniki, Thessaloniki 540 06, Greece

and

D. MENTZAFOS, A. HOUNTAS and A. TERZIS

X-ray Laboratory, NCR "Democritos", Athens, Greece

(*Received* 26 *September* 1989; *accepted* 13 *November* 1989)

Abstract—Following our earlier reports on copper(I) mixed-ligand complexes with heterocyclic thiones and triphenylphosphine, we now report the isolation of 12 new complexes of the general formula [$Cu(PPh_3)_2$(L)X] [L = 1-methyl-1,3-imidazoline-2-thione (meimtH), 5-methyl-2-benz-1,3-imidazoline-2-thione (mebzimtH_2), purine-6-thione (pur6SH), quinoline-2-thione (qn2SH) and X = Cl, Br, I], and their characterization by various physicochemical methods. The crystal structure of the complex [$Cu(PPh_3)_2$(meimtH)Br] is also reported. Crystals are prisms, space group $P\bar{1}$ with $a = 9.988(3)$, $b = 10.212(2)$, $c = 21.066(5)$ Å, $\alpha = 94.86(2)$, $\beta = 91.70(2)$, $\gamma = 119.16(2)°$ and $Z = 2$. The metal ion has a distorted tetrahedral geometry with bond lengths Cu—S = 2.375(1), Cu—Br = 2.509(0), Cu—P(1) = 2.268(1) and Cu—P(2) = 2.281(1) Å. The structure has been solved by single-crystal X-ray diffraction methods with a final R of 0.0330 for observed reflections with $F_o \geqslant 6.0\sigma(F_o)$.

In recent years the ligating properties of heterocyclic thiones have been extensively studied and an increasing number of mononuclear and dinuclear copper(I) complexes with trigonal or tetrahedral copper(I) are presented.[1] Our present research has been concerned with the mode of ligation of such ligands in connection with the presence of nucleophilic reagents, e.g. triphenylphosphine. In order to investigate the influence of bulky ligands (PPh_3) upon the environment of copper(I) we prepared and structurally characterized the complexes [$Cu(PPh_3)_2$(py2SH)Br],[2] (py2SH = pyridine-2-thione) and [$Cu(PPh_3)_2$ (tzdtH)$_2$]NO_3[3] (tzdtH = 1,3-thiazolidine-2-thione). To supplement our present knowledge we report in this paper results of the preparation and characterization of a new series of mononuclear complexes of the general formula [$Cu(PPh_3)_2$(L)X].

* Author to whom correspondence should be addressed.

EXPERIMENTAL

Physical measurements

IR, electronic and NMR spectra, conductivities, magnetic susceptibility measurements and elemental analyses of carbon, nitrogen, hydrogen and copper were performed as described previously.[3] Thermogravimetric analyses were performed on a Rigacu DTA/TG thermobalance in flowing air, with a heating rate of 10°C min^{-1}. Sample sizes were *ca* 15 mg.

Starting materials

All thione ligands, supplied by EGA or Aldrich, were purified by recrystallization from ethanol. Copper(I) halides, triphenylphosphine and all solvents were of reagent grade and were used without further purification.

Preparation of the complexes

A suspension of CuX in 20 cm^3 of THF was treated with a 50 cm^3 solution of 1 mmol of the appropriate thione and 2 mmol of PPh_3 in the same solvent. The reaction mixture was stirred for 2 h at 40°C, filtered and allowed to evaporate slowly at room temperature. The microcrystalline solid thus formed was collected by filtration, washed with small amounts of ethanol and ether and dried *in vacuo*.

Collection and reduction of intensity data

Complete crystal and intensity collection data are reported in Table 1. Preliminary oscillation and Weisenberg photographs indicated the space group $P\bar{1}$. Unit cell dimensions were derived from least-squares refinement of the setting angles of 15 automatically-centred reflections in the range $21° < 2\theta < 23°$ on a Syntex $P2_1$ diffractometer. The intensities of three standards monitored after every 67 reflections were stable, with a scatter of less than 3% from their respective means. Lorentz and polarization corrections were applied and the data were reduced using the SHELX 76 program.[4]

Solution and refinement of the structure

The positional coordinates of copper, bromine, sulphur and phosphorus atoms were deduced by

Table 1. Summary of crystal and intensity collection data

Formula	$Cu(P_2SC_{40}H_{36}N_2)_2Br$
*f*w	782.29
a (Å)	9.988(3)
b (Å)	10.212(2)
c (Å)	21.066(5)
α (°)	94.86(2)
β (°)	91.70(2)
γ (°)	119.16(2)
V (Å^3)	1863.5(8)
Z	2
D_{calc} (Mg m^{-3})	1.394
D_{meas} (Mg m^{-3})	1.35
Space group	$P\bar{1}$
Radiation	Mo-K_α (λ = 0.71069 Å)
μ (cm^{-1})	17.93
Scan speed (° min^{-1})	2.0–20.0
Scan range (°)	1.8 plus $\alpha_1-\alpha_2$ separation
Background counting (s)	0.5 of scan time
2θ limit (°)	50.0
Data collected/unique	6917/6503
Data used	5094 with $F_o > 6.0\sigma(F_o)$
Data form *h*, *k*, *l*	$0 \rightarrow 11$, $-12 \rightarrow 12$, $-25 \rightarrow 25$
Weighting scheme	Unit weights
F(000)	799.97
Number of refined parameters	454
$[\Delta/\sigma]_{max}$	0.143
$(\Delta p)_{max}//(\Delta p)_{min}$ (e Å^{-3})	0.758//−0.346
S^a	1.10
R^b (obsd/all data)	0.0330/0.0462
$R_w{}^c$ (obsd/all data)	0.0355/0.0469

[a] $S = [\Sigma w(\Delta F)^2/(N-P)]^{1/2}$; P = No. of parameters, N = No. of observed reflections.

[b] $R = \Sigma|\Delta F|/\Sigma|F_o|$.

[c] $R_w = [\Sigma w(\Delta F)^2/\Sigma w|F_o|^2]^{1/2}$.

the direct methods using the SHELX 76 program.[4] The rest of the non-hydrogen atoms were revealed by subsequent ΔF calculations. Refinement was carried out by blocked full-matrix least-squares, in which $\Sigma w\Delta^2$ was minimized. The hydrogen atoms of the phenyl groups were calculated as riding on carbon atoms at a distance of 0.98 Å. Non-hydrogen atoms were refined using anisotropic and hydrogen atoms using isotropic temperature factors. Seven reflections showing poor agreement were given zero weight during final refinement cycles. Atomic scattering factors were taken from *International Tables for X-ray Crystallography*.[5]

RESULTS AND DISCUSSION

Earlier reports from this laboratory showed[2,3] that some heterocyclic thiones reacts with PPh_3-containing copper(I) compounds such $[Cu(PPh_3)X]_4$, where X = Cl, Br, I, and $[Cu(PPh_3)_2NO_3]$ to give dimeric or monomeric complexes of the general formula $[Cu(PPh_3)(L)X]_2$ and $[Cu(PPh_3)_2(L)]NO_3$, respectively. Although, attempts to isolate complexes of the type $[Cu(PPh_3)_2(L)X]$ by reaction of the dimers with excess of PPh_3 were unsuccessful, these complexes can be achieved via the direct reaction of copper(I) halides with thiones in the presence of triphenylphosphine.[6]

The influence of the stereochemical bulkiness and the π-acidity of PPh_3 was demonstrated in the crystal structure of $[Cu(PPh_3)_2(py2SH)Br]$ and $[Cu(PPh_3)_2(pymtH)Br]$, where we showed that the stereochemistry on copper in both complexes became nearer to tetrahedral geometry than in the case of other copper(I) thione complexes wherein no PPh_3 is involved.[7,8]

The obtained coordination compounds, together with their melting points and elemental analyses, are listed in Table 2. The analytical data show good agreement with the suggested formulae. All the isolated complexes are diamagnetic, as would be expected for d^{10} species and their solutions show a non-electrolytic nature.

The predominant tautomeric form of the ligands investigated may be deduced from their IR spectra. They show the absence of ν(SH) at 2500 cm^{-1} and the presence of ν(NH), as well as the characteristic four "thioamide bands"[9,10] demonstrating that the thione form appears to be the predominant tautomer, in the solid state.

In the spectra of the complexes, the N—H stretching frequency is lowered to 3125–3180 cm^{-1} from 3180–3210 cm^{-1} for the solid free ligands. Such shifts are usually regarded as signifying that the ligand is non N-bonded to the metal.[11]

Analysis of the thioamide bands has been used in the past to differentiate between M—N and M—S contacts for various thione ligands.[12,13] Of the four thioamide bands, those showing the most significant changes upon coordination are I and IV, but in the present compounds they are partly masked by strong triphenylphosphine absorptions and therefore diagnostically useless. Thioamide II and thioamide III show in the spectra of the present complexes negative shifts ranging from 10 to 60 cm^{-1} which indicate that coordination occurs through the thione-S atom.

The new bands around 350 cm^{-1} in the far-IR

Table 2. Some physical properties and analytical data of the complexes

Compound	Yield (%)	Colour	Melting point (°C)	C (%)[a]	N (%)	H (%)	Cu (%)
$[Cu(PPh_3)_2(meimtH)Cl]$	62	Colourless	166	65.0(65.1)	3.8(3.8)	4.7(4.9)	8.4(8.6)
$[Cu(PPh_3)_2(meimtH)Br]$	66	Colourless	215	61.8(61.4)	3.2(3.6)	4.3(4.6)	8.2(8.1)
$[Cu(PPh_3)_2(meimtH)I]$	75	Colourless	165	58.3(57.9)	3.4(3.4)	4.4(4.4)	7.6(7.7)
$[Cu(PPh_3)_2(mebzimtH)Cl]$	60	Colourless	188	67.3(67.1)	3.4(3.5)	4.4(4.9)	7.9(8.0)
$[Cu(PPh_3)_2(mebzimtH)Br]$	68	Pale yellow	195	63.2(63.5)	3.2(3.4)	4.8(4.6)	7.7(7.6)
$[Cu(PPh_3)_2(mebzimtH)I]$	65	Pale yellow	164	60.7(60.1)	3.4(3.2)	4.6(4.3)	7.4(7.2)
$[Cu(PPh_3)_2(pur6SH)Cl]$	72	Yellow	142	63.5(63.5)	7.0(7.2)	4.3(4.4)	7.9(8.2)
$[Cu(PPh_3)_2(pur6SH)Br]$	70	Yellow	245	59.5(60.0)	6.6(6.8)	4.6(4.2)	7.6(7.7)
$[Cu(PPh_3)_2(pur6SH)I]$	78	Yellow	239	55.5(56.8)	6.3(6.5)	3.7(3.9)	7.3(7.3)
$[Cu(PPh_3)_2(qntH)Cl]$	84	Yellow	175	68.8(68.9)	1.7(1.8)	4.7(4.7)	8.2(8.1)
$[Cu(PPh_3)_2(qntH)Br]$	85	Orange	184	65.7(65.2)	1.6(1.7)	4.9(4.5)	8.0(7.7)
$[Cu(PPh_3)_2(qntH)I]$	88	Orange	203	62.0(61.7)	1.7(1.6)	4.3(4.2)	7.3(7.2)

[a] Calculated values in parentheses.

spectra are in the range previously reported for analogous copper(I) complexes[3] and can be assigned to Cu—S vibration.[14] In addition, there is no indication of any absorption for these complexes in the region where ν(Cu—N) generally lies. This fact further supports the monodentate nature of the ligands, although no activity assigned to the Cu—S vibration is observed in the cases of [Cu $(PPh_3)_2$(pur6SH)Cl] and [$Cu(PPh_3)_2$(meimtH)Cl].

All the complexes reported here exhibit electronic spectra typical of tetrahedrally-coordinated copper(I). Two strong absorptions are observed in the 260–285 and 315–385 nm ranges, respectively, which can be assigned as intraligand transitions.

The ^{1}H NMR spectra of the complexes in $CDCl_3$ solution also provided proof that ligands are (NH)-protonated. The presence of a peak for the NH-group at 10–14 ppm (sometimes very broad), together with the absence of any evidence for the thiol (SH)-proton (at δ = 3–5 ppm), indicate the thione tautomer as the dominant species in the complexes studied.

Thermal analysis in flowing air shows the complexes decompose in three or four stages. Figure 1 illustrates TG and DTG data curves for the complex [$Cu(PPh_3)_2$(qn2SH)Br]. The thermal decomposition of this compound is a typical example of a four-stage process. The first stage (195–260°C) is connected with a strong endothermic effect and involves a 62.5% mass loss, consistent with the evolution of two PPh_3 molecules (theoretical mass loss 63.2%). The burning of the ligand is accompanied by two exothermic peaks (275–330°C) suggesting the fractional decomposition of the heterocyclic thione and involves a 15% mass loss, corresponding to one chinoline molecule, C_9H_7N (theoretical mass loss 15.5%). The final stage (420–470°C) involves loss of the halogen atom.

Description of the structure

An ORTEP[15] diagram of the molecule is given in Fig. 2. Table 3 lists selected interatomic distances and valence angles.

The structure of [$Cu(PPh_3)_2$(meimtH)Br] is closely related to those of the other two analogous complexes [$Cu(PPh_3)_2$(py2SH)Br][2] and [$Cu(PPh_3)_2$(pymtH)Br],[6] which crystallize in the space group $P2_1/n$. The angles at the copper atom are nearly tetrahedral. This result is a consequence of the approximately equal steric factors near the copper coordination sphere.

The Cu—S bond length is 2.375 Å, as usually found for tetrahedrally-coordinated copper(I) with thione-S donors.[3,7,16] The Cu—P(1) and Cu—P(2) distances of 2.268(1) and 2.281(1) Å, respectively, are in agreement with the distances in [$Cu(PPh_3)_2$Br].[17] The Cu—Br distance of 2.509(0) Å is significantly longer than that observed in [$Cu(PPh_3)_2$Br] (2.35 Å), but similar to those found in two complexes of the type [$Cu(PPh_3)_2$(L) Br], where L = pyridine-2-thione and pyrimidine-2-thione.

For comparison purposes, selected interatomic distances and angles of the three related complexes [$Cu(PPh_3)_2$(py2SH)Br], [$Cu(PPh_3)_2$(pymtH)Br]

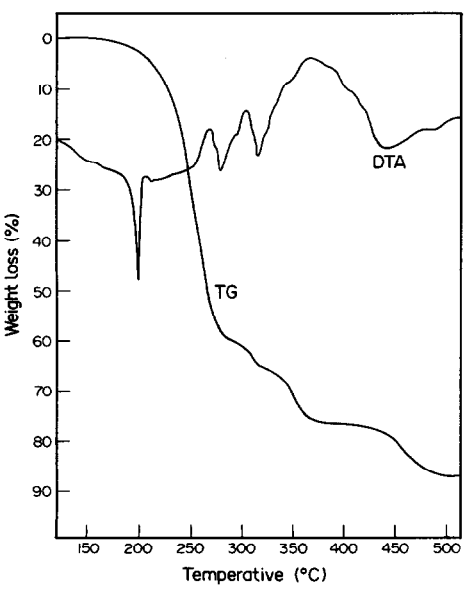

Fig. 1. TG and DTG curves for [$Cu(PPh_3)_2$(meimtH)Br].

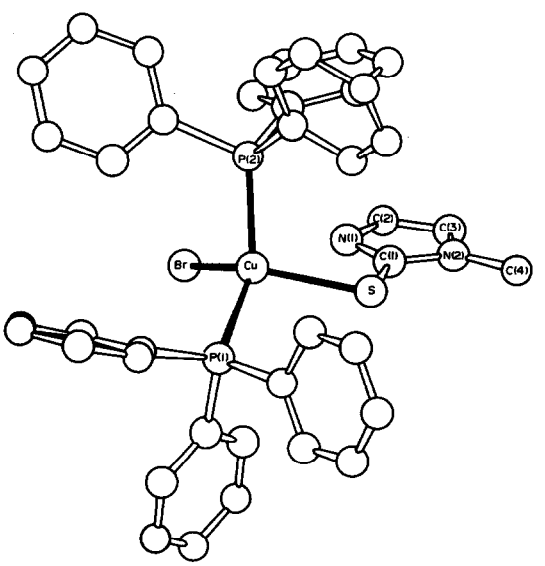

Fig. 2. Molecular structure of [$Cu(PPh_3)_2$(meimtH)Br].

Table 3. Selected interatomic distances (Å) and angles (°) with standard deviations in parentheses

Bonds			
Cu—Br	2.509(0)	N(1)—C(2)	1.367(9)
Cu—S	2.375(1)	C(2)—C(3)	1.302(11)
Cu—P(1)	2.268(1)	C(3)—N(2)	1.369(6)
Cu—P(2)	2.281(1)	N(2)—C(1)	1.347(7)
S—C(1)	1.685(4)	N(2)—C(4)	1.480(8)
C(1)—N(1)	1.345(4)		
Angles			
Br—Cu—S	112.6(0)	C(1)—N(1)—C(2)	109.6(5)
Br—Cu—P(1)	106.7(0)	N(1)—C(2)—C(3)	108.5(5)
Br—Cu—P(2)	98.3(0)	C(2)—C(3)—N(2)	106.8(7)
S—Cu—P(1)	102.9(0)	C(3)—N(2)—C(1)	110.5(5)
S—Cu—P(2)	105.3(0)	N(1)—C(1)—N(2)	104.7(4)
P(1)—Cu—P(2)	130.9(0)	S—C(1)—N(2)	127.2(3)
Cu—S(1)—C(1)	107.3(2)	C(3)—N(2)—C(4)	126.8(7)
S—C(1)—N(1)	128.1(4)	C(1)—N(2)—C(4)	122.8(6)

and $[Cu(PPh_3)_2(meimtH)Br]$ are included in Table 4. Three of the angles around copper in the two known complexes, as well as in the present, are nearly those of a regular tetrahedron. The P(1)—Cu—P(2) angle deviates considerably from the tetrahedral value of 109.47°. A possible explanation for the large value is the steric interaction between the PPh_3 group and the CuSBr entity; but as the angle has opened up considerably, these steric interactions are not likely to be the sole cause for the distortion.

The general trend of decreasing Cu—P bond lengths with the increasing P(1)—Cu—P(2) bond angle, as has been reported for the compounds $[Cu(PPh_3)_2X]$, is not evident in these complexes. In comparison with the pyridine-2-thione complex it is seen that the Cu—S distance is lengthened upon coordination, which suggests that the π-character in this bond is reduced.

Geometries within the phosphine and thione ligands are standard. The average P—C (1.823 Å) and S—C (1.685 Å) bond lengths are close to those found in other similar complexes. It appears that the exchange of the six-membered ring with a five-membered ring produces no significant changes in the $CuSP_2Br$ core.

Table 4. Interatomic distances (Å) and angles (°) in $[Cu(PPh_3)_2(meimtH)Br]$ (**A**), $[Cu(PPh_3)_2(pymtH)Br]$ (**B**) and $[Cu(PPh_3)_2(py2SH)Br]$ (**C**)

	A	**B**	**C**
Cu—S	2.375(1)	2.345(3)	2.302(4)
Cu—Br	2.509(0)	2.518(2)	2.462(2)
Cu—P	2.268(1)	2.303(2)	2.263(4)
	2.281(1)	2.306(2)	2.267(4)
P—Cu—P	130.9(0)	112.9(1)	125.0(2)
P—Cu—Br	98.3(0)	108.0(1)	104.4(1)
	106.7(0)	111.0(1)	105.9(1)
S—Cu—Br	112.6(0)	108.2(1)	114.9(1)
S—Cu—P	102.9(0)	106.5(1)	102.8(2)
	105.3(0)	110.0(2)	104.5(2)

REFERENCES

1. E. S. Raper, *Coord. Chem. Rev.* 1985, **61**, 115.
2. P. Karagiannidis, P. Aslanidis, D. P. Kessissoglou, B. Krebs and M. Dartman, *Inorg. Chim. Acta* 1989, **156**, 47.
3. P. Karagiannidis, P. Aslanidis, S. Papastefanou, D. Mentzafos, A. Hountas and A. Terzis, *Inorg. Chim. Acta* 1989, **156**, 277.
4. G. H. Sheldrick, SHELX 76, A program for crystal structure determination. University of Cambridge, U.K. (1976).
5. *International Tables for X-ray Crystallography*, Vol. IV. Kynoch Press, Birmingham (1974).
6. C. Lecomte, S. Skoulika, P. Aslanidis, P. Karagiannidis and S. Papastefanou, *Polyhedron* 1989, **8**, 1103.
7. S. C. Kokkou, V. Schramm and P. Karagiannidis, *Acta Cryst.* 1985, **C41**, 1040.
8. D. Mentzafos, A. Terzis, P. Karagiannidis and P. Aslanidis, *Acta Cryst.* 1989, **C45**, 54.
9. C. N. R. Rao and P. Venkataraghavon, *Spectrochim. Acta* 1962, **18**, 541.

10. B. Singh and K. P. Thakur, *J. Inorg. Nucl. Chem.* 1974, **36**, 1735.
11. P. P. Singh and R. Rivest, *Can. J. Chem.* 1968, **46**, 2361.
12. E. S. Raper and J. L. Brooks, *J. Inorg. Nucl. Chem.* 1977, **39**, 2163.
13. B. Singh, R. Singh, R. V. Chadhury and K. P. Thakur, *Ind. J. Chem.* 1973, **11**, 174.
14. L. J. Bellamy, *The Infrared Spectra of Complex Molecules*. John Wiley, New York (1966).
15. C. K. Johnson, ORTEP II. Report ORNL-5138. Oak Ridge National Laboratory, Tennessee (1976).
16. L. P. Battaglia, A. Bonamartini Corradi, M. Nardelli and M. E. Vidoli Tani, *J. Chem. Soc. A* 1976, 143.
17. P. H. Davis, R. L. Belford and I. C. Paul, *Inorg. Chem.* 1973, **12**, 213.

Polyhedron Vol. 9, No. 7, pp. 987–990, 1990
Printed in Great Britain

0277–5387/90 $3.00+.00
© 1990 Pergamon Press plc

THE PREPARATION AND CHARACTERIZATION OF $Pt(Se_3PPh)(PR_3)_2$; THE X-RAY CRYSTAL STRUCTURE OF $Pt(Se_3PPh)(dppe)\cdot CH_2Cl_2$

IVAN P. PARKIN, MARK J. PILKINGTON, ALEXANDRA M. Z. SLAWIN, DAVID J. WILLIAMS and J. DEREK WOOLLINS*

Department of Chemistry, Imperial College of Science and Technology, South Kensington, London SW7 2AY, U.K.

(*Received* 28 *September* 1989; *accepted* 13 *November* 1989)

Abstract—The reaction of the selenium analogue of Lawessons reagent, Ph(Se)PSe_2P(Se)Ph (**1**), with *cis*-$PtCl_2(PR_3)_2$ in either THF or liquid ammonia gives *cis*-$Pt(Se_3PPh)(PR_3)_2$ (**2–5**), the first examples of molecules containing a $PtSe_2P$ ring. Compounds **2–5** were characterized by ^{31}P-{^1H} NMR, IR, mass spectrometry and, in the case of PR_3 = 1/2 dppe (**2**), X-ray crystallography. Compound **2** has square-planar platinum coordination and a folded $PtSe_2P$ ring (dihedral angle 13.2°).

The coordination chemistry of phosphorus–sulphur species such as $R_2PS_2^-$ has been widely investigated. More recently, ourselves and other groups have studied the reaction of organoperthiophosphinic acid anhydride dimers (Lawessons reagent) with transition metal complexes.[1–3] We have recently reported the preparation of a selenium analogue of Lawessons reagent, Ph(Se)PSe_2P(Se)Ph (**1**), from the reaction of $(PhP)_5$ with selenium.[4] Here, we report on the preparation of $Pt(Se_3PPh)(PR_3)_2$, the first examples of complexes containing the $RPSe_3^{2-}$ ligand. The new compounds have been characterized by IR, NMR, microanalyses, and in the case of PR_3 = 1/2 dppe, X-ray crystallography.

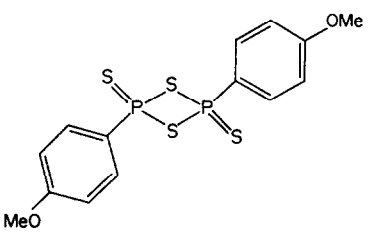

Lawessons reagent

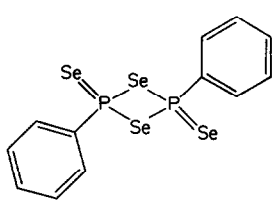

(1)

EXPERIMENTAL

$PtCl_2(PR_3)_2$ and $(PPh)_5$ were prepared as described in the literature.[5,6] All manipulations were carried out under argon or oxygen-free nitrogen, and all solvents were dried before use. THF and ethoxyethane were distilled from sodium/benzophenone and dichloromethane from calcium hydride. ^{31}P-{^1H} NMR were recorded on a JEOL FX90Q spectrometer, operating at 36.21 MHz, and are referred to an external standard of 85% H_3PO_4. IR spectra were obtained from KBr discs using a Perkin–Elmer 1720X spectrometer. Elemental analyses were performed by the microanalytical service of Imperial College.

Preparation of Ph(Se)PSe_2P(Se)Ph (1)

Degassed toluene (25 cm^3) was added to $(PPh)_5$ (1.35 g, 12.5 mmol) and grey selenium (1.97 g, 25 mmol). The suspension was heated, with stirring, and reflux maintained for 6 h. After cooling to room

* Author to whom correspondence should be addressed.

temperature, a red solid was filtered off, washed with toluene (4×10 cm^3) and dried *in vacuo*. Yield 1.86 g, 71%.

Preparation of Pt{$Se_2P(Se)(Ph)$}(dppe) (**2**)

Method 1. $PtCl_2$(dppe) (133 mg, 0.2 mmol) was dissolved in degassed THF (25 cm^3). $(PhPSe_2)_2$ (106 mg, 0.2 mmol) was then added and the suspension stirred at room temperature. After 15 min the $(PhPSe_2)_2$ had dissolved to give a yellow solution. On further stirring a cream–brown precipitate was deposited. After 2.5 h stirring the solid was filtered off, washed with further THF (2×15 cm^3) and dried *in vacuo*. Crystals suitable for X-ray analysis were obtained by slow diffusion of ethoxyethane into a CH_2Cl_2 solution of **2**. Yield 0.185 g, 70%. Compounds **3**–**5** were obtained by similar procedures.

Method 2. $(PPhSe_2)_2$ (60 mg, 0.11 mmol) was added to liquid ammonia at −78°C to generate a red solution/suspension. $PtCl_2(PR_3)_2$ (1 mmol) was then added and the solution stirred for 1/2 h at −78°C. The ammonia was then allowed to evaporate slowly as the solution warmed to room temperature. The solid was extracted with CH_2Cl_2 (5 cm^3). Filtering through a celite/glass-wool plug gave compounds **2**–**5** in *ca* 45% yield after the addition of *n*-hexane.

Crystal data

$C_{32}H_{29}P_3Se_3Pt \cdot CH_2Cl_2$, $M = 1023.4$, monoclinic, $a = 9.466(4)$, $b = 16.874(7)$, $c = 22.351(14)$ Å, $\beta = 101.35(5)°$, $U = 3500$ Å^3, space group $P2_1/n$, $Z = 4$, $D_c = 1.94$ g cm^{-3}. Straw-coloured, air-stable prisms, dimensions $0.6 \times 0.1 \times 0.4$ mm, μ(Cu-K_α) = 142 cm^{-1}, λ = 1.54178 Å, $F(000)$ = 1944.

Data collection and processing

Nicolet R3m diffractometer, ω-scan method, graphite monochromated Cu-K_α radiation; 4720 independent measured reflections ($2\theta \leqslant 116°$), 4244 observed [$|F_o| > 3\sigma(|F_o|)$], corrected for Lorentz and polarization factors; numerical absorption correction (face-indexed crystal). Maximum and minimum transmission factors 0.438 and 0.150, respectively.

Structure analysis and refinement

The structure was solved by direct methods and all the non-hydrogen atoms refined anisotropically. A ΔF map revealed the presence of a dichloromethane molecule. The positions of the hydrogen atoms were idealized (C—H = 0.96 Å), assigned isotropic thermal parameters $U(H) = 1.20$Ueq(C) and allowed to ride on their parent carbons. Refinement was by block-cascade full-matrix least squares to $R = 0.50$, ($R = \Sigma[|F_o| - |F_c|]/\Sigma|F_o|$), $R_w = 0.052$ ($w^{-1} = \sigma^2(F) + 0.00081F^2$). The maximum and minimum residual electron densities in the final ΔF map were 1.92 and −1.63 e Å^{-3} and the mean and maximum shifts/error in the final refinement cycle were 0.001 and 0.004, respectively. Computations were carried out on an Eclipse S140 computer using the SHELXTL program system.[7]

RESULTS AND DISCUSSION

Reaction of **1** with *cis*-$PtCl_2(PR_3)_2$ proceeds at room temperature as shown in eq. (1):

$$cis\text{-}PtCl_2(PR_3)_2 + Ph(Se)PSe_2P(Se)Ph \longrightarrow Pt(Se_3PPh)(PR_3)_2 + Ph(Se)PCl_2. \quad (1)$$

Apart from compounds **2**–**5** in the ^{31}P NMR we also observed a resonance at 73.6 ppm ($^1J\{^{31}P$–$^{77}Se\}$ 825 Hz) in the crude reaction mixtures from organic solvents and at 52.5 ppm (^1J 760 Hz) from the reactions in liquid ammonia and we assign this to the other product from the reactions, $Ph(Se)PCl_2$ and $Ph(Se)P(NH_2)_2$, respectively. The new metal complexes have been characterized by microanalyses, NMR (Table 1), mass spectrometry and IR spectroscopy. Their ^{31}P NMR spectra consist of

Table 1. Microanalyses (calculated values in parentheses) and ^{31}P NMR data

Compound	$\delta_{P^{III}}$	δ_{P^V}	$^1J_{Pt-P^{III}}$	$^2J_{Pt-P^V}$	PR_3	%C	%H	%P
(**2**)	45.7	13.4	3175	244	1/2 dppe (**2**)	41.1 (40.9)	3.4 (3.1)	10.8 (9.9)
(**3**)	4.1	8.7	3093	212	PEt_3 (**3**)	27.9 (27.8)	4.5 (4.5)	
(**4**)	−18.6	10.3	3093	217	PMe_2Ph (**4**)	35.2 (35.1)	3.1 (3.2)	
(**5**)	0.4	7.2	3125	232	PPh_2Me (**5**)[a]	—	—	

[a] This compound was only obtained as an oil which could not be freed of solvents and did not give satisfactory microanalyses.

Table 2. Selected bond lengths (Å) and angles (°) in **2**

Pt—Se(1)	2.471(1)	Pt—Se(2)	2.465(12)
Pt—P(2)	2.253(2)	Pt—P(4)	2.249(2)
Se(1)—P(1)	2.239(3)	P(1)—Se(2)	2.215(3)
P(1)—Se(3)	2.104(3)	P(1)—C(11)	1.845(10)
P(2)—C(3)	1.831(9)	P(2)—C(20)	1.831(9)
P(2)—C(26)	1.819(9)	P(4)—C(4)	1.843(9)
P(4)—C(40)	1.825(9)	P(4)—C(46)	1.833(10)
Se(1)—Pt—Se(2)	85.3(1)	P(2)—Pt—P(4)	86.3(1)
Se(2)—Pt—P(2)	92.0(1)	Se(1)—Pt—P(4)	96.3(1)
Se(1)—Pt—P(2)	176.7(1)	Se(2)—Pt—P(4)	176.4(1)
Pt—Se(1)—P(1)	87.6(1)	Pt—Se(2)—P(1)	88.3(1)
Se(1)—P(1)—Se(2)	97.3(1)	Se(1)—P(1)—Se(3)	118.2(1)
Se(2)—P(1)—Se(3)	115.3(1)	Se(1)—P(1)—C(11)	106.0(3)
Se(2)—P(1)—C(11)	110.5(3)	Pt—P(2)—C(3)	107.6(3)
Pt—P(2)—C(20)	115.8(3)	Pt—P(2)—C(26)	115.2(3)
Pt—P(4)—C(4)	106.9(3)	Pt—P(4)—C(40)	113.1(3)
Pt—P(4)—C(46)	121.4(3)		

two singlets each with platinum satellites with the expected coupling constants. In general, the ^2J $\{^{31}P-^{195}Pt\}$ couplings in **2–5** are higher in magnitude than in their sulphur analogues[4] (e.g. in the case of $PR_3 = PEt_3$ the values are 217 and 210 Hz for the sulphur and selenium cases, respectively). The IR spectra are dominated by the phosphine and aryl bands and it is not possible to assign the P—Se vibrations. The mass spectra of **2** and **3** (EI mode) reveal the parent ion and $\{M—P(Se)Ph\}^+$ ions with the expected isotopic distributions.

As was the case for the sulphur analogues[4] we noticed that **2–5** are somewhat air-/moisture-sensitive in solution. Thus, the ^{31}P NMR of a $CDCl_3$ solution of **4** following exposure to air revealed a new compound (δ −19.1 ppm, ^1J 3157 Hz, δ 38.2 ppm, ^2J 256 Hz) which appears to be of a similar type to **4**. The NMR data suggests that the terminal selenium has been replaced by oxygen to give P=O as part of a $PhPSe_2O^-$ ligand.

The X-ray structure of **2** reveals (Fig. 1, Table 2) square-planar coordination of the platinum by the dppe and a bidentate $Ph(Se)PSe_2^-$ ligand and is similar to that seen in the analogous $Pt\{S_2P(S)C_6H_4OMe\}(PPh_3)_2$ (**6**).[2] The ligand shell of the platinum [Pt, Se(1), Se(2), P(2) and P(4)] has a maximum deviation from planarity of 0.04 Å for Pt. The Pt—P distances in **2** (2.253(2) and 2.249(2) Å) are noticeably shorter than those in **6** (2.291(2) and 2.293(2) Å)[2] reflecting the difference in the *trans* donor atom (Se vs S). The dihedral angle between the $PtSe_2$ and PSe_2 planes is 13.2° compared to 19.4° in **6**. A consequence of this dihedral angle is that P(1) is displaced 0.21 Å from the ML_4 plane. The substituents on P(1) adopt a pseudo axial/equatorial

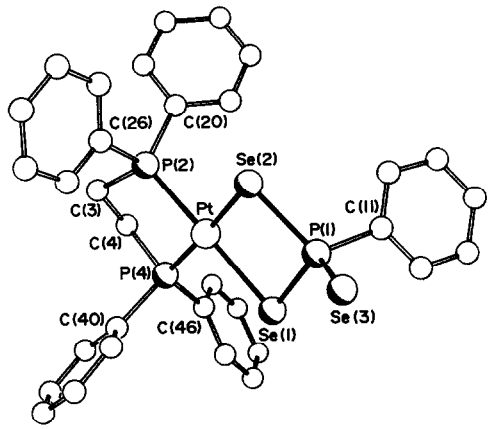

Fig. 1. The X-ray crystal structure of **2**.

conformation with respect to the PtP_2Se_2 coordination plane (Se equatorial). As was observed for the P—S distances in **6** the exocyclic P=Se bond length in **2** is only *ca* 0.1 Å shorter than those in the $PtSe_2P$ ring, thus implying substantial delocalization in the ring. The transannular Pt···P(1) and Se(1)···Se(2) distances are 3.27 and 3.34 Å, respectively. There are no significant short intermolecular contacts.

Acknowledgement—We are grateful to Johnson Matthey for loans of precious metals.

REFERENCES

1. G. A. Zank and T. B. Rauchfuss, *Organometallics* 1984, **3**, 1191.

2. R. Jones, D. J. Williams, P. T. Wood and J. D. Woollins, *Polyhedron* 1987, **6**, 539.
3. P. T. Wood and J. D. Woollins, *Trans. Met. Chem.* 1987, **12**, 405.
4. P. T. Wood and J. D. Woollins, *J. Chem. Soc., Chem. Commun.* 1988, 1190.
5. J. C. Bailar and H. Itatani, *Inorg. Chem.* 1965, **4**, 1618.
6. W. M. A. Henderson Jr, M. Epstein and F. S. Seichter, *J. Am. Chem. Soc.* 1963, **85**, 2462.
7. G. M. Sheldrick, SHELXTL, An Integrated System for Solving, Refining and Displaying Crystal Structures from Diffraction Data. University of Gottingen, F.R.G. (1978); Revision 4.1 (1983).

Polyhedron Vol. 9, No. 7, pp. 991–997, 1990
Printed in Great Britain

0277–5387/90 $3.00+.00
© 1990 Pergamon Press plc

X-RAY CRYSTAL STRUCTURE ANALYSIS AND REACTIVITY OF (2-CHLOROPHOSPHININE)PENTACARBONYLTUNGSTEN COMPLEXES

PASCAL LE FLOCH, LOUIS RICARD and FRANÇOIS MATHEY*

Laboratoire de Chimie du Phosphore et des Métaux de Transition DCPH,
Ecole Polytechnique, 91128 Palaiseau Cedex, France

(*Received* 4 *October* 1989; *accepted* 13 *November* 1989)

Abstract—The X-ray crystal structure analysis of (2-chlorophosphinine)pentacarbonyltungsten shows that the 2-chloro-substituent enhances the electronic cyclic delocalization within the ring by comparison with the parent phosphinine and its pentacarbonylmolybdenum complex. No nucleophilic substitution of this chloro-substituent is observed upon reaction with a variety of nucleophiles: $BuNH^-$, $i\text{-}Pr_2N^-$, HO^-, MeO^-, Me^-, Bu^-. In each case, a (2-chloro-1,6-dihydrophosphinine)pentacarbonyltungsten complex is obtained instead via initial attack at phosphorus. The subsequent reactions of $BuNH^-$, MeI and HCl with (2-chloro-4,5-dimethylphosphinine)pentacarbonyltungsten leads to (2-chloro-4,5,6-trimethylphosphinine)pentacarbonyltungsten.

In a previous paper, we described a very simple one-step synthesis of 2-chlorophosphinines,[1] eq. (1):

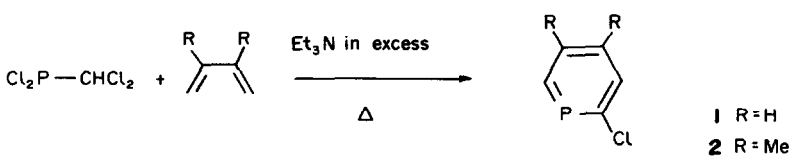

1 R=H
2 R=Me

(1)

The simplicity of this synthesis prompted us to investigate in more depth the properties of the resulting original and weakly substituted products.

RESULTS AND DISCUSSION

A series of experiments was first performed with the free phosphinines themselves. We tried without notable success to take advantage of the presence of a C—Cl bond. Thus, **1** and **2** were allowed to react with lithium, sodium and potassium in THF at room temperature, and red, paramagnetic, intractable products were obtained. No reaction was observed with magnesium in refluxing THF under ultrasonic irradiation. The zinc–copper couple in dimethylformamide at 140°C slowly converted **2** into the already described 3,4-dimethylphosphinine.[2] The formation of this compound was monitored by ^{31}P NMR analysis: δ +189 ppm [t, ^2J(P—H) = 34.2 Hz]. From this series of observations, it appears that the chloro-substituent of **1** and **2** stabilizes the phosphinine ring to a great extent (compare the thermal stability of **1** with the relative instability of the parent phosphinine[3]), but is practically unreactive. In order to enhance the reactivity of the halo substituent, we first decided

* Author to whom correspondence should be addressed.

to prepare a 2-bromophosphinine, eq. (2):

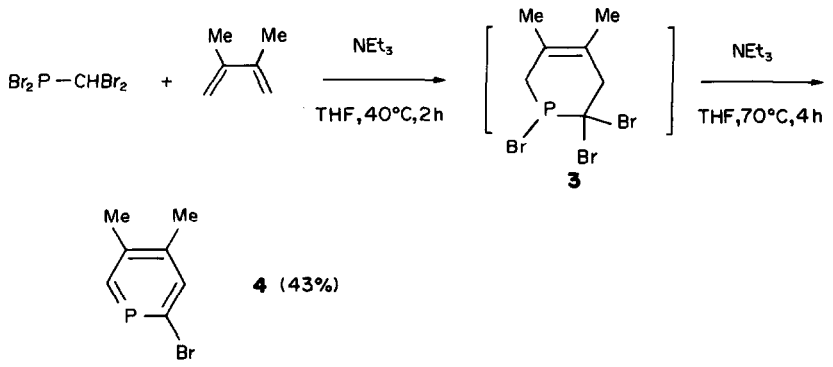

(2)

The intermediate product, **3**, gives a ^{31}P resonance at +74.7 ppm. As expected, the NMR parameters of the 2-bromophosphinine, **4**, are closely similar to those of **2** apart from a substantial shift of the ^{31}P resonance to low fields: δ ^{31}P (**4**) +194.6 ppm (hexane), $\Delta\delta$ (**4**−**2**) +15 ppm. Unfortunately, **4** proved to be as inert as **1** and **2**. In order to find an explanation for the stability of these 2-halophosphinines, we performed an X-ray crystal structure analysis of the P—$W(CO)_5$ complex of **1** (**5**).[1] The most significant structural parameters of **5** are collected in the caption of Fig. 1. A comparison of the ring parameters is made in Table 1 between **5**, $(C_5H_5P)Mo(CO)_5$,[4] and the parent phosphinine.[5] It must be recalled here that we have demonstrated, on the basis of chemical experiments,[6] that the aromaticity of the phosphinine ring is somewhat reduced when the phosphorus atom is complexed by a $M(CO)_5$ group. When comparing the data of C_5H_5P and $(C_5H_5P)Mo(CO)_5$, this loss of aromaticity can be monitored by a decrease of the P—C bond lengths from 1.73 to 1.70 Å (the P—C bonds acquire a higher double bond character and become able to give [2+4] cycloadducts with conjugated dienes[6]) and a decrease of the C—C bond lengths from 1.40 (mean) to 1.38 Å. The data in Table 1 show a striking structural similarity between **5** and the free phosphinine. It is quite clear that **5** is more aromatic than $(C_5H_5P)Mo(CO)_5$. Thus, the role of the 2-chloro-substituent is to enhance the electronic cyclic delocalization (and, hence, the stability) of the phosphinine ring. Only theoretical calculations could fully rationalize this phenomenon. Apparently, this stabilizing interaction between the halo-substituent and the phosphinine ring is specific of the 2-position. Märkl and Hock have indeed shown that 3-chlorophosphinines are able to react with strong nucleophiles such as lithium amides to give the corresponding 3-aminophosphinines.[7] We thus decided to investigate the reaction of **2** and its P—$W(CO)_5$ complex **6** with BuNHLi. A complex and intractable mixture were obtained with **2**, but **6** reacted very cleanly. However, no substitution took place at the C—Cl bond. A classical attack at phosphorus

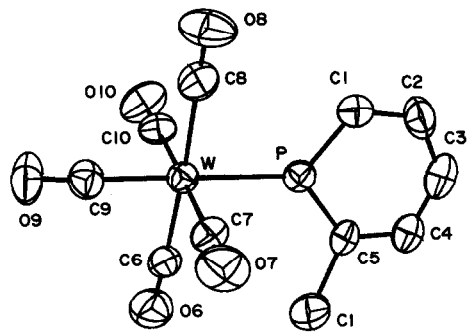

Fig. 1. ORTEP drawing of one molecule of **5**. Vibrational ellipsoids are scaled to enclose 50% of the electron density. Hydrogen atoms are omitted for clarity.

Principal bond distances (Å)

W—P	2.457(2)	P—C(5)	1.729(9)
W—C(6)	2.019(9)	Cl—C(1)	1.717(9)
W—C(7)	2.08(1)	C(1)—C(2)	1.39(1)
W—C(8)	2.09(1)	C(2)—C(3)	1.38(2)
W—C(9)	1.97(1)	C(3)—C(4)	1.38(1)
W—C(10)	2.026(9)	C(4)—C(5)	1.42(1)
P—C(1)	1.724(9)		

Selected bond angles (°)

W—P—C(1)	129.5(3)
W—P—C(5)	128.5(3)
C(1)—P—C(5)	101.8(5)
P—C(1)—Cl	118.5(5)
P—C(1)—C(2)	125.7(8)
Cl—C(1)—C(2)	115.6(7)
C(1)—C(2)—C(3)	120.5(9)
C(2)—C(3)—C(4)	127.0(9)
C(3)—C(4)—C(5)	121.1(9)
P—C(5)—C(4)	123.8(8)

was observed instead, eq. (3):

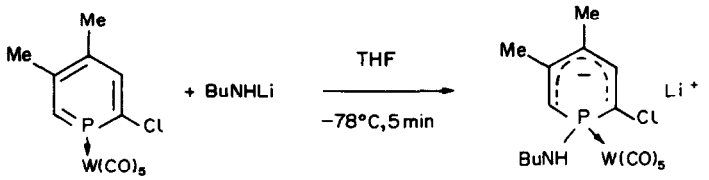

6 7 (3)

The delocalized anion **7** thus obtained was alkylated at the α-unsubstituted position by methyl iodide and at the γ-position by benzyl bromide or propyl iodide, eq. (4):

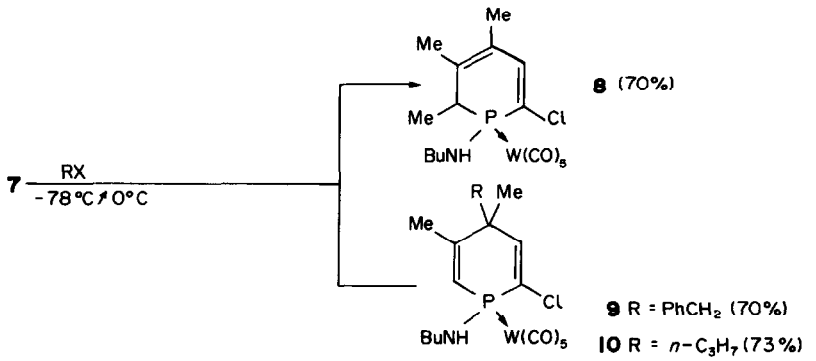

(4)

Treating **8** with HCl gave the corresponding phosphinine complex **12**, eq. (5):

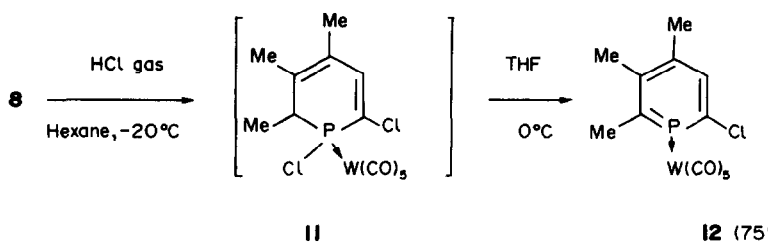

11 12 (75%) (5)

The formation of the intermediate dichloro complex **11** was monitored by ^{31}P NMR spectroscopy: δ ^{31}P (**11**) + 101.6 ppm. The compound is very unstable and spontaneously loses HCl in THF at 0°C. The aromaticity of 2-chlorophosphinine complexes is thus well evidenced. This two-step scheme (BuNHLi,IMe, then HCl) is a convenient method for methylating the 6-position of 2-chlorophosphinines. We also investigated the reaction of the more bulky lithium diisopropylamide with **6**. Our

Table 1. Structural comparison of various phosphinine derivatives

Bond or angle[a]	$(C_5H_5P)Mo(CO)_5$[b]	**5**	C_5H_5P[c]
P—C(1)	1.717(8)	1.724(9)	1.73
P—C(5)	1.695(8)	1.729(9)	1.73
C(1)—C(2)	1.381(9)	1.39(1)	1.41
C(2)—C(3)	1.348(10)	1.38(2)	1.38
C(3)—C(4)	1.353(10)	1.38(1)	1.38
C(4)—C(5)	1.396(10)	1.42(1)	1.41
C(1)—P—C(5)	103.1	101.8(5)	101

[a] Bond lengths in Å, bond angles in °; numbering as for **5**, see Fig. 1.
[b] See ref. 4.
[c] See ref. 5.

hope was to block attack at phosphorus by steric hindrance and to observe a substitution at C_2. In fact, the attack also took place at phosphorus but the amide acted as a masked lithium hydride, eq. (6):

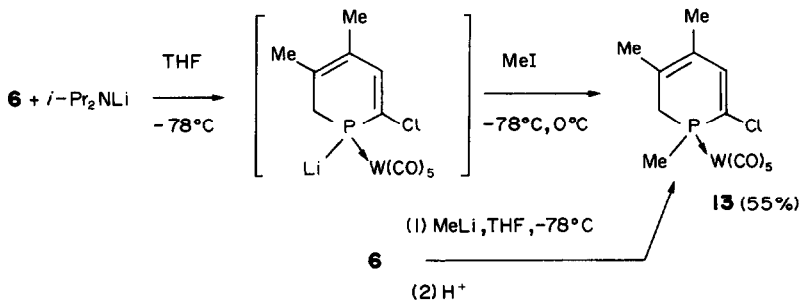

(6)

Complex **13** was independently synthesized by reaction of **6** with MeLi. We also investigated the reaction of **6** with other nucleophiles (HONa, MeONa, *n*-BuLi) and always observed an initial attack at phosphorus, eq. (7):

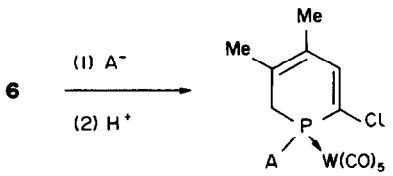

14, A = HO (95%)
15, A = MeO (85%)
16, A = *n*-Bu (95%)

(7)

These experiments clearly suggest that the 2-chloro- is less reactive than the 3-chloro-substituent on a phosphinine ring. The study of these interesting 2-halophosphinines is currently continuing.

EXPERIMENTAL

NMR spectra were recorded on a Bruker AC 200 SY spectrometer operating at 200.13 MHz for ^1H and 50.32 MHz for ^{13}C and on a Bruker WP 80 SY spectrometer operating at 32.44 MHz for ^{31}P. Chemical shifts are expressed in parts per million downfield from internal TMS (^1H and ^{13}C) and external 85% H_3PO_4 (^{31}P). Mass spectra were obtained at 70 eV with a Shimadzu GC–MS QP 1000 instrument by the direct inlet method. IR spectra were recorded with a Perkin–Elmer Model 297 spectrometer. Elemental analyses were performed by the "Service d'analyse du CNRS", at Gif-sur-Yvette, France. Silica gel (70–230 mesh) was used for chromatographic separations. All commercially available reagents were used as received from the suppliers.

4,5-*Dimethyl-2-bromophosphinine* (**4**)

Dibromomethyldibromophosphine (3.6 g, 10 mmol), triethylamine (2 g, 20 mmol) and 2,3-dimethylbutadiene (8.2 g, 10^{-1} mol) were heated in 60 cm^3 of THF at 40°C. After 2 h, triethylamine (5 g, 50 mmol) was added and the mixture heated at 70°C for 4 h. After evaporation of the solvent and the excess of amine and diene, the residue was dissolved in 100 cm^3 of hexane and then filtrated. After evaporation, the final product was quickly chromatographed on dry silica gel with hexane as eluent. Yield 0.86 g (43%).

4: colourless oil; ^{31}P NMR (hexane): δ +194.7 ppm; ^1H NMR ($CDCl_3$): δ 2.2 (s, 6H, CH_3), 7.82 (d, 1H, ^3J(H—P) = 4.3 Hz, H_3), 8.14 (d, 1H, ^2J(H—P) = 39.4 Hz, H_6); ^{13}C NMR ($CDCl_3$): δ 22.08 (s, CH_3), 22.8 (d, ^3J(C—P) = 2.7 Hz, CH_3), 140 (d, ^2J(C—P) = 14.2 Hz, C_3), 141.3 (d, ^2J(C—P) = 10.9 Hz, C_5), 141.6 (d, ^3J(C—P) = 10.2 Hz, C_4), 149.1 (d, ^1J(C—P) = 63 Hz, C_2), 157.1 (d, ^1J(C—P) = 53.5 Hz, C_6) ppm.

(1 - n - *Butylamino* - 2 - *chloro* - 4,5,6 - *trimethyl* - 1,6 - *dihydrophosphinine*)*pentacarbonyltungsten* (**8**)

Lithium *n*-butylamide (2.2 mmol in 2 cm^3 of THF) was added at −78°C to a solution of complex **6** (1 g, 2 mmol) in 10 cm^3 of dry THF. After a few minutes, methyl iodide (0.3 g, 2.2 mmol) was added and the reaction mixture was allowed to warm to room temperature. After evaporation of the solvent, the residue was chromatographed with hexane–CH_2Cl_2 (4 : 1) as eluent. Yield 0.8 g (70%).

8: yellow solid; m.p.: 108°C; ^{31}P NMR ($CDCl_3$): 70.5 ppm, $^1J(^{31}P-^{183}W)$ = 258.8 Hz; ^1H NMR ($CDCl_3$): δ 0.8 [t, 3H, CH_3 (butyl)], 1–1.5 (m, 6H), 1.65 (s, CH_3), 1.7 (s, CH_3), 2.8 (m, 2H, CH_2), 3.3 (m, 1H, N—H), 6.25 (d, ^3J(H—P) = 17.3 Hz, H_3); ^{13}C NMR ($CDCl_3$): δ 12.9 (d, ^2J(C—P) = 13.2 Hz, CH_3), 13.8 (s, CH_3), 16.65

(d, ^4J(C—P) = 5.3 Hz, CH_3), 19.3 (s, CH_3), 20 (s, CH_2), 34.0 (d, ^3J(C—P) = 5.1 Hz, CH_2), 37.5 (d, ^1J(C—P) = 36.4 Hz, P—CH), 44.0 (d, ^2J(C—P) = 9.2 Hz, N—CH_2), 126 (d, ^2J(C—P) = 10.4 Hz, C_5), 130.7 (d, ^1J(C—P) = 33.4 Hz, C_2), 133.1 (s, C_4), 137.6 (d, ^2J(C—P) = 6.5 Hz, C_3), 196.3 (d, ^2J(C—P) = 7.3 Hz, CO *cis*), 198.7 (d, ^2J(C—P) = 22.9 Hz, CO *trans*) ppm; IR (decalin): ν(CO) 2080, 1950 cm^{-1}; mass spectrum (^{184}W): *m/z* 570 (M, 15), 542 (M−CO, 4), 514 (M−2CO, 23), 486 (M−3CO, 6), 458 (M−4CO, 17), 430 (M−5CO, 28), 357 (M−5CO−$BuNH_2$, 100); Found: C, 36.0; H, 3.6. Calc. for $C_{17}H_{20}NO_5PWCl$: C, 35.8; H, 3.7%.

(1-n-Butylamino-2-chloro-4-benzyl-4,5-dimethyl-1,4-dihydrophosphinine)pentacarbonyltungsten (**9**)

Lithium *n*-butylamide (2.2 mmol in 2 cm^3 of THF) was added at −78°C to a solution of complex **6** (1 g, 2 mmol) in 10 cm^3 of THF. After a few minutes, benzyl bromide (0.5 g, 3 mmol) was added and the reaction mixture was allowed to warm to room temperature. After evaporation of the solvent, the residue was chromatographed quickly with hexane–CH_2Cl_2 (6:1) as eluent. Yield 0.9 g (70%).

9: colourless oil; ^{31}P NMR ($CDCl_3$): δ +24.48 ppm, $^1J(^{31}P-^{183}W)$ = 268.6 Hz; ^1H NMR ($CDCl_3$): δ 0.8 [t, 3H, CH_3 (butyl)], 1.21 (s, CH_3), 1.2–1.4 (m, 4H, $2CH_2$), 2.02 (s, CH_3), 2.5–2.9 (m, 4H, $2CH_2$), 5.64 (d, 1H, ^2J(H—P) = 23.4 Hz, H_6), 6.17 (d, 1H, ^3J(H—P) = 16 Hz, H_3), 6.9–7.3 (m, 5H, C_6H_5); ^{13}C NMR ($CDCl_3$): δ 13.8 (s, CH_3), 19.9 (s, CH_3), 21.9 (d, ^3J(C—P) = 11.9 Hz, CH_3), 26.45 (s, CH_2), 33.6 (s, CH_2), 43 (d, ^2J(C—P) = 10 Hz, N—CH_2), 46.54 (d, ^3J(C—P) = 5.6 Hz, C_4), 47.1 (s, CH_2), 121.9 (d, ^1J(C—P = 51.9 Hz, C_6), 127 [s, CH *para* (C_6H_5)], 128.55 [s, CH *meta* (C_6H_5)], 128.73 (d, ^1J(C—P) = 55.7 Hz, C_2), 129.88 [s, CH *ortho* (C_6H_5)], 136.1 [s, C *ipso* (C_6H_5)], 144.89 (d, ^2J(C—P) = 6.7 Hz, C_3), 153.06 (s, C_5), 196.55 (d, ^2J(C—P) = 11.8 Hz, CO *cis*), 199.7 (d, ^2J(C—P) = 22.1 Hz, CO *trans*) ppm; IR (decalin): ν(CO), 2090, 1950 cm^{-1}; mass spectrum (^{184}W): *m/z* 646 (M, 13), 618 (M−CO, 8), 562 (M−3CO, 66), 506 (M−5CO, 15), 343 (506−BuNH−$PhCH_2$, 98); Found: C, 43.5; H, 3.9. Calc. for $C_{23}H_{25}NO_5PWCl$: C, 42.8; H, 3.9%.

(1-n-Butylamino-2-chloro-4-n-propyl-4,5-dimethyl-1,4-dihydrophosphinine)pentacarbonyltungsten (**10**)

The same procedure as for **9** was used: lithium *n*-butylamide (2.2 mmol), 1 g of complex **6** and 0.5 g (3 mmol) of propyl iodide. The residue was chromatographed with hexane–CH_2Cl_2 (4:1) as eluent. Yield 0.87 g (73%).

10: colourless oil; ^{31}P NMR ($CDCl_3$): δ 26.59 ppm, $^1J(^{31}P-^{183}W)$ = 273.4 Hz; ^1H NMR ($CDCl_3$): δ 0.6–0.8 (m, 6H, $2CH_3$), 0.8–1 (m, 2H, CH_2), 1.12 (s, 3H, CH_3), 1.1–1.7 (m, 6H, $3CH_2$), 1.82 (s, 3H, CH_3), 2.52 (m, 2H, CH_2—N), 5.64 (d, 1H, ^2J(H—P) = 24.3 Hz, H_6), 6.09 (d, 1H, ^3J(H—P) = 15.75 Hz, H_3); ^{13}C NMR ($CDCl_3$): δ 13.8 (s, CH_3), 14.3 (s, CH_3), 18.5 (s, CH_3), 19.9 (s, CH_2), 21.2 (d, ^3J(C—P) = 11.8 Hz, CH_3), 27.6 (s, CH_2), 33.6 (s, CH_2), 43.0 (d, ^3J(C—P) = 10.4 Hz, N—CH_2), 43.27 (s, CH_2), 46.15 (d, ^3J(C—P) = 5.4 Hz, C_4), 121.7 (d, ^1J(C—P) = 52.8 Hz, C_6), 128.9 (d, ^1J(C—P) = 39.9 Hz, C_2), 145.46 (d, ^2J(C—P) = 6.6 Hz, C_3), 153.0 (s, C_5), 196.55 (d, ^2J(C—P) = 7.6 Hz, CO *cis*), 199.7 (d, ^2J(C—P) = 22.5 Hz, CO *trans*) ppm; IR (decalin): ν(CO) 2090, 1950 cm^{-1}; mass spectrum (^{184}W): *m/z* 597 (M, 34) 569 (M−CO, 13), 513 (M−3CO, 47), 485 (M−4CO, 6), 457 (M−5CO, 72), 341 (M−$BuNH_2$−C_3H_7, 100); Found: C, 38.4; H, 4.1. Calc. for $C_{19}H_{25}NO_5PWCl$: C, 38.2; H, 4.2%.

(4,5,6-Trimethyl-2-chlorophosphinine)pentacarbonyltungsten (**12**)

A stream of gaseous anhydrous HCl was bubbled for 5 min through a THF solution (10 cm^3) of complex **8** (0.57 g, 1 mmol) at 0°C. The mixture was then cooled to −20°C in order to allow a complete precipitation of the butylamine hydrochloride. The precipitate was removed by filtration on paper. The solvent was evaporated and the product was recrystallized from pentane. Yield: 0.37 g (75%).

12: yellow solid, m.p.: 95°C; ^{31}P NMR ($CDCl_3$): δ 162.3 ppm $^1J(^{31}P-^{183}W)$ = 273.4 Hz; ^1H NMR ($CDCl_3$): δ 2.35 (d, 3H, ^5J(H—P) = 3.1 Hz, CH_3), 2.4 (d, 3H, ^4J(H—P) = 6.3 Hz, CH_3), 2.65 (d, 3H, ^3J(H—P) = 21.3 Hz, CH_3), 7.8 (d, 1H, ^3J(H—P) = 12.9 Hz, H_3); ^{13}C NMR ($CDCl_3$): 18.12 (d, ^3J(C—P) = 5.9 Hz, CH_3), 22.66 (d, ^2J(C—P) = 25.6 Hz, CH_3), 23.43 (d, ^4J(C—P) = 3.5 Hz, CH_3), 138.29 (d, ^2J(C—P) = 9.1 Hz, C_3), 138.11 (d, ^2J(C—P) = 21.8 Hz, C_5), 143.9 (d, ^3J(C—P) = 13.1 Hz, C_4), 155.8 (d, ^1J(C—P) = 23.5 Hz, C_2), 160.16 (d, ^1J(C—P) = 16.72 Hz, C_6), 194.18 (d, ^2J(C—P) = 9.2 Hz, CO *cis*), 198.62 (d, ^2J(C—P) = 32.9 Hz, CO *trans*) ppm; IR (decalin): ν(CO) 2085, 1960, 1950 cm^{-1}; mass spectrum (^{184}W): *m/z* 496 (M, 21), 440 (M−2CO, 23), 384 (M−4CO, 13), 356 (M−5CO, 100); Found: C, 31.8; H, 2.1. Calc. for $C_{13}H_{10}O_5PWCl$: C, 31.4; H, 2.0%.

(2 - *Chloro* - 1,4,5 - *trimethyl* - 1,6 - *dihydrophosphinine*)*pentacarbonyltungsten* (**13**)

A solution of complex **6** (2 mmol) in THF (10 cm^3) was cooled to −78°C. Lithium diisopropylamide (2.2 mmol) in 2 cm^3 of THF or methyllithium (2.2 mmol) were then added. After a few minutes, methyl iodide (0.3 g, 2.2 mmol) was added and the reaction mixture was then allowed to warm to room temperature. After evaporation of the solvent, the residue was chromatographed with hexane–CH_2Cl_2 (9 : 1) as eluent. Yield : 0.55 g (55%).

10: colourless oil; ^{31}P NMR ($CDCl_3$): δ −10.8 ppm, $^1J(^{31}P–^{183}W) = 231.7$ Hz; ^1H NMR ($CDCl_3$): δ 1.8–2.0 (m, 9H, 3Me), 2.7 (d, 1H, $^2J(H—H) = 16.2$ Hz, CH_2—P), 3.6 (dd, 1H, $^2J(H—H) = 16.2$ Hz, $^2J(H—P) = 15.7$ Hz, CH_2—P), 6.42 (d, 1H, $^3J(H—P) = 16.9$ Hz, H_3). ^{13}C NMR ($CDCl_3$): δ 16.67 (d, $^1J(C—P) = 27.8$ Hz, CH_3—P), 19 (s, CH_3), 21.3 (d, $^3J(C—P) = 7.4$ Hz, CH_3), 38.3 (d, $^1J(C—P) = 29$ Hz, C_6), 125.7 (d, $^3J(C—P) = 9$ Hz, C_4), 127.2 (d, $^2J(C—P) = 10.2$ Hz, C_5), 127.2 (d, $^1J(C—P) = 39.5$ Hz, C_2), 136.75 (d, $^2J(C—P) = 4.5$ Hz, C_3), 196.2 (d, $^2J(C—P) = 7.1$ Hz, CO *cis*), 198.1 (d, $^2J(C—P) = 21.3$ Hz, CO *trans*) ppm; IR (decalin): ν(CO) 2085, 1950, 1960 cm^{-1}; mass spectrum (^{184}W): *m/z* 499 (M, 30), 443 (M−2CO, 17), 415 (M−3CO, 40), 387 (M−4CO, 42), 358 (M−5CO−H, 100); Found: C, 32.59; H, 2.73. Calc. for $C_{13}H_{12}O_5PWCl$: C, 31.9; H, 2.42%.

(1 - *Hydroxy* - 2 - *chloro* - 4,5 - *dimethyl* - 1,6 - *dihydrophosphinine*)*pentacarbonyltungsten* (**14**)

A solution of complex **6** (0.48 g, 1 mmol) in 10 cm^3 of THF was treated at room temperature with NaOH (1.5 mmol in 1 cm^3 of H_2O). After 15 min, the solvent was evaporated and the residue was chromatographed with benzene–acetone (1 : 1) as eluent. Yield : 0.48 g (95%).

14: yellow oil; ^{31}P NMR ($CDCl_3$): δ 98.47 ppm, $^1J(^{31}P–^{183}W) = 288$ Hz; ^1H NMR ($CDCl_3$): δ 1.74 (s, 3H, CH_3), 1.98 (s, 3H, CH_3), 2.8 (d, 1H, $^2J(H—H) = 17$ Hz, H_6), 3.3 (t, 1H, $^2J(H—H) \sim {}^2J(H—P) = 17$ Hz, H_6), 4.9 (m, 1H, OH), 6.4 (d, 1H, $^3J(H—P) = 16.2$ Hz, H_3); ^{13}C NMR ($CDCl_3$): δ 19.16 (s, CH_3), 21.49 (d, $^3J(C—P) = 6.7$ Hz, CH_3), 45.5 (d, $^1J(C—P) = 27.8$ Hz, CH_2—P), 126.32 (d, $^3J(C—P) = 8.8$ Hz, C_4), 128.82 (d, $^2J(C—P) = 8$ Hz, C_5), 131.1 (d, $^1J(C—P) = 36.4$ Hz, C—Cl), 137.2 (d, $^2J(C—P) = 6$ Hz, C_3), 195.56 (d, $^2J(C—P) = 8$ Hz, CO *cis*), 198.85 (d, $^2J(C—P) = 27.31$ Hz, CO *trans*) ppm; IR (decalin): ν(CO) 2090, 1950 cm^{-1}; mass spectrum (^{184}W): *m/z* 500 (M, 49), 472 (M−CO, 5), 444 (M−2CO, 38), 416 (M−3CO, 7), 388 (M−4CO, 21), 360 (M−5CO, 100).

(1 - *Methoxy* - 2 - *chloro* - 4,5 - *dimethyl* - 1,6 - *dihydrophosphinine*)*pentacarbonyltungsten* (**15**)

A solution of complex **6** (2 mmol) in 10 cm^3 of THF was cooled at −40°C. MeONa (3 mmol) in 2 cm^3 of MeOH was then added. The reaction mixture was then allowed to warm to room temperature. After hydrolysis and evaporation of the solvent, the final product was purified by chromatography with hexane–CH_2Cl_2 (4 : 1) as eluent. Yield : 0.87 g (85%).

15: yellow solid; m.p.: 112°C; ^{31}P NMR ($CDCl_3$): δ 107.3 ppm, $^1J(^{31}P–^{183}W) = 297.8$ Hz; ^1H NMR ($CDCl_3$): δ 1.71 (s, 3H, CH_3), 1.81 (s, 3H, CH_3), 2.85 (dd, 1H, $^2J(C—P) = 7.5$ Hz, $^2J(H—H) = 17.5$ Hz, H_6), 3.35 (dd, 1H, $^2J(C—P) = 12.5$ Hz, $^2J(H—H) = 17.5$ Hz, H_6), 3.34 (d, $^3J(H—P) = 11.8$ Hz, OCH_3), 6.58 (d, 1H, $^3J(H—P) = 15.4$ Hz, H_3); ^{13}C NMR ($CDCl_3$): δ 19.3 (s, CH_3), 21.0 (d, $^3J(C—P) = 6$ Hz, CH_3), 43.0 (d, $^1J(C—P) = 22.6$ Hz, CH_2—P), 55.5 (d, $^2J(C—P) = 12$ Hz, OCH_3), 125.7 (d, $^3J(C—P) = 7$ Hz, C_4), 127.6 (d, $^1J(C—P) = 31$ Hz, C_2), 130.4 (d, $^2J(C—P) = 9$ Hz, C_5), 139.8 (d, $^2J(C—P) = 6$ Hz, C_3), 195.85 (d, $^2J(C—P) = 8$ Hz, CO *cis*), 199.1 (d, $^2J(C—P) = 28$ Hz, CO *trans*) ppm; IR (decalin): ν(CO) 2085, 1950, 1945 cm^{-1}; mass spectrum: (*m/z*) 515 (M, 34), 487 (M−CO, 4), 459 (M−2CO, 49), 403 (M−4CO, 15), 375 (M−5CO, 74), 373 (100); Found: C, 30.62; H, 2.33. Calc. for $C_{13}H_{12}O_6PWCl$: C, 30.35; H, 2.35.

(1 - n - *Butyl* - 2 - *chloro* - 4,5 - *dimethyl* - 1,6 - *dihydrophosphinine*)*pentacarbonyltungsten* (**16**)

A solution of complex **6** (2 mmol) in 10 cm^3 of THF was cooled to −78°C. *n*-Butyllithium (1.25 cm^3, 1.6 M solution in hexane) was then added. After a few minutes, H_2O (0.2 cm^3) was added. After evaporation of the solvent at room temperature, the residue was chromatographed with hexane as eluent. Yield : 1 g (95%).

16: yellow solid; m.p.: 85°C; ^{31}P NMR ($CDCl_3$): δ −0.7 ppm, $^1J(^{31}P–^{183}W) = 236.8$ Hz; ^1H NMR ($CDCl_3$): δ 0.97 [t, 3H, CH_3 (butyl)], 1.5 (m, 4H, $2CH_2$), 1.6 (s, 3H, CH_3), 1.94 (s, 3H, CH_3), 2.1 (m, 2H, CH_2), 2.65 (d, 1H, $^2J(H—H) = 17.5$ Hz, H_6), 3.25 (dd, 1H, $^2J(H—H) = 17.5$ Hz, $^2J(H—P) = 15$ Hz, H_6), 6.43 (d, 1H, $^3J(H—P) = 19$ Hz, H_3); ^{13}C NMR ($CDCl_3$): δ 13.6 (s, CH_3), 19.0 (s, CH_3), 21.37 (d, $^3J(C—P) = 7$ Hz, CH_3), 24.1 (d, $^2J(C—P) = 13.5$ Hz, CH_2), 26.5 (s, CH_2), 30 (d, $^1J(C—P) = 25$ Hz, CH_2—P), 35.0 (d,

^1J(C—P) = 27.4 Hz, CH_2—P), 125.7 (d, ^3J(C—P) = 7.7 Hz, C_4), 126.3 (d, ^1J(C—P) = 34 Hz, C_2), 126.8 (d, ^2J(C—P) = 8.1 Hz, C_5), 137.3 (d, ^2J(C—P) = 3.5 Hz, C_3), 196.3 (d, ^2J(C—P) = 6.7 Hz, CO *cis*), 198.9 (d, ^2J(C—P) = 21.4 Hz, CO *trans*); IR (decalin): ν(CO) 2090, 1950 cm^{-1}; mass spectrum (^{184}W): *m/z* 540 (M, 19), 484 (M − 2CO, 20), 428 (M − 4CO, 43), 400 (M − 5CO, 13), 340 (M − 5CO − C_4H_{10}, 100); Found: C, 35.8; H, 3.4. Calc. for $C_{16}H_{18}O_5PWCl$: C, 35.5; H, 3.3%.

X-ray structure determination for **5**

Crystals of **5**, $C_{10}H_4ClO_5$ PW, were grown at −18°C from a pentane solution of the compound. Data were collected at 3 ± 1° on an Enraf–Nonius CAD4 diffractometer. The crystal structure was solved and refined using the Enraf–Nonius supplied SDP package. The compound crystallizes in space group *Pbca*, $a = 8.770(1)$, $b = 13.190(1)$, $c = 22.689(2)$ Å; $V = 2624.58(72)$ $Å^3$; $Z = 8$; $d_{calc} = 2.710$ g cm^{-3}; Mo-K_α radiation ($\lambda = 0.71073$ Å) graphite monochromator; $\mu = 93.7$ cm^{-1}; $F(000) = 2008$. A total of 3731 unique reflections were recorded in the range $2° \leqslant 2\theta \leqslant 60.0°$, of which 1643 were considered as unobserved [$F^2 < 3.0\sigma(F^2)$], leaving 2088 for solution and refinement. The structure was solved by Patterson methods, yielding a solution for the tungsten and phosphorus atoms. The hydrogen atoms were included as fixed contributions in the final stages of least-squares refinement while using anisotropic temperature factors for all other atoms. A non-Poisson weighting scheme was applied with a *p* factor equal to 0.08. The final *R* factors were $R = 0.034$, $R_w = 0.057$, G.O.F. = 1.20.

REFERENCES

1. P. Le Floch and F. Mathey, *Tetrahedron Lett.* 1989, **30**, 817.
2. J.-M. Alcaraz and F. Mathey, *Tetrahedron Lett.* 1984, **25**, 4659.
3. A. J. Ashe III, *J. Am. Chem. Soc.* 1971, **93**, 3293.
4. A. J. Ashe III, W. Butler, J. C. Colburn and S. Abu-Orabi, *J. Organomet. Chem.* 1985, **282**, 233.
5. A. J. Ashe III, *Accts Chem. Res.* 1978, **11**, 153.
6. J.-M. Alcaraz and F. Mathey, *Tetrahedron Lett.* 1984, **25**, 207.
7. G. Märkl and K. Hock, *Tetrahedron Lett.* 1983, **24**, 5055.

Polyhedron Vol. 9, No. 7, pp. 999–1007, 1990
Printed in Great Britain

0277–5387/90 $3.00+.00
© 1990 Pergamon Press plc

THE CHEMISTRY OF SIMPLE CERAMIC GLAZES—I. ^{57}Fe MÖSSBAUER STUDIES OF IRON-CONTAINING GLAZES AND GLASSES

NASSIF J. ALI, PETER A. GILLESPIE and WILLIAM R. McWHINNIE*

Department of Chemical Engineering and Applied Chemistry, Aston University, Aston Triangle, Birmingham B4 7ET, U.K.

(*Received* 25 *September* 1989; *accepted* 4 *December* 1989)

Abstract—A simple feldspathic glaze which matures at 1280°C and which contains iron as a colouring agent was examined by ^{57}Fe Mössbauer spectroscopy. When fired in air, oxidation of the iron (added as iron(II) oxalate) was complete and the iron(III) occupied a distorted octahedral site. By contrast a soda–lime–silica glass, fired under the same conditions, showed two iron sites, one octahedral [iron(III)], the other tetrahedral, although the oxidation state is uncertain. Firing under dinitrogen produced glazes containing iron(II) and iron(III); the iron was added as iron(II) oxalate or as a mixture of iron and Fe_2O_3. The chemical environment of the iron in the matured glaze was shown to be a function of the way in which the element is introduced into the raw batch, to the firing conditions, and may also be influenced by the replacement (gradual or complete) of $CaCO_3$ with $SrCO_3$ or $BaCO_3$. Using this simple glaze, good reproduction of Chinese "mirror black" and celadon were achieved by firing under dinitrogen and manipulating the form in which iron was added. Preliminary studies of iron–vanadium glazes are reported. Vanadium(IV), or VO^{2+}, was identified in the matured feldspathic glaze by ESR. The addition of iron (as metal) produced glazes, the ESR spectra of which were dominated by contributions from iron(III). The Mössbauer spectrum of a glaze containing 6% iron confirmed the presence of iron(III) but also revealed the presence of another iron site. The data are discussed in terms of an "FeO^{2+}" species.

The modern ceramic industry with its capacity for the manufacture of long runs of sophisticated and often intricate ware represents one of the triumphs of materials science. Craft pottery, whilst not untouched by advances in materials science remains a free form of expression in the sphere of ceramic art. The kiln of the craft potter is a cauldron in which much fascinating inorganic chemistry progresses. The potter, whilst able to exercise some control over the final result, often finds that serendipity remains an important ingredient of the process.

The reactant systems are complex, but it occurred to us that the examination of the chemical changes occurring during the firing of a simple glaze would provide a challenge which could be addressed via the resonance spectroscopies, in particular Mössbauer and solid-state magic angle spinning NMR (MASNMR). We recently attempted to demonstrate the power of the techniques by presenting our studies of the thermolysis of iron-containing minerals illite and montmorillonite[1] by ^{57}Fe Mössbauer spectroscopy and of the iron-free clays hectorite and laponite by ^{29}Si and ^{23}Na MASNMR spectroscopy.[2] In this paper we present some of our results on some iron-containing glazes of simple composition (together with data on simple glasses for comparison); we also investigate methods of obtaining glazes containing iron(II) other than by firing under a reducing atmosphere.

EXPERIMENTAL

Firing of specimens

Specimens were fired to temperatures up to 1280°C in a silicon carbide lined carbolyte MFHT furnace with a gas inlet facility to enable some firing

* Author to whom correspondence should be addressed.

to be carried out under a dinitrogen atmosphere. For such experiments the crucible containing the specimen was covered with a quartz sagger with a side arm which was attached to the gas inlet system. Samples were fired in platinum or unused porcelain crucibles. Materials were of reagent grade but some, for example, feldspar α-quartz and whiting were natural. All materials were subjected to XRD examination prior to use.

Physical measurements

X-ray diffraction (XRD) measurements were made on two instruments using Cu-K_α (1.54 Å) (JEOL) or Co-K_α (1.791 Å) (Philips) radiation. Exposure times of up to 4 h were necessary and identification of species was achieved via the powder diffraction file. Mössbauer spectra were obtained with a Centronic constant acceleration spectrometer as described by Fernandopulle,[3] other specimens were examined using the system recently described.[1] Spectra were computer fitted using a program written by Stone and co-workers[4] adapted for an ICL 1904S and HARRIS H800. The Gaussian non-linear regression method was used and the χ^2 criterion was used as a measure of the acceptability of fit. Spectra were recorded at room temperature. Electron spin resonance (ESR) spectra were measured with a JEOL PE-1X spectrometer using a Mn^{2+}/MgO standard.

RESULTS

Materials

XRD examination of starting materials gave the following results: reagent grade silica (amorphous), reagent grade sodium carbonate (amorphous), reagent grade calcium carbonate (calcite + aragonite), quartz (α-quartz), potash feldspar (no major impurity), whiting (calcite).

Firings in air

Iron was added as iron(II) oxalate dihydrate to both a simple soda glass and simple feldspathic glaze of the following composition:

GLASS I		GLAZE Ia	
10.9%	Na_2CO_3	54.4%	potash feldspar, $K_2O \cdot Al_2O_3 \cdot 6SiO_2$
11.1%	$CaCO_3$	19.1%	quartz (SiO_2)
58.1%	SiO_2	10.3%	whiting ($CaCO_3$)
19.9%	$Fe(COO)_2 \cdot 2H_2O$	16.2%	$Fe(COO)_2 \cdot 2H_2O$

Tables 1(a) (glass) and (b) (glaze) summarize the results of XRD and ^{57}Fe Mössbauer studies of specimens of the preceding composition fired to the indicated temperature. Heating rates were 400°C h^{-1}.

Observations from the data in Table 1 led to the design of experiments in which reagent grade calcium carbonate was heated in turn with X-ray amorphous silica and with α-quartz. The temperature was held at 1000°C for 2 h, after which the crucible was quenched. In both cases the composition was: 49.2% $CaCO_3$ (reagent grade); 50.8% silica (amorphous) *or* α-quartz. The results of XRD analyses are shown in Table 2.

Further experiments were carried out to assess the influence, if any, of the nature of the added alkaline earth ion, i.e. the substitution of Ca by Sr or Ba. One set of data (Table 3) were obtained for a glass, the other (Table 4) for the glaze, the compositions of which are recorded in the tables.

Firings under dinitrogen

"Reduced" glazes, i.e. those in the case of iron-containing glazes which might contain some iron(II), are usually formed by manipulation of the kiln atmosphere. We carried out two sets of experiments in one of which iron(II) was added to the initial glaze which was then fired under dinitrogen and in the other iron metal was added to the raw glaze. The results of the experiments are presented in Tables 5 and 6. The glaze compositions relevant to Table 5 are (weight %):

	Ia	Ib	Ic
Potash feldspar	55.0	55.0	55.0
Quartz	18.8	18.8	18.8
Whiting ($CaCO_3$)	10.7	7.2	3.6
Strontium oxalate	—	3.6	7.2
Iron(II) oxalate	15.5	15.4	15.4

For Table 6 the relevant compositions are:

	IVa	IVb
Potash feldspar	60.5	61.3
Quartz	21.2	21.5
Whiting ($CaCO_3$)	11.6	11.7
Haematite (α-Fe_2O_3)	5.0	—
Iron metal	1.7	5.5

Iron–vanadium glazes fired under dinitrogen

As a variant vanadium(V) oxide, V_2O_5, was included as an ingredient of the raw glaze together with iron metal. The glaze compositions were

Table 1. XRD and Mössbauer examination of iron-containing glass and feldspathic glaze

(a) Glass (for composition, see Results section)

Firing temperature (°C)	Components present identified by: XRD					^{57}Fe Mössbauer		
	Calcite	Aragonite	SiO_2[a]	$Fe(Ox)\cdot 2H_2O$	Others	α-Fe_2O_3	Unresolved	Others
400	√	√	×	×	α-Fe_2O_3	√	×	
600	√	×	×	×	α-Fe_2O_3	√	×	
800	×	×	×	×	α-Fe_2O_3	√	√	
900	×	×	×	×	α-Fe_2O_3, $CaSiO_3$	√	√	
1000	×	×	×	×	$CaSiO_3$	√	√	
1100	×	×	×	×		√	√	
1280	×	×	×	×		×	×	$\delta = 0.32$ $\Delta = 0.95$[c] $\delta = 0.03$ $\Delta = 0.97$

(b) Glaze **Ia** (for composition, see Results section)

Firing temperature (°C)	Components identified by: XRD						^{57}Fe Mössbauer		
	Potash feldspar	Quartz	Calcite	Aragonite	$Fe(Ox)\cdot 2H_2O$	Other	α-Fe_2O_3	Unresolved[b]	Other
400	√	√	√	×	×		√	×	
500	√	√	√	×	×	α-Fe_2O_3	—	×	
600	√	√	√	×	×	α-Fe_2O_3	√	×	
700	√	√	√	×	×	α-Fe_2O_3	—	×	
800	√	√	×	×	×	α-Fe_2O_3	√	×	
1000	√	√	×	×	×	α-Fe_2O_3	√	×	
1100	√	√	×	×	×		√	×	$\delta = 0.26$ $\Delta = 0.91$[c]
1200	√	√	×	×	×		—	—	—
1280	√	√	×	×	×		×	×	$\delta = 0.28$ $\Delta = 0.91$

[a] Amorphous to X-rays.

[b] Iron(III) resonances superimposed on α-Fe_2O_3 sextet.

[c] Mössbauer parameters (mm s^{-1}) relative to metallic iron, error in δ and Δ, ± 0.03 mm s^{-1}.

Table 2. Reaction products of the reaction of $CaCO_3$ with amorphous silica and α-quartz at 1000°C identified by XRD data

Species identified	$CaCO_3$+ α-quartz	$CaCO_3$+ amorphous silica
$CaCO_3$	×	×
CaO	√	×
α-Quartz	√	×
$CaSiO_3$	×	√
Others	×	×

(weight %):

	Va	Vb	Vc
Potash feldspar	57	58	50
Quartz	23	23	20
Whiting	14	15.2	10
V_2O_5	6	3	14
Iron metal	0	0.8	6

^{57}Fe Mössbauer data, together with some ESR data, are shown in Table 7.

DISCUSSION

Potash feldspar (orthoclase, $K_2O \cdot Al_2O_3 \cdot 6SiO_2$) can form the basis of many ceramic glazes. For this investigation we took a composition (**Ia** in Results section) which fires to an attractive opaque glaze maturing at 1280°C and which can be modified by the addition of various transition metal oxides to introduce colour to the final glaze. The frequency with which iron is used as a colouring oxide, and the availability of Mössbauer spectroscopy, make it an attractive element to study.

Iron glazes and glasses fired in air

The initial experiments were designed to compare the behaviour of iron in a feldspathic glaze and in a soda–lime–silica glass, both fired to the same maximum temperature of 1280°C. Iron was added as iron(II) oxalate (for consistency with subsequent experiments in which firings were carried out under dinitrogen). The glass components were laboratory reagent grade materials; the silica proved amorph-

Table 3. ^{57}Fe Mössbauer data for iron-containing alkaline earth glasses

Glass system	Mole % Quartz	Fe_2O_3	Whiting	SrO	BaO	Isomer shift (δ)[a] (mm s^{-1})	Quadrupole splitting (Δ)[b] (mm s^{-1}) or H_{eff}	Line width ($\Gamma_{1/2}$)[c] (mm s^{-1})
Ia	91	9	—	—	—	+1.821	H_{eff} = 525 kOe	0.275 0.262 0.245
IIa	74	8	18	—	—	+1.803	H_{eff} = 524 kOe 0.278	0.300 0.276
IIIa	74	8	—	18	—	0.283	1.178	0.613
IVa	74	8	—	—	18	0.200	0.875	0.451

[a] δ w.r.t. iron metal, error ±0.03 mm s^{-1}.
[b] Error in Δ, ±0.03 mm s^{-1}.
[c] Error in $\Gamma_{1/2}$, ±0.04 mm s^{-1}.

Table 4. ^{57}Mössbauer data for strontium and barium feldspathic glazes fired to 1280°C

Glaze number	Weight % Potash feldspar	Quartz	$Fe(COO)_2 \cdot 2H_2O$	$SrCO_3$	$BaCO_3$	Isomer shift (δ)[a] (mm s^{-1})	Quadrupole splitting (Δ)[b] (mm s^{-1})	Line width ($\Gamma_{1/2}$)[c] (mm s^{-1})
II	55.0	18.8	15.2	7.2		0.216	1.117	0.69
III	55.0	18.8	15.4		7.2	0.187	1.070	0.74

[a] δ w.r.t. iron metal, error ±0.06 mm s^{-1}.
[b] Error in Δ, ±0.06 mm s^{-1}.
[c] Error in $\Gamma_{1/2}$, ±0.01 mm s^{-1}.

Table 5. ^{57}Fe Mössbauer data[a] for some iron-containing feldspathic glazes fired to a maximum temperature of 1280°C under dinitrogen

Firing temperature (°C)	Glaze **Ia**			**Ib**	**Ic**
	α-Fe_2O_3	Fe_3O_4	Other (mm s^{-1})		
400	×	√			
600	×	√			
800	×	√			
1000	×	√			
1200	×	√			
1280	×	×	$\delta = 0.29$	$\delta = 0.22$	$\delta = 0.21$
			$\Delta = 1.16$	$\Delta = 0.96$	$\Delta = 1.00$
			$\delta = 1.06$	$\delta = 1.01$	$\delta = 0.96$
			$\Delta = 1.99$	$\Delta = 1.77$	$\Delta = 1.75$
				Under air	Under air
				$\delta = 0.32$	$\delta = 0.26$
				$\Delta = 1.01$	$\Delta = 1.09$

δ quoted relative to metallic iron; error in δ and $\Delta = \pm 0.03$ mm s^{-1}.

Fe_3O_4 identified from Mössbauer parameters in five cases. The "raw" materials, in the absence of iron(II) oxalate, failed to give evidence of this species.

Table 6. ^{57}Fe Mössbauer conclusions data for feldspathic glazes (raw glaze contains iron metal) (fired under dinitrogen)

Firing temperature (°C)	Glaze **IVa**			Glaze **IVb**	
	α-Fe_2O_3	Iron metal	Other (mm s^{-1})	Dinitrogen	Air
400	√	√			
600	√	√			
800	√	√			
1000	×	×		Iron metal	α-Fe_2O_3
1200	×	×			
1280	×	×	$\delta = 1.05$	$\delta = 0.99$	$\delta = 0.26$
			$\Delta = 2.36$	$\Delta = 1.78$	$\Delta = 0.91$

δ quoted w.r.t. iron metal; error in δ and $\Delta = \pm 0.03$ mm s^{-1}.

Table 7. ^{57}Fe Mössbauer and ESR data for mixed iron–vanadium feldspathic glazes fired under dinitrogen to 1280°C

Glaze number	Mössbauer data (mm s^{-1})	ESR data
Va	(No iron)	$g_{\parallel} = 1.959$, $A_{\parallel} = 163$ Hz $g_{\perp} = 1.986$, $A_{\perp} = 78.6$ Hz
Vb	No signal—iron concentration too low	$g = 1.995, 4.15, 6.3$
Vc	$\delta = 0.13$ $\delta = -0.59$ $\Delta = 1.31$ $\Delta = 4.10$	$g = 1.98, 4.20, 6.4$

δ quoted relative to metallic iron; error in δ and $\Delta = \pm 0.04$ mm s^{-1}.

ous to X-rays, whereas the calcium carbonate was shown by XRD to be a mixture of calcite and aragonite. By contrast, the whiting used in the glaze was pure calcite. Table 1 details the thermal history of the glass and glaze batches on firing to 1280°C in air.

Aragonite is lost from the glass batch between 400 and 600°C, this is in accord with published data which specifies a temperature of 510°C for the aragonite–calcite phase transition.[5] Calcite undergoes decomposition around 800°C and iron(II) oxalate has completely decomposed to haematite, α-Fe_2O_3, by 400°C. It is clear that additional reactions begin to occur around 800°C since weak unresolved Mössbauer features are seen to be superimposed on the central region of the dominant α-Fe_2O_3 sextet. Attempts to deconvolute this region were ultimately abandoned when no satisfactory χ^2 values were obtained, this presumably means that a range of iron(III) sites co-exist. At 900°C, XRD evidence for the formation of some β-$CaSiO_3$ is obtained consistent with the weight per cent of CaO and SiO_2 employed.[6,7] According to the Mössbauer data, haematite persists until 1100°C, but at 1280°C a glass has been formed and two iron sites are detected. The chemical isomer shift ($\delta = 0.32$ mm s^{-1}) of one site is consistent with the presence of iron(III) in an octahedral "FeO_6" environment. The fact that $\Delta > 0$ illustrates that the "octahedral" site must be distorted. The second site with $\delta = 0.03$ mm s^{-1} is of more interest. Tetrahedral iron(III) generally gives less positive values of δ,[8] but the value of 0.03 mm s^{-1} seems low even for the extended range of δ values seen in vitreous as opposed to crystalline systems.[9–14] Indeed it approaches the value, 0.01 mm s^{-1} w.r.t. iron metal, observed by Gallagher and Kurkjian[15] for the 700°C phase in their study of the thermal decomposition of $Sr_3[Fe(oxalate)_3]$, $2H_2O$ and attributed to iron(IV). Given that later in this paper evidence for iron(IV) in a glaze firing is presented, we suggest that this interpretation of the $\delta = 0.03$ mm s^{-1} resonance cannot be disregarded. Thus the second iron environment is probably stereochemically a distorted "FeO_4" site, however the oxidation state of the iron is not clearly defined by the Mössbauer technique.

By contrast, the feldspathic glaze (Table 1) seems more straightforward. Haematite persists until 1100°C, but even at that temperature there is evidence for the incorporation of some iron in a glassy matrix. By 1280°C all the iron has been incorporated into distorted octahedral sites which, within the cited errors, are very similar to the octahedral site in the soda–lime–silica glass. No evidence for a second iron site was obtained. A further difference between the glass and glaze firings is the identification of XRD of β-$CaSiO_3$ in the glass (but not glaze) batches fired to 800–1000°C. Table 2 reports experiments carried out on mixtures of $CaCO_3$ with amorphous silica and α-quartz. Firing to 1000°C produces β-$CaSiO_3$ in the former, but not in the latter case. This then is a kinetic phenomenon where the smaller particle size and greater surface activity of the amorphous material induces a more rapid reaction.

Table 3 investigates the influence of alkaline earth carbonates on the reaction between α-quartz and α-Fe_2O_3. Apparently no reaction occurs at 1280°C in the presence or absence of $CaCO_3$, however, $SrCO_3$ and $BaCO_3$ produce new iron species at that temperature. For $SrCO_3$ the parameters are consistent with iron(III) in a distorted octahedral environment, but the large value of $\Gamma_{1/2}$ suggests that a spectrum of environments is present. The value of δ for the barium system however (0.20 mm s^{-1}) could certainly indicate a tetrahedral site—the values of both Δ and $\Gamma_{1/2}$ are smaller then in the Sr case suggesting a narrower range of environments and suggesting the possibility of a barium ferrate(III) phase.

Substitution of $SrCO_3$ for $CaCO_3$ in glaze **I** (Table 4) produces a less positive isomer shift, but greater quadrupole splitting on firing to 1280°C, however, $\Gamma_{1/2}$ is again large suggesting once more that a spectrum of micro-environments is available to the iron(III). The substitution by $BaCO_3$ produces an even less positive value of δ but, within the errors, Δ is the same—$\Gamma_{1/2}$ at 0.74 mm s^{-1} is even larger. The sites are suggested to be tetrahedral, certainly the values of δ are consistent with this view,[8] and recently others have cited quadrupole splittings > 1.0 mm s^{-1} for tetrahedral sites in iron–silica glasses.[16] Thus it would appear, in the case of glaze **I**, that the alkaline earth cation may have a significant influence on the ultimate environment of the iron. This may occur via modification of the glass structure[17] or, as implied in Table 3, the precipitation of "ferrate(III)" phases.

Firing under dinitrogen

Many stoneware glazes have greater aesthetic impact if they are fired under reducing conditions. We decided to explore the possibility by adding, in this instance, iron in a lower oxidation state [iron(II) or iron(0)] and firing in an inert atmosphere to examine if "reduced" effects could be obtained. Table 5 contains experimental data for our basic feldspathic glaze (**Ia**) fired under nitrogen; also glazes **Ib** and **Ic** explore the influence of partial replacement of $CaCO_3$ by $SrCO_3$. Even at 400°C a magnetic hyperfine spectrum is seen for **Ia** but it

arises from magnetite, Fe_3O_4, rather than haematite. Magnetite persists to 1200°C but by 1280°C the iron has been incorporated into the matured glaze—octahedral iron(II) ($\delta = 1.06$ mm s^{-1}, $\Delta = 1.99$ mm s^{-1}) and iron(III) sites ($\delta = 0.29$ mm s^{-1}, $\Delta = 1.16$ mm s^{-1}); within the cited errors, the iron(III) site is clearly similar to that observed on firing in air (Table 1). The matured glaze fired in air to 1280°C is green, whilst that fired under nitrogen is mirror black. XRD showed the presence of α-quartz and potash feldspar in the mature black glaze (as was the case for firings in air); also XRD measurements confirmed, for batches fired to lower temperatures, that the oxide of iron present was indeed magnetite.

One of the summits of ceramic art was reached in the Chinese Sung Dynasty.[18] Hedges[19] has made Mössbauer studies of some authentic glazes from this period, the following comparison of parameters is of interest:

Glaze **Ia** (under N_2)		Chinese "Mirror Black"[19]	
δ	Δ	δ	Δ
0.29 ± 0.03	1.16 ± 0.03	0.30	1.29
1.06 ± 0.03	1.99 ± 0.03	1.08	2.02

The similarity is striking.

The partial replacement of $CaCO_3$ by $SrCO_3$ has little effect on the ultimate fate of the iron when **Ib** and **Ic** are fired in air, a single octahedral iron(III) environment being seen (Table 5). When fired under dinitrogen the Mössbauer parameters seem more sensitive to the substitution. Thus the iron(III) chemical isomer shift becomes less positive and comparable to that observed for glaze **II** in Table 4, thus the suggestion must again be made that, in the presence of strontium iron(III) prefers a tetrahedral environment. Although δ for iron(II) is not greatly influenced by the strontium for calcium substitution, Δ which is reduced to ~ 1.76 mm s^{-1}, is apparently sensitive to the change. This is unlikely to be an electronic effect, hence a modification of the site symmetry is implied.

Glazes **IVa** and **IVb** (Table 6) differ in that **IVa** contained, initially, both α-Fe_2O_3 and iron(0), whereas **IVb** contained iron metal as the sole source of the element. Bhatt *et al.*[20] have demonstrated the possibility of forming an iron(II) glass by mixing equimolar portions of iron and iron(III) oxide in the batch. Firing **IVa** under dinitrogen gave no evidence of reaction up to 800°C when XRD evidence for the continued presence of iron(0) and α-Fe_2O_3 was obtained. At 1280°C the glaze matured and a single iron(II) site was identified; the colour was a rich blue. The same iron(II) spectrum was in fact seen at 1000 and 1200°C even though the glaze was not mature. Although the isomer shift of the iron(II) resonance is similar to that of the iron(II) site in glaze **Ia** fired under dinitrogen, Δ is significantly larger suggesting that the ultimate location of the iron(II) is a function, amongst other variables, of the way in which the iron is introduced. When glaze **IVb** is fired in air, Mössbauer parameters essentially identical to those in Table 1 are obtained. This is not surprising since XRD shows that iron(II) oxalate decomposes to α-Fe_2O_3 by 400°C and that iron metal has completely oxidized to α-Fe_2O_3 by 1000°C, thus in both cases haematite is the effective source of iron. Firing under dinitrogen produces an iron(II) glaze with parameters closely similar to those obtained for **Ib** and **Ic** (Table 5). The matured glaze is pale green, again comparison with the data of Hedges[19] is instructive:

	δ	Δ
Pale green celadon glaze[19]	1.12	1.81
Glaze **IVb** under N_2	0.99 ± 0.03	1.78 ± 0.03

Hedges also reported a second site which he described as tetrahedral, but no evidence for a second iron site was found for **IVb**.

The colour of the "mirror black" glaze presumably arises from iron(II)/iron(III) charge-transfer between adjacent ions, whilst that of the celadon is typical of an $Fe^{II}O_6$ environment. The blue colour of **IVa** fired under N_2 is then probably a function of the more distorted ligand field apparent from the larger value of Δ, which gives some absorption in the red. Great variety may therefore be achieved from the same basic glaze composition by subtle variation in the firing conditions and in the manner of introduction of the iron.

Mixed iron–vanadium glazes

Glaze **Va** (see Results section) is similar to **Ia** except that V_2O_5 replaces iron(II) oxalate. The matured glaze is a creamy colour but it gives a well resolved ESR spectrum showing parallel and perpendicular components with evidence of hyperfine splitting (^{51}V has spin 7/2). The spectrum is characterized by $g_\parallel < g_\perp$ and $A_\parallel > A_\perp$. Early work by Bamford[21] predicted that vanadium should be incorporated in glasses primarily as vanadium(V) and vanadium(III), but others[22,23] allowed the possibility of vanadium(IV) also. Bandyopadhyag[24] has used ESR to detect the VO^{2+} ion in borate glass.

Fortunately a considerable body of experimental data exists for ESR studies of vanadium(IV); some useful comparative data are set out in Table 8. It is apparent that the spectrum of glaze **Va** is most similar to those in which the VO^{2+} ion is present

Table 8. Some comparative experimental data—ESR parameters for vanadium(II) in oxygen coordination environments

Ion	$g_{\parallel}$	$g_{\perp}$	$A_{\parallel}$	$A_{\perp}$	Reference	Interpretation
V^{4+} in tridymite	1.968	2.00	58	22	25	Tetrahedral
V^{4+} in TiO_2	1.957	1.915	142	37	26	Octahedral—weak tetragonal distortion
VO^{2+} in borosilicate glass	1.931	1.967	165.8	58.4	24	Octahedral sites with strong tetragonal distortion, i.e. VO^{2+} ion
VO^{2+} in lead silicate glass	1.906	1.969	170	60	27	
VO^{2+} in glaze **Va**	1.959	1.986	163	78.6	Present work	

as a network modifier. Thus it is clear that *some* vanadium(IV), probably in the form VO^{2+}, is present in the mature glaze **Va**; however, the colour of the final glaze suggests the concentration of VO^{2+} is small.

Glaze **Vb** and **Vc** contain iron; introduced as the metal **Vb** matures to an attractive blue violet colour and **Vc** to a lustrous brown. The ESR spectra are dominated by contributions from iron(III). Some ESR studies of Fe–V borosilicate glasses[24] have been published and the loss of hyperfine structure from the vanadium component was also noted; it was suggested that strong interactions between vanadium(IV) and iron(III) were responsible. Even the relatively low iron concentration that characterizes **Vb** results in the loss of the vanadium hyperfine structure, however, the use of a piece of glaze rather than the powdered glaze to record the spectrum did reveal some vanadium hyperfine structure superimposed on the broad high-field resonance, thus confirming, in our view, the continued presence of some vanadium(IV). The main spectral feature was at an apparent g value of 4.15. This feature is commonly observed in iron-containing minerals and glasses and is usually taken to arise from iron(III) in a rhombically distorted environment.[28] The iron content of **Vb** proved too low for a satisfactory Mössbauer spectrum to be obtained.

The ESR spectrum of **Vc** was very similar to that of **Vb**, hence there was the expectation that iron(III) in a distorted environment would be detected in the Mössbauer spectrum. In the event a most peculiar spectrum was obtained (even for this sample the iron content is not great and the spectral quality was poor). Four peaks only were seen and we pair these as indicated in Table 7. The anticipated distorted iron(III) site is, on this basis, tetrahedral ($\delta = 0.13$, $\Delta = 1.31$ mm s^{-1}). The second iron site is characterized by an isomer shift of -0.59 mm s^{-1} which is compatible with iron(IV),[8,9] however, the quadrupole splitting is massive (4.10 mm s^{-1}). A possible explanation is that the iron(IV) substitutes for vanadium(IV) in the VO^{2+} sites within the glaze, i.e. the implication is that a "FeO^{2+}" species must be considered. If such a species exists in the glaze it has been trapped on formation and the stability must be kinetic. There is no doubt that the Fe/V glass system will repay further investigation.

Acknowledgements—P.A.G. thanks the SERC and the Gladstone Pottery Museum for a CASE award.

REFERENCES

1. P. J. Michael and W. R. McWhinnie, *Polyhedron* 1989, **8**, 2709.
2. A-P. S. Mandair, P. J. Michael and W. R. McWhinnie, *Polyhedron* 1990, **9**, 517.
3. M. E. Fernandopulle, PhD thesis, University of Aston in Birmingham (1972).
4. G. M. Bancroft, A. G. Maddock, W. K. Ong, R. H. Prince and A. J. Stone, *J. Chem. Soc. A* 1967, 1966.
5. *The International Rubber Handbook*. The Rubber Co. Ltd (USA) (1972).
6. G. A. Rankin and F. E. Wright, *Am. J. Sci.* 1915, **39**, 5.
7. A. Muan and E. F. Osborn, *Am. Iron Steel Inst.* (1951), preprint; A. Muan and E. F. Osborn, *Ind. Heating* 1952, **19**, 317.
8. G. M. Bancroft, *Mössbauer Spectroscopy: An Introduction for Chemists and Geochemists*. McGraw Hill, Maidenhead (1973).
9. C. R. Kurkjian and D. N. E. Buchanan, *Phys. Chem. Glasses* 1964, **5**, 63.
10. A. A. Belyustin, Yu M. Ostanevich, A. H. Pisarevskii, S. B. Tomilov, U. Bai-shi and L. Cher, *Sov. Phys.–Solid State* 1965, **7**, 1163.
11. J. P. Gosselin, V. Shimony, L. Grodzins and A. R. Cooper, *Phys. Chem. Glasses* 1968, **9**, 73.

12. M. F. Taragin and J. C. Eisenstein, *J. Non-Cryst. Solids* 1970, **3**, 311.
13. M. F. Taragin and J. C. Eisenstein, *Phys. Chem. Glasses* 1967, **8**, 2.
14. Ch. Laber and P. Gielen, *J. Non-Cryst. Solids* 1973, **13**, 107.
15. P. K. Gallagher and C. R. Kurkjian, *Inorg. Chem.* 1966, **5**, 214.
16. E. De Grave and P. Van Isegham, in *Industrial Applications of the Mössbauer Effect* (Edited by G. J. Long and J. G. Stevens), p. 423. Plenum Press, New York (1986).
17. Yu G. Shteinberg, *Strontium Glazes*, 2nd edn, pp. 5–12. Stroiizdat, Leningrad, Moscow (1967).
18. W. B. Honey, *The Ceramic Plant of China*. Faber and Faber, London (1954).
19. R. E. M. Hedges, *Nature* 1975, **254**, 501.
20. V. K. Bhatt, C. R. Manning and L. H. Bowen, *J. Am. Ceram. Soc.* 1973, **56**, 459.
21. C. M. Bamford, *Phys. Chem. Glasses* 1960, **1**, 159; 1961, **2**, 163; 1962, **3**, 54.
22. T. Bates, *Modern Aspects of the Vitreous State*. Butterworth, London (1952).
23. W. A. Weyl, *Coloured Glasses*. Soc. Glass Technol., Sheffield (1951).
24. A. K. Bandyopadhyag, *J. Mater. Sci.* 1981, **16**, 189.
25. V. S. Grumin, V. A. Loffe and Z. N. Zonn, *J. Non-Cryst. Solids* 1973, **11**, 341.
26. H. J. Gerritsen and H. R. Lewis, *Phys. Rev.* 1960, **119**, 1010.
27. L. D. Bogomolova, V. A. Zhachkain, V. N. Lazukin and V. A. Shmucher, *J. Non-Cryst. Solids* 1978, **27**, 427.
28. W. R. McWhinnie, in *Chemical Bonding and Spectroscopy in Mineral Chemistry* (Edited by F. J. Berry and D. J. Vaughan), p. 209. Chapman and Hall, London (1985).

Polyhedron Vol. 9, No. 7, pp. 1009–1010, 1990
Printed in Great Britain

0277–5387/90 $3.00+.00
© 1990 Pergamon Press plc

COMMUNICATION

HOMOLEPTIC *t*-BUTYLIMIDO COMPOUNDS OF OSMIUM(VIII) AND CHROMIUM(VI)

ANDREAS A. DANOPOULOS and GEOFFREY WILKINSON*

Johnson Matthey Laboratory, Chemistry Department, Imperial College, London SW7 2AY, U.K.

(*Received* 16 *January* 1990; *accepted* 30 *January* 1990)

Abstract—The homoleptic imido compounds $Os(NBu^t)_4$ and $Li_2Cr(NBu^t)_4$ have been synthesized, the former by interaction of OsO_4 and $Bu^tNH(SiMe_3)$ where a tetrameric oxoimido compound $Os_4(NBu^t)_6(\mu\text{-}Bu^t)_4(\mu\text{-}O)_2$ is also formed, and the latter by methyllithium deprotonation of $Cr(NBu^t)_2(NHBu^t)_2$.

We recently described the first syntheses of homoleptic imido compounds, namely those of tungsten and rhenium, $Li_2W(NBu^t)_4$ and Li(TMED) $Re(NBu^t)_4$ (TMED = tetramethylethylenediamine). Details of the rhenium compound and of a second homoleptic compound of rhenium(VI), $[(Bu^tN)_2Re(\mu\text{-}NBu^t)]_2$ have been given.[2] X-ray structures of the three compounds were reported,[1,2] while the synthesis of the molybdenum analogue $Li_2Mo(NBu^t)_4$ has been described.[3]

We noted[1] that the only other similar transition metal imido compound was the non-homoleptic $Os(NBu^t)_3(Ntos)$ (tos = *p*-toluene sulphonate) made by K. B. Sharpless, details of which are not available.[4]

We now report the synthesis of $Os(NBu^t)_4$ and of $Li_2Cr(NBu^t)_4$, the latter completing the series of compounds for chromium, molybdenum and tungsten.

The osmium compound is obtained in *ca* 20% yield by interaction of OsO_4 in refluxing neat $Bu^tNH(SiMe_3)$ or, in lower yield using $Os(NBu^t)O_3$. Other compounds are formed and one of these, a red crystalline compound, m.p. 120°C, formed in *ca* 10% yield, has been fully characterized by analyses, spectra and by X-ray crystallography[5] as having the oxoimido formulation (**1**).

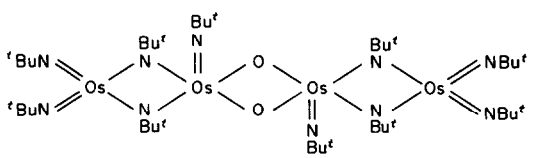

(1)

$Os(NBu^t)_4$ is an orange–brown, moisture-sensitive, low melting solid (m.p. *ca* 30°C; b.p. 90–100°C/0.01 mm Hg) that has correct analysis and cryoscopic molecular weight. The NMR spectra are invariant over the range −80 to +80°C: ^1H, 1.48 ppm (NBu^t); $^{13}C\text{-}\{^1H\}$, 30.25 ppm, $C(CH_3)_3$, 72.61 ppm, CMe_3. The mass spectrum shows the molecular ion (476) with structure due to osmium isotopes and peaks at lower mass due to loss of NBu^t and CH_3 groups. We have, so far, been unable to grow X-ray quality crystals.

The chromate(VI) analogue, $Li_2Cr(NBu^t)_4$, is made by a route similar to that used[3] for $Li_2Mo(NBu^t)_4$, starting from $Cr(NBu^t)_2(OSiMe_3)_2$[6] namely the sequence:

$$Cr(NBu^t)_2(OSiMe_3)_2 \xrightarrow[CH_2Cl_2]{BCl_3} Cr(NBu^t)_2Cl_2$$

$$\downarrow \text{LiNHBu}^t,\ \text{toluene}$$

$$Li_2Cr(NBu^t)_4 \xleftarrow[Et_2O/\text{hexane}]{MeLi} Cr(NBu^t)_2(NHBu^t)_2$$

* Author to whom correspondence should be addressed.

Satisfactory analyses were obtained for all the chromium compounds. The red $Li_2Cr(NBu^t)_4$, $d > 250°C$, forms crystals suitable for X-ray diffraction from diethyl ether. The ^1H NMR indicates that the structure is similar to that of the tungsten[1] and molybdenum[3] compounds having bands for linear and bent imido groups at 1.30 (9H) and 1.60 (27H) ppm, respectively. The intermediates were also fully characterized: $Cr(NBu^t)_2Cl_2$, m.p. 68–70°C, mass spectrum *m/e* 264 (M^+), ^1H NMR δ 1.60 ppm; $Cr(NBu^t)_2(NHBu^t)_2$, m.p. 57–60°C, IR ν(N—H) 3350, ^1H NMR δ 1.39 ppm (18H, $NHCMe_3$), mass spectrum *m/e* 338 (M^+).

Acknowledgements—We thank the SERC for support and Johnson Matthey plc for the loan of osmium.

REFERENCES

1. A. A. Danopoulos, G. Wilkinson, B. Hussain and M. B. Hursthouse, *J. Chem. Soc., Chem. Commun.* 1989, 896.
2. A. A. Danopoulos, C. J. Longley, G. Wilkinson, B. Hussain and M. B. Hursthouse, *Polyhedron* 1989, **8**, 2657.
3. A. A. Danopoulos, G. Wilkinson, M. B. Hursthouse and B. Hussain, *Polyhedron* 1989, **8**, 2947.
4. Quoted by W. A. Nugent and B. L. Haymore, *Coord. Chem. Rev.* 1980, **31**, 123.
5. By B. Hussain-Bates and M. B. Hursthouse, Queen Mary and Westfield College, London E1 4NS, U.K.
6. W. A. Nugent and R. L. Harlow, *Inorg. Chem.* 1980, **19**, 777.

Polyhedron Vol. 9, No. 8, pp. 1011–1015, 1990
Printed in Great Britain

0277–5387/90 $3.00+.00
Pergamon Press plc

BINUCLEAR DIOXOMOLYBDENUM(VI) COMPLEXES CONTAINING BRIDGING DIOXIME SCHIFF BASE LIGANDS

R. N. MOHANTY and K. C. DASH*

Department of Chemistry, Utkal University, Vani Vihar, Bhubaneswar-751004, India

(*Received* 29 *August* 1989; *accepted* 2 *November* 1989)

Abstract—$MoO_2(acac)_2$ reacts in EtOH with polydentate dioxime-based Schiff base ligands obtained by the condensation of biacetylmonoxime with ethylenediamine (H_2DMED), propylenediamine (H_2DMPD), diethylenetriamine (H_2DMDT) and triethylenetetramine (H_2DMTT) to form binuclear, ligand-bridged, six-coordinated *cis*-dioxomolybdenum(VI) complexes—[(acac)MoO_2(L)O_2Mo(acac)]. All the ligands essentially act as bridging tetradentate ligands. The complexes are characterized by analytical, conductivity, IR and NMR (^1H and ^{13}C) spectral measurements.

The biological activity of molybdenum mostly involves the molybdenum(VI) state, the coordination chemistry of which is to a large extent based on oxo complexes which are of importance for their role in oxidation catalysed by metals.[1,2] Among the transition metal oxocations, the oxovanadium(IV)[3] and dioxomolybdenum(VI)[4] have attracted particular attention. In the structural chemistry of molybdenum(VI) the MoO_2^{2+} has received wide attention and a near octahedral structure with *cis*-dioxo groups is a constant feature. $MoO_2(acac)_2$ is a good source of MoO_2^{2+} and is very convenient to prepare.[5,6] The reaction of $MoO_2(acac)_2$, in suitable solvents, with the multidentate Schiff bases obtained by the condensation of biacetylmonoxime with ethylenediamine (H_2DMED), propylenediamine (H_2DMPD), diethylenetriamine (H_2DMDT) and triethylenetetramine (H_2DMTT) results in the formation of binuclear, mixed-ligand, six-coordinated, *cis*-dioxomolybdenum(VI) complexes, [(acac)MoO_2(L)O_2Mo(acac)], by the partial displacement of the acetylacetone group from the starting $MoO_2(acac)_2$.

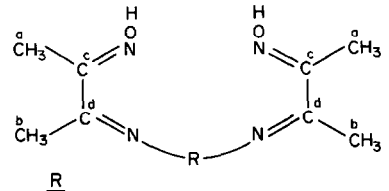

R	
$(CH_2)_2$	H_2DMED
$(CH_2)_3$	H_2DMPD
$(CH_2)_2$—NH—$(CH_2)_2$	H_2DMDT
$(CH_2)_2$—NH—$(CH_2)_2$—NH—$(CH_2)_2$	H_2DMTT

* Author to whom correspondence should be addressed.

EXPERIMENTAL

Materials and methods

FT–IR spectra in KBr phase and electrolytic conductance were obtained as reported earlier.[7] All NMR measurements in DMSO-d_6 medium were performed on a JEOL FT–NMR instrument operating at 270.05 MHz for ^1H and 67.80 MHz for ^{13}C. $MoO_2(acac)_2$ was prepared[5] from $(NH_4)_6Mo_7O_{24}\cdot 4H_2O$ (Merck) and acetylacetone (BDH). The multidentate Schiff bases, H_2L (H_2L = H_2DMED, H_2DMPD, H_2DMDT and H_2DMTT), were obtained by the condensation[7–9] of biacetylmonoxime (Loba Chemie) with ethylenediamine, propylenediamine, diethylenetriamine or triethylenetetramine in Et_2O or *i*-Pr_2O medium. The metal was estimated after digesting the complex in 3:4 vol/vol conc. HNO_3 and conc. H_2SO_4, extracting the residue in H_2O and precipitating as oxinate. C, H, N microanalyses were carried out by CDRI, Lucknow.

Synthesis of [(acac)MoO_2(L)O_2Mo(acac)] *complexes*

All these complexes were synthesized by a general synthetic technique. The solid ligand (H_2L) (1 mmol) was added in small amounts to a hot, stirred solution of $MoO_2(acac)_2$ (1 mmol) in EtOH (10 cm^3) and a white or pale yellow solid was formed. The mixture was further stirred under reflux for 8 h for completion of reaction. The solids were then collected on a glass frit, washed with small aliquots of EtOH followed by Et_2O and dried *in vacuo* at room temperature. Variation of the metal-to-ligand

ratio did not affect the stoichiometry of the complexes. The compounds were obtained in 70–75% yield.

RESULTS AND DISCUSSION

The chemistry of molybdenum(VI) is dominated by complexes containing the MoO_2^{2+} core,[2,10] the vast majority of which are six-coordinate with a distorted octahedral structure with the two Mo—O_t bonds *cis* to each other. In addition to the monomeric complexes, some polymeric structures are also known which have the Mo—O_t distances and O_t—Mo—O_t angles similar to those found in the mononuclear complexes. Complexes with MoO_2^{2+} core structures are prepared by using Na_2MoO_4, $(NH_4)_6Mo_7O_{24}$ or $MoO_2(acac)_2$ as the starting materials.[5,11] $MoO_2(acac)_2$ is a convenient starting material as one or both of the acac groups may be replaced by suitable ligands in a convenient reaction medium. The complexes formed may be mononuclear or binuclear containing the MoO_2^{2+} core or may also be binuclear containing the Mo_2O_3 and MO_2O_5 structures.[12,13] The polydentate oxime-based Schiff base ligands—the tetradentate H_2DMED, H_2DMPD; the pentadentate H_2DMDT and the hexadentate H_2DMTT—may coordinate to a single metal centre[9,14] or to two metal centres.[7,15,16] $MoO_2(acac)_2$ reacts with these ligands in EtOH medium to form stable, binuclear, diamagnetic, six-coordinated dioxomolybdenum(VI) complexes. That only one acac group is displaced from each $MoO_2(acac)_2$ is confirmed by the isolation of $Cu(acac)_2$ quantitatively from the filtrate after the reaction of $MoO_2(acac)_2$ with H_2L (H_2L = H_2DMED, H_2DMPD, H_2DMDT, H_2DMTT). Further confirmation of this is obtained from IR and NMR (^1H and ^{13}C) evidence as discussed below. The ligands, H_2L, behave as doubly-deprotonated tetradentate ligands bridging two $MoO_2(acac)^+$ centres. A similar partial displacement of acac groups from $MoO_2(acac)_2$ has also been observed in several complexes containing the MoO_2^{2+} core,[11,17,18] the VO^{2+} core[19] and in complexes of the type Co(acac)(Salen).[20]

The complexes isolated are reported in Table 1. They are rather poorly soluble in common organic solvents precluding the determination of molecular weight and isolation of a good quality crystal for structural determination. However, dilute solutions (10^{-4} M) in DMSO confirm their non-electrolytic behaviour.[21] All the complexes, [(acac)MoO_2 (L)O_2Mo(acac)], exhibit IR bands characteristic of the *cis*-MoO_2^{2+} core, the Schiff base ligands and the acac groups. In the complexes, a fairly sharp band in the 1580–1620 cm^{-1} region is assigned to the ν(C=N) of the Schiff base ligands.[22] The ν(N—O) in the complexes at 1140–1150 cm^{-1} suggests the oximes to be N-coordinated.[23] The ν'(N—O) and δ(N—O) bands appear at 1080 and 820 cm^{-1}, respectively. ν(C=O) for the coordinated acac group appears[24] at 1580 cm^{-1} and the methine C—H bending vibration is seen as a weak band at 1190 cm^{-1}. The formation of Mo—O bonds with acac groups and Mo—N bonds of the Schiff bases results in the appearance of a few medium-to-strong stretching frequencies in the 550–650 cm^{-1} region, which are absent in the free ligands. As for the *cis*-MoO_2^{2+} groups, the IR spectrum manifests itself in the form of an intense two-band pattern corresponding to the symmetric and antisymmetric Mo=O stretching vibrations[25] in the 880–920 cm^{-1} region. The *trans*-MoO_2^{2+} complex would have given only one absorp-

Table 1. Analytical, conductivity and prominent IR data of the molybdenum(VI) complexes

Complex	Colour	Melting point (°C)	Found (Calc.)%[a] Mo	C	H	δN	Λ_M[b] (Ω^{-1} cm^2 mol^{-1})	IR (cm^{-1}) ν(C=N)	ν(C=O)	ν(Mo=O)
$Mo_2O_4(acac)_2L$										
L = DMED	Pale yellow	> 240	28.8 (28.3)	35.6 (35.4)	4.1 (4.4)	8.1 (8.2)	9.76	1580	1570	890, 918
DMPD	White	> 240	27.9 (27.7)	36.3 (36.4)	4.5 (4.6)	7.9 (8.1)	10.58	1592	1574	886, 914
DMDT	Pale yellow	> 240	26.1 (26.6)	36.8 (36.6)	4.8 (4.9)	9.4 (9.7)	11.56	1600	1578	889, 904
DMTT	Pale yellow	> 240	24.9 (25.1)	37.6 (37.7)	5.1 (5.3)	10.8 (11.0)	11.39	1620	1580	896, 920

[a] Theoretical values in parentheses.

[b] All measurements in DMSO, 1 : 1 electrolyte in DMSO has Λ_M of 20–39.

Table 2. ^{1}H NMR[a] data for some of the molybdenum(VI) complexes

Compound	Schiff base protons				"acac" Protons	
	—CH_3[a]	—CH_3[b]	CH_2—CH_2	—NH	—CH_3	—CH
H_2DMED	1.88	2.04	3.75			
$Mo_2O_4(acac)_2$DMED	1.78	1.91	3.49		2.1	5.4
H_2DMDT	1.72	1.92	3.43 3.53	8.38		
$Mo_2O_4(acac)_2$DMDT	1.86	1.93	3.58 3.80	10.55	2.08	5.2
H_2DMTT	1.90	1.98	3.27 3.36 3.42	8.31		
$Mo_2O_4(acac)_2$DMTT	1.86	1.93	3.49 3.64 3.93	10.52	2.14	5.0

[a] All measurements in DMSO-d_6; all values in ppm downfield from TMS as internal standard.

tion band. That one or two secondary amine (—NH) functions remain uncoordinated in the complexes with the pentadentate H_2DMDT and the hexadentate H_2DMTT ligands is seen from the appearance of ν(NH) at *ca* 3150 cm^{-1}. This is further substantiated on the basis of the ^{1}H NMR spectra discussed below.

The ^{1}H and ^{13}C NMR spectra establish in a complementary way the disposition of the non-oxo ligands in the complexes. The ^{1}H NMR spectra of the Schiff base ligands and the complexes show two sharp signals due to the two non-equivalent CH_3 groups in the 1.7–2.0 ppm region and the CH_2—CH_2 signals at 3.3–3.9 ppm.[26] The ^{13}C NMR spectrum of the ligands have two ^{13}C signals due to the non-equivalent —CH_3 groups at 8.6 and 12.9–13.4 ppm which shift downfield in the complexes to *ca* 10.4 and 18.4 ppm, respectively. The CH_2—CH_2 carbons resonate in the 48.9–52.32 ppm region in the free ligands and shift to 42.5–48.9 ppm in the complexes. The carbons (C^c and C^d) in the diacetylmonoxime skeleton resonate at 156.48 and 164.1–165.1 ppm for the free ligands, respectively, and shift only slightly downfield in the complexes. Additional signals at *ca* 2.0 and 5.4 ppm in the ^{1}H NMR spectrum and at 30.6, 98.7 and 196.7 ppm in the ^{13}C NMR spectrum unequivocally demonstrate the presence of coordinated acetylacetonate[27] groups in all the complexes. The NH— proton signals in pentadentate H_2DMDT and the hexadentate H_2DMTT ligands appear at 8.3 ppm and in the complexes they shift to 10.5 ppm, providing proof for the presence of free NH— groups. The ^{1}H NMR and ^{13}C NMR data are presented in Tables 2 and 3, respectively, and Fig. 1 depicts the ^{13}C NMR of a typical complex.

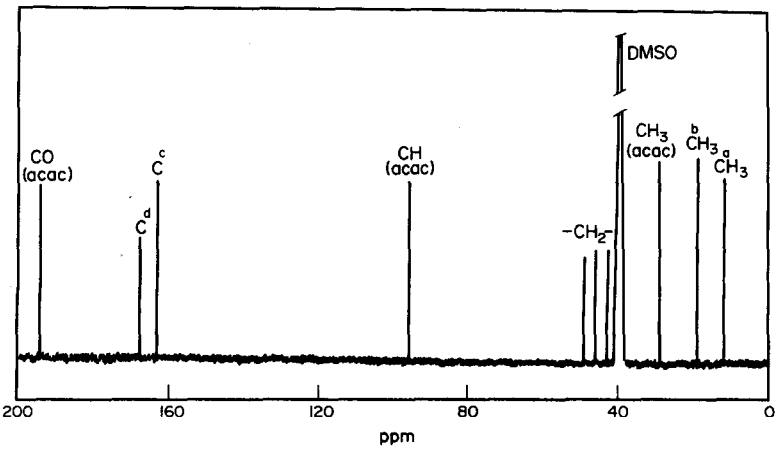

Fig. 1. ^{13}C NMR spectrum of [(acac)MoO_2(DMTT)O_2Mo(acac)] in DMSO-d_6.

Table 3. ^{13}C NMR[a] data for some of the molybdenum(VI) complexes

Compound	Schiff base carbons					"acac" Carbons		
	$—CH_3$[a]	$—CH_3$[b]	$CH_2—CH_2$	C[c]	C[d]	CH_3	CH	CO
H_2DMED	8.64	12.96	52.32	156.48	165.12			
$Mo_2O_4(acac)_2$DMED	10.4	18.22	48.51	164.30	168.54	30.6	98.7	196.7
H_2DMDT	8.64	12.96	49.92 51.36	156.48	164.64			
$Mo_2O_4(acac)_2$DMDT	10.07	18.41	46.52 47.65	162.70	166.46	28.9	95.9	194.1
H_2DMTT	8.64	13.44	48.96 49.92 51.84	156.48	164.16			
$Mo_2O_4(acac)_2$DMTT	10.25	18.42	42.59 45.81 48.92	162.81	167.27	28.6	95.5	193.7

[a] All measurements in DMSO-d_6; all values in ppm relative to internal DMSO-d_6 exhibiting a heptet centred at 39.6 ppm downfield from TMS.

The thermal analysis measurements clearly reveal the decomposition patterns of the complexes with increasing temperature, and ultimately in the 650°C region MoO_3 is formed as the stable end-product.[28] The analytical data, IR, ^1H and ^{13}C NMR spectral measurements establish the formation of binuclear, ligand-bridged, mixed-ligand, six-coordinated dioxomolybdenum complexes where each molybdenum(VI) is surrounded by two oxo-ligands, one bidentate acac group and two N-donor atoms (oxime N and imine N) of the Schiff bases. The potential pentadentate H_2DMDT and the hexadentate H_2DMTT ligands essentially function as bridging tetradentate ligands (like the tetradentate H_2DMED or H_2DMPD) with one or two secondary amine groups (—NH) remaining uncoordinated in the complexes. Similar observations have been previously[16] made by us for thorium(IV) and dioxouranium(VI) complexes.

Acknowledgements—The authors are grateful to Professor A. Schmidpeter, Munich University, Munich, F.R.G., for the FT–NMR (^1H and ^{13}C) spectra and to Dr C. R. Panda, Chemical Centre, Lund University, Sweden, for the FT–IR measurements. One of the authors (R.N.M.) thanks the Government of Orissa for leave of absence.

REFERENCES

1. J. K. Kochi, *Organometallic Mechanisms and Catalysis*, Ch. II. Academic Press, New York (1978).
2. M. S. Reynolds, J. M. Berg and R. H. Holm, *Inorg. Chem.* 1984, **23**, 3057.
3. L. Vilas Boas and J. Costa Pessoa, *Comprehensive Coordination Chemistry* (Edited by G. Wilkinson, R. D. Gillard and J. A. McCleverty), Vol. 3, p. 454. Pergamon Press, Oxford (1987).
4. E. I. Stiefel, *Comprehensive Coordination Chemistry* (Edited by G. Wilkinson, R. D. Gillard and J. A. McCleverty), Vol. 3, p. 1375. Pergamon Press, Oxford (1987).
5. O. A. Rajan and A. Chakravorty, *Inorg. Chem.* 1981, **20**, 660.
6. W. C. Fernelius, K. Terada and B. E. Bryant, *Inorg. Synth.* 1960, **6**, 147.
7. M. Mohapatra, V. Chakravortty and K. C. Dash, *Polyhedron* 1989, **8**, 1509.
8. E. Uhlig and M. Friedrich, *Z. Anorg. Allg. Chem.* 1966, **343**, 299.
9. A. V. Ablov, N. I. Belichuk and V. N. Kaftanat, *Russ. J. Inorg. Chem.* 1972, **17**, 392.
10. E. I. Stiefel, *Progress in Inorganic Chemistry* (Edited by S. J. Lippard), Vol. 22, p. 1. John Wiley, New York (1977).
11. J. Topich, *Inorg. Chem.* 1981, **20**, 3704.
12. C. Knobler, B. R. Penfold, W. T. Robinson, C. J. Wilkins and S. H. Yong, *J. Chem. Soc., Dalton Trans.* 1980, 248.
13. R. Colton, *Coord. Chem. Rev.* 1988, **90**, 29.
14. J. G. Mohanty, R. P. Singh and A. Chakravorty, *Inorg. Chem.* 1975, **18**, 1207.
15. N. I. Belichuk, A. V. Ablov and V. N. Kaftanat, *Russ. J. Inorg. Chem.* 1973, **18**, 1207.
16. S. Singh, V. Chakravortty and K. C. Dash, *Ind. J. Chem.* 1989, **28A**, 255.
17. M. Pasquali, A. Landi and C. Floriani, *Inorg. Chem.* 1979, **18**, 2397; S. Lee, C. Floriani, A. Chiesi-Villa and C. Guastini, *J. Chem. Soc., Dalton Trans.* 1989, 145.

18. R. L. Dutta and A. K. Pal, *Ind. J. Chem.* 1983, **22A**, 871; *J. Sci. Ind. Res.* 1984, **43**, 600; R. N. Hider and C. J. Wilkins, *J. Chem. Soc., Dalton Trans.* 1984, 495.
19. R. C. Aggarwal, R. A. Rai and T. R. Rao, *J. Inorg. Nucl. Chem.* 1981, **43**, 1927.
20. M. Caligaris, G. Manzini, G. Nardin and L. Randaccio, *J. Chem. Soc., Dalton Trans.* 1972, 543; R. J. Cozens and K. S. Murray, *Aust. J. Chem.* 1972, **25**, 911.
21. W. J. Geary, *Coord. Chem. Rev.* 1971, **7**, 81.
22. N. Yamazaki and Y. Hohokabe, *Bull. Chem. Soc. Jpn* 1971, **44**, 631.
23. K. Burger, I. Ruff and F. Ruff, *J. Inorg. Nucl. Chem.* 1965, **27**, 179.
24. B. Soptrajanov, A. Nikolovaski and I. Petrov, *Spectrochim. Acta* 1968, **24A**, 1617.
25. W. E. Newton and J. W. McDonald, *J. Less-Common. Met.* 1977, **54**, 51; L. Willis, T. Loehr, A. E. Bruce, K. Miller and E. I. Stiefel, *Inorg. Chem.* 1986, **25**, 4289.
26. *Handbook of NMR Spectrum and Data* (Edited by Asahi Research Centre Co. Ltd), Vol. 1, p. 242 and Vol. 2, p. 292 (1985).
27. G. Roychaudhury and K. C. Dash, *J. Molec. Struct.* 1980, **68**, 319.
28. P. K. Nath and K. C. Dash, *Transition Met. Chem.* 1985, **10**, 262.

Polyhedron Vol. 9, No. 8, pp. 1017–1020, 1990
Printed in Great Britain

0277–5387/90 $3.00+.00
© 1990 Pergamon Press plc

METAL ION INDUCED REARRANGEMENTS OF 1,3,4-THIADIAZOLIDINE-2-THIONES—I. THE REARRANGEMENTS OF 3-METHYL-5-(2-PYRIDYL)- AND 3-METHYL-5-(6-METHYLPYRID-2-YL)-1,3,4-THIADIAZOLIDINE-2-THIONES WITH NICKEL(II), ZINC(II) AND CADMIUM(II) IONS

S. M. M. H. MAJUMDER, M. AKBAR ALI* and KHANDKER M. M. RAHMAN

Department of Chemistry, University of Chittagong, Bangladesh

and

F. E. SMITH

Department of Chemistry, Laurentian University, Sudbury, Ontario, Canada

(*Received* 14 *September* 1987; *accepted after revision* 13 *November* 1989)

Abstract—3-Methyl-5-(2-pyridyl)- and 3-methyl-5-(6-methylpyrid-2-yl)-1,3,4-thiadiazolidine-2-thiones have been synthesized and characterized by spectroscopic techniques. The thiadiazolidine-2-thiones react with nickel(II), zinc(II) and cadmium(II) acetates producing intensely-coloured, stable metal complexes. Conductance, magnetic and spectroscopic evidences indicate that the rearrangement of the thiadiazolidine-2-thiones to the corresponding Schiff bases occurs. The complexes have been characterized by magnetic and spectroscopic techniques.

The phenomenon of tautomerization of the condensed products of thiolamines and carbonyl compounds to Schiff bases, promoted by metal ions, is well-known[1–4] and we report several further examples. The parent compounds (Fig. 1) and their metal complexes were prepared by extensions of standard methods.[4,5]

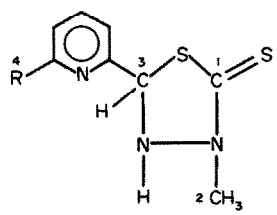

Fig. 1. R = H or CH_3.

EXPERIMENTAL

All the physical measurements and analytical methods were as described before.[6]

RESULTS AND DISCUSSION

The general structural formula of the two thiadiazolidine-2-thiones prepared in the present study is shown in Fig. 1 and their physical properties and characterization data are shown in Table 1.

The thiadiazolidine-2-thiones readily react with nickel(II), zinc(II) and cadmium(II) acetate salts producing stable complexes whose properties and other characterization data are summarized in Table 2. The magnetic and spectroscopic data in Table 2 support an octahedral geometry for the nickel complexes. The IR spectra of [Cd(NNS)ac] and [Cd(MeNNS)ac] show bands at *ca* 1540 and 1410 cm^{-1}, suggesting the presence of bridging acetate ligands.[9] The cadmium complexes most

* Author to whom correspondence should be addressed. Present address: Department of Chemistry, University of Brunei Darussalam, Bandar Seri Begawan, Negara Brunei Darussalam.

Table 1. Characterization data for the thiodiazolidine-2-thiones

Compound[a]	Colour	Melting point (°C)	Analytical data[b] C	H	N	Mol. wt[c]	^{1}H NMR data[d] δ, ppm	Assignment	^{13}C NMR data δ, ppm	Assignment	IR bands ν(NH)	ν(C—S—C)[7]	Electronic spectra[e] State	Band maxima, nm
TDT	White	95	45.3	4.3	19.9	211	8.59	—NH	189.71	C-1	3140	928	Solid	337, 278
			(45.5)	(4.36)	(19.9)		3.57	—NCH_3	66.74	C-2	(3122)[f]	(920)[g]	EtOH	345(4.1), 278(4.0)
							[8.14		116.91	C-3				
							8.18	Pyridine	23.8	C-4				
							8.27	protons	[120.52					
							8.30		122.84	Pyridine				
							8.40]		137.45	carbons				
									149.49					
									158.08]					
MTDT	Yellow	121	47.8	5.0	18.7	225	8.64	—NH	189.11	C-1	3142	930	Solid	344, 271
			(48.0)	(4.9)	(18.6)		3.60	—NCH_3	66.65	C-2				
							2.50	—CCH_3	119.95	C-3			EtOH	337(4.0), 271(3.8)
							[8.10		[120.52					
							8.18	Pyridine	123.42					
							8.30	protons	137.27	Pyridine carbon atoms				
							8.32]		149.49					
									157.09]					

[a] TDT = 3-Methyl-5-(2-pyridyl)-1,3,4-thiadiazolidine-2-thione; MTDT = 3-methyl-5-(6-methylpyrid-2-yl)-1,3,4-thiadiazolidine-2-thione.
[b] Calculated values are given in parentheses.
[c] Obtained by electron impact mass spectrometry.
[d] Relative to tetramethylsilane
[e] Log ε values in $dm^3\ mol^{-1}\ cm^{-1}$ are given in parentheses.
[f] Value reported in ref. 4.
[g] Value reported in ref. 8.

Table 2. Colour, decomposition temperatures, conductivity, magnetic moments, analytical data, IR and electronic spectral bands for metal complexes of the tautomeric Schiff bases

Compound[a]	Colour	Λ[b] (Ω^{-1} cm^2 mol^{-1})	μ (BM)	Decomposition temperature (°C)	Analytical data[c] C	H	M	IR absorption bands ν(C=N)	ν(M—S)	Others	Electronic spectra[d] State	Band maxima, nm
[Ni(NNS)$_2$]	Brown	0.4	3.20	284	42.5 (42.6)	4.1 (4.0)	11.4 (11.6)	1548s	308s	—	Solid	833, 430, 341
											DMSO	375(4.37), 280(4.06)
[Ni(MeNNS)$_2$]	Brown	0	3.21	240	40.3 (40.1)	3.7 (3.4)	12.1 (12.2)	1550s	315s	—	Solid	840sh, 455, 341
											DMSO	364(3.67), 293(3.47)
[Zn(NNS)$_2$]	Orange	0.4	Diamagnetic	230	42.0 (42.1)	4.0 (3.9)	12.6 (12.7)	1568s	317s	—	Solid	427,340
											DMSO	376(4.33), 286(4.08)
[Zn(MeNNS)$_2$]	Orange	0	Diamagnetic	229	39.4 (39.5)	3.7 (3.3)	13.3 (13.4)	1565s	320s	—	Solid	410, 342
[Cd(NNS)ac]	Yellow	3.1	Diamagnetic	235	33.1 (33.4)	3.6 (3.3)	28.3 (28.4)	1550s	365s	1540s,br [ν(C=O)]	Solid	389, 341
											DMSO	369(3.89), 281(3.50)
[Cd(MeNNS)ac]	Yellow	3.0	Diamagnetic	210	30.7 (31.2)	3.7 (3.7)	29.3 (29.2)	1550s	375s	1410s [ν(C—O)]	Solid	385, 341
											DMSO	375(4.19), 282(3.78)

[a] NNS = the uninegatively charged anion of the tautomeric Schiff base of 3-methyl-5-(2-pyridyl)-1,3,4-thiadiazolidine-2-thione; MeNNS = the uninegative anion of the tautomeric Schiff base of 3-methyl-5-(6-methylpyrid-2-yl)-1,3,4-thiadiazolidine-2- thione.

[b] Molar conductance of *ca* 10^{-3} M solutions in DMSO.

[c] Calculated values are given in parentheses.

[d] Log ε values (dm^3 mol^{-1} cm^{-1}) are given in parentheses.

probably have an acetato-bridged dimeric or polymeric structure.[10,11]

REFERENCES

1. L. F. Lindoy, *Quart. Revs* 1971, **25**, 379.
2. M. C. Thompson and D. H. Busch, *J. Am. Chem. Soc.* 1962, **84**, 1962.
3. H. Jadamus, Q. Fernando and H. Freiser, *Inorg. Chem.* 1964, **3**, 928.
4. M. Akbar Ali, S. E. Livingstone and D. J. Phillips, *Inorg. Chim. Acta* 1973, **7**, 553.
5. F. G. Heugebaert and J. F. Willems, *Tetrahedron* 1966, **22**, 913.
6. S. M. M. H. Majumder, M. Akbar Ali, F. E. Smith and M. A. U. Mridha, *Polyhedron* 1988, **7**, 2183.
7. C. A. Rice, C. G. Benson and C. A. McAuliffe, *Inorg. Chim. Acta* 1982, **59**, 33.
8. L. F. Capitan-Vallvey and P. Espinsosa, *Polyhedron* 1983, **2**, 1147.
9. K. Itoh and J. Bernstein, *Can. J. Chem.* 1956, **34**, 170.
10. M. M. Aly and Z. H. Khalil, *J. Inorg. Nucl. Chem.* 1980, **42**, 1261.
11. L. F. Capitan-Vallvey, C. Jiminez and L. Cuadros, *Can. J. Chem.* 1982, **60**, 1713.

Polyhedron Vol. 9, No. 8, pp. 1021–1026, 1990
Printed in Great Britain

0277–5387/90 $3.00+.00
Pergamon Press plc

COMPLEXES OF IRON AND COBALT TETRASULPHONATED PHTHALOCYANINES WITH HORSERADISH PEROXIDASE PROTEIN

ŁUCJA OSTROPOLSKA

Institute of Chemistry, University of Wrocław, Poland

(*Received* 3 *November* 1988; *accepted after revision* 13 *November* 1989)

Abstract—The interaction between the iron and cobalt tetrasulphonated phthalocyanines and the horseradish peroxidase protein leads to the formation of artificial peroxidase containing phthalocyanine derivative in place of protohaem. Such a modification has also been carried out by replacement of the haem in peroxidase by metal tetrasulphonated phthalocyanine. The complexes are not formed with apo-peroxidase previously modified by carboxymethylation at histidines. This suggests that the binding site of iron and cobalt phthalocyanines is a histidine residue, as is the case of the haem in the native peroxidase.

The visible absorption spectra show the main peak of the iron compound at 658 nm and that of the cobalt compound at 680 nm. The position of the main band and the properties of the cobalt compound suggest three oxidation states of the cobalt ion. It is shown by circular dichroism (CD) experiments that incorporation of $Fe^{III}L$ or $Co^{III}L$ into the peroxidase protein leaves the helical content of the protein virtually unchanged in spite of their larger sizes. It is, however, markedly lower than that of the native enzyme, which points to the lower stability of the model complexes. Molecular weight results indicate that the synthesized compounds are monomers. Both phthalocyanine-modified peroxidases are reduced by dithionite and ferrocytochrome *c* to give iron(II) and cobalt(II) complexes which are able to undergo reversible oxygen binding. Artificial peroxidases exhibit minimal enzymic activity and for this reason they cannot be regarded as physiological models of the native peroxidase.

The important role of metalloenzymes in the biological processes has led to the synthesis and study of their model analogues. One of the most important classes of metalloenzymes constitute the haem proteins. They are formed by conjugation of proteins with iron porphyrin which plays the role of the prosthetic group.[1] The interaction between the haem group and the surrounding protein is critical for the functional design of haem proteins.[2,3] The interaction has been investigated by comparing the reactivity of the physical properties of model systems with those of the proteins.[4,5]

The effect of metal substitution on peroxidase conformational stability and the effect of the protein on the haem centre have been reported for the following metallosubstituted peroxidases: Co–HRP, Cu–HRP, Mn–HRP and V–HRP.[6–9] Also, the effect of chemical modification of the porphyrin side chain and the role of peripheral substituents of the porphyrin in metalloporphyrin–apo-peroxidase complexes have been studied.[10–13] According to these results, the major role in the restoration of the helical content of a protein is played by the porphyrin ring itself, not by the metal component. For functionally active peroxidase a hydrophobic environment of the prosthetic groups is required.

The compounds which closely resemble metal-

Abbreviations:
L: tetrasulphonated phthalocyanine ligand, $C_{32}H_{12}N_8(SO_3Na)_4$.
$Fe^{III}L$: iron(III) tetrasulphonated phthalocyanine.
HRP: horseradish peroxidase.
apo-peroxidase: peroxidase protein, without its prosthetic haem group.
$Fe^{III}L$–apo-peroxidase: iron(III) tetrasulphonated phthalocyanine complex with peroxidase protein.
$Co^{II}L$: cobalt(II) tetrasulphonated phthalocyanine.
$Co^{III}L$–apo-peroxidase: cobalt(III) tetrasulphonated phthalocyanine complex with peroxidase protein.

loporphyrins are metal tetrasulphonated phthalocyanines. Recently it has been shown that iron and cobalt tetrasulphonated phthalocyanines are able to displace haem in haemoglobin and myoglobin to give complexes with properties resembling those of haemoglobin and myoglobin.[14,15] Iron and cobalt phthalocyanine-substituted cytochrome *c* has also been synthesized. The conformation of the protein in those compounds is significantly altered compared to that in the native cytochrome *c*. These phthalocyanine-substituted compounds are low-spin species with the metal ions in the trivalent state.[16,17]

In this article we report the results concerning the preparation, structure and properties of artificial peroxidase obtained by incorporation of iron and cobalt tetrasulphonated phthalocyanines into the haem binding site of the peroxidase protein.

EXPERIMENTAL

Materials and methods

Horseradish peroxidase, type I, was purchased from Sigma Chemical Co. and the isoenzyme *C* was separated and purified by the method of Shannon *et al.*[18] The purity index ($A_{403\,nm}:A_{278\,nm}$) of this enzyme was 3.4. The apo-peroxidase was prepared from horseradish peroxidase by a modification of Teale's acid butanone technique reported by Yonetani.[19] The concentration of the solutions was assayed spectrophotometrically using absorption coefficients, based on separate dry weight determinations: 9.2×10^4 M^{-1} cm^{-1} at 403 nm for the native protein and 1.3×10^4 M^{-1} cm^{-1} at 278 nm for the apo-protein. The preparation of the carboxymethylhistidine derivatives of apo-peroxidase was performed by iodoacetylation at pH 5.5 according to the method described previously.[20]

The preparation and purification of iron and cobalt tetrasulphonated phthalocyanines have been described by Fallab and co-workers.[21] The stock solution was obtained by weighing an appropriate amount of the solid and dissolving the latter in 100 cm^3 of an appropriate buffer.

Synthesis of the metal tetrasulphonated phthalocyanine-substituted peroxidase

The apo-peroxidase in 0.01 M Tris, pH = 8.4, was adjusted to 0.2 mM, mixed with a two-fold excess of iron or cobalt tetrasulphonated phthalocyanine, and allowed to stand at 4°C for 2 days. The mixture was passed through a DEAE–cellulose column equilibrated with 10 mM potassium phosphate buffer, pH = 7.4. The complexes of $Fe^{III}L$ and $Co^{II}L$ with the apo-peroxidase were not adsorbed on DEAE–cellulose, whereas free iron and cobalt tetrasulphonated phthalocyanines were firmly bound to this adsorbent. The complex fraction of the chromatographic separation was concentrated by lyophilization and stored at 0°C. The concentrations of the phthalocyanine complexes in the solutions were determined from the molar absorption coefficients: $Fe^{III}L$–apo-peroxidase $\varepsilon_{658} = 2.4\times10^4$ M^{-1} cm^{-1} and $Co^{III}L$–apo-peroxidase $\varepsilon_{680} = 3.8\times10^4$ M^{-1} cm^{-1}. Solid samples were obtained by lyophilization of the water solutions of the complexes.

The reduced forms of the complexes were prepared by addition of a few milligrams of sodium dithionite to their buffered solutions and removal of the reductant excess on a Sephadex G-50 column. All the chemicals used in the studies were of analytical purity. Absorption spectra and difference spectra were recorded on a Cary 15 spectrophotometer with a cell compartment thermostatically controlled at 4°C or on a Specord spectrophotometer.

Molecular weight measurements of the model complexes were carried out by gel-filtration on a Sephadex G-75 column according to the method of Andrews.[22] The following proteins were used as reference substances: cytochrome *c* (mol. wt 12,400), myoglobin (mol. wt 17,800), chymotrypsinogen (mol. wt 25,000), ovalbumin (mol. wt 45,000), serum albumin (mol. wt 67,000) and γ-globulines (mol. wt 160,000).

Circular dichroism spectra were recorded on a model ORD/UV-5 Japan Spectropolarimeter with CD attachment. The solutions of the complexes were prepared by dissolving the appropriate amount of lyophilized preparation in phosphate buffer, pH = 7.4.

Enzyme assay

Peroxidase activity was measured spectrophotometrically by following the change in absorbance at 460 nm due to *o*-dianisidine oxidation in the presence of H_2O_2 and the complexes.[23]

RESULTS

The reaction of $Fe^{III}L$ and $Co^{II}L$ with peroxidase indicates that haem is partially displaced by phthalocyanine compounds. This is shown by the difference spectra presented in Fig. 1. In both cases the Soret band at 403 nm, which is characteristic of peroxidase, disappears. The formation of phthalocyanine complexes is monitored by the appearance of a new characteristic band in the region of phthalocyanine absorption at 658 and 680 nm, respec-

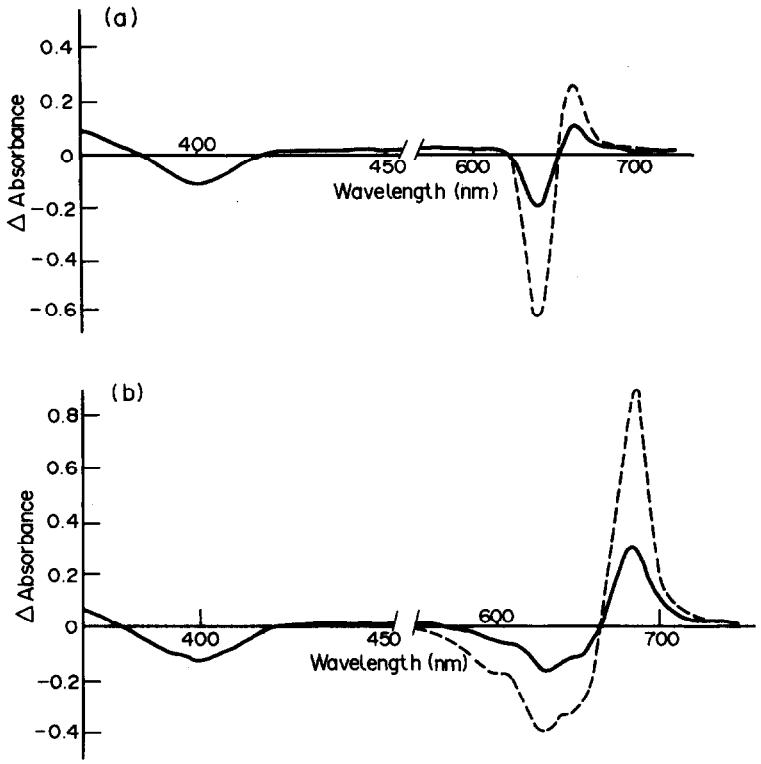

Fig. 1. Difference spectra of the mixture of HRP with (a) $Fe^{III}L$ and (b) $Co^{II}L$ against the same solution mixed (——). Difference spectra of (a) $Fe^{III}L$+apo-peroxidase and (b) $Co^{II}L$+apo-peroxidase mixtures against the same solution unmixed (– – –). Spectra were recorded after 24 h of the reaction run in 5 mM phosphate buffer, pH = 7.5. Concentrations: HRP = apo-peroxidase = 1×10^{-5} M, $Fe^{III}L = Co^{II}L = 2 \times 10^{-5}$ M.

tively, for iron and cobalt protein complexes. At the same time the characteristic absorption of $Fe^{III}L$ at 635 nm and $Co^{II}L$ at 625 nm decreases. The reaction of haem displacement in peroxidase by phthalocyanine derivatives was investigated in the pH range 4.5–9.5. The optimal pH for this reaction appeared to be 5.5. This fact suggested that displacement of haem by phthalocyanine was dependent on dissociation of the peroxidase into haem and apo-protein.[24] It is known from previous investigations[25] that tetrasulphonated phthalocyanine exists in aqueous solution in two forms: dimeric and monomeric. The stability of the dimers was found to decrease in the following way: $Fe^{III}L > Co^{II}L$. This could explain the higher displacement reaction rate in the case of $Co^{II}L$ than that of $Fe^{III}L$ and confirms previous suggestions that the monomer is a species which displaces haem from haemoproteins.[26]

Combination of $Fe^{III}L$ *and* $Co^{II}L$ *with peroxidase protein*

The reaction between metal tetrasulphonated phthalocyanine and apo-peroxidase was demonstrated by a difference absorption spectroscopy experiment (Fig. 1). The difference spectra of both systems in the visible region correspond closely to those of the systems with the native peroxidase. It is evident from these spectra that in the reaction of peroxidase apo-protein with phthalocyanine compounds new complexes are formed which are identical to those arising in the haem displacement process.

In contrast to free $Co^{II}L$, its complex with apo-peroxidase has very little ability to undergo reversible oxygen binding, which suggests that insertion of $Co^{II}L$ into the apo-protein under aerobic conditions leads to oxidation of the cobalt ion to its trivalent state.

Spectroscopic titration of an apo-peroxidase with $Fe^{III}L$ and $Co^{II}L$ points to a 1 : 1 molar ratio of the reagents. The new apo-peroxidase complexes were isolated as green–blue solids by separation of the reaction mixture on DEAE–cellulose and by lyophilization. The solids were stable for 4 weeks.

The incubation of iron and cobalt tetrasulphonated phthalocyanines with a carboxymethylhistidine derivative of the apo-peroxidase did not lead to the formation of the complexes.

This fact suggests that the metal phthalocyanine binding site in apo-peroxidase is the histidine group.

Properties of the $Fe^{III}L$*–apo-peroxidase and* $Co^{III}L$*–apo-peroxidase complexes*

The reduction of the $Fe^{III}L$–apo-peroxidase with dithionite involves direct attack of the reductant on the iron(III) atom. The spectrum of the reduced form of this complex exhibits a characteristic band at 690 nm. No degradation of the phthalocyanine ring is observed in this spectrum in contrast to that of free $Fe^{II}L$ where disappearance of the phthalocyanine characteristic bands occurs.[14] The results presented above suggest that the $Fe^{III}L$–apo-peroxidase compound is located deeply inside the protein.

A solution of $Fe^{II}L$–apo-peroxidase exhibits reversible combination with oxygen. Absorption spectra of this compound in argon and oxygen are shown in Fig. 2.

The reduction of $Co^{III}L$–apo-peroxidase with dithionite in argon results in the disappearance of the band at 680 nm and increased absorptivity at 635 nm. Bubbling oxygen through the solution gives rise to a new band at 690 nm. At the same time the band at 635 nm disappeared. In an argon atmosphere the reaction reverses. These results indicate that the reduced form of the $Co^{II}L$–apo-peroxidase complex is able to undergo reversible oxygen binding. The band at 690 nm corresponds to the oxygenated form of the complexes and that at 635 nm to its deoxygenated form. The oxygen displacement from the oxygenated form of the iron complex is more difficult than in the case of the cobalt complex, which suggests a stronger metal–oxygen bond in the iron complex.

The difference spectrum presented in Fig. 2 shows that $Fe^{III}L$–apo-peroxidase is able to oxidize ferrocytochrome *c* under anaerobic conditions. The increase in absorptivity at 406 nm and its decrease at 417 nm points to the transformation of ferrocytochrome *c* to ferricytochrome *c*. The simultaneous decrease of absorptivity at 658 nm and its increase at 690 nm indicates that $Fe^{III}L$–apo-peroxidase is reduced to $Fe^{II}L$–apo-peroxidase.

Both model complexes reacted slowly with hydrogen peroxide to form "peroxide compounds" with characteristic absorption bands at 662 and 682 nm for $Fe^{III}L$–apo-peroxidase and $Co^{III}L$–apo-peroxidase, respectively (Fig. 3). When catalase was added to the solution, H_2O_2 was decomposed and the original spectrum of $Fe^{III}L$–apo-peroxidase and $Co^{III}L$–apo-peroxidase was regenerated. This suggests that H_2O_2 coordinates to the metal atoms. However, the intensities of these spectra diminish with time, which is indicative of slow auto-oxidation of the phthalocyanine ligand. The purified $Fe^{III}L$–apo-peroxidase and $Co^{III}L$–apo-peroxidase gave activities of 500 and

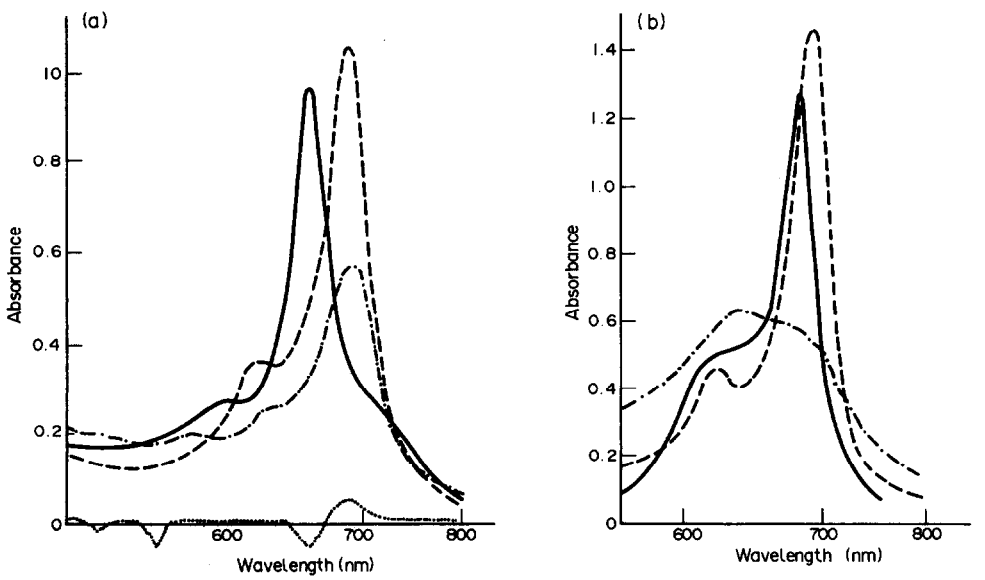

Fig. 2. The optical absorption spectra of (a) $Fe^{III}L$–apo-peroxidase and (b) $Co^{III}L$–apo-peroxidase in sodium phosphate buffer, pH = 7.5 with dithionite. $M^{III}L$–apo-peroxidase (——), $M^{III}L$–apo-peroxidase + $Na_2S_2O_4$ in oxygen (– – –), $M^{III}L$–apo-peroxidase + $Na_2S_2O_4$ in argon (–·–·–). Concentration: $Fe^{III}L$–apo-peroxidase = $Co^{III}L$–apo-peroxidase = 2×10^{-5} M. Difference spectra of the mixture $Fe^{III}L$–apo-peroxidase with ferrocytochrome *c* (a) against unmixed solution in anaerobic conditions (·····). Concentration of $Fe^{III}L$–apo-peroxidase = ferrocytochrome *c* = 5×10^{-6} M.

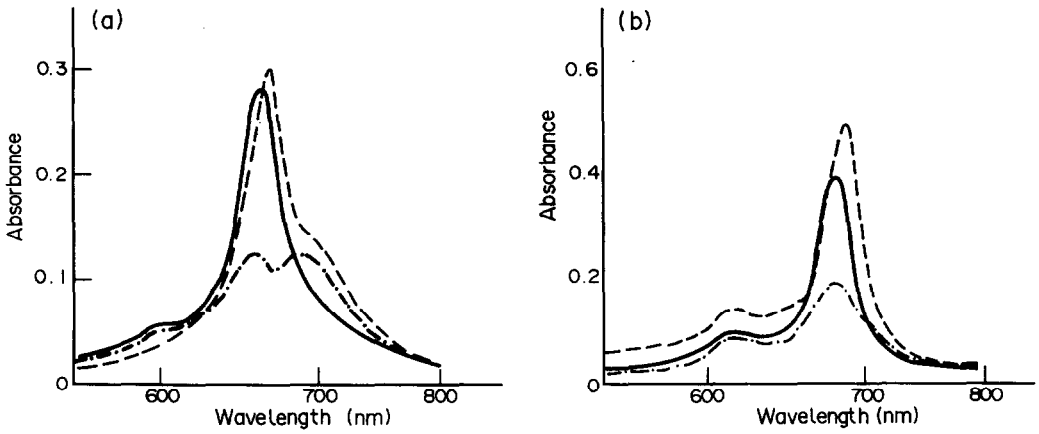

Fig. 3. Absorption spectra of (a) $Fe^{III}L$–apo-peroxidase and (b) $Co^{III}L$–apo-peroxidase in phosphate buffer, pH = 7.5 with hydrogen peroxide. $M^{III}L$–apo-peroxidase (——), $M^{III}L$–apo-peroxidase + H_2O_2 after 10 min of the reaction run (– – –), after 2 h of the reaction run (–·–·–). Concentrations: $Fe^{III}L$–apo-peroxidase = $Co^{III}L$–apo-peroxidase = 5×10^{-6} M, $H_2O_2 = 5 \times 10^{-6}$ M.

350 mol min^{-1} mg^{-1}, respectively, in the standard *o*-anisidine assay.

The results of the molecular weight estimation using Sephadex G-100 gel-filtration techniques demonstrated that the molecular weight of the iron complex is aproximately 42,500 and that of the cobalt one is 42,000. These values are comparable with that of peroxidase, which indicates that the model complexes are monomers.

To obtain information about whether the metal tetrasulphonated phthalocyanine incorporation in the peroxidase protein brings about perturbation of its helical structure, the UV CD spectra of the appropriate mixtures were taken. The results of these experiments, presented in Table 1, indicate that the helical content of the peroxidase apo-protein is virtually unchanged due to metal phthalocyanine coordination. CD spectra of the metal phthalocyanine-modified peroxidases exhibit molar ellipticities close to that of the peroxidase apo-protein. However, they are markedly lower than that of the native peroxidase.

Table 1. Comparison of CD results of the complexes. The medium contained 5 mM phosphate buffer, pH = 7.5

Compound	$\theta \times 10^6$ ° cm^2 $dmol^{-1}$ 221 nm	208 nm
$Fe^{III}L$–apo-peroxidase	−3.20	−3.75
$Co^{III}L$–apo-peroxidase	−3.25	−3.85
Apo-peroxidase	−2.90	−3.45
Peroxidase	−3.65	−4.15

CONCLUSIONS

Interaction between the iron and cobalt tetrasulphonated phthalocyanines and peroxidase protein results in the formation of the complexes $Fe^{III}L$–apo-peroxidase and $Co^{III}L$–apo-peroxidase with characteristic absorptivities at 658 and 680 nm, for iron and cobalt complexes, respectively. The same complexes were obtained by haem displacement in the native peroxidase with $Fe^{III}L$ and $Co^{II}L$. This suggests the same binding site on the protein for haem and phthalocyanine derivatives. The stoichiometry of this process was found to be 1 : 1 in the systems with both phthalocyanine complexes but the reaction rate was higher when $Co^{II}L$ was used. This suggests a different mechanism for the process with the cobalt complex. The position of the main absorption band of the cobalt phthalocyanine-modified peroxidase, as well as its lack of ability to undergo reversible oxygen binding, which is characteristic for free $Co^{II}L$, points to three oxidation state of the cobalt ion in this compound. According to the suggestions of Hoffman and Petering[27] reconstitution of the cobalt-substituted haemoglobin and the other haemoproteins depends markedly on the cobalt ion oxidation state. It is possible that in the case of the cobalt phthalocyanine-modified peroxidase, oxidation of the cobalt ion of $Co^{II}L$ results in its incorporation into the protein in the proper orientation at the haem binding site. Carboxymethylation of the histidyl residues of the peroxidase apo-protein renders it completely inactive towards metal tetrasulphonated phthalocyanine, which suggests that, like in the case of haem,[28] the histidine group constitutes the

phthalocyanine binding site. As is shown by molecular weight estimation, both phthalocyanine-modified peroxidases are monomers with molecular weights close to that of the native enzyme.

Incorporation of the metal tetrasulphonated phthalocyanines into the haem crevice of the peroxidase protein virtually does not change its helical conformation, in spite of their larger size. On the other hand, the helical content of the examined model complexes is markedly lower than that of the native peroxidase, which points to their lower stability.[29-31]

Both phthalocyanine-modified peroxidases reduced with dithionite under anaerobic conditions are able to undergo reversible oxygen binding to give oxygenated compounds. The cobalt oxygen adduct, however, is unstable and undergoes slow auto-oxidation with degradation of the phthalocyanine ring. Both model complexes exhibit extremely low activity toward H_2O_2 and *o*-dianisidine, which indicates that they cannot fulfill the physiological function of the native peroxidase and cannot be regarded as its model in this respect. In conclusion, it can be stated that the haem crevice of the peroxidase closely fits to the natural prosthetic group, to give a conformation which is essential for the physiological function of the enzyme.

REFERENCES

1. K. Kobayashi, M. Tamura and K. Hayoshi, *J. Biol. Chem.* 1980, **255**, 2239.
2. G. McLondon and K. Sandberg, *J. Biol. Chem.* 1978, **253**, 3913.
3. I. Morishima, S. Ogawa and T. Yonezawa, *Biochim. Biophys. Acta* 1978, **537**, 293.
4. F. Basolo, B. M. Hoffman and I. A. Ibers, *Accts Chem. Res.* 1975, **8**, 348.
5. I. Collman, *Accts Chem. Res.* 1977, **10**, 265.
6. R. K. Dinello and D. Dolphin, *Biochem. Biophys. Res. Commun.* 1978, **80**, 698.
7. M. Tamura, T. Asakura and T. Yonetani, *Biochim. Biophys. Acta* 1972, **268**, 292.
8. P. I. Ohlsson and K. G. Paul, *Biochim. Biophys. Acta* 1973, **315**, 293.
9. T. Yonetani, H. R. Drott, J. S. Leigh Jr., G. H. Reed, M. R. Waterman and T. Asakura, *J. Biol. Chem.* 1970, **245**, 2998.
10. M. R. Wang and B. H. Hoffman, *J. Biol. Chem.* 1977, **252**, 6268.
11. M. Tamura, N. Skimidzu and K. Hayoshi, *Biochem. Biophys. Res. Commun.* 1977, **75**, 1029.
12. M. Tamura, T. Asakura and T. Yonetani, *Biochim. Biophys. Acta* 1973, **295**, 467.
13. R. K. Dinello and D. Dolphin, *Biochem. Biophys. Res. Commun.* 1977, **86**, 190.
14. H. Przywarska-Boniecka, L. Trynda and E. Antonini, *Eur. J. Biochem.* 1975, **52**, 567.
15. L. Trynda, *Inorg. Chim. Acta* 1983, **78**, 229.
16. H. Przywarska-Boniecka and Ł. Ostropolska, *J. Inorg. Biochem.* 1982, **16**, 183.
17. H. Przywarska-Boniecka and Ł. Ostropolska, *J. Inorg. Biochem.* 1984, **20**, 103.
18. L. M. Shannon, E. Kay and I. Y. Lew, *J. Biol. Chem.* 1966, **241**, 2166.
19. T. Yonetani, *J. Biol. Chem.* 1967, **242**, 5008.
20. A. M. Crestfield, W. M. Stein and S. Moore, *J. Biol. Chem.* 1963, **238**, 2413.
21. D. Vonderschmidt, K. Bernauer and S. Fallab, *Helv. Chim. Acta* 1965, **48**, 951.
22. P. Andrews, *Biochem. J.* 1965, **96**, 595.
23. M. J. Frechold, *Enzymes, Enzyme Reagents and Related Biochemicals*. Worthington Enzyme Manual, Worthington Biochemical Corp. (1972).
24. N. N. Ugarova and O. V. Lebedeva, *Biochimia* 1978, **43**, 1731.
25. H. Sigel, P. Waldemeir and B. Prijs, *Inorg. Nucl. Chem. Lett.* 1971, **7**, 161.
26. H. Przywarska-Boniecka and L. Trynda, *Eur. J. Biochem.* 1978, **87**, 569.
27. B. M. Hoffman and D. H. Petering, *Proc. Natl. Acad. Sci. USA* 1970, **67**, 637.
28. K. G. Welinder, *FEBS Lett.* 1973, **30**, 243.
29. E. H. Strickland, E. Kay and L. M. Shannon, *J. Biol. Chem.* 1970, **245**, 1233.
30. E. H. Strickland, E. Kay, L. M. Shannon and J. Horowitz, *J. Biol. Chem.* 1968, **243**, 3560.
31. P. I. Ohlsson, K. G. Paul and I. Sjöholm, *J. Biol. Chem.* 1972, **252**, 8222.

Polyhedron Vol. 9, No. 8, pp. 1027–1028, 1990
Printed in Great Britain

0277–5387/90 $3.00+.00
Pergamon Press plc

SYNTHESIS AND ELECTROCHEMICAL STUDIES OF A MACROCYCLIC COMPLEX OF NICKEL(II) BEARING A PYRROLE UNIT

RANDHIR SINGH

Department of Chemistry, Gurukula Kangri University, Hardwar, India

(*Received* 16 *November* 1988; *accepted after revision* 13 *November* 1989)

Abstract—A saturated 13-membered C-substituted macrocycle containing a N-substituted pyrrole group and its nickel(II) complex have been synthesized and characterized. During electrochemical studies, electropolymerization of the macrocyclic complex was observed by cyclic voltammetry using a glassy carbon electrode in acetonitrile.

Since the publication of the first report on polypyrrole films, electrode surface deposition of redox polymers has received much attention.[1–4] In spite of the much lower conductivity of N-substituted polypyrrole films compared to polypyrrole itself,[5] one of the most appealing means of incorporating a catalytic species into an electroactive film[6,7] is by covalently linking the molecular electrocatalyst to pyrrole via its nitrogen atom. Recently, interesting work on ferrocene[8,9] and a few other complexes of nickel(II) and copper(II) has been published.[10,11] Keeping in view the interesting electrocatalytic properties of Ni^{II}(cyclam)$^{2+}$ and analogous complexes,[12–14] it has been planned to synthesize and carry out electrochemical studies of a [13]ane-N_4 macrocycle bearing a pendant pyrrole unit [Fig. 1(a)] and its nickel(II) complex.

EXPERIMENTAL

The macrocycle [Fig. 1(a)] and its nickel(II) complex were prepared by suitable modifications of published methods.[15,16] The combination of triethylene tetraamine and substituted diethylmalonate resulted in the 3-(4-amino-*n*-butyl)-1,5,8,11-tetraazacyclotridecane macrocycle which was then treated with *cis*-but-2-ene-1,4-diol in the presence of palladium black. This reaction mixture was stirred magnetically at 100°C for about 36 h under an inert atmosphere. The macrocycle was separated chromatographically as a white compound in very low yield. Found: C, 66.2; H, 10.3; N, 22.4. Calc. for $C_{17}H_{33}N_5$: C, 66.4; H, 10.3; N, 22.8%. The complex was prepared in good yield by mixing requisite amounts of macrocycle A and $Ni(ClO_4)_2 \cdot 6H_2O$ in MeOH. After filtering and drying *in vacuo*, a yellowish powder of the nickel(II) complex was obtained.

Cyclic voltammetry onto glassy carbon electrode vs SCE was performed in CH_3CN solution (deoxygenated by bubbling nitrogen gas) using a Cyclic Voltameter Princeton Applied Research Model 155 and tetrabutylammonium perchlorate, as supporting electrolyte.

RESULTS AND DISCUSSION

After the chromatographic separation the compound was characterized by ^{1}H NMR spectroscopy in CD_3OD and the characteristic pattern of the pyrrolic subunit showed two multiplets at δ 6.02 and 7.66. Cyclic voltammetric (CV) measurements have shown that redox potential values were found very close to those of Ni(cyclam)$^{2+}$.[17] The redox couples $Ni^{III}/Ni^{II}/Ni^{I}$ for the nickel(II) macrocyclic complex in CH_3CN showed E^0 values of +0.96 and −1.40 V, respectively. An irreversible and multielectronic oxidation of the pyrrolic group also gave a value of 1.34 V, which is close to N-substituted pyrroles.[18] In CH_3CN the macrocyclic complex showed electropolymerization by repeated cyclic scanning of the potential between 0.2 and 1.2 V on a glassy carbon electrode. The formation and growth of a polymer film on the electrode surface was observed with the increase in size of the CV peaks, Fig. 1. The redox couple Ni^{III}/Ni^{II}, to which the main electrochemical process corresponds, showed a peak separation of 100 mV. The peak current intensity is proportional to the potential sweep rate over a wide range (10–150 mV s^{-1}), as

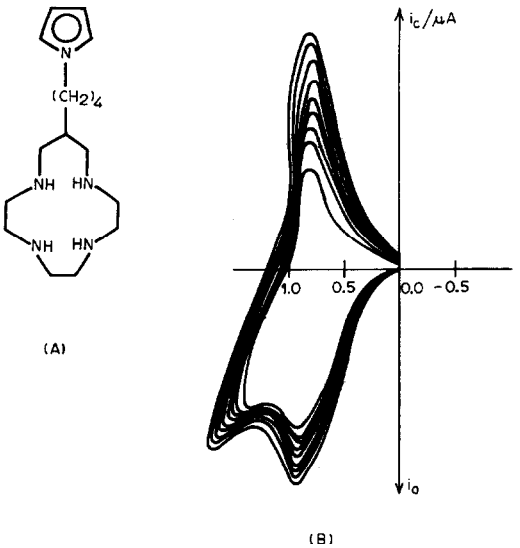

Fig. 1. Cyclic voltammogram showing polymerization of a macrocyclic complex of nickel(II) on to a glassy carbon electrode in acetonitrile using 0.1 M TBAP with a sweep rate of 50 mV s^{-1}.

expected for an electroactive compound which has deposited on the surface of an electrode.

The film becomes, interestingly, insulating as soon as a cathodic potential is applied. One point to be noted is that the present example deals with a non-aromatic electroactive species. The Ni^{II}/Ni^{I} redox couple involves a metal-localized redox processes.[19–21] It is well known that the nickel(II) cyclam-modified polypyrrole film does not lead to a redox process involving the Ni^{II}/Ni^{I} couple which may prevent its use in electroreduction processes. The reversibility of the redox couple Ni^{III}/Ni^{II} might be useful in the present polypyrrolic film for use in oxidative electrocatalysis.

Acknowledgements—The author is thankful to the Head, Department of Chemistry, University of Roorkee, Roorkee, for providing research facilities for the completion of this work. The author would also like to thank Dr D. P. Singh, R. E. C. Kurukshetra (Haryana), who helped me in this regard. Financial assistance from CSIR Grant No. 1(1105)/88-EMR-II is also acknowledged.

REFERENCES

1. C. J. R. Fookes, *J. Chem. Soc., Chem. Commun.* 1983, 1474.
2. E. K. Barefield, F. Wagner and K. D. Hodges, *Inorg. Chem.* 1976, **15**, 1370.
3. D. H. Busch and J. C. Bailar Jr, *J. Am. Chem. Soc.* 1956, **78**, 1137.
4. D. S. Eggleston and S. C. Jackels, *Inorg. Chem.* 1980, **19**, 1593.
5. A. F. Diaz, K. K. Kanazawa and G. P. Cardini, *J. Chem. Soc., Chem. Commun.* 1979, 635.
6. R. H. Schmehl and R. W. Murray, *J. Electroanal. Chem.* 1983, **152**, 97.
7. C. D. Ellis and T. J. Meyer, *Inorg. Chem.* 1984, **23**, 1748.
8. M. V. Rosenthal, T. Skotheim and J. Warren, *J. Chem. Soc., Chem. Commun.* 1985, 342.
9. A. Haimerl and A. Merz, *Angew. Chem. Int. Edn Engl.* 1986, **25**, 180.
10. J. P. Collin and J. P. Sauvage, *J. Chem. Soc., Chem. Commun.* 1987, 1075.
11. F. Daire, F. Bedioui, J. Devynck and C. Bied-Charreton, *J. Electroanal. Chem.* 1986, **205**, 309.
12. M. Beley, J. P. Collin, R. Ruppert and J. P. Sauvage, *J. Chem. Soc., Chem. Commun.* 1984, 1315; *J. Am. Chem. Soc.* 1986, **108**, 7461.
13. J. Y. Becker, J. B. Kerr, D. Pletcher and R. Rosas, *J. Electroanal. Chem.* 1981, **117**, 87.
14. B. Fisher and R. Eisenberg, *J. Am. Chem. Soc.* 1980, **102**, 7363.
15. I. Tabushi, Y. Taniguchi and H. Kato, *Tetrahedron Lett.* 1977, 1049.
16. S. I. Murahashi, T. Shumamura and I. Moritani, *J. Chem. Soc., Chem. Commun.* 1974, 931.
17. F. V. Lovecchio, E. S. Gore and D. H. Busch, *J. Am. Chem. Soc.* 1974, **96**, 3109.
18. A. F. Diaz, J. Castillo, K. K. Kanazawa, J. A. Logan, M. Salmon and O. Fajardo, *J. Electroanal. Chem.* 1982, **133**, 233.
19. S. Cosnier, A. Deronzier and J. C. Moutet, *J. Electroanal. Chem.* 1986, **198**, 187.
20. S. Cosnier, A. Deronzier and J. C. Moutet, *J. Electroanal. Chem.* 1986, **207**, 315.
21. G. Bidan, A. Deronzier and J. C. Moutet, *J. Chem. Soc., Chem. Commun.* 1984, 1185.

Polyhedron Vol. 9, No. 8, pp. 1029–1034, 1990
Printed in Great Britain

0277–5387/90 $3.00+.00
© 1990 Pergamon Press plc

THREE DIFFERENT COPPER(II) COORDINATION POLYHEDRA IN THE CRYSTAL STRUCTURE OF BIS(4-PICOLINE)DITHIOCYANATO COPPER(II) COMPLEX, $[Cu(4\text{-pic})_2(NCS)_2]$; EXPERIMENTAL EVIDENCE OF A NEW TYPE OF MUTUAL INFLUENCE OF LIGANDS IN COMPLEXES

Z. KOŽÍŠKOVÁ, J. KOŽIŠEK* and M. KABEŠOVÁ

Department of Inorganic Chemistry, Slovak Technical University, CS-812 37 Bratislava, Czechoslovakia

(*Received* 17 *August* 1989; *accepted* 13 *November* 1989)

Abstract—The crystal structure of bis(4-picoline)dithiocyanato copper(II) is reported. The compound crystallizes in space group $P2_1$, with $a = 9.808(6)$, $b = 26.752(10)$, $c = 9.927(4)$ Å, $\beta = 107.89(4)°$, $U = 2478(1)$ Å^3, $Z = 6$, $D_m = 1.48(2)$, $D_x = 1.47$ g cm^{-3}, μ(Cu-K_α) = 4.13 mm^{-1}, $F(000) = 1122$, $T = 293$ K. Final R is 0.043 ($R_w = 0.043$) for 2400 observed reflections. The complex compound exhibits three different pseudo-octahedral coordination polyhedra for copper(II). The polyhedra differ in the degree of their tetragonal distortion. While two of them show "symmetrical" shortening and elongation, respectively, the third presents both an elongated and a shortened axial bond.

Among others, the donor–acceptor properties of neutral ligands are factors influencing the coordination mode of the thiocyanate ligand in heterogeneous thiocyanate complexes.[1–3] Norbury[3] has generalized this knowledge for all transition metals by applying the π-bonding hypothesis. As we have shown,[4,5] the validity of the assumed hypothesis depends on the strength of the π-acceptor neutral ligand properties in conditions of the coordination sphere with various central atoms. Thiocyanato copper(II) complexes show an increasing sensitivity in this direction. This fact may be correlated with the plastic properties of their coordination polyhedra.[6,7] It was found that the ligands having different π-acceptor properties in thiocyanato copper(II) complexes can influence the bonding properties of thiocyanate ligands in several ways. For example, they cause changes in their coordination mode,[5] influence their interatomic distances to the copper(II) central atom[8] and they also affect the thermal properties in thiocyanato copper(II) complexes.[9] It was the differing thermal decomposition of compounds $[CuL_2(NCS)_2]$, where L = pyridine and all isomeric forms of picolines,[9,10] which led us to examine the crystal structure of $[Cu(4\text{-pic})_2(NCS)_2]$.

EXPERIMENTAL

Preparation

Dark green prism-shaped crystals of $[Cu(4\text{-pic})_2(NCS)_2]$ were prepared by the reaction of an aqueous solution of $CuSO_4$ with 4-picoline and ammonia, and an aqueous solution of KNCS (2 M), in the molar ratio of $[Cu^{II}]:[NH_3]:[4\text{-pic}]:[NCS^-] = 1:4:2.5:2$. Found: Cu, 17.3; N, 15.3; C, 45.9; H, 3.8. Calc: Cu, 17.4; N, 15.3; C, 45.9; H, 3.9%.

Crystal data

$[Cu(NC_6H_7)_2(NCS)_2]$, $M = 366.00$, monoclinic, space group $P2_1$, with $a = 9.808(6)$, $b = 26.752(10)$, $c = 9.927(4)$ Å, $\beta = 107.89(4)°$, $Z = 6$, $D_m = 1.48(2)$, $D_x = 1.47$ g cm^{-3}, Cu-K_α, $\lambda = 1.54178$ Å, graphite monochromator, $\mu = 4.13$ mm^{-1}, $F(000) = 1122$, room temperature.

The cell parameters were refined with a SYNTEX $P2_1$ diffractometer by the least-squares method

* Author to whom correspondence should be addressed.

using the angles of 10 selected reflections. The orientation matrix obtained was employed for further intensity measurements carried out within the range of $0 < 2\theta < 100°$ by applying the θ–2θ scanning technique with a variable scan rate ranging from 4.88 to 29.3° min^{-1}. The scan range for each reflection was from $2\theta(Cu\text{-}K_{\alpha 1}) - 1°$ to $2\theta(Cu\text{-}K_{\alpha 2}) + 1°$. Two standard reflections were re-measured after every 98 reflections.

The original total reflections were reduced to 2400 by rejecting reflections with $F < 4\sigma(F)$, $R_{Int} = 0.030$ for 376 reflections. Intensities were corrected for the Lorentz and polarization factors but not for absorption effects. The structure was solved by Patterson and Fourier methods.[11] Positional and thermal parameters for all non-hydrogen atoms were refined by the least-squares procedure. The hydrogen atoms located on Fourier synthesis were included in the F_c calculations with an idealized position and a fixed isotropic thermal parameter. Full-matrix least-squares refinement on F leads to $R = 0.043$ and $R_w = 0.043$ for the 568 parameters varied and 2400 observed reflections ($w^{-1} = k(\sigma^2(F) + gF^2)$, $k = 0.26$, $g = 0.00110$). Isotropic extinction correction, $F_c^* = F_c(1 - xF_c^2/\sin\theta)$ ($x = 2.7(6) \times 10^{-6}$) was carried out. The maximum residual electron density, max. $\Delta\rho = +0.50$ e $Å^{-3}$ and minimum, min. $\Delta\rho = -0.55$ e $Å^{-3}$. Scattering factors and anomalous dispersion corrections were obtained from *International Tables for X-ray Crystallography* (1974).

RESULTS AND DISCUSSION

The symmetry-independent section of the unit cell of the $[Cu(4\text{-pic})_2(NCS)_2]$ crystal structure exhibits three types of coordination polyhedra (Fig. 1). In

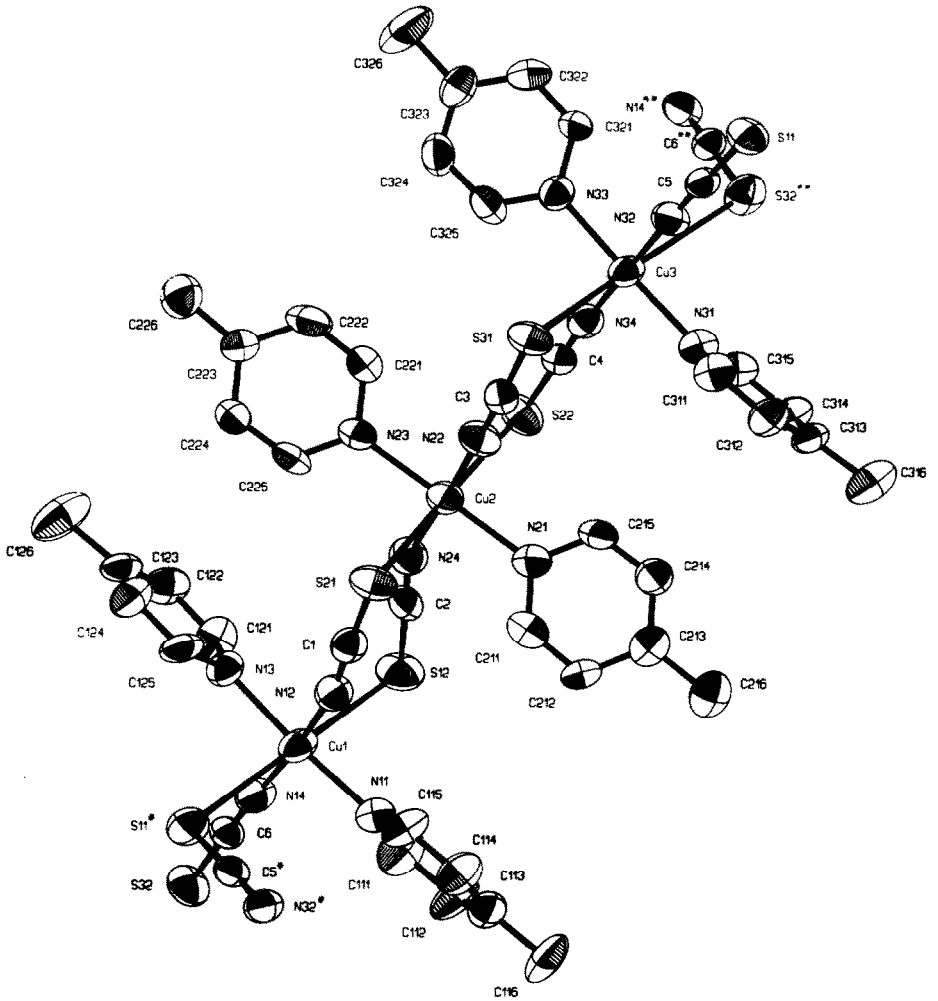

Fig. 1. An ORTEP drawing of the structure of $[Cu(4\text{-pic})_2(NCS)_2]$ and the atom numbering. The ellipsoids are drawn at the 50% probability level. The hydrogen atoms have been omitted. Symmetry code: (*) $1-x, -1/2+y, 1-z$; (**) $1-x, 1/2+y, 2+z$.

all three cases the central copper(II) atom appears to be octahedrally coordinated with the same ligand arrangement in the coordination sphere. Four nitrogen atoms are found in the equatorial planes of copper(II) coordination polyhedra; two of them are from the thiocyanate ligands (in *trans*-positions), while the other two are from the 4-picoline ligands. There are two sulphur atoms from the bidentate bridging thiocyanate ligands coordinated in axial positions of copper(II). The coordination mode found for copper(II) is analogous to that found in the crystal structure of $[Cu(py)_2(NCS)_2]$,[12] which, however, shows in its symmetry-independent section only one coordination polyhedron of copper(II).

The axial Cu—S distance in the crystal structure of $[Cu(py)_2(NCS)_2]$ is equal to 3.043(10) Å. Two of the three symmetry-independent copper(II) coordination polyhedra in the crystal structure of $[Cu(4\text{-pic})_2(NCS)_2]$ exhibit different values. The first polyhedron [Cu(1) central atom] shows a "symmetrical elongation" of this bond [3.109(4) and 3.124(4) Å] when compared with that of the pyridine complexes. In the second polyhedron [Cu(2) central atom] the Cu—S bond lengths remain constant [2.968(4) and 3.005(4) Å]. For the third polyhedron [Cu(3) central atom] one bond was found to be elongated [3.258(4) Å], while the other one remained unchanged [2.977(4) Å]—an "asymmetrical distortion". Based on the data obtained from electronic spectra, the differences in the degree of axial distortions in the copper(II) coordination polyhedra for the $[Cu(py)_2(NCS)_2]$ and $[Cu(4\text{-pic})_2(NCS)_2]$ compounds were expected.[13] The ligand-field band for $[Cu(py)_2(NCS)_2]$ with its maximum at 15,600 cm^{-1} was shifted and split for $[Cu(4\text{-pic})_2(NCS)_2]$. The maximum values were observed at 16,600 and 13,400 cm^{-1}.

In symmetry-independent coordination polyhedra the interatomic distances of Cu—N(NCS) and Cu—N(L) show minimal differences (Table 1). In all cases, however, the thiocyanate ligands in the equatorial plane are coordinated more strongly than the molecules of the heterocyclic base. This result is in good agreement with the published values for valence vibrations of ν(Cu—N)(NCS) = 321 cm^{-1} and ν(Cu—N)(4-pic) = 216 cm^{-1} observed in the IR spectra.[8] A comparison of the bonding properties of Cu—N(NCS) in the crystal structure both with 4-picoline and with pyridine indicates that the different bonding properties of heterocyclic ligands occur with no change in the coordination mode of the thiocyanate ligand and with only small differences in the strength of this bonding. As expected, the interatomic distance of Cu—N(L) in the coordination compound with 4-picoline is slightly greater than with pyridine.

The presence of the methyl substituent on the pyridine ring manifests itself significantly on the overall arrangement of structural units in the crystal structures. While the crystal structure of $[Cu(py)_2(NCS)_2]$ (Fig. 2) exhibits linear chains, that of $[Cu(4\text{-pic})_2(NCS)_2]$ (Fig. 2) shows chains of "zig-zag" form.

The numerical data (Table 1) indicating significant differences in the axial interatomic distances of Cu—S, are also in a good agreement with the known preferential sensitivity of axial bonds in copper(II) coordination polyhedra.[14]

In the three symmetry-independent structure units in the crystal structure of $[Cu(4\text{-pic})_2(NCS)_2]$, differences were also found in the orientation of the heterocyclic rings of 4-picoline (Table 2). The planes through the 4-picoline atoms and the equatorial plane of the copper(II) "symmetrically elongated" coordination polyhedron form dihedral angles of 151 and 126°, respectively.

The dihedral angles in coordination polyhedra with unchanged axial bonds have the values of 52 and 44° in accordance with the orientation of the pyridine rings in $[Cu(py)_2(NCS)_2]$.[12] It should be

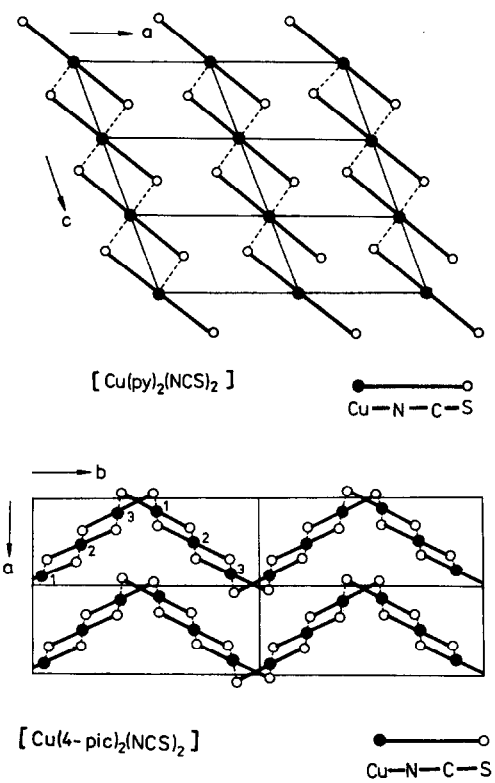

Fig. 2. Schematic representation of the chains of formula units in crystals of $[Cu(py)_2(NCS)_2]$ and $[Cu(4\text{-pic})_2(NCS)_2]$.

Table 1. Selected lengths (Å) and angles (°) with their ESDs

Cu(1)—N(11)	2.003(8)	Cu(2)—N(21)	2.054(8)	Cu(3)—N(31)	2.022(8)
Cu(1)—N(12)	1.956(8)	Cu(2)—N(22)	1.933(8)	Cu(3)—N(32)	1.973(9)
Cu(1)—N(13)	2.038(8)	Cu(2)—N(23)	2.074(8)	Cu(3)—N(33)	2.024(8)
Cu(1)—N(14)	1.939(8)	Cu(2)—N(24)	1.939(8)	Cu(3)—N(34)	1.952(8)
Cu(1)—S(11)	3.109(4)	Cu(2)—S(21)	3.005(4)	Cu(3)—S(31)	2.977(4)
Cu(1)—S(12)	3.124(4)	Cu(2)—S(22)	2.968(4)	Cu(3)—S(32)	3.258(4)
N(12)—C(1)	1.169(13)	N(22)—C(3)	1.156(13)	N(32)—C(5)	1.158(13)
C(1)—S(21)	1.602(11)	C(3)—S(31)	1.614(10)	C(5)—S(11)	1.591(10)
N(14)—C(6)	1.163(12)	N(24)—C(2)	1.158(14)	N(34)—C(4)	1.178(13)
C(6)—S(32)	1.614(10)	C(2)—S(12)	1.630(11)	C(4)—S(22)	1.618(10)
N(11)—C(111)	1.322(16)	N(21)—C(211)	1.329(13)	N(31)—C(311)	1.330(13)
N(11)—C(115)	1.304(12)	N(21)—C(215)	1.363(14)	N(31)—C(315)	1.336(15)
N(13)—C(121)	1.312(14)	N(23)—C(221)	1.365(13)	N(33)—C(321)	1.360(11)
N(13)—C(125)	1.330(17)	N(23)—C(225)	1.314(13)	N(33)—C(325)	1.321(13)
N(11)—Cu(1)—N(12)	91.0(4)	N(21)—Cu(2)—N(22)	90.8(4)	N(31)—Cu(3)—N(32)	89.8(4)
N(11)—Cu(1)—N(13)	175.8(4)	N(21)—Cu(2)—N(23)	179.1(4)	N(31)—Cu(3)—N(33)	177.4(4)
N(11)—Cu(1)—N(14)	92.5(3)	N(21)—Cu(2)—N(24)	90.1(3)	N(31)—Cu(3)—N(34)	90.2(4)
N(12)—Cu(1)—N(13)	87.5(4)	N(22)—Cu(2)—N(23)	89.9(4)	N(32)—Cu(3)—C(33)	89.9(4)
N(12)—Cu(1)—N(14)	175.9(4)	N(22)—Cu(2)—N(24)	178.9(4)	N(32)—Cu(3)—N(34)	177.0(4)
N(13)—Cu(1)—N(14)	89.2(4)	N(23)—Cu(2)—N(24)	89.3(3)	N(33)—Cu(3)—N(34)	89.9(4)
S(11)—Cu(1)—S(12)	173.6(2)	S(21)—Cu(2)—S(22)	177.8(1)	S(31)—Cu(3)—S(32)	171.6(2)
S(11)—Cu(1)—N(11)	95.0(3)	S(21)—Cu(2)—N(21)	88.3(3)	S(32)—Cu(3)—N(31)	84.7(3)
S(11)—Cu(1)—N(12)	92.4(3)	S(21)—Cu(2)—N(22)	87.6(3)	S(31)—Cu(3)—N(32)	90.7(3)
S(11)—Cu(1)—N(13)	89.0(3)	S(21)—Cu(2)—N(23)	91.2(3)	S(31)—Cu(3)—N(33)	90.5(3)
S(11)—Cu(1)—N(14)	85.1(3)	S(21)—Cu(2)—N(24)	91.7(3)	S(31)—Cu(3)—N(34)	92.3(3)
S(12)—Cu(1)—N(11)	85.6(3)	S(22)—Cu(2)—N(21)	89.8(3)	S(32)—Cu(3)—N(31)	84.7(3)
S(12)—Cu(1)—N(12)	93.9(3)	S(22)—Cu(2)—N(22)	91.4(3)	S(32)—Cu(3)—N(32)	81.5(3)
S(12)—Cu(1)—N(13)	90.5(3)	S(22)—Cu(2)—N(23)	90.8(3)	S(32)—Cu(3)—N(33)	92.7(3)
S(12)—Cu(1)—N(14)	88.5(3)	S(22)—Cu(2)—N(24)	89.3(3)	S(32)—Cu(3)—N(34)	95.5(3)
Cu(1)—N(12)—C(1)	159.4(8)	Cu(2)—N(22)—C(3)	171.3(8)	Cu(3)—N(32)—C(5)	168.2(8)
N(12)—C(1)—S(21)	176.1(10)	N(22)—C(3)—S(31)	179.3(10)	N(32)—C(5)—S(11)	177.4(10)
C(1)—S(21)—Cu(2)	96.3(4)	C(3)—S(31)—Cu(3)	95.7(4)	C(5)—S(11)—Cu(1)	106.9(4)
Cu(1)—N(14)—C(6)	169.5(8)	Cu(2)—N(24)—C(2)	157.6(8)	Cu(3)—N(34)—C(4)	169.3(8)
N(14)—C(6)—S(32)	178.5(10)	N(24)—C(2)—S(12)	176.9(10)	N(34)—C(4)—S(22)	177.8(10)
C(6)—S(32)—Cu(3)	110.0(4)	C(2)—S(12)—Cu(1)	91.4(4)	C(4)—S(22)—Cu(2)	98.1(4)

noted, that for the case of the coordination polyhedron with "asymmetrically distorted" axial bonds one value of the dihedral angle (130°) is between the dihedral angles of the "symmetrically-elongated" coordination polyhedron, while the other one (46°) is in the range of dihedral angles observed in unchanged coordination polyhedra of copper(II).

The results obtained by solving the crystal structure of $[Cu(4\text{-pic})_2(NCS)_2]$ have shown, however, that for copper(II)–cyanato complexes not every change in neutral ligand π-acceptor properties manifests itself in the bonding properties of thiocyanate ligands. In the case of $[Cu(4\text{-pic})_2(NCS)_2]$ the different π-acceptor properties of 4-picoline compared with those of pyridine in $[Cu(py)_2(NCS)_2]$ are shown in the changes of the degree of tetragonal distortion of the copper(II) coordination polyhedron.

The crystal structure of the complex compound under investigation exhibits three symmetry-independent coordination polyhedra of copper(II). They differ from each other in the values of the Cu—S interatomic distances and probably in the character of the molecular orbitals of Cu—N(4-picoline ring) due to the different orientation of the 4-picoline rings to the equatorial plane of copper(II) coordination polyhedron. The positions of the heavy atoms, copper and sulphur, are determinated very precisely, together with the position of the 4-picoline plane. Hence, it seems reasonable to assume that there is some connection between the changes in orientation of the 4-picoline rings and the values of Cu—S interatomic distances.

In connection with the conception of equatorial–axial interactions in complexes as a manifestation of the mutual influence of ligands,[14] it is possible to say, that the orientation of the 4-picoline rings

Table 2. The least-squares planes and the displacement (Å) of the atoms from the planes

Plane I: formed by N(11), N(12), N(13), N(14) atoms

$0.7494X-0.5369Y-0.3875Z-0.4167=0$

N(11)	−0.047(8)
N(12)	0.057(9)
N(13)	−0.057(9)
N(14)	0.056(9)
Cu(1)	0.017(3)

Plane II: formed by N(21), N(22), N(23), N(24) atoms

$0.6524X-0.5876Y-0.4783Z-5.0739=0$

N(21)	−0.001(9)
N(22)	0.001(9)
N(23)	−0.001(9)
N(24)	0.001(9)
Cu(2)	−0.011(3)

Plane III: formed by N(31), N(32), N(33), N(34) atoms

$0.7674X-0.4891Y-0.4146Z-7.0216=0$

N(31)	0.002(9)
N(32)	−0.003(9)
N(33)	0.002(8)
N(34)	−0.002(9)
Cu(3)	0.049(3)

Plane IV: formed by N(11), C(111), C(112), C(113), C(114), C(115) atoms

$-0.6630X+0.7467Y-0.0540Z-3.0134=0$

N(11)	0.006(3)
C(111)	0.001(14)
C(112)	−0.020(14)
C(113)	0.016(11)
C(114)	−0.007(13)
C(115)	−0.009(12)
C(116)	0.024(14)

Plane V: formed by N(13), C(121), C(122), C(123), C(124), C(125) atoms

$-0.5218X+0.7085Y-0.4752Z-6.0772=0$

N(13)	−0.001(9)
C(121)	−0.007(11)
C(122)	0.016(11)
C(123)	−0.018(11)
C(124)	0.014(13)
C(125)	−0.001(11)
C(126)	−0.109(14)

Plane VI: formed by N(21), C(211), C(212), C(213), C(214), C(215) atoms

$0.4227X-0.0143Y-0.9062Z-0.5.4341=0$

N(21)	0.013(7)
C(211)	−0.015(12)
C(212)	0.002(13)
C(213)	0.003(10)
C(214)	0.004(11)
C(215)	−0.016(11)
C(216)	0.035(11)

Plane VII: formed by N(23), C(221), C(222), C(223), C(224), C(225) atoms

$0.3404X+0.0850Y-0.9365Z-5.2128=0$

N(23)	−0.000(8)
C(221)	0.008(11)
C(222)	−0.007(13)
C(223)	−0.002(10)
C(224)	0.009(11)
C(225)	−0.007(10)
C(226)	−0.006(12)

Plane VIII: formed by N(31), C(311), C(312), C(313), C(314), C(315) atoms

$-0.5243X+0.7769Y-0.3486Z+6.0756=0$

N(31)	0.013(9)
C(311)	−0.009(11)
C(312)	−0.011(11)
C(313)	0.017(11)
C(314)	−0.005(11)
C(315)	−0.014(11)
C(316)	−0.023(14)

Plane IX: formed by N(33), C(321), C(322), C(323), C(324), C(325) atoms

$0.3931X-0.0249Y-0.9192Z-4.8014=0$

N(33)	−0.003(8)
C(321)	0.009(10)
C(322)	−0.010(10)
C(323)	0.007(10)
C(324)	−0.004(11)
C(325)	0.003(11)
C(326)	0.073(15)

Dihedral angles between planes (°)

I–IV	151.3(3)
I–V	126.0(3)
II–VI	44.1(3)
II–VII	51.7(3)
III–VIII	129.6(3)
III–IX	46.0(3)
IV–V	25.8(4)
VI–VII	7.6(4)
VIII–IX	84.6(3)

corresponds to the values of Cu—S interatomic distances, and vice versa. The 4-picoline rings have C_{2v} symmetry and have no steric hindrances to rotation around the Cu—N bond. They occupy a position with minimum energy and, in this way, affect the electronic properties of the nitrogen atom of the Cu—N bond. These changes via the central atom give rise to changes in the values of the Cu—S interatomic distances.

The above is experimental evidence of a new type of mutual influence of ligands in complexes.

REFERENCES

1. A. Turco and C. Pecile, *Nature (London)* 1961, **191**, 66.
2. A. M. Golub and H. Köhler, *Chemie der Pseudohalogenide*. VEB Deutscher Verlag der Wissenschaften, Berlin (1979).
3. A. H. Norbury, *Adv. Inorg. Chem. Radiochem.* 1975, **17**, 235.
4. M. Kabešová and J. Gažo, *Chem. Zvesti* 1980, **34**, 800.
5. M. Kabešová, L. Macášková and J. Gažo, *Koord. Chim.* 1982, **8**, 486.
6. J. Gažo, *Pure Appl. Chem.* 1974, **38**, 279.
7. J. Gažo, I. B. Bersuker, J. Garaj, M. Kabešová, J. Kohout, H. Langfelderová, M. Melník, M. Serátor and F. Valach, *Coord. Chem. Rev.* 1976, **19**, 253.
8. J. Kohout, M. Kabešová and J. Gažo, *Mh. Chem.* 1977, **108**, 1911.
9. M. Kabešová, T. Šramko, J. Gažo, E. K. Zumadilov and V. I. Nefedov, *J. Therm. Anal.* 1978, **13**, 55.
10. M. Kabešová, I. Vargová, T. Šramko and J. Gažo, *J. Therm. Anal.* 1978, **13**, 65.
11. G. M. Sheldrick, SHELX76, Program for crystal structure determination. University of Cambridge, U.K. (1976).
12. J. Soldánová, M. Kabešová and J. Gažo, *Inorg. Chim. Acta* 1983, **76**, L203.
13. M. Kabešová, J. Kohout and J. Gažo, *Mh. Chem.* 1976, **107**, 641.
14. J. Gažo, R. Boča, E. Jóna, M. Kabešová, L. Macášková and J. Šima, *Coord. Chem. Rev.* 1982, **43**, 87.

Polyhedron Vol. 9, No. 8, pp. 1035–1044, 1990
Printed in Great Britain

0277–5387/90 $3.00+.00
© 1990 Pergamon Press plc

BONDING IN BORANES

ALISON RODGER*

Physical Chemistry Laboratory, South Parks Road, Oxford OX1 3QZ, U.K.

and

SUSAN M. COLWELL and BRIAN F. G. JOHNSON

University Chemical Laboratory, Lensfield Road, Cambridge CB2 1EW, U.K.

(*Received* 7 *August* 1989; *accepted* 30 *November* 1989)

Abstract—The energetic results from molecular orbital calculations on fragments of boron hydrides and hydrocarbons illustrate the fundamental differences in bonding between these two types of compounds. Combining the results for boranes with an extension of Lipscomb's topological approach yields a procedure for constructing potentially stable boranes and understanding their bonding characteristics.

Bonding in boranes is often seen as rather unusual. For example, the regularity of carbon chemistry, and also of much of main group chemistry, with clearly defined bond types of approximately constant length and with predictable geometries does not hold for boranes. A number of schemes have been developed to account for the structure and bonding in boranes. Broadly speaking these can be divided into those based on molecular orbital (*mo*) arguments and those based on topological (connectivity) arguments. Philosophically the differences between these two types of approach lies in the fact that *mo*'s are delocalized over the whole molecule whereas topological approaches use localized bonds between nearest neighbour atoms. The idea of boranes being held together by a mixture of two- and three-centre bonds was first developed by Longuet-Higgins[1] and has been fruitfully exploited, in particular in the topological approach (TA) of Lipscomb *et al.*[2] and the work of Wade,[3] to rationalize the observed geometries of boranes. Some support for the topological approaches has come from calculations on various boranes and carboranes[4] where the electron density maps support the concepts of two- and three-centre bonds in boranes. In principle, an accurate *mo* calculation can always be performed, and in some cases symmetry constraints on *mo*'s enable *mo* theory to be used simply and semi-quantitatively to determine stable cluster geometries. Wade's rules[3] for *closo*-boranes are the classic example of this. However, this is by no means always the case. Recent thereotical work[5] on boranes has focused on rationalizing the geometry and reactivity of particular boranes using various semi-empirical *mo* formalisms. As with Wade's rules, wider applicability of these results rests on symmetry arguments, so for less symmetric boranes or fragments of boranes we still rely on the TA.

It is the aim of this work to develop, using *mo* calculations on simple boron hydride systems, an energetic rationale for the rules summarized in the TA, thus complementing it with a basis for choosing between different geometries for which localized bonding schemes can be proposed. In addition some extra rules are developed which simplify the application. The result is a scheme whereby potentially stable boranes can be "built" from component atoms, rather than the existence of known structures simply being rationalized or answers restricted to a limited series of compounds.

We shall begin by comparing the bonding in boron and carbon compounds to see why boron bonding does not accord with the chemists idea of "normal" bonding. We shall follow molecule formation by following how the molecular orbitals of atoms or groups of atoms change when they join to form molecules. Although individual *mo*'s have

* Author to whom correspondence should be addressed.

no reality in themselves, the changes in the orbitals of a molecular fragment upon molecule formation indicate how the wavefunction, and hence the electron density and bonding, changes upon molecule formation. The bonding of A to B can be understood in much the same manner as that of diatomic molecules. The *mo*'s of a molecule AB, composed of fragments A and B, can be expressed as linear combinations of A and B molecular fragment orbitals (*mfo*'s). The most important A and B *mfo* contributors to a given *mo* will be of comparable energy with significant overlap.[6] The main changes upon molecule formation are therefore due to occupied *mo*'s of AB which have a large component of unoccupied *mfo*'s—i.e. those resulting from the interaction of higher occupied *mfo*'s and lower unoccupied *mfo*'s, and often of the highest occupied (*ho*) and lowest unoccupied (*lu*) *mfo*'s. We denote a singly-occupied *mfo* (i.e. an orbital which is both *lu* and *ho*) as *somfo*, and a singly occupied *mo* as *somo*.

The calculations used in this work have been performed using MICROMOL,[7] which is an implementation for IBM PC's of a subset of a standard *ab initio* quantum chemistry program CADPAC.[7] This program performs self-consistent field (SCF) energy calculations using the Hartree–Fock–Roothan Linear Combination of Atomic Orbitals (HFRLCAO) method, i.e. the wavefunction is expressed as a single antisymmetrized product of molecular orbitals. These molecular orbitals are found as optimum LCAO's, which are represented by contracted Gaussian basis functions. MICROMOL also calculates the gradient of the energy of the molecule with respect to nuclear displacements, and so it is possible to calculate an optimized geometry for the molecule with a given basis set.

Unless otherwise noted, all the orbital energies presented in this work are results of MICROMOL calculations carried out with a double zeta basis set (i.e. two contracted Gaussian functions per orbital in the valence space) at the geometry optimized using MICROMOL with this basis set. A double zeta basis set SCF calculation is a very simple *ab initio* quantum chemical calculation, and one cannot hope to obtain quantitative accuracy: the basis set has little flexibility, and one is completely ignoring correlation (i.e. the instantaneous interaction between the electrons). However, we are concerned only with relative energies and with trends over a series of similar calculations on simple molecules, and so we believe that the qualitative picture given by these calculations should be adequate for our purposes.[8] (It should be noted that for open-shell species the orbital energies are not uniquely defined, though the total energy is.)

BORON AND CARBON COMPOUNDS

In this section we shall briefly look at the types of bonding which one might expect to be favourable for boron and why it differs from that for carbon. Boron and carbon are both first-row main group atoms with similar valence orbitals available for combining into molecular orbitals. The main differences between B and C which affect their bonding capabilities are that (i) carbon's orbitals are lower in energy than boron's, which affects the extent of interaction with heteroatoms, and (ii) carbon has one more electron than boron, which affects orbital occupancy. It is perhaps unfair to attach the somewhat derisory label "electron deficient" to boron compounds—they simply utilize fewer electrons than carbon compounds in the most efficient manner possible. Some results of these differences are illustrated by the simple molecules and fragments of molecules whose orbital energies and bond lengths are given in Figs 1 and 2.

Analysis of the results of the MICROMOL calculations enable the bonding and structure of boranes and their differences from hydrocarbons to be at least qualitatively understood. We shall proceed by first examining B_2H_6 and C_2H_6 systems in some detail, thus providing the groundwork for us to "build" stable boranes from component parts.

Ethane and diborane

A_2H_4 has the same optimized geometry for A = B or C, whereas the experimental structures for A_2H_6 are different for diborane and ethane (cf. Fig. 3). Let us consider the effect of adding two H atoms to A_2H_4. The H 1*s* *somo* has a bonding (and hence stabilizing) interaction with all occupied A_2H_4 orbitals (since less than half the valence *mo*'s of A_2H_4 are occupied). It is therefore apparent why C_2H_6 adopts the ethane structure: the *lumo* of C_2H_4 (which becomes a major component of the *homo* in both bridged and non-bridged C_2H_6) is a C—C antibonding π-orbital, $2\pi_g^*$, that has no interaction with a bridging H, but a stabilizing one with a terminal H.

The situation for B_2H_6 is less clear cut. The stabilizing nature of the interaction of H with all B—B orbitals ensures that each H, whether bridging or terminal, has nearly "two electrons-worth" ($\approx$ 2e) of electron density. In the non-bridged structure this means there is little valence electron density between the borons, so the electronic stabilization from having the B's close together (say < 2 Å) is not a sufficiently large contribution to the total energy to overcome the B—B internuclear repulsion at that distance. As a result the optimized non-

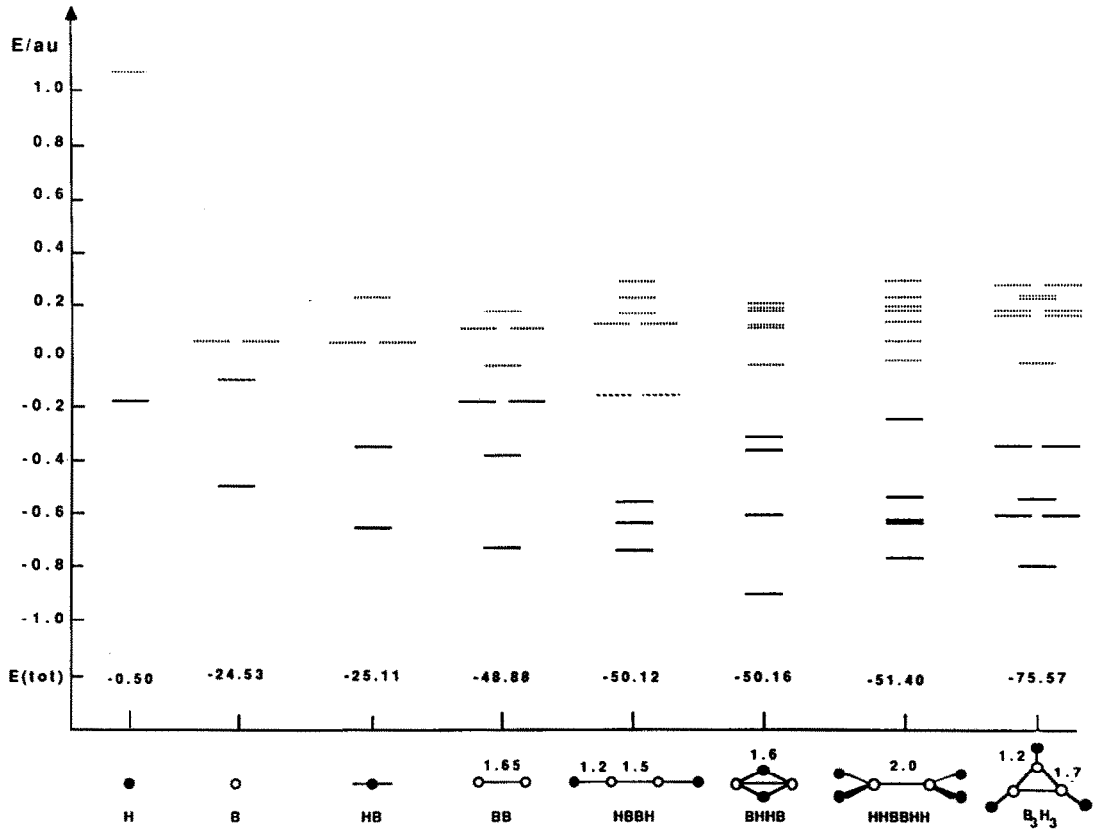

Fig. 1. Geometries and *mo* energy levels for some boron hydride fragments.

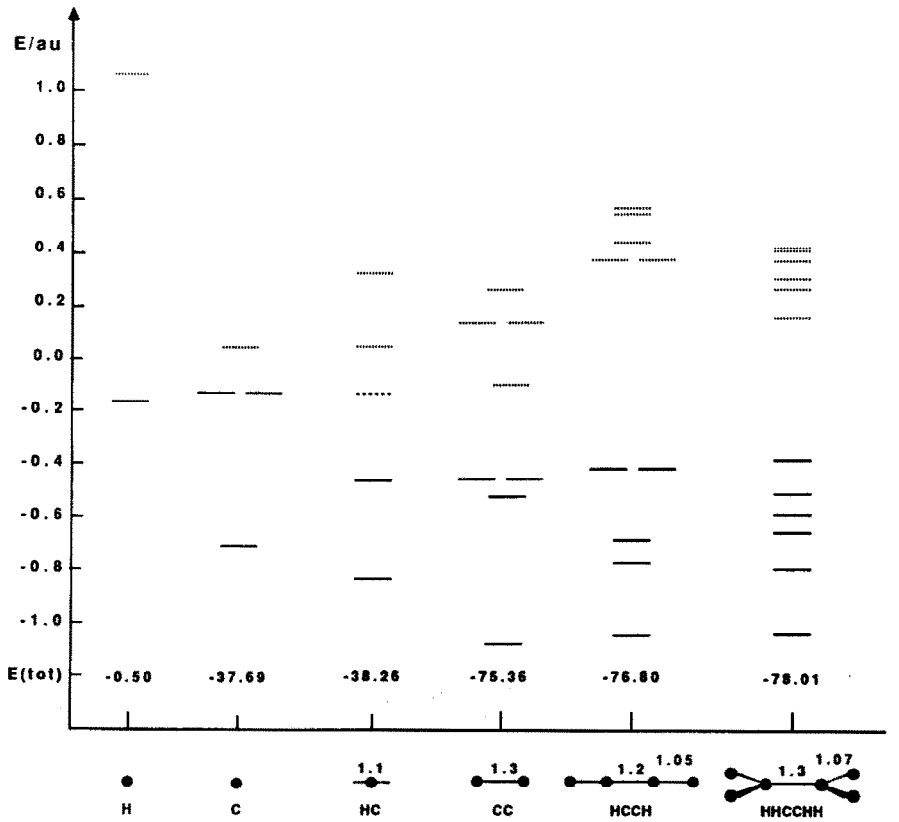

Fig. 2. Geometries and *mo* energy levels for some hydrocarbon fragments.

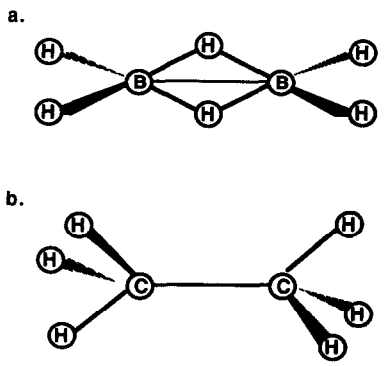

Fig. 3. Geometries of diborane and ethane.

bridged structure at the level of accuracy of our calculations did not converge. If however a bridged geometry is adoped, the electron density involved in boron-bridging hydrogen bonding is also involved in B—B bonding. Their combined stabilizing effect results in a B—B bond and a stable system.

In conclusion we can somewhat simplistically say that diborane adopts a geometry with two H bridges because it then gets both B—H and B—B bonding stabilization when there is insufficient electron density for a two electron/two atom bond. Equivalently this can be viewed as a consequence of the number of valence electrons and the variation principle (the more *ao*'s contributing to an *mo* the lower its energy is). Ethane on the other hand has sufficient electrons to have stabilizing contributions from six terminal C—H bonds and also one C—C bond. It should be noted that the calculations (Fig. 4) indicate that the comparative stability of the bridged structure of diborane is not as obvious as familiarity might lead one to believe. The whole of boron chemistry only just happens.

BUILDING BORANES

If a larger molecule is formed from diborane by replacing an H with a substituent A, similar types of bonding would be retained if A and H have *ho* and *lu* orbitals of similar energy and symmetry and A has ~ 1e available for bonding. If A does not satisfy

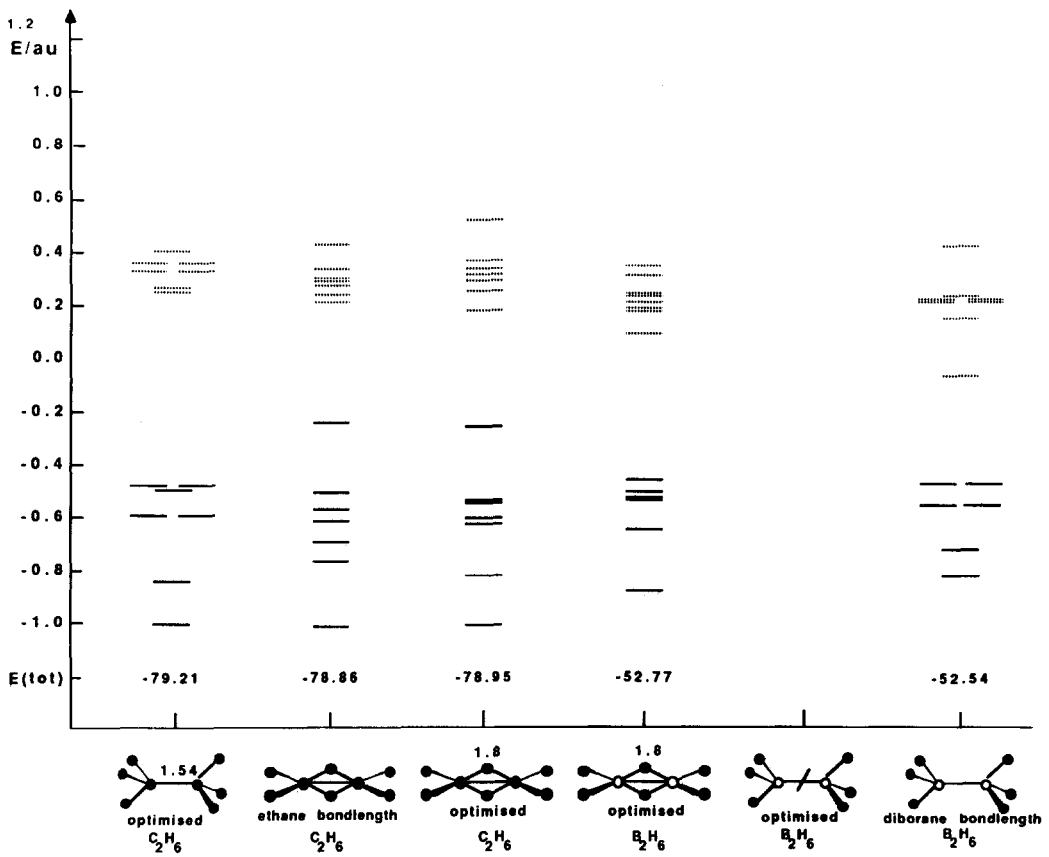

Fig. 4. *Mo* energy levels for possible geometries of diborane and ethane. (To make semi-quantitative deductions from orbital energy level diagrams it is best to compare different geometries with the same bond lengths so that the nuclear repulsion energy is the same.)

these criteria then a different bonding scheme, resulting in an ethane-type structure or two dissociated fragments, is almost certainly more stable. Both BH_2 and CH_3 fit these criteria so larger boranes (and carboranes) could in principle be built by substituting for H's in diborane resulting in additional BB and CB or BBB and BCB (by analogy with BHB) bonds. It should be noted that a particular geometry which one might build in this manner may never be observed experimentally if an alternative geometry is more stable, thus B_3H_7 with 6BH, 1BHB, and BBB is not observed since B_3H_9 with 6BH, 3BHB is more stable than $B_3H_7+H_2$.

Although somewhat artificial, it is helpful to consider the relative stabilities of two geometries to be determined by two factors: (i) the relative stabilities of the bonds which are formed, and (ii) steric considerations (i.e. does the proposed geometry force two nuclei so close together that repulsion due to overlapping electron clouds occurs). The artificiality of this situation is most obvious when one realizes that steric constraints can cause the distance between nearest neighbour (nn) atoms to be increased which in turn decreases the strength of the bond.

From the variation principle, and also from the results of *mo* calculations on borane fragments collected in Figs 1 and 2, one might expect contributions to borane stability to be in the order BBB $\geqslant$ BHB $\geqslant$ BB $\geqslant$ BH, with bonds which share an edge being less stable. This would be particularly true for BB or BH bonds so that any one nn link can be taken to have at most one two-centre bond. Each B of a BBB bond can notionally be seen to contribute $\sim$ 2/3e, since electron density in excess of $\sim$ 2e will be antibonding. Similarly, a B contributes $\sim$ 1/2e to a BHB, and $\sim$ 1e to a BB or BH (cf. ref. 3). Electron density can, however, easily be transferred between nn. Thus stable boranes will be held together by a mixture of two- and three-centre bonds, the ratio being such as to ensure all valence electrons are (at least nominally) bonding. The greater stability of three-centre bonds suggests that borane polyhedra with triangulated faces and as many bridging H's as possible are energetically desirable. We shall return to this below.

Let us first consider boranes whose B_p polyhedra are "convex", i.e. have each B such that other vertices lie on or beneath a tangential plane. This automatically limits the B polyhedron to having B's with at most six nn B's. In addition it excludes from our immediate consideration the polyhedra, which are in fact found for B_p, $p > 12$, where two convex boron fragments share an edge or a vertex. We denote a B vertex with i nn B's as B(i).

From the preceding discussion we can deduce stable bonding schemes for each vertex in a neutral borane, assuming each B has 3e to use in bonding. B(6) is most stably connected to its nn B's by 3BBB, so 1BH is required to use up its valence electrons (assuming no large charge displacements). The best bonds for connecting a B(5) to its nn B's are 2BBB and 1BHB, but steric factors preclude the additional BH or 2BHB then required. Thus B(5) is most stably bonded by 3BBB (two sharing an edge) and 1BH, or 2BBB, 1BB and 1BH. Thus both B(5) and B(6) are expected to always have a terminal H atom. Similarly B(4) is expected to have at least one terminal H, and probably no more. Ideally a B(3) would have 2BHB, 1BB and 1BH. Other combinations, some with 2BH, are possible and in fact more probable due to the requirements of the nn of a B(3) (see examples below). A B(2) will be most stable with 2BHB and 2BH.

Boranes with a net negative charge (a net positive charge is unlikely) must have more bonds than neutral boranes, thus fewer three-centre bonds. BHB bonds use least B valence electron per B per bond so are less likely in negatively-charged systems than in neutral systems. As charge increases one would expect first to lose BHB's, then gradually open out the triangulated faces to squares. In the limit of one or more extra electron per boron atom, were such a system able to exist, geometries like those in carbon chemistry might be expected.

The situation is somewhat different for the B atoms which are shared by two polyhedral fragments to make a larger borane than is possible with a single fragment. The nn of such a B are not restricted to one side of a plane containing the B, so for example, a B(5) can accommodate bridging H's. Borons of connectivity seven or higher will not have a terminal H as they do not have sufficient valence electron density. A B(6) or B(5) may have a terminal H. Alternatively they may have a bridging H.

At this stage it is appropriate to summarize the TA. The topological approach is based on the following assumptions: (i) in any borane 2e are required to make a stable bond to a terminal H, 2e per BHB bond, 2e per BBB bond and 2e per BB bond; (ii) each B has at least one terminal N and all B's, whose distance indicates a bond, are connected by one two-centre bond or one three-centre (BBB or BHB) bond or two three-centre bonds, and (iii) all B valence orbitals are involved in the bonding. Our previous discussion provides a semi-quantitative justification of these assumptions. As noted by Wade,[3] B's which connect two "convex" B polyhedral fragments do not necessarily have a terminal H. To be complete we therefore follow Wade and consider $B_{p+r}H_{p+q}^{c-}$, where r is the number of B's without a BH. Simple arithmetic to

balance electrons and orbitals gives

$$n_{BBB} = p+r-n_{BHB}-c \geqslant 0, \quad (1)$$

where n_{BBB} is the number of BBB, etc.

$$n_{BB} = n_{BHB}+r/2-q/2+3c/2 \geqslant 0. \quad (2)$$

For known or postulated single fragment boranes Lipscomb *et al.* determined all possible assignments of three-centre and two-centre bonds that satisfy their criterion. This provides a bonding scheme for B geometries and enables electron distribution, bond lengths and so on to be determined if the possible bond assignments are weighted in some way (usually equally in their work). Considering the weighting of assignments as a variational procedure (rather than an *ad hoc* average) supports the suggestion[2b] that greater stability corresponds to larger numbers of resonance structures. However, to make a significant contribution to the total electron density a given assignment of bonds must not be energetically unfeasible due to significant distortion of the charge distribution in the molecule.

Our extension to the TA (ETA) involves application of the preceding energetic arguments and the introduction of the additional structure parameters, n_e, the number of nn B—B links, i.e. polyhedral edges, n_d the number of edges shared by two three-centre bonds, and n_2 the number of B's with two BH's. We can then write:

$$n_d = n_{BB}+3n_{BBB}+n_{BHB}-n_e \geqslant 0$$
$$= 3p-n_{BHB}-3c/2-q/2-n_e \geqslant 0 \quad (3)$$
$$n_2 = q-n_{BHB}. \quad (4)$$

Closo-*boranes*

Let us consider boranes whose B_p polyhedra are *closo*, so $n_e = 3p-6$. A B(6) is not possible for $p = 7$ since the B—B bonds of a single vertex cannot be coplanar. For $p > 7$, B(6) is unfavourable relative to other options as it forces both small and large angles on the molecule. Thus one would expect a B(6) only in B_{11} polyhedron since a triangulated 11 vertex *closo*-polyhedron must contain at least one B(6) (10 B(5) and one B(4) cannot be formed into a *closo*-triangulated polyhedron). For structures between B_5 and B_{11} all vertices will then be B(5) or B(4). This dictates the polyhedra adopted to be the ones indicated in Fig. 5. For B_{12} we would expect an icosahedral boron polyhedron.

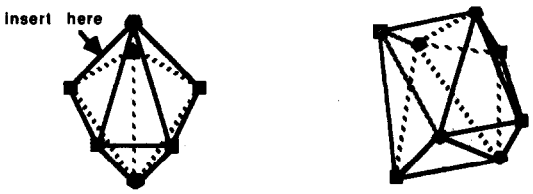

Fig. 6. Illustration of the insertion of an additional B atom into a boron polyhedron.

As an aside we note that the relationships between the polyhedra favoured by boranes is interesting as one can envisage synthesizing the *closo*-boranes in this manner. From $p = 4$ to $p = 11$ the successive triangulated polyhedra of Fig. 5 can be constructed from the preceding one by inserting an atom between nn B's as illustrated in Fig. 6. Insertion along an edge involves loss of only one stabilizing B—B contact so is most favourable. The choice of insertion point is, from the above discussion, that which, if possible, causes two of the B(4) (or B(3) for $p = 4$, 5) atoms to become B(5) [or B(4)] (Fig. 6). For $p = 11$ a B(6) is created, and as no B_{11} *closo*-polyhedron can be constructed without a B(6) it remains. If the same construction is followed to go from B_{11} to B_{12} two B(6) result.

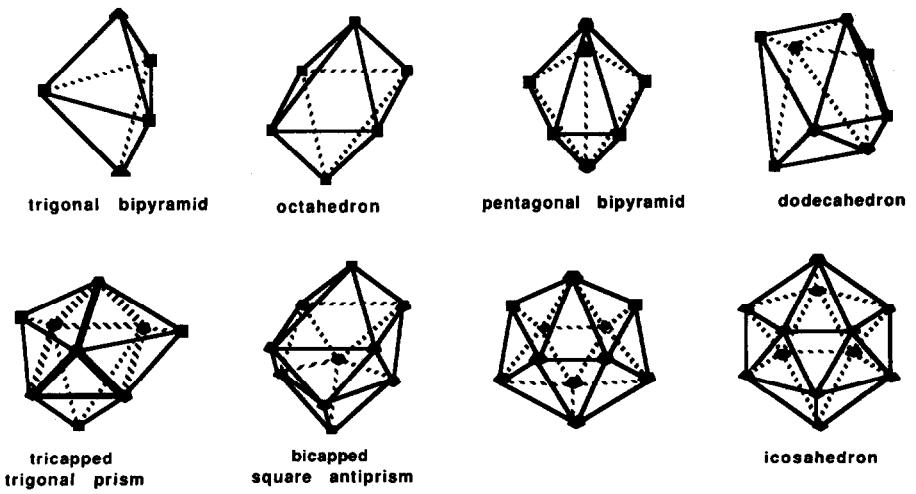

Fig. 5. B_p polyhedra.

The comparatively small curvature of the B_{11} polyhedron means that an alternative insertion point between the B(6), 2B(4) and 3B(5) atoms is possible. This gives the more stable icosahedron. Higher nuclearity "convex" *closo*-polyhedra either have lots of B(6) centres or low triangularity, so it is energetically more favourable to couple fragments of smaller polyhedra together for $p > 12$.

We have now deduced the geometries of the *closo*-borane polyhedra. We also know that each B will have one and only terminal H for $p > 5$. It remains only to determine c and hence the types of bonds. The stability of pairs of electrons in bonding orbitals suggests that $c = 0$, 2 or 4.

If $c = 0$, $n_{BBB} = p$, $n_{BB} = 0$, $n_d = 6$ and there is a total of $2p$ bonds. If $c = 2$, $n_{BBB} = p-2$, $n_{BB} = 3$, $N_d = 3$ and there is a total of $2p+1$ bonds. If $c = 4$, $n_{BBB} = p-4$, $n_{BB} = 6$, $n_d = 0$ and there is a total of $2p+2$ bonds. Now if BBB and BB were similar in energy, then the bond (or orbital) energy would favour $c = 4$, i.e. more bonds, and if they are quite different ($E_{BBB}/E_{BB} > 1.5$, where E denotes stabilizing energy) then bond energy favours $c = 0$. For some values of p, the required number of bonds for each c cannot be assigned[9] so one would not expect those to be observed. In those cases where more than one assignment is possible the following considerations apply. From Figs 1 and 3 it can be deduced that $E_{BBB}/E_{BB} > 1.5$ for unsubstituted boranes, where E denotes stabilizing energy. Thus bond energies favour $c = 4$. However, electron interaction terms are significantly different for molecules of different charge, and a minimum for neutral species. The observed value of $c = 2$ for *closo*-boranes is consistent with these conflicting trends. Thus $c = 2$, $n_{BBB} = p-2$, $n_{BB} = 3$, $n_d = 3$. The situation is different in substituted boranes, cf. ref. 9.

It is not possible to construct $B_4H_4^{2-}$ with the required types of bonds. Various other geometries, such as tetrahedral $B_4H_4^{4-}$ with 6BB+4BH, or $B_4H_8^{2-}$ with 2BBB+1BB+8BH, or $B_4H_7^-$ with 3BB+7BH are possible, however, only a small distortion of the tetrahedron takes the boron polyhedron to a butterfly shape. B_4H_{10}, which adopts this shape, has 4BHB, 6BH and 1BB, and is more stable than the other options.

Neutral boranes

A neutral borane has fewer electrons available for bonding than the negatively charged *closo*-boranes. This makes BHB bonds desirable. To construct a stable neutral borane, B_pH_{p+q}, one therefore considers p atom fragments of the *closo*-triangulated polyhedra illustrated in Fig. 5 and adds terminal and bridging H's. The maximum possible, though not necessarily desirable, number of bridging H's is determined by the space available in the "hole" of the polyhedron. Thus the removal of a single atom from the icosahedron does not leave enough room for bridging H's, so no B_{11} cluster whose B polyhedron is a fragment of an icosahedron exists. (Neutral B_{11} clusters are composed of two smaller fragments linked along a B—B edge.)

The B_p fragments which need be considered for a given p can be limited by the energetic considerations developed above. Firstly, those with nearest neighbour atoms missing will usually result in the most stable molecules as triangular faces are then retained. Which atoms are removed in forming a fragment is determined by two competing factors: (i) the creation of as many fragment edges as possible to enable the maximum number of bridging H's to be accommodated, and (ii) the retention of as many triangular faces as possible to maximize the number of BB links and hence maximize n_{BBB}. (i) Can be expected to dominate the formation of *arachno*-polyhedra, as more potential H bridging sites are created than BBB bonds lost. However, for *nido*, *hypo*, etc., polyhedra (ii) can be expected to dominate as few if any additional H bridging sites are created when the second or third B is removed. Thus the first atom removed from a *closo*-polyhedron will be one of highest connectivity. Subsequently, atoms of lowest connectivity are removed.

A BHB uses the least valence electron density from a boron atom, so a maximum value for n_{BHB} enables the formation of the largest total number of stabilizing bonds. Thus, unless it leads to an inconsistent result, we assume stability relates to the maximum number of BHB's possible for a given boron polyhedron fragment. By way of contrast a BH is expensive in electrons, so a minimum value of n_2 is usually appropriate, i.e. n_2 usually equals the number of B(2) in neutral boranes.

To construct stable neutral boranes we therefore proceed as follows. (i) For a given number of B's, construct all different boron fragment polyhedra from higher order *closo*-polyhedra by removing first a vertex of maximum connectivity and subsequently ones of minimum connectivity. (Molecular models considerably simplify this process. Cocktail sticks and small pieces of plastic tubing with holes punched in it are ideal.) (ii) Determine n_2(min) = the number of B(2), n_e and n_{BHB}(max) for each fragment. (iii) Starting with n_{BHB}(max) and n_2(min) determine n_{BB}, n_{BBB} and q for each n_{BHB} and n_2 until a consistent set of values is obtained. (iv) Determine whether the required number of BB and BBB bonds can be assigned in the proposed geometry, i.e. does

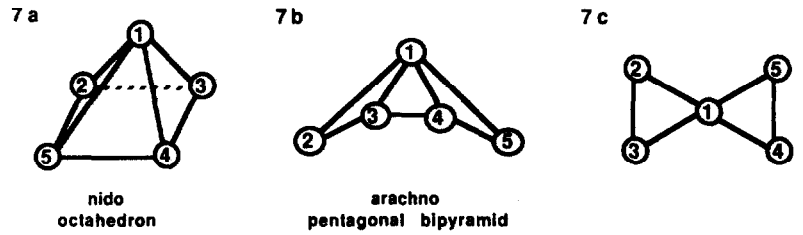

Fig. 7. The possible triangulated topologies for B_5.

each B—B link have 1BB, or 1BHB, or 1BBB, or 1BHB+1BBB, or 2BBB (ensuring n_d is correct facilitates this process). If an assignment cannot be made then one would not expect to observe the structure. (v) If all possible bond assignments lead to a significant distortion of the charge distribution from that represented by the unbonded atoms in the same shape, then that structure is energetically unfeasible. (Equations (1)–(3) only consider the total electron count—this is a more localized consideration.) (vi) Final determination of the most stable structure is made by considering the number of bonds of each type in a molecule. (It should be noted that in comparing stability of different structures with different numbers of H's, the energy of H—H bonds of the extra H's must be included where appropriate.) Step (iv) is precisely the topological approach of Lipscomb *et al.*[2] It is also the most tedious and error-prone step, which would be much simplified by implementation of the programs developed by Lipscomb *et al.* The main feature of the ETA compared with previous ones is the coupling of a topological approach used iteratively (previously done by Wade to a limited extent[3]) with a semiquantitative energetic discussion which enables potentially stable structures to be identified and unstable ones to be eliminated.

The following examples illustrate this procedure.

B_5H_{5+q}

The possible triangulated topologies for B_5 are illustrated in Fig. 7. The first is a *nido*-octahedron, and the second an *arachno*-pentagonalbipyramid.

The **7a** polyhedral fragment has $n_e = 8$, $n_2(\text{min}) = 0$, and $n_{\text{BHB}}(\text{max}) = 4$. If $n_{\text{BHB}} = 4$, then $n_2 = 0$ (for steric reasons), $n_{\text{BBB}} = 1$, $n_{\text{BB}} = 2$ and $n_d = 1$, and the molecular formula is B_5H_9. The bonds can be assigned as in Fig. 8(a). The average B charge assignment between the four equivalent bond assignments is 2.83e for B^2, B^3, B^4 and B^5, and 3.66e for B^1. Although B^+ has a nominal charge significantly above two, the balance of charge lies in its nn so a significant charge displacement is not in fact required to form the bonds of Fig. 8(a), and one might expect to observe this molecule, as is the case.

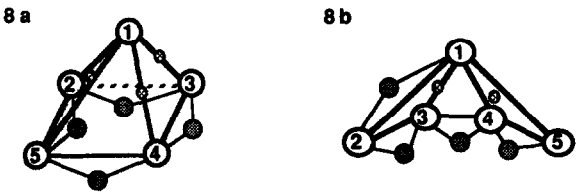

Fig. 8. The two possible neutral B_5 boranes.

The **7b** polyhedral fragment has $n_e = 7$, $n_2(\text{min}) = 2$, and $n_{\text{BHB}}(\text{max}) = 4$ (for steric reasons only one of the B(4)—B(2) edges can accommodate a BHB). If $n_{\text{BHB}} = 4$, and $n_2 = 2$ then $n_d = 1$, $n_{\text{BBB}} = 1$, $n_{\text{BB}} = 2$, and the molecular formula is B_5H_{11}. The bond assignment associated with this geometry is illustrated in Fig. 8(b). A "resonance" between this geometry and its mirror image would have additional stability since little or no geometry distortion is required. This derivation of the geometry of B_5H_{11} illustrates the usefulness of deriving borane geometries from first principles. When considering B_5H_{11}, Irving and Lipscomb assumed that the fourth bridging H was terminal on B^1. Although it is possible to derive a bond assignment for this geometry the electron distribution is more distorted than nn sharing can correct, and it does not correspond with the experimental bond lengths.[2b]

The two possible neutral B_5 boranes illustrated in Fig. 8: $B_5H_9+H_2$ with 4BHB+1BBB+2BB+5BH+1HH, $n_d = 1$, and B_5H_{11} with 4BHB+1BBB+BB+7BH, $n_d = 1$ are expected to be of comparable stability. A more quantitative analysis is required to differentiate between them. The existence of both molecules is consistent with this.

B_8H_{8+q}

B_8 systems are of sufficient complexity to illustrate how one should deal with the larger systems. Using the criteria for fragment formation given above we are able to limit our consideration to the fragment polyhedra illustrated in Fig. 9. They are,

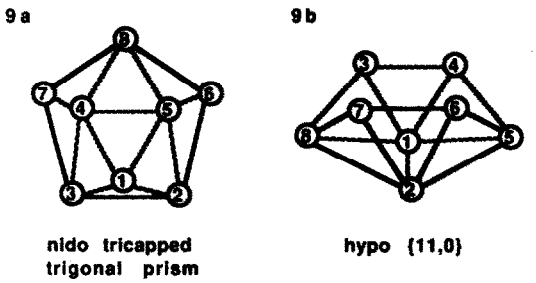

Fig. 9. The possible B_8 fragment polyhedra.

respectively, a *nido*-tricapped trigonal prism $\{9,-1\}$ or an *arachno*-bicapped antiprism $\{10,-2\}$, and a structure which can be viewed as either $\{11,-3\}$ or $\{12,-4\}$.

The polyhedral fragment of Fig. 9(a) has $n_e = 16$, $n_2(\text{min}) = 0$. $n_{BHB}(\text{max}) = 5$, however, this results in an odd number of electrons. So consider $n_{BHB} = 4$ and $n_2 = 0$, in which case $n_{BBB} = 4$, $n_{BB} = 2$ and $n_d = 2$. Although bond assignments can be made, all involve significant distortion of the electron distribution so are energetically unfavourable. If $n_2 = 2$ or 1 the geometries are also either electrostatically unfavourable or sterically crowded. So although in principle possible, such a geometry is unlikely to be energetically feasible.

The polyhedral fragment of Fig. 9(b) has $n_e = 15$, $n_2(\text{min}) = 0$. $n_{BHB}(\text{max}) = 6$, but eq. (3) then results in a negative value for n_d. $n_{BHB} = 5$, for steric reasons has $n_2 = 0$ and thus an odd number of electrons. So consider $n_{BHB} = 4$. If $n_2 = 0$, $n_{BBB} = 4$, $n_{BB} = 2$ and $n_d = 3$. The two possible assignments of BHB's for this B_8H_{12} cluster which both require only nn charge redistribution are illustrated in Fig. 10(b). If $n_{BHB} = 4$ and $n_2 = 2$, $n_{BBB} = 4$, $n_{BB} = 1$ and $n_d = 2$. Again two possible bond assignments for this B_8H_{14} cluster requiring only nn charge redistribution are possible, Fig. 10(c). We can therefore conclude that both of these clusters are feasible molecules and of comparable energy.

Charged boranes

Charged hydrogen-bridged boranes are observed when other factors overcome the repulsive electron interaction terms. For negatively-charged systems energetically feasible bond allocations may have a B requiring more than 3e for bonding to its nn's, however any positive charge must be able to be accounted for by nearest neighbour redistribution.

We considered above the neutral B_8 boranes which may be able to be synthesized. The first non-*closo*-B_8 borane to be observed was in fact $B_8H_{13}^-$. It has $n_e = 16$, $n_{BBB} = 4$, $n_{BB} = 2$, $n_{BHB} = 3$, $n_2 = 2$ and $n_d = 2$. Thus the additional electron makes a geometry with fewer BHB's favourable.

Another example is provided by $B_{10}H_{14}$ which is stable as an icosahedral or, equivalently, dodecaborane fragment with $n_2 = 0$ and four bridging H's (cf. figure). The bridged hydrogens are somewhat sterically crowded, and a small geometric distortion alters the position of two of the bridging H's to terminal positions on B(3)'s, and two to positions across the long bonds of the original structure. As B(3)'s in neutral boranes do not favour two BH's, additional electrons help stabilize this new geometry and it is found in both neutral and charged forms. Charged hydrogen-bridged boranes

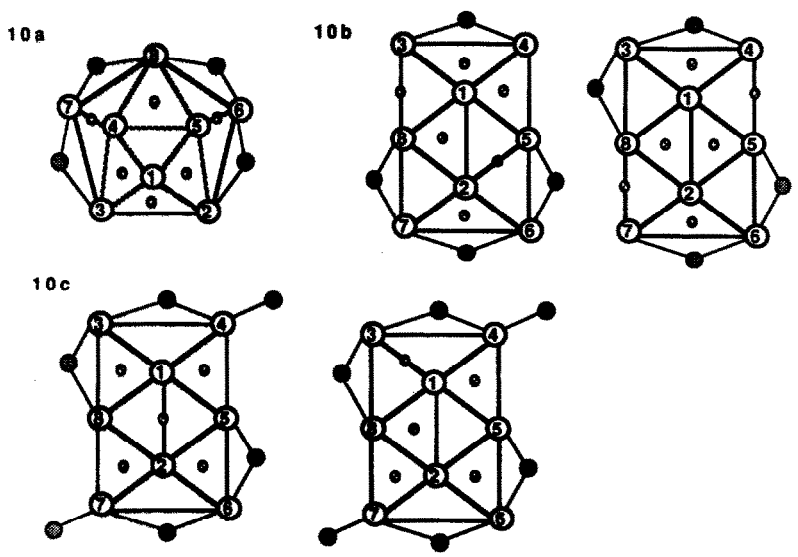

Fig. 10. Possible neutral B_8 boranes.

in fact often have more than one BH on a B(3) [or even on a B(4)].

CONCLUSION

By beginning our study of boron hydride clusters with small collections of B and H atoms and the corresponding C and H molecular fragments we were able to see why the bonding in boranes and organic molecules differs. This then enabled the development of a procedure to construct potentially stable boranes from component atoms. Much of the procedure coincided with the topological approach to borane bonding developed by Lipscomb *et al.*[2] The main differences are as follows.

(i) We are able to proceed by generating feasible boron hydride cluster frameworks from a knowledge of the atomic composition of a molecule.
(ii) The calculations on boron hydride fragments enabled comparisons of the stability of topologically feasible structures to be made.
(iii) Explicit inclusion of the number of bonds sharing edges facilitated the analysis.
(iv) The nearest neighbour charge redistribution discussion gives a rationale for weighting bond assignments in the determination of bond-lengths (cf. the work of Williams[10]).

The generality of our approach means that it does not always provide the final choice between a few remaining possible geometries. A more detailed analysis such as that of O'Neill and Wade on *closo*-structures with n, $n+1$ or $n+2$ skeletal electron pairs may then need to be undertaken.

Acknowledgements—Discussions with M. Yahawera, A. Brown and C. Housecroft are gratefully acknowledged.

REFERENCES

1. H. C. Longuet-Higgins, *J. Chim. Phys.* 1949, **46**, 275 and *Quart. Rev.* 1957, **11**, 121.
2. (a) W. N. Lipscomb, *Adv. Inorg. Chem. Radiochem.* 1959, **1**, 117; (b) I. R. Epstein and W. N. Lipscomb, *Inorg. Chem.* 1971, **10**, 1921.
3. K. Wade, *Electron Deficient Compounds*. Nelson, London (1971).
4. For example, I. R. Epstein, J. A. Tossell, E. Switkes, R. M. Stevens and W. N. Lipscomb, *Inorg. Chem.* 1971, **10**, 171; D. S. Marynick and W. N. Lipscomb, *J. Am. Chem. Soc.* 1972, **94**, 8699.
5. For example, B. J. Gimarc and J. J. Ott, *Inorg. Chem.* 1986, **25**, 83 and refs therein; D. J. Wales and A. J. Stone, *Inorg. Chem.* 1987, **26**, 3845.
6. L. Radom, *Australian National Theoretical Chemistry Summer School* (1985).
7. S. M. Colwell and N. C. Handy, *J. Molec. Struct. (Theochem.)* 1988, **170**, 197.
8. W. J. Hehre, L. Radom, P. v. R. Schleyer and J. A. Pople, *Ab Initio Molecular Orbital Theory*, Ch. 4. Wiley Interscience, New York (1986).
9. M. O'Neill and K. Wade, *Polyhedron* 1984, **3**, 199.
10. R. E. Williams, *Adv. Inorg. Chem. Radiochem.* 1976, **18**, 67.

Polyhedron Vol. 9, No. 8, pp. 1045–1049, 1990
Printed in Great Britain

0277–5387/90 $3.00+.00
© 1990 Pergamon Press plc

SULPHURATING AND COORDINATING PROPERTIES OF N,N′-THIOBISMORPHOLINE TOWARDS IRON CARBONYLS

CARLOS DIAZ*

Departamento de Química, Facultad de Ciencias, Universidad de Chile, Casilla 653, Santiago, Chile

(*Received* 9 *October* 1989; *accepted* 30 *November* 1989)

Abstract—The reactions of N,N′-thiobismorpholine, $S(N\bigcirc O)_2$, with $Fe(CO)_5$, $Fe_2(CO)_9$, $Fe_3(CO)_{11}$ and $[(\eta^5\text{-}C_5H_5)Fe(CO)_2THF]BF_4$ were examined. Thiobismorpholine undergoes desulphurization towards $Fe(CO)_5$ with formation of $Fe_3(CO)_9S_2$, while the novel complex $Fe(CO)_4S(N\bigcirc O)_2$ was isolated and characterized from the reaction with $Fe_2(CO)_9$. On the other hand, thiobismorpholine is somewhat unreactive towards $Fe_3(CO)_{11}$ but it undergoes S—N fission with $[(\eta^5\text{-}C_5H_5)Fe(CO)_2THF]BF_4$.

N,N′-thiobisamines, $(R_2N)_2S$, are known to be quite unreactive compounds.[1] They react neither with water nor with alcohols, but in the presence of H^+, ion metals or Lewis acid, redox[2,3] and substitution processes occur.[4] The low reactivity of N,N′-thiobisamines has been frequently explained by the diminished nucleophilicity of the sulphur and nitrogen atoms, arising from double bond character in the S—N linkage.[5] In spite of the expected coordinative properties arising from the lone electron pairs on the sulphur and nitrogen atoms the only metal complexes with N,N′-thiobisamines as ligands reported are $[M(CO)_5S(NR_2)_2]$ (M = Cr, Mo, W).[6] As part of our investigation of the coordinative properties of S^{II}—N compounds,[6,7] we now report the reaction of N,N′-thiobismorpholine with iron pentacarbonyl, enneacarbonyldiirons and triiron dodecacarbonyl.

RESULTS AND DISCUSSION

Reaction of $(O\bigcirc N)_2S$ *with* $Fe(CO)_5$

When iron pentacarbonyl was irradiated (UV) with N,N′-thiobismorpholine in methanol for 3 h at room temperature, dark red needles were produced. This compound was identified by elemental analysis, IR and mass spectroscopy as $Fe_3S_2(CO)_9$.[8] Its IR spectra were identical with those reported in the literature.[8–10] The mass spectrum of this compound showed the parent ion and the fragments arising from stepwise loss of all the carbonyl groups. Peaks at *m/z* 176, 144 and 120, corresponding to $Fe_2S_2^+$, Fe_2S^+ and FeS_2^+ fragments, were also observed.

The sulphur-transfer behaviour of N,N′-thiobismorpholine toward iron pentacarbonyl is unexpected but not surprising in view of the desulphurization behaviour shown by other organic sulphides toward iron carbonyls.[9,10] Furthermore, the compound $Fe_3S_2(CO)_9$ is a common product in the reaction of iron carbonyls with sulphur compounds.[9–11]

Reaction of $(O\bigcirc N)_2S$ *with* $Fe_2(CO)_9$

Reaction of diiron nonacarbonyl with N,N′-thiobismorpholine in THF at room temperature proceeds smoothly according to

$$(O\bigcirc N)_2S + Fe_2(CO)_9 \longrightarrow Fe(CO)_4S(N\bigcirc O)_2 + Fe(CO)_5.$$

* Present address: Departamento de Quimica Organometalica, Universidad de Oviedo, 33071 Oviedo, Spain.

The tetracarbonyliron (N,N′-thiobismorpholine) complex is a brown–orange solid, unstable to air. The compound was fully characterized by analysis, mass spectrometry as well as by IR, ^{1}H NMR and Mössbauer spectroscopy.

The IR spectrum of the complex $Fe(CO)_4S(N\bigcirc O)_2$ showed four terminal carbonyl bands with frequency and intensity values similar to those found for $Fe(CO)_4L$ complexes, where L is a sulphur-donor ligand.[12,13] Data for $Fe(CO)_4S(N\bigcirc O)_2$ and other $Fe(CO)_4L$ complexes are shown in Table 1.

In $Fe(CO)_4L$ complexes the ligand L could occupy an axial or equatorial site of the locally trigonal-bipyramidal geometry at iron. Quantitative group theoretical arguments indicate that axially-substituted $Fe(CO)_4L$ complexes (C_{3v} symmetry) should exhibit three IR-active CO stretching frequencies ($2A_1+E$), while equatorially substituted compounds (C_{2v} symmetry) should exhibit four such bands ($2A_1+B_1+B_2$). However, structural assays based solely on IR data could be misleading because, as pointed out by Darensbourg *et al.*,[14] the E mode of axially-substituted $Fe(CO)_4L$ compounds is often split, thus yielding a total of four distinct ν(CO) bands. An X-ray study of $Fe(CO)_4$(1,3-dithiane)[15] shows that the sulphur ligand adopts an axial site in a trigonal-bipyramidal array at iron.

In the complexes $Fe(CO)_4L$, with L = pyridine, pyrazine,[16] triphenylphosphine,[17] trimethylarsine and trimethylstibine,[18] the ligand also occupies an axial position in a trigonal-bipyramidal array. Given the similarity of the ν(CO) IR data of compound $Fe(CO)_4S(N\bigcirc O)_2$ with those for $Fe(CO)_4$(1,3-dithiane) and the other $Fe(CO)_4L$ compounds of known structure, it is reasonable to assume the persistence of the C_{3v} skeletal geometry in the N,N′-thiobismorpholine complex.

The $\nu(S—N)_{as}$ band which in the free ligand is observed at 950 cm^{-1},[19] is lowered to 940 cm^{-1} in the complex by coordination effects. Similar ν(N—S) shifts are observed in the $M(CO)_5S(N\bigcirc O)_2$ complexes.[6]

The ^{1}H NMR spectra of the complex $Fe(CO)_4S(N\bigcirc O)_2$ shows the expected signals slightly shifted downfield due to the coordination.

Mass spectral data provide support for the structure of the complex $Fe(CO)_4S(N\bigcirc O)_2$. The m/z fragments corresponding to the molecular ion, ions showing successive loss of CO, $S(N\bigcirc O)_2^+$, as well as other fragments expected from the proposed structure, are observed. An interesting feature of the spectrum of the tetracarbonyl(thiobismorpholine)iron complex is the apparent loss of morpholine from the fragment $Fe(CO)_2S(N\bigcirc O)_2^+$ to give an intense ion of m/z 232 and formulated as $Fe(CO)_2S—N\bigcirc O^+$.

Table 1. IR spectra of axially-substituted $LFe(CO)_4$ complexes

Complex	ν(CO)[a] cm^{-1} (n-hexane)				Reference
	$A_1^{(2)}$	$A_1^{(1)}$	E		
$Fe(CO)_4S(N\bigcirc O)_2$	2050(5.3)	1972(8.6)	1948(9.6)	1935(10)	This work
$Fe(CO)_4$(1,3-dithiane)	2056(7.7)	1981(7.1)	1954(10)	1943(9.7)	12
$Fe(CO)_4$(2-Me_3Si-1,3-dithiane)	2054(7.2)	1975(7.0)	1952(10)	1937(9.4)	12
$Fe(CO)_4$(2-Me_3Pb-1,3-dithiane)	2051(6.8)	1974(6.9)	1948(9.0)	1936(10)	12
$Fe(CO)_4$(1,3-dithia-5-cycloheptene)	2056 s	1979 s	1963 vs	1943 vs	13
$Fe(CO)_4PPh_3$	2050(3.5)	1977(2.2)	1945(10)		14
$Fe(CO)_4NC_5H_5$	2042 s	1970 s	1943 vs		16
$Fe(CO)N_2C_4H_4$	2043 s	1975 s	1948 vs		16
$Fe(CO)_4AsPh_3$	2051 s	1977 s	1947 vs		18

[a] Intensities values in parentheses relative to the strongest band as 10, using a per cent transmission scale.

Confirmation of the trigonal-bipyramidal structure of the complex $Fe(CO)_4S(NC_4H_8O)_2$ arises from its ^{57}Fe Mössbauer spectrum which is shown in Fig. 1. The spectrum consists of a single quadrupole splitting. The large quadrupole splitting value QS = 3.1 mm s^{-1} is typical of $Fe(CO)_4L$ complexes with a trigonal-bipyramidal structure, QS = 2.3–2.9 mm s^{-1}.[20,21] This result discards a binuclear structure of the type $Fe_2(CO)_6L_2$ for which QS = 0.6–1.4 mm s^{-1}, the other possible product found in the reaction of iron carbonyl with sulphur ligands. The isomer shift value, IS = 0.23 mm s^{-1}, is characteristic of iron(0) carbonyl derivatives.[20,21] The increase in the IS values in going from $Fe(CO)_5$, QS = 2.5mm s^{-1}, to $Fe(CO)_4S(NC_4H_8O)_2$ can be interpreted as a descrease in the σ-donor ability of N,N″-thiobismorpholine with respect to carbon monoxide. This is consistent with the weak nucleophilic character of N,N′-thiobisamines concluded from the IR[22] and structural data studied.[23] The highest value of the QS parameter for the $Fe(CO)_4S(NC_4H_8O)_2$ complex compared with those of $(Me_3N)_3PFe(CO)_4$, QS = 2.22, $PPh_3Fe(CO)_4$, QS = 2.44, $Ph_3SbFe(CO)_4$, QS = 2.63, $Ph_3AsFe(CO)_4$, QS = 2.68 and (*o*-Me $C_6H_4)_3AsFe(CO)_4$, QS = 2.93 mm s^{-1},[20] indicates a weaker π-acceptor ability than the phosphine, arsine and stilbine ligands. This agrees with the weak π-acceptor ability of N,N′-thiobisamines suggested from IR data of the $M(CO)_5S(NR_2)_2$ complexes.[6] We also find that the IS and QS values for the complex $Fe(CO)_4S(NC_4H_8O)_2$ occur in the poor π-acceptor region of the Collins–Pettit graph.[24]

Stability of the $Fe(CO)_4S(NC_4H_8O)_2$ *complex*

Similar to other $Fe(CO)_4L$ complexes where L = sulphur-donor ligand,[13] the complex $Fe(CO)_4S(NC_4H_8O)_2$ is very unstable. Mass and Mössbauer spectroscopic data indicate that this complex decomposes on standing to a mixture of $Fe_3S_2(CO)_9$[8] and $S(NC_4H_8O)_2$. The difficulty of preparing $Fe(CO)_4L$ complexes with L = nitrogen-donor ligand has been mentioned previously.[16] On the other hand, few examples of tetracarbonyl iron complexes with sulphur-donor ligands are known.[12–15] Hence the synthesis of the tetracarbonyl(thiobismorpholine)iron complex is relevant from the point of view of Fe—S compounds as well as from the coordination properties of S—N compounds

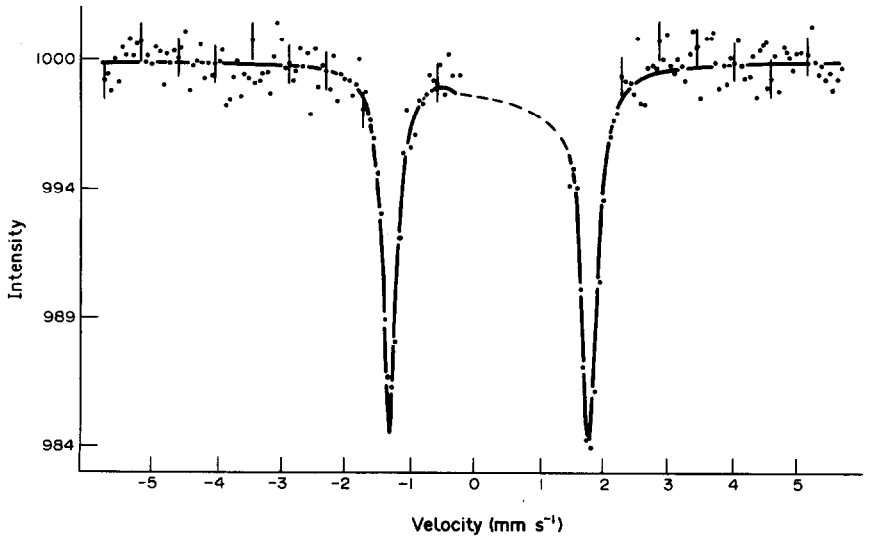

Fig. 1. The Mössbauer spectrum of $Fe(CO)_4S(NC_4H_8O)_2$. A small absorption (----) due to decomposition of the sample was subtracted (see text).

Reaction of S(N O)$_2$ *with* $Fe_3(CO)_{11}$

From the reaction of triiron dodecacarbonyl with thiobismorpholine in THF at 60°C, unchanged thiobismorpholine and a dark brown solid material were obtained. NMR spectroscopic examination of this product revealed the presence of thiobismorpholine and an unidentified carbonyl species. IR bands in the range 3600–3200 and at 2350 and 800 cm^{-1} [3] also suggest some S—N bond cleavage of the ligand.

Reaction of $[(\eta^5\text{-}C_5H_5)Fe(CO)_2THF]BF_4$ *with* S(N O)$_2$

From the reaction of (dicarbonyl)(η^5-cyclopentadienyl)(tetrahydrofuran)iron tetrafluoroborate[25] with thiobismorpholine a brown solid was isolated. Cleavage of the S—N linkage of the ligand is indicated by their IR spectrum which shows, among others, bands at 3410, 3290, 2040 and 1565 cm^{-1} typical of [O NH$_2$]X salts.[3] Similar behaviour leading to S—N cleavage has been reported in reactions of N,N′-thiobisamines with H^+ and with copper(II) salts.[2,3] Hence the S—N bond fission of thiobismorpholine in the presence of the $(\eta^5\text{-}C_5H_5)Fe(CO)_2THF^+$ cation, which is known to act as a Lewis organometallic acid,[26] is no surprise.

EXPERIMENTAL

Materials and general procedures

N,N′-thiobismorpholine[1] and $[(\eta^5\text{-}C_5H_5)Fe(CO)_2THF]BF_4$[25] were prepared according to literature methods. The iron carbonyls $Fe(CO)_5$ (Alfa), $Fe_2(CO)_9$ (Fluka) and $Fe_3(CO)_{11}$ (Fluka) were procured commercially and used without subsequent purifications. All solvents were carefully dried prior to use. All operations were performed under an inert atmosphere. Photochemical irradiation was carried out using a UV lamp, Hanau medium pressure, 150 W and a standard irradiation cell.

Spectroscopic measurements

IR spectra were obtained on a Perkin–Elmer 621 instrument. ^{1}H NMR spectra were measured on Varian T-60 apparatus. The mass spectra were determined on a Varian MAT 711 mass spectrometer at an ionizing voltage of 70 eV. The Mössbauer spectrum was determined using a constant acceleration drive system and the data were collected on a Canberra multichannel analyser. The source was ^{57}Co diffused in palladium and sodium nitroprusside was used as standard.

Reaction of S(N O)$_2$ *with* $Fe(CO)_5$

$Fe(CO)_5$ (4.37 g, 22.3 mmol) and S(N O)$_2$ (1.8 g, 8.8 mmol) in CH_3OH were irradiated for 3 h at room temperature. The solvent was then removed *in vacuo* and the residue chromatographed on a Florisil column and eluted with *n*-hexane. The resulting red solution was cooled to −20°C overnight to give dark red needles (0.5 g, 25% yield), m.p. 113–114°C (Refs 8, 9, 114°C). Found: C, 22.4. Calc. C, 22.3%. IR (*n*-hexane) 2060, 2045, 2024, 1985 cm^{-1}. Mass spectrum *m/z* 484 (M^+ 5%), 456 (M−CO) 428 (M−2CO) 400 (M−3CO), 372 (M−4CO), 344 (M−5CO) 316 (M−6CO), 288 (M−7CO), 260 (M−8CO) 232 (M−9CO), 176 (M−9CO−Fe), 144 (M−9CO−Fe−S).

Synthesis of $Fe(CO)_4$S(N O)$_2$

To $Fe(CO)_9$ (2.12 g, 5.82 mmol) was added a solution of S(N O)$_2$ (1.1 g, 5.4 mmol) in 50 cm^3 of THF. The mixture was stirred under a static argon atmosphere for 14 h and then solvent and $Fe(CO)_5$ were removed at room temperature *in vacuo*. The residue was extracted with *n*-hexane and after filtration the red–brown solution was cooled to −30°C overnight to give brown–orange solid (0.6 g, 30% yield), m.p. 69–70°C. Found: C, 38.9; H, 4.7; N, 7.9. Calc. for $C_{12}H_{16}O_6N_2SFe$: C, 38.7; H, 4.3; N, 7.5%. IR (*n*-hexane) 2050(s), 1972(s), 1948(vs), 1935(vs) cm^{-1}. NMR ($CDCl_3$) 3.66 (m, 4H, CH_2O), 3.33 ppm (m, 4H, CH_2N). Mass spectrum *m/z* 373 (M^+), 345 (M−CO), 316 (M−2CO), 232 (M−2CO−HN O) 176 (M−4CO−HN O).

Attempted reaction of $Fe_3(CO)_{11}$ *with* S(N O)$_2$

A solution of $Fe_3(CO)_{11}$ (1.15 g, 2.28 mmol) and

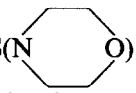
(0.60 g, 2.93 mmol) in THF were stirred at 60°C for 2 h, during which it assumed a red–brown colour. The solvent was removed under reduced pressure. The residue was dissolved in *n*-hexane and the solution filtered through Kieselguhr and cooled to −30°C overnight to give brownish-coloured crystals identified by IR and ^{1}H NMR as unreacted N,N′-thiobismorpholine (0.11 g). Following this the solution was evaporated to dryness to give a dark brown oil which solidified on standing. NMR ($CDCl_3$) 3.7 (m, 8H, OCH_2), 3.3 ppm (m, 8H, NCH_2). IR 3600–3200 (m, br), 3000 (m), 2350 (w), 2100–1850 (vs, br), 1600–1400 (m, br), 1260 (s), 1100 (vs), 1060 (vs), 1020 (vs), 920 (m), 800 (s).

Attempted reaction of $[(\eta^5\text{-}C_5H_5)Fe(CO)_2THF]BF_4$ *with* 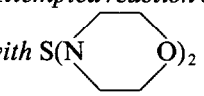

To a solution of $[(\eta^5\text{-}C_5H_5Fe(CO)_2THF]BF_4$[25] in CH_2Cl_2 (prepared from $\eta^5\text{-}C_5H_5Fe(CO)_2I$ and $AgBF_4$), was added 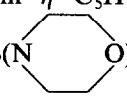 (1.1 g, 5.38 mmol) and stirred for 1 h. The reaction mixture changed from a red to brown–red colour. The resulting solution was evaporated *in vacuo* to dryness, and the solid redissolved in a mixture of *n*-hexane–CH_2Cl_2, filtered and cooled at −30°C. The brown solid residue was dried *in vacuo*. Found: C, 31.7; H, 4.1; N, 4.2. NMR [$(CD_3)_2CO$] 5.46 (s, 5M, C_5H_5), 3.91 (m, 6H), 3.43 (m, 10H). IR (KBr) 3410 (m), 3290 (m), 2420 (w), 2040 (vs), 1990 (vs), 1565 (m), 1430 (m), 1310 (m), 1150–1000 (vs, br), 905 (m), 890 (m), 880 (m), 873 (s), 610 (m, br).

Acknowledgements—I would like to thank Dr N. Yutronic and Dr R. Latorre for obtaining the mass and Mössbauer spectra.

REFERENCES

1. E. Thompson, *Q. Rep. Sulf. Chem.* 1970, **5**, 245.
2. C. Díaz, *Polyhedron* 1985, **4**, 1269.
3. C. Díaz, *Polyhedron* 1986, **5**, 655.
4. C. Díaz, S. Copaja and G. González, *Phosphorus Sulphur* 1985, **22**, 317.
5. G. González, M. A. Santa Ana and I. Chadwick, *J. Chem. Soc., Perkin Trans II* 1983, 1803.
6. C. Díaz and G. González, *Inorg. Chim. Acta* 1984, **85**, 61.
7. C. Díaz, *Sulfur Letts* 1989, **9**, 1.
8. W. Hieber and J. Gruber, *Z. Anorg. Allg. Chem.* 1958, **296**, 91.
9. N. S. Nametkin, V. D. Tyurin and M. A. Kukina, *J. Organomet. Chem.* 1978, **149**, 355.
10. A. J. Bard, A. M. Cowley, J. K. Leland, G. J. N. Thomas, N. C. Norman, P. Jutzi, C. P. Morley and F. Schluter, *J. Chem. Soc., Dalton Trans.* 1985, 1303.
11. R. B. King, *Inorg. Chem.* 1963, **2**, 326.
12. D. J. Cane, W. A. G. Graham and L. Vencea, *Can. J. Chem.* 1978, **56**, 1538.
13. A. Shaver, P. J. Fitzpatrick, K. Stelion and I. S. Butler, *J. Am. Chem. Soc.* 1979, **101**, 1313.
14. D. J. Darensbourg, H. H. Nelson and C. L. Hyde, *Inorg. Chem.* 1974, **13**, 2135.
15. F. A. Cotton, J. R. Kolb and B. R. Stults, *Inorg. Chim. Acta.* 1975, **15**, 239.
16. F. A. Cotton and J. M. Troup, *J. Am. Chem. Soc.* 1974, **96**, 3438.
17. P. E. Riley and R. E. Davis, *Inorg. Chem.* 1980, **19**, 159.
18. J. J. Legendre, C. Girard and M. Huber, *Bull. Soc. Chim. Fr.* 1971, 1998.
19. C. Díaz, E. Clavijo and G. González, *Spectrochimica Acta* 1983, **39A**, 537.
20. W. E. Carrol, F. A. Deeney, J. A. Delaney and F. J. Lalor, *J. Chem. Soc., Dalton Trans.* 1973, 719.
21. R. V. Parish, in *The Organic Chemistry of Iron* (Edited by E. A. Koerner von Gustorf, F. W. Grevels and I. Fischer), p. 175. Academic Press, New York (1978).
22. L. M. Epschtein, A. N. Zdanova, Y. A. Khazanova, M. S. Feldshtein and L. A. Kazitsyna, *Izv. Akad Nauk SSSR Ser. Khim.* 1974, 87.
23. C. Romming, G. O. Nevstad and O. Songtad, *Acta Chem. Scand.* 1982, **A36**, 393.
24. R. L. Collins and R. Pettit, *J. Chem. Phys.* 1963, **39**, 3433.
25. D. L. Reger and C. Coleman, *J. Organomet. Chem.* 1977, **131**, 153.
26. A. R. Cutler, P. K. Hanna and J. Vites, *Chem. Rev.* 1988, **88**, 1386.

Polyhedron Vol. 9, No. 8, pp. 1051–1058, 1990
Printed in Great Britain

0277–5387/90 $3.00+.00
© 1990 Pergamon Press plc

THE CYCLOMETALLATION OF 2,6-DIPHENYLPHENOXIDE (OAr-2,6Ph$_2$) LIGANDS AT NIOBIUM(V) AND TANTALUM(V) METAL CENTRES: THE SOLID STATE STRUCTURES OF THE MONOCYCLOMETALLATED COMPOUNDS Ta(OC$_6$H$_3$Ph-C$_6$H$_4$)(OAr-2,6Ph$_2$)$_2$(R) (R = CH$_3$, *n*-C$_4$H$_9$) AND Nb(OC$_6$H$_3$Ph-C$_6$H$_4$)(OAr-2,6Ph$_2$)$_2$(Cl)

ROBERT W. CHESNUT, JOYCE S. YU, PHILLIP E. FANWICK and IAN P. ROTHWELL*

Department of Chemistry, Purdue University, West Lafayette, IN 47907, U.S.A.

and

JOHN C. HUFFMAN

Department of Chemistry, Molecular Structure Center, Indiana University, Bloomington, IN 47405, U.S.A.

(*Received* 5 *September* 1989; *accepted* 20 *November* 1989)

Abstract—The dimethyl compounds M(OAr-2,6Ph$_2$)$_3$(CH$_3$)$_2$ (M = Nb, Ta; OAr-2,6Ph$_2$ = 2,6-diphenylphenoxide) undergo the thermal loss of methane in hydrocarbon solvents to generate the monocylometallated compounds M(OC$_6$H$_3$Ph-C$_6$H$_4$)(OAr-2,6Ph$_2$)$_2$(CH$_3$) (M = Nb, **1**; Ta, **2**). Kinetic studies show the reactions to be first-order with activation parameters $\Delta H^{\ddagger} = 25.3 \pm 0.8$ kcal mol^{-1} and $\Delta S^{\ddagger} = -15 \pm 5$ cal mol^{-1} K^{-1} for the tantalum compound. The use of the labelled compound Ta(OAr-2,6Ph$_2$)$_3$(CD$_3$)$_2$ shows no change in the rate of metallation and also the absence of a methylidene intermediate for the reaction. Attempts to generate a bis(*n*-butyl) compound by treatment of Ta(OAr-2,6Ph$_2$)$_3$Cl$_2$ with LiBu^n (2 equivs) led instead to the immediate formation of the metallated compound Ta(OC$_6$H$_3$Ph-C$_6$H$_4$)(OAr-2,6Ph$_2$)$_2$(Bu^n) (**3**) along with butane. Thermolysis of the bis(*p*-methylbenzyl) compound Ta(OAr-2,6Ph$_2$)$_3$(CH$_2$C$_6$H$_4$-4Me)$_2$ also leads to a monocyclometallated compound (**4**) and *p*-xylene. However, attempts to obtain a corresponding niobium bis(*p*-methylbenzyl) compound by treatment of Nb(OAr-2,6Ph$_2$)$_3$Cl$_2$ with Mg(CH$_2$C$_6$H$_4$-4Me)$_2$ led instead directly to the monocyclometallated derivatives Nb(OC$_6$H$_3$Ph-C$_6$H$_4$)(OAr-2,6Ph$_2$)$_2$(Cl) (**5**) and Nb(OC$_6$H$_3$Ph-C$_6$H$_4$)(OAr-2,6Ph$_2$)$_2$(CH$_2$C$_6$H$_4$-4Me) (**6**). Single-crystal X-ray diffraction studies of **2**, **3** and **5** show the molecules to be similar in the solid state. A trigonal bipyramidal environment about the metal atom is observed with *trans*,axial oxygen atoms. The new M—C(aryl) bond is chelated to an oxygen atom in one of the axial positions. Crystal data for TaC$_{64}$H$_{50}$O$_3$; **2**·3/2C$_6$H$_6$ at −155°C: $a = 13.497(3)$, $b = 17.033(6)$, $c = 10.744(2)$ Å, $\alpha = 94.76(1)$, $\beta = 96.34(1)$, $\gamma = 79.80(1)°$, $Z = 2$, $d_{calc} = 1.444$ g cm^{-3} in space group $P\bar{1}$; for TaC$_{64}$H$_{53}$O$_3$; **3**·C$_6$H$_6$ at −130°C: $a = 18.202(5)$, $b = 17.930(3)$, $c = 15.282(3)$ Å, $\beta = 96.05(2)°$, $Z = 4$, $d_{calc} = 1.408$ g cm^{-3} in space group $P2_1/c$; for NbC$_{54}$H$_{38}$ClO$_3$; **5** at 20°C: $a = 18.830(4)$, $b = 11.2856(9)$, $c = 20.725(5)$ Å, $\beta = 102.8(1)°$, $Z = 4$, $d_{calc} = 1.335$ g cm^{-1} in space group $P2_1/c$.

One of the most exciting recent developments in early transition metal organometallic chemistry has been the recognition that high valent, d^0-metal alkyl and related functional groups have the ability to intra- and intermolecularly activate carbon–hydrogen bonds under mild conditions.[1–6] A common

* Author to whom correspondence should be addressed.

feature of these reactions has been the need to carry out careful labelling studies in order to determine the actual pathway leading to C—H bond activation.[1-6] During our studies of the early transition metal chemistry associated with sterically bulky aryloxide ligation we have characterized a number of reactions involving the cyclometallation of 2,6-di-*tert*-butylphenoxide ligands.[7] A series of mechanistic studies of the reaction at tantalum(V) has shown that these reactions may proceed via indirect and sometimes competing reaction pathways.[8,9] More recent work has focussed on the related cyclometallation chemistry of 2,6-diphenylphenoxide ligands at various *p*- and *d*-block metal centres.[10,11] In this paper we wish to report on the cyclometallation of this ligand at niobium(V) and tantalum(V) metal centres, focussing on the mechanistic aspects of the reactivity as well as the structure of the metallated products.

$$M(OAr)_3(CH_3)_2 \longrightarrow M(OC_6H_3Ph{-}C_6H_4)(OAr)_2(CH_3) + CH_4$$

M = Nb (1); Ta (2)

OAr = 2,6-diphenylphenoxide

Scheme 1.

RESULTS AND DISCUSSION

The dimethyl compounds $M(OAr\text{-}2,6Ph_2)_3(CH_3)_2$ (M = Nb, Ta; OAr-2,6Ph$_2$ = 2,6-diphenylphenoxide) can be readily obtained in high yield from the corresponding dichloride.[12] Thermolysis of the alkyl compounds in hydrocarbon solvents at temperatures above 120°C leads to the formation of corresponding monocyclometallated compounds, **1** and **2**, and one equivalent of methane (Scheme 1). The reactions can be readily monitored in toluene-d_8 solution in sealed 5 mm NMR tubes by ^{1}H NMR spectroscopy. Although the aromatic region of the spectra is rather uninformative, the sharp M—CH_3 resonance of the dimethyl compound at δ +0.18 (Nb) and −0.21 ppm (Ta) is replaced by a new methyl resonance of **1** and **2** at δ −0.05 and −0.39 ppm, respectively, along with a corresponding peak for methane. In the ^{13}C NMR spectra of **1** and **2** highly characteristic resonances at δ 190.9 (Nb) and 199.9 ppm (Ta) can be assigned to the M—*C*(*ipso*) carbon atom of the new metallacycle ring. A single-crystal X-ray analysis of **2** confirms the stoichiometry of the compound as well as its mononuclearity (Fig. 1). Some selected bond distances and angles are collected in Table 1. The environment about the metal atom in **2** can best be described as trigonal bipyramidal with two axial oxygen atoms. The oxygen atom of the six-membered metallacycle ring occupies one of the axial sites while the new Ta–C bond lies in an equatorial position leading to a chelate bite at the metal of 80.8(2)°. As with other six-membered metallacycle rings formed by cyclometallation of aryloxide ligands, this small bite angle is readily accommodated with little puckering of the six-membered ring due to the large Ta—O—C angle, in this case 141.4(4)°.[7] The Ta—O distances of 1.883(4)–1.909(4) Å and Ta—C distances of 2.125(7) (alkyl) and 2.215(5) Å (aryl) are well within the range reported for related aryloxyl alkyl or aryl derivatives of tantalum(V).[13] The overall structure of **1** bears a close resemblance to that found for the monocyclometallated compound $Ta(OC_6H_3Bu^tCMe_2CH_2)(OAr\text{-}2,6Bu^t_2)(Ph)_2$ (OAr-2,6Bu$^t_2$ = 2,6-di-*tert*-butylphenoxide).[9]

A kinetic study of the formation of **2** was carried out by monitoring changes in the ^{1}H NMR spectrum in toluene-d_8 solution upon heating. The ring closure reaction was found to obey first-order kinetics over 3–4 half-lives yielding the following rate constants $10^5 k/s^{-1}$ at various temperatures (T/°C): 4.15(120); 10.1(130); 9.75(130); 18.0(139); 50.0 (151). These data yield activation parameters for the reaction of $\Delta H^{\ddagger} = 25.3(8)$ kcal mol^{-1} and

Table 1. Selected bond distances (Å) and angles (°) for $Ta(OC_6H_3Ph\text{-}C_6H_4)(OAr\text{-}2,6Ph)_2(CH_3)$ (**2**)

Ta—O(3)	1.909(4)	Ta—O(2)	1.883(4)
Ta—O(41)	1.899(4)	Ta—C(2)	2.125(2)
Ta—C(21)	2.215(5)		
O(3)—Ta—O(22)	92.6(2)	O(3)—Ta—O(41)	168.9(2)
O(3)—Ta—C(2)	87.3(2)	O(3)—Ta—C(21)	80.9(2)
O(22)—Ta—O(41)	98.0(2)	O(22)—Ta—C(2)	109.7(2)
O(22)—Ta—Cl(2)	131.2(2)	O(41)—Ta—C(2)	92.0(2)
O(41)—Ta—C(21)	89.7(2)	C(2)—Ta—C(21)	118.1(2)
Ta—O(3)—C(4)	141.4(4)	Ta—O(22)—C(23)	146.6(4)
Ta—O(41)—C(42)	169.5(4)		

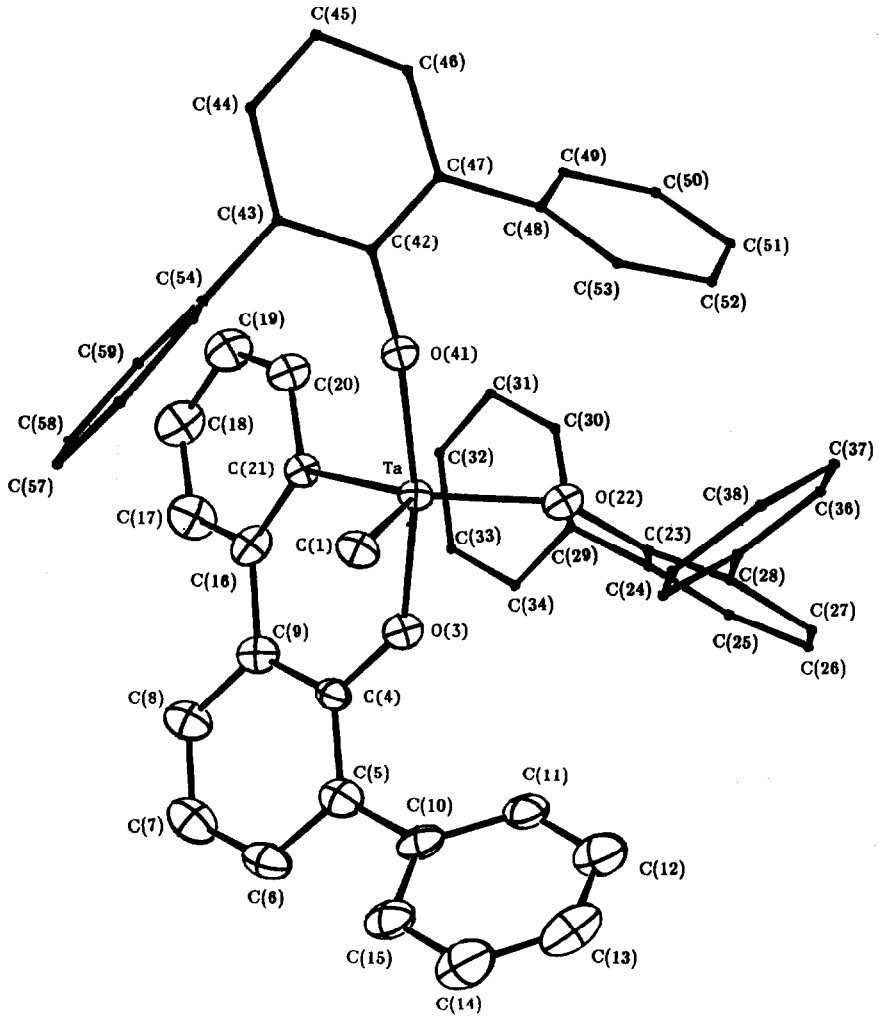

Fig. 1. ORTEP view of Ta(OC$_6$H$_3$Ph-C$_6$H$_4$)(OAr-2,6Ph$_2$)$_2$(CH$_3$) (**2**) emphasizing the central coordination sphere.

$\Delta S^{\ddagger} = -15(5)$ cal mol^{-1} K^{-1} (Fig. 2). The moderately large and negative entropy of activation for the reaction compares favourably with the other values reported for related reactions and appears to be a consistent characteristic of such cyclometallation reactions.[7]

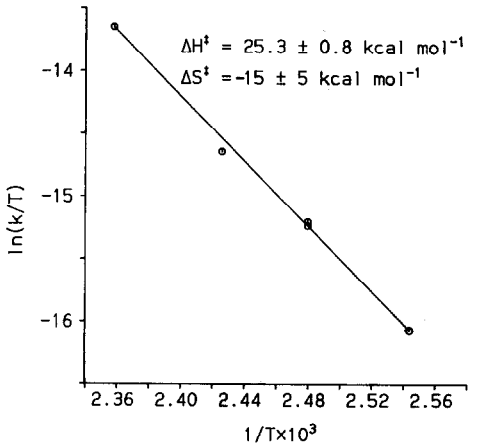

Fig. 2. Activated complex theory plot for the formation of **2** from Ta(OAr-2,6Ph$_2$)$_3$(CH$_3$)$_2$.

An important aspect of high-valent early transition metal alkyl chemistry is the possible formation of stable or intermediate alkylidene functional groups by α-hydrogen abstraction processes.[5,8,14,15] It is possible that the formation of **2** from Ta(OAr-2,6Ph$_2$)$_3$(CH$_3$)$_2$ proceeds via initial formation of a methylidene intermediate, [Ta(OAr-2,6Ph$_2$)$_3$(=CH$_2$)], which then undergoes rapid addition of the aromatic C—H bond to the tantalum methylide double bond to generate the product. This pathway has to be taken seriously given the fact that alkylidene compounds of the type Ta(OAr)$_2$(X)(=CHR) (X = OAr, CH$_2$R) have been isolated[13,16] and that a photogenerated tantalum methylidene intermediate was found to rapidly activate the aliphatic C—H bonds of OAr-2,6Bu$^t_2$ ligands.[8,17] In order to check this possibility

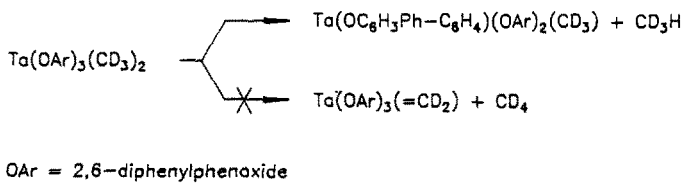

Scheme 2.

the compound $Ta(OAr\text{-}2,6Ph_2)_3(CD_3)_2$ was synthesized by reacting the dichloride with $LiCD_3$. Thermolysis of this compound in toluene was found to yield the monocyclometallated compound **2**. Analysis of this product by mass spectrometry clearly indicated the presence of only **2**-d_3. A simulation of the mass spectrum indicated < 5% of **2**-d_2, i.e. containing $TaCHD_2$, to be present. Hence, thermolysis of the labelled compound leads to loss of CD_3H and formation of only **1**-d_3. No loss of CD_4 to generate an intermediate $[Ta(OAr\text{-}2,6Ph_2)_3(=CD_2)]$ was detected in this experiment. Hence, it appears that the methyl leaving group in these reactions combines directly with the hydrogen of the aromatic C—H bond to yield the product **2** (Scheme 2). On the basis of work by many groups this process is believed to occur via a four-centre, four-electron transition state.[1–7]

Attempts to isolate a bis-*n*-butyl compound by treatment of $Ta(OAr\text{-}2,6Ph_2)_3Cl_2$ with Bu^{n}Li (2 equivs) led instead to the isolation of the monocyclometallated compound $Ta(OC_6H_4Ph\text{-}C_6H_4)(OAr\text{-}2,6Ph_2)_2(Bu^n)$ (**3**) in moderate yields. The dark brown reaction mixture contained numerous other unidentified components. Pale yellow crystals of **3** could be obtained from the reaction mixture by slow cooling of toluene solutions. The ^{13}C NMR spectrum of **3** clearly shows the Ta—*C*(*ipso*) resonance at δ 199.3 ppm along with the four non-equivalent Ta—$CH_2CH_2CH_2CH_3$ resonances. However, the ^1H NMR spectrum of **3** appears very complicated in the aliphatic region. In particular, a series of overlapping multiplets are observed in the δ −0.5 to +1.0 ppm region. This complexity of the Bu^n resonances can be explained by the molecular structure of **3** which lacks a plane of symmetry through the Ta—Bu^n bond, hence making all of the three methylene groups diastereotopic.

A solid-state structural analysis of **3** by single-

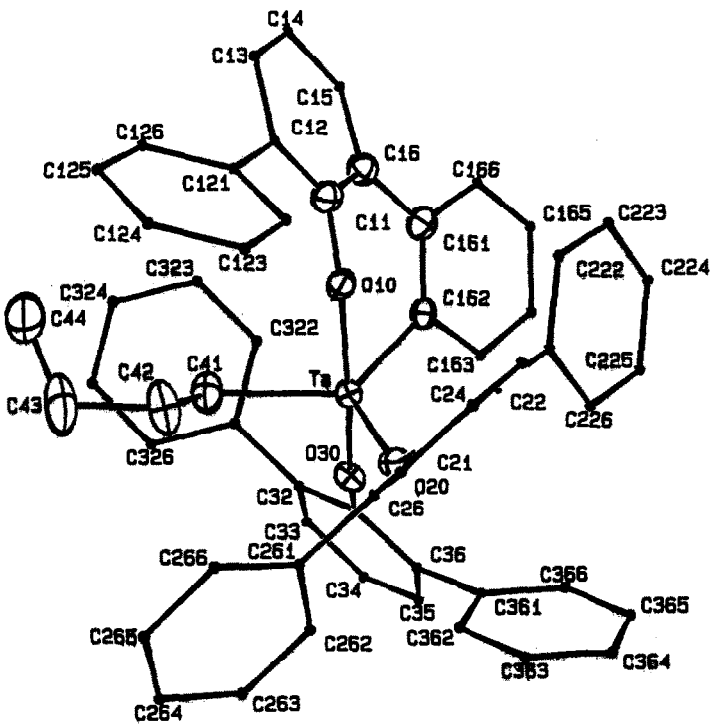

Fig. 3. ORTEP view of $Ta(OC_6H_3Ph\text{-}C_6H_4)(OAr\text{-}2,6Ph_2)_2(Bu^n)$ (**3**).

Table 2. Selected bond distances (Å) and angles (°) for Ta(OC$_6$H$_3$Ph-C$_6$H$_4$)(OAr-2,6Ph$_2$)$_2$(Bu^n) (3)

Ta—O(10)	1.913(3)	Ta—O(20)	1.910(3)
Ta—O(30)	1.890(3)	Ta—C(41)	2.149(4)
Ta—C(162)	2.182(4)		
O(10)—Ta—O(20)	95.6(1)	O(10)—Ta—O(30)	164.5(1)
O(10)—Ta—C(41)	85.6(1)	O(10)—Ta—C(162)	81.4(1)
O(20)—Ta—O(30)	99.6(1)	O(20)—Ta—C(41)	110.9(2)
O(20)—Ta—C(162)	125.4(1)	O(30)—Ta—C(41)	91.9(2)
O(30)—Ta—C(162)	87.2(1)	C(41)—Ta—C(162)	123.0(2)
Ta—O(10)—C(11)	136.5(3)	Ta—O(20)—C(21)	136.9(3)
Ta—O(30)—C(31)	160.7(3)		

crystal X-ray diffraction methods shows a molecular geometry almost identical to that of **2** (Fig. 3). Some selected bond distances and angles are collected in Table 2.

Treatment of the dichloride Ta(OAr-2,6Ph$_2$)$_3$Cl$_2$ with Mg(CH$_2$C$_6$H$_4$-4Me)$_2$ (where CH$_2$C$_6$H$_4$-4Me = 4-methylbenzyl) allows the isolation of the corresponding dialkyl compound in high yield.[12] Thermolysis of this compound at 120°C also leads to the formation of a monocyclometallated compound Ta(OC$_6$H$_3$Ph-C$_6$H$_4$)(OAr-2,6Ph$_2$)$_2$(CH$_2$C$_6$H$_4$-4Me) (**4**) along with one equivalent of *p*-xylene. In contrast, treatment of Nb(OAr-2,6Ph$_2$)$_3$Cl$_2$ with Mg(CH$_2$C$_6$H$_4$-4Me)$_2$ is found to initially yield the monocyclometallated chloro compound Nb(OC$_6$H$_3$Ph-C$_6$H$_4$)(OAr-2,6-Ph$_2$)$_2$(Cl) (**5**), which then undergoes further reaction to produce the *p*-methylbenzyl compound (**6**) (Scheme 3). Compounds **1**, **5** and **6** are of interest as they represent the first reported examples of cyclometallated aryloxide compounds of niobium. A single-crystal X-ray diffraction study of **5** was carried out for comparison with the related tantalum compounds (Fig. 4). Some selected bond distances and angles are collected in Table 3. Again a geometry about the central metal atom is found in **5** that is extremely close to those observed for **2** and **3**. In fact a comparison of the overall geometries of **2**, **3** and **5**, as well as the conformations adopted by the non-

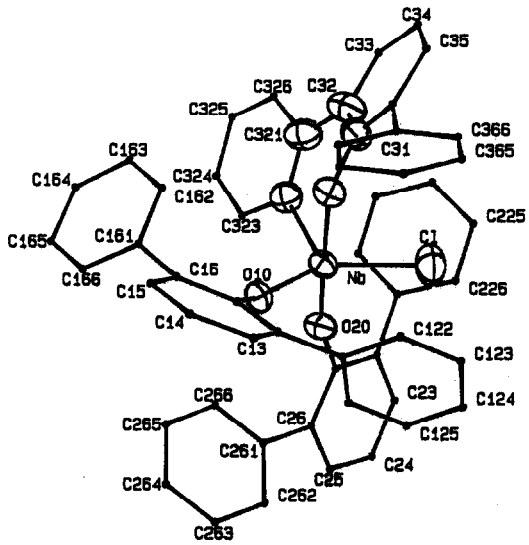

Fig. 4. ORTEP view of Nb(OC$_6$H$_3$Ph-C$_6$H$_4$)(OAr-2,6Ph$_2$)$_2$(Cl) (**5**).

metallated OAr-2,6Ph$_2$ ligands, shows a close similarity (Figs 1, 3 and 4).

Although variable-temperature analyses of the kinetics of the ring closure reactions of Nb(OAr-2,6Ph$_2$)$_3$(CH$_3$)$_2$ and Ta(OAr-2,6Ph$_2$)$_3$(CH$_2$C$_6$H$_4$-4Me)$_2$ were not carried out, first-order kinetics were found to be obeyed for the disappearance of both compounds at 120°C. Hence the following three half lives for the cyclometallation reactions are

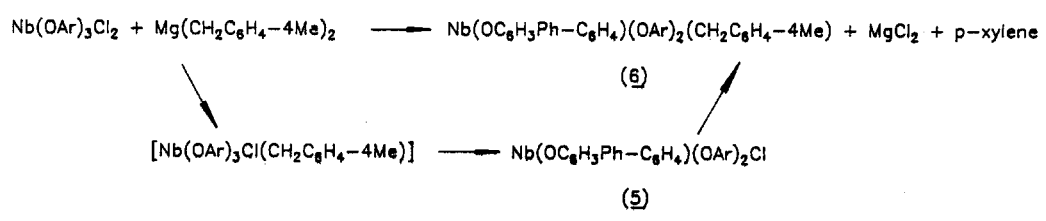

Scheme 3.

Table 3. Selected bond distances (Å) and angles (°) for $Nb(OC_6H_3Ph\text{-}C_6H_4)(OAr\text{-}2,6Ph_2)_2(Cl)$ (**5**)

Nb—Cl	2.316(1)	Nb—O(20)	1.898(3)
Nb—O(10)	1.872(3)	Nb—O(30)	1.918(3)
Nb—C(322)	2.122(5)		
Cl—Nb—O(10)	136.8(1)	Cl—Nb—O(20)	91.3(1)
Cl—Nb—O(30)	86.4(1)	Cl—Nb—C(322)	113.0(1)
O(10)—Nb—O(20)	96.7(1)	O(10)—Nb—O(30)	89.4(1)
O(10)—Nb—C(322)	108.8(2)	O(20)—Nb—O(30)	173.1(1)
O(20)—Nb—C(322)	93.5(2)	O(30)—Nb—C(322)	81.4(2)
Nb—O(10)—C(11)	141.5(3)	Nb—O(20)—C(21)	163.9(3)
Nb—O(30)—C(31)	131.1(3)		

available for comparison:

Compound	Half-life (min at 120°C)
$Nb(OAr\text{-}2,6Ph_2)_3Me_2$	22(2)
$Ta(OAr\text{-}2,6Ph_2)_3Me_2$	280(20)
$Ta(OAr\text{-}2,6Ph_2)_3(CH_2C_6H_4\text{-}4Me)_2$	65(5)

Hence it can be seen that cyclometallation occurs much faster at niobium than at tantalum for the same set of ligands. The difference in rates between the two metals, more than an order of magnitude, is much more pronounced than that observed for the cyclometallation of 2,6-di-*tert*-butylphenoxide ligands at titanium and zirconium. In that study a rate difference of only three (Ti > Zr) was found.[7,18] It can also be seen from the data that benzyl ligands are superior leaving groups to methyl ligands at tantalum. This difference in the rate may be attributable to the fact that early *d*-block metal bonds to benzyl ligands have been consistently found to be weaker than corresponding metal–methyl bonds.[19] Furthermore, this and related observations[7,9] may explain why treatment of $Nb(OAr\text{-}2,6Ph_2)_3Cl_2$ with $Mg(CH_2C_6H_4\text{-}4Me)_2$ leads to monocyclometallated **5** (Scheme 3). This reaction will initially produce the mono(benzyl) compound $Nb(OAr\text{-}2,6Ph_2)_3(CH_2C_6H_4\text{-}4Me)(Cl)$. Presumably cyclometallation occurs rapidly in this compound before further substitution can take place. The fact that the niobium bis(methyl) and tantalum bis(benzyl) compounds are isolable must be due to the slower rates of cyclometallation. A very similar situation was found for the reaction of $Ta(OAr\text{-}2,6Bu^t_2)_2Cl_3$ with LiPh, where rapid formation of a monocyclometallated compound $Ta(OC_6H_3Bu^tCMe_2CH_2)(OAr\text{-}2,6Bu^t_2)Cl_2$ was followed by the formation of corresponding phenyl derivatives.[9]

EXPERIMENTAL

All operations were carried out either under a dry nitrogen atmosphere or *in vacuo* using a Vacuum Atmosphere Dri-Lab or by standard Schlenck techniques. Hydrocarbon solvents were dried by distillation from sodium benzophenone and stored under DRY nitrogen. The compounds $M(OAr\text{-}2,6Ph_2)_3Cl_2$, and $M(OAr\text{-}2,6Ph_2)_3(CH_3)_2$ (M = Nb, Ta) were prepared by reported procedures.[12]

$Nb(OC_6H_3Ph\text{-}C_6H_4)(OAr\text{-}2,6Ph_2)_2(CH_3)$ (1)

A solution of $Nb(OAr)_3(CH_3)_2$ (0.20 g) dissolved in toluene (5 cm^3) was heated at 120°C for 2 h in a closed flask. Cooling and removal of solvent under vacuum yielded the product as a yellow powder. Yield = 0.18 g (90%). ^1H NMR (C_6D_6, 30°C): δ 6.60–7.85 (aromatics), −0.05 (s, Nb—CH_3). ^{13}C NMR (C_6D_6, 30°C): δ 190.9 (Nb—*C*), 62.0 (Nb—*C*H_3). Found: C, 78.4; H, 5.0. Calc. for $NbC_{55}H_{41}O_3$: C, 78.4; H, 4.9%.

$Ta(OC_6H_3Ph\text{-}C_6H_4)(OAr\text{-}2,6Ph_2)_2(CH_3)$ (2)

A solution of $Ta(OAr)_3(CH_3)_2$ (0.25 g) in toluene (5 cm^3) was heated for 7 h at 120°C in a closed flask. Removal of solvent under vacuum yielded the product as a pale white powder. The crude product was dissolved in a minimum amount of benzene. Slow evaporation of the benzene solvent inside the Dri-lab yielded colourless crystals of the product suitable for X-ray analysis. Yield = 0.24 g (87%). ^1H NMR (C_6D_6, 30°C): δ 7.74, 6.90 d, 7.4–6.4 (aromatics), −0.39 (s, Ta—CH_3). ^{13}C NMR (C_6D_6, 30°C): δ 199.9 (Ta—*C*), 64.3 (*C*H_3). Found: C, 72.8; H, 5.3. Calc. for $TaC_{65}H_{50}O_3$: C, 73.4; H, 4.8%.

$Ta(OC_6H_3Ph\text{-}C_6H_4)(OAr\text{-}2,6Ph_2)_2(Bu^n)$ (3)

To a solution of 20 g (2.0 mmol) of $Ta(OAr)_3Cl_2$ dissolved in 10 cm^3 of benzene was added, 2.0 cm^3 of a 2.2 M *n*-BuLi solution in hexane over 10 min. The mixture was cooled with an ice bath throughout

the *n*-BuLi addition. The reaction mixture was stirred for 40 min before being warmed to room temperature. A white precipitate that formed during stirring was filtered off, and the solvent was evaporated from the filtrate. The resulting crude solid was redissolved in a minimum amount of benzene, and crystals of product slowly formed over 24 h. Yield = 0.55 g (28.3%). Additional product could be obtained by concentrating the supernatant. ^{1}H NMR (C_6D_6, 30°C): δ 7.87 d, 7.82 d, 7.73 d, 7.35–6.20 (aromatics), 1.35 to −0.50 (m, Ta—C_4H_9). ^{13}C NMR: δ 199.3 (Ta—*C*), 87.3, 31.3, 28.8, 13.6 (Ta—C_4H_9). Found: C, 72.5; H, 4.9. Calc. for $TaC_{64}H_{53}O_3$ **3**·C_6H_6: C, 73.1; H, 5.1%.

Ta(OC$_6$H$_3$Ph - C$_6$H$_4$)(OAr - 2,6Ph$_2$)$_2$(CH$_2$C$_6$H$_4$ - 4Me) (**4**)

A solution of 0.25 g of Ta(OAr)$_3$(CH$_2$C$_6$H$_4$Me)$_2$ dissolved in toluene (5 cm^3) was heated at 120°C for 6 h in a sealed tube. The solvent was evaporated *in vacuo* to yield the crude product as a yellow solid. ^{1}H NMR (C_6D_6, 30°C): δ 0.71 (d), 2.39 (d, Ta—CH_2), 5.51 (d), 6.38 (d), 6.5–8.4 (m, aromatics). ^{13}C NMR (C_6D_6, 30°C): δ 200.7 (Ta—*C*), 86.6 (Ta—CH_2), 2.16 (4*Me*). Found: C, 72.0; H, 4.7. Calc. for $TaC_{62}H_{47}O_3$: C; 72.9; H, 4.6%.

Nb(OC$_6$H$_3$Ph-C$_6$H$_4$)(OAr-2,6Ph$_2$)$_2$(Cl) (**5**)

To a solution of Nb(OAr-2,6Ph$_2$)$_3$Cl$_2$ (1.50 g) in benzene (15 cm^3) was added Mg(CH$_2$C$_6$H$_4$-4Me)$_2$ (0.14 g) in small portions. The resulting mixture was stirred for 1 h, filtered and the deep red filtrate concentrated, whereupon deep-red crystals of the product were obtained. Yield = 1.1 g (78%). Found: C, 74.1; H, 4.6; Cl, 4.8. Calc. for $NbClO_3C_{54}H_{38}$: C, 75.1; H, 4.4; Cl, 4.1%. ^{1}H NMR (C_6D_6, 30°C): δ 6.6–7.8 (m, aromatics). ^{13}C NMR (C_6D_6, 30°C): δ 192.1 (Nb—*C*).

Nb(OC$_6$H$_3$Ph - C$_6$H$_4$)(OAr - 2,6Ph$_2$)$_2$(CH$_2$C$_6$H$_4$ - 4Me) (**6**)

To a solution of **5** (0.30 g) in benzene (15 cm^3) was added Mg(CH$_2$C$_6$H$_4$-4Me)$_2$ (0.05 g). The solution was stirred for 4 h, filtered and concentrated to yield

Table 4. Crystal data and data collection parameters

Compound	**2**	**3**	**4**
Formula	$TaC_{64}H_{50}O_3$	$TaO_3C_{64}H_{53}$	$NbClO_3C_{54}H_{38}$
fw	1048.05	1051.08	863.26
Space group	$P\bar{1}$	$P2_1c$ (No. 14)	$P2_1/c$ (No. 14)
a (Å)	13.497(3)	18.202(5)	18.830(4)
b (Å)	17.033(6)	17.930(3)	11.2856(9)
c (Å)	10.744(2)	15.282(3)	20.725(5)
β (°)	96.34(1)	96.05(2)	102.81(1)
V (Å^3)	2411.01	4959(3)	4294(2)
Z	2	4	4
d_{calc} (g cm^{-3})	1.444	1.408	1.335
Crystal size (mm)	0.15 × 0.15 × 0.18	0.60 × 0.45 × 0.28	0.49 × 0.45 × 0.44
Temperature (°C)	−155	−130	20
Radiation	Mo-K_α	Mo-K_α 22.35	Mo-K_α
Linear absorption coefficient (cm^{-1})	22.979	22.35	3.72
Monochromator	Graphite	Graphite	Graphite
Scan method	ω–2θ	ω–2θ	ω–2θ
h, *k*, *l* limits:	0 to 14, −17 to 18, −11 to 10	0 to 16, 0 to 19, −19 to 19	−20 to 19, 0 to 12, 0 to 22
2θ range (°)	6.00–45.00	4.00–45.00	4.00–45.00
Scan width (°)	2.0	0.42 + 0.35 tan (θ)	0.50 + 0.35 tan (θ)
Take-off angle (°)	2.0	1.90	2.30
Data collected	7429	6711	5958
Unique data	6354	6711	5958
Data with $I > 3.0\sigma(I)$	5659	5391	3502
Largest shift/ESD in final	0.05	0.00	0.00
R	0.0355	0.027	0.038
R_w	0.0356	0.038	0.045
Goodness-of-fit	0.840	1.232	1.246

the product as a fine yellow powder. ^{1}H NMR (C_6D_6, 30°C): δ 1.21 (d), 2.65 (d, Nb—CH_2); 5.62 (d), 6.35 (d), 6.6–8.0 (m, aromatics), 1.84 (s, 4-*Me*). ^{13}C NMR (C_6D_6, 30°C): δ 193.9 (Nb—*C*); 84.3 (Nb—CH_2).

X-ray crystallography

The X-ray diffraction analysis of **2** was carried out at the Indiana University Molecular Structure Center while those of **3** and **5** were obtained through the Purdue University Chemistry Department Facility. Crystal data and data collection parameters are gathered in Table 4. A more detailed account of the data collection and refinement is collected in the supplementary material.

Acknowledgements—We thank the National Science Foundation (Grant CHE 8612063) for support of this research. NSF support for the Chemistry Crystallographic Unit at Purdue is also gratefully acknowledged.

REFERENCES

1. I. P. Rothwell, in *Activation and Functionalization of Alkanes* (Edited by L. Hill), Ch. V. John Wiley, New York (1989).
2. M. E. Thompson, S. M. Baster, A. R. Bulls, B. J. Burger, M. C. Nolan, B. D. Santarsiero, W. R. Schaefer and J. E. Bercaw, *J. Am. Chem. Soc.* 1987, **108**, 203.
3. P. L. Watson and G. W. Parshall, *Accts Chem. Res.* 1985, **18**, 51 and refs therein.
4. J. W. Bruno, G. M. Smith, T. J. Marks, C. K. Fair, A. J. Schultz and J. M. Williams, *J. Am. Chem. Soc.* 1986, **108**, 40 and refs therein.
5. A. R. Bulls, W. P. Schaefer, M. Serfas and J. E. Bercaw, *Organometallics* 1987, **6**, 1219.
6. W. J. Evans, L. R. Chamberlain, T. A. Ulibarri and J. W. Ziller, *J. Am. Chem. Soc.* 1988, **110**, 6423.
7. I. P. Rothwell, *Accts Chem. Res.* 1988, **27**, 153.
8. L. R. Chamberlain, I. P. Rothwell and J. C. Huffman, *J. Am. Chem. Soc.* 1986, **108**, 1502.
9. L. R. Chamberlain, J. L. Kerschner, A. P. Rothwell, I. P. Rothwell and J. C. Huffman, *J. Am. Chem. Soc.* 1987, **109**, 6471.
10. R. W. Chesnut, B. D. Steffey, I. P. Rothwell and J. C. Huffman, *Polyhedron* 1988, **7**, 753.
11. G. D. Smith, P. E. Fanwick and I. P. Rothwell, *J. Am. Chem. Soc.* 1989, **111**, 750.
12. R. W. Chesnut, L. D. Durfee, P. E. Fanwick, I. P. Rothwell, K. Folting and J. C. Huffman, *Polyhedron* 1987, **6**, 2019.
13. (a) L. R. Chamberlain, I. P. Rothwell, K. Folting and J. C. Huffman, *J. Chem. Soc., Dalton Trans.* 1987, 155; (b) J. S. Yu, R. W. Chesnut and I. P. Rothwell, *Organometallics*, submitted.
14. R. R. Schrock, in *Reactions of Coordinated Ligands* (Edited by P. S. Bratermann). Plenum Press, New York (1968).
15. R. R. Schrock, *Accts Chem. Res.* 1979, **12**, 98.
16. M. R. Churchill, J. W. Ziller, J. H. Freudenberger and R. R. Schrock, *Organometallics* 1984, **3**, 1554.
17. C. McDade, J. C. Green and J. E. Bercaw, *Organometallics* 1982, **1**, 1629.
18. S. L. Latesky, A. K. McMullen, I. P. Rothwell and J. C. Huffman, *J. Am. Chem. Soc.* 1985, **107**, 5981.
19. J. Halpern, *Accts Chem. Res.* 1982, **15**, 238 and refs therein.

Polyhedron Vol. 9, No. 8, pp. 1059–1063, 1990
Printed in Great Britain

0277–5387/90 $3.00+.00
© 1990 Pergamon Press plc

CORRELATIONS OF CARBONYL STRETCHING FREQUENCIES AND ^{31}P AND ^{95}Mo NMR PARAMETERS FOR *FAC*-[$Mo(CO)_3(bipy)(PR_3)$] COMPLEXES

ELMER C. ALYEA,* ROBERT A. GOSSAGE, JOHN MALITO and ZURAIDAH A. MUNIR

Department of Chemistry and Biochemistry, University of Guelph, Guelph, Ontario N1G 2W1, Canada

(*Received* 11 *September* 1989; *accepted* 4 *December* 1989)

Abstract—Several complexes of the type [$Mo(CO)_3(bipy)(PR_3)$] [where bipy = 2,2′-dipyridine, R = *n*-Bu, Me, *p*-C_6H_4-X; X = F, Cl, H, CH_3, OCH_3, $N(CH_3)_2$] were synthesized and characterized by ^{31}P NMR, ^{95}Mo NMR and IR spectroscopy. Relationships are drawn between the bonding nature of the ligands and the ^{95}Mo and ^{31}P NMR chemical shifts and the $\nu(C{\equiv}O)$ values. Correlations of $\delta(^{95}Mo)$, $\Delta\delta(^{31}P)$ and $\nu(C{\equiv}O)$ to various parameters such as ligand pK_a, ligand cone angle (Θ), and the Kabachnik parameter ($\Sigma\sigma^{\phi}$) are discussed and indicate the interrelationship of the donor abilities of C≡O, dipy and the phosphine ligands. The importance of steric effects in influencing net metal electron density is demonstrated by the results.

IR data for the carbonyl region has been central to studies of the structural and electronic properties of transition metal carbonyl complexes for almost three decades.[1] Carbonyl stretching force constants were among the first parameters used to relate the σ-donor and π-acceptor ability of ligands in metal carbonyl complexes.[2] With the advent of Fourier transform NMR techniques, however, the bonding properties of ligands containing carbon (e.g. C≡O) or phosphorus [e.g. $P(C_6H_5)_3$] could be easily observed directly in terms of the NMR chemical shift.[3] Metal–ligand NMR coupling constants between the NMR active nuclei in the ligand (e.g. ^{31}P) and an NMR active nucleus of the central metal atom (e.g. ^{183}W) have also been widely employed to study metal–ligand interactions, especially for phosphorus donor ligands.[4] Metal–phosphorus bond properties are of great fundamental importance due to the widespread use of phosphorus-containing ligands in metal complexes used in various catalytic processes.[5]

The development of routine metal NMR spectroscopy has recently provided a direct probe of the metal environment[6] and enables one to observe metal–phosphorus coupling constants of metal nuclei which are difficult to observe via ^{31}P NMR spectroscopy (e.g. ^{95}Mo).[7] Studies in our laboratory over the past few years have centred on probing the effects of a number of ligand systems on the molybdenum metal centre in diamagnetic molybdenum metal complexes via ^{95}Mo NMR spectroscopy. ^{95}Mo NMR spectroscopy is well established as a sensitive probe of the molybdenum metal atom in several oxidation states.[8] Our studies on molybdenum(0) carbonyl complexes have shown the chemical shift range for $Mo(CO)_5L$ (L = P, As, Sb or N donating ligand) to exceed 400 ppm[9] and to exceed 800 ppm for $Mo(CO)_4L_2$ complexes.[10] Our recent study on $Mo(CO)_5L$ complexes (L = substituted pyridine ligands) have shown a direct correlation between the σ-bonding ability, as portrayed by the pK_a of the pyridine ligands, and the ^{95}Mo NMR chemical shift [$\delta(^{95}Mo)$] over a range of almost 70 ppm.[11] In contrast, $\delta(^{95}Mo)$ values were surprisingly similar for some [$Mo(CO)_5(p$-X-$C_6H_4)_3P$] complexes involving phosphines of varying basicity.[9] To investigate these effects further we have chosen the system $Mo(CO)_3(bipy)L$ (where bipy = 2,2′-bipyridine and L = various phosphine donor ligands). By systematically changing L, we hoped to probe the nature of the bonding between a d^6 metal centre in a low valent oxidation state, and carbon monoxide, a bidentate α-diimine ligand and various phos-

* Author to whom correspondence should be addressed.

phorus donor ligands. The reasons for choosing this system involve the fundamental importance of CO, α-diimine and phosphine ligands to coordination, catalytic and electrochemical chemical processes.[12,13] The ability of several commonly accepted parameters (e.g. cone angle (Θ), χ electronic parameter, pK_a, Kabachnik's $\Sigma\sigma^{\phi}$ values, etc.) in quantitatively describing the nature of metal–phosphorus bonding was also the subject of critical scrutiny[14] during this investigation.

EXPERIMENTAL

All reactions and manipulations were carried out under a dry oxygen-free dinitrogen atmosphere. The solvents used were all reagent grade. $Mo(CO)_6$, PMe_3, 2,2′-bipyridine, PBu_3 and trimethylamine oxide dihydrate (TMNO) were purchased from Aldrich Chemical Co. PPh_3 was purchased from Pressure Chemical Co. Tetrabutylammonium iodide (Bu_4NI) was purchased from Fisher Scientific Co. P(*p*-Me-C_6H_4)$_3$, P(*p*-N(CH_3)$_2$-C_6H_4)$_3$, P(*p*-F-C_6H_4)$_3$ and P(*p*-Cl-C_6H_4)$_3$ were acquired from Strem Chemical Co. and P(*p*-OCH_3-C_6H_4)$_3$ was bought from Columbia Organic Co. Inc. All were used without further purification. NMR measurements were performed in septum-capped 10 mm NMR tubes on freshly prepared samples at room temperature (23 ± 2°C). ^{31}P NMR spectra were recorded in CH_3CN solutions on a Bruker WH-400 spectrometer operating at 161.92 MHz. Chemical shifts are reported as positive to high frequency of external 85% phosphoric acid. ^{95}Mo NMR spectra were recorded on the same instrument or on a Bruker CXP-200 NMR spectrometer, operating at 26.08 or 13.04 MHz, respectively, from naturally abundant ^{95}Mo using saturated CH_3CN solutions. Chemical shifts are relative to external aqueous 2 M K_2MoO_4 at pH 11. Duplicate ^{95}Mo results were obtained at both operating fields, so field effects are termed to be negligible for this series. IR spectra were recorded on a Nicolet 20 DXC FT–IR spectrometer from CH_2Cl_2 solutions in 0.5 mm NaCl solution cells and are accurate to ±0.5 cm^{-1}. $Mo(CO)_4$bipy was prepared by a published method.[15] In a typical synthesis, 0.3 g of $Mo(CO)_4$ bipy in 20 cm^3 CH_3CN was heated to reflux for 15 min with an equimolar quantity of TMNO[16] or a catalytic amount of Bu_4NI and an equimolar quantity of the desired phosphine ligand. As the PPh_3 derivative of this series is known,[17] the species studied were not isolated but observed entirely *in situ* using at least duplicate repetitions. Note that although the reactions were carried out in CH_3CN, at no time was [$Mo(CO)_3$(bipy)(CH_3CN)] observed by IR spectroscopy, so it is assumed to be a short-lived intermediate in the decarbonylation–phosphine addition process.[18] The complexes synthesized are all the thermodynamically stable facial isomers as indicated by their IR spectra.[2]

RESULTS AND DISCUSSION

The ^{31}P NMR and reference data for the free phosphines and complexes appear in Table 1. For the complexes, the carbonyl stretching frequencies and the ^{95}Mo NMR data appear in Table 2. Several trends can be seen. First, the value of the CO stretching frequency representative of the A_1 mode does not greatly change throughout the series. In fact, any electronic differences between P(*p*-Me-C_6H_4)$_3$ and P(*p*-OCH_3-C_6H_4)$_3$ are not resolved by the A_1 mode. The sum of all CO stretching vibrations [$\Sigma\sigma$(CO)] may, in fact, be a better reflection of the net effect on the CO ligands of varying the phosphine.

Relationships between the measured values for ν(C≡O), $\Delta\delta(^{31}P)$ and $\delta(^{95}Mo)$ run from good to excellent within the series. The $\Delta\delta(^{31}P)$ values relate to the $\delta(^{95}Mo)$ values (correlation coefficient $r = 0.902$) and to the changes in the $\Sigma\nu$(C≡O) values ($r = 0.992$). In turn, the $\Sigma\nu$(C≡O) values relate well to the $\delta(^{95}Mo)$ values ($r = 0.962$). This trend is expected when the steric bulk of the phosphorus ligand remains constant,[21] as is the case here.

The $\Delta\delta(^{31}P)$ chemical shift values show a general decrease with increasing ligand substituent electron-donating ability, indicating less net electron donation by the phosphine with increasing ligand Brönsted basicity. This trend has also been observed for other molybdenum(0) carbonyl complexes.[22(a)] Electron density around the molybdenum atom, as indicated by $\delta(^{95}Mo)$, is not greatly affected by the changes in the electronic

Table 1. Data for P(X-C_6H_4)$_3$ phosphines and *fac*-[$Mo(CO)_3$(bipy){P(*p*-C_6H_4-X)$_3$}] complexes

X	$\delta(^{31}P)$ (ppm)[a]	pK_a[a]	$\Sigma\sigma^{\phi}$[b]	$\delta(^{31}P)$ (ppm)[c]	$\Delta(\delta^{31}P)$[d]
Cl	−8.7	1.03	−0.87	37.0	45.7
F	−9.3	1.97	−0.96	35.9	45.2
H	−6.3	2.73	−1.77	37.5	43.8
CH_3	−8.3	3.84	−2.16	35.2	43.5
OCH_3	−10.6	4.59	−2.22	33.1	43.5
$N(CH_3)_2$	−11.7	8.65	−3.51	30.3	42.0

[a] Free ligand values, ref. 19.
[b] Reference 20.
[c] Complex values, in CH_3CN solution.
[d] $\Delta(\delta^{31}P) = \delta(^{31}P)_{complex} - \delta(^{31}P)_{free\ ligand}$.

Table 2. IR spectral data of carbonyl region and ^{95}Mo NMR data of [Mo(CO)$_3$(bipy){P(*p*-C$_6$H$_4$-X)$_3$}] complexes

X	ν(C≡O) (cm^{-1})[a]	Σ[ν(CO)]	δ(^{95}Mo) (ppm)[b]	J_{Mo-P} (Hz)	$\Delta\nu_{1/2}$ (Hz)
Cl	1920, 1825, 1792	5537	−1061.1	127	51
F	1918, 1826, 1791	5535	−1060.0	132	30
H	1915, 1816, 1791, 1913, 1820, 1792,[c] 1919, 1822, 1789[d]	5522	−1062.8	127	18
CH_3	1913, 1815, 1788	5516	−1063.8	128	32
OCH_3	1913, 1814, 1787	5514	−1063.0	127	61
$N(CH_3)_2$	1908, 1806, 1783	5497	−1065.5	129	43

[a] In CH_2Cl_2 solution.
[b] In CH_3CN solution.
[c] Reference 17(a), in $C_2H_4Cl_2$ solution.
[d] Reference 17(b), in $CHCl_3$ solution.

properties of the phosphine since the δ(^{95}Mo) values span a range of only about 6 ppm. This slight shift is not adequately explained by plotting δ(^{95}Mo) vs the phosphine ligand pK_a (Table 1) (correlation coefficient (r) is only 0.880) nor by the Tolman χ_i value (r = 0.908).[13] This lends support to two conceptual ideas, one of which we discuss here, while the other has been discussed previously.[23] Firstly, the lack of good correlation with Tolman's χ_i values lends support to our idea that $\Sigma\nu$(CO) is a better reflection of the effect of the nature of PR$_3$ then the A_1 stretching mode is alone, since χ_i values are based solely on the A_1 stretching mode of various Ni(CO)$_3$L (L = phosphorus ligands) complexes.[13] Secondly, the lack of correlation with the measured value of the ligand's pK_a supports the argument that pK_a values are not an appropriate measure of the interaction between phosphines and soft acid species such as low-valent transition metal centres.[23] The justification here lies in the fact that pK_a values are dependent on the interaction between the phosphine and the hard acid, H^+. An acceptable correlation (r = 0.957) is found between δ(^{95}Mo) and the Kabachnik $\Sigma\sigma^\phi$ parameter (Fig. 1), indicating that $\Sigma\sigma^\phi$ may be the better experimental parameter for this type of series. The Kabachnik substituent parameters,[20] derived from ionization data of phosphorus acids using a Hammett-type relationship, have been noted by other workers[13,19] to be good measures of electronic effects for phosphines. The Mo—P coupling constants are basically uniform throughout the series indicating that molybdenum–phosphorus σ-bonding character is essentially the same throughout the series. Since the phosphines must be donating different amounts of electron density in total, as measured by $\Delta(\delta^{31}P)$,

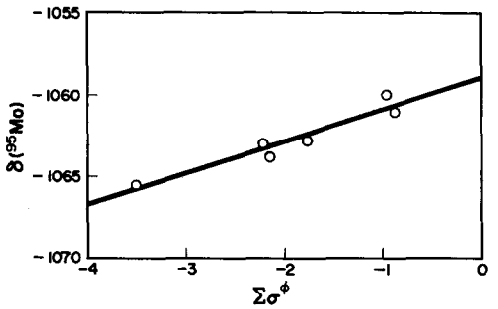

Fig. 1. Plot of δ(^{95}Mo) vs $\Sigma\sigma^\phi$ for [Mo(CO)$_3$(bipy){P(X-C$_6$H$_4$)$_3$}] complexes.

the other ligands present in the system must be serving in some way to compensate for the difference. A plot of $\Sigma\sigma^\phi$ vs $\Sigma\nu$(CO) yields an excellent correlation (r = 0.998) (Fig. 2), indicating that the electronic differences of the phosphines are adequately measured by summing the CO stretching frequency vibrations. This trend has been observed previously for a series of Mo(CO)$_5$(py-R)

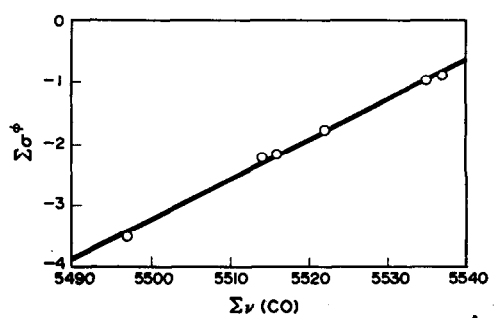

Fig. 2. Plot of $\Sigma\sigma^\phi$ vs $\Sigma\nu$(CO) for [Mo(CO)$_3$(bipy){P(X-C$_6$H$_4$)$_3$}] complexes.

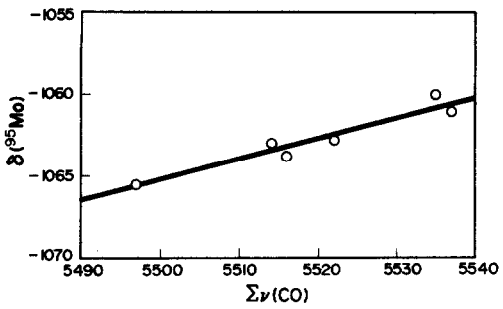

Fig. 3. Plot of $\delta(^{95}Mo)$ vs $\Sigma\nu(CO)$ for $[Mo(CO)_3(bipy)\{P(X\text{-}C_6H_4)_3\}]$ complexes.

(py-R = substituted pyridine ligand) complexes.[24] The $\delta(^{95}Mo)$ value is directly affected by the different electronic nature of $P(p\text{-}X\text{-}C_6H_4)_3$ and this trend is also reflected by the net change on the CO ligands (Fig. 3), but phosphorus σ-donor character is not significantly changed. This result tends to indicate that the CO ligands are responsible for compensating for the lesser or greater donating ability of $P(p\text{-}X\text{-}C_6H_4)_3$ compared to PPh_3. The effect of the bidentate α-diimine ligand, 2,2′-bipyridine, is likely uniform within this series since $\Sigma\sigma^{\phi}$ relates directly to $\Sigma\nu(CO)$. The general compensation of overall metal electron density by CO regardless of X in $P(p\text{-}X\text{-}C_6H_4)_3$ has the possibility of steric hindrance as its basis. The bulkiness of PPh_3 ($\Theta = 145°$),[13] compared to many other phosphine ligands, may not allow the phosphine to get close enough to the molybdenum centre for its full electronic character to greatly influence the metal's electron sphere. To test if this was indeed the case, we synthesized two other complexes $[Mo(CO)_3(bipy)(PMe_3)]$ and $[Mo(CO)_3(bipy)(PBu_3)]$, where the ligand PR_3 had a smaller steric size than PPh_3 but electronic capabilities, measured by $\Sigma\sigma^{\phi}$, within the same range.

The PBu_3 complex [ν(CO): 1908, 1806, 1784 cm^{-1}; $\delta(^{31}P)$: +3.70, $\Delta\delta(^{31}P) = 34.0$ ppm; $\delta(^{95}Mo) = -1071.2$ ppm, $^1J_{MoP} = 125$ Hz] produces a more pronounced effect on the molybdenum centre, shielding it by a further 5.7 ppm over the $P(p\text{-}NMe_2\text{-}C_6H_4)_3$ complex. PBu_3 is producing virtually the same net electronic effect on the CO ligands ($\Sigma\nu(CO) = 5498$) as compared to $P(p\text{-}NMe_2\text{-}C_6H_4)_3$ ($\Sigma\nu(CO) = 5497$) which is not unexpected since the $\Sigma\sigma^{\phi}$ values for these two ligands, −3.66 and −3.51,[20] respectively, are very similar. The further effects of PBu_3 over the PPh_3 derivatives in shielding the metal centre may therefore be a result of the smaller steric size of PBu_3 ($\Theta = 132°$) over PPh_3. This allows PBu_3 to move closer to the metal centre and hence produce stronger overall molybdenum shielding. This is also seen with the PMe_3 complex [ν(CO): 1910, 1810, 1785 cm^{-1}; $\delta(^{31}P)$: −15.2, $\Delta\delta^{31}P = 45.8$ ppm; $\delta(^{95}Mo) = -1076.8$ ppm, $^1J_{MoP} = 130$ Hz]. The poorer electron donor PMe_3 ($\Sigma\sigma^{\phi} = -2.88$ vs −3.66 for PBu_3), still puts considerably more electron density on the metal centre than does PPh_3 [$\delta(^{95}Mo) = -1062.8$ ppm, $\Sigma\sigma^{\phi} = -1.77$].

Thus, the CO ligands appear to restabilize net metal electron density only to some maximum extent, dictated not only by phosphine electronic but by steric properties. Only when the phosphine is small enough to get close to the metal centre can its electronic capabilities be seen to truly influence net metal electron density to a significant extent. This "push–pull" mechanism between phosphine σ-donor ability and steric ligand bulk is of great fundamental importance since it will greatly influence the design of metal catalytic molecules. The relative importance of steric vs electronic effects on molybdenum(0) carbonyl complexes has also been demonstrated in several earlier NMR studies by Gray and others.[21,22]

An interesting anomaly in this series is the fact that $P(p\text{-}OCH_3\text{-}C_6H_4)_3$ shields the molybdenum nucleus to a lesser extent than $P(p\text{-}CH_3\text{-}C_6H_4)_3$. This observation is also seen for the $Mo(CO)_5PR_3$ complexes,[9] although the shielding difference in that case is a more pronounced one. The reason for this is currently unclear, since steric effects in both cases are obviously uniform. It does indicate, however, that various groups may be less able to affect the metal nucleus than their $\Sigma\sigma^{\phi}$ (or pK_a) values would indicate. This dictates caution in describing metal electron density based solely on measured parameters of the free ligands only.

Our attempts to correlate relative shielding of the molybdenum metal nucleus to the Mo—P bond length have proved ineffective. The Mo—P bond lengths for $Mo(CO)_5PPh_3$ and $[Mo(CO)_5P(p\text{-}CH_3\text{-}C_6H_4)_3]$ are virtually identical, being 2.560 and 2.562 Å, respectively,[25,26] but $\delta(^{95}Mo)$ values differ by 7 ppm,[9] similar to the difference between $[Mo(CO)_3(bipy)\{P(p\text{-}CH_3O\text{-}C_6H_4)_3\}]$ and $[Mo(CO)_3(bipy)(PBu_3)]$. This similarity of bond lengths was noted in the recent related study of several iron(II) phosphine complexes where bond lengths and σ-donor/π-acceptor ability of the phosphine ligands do not appear to correlate.[14(a)]

Our results also show one other important factor. Giering and co-workers state in their discussion of the relative bonding ability of phosphine ligands that: "Undoubtedly, the terminal carbonyl stretching frequencies {of their $[(\eta^5\text{-}C_5H_5)Fe(CO)(COCH_3)(PR_3)]$ complexes} are directly dependent on the electron density of the metal to which the CO is bonded".[14(a)] However, we have clearly

shown, by comparing the $\delta(^{95}Mo)$ values of $[Mo(CO)_3(bipy)(PBu_3)]$ and $[Mo(CO)_3(bipy)\{P(p\text{-}NMe_2\text{-}C_6H_4)_3\}]$, both of which have virtually identical CO stretching frequencies, that their statement is not universally valid. Thus, the best probe of metal electron density is not by observation of the surrounding ligands but by observing the metal centre itself.

Related ^{95}Mo NMR studies currently underway in our laboratory are centred around further probing the nature of the effects of phosphines and phosphites on molybdenum environments.

Acknowledgements—We thank the Southwestern Ontario NMR Centre and W. P. Klimstra for assistance in operating the Bruker WH-400 spectrometer and NSERC Canada for continuing financial support to E.C.A.

REFERENCES

1. L. E. Orgel, *Inorg. Chem.* 1962, **1**, 25.
2. C. Kraihanzel and F. A. Cotton, *J. Am. Chem. Soc.* 1962, **84**, 4432.
3. For example: (a) G. M. Bodner, *Inorg. Chem.* 1975, **14**, 2694; (b) R. Mathieu, M. Lenzi and R. Poilblanc, *Inorg. Chem.* 1970, **9**, 2030; (c) S. O. Grim, R. M. Singer, A. W. Johnson and F. J. Randall, *Coord. Chem.* 1978, **8**, 121.
4. (a) S. O. Grim, D. A. Wheatland and W. McFarlane, *J. Am. Chem. Soc.* 1967, **89**, 5573; (b) G. G. Mather, A. Pidcock and G. J. N. Rapsey, *J. Chem. Soc., Dalton Trans.* 1973, 2095.
5. For example: (a) W. W. Porterfield, *Inorganic Chemistry*, Ch. 13. Addison-Wesley, Don Mills, Ontario (1984); (b) E. C. Alyea and D. W. Meek (Eds), *Catalytic Aspects of Metal Phosphine Complexes.* Advances in Chemistry Series **196**, American Chemical Society, Washington, D.C. (1982); (c) L. H. Pignolet (Ed.), *Homogeneous Catalysis with Metal Phosphine Complexes.* Plenum Press, New York (1983).
6. (a) J. J. Dechter, *Prog. Inorg. Chem.* 1985, **33**, 393; (b) J. B. Lambert and F. G. Riddell (Eds), *The Multinuclear Approach to NMR Spectroscopy.* Reidel Publishing Company, Dordrecht (1983); (c) J. Mason, *Chem. Rev.* 1987, **87**, 1299.
7. A. F. Masters, G. E. Bossard, T. A. George, R. T. C. Brownlee, M. J. O'Connor and A. G. Wedd, *Inorg. Chem.* 1983, **22**, 908.
8. M. Minelli, J. H. Enemark, R. T. C. Brownlee, M. J. O'Connor and A. G. Wedd, *Coord. Chem. Rev.* 1985, **68**, 169.
9. E. C. Alyea and A. Somogyvari, *Transition Met. Chem.* 1987, **12**, 310.
10. E. C. Alyea and A. Somogyvari, *Can. J. Chem.* 1988, **66**, 397.
11. E. C. Alyea, K. J. Fisher and R. A. Gossage, *Spectrochim. Acta* 1989, **45A**, 203.
12. M. S. Wrighton (Ed.), *Inorganic and Organometallic Photochemistry.* Advances in Chemistry Series **168**, American Chemical Society, Washington, D.C. (1978).
13. C. A. Tolman, *Chem. Rev.* 1977, 77, 313 and refs therein.
14. (a) M. M. Rahman, H. Y. Liu, K. Eriks, A. Prock and W. P. Giering, *Organometallics* 1989, **8**, 1; (b) M. M. Rahman, H. Y. Liu, A. Prock and W. P. Giering, *Organometallics* 1987, **6**, 650; (c) M. N. Golovin, M. M. Rahman, J. E. Belmonte and W. P. Giering, *Organometallics* 1985, **4**, 1981.
15. E. W. Abel, G. Bennett and G. Wilkinson, *J. Chem. Soc.* 1959, 2323.
16. T. S. A. Hor, *Inorg. Chim. Acta* 1988, **149**, 169.
17. (a) M. H. B. Stiddard, *J. Chem. Soc.* 1963, 756; (b) L. W. Houk and G. R. Dobson, *J. Chem. Soc. A* 1966, 317.
18. L. W. Houk and G. R. Dobson, *Inorg. Chem.* 1966, **5**, 2119.
19. T. Allman and R. Goel, *Can. J. Chem.* 1982, **60**, 716.
20. T. A. Mastryukova and M. I. Kabachnik, *Russ. Chem. Rev.* 1969, **38**, 795.
21. (a) G. M. Gray, *Inorg. Chim. Acta* 1984, **81**, 157; (b) G. M. Gray, R. J. Gray and D. C. Berndt, *J. Mag. Reson.* 1984, **57**, 347.
22. (a) G. M. Gray and R. J. Gray, *Organometallics* 1983, **2**, 1026; (b) G. M. Gray and C. S. Kraihanzel, *Inorg. Chem.* 1983, **22**, 2959; (c) A. M. Bond, S. W. Carr and R. Colton, *Organometallics* 1984, **3**, 541.
23. W. H. Thompson and C. T. Sears Jr, *Inorg. Chem.* 1977, **16**, 769.
24. H. O. Desseyn, B. J. van der Veken, J. R. Moss, B. J. Smith, P. Verhoeven and D. A. Thornton, *Spectrochim. Acta* 1984, **40A**, 467.
25. F. A. Cotton, D. J. Darensbourg and W. H. Ilsley, *Inorg. Chem.* 1981, **20**, 578.
26. E. C. Alyea, G. Ferguson and A. Somogyvari, *Organometallics* 1983, **2**, 668.

Polyhedron Vol. 9, No. 8, pp. 1065–1070, 1990
Printed in Great Britain

0277–5387/90 $3.00+.00
© 1990 Pergamon Press plc

SYNTHETIC, MAGNETIC AND SPECTRAL STUDIES OF IRON(III) COMPLEXES OF THIOHYDRAZIDES AND THIOHYDRAZONES

NAND K. SINGH, USHA SHARMA and SEEMA AGRAWAL

Department of Chemistry, Banaras Hindu University, Varanasi-221005, India

and

MICHEL J. M. CAMPBELL*

School of Chemistry, Thames Polytechnic, Wellington Street, London SE18 6PF, U.K.

(*Received* 20 *July* 1989; *accepted* 4 *December* 1989)

Abstract—2-Furanthiocarboxyhydrazide (Hfth), salicylaldehyde-2-furanthiocarboxyhydrazone (H_2L) and N-salicyl-N′-2-furanthiocarboxyhydrazine (H_2sfth) form complexes of the composition $[Fe(Hfth)_2Cl_2]Cl$, $Fe(fth)_3$, $[Fe(H_2sfth)_2Cl_2]Cl$, $Fe(HL)Cl_2$ and Fe(HL)L, which have been characterized on the basis of their elemental analyses, magnetic susceptibility, Mössbauer, UV–vis and IR spectral studies. The compounds $[Fe(Hfth)_2Cl_2]Cl$, $[Fe(H_2sfth)_2Cl_2]Cl$ and $Fe(fth)_3$ are all octahedral with coordination through sulphur and nitrogen. The compound $[Fe(H_2sfth)_2Cl_2]Cl$ exists in spin isomeric forms, $S = 5/2$ and $S = 1/2$, at room temperature as well as at liquid nitrogen temperature. The compound $Fe(HL)Cl_2$ is high-spin tetrahedral while the compound Fe(HL)L is low-spin octahedral.

Complexes of a number of metal ions with the condensation products of pyridine-2-carboxaldehyde and both S- and N-substituted dithiocarbazates have been reported.[1,2] These ligands react with iron to form a variety of high- and low-spin complexes of both iron(II) and iron(III)[2–4] and are potentially tridentate with an NNS donor atom set.

The basic SN chelate ring is similar to that of the thiosemicarbazide moiety, $=NNHCSNH_2$, which coordinates in most cases via the hydrazinic nitrogen and the sulphur to give a five-membered chelate ring. Thiosemicarbazones have long been known to constitute a class of compounds with a wide range of pharmacological activity which is thought to be connected to their chelation of trace metal ions.[5]

The iron(III) complexes of some α-N-heterocyclic carboxaldehyde thiosemicarbazones have recently been receiving attention in chelation therapy. A number of such thiosemicarbazones have strong antineoplastic activity,[6] while others show antimalarial action.[7] The role of chelation by metal ions in the mechanism of the action of such compounds has been discussed both by French and co-workers[8] and by Petering and co-workers.[9] Some iron(II) complexes of 5-substituted 2-formylpyridine and 1-formyl isoquinoline thiosemicarbazones are cytotoxic to tumour cells both *in vivo* and *in vitro*.[10–12]

Similarly, complexes of 2-formylpyridine thiosemicarbazone with iron(II) and other metal(II) ions have significant antitumour activity against Erhlich ascytes carcinoma and L1210 leukemia in mice.[13,14]

It is a logical extension of this work to prepare thiohydrazide and thiohydrazone complexes and to investigate their activity since they contain the same basic chelate ring =NNHCS— as thiosemicarbazones. We have previously reported the synthesis and properties of a few of these compounds[15–17] and now wish to report the synthesis and spectral properties of some iron(III) complexes of 2-furanthiocarboxyhydrazide (Hfth), salicylaldehyde-2-furanthiocarboxyhydrazide (H_2sfth) and N-salicyl-N′-2-furanthiocarboxyhydrazine (HL) (see Fig. 1).

* Author to whom correspondence should be addressed.

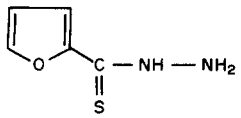

2– Furanthiocarboxyhydrazide (Hfth)

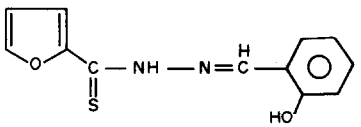

Salicylaldehyde — 2 — furanthiocarboxyhydrazone (H_2L)

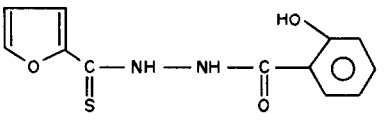

N – salicyl – N'–2–furanthiocarboxyhydrazine (H_2sfth)

Fig. 1. Structures of ligands.

EXPERIMENTAL

All the chemicals used were BDH or reagents of similar quality. The ligands were prepared as previously described.[15–17]

The compound $[Fe(Hfth)_2Cl_2]Cl$ was obtained by mixing chloroform solutions of anhydrous iron(III) chloride and the ligand in a 1:2 ratio at room temperature and with constant stirring. The compound $[Fe(fth)_3]$ was prepared by digesting a mixture of an ethanolic solution of ferric chloride and the ligand in a 1:3 molar ratio together with *ca* 1 g of sodium acetate. The precipitate was filtered and washed with a hot ethanol–water mixture.

The compound $[Fe(H_2Sfth)_2Cl_2]Cl$ was obtained by refluxing a chloroform solution of anhydrous iron(III) chloride with a suspension of H_2sfth in the same solvent, in a 1:2 molar ratio, for about 3 h. The complex $Fe(HL)Cl_2$ was prepared by mixing chloroform solutions of anhydrous iron(III) chloride and HL in a 1:1 molar ratio at room temperature. Stirring ethanolic solutions of iron(III) chloride and HL at room temperature for about 15 min, on the other hand, gave Fe(HL)L on evaporation of the solvent at room temperature.

The complexes were analysed for iron using a standard procedure[18] after first destroying the organic ligand with a mixture of nitric and hydrochloric acids followed by sulphuric acid. Sulphur was determined as $BaSO_4$. Carbon, hydrogen and nitrogen were determined by microanalysis using a Perkin–Elmer Analyser model 240C. The analytical data are shown in Table 1.

Electrical conductance was measured at room temperature on a WTW conductivity meter. Room temperature magnetic susceptibility was determined by the Faraday method using $HgCo(NCS)_4$ as calibrant and molar susceptibilities were corrected for diamagnetism.[19] The electronic reflectance spectra were recorded at room temperature on either a Cary 14 or a Perkin–Elmer model 330. The IR spectra were recorded on a Perkin–Elmer model 783. The Mössbauer spectra were measured using a Cryophysics microprocessor controlled spectrometer calibrated against iron foil. The spectra were fitted using a least-squares program developed by F. Woodham and supplied by Cryophysics.

RESULTS AND DISCUSSION

The analytical data on the complexes isolated are shown in Table 1 together with the colours, melting

Table 1. Analytical data of iron(III) complexes

Compound	Colour	Found (Calc.) (%)						μ_{eff} (BM)	Melting point (°C)	Molar conductance mhos cm^2 mol^{-1}
		Fe	Cl	N	S	C	H			
$[Fe(Hfth)_2Cl_2]Cl$	Bottle green	12.4 (12.5)	23.7 (23.8)	12.4 (12.5)	14.4 (14.3)	26.7 (26.9)	2.6 (2.7)	3.61	130	89.93 (DMF)
$[Fe(H_2sfth)_2Cl_2]Cl$	Brown	8.2 (8.1)	15.5 (15.5)	8.2 (8.2)	9.3 (9.3)	41.8 (42.0)	2.9 (2.9)	2.80	225	88.51 (DMF)
$Fe(HL)Cl_2$	Dark brown	15.2 (15.0)	19.1 (19.1)	7.5 (7.5)	8.7 (8.6)	38.7 (38.7)	2.6 (2.7)	6.0	219	165.02 (MeOH)
Fe(HL)L	Brown	10.3 (10.2)	—	10.2 (10.3)	11.8 (11.7)	52.7 (52.9)	3.1 (3.1)	2.37	240	—
$Fe(fth)_3$	Brown	11.6 (11.7)	—	17.5 (17.6)	20.1 (20.0)	37.7 (37.6)	3.7 (3.8)	3.22	> 300	—

point, magnetic moments and molar conductances in solution. The compound $Fe(HL)Cl_2$ is soluble in non-polar as well as polar organic solvents, while the other complexes are only soluble in polar organic solvents such as DMF and DMSO.

The IR spectra of both ligands and complexes were studied over the range 4000–200 cm^{-1} (see Table 2). Bands in the range 3400–3140 cm^{-1} due to ν(NH) modes show small negative shifts on coordination, indicating the involvement of the terminal hydrazine nitrogen in coordination to the metal. The largely ν(C=S) band of the ligands in the region 900–800 cm^{-1} is appreciably shifted to lower values in the spectra of the complexes confirming coordination through the thione sulphur. The ν(OH) and ν(C=O) bands in the spectrum of $Fe(H_2sfth)_2Cl_3$ appear at slightly higher frequencies than in the free ligand, indicating that neither the phenolic oxygen nor the carbonyl oxygen of this ligand is coordinated to the metal.

The room temperature magnetic moment of $Fe(Hfth)_2Cl_3$, 3.61 μ_B, would suggest either a strong magnetic interaction between coupled high-spin iron(III) ions or, less likely, an intermediate spin state, $S = 3/2$. However, all presently known well-characterized $S = 3/2$ species are five-coordinate and have Mössbauer spectra characterized by large quadrupole splittings with values greater than 2 mm s^{-1}, which is clearly not so in the present case (see Table 3). The molar conductance of $Fe(Hfth)_2Cl_3$ (see Table 1) lies in the range expected for a 1 : 1 electrolyte[20] if we assume that it is in fact a monomer, i.e. it should be formulated $[Fe(Hfth)_2Cl_2]Cl$. While a dimer structure $[Fe(Hfth)_2\text{-}\mu\text{-}Cl_2\text{-}Fe(Hfth)_2]Cl_4$ would account for the magnetic moment it is incompatible with the conductivity data. Furthermore, the far-IR band assigned to ν(Fe—Cl) at 315 cm^{-1} lies in the range expected for terminal Fe—Cl bands in six-coordinate species. The single ν(Fe—Cl) band indicates a *trans* structure. The Mössbauer isomer shift (Table 3) leaves no doubt that the compound contains iron(III). Unfortunately the decrease in isomer shift and quadrupole splitting at liquid nitrogen temperature suggests a crystal phase change and offers no real help. The compound obtained from Hfth in ethanolic solution, $Fe(fth)_3$, is a non-electrolyte with a magnetic moment of 3.22 μ_B. Thus its formulation as a six-coordinate ("octahedral") low-spin monomer is in little doubt. The far-IR bands assigned to ν(Fe—N) and ν(Fe—S) show the expected change, i.e. a decrease in the former and increase in the latter compatible with the bond rearrangement in the chelate ring. The *d–d* bands like those of $Fe(Hfth)_2Cl_3$ are characteristic of "octahedral" iron(III) coordination compounds with similar ligands.[21]

The compound $Fe(H_2sfth)_2Cl_3$ is a 1 : 1 electrolyte in DMF suggesting the formulation $[Fe(H_2sfth)_2Cl_2]Cl$. The Mössbauer data (Table 3) indicate the presence, both at room temperature and at liquid nitrogen temperature, of both high- and low-spin states, the latter characterized by its smaller isomer shift and much larger quadrupole splitting. The isomer shifts and quadrupole splittings are very similar to those found by Ablov, Goldanskii and their co-workers for iron(III) thiosemicarbazones and mixed complexes.[22] There are, however, two important differences. Firstly, the iron(III) species examined by Ablov and co-workers all contained iron(III) in the octahedral anionic form FeL^{2-} or $FeL'L^-$ and, secondly, only in one case, that of a mixed salicylaldehyde thiosemicarbazone–pyruvic acid species, $[FeL'L]^-$, did they observe both high- and low-spin states to be present at a detectable level at 300 K. Zelentsov and his co-workers have also discussed in detail the structural features and magnetic properties of iron(III) complexes of substituted salicylaldehyde thiosemicarbazones in the region of the $^6A_1$–$^2T_2$ spin crossover.[23] It is significant in the case of $[Fe(H_2sfth)_2Cl_2]^+$ that the hydrazine nitrogen is only mono-substituted —NH—NH— instead of —NH—N= in the case of salicylaldehyde thiosemicarbazones, and that the —OH group in the salicyl moiety is not involved in coordination. The far-IR and *d–d* spectra (Tables 2 and 4) of $Fe(H_2sfth)_2Cl_3$, $Fe(Hfth)_2Cl_3$ and $Fe(fth)_3$ are not greatly different, so that the crystal-field factors affecting spin crossover must be quite subtle. In fact the isomer shift values at room temperature of $Fe(Hfth)_2Cl_3$ and of the high-spin form of $Fe(H_2sfth)_2Cl_3$ are identical within experimental error and the difference in quadrupole splittings is relatively small.

The two complexes formed by the ligand H_2L are quite different. The compound $Fe(HL)Cl_2$ is high spin with $\mu = 6.0$ μ_B. The ν(NH) band is missing from the IR spectrum of the complex, indicating thioenolization of the ligand and coordination of the sulphur in the thiolato form. The Mössbauer data (Table 3) are compatible with a distorted tetrahedral geometry (low isomer shift combined with $\mu = 6.0$ μ_B and a relatively large quadrupole splitting) but not with a five-coordinate geometry which might be expected if the phenolic oxygen were also coordinated to the iron as well as the nitrogen and sulphur atoms. The positive shifts in the thioamide bands [β(NH) + ν(CN) and ν(CN) + β(NH)] and the ν(NN) band can be interpreted as support for bonding through the hydrazine nitrogen.[24] Consequently the ligand must be coordinated through nitrogen and sulphur and not through the phenolic oxygen.

Table 2. IR spectral data (cm^{-1}) and assignments

Compound	ν(NH)	$\nu(NH_2)$	$\delta(NH_2)$	Thioamide bands I: δ(NH)+ ν(CN)	Thioamide bands II: ν(CN)+ δ(NH)	Thioamide bands IV: ν(C═S)/ ν(C—S)	ν(N—N)	ν(M—N)	ν(M—S)	ν(M—Cl)	ν(M—O)
Hfth	3240	3180, 3140	1630	1535	1300	810	995	—	—	—	—
$[Fe(Hfth)_2Cl_2]Cl$	3220	3140, 3120	1600	1545	1360	765	1015	290	315	370	—
$Fe(fth)_3$	—	3130, 3100	1620	1570	1440	735	1010	305	340	—	—

Compound	ν(OH)	ν(NH)	ν(C═N)	Thioamide bands I: ν(C—O)/ ν(C—O—M)	Thioamide bands II: δ(NH)+ ν(CN)	Thioamide bands IV: ν(CN)+ δ(NH)	ν(C═S)/ ν(C—S)	ν(N—N)	ν(M—N)	ν(M—S)	ν(M—Cl)
H_2L	3160	3350	1620	1260	1465	1280	880	970	—	—	—
$Fe(HL)Cl_2$	—	—	1580	1540	1510	1300	710	1010	310	340	350
Fe(HL)L	—	—	1585	1530	1500	1320	725	1015	290	330	—

Compound	ν(NH)	ν(OH)	ν(C═O)/ ν(NCO)	Thioamide bands I: δ(NH)+ ν(CN)	Thioamide bands II: ν(CN)+ δ(NH)	Thioamide bands IV: ν(C═S)/ ν(C—S)	ν(N—N)	ν(M—N)	ν(M—S)	ν(M—Cl)
H_2sfth	3340	3070(br)	1630(s)	1520	1300	910	1080	—	—	—
$[Fe(H_2sfth)_2Cl_2]Cl$	3290	3400	1645	1540	1310	870	1120	290	325	380 340

Table 3. Mössbauer parameters

Compound	Room temperature IS (mm s^{-1})	Room temperature QS (mm s^{-1})	Liquid nitrogen temperature IS (mm s^{-1})	Liquid nitrogen temperature QS (mm s^{-1})
$[Fe(Hfth)_2Cl_2]Cl$	0.385	0.573	0.358	0.584
$Fe(fth)_3$	0.336	0.709	0.492	0.762
$[Fe(H_2sfth)_2Cl_2]Cl$	0.395	0.682	0.444	0.824 (High-spin species)
	0.171	2.804	0.209	2.814 (Low-spin species)
$Fe(HL)Cl_2$	0.282	0.854	0.455	0.960
Fe(HL)L	0.156	2.695	0.301	2.967

Table 4. Electronic spectral band positions and assignments

Compound	Band positions	Assignments	Geometry
$[Fe(Hfth)_2Cl]Cl_2$	11,300, 14,700, 24,670, 32,300	*d–d* transitions; CT	Octahedral
$[Fe(H_2sfth)_2Cl_2]Cl$	10,000, 11,300, 14,300, 19,000, 20,300, 28,700	*d–d* transitions; CT	Octahedral (low and high spin)
$Fe(HL)Cl_2$	14,000, 18,000, 21,700, 33,300, 36,700	*d–d* transitions; CT	Tetrahedral (high spin)
Fe(HL)L	11,000, 13,700, 21,000, 27,700	*d–d* transitions; CT	Octahedral (low spin)
$Fe(fth)_3$	11,000, 15,000, 20,700, 24,700, 29,000	$^2T_{2g} \rightarrow {}^4T_{1g}(^4G)$; $^2T_{2g} \rightarrow {}^4T_{2g}(^4G)$; $^2T_{2g} \rightarrow {}^2A_{2g}$; CT	Octahedral (low spin)

The *d–d* spectrum is compatible with a roughly tetrahedral geometry with the first band at 14,000 cm^{-1} (cf. Fe(HL)L where the first band occurs at 11,000 cm^{-1}). In methanol the compound is a 1 : 2 electrolyte but this probably results from solvent displacement of the chlorides. The compound Fe(HL)(L) is low spin with Mössbauer parameters which correspond well with those expected for a low-spin "octahedral" species, cf. the low-spin species of $[Fe(H_2sfth)Cl_2]Cl$ (see Table 3). The *d–d* (Table 4) and IR spectra (Table 2) support this formulation. (It is a non-electrolyte in MeOH and DMF as would be expected.) The donor atom set of each coordinated ligand must be SNO but the L^{2-} ligand must be in the thioenolato form, whereas the HL^- must be in the thionato form. In fact ν(OH) and ν(NH) bands are both missing from the IR spectrum.

REFERENCES

1. M. Akbar Ali, S. E. Livingstone and D. J. Phillips, *Inorg. Chim. Acta* 1971, **5**, 119.
2. M. Akbar Ali, S. E. Livingstone and D. J. Phillips, *Inorg. Chim. Acta* 1971, **5**, 493.
3. M. Akbar Ali, S. E. Livingstone and D. J. Phillips, *Inorg. Chim. Acta* 1972, **6**, 11; 1972, **6**, 39; 1972, **6**, 552; 1973, **7**, 179; 1973, **7**, 531.
4. S. E. Livingstone and J. D. Nolan, *J. Chem. Soc., Dalton Trans.* 1972, 218.
5. M. J. M. Campbell, *Coord. Chem. Rev.* 1975, **15**, 279; J. Kaufmann and S. Padhye, *Coord. Chem. Rev.* 1985, **63**, 127.
6. H. G. Petering, H. H. Buskirk and J. E. Underwood, *Cancer Res.* 1964, **24**, 367; A. Giner-Sorolla, M. McCravey, J. Longley-Cook and J. H. Burchenall, *J. Med. Chem.* 1973, **16**, 984; K. C. Agrawal, A. J. Lin, B. A. Booth, J. R. Wheaton and G. C. Sartorelli, *J. Med. Chem.* 1974, **12**, 631; J. A. French, E. J. Blanz, S. C. Shaddix and R. N. Brockman, *J. Med. Chem.* 1974, **13**, 1124; K. C. Agrawal, B. A. Booth, S. M. De Nuzoo and A. C. Sartorelli, *J. Med. Chem.* 1975, **18**, 308; W. J. Dunn and E. M. Hodnett, *Eur. J. Med. Chem., Chim. Ther.* 1977, **12**, 113; L. J. Linn, S. J. Lee and C. J. Chen, *Heterocycles* 1977, **7**, 347.
7. D. L. Klayman, J. F. Bartosevich, J. S. Griffin, C. J. Mason and J. P. Scovill, *J. Med. Chem.* 1979, **22**,

853; D. L. Klayman, J. P. Scovill, J. F. Bartosevich and C. J. Mason, *J. Med. Chem.* 1979, **22**, 1367.
8. E. J. Blanz, J. A. French, J. R. Do-Amaral and D. A. French, *J. Med. Chem.* 1970, **13**, 1117.
9. D. H. Petering, *Bioinorg. Chem.* 1972, **1**, 273; D. A. Winkelmann, Y. Bermke and D. H. Petering, *Bioinorg. Chem.* 1974, **3**, 261.
10. W. E. Antholine and D. H. Petering, *Proc. Am. Assoc. Cancer Res.* 1974, **15**, 289.
11. K. C. Agrawal, B. A. Booth, E. C. Moore and A. C. Sartorelli, *Proc. Am. Assoc. Cancer Res.* 1974, **15**, 289.
12. G. Atassi, P. Dumant and J. C. E. Hartell, *Eur. J. Cancer* 1979, **15**, 451.
13. W. E. Antholine, J. M. Knight and D. H. Petering, *J. Med. Chem.* 1976, **19**, 339.
14. L. A. Sarayan, E. Ankel, C. Krishnamurthi, W. E. Antholine and D. H. Petering, *Biochem. Pharmacol.* 1981, **30**, 1595.
15. N. K. Singh, S. Agrawal and R. C. Aggarwal, *Ind. J. Chem.* 1982, **21A**, 973.
16. N. K. Singh, S. Agrawal and R. C. Aggarwal, *Synth. React. Inorg. Met.-Org. Chem.* 1985, **15**, 75.
17. S. Agrawal and N. K. Singh, *Spectrochim. Acta* 1986, **42A**, 507.
18. A. I. Vogel, *Textbook of Quantitative Inorganic Analysis*, 4th Edn, Longman, London (1979).
19. B. N. Figgis and J. Lewis, *Modern Coordination Chemistry* (Edited by J. Lewis and R. C. Wilkins), p. 403. Interscience, N.Y. (1960).
20. W. J. Greary, *Coord. Chem. Rev.* 1971, **7**, 81.
21. M. J. M. Campbell, R. Grzeskowiak and G. D. Juneja, *J. Inorg. Nucl. Chem.* 1978, **40**, 1247 and 1507.
22. G. V. Ablov, V. I. Goldanskii, K. I. Turta, R. A. Stukan, V. V. Zelentsov, E. V. Ivanov and N. V. Gerbeleu, *Dokl. Phys. Chem.* (*Engl. Trans.*) 1971, **196**, 134; K. I. Turta, A. V. Ablov, V. I. Goldanskii, N. V. Gerbeleu and R. A. Stukan, *Dokl. Phys. Chem.* (*Engl. Transl.*) 1971, **196**, 190.
23. N. A. Ryabova, V. I. Ponomarev, V. V. Zelentsov and Z. O. Atomyan, *Dokl. Akad. Nauk SSSR* (*Engl. Transl.*) 1981, **4**, 715 and refs therein.
24. G. R. Burns, *Inorg. Chem.* 1968, **7**, 277; K. Geetharani and D. N. Sathyanarayana, *Aust. J. Chem.* 1977, **30**, 1617.

Polyhedron Vol. 9, No. 8, pp. 1071–1077, 1990
Printed in Great Britain

0277–5387/90 $3.00+.00
© 1990 Pergamon Press plc

ISOTOPE EFFECTS IN THE ACID-CATALYSED REACTIONS OF HYPOPHOSPHOROUS ACID

JOHN W. LARSON

Department of Chemistry, Marshall University, Huntington, WV 25755-2520, U.S.A.

(*Received* 8 *August* 1989; *accepted* 8 *December* 1989)

Abstract—Rate constants for four isotope exchange reactions and four oxidation reactions were measured at 25°C for protonated and deuterated hypophosphorous acid. For the acid-catalysed, rate-determining tautomerization of inactive $H_2PO(OH)$ to active $HP(OH)_2$, primary kinetic isotope effects (k^D/k^H) of 0.36 for the forward reaction and 0.24 for the reverse reaction were obtained. The secondary isotope effect was determined to be 1.45. These isotope effects are consistent with a transition state in which proton attachment occurs with a bond order of 0.2. This bond order is used, along with the Marcus theory of proton transfer, to calculate a free energy of tautomerization of 62 kJ.

The rate constants for a variety of acid-catalysed reactions involving the P—H bond of hypophosphorous acid are all approximately 3.5×10^{-3} M^{-1} s^{-1} at room temperature. These reactions range from simple isotope exchange with the solvent[1,2] to the oxidation of hypophosphorous acid with over 12 different oxidizing agents.[3–6] The common mechanism proposed to explain these rates involves the general acid-catalysed conversion of the inactive tautomer **I** to the active intermediate, tautomer **II**[1,2,5]

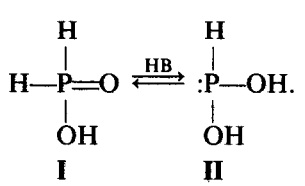

I II (1)

The present study involves examination of isotope effects on both the exchange reactions and the oxidation reactions with I_3^-. Detailed analysis of these isotope effects can reveal considerable information about the mechanism of the reaction and the structure of the transition state. Of particular interest is the fraction of protonation that occurs in the transition state structure as deduced from the isotope effect, α_I, and that deduced from the Brønsted coefficient,[5] α_B. No previous study of isotope effects on the reactions of hypophosphorous acid has been carried out.

Small but significant discrepancies also exist between the rates obtained for exchange versus oxidation reactions. In order to compare these results, a detailed experimental and theoretical analysis of the isotope effects is needed.

The larger temperature range and the better precision of the present study of the isotope exchange rates provides a more solid backdrop for interpretation of future kinetic experiments. In particular, this work was a necessary prelude to a planned quantitative study of Lewis acid catalysis of the isotope exchange reaction.

EXPERIMENTAL

Sodium hypophosphite monohydrate obtained from Fisher Scientific was analysed by heating to 200°C *in vacuo* followed by titration after elution from a strong acid ion exchange column. Hydrochloric and acetic acids were obtained commercially in the highest purity available and analysed by standard acidometric methods. The 99.8 atom % D_2O used was obtained from Aldrich.

Phosphorous magnetic resonance spectra were obtained using a Varian XL-200 spectrometer. Mole fractions of the $H_2PO(OL)$, $HDPO(OL)$ and $D_2PO(OL)$ species calculated from the spectra were generally reproducible to better than 2%. L is the symbol used for either H or D. Temperatures were controlled to within ±0.3°C. Temperature calibration was carried out with a mercury thermometer.

RESULTS AND DISCUSSIONS

Equilibrium isotope effect

Fifteen kinetic experiments were allowed to run to completion at stoichiometric mole fractions of deuterium between 0.1 and 0.9. Measurement of areas under the D_2PO_2 quintet, the $HDPO_2$ doublet of triplets and the H_2PO_2 triplet resulted in equilibrium constants for reactions (2) and (3) of $K_2 = 1.12 \pm 0.08$ and $K_3 = 0.305 \pm 0.015$:

$$DOL_l + H_2PO_2L_{aq} = DHPO_2L_{aq} + HOL_l \quad (2)$$

$$DOL_l + DHPO_2L_{aq} = D_2PO_{2aq} + HOL_l. \quad (3)$$

This value of K_2 is in good agreement with the value of $K_2 = 1.1 \pm 0.2$ obtained from the base-catalysed reaction.[7] K_2 and K_3 are consistent with statistical factors of 2 and 0.5, respectively, along with the deuterium fractionation factor, defined[8] by eq. (4), of $\phi_{PH} = 0.59 \pm 0.03$:

$$\phi_{PH} = (D—P/H—P)/(D—O/H—O)_{aq}. \quad (4)$$

A theoretical value for the deuterium fractionation factor may be estimated from bond stretching frequencies of 2400 cm^{-1} for P—H and 3300 cm^{-1} for O—H.[9] The estimated zero-point energy difference[8] of 132 cm^{-1} gives a value of ϕ_{PH} of 0.53 at 25°C, in good agreement with the measured value.

A value of 0.0176 for K_D, the acid ionization constant of $H_2PO(OD)$ in D_2O, is calculated from the PH coupling constants in various solutions following a previously discussed method.[10] The ratio of $K_D/K_H = 0.36$ is typical of that obtained for other acids in D_2O.[8] This ratio is equal to l^3/ϕ_{POH} where l is the fractionation factor for the hydronium ion and has a value of 0.69.[8] The calculated fractionation factor for the POH hydrogen of 0.9 is close to the value of 1.0 expected for a neutral OH group.

Determination of the rate constants for isotope exchange

The rate of disappearance of H_2P isotopic species at any particular acid concentration, ionic strength, isotope concentration and temperature is given by eq. (5):

$$d(H_2P)/dt = k_2(H_2PO_2L)(X_D) - k_{-2}(HDPO_2L)(1-X_D), \quad (5)$$

where X_D is the mole fraction of deuterated solvent. Dividing eq. (5) by the total hypophosphite concentration gives eq. (6):

$$dX_{H_2P}/dt = k_2F\,X_{H_2P}\,X_D - k_{-2}F\,X_{HDP}(1-X_D), \quad (6)$$

where F is the fraction of total hypophosphite in the acid form as determined from the PH coupling constant,[10] X_{H_2P} and X_{HDP} are the fractions of total P in these forms, and k_2 and k_{-2} represent the pseudo first-order rate constants obtained for the forward and reverse reaction (2). Similar expressions may be written for the rate of disappearance of $HDPO_2L$ and D_2PO_2L. The relations among k_2, k_{-2}, k_3 and k_{-3} are known from the equilibrium fractionation factors to be given by eq. (7):

$$k_2 = 2\phi_D k_{-2} = 2k_3 = k_{-3}\phi_D. \quad (7)$$

Experimental values of the mole fractions of the three L_2PO_2L species as a function of time were used to obtain k_2 by numerical integration of eq. (6). An example of typical results is shown in Fig. 1.

General acid catalysis of the exchange reaction means that k_2 is a sum of the products of individual acid rate constants and concentrations of acids LB, eq. (8):

$$k_2 = \Sigma k_2^{LB}(LB). \quad (8)$$

Even in the simplest system, involving only aqueous hypophosphorous acid, there are eight different, but related, rate constants that differ in the direction of the reaction, the acid catalysing the reaction, and the isotopic form of the acid. In this work, the subscript will indicate the isotope reaction taking place and the superscript indicates the catalytic acid for the reaction. Thus the acid-catalysed, pseudo first-order rate constant, k_{-3}, for the disappearance of D_2PO_2H in pure H_2O is given by eq. (9):

$$k_{-3} = k_{-3}^{H}(H_3O^+) + k_{-3}^{H_3PO_2}(H_3PO_2). \quad (9)$$

Dividing by (H_3O^+) yields eq. (10):

$$k_{-3}/(H_3O^+) = k_{-3}^{H} + k_{-3}^{H_3PO_2}(H_3PO_2)/(H_3O^+). \quad (10)$$

The values for the left-hand side of eq. (10) are plotted against $(H_3PO_2)/(H_3O^+)$ to give a straight line as shown in Fig. 2 for measurements made at 45°C and ionic strengths of 0.2 and 0.5. Values of k^H are obtained from the intercept and $k^{H_3PO_2}$ from the slope.

In making experimental measurements over a variety of temperatures and with various acids, it is necessary to use a considerable range of ionic strengths. As observed in Fig. 2, there is no appreciable dependence on ionic strength. This is expected from the fact that the transition state for the reaction will involve the same charge type species as the reactants.

In addition to the study of PD to PH exchange at 0, 25, 45 and 65°C, rates of disappearance of

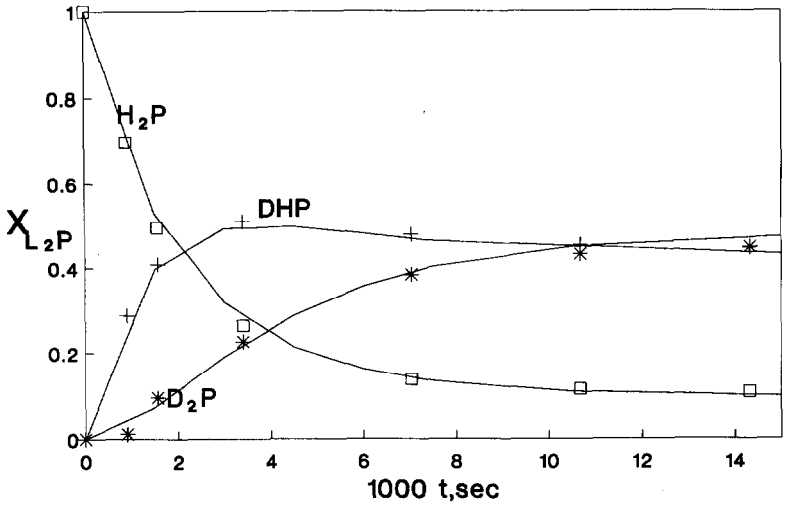

Fig. 1. Experimental and calculated mole fractions of H_2PO_2, $DHPO_2$ and D_2PO_2 as a function of time for Run No. 11, 25°C, $(H^+) = 0.077$ M, $(H_3PO_2) = 0.682$ M, $(H_2PO_2^-) = 0.581$, $X_D = 0.793$. $k_2 = 5.8 \times 10^{-4}$ used in calculating solid lines.

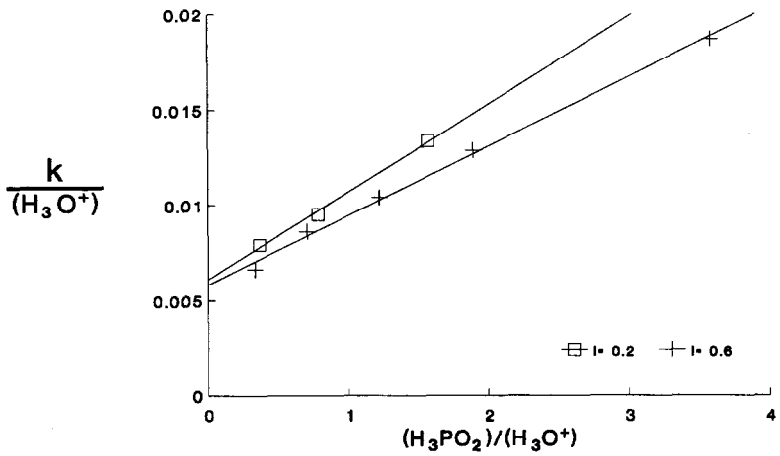

Fig. 2. Analysis of results at 45°C for the reaction $D_2PO_2 \rightarrow H_2PO_2$ via eq. (10) at ionic strengths of 0.2 and 0.6.

H_2PO_2L in pure D_2O were studied at these temperatures to obtain the values reported in Table 1.

The rate constants for the reverse exchange reactions in the same solvent system may be calculated from the relationships given in eq. (7). The four unique exchange rate constants for the L_3O^+-catalysed reactions at 25°C are summarized in the top half of Table 2. The uncertainties in these rate constants are ±15%.

Kinetic isotope effects for the oxidation reaction at 25°C and the mechanism of reaction

To assist in the detailed mechanistic analysis of the isotope effects, the rate of oxidation of hypophosphorous acid by I_3^-, eq. (11), was measured:

$$L_2O + L_2PO_2L + I_3^- = 3I^- + LPO_3L_2 + 2L^+. \quad (11)$$

The time dependence of oxidation was monitored from integration of the ^{31}P NMR of H_2PO_2 and HPO_3. Analysis of the results followed the method of Griffith *et al.*[5] Because of the changing pH during reaction (11), the experimental rates for the oxidation reaction were not precise enough to extract two independent rate constants as was done from the corresponding exchange rates. The experiments were therefore carried out under conditions where the reaction was predominantly catalysed by the hydronium ion, and the hydronium ion-catalysed rate constants were calculated by estimating the

Table 1. Measured rate constants[a] for exchange reactions

Temperature (°C)	Ionic strength	$k^{H}_{D\to H}$	$k^{D}_{H\to D}$	$k^{HL_2PO_2}_{D\to H}$	$k^{DL_2PO_2}_{H\to D}$
		($\times 10^3$ Ms)			
0	0.6–1.2	—	0.24	—	(0.12)[b]
25	0.2–1.0	1.19	4.09	1.01	1.87
45	0.2–0.6	11.0	27.6	6.14	17.9
65	0.8–1.4	—	(223)[b]	—	48.0

[a] Numerical subscripts have been replaced by explicit indication of the P bonding reaction being measured so that $k_{H\to D}$ indicates that PH is reacting to give PD and is equal to k_2.
[b] Extrapolated value.

Table 2. Measured and calculated rate constants for exchange and oxidation reactions at 25°C

Rate constant	Experimental value ($\times 10^3$ Ms)	Literature value ($\times 10^3$ Ms)	Expression for rate constant	Calculated value ($\times 10^3$ Ms)
$k^{H}_{H\to D}$	0.70		$k^0(k^{D}_{-13}/k^{H}_{-13})$	0.78
$k^{D}_{H\to D}$	4.09	4.62[a]	$k^0(K^{D}_{12}/K^{H}_{12})$	4.73
$k^{H}_{D\to H}$	1.19		$k^0(k^{D}_{13}/k^{H}_{13})$	1.17
$k^{D}_{D\to H}$	6.47		$k^0(K^{D}_{12}/K^{H}_{12})(k^{D}_{13}/k^{H}_{13})(k^{H}_{-13}/k^{D}_{-13})$	7.16
$k^{H}_{H\to OH}$	3.97	3.87[b]	k^0	3.26
$k^{D}_{H\to OD}$	5.86		$k^0(K^{D}_{12}/K^{H}_{12})$	4.73
$k^{H}_{D\to OH}$	1.13		$k^0(k^{D}_{13}/k^{H}_{13})$	1.17
$k^{D}_{D\to OD}$	2.07		$k^0(K^{D}_{12}/K^{H}_{12})(k^{D}_{13}/k^{H}_{13})$	1.67
$k^{H}_{T\to H}$	—	0.47[c]	$k^0(k^{D}_{-13}/k^{H}_{-13})^{1.4}$	0.44

[a] Value from ref. 1 corrected to 25°C.
[b] Average of five results corrected to 25°C from refs 5 and 21
[c] Value from ref. 2 corrected to 25°C.

hypophosphorous acid rate constant as being equal to 0.5 that of the rate constant for the hydronium ion-catalysed reaction. This ratio of 0.5 is equal to that determined in the isotope exchange work presented earlier and to the previously measured ratio[5] in the oxidation of H_2PO_2 by I_3^-. The values of the four rate constants obtained for the oxidation reactions from this work are given in Table 2. The total uncertainty in these rate constants is ±30%.

The data from the oxidation reactions reveal in a straightforward way the expected trends.[8,11-13] The primary isotope effect is to retard the reaction of PD relative to PH. The secondary or solvent isotope effect results in the reaction being faster in D_2O compared to H_2O, in accordance with the deuterium ion being a stronger acid in D_2O than the hydronium ion is in H_2O. The analysis of the exchange results is not as straightforward because it involves two different primary isotope effects, as will be shown by the following analysis.

Previous work[14] indicates hypophosphorous acid is protonated in a fast equilibrium, eq. (9), with $K_{12} = 0.02$. The fact that the reaction involves general acid catalysis suggests that the rate-determining step involves the conjugate base of the acid. This implies a mechanism classified[11] as A2 (Scheme 1). In this scheme H, D and L are used to indicate

$$H{-}P{=}O + LB \rightleftharpoons \overset{+}{H}{-}P{=}O{-}L + B \quad (12)$$

$$H{-}P{=}\overset{+}{O}{-}L + B \rightleftharpoons [B{\cdots}H{\cdots}P{=}O{-}L] \longrightarrow HB + :P{-}O{-}L \quad (13)$$

$$:P{-}O{-}L + \text{Oxidant} \longrightarrow [\,] \longrightarrow HO{-}P{-}OL \text{ (fast)} \quad (14)$$

$$:P{-}O{-}L + DB \longrightarrow D{-}P{=}\overset{+}{O}{-}L + B \quad (15)$$

$$D{-}P{=}\overset{+}{O}{-}L + B \longrightarrow D{-}P{=}O + LB \text{ (fast)}, \quad (16)$$

Scheme 1.

the three different hydrogens which may affect the reaction rate. The PH and the POH bonds that do not react are not shown in eqs (12)–(16).

Using the steady-state approximation, the concentration of the active tautomer is given by eq. (17):

$$(:POL) = \frac{k_{13}(B)(HPOL^+)}{k_{-13}(HB)+k_{14}(Ox)+k_{15}(DB)}. \quad (17)$$

Oxidation reactions. The overall rate for the oxidation is given by k_{14}(:POL)(Ox). Substituting for (:POL) under the conditions that k_{14}(Ox) is much greater than either of the two other terms in the denominator of eq. (17) and making use of the equilibrium constant to express the concentration $HOPOL^+$ and B in terms of K_{12}, the rate expression becomes eq. (18):

$$\text{rate} = k_{13}K_{12}(LB)(H_3PO_2). \quad (18)$$

If we designate k^0 as the value of $k_{13}K_{12}$ when all hydrogens are protons, we can express the rate constants of the other three oxidation reactions in terms of this value and the isotope effects on k_{13} and K_{12} as indicated in Table 2.

Exchange reactions. For the proton to deuterium exchange reactions, the overall rate is given by eq. (19):

$$\text{rate} = k_{15}(DB)(:POL). \quad (19)$$

Substituting for the active intermediate and rearranging yields eq. (20) for the rate and eq. (21) for k_2:

$$\text{rate} = \frac{k_{13}k_{15}K_{12}(H_3PO_2)(LB)X_D}{k_{-13}(1-X_D)+k_{15}X_D} \quad (20)$$

$$k_2 = \frac{k_{13}k_{15}K_{12}(LB)}{k_{-13}(1-X_D)+k_{15}X_D}. \quad (21)$$

Solving this in the limits of X_D equal to 0 and 1, with $k_{15} = k^D_{-13}$, gives two of the exchange expressions in Table 2. The two additional expressions are obtained in an identical manner by considering the deuterium to hydrogen exchange reaction.

Values of the individual kinetic isotope parameters, $K^D_{12}/K^H_{12} = 1.45$, $k^D_{13}/k^H_{13} = 0.36$ and $k^D_{-13}/k^H_{-13} = 0.24$, along with $k^0 = 3.26 \times 10^{-3}\ M^{-1}\ s^{-1}$, are obtained by best fit of the calculated to the experimental rate constants in Table 2.

Isotope effects and transition state structure

Following the procedure given by Schowen,[12] BH and PH bond orders in the transition state of eq. (13) may be estimated from the isotope effect on k_{13}. This procedure involves a linear interpolation from the maximum calculated isotope effect which is assumed to occur when the PH bond is half broken and the BH bond order is half formed. Bond orders of 0.83 and 0.17 are calculated for the BH and PH, respectively. A useful symbolism is to designate the PH bond order as α_I, the fraction of protonation of the transition state as determined by the kinetic isotope effect. Repeating the calculation for the reverse reaction from the k_{-13} isotope effect gives a value of $\alpha_I = 0.22$.

Extraction of the value of K^D_{12}/K^H_{12} from the experimental rates results in all isotope effects other than those involved indirectly in the P—H—B bond entering into this value. The theoretical estimate of these secondary isotope effects for hydronium ion catalysis will involve considering the fate of the three hydrogens from this ion as they are involved in the transition state.[15] Two of these are in the water molecule that serves as the base in eq. (13), and one is attached to the phosphorous oxygen in step (12). If the BH bond order is given as x, the extent to which the two water protons resemble the original OH^+ protons is also x and the extent to which the POH proton resembles OH^+ is $1-x$. The secondary isotope effect is calculated from the expression:

$$I^{2x}I^{1-x}/I^3,$$

where x is equal to $1-\alpha_I$. For $x = 0.8$, a solvent effect of 1.55 is calculated in good agreement with the experimental value of 1.45.

The fraction of transition state protonation determined for the kinetic isotope effect, α_I, is quite different from the fraction determined from the slope of the graph of $\ln(k)$ against the pK_a of the catalysing acid, α_B, the Brønsted coefficient. Griffith *et al.*[5] have determined the latter value to be 0.52. The value of α_I appears to give a more realistic indication of the transition state in that it is consistent with the Hammond postulate[16] that the transition state in the "uphill" reaction (13) should most closely resemble the product, **II**, which has zero proton transfer from the acid.

The Marcus theory[17,18] of proton transfer provides both a basis for analysing the reason for the discrepancy between the two α values and a method of estimating the free energy of tautomerization of hypophosphorous acid. The latter will be analysed first. The Marcus theory involves two key equations, eqs (22) and (23), that may be applied to eq. (13):

$$\Delta G^* = w_r + 1/4\lambda(1+\Delta G^0/\lambda)^2 \quad (22)$$

$$\alpha = (1+\Delta G^0/\lambda)/2. \quad (23)$$

For the hydronium ion-catalysed reaction, the solvation energy change on bringing the reactants of

eq. (13) together, w_R, should be approximately zero because the base is the solvent, water. The free energy of activation in eq. (22) is $\Delta G^{\ddagger}_{13} = 77$ kJ which is known from the difference in the overall free energy of activation (88 kJ) and ΔG^{0}_{12} (11 kJ). Using this activation energy and $\alpha = \alpha_I$, $\Delta G^{0}_{13} = 51$ kJ is calculated from eqs (22) and (23). The free energy of tautomerization, ΔG^{0}_{I}, is then obtained by adding ΔG_{12} to ΔG_{13} to obtain 62 kJ. This value is in excellent agreement with values estimated by very different methods of < 68[19] and 59 kJ.[20]

The large value of α_B in relation to α_I can be rationalized by some combination of three effects. (i) For negatively charged bases, w_R may be considerable; (ii) as the basicity of B in eq. (13) approaches that of :POH, ΔG^0 will decrease leading to a larger α; (iii) determination of α is made difficult by the fact that competing reactions become increasingly important as the pH increases, and part of the differences in these values may be due to the experimental error in α_B. Albery *et al.*[18] have discussed the first two effects in relation to a different reaction. Experimental support for the importance of these first two factors was obtained by measuring the rate of the exchange reactions at 45°C catalysed by acetic acid. The values obtained were $k^{AcOH}_{D\rightarrow H} = 3.4 \times 10^{-5}$ M^{-1} s^{-1} and $k^{AcOD}_{H\rightarrow D} = 3.0 \times 10^{-4}$ M^{-1} s^{-1}. A value of $k^{AcOH}_{H\rightarrow OH} = 3.1 \times 10^{-4}$ M^{-1} s^{-1} is calculated at 45°C from a measured value at 30°C.[5] Together these rate constants would indicate isotope effects of $K^{D}_{12}/K^{H}_{12} \sim 1$ and $k^{H}_{13}/k^{D}_{13} \sim 9$. This latter value is close to the maximum isotope effect possible which would occur at a value of $\alpha_I = 0.35$. The uncertainty in the acetic acid-catalysed rate constants is high ($\pm 30\%$) because over 50% of the reaction is still catalysed by H_3O^+ and H_3PO_2.

Temperature dependence of rate constants

The kinetic isotope expressions given in Table 2, along with the values of the parameters determined in this work, have been used to calculate k^0 from the rate constants for the exchange reactions. These are shown in Fig. 3 as a function of $1/T$ along with the directly measured rate constants for oxidation reactions. The rate constants for the tritium exchange reaction[2] were taken to apply to the rate of exchange of T_2PO_2 with H_2O and not $HTPO_2$ with H_2O as cited in the literature.[1,6] The original article seems to indicate that the statistical factor of two had been applied in order to arrive at the former rate constant. The good agreement of the values of k^0 obtained from the various oxidation reactions and those obtained from the exchange reactions confirm reaction (1) as the common rate-determining step in these reactions.

The energy of activation from all of these measurements is 81 kJ, in good agreement with the value of 84 kJ obtained by the careful work of Griffith *et al.*[5]

CONCLUSIONS

Experimental determinations were made of the isotope effects on both deuterium–hydrogen exchange of hypophosphorus acid and the oxidation of hypophosphorous acid with tri-iodide. Deuteration of either the hypophosphorous acid or the water reveals a primary isotope effect that decreases the exchange reaction rate constant. A secondary isotope effect is determined that indicates that the deuterium ion is more effective than the hydronium ion in catalysing the reaction.

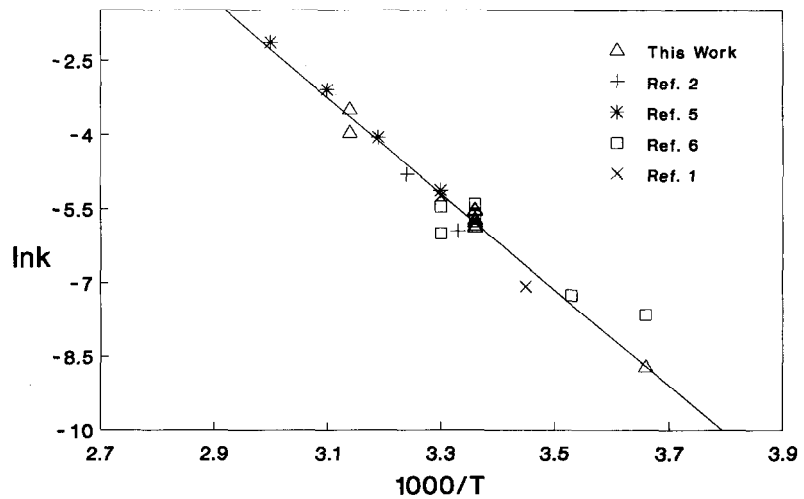

Fig. 3. Arrhenius analysis of kinetic results of this work and previous kinetic studies involving hypophosphorous acid.

The interpretation of these effects indicates that the rate-determining step of the reaction is the attack of a base on the PH proton of the protonated phosphorous acid. The theoretical calculation indicates that when the base is water the transition state occurs when the PH bond order is 0.2.

The Marcus theory is used to calculate a value of the free energy of tautomerization of hypophosphorous acid from $H_2PO(OH)$ to $HP(OH)_2$ as 62 kJ.

REFERENCES

1. A. Fratiello and E. W. Anderson, *J. Am. Chem. Soc.* 1963, **85**, 519.
2. W. A. Jenkins and D. M. Yost, *J. Inorg. Nucl. Chem.* 1959, **11**, 297.
3. P. Hayward and D. M. Yost, *J. Am. Chem. Soc.* 1949, **71**, 915.
4. K. S. Gupta and Y. K. Gupta, *Inorg. Chem.* 1975, **14**, 2000.
5. R. O. Griffith, A. McKeown and R. P. Taylor, *Trans. Faraday Soc.* 1940, **36**, 752.
6. I. R. Wilson, *Comprehensive Chemical Kinetics* (Edited by C. H. Bamford and C. F. H. Tipper), Vol. 6, Ch. 4. Elsevier, Amsterdam (1972).
7. G. C. Roper, T. E. Haas and H. D. Gillman, *Inorg. Chem.* 1970, **9**, 1049.
8. R. P. Bell, *The Proton in Chemistry*. Cornell University Press, Ithaca, New York (1973).
9. H. H. Bauer, G. D. Christian and J. E. O'Reilly, *Instrumental Analysis*, p. 218. Allyn and Bacon, Boston (1978).
10. J. W. Larson and M. Pippin, *Polyhedron* 1989, **8**, 527.
11. A. V. Willi, *Comprehensive Chemical Kinetics* (Edited by C. H. Bamford and C. F. H. Tipper), Vol. 8, Ch. 1. Elsevier, Amsterdam (1977).
12. R. L. Schowen, *Prog. Phys. Org. Chem.* 1974, **9**, 275.
13. N. S. Isaacs, *Physical Organic Chemistry*. Longman Scientific and Technical, Essex (1987).
14. T. E. Haas and H. D. Gillman, *Inorg. Chem.* 1968, **7**, 2051.
15. See reference 12, pp. 286–287.
16. G. S. Hammond, *J. Am. Chem. Soc.* 1955, **77**, 334.
17. R. A. Marcus, *J. Phys. Chem.* 1968, **72**, 891.
18. W. J. Albery, A. N. Campbell-Crawford and J. S. Curran, *J. Chem. Soc., Perkin Trans.* II 1972, 2206.
19. J. R. Van Wazer, *Phosphorous and its Compounds*, Vol. I, p. 365. Interscience, New York (1959).
20. J. P. Guthrie, *Can. J. Chem.* 1979, **57**, 236.

Polyhedron Vol. 9, No. 8, pp. 1079–1085, 1990
Printed in Great Britain

0277–5387/90 $3.00+.00
© 1990 Pergamon Press plc

THE SYNTHESIS AND ISOLATION OF THE STEREOSPECIFIC LIGAND, *N*-(2-AMINOETHYL)-2-[(2-AMINOETHYL)THIO]ACETAMIDE (egeH). COMPARISON OF THE CRYSTAL STRUCTURE OF $[Co(ege)(NO_2)_2]\cdot 4H_2O$ WITH RELATED SYSTEMS

PAUL J. TOSCANO* and KATHY J. FORDON

Department of Chemistry, State University of New York at Albany, Albany, NY 12222, U.S.A.

and

LUTZ M. ENGELHARDT, BRIAN W. SKELTON and ALLAN H. WHITE*

Department of Physical and Inorganic Chemistry, University of Western Australia, Perth 6009, Australia

and

PATRICIA A. MARZILLI

Department of Chemistry, Emory University, Atlanta, GA 30322, U.S.A.

(*Received* 15 *September* 1989; *accepted* 8 *December* 1989)

Abstract—A convenient synthetic scheme that utilizes readily available starting materials and leads to the isolation of the linear, stereospecific NSNN tetradentate ligand, *N*-(2-aminoethyl)-2-[(2-aminoethyl)thio]acetamide (egeH, **6**), as its dihydrobromide salt is reported. Ligand **6** deprotonates and forms octahedral complexes with cobalt(III) of only one geometric isomer, for example, $[Co(ege)(NO_2)_2]\cdot 4H_2O$ (**7**). Compound **7** crystallized in the monoclinic space group $I2/c$, $a = 25.83(2)$, $b = 7.896(6)$, $c = 15.703(8)$ Å, $\beta = 90.36(5)°$, $V = 3202(3)$ Å^3, $Z = 8$. Refinement was based on 3105 reflections and converged at $R = 0.038$, $R_w = 0.047$. The structural determination reveals that the geometry of the backbone ligand is *cis*-β. In addition, the structures of $[Co(egpy)(NO_2)_2]$ (**8**) (where egpyH = *N*-(2-aminoethyl)-2-[(2-pyridylmethyl)thio]acetamide) and $[Co(eee)(NO_2)_2]Br$ (**9**) (where eee = 1,8-diamino-3,6-dithiaoctane), which also contain stereospecific ligands, were also determined. Compound **8** crystallized in the monoclinic space group $P2_1/c$, $a = 7.628(3)$, $b = 12.347(4)$, $c = 16.433(8)$ Å, $\beta = 108.39(3)°$, $V = 1470(1)$ Å^3, $Z = 4$. Refinement was based on 2249 reflections and converged at $R = 0.034$, $R_w = 0.042$. Compound **9** crystallized in the monoclinic space group $P2_1/a$, $a = 12.719(9)$, $b = 13.855(4)$, $c = 8.033(6)$ Å, $\beta = 111.32(4)°$, $V = 1319(1)$ Å^3, $Z = 4$. Refinement was based on 2300 reflections and converged at $R = 0.029$, $R_w = 0.035$. The tetradentate ligand in the former adopts the *cis*-β conformation, while for the latter, the expected *cis*-α geometry is observed. The structural parameters are compared and the origins of the attendant stereospecificities are discussed in terms of the nature of the internal donor atoms of the tetradentate ligands.

Over the years, octahedral cobalt(III) complexes containing flexible, linear tetradentate ligands have been intensely studied.[1–3] Previous investigations of their reaction chemistry have centred upon the activation of coordinated amino acid derivatives, proteins, thiolates and related compounds.[1,4,5]

* Authors to whom correspondence should be addressed.

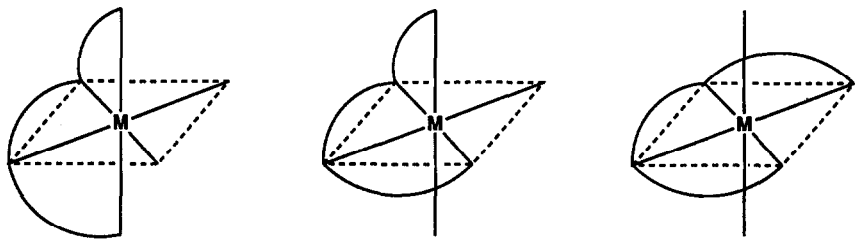

Fig. 1. The three possible coordination geometries for a flexible, linear tetradentate ligand in an octahedral metal complex.

Since three geometrical isomers (*cis*-α, *cis*-β and *trans*; see Fig. 1) are possible for such complexes, the synthetic design of ligands of high stereoselectivity, if not stereospecificity, is of special interest. The judicious incorporation of asymmetric centres into the backbone of the tetradentate ligand has met with varying degrees of success;[2,6,7] however, the exact geometry obtained has been difficult to predict and subsequent rearrangements under different reaction conditions have remained problematic.[8,9] We note that further isomers may result due to stereochemical considerations about planar, internal secondary amino donor atoms in linear chelating ligands such as triethylenetetramine (trien).[10]

Here we report on the synthesis and isolation of *N*-(2-aminoethyl)-2-[(2-aminoethyl)thio]acetamide (egeH). This compound is a linear, tetradentate ligand with an NSNN donor set containing internal thioether and amido groups, that belongs to the same class of ligands as egpyH (*N*-(2-aminoethyl)-2-[(2-pyridylmethyl)thio]acetamide), pygeH (*N*-[(2-pyridyl)methyl]-2-(2-aminoethyl)thioacetamide) and geeH (*N*-{2-[(2-aminoethyl)-thio]ethyl}-2-aminoacetamide), which coordinate to cobalt(III) with concomitant deprotonation of the amide moiety.[1]

It has been previously demonstrated[1] that each of these NSNN ligands, with the exception of egpy, generates a series of chemically interconvertible octahedral cobalt(III) complexes for which only one geometrical isomer is isolated in each case, as elucidated from ^{1}H and ^{13}C NMR spectroscopies. The lack of symmetry in the backbone ligands precludes identification of the gross geometry of the complexes by spectroscopic techniques. X-ray diffraction studies of $[Co(gee)(NO_2)_2]\cdot H_2O$[1] and $[Co(pyge)(NO_2)_2]\cdot H_2O$[11] have determined the stereochemistry as *cis*-β for complexes of these two ligands. In order to establish the geometry of cobalt(III) ege and egpy complexes, we have undertaken the structural determinations of $[Co(ege)(NO_2)_2]\cdot 4H_2O$ and $[Co(egpy)(NO_2)_2]$. In addition, the structure of $[Co(eee)(NO_2)_2]Br$, which is already known to adopt the *cis*-α geometry,[12,13] is reported for comparison. The chemical structures of the ligands in this article are depicted in Fig. 2.

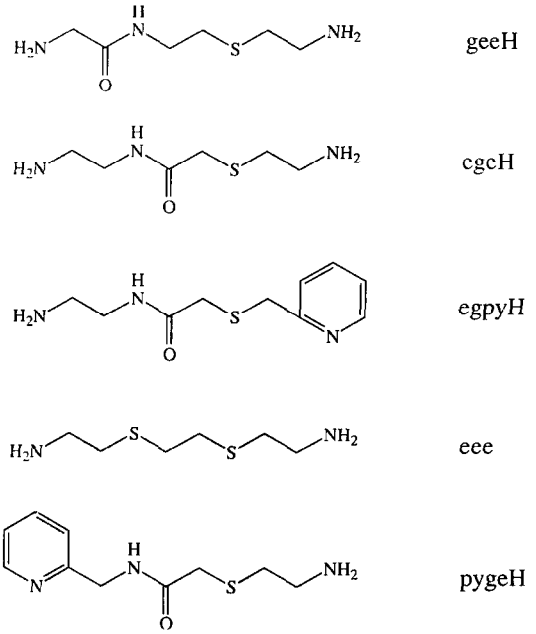

Fig. 2. Structural representations of the ligands in the present study.

EXPERIMENTAL

Materials and methods

^{1}H and ^{13}C NMR spectra were obtained on a Varian XL-300 spectrometer at 299.943 and 75.429 MHz, respectively. Spectra obtained in $CDCl_3$ or Me_2SO-d_6 solution were referenced to tetramethylsilane, while spectra obtained in D_2O solution were referenced to 3-(trimethylsilyl)propionic acid, sodium salt (^{1}H) or dioxane (^{13}C). A Varian DMS-80 spectrophotometer was utilized for visible

spectra at ambient temperature. All melting points are uncorrected. Elemental analyses were determined by Atlantic Microlabs Inc. (Atlanta, Georgia).

Preparation of compounds

Unless otherwise noted, all starting materials and solvents were obtained from standard sources and used without further purification.

N - {2 - [(*benzyloxy*)*carbonyl*]*aminoethyl*} - 2 - S-(*benzyloxy*)*carbonyl*]*mercaptoacetamide* (**2**)

A solution of benzyl chloroformate (17.93 g, 105 mmol) in toluene (25 cm^3) was added to a solution of *N*-(2-aminoethyl)-2-mercaptoacetamide (**1**)[1,14] (6.7 g, 50 mmol) in water at 0–5°C, followed quickly by a solution of $NaHCO_3$ (8.4 g, 100 mmol) in water (50 cm^3). The reaction was stirred vigorously for 35 min. Diethyl ether (20 cm^3) was added and the organic solvents removed on a rotary evaporator to give the white product in essentially quantitative yield. The material decomposed (turned pink) at 120–124°C without truly melting. An analytical sample was obtained from 95% ethanol as the monohydrate. Found: C, 57.33; H, 5.54. Calc. for $C_{20}H_{24}N_2O_6S$: C, 57.13; H, 5.75%. ^1H NMR ($CDCl_3$): δ 7.36 (broadened s, 10 H, aryl), 6.72 (br s, 1 H, NH), 5.26 (s, 2 H, OCH_2), 5.15 (br s, 1 H, NH), 5.11 (s, 2 H, OCH_2), 3.50 (s, 2 H, SCH_2CO), 3.36 (m, 4 H, NCH_2CH_2N). ^{13}C NMR ($CDCl_3$): 170.69, 168.56, 156.92, 136.38, 134.56, 128.79, 128.69, 128.54, 128.48, 128.16, 128.11, 70.00, 66.87, 40.64, 40.30, 34.48.

N - {2 - [(*benzyloxy*)*carbonyl*]*aminoethyl*} - 2 - *mercaptoacetamide* (**3**)

Sodium (1.27 g, 55.2 mmol) was dissolved carefully in absolute methanol (100 cm^3). Protected amino thiol (**2**) (20 g, 49.8 mmol) was added, along with methanol (200 cm^3). The reaction mixture was stirred for 3 h to give a light orange–pink solution. The methanol was removed on a rotary evaporator; then water (*ca* 100–150 cm^3) was added with stirring and the mixture was acidified to pH 3 by dropwise addition of conc. HCl. The off-white product was collected, washed well with water and petroleum ether and dried. Yield 7.88 g (59%); m.p. 109–111°C. Found: C, 53.89; H, 6.09. Calc. for $C_{12}H_{16}N_2O_3S$: C, 53.71; H, 6.01%. ^1H NMR ($CDCl_3$): δ 7.35 (broadened s, 5 H, aryl), 7.09 (br s, 1 H, NH), 5.25 (br s, 1 H, NH), 5.10 (s, 2 H, OCH_2), 3.38 (m, 4 H, NCH_2CH_2N), 3.16 (d, 2 H, SCH_2CO), 1.83 (t, 1 H, SH). ^{13}C NMR ($CDCl_3$): 170.17, 157.13, 136.38, 128.57, 128.24, 128.11, 66.92, 40.72, 40.59, 28.24.

N - {2 - [(*benzyloxy*)*carbonyl*]*aminoethyl*} - 2 - {(2 - [(*benzyloxy*)*carbonyl*]*aminoethyl*)*thio*}*acetamide* (**5**)

To a solution of NaOH (0.362 g, 9.1 mmol) in methanol–water (10 cm^3 : 2.5 cm^3) was added thiol (**3**) (2.43 g, 9.1 mmol) followed by 2-{[(benzyloxy)-carbonyl]amino}ethyl chloride (**4**)[15] (1.93 g, 9.1 mmol). The reaction mixture was heated at reflux for 2 h, then cooled to room temperature. The product precipitated and was collected and washed well with water. The crude product was recrystallized from hot absolute ethanol. Unoptimized yield, 1.21 g (30%); m.p. 131–133°C. Found: C, 58.99; H, 6.07. Calc. for $C_{22}H_{27}N_3O_5S$: C, 59.31; H, 6.11%. ^1H NMR ($CDCl_3$): δ 7.33 (broadened s, 10 H, aryl), 7.19 (br s, 1 H, NH), 5.38 (br s, 2 H, NH), 5.08 (s, 4 H, OCH_2), 3.36 (m, 6 H, NCH_2), 3.18 (s, 2 H, SCH_2CO), 2.65 (t, 2 H, SCH_2CH_2N). ^{13}C NMR ($CDCl_3$): 169.41, 156.61, 136.38, 128.53, 128.18, 128.10, 66.88, 40.91, 40.40, 40.10, 35.98, 33.36 (some accidental equivalences due to the similar environments of the (benzyloxy)carbonyl groups).

N - (2 - *aminoethyl*) - 2 - [(2 - *aminoethyl*)*thio*] *acetamide dihydrobromide* (egeH · 2HBr) (**6**)

Protected egeH (**5**) (1.11 g, 2.5 mmol) was stirred in 32% HBr–acetic acid (12.5 cm^3) for 1 h. At this time, diethyl ether (50 cm^3) was added, and the product collected. The crude material was stirred in absolute ethanol overnight, collected and washed with a little diethyl ether and dichloromethane. Yield 0.42 g (50%); m.p. 158–160°C. Found: C, 21.91; H, 5.13. Calc. for $C_6H_{17}Br_2N_3OS$: C, 21.25; H, 5.05%. ^1H NMR (D_2O): δ 3.55 (t, 2 H, CH_2NDCO), 3.39 (s, 2 H, SCH_2CO), 3.24 (t, 2 H, $SCH_2CH_2ND_2$), 3.17 (t, $D_2NCH_2CH_2ND$), 2.92 (t, 2 H, $SCH_2CH_2ND_2$). ^{13}C NMR (D_2O): 174.04, 39.85, 38.90, 38.01, 35.20, 30.03.

$Co(cge)(NO_2)_2$ (**7**)

To a solution of NaOH (0.05 g, 1.25 mmol) in methanol–water (3 cm^3 : 1.5 cm^3) was added **6** (0.22 g, 0.65 mmol). A solution of $NaNO_2$ (0.09 g, 1.30 mmol) in water (1.5 cm^3) was then added to the reaction mixture, followed by $CoCl_2 \cdot 6H_2O$ (0.15 g, 0.63 mmol). Air was bubbled through the solution for 4 h; after scratching and seeding, the orange product was collected. Yield 0.08 g (39%). Visible (H_2O) and ^{13}C NMR spectra (Me_2SO-d_6) were essentially identical to literature values.[1] ^1H NMR (Me_2SO-d_6): δ 5.60 (br s, 1 H, NH), 4.71 (br s, 1

Table 1. Crystal/refinement data

	7	8	9
Compound	$Co(ege)(NO_2)_2 \cdot 4H_2O$	$Co(egpy)(NO_2)_2$	$[Co(eee)(NO_2)_2]Br$
L	$C_6H_{14}N_3OS$	$C_{10}H_{14}N_3OS$	$C_6H_{16}N_2S_2$
Formula	$C_6H_{22}CoN_5O_9S$	$C_{10}H_{14}CoN_5O_5S$	$C_6H_{16}BrCoN_4O_4S_2$
Mol. wt	399.3	375.3	411.2
Crystal system	Monoclinic	Monoclinic	Monoclinic
Space group	*I2/c*, No. 15	$P2_1/c$, No. 14	$P2_1/a$, No. 14
a (Å)	25.83(2)	7.628(3)	12.719(9)
b (Å)	7.896(6)	12.347(4)	13.855(4)
c (Å)	15.703(8)	16.433(8)	8.033(6)
β (°)	90.36(5)	108.39(3)	111.32(4)
V (Å^3)	3202(3)	1470(1)	1319(1)
D_c (g cm^{-3})	1.66	1.69	2.07
Z	8	4	4
$F(000)$	1664	768	824
μ_{Mo} (cm^{-1})	13.0	13.8	45
Specimen (mm^3)	$0.30 \times 0.08 \times 0.20$	$0.50 \times 0.30 \times 0.25$	$0.45 \times 0.35 \times 0.22$
$2\Theta_{max}$ (°)	60	50	55
N_{unique}	5089	2591	3047
N_{obs}	3105	2249	2300
R	0.038	0.034	0.029
R_w	0.047	0.042	0.035
N_v	199	242	212

H, NH), 3.93 (br s, 1 H, NH), 3.74 (br s, 1 H, NH), 3.66 (d, 1 H, SCH_2CO), 3.31 (d, 1 H, SCH_2CO), 2.5–3.0 (complex m, 8H).

Crystals

Crystals of $[Co(ege)(NO_2)_2] \cdot 4H_2O$ (**7**), $[Co(egpy)(NO_2)_2]$ (**8**)[1] and $[Co(eee)(NO_2)_2]Br$ (**9**)[12] were obtained by slow evaporation of saturated aqueous solutions.

Structure determinations

Unique data sets ($h\ k\ \pm l$) were measured at ~ 295 K using a Syntex $P2_1$ four-circle diffractometer (graphite monochromated Mo-K_α radiation, $\lambda = 0.71069$ Å; 2θ–θ scan mode), yielding N independent reflections, N_0 with $I > 3\sigma(I)$ being considered "observed" and used in the full-matrix least-squares refinement after analytical absorption correction. Anisotropic thermal parameters were refined for the non-hydrogen atoms; for hydrogen atoms, x, y, z were refined in **8** and **9** (U_{iso} constrained) while for **7** all of (x, y, z, U_{iso})$_H$ were constrained at estimated values. Residuals at convergence are quoted on $|F|$; statistical weights derivative of $\sigma^2(I) = \sigma^2(I_{diff}) + 0.0005\sigma^4(I_{diff})$ were used. In no case was refinement of extinction necessary. Neutral atom complex scattering factors were employed;[16] computation used the X-RAY 76 program system[17] implemented by S. R. Hall. Crystallographic and refinement data for **7**, **8** and **9** are compiled in Table 1. Atomic positional parameters, anisotropic thermal parameters, complete tables of bond lengths and angles, hydrogen atom parameters, and tables of observed and calculated structure factors are available from the Editors or Cambridge Crystallographic Data Centre.

RESULTS AND DISCUSSION

New synthesis of the ligand, EgeH

The ligand, egeH (**6**), has been previously synthesized in solution by one of us,[1] but not isolated. The known amino thiol (**1**)[1,14] (Scheme 1) was protected at each terminus with benzyl chloroformate to give protected amino thiol (**2**). All attempts to introduce a (benzyloxy)carbonyl cap only at the amino end, with just one equivalent of protecting reagent, were not successful under various conditions of reaction. However, the desired protected thiol (**3**) could be obtained from **2** by selective cleavage of the thiocarbonate by sodium methoxide and subsequent work-up.

Thiol (**3**) was combined with the known protected alkyl chloride (**4**)[15] under basic conditions to give the protected egeH (**5**). The (benzyloxy)carbonyl caps on **5** were cleaved off with 32% HBr–acetic

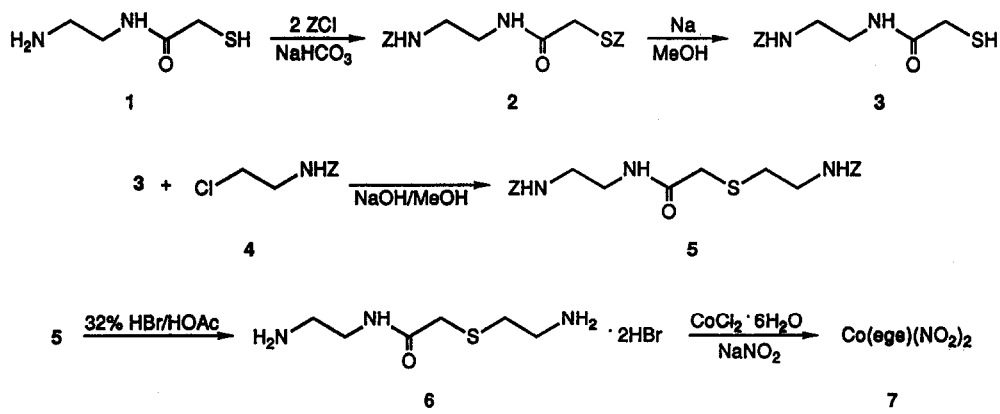

Scheme 1.

acid to provide **6**, from which **7** was prepared in good purity and modest yield.

Structural results

The ligands ege and egpy in this study are designed to coordinate only in the *cis-β* fashion in octahedral cobalt(III) complexes; on the other hand, the symmetrical eee is known to bind only in the *cis-α* mode from spectroscopic studies.[12,13] The control of geometry in these cases originates from the stereochemical preferences of the internal donor atoms of the tetradentate ligand.[1] Thioether donors overwhelmingly tend to coordinate in a pyramidal fashion when situated at the junction of two five-membered chelate rings, in which at least one of the adjacent donor atoms is nitrogen or oxygen.[12,13] This empirical observation likely stems from the longer metal-to-sulphur bond lengths due to the larger radius of sulphur vs nitrogen or oxygen. On the other hand, the atoms in the neighbourhood of a coordinated deprotonated amide nitrogen-donor atom have a strong proclivity for remaining in the same plane in order not to disturb electron delocalization into the carbonyl function.[18] Thus, these two propositions should lead us to anticipate the *cis-β* geometry for the NSNN lignds in this study and explains the previously observed *cis-α* stereochemistry for cobalt(III) eee complexes,[12] which have the NSSN donor set. We point out that for the ligands in the present study, no additional isomers can arise due to the nature of the internal donor atoms (amido or thioether).

The molecular structures of **7**, **8** and **9** are depicted in Figs 3, 4 and 5, respectively. For each of the three structure determinations, one formula unit comprises the asymmetric unit of the centrosymmetric unit cell. The ligand disposition in both **7** and **8** is *cis-β*, while in **9** it is *cis-α* as expected. The geometries of the cobalt environments are col-

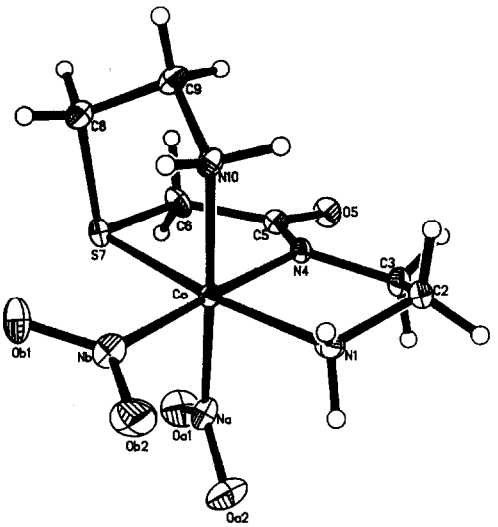

Fig. 3. Perspective view of the structure (20% probability ellipsoids) and atom labelling scheme for the non-hydrogen atoms of **7**; hydrogen atoms have arbitrary radii of 0.1 Å.

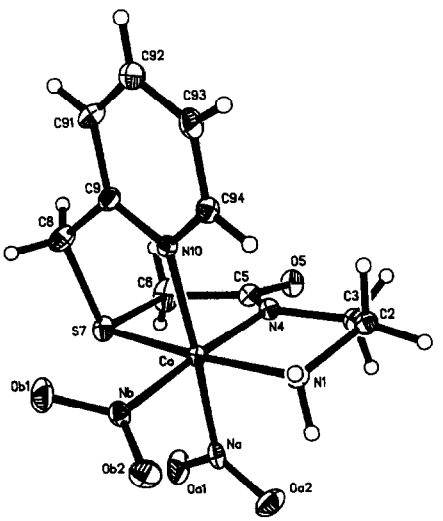

Fig. 4. Perspective view of the structure (20% probability ellipsoids) and atom labelling scheme for the non-hydrogen atoms of **8**; hydrogen atoms have arbitrary radii of 0.1 Å.

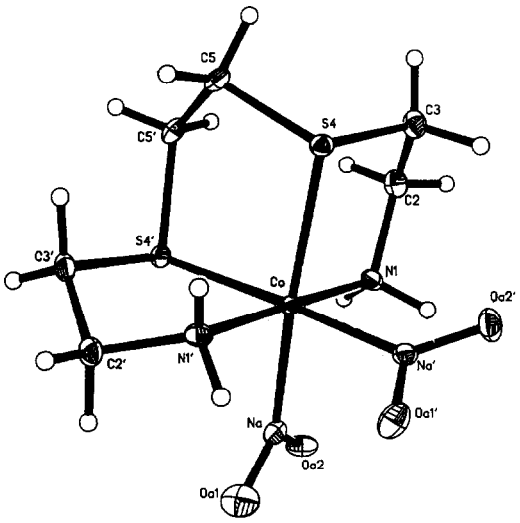

Fig. 5. Perspective view of the structure (20% probability ellipsoids) and atom labelling scheme for the non-hydrogen atoms of **9**; hydrogen atoms have arbitrary radii of 0.1 Å.

lected in Table 2; for the *cis*-β complexes, these are very similar, requiring the opposition of N(1) to S(7) and N(4,10) to N(b,a). For these latter, the geometrical parameters (Table 2) are generally very similar to those of $[Co(pyge)(NO_2)_2]\cdot H_2O$ (**10**)[11] and $[Co(gee)(NO_2)_2]\cdot H_2O$ (**11**).[1] Unusually large discrepancies noted are: (i) a large spread in the N(10)—Co—N(1,4) angles, presumably at least partly consequent upon the aliphatic or aromatic nature of N(10) and the presence or absence of H(94) in proximity to the hydrogen atom on N(1); (ii) an abnormally large N(1)—Co—N(b) angle in **10**[11] (compared to **7**, **8** or **11**) again presumably a consequence of the hydrogen atom *ortho* to the nitrogen atom of the aromatic ring in proximity to O(b2). Consistent large differences in Co—N(1) and Co—N(4) for compounds **7**, **8**, **10** and **11** are found throughout. It is notable that N(1) and N(4) are opposed to thioether and nitro ligating atoms, respectively; in addition, N(4) is deprotonated, which might lead to an anticipated shorter bond length.[1] As might be expected, the results for the ege derivative, **7**, most closely parallel those previously obtained for the gee analogue, **11**,[1] with the most significant differences being the angles N(4)—Co—N(10,a) (ege, 92.2(1), 88.9(1)°; gee, 90.5(1), 91.9(1)°).

The Co—NO_2 distances in **7** and **8** are within the usual range found in analogous cobalt(III) complexes.[19] The difference in Co—N(a,b) in the gee

Table 2. The cobalt environments

7	r^a	N(4)[b]	S(7)	N(10)	N(a)	N(b)
N(1)	1.952(3)	85.0(1)	171.9(1)	91.2(1)	90.9(1)	93.7(1)
N(4)	1.898(2)		87.12(9)	92.2(1)	88.9(1)	178.3(2)
S(7)	2.238(1)			87.62(8)	90.51(9)	94.3(1)
N(10)	1.985(3)				177.8(2)	88.8(1)
N(a)	1.930(3)					90.1(1)
N(b)	1.926(3)					
8	r^a	N(4)[b]	S(7)	N(10)	N(a)	N(b)
N(1)	1.955(3)	84.7(1)	171.56(7)	94.9(1)	88.7(1)	94.7(1)
N(4)	1.912(2)		86.9(1)	93.8(1)	87.6(1)	176.4(1)
S(7)	2.225(1)			86.90(9)	89.7(1)	93.6(1)
N(10)	2.007(3)				176.3(1)	89.7(1)
N(a)	1.939(3)					88.8(1)
N(b)	1.911(3)					
9	r^a	S(4)[b]	S(4′)	N(1′)	N(a)	N(a′)
N(1)	1.972(3)	87.4(1)	94.1(1)	179.3(6)	88.8(1)	90.7(1)
S(4)	2.271(2)		90.53(7)	93.3(1)	175.5(2)	90.5(1)
S(4′)	2.273(2)			86.1(1)	92.2(1)	175.1(2)
N(1′)	1.960(3)				90.5(1)	89.0(1)
N(a)	1.947(4)					87.2(1)
N(a′)	1.954(3)					

[a] Metal–ligand distance (Å).

[b] Other entries are the angles (°) subtended at the metal by the relevant atoms at the head of the row and column.

Table 3. Ligand torsion angles (°)[a]

Atoms	7	8	10[b]
Co—**1**—2—3	−36.1	−37.6	0.3
1—2—3—4	42.0	43.1	−7.0
2—3—**4**—Co	−30.6	−30.5	10.9
2—3—**4**—5	168.1	171.3	−171.2
3—**4**—5—6	173.2	172.5	−175.6
Co—**4**—5—6	13.6	16.6	2.1
4—5—6—S	−5.9	−9.1	8.9
5—6—S—Co	−2.1	−0.1	−13.1
5—6—S—8	98.0	102.1	87.3
6—S—8—9	−69.8	−89.6	−72.6
Co—S—8—9	30.0	11.2	28.4
S—8—9—**10**	−50.7	−15.4	−48.7
8—9—**10**—Co	48.0	11.3	46.5

[a] Carbon atoms are denoted by number only; nitrogen atoms are in bold type.

[b] Reference 11.

adduct (**11**) (1.941(2), 1.920(2) Å)[1] parallels that observed in **7** and **8**, possibly reflecting slightly different *trans* effects of amine and amide nitrogens.

The eee cation in **9** is potentially of C_2 symmetry;[13] this is reflected in the geometry of Table 2. Relative to the other complexes, significant elongations are noted in both the average Co—S and Co—NO_2 bond lengths, which now lie *trans* to each other.

In each complex, there is considerable strain in the vicinity of the coordinated thioether atom(s), as evidenced by small Co—S—C (97.9–104.4°) and C—S—C (101.4–104.2°) angles. Ligand torsion angles for **7**–**9** are provided in Table 3. The relative planarity about N(4) is quite apparent in these values. In addition, a possible explanation for why the egpy derivative (**8**) is less robust than the ege (**7**), pyge (**10**) and gee (**11**) complexes can be put forth. Previous work[1] had determined that **8** can not be derivatized like **7**, **10** and **11** with concentrated HCl to give violet $[Co(L)Cl_2]$ (L = tetradentate ligand). In the egpy case, green solutions resulted, suggesting that possibly the pyridyl donor was being displaced. The pyridyl donor in **8** causes the out-of-plane chelate ring to flatten by the nature of the aromatic ring. This presumably causes further strain around the coordinated thioether atom as evidenced by the torsion angles involving S(7). In the concentrated acid, this angular strain can be relieved by substitution and protonation of the pyridyl group by the HCl.

Of course, the in-plane chelate ring in the pyge analogue (**10**) is also flattened by the pyridyl donor here.[11] However, the other in-plane chelate ring is already very planar due to the constraints invoked by the deprotonated amide, N(4) (*vide supra*), so that apparently this additional flattening causes very little extra strain about N(4).

Acknowledgements—We gratefully acknowledge the generous support of the State University of New York at Albany Faculty Research Program (P.J.T.), the Australian Research Council (A.H.W.), and NIH Grant GM 29225 (to L. G. Marzilli) for work carried out at Emory University.

REFERENCES

1. P. J. Toscano and L. G. Marzilli, *Inorg. Chem.* 1983, **22**, 3342 and refs therein.
2. J. A. Chamber, T. J. Goodwin, P. A. Williams, F. S. Stephen and R. S. Vagg, *J. Coord. Chem.* 1988, **17**, 277 and refs therein.
3. M. Yashiro, S. Yano, M. Ajioka and S. Yoshikawa, *Inorg. Chem.* 1985, **24**, 3607 and refs therein.
4. P. A. Sutton and D. A. Buckingham, *Accts Chem. Res.* 1987, **20**, 357.
5. M. Yashiro, M. Ajioka, S. Yano, K. Toriumi, T. Ito and S. Yoshikawa, *Inorg. Chem.* 1986, **25**, 1709.
6. J. A. Muir, M. M. Muir, R. Saez and C. F. Campana, *Acta Cryst.* 1987, **C43**, 1487.
7. T. M. Suzuki, T. Kimura and J. Fujita, *Bull. Chem. Soc. Jpn* 1980, **53**, 77 and refs therein.
8. J. Cragel, Jr. and G. R. Brubaker, *Inorg. Chem.* 1972, **11**, 303.
9. R. G. Asperger, *Inorg. Chem.* 1969, **8**, 2127.
10. B. F. Anderson, J. D. Bell, D. A. Buckingham, P. J. Cresswell, G. J. Gainsford, L. G. Marzilli, G. B. Robertson and A. M. Sargeson, *Inorg. Chem.* 1977, **16**, 3233.
11. P. J. Toscano, K. A. Belsky, L. M. Englehardt, K. J. Fordon and A. H. White, *Inorg. Chem.*, 1990, in press.
12. (a) J. H. Worrell and D. H. Busch, *Inorg. Chem.* 1969, **8**, 1563; (b) J. H. Worrell and D. H. Busch, *Inorg. Chem.* 1969, **8**, 1572.
13. (a) B. Bosnich, W. R. Kneen and A. T. Phillip, *Inorg. Chem.* 1969, **8**, 2567; (b) B. Bosnich and A. T. Phillip, *J. Chem. Soc. A* 1970, 264.
14. E. R. Atkinson, G. R. Handrick, R. J. Bruni and F. E. Granchelli, *J. Med. Chem.* 1965, **8**, 29.
15. E. Katchalski and D. B. Ishai, *J. Org. Chem.* 1950, **15**, 1067.
16. *International Tables for X-ray Crystallography* (Edited by J. A. Ibers and W. C. Hamilton), Vol. 4. The Kynoch Press, Birmingham (1974).
17. J. M. Stewart (Ed.), The X-ray System-version of March 1976, Technical Report TR-446. Computer Science Center, University of Maryland (1976).
18. H. C. Freeman, *Adv. Protein Chem.* 1967, **22**, 257.
19. R. Herak, N. Juranic and M. B. Celap, *J. Chem. Soc., Chem. Commun.* 1980, 660.

Polyhedron Vol. 9, No. 8, pp. 1087–1090, 1990
Printed in Great Britain

0277–5387/90 $3.00+.00
© 1990 Pergamon Press plc

UV-VISIBLE AND IR SPECTRA OF IRON(II) PHTHALOCYANINE POLYMER COMPLEXES LINKED BY BIS-PYRIDINATO LIGANDS

KARIFA BAYO and GUY VENANCE OUEDRAOGO

I.N.C. Université de Ouagadougou, Burkina Faso

and

GEORGES TERZIAN and DAVID BENLIAN*

Laboratoire de Chimie de Coordination, Université de Provence D22,
Av. Escadrille Normandie-Niemen, 13397 Marseille Cedex 13, France

(*Received* 20 *September* 1989; *accepted* 8 *December* 1989)

Abstract—The spectra of iron(II) phthalocyanine polymer complexes $(FePcL)_n$ with bis-pyridinato bridging ligands, where L = 44′-bipyridine (bpy), *trans*-1,2-(4-pyridyl)ethylene (bpe), 1,2-bis-(4-pyridyl)ethane (bpa), are discussed in comparison with the spectra of $Fe^{II}Pc$ and $FePcL'_2$, where L′ = pyridine, 4-cyanopyridine (4CNpy), in reference to the π back-donation to the macrocycle.

Phthalocyaninato iron(II) is a widely investigated porphyrin-like molecule which exhibits a strong tendency to axial ligation. A former study of many of its adduct complexes with pyridine and substituted pyridines gave a consistent view of the axial and equatorial π-bonding in the series.[1,2]

Recently, many papers have reported on linear FePc polymers in which iron atoms are axially linked by conjugated π-electron-containing bridging ligands.[3–6] The main objective is to create conducting materials based on a linear chain arrangement of transition-metal centred molecules. However, the electronic properties of the iron atom in such complexes has to be completely established in relation with the observed spectral data.

We report on UV-vis and IR spectrometric results of $(FePcL)_n$, where L = bpy, bpe, bpa, and we compare them with the spectra of $Fe^{II}Pc$, $FePc(py)_2$ and $FePc(4CNpy)_2$. New information is provided on the interplay of axial and equatorial back-donation from the metal.

EXPERIMENTAL

The reagents for the syntheses are commercial grade and the solvents used in spectrometric experiments are spectral grade.

$Fe^{II}Pc$ and $FePcL'_2$ (L′ = py, 4CNpy) were prepared as previously described.[2]

Two routes were followed to prepare $(FePcL)_n$: L = 44′-bipyridine (bpy), *trans*-1,2-(4-pyridyl) ethylene (bpe), 1,2-bis(4-pyridyl)ethane (bpa).

(i) 0.5 g of $Fe^{II}Pc$ and 0.5 g of L were mixed in 50 cm^3 of acetonitrile and the mixture refluxed for 3 h. Then, the initially green solution became colourless and a blue solid compound precipitated. The solid was collected and washed several times.

(ii) A ground mixture of 0.5 g of FePc and 3 g of L were fused at 260°C and heated at this temperature for 3 h. After cooling, the blue solid residue was ground, washed several times with distilled water and ethanol and dried.

UV-vis spectra were recorded on a Philips PU 8800 spectrometer using the second derivative recording in saturated DMSO solutions or finely ground solid dispersed in KBr.

IR spectra were recorded on Nicolet FT 20SXB and 20F spectrometers, using KBr and PE pellets, collecting 128 scans at 1 cm^{-1} resolution.

RESULTS AND DISCUSSION

Both routes to $(FePcL)_n$ yield the same compound identified by IR, UV-vis and Mössbauer spectra. Analogous procedures have been used to

* Author to whom correspondence should be addressed.

prepare pyrazine (pyz) derivatives of FePc.[4] The Fe content of our compounds determined by atomic absorption spectroscopy agrees neither with $FePcL_2$ nor $(FePcL)_n$ with a defined n value. We think these compounds may be a mixture of different polymer species. However, Mössbauer spectroscopy revealed only one site for Fe nuclei in this type of compound.[6,7]

ELECTRONIC ABSORPTION SPECTRA

The electronic data are grouped in Table 1. We have compared, where possible, our spectra of finely ground solid dispersed in KBr to solution spectra of the same compound and observe an agreement within 2–3 nm for the band maxima.

The characteristic π–π^* transition band is observed both for $(FePcL)_n$ and $(FePcL'_2)$ at *ca* 652 nm except for L = bpe in which it appears at 680 nm.

Compared to FePc, several supplementary bands appear between 400 and 590 nm in all spectra. $FePc(py)_2$ and $(FePcbpa)_n$ show one band at 415 nm in the spectra while two bands are observed at 415 and 500 nm in the spectra of $FePc(4CNpy)_2$, $(FePcbpy)_n$ and $(FePcbpe)_n$.

In a previous study of an extended series of $FePcL'_2$ (L′ = py and substituted pyridine),[2] we showed that the band at 410 nm, initially attributed to an Fe–L′ charge-transfer band, is in fact L′–Pc CT *via* Fe d_π bonds. We also have attributed the band at 500 nm to Fe–L′ CT as it only appeared in the spectra of complexes where the axial pyridine is markedly "π-acceptor".

Our results on bridged polymers confirm these assignments. Besides, M–L charge-transfer bands have been observed with this type of bidentate ligand used in this work. As one needs a suitable basis for the comparison of their electronic overlap properties, we can use the data collected on carbonyl or ammine complexes of the same ligands which have been extensively investigated (M = Cr, Fe, Co, W, Ru, etc.). All these complexes have CT bands at 450–500 nm assigned to metal to ligand transfer.[8–11] In a similar way, M–L CT bands have been reported at 400–600 nm in axially substituted (Fe, Ru, Os) porphyrins[12–16] or porphyrin-type macrocyclic iron complexes.[17] Recent MO calculations have shown that ring π back-donation is stronger in $Fe^{II}Pc$ than in Fe^{II} porphyrins explaining the relatively easy oxidation of the latter.[18] In the case of axially coodinated FePc the charge transfer to the d_π (d_{xz}, d_{yz}) orbitals appears to be strong enough to increase the back-bonding from the metal to the ring LUMO. The extent of back-bonding in $FePcL_2$ is stronger than in $Fe^{II}Pc$.[18]

According to these considerations, our electronic absorption results are in good agreement with an analysis based on π back-donation in the $(FePcL)_n$ and $FePcL'_2$ compounds. The conjugation in the bpy and bpe ligands makes the pyridine rings behave, each with regard to the other, as a withdrawing group like the 4-cyano groups. However the CN group is a stronger π-electron acceptor than the pyridine ring. As 4CNpy is only linked to the metal by the ring nitrogen, there is no chain formation.[7,19]

We have shown in our previous Mössbauer studies that substituted pyridines behave mainly as "σ donors".[8] It seems that the conjugation in bpy and bpe does not markedly perturb this property, as the spectra of $(FePcbpy)_n$ and $[FePcbpe)_n$ exhibit a L–Pc CT band at 415 nm like those of $(FePcbpa)_n$ and $FePc(py)_2$. The position of this band at 406 nm in the spectrum of $FePc(4CNpy)_2$ is consistent with the stronger electron withdrawing property of the cyano group.

The band at 500 nm in the spectra of $(FePcbpy)_n$, $(FePcbpe)_n$ and $FePc(4CNpy)_2$ does not exist in the spectra of $Fe^{II}Pc$, $FePc(py)_2$ and $(FePcbpa)_n$. There is no conjugation between the two pyridine rings of bpa. Hence this ligand acts as two linked, but independent, pyridine molecules explaining the fact that the spectra of $(FePcbpa)_n$ and $FePc(py)_2$ are similar and only exhibit the L–Pc CT band.

Table 1. Electronic absorption spectra, λ_{max} (nm)

FePc	$FePc(Py)_2$	$FePc(4CNPy)_2$	$FePc(bpy)_n$	$FePc(bpa)_n$	$FePc(bpe)_n$
325	328	327	327	328	346
	415	406	415	416	416
		502	484		460
588	590	589	590	590	611
619	622	621	622	623	650
652	653	652	653	652	680

Table 2. Medium range IR bands (cm^{-1})

FePc	$FePc(Py)_2$	$FePc(4CNPy)_2$	$FePc(bpy)_n$	$FePc(bpa)_n$	$FePc(bpe)_n$
	1590[a]	1591[a]	1591[a]		1594[a]
1514m	1510s	1508s	1510s	1510s	1510s
1421m	1421s	1422s	1421s	1422s	1422s
			1403[a]		
1332vs	1328s	1329s	1330s	1331vs	1328s
1288s	1288s	1288s	1289s	1289s	1289s
	1218[a]				
1164m	1165s	1164s	1166s	1164s	1164s
1118vs	1120vs	1119vs	1119vs	1119vs	1119vs
1081s	1091s	1097s	1097s	1095s	1098s
			806[a]	821m[a]	823m[a]
779m	778m	778m	779m	779m	779m
753s	752s	752s	753s	753s	753s
729s	728vs	735s	733vs	733vs	734vs

vs: very strong, s: strong, m: medium intensity.
[a] Vibration band observed in the free ligand.

Table 3. Low frequency IR bands (cm^{-1})

FePc	$FePc(Py)_2$	$FePc(4CNPy)_2$	$FePc(bpy)_n$	$FePc(bpa)_n$	$FePc(bpe)_n$
	472	483	492	486	497
436	442	441	441	436	444
	403				403
365	366		365	365	
308	330	328	325	331	321
300	300	300	301	300	302
233	239	237	229	233	235

INFRARED SPECTRA

Infrared high-frequency and low-frequency data are listed in Tables 2 and 3.

The similarity between the IR spectra of phthalocyanine (H_2Pc) and metallophthalocyanines in the 1800–400 cm^{-1} region allows us to attribute the numerous vibrational bands to the macrocycle vibrational modes. All these bands consist of strongly coupled νCC, νCN, δCH and δCCN modes. Important modifications are noted in the 800–700 cm^{-1} region which corresponds to the CH deformations of the benzene and pyridine rings.[21–23]

The frequencies and the intensities of the peripheral CH deformation bands are sensitive to the stacking in the lattice. When the polymer is formed, the Pc molecules lie apart from each other with much less interaction than, for instance, in any crystalline modification of FePc.

The axially substituted species show bands of the ligands between 1600 and 1200 cm^{-1}. The strong band at 1590 cm^{-1} in the spectra of free ligands is slightly low shifted for $FePc(py)_2$ while it remains almost constant in frequency in the spectra of $(FePcbpy)_n$ and $(FePcbpe)_n$. An important loss of intensity in all the cases is the main feature.

We focus on two bands at 1332 and 1288 cm^{-1} in the Fe^{II} spectrum. In the $(FePcL)_n$ series the band at 1288 cm^{-1} appears to remain almost constant in frequency and intensity while the band at 1332 cm^{-1} varies in two ways: down shift to 1328 cm^{-1} and loss of relative intensity. We relate this effect to the π overlap in the chain. This influence on π bonding sensitive vibrations in the series of ligands can be referred to the similar effect observed in the spectra of $(CO)_5W$–L–$W(CO)_5$,[9] in which bpe appears to be the most effective in delocalizing the π charges between the $W(CO)_5$ moieties.

The remaining FePc bands are kept nearly constant except the group below 1110 cm^{-1} which derives from the composite band at 1081 cm^{-1} in $Fe^{II}Pc$. Under axial substitution, this band is split in 1098–1070 cm^{-1} in bpe, 1097–1071 cm^{-1} in

bpy, 1095–1081 cm^{-1} in bpa and 4CNpy through π coupling. The constancy is confirmed at 912, 820, 779, 753 and 730 cm^{-1}.

In the 500–50 cm^{-1} region, $Fe^{II}Pc$ has four characteristic bands (Table 3). Low frequency spectra are sensitive to the charge densities around the metal and supply useful data on the core structure of phthalocyanines.[24] The result of axial ligation of pyridine bases is a supplementary band at *ca* 400 cm^{-1} easily assigned to the ring deformations of L. Out of plane deformation modes of Pc assigned at 365 and 435 cm^{-1} remain nearly constant and show no obvious dependence on the ligands. On the other hand, the Fe–N_4 stretching at 308 cm^{-1} shifts largely towards the high frequencies in the spectra of axially substituted compounds. The observed shift is bpa > bpy > bpe for $(FePcL)_n$ and py > 4CNpy for $FePcL'_2$. This trend of variation follows the overall donor capacity of the bridging ligands. This mode of vibration involves the relative positions of Fe and ligand atoms in an almost constant "σ skeleton". The movement of Fe makes the π bonding region between Fe d_π orbitals and equatorial and axial π orbitals change markedly. The interplay of axial versus equatorial back-bonding determines the charge distribution in the complex.

Consequently the frequency of this vibrational mode is related to the importance of the π overlaps. Then the variation of νFe–N_4 is in good agreement with that of the Fe–L CT band in $(FePcL)_n$ electronic absorption spectra.

CONCLUSION

UV-vis and IR data on our homogeneous series of $(FePcL)_n$ polymers show evidence for three features depending on the conjugation of π bonds in the bridging ligands L:

(i) An Fe–L CT band near 500 nm is observed with bpa > bpy > bpe, showing that the π acceptor capacity is modulated by the extent of conjugation in the bridge.

(ii) The IR high-frequency bands of the axially substituted complexes of FePc remain almost constant except for the 1332 cm^{-1} absorption which shows strong dependence on the π overlaps between axial and equatorial systems through the d_π orbitals of Fe.

(iii) The Fe–N_4 stretching band at 308 cm^{-1} in FePc is remarkably sensitive to the interplay between axial and equatorial back-bonding as shown by the good correlation with the Fe–L CT electronic absorption.

REFERENCES

1. G. V. Ouedraogo, D. Benlian and L. Porte, *J. Chem. Phys.* 1980, **73**, 642.
2. G. V. Ouedraogo, C. More, Y. Richard and D. Benlian, *Inorg. Chem.* 1981, **20**, 4387.
3. C. W. Dick, T. Inabe, K. F. Schoch Jr. and T. J. Marks, *J. Am. Chem. Soc.* 1983, **105**, 1539.
4. O. Schneider and M. Hanack, *Angew.Chem.* 1980, **19**, 392.
5. J. Metz and M. Hanack, *J. Am. Chem. Soc.* 1983, **105**, 828.
6. H. H. Wei and H. L. Shyu, *Polyhedron* 1985, **6**, 979.
7. G. V. Ouedraogo, Thesis Université de Provence (1981).
8. J. J. Jwo, P. L. Gaus and A. Haim, *J. Am. Chem. Soc.* 1979, **101**, 6184.
9. M. M. Zulu and A. J. Lees, *Inorg. Chem.* 1988, **27**, 1139.
10. M. M. Zulu and A. J. Lees, *Inorg. Chem.* 1988, **27**, 3325.
11. J. C. Curtis, J. S. Bernstein and T. J. Meyer, *Inorg. Chem.* 1985, **24**, 385.
12. H. Ogoshi, E. Watanabe, Z. Yoshida, J. Kincaid and K. Nakamoto, *J. Am. Chem. Soc.* 1973, **95**, 2845.
13. G. A. Schick and D. F. Bocian, *J. Am. Chem. Soc.* 1984, **106**, 1682.
14. N. J. Boldt, K. E. Goodwill and D. F. Bocian, *Inorg. Chem.* 1988, **27**, 1188.
15. P. G. Wright, P. Stein, J. M. Burke and T. G. Spiro, *J. Am. Chem. Soc.* 1979, **101**, 3531.
16. S. Choi, T. G. Spiro, K. C. Languy, K. M. Smith, D. L. Budd and G. N. La Mar, *J. Am. Chem. Soc.* 1982, **104**, 4335.
17. D. Dolphin, J. R. Sans, T. B. Tsin and K. L. Wong, *J. Am. Chem. Soc.* 1976, **98**, 6970.
18. C. Fierro, A. B. Anderson and D. A. Scherson, *J. Phys. Chem.* 1988, **92**, 6902.
19. J. Burgess, *Spectrochim. Acta* 1968, **24A**, 1645.
20. K. Nakamoto, *Infrared and Raman Spectra of Inorganic and Coordination Compounds*, 4th edn. John Wiley, New York (1987).
21. M. Abkowitz, I. Chen and J. H. Sharp, *J. Chem. Phys.* 1968, **48**, 4561.
22. A. M. Ebert and B. Gotilieb, *J. Am. Chem. Soc.* 1952, **74**, 2806.
23. B. D. Berez, in *Coordination Compounds of Porphyrins and Phthalocyanines*. Nauka, Moscow (1978).
24. G. Terzian, B. Moubaraki, M. Mossoyan-Deneux and D. Benlian, *Spectrochim. Acta* 1989, **45A**, 675.

Polyhedron Vol. 9, No. 8, pp. 1091–1094, 1990
Printed in Great Britain

0277–5387/90 $3.00+.00
© 1990 Pergamon Press plc

A SCHIFF BASE DERIVED REDOX-RESPONSIVE RECEPTOR MOLECULE AND RELATED COMPOUNDS WITH POTENTIAL AS NON-LINEAR OPTICAL MATERIALS

PAUL D. BEER* and HARRISON SIKANYIKA

Department of Chemistry, University of Birmingham, P.O. Box 363, Birmingham B15 2TT, U.K.

(*Received* 31 *October* 1989; *accepted* 8 *December* 1989)

Abstract—A new Schiff base redox-responsive receptor molecule (**8**) containing a ferrocene redox-active centre and a benzo-15-crown-5 metal cation binding unit is reported. The reversible redox couple of **8** shifts anodically on addition of Na^+, K^+ and Mg^{2+} guest cations. The synthesis and electrochemical properties of two related ferrocenyl Schiff base compounds (**9** and **10**) possessing electron-donor and -acceptor moieties which have potential as non-linear optical materials are also reported.

We and others[1] have demonstrated that reducible[2–4] or oxidizable[5–7] redox-active macrocyclic receptor molecules can electrochemically recognize[1] cationic (metal, ammonium[8]) and anionic (bromide)[9] guests either "through space" electrostatic perturbation and/or via various conjugated bond linkages linking the heteroatoms of the ionophore to the redox centre. The magnitude and type (one- or two-wave) of the shift in the respective couple of these host systems produced by charged guest binding is dependent upon a combination of many factors[1] including: (i) redox-active host–guest complementarity; (ii) the charge/radius ratio or polarizing power of the guest; (iii) proximity of host binding site to redox centre; (iv) nature of redox centre; and (v) nature of bond linkage from host binding site to redox centre. With respect to studying the latter factor we report here the synthesis, coordination and electrochemical properties of a new redox-responsive receptor molecule (**8**) in which a ferrocene redox-active centre is linked to a benzo-15-crown-5 cation binding unit via a conjugated Schiff base covalent bond and two related compounds (**9** and **10**) possessing electron-donor and -acceptor moieties which have potential as new non-linear optical (NLO) materials.

* Author to whom correspondence should be addressed.

RESULTS AND DISCUSSION

4-Ferrocenylaniline (**2**) was prepared via the Sn/HCl reduction of 4-ferrocenylnitrobenzene (**1**).[10] Condensation of **2** with 3,4-dimethoxybenzaldehyde (**3**), 4-formylbenzo-15-crown-5 (**4**),[11] *p*-nitrobenzaldehyde (**5**) and 2,4-dinitrobenzaldehyde (**6**) gave the respective Schiff base products, **7**–**10**, in generally excellent yields (Scheme 1). The new, air-stable compounds were characterized by elemental analyses, fast atom bombardment mass spectrometry (FABMS), IR and ^1H NMR spectroscopy (see Experimental).

The elecrochemical properties of **7**–**10** were investigated using cyclic voltammetry in anhydrous acetonitrile with $[n\text{-}Bu_4N]BF_4$ as supporting electrolyte and the results are presented in Table 1. Each compound exhibits a reversible redox oxidation wave in the range +0.40 to +0.50 V (vs SCE) typical of a substituted ferrocene derivative. Comparing these values it is surprising that electrochemically the powerful electron-withdrawing nitro groups present in **9** and **10** have very little effect on the ferrocenyl redox couple of each compound, suggesting that inductive communication through the Schiff base bond linkage is extremely weak. Cyclic voltammograms were also recorded after progressive addition of stoichiometric molar equivalents of Na^+, K^+ and Mg^{2+} cations to the electrochemical solutions of **7** and **8**. The addition of any of the

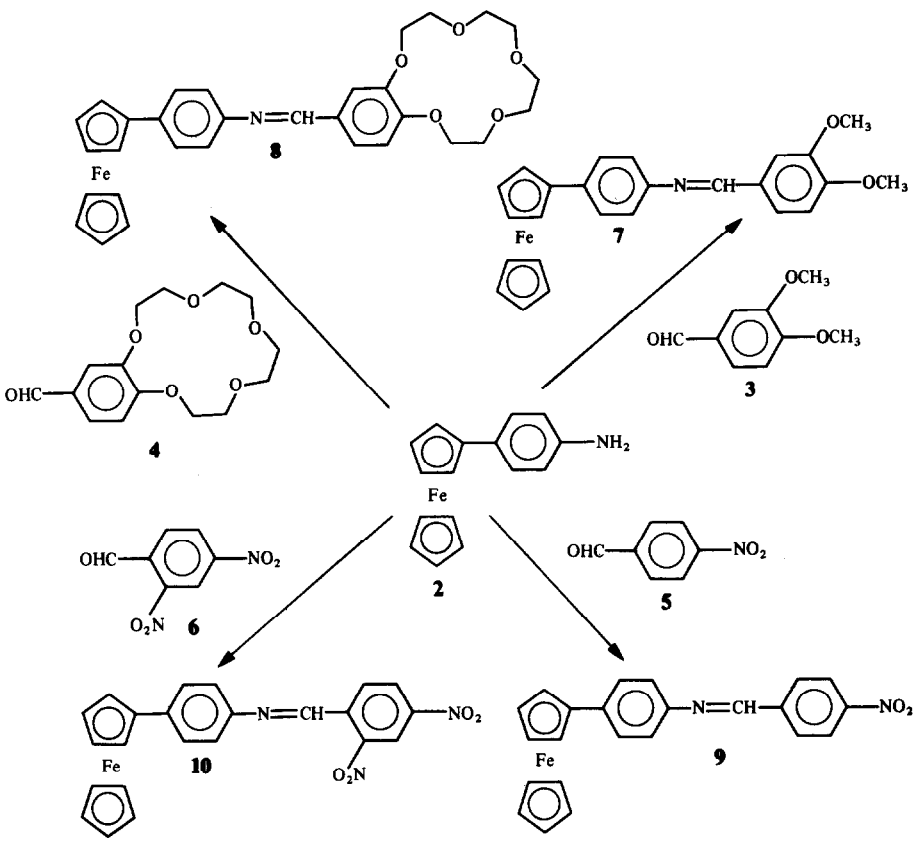

Scheme 1.

three metal cations to **7** had negligible effect on the ferrocene/ferricinium redox potential ($\Delta E_{1/2} \leqslant 5$ mV). The redox couple of **8**, however, shifted anodically by 10, 20 and 60 mV on addition of four equivalents of K^+, Na^+ and Mg^{2+} cationic guests, respectively. The magnitudes of these shifts reflect the differing polarizabilities of the bound metal cations, Mg^{2+} possessing the largest charge/radius ratio produces the greatest value of anodic shift, and K^+ the smallest. These findings are in agreement with those found with the *cis* and *trans* olefinic-linked ferrocene-benzo-15-crown-5 ionophores (**11a** and **11b**) in which K^+, and Na^+ produce modest shifts of 20 and 30 mV, respectively, whereas with Mg^{2+} a $\Delta E_{1/2}$ value of 70 mV is observed.[12] It is noteworthy that although compared to **11** receptor **8** contains an extended conjugated Schiff base bond linkage from the ferrocene redox centre to the benzo-crown-ether binding unit, the magnitude of $\Delta E_{1/2}$ values produced by metal cation binding are similar.

Table 1. Electrochemical data

Compound	$E_{1/2}$ (V)[a]	ΔE_p (mV)[b]
7	+0.44	80
8	+0.44	80
9	+0.46	80
10	+0.46	80

[a] Obtained in acetonitrile solution containing 0.2 M $[n\text{-}Bu_4N]BF_4$ as supporting electrolyte. Potentials were measured with reference to SCE at 24 ± 1°C at 0.2 V s^{-1} scan rate.

[b] Separation between anodic and cathodic peak potentials of cyclic voltammograms; values for ferrocene under the same conditions ranged from 75 to 85 mV.

Interestingly, addition of one equivalent of Mg^{2+} to **9** led to an unexpected anodic shift of 50 mV in the ferrocene/ferricinium redox couple accompanied by a large decrease in the peak current. Additional equivalents of Mg^{2+} did not induce any further shift in the redox potential but resulted in a progressive decrease in the peak current. These observations infer the Mg^{2+} cation interacts with the remote nitro group of **9** with the metal cation influencing the charge distributions of the respective canonical representations shown in Fig. 1.

Considerable interest is currently being shown in the synthesis of new materials with NLO properties

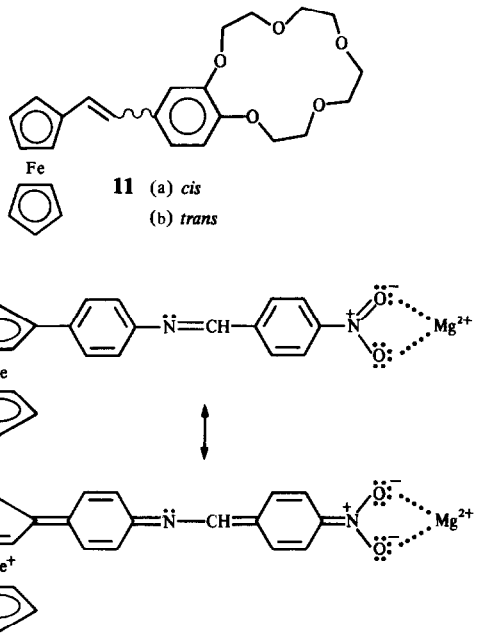

Fig. 1. Proposed interaction of Mg^{2+} with **9**.

which have applications in laser technology, telecommunications and integrated optical devices.[13] Non-centrosymmetric, highly polarizable organic[14] and organometallic[15] conjugated molecular systems bearing a donor group at one end and an acceptor group at the other have been shown to produce materials displaying large macroscopic optical nonlinearity.

Compounds **9** and **10** possess some of these features and an initial indication of potential NLO behaviour can be elucidated from solvation effects on solution UV–vis spectra. The UV–vis spectrum of **10** is markedly affected by varying the solvent. In hexane two absorptions at 390 and 530 nm are observed, whereas in N,N′-dimethylformamide large hypsochromic shifts to 380 and 500 nm are observed. In contrast, the analogous UV–vis spectra of the crown compound **8** was expectedly unaffected by solvent variation. As a result of this solvatochromic behaviour of **10** it is currently being screened for second-harmonic generation (SHG) and the results will be reported in a future paper.

EXPERIMENTAL

General

^{1}H NMR spectra were recorded at 400 and 270 MHz using TMS as internal standard. IR spectra were obtained on a Perkin–Elmer 297 instrument as KBr discs. Electrochemical measurements were carried out using a PAR 174 polarographic analyser.

4-Ferrocenylnitrobenzene (**1**)[10] and 4-formylbenzo-15-crown-5 (**4**)[11] were prepared according to literature methods. All elemental analyses were performed at the University of Birmingham's Microanalytical Department.

Syntheses

Preparation of 4-*ferrocenylaniline* (**2**). A three-necked, 500 cm^3, round-bottomed flask was equipped with a mechanical stirrer and a reflux condenser. To this, a solution of 4-ferrocenylnitrobenzene (1.88 g, 6.12 mmol) in concentrated HCl (25 cm^3) and absolute ethanol (40 cm^3) was added, followed by tin granules (4.5 g, 37.82 mmol), and the mixture was heated under reflux (N_2 atmosphere) for 4 h. The reaction mixture was allowed to cool to room temperature; water (200 cm^3), dichloromethane (200 cm^3) were added and the mixture basified with 40% NaOH to pH 14. The mixture was filtered through celite, extracted with dichloromethane and filtered again to remove residual $Sn(OH)_2$. After drying (Na_2SO_4) and removal of the solvent, the residue was recrystallized from dichloromethane–petroleum ether (60–80°C) to give **2** as orange crystals in 94.5% yield; m.p. 154–156°C; *m/z* 277; IR 1620 (—N—H bend), 3375, 3475 cm^{-1} (—N—H stretch); ^{1}H NMR ($CDCl_3$) δ: 3.45 (s, broad, 2H, NH_2), 4.0 (s, 5H, FcH), 4.21 (t, J = 1.8 Hz, 2H, FcH), 4.50 (t, J = 1.8 Hz, 2H, FcH), 6.50 (d, J = 9 Hz, 2H, ArH), 7.50 (d, J = 9 Hz, 2H, ArH).

Preparation of **7**. To a solution of **2** (0.30 g, 1.08 mmol) in dry toluene (150 cm^3) was added 3,4-dimethoxybenzaldehyde (0.18 g, 1.08 mmol), one drop of concentrated HCl and the mixture was refluxed under N_2 overnight using a Dean and Stark apparatus to azeotrope off the water formed during the reaction. The reaction mixture was allowed to cool to room temperature and the solvent removed *in vacuo*. The residue was chromatographed on an alumina column eluting with a petroleum ether (40–60°C)–dichloromethane gradient. The orange band was collected. After removal of the solvent mixture, recrystallization from *n*-hexane gave **7** as orange crystals, 0.37 g (80.4%); *m/z* 425; IR 1620 (—C=N— stretch), 1575, 1325 cm^{-1} (NO_2 asym. and sym. stretches, respectively); ^{1}H NMR ($CDCl_3$)δ: 3.94 (s, 3H, OCH_3), 3.98 (s, 3H, OCH_3), 405 (s, 5H, FcH), 4.30 (t, J = 1.8 Hz, 2H, FcH), 4.62 (t, J = 1.8 Hz, 2H, FcH), 6.88–7.65 (m, 7H, ArH), 8.41 (s, 1H, —N=CH—). Found: C, 67.3; H, 6.0; N, 3.2. Calc. for $C_{25}H_{23}O_2NFe \cdot H_2O$: C, 67.7; H, 5.6; N, 3.2%.

Preparation of **8**, **9** *and* **10**. Compounds **8**, **9** and **10** were prepared by slight modification of the above procedure for **7**. Thus, after removal of the solvent from the reaction mixture, the residue was exhaustively extracted with boiling hexane. Removal of the hexane gave the crude product which was recrystallized from dichloromethane–*n*-hexane to give the pure products in yields ranging from 55 to 94%.

Compound **8**: yield, 55%; m.p. 155–157°C; *m/z* 555; IR 1620 (—C═N— stretch), 1300–1100 cm^{-1} (C—O—C stretch); ^1H NMR ($CDCl_3$)δ: 3.75–4.20 (m, 16H, crown-H), 4.00 (s, 5H, FcH), 4.30 (t, $J = 1.8$ Hz, 2H, FcH), 4.66 (t, $J = 1.8$ Hz, 2H, FcH), 6.85–7.59 (m, 7H, ArH), 8.40 (s, 1H, —N═CH—). Found: C, 64.7; H, 5.2; N, 2.4. Calc. for $C_{31}H_{33}O_5NFe \cdot H_2O$: C, 64.9; H, 6.1; N, 2.4%.

Compound **9**: yield, 94%; m.p. 241°C (dec); *m/z* 410; IR 1620 (—C═N— stretch), 1575, 1340 cm^{-1} (NO_2 asym. and sym. stretches, respectively); ^1H NMR ($CDCl_3$)δ: 4.05 (s, 5H, FcH), 4.36 (t, $J = 1.8$ Hz, 2H, FcH), 4.68 (t, $J = 1.8$ Hz, 2H, FcH), 7.20 (d, $J = 9$ Hz, 2H, ArH), 7.55 (d, $J = 9$ Hz, 2H, ArH), 8.10 (d, $J = 9$ Hz, 2H, ArH), 8.35 (d, $J = 9$ Hz, 2H, ArH), 8.64 (s, 1H, —N═CH—). Found: C; 67.1; H, 4.2; N, 6.5. Calc. for $C_{23}H_{18}O_2N_2Fe$: C, 67.3; H, 4.4; N, 6.8%.

Compound **10**: yield, 71.4%; m.p. 206°C (dec); *m/z* 455; IR 1595 (—C═N— stretch), 1520, 1340 cm^{-1} (NO_2 asym. and sym. stretches, respectively); ^1H NMR ($CDCl_3$)δ: 4.08 (s, 5H, FcH), 4.38 (t, $J = 1.8$ Hz, 2H, FcH), 4.62 (t, $J = 1.8$ Hz, 2H, FcH), 7.32 (d, $J = 9$ Hz, 2H, ArH), 8.60 (t, $J = 0.9$ Hz, 2H, ArH), 8.94 (t, $J = 0.9$ Hz, 1H, ArH), 9.10 (s, 1H, —N═CH—). Found: C, 55.6; H, 4.0; N, 8.6. Calc. for $C_{23}H_{17}O_4N_3Fe \cdot 2H_2O$: C, 56.2; H, 4.3; N, 8.6%.

Acknowledgements—We thank the British Council for financial support and the SERC for use of the high-field NMR service at the University of Warwick, We also thank The Research Corporation Trust, L. and D. Blond for additional financial support.

REFERENCES

1. P. D. Beer, *Chem. Soc. Rev.* 1989, **18**, 409.
2. R. E. Wolf and S. R. Cooper, *J. Am. Chem. Soc.* 1984, **106**, 4646.
3. P. D. Beer, C. J. Jones, J. A. McCleverty and S. S. Salam, *J. Incl. Phenom.* 1987, **5**, 521.
4. A. Kaifer, D. A. Gustowski, L. Echegoyen, V. J. Gratto, R. A. Schultz, T. P. Cleary, C. R. Morgan, D. M. Goli, A. M. Rios and G. W. Gokel, *J. Am. Chem. Soc.* 1985, **107**, 1958.
5. T. Saji, *Chem. Lett.* 1986, 275.
6. P. D. Beer, H. Sikanyika, C. Blackburn, J. F. McAleer and M. G. B. Drew, *J. Organomet. Chem.* 1988, **356**, C19.
7. E. Fu, M. L. H. Green, V. J. Lowe and S. R. Marder, *J. Organomet. Chem.* 1988, **341**, C39.
8. P. D. Beer, D. B. Crowe and B. Main, *J. Organomet. Chem.* 1989, **375**, C35.
9. P. D. Beer and A. D. Keefe, *J. Organomet. Chem.* 1989, **375**, C40.
10. V. Weinmayr, *J. Am. Chem. Soc.* 1955, **77**, 3012.
11. E. M. Hyde, B. L. Shaw and I. Shephard, *J. Chem. Soc., Dalton Trans.* 1978, 1696.
12. P. D. Beer, C. Blackburn, J. McAleer and H. Sikanyika, *Inorg. Chem.* 1990, **29**, 378.
13. D. J. Williams, *Angew. Chem. Int. Edn Engl.* 1984, **23**, 690 and refs therein.
14. (a) A. F. Garito and A. J. Heeger, *Accts Chem. Res.* 1974, **7**, 232; (b) M. Blanchard-Desce, I. Ledoux, J. M. Lehn, J. Malthete and J. Zyss, *J. Chem. Soc., Chem. Commun.* 1988, 737.
15. M. L. H. Green, S. R. Marder, M. E. Thompson, J. A. Bandy, D. Bloor, P. V. Kolinsky and R. J. Jones, *Nature* 1987, **330**, 360.

Polyhedron Vol. 9, No. 8, pp. 1095–1097, 1990
Printed in Great Britain

0277–5387/90 $3.00+.00
Pergamon Press plc

A MODIFIED SYNTHESIS OF RUTHENIUM(II) HEXAAQUA SALTS

PAUL BERNHARD,* MARGRET BINER and ANDREAS LUDI†

Institut für Anorganische Chemie, Universität Bern, CH-3000 Bern 9, Switzerland

(*Received* 31 *October* 1989; *accepted* 8 *December* 1989)

Abstract—An efficient preparation of ruthenium aqua ions starts from the hydrated dioxide. Oxidation by periodate produces ruthenium tetroxide which is reduced by metallic lead to $[Ru(H_2O)_6]^{2+}$. Ion exchange and crystallization affords pure $[Ru(H_2O)_6](tos)_2$ (tos = *p*-toluenesulphonate) in 70–80% yield.

Some time ago we reported the first preparation of solid salts of the ruthenium aqua ions[1] as model systems for electron transfer[2] and ligand exchange[3] studies. The ruthenium(II) salt in particular was recognized as a very versatile and promising starting reagent for the synthesis of a wide variety of coordination compounds.[4] Surprisingly, this aqua ion could also be employed for very facile and efficient preparations of organoruthenium species, especially sandwich and half-sandwich compounds.[5] This reactivity of $[Ru(H_2O)_6]^{2+}$ toward unsaturated organic molecules evoked the interest of polymer chemists and stimulated its successful application as a catalyst in polymerization reactions.[6] Despite this remarkably rich chemistry the actual use of ruthenium aqua salts is rather limited owing to the quite difficult and tedious synthesis starting from ruthenium metal.[1] In order to make this potentially very useful compound more readily available, we have simplified the procedure as much as possible. This paper reports an improved and more efficient preparation of solid $[Ru(H_2O)_6]^{2+}$ salts.

EXPERIMENTAL

The overall reaction is summarized by the following equation

$$RuO_2 \xrightarrow[H_2SO_4]{NaIO_4} RuO_4 \xrightarrow[H_2SiF_6]{Pb} [Ru(H_2O)_6]^{2+}$$

$$\xrightarrow{\text{Ion exchange}} [Ru(H_2O)_6](tos)_2$$

$$\downarrow$$

$$PbSO_4$$

(tos = *p*-toluenesulphonate). Deionized water was used throughout. Chemicals were from Fluka, $RuCl_3 \cdot aq$ was a loan from Johnson Matthey.

(1) *Generation and reduction of* RuO_4

The complete arrangement displayed in Fig. 1 was swept with Ar for 20 min. H_2SO_4 was added over 1 h under continuous stirring of A and B and

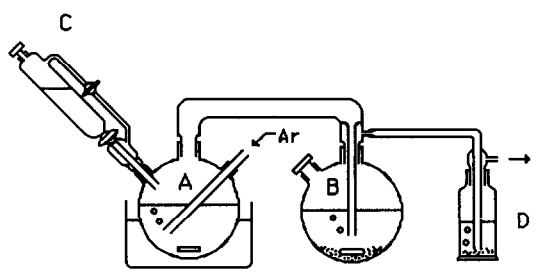

Fig. 1. Production of $[Ru(H_2O)_6]^{2+}$ solution. A: 500-cm^3 flask with 5 g of $RuO_2 \cdot aq$ and 25 g of $NaIO_4$ in 200 cm^3 of H_2O; B: 500-cm^3 flask containing 330 cm^3 of 1 M H_2SiF_6 and 35 g of Pb grains activated in 50 cm^3 of 50% HNO_3. A and B are stirred magnetically. C contains 100 cm^3 of icc-cold 50% H_2SO_4, D contains 70 cm^3 of 1 M H_2SiF_6 and 5 g activated Pb. Distance between A and B is as short as possible and all joints are without grease.

* Present address: CIBA–GEIGY AG, 1701 Fribourg, Switzerland.

† Author to whom correspondence should be addressed.

slow Ar bubbling (1 bubble per second). Formation of RuO_4 was indicated by a yellow colour in A. The Ar-stream was then increased three-fold until a dark colour appeared in B, then doubled in intensity. After complete addition of H_2SO_4, A was allowed to reach room temperature and Ar bubbling was continued until this solution was virtually colourless, which required about 2 days. If this did not occur another portion of 3 g of $NaIO_4$ was added. The colour in B should now be a deep purple–red. If it had a brownish tint another portion of 10 g of freshly activated Pb was added to B. The stirring of both solutions was continued for another day while A was gently warmed to 40°C.

Caution: Owing to the toxicity and sensitivity of RuO_4 the whole operation was carried out in a well ventilated, dark hood.

(2) *Removal of* $PbSO_4$, *ion exchange and crystallization*

The solution in B (Fig. 1) was decanted into an Ar-filled 1 dm^3 flask containing 100 cm^3 of Ar-saturated 2 M H_2SO_4 and stirred under Ar bubbling for 30 min. After standing for 15 min the mixture was quickly passed through a large ($\gtrsim$ 10 cm) G4 frit, and the filtrate was diluted to 4 dm^3 with Ar-saturated water. Ion exchange was then carried out under Ar using Schlenk techniques[7] (Fig. 2) adapted to the appropriate scale. After flushing the whole configuration with Ar connecting dropping funnel to collecting vessel (a to f in Fig. 2) maintained a constant Ar atmosphere throughout the ion-exchange process. The loaded column was washed first with 300 cm^3 of water and then with 700 cm^3 of 0.1 M Htos. Elution was achieved with 1.8 M Htos at a rate of about two drops per second. The resulting red solution ($\sim$ 400 cm^3) was rotatory concentrated at $\lesssim$ 40°C until precipitation of a solid began, i.e. to approximately 200 cm^3. Cooling to 0°C for 2 days afforded a crystalline mass which was collected on a G3 frit, thoroughly washed with ethyl acetate to remove solid Htos, then with ether, and dried *in vacuo* for 2 h. Yield: 12.98 g $[Ru(H_2O)_6](tos)_2$ (79%). Found: C, 30.6; H, 4.9; S, 11.2; H_2O, 19.7. Calc.: C, 30.5; H, 4.7; S, 11.6; H_2O, 19.6%.

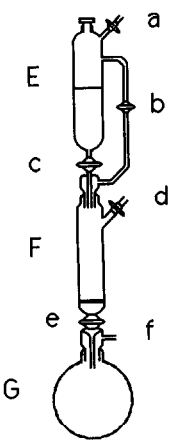

Fig. 2. Ion exchange of $[Ru(H_2O)_6]^{2+}$. E: 4000-cm^3 dropping funnel. F: ion-exchange column (30 × 3 cm) with G2 frit, 50 g of Dowex WX8 in H^+ form, Cl^- free by Ag^+ test. G: 1000-cm^3 flask. a, b, c, d, e: stopcocks.

Depending on the availability of starting materials the following adaptions can be made:

(i) Commercial $RuCl_3 \cdot aq$ (7.3 g) is heated in 300 cm^3 of 5 M NaOH to 60°C (30 min) then stirred at room temperature overnight. The extremely fine black powder is washed Cl^--free and used for the reaction with $NaIO_4$. Based on the Ru content of $RuCl_3(aq)$, yields for $[Ru(H_2O)_6](tos)_2$ are in the 50 to 70% range.

(ii) Ru sponge (3 g) is fused with 12 g of Na_2O_2 in a Ni crucible to red glow for 5 min. After cooling, the product is dissolved in 200 cm^3 of water to form a deep orange solution which is used to start the reaction with $NaIO_4$. Yields are between 70 and 75%.

DISCUSSION

General properties of $[Ru(H_2O)_6](tos)_2$

$[Ru(H_2O)_6](tos)_2$ is obtained as pink prismatic crystals. A simple test of sample purity is made by measuring the UV–vis spectrum of a freshly prepared solution under Ar in 0.5 M trifluoromethanesulphonic acid. The two ligand-field bands show the following absorption maxima and extinction coeffcients, respectively: 534 and 394 nm, with 12 and 15 $M^{-1}\,cm^{-1}$. Virtually identical values are measured in 0.5 M H_2SO_4.[4] Extinction measurements have to be made immediately after dissolving the solid complex salt in order to avoid errors owing to partial oxidation and subsequent hydrolysis of the ruthenium(III) species. Pink $[Ru(H_2O)_6]^{2+}$ is easily oxidized by atmospheric oxygen to yellow $[Ru(H_2O)_6]^{3+}$ (λ_{max} = 390 nm, ε = 30 $M^{-1}\,cm^{-1}$[4]). The corresponding reduction potential is 0.21 V. Crystalline $[Ru(H_2O)_6](tos)_2$ is surprisingly stable and is best stored under Ar at 0°C. No decomposition is observed for several weeks even at ambient conditions.

Since the tosylate salt of $[Ru(H_2O)_6]^{2+}$ is only very sparingly soluble in MeOH, EtOH and THF, it can be easily converted to the $CF_3SO_3^-$ salt by

ion exchange under Ar. After rotatory evaporation of the resulting $CF_3SO_3^-$ solution at 50°C to constant volume, cooling to −20°C for 2 days produces a pink–red precipitate which was collected by filtration and compressed with a glass stopper to remove occasionally occurring colourless crystals (presumably CF_3SO_3H hydrates). The solid was washed with a small amount of ice-cold ether, transferred into an Ar filled Schlenk vessel and stored at −20°C. This salt is stable at −20°C only for a few days but exhibits considerably higher solubility in non-aqueous solvents. The Tutton salt and its spectroscopic properties have also been reported.[8]

The conventional starting reagent in preparative ruthenium chemistry, $RuCl_3 \cdot aq$, is an ill-defined compound with varying composition and oxidation state. Syntheses are thus not very reproducible and produce low yields, quite often sacrificing organic ligands for the preparation of low-valent ruthenium–organic compounds. In contrast $[Ru(H_2O)_6](tos)_2$ and its $CF_3SO_3^-$ analogue are well defined ruthenium(II) species with a substitution lability[3] adapted for a variety of elegant synthetic routes.

Acknowledgements—We thank Johnson Matthey for a loan of ruthenium chloride, the Swiss National Science Foundation (Grant No. 20-5370.87) for support, and CIBA–GEIGY AG for the elemental analyses.

REFERENCES

1. P. Bernhard, H.-B. Bürgi, J. Hauser, H. Lehmann and A. Ludi, *Inorg. Chem.* 1982, **21**, 3936.
2. P. Bernhard, L. Helm, A. Ludi and A. Merbach, *J. Am. Chem. Soc.* 1985, **107**, 312.
3. I. Rapaport, I. Helm, A. E. Merbach, P. Bernhard and A. Ludi, *Inorg. Chem.* 1988, **27**, 873.
4. P. Bernhard, H. Lehmann and A. Ludi, *J. Chem. Soc., Chem. Commun.* 1981, 1216; P. Bernhard, H. Lehmann and A. Ludi, *Comm. Inorg. Chem.* 1983, **2**, 145.
5. O. H. Bailey and A. Ludi, *Inorg. Chem.* 1985, **14**, 2582; M. Stebler-Röthlisberger, A. Salzer, H.-B. Bürgi and A. Ludi, *Organometallics* 1986, **5**, 298.
6. B. M. Novak and R. H. Grubbs, *J. Am. Chem. Soc.* 1988, **110**, 7542.
7. D. F. Shriver and M. A. Drezdzon, *The Manipulation of Air Sensitive Compounds*, 2nd edn. Wiley, New York (1986).
8. P. Bernhard and A. Ludi, *Inorg. Chem.* 1984, **23**, 870.

Polyhedron Vol. 9, No. 8, pp. 1099–1105, 1990
Printed in Great Britain

0277–5387/90 $3.00+.00
© 1990 Pergamon Press plc

CARBONYL AND HALOCARBONYL COMPLEXES OF MOLYBDENUM AND TUNGSTEN WITH OXYGEN DONOR LIGANDS

P. PLANINIĆ* and H. MEIDER

Rudjer Bošković Institute, Department of Physical Chemistry, Zagreb, Croatia, Yugoslavia

(*Received* 20 *November* 1989; *accepted* 8 *December* 1989)

Abstract—Halogen oxidation of trisubstituted carbonyl complexes of molybdenum(0) and tungsten(0) containing bis[(diphenylphosphinyl)methyl]phenylphosphine oxide (RPPh) and methylenebis[diphenylphosphine oxide] (MDPO) under controlled conditions afforded diamagnetic, seven-coordinate compounds: $[M(CO)_3(RPPh)X_2]$ and $[M(CO)_3(MDPO)X_2]$, where M = Mo, W and X = Br, I. The reaction of molybdenum and tungsten hexacarbonyls with bis[(diphenylphosphinyl)methyl]ethyl phosphinate (RPOEt) was also investigated. Complexes of the type *cis*-$[M(CO)_4(RPOEt)]$ were isolated, which by treating with iodine released one molecule of carbon monoxide to give metal(II) derivatives, $[M(CO)_3(RPOEt)I_2]$.

Seven-coordinate complexes of molybdenum(II) and tungsten(II) continue to be an area of considerable interest. Amongst these, much attention has been paid to halocarbonyl derivatives containing amine, phosphine, stibine or arsine mono- and polydentate ligands.[1] Up until now, very few studies of analogous compounds with phosphine oxides as attached ligands have been conducted. The only hitherto known seven-coordinate halocarbonyl complexes of molybdenum and tungsten containing a phosphine oxide ligand have been those reported recently by Baker and Kendrick.[2] They prepared iodo-derivatives of molybdenum(II) and tungsten(II) with monodentate triphenylphosphine oxide starting from the corresponding highly reactive bis-acetonitrile diiodo tricarbonyl species.

In recent years we have investigated the synthesis and complexing ability of different organophosphorus ligands.[3–6] As a continuation of our work on metal carbonyl chemistry, in this paper we describe the preparation and properties of the new seven-coordinate halocarbonyl complexes of molybdenum(II) and tungsten(II) containing the following bidentate and potentially tridentate phosphine oxides: methylenebis[biphenylphosphine oxide] (MDPO), bis[(diphenylphosphinyl)methyl] phenylphosphine oxide (RPPh) and bis[(diphenylphosphinyl)methyl]ethyl phosphinate (RPOEt). We also report on the new molybdenum(0) and tungsten(0) tetracarbonyl complexes with the RPOEt ligand.

RESULTS AND DISCUSSION

Starting materials for the preparation of halocarbonyl complexes were trisubstituted carbonyl compounds $M(CO)_3(RPPh)$ and $M_2(CO)_6(MDPO)_3$[6] and tetracarbonyl species $M(CO)_4(RPOEt)$ (M = Mo, W). By halogen oxidation of the above complexes under controlled conditions the following compounds were isolated: $M(CO)_3(RPPh)X_2$, $M(CO)_3(MDPO)X_2$ and $M(CO)_3(RPOEt)I_2$ (M = Mo, W; X = Br, I) (Table 1).

Due to the insolubility of the starting carbonyl species or their highly unstable nature in most solvents, they were dispersed in a suitable solvent prior to halogen oxidation. Iodine or bromine dissolved in benzene or CCl_4 was then added dropwise into the suspension of the corresponding carbonyl complex in *n*-heptane or CCl_4 at temperatures below 0°C. The colour of the suspension began to change immediately with the addition of small portions of halogen. When all of the oxidizing agent had been added, the reaction mixture was additionally stirred

* Author to whom correspondence should be addressed.

Table 1. Analytical data for the complexes

Complex	Colour	M (%) Calc.	M (%) Found	P (%) Calc.	P (%) Found	Br/I (%) Calc.	Br/I (%) Found
$Mo(CO)_3(RPPh)Br_2$ (**1**)	Orange–yellow	10.7	10.4	10.4	10.2	17.9	17.9
$Mo(CO)_3(RPPh)I_2$ (**2**)	Orange	9.7	9.4	9.4	9.2	25.7	25.5
$W(CO)_3(RPPh)Br_2$ (**3**)	Orange–yellow	18.7	18.4	9.5	9.3	16.3	15.9
$W(CO)_3(RPPh)I_2$ (**4**)	Orange	17.1	16.8	8.6	8.5	23.6	23.6
$Mo(CO)_3(MDPO)Br_2$ (**5**)	Orange	12.7	12.4	8.2	8.4	21.1	20.9
$Mo(CO)_3(MDPO)I_2$ (**6**)	Orange–brown	11.3	11.1	7.3	7.2	29.8	29.7
$W(CO)_3(MDPO)Br_2$ (**7**)	Orange–yellow	21.8	21.5	7.3	7.2	18.9	19.1
$W(CO)_3(MDPO)I_2$ (**8**)	Orange	19.6	19.4	6.6	6.5	27.1	26.9
$Mo(CO)_3(RPOEt)I_2$ (**9**)	Yellow–brown	10.0	10.1	9.7	9.4	26.6	26.6
$W(CO)_3(RPOEt)I_2$ (**10**)	Yellow–brown	17.6	17.4	8.9	8.7	24.3	24.2
$Mo(CO)_4(RPOEt)$ (**11**)	Yellow–brown	13.1	13.1	12.7	12.6		
$W(CO)_4(RPOEt)$ (**12**)	Yellow–brown	22.5	22.3	11.4	11.2		

in the cold until the halogenated products were free from unreacted tricarbonyl or tetracarbonyl derivatives. The course of the reaction was followed by IR spectroscopy. The MDPO halocarbonyls were also prepared by a modified procedure using toluene as a solvent and a dispersing agent. As the complexes formed are soluble in toluene they were isolated by precipitation with *n*-heptane.

It has to be noted that further oxidation with expulsion of all the carbon monoxide occurs under more vigorous conditions yielding species of molybdenum and tungsten with higher oxidation states. Consequently, the preparation of bromocarbonyl derivatives proved to be extremely difficult. Very low temperatures are necessary to avoid oxidative decomposition of the reaction products.

The tetracarbonyl complexes $Mo(CO)_4(RPOEt)$ and $W(CO)_4(RPOEt)$ were prepared by allowing the RPOEt ligand to react with molybdenum and tungsten hexacarbonyls in toluene and xylene, respectively, under reflux for several hours. Tricarbonyl complexes like those obtained with RPPh[6] could not be isolated.

All of the new complexes are diamagnetic solids, yellow to brown in colour. The halocarbonyls are insoluble in aliphatic hydrocarbons, diethylether, benzene, CCl_4, but soluble in a variety of polar solvents such as $CHCl_3$, CH_2Cl_2, acetone, nitromethane or nitrobenzene, stable only for a limited period of time in solution. The tetracarbonyls, however, cannot be dissolved in any solvent without decomposition. The isolated complexes are also air-sensitive and thermally unstable, but they can be stored under argon at 0°C for several weeks. Generally, bromides are less stable than iodides, and molybdenum complexes are less stable than tungsten ones.

IR spectra

The most significant absorption bands in the spectra of the ligands and of the isolated complexes are listed in Tables 2 and 3.

Some representative IR spectra of the halocarbonyl complexes are shown in Fig. 1. It can be seen that the halocarbonyls, regardless of the attached ligand, exhibit three characteristic ν(CO) stretching modes at approx. 1900–1930, 2000–2020 and 2070–2090 cm^{-1} in the IR spectra. The highest

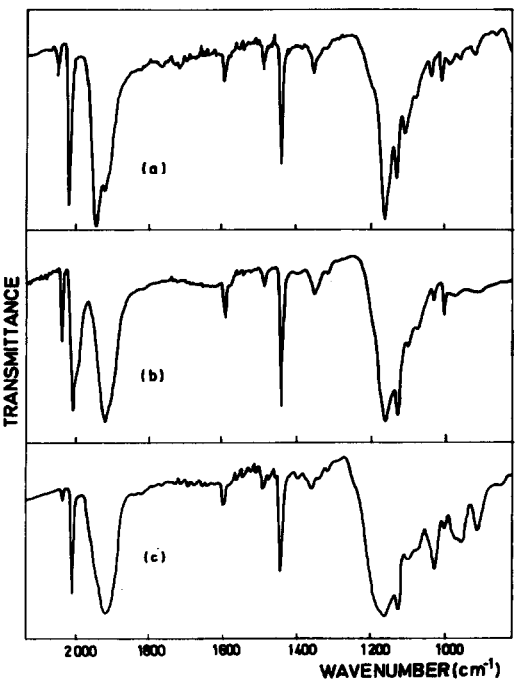

Fig. 1. IR spectra of (a) $Mo(CO)_3(MDPO)Br_2$, (b) $W(CO)_3(RPPh)I_2$ and (c) $Mo(CO)_3(RPOEt)I_2$ complexes.

Table 2. IR spectral[a] and molar conductivity[b] data for the ligands and the isolated halocarbonyl complexes

Compound	ν(CO) (cm^{-1})	ν(PO) (cm^{-1})	ν(M—Br) (cm^{-1})	Λ_M ($cm^2\,\Omega^{-1}\,mol^{-1}$)
RPPh		1215s, 1192vs, 1163s		
1	2092w–m, 2032s, sp; 1934vs	1159vs	250	4.0
2	2073w–m, 2020s, sp; 1935vs	1160vs		10.6
3	2090m, 2022s, sp; 1920vs	1158vs	256	3.2
4	2072m–s, 2015s, sp; 1917vs	1161vs		11.8
MDPO		1211m, 1194s, 1175vs		
5	2095w; 2032s, sp; 1943vs, 1918sh	1158vs	242	1.1
6	2074vw; 2025s, sp; 1941s, 1900m	1160vs		4.03
7	2092w; 2020s, sp; 1918vs	1160vs	247	3.18
8	2072w; 2014s, sp; 1915vs	1158vs		5.01
RPOEt		1245s, 1220m, 1190m		
9	2075vw, 2020m, 1919s	1163s		2.3
10	2075vw, 2022m, 1923s, 1905sh	1165s		1.7

[a] KBr pellets.
[b] Nitrobenzene, 10^{-3} M.

Table 3. IR spectral data and force constants for *cis*-$M(CO)_4$(RPOEt) complexes

Complex	ν(PO) (cm^{-1})	ν(CO) (cm^{-1})				Force constants (mdyn Å^{-1})		
		A_1	A_1	B_1	B_2	k_1	k_2	k_i
$Mo(CO)_4$(RPOEt)	1175 vs, br	2022m	1935s	1900vs	1849s	14.86	15.69	0.29
$W(CO)_4$(RPOEt)	1165 vs, br	1997m	1890m	1869vs	1813m	14.44	15.09	0.34
$Mo(CO)_4$(RPPh)[a]	1162 vs	2012w	1895vs	1850s	1805m	14.20	15.26	0.38
$W(CO)_4$(RPPh)[a]	1160 vs	2000w	1868vs	1845s	1802m	14.16	14.91	0.41

[a] From ref. 6.

energy band varies in intensity from medium to very weak, on going from one complex to another, suggesting to some extent different rigidity of the molecule in particular cases. The lowest of the three ν(CO) bands often has a shoulder, or as with $Mo(CO)_3(MDPO)X_2$ a resolved doublet (Fig. 1). Local site symmetry effects in the solid state can account for this difference, as the doublet disappears in solution. In general, the spectra are virtually identical whether measured using KBr pellets or using the substances in solution, and are consistent with the suggested structure which involves the $M(CO)_3$ moiety in a seven-coordinate arrangement. A similar IR pattern including both shape and position of the bands was obtained for analogous seven-coordinate species having different S-, N- or O-donor ligands,[2,7–9] although the frequencies are somewhat higher in the complexes studied indicating a higher bond order for the carbonyl groups. Generally, in these halocarbonyl species there is a shift of ν(CO) on oxidation by *ca* 150–200 cm^{-1} to higher energies compared with the tricarbonyl complexes in zero oxidation state. This shift is in accord with the expected decrease in metal-to-ligand π-backbonding as the positive charge at the metal centre increases by forming a M—X bond. The CO stretching frequencies in molybdenum complexes are slightly higher than in their tungsten analogues, compatible with a more effective π-electron donation from tungsten to the antibonding orbitals of the carbonyl ligands. Regarding halogens, as expected, the ν(CO) decreases in the following order: bromo complexes > iodo complexes.

It should be mentioned that the destroying of the $M(CO)_3$ moiety leading to the eventual formation of dicarbonyl species was not observed in any of the complexes studied, neither by aging of the samples nor by dissolution. Moreover, the initial IR pattern of the carbonyl region was preserved with-

out any shift of the absorption bands until the complete loss of carbon monoxide occurred, which takes place in particular complexes if kept in air. Similarly, the halocarbonyl species having IR spectra with the highest ν(CO) band extremely weak, especially RPOEt complexes, can not be considered as dicarbonyls since dicarbonyl species have distinct IR spectra with the absorption at lower frequencies. In addition, the highest energy band of the complexes under consideration becomes ordinarily more intense for solutions.

Absorption bands relating to the M—Br stretching modes in the bromocarbonyl complexes were found, as expected,[10] at ~ 250 cm^{-1} (Table 2). M—I stretching modes occur below 200 cm^{-1} and could not be observed.

The phosphoryl oxygen stretch, ν(PO), shifts by approximately 35–40 cm^{-1} to lower wavenumbers in comparison with the free ligands, which indicates the formation of a strong M—O(P) bond[11] in these complexes, in contrast to a weaker M—O(P) bond in the starting tricarbonyl species.[6]

The zerovalent tetracarbonyl complexes with the RPOEt ligand, $Mo(CO)_4$(RPOEt) and $W(CO)_4$(RPOEt) show four absorption bands in the CO stretching region of the spectra (2100–1800 cm^{-1}; Table 3) indicating a C_{2v} local symmetry around the metal.[12] Vibrations were assigned to $2A_1$, B_1 and B_2 modes in the order of decreasing frequency and force constants were calculated by use of approximations developed by Cotton and Kraihanzel.[13–15] The higher C—O stretching force constants obtained for the RPOEt complexes, in comparison to the RPPh complexes (Table 3), were ascribed to a more positive effective nuclear charge on the metal which is due to the different chemical nature of the substituent on the central phosphorus atom of the ligand.

Instead of three bands being present in the phosphoryl region of the spectrum of RPOEt at 1245, 1220 and 1190 cm^{-1}, only one intense, rather broad, absorption band is present in the spectra of its tetracarbonyl complexes. The ν(PO) is shifted to ~ 1175 cm^{-1} for molybdenum and to ~ 1165 cm^{-1} for tungsten complexes as a consequence of a strong M—O(P) bond which exists in these compounds, in contrast to the weaker M—C(O) bonds.

^{1}H *NMR spectra*

The ^{1}H NMR spectra of the halocarbonyl complexes show a downfield shift of the methylene proton signals as well as a slight downfield shift of the phenyl proton signals relative to those from the free ligands (Table 4). Phenyl proton resonances are, however, much less informative than the aliphatic proton signals because of the complexity of their patterns and the insensitivity towards structural changes. Thus, in the spectra of RPPh and MDPO, resonances due to phenyl protons appear as multiplets at ~ 7.5 ppm and shift in the spectra of their complexes to ~ 7.7 ppm.

Table 4. ^{1}H NMR (δ) data[a] for RPPh and MDPO and their complexes

Compound	$\delta(CH_2)$ (ppm)	$\delta(C_6H_5)$ (ppm)
RPPh	3.79 (t)	7.53 (m)
$W(CO)_3$(RPPh)I_2	4.14 (m)	7.75 (m)
MDPO	3.53 (t)	7.73–7.34 (m)
$Mo(CO)_3$(MDPO)I_2	4.42 (t)	7.99–7.46 (m)

[a] Spectra recorded in $CDCl_3$ at 22°C and referenced to TMS; t = triplet, m = multiplet.

The RPPh ligand shows fluxionality in solution by giving rise to a single PCH_2P resonance in the ^{1}H NMR spectrum at ambient temperatures, which appears as a triplet at 3.79 ppm. In the spectrum of the $W(CO)_3$(RPPh)I_2 complex, the CH_2 protons exhibit a multiplet centred at ~ 4.14 ppm. Had RPPh acted as a bidentate ligand two different CH_2 signals in a ratio of 1 : 1 should be present. If all three P=O groups were engaged in the same way only one CH_2 signal would arise. The appearance of a multiplet consisting of three triplets in a ratio of $\sim 2:1:1$ in the ^{1}H NMR spectrum of $W(CO)_3$(RPPh)I_2 indicates the presence of two different species in solution.

The CH_2 signal for the free MDPO ligand appears as a triplet at 3.53 ppm and shifts to 4.42 ppm in the spectrum of the $Mo(CO)_3$(MDPO)I_2 complex. This value is firmly associated with the chelating MDPO ligand.[16]

Other measurements and concluding remarks

RPPh *complexes.* During some previous investigations several types of transition metal complexes with this ligand were isolated, thus showing that RPPh can act as bidentate and tridentate complexing agents.[3–5] Since the bromocarbonyl complexes with RPPh are non-electrolytes in nitrobenzene and nitromethane solutions (Table 2) they are formulated as $[M(CO)_3(RPPh)Br_2]$ (M = Mo, W) rather than $[M(CO)_3(RPPh)Br]Br$. Thus, with regard to seven-coordination, presumably only two P=O groups from the ligand are attached to the metal in these species. The iodocarbonyl derivatives in nitrobenzene show conductance values which are

too high for non-electrolytes but too low for 1 : 1 electrolytes (Table 2). IR spectroscopy alone has been insufficient for distinguishing between bidentate or tridentate RPPh in the complexes studied, although only one main P=O stretching band is present (Table 2, Fig. 1). However, as the IR spectra of the iodocarbonyls are virtually identical to those of the bromo-derivatives it is very likely that the iodocarbonyls exist in the solid state as neutral complexes as well, i.e. $[M(CO)_3(RPPh)I_2]$. It is known that iodide ligands are more easily displaced than bromide ligands from neutral organotransition metal complexes due to a weaker M—I bond strength. Accordingly, there exists a probability that the third P=O group from RPPh re-enters the coordination sphere of the metal in solution via displacement of the weakly bound iodide ligand leading to the following equilibrium:

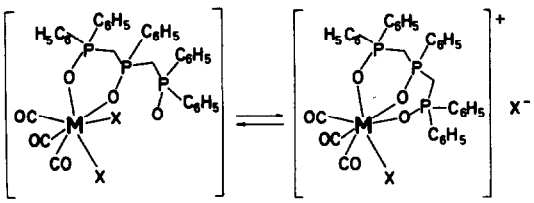

Evidence to support this hypothesis comes also from the ^1H NMR spectra discussed above.

Therefore, it is likely, as far as the halocarbonyls in the solid state are concerned, that RPPh behaves as a bidentate rather than tridentate complexing agent. It seems that the steric effects are predominant in determining the geometry of the molecule.

MDPO *complexes*. The isolated halocarbonyls containing MDPO ligand are essentially non-electrolytes (Table 2) in agreement with their formulation as $[M(CO)_3(MDPO)X_2]$. The ^1H NMR spectra confirmed MDPO to be bonded as a bidentate ligand. Molecular weight measurements for the molybdenum iodocarbonyl complex (in CH_2Cl_2) gave a value of $M_r = 829$, which is consistent with the formula $Mo(CO)_3(MDPO)I_2$ ($M_{theor.} = 850$). Neither spectral nor other evidence was found for the existence of a complex which would contain two ligand molecules. It is obvious that halogen oxidation under given circumstances causes the cleavage of the weak M—O(P) bridging bonds in the parent carbonyls liberating MDPO, according to the following equation:

$$M_2(CO)_6(MDPO)_3 \xrightarrow{2X_2} 2M(CO)_3(MDPO)X_2 + MDPO.$$

RPOEt *carbonyl and halocarbonyl complexes*. The formation of disubstituted neutral carbonyl species only, by reaction of RPOEt with the corresponding hexacarbonyls, implies presumably a bidentate nature of the RPOEt ligand in these six-coordinate complexes (Table 3). Under the same circumstances RPPh readily afforded trisubstituted compounds.[6] Electronic factors can account for the difference in the donor ability of the two structurally similar ligands.

cis-$Mo(CO)_4$(RPOEt) and *cis*-$W(CO)_4$(RPOEt) in reaction with iodine released one molecule of carbon monoxide, to give metal(II) derivatives, $M(CO)_3(RPOEt)I_2$, whose properties are listed in Tables 1 and 2. They are diamagnetic non-electrolytes, unstable to light and air, and according to the IR spectra certainly similar to the seven-coordinate complexes with RPPh and MDPO described above. Although the complexes $Mo(CO)_3(RPOEt)I_2$ and $W(CO)_3(RPOEt)I_2$ do not show initial conductance in nitrobenzene and nitromethane (Table 2) they do undergo dissociation to a certain degree since the conductivity increases slightly on standing of the solutions. At the same time in the IR spectra the solvent causes no significant shifts of the carbonyl frequencies.

The geometries of most seven-coordinate halocarbonyl complexes can be described in terms of a C_{3v} capped octahedron.[17] However, when the ligands are inequivalent and the actual symmetry lower, the assignment of a structure is ambiguous. Since the IR spectral properties of our $M(CO)_3(ligand)X_2$ complexes closely resemble the analogous seven-coordinate compounds it is likely that they will also have a capped octahedral structure, most of them probably with *Cs* local symmetry.

EXPERIMENTAL

Materials

The ligands, MDPO, RPPh and RPOEt, were prepared by literature procedures.[18,19]

Metal hexacarbonyls were purchased from commercial sources. The tricarbonyls, $M(CO)_3(RPPh)$ and $M_2(CO)_6(MDPO)_3$ (M = Mo, W), were prepared by reacting the metal hexacarbonyls and the corresponding ligand under reflux in appropriate solvent as described previously.[6]

Solvents were purified and dried in the usual manner and freshly distilled under argon before use. All reactions were carried out in an atmosphere of dry argon.

Physical measurements

IR spectra on nitromethane solution and KBr pellets were recorded in the region 4000–200 cm^{-1}

using a Perkin–Elmer Model 580B spectrometer. Far-IR samples were prepared as Nujol mulls supported between rigid polyethylene plates.

^{1}H NMR spectra were recorded on a JEOL FX90Q Fourier Transform spectrometer using tetramethylsilane as an internal standard.

Conductivity measurements were carried out at 25°C on 10^{-3} M nitrobenzene solutions using a Tacussel conductivity bridge, type Cd7.

Magnetic susceptibilities were measured at room temperature by the Gouy method with $CuSO_4 \cdot 5H_2O$ as calibrant. All the complexes were diamagnetic.

The molecular weight of the $Mo(CO)_3(MDPO)I_2$ complex was determined using a modified Signer's method.[20]

Preparation of complexes

Freshly prepared disubstituted or trisubstituted metal(0) carbonyl complexes[6] were dispersed in a suitable solvent. Adequate amounts of halogen dissolved in benzene, toluene or CCl_4 were added dropwise into the suspension under a stream of dry argon and with stirring at temperatures below 0°C. Completion of the reaction was monitored by IR spectroscopy. The resulting substances were filtered off, washed with appropriate solvent and dried over P_4O_{10} *in vacuo*.

$Mo(CO)_3(RPPh)Br_2$. To $Mo(CO)_3(RPPh)$ (0.184 g, 0.25 mmol) dispersed in 25 cm^3 of CCl_4, at −20 to −30°C with continuous stirring under a stream of dry argon, was added bromine (0.045 g, 0.28 mmol) dissolved in 5 cm^3 of benzene, over 1 h. The reaction mixture was stirred for a further 1/2 h and then the precipitate was filtered off, washed with a small amount of dry CCl_4 and dried over P_4O_{10} *in vacuo*. The yield was 0.157 g (70%).

$Mo(CO)_3(RPPh)I_2$. A suspension of the complex $Mo(CO)_3(RPPh)$ (0.147 g, 0.20 mmol) in CCl_4 (15 cm^3) was treated with iodine (0.061 g, 0.24 mmol) in CCl_4 (40 cm^3) over 4 h under argon with continuous stirring at −5°C. The orange product (0.170 g, 86%) was filtered off, washed with CCl_4 and dried.

$W(CO)_3(RPPh)Br_2$. To a suspension of $W(CO)_3$ (RPPh) (0.205 g, 0.25 mmol) in *n*-heptane (40 cm^3) at −30°C with continuous stirring under dry argon was added bromine (0.045 g, 0.28 mmol) in benzene (5 cm^3), over 2 h. After stirring for a further 1/2 h, the resulting orange–yellow precipitate was filtered off (0°C), washed with a small amount of cold heptane and dried in vacuum. The yield was 0.169 g (69%).

$W(CO)_3(RPPh)I_2$. The complex $W(CO)_3(RPPh)$ (0.164 g, 0.20 mmol) was dispersed in 10 cm^3 of CCl_4 at −10°C. Iodine (0.056 g, 0.22 mmol) in CCl_4 (30 cm^3) was added over 4 h under continuous stirring in a stream of dry argon. After the addition of iodine the reaction mixture was stirred for a further hour and then the complex (190 mg, 89%) was filtered off, washed with CCl_4 and dried.

$Mo(CO)_3(MDPO)Br_2$. To a suspension of $Mo_2(CO)_6(MDPO)_3$ (0.241 g, 0.15 mmol) in CCl_4 (20 cm^3) was added bromine (0.072 g, 0.45 mmol) in 20 cm^3 of the same solvent at −20 to −30°C over 1 h. The reaction mixture was stirred under dry argon. After completion of the reaction, the precipitate (0.180 g, 80%) was filtered off, washed with a few cm^3 of CCl_4 and dried.

$Mo(CO)_3(MDPO)I_2$. A CCl_4 solution (40 cm^3) of iodine (0.089 g, 0.35 mmol) was added dropwise into a suspension of the complex $Mo_2(CO)_6(MDPO)_3$ (0.241 g, 0.15 mmol) in CCl_4 (15 cm^3) under argon at −10°C over 4 h. The reaction mixture was vigorously stirred and after all the iodine had been added, it was left overnight. The orange–brown product was filtered off, washed and dried as usual. The yield was 0.216 g (85%).

$W(CO)_3(MDPO)Br_2$. Treatment of a suspension of $W_2(CO)_6(MDPO)_3$ (0.178 g, 0.1 mmol) in *n*-heptane (30 cm^3) with bromine (0.045 g, 0.28 mmol) dissolved in 6 cm^3 of benzene, with continuous stirring under argon at −25°C over 1 h, afforded 0.145 g (86%) of the orange–yellow complex $W(CO)_3(MDPO)Br_2$, which was filtered off, washed and dried as above.

$W(CO)_3(MDPO)I_2$. $W_2(CO)_6(MDPO)_3$ (0.178 g, 0.1 mmol) dispersed in 20 cm^3 of CCl_4 was treated with a solution (25 cm^3) of iodine (0.056 g, 0.22 mmol) in the same solvent with stirring under argon at −10 to −15°C over 3 h. The resulting precipitate (0.140 g, 75%) was filtered off, washed with a few cm^3 of CCl_4 and dried.

MDPO complexes were also obtained by an alternative procedure. As an example the preparation of $Mo(CO)_3(MDPO)I_2$ is given below.

$Mo(CO)_3(MDPO)I_2$. $Mo_2(CO)_6(MDPO)_3$ (0.161 g, 0.1 mmol) was dispersed in 20 cm^3 of toluene. Iodine (0.056 g, 0.22 mmol) in 30 cm^3 of toluene was added dropwise at −10°C. After stirring the reaction mixture for 2 h the oxidized products which separated on the sides of the flask were removed by filtration. Addition of a three-fold excess of *n*-heptane to the filtrate afforded a good yield (0.120 g; 70%) of orange $Mo(CO)_3(DMPO)I_2$, which was filtered off, washed with a small amount of toluene and dried as above.

$Mo(CO)_4(RPOEt)$. This was obtained by refluxing a mixture of $Mo(CO)_6$ (0.198 g, 0.75 mmol) and RPOEt (0.262 g, 0.5 mmol) in 20 cm^3 of toluene for 5 h. The brown product was collected by filtration from hot solution, washed with a few cm^3 of toluene and dried. The yield was 52% (0.190 g).

$W(CO)_4RPOEt$. A mixture of $W(CO)_6$ (0.176 g, 0.5 mmol) and RPOEt (0.157 g, 0.3 mmol) in 20 cm^3 of xylene was boiled under reflux for 4 h. The complex was collected from a hot solution as described above with a yield of 0.160 g (65%).

$Mo(CO)_3(RPOEt)I_2$. Freshly prepared $Mo(CO)_4$ (RPOEt) (0.146 g, 0.2 mmol) was dispersed in 20 cm^3 of *n*-heptane. An excess of iodine (0.35 mmol, 0.090 g) dissolved in 30 cm^3 of CCl_4 was added dropwise to the suspension over 4 h. The reacting mixture was stirred and cooled to $-20°C$. The resulting precipitate (0.128 g; 65%) was filtered off and washed with a few cm^3 of diethyl ether.

$W(CO)_3(RPOEt)I_2$. This was obtained in a yield of 70% using the same solvents and the same relative ratio of the reacting components as the analogous molybdenum complex described above.

All of the prepared RPOEt complexes are very sensitive and tend to loose carbon monoxide rather quickly if kept in air at room temperature.

Acknowledgement—The financial support from the Foundation of Scientific Research of SR Croatia is gratefully acknowledged.

REFERENCES

1. M. G. B. Drew, *Prog. Inorg. Chem.* 1977, **23**, 67.
2. P. K. Baker and D. ap. Kendrick, *J. Coord. Chem.* 1988, **17**, 355.
3. P. Bronzan-Planinić and H. Meider, *Polyhedron* 1983, **2**, 69.
4. P. Bronzan-Planinić and H. Meider, *Croat. Chem. Acta* 1984, **57**, 477.
5. M. Herceg, P. Bronzan-Planinić, H. Meider and B. Matković, *Polyhedron* 1986, **5**, 2013.
6. P. Planinić and H. Meider, *Polyhedron* 1989, **8**, 627.
7. S. C. Tripathi, S. C. Srivastava and A. K. Shrimal, *Inorg. Chim. Acta* 1976, **18**, 231.
8. P. K. Baker and S. G. Fraser, *Polyhedron* 1987, **6**, 2081.
9. R. Colton and I. B. Tomkins, *Aust. J. Chem.* 1967, **20**, 13.
10. K. Nakamoto, *Infrared and Raman Spectra of Inorganic and Coordination Compounds*. Wiley, New York (1978).
11. F. A. Cotton, R. D. Barnes and E. Bannister, *J. Chem. Soc.* 1960, 2199.
12. P. S. Braterman, *Metal Carbonyl Spectra*. Academic Press, New York (1975).
13. F. A. Cotton and C. S. Kraihanzel, *J. Am. Chem. Soc.* 1962, **84**, 4432.
14. C. S. Kraihanzel and F. A. Cotton, *Inorg. Chem.* 1963, **2**, 533.
15. F. A. Cotton, *Inorg. Chem.* 1964, **3**, 702.
16. A. Blagg, S. W. Carr, G. R. Cooper, I. D. Dobson, J. B. Gill, D. C. Goodall, B. L. Shaw, N. Taylor and T. Boddington, *J. Chem. Soc., Dalton Trans.* 1985, 1213.
17. D. L. Kepert, *Prog. Inorg. Chem.* 1979, **25**, 41.
18. C. R. White and M. D. Joesten, *J. Inorg. Nucl. Chem.* 1976, **38**, 2173.
19. T. Ya. Medved, Yu. M. Polikarpov, S. A. Pisareva, E. I. Matrosov and M. I. Kabachnik, *Izv. Akad. Nauk SSSR, Ser. Khim.* 1968, 2062.
20. E. P. Clark, *Ind. Eng. Chem.* 1941, **33**, 820.

Polyhedron Vol. 9, No. 8, pp. 1107–1112, 1990
Printed in Great Britain

0277–5387/90 $3.00+.00
© 1990 Pergamon Press plc

ACTIVATION OF AROMATIC C—H BONDS BY ZEROVALENT RUTHENIUM COMPLEXES OF BIS(DIMETHYLPHOSPHINO)METHANE

PILAR PALMA-RAMIREZ, DAVID J. COLE-HAMILTON,* PETER POGORZELEC (in part) and JUAN CAMPORA (in part)

Chemistry Department, University of St Andrews, St Andrews, Fife KY16 9ST, Scotland, U.K.

(*Received* 8 *December* 1989; *accepted* 15 *December* 1989)

Abstract—Reaction of $[RuCl_2(PPh_3)_3]$ with excess bis(dimethylphosphino)methane (dmpm) in petroleum produces *trans*-$[RuCl_2(dmpm)_2]$, whilst a similar reaction using $[OsCl_2(PPh_3)_3]$ in toluene produces only $[OsCl_2(dmpm)_2(PPh_3)_2]$ with *trans*-chlorine atoms or, under reflux in the presence of excess dmpm, $[OsCl_2(dmpm)_3]$. Reduction of $[RuCl_2(dmpm)_2]$ with sodium–potassium alloy in benzene or toluene produces *cis*-$[RuHR(dmpm)_2]$ (R = Ph or C_6H_4Me), together with small amounts of unidentified products, one of which is paramagnetic. The hydrido aryl complexes are characterized spectroscopically and the exchange of *cis*-$[RuHPh(dmpm)_2]$ with C_6D_6 is described.

Although zerovalent complexes of ruthenium containing tertiary phosphine ligands should be sufficiently electron rich to promote intermolecular activation of C—H bonds, their use in these reactions has been bedevilled by the tendency for internal metallation of C—H bonds of the phosphine to occur. This is especially true for triphenylphosphine complexes,[1,2] but even $[Ru(dmpe)_2]$ (dmpe = 1,2-bis(dimethylphosphino)ethane), although it does activate some C—H bonds,[3] also undergoes metallation reactions,[4] albeit intermolecularly.[5]

During studies[6] of zerovalent complexes of ruthenium containing bidentate phosphines, we noted that the rate of *ortho*-metallation of a phosphorus bound phenyl group was strongly dependent upon the length of the carbon chain separating the two phosphorus atoms. Thus, [Ru(styrene)(P—P)$_2$] could not be isolated for P—P = 1,3-bis(diphenylphosphino)propane (dppp), the only product of reactions of $[Ru(styrene)_2(PPh_3)_2]$ with dppp was $[RuH(C_6H_4P(Ph)(CH_2)_3PPh_2)(dppp)]$. For P—P = 1,2-bis(diphenylphosphine)ethane (dppe), [Ru(styrene)(dppe)$_2$] could be isolated but *ortho*-metallation occurred on standing in solution at room temperature for several hours, whilst for P—P = bis(diphenylphosphino)methane (dppm), [Ru(styrene)(dppm)$_2$] was stable to *ortho*-metallation even in refluxing toluene or on photolysis in benzene for 4 days.

We reasoned, therefore, that if $[Ru(dppm)_2]$ could be generated, it should be stable towards *ortho*-metallation reactions and should activate external C—H bonds. We now report studies aimed at generating this species, and the related $[Ru(dmpm)_2]$ (dmpm = bis(dimethylphosphino)methane) and show that the latter is capable of activating aromatic C—H bonds.

Certain dmpm complexes of ruthenium, including $[Ru(dmpm)_3]$ have been isolated[7] and during the course of this work it was shown[8] that the tetradentate phosphine, tris-3-(dimethylphosphino)propylphosphine (PP_3), which is also stabilized towards *ortho*-metallation, allows the production of a ruthenium(0) species which activates C—H bonds in aromatic compounds to give *cis*-[RuHPh(PP_3)].

RESULTS AND DISCUSSION

Preparation of $[RuCl_2(dmpm)_2]$

Attempts to prepare $[RuCl_2(dmpm)_2]$ by reaction of excess dmpm with $[RuCl_2(MeCN)_4]$, $[RuCl_2(DMSO)_4]$ (DMSO = dimethylsulphoxide) or the

* Author to whom correspondence should be addressed.

blue solution of chloro complexes of ruthenium(II), which can be generated by H_2 reduction of $[RuCl_3 \cdot xH_2O]$ in methanol, all failed to produce $[RuCl_2(dmpm)_2]$. $[RuCl_2(dmpm)_2]$ was successfully prepared, however, by the method pioneered by Stephenson[9] of phosphine exchange with $[RuCl_2(PPh_3)_3]$. Thus, stirring $[RuCl_2(PPh_3)_3]$ with excess dmpm* in petroleum produces a yellow solid from which pure $[RuCl_2(dmpm)_2]$ can be isolated on recrystallization from tetrahydrofuran (THF). Spectroscopic properties (Tables 1 and 2) indicate that this complex has *trans* stereochemistry.

Although ^{31}P NMR studies of the yellow solid obtained from petroleum show that it contains only *trans*-$[RuCl_2(dmpm)_2]$ and PPh_3, reasonable yields can only be obtained for small scale reactions (starting from *ca* 3 g of $[RuCl_2(PPh_3)_3]$) and even then substantial amounts of ruthenium remain in solution after recovering *trans*-$[RuCl_2(dmpm)_2]$.

Interestingly, the reaction of $[OsCl_2(PPh_3)_3]$ with dmpm did not lead to complete displacement of the triphenylphosphine ligands even under reflux. The isolated product was $[OsCl_2(dmpm)(PPh_3)_2]$ with *trans*-chlorine atoms (Tables 1 and 2). Using a large excess of dmpm, the product was similar, but spectroscopic properties suggested the formulation $[OsCl_2(dmpm)_3]$, containing two unidentate and one bidentate dmpm ligands. This compound was not obtained free from contaminating PPh_3.

Reduction of $[RuCl_2(dppm)_2]$ *and* $[RuCl_2(dmpm)_2]$

Attempts to reduce $[RuCl_2(dppm)_2]$ with sodium in refluxing toluene or potassium in refluxing benzene generally led to red solutions from which no clean products could be isolated. This was also the case for $[RuCl_2(dmpm)_2]$, but when sodium–potassium alloy, which is a liquid at room temperature, was employed as the reducing agent, cleaner reactions of $[RuCl_2(dmpm)_2]$ were observed and orange oily products could be isolated. Carrying out the reaction with benzene, 40–70°C, two products were observed, one of which was almost insoluble in light petroleum and the other was soluble. The petroleum-insoluble compound, which was obtained from toluene or benzene by precipitation with petroleum gave broad, temperature invariant, NMR signals and, although there were broad resonances in the phenyl and hydride regions of the ^1H NMR spectrum, we were unable fully to characterize the compounds but believe that they are paramagnetic complexes, possibly of ruthenium(I).

By contrast, the petroleum-soluble compounds, which were generally obtained as yellow–orange oils and were sometimes contaminated with small amounts of the paramagnetic species, described above, gave sharp NMR spectra and were identified spectroscopically as *cis*-$[RuHR(dmpm)_2]$ (R = Ph or C_6H_4Me), although they could not be obtained in an analytically pure state.

The phenyl and hydride resonances from the ^1H NMR spectrum of *cis*-$[RuHPh(dmpm)_2]$ are shown in Fig. 1. In the phenyl region separate resonances with the expected multiplicities are observed for the *ortho-*, *meta-* and *para*-protons of the coordinated phenyl group. Since all four phosphorus atoms are inequivalent,† the hydride resonance would be

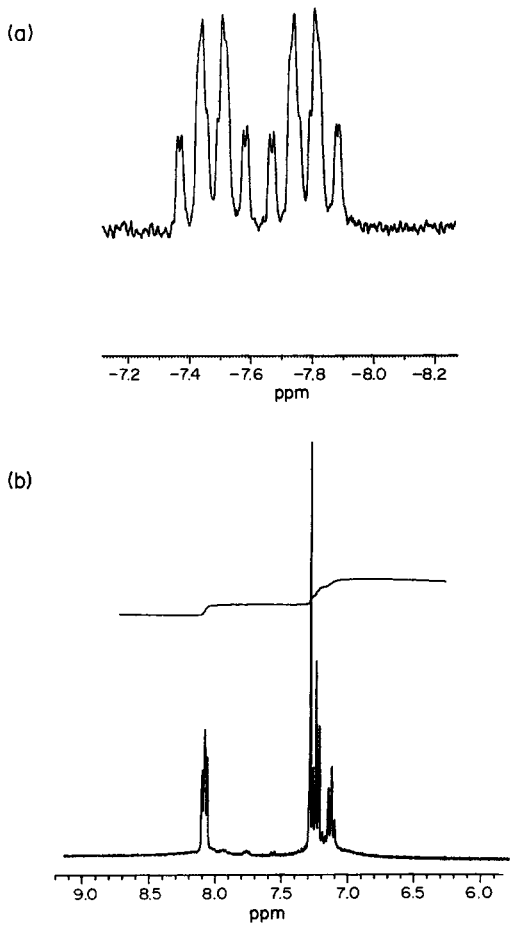

Fig. 1. 300 MHz ^1H NMR spectrum of *cis*-$[RuHPh(dmpm)_2]$ measured in C_6D_6: (a) hydride region and (b) phenyl region—the large singlet at δ 7.3 is from C_6D_5H and C_6H_6 and increases with time at the expense of the other resonances shown in A and B. Resonances are not drawn to scale.

*Carrying out this reaction in ethanol gives $[Ru(dmpm)_3]Cl_2$.[7]

†The mutually *trans*-phosphorus atoms are inequivalent by virtue of their being bound via the methylene groups to phosphorus atoms *trans* to H and *trans* to Ph, respectively. A similar non-equivalence also exists in, for example, *cis*-$[RuH(CO)(dppe)_2]^+$.[10]

Table 1. ^{1}H NMR spectra of new ruthenium complexes[a]

Complex	Ru—H						Ru—Ph							
		J(Hz)					δ			J (Hz)			CH_2	CH_3
	δ	HP_A	HP_B	HP_C	HP_D	HH	H_o	H_m	H_p	H_oH_m	H_mH_p	H_oP_D	$\delta(J_{PH})$	$\delta(J_{PH})$
trans-[$RuCl_2(dmpm)_2$]				—									3.52q(4)	1.46q(1.8)
cis-[$OsCl_2(PPh_3)_2$dmpm]				—									3.72bt(10)	1.15d(9)[b]
cis-[$OsCl_2(dmpm)_3$]				—									3.63tt(10,0.5)	1.15t(3)
														1.62d(9)[b]
														1.88d(8)
cis-[RuHPh(dmpm)$_2$]	−7.6	20	20	26	90	4	8.1dd	7.52t	7.12t	7	7	6	2.8m	1.1–1.7[c]
cis-[$RuH(C_6H_4Me)(dmpm)_2$]	−7.8br	21	21	21	90		7.87dd[d]	[e]	[e]	6		5		
							7.7dd[d]	[e]	[e]	7		6	2.8m	1.0–2.0[f]
							7.53d[d]	[e]	[e]			7		

[a] In C_6D_6 at 298 K, for assignments see Scheme 1, *o*, *m* and *p* are relative to the metal.
[b] Doublet with intensity between the lines, $J_{PH}+J_{PH'}=9$ Hz.
[c] Complex series of doublets.
[d] For assignments, see text.
[e] Not assigned.
[f] Complex series of doublets and singlets.

Table 2. ^{31}P NMR data for new dmpm complexes; measured in C_6D_6 at 298 K; chemical shifts are to high frequency of external 85% H_3PO_4. For assignments see Scheme 1

	δ					J (Hz)					
	P_A	P_B	P_C	P_D	P_E,P_F	P_AP_B	P_AP_C	P_AP_D	P_BP_C	P_BP_D	P_CP_D
trans-[$RuCl_2$(dmpm)$_2$]			−25.1								
cis-[$OsCl_2(PPh_3)_2$(dmpm)][a]	−12.6	−12.6	−80.6	−80.6				255	255		
cis-[$OsCl_2$(dmpm)$_3$][b]	−36.4	−36.4	−77.0	−77.0	−59.9			274	274[c]		
cis-[RuHPh(dmpm)$_2$]	−18.9	−21.0	−26.9	−35.3		299.5	33	49.3	33	37	12.3
cis-[RuH(C_6H_4Me)(dmpm)$_2$]	−19.2	−20.95	−26.9	−35.2		299.6	32	54	31	44	12

[a] AA′XX′type spectrum.
[b] AA′MM′XX′ type spectrum, $J(P_CP_E) = 22$ Hz.
[c] $J(P_AP_E) = J(P_BP_F) = 22$ Hz.

expected to be a doublet of doublets of doublets of doublets with one coupling of *ca* 100 Hz (from the *trans*-phosphorus atom) and three couplings of 20–30 Hz (from the *cis*-phosphorus atoms). This is exactly what is observed (Table 1), but there is an extra small coupling (4 Hz) which we have not been able to assign. It is possible that this coupling is either to another phosphorus atom, in which case the complex must not be mononuclear, although even with dinuclear species it is difficult to see how this particular coupling pattern or the observed ^{31}P NMR spectrum (see below) could be obtained. An alternative explanation is that the small coupling arises from coupling to a hydrogen atom. Being a four-bond coupling, this is not likely to be large but may be significant if the H—Ru—P—C—H skeleton holds a W configuration. The only such configurations possible in [RuHPh(dmpm)$_2$] are to two of the CH_3 hydrogen atoms and, although one of these methyl groups appears from models to be in such a position that steric crowding may restrict its rotation, we cannot be certain that this is responsible for the coupling.

Attempts to verify that this small coupling observed in the hydride resonance is to a dmpm methyl proton have been hampered by problems associated with the ready exchange of the complex with C_6D_6 (see below) which leads to loss of the relevant hydride signal, and by the complexity of the ^1H NMR spectrum in the methyl region.

As expected for a *cis*-bis(bidentate phosphine) complex in which the two other ligands are not identical, the ^{31}P NMR spectrum for *cis*-[RuHPh(dmpm)$_2$] is complex. However, it can be simulated and is totally consistent with the formulation proposed. The chemical shifts and coupling constants of the phosphorus atoms are collected in Table 2.

The petroleum-soluble compound obtained from reduction of [$RuCl_2$(dmpm)$_2$] in toluene has very similar spectroscopic properties of those of *cis*-[RuHPh(dmpm)$_2$], except that a more complex aromatic region is observed. From the signals in the region where the aromatic protons *ortho* to the metal resonate, it is possible to determine that the complexes in which the metal has added *para* to the methyl group (dd at 7.87 ppm, intensity 2), *ortho* to the methyl group (d at 7.7 ppm, intensity 1) are obtained in approximately equal amounts but that the product with the metal *meta* to the methyl group (d at 7.53 ppm intensity ~ 0.1, other dd not observed) is only a minor product. The assignment of the protons *meta* and *para* to the metal is complicated by signals from free toluene, which grow with time, presumably because of exchange with d^6-benzene. Once again this compound is contaminated with a paramagnetic species similar to that described above.

Reaction of cis-[RuHPh(dmpm)$_2$] *with* C_6D_6

On standing in C_6D_6 at room temperature for several hours, the signals from the hydride and the phenyl hydrogen atoms of *cis*-[RuHPh(dmpm)$_2$] diminish in intensity, whilst the residual benzene peak increases in intensity. No change is observed in the ^{31}P NMR spectrum so we interpret these observations as arising from an exchange of RuPhH with C_6D_6. Integration of the ^1H NMR spectrum after partial exchange has occurred shows that the ratio of Ph to H is still 1 : 1, suggesting that the exchange occurs via a concerted mechanism. All the reactions described are collected in Scheme 1.

EXPERIMENTAL

Microanalyses were by the University of St Andrews Materials Analysis services. IR spectra were obtained on Nujol mulls between ceasium iodide plates on a Perkin–Elmer 1310 spectrometer and

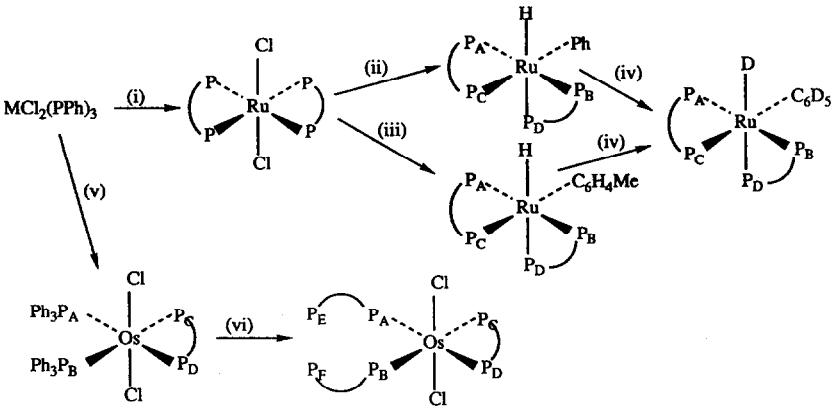

Scheme 1. Formation and reactions of dmpm complexes of ruthenium and osmium: (i) excess dmpm, M = Ru, petroleum, 20°C, 2 h; (ii) NaK, benzene; (iii) NaK, toluene; (iv) standing in C_6D_6 for several hours; (v) 3 mol dmpm, M = Os, toluene, 20°C, 20 min; (vi) excess dmpm, toluene, reflux, 3 h.

NMR spectra on a Bruker Associates A.M. 300 spectrometer working in the Fourier Transform Mode with (for ^{31}P) noise proton decoupling. All solvents were dried by distillation from sodium diphenylketyl and all manipulations were carried out under dry, deoxygenated nitrogen using standard Schlenk line and catheter tubing techniques. The petroleum used had boiling range 40–60°C.

$[RuCl_2(PPh_3)_3]$,[11] $[OsCl_2(PPh_3)_3]$[12] and dmpm[13] were synthesized by standard literature methods.

Sodium–potassium alloy

Sodium (0.5 g) and potassium (0.5 g) were suspended in THF (10 cm^3) and pressed together with a glass rod. The solvent was decanted and the liquid alloy washed with propan-2-ol (5 cm^3) to remove metal oxides and hydroxides. After decanting the propan-2-ol, the shiny alloy was washed with THF (2×5 cm^3) and the solvent to be used in the subsequent reaction (2×5 cm^3).

(1) trans-*Dichlorobisbis(dimethylphosphino)methaneruthenium*(II)

$[RuCl_2(PPh_3)_3]$ (2.9 g) was suspended in petroleum (30 cm^3) and dmpm (1.5 cm^3) was added. After stirring for 2 h, the yellow solid was collected by filtration, washed with petroleum (3×50 cm^3) and diethyl ether (1×20 cm^3) and dried *in vacuo* (yield *ca* 60%). Well-formed orange crystals of the product were obtained by dissolving the yellow solid in a minimum quantity of THF at room temperature and cooling to −30°C for 16 h. Yield. 30%. Analysis: Found: C, 27.2; H, 6.4. $C_{10}H_{28}Cl_2P_4Ru$ requires: C, 27.0; H, 6.3%. IR (λ_{max}/cm^{-1}) 288 (νRu—Cl). There are also medium features at 328 and 350 cm^{-1}.

(2) trans-*Dichlorobis(dimethylphosphino)methanebistriphenylphosphineosmium*(II)

A solution of $[OsCl_2(PPh_3)_3]$ (0.48 g, 0.5 mmol) in toluene (10 cm^3) was treated with dmpm (0.2 g, 1.5 mmol) and stirred for 20 min. The resulting yellow–green solution was evaporated to 1 cm^3 and treated with petroleum (30 cm^3). After filtration, the resulting yellow solid was washed with petroleum (2×20 cm^3) and dissolved in toluene (10 cm^3). The yellow solution was evaporated to 2 cm^3 and held at −30°C for 16 h. The yellow crystals so formed were collected and dried *in vacuo*. Yield *ca* 60%. Found: C, 53.6; H, 4.8. $C_{41}H_{44}Cl_2OsP_4$ requires: C, 53.4; H, 4.8%. IR (λ_{max}/cm^{-1}), 340 br, ν(Ru—Cl).

(3) trans-*Dichlorotrisbis(dimethylphosphino)methaneosmium*(II)

A solution of $[OsCl_2(PPh_3)_3]$ (0.48 g, 0.05 mmol) in toluene (5 cm^3) was refluxed with dmpm (0.41 g, 3 mmol) for 3 h. All of the osmium complex dissolved to give a yellow solution which was held at 50°C for 16 h. After evaporation to dryness, the product was extracted into petroleum (30 cm^3). Undissolved PPh_3 was removed by filtration and more PPh_3 crystallized on standing for 3 days. This was removed by filtration and the yellow solution evaporated to dryness. The product was obtained as yellow crystals by recrystallization from methanol at −30°C. ^{31}P NMR studies showed that, although the complex was the major product, it

still contained substantial quantities of PPh_3 (δ −6 ppm) and other impurities, the most important of which gave a singlet at δ −75.5.

(4) cis-*Bisbis(dimethylphosphino)methanehydridophenylruthenium*(II)

(i) $[RuCl_2(dmpm)_2]$ (0.67 g) in benzene (30 cm^3) was transferred onto a suspension of sodium–potassium alloy (1.0 g) in benzene (10 cm^3). The resulting suspension was stirred for 24 h using external heating from an oil bath at 70°C. The resulting deep red–orange suspension was filtered to remove NaK and metal chloride and evaporated to dryness to give a red–brown oil. This oil was extracted with petroleum (4 × 50 cm^3) to give a yellow solution and a pale brown solid. On evaporation to dryness, the yellow solution gave an orange oil which was identified as largely *cis*-$[RuHPh(dmpm)_2]$ by its ^{31}P and ^1H NMR spectra. The pale brown solid gave only broad signals in the ^1H and ^{31}P NMR spectra.

(ii) As above but at 60°C for 24 h.

(iii) As above but at 40°C for 42 h (contaminated with two other hydrido products, quintet at δ −16.17, J_{PH} = 20.3 Hz; quintet of triplets at δ −8.5, J_{PH} = 21q and 4.5t Hz).

(iv) As above but at 20°C for 5 days.

(5) cis-*Bis(bisdimethylphosphinomethane)hydridotolylruthenium*(II)

Was prepared as in (ii) above but using toluene (40 cm^3 total volume).

Acknowledgements—We thank the British Council for a Fleming Fellowship (P.P.R.), the British Council and the Spanish Ministerio de Educacion y Ciencias for funding of an Integrated Action programme (P.P.R. and J.C.) and the SERC for a grant to purchase the NMR spectrometer. We are also indebted to Johnson Matthey plc for generous loans of ruthenium salts.

REFERENCES

1. D. J. Cole-Hamilton and G. Wilkinson, *J. Chem. Soc., Dalton Trans.* 1979, 1283.
2. B. N. Chaudret, D. J. Cole-Hamilton and G. Wilkinson, *J. Chem. Soc., Dalton Trans.* 1978, 1739.
3. S. D. Ittel, C. A. Tolman, A. D. English and J. P. Jesson, *J. Am. Chem. Soc.* 1978, **100**, 7577.
4. J. Chatt and J. M. Davidson, *J. Chem. Soc.* 1965, 843.
5. F. A. Cotton, D. L. Hunter and B. Frenz, *Inorg. Chim. Acta* 1975, **15**, 155.
6. R. Obeso Rosete, D. J. Cole-Hamilton and G. Wilkinson, *J. Chem. Soc., Dalton Trans.* 1984, 2067.
7. W. K. Wong, K. W. Chiu, G. Wilkinson, A. J. Howes, M. Motevalli and M. B. Hursthouse, *Polyhedron* 1985, **4**, 603.
8. L. Dahlenburg and K-M. Frosin, *Chem. Ber.* 1988. **121**, 865.
9. P. W. Armit, A. S. F. Boyd and T. A. Stephenson, *J. Chem. Soc., Dalton Trans.* 1975, 1663.
10. G. Smith and D. J. Cole-Hamilton, *J. Chem. Soc., Dalton Trans.* 1984, 1206.
11. P. S. Hallman, T. A. Stephenson and G. Wilkinson, *Inorg. Synth.* 1970, **12**, 237.
12. P. R. Hoffmann and K. G. Caulton, *J. Am. Chem. Soc.* 1975, **97**, 4221.
13. H. H. Karsch and H. Schmidbaur, *Z. Naturfor.* 1977, **32b**, 762.

Polyhedron Vol. 9, No. 8, pp. 1113–1118, 1990
Printed in Great Britain

0277–5387/90 $3.00+.00
© 1990 Pergamon Press plc

SYNTHESIS AND REACTIONS OF ARENE–RUTHENIUM COMPLEXES CONTAINING NITROGEN-DONOR LIGANDS; CRYSTAL STRUCTURE OF (p-cymene)$_2$Ru$_2$Cl$_2$(N$_3$)$_2$

RICHARD S. BATES, MICHAEL J. BEGLEY and ANTHONY H. WRIGHT*

Chemistry Department, University of Nottingham, Nottingham NG7 2RD, U.K.

(*Received* 30 *October* 1989; *accepted* 21 *December* 1989)

Abstract—A range of nitrogen bases have been reacted with [(arene)RuCl$_2$]$_2$ complexes. The reaction with simple amines to give monomeric addition compounds (arene)RuCl$_2$NR$_3$ has been made rapid and quantitative using ultrasound. Steric factors predominate in determining the extent of the reactions. Trimethylsilylazide has been found to be a particularly suitable source of the azide ligand, generating the new dimer [(arene)Ru(μ-N$_3$)Cl]$_2$ which has been structurally characterized. This complex has been shown to undergo dimer cleavage and halide loss reactions.

The dimeric complexes of type **1** are very common and may be subdivided into two groups depending on whether the bridging ligands contribute two or three electrons.[1]

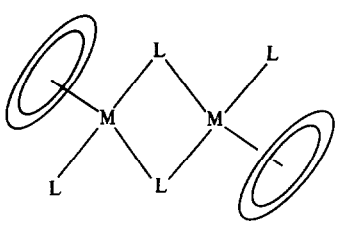

1

The reactivity of the former dimers, such as [CpFe(CO)$_2$]$_2$, is well established.[2] By comparison, the latter group of dimers such as [(arene)RuCl$_2$]$_2$ is much less understood.[3] We have begun a programme investigating the reactivity of these complexes, initially examining the range of different nitrogen-donor ligands that may be introduced to the metal centre.

Extensive investigations of the reactions of these dimers with oxygen-based ligands have been reported,[4] and the reaction with soft nitrogen-based ligands such as pyridine and acetonitrile has been investigated, particularly as sources of the [(arene)Ru]$^{2+}$ fragment.[5]

RESULTS AND DISCUSSION

Reactions with amines

One of the problems associated with using the dimers [(arene)RuCl$_2$]$_2$ (**1**), and especially the benzene-containing dimer, lies in the insolubility of these substrates in non-coordinating solvents. This can be readily overcome by carrying out the reactions at room temperature using a simple ultrasound bath.

Both aliphatic and aromatic primary amines react rapidly with [(C$_6$H$_6$)RuCl$_2$]$_2$ at room temperature when subjected to ultrasound in non-polar solvents (Scheme 1). The products are yellow crystalline solids and the initial product in each case is that of simple addition resulting in dimer cleavage (**2**, **3** and **4**). Analogous products such as (MeC$_6$H$_4$CHMe$_2$)RuCl$_2$(NH$_2$CMe$_3$) (**10**) can be obtained using substrate dimers containing other arenes.

In the case of p-toluidine, addition of excess ligand and longer reaction periods leads to increasing amounts of the product containing two amine ligands (**5**), resulting from subsequent halide substitution. The further substitution that is only observed with aromatic amines, indicates that in these reactions the softness (HSAB theory) of the nucleophile plays a more important role than basicity.

This conclusion is supported by the results of reactions with aliphatic secondary or tertiary

* Author to whom correspondence should be addressed.

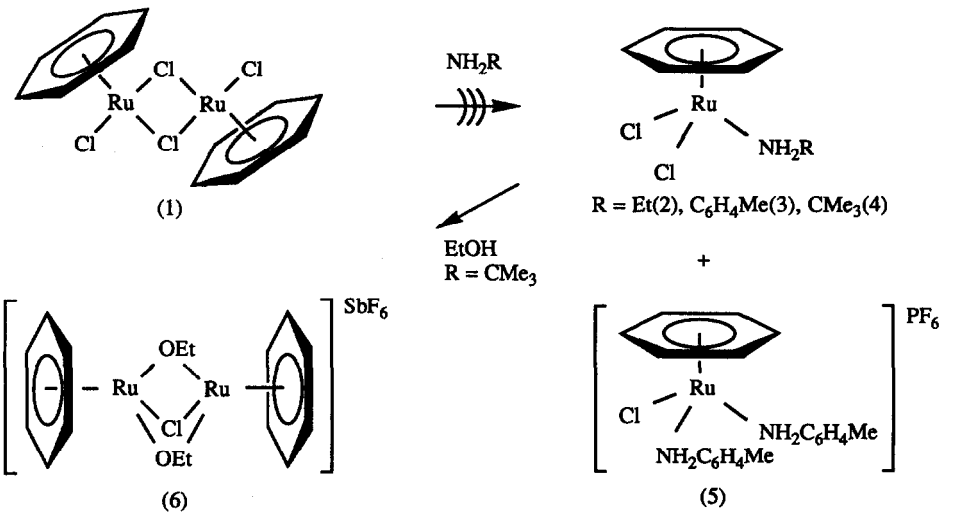

Scheme 1. Reactions of $(C_6H_6)_2Ru_2Cl_4$ with amines.

amines in which no addition reactions were observed. This result contrasts with the well-established reactions of the same substrates with tertiary phosphines and indicates that steric factors are much more important with the relative hard amines which are poorer ligands for the ruthenium centre. Softer nitrogen bases such as pyridine undergo the same reaction giving the addition product in the first step.

The recent report of addition reactions of primary aliphatic amines and a range of phosphine nucleophiles to the dimer adds further support for the reactivity pattern described.[6]

The relative weakness of the Ru—N bonds that are formed is illustrated in the reaction of $(C_6H_6)RuCl_2(NH_2CMe_3)$ with $AgSbF_6$ in ethanol, in which the only product that was detected was the triply-bridged cation **6**. In other reactions the only products isolated involve loss of the amine ligand.

Azide ligands

The azide ligand is a non-sterically demanding nitrogen-based pseudohalide. The reagent Me_3SiN_3 provides an excellent source of the azide moiety

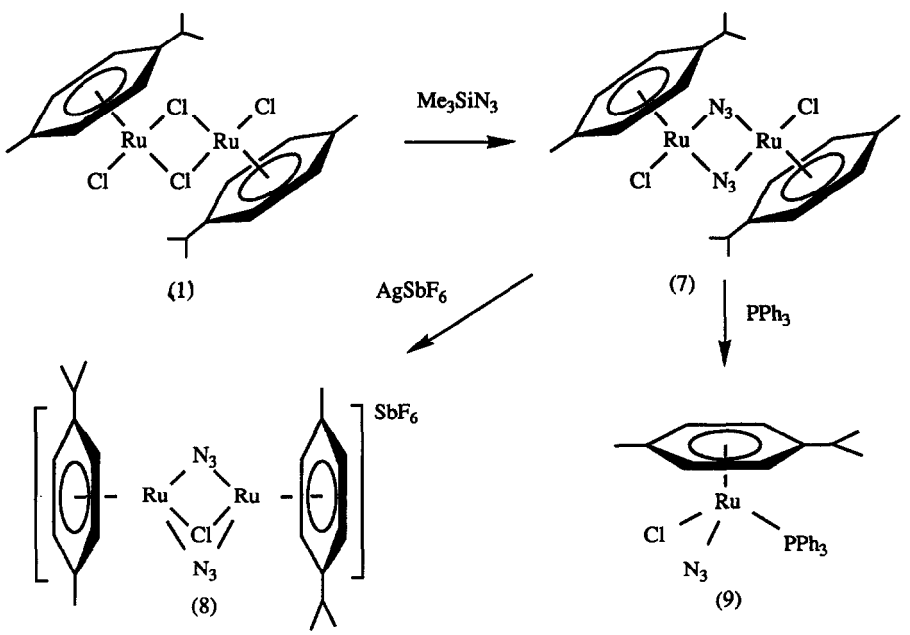

Scheme 2. Synthesis and reactions of $(cymene)_2Ru_2Cl_2(N_3)_2$.

and reacts rapidly with $[(cymene)_2RuCl_2]_2$ to give orange crystals of $[(cymene)_2Ru(N_3)Cl]_2$ (**7**).

IR spectra of **7** contain a single absorption assignable to the azide ligand and a single Ru—Cl stretch is observed. The ^1H NMR spectrum contains the absorption associated with a cymene ligand in only one environment. An X-ray crystal structure was carried out to confirm the dimeric nature of the product, Fig. 1.

No product involving further substitution of the chlorides has been detected. This result contrasts with the related reaction of $[(C_5Me_5)_2RhCl_2]_2$ with sodium azide, in which the product involving monosubstitution could only be obtained by limiting the amount of nucleophile to a 1 : 1 stoichiometry.[7]

A second difference between the related complexes lies in the thermal instability of the ruthenium complex. When **7** was heated in toluene, rapid loss of the arene ligand occurred (detected by NMR spectroscopy) and a brown product precipitated from solution that detonated on handling.

Unlike the amine ligands, the azide ligands remain in the coordination sphere when simple reactions are carried out. For example, addition of triphenylphosphine leads to simple bridge cleavage and formation of $(cymene)Ru(N_3)Cl(PPh_3)$ (**9**). The ^1H NMR spectrum of the product contains three sets of signals assignable to cymene ligands indicating that the complex exists in non-polar solutions in three conformations and there is steric hindrance to rotation of the arene ring.

Chloride rather than azide loss occurs when dimer **7** is reacted with $AgSbF_6$, leading to formation of the mixed ligand triply-bridged product **8**.

Structure of (p-*cymene*)$_2$Ru$_2$Cl$_2$(N$_3$)$_2$ (**7**)

The X-ray crystal structure determination of **7** shows that the molecule is dimeric with the two azide ligands bridging the two metals (Fig. 1), and bond lengths and angles are given in Table 1. The only crystallographically-imposed symmetry is an inversion centre midway between the metal atoms.

The surprising feature of the structure is that the ligating nitrogens are pyramidally coordinated, not planar, with the angles about the nitrogen summing to 351.6°. The ruthenium atoms and ligating nitrogens lie in a plane and N(2) and N(3) lie 0.514(2) and 0.992(3) Å, respectively, out of the plane. An examination of non-bonding interactions and a space filling model of the molecule failed to reveal any steric interactions that might cause the bending. Reactions aimed at exploring any reactivity associated with a lone pair on the ligating nitrogen were, however, unsuccessful. A related rhodium complex also contains a bridging azide ligand and has the same overall geometry, but in this case the angles about the ligating nitrogen do not differ significantly from those required for planarity.[7]

The cymene ring is essentially planar and the distance from the ring to the metal is 1.657(3) Å, a distance very similar to that found in $[(C_6Me_6)RuCl_2]_2$.[8] Likewise, the Ru—Cl distance of 2.395(1) Å is very close to that determined for the hexamethylbenzene complex.

EXPERIMENTAL

All reactions were carried out under nitrogen or argon using standard Schlenk techniques. Characterization of new compounds was achieved by means of elemental analysis, IR and NMR spectroscopy and mass spectrometry. Microanalytical data were obtained from the University of Nottingham's Microanalytical Laboratory. IR spectra were recorded on a Perkin–Elmer 983G spectrometer as Nujol mulls on CsI plates. NMR spectra were recorded on a Bruker 250 MHz spectrometer. A 500 W biological cell disruptor from Sonics and Materials Inc. was used for the experiments involving ultrasound.

Ruthenium trichloride was obtained from Johnson Matthey Chemicals Ltd and $[(C_6H_6)RuCl_2]_2$

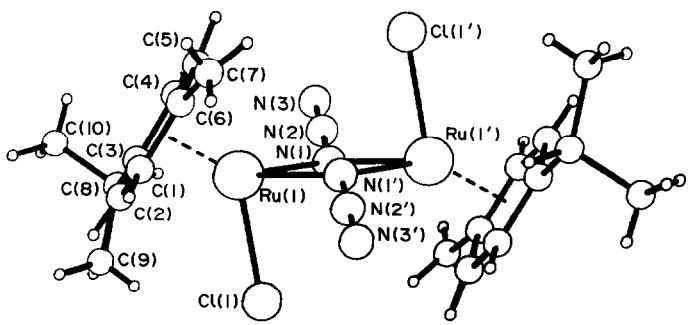

Fig. 1. Molecular structure of $(cymene)_2Ru_2Cl_2(N_3)_2$ showing the principal atomic numbering.

Table 1. Bond lengths (Å) and angles (°) for $(cymene)_2Ru_2Cl_2(N_3)_2$, with ESDs in parentheses

Bond lengths			
Ru(1)—Ru(1′)	3.448(1)	N(2)—N(3)	1.148(5)
Ru(1)—Cl(1)	2.395(1)	C(1)—C(2)	1.419(5)
Ru(1)—N(1)	2.165(3)	C(1)—C(6)	1.408(5)
Ru(1)—N(1′)	2.176(3)	C(2)—C(3)	1.409(5)
Ru(1)—C(1)	2.182(3)	C(3)—C(4)	1.412(5)
Ru(1)—C(2)	2.161(3)	C(3)—C(8)	1.518(6)
Ru(1)—C(3)	2.195(3)	C(4)—C(5)	1.409(5)
Ru(1)—C(4)	2.152(3)	C(5)—C(6)	1.409(5)
Ru(1)—C(5)	2.176(3)	C(6)—C(7)	1.495(5)
Ru(1)—C(6)	2.187(3)	C(8)—C(9)	1.534(7)
N(1)—N(2)	1.141(5)	C(8)—C(10)	1.513(7)
Bond angles			
Cl(1)—Ru(1)—N(1)	85.6(1)	C(2)—C(1)—C(6)	120.2(2)
Cl(1)—Ru(1)—N(1′)	85.4(1)	C(1)—C(2)—C(3)	121.7(1)
Cl(1)—Ru(1)—C(1)	104.2(1)	C(2)—C(3)—C(4)	116.8(2)
Cl(1)—Ru(1)—C(4)	137.3(1)	C(2)—C(3)—C(8)	123.4(2)
N(1)—Ru(1)—N(1′)	74.8(1)	C(4)—C(3)—C(8)	119.7(2)
N(1)—Ru(1)—C(1)	170.0(1)	C(3)—C(4)—C(5)	122.4(2)
N(1)—Ru(1)—C(4)	91.4(1)	C(4)—C(5)—C(6)	120.0(2)
N(1′)—Ru(1)—C(1)	107.4(1)	C(1)—C(6)—C(5)	118.8(2)
N(1′)—Ru(1)—C(4)	134.7(1)	C(1)—C(6)—C(7)	119.9(2)
Ru(1)—N(1)—Ru(1′)	105.2(1)	C(5)—C(6)—C(7)	121.2(2)
Ru(1)—N(1)—N(2)	122.4(1)	C(3)—C(8)—C(9)	109.0(2)
Ru(1′)—N(1)—N(2)	124.1(1)	C(3)—C(8)—C(10)	114.0(2)
N(1)—N(2)—N(3)	177.7(1)	C(9)—C(8)—C(10)	110.8(2)

and $[(cymene)RuCl_2]_2$ were prepared by literature methods.

$(C_6H_6)RuCl_2(NH_2Et)$ (2)

$[(C_6H_6)RuCl_2]_2$ (150 mg, 0.3 mmol) was suspended in THF (10 cm^3) and a solution of NH_2Et (100 mg, 2.2 mmol) in THF (5 cm^3) was added and subjected to ultrasound for approximately 90 min. The reaction mixture was allowed to stand at room temperature for 10 min and the yellow precipitate was collected and recrystallized from a dichloromethane–ethanol mixture to give $(C_6H_6)RuCl_2(NH_2Et)$ (71 mg, 40%). Found: C, 31.9; H, 4.3. Calc. for $RuC_8H_{13}Cl_2N$: C, 32.5; H, 4.4%. ν(NH) 3277, 3206 cm^{-1}, ν(RuCl) 273 cm^{-1} (Nujol mull); ^1H NMR ($CDCl_3$) 5.63 (s, 6H, C_6H_6), 3.2 (q, 2H, CH_2), 1.23 (t, 3H, CH_3).

$(C_6H_6)RuCl_2(NH_2C_6H_4Me)$ (3)

$[(C_6H_6)RuCl_2]_2$ (150 mg, 0.3 mmol) was suspended in THF (10 cm^3) and a solution of *p*-toluidine ($NH_2C_6H_4Me$) (230 mg, 2.2 mmol) in THF (5 cm^3) was added and subjected to ultrasound for approximately 90 min. The reaction mixture was allowed to stand at room temperature for 10 min and the yellow precipitate was collected and recrystallized from a dichloromethane–ethanol mixture to give $(C_6H_6)RuCl_2(NH_2C_6H_4Me)$ (162 mg, 76%). Found: C, 43.9; H, 4.35. Calc. for $RuC_{13}H_{15}Cl_2N$: C, 43.7; H, 4.2. ν(NH) 3255, 3223 cm^{-1}, ν(RuCl) 276 cm^{-1} (Nujol mull); ^1H NMR ($CDCl_3$) 7.32–7.14 (m, 4H, C_6H_4), 5.33 (s, 6H, C_6H_6), 2.33 (s, 3H, CH_3).

$[(C_6H_6)RuCl_2(NH_2CMe_3)]\cdot NH_2CMe_3$ (4)

Yield, 207 mg, 87%. Found: C, 42.3; H, 7.7. Calc. for $RuC_{14}H_{28}Cl_2N_2$: C, 42.4; H, 7.1%. ν(NH) 3273, 3215 cm^{-1}, ν(RuCl) 275 cm^{-1} (Nujol mull); ^1H NMR ($CDCl_3$) 5.72 (s, 6H, C_6H_6), 1.34 [s, 9H, $C(CH_3)_3$ (coord)], 1.11 [s, 9H, $C(CH_3)_3$ (free)].

$[(C_6H_6)RuCl(NH_2C_6H_4Me)_2]PF_6$ (5)

This product may also be isolated from the reaction described for **3**. The yield is increased if NH_4PF_6 is added to the reaction mixture to give $[(C_6H_6)RuCl(NH_2C_6H_4Me)_2]PF_6$. ν(NH) 3028 cm^{-1} (Nujol mull); ^1H NMR ($CDCl_3$) 7.34–7.06

(m, 8H, C_6H_4), 5.01 (s, 6H, C_6H_6), 2.29 (s, 6H, CH_3).

$(MeC_6H_4CHMe_2)RuCl_2(NH_2CMe_3)$ (**10**)

This compound was made using the method described for **2** (104 mg, 85%). Found: C, 44.2; H, 6.8. Calc. for $RuC_{14}H_{25}Cl_2N$: C, 44.3; H, 6.64%. ν(NH) 3266, 3209 cm^{-1}, ν(RuCl) 273 cm^{-1} (Nujol mull); ^1H NMR ($CDCl_3$) 5.50–5.43 (m, 4H, C_6H_4), 3.05 (sept, 1H, CH), 2.26 (s, 3H, $C_6H_4CH_3$), 1.33 (s, 9H, $C(CH_3)_3$), 1.29 and 1.26 (d, 3H, $CH(CH_3)_2$).

$[(C_6H_6)_2Ru_2Cl(OEt)_2]SbF_6$ (**6**)

$[(C_6H_6)RuCl_2(NH_2CMe_3)]\cdot NH_2CMe_3$ (300 mg, 0.76 mmol) was dissolved in MeCN (20 cm^3) and a solution of $AgSbF_6$ (286 mg, 0.84 mmol) in MeCN (5 cm^3) was added and the mixture stirred for 30 min. The precipitated AgCl was removed by filtration and the product precipitated as an orange solid by the gradual addition of EtOH to give $[(C_6H_6)_2Ru_2Cl(OEt)_2]SbF_6$ (96 mg, 35%). Found: C, 26.5; H, 3.1. Calc. for $Ru_2C_{16}H_{22}ClF_6O_2Sb$: C, 26.7; H, 3.1%. ν(RuCl) 258 cm^{-1} (Nujol mull).

$[(MeC_6H_4CHMe_2)_2Ru_2Cl_2(N_3)_2]$ (**7**)

$[(MeC_6H_4CHMe_2)RuCl_2]_2$ (200 mg, 0.33 mmol) was dissolved in dichloromethane (5 cm^3) and N_3SiMe_3 (530 mg, 4.6 mmol) was added dropwise and the mixture stirred for 30 min. An orange crystalline solid was obtained by addition of hexane and reduction of the volume under reduced pressure. Recrystallization was carried out from CH_2Cl_2–EtOH to give $[(MeC_6H_4CHMe_2)_2Ru_2Cl_2(N_3)_2]$ (186 mg, 90%). Found: C, 37.9; H, 4.5. Calc. for $Ru_2C_{20}H_{28}Cl_2N_6$: C, 38.4; H, 4.5%. ν(NN) 2057 cm^{-1}, ν(RuCl) 281 cm^{-1} (Nujol mull); ^1H NMR ($CDCl_3$) 5.33–5.22 (m, 4H, C_6H_4), 2.92 (sept., 1H, CH), 2.24 (s, 3H, $C_6H_4CH_3$), 1.28 and 1.25 (d, 3H, $CH(CH_3)_2$).

$[(MeC_6H_4CHMe_2)_2Ru_2Cl(N_3)_2]SbF_6$ (**8**)

$[(MeC_6H_4CHMe_2)_2Ru_2Cl_2(N_3)_2]$ (250 mg, 0.4 mmol) was dissolved in MeCN (10 cm^3) and $AgSbF_6$ (151 mg, 0.44 mmol) in MeCN, was added. The solution was stirred and then filtered to remove the AgCl precipitate. The product was crystallized by addition of ethanol to give $[(MeC_6H_4CHMe_2)_2Ru_2Cl(N_3)_2]SbF_6$ (208 mg, 63%). Found: C, 28.9; H, 3.5. Calc. for $Ru_2C_{20}H_{28}ClF_6N_6Sb$: C, 29.1; H, 3.4%. ν(NN) 2062 cm^{-1} (Nujol mull); ^1H NMR ($CDCl_3$) 5.57–5.36 (m, 4H, C_6H_4), 2.75 (sept., 1H, CH), 2.23 (s, 3H, $C_6H_4CH_3$), 1.29 and 1.28 (d, 3H, $CH(CH_3)_2$).

$[(MeC_6H_4CHMe_2)RuCl(N_3)PPh_3]$ (**9**)

PPh_3 (450 mg, 1.7 mmol) in CH_2Cl_2 (15 cm^3) was added dropwise to a stirred solution of $[(MeC_6H_4CHMe_2)_2Ru_2Cl_2(N_3)_2]$ (150 mg, 0.24 mmol) in CH_2Cl_2 (15 cm^3). A red solid was collected after treatment of the reaction mixture with hexane and the volume reduced under reduced pressure giving $[(MeC_6H_4CHMe_2)RuCl(N_3)PPh_3]$ (234 mg, 85%). Found: C, 58.8; H, 5.1. Calc. for $RuC_{28}H_{29}ClN_3P$: C, 58.5; H, 5.1%. ν(NN) 2039 cm^{-1}, ν(RuCl) 294 cm^{-1} (Nujol mull); ^1H NMR ($CDCl_3$) 5.50–4.80 (m, 4H, C_6H_4), 2.82 (sept., 1H, CH), 1.86–1.81 (s, 3H, $C_6H_4CH_3$), 1.29–1.08 (d, 6H, $CH(CH_3)_2$).

Crystal data

$C_{20}H_{28}Cl_2N_6Ru_2$, $M = 625.52$ g mol^{-1}, triclinic, $a = 7.586(2)$, $b = 8.376(2)$, $c = 9.689(2)$ Å, $\alpha = 101.40(1)$, $\beta = 87.00(1)$, $\gamma = 102.54(2)°$, $U = 589.07(3)$ $Å^3$, space group $P\bar{1}$ (No. 2), $Z = 1$, $D_c = 1.76$ g cm^{-3}, $F(000) = 312$, graphite-monochromated Mo-K_α radiation, $\lambda = 0.71069$ Å, μ(Mo-K_α) = 14.97 cm^{-1}, crystal dimensions $0.5 \times 0.25 \times 0.05$ mm.

Structure determination

Cell dimensions and their standard deviations were obtained by least-squares refinement of diffractometer setting angles for 12 centred reflections close to 13° in θ. Intensities of 3442 independent reflections ($1° < \theta < 25°$) were measured on a Hilger and Watts Y290 diffractometer in a ω–2θ scan mode.

The structure analysis used 3203 reflections with $I < 3\sigma(I)$ after correction for Lorentz and polarization factors. No correction was made for absorption.

Solution by Patterson and difference syntheses was followed by full-matrix least-squares refinement with anisotropic thermal parameters for all atoms except hydrogen using the CRYSTALS suite of programs. All the hydrogen atoms were located in difference maps and included, but not refined. The refinement for 192 parameters converged to $R = 0.039$ and $R_w = 0.046$, employing a weighting scheme based on Chebyshev polynomials. A final difference map contained no significant features. Complex neutral-atom scattering factors were cal-

culated from the analytical approximation and the coefficients given in ref. 9.*

Acknowledgements—We thank the SERC for support to R.S.B., the EEC for financial support and Johnson Matthey for the loan of ruthenium trichloride.

* Atomic coordinates, thermal parameters, full bond length and angle data and structure factor values have been deposited as supplementary material with the Editor, from whom copies are available on request. Atomic coordinates have also been deposited with the Cambridge Crystallographic Data Centre.

REFERENCES

1. G. Wilkinson, *Comprehensive Organometallic Chemistry*. Pergamon Press, Oxford (1987).
2. C. M. Lukehart, *Fundamental Transition Metal Organometallic Chemistry*, Ch. 85. Brooks/Cole, Belmont, California (1985).
3. H. Le Bozec, D. Touchard and P. H. Dixneuf, *Adv. Organomet. Chem.* 1989, **29**, 163.
4. R. O. Gould, C. L. Jones, D. R. Robertson and T. A. Stephenson, *J. Chem. Soc., Chem. Commun.* 1977, 222.
5. M. P. Gomez-Sal, B. F. G. Johnson, J. Lewis, P. R. Raithby and A. H. Wright, *J. Chem. Soc., Chem. Commun.* 1985, 1682.
6. P. Pertici, S. Bertozzi, R. Lazzaroni, G. Vitulli and M. A. Bennett, *J. Organomet. Chem.* 1988, **354**, 117.
7. W. Rigby, P. M. Bailey, J. A. McCleverty and P. M. Maitlis, *J. Chem. Soc., Dalton Trans.* 1979, 371.
8. F. B. McCormick and W. B. Gleason, *Acta Cryst.* 1988, **C44**, 603.
9. J. A. Ibers and W. C. Hamilton (Eds), *International Tables for X-Ray Crystallography*, Vol. 4. Kynoch Press, Birmingham (1974).

Polyhedron Vol. 9, No. 8, pp. 1119–1121, 1990
Printed in Great Britain

0277–5387/90 $3.00+.00
© 1990 Pergamon Press plc

HETEROLEPTIC POLYPYRAZOLYLBORATE DERIVATIVES OF YTTRIUM. THE SYNTHESES OF $[Y\{HB(C_3N_2H_3)_3\}_2(O_2CC_6H_4\text{-}p\text{-}Z)]$ (Z = NMe_2 AND NO_2) AND OF $[Y\{HB(C_3N_2H_3)_3\}(O_2CC_6H_4\text{-}p\text{-}Bu^t)_2]_2$

MICHAEL A. J. MOSS and CHRISTOPHER J. JONES*

Department of Chemistry, University of Birmingham, PO Box 363, Birmingham B15 2TT, U.K.

(*Received* 9 *November* 1989; *accepted* 21 *December* 1989)

Abstract—The new heteroleptic yttrium tris-pyrazolylborate complexes $[Y\{HB(C_3N_2H_3)_3\}_2(O_2CC_6H_4\text{-}p\text{-}Z)]$ (Z = NMe_2 and NO_2) and $[Y\{HB(C_3N_2H_3)_3\}(O_2CC_6H_4\text{-}p\text{-}Bu^t)_2]_2$ have been synthesized and characterized by spectroscopic methods, elemental analyses and solution molecular weight determinations.

As part of an investigation of heteroleptic lanthanide complexes containing the $\{LnL_2\}^+$ moiety (Ln = a lanthanide element or yttrium, L = hydrotris(pyrazol-1-yl)borate) we have prepared[1–5] the complexes $[YL_2X]$ (X = OC(Me)CHC(Me)O, $O_2C_7H_5$, O_2CMe and O_2CPh). The mass spectrum of the acetate complex suggested that this compound is oligomeric and solution molecular weight measurements made by Reger *et al.*[6] indicate a trimeric formulation $[YL_2(O_2CMe)]_3$ in CH_2Cl_2 solution. However, the related ytterbium benzoate complex, $[YbL_2(O_2CPh)]$, has been shown to be monomeric in the solid state containing a bidentate benzoate ligand.[4] This finding is somewhat unusual since those lanthanide carboxylate complexes which have been structurally characterized tend to be oligomeric, containing some bridging carboxylate ligands. In the case of acetate ligands the larger lanthanide ions form mono-, sesqui- and dihydrated tris(acetato) complexes, while the tetrahydrates predominate for the smaller lanthanide ions from samarium to lutetium.[7] Among the latter series $[Ln(O_2CMe)_3(H_2O)_2]\cdot 2H_2O$ (Ln = Ho, Er and Gd) have been structurally characterized.[8,9] These complexes consist of nine-coordinate lanthanide ions surrounded by three bidentate acetate ions, two water molecules and one oxygen of an acetate ligand bound to a neighbouring lanthanide ion. In the case of benzoate ligands several lanthanide complexes have been reported[10] but $[Dy(\mu\text{-}O_2CPh)(\kappa^1\text{-}O_2CPh)_2(H_2O)_4]\cdot H_2O$ is the only unsubstituted benzoate complex which has been structurally characterized.[11] The structure of this complex consists of eight-coordinate dysprosium ions bound to two monodentate benzoate ligands, four water molecules and two bridging benzoate ligands which lead to the formation of infinite chains.

Amongst the heteroleptic complexes, the bis(cyclopentadienyl)lanthanide acetates, benzoates and formates have been found to be dimeric,[12] as were the bis(cyclopentadienyl)ytterbium carboxylates $[(\eta^5\text{-}C_5H_5)_2Yb(O_2CR)]_2$ (R = Me, C_6F_5 and C_5H_4N).[13] The pentamethylcyclopentadienyl derivatives, $[(\eta^5\text{-}C_5Me_5)_2Yb(O_2CR)]$ were reported to be monomeric when R = CF_3 but oligomeric when R = Bu^t,[14] whilst the complexes $[(\eta^5\text{-}C_5Me_5)_2Yb(O_2CR)]_2$ (R = Ph, C_6F_5) are doubly benzoate bridged dimers.[13,15] Reger *et al.* have recently reported[6] the solid-state structure of $[YL(\mu\text{-}O_2CMe)_2]_2$ which contains four bridging acetate ligands linking two seven-coordinate yttrium ions. We have now synthesized three *para*-substituted benzoate complexes of yttrium which also contain the ligand L to further explore the heteroleptic tris-pyrazolylborate derivative chemistry of this element.

EXPERIMENTAL

Potassium hydrotris(pyrazol-1-yl)borate was prepared by the literature method.[16] Hydrated yttrium trichloride was obtained from Ventron

* Author to whom correspondence should be addressed.

GMBH. Water was distilled before use. ^{1}H NMR spectra were recorded using a JEOL JNM GX270 spectrometer. Deuterated NMR solvents were obtained from Aldrich Chemicals Ltd, and chemical shifts are reported with tetramethylsilane as internal reference at 293 K. IR spectra were recorded using potassium bromide pellets and a Perkin–Elmer 297 spectrometer. Mass spectra were obtained using a Kratos MS80RF mass spectrometer, ions being produced by electron impact. Elemental analyses were performed by the Microanalytical Service of the School of Chemistry, University of Birmingham, and osmometric solution molecular weight determinations by Ms S. Bradshaw, Department of Chemistry, University of Sheffield.

p-*Nitrobenzoatobis{hydrotris(pyrazol-1-yl)borato}yttrium*(III)

KL (0.75 g, 3 mmol), *p*-nitrobenzoic acid (0.25 g, 1.5 mmol), 0.1 mol dm^{-3} aqueous KOH (15 cm^3) and ethanol (15 cm^3) were mixed and added to a stirred solution of $YCl_3 \cdot 6H_2O$ (0.45 g, 1.5 mmol) in water (15 cm^3). The resulting white precipitate was collected by filtration, dried and recrystallized from CH_2Cl_2–hexane (yield, 0.50 g; 49%). M.p. 253–255°C. Found: C, 43.7; H, 3.4; N, 26.9. $C_{25}H_{24}B_2N_{13}O_4Y$ requires: C, 44.1; H, 3.5; N, 26.7%. IR spectrum: ν(BH) = 2460 cm^{-1} $\nu(NO_2)$ = 1540 cm^{-1}, also bands at 1605 and 1590 cm^{-1}; ^{1}H NMR spectrum:* pyrazolyl protons, δ_{TMS} = 7.67d(6), 7.16d(6), 6.01t(6) ppm ($^3J_{HH}$ = 2 Hz), phenyl protons δ_{TMS} = 7.60d, 7.05d ppm ($^3J_{HH}$ = 8 Hz). Mass spectrum: $\{[YL_2(O_2C\text{-}C_6H_4\text{-}NO_2)]-1\}^+$ m/z = 680 (7%), $\{[YL_2(O_2C\text{-}C_6H_4\text{-}NO_2)]-pz\}^+$ m/z = 615 (27%), $[YL_2]^+$ m/z = 515 (100%).

p-(*Dimethylamino*)*benzoatobis{hydrotris(pyrazol-1-yl)borato}yttrium*(III)

KL (0.50 g, 2 mmol), *p*-(dimethylamino)benzoic acid (0.17 g, 1 mmol), 0.1 mol dm^{-3} aqueous KOH (10 cm^3) and ethanol (15 cm^3) were mixed and added to a stirred solution of $YCl_3 \cdot 6H_2O$ (0.30 g, 1 mmol) in water (10 cm^3). The resulting white precipitate was collected by filtration, dried and recrystallized from CH_2Cl_2–hexane (yield, 0.38 g; 56%). M.p. 265–270°C. Found: C, 47.5; H, 4.2; N, 26.6. $C_{27}H_{30}B_2N_{13}O_2Y$ requires: C, 47.7; H, 4.4; N, 26.8%. IR spectrum: ν(BH) = 2460 cm^{-1}, also bands at 1604 and 1570 cm^{-1}. ^{1}H NMR spectrum: pyrazolyl protons δ_{TMS} = 7.64d(6), 7.13d(6), 5.98t(6) ppm, ($^3J_{HH}$ = 2 Hz), phenyl protons δ_{TMS} = 8.00d(2), 6.62d(2) ($^3J_{HH}$ = 9 Hz), methyl protons, δ_{TMS} = 2.98s(6). Mass spectrum: $[YL_2(O_2C\text{-}C_6H_4\text{-}NMe_2)]^+$ m/z = 697 (20%), $[YL_2]^+$ m/z = 515 (100%).

Hydrotris(pyrazol-1-yl)boratobis{p-(*tertiarybutyl*)*benzoato*}*yttrium*(III)

KL (0.75 g, 3 mmol) and *p*-(tertiarybutyl)benzoic acid (0.27 g, 1.5 mmol), 0.1 mol dm^{-3} KOH (15 cm^3) and ethanol (30 cm^3) were mixed and added to $YCl_3 \cdot 6H_2O$ (0.45 g, 1.5 mmol) in water (15 cm^3) with stirring. The resulting white precipitate was collected by filtration and dried (crude yield, 0.45 g; 91% with respect to *p*-Bu^t-C_6H_4-CO_2H), and recrystallized from CH_2Cl_2–hexane to give a white crystalline solid (yield, 0.22 g; 45%). M.p. 292–293°C. Found: C, 57.0; H, 5.6; N, 13.3. $C_{31}H_{36}BN_6O_4Y$ $[YL(O_2C\text{-}C_6H_4\text{-}Bu^t)_2]$ requires: C, 56.7; H, 5.5; N, 12.8%. IR spectrum: ν(BH) = 2460 cm^{-1}, also bands at 1630 and 1560 cm^{-1}. ^{1}H NMR spectrum: pyrazolyl protons, δ_{TMS} = 7.95d(3), 7.78d(3), 6.08t(3) ($^3J_{HH}$ = 2 Hz), phenyl protons, δ_{TMS} = 7.61d(4), 7.09d(4) ($^3J_{HH}$ = 8 Hz), methyl protons δ_{TMS} = 1.19s(18).

RESULTS

The new complexes could be precipitated in crude form by adding alkaline aqueous solutions containing KL and the appropriately substituted benzoic acid derivative in a 2:1 molar ratio to $YCl_3 \cdot 6H_2O$. They were isolated as colourless air- and moisture-stable solids which could be purified by recrystallization from CH_2Cl_2–hexane mixtures. All exhibited signals in their NMR spectra are attributable to the presence of the substituted benzoate ligand and the tripod ligand L. The ^{1}H NMR spectrum and elemental analyses of the tertiary-butylbenzoate complex were in accord with a formulation $[YL(O_2CC_6H_4\text{-}p\text{-}Bu^t)_2]$, involving only one ligand L but two benzoate ligands. This contrasts with the other two substituted benzoate ligands which afforded complexes of 1:2 benzoate:L stoichiometry as used in the synthesis procedure. The IR spectra of the new compounds contained ν(BH) at 2460 cm^{-1} in addition to bands attributable to the carboxylate moiety. In the cases of $[YL_2X]$ (X = NMe_2, NO_2) two bands were observed at *ca* 1605 and 1570–1590 cm^{-1}. However, in the case of the *p*-tertiary-butylbenzoate complex a band was observed at 1630 cm^{-1}. By analogy with $[YL(O_2CMe)_2]_2$ which was shown[6] to be a dimer,

*s, singlet; d, doublet; t, triplet; relative areas of signals are given in parentheses.

it might be expected that $[YL(O_2CC_6H_4\text{-}p\text{-}Bu^t)_2]$ might also be a dimer containing bridging benzoate groups. The dimeric nature of this complex was confirmed by an osmometric solution ($CHCl_3$) molecular weight determination which gave a value of 1423 compared with an expected value of 1312 for $[YL(O_2CC_6H_4\text{-}p\text{-}Bu^t)_2]_2$. The monocarboxylate complexes $[YL_2(O_2CC_6H_4\text{-}p\text{-}NMe_2)]$ and $[YL_2(O_2CC_6H_4\text{-}p\text{-}NO_2)]$ were expected to be monomeric by analogy with their structurally characterized[4] analogue $[YbL_2(O_2CPh)]$. This was again confirmed by osmometric solution ($CHCl_3$) molecular weight determinations which gave values of 646 and 699 compared with the respective values of 679 and 681 expected for the monomers.

The reason for the difference in benzoate : L stoichiometries found in these complexes is not entirely clear. The $—NMe_2$ and $—NO_2$ substituents lie at opposing extremes of the Hammett substituent parameter scale[17] yet afford similar products. Thus electronic factors do not appear to be involved. Similarly, steric effects do not offer a suitable explanation since the substituents are located well away from the metal ion and, in any event, although smaller than Bu^t, $—NMe_2$ and $—NO_2$ are nonetheless quite bulky. One possible explanation may lie in the solubility properties of the complexes. The hydrophobic $—Bu^t$ group may confer particularly low solubility on the complex $[YL(O_2CC_6H_4\text{-}p\text{-}Bu^t)_2]_2$ resulting in its rapid removal from the aqueous reaction medium and shifting the equilibrium distribution to favour this product. In the other cases it may be that the bis-carboxylate complex is not significantly different in properties from the mono-carboxylate so that the reactant stoichiometry is expressed in the product. ^1H NMR studies have shown[18] that facile intermolecular ligand exchange processes occur in complexes of this type so that the rapid removal of a 1:2 benzoate : L complex from solution may stimulate disproportionation of any 2 : 1 complex present.

Acknowledgements—We are grateful to Professor W. J. Evans for helpful discussions, to Dr D. W. Bruce and Ms S. Bradshaw for the molecular weight determinations, to the SERC and BP Chemicals for support (to M.A.J.M.) and to NATO for the provision of travel grant No. 175/84.

REFERENCES

1. M. A. J. Moss and C. J. Jones, *Abstr. XXIV Internat. Conf. Coord. Chem., Chimika Chronika*, Association of Greek Chemists, A7-488 (1986).
2. M. A. J. Moss, C. J. Jones and A. J. Edwards, *Polyhedron* 1988, **7**, 79.
3. M. A. J. Moss and C. J. Jones, *Polyhedron* 1989, **8**, 117.
4. M. A. J. Moss and C. J. Jones, *Polyhedron* 1989, **8**, 555.
5. M. A. J. Moss, C. J. Jones and A. J. Edwards, *J. Chem. Soc., Dalton Trans.* 1989, 1393.
6. D. L. Reger, J. A. Lindeman and L. Lebioda, *Inorg. Chem.* 1988, **27**, 3923.
7. D. G. Karraker, *Inorg. Nucl. Chem.* 1969, **31**, 2815.
8. J. W. Bats, R. Kalus and H. Fuess, *Acta Cryst.* 1979, **B35**, 1225.
9. M. C. Favas, D. L. Kepert, B. W. Skelton and A. H. White, *J. Chem. Soc., Dalton Trans.* 1980, 454.
10. M. J. Taylor, C. P. Carter and C. I. Winter, *J. Inorg. Nucl. Chem.* 1968, **30**, 1503.
11. M. S. Khiyalov, I. R. Amiraslanov, F. N. Musaev and Kh. S. Mamedov, *Koord. Khim.* 1982, **8**, 548.
12. J. M. Birmingham and G. Wilkinson, *J. Am. Chem. Soc.* 1954, **76**, 6210.
13. G. B. Deacon, G. D. Fallon, P. I. MacKinnon, R. H.Newnham, G. N. Pain, T. D. Tuong and D. L. Wilkinson, *J. Organomet. Chem.* 1984, **277**, C21.
14. T. D. Tilley, R. A. Andersen, A. Zalkin and D. H. Templeton, *Inorg. Chem.* 1982, **21**, 2644.
15. E. C. Baker, PhD thesis, University of California, Berkeley (1977).
16. S. Trofimenko, *Inorg. Synth.* 1970, **12**, 99.
17. M. Charlton, *Prog. Phys. Org. Chem.* 1981, **13**, 119.
18. M. A. J. Moss and C. J. Jones, *Polyhedron*, 1990, **9**, 697.

Polyhedron Vol. 9, No. 8, pp. 1123–1125, 1990
Printed in Great Britain

0277–5387/90 $3.00+.00
Pergamon Press plc

COMMUNICATION

FORMATION OF (η-CYCLOPENTADIENYL)(1,2-DISUBSTITUTED 1,2-ETHYLENEDITHIOLATO)COBALT(III) AND -RHODIUM(III) IN REACTIONS OF (η-CYCLOPENTADIENYL)COBALT(I) OR -RHODIUM(I) SPECIES WITH 1,4-DITHIINS

MASATSUGU KAJITANI,* RYUUJI OCHIAI, RIKA KIKUCHI, MIZUE OKUBO, TAKEO AKIYAMA and AKIRA SUGIMORI*

Department of Chemistry, Faculty of Science and Technology, Sophia University, Kioi-cho 7-1, Chiyoda-ku, Tokyo 102, Japan

(*Received* 13 *November* 1989; *accepted* 22 *December* 1989)

Abstract—The complexes, CpCo(cod), $CpCo(CO)_2$, $CpCo(CO)PPh_3$ and CpRh(cod), react with 1,4-dithiins having electron-attracting groups to give the title dithiolato complexes [$CpM(S_2C_2X,Y)$; M = Co or Rh]. 2-Nitro-3,5-diphenyl-1,4-dithiin reacts with $CpCo(CO)_2$ to afford selectively $CpCo(S_2C_2Ph,H)$.

The development of a facile synthetic method for (η-cyclopentadienyl)(1,2-disubstituted 1,2-ethylenedithiolato)cobalt(III) complexes [$CpCo(S_2C_2X,Y)$] in a one-pot reaction of $CpCo(CO)_2$ or CpCo(cod) (cod = 1,5-cyclooctadiene) with alkynes (X—C≡C—Y) and elemental sulphur[1] has enabled us to prepare a variety of dithiolatometal complexes of this type and to elucidate their unique physical and chemical properties.[2] Recently, Vollhardt and Walborsky found that trinuclear cobalt biscarbyne clusters react with elemental sulphur to give dithiolatocobalt complexes.[3] In this paper, we report that $CpM(S_2C_2X,Y)$ (M = Co or Rh) (**3**) complexes are formed in the reactions of CpM(I) complexes [CpM(cod), $CpM(CO)_2$ and $CpCo(CO)PPh_3$] with 1,4-dithiins (**2**).[4]

Only a few reports have appeared concerning the reactions of transition metal complexes with 1,4-dithiins or 1,4-diselenins. The reported reactions are those between $Fe_2(CO)_9$ and tetraphenyl-1,4-dithiin or its diselenin analogue to give the (dichalcogenato)(hexacarbonyl)diiron, together with ferracycle complexes, via the presumed expulsion of diphenylacetylene.[5,6]

Equimolar mixtures of CpM(cod) or $CpCo(CO)_2$ and 1,4-dithiins (each *ca* 0.37 mmol) in toluene (25 cm^3) were reacted at room temperature or at appropriate temperatures under an atmosphere of argon. The products were separated by means of silica gel column chromatogaphy (column, Wako Gel C300; eluent, hexane–dichloromethane) or preparative

(1)

2a : X = Y = CN
2b : X = Ph, Y = H
2c : X = C_6H_4-Cl (*p*), Y = H
2d : X = Ph, Y = NO_2

3a - Co: X = Y = CN
3a - Rh: X = Y = CN
3b - Co: X = Ph, Y = H
3c - Co: X = C_6H_4 - Cl (*p*), Y = H
3d - Co: X = Ph, Y = NO_2

* Authors to whom correspondence should be addressed.

Table 1. Reactions of CpM(cod) or $CpCo(CO)_2$ with symmetrical 1,3-dithiins

Starting complex	1,4-Dithiin reaction conditions X	Y	Temperature (°C)	Time (h)	Yields of recovery of $CpM(S_2C_2X,Y)$ (%)	1,4-dithiin (%)
CpCo(cod)	CN	CN	RT	5	**3a**-Co 23	32
CpCo(cod)	CN	CN	110	5	**3a**-Co 27	10
CpRh(cod)	CN	CN	110	5	**3a**-Co 17	17
CpIr(cod)	CN	CN	110	5	**3a**-Ir 0	> 99
$CpCo(CO)_2$	Ph	H	110	20	**3b**-Co trace	99
CpCo(cod)	Ph	H	110	72	**3b**-Co 0	> 99
CpCo(cod)	C_6H_4-Cl(*p*)	H	110	20	**3c**-Co trace	70
CpCo(cod)	Ph	NO_2	50	5	**3d**-Co trace	97
$CpCo(CO)_2$	Ph	NO_2	RT	70[a]	**3d**-Co 12	0[b]

[a] In benzene.
[b] 2,4-Dinitro-3,6-diphenylthiophene was obtained in a 50% yield.

HPLC (apparatus, LC-08 manufactured by Japan Analytical Industry Co. Ltd) which employed a column of GPC (eluent, chloroform). The products were identified spectroscopically (MS, NMR, and IR).*

The results in the reactions of CpM(cod) or $CpCo(CO)_2$ with 1,4-dithiins are summarized in Table 1.

The complex CpCo(cod) reacts with **2a** at room temperature for 5 h to give (η-cyclopentadienyl)(1,2-dicyano-1,2-ethylenedithiolato)cobalt(III) (**3a**-Co) and 2,3,4,5-tetracyanothiophene (**4a**) in 23 and < 1% yields, respectively. In the reaction of CpCo(cod) with **2a** at 110°C for 5 h, the yields of **3a**-Co and **4a** rise to 27 and 8%, respectively. The formation of thiopene, a by-product, was enhanced with an increase of temperature. The complex CpRh(cod) does not react with **2a** at room temperature but reacts at 110°C to afford $CpRh(S_2C_2(CN)_2)$ (**3a**-Rh) (17%) and **4a** (6%). However, CpIr(cod) does not react with **2a** even at 110°C, perhaps because of the strong coordination of cod to iridium atom. Thus, the reactivities of CpM(cod) for the formation of dithiolato complexes $[CpM(S_2C_2(CN)_2)]$ in the reaction between CpM(cod) and 2,3,4,5-tetracyano-1,4-dithiin are in the order of CpCo (cod) > CpRh(cod) ≫ CpIr(cod). This order is similar to the reactivities for the formation of the dithiolato complexes in the reactions of CpM(cod) with alkyne and S_8.[1] The complex CpIr(cod) gives no dithiolato complex in the reaction with dimethyl acetylenedicarboxylate and S_8 under similar conditions.

As seen in Table 1, the reactivities of symmetrically-substituted 1,4-dithiins with CpCo(cod) or $CpCo(CO)_2$ for the formation of dithiolato complexes increase with increasing electron-attracting abilities of substituents (X and Y) in the following order: X = Y = CN > X = NO_2, Y = Ph ≫ X = *p*-C_6H_4—Cl, Y = H > X = Ph, Y = H.

The leaving ligands also affect the reactivities of the complexes toward 1,4-dithiins. In the reaction with **2b** (at 140°C for 5 h), $CpCo(CO)PPh_3$ showed higher activity (4.4%) than CpCo(cod) or $CpCo(CO)_2$.

The reaction of the unsymmetrically-substituted 1,4-dithiins (**2e** and **2f**) is of interest. How fast do they react with $CpM(CO)_2$? Which moiety of 1,4-dithiins is incorporated in the dithiolatometal complexes as the ligand?

2-Nitro-3,6-diphenyl-1,4-dithiin (**2e**) reacts with $CpCo(CO)_2$ faster than 2,5-diphenyl-1,4-dithiin (**2b**): At 110°C, **2b** reacts with $CpCo(CO)_2$ only

* The novel complexes were identified by elemental analysis, MS, NMR and IR. $CpCo(S_2C_2PhCl,H)$ (**3c**-Co): m.p. 142–143°C; ^1H NMR ($CDCl_3$) δ = 5.38 (5H, s, Cp), 8.97 (^1H, s, dithiolene H), 7.72 (2H, d, J = 8.79 Hz), 7.28 (2H, d, J = 8.79 Hz); ^{13}C NMR ($CDCl_3$) δ = 79.41 (Cp); MS (70 eV) m/z 324 (M^+). Found: C, 48.2; H, 2.9. Calc. for $C_{13}H_{10}CoS_2Cl$: C, 48.1; H, 3.1%. $CpCo(S_2C_2Ph,NO_2)$ (**3d**-Co): m.p. 175–176°C; ^1H NMR ($CDCl_3$) δ = 5.51 (5H, s, Cp), 7.2–7.3 (2H, m, phenyl H), 7.3–7.4 (3H, m, phenyl H); ^{13}C NMR ($CDCl_3$) δ = 80.9 (Cp), 162.7 and 173.0 (dithiolene C); MS (70 eV) m/z 335 (M^+). Found: C, 46.3; H, 2.9; N, 4.0. Calc. for $C_{13}H_{10}CoO_2S_2N$: C, 46.6; H, 3.0; N, 4.2%. $CpRh(S_2C_2(CN)_2)$ (**3a**-Rh): m.p. 208–209°C; ^1H NMR [$(CD_3)_2CO$] δ = 6.22 (5H, s, Cp); IR (KBr) 2210 cm^{-1} (s) ν(—C≡N); MS (70 eV) m/z 308 (M^+). Found: C, 35.1; H, 1.6; N, 9.0. Calc. for $C_9H_5S_2N_2Rh$: C, 35.1; H, 1.6; N, 9.1%. Other dithiolato complexes (**3a**-Co and **3b**-Rh) were identified in a similar manner.

slightly, while **2e** reacts with $CpCo(CO)_2$ even at 50°C [eq. (2)]. The electron-attracting NO_2 should promote the reactivity of the dithiin. Interestingly, the moiety containing NO_2 is not incorporated in the dithiolato complex and $CpCo(S_2C_2Ph,H)$ is formed selectively. Similar results were obtained in the reaction of 2-nitro-3,6-di(*p*-chlorophenyl)-1,4-dithiin (**2f**) with $CpCo(CO)_2$: the nitro group in 1,4-dithiin accelerates the reaction, but the less electronegative moiety is incorporated in the dithiolato complex [eq. (3)].

In the reaction of **2e** with $CpCo(CO)PPh_3$, the benzene derivative which would be formed in the trimerization of 1-nitro-2-phenylacetylene under the catalyst of the phosphine-coordinated species was detected by MS, together with the increase of the yield of $CpCo(S_2C_2Ph,H)$ (about 20%) [eq. (4)].

The reactions of CpM(cod) or $CpCo(CO)_2$ with 1,4-dithiins afford a convenient method for the preparation of some new dithiolato complexes, such as $CpCo(S_2C_2Ph,NO_2)$, $CpCo(S_2C_2C_6H_4Cl(p),H)$, and $CpCo(S_2C_2(CN)_2)$, which could not be synthesized in the reactions of CpM(cod) with S_8 and alkynes (X—C≡C—Y) owing to the difficulty in the preparation of X—C≡C—Y.[1]

REFERENCES

1. H. Bönnemann, B. Bogdanovic, W. Brijoux, R. Brinkmann, M. Kajitani, R. Mynott, G. S. Natarajan and M. G. Y. Samson, Transition-Metal-Catalyzed Synthesis of Heterocyclic Compounds, in *Catalysis of Organic Reactions* (Edited by J. R. Kosak), 1st edn, pp. 31–62. Marcel Dekker, New York (1984).
2. A. Sugimori and M. Kajitani, *Kagaku Zokan* 1988, **115**, 113.
3. K. P. C. Vollhardt and E. C. Walborsky, *Polyhedron* 1988, 7, 1023.
4. The chemistry of 1,4-dithiins was reviewed by K. Kobayashi and C. L. Gajurel in *Sulfur Reports* 1986, 7, 123. 1,4-Dithiins were prepared according to pertinent references in this review. (a) **2a**: H. E. Simmons, R. D. Vest, D. C. Blomstrom, J. R. Roland and T. L. Cairus, *J. Am. Chem. Soc.* 1962, **84**, 4746; (b) **2b**: C. M. Buess, V. O. Brandt, R. C. Srivastave and W. R. Carper, *J. Heterocycl. Chem.* 1972, **9**, 887; (c) **2d**: W. E. Parham, I. Nicholson and V. J. Traynelis, *J. Am. Chem. Soc.* 1956, **78**, 850; (d) **2e**: W. E. Parham and V. J. Traynelis, *J. Am. Chem. Soc.* 1955, **77**, 68.
5. C. W. Bird and E. M. Hollins, *J. Organomet. Chem.* 1965, **48**, 254.
6. A. J. Mayr, H.-S. Liens, K. H. Ponnell and L. Parkanye, *Organometallics* 1985, **4**, 1580.

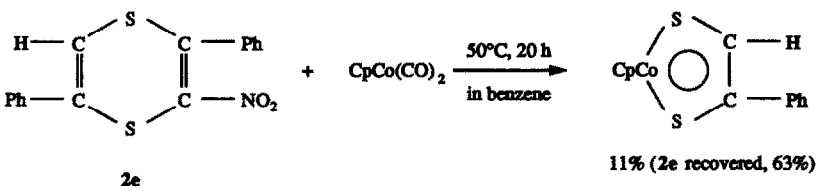

2e (2)

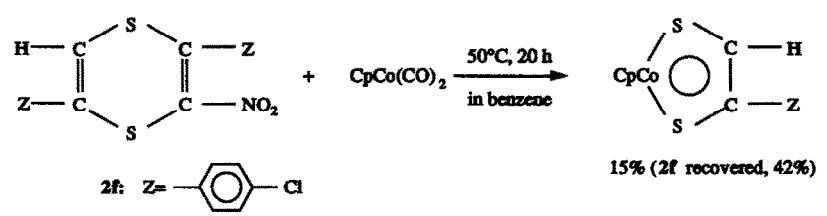

2f: Z= (3)

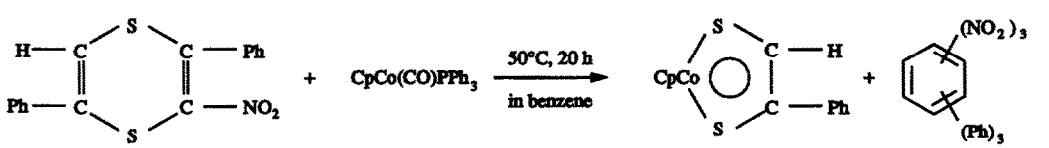

2e (4)

Polyhedron Vol. 9, No. 8, pp. 1127–1129, 1990
Printed in Great Britain

0277–5387/90 $3.00+.00
© 1990 Pergamon Press plc

COMMUNICATION

SYNTHESIS AND CHARACTERIZATION OF A PYRIDINE ADDUCT OF BIS(IRONTETRACARBONYL)GERMANIUM(IV)

D. LEI, M. J. HAMPDEN-SMITH* and E. N. DUESLER

Department of Chemistry and Center for Micro-Engineered Ceramics,
University of New Mexico, Albuquerque, NM 87131, U.S.A.

(*Received* 8 *November* 1989; *accepted* 9 *January* 1990)

Abstract—The reaction of $[(CO)_4FeGeBr_2]_2$ (**1**) with $Na_2Fe(CO)_4$ (**2**) in the presence of pyridine results in the formation of $[\{(CO)_4Fe\}_2Ge \cdot 2py]$ (**3**) in high yield. A single crystal X-ray diffraction study of **3** reveals that the local environment around germanium is severely distorted from tetrahedral coordination.

The chemistry of transition metal compounds containing bonds to heavier Group 14 elements has been extensively studied.[1] Multiply-bonded species, particularly of the types shown in **I** and **II** below that can be written in a form containing a formal transition metal–Group 14 element "double bond", (**I**), or as an ylide (**II**), are also well known.[2]

I **II**

The chemistry of *homoleptic* transition metal multiply-bonded Group 14 complexes has recently been reviewed[3] and is limited to the species of type **III**[4,5] and **IV**[4,6] below, where ML_5 represents $[W(CO)_5]$ or $[Mn(CO)_2Cp]$ and E = Ge or Sn. Type **III** species, where $ML_5 = Mn(CO)_2Cp$, contain Mn—E partial triple bonds, which accounts for their facile internal rotation about the Mn—E—Mn axis.[7] The metal–metal multiple bonds in these species seem to be surprisingly inert toward further oligomerization, probably as a result of coordinative saturation at the transition metal centres involved.

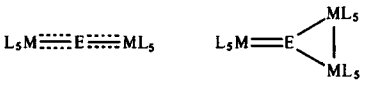

III **IV**

Zybill *et al.*[8] have recently reported the synthesis and structure of $[Si(Fe(CO)_4)_2] \cdot 2(Me_2N)_3PO$ prepared by the reaction of $SiCl_4$ with two equivalents of Collman's reagent. Here we report the high yield synthesis and characterization of a multiply-bonded homoleptic germanium–iron cluster, which can formally be considered as a base stabilized inorganic analogue of allene.

Treatment of a diethyl ether solution of **1** with a pyridine–diethyl ether solution of Collman's reagent **2**, according to eq. (1), resulted in the formation of a deep red–orange solution with the concomittant precipitation of sodium bromide.

After filtration, removal of the volatile components *in vacuo*, extraction into toluene, and crystallization at −30°C, red–orange crystals of **3** were isolated in 67% yield. Compound **3** was identified by its elemental analysis, NMR, IR and mass spectroscopic data.† The position of the germanium

* Author to whom correspondence should be addressed.

† ^1H NMR data (250.13 MHz, 20°C, C_6D_6): 8.67 ppm, s. br; 6.68 ppm, s. br; 6.38 ppm, s. br. ^{13}C NMR data (62.9 MHz, 20°C, C_6D_6): 126.1, 141.6, 146.8, 216.3 ppm. IR data (KBr disc, cm^{-1}): ν(C—O) 2036, m; 2011, s; 1914, s; ν(N—C) 1607, w; 1451, w; ν(M—C) 615. Mass spectral data (30 eV): no molecular ion observed, highest mass m/z 409 = $[Ge(Fe(CO)_4)_2]$ (10% relative abundance) then m/z = 381, 353, 325, 297, 269, 241, 213 and 185 corresponding to CO loss. Base mass m/z = 139 with Ge isotope distribution pattern. Elemental analysis: Found: C, 37.9; H, 1.7; N, 5.1. Calc. for $C_{18}H_{10}O_8N_2Fe_2Ge$: C, 38.1; H, 1.8; N, 4.9%.

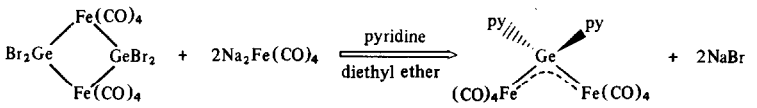

1 2 3 (1)

atom was assigned to an axial iron coordination site based on the observation of three IR active carbonyl stretching modes at 2036, 2011 and 1914 cm^{-1} in the solid state, characteristic of local C_{3v} symmetry ($2A_1 + E$) at each iron centre.[9] However, the single carbonyl resonance observed in the ^{13}C NMR spectrum indicates that the molecule is stereochemically non-rigid in solution on the NMR timescale.*

To unambiguously determine the ground state structure of this species, a single crystal X-ray diffraction study was carried out. Compound **3** crystallizes in the space group *Pccn* with two independent molecules in the unit cell, one type in a general position, and the other on a two-fold axis.† The structural parameters for both molecules are very similar, so only one type will be discussed in detail. The molecular structure of **3** is shown in Fig. 1, together with relevant bond distances and angles. Compound **3** possesses approximate C_{2v} molecular symmetry and local C_{3v} symmetry about the iron atoms with the germanium atom in axial positions, analogous to the structure adopted by $(CO)_4FeGeR_2 \cdot L$ species. The coordination environment about germanium is significantly distorted, with an enlarged Fe—Ge—Fe angle of 131° and a reduced N—Ge—N angle of 89°. The average Fe—Ge bond distances of 2.35 Å are over 0.1 Å shorter than the value expected for an Fe—Ge single bond.[10]

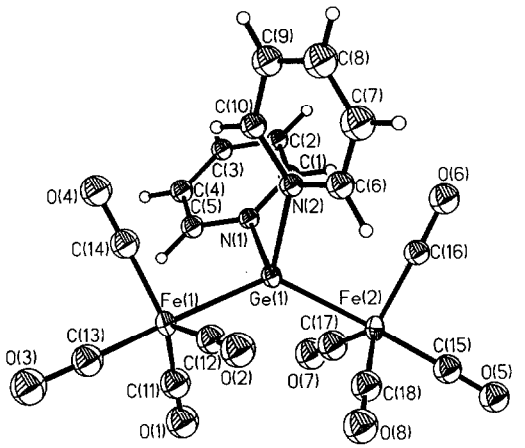

Fig. 1. Thermal ellipsoid plot of **3** emphasizing the enlarged Fe—Ge—Fe angle.

Relevant distances (Å):

Fe(1)—Ge(1)	2.339(4)	Fe(1)—C(11)	1.71(2)
Fe(2)—Ge(1)	2.351(3)	Fe(1)—C(12)	1.77(2)
Ge(1)—N(1)	2.05(1)	Fe(2)—C(15)	1.73(2)
Ge(1)—N(2)	2.08(1)	Fe(2)—C(16)	1.71(2)
Fe(1)—C(13)	1.69(3)	Fe(2)—C(17)	1.74(3)
Fe(1)—C(14)	1.74(2)	Fe(2)—C(18)	1.73(3)

Relevant angles (°):

Fe(1)—Ge(1)—Fe(2)	131.0(1)
N(1)—Ge(1)—N(2)	89.4(6)
N(2)—Ge(1)—Fe(1)	105.4(4)
N(2)—Ge(1)—Fe(2)	108.8(4)
N(1)—Ge(1)—Fe(1)	108.6(4)
N(1)—Ge(1)—Fe(2)	105.8(4)
Ge(1)—Fe(1)—C(13)	178.6(8)
Ge(1)—Fe(2)—C(15)	177.6(7)

These data are consistent with the representation of this species in either of the two canonical forms shown below: a double ylide (**V**) or as a base stabilized inorganic analogue of allene (**VI**).

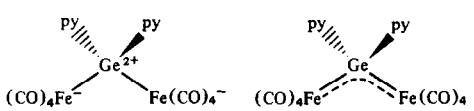

V **VI**

* No change in the ^{13}C NMR carbonyl resonance was observed on cooling a toluene-d_8 solution of **3** to −90°C.

† The red-orange crystal used for the X-ray study (0.092 × 0.184 × 0.575 mm) was sealed in a glass capillary under nitrogen. Crystal data: Empirical formula $C_{27}H_{15}N_3O_{12}Fe_3Ge_{1.5}$, orthorhombic space group Pccn, a = 23.840(5), b = 15.528(3), c = 17.977(4) Å, Z = 8. A total of 3113 independent reflections were measured on a Nicolet R3m/v diffractometer (293 K) using graphite monochromated Mo-K_α radiation, λ = 0.71073 Å, with ω scan node. 2θ max = 40°. The structure was solved by direct methods using SHELXTL PLUS (Microvax II) and was refined using full-matrix least-squares method. Positions of iron and germanium were refined anisotropically, other non-hydrogen atoms were refined isotropically and hydrogen atom positions were fixed. The final agreement factors were R = 10.11 and R_w = 6.94% for 2070 reflections having $F > 3.0\sigma(F)$. A final difference Fourier was featureless with the largest peak being 1.08 eÅ^{-3}. No unusual intermolecular interactions are observed. Atomic coordinates and equivalent isotopic displacement coefficients are available as supplementary material.

Considering this species as a derivative of inorganic allene {i.e. $[(CO)_4Fe{=}Ge{=}Fe(CO)_4]$ (**4**)} is consistent with the well-established isolobal analogy between $[:CH_2]$ and $[:Fe(CO)_4]$.[11] This explanation is also consistent with (i) the small N—Ge—N angle resulting from the donation of the pyridine lone pair into two empty, mutually orthogonal *p*-orbitals, (ii) the shortened Fe—Ge bonds, and (iii) the large Fe—Ge—Fe angle. The double ylide form (V) can be considered in two ways: either with the positive charge localized on Ge^{IV} or localized at the nitrogen centres analogous to a pyridinium salt. If this canonical form is dominant, tetrahedral geometry at germanium is expected.

The synthesis of this compound can be rationalized in terms of the rapid Ge—Fe bond homolysis in the presence of Lewis bases that has previously been observed in other systems containing four-membered rings,[12] together with a simple metathesis reaction. In the absence of pyridine, the reaction of eq. (1) results in the formation of a gel, which can be dried to form an orange polymeric material. The characterization and properties of this polymer will be reported separately.[13]

Thus far, we have been unable to isolate **4** by removing the pyridine ligands thermally from **3**.* Isolation and characterization of the ground state structure of **4** to determine the linearity of the Fe=Ge=Fe framework, the local coordination environment about iron (C_{2v} or C_{3v}), the relative orientation of the $[Fe(CO)_4]$ fragments, and the barrier to rotation about the Fe=Ge bonds, is of primary importance in understanding the chemistry of these species.

Further studies are in progress.

Acknowledgements—We thank Dr D. Doughty and Professor Vince Ortiz for helpful discussions, Eva Quesnell for typing this manuscript, the Sandia-University Research Program for Financial Support, and NSF for the purchase of a high-field NMR spectrometer.

* Thermal removal of pyridine has been demonstrated in the $(CO)_4FeER_2 \cdot py$ systems, see ref. 12(a).

REFERENCES

1. B. J. Aylett, in *Adv. Inorg. Chem. Radiochem.* 1982, **25**, 1; K. M. Mackay and B. K. Nicholson, in *Comprehensive Organometallic Chemistry* (Edited by G. Wilkinson, F. G. A. Stone and E. W. Abel), Vol. 6, Ch. 43, p. 1043. Pergamon Press, Oxford (1982).
2. For reveiews see, W. Petz, *Chem. Rev.* 1986, **86**, 1019; M. S. Holt, W. L. Wilson and J. H. Nelson, *Chem. Rev.* 1989, **89**, 11.
3. W. A. Herrmann, *Angew. Chem.* 1986, **25**, 56.
4. W. Gade and E. Weiss, *J. Organomet. Chem.* 1981, **213**, 451.
5. G. Magomeder, L. V. Morozova and Yu I. Markova, *Zh. Obshch. Khim.* 1983, **53**, 1684 (Engl. Transl. 1983, **53**, 1515).
6. G. Hultre, U. Weber, B. Sigworth, O. Scheidsteger, H. Long and L. Zsolrai, *J. Organomet. Chem.* 1985, **282**, 331; W. A. Hermann, *Angew. Chem.* 1986, **98**, 57.
7. N. M. Kostic and R. F. Fenske, *J. Organomet. Chem.* 1982, **233**, 337.
8. C. Zybill, D. L. Wilkinson and G. Muller, *Angew. Chem.* 1988, **27**, 574.
9. F. A. Cotton and R. V. Parish, *J. Chem. Soc.* 1960, 1440.
10. We have previously observed Fe—Ge bond distances in $[R_2GeFe(CO)_4]_2$ compounds of 2.48 Å, D. Lei, M. J. Hampden-Smith, E. Duesler and J. C. Huffman, *Inorg. Chem.* 1990, **29**, 795.
11. See for example, T. A. Albright, J. K. Burdett and M-H. Whangbo, *Orbital Interactions in Chemistry*. Wiley-Interscience, New York (1985).
12. (a) T. J. Marks and A. R. Newman, *J. Am. Chem. Soc.* 1973, **95**, 769; (b) T. J. Marks, *J. Am. Chem. Soc.* 1971, **93**, 7090; (c) A. B. Cornwell, P. G. Harrison and J. A. Richards, *J. Organomet. Chem.* 1976, **108**, 47; (d) A. B. Cornwell and P. G. Harrison, *J. Chem. Soc., Dalton Trans.* 1975, 2017.
13. M. J. Hampden-Smith, D. Lei and B. Wheeler, unpublished results.

Polyhedron Vol. 9, No. 9, pp. 1131–1134, 1990
Printed in Great Britain

0277–5387/90 $3.00+.00
© 1990 Pergamon Press plc

SYNTHESIS AND CHARACTERIZATION OF ALKOXYCARBONYLRHENIUM(III) COMPLEXES

A. HUGO KLAHN† and CAROLINA MANZUR

Instituto de Química, Universidad Católica de Valparaíso, Casilla 4059, Valparaíso, Chile

(*Received* 24 *July* 1989; *accepted* 6 *November* 1989)

Abstract—The reaction of the cationic complexes $[(\eta^5\text{-}C_5Me_5)Re(CO)_3X]^+$ (X = Cl, Br and I) with alkoxide anions in alcohol or dichloromethane results in the formation of the alkoxycarbonylrhenium(III) complexes, *trans*-$(\eta^5\text{-}C_5Me_5)Re(CO)_2(I)(COOR)$ (X = Cl and Br, R = Me and X = I, R = Me, Et and *i*-Pr). The *trans* orientation of the carbonyl groups in these complexes was assigned by IR spectroscopy.

Alkoxycarbonyl complexes of transition metals (i.e. metalloesters) have been proposed as intermediates in important catalytic reactions,[1,2] and more recently as "abnormal" insertion products in the reaction of metal–alkyl complexes with CO_2.[3] These compounds have usually been synthesized by reacting carbon monoxide coordinated to neutral or cationic complexes with alcohols or alkoxide anions. Some recent examples of alkoxycarbonyl complexes reported are: $[M(CO)_4(COOMe)]^-$ (M = Fe, Ru, Os);[4] $(\eta^5\text{-}C_5R_5)Re(CO)(N_2Ar)(COOR')$ (R = Me and H, R' = Me and *i*-Pr);[5] $(\eta^5\text{-}C_5Me_5)Ru(CO)_2(COOR)$ (R = Me, Et, *i*-Pr and *t*-Bu)[6] and $[Fe(CO)(PMe_3)_2(CNC_6H_{11})(C(Me){=}NHC_6H_{11})(COOMe)]^+$.[7] Nucleophilic attack at the CO ligand has been suggested in all cases.

In previous publications we described the synthesis of cationic pentamethylcyclopentadienyltricarbonylhalide complexes $[Cp^*Re(CO)_3X]^+$ ($Cp^* = \eta^5\text{-}C_5Me_5$, X = I[8] and X = Br and Cl).[9] We now wish to report the results of nucleophilic attack of RO^- on a carbonyl group of these cationic complexes. To our knowledge these reactions are the first examples of rhenium(III) cationic complexes possessing a four-legged pianostool type of structure where one of the CO groups has been transformed into an alkoxycarbonyl ligand. The assignment of the stereochemistry and the reaction of the alkoxycarbonyl complexes with HBF_4 are also included in this report.[10]

† Author to whom correspondence should be addressed.

EXPERIMENTAL

All reactions were carried out under nitrogen using Schlenk apparatus connected to a double manifold providing a low vacuum or nitrogen atmosphere. IR spectra were measured in solution (KBr cells) on a Perkin–Elmer 599 instrument. ^1H NMR spectra were recorded at 60 MHz on a Varian EM 360 instrument. Mass spectra (Hewlett–Packard model 5985), 400 MHz ^1H NMR spectra (Bruker WM-400) and elemental analyses were obtained using the Chemistry Department facilities at the Simon Fraser University, Canada.

Alcohols were distilled under nitrogen prior to use. $Cp^*Re(CO)_3$ was synthesized from $Re_2(CO)_{10}$ according to a literature procedure.[11]

Preparation of trans-$Cp^*Re(CO)_2(I)(COOR)$ (R = Me *and* Et)

The complex $[Cp^*Re(CO)_3I]I_3$ (about 200 mg), prepared by reacting $Cp^*Re(CO)_3$ with an excess of I_2 in hexane,[8] was dissolved in the corresponding alcohol (5.0 cm^3) and then treated with 0.1 cm^3 of NEt_3 at 0°C. The solution changed slowly from dark red to orange. After 1 h the alcohol was pumped off and the orange residue extracted with hexane (3 × 10 cm^3). Crystallization from hexane at −10°C yielded orange–yellow crystals of the corresponding alkoxycarbonyl complex (38% yield). In both cases (R = Me and Et) the complexes decomposed above 95°C without melting. Elemental analysis for $C_{14}H_{18}O_4IRe$: (R = Me) Found:

C, 30.1; H, 3.3. Calc.: C, 29.8; H, 3.2%. For $C_{15}H_{20}O_4IRe$: (R = Et) Found: C, 31.0; H, 3.5. Calc.: C, 31.1; H, 3.5%.

Preparation of trans-Cp*Re(CO)$_2$(I)(COOCHMe$_2$)

[Cp*Re(CO)$_3$I]I$_3$ (100 mg) was dissolved in 5.0 cm^3 of CH_2Cl_2 and cooled to 0°C. To this red solution, sodium isopropoxide (Alfa) (10 mg) dissolved in 2.0 cm^3 of isopropanol was slowly added and stirred for 2 h. Solvent evaporation *in vacuo*, extraction and crystallization in hexane yielded 22 mg (35%) of orange–yellow crystals, which decomposed without melting above 90°C. Elemental analysis for $C_{16}H_{22}O_4IRe$: Found: C, 32.3; H, 3.7. Calc.: C, 32.5; H, 3.7%.

Preparation of trans-Cp*Re(CO)$_2$(X)(COOMe) (X = Cl *and* Br)

A procedure similar to that described for the preceding compound, gave the chloro- and bromomethoxycarbonyl complexes as a crystalline yellow solid, in about 30% isolated yield. Both complexes decomposed without melting above 80°C. Elemental analysis for $C_{14}H_{18}O_4ClRe$: Found: C, 35.5; H, 3.7. Calc.: C, 35.6; H, 3.8%. For $C_{14}H_{18}O_4BrRe$: Found: C, 32.5; H, 3.4. Calc.: C, 32.5; H, 3.5%.

The spectroscopic data of these complexes are listed in Table 1.

Reaction of trans-Cp*Re(CO)$_2$(X)(COOMe) (X = Cl, Br, I *with* HBF$_4$)

The methoxycarbonyl complex *trans*-Cp*Re(CO)$_2$(X)(COOMe) (50 mg) was dissolved in 5.0 cm^3 of dry Et_2O and an excess (0.5 cm^3) of a 50% ether solution of HBF_4 (Alfa) was slowly added through a syringe, at room temperature with stirring. The precipitate of [Cp*Re(CO)$_3$X]BF$_4$ formed was washed three times with ether and dried *in vacuo*.

The isolated yields and melting points of the [Cp*Re(CO)$_3$X]BF$_4$ complexes are: X = I, 97%, > 140°C d.; X = Br, 96%, > 100 d.; X = Cl, 94%, > 80°C d.

RESULTS

The reaction of the cationic complex [Cp*Re(CO)$_3$X]$^+$ (X = Cl, Br and I) with alkoxide ions (as a solid, or generated *in situ* from the corresponding alcohol and Et_3N) as in eq. (1), yields after work-up, single orange–yellow crystals, characterized as the alkoxycarbonyl complexes *trans*-Cp*Re(CO)$_2$(X)(COOR) (X = Cl and Br, R = Me; X = I, R = Me, Et and *i*-Pr). The spectroscopic parameters are listed in Table 1.

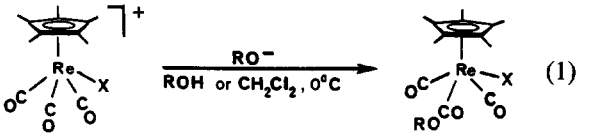

(1)

Table 1. IR and ^{1}H NMR spectral data for *trans*-Cp*Re(CO)$_2$(X)(COOR)

X	R	IR[a] (cm^{-1}) ν(CO)[b]	ν(CO)[c]	^{1}H NMR[d] (J in Hz) δ(C$_5$Me$_5$)	δ(R)
I	Me	2043 s 1960 vs	1635 m	2.11	3.65
I	Et	2045 s 1965 vs	1643 m	2.12	1.24 (t, J 7.1) 4.12 (q, J 7.1)
I	*i*-Pr	2047 s 1958 vs	1636 m	2.15	1.23 (d, J 6.0) 5.10 (Sep, J 6.0)
Br	Me	2050 s 1965 vs	1635	2.00[e]	3.60
Cl	Me	2065 s 1970 vs	1635	1.93[e]	3.58

[a] Measured in CH_2Cl_2 solution. s = strong; vs = very strong; m = medium.
[b] Terminal CO.
[c] Metalloester CO.
[d] Measured in $CDCl_3$ at 400 MHz.
[e] Measured in $CDCl_3$ at 60 MHz.

The IR spectrum (CH_2Cl_2 solution) of these complexes exhibits ν(CO) absorptions at *ca* 2065 and 1960 cm^{-1}, which can be attributed to two terminal CO groups in a neutral complex (see below), and a medium intensity absorption at about 1640 cm^{-1} assigned to the ν(C═O) of a metalloester group (—CO_2R). The latter value is in good agreement with the frequencies for this group observed in other related complexes.[4–7] The presence of the alkyl group of the alkoxycarbonyl ligands was also confirmed by ^1H NMR (see Table 1).

As a solid, the complexes decompose without melting at about 90°C. At room temperature under nitrogen atmosphere, they do not survive for periods longer than 3 days, the iodo derivatives being the most stable. The observed decomposition products (by IR), are the $Cp^*Re(CO)_3$ and $Cp^*Re(CO)_2X_2$ complexes (2:1). Similar decomposition products were observed for the iodo series by ^1H and ^{13}C NMR during an overnight run in $CDCl_3$ solution. The electron-impact MS do not show any parent peak even at 14 eV. Instead, the spectra show the presence of the tricarbonyl and $Cp^*Re(CO)_2X_2$ complexes. In spite of the thermal instability of the complexes at room temperature, they can be stored as solids at −10°C, under nitrogen, for months without visible deterioration.

As expected, an electrophilic attack on the alkoxy oxygen was observed in the reaction of the alkoxycarbonyl complexes with HBF_4 in ether solutions. The parent cationic complex, as a BF_4^- salt, could be isolated almost quantitatively as a red–orange (X = I) or orange–yellow (X = Cl and Br) solid, $\nu(BF_4)$ 1060 cm^{-1} (in CH_2Cl_2 solution). Evidence for the stereochemistry of the alkoxycarbonyl complexes was obtained from analysis of the intensity ratio of the symmetric and antisymmetric CO stretching vibrations of the terminal CO ligands, ν_s(CO) and ν_{as}(CO), respectively. The IR spectrum in each case consists of only two ν(CO) absorptions in the 1950–2070 cm^{-1} region, of which the lower frequency band [ν_{as}(CO)] is much more intense. Using this criterion, as well as the correspondence between our IR values and those reported for *trans*-$CpRe(CO)_2X_2$ (Cp = η^5-C_5H_5, X = Br and I[12]) and *trans*-$Cp^*Re(CO)_2X_2$ (X = Cl, Br and I[8]) we consider our products to be also the *trans* isomers.

We have used the relative ν(CO) IR intensities to calculate the angle between the CO groups using the relationship[13] $\tan^2\theta = I_{as}/I_s$, where I_{as} and I_s are the areas under the antisymmetric (at lower frequency) and symmetric (at higher frequency) bands, respectively, and 2θ is the angle between the two CO groups. The angles thus determined by this method are close to 130° in all cases, in accordance with their postulated *trans* or diagonal structure. It is important to note that angles between 104 and 147° have been determined by X-ray crystallography and by estimation from the ν(CO) intensities in the complexes containing a four-legged piano-stool type structure.[14]

DISCUSSION

The production of the dicarbonyl alkoxycarbonyl complexes, *trans*-$Cp^*Re(CO)_2(X)(COOR)$, from the tricarbonyl cations $[Cp^*Re(CO)_3X]^+$ evidently results from straightforward attack of the nucleophile on the relatively electrophilic carbonyl carbon atom in these cations.[15] These results are those expected according to Angelici's predictions[16] that carbonyl-containing compounds with $\nu(CO) > 2000$ cm^{-1} should yield these types of complexes. It is worth noting that possible products, which were *not* observed in these reactions, are the dicarbonyl alkoxides, $Cp^*Re(CO)_2(X)(OR)$, resulting from direct CO substitution or the tricarbonyl complex $Cp^*Re(CO)_3$ formed by reductive elimination of the halide ligand. Even though the tricarbonyl complex was not observed during the formation of the alkoxycarbonyl complexes it is the major decomposition product of these compounds. The manner in which these complexes are able to generate the tricarbonyl and dihalide complexes, $Cp^*Re(CO)_3$ and $Cp^*Re(CO)_2X_2$, when they decompose, is a matter of some interest but one about which presently we have no mechanistic information.

The exclusive appearance of the *trans* isomer in these rhenium alkoxycarbonyl complexes is not completely understood at the present time. Recently, we undertook a vibrational study of the cationic complexes[17] with the aim to determine which of the CO group (*cis* and *trans* to the halide ligand) is more likely to react with nucleophiles.

Acknowledgements—The authors express their gratitude to Professor D. Sutton and Ms Z. Xiaoheng for remaking some of the complexes and obtaining the NMR, MS and EA data at the Chemistry Department facilities of Simon Fraser University, Canada. The support of this research by D.G.I., Universidad Católica de Valparaíso and FONDECYT through operating grants to A.H.K., 125.709/87 and 155/89, respectively, are also appreciated.

REFERENCES

1. A. Mullen, Carbonylation catalyzed by metal carbonyls: *Reppe reactions* in *Syntheses with Carbon*

Monoxide (Edited by J. Falbe). Springer, Berlin (1980).
2. D. Milstein and J. L. Huckaby, *J. Am. Chem. Soc.* 1982, **104**, 6150.
3. P. Braunstein, D. Matt and D. Nobel, *Chem. Rev.* 1988, **88**, 747.
4. R. J. Trautman, D. C. Gross and P. C. Ford, *J. Am. Chem. Soc.* 1985, **107**, 2355.
5. C. F. Barrientos-Penna, A. H. Klahn-Oliva and D. Sutton, *Organometallics* 1985, **4**, 378.
6. H. Suzuki, H. Omori and Y. Moro-oka, *J. Organomet. Chem.* 1987, **327**, C47.
7. G. Cardaci, G. Bellachioma and P. F. Zanazzi, *J. Chem. Soc., Dalton Trans.* 1987, 473.
8. F. W. B. Einstein, A. H. Klahn-Oliva, D. Sutton and K. G. Tyers, *Organometallics* 1986, **5**, 53.
9. G. Díaz, A. H. Klahn and C. Manzur, *Polyhedron* 1988, **7**, 2743.
10. A. H. Klahn and C. Manzur, *XVIII Congreso Latinoamericano de Química*, Vol. II 2-269-O. Santiago, Chile (1988).
11. A. T. Patton, C. E. Strouse, C. B. Knobler and J. A. Gladysz, *J. Am. Chem. Soc.* 1983, **105**, 5804.
12. R. B. King and R. H. Reimann, *Inorg. Chem.* 1976, **15**, 183.
13. A. R. Manning, *J. Chem. Soc. A* 1967, 1984.
14. Some examples: *trans*-$Cp^*Re(CO)_2Br_2$, 104° (X-Ray);[8] *trans*-$CpMo(CO)_2PPh_3$)(COMe) 108° (X-ray), M. R. Churchill and J. P. Fennessey, *Inorg. Chem.* 1968, **7**, 953; [*trans*-$CpMo(CO)_2(PPh_3)(C_4H_6O)$]$^+$ 121° (IR), F. A. Cotton and C. M. Lukehart, *J. Am. Chem. Soc.* 1971, **93**, 2672; [*trans*-$CpRe(CO)_2[P(OEt)_3](SnCl_3)$]$^+$ 147° (IR), B. V. Lokshin, E. B. Rusach, N. E. Kolobova, Y. V. Makasov, N. A. Ustynyuk, V. I. Zdanobivh, A. Z. Zhakaeva and V. N. Setkina, *J. Organomet. Chem.* 1976, **108**, 353.
15. R. J. Angelici and L. Buseto, *J. Am. Chem. Soc.* 1969, **91**, 3197.
16. R. J. Angelici, *Accts Chem. Res.* 1972, **5**, 335.
17. G. Díaz and A. H. Klahn, manuscript in preparation.

Polyhedron Vol. 9, No. 9, pp. 1135–1140, 1990
Printed in Great Britain

0277–5387/90 $3.00+.00
© 1990 Pergamon Press plc

ELECTROCHEMICAL OXIDATION OF TETRA-(*S*)-MANDELATODIRHODIUM(II) AND TETRAFORMATODIRHODIUM(II)

A. SZYMASZEK and F. P. PRUCHNIK*

Institute of Chemistry, University of Wrocław, 50-383 Wrocław, Poland

(*Received* 9 *October* 1989; *accepted* 30 *November* 1989)

Abstract—Rhodium complexes $[Rh_2\{(S)\text{-}C_6H_5CHOHCOO\}_4]$ and $[Rh_2(O_2CH)_4]$ were investigated by electrochemical and spectral techniques in organic solvents and results were compared with those for $[Rh_2(O_2CCH_3)_4]$. The complexes were reversibly oxidized to yield Rh^{II}–Rh^{III} dimers. The half-wave potentials for $[Rh_2(O_2CR)_4L_2]$ (R = H, CH_3, $CH(OH)C_6H_5$) were found to bear a linear relationship with the RCOOH acid dissociation constant. The oxidation process becomes more favourable as the donor number of axial ligand increases. Electronic and ESR spectra of Rh^{II}–Rh^{III} complexes were investigated.

The binuclear rhodium(II) carboxylate complexes are widely studied, because of the interest in the theory of their electronic structure, reactivity and catalytic properties.[1,2] They also exhibit cytostatic and anticancer activity.[1–3]

Electrochemical investigations of the $[Rh_2(OORC)_4L_2]$ complexes allowed better recognition of their electronic structure and reactivity. Rhodium(II) carboxylates oxidate reversibly to Rh^{II}–Rh^{III} complexes, while their reduction is irreversible.[4–6] Oxidation potentials of $[Rh_2(OOCR)_4L_2]$ were discovered to decrease with an increase in the electron-donor properties of the R groups, and to decrease with an increase of the donor number of ligands, L, bound along the Rh—Rh axis (Fig. 1).

The rhodium(II) complexes with the chiral carboxylates are interesting from the point of view of their application in the asymmetric synthesis of the organic compounds. The interest in rhodium(II) chiral carboxylates has been maintained in recent years by their potential applications in chiral organic syntheses. Tetra-(*S*)-mandelatodirhodium catalyses cycloaddition reactions of dimethyl diazomalonate to 1-alkenes to give chiral cyclopropane compounds.[7]

The $[Rh_2(PhCHOHCOO)_4]$ and $[Rh_2(PhCHOHCOO)_2(N\text{-}N)_2Cl_2]$ (Ph = C_6H_5, N-N = 2,2′-bipyridine, 1,10-phenanthroline) complexes are precursors of the effective catalysts for reduction of olefins and ketones.[8] The $[Rh_2(O_2CR)_4]$ complexes also catalyse the oxidation of olefins and alkyl aromatic hydrocarbons.

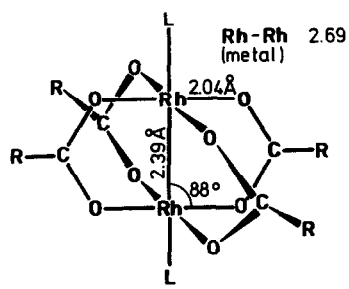

Fig. 1. Structure of tetracarboxylatodirhodium(II).

It seemed interesting to study the electrochemical oxidation of tetramandelatodirhodium(II) and compare its electrochemical properties with that of $[Rh_2(O_2CR)_4]$ dirhodium(II) carboxylates. Prior to this, we have examined the electrochemical properties of rhodium(II) mandelate in methanol.[9] To our knowledge, electrochemical properties of rhodium(II) formate were not investigated.

EXPERIMENTAL

$[Rh_2\{(S)\text{-}C_6H_5CHOHCOO\}_4(H_2O)_2]$,[10] $[Rh_2(O_2CCH_3)_4(H_2O)_2]$,[11] and $[Rh_2(O_2CH)_4]$,[12] were synthesized by the literature methods. All complexes were stored over molecular sieves (3 Å), at room temperature. Tetra-*n*-butylammonium tetrafluoroborate, $n\text{-}Bu_4NBF_4$ (Fluka), used as supporting

* Author to whom correspondence should be addressed.

electrolyte, was recrystallized from an acetone–ether (1 : 1) mixture and dried *in vacuo*. The solvents were dried over molecular sieves. Tetrahydrofuran (THF) and dimethylformamide (DMF) were distilled *in vacuo* over CaH_2 and dichloromethane and acetonitrile over P_4O_{10}. For both electrochemical and spectroscopic experiments all solvents contained 0.1 M *n*-Bu_4NBF_4. Measurements were performed on a Polarographic Analyser PA-4 (Laboratorni Pristroje) using a three-electrode system. The working electrode was a planar platinum electrode ($s = 0.98\ cm^2$). A coiled platinum wire served as the counter-electrode. Potentials were measured relative to a saturated calomel electrode (SCE), which was separated from the examined solution by a bridge filled with electrolyte. The solution in the bridge was periodically exchanged. Ferrocene ($Fecp_2^+/Fecp_2$)[13] was used as an internal standard. Coulometric measurements were made with a Radelkis OH-404 apparatus. The anode was platinum foil ($s = 6.5\ cm^2$), the cathode—mercury ($s = 8\ cm^2$). The coulometric electrolyses were carried out in an electrolyser with cells separated by a glass sinter (G-4). The reference electrode (SCE) was separated from the oxidation solution by means of an electrolytic bridge. Solutions in both cells were stirred magnetically. All measurements were performed at room temperature ($20 \pm 2°C$) in solutions deaerated by a stream of argon (p.a. grade).

Electronic absorption spectra were recorded on a Cary 14 spectrophotometer. The ESR spectra were measured at liquid nitrogen temperature, on a Jeol 3JSMX spectrophotometer.

RESULTS AND DISCUSSION

The cyclic voltammogram of the $[Rh_2\{(S)\text{-}C_6H_5CHOHCOO\}_4(H_2O)_2]$ solution in DMF on the platinum electrode vs SCE is shown in Fig. 2. In the potential range 0–1.5 V it shows a single wave, corresponding to one-electron oxidation (Fig. 2). Analogous voltammograms were obtained for $[Rh_2(C_6H_5CHOHCOO)_4]$ in CH_2Cl_2, CH_3CN and THF solutions and for $[Rh_2(O_2CH)_4]$ and $[Rh_2(O_2CCH_3)_4]$ in DMF solution. During the electro-oxidation of all dirhodium(II) carboxylates in each solution the potential separations ($E_{p,c} - E_{p,a}$) were in the range 60–70 mV, at the cyclic sweep rates $v = 0.02$–$0.5\ V\ s^{-1}$ (Table 1). The ratios of the

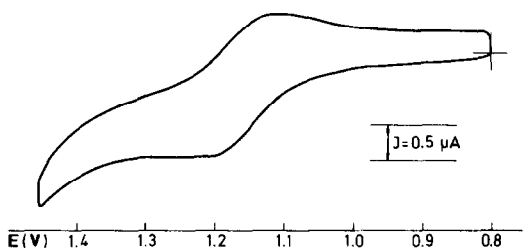

Fig. 2. Cyclic voltammogram of 6×10^{-4} M $[Rh_2\{(S)\text{-}C_6H_5CHOHCOO\}_4(H_2O)_2]$ in DMF/0.1 M *n*-Bu_4NBF_4 on the platinum electrode vs SCE, scan rate 200 mV s^{-1}.

Table 1. Electrochemical data for oxidation of $[Rh_2(O_2CR)_4(H_2O)_2]$ in DMF (0.1 M *n*-Bu_4NBF_4) on the platinum electrode (vs SCE); $v = 0.2\ V\ s^{-1}$

Compound	$E_{p,a}$[a] (V)	$E_{p,c} - E_{p,a}$ (mV)	$E_{1/2}$ (V)	Coulometric determination of the number of electrons transformed/ Mol of $[Rh_2(O_2CR)_4L_2]$
$[Rh_2(O_2CCH_3)_4L_2]$[b] (0.5 mM)	1.015	70	0.990	0.97 ± 0.05
$[Rh_2\{(S)\text{-}C_6H_5CHOHCO_2\}_4L_2]$ (0.5 mM)	1.200	70	1.170	0.97 ± 0.05
$[Rh_2(O_2CH)_4L_2]$[c] (0.1 mM)	1.240	70	1.215	0.95 ± 0.05

[a] Present potentials were determined at the presence of $Fecp^+/Fecp$ in the same electrolyte ($E_{formal}Fecp^+/Fecp = 0.540$ V vs SCE).

[b] Oxidation potential of $[Rh_2(O_2CCH_3)_4L_2]$ in DMF (0.1 M *n*-Bu_4NBF_4) is 40 mV lower than the literature value for oxidation of $[Rh_2(O_2CCH_3)_4L_2]$ in H_2O,[5] and 20 mV lower than its oxidation in 0.1 M H_2SO_4 given by Wilson and Taube.[4] $[Rh_2\{(S)\text{-}C_6H_5CHOHCO_2\}_4L_2]$ is insoluble in water.

[c] $[Rh_2(O_2CH)_4L_2]$ is slightly soluble in DMF.

$L = H_2O$.

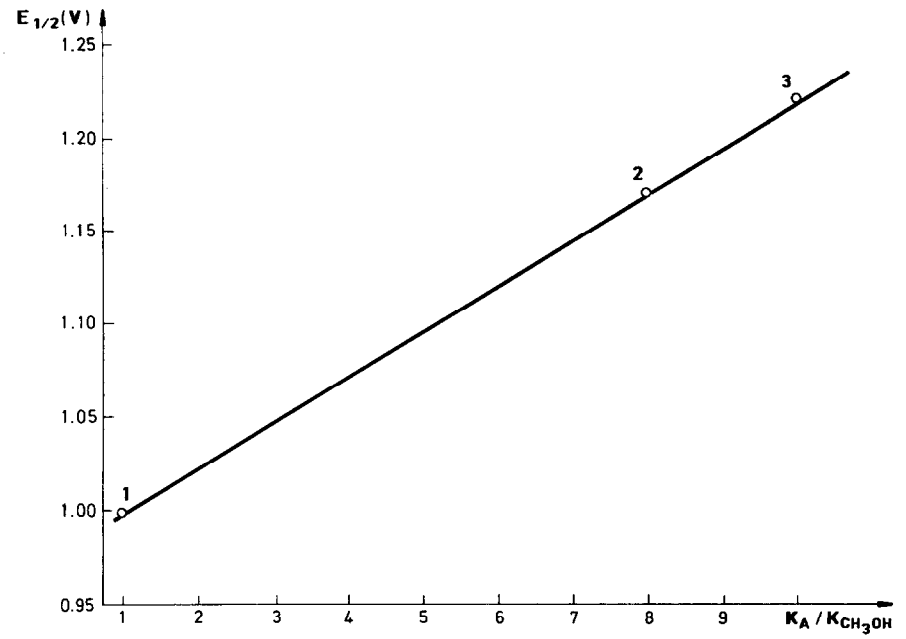

Fig. 3. Plot of the half-wave potentials (V) measured for electro-oxidation of $[Rh_2(O_2CR)_4(H_2O)_2]$ in DMF/0.1 M n-Bu_4NBF_4 vs the K_A/K_{CH_3COOH}: (1) R = CH_3; (2) R = PhC(OH)H; (3) R = H.

cathodic to the anodic peak currents, $i_{p,c}/i_{p,a}$, were close to unity at all scan rates, indicating the absence of coupled chemical reactions.[14] Moreover, the potentials of the anode peak ($E_{p,a/2}$) and formal potentials of all the complexes were independent of the scanning rate: the $i_{p,a}/v^{1/2}$ ratio was constant over the range of scan rates. Such properties are indicative of a one-electron diffusion-controlled Nernstian oxidation. Thus, the electrochemical oxidation of rhodium(II) mandelate and rhodium(II) formate proceed as for the other $[Rh_2(O_2CR)_4]$ complexes.

The stability of rhodium(II) carboxylato complexes, $[Rh_2(O_2CR)_4L_2]$, depends on dissociation constants of RCOOH acids. This is proved by the linear relationship of half-wave potentials with dissociation constants, K_{HA}, or with ratio K_{HA}/K_{CH_3COOH} (Fig. 3). The oxidation potentials are higher for complexes with stronger acids, which, therefore, stabilize the lower oxidation states of the metal.

The effect of axial ligand complexation on the electrode reactions was investigated. It was found that the half-wave potentials decrease with increasing donor number of the solvent (Fig. 4).[15] The donor number can be taken as a measure of the interaction of the axial ligand with the central atoms. The oxidation process becomes more favourable as the interaction of the axial ligand becomes stronger. The shift of the oxidation potential with strength of the axial ligand–rhodium bond indicates that the HOMO levels are destabilized with increasing binding ability of ligands. The differences in the peak potentials, $E = E_{p,c} - E_{p,a}$, for each solvent are near the theoretical value of

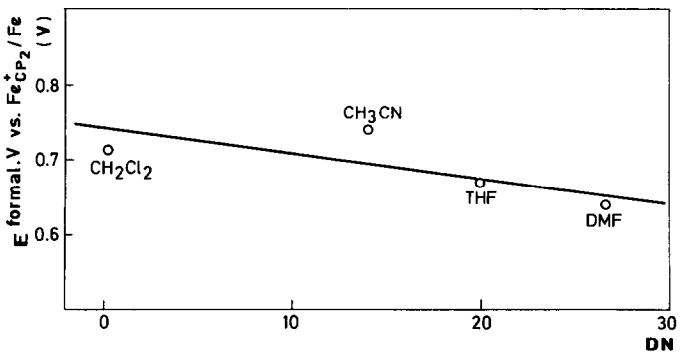

Fig. 4. Dependence of the formal electrode potential of $[Rh_2\{(S)\text{-}C_6H_5CHOHCOO\}_4(H_2O)_2]$ on the donor number of the solvent.

58 mV, corresponding to the reversible transfer of one electron.

$[Rh_2(O_2CR)_4]$ (R = H, Me, PhCHOH) were oxidized coulometrically at potentials 100 mV more anodic than $E_{1/2}$ (Table 1). The complete coulometric oxidation of complexes $[Rh_2(O_2CCH_3)_4(H_2O)_2]$ and $[Rh_2\{(S)\text{-}C_6H_5CHOHCOO\}_4(H_2O)_2]$ in DMF was followed by the change of colour of the solutions from blue to light brown. For $[Rh_2(O_2CCH_3)_2(H_2O)_2]$ the complex regained the blue colour after 24 h. Somewhat different behaviour occurred with $[Rh_2\{(S)\text{-}C_6H_5CHOHCOO\}_4(H_2O)_2]$. The colour of this solution also turned light brown after complete oxidation, but about 20 min after electrolysis was complete, the colour changed to yellow–celadon, under argon atmosphere. After 24 h the reduction process was almost completed and the solution changed to the original blue colour. Reversibility of the oxidation process of rhodium(II) formate, acetate and mandelate was confirmed by the complete reduction of $[Rh_2(O_2CR)_4]^+$ complexes at a potential of +0.6 V.

Similar to electro-oxidation, the consumption of 1.0 electron/dimer was observed, and the cyclic voltammetry of the obtained species gave identical current–voltage curves to those obtained from the original neutral complex.

During the coulometric oxidation of $[Rh_2(O_2CCH_3)_4(H_2O)_2]$ and $[Rh_2\{(S)\text{-}C_6H_5CHOHCOO\}_4(H_2O)_2]$ in DMF (0.1 M n-Bu_4NBF_4) the ESR and absorption spectra were recorded. The resulting absorption spectra are given in Figs 5 and 6 and in Table 2.

The absorption electronic spectra of the $[Rh_2(O_2CR)_4]$ type complexes consist of two weak bands in the visible region, band I (620–500 nm) and band II (450–425 nm). Whereas band II remains almost constant, band I is strongly influenced by changes in the axial ligands and shifts to lower wavelengths depending on the donor atom in the following sequence: I > Br > Cl > O > S > N ⩾ As > P.[1,2,8,10c,16–19] The electronic absorption spectra of the $[Rh_2(O_2CR)_4L_2]^+$ complexes, in addition to the band in the range 400–500 nm, exhibit a new band in the 600–800 nm range. The energy of the latter also depends on the type of ligands coordinated along the Rh—Rh axis. For $[Rh_2(O_2CCH_3)_4(H_2O)_2]^+$,[16–22] the band occurred at 770 nm and was assigned to the $\delta(RhRh) \rightarrow \delta^*(RhRh)$[21] transition. Whereas, in the $[Rh_2(O_2CCH_3)_4(NH_3)_2]^+$ complex this band is located at 570 nm.[22] Since in the spectra of $[Rh_2(O_2CR)_4(DMF)_2]^+$ (R = CH_3, PhCHOH) complexes the band is observed at 770 nm, the DMF molecules should be regarded as coordinated via the oxygen and not the nitrogen atom. In the latter case the strong shift of this band to lower wavelengths should be observed.

The $Rh^{II}Rh^{III}$ complexes in DMF solutions undergo reduction to $[Rh_2(O_2CR)_4]$, both in a

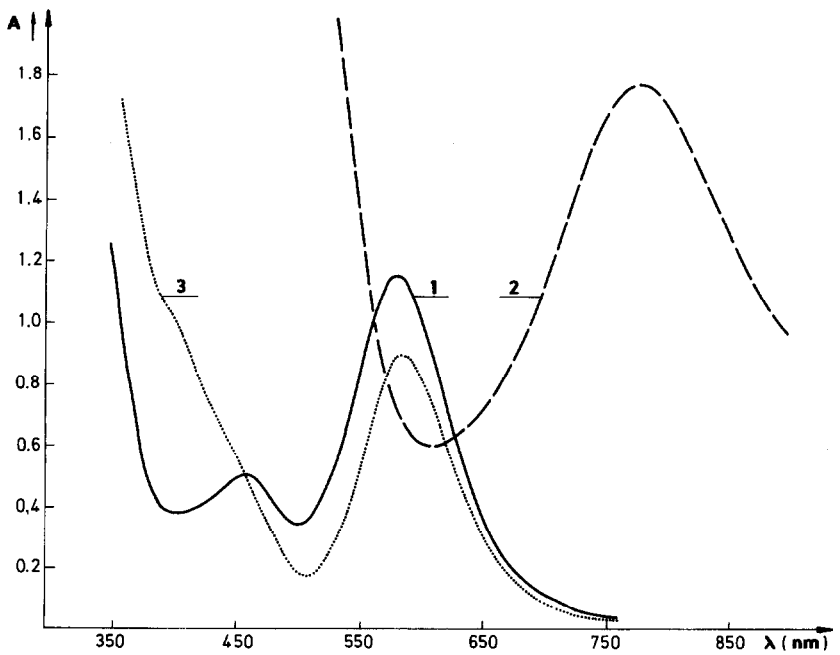

Fig. 5. Electronic absorption spectra obtained during the oxidation of 1×10^3 M $[Rh_2(O_2CCH_3)_4(H_2O)_2]$ in DMF/0.1 M n-Bu_4NBF_4, E_{app} = +1.1 V/SCE: (1) before electrolysis; (2) after electrolysis; (3) 24 h after electrolysis.

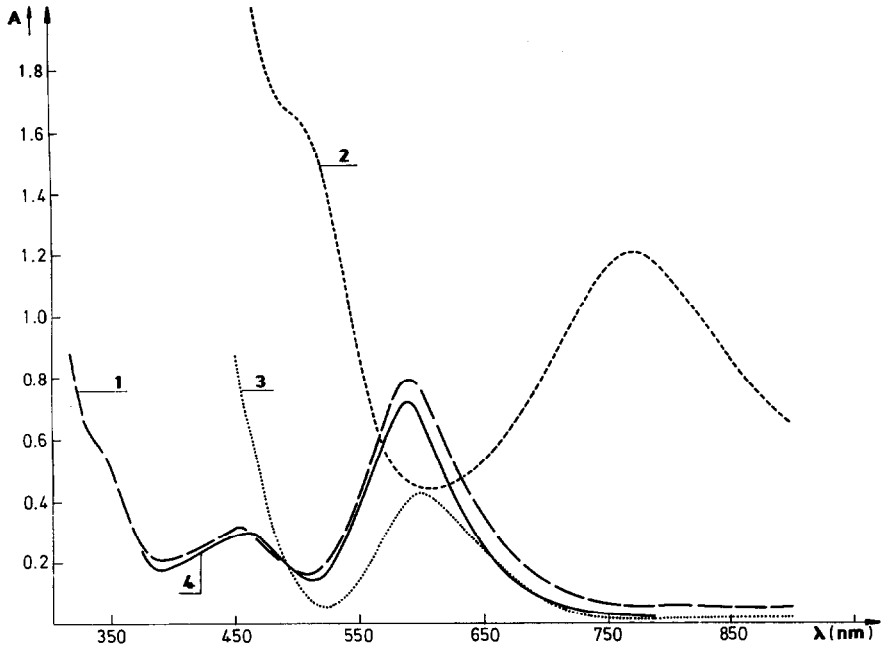

Fig. 6. Electronic absorption spectra obtained during the oxidation of 1×10^3 M $[Rh_2\{(S)\text{-}C_6H_5CHOHCOO\}_4(H_2O)]$ in DMF/0.1 M n-Bu_4NBF_4, $E_{app} = +1.270$ V/SCE: (1) before electrolysis; (2) after electrolysis; (3) 40 min after electrolysis; (4) 24 h after electrolysis.

Table 2. UV and visible absorption maxima of the $[Rh_2(O_2CR)_4L_2]$ complexes in DMF (0.1 M n-Bu_4NBF_4) on the platinum electrode vs SCE

Compound	Maxima, nm (ε, molar extinction coefficient) Before oxidation	After oxidation	Oxidation potential E (V)
$[Rh_2(O_2CCH_3)_4L_2]$ (1 mM)	580(285); 460(125)	770(450); 500sh(150); 410sh(275)	1.1 V
$[Rh_2\{(S)\text{-}C_6H_5CHOHO_2\}_4L_2]$ (1 mM)	580(195); 450(75)	770(150); 500sh(205) and 20 min after current was cut off 590(210) and no band at 450 nm	1.25 V

L = H_2O.

neutral atmosphere and in air. The rate of this process for the mandelate complex exceeds that for the acetate complex. The faster reduction of the mandelate complex is expected because the oxidation potential of the $[Rh_2(O_2CCHOHPh)_4(DMF)_2]^+$ is higher and this complex undergoes partial reduction after 20–30 min, while $[Rh_2(O_2CCH_3)_4(DMF)_2]^+$ is more stable, and even after 24 h its reduction was not complete (Figs 5 and 6).

REFERENCES

1. E. B. Boyar and S. D. Robinson, *Coord. Chem. Rev.* 1983, **50**, 109.
2. T. A. Felthouse, *Prog. Inorg. Chem.* 1982, **29**, 73.
3. (a) I. L. Bear, H. B. Gray, L. Rainen, I. M. Chang, R. A. Howard, G. Serio and A. P. Kimball, *Cancer Chemother. Rep., Pt* 1 1975, **59**, 611; (b) K. M. Kadish, K. Das, R. A. Howard, A. M. Dennis and I. L. Bear, *Bioelectrochem. Bioenerg.* 1978, **5**, 741; (c) R. G. Hughes, I. L. Bear and A. P. Kimball, *Cancer Res.* 1972, **13**, 20.
4. R. C. Wilson and H. Taube, *Inorg. Chem.* 1975, **14**, 405, 2276.
5. K. Das, K. M. Kadish and I. L. Bear, *Inorg. Chem.* 1978, **17**, 930.
6. (a) K. M. Kadish, D. Lancon, A. M. Dennis and I. L. Bear, *Inorg. Chem.* 1982, **21**, 2987; (b) I. Duncan, T. Malinski, T. P. Zhu, Z. S. Hu, K. M. Kadish and I. L. Bear, *J. Am. Chem. Soc.* 1982, **104**, 5507; (c)

M. Y. Chavan, T. P. Zhu, X. Q. Lin, M. Q. Ashan, I. L. Bear and K. M. Kadish, *Inorg. Chem.* 1984, **23**, 4538; (d) I. L. Bear, T. P. Zhu, T. Malinski, A. M. Dennis and K. M. Kadish, *Inorg. Chem.* 1984, **23**, 674.
7. F. P. Pruchnik, K. Wajda-Hermanowicz, M. Zuber and G. Kluczewska-Patrzałek, in preparation.
8. F. P. Pruchnik, *Pure Appl. Chem.* 1989, **61**, 795.
9. A. Szymaszek and F. P. Pruchnik, *Inorg. Chim. Acta* 1987, **131**, 143.
10. R. N. Shchelokov, A. G. Maiorova, S. S. Abdullaev, O. N. Evstafeva, I. E. Golovaneva and G. N. Emel'yanova, *Russ. I. Inorg. Chem.* (*Engl. Transl.*) 1981, **26**, 1774; (b) I. F. Golovaneva, S. S. Abdullaev and R. N. Shchelokov, *Russ. I. Inorg. Chem.* (*Engl. Transl.*) 1982, **27**, 1468; (c) F. P. Pruchnik, B. R. James and P. Kvintovics, *Can. J. Chem.* 1986, **64**, 936.
11. G. A. Rempel, P. Legzdins, H. Smith and G. Wilkinson, *Inorg. Synth.* 1979, **13**, 90.
12. F. P. Pruchnik, submitted for publication.
13. H. M. Koepp, H. Wendt and H. Z. Strehlow, *Z. Electrochem.* 1960, **64**, 483.
14. R. S. Nicholson, *Analyt. Chem.* 1964, **36**, 706.
15. V. Gutman, *The Donor–Acceptor Approach to Molecular Interactions*. Plenum Press, New York (1978).
16. F. P. Pruchnik and M. Zuber, *Roczniki Chemii* 1977, **51**, 1813.
17. V. Miskowski, W. P. Schaefer, B. Sadeghi, B. D. Santarsiero and H. B. Gray, *Inorg. Chem.* 1984, **23**, 1154.
18. I. W. Trexler, A. F. Schreiner and F. A. Cotton, *Inorg. Chem.* 1988, **27**, 3267.
19. L. Dubicki and R. L. Martin, *Inorg. Chem.* 1970, **9**, 673.
20. I. G. Norman and H. J. Kolari, *J. Am. Chem. Soc.* 1978, **100**, 791.
21. D. S. Martin, T. R. Weeb, G. A. Robbins and R. E. Fanwick, *Inorg. Chem.* 1979, **18**, 475.
22. R. D. Cannon, D. B. Powell, K. Sarawek and J. S. Stillman, *J. Chem. Soc., Chem. Commun.* 1976, 31.

Polyhedron Vol. 9, No. 9, pp. 1141–1146, 1990
Printed in Great Britain

0277–5387/90 $3.00+.00
© 1990 Pergamon Press plc

HETEROCYCLIC TELLURIUM COMPOUNDS AS LIGANDS; SOME COMPLEXES OF RHODIUM(III) AND RHODIUM(I)

ALI Z. AL-RUBAIE,* YASSIN N. AL-OBAIDI and LINA Z. YOUSIF

Department of Chemistry, College of Science, University of Basrah, Basrah, Iraq

(*Received* 17 *May* 1989; *accepted* 8 *December* 1989)

Abstract—The synthesis and characterization of new rhodium(III) complexes containing tellurium heterocyclic ligands are described. All complexes have the general formula of $RhCl_3L_3$ (where L = C_4H_8Te, $C_4H_8TeI_2$, C_4H_8OTe, C_5H_8Te, $C_6H_{10}Te$, C_8H_5ClTe, $C_{10}H_{12}Te$ and $C_{16}H_{10}Cl_2Te$). Reactions of $RhCl_3L_3$ complexes with carbon monoxide are shown to replace only one cyclic telluride by carbon monoxide under mild conditions. Reactions of square-planar rhodium(I) complexes with tellurium heterocycle ligands are reported.

Rhodium complexes containing organotellurium compounds, namely diphenyltelluride and dimethyltelluride, as donors have been previously prepared and characterized.[1–3]

Our current interest in heterocyclic tellurium compounds[4–7] together with the fact that heterocyclic tellurium compounds, as far as we are aware, have not been used as ligands with rhodium(III) compounds.[8] This prompted us to prepare and investigate properties of a number of new heterocyclic tellurium–rhodium complexes.

EXPERIMENTAL

(a) *Synthesis*

Reactions were carried out in a dry oxygen-free, nitrogen atmosphere. Solvents were dried and distilled before use.

Preparation of ligands. 1-Telluracyclopentane,[5] 1,1-diiodo-telluracyclopentane,[5] 1-oxa-4-telluracyclohexane,[6] 3-methyl-2,5-dihydrotellurophene,[9] 3,4-dimethyl-2,5-dihydrotellurophene,[9] 3-chloro-4,5-benzotellurophene,[10] 2-(chlorovinyl)-3-chloro-4,5-benzotellurophene,[10] di-μ-chlorobis(η^4-1,5-cyclooctadiene)dirhodium(I)[11] and chlorotris(triphenylphosphine)rhodium(I)[12] were prepared by reported methods.

Synthesis of 5,6-*dimethyl*-1,3-*dihydro*-2-*telluraindene*. This new telluride was prepared by the following method. To a suspension of $C_{10}H_{12}TeI_2$ (4.75 g, 7.5 mmol) (this orange compound was prepared by reaction of 1,2-bis(chloromethyl)-4,5-dimethylbenzene with tellurium powder and NaI in 2-butoxyethanol) in 250 cm^3 of ethanol was added dropwise a solution of hydrazine (0.88 g, 2.75 mmol) in 30 cm^3 of ethanol. The resulting solution was warmed gently until the red colour disappeared. The reaction solution was then poured into 1 dm^3 of water and extracted with ether (3 × 200 cm^3). The combined ether extracts were washed with water, dried over $CaCl_2$, and concentrated to dryness on a rotary evaporator. The resulting yellow powder was recrystallized from ethanol to give yellow flakes, m.p. 90–92°C. Found: C, 46.1; H, 4.5. Calc. for $C_{10}H_{12}Te$: C, 46.2; H, 4.7%.

Synthesis of rhodium(III) *complexes*, $RhCl_3L_3$. These complexes were all prepared by the reaction of rhodium(III) chloride trihydrate with the corresponding heterocyclic tellurium compounds. The general preparation route is illustrated by the following example.

Trichlorotris(5,6-*dimethyl*-1,3-*dihydro*-2-*telluraindene*)*rhodium*(III). Rhodium trichloride trihydrate (0.79 g, 3.0 mmol) in dry ethanol (50 cm^3) was added to an ethanolic solution of 5,6-dimethyl-1,3-dihydro-2-telluraindene (2.34 g, 9.0 mmol). The mixture was stirred at room temperature for 24 h. On cooling, a brownish-red solid was obtained, filtered off, washed with ethanol and dried *in vacuo*.

The rhodium(III)–heterocyclic tellurium complexes (along with melting points and elemental

* Author to whom correspondence should be addressed.

analyses), which were prepared by the above general route, are listed in Table 1.

Synthesis of carbonyltrichlorobis(1-telluracyclopentane)rhodium(III), $[RhCl_3(CO)(C_4H_8Te)_2]$. Carbon monoxide was passed through a chloroform solution of $RhCl_3(C_4H_8Te)_3$ (0.46, 4.4 mmol) for 4 h. The solution was filtered and evaporated to dryness. The product was washed several times with hexane to give a brown solid, m.p. 170°C.

Synthesis of carbonyltrichlorobis(3-chloro-4,5-benzotellurophene)rhodium(III), $[RhCl_3(CO)(C_8H_5ClTe)_2]$. Carbon monoxide was passed through a toluene solution of trichlorotris(3-chloro-4,5-benzotellurophene)rhodium(III) (1.32, 5.0 mmol) for 10 h. The solution was filtered and evaporated to dryness. Recrystallization from hexane gave a brown solid, m.p. 152°C.

Synthesis of chloro(η^4-1,5-cyclooctadiene)(1-telluracyclopentane)rhodium(III), $[Rh(COD)(C_4H_8Te)Cl]$. An excess of 1-telluracyclopentane (0.46 g, 2.5 mmol) was added to a solution of $[RhCl(COD)]_2$ (0.25 g, 0.5 mmol) in 30 cm^3 of hexane. The mixture was stirred for 24 h at room temperature. The yellowish-brown product was filtered, washed with hexane and dried *in vacuo*, m.p. 110°C.

Synthesis of di - μ - chloro - bis(1 - oxa - 4 - telluracyclohexane)bis(triphenylphosphine)dirhodium (I), $[Rh(C_4H_8OTe)(PPh_3)Cl]_2$. 1-Oxa-4-telluracyclohexane (0.30 g, 1.5 mmol) was added to 0.46 g (0.5 mmol) of chlorotris(triphenylphosphine) rhodium(I) dissolved in 45 cm^3 of toluene. The mixture was stirred for 12 h at room temperature. The yellowish-brown solid which formed was filtered, washed with dry toluene and dried *in vacuo*, m.p. 156°C.

Table 1. Analytical data, colours and conductivity of the new rhodium(III) complexes

Compound	Colour	Melting point (°C)	Analysis (%)[a] C	H	Conductivity[b] (Ω^{-1} cm^2 mol^{-1})
$RhCl_3$ 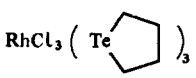	Orange	190	18.3 (18.9)	3.5 (3.2)	2.3
$RhCl_3$ 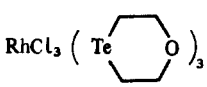	Orange	300	17.9 (17.8)	2.9 (2.9)	1.0
$RhCl_3$ 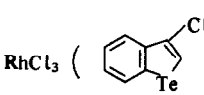	Red–brown	156	28.5 (28.8)	1.5 (1.5)	3.9
$RhCl_3$ 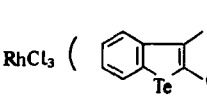	Red	145	41.6 (40.8)	2.1 (2.7)	1.7
$RhCl_3$ 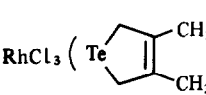	Brown	300	25.6 (25.8)	3.4 (3.6)	2.3
$RhCl_3$ 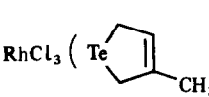	Brown	140(dec.)	22.4 (22.6)	2.9 (3.0)	0.85
$RhCl_3$ 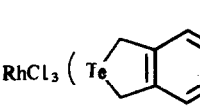	Red–brown	200	37.4 (36.4)	3.8 (3.7)	3.2
$RhCl_3$ 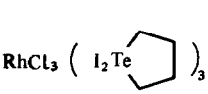	Brown	250	9.6 (9.5)	1.7 (1.6)	25.7

[a] Calculated values are in parentheses.
[b] In DMSO solution at 10^{-3} M.

(b) *Physical measurements*

IR spectra were recorded as KBr pellets or Nujol mulls in the range 4000–200 cm^{-1} using a Pye–Unicam SP3-300 IR spectrophotometer. ^1H NMR data were obtained with a Bruker WH-90DS spectrometer using DMF-d_7 as solvent and TMS as internal standard. UV–vis spectra were recorded on Pye–Unicam SP8-200 UV-vis spectrophotometers. Molar conductance of the complexes at 10^{-3} M dilution in DMSO was measured with a WTW conductivity meter LBR, using a standard conductivity cell with cell constant of 0.80.

Microanalyses for carbon and hydrogen were carried out by Heraeus, computer, H.P. 85. Tellurium analysis was carried out as described by Thavornytikarn[13] by use of a Pye–Unicam Spy flameless atomic absorption spectrometer. Melting points were determined on a Gallenkamp melting point apparatus and are uncorrected.

RESULTS AND DISCUSSION

Rhodium(III) *complexes*

Rhodium(III) chloride trihydrate reacted readily in ethanolic solution with tellurium-donor heterocycles (metal : ligand ratio varied between 1 : 6 and 1 : 3) to give complexes of the general formula $RhCl_3L_3$, which agrees well with previous reports.[2,3] All complexes are coloured solids and mostly soluble in DMF and DMSO. Their physical properties and elemental analyses are listed in Table 1.

Conductance measurements have been made for $RhCl_3L_3$ complexes (**1–7**) in DMSO and the low value of molar conductance (below 4 Ω^{-1} cm^2 mol^{-1}) reveals the non-electrolytic nature of these complexes. Complex **8** is an electrolyte (Table 1), thus it might be expected to dissociate into $RhCl_3$ and $C_4H_8TeI_2$ (see the discussion of the NMR spectra). So it seems probable, that in DMSO, the ligand has dissociated:

$$C_4H_8TeI_2 \rightleftharpoons C_4H_8TeI^+ + I^-.$$

On the other hand, the conductance behaviour of complex **8** could be due to its existence as $[C_4H_8TeI^+]_3[RhCl_3I_3]^{3-}$, since it is well known that dihaloheterocyclic tellurium compounds undergo monohalogen exchange reactions.[14,15a] Further support for this formula was obtained from the thermogravimetric study of complex **8** and some related complexes.[15b]

The IR spectra of complexes **1–8** show some characteristic bands between 320 and 385 cm^{-1} due to the terminal ν(Rh—Cl),[16] Table 2. The appearance of a medium band near 345 cm^{-1}, typical of asymmetric stretching vibration of a linear Cl—Rh—Cl group, indicates a *trans* arrangement of chlorine atoms.[17,18,19] Thus on the basis of the above evidence, the following structure can be assigned for these complexes:

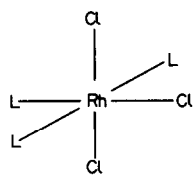

L = Heterocyclic tellurium ligands.

The weakness of the corresponding ν(Te—C) modes precludes direct verification of the proposed tellurium bonding. The essentially unchanged ν(C=C) in **5**, **6** and **7** (telluraindene is regarded as a special case of substituted 2,5-dihydrotellurophene)

Table 2. Selected IR data (cm^{-1}) of rhodium(III) complexes

Compound	ν(Rh—Cl)	Asym. ν(Cl—Rh—Cl)	ν(Te—C)	Other selected bands
1	322m, 380m	345m	545w	2900w, 2835w
2	322m, 385m	335m	515w	2900w, 2840m, 1090vs,[a] 815s[b]
3	320m, 370m	345m	445w	3060w, 3010w, 1500w, 1480m, 1250w, 915m, 750m, 740s, 720m, 685w
4	328m, 382m	340m	445w	3050w, 3030w, 1420m, 1280m, 1020w, 915m, 765s, 720m, 655w
5	325m, 382m	348m	520w	2960w, 2890w, 2840w
6	315m, 370m	345m	520w	3000w, 2900w, 2840w
7	322m, 380m	345m	520w	3055w, 2990w, 2945m, 2925w, 2900m
8	322m, 385m	335m	545w	2990w, 2940m, 2910w

[a] Asym. ν(C—O—C).
[b] Sym. ν(C—O—C).

of the heterocycle in complexes vs the free ligands supports tellurium bonding in these complexes. Moreover, the unchanged positions of the symmetric and non-symmetric C—O—C stretching modes of the heterocycle in the complex $RhCl_3(C_4H_8OTe)_3$ (**2**) vs the free ligands support Te-bonding,[20] see Table 2.

^1H NMR spectra of complexes **1**, **2**, **5**, **6** and **7** have been recorded in DMF-d_7 and show signal patterns similar to those shown by the free ligands (Table 3). This may be attributed to the dissociation of the ligands in solution. Furthermore, if these ligands coordinate, the α-protons become non-equivalent and we would expect an AB pattern.[4]

The electronic spectral data of complexes **1–8** are given in Table 4, with molar extinction values. The bands with lower molar extinction values could be assigned to *d–d* transitions and those with higher extinction values are assigned to charge-transfer transitions.[21] The electronic spectra of complex **2** are very different in $CHCl_3$ and DMSO (Table 4), which may be due to the existence of different species in the two solvents.

Carbonyl complexes

Bubbling carbon monoxide at atmospheric pressure through a chloroform solution of complex **1** for 4 h and through a toluene solution of complex **3** for 10 h gave $[RhCl_3(CO)(C_4H_8Te)_2]$ and $[RhCl_3(CO)(C_8H_5TeCl)_2]$ complexes, respectively (Table 5). The IR spectra of the complexes **9** and **10** exhibit strong bands at 2030 and 2060 cm^{-1}, respectively, assigned to the new ν(CO) group of rhodium(III) complexes.[3,19] The IR band at 325 cm^{-1} (in both complexes) is assigned to ν(Rh—Cl) (*trans* to CO) asymmetric stretching (Table 5). The relatively high value of ν(CO) observed for complex **10** (2060 cm^{-1}), as compared with complex **9** (2030 cm^{-1}), indicates an increased π-acidity of 3-chloro-4,5-benzotellurophene.[3]

Rhodium(I) *complexes*

The air-stable complex $[(COD)RhCl(C_4H_8Te)_2]$ was prepared by a bridge cleavage reaction analogous to the reaction of $SePPhMe_2$[22] and $P(p\text{-}C_6H_4F)_3$[23] with $[(COD)RhCl]_2$, as shown in the following equation:

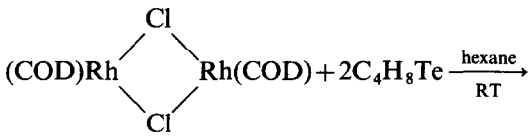

$$2(COD)RhCl(C_4H_8Te).$$

The stoichiometry of this complex has been deter-

Table 3. ^1H NMR spectral data of some new rhodium(III) complexes

Compound	Chemical shifts (ppm);[a] TMS = 0 ppm
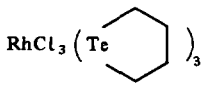	1.34(1.32) [m, 12H, CH_2], 2.45(2.14) [m, 12H, Te—CH_2]
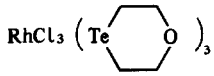	2.57(2.23) [t, 12H, Te—CH_2], 4.33(4.31) [t, 12H, O—CH_2]
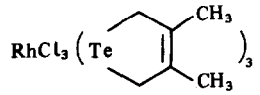	1.66(1.62) [s, 18H, CH_3], 4.53(4.11) [s, 12H, Te—CH_2]
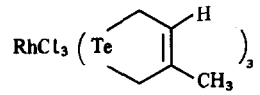	1.75(1.80) [s, 9H, CH_3], 4.35(3.93) [s, 12H, Te—CH_2], 5.65(5.57) [s, 3H, =C—H]
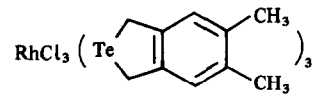	2.19(2.18) [s, 18H, CH_3], 3.95(3.62) [s, 12H, Te—CH_2], 6.95(7.01) [s, 6H, Ar—H]

[a] Values for the free ligand are in parentheses.

Table 4. Electronic spectral data of rhodium(III) complexes

1	CH_2Cl_2	232(22,502), 304(14,699), 360(1800)
2	CH_2Cl_2	236(17,997), 301(13,199), 367(1430)
	DMSO	261(13,998), 317(12,250)
3	CH_2Cl_2	230(45,996), 256(35,001), 324(4400)
	$CHCl_3$	243(49,003), 292(29,000)
4	CH_2Cl_2	242(47,109), 258(34,998), 290(20,000), 357(1720)
	DMSO	264(45,001), 283(35,989), 350(3600), 372(4500)
5	CH_2Cl_2	235(16,750), 300(8500), 358(1462)
6	CH_2Cl_2	238(11,125), 308(17,375), 476(500)sh
7	CH_2Cl_2	236(44,003), 299(15,400), 359(5700)
8	CH_2Cl_2	228(44,996), 272(49,002), 340(1260)

[a] Molar extinction values (M^{-1} cm^{-1}) are given in parentheses. sh = shoulder.

Table 5. Analytical data, colours and IR data of some new carbonylrhodium(III) and rhodium(I) complexes

Compound	Colour	Melting point (°C)	Analysis (%)[a] C	H	Ir (cm^{-1}) ν(Rh—Cl)	ν(Te—C)	Other bands
$[RhCl_3(CO)(C_4H_8Te)_2]$ (**9**)	Brown	179	21.6 (21.5)	3.3 (3.2)	325m, 295m	540w	2030s[b]
$[RhCl_3(CO)(C_8H_5ClTe)_2]$ (**10**)	Brown	152	26.4 (26.7)	1.3 (1.3)	325m, 300sh	255w	2060s[b]
$[RhCl(COD)(C_4H_8Te)]$ (**11**)[c]	Yellow–brown	110	33.0 (33.5)	4.4 (4.7)	280m, 270m	540w	2900[d]
$[RhCl(PPh_3)(C_4H_8OTe)]_2$ (**12**)	Yellow–brown	210	44.5 (44.0)	3.9 (3.9)	295m, 280m	528w	340m,[e] 1100vs,[f] 815s[f]

[a] Calculated values are in parentheses.
[b] ν(CO).
[c] Te: Found: 29.1. Calc.: 29.6%.
[d] $\nu(C—H)_{COD}$.
[e] ν(Rh—P).
[f] Sym. and asym. ν(C—O—C).

mined by IR and elemental analyses (Table 5). The IR spectrum of complex **11** exhibits a band at 340 cm^{-1} which is probably due to Rh—C_8H_{12} stretching mode,[12a] and bands at 270 and 280 cm^{-1} due to the monomeric rhodium(I) complex, which is slightly higher than the bridging Rh—Cl frequency in $[RhCl(COD)]_2$ (Table 5).[12]

Reaction of C_4H_8Te with $[RhCl(PPh_3)_3]$ produced complex **12** as a dimeric rhodium(I) complex (Table 5). This could be attributed to the displacement of one triphenylphosphine molecule by the telluride ligand and loss of another triphenylphosphine in the organic solvent to form complex **12**, as it is well known that $[RhCl(PPh_3)_3]$ loses one molecule of triphenylphosphine and the dimeric complex of the formula $[RhCl(PPh_3)_2]_2$ can be isolated.[12]

Acknowledgements—The Authors are grateful to the Department of Chemistry, College of Science, University of Basrah, for support. The Authors also thank Dr N. I. Al-Salim for helpful discussions.

REFERENCES

1. M. Sato and T. Yoshida, *J. Organomet. Chem.* 1973, **51**, 321.
2. S. J. Anderson, J. R. Barnes, P. L. Goggin and R. J. Goodfellow, *J. Chem. Res.* (*S*) 1979, 236; (*M*) 1978, 3601.
3. S. A. Gardner, *J. Organomet. Chem.* 1980, **190**, 289.

4. A. Z. Al-Rubaie, W. R. McWhinnie, P. Granger and S. Chapelle, *J. Organomet. Chem.* 1982, **234**, 287.
5. A. Z. Al-Rubaie, H. A. Al-Shirayda, P. Granger and S. Chapelle, *J. Organomet. Chem.* 1985, **287**, 321.
6. A. Z. Al-Rubaie, H. A. Al-Shirayda and A. I. Auoob, *Inorg. Chim. Acta* 1987, **134**, 139.
7. (a) A. Z. Al-Rubaie and H. A. Al-Shirayda, *J. Organomet. Chem.* 1985, **294**, 315; (b) A. Z. Al-Rubaie, H. A. Al-Shirayda and A. I. Auoob, *J. Organomet. Chem.* 1988, **356**, 49.
8. H. J. Gysling, in *The Chemistry of Organic Selenium and Tellurium* (Edited by S. Patai and Z. Rappoport), Vol. 1, p. 679. John Wiley, New York (1986).
9. J. Bergman and L. Engman, *J. Am. Chem. Soc.* 1981, **103**, 2715.
10. J. Bergman and L. Engman, *J. Organomet. Chem.* 1980, **201**, 377.
11. (a) G. Giordano and R. H. Crabtree, *Inorg. Synth.* 1979, **XIX**, 218; (b) L. Porri, A. Lionetti, G. Allegra and A. Immirzi, *J. Chem. Soc., Chem. Commun.* 1965, 336.
12. (a) M. A. Bennett and P. A. Longstaff, *Chem. Ind. (Lond)* 1965, 846; (b) J. A. Osborn, F. H. Jardine, J. F. Young and G. Wilkinson, *J. Chem. Soc. A* 1966, 1711.
13. P. Thavornytikarn, *J. Organomet. Chem.* 1973, **51**, 11.
14. Z. Zumbulyadis and H. J. Gysling, *J. Organomet. Chem.* 1980, **192**, 183.
15. (a) D. Dakterniek, R. DiGiacomo, R. W. Gable and F. H. Hoskins, *J. Organomet. Chem.* 1988, **356**, 49; (b) A. Z. Al-Rubaie, Y. N. Al-Obaidi and L. Z. Yousif, *Thermochim. Acta* 1990, in press.
16. M. M. T. Khan and E. R. Rao, *Polyhedron* 1988, **7**, 29.
17. M. A. Bennett, R. J. H. Clark and D. L. Milner, *Inorg. Chem.* 1967, **6**, 1647.
18. J. Browing, P. L. Goggin, R. J. Goodfellow, M. G. Norton, A. J. M. Rattary and B. F. Taylor, *J. Chem. Soc., Dalton Trans.* 1977, 2061.
19. N. I. Al-Salim, PhD thesis, Aston University, Birmingham (1987).
20. K. L. Baker and G. W. A. Fowles, *J. Chem. Soc. A* 1968, 801.
21. (a) L. Sacconi and G. P. Speroni, *Inorg. Chem.* 1968, **7**, 295; (b) D. M. Roundhill, S. G. N. Roundhill, W. B. Beaulieu and U. Bagchi, *Inorg. Chem.* 1980, **19**, 3365.
22. E. W. Ainscough, A. M. Brodie and E. Mentzer, *J. Chem. Soc., Dalton Trans.* 1973, 2167.
23. M. Iglesias, C. Del Pino, A. Corma, S. Garcia-Blanco and S. M. Carrera, *Inorg. Chim. Acta* 1987, **127**, 215.

Polyhedron Vol. 9, No. 9, pp. 1147–1153, 1990
Printed in Great Britain

0277–5387/90 $3.00+.00
© 1990 Pergamon Press plc

EXTRACTION EQUILIBRIUM OF COBALT(II) FROM SULPHATE SOLUTIONS BY DI(2-ETHYLHEXYL) PHOSPHORIC ACID DISSOLVED IN KEROSENE

TING-CHIA HUANG* and TEH-HUA TSAI

Department of Chemical Engineering, National Cheng Kung University, Tainan, Taiwan 70101, Republic of China

(*Received* 18 *October* 1989; *accepted* 8 *December* 1989)

Abstract—The distribution of cobalt(II) between 0.5 kmol m^{-3} aqueous sulphate medium and kerosene solutions of di(2-ethylhexyl)phosphoric acid (HDEHP) has been studied at 25°C. The extraction equilibrium is influenced by the total extractant concentration, equilibrium pH value and total metal concentration in the aqueous phase. The distribution data have been analysed both graphically and numerically. The results show that the species extracted into the organic phase have the composition $\overline{CoR_2(HR)_2}$ and $\overline{CoR_2(HR)_3}$. The stability constants of HSO_4^-, $NaSO_4^-$ and $CoSO_4$ in sulphate solutions have also been estimated from the extraction data.

Di(2-ethylhexyl)phosphoric acid (abbreviated as HDEHP or simply HR) has been studied extensively as an extraction reagent in hydrometallurgical processes for the separation and purification of a number of metals. It extracts first-row transition metals such as copper, cobalt, nickel and zinc, as well as uranium and rare earths in familiar nuclear fuel reprocessing, in a wide range of operating conditions.[1–7]

The extraction of cobalt with HDEHP has been studied by many investigators. Madigan[8] studied the distribution of cobalt between an aqueous sulphate solution and a solution of HDEHP in kerosene, and proposed that CoR_2 compounds are formed in the organic phase. Brisk and McManamey,[9] working in sulphate media, found that a single dimeric acid molecule was formed by the extracted species in aliphatic diluent. Grimm and Kolařík[10] and Komasawa *et al.*,[11] using both aliphatic and aromatic diluents, explained the extraction of Co^{2+} from nitrate medium by assuming the formation of $CoR_2(HR)_2$. Sato and Nakamura[12] proposed the extraction of $CoR_2(H_2O)_2$ after spectroscopic studies on the solid compound obtained by loading the metal in the organic phase. Komasawa *et al.*[13] studied the effect of diluents on extraction from nitrate media and showed the existence of $CoR_2(HR)_2$ formed in alcohol diluents and non-polar or weak polar diluents.

Further experimental studies seem necessary to clarify the uncertainties regarding species composition. In this work, the extraction of cobalt by HDEHP is studied in detail to determine the composition of the species extracted by HDEHP in kerosene. In order to obtain a complete understanding of the system, the extraction of cobalt was

* Author to whom correspondence should be addressed.

Nomenclature

D: Distribution ratio (−); K_a: acid dissociation constant of monomeric HDEHP in the aqueous phase (kmol m^{-3}); K_d: distribution constant of monomeric HDEHP between the organic and aqueous phases (−); K_2: dimerization constant of HDEHP in the diluent (m^3 $kmol^{-1}$); K_{mpq}: equilibrium constant of cobalt–HDEHP complexes; m: degree of aggregation of the extracted species (−); p: number of R group except HR molecule involved in the extracted species (−); q: number of free monomeric HDEHP involved in the extracted species (−); Co^{II}: metal species; U: error square sum (−); $[]_t$: total concentration of the species in the brackets (kmol m^{-3}).

Greek letters

β: Stability constants of sulphate complexes (m^3 $kmol^{-1}$); σ: standard deviation (−).

Superscripts

$\overline{\quad}$: Denotes the organic phase species or organic phase concentration.

Subscripts

min: Minimum value.

studied first by graphic and slope analysis, which assumed no complexes were in the aqueous phase. Then, by numerical analysis of the experimental data, values for the stability constants of the HSO_4^-, $NaSO_4^-$ and $CoSO_4$ complexes in the aqueous sulphate solutions can be obtained.

EXPERIMENTAL

Reagents and solutions

Di(2-ethylhexyl)phosphoric acid used in this work was the product of Daihachi Chemical Ind. Co. Ltd., Osaka, Japan. A purity of 95% was found by potentiometric titration with NaOH in ethanolic medium. HDEHP was further precipitated as a copper complex from toluene and acetone solution, and then dissolved in toluene and a 4 kmol m^{-3} sulphuric acid solution, following the procedure of McDowell *et al.*[14] Kerosene (Chinese Petroleum Co., Taiwan, R.O.C.) was washed twice with 1/5 volume 98% H_2SO_4, then with distilled water until it was neutral.[15] The other inorganic chemicals were analytical reagent grade supplied by Hayashi Pure Chemical Ind. Ltd., Osaka, Japan. Metal solutions were always prepared by weighing the appropriate volumes of the stock solution and making up with diluent.

Procedure

Twenty millilitres of the organic solution and an equal volume of aqueous solution were mixed in glass flasks with ground glass stoppers and shaken by a mechanical shaker for at least 30 min at 25.0 ± 0.2°C. Preliminary experiments have shown the time needed to reach equilibrium to be less than 15 min. The organic solutions containd a 0.01–0.35 kmol m^{-3} monomeric form of HDEHP in kerosene. The aqueous phase consisted of 0.5 kmol m^{-3} $(Na^+, H^+, Co^{2+})SO_4^{2-}$. The total anion concentrations were kept constant. The concentrations of cobalt ion in the initial aqueous solutions ranged from 8.5×10^{-4} to 1.7×10^{-2} kmol m^{-3}. The two phases were separated after they had been allowed to settle for 4 h in a thermostat at 25.0 ± 0.2°C.

After phase separation, the equilibrium hydrogen ion concentration was measured by a pH meter. The concentration of cobalt was measured with a IL-551 atomic absorption spectrophotometer (Instrumentation Laboratory Inc.) at a wavelength of 240.7 nm, coupled with background correction. Cobalt in the organic phases was stripped with 4 kmol m^{-3} sulphuric acid, and the metal concentration in the acidic solution was analysed by AAS. The process had been shown to be quantitative and the mass balance for the metal was always within ±2%.

RESULTS AND DISCUSSION

Extraction equilibrium of cobalt

Metal complexes of HDEHP tend to form very large polymeric species in a fully loaded organic phase. These polymers are strongly depolymerized in the presence of free HDEHP molecules and ethylene glycol.[16] Thus, it is necessary to assume that cobalt is extracted as an *m*-merized complex into the slightly loaded organic phase. The extraction of cobalt(II) with HDEHP can be represented by the following general reaction:

$$m\mathrm{Co}^{2+} + m(p+q)/2\overline{\mathrm{H_2R_2}} \rightleftharpoons \overline{(\mathrm{CoR}_p(\mathrm{HR})_q)_m} + mp\mathrm{H}^+ \quad (1)$$

where

$$K_{mpq} = \frac{\overline{[(\mathrm{CoR}_p(\mathrm{HR})_q)_m]}[\mathrm{H}^+]^{mp}}{[\mathrm{Co}^{2+}]^m[\overline{\mathrm{H_2R_2}}]^{m(p+q)/2}} \quad (2)$$

is the stoichiometric equilibrium constant referring to 0.5 kmol m^{-3} $(Na,H)SO_4$ with kerosene as diluent, and the bar indicates the species in the organic phase.

The distribution ratio of cobalt is defined as

$$D_{\mathrm{Co}} = \frac{[\overline{\mathrm{Co}^{\mathrm{II}}}]}{[\mathrm{Co}^{\mathrm{II}}]}. \quad (3)$$

Substituting eq. (2) into (3), we obtain

$$D_{\mathrm{Co}} = \frac{m\overline{[(\mathrm{CoR}_p(\mathrm{HR})_q)_m]}}{[\mathrm{Co}^{2+}]} = mK_{mpq}[\mathrm{Co}^{2+}]^{m-1}[\overline{\mathrm{H_2R_2}}]^{m(p+q)/2}[\mathrm{H}^+]^{-mp}. \quad (4)$$

At constant concentrations of HDEHP and low distribution ratio, $[Co^{2+}]^{m-1}[\overline{H_2R_2}]^{m(p+q)/2}$ will be approximately constant. Thus, a plot of $\log D_{Co}$ vs pH will give a straight line with a slope of *mp*. Figure 1 shows the relationships between D_{Co} and pH with HDEHP concentration as parameter for 0.5 kmol m^{-3} $(Na,H)SO_4$ and $[Co^{II}]_t = 0.0017$ kmol m^{-3} at 25°C. The straight lines have slopes = 2, i.e. $mp = 2$. Thus, eq. (4) can be simplified to

$$[\overline{\mathrm{Co}^{\mathrm{II}}}][\mathrm{H}^+]^2 = mK_{mpq}[\mathrm{Co}^{2+}]^m[\overline{\mathrm{H_2R_2}}]^{m(p+q)/2}. \quad (5)$$

At constant concentrations of HDEHP, the degree of aggregation of the cobalt–HDEHP complex in the organic phase, *m*, is obtained from the plot of $\log[\overline{Co^{II}}][H^+]^2$ vs $\log[Co^{2+}]$. The experimental results are shown in Fig. 2 for various HDEHP concentration and 0.5 kmol m^{-3} (Na, H)SO_4 at 25°C. The straight lines have unit slopes in Fig. 2.

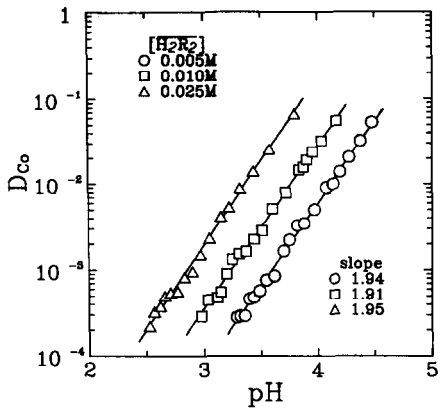

Fig. 1. Effect of pH on the extraction of cobalt between 0.5 kmol m^{-3} $(Na,H)SO_4$ and kerosene at 25°C. $[Co^{II}]_t = 0.0017$ kmol m^{-3}. (○) $[\overline{H_2R_2}] = 0.005$ kmol m^{-3}, slope = 1.94; (□) $[\overline{H_2R_2}] = 0.010$ kmol m^{-3}, slope = 1.91; (△) $[\overline{H_2R_2}] = 0.025$ kmol m^{-3}, slope = 1.95.

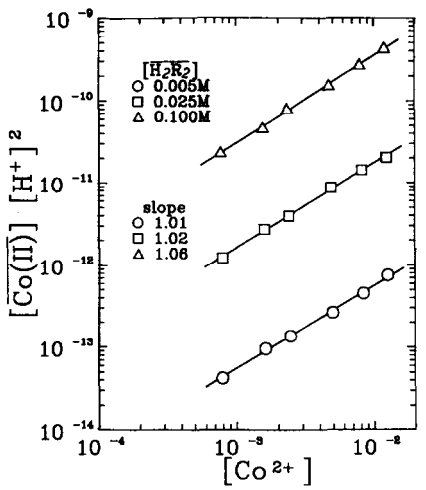

Fig. 2. Extraction of cobalt between 0.5 kmol m^{-3} $(Na,H)SO_4$ and kerosene at constant concentrations of HDEHP and 25°C. (○) $[\overline{H_2R_2}] = 0.005$ kmol m^{-3}, slope = 1.01; (□) $[\overline{H_2R_2}] = 0.025$ kmol m^{-3}, slope = 1.02; (△) = $[H_2R_2] = 0.10$ kmol m^{-3}, slope = 1.06.

Therefore, the extracted species is monomeric, i.e. $m = 1$. And then $p = 2$. Thus, eqs (2) and (4) can be simplified to

$$K_{2q} = \frac{[\overline{CoR_2(HR)_q}][H^+]^2}{[Co^{2+}][\overline{H_2R_2}]^{(2+q)/2}} \quad (6)$$

and

$$D_{Co} = K_{2q}[\overline{H_2R_2}]^{(2+q)/2}[H^+]^{-2}. \quad (7)$$

Rearranging eq. (7), it follows that

$$\log D_{Co} - 2\,pH = \log K_{2q} + (2+q)/2 \log[\overline{H_2R_2}]. \quad (8)$$

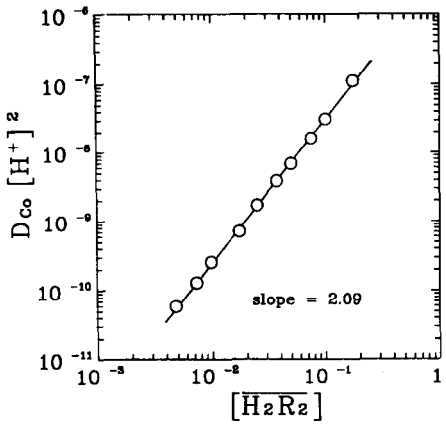

Fig. 3. Effect of HDEHP concentrations on the extraction equilibrium of cobalt between 0.5 kmol m^{-3} $(Na,H)SO_4$ and kerosene at 25°C. $[Co^{II}]_t = 0.0017$ kmol m^{-3}, slope = 2.09.

First, it could be assumed that only species of the type $\overline{CoR_2(HR)_q}$ are formed. Thus, a plot of $\log D_{Co}[H^+]^2$ vs $\log[\overline{H_2R_2}]$ would give a straight line with an intercept equal to K_{2q} and a slope equal to $(2+q)/2$.

Figure 3 shows the relationship between $D_{Co}[H^+]^2$ and $[\overline{H_2R_2}]$ for 0.5 kmol m^{-3} $(Na, H)SO_4$ and $[Co^{II}]_t = 0.0017$ kmol m^{-3} at 25°C. In Fig. 3, a straight line with a slope of 2.09 is obtained, i.e. $q = 2$. Thus, the species formed in the organic phase is $\overline{CoR_2(HR)_2}$. From Fig. 3, the intercept is -5.42, i.e. $K_{22} = 3.84 \times 10^{-6}$.

Reconfirmation of extraction equilibrium formation by slope analysis

Next, assuming two species are formed in the organic phase, e.g. $\overline{CoR_2(HR)_2}$ and $\overline{CoR_2(HR)_3}$, eq. (3) could be expressed as

$$D_{Co} = \frac{[\overline{CoR_2(HR)_2}] + [\overline{CoR_2(HR)_3}]}{[Co^{2+}]}. \quad (9)$$

Using eq. (6), eq. (9) becomes

$$D_{Co}[H^+]^2 = K_{22}[\overline{H_2R_2}]^2 + K_{23}[\overline{H_2R_2}]^{5/2} \quad (10)$$

or

$$\frac{D_{Co}[H^+]^2}{[\overline{H_2R_2}]^{5/2}} = K_{22}\frac{1}{[\overline{H_2R_2}]^{1/2}} + K_{23}. \quad (11)$$

Now, a plot of $D_{Co}[H^+]^2/[\overline{H_2R_2}]^{5/2}$ vs $[\overline{H_2R_2}]^{-1/2}$ would give a straight line with a slope equal to K_{22} and an intercept equal to K_{23}. Figure 4 shows the effect of HDEHP concentrations on the extraction equilibrium of cobalt between 0.5 kmol m^{-3} $(Na,H)SO_4$ and kerosene for $[Co^{II}] = 0.0017$ kmol m^{-3} at 25°C. In Fig. 4, a straight line with a

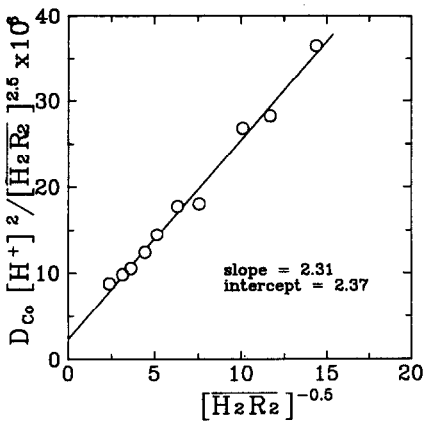

Fig. 4. Effect of HDEHP concentrations on the extraction equilibrium of cobalt between 0.5 kmol m^{-3} (Na,H)SO_4 and kerosene at 25°C. $[Co^{II}]_t = 0.0017$ kmol m^{-3}, slope = 2.31, intercept = 2.37.

slope of 2.31 and an intercept of 2.37 is obtained, i.e. $K_{22} = 2.31 \times 10^{-6}$ and $K_{23} = 2.37 \times 10^{-6}$ (kmol $m^{-3})^{-1/2}$.

Reconfirmation of extraction equilibrium formation by computer treatment

Numerical treatment of the data was performed by modifying the LETAGROP-DISTR program[17] in order to apply it to the five-component system in this work. The aim of these calculations was to confirm the results obtained with the previous graphic analysis and to refine the values of the equilibrium constants.

In this calculation, the computer searches for the best set of equilibrium constants that would minimize the error squares sum defined by

$$U = \sum (\log D_{calc} - \log D_{exp})^2 \qquad (12)$$

where D_{exp} is the distribution ratio of cobalt measured experimentally and D_{calc} is the corresponding value calculated by the program obtained by solving the mass balance equations for Co^{2+}, H_2R_2, SO_4^{2-}, Na^+, using a given set of complexes and their equilibrium constants. The optimal model is the one which minimizes the error squares sum function and gives the lowest mean standard deviation $\sigma(\log D)$, defined by

$$\sigma(\log D) = (U/Np)^{1/2} \qquad (13)$$

where Np is the degree of freedom, approximately equal to the number of data points.

The equilibrium constants for the different HDEHP species between 0.5 kmol m^{-3} (Na,H)SO_4 and kerosene system used in the present work are given from Huang and Juang[4] and shown in Table 1. Table 2 summarizes the results obtained with some of the models tried.

Table 1. Equilibrium constants for the different HDEHP species in the 0.5 kmol m^{-3} (Na,H)SO_4/HDEHP–kerosene system[4]

Reaction	Constant
$HR \rightleftharpoons R^- + H^+$	$pK_a = 1.27 \pm 0.03$
$HR \rightleftharpoons \overline{HR}$	$\log K_d = 3.54 \pm 0.02$
$2\overline{HR} \rightleftharpoons \overline{H_2R_2}$	$\log K_2 = 4.42 \pm 0.04$

Figure 5 presents the plot of U_{min} vs q for models I–VII given in Table 2; the optimal q values are between 2 and 3. And then, two species formed in organic phase (models VIII–XV) were tried, the result showed the optimal one turns out to be the set of species (p,q) equal to (2,2) and (2,3). Furthermore, several more than two species calculations were carried out to investigate the possibility of finding other complexes which could improve the fit of the experimental data (summarized as models XVI and XVII). From Table 2, the optimal fit for sulphate systems was obtained when the species were the same as those suggested by the graphic treatment, i.e. $\overline{CoR_2(HR)_2}$ and $\overline{CoR_2(HR)_3}$ with $\log K_{22} = -5.56 \pm 0.04$ and $\log K_{23} = -5.65\,\max - 5.37$.

The experimental data for the above numerical calculation are given in Figs 1, 2 and 3. The mass balance equation for H_2R_2 in the optimal model is given by

$$[\overline{H_2R_2}]_t = [\overline{H_2R_2}] + 1/2K_2^{-1/2}[\overline{H_2R_2}]^{1/2} + 2K_{22}[Co^{2+}][\overline{H_2R_2}]^2[H^+]^{-2} + 5/2K_{23}[Co^{2+}][\overline{H_2R_2}]^{5/2}[H^+]^{-2}. \qquad (14)$$

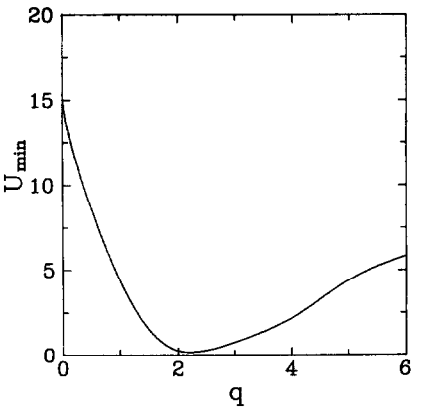

Fig. 5. Variation of U_{min} with number of free monomeric HDEHP involved in the extracted species. (Table 2 models I–VII.)

Table 2. Results of the numerical calculation for the various model species, $\overline{CoR_p(HR)_q}$

Model	Species (p,q)	$\log K_{pq}$	U_{min}	$\sigma(\log D)$
I	(2,0)	-7.39 ± 0.16^a	15.4	0.457
II	(2,1)	-6.45 ± 0.09	4.42	0.244
III	(2,2)	-5.52 ± 0.02	0.267	0.060
IV	(2,3)	-4.58 ± 0.07	2.76	0.193
V	(2,4)	-3.63 ± 0.14	11.4	0.393
VI	(2,5)	-2.67 ± 0.21	25.7	0.589
VII	(2,6)	-1.71 max -1.49^b	44.9	0.779
VIII	(2,2), (2,0)*		0.267	0.060
IX	(2,2), (2,1)*		0.267	0.060
X	(2,2)	-5.56 ± 0.04	0.228	0.056
	(2,3)	-5.65 max -5.37		
XI	(2,2)	-5.53 ± 0.03	0.235	0.057
	(2,4)	-5.29 max -4.98		
XII	(2,2)	-5.53 ± 0.02	0.240	0.057
	(2,5)	-4.88 max -4.55		
XIII	(2,2)	-5.52 ± 0.02	0.243	0.058
	(2,6)	-4.47 max -4.12		
XIV	(2,3), (2,4)*		2.76	0.195
XV	(2,3), (2,5)*		2.76	0.196
XVI	(2,2), (2,3), (2,4)*		0.228	0.056
XVII	(2,0)*, (2,1)*, (2,2), (2,3), (2,4)*, (2,5)*, (2,6)*		0.228	0.058

* Rejected species.

[a] The error given corresponds to $3\cdot\delta(\log K)$.

[b] The value after max corresponds to $\log[K+3\sigma(K)]$.

Complexation of cobalt in sulphate solutions

In the sulphate medium, the equilibrium constants obtained are a sort of "conditional" constant, since cobalt is complexed by sulphate ions. Considering also the species SO_4^{2-}, eq. (9) should be written as follows:

$$D_{Co} = \frac{K_{22}[\overline{H_2R_2}]^2[H^+]^{-2} + K_{23}[\overline{H_2R_2}]^{5/2}[H^+]^{-2}}{1+\beta_1[SO_4^{2-}]} \tag{15}$$

where the stability constant of $CoSO_4$ is defined by

$$\beta_1 = \frac{[CoSO_4]}{[Co^{2+}][SO_4^{2-}]}. \tag{16}$$

$[SO_4^{2-}]$ can be calculated from the mass balance expression for the sulphate concentration as given by eq. (17)

$$[SO_4^{2-}]_t = [SO_4^{2-}]+[CoSO_4] + \beta_2[Na^+][SO_4^{2-}]+\beta_3[H^+][SO_4^{2-}] \tag{17}$$

where β_2 and β_3 are the stability constants of $NaSO_4^-$ and HSO_4^-, respectively, defined by

$$\beta_2 = \frac{[NaSO_4^-]}{[Na^+][SO_4^{2-}]} \tag{18}$$

and

$$\beta_3 = \frac{[HSO_4^-]}{[H^+][SO_4^{2-}]}. \tag{19}$$

The values of $\log\beta_1$, $\log\beta_2$ and $\log\beta_3$ were taken to be 2.4, 1.06 and 1.99 at zero ionic strength.[18] Table 3 summarizes the results of the graphic and computer calculations. However, in the 0.5 kmol m^{-3} $(Na^+, H^+, Co^{2+})SO_4^{2-}$ system, the ionic strength is not zero. Therefore, for minimizing error square sum calculations, the best log values of K_{23}, K_{24}, β_1, β_2 and β_3 were obtained and shown in Table 3.

The published values for the equilibrium constants are compiled in Table 4.

Figure 6 represents the distribution diagram of Co^{II} as a function of the total HDEHP concentration at various total concentrations of cobalt and pH values. It is worth noting the increasing predominance of the $\overline{CoR_2(HR)_2}$ species as the total concentration of HDEHP is increased.

Table 3. Equilibrium constants for species $\overline{CoR_2(HR)_2}$ and $\overline{CoR_2(HR)_3}$ calculated by different methods for sulphate solutions

Method of calculation	$\log K_{22}$	$\log K_{23}$
Conditional constants		
Graphic	−5.64	−5.63
Numerical	−5.56±0.04	−5.65 max −5.37
Corrected for $CoSO_4$ complexation at zero ion strength[a]		
Numerical	−4.31±0.04	−4.23 max −4.16
Corrected for $CoSO_4$ complexation at 0.5 kmol m^{-3} $(Na,H)SO_4$ solutions[b]		
Numerical	−4.67±0.13	−4.98 max −4.59

[a] $\log\beta_1 = 2.4$, $\log\beta_2 = 1.06$ and $\log\beta_3 = 1.99$ obtained from Morel.[18]

[b] The optimal values of stability constants from calculation were $\log\beta_1 = 2.01\pm0.20$,[c] $\log\beta_2 = 1.06\pm0.19$ and $\log\beta_3 = 1.79$ max 3.00.

[c] The value after max corresponds to $\log[K+3\sigma(K)]$ and the error given corresponds to $3\cdot\sigma(\log K)$.

CONCLUSION

For the sulphate system, the cobalt distribution data could be best explained by assuming the formations of two species: $\overline{CoR_2(HR)_2}$ and $\overline{CoR_2(HR)_3}$. Graphic and computer modelling of the data excluded the existence of the species $\overline{CoR_2}$. It could also be established that the existence of these two species together gives the best fit for the distribution data, whereas the assumption that either of them exists alone gives a considerably worse fit.

Grimm and Kolařík[10] and Komasawa *et al.*[11] also reported the existence of the $\overline{CoR_2(HR)_2}$ we identified, although the aqueous phase contained nitrate solutions. However, in the sulphate solutions, $\overline{CoR_2(HR)_3}$ existed at the same time from the above graphic and numerical analysis.

On the other hand, the numerical values of the "conditional" equilibrium constants determined for these two species depend on the composition of the aqueous phase. This is due to the possible complexation of cobalt in the aqueous phase. In this work, we adopted two approaches for considering the existence of $CoSO_4$, $NaSO_4^-$ and HSO_4^- complexations. In the first approach, computer calculations on all sulphate system data were performed by introducing the values of the stability constants of the sulphates in the literatures. In the second approach, the equilibrium constants of Co–

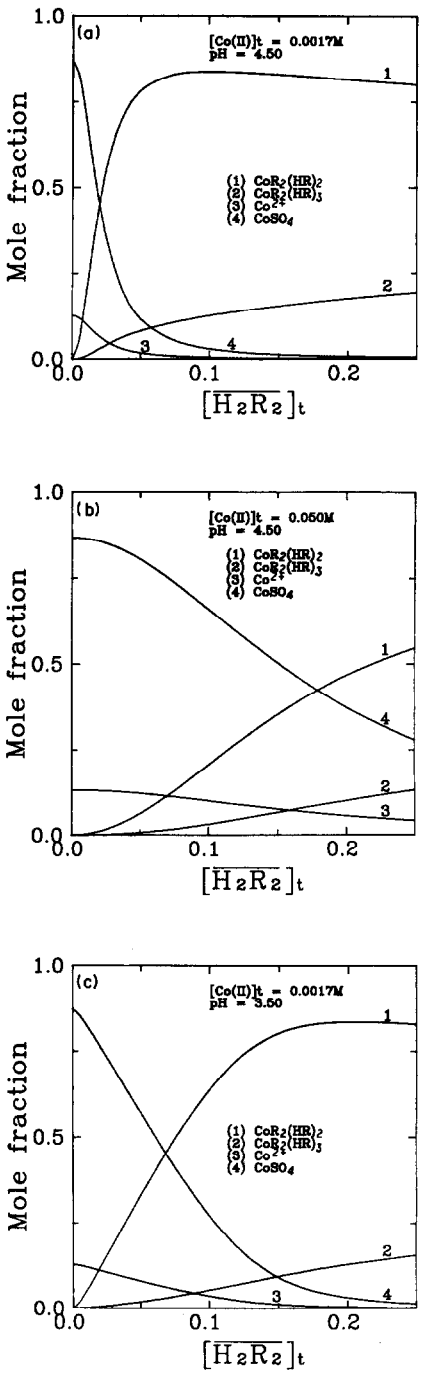

Fig. 6. Cobalt distribution diagrams as a function of the total HDEHP concentration at two different total concentrations of cobalt and two different pH values. Lines 1, 2, 3 and 4 represent $\overline{CoR_2(HR)_2}$, $\overline{CoR_2(HR)_3}$, Co^{2+} and $CoSO_4$, respectively. (a) $[Co^{II}]_t = 0.0017$ kmol m^{-3}, pH = 4.50; (b) $[Co^{II}]_t = 0.05$ kmol m^{-3}, pH = 4.50; (c) $[Co^{II}]_t = 0.0017$ kmol m^{-3}, pH = 3.50.

HDEHP complexes and sulphates were calculated at the same time. New values of K_{22}, K_{23}, β_1, β_2 and β_3 were calculated and are given in Table 3. As can be seen in Table 4, the value of K_{22} obtained agrees

Table 4. The equilibrium constants for $CoR_p(HR)_q$ extracted by HDEHP found in the literature

Aqueous phase	Temperature (°C)	Diluent	$\log K_{pq}$ (2,2)	$\log K_{pq}$ (2,3)	References
0.5 M (Na,H)SO_4	25±0.2	Kerosene	−4.67±0.13	−4.98 *max* −4.59	This work
1.0 M (Na,H)NO_3	—	*n*-Dodecane	−4.41		10
0.5 M (Na,H)NO_3	25±0.2	*n*-Heptane	−4.40		11
No medium	25±0.2	*n*-Heptane	−4.22		11
0.5 M (Na,H)NO_3	25±0.2	Toluene or benzene	−5.35		11
No medium	25±0.2	Toluene or benzene	−5.19		11
(Na,H)NO_3	—	2-Ethylhexyl alcohol	−4.59		13
(Na,H)NO_3	—	Isodecanol	−3.89		13
(Na,H)NO_3	—	Nitrobenzene	−5.20		13
(Na,H)NO_3	—	Ether	−5.13		13

well with those obtained for the nitrate systems and aliphatic diluents. It is worth mentioning that some other models were tested and the optimal fit remained the same as that obtained by assuming the same species (p,q) equal to (2,2) and (2,3).

Acknowledgements—This work was performed under the auspices of the National Science Council of the Republic of China, under contract number NSC76-0402-E006-04, to which the authors wish to express their thanks.

REFERENCES

1. T. Sekine and Y. Hasegawa, *Solvent Extraction Chemistry: Fundamentals and Applications*, Ch. 7. Marcel Dekker, New York (1977).
2. G. M. Ritcey and A. W. Ashbrook, *Solvent Extraction: Principles and Applications to Process Metallurgy*, Part II. Elsevier, Amsterdam (1984).
3. T. C. Huang and R. S. Juang, *Hydrometall. Symp.* 1985, 79.
4. T. C. Huang and R. S. Juang, *Ind. Eng. Chem. Fundam.* 1986, **25**, 752.
5. T. C. Huang and R. S. Juang, *J. Chem. Eng. Japan* 1986, **19**, 379.
6. C. T. Huang and T. C. Huang, *Solvent Extr. Ion Exch.* 1987, **5**, 611.
7. T. C. Huang and C. T. Huang, *Ind. Eng. Chem. Res.* 1988, **27**, 1675.
8. D. C. Madigan, *Aust. J. Chem.* 1960, **13**, 58.
9. M. L. Brisk and W. J. McManamey, *J. Appl. Chem.* 1969, **19**, 103.
10. R. Grimm and Z. Kolařík, *J. Inorg. Nucl. Chem.* 1974, **36**, 189.
11. I. Komasawa, T. Otake and Y. Higaki, *J. Inorg. Nucl. Chem.* 1981, **43**, 3351.
12. T. Sato and T. Nakamura, *J. Inorg. Nucl. Chem.* 1972, **34**, 3721.
13. I. Komasawa, T. Otake and Y. Ogawa, *J. Chem. Eng. Japan* 1984, **17**, 410.
14. W. J. McDowell, P. T. Perdue and G. N. Case, *J. Inorg. Nucl. Chem.* 1976, **38**, 2127.
15. T. Sato, *J. Inorg. Nucl. Chem.* 1965, **27**, 1395.
16. Z. Kolařík and R. Grimm, *J. Inorg. Nucl. Chem.* 1976, **38**, 1721.
17. D. H. Liem, *Acta Chem. Scand.* 1971, **25**, 1521.
18. F. M. M. Morel, *Principles of Aquatic Chemistry*. Wiley-Interscience, New York (1983).

Polyhedron Vol. 9, No. 9, pp. 1155–1164, 1990
Printed in Great Britain

0277–5387/90 $3.00+.00
© 1990 Pergamon Press plc

SYNTHESIS, CHARACTERIZATION AND CRYSTAL STRUCTURE OF COPPER(I) THIOLATES: $[(C_6H_5)_4P^+]_2[Cu_4(C_2H_5S^-)_6]\cdot 0.5C_2H_6O_2$ AND $[(C_6H_5)_4P^+][Cu_7(C_2H_5S^-)_8]$

MARKUS BAUMGARTNER, HELMUT SCHMALLE and ERICH DUBLER*

Institute of Inorganic Chemistry, University of Zürich, Winterthurerstrasse 190, CH-8057 Zürich, Switzerland

(*Received* 20 *October* 1989; *accepted* 8 *December* 1989)

Abstract—The reaction of the monodentate ligand thioethane with $(C_6H_5)_4PBr$ and Cu_2O in organic solvents results in the crystallization of two new homoleptic polynuclear copper(I) thiolates: $[(C_6H_5)_4P^+]_2[Cu_4(C_2H_5S^-)_6]\cdot 0.5C_2H_6O_2$ (**1**) and $[(C_6H_5)_4P^+][Cu_7(C_2H_5S^-)_8]$ (**2**). Both compounds have been characterized by X-ray crystallography, thermal analysis, luminescence spectroscopy and IR spectroscopy. Compound **1** is triclinic, space group $P\bar{1}$ with $a = 12.066(5)$, $b = 13.824(5)$, $c = 19.112(3)$ Å, $\alpha = 90.82(2)$, $\beta = 101.85(2)$, $\gamma = 93.53(3)°$ and $Z = 2$. Compound **2** is monoclinic, space group $P2_1/c$ with $a = 19.208(3)$, $b = 16.975(4)$, $c = 16.394(6)$ Å, $\beta = 108.68(2)°$ and $Z = 4$. The structure of **1** is built up by $[(Cu_4(RS^-)_6)^{2-}]$ adamantane-type cluster units, separated by $[(C_6H_5)_4P^+]$ cations. Compound **2** consists of copper(I) thiolate chains, also separated by $[(C_6H_5)_4P^+]$ cations. In **2**, structural units of the stoichiometry $Cu_7(C_2H_5S^-)_{10}$ are connected by common sharing of four sulphur atoms, leading to a chain of the stoichiometry $Cu_7(C_2H_5S^-)_8$. The shortest Cu—Cu distance is 2.692(1) Å in **1** and 2.736(2) Å in **2**. Excitation at 450 nm of **1** in the solid state results in a weak emission at 665 nm, compound **2** exhibits in the solid state an intense luminescence at 591 nm upon excitation at 365 nm.

The coordination chemistry of thiolates, a fundamental ligand type in transition metal chemistry,[1,2] is of much current interest in view of forming appropriate model compounds of active sites in metalloproteins.

We are interested in crystallizing metal-rich copper(I) thiolates as model compounds of copper(I) thioneins. Metallothioneins (MT) are believed to play a role in the metabolism and in the detoxification of a number of essential and non-essential trace metals in animals and plants, mainly of the metals zinc, cadmium, mercury and copper.[3] They are characterized by an unusually high cysteinate content of the peptide and a metal-to-cysteinate ratio of 1:3 for Zn– and Cd–MT. In copper(I) thioneins, the metal content found is even higher. In the case of only copper(I)-containing MTs, cluster core types of the stoichiometries Cu_6S_9 and Cu_8S_{12} are often suggested.[4,5] A copper-to-sulphur ratio of 2:3 seems to be a characteristic feature of Cu^I–MTs as well as of synthetic polynuclear copper(I) complexes with mono- or bidentate thiolates.[6,7] The MT with the highest metal content is a fungal MT found in *Neurospora crassa* with a copper(I)-to-cysteinate ratio of 6:7.[8] Syntheses of copper(I) thiolates with *mono*dentate ligands RS^- revealed species that contain core units of the stoichiometries Cu_4S_6 ($R = C_6H_5, CH_3$), Cu_5S_6 ($R = (CH_3)_3C$) and Cu_5S_7 ($R = C_6H_5$).[9] The most favoured Cu_4S_6 "adamantane" type can also be obtained with *bi*dentate ligands ($^-SRS^-$) like 1,2-dithioethane, 1,3-dithiopropane or *o*-xylene-α-α′-dithiol.[10,11] In addition, the formation of core units of the type Cu_3S_6, Cu_8S_{12} and $Cu_{10}S_{16}$ has been observed with bidentate dithiol ligands.[12–14] Our syntheses using the monodentate ligand thioethane (TE) revealed two new homoleptic polynuclear copper(I) thiolates: One with the well-known adamantane-type Cu_4S_6 cluster, the other with a non-molecular one-dimensional Cu_7S_8 chain structure. In both structures, all the copper atoms are trigonally coordinated by

* Author to whom correspondence should be addressed.

bridging thiolates. We report here on synthesis, structure, spectroscopical and thermoanalytical data of these new copper(I) thiolates.

EXPERIMENTAL

Syntheses and thermal analysis

Thioethane (TE), $(Ph)_4PBr$ and Cu_2O were purchased from Fluka AG, Buchs/Switzerland and used without further purification. The 1 M solution of NaOMe was obtained by adding 23.0 g (1 mol) of sodium to 1000 cm^3 of methanol, stirred on an ice bath. The syntheses were performed in a Schlenk-type apparatus in a nitrogen atmosphere. Thermogravimetric (TG) data in the temperature range 30–700°C were recorded in a flowing N_2-atmosphere, using heating rates of 10°C min^{-1} and sample weights of 4–15 mg on a Perkin–Elmer TGS-2 thermobalance. X-ray powder diffraction diagrams of the final products were produced by a Guinier-type camera with a Johansson monochromator (Cu-$K_{\alpha 1}$ radiation).

$[(C_6H_5)_4P^+]_2[Cu_4(TE^-)_6]\cdot 0.5C_2H_6O_2$ (**1**)

To a solution of 3.34 g (7.8 mmol) of $(Ph)_4PBr$ in ethylene glycol (20 cm^3), MeOH (33 cm^3) and 1 M NaOMe/MeOH (7 cm^3), 1.05 g (16.9 mmol) of TE was added. After warming up to a reaction temperature of 55°C and addition of 400 mg (2.8 mmol) of Cu_2O, a clear yellow solution was obtained. Slow evaporation at room temperature first yielded dark red bulky crystals of **1**. Later on, yellow crystals of compound **2** could also be isolated from the same solution. The red crystals of **1** were separated manually. Found: C, 54.2; H, 5.6; Cu, 20.1 (TG analysis); S, 15.1. Calc. for $C_{61}H_{73}Cu_4OP_2S_6$ (1330.8): C, 55.1; H, 5.5; Cu, 19.1; S, 14.5%.

$[(C_6H_5)_4P^+][Cu_7(TE^-)_8]$ (**2**)

To a solution of 2.5 g (6.0 mmol) of $(Ph)_4PBr$ in ethylene glycol (20 cm^3), MeOH (33 cm^3) and 1 M NaOMe/MeOH (8 cm^3), 1.11 g (17.9 mmol) of TE was added. After addition of 400 mg (2.8 mmol) of Cu_2O, the solution was kept at 60°C for 30 min until it became clear yellow. Slow evaporation at room temperature yielded yellow crystals of **2**. Found: C, 37.7; H, 4.9; Cu, 34.6 (TG analysis). Calc. for $C_{40}H_{60}Cu_7PS_8$ (1273.8): C, 37.7; H, 4.7; Cu, 34.9%.

X-ray crystallography

Symmetry, preliminary cell parameters and space groups of the complexes investigated were established by precession and Weissenberg photography. Final lattice parameters and crystal orientations were obtained from least-squares refinement of the θ values of 25 reflections on an Enraf–Nonius CAD-4 diffractometer.

Intensity data were collected by using graphite-monochromated Mo-K_α radiation. Four standard reflections lying in different regions of the reciprocal space were monitored periodically. A total loss in intensity of −2.3% (**1**) and −1.3% (**2**) was observed and corrected for in data reduction. The intensities were reduced to F_o by applying corrections for Lorentz and polarization effects. A numerical absorption correction based on carefully indexed crystal faces was carried out for both compounds.

The structure of **1** was solved by using the Patterson interpretation routine in SHELXS-86[15] and by conventional Fourier techniques, and refined with full-matrix least-squares methods including anisotropic temperature factors for copper, sulphur, phosphorus and the carbon atoms of the ligands. The phenyl rings were refined as rigid groups with free varying isotropic temperature factors. The atoms of the inserted solvent molecule were also treated with isotropic temperature factors. Due to a disordered arrangement of the terminal carbon atom C(22), the C(21)—C(22) distance was treated with a constrained length in the refinement. The positions of the hydrogen atoms of the phenyl rings and of the ligand molecules were calculated, and the hydrogen atoms were included as fixed contributions in the refinement.

The structure of **2** could be solved with direct methods using 937 negative quartets in SHELXS-86. For the structure refinement of **2** (full-matrix least-squares methods including anisotropic temperature factors for copper, sulphur, phosphorus and the carbon atoms of the ligands) it was not necessary to fix the phenyl ring atoms. These carbon atoms were used with free varying isotropic temperature factors. Due to a disordered arrangement, some of the terminal carbon atoms [C(52), C(62), C(72), C(82)] of the thiolate ligands were treated with a constrained bond length to the adjacent carbon atom in the refinement. The position of all the hydrogen atoms was calculated and the hydrogen atoms included as fixed contributions in the refinement.

The structure of **1** was finally refined with unit weights. The weighting scheme for **2** was $w = 1.0/\sigma^2(F)$. Interatomic distances and angles have

been calculated with the ORFFE3 program.[16] The calculations were performed with the programs SHELXS-86 and SHELX-76[17] on an IBM 3033 and a NAS AS/XL V60 computer at the University of Zürich. Crystal parameters, data collection details, and results of the refinements are summarized in Table 1.

Atomic coordinates and thermal parameters for the two structures have been deposited with the Editor as supplementary material, from whom copies are available on request.

Luminescence spectroscopy

Emission spectra were recorded on a Perkin–Elmer Model 204 fluorescence spectrophotometer using a Xenon lamp as exciting source. Powder samples were fixed on a quartz plate with a non-fluorescing glue.

IR spectroscopy

Solid-state IR spectra in the range 400–180 cm^{-1} were obtained on a Perkin–Elmer spectrophotometer type 983. Spectra were run on Nujol mulls between CsI or polyethylene plates.

RESULTS AND DISCUSSION

The structures of $[(C_6H_5)_4P^+]_2[Cu_4(C_2H_5S^-)_6]\cdot 0.5C_2H_6O_2$ **(1)** *and* $[(C_6H_5)_4P^+][Cu_7(C_2H_5S^-)_8]$ **(2)**

The structure of **1** is built up by $[(Cu_4S_6)^{2-}]$ adamantane-type cluster units, separated by bulky $[(C_6H_5)_4P^+]$ cations, as shown in Fig. 1. The structure of the cluster anion can be considered as a tetrahedron of copper atoms inscribed in a distorted octahedron formed by six μ_2-sulphur atoms (Fig. 2). This cluster type is very common for copper(I) thiolates.[1,2,9] The Cu—Cu distances range from 2.692(1) to 2.780(1) Å, with a mean distance of

Table 1. Crystal data and structure determination parameters for **1** and **2**

	1	**2**
Formula	$C_{61}H_{73}Cu_4OP_2S_6$	$C_{40}H_{60}Cu_7PS_8$
Mol. wt	1330.8	1273.8
Data crystal (mm)	0.52 × 0.50 × 0.65	0.18 × 0.22 × 0.55
Colour	Orange–red	Yellow, transparent
a (Å)	12.066(5)	19.208(3)
b (Å)	13.824(5)	16.975(4)
c (Å)	19.112(3)	16.394(6)
α (°)	90.82(2)	90.0
β (°)	101.85(2)	108.68(2)
γ (°)	93.53(3)	90.0
V (Å^3)	3112.9	5063.8
Crystal system	Triclinic	Monoclinic
Z	2	4
d_{calc} (g cm^{-3})	1.42	1.68
Space group	$P\bar{1}$	$P2_1/c$
Scan method	ω–2θ	ω–2θ
2θ range (°)	2.0–52.0	2.0–50.0
hkl range	±14, ±17, +23	+22, +20, ±19
Max time/rfln (s)	30	30
μ(Mo-K_α) (cm^{-1})	15.66	31.62
Transmission factors (max/min)	0.514/0.363	0.621/0.492
Data measured (incl. stds.)	11,934	9645
R_{av}/ No. of refln av.	0.027/614	0.024/1274
Unique data	11,499	8884
Observed data [$I \geqslant 3\sigma(I)$]	6976	3538
Number of variables	321	385
Max/min $\Delta\rho$ (e^3/Å^3)	1.01/−0.71	0.71/−0.53
R	0.065	0.054
R_w	0.068	0.049
Weight	w = 1 (unit weight)	$w = 1/\sigma^2(F_o)$

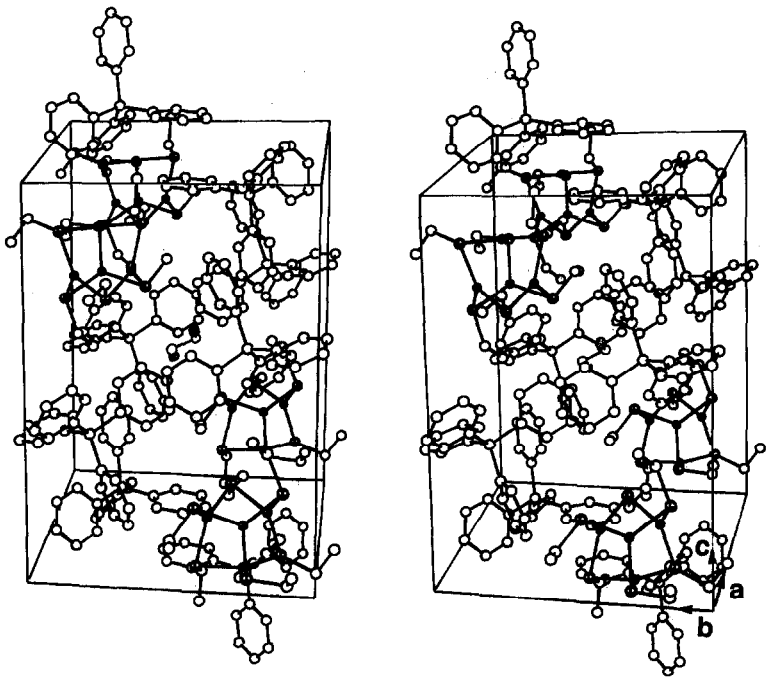

Fig. 1. Stereoview of the unit cell of **1**.

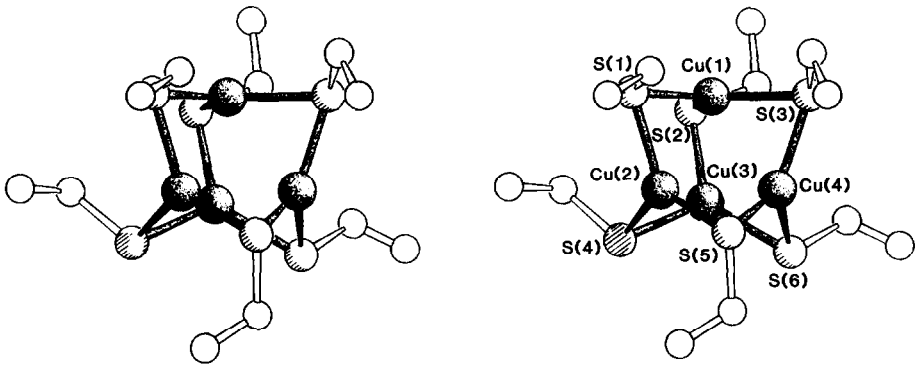

Fig. 2. Stereoview of the adamantane-type $[(Cu_4(TE^-)_6)^{2-}]$ cluster anion in **1**.

2.725 Å. The 12 crystallographically-independent Cu—S distances range from 2.248(3) to 2.309(3) Å, with a mean distance of 2.281 Å (Table 2). Five of the six Cu—S—Cu angles range from 72.6(1) to 73.8(1)°, whereas an increased angle of 75.1(1)° is observed at the sixth sulphur atom as a consequence of a hydrogen bond linking this sulphur atom to the solvate molecule.

The two $[(Cu_4S_6)^{2-}]$ clusters within the unit cell are linked by two hydrogen bonds of the type S···H—O to the ethylene glycol solvate molecule at the inversion centre in the middle of the cell. The corresponding S(4)···O acceptor–donor distance is 3.170(7) Å. The hydrogen atom of the hydroxy group of the inserted solvate molecule could be located in a difference Fourier map. The resulting distances, O—H of 1.05 Å (with a C—O—H angle of 108.1°) and S···H of 2.27 Å, are within the range found for solvate molecules linked to metal coordinating thiolates.[18,19] The O—H···S angle of 142.4° is comparable with values found in a neutron diffraction study.[20]

The structure of **2** consists of copper(I) thiolate chains parallel to the *c*-axis (see Figs 3 and 4) separated by bulky $[(C_6H_5)_4P^+]$ cations. The shortest Cu—Cu distance within the chain is 2.736(2) Å. Structural units of the stoichiometry $Cu_7(TE^-)_{10}$ are connected by common sharing of four sulphur atoms, leading to a chain of the overall stoichiometry $Cu_7(TE^-)_8$. Adjacent units within the chain are generated by a glide-plane operation. This structure type is unique within copper(I) thiolates,

Table 2. Cu—Cu distances (Å) and Cu—S bond lengths (Å) in **1** and **2**

1		**2**		**2**	
Cu(1)—S(1)	2.253(3)	Cu(1)—S(3)	2.280(4)	Cu(1)—Cu(2)	2.802(2)
Cu(1)—S(2)	2.295(3)	Cu(1)—S(4)	2.219(4)	Cu(1)—Cu(3)	4.243(3)
Cu(1)—S(3)	2.306(3)	Cu(1)—S(5)	2.304(4)	Cu(1)—Cu(4)	2.758(2)
Cu(2)—S(1)	2.292(3)	Cu(2)—S(1)	2.359(3)	Cu(1)—Cu(5)	4.066(3)
Cu(2)—S(4)	2.274(2)	Cu(2)—S(4)	2.236(4)	Cu(1)—Cu(6)	3.657(2)
Cu(2)—S(5)	2.271(2)	Cu(2)—S(6)	2.241(4)	Cu(2)—Cu(4)	2.761(3)
Cu(3)—S(2)	2.283(3)	Cu(3)—S(2)	2.273(4)	Cu(2)—Cu(5)	4.347(3)
Cu(3)—S(4)	2.287(2)	Cu(3)—S(3)	2.263(3)	Cu(2)—Cu(7)	3.028(2)
Cu(3)—S(6)	2.248(3)	Cu(3)—S(8)	2.247(4)	Cu(3)—Cu(4)	3.266(3)
Cu(4)—S(3)	2.257(3)	Cu(4)—S(1)	2.246(4)	Cu(3)—Cu(5)	2.736(2)
Cu(4)—S(5)	2.295(3)	Cu(4)—S(3)	2.267(4)	Cu(3)—Cu(6)	2.759(3)
Cu(4)—S(6)	2.309(3)	Cu(4)—S(7)	2.298(4)	Cu(3)—Cu(7)	4.032(2)
		Cu(5)—S(1)	2.286(4)	Cu(4)—Cu(5)	3.043(2)
		Cu(5)—S(2)	2.310(4)	Cu(4)—Cu(6)	3.969(3)
		Cu(5)—S(5)	2.270(4)	Cu(4)—Cu(7)	3.529(3)
Cu(1)—Cu(2)	2.692(1)	Cu(6)—S(5)	2.262(4)	Cu(5)—Cu(6)	2.813(2)
Cu(1)—Cu(3)	2.748(2)	Cu(6)—S(8)	2.228(4)	Cu(5)—Cu(7)	2.834(2)
Cu(1)—Cu(4)	2.701(2)	Cu(6)—S(7)	2.291(4)	Cu(6)—Cu(7)	3.129(3)
Cu(2)—Cu(3)	2.780(1)	Cu(7)—S(2)	2.310(4)		
Cu(2)—Cu(4)	2.712(1)	Cu(7)—S(6)	2.206(4)		
Cu(3)—Cu(4)	2.718(2)	Cu(7)—S(7)	2.284(4)		

and it can obviously only be realized with the ligand molecule ethanethiolate. On the one hand, the terminal C_2H_5 group of this ligand is able to separate and stabilize the well-known $[(Cu_4S_6)^{2-}]$ cluster found in **1**, on the other hand, this ligand seems to have an optimal size and flexibility to favour the building of the chain structure found in **2**. Using the smaller CH_3S^- molecule as a ligand, the adamantane-type $[(Cu_4S_6)^{2-}]$ is the only structure realized.[21] Syntheses with the more space-filling ligands 2-propanthiolate $[(CH_3)_2CH—S^-]$ or $^tBuS^-$ thiolate with copper(I) under the same reaction conditions always lead to the well-known $[Cu_5(RS^-)_6]$ cluster,[10,22] albeit several enlarged molecular clusters and one-dimensional chain structures are known with $^tBuS^-$ or with even more

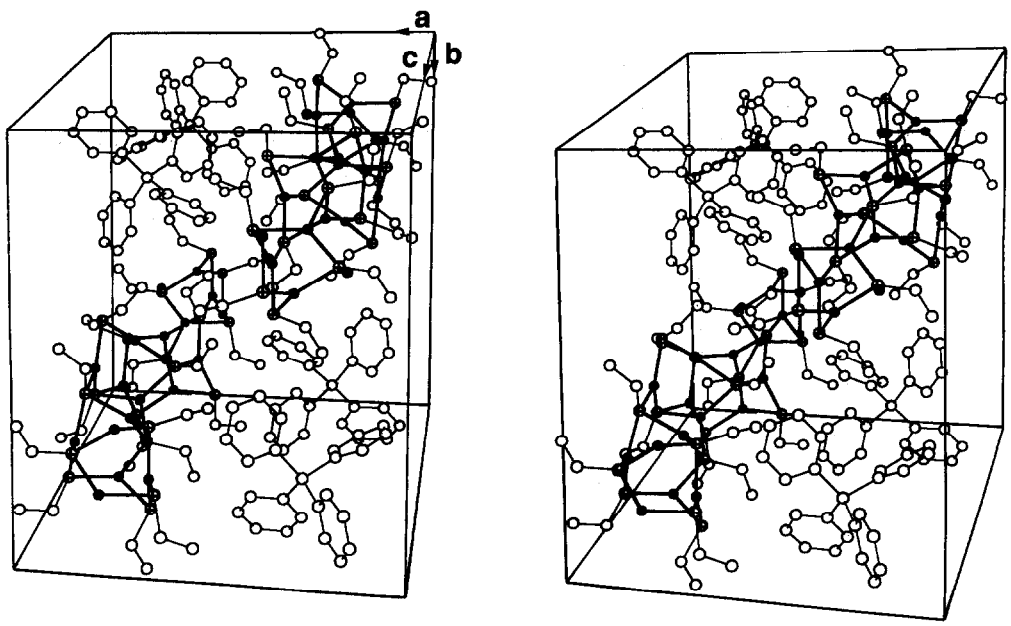

Fig. 3. Stereoview of the unit cell of **2**.

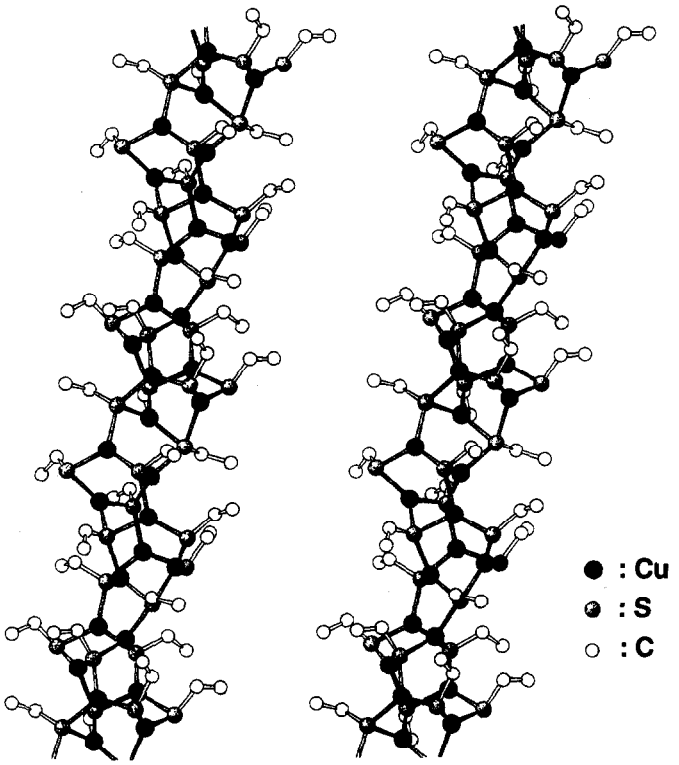

Fig. 4. Stereoview of the $[(Cu_7(TE^-)_8)]_\infty$ chain in **2**.

space-filling thiolates in the case of cadmium(II), silver(I) and other metals.[1,23]

The copper(I) thiolate chain in **2** exhibits two different types of thiolates, involving μ_2- and μ_3-bridging RS^- (see Fig. 5). The latter μ_3-$S(Cu)_3$ unit, exhibiting a RS^- bridging three copper atoms with an approximately tetrahedral C—$S(Cu)_3$ arrangement, is only rarely reported in pure copper(I) thiolates.[13,24] The mean value of all Cu—(μ_3-S)—Cu angles is 99.3°; the mean value of the corresponding angles around the μ_2-S atoms is 79.9°. The μ_2-S—Cu bond distances range from 2.206(4) to 2.247(4) Å, with a mean distance of 2.230 Å, whereas the μ_3-S—Cu bond distances range from 2.246(4) to 2.359(3) Å, with a mean distance of 2.287 Å (Table 2).

Using an alternative description of the structures of **1** and **2**, the CuS_3 group is regarded as a rigid triangle with the copper atoms located a little above or below the S_3 plane. The geometry of these triangles in both structures is determined by a set of three S—Cu—S angles which range from 102.9(1) to 137.3(2)°, with a mean value of 119.9°, and by three Cu—S distances ranging from 2.206(4) to

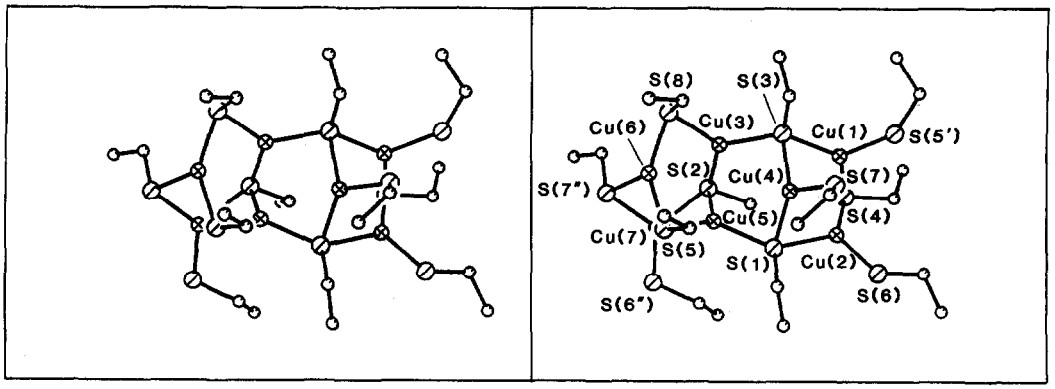

Fig. 5. Stereoview of a cut out of the $[(Cu_7(TE^-)_8)]_\infty$ chain in **2**, representing the coordination sphere around the copper atoms in the asymmetric unit.

Table 3. S—Cu—S coordination angles (°) and deviation (Å) of the Cu atoms from the corresponding S_3 planes in **1** and **2**

1	Angles	Deviation	2	Angles	Deviation
S(2)—Cu(1)—S(1)	114.4(1)		S(3)—Cu(1)—S(4)	122.8(1)	
S(3)—Cu(1)—S(1)	128.3(1)	0.045	S(3)—Cu(1)—S(5)	116.4(1)	0.031
S(3)—Cu(1)—S(2)	117.2(1)		S(4)—Cu(1)—S(5)	120.9(1)	
S(4)—Cu(2)—S(1)	113.6(1)		S(1)—Cu(2)—S(4)	120.0(1)	
S(5)—Cu(2)—S(1)	124.8(1)	0.067	S(1)—Cu(2)—S(6)	107.8(1)	0.092
S(5)—Cu(2)—S(4)	121.3(1)		S(4)—Cu(2)—S(6)	131.6(2)	
S(4)—Cu(3)—S(2)	110.5(1)		S(2)—Cu(3)—S(3)	116.2(1)	
S(6)—Cu(3)—S(2)	129.4(1)	0.085	S(2)—Cu(3)—S(8)	118.3(2)	0.048
S(6)—Cu(3)—S(4)	119.6(1)		S(3)—Cu(3)—S(8)	125.4(2)	
S(5)—Cu(4)—S(3)	127.6(1)		S(1)—Cu(4)—S(3)	126.2(1)	
S(6)—Cu(4)—S(3)	118.7(1)	0.043	S(1)—Cu(4)—S(7)	122.6(1)	0.213
S(6)—Cu(4)—S(5)	113.6(1)		S(3)—Cu(4)—S(7)	108.6(1)	
			S(1)—Cu(5)—S(2)	111.8(1)	
			S(1)—Cu(5)—S(5)	123.0(1)	0.008
			S(2)—Cu(5)—S(5)	125.3(1)	
			S(5)—Cu(6)—S(7)	102.9(1)	
			S(5)—Cu(6)—S(8)	137.3(2)	0.046
			S(7)—Cu(6)—S(8)	119.5(2)	
			S(2)—Cu(7)—S(6)	126.4(1)	
			S(2)—Cu(7)—S(7)	105.3(1)	0.051
			S(6)—Cu(7)—S(7)	127.8(1)	

2.359(3) Å, with a mean value of 2.274 Å (Tables 2 and 3). Table 3 summarizes the deviation of the copper atoms from the corresponding S_3 plane. Using this point of view, the structure of **1** is built up by four CuS_3 groups, each triangle being linked by corner-sharing to the three other triangles. All copper atoms in **1** are systematically displaced from the plane through the three sulphur atoms in a direction away from the centroid of the cage. The connection in structure **2** is similar with the restriction that three triangles instead of two only may be linked by corner-sharing (Fig. 6). The Cu_4S_6 structural entity of **1** can be found in an expanded form as a Cu_5S_8 substructure in **2**. The four-triangle polyhedron of the Cu_4S_6 core is modified by breaking the linkage of two corner-shared S_3 triangles and by insertion of an additional S_3 triangle. A similar transformation is observed in the formation of the M_5S_7 cage ($M = Ag^I$, Cu^I) from a M_4S_6 polyhedron by replacing a sulphur vertex by a linear S—Cu—S bridge.[23,25]

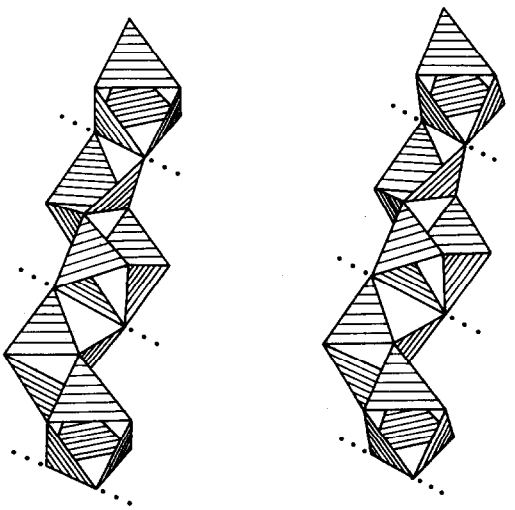

Fig. 6. Schematic stereoview of the $[(Cu_7(TE^-)_8)]_\infty$ chain in **2**. Each hatched triangle represents a CuS_3 unit with the sulphur atoms at the corner of the triangle and the copper(I) lying slightly above or below the S_3 plane. The structural units are separated by dotted lines.

A summary of interatomic bond distances and angles involving the μ_2- and μ_3-sulphur atoms in **1** and in **2** is given in Table 4.

In both structures, the geometry of the $[Ph_4P^+]$ cations as well as of the terminal C_2H_5 groups of the ligands shows no unusual features. The P—C distances range from 1.779(13) to 1.812(13) Å, and the C—P—C angles give no indication for a distinct distortion of the tetrahedral environment about the phosphorus atoms. The C—C bond lengths range

Table 4. Stereochemistry of the μ_2- and the μ_3-bridging thiolates

$[Ph_4P^+]_2[Cu_4(TE^-)_6]\cdot 0.5C_2H_6O_2$ (1)					
Ligand	Type	Cu—S—Cu (°)		Cu—S—C (°)	S—C (Å)
1	μ_2	Cu(1)—S(1)—Cu(2)	72.6(1)	112.4(4)	1.817(10)
				103.4(4)	
2	μ_2	Cu(1)—S(2)—Cu(3)	73.8(1)	103.8(3)	1.818(9)
				110.0(3)	
3	μ_2	Cu(1)—S(3)—Cu(4)	72.6(1)	105.7(4)	1.901(13)
				113.8(4)	
4	μ_2	Cu(2)—S(4)—Cu(3)	75.1(1)	104.4(3)	1.839(9)
				104.8(3)	
5	μ_2	Cu(2)—S(5)—Cu(4)	72.9(1)	107.1(3)	1.847(9)
				101.5(3)	
6	μ_2	Cu(3)—S(6)—Cu(4)	73.2(1)	107.0(4)	1.826(11)
				109.1(5)	
$[Ph_4P^+][Cu_7(TE^-)_8]$ (2)					
Ligand	Type	Cu—S—Cu (°)		Cu—S—C (°)	S—C (Å)
1	μ_3	Cu(2)—S(1)—Cu(4)	73.6(1)	106.6(4)	1.848(11)
		Cu(2)—S(1)—Cu(5)	138.7(2)	109.0(4)	
		Cu(4)—S(1)—Cu(5)	84.4(1)	113.6(4)	
2	μ_3	Cu(3)—S(2)—Cu(5)	73.3(1)	113.3(5)	1.817(13)
		Cu(3)—S(2)—Cu(7)	123.3(2)	100.6(5)	
		Cu(5)—S(2)—Cu(7)	75.7(1)	118.3(5)	
3	μ_3	Cu(1)—S(3)—Cu(3)	138.1(1)	110.2(4)	1.800(12)
		Cu(1)—S(3)—Cu(4)	74.7(1)	111.6(4)	
		Cu(3)—S(3)—Cu(4)	92.3(1)	107.9(5)	
4	μ_2	Cu(1)—S(4)—Cu(2)	77.9(1)	106.4(5)	1.812(12)
				108.1(5)	
5	μ_3	Cu(1)—S(5)—Cu(5)	125.4(2)	118.5(6)	1.804(15)
		Cu(1)—S(5)—Cu(6)	106.4(2)	103.9(6)	
		Cu(5)—S(5)—Cu(6)	76.7(1)	120.0(6)	
6	μ_2	Cu(2)—S(6)—Cu(7)	85.9(1)	109.2(6)	1.842(16)
				104.0(5)	
7	μ_3	Cu(4)—S(7)—Cu(6)	119.8(2)	129.1(5)	1.810(15)
		Cu(4)—S(7)—Cu(7)	100.8(1)	105.9(6)	
		Cu(6)—S(7)—Cu(7)	86.3(2)	108.2(7)	
8	μ_2	Cu(3)—S(8)—Cu(6)	76.1(1)	104.4(6)	1.760(19)
				106.6(8)	

from 1.407(16) to 1.482(16) Å, the S—C—C angles are between 108.0(10) and 115.9(14)°.

Thermal analytical results

Thermogravimetric investigations allow a characterization referring to the stoichiometry of the compounds investigated and to possible decomposition mechanisms. For different copper(I) thiolate clusters, the final product of the degradation is $Cu_{1.96}S$, as identified by X-ray powder diffraction. The patterns were in agreement with those reported in ref. 26 for a synthetic form of Chalcocite, $Cu_{1.96}S$.

The thermal decomposition of $[Ph_4P^+]_2[Cu_4(TE^-)_6]\cdot 0.5C_2H_6O_2$ (1) can be described as a two-step reaction. Within the first step in the range 100–180°C, the inserted solvate molecule is evolved. The second step, partly overlapping with the first one, involves the decomposition of the solvent free species $[Ph_4P^+]_2[Cu_4(TE^-)_6]$ and leads to the final product $Cu_{1.96}S$. Because this degradation is not dependent on the Cu^I—S score type,[9] the thermal decomposition of $[Ph_4P^+][Cu(TE^-)_8]$ (2) shows a pattern very similar with the second decomposition step of $[Ph_4P^+]_2[Cu_4(TE^-)_6]$. The thermal stability of copper(I) ethanethiolates is much smaller than those of copper(I) thiophenolates. The final decomposition temperatures of both compounds investigated are about 270°C, compared to 340–

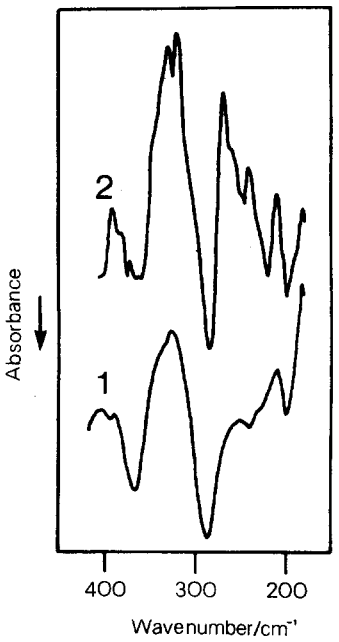

Fig. 7. IR spectra of **1** and **2**.

390°C for copper(I) thiophenolates decomposed under the same reaction conditions.

Spectroscopic results

Copper-containing metallothioneins have been found to exhibit significant luminescence which is related to the copper(I) thiolate chromophore.[27,28] Excitation of the *Neurospora crassa* Cu—MT at 305 nm leads to luminescence at 565 nm.[8] A similar luminescence in the visible region results in a maximum at 609 nm upon excitation of yeast Cu—MT with UV light.[7] This luminescence from copper(I)-containing species at room temperature in solution is highly unusual and is a further remainder of the remarkable coordination properties of MT.

Luminescence emission is well known for d^{10} systems, with most reports concerning solids. Investigations of the luminescence properties of copper(I) species showed that luminescence in the range 500–700 nm is related in solution as well as in the solid state, to the triplet–singlet emission observed for isolated Cu^+ ions.[29–32]

The colour and intensity of the emission of the two homoleptic copper(I) complexes, **1** and **2**, differ considerably. Excitation at 450 nm of **1** in the solid state at about −50°C results in a weak emission at 665 nm. Compound **2** exhibits in the solid state an intense luminescence at 591 nm upon excitation at 365 nm. This emission can be seen at room temperature by the naked eye whilst the luminescence appearance of **1** is only weak even at liquid nitrogen temperature. The intensities increase while cooling the samples. The emission spectra of both compounds are broad and structureless.

The IR spectra in the range 420–180 cm^{-1} of **1** and **2** are given in Fig. 7. The bands above 420 cm^{-1} can be assigned to internal vibrations of the thiolate ligand and of the $[Ph_4P^+]$ ion. The bands in the range given in Fig. 7 are expected to arise mainly from metal–ligand vibrations, e.g. copper–sulphur stretching, $\nu_{(Cu-S)}$.[33] The two spectra differ considerably. The spectrum of **2** (symmetry group of the Cu—S core: C_1) reveals at least two bands more than the spectrum of **1** (symmetry group of the Cu—S core: approximately T_d) (see Table 5). This difference could be a consequence of the different symmetries as well as of the different bridging types of sulphur atoms within the two structures.

Supplementary material including tables of observed and calculated structure factors and of anisotropic thermal parameters may be obtained on request from one of the authors (E.D.).

Table 5. IR spectra (400–180 cm^{-1}) of **1** and **2** at room temperature

Compound	Wavenumber (cm^{-1})
1	395(w), 368(m), 288(s), 240(w), 223(w,sh), 201(m)
2	383(w,sh), 376(w), 363(m), 326(w), 305(m,sh), 283(s), 244(w), 221(m), 198(m)

Acknowledgements—We thank Professor H. R. Oswald for supporting this project and Professor H. U. Güdel for helpful discussions concerning the luminescence investigation. Research grants from the Swiss National Science Foundation (No. 2000–5.422) are gratefully acknowledged.

REFERENCES

1. I. G. Dance, *Polyhedron* 1986, **5**, 1037.
2. P. J. Blower and J. R. Dilworth, *Coord. Chem. Rev.* 1987, **76**, 121.
3. J. H. R. Kägi and Y. Kojima, *2nd Int. Meet. Metallothionein, Zürich, Switzerland* (1985), Abstr. Book, p. 25.
4. K. B. Nielson, C. L. Atkin and D. R. Winge, *J. Biol. Chem.* 1985, **260**, 5342.
5. G. N. George, J. Byrd and D. R. Winge, *J. Biol. Chem.* 1988, **263**, 8199.
6. F. J. Hollander and D. Coucouvanis, *J. Am. Chem. Soc.* 1974, **96**, 5646.
7. J. Byrd, R. M. Berger, D. R. McMillin, C. F. Wright, D. Hamer and D. R. Winge, *J. Biol. Chem.* 1988, **263**, 6688.

8. M. Beltramini and K. Lerch, *Environ. Health Perspect.* 1986, **65**, 21, and refs therein.
9. M. Baumgartner, W. Bensch, P. Hug and E. Dubler, *Inorg. Chim. Acta* 1987, **136**, 139, and refs therein.
10. M. Baumgartner, H. Schmalle and E. Dubler, to be published.
11. G. Henkel, B. Krebs, P. Betz, H. Fietz and K. Saatkamp, *Angew. Chem.* 1988, **100**, 1373.
12. Ch. P. Rao, J. R. Dorfman and R. H. Holm, *Inorg. Chem.* 1986, **25**, 428.
13. R. K. Chadha, R. Kumar and D. G. Tuck, *Polyhedron* 1988, **7**, 1121.
14. D. Coucouvanis, D. Swenson, N. C. Baenziger, R. Pedelty, M. L. Caffery and S. Kanodia, *Inorg. Chem.* 1989, **28**, 2829.
15. G. M. Sheldrick, SHELXS-86. *Crystallographic Computing* (Edited by G. M. Sheldrick, C. Krüger and R. Goddard), p. 175. Oxford University Press, Oxford, U.K. (1985).
16. W. R. Busing, K. O. Martin, H. A. Levy, G. M. Brown, C. K. Johnson and W. A. Thiessen, ORFFE3—A Fortran Function and Error Program. Oak Ridge National Laboratory, Tennessee (1971).
17. G. M. Sheldrick, SHELX-76—Program for Crystal Structure Determination. University of Cambridge, Cambridge, U.K. (1976).
18. J. K. Money, J. C. Huffman and G. Christou, *Inorg. Chem.* 1985, **24**, 3297.
19. I. G. Dance, *J. Am. Chem. Soc.* 1980, **102**, 3445.
20. V. M. Padmanabhan, V. S. Yadava, Q. Q. Navarro, A. Garcia, K. Karsono, I-H. Suh and L. S. Chien, *Acta Cryst.* 1971, **27B**, 253.
21. I. G. Dance, G. A. Bowmaker, G. R. Clark and J. K. Seadon, *Polyhedron* 1983, **2**, 1031.
22. G. A. Bowmaker, G. R. Clark, J. K. Seadon and I. G. Dance, *Polyhedron* 1984, **3**, 535.
23. I. G. Dance, *Inorg. Chem.* 1981, **20**, 1487.
24. G. Henkel, P. Betz and B. Krebs, *XXIV Int. Conf. Coord. Chem., Athens, Greece* (1986), Abstr. Book, p. 737.
25. I. G. Dance, *Aust. J. Chem.* 1978, **31**, 2195.
26. *JCPDS, Powder Diffraction File*, Card No. 29-578, Swarthmore, Pa, U.S.A.
27. Z. Gasyna, A. Zelazowski, A. R. Green, E. Ough and M. J. Stillman, *Inorg. Chim. Acta* 1988, **153**, 115, and refs therein.
28. M. J. Stillman, A. J. Zelazowski, J. Szymanska and Z. Gasyna, *Inorg. Chim. Acta* 1989, **161**, 275.
29. P. A. Breddels, P. A. M. Berdowski, G. Blasse and D. R. McMillin, *J. Chem. Soc., Faraday Trans. II* 1982, **78**, 595.
30. A. Vogler and H. Kunkely, *J. Am. Chem. Soc.* 1986, **108**, 7211.
31. G. Blasse, P. A. Breddels and D. R. McMillin, *Chem. Phys. Lett.* 1984, **109**, 24.
32. S. A. Payne, L. L. Chase and L. A. Boatner, *J. Luminescence* 1986, **35**, 171.
33. A. J. Canty, R. Kishimoto, G. B. Deacon and G. J. Farquharson, *Inorg. Chim. Acta* 1976, **20**, 161.

Polyhedron Vol. 9, No. 9, pp. 1165–1173, 1990
Printed in Great Britain

0277–5387/90 $3.00+.00
© 1990 Pergamon Press plc

STRUCTURAL AND SPECTROSCOPIC STUDIES ON THE TRINUCLEAR CLUSTERS $Re_3Cl_9(PMe_3)_3$ AND $Re_3Cl_9(\eta^1\text{-dppm})_3$ (dppm = $Ph_2PCH_2PPh_2$)

SYLVIA M. V. ESJORNSON, PHILLIP E. FANWICK and RICHARD A. WALTON*

Department of Chemistry, Purdue University, West Lafayette, IN 47907, U.S.A.

(*Received* 10 *October* 1989; *accepted* 14 *December* 1989)

Abstract—The reactions of the trinuclear cluster Re_3Cl_9 with various phosphine ligands in ethanol have been used to prepare the new complexes $Re_3Cl_9(PMe_2Ph)_3$, $Re_3Cl_9(\eta^1\text{-dppm})_3$, $Re_3Cl_9(dmpm)_{1.5}$, $Re_3Cl_9(\eta^1\text{-arphos})_3$ and $Re_3Cl_9(arphos)_{1.5}$, where dppm = $Ph_2PCH_2PPh_2$, dmpm = $Me_2PCH_2PMe_2$ and arphos = $Ph_2PCH_2CH_2AsPh_2$. The ^1H and $^{31}P\{^1H\}$ NMR spectra of several of these complexes and of $Re_3Cl_9(PMe_3)_3$ and $Re_3Cl_9(PMePh_2)_3$ are described, including studies of the dissociative ligand exchange in $Re_3Cl_9(\eta^1\text{-dppm})_3$. The structures of $Re_3Cl_9(PMe_3)_3$ and $Re_3Cl_9(\eta^1\text{-dppm})_3$ have been established by X-ray crystallography. Crystallographic data for $Re_3Cl_9(PMe_3)_3$: hexagonal space group $P6_3/m$, $a = b = 11.614(1)$, $c = 11.209(2)$ Å, $\alpha = \beta = 90$, $\gamma = 120°$, $V = 1309.4(5)$ Å^3 and $Z = 2$. The structure was refined to $R = 0.038$ ($R_w = 0.064$) for 524 data with $I > 3.0\sigma(I)$. Crystallographic data for $Re_3Cl_9(\eta^1\text{-dppm})_3 \cdot C_7H_8$: triclinic space group $P\bar{1}$, $a = 11.883(3)$, $b = 18.233(4)$, $c = 20.102(5)$ Å, $\alpha = 103.32(1)$, $\beta = 99.18(1)$, $\gamma = 95.88(1)°$, $V = 4139(3)$ Å^3 and $Z = 2$. The structure was refined to $R = 0.039$ ($R_w = 0.050$) for 7190 data with $I > 3.0\sigma(I)$. Both structures resemble that of the previously reported $Re_3Cl_9(PEt_2Ph)_3$, with Re—Re double bond distances spanning the narrow range of 2.471(1)–2.488(1) Å. The Re—P bond lengths are 2.634(4) Å for the Me_3P complex, and between 2.693(3) and 2.727(3) Å for $Re_3Cl_9(\eta^1\text{-dppm})_3$; the presence of three monodentate dppm ligands is confirmed in the latter structure.

Trinuclear derivatives of the type $Re_3X_9(L)_3$ are known to form readily when the rhenium(III) halides are treated with donor molecules.[1–3] In the case of monodentate tertiary phosphine ligands, the complexes $Re_3Cl_9(PR_3)_3$ (PR_3 = PMe_3, PEt_2Ph, $PMePh_2$, $PEtPh_2$, PPh_3, 3-methyl-1-phenylphosphole and 3,4-dimethyl-1-phenylphosphole) and $Re_3Br_9(PR_3)_3$ (PR_3 = PEt_2Ph and PPh_3) have been prepared[4–11] but in only one instance, viz. $Re_3Cl_9(PEt_2Ph)_3$,[12] has the structure been established by X-ray crystallography. While several polydentate phosphines have been reacted with Re_3Cl_9, the products are generally not very well defined structurally,[13] although in the case of the insoluble complex $Re_3Cl_9(dppe)_{1.5}$ (dppe = $Ph_2PCH_2CH_2PPh_2$) it seems likely that intermolecular dppe bridges link Re_3Cl_9 units in the solid state.[14]

In the present report we describe the synthesis and characterization of the complexes $Re_3Cl_9(PMe_3)_3$ and $Re_3Cl_9(PMe_2Ph)_3$, as well as $Re_3Cl_9(\eta^1\text{-dppm})_3$ (dppm = $Ph_2PCH_2PPh_2$); the latter is the first example of a structurally characterized complex that contains three pendant dppm ligands. Other reactions studied include those of Re_3Cl_9 with $Me_2PCH_2PMe_2$(dmpm) and $Ph_2PCH_2CH_2AsPh_2$ (arphos) which afford $Re_3Cl_9(dmpm)_{1.5}$, $Re_3Cl_9(\eta^1\text{-arphos})_3$ and $Re_3Cl_9(arphos)_{1.5}$. The ^1H and ^{31}P NMR spectra of these complexes and of the previously reported complex $Re_3Cl_9(PMePh_2)_3$[9] provide the first such spectroscopic data on phosphine complexes of the Re_3X_9 halides with the exception of $Re_3Cl_9(PMe_3)_3$.[11]

* Author to whom correspondence should be addressed.

EXPERIMENTAL

Starting materials

Rhenium(III) chloride was prepared from $Re_2(O_2CCH_3)_4Cl_2$ by the published procedure.[15] The ligands PMe_3, PMe_2Ph, $PMePh_2$, $Me_2PCH_2PMe_2$(dmpm), *cis*-$Ph_2PCH{=}CHPPh_2$ (*cis*-dppee), and $Ph_2PCH_2CH_2AsPh_2$(arphos) were purchased from Strem Chemicals; $Ph_2PCH_2PPh_2$(dppm), was purchased from the Pressure Chemical Company.

Reaction procedures

A. *Reactions of* Re_3Cl_9 *with monodentate phosphines.* (i) $Re_3Cl_9(PMe_3)_3 \cdot 0.5EtOH$. A solution of Re_3Cl_9 (0.169 g, 0.19 mmol) in 10 cm^3 of absolute ethanol was purged of oxygen by the freeze–thaw method of degassing. This solution was then frozen in a Schlenk tube immersed in liquid nitrogen. A quantity of trimethylphosphine (0.70 cm^3, 6.8 mmol) was introduced via syringe onto the frozen solution and the reaction tube removed from the liquid nitrogen and allowed to warm. Just as soon as the ethanol solution had melted, the mixture was agitated briefly, and a red precipitate formed. This precipitate was quickly filtered off, washed with diethyl ether, and dried *in vacuo*; yield 0.143 g (70%). The pale red filtrate did not yield additional product and was discarded. Found: C, 10.9; H, 3.0. Calc. for $C_{10}H_{30}Cl_9O_{0.5}P_3Re_3$: C, 10.6; H, 2.7%. The presence of lattice ethanol in this product was confirmed by ^1H NMR spectroscopy. $Re_3Cl_9(PMe_3)_3$ is soluble in dichloromethane, chloroform and benzene, soluble with some decomposition in acetone and acetonitrile, and insoluble in methanol, ethanol, diethyl ether, hexane and water.

(ii) $Re_3Cl_9(PMe_2Ph)_3 \cdot 2EtOH$. This complex was prepared in a manner analogous to that described in section A(i); Re_3Cl_9 (0.20 g, 0.2 mmol) was reacted with dimethylphenylphosphine (0.15 cm^3, 1.0 mmol) to afford a red powder; yield 0.236 g (80%). Found: C, 24.8; H, 3.1. Calc. for $C_{28}H_{45}Cl_9O_2P_3Re_3$: C, 24.3; H, 3.3%. The presence of lattice ethanol was confirmed by ^1H NMR spectroscopy.

(iii) $Re_3Cl_9(PMePh_2)_3$. This complex was prepared with the use of a procedure similar to that described in section A(i). A small quantity of Re_3Cl_9 (0.071 g, 0.08 mmol) was reacted with methyldiphenylphosphine (0.25 cm^3, 1.3 mmol) to yield a red powder; yield 0.088 g (75%). Found: C, 31.3; H, 2.7. Calc. for $C_{39}H_{39}Cl_9P_3Re_3$: C, 31.7; H, 2.7%.

B. *Reactions of* Re_3Cl_9 *with bidentate phosphines.* (i) $Re_3Cl_9(dmpm)_{1.5}$. A procedure similar to that described in section A(i) was used to react Re_3Cl_9 (0.102 g, 0.12 mmol) with 0.7 cm^3 of a 0.73 M toluene solution of dmpm (4.5 equivalents). This afforded a red insoluble product; yield 0.035 g (28%). Found: C, 8.3; H, 2.7. Calc. for $C_{7.5}H_{21}Cl_9P_3Re_3$: C, 8.3; H, 2.0%.

(ii) $Re_3Cl_9(dppm)_3 \cdot C_7H_8$. A solution of Re_3Cl_9 (0.102 g, 0.12 mmol) in 10 cm^3 of absolute ethanol was purged of oxygen by the freeze–thaw method of degassing. After the third cycle, a quantity of dppm (0.147 g, 0.38 mmol) dissolved in 5 cm^3 of deoxygenated toluene was added and the mixture frozen. When this mixture was allowed to slowly warm, a red solution resulted. The quick addition of an equal volume of hexanes, followed by centrifugation, yielded a pink solid (0.128 g). Upon allowing the supernate to stand for *ca* 10 min, an additional quantity of solid was obtained (0.043 g); the combined yield was 70%. Found: C, 47.1; H, 3.7. Calc. for $C_{82}H_{74}Cl_9P_6Re_3$: C, 46.4; H, 3.5%. Lattice toluene was evident in the structural analysis of a single crystal of this complex as well as in the ^1H NMR spectrum. $Re_3Cl_9(dppm)_3$ is soluble in dichloromethane but insoluble in acetone, ethanol, diethyl ether and benzene.

When a reaction mixture comprising Re_3Cl_9 (0.066 g, 0.075 mmol) dissolved in EtOH, and dppm (0.134 g, 0.35 mmol) dissolved in toluene was not treated with hexanes, a mixture of compounds slowly precipitated. When the resulting solid was washed with diethyl ether, $Re_3Cl_9(dppm)_3$ remained undissolved on the filter pad; yield 0.016 g (10%). The red filtrate was allowed to stand for *ca* 1 h, whereupon a red solid precipitated; yield 0.050 g. This material was sparingly soluble in acetone, but it was insoluble in dichloromethane. Elemental carbon and hydrogen microanalyses were consistent with a composition between that for $Re_3Cl_9(dppm)_3$ and $Re_3Cl_9(dppm)_2$. Found: C, 40.0; H, 3.4%.

(iii) $Re_3Cl_9(arphos)_3$. An ethanol solution (10 cm^3) of Re_3Cl_9 (0.120 g, 0.14 mmol) was added dropwise to a solution of arphos (0.5 g, 1.1 mmol) in diethyl ether (10 cm^3). After the addition of only one third of the rhenium chloride solution, a red precipitate had already formed. This solid was separated from the solution by filtration, washed with ethanol and diethyl ether and dried; yield 0.088 g. Found: C, 42.0; H, 3.4; Cl, 14.9. Calc. for $C_{78}H_{72}As_3Cl_9P_3Re_3$: C, 42.5; H, 3.3; Cl, 14.5%. $Re_3Cl_9(arphos)_3$ is soluble in dichloromethane but insoluble in ethanol and diethyl ether.

The remaining portion of the Re_3Cl_9 was then added to the arphos in the reaction filtrate. No precipitate was observed initially, but after *ca* 1 h a

second red solid precipitated from this red solution; yield 0.077 g. Elemental carbon and hydrogen microanalyses were fairly close to those expected for $Re_3Cl_9(arphos)_2$. Found: C, 37.3; H, 3.0%. This product is insoluble in dichloromethane, acetone and diethyl ether.

When a different synthetic strategy was used, whereby Re_3Cl_9 (0.021 g, 0.02 mmol) and arphos (0.032 g, 0.08 mmol) were combined as solids to which the solvent EtOH (8 cm^3) was then added, the insoluble product appeared to be of the stoichiometry $Re_3Cl_9(arphos)_{1.5}$; yield 0.030 g (80%). Found: C, 30.2; H, 2.3. Calc. for $C_{39}H_{36}As_{1.5}Cl_9P_{1.5}Re_3$: C, 30.4; H, 2.3%.

Crystallography

Preparation of single crystals for structure determinations. Single crystals of $Re_3Cl_9(PMe_3)_3$ were obtained by the slow evaporation of CD_2Cl_2 from a solution of this complex contained in a 5-mm quartz NMR tube that had been kept under a dinitrogen atmosphere for a period of 1 week. Single crystals of $Re_3Cl_9(dppm)_3$ were obtained by the slow evaporation of the solvent from an ethanol–toluene reaction filtrate under a gentle stream of nitrogen gas over a period of *ca* 4 h.

X-ray data collection and structure refinement. The structure of crystals of composition $Re_3Cl_9(PMe_3)_3$ and $Re_3Cl_9(dppm)_3\cdot C_7H_8$ were determined by standard procedures. A summary of the crystallographic data for these two structures is given in Table 1. The cell parameters are based on 25 reflections with $21.9 < \theta < 22.4°$ for $Re_3Cl_9(PMe_3)_3$ and $17.9 < \theta < 19.5°$ for $Re_3Cl_9(dppm)_3\cdot C_7H_8$. Three standard reflections were measured every 5000 s of beam time during data collection and displayed no systematic variations in intensity. Calculations were performed on a MicroVAX II computer using the Enraf–Nonius structure determination package.

(i) $Re_3Cl_9(PMe_3)_3$. The crystal selected for the structure determination belonged to the hexagonal space group $P6_3/m$ with $Z = 2$. The position of the crystallographically unique rhenium atom was determined from a three-dimensional Patterson map. The molecule resides about the special position 2/3, 1/3, 1/4 which has site symmetry $\bar{6}$. The molecule possess C_{3h} point symmetry where one carbon on each PMe_3 ligand lies in the $Re_3(\mu\text{-}Cl)_3P_3$ plane. One hydrogen, attached to this carbon, was constrained by symmetry to lie in the $Re_3(\mu\text{-}Cl)_3P_3$ plane as well. One other hydrogen, in a methyl group not on the mirror plane, was uniquely determined. The positions of these hydrogens were idealized, and the remaining hydrogen positions were calculated assuming idealized geometry and a C—H bond distance of 0.95 Å. The value of B[H], i.e. the isotropic equivalent thermal parameter, was assumed to be 4 $Å^2$. Scattering factors for hydrogens in these idealized positions were used as a fixed contribution to F_{calc}; the hydrogens were not included in the least-squares refinement (their relative positions were fixed and did not vary as a result of refinement). Lorentz and polarization corrections were applied to the data. An empirical absorption correction was applied,[16] the linear absorption coefficient being 151.35 cm^{-1}. No correction for extinction was applied. The structure was refined in full-matrix least-squares where the function minimized was $\Sigma w(|F_o|-|F_c|)^2$, and w is the weighting factor defined as $w = 1/\sigma^2(F_o)$.

All non-hydrogen atoms were refined anisotropically; corrections for anomalous scattering were applied to all atoms so refined.[17] The highest peak in the final difference Fourier map was 1.54 e $Å^{-3}$; this is a ghost of the rhenium atom.

(ii) $Re_3Cl_9(dppm)_3\cdot C_7H_8$. The crystal of this complex belonged to the triclinic space group $P\bar{1}$ with $Z = 2$. Consequently there was no crystallographically-imposed symmetry for the trirhenium molecule. The positions of the three rhenium atoms were determined from a three-dimensional Patterson map. The remaining atoms were located in succeeding difference Fourier syntheses. The presence of lattice toluene, which was observed in the ^1H NMR spectrum, was confirmed by the crystal structure analysis. Both the trirhenium molecule and the toluene reside in general positions. Lorentz and polarization corrections were applied to the data. An empirical absorption correction was applied,[16] the linear absorption coefficient being 48.85 cm^{-1}. No correction for extinction was applied.

The Re, Cl, P, and bridgehead C atoms were refined anisotropically. Corrections for anomalous scattering were applied to these atoms.[17] The phenyl ring carbon atoms and the carbon atoms in the toluene were refined isotropically. Hydrogen atoms were not refined. The highest peak in the final difference Fourier map was 1.88 e $Å^{-3}$ and did not appear to be of any chemical significance.

Further details concerning the data sets and the structure solutions and refinements may be obtained from Dr P. E. Fanwick. Tables 2 and 3 list important bond distances and angles.*

* Atomic positional and thermal parameters and full listings of bond lengths and angles have been deposited with the Editor and with the Director, Cambridge Crystallographic Data Centre.

Table 1. Crystallographic data and data collection parameters for $Re_3Cl_9(PMe_3)_3$ and $Re_3Cl_9(\eta^1\text{-dppm})_3 \cdot C_7H_8$[a]

	$Re_3Cl_9(PMe_3)_3$	$Re_3Cl_9(\eta^1\text{-dppm})_3 \cdot C_7H_8$
Formula	$Re_3Cl_9P_3C_9H_{27}$	$Re_3Cl_9P_6C_{82}H_{74}$
Formula weight	1105.91	2123.03
Space group	$P6_3/m$ (No. 176)	$P\bar{1}$ (No. 2)
a (Å)	11.614(1)	11.883(3)
b (Å)	11.614(1)	18.233(4)
c (Å)	11.209(2)	20.102(5)
α (°)	90	103.32(1)
β (°)	90	99.18(1)
γ (°)	120	95.88(1)
V (Å^3)	1309.4(5)	4139(3)
Z	2	2
D_c (g cm^{-3})	2.805	1.703
Crystal dimensions (mm)	$0.38 \times 0.15 \times 0.09$	$0.13 \times 0.11 \times 0.08$
Temperature (°C)	21	20
Radiation (wavelength)	Mo-K_α (0.71073 Å)	Mo-K_α (0.71073 Å)
Monochromator	Graphite	Graphite
Linear absorption coefficient (cm^{-1})	151.35	48.85
Absorption correction applied	Empirical[b]	Empirical[b]
Transmission factors: min, max	0.63, 1.00	0.83, 1.00
Diffractometer	Enraf–Nonius CAD4	Enraf–Nonius CAD4
Scan method	ω–2θ	ω–2θ
h, k, l limits	-12 to 0, 0 to 12, 0 to 12	-12 to 12, -19 to 19, 0 to 21
2θ range (°)	4.00–45.00	4.00–45.00
Scan width (°)	$0.35+0.35\tan(\theta)$	$0.42+0.35\tan(\theta)$
Take-off angle (°)	1.90	1.90
Programs used	Enraf–Nonius SDP	Enraf–Nonius SDP
$F(000)$	1008.0	2068.0
p-Factor used in weighting	0.040	0.040
Data collected	1320	10,816
Unique data	615	10,816
Data with $I > 3.0\sigma(I)$	524	7190
Number of variables	43	506
Largest shift/ESD in final cycle	0.00	0.02
R[c]	0.038	0.039
R_w[d]	0.064	0.050
Goodness-of-fit[e]	2.103	1.027

[a] Number in parentheses following certain data are estimated standard deviations occurring in the least significant digit.

[b] See ref. 16.

[c] $R = \Sigma \| |F_o| - |F_c| \| / \Sigma |F_o|$.

[d] $R_w = [\Sigma w(|F_o| - |F_c|)^2 / \Sigma w|F_o|^2]^{1/2}$; $w = 1/\sigma^2(F_o)$.

[e] Goodness-of-fit $= [\Sigma w(|F_o| - |F_c|)^2 / (N_{obs} - N_{param})]^{1/2}$.

Physical measurements. IR spectra (4000–150 cm^{-1}) were recorded as Nujol mulls with a Perkin–Elmer 1800 Fourier transform spectrometer. Electronic absorption spectra were recorded on an IBM Instruments 9420 UV–vis (900–200 nm) spectrophotometer. ^{1}H NMR spectra were recorded on a Varian XL-200 spectrometer. Resonances were referenced internally to the residual protons in the incompletely deuteriated solvent. $^{31}P\{^1H\}$ spectra were recorded on a Varian XL-200 spectrometer operating at 80.98 MHz with an internal deuterium lock using aqueous 85% H_3PO_4 as an external standard.

Elemental microanalyses were performed by Dr H. D. Lee of the Purdue University Microanalytical Laboratory.

Table 2. Some important bond distances (Å) and bond angles (°) for $Re_3Cl_9(PMe_3)_3$[a]

Distances			
Re—Re	2.481(1)	Re—P	2.634(4)
Re—Cl(B)	2.418(4)	P—C(1)	1.80(1)
Re—Cl(T)	2.310(3)	P—C(2)	1.79(2)
Angles			
Re—Re—Re	60.0	Cl(T)—Re—Cl(T)	157.8(2)
Re—Re—Cl(B)	59.0(1)	Cl(T)—Re—P	79.07(8)
Re—Re—Cl(B)	119.2(1)	Re—Cl(B)—Re	61.8(1)
Re—Re—Cl(T)	98.94(8)	Re—P—C(1)	117.3(5)
Re—Re—P	153.6(1)	Re—P—C(2)	112.7(7)
Cl(B)—Re—Cl(B)	178.2(1)	C(1)—P—C(1)	101(1)
Cl(B)—Re—Cl(T)	89.03(8)	C(1)—P—C(2)	103.3(7)
Cl(B)—Re—P	94.6(1)		

[a] Numbers in parentheses are ESDs in the least significant digits.

RESULTS AND DISCUSSION

(a) *Synthesis and preliminary characterization*

The reactions of Re_3Cl_9 with PMe_3 and PMe_2Ph in ethanol to afford $Re_3Cl_9(PMe_3)_3$ and $Re_3Cl_9(PMe_2Ph)_3$ complete the series of complexes $Re_3Cl_9(PMe_{3-x}Ph_x)_3$ ($x = 0$–3). A recent report that also describes the isolation of $Re_3Cl_9(PMe_3)_3$ used the reaction between $Re_3Cl_9(THF)_3$ and PMe_3 in dichloromethane.[11] A similar reaction between Re_3Cl_9 and bis(diphenylphosphino)methane in an ethanol–toluene mixture gave pure $Re_3Cl_9(\eta^1\text{-dppm})_3$ when the product was isolated quickly from the cold reaction mixture by the addition of hexanes. Slow precipitation of the product at room temperature afforded a material whose composition was between those expected for $Re_3Cl_9(dppm)_3$ and $Re_3Cl_9(dppm)_2$, thereby indicating that polymerization through intermolecular dppm bridges was beginning to occur. An analogous reaction between Re_3Cl_9 and dmpm in ethanol–toluene gave $Re_3Cl_9(dmpm)_{1.5}$ as the only reproducibly identifiable product, i.e. a product in which polymerization through dmpm bridges appears to be complete. This compound probably bears a close structural relationship to $Re_3Cl_9(dppe)_{1.5}$.[14] In the case of the reactions between Re_3Cl_9 and dppee and 1,2-$C_6H_4(PPh_2)_2$ (dppbe), the insoluble red or purple solids that were formed had compositions (based upon carbon and hydrogen microanalyses) approximating to $Re_3Cl_9(dppee)_2$ and $Re_3Cl_9(dppbe)_{0.75}$, respectively; this indicates that polymerization through phosphine ligand bridges and/or incomplete coordination at the three acceptor sites per cluster had occurred.

When a solution of Re_3Cl_9 in ethanol is added to a large excess of arphos in diethyl ether the red 1:3 adduct $Re_3Cl_9(arphos)_3$ is formed. Reactions between Re_3Cl_9 and arphos in ethanol under conditions where the arphos ligand was not present in such a large excess gave a product that analysed as $Re_3Cl_9(arphos)_{1.5}$.

In the preceding syntheses, the isolations of $Re_3Cl_9(PMe_3)_3$, $Re_3Cl_9(PMe_2Ph)_3$ and $Re_3Cl_9(PMePh_2)_3$ were carried out at low temperatures to avoid the possibility of contamination by the dirhenium derivatives $Re_2Cl_4(PR_3)_4$ ($PR_3 = PMe_3$ or PMe_2Ph) and $Re_2Cl_5(PMePh_2)_3$ that can be formed by disruption of the Re_3 cluster unit under more forcing reaction conditions.[9] In the case of $Re_3Cl_9(dppm)_3$ and $Re_3Cl_9(arphos)_3$, the reaction conditions were adjusted so as to favour the coordination of these ligands in a monodentate η^1-fashion. The isolation of $Re_3Cl_9(\eta^1\text{-dppm})_3$ can be compared with our earlier success in preparing *trans*-$ReCl_4(\eta^1\text{-dppm})_2$.[18] We have observed previously the ability of arphos to bind in a monodentate or bridging bidentate fashion to rhenium as in the complexes *trans*-$ReCl_4(\eta^1\text{-arphos})_2$ and [*trans*-$ReCl_4(arphos)]_\infty$.[18]

The electronic absorption spectra of the complexes (Table 4) are typical of derivatives of the Re_3X_9 halides,[12,14,19] the transitions being primarily metal-based.[20] The spectra of $Re_3Cl_9(PMe_3)_3$ in deoxygenated solutions of dichloromethane and in benzene, were unchanged over a period of 30 min, whereas solutions in acetone and acetonitrile were much less stable. The low-frequency IR spectra of each of these derivatives show a very similar group of bands below *ca* 350 cm^{-1} that, in turn, resemble the spectra of other complexes of Re_3Cl_9.[19] The bands between 360 and 300 cm^{-1} are primarily due to ν(Re—Cl) modes.

Table 3. Some important bond distances (Å) and bond angles (°) for $Re_3Cl_9(\eta^1\text{-dppm})_3$[a]

Distances			
Re(1)—Re(2)	2.4808(7)	Re(2)—Cl(23)	2.392(3)
Re(1)—Re(3)	2.4710(7)	Re(2)—Cl(2A)	2.306(3)
Re(1)—Cl(12)	2.390(3)	Re(2)—Cl(2B)	2.309(3)
Re(1)—Cl(13)	2.405(3)	Re(2)—P(21)	2.693(3)
Re(1)—Cl(1A)	2.299(3)	Re(3)—Cl(13)	2.410(3)
Re(1)—Cl(1B)	2.306(3)	Re(3)—Cl(23)	2.402(3)
Re(1)—P(11)	2.693(3)	Re(3)—Cl(3A)	2.301(3)
Re(2)—Re(3)	2.4881(7)	Re(3)—Cl(3B)	2.314(3)
Re(2)—Cl(12)	2.382(3)	Re(3)—P(31)	2.727(3)
Angles			
Re(2)—Re(1)—Re(3)	60.33(2)	Cl(1A)—Re(1)—P(11)	80.5(1)
Re(2)—Re(1)—Cl(12)	58.51(8)	Cl(1B)—Re(1)—P(11)	77.7(1)
Re(2)—Re(1)—Cl(13)	119.55(9)	Re(1)—Re(2)—Re(3)	59.64(2)
Re(2)—Re(1)—Cl(1A)	99.90(9)	Re(1)—Re(2)—Cl(12)	58.83(8)
Re(2)—Re(1)—Cl(1B)	98.42(8)	Re(1)—Re(2)—Cl(23)	118.54(9)
Re(2)—Re(1)—P(11)	147.90(8)	Re(1)—Re(2)—Cl(2A)	99.29(8)
Re(3)—Re(1)—Cl(12)	118.84(9)	Re(1)—Re(2)—Cl(2B)	98.74(8)
Re(3)—Re(1)—Cl(13)	59.23(8)	Re(1)—Re(2)—P(21)	147.84(8)
Re(3)—Re(1)—Cl(1A)	100.31(9)	Re(3)—Re(2)—Cl(12)	118.47(8)
Re(3)—Re(1)—Cl(1B)	98.91(9)	Re(3)—Re(2)—Cl(23)	58.92(8)
Re(3)—Re(1)—P(11)	151.63(8)	Re(3)—Re(2)—Cl(2A)	99.89(9)
Cl(12)—Re(1)—Cl(13)	178.0(1)	Re(3)—Re(2)—Cl(2B)	99.64(8)
Cl(12)—Re(1)—Cl(1A)	90.0(1)	Re(3)—Re(2)—P(21)	152.41(8)
Cl(12)—Re(1)—Cl(1B)	89.6(1)	Cl(12)—Re(2)—Cl(23)	177.2(1)
Cl(12)—Re(1)—P(11)	89.4(1)	Cl(12)—Re(2)—Cl(2A)	89.8(1)
Cl(13)—Re(1)—Cl(1A)	90.9(1)	Cl(12)—Re(2)—Cl(2B)	89.2(1)
Cl(13)—Re(1)—Cl(1B)	90.2(1)	Cl(12)—Re(2)—P(21)	89.1(1)
Cl(13)—Re(1)—P(11)	92.5(1)	Cl(23)—Re(2)—Cl(2A)	89.6(1)
Cl(1A)—Re(1)—Cl(1B)	158.2(1)	Cl(23)—Re(2)—Cl(2B)	92.3(1)
Cl(23)—Re(2)—P(21)	93.6(1)	Re(2)—Re(3)—P(31)	153.68(8)
Cl(2A)—Re(2)—Cl(2B)	158.3(1)	Cl(13)—Re(3)—Cl(23)	177.5(1)
Cl(2A)—Re(2)—P(21)	80.9(1)	Cl(13)—Re(3)—Cl(3A)	91.1(1)
Cl(2B)—Re(2)—P(21)	77.4(1)	Cl(13)—Re(3)—Cl(3B)	92.5(1)
Re(1)—Re(3)—Re(2)	60.03(2)	Cl(13)—Re(3)—P(31)	87.0(1)
Re(1)—Re(3)—Cl(13)	59.02(8)	Cl(23)—Re(3)—Cl(3A)	88.6(1)
Re(1)—Re(3)—Cl(23)	118.57(9)	Cl(23)—Re(3)—Cl(3B)	88.7(1)
Re(1)—Re(3)—Cl(3A)	100.74(9)	Cl(23)—Re(3)—P(31)	95.5(1)
Re(1)—Re(3)—Cl(3B)	99.56(9)	Cl(3A)—Re(3)—Cl(3B)	158.2(1)
Re(1)—Re(3)—P(31)	145.84(8)	Cl(3A)—Re(3)—P(31)	81.8(1)
Re(2)—Re(3)—Cl(13)	119.06(8)	Cl(3B)—Re(3)—P(31)	77.0(1)
Re(2)—Re(3)—Cl(23)	58.55(8)	Re(1)—Cl(12)—Re(2)	62.66(8)
Re(2)—Re(3)—Cl(3A)	100.18(8)	Re(1)—Cl(13)—Re(3)	61.75(8)
Re(2)—Re(3)—Cl(3B)	96.79(8)	Re(2)—Cl(23)—Re(3)	62.53(8)

[a] Numbers in parentheses are ESDs in the least significant digits.

(b) *Crystal structures of* $Re_3Cl_9(PMe_3)_3$ (**1**) *and* $Re_3Cl_9(\eta^1\text{-dppm})_3$ (**2**)

The structures of these two complexes have been confirmed by X-ray crystallography. ORTEP representations of the structures are shown in Figs 1 and 2, while important bond distances and angles are listed in Tables 2 and 3. A close similarity with the previously reported structure of $Re_3Cl_9(PEt_2Ph)_3$ is revealed. Of importance is our finding that the Re—Re distances for **1** and **2** encompass the narrow range of 2.471(1)–2.488(1) Å, and are similar to the distance of 2.493(4) Å reported for $Re_3Cl_9(PEt_2Ph)_3$.[12]

The Re—P bond lengths of 2.634(4) Å for **1** and 2.693(3)–2.727(3) Å for **2** are not significantly different from the value of 2.700(19) Å for $Re_3Cl_9(PEt_2Ph)_3$.[12] The constancy of the latter

Table 4. Electronic absorption and IR spectral data for phosphine complexes of Re_3Cl_9

Complex	Electronic absorbance spectra[a] Medium	λ_{max}, nm (ε)[b]			Low-frequency IR spectra[c] ν(Re—Cl)
$Re_3Cl_9(PMe_3)_3$	Nujol mull	442	540	812	347(s) 335(sh) 325(w) 203(w)[d]
	C_6H_6	440 (1380)	535 (1690)	807 (550)	
	CH_2Cl_2	445 (1240)	535 (1540)	812 (485)	
$Re_3Cl_9(PMe_2Ph)_3$	CH_2Cl_2	446 (1510)	539 (1470)	813 (450)	350(s) 331(sh) 307(sh) 204(w)
$Re_3Cl_9(PMePh_2)_3$	CH_2Cl_2	436 (1850)	540 (1710)	818 (570)	351(s) 336(sh) 328(m) 200(w)
$Re_3Cl_9(dppm)_3$	CH_2Cl_2	430 sh	537 (2210)	814 (620)	≃ 365(sh) 354(s) ≃ 340(sh) 330(m) 269(vw) 201(w)
$Re_3Cl_9(arphos)_3$	CH_2Cl_2	435 (2390)	539 (2220)	816 (720)	357(s) 327(w) 306(vw) 289(vw) 200(w)
$Re_3Cl_9(arphos)_{1.5}$	Nujol mull	≃ 430 sh	539	805	353(s) 330(w) 322(w) 200(w)
$Re_3Cl_9(dppe)_{1.5}$	Nujol mull[e]	420	538	813	356(m) 348(sh) 326(w) 200(w)[f]

[a] Spectra recorded from 900 to 400 nm.
[b] Molar extinction coefficients given in parentheses.
[c] Relative intensities are given in parentheses.
[d] Similar to spectrum reported in ref. 11.
[e] Diffuse reflectance spectrum shows bands at 550 and 820 nm (see ref. 19).
[f] Similar to spectrum reported in ref. 19.

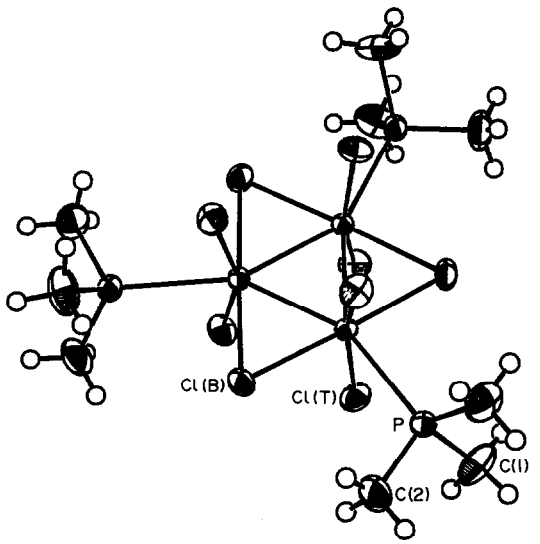

Fig. 1. ORTEP representation of the structure of $Re_3Cl_9(PMe_3)_3$ showing the atomic numbering scheme. The thermal ellipsoids are drawn at the 50% probability level.

values supports the notion that these long distances are a consequence of steric crowding about the rhenium atoms. The slightly shorter Re—P bonds of **1** are doubtless a reflection of the greater basicity of the PMe_3 ligand (compared to PEt_2Ph and dppm) together with some slight relief of steric pressure. These Re—P bond lengths can be contrasted with those of 2.401(6) and 2.458(6) Å reported for *mer*-$ReCl_3(PMe_2Ph)_3$.[21] The effect of reducing the steric compression is seen in the structure of the bis(phosphine) complex $Re_3Me_9(PEt_2Ph)_2$.[22] In this molecule, the Re—Re distances of 2.433(1)–2.474(1) Å are still compatible with Re—Re double bonds, but the Re—P distances are now considerably shorter (2.546(3) and 2.569(3) Å).

The terminal Re—Cl bonds are, as expected, shorter than the Re—Cl bridging bonds (e.g. 2.310(3) vs 2.418(4) Å for **1**), a trend that is also seen in the structure of $Re_3Cl_9(PEt_2Ph)_3$. The angular distortions in all three molecules are generally very similar and will not be discussed further.

(c) *NMR spectroscopic properties*

The ^1H NMR spectra of $Re_3Cl_9(PMe_3)_3$ in CD_2Cl_2 and C_6D_6 consist of a virtual triplet at δ +1.57 and +1.06, respectively, with $J_{P-H} = 8.4$ Hz. This compares well with the data reported by Wilkinson and co-workers[11] for a solution of $Re_3Cl_9(PMe_3)_3$ in CD_2Cl_2 (δ +1.50(t) with $J_{P-H} = 8.3$ Hz). In the case of $Re_3Cl_9(PMe_2Ph)_3$ and $Re_3Cl_9(PMePh_2)_3$, singlets at δ +1.80 and +2.08, respectively, were observed for CD_2Cl_2 solutions, together with phenyl resonances (showing the correct relative intensities) between δ +7.4 and +7.6. The $^{31}P\{^1H\}$ NMR spectra of these three complexes (recorded in CD_2Cl_2) show singlets at δ −35.2, −30.8 and −20.6, respectively, which are shifted downfield of the free phosphines (δ −63,

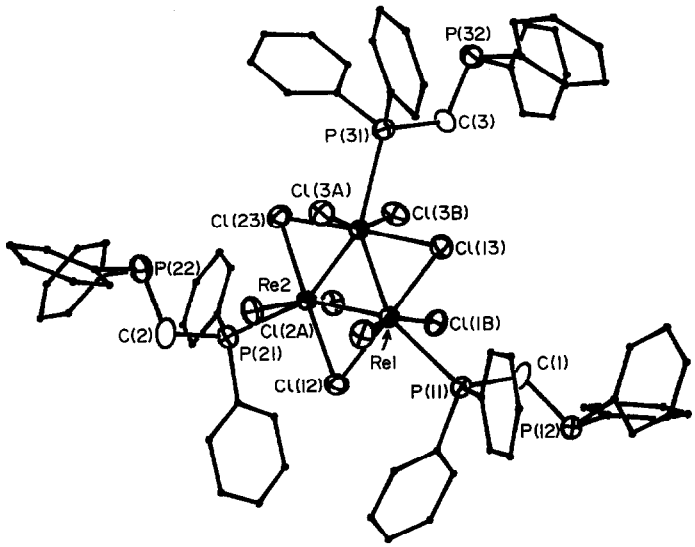

Fig. 2. ORTEP representation of the structure of $Re_3Cl_9(\eta^1\text{-dppm})_3$ showing the atomic numbering scheme for the non-phenyl group atoms. The thermal ellipsoids are drawn at the 50% probability level.

-47 and -28);[23] a previous citation of the $^{31}P\{^1H\}$ NMR spectrum of $Re_3Cl_9(PMe_3)_3$ reported a singlet at δ -38.38.

The NMR spectral properties of $Re_3Cl_9(dppm)_3$ are of interest in view of the monodentate coordination of the dppm ligands. The ^1H NMR spectrum of the crystals of stoichiometry $Re_3Cl_9(dppm)_3 \cdot C_7H_8$ in CD_2Cl_2 at $+20°C$ exhibits a fairly narrow phenyl multiplet centred at δ $+7.25$, a broad singlet at δ $+3.10$ due to the bridgehead —CH_2— groups of the dppm ligands (P—H coupling is not resolved), and a sharp methyl resonance at δ $+2.32$ arising from the lattice toluene molecule. At $-60°C$ the spectrum is little changed, with the exception that the phenyl resonances now display a much more complex pattern as the conformational changes resulting from rotation about the CH_2—P bonds are slowed, as is the dissociative exchange of the dppm ligands (*vide infra*). At $+20°C$, the $^{31}P\{^1H\}$ spectrum shows no discernible features with the exception of two extremely broad humps near δ -14 and -26. As the temperature is lowered to $-50°C$ in 10 degree intervals, the spectral changes shown in Fig. 3 occur with the growth of multiplets centred at δ -12.7 and -27.4 that are assigned to the bound and free phosphorus atoms, respectively. These features are characteristic of a fluxional process such as that involving exchange of bound and free phosphorus ligand atoms; in the present case coalescence occurs just above room temperature. In view of the coordinative saturation at the rhenium atoms of this trinuclear cluster, this process must involve the dissociative exchange of dppm [eq. (1)]:

$$Re_3Cl_9(dppm)_3 \rightleftharpoons Re_3Cl_9(dppm)_2 + dppm \quad (1)$$

with a rate of *ca* 2700 s^{-1} (calculated from rate $= \pi\Delta\nu/\sqrt{2}$, with $\Delta\nu = 1200$ Hz).[24]

In a separate NMR experiment, additional dppm was added to a CH_2Cl_2–CD_2Cl_2 solution of $Re_3Cl_9(dppm)_3$. At room temperature, three broad

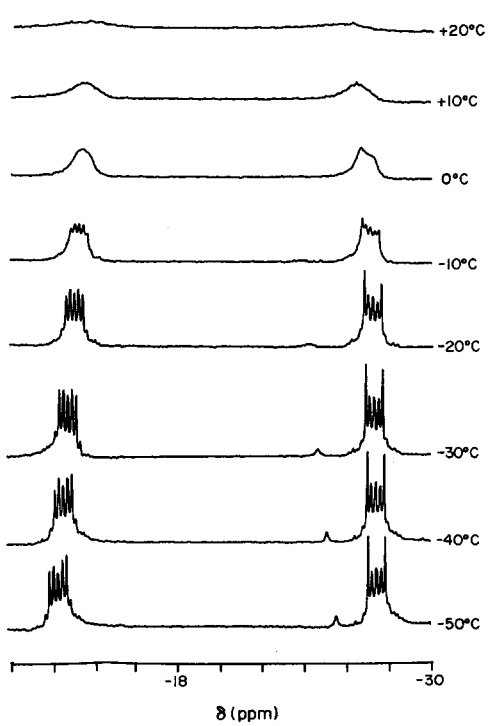

Fig. 3. $^{31}P\{^1H\}$ NMR spectrum of $Re_3Cl_9(\eta^1\text{-dppm})_3$ recorded in CD_2Cl_2 over the temperature range $+20°$ to $-50°C$.

^{31}P signals were observed that correspond to the coordinated (δ −14) and dangling (δ −27) phosphorus atoms of the complex as well as the phosphorus atoms of free dppm (δ −23). These signals, while broad, were considerably sharper than the signals observed at room temperature in the absence of added dppm. This result suggests that, in the presence of excess dppm, the equilibrium of eq. (1) lies well to the left.

Finally, we note that in the room temperature $^{31}P\{^1H\}$ NMR spectrum of $Re_3Cl_9(\eta^1\text{-arphos})_3$ (recorded in CD_2Cl_2), the phosphorus signal at δ −9.0 is downfield of free arphos (δ −12.6 in CD_2Cl_2). While we cannot rule out the presence of small amounts of arsenic-bound arphos in this product, the major species apparently contains phosphorus-bound ligands.

(d) *Concluding remarks*

The reactions of Re_3Cl_9 with the ligands $R_2PCH_2PR_2$ (R = Me or Ph), $Ph_2PCH_2CH_2PPh_2$ and $Ph_2PCH_2CH_2AsPh_2$ have been shown in the present study, and in earlier investigation,[14] to afford polymeric complexes of the type $Re_3Cl_9(LL)_{1.5}$, in which the Re_3Cl_9 cluster units are linked by L—L bridges (LL = $Me_2PCH_2PPh_2$, $Ph_2PCH_2CH_2PPh_2$ and $Ph_2PCH_2CH_2AsPh_2$). For the first time, we have isolated complexes of the type $Re_3Cl_9(\eta^1\text{-LL})_3$ in the case of LL = $Ph_2PCH_2PPh_2$ and $Ph_2PCH_2CH_2AsPh_2$, and confirmed the monodentate nature of these ligands through a single crystal X-ray structure analysis of $Re_3Cl_9(\eta^1\text{-}Ph_2PCH_2PPh_2)_3$. This structure, and that of $Re_3Cl_9(PMe_3)_3$, resemble the previously determined structure of $Re_3Cl_9(PEt_2Ph)_3$.[12]

Acknowledgements—Support from the National Science Foundation, through Grant Nos CHE88-07444 to R.A.W., and Grant No. CHE86-15556 for the purchase of the MicroVAX II computer and diffractometer, is gratefully acknowledged. We also acknowledge the National Institutes of Health (Grant No. RR-01077) and the National Science Foundation (Grant No. 8714258) for funds for the purchase of the NMR spectrometers.

REFERENCES

1. F. A. Cotton and R. A. Walton, *Multiple Bonds Between Metal Atoms*, pp. 268–280 and refs cited therein. John Wiley, New York (1982).
2. K. A. Conner and R. A. Walton, in *Comprehensive Coordination Chemistry*, Vol. 4, Ch. 43, pp. 160–164 and refs cited therein. Pergamon Press, Oxford (1987).
3. A. Perrin and M. Sergent, *New J. Chem.* 1988, **12**, 337.
4. R. Colton, R. Levitus and G. Wilkinson, *J. Chem. Soc.* 1960, 4121.
5. J. Chatt and G. A. Rowe, *J. Chem. Soc.* 1962, 4019.
6. N. P. Johnson, C. J. L. Lock and G. Wilkinson, *J. Chem. Soc.* 1964, 1054.
7. F. A. Cotton, S. J. Lippard and J. T. Mague, *Inorg. Chem.* 1965, **4**, 508.
8. B. H. Robinson and J. E. Fergusson, *J. Chem. Soc.* 1964, 5683.
9. J. R. Ebner and R. A. Walton, *Inorg. Chem.* 1975, **14**, 1987.
10. D. G. Holah, A. N. Hughes, B. C. Hui and P. K. Tse, *J. Heterocyclic Chem.* 1978, **15**, 1239.
11. A. C. C. Wong, P. G. Edwards, G. Wilkinson, M. Montevalli and M. B. Hursthouse, *J. Chem. Soc., Dalton Trans.* 1988, 219.
12. F. A. Cotton and J. T. Mague, *Inorg. Chem.* 1964, **3**, 1094.
13. (a) Reference 1, pp. 276–277; (b) reference 2, p. 162.
14. F. A. Cotton and R. A. Walton, *Inorg. Chem.* 1966, **5**, 1802.
15. H. D. Glicksman and R. A. Walton, *Inorg. Synth.* 1980, **20**, 46.
16. N. Walker and D. Stuart, *Acta Cryst.* 1983, **A39**, 158.
17. D. T. Cromer, *International Tables for X-ray Crystallography*, Vol. IV, Table 2.3.1. Kynoch Press, Birmingham, U.K. (1974); (b) For the scattering factors used in the structure solution see: D. T. Cromer and J. T. Waber, *Ibid.* Table 2.2B.
18. R. E. Myers and R. A. Walton, *Inorg. Chem.* 1976, **15**, 3065.
19. D. G. Tisley and R. A. Walton, *Inorg. Chem.* 1973, **12**, 373.
20. B. E. Bursten, F. A. Cotton, J. C. Green, E. A. Seddon and G. G. Stanley, *J. Am. Chem. Soc.* 1980, **102**, 955.
21. L. Aslanov, R. Mason, A. G. Wheeler and P. O. Whimp, *Chem. Commun.* 1970, 30.
22. P. Edwards, K. Mertis, G. Wilkinson, M. B. Hursthouse and K. M. Abdul Malik, *J. Chem. Soc., Dalton Trans.* 1980, 334.
23. D. G. Gorenstein and D. O. Shah, in *Phosphorus-31 NMR Principles and Applications*, Ch. 18, p. 553. Academic Press, New York (1984).
24. R. H. Crabtree, *The Organometallic Chemistry of the Transition Metals*. p. 221. John Wiley, New York (1988).

Polyhedron Vol. 9, No. 9, pp. 1175–1179, 1990
Printed in Great Britain

0277–5387/90 $3.00+.00
© 1990 Pergamon Press plc

A STUDY OF THE ANATION REACTION OF $[Cr(NH_3)_6][C_2O_4]_{1.5} \cdot 2H_2O$ IN THE SOLID STATE

PAUL O'BRIEN* and NIGEL B. SELLERS

Department of Chemistry, Queen Mary and Westfield College, University of London, Mile End Road, London E1 4NS, U.K.

(*Received* 14 *September* 1989; *accepted* 15 *December* 1989)

Abstract—The crystalline oxalate salts of chromium(III) and cobalt(III) hexaammines $[M(NH_3)_6][C_2O_4]_{1.5} \cdot 2H_2O$ have been prepared. The chromium salt readily dehydrates and deamminates at 140°C losing four equivalents of ammonia to yield an amorphous product, $[Cr(NH_3)_2(C_2O_4)_{1.5}]$, in which bridging oxalates are coordinated to chromium.

The anation reactions of trivalent metal complexes are amongst the most widely studied of solid-state reactions of coordination complexes.[1–4] As such they have been widely used in discussions of the mechanisms of such reactions, on the whole such debate has tended to ignore solid-state effects. It is unusual for any information on the crystallinity of the reaction product to be reported and mechanisms are usually interpreted in terms of SN 1 (D) or SN 2 (A) processes at the metal centre.[1–4] However, LeMay and Babich[1] have pointed out many of the difficulties in determining mechanisms due to the effects of procedural variables, and House[5] has emphasized the importance, in controlling anation reactions, of defects in the solids.

We have, for some time, been interested both in the reactions of various coordination complexes in the solid state,[6–9] and in the coordination chemistry of chromium(III).[10–14] We were keen to study a system in which a well-defined salt of a cationic chromium(III) complex reacted in the solid state with an anionic chelating ligand, present as the counter ion, but salts of this kind have proved difficult to synthesize. However, the oxalate salts of both chromium and cobalt hexaammines were easy to prepare; in this paper we report on their solid-state reactivity.

RESULTS AND DISCUSSION

Preparation and characterization of the hexaammine salts

The oxalate salts of the hexaammines were prepared by the direct reaction of a cold solution of the nitrate salt of the hexaamine with a solution of potassium oxalate (see Experimental). The oxalate salts of both of the hexaammines were microcrystalline and isomorphous. Many attempts to crystallize the salts, e.g. by diffusion methods, were made and although crystalline material could be obtained the compounds formed as "star bursts" of very fine needles unsuitable for a single-crystal X-ray structure determination.

The IR and electronic spectra of the chromium salt with oxalate are summarized in Tables 1 and 2. The IR spectra (Fig. 1) of the salt before heating is close to an addition of that of the oxalate dianion (e.g. as in $K_2C_2O_4$) and the metal hexaammine; the main bands can be assigned by reference to the parent compounds and the literature,[15] Table 1. The ligand-field strength, as judged from the electronic spectrum,[16] is similar to that in other hexaammine salts of chromium(III) (Table 2), indicating that no anation has occurred during the preparation of the complex. The magnetic moment is typical of that found for a monomeric chromium(III) complex, Table 2.

Thermal analysis of the chromium salt (10°C min^{-1}, N_2 25 cm^3 min^{-1}) gave a single mass loss (120–180°C) of 30%, which is close to that theoretically required for the loss of two molecules of water and four of ammonia (32%). The product and kinetics of the decomposition are discussed later in this paper. Differential thermal analysis of the chromium salt (10°C min^{-1}, static air) resulted in a single endotherm concurrent with deammination and dehydration, $\Delta H = 22(\pm 3)$ kJ mol^{-1} (110–164°C, extrapolated onset temperature 108°C).

The cobalt(III) salt had analogous spectroscopic properties to that of chromium(III), but thermal decomposition took place in three steps: 10.5%,

* Author to whom correspondence should be addressed.

Table 1. Selected IR spectra assignments

$[Cr(NH_3)_6][C_2O_4]_{1.5}\cdot 2H_2O$	Product	Literature $K_2(C_2O_4)^a$ $([Cr(NH_3)_6][NO_3]_3)^b$ $\{K_3[Cr(C_2O_4)_3]\}\cdot 3H_2O^b$
1596		1606, ν_a(C═O)
	1708, 1678, 1650	{1708, 1684, 1660}, ν_a(C═O)
	1620	(1630), $\delta_a(H_3N)$
1372	1377, 1300	{1398}, ν_s(CO)+ν(C—C)
		1311, ν_s(C—O)+δ(O—C═O)
1289	1275, 1258	{1253}, ν_s(C—O)+δ(O—C═O)
767		772, ν_s(C—O)+δ(O—C═O)
757	762	(748), $\mu_r(NH_3)$
	896	{893}, ν_s(C—O)+δ(O—C═O)
	845	
807	804	{810, 798}, δ(O—C═O)+ν(MO)
834		
581		{595}, crystal water?
	541	{543}, ν(MO)+ν(C—C)
		526, ν(C—C)
470	479	{485}, ring def.+δ(O—C═O)
		(495, 473, 465), ν(MN)
	408	{415}, ν(MO)+ring def.
	360	{358}, δ(O—C═O)+ν(C—C)

[a] This work.

[b] For details of assignments see ref. 14; ν, stretching, μ_w, wagging, μ_r, rocking, μ_t, twisting, δ, in-plane bending deformation.

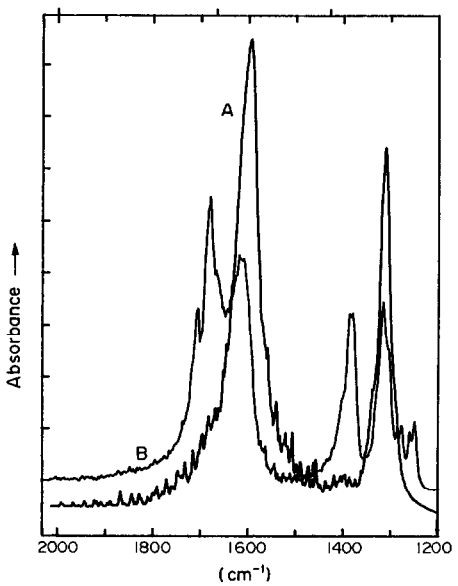

Fig. 1. The IR spectrum of $[Cr(NH_3)_6][C_2O_4]_{1.5}\cdot 2H_2O$ and the product of deammination. The spectra were obtained as KBr disks (1% 100 mg); the spectrum of the salt (A) was first recorded, then the disk was placed in an oven at 140°C for 45 min and spectrum (B) was recorded after the disk had cooled. The results are similar to those obtained for a sample decomposed in an oven, Table 1.

Table 2. Electronic spectra[a]

Compound	Energy	μ_{BM}
$[Cr(NH_3)_6]^{3+}[NO_3]$[16]	21.6, 28.3	—
$[Cr(NH_3)_6][C_2O_4]_{1.5}\cdot 2H_2O$	21.7, 28.4	3.9
$[Cr(NH_3)_6][C_2O_4]_{1.5}\cdot 2H_2O$ after deammination	18.3, 24.8	3.5
$K[Cr(NH_3)_2(C_2O_4)_2]$[b]	18.7, 26.7	—
fac-$[Cr(glyO)_3]$[14]	19.2, 25.3	—
$K_3[Cr(C_2O_4)]\cdot 3H_2O$	17.4, 24.3	—

[a] 10^3 cm^{-1}, by diffuse reflectance, for the two lowest energy bands.

[b] E. Kyuno, M. Kamada and N. Tanaka, *Bull. Chem. Soc. Jpn* 1967, **40**, 1848.

107–145°C ($2H_2O$, 10.9%), 41%, 155–290°C ($6NH_3+CO$, 40%) and 20.5% up to 500°C ($CO+CO_2$, 21.9%) (10°C min^{-1}, N_2 25 cm^3 min^{-1}). The oxalate anion decomposed concurrent with deammination and the deammination did not lead to a simple reaction of the oxalate with the metal centre; further studies of this compound were not undertaken. However, it is interesting to note

the difference in the reactivity of these isomorphous salts.

Characterization of the reaction product

The product of the deammination of the chromium complex was always found to be amorphous. In the product of the reaction the antisymmetric stretch of the COO^- group is shifted from a single peak at 1596 cm^{-1}, in the salt, to a series of peaks between 1708–1660 cm^{-1}; the new bands are consistent with coordination of the carboxylate function to the metal[15] and resemble the antisymmetric carboxylate stretches in trisoxalatochromate(III). The symmetric carboxylate stretches are also more complicated in the reaction product (Table 1) but show no obvious resemblance to the frequencies in the tris-oxalate. The separation of the symmetric and antisymmetric oxalate stretches is greater than in the chelating oxalates of chromium(III); this observation may suggest bridging oxalate groups in the reaction product.[15,16] A new band is observed at 408 cm^{-1} and may be assigned tentatively as an M—O stretch.[15]

The electronic spectra of various complexes with chromophores from CrN_6 to CrO_6 are summarized in Table 2; the lowest energy *d–d* transition ($^4A_{1g} \rightarrow {}^4T_{2g}$ in *Oh* symmetry) gives an approximate measure of the ligand-field strength.[17] The initial product of the reaction can be assigned as a CrN_2O_4 chromophore. The fact that the lowest energy transition is not split suggests a single product (or products with remarkably similar ligand-field strengths) and that a *cis* arrangement of similar donor atoms predominates.[13,18] The magnetic moment of the salt is slightly below that expected for a monomeric chromium(III) complex (Table 2), supporting the suggestion made above that the product involves bridging ligands.

On dissolution of the product in water the resulting solution had a conductivity of 56 Ω^{-1} cm^2 mol^{-1} (per chromium), typical of a 1 : 1 electrolyte. On standing for 3–4 h the conductivity of the solution gradually increased to 213 Ω^{-1} cm^2 mol^{-1} consistent with a 2 : 1 electrolyte. Solutions of the product separated into two bands on a Sephadex A-25 anion-exchange column, a rapidly moving purple band and a more firmly bound green fraction. The two fractions were characterized by bands in the electronic spectra at 18.5 and 25.0×10^3 cm^{-1} and 17.5 and 24.4×10^3 cm^{-1}, respectively, suggesting CrN_3O_3 and CrO_6 chromophores.

The product of the reaction is probably a chromium(III) complex involving bridging oxalates; a structure such as the neutral dimer $[(NH_3)_2(C_2O_4)Cr(C_2O_4)Cr(C_2O_4)(NH_3)_2]$ with a catenaoxalate bridge fits well with all of the spectroscopic properties of the product, but fails to explain the facile hydrolysis in aqueous solution. A more random polymeric structure involving extended chains of singly (μ) bridging oxalato ligands is more likely. Structures involving two different chromium chromophores seem unlikely as the electronic spectrum of the product has a symmetrical band at low energy.

Isothermal kinetic studies

Isothermal studies of the decomposition were then carried out to determine the mechanism of the solid-state reaction. In order to determine the most appropriate rate law the kinetic results were investigated using various models.[6,9,19,20] Reduced time plots,[21] in which progress of the reaction (α) is plotted against $t/t_{0.5}$ (α, fraction of reaction, $\alpha = 1$, 100% reaction, corresponding to the loss of two molecules of water and four of ammonia from each hexaammine, $t/t_{0.5}$ the absolute time divided by the estimated half-life), are a useful way of assessing the appropriate rate law. Results from a range of temperatures may be compared on a single plot; Fig. 2 shows a reduced time plot. The reaction profile is close to that required for a reaction which obeys the concept of an order (usually for a solid-state process 1, 0.5 or 0.333). Closer inspection of various reduced time plots, and the fitting of the results to these various rate laws as previously described (Table 3),[6,18,19] strongly supports a first-order model. The activation energy, derived from an Arrhenius plot of the first-order rate constants, is 84(±5) kJ mol^{-1}.

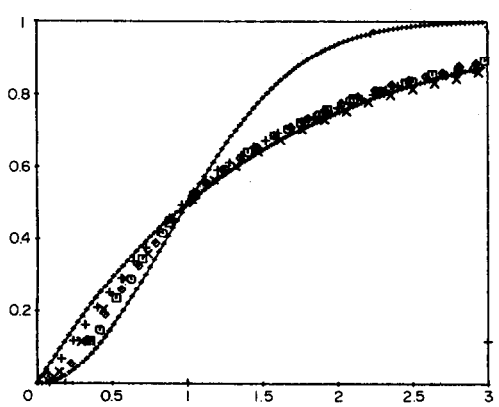

Fig. 2. Reduced time plot. The graph incorporates data at the following temperature (°C): +, 117; ×, 125; ◇, 136; □, 142; ○, 147. The solid lines are the theoretical curves for (a) a first-order process and (b) nucleation and growth in two-dimensions (Avrami/Eroveev kinetics, see refs 20 and 21).

Table 3. First-order rate constants

Temperature (°C)	$10^4 k$ (s^{-1})	
117	8.5	
125	16.8	$\Delta H = 22(\pm 3)$ kJ mol^{-1}
129	17.2	$\Delta H^{\ddagger} = 80(\pm 5)$ kJ mol^{-1}
136	29.2	$\Delta S^{\ddagger} = -100(\pm 25)$ J K^{-1} mol^{-1}
142	45.0	
147	52.5	

The overall process models as a single first-order process. The most logical explanation for this observation is that we are following a random process within the solid in which the loss of various constituents occurs with a single rate-determining step, probably Cr—N bond breaking. Our experience has indicated that genuine first-order reactions are rare in the solid state, but the majority of reactions we are aware of involve crystalline products and reactants. One reason for the lack of a crystalline product may be the large volume change in this reaction, the loss of six molecules overall and the substitution of a chelating ligand into the first coordination sphere of chromium producing too much structural change for the retention of crystallinity.

Consequently it is difficult to draw firm conclusions from our kinetic study, especially as procedural variables can have a marked effect on activation parameters.[4] However, the results do clearly indicate:

(1) a first-order rate,
(2) a modest enthalpy of activation and entropy of activation.

The reaction may proceed by a dissociative mechanism in which the rate-determining step is the loss of ammonia molecules from the ammine complex and resembles the reaction of glycine with $[Cr(NH_3)_6]^{3+}$, in a melt[14] ($\Delta H^{\ddagger}$ 106 kJ mol^{-1}).

EXPERIMENTAL

Materials

All reagents were purchased from BDH Chemicals Ltd. $[Cr(NH_3)_6](NO_3)_3$ and $[Co(NH_3)_6](NO_3)_3$ were prepared by the literature method.[22,23]

Synthesis of $[M(NH_3)_6][C_2O_4]_{1.5}\cdot 2H_2O$ (M = Co *or* Cr)

$[M(NH_3)_6](NO_3)_3$ (1.0 g) was dissolved in cold water (10 cm^3) and 5 cm^3 of a saturated solution of potassium oxalate was added with continuous stirring. A bright yellow microcrystalline precipitate formed almost immediately, the solid was air-dried and stored in a deep freeze. The chromium complex effloresced in air losing one water of hydration. Major *d*-spacings (Å) are as follows for $[Cr(NH_3)_6][C_2O_4]_{1.5}\cdot 2H_2O$, (Co): 4.39, (4.36), 4.15, (4.06), 2.83, (2.80), 2.32, (2,30), 2.23, (2.27), 1.89, (1.86), 1.76, (1.76), 1.40, (1.49), 1.38, (1.35). Both salts gave satisfactory microanalysis: $[Cr(NH_3)_6][C_2O_4]_{1.5}\cdot 2H_2O$ %C 11.1 (11.4), %H 6.8 (6.7), %N 26.0 (25.7); $[Co(NH_3)_6][C_2O_4]_{1.5}\cdot 2H_2O$: %C 10.9 (10.8), %H 6.7 (6.5), %N 25.5 (24.4).

Physical measurements

Electronic spectra were recorded with a Perkin–Elmer 330 spectrophotometer; IR spectra were recorded on a Mattson Polaris FT–IR spectrometer; as Nujol mulls or KBr disks (*ca* 2%, 100 mg). Magnetic moments were measured with an Evans' Balance (Sherwood Scientific, Cambridge, U.K.). Thermogravimetric studies were carried out using a Stanton Redcroft TG-750 (in static air). Differential thermal analysis was undertaken using a DTA 671B, calibrated with high purity indium metal. Activation parameters were calculated as described by Edwards *et al.*[24]

Acknowledgements—N.B.S. wishes to thank the SERC for a research studentship. We thank the University of London Central Research Fund for their support of our work.

REFERENCES

1. H. E. LeMay Jr and M. W. Babich, *Thermochim. Acta* 1980, **48**, 147.
2. H. Oki and K. Orsuka, *Bull. Chem. Soc. Jpn* 1976, **49**, 1841.
3. R. Tsuchiya, A. Uehara and K. Kobayashi, *Bull. Chem. Soc. Jpn* 1980, **53**, 921.
4. H. E. LeMay, in *Comprehensive Coordination Chemistry* (Edited by G. Wilkinson, R. D. Gillard and J. A. McCleverty), Vol. 1, Ch. 7.5. Pergamon Press, Oxford (1987).

5. J. E. House Jr, *Thermochim. Acta* 1980, **38**, 59.
6. P. O'Brien, *Polyhedron* 1983, **2**, 233.
7. P. O'Brien, *Transition Met. Chem.* 1980, **5**, 314.
8. P. O'Brien, *Inorg. Chim. Acta* 1981, **55**, L27.
9. P. O'Brien, *Polyhedron* 1986, **5**, 659.
10. M. Abdullah, J. Barrett and P. O'Brien, *J. Chem. Soc., Dalton Trans.* 1984, 1647.
11. J. Barrett, P. O'Brien and J. Pedrosa de Jesus, *Polyhedron* 1985, **4**, 1.
12. L. F. Larkworthy, K. B. Nolan and P. O'Brien, in *Comprehensive Coordination Chemistry* (Edited by G. Wilkinson, R. D. Gillard and J. A. McCleverty), Vol. 3, Ch. 35. Pergamon Press, Oxford (1987).
13. M. Abdullah, J. Barrett and P. O'Brien, *J. Chem. Soc., Dalton Trans.* 1985, 2085.
14. P. O'Brien and N. B. Sellers, *Polyhedron* 1990, **9**, 119.
15. K. Nakamoto, *Infrared and Raman Spectra of Inorganic and Coordination Compounds*, 4th edn, pp. 192, 234 and 245. John Wiley, New York (1986).
16. P. O'Brien, *J. Chem. Soc., Dalton Trans.* 1981, 1540.
17. R. S. Drago, *Physical Methods in Chemistry*, p. 387. Holt Saunders, New York (1977).
18. R. G. Wilkins and M. G. Williams, in *Modern Coordination Chemistry* (Edited by J. Lewis and R. G. Wilkins), p. 187. Interscience, New York (1960).
19. M. Watabe, H. Yano, Y. Odaka and H. Kobayashi, *Inorg. Chem.* 1981, **20**, 3623.
20. P. O'Brien, *J. Chem. Soc., Dalton Trans.* 1982, 1173.
21. J. H. Sharp, G. W. Brindley and B. N. Narahari Achar, *J. Am. Ceram. Soc.* 1966, **49**, 379.
22. A. L. Oppegard and J. C. Bailar Jr, *Inorg. Synth.* 1950, **3**, 153.
23. A. A. Blanchard, *Inorg. Synth.* 1949, **2**, 126.
24. J. O. Edwards, F. Monacelli and G. Ortaggi, *Inorg. Chim. Acta* 1974, **11**, 47.

Polyhedron Vol. 9, No. 9, pp. 1181–1186, 1990
Printed in Great Britain

0277–5387/90 $3.00+.00
© 1990 Pergamon Press plc

REDOX CHEMISTRY AND SPECTROSCOPY OF 2-MERCAPTOBENZOIC ACID AND ITS MANGANESE(II) AND (III) COMPLEXES IN DIMETHYLSULPHOXIDE

MARIO E. BODINI* and M. ANGÉLICA DEL VALLE

Laboratorio de Electroquímica, Facultad de Química,
Pontificia Universidad Católica de Chile, Casilla 6177, Santiago, Chile

(*Received* 31 *August* 1989; *accepted* 15 *December* 1989)

Abstract—The redox behaviour of the ligand 2-mercaptobenzoic acid has been studied in dimethylsulphoxide. The combination of the dianion of the ligand with manganese(II) in a 1:2 mole ratio forms a colourless complex whose stability constant has been determined polarographically as 2.8×10^9 M^{-2}. Oxidation of this complex at -0.45 V vs SCE yields a red complex of manganese(III) whose stoichiometry is also 1:2. The complexes have been characterized by cyclic voltammetry, controlled-potential electrolysis, optical spectroscopy and magnetic susceptibility measurements. The formation constant of the $[Mn^{III}(2\text{-MBA})_2]^-$ complex has been evaluated spectrophotometrically as 9.3×10^7 M^{-2}. These results may be relevant to the development of an adequate model for the active centre of acid phosphatases.

The coordination chemistry of manganese in the +2, +3 and +4 oxidation states is useful for understanding the structure and reactivity of manganese sites in biological systems. It is now well established that manganese plays an important role in numerous redox processes: at least superoxide dismutase,[1,2] acid phosphatases,[3] pseudo-catalase[4] and the photosynthetic oxygen-evolving complex[5–7] contain manganese in their catalytic centre. Therefore, an important area of investigation of the bioinorganic chemistry of manganese is the study of the structure and reactivity of manganese complexes with biologically relevant heteroatom donor ligands.

Previous papers from our group have been concerned with the redox properties of manganese complexes to serve as models for the centre that catalyses the oxidation of water to dioxygen in Photosystem II of green-plant photosynthesis.[8–11] Transition metal dithiolate complexes have also attracted our attention[12] because of the common occurrence of metal–sulphur bonding in biological systems.[13–15] Therefore, we have undertaken the study of the redox chemistry of the ligand 2-mercaptobenzoic acid (2-MBA) and its complexes with manganese in order to determine their stability and stoichiometry, as well as the possibility of stabilizing higher oxidation states of the metal. This ligand represents an analogue of a cysteine residue—with a second coordinating group to enhance the stability of the complexes. It is thus of interest to determine the properties of its complexes with manganese to mimic the ligation properties of cysteinyl residues in proteins.

EXPERIMENTAL

Equipment

A three-electrode potentiostat (Tacussel Model PRT 20-2X potentionstate/galvanostat with Model GSTP wave generator) was used for the cyclic voltammetric and controlled-potential electrolysis experiments.

A current integrator based on operational amplifiers was used as coulometer in the controlled-potential electrolyses.

Cyclic voltammograms were recorded on a Hewlett–Packard Model 7004 A X–Y recorder. The electrochemical cell was equipped with a Beckman platinum-inlay working electrode (area 0.23 cm^2), a platinum coil auxiliary electrode, and an Ag/AgCl

* Author to whom correspondence should be addressed.

reference electrode filled with an aqueous tetramethylammonium chloride solution and adjusted to 0.00 V vs SCE.[16] The latter was contained in a Pyrex tube with a soft-glass cracked tip; this electrode was placed inside a Luggin capillary. For controlled-potential electrolysis, a platinum-mesh working electrode was employed.

A Beckman Model ACTA CV spectrophotometer was used for UV–vis spectrophotometric measurements. The magnetic susceptibility measurements were made with a Varian XL-100 NMR spectrometer by the method of Evans[17] as modified by Retting.[18] Diamagnetic corrections were made.[19]

Air-sensitive compounds were handled in a glove bag (Aldrich) under a nitrogen atmosphere and the oxygen content was monitored with a Beckman Model Monitor II Oxygen Analyser.

Reagents

The reagents for the investigation and syntheses included $Mn(ClO_4)_2 \cdot 6H_2O$ (G. Frederick Smith), tetraethylammonium hydroxide (TEAOH) (25% in methanol, Eastman), tetramethylammonium chloride (Aldrich) and tetraethylammonium perchlorate (TEAP) (G. Frederick Smith). The ligand 2-mercaptobenzoic acid was obtained from Aldrich and was purified by sublimation.

Burdick and Jackson Laboratories "distilled-in-glass" grade solvents were used without further purification for all of the experiments. High purity argon was used to deaerate solutions.

Because the solvation water of the $Mn(ClO_4)_2 \cdot 6H_2O$ salt interfered with the stoichiometric formation of the complexes under study, $[Mn^{II}(DMU)_6][ClO_4]_2$ (DMU = dimethylurea)[20] was used in all the experiments in which the manganese(II) complexes were formed *in situ*. As a source of manganese(III) $[Mn^{III}(urea)_6][ClO_4]_3$[21] was used in all the experiments.

RESULTS AND DISCUSSION

A preliminary study of the ligand showed that this compound is very sensitive to air, and is oxidized by molecular oxygen to the corresponding dimer. Therefore, it was purified by sublimation at reduced pressure. White crystals were obtained whose purity was verified by controlled potential coulometry.

Figure 1 shows the cyclic voltammograms of solutions of 2-MBA in dimethylsulphoxide. In Fig. 1(A) it is observed that in a negative scan a reduction peak at −0.65 V vs SCE appears corresponding to the following process:

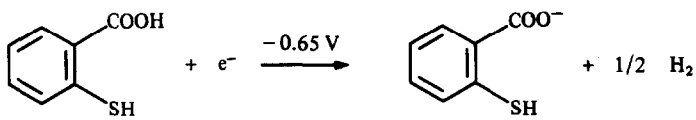

(1)

A study of the peak current as a function of the square root of the scan rate indicates that this is a diffusion-controlled process, and controlled-potential electrolysis at −0.90 V vs SCE allowed us to determine that one equivalent of charge per mole of ligand has been transferred in this process. Peak 1b can be assigned to the oxidation of hydrogen that has been produced in process (1) and that remains at the electrode. In this case the peak current does not show a linear dependence with the square root of the scan rate. This phenomenon is commonly observed in aprotic solvents and has been reported in a study of the activation of molecular hydrogen at a platinum disc electrode in non-aqueous solvents.[22]

The positive scan [Fig. 1(B)] shows an anodic peak (peak 1c) at 0.45 V vs SCE, which corresponds to the oxidation of the ligand in solution to the corresponding dimer according to process (2). The electron stoichiometry of this process has been confirmed by controlled-potential electrolysis.

Peaks 1d and 1e are the reductions of the dimeric species generated before. The first peak (1e) overlaps with process (1) and therefore it cannot be observed very easily. However, peak 1d allows the determination of the purity of the ligand because the absence of this peak in a negative scan indicates the absence of oxidized ligand.

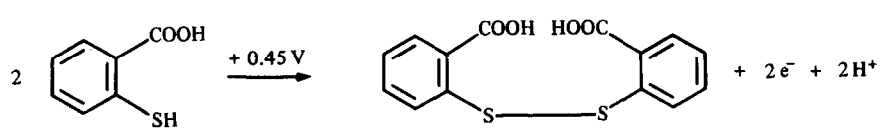

(2)

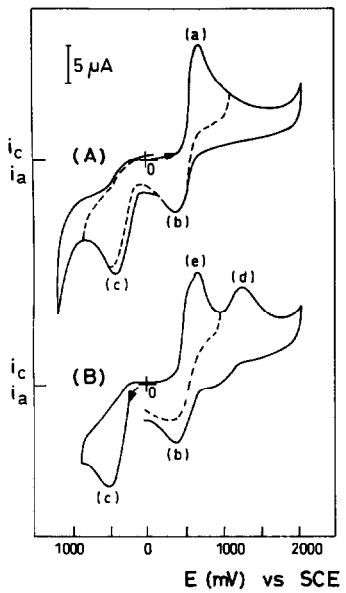

Fig. 1. Cyclic voltammograms in Me_2SO (0.1 M TEAP; $v = 0.1$ V s^{-1}) of a solution that is 1 mM in 2-MBA. (A) initial negative scan; (B) initial positive scan.

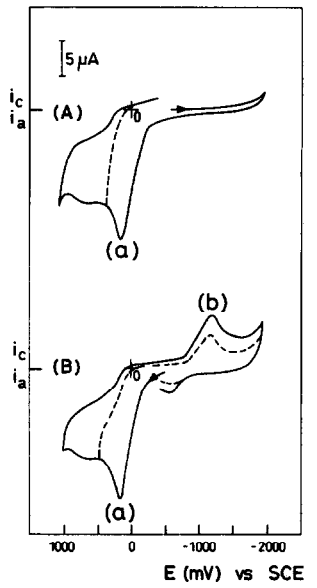

Fig. 2. Cyclic voltammograms in Me_2SO (0.1 M TEAP; $v = 0.1$ V s^{-1}) of a solution that is 1 mM in 2-MBA and 1 mM in base (TEAOH). (A) initial negative scan; (B) initial positive scan.

The two reduction steps of the dimeric species are illustrated by processes (3) and (4). In these cases the electron stoichiometries of the reactions have been confirmed by controlled-potential electrolysis.

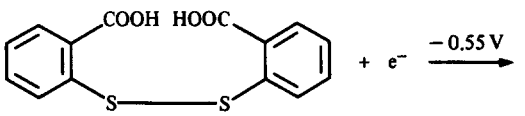

(3)

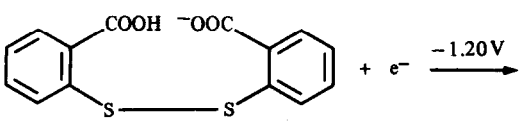

(4)

Figure 2 shows the voltammetric study of the ligand in the presence of one equivalent of base. In a negative scan [Fig. 2(A)] no reduction peak is observed which confirms that process (1) is equivalent to the neutralization of a proton of the ligand.

In the monoanionic species in this case, the proton that remains in the molecule is shared between the carboxylate and the mercapto groups, as a consequence of the *ortho*-effect present, weakening the S—H bond and facilitating its oxidation to produce the dimeric species, as can be inferred by the appearance of peak 2a. In this case the oxidation takes place at a less positive potential than when neutral 2-MBA is present.

On the other hand, the potential of peak 2b is equivalent to that of peak 1d, which would confirm that the ligand is oxidized in 2a to the corresponding disulphide according to process (5), indicating that the protons generated in this process permit the obtention of the species that is reduced in 1d.

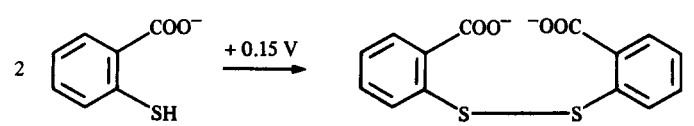

(5)

Figure 3 shows the voltammograms corresponding to a solution of 2-MBA in the presence of two equivalents of base. The most relevant observation in this case is that the oxidation to the cor-

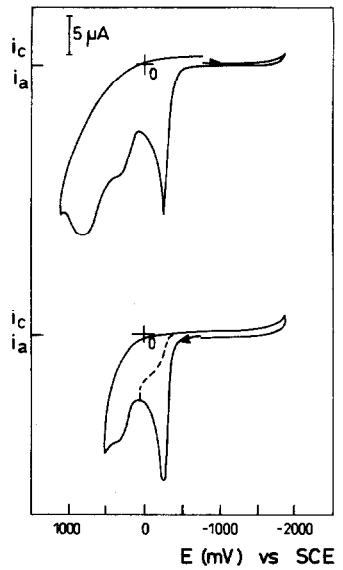

Fig. 3. Cyclic voltammograms in Me_2SO (0.1 M TEAP; $v = 0.1$ V s^{-1}) of a solution that is 1 mM in 2-MBA and 2 mM in base (TEAOH). (A) initial negative scan; (B) initial positive scan.

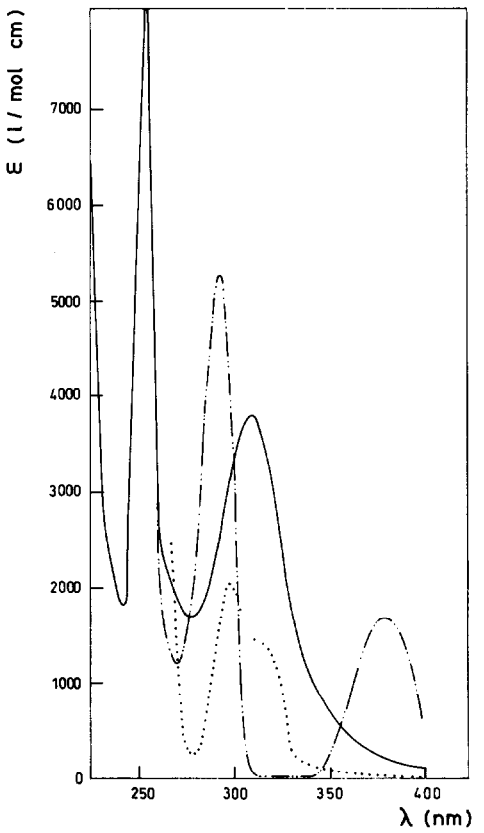

Fig. 4. UV spectra in Me_2SO of solutions that are: (——) 1 mM in the dianion of 2-MBA; (–·–·–·–) 1 mM in the monoanion of 2-MBA; (·····) 1 mM in the neutral form of 2-MBA.

responding disulphide becomes even easier because the dianionic species are now in solution. The absence of cathodic processes when the potential is scanned in any direction should also be noted. This confirms the above mentioned reduction processes for the oxidized ligand because they cannot take place when both protons have been neutralized.

Figure 4 shows the absorption spectra of solutions of 2-MBA in its neutral, monoanionic and dianionic forms. The neutral protonated form presents an absorption maximum at 295 nm ($\varepsilon = 2100$ M^{-1} cm^{-1}) with a sort of shoulder at 315 nm, which may be due in part to the *B* band of the benzene ring of the ligand. The addition of one equivalent of base causes a bathochromic shift due to the presence of the unshared electrons of the monoanion. Therefore, the E_2 band of the ligand is observed at 290 nm ($\varepsilon = 5350$ M^{-1} cm^{-1}), whereas the *B* band shows up at 380 nm ($\varepsilon = 1670$ M^{-1} cm^{-1}). The dianion of the species shows a hypsochromic shift with a great increase in the extinction coefficients. The absorption maximum corresponding to the E_2 band of the benzene ring of the ligand appears at 260 nm ($\varepsilon = 8000$ M^{-1} cm^{-1}) and the *B* band at 310 nm ($\varepsilon = 3700$ M^{-1} cm − 1).

Finally, with respect to the study of the ligand, it should be stated that the observed behaviour in the presence of base is analogous to that found when the protons are removed by previous controlled-potential electrolysis [Process (1)]. This indicates that the amount of water produced upon chemical neutralization of a proton does not affect the above mentioned processes. However, it is very important to avoid the presence of oxygen in the system as the anionic ligand oxidizes very easily to the corresponding disulphide [Process (2)].

The addition of manganese(II) to the ligand, both in its neutral and monoanionic forms, does not produce any change either in the spectra or the cyclic voltammograms of the latter. Only the reduction processes corresponding to the free metal are observed to be independent of the electrochemical behaviour of the ligand. Therefore, we can conclude that under these conditions no complex is being formed.

The voltammetric behaviour of the ligand upon addition of two equivalents of base and in the presence of manganese(II) is illustrated in Fig. 5. In this case a 1 : 2 complex is formed, because the reduction of free manganese(II) is observed when a stoichiometric ratio of 1 : 1 is used [Fig. 5(C)]. In the latter case the free manganese(II) is in excess with respect to the ligand.

The cyclic voltammogram of a solution of the complex [Fig. 5(B)] shows a fairly reversible couple

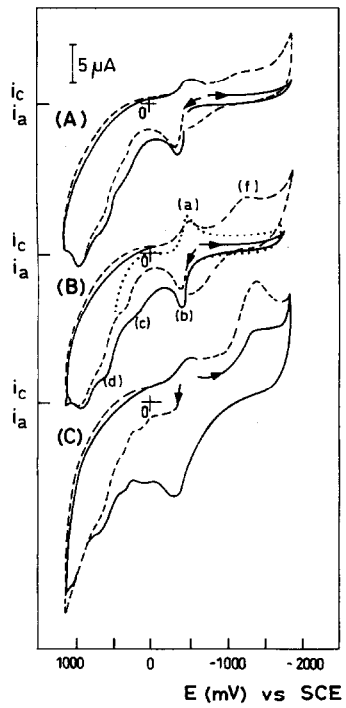

Fig. 5. Cyclic voltammograms in Me_2SO (0.1 M TEAP; $v = 0.1$ V s^{-1}) of solutions that are 1 mM in the dianion of 2-MBA plus: (A) 1/3 mM Mn^{2+}; (B) 1/2 mM Mn^{2+}; and (C) 1mM Mn^{2+}. The metal ion has been added as $[Mn^{II}(DMU)_6](ClO_4)_2$.

(peaks 5a and 5b) when an initial negative scan is made. On the other hand, when the initial scan is made positive, the reduction of free manganese(II) at -1.25 V vs SCE is observed clearly only if the potential scan is reversed after peaks 5d or 5e. Therefore, we can conclude that the processes corresponding to these two peaks are oxidations of the ligand with the subsequent destruction of the complex.

On the other hand, peak 5b corresponds to an oxidation process that leads to another complex. Controlled-potential electrolysis at -0.2 V vs SCE produces a red species with one equivalent of charge being transferred per mole of metal ion. Therefore, this result indicates that this voltammetric peak corresponds to the oxidation of manganese(II) to manganese(III). Controlled-potential electrolysis of a solution of the red complex at -0.7 V vs SCE yields a colourless solution which shows the same voltammetric behaviour as the initial one. In this case, one equivalent of charge per mole of metal ion is transferred in the reduction process. The voltammetric behaviour of these solutions indicates that the following process is reversible:[23]

$$[Mn^{II}(2\text{-MBA})_2]^{2-} \underset{-0.50\,V}{\overset{-0.45\,V}{\rightleftharpoons}} [Mn^{III}(2\text{-MBA})_2]^{-} + e^{-}. \quad (6)$$

Figure 6(A) illustrates the UV spectra of the solutions of the complexes of manganese with 2-MBA. In the case of manganese(II) an absorption maximum is observed at 300 nm ($\varepsilon = 3300$ M^{-1} cm^{-1}) which is probably the same *B* band of the benzene ring of the ligand that has shifted hypsochromically by the interaction of the metal ion with the electrons of the donor groups. In the presence of manganese(III) this band is not observed

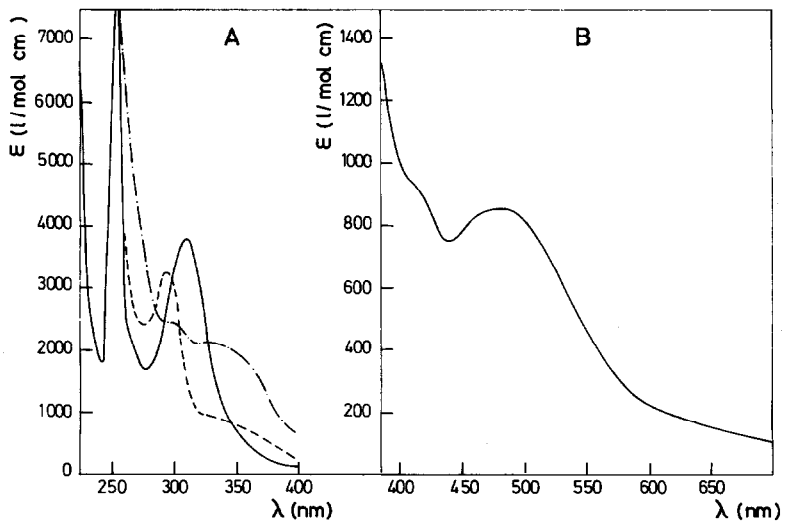

Fig. 6. (A) UV spectra in Me_2SO of solutions that are: (——) 1 mM in the dianion of 2-MBA; (– – – –) 1 mM in the dianion of 2–MBA plus 0.5 mM $[Mn^{II}(DMU)_6](ClO_4)_2$; (–·–·–) 1 mM in the complex of manganese(III) obtained by oxidation at -1.2 V vs SCE. (B) Visible spectrum of a solution 1 mM in the complex of manganese(III).

probably because it has shifted further to shorter wavelengths as a consequence of stronger interaction of these electrons with the oxidized metal. In the visible region, only the red species shows an absorption maximum at 480 nm ($\varepsilon = 840$ M^{-1} cm^{-1}) which could be due to a *d–d* transition in the metal ion, and this is illustrated in Fig. 6(B).

The spectrophotometric behaviour of the red complex of manganese(III) allowed the determination of its formation constant by Job's method (9.3×10^7 M^{-2}). The stoichiometry of the complex was confirmed.

For the manganese(II) complex the determination of the formation constant by this method was not possible because both the ligand and the complex present absorption maxima that are too close to each other. Therefore, its value was evaluated polarographically[24] as 2.8×10^9 M^{-2}.

Finally, the magnetic susceptibility of solutions of these complexes was measured using Evans' method in order to confirm the oxidation state of the metal ion. The colourless solution gave a value of 5.89 BM which indicates that it is manganese(II), whereas the red complex gave a value of 5.28 BM which is closer to the theoretical value for manganese(III).

The oxidation state of the metal ion in the red complex was further confirmed by preparing a solution using $[Mn^{III}(urea)_6(ClO_4)_3]$ as starting material. This solution presented the same voltammetric, spectrophotometric and magnetic behaviour as the one obtained by oxidation of the manganese(II) complex.

These results may be relevant for the development of a model system for the active centre of acid phosphatases. It is believed that this enzyme—isolated from plants such as sweet potato[3] and spinach[25]—appears to contain a mononuclear manganese(III) site with thiolate (cysteine) and phenoxide (tyrosine) ligation.[3,26]

Acknowledgement—This work was supported by CONICYT–Chile through the FONDECYT No. 309/88 Research Grant.

REFERENCES

1. W. C. Stallings, K. A. Pattridge, R. K. Strong and M. L. Ludwig, *Manganese in Metabolism and Enzyme Function*, p. 405. Academic Press, New York (1986).
2. Y. Kono and I. Fridovich, *J. Biol. Chem.* 1983, **258**, 13,646.
3. Y. Sugiura, H. Kawabe, H. Tanaka, S. Fujimoto and A. Ohara, *J. Biol. Chem.* 1981, **256**, 10,664.
4. W. F. Beyer and I. Fridovich, *Manganese in Metabolism and Enzyme Function*, p. 193. Academic Press, New York (1986).
5. J. C. de Paula and G. W. Brudvig, *J. Am. Chem. Soc.* 1985, **107**, 2643.
6. J. A. Kirby, S. A. Robertson, J. P. Smith, A. C. Thompson, S. R. Copper and M. P. Kelin, *J. Am. Chem. Soc.* 1981, **103**, 5529.
7. G. C. Dismukes, *Photochem. Photobiol.* 1986, **43**, 99.
8. M. Bodini, L. Willis, T. Riechel and D. T. Sawyer, *Inorg. Chem.* 1976, **15**, 1538.
9. M. Bodini and D. T. Sawyer, *J. Am. Chem. Soc.* 1976, **98**, 8366.
10. V. Arancibia and M. E. Bodini, *Am. Quim.* 1986, **82B**, 309.
11. M. Bodini and V. Arancibia, *Polyhedron* 1989, **8**, 1407.
12. D. T. Sawyer, G. S. Srivatsa, M. E. Bodini, W. P. Schaefer and R. M. Wing, *J. Am. Chem. Soc.* 1986, **108**, 936.
13. T. G. Spiro (Ed.), *Iron Sulfur Proteins*, Vol. 4. John Wiley, New York (1982).
14. G. L. Lawrence and D. T. Sawyer, *Coord. Chem. Rev.* 1978, **27**, 173.
15. H. Siegel (Ed.), *Copper Proteins*, Vol. 13. Marcel Dekker, New York (1981).
16. D. T. Sawyer and J. L. Roberts, *Experimental Electrochemistry for Chemists*, pp. 144–145. Wiley-Interscience, New York (1974).
17. D. F. Evans, *J. Chem. Soc.* 1959, 2003.
18. M. F. Rettig, private communication, University of California, Riverside, California.
19. B. N. Figgis and J. Lewis, *Modern Coordination Chemistry* (Edited by J. Lewis and R. G. Wilkins). Interscience, New York (1960).
20. P. W. van Loenwen and W. L. Groenweld, *J. Inorg. Nucl. Chem. Lett.* 1967, **3**, 145.
21. H. Oghakozorg and J. Summers, *Inorg. Chem.* 1982, **21**, 3903.
22. D. T. Sawyer and W. C. Barrette, *Analyt. Chem.* 1984, **56**, 653.
23. J. A. Plambeck, *Electroanalytical Chemistry*, pp. 317–318. John Wiley, New York (1982).
24. Z. Galus, *Fundamentals of Electrochemical Analysis*, pp. 361–362, Halsted Press, New York (1976).
25. S. Fujimoto, T. Nakagawa, S. Ishimitsu and A. Ohara, *Chem. Phar. Bull.* 1977, **25**, 1459.
26. J. S. Bashkin, J. C. Huffman and G. Christou, *J. Am. Chem. Soc.* 1986, **108**, 5038.

Polyhedron Vol. 9, No. 9, pp. 1187–1189, 1990
Printed in Great Britain

0277-5387/90 $3.00+.00
© 1990 Pergamon Press plc

REACTION OF THE $M(CO)_3(NN)$ FRAGMENTS (M = Mo, W; NN = bipy, phen, dipyam) WITH SOME ORGANOMETALLIC HALOTIN DERIVATIVES. POLYNUCLEAR COMPLEXES CONTAINING Sn–M–X MOIETIES (X = Cl, Br, I)

J. GRANIFO

Departamento de Ciencias Químicas, Facultad de Ingeniería y Administración, Universidad de La Frontera, Casilla 54-D, Temuco, Chile

(*Received* 8 *September* 1989; *accepted* 15 *December* 1989)

Abstract—The compounds $[Fe_2(\mu\text{-}SnX_2)(CO)_4(\eta^5\text{-}C_5H_5)_2]$ and $[Fe(SnX_3)(CO)_2(\eta^5\text{-}C_5H_5)]$ (X = Cl, Br, I) were used as probes to react with the $[M(CO)_3(bipy)(NCMe)]$ complexes (M = Mo, W; bipy = 2,2′-bipyridine). The results show that only the trihalide species interact to produce trimetallic complexes $[(\eta^5\text{-}C_5H_5)(OC)_2Fe(\mu\text{-}SnX_2)M(X)(CO)_3(bipy)]$. These new substances were characterized by IR and electronic spectroscopy. The reaction can be interpreted as an insertion of the $M(CO)_3(bipy)$ fragments into Sn—X bonds to give Fe—Sn—M—X arrays. Complexes of similar formula (X = Cl) are obtained when bipy is replaced either by phen (1,10-phenanthroline) or dipyam (di-2-pyridylamine). The mono-insertion also was verified in other organometallic systems containing SnX_3 groups. In particular, the $[M(Cl)(SnCl_3)(CO)_3(bipy)]$ complexes yield only the trinuclear compounds $[(bipy)(OC)_3(Cl)M(\mu\text{-}SnCl_2)M'(Cl)(CO)_3(bipy)]$ (M′ = Mo, W) when they react with $[M(CO)_3(bipy)(NCMe)]$.

Previous papers from this laboratory[1,2] have shown that the reaction of the $M(CO)_3(NN)$ fragments [M = Mo, W; NN = 2,2′-bipyridine (bipy), 1,10-phenanthroline (phen), ethylenediamine (en)] with mercury halide derivatives, can be interpreted as the insertion of the former into the mercury–halide bonds. This characteristic was demonstrated by isolating the trimetallic complexes X—M—Hg—M—X and Fe—Hg—M—X (X = halide), using as source of the insertion fragments the $[M(CO)_3(NN)(NCMe)]$ complexes.

In this paper we describe the extension of the above insertion concept to metal centres different from mercury, with the aim to clarify a new route for preparing multinuclear organometallic complexes. Accordingly, in this work we chose to apply this property to compounds with transition metal—tin—halide bonds. The tin selection was done taking into account the recently reported[3] reaction of the $[Mo(CO)_3(bipy)(phosphine)]$ complexes with organotin halides $SnCl_3R$ (R = Cl, CH_3, C_6H_5) to produce, depending upon the phosphine, the tricarbonyl complexes $[Mo(Cl)(SnCl_2R)(CO)_3(bipy)]$. These bimetallic compounds have the $Mo(CO)_3(bipy)$ unit acting as a bridge between the chloride and tin atoms.

For the present study, the tin halide derivatives $[Fe_2(\mu\text{-}SnX_2)(CO)_4(\eta^5\text{-}C_5H_5)_2]$ and $[Fe(SnX_3)(CO)_2(\eta^5\text{-}C_5H_5)]$ were used as probes to react with the $[M(CO)_3(NN)(NCMe)]$ complexes. It was observed that the insertion occurs solely with the complexes $[Fe(SnX_3)(CO)_2(\eta^5\text{-}C_5H_5)]$ to give only trimetallic arrays. A possible explanation for this behaviour and the results using as an additional probe the complexes $[M(Cl)(SnCl_3)(CO)_3(bipy)]$, is also reported herein.

RESULTS AND DISCUSSION

Refluxing mixtures of $[Fe(SnX_3)(CO)_2(\eta^5\text{-}C_5H_5)]$ (X = Cl, Br, I) and $[M(CO)_3(bipy)(NCMe)]$ (M = Mo, W) in methanol in the molar ratio 1:1 or more gave, in all cases, only the trimetallic complexes $[(\eta^5\text{-}C_5H_5)(OC)_2Fe(\mu\text{-}SnX_2)M(X)(CO)_3(bipy)]$ according to the reaction:

$$[Fe(SnX_3)(CO)_2(\eta^5\text{-}C_5H_5)] + [M(CO)_3(bipy)(NCMe)] \longrightarrow [FeM(\mu\text{-}SnX_2)(X)(CO)_5(bipy)(\eta^5\text{-}C_5H_5)] + MeCN. \quad (1)$$

Table 1. Analytical data and IR spectra for the $[(\eta^5\text{-}C_5H_5)(OC)_2Fe(\mu\text{-}SnX_2)M(X)(CO)_3(NN)]$ (**1**) and $[(bipy)(OC)_3(Cl)M(\mu\text{-}SnCl_2)M'(Cl)(CO)_3(bipy)]$ (**2**) complexes

Compound				Colour	Analysis (%)[a] C	H	N	IR data (cm^{-1})[b] ν(CO)
		(1)						
	M	NN	X					
(a)	Mo	bipy	Cl	Orange	32.2(32.5)	1.7(1.8)	4.1(3.8)	2000, 1970b, 1890, 1855
(b)	Mo		Br	Red	28.0(27.6)	1.6(1.5)	3.1(3.2)	2010, 1970b, 1880b
(c)	Mo		I	Dark red	23.4(23.7)	1.2(1.2)	2.7(2.8)	2010, 1970b, 1880b
(d)	W		Cl	Red	28.8(29.1)	1.5(1.6)	3.4(3.4)	2020, 1980, 1960, 1870b
(e)	W		Br	Red	25.2(25.0)	1.4(1.4)	3.0(2.9)	2020, 1980, 1960, 1875b
(f)	W		I	Dark red	22.0(21.8)	1.2(1.2)	2.7(2.6)	2000, 1970, 1960, 1900, 1870
(g)	Mo	phen	Cl	Orange	34.5(34.7)	1.7(1.7)	3.8(3.7)	2030, 1980b, 1900, 1880
(h)	W		Cl	Orange	31.2(31.1)	1.4(1.5)	3.2(3.3)	2000, 1970, 1965, 1900, 1885
(i)	Mo	dipyam	Cl	Orange	32.1(31.9)	1.8(1.9)	5.7(5.6)	2015, 1970b, 1895, 1860
(j)	W		Cl	Orange	28.8(28.6)	1.7(1.7)	4.9(5.0)	2020, 1970b, 1870b
		(2)						
	M		M′					
(a)	Mo		Mo	Orange–red	33.7(33.5)	1.9(1.7)	6.2(6.0)	1990b, 1910, 1880, 1860
(b)	Mo		W	Orange	30.9(30.6)	1.7(1.6)	5.7(5.5)	1990, 1970, 1910, 1880, 1870
(c)	W		W	Orange	28.4(28.2)	1.5(1.5)	5.0(5.1)	1980, 1970, 1890, 1870, 1860

[a] Required values are given in parentheses.
[b] KBr discs.

The new compounds are air-stable, but decompose slowly in the solid state and in solution in the presence of light. They are orange to dark red crystalline solids, with the colour darkening through the sequence X = Cl < Br < I.

The behaviour in solution of the $[FeM(\mu\text{-}SnX_2)(X)(CO)_5(bipy)(\eta^5\text{-}C_5H_5)]$ complexes depends on the metal M. The tungsten derivatives are soluble in organic solvents such as methylene chloride, chloroform or acetone. The molybdenum analogous are unstable in solution. In addition, they react with donor solvents or Lewis bases (L) to produce the complexes $[Fe(SnX_3)(CO)_2(\eta^5\text{-}C_5H_5)]$ and $[Mo(CO)_3(bipy)L]$. Hence, the following equilibrium seems to be operative:

$$[FeM(\mu\text{-}SnX_2)(X)(CO)_5(bipy)(\eta^5\text{-}C_5H_5)] + L \longrightarrow [Fe(SnX_3)(CO)_2(\eta^5\text{-}C_5H_5)] + [Mo(CO)_3(bipy)L]. \quad (2)$$

The IR spectra of the $[(\eta^5\text{-}C_5H_5)(OC)_2Fe(\mu\text{-}SnX_2)M(X)(CO)_3(bipy)]$ complexes in the CO stretching region (Table 1, compounds **1a–f**) show bands assignable to the $(\eta^5\text{-}C_5H_5)(OC)_2FeSn$[4] and $SnM(X)(CO)_3(bipy)$[3] moieties. Thus, it is concluded that the insertion into the Sn—X bonds has occurred to give the Fe—Sn—M—X arrangements.

The dihalotin derivatives $[Fe_2(\mu\text{-}SnX_2)(CO)_4(\eta^5\text{-}C_5H_5)_2]$ fail to react with the $[M(CO)_3(bipy)(NCMe)]$ complexes. These and the above results showing that the insertion occurs only once, can be understood by considering adduct formation[5] as the initial step of the reaction and the Lewis acid character of the tin atom. The tin acidity decreases in the series of compounds $[(\eta^5\text{-}C_5H_5)(OC)_2Fe]_nSnX_{4-n}$ (n = 1–4) by replacing the halide atoms for the metal groups $(\eta^5\text{-}C_5H_5)(OC)_2Fe$.[6] Then, it would be expected that the strongest acid–base interaction involves the trihalide complexes $[Fe(SnX_3)(CO)_2(\eta^5\text{-}C_5H_5)]$.

The visible spectra of the solution-stable complexes $[(\eta^5\text{-}C_5H_5)(OC)_2Fe(\mu\text{-}SnX_2)W(X)(CO)_3(bipy)]$ were recorded in CH_2Cl_2. They present a unique band localized in the 400–500 nm region. The position of this broad band is related to the X electronegativity, since it is shifted to shorter wavelength in the order Cl(λ_{max} = 440 nm) > Br (λ_{max} = 450 nm) > I(λ_{max} = 440 nm). This absorption is characteristic of the $W(X)(CO)_3(bipy)$ moiety and is associated to the metal ligand charge transfer transition bipy (π^*) ← W($d\pi$)[2].

The complexes $[M(CO)_3(NN)(NCMe)]$ [NN = phen, di-2-pyridylamine (dipyam)] were also found to react with $[Fe(SnCl_3)(CO)_2(\eta^5\text{-}C_5H_5)]$ to yield only trimetallic species $[(\eta^5\text{-}C_5H_5)(OC)_2Fe(\mu\text{-}SnCl_2)M(Cl)(CO)_3(NN)]$ (Table 1, compounds **1g–j**).

The above results prompted us to check the syn-

thetic applicability of the insertion reaction in organometallic systems containing SnX_3 groups by using the $[M(Cl)(SnCl_3)CO_3(bipy)]$ complexes. The insertion takes place and again the reaction is stopped affording only trimetallic complexes $[(bipy)(OC)_3(Cl)M(\mu\text{-}SnCl_2)M'(Cl)(CO)_3(bipy)]$ (M′ = Mo, W). The IR spectra (Table 1, compounds **2a–c**) confirm the existence of M—Sn—M′ arrays[2] and the low solubility of these compounds precluded the measurement of the electronic spectra.

EXPERIMENTAL

All operations were carried out in a nitrogen atmosphere using standard Schlenk line techniques. The starting materials, $[Fe(SnCl_3)(CO)_2(\eta^5\text{-}C_5H_5)]$,[7] $[Fe_2(\mu\text{-}SnCl_2)(CO)_4(\eta^5\text{-}C_5H_5)_2]$,[7] $[M(Cl)(SnCl_3)(CO)_3(bipy)]$,[8] $[M(CO)_4(bipyam)]$,[9] $[M(CO)_3(NN)(NCMe)]$[1] [M = Mo, W; NN = 2,2′-bipyridine (bipy), 1,10-phenanthroline (phen), di-2-pyridylamine (dipyam)] were prepared by similar methods to those described in the literature. The $[Fe(SnX_3)(CO)_2(\eta^5\text{-}C_5H_5)]$ complexes (X = Br, I) were precipitated by treating an acetonitrile solution of $[Fe(SnCl_3)(CO)_2(\eta^5\text{-}C_5H_5)]$ with an excess of KI salt dissolved in water or with a HBr solution respectively; the crystalline solids were filtered off and washed with water. The IR spectra were recorded on a Perkin–Elmer 577 spectrophotometer. The electronic spectra were registered on a Carl–Zeiss DMR 22 instrument.

Synthesis of $[(\eta^5\text{-}C_5H_5)(OC)_2Fe(\mu\text{-}SnX_2)M(X)(CO)_3(bipy)]$ (M = Mo, W; X = Cl, Br, I)

The complexes were obtained from the reaction of equimolar quantities of $[Fe(SnX_3)(CO)_2(\eta^5\text{-}C_5H_5)]$ and $[M(CO)_3(bipy)(NCMe)]$ in refluxing methanol. The following procedure is typical. $[(\eta^5\text{-}C_5H_5)(OC)_2Fe(\mu\text{-}SnCl_2)W(Cl)(CO)_3(bipy)]$: a methanol solution of $[Fe(SnCl_3)(CO)_2(\eta^5\text{-}C_5H_5)]$ (69.1 mg, 0.172 mmol) and freshly prepared $[W(CO)_3(bipy)(NCMe)]$ (80 mg, 0.172 mmol) was refluxed under nitrogen in the dark for 0.25 h. The red crystals were collected by filtration, washed repeatedly with methanol and dried *in vacuo* (90 mg, 63.3% yield). The results of the elemental analysis are presented in Table 1 (compounds **1a–f**).

Synthesis of $[(\eta^5\text{-}C_5H_5)(OC)_2Fe(\mu\text{-}SnCl_2)M(Cl)(CO)_3(NN)]$ (M = Mo, W; NN = phen, dipyam)

The same above procedure was used to prepare the $[(\eta^5\text{-}C_5H_5)(OC)_2Fe(\mu\text{-}SnCl_2)M(Cl)(CO)_3(phen)]$ complexes. To isolate the $[(\eta^5\text{-}C_5H_5)(OC)_2Fe(\mu\text{-}SnCl_2)M(Cl)(CO)_3(dipyam)]$ compounds the reaction was carried out at room temperature with stirring for 1 h. Then, the solvent was partially evaporated off to give the orange precipitate. The colours and analytical data for all the complexes are given in Table 1 (compounds **1g–j**).

Synthesis of $[(bipy)(OC)_3(Cl)M(\mu\text{-}SnCl_2)M'(Cl)(CO)_3(bipy)]$ (M,M′ = Mo, W)

A similar method was used to prepare these complexes by refluxing for 0.25 h a methanol solution of the starting materials $[M(Cl)(SnCl_3)(CO)_3(bipy)]$ and $[M'(CO)_3(bipy)(NCMe)]$. The precipitate was filtered off, washed with methanol and then dried *in vacuo*. The analytical data are given in Table 1 (compounds **2a–c**).

Acknowledgements—Financial support given by the Dirección de Investigación y Desarrollo de la Universidad de La Frontera (Project No. 8921) to carry out this work is gratefully acknowledged.

REFERENCES

1. P. Correa, M. E. Vargas and J. Granifo, *Polyhedron* 1987, **6**, 1781.
2. J. Granifo and M. E. Vargas, *Polyhedron* 1989, **8**, 1471.
3. M. Panizo and M. Cano, *J. Organomet. Chem.* 1985, **287**, 221.
4. P. Hackett and A. R. Manning, *J. Chem. Soc., Dalton Trans.* 1972, 1487.
5. P. Donegan and A. R. Manning, *J. Organomet. Chem.* 1987, **336**, 115.
6. M. S. Holt, W. L. Wilson and J. H. Nelson, *Chem. Rev.* 1989, **89**, 11.
7. F. Bonati and G. Wilkinson, *J. Chem. Soc.* 1964, 179.
8. R. Kummer and W. A. G. Graham, *Inorg. Chem.* 1968, **7**, 310.
9. R. A. Howie, G. Izquierdo and G. P. McQuillan, *Inorg. Chim. Acta* 1983, **72**, 165.

Polyhedron Vol. 9, No. 9, pp. 1191–1197, 1990
Printed in Great Britain

0277–5387/90 $3.00+.00
© 1990 Pergamon Press plc

STUDY OF COMPLEX FORMATION EQUILIBRIA OF PAMOATE ION WITH COPPER(II) ION IN A DIOXANE–WATER SOLUTION

E. CASASSAS* and A. IZQUIERDO-RIDORSA

Department of Analytical Chemistry, University of Barcelona, Av. Diagonal 647, 08028 Barcelona, Spain

(*Received* 1 *March* 1989; *accepted* 21 *December* 1989)

Abstract—Protonation constants of the carboxylate groups in pamoic acid and stability constants of copper(II) complexes with pamoic acid have been determined from EMF data in a 50% (v/v) dioxane–water solution at 25°C and 0.1 M KNO_3, and protonation constants for the hydroxyl groups have been determined spectrophotometrically in 1 M KCl aqueous medium. The values obtained for the constants are: protonation constants for the carboxylate groups: $\log\beta_1 = 4.352 \pm 0.001$ and $\log\beta_2 = 7.706 \pm 0.001$; for the hydroxyl groups: $\log K_1 = 14.80 \pm 0.24$ and $\log K_2 = 13.05 \pm 0.065$. For the complex-forming reactions $Cu^{II} + nH_2pam \rightleftarrows Cu(pamH)_n + nH$ ($n = 1$ or 2), the equilibrium constants are: $\log\beta_{11-1} = -1.96 \pm 0.02$ and $\log\beta_{21-2} = -5.28 \pm 0.02$. An insoluble 3:2 copper(II)–pamoate complex is identified.

The study of the acid–base properties of aromatic *ortho*-hydroxycarboxylic acids and that of their complex formation equilibria with several metallic ions is important due to the great application that these compounds have in very different fields; they are considered some of the most important model compounds in the study of humic and fulvic acids,[1,2] they are the main constituents in many mordent dyes,[3] they have a very wide pharmaceutical application due to the anti-inflammatory properties of some of their copper(II) complexes,[4–7] and they find a diversity of applications in analytical chemistry.[8,9]

Since many natural compounds contain the aromatic *ortho*-hydroxycarboxylic grouping more than once in their structure, it seems interesting to study model molecules which derive from the most simple aromatic *ortho*-hydroxycarboxylic acids (salicylic acid and 3-hydroxy-2-naphthoic acid) but which contain two such groupings. One of these compounds is 2,2′-dihydroxy-3,3′-dicarboxy-1,1′-dinaphthylmethane (pamoic acid).

In this work, the acid–base properties of pamoic acid and its complex formation equilibria with copper(II) ions were studied. While protonation constants for both hydroxyl groups in pamoic acid must be determined in aqueous medium and at high ionic strength in order to attain pH values high enough to have a measurable amount of deprotonated hydroxyl groups, protonation constants for the carboxylic groups and stability constants for the copper(II) complexes must be determined in dioxane–water mixtures due to the low solubility in water of the neutral ligand and of its metallic complexes.

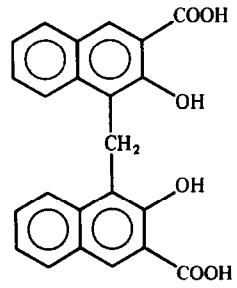

Pamoic acid

EXPERIMENTAL

Reagents and solutions

Pamoic acid disodium salt (Eastman AR), nitric acid (Merck AR) and copper(II) oxide (Merck AR) were used without further purification. Potassium nitrate (Probus AR) and potassium chloride (Probus

* Author to whom correspondence should be addressed.

AR) were purified by recrystallization in water. CO_2-free potassium hydroxide (Merck AR) solutions were prepared and standardized as usual.[10] Doubly-distilled freshly boiled water was used for the preparation of the solutions. In the potentiometric study the mixed solvent used was prepared from dioxane (Carlo Erba, RPE) purified by Eigenberger's method.[11]

In the spectrophotometric study, aqueous ligand solutions and potassium hydroxide solutions were prepared at 1 M ionic strength adjusted with potassium chloride. In the potentiometric study, ligand solutions, metal ion solutions, nitric acid solutions and potassium hydroxide solutions were prepared in dioxane–water (1 : 1, v/v) mixtures, at 0.1 M ionic strength adjusted with potassium nitrate. Metal ion solutions were standardized iodometrically and by the electrodeposition procedure. Nitric acid solutions were standardized volumetrically with tris(hydroxymethyl)aminomethane.

A flow of N_2 (previously purified with vanadous perchlorate and barium hydroxide) was bubbled continuously through the solution in the potentiometric cell.

Apparatus

(a) Beckman DU-7 single-beam spectrophotometer, equipped with 1-cm silica cells thermostatized at 25.0 ± 0.1°C.

(b) Radiometer PHM 64 pH-Meter equipped with a wide-range glass electrode (Radiometer G202B) and a silver–silver chloride electrode, prepared as described by Brown,[12] in a Wilhelm-type salt bridge.[13] The titrant was added with a Metrohm 655 Multi-Dosimat automatic burette with 1.0 and 5.0 cm^3 exchanging units. Sample solutions were titrated in a double-walled vessel maintained at 25.0 ± 0.1°C by circulating water and stirred magnetically under a continuous flow of N_2. The potentiometric assembly was controlled by an HP 9816 microcomputer via an HP 3421A data acquisition control unit (for details see ref. 14).

(c) IR spectra (KBr pellets) were recorded on a Perkin–Elmer 1330 spectrophotometer.

(d) EPR spectra (of solid samples and DMSO solution) were recorded on a VARIAN E-109 E Spectrometer. The spectra in solution were recorded in capillary quartz tubes of 1 mm diameter (Wilmad, Cat. Nr. 800).

(e) ^{1}H NMR spectra were recorded on a GEMINI 200 (200 MHz) spectrometer. In the ^{1}H NMR experiments, deuterated DMSO was used as solvent, because it provided adequate solubility without proton transfer.

Procedure

(a) *Spectrophotometric determination.* The protonation constants of both hydroxyl groups in pamoic acid were determined by the spectrophotometric method, in 1 M KCl aqueous medium. The spectrophotometric determination was carried out from the absorbance readings taken, between 230 and 275 nm at 5 nm increments, for different solutions of pamoic acid (concentration between 1.6×10^{-4} and 4.2×10^{-6} mol dm^{-3}) in 1 M KCl, in which the pH was varied, between 11.3 and 13.8, by addition of a measured volume of a titrant solution of potassium hydroxide in 1 M KCl. The pH of the solutions was calculated from the known amount of potassium hydroxide added and the value of the autoprotolysis constant of the working medium[15] ($pK_w = 13.93$).

(b) *Potentiometric determinations.* The protonation constants of both carboxylate groups in pamoic acid and the stability constants of its copper(II) complexes have been determined from EMF data obtained according to the previously described method.[16] The calibration parameters (standard potential of the cell, pH dependence of the liquid junction potential and value of the ionic product of the medium) were obtained from a strong acid–strong base titration by the Gran method,[17] using a multiparametric data-fitting procedure.[18] This calibration procedure allows direct correlation of the EMF reading with the hydrogen ion concentration. In a 1 : 1 v/v dioxane–water medium, with 0.1 M ionic strength at 25°C, the value of the ionic product of the medium is: $-\log K_w = 15.322 \pm 0.001$. In this medium, the liquid junction potential, $E_j = j_H[H]$, must be taken into account in acid solutions of $pH < 3.0$: $j_H = -435 \pm 4$ mV M^{-1}.

Protonation curves were obtained at several ligand concentrations, and complex formation curves were obtained at several metal ion concentrations and different ligand-to-metal ion concentration ratios. The experimental conditions of the titrations performed are listed in Table 1. When the ligand–metal ion ratio is 10 : 1 or lower, there is formation of a red precipitate at pH values near 5. When the ligand–metal ion ratio is higher than 10 : 1, the titration with potassium hydroxide can be performed up to basic pH values without any precipitation.

Data treatment

The numerical analysis of the experimental spectrophotometric data has been carried out with the program SQUAD,[19] which determines sim-

Table 1. Experimental conditions of potentiometric titrations

Titration number	$[Ligand]_0$ (mM)	$[Cu]_0$ (mM)	Ligand–metal ratio	Range of $-\log[H]$
1	3.538	—	—	3.7–4.7
2	3.538	—	—	3.7–4.7
3	1.572	—	—	3.7–4.8
4	2.854	—	—	3.8–4.4
5	0.685	0.259	2.6:1	3.9–4.7
6	0.500	0.505	1:1	3.1–4.5
7	0.500	0.505	1:1	3.1–4.5
8	0.493	0.497	1:1	3.7–4.5
9	4.205	0.423	10:1	4.3–4.9
10	4.205	0.423	10:1	4.3–4.9
11	6.417	0.275	23.5:1	4.6–6.1
12	4.115	0.278	15:1	4.1–5.9
13	5.285	0.258	20.5:1	4.3–5.2

ultaneously the stability constants of the formed species and their individual molar absorptivities in the whole working wavelength range.

The numerical analysis of the experimental EMF data has been performed with the computer programs SUPERQUAD[20] and MINIGLASS.[18] The SUPERQUAD program indicates the goodness of the results by the value of the parameter SIGMA, which is the ratio of the root-mean-square of the weighted residuals to the estimated error in our working conditions (0.001 cm^3 for the autoburette volume readings and 0.1 mV for the EMF readings), and by the value of the statistic parameter, χ^2, which is based on weighted residuals of EMF readings.[20] The reliability of the results obtained with the MINIGLASS program is indicated by the standard deviation of the residuals either with respect to added volumes or with respect to measured $[H^+]$, and by the sum of squared residuals.

RESULTS AND DISCUSSION

The values for the protonation constants of both hydroxyl groups in pamoic acid, obtained in aqueous solution at 1 M KCl ionic strength and 25°C are: $\log K_1 = 14.80 \pm 0.24$ and $\log K_2 = 13.05 \pm 0.065$. The standard deviation of the residuals in absorbance units is 2.05×10^{-2} and the sum of residual squares is 1.09×10^{-1}. The calculated individual absorption spectra are given in Fig. 1.

The values for the protonation constants of both carboxylate groups in pamoic acid and for the formation constants of the copper(II) complexes of pamoic acid, obtained in dioxane–water (1 : 1, v/v) solution at 0.1 M KNO_3 ionic strength and at 25°C, are given in Tables 2 and 3, respectively, together with the resulting statistical parameters.

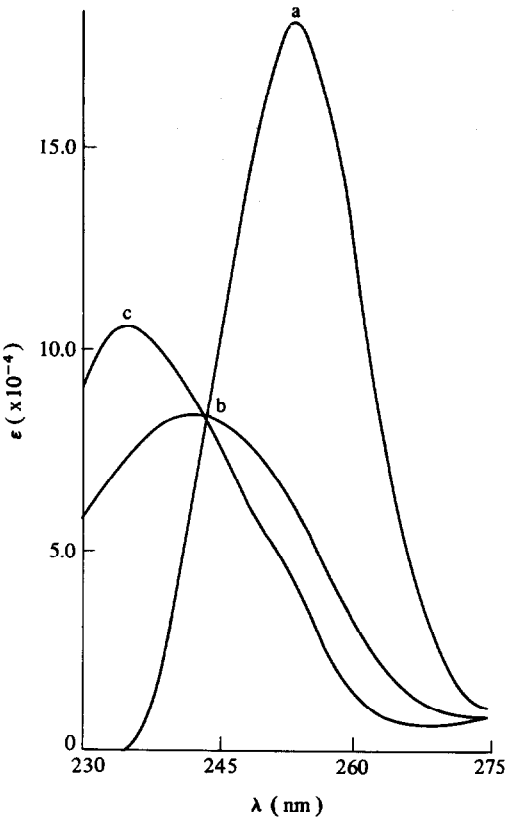

Fig. 1. Individual absorption spectra of (a) pam, (b) Hpam and (c) H_2pam species, where pam refers to the fully deprotonated pamoate ligand.

In the complexation study, the best fits were found with the model containing the species 1 : 1 and 1 : 2 metal ion–ligand. From the values of the constants obtained, the distribution of species which contain copper(II) as a function of pH was evaluated (Fig. 2).

Table 2. Values of the protonation constants of the carboxylate groups in pamoic acid at 25°C in dioxane–water (1 : 1, v/v) at 0.1 M KNO_3 ionic strength

	SUPERQUAD (Mode 0)	MINIGLASS
$\log\beta_1$	4.352±0.001	4.352±0.001
$\log\beta_2$	7.707±0.001	7.706±0.001
Sigma	1.881	—
χ^2	33.19	—
Standard deviation[a]	—	4.21×10^{-3}
ΣU^2	—	2.04×10^{-3}

[a] Standard deviations of the residuals respect added volumes.

Table 3. Formation constants of copper(II)–pamoate complexes at 25°C in dioxane–water (1 : 1, v/v) at 0.1 M KNO_3 ionic strength

	SUPERQUAD (Mode 0)	MINIGLASS
$\log\beta_{11-1}$[a]	−1.97±0.02	−1.96±0.01
$\log\beta_{21-2}$[b]	−5.30±0.02	−5.27±0.01
Sigma	4.17	—
χ^2	35.18	—
Standard deviation[c]	—	1.53×10^{-2}
ΣU^2	—	4.54×10^{-2}

[a] Value of the logarithm of the equilibrium constant for the reaction: $Cu^{II}+H_2pam \leftrightarrows Cu(Hpam)+H$, where pam is the fully deprotonated pamoate ligand. The negative subscript shows the number of hydrogen ions split-off in the complex-forming reaction.

[b] Value of the logarithm of the equilibrium constant for the reaction: $Cu^{II}+2H_2pam \leftrightarrows Cu(Hpam)_2+2H$.

[c] Standard deviations of the residuals respect measured $-\log[H^+]$.

Although pamoic acid contains two *ortho*-hydroxycarboxylic groupings in its molecule, they cannot coordinate simultaneously to a single metal ion due to the steric features of the ligand molecule, where both naphthalene rings lay in different planes because of the sp^3 hybridization of the bridging $-CH_2-$. So, the complexation behaviour of pamoic acid can be compared with that of other related ligands which contain only once the *ortho*-hydroxycarboxylic grouping, like salicylic acid and 3-hydroxy-2-naphthoic acid.

Previous studies on complexation of the copper(II) ion with salicylic acid[16,21] and 3-hydroxy-2-naphthoic acid[14] also show the formation of the 1 : 1 and 1 : 2 metal ion–ligand complexes. A comparison between the values obtained for the 1 : 1 complexes with these ligands show that there is a relationship between the stability of the 1 : 1 complexes and the acidic character of the

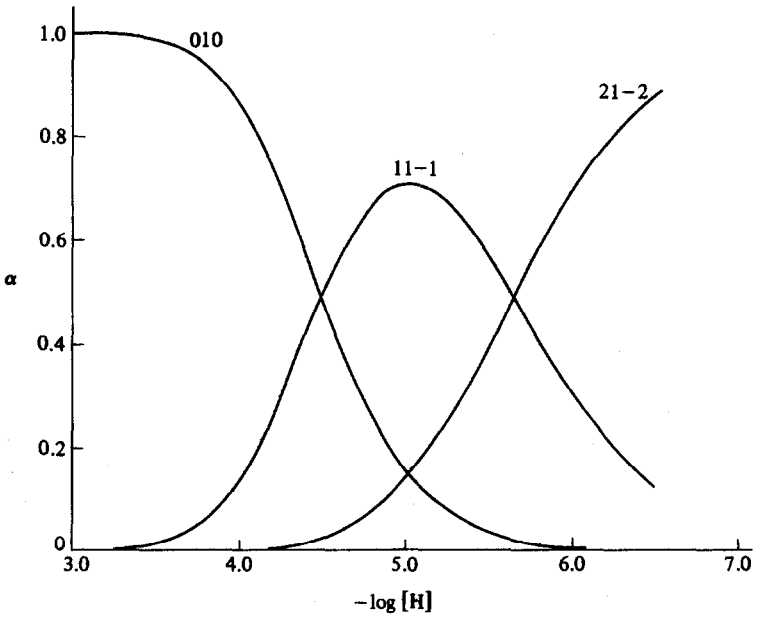

Fig. 2. Distribution plot as a function of $-\log[H]$ for the species which contain copper(II) ion in the Cu^{II}–pamoate system. Alpha is the ratio of each species concentration to the total copper(II) concentration. In the figure, 010, 11−1 and 21−2 refer, respectively, to Cu^{II}, Cu(Hpam) and $Cu(Hpam)_2$. Ligand concentration = 5.3×10^{-3} mol dm^{-3}; metal concentration = 2.6×10^{-4} mol dm^{-3}.

Table 4. Summary of hydroxyl group deprotonation constants and of copper(II) complex formation constants for similar ligands

Ligand	Species[a] ligand–Cu–H	Log β	Ionic strength (mol dm^{-3})	Reference
Salicylate	1:0:−1	−12.9	1.0	16
	1:1:−1	−0.33	0.1	21
	2:1:−2	−6.40	0.1	21
Hydroxynaphthoate	1:0:−1	−12.5	0.1	22
	1:1:−1	−3.10	0.2	14
	2:1:−2	−8.84	0.2	14
Pamoate	1:0:−1	−13.0	1.0	[b]
	1:1:−1	−1.96	0.1	[b]
	2:1:−2	−5.27	0.1	[b]

[a] The formation constants include the deprotonation of the hydroxyl groups in the ligands. Thus, the negative digit indicates the number of hydrogen ions split-off in the complex-forming reaction.
[b] This work.

hydroxyl group of the ligand; the more acidic this group is, the less stable is its related 1 : 1 copper(II) complex (see Table 4). The stability of the 1 : 1 complex with pamoic acid, however, compared with that with salicylate, is much lower than would be expected from only the acidities of the hydroxyl groups of the respective ligands, probably due to the effect of steric hindrance, which must have a certain influence with the pamoate ligand.

The 1 : 2 metal ion–ligand complexes with salicylate and 3-hydroxy-2-naphthoate ions show the same order of stability as the 1 : 1 complexes. With the pamoate ligand, however, the 1 : 2 complex is even more stable than the 1 : 2 copper(II)–salicylate complex. Part of this additional stabilization must be attributed to entropic effects related with the change in electric charge associated with complex formation; while with salicylate and 3-hydroxy-2-naphthoate the 1 : 2 species is formed from a neutral 1 : 1 species, with pamoate both 1 : 1 and 1 : 2 complexes are negatively charged due to the second *ortho*-hydroxycarboxylic grouping which does not participate in complexation.

Studies of the complexation of copper(II) ions with salicylate or 3-hydroxy-2-naphthoate ions showed, at certain conditions of pH and certain ligand-to-metal ion concentration ratios, the formation of a precipitate consisting of the neutral 1 : 1 metal ion–ligand species. In the copper(II)–pamoate system, however, when the concentration ratio copper(II)–pamoate ion is 1 : 10 or lower, there is formation of a precipitate of a different nature at pH values higher than 4. In order to determine the nature of this precipitate, the elemental analysis for several samples obtained at total concentrations much higher than those used in the potentiometric experiments has been carried out. Their IR, EPR and ^1H NMR spectra have also been obtained.

Elemental analysis

The experimental values for %Cu, %C and %H of samples obtained at different working conditions are given in Table 5. The dispersion obtained in the experimental results is due to the critical conditions at which there is precipitation; coprecipitation of copper(II) hydroxide can take place simultaneously. If a somewhat lower pH is used, coprecipitation of pamoic acid occurs. The average percentages are in agreement with the calculated ones for the 3 : 2 copper(II)–pamoate complex, which are also included in Table 5. The 3 : 2 complex with all the hydroxyl groups deprotonated is a negatively-charged species. So, the precipitate must have two hydroxyl groups that do not participate in complexation, or be the sodium salt of the complex. The dispersion of the results does not allow a decision to be made in this respect.

IR absorption spectra

A comparison of the IR absorption spectrum of the insoluble complex and that of pure pamoic acid shows the variation of some IR bands due to complexation. The most characteristic is the disappearance of the acute band at 3600 cm^{-1}, which is due to the —OH stretching vibrations in the free

Table 5. Elemental analysis of the insoluble precipitate

Sample	Copper–ligand	%Cu[a]	%C[b]	%H[b]
1	1:2	18.8	51.2	2.6
2	1:2	15.3	52.7	3.7
3	1:5	17.8	47.6	3.2
4	1:1	15.7	51.8	3.6
5	1:2	18.6	48.8	3.4
Average		17.2±1.6	50.4±2.2	3.3±0.4
$Cu(pamH)_2 \cdot 2H_2O$		13.1	56.8	3.7
$Cu_2pam \cdot 4H_2O$		21.8	47.3	3.4
$Cu_3(pamH)_2 \cdot 4H_2O$		18.4	53.5	3.3
$Cu_3(pamNa)_2 \cdot 4H_2O$		17.7	51.3	3.0

[a] Iodometrically determinated after mineralization of the precipitate with sulphuric acid.

[b] Analysed by automated microanalytical techniques.

hydroxyl groups that participate in intramolecular hydrogen bonds. There is also variation in the bands between 1300 and 1700 cm^{-1} and those between 700 and 900 cm^{-1}.

EPR absorption spectra

The EPR experiments have been performed on the powder obtained and on its DMSO solution.

The solution yields a highly asymmetrical EPR spectrum where, of the four bands due to the hyperfine splitting, only the one that appears at higher magnetic field is well defined. This spectrum is characterized by a g_{av} value around 2.13. The bulk of the copper(II) complexes influences the asymmetry of the spectral shape; the more bulky the complex is, the more difficult is its tumbling in solution and the relaxation must go through a spin–spin process which yields asymmetric spectra.

The fact that for the studied copper(II) complex an EPR spectrum is observable indicates the presence of an odd number of copper(II) ions in the insoluble complex, which is, therefore, consistent with the assigned 3:2 copper(II)–pamoate compound.

In order to ascertain if there is any interaction between the copper(II) ions, which could lead to a triplet state, the EPR spectrum of the powder has been obtained. This spectrum exhibits parallel and perpendicular features typical of copper(II) ions in an axial ligand field with tetragonal distortion by elongation along the axial direction. It is composed of an acute band at $g_\perp = 2.003$ and two broad bands at lower magnetic field with an approximated $g_\parallel$ value of about 2.15–2.20. The poor resolution of this region of the spectrum could be due to the presence in the studied compound of more than one copper(II) ion having similar but not identical surroundings. For this studied solid no EPR spectrum is observable in the region between 600 and 2600 G (i.e. in the forbidden transition region with $\Delta M_s = 2$, where the appearance of an EPR spectrum would characterize a triplet state), and thus, there is no evidence of a dipole–dipole interaction between two copper(II) ions in the compound. In the proposed 3:2 copper(II)–pamoate structure the three copper(II) ions lie in different planes due to the sp^3 hybridization of the methylene bridge in the pamoate ligands, and they probably cannot interact with each other.

^{1}H NMR absorption spectra

The ^{1}H NMR resonance technique has been used by several authors to study the binding of copper(II) ions to different ligands by following the broadening effects of the paramagnetic copper(II) ions on the ligand proton resonances.[23,24] Only when a diamagnetic dimeric copper(II) species is formed is no broadening effect observed.[25] For the copper(II)–pamoate insoluble complex all the proton resonance bands of the pamoate ligand are severely broadened, which indicates the paramagnetism of the studied complex.

CONCLUSIONS

The complexing behaviour of pamoate ion with copper(II) ion is very similar to that of other *ortho*-hydroxycarboxylic acids, like salicylic acid and 3-hydroxy-2-naphthoic acid, which is in accordance with the fact that they have the same

active coordination centres in front of metal ions. Due to the steric features of the pamoate ligand, both *ortho*-hydroxycarboxylic groupings lie in different planes and cannot coordinate simultaneously to a single metal ion. The differences observed in the stability of their metal complexes are mainly attributed to the different molecular dimensions and to the indirect effect of the second *ortho*-hydroxycarboxylic grouping in the pamoate molecule.

The insoluble complex formed at certain working conditions has been identified as a 3 : 2 copper(II)–pamoate species and it could be assigned to the second ($n = 1$) member of a series of *core-and-links* complexes with the general formula $(Cu_2PX)(CuPX)_n$, where P is the fully deprotonated pamoate ligand and X is H or Na.

Acknowledgement—This research is supported by CICYT grant number PB87-0061.

REFERENCES

1. F. M. Morel, J. C. Westall, C. R. O'Melia and J. J. Morgan, *Environ. Sci. Technol.* 1975, **9**, 757.
2. W. Stumm and J. J. Morgan, *Aquatic Chemistry. An Introduction Emphasizing Chemical Equilibria in Natural Waters*. Wiley Interscience, New York (1981).
3. F. D. Snell and L. S. Ettre, *Encyclopaedia of Industrial Chemical Analysis*, Vol. 12. Interscience, New York (1971).
4. L. R. De Alvare, K. Goda and T. Kimura, *Biochem. Biophys. Res. Commun.* 1976, **69**, 687.
5. J. R. J. Sorenson, *J. Med. Chem.* 1976, **19**, 135.
6. J. R. J. Sorenson, *Prog. Med. Chem.* 1978, **15**, 211.
7. W. M. Willingham and J. R. J. Sorenson, *Trace Elem. Med.* 1986, **3**, 139.
8. E. Casassas, A. Izquierdo-Ridorsa, L. García-Puignou and J. Duñach, *Analyt. Lett.* 1985, **18**, 2239.
9. E. Casassas, A. Izquierdo-Ridorsa and L. Puignou, *Talanta* 1988, **35**, 199.
10. J. E. Powell and M. A. Hiller, *J. Chem. Ed.* 1957, **34**, 330.
11. A. I. Vogel, *Textbook of Practical Organic Chemistry*, p. 177. Longmans, London (1961).
12. A. S. Brown, *J. Am. Chem. Soc.* 1934, **56**, 646.
13. W. Forsling, S. Hietanen and L. G. Sillén, *Acta Chem. Scand.* 1952, **6**, 601.
14. E. Casassas, G. Fonrodona and R. Tauler, *Polyhedron* 1987, **6**, 1517.
15. G. Veliniv, P. Zikolov, P. Tchakarova and O. Budevsky, *Talanta* 1974, **21**, 163.
16. E. Casassas and R. Tauler, *J. Chim. Phys.* 1984, **81**, 233; 1984, **81**, 557; 1985, **82**, 1067.
17. G. Gran, *Analyst* 1952, **77**, 661.
18. A. Izquierdo and J. L. Beltrán, *Anal. Chim. Acta* 1986, **181**, 87.
19. D. J. Leggett, S. L. Kelly, L. R. Shiue, Y. T. Wu, D. Chang and K. M. Kadish, *Talanta* 1983, **30**, 579.
20. P. Gans, A. Sabatini and A. Vacca, *J. Chem. Soc., Dalton Trans.* 1985, 1195.
21. E. Casassas, G. Fonrodona, A. Izquierdo-Ridorsa and R. Tauler, *Anal. Quím., Serie B*, in press.
22. E. Casassas and G. Fonrodona, *J. Chim. Phys.* 1989, **86**, 391.
23. N. A. Berger and G. L. Eichhorn, *Biochemistry* 1971, **10**, 1857.
24. G. V. Fazakerley, G. E. Jackson, M. A. Phillips and J. C. Van Niekerk, *Inorg. Chim. Acta* 1979, **35**, 151.
25. Y. H. Chao and D. R. Kearns, *J. Am. Chem. Soc.* 1977, **99**, 6425.

Polyhedron Vol. 9, No. 9, pp. 1199–1208, 1990
Printed in Great Britain

0277–5387/90 $3.00+.00
© 1990 Pergamon Press plc

^{77}Se-NMR AND RAMAN SPECTROSCOPIC CHARACTERIZATION OF SELENIUM DIBROMIDE ($SeBr_2$) AND ITS REACTION WITH TITANOCENE PENTASULPHIDE TO GIVE CYCLIC SELENIUM SULPHIDES OF RING SIZE 6, 7, 8, AND 12*

RALF STEUDEL† and DETLEF JENSEN

Institut für Anorganische und Analytische Chemie, Technische Universität Berlin, Sekr. C 2, D-1000 Berlin, F.R.G.

and

FRANK BAUMGART

Iwan-N.-Stranski-Institut für Physikalische und Theoretische Chemie, Technische Universität Berlin, D-1000 Berlin 12, F.R.G.

(*Received* 29 *November* 1989; *accepted* 21 *December* 1989)

Abstract—Selenium dibromide prepared from Se and $SeBr_4$ in acetonitrile shows a singlet at 1496 ppm in the ^{77}Se-NMR spectrum and Raman lines at 291, 265, and 105 cm^{-1}. Selenium dibromide which is in equilibrium with Se_2Br_2 and Br_2 reacts with titanocene-pentasulphide at 20°C in CS_2 to give SeS_5 which partly dimerizes to give 1,2-Se_2S_{10} and 1,7-Se_2S_{10}. Raman spectra of Se_2S_{10} and $Se_2S_{10}\cdot CS_2$ are reported and their formation from SeS_5 is discussed. Other products of the $SeBr_2$-titanocenepentasulphide reaction are 1,2-Se_2S_5 (from Se_2Br_2), S_{10} (from Br_2), 1,2-Se_2S_6, 1,5-Se_2S_6, and 1,2,5,6-Se_4S_4.

Selenium and bromine form three binary compounds: $SeBr_2$, Se_2Br_2, and $SeBr_4$.[2] While the molecular structure, spectra, and chemical reactions of Se_2Br_2 are well known the other two compounds are less well studied which may be explained by their thermal instability. $SeBr_4$ exists as solid phases (two allotropes) only and completely decomposes both in solution in various solvents[3,4] and in the vapour phase[5] according to eq. (1):

$$SeBr_4 \longrightarrow SeBr_2 + Br_2. \quad (1)$$

Selenium bromide, on the other hand, has never been prepared as a pure substance but exists only in solutions[6] and the vapour phase[5,7] in equilibrium with Se_2Br_2 according to eq. (2):

$$2SeBr_2 \rightleftharpoons Se_2Br_2 + Br_2. \quad (2)$$

The equilibrium constant $K_2 = [Se_2Br_2][Br_2]/[SeBr_2]^2$ has been determined by spectrophotometric measurements at room temperature as 0.0252 for a solution in carbon tetrachloride[3] and as 0.014 for acetonitrile.[6] The lower value observed for CH_3CN indicates some solvent/solute interaction. However, since SCl_2 interacts only weakly with CH_3CN[8] the same is likely for $SeBr_2$. The dissolved $SeBr_2$ has so far only been detected directly by Raman spectroscopy. Milne[6] observed three Raman lines at 290, 260, and 96 cm^{-1} and, using polarization measurements, assigned them to the asymmetric and symmetric stretching and the bending modes of the C_{2v} molecule $SeBr_2$, respectively. No Raman lines due to Br_2 or Se_2Br_2 were observed for acetonitrile solutions with an Se : Br ratio of 1 : 2.

The aim of the present work was to confirm the Raman data of $SeBr_2$, to measure for the first time the ^{77}Se-NMR spectrum of this molecule, and to check whether $SeBr_2$ reacts with titanocene-

* Part 132 of the Series "Sulphur Compounds"; for Part 131 see Ref. 1.

† Author to whom correspondence should be addressed.

pentasulphide in a similar fashion as sulphur and selenium chlorides do, i.e. according to eq. (3):

$$(C_5H_5)_2TiS_5 + SeBr_2 \longrightarrow SeS_5 + (C_5H_5)_2TiBr_2. \quad (3)$$

SCl_2 is known to react with $(C_5H_5)_2TiS_5$ to give a mixture of mainly S_6 and some S_{12},[9] while S_2Cl_2 yields S_7,[9] and Se_2Cl_2 reacts to give primarily 1,2-Se_2S_5 which then slowly decomposes according to eq. (4):[10]

$$2\ 1,2\text{-}Se_2S_5 \longrightarrow SeS_5 + 1,2,3\text{-}Se_3S_5. \quad (4)$$

The two selenium sulphides 1,2-Se_2S_5 and 1,2,3-Se_3S_5 contain the Se atoms in neighbouring positions as has been shown by X-ray crystallography of single crystals as well as by ^{77}Se-NMR spectroscopy.[10–13]

EXPERIMENTAL

Materials

Carbon disulphide (CS_2; tech. grade) and acetonitrile (CH_3CN; tech. grade) were purified by distillation from phosphorus pentoxide (P_4O_{10}; anal. grade). Grey elemental selenium (Fluka; 99.5%) and bromine (Merck; anal. grade) were used as received. Orange selenium tetrabromide (β-$SeBr_4$),[14] diselenium dibromide (Se_2Br_2),[14] and titanocenepentasulphide (Cp_2TiS_5; Cp = η^5-C_5H_5)[15] were prepared according to literature methods. Methanol used as an eluent for HPLC was distilled from anhydrous magnesium sulphate and degassed in a vacuum immediately prior to use. A solution of $SeBr_2$ was obtained by adding 0.88 g of grey Se (11.1 mmol) to a solution of 4.43 g $SeBr_4$ (11.1 mmol) in 15 cm^3 acetonitrile and stirring until the Se had dissolved quantitatively.[6] If the reaction proceeded quantitatively according to eq. (5), this solution would contain 1.48 mol $SeBr_2$ per litre.

$$SeBr_4 + Se \longrightarrow 2SeBr_2. \quad (5)$$

Procedures

^{77}Se-NMR spectra were recorded with a Bruker WM 360 spectrometer equipped with Aspect 3000 computer for spectrometer control and data processing (frequency 68.679 MHz; temperature 23°C; sample tube diameter 20 mm). Raman spectra were obtained with an Instruments S.A. spectrometer which is based on a Jobin Yvon U 1000 double monochromator and controlled by a MAC 80 computer. Raman scattering was excited with a Spectra Physics krypton ion laser (647.1 nm) and measured by a Hamamatsu R943-02 GaAs photomultiplier. The wavenumbers were reproducible to within ± 1 cm^{-1}. To prevent the Raman samples from thermal or photolytic decomposition during the measurements they were usually cooled to well below 0°C using a self-made cryostat in which the vapour of liquid nitrogen was used as a coolant. Evaporation of the nitrogen by an electric heater was controlled by a Pt 100 temperature sensor placed next to the sample which was contained in a glass capillary inside a glass Dewar vessel.

High pressure liquid chromatography (HPLC) was performed with the following equipment: Perkin–Elmer Liquid Chromatograph (Series 2 with two pumps), Rheodyne Syringe Loading Injector (Model 7125 with 10 μl sample loop), Waters–Millipore Radial-Pak column cartridges filled with C18 phase for reversed-phase chromatography (column length 10 cm, inner diameter 8 mm; particle size 5 or 10 μm) and contained in a RCM-100 compression module, Perkin–Elmer LC75 UV spectrophotometer with autocontrol (variable wavelength detector with deuterium lamp), Hewlett–Packard 3390A electronic integrator with integrated recorder and printer.

To measure UV absorption spectra of chromatographically separated substances during the continuing HPLC analysis a Waters 990 diode-array detector with NEC APC III computer was employed (array of 512 diodes, range 190–800 nm). This equipment does not result in spectra distorted due to photodecomposition of the solute in the methanolic liquid phase as has repeatedly been observed when the stopped-flow technique was used.

RESULTS AND DISCUSSION

^{77}Se-*NMR spectrocopy*

Selenium compounds may be analysed by NMR-spectroscopy[16] since the isotope ^{77}Se (natural abundance 7.6%) has $I = 1/2$. However, the sensitivity of ^{77}Se is relatively low and in the case of selenium bromides the nuclear quadrupole moments of ^{79}Br and ^{81}Br ($I = 3/2$; natural abundance *ca* 50% each) create additional difficulties due to line broadening. We nevertheless succeeded in recording a ^{77}Se-NMR spectrum of a solution of $SeBr_2$ in acetonitrile obtained as described above.

In the range 1050–1700 ppm (relative to dimethyl selenide) only one signal was observed at 1496 ppm, which we assign to $SeBr_2$. The known resonance of Se_2Br_2 at 1176 ppm[17] was not detected which is in agreement with the low equilibrium concentration of this species as mentioned in the Introduction.

The half-width of the line at 1496 ppm was 860 Hz which is much larger than in the case of Se_2Br_2. The reason may be the interactions with both the two bromine nuclei and the nitrogen nuclei ($I = 1$) of the coordinated acetonitrile molecules. The larger chemical shift of $SeBr_2$ compared to Se_2Br_2 is caused by the two bromine atoms attached to one selenium atom but may also be influenced by solvation. These results show that NMR spectroscopy is a suitable technique to analyse selenium bromide solutions.

Raman spectroscopy

Raman spectra of $SeBr_2$ (in CH_3CN), Se_2Br_2 (neat), and β-$SeBr_4$ (solid) were recorded; the results are listed in Table 1. The data obtained for Se_2Br_2 agree with the literature spectra[2] and therefore are not shown. In the case of $SeBr_2$ we agree with Milne[6] as far as the stretching vibrations are concerned. However, we find the bending mode at 105 cm^{-1} rather than at 96 cm^{-1} which may be a plasma line of the krypton laser used by Milne. The Raman spectrum of $SeBr_4$ has so far been known only at > 130 cm^{-1} (allotrope not specified);[18] our data in this region agree with the previously reported values. The spectrum shows the typical lines[19] of $SeBr_3^+$ which is present in both α- and β-$SeBr_4$ and the site symmetry of which is approximately C_s.[20]

Table 1. Raman spectra of $SeBr_2$ and $SeBr_4$ at 23°C

$SeBr_2$ (in CH_3CN)	β-$SeBr_4$ (solid)
	21 m
	30 vw
	47 w
	54 m
	63 vw
	69 vw
	86 m
	95 w
	102 vw
105 m (δ)	110 vw
	123 vw
	132 w
	141 m (δ_s of $SeBr_3^+$)
	228 vs (ν_s of $SeBr_3^+$)
265 s (ν_s)	248 vs (ν_{as} of $SeBr_3^+$)
291 vs (ν_{as})	267 s (ν_{as} of $SeBr_3^+$)
380 w,b (CH_3CN)	

[a] Region below 90 cm^{-1} obscured by strong continuous scattering.

vs = very strong, s = strong, m = medium, w = weak, vw = very weak, b = broad, sh = shoulder.

Reaction of $SeBr_2$ with titanocene pentasulphide

To follow this reaction by ^{77}Se-NMR spectroscopy 500 mg Cp_2TiS_5 (1.47 mmol) were dissolved in 20 cm^3 CS_2 and reacted with 1 cm^3 of the $SeBr_2$ solution described above (1.48 mmol dm^{-3} $SeBr_2$). After stirring for 10 min the CS_2 phase was filtered into an NMR tube, 0.1 cm^3 each of cyclohexane and deuterobenzene were added and the spectrum recorded immediately in the ranges 502–848 and 999–1302 ppm which are typical for cyclic selenium sulphides. The five signals observed could all be assigned by comparison with literature data.[11-13] The results (Fig. 1; Table 2) show SeS_5 as the major product accompanied by 1,2-Se_2S_5 and three eight-membered SeS rings in small concentrations. The formation of 1,2-Se_2S_5 can be explained from the reaction of Se_2Br_2 with Cp_2TiS_5 which should proceed analogously to the above mentioned corresponding reaction of Se_2Cl_2:

$$Se_2Br_2 + Cp_2TiS_5 \longrightarrow 1,2\text{-}Se_2S_5 + Cp_2TiBr_2. \quad (6)$$

The occurrence of Se_4S_4 and of the two isomers of Se_2S_6 will be discussed below.

To confirm the NMR spectroscopic results the reaction mixture has been analysed also by HPLC. The retention times of cyclic selenium sulphides reflect the ring size and atomic arrangement in a characteristic manner.[21-23] To 53 mg Cp_2TiS_5 (156 μmol) dissolved in 50 cm^3 CS_2 were added 7 cm^3 $SeBr_2$ solution (20 mmol l^{-1}) formally containing 141 μmol $SeBr_2$ (a slight excess of Cp_2TiS_5 is necessary to avoid free selenium bromides which would react with the methanol eluent and result in additional chromatographic peaks). After stirring for 10 min the solution was injected into the HPLC apparatus without further dilution. Most of the chromatographic peaks observed could be assigned using reference substances prepared by literature methods.[10,11,21-26] In addition to SeS_5, 1,2-Se_2S_5, and eight-membered selenium sulphide rings the chromatograms show the presence of S_{10} and of two 12-membered SeS rings (see Table 3, Fig. 2), which may arise from the following reactions:

$$2Br_2 + 2Cp_2TiS_5 \longrightarrow S_{10} + 2Cp_2TiBr_2 \quad (7)$$

$$2SeS_5 \longrightarrow Se_2S_{10}. \quad (8)$$

The concentrations of SeS_5 and 1,2-Se_2S_5 were high enough to measure their UV absorption spectra for the first time. The results are shown in Fig. 3 together with the spectra of the corresponding sulphur rings S_6 and S_7;[27] also shown are the spectra of 1,2,3-Se_3S_5 and S_8. All spectra apply to chromatographically pure substances dissolved in methanol recorded using diode-array detectors. As can

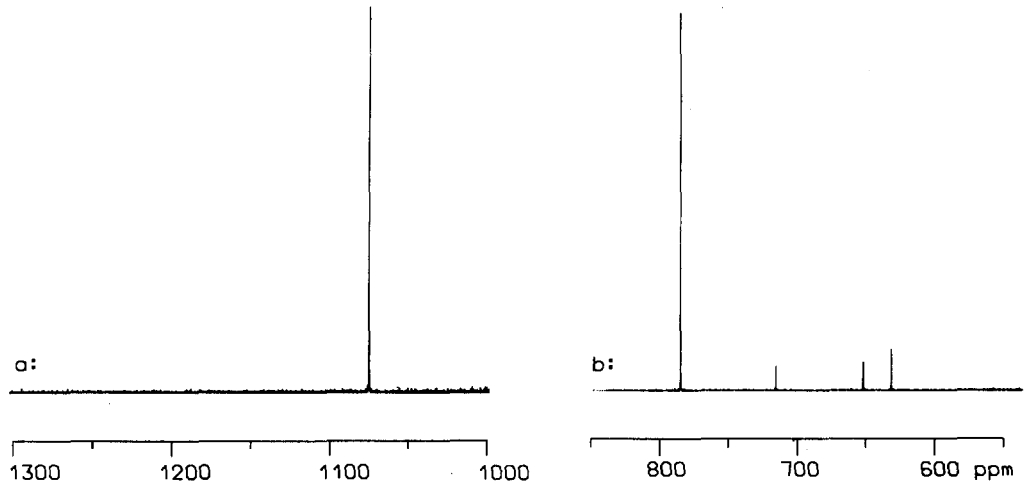

Fig. 1. ^{77}Se-NMR spectra of the reaction mixture of $SeBr_2$ and titanocenepentasulphide showing the presence of 1,2-Se_2S_5 (a) and of SeS_5, 1,5-Se_2S_6, 1,2-Se_2S_6, and 1,2,5,6-Se_4S_4 (b). For details see Table 2.

be seen from Fig. 3 the substitution of S by Se shifts the maxima to higher wavelengths and increases the absorbance at most wavelengths compared to the maximum near 220 nm; the spectra of species of identical ring size are similar. However, S_8 is an exception since this molecule exhibits a rather unique double absorption maximum near 280 nm which is not observed for eight-membered Se–S rings.

To determine the composition and to measure the Raman spectra of the chromatographically detected Se_nS_{12-n} rings a larger sample was prepared. Five grams of Cp_2TiS_5 (14.8 mmol), dissolved in 50 cm^3 CS_2 were reacted with 10 cm^3 $SeBr_2$ solution (14.8 mmol) at 20°C by stirring for 15 min. The precipitate formed was isolated and shown to consist of Cp_2TiBr_2 with traces of six-, seven- and eight-membered selenium sulphide rings (IR spectrum, HPLC analysis, CH content by combustion analysis). The filtrate was separated into CH_3CN and CS_2 phases and the latter cooled to −60°C for 15 h. The precipitate formed (1.42 g) was isolated, washed with a little dried pentane, and analysed by HPLC and IR spectroscopy which showed a mixture of Cp_2TiS_5, Cp_2TiBr_2, Se_nS_{8-n} and Se_xS_{12-x}. To isolate the latter in a pure state the mixture was extracted by 50 cm^3 CH_2Cl_2 for 2 h and the residue (118 mg) by 35 cm^3 CS_2 for 30 min at 20°C. Cooling of the CS_2 extract to −18°C for 15 h resulted in yellow

Table 2. ^{77}Se-NMR chemical shifts of the products of the reaction of $SeBr_2$ with titanocenepentasulphide; cf. Fig. 1

	Shift (ppm)	Relative intensity	Assignment
a	1075	100	1,2-Se_2S_5
b	784	100	SeS_5
	715	6.7	1,5-Se_2S_6
	652	7.7	1,2,5,6-Se_4S_4
	632	11.0	1,2-Se_2S_6

Range a: 919–1302 ppm, 9064 scans; range b: 502–849 ppm, 36,938 scans. Pulse width 20 μs, excitation frequency 68.675 MHz, line broadening factor 2 Hz, acquisition time *ca* 1.5 s/point.

Table 3. Chromatographic analysis of the reaction of $SeBr_2$ with titanocenepentasulphide (dead time: 1.38 min); cf. Fig. 2

Retention time (min)	Assignment
2.55	CS_2
3.44	Cp_2TiS_5
3.77	SeS_5
4.65	1,2-Se_2S_5
6.00	1,*n*-Se_2S_6 ($n \neq 2,8$)
6.39	1,2-Se_2S_6
6.65 (shoulder)	1,2,5,6-Se_4S_4
8.93	?
11.37	S_{10}
11.80	S_{11} (?)
13.51	?
17.04	1,7-Se_2S_{10}
18.45	1,2-Se_2S_{10}

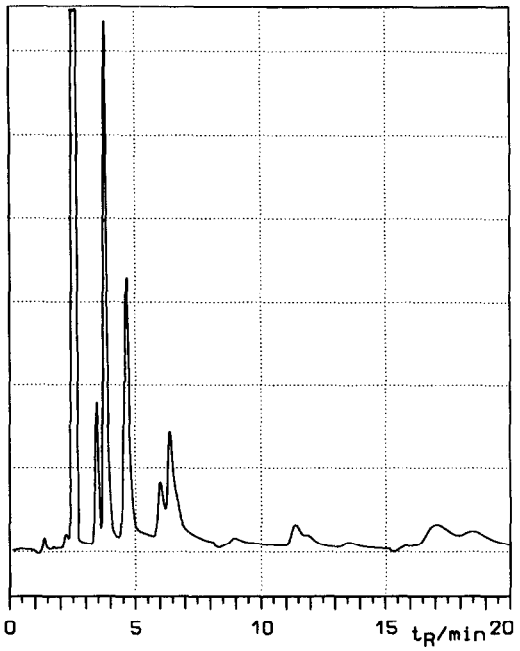

Fig. 2. Chromatographic separation of the products of the reaction between $SeBr_2$ and titanocenepentasulphide showing the presence of rings of sizes 6–12 (see Table 3). t_R retention time, ordinate: absorbance at 254 nm.

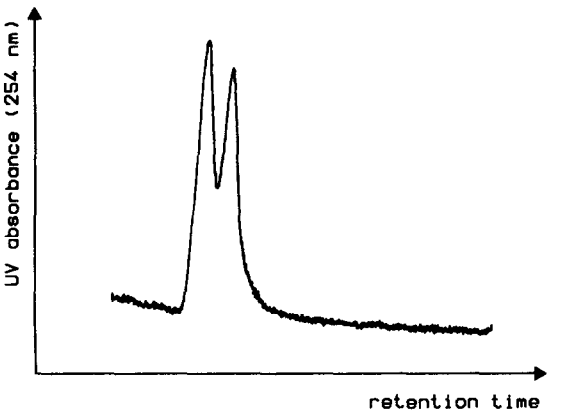

Fig. 4. Chromatographic separation of two isomeric 12-membered rings Se_2S_{10} (retention times see Table 4).

crystals, the HPLC analysis (Fig. 4) and Raman spectra (Fig. 5) of which showed that almost pure 12-membered selenium sulphide rings had been obtained. The analytical composition of several of the Se_xS_{12-x} crystals was determined by energy-dispersive X-ray spectroscopy. Only lines due to S and Se were detected, and using ZnS and elemental selenium as reference materials the atomic ratio S:Se was determined as 5.29:1 resulting in a formula of $Se_{1.89}S_{10}$. Obviously, the compound prepared is Se_2S_{10}. The crystals formed right parallelepipeds.

The HPLC chromatogram of the Se_2S_{10} sample shows two peaks with an intensity ratio of *ca* 1:1 (peak areas). The retention times of a number of sulphur and selenium sulphide rings measured under identical conditions are shown in Table 4. From this table and literature data[21–23] it can be seen that the retention times depend on

(a) the ring size,
(b) the selenium content, and
(c) the number of SeS bonds per molecule.

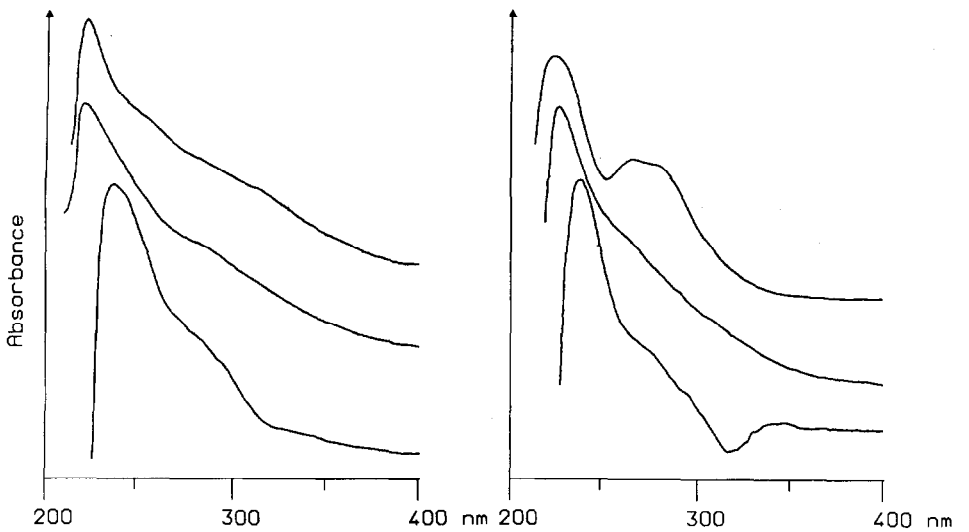

Fig. 3. Left: UV absorption spectra of SeS_5 (bottom), 1,2-Se_2S_5 (centre), and 1,2,3-Se_3S_5 (top). Right: UV spectra of S_6 (bottom), S_7 (centre), and S_8 (top) for comparison. All spectra were recorded with a diode array detector using methanol as a solvent.

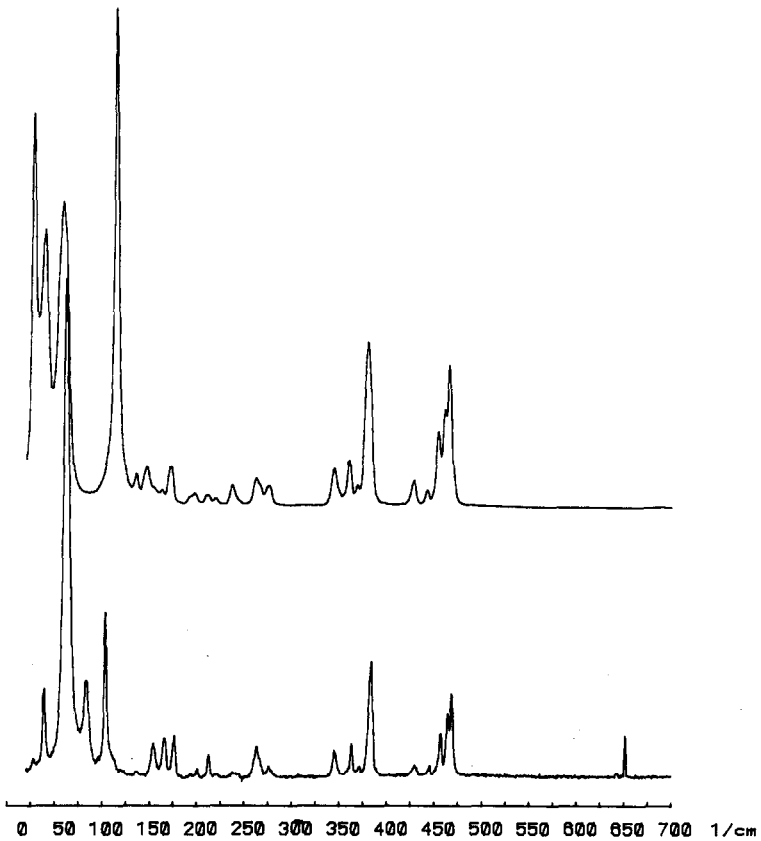

Fig. 5. Raman spectra of solid samples of Se_2S_{10} (top) and $Se_2S_{10} \cdot CS_2$ (bottom). For wavenumbers see Table 5.

While an increase of (a) or (b) enhances the retention time (t_B), an increase of (c) lowers t_B. The two Se_2S_{10} rings prepared in this work show t_B values of which one is distinctly lower than that of S_{12}, while the other one is slightly higher (almost identical) than that of S_{12}. We interpret the first peak as caused by 1,7-Se_2S_{10} (compare 1,4-Se_2S_4 vs S_6) and the second as caused by 1,2-Se_2S_{10} (compare 1,2-Se_2S_5 vs S_7). Both retention times are too different from those of S_{11} (calc. t_B: 13.3 min) and S_{13} (calc. t_B: 20.4 min)[28] to justify any other ring size than 12. A chromatograhic separation of 1,2- and 1,7-Se_2S_{10} on a preparative scale seems to be impossible due to the extremely low solubility of both compounds in methanol.

A dimerization of SeS_5 may result in either

Table 4. Retention times t_B (min) of two Se_xS_{12-x} rings and of 12 reference compounds to illustrae the dependence of t_B on ring size, selenium content, and number of SeS bonds per molecule

Ring size	Increasing t_B
6	1,4-Se_2S_4: 3.38 SeS_5: 3.46 S_6: 3.60
7	1,2-Se_2S_5: 4.28 1,2,5-Se_3S_4: 4.32 S_7: 4.38
8	S_8: 5.86 1,2,3-Se_3S_5: 6.21 1,2,5,6-Se_4S_4: 6.25
9	S_9: 8.80
10	S_{10}: 10.76
12	1,7-Se_2S_{10}: 15.66 S_{12}: 16.41 1,2-Se_2S_{10}: 16.52

Flow: 2 cm^3 min^{-1}; dead time: 1.41 min; eluent: CH_3OH/H_2O: 95/5 v/v.

1,2-Se_2S_{10} or 1,7-Se_2S_{10}. Assuming an analogous molecular structure for 1,7-Se_2S_{10} as is known for S_{12}[29] the latter heterocycle may exist as two isomers since the atomic positions in the 12-membered ring are not all equivalent (S_{12}: two sets of 6 equivalent atoms each; symmetry D_{3d}). Therefore, the two atoms in 1,7-Se_2S_{10} may be both in the central plane of the molecule (isomer 1) or one in the upper and one in the lower of the three parallel planes of atoms (isomer 2). Both isomers are of C_{2h} symmetry, while 1,2-Se_2S_{10} is of C_1 symmetry (Fig. 6).

The Raman spectra of the yellow Se_2S_{10} crystals, when still wet from CS_2, and of the dried sample are listed in Table 5. S_{12} forms a stoichiometric solid solution with CS_2, the crystal structure[29] and Raman spectrum[30] of which are known and are distinctly different from those of pure S_{12}. A similar behaviour is to be expected for Se_2S_{10} molecules. The crystals obtained from CS_2 show the symmetrical stretching vibration of the structural CS_2 at 651 cm^{-1} and its strongest ^{34}S satellite at 642 cm^{-1} indicating that they consist of $Se_2S_{10}\cdot CS_2$ (Table 5). The corresponding wavenumbers of liquid CS_2 are 654 and 645 cm^{-1}. There are five Raman lines to be assigned to SS stretching modes (500–400 cm^{-1}), four in the region typical for SeS stretching modes (390–330 cm^{-1}), and a number of bending modes below 250 cm^{-1}. The two relatively weak lines at 276 and 262 cm^{-1} may be assigned to either SeSe stretching or SSS bending vibrations (see the vibrational spectra of S_8,[30] S_{12}[30] and Se_nS_{8-n}[31]). If an equimolar mixture of 1,2- and 1,7-Se_2S_{10} was present, only one out of 24 bonds was an SeSe bond resulting in a very weak Raman line for the SeSe stretching mode.

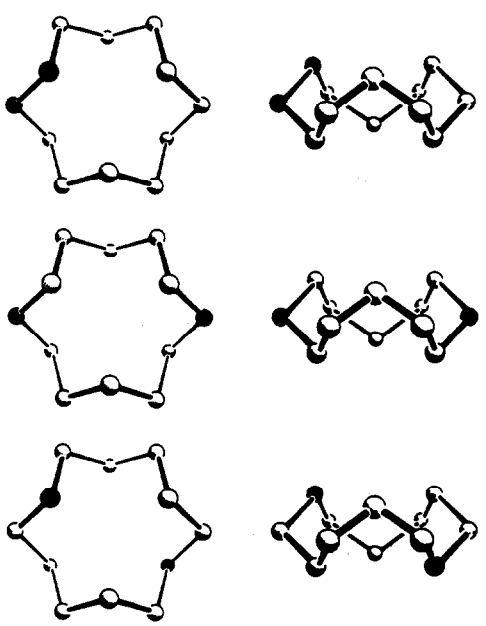

Fig. 6. Likely molecular structures of 1,2-Se_2S_{10} (top) and of two isomers of 1,7-Se_2S_{10} (centre and bottom; black balls = selenium atoms).

On storage of $Se_2S_{10}\cdot CS_2$ in air the Raman spectrum changes to that of Se_2S_{10} which has its most intense line at 114 cm^{-1} (Table 5). This line observed at 127 cm^{-1} for S_{12}, at 117 cm^{-1} for $S_{12}\cdot CS_2$, at 114 cm^{-1} for Se_2S_{10}, and at 103 cm^{-1} for $Se_2S_{10}\cdot CS_2$ has to be assigned to the totally symmetrical ring bending vibration.[30,32] Its position is a function of both the ring size[33] and the Se content, and its high Raman intensity may be utilized to detect these ring molecules in mixtures.

The striking similarities between the spectra of S_{12} and Se_2S_{10} on one hand and of $S_{12}\cdot CS_2$ and $Se_2S_{10}\cdot CS_2$ on the other hand demonstrate that these species do not only agree in molecular structure but the crystal structures must also be analogous. In fact, Weiss *et al.*[34] have prepared solid solutions of S_{12} and Se_xS_{12-x} which crystallize from benzene as orthorhombic needles; the maximum selenium content of 29% (by weight) corresponds to the formula $Se_{1.7}S_{10.3}$. On the other hand, Kutoglu[35] determined the structure of $Se_2S_{10}\cdot CS_2$ by X-ray diffraction at 25°C and found it extremely similar to that of $S_{12}\cdot CS_2$. Both compounds crystallize in space group $R3m-D_{3d}^5$ with $Z = 3$. The lattice constants of $Se_2S_{10}\cdot CS_2$ were $a = 1086.9(3)$ and $c = 1177.9(3)$ pm resulting in a cell volume of 1205.1(9) pm^3. It is not known whether the samples investigated by Weiss *et al.* and by Kutoglu also consisted of isomeric Se_2S_{10} molecules as our sample does. But as has been observed for a large number of eight-membered rings Se_nS_{8-n}, the atomic positions in the crystals of both $Se_{1.7}S_{10.3}$ and $Se_2S_{10}\cdot CS_2$ are occupied statistically by S and Se due to rotational disorder of the ring molecules. The shape of the 12-membered rings agrees with that of S_{12}.

The proposed dimerization of SeS_5 with formation of 1,2- and 1,7-Se_2S_{10} may proceed by two different mechanisms:

(1) Via a hypervalent intermediate as has been proposed before for the interconversion of sulphur rings[36] and for the formation of SeS_5 and 1,2,3-Se_3S_5 by decomposition of 1,2-Se_2S_5.[10] The first step will be an insertion of an Se atom of one molecule into the weakest bond (Se—S) of the second molecule:

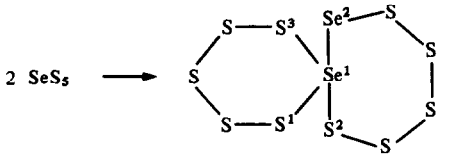

Table 5. Raman spectra of S_{12}, Se_2S_{10}, $S_{12}\cdot CS_2$, and $Se_2S_{10}\cdot CS_2$ at low temperatures[a]

S_{12} (−80°C)	Se_2S_{10} (−100°C)	$S_{12}\cdot CS_2$ (−80°C)	$Se_2S_{10}\cdot CS_2$ (−100°C)	Assignment
31 vs	27 vs			lattice
43 vs	39 s		39 w	
58 m-s	58 vs	64 vvs	62 vs	lattice and torsions
63 vs				
67 s		85 s	83 w	
127 vs	114 vvs	117 s-vs	103 m	δ (ring)
	134 vw			SeSeS, SSeS, and SSS bending modes
156 vvw	146 w		154 w	
170 m	171 w		165 w	
177 m-s			175 w	
180 sh	197 w,b	188 s-vs		
	210 vw		212 vw	
221 vw	219 vw			
238 m	236 w	245 w		
245 m	261 w		262 w, b	δ (SSS) and ν (SeSe)
	266 sh			
289 m	274 w	287 m	276 vw	
	344 w		344 w	ν(SeS)
	359 w		362 w	
	368 vw		371 vvw	
	379 s		382 m	
	427 w		429 vw	ν(SS)
	441 vw		445 vw	
449 s	453 m	451 m-s	456 w	
460 vs	460 sh	461 vs	468 m	
475 vw	465 s	476 vw		
			642 vvw	CS_2
		651 w	651 w	

[a] For symbols, see Table 1.

The intermediate may decompose by formation of a bond between S^1 and S^2 at the expense of the two SeS bonds S^1Se and S^2Se in which case 1,2-Se_2S_{10} is formed. On the other hand, the atoms S^3 and Se^2 may combine with rupture of bonds S^3Se^1 and Se^1Se^2 in which case 1,7-Se_2S_{10} is formed. Quantum chemical calculations on model compounds have shown that the two axial bonds in hypervalent species of this type are extremely weak;[37] their dissociation may therefore require very little energy.

This mechanism does not explain the formation of the eight-membered rings observed as side products (see Table 2).

(2) By nucleophilic attack and ring opening followed by formation of new rings of stable sizes like eight- and 12-membered species.[36,38] In this case the SeS_5 molecule is opened up by attack from a nucleophilic impurity (Nu) in the solution and the zwitterion formed attacks a second molecule. The weakest bond of the molecule will be broken easiest and several products are to be expected:

(a) $Nu + SeS_5 \longrightarrow$

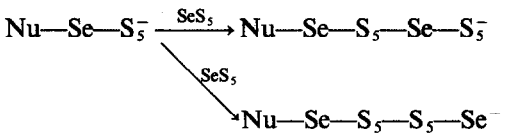

(b) $Nu + SeS_5 \longrightarrow$

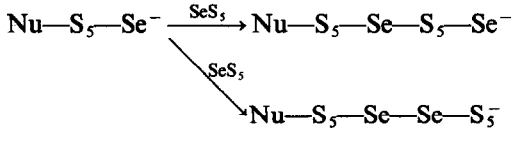

The four species of composition $NuSe_2S_{10}$ may

dissociate into Nu and Se_2S_{10} and it can be seen that only 1,2-Se_2S_{10} and 1,7-Se_2S_{10} are formed. If the $NuSe_2S_{10}$ species split off an eight-membered ring by attack of the tail on the chain the following species could form: SeS_7 from reaction (a) and 1,3-Se_2S_6 as well as 1,2-Se_2S_6 from reaction (b). Only the last of these rings has been observed (Table 2). This may indicate that reactions (a) and (b) proceed with a different rate, but additional and presently unknown reactions must occur to explain the products 1,5-Se_2S_6 and 1,2,5,6-Se_4S_4. In general, it is likely that other reactive species present in the reaction mixture like 1,2-Se_2S_5 take part in the above discussed interconversion reactions.

Another route to explain the formation of Se_2S_{10} takes the formation of S_{12} from SCl_2 and Cp_2TiS_5 into consideration. The first product from this reaction may either split off S_6 or react as follows:

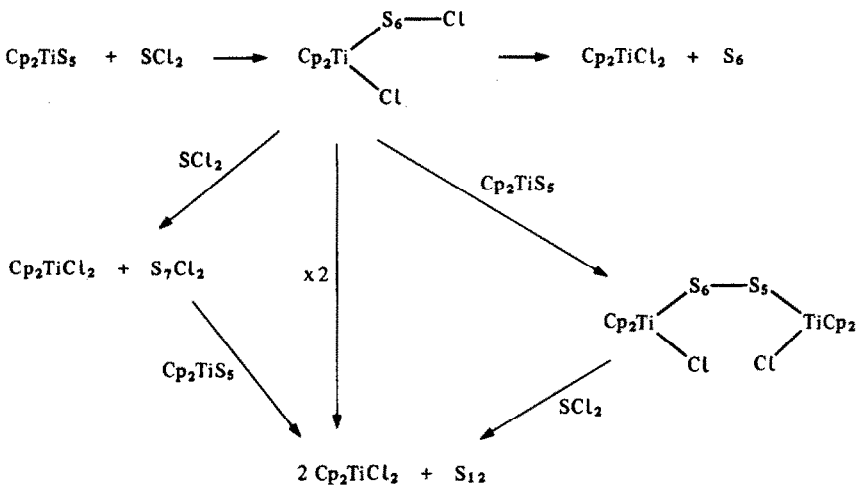

Applied to the reaction of $SeBr_2$ with Cp_2TiS_5 the only product would be 1,7-Se_2S_{10} which is in contrast to the observation of 1,2-Se_2S_{10}. We therefore believe that at least this 12-membered ring results from the dimerization of SeS_5.

The present work shows that the combination of HPLC and NMR analysis provides complete information about the species present in reaction mixtures of selenium sulphides. The higher sensitivity of HPLC allows the detection of species present in low concentration or of low solubility, while the very specific dependence of the ^{77}Se chemical shift on ring size and neighbouring atoms helps to identify the species involved provided a sufficiently high solubility.

Acknowledgements—We are grateful to Ulrich Gernert for the X-ray analysis and to the Deutsche Forschungsgemeinschaft and the Verband der Chemischen Industrie for support.

REFERENCES

1. R. Steudel, G. Holdt, P. T. Visscher and H. van Gemerden, *Arch. Microbiol.*, in press.
2. *Gmelin Handbook of Inorganic Chemistry, Selenium*, Suppl. Vol. B2, pp. 219–251. Springer, Berlin (1984).
3. N. W. Tideswell and J. D. McCullough, *J. Am. Chem. Soc.* 1956, **78**, 3026.
4. N. Katsaros and J. W. George, *Inorg. Chem.* 1969, **8**, 759.
5. D. M. Yost and J. B. Hatcher, *J. Am. Chem. Soc.* 1931, **53**, 2549.
6. J. Milne, *Polyhedron* 1985, **4**, 65.
7. E. Nagy-Felsobuki and J. B. Peel, *Chem. Phys.* 1980, **45**, 189.
8. H. G. Heal and J. Kane, *J. Inorg. Nucl. Chem.* 1967, **29**, 1539.
9. M. Schmidt, B. Block, H. D. Block, H. Köpf and E. Wilhelm, *Angew. Chem.* 1968, **80**, 660; *Angew. Chem. Int. Ed. Engl.* 1968, **7**, 632.
10. R. Steudel and E.-M. Strauss, *Angew. Chem.* 1984, **96**, 356; *Angew. Chem. Int. Ed. Engl.* 1984, **23**, 362.
11. R. S. Laitinen, N. Rautenberg, J. Steidel and R. Steudel, *Z. Anorg. Allg. Chem.* 1982, **486**, 116.
12. R. Steudel, M. Papavassiliou, D. Jensen and K. Seppelt, *Z. Naturforsch.* 1988, **43b**, 245.
13. R. S. Laitinen and T. A. Pakkanen, *Inorg. Chem.* 1987, **26**, 2598; *J. Chem. Soc., Chem. Commun.* 1986, 1381.
14. F. Fehér, *Handbuch der Präparativen Anorganischen Chemie* (Edited by G. Brauer), 3rd edn, Vol. 1, pp. 418–419. F. Enke, Stuttgart (1975).
15. R. Steudel and R. Strauss, *J. Chem. Soc., Dalton Trans.* 1984, 1775.
16. H. C. E. MacFarlane and W. MacFarlane, in *Multi-*

nuclear NMR (Edited by J. Mason), Chap. 15, p. 417. Plenum Press, New York (1987).
17. T. Birchall, R. J. Gillespie and S. L. Vekris, *Can. J. Chem.* 1965, **43**, 1672.
18. J. W. George, N. Katsaros and K. J. Wynne, *Inorg. Chem.* 1967, **6**, 903.
19. Cf. the Raman spectra of $SeBr_3^+X^-$ with X = $AlCl_4$, $AlBr_4$, AsF_6, SbF_6.[2]
20. P. Born, R. Kniep and D. Mootz, *Z. Anorg. Allg. Chem.* 1979, **451**, 12.
21. R. Steudel and E.-M. Strauss, *Z. Naturforsch.* 1983, **38b**, 719.
22. E.-M. Strauss, Doctoral Dissertation, Techn. Univ. Berlin (1986).
23. D. Jensen, Doctoral Dissertation, Techn. Univ. Berlin (1989).
24. R. Steudel, M. Papavassiliou, E.-M. Strauss and R. S. Laitinen, *Angew. Chem.* 1986, **98**, 81; *Angew. Chem. Int. Ed. Engl.* 1986, **25**, 99.
25. D. M. Giolando, M. Papavassiliou, J. Pickardt, T. B. Rauchfuss and R. Steudel, *Inorg. Chem.* 1988, **27**, 2596.
26. R. Steudel, D. Jensen and M. Papavassiliou, *Phosphorus Sulfur Silicon* 1989, **41**, 349.
27. R. Steudel, D. Jensen, P. Göbel and P. Hugo, *Ber. Bunsenges. Phys. Chem.* 1988, **92**, 118.
28. R. Strauss and R. Steudel, *Fresenius' Z. Anal. Chem.* 1987, **326**, 543.
29. J. Steidel, R. Steudel and A. Kutoglu, *Z. Anorg. Allg. Chem.* 1981, **476**, 171.
30. R. Steudel and H.-J. Mäusle, *Z. Naturforsch.* 1978, **33a**, 951.
31. R. Steudel and R. Laitinen, *J. Mol. Struct.* 1980, **68**, 19.
32. R. Steudel and D. F. Eggers, *Spectrochim. Acta* 1975, **31A**, 879.
33. R. Steudel, *Spectrochim. Acta* 1975, **31A**, 1065.
34. J. Weiss and W. Bachtler, *Z. Naturforsch.* 1973, **28b**, 523.
35. A. Kutoglu, personal communication to R.S. (1980).
36. R. Steudel, *Top. Curr. Chem.* 1982, **101**, 149.
37. R. Laitinen, T. A. Pakkanen and R. Steudel, *J. Am. Chem. Soc.* 1987, **109**, 710.
38. R. Steudel, *Nova Acta Leopoldina* 1985, **59**, 231.

Note added in proof: After this work had been submitted, the ^{77}Se-NMR spectrum of $SeBr_2$ in equilibrium with liquid Se_2Br_2 at 20°C was reported (singlet at 1446 ppm); M. Lamoureux and J. Milne, *Can. J. Chem.* 1989, **67**, 1936.

Polyhedron Vol. 9, No. 9, pp. 1209–1215, 1990
Printed in Great Britain

0277–5387/90 $3.00+.00
© 1990 Pergamon Press plc

TETRAHALODIMOLYBDATE(II) COMPLEXES WITH ALKYL SUBSTITUTED PYRIDINES. A STRUCTURAL AND SPECTROSCOPIC STUDY

K. J. EWING† and S. I. SHUPACK‡

Department of Chemistry, Villanova University, Villanova, PA 19085, U.S.A.

and

A. L. RHEINGOLD

Department of Chemistry, The University of Delaware, Newark, DE 19716, U.S.A.

(*Received* 21 *August* 1989; *accepted* 2 *January* 1990)

Abstract—Tetrahalodimolybdate(II) complexes with pyridine (PY), 3-methylpyridine (3PIC), 4-methylpyridine (4PIC), 3,4-dimethylpyridine (34LUT) and 4-tert-butylpyridine (4TBP) have been spectroscopically characterized. Additionally, the X-ray diffraction structure of the complex $Mo_2Br_4(4TBP)_4 \cdot 2C_6H_6$ is reported and compared to the previously reported structure of the complex $Mo_2Br_4(4PIC)_4 \cdot CHCl_3$. The 4TBP complex crystallizes in the $P2_1/n$ space group ($a = 9.143(3)$, $b = 15.305(5)$, $c = 18.766(4)$ Å, $\beta = 93.46°$, $V = 2621.9(9)$ Å^3, $Z = 4$) in the eclipsed conformation, giving the complex an overall D_{2h} symmetry. The Mo—Mo bond distance is 2.148(2) Å. These structural features are very similar to those found in $Mo_2Br_4(4PIC)_4 \cdot CHCl_3$ according to the published atomic coordinates rather than the depicted complex geometry. A plot of the $\delta \rightarrow \delta^*$ transition energy versus ligand gas-phase basicity shows that the $\delta \rightarrow \delta^*$ transition energy varies with respect to the position and type of alkyl substituent on the pyridine ring.

There is presently little spectroscopic or structural data available for dimolybdenum complexes containing substituted pyridine ligands. This is surprising when one considers that the variability in both the ligand basicity and steric bulk makes the substituted pyridines excellent ligands for probing the nature of the quadruple metal–metal bond and its interactions with such ligands. To our knowledge, the only structural study reported to date for this class of complex is of the tetrakis(4-methylpyridine)tetrahalodimolybdate(II) complexes.[1] This study showed that both chloride and bromide forms exist in the eclipsed conformation with overall D_{2h} symmetry. The coordination about each molybdenum atom was reported to be square-planar. The authors speculated that, based on IR data, $Mo_2Cl_4(4PIC)_4 \cdot CHCl_3$ underwent a structural rearrangement from D_{2h} to D_{2d} symmetry upon loss of chloroform.

Recently, Cotton *et al.*[2] reported on the influence the π-acidity of various phosphine ligands in $Mo_2Cl_4(PR_3)_4$ have on the electronic spectra of these complexes. They showed that there is a correlation between the $\delta \rightarrow \delta^*$ transition energy and the π-acidity for 15 phosphine ligands. In a related paper Hanselman and Smith[3] studied the relationship between spectroscopic properties of $Mo_2Cl_4(PR_3)_4$ complexes and their electrochemical behaviour. They reported that the $Mo_2Cl_4(PR_3)_4$ complexes became more difficult to oxidize as the $\delta \rightarrow \delta^*$ transition energy decreased due to the increased π-acidity of the phosphine ligands. They noted that with more strongly electron-withdrawing phosphine ligands Mo—P backbonding will primarily affect the $\delta \rightarrow \delta^*$ transition energy, while with trialkyl phosphines the $\delta \rightarrow \delta^*$ transition energy is more dependent on the electron-donating ability of the phosphine ligand.

† Currently at The U.S. Naval Research Laboratory, Optical Sciences Division, Code 6505, Washington, D.C. 20375, U.S.A.

‡ Author to whom correspondence should be addressed.

In a previous paper[4] the preparation of tetrahalodimolybdate(II) complexes with the ligands 3-methylpyridine, 3,4-dimethylpyridine, 3,5-dimethylpyridine and 4-tert-butylpyridine was reported. The current thrust of this work is in determining which factors, electronic or steric, play the predominant role in determining the complex geometry and spectroscopic characteristics. In similar fashion to Cotton[2] and Smith[3] the $\delta \rightarrow \delta^*$ transition energy of the pyridine complexes is evaluated with respect to the change in ligand gas-phase basicity.

EXPERIMENTAL

Synthesis

The complexes were prepared from $Cs_3Mo_2Cl_8H$ and $Cs_3Mo_2Br_8H$ as described by San Filippo *et al.*[5] All solvents and ligands were dried and distilled via literature methods under nitrogen. The dimolybdenum complex containing 2-methylpyridine, the most sterically restrictive ligand, was not isolable. Instead, a brown solid which did not exhibit the characteristic electronic absorption attributable to the $\delta \rightarrow \delta^*$ transition was obtained. This suggests that the resulting product is monomeric in nature, formation of which is due to decomposition of the sterically unstable dimer.

Slow recrystallization of $Mo_2Br_4(4TBP)_4$ from a benzene–pentane solution at 0°C resulted in the formation of a mixture of blue and green crystals. Recrystallization from tetrahydrofuran or excess ligand (4TBP) led to an almost exclusive formation of the green crystals. The green crystals were found to change back to the blue material upon leaving under argon for about a month. X-ray structural data are reported for the blue crystalline form, while X-ray quality crystals of the green form have yet to be obtained.

Spectroscopic measurements

Visible spectra of Nujol mulls of the complexes were recorded on a Cary 219 spectrophotometer with an Apple IIC computer interface. Raman spectra were recorded as described elsewhere.[6]

X-ray crystallography procedures

A crystal (0.12 × 0.17 × 0.37 mm) of the blue form of $Mo_2Br_4(4TBP)_4 \cdot 2C_6H_6$ (red by transmitted light) was sealed in epoxy cement and mounted on a glass fibre. The space group, $P2_1/n$, was uniquely determined from systematic absences. Unit cell parameters were derived from a least-squares fit of the angular settings of 25 reflections ($22° \leqslant 2\theta \leqslant 26°$). The data were corrected for absorption by an empirical method (max/min transmission = 0.198/0.181); R(int) = 0.024. Pertinent crystal data and parameters are collected in Table 1.

The structure was solved by direct methods (SOLV–SHELXTL) which located the molybdenum and two bromine atoms. The remaining non-hydrogen atoms were located from subsequent difference Fourier synthesis. The asymmetric unit consists of 1/2 of the Mo_2 complex (an inversion centre is midway in the Mo—Mo bond) and a molecule of benzene (the recrystallization solvent).

All non-hydrogen atoms were refined with anisotropic thermal parameters, with hydrogen atoms treated as idealized isotropic contributions (d(C—H) = 0.96 Å) and the benzene molecule as a rigid hexagon (d(C—C) = 1.395 Å). Selected bond distances are given in Table 2. Additional crys-

Table 1. Crystal and data collection parameters: $Mo_2Br_4(4TBP) \cdot 2C_6H_6$ (blue form)

Crystal data	
Formula	$Mo_2Br_4C_{48}H_{64}N_4$
Z	2
Size (mm)	0.12 × 0.17 × 0.37
Crystal system	Monoclinic
D(calc) (g cm^{-3})	1.534
μ(Mo-K_α) (cm^{-1})	35.2
Temperature (°C)	22
Max/min transmission	0.198/0.181
Space group	$P2_1/n$
a (Å)	9.143(3)
b (Å)	15.305
c (Å)	18.766(4)
β (°)	93.46(2)
V (Å^3)	2621.2(9)
Data collection	
Diffractometer	Nicolet R3
Standard reflections	3 std/97 rflns
Radiation	Mo-K_α (λ = 0.71073 Å)
Data collected	3707
Monochromator	Graphite
Scan technique	θ–2θ
Unique data	3424 ($\pm h$, $+k$, $+l$)
Scan speed (° min^{-1})	Var. 5–20
Unique $3\sigma F_o$ data	2460
Scan range (°)	$4 \leqslant 2\theta \leqslant 45°$
Structure refinement	
R_F (%)	6.68
$R_{\omega F}$ (%)	6.33
GOF	1.51
$\Delta(\rho)$ (e Å^{-3})	0.88
Mean Δ/σ	0.031

Table 2. Selected bond distances (Å) and angles (°) for $Mo_2Br_4(4TBP)_4 \cdot 2C_6H_6$

Bond distances			
Mo—Mo(a)	2.148(2)	Mo—N(1)	2.237(9)
Mo—Br(1)	2.569(2)	Mo—N(2)	2.233(9)
Mo—Br(2)	2.572(2)		

Bond angles			
Br(1)—Mo—Br(2)	144.5(1)	N(1)—Mo—N(2)	155.4(3)
Br(1)—Mo—N(1)	90.6(2)	Br(1)—Mo—Mo(a)	103.0(1)
Br(2)—Mo—N(1)	80.8(2)	Br(2)—Mo—Mo(a)	112.4(1)
Br(1)—Mo—N(2)	91.4(1)	N(1)—Mo—Mo(a)	102.8(2)
Br(2)—Mo—N(2)	83.4(2)	N(2)—Mo—Mo(a)	100.6(2)

tallographic data are available as supplementary material.

RESULTS AND DISCUSSION

Structure of $Mo_2Br_4(4TBP)_4 \cdot 2C_6H_6$

The structure, as well as the atomic numbering scheme are shown in Fig. 1, bond distances and angles are presented in Table 2. The molecule crystallizes in the $P2_1/n$ space group exhibiting features common to dimolybdenum complexes containing an Mo—Mo quadruple bond.[7] It possesses an eclipsed conformation about the quadruple bond with two 4TBP ligands on each molybdenum atom *trans* to one another giving the complex an overall D_{2h} symmetry. The unit cell contains two molecules of the complex along with four molecules of benzene solvate arranged as shown in Fig. 2. The Mo—Mo and Mo—N bond lengths, 2.148(2) and 2.35(9) Å, respectively, are virtually the same as the Mo—Mo and Mo—N bond lengths found[1] in $Mo_2Br_4(4PIC)_4$. The average Mo—Br bond length, 2.571(2) Å, is slightly longer than that reported for the 4PIC complex, being closer to the Mo—Br (terminal) bond length of 2.57 Å in $MoBr_3$.[8]

Brencic *et al.*,[1] reported that in the $MoBr_2(4PIC)_2$ moiety, the two ring nitrogen atoms, two bromide atoms and the molybdenum atom were in a common plane, while the 4PIC ring was tilted 35° out of this plane. In the 4TBP complex, both the bromide ions and pyridine ligands are bent away from the quadruple bond forming Br(1)—Mo—Br(2) and N(1)—Mo—N(2) angles of 144.5(1) and 155.4(1)°, respectively. Initially, the difference between the geometry of the two complexes was thought to be due to steric interactions between opposing 4TBP groups. However, using Brencic's original published atomic coordinates,[1] the structure of $Mo_2Br_4(4PIC)_4 \cdot CHCl_3$ was re-examined. It was determined that the original structural rep-

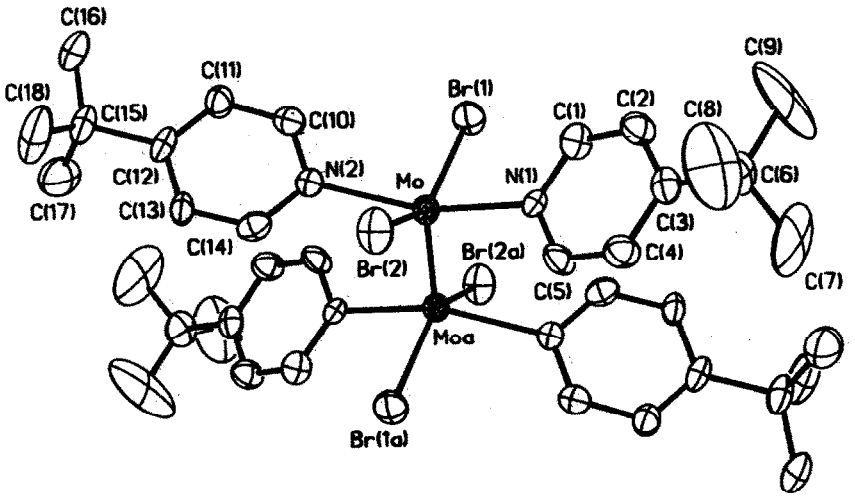

Fig. 1. Molecular structure and labelling scheme for $Mo_2Br_4C_{36}H_{52}N_4$ with 35% probability ellipsoids and the crystallographic numbering scheme. Hydrogen atoms omitted for clarity.

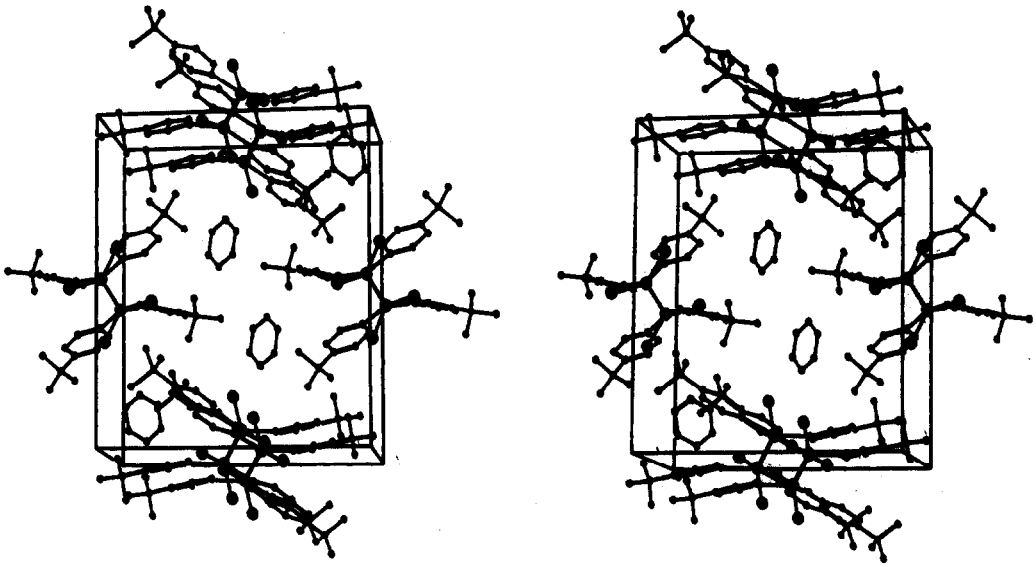

Fig. 2. Stereoview of the unit cell for $Mo_2Br_4(4TBP)_4 \cdot 2C_6H_6$ as viewed down the *a* axis (*b*, vertical; *c*, horizontal).

resentation was in error (see Fig. 2 in ref. 1). Comparison of the structures for the 4PIC and 4TBP complexes (this work) shows these complexes to be isostructural. This indicates that the complex geometry is unaffected by the presence of the bulky tert-butyl group on the pyridine rings.

Both blue and green forms of $Mo_2Br_4(4TBP)_4$ possess identical IR spectra but have different solid-state visible spectra. In the visible region where the absorption due to the $\delta \rightarrow \delta^*$ transition usually appears,[7] the blue form has its lowest energy electronic transition at 17,544 cm^{-1}, while the green form has this transition at 17,182 cm^{-1}. Similarly, $Re_2(N_2CPh_3)_2Cl_4$ crystallizes from tetrahydrofuran as a mixture of ruby red and dark purple crystals.[9] An X-ray study of both crystalline forms show the ruby red complex has a totally eclipsed conformation while the dark purple complex exhibits a 6° twist from the eclipsed conformation. It was proposed that this twist in the Mo—Mo quadrule bond was due to coordination of tetrahydrofuran to one of the rhenium atoms. Elemental analysis of the green form† of $Mo_2Br_4(4TBP)_4$, recrystallized from a 4TBP/hexane mixture, indicates the presence of an additional 4TBP ligand in the molecule. Hence the formula of the green form is best represented as $Mo_2Br_4(4TBP)_4 \cdot L$, where L = 4TBP. The conformation about the quadruple bond may be twisted due to axial coordination of 4TBP to one of the molybdenum atoms in the dimer. This would cause the energy of the $\delta \rightarrow \delta^*$ transition to be lower in the green form than in the blue form, as is observed.

†Found: C, 45.5; H, 5.6; N, 5.4; Br, 28.8. Calc. for $C_{45}H_{65}N_5Br_4Mo_2$: C, 45.5; H, 5.5; N, 5.9; Br, 27.0%.

Spectral data

It is known[10] that the $\delta \rightarrow \delta^*$ transition energy is dependent upon the degree of departure from the eclipsed conformation, as determined by the twist angle χ. The twisting of the quadruple bond can be brought about via torsional forces exerted by bridging bidentate phosphine ligands such as bis(dimethylphosphino)ethane. More recently, the $\delta \rightarrow \delta^*$ transition energy has been shown to vary with either the π-acidity[2] or basicity[3] of different phosphine ligands. In this light, the complexes $Mo_2Cl_4L_4$, where L = PY, 3PIC, 4PIC, 34LUT, 35LUT and 4TBP (blue form), have been studied to determine whether electronic or steric factors primarily affect the $\delta \rightarrow \delta^*$ transition energy.

As shown in Table 3, the measured $\delta \rightarrow \delta^*$ transition energy varies in the order: 35LUT > 4TBP (blue form) > 34LUT > 3PIC > 4PIC < PY. Both the 4PIC[1] and 4TBP (blue form) complexes possess an eclipsed conformation indicating negligible steric interaction across the quadruple bond. The frequencies of the metal–metal stretch in the Raman spectra of the PY, 3PIC, 34LUT and 35LUT complexes (Table 3) are all within 7 cm^{-1} of that for the 4PIC and 4TBP complexes, indicating an eclipsed conformation[7] for all complexes. This evidence suggests that the variation in the $\delta \rightarrow \delta^*$ transition

Table 3. Spectral data for $Mo_2Br_4L_4$

Ligand (L)	Gas-phase basicity (kcal mol^{-1})[a]	$\delta \rightarrow \delta^*$ (cm^{-1})	$\bar{\nu}$M—M (cm^{-1})
PY	212.6	16,667	343
4PIC	215.8	16,807	348
3PIC	215.0	17,331	346
34LUT	218.4	17,391	350
4TBP	218.3	17,544	350
35LUT	217.7	17,986	349

[a] As defined in ref. 11.

energy over the range of ligands employed is not due to a twisting of the quadruple bond.

Therefore, electronic factors associated with the different ligands are expected to be of primary importance in determining the spectroscopic properties of the complexes. Because the electronic spectrum of each complex is measured in a Nujol mull, solvation effects would appear to be insignificant. Furthermore, since the differences between the two known crystal structures (i.e. the 4PIC[1] and 4TBP (this work), which are crystallized from two different solvents) are minimal, it seems reasonable to rule out differences due to crystal lattice effects. In Table 3 are listed the gas-phase basicities[11] of the ligands and the measured $\delta \rightarrow \delta^*$ transition energies. In Fig. 3 a plot of the $\delta \rightarrow \delta^*$ transition energy vs the ligand gas-phase basicity indicates that as the gas-phase basicity increases the $\delta \rightarrow \delta^*$ energy generally increase for all complexes. Also, the transition energy is dependent upon the position of alkyl substituents on the pyridine ring.

The variation in the $\delta \rightarrow \delta^*$ energies with respect to both the donor strength of the ligand and

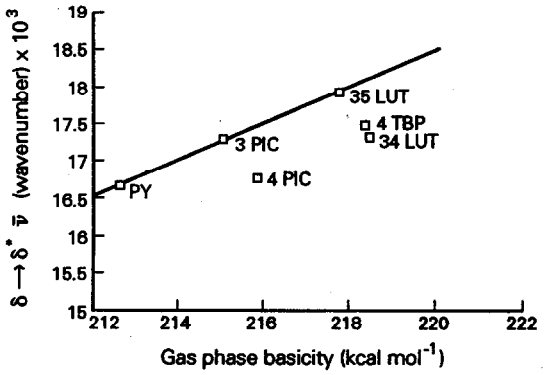

Fig. 3. Plot of the ligand gas-phase basicity of the ligand L = PY, 3PIC, 34LUT, 35LUT and 4TBP in $Mo_2Cl_4L_4$ vs the $\delta \rightarrow \delta^*$ transition energy.

location of the alkyl substituent suggests a complex bonding scenario with at least two possible explanations. Metal-*d* to ligand-*d* backbonding in the complexes $Mo_2X_4(PMe_3)_4$, X = Cl, Br, I, has been proposed[12] to affect the ease of oxidation and difficulty of reduction in the order Cl < Br < I. This order is the opposite to what one would expect based on simple electronegativity arguments. Smith[3] noted that in the trialkyl phosphine complexes, $Mo_2Cl_4(PR_3)_4$, variation in ligand basicity strongly affects the $\delta \rightarrow \delta^*$ transition energy, while in phosphines containing more electronegative substituents Mo(δ) to P(*d*) backbonding has more of an effect on the $\delta \rightarrow \delta^*$ energy.

In the current system, the empty ligand π^*-orbitals with local b_2 symmetry span b_{2g} (δ) symmetry in a D_{2h} complex (note the centre of symmetry in the molecule), allowing for δ-to-ligand π^* backbonding.[13] Assuming δ to ligand π^* backbonding does occur throughout the present series of complexes, the observed $\delta \rightarrow \delta^*$ transition energy is actually a transition between linear combinations of the δ and ligand π^*-orbitals, $\delta + \pi_L^* \rightarrow \delta - \pi_L^*$. Thus, as the σ-basicity of the ligand increases, the effective nuclear charge of the molybdenum is reduced causing the 4*d* orbitals to expand allowing increased δ to π_L^* overlap. As in previous work,[2,3] the observed $\delta \rightarrow \delta^*$ transition energy increases with ligand basicity, but in this case it is due to an increase in the δ-to-ligand π^* overlap. In the case of the 4-alkyl substituted pyridine ligands, hyperconjugative electron release[14] by the 4-methyl, and to a lesser exent the 4-tert-butyl groups will decrease the δ to π_L^* overlap. This will cause a decrease in δ to π_L^* overlap making the observed $\delta \rightarrow \delta^*$ transition lower than expected based on σ-donation arguments alone. Physical manifestation of the δ to π^* backbonding is shown in Fig. 4. Here each tert-butylpyridine ring in $Mo_2Br_4(4TBP)_4 \cdot 2C_6H_6$ is twisted 30° from the plane perpendicular to the metal–metal bond. The analogous 4PIC[1] complex also shows a 30.9° (av.) twist angle, which is not significantly different from the angle found in the 4TBP complex; this twisting of the ligands probably allows for stronger interaction to occur between the δ and ligand π^*-orbitals. A second explanation for the anomalous behaviour of the four-substituted pyridine complexes is that their π-acidity is greater than that of the other pyridine ligands. While data is scarce, Drago and coworkers[15] determined the π-acidity of pyridine and 4PIC to be the same based on observation of the CO stretching frequencies of (B)$Rh_2(pfb)_4(CO)$ (pfb = $O_2C_4F_7^-$, B = pyridine, 4PIC).

Cotton *et al.*[2] have shown that there is a linear relationship between the π-acidity parameters, delta

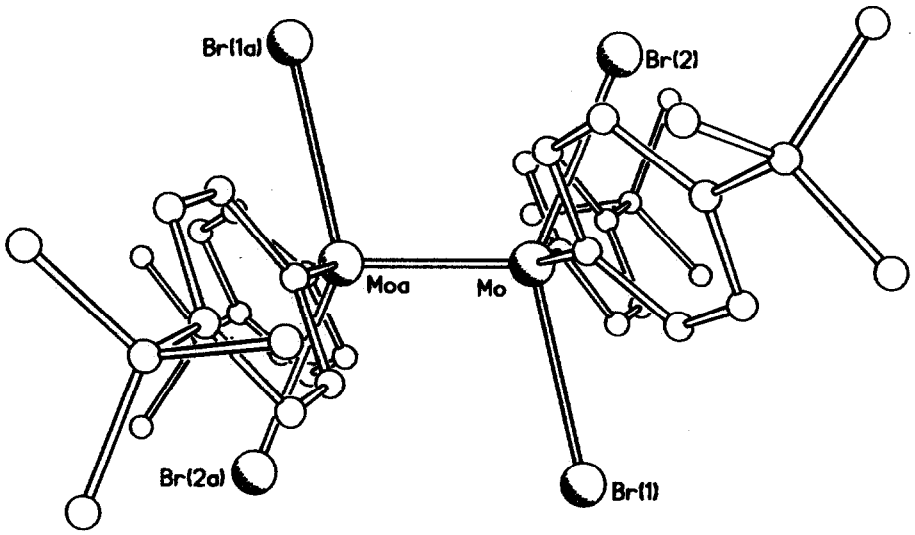

Fig. 4. View of $Mo_2Br_4(4TBP)_4 \cdot 2C_6H_6$ along the *b* axis showing the 30° twist of the pyridine rings with respect to a plane perpendicular to the metal–metal bond.

δ(CO) and $\bar{\nu}$(CO), with the $\delta \rightarrow \delta^*$ transition energy for the complexes $Mo_2Cl_4(PR_3)_4$, where the R group is varied producing 20 different compounds. The data suggest that, as the phosphine's ability to remove electron density increases, the $\delta \rightarrow \delta^*$ energy difference decreases. This effect should then be accompanied by a weakening of the δ bond. However, as the authors point out, it is difficult to estimate the contributions of electron correlation and relaxation effects. Furthermore, the deviation of the phosphines PMe_3, PH_2Ph and $PHPh_2$ from the other ligands presented in previous work[2] is not clearly understood, though perhaps the R group size may play a role.

By way of comparison to previous work,[2] this work has considered the electron-donating ability of the ligand unencumbered by solvent effects and, as it turned out, any steric effects. Thus presumably, as the ability of the ligand to donate electron density increases, the δ to π_L^* overlap increases, consequently increasing the observed $\delta \rightarrow \delta^*$ transition energy as seen in Table 3. However, as was pointed out above, the effect of the position of the R group on the pyridine ring can cause deviation in the expected $\delta \rightarrow \delta^*$ transition energy. Perhaps some mechanism similar to that proposed in this work, encompasing the R groups on the phosphines that show aberrant behaviour may be involved.

Lastly, if electron donation strengthens the δ bond, or if electron back donation weakens it,[2] it would be expected that this would be reflected in the metal–metal fundamental vibration if bond length and bond strength are directly proportional. The Raman spectral data in Table 3 show no significant change or trend, as compared to the gas-phase basicity data. Here again, as previously pointed out,[2] it is difficult to assess the contributions of the many factors to the metal–metal quadruple bond such as electron correlation and relaxation effects.

In conclusion, the results of this study indicate that the spectroscopic behaviour of these complexes is predominately determined by electronic, rather than steric effects. It is shown that the $\delta \rightarrow \delta^*$ transition energy varies with respect to the ligand gas-phase basicity as well as the position of the alkyl substituent on the pyridine ring. The structure of $Mo_2Br_4(4TBP)_4 \cdot 2C_6H_6$ has been determined and found to be isostructural with $Mo_2Br_4(4PIC)_4 \cdot 2CHCl_3$.

Acknowledgements—We would like to thank Drs Roman Czernuszewicz, and Thomas Spiro of Princeton University, and Dr Daniel DeLillo of the Naval Research Laboratory for help in obtaining Raman spectra.

REFERENCES

1. J. V. Brencic, L. Golic, I. Leban and P. Segedin, *Monatsh. Chem.* 1979, **110**, 1221.
2. F. A. Cotton, L. M. Daniels, G. L. Powell, A. J. Kahaian, T. J. Smith and E. Fiore Vogel, *Inorg. Chim. Acta* 1988, **144**, 109.
3. D. S. Hanselman and T. J. Smith, *Polyhedron* 1988, **7**, 2679.
4. K. J. Ewing and S. I. Shupack, *Polyhedron* 1985, **4**, 2069.
5. J. San Filippo Jr, H. J. Sniadoch and R. L. Grayson, *Inorg. Chem.* 1974, **13**, 2121.

6. R. S. Czernuszewiez and M. K. Johnson, *Applied Spec.* 1983, **37**, 297.
7. F. A. Cotton and R. A. Walton, *Multiple Bonds Between Metal Atoms*. Wiley-Interscience, New York (1982).
8. D. J. Babel, *Solid State Chem.* 1972, **4**, 410.
9. F. A. Cotton and L. W. Shive, *Inorg. Chem.* 1975, **14**, 2027.
10. F. L. Campbell III, F. A. Cotton and G. L. Powell, *Inorg. Chem.* 1985, **24**, 177.
11. (a) H. P. Hopkins Jr, D. V. Jahagiradr, P. S. Moulik, D. H. Aue, H. M. Webb, W. R. Davidson and M. D. Pedly, *J. Am. Chem. Soc.* 1984, **106**, 4341; (b) D. H. Aue and M. T. Bowers, *Gas Phase Ion Chemistry* (Edited by M. T. Bowers), Vol. 2. Academic Press, New York (1979).
12. T. C. Zietlow, M. D. Hopkins and H. B. Gray, *J. Am. Chem. Soc.* 1986, **108**, 8266.
13. F. A. Cotton, *Chemical Applications of Group Theory*. Wiley-Interscience, New York (1971).
14. J. Burgess, *Spectrochim. Acta* 1968, **24A**, 277.
15. C. Bilgrien, R. S. Drago, G. C. Vogel and J. Stahlbush, *Inorg. Chem.* 1986, **25**, 2864.

Polyhedron Vol. 9, No. 9, pp. 1217–1220, 1990
Printed in Great Britain

0277–5387/90 $3.00+.00
© 1990 Pergamon Press plc

DIBENZO[b,i][1,4,8,11]TETRA-AZACYCLOTETRADECINE COMPLEXES—I. $W(CO)_4$(tmtaa)

F. ALBERT COTTON* and JOANNA CZUCHAJOWSKA

Department of Chemistry and Laboratory for Molecular Structure and Bonding, Texas A&M University, College Station, TX 77843, U.S.A.

(*Received* 6 *November* 1989; *accepted* 2 *January* 1990)

Abstract—The title compound (which has been previously reported and an unusual structure postulated) has been prepared by essentially the previous method and its structure determined by X-ray crystallography. It has the previously proposed structure in which there is a diimide group, —N=C(CH_3)CH_2C(CH_3)=N— coordinated to *cis* positions of the $W(CO)_4$ group. The other side of the macrocycle takes on the —NHC(CH_3)CHC(CH_3)NH— structure and is not bonded to the $W(CO)_4$ group. Crystal data: space group *Pcab* (No. 61) with $a = 16.387(8)$, $b = 21.435(8)$, $c = 14.529(5)$ Å, $V = 5104(3)$ Å^3, $Z = 8$.

This report is concerned with the structure of a novel complex of the title ligand, whose normal structure[1] is that shown as **I**, and which may be abbreviated tmtaa. The conventional role played by this ligand[2] is that of a tetra-aza macrocyclic dianion. However, there are a few reports of compounds in which this ligand is believed to behave differently, and one of these struck us as being sufficiently novel as to merit further study. In 1975 Bell and Dabrawiak[3] prepared the two compounds $M(CO)_4$(tmtaa) (M = Mo, W) and proposed, on the basis of spectroscopic evidence the type of structure represented schematically in **II**. Although we saw no reason to doubt the conclusion of Bell and Dabrawiak, we thought it worth establishing with certainty and at a quantitative level of structural detail the occurrence of such an unconventional mode of coordination of tmtaa. It should be noted that in **II** the ligand remains neutral, but has undergone a proton shift from one of the nitrogen atoms to a ring carbon atom, thus generating a —N=C(CH_3)—CH_2—C(CH_3)=N— chain, a 1,3-diimino propane unit, which is the entity that coordinated to the metal atom.

We have prepared the tungsten compound, $W(CO)_4$(tmtaa), and shown that it does indeed have a structure of type **II**. The structure determination and structural details are reported here.

* Author to whom correspondence should be addressed.

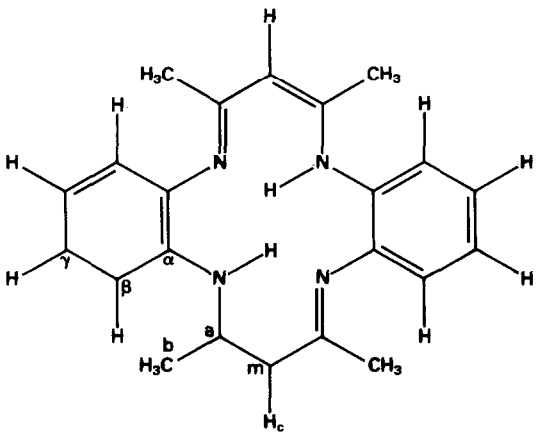

I

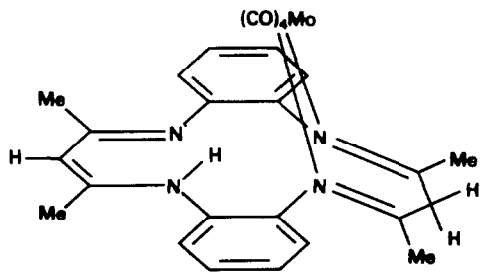

II

EXPERIMENTAL

All manipulations were carried out under an argon atmosphere, using standard vacuum-line and Schlenk techniques. The solvents were freshly distilled under nitrogen from the appropriate drying agents. $W(CO)_6$ was obtained from the Pressure Chemical Company and tmtaa[4] was prepared according to the literature.

Preparation

Equimolar quantities of tungsten hexacarbonyl (0.08 g, 0.23 mmol) and tmtaa (0.08 g, 0.23 mmol) were mixed and refluxed in toluene (18 cm^3) for 48 h. The yellow, crystalline product was isolated by layering the reaction solution with hexanes. The product is air-stable. It displayed four IR peaks at 2000, 1890, 1872 and 1830 cm^{-1}, in good agreement with the original paper.

X-ray crystallography

The unit cell determinations and collection of intensity data were carried out by following routine procedures which have been previously described elsewhere.[5] The intensity data were corrected for Lorentz and polarization effects. An empirical absorption correction based upon azimuthal scans of six reflections near $\chi = 90°$ was applied to the data. Pertinent crystallographic data are given in Table 1.

Inspection of the systematic absences led to the inference that the correct space group would be *Pcab*, a non-standard setting of *Pbca* (No. 61). Successful solution and refinement confirmed that choice.

The positions of tungsten, carbonyl groups and the entire macrocyclic ligand were located from the Patterson map. All hydrogen atoms were located from difference Fourier maps and refined with an

Table 1. Crystal data for $W(CO)_4(C_{22}H_{24}N_4)$

Formula	$W(CO)_4(C_{22}H_{24}N_4)$
Formula weight	638.34
Space group	*Pcab*
a (Å)	16.387(8)
b (Å)	21.435(8)
c (Å)	14.529(5)
α (°)	90.00(3)
β (°)	90.00(3)
γ (°)	90.00(3)
V (Å^3)	5104(3)
Z	8
d_{calc} (g cm^{-3})	1.661
Crystal size (mm)	$0.40 \times 0.49 \times 0.10$
μ(Mo-K_α) (cm^{-1})	7.50
Data collection instrument	AFC5R
Radiation monochromated in incident beam (Mo-K_α, Å)	0.71073
Orientation reflections number; range (2θ)	25; $21.1 < 2\theta \leqslant 31.6$
Temperature (°C)	23 ± 1
Scan method	2θ–ω
Data collection range, 2θ (°)	$4 \leqslant 2\theta \leqslant 50$
Number of unique data, total with $F_o^2 > 3\sigma(F_o^2)$	5014, 2476
Number of parameters refined	398
Transmission factors, max., min.	100, 0.48
R^a	0.0319
$R_w{}^b$	0.0458
Quality-of-fit indicator^c	0.963
Largest shift/ESD, final cycle	0.42
Largest peak (e/Å^3)	0.98

$^a R = \Sigma \| |F_o| - |F_c| \| / \Sigma |F_o|$.
$^b R_w = [\Sigma w(|F_o| - |F_c|)^2 / \Sigma w|F_o|^2]^{1/2}$; $w = 1/\sigma^2(|F_o|)$.
^{c} Quality-of-fit $= [\Sigma w(|F_o| - |F_c|)^2 / (N_{observed} - N_{parameters})]^{1/2}$.

overall isotropic temperature factor. In the later stage, restraints were put on four C—H interatomic distances and added to least-squares refinements. Finally, three models were created to test the position of H(1) with respect to the two nitrogens, N(3) and N(4). In model 1, H(1) was located by the difference Fourier map and refined to convergence at a distance of *ca* 0.9 Å from N(3). In model 2, a hydrogen atom, H(1′), was added to a calculated position at *ca* 0.9 Å from N(4). The atoms H(1′) and H(1) were assigned a fractional occupancy factor of 0.5 and refined to convergence. In model 3, H(1) was deleted, leaving H(1′) at a multiplicity of one. All these models pointed to the fact that, in reality, H(1) and H(1′) have a fractional occupancy factor of 0.5, as described in model 2. The results of model 2 are reported here.

RESULTS AND DISCUSSION

ORTEP drawings of $W(CO)_4$(tmtaa) are shown in Figs 1 and 2, which also define the atomic numbering scheme used in the tables and the following discussion.

The molecule resides on a general position in the unit cell, but has idealized C_s symmetry, with the mirror plane passing through W, C(25)—O(3), C(23)—O(1), C(2) and C(11). If the hydrogen atom spent 100% of its time at either of the nitrogens, N(3) or N(4), then we should see an appropriate shortening of some C—C and C—N bonds, as shown schematically below.

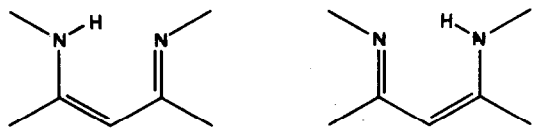

In our case however, H(1) and H(1′) are bonded to N(3) and N(4) respectively, at a distance of *ca* 0.7 Å. We observe a superposition of both of these structures, which explains why the entire C(9)—N(3)—C(10)—C(11)—C(12)—N(4)—C(13) group shows no bond alternation, as would be expected for either one of the above structures. Finally, H(1) and H(1′) participate in hydrogen bond interactions to N(4) and N(3), respectively, with H(1)—N(4) and H(1′)—N(3) distances of 1.964 and 2.024 Å.

The metal atom is indeed bonded to only two of the four nitrogens of tmtaa, N(1) and N(2). Interestingly enough, the ligand remains neutral upon coordinating to the $W(CO)_4$ moiety, due to the migration of one of the nitrogen protons to the methine carbon, C(2). The resulting 1,3-diimino propane unit displays shortened N—C distances of 1.28(1) Å for N(2)—C(3) and N(1)—C(1).

Finally, tmtaa takes on the familiar saddle-shape conformation, but much more pronounced than in the free ligand. Large dihedral angles between planes defined by atoms: (i) N(2)—C(4)—C(5) and C(3)—N(2)—C(4), and (ii) C(1)—N(1)—C(18) and N(1)—C(18)—C(17) of 72.98 and 74.50°, respec-

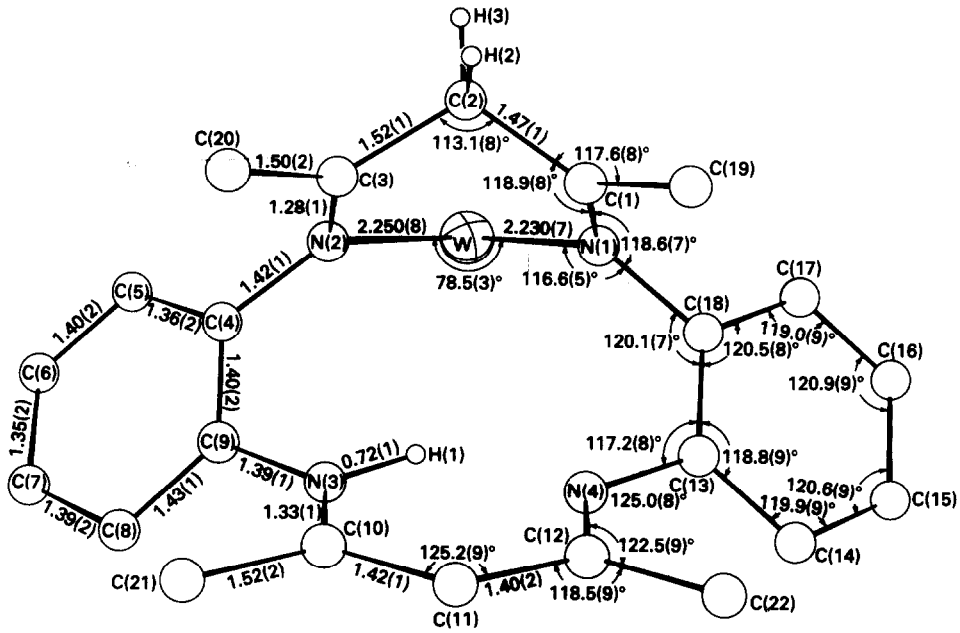

Fig. 1. The molecular structure (ORTEP plot), labelling scheme, and interatomic distances of $W(CO)_4$(tmtaa). (H(1′) and the four carbonyl groups have been omitted for clarity.)

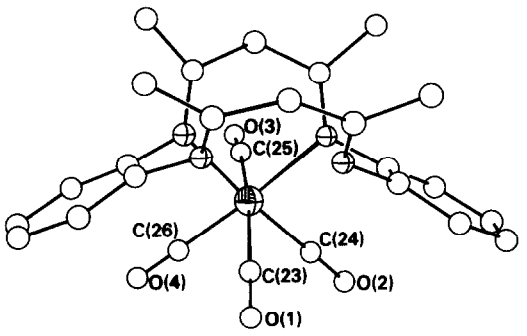

Fig. 2. An ORTEP diagram of $W(CO)_4$(tmtaa) showing the side-view of the molecule.

tively, show a 30° increase as compared to the free tmtaa.

This report established with certainty an unconventional mode of coordination of tmtaa to tungsten, as previously postulated by Bell and Dabrawiak. Tmtaa is also capable of taking on other, equally interesting coordination geometries as shown by some further studies carried out in our laboratory, to be reported presently.

Acknowledgement—We thank the National Science Foundation for support.

Supplementary material available. Tables of positional and isotropic equivalent displacement parameters, anisotropic displacement parameters, observed and calculated structure factors, as well as full lists of bond distances and bond angles, have been deposited as supplementary material with the Editor.

REFERENCES

1. V. L. Goedken, J. J. Pluth, S.-M. Peng and B. E. Bursten, *J. Am. Chem. Soc.* 1976, **98**, 8014.
2. A. R. Cutler, C. S. Alleyne and D. Dolphin, *Inorg. Chem.* 1985, **24**, 2276 and refs therein.
3. L. G. Bell and J. C. Dabrawiak, *J. Chem. Soc., Chem. Commun.* 1975, 512.
4. V. L. Goedken, J. Molin-Case and Y. A. Whang, *J. Chem. Soc., Chem. Commun.* 1973, 337.
5. See, for example, A. Bino, F. A. Cotton and P. E. Fanwick, *Inorg. Chem.* 1979, **18**, 3558.

Polyhedron Vol. 9, No. 9, pp. 1221–1224, 1990
Printed in Great Britain

0277–5387/90 $3.00+.00
© 1990 Pergamon Press plc

DIBENZO[b,i][1,4,8,11]TETRA-AZACYCLOTETRADECINE COMPLEXES—II. Ru(tmtaa)($PMePh_2$)$_2$

F. ALBERT COTTON* and JOANNA CZUCHAJOWSKA

Department of Chemistry and Laboratory for Molecular Structure and Bonding, Texas A&M University, College Station, TX 77843, U.S.A.

(*Received* 13 *November* 1989; *accepted* 2 *January* 1990)

Abstract—The title compound has been prepared via an unusual synthetic route and structurally characterized. The compound crystallizes in space group $P\bar{1}$ with unit cell dimensions $a = 10.928(3)$, $b = 11.030(2)$, $c = 10.035(3)$ Å, $\alpha = 116.70(1)$, $\beta = 113.10(2)$, $\gamma = 85.94(2)°$, $V = 985.7(5)$ Å^3 and $Z = 1$. This ruthenium monomer is the first Ru–tmtaa compound to be crystallographically characterized. The usual saddle-shape geometry of the macrocyclic ligand is destroyed due to the presence of bulky $PMePh_2$ phosphines. This complex is the first example of such an occurrence.

The title macrocyclic ligand[1] has long been known to take on a characteristic saddle-shape geometry both as the free ligand and upon coordination to a metal atom. The inherent predisposition of tmtaa to adopt such a geometry is due to steric interactions of the methyl groups with the benzenoid rings.[2] There are numerous examples of early[3] and late[4] transition metal complexes with this macrocyclic ligand in which the saddle-shape geometry is evident. The largest observed displacement of the metal out of the N_4 plane is 1.070(2) Å for tmtaa^{2-}, [Zr(tmtaa)Cl_2][4] and 1.5 Å for tmtaa^0, [W(CO)$_4$(tmtaa)].[5]

This report is concerned with the synthesis and crystallographic characterization of a novel Ru–tmtaa complex in which the conventional geometry of the ligand is destroyed. Reaction of $Ru_2(O_2CCH_3)_4$ with tmtaa, in the presence of $PMePh_2$ phosphine, gives a monomeric species, Ru(tmtaa)($PMePh_2$)$_2$. The octahedral environment of the ruthenium atom consists of four equatorially bound nitrogen atoms of tmtaa and two axially bound phosphorus atoms of $PMePh_2$. Presumably, the axially bound, bulky phosphines force the ligand out of the saddle-shape and into a "step-like" geometry, with the two benzenoid rings *trans* to each other, relative to the N_4 plane.

* Author to whom correspondence should be addressed.

EXPERIMENTAL

All manipulations were carried out under an argon atmosphere, using standard vacuum-line and Schlenk techniques. The solvents were freshly distilled under nitrogen from the appropriate drying agents. Starting materials, $Ru_2(O_2CCH_3)_4$[6] and tmtaa[1] were prepared according to the literature. $PMePh_2$ was purchased from Strem, Inc. The UV–vis spectrum was measured on a Cary 17D spectrophotometer at room temperature. The ^{1}H NMR was run on a Varian XL-200A spectrophotometer.

Preparation

A solution of $Ru_2(O_2CCH_3)_4$ (0.06 g, 0.13 mmol) and tmtaa (0.09 g, 0.26 mmol) in ethanol (15 cm^3) was refluxed for 2 h. To this hot solution, $PMePh_2$ (0.20 cm^3, 1.06 mmol) was quickly added. After an additional 12 h of vigorous refluxing, the reaction solution was evaporated to dryness and the remaining solid was dissolved in benzene (12 cm^3). After 12 h, the tube was shaken and green, block-like crystals formed over several hours. The material is air-sensitive, becoming brown within minutes upon exposure to air. Yield: 0.12 g; 60%. Visible spectrum (benzene, λ, nm) of Ru(tmtaa)($PMePh_2$)$_2$: 670, 456, 358 (sh). ^{1}H NMR (C_6D_6, 298 K): δ 8.02–7.10 (m, 10H, $PCH_3(C_6H_5)_2$), 6.051 (m, 8H, Ar*H*), 3.88 (s, 2H, γ-C*H*), 2.31 [s, 3H, $PCH_3(C_6H_5)_2$] and 1.74 (s, 12H, CH_3).

X-ray crystallography

General procedures that have already been fully described elsewhere[7] were used to determine the crystal structure. Information about data collection and structure refinement for the compound is given in Table 1. The intensity data were corrected for Lorentz and polarization effects. An empirical absorption correction based upon azimuthal scans of six reflections near $\chi = 90°$ was applied to the data.

The position of the ruthenium atom in the unit cell (space group $P\bar{1}$) was determined by the Patterson method; it resides on a crystallographic inversion centre. The subsequent development of the structure was done by an alternating sequence of least-squares refinements and difference Fourier maps. All hydrogen atoms were found the same way and refined freely.

Table of positional and isotropic equivalent displacement parameters, anisotropic displacement parameters, observed and calculated structure factors, as well as full lists of bond distances and angles, have been deposited as supplementary material with the Editor.

RESULTS AND DISCUSSION

Figures 1 and 2 show ORTEP drawings of $Ru(tmtaa)(PMePh_2)_2$ and define the atomic numbering scheme used in the tables and the following discussion. Important interatomic dimensions are presented in Table 2.

The ruthenium atom resides on a crystallographic inversion centre and thus is constrained to be in the plane of the four nitrogen atoms of tmtaa. The metal is in an octahedral environ-

Table 1. Crystal data for $Ru(C_{22}H_{22}N_4)(PMePh_2)_2$

Formula	$Ru(C_{22}H_{22}N_4)(PMePh_2)_2$
Formula weight	843.96
Space group	$P\bar{1}$
a (Å)	10.928(3)
b (Å)	11.030(2)
c (Å)	10.035(3)
α (°)	116.70(1)
β (°)	113.10(2)
γ (°)	85.94(2)
V (Å^3)	985.7(5)
Z	1
d_{calc} (g cm^{-3})	1.421
Crystal size (mm)	$0.40 \times 0.35 \times 0.30$
μ(Mo-K_α) (cm^{-1})	5.077
Data collection instrument	AFC5R
Radiation monochromated in incident beam [Mo-K_α (Å)]	0.71073
Orientation reflections, number; range (2θ)	25; $20.0 < 2\theta \leqslant 32.0$
Temperature (°C)	23 ± 1
Scan method	2θ–ω
Data collection range, 2θ (°)	$4 \leqslant 2\theta \leqslant 50$
Number of unique data, total with $F_o^2 > 3\sigma(F_o^2)$	3462, 3217
Number of parameters refined	349
Transmission factors, max., min	1.00, 0.94
R^a	0.0291
$R_w{}^b$	0.0403
Quality-of-fit indicator^c	1.064
Largest shift/ESD, final cycle	0.10
Largest peak, e/Å^3	0.48

$^a R = \Sigma ||F_o| - |F_c|| / \Sigma |F_o|$.

$^b R_w = [\Sigma w(|F_o| - |F_c|)^2 / \Sigma w|F_o|^2]^{1/2}$; $w = 1/\sigma^2(|F_o|)$.

^{c} Quality-of-fit $= [\Sigma w(|F_o| - |F_c|)^2 / (N_{observed} - N_{parameters})]^{1/2}$.

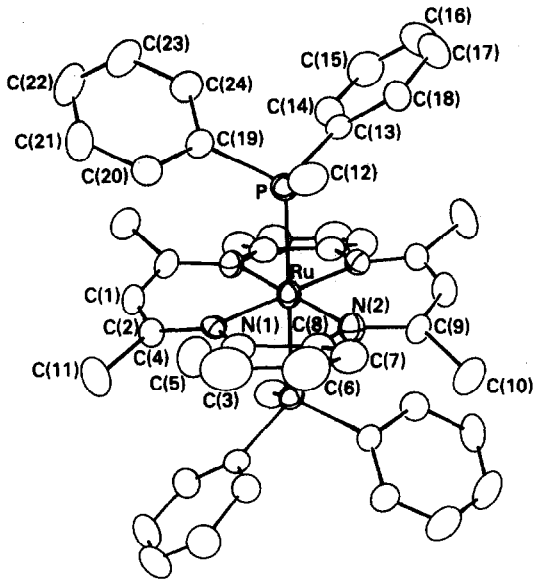

Fig. 1. An ORTEP drawing of the molecular structure showing the atom labelling scheme. Unlabelled atoms are related to labelled ones by the inversion centre at the ruthenium atom.

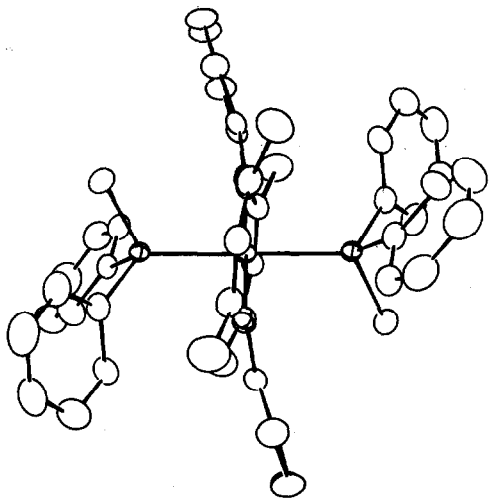

Fig. 2. An ORTEP drawing from a point of view that emphasizes the shape of the tmtaa ligand and the internal contacts that give rise to it.

ment, with the two phosphines in axial positions. The Ru—P distance, 2.382(1) Å, is not atypical, and the Ru—N distances are also normal and equal to 2.029(2) and 2.032(1) Å. These parameters may be compared with those of the structurally characterized ruthenium tetraphenylporphyrinato complex,[8] Ru(TPP)(PPh$_3$)$_2$, in which the Ru—P and Ru—N distances are 2.428 and 2.050 Å, respectively. The NMR data agree well with the crystal structure of our compound, clearly showing the retention of structure with its dianionic ligand and the two equivalent PMePh$_2$ phosphines, in solution.

As mentioned in the introduction, the conventional saddle-shape geometry of tmtaa is destroyed in this ruthenium monomer. The phenyl groups of each axially bound phosphine sterically interact with the benzenoid ring directly below it. This benzenoid ring is being pushed downwards to minimize the steric crowding. That, in turn, causes the two methyl groups of tmtaa, C(10) and C(11), to direct themselves the opposite way to avoid steric interaction with the benzenoid ring. What results is a "step-like" geometry of the macrocycle, in which the two benzenoid rings are *trans* to each other, relative to the N_4 plane. This is clearly seen in Fig. 2.

This report provides a new entry into the formation of novel Ru–tmtaa complexes. It establishes with certainty an unconventional geometry of tmtaa, as it takes on a "step-like" shape to minimize steric crowding with other ligands. We believe that

Table 2. Important bond distances (Å) and bond angles (°) for Ru(tmtaa)(PMePh$_2$)$_2$

Distances			
Ru—P	2.382(1)	P—C(12)	1.832(2)
Ru—N(1)	2.031(1)	P—C(13)	1.831(2)
Ru—N(2)	2.028(2)	P—C(19)	1.845(2)
Angles			
P—Ru—N(1)	90.89(5)	Ru—P—C(13)	117.00(7)
P—Ru—N(1′)	89.10(5)	Ru—P—C(19)	116.81(8)
P—Ru—N(2)	89.33(5)	C(12)—P—C(13)	102.3(1)
P—Ru—N(2′)	90.68(5)	C(12)—P—C(19)	99.9(1)
N(1)—Ru—N(2)	81.00(6)	C(13)—P—C(19)	102.82(8)
Ru—P—C(12)	115.51(6)		

Numbers in parentheses are ESDs in the least significant digits.

the axially bound phosphines can be easily replaced by other σ-donating groups. Such chemistry has been seen with $Ru(TPP)(PPh_3)_2$ and $Ru(OEP)(PPh_3)_2$.[8] Finally, it is of interest to see if a less sterically demanding phosphine like PMe_3, can also destroy the saddle-shape of tmtaa. Chemistry of this kind is presently under investigation.

Acknowledgement—We thank the National Science Foundation for support.

REFERENCES

1. V. L. Goedken, J. Molin-Case and Y.-A. Whang, *J. Chem. Soc., Chem. Commun.* 1973, 337.
2. V. L. Goedken, J. J. Pluth, Shie-Ming Peng and B. Bursten, *J. Am. Chem. Soc.* 1976, **98**, 8014.
3. See, for example, S. Ciurli, C. Floriani, A. Chiesi-Villa and C. Guastini, *J. Chem. Soc., Chem. Commun.* 1986, 1401.
4. See, for example, M. C. Weiss, B. Bursten, Shie-Ming Peng and V. L. Goedken, *J. Am. Chem. Soc.* 1976, **98**, 8021; C. Floriani, S. Ciurli, A. Chiesi-Villa and C. Guastini, *Angew. Chem. Int. Ed. Engl.* 1987, **26**, 70.
5. F. A. Cotton and J. Czuchajowska, *Polyhedron* 1990, **9**, 1217.
6. A. J. Lindsay and G. Wilkinson, *J. Chem. Soc., Dalton Trans.* 1985, 2321.
7. See, for example, A. Bino, F. A. Cotton and P. E. Fanwick, *Inorg. Chem.* 1979, **18**, 3558.
8. S. Ariel, D. Dolphin, G. Damazetis, B. R. James, T. W. Leung, S. J. Rettig, J. Trotter and G. M. Williams, *Can. J. Chem.* 1984, **62**, 755.

Polyhedron Vol. 9, No. 9, pp. 1225–1234, 1990
Printed in Great Britain

0277–5387/90 $3.00+.00
© 1990 Pergamon Press plc

RELATIONSHIP BETWEEN STRUCTURES AND STABILITIES OF MOLYBDATE COMPLEXES OF ALDITOLS: A POTENTIOMETRIC, ^{13}C AND ^{95}Mo NMR STUDY

S. CHAPELLE*

Laboratoire de RMN de l'Université de Rouen, URA 464 du CNRS, Faculté des Sciences, B.P. 118, 76134 Mont-Saint-Aignan Cedex, France

and

J. F. VERCHERE and J. P. SAUVAGE

Laboratoire de Chimie Macromoléculaire, URA 500 du CNRS, Université de Rouen, Faculté des Sciences, B.P. 118, 76134 Mont-Saint-Aignan Cedex, France

(*Received* 9 *November* 1989; *accepted* 15 *January* 1990)

Abstract—Dinuclear molybdate complexes of alditols have been studied in aqueous acidic solution by ^{95}Mo and ^{13}C NMR. Their formation constants were determined by potentiometry. In all complexes, the dimolybdate group was chelated by four vicinal hydroxyls. Two types of complexes were characterized by NMR, depending on the *erythro* or *threo* configuration of the central diol group. Their structures were precised using literature crystal data. A single asymmetrical complex of the first type was formed by symmetrical *erythro* ligands (erythritol, galactitol), while the asymmetrical D-arabinitol and D-mannitol formed pairs of isomeric species of this type. Ligands with complexing sites involving a central *threo* group (DL-threitol, xylitol) were complexed in a symmetrical manner. D-Glucitol formed four complexes as pairs of each type. Rules relating the stabilities of the complexes to the structures of the ligands are presented.

In aqueous acidic solution, molybdate ions MoO_4^{2-} react with many polyhydroxy organic compounds to form soluble complexes. Sugars and alditols form a particular class of dinuclear anionic complexes, as demonstrated by a series of polarimetric and potentiometric studies.[1–4] The enhancement of optical rotation of alditols by molybdate has been used for their identification[1] and determination,[5] and sugars were separated by paper electrophoresis in molybdate solution.[2] The crystal structures of D-mannitol complexes have been described.[6] Monosaccharide complexes in solution have been studied by ^1H and ^{13}C NMR. Some aldoses have been shown[7–10] to complex with molybdate in cyclic structures as tridentate donors. ^{95}Mo NMR has been used to demonstrate the presence of two non-equivalent Mo atoms[11] in complexes of aldoses of the *lyxo–manno* series, which chelated molybdate as tetradentate donors.

While our work on homologous complexes of alditols, including ^{95}Mo NMR spectroscopy, was in progress, a paper was published describing a ^1H and ^{13}C NMR investigation on such compounds.[12] It was stated that "alditols form four types of dinuclear molybdate complexes in which they serve as tetradentate donors with four vicinal hydroxyl groups". Although our results were mainly in agreement, important differences are presented in this paper. Several alditols were found to form small proportions of complexes unreported or poorly characterized up to now, allowing us to compare the stabilities of complexes involving various chelating sites. A specificity of our approach was the simultaneous determination of both the structures and the formation constants of the complexes, in order to establish correlations between their stabilities and the configurations of the ligands.

* Author to whom correspondence should be addressed.

EXPERIMENTAL

Materials

A stock solution of disodium molybdate (Prolabo, 0.1 mol dm^{-3}) was prepared and kept in polyethylene bottles. All products were of analytical grade. Commercial alditols (Fluka or Aldrich) were used as received. Water was de-ionized in a Millipore apparatus. Potentiometric measurements were made at constant ionic strength (KCl, 0.1 mol dm^{-3}). The acid used either in potentiometric or NMR experiments was HCl.

Determination of formation constants

They were measured by potentiometry according to a procedure described previously,[11] based on the determination of the half-equivalence $pH_{1/2}$ values in acidimetric titrations of molybdate–alditol mixtures.

NMR experiments

All 1-D and 2-D NMR spectra were recorded on a Bruker AM 400 spectrometer equipped with a 5 mm multinuclear probe. Solution samples were prepared by dissolving weighed amounts of alditol (0.5 mmol) and disodium molybdate dihydrate (1.5 mmol) in 0.5 cm^3 of D_2O. Then HCl (0.75 mmol) was added. The samples were stable for several weeks at 4°C in the dark. The ^{95}Mo NMR experiments were made as before.[11]

For the ^{13}C NMR experiments, the proton coupled and decoupled spectra were obtained with nuclear overhauser enhancement. The chemical shifts were determined by the substitution method[13] using the TMPS reference signal in D_2O. 2-D heteronuclear experiments were classically performed[14] with polarization transfer from ^{1}H to ^{13}C, the number of experiments being 64×1 K. Initial assignment of ^{1}H spectra in the case of mixtures of complexes, made necessary 2-D homonuclear experiments (COSY-45).[15,16]

RESULTS

^{95}Mo *NMR*

Using an excess of molybdate, the spectra of alditol–molybdate–HCl mixtures were recorded for a series of tetritols, pentitols and hexitols, showing in every case the sharp signal of free molybdate at $\delta \simeq 0$ ppm and a new broad signal ($\Delta\nu \geqslant 270$ Hz) attributed to the complex(es) (Table 1). No individual signals could be characterized in these spectra, contrary to those of complexes of some aldoses which displayed two sharper signals[11] attributed to the dinuclear Mo core. The broader signals were given by hexitol complexes, which could be a consequence of their larger molecular radii and/or of the formation of a mixture of species giving unresolved spectra. It is shown below that while galactitol formed a single complex, D-mannitol and D-glucitol formed at least two complexes. Similarly, the broad signal of the D-arabinitol complex, compared to other pentitols, can result from the formation of two different complexes.

Table 1. 26.076 MHz ^{95}Mo NMR chemical shifts and linewidths in molybdate–alditol complexes; n is the number of complexes[a]

Alditol	δ (ppm)	$\Delta\nu$ (Hz)	n
Erythritol	33.5	290	1
DL-Threitol	22.5	270	1
Ribitol	34	290	1
Xylitol	21	350	1
D-Arabinitol	29.5	450	2
D-Mannitol	31	530	2
D-Glucitol	33	730	4
Galactitol	34	550	1

Reference: Na_2MoO_4 in D_2O. Accuracy: $\delta \pm 1$ ppm.
[a] From ^{13}C NMR data.

The range of chemical shifts for all the complexes was narrow, $\delta = 21$–34 ppm, in agreement with molybdenum being in the +VI oxidation state.[17]

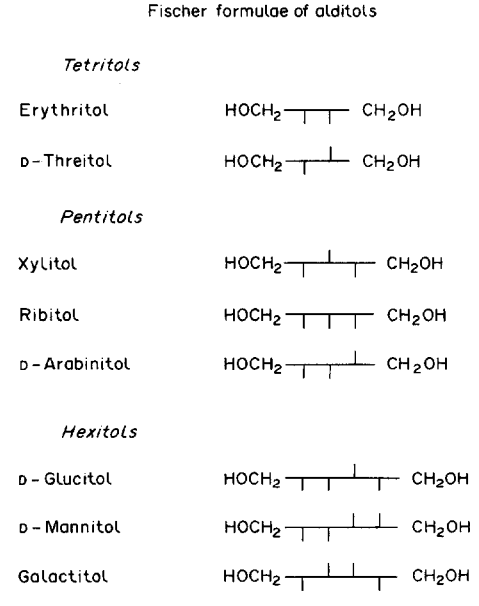

Scheme 1.

In fact, two polyols, namely DL-threitol and xylitol, were characterized by δ values lower than other alditols (22.5 and 21 ppm respectively) and probably formed complexes of a distinct structural type. Besides, the complexes of all other alditols had δ values varying between 29.5 and 34 ppm, which is the same range as one signal given by the complexes of aldoses of the *lyxo–manno* series[11] (two signals at 30 ± 4 ppm and 42 ± 1 ppm). The aldose 42 ppm signal had been attributed to the Mo atom bound to the anomeric HO-1 and neighbouring hydroxyls, which obviously was not possible with alditols.

It was remarked that DL-threitol and xylitol, which gave Mo signals at $\delta \simeq 22$ ppm, did not possess *erythro* diol groups, while D-mannose and D-lyxose, which gave signals at $\delta \simeq 30$ ppm, possessed an *erythro* diol group at C-2,3. This suggested that alditols giving rise to signals at $\delta \simeq 30$ ppm had a related complexing site involving also an *erythro* diol group.

^{13}C *NMR*

The spectrum of an alditol possessing *n* carbon atoms showed at most *n* signals, depending on the molecular symmetry. The assignments were readily made from literature.[18] The addition of molybdate and acid gave rise to new signals, the number and intensity of which indicated the number and relative proportions of complexes formed. Depending on the stabilities of the complexes, signals of the uncomplexed ligand could also be observed in variable proportions.

When the molybdate/alditol ratio varied from 3 to 10, the complex/free ligand ratio increased, but the chemical shifts and relative intensities of the signals remained unchanged, indicating that the ratio of the complex species and their nature was not modified.

In agreement with a previous work,[12] it was found that erythritol, ribitol, xylitol and galactitol gave only one complex each. The same result was obtained with DL-threitol. Besides, D-arabinitol and D-mannitol were found to give two complexes each, in unequal proportions, and up to four complexes were identified in the case of D-glucitol. This contrasted with the same reference[12] in which only one complex was reported for D-mannitol and three for D-glucitol.

The principle of the ^{13}C NMR identification of the chelating sites of the ligands lies on the important deshielding effect on carbons bearing the hydroxyls bound to molybdate.[7–12] These carbons also show increased direct coupling constants $^1J_{CH}$. Consequently, our study required the assignment of the different carbons in the complexes, which was achieved through 2-D heterocorrelated C–H NMR experiments. In every case, the comparison of the spectra of the free and complexed alditol demonstrated that four vicinal carbons were deshielded. The variations of chemical shifts due to complexation ($\Delta\delta$) were calculated and are given in Tables 2–5. The assignments were confirmed by the corresponding variations of the direct coupling constants $^1J_{CH}$. Unless contrary mention, the results were in agreement with literature data.[12]

Galactitol. The spectra (Table 2) of the single complex showed that the characteristic signals of the CH_2OH groups were almost unchanged, proving that complexation involved the four central secondary hydroxyls, which were in a symmetrical (*meso*) configuration. However, the ligand symmetry was destroyed in the complex, since the chemical shift for C-4 (+19.7 ppm) was much higher than those for C-2,3,5 (+7.9–11.8 ppm). This result was unexpected, because the dinuclear Mo core also had a symmetrical structure. Possible reasons for this finding are presented in the Discussion.

Erythritol. This tetritol formed a single asymmetrical complex involving all four hydroxyls. A comparison (Table 2) with the $\Delta\delta$ values calculated for the CHOH groups of galactitol showed a strong analogy, which was not unexpected because both alditols have a central *erythro* diol group. It was remarked that the deshielding effect of complexation on a carbon of the chelating site was nearly the same, whether it bore a central secondary or a terminal primary hydroxyl.

Ribitol. The formation of an asymmetrical complex was expected for this pentitol, because one of the terminal hydroxyls must be involved in complex formation. Accordingly, carbons C-2,3,4,5 were deshielded (Table 2) and displayed increased coupling constants. As in the galactitol and erythritol complexes, one carbon was more strongly deshielded than the others ($\delta \simeq 17$ ppm for C-4), suggesting the ribitol complex to belong to the same type.

Xylitol. Like ribitol, this symmetrical *meso* pentitol formed an asymmetrical complex involving one terminal hydroxyl (Table 3). The chelating site involved carbons C-1,2,3,4. Contrary to that found in the above complexes, the central carbons C-2,3 were equally deshielded ($\Delta\delta \simeq 10.3$ ppm) but less than the lateral carbons C-1,4, which were also equally deshielded ($\Delta\delta \simeq 12.5$ ppm).

DL-*Threitol.* This compound formed a single complex which has not been described heretofore. Data in Table 3 showed a strong analogy with the xylitol complex, when carbons C-1,2,3,4 having related positions were compared. The internal C-4 of xylitol had a $\Delta\delta$ value (> 12 ppm) close to that

Table 2. 100.13 MHz ^{13}C NMR chemical shifts and $^{1}J_{CH}$ direct coupling constants of alditols and of their molybdate complexes (*erythro* type)

Alditol	Carbon position					
Galactitol	1	2	3	4	5	6
δ (ppm)[a]	65.5	71.5	72.1	72.1	71.5	65.5
δ (ppm)[b]	65.5	83.3	83.7	91.8	79.4	64.7
$^{1}J_{CH}$ (Hz)[b]	143	146	147	149	144	143
$\Delta\delta$ (ppm)	0	11.8	11.6	19.7	7.9	−0.8
Erythritol		1	2	3	4	
δ (ppm)[a]		64.7	74.3	74.3	64.7	
δ (ppm)[b]		74.3	83.5	92.8	71.3	
$^{1}J_{CH}$ (Hz)[b]		144	147	147	144	
$\Delta\delta$ (ppm)		9.6	9.2	18.5	6.6	
Ribitol	1	2	3	4	5	
δ (ppm)[a]	64.6	74.1	74.4	74.1	64.6	
δ (ppm)[b]	63.9	87.9	83.7	91.0	72.1	
$^{1}J_{CH}$ (Hz)[b]	141	147	147	147	142	
$\Delta\delta$ (ppm)	−0.7	13.8	9.3	16.9	7.5	

[a] Uncomplexed alditols. $^{1}J_{CH}$ = 141 Hz for all carbons. δ assigned from literature.[18]

[b] Molybdate complexes. Carbons in the same column have related positions. Accuracy: $\delta \pm 0.1$ ppm; $J \pm 1$ Hz.

Table 3. 100.13 MHz ^{13}C NMR chemical shifts and $^{1}J_{CH}$ direct coupling constants of alditols and of their molybdate complexes (*threo* type)

Alditol	Carbon position				
Xylitol	1	2	3	4	5
δ (ppm)[a]	64.8	74.0	72.8	74.0	64.8
δ (ppm)[b]	77.1	84.3	83.4	86.6	64.1
$^{1}J_{CH}$ (Hz)[b]	146	148	149	149	142
$\Delta\delta$ (ppm)	12.3	10.3	10.6	12.6	−0.7
DL-Threitol	1	2	3	4	
δ (ppm)[a]	64.8	73.6	73.6	64.8	
δ (ppm)[b]	77.0	83.4	83.4	77.0	
$^{1}J_{CH}$ (Hz)[b]	144	147	147	144	
$\Delta\delta$ (ppm)	12.2	9.8	9.8	12.2	

[a] Uncomplexed alditols. $^{1}J_{CH}$ = 141 Hz for all carbons. δ assigned from literature.[18]

[b] Molybdate complexes. Carbons in the same column have related positions. Accuracy: $\delta \pm 0.1$ ppm, $J \pm 1$ Hz.

of the terminal C-4 of threitol, i.e. higher than the typical value ($\simeq$ 10 ppm) for other CHOH groups. Thus the deshielding effects were similar for a CHOH or CH_2OH group in related position, as in galactitol and erythritol complexes. Moreover, the similar deshielding effects at C-1,4 ($\Delta\delta$ = 12.2 ppm) and C-2,3 ($\Delta\delta$ = 9.8 ppm) indicated that the ligand was complexed in a symmetrical fashion, contrary to galactitol and erythritol. The same was probably true for the above xylitol complex.

These results indicated the existence of at least two types of molybdate complexes, depending on the alditol configurations. One type corresponded to *threo* compounds (xylitol and DL-threitol). The second type was obtained with *erythro* compounds, typically erythritol and galactitol, and probably included ribitol.

D-*Arabinitol.* Two complexes in 60 : 40 ratio were detected in the ^{13}C NMR spectrum, in accordance with literature results. The first one, symbolized as A_1 was that previously identified,[12] involving C-2,3,4,5, since the C-1 signal remained almost unchanged (Table 4). A comparison with the chemical shifts in the galactitol complex showed a striking similarity, indicating an analogous structure of both ligands, as expected because of the identical configurations of the three carbons C-2,3,4. The second minor complex, noted A_2, which had not been characterized in literature, was formed by the same tetritol group, C-2,3,4,5 (the C-1 signal was slightly modified) but the chemical shifts were different from those of the major A_1 complex. The most striking feature was that the more deshielded carbon ($\Delta\delta \simeq 20$ ppm) was C-3 in A_2 instead of C-4 in A_1 and that the overall deshielding patterns were reversed, the variations of chemical shifts

Table 4. 100.13 MHz ^{13}C NMR chemical shifts and $^{1}J_{CH}$ direct coupling constants of D-arabinitol, D-mannitol and of their molybdate complexes

Alditol	Carbon position					
D-Arabinitol		1	2	3	4	5
δ (ppm)		65.3	72.4	72.6	73.1	65.1
Complex A_1						
δ (ppm)		65.1	84.1	84.0	92.9	71.7
$^{1}J_{CH}$ (Hz)		143	146	146	148	146
$\Delta\delta$ (ppm)		−0.2	11.7	11.4	19.8	6.6
Complex A_2						
δ (ppm)		66.1	79.9	92.4	83.7	74.1
$^{1}J_{CH}$ (Hz)		142	143	148	148	148
$\Delta\delta$ (ppm)		0.8	7.5	19.8	10.6	9.0
D-Mannitol	1	2	3	4	5	6
δ (ppm)	65.8	74.2	71.6	71.6	74.2	65.8
Complex M_1						
δ (ppm)	65.4	73.1	83.3	83.8	93.1	71.7
$^{1}J_{CH}$ (Hz)	142	142	145	149	148	145
$\Delta\delta$ (ppm)	−0.4	−0.9	11.7	12.2	18.9	5.9
Complex M_2						
δ (ppm)	65.9	74.1	80.3	92.3	83.8	74.1
$^{1}J_{CH}$ (Hz)	142	142	143	148	149	145
$\Delta\delta$ (ppm)	0.1	−0.1	8.7	20.7	9.6	8.3

$^{1}J_{CH}$ = 141 Hz for all carbons of uncomplexed alditols. δ assigned from literature.[18] Carbons in the same column have related positions. Accuracy: $\delta \pm 0.1$ ppm; $J \pm 1$ Hz.

Table 5. 100.13 MHz ^{13}C NMR chemical shifts and $^{1}J_{CH}$ direct coupling constants of D-glucitol and of its molybdate complexes

Alditol	Carbon position					
D-Glucitol	1	2	3	4	5	6
δ (ppm)[a]	64.7	75.0	71.7	73.2	73.2	65.0
Complex G_1						
δ (ppm)	77.2	84.2	83.1	85.7	72.1	65.3
$^{1}J_{CH}$ (Hz)	143	149	146	146	147	144
$\Delta\delta$ (ppm)	12.5	9.2	11.4	12.5	−1.1	0.3
Complex G_2						
δ (ppm)	64.8	75.2	83.8	83.7	92.9	71.3
$^{1}J_{CH}$ (Hz)	142	143	146	146	148	148
$\Delta\delta$ (ppm)	0.1	0.2	12.1	10.5	19.7	6.3
Complex G_3						
δ (ppm)	63.5	86.6	80.4	83.7	86.4	64.1
$^{1}J_{CH}$ (Hz)	ND	147	143	146	148	144
$\Delta\delta$ (ppm)	−1.2	11.6	8.7	10.5	13.2	−0.9
Complex G_4						
δ (ppm)	64.5	76.1	78.9	92.2	84.7	74.1
$^{1}J_{CH}$ (Hz)	ND	143	146	147	145	148
$\Delta\delta$ (ppm)	−0.2	1.1	7.2	19.0	11.5	9.1

[a] $^{1}J_{CH}$ = 141 Hz for all carbons of uncomplexed D-glucitol. δ assigned from literature.[18] ND: not determined. Accuracy: $\delta \pm 0.1$ ppm; $J \pm 1$ Hz.

being related in the sequences C-2,3,4,5 in A_1 and C-5,4,3,2 in A_2.

D-*Mannitol.* Two complexes in 70:30 ratio, which were called M_1 (major species) and M_2, could be identified (Table 4). Both species involved the tetritol group at C-3,4,5,6 and were analogous to those described for D-arabinitol, in accordance to the related configurations of C-2,3,4 of arabinitol and C-3,4,5 of mannitol.

This makes surprising the report that only one complex (the M_1 species) was formed by D-mannitol, while both A_1 and A_2 species had been detected for D-arabinitol in the same study.[12] Such discrepancies may be due to the difference in techniques for preparing the complexes, since we used sodium molybdate acidified with varying amounts of HCl instead of ammonium molybdate.

D-*Glucitol.* The spectrum of this hexitol in acidified molybdate showed 24 new signals in addition to those of uncomplexed ligand, due to the formation of four complexes referred as G_1 (32%), G_2 (26%), G_3 and G_4 (21% each) (Table 5). The spectra of species G_1 (molybdate bound to C-1,2,3,4) and G_2 (molybdate bound to C-3,4,5,6) have been already reported in literature, a third complex being believed to involve all secondary hydroxyl groups, from the products of its periodate oxidation.[12] The patterns of variations of chemical shifts were typical of the "xylitol type" for G_1 and of the "arabinitol type" for G_2

Unambiguous assignments for the G_3 and G_4 complexes were not possible because homonuclear ^1H 2-D experiments were precluded, owing to the large number of overlapping signals. However, using only ^{13}C NMR data, we found that the G_3 species was characterized by two unchanged signals for the CH_2OH groups, and therefore involved C-2,3,4,5 as the chelating system. The G_4 species had one unchanged CH_2OH signal and since only one complex could be imagined when C-1 was involved (the "xylitol type" G_1), the complexed hydroxyl was assigned to C-6. Thus G_4 had the same complexing site as G_2 at C-3,4,5,6 (arabinitol-like configuration) and the G_2–G_4 couple corresponded to the homologous couples of complexes observed with D-arabinitol and D-mannitol.

Tentative assignments for G_4 were made by considering that the C-3,4,5 systems had the same configurations in D-glucitol and in D-mannitol. Thus the variations of chemical shifts were assumed to be similar in complexes M_2 and G_4, as they were in the M_1–G_2 pair.

Possible assignments for G_3 were proposed by analogy with the xylitol-type complex G_1, since the chelating sites of both species involved the same *xylo* group at C-2,3,4.

Formation constants of the complexes

The potentiometric determination of the formation constants was made according to the method described previously.[11] Two equilibria were observed in molybdate–alditol(L)–H^+ systems:

$$2MoO_4^{2-} + L + 2H^+ \rightleftharpoons (2,1,2)^{2-}$$

$$2MoO_4^{2-} + L + 3H^+ \rightleftharpoons (2,1,3)^{-}.$$

The corresponding equilibrium constants K_{212} and K_{213} defined the formation constants of the complexes in the classical way.[11] The equilibrium between the (2,1,2) and (2,1,3) species was characterized by the pK_a value relative to reaction:

$$(2,1,3)^- \rightleftharpoons (2,1,2)^{2-} + H^+.$$

The values of the formation constants are presented in Table 6. Good agreement was observed with literature values[19–21] when available.

DISCUSSION

This part will be devoted to the examination of factors governing the relative stabilities of the molybdate complexes, with emphasis on those related to the structures of the ligands. Only the (2,1,2) species will be considered, since the acidic (2,1,3) complexes were not characterized by NMR. However, the stabilities of both series of complexes should be strongly related, because the corresponding pK_a values show little differences.

The first problem to be considered was the origin of the different behaviours of the homologous tetritols, erythritol and threitol, which differed only by the configuration of one CHOH group. It resulted in two important effects, first the existence of a symmetrical complex with threitol, while the erythritol one was asymmetrical, and second the higher stability of the erythritol complex. The former result was surprising because both ligands have symmetrical structures. The relationship between stabilities and structures is not simple and is discussed below. Besides, the problem of symmetry, which concerned also pentitols and hexitols, was discussed using available literature data[6,23–26] on the structures of related molybdate complexes.

Molybdate complexes of D-lyxose[23] and polyols[6,26] possess a dinuclear core bridged by three oxygen atoms, two of them being triply-bonded. Each molybdenum atom is also bound to one oxygen atom of the ligand. This unusual dimolybdate group is not typical of carbohydrate complexes, as similar structures have been reported for some complexes of quinones[24] and catechol[25] derivatives. The geometry of the acceptor site can be

Table 6. Formation constants of molybdate–alditol complexes (KCl 0.1 M, 25°C) determined by potentiometry. $\log K_{xyz}$ refers to the formation of the (x,y,z) species from x MoO_4^{2-} y alditol and z H^+. K_a is the acidity constant of the (2,1,3) complex

Alditol	$\log K_{212}$	$\log K_{213}$	pK_a	$\log K_{212}$ (lit.)	$\log K_{213}$ (lit.)
Erythritol	15.20	19.50	4.30		
DL-Threitol	14.60	18.20	3.60		
Ribitol	15.55	19.45	3.90	15.57[a]	19.52[a]
Xylitol	16.25	19.65	3.40		
D-Arabinitol	16.35	20.45	4.10		
D-Mannitol	16.70	20.80	4.10	16.89[b]	20.77[b]
				17.49[c]	21.55[c]
D-Glucitol	16.60	20.50	3.90	16.90[b]	20.72[b]
Galactitol	17.30	20.90	3.60	17.50[a]	20.93[a]

Accuracy: $\log K_{212} \pm 0.06$; $\log K_{213} \pm 0.11$; $pK_a \pm 0.05$.
[a] Ref. 21.
[b] Ref. 20.
[c] By potentiometry and polarimetry[19] in $NaClO_4$ 3 M.

schematized by projecting, perpendicularly to the medium plane of the dimolybdate core, the four bonded oxygens which form either a stretched diamond[6,23,26] or a parallelogram (naphthalenediol complex[25]) as shown in Fig. 1. The fitting of this quadrilateral with the figure drawn by the donor groups of a ligand was checked using molecular models.

A first type of complex was characterized with alditols possessing a complexing site involving a central *erythro* group (erythritol, galactitol, ribitol). As established by NMR, D-mannitol and D-arabinitol belonged to this type, corresponding to types *A* and *C* in the literature.[12] The known crystal structures of the D-mannitol[6] and erythritol complexes[26] could then be used as models for the whole series. The four carbons of the complexing site must adopt a sickle arrangement allowing their four hydroxyls to point in the same direction, forming a trapeze which did not match exactly the acceptor site. Accordingly, the molecule must twist at one internal carbon as shown in Fig. 1(a). It agreed with the NMR result that one of the central carbons in the ligands was more strongly deshielded (Tables 2 and 4) than the other one.

In fact, we observed that two ligands (D-mannitol, D-arabinitol) formed a pair of complexes, with reversed deshielding patterns, involving the same chelating site: C-2,3,4,5 for arabinitol complexes A_1–A_2 and C-3,4,5,6 for mannitol complexes M_1–M_2. Accordingly, the scheme in Fig. 1(a) predicted that two isomers could be formed when the lateral carbons of the complexing site bore different substituents R and R′, depending on the site of twisting. Their proportions were not equal, the favoured isomer being that in which the more deshielded carbon bore the shortest side chain, i.e. a CH_2OH group. In contrast, one isomer only could be formed by symmetrical ligands (R = R′) like erythritol and galactitol.

Ribitol was remarkable among ligands forming asymmetrical complexes of the *erythro* type, since it gave a single complex instead of two. It was assumed that one complex was much less stable than the other, for reasons similar to those invoked in the case of D-arabinitol. Moreover, the existing complex had a low stability because in the sickle arrangement of the C-2,3,4,5 complexing site, an unfavourable steric interaction existed between C-1 and C-5. The high $\Delta\delta$ value at C-2 (Table 2) may reflect some strain due to this interaction, which did not occur in the D-arabinitol complex possessing the opposite C-2 configuration.

Considering that types *A* and *C* differed only by the possible substitution of one external carbon, which was not associated with a particular deshielding effect, no reason was found to make a distinction between them.

A second type of complex was formed by ligands possessing only *threo* diol groups (DL-threitol and xylitol) which had a carbon chain in a zig-zag arrangement. They were referred to as type *B* and type *D* in the literature.[12] Four hydroxyls already point towards the four tops of a parallelogram, which could not match the acceptor site described above for the *erythro* series. Considering the symmetry of the complexation site, demonstrated by NMR, it seemed likely that the acceptor

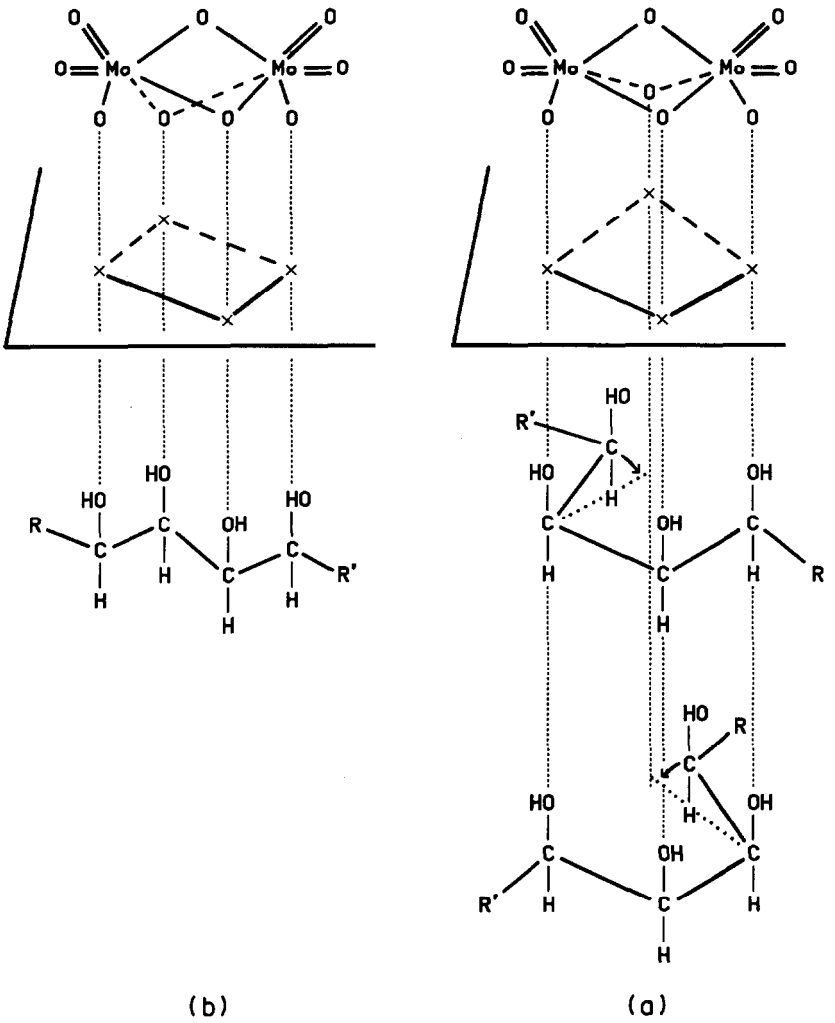

Fig. 1. Schematic representation of the chelation of the dimolybdate core by four vicinal hydroxyls of an alditol molecule. R and R′ are either H or CH_2OH groups. (a) Complexes of *erythro* type, showing the formation of a pair of isomers depending on the site of twisting. The dimolybdate structure is that reported in the D-mannitol,[6] D-lyxose[23] and erythritol[26] complexes. (b) Complex of *threo* type. The proposed symmetrical dimolybdate structure is that observed in the naphthalene-2,3-diol[25] complex.

site had rather a parallelogram shape (in planar projection), allowing the ligands to complex molybdate without appreciable loss of symmetry. The proposed structure, which had never been characterized by X-ray studies in literature, was in agreement with NMR data. Figure 1(b) shows that the triply-bonded oxygens are borne by the internal carbons of the ligand complexing sites, and that the doubly-bonded oxygens are borne by the external carbons. Accordingly, these pairs of carbons were found to be respectively equally deshielded.

Finally, there is no more reason to differentiate between types *B* and *D* than between types *A* and *C*. Moreover, ^{95}Mo NMR afforded a supplementary criterion to distinguish between both types, since complexes of the *threo* type (*B–D*) gave a Mo signal at $\simeq$ 22 ppm while those of the *erythro* type (*A–C*) gave a Mo signal at $\simeq$ 30–34 ppm.

D-Glucitol had a unique behaviour, forming complexes belonging to both types in comparable proportions. All four possible complexes allowed by the structure of this hexitol were detected by ^{13}C NMR:

(1) A *threo* complex G_1, in which the complexing site involved C-1 and the C-2,3,4 *xylo* system.

(2) and (3) A pair of *erythro* complexes G_2 and G_4, in which the complexing site involved C-6 and the C-3,4,5 *arabino* system.

(4) A *threo* complex G_3, involving the four internal CHOH (the *gluco* system) at C-2,3,4,5.

Thus three different sites competed to complex molybdate, and formed species of comparable stabilities. The following discussion examines the relationship between the formation constants and the structural types of the various complexes.

In the *erythro* series, the stability order was: erythritol < ribitol < arabinitol < mannitol < galactitol. The favourable effect of increasing the chain length was correlated with the replacement of CH_2OH groups by CHOH groups in the chelating site. Among hexitols, the highest stability of the galacticol complex was attributed to the favourable configurations of C-2,5, which orientated the terminal CH_2OH groups far away from the complexing site. Such influence of the C-2 configuration also accounted for the relative stabilities of pentitol complexes: D-arabinitol > ribitol. The D-arabinitol complexes were almost as stable as the D-mannitol ones, probably because their complexing sites differed only by the size of the substituent on a lateral carbon.

Thus two rules appeared to govern the stabilities of *erythro* complexes. Rule 1: complexing sites in which the lateral carbons bore secondary hydroxyls gave more stable complexes than those using terminal CH_2OH groups, because of corresponding entropy gain.[22] Rule 2: alditols possessing lateral CHOH groups orientated *threo* with respect to the central *erythro* groups formed complexes of higher stabilities than those with lateral groups orientated *erythro*, since no steric interaction took place between the complexing site and the uncomplexed side chains.

In the *threo* series, the order of stabilities of the complexes xylitol > threitol, was in agreement with Rule 1. The presence of a *threo–threo* system in xylitol resulted in a high stability of the complex, indicating that Rule 2 probably applied. However, the corresponding enhancement of the formation constants (Table 6) seemed more important in this series than in the *erythro* one, making the xylitol complex almost as stable as the D-arabinitol ones. It was concluded that Rules 1 and 2 were also valid in the *threo* series.

We also examined the relative stabilities of complexes belonging to both series. An essential result was that the erythritol complex was more stable than the threitol one, suggesting that an *erythro* diol group had a stronger affinity towards molybdate than a *threo* group. In this respect, the reactions of D-arabinitol and D-mannitol afforded an interesting comparison of the reactivities of *erythro* and *threo* diol groups borne by the same ligand. Both alditols formed two complexes, but none involved the *threo* group in the central position of the four chelating hydroxyls. The complexing sites in both pairs of complexes had a central *erythro* group (C-3,4 in arabinitol and C-4,5 in mannitol). In the case of D-mannitol, the *threo* type complex, involving C-2,3,4,5, was not detected, although it would involve only CHOH groups and should be stabilized according to Rule 1.

These results were formulated as Rule 3: complexes involving a central *erythro* group were generally of higher stabilities than those involving central *threo* groups.

The combined effects of Rules 2 and 3 were unfavourable to the formation of complexes of the *threo* series: when a ligand bore simultaneously an *erythro* group and a *threo* group, (a) complex(es) in which the complexing site(s) involved a central *erythro* group and a lateral *threo* group was stabilized with regard to complexes with a central *threo* group and a lateral *erythro* group. Only in the case of D-glucitol, we were able to detect a complex involving an *erythro–threo* system with the *threo* group in the central position. This G_3 species was expected to have a higher stability, because its complexing site C-2,3,4,5 did not involve any CH_2OH group (Rule 1). Therefore a complexing site of *gluco* configuration (*erythro–threo–threo*) had probably a low affinity for molybdate. Besides, in D-mannitol, the complexing site C-2,3,4,5 of *manno* configuration (*erythro–threo–erythro*) had even lower affinity for molybdate, in agreement again with predictions made by combining Rules 2 and 3.

Finally, the formation constants showed a close correlation with those reported for homologous tungstate complexes,[22] molybdate complexes being about three orders of magnitude less stable. This stability difference did not depend on the nature of the ligand and was ascribed[11] to the easier dimerization of tungstate. Consequently, it was concluded that the structural characteristics of an alditol similarly affected the stabilities of the complexes of both elements.

REFERENCES

1. N. K. Richtmyer and C. S. Hudson, *J. Am. Chem. Soc.* 1951, **73**, 2249.
2. E. J. Bourne, D. H. Hutson and H. Weigel, *J. Chem. Soc.* 1960, 4252; 1961, 35.
3. H. J. F. Angus and H. Weigel, *J. Chem. Soc.* 1964, 3994.
4. W. Voelter, E. Bayer, R. Records, E. Bunnenberg and C. Djerassi, *Chem. Ber.* 1969, **102**, 1005.
5. M. Hamon, C. Morin and R. Bourdon, *Anal. Chim. Acta* 1969, **46**, 255.

6. J. E. Godfrey and J. M. Waters, *Cryst. Struct. Commun.* 1975, **4**, 5; B. Hedman, *Acta Cryst.* 1977, **B33**, 3077.
7. J. Alfoldi, L. Petrus and V. Bilik, *Collect. Czech. Chem. Commun.* 1978, **43**, 1476.
8. J. Alfoldi, V. Bilik and L. Petrus, *Collect. Czech. Chem. Commun.* 1980, **45**, 123.
9. V. Bilik, J. Alfoldi and E. Sookyova, *Chem. Zvesti* 1984, **38**, 499.
10. V. Bilik, J. Alfoldi and M. Matulova, *Chem. Papers* 1986, **40**, 763.
11. J. F. Verchère and S. Chapelle, *Polyhedron* 1989, **8**, 333.
12. M. Matulova, V. Bilik and J. Alfoldi, *Chem. Papers* 1989, **43**, 403.
13. G. Brévard and P. Granger, *Handbook of High Resolution Multinuclear NMR*, p. 40. Wiley, New York (1981).
14. A. Bax and G. Morris, *J. Magn. Res.* 1981, **42**, 501.
15. W. P. Aue, E. Bartholdi and R. R. Ernst, *J. Chem. Phys.* 1976, **64**, 2229.
16. K. Nagayama, *J. Magn. Res.* 1980, **40**, 321.
17. R. T. C. Brownlee, M. J. O'Connor and A. G. Wedd, *Coord. Chem. Rev.* 1985, **68**, 194.
18. K. Bock and C. Pedersen, *Adv. Carbohydr. Chem. Biochem.* 1983, **41**, 27.
19. L. Pettersson, *Acta Chem. Scand.* 1972, **26**, 4067 and references therein.
20. M. Mikesova and M. Bartusek, *Collect. Czech. Chem. Commun.* 1978, **43**, 1867.
21. E. Mikanova and M. Bartusek, *Scr. Fac. Sci. Nat. Univ. Purk. Brun.* 1981, **11**, 451.
22. J. F. Verchère and J. P. Sauvage, *Bull. Soc. Chim. Fr.* 1988, 263.
23. G. E. Taylor and J. M. Waters, *Tetrahedron Lett.* 1981, **22**, 1277.
24. C. G. Pierpont and R. M. Buchanan, *J. Am. Chem. Soc.* 1975, **97**, 6450.
25. A. M. El-Hendawy, W. P. Griffith, C. A. O'Mahoney and D. J. Williams, *Polyhedron* 1989, **8**, 519.
26. L. Ma, S. Liu and J. Zubieta, *Polyhedron* 1989, **8**, 1571.

Polyhedron Vol. 9, No. 9, pp. 1235–1236, 1990
Printed in Great Britain

0277–5387/90 $3.00+.00
© 1990 Pergamon Press plc

COMMUNICATION

ALCOHOLS AS SOURCES OF HYDROGEN IN HYDROFORMYLATION OF ALKENES

JOANNA K. MacDOUGALL and DAVID J. COLE-HAMILTON*

Chemistry Department, University of St Andrews, St Andrews, Fife KY16 9ST, Scotland, U.K.

(*Received* 1 *February* 1990; *accepted* 14 *February* 1990)

Abstract—Heating hex-1-ene in the presence of alcohols, CO and $[RhH(PEt_3)_3]$ gives, as the major products, heptanol and 2-methoxyhexanol with the hydrogen source being the alcohol.

In successful catalysed reactions of alkenes with CO in the presence of alcohols, the normal products are esters formed by Reppe type chemistry [eq. (1)][1]

$$RCH{=}CH_2 + CO + R'OH \longrightarrow RCH_2CH_2COOR'. \quad (1)$$

We have recently demonstrated that certain group 8 metal complexes are highly efficient for the dehydrogenation of alcohols,[2–4] and have extended the investigation to the use of such catalysts in reactions of alcohols with alkenes in the presence of CO. We now report for the first time, the selective formation of higher alcohols from alkenes, the extra carbon atom coming from CO and the hydrogen from the alcohol solvent. The only related reactions that have been reported are those in which alcohols act as hydrogen sources in the formation of diethylketone from ethene, CO and the alcohol [eq. (2)][5]

$$2C_2H_4 + CO + R''_2CHOH \longrightarrow Et_2CO + R''_2CO. \quad (2)$$

Water has been used as a hydrogen source in rhodium-catalysed hydroformylation reactions, and alcohols can be the major products,[6] although in these systems addition of excess base is essential.

Table 1 lists the products formed when various alcohols are heated with hex-1-ene in the presence of CO and $[RhH(PEt_3)_3]$. In all cases, the major products are heptanol and 2-methylhexanol. The formation of alcohols rather than aldehydes has also been observed[7] in conventional hydroformylation reactions, carried out in alcohol solvents, catalysed by $[RhH(PEt_3)_3]$.

The formation of heptanol from the reaction of hex-1-ene, CO and alcohols can be represented by eq. (3). 2-Methylhexanol is formed similarly by Markownikoff addition across the double bond

$$C_4H_9CH{=}CH_2 + CO + 2RCH_2OH \longrightarrow C_4H_9CH_2CH_2CH_2OH + 2RCHO. \quad (3)$$

Examination of Table 1 shows that the yield of C_7 alcohol decreases as the steric bulk of the donor alcohol increases, whilst the selectivity to straight-chain C_7 alcohol (heptanol) increases. Adding excess PEt_3 to the reaction using alcohols as the hydrogen source generally has little effect on the straight-branched selectivity of the reaction, although in all cases the yield of C_7 alcohol increases. This observation, together with the finding that the conversion also increases as the CO pressure is reduced at least above 20 atm (see Table 2), suggests that the most active catalytic species has a high PEt_3 content and a low CO content.

Although for linear donor alcohols, C_7 aldehydes are only observed in trace amounts in this reaction, other products are present mostly in $< 10\%$ yield although their yields are higher in the presence of excess PEt_3 than in its absence. For ethanol, these products include the Reppe products, ethyl heptanoate (EH) and ethyl(2-methyl)hexanoate

* Author to whom correspondence should be addressed.

Table 1. Reaction of hexene with CO and alcohols in the presence of $[RhH(PEt_3)_3]$; effect of donor alcohol and added PEt_3 on yield and selectivity[a]

Alcohol	$[PEt_3]/10^{-2}$ (mol dm^{-3})	C_7 alcohols (%)	$n:i$ Ratio	C_7 aldehydes (%)	$n:i$ Ratio	Hexenes (%)	Other products[b]
MeOH	0	66.3	1.4	—	—	17.3	MH, M2MH, HH, MF
	8	73.5	1.4	—	—	10.9	MH, M2MH, HH, MF
EtOH	0	45.3	1.7	—	—	39.6	EE, EH, E2MH
	8	66.3	1.7	—	—	21.4	EE, EH, HE, E2MH, 2MHE, HH
n-BuOH	0	32.4	2.0	—	—	56.0	BB, BH, B2MH, butanal
	8	49.5	2.9	—	—	50.0	BB, BH, B2MH, HH, butanal
i-PrOH	0	7.9	4.6	6.5	1.5	77.4	*i*-PrH, HH
	8	11.7	4.1	7.5	1.5	44.1	*i*-PrH, HH

[a] $[RhH(PEt_3)_3]$ (0.008 mol dm^{-3}); alcohol (4 cm^3); hex-1-ene (1 cm^3); 16 h; 30 atm CO; 144°C.

[b] MH, methyl heptanoate; EH, ethyl heptanoate; BH, butyl heptanoate; *i*-PrH, isopropyl heptanoate; HH, heptyl heptanoate; MF, methyl formate; EE, ethyl ethanoate; BB, butyl butanoate; M2MH, methyl(2-methyl)hexanoate; E2MH, ethyl(2-methyl)hexanoate; B2MH, butyl(2-methyl)hexanoate; HE, heptyl ethanoate; 2MHE, (2-methyl)hexyl ethanoate.

(E2MH) and straight and branched isomers of heptylheptanoate (HH), as well as heptyl ethanoate (HE) and 2-methylhexylethanoate (2MHE). The origin of the last two products is less certain, but is currently under active study. One other type of product, ethylethanoate in the case of ethanol, is also produced, in quite high yield if excess PEt_3 is present. It is probable that this product arises from acetaldehyde, formed from the dehydrogenation of ethanol.

Detailed speculation on the mechanisms of these unusual reactions is not possible at this stage, but the observation that the rate of reaction is low for propan-2-ol, which is normally considered to be the best of the hydrogen donors, but substantially higher for methanol, the least good hydrogen donor studied, suggests that steric effects may be very important in determining the rate of the reaction. This and other mechanistic aspects are currently under active investigation.

Table 2. Effect of pressure on yield and selectivity for C_7 alcohols[a]

	Pressure (CO)	Temperature (°C)	C_7 alcohols (%)	$n:i$ Ratio
MeOH	40	144	65.5	1.7
	30	144	73.5	1.4
	20	144	84.6	1.4
EtOH	40	120	49.2	2.4
	30	120	61.5	2.4
	20	120	69.2	2.4
	10	120	60.0	2.6

[a] Conditions as Table 1 with $[PEt_3]$, 0.08 mol dm^{-3}.

Acknowledgements—We thank M. Green of BP Research International for the original idea and helpful discussions, BP Research International and the SERC for a Studentship (J.K.M.) and Johnson Matthey plc for generous loans of rhodium salts.

REFERENCES

1. See, for example, J. F. Knifton, *J. Org. Chem.* 1976, **41**, 2885 and refs therein.
2. D. Morton, D. J. Cole-Hamilton, I. D. Utuk, M. Paneque-Sosa and M. Lopez-Poveda, *J. Chem. Soc., Dalton Trans.* 1989, 489.
3. D. Morton and D. J. Cole-Hamilton, *Polyhedron* 1987, **6**, 2187.
4. D. Morton and D. J. Cole-Hamilton, *J. Chem. Soc., Chem. Commun.* 1988, 1154.
5. P. Isnard, B. Denise, R. P. A. Sneeden, J. M. Cognion and P. Durnal, *J. Organomet. Chem.* 1982, **240**, 169.
6. K. Kameda, M. Yasumura, M. Hiraki, T. Imanaka and S. Teranishi, *Chem. Lett.* 1981, 1763.
7. J. K. MacDougall and D. J. Cole-Hamilton, *J. Chem. Soc., Chem. Commun.* 1990, 165.

Polyhedron Vol. 9, No. 9, pp. 1237–1239, 1990
Printed in Great Britain

0277–5387/90 $3.00+.00
© 1990 Pergamon Press plc

COMMUNICATION

PREPARATION OF $[Mo_2(O_2CCH_3)_4]$ AND $[CrMo(O_2CCH_3)_4]$ FROM M^{II} DERIVATIVES (M = Cr, Mo)

JOSÉ C. MENEZES and CARLOS C. ROMÃO*

Laboratório de Química Inorgânica, Instituto Superior Técnico, Av. Rovisco Pais, 1096 Lisboa Codex, Portugal

(*Received* 7 *November* 1989; *accepted* 27 *February* 1990)

Abstract—The compounds $[Mo_2(O_2CCH_3)_4]$ and $[CrMo(O_2CCH_3)_4]$ are conveniently prepared in 40–50% yields from acetic acid/acetic anhydride solutions and, respectively, $[Mo_2Br_4(CO)_8]$ or a mixture of $[Mo_2Br_4(CO)_8]$ and $CrCl_2$. An improvement in the preparation of $[Mo_2(O_2CCH_3)_4]$ from $Mo(CO)_6$ and acetic acid is also described.

In the course of a project aimed at the study of the chemistry of $[Mo_2(Allyl)_4]$ and the possible preparation of the heteronuclear analogues $[CrMo(Allyl)_4]$ and $[MoW(Allyl)_4]$,[1] we were faced with the repeated preparation of $[Mo_2(O_2CCH_3)_4]$ (**1**) and $[CrMo(O_2CCH_3)_4]$ (**2**). As Cotton and other workers pointed out,[2] the classical preparation of **1**, from $Mo(CO)_6$ and acetic acid,[3] gives rather low yields. The use of carefully purified diglyme as solvent improves the yield of this synthetic method, but is rather time consuming.[4] We also found that the preparation of **2**, by the original method of Garner and Senior[5] gave erratic and low yields well below the 30% originally reported.

Recently, Cotton and Poli reported a new approach to the formation of Mo≡Mo bonds starting from molybdenum(II) carbonyl complexes, namely $[Mo_2X_4(CO)_8]$ (X = Cl, Br, I).[6] In the following we describe our results on the use of this method for the preparation of **1** and **2**, which also led to a very simple and effective improvement of the classical preparation of **1**.

RESULTS AND DISCUSSION

A mixture of acetic acid (HOAc) and acetic anhydride (Ac_2O) was added to freshly prepared $[Mo_2Br_4(CO)_8]$ (**3**), at −40°C, and the resulting slush warmed to room temperature, stirred overnight and finally refluxed for 4 h. After concentration and filtration, **1** was isolated as yellow microcrystals in 57% yield. This convenient preparation of **1** from a molybdenum(II) complex, formally a $MoBr_2$ derivative, suggested that the heteronuclear analogue **2** could be prepared from **3** and $CrCl_2$. A mixture of freshly prepared **3** and a six-fold excess of $CrCl_2$ was therefore treated with HOAc at −40°C, warmed and further refluxed for 2 h. Sublimation of the solid residue left after solvent evaporation allowed the isolation of **2** in 11% yield. However, we found out that this yield can be easily and reproducibly increased to 40% if the cold reaction mixture is brought from −40°C directly into a pre-heated silicone bath at 120°C and left at reflux for 2 h. The better yield and the much shorter reaction time needed make this a very convenient preparation of the heteronuclear complex $[CrMo(OAc)_4]$ (**2**).

Interestingly, a similar effect of the sudden temperature rise was observed in the already mentioned classical preparation of **1**. Indeed, when the suspension of $Mo(CO)_6$ in $HOAc/(Ac)_2O$ is brought directly from room temperature into a pre-heated silicone bath at 120–130°C, the yield of recovered **1** increases from the normal 15–25%,[2] obtained through gradual heating of the reaction mixture, to a reproducible 52–53% yield. Using a 20 g scale of $Mo(CO)_6$, the yield can only be kept at the latter level if a small amount of toluene is added to the

* Author to whom correspondence should be addressed.

reaction mixture in order to wash the sublimed hexacarbonyl back into the reaction vessel.

The origin of the influence of the sudden temperature jump upon the observed yield is unclear. It certainly reflects the existence of a balance between thermodynamically and kinetically controlled reaction pathways for the evolution of the reaction intermediates. In fact, the complexity of this reaction system is confirmed by the wide variety of by-products that have been isolated from it.[2b] However, the organometallic literature provides examples of the clean preparation of $[Mo_2(O_2CR)_4]$ from $[Mo(\eta^6\text{-}C_7H_8)(\eta^3\text{-}C_3H_5)_2]$ and $[Mo(\eta^6\text{-}C_7H_8)(\eta^3\text{-}C_3H_5)X]_2$ (X = Cl, O_2CR) and the corresponding carboxylic acids.[7] The yields exceed 80% and the chemistry seems to imply the formation of a stabilized "$Mo(O_2CR)_2$" fragment, $[Mo(\eta^6\text{-}C_7H_8)(O_2CR)_2]$, that decomposes at room temperature to give $[Mo_2(O_2CR)_4]$.

It is therefore tempting to speculate that the sudden temperature rise favours the formation of a carbonyl stabilized "$Mo(O_2CR)_2$" species, e.g. "$Mo(O_2CR)_2(CO)_4$" (or the carboxylato bridged dimer $[\{Mo(CO)_4\}_2(\mu\text{-}O_2CCH_3)_2]$) and/or a rapid decarbonylation of these species to give $[Mo_2(O_2CR)_4]$. In either case the formation of side products is expected to be disfavoured.

A similar effect can be present when one starts from **3** in which case, to the further advantage of the Mo≡Mo bond formation process, a pre-existing bridging situation between the two molybdenum atoms already exists. The likely formation of halide bridges between chromium and molybdenum in the mixture of **3** and $CrCl_2$ can possibly improve the formation of the heteronuclear quadruple Cr—Mo bonds in **2**.

EXPERIMENTAL

All reactions were performed under an argon atmosphere using standard vacuum line and Schlenk techniques. Solvents were dried by standard techniques and distilled under argon atmosphere.

Samples of $[Mo_2(O_2CCH_3)_4]$,[3] $[CrMo(O_2CCH_3)_4]$[5] and $[Cr_2(O_2CCH_3)_4]\cdot(H_2O)_2$[8] were prepared according to published procedures. Anhydrous $CrCl_2$ was prepared from dehydrated $[Cr_2(O_2CCH_3)_4]\cdot(H_2O)_2$ by bubbling dry gaseous HCl through a suspension in CH_2Cl_2 for 4 h. The white precipitate was filtered, washed with CH_2Cl_2 and dried *in vacuo*. $[Mo_2Br_4(CO)_8]$ was prepared according to the published procedure.[9] After addition of Br_2 to $Mo(CO)_6$ the solvent (CH_2Cl_2) was evaporated at low temperature and the residue used immediately without further purification.

Perkin-Elmer 457, 683 and 1330 IR spectrometers were used to record the IR spectra of the compounds in KBr pellets prepared under Argon. Mass spectra were obtained on a Varian Mat 112S apparatus.

Preparation of $[Mo_2(O_2CCH_3)_4]$ (**1**)

(a) *From* $[Mo_2Br_4(CO)_8]$ (**3**). Acetic acid (110 cm^3) and acetic anhydride (40 cm^3) were added to solid **3**, at −40°C, freshly prepared from $Mo(CO)_6$ (1 g, 3.8 mmol). The mixture was stirred, left to warm to room temperature overnight and finally refluxed for 4 h. Upon slow cooling to room temperature a fine yellow precipitate formed. The mixture was further concentrated to *ca* 1/4 of the initial volume and filtered. The residue was washed several times with benzene and dried *in vacuo*. It was identified as $[Mo_2(O_2CCH_3)_4]$ by its IR and mass spectra. The yield was 0.46 g, 57% referred to $Mo(CO)_6$.

(b) *From* $Mo(CO)_6$. A mixture of $Mo(CO)_6$ (20 g, 76 mmol), acetic acid (100 cm^3), acetic anhydride (70 cm^3) and toluene (10 cm^3) was made at room temperature. The Schlenk tube containing this reaction mixture was fitted with a reflux condenser and transferred to a pre-heated silicone bath at 120°C. Reflux was maintained for 20 h. The reaction mixture was cooled to room temperature and concentrated to 1/2 of the original volume. A brownish precipitate was filtered off and thoroughly washed with CH_2Cl_2 and dried *in vacuo*. The yield of pure $[Mo_2(O_2CCH_3)_4]$ was 8.5 g or 52% referred to $Mo(CO)_6$.

Preparation of $[CrMo(O_2CCH_3)_4]$ (**2**)

To a Schlenk tube containing freshly prepared $[Mo_2Br_4(CO)_8]$ (0.28 g, 0.4 mmol), a six-fold excess of $CrCl_2$ (0.56 g, 4.6 mmol) was added. Acetic acid (100 cm^3) was added to this mixure at −40°C. The flask was then transferred to a pre-heated silicone bath at 120°C and left to reflux gently for 2 h with stirring. After cooling to room temperature the reaction mixure was taken to dryness and the solid residue sublimed *in vacuo*. The pale yellow product, sublimed at 170–200°C and 10^{-2} torr, was resublimed to give 0.12 g (40% referred to molybdenum) of pure $[CrMo(O_2CCH_3)_4]$, identified by comparison of the IR and mass spectra with those of an authentic sample.

Acknowledgement—We thank Professor A. Ferrer Correia of the Universidade de Aveiro for the use of mass spectral facilities.

REFERENCES

1. J. C. de Menezes, MSc dissertation. Instituto Superior Técnico, Lisboa (1988).
2. (a) F. A. Cotton and R. A. Walton, *Multiple Bonds between Metal Atoms*, p. 86. John Wiley, New York (1982); (b) A. Bino, F. A. Cotton and Z. Dori, *J. Am. Chem. Soc.* 1981, **103**, 243; (c) F. A. Cotton, *Polyhedron* 1986, **5**, 3.
3. A. B. Brignole and F. A. Cotton, *Inorg. Synth.* 1972, **13**, 81.
4. G. Holste and H. Schäfer, *Z. Anorg. Allg. Chem.* 1972, **391**, 264.
5. (a) C. D. Garner and R. G. Senior, *J. Chem. Soc., Chem. Commun.* 1974, 580; (b) C. D. Garner, R. G. Senior and T. J. King, *J. Am. Chem. Soc.* 1976, **98**, 3526.
6. F. A. Cotton and R. Poli, *J. Am. Chem. Soc.* 1986, **108**, 5628.
7. (a) M. L. H. Green, L. C. Mitchard and W. E. Silverthorn, *J. Chem. Soc., Dalton Trans.* 1973, 1952; (b) A. W. Coleman, J. C. Green, A. J. Hayes, E. A. Seddon, D. R. Lloyd and Y. Niwa, *J. Chem. Soc., Dalton Trans.* 1979, 1057.
8. M. Kranz and A. Witowska, *Inorg. Synth.* 1960, **6**, 144.
9. R. Colton and I. B. Tomkins, *Aust. J. Chem.* 1966, **19**, 1519.

Polyhedron Vol. 9, No. 9, p. 1241, 1990
Pergamon Press plc. Printed in Great Britain

CORRIGENDUM

Complexes of vitamin B_6—XXI. The affinity of the binary complexes of the 2,2′-bipyridyl copper(II) system to the vitamin B_6 compounds. N. M. Shuaib, M. S. El-Ezaby and R. Ghodsian (*Polyhedron*, Vol. 9, No. 5, pp. 629–638, 1990).

In Figure 2(c) of the above paper, the formation percentage scale should be doubled and $T_{BP} = T_{PM} = \frac{1}{2}T_{Cu} = 2 \times 10^{-3}$ should read $T_{BP} = T_{PM} = 2T_{Cu} = 2 \times 10^{-3}$.

Polyhedron Vol. 9, No. 10, pp. 1243–1248, 1990
Printed in Great Britain

0277–5387/90 $3.00+.00
© 1990 Pergamon Press plc

RUTHENIUM(II)–BIPYRIMIDINE COMPLEXES: CHARACTERIZATION, SPECTROSCOPY AND PHOTOANATION STUDIES

MIRZA M. TAQUI KHAN,* RAMESH C. BHARDWAJ and CHHAYA BHARDWAJ

Central Salt & Marine Chemicals Research Institute, Bhavnagar—364 002, India

(*Received* 13 *April* 1989; *accepted* 2 *November* 1989)

Abstract—Preparation, characterization and photoanation studies of ruthenium(II) complexes with bipyrimidine are reported. Fluorescence and electrochemical studies have also been conducted. The quantum yield has been calculated for photoanation studies of the complex $[Ru(bipym)_3](PF_6)_2$.

The photochemistry and photophysics of the $Ru(bpy)_3^{2+}$ cation have been intensely investigated[1] during the past decade with a view to develop suitable solar energy conversion catalysts. The study of this species in the excited state has contributed greatly to the understanding of other related photocatalytic molecules[2,3] such as $Ru(bpz)_3^{2+}$ (bpz = bipyrazyl) cation. The $Ru(bipym)_3^{2+}$ (**1**) (bipym = bipyrimidine) cation, which is analogous to $Ru(bpy)_3^{2+}$, is also an excellent photocatalyst[4] and has an added advantage over $Ru(bpy)_3^{2+}$ and $Ru(bpz)_3^{2+}$ as there is no quenching[3] of its emission by molecular oxygen. As in the case of $Ru(bpz)_3^{2+}$ the emission of $Ru(bipym)_3^{2+}$ is quenched by protons at pH < 1, indicating a slightly enhanced basicity of its excited state compared to the ground state. There is, however, no change[4] in the emission of **1** at pH 4.5–8; the formal reduction potential of $Ru(bipym)_3^{2+}$. The presence of the bipyrimidine ligand thus shifts the redox potential to a more positive value compared to the corresponding bipyridine and bipyrazine complexes.

Protonation studies of bipyridine, bipyrazine and their ruthenium(II) complexes have been reported.[3] Recently, protonation of 1,10-phenanthroline in aqueous dioxane was conducted by Ishiguro *et al.*[5] Protonation of 2-pyrimidyl and the 2-pyrazylpalladium(II) complex was reported by Crociani *et al.*[6]

The complexes of bipyrimidine, therefore, have the inherent potential to be better oxidizing photocatalysts than the analogous complexes of bipyridine and bipyrazine. Besides, protonation of bipyrimidine is expected to yield species with even more positive oxidizing potentials than the neutral species, providing a handle to change its redox behaviour in suitable photoreactions.

In this paper we report the synthesis, characterization, fluorescence and electrochemical studies and photoanation (quantum yield) studies of ruthenium(II)–bipyrimidine complexes.

RESULTS AND DISCUSSION

The elemental analysis and conductivity of the complexes are given in Table 1. The conductivity of the acetonitrile complexes shows that complexes **1** and **2** are 1:2 electrolytes, complex **5** is a 1:1 electrolyte and complexes **3**, **4** and **6** are non-electrolytes.

The IR spectra of the complexes show a weak peak at 480–495 cm^{-1} assigned to the (Ru—N) stretching frequency. The absence of a peak at 310 cm^{-1} in complexes **1** and **2** suggests that the chlorides are in the outer coordination sphere of the metal ion. The peaks at 320 and 310 cm^{-1} in complex **3** can be assigned to the (Ru—Cl) stretching of *cis*-chlorides. The peak at 510 cm^{-1} in **3** can be assigned to the (Ru—P) stretching. The ^{31}P NMR of **3** gives a singlet at 21.49 ppm suggesting a *trans* disposition of the coordinated triphenylphosphine. Complex **4** exhibits a single peak at 315 cm^{-1} corresponding to the (Ru—Cl) stretching of *trans*-

* Author to whom correspondence should be addressed.

Table 1. Analytical data for ruthenium–bipyrimidine complexes. Experimental values are given in parentheses

Complex	Colour	Melting point (°C)	%C	%H	%N	Molar conductivity (acetonitrile) (1×10^{-4} M)
$[Ru(bipym)_3]Cl_2$ (**1**)	Reddish	180–185	40.6 (41.0)	2.5 (3.0)	23.7 (23.8)	105
$[Ru(bipym)_3](PF_6)_2$ (**2**)	Orange	—	33.3 (33.6)	2.1 (2.0)	19.2 (18.9)	115
$[Ru(bipym)(PPh_3)_2Cl_2]$ (**3**)	Brownish red	Decomposes at 110	61.8 (61.3)	4.2 (4.4)	6.5 (6.5)	000
$[Ru(bipym)_2Cl_2]$ (**4**)	Black	210–215	36.3 (35.7)	3.1 (3.4)	21.4 (20.9)	005
$[Ru(bipym)_2(CH_3CN)(Cl)]^+[PF_6]^-$ (**5**)	Dark red	—	33.8 (33.6)	2.3 (2.0)	19.7 (19.6)	098
$[Ru(bipym)_2(NO_2)_2]\cdot 0.5H_2O$ (**6**)	Red	—	37.7 (37.3)	2.4 (2.6)	27.5 (25.1)	000

chlorides. Complex **5** exhibits (Ru—Cl) at 315 cm^{-1}. The IR spectral data are given in Table 2.

The electronic spectra of complexes **1–6** show low-energy bands in the visible region at 24,271 cm^{-1} assigned to ruthenium(II) to bipyrimidine MLCT charge-transfer. The higher energy bands at 30,120 and 40,650 cm^{-1} are π–π^* transitions within the bipyrimidine molecule. The band at 22,123 cm^{-1} in the spectrum of complex **1** is a *d* π–π^* MLCT transition. Similar bands were reported for analogous ruthenium(II) bipyridyl complexes.[7] The two major peaks in the UV spectra are essentially independent of the nature of the complex and are assigned to π–π^* transitions within the bipyrimidine rings. The weaker absorption near 40,650 cm^{-1} can be assigned to a higher energy MLCT. The major shoulder near 22,123 and 24,271 cm^{-1} can be either a *d–d* band or a second MLCT transition. The results are tabulated in Table 2.

Luminescence studies

Luminescence spectra of the complexes were taken in aqueous solution and are uncorrected. The

Table 2. IR spectra of the ruthenium complexes

Complex	ν(Ru—X), (cm^{-1}) X = Cl, PF_6, NO_2	ν(Ru—P), (cm^{-1})	ν(Ru—N), (cm^{-1})	Other characteristic peaks
$[Ru(bipym)_3]Cl_2$ (**1**)	—	—	480(w)	3100(s), 1550(s), 1400(vs), 1030(w), 750(m)
$[Ru(bipym)_3](PF_6)_2$ (**2**)	—	—	480(w)	3100(s), 1570(m), 1400(vs), 850(s), 750(w)
$[Ru(bipym)(PPh_3)_2Cl_2]$ (**3**)	320(m) 310(m)	510(s)	490(w)	3100(s), 1610(m), 1470(w), 1390(vs), 1090(m), 740 (m)
$[Ru(bipym)_2Cl_2]$ (**4**)	315(m)	—	480(w)	3100(s), 1550(m), 1400(vs), 1030(w), 810(m)
$[Ru(bipym)_2(CH_3CN)(Cl)]^+[PF_6]^-$ (**5**)	315(m)	—	490(w)	3100(s), 1550(m), 1400(vs), 1090(m), 740(m)
$[Ru(bipym)_2(NO_2)_2]\cdot 0.5H_2O$ (**6**)	1250(s)	—	495(w)	3100, 1615(m), 1410(vs), 1020(w), 800(m)

Key: s = strong; vs = very strong; w = weak and m = medium.

emission spectra of complex **1** shows a strong intensity peak at 611 nm which seems to be $d\pi^*$ in origin. The substitution of chloride by PF_6 shows a blue shift of the λ_{em} maximum which is observed at 602 nm with slightly lower intensity. The emission intensity of complexes **1** and **2** does not change in the pH range 4.5–8. At lower pH the emission intensity rapidly decreased and no emission was observed below pH 1, indicating a slightly enhanced basicity of the excited state of $Ru(bipym)_3^{2+}$. Complex **3** gave λ_{em}(max) at 546 nm which is due to replacement of two bipyrimidine molecules, responsible for fluorescence. The removal of one bipyrimidine molecule has shown a blue shift in complex **4**, where λ_{em}(max) is at 533 nm. The addition of CH_3CN and Cl to the coordination sphere of the metal ion in complex **5** shows a red shift for the emission wavelength at 644 nm. Addition of NO_2 also exhibits a red shift at 750 nm. The red shift in the emission wavelength is very important because the energy utilized for the excitation wavelength is also less. This fact is helpful for the utilization of these complexes in the visible part of the solar spectrum (with less energy) to realize the harnessing of solar energy. The λ_{em} maximum of complexes **1–6** is given in Table 3.

Electrochemical studies

Polarographic $E_{1/2}$ data for ruthenium(II) bipyridimine complexes in aqueous solution with SCE as reference electrode in 0.1 M KNO_3 as supporting electrolyte are compared with those of their bipyridyl analogues. The $E_{1/2}$ value of $Ru(bipym)_3^{2+}$ with bipyrimidine results in a shift of the reduction potentials to more positive values by about 0.5 V. Similar results were reported when bipyridyl was replaced by bipyrazyl ligand.[8] The replacement of bipyrimidine in complex **4** by CH_3CN or NO_2 shows a less positive (more negative) reduction potential because of good σ-donor and poor π-acceptor behaviour of CH_3CN and NO_2 compared to Cl^-, PPh_3 or bipyridine. The shift of the reduction potential to negative values by the replacement of a halogen with good σ-donor groups was reported earlier by Crutchley and Lever.[7] We did not notice the solvolysis of complex **4**.

The diffusion currents for complexes **1–6** were calculated using differential pulse polarography and the results are tabulated in Table 4. As expected, higher diffusion currents were observed in complexes **5** and **6** by the replacement of halogen or bipyrimidine in the coordination sphere of the metal ion by the strong σ-donor CH_3CN or NO_2 groups. The more positive potentials of complexes **1–4** compared to **5** and **6** are due to the presence of less σ-basic or π-acidic ligands like bipyrimidine, PPh_3 and Cl ligands. The π-acidities decrease in the order PPh_3 > bipyrimidine > Cl^-. This is reflected in the increase of i_d for complexes **1–4** in the order **3** < **1** < **2** < **4**.

Photoanation studies

Photoanation studies of $[Ru(bipym)_3](PF_6)_2$ (**2**) in acetonitrile shows the formation of $[Ru(bipym)_2(CH_3CN)(Cl)]PF_6$ (**5**) which corresponds to a quantum yield of 0.14. The results can be compared with the reports of Jones and Cole-Hamilton[9] for the photoanation of the ruthenium(II)–tris-(bipyridyl) dication, $Ru(bipy)_3^{2+}$, by chloride ion in acetonitrile. The only photoproduct reported[9] was $[Ru(bpy)_2(CH_3CN)(Cl)]Cl$ with a maximum quantum yield of 0.01. In solvents of lower polarity such as acetone and CH_2Cl_2 the photoproduct formed was $Ru(bpy)_2Cl_2$ with a slightly higher quantum yield of 0.02.[10,11] These facts are suggestive of an ion-paired mechanism for photoanation. The mech-

Table 3. Electronic and emission spectra of the bipyrimidine complexes of ruthenium(II) in aqueous solution

$[Ru(bipym)_3]Cl_2$ (**1**)	22,123(3.82), 24,271(3.8), 30,120(4.13)	452, 412 332	40,650(4.59)	246	611
$[Ru(bipym)_3](PF_6)_2$ (**2**)	22,075(3.86), 24,271(3.8), 30,180(4.16)	453, 412 331	40,650(4.66)	246	602
$[Ru(bipym)(PPh_3)_2Cl_2]$ (**3**)	24,630(3.68)	406	41,152.2(4.089)	243	546
$[Ru(bipym)_2Cl_2]$ (**4**)	25,315(3.94), 27,178(3.91)	395, 368	41,152(4.43) 51,813(4.50)	243 193	533
$[Ru(bipym)_2(CH_3CN)(Cl)]^+[PF_6]^-$ (**5**)	20,202(3.8), 26,809(4.22)	495, 373	—	—	644
$[Ru(bipym)_2(NO_2)_2]\cdot 0.5H_2O$ (**6**)	28,735(3.97), 20,660(3.94)	484, 348	42,020(4.29) 32,364(4.5)	238 309	750

Table 4. Electrochemical data of ruthenium–bipyrimidine complexes

Complex	Oxidation $E_{1/2}$ (V)	Reduction $E_{1/2}$ (V)			Differential pulse i_d (μA)
$[Ru(bipym)_3]Cl_2$ (1)	1.69	−0.80	−0.95	−1.2	7.0
					7.5
$[Ru(bipym)_3](PF_6)_2$ (2)	1.67	−0.92	−1.06	−1.09	5.5
					5.75
$[Ru(bipym)(PPh_3)_2Cl_2]$ (3)	—	−0.76	—	—	3.6
$[Ru(bipym)_2Cl_2]$ (4)	—	−0.75	−1.16	—	4.9
					7.25
$[Ru(bipym)_2(CH_3CN)(Cl)]^+[PF_6]^-$ (5)	—	−1.37	—	—	27.5
$[Ru(bipym)_2(NO_2)_2]\cdot 0.5H_2O$ (6)	—	−1.18	−1.45	—	7.9
					12.75

anism of photoanation of $Ru(bipym)_3^{2+}$ by analogy to that of $Ru(bpy)_3^{2+}$ is believed to be dissociative, resulting in a five-coordinate intermediate with an end-bonded bipyrimidine ligand. Monodentate bipyridyl intermediates have been isolated and their electronic spectra recorded.[12,13] However, these intermediates are unstable and it is probably that in the case of $Ru(bipym)_3^{2+}$, the formation of a monodentate bipyrimidine complex is not detected spectrophotometrically because of its rapid conversion of $Ru(bipym)_3^{2+}$ to $[Ru(bipym)_2(CH_3CN)(Cl)]^+$. As soon as the five-coordinate intermediate is formed, anation results from the Cl^- associated in the ion pair. The difference in the quantum yields of $Ru(bipym)_3^{2+}$ ($\phi = 0.14$) and $Ru(bpy)_3^{2+}$ ($\phi = 0.01$) may be due to the conversion of the latter species to $[Ru(bpy)_2(solvent)(Cl)]^+$ in solution as observed by Van Houten and Watts.[12]

Our interest in the bipyrimidine(II) species is in the design of the highly photo-oxidizable photocatalyst and it is pertinent that the redox couples associated with $Ru(bpy)_3^{2+}$ do shift to positive values in sulphuric acid by a significant amount.[14] The excited state protonation studies using fluorescence spectroscopy are also of interest to us and are under investigation. The electrochemical properties of these complexes and the replacement of Cl^- by ligands such as NCS, Br_2, I_2, oxalate etc. also falls under our future interest of work.

EXPERIMENTAL

Preparation of complexes

(1) *Tris(bipyrimidine)ruthenium*(II) *dichloride.* The complex was prepared by refluxing $Ru(Me_2SO)_4Cl_2$ (0.4 g) and bipyrimidine (0.8 g) in water (50 cm^3) for 20 h. The reaction mixture was filtered and evaporated to dryness. The residue was washed with acetone and chloroform and again with acetone. The crude product (0.6 g) was dissolved in water (10 cm^3) and filtered. To the boiling filtrate was added slowly a 1:2 mixture of ethanol and propanol (20 cm^3). On cooling the solution, reddish crystalline $[Ru(bipym)_3]Cl_2$ precipitated out (0.55 g); yield: 80%.

(2) *Tris(bipyrimidine)ruthenium*(II) *hexafluorophosphate.* A solution of $[Ru(bipym)_3]Cl_2$ (0.4 g in water to cm^3) was heated to boiling. To this was added an aqueous solution of 0.2 M (50 cm^3) NH_4PF_6 and an orange precipitate was immediately formed. The solution was allowed to cool to room temperature and then filtered. The crude product was washed with water and recrystallized with acetone–ethanol solution to give the orange-coloured crystalline $[Ru(bipym)_3](PF_6)_2$; yield: 76%.

(3) *Dichlorobis(triphenylphosphine)bipyrimidineruthenium*(II). A solution of $RuCl_2(PPh_3)_2$ (0.6 g) and bipyrimidine (0.36 g) in acetone (50 cm^3) was refluxed for 6 h to give a reddish-brown precipitate which was filtered and dissolved in chloroform (100 cm^3). The solution was concentrated to 20 cm^3 and $[Ru(bipym)(PPh_3)_2Cl_2]$ crystallized out on cooling. The complex was recrystallized from chloroform; yield: 42%.

(4) *Dichlorobis(bipyrimidine)ruthenium*(II). The complex was prepared by refluxing $RuCl_3\cdot xH_2O$ (0.25 g) and bipyrimidine (0.3 g) in DMF (20 cm^3) for 2 h. The purple solution obtained was filtered and evaporated to dryness in a roto-evaporator. The dry mass was dissolved in 50 cm^3 of acetonitrile and concentrated to 10 cm^3, when black crystalline $[Ru(bipym)_2Cl_2]$ was obtained. The complex was recrystallized from water; yield: 62%.

(5) *Chlorobis(bipyrimidine)acetonitrileruthenium*(II) *hexafluorophosphate.* To a solution of [Ru(bipym)$_3$](PF$_6$)$_2$ (0.3 g) in CH$_3$CN (100 cm^3) was added slowly over 30 min, tetrabutyl ammonium chloride (TBA)Cl (0.07 g). The solution was irradiated at 350 nm when the orange-coloured solution started to turn deep red. After 3 h the excess of acetonitrile was removed over a roto-evaporator and the crude product was digested in boiling propanol. The residue was dissolved in acetone (20 cm^3), and on cooling dark red crystalline [Ru(bipym)$_2$(CH$_3$CN)(Cl)]PF$_6$ separated out. The complex was recrystallized from water; yield: 37%.

(6) *Bis(dinitrito)bis(bipyrimidine)ruthenium*(II). A solution of Ru(bipym)$_2$Cl$_2$ (0.2 g) and NaNO$_2$ (0.4 g) in a 1:1 ethanol–water mixture (30 cm^3) was refluxed for 8 h and the orange solution turned deep red. The deep red solution was concentrated and the complex precipitated by an excess of acetone, when red crystals of [Ru(bipym)$_2$(NO$_2$)$_2$]·0.5 H$_2$O were obtained. The complex was recrystallized from a water–alcohol mixture; yield: 78%.

Acetonitrile was distilled over anhydrous AlCl$_3$ and P$_2$O$_5$. Tetrabutylammonium chloride was used without purification. Bipyrimidine and tetrabutylammonium chloride was used as purchased from Lancaster Chemicals and Aldrich without further purification. RuCl$_2$(Me$_2$SO$_4$) was prepared as reported earlier.[15] Photoanation studies were conducted using a 450 W Xenon lamp from Applied photo physics in a quartz cell of 1 cm path length. All the solutions were made in double-distilled water or acetonitrile. Fresh stock solutions were prepared for spectroscopic studies.

Electrochemical studies were conducted on a PAR Model 174 electrochemical analyser using DME. The solutions contained 9×10^{-4} M ruthenium complex in 0.1 M KNO$_3$ as the supporting electrolyte. All measurements were performed at 26°C in degassed (N$_2$) aqueous solution and all potentials are reported against a SCE.

Electronic spectra of all the complexes were recorded with a Beckman DU-7 UV–vis spectrometer. IR spectra were recorded on a Nicolet 200 SX FT–IR spectrophotometer. Fluorescence emission spectra were recorded on a Hitachi Model 650 Fluorometer with microprocessor. Irradiation of a vacuum degassed solution of [Ru(bipym)$_3$](PF$_6$)$_2$ (8.0×10^{-5} M) and (TBA)Cl (2×10^{-4} M) was carried out in a 1 cm quartz cell under N$_2$. The light source was a 450 W xenon lamp with an interference filter of 436 nm for photoanation of **2**. The light intensity was calculated using ferrioxalate actinometry.[16] The photolysis was interrupted periodically and the absorption spectra recorded. Quantum yields were calculated on the basis of the

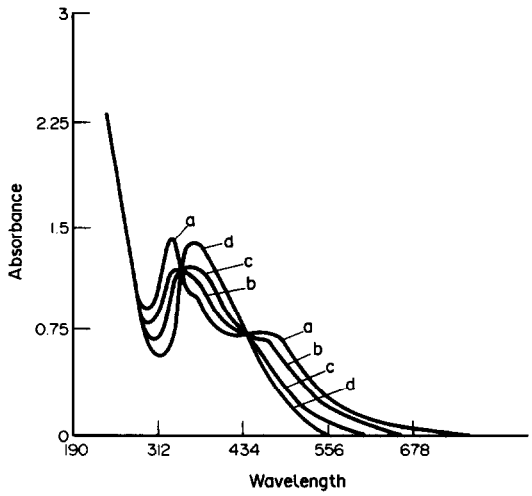

Fig. 1. Absorption spectrum of photoanation studies, Ru(bipym)$_3^{2+}$ (10^{-5} M) and (TBA)Cl (10^{-4} M) in acetonitrile: (a) without illumination; (b) 5 min; (c) 30 min; (d) 45 min for illuminated.

disappearance of the peak corresponding to Ru(bipym)$_3^{2+}$ at 30,120 cm^{-1}.

For the photoanation studies a solution of the complex [Ru(bipym)$_3$](PF$_6$)$_2$ (**2**) in acetonitrile is relatively stable when irradiated at $\lambda = 436$ nm even in the presence of Cl$^-$. However, on irradiation at 350 nm in the presence of Cl$^-$, photoanation takes place as shown in Fig. 1. Figure 1 shows the spectrum of a typical photoanation experiment. The presence of two isobestic points at 356 and 456 nm suggests the formation of two intermediates but only one photoproduct could be isolated. Photolysed solutions of **2** in the presence of Cl$^-$ were extracted with hexane. The UV–vis spectrum before and after hexane extraction showed no change in the position of MLCT bands and a drop in intensity and a narrowing of the ligand π–π^* bands. The hexane extract was evaporated and the melting point and UV–vis spectrum of the residue confirmed the product to be bipyrimidine. The elemental analysis of the photoproduct agrees with the formation [Ru(bipym)$_2$(CH$_3$CN)(Cl)]PF$_6$.

The photolysis at 359 nm seems to give rise to an ion-paired five-coordinate intermediate [Ru(bipym)$_2$bipy)]$^+$Cl$^-$ (**1**), where one of the bipyrimidines is monodentate. This intermediate then collapses to the product [Ru(bipym)$_2$(CH$_3$CN)(Cl)]PF$_6$ (**5**). Irradiation at 350 nm seems to be essential to obtain **1** since irradiation at 450 nm cannot give the photoanation product.

REFERENCES

1. K. Kalyanasundaram, *Coord. Chem. Rev.* 1979, **46**, 159.

2. R. J. Crutchley and A. B. P. Lever, *J. Am. Chem. Soc.* 1980, **102**, 7128.
3. R. J. Crutchley, N. Kress and A. B. P. Lever, *J. Am. Chem. Soc.* 1983, **105**, 1170.
4. M. Hunziker and A. Lundi, *J. Am. Chem. Soc.* 1977, **99**, 7370.
5. Shin-ichi Ishiguro, Hides Wada and Hitoshi Ohtaki, *Bull. Chem. Soc. Jpn* 1985, **58**, 982.
6. B. Crociani, F. Bibianca, A. Giovenco and S. Scri Vanti, *J. Organomet. Chem.* 1985, **291**, 259.
7. R. J. Crutchley and A. B. P. Lever, *Inorg. Chem.* 1983, **22**, 2647.
8. R. J. Crutchley and A. B. P. Lever, *Inorg. Chem.* 1982, **21**, 2276.
9. R. F. Jones and D. J. Cole-Hamilton, *Inorg. Chim. Acta* 1981, **53**, L3.
10. M. Gleria, F. Minto, G. Beggiato and P. Bortous, *J. Chem. Soc., Chem. Commun.* 1978, 285.
11. P. E. Hoggard and G. B. Porter, *J. Am. Chem. Soc.* 1978, **100**, 1457.
12. J. Van Houten and R. J. Watts, *Inorg. Chem.* 1978, **17**, 3381.
13. B. Durham, J. L. Walsh, C. L. Carter and J. J. Meyer, *Inorg. Chem.* 1980, **19**, 860.
14. P. G. Bradley, N. Kress, B. A. Horbuyer, R. F. Dallinger and W. H. Woodruff, *J. Am. Chem. Soc.* 1981, **103**, 7441.
15. I. P. Ivan and G. Wilkinson, *J. Chem. Soc., Dalton Trans.* 1973, 204.
16. C. G. Hatchard and C. A. Parker, *Proc. R. Soc. A.* 1956, **235**, 518.

Polyhedron Vol. 9, No. 10, pp. 1249–1256, 1990
Printed in Great Britain

0277–5387/90 $3.00+.00
© 1990 Pergamon Press plc

^{17}O, ^{31}P AND ^{183}W NMR SPECTRA OF PARAMAGNETIC COMPLEXES WITH THE HETEROPOLYTUNGSTATE ANION $[Ln(PW_{11}O_{39})_2]^{11-}$ AND THEIR CONSTITUTION IN AQUEOUS SOLUTION. Ln—RARE EARTH ELEMENT

MARTIN A. FEDOTOV*

Institute of Catalysis, 630090 Novosibirsk, U.S.S.R.

and

BORIS Z. PERTSIKOV

Irkutsk Polytekhnik Institute, Irkutsk, U.S.S.R.

and

DAVID K. DANOVICH

Irkutsk Institute of Organic Chemistry, Irkutsk, U.S.S.R.

(*Received* 18 *September* 1989; *accepted* 8 *December* 1989)

Abstract—Lanthanide complexes from La to Yb with $[PW_{11}O_{39}]^{7-}$ ligands were studied by ^{17}O, ^{31}P and ^{183}W NMR methods. The complexes are non-labile on the NMR time scale, and their 1:2 composition in solution was confirmed by ^{31}P NMR. Contact and dipolar contributions to the lanthanide induced shift (LIS) of ligand nuclei have been estimated. The geometry of the ligand was shown to change in the lanthanide series and the dipolar contribution to LIS increases compared to the contact contribution, as the distance from the lanthanide ion increases.

Lanthanide(III) complexes, known as lanthanide shift reagents (LSR), are tools for the simplification and interpretation of NMR spectra and the structural analysis of organic molecules in solution.[1] On the other hand, ^{17}O and ^{183}W NMR can give some information about the structure of polytungstates in solution.[2–4] Comparison of X-ray and ^{17}O NMR data shows a change of bond length in heteropolyanions (HPA) of tungsten and molybdenum on dissolution. Equivalent bonds of NPA become more equal in solution than in the crystal.[2,4] ^{17}O and ^{183}W NMR studies of the lanthanide complexes of $[PW_{11}O_{39}]^{7-}$–HPA (PW_{11}) were expected to give additional information about the structure and NMR spectra of HPA.

The inorganic tetradentate macroligand PW_{11} is known[5] to form $Ln(PW_{11})_2$ complexes with lanthanide ions, which are HPA with two heteroatom types. We are not aware of structural or NMR ^{17}O studies which can give structural information[3] on these HPA. In the present paper ^{17}O, ^{31}P and ^{183}W NMR spectra of $Ln(PW_{11})_2HPA$ and their constitution in aqueous solution were studied for all stable lanthanides.

EXPERIMENTAL

The $Ln(PW_{11})_2$ complexes were prepared with solid chloride or nitrate lanthanide salts added to a 0.3 M aqueous solution of the sodium salt of $PW_{11}HPA$ in the ratio $Ln:PW_{11} = 1:2$. The natural abundance of ^{31}P, ^{17}O and ^{183}W NMR spectra was recorded with a Bruker CXP-300 spectrometer at 121.47, 40.7 and 12.5 MHz, respectively. Chemical shifts (CS) in δ scale are given to external references H_2O (^{17}O), 85% H_3PO_4 (^{31}P)

* Author to whom correspondence should be addressed.

Table 1. ^{31}P and ^{17}O NMR data of complexes $Ln(PW_{11}O_{39})_2^{n-}$

Ion	$\delta^{14}N^a$ (ppm)	$\delta^{31}P$ (ppm) 293 K	323 K	$W_{1/2}{}^b$ 293 K	$\delta^{17}O$ (ppm) $\delta_{aq}^{c,d}$	$\delta(H_2O)_{bulk}^{a,d}$	$\delta^{17}O$ oxygen atoms of type^{d,e} (ppm) O=W	Ln—O—W	W—O—W
La^{3+}	0	−11.9	—	15	0	0	708 685 670	632 614	432 386 360
Ce^{3+}	−0.7	−19.3	−17.6	18	1	−0.3	711 686 669	782 737	430 385 355
Pr^{3+}	−0.7	−14.6	−15.2	25	5.5	−0.4	711 689 677	1000 916	432 389 356
Nd^{3+}	−0.7	−24.2	−22.1	23	6.7	0.5	713 688 677	1084 988	430 387 356
Sm^{3+}	0.4	−15.4	−14.8	16	−0.4	−1.0	710 689	614 559	422 388 356
Eu^{3+}	−0.4	−1.2	−2.4	27	−13.6	−2.1	710 689	655 632	410 387 359
Gd^{3+}	−3.7	—	−3[g]	—	−46.9	−1.9	709 689	— —	393 372 355
Tb^{3+}	−7.1	−223	−169	210	−34.3	−0.9	710 683 672	— —	413 381 357
Dy^{3+}	−10.1	−108	−98	410	−39	1.1	711 687 679	— —	401 372 352
Ho^{3+}	−11.1	−109	−90	530	−41	−2.0	710 692 685 678	433 427	396 380 373 355
Er^{3+}	−10.3	61.4	48.8	270	−22.4	−4.2	712 687 675	664 641	398 378 352
Tm^{3+}	−6.4	217	164	200	−21.1	−3.8	717 708 684	670 616	400 391 360
Yb^{3+}	−1.7	32	26.1	50	−4.7	−1.6	711 695	— —	394 352

[a] 293 K.
[b] $W_{1/2}$ linewidth (Hz) at half height (field inhomogeneity = 15 Hz).
[c] LIS ^{17}O of H_2O of 0.1 M water solutions of $Ln(NO_3)_3$.
[d] Sample susceptibility correction is included.
[e] 323 K.
[g] $W_{1/2}$ = 4 kHz.

and 2 M solution of Na_2WO_4 in H_2O (^{183}W). About 10,000 accumulated scans were used for ^{183}W NMR spectra with a delay of 3–5 s. Correction of CS for magnetic susceptibility of samples was made using the ^{14}N NMR CS of the NO_3^- ion, neglecting its paramagnetic shifts. LIS values are taken as the difference between the CS of the atom of interest in paramagnetic and diamagnetic complexes. For ^{31}P NMR the last value for a given Ln was changed from −11.9 (La) to −13.2 ppm (Lu) proportional to the number of *f*-electrons of Ln. ^{31}P and ^{17}O NMR data are listed in Table 1.

RESULTS AND DISCUSSION

The stoichiometry of the $Ln(PW_{11})_2$ complexes was established in solution by the ^{31}P NMR method as follows. After addition of a stoichiometric amount of lanthanide salt to the solution of PW_{11}HPA the ^{31}P NMR peak of PW_{11} diminished and the $Ln(PW_{11})_2$ peak complex increased. Dissolution of half of the amount of Ln gave two NMR peaks of equal intensity arising from free ligand PW_{11} ($\delta = -10.7$ ppm) and the ligand in the complex. The existence of two peaks means a slow exchange of ligand (or absence of exchange). The life-time of the ligand in the complex, as estimated from NMR spectra, is more than 10–100 ms depending on the Ln.

A study of any salt HPA $Ln(PW_{11})_2$ structure is lacking. A unique X-ray crystal structure determination of the relative HPA (ref. 6) has shown that the two anions α-$GeW_{11}O_{39}^{8-}$ (see Fig. 1) form an oxygen square antiprism around the central atom. In the crystal the square facets of the antiprism differ from each other, and the sides of each square facet differ by about 10%. If this distortion of HPA was present in solution, ^{31}P peaks of different P atoms of the complex should be resolved, especially for a complex with a large LIS. The single peak of ^{31}P NMR demonstrated a uniform construction and connection of the ligands to the lanthanide ion.

LIS of nucleus *i* of the ligand upon coordination to the Ln^{3+} ion is known to be expressed as the sum of the contact shift Δ^c (the first term) and the pseudocontact (dipolar) shift Δ^{pc} (the other terms):

$$\delta_i = \Delta^c + \Delta^{pc} = 2\pi\beta\langle S_z\rangle A_i/3kTh\gamma_N + D'(3\cos^2\theta - 1)r_i^{-3} + D''\sin^2\theta\cos 2\phi_i r_i^{-3}, \quad (1)$$

where $\langle S_z\rangle$ is the Golding constant[7] and A_i the hyperfine coupling constant. Factors D' and D'' are anisotropy components of the magnetic susceptibility tensor, r, θ, ϕ are the spherical coordinates of the observed nucleus with respect to Ln^{3+} at the origin and with the principal magnetic axis as the z axis (Fig. 1). The $\langle S_z\rangle$ value is characteristic of the Ln^{3+} ion only and defines the contact term Δ^c.

The dependence of Δ^{pc} on the Ln^{3+} ion characteristics is defined by the Bleany factor C_B,[9] and LIS must follow C_B along the lanthanide series, if

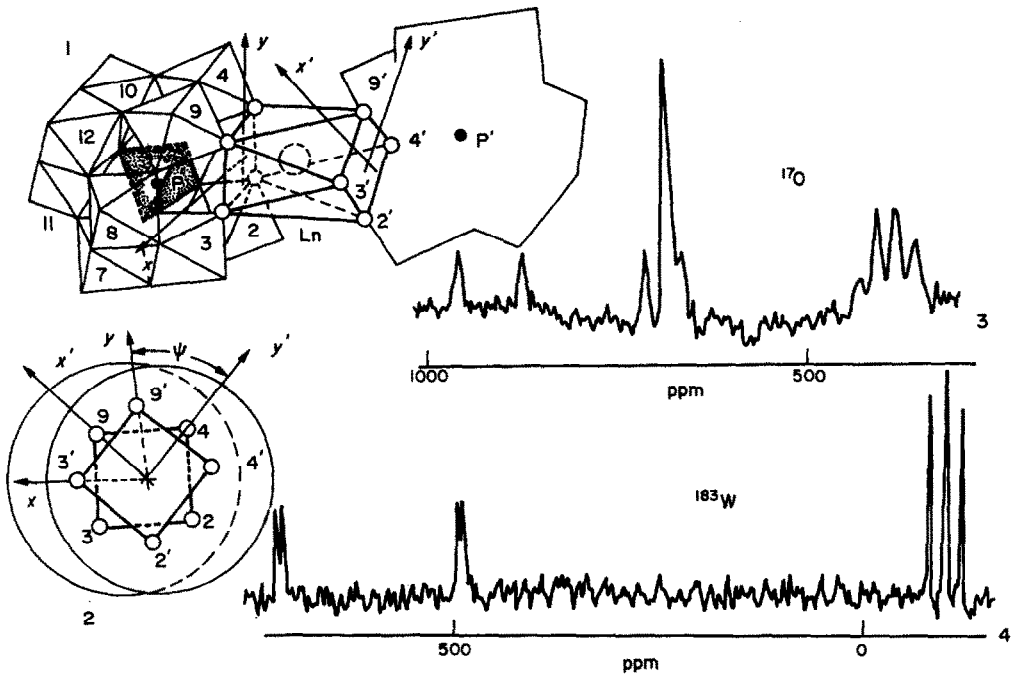

Fig. 1. (1) Schematic representation of the $Ln(PW_{11}O_{39})_2^{11-}$ complex. (Figures denote tungsten atom numbers.) (2) Side view of the complex showing the rotation angle ϕ. (3) ^{17}O NMR spectrum of $Pr(PW_{11}O_{39})_2^{11-}$ at 323 K. (4) ^{183}W NMR spectrum of the same complex.

structural changes are absent. As usual, Δ^{pc} predominates in LIS of atoms further than four bonds away from a paramagnetic ion. Atom P is four bonds away from Ln; furthermore, the W—O—P bond is longer (244 pm[10]) than other W—O bonds (190–192 pm), and the Δ^c value must be less than that of other atoms four bonds away from Ln. Comparison of the C_B and LIS dependences of $Ln(PW_{11})_2$ complexes on Ln shows an appreciable, if not predominant, Δ^{pc} value in LIS.

The geometry of the coordination sphere of the Ln^{3+} ion can change along the lanthanide series.[8] If Δ^c is small in comparison to Δ^{pc} and if structural changes are negligible, we must expect a linear dependence between LIS and C_B values.[8] We did not observe a linear dependence of these values either between light Ln-HPA or heavy Ln-HPA, or even the Ce–Pr–Nd series. Gadolinium HPA LIS is contact in nature, and its ^{31}P value is about 10 ppm. The Δ^c value of Ce-, Pr- and Nd-HPA must be less than in Gd-HPA, therefore a dipolar Δ^{pc} contribution predominates in ^{31}P LIS of Ce-, Pr- and Nd-HPA. This means that the HPA structure changes along the lanthanide series.

The P atoms are equivalent and situated symmetrically with respect to Ln in HPA $Ln(PW_{11})_2$, because only one ^{31}P peak is observed. Estimation of the difference in Ln—P distances in HPA with maximal LIS (Tb- or Tm-HPA) gives a value of less than 0.1 pm, taking into account the cubic dependence of LIS on the Ln—P distance and a linewidth for ^{31}P NMR of 200 Hz.

The Δ^{pc} contribution depends on the coordinates of the nucleus of interest only in the given complex. Variation of Δ^{pc} from one nucleus of PW_{11} to another can be estimated from the coordinates of the HPA atoms (from ref. 6) as a first approximation. Supposing the LIS ^{31}P of HPA to be fully dipolar, we calculated maximal values Δ^{pc} in LIS for other nuclei and used them to determine the character of LIS of each nucleus.

^{17}O NMR spectra of $Ln(PW_{11})_2HPA$ consist of a set of peaks of terminal O=W atoms (725–685 ppm) and a set of W—O—W bridging atom peaks (430–350 ppm, see Fig. 1). They are situated near their position in the free ligand spectrum.[11] Diamagnetic and paramagnetic HPA spectra differ insignificantly except in the peaks for Ln—O—W bridging atoms. Peaks for terminal and bridging O atoms change position negligibly along the lanthanide series.

As is known,[3] the down-field shift of ^{17}O NMR peaks of O=W terminal atoms of polytungstate corresponds to a shortening of the O=W— bond. The average bond length increases from 163 to 183 ppm in the series $O{=}W_{4,9}$, $O{=}W_{5,8}$, $O{=}W_{2,3}$,

O=$W_{6,7}$, O=$W_{10,12}$, O=W_{11}, as follows from structural data.[6] CS ^{17}O of O=$W_{4,9}$ must change along the Ln series, because their LIS is significant. Apparently, the down-field 710 ppm peak belongs to O=$W_{5,8}$ atoms, taking into account that the ^{183}W CS of the $W_{5,8}$ atom changes insignificantly along the Ln series.

Water molecules do not enter the coordination sphere of Ln in HPA, as follows from comparison of ^{17}O CS of water in the solution studied {$\delta(H_2O)$, Table 1, [Ln] = 0.3 M} and a 0.1 M solution of $Ln(NO_3)_3(\delta_{aq})$. Therefore, the coordination sphere of Ln in $Ln(PW_{11})_2$–HPA consists of $O_{2,3,4,9}$ atoms of the PW_{11} ligand only, which are connected with $W_{2,3,4,9}$ atoms. The NMR ^{17}O peaks of $O_{2,3,4,9}$ atoms are not observed for all Ln. These peaks are situated between a set of peaks of O=W terminal atoms and a set of peaks of W—O—W bridging atoms of the MPW_{11} complex (ref. 12, M = M^+, M^{2+}, M^{3+}).

LIS ^{17}O of Ln—O—W atoms depend on the magnetic properties of Ln and the structural parameters of the coordination sphere of Ln (e.g. Ln radius). ^{17}O NMR peaks of Ln—O—W atoms in Ce-, Pr-, Nd-HPA are shifted more than 100 ppm from their position in $Ln(PW_{11})_2$, and these shifts are mainly paramagnetic. LIS of Ln—O—W atoms increase successively in the series Ce, Pr, Nd and do not correlate with C_B. ^{17}O NMR peaks lie near the peaks of La- and Lu-HPA. Oxygen-17 peaks of Ho-, Er- and Tm-HPA, which are situated between the peaks of terminal and bridging atoms (Table 1), apparently belong to O atoms W_4—O—W_{10}, W_9—O—W_{12} and so on, or W_4—O—W_9, W_2—O—W_3 atoms, because ^{183}W LIS of the HPA $W_{2,3,4,9}$ atoms are much more than LIS of those atoms of Ce-HPA (Table 2) and LIS of Ho- and Tm-HPA Ln—O—W atoms must be more than LIS of analogous atoms of Ce-HPA.

The contributions Δ^c and Δ^{pc} for P atoms and $W_{4,9}$—O—Ln and $W_{2,3}$—O—Ln oxygen atoms in Ce-, Pr- and Nd-HPA were calculated using eq. (1) and LIS ^{31}P and ^{17}O with the projection of the Ln atom on O_2, O_3, O_4, O_9 plane taken as the origin of coordinates. The non-linear minimization program LISMIN[13] was explored and calculated results are listed in Table 3.

If k nuclei are taken, a system of k equations arises with j unknowns, which are the Cartesian coordinates of nuclei x, y, z, susceptibility tensor anisotropy constants D' and D'' and the hyperfine coupling constant A. The system is solved if $j < k$. As usual one supposes that x, y, z and A are equal in LIS complexes of light or heavy lanthanides, and the system is solved with a definite number of Ln. This approach is not suitable in this case due to insufficient experimental data. Therefore, a minimization procedure with the minimum criterion R was used

$$R = \left[\sum_k (\delta_{\mathrm{calc},k} - \delta_{\mathrm{obs},k})^2 \Big/ \sum_k (\delta_{\mathrm{obs},k})^2\right]^{1/2},$$

where δ_{calc} was calculated from eq. (1) and δ_{obs} was the observed LIS. Because of the non-linearity of eq. (1), the existence of several minima is possible,

Table 2. ^{183}W NMR chemical shifts[a] of $Ln(PW_{11}O_{39})_2^{n-}$

Ion	T (K)	$-\delta$ ^{183}W (ppm) of atoms[a]					
		$W_{4,9}$ ($W_{2,3}$)	$W_{2,3}$ ($W_{4,9}$)	$W_{10,12}$	$W_{5,8}$	$W_{6,7}$	W_{11}
La^{3+}	295	144	130	150	128	104	117
Ce^{3+}	308	−325	−181	141	118	96	113
Pr^{3+}	297	−829	−574	133	114	93	113
Nd^{3+}	291	−1027	−999	131	115	94	113
Sm^{3+}	304	159	140	148	125	103	116
Eu^{3+}	313	1761	1635	179	136	119	124
Gd^{3+}	293	—	—	248	170	152	154
Tb^{3+}	293	3604 3318	2842 2779	290 277	203 206	164 167	188
Dy^{3+}	293	2657 2429	2141 2029	246 240	172 164	138[b]	161
Ho^{3+}	293	1830 1681	1572 1427	213 225	159 163	131 135	154
Er^{3+}	293	1124 1007	905 887	157 163	114 119	103 109	116
Tm^{3+}	295	484 407	420 408	103 102	82 89	72 77	80
Yb^{3+}	293	151 140	136 132	122[b]	112 114	94 101	122
Lu^{3+}	293	159 184	135 133	144 146	123 124	102 104	115
Th^{4+}	293	142	130	142	124	105	111

[a] Correction for sample susceptibility is made.

[b] Double intensity peak.

Table 3. Calculated contributions of Δ^c and Δ^{pc} of $Ln(PW_{11}O_{39})_2^{n-}$

Ion Ln^{3+}	Atom	δ_{obs} (ppm)	D' (cm^{-1})	$A \times 1000$ (Oe)	Δ^c (ppm)	Δ^c (%)	Δ^{pc} (ppm)	Δ^{pc} (%)
Ce^{3+}	$O_{4,9}$	149	44	435	148	99	1.5	1
	$O_{2,3}$	122		355	120	99	1.5	1
	P	−5.6		178	−20.2	58	14.6	42
Pr^{3+}	$O_{4,9}$	367	30	344	360	98	7.1	2
	$O_{2,3}$	301		272	294	98	7.1	2
	P	−3.2		165	−59.5	51	56.3	49
Nd^{3+}	$O_{4,9}$	451	5.3	272	450	100	0.7	0.2
	$O_{2,3}$	373		225	372	100	0.7	0.2
	P	−10.1		46	−25.3	62.5	15.2	37.5

depending on the initial set of parameters. If LIS is contact by nature, eq. (1) transforms into $\delta_{calc.i} = FA_i$, from which a set of A_i for all nuclei with measured LIS can be obtained. In the case of Ce-, Pr- and Nd-HPA A_i is $\simeq 0.3$ Oe for $O_{2,3,4,9}$ atoms and A is $\simeq 0.01$ Oe for P atom. The geometry of HPA from ref. 6 was taken as the initial geometry for the calculations.

A dipolar axial model of the complex cannot explain the ^{183}W and ^{31}P LIS values observed. Calculations for the non-axial complex led us to $D' < D''$, which means that the z axis is not the principal magnetic axis of the complex. This disagreement led us to the axial model with Δ^c and Δ^{pc} contributions of LIS, and eq. (1) transforms the forms into $\delta_{calc.i} = D'(3\cos^2\theta_i - 1)r_i^{-3} + FA_i$. Agreement of calculated and observed parameters is achieved, if the contact contribution dominates for O atoms (about 99%) and both Δ^c and Δ^{pc} are comparable in the LIS of the P atom.

The presence of the paramagnetic ion in the HPA shortens the magnetic relaxation times of ^{183}W nuclei and makes conditions for obtaining NMR spectra more favourable in general. Except for Gd-HPA, distant atoms peaks observed are narrow (≤ 10 Hz) and peaks of neighbouring $W_{2,3,4,9}$ atoms are broader. The ^{183}W NMR data are listed in Table 2. HPA may be divided into four groups, which have similar ^{183}W NMR spectra: La—Nd, Sm—Gd, Tb—Er, Tm—Lu. The first and second HPA groups have six-peak spectra typical of PW_{11} complexes with other cations.[11] These spectra have five double intensity peaks of the atom pairs $W_{4,9}$, $W_{2,3}$ $W_{5,8}$, $W_{6,7}$ and $W_{10,12}$, which are situated symmetrically from the plane of atoms La, P, W_{11}, and the peak of atom W_{1} (Fig. 1). $W_{2,3,4,9}$ atom peaks are arranged either away from other peaks of the spectrum or are broader (the spectrum of Gd-HPA is not full). Supposing the order of peaks for all W atoms except $W_{2,3,4,9}$ is the same as in the La-HPA

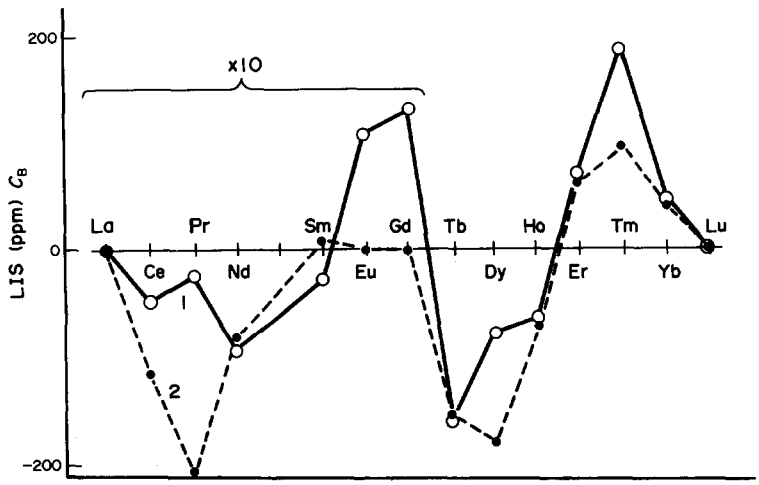

Fig. 2. ^{31}P LIS (323 K, solid line) of $Ln(PW_{11}O_{39})_2^{11-}$ and Bleany factor C_B of lanthanide ions (dotted line).

Table 4. Spherical coordinates,[a] observed LIS[b] and calculated Δ^{pc} (in parentheses) of $Ln(PW_{11}O_{39})_2^{11-}$

Coordinates, parameters	Atoms: $W_{4,9}$	$W_{2,3}$	$W_{5,8}$	$W_{6,7}$	$W_{10,12}$	W_{11}	P
$r_{A\text{-}Ln}$ (pm)	387	416	573	687	688	796	439
$\cos\theta$	0.794	0.718	0.748	0.741	0.958	0.977	0.959
$\Delta_W^{pc}/\Delta_P^{pc}$	0.74	0.36	0.17	0.10	0.26	0.18	1.00
LIS,							
Ln = Ce	469 (−5.0)	311 (−2.4)	10 (−1.4)	8 (−0.7)	9 (−1.7)	2.7 (−1.2)	−6.7
Pr	973 (−1.4)	704 (−0.7)	14 (−0.3)	11 (−0.2)	17 (−0.5)	3.7 (−0.3)	−1.9
Nd	1171 (−8.4)	1121 (−4.1)	19 (−1.9)	10 (−1.1)	19 (−2.0)	3.7 (−2.0)	−11.9
Eu	−1617 (8.7)	−1505 (4.2)	−8 (2.2)	−15 (1.3)	−29 (3.0)	−6.5 (2.1)	11.8
Tb	−3422 −3160 (−150)	−2705 −2649 (−70)	−82 −78 (−35)	−63 −62 (−20)	−143 −132 (−54)	−72 (−36)	−203
Dy	−2475 −2281 (−63)	−2004 −1849 (−31)	−49 −39 (−14)	−34 −32 (−8.5)	−99 −32 (−22)	−44 (−15)	−85
Er	−942 −849 (63)	−768 −757 (31)	5 11 (14)	−4 −1 (8.5)	−16 −12 (22)	1.3 (15)	85
Yb	31 18 (35)	1 2 (17)	10 13 (8)	3 8 (4.7)	25 23 (12)	−5.3 (8.3)	47

[a] Calculated from data from ref. 6.
[b] In ppm.

spectrum (it is evident for La-, Ce-, Pr- and Nd-HPA[12]), we assigned peaks to definite W atoms of HPA. For diamagnetic $La(PW_{11})_2$-HPA the assignment has been carried out earlier[12]: Ce-, Pr-, Nd-HPA atoms W_4 and W_9, W_2 and W_3 are slightly non-equivalent, because their peaks are resolved at 323 K as doublets (Fig. 1). Their location can be supposed to be not fully symmetrical.

The sign of LIS changes in the Sm–Gd group compared to groups 1 and 2. The peak positions of Sm-HPA are nearly the same as those of La-HPA. Besides narrow peaks with an intensity corresponding to 1, 2, 2, 2 W atoms we observed two broader peaks with $\delta = -140$ and -159 ppm (2 and 2 atoms); the last peak is broader. We suppose that these peaks belong to $W_{2,3,4,9}$ atoms. The Gd-HPA spectrum consists of four broad peaks. They are assigned to seven distant ligand atoms. In contrast to the spectra mentioned above those of Tb-Yb-HPA consist of 11 peaks. They correspond to fully non-equivalent W atoms in each PW_{11} ligand, while the single ^{31}P NMR peak demonstrates that the ligands are identical.

The change of ^{183}W spectra character in the lanthanide series (Table 2) is similar to the "gadolinium break" in the other properties of lanthanide compounds. One may suppose that the appearance of an 11-peak spectrum is caused by distortion of the ligand in the Ln-HPA series after Gd. This distortion corresponds to a square antiprism surrounding of Ln, *ie.* absence of the symmetry plane of the whole complex ($\phi = 45°$ or 135°, Fig. 1), and $Ln(PW_{11})_2$ complexes before Gd have the symmetry plane and cubic surrounding of Ln ($\phi = 0°$ or 180°). The structure of HPA[6] supports this suggestion, because it has a square antiprism surrounding of the central ion, with the radius corresponding to the heavy lanthanide radii.

Comparison of the Golding constant $\langle S_z \rangle$ and ^{183}W CS of atoms $W_{2,3}$, $W_{10,12}$, $W_{6,7}$ and W_{11} (Fig. 3) shows that contribution of Δ^c predominates in the LIS. LIS and $\langle S_z \rangle$ do not exactly correspond to one another. However, the contribution of Δ^c appears to predominate in the LIS of atoms $W_{2,3}$ and $W_{4,9}$. LIS ^{183}W Tb-HPA have an opposite sign to LIS Tm-HPA for distant W atoms, which is typical for a dipolar contribution, which is more important for more distant W atoms.

As was shown above, LIS ^{31}P Ln-HPA are mainly dipolar and the change of Ln radius is included in them. Because Δ^{pc} is a function only of geometry for a given Ln, we calculated the ratio $\Delta^{pc}_W/\Delta^{pc}_P$ and list them in Table 4. LIS ^{183}W and Δ^{pc} of HPA with full ^{183}NMR spectra are also listed. It is seen from Table 4 that Δ^c predominates in LIS of atoms $W_{2,3,4,9}$ neighbouring Ln. Apparently it predominates in LIS of Ce-, Pr- and Nd-HPA for the distant atoms $W_{5,8}$, $W_{6,7}$ and $W_{10,12}$. Both Δ^c and Δ^{pc} are comparable in LIS of atoms $W_{10,12}$ of Er-, Tm- and Yb-HPA, but Δ^c in LIS of $W_{10,12}$ predominates for other Ln-HPA. The importance of both contributions is seen for all W atoms of Yb-HPA. The data obtained allow the peaks of the ^{183}W NMR spectrum of Th^{IV}-HPA to be assigned as it is isostructural to Ln-HPA. Because LIS ^{31}P of Ln-HPA are very different (see Tables 1 and 4) and the sensitivity of ^{31}P NMR is quite high, the method of lanthanide mixture analysis can be developed when lanthanide compounds are transformed into $Ln(PW_{11})_2$ complexes and their relation can be determined from peak intensities of the ^{31}P NMR spectra (as in ref. 14).

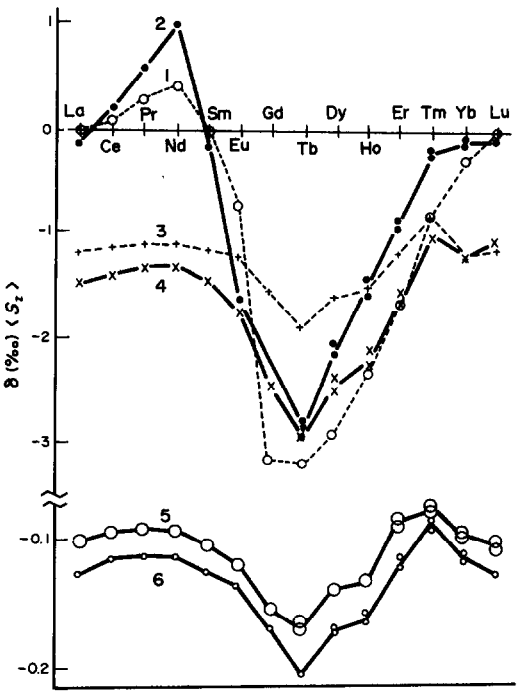

Fig. 3. Golding constants $\langle S_z \rangle$ of lanthanide ions and ^{183}W NMR chemical shifts of different W atoms of $Ln(PW_{11}O_{39})_2^{11-}$. (1) $\langle S_z \rangle$: 10; (2) $\delta(W_{2,3})$; (3) $\delta(W_{11}) \times 10$; (4) $\delta(W_{10,12}) \times 10$; (5) $\delta(W_{6,7})$; (6) $\delta(W_{5,8})$.

REFERENCES

1. V. T. Paniushkin, *Spektroskopiya koordinatsionnykh soyedinenii RZE.* Rostov University Publ., Rostov on Don (1984).
2. M. A. Fedotov, R. I. Maksimovskaya, O. A. Molchanova and A. K. Il-yasova, *Izv. AN SSSR, Ser. Khim.* 1980, 709.
3. M. A. Fedotov, L. P. Kazansky and V. I. Spitsyn, *Dokl. AN SSSR* 1983, **272**, 1179.

4. R. I. Maksimovskaya, M. A. Fedotov and G. M. Maksimov, *Izv. AN SSSR, Ser. Khim.* 1983, 247.
5. R. D. Peacock and T. J. R. Weakley, *J. Chem. Soc. A.* 1971, 1836.
6. C. M. Tourne, G. P. Tourne and M.-C. Brianso, *Acta Cryst.* 1980, **36b**, 2012.
7. R. M. Golding and M. P. Halton, *Aust. J. Chem.* 1972, **25**, 2577.
8. J. P. Peters, *J. Magn. Reson.* 1986, **68**, 240.
9. B. Bleany, *J. Magn. Reson.* 1972, **8**, 91.
10. M. T. Pope, *Heteropoly and Isopoly Oxometallates.* Springer, Berlin (1983).
11. R. I. Maksimovskaya, M. A. Fedotov and G. M. Maksimov, *Z. Neorgan. Khim.* 1985, **30**, 918.
12. M. A. Fedotov, G. M. Maksimov and K. I. Matveyev, *Koord. Khim.* 1989, **15**, 1291.
13. D. K. Danovich, V. G. Zakzhevsky and V. K. Voronov, *Zh. Strukt. Khim.* 1986, **27**, 165.
14. L. A. Fedorov, B. F. Myasoyedov, S. A. Sokolovsky, M. S. Milyukova and D. A. Malikov, *Dokl. AN SSSR* 1988, **298**, 1174.

Polyhedron Vol. 9, No. 10, pp. 1257–1262, 1990
Printed in Great Britain

0277–5387/90 $3.00+.00
Pergamon Press plc

MIXED-LIGAND COMPLEXES OF COPPER(II) WITH PYRIDINE

EDUARDO ALMEIDA NEVES* and MORENA PINTO PETERS

Instituto de Química da Universidade de São Paulo, Cx. Post. 20780, São Paulo, Brazil

(*Received* 21 *November* 1988; *accepted* 15 *December* 1989)

Abstract—The copper(II)–pyridine–azide system was studied at 1.0 M ionic strength (sodium methanesulphonate) and 25°C under conditions which favour the formation of CuN_3^+ and mixed species up to $[Cu(py)_4N_3]^+$. The treatment of data led to several types of equilibrium constant (also for the binary copper(II)–pyridine complexes), spectral data and evidence that the formation of mixed complexes overcomes statistical effects.

This paper is an extension of the systematic studies carried out in this laboratory for the copper(II)–azide reaction[1–7] from an analytical or inorganic viewpoint. The affinity of azide ion for copper(II) complexed with pyridine, to form monoazide species is presented and possible analytical application discussed. All equilibrium studies were performed at 1.0 M ionic strength, held constant with sodium methanesulphonate.

We also tested a new experimental condition for studying the mixed-ligand complex equilibrium using methods of calculation which made the data treatment unusually simple and accurate.

Experimental values of equilibrium constants of mixed-ligand complexes are important for the development of coordination chemistry in a number of ways. In fact, there is an up-to-date trend in equilibrium studies, as has been pointed out by specialists such as Beck[8] and Marcus and Eliezer.[9]

EXPERIMENTAL

CP or AR chemicals were normally used.

Copper(II) methanesulphonate was prepared by reaction of 2 M methanesulphonic acid with excess of copper(II) carbonate under constant stirring for 24 h, at room temperature. After filtering, strong acid was added in millimolar quantities to avoid hydrolysis. Standardization was carried out electrogravimetrically.

Sodium methanesulphonate was prepared by neutralization of the acid with sodium hydroxide, followed by evaporation. The solid was recrystallized twice from water, and standardization of a 3 M solution was carried out by titration of the acid eluted from a cationic exchanger (Amberlite I-R-30).

Pyridine was purified according to Vogel,[10] distilled and kept in dark bottles. Aqueous solutions were prepared with water previously bubbled with nitrogen. Standardization was performed potentiometrically with hydrochloric acid.

Sodium azide was standardized by boiling an aliquot with excess of 0.1 N H_2SO_4 and back-titrating the excess with sodium hydroxide.

All equilibrium studies (potentiometric or spectrophotometric) were performed at a controlled temperature, 25.0±0.1°C.

A digital potentiometer, Orion Research 801 A, was used for the pH measurements with a glass electrode combined with a reference electrode of Ag/AgCl/NaCl(sat). In the equilibrium studies the glass electrode was calibrated with 0.01000 M $HClO_4$ in 0.99 M $NaClO_4$ (conditional pH = 2.000), as described in previous studies,[3,11] in order to measure the hydrogen ion concentration rather than its activity. A precision of 0.002 pH units was attained.

The spectrophotometric equilibrium studies were carried out with an initial solution of pH 5.5–6, 10 mM $C_{Cu^{II}}$ with a C_{py} containing the desired $\bar{n}$ level (ionic strength 1.0 M). A sodium azide concentration, usually lower than 1 mM, was maintained so that the transmittance obtained was never lower than 15% in the 370–400 nm range. 3.00 cm^3 of this

* Author to whom correspondence should be addressed.

solution were placed in a quartz cuvette (1 cm light path) which was modified to hold a few more cm^3 of added reagent. Measurements at eight different wavelengths were carried out vs the blank with the background electrolyte. The initial solution was diluted with 0.5 cm^3 volumes of a blank with the same free pyridine concentration and measured. The copper(II) and azide concentrations in this solution were decreased but the $C_{Cu^{II}}/C_{N_3^-}$ ratio as well as the $\bar{n}$ value were maintained. The pH was slightly changed but could be followed by using the glass electrode in a parallel experiment. The transmittance of the initial solution increased with dilution to a maximum value of 70%. This procedure has proved to be very rapid and accurate.

Other instruments used were a Zeiss PM QII spectrophotometer, and the treatment of data required the use of programmable calculators (e.g. HP 97 or HP 41 CV from Hewlett Packard).

RESULTS AND DISCUSSION

An outline of the equilibrium studies

A number of spectrophotometric studies of complex formation have been shown in the literature as performed at conditions which favour the mono-ligand species by maintaining an excess of metal cations over the total ligand concentration. It is expected that if an excess of copper(II), complexed with pyridine, is in equilibrium with a lower azide concentration, a mixture of monoazide mixed complexes, $Cu(py)_iN_3^+$, is formed. The composition of the excess copper(II) is controlled by the free ligand, pyridine, and is expressed by its $\bar{n}$ values (Bjerrum's function), average ligand number:

$$\bar{n} = \frac{\beta_{10}[py]+2\beta_{20}[py]^2+3\beta_{30}[py]^3+4\beta_{40}[py]^4}{1+\beta_{10}[py]+\cdots+\beta_{40}[py]^4}, \quad (1)$$

where β_{i0} is the well known overall formation constant[8,12] with i pyridine ligands and no azide

$$\beta_{i0} = \frac{[Cu(py)_i^{2+}]}{[Cu^{2+}][py]^i}. \quad (2)$$

The following conditional equilibrium takes place for a $C_{Cu^{II}} \gg C_{N_3^-}$:

$$Cu(py)_{\bar{n}}^{2+} + N_3^- \rightleftharpoons Cu(py)_{\bar{n}}N_3^+.$$

A conditional equilibrium constant is defined at each $\bar{n}$ value,

$$K_{\bar{n}1} = \frac{[Cu(py)_{\bar{n}}N_3^+]}{[Cu(py)_{\bar{n}}^{2+}]N_3^-} = \frac{[Cu(py)_{\bar{n}}N_3^+]}{C_{Cu^{II}}[N_3^-]} \quad (3)$$

and represent the average tendency of azide to be added to a copper(II) concentration, $C_{Cu^{II}}$, complexed with pyridine at a particular $\bar{n}$ condition, in order to form a mixture of monoazide complexes such as CuN_3^+, $Cu(py)N_3^+$, $Cu(py)_2N_3^+$, etc. As $C_{Cu^{II}}$ is relatively high, the complexation with azide has no significant effect on its $\bar{n}$ value. This $K_{\bar{n}1}$ constant can be spectrophotometrically determined as for the CuN_3^+ species[5,13] with excess of Cu^{2+}, with the only difference being that now copper(II) is complexed with pyridine at a desired $\bar{n}$ level. However, this constant changes with $\bar{n}$ because the per cent distribution of the copper(II) species is altered and each species is expected to have a different affinity for the azide ion. The free pyridine concentration used to set the copper(II) at a $\bar{n}$ level can be calculated iteratively by eq. (1) if the β_{i0} formation constants are known.

The following equation can be developed with mass balance and equilibrium constants for the copper(II)/pyridine complexes:

$$C_{Cu^{II}} = [Cu(py)_{\bar{n}}^{2+}] = [Cu^{2+}]+[Cu(py)^{2+}] + [Cu(py)_2^{2+}]+[Cu(py)_3^{2+}]+[Cu(py)_4^{2+}]. \quad (4)$$

Each complex concentration is related to β_{10} [eq. (2)]. For the monoazide complexes in equilibrium with this $C_{Cu^{II}}$ the following mass balance is applied:

$$[Cu(py)_{\bar{n}}N_3^+] = [CuN_3^+] + [Cu(py)N_3^+]+\cdots+[Cu(py)_4N_3^+]. \quad (5)$$

From eq. (3) the total concentration of the monoazido complexes is:

$$[Cu(py)_{\bar{n}}N_3^+] = C_{Cu^{II}}[N_3^-]K_{\bar{n}1}. \quad (6)$$

Each monoazido complex concentration is related to an addition constant referred to a copper(II) cation with i pyridine ligands:

$$K(+N_3)_{i1} = \frac{[Cu(py)_iN_3^+]}{[Cu(py)_i^{2+}][N_3^-]} \quad (7)$$

and to the equilibrium

$$Cu(py)_i^{2+} + N_3^- \rightleftharpoons Cu(py)_iN_3^+.$$

Of course, if $i = 0$, $K(+N_3)_{0i}$ is the conventional formation constant of CuN_3^+. The combination of eqs (5), (6) and (7) leads to

$$[N_3^-]K_{\bar{n}1}C_{Cu^{II}} = \{K(+N_3^-)_{01}[Cu^{2+}] + K(+N_3^-)_{11}[Cu(py)_1^{2+}]+\cdots+K(+N_3^-)_{41} \times [Cu(py)_4^{2+}]\}[N_3^-]. \quad (8)$$

By eliminating $[N_3^-]$ and considering that the following function can be taken for the copper(II)/

pyridine complexes,

$$\frac{[Cu^{2+}]}{C_{Cu^{II}}} = \alpha_0 \qquad (9)$$

and

$$\frac{[Cu(py)_i^{2+}]}{C_{Cu^{II}}} = \alpha_i, \qquad (10)$$

eq. (8) can be modified to

$$K_{\bar{n}1} = \alpha_0 K(+N_3^-)_{01} + \alpha_1 K(+N_3^-)_{11} + \cdots + \alpha_4 K(+N_3^-)_{41}. \qquad (11)$$

This is the final equation, and is surprisingly simple for dealing with mixed-ligand complexes. Simultaneous equations can be used to solve the $K(+N_3^-)_{i1}$ constants from α_1 and the experimental $K_{\bar{n}1}$ data. These α_1 data are calculated with the free ligand which places copper(II) as the derived $\bar{n}$, and the β_{i0} constants:

$$(\alpha_0)^{-1} = 1 + \beta_{10}[py] + \cdots + \beta_{40}[py]^4 \qquad (12)$$

$$\alpha_i = \beta_{i0}\alpha_0[py]^i. \qquad (13)$$

Determination of β_{i0} constants

The overall formation constants in the copper(II)/pyridine system, β_{10}, has been studied[14-18] and the majority of the authors agree with the existence of four stepwise species.

We obtained the formation constants at 1.0 M ionic strength, held with sodium methanesulphonate. The main reason for using this medium is the low tendency of this anion to precipitate with the $Cu(py)_i^{2+}$ cations. Perchlorate precipitates for some copper(II) concentrations used in the spectrophotometric study. As methanesulphonic acid is recognized as a strong one, its salts can eventually be used to adjust the ionic strength in equilibrium studies, preferably to nitrate.

Experimental $\bar{n}$ data vs the free ligand (formation curve) presented in Fig. 1 were taken from an indirect method based on the pH change in several py/Hpy^+ buffers by addition of Cu^{2+}. The experimental procedure, calculation and advantages of the method are described in detail by Neves *et al.*[11] The Leden function, $F_o(X)$, was obtained and treated by the classical graphical method[8,12] and by the modern process of weighted simultaneous equations.[19] The log β_{i0} data are given in Table 1 along with literature values for comparison. Good agreement with literature data is found at 1.0 M ionic strength and supports the use of methanesulphonate ion as the background electrolyte.

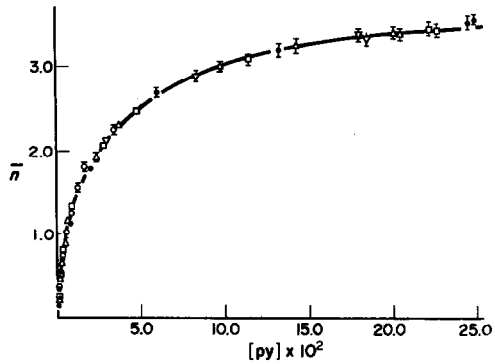

Fig. 1. Formation curve of the copper(II)/pyridine complexes in 1.0 M ionic strength held constant with NaO_3S–CH_3 at 25°C.

Spectrophotometric study

The monoazido species was formerly studied under conditions of low and high ionic strength.[3,13] The McConnel and Davidson[20] spectrophotometric method was applied at constant pH by Saini and Ostacoli[13] in order to correct for HN_3 formation. As this is a cumbersome process, the introduction of a correction factor, $F = 1 + [H^+]/K_i$, with the ionization constant (K_i) of the hydrazoic acid, directly into the equation allows us to work at variable pH,[3]

$$\underbrace{\underbrace{\frac{C_{Cu^{II}}C_{N_3^-}}{AF}}_{y} + \frac{A}{\varepsilon_1^2 F}}_{y'} = \frac{1}{\varepsilon_1\beta_1} + \frac{1}{\beta_1}\underbrace{\frac{C_{Cu^{II}} + C_{N_3^-}}{F}}_{x}, \qquad (14)$$

where A is the absorbance and ε_1 the molar absorptivity of the complex (or an average value $\bar{\varepsilon}_1$, for the mixture of monoazide mixed complexes).

The term including ε_1^2 is normally neglected, as a virtually linear relationship is maintained between "y" and "x". However we found it convenient to find the true "y" value iteratively, and more accurate final values were obtained. The final β_1 is about 10% higher than the initial value.

The $C_{Cu^{II}}/C_{N_3^-}$ ratio was about ten (see Experimental) in the working solution containing pyridine. In order to maintain the desired $\bar{n}$ level the following total pyridine concentration is required:

$$C_{py} = C_{Cu^{II}}\bar{n} + [py] + [Hpy^+]. \qquad (15)$$

At pH 6–6.5, $[Hpy^+]$ is a small fraction of [py] as can be inferred from the $pK = 5.45$ (Table 1) and $C_{Cu^{II}} = 10$ mM.

The ionization constant of hydrazoic acid,

Table 1. Literature values for pK of Hpy^+ and overall formation constants in the copper(II)/pyridine system at 25°C in aqueous medium

Medium, I; strength, M	pK Hpy^+	log β_i 1	2	3	4	5	Reference
KNO_3, 0.50	5.45	2.52	4.38	5.69	6.54	—	14
KNO_3, 1.0	5.5	2.59	4.64	5.93	6.54	7.0	15
$NaClO_4$, 1.0	—	2.46	4.41	5.68	6.52	—	16
$NaClO_4$, 1.0	5.75	2.86	4.78	—	—	—	17
$PyHNO_3$, 0.50	5.22	2.41	4.29	5.45	6.03	—	18
$NaCH_3SO_3$, 1.0	5.42	2.551	4.474	5.687	6.592	—	[a]

[a] Present paper.

measured as described in ref. 3, is $(3.94+0.04)\times 10^{-5}$ M^{-1} taken at 1.0 M ionic strength held constant with sodium methanesulphonate.

The $K_{\bar{n}1}$ constants were obtained for $\bar{n}$ levels from 0 to 3.5 using this spectrophotometric method, with iterative correction of the "y" term in eq. (14). Measurements were taken at eight wavelengths in the region around the maximum (370–400 nm). The standard deviation of each average result is $\pm 1.7\%$. The graphical interpolations of the constants at small increments are presented in Table 2 and these were used in simultaneous equations (see next section).

The constant in the absence of pyridine is the conventional β_1, but has other notations when mixed-ligand equilibria are considered:

$$\beta_1 = \beta_{01} = K_{01} = K(+N_3^-)_{01} = \frac{[CuN_3^+]}{[Cu^{2+}][N_3^-]} = 111.5\,M^{-1}. \quad (16)$$

This value agrees, within experimental error, with that found by Maggio *et al.*,[21] 112 M^{-1}, at the same ionic strength (held constant with sodium perchlorate).

The spectra of the CuN_3^+ species in the UV region[3] are similar to those obtained for the mixed complexes with pyridine, as the round maxima of charge-transfer are always observed. Although the $K_{\bar{n}1}$ constants decrease for $\bar{n} > 1$, the $\bar{\varepsilon}_1$ (average molar absorptivity) increases markedly with the level of $\bar{n}$, with a discrete shift of λ_{max} to higher wavelengths. This means that the power of oscillation ($N_3^- \rightarrow Cu^{II}$) is increased under mixed-ligand conditions.

From an analytical viewpoint the spectral shift to higher wavelengths favours the sensitivity of a qualitative test for the azide on the basis of mixed species formation. However, a compromise exists between the stability of the mixed complexes, its $\bar{\varepsilon}_1$ and the masking effect of the deeper blue colour of the pyridine mixed complexes, when the sensitivity of the human sight is considered. In fact, the best conditions for a qualitative test of azide is found at $\bar{n} = 2$ for copper(II) complexed with pyridine.[22] In

Table 2. $K_{\bar{n}1}$ vs $\bar{n}$ taken by interpolation from experimental data, and the corresponding [py] calculated from eq. (1)

$\bar{n}$	$K_{\bar{n}1}$	[py] $\times 10^3$
0.500	127.5	1.878
0.575	129.0	2.266
0.675	130.8	2.843
0.750	131.9	3.326
0.825	133.0	3.858
0.900	133.8	4.444
1.000	134.5	5.325
1.100	135.0	6.325
1.200	135.0	7.475
1.300	134.5	8.795
1.400	134.0	10.30
1.500	133.0	12.05
1.600	131.5	14.04
1.700	129.7	16.31
1.800	127.4	18.91
1.900	124.8	21.87
2.000	121.5	25.23
2.100	118.0	29.01
2.200	113.5	33.30
2.300	109.0	38.13
2.400	103.7	43.59
2.500	98.0	49.77
2.600	92.5	56.80
2.700	87.0	64.84
2.800	81.5	74.12
2.900	76.0	85.00
3.000	70.0	97.80
3.100	65.0	113.3
3.200	59.2	132.3
3.300	54.0	156.4
3.400	48.5	188.2
3.500	43.5	232.0

Table 3. Simultaneous equations calculated using the data of Table 2, β_{01} and eqs (9), (10) and (17)

$5.4061 = 2.7740\times10^{-2}\,K(+N_3^-)_{11} + 8.9858\times10^{-3}\,K(+N_3^-)_{21} + 6.4398\times10^{-4}\,K(+N_3^-)_{31} + 2.5008\times10^{-5}\,K(+N_3^-)_{41}$
$7.3666 = 2.3283\times10^{-2}\,K(+N_3^-)_{11} + 2.5257\times10^{-2}\,K(+N_3^-)_{21} + 6.0048\times10^{-3}\,K(+N_3^-)_{31} + 7.7485\times10^{-4}\,K(+N_3^-)_{41}$
$7.9089 = 1.0334\times10^{-2}\,K(+N_3^-)_{11} + 3.3586\times10^{-2}\,K(+N_3^-)_{21} + 2.3381\times10^{-4}\,K(+N_3^-)_{31} + 8.7251\times10^{-5}\,K(+N_3^-)_{41}$
$7.9915 = 2.6868\times10^{-3}\,K(+N_3^-)_{11} + 2.4666\times10^{-2}\,K(+N_3^-)_{21} + 4.9948\times10^{-2}\,K(+N_3^-)_{31} + 5.6737\times10^{-2}\,K(+N_3^-)_{41}$

Solution $K(+N_3^-)_{11} = 1.486\times10^{-2}$ $K(+N_3^-)_{21} = 1.375\times10^{2}$ $K(+N_3^-)_{31} = 7.06\times10$ $K(+N_3^-)_{41} = 1.19\times10$

a quantitative spectrophotometric procedure higher $\bar{n}$ levels can be maintained for higher sensitivity in the UV range at 380 nm.

Calculations of equilibrium constants from $K_{\bar{n}1}$

As the $K(+N_3^-)_{01}$ constant is known, 112 M^{-1}, it can be introduced into eq. (11) to decrease the number of unknowns in each simultaneous equation. A weighting factor $1/K_{\bar{n}1}$ can be introduced in order to ensure that all dependent terms are of the same magnitude. This is justifiable on the basis that the same relative uncertainty can be attributed to the experimental $K_{\bar{n}1}$ constants and the intermediate data obtained by interpolation (Table 2). The free concentrations of pyridine at defined $\bar{n}$ levels corresponding to the interpolated constants, calculated iteratively from eq. (1), are also included in Table 2. These [py] data were then used in eqs (12) and (13) to obtain the fraction of all species containing pyridine in order to prepare the simultaneous equations.

In the treatment of data two possibilities were considered: whether the $Cu(py)_4N_3^+$ species exists or not, defining a system with four or three unknowns. The best solution is consistent with the contribution of the $Cu(py)_4N_3^+$ complex. Thus, a 4×4 matrix was built with four simultaneous equations with the available $K_{\bar{n}1}$ and α_i data:

$$\sum\frac{K_{\bar{n}1}-\alpha_0\cdot K(+N_3^-)_{01}}{K_{\bar{n}1}} = K(+N_3^-)_{11}\sum\frac{\alpha_1}{K_{\bar{n}1}} + \cdots + K(+N_3^-)_{41}\sum\frac{\alpha_4}{K_{\bar{n}1}}. \quad (17)$$

The four simultaneous equations are shown in Table 3 with the solution for the $K(+N_3^-)_{i1}$ constants. The obtained equilibrium constants are in agreement with interpolated $K_{\bar{n}1}$ data within $\pm0.7\%$.

Final comments on the results

Figure 2 shows that the formation of $Cu(py)N_3^+$ is particularly favoured and that a marked decrease in affinity for azide occurs when more than two pyridine ligands fill coordination sites on Cu^{2+}. Conversely, the average molar absorptivities increase in the reverse direction as already stated.

Interesting relationships can also be seen in Fig. 3, where other equilibrium situations are considered, indicating the spontaneous processes. The backbonding copper(II)/pyridine favours the

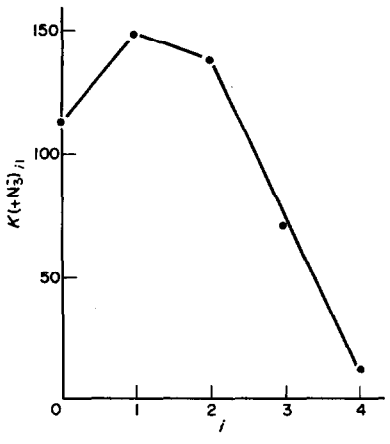

Fig. 2. Change of $K(+N_3^-)_{i1}$ constants vs the number of pyridine molecules coordinated to copper(II).

Table 4. Stabilization constants K_e, eq. (19), for some monoazido complexes

Equilibrium	log $K_{M(i1)}$	log $K_{Stat(i1)}$	log $K_{E(i1)}$
$1/2\ Cu(py)_2^{2+} + 1/2\ Cu(N_3)_2 \rightleftharpoons Cu(py)(N_3)^+$	0.445	0.301	0.144
$2/3\ Cu(py)_2^{2+} + 1/3\ Cu(N_3)_3^- \rightleftharpoons Cu(py)_2(N_3)^+$	0.809	0.477	0.333
$3/4\ Cu(py)_4^{2+} + 1/4\ Cu(N_3)_4^{2-} \rightleftharpoons Cu(py)_3(N_3)^+$	0.859	0.602	0.257

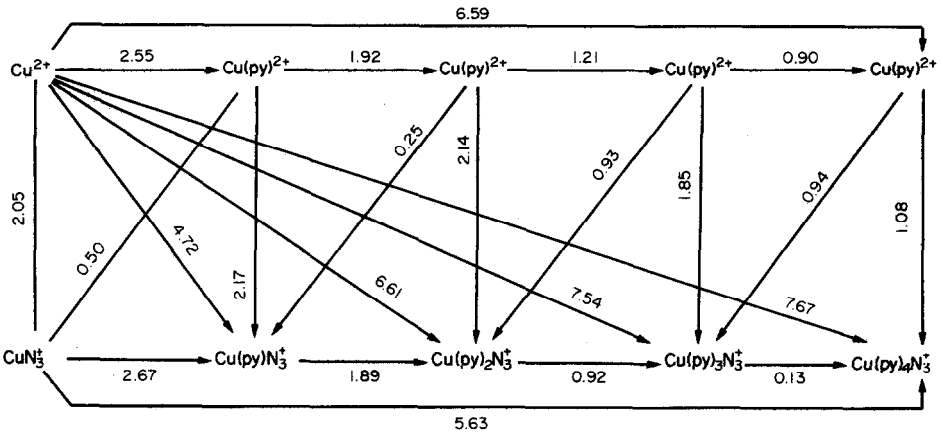

Fig. 3. Spontaneous processes of complex formation in copper(II) systems, on the basis of positive values of log K.

azide bond more than predicted by statistical effects, and is considered as follows.

When two complexes of the same cation MA_m and MB_n exchange ligands according to

$$(i/n)\,MA_n + (j/n)\,MB_n \rightleftharpoons MA_iB_j$$

to form one mole of MA_iB_j, an equilibrium constant $KM_{(ij)}$ is

$$K_{M(ij)} = \frac{\beta_{ij}}{\beta_{n0}(\beta_{0n})^{j/n}} = \frac{\beta(+j\beta - jA)_{ij}}{(\beta(+n\beta - nA)_{0n})^{j/n}}. \quad (18)$$

With regard to such equilibrium, Marcus and Eliezer[9] have proposed a stabilization constant K_e

$$\log K_e = \log K_{M(ij)} - \log \frac{n!}{i!j!}, \quad (19)$$

where

$$K_{stat} = \frac{n!}{i!j!}. \quad (20)$$

A positive value for log K_e indicates a true stabilization of the mixed-ligand complex, higher than predicted by statistical factors.

The combination of present equilibrium data with that from the copper(II)/azide system,[7] although taken at an ionic strength of 2.0 M, leads to the conclusion that there is a true stabilization of the monoazido mixed species, as shown in Table 4.

Acknowledgements—The authors are greatly indebted to CNPq, FAPESP, FINEP and CAPES agencies (Brazil) for support.

REFERENCES

1. E. F. A. Neves and P. Senise, *Anal. Chim. Acta* 1969, **48**, 177.
2. E. F. A. Neves, *J. Inorg. Nucl. Chem.* 1971, **33**, 351.
3. P. Senise and E. F. A. Neves, *J. Inorg. Nucl. Chem.* 1971, **33**, 351.
4. P. Senise and E. F. A. Neves, *J. Inorg. Nucl. Chem.* 1972, **34**, 1923.
5. E. F. A. Neves and P. Senise, *J. Inorg. Nucl. Chem.* 1972, **34**, 1915.
6. E. F. A. Neves, E. Oliveira and L. Sant'Agostino, *Anal. Chim. Acta* 1976, **87**, 243.
7. E. A. Neves, E. Oliveira and Z. Santos, *Talanta* 1980, **27**, 609.
8. M. T. Beck, *Chemistry of Complex Equilibria*. Van Nostrand, London (1969).
9. Y. Marcus and I. Eliezer, *Coord. Chem. Rev.* 1969, **4**, 273.
10. A. I. Vogel, *Practical Organic Chemistry*, 2nd edn, p. 173. Longmans, London (1951).
11. E. A. Neves, R. Tokoro and M. E. V. Suarez, *J. Chem. Res.* (*M*), 1979, 4401; (*S*), 1979, **11**, 376.
12. K. B. Yatsimirskii and V. P. Vasil'ev, *Instability Constant of Complex Compounds*. Pergamon Press, Oxford (1960).
13. G. Saini and G. Ostacoli, *J. Inorg. Nucl. Chem.* 1958, **8**, 346.
14. R. J. Bruehlman and F. H. Verhoek, *J. Am. Chem. Soc.* 1948, **70**, 1401.
15. D. L. Leussig and R. C. Hansen, *J. Am. Chem. Soc.* 1957, **79**, 4270.
16. G. Atkinson and J. E. Bauman Jr, *Inorg. Chem.* 1963, **2**, 64.
17. V. Mihailova and M. Bonnet, *Bull. Soc. Chim. Fr.* 1969, **12**, 4258.
18. J. Bjerrum, *Acta Chem. Scand.* 1964, **18**, 843.
19. E. A. Neves, N. Milcken and D. W. Franco, *J. Inorg. Chem.* 1981, **43**, 2081.
20. H. McConnel and N. Davidson, *J. Am. Chem. Soc.* 1950, **72**, 3164.
21. F. Maggio, V. Romano and L. Pellerito, *Ann. Chim.* 1967, **57**, 191.
22. E. A. Neves and M. Peters, unpublished results.

Polyhedron Vol. 9, No. 10, pp. 1263–1270, 1990
Printed in Great Britain

0277-5387/90 $3.00+.00
© 1990 Pergamon Press plc

FLUOROGERMANATE(IV) EQUILIBRIA IN ACID MEDIA

LIBERATO CIAVATTA,† MAURO IULIANO, RAFFAELLA PORTO and ERMANNO VASCA

Dipartimento di Chimica dell'Università, Via Mezzocannone 4, 80134 Napoli, Italy

(*Received* 21 *November* 1989; *accepted* 22 *December* 1989)

Abstract—The equilibria between $Ge(OH)_4$, HF and H^+ ions in aqueous solution have been investigated, at 25°C in $NaClO_4$ as well as in $LiClO_4$ media, by potentiometric measurements with a fluoride ion-selective electrode. The perchlorate ion molal concentration was kept constant at 3. The molalities of Ge^{IV} and of the H^+ ion were chosen, respectively, between 10^{-3} and 10^{-2} and from 0.03 to 2.9.

The potentiometric data have been explained by the presence of GeF_4, $Ge(OH)F_4^-$, GeF_6^{2-}, $HGeF_6^-$ and a minor complex to which the composition $Ge(OH)F_2^+$ has been tentatively ascribed. Equilibrium constants for their formation in the inert 3 molal $NaClO_4$ and in 3 molal $LiClO_4$ are reported.

Little quantitative information exists on the reaction between the fluoride ion and $Ge(OH)_4$, the relevant form in which germanium(IV) is present in acid non-complexing media.[1] The most extensive investigation is that of Benoit and Place[2] who employed solvent extraction, solubility and potentiometry to establish the composition of the reaction products and their formation constants. The results from solutions of acidities exceeding 0.5 molar were interpreted with $Ge(OH)_rF_4^{r-}$ and $Ge(OH)_rF_5^{(r+1)-}$, but no attempt was made to estimate the most probable number of OH^- groups in the complexes. On the other hand, the existence of GeF_6^{2-} is supported by Raman spectroscopy[3] in concentrated H_2GeF_6 solutions as well as by Raman, IR and NMR measurements[4] in concentrated $(NH_4)_2GeF_6$ solutions. Further evidence comes from the potentiometric studies by Ryss and Kulish.[5,6] These authors calculated (25°C in dilute solution and in molar units) a constant of $10^{-5.3}$ for

$$GeF_6^{2-} + H_2O \rightleftharpoons Ge(OH)F_4^- + HF + F^-$$

using acidity measurements and chemical analysis, and a constant of $10^{-25.8}$ for

$$GeF_6^{2-} + 2H_2O \rightleftharpoons GeO_2(s) + 6F^- + 4H^+$$

through activity determinations of the H^+ and F^- ions.

The aim of the present work was to investigate the fluorogermanate(IV) equilibria by methods developed in this laboratory and concerning the complex formation of titanium(IV)[7] and silicon(IV)[8] with fluoride ions.

METHOD

The equilibria were studied at 25°C by measurements with cell(I)

$$-EF/TS,QQH_2(s)/Au+ \qquad (I)$$

where EF and QQH_2 stand, respectively, for a fluoride ion-selective electrode and quinhydrone, while TS designates a test solution of the general composition (molal units and $Me^+ = Li^+$ or Na^+)

$$TS = Ge^{IV}: m_M,\ MeF: m_F,$$

$$HClO_4: (m_H + m_F),\ MeClO_4: (3 - m_H - m_F).$$

In TS the molality of the perchlorate ion was kept constant in order to minimize variations of activity coefficients. In the initial stage of the work $LiClO_4$ was chosen as the inert salt. In the course of the measurements, with the main purpose to extend the acidity range to m_H values inferior to 0.3 molal, where LiF is of limited solubility in an excess of Li^+ ions, it was thought of value to carry out experi-

† Author to whom correspondence should be addressed.

ments also in 3 molal $(Na)ClO_4$. The standard states are so chosen that the activity of solute species tends to molality as the composition of TS approaches 3 molal $MeClO_4$.

The molality of germanium was varied from 10^{-3} to 10^{-2}. Values of m_H, the analytical molality excess of H^+ counting HF, H_2O, $MeClO_4$ and $Ge(OH)_4$ as zero level, were chosen in the intervals 0.03–2.9, in $NaClO_4$, and 0.3–2.9 in $LiClO_4$.

The EMF of cell(I) at 25°C can be expressed by (1)

$$E = E'_0 + 0.05916 \log([HF] y_{HF}) + E_q \quad (1)$$

where E'_0 is a constant, y is the symbol of the activity coefficient and E_q is a correction term for the basicity of p-benzoquinone.[9] In our solutions y_{HF} can be assumed to be a function of $[H^+]$ and of [HF]. In order to gain an idea of the dependence of y_{HF} on $[H^+]$ the EMF of cell(I), containing no Ge^{IV}, was measured as a function of m_H ranging from 0.1 to 2.9, while m_F was kept constant at 10^{-2}. These data could be explained by the relationships (2a,b), by assuming for $Q + H^+ \leftrightarrows QH^+$ a constant of 0.1 as proposed by Biedermann,[9]

$$\log y_{HF}([H^+]) = (0.061 \pm 0.005)[H^+] \quad (\text{in } NaClO_4) \quad (2a)$$

$$\log y_{HF}([H^+]) = (0.020 \pm 0.010)[H^+] \quad (\text{in } LiClO_4). \quad (2b)$$

The dependence of y_{HF} on [HF] was determined by measuring at constant m_H and for $m_M = 0$ the EMF of cell(I) where $10^{-3} \leqslant [HF] \leqslant 0.1$. The data were described by eq. (3)

$$0.05916 \log y_{HF}([HF]) = (9 \pm 2) \times 10^{-3}[HF]. \quad (3)$$

In each experiment, carried out conveniently as a potentiometric titration, m_H was kept constant, while [HF] was varied. According to $Ge(OH)_4 + nHF \leftrightarrows Ge(OH)_t F_n^{(4-t-n)} + pH^+$, hydrogen ions are formed when the complex formation proceeds. Since, however, $m_M < 0.1 m_H$, the concentration of the H^+ ion did not change sensibly during a run to cause variations in $y_{HF}([H^+])$ and E_q. Consequently, the EMF of cell(I) can be expressed as eq. (4)

$$E = E_0 + 0.05916 \log[HF] + 9 \times 10^{-3}[HF] \quad (4)$$

where $E_0 = E_o(m_H)$ includes E_q and $y_{HF}([H^+])$.

Each titration was divided into two parts. In the first, E_0 was determined in the absence of Ge^{IV}. For $m_H \geqslant 0.3$, [HF] was approximated with m_F to calculate E_0. At lower acidities the equilibria

$$H^+ + F^- \leftrightarrows HF, \quad [HF] = 1.4 \times 10^3 [H^+][F^-] \quad (5)$$

$$HF + F^- \leftrightarrows HF_2^-, \quad [HF_2^-] = 5.5[HF][F^-] \quad (6)$$

were assumed to find [HF] from the m_F and m_H values. The constants in eqs (5) and (6) were evaluated for 3 molal $NaClO_4$ by interpolation of literature data.[10] E_0 values constant to within $\pm 10^{-4}$ V were obtained in the m_F range from 5×10^{-4} to 0.1.

In the second part, germanium(IV) was added and the complex formation was followed by varying the m_F/m_M ratio. With E_0 being known, [HF] could be evaluated from (4) and $\bar{n}$, the average number of fluoride ions bound per Ge^{IV}, could be obtained, using (5) and (6), by

$$\bar{n} = (m_F - [HF] - [F^-] - 2[HF_2^-])/m_m. \quad (7)$$

In (7), $[F^-]$ and $[HF_2^-]$ represent only small correction terms and were neglected for $m_H \geqslant 0.3$.

EXPERIMENTAL

Materials and analysis

The germanium source was the hexagonal form of GeO_2, Fluka, 99.9% purity. Stock solutions were obtained by dissolving weighed amounts of the product previously ignited at 1000°C.

Sodium perchlorate was prepared and analysed as described by Biedermann.[11]

Sodium fluoride, lithium fluoride, lithium perchlorate, perchloric acid and quinhydrone were obtained as described previously.[7,8]

Details of the EMF measurements

The cell arrangement, electrodes and titration procedure were the same as described in preceding papers.[7,8] The EMF values of cell(I) were measured to within 10^{-5} V with a computer-controlled data acquisition unit 3421 A, furnished by Hewlett and Packard. The silicon oil thermostat, in which cell(I) was immersed, had a temperature of 25.00 ± 0.02°C.

DATA AND CALCULATIONS

The $\bar{n}(\log[HF], m_M)_{m_H}$ data, which are the basis for the calculation of the composition of the reaction products and their formation constants, are collected in Table 1. The graph in Fig. 1, representing the measurements at $m_H = 0.1$, indicates that the points for different m_M and for $m_M \ll m_H$, within the limits of experimental error, fall on the same curve and the $\bar{n}$ values tend to 6 as [HF] increases. Hence, $Ge(OH)_t F_n^{4-t-n}$ species with $n \leqslant 6$ predominate. Furthermore, data of forward titrations (m_F/m_M increasing) practically coincide with those of back tirations (m_F/m_M decreasing) which implies that we are measuring true equilibria.

To assess the prevailing t and n in the complexes

Table 1. Survey of the $\bar{n}$ ($-\log[HF]$, $m_M \times 10^3$) data at various m_H

(Na)ClO_4 media
$m_H = 0.0300$
(a) 0.102 (2.483, 0.957); 0.167 (2.434, 0.951); 0.355 (2.363, 0.943); 0.693 (2.298, 0.933); 1.09 (2.252, 0.923); 1.49 (2.218, 0.915); 1.96 (2.184, 0.906); 2.50 (2.151, 0.896); 2.82 (2.131, 0.890); 3.23 (2.107, 0.882); 3.57 (2.086, 0.876); 3.80 (2.071, 0.871); 4.00 (2.055, 0.866); 4.26 (2.036, 0.860); 4.48 (2.015, 0.854); 4.71 (1.998, 0.849); 4.92 (1.972, 0.841); 5.05 (1.950, 0.834); 5.16 (1.928, 0.828); 5.24 (1.904, 0.820).
(b) back titration 5.29 (1.893, 1.14); 4.75 (1.989, 1.67); 4.06 (2.048, 2.13); 3.45 (2.088, 2.56); 3.02 (2.113, 2.92); 2.43 (2.147, 3.53); 2.05 (2.170, 4.03).
(c) 0.132 (2.465, 1.16); 0.236 (2.404, 1.15); 0.377 (2.357, 1.14); 0.661 (2.299, 1.13); 0.904 (2.269, 1.12); 1.21 (2.239, 1.11); 1.53 (2.214, 1.10); 1.94 (2.185, 1.09); 2.36 (2.159, 1.08); 2.75 (2.134, 1.07); 3.12 (2.111, 1.06); 3.55 (2.085, 1.05); 3.89 (2.062, 1.04); 4.26 (2.031, 1.03); 4.51 (2.005, 1.02); 4.73 (1.978, 1.01); 5.03 (1.926, 0.994); 5.2 (1.874, 0.974).
$m_H = 0.100$
(a) 0.164 (2.316, 8.02); 0.231 (2.279, 7.94); 0.472 (2.207, 7.70); 0.892 (2.140, 7.36); 1.63 (2.071, 6.86); 2.52 (2.006, 6.33); 3.03 (1.970, 6.05); 3.55 (1.936, 5.79); 3.96 (1.905, 5.58); 4.34 (1.869, 5.39); 4.65 (1.833, 5.21); 4.83 (1.803, 5.09); 5.09 (1.748, 4.88); 5.24 (1.697, 4.71).
0.156 (2.314, 2.67); 0.326 (2.240, 2.63); 0.539 (2.190, 2.59); 0.761 (2.155, 2.56); 1.02 (2.124, 2.53); 1.41 (2.086, 2.48); 1.81 (2.055, 2.44); 2.29 (2.021, 2.39); 2.85 (1.984, 2.33); 3.36 (1.949, 2.28); 3.79 (1.918, 2.23); 4.23 (1.876, 2.18); 4.58 (1.838, 2.13); 4.79 (1.804, 2.09); 4.96 (1.767, 2.04); 5.10 (1.733, 2.00).
(c) back titration 5.13 (1.724, 2.47); 4.91 (1.788, 2.99); 4.70 (1.824, 3.31); 4.29 (1.874, 3.86); 3.89 (1.908, 4.36); 3.39 (1.942, 5.05); 2.82 (1.977, 5.98).
$m_H = 0.300$
(a) 0.012 (2.509, 4.82); 0.033 (2.408, 4.77); 0.106 (2.290, 4.69); 0.213 (2.213, 4.62); 0.332 (2.164, 4.56); 0.499 (2.118, 4.48); 0.786 (2.067, 4.38); 1.01 (2.038, 4.30); 1.24 (2.012, 4.23); 1.56 (1.983, 4.14); 1.94 (1.951, 4.03); 2.37 (1.916, 3.91); 2.77 (1.885, 3.80); 3.10 (1.859, 3.71); 3.40 (1.833, 3.63); 3.69 (1.804, 3.54); 3.92 (1.779, 3.47); 4.14 (1.751, 3.39); 4.33 (1.722, 3.32); 4.46 (1.696, 3.25); 4.60 (1.664, 3.17).
(b) back titration 4.59 (1.663, 3.76); 4.17 (1.740, 4.66); 3.54 (1.810, 5.77); 2.78 (1.875, 7.29); 1.94 (1.938, 9.57).
$m_H = 1.00$
0.043 (2.456, 4.74); 0.065 (2.399, 4.71); 0.090 (2.354, 4.68); 0.142 (2.291, 4.64); 0.217 (2.233, 4.58); 0.293 (2.193, 4.54); 0.402 (2.152, 4.48); 0.543 (2.112, 4.42); 0.767 (2.064, 4.33); 1.02 (2.026, 4.24); 1.31 (1.988, 4.15); 1.58 (1.958, 4.06); 1.83 (1.932, 3.98); 2.09 (1.906, 3.91); 2.33 (1.882, 3.83); 2.61 (1.855, 3.75); 2.87 (1.831, 3.67); 3.10 (1.808, 3.60); 3.34 (1.782, 3.53); 3.56 (1.755, 3.45); 3.76 (1.727, 3.37); 3.94 (1.701, 3.30); 4.14 (1.666, 3.20); 4.30 (1.634, 3.11); 4.61 (1.589, 2.98); 4.78 (1.545, 2.85); 4.90 (1.508, 2.73); 4.99 (1.476, 2.63); 5.06 (1.447, 2.53).
$m_H = 2.90$
(a) 0.126 (2.509, 6.77); 0.232 (2.403, 6.66); 0.368 (2.325, 6.54); 0.518 (2.267, 6.43); 0.679 (2.222, 6.32); 0.857 (2.183, 6.21); 1.03 (2.151, 6.10); 1.20 (2.122, 6.01); 1.37 (2.094, 5.91); 1.56 (2.066, 5.80); 1.75 (2.040, 5.70); 1.95 (2.013, 5.59); 2.14 (1.987, 5.49); 2.34 (1.959, 5.38); 2.55 (1.931, 5.27); 2.76 (1.901, 5.16); 2.96 (1.870, 5.04); 3.16 (1.837, 4.92); 3.34 (1.806, 4.81); 3.51 (1.774, 4.70); 3.66 (1.743, 4.59); 3.81 (1.711, 4.47); 3.94 (1.683, 4.37); 4.09 (1.653, 4.25); 4.34 (1.622, 4.11); 4.44 (1.582, 3.96); 4.56 (1.548, 3.82); 4.75 (1.504, 3.62).
(b) 0.336 (2.348, 2.80); 0.467 (2.291, 2.77); 0.622 (2.241, 2.74); 0.803 (2.196, 2.71); 1.01 (2.154, 2.67); 1.23 (2.115, 2.64); 1.49 (2.074, 2.60); 1.92 (2.016, 2.53); 2.24 (1.975, 2.48); 2.58 (1.928, 2.43); 2.94 (1.877, 2.36); 3.31 (1.819, 2.29); 3.67 (1.760, 2.21); 3.89 (1.697, 2.12); 4.20 (1.641, 2.03).
(c) back titration 3.92 (1.698, 2.73); 3.66 (1.751, 3.37); 3.45 (1.802, 3.98); 3.14 (1.852, 4.70); 2.88 (1.894, 5.36).
(Li)ClO_4 media
$m_H = 0.300$
(a) 0.068 (2.361, 1.66); 0.165 (2.299, 1.65); 0.267 (2.252, 1.63); 0.421 (2.203, 1.62); 0.635 (2.158, 1.60); 0.880 (2.120, 1.58); 1.23 (2.078, 1.56); 1.62 (2.040, 1.54); 2.01 (2.007, 1.52); 2.44 (1.973, 1.49); 2.95 (1.933, 1.46);

Table 1—*cont.*

3.42 (1.893, 1.43); 3.77 (1.859, 1.41); 4.06 (1.825, 1.38); 4.37 (1.784, 1.35); 4.53 (1.753, 1.33); 4.69 (1.718, 1.30); 4.82 (1.684, 1.27); 4.91 (1.653, 1.25); 4.99 (1.616, 1.21).

(b) back titration 4.93 (1.650, 1.50); 4.82 (1.690, 1.83); 4.64 (1.733, 2.18); 4.41 (1.775, 2.54); 4.13 (1.813, 2.90); 3.83 (1.848, 3.28); 3.46 (1.882, 3.72); 3.01 (1.921, 4.31); 2.57 (1.955, 4.96); 2.19 (1.984, 5.63); 1.78 (2.016, 6.49); 1.47 (2.043, 7.30); 1.16 (2.073, 8.32); 0.918 (2.100, 9.27); 0.709 (2.130, 10.3); 0.573 (2.151, 11.1); 0.445 (2.179, 11.9).

$m_H = 1.00$

(a) 0.01 (2.761, 19.3); 0.038 (2.517, 19.2); 0.083 (2.433, 19.2); 0.180 (2.321, 19.0); 0.392 (2.219, 18.8); 0.613 (2.160, 18.5); 0.921 (2.103, 18.2); 1.21 (2.059, 17.9); 1.59 (2.014, 17.6); 1.93 (1.979, 17.3); 2.35 (1.933, 16.9); 2.88 (1.879, 16.5); 3.35 (1.825, 16.1); 3.77 (1.765, 15.7); 4.21 (1.675, 15.3); 4.54 (1.581, 14.9).

(b) back titration 4.90 (1.569, 1.12); 4.57 (1.641, 1.87); 4.10 (1.726, 2.80); 3.66 (1.793, 3.51); 3.24 (1.844, 4.20); 2.99 (1.870, 4.62); 2.65 (1.907, 5.27); 2.37 (1.935, 5.85); 2.12 (1.956, 6.41); 1.92 (1.977, 6.93); 1.80 (1.989, 7.29); 1.48 (2.021, 8.31); 1.22 (2.050, 9.35); 1.05 (2.071, 10.1).

as well as the $^*\beta_{n,p}$ constants for their formation according to (8)

$$Ge(OH)_4 + nHF \rightleftharpoons Ge(OH)_tF_n^{4-t-n} + pH^+ + (4-t)H_2O \quad (8)$$

where $p = n+t-4$, the experimental data were treated as follows. By considering, firstly, data at a given m_H, the most important n values and the conditional constants K_n, eq. (12), were ascertained. Then, the t and $^*\beta_{n,p}$ values were calculated by examining the dependence of the K_n-s on m_H.

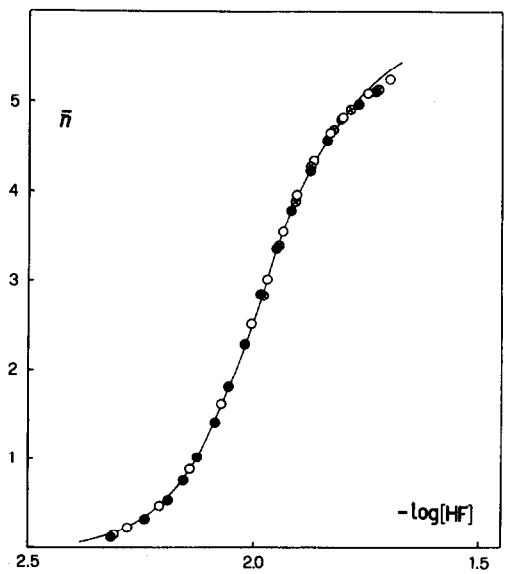

Fig. 1. Experimental data at $m_H = 0.1$ in $NaClO_4$ media. $\bar{n}$, the average number of fluoride ions bound per germanium, as a function of log [HF] for different m_M. Dots: titration (a), points: titration(b), crosses: back titration (c). The curve has been calculated with the constants of Table 3 setting $[H^+] = 0.103$.

Treatment of the data at constant m_H

If only mononuclear complexes in germanium are present $\bar{n}$ may be expressed as (9)

$$\bar{n} = \sum nQ_{n,p}[HF]^n[H^+]^{-p} \Big/ \left(1 + \sum Q_{n,p}[HF]^n[H^+]^{-p}\right) \quad (9)$$

where for brevity $Q_{n,p}$ stands for

$$Q_{n,p} = {}^*\beta_{n,p} y_{HF}^n y_H^{-p} y_M y_{n,p}^{-1} a_W^{(t-4)} \quad (10)$$

a_W is the water activity and y_H, y_M, $y_{n,p}$ are, respectively, the activity coefficients of H^+, $Ge(OH)_4$, $Ge(OH)_tF_n^{4-t-n}$.

For a constant m_H value, since $m_M < 0.1m_H$, $Q_{n,p}$ is with good approximation constant and $[H^+]$ must be very close to m_H. As a consequence, we have from (9)

$$\bar{n} = \sum nK_n[HF]^n \Big/ \left(1 + \sum K_n[HF]^n\right) \quad (11)$$

in which

$$K_n = K_n([H^+]) = \sum Q_{n,p}[H^+]^{-p}. \quad (12)$$

The graphical approach, described in detail in preceding papers[7,8] and founded on the comparison of the experimental data with normalized functions,[12] indicated the predominance of complexes with $n = 4$ and 6 at $m_H \leqslant 0.3$ and of additional species with $n = 2$ at higher acidities. The conditional constants, K_n, evaluated by curve-fitting are listed in Table 2. The errors represent maximal deviations from mean values.

Table 2. Survey of the conditional constants, K_n

m_H	log K_2	Graphical log K_4	log K_6	$[H^+]$	log K_2	Letagrop log K_4	log K_6
			$NaClO_4$ media				
0.0300		8.26±0.10	12.59±0.05	0.0317		8.20±0.05	12.63±0.02
0.100		7.83±0.10	11.66±0.05	0.103		7.82±0.05	11.68±0.03
0.300		5.57±0.05	10.95±0.10	0.302		7.57±0.04	10.86±0.06
1.00	2.95±0.10	7.56±0.05	10.47±0.05	1.00	2.94±0.10	7.55±0.01	10.54±0.02
2.90	3.76±0.05	7.98±0.05	10.68±0.10	2.90	3.83±0.06	7.96±0.02	10.82±0.06
			$LiClO_4$ media				
0.300		7.76±0.05	11.30±0.10	0.302		7.76±0.03	11.26±0.05
1.00	3.18±0.18	7.78±0.05	10.82±0.10	1.00	3.1±0.2	7.81±0.01	10.86±0.04

As a check, the experimental data were treated with the general minimizing program Letagrop.[13] To avoid the introduction of uncertainties connected with the estimation of activity coefficients the least-squares procedure separately considered data at constant m_H. The minimum of the sum

$$U = \sum (m_{F_{calc}} - m_F)^2 \qquad (13)$$

where $m_{F_{calc}}$ denotes a value calculated with a given set of constants, was sought for by assuming a series of species with various n and t. Owing to the essential constancy of $[H^+]$ comparable minima were recorded in testing complexes with identical n but different t. Furthermore, the constant $Q_{n,p}$ computed for a given set (n,p) is in reality the series: $Q_{n,p} + Q_{n,p-1}[H^+] + \cdots = K_n[H^+]^p$. Therefore, from the numerical treatment of data at constant m_H only conclusions concerning the most probable n and K_n values can be drawn.

The minimizing procedure yielded results in perfect agreement with those found graphically. No significant lower minima were recorded on testing hypotheses including also species with $n = 1$, 3 and 5. The constants reported in Table 2 are averages of K_n deduced from a series of $K_n[H^+]^p$ calculated by assuming the same n, *i.e.* 2, 4 and 6, but various p for each n. The errors represent three times the standard deviation. These were found to exceed the deviations from the average of every single K_n. Mean $[H^+]$ values, as furnished by Letagrop, were employed to obtain K_n from $K_n[H^+]^p$. In Table 2 are listed $[H^+]$ values calculated as mean when assuming $Ge(OH)_2F_4^{2-}$ and GeF_6^{2-}, *i.e.* the species producing the largest changes in the medium acidity. This may serve to get an idea on the constancy of the hydrogen ion concentration at a given m_H. The mean $[H^+]$ and the K_n values derived from the least-squares procedure were selected for the following treatment.

Calculation of the most important t *and* $*\beta_{n,p}$ *values*

To determine t and $*\beta_{n,p}$ the dependence of K_n with $[H^+]$ [eqs (10) and (12)] was examined. The correct treatment requires the knowledge of the medium changes when Me^+ is replaced by H^+. The activity coefficient of HF was accounted for by eq. (2a,b) and the water activity was evaluated from

$$\log a_W = -7.0 \times 10^{-3}[H^+]\,(\text{in } NaClO_4)$$
$$= 2.1 \times 10^{-4}[H^+]\,(\text{in } LiClO_4). \qquad (14)$$

Relationships (14) were established from the osmotic coefficients listed by Robinson and Stokes[14] by assuming a linear change with composition from values relevant to the pure 3 molal $MeClO_4$ and $HClO_4$ solutions. Medium effects on other reagents were estimated by the specific interaction theory SIT.[15] Thus, due to the unchanged ionic strength and ClO_4^- molality, the activity coefficient of positively charged ions was taken as unity in the medium scale. For anions and uncharged species we put

$$y_i = 10^{b_i[H^+]} = 1 + 2.3 b_i[H^+] + \cdots \qquad (15)$$

where b_i is the difference of the interaction coefficient of i with $HClO_4$ and $MeClO_4$. Since b_i is expected to be less than 0.1 higher terms in (15) can be neglected. The b_i values were considered as unknown parameters to be established simultaneously with $*\beta_{n,p}$.

With these assumptions eqs (12) and (10) for

$n = 6$ may be rearranged to give eq. (16)

$$K_6 a_W^4 [H^+] y_{HF}^{-6} = {}^*\beta_{6,1} y_M y_{6,1}^{-1} + {}^*\beta_{6,2} [H^+]^{-1} y_M y_{6,2}^{-1} + \cdots$$
$$= {}^*\beta_{6,1} + 2.3 {}^*\beta_{6,2} (b_M - b_{6,2}) + {}^*\beta_{6,2} [H^+]^{-1} + 2.3 {}^*\beta_{6,1} (b_M - b_{6,1}) [H^+]. \quad (16)$$

Figure 2 shows the dependence of $K_6 a_W^4 [H^+] y_{HF}^{-6}$ on $[H^+]^{-1}$ for data in $NaClO_4$ media. Within the limits of experimental error the points form a straight line, thus indicating the presence of GeF_6^{2-} and $HGeF_6^-$ and that the last term of eq. (16) is small. Furthermore, the slope of the straight line (${}^*\beta_{6,2}$) is about 0.45 times the intercept $[{}^*\beta_{6,1} + 2.3 {}^*\beta_{6,2} (b_M - b_{6,2})]$ which, being $b_M - b_{6,2}$ expected inferior than 0.1, can be approximated with ${}^*\beta_{6,1}$. The neglect of the $(b_M - b_{6,2})$ term does not introduce an uncertainty greater than the error of the intercept. The most probable ${}^*\beta_{6,1}$ and ${}^*\beta_{6,2}$ constants are given in Table 3.

A similar treatment of data in $LiClO_4$ led to the presence of $HGeF_6^-$ with the constants of Table 3. The absence of GeF_6^{2-} in $LiClO_4$ solutions seems understandable due to the high acidities investigated.

Equation (12) for $n = 4$ can be written as (17)

$$K_4 a_W^4 y_{HF}^{-4} = {}^*\beta_{4,0} y_M y_{4,0}^{-1} + {}^*\beta_{4,1} [H^+]^{-1} y_M a_W y_{4,1}^{-1} + \cdots$$
$$= {}^*\beta_{4,0} + {}^*\beta_{4,1} 2.3 (b_M - b_{4,1}) a_W + {}^*\beta_{4,1} a_W [H^+]^{-1} + {}^*\beta_{4,0} [H^+] 2.3 (b_M - b_{4,0}). \quad (17)$$

From the plot of $K_4 a_W^4 y_{HF}^{-4}$ against $a_W [H^+]^{-1}$, Fig. 3, it is concluded that GeF_4 and $Ge(OH)F_4^-$ are formed and the last term of (17) must be negligible. From the slope and intercept of the best straight line the ${}^*\beta_{4,1}$ and ${}^*\beta_{4,0} \simeq {}^*\beta_{4,0} + {}^*\beta_{4,1} 2.3 (b_M - b_{4,1}) a_W$ listed in Table 3 were evaluated.

Table 3. The equilibrium constants, ${}^*\beta_{n,p}$

	$NaClO_4$ media	$LiClO_4$ media
$\log {}^*\beta_{2,-1}$	2.9±0.1	3.2±0.2
$\log {}^*\beta_{4,0}$	7.18±0.10	7.73±0.02
$\log {}^*\beta_{4,1}$	6.65±0.05	
$\log {}^*\beta_{6,1}$	9.94±0.10	10.8±0.1
$\log {}^*\beta_{6,2}$	9.59±0.05	

The K_4 values in $LiClO_4$ yielded as predominant GeF_4.

Lastly, we attempted to ascribe a plausible t in the $Ge(OH)_t F_2^{2-t}$ species which are important only at $m_H \geqslant 1$. Assuming a single t, eq. (12) can be written

$$\log {}^*\beta_{2,p} = \log K_2 + p \log [H^+] - 2 \log y_{HF} - \log y_M + \log y_{2,p} + (4-t) \log a_W \quad (18)$$

from which values of ${}^*\beta_{2,p}$ were computed by putting $y_M = y_{2,p} = 1$ and $p = 0, 1, 2, -1, -2$. Approximately constant ${}^*\beta_{2,-1}$ values were obtained, thus the $Ge(OH)F_2^+$ species would be present. In consideration, however, of the various sources of uncertainty, the proposal of such a complex must be understood as tentative.

DISCUSSION

The main conclusion of this investigation is that in the acidity interval from 0.03 to 3 molal the

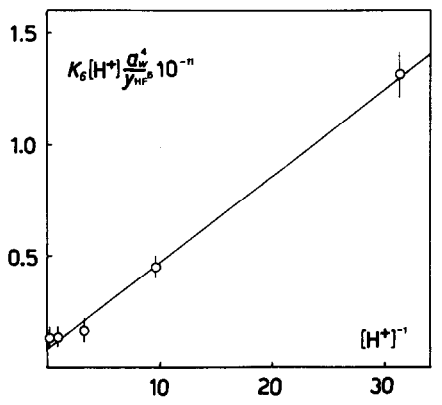

Fig. 2. $K_6 [H^+] a_W^4 y_{HF}^{-6}$, eq. (16), as a function of $[H^+]^{-1}$ for data in $NaClO_4$. The straight line represents: $8.7 \times 10^9 + 3.9 \times 10^9 [H^+]^{-1}$.

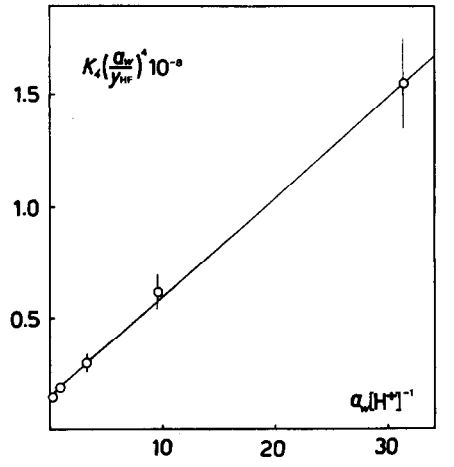

Fig. 3. $K_4 a_W^4 y_{HF}^{-4}$, eq. (17), as a function of $a_W [H^+]^{-1}$ for data in $NaClO_4$. The line is: $1.5 \times 10^7 + 4.5 \times 10^6 a_W [H^+]^{-1}$.

fluorogermanate(IV) equilibria lead to the formation of GeF_4, $Ge(OH)F_4^-$, GeF_6^{2-}, $HGeF_6^-$ and a minor species $Ge(OH)F_2^+$ which becomes significant only at the highest m_H. Figure 4 illustrates the distribution of the complex species. It is evident how at increasing m_H the curves representing GeF_6^{2-} and $HGeF_6^-$ are displaced to leave room for intermediate species.

The remarkable differences between constants deduced in $NaClO_4$ and $LiClO_4$ solutions are accounted for mainly by the salting effect on the activity of HF. It is recalled that according to the SIT,[15] 0.061 in eq. (2a) is the difference between the interaction coefficient of HF with $HClO_4$ and that of HF with $NaClO_4$. The analogous quantity for $LiClO_4$ is given by 0.020 in eq. (2b). Consequently, for a 3 molal salt concentration we have

$$\log y_{HF}(LiClO_4) - \log y_{HF}(NaClO_4) = (0.061 - 0.020) \times 3 = 0.123. \quad (19)$$

By assuming no appreciable changes in the activity coefficient of other reagents, the differences between

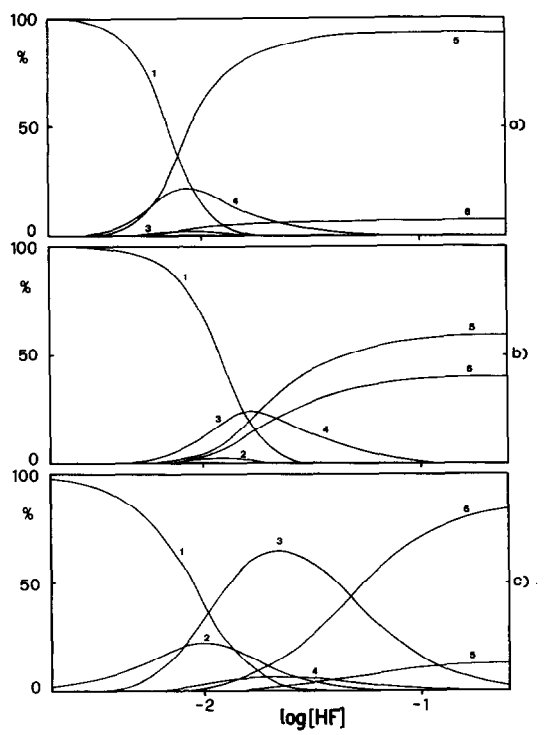

Fig. 4. Distribution of the fluorogermanates as a function of the free hydrofluoric acid concentration at different acidities: 0.03 (a), 0.3 (b), 3 (c). (1) $Ge(OH)_4$ (2) $Ge(OH)F_2^+$ (3) GeF_4 (4) $Ge(OH)F_4^-$ (5) GeF_6^{2-} (6) $HGeF_6^-$. The curves have been calculated with the constants relevant to the inert 3 molal $NaClO_4$ medium, Table 3, and assuming y_{HF} of eq. (2a) and a_w from eq. (14). Other activity coefficients have been set equal to unity.

$^*\beta_{n,p}$ values determined in $NaClO_4$ and $LiClO_4$ are explained, within the limits of error, by relationship (19).

The results of the present work are to a certain extent in contrast with those by Benoit and Place[2] who proposed species with 5 instead of 6 fluoride ions. The serious discrepancy led us to undertake a recalculation of their potentiometric measurements in 0.5 molar $HClO_4$. Comparison of the $\bar{n}(\log[HF])$ data with normalized functions,[12] constructed by assuming only two predominating complexes, clearly indicates that the curves representing $n = 4$ and 6 fit the data much better than those calculated with $n = 5$ and 6. In position of best agreement values of $\log K_4 = 7.5 \pm 0.1$ and $\log K_6 = 10.2 \pm 0.1$ were determined which on account of the different experimental conditions are not very far from the constants of Table 2.

The complexation pattern of the Ge^{IV}–HF, Si^{IV}–HF and Ti^{IV}–HF systems has close resemblance. Apparently, a very stable MF_6^{2-} complex is formed by all of these metals and the formation function is accomplished within less than 2 logarithm units of the ligand concentration, which involves a narrow range of existence for intermediate species. We have been able to detect some of the complexes bearing less than 6 fluoride ions by exploring the equilibria in acid media where the formation of MF_6^{2-} is disfavoured. Notwithstanding this, even at $m_H = 3$, the highest acidity studied, every complexation step could not be characterized with an equilibrium constant. Noticeably, in no case could species with 3 and 5 fluoride ions be identified. The irregularities in the stepwise addition of ligand has to be connected probably to structural changes on passing from lower to higher complexes.

Finally, in all of the systems investigated the existence of HMF_6^-, with an acid constant ranging from 0.1 to 1, has been demonstrated. This seems unexpected on account of the generalized belief that the H_2MF_6 acids behave as strong electrolytes.

Acknowledgement—This work was financially supported by Ministero della Pubblica Istruzione, Rome.

REFERENCES

1. C. F. Baes and R. E. Mesmer, *The Hydrolysis of Cations*, J. Wiley and Sons, New York (1976).
2. R. L. Benoit and J. Place, *Canad. J. Chem.* 1963, **41**, 1170.
3. J. E. Griffiths and D. E. Irish, *Inorg. Chem.* 1964, **3**, 1134.
4. P. A. W. Dean and D. F. Evans, *J. Chem. Soc. A* 1967, 698.

5. I. G. Ryss and N. F. Kulish, *Russ. J. Inorg. Chem.* 1964, **9**, 752.
6. I. G. Ryss and N. F. Kulish, *Russ. J. Inorg. Chem.* 1965, **10**, 996.
7. L. Ciavatta and A. Pirozzi, *Polyhedron* 1983, **2**, 769.
8. L. Ciavatta, M. Iuliano and R. Porto, *Polyhedron* 1988, **7**, 1773.
9. G. Biedermann, *Acta Chem. Scand.* 1956, **10**, 1340.
10. L. G. Sillén and E. A. Martell, *Stability Constants*, The Chemical Soc., Special Publ. N° 17(1964) and N° 25(1971), London.
11. G. Biedermann, *Arkiv Kemi* 1956, **9**, 277.
12. L. G. Sillén, *Acta Chem. Scand.* 1956, **10**, 186.
13. L. G. Sillén and B. Warnqvist, *Arkiv Kemi* 1969, **31**, 315.
14. R. A. Robinson and R. H. Stokes, *Electrolyte Solutions*, Butterworths, London (1955).
15. L. Ciavatta, *Ann. Chim.* (*Rome*) 1980, **70**, 551.

Polyhedron Vol. 9, No. 10, pp. 1271–1276, 1990
Printed in Great Britain

0277–5387/90 $3.00+.00
© 1990 Pergamon Press plc

A CONVENIENT SYNTHESIS OF TRIALKYLALKYLIDYNE TUNGSTEN (6+) COMPOUNDS AND THE X-RAY CRYSTAL STRUCTURE OF $(Me_3CCH_2)_3W{\equiv}CPh(py)$

MALCOLM H. CHISHOLM,* JOHN C. HUFFMAN and JEFFREY A. KLANG

Department of Chemistry and Molecular Structure Center, Indiana University, Bloomington, IN 47405, U.S.A.

(*Received* 27 *September* 1989; *accepted* 9 *January* 1990)

Abstract—A convenient synthesis for trialkylalkylidyne tungsten compounds is reported based on the metathetic reaction between alkyllithium or alkyl-Grignard reagents and $(^tBuO)_3W{\equiv}CR$ compounds. The success of the strategy is limited to alkyl ligands that lack β-hydrogen atoms. The X-ray crystal structure of $(Me_3CCH_2)_3W{\equiv}CPh(py)$ is reported. Cell dimensions at $-155°C$: $a = 13.657(7)$, $b = 13.897(9)$, $c = 14.115(7)$ Å, $Z = 4$ and space group $P2_12_12_1$. The central WC_4N unit is based on a distorted trigonal bipyramid with axial alkylidyne and pyridine ligands, with W—C = 1.74(3) and W—N = 2.57(3) Å, respectively.

As part of our long-standing interest in Group VI organometallic and inorganic chemistry we have become interested in exploring new, molecular routes to carbides, nitrides and oxides of molybdenum and tungsten.[1] We believe that trialkyltungstenalkylidynes, R'_3WCR, will serve as low temperature precursors to tungsten carbides (WC or W_2C). Girolami and his co-workers[2] have reported the formation of titanium carbide in the decomposition of $Ti(CH_2CMe_3)_4$ at temperatures as low as 150°C.

As we begin this work there are only a few examples of tungsten alkylidynes supported exclusively by alkyl ligands. These are prepared by reactions involving multiple α-hydrogen abstractions and are specific for Me_3SiCH_2 and Me_3CCH_2 ligands.[2] We require a more general method and chose to investigate metathetic reactions involving $(^tBuO)_3WCR$ complexes.

RESULTS AND DISCUSSION

Synthesis

Reaction of the alkoxide supported alkylidyne $(^tBuO)_3WCR$ with alkyl-Grignard or alkyl-lithium reagents of the type RCH_2M results in the formation of the desired trialkylalylidynes as shown in eq. (1). As the complexes $(^tBuO)_3WCR$ can be made with a wide variety of different R groups by the reaction of $W_2(O^tBu)_6$ with RCCR,[3] this route has the potential to be quite general. Table 1 lists the compounds made by this route so far, along with selected ^{13}C NMR data for their alkylidyne ligands. All of the new compounds have been characterized by ^1H and ^{13}C NMR spectroscopies, elemental analysis in most cases, and for $(Me_3CCH_2)_3WCPh(py)$ by single crystal X-ray crystallography.

Table 1. New alkylalkylidyne tungsten compounds with selected ^{13}C NMR data for the alkylidyne carbon

	Chemical shift (ppm)	J_{WC} (Hz)
$(PhCH_2)_3WC^tBu$	297.5	n.o.
$(Me_3CCH_2)_3WCSiMe_3$	338.3	188.7
$(Me_3SiCH_2)_3WCPh$	303.6	221.0
$((Me_3SiCH_2)_3WC)_2$	314.4	n.o.
$(Me_3CCH_2)_3WCPh \cdot py$	283.4	n.o.
$(Me_3SiCH_2)_3WCPh \cdot py$	n.o.	—
$((Me_3CCH_2)_3WC)_2$	n.o.	—
$(py(Me_3CCH_2)_3WC)_2$	305.3	n.o.
$(Me_3SiCH_2)_3WC^tBu$	319.5	215.0

n.o. = not observed.

* Author to whom correspondence should be addressed.

$$(^tBuO)_3W{\equiv}CR + 3\,LiR' \longrightarrow (R')_3W{\equiv}CR + 3\,{}^tBuOLi. \quad (1)$$

Compounds containing benzyl or neopentyl ligands have only been prepared using the Grignard or lithium reagents, respectively. This is simply due to the convenience of these reagents relative to benzyllithium or neopentyl-Grignard. Compounds with Me_3SiCH_2 ligands can be made equally well from Me_3SiCH_2MgCl or Me_3SiCH_2Li. In some cases, when alkyl-lithium reagents were used it was difficult to separate the ^tBuOLi formed from the desired product. A useful procedure in this situation was to add a stoichiometric amount of $BF_3 \cdot OEt_2$ to a cooled hexane solution of the mixture. This quantitatively precipitated $BF_3(^tBuO)Li$ which was then removed by filtration.

As expected, the stability and physical properties of the trialkylalkylidynes depended markedly on the substituents R and R′. Although combinations of large R and R′ groups give the best stability, steric and electronic factors cannot be separated at this point. The importance of the alkylidyne substituent, R, in determining the stability of these complexes is underscored by the relative stabilities of $(PhCH_2)_3WCR$ (R = ^tBu, Me_3Si, Ph). The neopentylidyne is a yellow crystalline solid which is indefinitely stable in the absence of air or moisture. The trimethylsilylmethylidyne can be detected in solution (^1H NMR: $PhCH_2$ 2.18 ppm, J_{WH} = 7.7 Hz) but decomposes at a rate similar to that of its formation from $(^tBuO)_3WCSiMe_3$ and $PhCH_2MgCl$ and cannot be isolated. The benzylidyne has never been detected. Likewise, no evidence for a complex with an ethylidyne ligand $(RCH_2)_3WCMe$ has ever been seen with any alkyl ligand.

Of the alkyl ligands investigated, Me_3CCH_2 and Me_3SiCH_2 most effectively stabilize the alkylalkylidynes. In these series even compounds with relatively small alkylidyne substituents such as phenyl, and the dimers $(RCH_2)_3WC\text{-}CW(CH_2R)_3$, can be made and are relatively stable. The mixed neopentyl/trimethylsilylmethyl complexes $(Me_3CCH_2)_3WCSiMe_3$ and $(Me_3SiCH_2)_3WCCMe_3$ are both quite volatile, the latter subliming with little or no decomposition at *ca* 10^{-3} Torr and 50–55°C. The former compound is an oil and although small amounts of it can be distilled onto a cold finger condenser, attempted distillation on larger scales causes extensive decomposition. The benzylidynes, $(Me_3SiCH_2)_3WCPh$ and $(Me_3CCH_2)_3WCPh$, are oils at room temperature and decompose upon attempted distillation. Their pyridine adducts are, however, crystalline allowing purification of these compounds. The X-ray crystal structure of one of these is presented below.

We have not had as much success with other alkyl ligands. Only one complex containing benzyl ligands has been isolated, and with smaller alkyl groups or those with β-hydrogens (Me_2CHCH_2, Me_2CH) we have found no evidence for formation of R'_3WCR complexes.

NMR studies

The ^1H and ^{13}C NMR spectra are consistent with the formulation of these complexes as being monomeric with C_3 symmetry. The ^{13}C NMR spectra show characteristic far downfield chemical shifts and large values of J_{WC} for the alkylidyne carbon atoms (see Table 1). The alkylidyne chemical shifts range from 283.8 to 327.0 ppm; in each case this is about 30 ppm downfield of the corresponding $(^tBuO)_3WCR$ complex. Tungsten coupling of 75–90 Hz is also observed to the carbon atoms of the methylene groups. In the ^1H NMR spectra, small ^{183}W–^1H couplings (6–11 Hz) are seen to the hydrogen atoms of the methylene groups.

Molecular structure of $(Me_3CCH_2)_3W{\equiv}CPh(py)$

A summary of crystal data is given in Table 2 and selected bond distances and bond angles are given in Table 3. A ball-and-stick drawing of the molecule is shown in Fig. 1.

The central WC_4N core is a distorted trigonal pyramid in which the alkylidyne carbon and pyridine nitrogen occupy *trans* positions: N(15)—W—C(21) = 179.5(10)°. The W—C triple bond distance, 1.74(3) Å, and the W—C (neopentyl) distances, 2.13(4) Å, are well within the range expected based on other alkylalkylidyne compounds of tungsten (6+). The W—N (pyridine) distance of 2.575(25) Å is very long, indicative of a relatively weak donor interaction. The alkylidyne—C—W—C (alkyl) angles of *ca* 100° are similar to those seen in related trigonal bipyramidal structures such as $[(^tBuO)_3W{\equiv}N]_\infty$[3] and $(^tBuO)_3W(NO)(py)$[4] where the equatorial ligands bend away from the multiple bond in one axial site and toward the weak donor ligand in the other axial position.

Concluding remarks

The reported procedure provides a convenient synthesis for a number of trialkylalkylidyne tungsten compounds. Studies of their modes of thermal decomposition are currently underway.

Table 2. Summary of crystal data for $(Me_3CCH_2)_3W{\equiv}CPh(py)$

Empirical formula	$WC_{27}H_{43}N$
Colour of crystal	Reddish green?
Crystal dimensions (mm)	$0.25 \times 0.25 \times 0.25$
Space group	$P2_12_12_1$
Cell dimensions	
Temperature (°C)	−155
a (Å)	13.657(7)
b (Å)	13.897(9)
c (Å)	14.115(7)
Z (molecules/cell)	4
Volume (Å^3)	2679.03
Calculated density (g cm^{-3})	1.402
Wavelength (Å)	0.71069
Molecular weight	565.49
Linear absorption coefficient (cm^{-1})	44.148
Detector to sample distance (cm)	22.5
Sample to source distance (cm)	23.5
Average omega scan width at half height	0.25
Scan speed (deg min^{-1})	4.0
Scan width (deg + dispersion)	1.8
Individual background (s)	8
Aperture size (mm)	3.0×4.0
2θ Range (deg)	6–45
Total number of reflections collected	2744
Number of unique intensities	2000
Number with $F > 0.0$	1896
Number with $F > 2.33\sigma(F)$	1754
$R(F)$	0.0649
$Rw(F)$	0.0594
Goodness-of-fit for the last cycle	1.240
Maximum δ/σ for last cycle	0.45

Table 3. Selected bond distances and bond angles for $(Me_3CCH_2)_3W{\equiv}CPh(py)$

A	B	Distance
W(1)	N(15)	2.575(26)
W(1)	C(2)	2.165(26)
W(1)	C(6)	2.12(3)
W(1)	C(11)	2.101(21)
W(1)	C(21)	1.74(3)

A	B	C	Angle
N(15)	W(1)	C(2)	80.8(10)
N(15)	W(1)	C(6)	77.1(10)
N(15)	W(1)	C(11)	79.7(9)
N(15)	W(1)	C(21)	179.5(10)
C(2)	W(1)	C(6)	113.4(13)
C(2)	W(1)	C(11)	116.8(14)
C(2)	W(1)	C(21)	99.6(11)
C(6)	W(1)	C(11)	119.0(14)
C(6)	W(1)	C(21)	102.7(11)
C(11)	W(1)	C(21)	100.8(11)
W(1)	C(2)	C(3)	131.1(20)
W(1)	C(6)	C(7)	128.4(23)
W(1)	C(11)	C(12)	131.5(19)
W(1)	C(21)	C(22)	174.6(20)

EXPERIMENTAL

General operating procedures and techniques have been given previously.[5] Elemental analyses were performed by Oneida Research Services, Whitesboro, New York.

Crystallographic studies

General operating procedures and listings of programs have been described previously.[7] A summary of crystal data is given in Table 2. A suitable crystal was cleaved from a larger multicrystalline conglomerate and transferred to the goniostat using standard inert atmosphere handling techniques employed by the Indiana University Molecule Structure Center and cooled to −155°C for characterization and data collection.

A systematic search of a limited hemisphere of reciprocal space located a set of diffraction maxima with symmetry and systematic absences corresponding to the unique orthorhombic space group $P2_12_12_1$. Subsequent solution and refinement

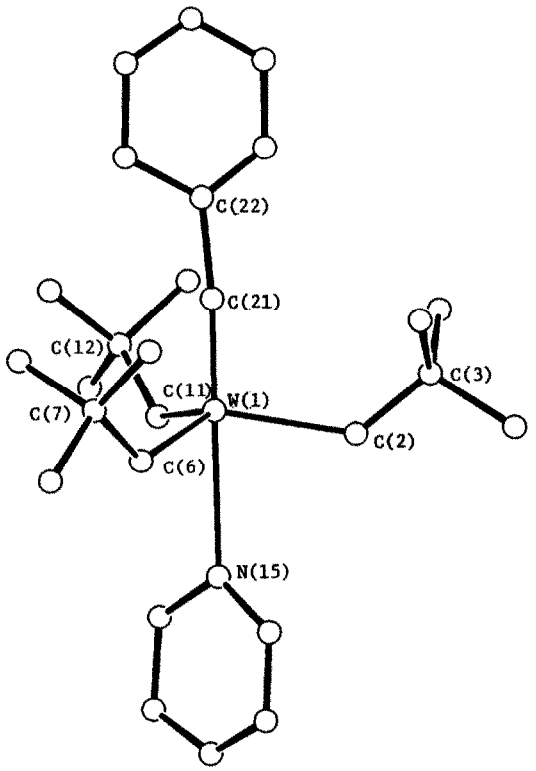

Fig. 1. A ball-and-stick drawing of the $(Me_3CCH_2)_3W{\equiv}CPh(py)$ molecule.

of the structure confirmed this choice. There were several weak peaks present which could not be accounted for based on the chosen cell, or a supercell based on the known cell. Some of these were identified as a second well-ordered fragment of *ca* 10% the intensity of the located cell, and other peaks indicated other fragments were possibly present. Examination of the bulk sample indicated that it would be difficult to find a more homogenous sample, so the mounted specimen was utilized.

Data were collected using a continuous θ–2θ scan with fixed backgrounds and reduced to a unique set of intensities and associated sigmas in the usual manner. The structure was solved by a combination of direct methods (MULTAN78) and Fourier techniques. A difference Fourier synthesis revealed the location of some, but not all, hydrogen atoms. All hydrogen atom positions were therefore calculated using idealized geometries and d(C—H) = 0.95 Å. These calculated positions were fixed for the final cycles of refinement. The data were corrected for absorption based on measurements made on the diffractometer, but use of the absorption corrected data led to non-positive definite thermal parameters for many of the atoms. For the final cycles, the uncorrected data were used. The poor quality of the refinement is partially due to the large thermal motion present, as well as to interference from the fragments known to be present.

Chemicals

The alkylidynes $(^tBuO)_3WCR$ were made by the method of Schrock;[6b] $(CH_3)_3CCH_2Li$ and Me_3SiCH_2Li were made by published procedures. $PhCH_2MgCl$ and Me_3SiCH_2MgCl were purchased from Aldrich Chemical Co.

Preparation of $(PhCH_2)_3WC^tBu$

In a 50 cm^3 Schlenk flask, $(^tBuO)_3WC^tBu$ (1.56 g, 3.3 mmol) was dissolved in Et_2O (20 cm^3), the solution was cooled to 0°C and $PhCH_2MgCl$ (3.3 equiv, 2.0 M in THF) was added via syringe. After stirring for 1 h at 0°C, the volatile components were removed *in vacuo* and the residue was extracted with 4×10 cm^3 of hexane at room temperature. The combined hexane filtrates were concentrated and cooled to *ca* −20°C for 2 days to give 1.05 g (60% yield) of $(PhCH_2)_3WC^tBu$ as yellow crystals.

$(PhCH_2)_3WC^tBu$: ^1H NMR (C_6D_6) δ: C_6H_5 7.18 (m, 3H); 6.93 (m, 6H); 6.78 (m, 6H); $PhCH_2$ 1.95 (s, J_{WC} = 6.5 Hz, I = 20%, 6H); $C(CH_3)_3$ 1.36 (s, 9H). $^{13}C\{^1H\}$ NMR (C_6D_6) δ: $WCC(CH_3)_3$ 297.5 (s); C_6H_5 131.6(s); 131.1(s); 129.7(s); 127.1(s); $PhCH_2$ 57.1 (s, J_{WC} = 77.1 Hz, I = 15%); $C(CH_3)_3$ 38.1 (s); $C(CH_3)_3$ 30.9 (s). IR (KBr) cm^{-1}: 2960(s); 2940(s); 2900(m); 1580(m); 1485(s); 1450(s); 1155(m); 1030(m); 1005(m); 980(m); 815(m); 800(m); 710(s); 695(s); 515(s). Found: C, 59.5; H, 5.7. Calc. for $WC_{26}H_{30}$: C, 59.3; H, 5.7%.

Preparation of $(Me_3CCH_2)_3WCSiMe_3$

A solution of $(^tBuO)_3WC(SiMe_3)$ (0.466 g, 0.96 mmol) in Et_2O (10 cm^3) was cooled to 0°C and an Et_2O (5 cm^3) solution of Me_3CCH_2Li (0.246 g, 3.15 mmol) was added via cannula. The mixture was stirred at 0°C for 1.5 h and the volatile components were removed *in vacuo*. Sublimation of the residue onto a water cooled cold-finger at *ca* 10^{-3} Torr and 50–55°C provided 315 mg (68% yield) of analytically pure $(Me_3CCH_2)_3WCSiMe_3$.

$(Me_3CCH_2)_3WCSiMe_3$: ^1H NMR (C_6D_6) δ: $C(CH_3)_3$ 1.15 (s, 27H); 0.91 (s, J_{WH} = 11.0 Hz, I = 20%, 6H); $Si(CH_3)_3$ 0.44 (s, J_{SiH} = 6.6 Hz, I = 8.6%, 9H). $^{13}C\{^1H\}$ NMR (C_6D_6) δ: $CSi(CH_3)_3$ 338.3 (s, J_{WC} = 188.7 Hz, J_{SiC} = 42.7 Hz); $^tBuCH_2$ 105.2 (s, J_{WC} = 91.7 Hz); $C(CH_3)_3$ 34.7(s); $C(CH_3)_3$ 33.9(s); $Si(CH_3)_3$ 1.95 (s, J_{SiC} = 41.9 Hz). IR (KBr) cm^{-1}: 2975(s); 2900(m); 2865(m); 1460(m); 1385(m); 1360(s); 1265(m); 1245(s);

1235(s); 1195(s); 1120(m); 840(s); 755(m). Found: C, 47.0; H, 8.7. Calc. for $WC_{19}H_{42}Si$: C, 47.3; H, 8.8%.

Preparation of $(Me_3SiCH_2)_3WCPh$

A solution of $(^tBuO)_3WCPh$ (0.70 g, 1.4 mmol) in Et_2O (10 cm^3) was cooled to 0°C and Me_3SiCH_2MgCl (1.0 M in Et_2O, 4.3 cm^3) was added via syringe. The mixture was stirred at 0°C for 1.5 h and the volatile components were removed *in vacuo*. The residue was extracted with 2×10 cm^3 hexane, filtered through a Celite pad and the hexane removed *in vacuo* to give $(Me_3SiCH_2)_3WCPh$ as a dark red oil. This oil could not be induced to crystallize and decomposed upon attempted sublimation/distillation but was approximately 95% pure as judged by ^1H NMR. The pyridine adduct $(Me_3SiCH_2)_3WCPh \cdot py$ was made by adding 1 cm^3 of pyridine and 5 cm^3 of DME to the oil obtained above. The dark red solution was reduced in volume by about 1/2 and cooled to −20°C overnight to give 410 mg (48% yield) of yellow–brown $(Me_3SiCH_2)_3WCPh \cdot py$ as a tacky solid.

$(Me_3SiCH_2)_3WCPh$: ^1H NMR (C_6D_6) δ: C_6H_5 7.44 (m, 2H); 7.29 (m, 2H); 6.93 (m, 1H); CH_2 0.69 (s, $J_{WH} = 9.3$ Hz, $I = 20\%$, 6H); $Si(CH_3)_3$ 0.15 (s, $J_{SiH} = 7.6$ Hz, $I = 8.0\%$, 27H). $^{13}C\{^1H\}$ NMR (C_6D_6) δ: $C(C_6H_6)$ 303.6 (s, $J_{WC} = 221.0$ Hz, $I = 14.4\%$); phenylipso 150.0 (s, $J_{WC} = 51.7$ Hz, $I = 15.1\%$); C_6H_5 130.4(s); 126.3(s); CH_2 76.2 (s, $J_{WC} = 76.4$ Hz, $I = 13.5\%$; $J_{SiC} = 40.0$ Hz, $I = 6.6\%$); $Si(CH_3)_3$ 2.7 (s, $J_{SiC} = 51.5$ Hz, $I = 7.8\%$). IR (film on NaCl) cm^{-1}: 2980(s); 2900(m); 1360(m); 1245(s); 1195(m); 945(s); 840(s); 750(s); 690(s). No analysis was attempted; compound is an oil.

$(Me_3SiCH_2)_3WCPh \cdot py$: ^1H NMR (C_6D_6) δ: C_6H_5 and py 8.89 (m, 2H); 7.65 (m, 2H); 7.38 (m, 2H); 6.96 (m, 1H); 6.92 (m, 1H); 6.67 (m, 2H); CH_2 1.17 (s, $J_{WH} = 9.1$ Hz, $I = 18\%$, 6H); $Si(CH_3)_3$ 0.21 (s, $J_{SiH} = 6.0$ Hz, $I = 8.3\%$, 27H). $^{13}C\{^1H\}$ NMR (C_6D_6) δ: C_6H_5 and py 150.5(s); 149.8(br, s); 131.5(s); 125.9(s); 124.5(br, s); CH_2 72.3 (s, $J_{WC} = 81.8$ Hz, $I = 16\%$); $Si(CH_3)_3$ 3.2(s).

Preparation of $((Me_3SiCH_2)_3W{\equiv}C)_2$

An Et_2O (10 cm^3) solution of $((^tBuO)_3WC)_2$ (0.50 g, 0.60 mmol) was cooled to 0°C and solid Me_3SiCH_2Li (0.34 g, 3.6 mmol) was added from a side arm over about 20 min. The mixture was stirred at 0°C for 3 h, and volatiles removed *in vacuo*, the residue dissolved in *ca* 3 cm^3 hexane and placed in a −20°C freezer. After about 24 h black crystals (290 mg, 52% yield) of $((Me_3SiCH_2)_3WC)_2$ were isolated by filtration and dried *in vacuo*.

$((Me_3SiCH_2)_3W{\equiv}C)_2$: ^1H NMR (C_6D_6) δ: CH_2 1.13 (s, $J_{WH} = 7.7$ Hz, $I = 22\%$, 12H); $(CH_3)_3Si$ 0.30 (s, $J_{SiH} = 6.2$ Hz, $I = 12\%$, 54H). $^{13}C\{^1H\}$ NMR (C_6D_6) δ: W≡*C*— 314.4(s); CH_2 77.8 (s, $J_{WC} = 79.4$ Hz, $I = 14.6\%$). IR (KBr) cm^{-1}: 2970(s); 2880(m); 2820(m); 1395(m); 1380(m); 1245(s); 1210(m); 940(s); 840(s); 750(s); 685(s). Found: C, 33.8; H, 7.0. Calc. for $W_2C_{26}H_{66}Si_6$: C, 34.1; H, 7.2%.

Preparation of $(Me_3CCH_2)_3WCPh \cdot py$

An Et_2O (10 cm^3) solution of $(^tBuO)_3WCPh$ (0.4 g, 0.813 mmol) was cooled to 0°C and solid Me_3C-CH_2Li (0.176 g, 2.26 mmol) was added from a side arm over about 20 min. The mixture was stirred at 0°C for 1 h and the volatile components were removed *in vacuo*. The residue was dissolved in hexane (3 cm^3) at 0°C and $BF_3 \cdot OEt_2$ (0.2 cm^3, 3.25 mmol) was added via syringe to precipitate $BF_3 \cdot O^tBu^-Li^+$ as a light brown solid which was filtered off and discarded. The filtrate was reduced in volume to about 1 cm^3 and pyridine (0.2 cm^3) was added. Cooling to −20°C overnight caused 244 mg (54% yield) of $(Me_3CH_2)_3WCPh \cdot py$ to precipitate as a light brown solid.

Crystals of $((CH_3)_3CCH_3)_3WCPh \cdot py$ suitable for X-ray diffraction analysis were obtained by cooling a solution of *ca* 250 mg of the compound in *ca* 2 cm^3 of 1 : 1 hexane–pyridine to −20°C for several days.

$(Me_3CCH_2)_3WCPh \cdot py$: ^1H NMR (C_6D_6) δ: C_6H_5 and py 8.69 (m, 2H); 7.82 (m, 2H); 7.32 (m, 2H); 7.0 (m, 1H); 6.93 (m, 1H); 6.63 (m, 2H); $C(CH_3)_3$ 1.28 (s, 27H); CH_2 1.11 (s, $J_{WH} = 10.1$ Hz, $I = 25\%$, 6H). $^{13}C\{^1H\}$ NMR (C_6D_6) δ: ≡*C*(C_6H_5) 283.4 (br. s); C_6H_5 and py 150.5(s); 149.8(s); 136.8(s); 132.5(s); 125.6(s); 124.4(s); CH_2 104.2 (s, $J_{WC} = 89.2$ Hz, $I = 13.7\%$); $C(CH_3)_3$ 36.4(s); $C(CH_3)_3$ 34.6(s). IR (KBr) cm^{-1}: 2945(s); 2850(s); 1595(m); 1580(m); 1480(s); 1440(s); 1380(s); 1355(s); 1235(s); 1225(s); 1115(m); 1065(m); 940(m); 750(s); 690(s). Found: C, 57.1; H, 7.5; N, 2.4. Calc. for $WC_{27}H_{43}N$: C, 57.4; H, 7.6; N, 2.5%.

Preparation of $((Me_3CCH_2)_3WC)_2$ *and* $((Me_3CCH_2)_3WC)_2 \cdot py_2$

An Et_2O (5 cm^3) solution of $((^tBuO)_3WC)_2$ (0.875 g, 1.05 mmol) was cooled to 0°C and an Et_2O (5 cm^3) solution of Me_3CCH_2Li (0.532 g, 6.82 mmol) added via cannula. The mixture was stirred at 0°C for 1.5 h, the volume of the solution reduced by

about 1/2 and placed in a −20°C freezer. After 2 days 608 mg (71% yield) of dark red $((Me_3CCH_2)_3WC)_2$ was collected by filtration and dried *in vacuo*. The bis-pyridine adduct was formed by addition of excess pyridine to a suspension of $((Me_3CCH_2)_3WC)_2$ in toluene and by removing the volatile components *in vacuo*.

$((Me_3CCH_2)_3WC)_2$: ^1H NMR (C_6D_6) δ: $C(CH_3)_3$ 1.28 (s, 54H); CH_2 1.18 (s, J_{WH} = 9.2 Hz, I = 16.6%, 12H). $^{13}C\{^1H\}$ NMR (C_6D_6) δ: CH_2 105.5 (s, J_{WC} = 91 Hz, I = 15%); $C(CH_3)_3$ 35.9(s); $C(CH_3)$ 34.5(s). IR (KBr) cm^{-1}: 2950(s); 2895(s); 2875(s); 2750(m); 1465(m); 1360(s); 1340(s); 1230(s); 1220(m); 1105(m); 750(m); 600(m); 520(m). Satisfactory analysis not obtained.

$((Me_3CCH_2)_3WC)_2 \cdot py_2$: ^1H NMR (C_6D_6) δ: py 8.63 (m, 2H); 6.97 (m, 1H); 6.64 (m, 2H); $C(CH_3)_3$ 1.43 (s, 27H); CH_2 1.34 (s, 6H). $^{13}C\{^1H\}$ NMR (C_6D_6) δ: $\equiv C-$ 305.3(s); py 150.0(s); 136.0(s); 124.0(s); CH_2 105.3 (s, J_{WC} = 89.8 Hz, I = 12.8%); $C(CH_3)_3$ 35.9(s); $C(CH_3)_3$ 34.5(s).

Preparation of $(Me_3SiCH_2)_3WC^tBu$

An Et_2O (5 cm^3) solution of $(^tBuO)_3WC^tBu$ (0.643 g, 1.4 mmol) was cooled to 0°C and Me_3SiCH_2MgCl (5.0 mmol, 1.0 M in Et_2O) was added via syringe. The mixture was stirred at 0°C for 1.75 h and the volatile components were removed *in vacuo*. The residue was extracted with 2×5 cm^3 hexane and the solid filtered off and discarded. The volatile components were removed from the filtrate under a dynamic vacuum to leave a red oil that is approximately 95% pure as judged by ^1H NMR. Small amounts can be distilled onto a water cooled cold finger at *ca* 10^{-3} Torr and 55–60°C but, attempts to purify $(Me_3SiCH_2)_3WC^tBu$ by short path distillation lead to decomposition.

$(Me_3SiCH_2)_3WC^tBu$: ^1H NMR (C_6D_6) δ: CMe_3 1.55 (s, 9H); CH_2 0.78 (s, J_{WH} = 9.8 Hz, I = 16%, 6H); $SiMe_3$ 0.14 (s, 27H). $^{13}C\{^1H\}$ NMR (C_6D_6) δ: WC^tBu 319.5 (s, J_{WC} = 215.0 Hz, I = 15%); CH_2 74.7 (s, J_{WC} = 78.9 Hz, I = 16%, J_{SiC} = 40.6, I = 11%); $C(CH_3)_3$ 33.2(s); $C(CH_3)$ 32.5(s): $Si(CH_3)_3$ 2.9(s).

Acknowledgements—We thank the National Science Foundation for support. J.A.K. acknowledges support as a Chester Davis Fellow for 1988/89.

Supplementary materials. Atomic positional parameters have been deposited with the Cambridge Crystallographic Data Centre.

REFERENCES

1. R. K. Viswanadham, D. J. Rowcliffe and J. Gurland (Eds), *Science of Hard Materials*. Plenum Press, New York (1983).
2. G. S. Girolami, J. A. Jensen, D. M. Pllina, W. S. Williams, A. E. Kaloyeros and C. M. Alloca, *J. Am. Chem. Soc.* 1987, **109**, 1579.
3. R. R. Schrock, *Accts Chem. Res.* 1986, **19**, 342.
4. M. H. Chisholm, D. M. Hoffman and J. C. Huffman, *Inorg. Chem.* 1983, **22**, 2903.
5. M. H. Chisholm, F. A. Cotton, M. W. Extine and R. L. Kelly, *Inorg. Chem.* 1979, **18**, 116.
6. (a) $W_2(O^tBu)_6$: M. Akiyama, M. H. Chisholm, F. A. Cotton, M. W. Extine, D. A. Haitko, D. Little and P. E. Fanwick, *Inorg. Chem.* 1979, **18**, 2266; (b) $(^tBuO)_3W{\equiv}CR$: M. L. Listemann and R. R. Schrock, *Organometalics* 1985, **4**, 74.
7. M. H. Chisholm, K. Folting, J. C. Huffman and C. C. Kirkpatrick, *Inorg. Chem.* 1984, **23**, 1021.

Polyhedron Vol. 9, No. 10, pp. 1277–1286, 1990
Printed in Great Britain

0277–5387/90 $3.00+.00
© 1990 Pergamon Press plc

CRITICAL EVALUATION OF EMPIRICAL FORCE-FIELD MODELS FOR SIMULATION OF PLASTICITY OF COPPER(II) COORDINATION

J. SABOLOVIĆ and N. RAOS*

Institute for Medical Research and Occupational Health, University of Zagreb, M. Pijade 158, 41001 Zagreb, Croatia, Yugoslavia

(*Received* 18 *May* 1989; *accepted* 11 *January* 1990)

Abstract—The plasticity of the copper(II) coordination sphere was simulated with the empirical force-field (molecular mechanics) method. Altogether five models for copper coordination were checked on the *trans*-CuN_2O_2 "complex": (1) a simple model with an angle-bending potential for only *cis* (N–Cu–O) angles, (2) a "dummy" atom model with two apically placed "dummy" atoms, (3) a model with a distortion potential (defined as quadratic function of the angle between bisectors of two opposite valence angles) and a quadratic function for bending of *cis* angles, (4) a model with a distortion potential and an angle-bending potential with two minima (at 90 and 109.47°) for O–Cu–N angles and (5) a newly proposed model with a distortion angle and an angle-bending potential with two minima for all valence angles around copper. The simplest model (1) did not give geometrically defined minima, and model (2) yielded besides the *trans* configuration three minima with superimposed atoms. Models with a distortion potential yielded better results: with model (3) only the *trans* configuration was obtained upon minimization, and model (4) yielded *trans* and tetrahedral configurations besides three "false" configurations of the same (zero) energy. Improving model (4), by proposing model (5), only two configurations (*trans* and tetrahedral) with zero energy were obtained. Model (5) was also proved best in reproducing the crystal geometry and diastereoselectivity of copper(II) bis-aminoacidates.

The plasticity of the copper(II) coordination sphere,[1] i.e. the fact that copper usually does not form "regular" (planar, tetrahedral or octahedral) coordination polyhedra, is a well-known feature of copper stereochemistry.[2] Because of plasticity, copper compounds form crystal modifications with differently distorted coordination polyhedra (distortion isomerism),[3] and show less pronounced stereoselectivity effects than corresponding complexes of nickel(II) and cobalt.[4,5]

Besides classical model compounds for the study of tetracoordinated copper(II) distortion (planar/tetrahedral), bis-(N-alkylsalicylaldiminato)copper (II) complexes,[6] most of our research was done on copper(II) complexes with N,N-dimethylated β-branched amino acids (valine[6–9] and isoleucine[10,11]). In those complexes,[12] as well as in the other chelates with N-alkylated amino acids,[12–14] there is a very pronounced diastereoselectivity effect.†[15–17] In apolar solvents, incapable of coordinating, the diastereoselectivity effect could be totally attributed to the steric strain in the molecule; therefore it can be estimated from the difference in conformational energy between diasteroisomers.

In order to estimate the energy and geometry of those complexes, we used two kinds of empirical force fields: (1) a "dummy" atom model which treats tetracoordinate, a virtually planar complex, as pseudo-octahedral by placing two "dummy" atoms in apical positions[18] and (2) a model with a distortion coordinate potential,[9] dependent on distortion coordinate (defined as an angle between bisectors of two opposite valence angles around the

* Author to whom correspondence should be addressed.

† Defined as $\Delta G = -RT\ln(\beta_{MLL}/\beta_{MDL})$, L and D denoting ligand diastereomers (usually enantiomers) and β cumulative stability constants.

central atom). The "dummy" atom model proved good for predicting thermodynamic stability of bis-(N,N-dimethylvalinato)copper(II),[6,8] but not so good for predicting its crystal geometry.[8] It seems that the sterical strain in the molecule, computed with such a model, leads to a distorted pyramid instead of to a distorted tetrahedron. Recently proposed models[9] with a distortion coordinate potential (Models 3 and 4), overcome that obstacle, but the angles around copper and the thermodynamic stability of the complex do not seem to be reproduced with higher accuracy.

The aim of this paper is to critically evaluate all of the proposed models by analysing the surface of potential (i.e. conformational) energy for planar/tetrahedral distortion. For that purpose we used the simplest system, "complex" *trans*-CuN_2O_2, which corresponded to the coordination polyhedron in copper(II) chelates with amino acids.

METHODS

The conformational (strain) potential energy was calculated from the basic formula:

$$V = 1/2\sum_i k_{b,i}(b_i - b_{0,i})^2 + 1/2\sum_j k_{\theta,j}(\theta_j - \theta_{0,j})^2 + 1/2\sum_k V_n(1 \pm \cos n\varphi_k) + \sum_l [A_l \exp(-B_l r_l) - C_l r_l^{-6}] + 1/2\sum_m k_{\chi,m}\chi_m^2 + 1/2k_\beta(\beta - \beta_0)^2 + V_{XMY} \quad (1)$$

in which b, θ, φ, and χ stand for bond lengths, valence, torsional and out-of-plane angles, respectively; r is non-bonded distance, and β is a distortion coordinate defined as an angle between bisectors of two opposite (N–Cu–O and N′–Cu–O′, see Fig. 4) valence angles around copper. K_b is an empirical parameter for bond stretching and k_θ for valence angle bending. Torsional interactions were determined with parameters V_n and n (height and multiplicity of the torsional barrier, respectively) and non-bonded interactions were computed from a Buckingham function with parameters A, B and C. In addition, the out-of-plane deformation potential for the carboxyl groups and aromatic rings with a quadratic function dependent on parameter k_χ and distortion potential (parameters k_β and β_0) in Models 3–5 (Table 1) were also computed.

The last term in eq. (1) is angle-bending potential for the angles around copper, which can be quadratic (Models 1–3) or in the form of cosine power series (Models 4 and 5), see below (eqs 2 and 3). Contrary to models with a quadratic angle-bending function which have only one minimum (for planar configuration), models with an angle-bending function in the form of cosine power series have two minima which correspond to planar and tetrahedral configurations.

The parameters not shown in Table 1 were the same as those used in our first paper,[18] with the exception of C–N–C bending parameters which were taken to be equal to the parameters for C–C–C bending. The empirical constant k_χ is taken to be

Table 1. Parameters for force-field calculations[a]

Bond	Bonding potential k_b (kcal mol^{-1} Å^{-2})	b_0 (Å)
Cu–N (all models)	251.65	2.000
Cu–O (all models)	270.00	1.950
Cu–*X* (Model 2)	270.00	2.475
Angle	**Angle-bending potential k_θ (kcal mol^{-1} rad^{-2})**	**θ_0 (rad)**
N–Cu–O (Models 1, 3)	250.00	1.571
(Model 2)	97.00	1.571
X–Cu–N (Model 2)	9.00	1.571
X–Cu–O (Model 2)	9.00	1.571
	k_z (kcal mol^{-1})	k_s (kcal mol^{-1})
N–Cu–O (Model 4)	500.00	
(Model 5)	180.00	
N–Cu–N (Model 5)		22.50
O–Cu–O (Model 5)		22.50
Angle	**Distortion potential k_β (kcal mol^{-1} rad^{-2})**	**β_0 (rad)**
β (Models 3–5)	37.50	3.142

[a] "Dummy" atom is denoted with *X*. Only the most specific parameters were presented here, for other parameters see Methods. The parameters for Model 2 were taken from Ref. 6 and for Models 3 and 4 from Ref. 9. Parameters for models with distortion coordinate potential (Models 3, 4 and 5) were obtained by systematical variation of parameters k_θ, k_s, k_z and k_β until the best reproduction of crystal structure of bis-(L-N,N-dimethylvalinato)copper(II) in terms of $\varepsilon_{r.m.s.}(\Delta\theta)$ and $\varepsilon_{r.m.s.}(\Delta\theta, \Delta\varphi, \Delta\beta)$ was obtained. Bonding parameters for all models were taken from Ref. 18.

100 kcal mol^{-1} rad^{-2} for both kinds of out-of-plane deformation. Other empirical parameters specific to aromatic compounds were taken from modified Dashevsky force field (FF2).[19]

Calculations were performed with a program developed by Kj. Rasmussen and co-workers,[20] which was further modified to cope with new empirical potentials (distortion potential and two-well angle-bending potential).[9]

The two-well angle-bending potential for the N–Cu–O angle (with minima at 90 and 109.47°) is given by the expression:

$$V_z = 1/2k_z(9z^4+6z^3+z^2) \qquad (2)$$

where k_z is empirical parameter (Table 1) and $z = \cos\theta$. For angles N–Cu–N and O–Cu–O (with minima at 109.47 and 180°) the two-well angle-bending function has the form:

$$V_s = 1/2k_s(9/8s^4+3\sqrt{2}/2s^3+s^2) \qquad (3)$$

where k_s is empirical parameter (Table 1) and $s = \sin\theta$. Both potentials, V_z and V_s, have two minima of equal (zero) energy and a maximum at symmetry axis between them. The parameters for the potential (3) were chosen so that potential (3) had the same maximum value as potential (2). The full mathematical description of the potentials is given elsewhere.[9]

Root-mean-square deviation between crystal and theoretical structures was calculated from:

$$\varepsilon_{\text{r.m.s}}(\Delta X) = \left(1/N \sum_{i=1}^{N} (\Delta X_i)^2\right)^{1/2} \qquad (4)$$

where X stands for angles around copper [valence angles, θ, distortion angle β and "torsional angle" φ(ONNO)] when comparing the copper coordination geometry, or the interatomic distance, r, when checking the overall similarity. Mark Δ denotes the difference between the values of the observable X in two structures.

The average Gibbs energy of the diastereomer (MLL or MDL) was calculated from the formula:

$$\langle G \rangle = \sum w_i G_i \Big/ \sum w_i \qquad (5)$$

where G_i denotes the Gibbs energy of the ith conformer, and w_i stands for the statistical weight calculated from Boltzmann formula. Details of calculations were given elsewhere.[10]

The potential energy surface for distortion of the copper coordination polyhedron was constructed from the values of potential energy and appropriate values of two internal coordinates obtained after every iteration during the minimization of potential energy (procedure of Rasmussen and co-workers,[21] modified). As the starting points for minimization, arbitrary conformations of the "complex" CuN_2O_2 in the whole conformational space were constructed. The value of potential energy on the conformational hypersurface (i.e. on the energy diagram) was taken to be equal to the lowest energy value obtained in the given region of the conformational space. The procedure was repeated until a stable shape of energy diagrams (in the frame of different internal coordinates) was reached.

For construction of an energy diagram it was necessary to perform 200–300 minimizations, with 80 steepest descent and approximately 20 Newton-Raphson iterations; therefore some 100 energy values per point (covering an area of $12.5 \times 12.5°$) on the diagram were needed.

RESULTS AND DISCUSSION

In order to check our empirical force-field models, we had to answer four principal questions: (1) did the minima of the CuN_2O_2 system correspond to the experimentally obtained configurations (planar, tetrahedral) of copper(II) coordination, (2) did the shape of the potential energy surface show that the tetrahedral distortion was preferred to the pyramidal one (Fig. 1), (3) how well were theoretical models able to reproduce the geometry of real molecules and, finally, (4) did they give values of the diastereoselectivity effect close to the experimental results.

We checked altogether five models (Fig. 2, Tables 1 and 2). The simplest model, Model 1 (harmonic potential only for N–Cu–O bending) yielded an indefinite number of conformations with zero potential energy. All of the conformations were characterized by N–Cu–N = 0 or 180° or O–Cu–O = 0 or 180°. That means that the model permits more degrees of freedom than the real system, i.e. $V = 0$ for every configuration with all N–Cu–O angles equal to 90°.

Model 2 ("dummy atom" model) yielded four minima, all with N–Cu–O = 90°, but only one of the minima (No. 4) corresponded to the real molecular conformation, i.e. to the *trans*-configuration (N–Cu–N = O–Cu–O = 180°). Another three minima of potential energy had superposed ligand atoms.

Model 3 (distortion potential included) seems to satisfy our conditions because it yielded only the *trans*-configuration upon minimization. However, it failed to converge to the tetrahedral configuration, although it yielded tetrahedral distortion when applied to bis-(L-N,N-dimethylvalinato)copper (II).[9] In our previous paper[9] we improved Model 3 by introducing a two-well angle-bending poten-

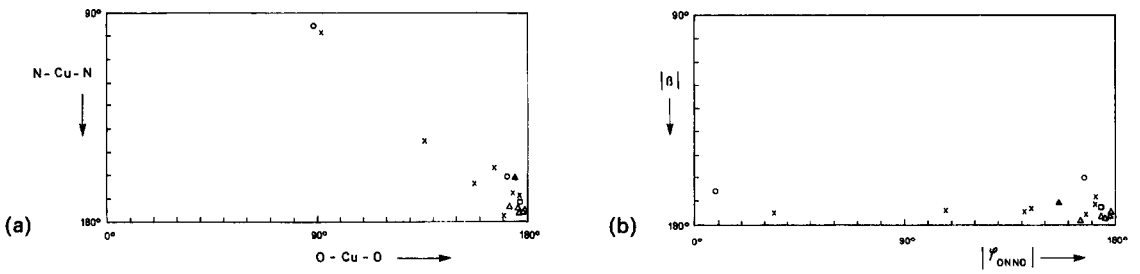

Fig. 1. The coordination polyhedra of copper(II) complexes with CuO_2N_2 chromophore: in the space of *trans* angles (a) and in the space of internal coordinates β (angle between bisectors of O–Cu–N angles in opposite chelate rings) and "torsional" angle O–N–N–O (b). Mark × denotes N-alkylsalicylaldiminates,[22] mark △ stands for tetracoordinated aminoacidates and N-alkylated aminoacidates [see Table 3; bis-(L-N,N-dimethylvalinato)copper(II)[9] is marked with ▲], and mark ⊙ for pentacoordinated bis-(L-isoleucinato)aquacopper(II)[25] and bis(N-benzylvalinato)copper(II).[15] Mark □ denotes hexacoordinated bis-(L-threoninato)copper(II) monohydrate.[26] Symmetrical distortion of coordination polyhedron (a) and very small variation of β angle comparing with O–N–N–O angle (b) show preference for tetrahedral distortion.

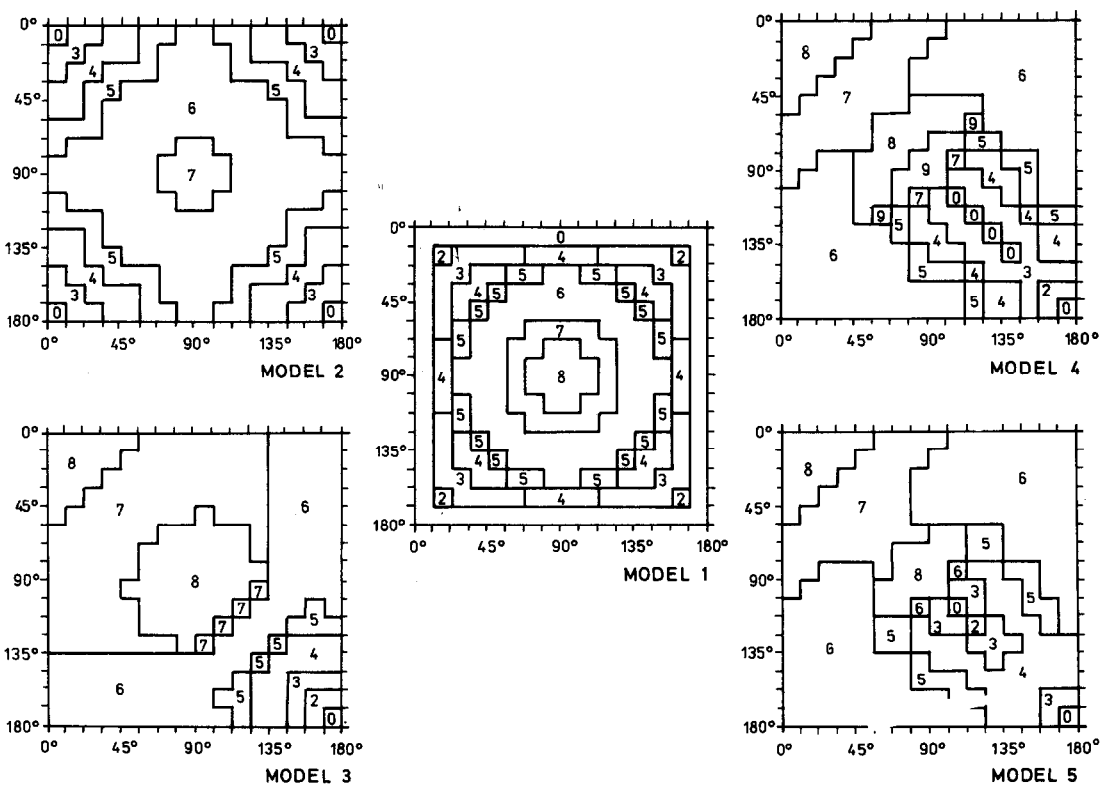

Fig. 2. The diagram of potential (conformational) energy of the *trans*-CuO_2N_2 "complex" in the frame of O–Cu–O and N–Cu–N coordinates obtained by five models for simulation of distortion of the copper coordination polyhedron (see Table 1 and Methods). Ranges of energy in appropriate regions of diagrams are denoted with numbers (values given in parentheses are expressed in kcal mol^{-1}): 0 (< 0.001), 1 (0.001–0.01), 2 (0.01–0.1), 3 (0.1–1), 4 (1–5), 5 (5–10), 6 (10–50), 7 (50–100), 8 (100–1000), 9 (> 1000).

Table 2. Minima with zero conformational energy for "complex" CuN_2O_2[a]

Model No.	Internal coordinate (°)				
	N–Cu–N	O–Cu–O	N–Cu–O	β	O–N–N–O
1	0	0–180	90	0–180	0–180
	180	0–180	90	0–180	0–180
	0–180	0	90	0–180	0
	0–180	180	90	0–180	0
2	0	0	90	0	0
	0	180	90	90	0–90
	180	0	90	90	0
	180	180	90	180	180
3	180	180	90	180	190
4	109.47	109.47	109.47	180	69.8
	118.89	118.89	109.47(1)	180	80.11
			90.00(3)		
	131.81	131.81	109.47(2)	180	94.49
			90.00(2)		
	114.74	114.74	109.47(1)	180	116.23
			90.00(3)	180	
	180.00	180.00	90.00	180	180.00
5	109.47	109.47	109.47	180	69.8
	180.00	180.00	90.00	180	180.0

[a] The number of angles with the specified value is given in parentheses.

Table 3. Comparison of experimental and theoretical geometries of copper(II) bis-aminoacidates[a]

Angle	Crystal structure[b]	Model 3	Model 4	Model 5	Crystal structure[b]	Model 3	Model 4	Model 5
	bis-(L-N,N-dimethylvalinato)copper(II) (8)				bis-(L-N-benzylprolinato)copper(II) (24)			
N–Cu–N′	161.45	159.90	160.10	161.41	172.72	178.22	178.25	178.92
N–Cu–O	84.32	88.41	89.10	87.62	85.58	88.75	89.30	88.36
N–Cu–O′	97.07	92.68	91.90	93.34	96.16	91.39	90.84	91.64
N′–Cu–O	95.30	92.68	92.90	93.34	93.40	91.46	90.89	91.82
N′–Cu–O′	84.75	88.41	89.10	87.62	85.68	88.68	89.26	88.29
O–Cu–O′	175.51	173.78	174.22	174.04	173.29	170.77	170.73	173.50
O′–N′–N–O	156.14	153.74	154.36	155.44	−165.54	168.95	168.95	172.39
β	170.49	170.38	170.15	171.29	−178.56	−174.79	−174.72	−176.21
$\varepsilon_{r.m.s.}$ ($\Delta\theta$)		3.20	3.73	2.55		3.70	4.05	3.56
$\varepsilon_{r.m.s.}$ ($\Delta\theta$, $\Delta\varphi$, $\Delta\beta$)		2.90	3.29	2.21		9.66	9.77	8.43
$\varepsilon_{r.m.s.}$ (Δr)		0.141	0.148	0.136		0.374	0.350	0.333
	bis-(L-leucinato)copper(II) (23)				bis-(L-alaninato)copper(II) (27)			
N–Cu–N′	174.56	179.22	179.22	179.72	175.47	179.57	179.57	180.00
N–Cu–O	84.19	88.49	89.15	88.13	83.83	88.66	89.24	88.30
N–Cu–O′	95.66	91.44	90.81	91.81	95.51	91.41	90.79	91.77
N′–Cu–O	95.95	91.43	90.81	91.79	96.18	91.41	90.80	91.77
N′–Cu–O′	84.17	88.65	89.23	88.27	84.44	88.52	89.17	88.16
O–Cu–O′	179.71	180.00	180.00	180.00	179.25	180.00	180.00	180.00
O′–N′–N–O	174.71	−179.27	−179.27	−179.98	175.79	−179.69	−179.68	−179.95
β	176.16	−179.41	−179.41	−179.64	176.66	−179.62	−179.62	−179.69

Table 3—*continued*

$\varepsilon_{r.m.s.}$ ($\Delta\theta$)		4.05	4.51	3.90		4.02	4.48	3.84
$\varepsilon_{r.m.s.}$ ($\Delta\theta$, $\Delta\varphi$, $\Delta\beta$)		4.39	4.71	4.14		4.05	4.40	3.87
$\varepsilon_{r.m.s.}$ (Δr)		0.302	0.310	0.293		0.212	0.220	0.207
	bis-(L-phenylalaninato)copper(II) (28)				(L-serinato)(glycinato)copper(II) (29)			
N–Cu–N′	175.86	180.00	180.00	179.69	175.23	179.64	179.64	180.00
N–Cu–O	84.82	88.41	89.11	88.06	82.93	88.51	89.16	88.15
N–Cu–O′	96.43	91.42	90.80	91.76	94.41	91.42	90.80	91.79
N′–Cu–O	94.62	91.46	90.83	91.86	101.13	91.42	90.80	91.79
N′–Cu–O′	83.93	88.71	89.26	88.31	81.53	88.64	89.23	88.27
O–Cu–O′	176.85	178.22	178.22	179.28	177.33	180.00	180.00	180.00
O′–N′–N–O	178.63	178.26	178.23	179.61	177.53	179.87	179.87	179.97
β	175.22	−178.74	−178.75	−179.31	176.20	179.59	179.59	179.67
$\varepsilon_{r.m.s.}$ ($\Delta\theta$)		3.87	4.32	3.64		5.94	6.38	5.73
$\varepsilon_{r.m.s.}$ ($\Delta\theta$, $\Delta\varphi$, $\Delta\beta$)		3.97	4.31	3.72		5.34	5.72	5.18
$\varepsilon_{r.m.s.}$ (Δr)		0.752	0.750	0.748		0.231	0.238	0.226
	(L-N,N-diethylalaninato)(D-N,N-diethylalaninato)copper(II) (30)				bis-(1-aminocyclopentane-1-carboxylato) copper(II) (27)			
N–Cu–N′	180.00	180.00	180.00	180.00	180.00	180.00	180.00	180.00
N–Cu–O	84.07	88.37	88.05	87.99	83.84	88.76	89.30	88.44
N–Cu–O′	95.93	91.63	90.95	92.01	96.16	91.24	90.70	91.56
N′–Cu–O	95.93	91.63	90.95	92.01	96.16	91.24	90.70	91.56
N′–Cu–O′	84.07	88.37	89.05	87.99	83.84	88.76	89.30	88.44
O–Cu–O′	180.00	180.00	180.00	180.00	180.00	180.00	180.00	180.00
O′–N′–N–O	180.00	180.00	180.00	180.00	180.00	180.00	180.00	180.00
β	180.00	180.00	180.00	180.00	180.00	180.00	180.00	180.00
$\varepsilon_{r.m.s.}$ ($\Delta\theta$)		3.51	4.07	3.20		4.02	4.46	3.76
$\varepsilon_{r.m.s.}$ ($\Delta\theta$, $\Delta\varphi$, $\Delta\beta$)		3.04	3.52	2.77		3.48	3.86	3.25
$\varepsilon_{r.m.s.}$ (Δr)		0.097	0.106	0.089		0.242	0.249	0.238
	(L-N-benzylprolinato)(D-N-benzylprolinato)copper(II) (31)				bis-(α-aminoisobutyrato)copper(II) (32)			
N–Cu–N′	180.00	180.00	180.00	180.00	180.00	180.00	180.00	180.00
N–Cu–O	87.89	88.55	89.17	88.20	83.92	88.56	89.19	88.19
N–Cu–O′	92.11	91.45	90.83	91.80	96.08	91.44	90.81	91.81
N′–Cu–O	92.11	91.45	90.83	91.80	96.08	91.44	90.81	91.81
N′–Cu–O′	87.89	88.55	89.17	88.20	83.92	88.56	89.19	88.19
O–Cu–O′	180.00	180.00	180.00	180.00	180.00	180.00	180.00	180.00
O′–N′–N–O	180.00	180.00	180.00	180.00	180.00	180.00	180.00	180.00
β	180.00	180.00	180.00	180.00	180.00	180.00	180.00	180.00
$\varepsilon_{r.m.s.}$ ($\Delta\theta$)		0.54	1.05	0.25		3.79	4.30	3.49
$\varepsilon_{r.m.s.}$ ($\Delta\theta$, $\Delta\varphi$, $\Delta\beta$)		0.47	0.91	0.22		3.28	3.73	3.02
$\varepsilon_{r.m.s.}$ (Δr)		0.334	0.336	0.333		0.106	0.118	0.100
	(L-2-aminobutyrato)(D-2-aminobutyrato) copper(II) (23)				(L-N-benzylvalinato)(D-N-benzylvalinato) copper(II)dihydrate (33)			
N–Cu–N′	180.00	180.00	180.00	180.00	180.00	180.00	180.00	180.00
N–Cu–O	84.55	88.51	89.16	88.13	85.02	88.69	89.25	88.35
N–Cu–O′	95.45	91.49	90.84	91.87	94.98	91.31	90.75	91.65
N′–Cu–O	95.45	91.49	90.84	91.87	94.98	91.32	90.75	91.65
N′–Cu–O′	84.55	88.51	89.16	88.13	85.02	88.69	89.25	88.35
O–Cu–O′	180.00	180.00	180.00	180.00	180.00	180.00	180.00	180.00
O′–N′–N–O	180.00	180.00	180.00	180.00	180.00	−179.90	−179.90	−179.89
β	180.00	180.00	180.00	180.00	180.00	−179.99	−179.99	−179.99
$\varepsilon_{r.m.s.}$ ($\Delta\theta$)		3.23	3.76	2.92		2.99	3.45	2.72
$\varepsilon_{r.m.s.}$ ($\Delta\theta$, $\Delta\varphi$, $\Delta\beta$)		2.80	3.26	2.53		2.59	2.99	2.35
$\varepsilon_{r.m.s.}$ (Δr)		0.324	0.329	0.321		0.217	0.220	0.216

[a] All angles are expressed in ° and $\varepsilon_{r.m.s.}$ (Δr) values in Å (only non-hydrogen atoms were taken into account).
[b] References for crystal structures are given in parentheses.

tial for N–Cu–O angles (minima at 90 and 109.47°). The improved model, Model 4 (Table 2, Fig. 2), yielded not only minima with *trans* and tetrahedral configuration, but all combinations (altogether five) of values 90 and 109.47° for N–Cu–O angles. Transition from *trans* to tetrahedral conformation was characterized with trajectory $\beta = 180°$ with a very low transition barrier.

With Model 5 we went a step further by introducing to Model 4 a two-well angle-bending potential (with minima at 109.47 and 180°) for "*trans*" (N–Cu–N and O–Cu–O) angles. The model yielded only two minima (*trans* and tetrahedral) with zero potential energy; however, "false" minima (combination of 90 and 109.47° for N–Cu–O angles) again appeared but with a higher energy (1–5 kJ mol^{-1}).

The models were further checked on crystal structures of all tetracoordinated *trans* copper(II) bisaminoacidates which showed no pronounced inter-

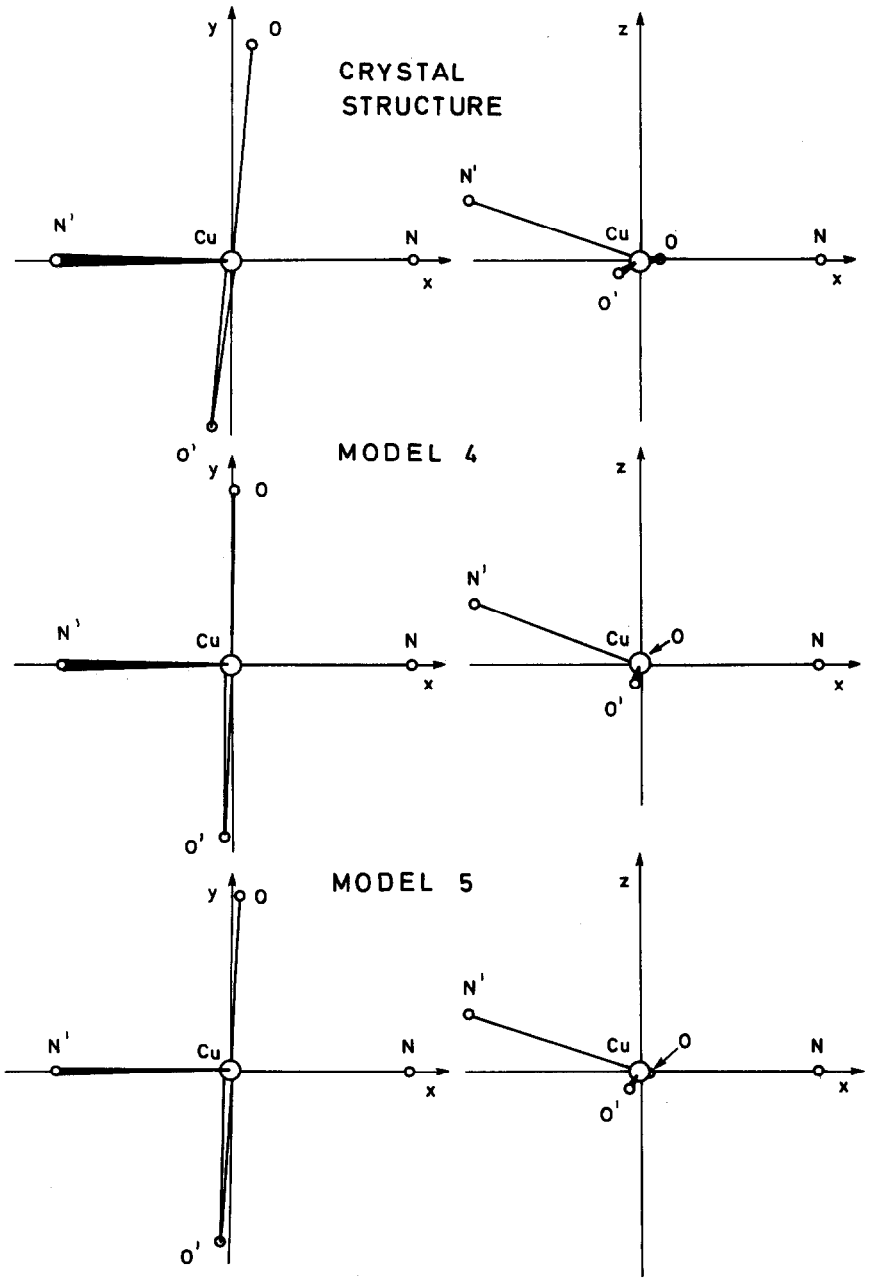

Fig. 3. Coordination polyhedra of bis-(N,N-dimethylvalinato)copper(II) as obtained experimentally[8] and using the models with a distortion coordinate potential (Model 4[9] and Model 5, this paper). Mark ′ denotes Ring 1 (see Fig. 4).

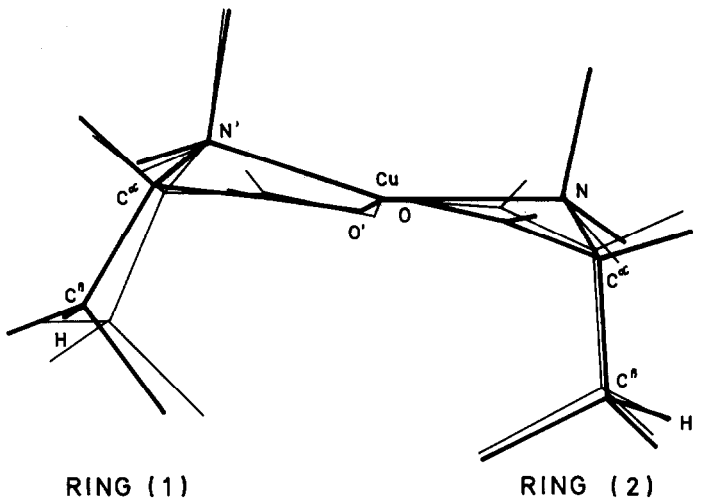

Fig. 4. Comparison of X-ray structure[8] (heavy line) and theoretical structure, Model 5 (thin line) of bis-(L-N,N-dimethylvalinato)copper(II).

Table 4. Estimation of conformational potential, Gibbs energy and statistical weights of the two isomers of bis-(N,N-dimethylvalinato)copper(II) with Model 5[a]

No.	Conformational potential MLL	MDL	ΔV	Gibbs energy MLL	MDL	ΔG
1–3	28.959	24.630	4.329	20.765	23.827	−3.062
	(0.0000)	(0.0000)		(0.0002)	(0.0000)	
1–6	10.458	9.774	0.684	10.229	8.925	1.304
	(0.0132)	(0.0008)		(0.0141)	(0.0039)	
3–3	15.164	16.643	−1.479	13.538	15.693	−2.155
	(0.0020)	(0.0001)		(0.0037)	(0.0003)	
3–4	26.673	22.880	3.793	23.485	18.243	5.242
	(0.0000)	(0.0000)		(0.0000)	(0.0001)	
3–6	12.572	11.189	1.383	11.527	11.064	0.463
	(0.0056)	(0.0005)		(0.0084)	(0.0017)	
4–6	5.939	5.589	0.350	5.758	5.753	0.005
	(0.0815)	(0.0044)		(0.0858)	(0.0141)	
5–5	29.352	23.410	5.942	32.328	26.965	5.363
	(0.0000)	(0.0000)		(0.0000)	(0.0000)	
6–6	0.0000	−7.860	7.860	0.000	−4.752	4.752
	(0.8941)	(0.9924)		(0.8755)	(0.9780)	
Estimated diastereoselectivity			8.53		5.42	
Experimental value[12]				2.9...4.0		

[a] All energy values are expressed in kJ mol^{-1}. Statistical weights are given in parentheses. The minima of the conformational energy are denoted as in Ref. 7. Zero points: $V = 33.957$ kJ mol^{-1}, $G = 1099.101$ kJ mol^{-1}. Diastereoselectivity was calculated from the energy of all 21 conformers; for conformers with high energy (not referred to here) energies were not computed after minimization, but approximative values for both strain and Gibbs energy were taken (approximation $E(n-m) = 1/2[E(n-n)+E(m-m)]$, where n and m were code numbers of the conformers).

molecular interactions (Table 3). The geometry of the copper(II) coordination polyhedron was best reproduced with Model 5 and worst with Model 4 for all, both planar and non-planar molecules. That also holds true for overall structure agreement expressed as r.m.s.-deviation with respect to all interatomic distances between non-hydrogen atoms. The only exception was bis-(L-N-benzylprolinato) copper(II), and to some degree bis-(L-phenylalaninato)copper(II), which showed preference (in decreasing order) for Models 5, 4 and 3. The very high $\varepsilon_{r.m.s.}(\Delta r)$ for the latter molecule is due to altered orientation of the phenyl ring in theoretical structures. Inspection of crystal structure[28] revealed that orientation of phenyl rings was determined by crystal packing, i.e. by stacking of phenyl rings.

All three models better reproduced geometry of planar than of non-planar molecules. Of all non-planar molecules the geometry of heavily distorted bis-(L-N,N-dimethylvalinato)copper(II) was most successfully reproduced (Figs 3 and 4), which was not surprising having in mind that all force fields were adjusted on that molecule. The angles determining the copper(II) coordination geometry did not fit equally well. The experimental vs theoretical values for *trans* angles (O–Cu–O and N–Cu–N) and distortion angle were highly correlated ($r > 0.8$ for non-planar molecules), less successfully correlated was the angle O′–N′–N–O ($r = 0.6$), and the worst correlation coefficients were obtained for *cis*-angles O–Cu–N ($r = 0.1$). The force fields appear to be "too stick"; they gave values for valence angles systematically closer to their equilibrium values (90 and 180°). That is possibly due to the fact that parameters determining the force fields were adjusted mostly to reproduce the *trans* angles and distortion coordinate β, which are the most critical internal coordinates for description of coordination polyhedron distortion.

The diastereoselectivity effect in copper(II)/N,N-dimethylvaline system was estimated with Model 5 (Table 4) nearly in the range of experimental error. It gave substantially better results than other models with distortion coordinate potential (Model 3 gave 7.43 and Model 4 gave 6.56 kJ mol^{-1}).[9]

In conclusion, we can state that of all the models checked, Model 5 seemed to be best because: (1) it yielded only two (planar and tetrahedral) minima with zero potential energy for "complex" CuN_2O_2, (2) it showed tetrahedral distortion to be preferred over the pyramidal one, (3) it reproduced the crystal geometry of *trans* copper(II) bis-aminoacidates with the highest accuracy and (4) it gave the best value for the diastereoselectivity effect of copper(II) N,N-dimethylvalinates of all models with distortion coordinate potential. Therefore, we recommend Model 5 for further development of force field for coordination compounds with distorted geometry.

REFERENCES

1. J. Gažo, I. B. Bersuker, J. Garaj, M. Kobašova, J. Kohout, H. Langefelderova, M. Melnik, M. Serator and F. Valach, *Coord. Chem. Rev.* 1976, **19**, 253.
2. B. J. Hathaway, *Coord. Chem. Rev.* 1982, **41**, 423.
3. J. Gažo, *Pure Appl. Chem.* 1974, **38**, 279.
4. J. H. Ritsma, G. A. Wiegers and F. Jellinek, *Rec. Trav. Chim.* 1965, **84**, 1577.
5. G. Brookes and L. D. Pettit, *J. Chem. Soc., Dalton Trans.* 1976, 1224.
6. N. Raos and Vl. Simeon, *Croat. Chem. Acta* 1985, **58**, 127.
7. N. Raos and Vl. Simeon, *Croat. Chem. Acta* 1983, **56**, 79.
8. B. Kaitner, B. Kamenar, N. Paulić, N. Raos and Vl. Simeon, *J. Coord. Chem.* 1987, **15**, 373.
9. J. Sabolović, N. Raos and Kj. Rasmussen, *Croat. Chem. Acta* 1989, **62**, 495.
10. N. Raos and Vl. Simeon, *Croat. Chem. Acta* 1984, **57**, 1217.
11. B. Kamenar, M. Penavić, A. Škorić, N. Paulić, N. Raos and Vl. Simeon, *J. Coord. Chem.* 1988, **17**, 85.
12. V. A. Davankov, S. V. Rogozhin, A. A. Kurganov and L. Ya. Zhuchkova, *J. Inorg. Nucl. Chem.* 1975, **37**, 369.
13. V. A. Davankov, S. V. Rogozhin and A. A. Kurganov, *Izv. Akad. Nauk. SSSR, Ser. Khim.* 1971, 204A.
14. V. A. Davankov, S. V. Rogozhin, Yu. T. Struchkov, G. G. Alexandrov and A. A. Kurganov, *J. Inorg. Nucl. Chem.* 1976, **38**, 631.
15. A. A. Kurganov, V. A. Davankov and L. Ya. Zhuchkova, *Koord. Khim.* 1977, **3**, 988.
16. K. Bernauer, *Top. Curr. Chem.* 1976, **65**, 1.
17. V. A. Davankov, A. A. Kurganov and S. V. Rogozhin, *Usp. Khim.* 1974, **43**, 1610.
18. N. Raos, S. R. Niketić and Vl. Simeon, *J. Inorg. Biochem.* 1982, **16**, 1.
19. N. Raos and S. M. Shevchenko, *J. Mol. Struct. (Theorchem.)* 1988, **164**, 407.
20. S. R. Niketić and Kj. Rasmussen, *The Consistent Force Field: A Documentation*, Springer, Berlin (1977).
21. S. Melberg and Kj. Rasmussen, *Carbohydrate Res.* 1979, **69**, 27; S. R. Niketić and Kj. Rasmussen, *Acta Chem. Scand.* 1981, **A35**, 213.
22. G. R. Clark, D. Hall and T. N. Waters, *J. Chem. Soc. (A)* 1969, 2808; T. P. Cheeseman, D. Hall and T. N. Waters, *ibid.* 1966, 685; D. Hall, S. V. Sheat and T. N. Waters, *ibid.* 1968, 460; T. P. Cheeseman, D. Hall and T. N. Waters, *ibid.* 1966, 1396; H. Tamura, K. Ogawa, A. Takeuchi and S. Yamada, *Bull. Chem. Soc. Japan* 1979, **52**, 3522; C. Panattoni, G. Bombieri and R. Graziani, *Acta Cryst.* 1967, **23**, 537.
23. T. G. Fawcett, M. Ushay, J. P. Rose, R. A. Lalan-

cette, J. A. Potenza and H. J. Schugar, *Inorg. Chem.* 1979, **18**, 327.
24. G. G. Aleksandrov, T. Struchkov and A. A. Kurganov, *Zh. Strukt. Khim.* 1973, **14**, 492.
25. C. M. Weeks, A. Cooper and D. A. Norton, *Acta Cryst.* 1969, **B25**, 443.
26. H. C. Freeman and R. J. Floor, personal communication (1978); V. Amirthalingam and K. V. Muralindharan, *Pramana* 1975, **4**, 83.
27. M. A. Hitchman, L. Kwan, L. M. Engelhardt and A. H. White, *J. Chem. Soc., Dalton Trans.* 1987, 457.
28. D. van der Helm, M. B. Lawson and E. L. Enwall, *Acta Cryst.* 1971, **B27**, 2411.
29. I. A. Dyakon, S. V. Donu, L. F. Chapurina and A. S. Avilov, *Kristallografia* 1984, **29**, 384.
30. C. P. Nash and W. P. Schaefer, *J. Am. Chem. Soc.* 1969, **91**, 1319.
31. G. G. Aleksandrov, Yu. T. Struchkov, A. A. Kurganov, S. V. Rogozhin and V. A. Davankov, *Zh. Strukt. Khim.* 1972, **13**, 671.
32. R. Calvo, M. A. Mesa, G. Oliva, J. Zukerman-Schpector, O. R. Nascimento, M. Tovar and R. Arce, *J. Chem. Phys.* 1984, **81**, 4584.
33. G. G. Aleksandrov and Yu. T. Struchkov, *Zh. Strukt. Khim.* 1975, **16**, 228.

Polyhedron Vol. 9, No. 10, pp. 1287–1292, 1990
Printed in Great Britain

0277–5387/90 $3.00+.00
© 1990 Pergamon Press plc

THIOPHENE RING CYCLOPALLADATION OF N,N-DIMETHYL-2(OR 3)-THIOPHENECARBOTHIOAMIDE

HIROYUKI MIZUNO and MATSUO NONOYAMA*

Department of Chemistry, Faculty of Science, Nagoya University, Chikusa, Nagoya, 464 Japan

(*Received* 26 *September* 1989; *accepted* 11 *January* 1990)

Abstract—N,N-Dimethyl-2(or 3)-thiophenecarbothioamide [abbreviated as Hatt (or Hbtt)] was conveniently prepared by the reaction of the corresponding carboxaldehyde with dimethylamine hydrochloride and sulfur. The thioamides reacted with lithium tetrachloroplalladate(II) in methanol to give PdCl(att) and PdCl(btt). Their derivatives of tri-n-butylphosphine, pyridine, and pentane-2,4-dione were prepared. The new complexes were characterized spectroscopically. The palladium atom is bound to the thiophene ring 3(or 2)-carbon atom and simultaneously coordinated with the sulfur atom of the thioamide group to form a five membered palladathiaheterocycle. Geometrical isomers [*cis*(C,X) and *trans*(C,X)] were identified for $PdX(att)(PBu_3)$ (X = Cl, I; PBu_3 = tri-n-butylphosphine) and some other derivatives in $CDCl_3$ solutions.

Thiophene lies in chemical reactivity between benzene and furan.[1] The latter two substituted with an N,N-dimethylthiocarbamoyl group, that is, N,N-dimethylbenzthioamide (abbreviated as Hpht), and N,N-dimethyl-2(or 3)-furancarbothioamide [Haft (or Hbft)], are cyclopalladated with lithium tetrachloropalladate(II) in methanol to give, respectively, PdCl(pht) and PdCl(aft) [or PdCl(bft)]. The compositions are apparently similar to each other but the site of palladation is quite different: Hpht is palladated at the N-methyl substituent of the thioamide group[2] while Haft (or Hbft) at the furan ring[3] [Structures I and II (or III), respectively].

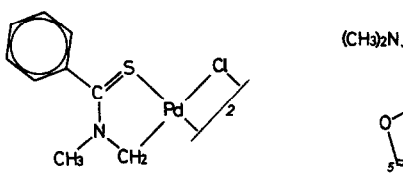

I

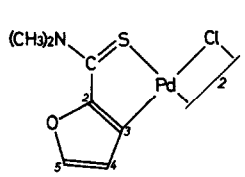

II

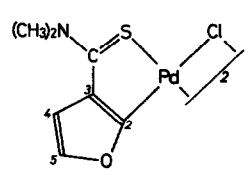

III

* Author to whom correspondence should be addressed.

These results indicate that the benzene ring is less reactive than the N-methyl group but the furan ring is more reactive than that. How the thiophene analogue reacts attracts our interest: N,N-dimethyl-2(or 3)-thiophenecarbothioamide [abbreviated as Hatt(or Hbtt)] will be cyclopalladated either at the N-methyl group or at the thiophene ring.

RESULTS AND DISCUSSION

N,N-Dimethylthiophenecarbothioamide has been prepared by thiation of the carboxamide with diphosphorus pentasulfide[4] but one pot reaction of commercially available thiophenecarbaldehyde with dimethylamine hydrochloride and sulfur affords the thioamide more conveniently.[5] The thioamide reacted easily with lithium tetrachloropalladate(II) in methanol at room temperature to give PdCl(att) or PdCl(btt) (Table 1). Their solubilities are generally poor but they are slightly soluble in dmso (dimethylsulfoxide).

The ^1H NMR spectra of dmso-d_6 solutions of PdCl(att) and PdCl(btt) (Table 2) show clearly that one of the thiophene ring protons is lost in the complexes while the N-methyl substituent of the thioamide group remains intact. In the $^{13}C\{^1H\}$ NMR spectra (Table 3) the 3-C signal of the thiophene ring of PdCl(att) and the 2-C signal of

Table 1. Yields, melting points, analytical results and the IR spectra of the complexes

Complex[a]	Yield (%)	M.p.[b] (°C)	Analysis: Found(Calc.), % C	H	N	IR spectra[c] ν(Pd—Cl)	ν(C—N)
Hatt	68	124–127[d]	48.8(49.1)	5.2(5.3)	8.4(8.2)		1503
Hbtt	93	45–46	49.4(49.1)	5.4(5.3)	8.3(8.2)		1525
PdCl(att)	82	235(dec)	26.7(26.9)	2.5(2.6)	4.4(4.5)	218, 297	1560
PdCl(att)(PBu_3)	61	111–116	44.6(44.4)	6.8(6.9)	2.4(2.7)	297	1546
PdI(att)(PBu_3)	62	146–147	37.8(37.7)	5.9(5.8)	2.3(2.3)		1549
PdCl(att)($Ptol_3$)	89	208–210	54.6(54.6)	4.8(4.7)	2.2(2.3)	304	1552
PdCl(att)(py)	88	187(dec)	36.7(36.8)	3.3(3.4)	7.2(7.2)	313	1552
PdI(att)(py)	83	215(dec)	29.7(29.9)	2.7(2.7)	5.9(5.8)		1551
Pd(att)$(py)_2(BF_4)$	60	153–156	39.2(39.1)	3.4(3.5)	8.3(8.1)		1560
Pd(att)(acac)	82	174(dec)	38.2(38.4)	4.1(4.0)	3.7(3.7)	246, 439[e]	1551
PdCl(btt)	80	204(dec)	26.9(26.9)	2.5(2.6)	4.6(4.5)	218, 300	1562
PdCl(btt)(PBu_3)	60	121–124	44.4(44.4)	6.8(6.9)	2.8(2.7)	304	1549
PdCl(btt)(py)	83	182(dec)	36.8(36.8)	3.4(3.4)	7.2(7.2)	321	1551
Pd(btt)(acac)	54	176(dec)	38.2(38.4)	4.1(4.0)	3.9(3.7)	248, 441[e]	1553

[a] Abbreviations: Hatt = N,N-dimethyl-2-thiophenecarbothioamide, Hbtt = N,N-dimethyl-3-thiophenecarbothioamide, PBu_3 = tri-n-butylphosphine, $Ptol_3$ = tri-p-tolylphosphine, py = pyridine, and acac = pentane-2,4-dionate ion.

[b] dec = decomposition.

[c] Nujol mull and frequencies in cm^{-1}.

[d] Boiling point under 2 mm Hg.

[e] ν(Pd—O).

PdCl(btt) are significantly deshielded compared with those of free Hatt and Hbtt. The deshielding is very similar to that observed for cyclopalladation of Haft and Hbft (c.f. Structures II and III).[3] The chemical shifts of 4-C and 5-C coincide for each complex.

In the IR spectra (Nujol mull) of the complexes a higher frequency shift of ν(C–N) for the thioamide group is notable (Table 1). The shift is characteristic of S-coordination of the thioamide group and originates from an increase in double bond character of the C–N bond in a coordinated form (eq. 1, B).[6]

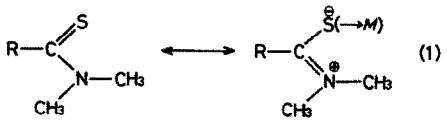

(1)

A B

The above data suggest Structures IV and V for PdCl(att) and PdCl(btt), respectively. Coordination of Cl is supported by the presence of strong ν(Pd–Cl) bands (Table 1).

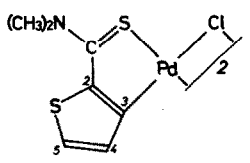

IV

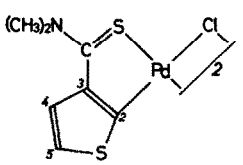

V

The spectroscopic data of the pentane-2,4-dionato derivatives, Pd(att)(acac) and Pd(btt)(acac), show that the acac ligand is coordinated in a normal way, while the two halves of acac are not spectroscopically equivalent: one half is *trans* to C and the other to S donor atoms. The palladated att and btt remain in the same coordination modes as those of the parent complexes (Tables 2 and 3). Structure VI (X,L = acac) is proposed for Pd(att)(acac) and

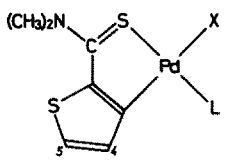

trans(C,X)
VI

a similar one for Pd(btt)(acac). The structures, where the Pd—O bonds are arranged *trans* to the C and S atoms, are compatible with the lower frequencies of ν(Pd–O) (Table 1) than those of Pd $(acac)_2$ because the *trans* influences of the C and S atoms are superior to that of the O atoms of acac.[7]

The ^1H NMR spectrum of PdCl(att)(PBu_3), measured a few hours after dissolution in $CDCl_3$, is shown in Fig. 1. The spectrum measured immediately after dissolution gives, however, no lower field weak signals and changes into the above spectrum

Table 2. ^1H (90 MHz) and $^{31}P\{^1H\}$ (36.4 MHz) NMR spectra of the ligands and complexes

Compound	Solvent	$\delta(^1H)$, ppm[a]			$\delta(^{31}P)$[b] (ppm)
		4-H	5-H	N—CH_3[b]	
Hatt[c]	$CDCl_3$	6.94dd(5.0, 3.7)	7.37dd(5.0, 1.3)	3.46	
Hbtt[d]	$CDCl_3$	7.12dd(5.0, 1.3)	7.26dd(5.0, 3.1)	3.55, 3.25	
PdCl(att)	dmso-d_6	8.01d(5.2)	7.79d(5.2)	3.73, 3.63	
PdCl(att)(PBu_3)	$CDCl_3$				
trans(C,Cl)		7.05dd(5.1)[1.8]	7.66dd(5.1)[1.5]	3.74, 3.65	14.9
cis(C,Cl)		8.02dd(4.8)[2.2]	7.74dd(4.8)[3.5]	3.74, 3.68	2.4
PdI(att)(PBu_3)	$CDCl_3$				
trans(C,I)		7.10dd(5.1)[1.8]	7.78dd(5.1)[1.5]	3.71, 3.60	13.8
cis(C,I)		8.45dd(5.0)[2.0]	7.58dd(5.0)[3.6]	3.71, 3.63	−1.0
PdCl(att)($Ptol_3$)	$CDCl_3$	6.30dd(5.2)[2.3]	[e]	3.72, 3.68	32.4[f]
PdCl(att)(py)[g]	$CDCl_3$	8.09d(5.0)	7.70d(5.0)	3.74, 3.64	
PdI(att)(py)	$CDCl_3$	8.47d(5.1)	7.57d(5.1)	3.73, 3.61	
Pd(att)(py)$_2$(BF_4)	CD_3NO_2	6.15d(5.1)	7.67d(5.1)	3.80, 3.69	
Pd(att)(acac)	$CDCl_3$	7.64d(5.2)	7.72d(5.2)	3.70, 3.66	
PdCl(btt)	dmso-d_6	7.39s	7.39s	3.71, 3.58	
PdCl(btt)(PBu_3)	$CDCl_3$	7.18m	7.18m	3.67	15.6[h]
				3.57d(0.7)	
PdCl(btt)(py)	$CDCl_3$	7.19s	7.19s	3.70, 3.60	
Pd(btt)(acac)	$CDCl_3$	7.13d(5.5)[i]	7.16d(5.5)[i]	3.68, 3.63	

[a] Only the signals due to Hatt and Hbtt are given in this Table. Figures in parentheses are coupling constants, J(H—H) and those in square brackets J(P—H) in Hz. Abbreviations: s = singlet, d = doublet, m = multiplet, and dmso-d_6 = deuterated dimethylsulfoxide.

[b] These signals are singlets unless otherwise noted.

[c] The 3-H signal is at 7.09 ppm (dd: 3.7, 1.3 Hz).

[d] The 2-H signal is at 7.35 ppm (dd: 3.1, 1.3 Hz).

[e] Obscured by the signals due to $Ptol_3$.

[f] Accompanied by a very weak signal at 14.7 ppm.

[g] Very weak signals are observed at 6.35 ppm (d: 5.1 Hz, 4-H) and 7.60 (d: 5.1, 5-H).

[h] Accompanied by a very weak signal at 4.1 ppm.

[i] Assignment is not definite.

within a few hours. This fact indicates that PdCl(att)(PBu_3) in the solid state consists only of one species which gives the major signals in the spectrum of Fig. 1 and dissolution results in an equilibrium between one major and the other minor isomers (the ratio is about 85:15). The ^1H NMR spectrum of the corresponding iodo complex PdI(att)(PBu_3) is unchangeable with time and shows that nearly equal amounts of two isomers are present in a $CDCl_3$ solution (Fig. 1). The assignment of the spectra is given in Table 2.

The $^{13}C\{^1H\}$ NMR spectrum of PdCl(att)(PBu_3) (Table 3) suggests that the minor isomer is *cis*(C,Cl), because J(P–C) for the 3-C signal is very large: PBu_3 is *trans* to the palladated 3-C atom (Structure VII, L = PBu_3). The two isomers of PdI(att)(PBu_3) are similarly assigned. The ^1H chemical shift difference (Δ) of 4-H of the *cis*(C,X) isomers between X = Cl and I is remarkable: Δ = 0.43 ppm. A similar downfield shift upon replacement of Cl with I has been reported for related cyclopalladated complexes[8] and attributed to the fact that the hydrogen in question is situated in the proximity of X. In Structure VII, proposed on the basis of the ^{13}C NMR spectra, the 4-H is also situated near to X. In contrast, in Structure VI the 4-H is far away from X and should be insensitive to X. The major isomer of PdCl(att)(PBu_3) has, therefore, a *trans*(C,Cl) arrangement (Structure VI, X = Cl, L = PBu_3). For this complex the assignment of the ^{13}C signals is certified by the ^1J(C—H) values: 167.4 Hz for 4-C

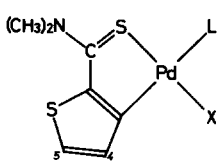

cis (C, X)
VII

Table 3. $^{13}C\{^1H\}$ NMR spectra (22.6 MHz) of the ligands and complexes

Compound	Solvent	$\delta(^{13}C)$, ppm[a]					
		2-C	3-C	4-C	5-C	C(=S)	CH_3
Hatt	$CDCl_3$	145.0	126.3	126.3	129.0	191.4	44.5
Hbtt	$CDCl_3$	123.6	143.0	127.0	125.3	195.0	44.1, 43.4
PdCl(att)	dmso-d_6[b]	136.2	160.7	134.7	134.7	188.0	46.8
PdCl(att)(PBu_3)	$CDCl_3$						
trans(C,Cl)		138.3(1.4)	162.1(1.0)	135.3(11.4)	132.3(5.5)	190.8(3.1)	45.1, 46.1(3.1)
cis(C,Cl)		135.8(5.2)	177.7(140)	133.1(12.8)[c]	135.3[c]	191.9(14.5)	[d]
PdI(att)(PBu_3)	$CDCl_3$						
trans(C,I)		137.8(1.7)	166.6	134.6(10.7)	132.9(4.8)	192.9(3.1)	45.3, 46.1(2.8)
cis(C,I)		143.5(4.5)	174.6(141)	134.4(12.4)[c]	136.8[c]	191.8(13.5)	45.9, 45.5
PdCl(att)($Ptol_3$)	$CDCl_3$	138.0(1.4)	161.7	137.7(10.0)	131.3(6.2)	190.5(3.5)	45.1, 46.2(2.8)
Pd(att)$(py)_2(BF_4)$	CD_3NO_2	136.2	160.7	133.6	134.6	187.7	45.3
Pd(att)(acac)	$CDCl_3$	133.8	164.0	132.0	132.0	190.7	45.0, 44.8
PdCl(btt)	dmso-d_6[b]	164.7	142.6	125.8	125.8	188.3	45.2, 44.9
PdCl(btt)(PBu_3)	$CDCl_3$	165.3	147.0	125.5(0.7)	124.7(3.5)	193.3(3.5)	45.7
Pd(btt)(acac)	$CDCl_3$	170.5	142.3	124.7[c]	123.5[c]	192.1	45.4, 45.2

[a] Only the signals due to Hatt and Hbtt are given in this Table. Figures in parentheses are coupling constants J(P—C) in Hz.
[b] Measured at 80°C.
[c] Assignment of 4-C and 5-C is uncertain.
[d] Obscured by strong signals of the *trans*(C,Cl) isomer.

at 135.3 ppm and 185.3 Hz for 5-C at 132.3 ppm.[9]

The $^{31}P\{^1H\}$ NMR spectrum of PdCl(att)($Ptol_3$) (Table 2) shows that there are also two isomers in a $CDCl_3$ solution: one major and the other minor (less than 10%). The ^1H signals of att and $Ptol_3$ overlap in the region of aromatic proton resonances but the 4-H of the major isomer resonates separately significantly to higher field. This shielding may be attributed to the anisotropic effect of the neighbouring aromatic ring of $Ptol_3$ (Structure VI, L = $Ptol_3$). The minor isomer is not characterized so far because of its low concentration in the solution but may be a *cis*(C,Cl) isomer (Structure VII). The presence of its weak ^{31}P signal at a higher field (δ = 14.7 ppm) than that of the major isomer supports the structure by analogy with the ^{31}P NMR chemical shifts of PdCl(att)(PBu_3): the P atom *trans* to the palladated C atom resonates at a higher field than that *cis* to the C atom.

The shielding of the 4-H is similarly remarkable for Pd(att)$(py)_2(BF_4)$ (Table 2) where the 4-H is in the shielding region of py (Structure VI, X = L = py), because the py ring is sterically restricted perpendicular to the coordination plane. Contrastingly the signal of the 4-H of PdX(att)(py) is deshielded and depends strongly upon X like that of *cis*(C,X)-PdX(att)(PBu_3). Structure VII (L = py, X = Cl, I) is suggested for PdX(att)(py). The weak signal at 6.35 ppm indicates the presence of a second isomer (less than 10%) and the shielding of the 4-H signal suggests Structure VI (X = Cl, L = py) for the isomer because the 4-H is in the shielding region of py as in the case of Pd(att)$(py)_2(BF_4)$.

The isomer ratios of PdCl(att)(L) (L = py, PBu_3) in $CDCl_3$ solutions depend markedly upon L: the dominant isomer is *cis*(C,Cl) for L = py but *trans* (C,Cl) for PBu_3. The donor properties of L (py or PBu_3) may be a major influence. The ratios are also affected by X as observed for PdX(att)(PBu_3) [*trans*/*cis*(C,X) = 85/15 (X = Cl) and 45/55 (I)]. We have no certain explanation for these trends at present and more investigations will be required.

Spectroscopic information available for PdCl (btt)(PBu_3) and PdCl(btt)(py) is less revealing because the signals due to 4-H and 5-H are overlapped (Table 2). The ^{31}P NMR spectrum of PdCl(btt)(PBu_3) shows that in a $CDCl_3$ solution two isomers [one major and the other minor (less than 10%)] coexist and the chemical shifts [15.6 (strong) and 4.1 (weak) ppm] suggest that the major isomer is *trans*(C,Cl) and the minor one *cis*(C,Cl) by analogy with the isomerism of PdCl(att)(PBu_3). The *trans*(C,Cl) structure is consistent with the fact that no J(P—C) is detected for the 2-C signal of the major isomer of PdCl(btt)(PBu_3) (Table 3). The assignment of 4-C and 5-C of the major isomer is

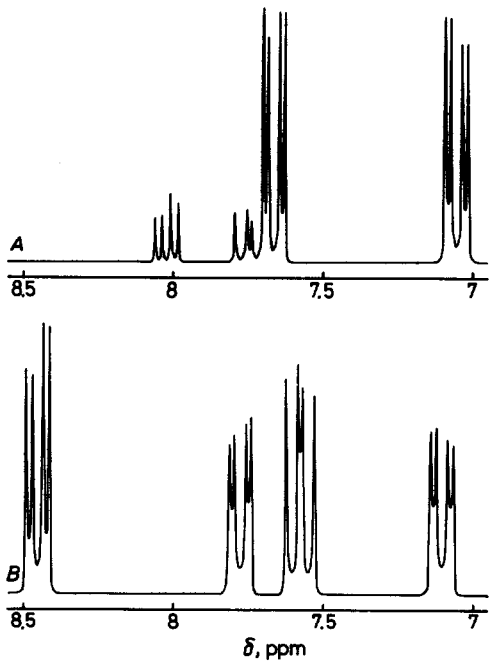

Fig. 1. ^{1}H NMR spectra (90 MHz) of A : PdCl(att)(PBu_3) and B : PdI(att)(PBu_3) measured a few hours after dissolution in $CDCl_3$ at room temperature.

confirmed by the values of ^1J(C—H) : 167.5 Hz for 4-C at 125.5 ppm and 187.7 Hz for 5-C at 124.7 ppm.[9] The structure of PdCl(btt)(py) cannot be assigned unambiguously.

In summary, under the conditions of this experiment both Hatt and Hbtt are cyclopalladated at the thiophene ring and there are no indications of cyclopalladation of the N-methyl substituent of the thioamide group. The thiophene derivatives are similar to the furan derivatives,[3] Haft and Hbft, in that the aromatic heterocycles are exclusively cyclopalladated, but quite different from the benzene derivative, Hpht, where the N-methyl substituent is cyclopalladated.[2] All these thioamides are sterically similar and the quite different reactivity should be attributed to electronic origin.[1]

EXPERIMENTAL

Measurements

IR spectra were recorded on JASCO IR-A3 and HITACHI EPI-L spectrometers. NMR spectra were recorded on HITACHI R-90H (^{1}H, 90 MHz; ^{13}C, 22.6 MHz; ^{31}P, 36.4 MHz) and JEOL PMX-60 (^{1}H, 60 MHz) spectrometers. Chemical shifts, δ ppm, were relative to internal tetramethylsilane (^{1}H, ^{13}C) and to external 85% H_3PO_4(^{31}P). Melting points were not corrected.

Synthesis of ligands, Hatt and Hbtt

Analytical results, yields, and melting points are given in Table 1 and spectroscopic data in Tables 2 and 3.

The two thioamides were prepared from appropriate aldehydes by application of the method of Amupitan.[5] Hatt was obtained as a yellow oily substance and Hbtt as yellow crystals (from dichloromethane/n-hexane).

Synthesis of complexes

PdCl(att) *and* PdCl(btt). To a solution of 1 mmol of lithium tetrachloropalladate in 30 cm^3 of methanol, prepared *in situ* from 1 mmol of palladium(II) chloride and 2 mmol of lithium chloride, was added 1 mmol or Hatt (or Hbtt) and the mixture was stirred at room temperature overnight. The yellow precipitate was washed with methanol and dried in air.

PdCl[att(*or* btt)](L) (L = PBu_3, $Ptol_3$, *and* py). To a suspension of PdCl[att(or btt)] in dichloromethane was added a stroichiometric amount of PBu_3 (or $Ptol_3$) or an excess of py and the mixture was stirred until it had become clear. The filtrate was concentrated to a small volume and addition of n-hexane precipitated the yellow product, which was washed with n-hexane and dried in air. The iodo complexes were obtained by metathesis of the chloro complexes with a fourfold excess of lithium iodide in acetone.

Pd(att)$(py)_2(BF_4)$. To a suspension of 1 mmol of PdCl(att) in a mixture of 20 cm^3 of acetone and 20 cm^3 of water was added an excess of py and the mixture was stirred until it had become clear. To the solution was added 1 mmol of silver tetrafluoroborate and the mixture was stirred for a few hours. The silver chloride precipitated was removed and the filtrate was concentrated to a small volume to give the product, which was washed with water and dried in air.

Pd(att)(acac) *and* Pd(btt)(acac). To a solution of 1 mmol of sodium pentane-2,4-dionate in a mixture of 25 cm^3 of methanol and 50 cm^3 of dichloromethane was added 1 mmol of PdCl[att(or btt)] and the mixture was stirred for 4 h. The filtered solution was evaporated to dryness and the residue was dissolved in dichloromethane. The undissolved material was removed by filtration and the filtrate was concentrated to a small volume. Upon addition of n-hexane a yellow precipitate was obtained, which was washed with n-hexane and dried in air.

The IR and NMR data due to the acac moiety are as follows: ν(C=O, C=C) at 1572 and 1516 cm^{-1}(att) and at 1567 and 1515(btt). δ(^{1}H) = 1.98,

2.09, and 5.38 ppm(att), and 1.98, 2.09, and 5.39(btt). $\delta(^{13}C\{^{1}H\}) = 27.7$, 27.8, 100.1, 186.1, and 187.5 ppm(att), and 27.4, 27.7, 100.4, 186.2, and 187.5(btt).

Acknowledgement—This work was supported in part by a Grant-in-Aid for Scientific Research from the Ministry of Education, Science, and Culture (No. 61430013).

REFERENCES

1. C. W. Bird and G. W. H. Cheeseman (Eds), *Comprehensive Heterocyclic Chemistry*, Vol. 4, Part 3, p. 39. Pergamon Press, Oxford (1984).
2. T. J. Grinter, D. Leaver and R. M. O'Neil, *Inorg. Nucl. Chem. Lett.* 1980, **16**, 145.
3. M. Nonoyama, *Inorg. Chim. Acta* 1989, **157**, 9.
4. F. Bernardi, L. Lunazzi and P. Zanirato, *Tetrahedron* 1977, **33**, 335.
5. J. O. Amupitan, *Synthesis* 1983, 730.
6. K. A. Jensen and P. H. Nielsen, *Acta Chem. Scand.* 1966, **20**, 597.
7. T. G. Appleton, H. C. Clark and L. E. Manzer, *Coord. Chem. Rev.* 1973, **10**, 335.
8. M. Nonoyama and H. Takayanagi, *Transition Met. Chem.* 1975, **1**, 10.
9. Ref. 1, p. 733.

Polyhedron Vol. 9, No. 10, pp. 1293–1296, 1990
Printed in Great Britain

0277–5387/90 $3.00+.00
© 1990 Pergamon Press plc

MIXED-LIGAND COMPLEXES OF COPPER(II) CONTAINING A MONOCONDENSED SCHIFF BASE AND AN AMINO ACID OR AMINE

W. L. KWIK* and ALICE W. N. TAY

Department of Chemistry, National University of Singapore, Lower Kent Ridge Road, Singapore 0511, Republic of Singapore

(*Received* 9 *June* 1989; *accepted* 15 *January* 1990)

Abstract—A series of mixed-ligand complexes of Cu^{II} containing a monocondensed Schiff base and an amino acid/amine have been isolated and characterised via molar conductance, magnetic susceptibility, IR and electronic spectral measurements.

As part of our continuing interest in the study of four-coordinate Schiff bases,[1,2] condensation reactions of 1,3-diacetylbenzene with phenylalanine methyl ester, tyrosine ethyl ester, histamine, histidine methyl ester and 2-(2-aminoethyl)pyridine, have now been examined. Whereas benzene 1,3-dicarbaldehyde condenses with two moles of l-histidine methyl ester or N-methylhistidine methyl ester[3] along with hydroxylation of the aromatic nucleus at position 2 producing binuclear phenoxy-bridge copper(II) complexes, 1,3-diacetylbenzene forms only monocondensed Schiff bases under similar experimental conditions. The resultant mono-Schiff base in each case readily forms mixed-ligand complexes of copper(II) with a second amino acid or amine molecule. In the following we report on the synthesis and spectral properties of several such mixed-ligand complexes of copper(II).

EXPERIMENTAL

Synthesis

Both 1,3-diacetylbenzene and 2-(2-aminoethyl) pyridine (Aldrich Chemical Co.) were used as received. Phenylalanine methyl ester hydrochloride, tyrosine ethyl ester hydrochloride, histidine methyl ester dihydrochloride and histamine dihydrochloride (Sigma Chemical Co.) were treated to remove the hydrochloride.

The syntheses of all the copper(II) and zinc(II) complexes are similar to those described previously.[1] The complexes 1–5 (Table 1) containing the mono-Schiff bases L^1–L^5 (Scheme 1) were prepared by prolonged reflux of a dry methanolic solution of 1,3-diacetylpyridine and two moles of an appropriate amino acid or amine, in the presence of a stoichiometric amount of the metal salt. The complex was recrystallised twice using 5 : 1 MeOH : isopropanol. The Cu^{II} complexes have been characterised by elemental analysis, conductance measurements in MeOH and DMSO, magnetic susceptibilities and electronic spectral determinations (Table 1).

Physical and spectral measurements

Conductivities of 10^{-3} M solutions of the complexes were measured at 30°C using a CM-115 conductivity bridge meter. Infrared spectra in the region 4000–400 cm^{-1} were recorded on a Perkin–Elmer model 1710 Fourier Transform Infrared spectrometer. Spectra extending into the Far IR region of 200 cm^{-1} were recorded on a Perkin–Elmer model 567 spectrometer calibrated with polystyrene film. CsI and KBr pellets were employed throughout. Electronic spectra were recorded on a Perkin–Elmer Lambda 9 UV–vis/near IR spectrophotometer. Magnetic susceptibilities for the complexes in the solid state were determined by the Faraday technique at 25°C on a Cahn Model RTL No. 7050 magnetic susceptibility system. Both ^1H and ^{13}C NMR spectra were recorded on a Joel 90 MHz spectrophotometer.

* Author to whom correspondence should be addressed.

Table 1. Microanalysis (%), conductivity data and magnetic moment

Complex	Microanalysis (%) Found C	H	N	Cu/Zn	Calculated C	H	N	Cu/Zn	Conductivity data and magnetic moment at 30°C Λ_M[a] MeOH	DMSO	μ (BM)
1 $[CuL^1(PHE)](BF_4)_2$[b]	48.1	4.7	3.8	8.27	48.1	4.7	3.7	8.48	244	89	1.75
2 $[CuL^2(TYR)](BF_4)_2$[b]	49.2	4.8	4.0	8.53	49.1	4.6	3.6	8.13		76	1.74
3 $[CuL^3(HME)](BF_4)_2$	37.2	4.5	10.4	8.36	37.2	4.6	10.9	8.21	256	96	1.82
4 $[CuL^4(HMN)](BF_4)_2$	37.7	4.8	13.0	9.83	37.5	4.7	13.1	9.93	120	60	2.11
5 $[CuL^5(AEP)](BF_4)_2$ $[Cu(CH_3CN)_4](BF_4)_2$	41.3	3.9	11.8	13.01	41.6	4.1	12.1	13.77	151		2.05
6. $[ZnL^2(TYR)](ClO_4)_2$	42.1	4.6	3.6	7.56	42.3	4.6	3.3	7.68	150	50	

[a] Unit for molar conductance is $\Omega^{-1}\,cm^2\,mol^{-1}$.
[b] Abbreviations: PHE = phenylalanine; TYR = tyrosine.

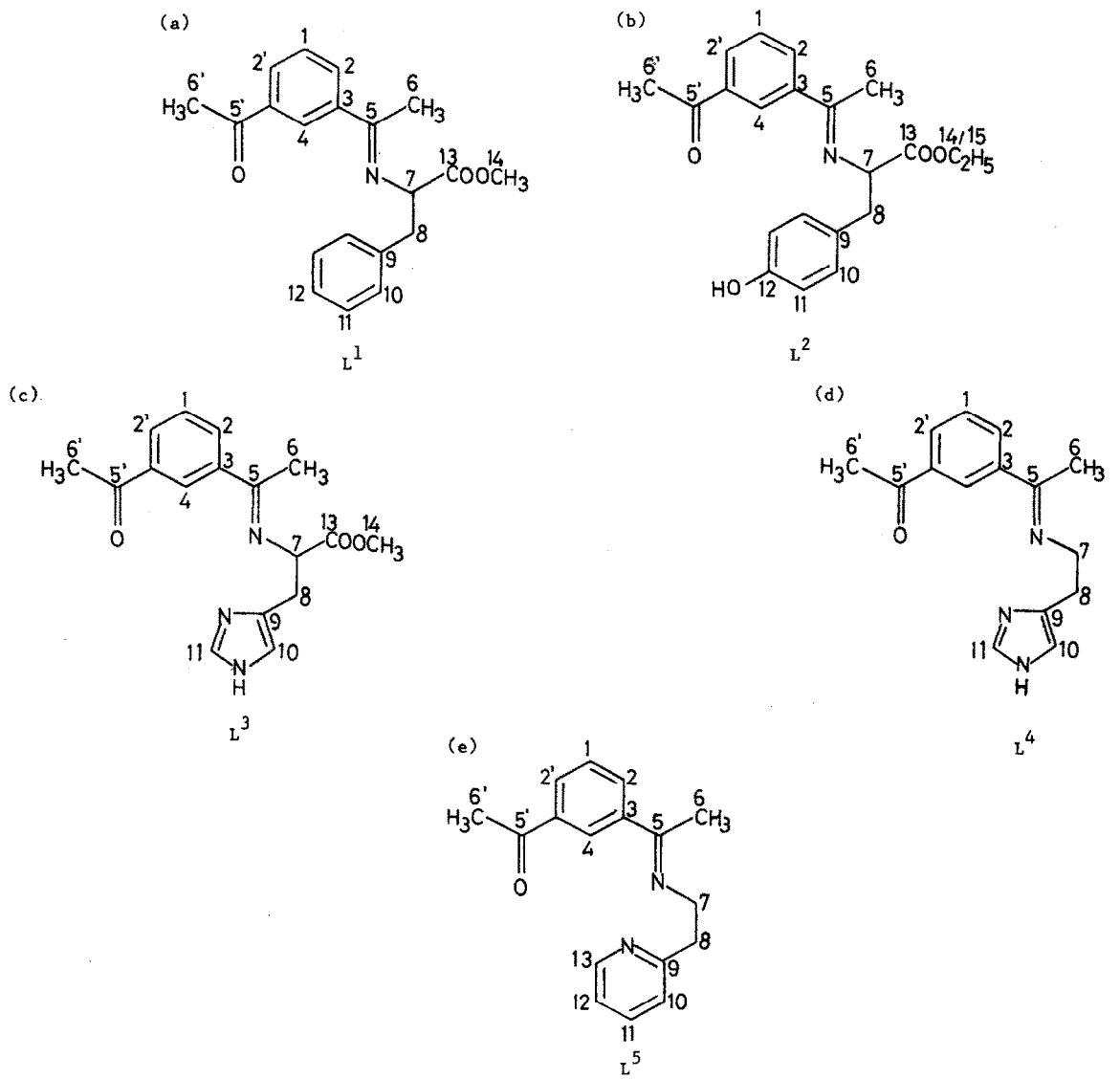

Scheme 1. Schiff bases derived from 1,3-diacetylbenzene and (a) phenylalanine methyl ester; (b) tyrosine ethyl ester; (c) histidine methyl ester; (d) histamine; (e) 2-(2-aminoethyl)pyridine.

RESULTS AND DISCUSSION

Evidence for the presence of a monocondensed Schiff base in the coordination sphere of Cu^{II} with an amino acid or an amine taking up the remaining coordination sites, are derived from a careful analysis of the IR spectral data. Thus all the complexes are characterised by a strong absorption at 1685 cm^{-1} attributable to the $\rangle C{=}O$ stretching and at 1620/1597 cm^{-1} due to the imino $\rangle C{=}N$ stretching of the mono-Schiff base.[5,6] The $-NH_2$ vibrational modes[5,6] due to the coordinated amino acid or amine appear at 3320–3260 and 1608 (ν_{NH_2}), 1151/1058 (δ_{NH_2}) and 644 (ρ_{NH_2}) cm^{-1}. Furthermore in complexes containing the PME/TEE* moieties the absorption band at 1740 cm^{-1} characteristic of the uncoordinated carboxylate group[7] is of reduced intensity relative to that of $\nu_{C=N}$. This implies that the carboxylate ester group in the amino acid ester of complexes 1 and 2 are probably hydrolysed as has previously been observed.[1,2] The stretching of the coordinated carboxylate occurs at 1610–1590 cm^{-1} which overlaps with those of the $\rangle C{=}N$. However from the electronic spectral data as well as the known preferred coordination geometry for Cu^{II}, complexes containing PME/TEE attain at least four coordination with the carboxylate oxygen of the amino acid being one of the donor atoms (Fig. 1). Those of HME, HMN and AEP* contain at least four-coordinated $Cu^{II}N_4$ chromophore with possible interaction of the carbonyl oxygen (Fig. 2).

The expected absorptions[8] for ν_{Cu-N} and ν_{Cu-O} are found at 480, 415, 340, 318 and 280 cm^{-1}.

Isolation of the corresponding Zn^{II} complexes proves to be elusive. However the ^1H and ^{13}C NMR spectral data for the complex derived from L^2 and TYR are consistent with the formula $Zn[L^2(TYR)](ClO_4)_2$ which was first established from elemental analysis. Thus the two groups of methyl protons of the dicarbonyl became inequivalent in the complex, appearing at 2.52 and 2.65 ppm;[9,10] the change of 0.13 ppm in going from the free carbonyl to the imino group is consistent with the fact that the oxygen atom of 1,3-diacetylbenzene is replaced[2] by the less electronegative nitrogen in the Schiff base formed. The non-equivalence of the two methine

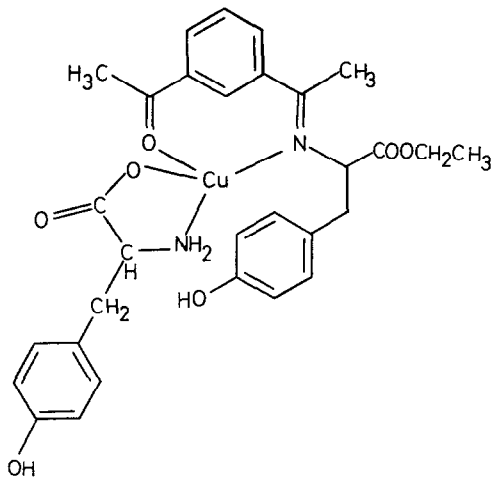

Fig. 1.

H(7) as well as the methylene H(8) protons due to the two different TYR moieties resulted in the somewhat broad absorption peaks at 4.1 and 3.0 ppm respectively, whereas in the Schiff base complexes derived from the 2,6-diacetylpyridine[1,2] one sharp absorption each was observed. The shifts of 0.5 ppm for H(7) and of 0.3 ppm for H(8) in going from the precursor to the complex are, however, comparable in these cases.[1,2]

The imino and carbonyl carbons C(5) of the monocondensed Schiff base L^2 in the Zn^{II} complex appear at 169 and 197 ppm respectively, in contrast to those of the bis-Schiff bases Zn^{II} complexes[1,2] displaying only one signal at 172 ppm. Two absorptions at 176 and 197 ppm are observed for C(13) in the mono-Schiff base and the coordinated amino acid, respectively. The relatively large shift of the latter from that of the precursor clearly demonstrates interaction of the carboxylate oxygen with the Zn^{II}.

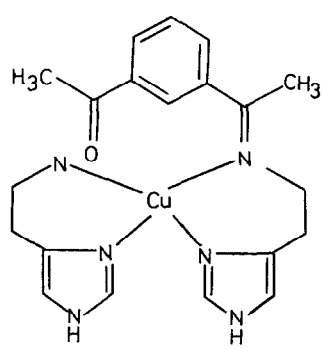

Fig. 2.

*Abbreviations: PME = phenylalanine methyl ester; TEE = tyrosine ethyl ester; HME = histidine methyl ester; HMN = histamine; AEP = 2-(2-aminoethyl) pyridine.

REFERENCES

1. W. L. Kwik, K. P. Ang and Alice W. N. Tay, *Polyhedron* 1988, **7**, 695.
2. W. L. Kwik and Alice W. N. Tay, *Polyhedron* 1989, **8**, 1321.
3. Luigi Casella and Luigi Rigoni, *J. Chem. Soc., Chem. Commun.* 1985, 1668.
4. W. J. Geary, *Coord. Chem. Rev.* 1971, 81.
5. A. D. Cross and R. A. Jones, *An Introduction to Practical Infrared Spectroscopy*. Butterworth, London (1969).
6. L. J. Bellamy, *The Infrared Spectra of Complex Molecules*. Chapman and Hall, London (1975).
7. K. Nakamoto, *Infrared and Raman Spectra of Inorganic and Coordination Compounds*. John Wiley, New York (1986).
8. David M. Adams, *Metal-Ligand Related Vibrations*. Edward Arnold (Publishers) Ltd., London (1967).
9. R. H. Bible, *Interpretation of N.M.R. Spectra*. Plenum Press, New York (1966).
10. R. J. Abraham and P. Loftus, *Proton and C-13 NMR Spectroscopy*. Heydon, London (1978).

Polyhedron Vol. 9, No. 10, pp. 1297–1303, 1990
Printed in Great Britain

0277–5387/90 $3.00+.00
© 1990 Pergamon Press plc

CRYSTAL AND MOLECULAR STRUCTURE OF 10-(4′-N-PYRIDYL)-5,15,20-TRIPHENYLPORPHINATO INDIUM(III) CHLORIDE

C. H. BEDEL-CLOUTOUR,* L. MAUCLAIRE and M. PEREYRE

Laboratoire de Chimie Organique et Organométallique, URA 35, CNRS, Université Bordeaux I, 351 cours de la Libération, F-33405 Talence Cedex, France

and

S. ADAMS and M. DRAGER

Institut für Anorganische Chemie und Analytische Chemie der Johannes Gutenberg-Universität, Johann Joachim Becher-Weg 24, D-6500 Mainz, F.R.G.

(*Received* 20 *March* 1989; *accepted* 17 *January* 1990)

Abstract—A study of the metallation of *meso* 10-(4′-N-pyridyl)-5,15,20-triphenylporphyrin with indium is reported. The crystal structure of the title compound has been determined by single-crystal X-ray diffraction. The complex crystallizes in the space group $P2_1/n$ with $Z = 4$ and $a = 10.146(2)$, $b = 16.096(4)$, $c = 20.861(2)$ Å, $\beta = 90.33(1)°$ and $V = 3407$ Å^3. The crystal structure was refined to a conventional $r(F) = 0.059$ for 6355 out of 8613 reflections having $\sigma(I)/I < 0.5$. The indium–chlorine distance is 2.374(2) Å, whereas the indium atom lies 0.608 and 0.7214 Å from the plane of the four porphyrin nitrogens and the 24-atom porphyrin plane, respectively. The four outer-sphere aromatic substituents exhibit some degree of distributional disorder.

The extensive electronic delocalization which occurs in the porphinato ligand leads to a substantial planarity of the macrocycle and an essentially square-planar environment for the metal ion in four-coordinated complexes. Coordination numbers greater than four occur by addition of extra ligands. As with the indium derivative, 5,10,15,20-(tetraphenylporphynato)indium(III) chloride,[1] the five-coordinate complex obtained has a square-pyramidal geometry with the single axial ligand occupying the apex. The In—N bonds are restricted by the constraints of the macrocycle ring which limits the radial expansion or contraction of the core.

In addition to this, the porphinato core has been observed to undergo substantial deformations normal to the mean plane. As it possesses some flexibility and variability in size, structural changes in the core must produce variations in the size of the central hole characterized by the average distance between the centre of the ring and nitrogen atoms.

The present analysis was undertaken to elucidate the consequences of the presence of a dissymmetry at the periphery of the porphinato core. We have chosen to study 10-(4′-N-pyridyl)-5,15,20-triphenylporphinato indium chloride ($P_3PyPInCl$).

EXPERIMENTAL

Physicochemical measurements

^{1}H NMR spectra were obtained at room temperature on a Brucker AC 200 in the Fourier transform mode using 32 K data points; chemical shifts in ppm were referenced to internal tetramethylsilane (TMS); abbreviations used were: S: singlet, D: doublet, M: multiplet. Optical spectra in the Soret and visible region were recorded on a Beckman-25 spectrophotometer using 2×10^{-4} mol dm^{-3} chloroformic solutions. The IR spectrum was obtained on a Perkin–Elmer 683 spectrometer; the sample was prepared as a 0.5% dispersion in KBr pellets. Desorption chemical ionization mass spec-

* Author to whom correspondence should be addressed.

tra (DCI) were obtained on a Nermag R10-10B; samples were dissolved in methylene chloride and an aliquot was deposited on the desorption ("in beam") probe; the solvent was then evaporated; ammonia was used as the DCI reactant gas.

Synthesis of the free base P_3PyPH_2

P_3PyPH_2 was obtained from the mixed condensation of 4-pyridine carboxaldehyde (0.42 mol), benzaldehyde (0.11 mol) and pyrrole (0.4 mol) in refluxing propionic acid (1.2 dm^3). Reflux was maintained for 1 h and subsequently propionic acid was removed under reduced pressure. The solid obtained was dissolved in DMF and the resulting solution kept at 0°C overnight; porphyrinic materials precipitated. After filtration the crude mixture contained the six possible macrocycles $P_{4-x}Py_xPH_2$, $x = 0$–4, as seen by CCM on silica gel (eluent: MeOH–$CHCl_3$, 2.5%).

The separation was realized by flash chromatography on silica gel (230–400 mesh) with a gradient elution. The first fraction contained tetraphenylporphyrin (eluent: light petroleum–$CHCl_3$, 80:20). A subsequent elution with light petroleum–$CHCl_3$, 60:40, gave a violet moving band from which, on evaporation, was obtained P_3PyPH_2 as violet crystals in 3.6% yield.

Electronic absorption spectrum ($CHCl_3$): λ_{max} nm ($\varepsilon\ 10^{-3}$): 418.5 (385), 515.5 (15.9), 550 (6.3), 590 (4.9), 646 (3). IR (cm^{-1}):[2] ν(N—H) 3333, ν(aromatic CH) 3065, ν8a (phenyl and pyridyl) 1603, ν(C=C pyrrole) 1567, ν(C=N pyrrole) 1480, ν19b (pyridyl) 1410, ν(=C—N pyrrole) 1357, ν9a (phenyl) 1160, δ(NH pyrrole) 1077, δ (skeleton) 1008, ν11 (pyrrole) 972, γ(CH pyridyl) 855, δ (ring) and δ(CH pyrrole) 805, ν4 (mono substituted phenyl) 707, ν6b (pyridyl) 662. DCI MS m/z (relative intensity): 616 $(M+1)^{+\cdot}$, 100.

Metallation of P_3PyPH_2 *with indium*

The free base (1.22×10^{-3} M) was dissolved in acetic acid; three equivalents of indium trichloride were added and the solution was maintained under stirring and heated at 140°C for 2 h. The cooled reaction mixture was then poured into water and extracted with chloroform to eliminate unreacted indium salts. After neutralization with a saturated solution of sodium hydrogenosulphate, the organic phase was dried ($MgSO_4$), filtered and evaporated to dryness. The crude product was chromatographed on a silica gel column prepared in chloroform. A first elution with chloroform removed the free base; a subsequent elution with MeOH 5% in chloroform gave pure $P_3PyPInCl$. After evaporation of the solvent, the violet crystals of the indium derivative were dried at 180°C, *in vacuo* (0.05 mmHg) for 8 h (yield: 87%).

Electronic absorption spectrum ($CHCl_3$): λ_{max} nm: 423 (Soret), 518.5, 557, 596. DCI MS m/z (relative intensity): 764 $(M+1)^{+\cdot}$, 91.9, 728 $(M-35)^+$, 100.

Crystal structure determination

A suitable crystal of $P_3PyPInCl$ was obtained from very slow evaporation of a methylene chloride solution of the complex, at room temperature (several weeks). The crystallographic data and the experimental conditions are given in Table 1. Reference reflections showed a loss of intensity at about 7%; for which a correction was applied.

The structure was solved by direct methods (SHELX-86).[3] Indium scattering factors were taken from ref. 5. Indium, chlorine and N(1)—C(20) were refined with anisotropic temperature factors and isotropic ones for the remaining carbon and nitrogen atoms of the phenyl and pyridyl substitutents. Positions of hydrogens were calculated geometrically and considered with one isotropic temperature factor for all porphinato hydrogens, and one for all phenyl/pyridyl hydrogens.

Tables of final coordinates and thermal parameters and a list of observed and calculated structure factor amplitudes have been deposited as supplementary data with the Editor, from whom copies are available.

RESULTS AND DISCUSSION

Synthesis of $P_3PyPInCl$ (*Fig.* 1)

The starting free base was synthesized by a modification of the method reported by Hambright and co-workers[6] based on the porphyrin condensation procedure of Loach and co-workers.[7]

For metallation with indium, we applied the method we have already used for substituted phenylporphyrins by refluxing an excess of the metal salt

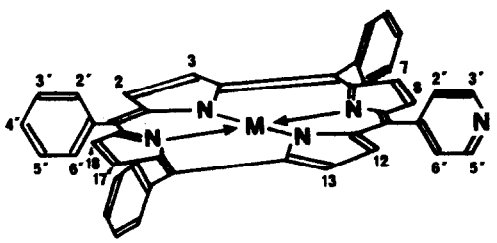

Fig. 1. P_3PyPM. Free base: M = 2H; indium derivative: M = InCl.

Table 1. Crystallographic data and experimental conditions

Formula	$C_{43}H_{27}N_5InCl$
Mol. wt	764.001
Space group	$P2_1/n$ (No. 14)
Crystal size (mm^3), form	$0.12 \times 0.34 \times 0.62$, {100, 010, 001}
Crystal colour	Violet
Lattice parameters	
a, b, c (Å)	10.146(2), 16.096(4), 20.861(2)
β (°)	90.33(1)
V (Å^3), Z	3407, 4
D_{calc}, D_{exp} (g cm^{-3})[a]	1.489, 1.47(1)
μ(Mo-K_{α}) (cm^{-1})	7.30
Diffractometer	Enraf–Nonius CAD-4
Radiation	Mo-K_{α} (graphite monochromatized)
λ (Å)	70.926
Scan type $(\sin\theta/\lambda)_{max}$ (Å^{-1})	ω–2θ, 0.67
Scan range (°)	$1.00 < \theta < 28.50$; $0.80 + 0.50$ tg θ
Detector aperture (mm)	Horizontal $2 + 1.0$ tg θ
	Vertical 4
h, k, l limits	$0 \leqslant h \leqslant 13$, $0 \leqslant k \leqslant 21$, $-28 \leqslant l \leqslant 28$
Numbers of reflections measured	8613
Numbers of reflections used (N)	6355 [$I > 2\sigma(I)$]
Numbers of parameters (N_p)	335
N/N_p	18.97
Programs used[b]	SHELX-86,[3] SHELX-76[4]
$r(F)$, $r_w(F)$	0.059, 0.098
w	$0.935/[\sigma^2(F) + 0.00707F^1]$

[a] Flotation in Thoulet's solution.

[b] Calculations at Rechenzentrum Universität Mainz on a HB-DPS-8170 computer.

with the porphyrin base in glacial acetic acid.[8] This reaction was conducted with indium trichloride:

$$P_3PyPH_2 + InCl_3 \xrightarrow{CH_3COOH} P_3PyPInCl.$$

Progress of the metallation was monitored by visible spectrometry following the disappearance of the 418.5 and 515.5 nm bands in the free base and the concomitant increased bands of the indium derivative, e.g. α- and β-bands between 500 and 600 nm. Metallation reaction times were optimized as a function of free base concentration and temperature. Results are summarized in Tables 2 and 3, respectively.

Metallation is fastest when a concentration of 1.22×10^{-3} M and a temperature of 140°C are used. Using these experimental conditions and after purification, $P_3PyPInCl$ was synthesized in 87% yield.

Spectral measurements

The desorption chemical ionization mass spectrometry (DCI MS) with ammonia as the reagent gas confirmed the formation of the indium derivative. Initial attack by the reactant gas results in the formation of the protonated metalloporphyrin molecular ion $(M+1)^{+\cdot}$, m/z 764, while the base

Table 2. Metallation times as a function of concentration of P_3PyPH_2 (P_3PyPH_2: 5×10^{-5} mol, $InCl_3$: 1.5×10^{-4} mol)

M	t (min)
1.627×10^{-3}	105
1.22×10^{-3}	45
0.813×10^{-3}	55

Table 3. Metallation of P_3PyPH_2 (1.22×10^{-3} M) as a function of temperature

T (°C)	t (min)
100	$\gg 45$
120	45
140	30

Table 4. ^{1}H NMR chemical shifts of P_3PyPInCl and its free base

P_3PyPM	Pyrrole	Pyridyl	Phenyl	NH
M = 2H	8.89 (D, 2H) 8.86 (S, 4H) 8.79 (D, 2H)	9.02 (D, 2H) 8.16 (D, 2H)	8.20 (M, 6H) 7.76 (M, 9H)	−2.80 (S, 2H)
M = InCl	9.11 (D, 2H) 9.08 (S, 4H) 9.01 (D, 2H)	9.04 (M, 2H) 8.36 (M, 1H) 8.08 (M, 1H)	8.36 (M, 3H) 8.08 (M, 3H) 7.79 (M, 9H)	

peak (*m/z* 728) corresponds to the loss of the axial chloride ligand.

^{1}H NMR characteristics of P_3PyPInCl at ambient temperature are listed in Table 4 with those of its corresponding free base.

As in other dissymmetrically substituted macrocycles,[8] a splitting pattern for the pyrrolic protons is observed in the free base. H(7) and H(8) are, respectively, pairwise equivalent to H(12) and H(13) and lead to two asymmetrical doublets, each corresponding to two protons. The equivalent H(2), H(3), H(17), H(18) lead to a singlet. Chemical shifts of these protons in the free base are in disagreement with the values observed in literature[6] which are roughly 0.4 ppm smaller. However, our values fit much better with what is expected for pyrrolic protons (around 9 ppm).

The pyridyl protons give two doublets corresponding to H(3′), H(5′) and H(2′), H(6′), respectively; the more deshielded doublet, centred at 9.02 ppm, corresponds to protons 3′ and 5′ in α-position from nitrogen. The doublet at higher field [8.16 ppm, H(2′), H(6′)] in superposed to the resonance peak of *ortho* phenyl protons (8.2 ppm). *Meta* and *para* phenyl protons resonate at 7.76 ppm. To higher field than TMS, is the signal of pyrrolic N—H protons.

Upon formation of the chloro indium porphyrin complex, the ^{1}H NMR spectrum of pyrrolic protons retains the same multiplicity of signals with a downfield chemical shift of *ca* 0.22 ppm.

At room temperature, the resonance of the *ortho* aryl protons is theoretically split into two signals, this inequivalence being due to the restricted rotation of the aryl groups;[9] in our case, the resonance of these protons is broad, this broadening being enhanced by the superposition of phenyl and pyridyl proton signals at 8.36 and 8.08 ppm. The splitting difference between the resonance frequencies of the non-equivalent *ortho* protons (0.24 ppm) agrees with those observed in the literature (0.25 ppm).[10]

Molecular structure description

Figures 2 and 3 show the structure of P_3PyPInCl in directions perpendicular and parallel to the porphyrin plane. Table 5 gives the bond lengths and angles within the coordination polyhedron. Those for the porphyrinic system are all within three ESDs the same as in TPPInCl.[1]

Indium is five-coordinated in a square pyramid by the porphinato ligand and chlorine. The essentially equivalent In—N distances of 2.154 Å are

Table 5. Selected interatomic distances (Å) and angles (°) around In(1) with ESDs in parentheses

Bond lengths			
In(1)—N(1)	2.157(4)	In(1)—Cl(1)	2.374(2)
In(1)—N(2)	2.151(5)	N(1)—N(3)	4.149(6)
In(1)—N(3)	2.159(5)	N(2)—N(4)	4.117(6)
In(1)—N(4)	2.150(4)		
Bond angles			
N(1)—In(1)—N(2)	85.4(2)	N(2)—In(1)—N(4)	146.4(2)
N(2)—In(1)—N(3)	85.4(2)	Cl(1)—In(1)—N(1)	105.8(2)
N(3)—In(1)—N(4)	85.5(2)	Cl(1)—In(1)—N(2)	106.8(2)
N(4)—In(1)—N(1)	85.4(2)	Cl(1)—In(1)—N(3)	106.2(2)
N(1)—In(1)—N(3)	148.1(2)	Cl(1)—In(1)—N(4)	106.8(2)

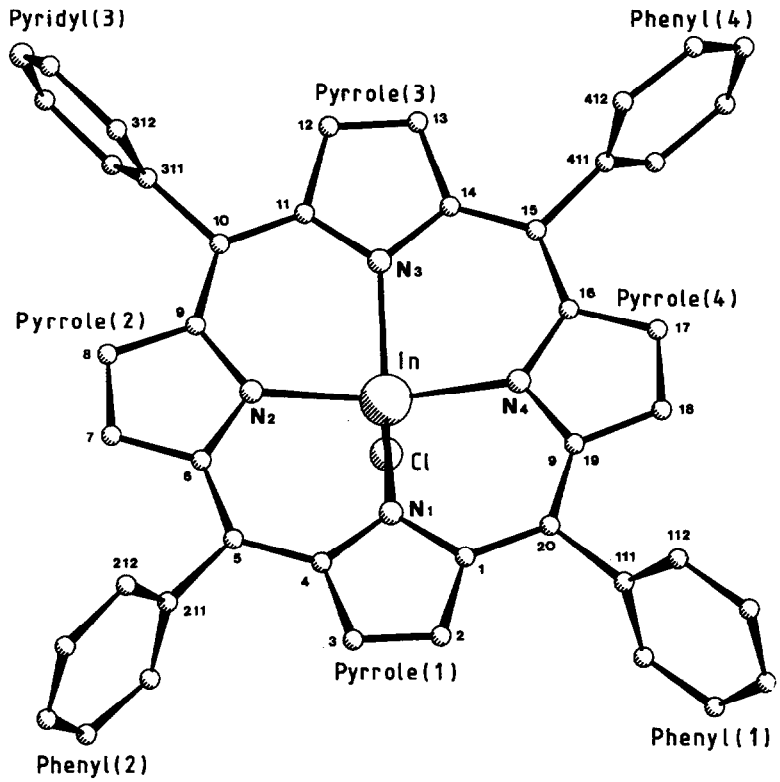

Fig. 2. Molecular structure of $P_3PyPInCl$ with the atom numbering scheme.

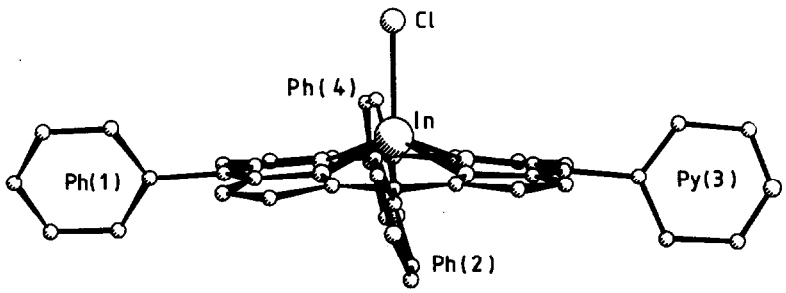

Fig. 3. View of $P_3PyPInCl$, parallel to the porphyrin plane, showing the "doming" of the molecule.

comparable to those in TPPInCl;[1] the average N—In—N bond angles are 85 and 147°. The four pyrrole nitrogens are approximately coplanar, the indium atom is displaced out of this Δ(4N) mean plane by 0.608(1) Å toward the chlorine ligand and lies 0.721(1) Å above Δ (porphyrin). Thus, the porphinato core displays a net doming of 0.11 Å away from the indium atom as illustrated in Fig. 3. The chlorine atom occupies the apical position of the square pyramid with In—Cl = 2.374(2) Å. This bond is considerably shorter than in the five-coordinate anionic chloro complex $InCl_5^{2-}$ (square-pyramidal arrangement with apical In—Cl = 2.415 Å[11]).

Structural changes in the porphinato core do not produce variation in the size of the central hole. The main distance between Ct, the centre of the nitrogens, and N is 2.07 Å, which is in the normal range of values for Ct—N suggested by Collins and Hoard.[12]

The distribution of the four outer-sphere aromatic substituents at carbons (5), (10), (15) and (20) demands some special comment. Table 6 lists their geometrical data. The aromatic group in the four-position is definitely phenyl. The group in the three-position exhibits the normal geometry of *p*-pyridyl.[12,13] The rings in the two- and one-positions are both somewhat distorted from regular

Table 6. Bond lengths (Å) and angles (°) of the outer-sphere substituents; ESDs 0.01 Å and 0.7°

Assignment	Phenyl(1)[a]	Phenyl(2)[a]	Pyridyl(3)	Phenyl(4)
i–o	1.39, 1.39	1.39, 1.37	1.36, 1.38	1.37, 1.39
o–m	1.38, 1.39	1.42, 1.41	1.45, 1.45	1.41, 1.39
m–p	1.35, 1.35	1.33, 1.30	1.29, 1.27	1.37, 1.37
o–i–o	117.8	118.5	118.6	119.6
i–o–m	121.0, 119.7	118.5, 118.3	121.9, 116.3	119.8, 119.7
o–m–p	120.1, 121.1	121.9, 123.8	116.1, 121.4	120.4, 120.8
m–p–m	120.3	118.8	125.7	119.7

[a] Some adding of pyridyl: distributional disorder.

phenyl geometry. A low degree of disorder must be assumed for the distribution of the four substituents.

As normal for a metallotetraarylporphyrin[14] the aryl rings are rotated considerably out of plane of the macrocycle (local torsion angles 63–104°).

Crystal structure description

The crystal structure of $P_3PyPInCl$ contains discrete molecules with no short In... Cl interactions. The intermolecular distribution of the pyridyl substituents is noticeable.

In Fig. 4, the $P_3PyPInCl$ molecule is divided into shells for the indium, chlorine, nitrogen and carbon atoms of the porphyrinic system and the *ortho*, *meta* and *para* atoms of the aromatic *meso* substituents. The shortest intermolecular distances are given from each of these shells to the *para* positions of the four different aromatic substituents in the surrounding $P_3PyPInCl$ molecules. All of these distances are longer than van der Waals' distances.

Regardless of this reservation, the position of the pyridyl(3) group is a special one: the N... In distance of 4.58 Å is the shortest, the N... Cl distance of 5.58 Å is the longest of these distances. Further, some of the intermolecular contacts between atoms of the porphyrinic system and the pyridyl nitrogen are shorter than 4 Å, all related distances to the phenyl groups are longer than 4 Å.

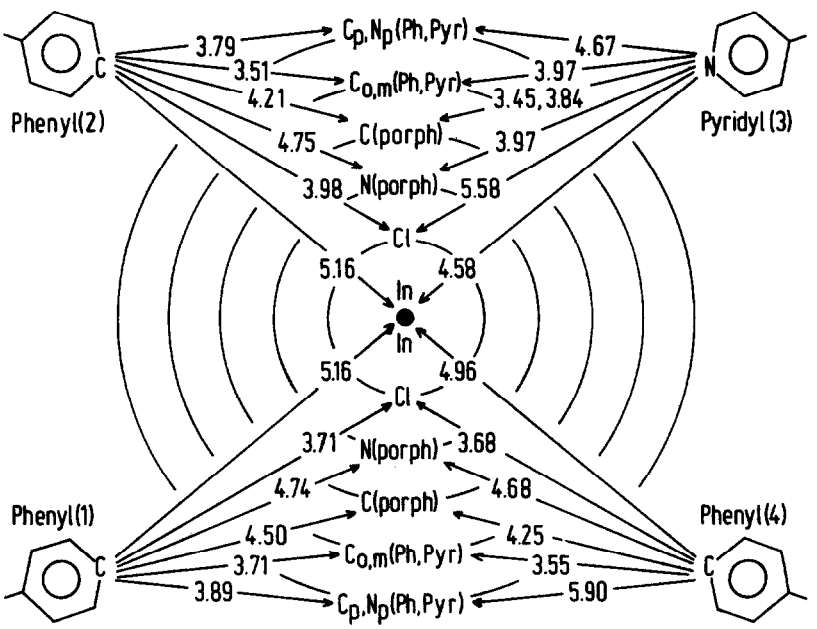

Fig. 4. Shortest intermolecular distances (Å) from the *para* positions of the four aromatic substituents to different regions of the neighbouring $P_3PyPInCl$ molecule.

CONCLUSION

$P_3PyPInCl$ crystallizes in the monoclinic crystal system; it is isomorphic to a series of tetraphenylporphyrin derivatives of the $P2_1/n$ series very recently presented by Scheidt and Lee.[15] No strong degree of overall distortion of the macrocyclic ligand is induced by introduction of a pyridyl group at C(10). Nevertheless, this pyridyl group is in a very special site seen from an intermolecular point of view. We can suppose a complete change of the crystal structure on going to the *cis* and *trans* dipyridyl derivatives; their crystal structures are under investigation.

Acknowledgements—Financial support of this work by ORIS INDUSTRIE Company and Etablissement Public Régional d'Aquitaine (Pole Génie Biologique et Médical) are gratefully acknowledged.

REFERENCES

1. R. G. Ball, K. M. Lee, A. G. Marshall and J. Trotter, *Inorg. Chem.* 1980, **19**, 1463.
2. (a) S. Sugata, S. Yamanouchi and Y. Matsushima, *Chem. Pharm. Bull.* 1977, **25**, 884; (b) C. H. Bedel-Cloutour, C. Barois-Gacherieu and A. Marchand, *Spectrochim. Acta* 1988, **44A**, 567 and refs therein.
3. G. M. Sheldrick, SHELX-86, Program for Crystal Structure Determinations. University of Göttingen, F.R.G. (1986).
4. G. M. Sheldrick, SHELX-76, Program for Crystal Structure Determinations. University of Cambridge, U.K. (1976).
5. (a) P. A. Doyle and P. S. Turner, *Acta Cryst.* 1968, **A24**, 390; (b) D. T. Cromer and D. Liberman, *J. Chem. Phys.* 1970, **53**, 1891.
6. A. Shamin, P. Worthington and P. Hambright, *J. Chem. Soc. Pak.* 1981, **3**, 1.
7. (a) J. A. Anton, J. Kwong and P. A. Loach, *J. Heterocycl. Chem.* 1976, **13**, 717; (b) J. L. Y. Kong and P. A. Loach, *J. Heterocycl. Chem.* 1980, **17**, 737.
8. C. H. Bedel-Cloutour and C. Barois-Gacherieu, *Main Group Met. Chem.* 1987, **10**, 109 and refs therein.
9. (a) S. S. Eaton and G. R. Eaton, *J. Am. Chem. Soc.* 1977, **99**, 6594; (b) A. L. W. Shroyer, C. Lorberau, S. S. Eaton and G. R. Eaton, *J. Org. Chem.* 1980, **45**, 4296.
10. M. Bhatti, W. Bhatti and E. Mast, *Inorg. Nucl. Chem. Lett.* 1972, **8**, 133.
11. D. S. Brown, F. W. B. Einstein and D. G. Tuck, *Inorg. Chem.* 1969, **8**, 14.
12. D. M. Collins and J. L. Hoard, *J. Am. Chem. Soc.* 1970, **92**, 3761.
13. (a) M. Laing, N. Sparrow and P. Sommerville, *Acta Cryst.* 1971, **B27**, 1986; (b) G. O. Soerensen, L. Mahler and N. Rastrup-Andersen, *J. Molec. Struct.* 1974, **20**, 119.
14. E. B. Fleischer, *Accts Chem. Res.* 1970, **3**, 105.
15. W. R. Scheidt and Y. J. Lee, *Struct. Bond. (Berlin)* 1987, **64**, 1.

Polyhedron Vol. 9, No. 10, pp. 1305–1310, 1990
Printed in Great Britain

0277–5387/90 $3.00+.00
© 1990 Pergamon Press plc

UNEXPECTED CLEAVAGE OF ACETYLACETONE INDUCED BY YTTRIUM OXOISOPROPOXIDE: SYNTHESIS AND MOLECULAR STRUCTURE OF $Y_2(\mu_2\text{-}OAc)_2(acac)_4(H_2O)_2$

OLIVIER PONCELET and LILIANE G. HUBERT-PFALZGRAF*

Laboratoire de Chimie Moléculaire, Unité de Recherche Associée au CNRS, Université de Nice, Parc Valrose, 06034 Nice, France

and

JEAN-CLAUDE DARAN

Laboratoire de Chimie des Métaux de Transition, Unité de Recherche Associée au CNRS, 4, Place Jussieu, 75230 Paris, France

(*Received* 10 *November* 1989; *accepted* 17 *January* 1990)

Abstract—Reaction between $Y_5O(O^iPr)_{13}$ and acetylacetone at room temperature under anhydrous conditions, produced in high, reproducible yield a compound characterized—by ^1H and ^{13}C NMR, as well as X-ray diffraction—as $Y_2(\mu_2\text{-}OAc)_2(acac)_4(H_2O)_2$. It crystallizes in the orthorhombic *Pcnb* system, with unit cell dimensions $a = 13.385(3)$, $b = 15.107(4)$, $c = 16.100(4)$ Å and $Z = 4$. Least-squares refinement converged to a final $R = 0.0356$. The molecule is a centrosymmetric dimer with chelating tridentate acetato groups in the bridging positions. The yttrium atoms are eight-coordinated, with a distorted square antiprism geometry. Intra- as well as intermolecular hydrogen bonding between the water molecules and the β-diketonato ligands is observed. The formation of this acetatoacetylacetonate derivative as well as its behaviour in solution are discussed.

Yttrium and lanthanide oxides are of great interest for a variety of high technology materials such as superconductors, yttrium iron garnets (YIG), etc.[1] Chemical routes to such materials using well-defined molecular precursors should allow better control of their properties and larger flexibility of the products (ceramics, coatings, etc.) in comparison with the solid-state synthesis.[2] The structural characterization of a pentanuclear oxoisopropoxide, $Y_5O(O^iPr)_{13}$,[3] prompted us to investigate its reactivity, especially towards ligands such as β-diketones, which can offer volatile precursors of oxides for use in MOCVD techniques,[4] or which may act as additives in order to control the sol–gel process.[5]

Reaction between $Y_5O(O^iPr)_{13}$ and acetylacetone at room temperature under anhydrous conditions, produced in high, reproducible yield a compound characterized by X-ray diffraction as $Y_2(\mu_2\text{-}OAc)_2(acac)_4(H_2O)_2$ (acacH = $C_5H_8O_2$, acetylacetone).

EXPERIMENTAL

All operations were carried out under an argon atmosphere using standard Schlenk techniques. All solvents were dried, degassed and distilled prior to use. Acetylacetone was purified as reported in the literature in order to remove trace amounts of acetic acid as well as water.[6] IR spectra were recorded on a Bruker IR S45 spectrometer. The ^1H and ^{13}C NMR spectra were measured on a Bruker AC-200E spectrometer. Elemental analyses were performed by the Centre de Microanalyse du CNRS.

Synthesis of $Y_2(OAc)_2(acac)_4(H_2O)_2$

Excess acetylacetone (4.5 cm^3, 43.3 mmol) in 10 cm^3 toluene was added slowly to a solution of $Y_5O(O^iPr)_{13}$ (1.6 g, 1.30 mmol) in 30 cm^3 of toluene.

* Author to whom correspondence should be addressed.

Stirring at room temperature was maintained for 24 h, and the reaction medium evaporated to dryness. Recrystallization in acetone led to 1.12 g (87%) of white, air-sensitive crystals of $Y_2(OAc)_2(acac)_4(H_2O)_2$, slightly soluble in hexane or toluene, more soluble in alcohol, acetone, CH_2Cl_2 and $CHCl_3$. Found: C, 40.7; H, 5.7. Calc. for $C_{24}H_{38}O_{14}Y_2$: C, 39.6; H, 5.5%. IR (Nujol, cm^{-1}): 3438 $\nu(H_2O)$, 1607, 1590 sh $\nu_s(C{=}O)$, 1522 $\nu_s(C{-}C)$; 1460, 1263 $\nu_{as}(C{-}O)$; 1168, 1099, 1016, 922, 760, 727, 656 $\delta(CO_2)$, 535 $\nu(M{-}O)$. ^1H NMR ($CDCl_3$, ppm): 5.55 (CH, 4H), 4.40 (H_2O, 4H), 2.28 (OAc, 6H), 2.08 (CH_3(acac), 24H). $^{13}C\{NMR\}$ ($CDCl_3$, ppm): 205 (CO_2), 192 (CO); 100 (CH); 27.5 [$CH_3(CO_2)$]; 25 [$CH_3(CO)$].

Crystallography of $Y_2(OAc)_2(acac)_4(H_2O)_2$

Crystals suitable for X-ray were obtained from recrystallization in acetone at room temperature. A transparent crystal was mounted on a Nonius CAD-4 diffractometer and cooled at −105°C for characterization and data collection. Accurate unit cell dimensions and crystal orientation matrix were obtained from least-squares refinements of the setting angles of 25 reflections. Three standard reflections were monitored periodically; they showed no change during data collection. Crystallographic data and other pertinent information are summarized in Table 1. Corrections were made for Lorentz, polarization and absorption[7] effects.

Computations were performed using CRYSTALS' adapted on a MICROVAX II.[8] Atomic-form factors for neutral Y, O, C and H atoms were taken from *International Tables for X-ray Crystallography*.[9] The structure was solved using SHELXS.[10] Hydrogen atoms were located on difference electron density maps. Their coordinates were refined with an overall isotropic thermal parameter. Anisotropic temperature factors were introduced for all non-hydrogen atoms. Least-squares refinements were carried out by minimizing the function $\Sigma w([F_o]-[F_c])^2$. Heavy atoms (Y, O and C) and H atoms were refined alternately. The criteria for a satisfactory complete analysis were the ratio of the rms shift to standard deviation being less than 0.1 and no significant features in the final

Table 1. X-ray crystal data and data collection of $Y_2(OAc)_2(acac)_4(H_2O)_2$

Compound	$C_{24}H_{38}O_{14}Y_2$
Colour	Colourless
Molecular weight	728.36
Crystal system	Orthorhombic
Space group	*Pcnb*
a (Å)	13.385(3)
b (Å)	15.107(4)
c (Å)	16.100(4)
V (Å^3)	3255
Z	4
Linear absorption coefficient	36.36
Density (calc.) (g cm^{-3})	1.628
Temperature (°C)	−105
Diffractometer	Enraf–Nonius CAD-4
Radiation	Mo-K_α (graphite monochromator)
Scan type	$\omega/0.66$
Scan range (°)	$1.2+0.345\tan\theta$[a]
2θ range (°)	4–50θ
Speed range (° min^{-1})	0.9–5.5
Standard reflections	0 0 −6; 0 80; 0 34
Reflection collection	3219
Reflections used	1135 [$I \geqslant 3\sigma(I)$]
Absorption	DIFABS[7]
R[b]	0.0356
R_w	0.0334
Weighting scheme[8]	$w = 1/\Sigma_{r=1} ArTr(X)\lvert 1-\Delta F/6\sigma(F)^2\rvert^2$
Coefficients Ar	3.13; −2.81; 1.84
Ratio of observed to parameters	6

[a] Scan extended by 25% on either side for background determination.
[b] $R = \Sigma(\lvert F_o\rvert-\lvert F_c\rvert)/\Sigma\lvert F_o\rvert$; $R_w = \{\Sigma_w(\lvert F_o\rvert-\lvert F_c\rvert)^2/\Sigma_w(\lvert F_o\rvert)^2\}^{1/2}$.

Table 2. Selected bond lengths and angles for $Y_2(OAc)_2(acac)_4(H_2O)_2$ (coordination polyhedron)

Bond lengths (Å)			
Y(1)′—Y(1)	4.054(1)	Y(1)—O(11)	2.325(4)
Y(1)—O(1)	2.322(5)	Y(1)—O(12)	2.271(5)
Y(1)—O(2)	2.503(5)	Y(1)—O(21)	2.283(4)
Y(1)—O(2)′	2.364(4)	Y(1)—O(22)	2.312(4)
Y(1)—O(3)	2.410(5)		
Bond angles (°)			
O(2)—Y(1)—O(1)	72.2(1)	O(21)—Y(1)—O(1)	136.4(2)
O(2)′—Y(1)—O(1)	74.2(2)	O(21)—Y(1)—O(2)	117.3(2)
O(2)′—Y(1)—O(2)	67.2(2)	O(21)—Y(1)—O(2)′	149.3(1)
O(3)—Y(1)—O(1)	79.8(2)	O(21)—Y(1)—O(3)	76.2(2)
O(3)—Y(1)—O(2)	52.7(1)	O(21)—Y(1)—O(11)	74.5(2)
O(3)—Y(1)—O(2)′	119.3(2)	O(21)—Y(1)—O(12)	84.4(2)
O(11)—Y(1)—O(1)	71.3(2)	O(22)—Y(1)—O(1)	145.9(2)
O(11)—Y(1)—O(2)	134.0(1)	O(22)—Y(1)—O(2)′	78.3(1)
O(11)—Y(1)—O(2)′	126.2(2)	O(22)—Y(1)—O(2)	78.7(2)
O(11)—Y(1)—O(3)	93.7(2)	O(22)—Y(1)—O(3)	96.0(2)
O(12)—Y(1)—O(1)	110.9(2)	O(22)—Y(1)—O(11)	142.7(2)
O(12)—Y(1)—O(2)	146.3(2)	O(22)—Y(1)—O(12)	84.7(2)
O(12)—Y(1)—O(2)′	81.1(2)	O(22)—Y(1)—O(21)	73.1(2)
O(12)—Y(1)—O(3)	159.4(2)	Y(1)′—O(2)—Y(1)	112.8(2)
O(12)—Y(1)—O(11)	74.3(2)		

Atoms labelled ′ are related by a centre of symmetry.

difference map. Atomic coordinates are given in Table 2.

Positional parameters and equivalent isotropic parameters are given as Supplementary Material.

RESULTS AND DISCUSSION

Although reactions between alkoxides and β-diketones often lead to partial substitution with formation of mixed alkoxo β-diketonate derivatives as a result of steric hindrance,[11] the reaction between $Y_5O(O^iPr)_{13}$ and excess acetylacetone in toluene, proceeds to complete substitution of the isopropoxo groups even at room temperature. The reaction, achieved in anhydrous conditions, offered in high, reproducible yield (≃ 85%), an acetylacetonate derivative whose IR spectra appeared to be different from that reported for $Y(acac)_3$ or $Y(acac)_3,3H_2O$.[12] The main modification is the presence of additional absorption around 660 cm^{-1}. ^1H NMR spectra are also puzzling, especially regarding the integration between methyl and methine groups and the presence of an additional peak at 4.40 ppm.

The structure of the compound was established by X-ray diffraction, which showed it to be an acetatoacetylacetonate compound of formula $Y_2(\mu_2\text{-}OAc)_2(acac)_4(H_2O)_2$. It is, to our knowledge, the first example of a lanthanide carboxylatodiketonate reported.

Molecular structure of $Y_2(OAc)_2(acac)_4(H_2O)_2$

The molecule is a centrosymmetric dimer, the most salient feature being the presence of acetate ligands, which bridge the yttrium atoms in a bridging tridentate mode; this coordination mode has previously been observed for lanthanide derivatives.[13] Table 2 lists selected bond lengths and angles, while Fig. 1 shows an ORTEP diagram. The yttrium atoms are octacoordinated and separated by 4.054(1) Å. The metal atoms have a distorted square antiprism geometry and bear two chelating acetylacetone ligands and a water molecule. The Y—O bond lengths range from 2.271(5) to 2.505(5) Å, the longest one corresponding to the bridging, chelating acetato ligand. The Y—O distances involving the acetate ligand are significantly different (2.412(5) and 2.505(5) Å), and longer than those observed for simply bridging acetate groups, as in $\{[HB(pz)_3]Y(\mu\text{-}O_2CCH_3)_2\}_2$ (2.279(6) Å).[14] The Y—O(acac) values are close to those observed for $Y(acac)_3,3H_2O$.[15] Intra- as well as intermolecular hydrogen bonding is observed between water and the oxygen atoms of the β-diketonato ligands. The intermolecular interactions (H(11)···O(11):

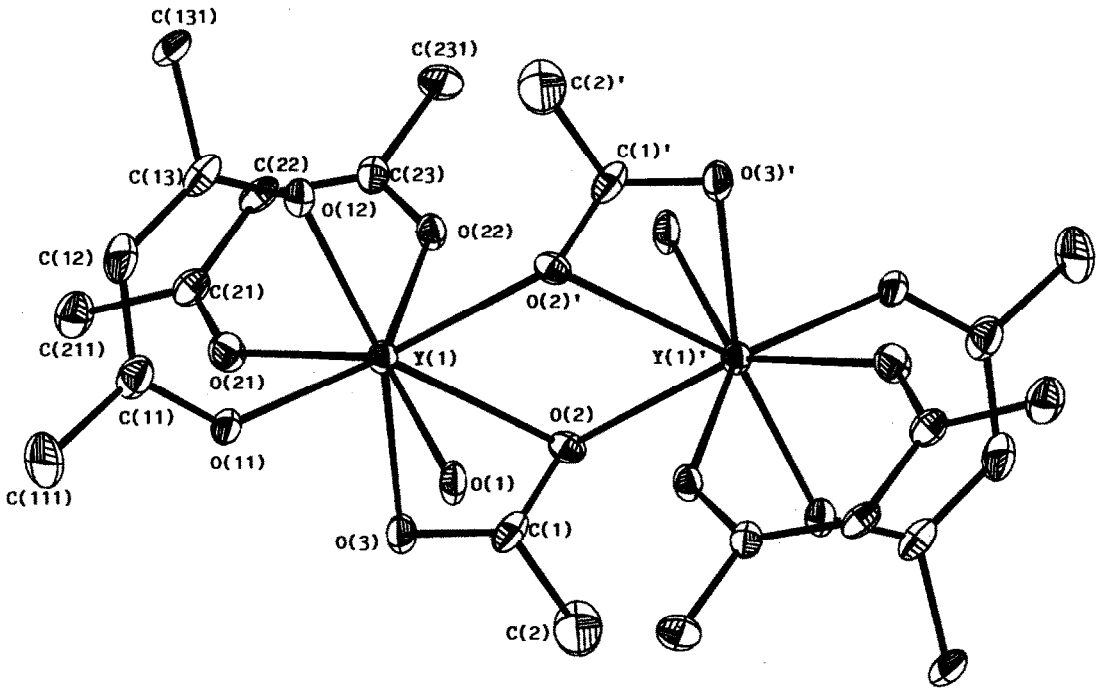

Fig. 1. ORTEP view of $Y_2(\mu\text{-OAc})_2(acac)_4(H_2O)_2$, showing the numbering of atoms other than C and H. The hydrogens of the water molecule [O(1)] interact with O(22) and O(11) via intra- and intermolecular hydrogen-bonding, respectively.

2.015(4) Å) appear weaker than the intramolecular one (H(12)···O(22): 1.866(4) Å), but give rise to extended chains along the *b* axis (Fig. 2).

The rest of the bonding of the β-diketone ligand appears normal, with C—O and C—C bond lengths ranging from 1.257(8) to 1.273(8) and from 1.38(1) to 1.53(1) Å, respectively. Close intermolecular contacts are noted between most oxygen atoms, as often observed for β-diketonate derivatives.

The question which arises concerns the origin of the acetato and water ligands. Although other hypotheses might be considered, acetylacetone is most probably the source of the acetato ligand. Comparison of the spectroscopic data (IR, ^1H NMR) of the crude and recrystallized product established that the transformation of the β-diketone had already occurred in the crude product. ^1H NMR monitoring experiments have shown that an excess of β-diketone is not required for the formation of $Y_2(\mu\text{-OAc})_2(acac)_4(H_2O)_2$ from $Y_5O(O^iPr)_{13}$, since this compound is already formed in a large amount for a molar ratio such as acacH/Y = 10, and its formation is probably favoured by its poor solubility in toluene. Generation of the acetato moieties is probably due to retro-Claisen type reactions,[16] induced either by trace amounts of alkoxo or hydroxo anions (water may result from the reaction of the oxo ligand) stabilized by a highly basic medium. Further esterification can then provide additional water molecules. Formation of carboxylatodiketonato derivatives from a yttrium oxoalkoxide seems relatively specific to acetylacetonates: the reaction between $Y_5O(O^iPr)_{13}$ and dipivaloylmethane (dpmH) yielded only $Y(dpm)_3$. However, reaction between an oxo neodymium isopropoxide and excess of acetylacetone also offered an unexpected derivative, a hydroxoacetylacetonate $Nd(\mu_3\text{-OH})_2(acac)_{10}$, as established by X-ray structure determination.[17] The remarkable behaviour of the lanthanide acetylacetonates, as compared with their more crowded counterparts, may thus be related to a higher susceptibility to the water molecules generated during their synthesis from oxoalkoxides. These observations are also in agreement with their behaviour when used as MOCVD precursors.

The $Y_2(\mu_2\text{-OAc})_2(acac)_4(H_2O)_2$ hydrate is stable in the solid state at room temperature and under an inert atmosphere for periods of up to one year. However, its stability in solution and in the absence of additional acetylacetone is more limited. Rapid evolution of the NMR spectra requires characterization in fresh as well as concentrated solutions. Indeed, the presence of water molecules in the coordination sphere induces spontaneous hydrolysis—and probably also condensation—reactions upon dissolution, thus giving several molecular species in rapid equilibrium on the NMR

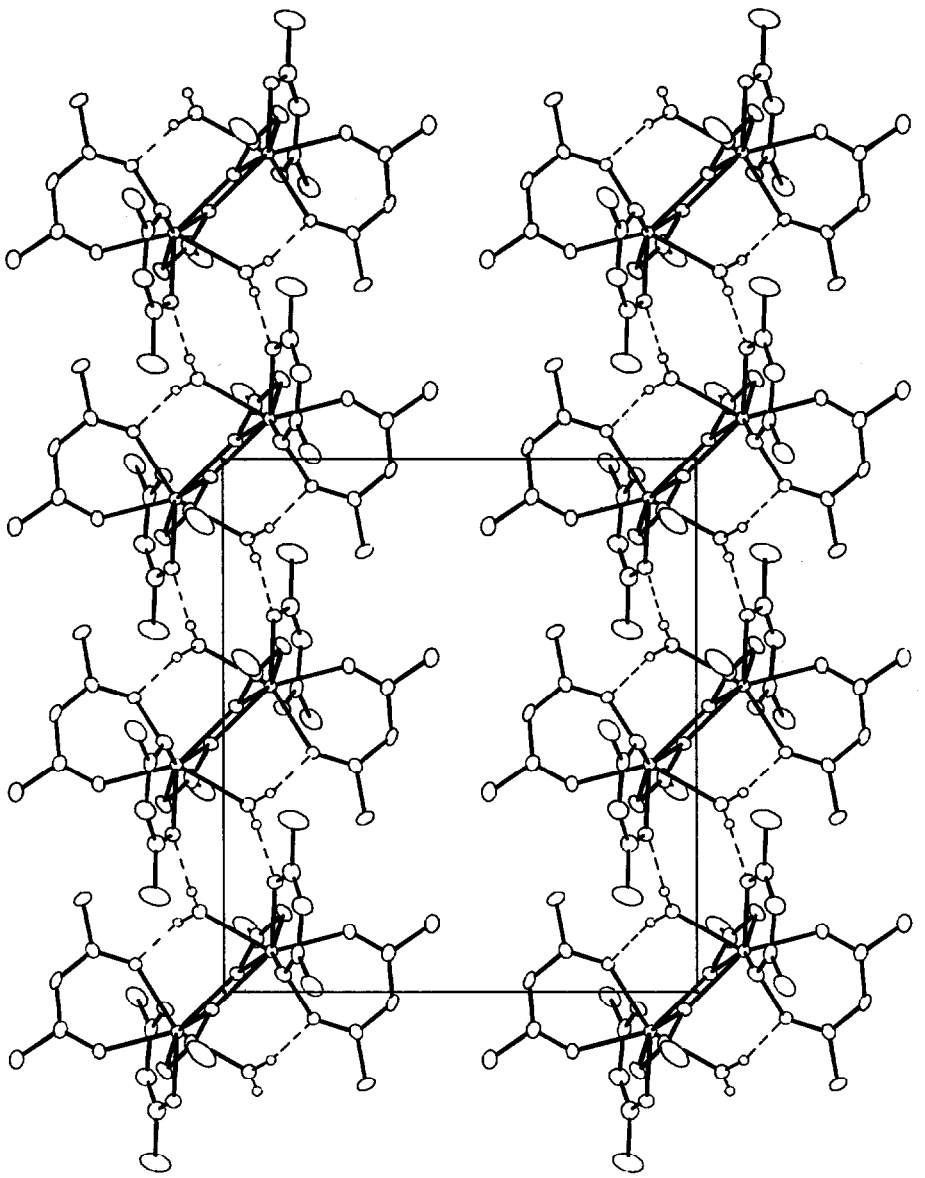

Fig. 2. Packing of $Y_2(\mu_2\text{-}OAc)_2(acac)_4(H_2O)_2$ showing the intra- and intermolecular hydrogen-bonding (dotted lines).

time scale and a complex behaviour. Formation of $Y_2(\mu_2\text{-}OAc)_2(acac)_4(H_2O)_2$ is evidenced in the ^1H NMR by the appearance of free acetylacetonate and its enol (OH = 15.6, CH_2 = 3.6, CH_3 = 2.02 ppm), as well as by the progressive disappearance of the peak of the water molecules at 4.4 ppm. A very broad resonance, located between 6.8 and 2.7 ppm, has been tentatively attributed to the hydrogen of the metal hydroxo bond. Thus although β-diketones are generally considered as poorly hydrolysable ligands,[18] they appear more susceptible to hydrolytic attack than acetato ligands in $Y_2(\mu_2\text{-}OAc)_2(acac)_4(H_2O)_2$. Its thermal decomposition gives $[Y(acac)_3]_m$ as volatile, metallic derivatives, as shown by mass spectrometry.

The facile, total substitution, at room temperature, of the alkoxo groups of rare earth oxoalkoxides, even with a polynuclear *closo*-framework, by β-diketones might be attributed to the propensity of these metals to achieve octacoordination. The results, obtained on yttrium and neodymium derivatives, also suggest further investigation on acetylacetonate derivatives obtained by using oxo compounds as starting material and might bring some insight into the degradation of acetylacetonates during catalysis experiments. In addition, acetylacetonate is often used in the sol–gel process as a "modifier";[19] more careful investigation of the metallic species formed in the presence of this ligand and water seems warranted.

Acknowledgements—We thank Dr R. Astier (Montpellier) for the X-ray data collection. Financial support by the CNRS (AIR and GRECO 93) is acknowledged.

REFERENCES

1. P. Falconnet, *J. Less Common Met.* 1985, **111**, 9.
2. L. G. Hubert-Pfalzgraf, *New J. Chem.* 1987, **11**, 662.
3. O. Poncelet, W. Sartain, L. G. Hubert-Pfalzgraf, K. Folting and K. G. Caulton, *Inorg. Chem.* 1989, **28**, 263.
4. H. Abe, T. Tsuruoka and T. Nakamori, *Jap. J. Appl. Phys.* 1988, **27**, L1473; H. Yamane, H. Mabumoto, T. Hirai, H. Iwasaki, K. Watanabe, N. Kobayashi, Y. Muto and H. Kurosawa, *Appl. Phys. Lett.* 1988, **53**, 1548.
5. K. Yamada, T. Y. Chow, T. Horihata and M. Nagata, *J. Non-Cryst. Solids* 1988, **100**, 316; C. Sanchez, J. Livage, M. Henry and F. Babonneau, *J. Non-Cryst. Solids* 1988, **100**, 65.
6. D. D. Perrin, W. L. F. Armarego and D. W. Perrin, *Purification of Individual Organic Chemicals*, 2nd edn. Pergamon Press, Oxford (1980).
7. N. Walker and D. Stuart, *Acta Cryst.* 1983, **A39**, 158.
8. D. J. Watkin, D. J. Carruthers, J. R. and T. W. Betridge, *CRYSTALS, User's Guide. Chemical Crystallography Laboratory*. University of Oxford, U.K. (1987); E. Prince (Ed.), *Mathematical Techniques in Crystallography*. Springer, Berlin (1982).
9. D. T. Cromer, *International Tables for X-ray Crystallography*, Vol. IV. Kynoch Press, Birmingham, U.K. (1974).
10. G. M. Sheldrick, SHELXS 86, Program for Crystal Solution. University of Göttingen, F.R.G. (1986).
11. D. C. Bradley, R. C. Mehrotra and D. P. Gaur, *Metal Alkoxides*. Academic Press, London (1978).
12. J. K. Przystal, W. G. Bos and I. B. Liss, *J. Inorg. Nucl. Chem.* 1971, **33**, 679.
13. A. Ouchi, Y. Suzuki, Y. Olki and J. Koizumi, *Coord. Chem. Rev.* 1988, **92**, 29; S. P. Bone, D. B. Sowerby and R. D. Verma, *J. Chem. Soc., Dalton Trans.* 1978, 1544; S. Ganapathy, V. P. Chacko, R. G. Bryant and M. C. Ether, *J. Am. Chem. Soc.* 1986, **108**, 3159.
14. D. L. Reger, J. A. Linderman and L. Lebioda, *Inorg. Chem.* 1988, **27**, 3923.
15. J. A. Cunningham, D. E. Sands and W. F. Wagner, *Inorg. Chem.* 1967, **6**, 499.
16. M. March, *Advanced Organic Chemistry: reactions, mechanisms and structure*, 2nd edn. McGraw-Hill, New York (1977).
17. O. Poncelet and L. G. Hubert-Pfalzgraf, *Polyhedron* 1989, **8**, 2183.
18. M. Guglielmi and C. Carturan, *J. Non-Cryst. Solids* 1988, **100**, 16.
19. A. Leaustic, F. Babonneau and J. Livage, *Chem. Mater.* 1989, **1**, 240; 248.

Polyhedron Vol. 9, No. 10, pp. 1311–1315, 1990
Printed in Great Britain

0277–5387/90 $3.00+.00
© 1990 Pergamon Press plc

SYNTHESIS AND X-RAY STRUCTURE OF MONOMERIC ARYLOXIDE COMPLEXES OF MANGANESE(II) AND CHROMIUM(II)

D. MEYER, J. A. OSBORN* and M. WESOLEK

Institut Le Bel, Université Louis Pasteur, 4, rue Blaise Pascal, 67070 Strasbourg, France

(*Received* 20 *November* 1989; *accepted* 17 *January* 1990)

Abstract—Two monomeric alkoxide complexes of manganese(II) and chromium(II) have been synthesized and their structure determined by X-ray methods. In both cases, the bond distances and, in particular, the large M—O—C angles are most consistent with a dominant role of steric effects.

In recent years alkoxo- and aryloxo-ligands have been used in the stabilization of high oxidation state organometallic complexes.[1] The origin of the stabilizing effect, which is accompanied by shortening of the metal–oxygen bond lengths and opening of the bond angle at oxygen, is attributed to the existence of a π-donor interaction from the non-bonding oxygen electrons to an empty *d* orbital of the metal. For intermediate oxidation states where the *d* orbitals are partially occupied, the effects of such a π-interaction on the structure and on the stabilization (or destabilization) of the molecule is less evident.[1a]

We report here the synthesis and structure of two monomeric alkoxide compounds of manganese(II) (d^5) and chromium(II) (d^4). Few simple monomeric alkoxide complexes of these metals in their divalent state have, until recently, been reported, since, for the most part, oligomers or polymers are formed. The use of sterically bulky aryloxide ligands originally developed by Horvath[2] appears to impede polymer formation, although full characterization of these apparently monomeric complexes by X-ray diffraction methods had not been carried out.

We have isolated two such derivatives, $Mn(OR)_2(CH_3CN)_2$ (**1**) and $Cr(OR)_2(Py)_2$ (**2**) (where R = 2,4,6-tri-t-butylphenoxide) and characterized them using X-ray analysis. Very recently, the structure of a closely analogous complex of chromium(II) has been described.[3]

* Author to whom correspondence should be addressed.

RESULTS AND DISCUSSION

The complexes are simply prepared by treating $MnCl_2(CH_3CN)_2$ or $CrCl_3(THF)_3$ with, respectively, two or three equivalents of the phenolate as the sodium salt in an ether solvent. The manganese acetonitrile derivate gave colourless crystals of **1** suitable for a structural determination, whereas for chromium(II), addition of pyridine yielded the light blue–green crystalline adduct, **2**. Both complexes are extremely sensitive to oxygen and manipulations were carried out under nitrogen in a glovebox.

The ORTEP diagram of **1** is shown in Fig. 1 and selected bond distances and angles are given in Table 1. The complex crystallizes as a discrete monomer unit, along a two-fold axis, with a distorted tetrahedral arrangement about manganese. Although the organometallic chemistry of manganese(II) with alkoxo- and aryloxo-ligands has been widely developed during the last few years,[4] only recently have monomeric[5] alkoxo-complexes of manganese(II), $[Li_2(THF)_2MnBr_2(OC^tBu_3)_2]$ and $[LiMn(OC^tBu_3)_2(N(SiMe_3)_2)]$ been reported. The first of these complexes shows the expected quasi-tetrahedral arrangement about manganese, but the angles subtended at manganese show clear differences with those in **1**. Whereas the $\angle$ O—Mn—O in **1** is 121.2(3)°, the corresponding angle in $[Li_2(THF)_2MnBr_2(OC^tBu_3)_2]$ is 87.9(3)°, chelation of the lithium cation by the alkoxy ligands causing the severe reduction of this angle in the complex. The smallest subtended angle about

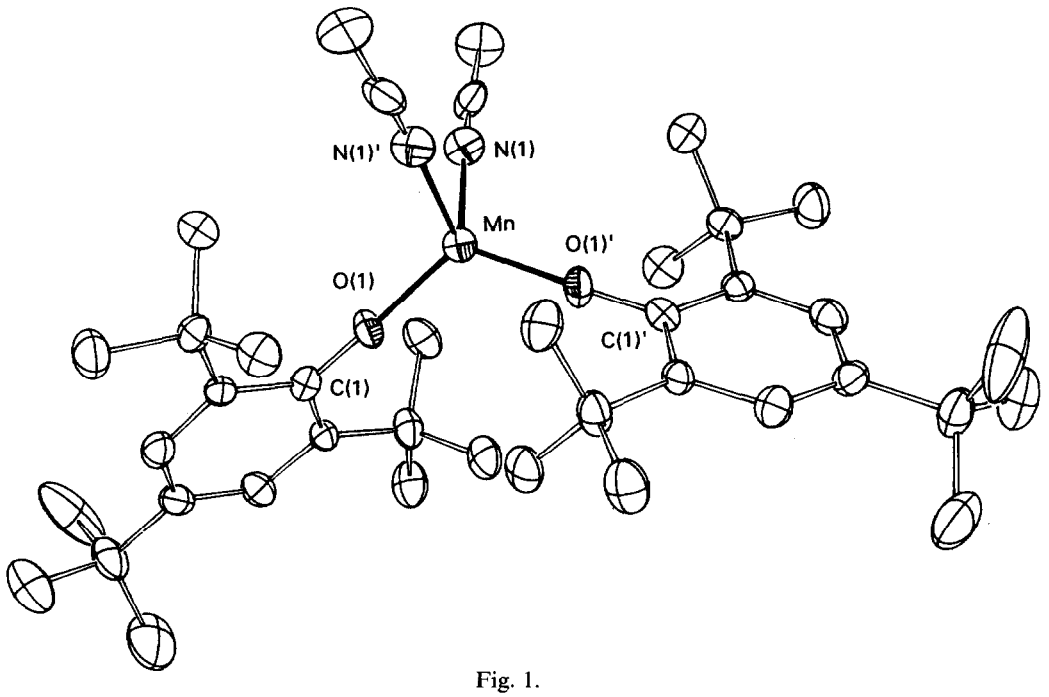

Fig. 1.

manganese in **1** is that between the two CH_3CN ligands (93.8(4)°).

However, the most interesting aspect of **1** is the almost linear Mn—O—C entity (179.1(5)°), the largest yet reported, although in $Cr_2(OCH(^tBu)_2)_4$,[4e] angles of 171.0(3) and 174.9(3)° were found. The Mn—O bond distances for **1**, however, show no real shortening (1.910(6) Å), being effectively longer than the terminal alkoxy–manganese(II) bonds in $Mn_3(OCH(^tBu)_2)_6$ (1.856(4) and 1.852(4) Å), although it could be argued,[6] that these complexes show values that are a little lower than expected for manganese(II) complexes. However, the terminal Mn—O—C bond angles in $Mn_3(OCH(^tBu)_2)_6$ are much smaller (151.2(5) and 148.2(4)°) than in **1** despite the presemnce of shorter Mn—O bond lengths. Clearly it is difficult to make comparisons between complexes of different structures, but it would seem that the bond length/bond angle variations are not consistent with the existence of a classical π-donor interaction, and probably result from steric effects. Finally, the magnetic susceptibility using Evans' method in C_6D_6 ($\mu_{eff} = 5.8\mu_B$) is in agreement with a normal high-spin manganese(II) in a tetrahedral environment.

The X-ray structure of the chromium compound $Cr(OR)_2(Py)_2$ (**2**) is shown in Fig. 2, with selected bond distances and angles presented in Table 2. These compounds were originally synthesized and proposed to be monomeric by Horvath,[2b] and this was recently confirmed by an X-ray diffraction analysis of an analogue[3] whose structural features are very similar to those we describe here. Compound **2** consists of a square arrangement of ligands about chromium; the two oxygen atoms, the two nitrogen atoms and the chromium atom being coplanar. The phenoxo-ligands occupy *trans* positions and the N—Cr—N vector is nearly perpendicular to the O—Cr—O axis (84.45(7)°).

As was found for $Cr(OR)_2(THF)_2$ (R = 2,6-$(^tBu)_2$ 4-Me),[3] the Cr—O bond lengths in **2** are also long (1.952(2) Å) despite the rather open Cr—O—C bond angles (143.4(1)°). The Cr—N bond lengths (2.201(2) Å) are notably longer than in (lutidine)$_2$Cr$(CF_3COO)_2$ (2.111(3) Å)[7] with the plane of the pyridine ligand lying almost in the plane of the

Table 1. Selected bond distances and angles for **1**

Bond distances (Å)		Bond angles (°)	
Mn—O(1)	1.910(6)	O(1)—Mn—O(1′)	121.2(3)
Mn—N(1)	2.18(1)	O(1)—Mn—N(1)	105.5(3)
O(1)—C(1)	1.31(1)	O(1)—Mn—N(1′)	113.9(3)
		N(1)—Mn—O(1)	93.8(4)
		Mn—O(1)—C(1)	179.1(5)

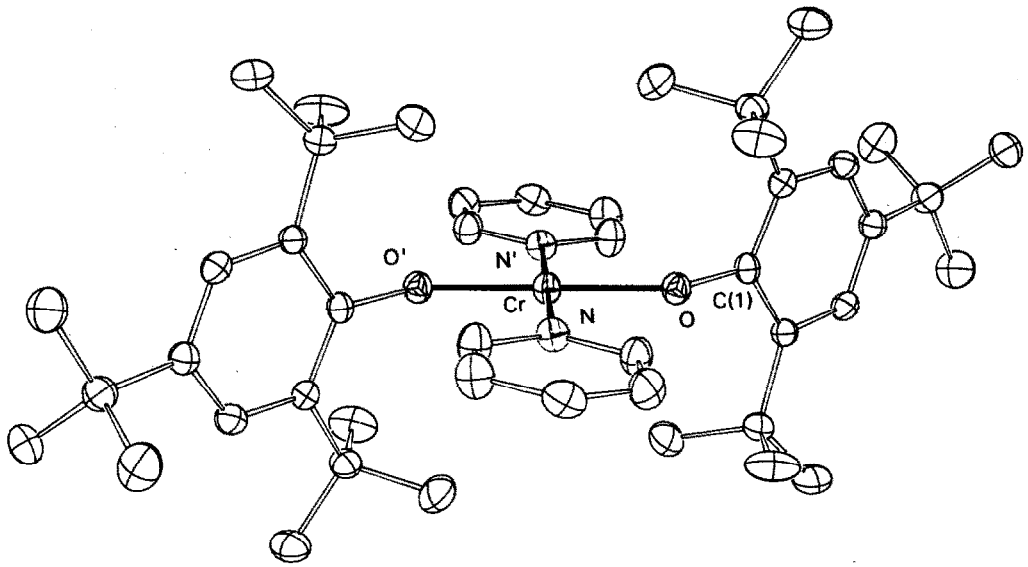

Fig. 2.

Table 2. Selected bond distances and angles for **2**

Bond distances (Å)		Bond angles (°)	
Cr—O	1.952(2)	O—Cr—N	84.45(7)
Cr—N	2.201(2)	Cr—O—C(1)	143.4(1)
O—C(1)	1.342(3)		

complex, making an angle of only 6.29(3)° to it. These results again do not point to any significant π-interactions, steric effects sufficing to explain the small distortions observed.

Hence **2** provides a further example of simple monomeric tetracoordinate chromium(II) species with a square-planar ligand arrangement which has become relatively common in recent years.[3,8] The square arrangement is expected for a d^4 high-spin tetracoordinate complex where (as in d^8 low-spin systems) electron occupancy of the antibonding $d_{x^2-y^2}$ orbital is avoided.

Conclusion

The structural features found for the two alkoxide compounds indicate that at least for high-spin d^4 and d^5 electronic configurations, the π-donor effects are either small or largely dominated by steric factors. However, the effect of the presence of the alkoxide ligands on the chemical reactivity of such compounds, particularly in oxidative processes, is important and under study.

EXPERIMENTAL

All manipulations were carried out in a Vacuum Atmosphere glove-box under a nitrogen atmosphere. Solvents were distilled under nitrogen over sodium/benzophenone for THF, pentane and diethyl ether, and over calcium hydride for acetonitrile and pyridine.

$[(2,4,6\text{-}(^tBu)_3C_6H_2O)_2Mn(CH_3CN)_2] \cdot 2[CH_3CN]$ (1)

A slurry of $MnCl_2(CH_3CN)_2$ (1.0 g, 4.8 mmol) in 100 cm^3 of THF was magnetically stirred and two equivalents of $Na[2,4,6\text{-}(^tBu)_3C_6H_2O)] \cdot THF$ (3.43 g), dissolved in 50 cm^3 of THF, were added, and the solution stirred for 3 h at room temperature. The NaCl precipitate was removed by decantation and the solution filtered through celite, and evaporated to dryness. The resultant solid was crystallized from acetonitrile to give colourless crystals of the biacetonitrile adduct (yield: 2.85 g, 80%).

The IR spectrum (Nujol mull) shows, in particular, absorptions at 2310, 2285 and 2255 cm^{-1}. The magnetic moment was determined by Evans' method[9] in C_6D_6 ($\mu_{eff} = 5.8\ \mu_B$). The compound is slightly soluble in benzene and reacts rapidly with oxygen, changing from a colourless to a black solution.

$[(2,4,6\text{-}(^tBu)_3C_6H_2O)_2Cr(Py)_2]$ (2)

$CrCl_3(THF)_3$ (2 g, 2.67 mmol) was dissolved in 100 cm^3 of THF and three equivalents of $Na[2,4,6\text{-}(^tBu)_3C_6H_2O] \cdot THF$ (2.85 g), dissolved in 50 cm^3 of

THF, were slowly added under magnetic agitation. A deep blue–black solution was obtained after complete addition of the sodium salt, pyridine (3 cm^3, 37 mmol) was added over 2 h with stirring, and the colour changed slowly to green. After filtration over celite the solvent was evaporated under vacuum and a crude green product obtained. The major part was very soluble in pentane and green needles could be recovered at low temperature. Further recrystallization of the green needles in pentane at low temperature, in order to produce crystals suitable for X-ray analysis, led to compound **2**, as well as some white crystalline material.

X-ray crystallographic studies

All X-ray data were collected on a Philips PW1100/16 automated diffractometer with a local-built gas flow device for low temperature measurements. The resulting data-set was transferred to a VAX computer, and for all subsequent calculations the Enraf–Nonius SDP/VAX[10] package was used, with the exception of a local data reduction program which converts the raw step-scan data to intensities using the Lehmann–Larson method,[11] and then corrected for Lorentz and polarization factors. For both structures absorption corrections using empirical methods were performed.[12] Details of the crystal data are given in Table 3.

Crystal data for $C_{44}H_{70}N_4O_2Mn$ (**1**). $M_R = 742.01$, orthorhombic, space group *Iba*2, $a = 19.519(6)$, $b = 15.364(5)$, $c = 15.717(5)$ Å, $V = 4713.4$ Å^3, $Z = 4$, $D_c = 1.046$ g cm^{-3}, graphite monochromized Cu-K_α with $\lambda = 1.5404$ Å and $\mu = 25.339$. Intensities of 1045 reflections were collected ($2\theta_{max} = 50°$, ω–2θ flying step scan) at -100°C. A total of 794 independent reflections with $I > 3\sigma(I)$ were used in the structure determination. The structure was solved by direct methods (MULTAN) and refined by full-matrix least-square techniques (SDP) to $R = 0.039$ ($R_w = 0.052$). Hydrogen atoms were included in structure factor calculations at idealized positions ($d_{C-H} = 0.95$ Å) and were assigned isotropic thermal parameters $B(H) = 1.3\ B_{equ}(C)$ Å^2.

Crystal data for $C_{46}H_{68}N_2O_2Cr$ (**2**). $M_R = 733.06$, monoclinic, space group $P2_1/c$, $a = 9.567(3)$, $b = 10.6373(6)$, $c = 21.502(6)$ Å, $\beta = 93.20(2)°$, $V = 2184.7$ Å^3, $Z = 4$, $D_c = 1.114$ g cm^{-3}, graphite monochromized Cu-K_α with $\lambda = 1.5404$ Å and $\mu = 24.363$. Intensities of 2790 reflections were collected ($2\theta_{max} = 50°$, ω–2θ flying step scan) at -100°C. A total of 2044 independent reflections with $I > 3\sigma(I)$ were used in the structure determination. The structure was solved by Patterson function interpretation and Fourier synthesis, and refined by full-matrix least-square techniques (SDP) to $R = 0.036$ ($R_w = 0.062$). Hydrogen atoms were included in structure factor calculations at idealized positions ($d_{C-H} = 0.95$ Å) and were assigned isotropic thermal parameters $B(H) = 1.3\ B_{equ}(C)$ Å^2.

Supplementary material available. Complete listings of crystal data, positional atomic param-

Table 3. Data collection and structure refinement information

	1	**2**
Space group	*Iba*2	$P2_1/c$
Crystal system	Orthorhombic	Monoclinic
a (Å)	19.519(6)	9.567(3)
b (Å)	15.364(5)	10.637(3)
c (Å)	15.717(5)	21.502(6)
β (°)	—	93.20(2)
V (Å^3)	4713.4	2184.7
Z	4	2
ρ	1.046	1.114
Crystal dimensions (μm)	150 × 200 × 200	180 × 220 × 100
Chemical formula	$C_{44}H_{70}N_4O_2Mn$	$C_{46}H_{68}N_2O_2Cr$
M_w	742.01	733.06
Radiation	Cu-K_α (1.5404 Å) graphite monochromized	
Temperature (°C)	−100	−100
Scanning range	$3° < \theta < 50°$	$3° < \theta < 53°$
Scan mode	ω–2θ flying step scan	
Absorption coefficient (μ cm^{-1})	25.339	24.363
R	0.039	0.036
R_w	0.052	0.062

eters, thermal parameters, observed and calculated structure factors, and bond distances and angles.

Acknowledgements—The CNRS is thanked for financial support and the MRT for a fellowship (D.M.).

REFERENCES

1. (a) M. H. Chisholm and D. C. Clark, *Comm. Inorg. Chem.* 1987, **6**, 23; (b) M. T. Youinou, J. Kress, J. Fischer, A. Aguero and J. A. Osborn, *J. Am. Chem. Soc.* 1988, **110**, 1488.
2. (a) B. Horvath, R. Möseler and E. G. Horvath, *Z. Anorg. Allg. Chem.* 1979, **449**, 41; B. Horvath and E. G. Horvath, *Z. Anorg. Allg. Chem.* 1979, **457**, 51.
3. J. J. H. Edema, S. Gambarotta, F. Bolhuis, W. J. J. Smeets and A. L. Spek, *Inorg. Chem.* 1989, **28**, 1407.
4. (a) D. C. Bradley, *Adv. Inorg. Chem. Radiochem.* 1972, **15**, 259; (b) D. C. Bradley, R. C. Mehrotra and D. P. Gaur, *Metal Alkoxides*. Academic Press, London (1980); (c) R. C. Mehrotra, *Adv. Inorg. Chem. Radiochem.* 1983, **26**, 269; (d) M. Bochmann, G. Wilkinson, G. B. Young and M. B. Hursthouse, *J. Chem. Soc., Dalton Trans.* 1980, 1863; (e) B. D. Murray, H. Hope and P. P. Powers, *J. Am. Chem. Soc.* 1985, **107**, 169.
5. B. D. Murray and P. P. Powers, *J. Am. Chem. Soc.* 1984, **106**, 7011.
6. M. W. Lynch, D. N. Hendrickson, B. J. Fitzgerald and C. G. Pierpont, *J. Am. Chem. Soc.* 1984, **106**, 2041.
7. I. L. Eremenko, A. A. Pasynskii, V. T. Kalinnikov, G. G. Aleksandrov and Yu. T. Struchkov, *Inorg. Chim. Acta* 1981, **54**, L85.
8. A. R. Hermes, R. J. Morris and G. S. Girolami, *Organometallics* 1988, **7**, 2372.
9. (a) D. F. Evans, *J. Chem. Soc.* 1959, 2003; (b) D. F. Evans, G. V. Fazakerley and R. F. Phillips, *J. Chem. Soc. A* 1971, 1931; (c) I. Bertini and C. Luchinat, *NMR of Paramagnetic Molecules in Biological Systems*, p. 132. Physical Bioinorganic Chemistry Series No. 4. The Benjamin/Cummings Publishing Company, Inc., California (1986).
10. B. A. Frenz, The Enraf–Nonius CAD4-SDP, in *Computing in Crystallography* (Edited by H. Schenk, R. Olthof-Hazekamp, H. Van Koningveld and G. C. Bassi), pp. 64–71. Delft University Press, Holland (1978).
11. M. S. Lehmann and F. K. Larsen, *Acta Cryst.* 1974, **A30**, 580.
12. N. Walker and D. Stuart, *Acta Cryst.* 1983, **A39**, 158.

Polyhedron Vol. 9, No. 10, pp. 1317–1321, 1990
Printed in Great Britain

0277–5387/90 $3.00+.00
© 1990 Pergamon Press plc

THE SYNTHESIS OF HETEROBIMETALLIC SYSTEMS BASED ON A HEXATERTIARYPHOSPHINE LIGAND SYSTEM: COBALT–NICKEL AND NICKEL–PLATINUM COMPLEXES

SUZANNE E. SAUM and FREDRIC R. ASKHAM

Department of Chemistry, Washington University, St. Louis, MO 63130, U.S.A.

and

SCOTT A. LANEMAN and GEORGE G. STANLEY*

Department of Chemistry, Louisiana State University, Baton Rouge, LA 70803-1804, U.S.A.

(*Received* 14 *November* 1988 ; *accepted* 18 *January* 1990)

Abstract—Heterobimetallic complexes can be prepared in an extremely straightforward fashion by the use of the binucleating hexatertiaryphosphine ligand $(Et_2PCH_2CH_2)_2PCH_2P(CH_2CH_2PEt_2)_2$, eHTP. The following mixed-metal dimers have been prepared in at least 50% yields: $NiPtCl_2(eHTP)^{2+}$ and $Co(CO)_2NiCl(eHTP)^{2+}$. The CoNi mixed-metal complex is the first example of these metals bridged by a bis(phosphino)methane-type linkage. Two-dimensional ^{31}P COSY NMR spectra are presented to conclusively demonstrate the formation of mixed-metal dimer species. The yields of the heterobinuclear complexes in some cases are dependent upon the reaction conditions and the order of reagent addition. The $NiPtCl_2(eHTP)^{2+}$ complex, for example, is produced statistically in about 50% yield when K_2PtCl_4 is added first to eHTP, whereas it is produced in 67% yield when $NiCl_2 \cdot 6H_2O$ is added first. Reasons for this effect on the yield of the mixed-metal dimer species are discussed. The production of an unusual tetrametallic intermediate $Ni_2Pt_2Cl_8(eHTP)$ is also presented.

Heterobimetallic compounds have attracted a considerable amount of attention over the last few years for applications in both homogeneous[1] and heterogeneous catalysis.[2] Most rational syntheses rely on the use of bridging ligand systems that can act as templates for dimers. High yields are generally only obtained when one is using a mixed functionality hybrid ligand such as Pr_2–$C_5H_4^-$ which has a large difference in binding abilities for two different metal centres.[3] The syntheses of mixed-metal dimers using bridging ligands with similar donor functionalities such as $Ph_2PCH_2PPh_2$ (dppm) are usually only readily accessible if an η^1-dppm metal complex for one of the metal centres can be prepared.[4] We would like to report the straightforward synthesis of heterobimetallic transition metal systems based on the powerful binucleating hexatertiaryphosphine ligand eHTP, which we have used in the past to prepare a variety of homobimetallic complexes.[5–9]

The reaction of one equivalent of $NiCl_2 \cdot 6H_2O$ with eHTP in ethanol followed by one equivalent of $CoCl_2$ produces a mixture of the heterobimetallic complex $CoNiCl_2(eHTP)^{2+}$ and the analogous two homobimetallic systems. This red–brown solution was reacted with H_2/CO (50 bar, 80°C, 24 h) which selectively carbonylated and reduced the cobalt centres to cobalt(I), producing an orange mixture of $Co(CO)_2NiCl(eHTP)^{2+}$ and the previously characterized dimers: $Co_2(CO)_4(eHTP)^{2+}$ (yellow)[5] and $Ni_2Cl_2(eHTP)^{2+}$ (red).[6] ^{31}P NMR on the crude reaction mixture shows that the mixed cobalt–nickel eHTP dimer is produced in *ca* 50% yield while the homobinuclear cobalt and nickel systems are each present in 25% yield.† These are the yields

* Author to whom correspondence should be addressed.

† Spectroscopic data on $Co(CO)_2NiCl(eHTP)^{2+}$: IR (KBr) ν_{CO}: 2005 and 1955 cm^{-1}; $^{31}P\{^1H\}$ NMR (acetone-d_6, δ ppm, H_3PO_4 ref.): 58.5 ($2P_{ext}$—Ni, d, J_{P_P} = 39.3 Hz), 84.3 ($2P_{ext}$—Co, d, J_{P_P} = 48.8 Hz), 110.1 (P_{int}—Ni, pseudo-quartet, J_{P_P} = 34.7 Hz) 121.8 (P_{int}—Co, pseudo-quartet, J_{P_P} = 34.7).

expected based on simple statistical distributions of the metal centres in the eHTP ligand.

The presence of the heterometallic $Co(CO)_2NiCl(eHTP)^{2+}$ dimer is most clearly seen through the use of two-dimensional $^{31}P\{^1H\}$ COSY NMR spectroscopy. Figure 1 shows an expanded portion of the $^{31}P\{^1H\}$ COSY spectrum on $Co(CO)_2NiCl(eHTP)^{2+}$ for the two internal methylene-bridged phosphorus atoms of the eHTP ligand. The mixed-metal $Co(CO)_2NiCl(eHTP)^{2+}$ dimer is uniquely identified by two features in this spectrum: the off-diagonal connectivities which clearly demonstrate that the two internal phosphorus centres are coupled to one another; and from the fact that cobalt is a quadrupolar nucleus that selectively broadens the phosphorus atoms bound to the cobalt, as can be plainly seen in the spectrum. This quadrupolar broadening is also seen for the terminal phosphorus groups bound to the cobalt atom and all the expected off-diagonal couplings from the ^{31}P COSY spectrum consistent with the $Co(CO)_2NiCl(eHTP)^{2+}$ formulation are observed. The pseudo-quartet pattern observed for the central phosphines arises from essentially equivalent coupling of the internal phosphorus atom to the two equivalent linked terminal phosphines and the other methylene-bridged internal phosphorus centre.

Transition metal dimers based on eHTP usually

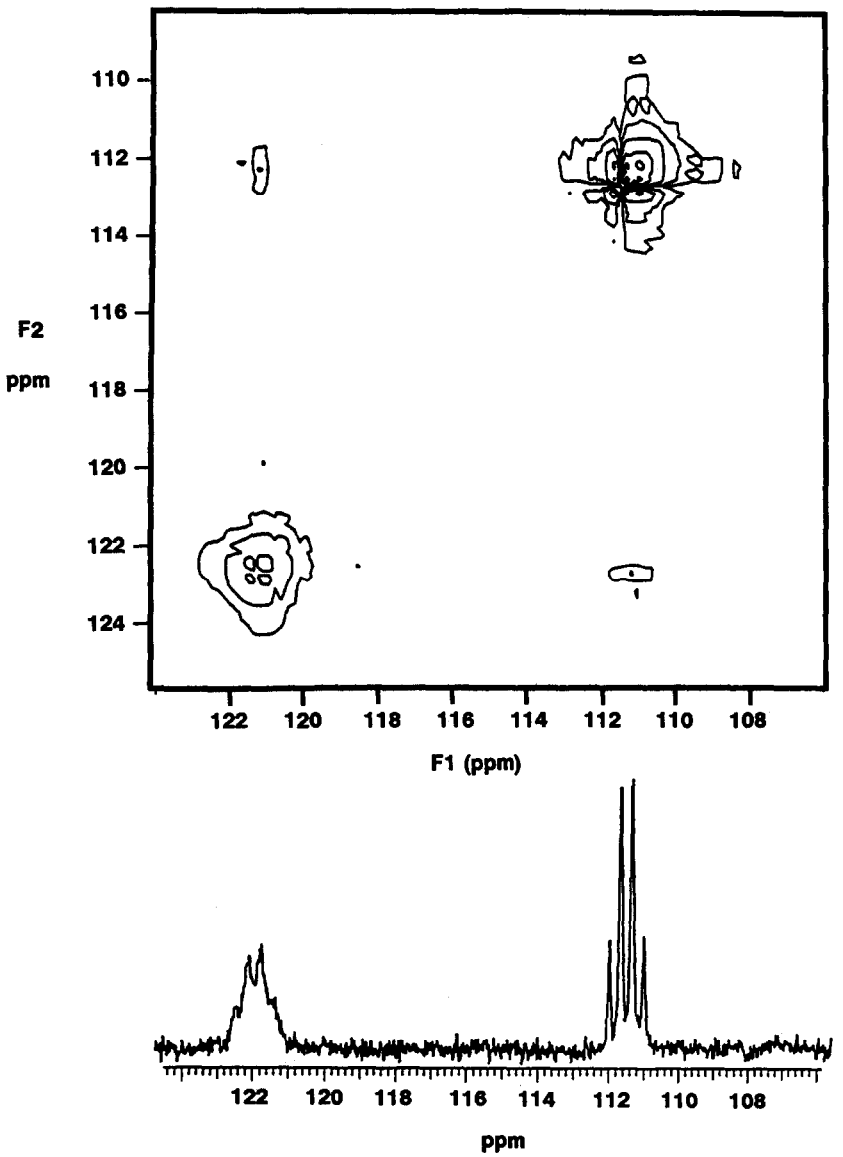

Fig. 1. Expanded portion of the two-dimensional ^{31}P–^{31}P shift correlated (COSY) spectrum for the two inner phosphorus atoms of $Co(CO)_2NiCl(eHTP)^{2+}$ in acetone-d_6. The 1-D $^{31}P\{^1H\}$ NMR spectrum of the same region is shown below the 2-D spectrum for reference.

form open-mode conformations in which the metal centres are separated by 4–7 Å with a variety of rotational orientations about the central methylene bridge. Van der Waals' (VDW) energy calculations have proved to be extremely valuable in probing the possible low-energy conformations for eHTP dimer complexes[6,9,10] and the $Co(CO)_2NiCl(eHTP)^{2+}$ dimer represents an ideal system to probe since the crystal structures on both homobimetallic parent systems are known.[5,6] We used the SYBYL[11] molecular graphic/mechanics program set to fuse half of the $Ni_2Cl_2(eHTP)^{2+}$ structure with half of the $Co_2(CO)_4(eHTP)^{2+}$ structure to create a computer model of the hybrid $Co(CO)_2NiCl(eHTP)^{2+}$ dimer. Terminal methyl groups were used instead of the existing ethyl groups on eHTP as in previous VDW calculations and calculations were carried out with central methylene bridge angles of 123, 125 and 127°, with similar results being obtained. The VDW energy calculation predicts that there are two low energy conformers connected by a pathway with a 34 kcal mol^{-1} barrier (P—CH_2—P = 125°). Parallel and perpendicular views of these two conformers are shown in Fig. 2. Conformer **A** has a structure analogous to $Co_2(CO)_4(eHTP)^{2+}$,[5] while conformer **B** has a structure most similar to that observed for $[Ni_2Cl_2(eHTP)^{2+}][2BF_4^-]$.[6] We are attempting to grow X-ray quality single crystals for a structural analysis on this system.

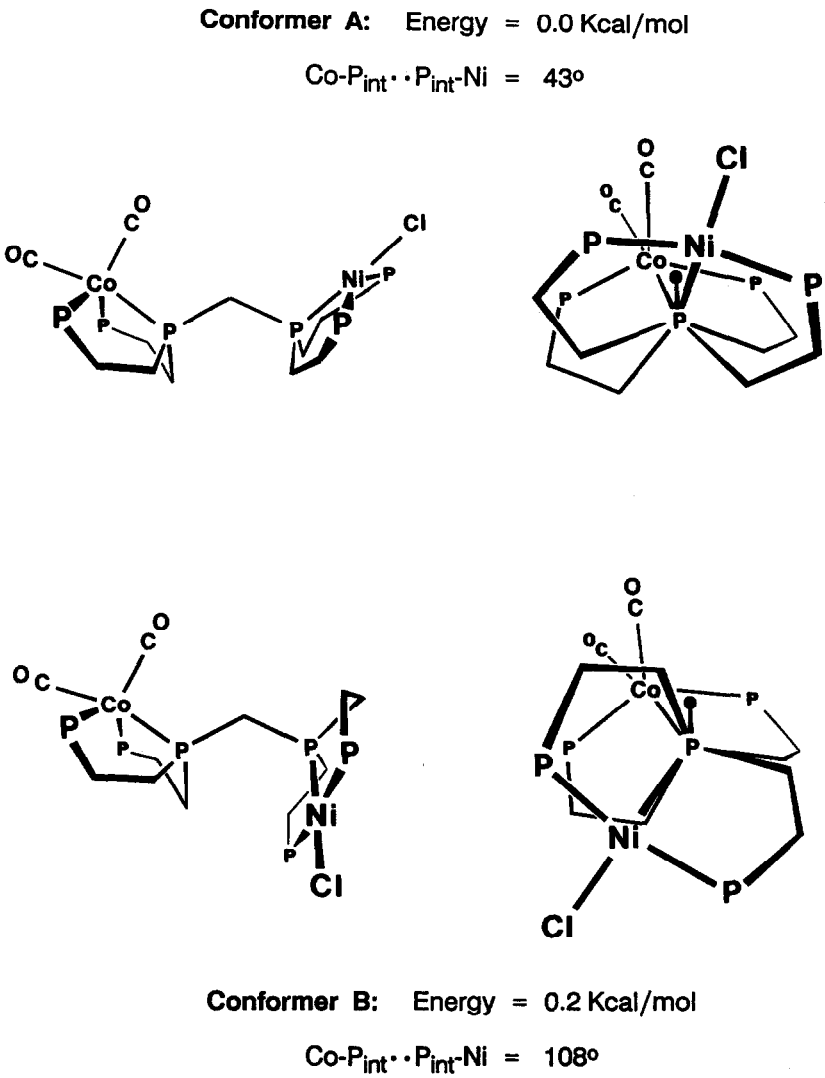

Fig. 2. Calculated low-energy rotational conformations for $Co(CO)_2NiCl(eHTP)^{2+}$ from a van der Waals' (VDW) energy calculation on a model complex using the SYBYL molecular mechanics program package. Views which are parallel and perpendicular to the $P_{int}\cdots P_{int}'$ vector are shown for each conformer to clearly show the rotational orientations. The relative VDW energy and $M—P_{int}\cdots P_{int}'—M'$ torsional angle for each conformer is also listed.

A nickel–platinum(II) mixed-metal dimer system was obtained in a similar fashion to the cobalt–nickel complex. One equivalent of K_2PtCl_4 was reacted with one equivalent of eHTP followed by the addition of one equivalent of $NiCl_2 \cdot 6H_2O$ in ethanol. This gives a statistical product distribution of $NiPtCl_2(eHTP)^{2+}$ (orange, 50%), $Ni_2Cl_2(eHTP)^{2+}$ (red, 25%)[6] and $Pt_2Cl_2(eHTP)^{2+}$ (colourless, 25%).[7] The production of the heterobimetallic $NiPtCl_2(eHTP)^{2+}$ system was confirmed once again by ^{31}P COSY NMR.* Most interestingly, there are deviations observed from the statistical product distribution depending on reaction conditions, particularly with respect to the order of metal reagent addition. Use of $NiCl_2 \cdot 6H_2O$ first instead of K_2PtCl_4, for example, gives a higher production of the mixed-metal species with a product ratio for $Ni_2/Pt_2/NiPt$ of 1 : 1 : *4* (67% yield of the heterobinuclear complex).

We initially believed that this selectivity came about from the partial deactivation of the polyphosphine ligand to the coordination of a second metal centre after complexation of the first metal atom. Optimum formation of mixed-metal dimers occurs for the case when the metal species which has the *weakest* M—P coordination is added *first*, followed by some equilibrium period to allow distribution of the metal centres into the maximum number of monomer species. The metal species which has the weakest M—P bonds will be the most selective at coordinating to the most electron-rich eHTP ligand which will, of course, be one that has *not* coordinated to another metal atom. Metal atoms (such as platinum) which have a considerably higher binding affinity for phosphines will be less sensitive and selective to whether they are coordinating to an empty eHTP or one that already has a bound metal centre.

It was suggested to us by a NSF proposal reviewer, however, that what might actually be happening to produce enhanced yields of the Ni/Pt mixed-metal system when nickel(II) is added

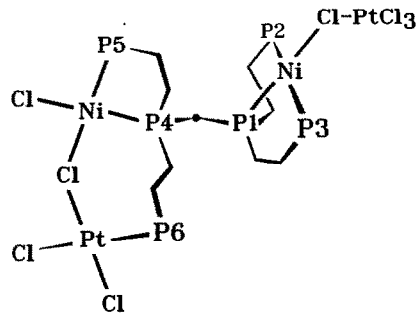

Scheme 1.

first to eHTP is that some of the homobimetallic $Ni_2Cl_2(eHTP)^{2+}$ complex formed can react directly with platinum(II) to form $NiPtCl_2(eHTP)^{2+}$. We tested this by taking pure $Ni_2Cl_2(eHTP)^{2+}$ and adding three equivalents of K_2PtCl_4 in H_2O. There was an immediate reaction with the precipitation of an orange–red material. Based on the elemental analysis and ^{31}P NMR spectral data† of this orange–red material we have assigned this new molecule to the *tetra*metallic species $Ni_2Pt_2Cl_8(eHTP)$, which is shown above.

On standing in CH_3CN solution, $Ni_2Pt_2Cl_8(eHTP)$ slowly and almost quantitatively converts to $Pt_2Cl_2(eHTP)^{2+}$ and $NiCl_2 \cdot 6H_2O$ over the course of 1–2 weeks. This observation is consistent with the proposed presence of two platinum atoms in the complex. Interestingly, we do see small quantities of the heterobimetallic system $NiPtCl_2(eHTP)^{2+}$ in the ^{31}P NMR spectra during the conversion of $Ni_2Pt_2Cl_8(eHTP)$ to $Pt_2Cl_2(eHTP)^{2+}$. It is, therefore, quite reasonable to assume that in the reaction of $NiCl_2 \cdot 6H_2O$ with eHTP, followed by the addition of K_2PtCl_4, some $PtCl_4^{2-}$ (or $PtCl_3(solvent)^-$) did directly attack some of the bimetallic $Ni_2Cl_2(eHTP)^{2+}$ present to form the tetrametallic species $Ni_2Pt_2Cl_8(eHTP)$. This could then further react to displace one of the nickel atoms to form the heterobimetallic complex $NiPtCl_2(eHTP)^{2+}$, resulting in an enhanced yield of the heterobimetallic product. This raises the intriguing possibility of obtaining nearly quantitative yields of the mixed NiPt complex by starting with pure $Ni_2Cl_2(eHTP)^{2+}$ and reacting it with only a *single* equivalent of K_2PtCl_4. We are currently exploring this possibility.

Although this general method for preparing heterobimetallic complexes may appear to be somewhat inelegant, it should be noted that it is virtually assured to work for any pair of transition metal centres that will coordinate a bis(phosphino)-ethane-type moiety to give at least a 50% yield of the mixed-metal compound. The NiCo bimetallic complex reported here is the first example of these

* Spectroscopic data on $NiPtCl_2(eHTP)^{2+}$: $^{31}P\{^1H\}$ NMR (CD_2Cl_2, δ ppm, H_3PO_4 ref.): 52.2 ($2P_{ext}$—Pt, s, J_{Pt-P} = 1145.2 Hz), 57.5 ($2P_{ext}$—Ni, d, J_{P-P} = 27.5 Hz), 80.0 (P_{int}—Pt, d, J_{P-P} = 27.1 Hz, J_{Pt-P} = 1580.9 Hz), 104.9 (P_{int}—Ni, pseudo-quartet, J_{P-P} = 27.3 Hz).

† $^{31}P\{^1H\}$ NMR data for $Ni_2PtCl_6(eHTP)$, CD_3CN (numbering of the phosphorus atoms corresponds to those used in the text figure): 20.4 (P6, dd, J_{P-P} = 24.3 Hz, J_{Pt-P} = 1215.4 Hz), 61.6 (P2, 3, d, J_{P-P} = 55.3 Hz), 74.3 (P4, m, J_{P-P} = unresolvable), 82.8 (P5, dd, J_{P-P} = 64.1, 15.5 Hz), 110.1 (P1, dt, J_{P-P} = 55.3, 15.5 Hz). Calc. for $C_{25}H_{58}Cl_8Ni_2P_6Pt_2$: C, 22.48; H, 4.38; P, 13.91. Found: C, 23.51; H, 4.96; P, 12.85.

two metal centres linked by a bis(phosphino)-methane group, and there are only two recently reported examples of bis(phosphino)methane-bridged NiPt dimers: $NiPtCl_2(\mu\text{-dppm})_2(\mu\text{-CO})$ by Holah *et al.*,[12] and $[Ni(CH_3CN)_2(\mu\text{-dppm})Pt(\eta^2\text{-dppm})]^{2+}$ by Miedaner and DuBois.[13]

One reaction that is potentially well suited to mixed-metal binuclear systems is hydroformylation and there have been several reports on the effects of heterobimetallic homogeneous catalysts on the rate and selectivity of hydroformylation reactions.[14] We are particularly interested in studying the hydroformylation activity of homo- and heterobimetallic Group VIII metal complexes based on our new, less sterically hindered binucleating tetratertiaryphosphine ligand system $(Et_2PCH_2CH_2)(Ph)PCH_2P(Ph)(CH_2CH_2PEt_2)$, eLTTP.[15-17] This ligand should have extremely similar coordinating properties as eHTP and we plan to study the reaction conditions required to optimize the syntheses of heterobimetallic eHTP and eLTTP bimetallic complexes.

Acknowledgement—We would like to thank the National Science Foundation (CHE-86-13089 and CHE-88-23041) for supporting this research.

REFERENCES

1. (a) E. L. Muetterties, *Bull. Soc. Chim. Belg.* 1976, **85**, 451; (b) A. K. Smith and J. M. Basset, *J. Molec. Catal.* 1977, **2**, 229.
2. (a) J. R. Anderson, P. S. Elmes, R. F. Howe and P. E. Mainwaring, *J. Catal.* 1977, **50**, 508; (b) M. Ichikawa, *J. Catal.* 1979, **56**, 127.
3. Cf. R. M. Bullock and C. P. Casey, *Accts Chem. Res.* 1987, **20**, 167.
4. Cf. most recent review on $M_2(dppm)_2$ complexes: C. P. Kubiak, *Polyhedron*, submitted.
5. F. R. Askham, G. G. Stanley and E. C. Marques, *J. Am. Chem. Soc.* 1985, **107**, 7423.
6. S. A. Laneman and G. G. Stanley, *Inorg. Chem.* 1987, **26**, 1177.
7. S. E. Saum and G. G. Stanley, *Polyhedron* 1987, **6**, 1803.
8. F. R. Askham, A. W. Maverick and G. G. Stanley, *Inorg. Chem.* 1987, **26**, 3963.
9. S. E. Saum, F. R. Askham, F. R. Fronczek and G. G. Stanley, *Organometallics* 1988, **7**, 1409.
10. A. D'Avignon, F. R. Askham and G. G. Stanley, *Inorg. Chem.*, submitted.
11. (a) S. Naruto, I. Motoc, G. R. Marshall, S. B. Daniels, M. J. Sofia and J. A. Katzenellenbogen, *J. Am. Chem. Soc.* 1985, **107**, 5262; (b) The SYBYL program set (version 5.1) is available from TRIPOS Associates, Inc., 1699 S. Hanley Road, Suite 303, St. Louis, MO 63144, U.S.A.
12. D. G. Holah, A. N. Hughes, V. R. Magnuson, H. A. Mirza and K. O. Parker, *Organometallics* 1988, **7**, 1233.
13. A. Miedaner and D. L. DuBois, *Inorg. Chem.* 1988, **27**, 2479.
14. (a) L. Gelmini and D. W. Stephan, *Organometallics* 1988, **7**, 849; (b) I. Kovacs, C. D. Hoff, F. Ungvary and L. Marko, *Organometallics* 1985, **4**, 1347; (c) M. Hidai, A. Fukoka, Y. Koyasu and Y. Uchida, *J. Chem. Soc., Chem. Commun.* 1984, 516; (d) P. Pino and D. A. von Bezard, *Swiss Patent* 625,233, 1981; (e) P. Pino and G. Consiglio, *Proc. Symp. Rhodium Homogeneous Catal.* p. 98. Veszprem (1978).
15. S. A. Laneman, F. R. Fronczek and G. G. Stanley, *J. Am. Chem. Soc.* 1988, **110**, 5585.
16. S. A. Laneman, F. R. Fronczek and G. G. Stanley, *Inorg. Chem.* 1989, **28**, 1206.
17. S. A. Laneman, F. R. Fronczek and G. G. Stanley, *Inorg. Chem.* 1989, **28**, 1872.

Polyhedron Vol. 9, No. 10, pp. 1323–1329, 1990
Printed in Great Britain

0277–5387/90 $3.00+.00
© 1990 Pergamon Press plc

THE SYNTHESIS, CHARACTERIZATION AND REDOX PROPERTIES OF OXO-COMPLEXES OF RHENIUM(V) AND (VII) WITH CATECHOL LIGANDS. THE X-RAY CRYSTAL STRUCTURE OF $[ReO_2(O_2C_6H_4)_2]^-$

JONATHAN R. DILWORTH,* SAAD K. IBRAHIM and SHAH ROZ KHAN

Department of Chemistry and Biological Chemistry, University of Essex, Colchester CO4 3SQ, U.K.

and

MICHAEL B. HURSTHOUSE* and ALEXANDER A. KARAULOV

Department of Chemistry, Queen Mary and Westfield College, Mile End Road, London E1 4NS, U.K.

(*Received* 29 *November* 1989; *accepted* 18 *January* 1990)

Abstract—The rhenium(V) complex $[ReO(O_2C_6H_4)_2]^-$ has been synthesized by reaction of $[ReOCl_3(PPh_3)_2]$ with excess catechol in methanol in the presence of triethylamine under N_2. If the reaction is carried out in air the rhenium(VII) complexes $[ReO_2(O_2C_6H_2R_2)_2]^-$ (R = H, Bu^t) can be isolated with a range of cations. Cyclic voltammetry coupled with convolution analysis showed that the rhenium(VII) complexes undergo a reversible diffusion-controlled one-electron reduction. The X-ray crystal structure of the rhenium(VII) derivative with R = H revealed a distorted octahedral geometry with *cis*-oxo groups.

Catechol complexes are well known for most of the transition elements, including iron, molybdenum, osmium, manganese and chromium and a comprehensive review has appeared.[1] The recent research effort in this area has in part been due to the established wide occurrence of catechol-based metal ion siderophores in biological systems. However, catechol complexes are also of intrinsic interest from the standpoint of their redox chemistry. Catecholate† ligands are suspect in Jorgensen's classification and redox reactions may occur either at the metal centre or within the catecholate ligand. We are currently interested in the chemistry of rhenium due to its close analogy with technetium which is used extensively as a radionuclide imaging agent.

Recently some six-coordinate cathecholate complexes of rhenium of the type $[Re(O_2C_6H_4)_3]^{2-}$ were reported,[2] prepared by reaction of $[ReCl_6]^{2-}$ with catechol in the presence of base. The synthesis of neutral, formally rhenium(VI) complexes $[Re(O_2C_6H_2Bu^t_2)_3]$ and $[Re(O_2C_6Cl_4)_3]$ have also recently been reported by oxidative addition of the corresponding quinones to $[Re_2(CO)_{10}]$.[3] Monomeric oxo-catecholato-complexes are comparatively rare, being restricted to $[OsO_2(cat)_2]^{2-}$,[4] $[OsO_2(cat)py_2]$,[4] $[MoO_2(cat)_2]^{2-}$ [5] and $[WO_2(cat)_2]^{2-}$.[4] We here report the synthesis and characterization of some simple monomeric oxo- and dioxo-catecholato-complexes of rhenium.

RESULTS AND DISCUSSION

Synthesis of complexes

The reaction of $[ReOCl_3(PPh_3)_2]$ with excess catechol under N_2 in the presence of base in refluxing ethanol yields a pale olive-green anionic complex of apparent stoichiometry $[ReO(cat)_2]^-$ (**I**). This can be isolated as a microcrystalline, somewhat air-sensitive solid by the addition of

* Authors to whom correspondence should be addressed.

† We have adopted previously suggested nomenclature in using the term catecholato-complexes as X-ray crystal structural and spectroscopic data are consistent with the dianionic bonding mode.

Table 1. Mono- and dioxo-catecholato-complexes of rhenium

Complex	Colour	Melting point[a]	Analysis[b] C	H	N	^{1}H NMR[c] (ppm)	^{31}P NMR[d] (ppm)	IR[e] ν(R=O)
$[Me_4N][ReO(O_2C_6H_4)_2]$	Green	285	38.8 (39.0)	4.4 (4.7)	2.1 (2.2)	7.50s, 6.60s (phenyl) 1.1s (Me)	—	987
$[Et_4N][ReO_2(O_2C_6H_4)_2]$	Purple	200	40.3 (39.5)	5.3 (5.6)	2.5 (2.3)	7.505, 6.60s (phenyl) 3.00–3.40q (CH_2) 1.20–1.40t (CH_3)	—	923 985
$[Ph_4P][ReO_2(O_2C_6H_4)_2]$	Purple	360	55.6 (55.8)	3.7 (3.6)	0.0 (0.0)	7.50s, 6.60s (phenyl) 7.25m, (PPh_4 phenyl)	20s	922 985
$[Et_4N][ReO_2(O_2C_6H_3Bu^t)_2]$	Purple	180	50.2 (49.1)	7.1 (6.5)	2.1 (2.0)	7.55s, 6.65s (phenyl) 3.00–3.45q (CH_2) 1.00–1.45t (CH_3) 1.25s (Bu^t)	—	923 982
$[Et_4N][ReO_2(O_2C_6H_2Bu^t_2)_2]$	Purple	165	55.0 (54.8)	7.8 (7.6)	1.9 (1.8)	7.50s, 6.60s (phenyl) 3.00–3.40q (CH_2) 1.00–1.40t (CH_3) 1.20s, 1.70s (Bu^t)	—	922 979
$[Ph_4P][ReO_2(O_2C_6H_2Bu^t_2)_2]$	Purple	195	61.9 (62.9)	5.7 (6.0)	0.0 (0.0)	7.60s, 6.55s (phenyl) 7.25m (PPh_4 phenyl) 1.30s, 1.90s (Bu^t)	—	919 981

[a] Unconnected with decomposition.
[b] Calculated values in parentheses.
[c] In $CDCl_3$ or $(CD_3)_2CO$ relative to TMS, s = singlet, t = triplet, q = quartet.
[d] Relative to H_3PO_4.
[e] As Nujol mulls.

$[Me_4N]Cl$, and analogues with other substituted catechols can be prepared in a similar manner. These complexes and others discussed below are summarized in Table 1, together with relevant analytical and spectroscopic properties.

If the above reaction was carried out in air, or the mono-oxo-complex allowed to stand in air, the deep purple rhenium(VII) dioxo-anion $[ReO_2(cat)_2]^-$ (**II**) is formed in high yield. These could be precipitated from solution with a range of large cations, and their properties are summarized in Table 1.

A range of other rhenium precursors with metal nitrogen multiple bonds such as $[ReCl_2N(PPh_3)_2]$, $[ReCl_3(NPh)(PPh_3)_2]$ and $[ReCl_2(N_2COPh)(PPh_3)_2]$ were reacted under similar conditions with the catecholate anion generated *in situ*. No nitrogen-containing products could be isolated and in air the dioxo-rhenium(VII) complex was formed. It seems probable that anionic species such as $[ReN(cat)_2]^{2-}$ may be transiently generated but that the overall negative charge activates the nitrogen ligand to protonation and subsequent loss as ammonia or amine. Similar results have been observed for the reaction of such species with anionic thiolato-ligands.[6]

SPECTROSCOPIC PROPERTIES

(i) *IR and UV–vis spectra*

Both types of anion exhibit intense bands in the 1250–1270 cm^{-1} region attributable to the C—O stretching frequencies for coordinated catecholato-anions. There was no evidence for bands assignable to ν(O—H) confirming that the catecholate ligands are completely deprotonated.

The mono-oxo-complexes such as **I** show a single intense band in the region 980–1000 cm^{-1} due to a terminal Re=O group. By contrast, the rhenium(VII) complexes such as **II** have two strong bands at 925 and 985 cm^{-1} confirming the presence of a *cis*-ReO_2 dioxo-moiety.

The rhenium(VII) dioxo-complexes are an intense purple colour in solution which is reflected in the presence of intense charge-transfer absorptions in the region 540–550 nm.

(ii) *NMR spectra*

The rhenium(VII) dioxo-catecholato-anion shows two broad resonances at 6.6 and 7.5 ppm assigned to the 3,6- and 4,5-phenyl protons of the catecholate ligand, respectively. By contrast, the complex $[MoO_2(cat)_2]^{2-}$ shows only one broad multiplet at 6.59 ppm assigned to coordinated catechol.

For the corresponding rhenium(VII) complex of 3,5-ditertiarybutyl catechol, two sharp singlets are observed for the Bu^t hydrogens. This indicates that at room temperature only one of the two possible stereoisomers is present in solution. There was no sign of broadening of these resonances on lowering the temperature suggesting that the system is not fluxional. Presumably steric effects are responsible for the selection of one isomer and we propose the structure shown in Fig. 1. Here the catechol is ligated so that the oxygens at position two are *trans* thereby minimizing repulsions between Bu^t groups at the *cis*-oxygen positions. Similarly only one singlet resonance is observed for the complex of monotertiarybutyl catechol, again suggesting the presence of a single isomer in solution.

Structure of rhenium(V) *mono-oxo-complex* [ReO $(O_2C_6H_4)_2]^-$

This complex is formally analogous to $[\{MoO(O_2C_6H_4)_2\}_2]$ which has been shown to have a dimeric catechol oxygen-bridged structure in the solid state.[7] The molybdenum complex shows *four* resonances due to Bu^t groups which decrease to two on solution in coordinating solvents such as acetone due to the formation of mono-oxo-complex monomers. However, the rhenium(V) complex shows no colour change in solution on addition of donor

$[ReO_2(C_6H_2(t.Bu)_2)_2]$

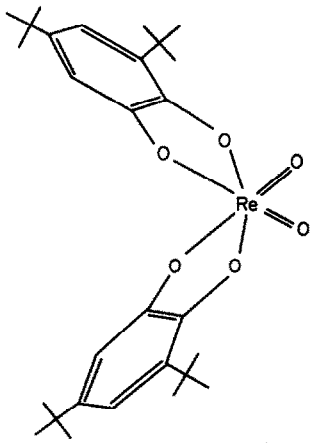

Fig. 1.

$[ReO(O_2C_6H_4)_2]$

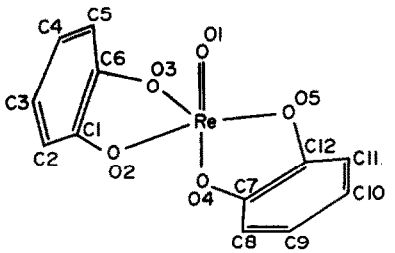

Fig. 2.

solvents and we tentatively propose the monomeric square-pyramidal structure in Fig. 2.

Structure of $[ReO_2(O_2C_6H_4)_2]^-$

Crystals of $[Et_4N][ReO_2(O_2C_6H_4)_2]$ suitable for an X-ray crystal structure determination were grown from dichloromethane–diethyl ether as purple needles. Data pertinent to the structure determination are summarized in Table 2 and selected bond lengths and angles appear in Table 3. Tables of atomic coordinates and full bond lengths and angles have been deposited as supplementary data. An ORTEP representation of the structure is shown in Fig. 3 together with the atom labelling scheme. Both ions lie on two-fold axes of symmetry.

The overall geometry about the rhenium is distorted octahedral with the two terminally bonded oxo-groups occupying *cis* positions. Two distortions from idealized octahedral geometry are evident. Repulsion between the two *cis*-oxo-groups occurs due to the high concentration of electron density in the Re=O bonds and the O(3)—Re—O(3)′ angle is 99.4(5)°. The high *trans*-influence of the oxo-ligands causes the catecholato-ligands to be asymmetrically coordinated with Re—O(1) = 2.031(7) Å and Re—O(2) = 1.952(6) Å.

The Re—O distances for the catecholate ligand not lengthened by the *trans*-influence are very similar to those found in other related catecholato-complexes such as $[\{MoO(S_2C_6H_2Bu^t_2)_2\}_2]$ (1.945 Å). The C—O distances of 1.324(9) and 1.357(9) Å are consistent with the presence of the dianionic catecholato- rather than ligated semiquinone or benzoquinone ligands. The lengthening of the Re—O distances *trans* to the oxo-groups is reflected in a concomitant slight decrease in the C—O bonds.

Examples of complexes with the *cis*-ReO_2 moiety are rare although many are known for molybdenum and tungsten. To our knowledge this is the first structurally characterized example of such a complex.

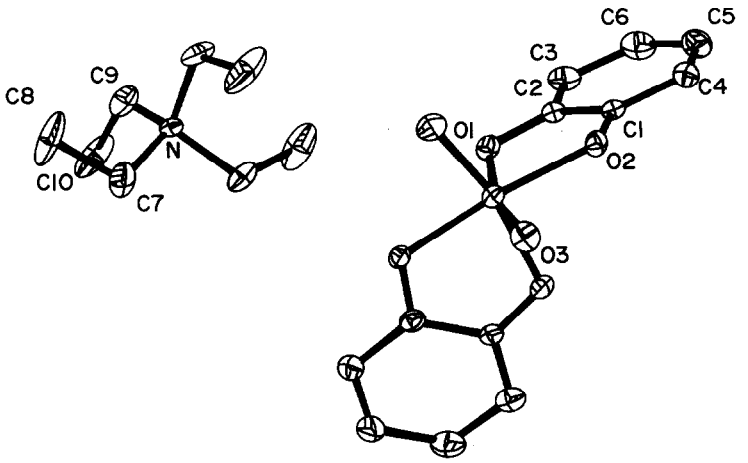

Fig. 3.

Table 4 compares X-ray structural data for isoelectronic $[ReO_2(O_2C_6H_4)_2]^-$ and $[MoO_2(O_2C_6H_4)_2]^{2-}$.[8] The general features of the complexes are very similar with asymmetric coordination of the catecholato-ligands due to the *trans*-influence of the oxo-ligands. A surprising feature of the molybdenum complex is the Mo—O distance of the Mo=O groups of 1.77 Å, which is about

Table 2. Crystal data and details of data collection and structure refinement for $[Et_4N][ReO_2(O_2C_6H_4)_2]$

Crystal data	
Formula	$[C_{12}H_8O_6Re][C_8H_{20}N]$
Formula weight	564.66
Crystal system	Monoclinic
a (Å)	11.351(4)
b (Å)	16.073(3)
c (Å)	11.625(5)
α (°)	90
β (°)	100.29(3)
γ (°)	90
V (Å^3)	2086.98
Space group	$C2/c$
Z	4
D_c	1.796
$F(000)$	1112
μ (cm^{-1})	59.33
Data collection	
Radiation	Mo-K_α (monochromated); $\lambda = 0.71069$ Å
Temperature	293
Crystal size (mm^3)	$0.15 \times 0.20 \times 0.30$
θ min, max (°)	1.5, 25.0
Scan mode	ω–2θ
No. data collected	3664 (2 asymm. units)
No. unique; R_{int}	1836; 0.023
No. observed	1654
Sigma cut-off	$I > 3\sigma(I)$
Absorption correction	Psi scans
Refinement	
No. of parameters	141
Weighting scheme	$[\sigma^2]^{-1}$
Final R value	0.0359
Final R_w value	0.0334

Table 3. Selected bond lengths and angles for $[NEt_4][ReO_2(O_2C_6H_4)_2]$

Bond lengths (Å)			
O(1)—Re	2.031(7)	O(2)—Re	1.952(6)
O(3)—Re	1.681(7)	C(2)—O(1)	1.319(9)
C(1)—O(2)	1.357(9)	C(2)—C(1)	1.385(10)
C(4)—C(1)	1.385(11)	C(3)—C(2)	1.386(11)
C(6)—C(3)	1.399(15)	C(5)—C(4)	1.371(14)
C(6)—C(5)	1.349(16)	C(7)—N	1.498(11)
C(9)—N	1.513(11)	C(8)—C(7)	1.548(22)
C(10)—C(9)	1.428(18)		
Bond angles (°)			
O(2)—Re—O(1)	77.1(3)	O(3)—Re—O(1)	164.2(2)
O(3)—Re—O(2)	88.7(3)	C(2)—O(1)—Re	116.7(5)
O(1)—Re—O(1)	81.2(4)	C(1)—O(2)—Re	117.3(5)
O(3)—Re—O(3)	99.4(5)	C(2)—C(1)—O(2)	114.9(7)
C(4)—C(1)—O(2)	123.6(8)	C(4)—C(1)—C(2)	121.5(8)
C(1)—C(2)—O(1)	113.6(7)	C(3)—C(2)—O(1)	126.9(8)
C(3)—C(2)—C(1)	119.5(9)	C(6)—C(3)—C(2)	117.9(11)
C(5)—C(4)—C(1)	118.2(10)	C(6)—C(5)—C(4)	121.1(12)
C(5)—C(6)—C(3)	121.7(11)	C(9)—N—C(7)	112.3(8)
C(8)—C(7)—N	111.5(11)	C(7)—N—C(7)	111.3(15)
C(10)—C(9)—N	119.5(12)	C(9)—N—C(9)	111.1(10)

Table 4. X-ray structural data for oxo-catecholato-complexes

Complex	Bond lengths (Å) M=O	M—O[a]	M—O[b]	C—O[c]	Bond angles (°) O=M̂=O	Reference
$[ReO_2(O_2C_6H_4)_2]^-$	1.68	1.95	2.03	1.36	99.4	This work
$[MoO_2(O_2C_6H_4)_2]^{2-}$	1.77	2.05	2.15	1.39	101.0	8

Bond lengths are all corrected to two figures to compare data, as the data set for $[MoO_2(O_2C_6H_4)_2]^{2-}$ is comparatively poor.

[a] *Trans* to catecholate oxygen.

[b] *Trans* to M=O.

[c] Averaged value.

0.1 Å longer than that found in other molybdenum oxo-complexes. The reasons for this are far from clear, but the potassium ions are co-ordinated by water molecules and the oxygen atoms of the Mo=O groups. This interaction might possibly remove sufficient electrons from the Mo=O bond to rationalize the observed long Mo—O distance.

Cyclic voltammetric studies

The redox characteristics of the $[ReO_2(cat)_2]^-$ complexes were studied using convolution analysis coupled to cyclic voltammetry. The measurements were carried out in a standard three-electrode cell under dinitrogen, using platinum wire working and auxilliary electrodes and a silver wire pseudo-reference electrode. Generally dry acetonitrile was used as solvent with $[Bu^n_4N][BF_4]$ as support electrolyte, measurements of peak potential were made relative to ferrocene ($E_{1/2}$ for oxidation +0.54 V relative to SCE in THF). A standard commercial software package CONDECON was used to analyse the cyclic voltammetric responses by convolution analysis. Full details of the theory of convolution analysis have appeared elsewhere[9,10] and will not be discussed here.

The complexes all undergo a complex series of irreversible oxidation processes which will not be considered further. In addition each complex undergoes a fully reversible diffusion-controlled one-electron reduction process between −0.78 and −1.01 V depending on the catechol substituent. The observed $E_{1/2}$ values observed at a scan rate of

Table 5. Cyclic voltammetric data for complexes of the type $[ReO_2(cat)_2]^-$

Compound	$E_{1/2}$ V[a]	Half-height widths for deconvolution dI_1/dt (mV)	No. of electrons involved
$[ReO_2(O_2C_6H_4)_2]^-$	−0.788	91.0	1
$[ReO_2(O_2C_6H_3Bu^t)_2]^-$	−0.880	92.0	1
$[ReO_2(O_2C_6H_2Bu^t_2)_2]^-$	−1.010	92.0	1

[a] Relative to SCE calibrated vs ferrocene.

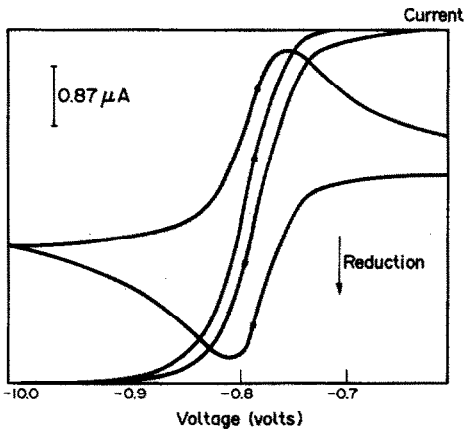

Fig. 4.

50 mV s^{-1} are summarized in Table 5 together with convolution/deconvolution data. The cyclic voltammogram of $[ReO_2(O_2C_6H_4)_2]^-$ is shown in Fig. 4 with the convolution I_1 superimposed.

A number of factors confirm that the reduction is indeed a fully reversible, diffusion-controlled, one-electron process. Table 6 summarizes data for three complexes over a wide range of scan rates. The $[ReO_2(cat)_2]^-$ complexes become progressively harder to reduce with increasing alkyl substitution of the catecholato-ligand as expected with the inductive effect of the alkyl groups. Virtually independent of scan rate all complexes show a peak separation of about 60 mV, close to the theoretical value of 59 mV for the Nernstian process. The fact that the I_1 convolution returns to the same point confirms that there are no homogeneous kinetic processes accompanying the simple electron-transfer. The deconvolution (dI/dt) vs E plot gives maxima at identical E values, indicating that the heterogeneous electron-transfer processes are fast. Moreover, the half-height peak widths of about 90 mV (Table 1) confirm that one electron is involved in the reduction process. These data suggest reasonable stability for the formally 17-electron rhenium (VI) species $[ReO_2(cat)_2]^{2-}$. Experiments are currently in progress to attempt to isolate this species by controlled potential electrolysis and to examine the EPR spectrum of the d^1 complex.

The rhenium(V) complexes $[ReO(cat)_2]^-$ proved to be too unstable in solution for detailed investigation of their redox characteristics.

Table 6. Convolution data for complexes of the type $[ReO_2(cat)_2]^-$

Scan rate	$[ReO_2(O_2C_6H_4)_2]^-$ ΔE_p (mV)	$(dI_1/dt)\ P_a/(dI_1/dt)\ P_c$	$[ReO_2(O_2C_6H_3Bu^t)_2]^-$ ΔE_p (mV)	$(dI_1/dt)\ P_a/(dI_1/dt)\ P_c$	$[ReO_2(O_2C_6H_2Bu^t_2)_2]^-$ ΔE_p (mV)	$(dI_1/dt)\ P_a/(dI_1/dt)\ P_c$
20	57	1.00	60	0.99	60	0.99
50	60	1.02	59	1.00	60	0.99
100	60	1.01	61	1.02	62	1.02
200	60	1.01	61	1.03	62	1.02
500	61	1.02	63	1.04	65	1.04
1000	63	1.04	70	1.05	70	1.05
2000	73	1.05	72	1.05	65	1.04
5000	75	1.05	78	1.05	75	1.06

P_a—anodic peak; P_c—cathodic peak.

In 0.2 M $[Bu^n_4N][BF_4]$ in acetonitrile at 20°C using a platinum wire as working electrode and a silver wire pseudo-reference electrode. Potentials calibrated vs the ferrocene/ferrocenium couple.

Reactions of complexes $[ReO_2(cat)_2]^-$

The purple rhenium(VII) complexes, $[ReO_2(cat)_2]^-$, react rapidly with triphenylphosphine or hydrazine hydrate in refluxing ethanol to give the rhenium(V) species $[ReO(cat)_2]^-$ in high yield. This reaction is rapidly reversed by aerobic oxidation. Attempts to synthesize hydrazido- or diazenido-complexes by reaction of $[ReO_2(cat)_2]^-$ with 1,1-dialkylhydrazines or phenylhydrazine, gave distinct colour changes but no pure complexes could be isolated.

EXPERIMENTAL

All reactions were carried out under dinitrogen in conventional Schlenk apparatus using dry solvents. Elemental analyses were carried out by the analytical services of The University of Sussex. IR spectra were recorded on a Perkin–Elmer 1330 spectrophotometer as Nujol mulls or KBr discs and NMR spectra were measured on a Brukker WP80SY spectrometer.

Cyclic voltammetry was performed using a PAR 362 potentiostat interfaced to an OPUS 2 IBM-compatible computer system via an *A/D* converter. The data was analysed using the CONDECON software package. A standard three-electrode cell was used with platinum wire working and auxiliary electrodes and a silver wire pseudo-reference electrode. Dry acetonitrile was used as solvent with recrystallized $[Bu^n_4][BF_4]$ as support electrolyte (10^{-1} M).

The rhenium precursors $[ReOCl_3(PPh_3)_2]$,[11] $[ReCl_2N(PPh_3)_2]$[12] and $[ReCl_2(N_2COPh)(PPh_3)_2]$[13] were prepared using standard literature methods.

Tetraethylammonium bis(catecholato)di(oxo)rhenate(VII)

$[ReOCl_3(PPh_3)_2]$ (0.5 g), catechol (0.17 g) and diethylamine (0.35 cm^3) in ethanol (25 cm^3) were heated under reflux for 3 h in air. The clear purple solution was cooled and tetraethylammonium chloride (0.5 g) dissolved in ethanol (10 cm^3) was added. The solution was left to stand for 20 h, depositing purple crystals of the dioxo-complex which were then recrystallized from dichloromethane–diethyl ether.

The tetraphenylphosphonium analogue was prepared similarly by addition of tetraphenylphosphonium bromide. Analogues with 4-tert-butylcatechol and 3,5-ditert-butylcatechol were also prepared in a directly similar manner.

Use of $[ReCl_2N(PPh_3)_2]$ or $[ReCl_2(N_2COPh)(PPh_3)_2]$ as precursors under similar conditions also gives the rhenium(VII) dioxo-complexes in high yield.

Tetramethylammonium bis(catecholato)oxorhenate (V)

$[ReOCl_3(PPh_3)_2]$ (0.65 g), catechol (0.17 g) and triethylamine (0.35 cm^3) in methanol (20 cm^3) were heated under reflux under dinitrogen for 3 h to give a clear green solution. A solution of 0.5 g of tetramethylammonium chloride in methanol was added under dinitrogen to give a green microcrystalline precipitate. This was washed with methanol after filtration under N_2 and dried *in vacuo*.

The tetraphenylphosphonium complex was prepared analogously by addition of tetraphenylphosphonium bromide.

REFERENCES

1. C. G. Pierpont and R. M. Buchanan, *Coord. Chem. Rev.* 1981, **38**, 45.
2. A. J. Nielson and W. P. Griffith, *J. Chem. Soc., Dalton Trans.* 1986, 1125.
3. L. A. de Learie and C. G. Pierpont, *J. Am. Chem. Soc.* 1986, **108**, 6393.
4. A. J. Nielson and W. P. Griffith, *J. Chem. Soc., Dalton Trans.* 1978, 1501.
5. V. R. Weinland, A. Babel, K. Gross and H. Mai, *Z. Anorg. Chem.* 1926, **130**, 177.
6. J. R. Dilworth and P. J. Blower, unpublished results.
7. R. M. Buchanan and C. G. Pierpont, *Inorg. Chem.* 1979, **18**, 1617.
8. V. V. Tkachev and L. O. Atovmyan, *Koord. Khim.* 1975, **1**, 845.
9. K. B. Oldham, *J. Chem. Soc., Faraday Trans.* 1986, **82**, 1099.
10. A. Blagg, S. W. Carr, G. R. Cooper, I. D. Dobson, J. B. Gill, B. L. Shaw, N. Taylor and T. Boddington, *J. Chem. Soc., Dalton Trans.* 1985, 1213.
11. J. Chatt, J. D. Carfarth, N. P. Johnson and G. A. Rowe, *J. Chem. Soc.* 1964, 601.
12. J. Chatt, C. D. Falk, G. J. Leigh and R. J. Paske, *J. Chem. Soc. A* 1969, 2288.
13. J. Chatt, J. R. Dilworth, G. J. Leigh and V. D. Gupta, *J. Chem. Soc. A* 1971, 2631.

Polyhedron Vol. 9, No. 10, pp. 1331–1336, 1990
Printed in Great Britain

0277–5387/90 $3.00+.00
© 1990 Pergamon Press plc

TIN(IV) PORPHYRIN COMPLEXES—III.* NMR *TRANS*-INFLUENCES IN TIN(IV) TETRAPHENYLPORPHYRIN COMPLEXES

DENNIS P. ARNOLD† and ELIZABETH A. MORRISON

Department of Chemistry, Queensland University of Technology, G.P.O. Box 2434, Brisbane 4001, Australia

and

JOHN V. HANNA

Brisbane NMR Centre, Griffith University, Nathan 4111, Australia

(*Received* 2 *January* 1990; *accepted* 29 *January* 1990)

Abstract—^{1}H NMR data are reported for the series of octahedral tin(IV) complexes Sn(TPP)(OCOH)X, where TPP is 5,10,15,20-tetraphenylporphyrin and X = OSO_2CF_3, ONO_2, NCS, $OCOCF_3$, OCOH, $OCOC_6H_4$-*o*-OH, $OCOC_6H_5$, $OCOCH_3$, OC_6H_4-*p*-CH_3, OH, OCH_3, F, Cl, Br and I. The mixed-ligand complexes were generated as mixtures also containing the symmetrical complexes Sn(TPP)$(OCOH)_2$ and Sn(TPP)X_2. The chemical shifts of the formate protons and the tin–proton coupling constants, ^3J(Sn—O—C(O)—H), show a fair correlation with the basicity of the ligand X for the O-bound ligands, but the halide complexes demonstrate the importance of π-bonding. The *trans*-influence and *cis*-influence are in the same direction, ie. a ligand which weakens the bond to the *trans*-formate ligand, also weakens the tin–porphyrin coordination.

The tin(IV) complexes of porphyrins and related ligands are proving useful in a range of chemical and biological fields. For example, tin(IV) protoporphyrin is an inhibitor of haem oxygenase, making it a possible agent for treatment of neonatal jaundice.[1,2] Tin complexes of modified porphyrins such as purpurins are being studied as photodynamic therapy drugs, and show good efficacy *in vitro*.[3] Meyerhoff and co-workers reported that poly(vinyl chloride) membrane electrodes impregnated with tin porphyrins display excellent but unexplained selectivity for salicylate over various other anions.[4,5] The determination of salicylate in blood and urine is an important measurement for patients undergoing aspirin therapy. The complexes of water-soluble synthetic porphyrins such as tetrakis(N-methyl-4-pyridyl)porphyrin were studied as possible solar energy capture agents.[6] Lastly, the favourable chemical and spectroscopic properties of tin(IV) porphyrins enable the study of metal–ligand interactions and electronic effects of porphyrin substituents. An understanding of these properties should be useful in extending the uses of these complexes.

Previous investigations have generated an NMR and electronic absorption spectroscopic *cis*-influence series for a number of anionic axial ligands, especially O-donors.[7] A preliminary report suggested the use of the formato ligand as an NMR probe of *trans*-influences,[8] while the instructional value of these complexes has also been pointed out.[9] We now report the results of studies of a series of formato complexes, Sn(TPP)(OCOH)X (Table 1), which yield the *trans*-influence data and allow the comparison of *cis*- and *trans*-influences in the same series.

RESULTS AND DISCUSSION

Preparations of complexes

The most general method for the preparation of tin(IV) porphyrins with identical axial ligands, Sn(TPP)X_2, is the acidolysis of Sn(TPP)$(OH)_2$

* For Part II, see ref. 7.

† Author to whom correspondence should be addressed.

Table 1. Selected NMR data for Sn(TPP)(OCOH)X complexes[a]

Number in text	X	Pyrrole β-H δ	Pyrrole β-H ^4J(Sn—H)	Formate H δ	Formate H ^3J(Sn—H)	X Ligand
1	OSO_2CF_3	9.35	17.6	3.67	70.8	
2	ONO_2	9.29	16.6	3.08	53.1	
3	NCS	9.30	15.9	2.82	46.1	
4	$OCOCF_3$	9.27	16.1	2.88	45.7	
5	OCOH	9.29[b]	15.5[b]	2.70[b]	42.9[b]	
6	$OCOC_6H_4$-*o*-OH	9.30	15.9	2.70	37.8	4.04 (br d, 6″), 5.74 (t, 5″), 6.04 (d, 3″), 6.63 (dt, 4″), 9.38 (br, OH)
7	F	9.32	—[c]	2.48	34.5	
8	$OCOC_6H_5$	9.28	15.9	2.45	31.1	4.97 (br d, 2″, 6″), 6.37 (t, 3″, 5″), 6.67 (dt, 4″)
9	Cl	9.30	—[c]	2.33	30.5	
10	I	9.24	14.4	2.30	29.9	
11	Br	9.23	15.4	2.28	29.7	
12	$OCOCH_3$	9.26	14.7	2.19	28.6	−0.88, ^4J(Sn—H) 4 Hz
13	OC_6H_4-*p*-CH_3	9.17	13.7	2.10	25.4	1.72 (s, CH_3), 1.79 (d, 2″, 6″), 5.49 (d, 3″, 5″)
14	OH	9.26	13.2	1.90	23.5	−6.9 (v br)[d]
15	OCH_3	9.28	12.8	1.89	22.4	−1.79, ^3J(Sn—H) 70.8 Hz

[a] Chemical shifts in ppm relative to $CHCl_3$ at 7.24. Protons of the *meso*-phenyl groups appeared at *ca* 7.8 (3′, 4′, 5′) and *ca* 8.2–8.4 (2′, 6′) ppm. Tin–proton coupling constants (Hz) are the average of the $J(^{119}Sn—H)$ and $J(^{117}Sn—H)$ values, where these were resolved.

[b] Averages of all determinations (see text).

[c] Obscured by other peaks.

[d] Literature value.[8]

with excess HX.[8,9] Reactions are rapid and quantitative even with carboxylic acids and phenols. The corresponding reaction of the mixed complex Sn(TPP)(OCOH)(OH) with one equivalent of HX, was investigated as a route to the required complexes Sn(TPP)(OCOH)X. Since the complex Sn(TPP)(OCOH)(OH) is always contaminated with the symmetrization products $Sn(TPP)(OCOH)_2$ and $Sn(TPP)(OH)_2$, the resulting product will likewise be contaminated with the diformato species and $Sn(TPP)X_2$. In any case, redistribution will occur to give more or less of these complexes. These will be the only three complexes present as long as (i) acidolysis is fast and (ii) only OH groups are protonated and displaced by X^-. This method was found to be satisfactory for the carboxylic acids, which could be added as solutions in CH_2Cl_2 or $CHCl_3$, and complexes **6**, **8** and **12** were prepared by this route.

When stronger acids (eg. HNO_3, HCl, HBr) were used as aqueous solutions in a two-phase reaction, the other two possible products, $Sn(TPP)(OH)_2$ and Sn(TPP)(OH)X, were also found as products. This could be due to either incomplete reaction with the dihydroxo complex or displacement of formic acid rather than water because of locally distorted stoichiometric ratios at the water–CH_2Cl_2 interface. The presence of five complexes in such cases was considered undesirable, so this method was subsequently abandoned. A cleaner method applicable to all species is the redistribution reaction between the two bis(acido) complexes

$$Sn(TPP)(OCOH)_2 + Sn(TPP)X_2 \rightleftharpoons 2Sn(TPP)(OCOH)X.$$

The extents and rates of these reactions varied considerably with the ligand X. More rigorous studies will be required before the significance of such variation can be determined. The redistribution reaction makes it virtually impossible to purify the mixed complexes, as the latter are usually the most soluble components in the mixtures. Since the complexes of interest in this study give unmistakable NMR spectra, the mixtures are just as suitable as the pure complexes for our purposes, provided there is no exchange broadening nor any extreme concentration dependence (see below).

NMR spectra (*Table* 1)

General

The formate resonances of the mixed complexes were easily assigned in all cases, since the diformato

complex (**5**) was present in all samples. Comparison of peak heights and knowledge of chemical shift trends enabled assignment of the β-pyrrole resonances. In some cases, there was severe overlap of β-pyrrole peaks and/or satellites, making measurements of ^4J(Sn—H) difficult or impossible (eg. in **7** and **9**). Other axial ligand resonances were assigned by expected coupling patterns, peak heights, and comparison with pure samples of Sn(TPP)X_2 complexes.[7-10]

Concentration effects on chemical shifts and coupling constants were assessed by observing the signals due to the diformato complex. Over all the mixed samples, the range was 2.65–2.75 ppm, while pure samples of **5** gave a chemical shift of 2.75 ppm at 0.1 M and 2.63 ppm at 0.01 M. Comparisons of peak heights and known starting concentrations gave approximate values for the concentration of **5** in the mixed samples, but these showed extreme scatter when plotted against the chemical shift. The conclusion must therefore be that specific intermolecular effects are blurring the concentration dependence of this shift. As there are no apparent line broadening effects, this is presumably not a shift due to chemical exchange. Since the individual concentrations of the various species in each mixture are uncontrollable because of variations in equilibrium constants, the quoted shifts must be regarded as precise to only *ca* ±0.05 ppm. The extreme values of the ^3J(Sn—H) values for **5** were 42.6 and 43.2 Hz (average of ^{119}Sn and ^{117}Sn coupling constants), so concentration and ligand specific effects on the coupling constants appear to be of less significance, and the precision is *ca* ±0.2 Hz. The chemical shifts of the β-pyrrole protons also show a concentration dependence, for example, for **5**, $\delta = 9.33$ at 0.1 M and 9.24 at 0.01 M. This explains the small discrepancies between the present data and those reported previously,[7,8] the latter having been recorded at concentrations less than 0.02 M. Concentration effects on porphyrin chemical shifts are well known.[11]

The trans-*influence*

The *trans*-influence gives a relative estimate of the ability of a ligand to weaken the bond *trans* to itself in the ground-state of a complex.[12] In this series, the relative strengths of the tin–formate bonds are being studied. The *trans*-influence of a ligand can be examined by considering the chemical shift of the formate proton and the coupling constant ^3J(Sn—H). There is a strong correlation between these two parameters (Fig. 1, $r = 0.986$). It should be noted that the coordination of carboxylate anions to tin(IV) porphyrins is unidentate.

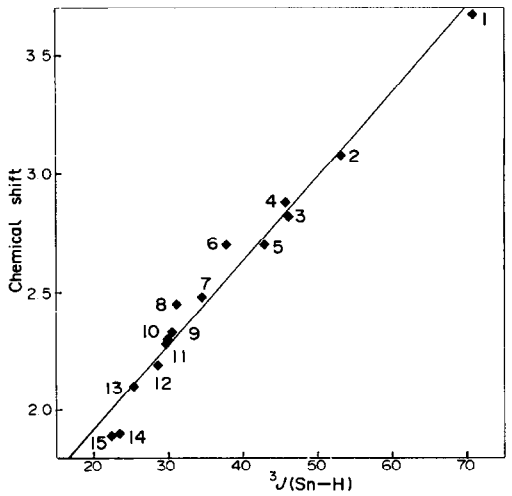

Fig. 1. Plot of chemical shift (δ, ppm) of the formate protons vs ^3J(Sn—H) (Hz) for Sn(TPP)(OCOH)X complexes. Numbering as in Table 1.

This has been shown by IR spectra[13] and crystal structures.[10] The chemical shift presumably reflects the electron density at the nucleus of the formate proton, effects of *trans* ligands being transmitted by contact interactions through the σ-bonds of the Sn—O—C(O)—H fragment. Lengthening of the Sn—O bond (reflecting a strong *trans*-influence of X) might be expected to shift the formate signal downfield, as it would reside on average farther out in the shielding zone of the macrocycle. Clearly this is outweighed by the electronic effects. There is a limit to such lengthening, but bases stronger than methoxide would be required to probe any curvature in Fig. 1. The determination of bond distances in mixed complexes may prove impossible as they cannot be crystallized pure, so the relative magnitudes of these effects may not be assessable. Because of the relationship between δ_H and ^3J(Sn—H), discussion of the reasons for the *trans*-influence order will be confined from now on to the coupling constants, as these enable more precise comparison with *cis*-influences.

The coupling constant ^3J(Sn—H) is quite sensitive to changes in the *trans* ligand, varying from 22.4 to 70.8 Hz. Figure 2 shows the relationship between ^3J(Sn—H) and the pK_a of the conjugate acid of the ligand X.[14-16] The O-bound ligands and thiocyanate yield a fair correlation ($r = -0.940$), while the halides are quite different and appear to fit on another line of near-zero slope. The behaviour of the O-bound ligands appears to be broadly explicable in terms of the proton basicity of X^-. It has been assumed that the triflate ion is coordinated to the tin atom in complex **1**. The Sn(TPP) complexes containing triflate or perchlorate have very

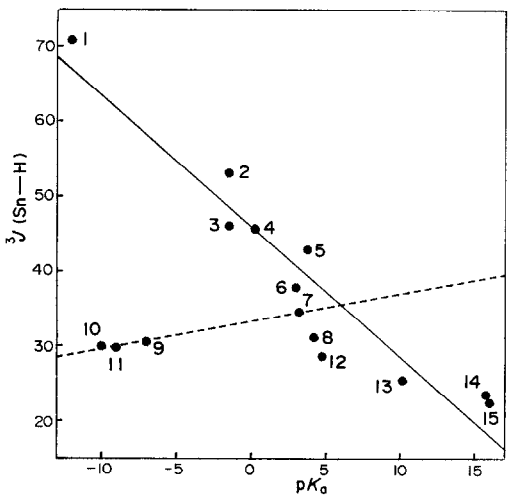

Fig. 2. Dependence of ^3J(Sn—H) (Hz) for formate protons in Sn(TPP)(OCOH)X complexes on the pK_a of the conjugate acids HX. Numbering as in Table 1. Solid line: linear regression for O-ligands; dashed line: linear regression for halides.

low solubility in chloroform, while they are readily soluble in acetone and THF. This is presumably due to coordination of solvent molecules (or adventitious water), with dissociation of the weakly basic anions. No other complexes in these series exhibit such behaviour. Kadish *et al.* have reported perchlorate dissociation in electrochemical studies of similar complexes.[17] The major species giving rise to sharp NMR lines in $CDCl_3$ solutions of **1** does seem to be the "covalent" form, since the chemical shifts and coupling constants fit in with other O-bound ligands for a pK_a of -12 rather than -1.74 as would be expected for X = H_2O. Slow crystallization of the bis(triflate) complex led, on the other hand, to the bis(aqua) salt.[10] In the present study, we could not obtain the data for the mixed formato/perchlorato complex because of dissociation and consequent precipitation.

The σ-bonding capacity of the ligands (as reflected by their donor strength to the proton) is probably the dominant factor for the first row donors. In fact, fluoride and N-bound thiocyanate also fit well with the trend shown by the O-donors. There are some notable deviations. The most surprising is the large difference between formate (**5**) and acetate (**12**). Complex **12** was prepared by both methods described above, with identical results. The scatter exhibited by the O-bound ligands is such that there are some less obvious effects at work, but the reasons for the formate/acetate discrepancy are particularly elusive. The difference between these ligands is apparent not only in the formate and β-pyrrole signals, but also in the acetate signals. The methyl group appears at -0.88 ppm in **12** and at -0.99 ppm in Sn(TPP)$(OCOCH_3)_2$, a shift consistent with that shown by the other protons.

The halides clearly exhibit very different effects from the O-donors. This is the first series of tin(IV) porphyrins examined by NMR which includes (i) all the halides and (ii) a range of O-ligands which spans such a spectrum of donor strengths. Gouterman *et al.* studied excited-state properties of the dihalo complexes of electron-rich porphyrins,[18] while other reports have examined more restricted sets of ligands.[7,17,19] The *trans* bond weakening abilities of Cl^-, Br^- and I^- are much greater than their proton basicity would suggest. This is not surprising since they possess unfilled *d*-orbitals available for π-backbonding from the filled tin d_{z^2} orbital, or molecular orbitals derived from it. However, the similarity of the coupling constants (and chemical shifts) for **9**, **10** and **11** argues that π-donation from filled p_π ligand orbitals to empty p_π and d_π orbitals on Sn is also important. The exact energies of the various orbitals will control the interplay of these effects. The ability of the TPP ligand to act as a π-acceptor presumably "softens" the tin centre (ie. it is very unlike a hard Sn^{4+} ion), and hence relatively strong interactions would be expected for the softer halides Br and I.

The cis-*influence vs the* trans-*influence*

These two effects can now be assessed *in the one series* of complexes Sn(TPP)(OCOH)X, by comparing ^4J(Sn—H) (β-pyrroles) with ^3J(Sn—H) (formates). The chemical shifts could also be used, but suffer from the concentration effects noted above. Unfortunately, the changes in the former coupling constants are rather small compared with their precision. Figure 3 shows this comparison, and the clustering of values around *ca* 15.5 Hz is apparent. There is a broad trend, although the correlation is not well defined. Greater sensitivity would be possible by using ^4J(Sn—H) in the series Sn(TPP)X_2, as the range of values is wider, but this is not a valid comparison, since the *trans*-interactions of the X ligands may be convoluted with the *cis*-influences. Figure 3 does show that the two influences are generally in the *same direction*, which is not necessarily the case for other complexes, for example, in various platinum(II) alkylbis(tertiary phosphine) and similar complexes, the two influences are often in opposite directions.[20] This implies that a ligand which weakens the *trans* Sn—O bond also weakens the bonding in the porphyrin plane, presumably by placing a higher demand on the electrons of the tin atom. The quantities being mea-

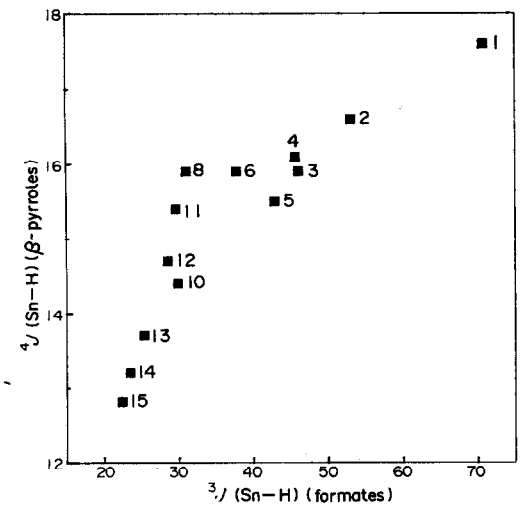

Fig. 3. Relationship between ^4J(Sn—H) (Hz) for the β-pyrrole protons and ^4J(Sn—H) (Hz) for the formate protons in Sn(TPP)(OCOH)X complexes. Numbering as in Table 1. The data for complexes **7** and **9** are missing because of peak overlap.

sured, ie. tin–proton coupling constants, are intrinsically dependent only on *s* orbital electron density or the *s* character of relevant molecular orbitals, since these are the only orbitals with non-zero coefficients at the nuclei.[12] However, it is clear from these data that π-effects are transmissible through the tin–porphyrin and tin–formate bonding orbitals, and can be felt at the β-pyrrole and formate proton nuclei.

In summary, the two series Sn(TPP)X_2[7] and Sn(TPP)(OCOH)X have demonstrated the utility of NMR chemical shifts and metal–proton coupling constants in probing metal–ligand binding. Further studies are now required to relate these ground state effects to data such as redistribution and ligand substitution equilibrium constants.

EXPERIMENTAL

General

Instruments were as described previously.[7] Chloroform was distilled from anhydrous Na_2CO_3. Other solvents, acids, etc., were A.R. or "zur Synthese" grade. Starting materials (Sn(TPP)$(OH)_2$, Sn(TPP)(OCOH)(OH), and various Sn(TPP)X_2 complexes) were available from previous studies.[7,8] The preparations and crystal structures of Sn(TPP)$(OSO_2CF_3)_2$, Sn(TPP)$(OCOC_6H_5)_2$ and Sn(TPP)$(OCOC_6H_4$-*o*-$OH)_2$ will be described elsewhere.[10]

Preparation of new Sn(TPP)X_2 *complexes*

X = F. A solution of Sn(TPP)$(OH)_2$ (38 mg, 0.05 mmol) in CH_2Cl_2 (20 cm^3) was shaken in a separating funnel with aqueous HF (1 M, 5 cm^3) for 30 min. The organic layer was separated, dried over anhydrous Na_2SO_4 and the solvent was evaporated. The residue was recrystallized from CH_2Cl_2–hexane to yield shiny purple prisms (31 mg, 80%). (Found: C, 68.8; H, 3.6; N, 7.3. $C_{44}H_{28}F_2N_4Sn$ requires: C, 68.7; H, 3.7; N, 7.3%); δ_H *ca* 7.8 (m, *meta-*, *para*-H), *ca* 8.4 (m, *ortho*-H) and 9.24 (s, β-pyrrole, ^4J(Sn—H) 14.9 Hz); λ_{max} ($\varepsilon \times 10^{-3}$) ($CHCl_3$) 419 (695), 514 (3.5), 553 (24.4) and 591 (9.8) nm.

X = $OCOCF_3$. Trifluoroacetic acid (3.1×10^{-2} cm^3, 0.4 mmol) was added dropwise with stirring to a solution of Sn(TPP)$(OH)_2$ (77 mg, 0.1 mmol) in CH_2Cl_2 (10 cm^3). After 15 min, the solution was dried over anhydrous Na_2SO_4 and the solvent was evaporated. The residue was recrystallized from CH_2Cl_2–hexane to yield sparkling purple prisms (52 mg, 54%). (Found: C, 61.1; H, 2.9; N, 5.7. $C_{48}H_{28}F_6N_4O_4Sn$ requires: C, 60.2; H, 3.0; N, 5.9%); δ_H *ca* 7.8 (m, *meta-*, *para*-H), *ca* 8.3 (m, *ortho*-H) and 9.25 (s, β-pyrrole, ^4J(Sn—H) 16.9 Hz); λ_{max} ($\varepsilon \times 10^{-3}$) ($CHCl_3$) 420 (622), 514 (3.4), 553 (23.1) and 592 (8.3) nm; ν_{max} (KBr) 1718, 1202, 1174 and 1148 (all vs) cm^{-1} ($OCOCF_3$).

Preparations of Sn(TPP)(OCOH)X *complexes*

(a) *By acidolysis of* Sn(TPP)(OCOH)(OH). A solution of the acid HX (one equivalent) in CH_2Cl_2 was added dropwise to a solution of Sn(TPP)(OCOH)(OH) (38 mg, 0.05 mmol) in CH_2Cl_2 (5 cm^3). After stirring for 30 min, the solution was filtered through anhydrous Na_2SO_4, and the solvent was evaporated. The vacuum-dried residue was dissolved in $CDCl_3$ (0.5 cm^3) and filtered into an NMR tube.

(b) *By redistribution of* Sn(TPP)$(OCOH)_2$ *and* Sn(TPP)X_2. Equimolar amounts of the two complexes (0.01–0.025 mmol) were separately dissolved in $CDCl_3$, mixed, filtered into an NMR tube, and the volume was made up to *ca* 0.5 cm^3. In this way, the *total* Sn(TPP) concentration was in the range 0.02–0.1 M. The reactions were monitored by NMR until no further change was apparent.

REFERENCES

1. G. S. Drummond, R. A. Galbraith, M. K. Sardana and A. Kappas, *Arch. Biochem. Biophys.* 1987, **255**, 64.
2. G. S. Drummond and A. Kappas, *J. Clin. Invest.* 1986, **77**, 971.

3. A. R. Morgan, G. M. Garbo, R. W. Keck and S. H. Selman, *Cancer Res.* 1988, **48**, 194.
4. S. C. Ma, N. A. Chan and M. E. Meyerhoff, *Analyt. Chem.* 1988, **60**, 2293.
5. N. A. Chaniotakis, S. B. Park and M. E. Meyerhoff, *Analyt. Chem.* 1989, **61**, 566.
6. A. Harriman, G. Porter and P. Walters, *J. Chem. Soc., Faraday Trans. I.* 1983, **79**, 1335.
7. D. P. Arnold, *Polyhedron* 1986, **5**, 1957.
8. D. P. Arnold, *Polyhedron* 1988, **7**, 2225.
9. D. P. Arnold, *J. Chem. Educ.* 1988, **65**, 1111.
10. D. P. Arnold, G. Smith, C. H. L. Kennard and T. W. Mak, unpublished results.
11. T. R. Janson and J. J. Katz, in *The Porphyrins* (Edited by D. Dolphin), Vol. IV, p. 12. Academic Press, New York (1978).
12. L. E. Manzer, H. C. Clark and T. G. Appleton, *Coord. Chem. Rev.* 1973, **10**, 335.
13. J. W. Buchler, in *The Porphyrins* (Edited by D. Dolphin), Vol. I, p. 438. Academic Press, New York (1978).
14. J. March, *Advanced Organic Chemistry*, 2nd edn, p. 227 and refs therein. McGraw-Hill, Tokyo (1977).
15. E. P. Serjeant and B. Dempsey, *Ionization Constants of Organic Acids in Aqueous Solution.* Pergamon Press, Oxford (1979).
16. D. D. Perrin, *Ionization Constants of Inorganic Acids and Bases in Aqueous Solution*, 2nd edn. Pergamon Press, Oxford (1982).
17. K. M. Kadish, Q. Y. Y. Xu, G. B. Maiya, J.-M. Barbe and R. Guilard, *J. Chem. Soc., Dalton Trans.* 1989, 1531.
18. M. Gouterman, F. P. Schwarz, P. D. Smith and D. Dolphin, *J. Chem. Phys.* 1973, **59**, 676.
19. L. R. Milgrom and R. N. Sheppard, *J. Chem. Soc., Chem. Commun.* 1985, 351.
20. D. P. Arnold and M. A. Bennett, *Inorg. Chem.* 1984, **23**, 2117.

Polyhedron Vol. 9, No. 10, pp. 1337–1340, 1990
Printed in Great Britain

0277–5387/90 $3.00+.00
© 1990 Pergamon Press plc

COMMUNICATION

CRYSTAL STRUCTURES OF THE PPN SALTS OF THE ANIONS *TRANS*-$[SiCl_3(PPh_3)Fe(CO)_3]^-$ AND *TRANS*-$[SiCl_3\{P(OPh)_3\}Fe(CO)_3]^-$

JOHN W. CONNOLLY*

Department of Chemistry, University of Missouri–Kansas City, Kansas City, MO 64110, U.S.A.

and

ALAN H. COWLEY and CHRISTINE M. NUNN

Department of Chemistry, University of Texas at Austin, Austin, TX 78712, U.S.A.

(*Received* 13 *November* 1989; *accepted* 26 *February* 1990)

Abstract—PPN salts of $[SiCl_3(PPh_3)Fe(CO)_3]^-$ (I) and $[SiCl_3\{P(OPh)_3\}Fe(CO)_3]^-$ (II) have been prepared by literature procedures from the hydride precursors. Each crystallizes in the monoclinic space group $P2_1/c$ with the following respective unit cell constants: I, $a = 16.087(3)$, $b = 15.334(2)$, $c = 22.804(2)$ Å, $\beta = 109.45(1)°$, $V = 5304.0(1)$ Å^3, $Z = 4$; II, $a = 18.623(3)$, $b = 13.449(6)$, $c = 23.447(6)$ Å, $\beta = 109.91(2)°$, $V = 5528.8(1)$ Å^3, $Z = 4$. Both anions are trigonal bipyramidal with the silicon and phosphorus ligands in the axial positions.

Hydridophosphine-and-phosphite iron tricarbonyl anions were synthesized recently. Crystal structure determination showed that in $[H(PPh_3)Fe(CO)_3]^-$ the hydrido and phosphine ligands are *trans*, while in $[H\{P(OPh)_3\}Fe(CO)_3]^-$ the hydrido and phosphite ligands are *cis*.[1,2] By contrast, we report here the structures of the trichlorosilyltriphenylphosphine and trichlorosilyltriphenylphosphite iron carbonyl anions, I and II, both of which are *trans* in the solid state.

EXPERIMENTAL

Standard vacuum line techniques were used throughout. All solvents were dried and deaerated prior to use.

Photochemical preparation of the hydride precursor of I has been reported.[3] The precursor to II, OC-6-23-$H(SiCl_3)\{P(OPh)_3\}Fe(CO)_3$, was prepared similarly. Tetracarbonylirontriphenylphosphite (5.0 g, 10.4 mmol) was dissolved in 200 cm^3 of hexane along with 4 cm^3 of trichlorosilane (excess). Photolysis of this mixture in a glass Schlenk tube with a 150 W mercury lamp for 2 h gave a cloudy red solution. This solution was filtered and reduced to 50 cm^3 by evaporation. The resulting solution was stored at −15°C for several weeks and 2.0 g (3.4 mmol) of product (33%) crystallized out. Found: C, 43.3; H, 3.0. Calc.: C, 43.1; H, 2.8%. NMR ^{1}H (300 MHz) Fe—H −8.9 ppm (d) $^2J_{P-H}$ 36 Hz; $^{13}C\{H\}$ (75.4 MHz) 204.7 ppm (d), $^2J_{P-C}$ 26 Hz *axial CO*, 203.7 ppm (d), $^2J_{P-C}$ 13 Hz *equatorial CO* (axial and equatorial CO assignments are based on the 2:1 intensity ratio); $^{31}P\{H\}$ (121.4 MHz) 160 ppm; $^{29}Si\{H\}$ (59.6 MHz) 54.6 ppm (d), $^2J_{P-Si}$ 95 Hz; m.p. 75°C; $\bar{\nu}$(CO) (hexane) 2085 (w), 2050 (sh), 2040 (s) cm^{-1}.

PPN salts I and II were prepared from their hydride precursors by treating the hydride with PPNCl and sparging the solution with argon until the reaction was complete. In a typical experiment 1.2 g (2.05 mmol) of $H(SiCl_3)\{P(OPh_3)\}Fe(CO)_3$

* Author to whom correspondence should be addressed.

Table 1. Summary of crystallographic data

	I	II
Formula	$FeP_3Cl_3NSiO_3C_{57}H_{45}$	$FeP_3Cl_3NSiO_6C_{57}H_{45}$
Formula weight	1075.21	1123.21
Crystal system	Monoclinic	Monoclinic
Space group	$P2_1/C$	$P2_1/C$
Cell parameters		
a (Å)	16.087(3)	18.623(3)
b (Å)	15.34(2)	13.449(6)
c (Å)	22.804(2)	23.447(6)
β (°)	109.45(1)	109.91(2)
Cell volume (Å^3)	5304.00	5528.76
Z	4	4
Calculated density g (cm^{-1})	1.346	1.349
Corrections	Lorentz-polarization	
Absorption coefficient (cm^{-1})	5.9	5.7
Radiation Mo (Å)	0.71073	0.71073
2θ range (°)	3–45	3–45
Data rejected if $I_- >$	3σ	3σ
Total reflections	7220	7832
Observed reflections	4088	4629
Largest peak in final difference Fourier (e/Å^3)	0.66(5)	0.76(10)
Smallest peak in final difference Fourier	0.00(8)	0.00(10)
ESD of obs. of unit weight	2.50	1.49
Convergence	0.050	0.28
R	0.068	0.094
R_w	0.089	0.101

was dissolved in 30 cm^3 of methylene chloride along with a 20% excess of PPNCl in a Schlenk tube under argon. Argon was bubbled through the solution and the solvent was replenished periodically. The reaction was worked-up when the carbonyl bands of the starting material (*vide supra*) were replaced by the 1875 cm^{-1} band of **II** (1 h in this experiment). Work-up was accomplished by cannulating 30 cm^3 of hexane onto the reaction mixture, causing the ionic materials to precipitate. After removal of the liquid, 50 cm^3 of THF was added and the resulting cloudy solution was filtered through celite. The product was then precipitated from solution by addition of 50 cm^3 of hexane. In this way 1.8 g (1.6 mmol) of **II** were obtained (78%).

Preparation of **I** this way gave only a 39% yield since it was necessary to repeat the solution–precipitation cycle several times. Crystals were grown by diffusing gaseous hexane into a methylene chloride solution of the salts.

Data for the PPN salts are as follows. **I**, Found: C, 62.6; H, 4.5. Calc.: C, 63.5; H, 4.5%. **II**, Found: C, 60.4; H, 4.2. Calc.: C, 60.9; H, 4.0%. NMR $^{13}C\{H\}$: **I**, 214.9 ppm (d), $^2J_{P-C}$ 23.4 Hz; **II**, 211 ppm (broad); $^{31}P\{H\}$: **I**, 81.5 ppm; **II**, 187 ppm (broad). $\bar{\nu}$(CO) (CH_2Cl_2): **I**, 1850; **II**, 1875 cm^{-1}.

The structures were determined by X-ray crystallography according to procedures already described.[4]*

A small crystal of **I** or **II** was mounted in a glass capillary and the capillary was then mounted on the goniometer head of a CAD-4 diffractometer. Preliminary examination showed the space group to be $P2_1/c$ and data collection was carried out in each case as indicated in Table 1. Phenyl groups were refined isotropically, the other atoms were refined anisotropically.

RESULTS AND DISCUSSION

ORTEP diagrams for anions **I** and **II** are shown in Fig. 1 and the relevant bond lengths and angles are listed in Table 2. The PPN structures are unexceptional and the cation is well separated from the anion in both **I** and **II**. The Fe—Si bond lengths of

* Supplementary material available: tables of atomic coordinates, thermal parameters, and bond lengths and angles have been deposited with the Director, Cambridge Crystallographic Centre.

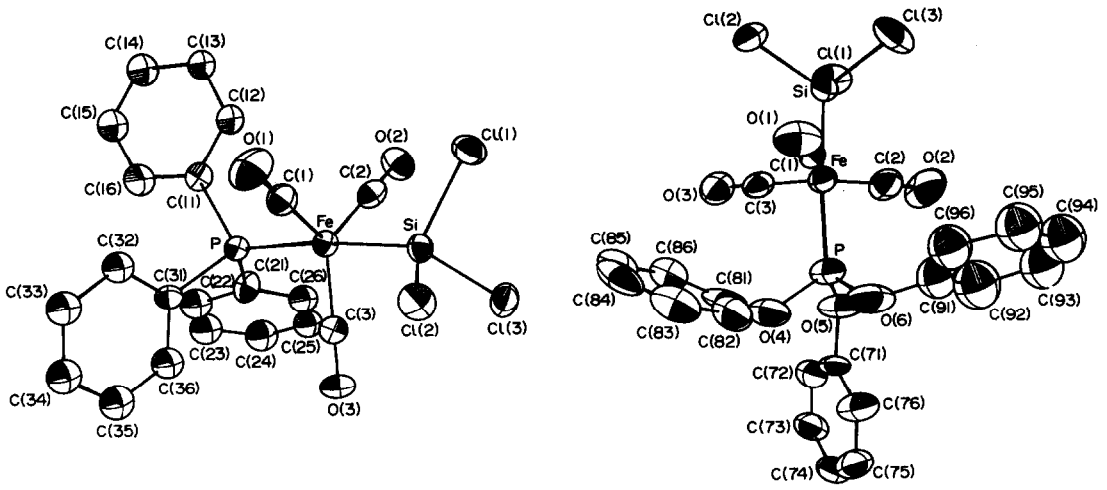

Fig. 1. ORTEP diagrams of I (left) and II (right).

Table 2. Selected bond lengths and angles for I and II

	I	II
Bond lengths		
Fe—P	2.207(3)	2.121(4)
Fe—Si	2.197(3)	2.206(4)
Fe—C(1)	1.754(8)	1.73(1)
Fe—C(2)	1.765(7)	1.70(1)
Fe—C(3)	1.744(8)	1.76(1)
C(1)—O(1)	1.17(1)	1.21(2)
C(2)—O(2)	1.53(9)	1.21(2)
C(3)—O(3)	1.17(1)	1.14(2)
Bond angles		
P—Fe—Si	174.19(9)	173.7(1)
P—Fe—C(1)	92.7(3)	95.4(4)
P—Fe—C(2)	97.1(3)	96.1(4)
P—Fe—C(3)	89.9(3)	88.6(5)
Si—Fe—C(1)	86.9(3)	88.2(4)
Si—Fe—C(2)	88.2(3)	86.9(4)
Si—Fe—C(3)	85.3(4)	85.2(5)
C(1)—Fe—C(2)	117.3(4)	125.7(8)
C(1)—Fe—C(3)	120.5(3)	115.0(6)
C(2)—Fe—C(3)	121.3(3)	118.3(8)

I and II are comparable to the value of 2.224(9) Å reported for $[SiCl_3Fe(CO)_4]^-$, the Fe—C bond lengths of I and II are similar to the value of 1.75(4) Å reported for $[HFe(CO)_4]^-$ [6] and the Fe—P bond length in I is longer than the value of 2.187(1) Å reported for $[H(PPh_3)Fe(CO)_3]^-$.[1] It is reasonable to assume that the *trans*-$SiCl_3$ group has a greater share in the π-electron density along the z-axis in I than the hydrogen atom does in $[H(PPh_3)Fe(CO)_3]^-$. Therefore, the Fe—P π-bond will be weaker in I and it is to be expected that the Fe—P distance in I will be longer. In II, both the range of C—O bond lengths and the unexpectedly large C(1)—Fe—C(2) bond angle indicate a greater distortion from the ideal trigonal bipyramidal configuration than in I. That is probably due to the location of the phenyl groups. From the figure it can be seen that the plane of each phenyl group in I nearly bisects the CO—Fe—CO angle directly above it. This is reflected in an oxygen to nearest phenyl carbon distance of 3.8 ± 0.3 Å for each carbonyl oxygen. In the case of anion II, two of the phenoxy-phenyl groups are directed toward the iron–carbonyl plane, while the third one is directed away from it. Therefore in II the shortest carbonyl-oxygen to phenyl-carbon distances are (respectively) O(1): 6.8 Å, O(2): 3.3 Å and O(3): 3.6 Å.

These structures (I and II) do not show the remarkable *trans*-to-*cis* configuration change which has been observed with $[H(PPh_3)Fe(CO)_3]^-$ and $[H\{P(OPh)_3\}Fe(CO)_3]^-$. Since the trichlorosilyl group differs from the hydrido group both sterically and electronically, it is not possible to determine at this point what causes these structural differences.

Solution IR measurements on both I and II show only a single intense band in the carbonyl region, consistent with approximate C_{3v} symmetry in solution as well as in the solid state. The broad NMR signals observed for II, which are not due to paramagnetic impurities since the cation signals in this solution are sharp, indicate the occurrence of a rearrangement which is slow on the NMR time scale. Investigation of the nature of this rearrangement process is planned.

Acknowledgements—J.W.C. gratefully acknowledges the support of this work by UMKC in the form of a Weldon Springs Foundation grant, and the assistance of Dr Evelyn Murrill, Midwest Research Corporation, Kansas

City, MO 64110, for assistance in obtaining the NMR spectra reported here. A.L.H. wishes to acknowledge the financial assistance of the National Science Foundation and the Robert A. Welch Foundation.

REFERENCES

1. C. E. Ash, T. Delord, D. Simmons and M. Y. Darensbourg, *Organometallics* 1986, **5**, 17.
2. C. E. Ash, C. M. Kim, M. Y. Darensbourg and A. L. Rheingold, *Inorg. Chem.* 1987, **26**, 1357.
3. M. Knorr and U. Schubert, *Transition Met. Chem.* 1986, **11**, 268.
4. A. M. Arif, A. H. Cowley, N. C. Norman, A. G. Orpen and M. Pakulski, *Organometallics* 1988, **7**, 309.
5. P. R. Jansen, A. Oskam and K. Olie, *Cryst. Struct. Commun.* 1975, **4**, 667.
6. M. B. Smith and R. Bau, *J. Am. Chem. Soc.* 1973, **95**, 2388.

Polyhedron Vol. 9, No. 10, pp. 1341–1343, 1990
Printed in Great Britain

0277–5387/90 $3.00+.00
© 1990 Pergamon Press plc

COMMUNICATION

X-RAY CRYSTAL STRUCTURE OF $[Ni(S_2COC_6H_{11})_2(PMePh_2)]$. ASYMMETRIC COORDINATION OF THE O-CYCLOHEXYLXANTHATE LIGAND

L. BALLESTER, A. GUTIERREZ-ALONSO and M. F. PERPIÑÁN*

Departamento de Química Inorgánica, Facultad de Ciencias Químicas, Universidad Complutense, 28040 Madrid, Spain

and

E. GUTIERREZ-PUEBLA and C. RUIZ-VALERO

Instituto de Ciencias de Materiales, Sede D., Serrano 113, 28006 Madrid and Laboratorio de Difración de Rayos X, Facultad de Ciencias Químicas, Universidad Complutense, 28040 Madrid, Spain

(*Received* 29 *January* 1990; *accepted* 1 *March* 1990)

Abstract—The structure determination of $[Ni(S_2COC_6H_{11})_2(PMePh_2)]$ shows the presence of one asymmetrically coordinating O-cyclohexylxanthate ligand in this complex, which presents a distorted square-pyramidal geometry.

We have previously studied the behaviour of O-alkyldithiocarbonato complexes, $[Ni(S_2COR)]_2$, towards several phosphines.[1] Depending on the S_2COR derivative (xanthate) and phosphine used, complexes with different stoichiometries and geometries have been obtained. The reaction of $[Ni(S_2COC_6H_{11})]_2$ with $PMePh_2$ gives a dark brown compound, $[Ni(S_2COC_6H_{11})_2(PMePh_2)]$, with IR spectroscopic and magnetic properties similar to those found for square-planar complexes of palladium(II) and platinum(II). These compounds contain mono- and bidentate xanthate ligands. Since this type of complex had not been reported for nickel, it was important to determine its crystal structure.

Figure 1 shows the geometry of the structure and the atom labelling of the title complex. The structure† consists of individual molecules of the title compound held together by van der Waals' forces. The structure determination confirms the stoichiometry of the complex but shows that the nickel atom is five-coordinated in a distorted square-pyramidal geometry, in which the four atoms, S(1), S(2), S(3) and P, describe an approximate basal plane and the apical position is occupied by the S(4) atom from an asymmetrically coordinating xanthate ligand. The nickel atom exhibits a deviation from the basal plane of −0.1455 Å.

* Author to whom correspondence should be addressed.

† Crystal data: $C_{27}H_{35}NiO_2PS_4$, M = 609.496, triclinic, space group $P\bar{1}$, with $a = 9.704(3)$, $b = 10.733(1)$, $c = 14.533(2)$ Å; $\alpha = 81.94(12)$, $\beta = 79.00(23)$, $\gamma = 84.65(6)°$; $U = 146.7$ Å^3, $Z = 2$, $D_c = 1.35$ g cm^{-3}; μ(Mo-K_α) = 7.49 cm^{-1}, $F(000) = 640$. A total of 4154 unique reflections were measured in the range $0 < \theta < 26$ on an Enraf–Nonius CAD 4 diffractometer using ω–2θ scans and Mo-K_α radiation ($\lambda = 0.71069$ Å); 2708 reflections were considered observed [$I < 2\sigma(I)$] after data reduction, and used in subsequent calculations. The structure was solved by Patterson and Fourier techniques and refined by full-matrix least-squares procedures in the XRAY 80 system to $R = 0.033$ and $R_w = 0.032$. The hydrogen atoms were refined with fixed atomic coordinates and isotropic temperature factors.

Atomic coordinates, bond lengths and angles, and thermal parameters have been deposited with the Cambridge Crystallographic Data Centre.

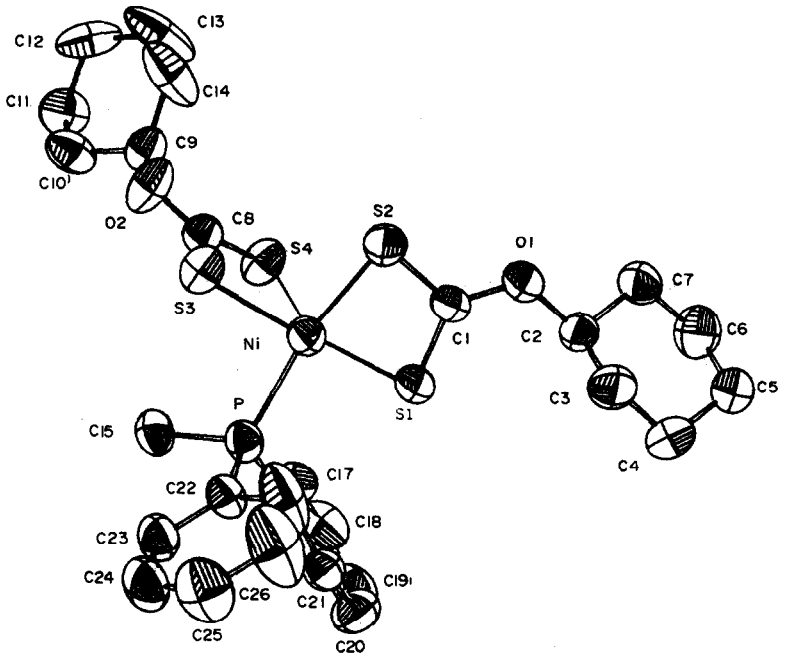

Fig. 1. ORTEP perspective of $[Ni(S_2COC_6H_{11})_2(PMePh_2)]$, showing the atom numbering scheme. Important bond distances and angles:

Bond distances (Å)

Ni—P	2.1746(23)	C(1)—S(1)	1.6826(55)
Ni—S(1)	2.2099(18)	C(8)—S(3)	1.7085(53)
Ni—S(2)	2.2441(27)	C(8)—S(4)	1.6570(44)
Ni—S(3)	2.2221(20)	O(1)—C(1)	1.3312(54)
Ni—S(4)	2.7223(43)	O(2)—C(8)	1.3267(53)
C(1)—S(2)	1.6645(43)		

Bond angles (°)

S(1)—Ni—S(2)	78.14(29)	C(1)—O(1)—C(2)	119.79(59)
S(3)—Ni—S(4)	71.92(27)	C(8)—O(2)—C(9)	120.75(82)

In the complex, the two xanthates are chelate ligands, however, one of the ligands presents gross asymmetry in its sulphur–nickel bonding, e.g. Ni—S(3) = 2.2221(20) and Ni—S(4) = 2.7223(43) Å, compared to the near equivalence of the Ni—S bonds, Ni—S(1) = 2.2099(18) and Ni—S(2) = 2.2441(27) Å in the second xanthate.

In the transition metal compounds, the asymmetric xanthate coordination occurs infrequently. To date, this type of coordination has only been described for the complex $[Ni(S_2COEt)_2(PPh_3)]$.[2] A comparison of the Ni—S distances in both complexes indicates a higher asymmetry in the O-cyclohexylxanthate ligand of the complex reported by us. In the platinum(II) complexes of analogous stoichiometry, $[Pt(S_2CNEt)_2(PPh_3)]$, the Pt—S(4) = 3.457 Å distance shows clearly the existence of a monodentate dithiocarbamate.[3] On the other hand, the bond lengths and angles are different in the complex studied in this work with respect to those found in the $[Ni(\eta^5\text{-}C_5H_5)(S_2COEt)(PPh_3)]$ complex, which contains one monodentate xanthate.[4]

The Ni—P distance of 2.1746(23) Å lies in the range 2.16–2.24 Å found in other related systems.[2,4,5]

The structure solution leads to an explanation of the reported IR spectroscopic and magnetic data.[1] Thus, the compound is a five-coordinated complex of low spin, in which the two IR ν(C—OR) vibrations observed (1275 and 1190 cm^{-1}) are consistent with the two different modes of coordination exhibited by the xanthate ligands.

We are currently investigating other five-coordinated nickel complexes.

Acknowledgement—We thank the Comisión Interministerial de Ciencia y Tecnología (Project No. PS87-0028) for financial support.

REFERENCES

1. M. F. Perpiñán, L. Ballester and M. E. González-Casso, *J. Chem. Soc., Dalton Trans.* 1987, 281.
2. E. R. T. Tiekink and G. Winter, *Aust. J. Chem.* 1986, **39**, 813.
3. J. P. Fackler Jr, L. D. Thompson, I. J. B. Lin, T. A. Stephenson, R. O. Gould, J. M. C. Alison and A. J. F. Fraser, *Inorg. Chem.* 1982, **21**, 2397.
4. C. Tsipis, G. E. Manoussakis, D. P. Kessissoglou, J. C. Huffman, L. N. Lewis, M. A. Adams and K. G. Caulton, *Inorg. Chem.* 1980, **19**, 1458.
5. I. A. Fanariotis, P. C. Christidis and P. J. Rentzeperis, *Z. Krist.* 1983, **164**, 109.

Polyhedron Vol. 9, No. 11, pp. 1345–1362, 1990
Printed in Great Britain

0277–5387/90 $3.00+.00
© 1990 Pergamon Press plc

POLYHEDRON REPORT NUMBER 31

NEW DEVELOPMENTS IN THE ORGANOMETALLIC CHEMISTRY OF CALCIUM, STRONTIUM AND BARIUM

TIMOTHY P. HANUSA

Department of Chemistry, Vanderbilt University, Nashville, TN 37235, U.S.A.

CONTENTS

1. INTRODUCTION 1345

2. DISTINCTIVENESS OF THE HEAVY ALKALINE-EARTH METALS 1346
2.1. Properties of the divalent ions 1346
2.2. Comparisons with the lanthanide elements 1346

3. SYNTHETIC APPROACHES TO ORGANOALKALINE-EARTH COMPLEXES . . 1347
3.1. Metal vapour methods 1347
3.2. Activated metal powders 1348
3.3. Halide metathesis 1349

4. ORGANOALKALINE-EARTH COMPLEXES 1349
4.1. Bis(cyclopentadienyl) complexes 1349
4.1(a). Metallocenes containing unsubstituted cyclopentadienyl rings 1349
4.1(b). Decamethylmetallocenes 1350
4.1(c). Base-free decamethylmetallocenes 1351
4.1(d). Adducts of the decamethylmetallocenes with Lewis bases 1352
4.1(d).1. Phosphine and isonitrile adducts 1352
4.1(d).2. Aromatic amine adducts 1352
4.1(d).3. Adducts with unsaturated hydrocarbons 1353
4.1(e). Metallocenes containing alkyl-substituted cyclopentadienyl rings 1355
4.1(f). Metallocenes containing trimethylsilyl-substituted cyclopentadienyl rings . . . 1356
4.2. Monocyclopentadienyl complexes 1357
4.3. Cyclooctatetraenyl complexes 1358
4.4. Organoalkaline-earth species containing monovalent calcium and strontium 1359

5. STRUCTURAL STUDIES 1359

6. APPLICATIONS 1360

7. CONCLUSIONS 1360

1. INTRODUCTION

Although the well-known Grignard reagents (RMgX) are perhaps the most widely used of any organometallic species in the modern synthetic laboratory, their heavier Group II analogues, compounds of calcium, strontium and barium, have until very recently languished in the backwaters of organometallic chemistry. First described in 1905 by Beckman,[1] the dialkyls and alkyl halides of the heavy alkaline-earth metals were studied by Gilman and his co-workers from the mid-1920s through the mid-1940s with a view toward developing more active versions of Grignard reagents.[2] These investigations were generally disappointing, as many of the compounds prepared were therm-

ally unstable and either insoluble or only slightly soluble in organic media. Their difficult synthesis and apparently limited usefulness provided little incentive to develop and refine their chemistry.

Despite the impetus given to the field of inorganic chemistry by the discovery of ferrocene in the early 1950s, progress with organoalkaline-earth complexes remained slow. Cp_2Ca was described in 1956,[3] and the strontium and barium analogues followed in 1961,[4] but the metallocenes were not easy to obtain [e.g. Cp_2Ba was only available through a high-temperature synthesis which provided a yield of 0.2%(!)]. Not until 1974 was the solid state structure of Cp_2Ca published,[5] and it remained the only structurally characterized heavy organoalkaline-earth compound until the gas-phase structure of $(Me_5C_5)_2Ca$ was reported in 1986.[6] With a fair degree of accuracy, an inorganic chemistry textbook summarized the state of the field in 1980 with the observation that "the organic compounds of calcium, strontium and barium are relatively obscure and of little utility . . .".[7]

With increased understanding of the principles required to synthesize and manipulate the compounds of these large, electropositive metals, this situation is now rapidly changing, and the organometallic chemistry of calcium, strontium and barium is poised for considerable expansion in the coming years as the distinctive attributes of these compounds become more accessible and appreciated. The area was last comprehensively surveyed in 1982,[8] although several earlier reviews are available.[9,10] This Report will concentrate on developments in the area since 1982. As the organometallic chemistry of magnesium and beryllium differs considerably from that of the heavier metals, their compounds will not be explicitly covered here, except where useful comparisons can be made.

2. DISTINCTIVENESS OF THE HEAVY ALKALINE-EARTH METALS

2.1. *Properties of the divalent ions*

In retrospect, one of the most serious impediments to the development of organoalkaline-earth chemistry was the expectation that the behaviour of calcium, strontium and barium compounds should parallel that of their organomagnesium counterparts. Attempts dating from the turn of the century to prepare synthetically useful "pseudo-Grignard reagents", RAeX (R = Me, Et, etc.; Ae = Ca, Sr, Ba; X = Cl, Br, I) from the Ae metals were repeatedly frustrated by their low solubility and poor stability, and the production of Wurtz-coupled species during their synthesis.[11]

Many of the observed differences in reactivity can be traced to the small size of the Mg^{2+} ion (0.72 Å) relative to that of the other Ae cations [1.00 Å (Ca^{2+})–1.35 Å (Ba^{2+})].[12] The consequences of this are at least two-fold. To begin with, the lower charge/size ratios of Ca^{2+}, Sr^{2+} and Ba^{2+} suggest that their compounds will be even more ionic than those of Mg^{2+}. With little or no orbital involvement from their $ns^0(n-1)d^0$ cores, kinetic lability and the possibility of ligand loss will be high. Secondly, the small ligands such as methyl or ethyl which are typically found in Grignard reagents will leave the large Ae cations coordinatively unsaturated. As has been frequently observed in organolanthanide and actinide chemistry, the lack of steric saturation can lead to irreversible oligomerization or decomposition of compounds (e.g. via hydrogen abstraction reactions).[13–15] Evidence of such coordinative unsaturation in an Ae complex is provided by the solid-state structure of Cp_2Ca; unlike the monomeric sandwich geometry possessed by Cp_2Mg,[16] Cp_2Ca is an insoluble, polymeric solid, in which each calcium ion is surrounded by various bridging cyclopentadienyl rings [see Section 4.1(a)].[5]

As will be examined in more detail below, the use of large, sterically bulky ligands has allowed the preparation of a wide range of thermally stable, hydrocarbon-soluble complexes.

2.2. *Comparisons with the lanthanide elements*

Although the chemistry of the heavy alkaline-earth elements was originally developed along the lines established by organomagnesium compounds, a compelling case can be made that a natural relationship exists between calcium, strontium and barium and the *f*-elements, especially with the divalent lanthanide ions.[15] The alkaline-earth, lanthanide and actinide families of metals are large

and highly electropositive, and the similarity in radii between Ca^{2+} and Yb^{2+} (1.00 and 1.02 Å, respectively) and between Sr^{2+} (1.22 Å) and Sm^{2+} or Eu^{2+} (1.22 and 1.21 Å, respectively)[12] is noteworthy. The restricted radial functions of the *f*-orbitals insure that they are not energetically accessible enough to participate significantly in bonding,[17] and hence organolanthanide compounds, like those of the alkaline earths, tend to be highly ionic. The similarity in size has also permitted the construction of compounds with related structures, especially among the pentamethylcyclopentadienyl derivatives (see Sections 4.1(b), 4.2). The combination of similar size and ionic bonding means that many of the problems encountered by early workers in the organolanthanide and actinide fields, including poor solubility and low volatility of compounds, are identical to those found with the organoalkaline-earth systems. For both the Ae and the *f*-element metals, the remedy was the same—the employment in complexes of large, sterically bulky ligands, which help to block open coordination sites, thus attenuating strong intermolecular interactions. Both decomposition via hydrogen-elimination pathways and the insolubility arising from polymerized materials are thus minimized.

Although instructive, the analogy with the lanthanides has limitations. Only the divalent oxidation state is readily accessible in Ae compounds, although species containing monovalent calcium and strontium have been identified in the gas phase (see Section 4.4). In contrast, oxidation states ranging from +2 to +4 and from +3 to +6 are known in organolanthanide and organoactinide complexes, respectively.[14,18] In addition, the change in ionic radii from Ca^{2+} to Ba^{2+} is approximately 35%, considerably larger than the difference between the smallest and largest trivalent lanthanides (Lu^{3+} (0.86 Å)–La^{3+} (1.03 Å); 20% change), or the nearly equally sized U^{4+} (0.89 Å) and Th^{4+} (0.94 Å) (a 6% difference).[12] In particular, Ba^{2+} is approximately 15% larger than that of the largest divalent lanthanide (Sm^{2+}). The large size differential between Ca^{2+} and Ba^{2+} significantly affects their relative Lewis acidities. The Ca^{2+} ion is the most acidic of the three Ae^{2+} species, and is observed to form more robust adducts with Lewis bases than does Ba^{2+}. This becomes of synthetic importance when removing coordinated ethers from organocalcium and -barium complexes, or when attempting to isolate organobarium adducts of particularly weak bases, such as unsaturated hydrocarbons (see Section 4.1(d).3).

A further difference between the chemistry of the alkaline-earth metals and that of the *f*-elements is that the noble gas configuration of the Ca^{2+}, Sr^{2+} and Ba^{2+} cations insures that nearly all of their compounds will be diamagnetic, and therefore easily studied by NMR spectroscopy. In contrast, with the exception of Ce^{4+}, La^{3+}, (Y^{3+}),[19] Yb^{2+}, Lu^{3+} and Th^{4+}, the paramagnetism of the majority of lanthanide and actinide ions may restrict detailed spectroscopic analysis of reaction rates and mechanisms.

Even though the comparisons which can be drawn between calcium, strontium and barium and the *f*-elements are more revealing than with magnesium, it is probably best to regard the organometallic compounds of the Ae metals as a distinct class of complexes, related to, but not identical with, their ionically-bonded neighbours.

3. SYNTHETIC APPROACHES TO ORGANOALKALINE-EARTH COMPLEXES

The traditional starting point for organoalkaline-earth chemistry has been the bulk metals, either used alone or activated by amalgamation or iodine.[8] Impurities in the common grades of calcium and the other metals have been cited as the source of some of the variability in reaction rates and yields for RAeX species,[20,21] but higher purity metals are now commercially available (up to 99.98% for calcium). Nevertheless, other synthetic methods have appeared during the period under review. Those compounds discussed elsewhere will be given only brief mention here.

3.1. *Metal vapour methods*

The use of metal vapour methods to prepare organoalkaline-earth compounds was first described for the synthesis of solvent-free alkyl metal halides, metallocenes and bis(indenyls), for which yields were gratifyingly high ($\geq 90\%$).[11] Condensation of calcium vapour and aryl halides, ArX (Ar = C_6H_5, *o,m,p*-$(CH_3)C_6H_4$ and *o,m,p*-$(CF_3)C_6H_4$ for X = F, Cl; Ar = C_6H_5 for X = F, Cl, Br),

produces the solvent-free aryl calcium halides in 38–50% yield for all except the trifluorotolylcalcium chlorides, where the yields are < 10%.[22] Although phenylcalcium bromide and chloride have been prepared by solution methods, the metal vapour route is currently the only one to arylcalcium fluorides. Subsequent studies have extended these results to various aryldihalides, benzylhalides and β-napthylhalides, and underscored the dramatic effects of solvents and metal vapour techniques on the yields of products.[23] Thus chlorobenzene and calcium vapour produces no phenylcalcium chloride in the presence of THF, although a 42% yield is obtained in its absence.[22] Conversely, *n*-octylbromide yields the corresponding RCaBr species in 70% yield in the presence of THF, but only in 0.5% yield if toluene is used as the solvent.[23]

Condensation of calcium vapours into an excess of solvent so as to generate metal slurries, rather than adding solvents after the metal has been deposited, also affects yields. For example, when added to a slurry of calcium metal in THF, chlorobenzene produces phenylcalcium chloride in 32% yield, although, as noted above, no reaction is observed if the chlorobenzene and THF are added after the condensation of the metal.[24]

Benzene and calcium vapour will react with organic halides (RCl, RBr) to yield on work-up both phenyl-substituted products (PhR) and reduced species (RH), and with ketones (RR'CO) to yield the alcohols PhRR'COH and RR'CHOH. With benzaldehyde, Ph_2CHOH and $PhCH_2OH$ are generated.[25] Further study of this reaction with other aromatic hydrocarbons (alkylbenzenes, phenyltrimethylsilane, xylenes) has determined that the initial condensation product gives an ESR signal at −60°C, but becomes diamagnetic on warming to room temperature. Decomposition and deuteration experiments suggest that the room temperature materials are arylcalcium hydrides, formed by insertion of Ca^+ into the arene C—H bond, and it is the latter which reacts with organic halides and carbonyls, eq. (1):[26,27]

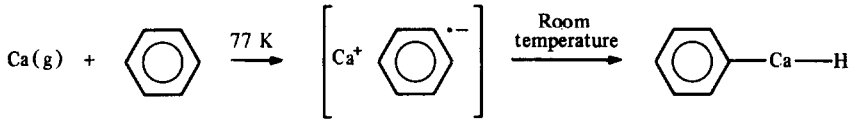

(1)

Slurries of calcium and barium prepared by co-condensation of the metal vapour with toluene at −196°C were allowed to react with various organotransition metal complexes at room temperature.[28] A number of reduced organotitanium species were identified, and a benzyl–calcium species was suggested as a product from a calcium–toluene slurry, but no organoalkaline-earth complexes were isolated.

Co-condensation of $(SiMe_3)_2C_5H_4$ and calcium, strontium or barium vapour at −196°C followed by warming to room temperature yields the base-free metallocenes $[(SiMe_3)_2C_5H_3]_2Ae$ in moderate to good yields [see Section 4.1(f)].[29]

Cyclooctatetraenyl complexes can be formed from the condensation of calcium, strontium and barium vapour with cyclooctatetraene (COT) and THF at −196°C. The cream-coloured Ae(COT)$(THF)_n$ complexes release THF on heating (see Section 4.3).[30]

Reaction of alkaline-earth metal vapours with the cyclopentadiene monomer,[31] pyrrole,[32] Me_4Sn and Me_2Hg[33] produces a variety of organometallic free radicals which have been characterized by laser excitation spectroscopy. These are discussed in Section 4.4.

3.2. *Activated metal powders*

Alkali metal reduction in organic solvents of many main group and transition metal halides will produce powders which are substantially more reactive than bulk or amalgamated metals.[34] Although the first application of this method was to magnesium,[35] only recently has an extension of the technique to the heavier alkaline-earth metals been reported.

Stirring a mixture of potassium metal and an anhydrous alkaline-earth diiodide in dry THF or toluene under nitrogen at ambient or reflux temperatures produces suspensions of black or grey powders, eq. (2):[36]

$$2K + AeX_2 \rightarrow Ae\downarrow + 2KX\downarrow. \quad (2)$$

The metal powders react with triphenylmethylchloride to generate the corresponding $Ph_3CAeCl(THF)_n$ complexes 12–16 times more rapidly than the analogous syntheses using metal amalgams.[37,38] Activated calcium powder reacts with trifluoroacetylacetone {H[TFA]} and hexafluoroacetylacetone {H[HFA]} to form the respective $Ca[TFA]_2$ and $Ca[HFA]_2$ salts in 1 h, compared to the 5 days or greater required from the use of bulk calcium and the parent acid.[39] Barium powder reacts with Cp*H in THF to produce the $Cp^*_2Ba(THF)_2$ metallocene; bulk barium, in contrast, does not react with Cp*H.[40]

3.3. *Halide metathesis*

The reaction of the anhydrous metal halides with the alkali metal salt of an organic anion in THF or ether has become one of the most extensively used methods for the preparation of organoalkaline-earth compounds; metallocenes, alkoxides and amides, among others, have been prepared via this route, eq. (3):

$$2\,RM + AeX_2 \xrightarrow{\text{ether}} R_2Ae(THF)_2\,(\text{or } RAeX) + 2\,MX\downarrow \quad (M = Li, Na, K). \tag{3}$$

With the proper systems, this method has the advantage of offering high, reproducible yields, and if the organometallic product is soluble in aromatic hydrocarbons or can be sublimed, removal of residual halides is simplified. If not, halide by-products can represent significant contamination.[41]

4. ORGANOALKALINE-EARTH COMPLEXES

4.1. *Bis(cyclopentadienyl) complexes*

The cyclopentadienyl ligand (Cp) and its substituted analogues serve organoalkaline-earth chemistry as well as they do *d*- and *f*-block organometallics, by obstructing coordination sites which might otherwise serve as sites for decomposition, by offering a range of steric bulk, and by improving the crystallinity of complexes. Not too surprisingly, the greatest increase in the number of organoalkaline-earth compounds in recent years has been with those containing Cp ligands, and most of these are derivatives of the decamethylmetallocenes, Cp^*_2Ae ($Cp^* = Me_5C_5$). The chemistry of Cp derivatives will probably continue to experience considerable growth in the coming years.

4.1(a). *Metallocenes containing unsubstituted cyclopentadienyl rings*

Although "calciocene" (Cp_2Ca), "strontiocene" (Cp_2Sr) and "bariocene" (Cp_2Ba) have been known for over 25 years and are thermally stable, only recently have the strontium and barium derivatives been available in quantities which make them more than curiosities. A metal vapour route to these compounds has been developed,[11] but they are also readily prepared by the metathetical exchange of an alkali metal cyclopentadienide with an Ae dihalide. The reaction of CaI_2 or $CaCl_2$ with two equivalents of KCp or TlCp in THF produces crude $Cp_2Ca(THF)_2$ in 75% (CaI_2) or 14% ($CaCl_2$) yield along with the alkali halide which is removed by filtration, eq. (4):[41]

$$2\,KCp + CaX_2 \xrightarrow{THF} Cp_2Ca(THF)_2 + 2\,KX\downarrow. \tag{4}$$

The lower yield from the chloride probably stems from the lower solubility of $CaCl_2$ in THF.

The insolubility of strontiocene and bariocene in ethers requires that the alkali metal halide, rather than the metallocene, be extracted from the reaction mixture. This can be accomplished by reacting lithium cyclopentadienide with the alkaline-earth metal halide; the resulting LiI is then removed with THF, eq. (5):[41]

$$2\,LiCp + AeI_2 \xrightarrow{THF} Cp_2Ae(THF)_x\downarrow + 2\,LiI \quad (Ae = Sr, Ba). \tag{5}$$

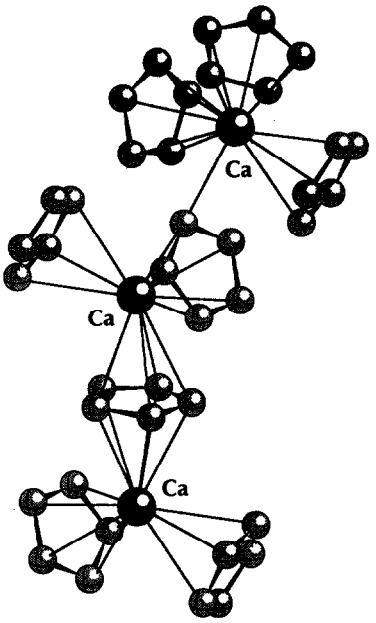

Fig. 1. A portion of the structure of Cp_2Ca, indicating the polymerized nature of the complex. Four Cp rings surround each calcium in the extended structure, displaying $2 \times \eta^5, \eta^3$ and $\eta^1(\sigma)$ coordination.

Interestingly, the strontium and barium derivatives are isolated from the reaction mixtures with less than two equivalents of THF; $x \approx 1$ for Sr and ≈ 0.25 for Ba. The size of the strontium and barium ions may preclude the formation of stable monomeric disolvated complexes, so that oligomerized structures form.

Cp_2Ca has also been prepared in 46% yield from the reaction of either $(Me_3Si)C_5H_5$ or $(Me_3Si)_2C_5H_4$ and $Ca(NH_2)_2$ in liquid ammonia, eq. (6):[42]

$$Ca(NH_2)_2 + 2(Me_3Si)_nC_5H_{6-n} \xrightarrow[-n(Me_3Si)_2NH\uparrow]{THF,\ NH_{3(l)}} Cp_2Ca(THF)_2 \qquad (6)$$

$$(n = 1, 2).$$

All of the metallocenes exhibit well-resolved ^1H and ^{13}C NMR spectra, with highly solvent-dependent chemical shifts. Ring exchange occurs between Cp_2Ca and KCp in THF.[41]

Some of the reactions of Cp_2Ca with nitrogen and oxygen donors have been examined,[43] and the oligomeric nature of the unsolvated complex has been established by X-ray crystallography (Fig. 1).[5] The low volatility and the insolubility of the strontium and barium analogues in any but the most polar liquids (DMSO, HMPA) has made their chemistry difficult to study.

4.1(b). *Decamethylmetallocenes*

The increase in steric bulk provided by the Cp* ring greatly improves the solubility, volatility and kinetic stability of its associated compounds. All three Cp^*_2Ae complexes have been prepared in > 65% yield from the reaction of sodium or potassium pentamethylcyclopentadienide and the metal diiodides in THF or ether, eq. (7):[41,44]

$$2(Na, K)Cp^* + AeI_2 \xrightarrow{ether} Cp^*_2Ae(ether)_2 + 2(Na, K)I\downarrow. \qquad (7)$$

An alternate preparation of Cp^*_2Ba, although in lower yield, is from finely divided metal powders and the diene (see Section 3.2).

Cp^*_2Ca has been prepared in moderate yield from the reaction of Cp*H and $Ca(NH_2)_2$ in liquid ammonia, eq. (8):[42]

$$Ca(NH_2)_2 + 2\,Cp^*H \xrightarrow{THF,\ NH_{3(l)}} Cp^*_2Ca(THF)_2 \quad (48\%). \qquad (8)$$

The THF can be displaced from $Cp^*_2Ca(THF)_2$ by dissolution in DME to yield the $Cp^*_2Ca(DME)$ solvate,[42] although complete removal of ethers is more difficult [see Section 4.1(c)]. The disolvated decamethylmetallocenes of all three elements are white, thermally stable solids, slightly (Ba) to moderately (Ca) soluble in alkanes, and readily soluble in aromatics. Their solubility in non-polar solvents greatly eases their purification, since they can be obtained free of insoluble by-products by extracting them into hydrocarbons. As expected for diamagnetic compounds, they display well-resolved NMR spectra, with appreciable chemical shift dependences on the solvent; as the polarity of the solvents increases ($C_6D_6 \rightarrow$ THF-$d_8 \rightarrow$ DMSO-d_6) the ^1H NMR methyl proton resonances move upfield.

The decamethylmetallocenes are highly air- and moisture-sensitive, and $Cp^*_2Ca(THF)_2$ decomposes in solution on contact with O_2 or N_2O to form intractable oily yellow solids. No reaction is observed with CO in THF or toluene solution.[40]

4.1(c). *Base-free decamethylmetallocenes*

Removal of coordinated ether from $Cp^*_2Ae(OEt_2)$ can be accomplished by refluxing the compounds in toluene under vacuum[44] or at atmospheric pressure.[45] Removal of coordinated THF from $Cp^*_2Ba(THF)_2$ has also been accomplished by slow sublimation at 190°C under a dynamic vacuum of 10^{-6} torr.[45,46] Coordinated THF is difficult to remove from $Cp^*_2Ca(THF)_2$; prolonged heating at 100°C and 10^{-5} bar will remove one of the THF ligands; the resulting monosolvate $Cp^*_2Ca(THF)$ is even more air- and moisture-sensitive than the starting material.[42] Complete removal of THF from the calcium complex by sublimation has not been accomplished.[45]

The decamethylmetallocenes, because of their position as archetypal organoalkaline-earth complexes, have received considerable attention. Their structures have been examined by both gas electron diffraction and by X-ray crystallography. Cp^*_2Ca, Cp^*_2Sr and Cp^*_2Ba are bent in the gas phase, with ring centroid–metal–ring centroid angles ranging from 148 to 156°.[6,47,48] In the solid state, Cp^*_2Ca and Cp^*_2Ba are somewhat more bent (147 and 131°, respectively) (Figs 2 and 3).[45,46] Although the monomeric Cp^*_2Ca units are well separated in the crystalline state, and individual Cp^*_2Ba units can be identified in the lattice, the latter are grouped together to form "quasi-polymeric" chains (Fig. 3). Within a chain, the shortest intermolecular Ba—C(methyl) distance is 3.349(5) Å; this is only 0.28 Å longer than the shortest intramolecular Ba—C distance, and there is probably some degree of solid-state interaction between the complexes.

A comparison of the bending angles in the solid-state structures of Cp^*_2Ca and Cp^*_2Ba with that of the similarly bent organolanthanide species Cp^*_2Sm, Cp^*_2Eu[49,50] and Cp^*_2Yb[51] reveals a linear relationship between the bending angles and the metal ionic radii.[45] There is no intuitively obvious explanation for the bending of any of the Ae or Ln decamethylmetallocenes, as simple steric

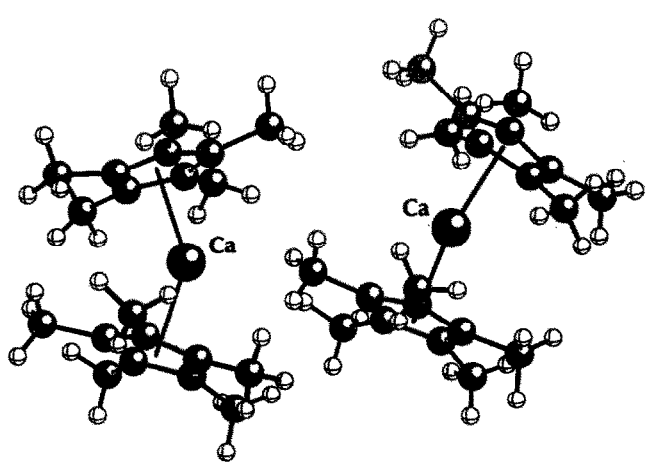

Fig. 2. Solid-state structure of Cp^*_2Ca, indicating the relative orientation of the two independent molecules in the unit cell.

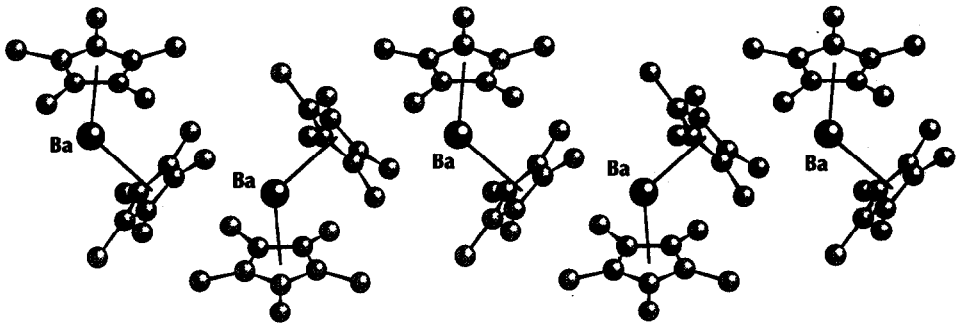

Fig. 3. Structure of Cp^*_2Ba, indicating the "chain-like" structure observed in the solid state.

considerations would suggest that structures with parallel rings should be favoured, thus minimizing intramolecular repulsions. No energetic reason for the bending in these molecules has emerged from molecular orbital calculations on the structures of Cp_2Sm, Cp_2Eu and Cp_2Yb, performed at the extended Hückel[52] and quasi-relativistic SW-Xα levels.[53]

The gas-phase structural studies have established that if the equilibrium structures of Cp^*_2Ca, Cp^*_2Sr and Cp^*_2Ba do have parallel rings, then less than 2 kJ mol^{-1} would be required to bend the complexes by 20°;[47,48] crystal packing forces or other intermolecular interactions might be able to supply this small amount of energy. Detailed comparisons between the solid-state structures of the alkaline-earth and organolanthanide molecules have not revealed any pattern in the intermolecular contacts that would provide an adequate rationalization for the bent geometries, however. Explanations for the bending based on "reverse polarization" effects have been proposed; viz. that negatively charged Cp^- rings will induce a dipole in a large, polarizable cation, thus favouring a bent geometry.[50,53] This is the same reasoning offered for the bending observed in the gas-phase Ae dihalides.[54] Recent Hartree–Fock–Slater calculations on CaH_2, CaF_2, CeO_2 and $YbCl_2$ have successfully predicted bent geometries for these species, and related explanations for the bending in the metallocenes based on *sd* hybrid orbitals have been suggested.[55]

4.1(d). *Adducts of the decamethylmetallocenes with Lewis bases*

The decamethylmetallocenes, either solvated or base-free, form adducts with a variety of Lewis bases, including ethers, aromatic amines, phosphines, isonitriles and unsaturated hydrocarbons. These can generally be formed by dissolving the base-free complex in the neat bases or in a solution of the base in a hydrocarbon solvent.

4.1(d).1. *Phosphine and isonitrile adducts.* Reaction of excess PEt_3 with base-free Cp^*_2Ae (Ae = Ca, Sr, Ba) produces 1 : 1 adducts as white, crystalline solids.[44] The $^{31}P\{^1H\}$ NMR shifts of the phosphine ligands, close to that of free PEt_3, indicates that the complexes may be extensively dissociated in solution. Variable-temperature NMR studies down to −80°C were not successful in halting the exchange.

2,6-Dimethylphenylisonitrile reacts with the decamethylmetallocenes to produce yellow 2:1 adducts, $Cp^*_2Ae(C{\equiv}NC_6H_3Me_2\text{-}2,6)_2$.[44] These all display two $\nu(C{\equiv}N)$ stretching frequencies in the solid state, one at 2115 cm^{-1}, and a second in the range 2138–2145 cm^{-1}. The former is close to the value for the free isonitrile (2120 cm^{-1}), suggesting that some dissociation may be occurring. NMR studies again indicate that the free and coordinated ligand are in fast exchange, which is not completely suppressed at −80°C.

4.1(d).2. *Aromatic amine adducts.* Adducts have been generated from the decamethylmetallocenes and a number of aromatic nitrogen heterocycles, including pyridine, pyrazine and dimethyl- and tetramethyl-substituted pyrazines, pyridazine, 2,2-bipyridine (bipy) and 2,2′:6′,2″-terpyridine (terpy).[40] In aromatic solvents, pyrazine will displace one THF from $Cp^*_2Ba(THF)_2$ to yield the orange complex $[Cp^*_2Ba(THF)]_2(\mu\text{-}NC_6H_4N)$. Bipy will displace both coordinated THF ligands from $Cp^*_2Ba(THF)_2$ to yield an orange adduct.[40] Bipy complexes can also be formed from reaction of the base-free metallocenes with the ligand in toluene.[44]

The base-free Cp^*_2Ae(Ca, Sr, Ba) complexes react readily with pyrazine and alkyl-substituted

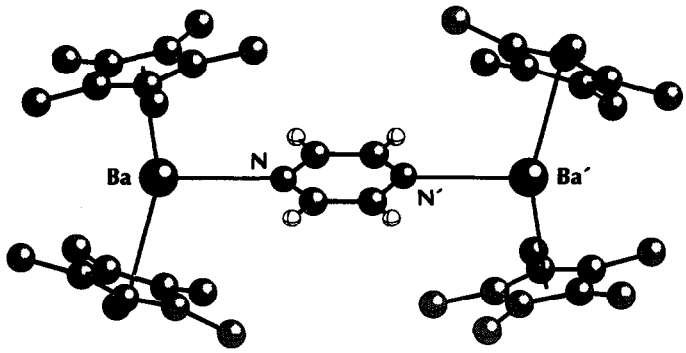

Fig. 4. Structure of the $[Cp^*_2Ba]_2(\mu\text{-}NC_6H_4N)$ dimer.

pyrazines to form the corresponding 2 : 1 adducts. The solid-state structure of the barium pyrazine adduct has been determined, and it is found to be a centrosymmetric dimer (Fig. 4).[56] The pyrazine unit is coordinated to the barium at a distance of 2.867(7) Å, with a Ba—N—N′ angle of 175°. The two N—C distances average 1.34(2) Å and the unique C—C′ distance is 1.381(19) Å, values which are indistinguishable from those in free pyrazine.

The stability of the adducts does not depend solely on the basicity of the heterocycles; excess THF will displace both pyrazine ($pK = 0.65$) and tetramethyl pyrazine ($pK = 3.55$) from the barium centre, but leaves the pyridazine adduct ($pK = 2.24$) unaffected; a chelate effect may be operating here.[40] An interesting point of comparison with the Ca—Ba systems is provided by Cp^*_2Mg, which forms a 1 : 1 complex with bipy, although no adducts with PMe_3 or 2,6-dimethylphenylisonitrile have been identified. Cp^*_2Mg may be too sterically crowded to permit adduct formation with comparatively bulky ligands.[44]

4.1(d).3. *Adducts with unsaturated hydrocarbons.* It might initially be surprising that organo-alkaline-earth complexes should display any appreciable interaction with hydrocarbons, a realm of organometallic chemistry usually restricted to the *d*-block and some *f*-block metal complexes.[57] These elements lack the orbitals of appropriate energy considered to be a prerequisite for covalent metal–ligand interactions, and particularly for the π-backbonding so characteristic of olefin and alkyne complexes. Nevertheless, some evidence for interaction is available from the fact that base-free Cp^*_2Ba, colourless in the solid state, is yellow in aromatic hydrocarbons. The yellow colour arises from a broad tailing from the UV to the blue region of the spectrum; removal of the solvent leaves the colourless metallocene, and no adducts have been isolated.[40]

Alkynes display somewhat stronger interactions than do alkenes. The reaction of 2-butyne with Cp^*_2Ca in pentane produces the 1 : 1 adduct $Cp^*_2Ca(\eta^2\text{-}MeC{\equiv}CMe)$ as a colourless solid. Proton NMR in C_6D_6 reveals only a single peak for the butyne, and no $\nu(C{\equiv}C)$ stretch is evident in the IR spectrum, an indication that the symmetry of the alkyne is not degraded on coordination.[51]

The first structurally characterized alkyne complex was formed from the reaction of Cp^*_2Ca and $Me_3SiC{\equiv}C{-}C{\equiv}CSiMe_3$ (BTMSBD) in toluene.[58] NMR evidence supports a 1 : 1 stoichiometry for the yellow adduct; addition of extra BTMSBD generates an averaged set of resonances for the alkyne carbons, indicating that the free and complexed diyne are in fast exchange even at −80°C. In the solid-state IR spectrum of the complex, $\nu(C{\equiv}C)$ appears at 2068 and 2053 cm^{-1}, a change from the uncomplexed value of 2067 cm^{-1}, and an indication that the symmetry around the triple bonds has been reduced. The diyne is readily displaced by oxygen and nitrogen donors, such as ethers and amines.

Details of the alkyne coordination were revealed in a single-crystal X-ray structure determination at −155°C.[58] Two crystallographically independent molecules are present in the asymmetric unit; both contain a calcium atom flanked by two η^5-Cp* rings, with the BTMSBD unit wedged between them (Fig. 5). In the "A" adduct, the diyne is symmetrically disposed around the ring centroid—Ca—ring centroid plane, with the two centre methyne carbons at nearly identical distances to the calcium (3.02 and 2.99 Å), and the outer methyne carbons substantially farther away (3.53 and 3.60 Å) (see Table 1). In the "B" adduct, the diyne has slipped *ca* 0.8 Å to one side of the plane,

Table 1. Structural data for organoalkaline-earth complexes

Complex	Average Ae—C distance (Å)	Ring centroid–Ae–ring centroid (°)	Ae—L distance (Å), donor atom	Method[a]	References
Cp^*_2Ba	2.898(17)	158(4)	—	E	48
Cp^*_2Ba[b]	2.99(2)	131.0	—	X	45, 46
$[Cp^*_2Ba(\mu\text{-pyrazine})]_2$[b]	2.96(2)	138.0	2.867(7), N	X	56
Cp_2Ca	2.800[c]	118.9[d]	—	X	5
Cp^*_2Ca	2.609(6)	154(3)	—	E	6, 47
Cp^*_2Ca[b]	2.64(2)	147.0	—	X	45
$Cp^*_2Ca(Me_3SiC{\equiv}C{-}C{\equiv}CSiMe_3)$[b]	2.65(3)	144.4	2.991(5), C 3.024(5), C (in "Å")[e] 2.878(5), C 3.104(5), C (in "B")[e]	X	58
$(MeCp)_2Ca(DME)$	2.676(9)	134.8	2.404(1), O	X	59
$[(C_3H_7)_4C_5H]_2Ca$	2.64(1)	162.3	—	X	61
$\{C_5H_3\text{-}1,3\text{-}(SiMe_3)_2\}_2Ca(THF)$	2.68[f]	135.3[f]	2.32(1), O	X	29, 42
$[Cp^*CaI(THF)_2]_2$[b]	2.67(1)	n/a	2.422(6), O 2.387(7), O[g]	X	62
Cp^*_2Sr	2.750(8)	149(3)	—	E	48
$\{C_5H_3\text{-}1,3\text{-}(SiMe_3)_2\}_2Sr(THF)$	2.82	134	2.49(3), O	X	29

[a] E = gas electron diffraction; X = single crystal X-ray diffraction.
[b] Two independent molecules exist in the unit cell; the average values are given.
[c] Distance to η^5-Cp rings.
[d] Ring centroid–metal–ring centroid angle between η^5-Cp rings.
[e] The two closest Ca—C(methyne) contacts.
[f] Average for two independent structure determinations.
[g] Average distance in each dimer.

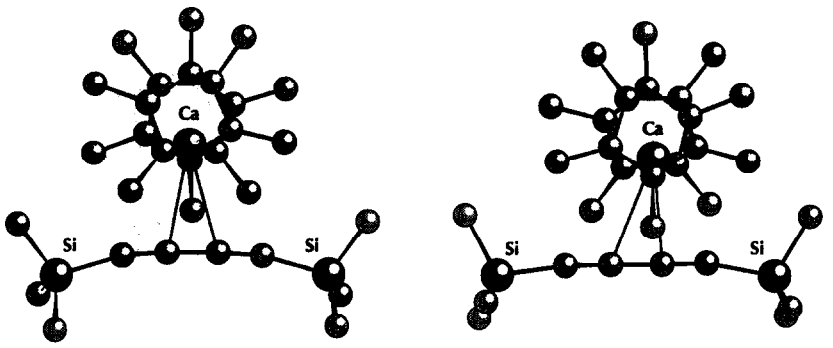

Fig. 5. Schematic view of the two independent complexes of $Cp^*_2Ca(Me_3SiC{\equiv}C{-}C{\equiv}CSiMe_3)$, indicating the different bonding modes of the diyne.

so that the distances from the calcium to the centre methyne carbons now differ significantly (2.88 and 3.10 Å), and a third methyne carbon is brought to within 3.17 Å of the metal centre. Crystal packing forces may be responsible for the occurrence of two conformers.

Interestingly, although adduct formation apparently occurs between Cp^*_2Ba and BTMSBD in alkanes, as evidenced by the formation of orange-coloured solutions, evaporation of the solutions causes Cp^*_2Ba to precipitate, and attempts to crystallize an adduct have not been successful.[40]

4.1(e). *Metallocenes containing alkyl-substituted cyclopentadienyl rings*

By using metathesis procedures analogous to those for the unsubstituted metallocenes, the bis(methylcyclopentadienyl) metallocenes, $(MeCp)_2Ae(THF)_n$, have been produced from (MeCp)(Li, K) and (Ca, Sr, Ba)I_2.[41] The calcium compound has also been prepared from the reaction of calcium metal in liquid ammonia with methylcyclopentadiene, and isolated as the DME adduct; its IR spectrum has been assigned.[59] The change in solubility from the parent compounds is slight: $(MeCp)_2CaL$ (L = 2THF, DME) has some solubility in aromatic hydrocarbons, $(MeCp)_2Sr(THF)_x$ is slightly soluble in THF, and $(MeCp)_2Ba(THF)_x$, like $Cp_2Ba(THF)_x$, is insoluble in THF. Loss of DME from $(MeCp)_2Ca(DME)$ begins at 65–70°C; the unsolvated complex is insoluble in hydrocarbons. The X-ray crystal structure of $(MeCp)_2Ca(DME)$ reveals calcium in a pseudo-tetrahedral coordination environment, with distances to the ring centroids and the oxygen atoms of the DME ligand of 2.399 and 2.404 Å, respectively (Fig. 6).[59] The compound is isostructural with the $Cp_2Yb(DME)$ analogue.[60]

The benzene-soluble t-butyl-substituted $[1,3\text{-}(Me_3C)_2C_5H_3]_2Ca(THF)$ has been prepared in 11% yield from the reaction of $[1,3\text{-}(Me_3C)_2C_5H_4]$ and $Ca(NH_2)_2$ in liquid ammonia/THF, eq. (9):[42]

$$Ca(NH_2)_2 + 2[1,3\text{-}(Me_3C)_2C_5H_4] \xrightarrow{THF,\ NH_{3(l)}} [1,3\text{-}(Me_3C)_2C_5H_3]_2Ca(THF). \qquad (9)$$

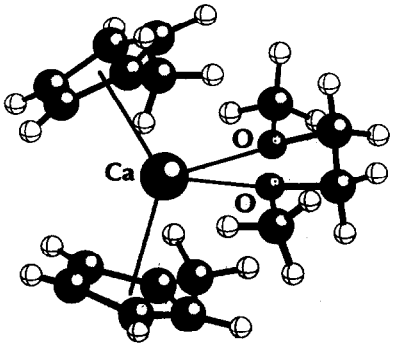

Fig. 6. Structure of $(MeCp)_2Ca(DME)$. The two ring centroids and the oxygen atoms of the DME ligand are at nearly identical distances from the calcium centre (*ca* 2.40 Å).

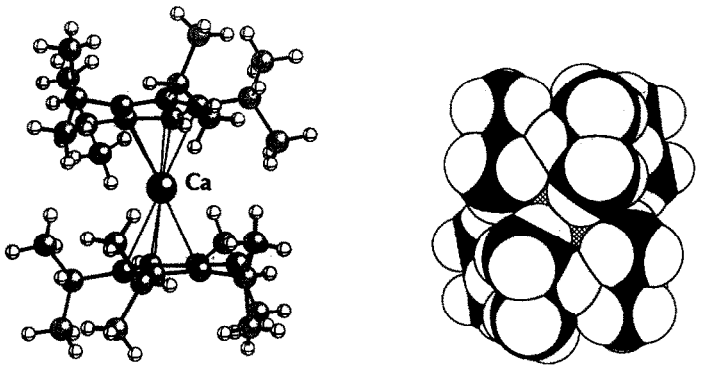

Fig. 7. Ball and stick drawing of $[(i\text{-}Pr)_4C_5H]_2Ca$ on the left; on the right, a space-filling view of the same complex, indicating the near-total encapsulation of the calcium (crosshatched area).

The complex $[(i\text{-}Pr)_4C_5H]_2Ca$ has been synthesized via halide metathesis from $K[(i\text{-}Pr)_4C_5H]$ and CaI_2 in diethyl ether, and purified by sublimation.[61] It provides an interesting example of the kinetic stability which can be produced in an organoalkaline-earth complex with ligands of sufficient steric bulk. In stark contrast to the extreme air sensitivity of the decamethylmetallocenes, crystalline bis(tetraisopropylcyclopentadienyl)calcium can be handled for several minutes in dry air without decomposition. A space-filling drawing based on the X-ray crystal structure of the complex reveals that the steric bulk of the $(i\text{-}Pr)_4Cp$ rings effectively encapsulates the metal centre (Fig. 7). The resulting blockage is presumably responsible for the inability of $[(i\text{-}Pr)_4C_5H]_2Ca$ to form adducts with ethers and aromatic amines, unlike the analogous Cp^*_2Ca species [see Section 4.1(c)]. Also of note is the ring centroid–metal–ring centroid bending angle of 162°; this represents a smaller deviation from a structure with parallel rings than is observed with Cp^*_2Ca (147°); the bulk of the rings may serve to force a more open angle.

4.1(f). *Metallocenes containing trimethylsilyl-substituted cyclopentadienyl rings*

A variety of trimethylsilyl-substituted metallocenes have been prepared by both solution routes and metal vapour methods. Calcium amide reacts with trimethylsilyl cyclopentadienes in THF with loss of NH_3 and formation of the corresponding metallocenes, eq. (10):[42]

$$Ca(NH_2)_2 + 2(Me_3Si)_nC_5H_{6-n} \xrightarrow[-2NH_3]{THF} [(Me_3Si)_nC_5H_{5-n}]_2Ca(THF) \qquad (10)$$

$$n = 1\ (12\%)$$

$$n = 2\ (30\%).$$

Displacement of the indenyl rings from $(C_9H_7)_2Ca$ with $Me_3SiC_5H_5$ also yields the trimethylsilyl-substituted metallocene, eq. (11):

$$(C_9H_7)_2Ca + 2\,Me_3SiC_5H_5 \xrightarrow[-2C_9H_8]{THF} (Me_3SiC_5H_4)_2Ca(THF). \qquad (11)$$

Bis(indenyl)calcium will not react with bis(trimethylsilyl)cyclopentadiene to form the corresponding metallocene.

Co-condensation of $1,3\text{-}(SiMe_3)_2C_5H_4$ and calcium, strontium or barium vapour at −196°C, followed by warming to room temperature, yields the base-free metallocenes $[(SiMe_3)_2C_5H_3]_2Ae$ in moderate to good yields.[29] Recrystallization of the metallocenes from THF yields the mono-THF adducts, which can be rendered base-free again by sublimation under vacuum. For the calcium derivative, repeated sublimations are necessary to obtain a base-free material; this is similar to the behaviour observed with $Cp^*_2Ca(THF)_2$, although the latter cannot be obtained completely base-free by sublimation. The calcium and strontium derivatives, whether solvated or base-free, are readily soluble in C_6D_6 and THF; curiously, the unsolvated barium metallocene is reported as more soluble than the THF adduct, for which NMR spectra could not be obtained.[29]

The X-ray crystal structures of $\{C_5H_3\text{-}1,3\text{-}(SiMe_3)_2\}_2Ca(THF)$[29,42] (Fig. 8) and $\{C_5H_3\text{-}1,3\text{-}$

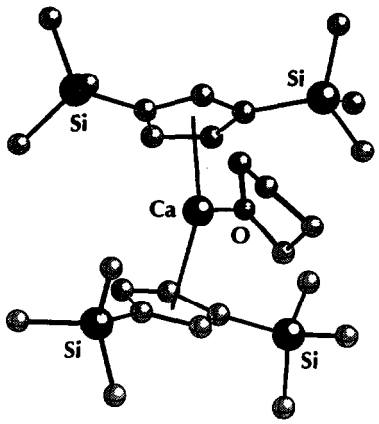

Fig. 8. Structure of $\{C_5H_3\text{-}1,3\text{-}(SiMe_3)_2\}_2Ca(THF)$.

$(SiMe_3)_2\}_2Sr(THF)$[29] have been obtained. The calcium and strontium compounds are isomorphous and isostructural, and possess crystallographically imposed C_2 symmetry. They display typical "bent metallocene" geometries, with ring centroid–metal–ring centroid angles of 135° (Ca) and 134° (Sr). These are, not unexpectedly, smaller than in the unsolvated Cp^*_2Ca and Cp^*_2Sr metallocenes (Table 1), a reflection of the steric demands imposed by the THF ligand.

4.2. *Monocyclopentadienyl complexes*

Interest in monocyclopentadienyl complexes (CpAeX) stems from the potential richness of the chemistry from these complexes. In the ideal case, the single Cp ring would supply solubility by blocking extensive oligomerization, while the X group would supply functionality not available from the metallocenes.

A general difficulty with the synthesis of monocyclopentadienyl complexes is the occurrence of Schlenk equilibria, which causes disproportionation into a metallocene and a metal salt, for example, eq. (12):

$$2\,CpAeX \rightleftharpoons Cp_2Ae + AeX_2. \tag{12}$$

The position of the equilibrium is sensitive to the nature of the solvent and the temperature; in those cases where all three components of the Schlenk equilibria are comparably soluble, the equilibrium constant for the exchange approaches that expected from complete scrambling of the ligands.[62]

Monopentamethylcyclopentadienyl complexes have been prepared in solution by a variety of routes:

(1) Reaction of an alkali metal cyclopentadienide with an Ae dihalide, for example, eq. (13):[62]

$$KCp^* + CaI_2 \xrightarrow{THF} Cp^*CaI(THF)_2 + KI. \tag{13}$$

(2) Reaction of a metallocene with an Ae dihalide, for example, eq. (14):[62]

$$Cp^*_2Ca + CaI_2 \xrightarrow{THF} 2\,Cp^*CaI(THF)_2. \tag{14}$$

Methods (1) and (2) are functionally related because of the Schlenk equilibrium which exists between Cp^*CaI, Cp^*_2Ca and CaI_2. In order to obtain pure $Cp^*CaI(THF)_2$, a reaction can be run according to eq. (13), but with excess KCp^*; this insures that the amount of free CaI_2 will be negligible. The resulting mixture of Cp^*CaI and Cp^*_2Ca can be freed from the decamethylmetallocene by a hexane wash.[62] $Cp^*CaI(THF)_2$ was found to dissociate in dioxane-d_8 to form Cp^*_2Ca and a white precipitate, presumably the solvate $CaI_2(dioxane)_n$. Such behaviour is reminiscent of Grignard reagents.[63] Dilute hydrocarbon solutions are unstable, yielding a precipitate of CaI_2 and a solution of Cp^*_2Ca.

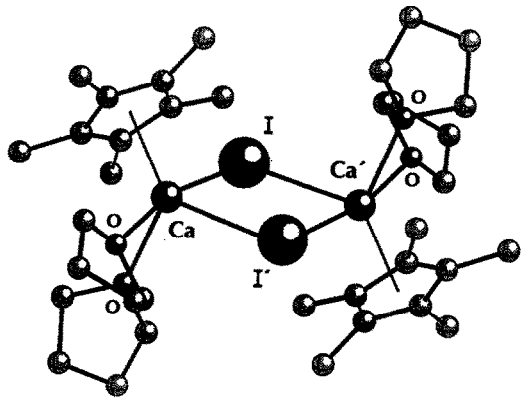

Fig. 9. Structure of $[Cp^*Ca(\mu\text{-}I)(THF)_2]_2$.

(3) Selective precipitation of a Cp* ring from a metal centre, eq. (15):[64]

$$Cp^*_2Ca + LiR \xrightarrow{THF} Cp^*CaR(THF)_n + LiCp^*\downarrow \quad (15)$$
$$[R = N(SiMe_3)_2,\ CH(SiMe_3)_2].$$

Interestingly, similar reactions performed with Cp^*_2Ba yield organometallic salts rather than monocyclopentadienyl species, eq. (16):

$$Cp^*_2Ba + LiR \xrightarrow{THF} Li^+[Cp^*_2BaR(THF)_n]^- \quad (16)$$
$$[R = N(SiMe_3)_2,\ CH(SiMe_3)_2].$$

The organobarium salts are not soluble in hydrocarbons, but disproportionate in THF to produce the metallocenes and LiR.[64] The difference between the calcium and barium reactions may be an indication that a "Cp*BaR" complex may be too coordinatively unsaturated to be stable under these conditions.

$[Cp^*Ca(\mu\text{-}I)(THF)_2]_2$ crystallizes from toluene as a halide-bridged dimer, in which each calcium atom is coordinated by a single pentamethylcyclopentadienyl ring, two THF molecules and two bridging iodides (Fig. 9). The complex is isostructural with a divalent organosamarium compound.[65] Two independent dimers appear in the asymmetric cell, each with a crystallographically imposed centre of inversion. The average (η^5-Cp*)—Ca distances for both species is 2.67 Å, whereas the average Ca—O(THF) distance is 2.422(6) Å in one dimer and 2.387(7) Å in the second dimer. The $[Ca(\mu\text{-}I)]_2$ core is asymmetric, the Ca—I distances differing by 0.062 Å in one dimer and by 0.146 Å in the other. The significance of these distances has been discussed in terms of a parameter based on relative bond lengths (see Section 5).

A species identified as $[(MeCp)CaNH_2]_n$ has been prepared by the careful addition of MeCpH to a solution of calcium in liquid ammonia; it is believed to be an intermediate in the formation of $(MeCp)_2Ca$.[59]

4.3. *Cyclooctatetraenyl complexes*

The bis(cyclooctatetraenyl)calcium anion $[(C_8H_8)_2Ca]^{2-}$ has been prepared in 90% yield from the reaction of C_8H_8 with Ca and K in liquid ammonia, and isolated as a THF adduct, eq. (17):[66]

$$Ca + K + C_8H_8 \xrightarrow{THF,\ NH_{3(l)}} [K(THF)_2]_2[(C_8H_8)_2Ca]. \quad (17)$$

The same compound can also be prepared from the reaction of K_2COT and CaI_2 in THF.[67] The solvated complex easily loses THF to generate the base-free complex, which can be recrystallized from DME to produce the stable monosolvate $[K(DME)]_2[(C_8H_8)_2Ca]$. The IR spectra of both the base-free material and the DME solvate are identical to those of the corresponding Yb^{2+} complex; the X-ray powder patterns of the calcium and ytterbium DME adducts are also similar, suggesting

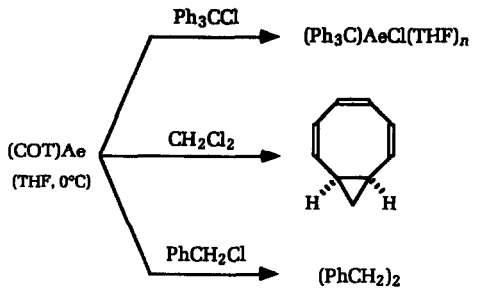

Scheme 1.

that the calcium species possesses a symmetrical sandwich geometry analogous to the structurally characterized $[(\eta\text{-}C_8H_8)_2Yb]^{2-}$ complex.[66]

Monocyclooctatetraenyl complexes can be formed from the condensation of calcium, strontium and barium vapour with cyclooctatetraene (COT) and THF at $-196°C$.[30] The calcium compound has also been isolated from the reaction of calcium metal in liquid ammonia with COT.[59] The sparingly-soluble, pyrophoric (COT)Ae$(THF)_n$ complexes can be rendered base-free by heating at 60°C under vacuum. (COT)Ca is stable up to 350°C, and its IR spectrum is similar to that of K^+, La^{3+} and Th^{4+} analogues.[68] These complexes form orange adducts with pyridine and can act as a source of soluble Ae^{2+} or as an organic nucleophile (Scheme 1).

Reaction of (COT)Ae with $RPCl_2$ produces a stable phosphacyclopropane which has been structurally characterized, eq. (18):[30]

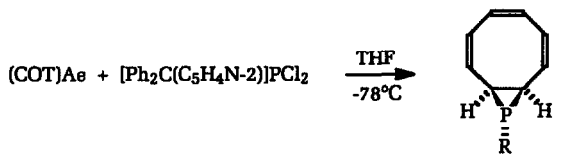

(18)

4.4. *Organoalkaline-earth species containing monovalent calcium and strontium*

A relatively recent development in alkaline-earth chemistry has been the production and characterization of radical species containing formal calcium(I) and strontium(I). These have been generated from the gas-phase reactions of calcium and strontium metal vapours with the organic oxidizing agent, and include monoalkoxides,[69,70] monoalkylamides,[71] monomethyl,[33,72] monoacetylide,[73,74] monoisocyanate,[75,76] monoazide,[77] monocyclopentadienide,[31] monopyrrolate,[32] monoformamidate[78] and monocarboxylate complexes.[79] Of those species containing Ae—C bonds, the monocyclopentadienyl free radicals CpCa$^\bullet$ and CpSr$^\bullet$ are of special interest, as laser-induced fluorescence spectroscopy indicates that these gas-phase species are "half-sandwich" complexes with C_{5v} symmetry.[31] Comparisons of the spectra obtained for these species with that from the reaction of calcium and strontium vapour with pyrrole indicates that the latter should be formulated as $(\eta^5\text{-}C_4H_4N)Ae^\bullet$ species rather than as σ-bonded complexes.[32]

Rotational analysis of gas-phase $HC{\equiv}CCa^\bullet$ [74] and $CH_3Ca^\bullet$ [33] have found Ca—C bond lengths of 2.25 and 2.349(13) Å, respectively. The longer length of the Ca—methyl bond was taken as a reflection of the weakness of the Ca—C interaction, estimated at < 45 kcal mol^{-1}.

5. STRUCTURAL STUDIES

The number of structural studies of organoalkaline-earth complexes increased considerably during the period under review; many of these represent decamethylmetallocenes and their adducts with various neutral donors. A complete listing of the available structures is given in Table 1.

An analysis of over 200 structurally characterized compounds of the alkaline-earth and *f*-elements revealed that metal–ring centroid distances can be predicted with high accuracy in those

complexes with divalent metal centres by adding an effective Cp radius of 1.33(3) Å to the coordination number-adjusted metal ionic radii. This correlation was found to hold regardless of the coordination environment. In contrast, equally effective correlations could only be established for trivalent complexes if their coordination numbers were eight or higher.[80]

By assuming that the Cp ligand is a "ball" of radius 2.04 Å attached to a metal centre, various structural features of di-, tri-, and tetravalent ionic cyclopentadienyl complexes have been rationalized.[59] This model has been used to predict the values of ring centroid–metal–ring centroid angles and the tendency of certain metal/ligand combinations to exist as monomeric or polymeric solids.

A method for ranking structural distortions in bridged homometallic dimers based on calculations of the relative difference in effective ionic radii of the ligands has been proposed.[62] It uses relative differences in metal–ligand bond lengths in order to compensate for changes in metal radii and coordination numbers. The method has been used to compare the Ca—I bond lengths in $[Cp^*CaI(THF)_2]_2$ with those in related organolanthanide complexes.

6. APPLICATIONS

The applications of organoalkaline-earth compounds have traditionally been limited to the use of the RAeX species as adjuncts to Grignard reagents in organic synthesis,[8,81] and a review in this area has recently appeared.[82] Organoalkaline-earth species, especially those with barium, have found a small niche as initiators of anionic polymerization reactions; studies of such systems and the ion pairing processes associated with them continue to appear.[83–85]

A potentially vast new field of use may exist for organoalkaline-earth compounds in chemical vapour deposition (CVD) technology. The gas-phase decomposition of volatile organometallic substances may be useful in the preparation of thin films of alkaline-earth containing materials, including the recently discovered high-temperature superconducting ceramics.[86,87] The vapour-phase reaction of Cp^*_2Ca with SiF_4 or NF_3 at 150°C has been used to deposit polycrystalline films of CaF_2 on glass and Si(100) surfaces.[88] Depending on the deposition conditions, such films can be varied in thickness from 10 to 100 μm. The calcium, barium and strontium complexes of trifluoroacetylacetone {H[TFA]} and hexafluoroactylacetone {H[HFA]} have been prepared and show promise in CVD applications.[39]

7. CONCLUSIONS

The compounds of the heavy alkaline-earth metals, which for many years represented a nearly dormant branch of organometallic chemistry, have steadily grown in number and interest as the special steric and electronic requirements of these metals have been recognized. These advances have forced the realization that the compounds of calcium, strontium and barium possess attributes distinct from those of magnesium or the alkali metals, and that their combination of large size, high Lewis acidity and dipositive charge can generate chemistry with distinct differences from that of their neighbouring metal families. Much remains to be done in extending and systematizing organoalkaline-earth reactions and structures and refining their relationships with the alkali metals and the lanthanides and actinides, but the potential for growth in this field looks bright.

Acknowledgements—Acknowledgement for support of the research from my laboratory is made to the donors of the Petroleum Research Fund, administered by the American Chemical Society, and to the Natural Science Committee of Vanderbilt University. Professor Peter F. Bernath is thanked for preprints of refs 32, 78 and 79.

REFERENCES

1. E. Beckman, *Chem. Ber.* 1905, **38**, 904.
2. H. Gilman and F. Schulze, *J. Am. Chem. Soc.* 1926, **48**, 2463.
3. K. Ziegler, H. Froitzheim-Kühlhorn and H. Hafner, *Chem. Ber.* 1956, **89**, 434.
4. E. O. Fischer and G. Stölzle, *Chem. Ber.* 1961, **94**, 2187.
5. R. Zerger and G. Stucky, *J. Organomet. Chem.* 1974, **80**, 7.
6. R. A. Andersen, J. M. Boncella, C. J. Burns, R. Blom, A. Haaland and H. V. Volden, *J. Organomet. Chem.* 1986, **312**, C49.

7. F. A. Cotton and G. Wilkinson, *Advanced Inorganic Chemistry*, p. 286. Wiley, New York (1980).
8. W. E. Lindsell, in *Comprehensive Organometallic Chemistry* (Edited by G. Wilkinson, F. G. A. Stone and E. W. Abel), Ch. 4.2. Pergamon Press, Oxford (1982).
9. S. T. Ioffe and A. Nesmeyanov, *The Organic Compounds of Magnesium, Beryllium, Calcium, Strontium and Barium*. North-Holland, Amsterdam (1967).
10. B. G. Gowenlock and W. E. Lindsell, *J. Organomet. Chem. Library, Organomet. Chem. Rev.* 1977, **3**, 1.
11. B. G. Gowenlock, W. E. Lindsell and B. Singh, *J. Chem. Soc., Dalton Trans.* 1978, 657.
12. R. D. Shannon, *Acta Cryst.* 1976, **A32**, 751.
13. T. J. Marks, *Science* 1982, **217**, 989.
14. W. J. Evans, *Adv. Organomet. Chem.* 1985, **24**, 131.
15. W. J. Evans, *Polyhedron* 1987, **6**, 803.
16. W. Bünder and E. Weiss, *J. Organomet. Chem.* 1975, **92**, 1.
17. A. J. Freeman and R. E. Watson, *Phys. Rev.* 1976, **9**, 217.
18. T. J. Marks and R. D. Ernst, in *Comprehensive Organometallic Chemistry* (Edited by G. Wilkinson, F. G. A. Stone and E. W. Abel), Ch. 21. Pergamon Press, Oxford (1982).
19. W. J. Evans, T. P. Hanusa, J. H. Meadows, W. E. Hunter and J. L. Atwood, *Organometallics* 1987, **6**, 295.
20. D. Bryce-Smith and A. C. Skinner, *J. Chem. Soc.* 1963, 577.
21. N. Kawabata, A. Matsumura and S. Yamashita, *J. Org. Chem.* 1973, **38**, 4268.
22. K. Mochida and H. Ogawa, *J. Organomet. Chem.* 1983, **243**, 131.
23. K. Mochida, S.-I. Ogura and T. Yamanishi, *Bull. Chem. Soc. Jpn* 1986, **59**, 2633.
24. K. Mochida and T. Yamanishi, *J. Organomet. Chem.* 1987, **332**, 247.
25. K. Mochida, H. Takeuchi, Y. Hiraga and H. Ogawa, *Chem. Lett.* 1984, 1989.
26. K. Mochida and Y. Mizuno, *Chem. Lett.* 1986, 1125.
27. K. Mochida, H. Takeuchi, Y. Hiraga and H. Ogawa, *Organometallics* 1987, **6**, 2293.
28. W. E. Lindsell and R. A. Parr, *Polyhedron* 1986, **5**, 1259.
29. L. M. Engelhardt, P. C. Junk, C. L. Raston and A. H. White, *J. Chem. Soc., Chem. Commun.* 1988, 1500.
30. D. S. Hutchings, P. C. Junk, W. C. Patalinghug, C. L. Raston and A. H. White, *J. Chem. Soc., Chem. Commun.* 1989, **15**, 973.
31. L. C. O'Brien and P. F. Bernath, *J. Am. Chem. Soc.* 1986, **108**, 5017.
32. A. M. R. P. Bopegedera, W. T. M. L. Fernando and P. F. Bernath, *J. Phys. Chem.* in press.
33. C. R. Brazier and P. F. Bernath, *J. Chem. Phys.* 1989, **91**, 4548.
34. R. D. Rieke, T. P. Burns, R. M. Wehmeyer and B. E. Kahn, *Am. Chem. Soc., Symp. Ser.* 1987, **333**, 223.
35. R. D. Rieke and P. M. Hudnall, *J. Am. Chem. Soc.* 1972, **94**, 7178.
36. M. J. McCormick, K. B. Moon, S. R. Jones and T. P. Hanusa, *J. Chem. Soc., Chem. Commun.* in press.
37. R. Masthoff, H. Schüler and G. Krieg, *J. Organomet. Chem.* 1968, **13**, 37.
38. W. E. Lindsell, F. C. Robertson, I. Soutar and D. H. Richards, *Eur. Polym. J.* 1981, **140**, 107.
39. A. P. Purdy, A. D. Berry, R. T. Holm, R. T. Fatermi and D. K. Gaskill, *Inorg. Chem.* 1989, **28**, 2799.
40. R. A. Williams and T. P. Hanusa, unpublished results.
41. M. J. McCormick, R. A. Williams, L. J. Levine and T. P. Hanusa, *Polyhedron* 1988, **7**, 725.
42. P. Jutzi, W. Leffers, G. Müller and B. Huber, *Chem. Ber.* 1989, **122**, 879.
43. K. A. Allen, B. G. Gowenlock and W. E. Lindsell, *J. Organomet. Chem.* 1973, **55**, 229.
44. C. J. Burns and R. A. Andersen, *J. Organomet. Chem.* 1987, **325**, 31.
45. R. A. Williams, T. P. Hanusa and J. C. Huffman, *Organometallics* 1990, **9**, 1128.
46. R. A. Williams, T. P. Hanusa and J. C. Huffman, *J. Chem. Soc., Chem. Commun.* 1988, 1045.
47. R. A. Andersen, R. Blom, J. M. Boncella, C. J. Burns and H. V. Volden, *Acta Chem. Scand.* 1987, **A41**, 24.
48. R. A. Andersen, R. R. Blom, C. J. Burns and H. V. Volden, *J. Chem. Soc., Chem. Commun.* 1987, 768.
49. W. J. Evans, L. A. Hughes and T. P. Hanusa, *J. Am. Chem. Soc.* 1984, **106**, 4270.
50. W. J. Evans, L. A. Hughes, T. P. Hanusa and R. J. Doedens, *Organometallics* 1986, **5**, 1285.
51. C. J. Burns, PhD thesis. University of California at Berkeley (1987).
52. J. V. Ortiz and R. Hoffman, *Inorg. Chem.* 1985, **24**, 2095.
53. J. C. Green, D. Hohl and N. Rösch, *Organometallics* 1987, **6**, 712.
54. M. Guido and G. Gigli, *J. Chem. Phys.* 1976, **65**, 1397.
55. R. L. DeKock, L. K. Timmer, E. J. Baerends and P. Vernooijs, *Abstracts of Papers*, 198th National Meeting of the American Chemical Society, Miami Beach, Florida; American Chemical Society: Washington, D.C. (1989); INOR 234.
56. R. A. Williams, T. P. Hanusa and J. C. Huffman, manuscript in preparation.
57. F. A. Cotton and G. Wilkinson, *Advanced Inorganic Chemistry*, Ch. 26. Wiley, New York (1988).
58. R. A. Williams, T. P. Hanusa and J. C. Huffman, *J. Am. Chem. Soc.* 1990, **112**, 2454.

59. A. Hammel, W. Schwarz and Weidlein, *J. Organomet. Chem.* 1989, **378**, 347.
60. G. B. Deacon, P. I. MacKinnon, T. C. Hambley and J. C. Taylor, *J. Organomet. Chem.* 1983, **259**, 91.
61. R. A. Williams and T. P. Hanusa, manuscript in preparation.
62. M. J. McCormick, S. C. Sockwell, C. E. H. Davies, T. P. Hanusa and J. C. Huffman, *Organometallics* 1989, **8**, 2044.
63. W. Schlenk and W. Schlenk, *Chem. Ber.* 1929, **62**, 920.
64. S. C. Sockwell and T. P. Hanusa, manuscript in preparation.
65. W. J. Evans, J. W. Grate, H. W. Choi, I. Bloom, W. E. Hunter and J. L. Atwood, *J. Am. Chem. Soc.* 1985, **107**, 841.
66. S. A. Kinsley, A. Streitwieser Jr and A. Zalkin, *Organometallics* 1985, **4**, 52.
67. M. J. McCormick and T. P. Hanusa, unpublished results.
68. V. T. Aleksanyan, I. A. Garbuzova, T. M. Chernyshova, Z. V. Todres, M. R. Leonov and N. I. Gramateeva, *J. Organomet. Chem.* 1981, **217**, 169.
69. C. R. Brazier, L. C. Ellingboa, S. Kinsey-Neilsen and P. F. Bernath, *J. Am. Chem. Soc.* 1986, **108**, 2126.
70. L. C. O'Brien, C. R. Brazier and P. F. Bernath, *J. Molec. Spectrosc.* 1988, **130**, 33.
71. A. M. R. P. Bopegedera, C. R. Brazier and P. F. Bernath, *J. Phys. Chem.* 1987, **91**, 2779.
72. C. R. Brazier and P. F. Bernath, *J. Chem. Phys.* 1987, **86**, 5918.
73. A. M. R. P. Bopegedera, C. R. Brazier and P. F. Bernath, *Chem. Phys. Lett.* 1987, **136**, 97.
74. A. M. R. P. Bopegedera, C. R. Brazier and P. F. Bernath, *J. Molec. Spectrosc.* 1988, **129**, 268.
75. L. C. Ellingboe, A. M. R. P. Bopegedera, C. R. Brazier and P. F. Bernath, *Chem. Phys. Lett.* 1986, **126**, 285.
76. L. C. O'Brien and P. F. Bernath, *J. Chem. Phys.* 1988, **88**, 2117.
77. C. R. Brazier and P. F. Bernath, *J. Chem. Phys.* 1988, **88**, 2112.
78. A. M. R. P. Bopegedera, W. T. M. L. Fernando and P. F. Bernath, *J. Phys. Chem.*, in press.
79. L. C. O'Brien, C. R. Brazier, S. Kinsey-Nielsen and P. F. Bernath, *J. Phys. Chem.*, in press.
80. S. C. Sockwell and T. P. Hanusa, *Inorg. Chem.* 1990, **29**, 76.
81. L. Miginiac, *J. Organomet. Chem.* 1982, **238**, 235.
82. C. L. Raston and G. Salem, in *Chemistry of the Metal Carbon Bond* (Edited by F. R. Hartley), Vol. 4, Ch. 2. John Wiley, Chichester (1987).
83. L. C. Tang, C. Mathis and B. Francois, *J. Organomet. Chem.* 1983, **243**, 356.
84. C. Mathis, B. François and J. Smid, *J. Organomet. Chem.* 1981, **217**, 291.
85. W. E. Lindsell, F. C. Robertson and I. Soutar, *Eur. Polym. J.* 1983, **19**, 115.
86. V. Mantese, A. B. Catalan, A. H. Hamdi and A. L. Micheli, *Appl. Phys. Lett.* 1988, **52**, 1741.
87. A. Gupta, E. I. Jagannathan, E. A. Cooper, E. A. Giess, J. I. Landman and B. W. Hussey, *Appl. Phys. Lett.* 1988, **52**, 2077.
88. M. J. Benac, A. H. Cowley, R. A. Jones and A. F. Tasch Jr, *Chem. Mater.* 1989, **1**, 289.

Note added in proof: A recent report describes in detail the gas-phase structures of Cp^*_2Sr and Cp^*_2Ba (R. Blom, K. Faegri Jr and H. V. Volden, *Organometallics* 1990, **9**, 372). *Ab initio* calculations were performed on Cp_2Mg and Cp_2Ca; structures with parallel rings represented energy minima for both molecules. The failure of the calculations to identify a bent structure for Cp_2Ca (as occurs with Cp^*_2Ca) was ascribed to the inability to model *d*-orbital interactions adequately.

Polyhedron Vol. 9, No. 11, pp. 1363–1367, 1990
Printed in Great Britain

0277–5387/90 $3.00+.00
© 1990 Pergamon Press plc

THE 1,2-DIHYDRO-1,2-DIPHOSPHETE–1,4-DIPHOSPHADIENE EQUILIBRIUM. X-RAY STRUCTURES OF $[\mu^2,\mu^2,\eta^1,\eta^1\text{-}(Ph)_8C_4P_4]W_2(CO)_6$ AND $[\eta^1,\eta^1\text{-}(Ph)_4C_2P_2]W_2(CO)_{10}$

NICOLE MAIGROT, CLAUDE CHARRIER, LOUIS RICARD and FRANÇOIS MATHEY*

Laboratoire de Chimie du Phosphore et des Métaux de Transition DCPH, Ecole Polytechnique, 91128 Palaiseau Cedex, France

(*Received* 4 *September* 1989; *accepted* 15 *December* 1989)

Abstract—As its $P_2W_2(CO)_{10}$ dicomplex, the ring of 1,2,3,4-tetraphenyl-1,2-dihydro-1,2-diphosphete undergoes a reversible conrotatory opening to give the corresponding 1,4-diphosphadiene dicomplex which can be trapped as [4+2] cycloadducts with *N*-phenylmaleimide, maleic anhydride, acrylonitrile and benzaldehyde. X-ray crystal structure analysis indicates a weakening of the P—P bond of the 1,2-dihydro-1,2-diphosphete upon complexation: the P—P bond length increases from 2.248(1) Å in the free ring to 2.281(3) Å in the complex explaining why this reversible opening takes place only in the complex.

Several indications in the literature pointed to a possible equilibrium between the 1,2-dihydro-1,2-diphosphete ring and its 1,4-diphosphadiene open-chain isomer [eq. (1)]:

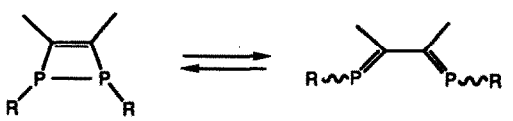

(1)

Indeed, one of the various syntheses of the 1,2-dihydro-1,2-diphosphete ring involves the spontaneous ring-closure of a transient 1,4-diphosphadiene.[1,2] When using the same synthetic scheme with bulky R-substituents at phosphorus, the 1,4-diphosphadiene can be isolated because it does not spontaneously cyclize anymore.[3] Unfortunately, the Diels–Alder reactivity is simultaneously lost as a consequence of the steric hindrance at the terminal 1,4-positions. On the other hand, the related 1,2-dihydrophosphete ring can similarly be prepared via the spontaneous cyclization of the corresponding 1-phosphadienes.[4,5] Besides, as a P—$W(CO)_5$ complex, this ring is in equilibrium with its phosphadienic isomer. The existence of this equilibrium was demonstrated by a series of trapping reactions of the open-chain complex.[6,7] These results strongly suggested the possibility of using 1,2-dihydro-1,2-diphosphetes as synthetic equivalents of 1,4-diphosphadienes. This idea has been successfully checked as hereafter reported.

RESULTS AND DISCUSSION

Our starting product was the easily prepared 1,2,3,4-tetraphenyl-1,2-dihydro-1,2-diphosphete **1**.[8] A preliminary attempt involved the reaction of **1** with *N*-phenylmaleimide. The expected cycloadduct **2** was not obtained [eq. (2)]:

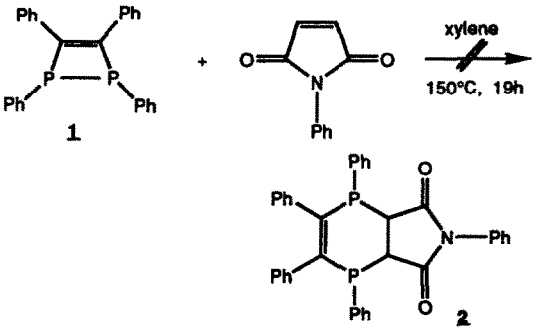

(2)

A complicated and useless mixture of oxidized products was recovered instead. Modelling our approach on the 1,2-dihydrophosphete case,[6] we thus prepared the *P,P* dicomplex **3** from **1**. According to the results of a X-ray crystal structure analy-

* Author to whom correspondence should be addressed.

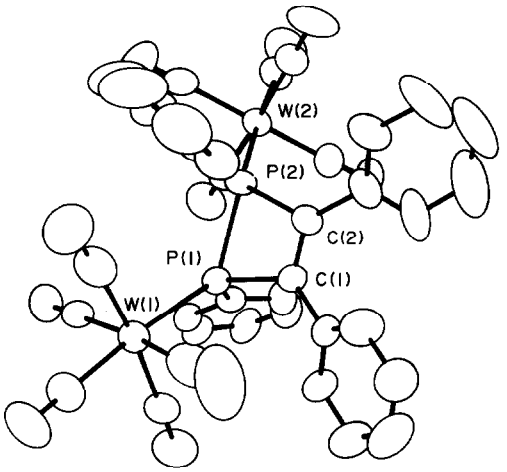

Fig. 1. X-ray structure of **3**.

sis of **3** (Fig. 1), the prospects of achieving an equilibrium such as the one depicted in eq. (1) were far better with **3** than with **1**. Indeed, the P—P bond distance in **3** [2.281(3) Å] is significantly longer than in **1** [2.248(1) Å].[9] Besides, the complexation of the two phosphorus atoms prevents side-reactions such as oxidation at the phosphorus lone pairs and stabilizes the P=C double bonds of the postulated open-chain isomer.[10] In line with our expectations, the reaction of **3** with *N*-phenylmaleimide indeed produces the corresponding cycloadduct as a mixture of two isomers **4a,b** [eq. (3)] which have been separated by chromatography and completely characterized:

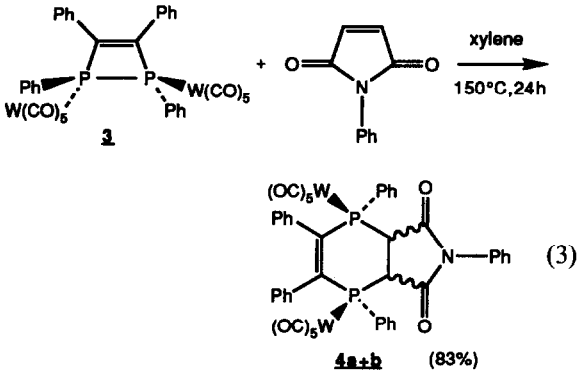

(3)

The various spectroscopic data unambiguously indicate that both isomers have a plane of symmetry bisecting the (Ph)C=C(Ph) double bond of the former 1,2-dihydro-1,2-diphosphete ring. For example, only one resonance is observed on the ^{31}P NMR spectra of **4a** and **4b** respectively at +49.9 and +53.7 ppm in CD_2Cl_2. On the other hand, the C*H* protons at the junction of the two heterocycles give either a pseudo-triplet at 4.57 ppm for **4a** or a singlet at 4.59 ppm for **4b** ($CDCl_3$). Thus, it appears that **4a** and **4b** have the stereochemistries depicted in eq. (3). This result demonstrates that a conrotatory opening of the ring of **3** has taken place in agreement with the classical Woodward–Hoffmann rules [eq. (4)]:

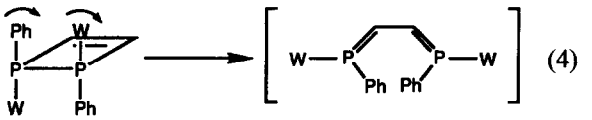

(4)

Very similar results have been obtained with maleic anhydride [eq. (5)]:

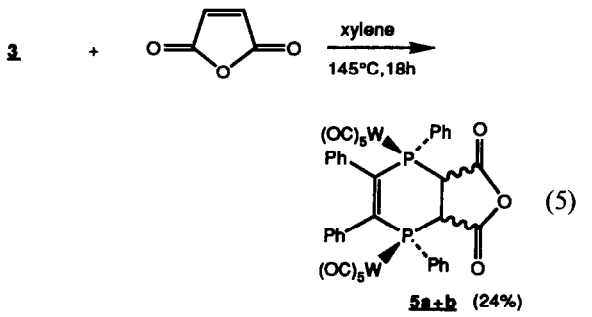

(5)

In that case, it is necessary to purify the products by recrystallization and the final low yields result from heavy losses during the purification procedure. This kind of chemistry has also been extended to acrylonitrile and benzaldehyde [eqs (6) and (7)]:

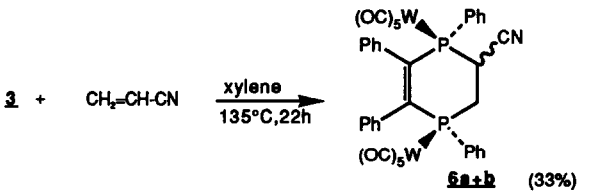

(6)

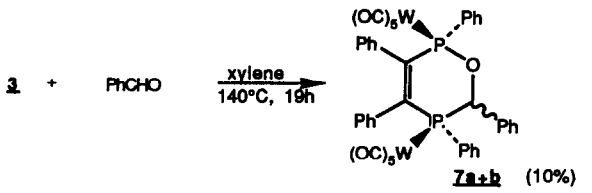

(7)

In these cases, a part of the starting product can be recovered due to the lower reactivity of the dienophiles.

It was, of course, interesting to study what happens when complex **3** is heated alone under the same conditions which are used for performing the [4+2] cycloadditions. At 135°C for 3 days, **3** loses one of its $W(CO)_5$ complexing groups to give the mono complex **8** [eq. (8)] which was partly characterized

by ^{31}P NMR and mass spectrometry:

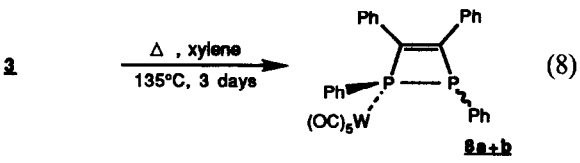

(8)

At 150°C, a further evolution takes place with loss of CO to give a green complex **9** whose structure has been studied by X-ray analysis [eq. (9)]. Due to a substantial decomposition of the crystal during the data collection, it has been impossible to calculate significant structural parameters but the overall geometry of the central skeleton of the molecule has been unambiguously established (Fig. 2). Complex **9** probably results from the dimerization of a transient diradical as shown in eq. (9):

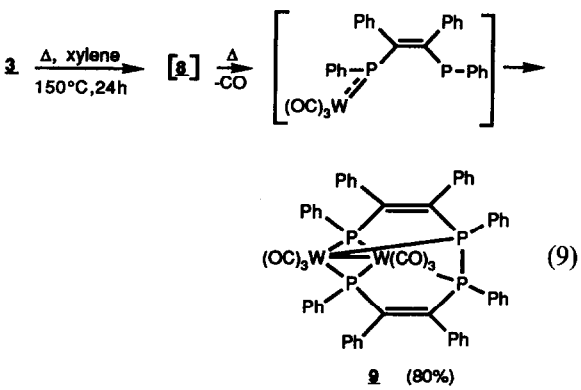

(9)

Since **9** is diamagnetic, electron book-keeping implies the existence of a W—W bond as indicated.

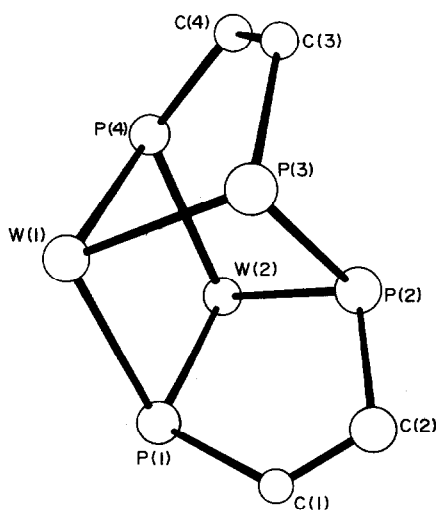

Fig. 2. Central skeleton of complex **9** as established by X-ray crystal structure analysis.

EXPERIMENTAL

All reactions were carried out under argon. Chromatograhic separations were performed on silica gel columns (70–230 mesh Merck) under argon. NMR spectra were recorded on Brucker WP 80 and AC 200. Chemical shifts are reported in parts per million from internal Me_4Si for ^1H and ^{13}C and from external 85% H_3PO_4 for ^{31}P. Downfield shifts are noted positive in all cases. IR spectra were recorded on a 297 Perkin–Elmer spectrometer and mass spectra on a Shimadzu GCMS-QP 1000 spectrometer at 70 eV.

1,2,3,4-*Tetraphenyl*-1,2-*dihydro*-1,2-*diphosphete*-1,2-*bis*(*pentacarbonyl*)*tungsten* **3**

A solution of 7.9 g of **1** in 30 cm^3 of anhydrous THF was added to 4/100 mol of $W(CO_5)THF$.[11] The mixture was stirred for 2 h. The solvent was removed by evaporation and complex **3** was purified by chromatography with hexane: Yield: 60%, m.p. 228°C. Found: C, 41.6; H, 1.7. Calc. for $C_{36}H_{20}O_{10}P_2W_2$: C, 41.5; H, 1.9%. ^{31}P NMR ($CDCl_3$) δ 46.2 ($^1J_{P-^{183}W} = 249$ Hz, $^2J_{P-^{183}W} = 17$ Hz). X-ray structure: for $C_{36}H_{20}O_{10}P_2W_2$ (Fig. 1).

X-ray structure determination for **3**

Crystals of **3**, $C_{36}H_{20}O_{10}P_2W_2$, were grown at room temperature by slow diffusion of hexane into a toluene solution of the compound. Data were collected at $18 \pm 1°$ on an Enraf Nonius CAD4 diffractometer. The crystal structure was solved and refined using the Enraf Nonius supplied SDP package. The compound crystallizes in space group $P2_1/c$, $a = 16.108(1)$, $b = 11.981(1)$, $c = 20.367(2)$ Å, $\beta = 112.19(1)°$, $V = 3639.64(1.1)$ Å^3; $Z = 4$; $D_{calc} = 1.902$ g cm^{-3}; Mo-K_α radiation ($\lambda = 0.71073$ Å) graphite monochromator; $\mu = 65.9$ cm^{-1}; $F(000) = 1976$. A total of 10,579 unique reflections were recorded in the range $2° \leqslant 2\theta \leqslant 60°$ of which 5019 were considered as unobserved [$F^2 < 3\sigma(F^2)$], leaving 5560 for solution and refinement. The structure was solved by Patterson methods, yielding a solution for the tungsten and phosphorus atoms. The hydrogen atoms were included as fixed contribution in the final stages of least-squares refinement while using anisotropic temperature factors for all other atoms. A non-Poisson weighting scheme was applied with a p factor equal to 0.08. The final R factors were $R = 0.038$, $R\omega = 0.054$, G.O.F. = 1.04.

2,3,4,5,8 - *Pentaphenyl* - 7,9 - *dioxo* - 8 - *aza* - 2,5 - *diphosphabicyclo*[4,3,0] - 3 - *nonene* - 2,5 - *bis(pentacarbonyl)tungsten.* **4a,b** $C_{46}H_{27}NO_{12}P_2W_2$

The bis complex **3** (1.3 g, 1.2 mmol) and *N*-phenylmaleimide (1.04 g, 6 mmol) were heated in a sealed tube at 150°C for 24 h in 2 cm^3 of xylene. After removal of the solvent, the residue was chromatographed on silica gel with hexane–dichloromethane (40 : 60) as eluent. The isomers **4a** and **4b** (83% total-yield) were separated.

4a: yellow solid ^{31}P NMR ($CDCl_3$) δ 48.1 ($^1J_{P-^{183}W}$ = 229 Hz); ^1H NMR ($CDCl_3$) δ 4.57 (dd, $|^2J_{HP}+{}^3J_{HP}|$ = 4.9 Hz, 2H, PCH) 6.4–7.7 (m, 25H, Ph); ^{13}C NMR ($CDCl_3$) δ 49.74 (pseudo t $|^1J_{CP}+{}^2J_{CP}|$ = 23 Hz, CHP); 157 (s, :C—P), 171.4 (s, NC=O); mass spectrum (^{184}W), *m/z* (relative intensity) 835 [M—W(CO)$_7$, 25] 751 [M—W(CO)$_{10}$, 20] 578 ($WP_2C_2Ph_4$, 100).

4b: yellow solid ^{31}P NMR ($CDCl_3$) δ 51.6 ($^1J_{P-^{183}W}$ = 232 Hz); ^1H NMR ($CDCl_3$) δ 4.59 (s, 2H, PCH); 6.5–7.8 (m, 25H, Ph); ^{13}C NMR ($CDCl_3$) δ 47.32 (pseudo triplet $|^1J_{CP}+{}^2J_{CP}|$ = 28.7 Hz, CHP), 160.97 (pseudo triplet, :C—P), 171.17 (s, N—C=O); mass spectrum (^{184}W), *m/z* (relative intensity) 835 [M—W(CO)$_7$, 21] 751 [M—W(CO)$_{10}$, 13] 578 ($WP_2C_2Ph_4$, 100).

2,3,4,5 - *Tetraphenyl* - 7,9 - *dioxo* - 8 - *oxa* - 2,5 - *diphosphabicyclo*[4,3,0] - 3 - *nonene* - 2,5 - *bis(pentacarbonyl)tungsten.* **5a,b** $C_{40}H_{22}O_{13}P_2W_2$

Compound **3** (0.5 g, 0.48 mmol) and maleic anhydride (0.5 g, 5 mmol) dissolved in 2 cm^3 of xylene were heated in a sealed tube at 145°C for 18 h. The reaction mixture was extracted with dichloromethane. Fractional crystallization in hexane yields a mixture of the pure isomers **5a–5b** (24% yield).

5a: major isomer, yellow solid; ^{31}P NMR (CD_2Cl_2) δ 53.0 ($^1J_{P-^{183}W}$ = 234 Hz); ^1H NMR (CD_2Cl_2) δ 4.68 (pseudo triplet, 2H, CHP), 6.8–7.6 (m, 20H, Ph); ^{13}C NMR (CD_2Cl_2) δ 51.12 (pseudo triplet, CHP), 159.1 (s, :C—P), 166.9 (s, O—C=O).

5b: minor isomer, yellow solid; ^{31}P NMR (CD_2Cl_2) δ 55.8; ^1H NMR (CD_2Cl_2) δ 4.82 (pseudo triplet, 2H, CHP), 6.6–7.5 (m, 20H, Ph).

1,2,3,4 - *Tetraphenyl* - 5 - *cyano* - 1,4,5,6 - *tetrahydro* - 1,4 - *diphosphinine* - 1,4 - *bis(pentacarbonyl)tungsten.* **6a,b** $C_{39}H_{23}NO_{10}P_2W_2$

Compound **3** (1 g, 0.96 mmol) and acrylonitrile (0.15 cm^3) in 2 cm^3 of xylene were heated at 135°C for 22 h in a sealed tube. After work-up, the residue was chromatographed on silica gel with toluene to yield 0.3 g of **1** followed by 0.250 g of **6a** (1st isomer). The second isomer 0.100 g of **6b** was obtained using dichloromethane as eluent. The global yield amounts to 33%.

6a: yellow solid, m.p. 210°C dec.; ^{31}P NMR ($CDCl_3$) δ 53.7 ($^1J_{P1-^{183}W}$ = 231 Hz, $^1J_{P1P2}$ = 58.6 Hz, P_1), 35.2 ($^1J_{P2-^{183}W}$ = 224 Hz, P_2); ^1H NMR ($CDCl_3$) δ 3.25 ($^2J_{HAHB}$ = 12.9 Hz, $^3J_{HAHC}$ = 3.8 Hz, J_{HAP1} = 9.7 Hz, J_{HAP2} = 5.0 Hz, 1H, H_ACH), 3.04 ($^3J_{HBHC}$ = 10.8 Hz, J_{HBP1} = 7.8 Hz, J_{HBP2} = 0.3 Hz, 1H, H_BCH), 3.72 (J_{HCP1} = 2.4 Hz, J_{HCP2} = 7.1 Hz, 1H, H_CCCN); ^{13}C NMR ($CDCl_3$), 33.62 (J_{CP} = 24.4 Hz, J_{CP} = 10.3 Hz, CH_2), 30.84 (J_{CP} = 14.0 Hz, J_{CP} = 12.8 Hz, HCCN), 120.76 (J_{CP} = 7 Hz, J_{CP} = 7 Hz, C≡N), 157.2 (J_{CP} = 25 Hz, J_{CP} = 18 Hz, :C), 160.9 (J_{CP} = 25 Hz, J_{CP} = 18 Hz, :C); 200.8 (C≡O), 208.5 (C≡O).

6b: yellow solid, m.p. 210°C dec.; ^{31}P NMR ($CDCl_3$) δ 60.83 ($^1J_{P1-^{183}W}$ = 239 Hz, $^1J_{P1P2}$ = 53.7 Hz, P_1), 37.81 ($^1J_{P2-^{183}W}$ = 224 Hz, P_2); ^1H NMR ($CDCl_3$) δ 3.5 ($^2J_{HAHB}$ = 11.9 Hz, $^3J_{HAHC}$ = 10.5 Hz, J_{HAP1} = 12.6 Hz, J_{HAP2} = 10.4 Hz, 1H, H_ACH), 2.83 ($^3J_{HBHC}$ = 4.5 Hz, J_{HBP1} = 2.8 Hz, J_{HBP2} = 2.5 Hz, 1H, H_BCH), 3.89 (J_{HCP1} = 9.9 Hz, J_{HCP2} = 3.9 Hz, 1H, H_CCCN); ^{13}C NMR ($CDCl_3$) δ 32.3 (J_{CP} = 24.3 Hz, J_{CP} = 11.3 Hz, CH^2), 30.1 (J_{CP} = 18.8 Hz, J_{CP} = 13.3 Hz, HCCN), 118.15 (J_{CP} = 9 Hz, CN), 158.9 (J_{CP} = 25 Hz, J_{CP} = 24 Hz, :C), 160.0 (J_{CP} = 24.5 Hz, J_{CP} = 22 Hz, :C), 200.1 (C≡O), 208.7 (C≡O).

1,3,4,5,6 - *Pentaphenyl* - 1,2,3,4 - *tetrahydro* - 2 - *oxa* - 1,4 - *diphosphinine* - 1,4 - *bis(pentacarbonyl)tungsten.* **7a,b** $C_{34}H_{26}O_{11}P_2W_2$

Benzaldehyde (0.2 cm^3, 2 mmol) and complex **3** (1 g, 0.9 mmol) in 2 cm^3 of xylene were heated at 140°C in a sealed tube for 19 h. After evaporation of the solvent, chromatography of the residue on silica gel with hexane–dichloromethane (1 : 1) as eluent, yields 50% unreacted **3** and 0.100 g (10%) **7a** and **7b** as a mixture of isomers.

7a major isomer (90%); ^{31}P NMR ($CDCl_3$) δ 153.0 ($^3J_{P1P4}$ = 29.3 Hz, $^1J_{P1-^{183}W}$ = 261 Hz, P_1), 52.7 ($^1J_{P4-^{183}W}$ = 216 Hz, P_4); ^1H NMR (CD_2Cl_2) δ 5.58 (J_{HP1} = 3.7 Hz, J_{HP4} = 9.3 Hz, 1H, HCO); ^{13}C NMR (CD_2Cl_2) δ 82.6 (J_{CP4} = 18 Hz, OCP_4), 155.9 (:C), 166.5 (:C), 196.1 (C≡O), 209.9 (C≡O); mass spectrum (^{184}W), *m/z* (relative intensity) 796 [M—W(CO)$_6$, 14], 684 [M—W(CO)$_{10}$, 52].

7b: minor isomer (10%); ^{31}P NMR ($CDCl_3$) δ 154.4 ($^3J_{P1P4}$ = 24.4 Hz, P_1), 60.9 (P_4).

1,2,3,4-Tetraphenyl-1,2-dihydro-1,2-diphosphete-1-(pentacarbonyl)tungsten **8a,b** $C_{31}H_{20}O_5P_2W$ *and complex* **9** $C_{58}H_{40}O_6P_4W_2$

Complex **3** was heated for 3 days at 135°C in xylene. The mono complex (**8a**, **8b**) is produced as a mixture of two isomers.

8a: ^{31}P NMR ($CDCl_3$) δ 8.0 ($^1J_{P1P2} = 85$ Hz, P_1), −3.5 (P_2); **8b**: δ 5.0 ($^1J_{P1P2} = 73$ Hz, P_1), −0.5 (P_2); mass spectrum (^{184}W), *m/z* (relative intensity) 718 (M^+, 12) 690 (M—CO, 29) 634 (M—3CO, 30) 606 (M—4CO, 10) 578 (M—5CO, 100).

The same reaction conducted at 150°C yields the green complex **9**. Compound **9** crystallizes in the monoclinic space group $P2_1/n$ with $a = 13.635(1)$, $b = 26.026(2)$, $c = 18.046(1)$ Å, $\beta = 106.02(1)°$, $V = 6155.3(1.6)$ Å^3, $Z = 4$. Mo-K_α radiation ($\lambda = 0.71073$ Å). Due to extensive decomposition under X-ray irradiation (60% over 2 days) data collection was conducted at high speed (20 s reflection^{-1}) in a limited θ range (2–18°).

The data set so obtained allows establishment of the formulation of the compound as $C_{58}H_{40}O_6P_4W_2$ (present isotropic $R = 0.092$). Poor resolution does not allow location of the solvent molecules or further refinement. The structure will be redetermined at low temperatures in the near future.

REFERENCES

1. R. Appel, V. Barth and F. Knoch, *Chem. Ber* 1983, **116**, 938.
2. R. Appel and V. Barth, *Tetrahedron Lett.* 1980, **21**, 1923.
3. R. Appel, J. Hünerbein and N. Siabalis, *Angew. Chem., Int. Ed. Engl.* 1987, **26**, 779.
4. B. A. Boyd, T. J. Thoma and R. H. Neilson, *Tetrahedron Lett.* 1987, **28**, 6121.
5. N. H. Tran Huy, L. Ricard and F. Mathey, *Organometallics* 1988, **7**, 1791.
6. N. H. Tran Huy and F. Mathey, *Tetrahedron Lett.* 1988, **29**, 3077.
7. N. H. Tran Huy and F. Mathey, *Heteroatom. Chem.* 1990, **1**, 33.
8. L. Ricard, N. Maigrot, C. Charrier and F. Mathey, *Angew. Chem., Int. Ed. Engl.* 1987, **26**, 548.
9. C. Charrier, J. Guilhem and F. Mathey, *J. Org. Chem.* 1981, **46**, 3.
10. The stabilization of the P=C double bonds by complexation of the phosphorus lone pairs is well documented, see: A. Marinetti and F. Mathey, *Angew. Chem., Int. Ed. Engl.* 1988, **27**, 1382.
11. W. Strohmeier, *Angew. Chem., Int. Ed. Engl.* 1964, **3**, 730.

Polyhedron Vol. 9, No. 11, pp. 1369–1374, 1990
Printed in Great Britain

0277–5387/90 $3.00+.00
© 1990 Pergamon Press plc

MACROHETEROCYCLES—LVI.* COMPLEX FORMATION OF THE CRYPTANDS CONTAINING TWO PROPYLENE FRAGMENTS IN ONE OF THE BRIDGES WITH ALKALI AND ALKALINE-EARTH CATIONS

NIKOLAI G. LUKYANENKO,† NATALIE Yu. NAZAROVA, VIKTOR I. VETROGON, NATALIE I. VETROGON and ANATOLY S. REDER

A. V. Bogatsky Physico-Chemical Institute, Academy of Sciences of the Ukrainian SSR, 86, Chernomorskaya doroga, 270080, Odessa, U.S.S.R.

(*Received* 21 *November* 1989; *accepted* 15 *January* 1990)

Abstract—The stability constants of the complexes of the alkali and alkaline-earth cations with the cryptands containing two propylene (L-H) or 2-hydroxypropylene (L-OH) chains between the nitrogen bridgeheads and the adjacent oxygen atoms in one of the bridges were determined by pH-metry in 95% aqueous methanol.

In most cases (L-H) and (L-OH) form less stable complexes as compared to classic cryptands (L) with the same number of donor atoms. Unlike the latter compounds the (L-H) and (L-OH) series do not show any regular alteration of complex stability dependent on the ratio of cavity and complexed cation sizes. All (L-H) and (L-OH) form the most stable complexes with Na^+ and K^+ in the series of alkali cations, and with Sr^{2+} and Ba^{2+} along the alkaline-earth cation series. Complexes of alkali cations with cryptands (L-H) are more stable than those with (L-OH). For the complexes of the alkaline-earth cations the opposite dependence is observed. Stability of alkaline-earth cryptates of (L-OH) increases with the increase of a ligand's conformational flexibility and decreases with the increasing radius of a cation. The cause of this is the possibility of endo–endo and exo–exo cryptates formation, differing by the orientation of hydroxyl groups toward the inside or the outside of the cryptands cavity. Conformational changes of an exo–exo form into endo–endo one lead to a decrease of the ligand's cavity size changing the number and nature of the binding sites.

Preferable interaction of more charge-dense cations with the polar OH-groups in endo–endo cryptates results in unusually high M^{2+}/M^+ complexation selectivity of (L-OH). As opposed to (L-OH), (L-H) cryptands exhibit the unique for neutral ligands Na^+/Ca^{2+} selectivity which is probably due to kinetic reasons.

Complexation of mono- and divalent cations by cryptands has been intensively investigated since the discovery of their ability to form very stable complexes.[2] The stability of cryptand complexes as well as the selectivity of complexation depend on a number of factors including the size of the intramolecular cavity. Generally, it is suggested that metal ions which better fit the cryptand cavity will form the most stable complexes. However, these classical considerations explain only partly the observed complexation selectivity.[3–5]

It is known that the decrease of molecular symmetry and the increase of the crown ether size by the introduction of one or several propylene chains between the oxygen atoms have drastic and different effects on its cation binding ability.[6]

One should expect that complexing properties of classic cryptands will also change with the introduction of extra methylene groups between two adjacent donor atoms, though this effect was not studied.

We have recently described a convenient synthesis of cryptands with two propylene (L-H) and 2-hydroxypropylene (L-OH) chains between the nitrogen bridgeheads and the adjacent oxygen atoms in one of the bridges.[7] Now we discuss the

* For Part LV, see Ref. 1.

† Author to whom correspondence should be addressed.

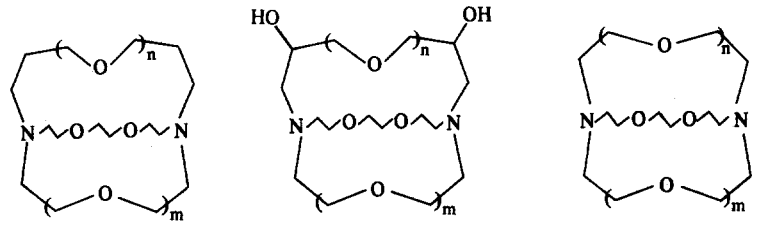

L-H

$n = 1, m = 1$: 121-H
$n = 2, m = 1$: 221-H
$n = 3, m = 3$: 321-H
$n = 1, m = 2$: 122-H
$n = 2, m = 2$: 222-H
$n = 3, m = 2$: 322-H

L-OH

$n = 1, m = 1$: 121-OH
$n = 2, m = 1$: 221-OH
$n = 3, m = 3$: 321-OH
$n = 1, m = 2$: 122-OH
$n = 2, m = 2$: 222-OH
$n = 3, m = 2$: 322-OH

L

$n = 1, m = 1$: 211
$n = 2, m = 1$: 221
$n = 2, m = 2$: 222
$n = 3, m = 2$: 322

Fig. 1. Cryptands (L-H) and (L-OH) studied and the classic cryptands (L).

results of a pH-metric study of the stability of their complexes with the alkali and alkaline-earth cations in 95% aqueous methanol.

EXPERIMENTAL

Synthesis and properties of the studied cryptands (L-H) and (L-OH) were described earlier.[7] Dihydroxycryptands (L-OH) were obtained and studied as a mixture of meso- and (±)stereoisomers. For (L-H) and (L-OH) we use the nomenclature which is shown in Fig. 1. This nomenclature is very close to that proposed for the classic cryptands (L) but unlike it the first figure always represents the number of oxygen atoms in the bridge with two propylene fragments.

Alkali and alkaline-earth metals chlorides of reagent grade were used. The protonation constants of the ligands and the formation constants of the complexes β_{xyz} referring to the general equilibrium of complexation:

$$xM^{n+} + yL + zH^{+} \rightleftharpoons M_xL_yH_z^{(nx+z)+},$$

$$\beta_{xyz} = \frac{[M_xL_yH_z]^{(nx+z)+}}{[M^{n+}]^x[L]^y[H^+]^z}$$

have been determined from pH-metric data during the neutralization by $N(C_4H_9)_4OH$ of acidic solution of ligands dihydrochloride in 95% aqueous methanol with or without metal salts at 25.0 ± 0.1°C under an argon stream as described in Ref. 5. During the titration the ionic strength was kept constant at 0.05 M using $N(C_4H_9)_4Br$ as the supporting electrolyte. The ratio of metal to ligand concentrations C_M/C_L was generally 0.8–1.2.

Measurements have been performed using pH-meter OP208/1 (Radelkis) connected to a combined glass electrode OP0808P (Radelkis) in which the standard solution in the reference cell was replaced by a 0.05 M $N(C_2H_5)_4Cl$ methanol solution saturated with AgCl. Parameters (a and S) of electrode function $pH_{meas} = a + S * \log[H^+]$, activity coefficients of H^+ in 95% methanol and the ionic product $[H^+][OH^-]$ were determined by measuring the standard buffer for 95/5 (v/v) methanol/water mixture with the reference value of pH 7.10 (0.01 M succinic acid plus 0.01 M lithium hydrogensuccinate in 95% methanol)[8] and from the titration curve of 0.01 M $N(C_4H_9)_4OH$ plus 0.05 M $N(C_4H_9)_4Br$ solution by a 0.01 M HCl solution in 95% methanol. $\log[H^+][OH^-]$ was found to be $-15.2 + 0.1$. pH-Metric data were treated by the least squares method using the program SIRKO allowing simultaneous adjustment of the electrode parameters, ligand and cation concentrations.[9] For computer processing the whole titration curve over the pH range 2.5–10.5 was used. Within this pH range only complexes 1 : 1 have been found. Results are expressed as the consequent ligands' protonation constants K_i* and complexes' stability constants K_s* are listed in Table 1.

The confidence interval calculated by the program was not more than 0.1 for all cases.

RESULTS AND DISCUSSION

CPK molecular models analysis shows that the extention of one of the cryptand bridges by introducing two propylene fragments between the nitrogen bridgeheads and adjacent oxygen atoms leads to an increase of the radius of the cryptand intramolecular cavity by 0.1–0.2 Å (Table 2) and makes the spatial arrangement of donor atoms less symmetrical as compared with the classic cryptands with the same number of donor atoms.

* $K_1 = \beta_{011}$ and $K_2 = \beta_{012}/\beta_{011}$; $K_s = \beta_{110}$.

Table 1. Stability constants (log K_s; K_s in M^{-1}) for the complexation of alkali and alkaline-earth cations by cryptands and (L) in 95% methanol at 25°C

Ligand	pK_1	pK_2	log K_s								
			Li^+	Na^+	K^+	Rb^+	Cs^+	Mg^{2+}	Ca^{2+}	Sr^{2+}	Ba^{2+}
121-H	9.84	8.17	4.21	5.20	2.60	< 2	< 2	< 2	4.01	3.57	3.34
221-H	9.50	8.19	< 2	4.83	4.14	3.12	< 2	< 2	4.36	4.33	4.92
321-H	9.27	7.04	< 2	4.46	3.23	3.15	2.86	< 2	3.72	4.64	5.21
122-H	9.94	8.25	< 2	6.13	5.11	3.41	2.32	< 2	5.20	5.81	5.05
222-H	9.68	7.52	< 2	4.36	5.47	5.14	3.71	< 2	3.75	4.81	7.53
322-H	9.36	6.80	< 2	4.65	5.15	5.08	4.05	< 2	4.12	6.53	6.64
121-OH	9.41	5.82	< 2	3.15	< 2	< 2	< 2	< 2	4.55	4.61	< 2
221-OH	9.11	6.28	< 2	3.07	2.44	< 2	< 2	4.32	5.63	5.72	5.51
321-OH	9.04	6.72	3.59	5.12	3.78	3.25	2.74	3.24	6.81	7.37	7.08
122-OH	9.77	5.91	< 2	4.01	3.40	< 2	< 2	< 2	5.92	5.95	3.63
222-OH	9.43	6.32	< 2	5.75	5.13	4.31	< 2	3.63	6.64	7.21	8.62
322-OH	9.05	6.45	< 2	5.15	5.63	4.03	< 2	3.71	8.73	8.94	8.43
211[a]	11.00	6.56	7.58	6.08	2.26	< 2	< 2	4.00	4.34	2.90	< 2
221[a]	10.42	6.60	4.18	8.84	7.45	5.80	3.90	< 2	9.61	10.65	9.70
222[a]	9.85	6.64	1.8	7.21	9.75	8.40	3.54	< 2	7.60	11.5	12
322[a]	9.14	6.55	< 2	4.57	7.0	7.30	7.0	< 2	4.74	7.06	10.40

[a] From Ref. 3.

Table 2. Cation and cryptands cavity radius (in Å)

Cation	Ionic radius[a]	L-H and exo–exo L-OH	Cavity radius[b]	Endo–endo L-OH	Cavity radius[b]	L	Cavity radius[a]
Li^+	0.78	121-H, 121-OH	1.0–1.1	121-OH[c]	0.8–0.9	211	0.8
Na^+	0.98	221-H, 221-OH	1.2–1.3	221-OH	1.0–1.1	221	1.1
K^+	1.33	321-H, 321-OH	1.5–1.6	321-OH	1.1–1.2	222	1.4
Rb^+	1.49	122-H, 122-OH	1.2–1.3	122-OH[c]	0.9–1.0	322	1.8
Cs^+	1.65	222-H, 222-OH	1.5–1.6	222-OH	1.3–1.4		
Mg^{2+}	0.78	322-H, 322-OH	1.9–2.0	322-OH	1.4–1.5		
Ca^{2+}	1.06						
Sr^{2+}	1.27						
Ba^{2+}	1.43						

[a] From Ref. 3.
[b] Measured on CPK models.
[c] Exo–endo form.

Dihydroxycryptands (L-OH) and their complexes may exist in three forms: exo–exo, exo–endo, and endo–endo differing by orientation of hydroxyls toward the inside or the outside of the intramolecular cavity.

Endo–endo conformation is readily realized in (322-OH) and (321-OH). In (222-OH) and especially in (221-OH) this conformation is more rigid. For (122-OH) and (121-OH) only endo–exo and endo–endo forms can exist. Conformational transformation of exo–exo form of (L-OH) into endo–endo form leads to the decrease of the intramolecular cavity radius by 0.2–0.5 Å (Table 2). In the exo–exo cryptates of (L-OH) the cation may interact with all the ether oxygen atoms. However, in endo–exo and endo-endo cryptates the interaction of cation with the ether oxygens of the extended bridge is impossible (Fig. 2).

Thus, the main features of the studied cryptands distinguishing them from the classic ones, are: (i) large radius of intramolecular cavity of (L-H) and exo–exo (L-OH), (ii) less symmetric spatial arrangement of donor atoms, and (iii) possibility to realize the endo–endo forms of (L-OH) which results in

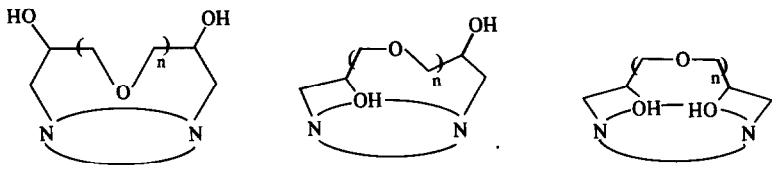

exo–exo exo–endo endo–endo

Fig. 2. Different conformational forms of dihydroxycryptands (L-OH).

the decrease of the radius of their intramolecular cavity and changes the number and the nature of the binding sites. These factors will perhaps determine the differences in the complexing abilities of the studied and classic cryptands.

The additional effect on the cryptand complexing ability should be also contributed by the change of nitrogen atom basicity due to the introduction of two propylene or 2-hydroxypropylene fragments into one of the bridges. As compared with the classic cryptands with the same number of donor atoms, (L-H) in most cases form less stable complexes with alkali and alkaline-earth cations (Table 1). This may be due to at least two reasons: (i) the less symmetrical spatial arrangement of the binding sites and (ii) the presence of less favourable for complexation fragments $N\text{-}(CH_2)_3\text{-}O$, since it is known that five-membered ring chelates are more stable than six-membered ones.

Linking our results with those obtained earlier for crown ethers[6] it can be concluded that the observed decrease of the complex stability by substitution of the ethylene chain between the adjacent heteroatoms for the propylene one is a general feature of the macrocyclic ligands. However, there are some exceptions in the series of cryptands (L-H): cryptand (121-H) gives more stable complexes with K^+, Sr^{2+}, Ba^{2+}, and (222-H) with Cs^+, as compared with (211) and (222) (Table 1). Probably, in these cases the relative complex stability is determined by a better size correspondence of the ligand cavity and the cation (Table 2). For example, the ratio of the cation ionic radius and the (121-H) cavity radius is equal to 0.89, 1.15 and 1.3 for Na^+, Sr^{2+}, and Ba^{2+}, respectively. For the cryptand (211) these values are considerably higher: 1.23, 1.59, and 1.79, respectively. Thus, the unfavourable effect of the ligand propylene fragments may be compensated and even exceeded due to the better cation–cavity size relation.

Electronegative hydroxyls in cryptands (L-OH) decrease basicity of the adjacent nitrogen and oxygen atoms and as a result, should lead to the decrease of the complex stability of these ligands as compared with (L-H). Indeed, in most cases stability of alkali cation complexes with cryptands (L-H) is larger than with cryptands (L-OH) (Table 3).

As opposed to this, alkaline-earth cation complexes with (L-OH) are more stable than with (L-H). This contradiction becomes clear if one takes into consideration the possibility of the formation of endo- and exo-cryptates of (L-OH), differing in their stability. In general, the measured stability constants of (L-OH) complexes reflect the thermodynamic equilibrium with respect to conformation as well as to complexation.

$$[\text{L-OH}]+[\text{M}]^{n+} \rightleftharpoons [(\text{exo–exo})\text{ML-OH}]^{n+} + [(\text{exo–endo})\text{ML-OH}]^{n+} + [(\text{endo–endo})\text{ML-OH}]^{n+}.$$

In exo–exo cryptates of (L-OH) the size of the intramolecular cavity is equal to that of (L-H). However, due to the lower basicity of the binding sites of (L-OH), their complexes, in principle, should be less stable than (L-H) ones. In endo-cryptates (L-OH) the cavity size and the nature of binding sites differ from those of (L-H): in endo-cryptates the cavity radius is less, and the cation interacts with the oxygen atoms of hydroxyls. The most important factors determining the relative stability of endo- and exo-cryptates of (L-OH) are: (i) correspondence of the ligand cavity and cation sizes, (ii) energies of the conformational changes of exo–exo form into endo–endo or endo–exo form, and (iii) energy difference of cation interaction with ether or hydroxyl oxygens. The latter can be of great importance for the stability of complexes with high charge density cations. The preferred interaction of such cations with the polar hydroxyl is clearly shown for N,N′-bis(2-hydroxyethyl)diaza crown ethers.[10]

Cryptands (121-H), (221-H), and (122-H) give more stable complexes with the alkali cations than their (L-OH) partners. However, (321-OH) form more stable complexes with Li^+, Na^+, K^+ and Rb^+, (322-OH) with Na^+ and K^+; (222-OH) with Na^+, as compared with the corresponding (L-H). This suggests that depending on the cycle size, (L-OH) form the cryptates of the different structures. Probably, the cause of this is the differing ligand flexibility. As we have noted, endo–exo conformations

Table 3. Difference (δ) between the stability constants of the complexes of cryptands (L-H) and (L-OH) with cations, $\delta = \log K_s(ML\text{-}H^{n+}) - \log K_s(ML\text{-}OH^{n+})$

L / Cation	121	221	321	122	222	322
Li^+	> 2.21		> −1.59			
Na^+	2.05	1.76	−0.66	2.12	−1.39	−0.50
K^+	> 0.60	1.70	−0.55	1.71	0.34	−0.48
Rb^+	1.12	−0.05	> 1.41	0.83	1.05	
Cs^+			0.12	> 0.32	> 1.71	> 2.05
Mg^{2+}		> −2.32	> −1.24		> −1.63	> −1.71
Ca^{2+}	−0.54	−1.27	−3.09	−0.72	−2.89	−4.61
Sr^{2+}	−1.04	−1.39	−2.73	−0.14	−2.40	−2.41
Ba^{2+}	> 1.34	−0.59	−1.87	1.42	−1.09	−1.79

of (121-OH) and (122-OH) and endo–endo form (221-OH) are quite rigid, while endo–endo conformation of (222-OH), (321-OH) and (322-OH) are readily realized. It gives evidence for the preferable formation of exo-cryptates by the former which are less stable than the complexes of the corresponding (L-H). In the case of more flexible (222-OH), (321-OH), and (322-OH) the possibility of endo-cryptate formation increases which leads to the increase of the observed stability constant of the complexes with charge-dense cations. Along the series of alkaline-earth cations all (L-OH) form more stable complexes than their (L-H) analogues with the exception of Ba^{2+} complexes with (121-OH) and (122-OH). Since the divalent cations are more charge dense than monovalent ones, the former should interact more strongly with the polar hydroxyls in endo-cryptates. Thus, achieved energetic advantage is probably more than the energy of unfavourable conformational transformation of exo–exo forms of small cryptands (121-OH), (122-OH), and (221-OH) into endo–exo or endo–endo forms. As a result, these cryptands form preferably endo-cryptates of the alkaline-earth cations in contrast to exo-cryptates of the alkali cations. The formation of endo–endo alkaline-earth cryptates is more evident for (222-OH), (321-OH), and (322-OH). This is proved by the increase of the relative stability of cryptates of each alkaline-earth cation in the series: (121-OH) < (221-OH) < (321-OH) and (122-OH) < (222-OH) < (322-OH). This sequence corresponds to the decreased energy of the exo–endo conformational changes of the ligands. The formation of alkaline-earth endo-cryptates is also in agreement with the observed decrease of their relative stabilities with the increase of cation radius and thus with the decrease of the charge density on it (Table 3).

Thus, the stability of dihydroxycryptand complexes is determined by the ligand flexibility and the cation charge density. The latter is the cause of high preference of (L-OH) interaction with divalent cations as compared with the monovalent ones of the same size (Li^+ and Mg^{2+}; Na^+ and Ca^{2+}; K^+ and Ba^{2+}) (Table 4). The only exception is the relative stability of Mg^{2+} and Li^+ complexes with (321-OH). M^{2+}/M^+ selectivity of most dihydroxy-cryptands is much larger than that for the classic cryptands and crown ethers.

Cryptands (L-H) show less Ba^{2+}/K^+ selectivity as compared with the corresponding (L-OH). However, in contrast to (L-OH) all (L-H) form more stable complexes with Na^+ than with Ca^{2+}. This selectivity is the unique feature of these cryptands, since as we know amongst those previously described only (211) exhibits Na^+/Ca^{2+} selectivity.[5]

As was shown earlier[11] the formation rate constants k_f of alkaline-earth cation complexes and their dissociation rate constants k_d are lower than those of the alkali complexes. So, the relation may assume different values depending on the ratio of constants k_f and k_d. This means that Na^+/Ca^{2+} selectivity of (L-H) may result from $k_f(CaL\text{-}H^{2+})/k_f(NaL\text{-}H^+) < k_d(CaL\text{-}H^{2+})/k_d(NaL\text{-}H^+)$. The preferable complexation of Li^+ as compared to Mg^{2+} with cryptands (121-H) and (321-OH) is probably due to the same reasons.

By comparison of the cryptands (L-H) and (L-OH) with the same number of donor atoms it is obvious that the stability of their complexes depends considerably on the ligand symmetry. The less symmetrical (221-H), (221-OH), (321-H) and (321-OH) in most cases form less stable complexes as compared to the more symmetrical (122-H), (122-OH), (222-H) and (222-OH), respectively (Table 1).

Unlike the classic cryptands the stability of complexes of (L-H) and (L-OH) does not change regu-

Table 4. M^{2+}/M^{+} Selectivity of the cryptands (L-OH) and (L-H). Selectivity $\delta = \log K_s(ML^{2+}) - \log K_s(ML^{+})$

	$\log K_s$			$\log K_s$			$\log K_s$		
L	Mg^{2+}	Li^{+}	δ	Ca^{2+}	Na^{+}	δ	Ba^{2+}	K^{+}	δ
121-OH	< 2	< 2		4.55	3.15	1.40	< 2	< 2	
221-OH	4.32	< 2	> 2.32	5.63	3.07	2.56	5.51	2.44	3.07
321-OH	3.24	3.59	−0.35	6.81	5.12	1.69	7.08	3.78	3.22
122-OH	< 2	< 2		5.92	4.01	1.91	3.63	3.40	0.23
222-OH	3.63	< 2	> 1.63	6.64	5.75	0.89	8.62	5.13	3.49
322-OH	3.71	< 2	> 1.71	8.73	5.15	3.58	8.43	5.63	2.80
121-H	< 2	4.21	> −2.20	4.01	5.20	−1.19	3.34	2.60	0.74
221-H	< 2	< 2		4.36	4.83	−0.47	4.92	4.14	0.78
321-H	< 2	< 2		3.72	4.46	−0.74	5.21	3.23	1.98
122-H	< 2	< 2		5.20	6.13	−0.93	5.05	5.11	−0.06
222-H	< 2	< 2		3.75	4.36	−0.61	7.53	5.47	2.06
322-H	< 2	< 2		4.12	4.65	−0.55	6.64	5.15	1.4

larly with the increase of the cavity size. Irrespective of the cavity size (L-H) and (L-OH) form the most stable complexes with Na^{+} and K^{+} in the series of alkali cations and with Sr^{2+} and Ba^{2+} [with the exception of (121-H) and (121-OH) which interact preferably with Ca^{2+}] in the series of alkaline-earth cations (Table 1).

Thus, the studied cryptands (L-OH) and (L-H) are novel macrocyclic ligands forming rather stable complexes with alkali and alkaline-earth cations and showing the striking complexation selectivity in most cases.

REFERENCES

1. N. G. Lukyanenko, N. Yu. Nazarova, V. I. Vetrogon, N. I. Vetrogon, A. S. Reder, S. S. Basok and E. Yu. Kulygina, *Zh. Obsch. Khim.*, in press.
2. J. M. Lehn and J. P. Sauvage, *J. Chem. Soc., Chem. Commun.* 1971, 440.
3. J. M. Lehn and J. P. Sauvage, *J. Am. Chem. Soc.* 1975, **97**, 6700.
4. R. M. Izatt, J. S. Bradshaw, S. A. Nielsen, J. D. Lamb and J. J. Christensen, *Chem. Rev.* 1985, **85**, 271.
5. F. Arnaud-Neu, R. Yahya and M. J. Schwing-Weil, *J. Chim. Phys.* 1986, **83**, 403.
6. M. Ouchi, U. Inoe, H. Sakamoto, A. Yamahira, M. Yoshinaga and T. Hakushi, *J. Org. Chem.* 1983, **48**, 3168; M. Ouchi, Y. Inoe, T. Kanzaki and T. Hakushi, *J. Org. Chem.* 1984, **49**, 1408; K. Kimura, M. Tanaka, S. Iketani and T. Shono, *J. Org. Chem.* 1987, **52**, 836.
7. N. G. Lukyanenko and A. S. Reder, *J. Chem. Soc., Perkin Trans.* 1988, **1**, 2533.
8. T. Wickstrom, J. Dale and W. Lund, *Anal. Chim. Acta* 1988, **211**, 223.
9. V. I. Vetrogon, N. Yu. Nazarova, N. I. Vetrogon and N. G. Lukyanenko, *Anal. Chim. Acta*, in press.
10. V. J. Gatto, K. A. Arnold, A. M. Viseariello, S. R. Miller, C. R. Morgan and G. W. Gokel, *J. Org. Chem.* 1986, **51**, 5377.
11. B. G. Cox, Ng. V. Truong, J. Garsia-Rosas and H. Shneider, *J. Phys. Chem.* 1984, **88**, 996.

Polyhedron Vol. 9, No. 11, pp. 1375–1378, 1990
Printed in Great Britain

0277–5387/90 $3.00+.00
© 1990 Pergamon Press plc

COORDINATION STATE OF $Co(NCS)_2$ IN ACETONE

MICHAŁ PILARCZYK,* WACŁAW GRZYBKOWSKI and LUCYNA KLINSZPORN

Department of Physical Chemistry, Technical University of Gdańsk, 80-952 Gdańsk, Poland

(*Received* 18 *December* 1989; *accepted* 15 *January* 1990)

Abstract—The visible absorption spectra and molar conductance curve for $Co(NCS)_2$ in acetone, together with the spectra for $Co(ClO_4)_2$–$Co(NCS)_2$–acetone, $Co(NCS)_2$–KNCS–acetone and $Co(NCS)_2$–acetone–benzene, have been determined at 25°C. The results indicate that $Co(NCS)_2$ probably exists in acetone as the complex electrolyte $Co(NCS)(acetone)_5^+Co(NCS)_3(acetone)^-$.

Our previous work on $Co(NCS)_2$ in N,N-dimethylformamide and dimethylsulphoxide has shown that in extremely dilute solutions the salts dissociate into the simplest ions, while the formation of mono- and tetra-thiocyanate complexes was observed even in dilute solution.[1,2] It has been shown by Libuś that the dissolution of anhydrous $Co(NCS)_2$ in acetonitrile results in formation of two complexes of cobalt(II), the octahedral $Co(NCS)(CH_3CN)_5^+$ cation, and the tetrahedral $Co(NCS)_3(CH_3CN)^-$ anion, both being considered as the 1 : 1 complex electrolyte.[3]

The present work was undertaken in order to establish a mode of ionization of $Co(NCS)_2$ in acetone solution. It has been reported previously[4] that $CoCl_2$ and $CoBr_2$ exist in acetone in the form of the electrically neutral tetrahedral species, $CoCl_2(acetone)_2$ and $CoBr_2(acetone)_2$, respectively.

EXPERIMENTAL

Acetone was purified by means of $KMnO_4$, dried over a molecular sieve, and distilled. The product was kept under dry-air. The specific conductance of the purified solvent was in the range of 8.2×10^{-9}–1.8×10^{-8} S cm^{-1}.

Ethanol solution of $Co(NCS)_2$ was obtained by metathesis of strictly equivalent amounts of ethanol solution of corresponding nitrate and KNCS. On cooling, the solid KNO_3 was filtered off. After removing any excess of solvent under reduced pressure the solid $Co(NCS)_2$ was obtained, recrystallized twice and dried *in vacuo*. KNCS was recrystallized twice from ethanol and dried *in vacuo* at 80°C.

The $Co(ClO_4)_2 \cdot 6H_2O$ was recrystallized from water, dried over phosphoric oxide *in vacuo* and dissolved in dry acetone. The resulting solution was dried using molecular sieves. After removing any excess of solvent the crystalline solvate was isolated and recrystallized from anhydrous acetone.

All details of the procedures for preparations of solutions and measurements were described previously.[1,2]

RESULTS AND DISCUSSION

Figure 1 shows the plot of the molar conductivity of $Co(NCS)_2$ in acetone at 25°C. In the same figure is presented the molar conductance curve of $Co(ClO_4)_2$ reported previously.[4] It has been shown recently that $Co(ClO_4)_2$ in acetone exhibits pronounced tendency to associate. However, as can be seen, the molar conductance curve for this highly associated electrolyte runs well above the points for $Co(NCS)_2$ indicating a high degree of complex formation over the range of $Co(NCS)_2$ concentration, and unusually high stability of the complexes, even in the lowest concentration range.

The most striking feature of the acetone solutions of $Co(NCS)_2$ consists in the fact that their visible absorption spectra are practically independent of

* Author to whom correspondence should be addressed.

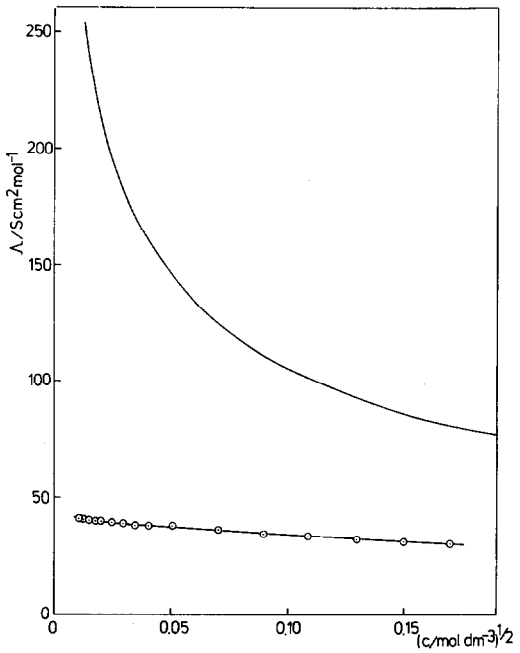

Fig. 1. Concentration dependence of the molar conductivity of $Co(NCS)_2$ in acetone solutions at 25°C. The solid line shows the molar conductance curve of $Co(ClO_4)_2$.

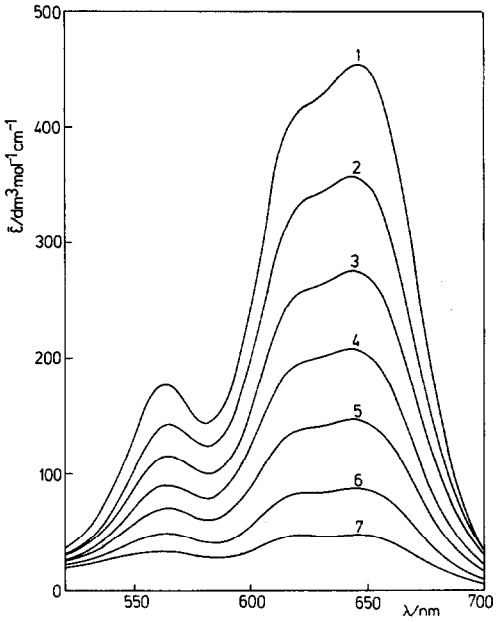

Fig. 2. Absorption spectra of cobalt(II) for a series of equimolar mixtures of $Co(ClO_4)_2$ with $Co(NCS)_2$ at 25°C. The total metal concentration is constant (*ca.* 0.012 mol dm^{-3}), while the NCS^-/Co^{2+} ratios are: (1) 2.0, (2) 1.770, (3) 1.571, (4) 1.371, (5) 1.185, (6) 0.972 and (7) 0.779.

the solute concentration, i.e. display optical constancy. However, they are very sensitive to change in a solvent composition as well as to change of the NCS^-/Co^{2+} ratio.

Figure 2 presents the visible absorption spectra of cobalt(II) for a series of equimolar mixtures of $Co(NCS)_2$ with $Co(ClO_4)_2$ covering the 2.0–0.8 range of the NCS^-/Co^{2+} ratio, with the total concentration of cobalt(II) being constant, *ca.* 0.012 mol dm^{-3}. The spectrum of cobalt(II) for pure $Co(NCS)_2$ is indicated by curve 1. As is seen, the latter spectrum of cobalt(II) consists of a broad band with maxima located at 564 and 646 nm. The band shows characteristics of the four-coordinated complexes of cobalt(II). Moreover, the spectrum is very similar to the spectrum of the $Co(NCS)_3(CH_3CN)^-$ complex reported by Libuś.[3] As is seen, substitution of $Co(ClO_4)_2$ for $Co(NCS)_2$ brings about distinct changes in the spectrum of cobalt (II). It is obvious that the spectrum of Co $(NCS)_2$ is gradually transformed into the known spectrum of $Co(ClO_4)_2$, due to the $Co(acetone)_6^{2+}$ solvate and exhibiting very low molar absorptivity.[4] However, the total decrease in intensity of the band with a decrease of the NCS^-/Co^{2+} is accompanied by a distinct broadening of the band, suggesting the coexistence of the second four-coordinated complex of cobalt(II) at a NCS^-/Co^{2+} ratio lower than 2.0.

Similar spectral changes were observed when the effect induced by a non-coordinating diluent of low polarity on the spectrum of $Co(NCS)_2$ dissolved in acetone was studied. The effects generated by addition of benzene up to mole fraction 0.75 are shown in Fig. 3. As is seen, the addition of diluent causes a decrease in intensity accompanied by the disappearance of the maximum at 564 nm and the broadening of the second component of the band. When the mole fraction of diluent exceeds 0.50, a further addition of benzene does not affect the spectrum of cobalt(II). It may be expected that the dilution of acetone with coordinatively inactive and non-polar solvent will shift the equilibria in solution towards existence of electrically neutral species. Thus, we infer that the four-coordinated species existing in the presence of benzene is the pseudo-tetrahedral $Co(NCS)_2(acetone)_2$ complex, and the identical spectra of cobalt(II) observed for 0.54 and 0.75 mole fractions of benzene is the single species spectrum. The same complex seems to be responsible for the broadening of the band observed for the $Co(NCS)_2$–$Co(ClO_4)_2$–acetone system, while the spectrum observed at the $NCS^-/Co^{2+} = 2.0$, i.e. for the $Co(NCS)_2$–acetone solution is due to the presence of $Co(NCS)_3(acetone)^-$.

Figure 4 shows the visible absorption spectra of

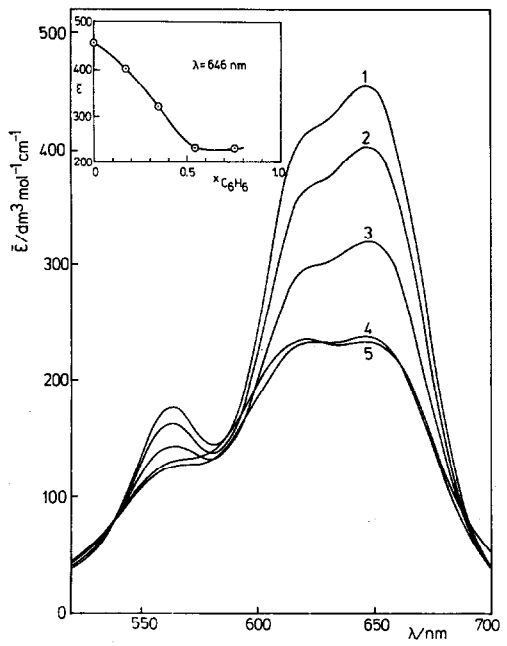

Fig. 3. Absorption spectra of $Co(NCS)_2$ in acetone–benzene mixtures at 25°C. The concentrations (mol dm^{-3}) of $Co(NCS)_2$ and the mole fractions of benzene in the mixed solvent are, respectively: (1) 0.00109, 0.00; (2) 0.00107, 0.169; (3) 0.00113, 0.349; (4) 0.00112, 0.544 and (5) 0.00110, 0.753.

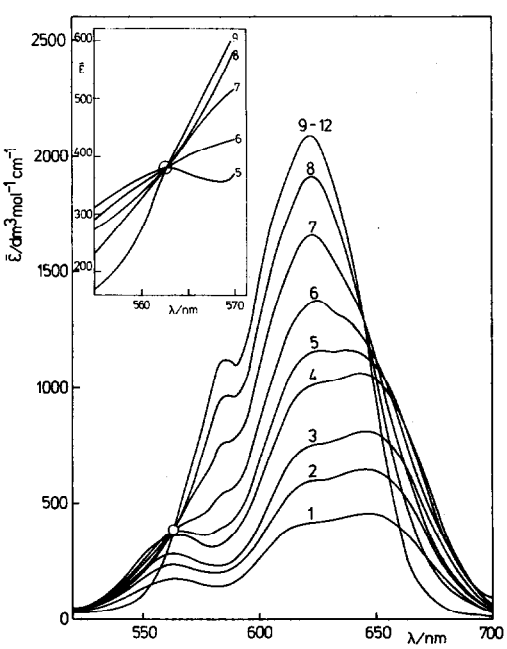

Fig. 4. Absorption spectra of $Co(NCS)_2$–KNCS solutions in acetone at 25°C. The concentration of $Co(NCS)_2$ is constant (0.001 mol dm^{-3}), the NCS^-/Co^{2+} ratios are: (1) 2.0, (2) 2.286, (3) 2.550, (4) 2.858, (5) 3.067, (6) 3.267, (7) 3.531, (8) 3.716, (9) 4.053, (10) 4.684, (11), 5.073 and (12) 10.701.

a series of solutions containing $Co(NCS)_2$ at an approximately constant concentration of 0.001 mol dm^{-3}, and KNCS at a number of different concentrations up to *ca.* 0.011 mol dm^{-3}. The addition of KNCS initially causes an increase in intensity of the band of the $[Co(NCS)_3(acetone)]^-$ complex. Further addition results in a marked change consisting of the disappearance of the maximum at 564 nm and the gradual shift of the second maximum from 646 nm to 623 nm. The changes are accompanied by the appearance of the maximum at 586 nm and the well-defined isosbestic point at 562 nm. When the NCS^-/Co^{2+} ratio exceeds 4.0, further increase in the KNCS concentration does not affect the spectrum, and the spectrum of cobalt(II) becomes almost identical to those of $Co(NCS)_4^{2-}$ in N,N-dimethylformamide,[1] dimethylsulphoxide[2] and acetonitrile.[3] However, it should be noted that the limiting spectrum of $Co(NCS)_4^{2-}$ was obtained at a NCS^-/Co^{2+} ratio as low as 4.0, while the values exceeding 190 were necessary for the transformation of cobalt(II) into $Co(NCS)_4^{2-}$ in DMF and DMSO, and higher than 7.0 in acetonitrile solutions. Analogous observations were reported by Gutmann and discussed in terms of the relative donor properties of both solvent molecules and pseudohalide anions.[5] The donor numbers of DMF and DMSO, 26.6 and 29.8, respectively, are much higher than the respective values of 14.1 for acetonitrile and 17.0 for acetone.[6] Unfortunately, the differences in the donor number explain the general trend only. As is seen, acetone exhibits a donicity higher than that of acetonitrile, while the respective NCS^-/Co^{2+} ratio form the opposite order. Furthermore, the donor number of N,N-dimethylacetamide (DMA) amounts to 28, while the NCS^-/Co^{2+} ratio higher than 13 is sufficient for the replacement of the solvent molecules of the Co^{2+} solvation sphere by the NCS^- anions and the change of the coordination number of the central metal atom from 6 to 4. The properties of the Co^{2+}–NCS^-–DMA system may be explained in terms of a relatively low stability of the $Co(DMA)_6^{2+}$ solvent-cation arising from the bulk properties of the solvent molecule.[7] The same factors seem to be responsible for the formation of the $Co(NCS)_3L^-$ (L = acetone or acetonitrile molecule) complexes, while only one tetrahedral complex, i.e. the $Co(NCS)_4^{2-}$ anion is present in the Co^{2+}–NCS^-–DMSO and Co^{2+}–NCS^-–DMF systems.

Further attempts to describe a coordination state of $Co(NCS)_2$ in acetone consists of a more detailed analysis of the electronic spectra. It may be seen that the molar absorption coefficient of cobalt(II) at the isosbestic point at 562 nm equals twice that of

a solution of $Co(NCS)_2$ at the same wavelength. As is known, an existence of the isosbestic point indicates a two-species equilibrium and is a consequence of the fact that the molar absorption coefficient of both the species are the same at the wavelength of this point. From the above and an assumption that a light absorption due to the octahedral species may be ignored, follows that 50% of cobalt(II) in acetone solution of $Co(NCS)_2$ is present in the form of the $Co(NCS)_3(acetone)^-$ complex. Assuming complete binding of the NCS^- anions the acetone solution of $Co(NCS)_2$ may be considered as a solution of the $Co(NCS)(acetone)_5^+ \cdot Co(NCS)_3(acetone)^-$ complex electrolyte. The appreciable stability of the monothiocyanate octahedral complexes of cobalt(II) was discussed previously.[3]

Using the values of the molar absorption coefficient of cobalt(II) at the isosbestic point the mole fraction of $Co(NCS)_3(acetone)^-$ may be calculated as

$$\frac{c_3}{c} = \frac{\bar{\varepsilon}}{\varepsilon_{34}} \quad (1)$$

where ε_{34} is the molar absorption coefficient at the isosbestic point and $\bar{\varepsilon}$ denotes the mean molar absorption coefficient of cobalt(II) at the same wavelength for the solutions in which only one tetrahedral complex of cobalt exists. Moreover, the values of the molar absorption coefficient for any other wavelength may be extracted from this spectra, and the spectrum of the $Co(NCS)_3(acetone)^-$ may be reconstructed. Figure 5 shows the results of such a treatment of the spectrophotometric data, presenting the spectra of the three tetrahedral complexes of cobalt(II) known to be formed in the Co^{2+}–NCS^-–acetone system. The respective mole fraction of the particular complexes were used to prepare the distribution diagram shown in Fig. 6.

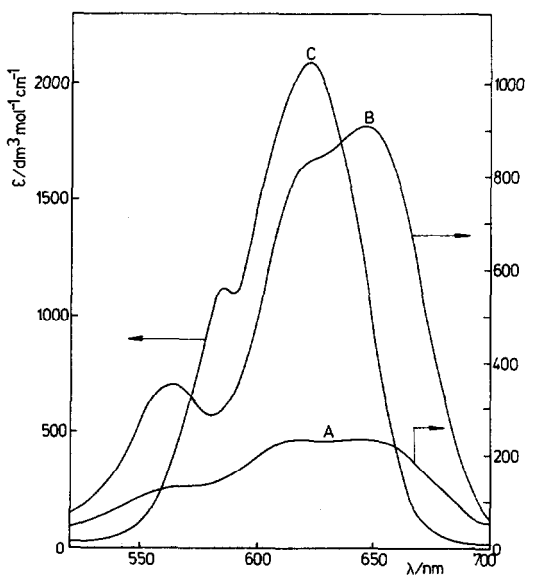

Fig. 5. Absorption spectra of the individual complexes of cobalt(II) in the Co^{2+}–NCS^2–acetone system: (a) $Co(NCS)_2(acetone)_2$, (b) $Co(NCS)_3(acetone)^-$, (c) $Co(NCS)_4^{2-}$.

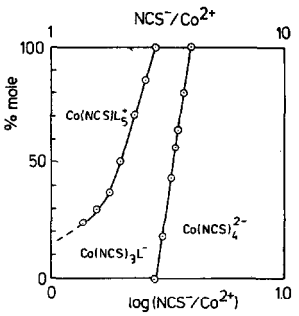

Fig. 6. Formation diagram of the thiocyanate complexes of cobalt(II) in the Co^{2+}–NCS^-–acetone system at 25°C.

Concluding, the results presented in this paper are an illustration of the fact that the electrolytic properties of the transition metal halides and pseudohalides in strongly polar donor solvents may be rationalized in terms of a relatively small number of modes of ionization.

Acknowledgement—This work was supported by Program CPBP-01.15.

REFERENCES

1. M. Pilarczyk, W. Grzybkowski and L. Klinszporn, *J. Chem. Soc., Faraday Trans.* 1 1987, **83**, 2261.
2. M. Pilarczyk, W. Grzybkowski and L. Klinszporn, *J. Chem. Soc., Faraday Trans.* 1 1989, **85**, 3395.
3. W. Libuś, *Roczn. Chem.* 1961, **35**, 411.
4. W. Grzybkowski and M. Pilarczyk, *Electrochim. Acta* 1990, in press.
5. V. Gutmann and O. Bohunovsky, *Monatsh. Chem.* 1968, **99**, 751.
6. V. Gutmann, *Topics in Current Chem.* 1972, **27**, 59.
7. S. F. Lincoln, A. M. Hounslow and A. N. Boffa, *Inorg. Chem.* 1986, **25**, 1038.

Polyhedron Vol. 9, No. 11, pp. 1379–1382, 1990
Printed in Great Britain

0277–5387/90 $3.00+.00
© 1990 Pergamon Press plc

LINKAGE ISOMERISM IN COBALT(III) COMPLEXES

T. Sh. KAPANADZE, G. V. TSINTSADZE, Yu. V. KOKUNOV and Yu. A. BUSLAEV*

N.S.Kurnakov Institute of General and Inorganic Chemistry, U.S.S.R. Academy of Sciences, Moscow, U.S.S.R.

(*Received* 22 *November* 1984; *accepted after revision* 11 *January* 1990)

Abstract—Interaction of *cis*-$[Co(AA)_2Cl_2]Cl$, *cis–trans*-$[Coen_2(H_2O)_2]Br_3$ and $[Co(CN)_5H_2O]^{2-}$ (where AA is α,α^1-bipyridyl or 1,10-phenanthroline, en—ethylenediamine) with NO_2^-, SO_3^{2-} ambidentate ligands and thiourea was studied by ^{59}Co NMR and linkage O,N-, O,S- and N,S-isomerization in bis-ethylenediamine Co^{III} complexes was found. No similar linkage isomerization was observed for bipyridyl or phenanthroline Co^{III} complexes.

At present there are many experimental data proving the existence of O,N and O,S linkage isomerism in aqueous solutions of Co^{III} complexes containing the NO_2^- and SO_3^{2-} groups.[1–7] It was found that the reactions of nitrito-nitro linkage isomerization in aqueous solutions occur spontaneously by an intramolecular mechanism[8] or are catalysed by bases.[9,10] We have also discovered linkage isomerism in the case of the reactions of different Co^{III} amine complexes and molecular ligands (urea, thiourea, acetamide, thioacetamide and thiosemicarbazide),[11,12] in which we assume O,N-linkage isomerism is caused by deprotonation of amine ligands and changing of electron density of the central atom.[13]

It seemed of interest to us to find out whether the linkage isomerism of Co^{III} complexes in which proton dissociation of coordinated ligands is improbable. We studied the interaction of NO_2^--, SO_3^{2-}- and thiourea with $[Cophen_2Cl_2]Cl$, $[Codipy_2Cl_2]Cl$, $[Coen_2(H_2O)_2]X_3$ ($X = ClO_4^-$ and Br^-) and $[Co(CN)_5H_2O]^{2-}$.

EXPERIMENTAL

The initial compounds were synthesized according to the known procedure: $[Co(AA)_2Cl_2]Cl$,[14,15] *cis*- and *trans*-$[Coen_2(H_2O)_2]X_3$[16] and aqueous solution containing 0.1 mol dm^{-3} of $[Co(CN)_5H_2O]^{2-}$.[17] ^{59}Co NMR spectra were recorded on "РЯ 2311" (19.76 MHz) and "BRUKER" AM-400 (95.45 MHz) spectrometers. Chemical shifts are presented relative to $[Co(NH_3)_6]Cl_3$. The attribution of resonance lines of ^{59}Co NMR spectra was based on the additivity method proposed by authors.[18] The constant of the nitrito-nitro isomerism rate was determined in buffer solution of (KH_2PO_4/Na_2HPO_4) at pH = 6.86 according to the changes in time of the integral intensity ratio of signals δ ^{59}Co of nitrito- and nitro- forms.

RESULTS AND DISCUSSION

Linkage O,N-isomerism (at different pH) was observed in the case of NO_2^--ions reaction with *cis*- and *trans*-$[Coen_2(H_2O)_2]X_3$. In basic solution coordination of the nitro-group with cobalt took place only through the nitrogen atom. Both isomers of diaqua-complex underwent hydrolysis, and the process was accompanied by *cis–trans*-isomerization (*cis*:*trans* = 1:2). While adding $NaNO_2$ ($Co:NO_2 = R = 1:2$) the formation of *trans*-isomers $[Coen_2(OH)NO_2]^+$ (363, 583 ppm *cis*:*trans* = 1:3) and $[Coen_2(NO_2)_2]^+$ (−1637, −1835 ppm, *cis*:*trans* = 1:5) took place mainly independently of the primary geometric configuration of the initial bis-ethylenediamine complexes. The period of semi-conversion of *cis*-$[Coen_2(NO_2)_2]^+$ complexes into the *trans*- form, as was found before[13] is 20 h at 86°C. The *trans*-isomer $[Coen_2(NO_2)_2]^+$ is not converted to the *cis*-configuration and is not catalytically effected by the bases due to the concurrent hydrolysis process. At

* Author to whom correspondence should be addressed.

the same time similar to the reaction of *trans*-$[Coen_2(H_2O)_2]^{3+}$ with the nitro group in basic solution, both *cis*- and *trans*-$[Coen_2(NO_2)OH]^+$ are easily formed and then both *cis*- and *trans*-$[Co(en)_2(NO_2)_2]^+$ geometric isomers are produced in the presence of NO_2^- ions. The equilibrium observed in the process of nitrogen-complexes formation (*cis* $\rightleftharpoons$ *trans*) can be explained by the hydrolysis of the initial diaqua-complexes and regrouping of chelate rings.

Dinitrito-complexes of *cis*- and *trans*-$[Coen_2(ONO)_2]^+$ in neutral solution (pH = 7) are isomerized in time into nitrito-nitro- and dinitro- forms without changing its geometric configuration

$$\underset{\text{(or } trans\text{)}}{cis\text{-}[Coen_2(ONO)_2]^+} \xrightarrow[H_2O]{} \underset{\text{(or } trans\text{)}}{cis\text{-}[Coen_2(ONO)NO_2]^+} \xrightarrow[H_2O]{} \underset{\text{(or } trans\text{)}}{cis\text{-}[Coen_2(NO_2)_2]^+}.$$

When the solutions are alkalized (pH = 9) the rate of linkage isomerization increases considerably. Kinetic parameters of these reactions were discussed elsewhere.[13] Isomerization rate constants at 25°C determined by us for *cis*- and *trans*-$[Coen_2(X)ONO]^+$ (X = NH_3, Py and CH_3NH_2) are in good agreement with the results obtained[13,19] for similar complexes where X = ONO^-, NCS^-, NO_2^-, CN^-. As follows from Table 1, the isomerization rate for *cis*-complexes depends slightly on the nature of X and increases in the order Py < NH_3 < CH_3NH_2. The rate of isomerization of *trans*-complexes changes considerably for different X. Speeding up of the reaction of *trans*-$[Coen_2(ONO)CH_3NH_2]^{2+}$ isomerization can be evidently explained by stronger *trans*-effect of CH_3NH_2 as compared with ammonia and pyridine.

Reaction of *cis*-$[Coen_2(H_2O)_2]Br_3$ with thiourea (ratio = 2 and pH = 7) starts with the replacement of water and addition of thiourea through the nitrogen atom and then N,S-linkage isomerism occurs without changing its *cis*-configuration in time or on making the solution alkaline.

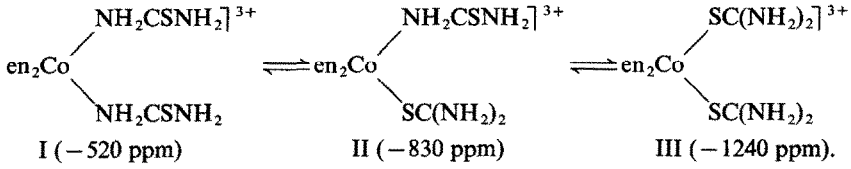

The isomer containing thiourea molecules coordinated to Co through the nitrogen atom is the dominating form in acid solutions (pH = 5; I : II : III = 5 : 2 : 1), but at pH = 9 the equilibrium shifts and complexes with Co—S bond are formed (I : II : III = 1 : 3 : 4). In the range of 3 < pH < 12 both N- and S-linkage isomers are present in the solution in commensurable quantities, while

$[Coen_2(ONO)_2]^+$ under similar conditions isomerizes in a more stable nitro-form in time.

It is known,[20-23] that in the reaction of $[Co(NH_3)_5H_2O]^{3+}$ and *cis*- and *trans*-$[Coen_2(H_2O)_2]^{3+}$ with SO_2 or $Na_2S_2O_5$, $NaHSO_3$ or Na_2SO_3 when 4 < pH < 7 the monosulfite complexes $[(NH_3)_5CoOSO_2]^+$[20,21] are formed, as well as *cis*-[22] and *trans*-[23] $[en_2CoOSO_2(H_2O)]^+$ in which coordination of SO_3-group is realized through the oxygen atom. But at pH < 6 they are not stable and decompose with the formation of Co^{2+} complexes. At pH > 6 only Co—SO_3 bonded complexes are formed in similar reactions.[24,25] O,S-linkage isomerism was previously observed at 6 < pH < 7.5 for α,β-$[Co(tetren)OSO_2]^+$[4] and $[Codien(OSO_2)_3]^{3-}$.[12]

Interaction of *cis*- and *trans*-$[Coen_2(H_2O)_2](ClO_4)_3$ with sodium sulfite (pH = 7, R = I) resulted in the formation of three complexes: two isomers $[Coen_2SO_3(H_2O)]^+$ (*cis*-, −1320 ppm; *trans*-, −1435 ppm) with the concentration ratio *cis* : *trans* = 1 : 3 and $[Coen_2SO_3]^+$ (−1538 ppm). Assumption of SO_3-group coordination as chelate ligand suggested previously[26]

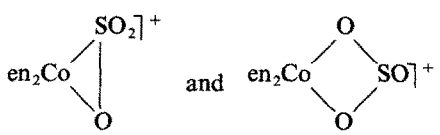

was not confirmed because deshielding of the central atom would be observed in this case as was noted for $[Coen_2CO_3]^+$ (800 ppm). One can rather assume that $[Coen_2SO_3]^+$ is a pentacoordinated complex. High donor SO_3-group activity decreases the lifetime of the water molecule in the coordination sphere of *trans*-$[Coen_2(SO_3)H_2O]^+$ so that ^{59}Co NMR registers pentacoordinated monosulfite complex $[Coen_2SO_3]^+$ in equilibrium $[Coen_2(SO_3)H_2O]^+ \rightleftharpoons [Coen_2SO_3]^+ + H_2O$. The stable pentacoordinated complex of pseudo-tetragonal configuration was studied previously when *trans*-

Table 1. Isomerization rate constants at 25°C for *cis*- and *trans*-$[Co(en)_2X(ONO)]^{2+}$ complexes and parameters of NMR spectra

X	10^4 K, s^{-1} *cis*	10^5 K, s^{-1} *trans*	δ ppm ^{59}Co *cis* ONO	*trans* ONO	*cis* NO_2	*trans* NO_2
CH_3NH_2	1.87	88	−360	−430	−1605	−1895
NH_3	1.65	5.5	−145	−230	−1265	−1315
Py	1.11	0.32	−95	−160	−1115	−1135

$[Coen_2(SO_3)_2]^-$ were investigated.[27] It should be noted that for complexes $[Coen_2(H_2O)SO_3]^+$ and $[Coen_2SO_3]^+$ the *trans*-configuration is much preferable. *Cis*-$[Coen_2(H_2O)SO_3]^+$ was synthesized and its *cis*- to *trans*-isomerization was studied.[28] On substitution of the water molecule in *trans*-$[Coen_2(H_2O)SO_3]^+$ for the sulfite group (pH = 7.2) the latter is bonded to cobalt through oxygen atom and then O,S-isomerization occurs resulting in the formation of a complex with two Co—S bonds.

The equilibrium is given by the following scheme:

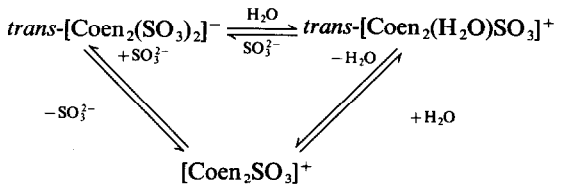

The presence in the Co^{III} coordination sphere of α,α′-bipyridyl or 1,10-phenanthroline chelate rings, being rather rigid, makes the formation of Co—NO_2 and Co—ONO bonds equally possible but for pentacyanide complex the equilibrium of O,N-linkage isomers shifts completely to the formation of the nitrito-complex.

It should be noted that all known tetramines $[Co(AA)_2X_2]^{n\pm}$ (AA = bipy or phen) exist only in the *cis*-configuration, due to steric reasons.[29–31] For $[Cophen_2(NO_2)_2]Cl$ and $[Codipy_2(NO_2)_2]Cl$[13,14] authors[32] made the assumption that both NO_2-groups are coordinated to cobalt through nitrogen atom. However, according to the values of chemical shifts of $[Cophen_2(NO_2)_2]^+$ (−1078 ppm) and $[Codipy_2(NO_2)_2]^+$ (−1212 ppm) both complexes are the compounds $[Co(AA)_2(NO_2)ONO]^+$, where one NO_2-group is coordinated to cobalt through nitrogen atom and another through oxygen atom. Unlike similar nitrito-nitro $[Coen_2(NO_2)ONO]^+$ complex, $[Co(AA)_2(NO_2)ONO]^+$ complexes are stable and do not undergo spontaneous O,N-linkage isomerization and are not affected catalytically by bases. On making the solutions of $[Co(AA)_2(NO_2)ONO]^+$ alkaline (diluted NaOH or ammonia up to pH = 9) hydrolysis of the nitrito-group easily occurs with the formation of $[Cophen_2(NO_2)OH]^+$ (δ = 525 ppm); $[Codipy_2(NO_2)OH]^+$ (δ = −694 ppm), and on further increase of alkaline concentration in the solutions of $[Co(AA)_2(NO_2)OH]^+$ (up to 2% NaOH) nitro-group undergoes hydrolysis accompanied by $[Co(AA)_2(OH)_2]^+$ dihydroxo-complexes formation.

Data available in the literature concerning displacement of the nitro-group for hydroxo-group in ethylenediamine Co^{III} complexes is related only to the alkaline concentration equal to 20%[31]; in that case both nitro-groups are replaced in isomeric *cis*- and *trans*-$[Coen_2(NO_2)_2]^+$ with the formation of *cis–trans*-$[Coen_2(OH)_2]^+$. In acid solution the Co—ONO bond is more stable than Co—NO_2. Short heating (for 12–15 min) of the solutions of $[Co(AA)_2(NO_2)ONO]^+$ with concentrated HCl up to 90°C resulted in the precipitation from the solution of the insoluble chloronitrito-complexes of $[Co(AA)_2(ONO)Cl]^+$. ^{59}Co NMR spectra of these complexes in DMFA and DMSO (δ = 388 ppm for $[Cophen_2(ONO)Cl]^+$) and (δ = 185 ppm for $[Codipy_2(ONO)Cl]^{\pm}$) showed that the NO_2-group is coordinated to cobalt through the oxygen atom.

Coordination of thiourea and sulfito-group to cobalt in phenanthroline and dipyridyl complexes of Co^{III} is realized through the sulfur atom and in all cases the changing of temperature or pH of the solution did not result in the formation of linkage isomers.

Deprotonation of aminoligand (en) causing the increase of electron density on Co^{III} atom and stabilization of Co—NO_2, Co—SO_3 and Co—SC

bonds play the essential role for linkage isomerization in bis-ethylenediamine complexes with NO_2^-, SO_3^{2-} and thiourea. No linkage isomerization was found in bipyridyl or phenanthroline complexes having no mobile protons at the nitrogen atoms coordinated to cobalt.

The interaction of SO_3-group with $[Co(CN)_5H_2O]^{2-}$ resulted in the formation of $[Co(CN)_5OSO_2]^{4+}$ ($\delta = -6385$ ppm) with Co—OSO_2 bond, which does not undergo isomerization within 7 days, but in the complexes with amine ligands the SO_3-group acts as a strong S-donor ligand.

Interaction of $[Co(CN)_5H_2O]^{2-}$ with KNO_2 is accompanied by coordination of NO_2-group to cobalt through the oxygen atom of $[Co(CN)_5ONO]^{3-}$ ($\delta = -6833$ ppm) and decrease of pH (< 12) does not result in the formation of the nitro-isomer, as was observed for $[Co(NH_3)_5ONO]^{2+}$.

However, when heating the solution of $[Co(CN)_5OSO_2]^{4-}$ and $[Co(CN)_5ONO]^{3-}$ (90°C, for 2–3 h) we observed the formation of linkage isomers of $[Co(CN)_5SO_3]^{4-}$ ($\delta = -7518$ ppm) and $[Co(CN)_5NO_2]^{3-}$ ($\delta = -7600$ ppm) which were isomerized into the initial oxygen coordinated forms upon cooling of the solutions.

REFERENCES

1. G. B. Kauffman, *Coord. Chem. Rev.* 1973, **11**, 161.
2. R. G. Jackson, P. A. Lay and A. M. Sargeson, *Aust. J. Chem.* 1982, **35**, 1561.
3. R. Van Eldick, *Inorg. Chim. Acta* 1982, **65**, 125.
4. A. C. Dash, A. A. El-Awady and G. M. Harris, *Inorg. Chem.* 1981, **20**, 3160.
5. W. G. Jackson, G. A. Lawrance, P. A. Lay and A. M. Sargeson, *J. Chem. Soc., Chem. Commun.* 1982, **1**, 70.
6. W. J. Jackson, *Inorg. Chem.* 1987, **26**, 3857.
7. W. J. Jackson, *Inorg. Chim. Acta* 1988, **149**, 101.
8. W. Rindermann, R. Van Eldik and H. Kelm, *Inorg. Chim. Acta* 1982, **61**, 173.
9. W. G. Jackson, G. A. Lawrance, P. A. Lay and A. M. Sargeson, *Inorg. Chim. Acta.* 1980, **19**, 904.
10. W. G. Jackson, G. A. Lawrance, P. A. Lay and A. M. Sargeson, *J. Chem. Educ.* 1981, **58**, 734.
11. V. P. Tarasov, T. Sh. Kapanadze, G. V. Tsintsadze and Yu. A. Buslaev, *Koord. Khim.* 1983, **9**, 647.
12. V. P. Tarasov, T. Sh. Kapanadze, I. B. Baranovsky, G. B. Tsintsadze, S. G. Drobyshev and Yu. A. Buslaev, *Dokl. AN SSSR* 1983, **270**, 4,894.
13. W. Rindermann and R. Van Eldik, *Inorg. Chim. Acta.* 1983, **68**, 35.
14. A. V. Ablov, *Zhurnal Neorg. Khimii.* 1961, **6**, 309.
15. D. M. Palade and A. V. Ablov, *Zhurnal Neorg. Khimii.* 1969, **14**, 445.
16. J. W. Vaughn and R. D. Lindholm, *Inorg. Syntheses* 1967, **9**, 163.
17. A. Haim and W. K. Wilmarth, *J. Am. Chem. Soc.* 1961, **83**, 509.
18. R. J. Buist, S. C. F. Au-Yeung and D. R. Eaton, *Canad. J. Chem.* 1985, **63**, 3558.
19. K. Miyoshi, N. Katoda and H. Yoneda, *Inorg. Chem.* 1983, **22**, 1839.
20. R. Van Eldik and G. M. Harris, *Inorg. Chem.* 1980, **19**, 880.
21. R. Van Eldik, *Inorg. Chem.* 1983, **22**, 352.
22. T. P. Dasgupta and G. M. Harris, *Inorg. Chem.* 1984, **23**, 4399.
23. A. A. El-Awady and G. M. Harris, *Inorg. Chem.* 1986, **25**, 1323.
24. R. C. Elder, M. J. Heeg, M. D. Payne, M. Trkula and E. Deutsch, *Inorg. Chem.* 1978, **17**, 2, 431.
25. S. M. Farrell and R. S. Murray, *J. Chem. Soc., Dalton Trans.* 1977, 322.
26. M. E. Baldwin, *J. Chem. Soc.* 1961, **7**, 3123.
27. M. C. Ghash, P. Bhattacharya and P. Baherjee, *Coord. Chem. Rev.* 1988, **91**, 1.
28. W. G. Jackson, *Inorg. Chem.* 1988, **27**, 777.
29. A. V. Ablov, Yu. Khon and T. I. Malinovsky, *Dokl. AN SSSR* 1966, **167**, 1051.
30. D. M. Palade, *Zhurnal Neorg. Khimii.* 1969, **14**, 1438.
31. D. M. Palade, *Zhurnal Neorg. Khimii.* 1969, **14**, 452.
32. M. Davidson, T. W. Faulkner, M. A. Green and E. D. McKenzie, *Inorg. Chim. Acta.* 1974, **9**, 231.
33. A. V. Ablov and N. I. Lobanov, *Zhurnal Neorg. Khimii.* 1957, **2**, 2570.

Polyhedron Vol. 9, No. 11, pp. 1383–1388, 1990
Printed in Great Britain

0277-5387/90 $3.00+.00
© 1990 Pergamon Press plc

ELECTRONIC AND MAGNETIC PROPERTIES OF SOME DIVALENT METAL SACCHARINATES

ENRIQUE J. BARAN* and PATRICIA A. M. WILLIAMS

Departamento de Química, Facultad de Ciencias Exactas, Universidad Nacional de La Plata, Calles 47 y 115, 1900-La Plata, Argentina

and

REGINO SAEZ PUCHE

Departamento de Química Inorgánica, Facultad de Ciencias Químicas, Universidad Complutense, 28040 Madrid, Spain

and

JAVIER SORIA

Instituto de Catálisis y Petroleoquímica, CSIC, 28006 Madrid, Spain

(*Received* 28 *September* 1989; *accepted* 11 *January* 1990)

Abstract—The electronic absorption spectra of a series of divalent metal saccharinates of the type $[M^{II}(C_7H_4NO_3S)_2(H_2O)_4]\cdot 2H_2O$ (with M^{II} = Mn, Fe, Co, Ni, Cu) were recorded and briefly discussed. The obtained 10Dq-values were comparable to that of the respective hexaaqua complexes. Magnetic susceptibility measurements of these samples, in the temperature range between 4.2 and 300 K, were also undertaken and complemented, in some cases, with ESR data. The results of all these measurements could be explained on the basis of octahedral coordination of the metal centres, showing that the axial distortion introduced by the two saccharinate-ligands is very small.

The chemistry of saccharin (p-sulphobenzimide), commonly used as a non-nutritive sweeting agent, has attracted the attention in recent years due to its suspected carcinogenic nature (cf. for example ref. 1). Notwithstanding, studies on general physicochemical properties of saccharin complexes of transition metals of biological relevance are scanty.

We have recently investigated the ^{57}Fe-Mössbauer spectrum of the respective Fe^{II} complex and advanced some aspects of the magnetic behaviour of this and the corresponding Ni^{II} compound.[2]

Now we have investigated the electronic spectra of the Mn^{II}, Fe^{II}, Co^{II}, Ni^{II} and Cu^{II} saccharinate complexes as well as their magnetic behaviours in the temperature range between 4.2 and 300 K. The results are also complemented, in some cases with ESR measurements.

EXPERIMENTAL

The five complexes were obtained from the sodium salt of saccharine and the respective metal sulphates or acetates, in aqueous solution, according to the procedure described by Haider *et al.*[3] They were purified by double recrystallization from water and characterized by chemical analysis and IR spectroscopy.

The electronic spectra were recorded on a Shimadzu UV-300 spectrophotometer (UV–vis-range) and on a Cary 14 instrument (near IR-range) using freshly prepared solutions of the complexes in DMF, and concentrations ranging from 0.6 to 0.01 M.

* Author to whom correspondence should be addressed.

Magnetic susceptibility measurements in the temperature range 4.2–300 K were made using a fully automatic DSM 5 pendule susceptometer. The setup was calibrated with $NH_4Mn(SO_4)_2 \cdot 12H_2O$ and $Hg[Co(SCN)_4]$ as standards. The maximum field was 15 kG with $H\delta H/\delta z = 30\ kG^2 \cdot cm^{-1}$. In all cases the magnetic susceptibility was independent of the magnetic field strength. The susceptibilities were corrected for ionic diamagnetism.[4]

The ESR spectra were recorded at 77 and 300 K with a Bruker (Model ER 200D, X band) spectrometer. Only spectra measured at liquid nitrogen temperature, show adequate resolution and structure.

RESULTS AND DISCUSSION

1. *Structural characteristics*

The complexes have the general formula $[M(C_7H_4NO_3S)_2(H_2O)_4] \cdot 2H_2O$. They belong to the monoclinic space group $P2_1/c$ and $Z = 2$, as determined by single crystal X-ray diffraction methods.[5] The metal ions are located on crystallographic inversion centres and have distorted octahedral geometry. Each ion is bounded to four H_2O molecules and two nitrogen atoms, from the saccharinate ligands, in *trans* positions.

2. *Electronic spectra*

The electronic spectra of all these complexes can be discussed in terms of the tetragonally distorted octahedral configuration mentioned above. Data of the absorption maxima, and the proposed band assignments, together with the calculated 10Dq values are summarized in Table 1. Figure 1 shows the spectra of the cobalt and nickel complexes.

The proposed assignments were made by comparison with those of the respective hexaaqua-complexes which show very similar band positions and 10 Dq values.[6]

In the case of the Mn^{II} complexes, the $^6A_{1g} \rightarrow {}^4E_g(D)$ transition is overlapped by the tail of a charge transfer band located in the UV region, so direct calculation of the Racah parameters B and C was not possible. However, taking $C = 4.477B$ for an octahedral field[6] we were able to calculate $B = 760.5\ cm^{-1}$ and 10Dq (cf. Table 1).

$[Fe(Sac)_2(H_2O)_4] \cdot 2H_2O$ shows a broad absorption resolved into two components, due to the splitting of the excited ^5E_g state ($^5E_g \rightarrow {}^5A_{1g} + {}^5B_{1g}$). The value of 10Dq cannot be derived directly from that spectrum, except under the following suppositions: as there exists a *trans*-tetragonal distortion, and the axial field has lower σ-force than the equatorial one, the energy of the $^5A_{1g}$ level lies lower than that of

Table 1. Electronic spectra of the investigated divalent-metal saccharinates of the type $[M(sac)_2(H_2O)_4] \cdot 2H_2O$

M^{II}	Band positions nm	cm^{-1}	ε^a	Assignment	10Dq[b]
Mn	406	24,630	0.13	$^6A_{1g} \rightarrow {}^4A_{1g}, {}^4E_g(G)$	
	443	22,573	0.04	$^6A_{1g} \rightarrow {}^4T_{2g}(G)$	8366
	530	18,868	0.04	$^6A_{1g} \rightarrow {}^4T_{1g}(G)$	
Fe	995	10,050	7.70	$^5B_{2g} \rightarrow {}^5B_{1g}$	10,050
	1250	8000	5.70	$^5B_{2g} \rightarrow {}^5A_{1g}$	
Co	475	21,052		see text	
	490	20,408			
	524	19,084	21.83	$^4T_{1g} \rightarrow {}^4T_{1g}(P)$	8496
	620	16,130	1.90	$^4T_{1g} \rightarrow {}^4A_{2g}$	
	1310	7634	4.70	$^4T_{1g} \rightarrow {}^4T_{2g}$	
Ni	400	25,000	13.67	$^3A_{2g} \rightarrow {}^3T_{1g}(P)$	
	668	14,970	4.90	$^3A_{2g} \rightarrow {}^3T_{1g}$	8885
	1160	8621	6.12	$^3A_{2g} \rightarrow {}^3T_{2g}$	
Cu	785	12,738	66.00	$^2B_{1g} \rightarrow {}^2E_g$	
	1100	9091	14.10	$^2B_{1g} \rightarrow {}^2B_{2g}$	9091
	1280	7812	9.10	$^2B_{1g} \rightarrow {}^2A_{1g}$	

[a] $mol^{-1}\ dm^3\ cm^{-1}$.
[b] cm^{-1}.

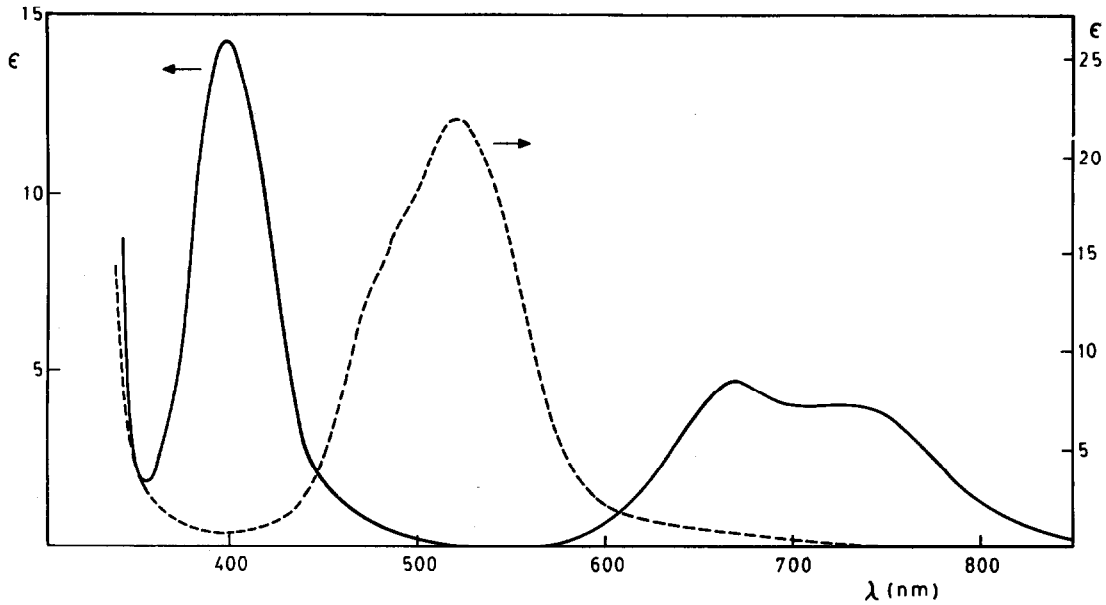

Fig. 1. Electronic absorption spectra of $[Co(sac)_2(H_2O)_4]$ (----) and $[Ni(sac)_2(H_2O)_4]$ (———).

the $^5B_{1g}$. Assuming that the ground state is $^5B_{2g}$, the transition $^5B_{2g} \rightarrow {}^5B_{1g}$ (= 10,050 cm^{-1}) gives the value of 10Dq directly.[6]

For the Co^{II} complex there are three possible electronic transitions: ν_1 ($^4T_{1g} \rightarrow {}^4T_{2g}$) = 7634 cm^{-1}, ν_2 ($^4T_{1g} \rightarrow {}^4A_{2g}$) = 16,130 cm^{-1} and ν_3 [$^4T_{1g} \rightarrow {}^4T_{1g}(P)$] = 19,084 cm^{-1} with $10Dq = \nu_2 - \nu_1$ = 8496 cm^{-1}.

The irregularity of the ν_3 band at higher frequencies (see Fig. 1) is due to spin-orbit coupling of the $^4T_{1g}(P)$ state. The ν_2-transition is, as expected, very weak, because it involves a two-electron transition.

The presented data allow the calculation of a mean value of B = 821 cm^{-1} and C = 3804 cm^{-1} (assuming C = 4.633B).[6]

Three electronic transitions are also expected in the case of $[Ni(sac)_2(H_2O)_4] \cdot 2H_2O$. The spin-forbidden $^3A_{2g} \rightarrow {}^1E_g$ transition is expected to lie near the ν_2 band and this is the reason for the doublet structure observed in this region (cf. Fig. 1). ^1E_g and $^3T_{1g}$ states are scrambled by spin-orbit coupling and ν_2 was taken as the most intense band of the doublet.

The $^3A_{2g} \rightarrow {}^3T_{2g}$ transition gives the 10Dq value directly and the mean value for B calculated from all these data is 890 cm^{-1}. Considering C = 4.70B[6] gives C = 4193 cm^{-1}.

The spectrum of the Cu^{II} complex consists of a band with a main peak and a shoulder on the low energy side. Deconvolution of these bands, using Gaussian line-shapes and a least squares fitting procedure, suggested the assignments shown in Table 1. The calculated values for the tetragonal distortion parameters D_s and D_t were 78.8 and −682.5 respectively.

A comparison of the calculated 10Dq values with those known for the respective $[M(H_2O)_6]^{2+}$ complexes[6] is shown in Table 2. As can be seen, the absolute values are very similar in both series of compounds. Saccharinate values are slightly higher in the case of Mn^{II}, Co^{II} and Ni^{II} compounds and lower in the other two cases.

These results clearly show that the replacement of two of the water molecules in the hexaaqua moieties, by two saccharinate nitrogens has only a very small effect on the crystal fields of these cations. The spectroscopic results also show that the distortive effects on the overall octahedral symmetry are very low.

3. *Magnetic properties*

The magnetic behaviour of all these complexes is rather simple and could be directly explained on the

Table 2. Comparison of 10Dq values of the $[M(sac)_2(H_2O)_4]$ and the corresponding $[M(H_2O)_6]^{2+}$ complexes (values in cm^{-1})

	Mn	Co	Ni	Fe	Cu
$[M(sac)_2(H_2O)_4]$	8366	8496	8885	10,050	9091
$[M(H_2O)_6]^{2+}$	8000	7900	8500	10,400	10,650

Table 3. Magnetic parameters for the different investigated $[M(sac)_2(H_2O)_4]\cdot 2H_2O$ complexes

M	μ_S (B.M.)	μ_{S+L} (B.M.)	μ_{exp} (B.M)	θ (K)
Mn	5.92	5.92	5.98	−0.05
Fe	4.90	5.84	5.26	−5.16
Co	3.87	5.20	4.80	−3.08
Ni	2.83	4.47	2.99	−8.47
Cu	1.73	3.00	1.76	+9.10

basis of octahedral coordination of the different metal centres. The magnetic behaviour can also be interpreted neglecting the small axial distortion of the ligand field, in agreement with the results obtained from the electronic spectra discussed in the preceeding section.

Table 3 shows the relevant magnetic parameters including calculated spin-only values, $\mu_S = 2[S(S+1)]^{1/2}$ and values resulting by considering spin-orbit coupling, $\mu_{S+L} = [L(L+1)+4S(S+1)]^{1/2}$, which are compared with the experimental μ_{exp}-data. Values of the Weiss constant θ, are also included in this table.

The temperature dependence of the reciprocal molar susceptibility of $[Mn(sac)_2(H_2O)_4]\cdot 2H_2O$ is shown in Fig. 2. The magnetic susceptibility obeys a quasi-Curie law, $\chi = 0.22/T$ in the whole temperature range of measurements. The magnetic moment of 5.98 B.M. fairly agrees with that expected for the octahedral crystal field $^6A_{1g}$ term. This term arises from the free ion ^6S term associated with the Mn^{II} ion for which only a spin contribution is expected.

The ESR spectrum of this complex measured at 77 and 300 K shows a single broad isotropic signal with $g_{eff.} = 2.00$.

The magnetic susceptibility of $[Fe(sac)_2(H_2O)_4]\cdot 2H_2O$ follows a behaviour which is characteristic of the $^5T_{2g}$ term arising from a free ^5D term under octahedral field splitting. Although the susceptibility appears to follow a Curie–Weiss law, $\chi = 3.84/T - 5.2$, the magnetic moment slightly increases with decreasing temperature below 100 K, rising to a maximum of 5.83 B.M. in the temperature range between 90 and 30 K. The magnetic moment steadily decreases below this temperature taking a value of 5.56 B.M. at 12 K.

The average magnetic moment of 5.26 B.M. obtained from the Curie–Weiss behaviour is in good agreement with that usually observed for Fe^{II} complexes in octahedral environments[4,7] in which small spin-orbit coupling effects are present. The negative value of the Weiss-constant, $\theta = -5.2$ K can be primarily related to crystal field effects, and cooperative interactions, such as antiferromagnetic couplings, need not be considered.

The magnetic susceptibility also obeys a Curie–Weiss law, $\chi = 2.89/T - 3.08$, in the case of the cobalt complex in the temperature range between 300 and 60 K (see Fig. 3). Deviations from the

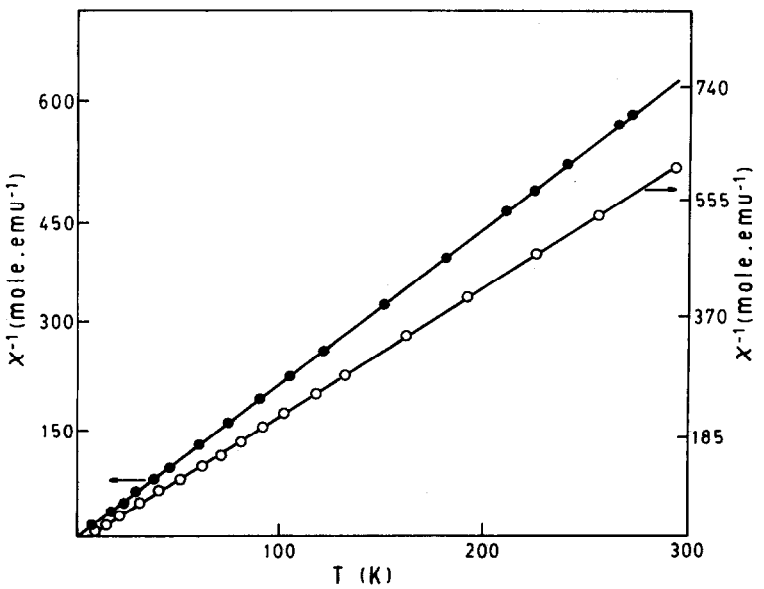

Fig. 2. Temperature dependence of the reciprocal molar susceptibility of $[Mn(sac)_2(H_2O)_4]\cdot 2H_2O$ (●) and $[Cu(sac)_2(H_2O)_4]\cdot 2H_2O$ (○).

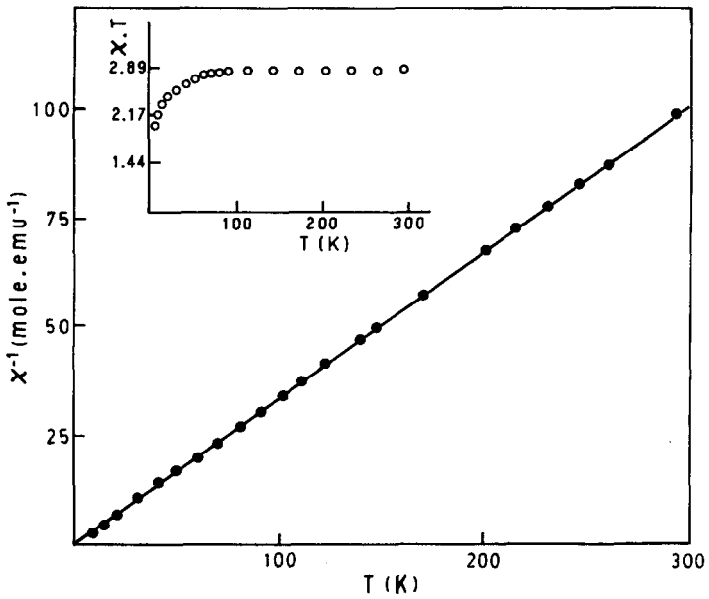

Fig. 3. Temperature dependence of the reciprocal molar susceptibility for $[Co(sac)_2(H_2O)_4]\cdot 2H_2O$. Inset: $\chi \cdot T$ vs T plot.

linearity are observed below 60 K, and the magnetic susceptibility increases more rapidly than required by this Curie–Weiss law. The magnetic moment remains almost constant between 300 and 60 K, taking a value of 4.80 B.M., which is indicative of important orbital contributions. The magnetic moment gradually decreases, below 60 K, taking a value of 3.56 B.M. at 4.2 K (cf. inset of Fig. 3).

Both the magnetic moment and the negative Weiss-constant are characteristic for a $^4T_{1g}$-term arising from the ^4F free ion state and, as in the case of iron-saccharinate, no magnetic interactions are operative for this compound.

The $[Ni(sac)_2(H_2O)_4]\cdot 2H_2O$ has been investigated earlier[2] and its magnetic susceptibility also follows a Curie–Weiss law, $\chi = 1.07/T - 8.47$, between 78 and 300 K. The magnetic moment of 2.99 B.M. points only to a very weak spin-orbit coupling, as is usual for octahedral Ni^{II} complexes.[4,7]

The variation of the reciprocal molar susceptibility against the temperature for the copper complex is shown in Fig. 2. The data are compatible with a Curie–Weiss behaviour, $\chi = 2.57/T + 9.10$. The value obtained for the magnetic moment (1.76 B.M.) is unusually low, suggesting some spin-orbit coupling.

The corresponding ESR spectrum (Fig. 4) shows a Lorentzian axial signal with $g_\parallel = 2.347$ and $G_\perp = 2.073$, $A_\parallel = 150 \times 10^{-4}$ and $A_\perp$ unobserved. Such signals are characteristic for the Cu^{II} ion with the unpaired electron placed in the $d_{x^2-y^2}$ orbital and is also typical for an axially distorted octahedral coordination sphere.[8] The broadening of the signal

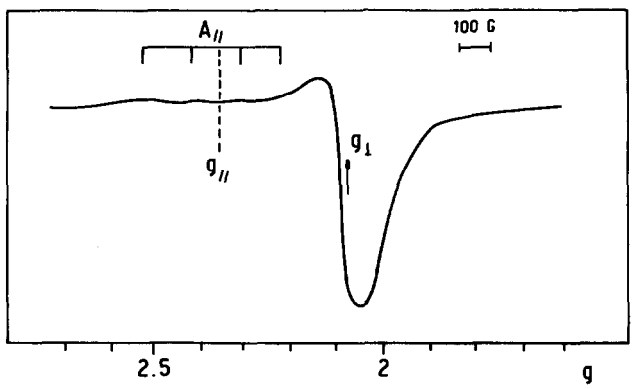

Fig. 4. ESR spectrum of a polycrystalline sample of $[Cu(sac)_2(H_2O)_4]\cdot 2H_2O$ at 77 K.

can be attributed to non-solved superhyperfine structure arising from the coupling of the copper-spin with those of the two coordinated nitrogen atoms ($I = 1$).

Using the known relations between g-values and electronic transition energies,[8] assuming the value of $-830\ cm^{-1}$ for the spin-orbit coupling constant[6] and values between 0.5 and 0.6 for the squares of the orbital reduction factors k, we calculated $g_\perp = 2.07$ and $g_\parallel = 2.36$, in excellent agreement with the experimental values.

Acknowledgements—This work is part of a joint research project of the inorganic chemistry groups in La Plata and Madrid, which is supported by the Ministry of Education and Science of Spain. E.J.B. and P.A.M.W. acknowledge also the support of CONICET (Argentina).

REFERENCES

1. M. J. Allen, E. Bayland, C. E. Dukes, E. S. Horning and J. G. Watson, *Brit. J. Cancer* 1957, **11**, 212; J. M. Price, C. G. Biava, B. L. Oser, E. E. Vogin, J. Steinfield and H. J. Ley, *Science* 1970, **167**, 1131; J. T. Bryan, E. Ertück and O. Yoshida, *Science* 1971, **168**, 1238; J. C. Munro, C. A. Modie, D. Krewski and H. G. Grise, *Toxicol. Appl. Pharmacol.* 1975, **32**, 513.
2. A. L. Rocha, G. Urretaviscaya and E. J. Baran, *J. Inorg. Biochem.* 1987, **31**, 81.
3. S. Z. Haider, K. M. A. Malik and K. J. Ahmed, *J. Bangladesh Acad. Sci.* 1951, **5**, 81.
4. A. Weiss and H. Witte, *Magnetochemie*, Verlag Chemie, Weinheim (1973).
5. S. Z. Haider, K. M. A. Malik, K. J. Ahmed, H. Hess, H. Riffel and M. B. Hursthouse, *Inorg. Chim. Acta* 1983, **72**, 21.
6. A. B. P. Lever, *Inorganic Electronic Spectroscopy*, 2nd edn, Elsevier, Amsterdam (1984).
7. F. E. Mabbs and D. C. Machin, *Magnetism and Transition Metal Complexes*, Chapman and Hall, London (1973).
8. B. J. Hathaway and A. A. G. Tomlinson, *Coord. Chem. Rev.* 1970, **5**, 1.

Polyhedron Vol. 9, No. 11, pp. 1389–1395, 1990
Printed in Great Britain

0277-5387/90 $3.00+.00
© 1990 Pergamon Press plc

SYNTHESIS, STRUCTURE AND $^{77}Se/^{119}Sn$ NMR SPECTROSCOPY OF THE NEW POLYSELENIDE, TRIS(TETRASELENIDO)STANNATE(IV), $[Sn(Se_4)_3]^{2-}$

SONG-PING HUANG, SANDEEP DHINGRA and MERCOURI G. KANATZIDIS*

Department of Chemistry, Michigan State University, East Lansing, MI 48824, U.S.A.

(*Received* 11 *September* 1989; *accepted* 18 *January* 1990)

Abstract—The reaction of sodium pentaselenide with $SnCl_4$ or $SnCl_2 \cdot 2H_2O$ in dimethylformamide (DMF), in a 3:1 ratio, forms the new soluble anion $[Sn(Se_4)_3]^{2-}$ in high (> 79%) yields. The compound $(Ph_4P)_2[Sn(Se_4)_3]$ (I) crystallizes in the monoclinic space group $P2_1/c$ with unit cell dimensions, $a = 13.320(2)$, $b = 11.678(3)$, $c = 34.817(9)$ Å, $\beta = 98.85(2)°$ and $V = 4535$ Å^3. A single-crystal X-ray diffraction study of I shows that three chelating Se_4^{2-} ligands provide an octahedral coordination about the central Sn^{4+} atom. The crystal structure was solved and refined with conventional techniques to $R = 6.0\%$ and $R_w = 7.0\%$. The average Sn—Se distance is 2.709(13) Å, while the average Se—Se bond distance is 2.324(12) Å. The IR spectrum of I (CsI pellet) shows two sets of absorptions at 273, 256 cm^{-1} and 181, 173 cm^{-1}, respectively, assigned tentatively to ν(Se—Se) and ν(Sn—Se) vibrations. The ^{119}Sn NMR spectrum of I in DMF, shows a single resonance at −723 ppm (vs Me_4Sn). The ^{77}Se NMR spectrum of I in DMF, shows two resonances at 618 and 459 ppm. Thermal decomposition of I results in formation of $SnSe_2$ at 510°C. Further heating, above 600°C, results in SnSe.

Interest in the synthesis of soluble transition-metal polychalcogenide compounds remains intense because of their astonishing tendency for structural and stoichiometric diversity. As a result, a number of polysulphide and to a lesser extent polyselenide and polytelluride complexes with transition metals have been isolated and structurally characterized.[1–8] By contrast, the preparation of soluble polychalcogenide compounds containing main-group elements has not been pursued to any considerable degree. The few existing examples are, the $[Bi_2S_{34}]^{4-}$,[9] $[Sn(S_4)_2(S_6)_{0.6}(S_4)_{0.4}]^{2-}$,[10] $[In_2Se_{21}]^{4-}$,[11] $[In_3Se_{15}]^{3-}$ [12] and $[Tl_3Se_{15}]^{3-}$.[12] Recently we have undertaken a systematic investigation of polychalcogenide chemistry of the late transition and main group metals.[11–15] Except for some cases, the solution chemistry of polyselenide or polytelluride complexes has proven to be at considerable variance from that of polysulphide chemistry. For example, while group 12 metals form isostructural complexes with all types of Q_4^{2-} ligands, group 11 metals form different structures with different polychalcogenide ligands.[3,13] The reasons for this deviation from polysulphide chemistry are not completely understood, although the size difference between sulphur and the heavier chalcogens is probably a strongly influencing factor. It would be useful to understand the role of the metal ion in determining similarities and differences in the chemistry of the various polychalcogenide ligands. ^{77}Se NMR spectroscopy appears to be a useful or even unique tool (not applicable to polysulphides) for the investigation of metal–polyselenide complexes.[5,8] In this paper we report the synthesis, molecular structure, ^{77}Se, ^{119}Sn NMR and other spectroscopic characterization of the new complex $[Sn(Se_4)_3]^{2-}$, the first group 14 polyselenide.

EXPERIMENTAL

All work was done in a glovebox (Vacuum Atmospheres, Inc.) under a nitrogen atmosphere. Dimethylformamide (DMF) was stored over 4 Å Linde molecular sieves for several days and distilled under vacuum. Ether was distilled over sodium (or potassium)/benzophenone under a nitrogen blanket. $SnCl_4$ (anhydrous) and $SnCl_2 \cdot 2H_2O$ were pur-

* Author to whom correspondence should be addressed.

chased from Alpha Products. Elemental analyses were performed by Galbraith Laboratories, Knoxville, Tennessee. Satisfactory elemental analyses were obtained. Sodium pentaselenide (Na_2Se_5) was prepared in liquid ammonia from sodium metal and elemental selenium in a 2:5 ratio. The X-ray powder diffraction patterns were recorded either with a standard Debye-Scherrer powder camera mounted on a Phillips Norelco XRG-5000 X-ray generator operating at 40 kV/20 mA, or a Phillips XRG-3000 computer-controlled powder diffractometer. Nickel filtered, copper radiation was used. Thermal gravimetric analyses were performed on a Cahn TG System 121 under flowing nitrogen. A typical heating rate of 5°C min^{-1} was used. IR spectra were recorded as KBr and CsI pellets on a Nicolet 740 FT–IR spectrometer. UV–vis spectra were recorded on a Hitachi U-2000 spectrophotometer.

Synthesis of $(Ph_4P)_2[Sn(Se_4)_3]$ **(I)**

Method A. A 10 cm^3 DMF solution of 0.051 g (~ 0.2 mmol) liquid $SnCl_4$ was added to a 50 cm^3 DMF solution of 0.270 g (~ 0.61 mmol) Na_2Se_5 in the presence of 0.150 g (0.40 mmol) Ph_4PCl. Filtration of NaCl precipitate, followed by slow addition of *ca* 60 cm^3 of ether, and storage at room temperature for several days, afforded analytically-pure red–brown hexagonal platelets in 85%. The X-ray diffraction (XRD) powder pattern obtained from this material matches extremely well that obtained from calculating the same pattern from the single-crystal coordinates, confirming the purity of the compound. A comparison between the calculated and observed *d* spacings for this material is shown in Table 1.

Method B. A 20 cm^3 DMF solution of 0.045 g (0.2 mmol) $SnCl_2 \cdot 2H_2O$ was added to a 30 cm^3 DMF solution of 0.270 g (0.61 mmol) Na_2Se_5 in the presence of 0.220 g (0.60 mmol) Ph_4PCl. The resulting red–brown solution was filtered to remove NaCl and the filtrate was diluted with 50 cm^3 ether to incipient crystallization. Upon standing at room temperature for a week, red–brown microcrystalline powder was obtained (0.275 g). Yield 79%. The product was recrystallized from DMF–ether to obtain large, hexagonal-shaped crystals. The XRD powder pattern of this product is identical to that obtained in method A.

Thermal decomposition of $(Ph_4P)_2[Sn(Se_4)_3]$ *to* $SnSe_2$

This decomposition was carried out inside an alumina boat in a tube furnace under flowing nitrogen at 510°C. The final black–grey microcrystalline product corresponds, by weight, to $SnSe_2$. It was characterized by X-ray diffraction. X-ray diffraction powder pattern spacings (in Å) follow; intensities are shown in parentheses: 6.17 (100.0), 3.076 (7), 2.25 (21), 2.050 (40), 1.906 (6), 1.742 (13).

Table 1. Observed and calculated X-ray powder pattern of $(Ph_4P)_2[Sn(Se_4)_3]$

h	*k*	*l*	D_{calc}	D_{obs}	I/I_{max} (Obs)
1	0	0	13.16	13.39	38
−1	0	2	11.33	11.43	100
1	0	2	9.75	9.79	85
1	1	0	8.73	8.82	85
−1	1	1	8.68	8.65	65
0	0	4	8.60		
1	1	1	8.30	8.36	28
0	1	3	8.18	8.20	31
−1	1	2	8.13		
0	1	4	6.962	6.925	14
1	0	4	6.740	6.779	22
−1	1	4	6.467	6.499	32
−2	1	1	5.782	5.817	33
−2	0	4	5.663	5.689	19
0	2	2	5.529	5.577	14
1	2	1	5.225	5.257	23
−1	1	6	5.035	4.998	25
−1	2	3	4.958		
2	1	3	4.873	4.897	36
−2	0	6	4.695	4.699	25
−2	2	5	3.870	3.888	26
0	3	1	3.867		
3	1	3	3.700	3.708	35
0	3	3	3.686		
2	2	5	3.528	3.522	29
−1	2	8	3.455	3.459	15
−2	3	1	3.360	3.369	31
3	2	2	3.356		
2	3	0	3.350		
−3	0	8	3.338	3.339	27
−2	0	10	3.261	3.264	29
−4	1	1	3.197	3.207	39
2	3	3	3.150	3.164	25
−3	2	7	3.037	3.046	24
2	2	8	2.918	2.922	25
−3	1	10	2.846	2.848	41
3	2	6	2.840		
−4	1	8	2.752	2.758	26
2	3	7	2.672	2.677	14
3	3	5	2.588	2.589	26
5	0	2	2.544	2.537	8
2	4	5	2.437	2.439	20
2	1	12	2.436		
−5	1	8	2.366	2.370	7
1	5	1	2.290	2.297	13
5	2	5	2.173	2.174	11
−1	4	13	1.972	1.972	9

Thermal decomposition of $(Ph_4P)_2[Sn(Se_4)_3]$ *to* SnSe

This decomposition was carried out inside an alumina boat in a tube furnace under flowing nitrogen at 600°C. The final black–grey microcrystalline is, by X-ray diffraction, SnSe. *d* Spacings (in Å) follow; intensities are shown in parentheses: 5.76 (1), 3.514 (3), 3.033 (2), 2.934 (10), 2.874 (100), 2.380 (6), 2.087 (4), 2.042 (3), 1.920 (1), 1.833 (7), 1.761 (3), 1.684 (2).

X-ray crystallographic studies

The crystallographic data for **I** were collected on a Nicolet four-circle diffractometer using a ω–2θ scan mode and Mo-K_α radiation (at Crystalytics Co., Lincoln, Nebraska by Dr C. S. Day). The crystals were mounted inside glass capillaries and sealed. Crystal data and details for data collection and refinement are shown in Table 2. The intensities of three check reflections were monitored every 100 reflections and did not show any appreciable decay during the data collection period. An empirical absorption correction was applied to all data based on ψ scans for seven reflections. The structure was solved with direct methods using SHELXS-86[16] and was refined with the SDP[17] package of crystallographic programs, using a VAXstation 2000 computer. All non-carbon and non-hydrogen atoms were refined anisotropically. The carbon atoms were refined isotropically. The hydrogen atom positions were calculated and included in the structure factor calculation but were not refined. There were no significant residual peaks in the final electron density difference map. The XRD powder pattern was calculated using the atom coordinates determined from the single-crystal data using the program POWD 10[18] (see Table 1).

Table 2. Data for crystal structure analysis[a] of $(Ph_4P)_2[Sn(Se_4)_3]$

Formula	$C_{48}H_{40}P_2SnSe_{12}$
FW	1744.6
a (Å)	13.320(2)
b (Å)	11.678(3)
c (Å)	34.817(9)
α (°)	90.00
β (°)	98.85(2)
γ (°)	90.00
Z, V (Å^3)	4, 5351(2)
Space group	$P2_1/c$ (No. 14)
D_{calc} (g cm^{-3})	2.17
μ(Mo-K_α) (cm^{-1})	86.5
Crystal size (mm)	$0.11 \times 0.60 \times 0.88$
θ range (°)	4.0–48.0
Data collected	$h, k, \pm l$
Number of data collected	9412
Number of data unique	9220
Data used [$F_o > 3\sigma(F_o)$]	3898
Min, max abs. correction	0.41, 0.99
Number of variables	328
Number of atoms per asym. unit (including H)	103
Final R/R_w (%)	6.0/7.0

[a] At 25°C.

NMR spectroscopy

^{77}Se ($I = 1/2$, nat. abund. 7.58%) and ^{119}Sn ($I = 1/2$, nat. abund. 8.58%) NMR spectra were obtained on a Varian VXR-500 (superconducting cryomagnet 11.74 Tesla) pulse spectrometer equipped with Sun/360 workstation. The spectra were recorded at ambient temperature using a broad band 5 mm probe (frequency range 50–202 MHz). The observing frequencies were 95.358 MHz for ^{77}Se and 186.250 MHz for ^{119}Sn. The aquisition time was 0.32 s with a spectral width of 38.35 KHz for ^{77}Se and 37.393 KHz for ^{119}Sn which gave data point resolution of 1.14 and 1.17 Hz, respectively. The pulse width used in these experiments was 6 μs for both ^{77}Se and ^{119}Sn spectra, and no relaxation delay was applied. The number of free induction decays accumulated was 30,000 and 72,000 for ^{77}Se and ^{119}Sn, respectively. A line broadening of 50 Hz was typically applied.

The spectra were referenced to Me_2Se for ^{77}Se and Me_4Sn for ^{119}Sn at $\delta = 0$ ppm in DMF. Solutions of Ph_2Se_2 ($\delta = 460$ ppm) and Me_4Sn in DMF were used as external reference. The convention used for the chemical shifts is that a positive sign signifies a shift to high frequency compared to the reference compound.

RESULTS AND DISCUSSION

Synthesis

The preparation of $(Ph_4P)_2[Sn(Se_4)_3]$ was carried out by reacting $SnCl_4$ with Na_2Se_5 in DMF in the presence of Ph_4P^+ according to eq. (1):

$$SnCl_4 + 3Na_2Se_5 + 2Ph_4PCl \longrightarrow (Ph_4P)_2[Sn(Se_4)_3] + 6NaCl. \quad (1)$$

The reaction was accompanied by a sharp colour change from dark green to red–brown. Interestingly the same compound can be obtained by using $SnCl_2 \cdot 2H_2O$ as starting material which indicates that possible Sn^{2+}–Se_x^{2-} ($x > 1$) complexes are unstable towards internal redox chemistry resulting in the formation of Sn^{4+} species. This is similar to

the behaviour of the corresponding Fe^{2+}/Se_x^{2-},[2] Au^{+}/Se_x^{2-}[14,15] and Tl^{+}/Se_x^{2-}[12] systems from which only Fe^{3+}, Au^{3+} and Tl^{3+} complexes have been isolated.

The UV–vis spectrum of **I** in DMF solution has no characteristic absorption bands (300–800 nm) and features a rising absorbance at higher energies. The absence of a band around 650 nm suggests that the complex does not dissociate in this solvent to form Se_x^{-} radical anions (as has been observed in $[In_2Se_{21}]^{4-}$[11]) which are responsible for this absorption.[11,19] In the far-IR region of the spectrum we observe two sets of two absorptions at 273, 256 cm^{-1} and 181, 173 cm^{-1}, respectively. According to other literature data[2,20] we assign these sets, respectively, to Se—Se and Sn—Se vibrations.

The ^{77}Se NMR spectrum of **I** in DMF solution at room temperature, shows two peaks at 618 and 459 ppm, respectively, indicating that all three Se_4^{2-} ligands in the complex are equivalent [Fig. 1(A)]. The various conformations of the $SnSe_4$ five-membered rings (*vide infra*) interconvert in solution at room temperature. This is common in complexes containing Se_4^{2-} ligands, as in the series $[MQ(Se_4)_2]^{2-}$ (Q = O, S, Se)[2] where the fluxional behaviour persists down to −60°C. Table 3 summarizes pertinent ^{77}Se NMR chemical shifts from MSe_4 systems known thus far. In all cases but one, the metal-bound selenium atom resonance occurs at lower field than the corresponding ring-selenium resonance.[5,8] It was found in the isostructural (but not isomorphous) $[Pt(Se_4)_3]^{2-}$, the platinum-bound ^{77}Se resonance occurs at higher field than the corresponding non-platinum-bound ^{77}Se resonance.[21] Since we could not observe Sn—Se satellite peaks, we cannot unequivocally assign the resonances for $[Sn(Se_4)_3]^{2-}$.

The ^{119}Sn NMR spectrum of $[Sn(Se_4)_3]^{2-}$, in DMF solution at room temperature, shows a single peak at −723 ppm, as expected, consistent with the notion that the integrity of the complex is maintained in solution [Fig. 1(B)]. We did not observe satellite peaks that could be attributed to ^{119}Sn–^{77}Se coupling. The observed ^{119}Sn NMR chemical

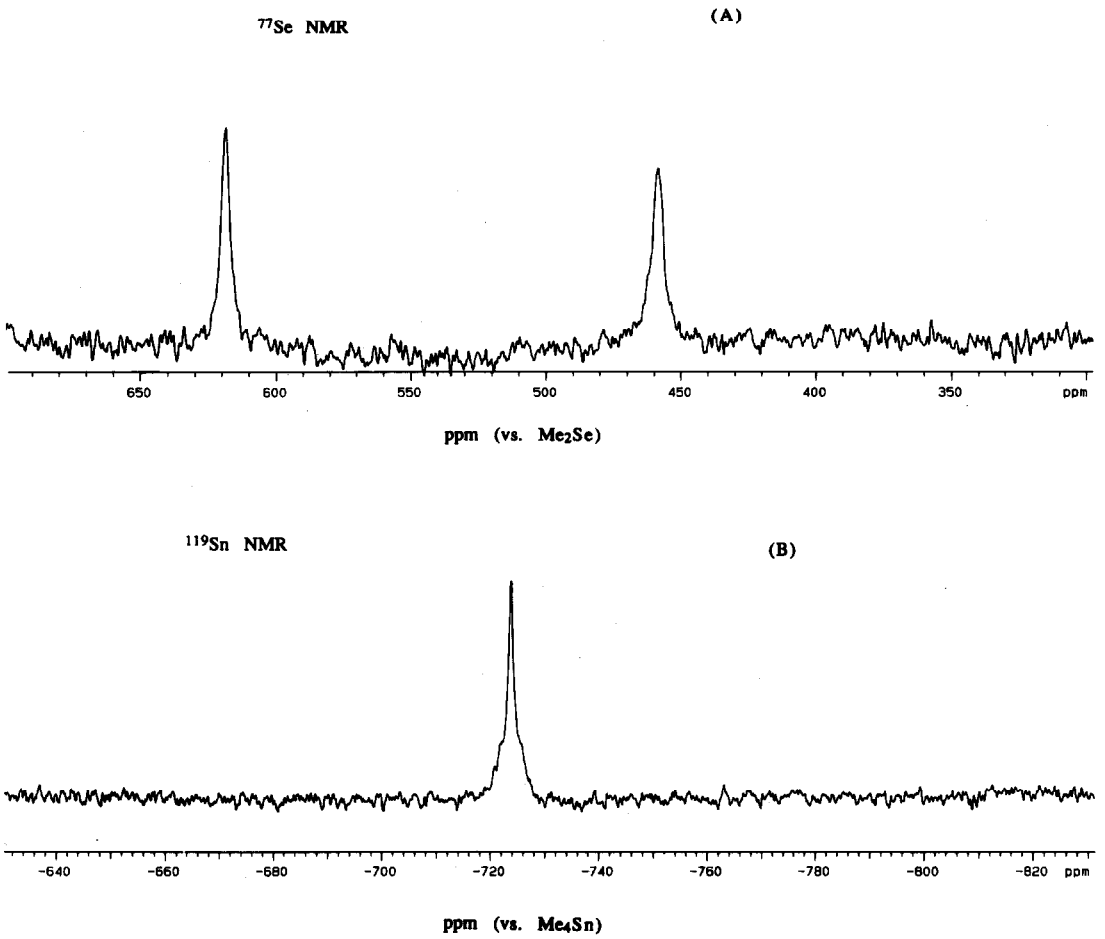

Fig. 1. (A) ^{77}Se NMR spectrum of $(Ph_4P)_2[Sn(Se_4)_3]$ in DMF at 25°C; (B) ^{119}Sn NMR spectrum of $(Ph_4P)_2[Sn(Se_4)_3]$ in DMF at 25°C.

Table 3. ^{77}Se NMR chemical shifts (in ppm) for metal–polyselenide compounds containing Se_4^{2-} ligands in DMF

Compound	Se_a[a]	Se_b[a]	Reference
$(Et_4N)_2[MoO(Se_4)_2]$	946	380	8
$(Et_4N)_2[MoS(Se_4)_2]$	1122	396	8
$(Et_4N)_2[MoSe(Se_4)_2]$	1163	403	8
$(Ph_4As)_2[WO(Se_4)_2]$	828	280	8
$(Ph_4As)_2[WS(Se_4)_2]$	993	313	8
$(Ph_4As)_2[WSe(Se_4)_2]$	1034	324	8
$(Ph_4P)_2[Zn(Se_4)_2]$	598	127	8
$(Ph_4P)_2[Zn(Se_4)_2]$	607	137	12
$(Ph_4P)_2[Cd(Se_4)_2]$	617	75	12
$(Et_4N)_2[Hg(Se_4)_2]$	604	86	12
$(Ph_4P)_2[Ni(Se_4)_2]$	829	759	12
$(Et_4N)_3[In_3Se_3(Se_4)_3]$	644	197	12
$(Ph_4P)_2[Sn(Se_4)_3]$	619	459	This work
$(Ph_4P)_2[Pt(Se_4)_2]$	680	790	21

[a] Labelling scheme of the MSe_4 ring system:

shift for $[Sn(Se_4)_3]^{2-}$, correlates well with those of $[SnSe_3]^{2-}$ and $[SnSe_4]^{4-}$ anions[22] which occur at −264.3 and −476.6 ppm, respectively. The successive shift of the ^{119}Sn resonance toward more negative values with increasing tin coordination number is evident and suggests increased shielding on the tin centre. This is consistent with similar trends observed for other tin complexes (e.g. the tin–halide series).[23]

TGA examination of the thermolysis of **I** under flowing nitrogen shows that the compound begins to lose weight at ~ 335°C as shown in Fig. 2. This onset temperature of initial weight loss, is shared by other Ph_4P^+ salts of polyselenide complexes and is due to the nucleophilic attack on the Ph_4P^+ cation by the Se_x^{2-} ligands to generate the volatile Ph_3P, Ph_3PSe, Ph_2Se, Ph_2Se_2, etc. Following a smooth and continuous weight loss, the decomposition of **I** results, at 520°C, in the formation of $SnSe_2$. Further heating results in the loss of one selenium to yield SnSe at ~ 660°C. $SnSe_2$ and SnSe were unequivocally identified by X-ray powder diffraction.

Description of the structure of **I**

The monoclinic unit cell contains well-separated $[Sn(Se_4)_3]^{2-}$ anions and Ph_4P^+ cations. The latter have the usual tetrahedral structure and will not be discussed further. The structure of the anion in **I** is similar to the recently reported $[Pt(Se_4)_3]^{2-}$[21] and $[Sn(S_4)_3]^{2-}$.[10] However, the latter was not isolated in pure form. It was found co-crystallized in the same crystallographic site (and therefore disordered) with $[Sn(S_4)_2(S_6)]^{2-}$, respectively, in a 4:6 ratio. No such disorder was detected in the present study. The structure of the $[Sn(Se_4)_3]^{2-}$ anion is shown in Fig. 3, and consists of three four-membered selenium chains chelated to a central Sn^{4+}. The coordination geometry of the Sn^{4+} is octahedral approaching D_3 symmetry, with an average Sn—Se bond distance of 2.709(13) Å, and a Se—Sn—Se angle of roughly 90°. A listing of selected bond distances and angles for $[Sn(Se_4)_3]^{2-}$ is given in Table 4. The observed Se—Se bonds are in the normal range of single Se—Se bond distances reported for other metal–polyselenide compounds. To the best of our knowledge $[Sn(Se_4)_3]^{2-}$ is the first

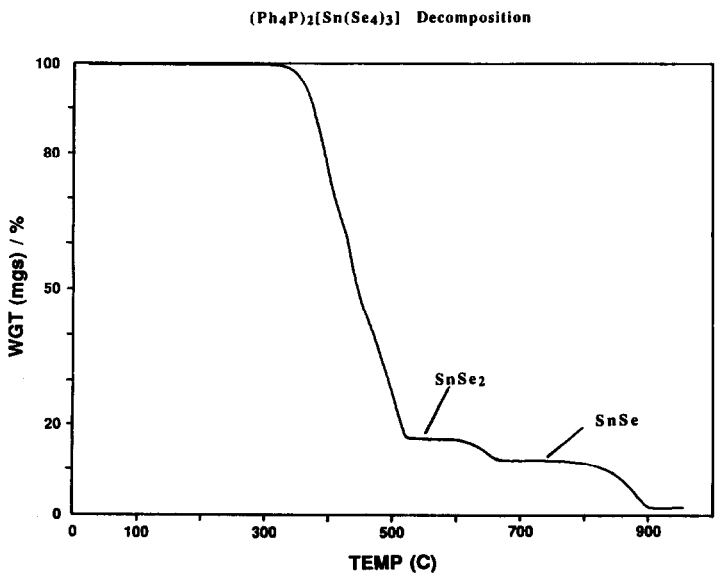

Fig. 2. Typical TGA diagram of **I** under flowing nitrogen.

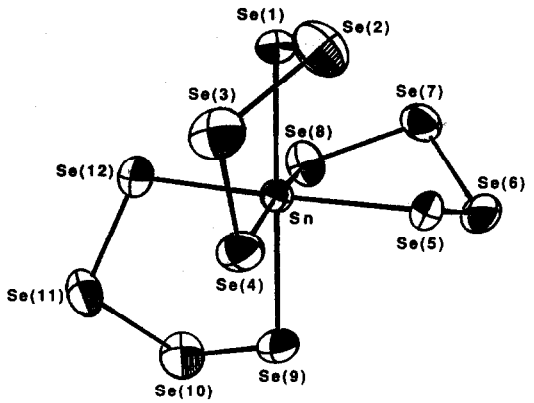

Fig. 3. ORTEP representation and labelling scheme of the structure of the $[Sn(Se_4)_3]^{2-}$ anion.

molecular example of a Sn^{4+} centre being coordinated in an octahedral fashion by six selenide atoms. A solid-state analogue is $SnSe_2$, in which the tin is coordinated octahedrally. The Sn—Se bond lengths in the anion of **I** are comparable to those found in $SnSe_2$[24] (2.683(2) Å) but shorter than those observed for SnSe[25] (2.793(2) and 2.744(3) Å). This difference is expected due to the Sn^{2+} oxidation state in SnSe. The Sn—Se bond, however, in $[Sn(Se_4)_3]^{2-}$ is much longer than that found in $[Sn_2Se_6]^{4+}$ (av. 2.508 Å) in which tin features a tetrahedral coordination.[26] The SnSe(1)Se(2)Se(3)Se(4) ring adopts the envelope comformation while the other two SenSe(5)Se(6)Se(7)Se(8) and SnSe(9)Se(10)Se(11)Se(12) adopt puckered conformations. Both of these conformations are common in Q_4^{2-} chemistry. For example, the envelope conformation is notable in the series $[M(Se_4)_2]^{2-}$[3] (M = Zn, Cd, Hg), while the puckered one is characteristic in the $[MQ(Se_4)_2]^{2-}$ (M = Mo, Q = Q, S, Se) series.[5]

With three *cis*-coordinated bidentate ligands, **I** can exist as optical isomers. The complex is a racemic mixture similar to the $[Pt(S_5)_3]^{2-}$[27] where

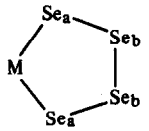

Table 4. Selected distances (Å) and angles (°) in the $[Sn(Se_4)_3]^{2-}$ anion. Standard deviations are shown in parentheses

Sn—Se(1)	2.694(3)	Se(1)—Se(2)	2.341(4)
Sn—Se(4)	2.705(3)	Se(2)—Se(3)	2.302(4)
Sn—Se(5)	2.718(3)	Se(3)—Se(4)	2.327(4)
Sn—Se(8)	2.697(3)	Se(5)—Se(6)	2.337(4)
Sn—Se(9)	2.733(3)	Se(6)—Se(7)	2.328(4)
Sn—Se(12)	2.708(3)	Se(7)—Se(8)	2.320(4)
		Se(9)—Se(10)	2.308(4)
Sn—Se(mean)	2.709(13)	Se(10)—Se(11)	2.332(4)
		Se(11)—Se(12)	2.319(4)
		Se—Se(mean)	2.324(12)
Intrachelate			
Se(1)—Sn—Se(4)	95.30(8)	Sn—Se(1)—Se(2)	100.6(1)
Se(5)—Sn—Se(8)	96.73(8)	Sn—Se(4)—Se(3)	104.9(1)
Se(9)—Sn—Se(12)	95.40(9)	Sn—Se(5)—Se(6)	101.9(1)
		Sn—Se(8)—Se(7)	101.6(1)
Interchelate		Sn—Se(9)—Se(10)	101.9(1)
Se(1)—Sn—Se(5)	91.15(9)	Sn—Se(12)—Se(11)	103.5(1)
Se(1)—Sn—Se(8)	91.31(9)		
Se(1)—Sn—Se(9)	172.51(9)	Sn—Se—Se(mean)	102(2)
Se(1)—Sn—Se(12)	87.53(9)		
Se(4)—Sn—Se(5)	84.18(9)	Se(1)—Se(2)—Se(3)	101.0(1)
Se(4)—Sn—Se(8)	173.31(9)	Se(2)—Se(3)—Se(4)	103.1(1)
Se(4)—Sn—Se(9)	77.49(9)	Se(5)—Se(6)—Se(7)	102.2(1)
Se(4)—Sn—Se(12)	79.91(9)	Se(6)—Se(7)—Se(8)	101.0(1)
Se(5)—Sn—Se(9)	86.15(9)	Se(9)—Se(10)—Se(11)	102.4(1)
Se(5)—Sn—Se(12)	177.62(9)	Se(10)—Se(11)—Se(12)	100.5(1)
Se(8)—Sn—Se(9)	95.94(9)		
Se(8)—Sn—Se(12)	81.32(9)	Se—Se—Se(mean)	101(1)

partial resolution of the optical isomers using (+)-$[Ru(Phen)_3]^{2+}$ as the counterion provided a carbon-free optically active inorganic molecule. Although we did not attempt it, the resolution of the optical isomers of $[Sn(Se_4)_3]^{2-}$ by a similar method should also be possible.

Acknowledgements—Financial support from the Donors of the Petroleum Research Fund, administered by the American Chemical Society, the Center for Fundamental Materials Research (CFMR) at Michigan State University and the NSF (for a Presidential Young Investigator Award) is gratefully acknowledged.

Supplementary material. Tables of atomic coordinates of all atoms and anisotropic and isotropic thermal parameters of all non-hydrogen atoms have been deposited with the Cambridge Crystallographic Data Centre.

REFERENCES

1. (a) A. Müller, *Polyhedron* 1986, **5**, 323; (b) M. Draganjac and T. B. Rauchfuss, *Angew. Chem. Int. Ed. Engl.* 1985, **24**, 742.
2. H. Strasdeit, B. Krebs and G. Henkel, *Inorg. Chim. Acta* 1984, **89**, L11.
3. J. Adel, F. Weller and K. Dehnicke, *Z. Naturfor.* 1988, **43b**, 1094.
4. M. G. Kanatzidis and S.-P. Huang, *J. Am. Chem. Soc.* 1989, **111**, 760.
5. (a) R. W. M. Wardle, C.-N. Chau and J. A. Ibers, *J. Am. Chem. Soc.* 1987, **109**, 1859; (b) C.-N. Chau, R. W. M. Wardle and J. A. Ibers, *Inorg. Chem.* 1987, **26**, 2740; (c) R. W. M. Wardle, S. Chaduri, C.-N. Chau and J. A. Ibers, *Inorg. Chem.* 1988, **27**, 1747; (d) R. W. M. Wardle, C. H. Mahler, C.-N. Chau and J. A. Ibers, *Inorg. Chem.* 1988, **27**, 2790.
6. (a) W. A. Flomer and J. W. Kolis, *J. Am. Chem. Soc.* 1988, **110**, 3682; (b) W. A. Flomer, S. C. O'Neal, W. T. Pennington, D. Jeter, A. W. Cordes and J. W. Kolis, *Angew. Chem. Int. Ed. Engl.* 1988, **27**, 1702; (c) S. C. O'Neal and J. W. Kolis, *J. Am. Chem. Soc.* 1988, **110**, 1971.
7. R. D. Adams, T. A. Wolfe, B. W. Eichhorn and R. C. Haushalter, *Polyhedron* 1989, **8**, 701.
8. (a) M. A. Ansari and J. A. Ibers, *Coord. Chem. Rev.* 1990, in press; (b) M. G. Kanatzidis, *Comm. Inorg. Chem.* 1990, in press.
9. A. Müller, M. Zimmermann and H. Bögge, *Angew. Chem. Int. Ed. Engl.* 1986, **25**, 273.
10. A. Müller, J. Schimanski *et al. Chimia* 1985, **39**, 25.
11. M. G. Kanatzidis and S. Dhingra, *Inorg. Chem.* 1989, **28**, 2024.
12. M. G. Kanatzidis and S. Dhingra, manuscript in preparation.
13. (a) M. G. Kanatzidis, *Abstr. 196th ACS Nat. Meet.*, Los Angeles 1988, INOR 469; (b) S. Dhingra, S.-P. Huang and M. G. Kanatzidis, manuscript in preparation.
14. M. G. Kanatzidis and S.-P. Huang, unpublished.
15. M. G. Kanatzidis and S.-P. Huang, *Inorg. Chem.* 1989, **28**, 4667.
16. G. M. Sheldrick, in *Crystallographic Computing* 3 (Edited by G. M. Sheldrick, C. Kruger and R. Goddard), pp. 175–189. Oxford University Press, Oxford (1985).
17. B. A. Frenz, *The Enraf–Nonius CAD4 SDP System.* In *Computing in Crystallography*, pp. 64–71. Delft University Press, Delft, Holland (1978).
18. D. K. Smith, M. C. Nichols and M. E. Zolensky, POWD 10: A FORTRAN Program for Calculating X-ray Powder Diffraction Patterns, Version 10. Pennsylvania State University (1983).
19. P. Dubois, J. P. Lelieur and G. Lepourte, *Inorg. Chem.* 1988, **27**, 73.
20. F. Weller, J. Adel and K. Dehnicke, *Z. Anorg. Allg. Chem.* 1987, **548**, 125.
21. M. A. Ansari and J. A. Ibers, *Inorg. Chem.* 1989, **28**, 4068.
22. R. C. Burns, L. A. Devereux, P. Granger and G. Schrobilgen, *Inorg. Chem.* 1985, **24**, 2615.
23. (a) J. D. Kennedy and W. McFarlane, in *Multinuclear NMR* (Edited by J. Mason), pp. 305–333. Plenum Press, New York (1987); (b) A. G. Davies, P. G. Harrison, J. D. Kennedy, R. J. Puddephatt, T. N. Mitchell and W. McFarlane, *J. Chem. Soc. A.* 1969, 1136.
24. B. L. Evans and R. A. Hazelwood, *J. Appl. Phys.* 1969, **2**, 1507.
25. H. Wiedemeier and H. G. von Schnering, *Z. Krist.* 1978, **148**, 295.
26. W. S. Sheldrick and H. G. Braunbeck, *Z. Naturfor.* 1989, **44b**, 851.
27. R. D. Gillard and F. L. Wimmer, *J. Chem. Soc., Chem. Commun.* 1978, 936.

Polyhedron Vol. 9, No. 11, pp. 1397–1400, 1990
Printed in Great Britain

0277–5387/90 $3.00+.00
© 1990 Pergamon Press plc

SYNTHESIS AND STUDY OF OXOVANADIUM(IV) COMPLEXES WITH DITHIOBIS(2,4-PENTANEDIONE)

RYSZARD GRYBOŚ* and WITOLD PAW

Faculty of Chemistry, Jagiellonian University, 30-060 Kraków, Poland

(*Received* 27 *February* 1989; *accepted after revision* 19 *January* 1990)

Abstract—Two vanadyl complexes of dithiobis(2,4-pentanedione), $H_2acac_2S_2$, with 1 : 1 : 1 (metal–$acac_2S_2$–L, where L = DMSO, py) stoichiometry have been characterized by elemental analysis, IR and optical spectral studies, field desorption mass spectrometry and magnetic susceptibility measurements. It is concluded that trinuclear complexes $[VO(acac_2S_2)DMSO]_3$ (**A**) and $[VO(acac_2S_2)py]_3$ (**B**) are formed, for which cyclic structural forms are proposed.

Polynuclear metal complexes in which metal ions are linked together by di- or polyfunctional organic ligands are an area of intense studies due to the potential possibility of applications of these complexes in electronics, microlithography or catalysis.[1] Various bis(β-diketones) and metal ions have been used for the synthesis of these complexes.[2–5] However, polynuclear metal complexes containing thiobis(β-diketones) as bridging ligands have not been numerous.[2,6,7] These complexes are insoluble in water and organic solvents, making difficult the study of their properties. In an attempt to explore in some detail the coordination chemistry of these ligands, vanadyl complexes were synthesized and characterized by spectroscopic methods in addition to the data based on analyses and magnetic susceptibility.

EXPERIMENTAL

Materials

3,3′-Dithiobis(2,4-pentanedione), $H_2acac_2S_2$, was prepared by the method described in the literature[6] and gave satisfactory analyses, ^1H NMR and IR spectra. Oxobis(2,4-pentanedionato)vanadium(IV), $VO(acac)_2$ (Alfa Products) was recrystallized from acetone. Dimethyl sulphoxide (DMSO) (Reachim, U.S.S.R.) was dried over CaO and distilled under reduced pressure. Pyridine (py) (POCh, Gliwice) was used without further purification.

* Author to whom correspondence should be addressed.

Preparation of $[VO(acac_2S_2)DMSO]_3$ (A)

Equivalent amounts of $VO(acac)_2$ (10 mmol) and $H_2acac_2S_2$ (10 mmol) were added to 200 cm^3 DMSO. The mixture was stirred until both reagents were completely dissolved. The solution was heated to 45°C using a hot plate. DMSO and 2,4-pentanedione were evaporated under reduced pressure until no solvent remained. The powder obtained was washed three times with 15 cm^3 portions of benzene to remove the brown by-product and/or unreacted reagents, then filtered and dried *in vacuo* at room temperature. The yield of crude product was 95%. The pure product was obtained by recrystallization from DMSO, washed with diethyl ether and dried *in vacuo* at room temperature. Found: V, 12.2; C, 34.7; H, 4.56; S, 23.6. Calc. for $[VO(acac_2S_2)DMSO]_3$: V, 12.6; C, 35.5; H, 4.48; S, 23.7%. The complex does not melt but decomposes on heating at about 150°C.

The same product was obtained when the reaction was carried out at the molar ratio $VO(acac)_2$–$H_2acac_2S_2$ equal to 1.5 : 1.

Preparation of $[VO(acac_2S_2)py]_3$ (B)

$[VO(acac_2S_2)DMSO]_3$ (1 g) was dissolved in 50 cm^3 of warm pyridine and then the solution was stored in a refrigerator for a few days. The solid obtained was filtered off, washed with diethyl ether and dried *in vacuo* at room temperature. Found: V, 12.3; C, 44.4; H, 4.55; S, 15.6; N, 3.8. Calc. for $[VO(acac_2S_2)py]_3$: V, 12.6; C, 44.3; H, 4.18; S,

15.8; N, 3.45%. The complex does not melt but decomposes on heating at about 200°C.

Analytical methods

Carbon, hydrogen, nitrogen and sulphur were determined by organic microanalysis procedures. Vanadium was determined by manganometric titration after decomposition of the complex with hot 3 M H_2SO_4.

Physical measurements

The attempted determination of melting points was performed on "Boetius" apparatus (MLW, VEB Analytik, G.D.R.). A Carl Zeiss Jena (G.D.R.) Model UR-10 IR spectrophotometer was used to obtain the spectra in the range 4000–400 cm^{-1}. The KBr disc method was employed for the preparation of the sample. The electronic absorption spectra in the range 400–1300 nm were recorded using a Perkin–Elmer, Lambda 9, UV–vis–NIR spectrophotometer. The field desorption (FD) mass spectra were obtained on a Varian MAT-711 mass spectrometer by desorption of the samples from 10 μm tungsten wire at 20 mA. Magnetic measurements were carried out on Bruker (F.R.G.) apparatus using the Faraday technique over the temperature range 98–293 K, with $Hg[Co(NCS)_4]$ as a calibrant. Diamagnetic corrections were estimated from Pascal's constants.[8]

RESULTS AND DISCUSSION

$[VO(acac_2S_2)DMSO]_3$ (**A**) and $[VO(acac_2S_2)py]_3$ (**B**) are yellow–green powders which are stable in air. They are soluble in pyridine and DMSO but insoluble in hydrocarbons, CCl_4, H_2O and benzene. Complexes **A** and **B** decompose in alcohols, acetone, THF and $CHCl_3$, and the rate of decomposition depends on the solvent, being very rapid in $CHCl_3$ and slow in acetone.

It is evident from the elemental analyses that oxovanadium(IV) forms complexes with 1:1:1 (metal–ligand–solvent) stoichiometry. Jones and Power[6] suggested a polymeric helical type structure for insoluble 1:1 complexes of cobalt, copper and nickel of $acac_2S_2^{2-}$ based on the spectral data in the visible region. Two structural forms which satisfied the metal to ligand ratio (1:1) are possible: polymeric and cyclic oligomeric. For the polymeric structure containing a chain of alternate ($acac_2S_2$) and (VOL) units this ratio is reached for the average degree of polymerization higher than ten. For the cyclic form, the metal to ligand ratio is equal 1:1 and is independent of the degree of polymerization. The best resolution of this problem would be to determine the molecular weight of the complexes. Unfortunately, attempts to determine the molecular weights of **A** and **B** in DMSO or pyridine by vapour pressure osmometry were unsuccessful due to the hygroscopic properties of the solvents and/or partial decomposition of the complexes under experimental conditions.

We tried to resolve this problem using FD technique. The mass spectral studies on $VO(acac)_2$[9] showed that electron ionization produced both parent and fragment ions, whereas field desorption produced molecular and dimeric ions (dimeric ions were present in low relative abundance). Thus the FD technique can be useful for the molecular weight determination of neutral complexes.[10] FD mass spectra of **A** and **B** show a signal for the molecular ion $[VO(acac_2S_2)]_3^+$ at m/z 981. Assuming that under FD conditions the solvent molecules (DMSO or pyridine) are liberated, both complexes could be regarded as trimeric species, $[VO(acac_2S_2)]_3$. It appears that the cyclic trimeric structure (Fig. 1) is more reliable for complexes **A** and **B** than the polymeric structure.

The IR spectroscopic data in the interesting 400–1700 cm^{-1} range and the possible assignments are given in Table 1.

The spectra exhibit two intense closely-spaced bands in the 1583–1560 cm^{-1} region. The high-frequency band is assigned to C···O and the lower-frequency one to the C···C stretching modes.[11,12] This is characteristic for chelation of the β-diketone to metal ion through oxygen atoms.

Interpretation of the spectrum of **A** in the 1100–900 cm^{-1} range is difficult because the V=O and S=O stretching, as well as CH_3 rocking modes, are expected to appear in this region. The strong absorption band observed in the spectrum of **A** at 990 cm^{-1} is assigned to ν(S=O). It is expected that the attachment of the DMSO molecule to a vanadium ion through oxygen should cause a

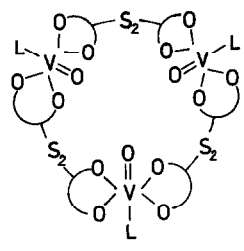

Fig. 1. Schematic representation of trinuclear vanadyl-$acac_2S_2$ complexes.

Table 1. IR data (cm^{-1}) for $[VO(acac_2S_2)DMSO]_3$ (**A**) and $[VO(acac_2S_2)py]_3$ (**B**)[a]

A	B	Tentative assignments[b]
1583 s	1580 vs	ν(C⋯O)
1563 vs	1560 vs	ν(C⋯C)
1412 s	1410 s	CH_3 deg. def.
1365 vs	1365 vs	CH_3 sym. def.
1332 s	1335 vs	
1325 s	—	
1255 w	1262 vw	ν(C—C)+ν(C—CH_3)
1068 m	1075 m	
1020 m	1025 m	CH_3 rock
990 s	—	ν(S=O)
—	965 s	ν(V=O)
945 s	—	ν(V=O)+CH_3 rock (DMSO)
910 vw	918 vw	ν(C—CH_3)
720 vw	—	ν(C—S) antisym. (DMSO)
700 vw	—	ν(C—S) sym. (DMSO)
685 vw	—	ν(V—O)+ring def.
660 vw	665 vw	π
605 w	608 w	ν(V—O)
570 vw	575 vw	
492 w	495 s	ν(V—O)+δ(C—CH_3)
475 vw	460 m	
450 w	445 w	ν(S—S)
435 w	—	δ(O—V—O) in-plane

[a] Intensity designations: vs—very strong, s—strong, m—medium, w—weak, vw—very weak.

[b] ν, δ and π denote stretching, bending and out-of-plane bending modes, respectively. Not all the pyridine bands are listed.

decrease in the electron density on the DMSO oxygen atom, this results in the lowering of the S=O bond order and hence ν(S=O). The assignment is in agreement with the observed lowering of the ν(S=O) band from 1045 in free DMSO to the 1000 cm^{-1} region for transition metal complexes with DMSO.[13] It is also known that coordination of the additional ligand (e.g. substituted pyridines[14]) to $VO(acac)_2$ shifts the ν(V=O) band to lower frequencies, thus the strong band observed for **A** and **B** at 945 and at 965 cm^{-1}, respectively, is assigned to ν(V=O).

Two weak bands at 720 and 700 cm^{-1} which are observed in the spectrum of **A** can be assigned to the C—S stretching mode of DMSO.[15]

The weak band at 450 cm^{-1} observed in both the complexes and $H_2acac_2S_2$ we propose to assign to the —S—S— stretching mode which should occur in the 500–400 cm^{-1} region.[16] For S_2Cl_2 this band appears at 448 cm^{-1}.[17]

The spectrum of **B** shows the pyridine bands,[18] which are not listed in Table 1.

The electronic spectra of vanadyl complexes having a square pyramidal or a distorted octahedral structure are most often interpreted in terms of the energy level scheme proposed by Ballhausen and Gray.[19] Usually three optical bands are observed in the visible region, assigned to (I) $^2B_2(d_{xy}) \rightarrow {}^2E(d_{xz}, d_{yz})$; (II) $^2B_2(d_{xy}) \rightarrow {}^2B_1(d_{x^2-y^2})$; and (III) $^2B_2(d_{xy}) \rightarrow {}^2A_1(d_{z^2})$. Band III is often obscured by intense absorption tailing in from the UV.

The electronic spectra in the range 400–1300 nm of $[VO(acac_2S_2)DMSO]_3$ and $[VO(acac_2S_2)py]_3$ in DMSO and pyridine, respectively, are shown in Fig. 2 together with the spectra of $VO(acac)_2$. All the spectra show two bands and only the spectrum of $VO(acac)_2$ in DMSO exhibits three bands.

The first band, assigned to a $^2B_2 \rightarrow {}^2E$ transition, observed in the spectrum of $VO(acac)_2$ in DMSO at 784 ($\varepsilon = 45$) and in pyridine at 765 nm ($\varepsilon = 42$ $dm^3\ mol^{-1}\ cm^{-1}$) is displaced to 807 ($\varepsilon/V^{4+} = 40$) and 750 nm ($\varepsilon/V^{4+} = 46$) in complexes **A** and **B**, respectively.

The second band, assigned to a $^2B_2 \rightarrow {}^2B_1$ transition, observed for $VO(acac)_2$ in DMSO at 594 ($\varepsilon = 16$) and in pyridine at 580 ($\varepsilon = 29$) is shifted to 629 ($\varepsilon/V^{4+} = 21$) and 581 nm ($\varepsilon/V^{4+} = 29$ $dm^3\ mol^{-1}\ cm^{-1}$) in complexes **A** and **B**, respectively.

The electronic spectral data suggest that the vanadium(IV) ion in complexes **A** and **B** exists in the distorted octahedral local environment in agreement with Fig. 1.

The magnetic moments of both the complexes are found to be practically constant in the range 98–293 K. Complexes **A** and **B** have magnetic moment values of 1.78 and 1.77 BM (293 K) per metal atom, respectively, which are consistent with the spin-only value for a d^1 case. Furthermore, they are very

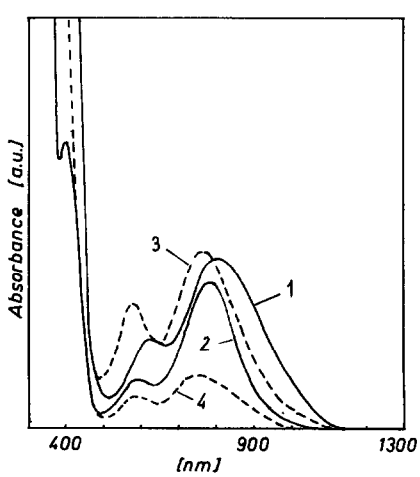

Fig. 2. The electronic spectra of (1) $[VO(acac_2S_2)DMSO]_3$ and (2) $VO(acac)_2$ in DMSO, and (3) $[VO(acac_2S_2)py]_3$ and (4) $VO(acac)_2$ in pyridine.

close to the reported values, 1.71–1.76 BM, for the oxovanadium(IV) β-diketones.[20] These results suggest that there are no direct V—V interactions in the solid complexes.

Acknowledgements—The authors wish to express their sincere thanks to Professor A. Samotus (Jagiellonian University, Kraków) for her interest, helpful suggestions and useful discussions, and to Professor K. Wieghardt (Ruhr University, Bochum), for the use of the Perkin–Elmer spectrophotometer and the Bruker apparatus for magnetic measurements. This work was supported in part by the Polish Academy of Sciences under Contract CPBP 01.12.9.5.

REFERENCES

1. J. E. Sheats, C. E. Carraher Jr and C. U. Pittman Jr, *Metal-containing Polymeric Systems*. Plenum Press, New York (1985).
2. J. S. Oh and J. C. Bailar Jr, *J. Inorg. Nucl. Chem.* 1962, **24**, 1225.
3. E. S. Krongauz and A. M. Berlin, *Russ. Chem. Rev.* 1969, **38**, 655.
4. D. E. Fenton, J. R. Tate, U. Casellato, S. Tamburini, P. A. Vigato and M. Vidali, *Inorg. Chim. Acta* 1984, **83**, 23.
5. A. W. Maverick and F. E. Klavetter, *Inorg. Chem.* 1984, **23**, 4129.
6. R. D. G. Jones and L. F. Power, *Aust. J. Chem.* 1971, **24**, 735.
7. R. D. Archer, C. J. Hardiman, R. Gryboś and J. C. W. Chien, *US Pat.* 4,693,957 sep. 15 (1987).
8. C. J. O'Connor, *Prog. Inorg. Chem.* 1982, **29**, 203.
9. S. E. Unger, *Analyt. Chem.* 1985, **57**, 776.
10. R. L. Cerny, B. P. Sulivan, M. M. Bursey and T. J. Meyer, *Analyt. Chem.* 1983, **55**, 1954.
11. K. Nakamoto, Y. Marimoto and A. E. Martell, *J. Am. Chem. Soc.* 1961, **83**, 4533.
12. R. C. Mehrotra, R. Bohra and D. P. Gaur, *Metal-diketones and Allied Derivatives*, p. 109. Academic Press, London (1978).
13. R. S. Drago and D. W. Meek, *J. Phys. Chem.* 1961, **65**, 1446.
14. M. R. Caira, J. M. Haigh and L. R. Nassimbeni, *J. Inorg. Nucl. Chem.* 1972, **34**, 3171.
15. W. D. Horrocks Jr and F. A. Cotton, *Spectrochim. Acta* 1961, **17**, 134.
16. L. J. Bellamy, *The Infrared Spectra of Complex Molecules*, p. 397. Chapman and Hall, London (1975).
17. K. Isobe, Y. Nakamura and S. Kawaguchi, *J. Inorg. Nucl. Chem.* 1978, **40**, 607.
18. I. S. Perelygin and M. A. Klimchuk, *Zh. Prikl. Spektrosk.* 1976, **24**, 65.
19. C. J. Ballhausen and H. B. Gray, *Inorg. Chem.* 1962, **1**, 111.
20. K. S. Patel, *J. Inorg. Nucl. Chem.* 1981, **43**, 667.

Polyhedron Vol. 9, No. 11, pp. 1401–1403, 1990
Printed in Great Britain

0277-5387/90 $3.00+.00
Pergamon Press plc

SYNTHESIS, CHARACTERIZATION AND CATALYTIC BEHAVIOUR OF THORIUM PEROXO COMPLEXES

D. D. AGARWAL,* SAVITA SRIVASTAVA and POONAM CHADHA

School of Studies in Chemistry, Jiwaji University, Gwalior 474011 (M.P.), India

(*Received* 18 *September* 1989; *accepted* 29 *January* 1990)

Abstract—Stable peroxo complexes of thorium are formed which are unreactive as stoichiometric reagents but active as catalysts in the presence of tert-butylhydroperoxide, resulting in the formation of cyclohexenone and cyclohexenol in substantial yields together with cyclohexene oxide. Competitive epoxidation of cyclo-olefins suggests that coordination of olefins to the metal centre does not take place.

In recent years there has been considerable interest in the investigation of peroxo complexes of transition metals.[1] The peroxo complexes of molybdenum,[2] titanium,[3–5] uranium,[6] chromium,[7,8] vanadium,[9] zirconium,[10] thorium,[11,12] etc., have been studied. In continuation of our efforts[13,14] to find new oxidizing systems we report here the synthesis, characterization and catalytic behaviour of some thorium peroxo complexes synthesized using the ligands, bis(salicylaldehyde)ethylene diamine (SALEN), bis(acetylacetone)ethylenediamine (ACEN), bis(anthranilic acid)acetylacetone (ANAC), 2 - carboxyphenylhydrazonopentane - 2,4 - dione (ANAC hydrazone), salicylaldehyde-O-aminophenyl (SAP), salicylaldehyde anthranilic acid (SAC), bis(salicylaldehyde)-1,3-diamino propane (SAPEN), bis(salicylaldehyde)-O-phenylene diamine (SALPHEN).

EXPERIMENTAL

All ligand components were used as obtained from commercial sources. Absolute alcohol was prepared following the method in ref. 15. $Th(NO_3)_4 \cdot 6H_2O$ was obtained from Loba Chemical Laboratories and 30% H_2O was purchaed from Glin India Ltd. All alkenes were checked by gas chromatography, and if needed purified[15] and stored under N_2. Tert-butylhydroperoxide (TBHP), Aldrich, was dried and estimated.[16] The reference sample of the epoxides were prepared following the methods in refs 17 and 18. Elemental analysis (C H N) was performed using a Carlo-Erba elemental analyser, and IR spectra were recorded using a Perkin–Elmer spectrophotometer in the range 4000–250 cm^{-1}. Analytical gas chromatography was carried out using a Nucon-Amil-5700 series gas chromatograph fitted with a Shimadzu CR-3A data processor. XE-60 and Carbowax-20M columns were used.

Synthesis of the complexes

The ligands were synthesized by literature procedures.[19] The complexes were synthesized by taking $Th(NO_3)_4 \cdot 6H_2O$ (0.02 mol) in water (10 cm^3) and adding the ligand (0.02 mol) in methanol (25 cm^3). To this mixture 12.5 cm^3 of 30% H_2O_2 was added. The resulting mixture was stirred and heated on a water bath for 15 min. The precipitated complex was filtered, washed with water, ether and then dried. The complexes of anthanilic acid and O-aminophenol were synthesized by the reported[12] method. The conductance, melting point and elemental analysis data are given in Table 1.

Epoxidation

Cyclohexene (0.02 mol), TBHP (0.002 mol), a catalyst (0.002 mmol) and benzene (20 cm^3) were heated at 70°C under N_2 for 4 h. The hydroperoxide was decomposed, the contents were than extracted in ether and the products identified. The effect of $NaHCO_3$ and NaH_2PO_4 was studied by adding 100 mg of the same.

* Author to whom correspondence should be addressed.

Table 1. Elemental analysis[a] and conductance data for peroxo thorium(IV)

S. No.	Complex	Melting point (°C)[b]	C (%)	H (%)	N (%)	Molar conductance
1.	ThO_2(SALEN)	250(d)	36.1 (36.2)	2.7 (2.6)	5.2 (5.3)	2.02
2.	ThO_2(ACEN)	260(d)	30.1 (29.6)	3.6 (3.7)	5.8 (5.8)	1.50
3.	ThO_2(ANAC)	250(d)	38.1 (38.0)	2.5 (2.7)	4.8 (4.7)	1.20
4.	ThO_2(ANAC hydrazone)·H_2O	280(d)	27.1 (27.1)	2.3 (2.3)	5.4 (5.3)	0.54
5.	ThO_2(SAP)·H_2O	280(d)	31.5 (31.6)	2.3 (2.2)	2.7 (2.8)	0.62
6.	ThO_2(SAC)·H_2O	280(d)	32.3 (32.2)	2.1 (2.1)	2.7 (2.7)	1.00
7.	ThO_2(SAPEN)	240(d)	37.3 (37.5)	3.0 (2.9)	5.1 (5.1)	0.08
8.	ThO_2(SALPHEN)	240(d)	41.6 (41.5)	2.5 (2.4)	4.7 (4.8)	1.82
9.	ThO_2(anthranilic acid)$_2$	280(d)	31.2 (31.3)	2.2 (2.2)	5.2 (5.2)	1.42
10.	ThO_2(O-aminophenol)$_2$	280	30.1 (30.0)	2.6 (2.5)	5.8 (5.8)	2.00

[a] Calculated values are given in parentheses.
[b] d = decompose.

Competitive epoxidation

The competitive epoxidation of cyclopentene, cyclohexene, cycloheptene, cyclo-octene and norbornene was studied by mixing cyclohexene (20 mmol), another olefin (20 mmol), catalyst (0.004 mmol) and TBHP (0.004 mol) in benzene (10 cm^3) and heating this at 70°C under N_2 for 4 h.

RESULTS AND DISCUSSION

Elemental analyses (Table 1) (C, H and N) are in accordance with the calculated values. The molar conductance data in DMSO (10^{-3} M) show that they are non-electrolytes[12] (1.5–4.5 Ω^{-1} cm^2 mol^{-1}), Table 1.

The IR spectra of ThO_2(SALEN) display the ν(C=N) band 20 cm^{-1} lower (1600 cm^{-1}) than in ligand.[20] The shifted stretching band at 1220 cm^{-1} suggests involvement of ν(C—O). The ν(OH) stretching dimer at 2690 cm^{-1} disappears in the ThO_2(ANAC) complex. The ν(C=O) band at 1660 cm^{-1}, due to the internally hydrogen-bonded carboxylic group, and the ν(OH) in-plane bending at 1320 cm^{-1} disappear, suggesting that the carboxyl group is involved. The IR spectra of ThO_2(ANAC hydrazone)·H_2O show a band at 1620 cm^{-1} [ν(C=O)], lower by 20 cm^{-1}. In this complex the possible involvement of C=O, NH and COOH takes place. The non-electrolytic nature of the complex also suggests that NH is coordinated.[14] The IR spectra of ThO_2(SAP)·H_2O show a band at 1625 cm^{-1}, lower by 25 cm^{-1}. Also, a band at 1230 cm^{-1} is assigned to the C—O group suggesting that C=N and OH groups are involved in coordination. The bands in the Raman spectra for all the complexes in the region 830–815 cm^{-1} are assigned to O—O and Th—O—O frequencies. The band at 405–390 cm^{-1} suggests a Th—O mode.[11] The IR spectra of ThO_2(SAPEN), ThO_2(ACEN) and ThO_2(SALPHEN) are similar to that observed for ThO_2(SALEN). The IR spectra of ThO_2(SAC)·H_2O, ThO_2(anthranilic acid)$_2$, ThO_2(O-aminophenol)$_2$ are the same as those reported by Tarafdar and co-workers.[11,12] The two representative structures are as follows:

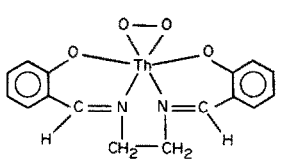

ThO_2(SALEN)

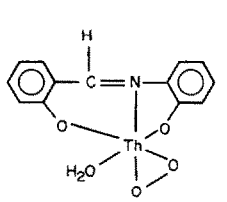

ThO_2(SAP)·H_2O

Epoxidation

When thorium peroxo complexes were subjected to stoichiometric reaction with cyclohexene no product was observed even after 10 h. When the formation of products was followed using the ThO_2(anthranilic acid)$_2$/TBHP system it was observed that the yield of cyclohexenol and cyclohexenone was the same for the first 60 min, but as time passed the yield of cyclohexenone increased and after 4 h the yield of cyclohexenone (0.050 mmol) was 12.5 times greater than cyclohexenol (0.004 mmol). The yield of epoxide was 0.01 mmol and the catalyst turnover number 150. Similar behaviour was observed with the CrO_3/TBHP system.[21] ThO_2(O-aminophenol)$_2$, ThO_2(SAC)·H_2O and ThO_2(SALPHEN) produced no epoxide, but the allylic oxidation produced cyclohexenol (0.018, 0.006, 0.012 mmol) and cyclohexenone (0.055, 0.014, 0.040 mmol), respectively. ThO_2 (ACEN) and ThO_2(ANAC hydrazone)·H_2O produced epoxide (0.013, 0.002 mmol) together with cyclohexenol (0.081, 0.014 mmol) and cyclohexenone (0.202, 0.026 mmol), respectively. The high yield of allylic oxidation products shows that the peroxo complex/TBHP is a good system for the hydroxylation of alkenes.

Epoxidation of cyclo-olefins shows the relative rate of reactivity: cyclo-octene (13.65) > norbornene (11.0) > cyclopentene (3.20) > cycloheptene (1.60) > cyclohexene (1.0). The higher rates for norbornene, cyclo-octene and cycloheptene compared to cyclohexene show that the olefin is not coordinated to the metal centre during epoxidation.[9] Similar results to those for the ThO_2 (ACEN)/TBHP system have been observed with the O=Mo(TPP)OMe/cumene hydroperoxide[22] and the MoO_2(SALEN)/TBHP[13] systems. This shows that conformation bond angle strain and torsional strain play important roles in determining the relative rates for cyclic olefins.

Effect of additives

The addition of $NaHCO_3$ and NaH_2PO_4 reduces the yield of epoxide. This is explained by the fact, as observed in O=Mo(TPP)OMe,[22] O=Ti (TPP)/TBHP[5] and MoO_2(SALEN)/TBHP[13] systems, that $NaHCO_3$ retards the yield of epoxide because it promotes peroxo complex formation, which is inactive.[23] In the present case also it is preventing the opening of the peroxo linkage thereby reducing the yield.

A mechanism similar to the vanadium-catalysed reaction[24] is proposed.

Acknowledgements—The authors are thankful to Professor R. P. Bhatnagar for facilities and CSIR, New Delhi, for financial assistance.

REFERENCES

1. H. Mimoun, *J. Molec. Catal.* 1980, **7**, 1.
2. H. Mimoun, *Rev. Inst. Fr. Petrol.* 1978, **33**, 259.
3. D. Schwarzenbach, *Helv. Chim. Acta* 1972, **55**, 2990.
4. H. Mimoun, M. Postel, F. Casabianca, J. Fischer and A. Mitsnler, *Inorg. Chem.* 1982, **21**, 1303.
5. H. J. Ledon and F. Varescon, *Inorg. Chem.* 1984, **23**, 2735.
6. A. D. Westland and M. T. H. Tarafdar, *Inorg. Chem.* 1981, **20**, 3992.
7. D. A. House, R. G. Hughes and C. S. Garner, *Inorg. Chem.* 1967, **6**, 1077.
8. S. H. Caldwell and D. A. House, *Inorg. Chem.* 1969, **8**, 151.
9. H. Mimoun, M. Mignard, P. Brechot and L. Saussine, *J. Am. Chem. Soc.* 1986, **108**, 3711.
10. M. T. H. Tarafdar and M. A. L. Miah, *Inorg. Chem.* 1986, **25**, 2265.
11. A. D. Westland and M. T. H. Tarafdar, *Inorg. Chem.* 1982, **21**, 3228.
12. M. T. H. Tarafdar, *Ind. J. Chem.* 1987, **26A**, 874.
13. D. D. Agarwal, *J. Molec. Catal.* 1988, **44**, 65.
14. D. D. Agarwal and Savita Srivastava, *Polyhedron* 1988, **7**, 2569.
15. D. D. Perrin, W. L. Armarego and D. R. Perrin, *Purification of Laboratory Chemicals.* Pergamon Press, New York (1980).
16. K. B. Sharpless and T. R. Verhoeven, *Aldrichim. Acta* 1979, **12**, 63.
17. D. Swern, *Org. React.* 1953, **7**, 378.
18. L. F. Fieser and M. Fieser, *Reagents for Organic Synthesis*, Vol. I. John Wiley, New York (1967).
19. G. Wilkinson (Ed.), *Comprehensive Inorganic Chemistry*, Vol. 3. Pergamon Press, Oxford (1987).
20. J. R. Dyer, *Application of Absorption Spectroscopy of Organic Compounds.* Prentice Hall of India (1974).
21. D. D. Agarwal, Savita Srivastava and Poonam Chadha, *Polyhedron* 1990, **9**, 487.
22. F. Varescon, Thesis L'Universite Claude Bernard, Lyon, France (1982).
23. M. Inamo, S. Funahashi and M. Tamaka, *Inorg. Chem.* 1985, **24**, 2475.
24. H. Mimoun, *Comprehensive Coordination Chemistry* (Edited by G. Wilkinson, R. D. Gillard and J. A. McCleverty), Vol. 6. Pergamon Press, New York (1987).

Polyhedron Vol. 9, No. 11, pp. 1405–1409, 1990
Printed in Great Britain

0277–5387/90 $3.00+.00
Pergamon Press plc

SYNTHESIS AND CHARACTERIZATION OF SOME PEROXO COMPLEXES OF ZIRCONIUM

D. D. AGARWAL,* RAJEEV JAIN, R. P. BHATNAGAR and SAVITA SRIVASTAVA

School of Studies in Chemistry, Jiwaji University, Gwalior 474011 (M.P.), India

(*Received* 14 *September* 1989; *accepted* 8 *February* 1990)

Abstract—The peroxo complexes of zirconium using bidentate, tridentate and tetradentate ligands have been synthesized and characterized. Oxidation studies showed that when Ph_3P, cyclohexene and allylalcohol were involved, the peroxo complexes with the tetradentate ligand failed to oxidize Ph_3P while the one with the bidentate ligand did. The peroxo complexes involving bidentate and tetradentate ligands gave peroxide when cyclohexene (the substrate) in the presence of tert-butyl hydroperoxide as oxidant was oxidized. The peroxo complexes with the bidentate ligand gave higher yields of peroxide compared with the tetradentate ligand complex. The peroxo complexes failed to oxidize stoichiometrically allylalcohol and cyclohexene. This shows that peroxo complexes containing the tetradentate moiety are more stable.

The chemistry of oxo and peroxo complexes is of interest as they may be potential oxidants or oxidation catalysts for the oxygen atom transfer reaction to organic substrates.[1–16] The peroxo complexes of molybdenum tungsten, uranium, thorium and titanium have been studied.[17–21] Titanium compounds have been found to be potential catalysts for asymmetric synthesis, while O=Ti(TPP)[9] has been found to be a potential catalyst for olefin epoxidation,[22] and at the end of the reaction a peroxotitanium complex is obtained. Studies of zirconium peroxo complexes and their reactivity were needed to discover the catalytic potential of zirconium complexes. We have studied the catalytic behaviour of various oxo complexes of molybdenum and titanium[23,24] and we now report our studies on zirconium peroxo complexes of some tri- and tetradentate ligands and their reactivities with various substrates to test their oxygen atom transfer capabilities.

EXPERIMENTAL

Physical measurements

The elemental analyses (C, H, N) were determined using a Carlo-Erba elemental analyser. IR spectra were recorded with Perkin–Elmer IR spectrophotometer. Conductivities of the solutions in dimethylsulphoxide were measured using a conductivity bridge. The oxidation products were followed with a NUCON-Amil-5700 series gas chromatograph fitted with a CR-3A Shimadzu data processor. XE-60 was used as the column at 120°C.

Reagents

Zirconium nitrate dihydrate, anthranalic acid, acetylacetone, salicylaldehyde, ethylenediamine, *o*-aminophenol, acetoacetanilide, triphenylphosphine, cyclohexene, dodecane, etc., were from Aldrich, Merk or Fluka. Dry tert-butylhydroperoxide was prepared by a literature method.[25]

Preparation of the Schiff bases

All the Schiff bases were synthesized by condensing the respective aldehyde or ketone with amine in methanol following a published procedure.[24]

Preparation of the complexes

A solution of $Zr(NO_3)_4 \cdot 2H_2O$ (0.01 mol) in 30% H_2O_2 (30 cm^3) was added to a solution of the bidentate ligand (0.02 mol) in boiling acetone (50 cm^3). The contents were heated for *ca* 1 h. On cooling, a

* Author to whom correspondence should be addressed.

precipitate appeared which was washed successively with water and *n*-hexane and then dried *in vacuo*.

Peroxozirconium complexes of tridentate and tetradentate ligands were prepared by mixing $Zr(NO_3)_4 \cdot 2H_2O$ (0.01 mol) in 30% H_2O_2 (30 cm^3) and the ligand (0.01 mol) in boiling acetone (50 cm^3). The contents were heated for *ca* 1 h and on cooling a precipitate appeared which was washed successively with water, *n*-hexane and then dried.

Oxidation of triphenylphosphine

To a solution of triphenylphosphine (0.006 mol) in tetrahydrofuran (100 cm^3) was added the suspension of the peroxozirconium anthralinic acid complex (0.006 mol) to study stoichiometric oxidation. The contents were heated for 4 days. The thin-layer chromatographic study shows the conversion of triphenylphosphine to triphenylphosphine oxide. The product was isolated and purified and the melting point noted (153°C). In another set of reactions peroxozirconium salen (0.006 mol) was used and analysed.

Oxidation of cyclohexene using tert-butylhydroperoxide

The possible oxidation of cyclohexene using tert-butylhydroperoxide as oxidant and peroxozirconium salen as well as the peroxozirconium aniline 2-carboxylato complex was studied. The reaction was carried out in dry benzene using dodecane as internal standard. The product was followed by gas chromatographic analysis. The complex was isolated after the reaction and characterized by m.p. and IR studies.

Oxidation of allylalcohol using the peroxozirconium salen complex

To the peroxozirconium salen (0.006 mol) complex in dichloromethane was added allylalcohol (0.006 mol). The contents were refluxed at 70°C for 2 days, and at the end of the reaction the mixture was analysed, and the complex isolated and characterized by m.p. and IR studies.

Stoichiometric oxidation of cyclohexene

The possible oxidation of cyclohexene using stoichiometric amounts of peroxozirconium salen complex in benzene at 80°C for 24 h was studied. After the reaction the complex was isolated and characterized.

RESULTS AND DISCUSSION

The elemental analysis data (Table 1) obtained agree with the calculated values, suggesting a six-coordinate zirconium atom. The molar conductance values show these peroxo complexes to be non-electrolytes. Titration of methanolic solutions of the peroxo complexes with aqueous acidified standard ceric sulphate solution (~ 2) showed (Table 1) that the complexes were monoperoxo complexes. These peroxo complexes are quite stable and their reduction by iodide was slow and needed 10–12 h to impart a brown colouration to the solution.

The IR spectral data are shown in Table 1. The $Zr(O_2)$(ACEN) complex shows an absorption at 1620 cm^{-1} assigned to a C=N stretching, which decreased by 10 cm^{-1} on coordination, therefore, suggesting its involvement. The metal peroxo grouping gives rise to three IR vibration modes. These are predominantly O—O stretching (ν_1 850 cm^{-1}), symmetric M—O stretching (ν_3 650 cm^{-1}) and antisymmetric M—O stretching (ν_2 595 cm^{-1}), respectively.[26–28] The absorption bands at 412 and 390 cm^{-1} are assigned to Zr—O and Zr—N bonds in the complexes.[29–31]

The IR spectrum of the $Zr(O_2)$(salen) complex shows an absorption at 1620 cm^{-1} which is 15 cm^{-1} lower than the absorption found in the ligands, suggesting the involvement of the C=N group in coordination. The absorption bands observed in the complex at 810, 650 and 580 cm^{-1} are assigned to peroxo symmetric and antisymmetric O—O stretching modes. The absorption bands at 410 and 390 cm^{-1} may have arisen due to ligand-to-metal bond formation through the OH and C=N groups. The IR absorption bands of the ligand (ANAC) at 2699, 1660, 1440 and 1320 cm^{-1} are assigned to the ν(OH) stretching (dimer), the ν(C=O) frequency of the internally hydrogen-bonded carboxylic group, the ν(C—O) stretching and the OH in-plane bending of the carboxylic group, respectively. All these bands except that at 1440 cm^{-1} disappear on coordination. The peak at 1610 cm^{-1} is assigned to C=N in the ligand which moves to 1600 cm^{-1}, supporting its involvement in coordination. The absorption bands at 830, 645 and 575 cm^{-1} are assigned to various modes of the peroxo group, while the bands at 415 and 390 cm^{-1} are assigned to Zr—O and Zr—N modes.

The IR spectrum of $Zr(O_2)(SAP) \cdot H_2O$ contains bands at 1600, 840, 638 and 580 cm^{-1} which are assigned to —N=C, peroxo stretching, symmetric and antisymmetric modes, respectively. The bands at 420 and 375 cm^{-1} are assigned to Zr—O and Zr—N bonds, respectively.

Table 1. Analytical and IR spectral data of zirconium(III) peroxo complexes

S. No.	Complexes	Melting point (°C)	Analyses[a] C	H	N	Zr	IR (cm^{-1}) C=N	O—O	ν_3 Zr (O—O)	ν_2 Zr (O—O)	Zr—O	Zr—N	Equivalent cerric sulphate/mol of complex
1	$ZrO_2(C_{16}H_{14}N_2O_2)$	210(d)	49.1 (49.4)	3.6 (3.6)	7.0 (7.2)	23.8 (23.4)	1620	810	650	580	410	390	2.15
2	$ZrO_2(C_{12}H_{18}N_2O_2)$	170(d)	41.7 (41.7)	5.1 (5.2)	8.2 (8.1)	26.6 (26.3)	1620	850	650	595	412	390	1.95
3	$ZrO_2(C_{19}H_{16}N_2O_4)$	235(d)	49.4 (49.6)	3.7 (3.7)	6.0 (6.1)	19.6 (19.8)	1600	830	645	575	415	390	2.00
4	$ZrO_2(C_{17}H_{16}N_2O_2)$	170(d)	50.4 (50.6)	4.0 (4.0)	6.8 (6.9)	22.5 (22.6)	1610	820	660	590	420	385	2.20
5	$ZrO_2(C_{13}H_9NO_2)H_2O$	240(d)	44.9 (44.3)	3.3 (3.1)	3.9 (4.0)	25.8 (25.9)	1600	840	650	590	420	375	2.12
6	$ZrO_2(C_{22}H_{24}N_4O_2)$	205(d)	53.8 (52.9)	4.6 (4.8)	11.2 (11.2)	18.1 (18.2)	1600	850	650	590	410	380	1.98
7	$ZrO_2(C_{14}H_9NO_3)H_2O$	170(d)	44.2 (44.2)	2.6 (2.9)	3.6 (3.7)	23.6 (23.9)	1570	850	685	582	405	385	2.05
8	$ZrO_2(C_{24}H_{19}N_3O_4)$	210(d)	53.8 (53.7)	3.5 (3.5)	7.7 (7.8)	16.8 (17.0)	1602	820	675	580	410	390	2.10
9[b]	$ZrO_2(C_{14}H_{12}N_2O_4)$	—	(42.53)	(3.0)	(7.1)	(23.0)	—	825	645	500	400	375	2.08

[a] Calculated values in parentheses.
[b] Reference 32.

The IR spectrum of $Zr(O_2)$(A ACEN) contains bands at 1600, 850, 650 and 590 cm^{-1} which are assigned to C=N and three modes of the peroxo group. The bands at 410 and 380 cm^{-1} are assigned to Zr—O and Zr—N modes.

The IR spectral studies of the $Zr(O_2)(SAC)\cdot H_2O$ and $ZrO_2(AN)_2$ compounds are reported elsewhere.[32]

The IR spectrum of $Zr(O_2)$(SALPA) shows similar characteristics to those observed for $Zr(O_2)$ (salen), while the IR spectral bands of $Zr(O_2)$ (ANAAC) are similar to those observed for $Zr(O_2)$ (ANAC) (Table 1).

The IR studies suggest that all the complexes are six-coordinate and one peroxo group per ligand molecule is present.

The zirconium peroxo complexes with bidentate ligands were found to be active towards Ph_3P as it directly inserts into the metal–peroxide bond.[7,33]

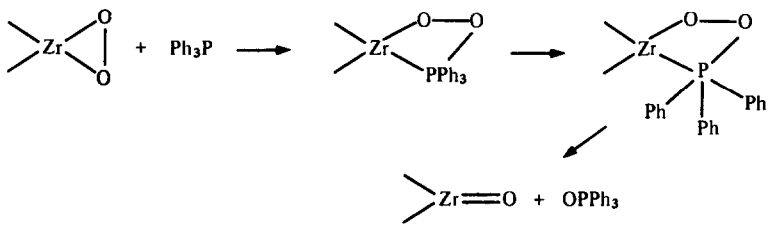

The formation of Ph_3PO (> 90%) was confirmed by the appearance of the IR band at 1190 cm^{-1} (P—O).[34] The zirconium complex after the reaction was separated and its IR spectra studied. The appearance of a band at 930 cm^{-1} is attributed to Zr—O and this has appeared due to the disappearance of the O—O band. In the absence of the zirconium peroxo complex no oxidation product was obtained. Zirconium peroxo complexes prepared with tetradentate ligands did not oxidize Ph_3P.

Zirconium peroxo complexes have been found to be excellent catalysts for the homolytic decomposition of hydroperoxide. When the oxidation of cyclohexene was studied using tert-butylhydroperoxide as oxidant and a zirconium peroxo complex as the catalyst, some epoxide formation takes place but the yield was very low and decomposition of tert-butylhydroperoxide gave a peroxide mixture as the major product. This reaction justifies a possible radical mechanism.[35]

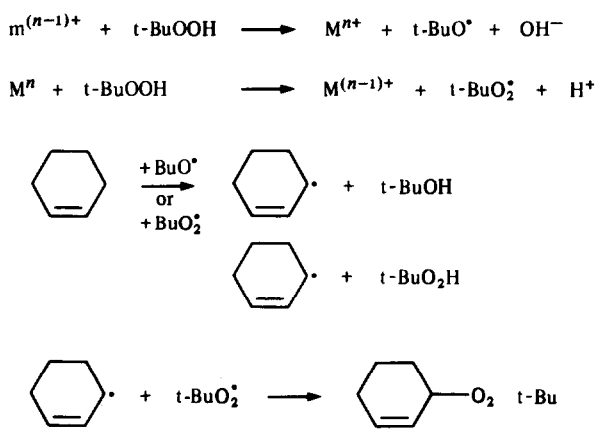

The epoxide which is obtained in small amounts may be due to the following mechanism:

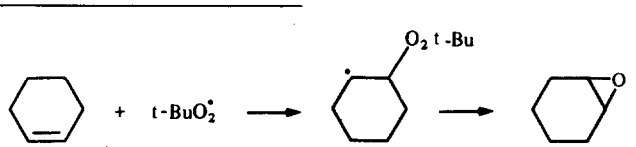

(1)

or to:

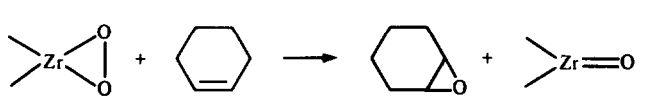

(2)

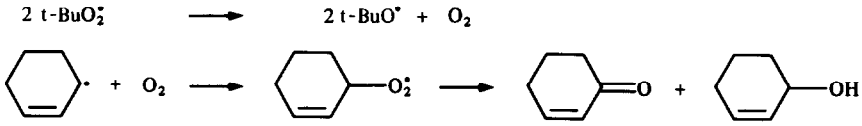

but when cyclohexene was stoichiometrically oxidized using a zirconium peroxo complex in benzene no epoxide was obtained, confirming that a mechanism, similar to eq. (1), is respnsible for the trace of epoxide obtained. Cyclohexene-2-ol and cyclohexene-2-one-1 were observed as products in small quantities. This formation can be explained by the mechanism above.

The evolution of peroxide increased rapidly 2 h after the reaction. Initially an induction period was observed, which shows that during this period free radical decomposition of hydroperoxide takes place. The peroxo complexes using a bidentate ligand (anthanilic acid) gave a higher conversion to peroxide compared with the tetradentate salen complex ($K_1/K_2 = 3.2$); this may be due to the enhanced stability of the zirconium peroxo moiety afforded by the tetradentate salen ligand. At the end of the reaction the complex was isolated and it was found that it had identical IR and m.p. values to those observed before the reaction, thereby showing that peroxo zirconium salen is not decomposed during this reaction. The peroxo zirconium salen complex was found to fail in the stoichiometric oxidation of cyclohexene and at the end of the reaction the unaltered complex was obtained (as is evident by its m.p. and IR spectra). The peroxo zirconium salen complex also failed to oxidize the allylalcohol. All these studies suggest that peroxo zirconium complexes are stable and peroxo complexes with tri- and tetradentate ligands are almost unreactive.

Acknowledgement—The authors are thankful to CSIR, New Delhi, for financial assistance.

REFERENCES

1. R. A. Sheldon and J. K. Kochi, *Metal Catalysed Oxidation of Organic Compounds*. Academic Press, New York (1981).
2. H. J. Ledon, P. Durbut and F. Varescon, *J. Am. Chem. Soc.* 1981, **103**, 3601.
3. H. J. Ledon and M. Bonnet, *J. Molec. Catal.* 1980, 7, 309.
4. A. D. Westland, F. Haque and J. M. Bouchard, *Inorg. Chem.* 1980, **19**, 225.
5. D. A. Muccigrosso, S. E. Jacobson, P. A. Apgar and P. Mates, *J. Am. Chem. Soc.* 1978, **100**, 7063.
6. H. Mimoun, I. S. de Roch and L. Sajus, *Tetrahedron* 1970, **26**, 37.
7. H. Mimoun, *J. Molec. Catal.* 1980, 7, 1.
8. G. A. Olah and J. Welch, *J. Org. Chem.* 1978, **43**, 2830.
9. H. J. Ledon and F. Varescon, *Inorg. Chem.* 1984, **23**, 2735.
10. Chi-Ming Che and V. W. W. Yam, *J. Am. Chem. Soc.* 1987, **109**, 1262.
11. T. J. Meyer, *Electrochem. Soc.* 1984, **131**, 221C.
12. S. Torii, T. Inokuchi and T. Sugiura, *J. Org. Chem.* 1986, **51**, 155.
13. J. T. Groves and R. Quinn, *J. Am. Chem. Soc.* 1985, **107**, 5795.
14. Chi-Ming Che, T. F. Lai and K. Y. Wong, *Inorg. Chem.* 1987, **26**, 2289.
15. C. L. Bailey and R. S. Drago, *J. Chem. Soc., Chem. Commun.* 1987, 179.
16. T. C. Lan and J. K. Kochi, *J. Chem. Soc., Chem. Commun.* 1987, 798.
17. H. Mimoun, I. S. de Roch and L. Sajus, *Bull. Soc. Chim. France* 1969, 1481.
18. S. Jacobson, R. Tang and F. Mares, *Inorg. Chem.* 1978, **17**, 3055.
19. A. D. Westland and M. T. H. Tarafdar, *Inorg. Chem.* 1982, **21**, 3228.
20. H. Mimoun, M. Poster, F. Casabianca, J. Fischer and A. Mitschler, *Inorg. Chem.* 1982, **21**, 803.
21. A. D. Westland and M. T. H. Tarafdar, *Inorg. Chem.* 1981, **20**, 3992.
22. T. Katsuki and K. B. Sharpless, *J. Am. Chem. Soc.* 1980, **102**, 5974.
23. D. D. Agarwal, *J. Molec. Catal.* 1988, **44**, 65.
24. D. D. Agarwal and Savita Srivastava, *Polyhedron* 1988, 7, 2569.
25. K. B. Sharpless and T. R. Verhoeven, *Aldrichim. Acta* 1979, **12**, 63.
26. G. V. Jere and M. T. Santhamma, *Inorg. Chim. Acta* 1977, **24**, 57.
27. W. P. Griffith, *J. Chem. Soc.* 1964, 5248.
28. W. P. Griffith and T. D. Wickins, *J. Chem. Soc. A* 1968, 397.
29. N. M. Karaynnis, C. M. Mikulski, M. J. Stroko, L. L. Pytlewski and M. M. Labes, *Inorg. Chim. Acta* 1970, **4**, 455.
30. R. K. Agarwal, M. Srivastava and A. K. Srivastava, *J. Inorg. Nucl. Chem.* 1981, **43**, 204.
31. R. K. Agarwal, A. K. Srivastava, M. Srivastava, N. Bakru and T. N. Srivastava, *J. Inorg. Nucl. Chem.* 1980, **42**, 1778.
32. M. T. H. Tarafdar and M. A. L. Miah, *Inorg. Chem.* 1986, **25**, 2265.
33. R. A. Sheldon and J. A. Van Doorn, *J. Organomet. Chem.* 1975, **94**, 115.
34. D. Brown, J. Hill and C. E. F. Rickard, *J. Chem. Soc. A* 1970, 499.
35. R. A. Sheldon and J. A. Van Doorn, *J. Catal.* 1973, **31**, 427.

Polyhedron Vol. 9, No. 11, pp. 1411–1422, 1990
Printed in Great Britain

0277–5387/90 $3.00+.00
© 1990 Pergamon Press plc

X-RAY CRYSTAL STRUCTURES AND NUCLEAR MAGNETIC RESONANCE SPECTRA OF MACROCYCLIC COMPLEXES OF NEODYMIUM(III) AND EUROPIUM(III)

F. BENETOLLO* and A. POLO

Istituto di Chimica e Tecnologia dei Radioelementi, C.N.R., Corso Stati Uniti 4, Padova, Italy

and

G. BOMBIERI

Istituto di Chimica Farmaceutica, Universitá di Milano, Milano, Italy

and

K. K. FONDA and L. M. VALLARINO*

Department of Chemistry, Virginia Commonwealth University, Richmond, VA 23284, U.S.A.

(*Received* 4 *October* 1989; *accepted* 8 *February* 1990)

Abstract—The compounds of formula $[M(CH_3COO)_2L_I]Cl \cdot 4H_2O$, in which M is neodymium(III) or europium(III) and L_I is a six-nitrogen-donor macrocyclic ligand ($C_{22}H_{26}N_6$), have been investigated by single crystal X-ray diffraction, thermogravimetric analysis and nuclear magnetic resonance spectroscopy. The two compounds are isostructural and crystallize in the triclinic system, space group $P\bar{1}$. The complex cations present in the crystal lattice consist of a 10-coordinate metal centre linked to the six nitrogen-donor atoms of the macrocyclic ligand and to two bidentate chelating acetates, situated on opposite sides of the macrocycle and staggered by approximately 90°; an ionic chloride balances the residual metal charge. The paramagnetic-shifted NMR spectra of the complexes were measured in various solvents, and confirm that the metal–macrocycle moieties remain undissociated. Also, the spectra depend on the counterions, showing that, on average, at least one of the labile acetate ligands is bound to the metal ion even in aqueous solution.

The ability of the lanthanide(III) and yttrium(III) ions to act as templates for the cyclic (2+2) Schiff base condensation of 1,2-diaminoethane with 2,6-diacetylpyridine is well established and a considerable number of complexes of the resulting macrocycle L_I [Fig. 1(a)] have been described.[1–9] These complexes are unique among the compounds of the lanthanides in that the metal–macrocyclic entity is extremely inert with respect to release of the metal ion, whereas the exocyclic ligands (anions or solvent molecules) are labile and easily exchangeable. The inertness of the metal–L_I entity must arise from an especially favourable combination of metal ionic radius, cavity size of the 18-membered macrocyclic ligand L_I, and bonding ability of the six nitrogen-donor atoms. This suggestion is supported by the observation that the lanthanide complexes of an 18-membered tetraimine macrocycle similar to L_I, but having furan instead of pyridine head-units, are labile and decompose rapidly when dissolved in water.[10] Also, a lanthanum(III) complex of the L_{II} macrocycle [20-membered cavity, pyridine head-units, Fig. 1(b)] was found to undergo transmetallation with

* Authors to whom correspondence should be addressed.

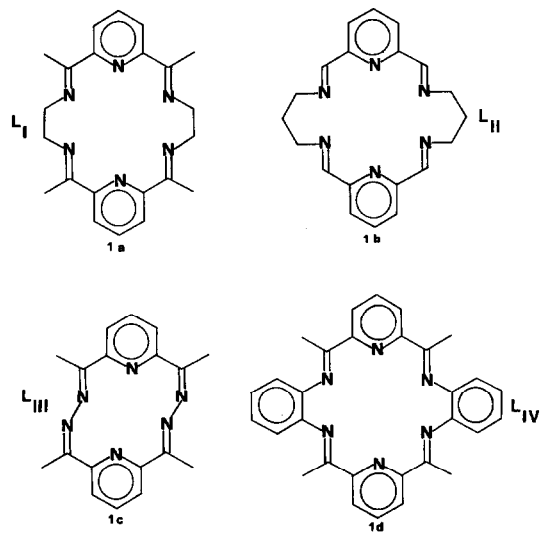

Fig. 1. Schematic formulae of macrocyclic ligands: $L_I = C_{22}H_{26}N_6$, $L_{II} = C_{18}H_{22}N_6$, $L_{III} = C_{18}H_{18}N_6$, $L_{IV} = C_{30}H_{26}N_6$.

copper(II),[11] while complexes of the smaller lanthanides (Tb–Lu) with the L_{III} macrocycle [14-membered cavity, pyridine head-units, Fig. 1(c)] are readily hydrolysed to complexes of an open-cycle diketone.[12] The flexibility of the $—CH_2—CH_2—$ diimine side-chains of the L_I macrocycle must also represent a favourable factor in the stabilization of its lanthanide complexes, as the derivatives of the L_{IV} macrocycle [18-membered cavity, pyridine head-units, rigid O-phenylenediamine side-chains, Fig. 1(d)] are both more difficult to synthesize and less inert to metal release or rearrangement.[13]

Crystal structures have been reported for a number of complexes of the lanthanide(III) and yttrium(III) ions with the L_I macrocycle and some trends begin to emerge. The 12-coordinate, neutral species $[La(NO_3)_3L_I]$, containing three bidentate chelating nitrates, was obtained by template synthesis with lanthanum(III) nitrate in methanol.[1,7] The 11-coordinate $[Ce(NO_3)_2(H_2O)L_I]^+$ cation, isolated as the nitrate salt, was formed by metal exchange from $Ba(ClO_4)_2L_I$ and cerium(III) nitrate in water.[7] Under similar conditions, the neodymium(III) ion gave instead a 10-coordinate (2+) cation,[7] isolated as a mixed nitrate–perchlorate salt of formula $[\{Nd(NO_3)(H_2O)_2L_I\}_2]NO_3(ClO_4)_3 \cdot 4H_2O$. With yttrium(III) and acetate ions, the metal-templated synthesis yielded crystals containing two nine-coordinate cationic species, $[Y(CH_3COO)(H_2O)L_I]^{2+}$ and $[Y(CH_3COO)_2L_I]^+$, the latter containing one bidentate and one monodentate acetate.[8] With europium(III) and yttrium (III), a pair of isostructural neutral complexes, $[Eu(NCS)_3L_I]$ and $[Y(NCS)_3L_I]$, were isolated by anion exchange from the diacetate–chlorides in methanol.[9] Finally the smallest lanthanide, lutetium(III), gave the two nine-coordinate monoacetate cationic species $[Lu(CH_3COO)(CH_3OH)L_I]^{2+}$ and $[Lu(CH_3COO)(H_2O)L_I]^{2+}$, obtained by template synthesis of the diacetate–chlorides followed by partial anion metathesis.[5] Thus, ligand L_I can form neutral or cationic complexes of coordination numbers ranging from 12 to nine, depending on the combination of metal ion, anion, and method of preparation.

To investigate how the structural aspects of the lanthanide–L_I complexes may relate to their solution properties, we carried out a crystallographic analysis of two representative examples, the diacetate–chlorides of Nd^{III}–L_I and Eu^{III}–L_I, which are very soluble in both water and organic solvents, and investigated their ^1H and ^{13}C NMR spectra. An understanding of the relationship among structure, metal–macrocycle inertness, and lability of exocyclic ligands is essential in the future design of functionalized complexes that may allow the attachment to biological substrates of selected lanthanides, such as europium(III) and terbium(III) as luminescent markers,[14] or Gadolinium(III) as a contrast agent for NMR imaging.[15]

EXPERIMENTAL

Diacetate–chloride complexes of europium(III) *and terbium*(III) *with the* L_I *macrocycle*

These compounds were prepared as previously described.[4] Single crystals suitable for X-ray analysis were obtained by slow crystallization from methanol–diethyl ether at *ca* 4°C.

$[Pr(NO_3)_2(H_2O)(L_I)](NO_3) \cdot 2H_2O$

This compound[7] was prepared as follows: the diacetate–chloride complex (0.5 mmol, *ca* 360 mg) was dissolved in water (10 cm^3) and mixed with $LiNO_3$ (3.0 mmol, *ca* 210 mg in 2 cm^3 of water). The resulting mixture was repeatedly filtered over a tight wad of cotton wool and the clear solution was allowed to stand undisturbed in an open container for several days at room temperature. The trinitrate complex precipitated as pale yellow crystals which were decanted, carefully washed with ice-cold water, and dried at 60°C. The compound had correct chemical analysis. IR absorption frequencies (cm^{-1}) and selected assignments: 3542s, sharp: 3510m $\nu(OH_2)$ of lattice water; 3366s, br; 3300sh $\nu(OH_2)$ of coordinated water; 3072w;

2955vw; 1637s ν(C=N) of imine; 1584s ν(C=N) of pyridine; 1443vs ν(coord. NO_3^-); 1378vs ν(ionic NO_3^-); 1314s ν(coord. NO_3^-); 1190s; 1120w; 1067w; 1038w; 1002m; 920w; 814 ν(ionic NO_3^-); 703w; 644w; 591w.

X-ray measurements and structure determination

Neodymium complex. A transparent, pale violet, prismatic single crystal of dimensions $0.14 \times 0.28 \times 0.40$ mm was used for data collection on a four-circle Philips PW 1100 diffractometer with graphite-monochromated Mo-K_α radiation. The intensity data were corrected for Lorentz-polarization effects and for absorption, following the method of North *et al.*[16] The structure was solved using three-dimensional Patterson and Fourier techniques and refined with full-matrix least-squares. Hydrogen atoms were introduced at the positions indicated from the final difference Fourier map and were refined with a fixed unique thermal parameter ($U = 0.08$ Å^2); however, the hydrogen atoms of the water molecules, which were disordered among two or three positions, were not introduced. The non-hydrogen atoms, except for the oxygens of the water molecules (refined isotropically), were allowed to vibrate anisotropically. The final difference Fourier map showed a few residuals of the order of 0.6e/Å^3, close to the water positions and assigned to the disordered hydrogens. The programs used were SHELX-76[17] for structure solution and refinement, ORTEP[18] and PLUTO[19] for drawings, and PARST[20] for geometrical calculations. Atomic scattering factors were taken from ref. 21.

Europium complex. A single crystal of dimensions $0.30 \times 0.44 \times 0.50$ mm was used for analysis; data collection and treatment were carried out as described for the neodymium analogue except for the hydrogen atoms of the macrocycle being introduced at calculated positions. In the final difference Fourier map two major residuals of about 1e/Å^3 were present near the europium(III) position. Crystallographic parameters are reported in Table 1. Bond lengths and bond angles are given in Table 2; torsion angles are given in Table 3;

Table 1. Crystal data for $[Ln(CH_3COO)_2L_1](Cl)(H_2O)_4$ (Ln = Nd and Eu)

Formula	$NdClO_8N_6C_{26}H_{40}$	$EuClO_8N_6C_{26}H_{40}$
M_r	744.33	752.05
Crystal system	Triclinic	Triclinic
a (Å)	13.271(2)	13.692(2)
b (Å)	12.788(2)	12.758(2)
c (Å)	10.089(2)	10.058(2)
α (°)	73.75(2)	73.94(2)
β (°)	107.72(3)	107.73(3)
γ (°)	111.15(3)	110.83(3)
U (Å^3)	1492.99	1535.88
Space group	$P\bar{1}$	$P\bar{1}$
D_c (g cm^{-3})	1.66	1.63
Z	2	2
F(000)	758	764
Radiation	Mo-K_α	Mo-K_α
μ (cm^{-1})	17.60	20.48
Reflection measured	6435	6938
Scan method	θ–2θ	θ–2θ
Scan speed (° min^{-1})	1.8	1.8
Scan width (°)	1.2	1.2
Background counts (s)	20	20
$2\theta_{max}$ (°)	50	50
σ Limit [$I \geq n\sigma(I)$]	3	3
Unique observed data with [$I \geq n\sigma(I)$]	5475	6204
Number of parameters	456	378
Weighting scheme w	unit	$[\sigma^2(F_o)+0.002549(F_o^2)]^{-1}$
$R = \Sigma[\|F_o\|-\|F_c\|]/\Sigma\|F_o\|$	0.0297	0.0325
$R_w = [\Sigma w(\|F_o\|-\|F_c\|)^2/\Sigma w\|F_o\|^2]^{1/2}$	—	0.0380
Max Δ/σ	0.08	0.09
GOF	1.41	1.05
Standard reflections	121 −151	−232 261

Table 2. Bond lengths (Å) and angles (°) for $[Ln(CH_3COO)_2L_I](Cl)(H_2O)_4$ (Ln = Nd and Eu) with ESDs in parentheses

(a) Neodymium environment		(a′) Europium environment	
Nd—N(1)	2.619(4)	Eu—N(1)	2.651(3)
Nd—N(2)	2.609(3)	Eu—N(2)	2.590(3)
Nd—N(3)	2.587(4)	Eu—N(3)	2.638(3)
Nd—N(4)	2.628(4)	Eu—N(4)	2.665(3)
Nd—N(5)	2.640(3)	Eu—N(5)	2.624(3)
Nd—N(6)	2.591(4)	Eu—N(6)	2.639(4)
Nd—O(1)	2.511(3)	Eu—O(1)	2.505(3)
Nd—O(2)	2.500(4)	Eu—O(2)	2.460(3)
Nd—O(3)	2.545(3)	Eu—O(3)	2.500(3)
Nd—O(4)	2.498(4)	Eu—O(4)	2.458(3)
N(1)—Nd—N(2)	63.2(1)	N(1)—Eu—N(2)	64.1(1)
N(1)—Nd—N(6)	61.7(1)	N(1)—Eu—N(6)	60.4(1)
N(2)—Nd—N(3)	60.3(1)	N(2)—Eu—N(3)	61.3(1)
N(3)—Nd—N(4)	61.2(1)	N(3)—Eu—N(4)	59.7(1)
N(4)—Nd—N(5)	61.7(1)	N(4)—Eu—N(5)	63.0(1)
N(5)—Nd—N(6)	59.9(1)	N(5)—Eu—N(6)	60.3(1)
O(1)—Nd—O(2)	50.2(1)	O(1)—Eu—O(2)	52.5(1)
O(3)—Nd—O(4)	51.6(1)	O(3)—Eu—O(4)	52.3(1)
(b) Macrocycle		(b′) Macrocycle	
N—$C(py)_{av}$	1.333(5)	N—$C(py)_{av}$	1.348(4)
C—$C(py)_{av}$	1.360(7)	C—$C(py)_{av}$	1.363(6)
C—$C(aliphatic)_{av}$	1.483(7)	C—$C(aliphatic)_{av}$	1.495(6)
Nd—N(py)—C_{av}	119.6(3)	Eu—N(py)—C_{av}	120.2(2)
Nd—N(aliphatic)—C_{av}	119.4(3)	Eu—N(aliphatic)—C_{av}	118.6(2)
Nd—N(1)—C(1)	117.3(3)	Eu—N(1)—C(1)	116.2(3)
Nd—N(4)—C(10)	119.9(3)	Eu—N(4)—C(10)	121.0(3)
Nd—N(1)—C(21)	122.1(3)	Eu—N(1)—C(21)	123.2(2)
Nd—N(4)—C(12)	119.1(3)	Eu—N(4)—C(12)	117.6(3)
Nd—N(2)—C(2)	114.0(3)	Eu—N(2)—C(2)	113.6(2)
Nd—N(5)—C(13)	114.5(3)	Eu—N(5)—C(13)	113.6(2)
Nd—N(2)—C(3)	126.2(3)	Eu—N(2)—C(3)	124.4(2)
Nd—N(5)—C(14)	122.0(3)	Eu—N(5)—C(14)	122.5(2)
N(2)—C(3)—C(4)	127.3(5)	N(2)—C(3)—C(4)	125.4(4)
N(5)—C(14)—C(15)	126.7(5)	N(5)—C(14)—C(15)	127.2(4)
C(4)—C(3)—C(5)	118.7(5)	C(4)—C(3)—C(5)	117.8(4)
C(15)—C(14)—C(16)	117.7(4)	C(15)—C(14)—C(16)	117.0(4)
N(3)—C(5)—C(6)	122.4(4)	N(3)—C(5)—C(6)	121.8(4)
C(14)—C(16)—C(17)	121.0(4)	C(14)—C(16)—C(17)	121.6(3)
C(3)—C(5)—C(6)	119.9(4)	C(3)—C(5)—C(6)	121.7(4)
N(6)—C(16)—C(17)	122.6(4)	N(6)—C(16)—C(17)	122.4(4)
Nd—N(3)—C(5)	120.6(3)	Eu—N(3)—C(5)	120.0(3)
Nd—N(6)—C(16)	119.9(3)	Eu—N(6)—C(16)	119.2(3)
Nd—N(3)—C(9)	118.6(3)	Eu—N(3)—C(9)	120.9(3)
Nd—N(6)—C(20)	119.2(3)	Eu—N(6)—C(20)	120.6(2)
C(5)—C(6)—C(7)	117.1(5)	C(5)—C(6)—C(7)	119.7(4)
C(16)—C(17)—C(18)	118.1(5)	C(16)—C(17)—C(18)	118.0(4)
C(6)—C(7)—C(8)	120.9(6)	C(6)—C(7)—C(8)	118.6(5)
C(17)—C(18)—C(19)	119.6(5)	C(17)—C(18)—C(19)	120.8(5)
C(7)—C(8)—C(9)	119.9(5)	C(7)—C(8)—C(9)	119.1(4)
C(18)—C(19)—C(20)	119.4(5)	C(18)—C(19)—C(20)	117.8(4)
N(3)—C(9)—C(8)	119.5(4)	N(3)—C(9)—C(8)	122.3(4)
C(19)—C(20)—C(21)	121.8(4)	C(19)—C(20)—C(21)	121.9(4)
C(8)—C(9)—C(10)	123.0(4)	C(8)—C(9)—C(10)	122.3(4)
C(19)—C(20)—N(6)	121.4(4)	C(19)—C(20)—N(6)	122.5(3)
C(9)—C(10)—N(4)	116.8(4)	C(9)—C(10)—N(4)	116.6(3)
C(20)—C(21)—C(22)	117.3(4)	C(20)—C(21)—C(22)	115.7(4)
C(9)—C(10)—C(11)	121.3(4)	C(9)—C(10)—C(11)	119.8(4)
C(22)—C(21)—N(1)	125.4(4)	C(22)—C(21)—N(1)	126.9(4)

Table 2—*continued*

(c) Acetate ligands		(c′) Acetate ligands	
O(1)—C(23)	1.227(7)	O(1)—C(23)	1.248(6)
O(2)—C(23)	1.242(5)	O(2)—C(23)	1.267(4)
O(3)—C(25)	1.268(6)	O(3)—C(25)	1.251(5)
O(4)—C(25)	1.255(5)	O(4)—C(25)	1.254(5)
C(23)—C(24)	1.498(8)	C(23)—C(24)	1.514(6)
C(25)—C(26)	1.501(9)	C(25)—C(26)	1.518(7)
O(1)—C(23)—O(2)	118.7(4)	O(1)—C(23)—O(2)	121.7(4)
O(3)—C(25)—O(4)	120.8(4)	O(3)—C(25)—O(4)	121.4(4)
Nd—O(1)—C(23)	95.5(3)	Eu—O(1)—C(23)	92.1(3)
Nd—O(3)—C(25)	92.2(3)	Eu—O(3)—C(25)	91.9(2)
Nd—O(2)—C(23)	95.6(3)	Eu—O(2)—C(23)	93.7(3)
Nd—O(4)—C(25)	94.8(3)	Eu—O(4)—C(25)	93.8(2)
O(1)—C(23)—C(24)	122.2(5)	O(1)—C(23)—C(24)	119.0(4)
O(2)—C(23)—C(24)	119.2(5)	O(3)—C(25)—C(26)	119.7(4)
O(3)—C(25)—C(26)	119.3(4)	O(2)—C(23)—C(24)	119.3(4)
O(4)—C(25)—C(26)	119.9(4)	O(4)—C(25)—C(26)	118.9(4)

Table 3. Macrocycle torsion angles (°) for $[Ln(CH_3COO)_2L_1](Cl)(H_2O)_4$ (Ln = Nd and Eu)

Atoms	Neodymium	Europium
N(1)—C(1)—C(2)—N(2)	−55.8(5)	−55.5(4)
C(1)—C(2)—N(2)—C(3)	−127.9(5)	−126.1(4)
C(2)—N(2)—C(3)—C(5)	177.3(4)	177.1(4)
N(2)—C(3)—C(5)—N(3)	12.6(6)	11.1(6)
C(3)—C(5)—N(3)—C(9)	−176.6(4)	−177.2(4)
C(5)—N(3)—C(9)—C(10)	−173.1(4)	−172.3(4)
N(3)—C(9)—C(10)—N(4)	4.8(6)	4.4(5)
C(9)—C(10)—N(4)—C(12)	174.6(4)	173.3(4)
C(10)—N(4)—C(12)—C(13)	−163.1(5)	−164.4(4)
N(4)—C(12)—C(13)—N(5)	−58.0(5)	−56.6(5)
C(12)—C(13)—N(5)—C(14)	−102.2(5)	−102.2(4)
C(13)—N(5)—C(14)—C(16)	178.4(4)	177.4(3)
N(5)—C(14)—C(16)—N(6)	−0.5(6)	−1.2(5)
C(14)—C(16)—N(6)—C(20)	177.4(4)	176.6(3)
C(16)—N(6)—C(20)—C(21)	176.7(4)	175.8(3)
N(6)—C(20)—C(21)—N(1)	−12.1(6)	−11.4(5)
C(20)—C(21)—N(1)—C(1)	178.3(4)	179.3(4)
C(21)—N(1)—C(1)—C(2)	−152.6(4)	−153.1(4)

relevant intermolecular contacts are given in Table 4.

Supplementary material (tables of atomic coordinates, atomic vibrations and calculated structure amplitudes) has been deposited with the Editor, and coordinates also at the Cambridge Data Centre.

Other measurements

Microanalyses were performed by Atlantic Microlab, Atlanta, Georgia. Water content was determined by thermogravimetic analysis with a Perkin–

Table 4. Relevant intermolecular contacts

	Neodymium	Europium
Ow(2)···Ow(4)	2.768(7)	2.867(6)
O(3)···Ow(1)′	2.844(5)	2.872(4)
O(2)···Ow(4)′	2.797(7)	2.851(6)
Cl···Ow(1)′	3.158(5)	3.236(5)
Cl···Ow(3)″	3.082(4)	3.198(4)
Cl···Ow(3)′	3.246(4)	3.249(4)

(′ $1-x, 1-y, 1-z$; ″ $-1+x, y, z$).
All the distances are in Å.

Elmer TGS-4 system, under a dry helium flow of 60 cm^3 min^{-1}. IR spectra of the solid samples, as Nujol/hexachlorobutadiene mulls and KBr pellets, were recorded with a Perkin–Elmer Model 1500 FTIR instrument. NMR spectra were recorded on a GE QE-300 FT–NMR spectrometer in high-precision 5 mm glass NMR tubes. Observed frequencies were 300.65 MHz for ^1H and 75.60 MHz for ^{13}C. Internal standards were TMS for non-aqueous solutions and DSS for aqueous solutions.

RESULTS AND DISCUSSION

Crystal structures

In the series of diacetate–chloride complexes, $[Ln(CH_3COO)_2L_I]Cl \cdot nH_2O$ (Ln = La–Lu), the number of H_2O molecules varies from 3 to 6 depending on the metal ion and ambient conditions;[4] for the crystalline neodymium(III) and europium(III) complexes examined in this work, *n* is 4. The two complexes have the same coordination formula, $[M(CH_3COO)_2L_I]Cl \cdot 4H_2O$ (M = Nd or Eu), and are isostructural. Selected bond distances and angles are reported in Table 2; an ORTEP view of the $[Nd(Ac)_2L_I]^+$ complex cation is shown in Fig. 2. In these complexes the metal ion is 10-coordinated, being linked to the six nitrogen atoms of the macrocycle and to two bidentate chelating acetates situated on opposite sides of the macrocycle. The two acetates are staggered and the angle between their planes is 94.8(2)° for Nd and 94.8(2)° for Eu. The macrocycle itself has the "folded butterfly" configuration usually found in lanthanide complexes of the L_I ligand.[1–9] The structure consists of two approximately planar sections containing the pyridine rings and hinged at the $—CH_2—CH_2—$ side-chains, with dihedral angles of 132.82(6)° for Nd and 132.37(6)° for Eu.

The orientation of the coordinated acetates appears to be dictated primarily by steric requirements, as the OCO plane is aligned with the fold of the macrocycle for the acetate on the concave side and is perpendicular to it for the acetate on the opposite side. However, the plane of the acetate on the concave side is not symmetrically located but leans toward one of the two quasi-planar sections of the macrocycle. In the neodymium complex, the acetate plane [O(3), C(25), C(26), O(4)] forms a dihedral angle of 54.7(2)° with the C(1)···N(6)···C(13) macrocycle section and an angle of 101.8(2)° with the C(2)···N(3)···C(12)

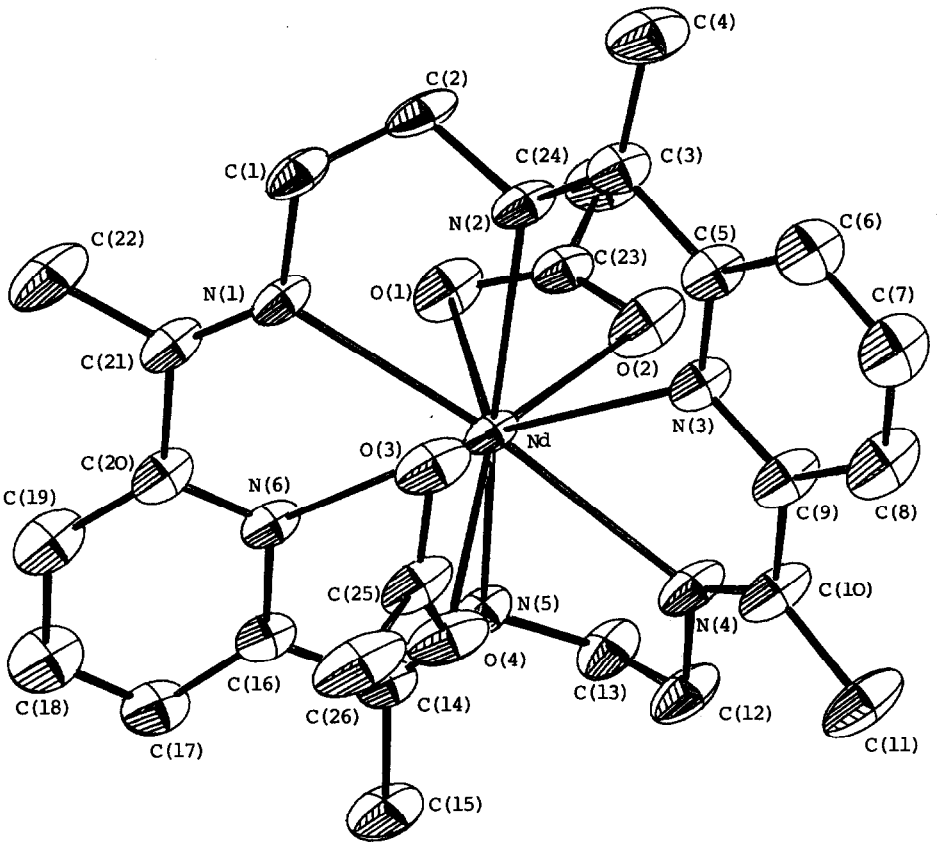

Fig. 2. ORTEP view of the $[Nd(CH_3COO)_2L_I]^+$ complex cation.

section; in the europium complex, the corresponding angles are 55.1(2) and 102.6(2)°. This lack of symmetry contrasts with the situation found in the $[Nd(NO_3)_2(18\text{-crown-6})]_3[Nd(NO_3)_6]$ complex.[22] The latter compound contains two cationic entities that have the same stoichiometry but differ slightly in their overall symmetry due to different conformations of the crown-ether ligand; in each entity, however, the two bidentate chelating nitrates on opposite sides of the crown-ether are essentially coplanar and perpendicular to the $\{NdO_6\}$ best plane of the macrocycle. A staggered arrangement of two bidentate chelating oxygen-donor anions is present in the pair of isostructural neodymium(III) and europium(III) complexes of formula $[M(NO_3)_2(C_{14}H_{30}N_2O_4)]_3[M(NO_3)_6]$ containing a diaza-crown-ether ligand.[23] Each of these compounds contains two $[M(NO_3)_2(ligand)]^+$ cations of different symmetry, one (C_{2v} symmetry) with the two N-methyl groups on the same side of the $\{MN_2O_4\}$ coordination plane, and the other (C_2 symmetry) with the N-methyl groups on opposite sides. In the C_2 cation, the angle between the planes of the two opposite NO_3^- groups is *ca* 90°, whereas in the C_{2v} cation the angle is *ca* 60°; in both cations, however, the planes of the NO_3^- groups are essentially perpendicular to the $\{MN_2O_4\}$ best plane of the macrocycle. A close examination of the crystal packing of the diacetate–chloride complexes described in the present work shows short intermolecular contacts among water oxygens, acetate oxygens and chloride ions (see Table 4 and Fig. 3). These non-bonding interactions may be responsible for the asymmetric arrangement of the concave-side acetate with respect to the folded macrocycle.

A ring-puckering analysis[24] for the six-nitrogen donor moieties of the Nd—L_I and Eu—L_I diacetate–chloride complexes showed that in each case the 6-N has a slightly twisted boat conformation with the boat vertices, N(2) and N(5), on the convex side of the macrocycle. The two sets of puckering constants were also quite similar: $Q = 0.907(4)$,

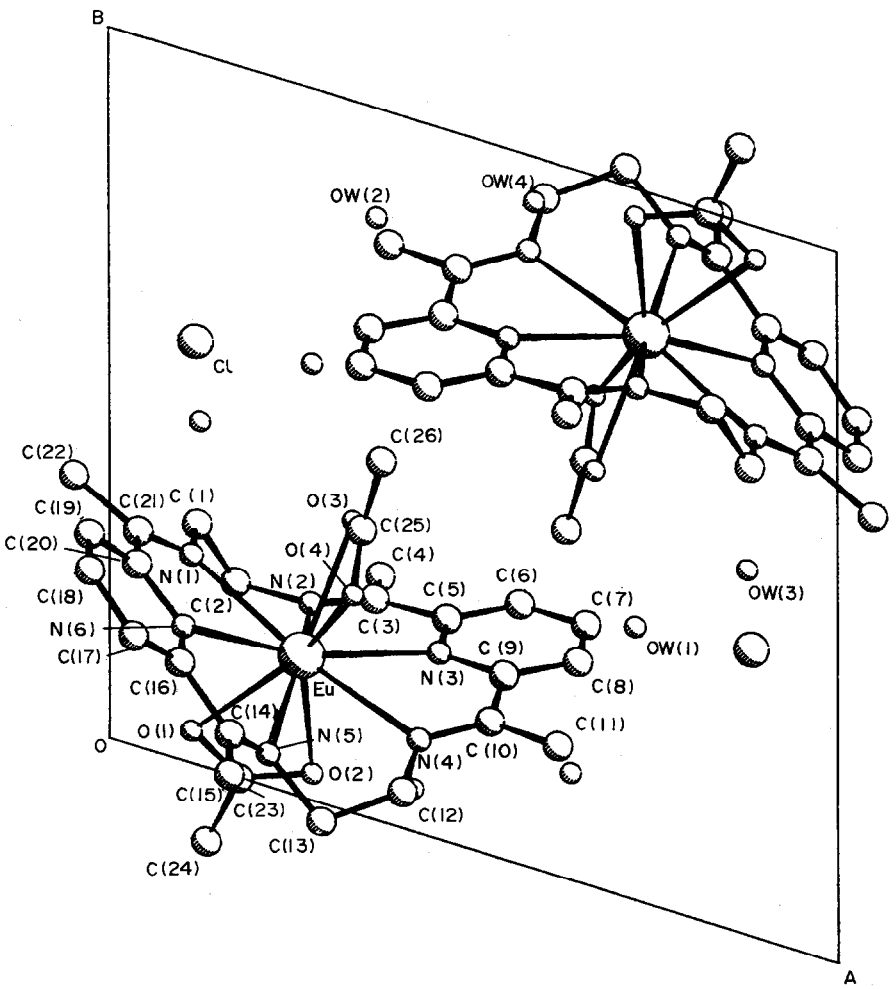

Fig. 3. PLUTO view down *c* of the cell content (europium derivative).

$\Theta = 91.8(2)$, $\Phi = 70.4(2)°$ for neodymium, and $Q = 0.957(3)$, $\Theta = 91.6(2)°$, $\Phi = 71.1(2)°$ for europium. Thus the difference in ionic radius between neodymium (1.303 Å) and europium (1.260 Å)[27] does not appreciably affect the 6-N ring conformation.

Comparison among the bond lengths listed in Table 2 shows that the metal–acetate distances are longer for neodymium (average Nd—$O_{acetate}$ = 2.514 Å) than for europium (average Eu—$O_{acetate}$ = 2.481 Å), in agreement with the decrease in metal ionic radius from neodymium to europium. In contrast, all metal–nitrogen distances are appreciably shorter for neodymium than for europium (average M—$N_{pyridine}$ = 2.589(4) Å for Nd; 2.639(4) Å for Eu; range of M—N_{imine} = 2.591(4)–2.641(3) Å for Nd; 2.590(3)–2.665(4) Å for Eu). For comparison, the following values were found in neodymium(III) and europium(III) complexes with the same L_I macrocycle but different counterions: Nd—$N_{pyridine}$ = 2.621 Å and Nd—N_{imine} = 2.1610 Å for $[\{Nd(NO_3)(H_2O)_2L_I\}_2](NO_3)(ClO_4)_3 \cdot 4H_2O$;[7] Eu—$N_{pyridine}$ = 2.622 Å and Eu—N_{imine} = 2.586 Å for $[Eu(NCS)_3L_I]$.[9] In the diacetate–chloride complexes considered in the present work, the intermolecular contacts (Table 4) are also on average shorter for the neodymium complex than for the europium analogue, and the cell volume is more compact. A comparative analysis of the thermal parameters of both compounds does not reveal particular features which might explain these irregularities. A smaller cell volume for the neodymium derivative has been also found in the isomorphous pair of neodymium and europium nitrate complexes with the macrocycle 4,13-dimethyl-1,7,10,16-tetraoxa-4,13-diazacyclooceadecane $Me_2(2,2)$.[25]

NMR spectra

The ^1H NMR spectra of the neodymium(III) and europium(III) diacetate–chloride complexes were recorded in three solvents of different coordinating abilities: deuterium oxide, deuterodimethylsulphoxide and deuterochloroform. ^1H resonances were assigned on the basis of integration and coupling (for the pyridine protons); they are reported in Table 5. Unlike the spectra of the diamagnetic complex of lanthanum(III)[4,7] and lutetium(III),[5] those of the paramagnetic neodymium(III) and europium(III) complexes were found to be strongly dependent upon the solvent. The CH_2 resonance of the europium complex, for example, occurs at −7.65 ppm in D_2O, at 1.47 ppm in DMSO-d_6 and at 0.62 ppm in $CDCl_3$. The ^1H spectra of the Eu—L_I complex were also recorded at several different concentrations, ranging from near saturation to the lower limit of convenient measurement; within this range, the spectra remained nearly constant.

Table 5 also lists the ^1H spectra of the diacetate–chloride and trinitrate complexes of lanthanum(III), as well as the spectra of the nitrate complexes of several paramagnetic lanthanides reported by Hart and co-workers.[7] We were initially surprised to find that the macrocycle resonance of the diacetate–chloride and nitrate complexes, which are virtually identical for the lanthanum(III) species, differ appreciably from one another in both the neodymium(III) and the europium(III) species. To eliminate the possibility of unaccounted experimental differences between our results and those in the literature, we prepared as a check a sample of the $[Pr(NO_3)_2(H_2O)(L_I)](NO_3) \cdot 2H_2O$ complex, which is isostructural with the cerium(III) complex of the same formula (analysed by single crystal X-ray diffraction[7]) and measured its ^1H spectrum in D_2O. The values we obtained were identical to those of Hart and co-workers, showing that for any given solvent the differences observed among macrocycle resonances of paramagnetic M—L_I entities associated with different counterions are indeed real. It may be concluded that for each metal the bonding and overall symmetry of the metal–macrocycle entity are essentially independent of the exocyclic ligands (anions and/or solvent molecules). In contrast, the folding of the macrocycle is affected both by the the nature and by the number of exocyclic ligands, resulting in different spatial positions of the hydrogen atoms relative to the paramagnetic centre and hence in different chemical shifts.

The ^{13}C spectra of the neodymium(III) and europium(III) diacetate–chloride complexes were recorded in $CDCl_3$ and D_2O; they are summarized in Table 6. This table also includes for comparison the spectra of the lanthanum(III) diacetae–chloride and of the praseodymium(III) diacetate–chloride and trinitrate. For the paramagnetic complexes, assignments of the resonances of the hydrogen-bound carbons were confirmed by heteronuclear correlation (HETCOR) experiments. The HETCOR spectrum and Attached Proton Test of the praseodymium(III) diacetate–chloride complex are shown in Fig. 4. The ^{13}C resonances of the paramagnetic species examined in this work appear to be much less sensitive than the ^1H resonances to changes in counterions; they still are, however, strongly solvent-dependent.

These results show that solvent and counterion effects are important in determining the NMR spectra of paramagnetic macrocyclic complexes

Table 5. ^1H chemical shifts (ppm)

Complex	Solvent[a]	βH-py	γH-py	CH_2	CH_3 (ring)	CH_3 (acetate)	Reference
$La(CH_3COO)_2Cl(L_I)\cdot nH_2O$	$CDCl_3$	8.02 d[b]	8.19 t[b]	3.96	2.46	1.55	4, This work
	D_2O	8.25 d	8.35 t	4.06	2.59	1.75	4, This work
$[La(NO_3)_3(L_I)]$	D_2O	8.21	8.21	4.04	2.59	—	7
$[Nd(CH_3COO)_2(L_I)]Cl\cdot 4H_2O$	$CDCl_3$	9.56 d	9.00 t	7.66	1.69	1.26	This work
	D_2O	12.59 d	10.75 t	12.52	4.91	−2.59	This work
$[\{Nd(NO_3)(H_2O)_2(L_I)\}_2](NO_3)(ClO_4)_3\cdot 4H_2O$	D_2O	13.81	11.70	11.88	5.35	—	7
$[Eu(CH_3COO)_2(L_I)]Cl\cdot 4H_2O$	D_2O (27.6 mg/g)	1.97 d	5.24 t	−7.64	0.24	6.73	This work
	D_2O (13.8 mg/g)	1.96 d	5.24 t	−7.65	0.23	6.70	This work
	D_2O (9.2 mg/g)	1.96 d	5.24 t	−7.65	0.24	6.71	This work
	DMSO-d_6	6.52 d	7.56 t	1.47	5.55	−1.11 br, 3.44 br	This work
	$CDCl_3$ (13.1 mg/g)	6.31 d	7.59 t	0.62	5.28	−0.02 br, 3.23 br	This work
	$CDCl_3$ (6.6 mg/g)	6.33 d	7.60 t	0.70	5.31	−0.13 br, 3.09 br	This work
	$CDCl_3$ (4.4 mg/g)	6.31 d	7.60 t	0.74	5.31	−0.12 br, 2.71 br	This work
$[\{Eu(NO_3)(H_2O)_2(L_I)\}_2](NO_3)(ClO_4)_3\cdot 4H_2O$	D_2O	1.07	4.52	−7.60	−0.05	—	7
$Pr(CH_2COO)_2Cl(L_I)\cdot nH_2O$	$CDCl_3$	8.01 d	8.62 t	−4.01	−1.52	9.45 br	This work
	D_2O	16.38	14.22	4.01	5.50	−3.90	This work
$[Pr(NO_3)_2(H_2O)(L_I)](NO_3)\cdot 2H_2O$	D_2O	18.60	15.90	3.92	6.71	—	This work
	D_2O	18.13	15.63	3.92	6.60	—	7

[a] For reference, see Experimental. [b] $J = 8$ Hz.

Table 6. ^{13}C chemical shifts (ppm)

Complex	Solvent[a]	C=O (acetate)	C=N	αC-py	γC-py	βC-py	CH_2	CH_3 (ring)	CH_3 (acetate)	References
$La(CH_3COO)_2Cl(L_1)\cdot nH_2O$	$CDCl_3$	182.20	168.32	154.68	140.94	125.71	52.66	16.55	24.54	4, This work
$La(CH_3COO)_2Cl(L_1)\cdot nH_2O$	D_2O	[b]	171.12	154.38	141.64	126.42	51.96	15.71	[b]	4, This work
$[La(NO_3)_3(L_1)]$	D_2O	—	171.8	154.5	142.0	126.7	52.0	15.9	—	7
$[Nd(CH_3COO)_2(L_1)]Cl\cdot 4H_2O$	$CDCl_3$	[b]	[171.16, 163.51]		139.50	137.58	46.84	37.52	[b]	This work
$[Nd(CH_3COO)_2(L_1)]Cl\cdot 4H_2O$	D_2O	[b]	[185.13, 174.25]		143.40	142.45	55.86	42.05	[b]	This work
$[Eu(CH_3COO)_2(L_1)]Cl\cdot 4H_2O$	$CDCl_3$	[b]	[161.58, 136.19]		148.31	104.58	57.26	−17.77	[b]	This work
$[Pr(CH_3COO)_2(L_1)]Cl\cdot 4H_2O$	$CDCl_3$	164.78[c]	[157.03, 155.08]		139.64	132.78	26.05	27.75	54.45[c]	This work
$[Pr(CH_3COO)_2(L_1)]Cl\cdot 4H_2O$	D_2O	[199.13, 191.97, 191.57]			153.41	149.57	48.52	40.63	—	This work
$[Pr(NO_3)_2(H_2O)(L_1)](NO_3)\cdot 2H_2O$	D_2O	—	[193.6]		152.6	148.7	46.7	37.5	—	7

[a] For reference, see Experimental. [b] Not observed. [c] Extremely weak signal after 24 h data accumulation.

and cannot be ignored when comparing spectra of such complexes from different literature sources.

CONCLUSIONS

The X-ray analysis of these neodymium(III) and europium(III) diacetate–chloride macrocyclic complexes, when taken in conjunction with the structural data available for related compounds of the same or other lanthanides, points to some interesting generalizations. First, in the crystalline compound the coordinated exocyclic anions are bound to the central metal ion more strongly than are the six nitrogen-donor atoms of the uncharged macrocyclic ligand, and this is true for both oxygen-donor and nitrogen-donor anions. This observation confirms the kinetic origin of the extreme resistance to decomposition of the $\{ML_1\}$ entity, compared to the ease of exchange of the exocyclic anions. Second, the departure from planarity which exists, although in different measures, in all members of this macrocyclic series appears to result primarily from the requirement that all six nitrogen-donor atoms of the macrocycle remain within bond-distance from the central metal ion, while allowing close approach of as many exocyclic donor atoms as possible. Third, the fact that every compound of this series for which the crystal structure is known contains at least one anionic exocyclic ligand, suggests that its coordination greatly contributes to the stability of the complex and will occur whenever a suitable anion is available. Coordination of additional anionic ligands appears instead to be controlled by a fine balance of steric requirements and/or crystal lattice (solubility) effects, and may not take place even when "free" anions are present. For example, the mono-nitrato-diaquo complex $[\{Nd(NO_3)(H_2O)_2L_1\}_2](NO_3)(ClO_4)_3\cdot 4H_2O$ is obtained from solutions that contain a 1:3 $Nd:NO_3$ mole ratio,[7] even though there should be no forbidding steric hindrance to the coordination of two chelating oxygen-donor anions, as shown by the easy formation of the $[Nd(CH_3COO)_2L_1]Cl\cdot 4H_2O$ species.

These generalizations based on X-ray results are in good agreement with the NMR experiments, which show that the nature of the counterion affects the geometry of the macrocyclic moiety even in dilute aqueous solutions. Therefore the species present in these solutions cannot be the simple aquo-macrocycles, $[M(H_2O)_nL_1]^{3+}$, as previously postulated,[7] but rather must include at least one coordinated counterion, possibly in rapid exchange with the solvent. This conclusion provides a satisfactory rationalization for the observed fluorescence behaviour of the diacetate–chloride

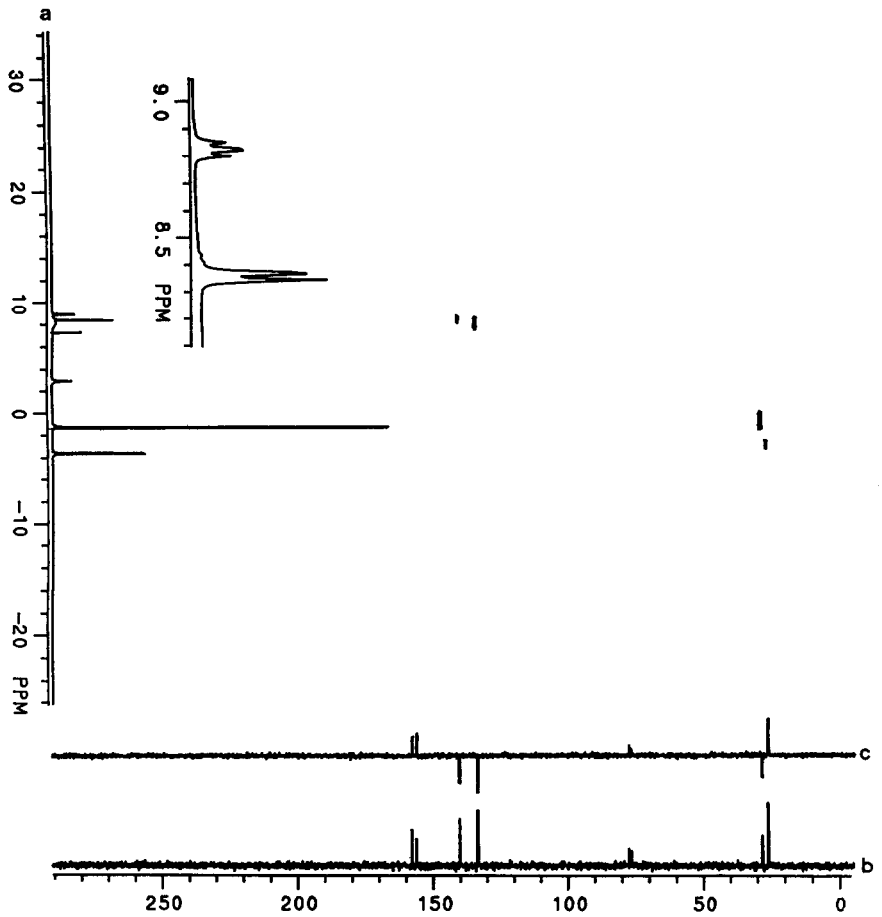

Fig. 4. Heteronuclear correlation spectrum (a = ^1H, with inset showing coupling of pyridine protons; b = ^{13}C) and attached ^1H test (c) for $[Pr(CH_3COO)_2L_1]Cl \cdot nH_2O$ in $CDCl_3$.

of the europium(III) macrocycle[6] and related carboxylates.[26]

REFERENCES

1. J. D. J. Backer-Dirks, C. J. Gray, F. A. Hart, M. B. Hursthouse and B. C. Schopp, *J. Chem. Soc., Chem. Commun.* 1979, 774.
2. W. Radecka-Paryzek, *Inorg. Chim. Acta* 1980, **45**, L147.
3. G. Wang and L. Miao, *Gaodeng Xnexiao Huaxue Xuebao* 1984, **5**, 281; *Chem. Abstr.* 1984, **101**, 182591C.
4. L. De Cola, D. L. Smailes and L. M. Vallarino, *Inorg. Chem.* 1986, **25**, 1729.
5. G. Bombieri, F. Benetollo, A. Polo, L. De Cola, D. L. Smailes and L. M. Vallarino, *Inorg. Chem.* 1986, **25**, 1127.
6. N. Sabbatini, L. De Cola, L. M. Vallarino and G. Blasse, *J. Phys. Chem.* 1987, **18**, 4681.
7. A. M. Arif, J. D. J. Backer-Dirks, C. J. Gray, F. A. Hart and M. B. Hursthouse, *J. Chem. Soc., Dalton Trans.* 1987, 1665.
8. G. Bombieri, F. Benetollo, W. T. Hawkins, A. Polo and L. M. Vallarino, *Polyhedron* 1989, **8**, 1923.
9. G. Bombieri, F. Benetollo, A. Polo, L. De Cola, W. T. Hawkins and L. M. Vallarino, *Polyhedron* 1989, **8**, 2157.
10. K. K. Abid and D. E. Fenton, *Inorg. Chim. Acta* 1984, **82**, 223.
11. K. K. Abid and D. E. Fenton, *Inorg. Chim. Acta* 1984, **95**, 119.
12. W. Radecka-Paryzek, *Inorg. Chim. Acta* 1981, **52**, 261.
13. F. Benetollo, G. Bombieri, L. De Cola, A. Polo, D. L. Smailes and L. M. Vallarino, *Inorg. Chem.* 1989, **28**, 3447.
14. (a) R. C. Leif, S. P. Clay, H. G. Gratzner, H. G. Haines and L. M. Vallarino, *The Automation of Uterine Cancer Cytology*, p. 313. Tutorials of Cytology, Chicago, Illinois (1976); (b) L. M. Vallarino, *J. Less-Common. Met.* 1989, **149**, 121.
15. R. B. Lauffer, *Chem. Rev.* 1987, **87**, 902.
16. A. C. T. North, D. C. Phillips and F. S. Mathews, *Acta Cryst.* 1968, **24A**, 351.
17. G. M. Sheldrick, SHELX Program for Crystal Structure Determination. University of Cambridge (1976).
18. C. K. Johnson, ORTEP II, Report ORNL-5138. Oak Ridge National Laboratory, Tennessee (1976).
19. W. D. S. Motherwell and W. Clegg, PLUTO, Pro-

gram for Molecular and Crystal Structures. University of Cambridge (1978).
20. M. Nardelli, *Comput. Chem.* 1983, **7**, 95.
21. *International Tables for X-Ray Crystallography*, Vol. 4. Kynoch Press, Birmingham (1974).
22. J. C. G. Bünzli, B. Klein, D. Wessner, K. J. Schenk, G. Chapuis, G. Bombieri and G. De Paoli, *Inorg. Chim. Acta* 1981, **54**, L43.
23. F. Nicolo', D. Plancherel, G. Chapuis and J. C. G. Bünzli, *Inorg. Chem.* 1988, **27**, 3518.
24. D. Cremer and J. A. Pople, *J. Am. Chem. Soc.* 1975, **97**, 1354.
25. G. J. D. Dunitz, M. Dobler, P. Seiler and R. P. Phizackerley, *Acta Cryst.* 1974, **30B**, 2733.
26. L. De Cola, D. D. Shillady, D. L. Smailes and L. M. Vallarino, Abstract 252. ACS 36th South-eastern Regional Meeting, Raleigh, N. C. (1984).
27. R. D. Shannon, *Acta Cryst.* 1976, **32A**, 751.

Polyhedron Vol. 9, No. 11, pp. 1423–1427, 1990
Printed in Great Britain

0277–5387/90 $3.00+.00
Pergamon Press plc

SYNTHESIS, PHOTOCHEMISTRY AND X-RAY CRYSTAL STRUCTURES OF THE METHYLTRIS[BIS(TRIMETHYLSILYL)AMIDO] COMPOUNDS $MeTi[N(SiMe_3)_2]_3$ AND $MeZr[N(SiMe_3)_2]_3$

DONALD C. BRADLEY,* HALINA CHUDZYNSKA, JULIUS D. J. BACKER-DIRKS, MICHAEL B. HURSTHOUSE,* ALI A. IBRAHIM, MAJID MOTEVALLI and ALICE C. SULLIVAN

Department of Chemistry, Queen Mary and Westfield College, London E1 4NS, U.K.

(*Received* 12 *January* 1990; *accepted* 8 *February* 1990)

Abstract—The synthesis and characterization of the compound methyltris[bis(trimethylsilyl)amido]titanium, $MeTi[N(SiMe_3)_2]_3$ (**1**), is reported. In the presence of UV radiation or sunlight, **1** decomposed rapidly to the titanium(III) species $Ti[N(SiMe_3)_2]_3$ (**2**). The X-ray crystal structures of the compounds $MeM[N(SiMe_3)_2]_3$, M = Ti and Zr (**3**), are reported. Compound **3** was stable in sunlight, but the cyclometallated product $[(Me_3Si)_2N]_2ZrN(SiMe_3)SiMe_2CH_2$ (**4**) was apparently formed (from ^1H and ^{13}C NMR data) when solutions of **3** were exposed to a source of UV radiation.

In the last decade or so there has been considerable interest in metal amide compounds incorporating the bulky bis(trimethylsilyl)amido—$N(SiMe_3)_2$, "silylamido", group. A number of reasons account for this interest, the most notable concerning the ability of the ligand to stabilize low coordination in transition metals and the lanthanides,[1] the utility of these compounds as precursors for a range of metalloorganic derivatives,[2] and of course the unusual intramolecular reactivity displayed by a number of bis(trimethylsilyl)amido species. A number of unusual thermally-promoted intramolecular reactions have been reported; for example, the thermal elimination of alkanes from compounds $R_2Zr[N(SiMe_3)_2]_2$, R = Me, Et or CH_2SiMe_3, and the isolation of a cyclometallated product $Cp_2TiN(SiMe_3)SiMe_2CH_2$ from the reaction between Cp_2TiCl_2 and $Li[N(SiMe_3)_2]$.[3] In this paper we report on the photoreactivity we have observed for the silylamido compounds $MeM[N(SiMe_3)_2]_3$ along with the X-ray crystal structures of the titanium and zirconium derivatives.

RESULTS AND DISCUSSION

The compound $MeTi[N(SiMe_3)_2]_3$ (**1**) was prepared by the reaction of methyllithium with the corresponding chloride (see Scheme 1) at temperatures in the range 0–7°C. Compound **1** was found to be photoactive in both the solid state and in solution, changing from colourless to blue on exposure to sunlight or a UV source. The formation of the titanium(III) compound $Ti[N(SiMe_3)_2]_3$ (**2**) was confirmed by comparison of its UV and ESR spectra with those of an authentic sample.[4] Photo-assisted reduction of titanium(IV) species is not unprecedented.[5] Hunt and Winter have shown that exposure to sunlight of a solution of $TiCl_4$ and butanol in petroleum-ether led to the formation

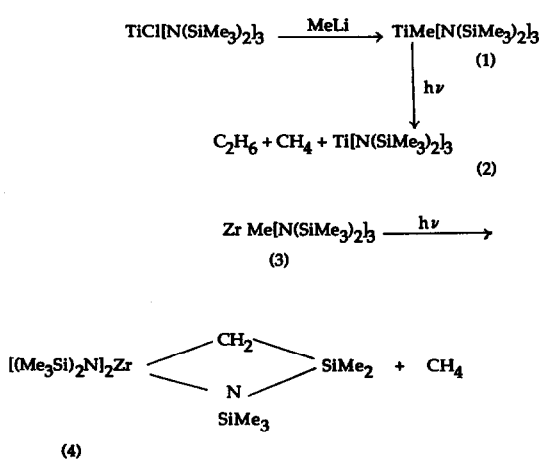

Scheme 1.

* Author to whom correspondence should be addressed.

of the compound $TiCl_3 \cdot 3BuOH$. Also mixtures of compounds $Ti(OR)_4$ and lithium halide in the parent alcohols were said to give insoluble titanium (III) species, $Ti(OR)_3$, on exposure to sunlight. Interestingly, sensitivity to sunlight was not a feature of the related dimethyl compound $Me_2Ti[N(SiMe_3)_2]_2$. The zirconium compound $MeZr[N(SiMe_3)_2]_3$ (**3**) was prepared as previously described.[6] Unlike the titanium analogue **1**, compound **3** was stable in the presence of sunlight. However the exposure of toluene solutions of **3** to a source of UV radiation for a period of approximately 25 min apparently resulted in the formation of the metallocycle **4** (from ^1H and ^{13}C NMR data), presumably via intramolecular elimination of methane. Similar thermally promoted cyclometallation reactions were reported for the compounds $R_2Zr[N(SiMe_3)_2]_2$[7] and $MeM[N(SiMe_3)_2]_3$,[8] M = U and Th, giving, respectively, $\{Zr[N(SiMe_3)SiMe_2CH]N(SiMe_3)_2\}_2$ and $MN(SiMe_3)SiMe_2CH_2[N(SiMe_3)_2]_2$, presumably via elimination of alkane. In contrast to the zirconium analogue, the compound $Me_2Ti[N(SiMe_3)_2]_2$ was found to be remarkably thermally stable, a feature which led Andersen to rule out the possibility of a radical mechanism for the thermal reactivity of the zirconium species. Our studies of the photoactivity of compound **1**, however, which resulted in the formation of the paramagnetic titanium(III) compound **2**, suggested a radical mechanism in this particular case. In an attempt to investigate the possibility of a radical mechanism, solutions of **1** and the radical trap nitrosotertiarybutane, Bu^tNO, in benzene, were exposed to sunlight until the blue colour of compound **2** appeared. The ESR spectrum was recorded at 15 min intervals from that point and while a strong signal due to the titanium(III) species (**2**) was observed, no signals associated with the nitroxide $MeBu^tNO$[9] or indeed $PhBu^tNO$ were detected.

In another experiment a solution of **1** in C_6D_6 was exposed to a source of UV light for 30 min and the gases produced examined by mass spectrometry. Peaks were observed at *m/z* 17 and 30 which may be tentatively assigned to CH_3D and C_2H_6, respectively. While the failure to trap any methyl radical in the previous experiment at best suggested the absence of a dissociated radical pair process, the observation of CH_3D and C_2H_6 formation was indicative of precursor methyl radical formation. The formation of a diamagnetic photoelimination zirconium(IV) product (**4**) from the zirconium compound (**3**) was in keeping with the relative inaccessibility of the lower oxidation state for zirconium compared with titanium and probably did not involve radical intermediates. However, the driving force for these photoeliminations of the methyl function from **1** and **3** was probably steric in both cases.

Restricted rotation of the silylamido ligands in compounds $[MCl\{N(SiMe_3)_2\}_3]$, M = Ti, Zr and Hf, was observed in solution at low temperature by NMR spectroscopy.[10] Similar fluxional behaviour was observed for the compounds $[MMe\{N(SiMe_3)_2\}_3]$, M = Ti and Hf. Lowering the temperature resulted in line broadening and the eventual splitting into a doublet of the single resonance, due to the silylamide group, observed at room temperature. This is consistent with the presence of a configuration having three equivalent silylamido ligands each with magnetically distinct trimethylsilyl groups, where one is distal and the other proximal to the coordinated methyl group. Andersen[6] has previously reported the coalescence temperature of *ca* −25°C for the hafnium complex and we have found, as expected, that the titanium compound has a much higher coalescence temperature (i.e. *ca* −2°C). This is consistent with a decrease in steric congestion with an increase in atomic radius from titanium to hafnium.

It is noteworthy that our attempts to introduce alkyl groups larger than methyl failed for a range of conditions and reagents explored in the case of zirconium.

The intramolecular ligand steric relationships were further highlighted by single crystal X-ray crystallographic analysis. The essential structural features closely resemble those of the related monochloride derivatives, $MCl[N(SiMe_3)_2]_3$, M = Ti, Zr and Hf.[10] The geometry in the isostructural compounds $MMe[N(SiMe_3)_2]_3$, M = Ti and Zr, was found to be distorted tetrahedral with the metal–methyl bond coincident with a three-fold rotation axis. The molecular structure is shown in Fig. 1

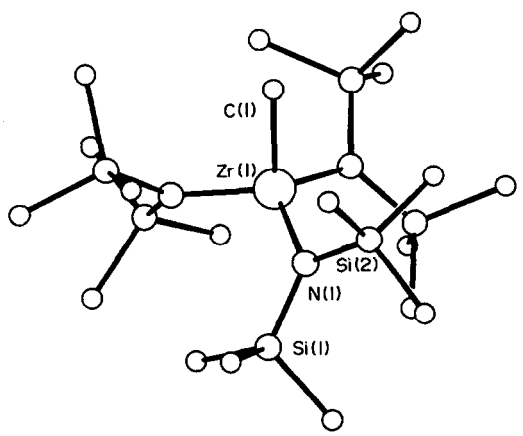

Fig. 1. The molecular structure of $MMe\{N(SiMe_3)_2\}_3$ (M = Zr).

Table 1. Selected bond lengths and bond angles for $[MMe\{N(SiMe_3)_2\}_3]$, M = Ti or Zr

	Ti	Zr
(a) Bond lengths (Å)		
C(1)—M	2.127(13)	2.262(11)
N(1)—M	1.935(7)	2.080(5)
Si(1)—N(1)	1.775(7)	1.758(6)
Si(2)—N(1)	1.777(7)	1.758(6)
C(11)—Si(1)	1.866(10)	1.869(8)
C(12)—Si(1)	1.871(10)	1.849(8)
C(13)—Si(1)	1.895(10)	1.864(8)
C(21)—Si(2)	1.874(10)	1.871(8)
C(22)—Si(2)	1.861(10)	1.862(7)
C(23)—Si(2)	1.881(9)	1.879(8)
(b) Bond angles (deg.)		
N(1)—M—C(1)	102.4(3)	102.6(2)
N(1)—M—N(1a)	115.6(2)	115.4(2)
Si(1)—N(1)—M	126.7(4)	125.8(3)
Si(2)—N(1)—M	118.0(4)	117.4(3)
Si(2)—N(1)—Si(1)	115.0(4)	116.7(3)
C(11)—Si(1)—N(1)	112.4(4)	111.8(3)
C(12)—Si(1)—N(1)	112.3(4)	111.0(3)
C(12)—Si(1)—C(11)	106.8(5)	108.0(4)
C(13)—Si(1)—N(1)	115.6(4)	115.0(3)
C(13)—Si(1)—C(11)	103.8(5)	106.5(4)
C(13)—Si(1)—C(12)	105.1(5)	104.0(4)
C(21)—Si(2)—N(1)	113.5(4)	112.4(3)
C(22)—Si(2)—N(1)	112.2(4)	114.2(3)
C(22)—Si(2)—C(21)	104.0(5)	105.4(4)
C(23)—Si(2)—N(1)	111.7(4)	111.2(3)
C(23)—Si(2)—C(21)	105.3(5)	108.0(4)
C(23)—Si(2)—C(22)	109.6(5)	105.1(4)

along with the atom numbering scheme, and the main bond lengths and angles are given in Table 1. Interligand repulsion was seen to be minimized in the manner previously found for the monochloride systems. Thus there was widening from tetrahedral values of the N—M—N angles to 115.6(2)° (Ti) and 115.4(2)° (Zr), and narrowing of the C—M—N angles to 102.4(3)° (Ti) and 102.6(3)° (Zr).

The trimethylsilyl groups of each silylamide had either a proximal or distal disposition, respectively, with respect to the coordinated methyl groups and a staggered arrangement in the distal and proximal directions.

The M—N—Si(1) (distal) angles were opened up to 126.7(4)° (Ti) and 125.8(3)° (Zr), while the M—N—Si(2) (proximal) angles were slightly compressed to 118.0(4)° (Ti) and 117.4(3)° (Zr), from trigonal planar values, probably to accommodate the tetrahedral distortion at the metal centres. Despite the C—M—N angle narrowing, the M—C bond distances were normal, being close to those previously observed in a range of titanium[11] or zirconium[12] compounds with metal–C(sp^3) bonds. The proposed photoelimination of methane from the zirconium compound (**4**) prompted a search for hydride type interactions but no such contacts were found.

EXPERIMENTAL

The compounds $[MCl\{N(SiMe_3)_2\}_3]$, M = Ti or Zr,[10] and $MeZr[N(SiMe_3)_2]_3$[6] were prepared as previously described. Solvents were dried over and distilled from the sodium ketyl of benzophenone. Microanalytical data was obtained from University College London. Instruments: NMR, Bruker WP80 and WM-250; ESR, Bruker 200D (X-Band); mass spectrometer, MS-902, EI, recorded at 70 eV. All reactions were carried out in an atmosphere of purified nitrogen using standard Schlenk techniques.

Methyltris[bis(trimethylsilyl)amido]titanium (1)

With exclusion of light a cooled (0–7°C) solution of $[TiCl\{N(SiMe_3)_2\}_3]$ (4.6 g, 8 mmol) in diethyl ether (150 cm^3) was treated with methyllithium (4.5 cm^3 of a 1.8 mol dm^{-3} solution in diethyl ether, 8 mmol). The reaction mixture was stirred for 16 h at 0–7°C, the ether evaporated and pentane (150 cm^3) added. The filtered pentane solution was concentrated to about 50 cm^3 and on cooling to −25°C colourless needles of **1** (3.14 g, 71%) were deposited (m.p. 202–205°C; sublimes 140°C/10^{-4} mm Hg). Found: C, 41.7; H, 10.0; N, 7.7; Ti, 8.8. Calc. for $C_{19}H_{57}N_3Si_6Ti_2$: C, 41.9; H, 10.6; N, 7.2; Ti, 8.8%. ^1H NMR (C_6D_6): δ 0.48 (54H, s, Me_3Si), 1.68 (3H, s, MeTi).

Photolysis of $MeZr[N(SiMe_3)_2]_3$

Solutions of $MeZr[N(SiMe_3)_2]_3$ in toluene in a quartz flask were exposed to a UV source (Hanovia Type 504/4 operating at 250 W) for 25 min. The colourless solution slowly changed to pale yellow. Removal of the toluene afforded a gold-coloured gummy residue. ^1H NMR (tol-d^8): δ 0.38 (36H, s, $(Me_3Si)_2N$), 0.40 (9H, s, Me_3SiN), 0.48 (6H, s, Me_2SiN), 1.4 (2H, s, CH_2). ^{13}C NMR (C_6D_6): δ 0.27 (q, Me_3SiN), 3.81 (q, Me_2SiN), 4.21 (q, $(Me_3Si)_2N$), 53.4 (t, CH_2); $J(^1H, ^{13}C)$ = 121 Hz

Crystallography

Measurements were made on crystals sealed under nitrogen in glass capillaries using a CAD4 diffractometer operating in the ω–2θ scan mode with graphite-monochromated Mo-K_α radiation

Table 2. Crystal data and details of intensity measurement and structure refinement for $[MMe\{N(SiMe_3)_2\}_3]$, M = Ti or Zr

	Ti	Zr
(a) *Crystal data*		
M_r	544.098	587.436
Crystal system	Rhobohedral (hexagonal axes)	
a (Å)	18.125(1)	18.345(2)
c (Å)	17.170(4)	17.091(4)
U (Å^3)	4883.54	4981.31
Space group	$R3c$	$R3c$
D_c (g cm^{-3})	1.11	1.17
Z	6	6
$F(000)$	1877	1896
(Mo-K_α)	0.71069	0.71069
(Mo-K_α) (cm)	4.06	5.49
(b) *Data collection*		
θ, min/max (°)	1.5, 25	1.5, 25
Total data measured	3021	3189
Total data unique	951	1013
Total data observed	839	893
Significance test	$F_o > 3\sigma(F_o)$	$F_o > 6\sigma(F_o)$
(c) *Refinement*		
Number of parameters	109	163
Weighting scheme parameters, g[a]	0.000012	0.001177
Final R[b]	0.0381	0.0257
Final RG[c]	0.0425	0.0344

[a] $\omega = 1/[\sigma^2(F_o)+gF_o^2]$.
[b] $R = \Sigma|\Delta F|/\Sigma|F_o|$.
[c] $RG = [\Sigma w|\Delta F|^2/\Sigma w|F_o^2|]^{1/2}$.

($\lambda = 0.71069$ Å) as previously described.[13] The intensity data were corrected for absorption empirically using psi-scan profiles. The structures were solved using standard heavy-atom procedures and refined using full-matrix least-squares methods[14] with scattering factors calculated from data obtained from ref. 15. All non-hydrogen atoms were refined with anisotropic displacement factor coefficients. For structure **1**, hydrogens were included in idealized positions and refined as components of rigid groups and assigned a common isotropic displacement factor coefficient. For structure **3**, hydrogens were freely refined with individual U_{iso} values. Crystal data for **1** and **3** are given in Table 2.

Acknowledgements—We thank SERC and Queen Mary College for equipment grants and one of us (A.C.S.) thanks SERC for an Advanced Fellowship. The Sudan Government and the British Council are thanked for financial support (A.A.I.). We are also grateful to Mr Greg Coumbarides for the NMR spectra, Dr A. Oduwole for ESR spectra and Mr Peter Cook for mass spectra.

REFERENCES

1. E. C. Alyea, D. C. Bradley and R. G. Copperthwaite, *J. Chem. Soc., Dalton Trans.* 1972, 1580; D. C. Bradley, J. S. Ghotra and F. A. Hart, *J. Chem. Soc., Dalton Trans.* 1973, 1021.
2. M. Bochmann, M. B. Hursthouse and G. Wilkinson, *J. Chem. Soc., Dalton Trans.* 1980, 1863; D. Barr, R. A. Bartlett, D. Decker, M. M. Olmstead and P. P. Power, *Inorg. Chem.* 1987, **26**, 1773.
3. C. R. Bennett and D. C. Bradley, *J. Chem. Soc., Chem. Commun.* 1974, 29.
4. E. C. Alyea, D. C. Bradley, R. G. Copperthwaite and K. D. Sales, *J. Chem. Soc., Dalton Trans.* 1973, 185; D. C. Bradley, R. G. Copperthwaite, S. Cotton, J. D. Gibson and K. D. Sales, *J. Chem. Soc., Dalton Trans.* 1973, 191.
5. M. R. Hunt and G. Winter, *Inorg. Nucl. Chem. Letts* 1970, **6**, 529.
6. R. A. Andersen, *Inorg. Chem.* 1979, **18**, 1724.
7. R. P. Planalp, R. A. Andersen and A. Zalkin, *Organometallics* 1983, **2**, 16.
8. S. J. Simpson, H. W. Turner and R. A. Andersen, *J. Am. Chem. Soc.* 1979, **101**, 7728.
9. M. J. Perkins, *Chem. Soc. Spec. Publ. No.* 24, p. 97 (1970).

10. C. Airoldi, D. C. Bradley, H. Chudzynska, M. B. Hursthouse, K. M. A. Malik and P. R. Raithby, *J. Chem. Soc., Dalton Trans.* 1980, 2010.
11. I. W. Bassi, G. Allegra, R. Scordamaglia and G. Chioccola, *J. Am. Chem. Soc.* 1971, **93**, 3788; J. L. Atwood, W. E. Hunter, D. S. Hrncir, E. Samuel, H. Alt and M. D. Rausch, *Inorg. Chem.* 1975, **14**, 1757.
12. G. S. Girolami, G. Wilkinson, M. Thornton-Pett and M. B. Hursthouse, *J. Chem. Soc., Dalton Trans.* 1984, 2789.
13. R. A. Jones, M. B. Hursthouse, K. M. A. Malik and G. Wilkinson, *J. Am. Chem. Soc.* 1979, **101**, 4128.
14. G. M. Sheldrick, SHELX 76, Program for Crystal Structure Determination. University of Cambridge (1976).
15. *International Tables for X-ray Crystallography*, Vol. 4. Kynoch Press, Birmingham (1974).

Polyhedron Vol. 9, No. 11, pp. 1429–1432, 1990
Printed in Great Britain

0277–5387/90 $3.00+.00
© 1990 Pergamon Press plc

COMMUNICATION

SILVER(I) CLUSTERS OF THE STERICALLY-HINDERED BIDENTATE LIGAND, 3-(DIMETHYLPHENYL)SILYL-2-PYRIDINETHIOL. THE CRYSTAL AND MOLECULAR STRUCTURES OF $[Ag(SC_5H_3N\text{-}3\text{-}SiMe_2Ph)]_6$ AND $[Ag_8(SC_5H_3N\text{-}3\text{-}SiMe_2Ph)_6][Ag(NO_3)_2]_2 \cdot 2CH_3OH \cdot CH_2Cl_2$

ERIC BLOCK, DEBORAH MACHERONE, SHAHID N. SHAIKH and JON ZUBIETA*

Department of Chemistry, State University of New York at Albany, Albany, NY 12222, U.S.A.

(*Received* 22 *January* 1990; *accepted* 26 *March* 1990)

Abstract—The reaction of $Ag(NO_3)$ with excess $HSC_5H_3N\text{-}3\text{-}SiMe_2Ph$ yields the hexanuclear $[Ag_6(SC_5H_3N\text{-}3\text{-}SiMe_2Ph)_6]$, a species exhibiting a molecular "paddlewheel" structure with a central Ag_6S_6 drum. In contrast, the reaction of excess $Ag(NO_3)$ with $HSC_5H_3N\text{-}3\text{-}SiMe_2Ph$ under otherwise identical conditions produces $[Ag_8(SC_5H_3N\text{-}3\text{-}SiMe_2Ph)_6][Ag(NO_3)_2]_2 \cdot 2CH_3OH \cdot CH_2Cl_2$. The eight silver centres of the $[Ag_8(SR)_6]^{2+}$ central core exhibit hexagonal bipyramidal geometry, with the two silver ions of the $[Ag(NO_3)_2]^-$ units associated as two weakly interacting appendages. Crystal data $[Ag_6(SC_5H_3N\text{-}3\text{-}SiMe_2Ph)_6]$: orthorhombic *Pbca*, $a = 17.576(3)$, $b = 18.634(3)$, $c = 25.845(6)$ Å, $V = 8464.4(11)$ Å^3, $Z = 4$, $D_{calc} = 1.66$ g cm^{-3}; structure solution and refinement based on 2945 reflections (Mo-K_α, $\lambda = 0.71073$ Å) converged at $R = 0.0420$. $[Ag_8(SC_5H_3N\text{-}3\text{-}SiMe_2Ph)_6][Ag(NO_3)_2]_2$: triclinic $P\bar{1}$, $a = 13.103(3)$, $b = 14.766(3)$, $c = 15.600(3)$ Å, $\alpha = 63.88(1)$, $\beta = 80.27(2)$, $\gamma = 72.35(1)°$, $V = 2580.5(9)$ Å^3, $Z = 1$, $D_{calc} = 1.95$ g cm^{-3}; 5251 reflections, $R = 0.0392$.

Thiolate ligands are of continuing interest in the modelling of enzyme active sites and in the synthesis of metal complexes of diversified structural types with varying nuclearities.[1] Although the chemistry of silver thiolates has been extensively studied in recent years, the types and structural patterns have not been fully realized. The silver thiolates described to date are exclusively anionic or neutral oligomers of the types $[Ag_x(SR)_y]^{x-y}$ or $[Ag(SR)]_n$, respectively. The anionic complexes $[Ag_5(SPh)_7]^{2-}$,[2] $[Ag_5(S\text{-}t\text{-}Bu)_6]^-$[3] and $[Ag_4(SRS)_3]^{2-}$[4,5] occur as molecular cages, while the hexaargentate species $[Ag_6(SPh)_8]_n^{2-}$ consists of a tubular framework of weakly associated $[Ag_{12}(SPh)_{16}]^{4-}$ units.[6] The uncharged compounds are frequently insoluble, polymeric materials or oligomers, of which the cyclic $[AgSC_6H_{11}]_{12}$ and the non-molecular $[AgSCMeEt_2]_n$ are examples.[7,8] However, the degree of aggregation of silver thiolate species may be controlled by tuning the steric bulk of the thiolate substituents R, as demonstrated by us in the structural characterization of the series of polynuclear species $[AgSC(SiPhMe_2)_3]_3$, $[AgSC(SiMe_3)_3]_4$, $[AgSCH(SiMe_3)_2]_8$ and $[Ag_4\{SCH_2(SiMe_3)\}_3]_n(OMe)_n$.[9] Furthermore, we would anticipate that the presence of a potentially chelating group on the substituent, such as a pyridine nitrogen donor, in addition to the steric bulk of the triorganosilyl substituent, should result in unusual structural types. Consequently, 3- and 3,6-silylated 2-pyridinethiols **1** and **2** were designed.[10] The reactions of the 3-(dimethylphenyl)silyl-2-pyridinethiol (**1b**) with $AgNO_3$ under various conditions yielded the complexes $[Ag(SC_5H_3N\text{-}3\text{-}SiMe_2Ph)]_6$ (**3**) and $[Ag_8(SC_5H_3\text{-}3\text{-}SiMe_2Ph)_6][Ag(NO_3)_2]_2 \cdot 2CH_3OH \cdot CH_2Cl_2$

* Author to whom correspondence should be addressed.

(**4**), whose preparations and structures we report in this paper. Although the structure of **3** is related to that of the previously reported copper complex $[Cu_6(SC_5H_3NSiMe_3)_6]$,[10] the structure of **4** is unique, exhibiting a cationic central core $[Ag_8(SC_5H_3N\text{-}3\text{-}SiMe_2Ph)_6]^{2+}$ weakly interacting with two $[Ag(NO_3)_2]^-$ units and two CH_3OH molecules.

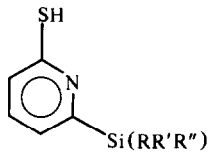

1a R = R' = R" = $-CH_3$
1b R = R' = $-CH_3$, R" = $-C_6H_5$

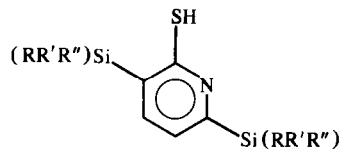

2a R = R' = R" = $-CH_3$
2b R = R' = $-CH_3$, R" = $-C_6H_5$

The reaction of $Ag(NO_3)$ with an excess of **1b** yields the hexanuclear complex $[Ag_6(SC_5H_3N\text{-}3\text{-}SiMe_2Ph)_6]$,* whose structure is illustrated in Fig. 1.† The discrete molecular structure possesses a centre of symmetry at the centroid of the Ag_6S_6 drum, with a pseudo-three-fold axis passing through the centroids of the Ag_3S_3 rings. The overall geometry has been described as a molecular paddlewheel, a structure reminiscent of the cyclophanes.[11] The central drum of the paddlewheel is constructed from the two Ag_3S_3 rings, while the $-C_5H_3N(SiMe_2Ph)$ fragments of the ligands provide the six paddles. The organosilylated pyridinethiolate ligands bridge the Ag_3S_3 rings, alternating such that three thiolate donors and three pyridine donors ligate to each ring. The thiolate sulphur atoms bridge adjacent metal sites within an Ag_3S_3 ring, while a pyridine nitrogen provides the third ligand in the distorted trigonal planar geometry about each metal site.

In contrast, the reaction of excess $Ag(NO_3)$ with **1b** in CH_3CN, followed by crystallization from CH_2Cl_2–CH_3OH yields the unusual dodecanuclear aggregate **4**,‡ whose structure is illustrated in Fig. 2.§ The structure is best described as a $[Ag_8(SC_5H_3N\text{-}3\text{-}SiMe_2Ph)_6]^{2+}$ cation, associated via secondary interactions to two $[Ag(NO_3)_2]^-$ anions and two methanol molecules. Since there is a crystallographically imposed centre of symmetry at the midpoint of the Ag(1)···Ag(1a) vector, there are five chemically and crystallographically unique silver sites: Ag(1) enjoys distorted trigonal planar coordination to three thiolate donors; Ag(2) exhibits highly distorted trigonal planar geometry via coordination to a sulphur donor and a pyridyl nitrogen donor from different ligands and long, secondary bonding to O(3) of the nitrate group; Ag(3) is essentially digonally coordinated to a sulphur and a nitrogen from different ligand groups; Ag(4) presents [SNO] coordination geometry as a consequence of thiolate sulphur, pyridyl nitrogen and methanol oxygen bonding; Ag(5) bonds to oxygen donors from two nitrate groups and in a secondary interaction to a thiolate sulphur, producing $[SO_2]$ distorted trigonal planar geometry. Although the overall molecular geometry appears quite irregular, the arrangement of silver centres is elegantly simple

*All manipulations were carried out under argon atmosphere. Compound **3**: a degassed solution of **1b** (0.362 g, 1.48 mmol) and an equivalent amount of Et_3N in CH_3CN (15 cm^3) was added to a solution of $AgNO_3$ (0.25 g, 1.47 mmol) in CH_3CN (15 cm^3). A light yellow suspension formed immediately, and upon stirring at room temperature for 5 h, a bright yellow powder precipitated. After filtration and drying *in vacuo*, this yellow material was recrystallized from CH_2Cl_2–CH_3OH (1:4, v:v) to give bright yellow plates in 45% yield. Found: C, 44.0; H, 4.1; N, 4.1. Calc. for $C_{78}H_{84}N_6Si_6S_6Ag_6$: C, 44.3; H, 4.0; N, 4.0%. IR (KBr pellet, cm^{-1}): 2962(w), 1555(m), 1432(w), 1763(vs), 1131(s), 1105(m), 1069(s), 1022(s), 821(vs), 781(m), 740(m), 704(s), 470(w).

†Compound **3**: orthorhombic space group *Pbca*, $a = 17.576(3)$, $b = 18.634(3)$, $c = 25.845(6)$ Å, $V = 8464.4(11)$ $Å^3$, $Z = 4$, $D_{calc} = 1.66$ g cm^{-3}; structure solution and refinement based on 2945 reflections with $F_o \geqslant 6\sigma(F_o)$ (Mo-K_α, $\lambda = 0.71073$ Å), $R = 0.0420$ (265 variables).

‡Compound **4**: a degassed solution of **1b** (0.181 g, 0.74 mmol) and an equivalent amount of Et_3N in CH_3CN (15 cm^3) was added to a solution of $Ag(NO_3)$ (0.25 g, 1.47 mmol) in CH_3CN (15 cm^3). After stirring for 5 h, the yellow precipitate was filtered, dried *in vacuo*, and recrystallized from CH_2Cl_2–CH_3OH (1:2, v:v). Bright yellow block-shaped crystals of **4** were obtained in 40% yield. Found: C, 33.3; H, 3.0; N, 4.8. Calc. for $C_{81}H_{94}N_{10}Cl_2O_{14}Si_6S_6Ag_{10}$: C, 33.1; H, 3.2; N, 4.8%. IR (KBr pellet, cm^{-1}): 3041(w), 2957(w), 1562(m), 1548(m), 1422(m), 1365(vs), 1279(m), 1204(m), 1132(m), 1111(m), 1072(m), 1028(m), 819(s), 776(s), 737(s), 702(s), 648(m), 475(m).

§Compound **4**: triclinic space group $P\bar{1}$, $a = 13.103(3)$, $b = 14.766(3)$, $c = 15.600(3)$ Å, $\alpha = 63.88(1)$, $\beta = 80.27(2)$, $\gamma = 72.35(1)°$, $V = 2580.5(9)$ $Å^3$, $Z = 1$, $D_{calc} = 1.95$ g cm^{-3}; structure solution and refinement based on 5251 reflections with $F_o \geqslant 6\sigma(F_o)$ (Mo-K_α, $\lambda = 0.71073$ Å), $R = 0.0392$ (390 variables).

Tables of atomic coordinates, thermal parameters, bond lengths and bond angles have been deposited with the Editor and with the Cambridge Crystallographic Data Centre.

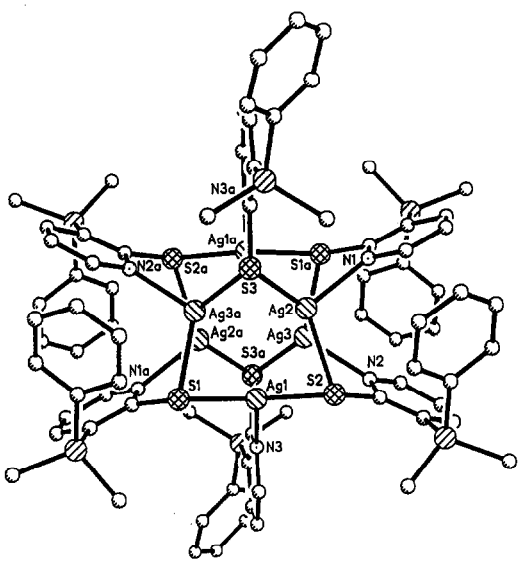

Fig. 1. ORTEP view of the structure of $[Ag_6(SC_5H_3N\text{-}3\text{-}SiMe_2Ph)_6]$ (**3**) viewed parallel to the pseudo-three-fold axis passing through the centroids of the Ag_3S_3 rings. Relevant bond lengths (Å) and angles (°):

Ag(1)—S(1)	2.472(3)	Ag(3)—S(3a)	2.472(3)
Ag(1)—S(2)	2.493(3)	Ag(3)—N(2)	2.321(10)
Ag(1)—N(3)	2.300(10)	Ag···Ag(av)	3.157(2)
Ag(2)—S(2)	2.495(3)	(within an Ag_3S_3 cycle)	
Ag(2)—S(3)	2.485(3)	and	3.016(2)
Ag(2)—N(1)	2.329(10)	(between Ag_3S_3 cycles)	
Ag(3)—S(1a)	2.464(3)		

S(1)—Ag(1)—S(2)	122.7(1)
S(1)—Ag(1)—N(3)	112.4(3)
S(2)—Ag(1)—N(3)	114.1(3)
S(2)—Ag(2)—S(3)	126.1(1)
S(2)—Ag(2)—N(1)	109.7(3)
S(3)—Ag(2)—N(1)	113.6(3)
S(1a)—Ag(3)—S(3a)	125.1(1)
N(2)—Ag(3)—S(1a)	110.6(2)
N(2)—Ag(3)—S(3a)	117.1(2)

as shown in Fig. 3. The eight silver atoms of the $[Ag_8(SR)_6]^{2+}$ central core exhibit a hexagonal bipyramidal geometry, with the two silver ions of the $[Ag(NO_3)_2]^-$ units associated as two weakly interacting arms. The pyridinethiol ligands are disposed three above and three below the equatorial plane. Alternate "spokes" to the axial silver centres from the equatorial sites are bridged by thiolate donors, while the pyridine nitrogens provide connectivity to the adjacent silver ions of the hexagonal plane. Thus, the axial silver sites exhibit trigonal planar coordination geometry to an $[S_3]$ donor set, while the equatorial sites display [SN] coordination, more or less distorted by secondary bonding interactions.

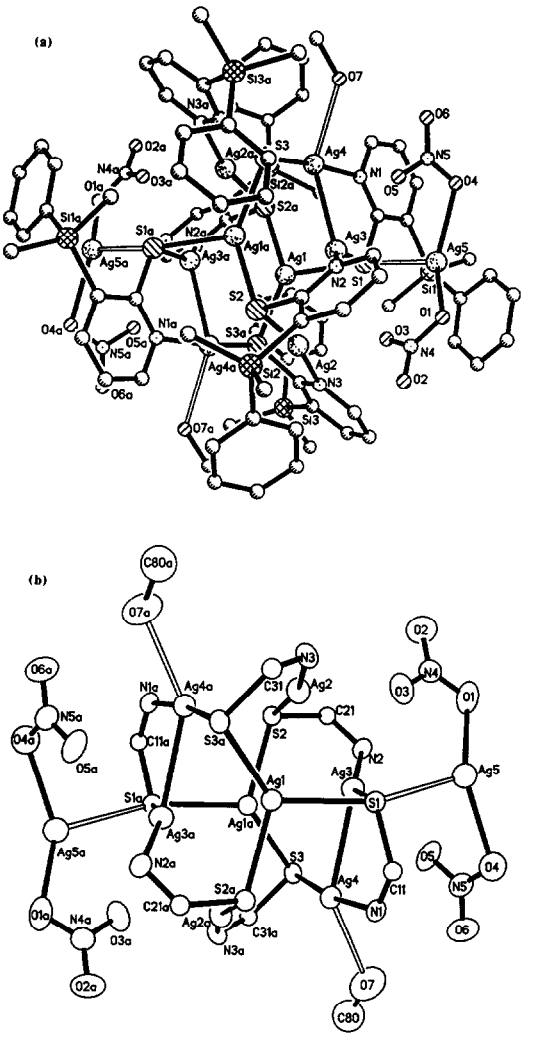

Fig. 2. (a) ORTEP view of the structure of the $[Ag_8(SC_5H_3N\text{-}3\text{-}SiMe_2Ph)_6][Ag(NO_3)]_2 \cdot 2CH_3OH$ unit of **4**. (b) Schematic view of the unit showing only the S—N—C moieties of the pyridine–thiolate ligands and the $[Ag_8][Ag(NO_3)_2]_2 \cdot 2CH_3OH$ framework. Relevant bond lengths (Å) and angles (°):

Ag(1)—S(1)	2.537(2)	Ag(3)—N(2)	2.200(5)
Ag(1)—S(2a)	2.504(2)	Ag(4)—S(3)	2.417(2)
Ag(1)—S(3a)	2.473(3)	Ag(4)—N(1)	2.208(5)
Ag(2)—S(2)	2.382(2)	Ag(4)—O(7)	2.623(5)
Ag(2)—N(3)	2.179(5)	Ag(5)—S(1)	2.784(2)
Ag(2)—O(3)	2.624(5)	Ag(5)—O(1)	2.360(7)
Ag(3)—S(1)	2.403(2)	Ag(5)—O(4)	2.430(8)

S(1)—Ag(1)—S(2a)	104.5(1)
S(1)—Ag(1)—S(3a)	122.9(1)
S(2a)—Ag(1)—S(3a)	123.7(1)
S(2)—Ag(2)—N(3)	167.1(2)
S(1)—Ag(3)—N(2)	150.1(1)
S(2)—Ag(2)—O(3)	107.6
N(3)—Ag(2)—O(3)	84.0
S(3)—Ag(4)—N(1)	171.6(2)
O(1)—Ag(5)—O(4)	139.2(2)
S(1)—Ag(5)—O(1)	120.9(2)
S(1)—Ag(5)—O(4)	94.3(2)

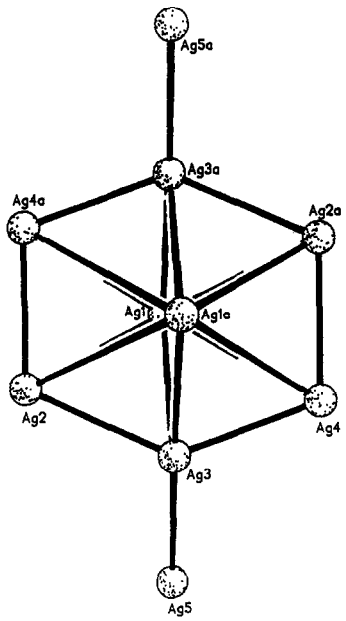

Fig. 3. Schematic representation of the geometry of the silver centers of **4**. Non-bonding distances (Å):

Ag(1)—Ag(2) 3.271(1)	Ag(1)—Ag(1a) 3.660(1)
Ag(1)—Ag(3) 3.320(1)	Ag(2)—Ag(3) 3.041(1)
Ag(1)—Ag(4) 3.867(1)	Ag(2)—Ag(4a) 2.928(1)
Ag(1)—Ag(2a) 3.787(1)	Ag(3)—Ag(4a) 2.856(1)
Ag(1)—Ag(3a) 2.992(1)	Ag(3)—Ag(5) 2.976(1)
Ag(1)—Ag(4a) 3.404(1)	

The isolation and characterization of **3** and **4** demonstrate that variations in reaction conditions, as well as the introduction of steric constraints, can have profound influences on the structures of metal–thiolate complexes. The unique structure of **4** suggests that the presence of coordinating anions results in unexpected structural consequences, such that the already rich and varied chemistry of the group IIb thiolates may be further developed.

Acknowledgement—This work was supported by a grant from the National Institutes of Health (GM2256610 to E.B. and J.Z.).

REFERENCES

1. (a) I. G. Dance, *Polyhedron* 1986, **5**, 1037; (b) P. G. Blower and J. R. Dilworth, *Coord. Chem. Rev.* 1987, **76**, 121.
2. G. A. Bowmaker and L.-C. Tan, *Aust. J. Chem.* 1979, **32**, 1443.
3. I. G. Dance, *Aust. J. Chem.* 1978, **31**, 2195.
4. G. Henkel, P. Betz and B. Krebs, *Angew. Chem. Int. Edn Engl.* 1987, **26**, 145.
5. G. Henkel, B. Krebs, P. Betz, H. Fietz and K. Saatkamp, *Angew. Chem. Int. Edn Engl.* 1988, **27**, 1326.
6. (a) S. Hong, A. Olin and R. Hesse, *Acta Chem. Scand.* 1975, **A29**, 583; (b) I. G. Dance, *Inorg. Chim. Acta* 1977, **25**, L17.
7. I. G. Dance, L. J. Fitzpatrick, A. D. Rae and M. L. Scudder, *Inorg. Chem.* 1983, **22**, 3785.
8. I. G. Dance, *Polyhedron* 1988, **7**, 2205.
9. K. Tang, M. Aslam, E. Block, T. Nicholson and J. Zubieta, *Inorg. Chem.* 1987, **10**, 1488.
10. E. Block, M. Gernon, H. Kang and J. Zubieta, *Angew. Chem. Int. Edn Engl.* 1988, **27**, 1342.
11. P. M. Keehn, in *Cyclophanes* (Edited by P. M. Keehn and S. M. Rosenfeld), Vol. I, pp. 69–239. Academic Press, New York (1983).

Polyhedron Vol. 9, No. 12, pp. 1433–1440, 1990
Printed in Great Britain

0277–5387/90 $3.00+.00
© 1990 Pergamon Press plc

CYCLIC S–N COMPOUNDS AND PHOSPHORUS REAGENTS—VII. REACTIONS OF S_4N_4 WITH TERTIARY (AMINO)PHOSPHINES: SYNTHESIS AND CHARACTERIZATION OF $(R_2N)_3PN\text{-}S_3N_3$ DERIVATIVES AND THEIR ADDITION PRODUCTS WITH NORBORNADIENE. X-RAY CRYSTAL STRUCTURE OF $(C_5H_{10}N)_3PN\text{-}S_3N_3$

ANIL JACOB ELIAS and M. N. SUDHEENDRA RAO*

Department of Chemistry, Indian Institute of Technology, Madras, 600 036, India

and

BABU VARGHESE

Regional Sophisticated Instrumentation Centre, Indian Institute of Technology, Madras, 600 036, India

(*Received* 26 *June* 1989; *accepted* 15 *January* 1990)

Abstract—The reactions of the tertiary (amino)phosphines $(R_2N)_3P$ [$R_2N = C_4H_8N$-, $C_5H_{10}N$-, $C_6H_{12}N$-, OC_4H_8N-, and $CH_3NC_4H_8N$-] with S_4N_4 are described. The phosphiniminocyclotrithiazenes $(R_2N)_3PN\text{-}S_3N_3$ (**1–5**) are the only heterocyclic products isolated (60–80% yield). Excess (amino)phosphines cleave the heterocycles readily while norbornadiene reacts with them to give rise to the addition products, $(R_2N)_3PN\text{-}S_3N_3 \cdot C_7H_8$ (**6–9**) in small yields. The single crystal X-ray structure of $(C_5H_{10}N)_3PN\text{-}S_3N_3$ (triclinic system, space group $P_{\bar{1}}$) gave the unit cell dimensions: $a = 9.573(5)$, $b = 10.372(6)$, $c = 10.916(6)$ Å, $\alpha = 85.46(3)$, $\beta = 81.13(4)$, $\gamma = 79.73(4)°$, $V = 1052.25$ Å^3 and $Z = 2$. The structure has been compared with that of $Ph_3PN\text{-}S_3N_3$ which is the only other compound of this type ($R_3PN\text{-}S_3N_3$) whose X-ray structure is known.

Prior to our work, Ph_3P,[2–4] $(C_6H_{11})_3P$[4] and $(PhO)_3P$[5] are the only examples of symmetrically substituted tertiary phosphines, R_3P to be reacted with S_4N_4. Recently we have carried out a similar investigation using a few phosphines of this type (P–C bonded only) which have shown noticeable variation in their behaviour,[1] compared to Ph_3P, which is the only well studied example. Tertiary (amino) phosphines, $(R_2N)_3P$ by virtue of their labile P–N bonds and more basic nature also offer suitable examples for such studies.[6] To date, besides a brief mention on the formation of an acyclic species from the reaction of S_4N_4 with $(Me_2N)_3P$[7], no other information on such reactions is available in the literature.

In this paper we report the detailed study of five different tertiary (amino)phosphines, $(R_2N)_3P$ [R_2N = (i) C_4H_8N-, (ii) $C_5H_{10}N$-, (iii) $C_6H_{12}N$-, (iv) OC_4H_8N- and (v) $CH_3NC_4H_8N$-] which has led to the isolation of phosphiniminocyclotrithiazene derivatives, $(R_2N)_3PN\text{-}S_3N_3$ (**1–5**) and their characterization and conversion to norbornadiene adducts (**6–9**). In addition, the X-ray crystal structure of $(C_5H_{10}N)_3PN\text{-}S_3N_3$ has been determined and compared with that of $Ph_3PN\text{-}S_3N_3$.[8]

EXPERIMENTAL

General procedures and materials

Spectrophotometers were as follows: IR, Perkin–Elmer 983G and 1430 (spectra in Nujol mull, values in cm^{-1}); NMR, ^{1}H-Varian EM 390 and Bruker

* Author to whom correspondence should be addressed.

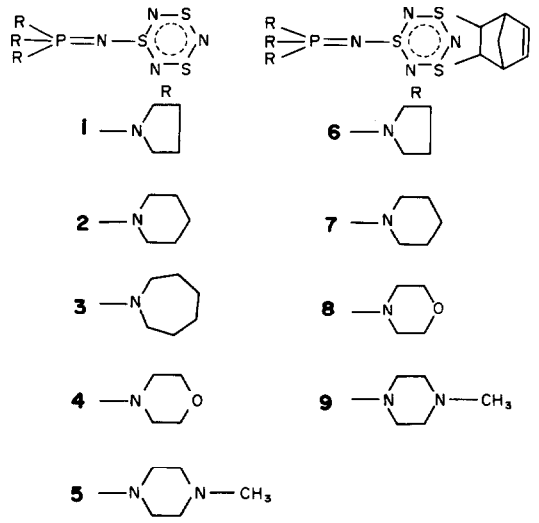

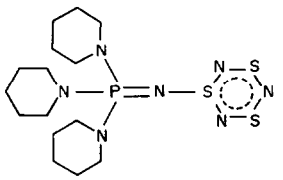

WH 250 (chemical shifts in ppm, relative to $SiMe_4$); ^{31}P-Varian XL 100, Varian FT 80A and Bruker WH 400 (chemical shifts in ppm, positive values downfield relative to 85% H_3PO_4); UV–vis, Shimadzu UV240 and Hitachi 220A (CH_2Cl_2 solutions); and mass spectra, Finnigan Matt 8280 GC-MS. CHN analyses were done by Messrs Beller, Goettingen, W. Germany and Department of Chemistry, University of Calgary, Calgary, Canada. Melting points were determined in sealed tubes and are uncorrected. All operations were performed under dry oxygen free argon atmosphere using glove bag/dry box and standard Schlenck techniques. Acetonitrile was twice distilled over P_4O_{10}, then over CaH_2 and stored over CaH_2 under argon. Benzene (AR) (**Caution!** potential carcinogen) was refluxed, distilled and stored over sodium wire.

S_4N_4 prepared by the literature method[9] was recrystallized from hot toluene before use. (**Caution!** S_4N_4 may explode. Recommended safety precautions have to be adopted.[10]) Aminophosphines (i)–(v) were prepared by employing the reported procedures.[11,12] $(C_5H_{10}N)_3P$, $(OC_4H_8N)_3P$ and $(CH_3NC_4H_8N)_3P$ were purified by recrystallization from a benzene–hexane (1 : 1) mixture and $(C_4H_8N)_3P$ and $(C_6H_{12}N)_3P$ by low pressure distillation. The physical and spectral properties of these phosphines have been published elsewhere.[12]

Reactions of S_4N_4 *and (amino)phosphines*

Reactions were carried out both in acetonitrile and benzene using different mole ratios of S_4N_4 and phosphine (1 : 2, 1 : 3.5 and 1 : 5) and different temperatures, [−5, 15, RT (*ca.* 30) and 45°C] with each of the phosphines. Only R_3PN–S_3N_3 and/or the corresponding phosphine sulphide were isolated from these reactions. The results of the reactions studied with each phosphine have been summarized in Table 1. Details of the synthesis in two specific cases are described here. The procedure given is adequate for the isolation of the corresponding derivatives in the other cases.

(a) *Reaction of* S_4N_4 *with tris(pyrrolidino)phosphine* [1 : 2, C_6H_6, RT]. Tetrasulphurtetranitride (0.56 g, 3.05 mmol) was added at room temperature as solid in aliquots to a stirred solution of $(C_4H_8N)_3P$ (1.47 g, 6.10 mmol) in benzene (30 cm^3). [WARNING: Direct addition of S_4N_4 to this liquid phosphine can cause sudden fire.] The reaction started at once with the evolution of heat and formation of a red colour which darkened with time. No precipitate formation was observed. The resulting dark

Table 1. Reactions of tertiary (amino)phosphines with S_4N_4 leading to R_3PN-S_3N_3 heterocycles (1–5)[a]

S. No.	Phosphine	C_6H_6 1:2 RT	CH_3CN 1:2 RT	CH_3CN 1:2 −5°C	CH_3CN 1:2 45°C	CH_3CN 1:3.5 15°C	CH_3CN 1:5 RT
1.	$(Pyrrolidino)_3P$	80	60	44	45		
2.	$(Piperidino)_3P$	62	51		26		
3.	$(Hexamethylenimino)_3P$	60	55		18		
4.	$(Morpholino)_3P$	60	73	[b]	22		
5.	$(N\text{-}Methylpiperazino)_3P$	67	70	16	24		

[a] The numbers shown correspond to the percentage yield of the R_3PN-S_3N_3 heterocycle isolated. Phosphine sulphide was a product of all the reactions. Yields are calculated based on percentage nitrogen content of S_4N_4.

[b] No reaction. S_4N_4 recovered unchanged.

Table 2. Analytical and physical data for the cyclotrithiazenes (**1–5**) and their norbornadiene adducts (**6–9**)

Compound	M.p. (°C)	Colour	Maximum yield (%)	Analysis (%) Calculated C	H	N	Found C	H	N
$(C_4H_8N)_3PN\text{-}S_3N_3$ (**1**)	96	Red	80	36.6	6.1	24.9	36.7	6.2	25.0
$(C_5H_{10}N)_3PN\text{-}S_3N_3$ (**2**)	102	Dark red	62	41.3	6.9	22.5	41.5	7.0	22.9
$(C_6H_{12}N)_3PN\text{-}S_3N_3$ (**3**)	92	Red	60						
$(OC_4H_8N)_3PN\text{-}S_3N_3$ (**4**)	131	Red	73	32.6	5.5	22.2	32.8	5.7	22.2
$(CH_3NC_4H_8N)_3PN\text{-}S_3N_3$ (**5**)	136	Dark red	70						
$(C_4H_8N)_3PN\text{-}S_3N_3\cdot C_7H_8$ (**6**)	97	Dull white	11						
$(C_5H_{10}N)_3PN\text{-}S_3N_3\cdot C_7H_8$ (**7**)	118	Dull white	5						
$(OC_4H_8N)_3PN\text{-}S_3N_3\cdot C_7H_8$ (**8**)	136	Dull white	45	42.8	6.0	18.4	43.1	6.2	18.2
$(CH_3NC_4H_8N)_3PN\text{-}S_3N_3\cdot C_7H_8$ (**9**)	108	Dull white	39	46.1	7.2	24.5	46.8	6.7	24.0

red solution was concentrated to one fourth the original volume and acetonitrile (20 cm^3) was added and cooled at 0°C (24 h). The red crystalline solid formed was separated by filtration under argon and recrystallized from CH_3CN–C_6H_6 (1 : 1, v/v) to obtain $(C_4H_8N)_3PN\text{-}S_3N_3$ (**1**) (0.96 g, 80%). [See Tables 2–4 for physical and spectral data.] From the residual mother liquor a colourless oily liquid was obtained by distillation under reduced pressure [b.p. 110°C/0.04 mm] which was identified as $(C_4H_8N)_3PS$ (see Table 4).

(b) *Reaction of* S_4N_4 *with tris(morpholino)phosphine* [1 : 2, CH_3CN, RT]. To a stirred solution of the phosphine (1.05 g, 3.62 mmol) in acetonitrile (25 cm^3) at room temperature, tetrasulphurtetranitride (0.33 g, 1.81 mmol) was added as solid in portions over a period of 15 min. The red colour formation was slow in this case. After *ca.* 8 h the formation of a red precipitate was observed which increased with time. After 24 h the reaction mixture was filtered under argon to isolate the red precipitate which on recrystallization from a mixture of CH_3CN–C_6H_6 (1 : 1, v/v) gave crystalline red blocks of $(OC_4H_8N)_3PN\text{-}S_3N_3$ (**4**) (0.41 g, 51%) (Tables 2–4).

The filtrate was concentrated to two thirds of the original volume and cooled in the refrigerator for 1 day to obtain further quantities of **4** (0.17 g, 21%). The concentrated residual mother liquor gave a small amount of S_4N_4 (10 mg) and $(OC_4H_8N)_3PS$ (0.39 g) when cooled at 0°C for 1 day.

(c) *Reaction of* $(OC_4H_8N)_3PN\text{-}S_3N_3$ *with* C_7H_8 [1 : 18, CH_2Cl_2, RT]. Tris(morpholino)phosphiniminocyclotrithiazene (0.35 g, 0.79 mmol) was stirred in CH_2Cl_2 (20 cm^3) in a side arm flask under argon and norbornadiene (1.31 g, 14.22 mmol) was added into it all at once. While it was stirred at room temperature, the intense red colour of the solution faded gradually and at the end of 36 h a pale red brown solution resulted. The solvent was removed *in vacuo* from this to obtain a pale brown semisolid which was vigorously stirred in diethylether (30 cm^3) for 30 min and filtered to get a slightly coloured powdery solid. This was recrystallized from a mixture of CH_2Cl_2–Et_2O (1 : 1, v/v) at 0°C to obtain $(OC_4H_8N)_3PN\text{-}S_3N_3\cdot C_7H_8$ (0.19 g, 45%) (Tables 2–4 for physical and spectral characteristics).*

X-ray crystallographic analysis

Crystal and refinement data for $(C_5H_{10}N)_3PN\text{-}S_3N_3$ are summarized in Table 5. Crystals suitable for X-ray analysis were prepared by slow recrystallization of the compound from a mixture of benzene and acetonitrile (1 : 1, v/v) at 0°C. Diffraction intensities were collected at 23°C using an Enraf–Nonius CAD 4 X-ray diffractometer with Cu-K_α radiation (λ = 1.5418 Å) and were corrected for Lorentz and polarization effects. Numerical absorption correction was applied using SHELX-76 program. The structure was solved by direct methods using SHELX-86 program and refined by full matrix least squares method, the minimized function being $\Sigma w(|F_o|-|F_c|)^2$. The weighting scheme employed was $w = 1/[\sigma^2(F_o)+0.0046F_o^2]$. The analytical scattering factors corrected for the real and imaginary parts of anomalous dispersions were taken from literature.[13,14] All hydrogens were located in difference Fourier maps synthesized after anisotropic refinement of non-hydrogen atoms. All computations were performed on a SIEMENS 7580 E computer.

* In the case of $(C_6H_{12}N)_3PN\text{-}S_3N_3$ the norbornadiene adduct could not be isolated.

Table 3. Spectral data for the cyclotrithiazenes (**1–5**) and their norbornadiene adducts (**6–9**)

Compound	IR[a] ν_{max}/cm^{-1}	UV–vis λ_{max} [dm^3 mol^{-1} cm^{-1}]	^{1}H-NMR δ (in ppm)	$^3J_{PH}$	$^3J_{HH}$ (Hz)
(**1**)	1460m, 1355s, 1250m, 1235m, 1200s, 1165s, 1120s, 1085vs, 1020vs, 935vs, 915vs, 865m, 775m, 715m, 680m.	485[2.5×10^3] 335[2.1×10^3] 288[2.0×10^3]	1.76[12H,m,C-CH_2] 3.06[12H,m,N-CH_2]	3.1	6.0
(**2**)	1364m, 1339m, 1320m, 1206s, 1198s, 1155vs, 1134s, 1118s, 1110s, 1071vs, 1026m, 945vs,b, 855m, 850m, 838m, 730s.	485[1.2×10^4] 335[9.1×10^3] 285[8.2×10^3]	1.54[18H,m,C-CH_2] 2.90[12H,m,N-CH_2]	[b]	[b]
(**3**)	1465m, 1448m, 1230m, 1155s, 1140vs, 1120vs, 1105s, 1070vs, 1055s, 1005m, 950s, 932s, 900m, 730m.	483[4.9×10^3] 338[4.2×10^3] 280[3.5×10^3]	1.59[24H,s,C-CH_2] 3.06[12H,m,N-CH_2]	4.0	5.5
(**4**)	1348m, 1333m, 1297s, 1261s, 1252vs, 1208m, 1152vs, 1133vs, 1112vs, 1088vs, 1070s, 1019s, 967vs, 930vs, 915s, 845m, 782m, 690m, 608m.	483[4.3×10^3] 330[3.5×10^3] 288[3.1×10^3]	3.07[12H,m,N-CH_2] 3.54[12H,t,O-CH_2]	4.0	3.6
(**5**)	2780m, 2735m, 2680m, 1465vs, 1370s, 1360m, 1345m, 1335m, 1285vs, 1225m, 1215m, 1205m, 1160vs, 1140vs, 1100vs, 1070s, 1060s, 1050m, 965vs, 930vs, 790m, 740s, 730s, 610s.	481[4.0×10^3] 332[3.1×10^3] 287[2.6×10^3]	2.18[9H,s,N-CH_3] 2.24[12H,t,C-NCH_2] 3.00[12H,m,P-NCH_2]	5.0	4.5
(**6**)	1365m, 1320m, 1250s, 1208vs, 1160s, 1120vs, 1085vs, 1015vs, 920vs,b, 870s, 862vs, 782m, 770m, 750m, 732vs, 640s.		6.32[2H,s], 5.25[2H,s] 3.14[2H,s], 3.06[12H,m] 1.90, 1.19[2H,m] 1.76[12H,m]		
(**7**)	1368vs, 1338s, 1320m, 1205s, 1113s, 1085s, 1065vs, 1020s, 955vs, 930s, 920vs, 910vs, 865s, 712s, 632vs, 615s.		6.35[2H,s], 5.25[2H,s] 3.14[2H,s], 2.98[12H,m] 1.60–1.40[18H,m] 1.90, 1.20[2H,m]		
(**8**)	1368s, 1258s, 1170m, 1135s, 1115vs, 1090vs, 1070m, 965vs, 919vs, 865s, 775s, 730s, 645s, 620s.		6.40[2H,s], 5.25[2H,s] 3.59[12H,m], 3.10[16H,m] 1.95, 1.20[2H,m]		
(**9**)	1290s, 1210m, 1165s, 1150s, 1135s, 1100s, 1070m, 970vs, 930m, 915vs, 870m, 865m, 722vs, 670m, 650s.		6.38[2H,s], 5.11[2H,s] 3.10[16H,m], 2.23[21H,m] 1.90, 1.20[12H,m]		

[a] Weak and very weak peaks have been omitted.
[b] J values could not be measured due to poor resolution of peaks.

Table 4. $\{^1H\}$ ^{31}P-NMR spectral data of tertiary (amino)phosphines and their sulphides, phosphiniminocyclotrithiazenes (**1–5**) and their norboranadiene adducts (**6–9**)

R	R_3P	R_3PS	$R_3PN\text{-}S_3N_3$	$R_3PN\text{-}S_3N_3\cdot C_7H_8$
C_4H_8N-	121.1	82.6	22.3	21.2
$C_5H_{10}N$-	115.7	76.0	25.8	24.7
$C_6H_{12}N$-	108.0	98.0	33.2	
OC_4H_8N-	114.5	74.8	23.1	22.2
$CH_3NC_4H_8N$-	116.8	92.6	26.7	23.1

$(C_4H_8N)_3PS$ (b.p., 110°C/0.04 mm), $(C_6H_{12}N)_3PS$ (m.p., 84°C) and $(CH_3NC_4H_8N)_3PS$ (m.p., 94°C) are new phosphine sulphides not reported so far.

RESULTS AND DISCUSSION

The reaction between the tertiary (amino)phosphines and S_4N_4 that proceed exothermically at room temperature can be represented as in eq. (1).

$$2(R_2N)_3P + S_4N_4 \longrightarrow (R_2N)_3PN\text{-}S_3N_3 + (R_2N)_3PS \quad (1)$$
(1–5)

[R_2N = (i) C_4H_8N-, (ii) $C_5H_{10}N$-, (iii) $C_6H_{12}N$-, (iv) OC_4H_8N- and (v) $CH_3NC_4H_8N$-].

Compounds **1–5** are the first examples of mono-substituted $-S_3N_3$ heterocycles to contain tertiary (amino)phosphine residues whose isolable yields lie in the range 60–80% and are best obtained from 1 : 2 [S_4N_4 : $(R_2N)_3P$] reactions. It is observed that only in the case of $(C_4H_8N)_3P$ and $(CH_3NC_4H_8N)_3P$, the corresponding $-S_3N_3$ derivatives were isolable from the reactions carried out at −5°C. Neither improvement in the yield nor any new heterocyclic product was observed when the reactions are done at higher temperature and mole ratio of reactants (Table 1). It may be noted that Ph_3P affords three types of cyclic derivatives [cf. $Ph_3PN\text{-}S_3N_3$; 1,5-$(Ph_3PN)_2S_4N_4$ and $(Ph_3PN)_3S^+S_4N_5^-$].[3] Also, the reaction of S_4N_4 with the phosphine containing only one amino residue, $(OC_4H_8N)Ph_2P$, gives $(OC_4H_8N)Ph_2PN\text{-}S_3N_3$ and $[(OC_4H_8N)Ph_2PN]_2S_4N_4$.[15] A ^{31}P-NMR spectrum of 1 : 5 reaction mixture [S_4N_4 : $(OC_4H_8N)_3P$] gives rise to only three signals (δ_P at 74.8, 34.9 and 18.8 ppm) with the most intense signal at 74.8 ppm which corresponds to $(OC_4H_8N)_3PS$.* It is noteworthy

* The origin of the other two peaks is not clear. Probably indicates decomposition products of **4**.

Table 5. Crystal and refinement data of $(C_5H_{10}N)_3PN\text{-}S_3N_3$

Formula	$C_{15}H_{30}N_7PS_3$
M	435.67
Crystal system	Triclinic
Space group	$P_{\bar{1}}$
a (Å)	9.573(5)
b (Å)	10.372(6)
c (Å)	10.916(6)
α (°)	85.46(3)
β (°)	81.13(4)
γ (°)	79.73(4)
U (Å^3)	1052.25
Z	2
D_c (g cm^{-3})	1.37
μ(Cu-K_α) (cm^{-1})	39.02
Crystal size (mm)	0.35 × 0.27 × 0.20
Scan mode	ω–2θ
θ range (°)	2–70
Octants of reciprocal/ space explored	h, $\pm k$, $\pm l$
Measured reflections	4230
Observed unique reflections [$I > 3\sigma(I)$]	3268
F(000)	464.00
Final R and R' indices	0.0624, 0.0672
ω scan width (°)	0.85+0.35 tan θ
Prescan speed (° min^{-1})	6.66
Prescan acceptance $\sigma(I)/I$	1/3
Maximum scan time (s)	60
Requested $\sigma(I)/I$	0.03
Parameters refined	355
Transmission factors	max = 0.3526 min = 0.1665
Maximum shift/ESD in final cycle	0.09
Diameter of incident beam collimeter	0.5 mm

that the presence of either $(OC_4H_8N)_3P$ or $(OC_4H_8N)_3PN\text{-}S_3N_3$ was not detected. In addition, independent reactions of **1–5** with the corresponding phosphines lead to the destruction of the heterocycle. Only the sulphide of the respective phosphine was isolated from these reactions.

In all the cases, the corresponding phosphine sulphide $(R_2N)_3PS$ has been readily isolated and to the best of our knowledge $(C_4H_8N)_3PS$, $(C_6H_{12}N)_3PS$ and $(CH_3NC_4H_8N)_3PS$ were hitherto unknown.

Characterization of $R_3PN\text{-}S_3N_3$ *compounds* (**1–5**)

Characterization data on compounds **1–5** are given in Tables 2–4.

Similar to $R_3PN\text{-}S_3N_3$ (R = c-C_6H_{11}- and t-C_4H_9-)[1] the UV–vis spectra of compounds **1–5** also show the 285 nm absorption.[16] The failure to detect this absorption in the previously reported examples is conceivably due to its masking by the absorption of the phenyl groups. Phosphorus chemical shift data (Table 4) reveal that the phosphorus atom in a given series experiences increased shielding in going from the phosphine to the corresponding $R_3PN\text{-}S_3N_3 \cdot C_7H_8$. The changing amino substituents seem to exert only a modest influence on the observed chemical shift values. EI mass spectra of compounds **2**, **3** and **4** similar to $Ph_3PN\text{-}S_3N_3$ show the presence of the [M-SN_3] ion. A characteristic feature in these cases is that the mass peak due to R^+ appears in very high intensity [base peak in the cases of **2** and **4**] while that of R_3PN^+ is insignificant which is suggestive of a facile P—N< (amino) bond cleavage. The mass spectra of tertiary (amino)phosphines also exhibit similar features.[17]

Norbornadiene adducts of compounds **1–5**

$Ph_3PN\text{-}S_3N_3$ reacts with norbornadiene in refluxing methylenechloride to give rise to the addition product $Ph_3PN\text{-}S_3N_3 \cdot C_7H_8$.[18] Compounds **1–5** fail to afford the corresponding adducts under these conditions. However, these derivatives **6–9** are isolated in low yield (5–45%) from room temperature reactions. They are comparatively less stable than the parent heterocycles. The number of proton signals and their chemical shift values for the norbornadiene moiety in their ^{1}H-NMR spectra are in good agreement with those observed for $Ph_3PN\text{-}S_3N_3 \cdot C_7H_8$[18] (Table 3). A comparison of the ^{31}P-chemical shift values for the parent heterocycles **1–5** and the norbornadiene adducts **6–9** suggests only little influence by the olefin on the phosphorus shielding in these cases.

X-ray crystal structure of $(C_5H_{10}N)_3PN\text{-}S_3N_3$ (**2**)

Among the four crystal structure data reported on the monosubstituted cyclotrithiazenes,[8,19–21]

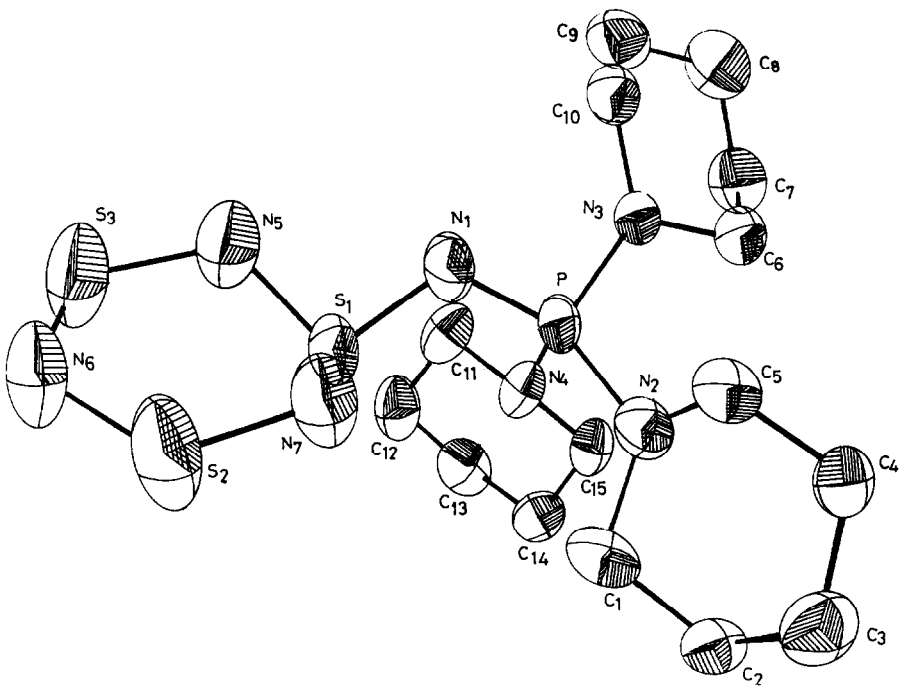

Fig. 1. ORTEP plot (50% probability ellipsoids) of $(C_5H_{10}N)_3PN\text{-}S_3N_3$ showing the atomic numbering scheme.

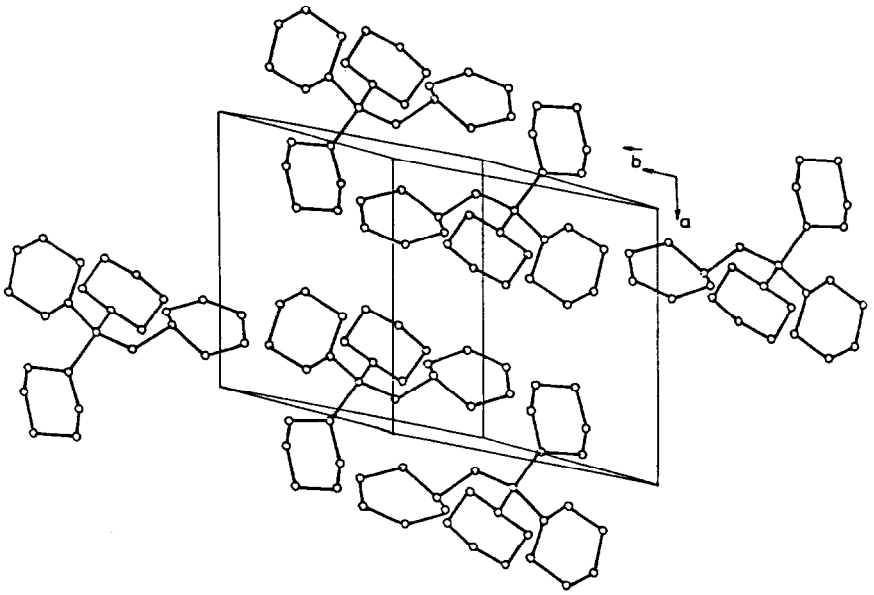

Fig. 2. Packing of the molecule in the unit cell (view down c^* axis).

$Ph_3PN\text{-}S_3N_3$ is the only example to possess a phosphinimino group. The ORTEP plot, the unit cell diagram (Fig. 2) and the selected bond distances and bond angles of the second example of such a type, $(C_5H_{10}N)_3PN\text{-}S_3N_3$ are given in Fig. 1 and Table 6 respectively. As in $Ph_3PN\text{-}S_3N_3$ the tricoordinate sulphur atom S(1) is deviated (by 0.65 Å) from the mean plane constituted by the other skeletal atoms N(5)—S(3)—N(6)—S(2)—N(7). In contrast to $Ph_3PN\text{-}S_3N_3$, the endocyclic bonds N(5)—S(3)—N(6)—S(2)—N(7) within experimental error have the same lengths (*ca.* 1.59 Å). In general the endocyclic bond lengths of the $\text{-}S_3N_3$ ring as well as the exocyclic bonds S(1)—N(1) and N(1)—P in **2** are shorter than the corresponding single bond distances[22,23] and $Ph_3PN\text{-}S_3N_3$. Interestingly, the three phosphorus–nitrogen distances P—N(2), P—N(3) and P—N(4) [1.638, 1.619 and 1.639 Å] of the phosphine moiety in **2** are noticeably shorter than the corresponding distances in the free phosphine [1.727, 1.692 and 1.705 Å][11] which is suggestive of more extended delocalization in $(C_5H_{10}N)_3PN\text{-}S_3N_3$. Another feature of the present structure is that the distance P—S(1) (non bonded)

Table 6. Selected bond distances (Å) and angles (°) with ESDs in parentheses for $(C_5H_{10}N)_3PN\text{-}S_3N_3$

Bond distances (Å)			
P—N(1)	1.595(3)	S(3)—N(6)	1.579(5)
N(1)—S(1)	1.574(3)	S(3)—N(5)	1.594(4)
S(1)—N(7)	1.640(4)	P—N(2)	1.638(3)
S(1)—N(5)	1.633(5)	P—N(3)	1.619(3)
S(2)—N(7)	1.602(3)	P—N(4)	1.639(3)
S(2)—N(6)	1.594(5)	P—S(1)	2.745(1)

Bond angles (°)			
P—N(1)—S(1)	120.0(2)	S(3)—N(5)—S(1)	117.1(3)
N(1)—S(1)—N(5)	100.6(2)	N(1)—P—N(3)	104.3(2)
N(1)—S(1)—N(7)	103.5(2)	N(1)—P—N(4)	111.5(2)
N(5)—S(1)—N(7)	107.3(2)	N(1)—P—N(2)	117.3(2)
S(1)—N(7)—S(2)	117.3(2)	N(2)—P—N(3)	105.9(2)
N(7)—S(2)—N(6)	115.4(2)	N(2)—P—N(4)	104.0(2)
S(2)—N(6)—S(3)	123.2(2)	N(3)—P—N(4)	114.1(2)
N(6)—S(3)—N(5)	115.7(2)		

has reduced to 2.745 Å from 2.826 Å in $Ph_3PN\text{-}S_3N_3$[8] which is presumably a reflection of the shortened adjacent bonds to N(1). The piperidino groups are found to be in an approximately chair conformation.

Acknowledgements—One of the authors (A.J.E.) thanks the Council of Scientific and Industrial Research (India) for a Senior Research Fellowship. We thank Monika Moertter, Bruker Analytische Messetechnik GmbH Rheinstetten, W. Germany for recording ^{31}P-NMR spectra and Dr. Yamadagni, Department of Chemistry, University of Calgary, Calgary, Canada for providing microanalysis data. Spectral facilities of RSIC, IIT, Madras are gratefully acknowledged.

REFERENCES

1. Part VI: A. J. Elias and M. N. Sudheendra Rao, *Inorg. Chim. Acta* 1989, **164**, 45.
2. J. Bojes, T. Chivers, A. W. Cordes, G. MacLean and R. T. Oakley, *Can. J. Chem.* 1979, **57**, 3171.
3. J. Bojes, T. Chivers, A. W. Cordes, G. MacLean and R. T. Oakley, *Inorg. Chem.* 1981, 2016.
4. H. L. Krauss and H. Jung, *Z. Naturforsch B.* 1961, **16B**, 624.
5. N. Burford, T. Chivers, A. W. Cordes, W. G. Laidlaw, M. C. Noble, R. T. Oakley and P. W. Swepston, *J. Am. Chem. Soc.* 1982, **104**, 1282.
6. W. Gerrard and H. R. Hudson, in *Organic Phosphorus Compounds* (Edited by G. M. Kosolopoff and L. Maier), Vol. 5, p. 21. Wiley Insterscience, New York (1973).
7. M. Witt, Ph.D thesis, University of Frankfurt (1981).
8. E. M. Holt and S. L. Holt, *J. Chem. Soc., Dalton Trans.* 1974, 1990.
9. M. Villena Blanco and W. L. Jolly, *Inorg. Synth.* 1967, **9**, 98.
10. A. J. Banister, *Inorg. Synth.* 1977, **17**, 197.
11. C. Romming and J. Songstad, *Acta Chem. Scand.* 1978, **A32**, 689.
12. L. A. Hussain, A. J. Elias and M. N. S. Rao, *Tetrahedron Lett.* 1988, **29**, 5983.
13. D. T. Cromer and J. B. Mann, *Acta Cryst.* 1968, **A24**, 321.
14. D. T. Cromer and D. Libermann, *J. Chem. Phys.* 1970, **53**, 1891.
15. C. J. Thomas and M. N. Sudheendra Rao, *J. Chem. Soc., Dalton Trans.* 1988, 1445.
16. F. G. Sherif and C. D. Schmulbach, *Inorg. Chem.* 1966, **5**, 322.
17. I. Granoth, in *Topics in Phosphorus Chemistry*, Vol. 8, p. 60. Wiley Interscience, New York (1976).
18. S. W. Liblong, R. T. Oakley, A. W. Cordes and M. C. Noble, *Can. J. Chem.* 1983, **61**, 2062.
19. T. Chivers, R. T. Oakley, A. W. Cordes and W. T. Pennington, *J. Chem. Soc., Chem. Commun.* 1981, 1214.
20. E. M. Holt, S. L. Holt and K. J. Watson, *J. Chem. Soc., Dalton Trans.* 1977, 514.
21. C. Spang, F. T. Edelmann, M. Noltemeyer and H. W. Roesky, *Chem. Ber.* 1989, **122**, 1247.
22. R. L. Sass, *Acta Cryst.* 1960, **13**, 320.
23. D. W. J. Cruckshank, *Acta Cryst.* 1964, **17**, 671.

Polyhedron Vol. 9, No. 12, pp. 1441–1445, 1990
Printed in Great Britain

0277-5387/90 $3.00+.00
© 1990 Pergamon Press plc

PREPARATION AND SPECTROSCOPIC CHARACTERIZATION OF SOME HETEROBIMETALLIC COMPLEXES OF 1,1-DICARBOETHOXY-2,2-ETHYLENE DITHIOLATE INVOLVING DIVALENT AND MONOVALENT METAL IONS

NANHAI SINGH,* RAGINI VERMA and N. K. SINGH

Department of Chemistry, Faculty of Science, Banaras Hindu University, Varanasi—221005, India

(*Received* 14 *August* 1989; *accepted* 29 *January* 1990)

Abstract—Reaction of the anionic dithiolato complexes $[M'(DED)_2]^{2-}$ (M' = Cd^{II} or Pd^{II}; DED = 1,1-dicarboethoxy-2,2-ethylene dithiolate) with metal ions occurs forming a new series of heterobimetallic complexes $M[M'(DED)_2]$ (M = Co^{II}, Ni^{II}, Cu^{II}, Pb^{II}, $2Ag^{I}$ or $2Tl^{I}$). The precursor ions $[M'(DED)_2]^{2-}$ used for the synthesis of heterobimetallic complexes have been isolated as $(Et_4N)_2[M'(DED)_2]$ salts for the first time. The composition of the complexes has been determined by elemental analysis. The tendency for the anionic dithiolato complexes, $[M'(DED)_2]^{2-}$, to act as a bridging moiety via the sulphur atoms to form heterobimetallic complexes has been explored. Heterobimetallic compounds are non-conducting, while $(Et_4N)_2[M'(DED)_2]$ salts exhibit 2:1 electrolytic behaviour in nitrobenzene. The IR spectra indicate dinegative bidentate behaviour of DED with the presence of non-equivalent ester groups, while ^1H and ^{13}C NMR spectral studies suggest that the non-equivalent nature of the ester groups is not retained in solution. Magnetic moment and electronic spectral studies suggest a square-planar environment around cobalt(II), nickel(II), palladium(II) and copper(II).

The chemistry associated with low-dimensional heterometal assemblies in polynuclear complexes has attracted much attention owing to their potential to exhibit unique physicochemical properties. A resurgence of interest in heterobinuclear transition metal complexes has occurred for several reasons,[1–6] for example, in catalysis, models for active sites of many enzyme systems, magnetic exchange behaviour, electron-transfer reactions and electrically conducting materials. Planar transition metal bis(dithio) complexes have long been known as attractive precursors for the synthesis of highly conducting[7–9] molecular solids due to their highly delocalized electronic structure, range of stable oxidation states and propensity to adopt linear-chain structures in the solid state. Very interesting and novel mixed-metal polymeric catalysts containing dithiolene, porphoryn, acetamide and carboxylate units have evolved.[10]

Although much work[11] has been carried out on binary and ternary complexes of 1,1-dithio ligands including 1,1-dicarboethoxy-2,2-ethylene dithiolate (DED), comparatively less has been carried out on the heterobimetallic complexes of 1,1-dithio ligands. Coucouvanis[12] and co-workers have demonstrated that the substitution of the inert cations that accompany certain anionic 1,1- or 1,2-dithiochelates by coordinately unsaturated complex cations as Lewis acids, has proved to be a satisfactory approach to the synthesis of heteronuclear complexes. A few papers[13,14] from our laboratory have also been published on heterobimetallic complexes of some 1,1-dithio ligands, for example, xanthate and dithiocarbamate, where the two identical sulphur donor atoms of these ligands bridge the two different metal ions.

Compared to other 1,1-dithio ligands, the DED ligand is quite unique in its properties and appears to be more effective than other 1,1-dithio ligands in stabilizing[15,16] metal ions in unusually high oxi-

* Author to whom correspondence should be addressed.

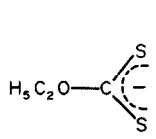

Xanthate

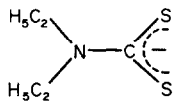

Dithiocarbamate

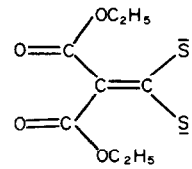

DED

dation states. The DED ligand by virtue of its conjugated π-system appears to exhibit different behaviour from that of the xanthate or dithiocarbamate.

We present here the synthetic and spectral properties of some novel heterobinuclear complexes formed with 1,1-dicarboethoxy-2,2-ethylene dithiolate.

EXPERIMENTAL

Materials and methods

The chemicals used were BDH (AR) or equivalent grades. The solvents were freshly distilled and where necessary dried before use. The ligand K_2DED was prepared according to the literature[17] procedure.

Preparation of the complexes

(i) $(Et_4N)_2[Cd(DED)_2]$. $K_2[Cd(DED)_2]$ was prepared *in situ* by gradual addition of 5 cm^3 of an aqueous solution of cadmium nitrate (0.61 g, 2 mmol) to a 30 cm^3 solution of K_2DED (1.25 g, 4 mmol) in 50 : 50 ethanol–water (v/v) with vigorous stirring. The dirty white precipitate which formed initially immediately dissolved giving a pale yellow solution of $K_2[Cd(DED)_2]$. The $K_2[Cd(DED)_2]$ thus obtained was added to a 10 cm^3 aqueous solution containing tetraethylammonium bromide (1.00 g, 4.5 mmol), whereby a yellow precipitate of the compound formed immediately. This was filtered off, washed with the above solvent mixture and air dried.

(ii) $(Et_4N)_2[Pd(DED)_2]$. $K_2[Pd(DED)_2]$ was prepared *in situ* by adding, with constant stirring, a 2 cm^3 aqueous solution of palladous chloride (0.18 g, 1 mmol) and potassium chloride (0.15 g, 2 mmol) to a 5 cm^3 solution of K_2DED (0.65 g, 2 mmol) in 60 : 40 ethanol–water (v/v). The orange–brown precipitate formed initially dissolved to give a brown solution of $K_2[Pd(DED)_2]$. This was immediately added to an aqueous solution containing tetraethylammonium bromide (0.5 g, 2.5 mmol). The orange–brown precipitate which formed immediately was filtered off, washed with the above solvent mixture and air dried.

(iii) $M[M'(DED)_2]$. In general, the heterobimetallic complexes were prepared by gradual addition of a 5–10 cm^3 aqueous solution containing $Co(NO_3)_2 \cdot 6H_2O$, $NiCl_2 \cdot 6H_2O$, $CuSO_4 \cdot 5H_2O$, $Pb(NO_3)_2$, Tl_2SO_4 or $AgNO_3$ (1 mmol/2 mmol), with constant stirring, to a solution of $K_2[Cd(DED)_2]$ or $K_2[Pd(DED)_2]$ prepared *in situ* as described above. All the heterobimetallic complexes which precipitated as microcrystalline material were suction filtered, washed with an ethanol–water mixture and air dried.

Analysis and physical measurements

Except for the palladium complexes all the others were analysed for their metal and sulphur contents following standard literature procedures.[18] Carbon, hydrogen and nitrogen were determined microanalytically on a Perkin–Elmer 240C model microanalyser.

The conductivity of soluble complexes was recorded in 10^{-3} M nitrobenzene solution on a WTW conductivity meter. Magnetic susceptibility measurements were made at room temperature on a Cahn–Farday electrobalance using $Hg[Co(NCS)_4]$ as calibrant. IR spectra were recorded in the region 4000–200 cm^{-1} in Nujol mulls using a Perkin–Elmer 783 spectrophotometer. Electronic spectra were recorded on a Cary-14 spectrophotometer as Nujol mulls following the procedure of Lee *et al.* ^1H and ^{13}C NMR spectra of $(Et_4N)_2[Cd(DED)_2]$ and $(Et_4N)_2[Pd(DED)_2]$ were obtained in $CDCl_3$ while that of K_2DED was obtained in $DMSO(d_6)$ on a JEOL FX 90Q spectrophotometer using TMS as internal reference. The relevant analytical and physicochemical data are given in Table 1.

RESULTS AND DISCUSSION

The formation of $(Et_4N)_2[M'(DED)_2]$ and the heterobimetallic complexes $M[M'(DED)_2]$ may be represented by the following equations:

$$Cd(NO_3)_2 + 2\,K_2DED \longrightarrow K_2[Cd(DED)_2] + 2\,KNO_3 \quad \text{(i)}$$

$$PdCl_2 + 2\,KCl + 2\,K_2DED \longrightarrow K_2[Pd(DED)_2] + 4\,KCl \quad \text{(ii)}$$

Table 1. Analytical data, physical properties and electronic spectral data of the complexes

Complex	Colour	Decomposition temperature (°C)	Analysis: Found (calc.) %						S ($cm^2\,\Omega^{-1}\,mol^{-1}$)	Electronic band position (cm^{-1})	Assignment	Splitting parameter (cm^{-1})
			M	Cd	S	C	H	N				
$(Et_4N)_2[Cd(DED)_2]$	Light yellow	146	—	12.8 (13.3)	14.8 (15.2)	11.2 (11.4)	1.1 (1.1)	3.2 (3.3)	52.25	—	—	—
$Ni[Cd(DED)_2]$	Reddish-brown	165	8.9 (9.2)	16.9 (17.5)	19.2 (20.0)	14.6 (15.0)	1.4 (1.5)	—	2.25	16,600 28,600	$^1A_{1g} \rightarrow {}^1B_{1g}$ M–L	19,400
$Co[Cd(DED)_2]$	Greyish-green	182	8.8 (9.2)	16.8 (17.5)	19.5 (20.0)	14.5 (15.0)	1.4 (1.5)	—	4.54	10,250 16,200	$^2A_{1g} \rightarrow {}^2E_{2g}$	680
$Pd[Cd(DED)_2]$	Brown	180	—	—	—	13.6 (13.9)	1.4 (1.4)	—	2.52	24,800	M–L	
$Cu[Cd(DED)_2]$	Dark brown	144	9.5 (9.8)	16.5 (17.4)	19.1 (19.9)	14.5 (14.9)	1.5 (1.5)	—	1.86	16,150 22,200	*d–d* M–L	
$Pb[Cd(DED)_2]$	Yellow	170	25.5 (26.3)	13.6 (14.2)	15.8 (16.2)	11.8 (12.1)	1.2 (1.2)	—	2.45	—	—	
$Ag_2[Cd(DED)_2]$	Light yellow	131	26.1 (26.9)	13.5 (14.1)	15.4 (16.1)	11.6 (12.0)	1.2 (1.2)	—	1.51	—	—	
$Tl_2[Cd(DED)_2]$	Light yellow	138	40.3 (41.2)	10.7 (11.3)	12.2 (12.9)	9.4 (9.7)	1.0 (1.0)	—	2.25	—	—	
$(Et_4N)_2[Pd(DED)_2]$	Orange	140	—	—	—	11.0 (11.5)	1.1 (1.1)	3.3 (3.35)	48.82	24,500	M–L	
$Ni[Pd(DED)_2]$	Orange–brown	224	—	—	—	14.7 (15.1)	1.4 (1.5)	—	4.52	16,500 24,200	$^1A_{1g} \rightarrow {}^1B_{1g}$ M–L	19,300
$Cu[Pd(DED)_2]$	Brown	137	—	—	—	14.7 (15.0)	1.4 (1.5)	—	4.50	12,500–23,000 (br)	*d–d* and M–L	

$$K_2[M'(DED)_2] + 2\,Et_4NBr \longrightarrow (Et_4N)_2[M'(DED)_2] + 2\,KBr \quad \text{(iii)}$$

$$K_2[M'(DED)_2] + M(NO_3)_2/MSO_4 \longrightarrow M[M'(DED)_2] + 2\,KNO_3/K_2SO_4. \quad \text{(iv)}$$

All the complexes decompose in the temperature range 131–224°C. Except for the $(Et_3N)_2[M'(DED)_2]$ salts which are soluble in polar as well as non-polar solvents such as methanol, actone, DMF, DMSO, chloroform or nitrobenzene, all of the other complexes are insoluble in water and common organic solvents but slightly soluble in nitrobenzene. The electrical conductances[19] (Λ_M = 48–52 $cm^2\ \Omega^{-1}\ mol^{-1}$) in nitrobenzene at 10^{-3} M concentration are consistent with 2:1 electrolytic behaviour of $(Et_4N)_2[M'(DED)_2]$, whilst the heterobimetallic complexes (Λ_M = 2–4 $cm^2\ \Omega^{-1}\ mol^{-1}$) are non-conducting.

The diamagnetic nature and electronic spectral bands (Table 1) of $(Et_4N)_2[Pd(DED)_2]$, Pd[Cd $(DED)_2$], Ni[$Pd(DED)_2$] and Ni[$Cd(DED)_2$] suggest square-planar geometry[12,20] around nickel(II) and palladium(II) in these complexes.

The magnetic moment (2.2 BM) and the electronic spectral bands (Table 1) suggest square-planar geometry[21,22] around cobalt(II) in Co[Cd $(DED)_2$].

The μ_{eff} values of 1.66 and 1.70 BM for Cu[Cd $(DED)_2$] and Cu[$Pd(DED)_2$], respectively, indicate the presence of one unpaired electron. The somewhat lower magnetic moments as compared to the spin-only value may be attributed to metal–metal interaction or the presence of antiferromagnetism in the copper(II) complexes. The presence of bands in the visible region (Table 1) suggest the planar CuS_4 chromophore.[23]

The occurrence in general of two absorptions in the IR spectra of $(Et_4N)_2[M'(DED)_2]$ in the 1675–1730 cm^{-1} region is due to the C=O stretching vibration.[11,12] The presence of two bands in the carbonyl region was attributed to the twisting of one of the ester groups out of the plane containing the ethylene carbons.[12,16,17] There is little change of the ν(C=O) frequency in the heterobimetallic complexes $M[M'(DED)_2]$ indicating that the bonding mode of the carbonyl group is virtually unchanged on formation of the heterobimetallic complex.

The $\nu(C{=}CS_2)$ absorption band appearing at 1450 cm^{-1} in $(Et_4N)_2[M'(DED)_2]$ is observed in the range 1465–1470 cm^{-1} in the bimetallic complexes.[12,17] The appearance of the $C{=}CS_2$ stretching vibrations at somewhat higher frequencies in the heterobimetallic complexes, as compared to $(Et_4N)_2[M'(DED)_2]$, may be indicative of interaction of the sulphur atoms of the chelating group attached to M′ with the added metal ions, M, in a polymeric fashion.[12,24]

Three bands which are generally found for these complexes in the 890–1030 cm^{-1} region may be assigned to the $\nu(CS_2)$ group.[17] The occurrence of a single band in the 1010–1030 cm^{-1} region is related to the $\nu_s(=CS_2)$ group, while the presence of two bands in the 890–990 cm^{-1} region may be attributed to the $\nu_{as}(=CS_2)$ group. In all the complexes the bands occurring below 400 cm^{-1} have been tentatively assigned to metal–sulphur stretching vibrations. The lower one may be related to Tl—S, Pb—S, Ag—S, Cd—S, Pd—S and the higher one to Co—S, Ni—S or Cu—S stretching modes.[12]

The ^1H NMR spectra of $(Et_4N)_2[Cd(DED)_2]$ and $(Et_4N)_2[Pd(DED)_2]$ yield a triplet at δ 1.27 ppm for the CH_3 protons of Et_4N and the ester groups of the ligand which are mixed together. The protons of the $-NCH_2$ and $-OCH_2$ groups are not resolved as a sharp quartet but are observed as a doublet at δ 3.36 and 4.06 ppm, respectively, in both the complexes. The downfield shift observed for the protons compared to K_2DED ($CH_3 = \delta$ 1.11 ppm; $-OCH_2 = \delta$ 3.93 ppm) clearly indicates the deshielding of ethoxy protons in these complexes.

The ^{13}C NMR spectra gave signals at δ 8.0 and 53.04 ppm for $-CH_3$ and $-NCH_2(NEt_4)$. The $-CH_3$ and $-OCH_2$ carbons of the ester groups are observed at δ 14.25 and 60.08 ppm as singlets. The carbonyl carbon has δ 168.43 ppm in these complexes compared to δ 167.89 ppm in K_2DED, suggesting non-involvement of the C=O group in bonding on complex formation.

The number of peaks in the ^1H and ^{13}C NMR spectra clearly indicate that the non-equivalent nature of the ester group is not retained in solution in the above complexes.

Based on the chemical composition and physical measurements, the ionic structure $(Et_4N)_2[M'(DED)_2]$ and polymeric structure $M[M'(DED)_2]$ may be suggested for the complexes.

On the basis of the foregoing studies the following conclusions may be drawn regarding the present series of complexes:

(i) The S—S chelating site of the DED ligand in its anionic complexes shows a tendency to act as a bridging ligand via the sulphur atoms to form heterobimetallic complexes.
(ii) The low-spin planar geometry of cobalt(II), nickel(II) or palladium(II) are stabilized in their heterobimetallic complexes.
(iii) The average value of the ligand-field splitting

parameter, $\sim 19{,}350\ cm^{-1}$, for the planar NiS_4 chromophore places DED between trithiocarbonate and 1,1-cyanocarboethoxyethylenedithiolate[25] in the spectrochemical series of the sulphur donors.

(iv) IR spectral studies clearly indicate the dinegative bidentate behaviour of DED and the non-equivalent nature of the ester groups of the ligand in the complex.

(v) NMR studies indicate that non-equivalent nature of the ester group is not retained in solution.

Acknowledgement—The authors thank CSIR, New Delhi for financial support in the form of a research project.

REFERENCES

1. G. B. Jacobsen and B. L. Shaw, *J. Chem. Soc., Dalton Trans.* 1987, 151; C. P. Garey, R. E. Palermo and A. L. Rheingold, *J. Am. Chem. Soc.* 1986, **108**, 549; T. A. Wark and D. W. Stephan, *Inorg. Chem.* 1987, **26**, 363; I. E. Maxwell, *Adv. Catal.* 1981, **30**, 1.
2. A. B. Grey and E. Sinn, *Inorg. Chem.* 1987, **26**, 1529; G. S. White and D. W. Stephan, *Inorg. Chem.* 1985, **24**, 1499.
3. W. M. Davis, J. C. Dewan and S. J. Lippard, *Inorg. Chem.* 1981, **20**, 2928.
4. E. Sinn, in *Biochemical Inorganic Copper Chemistry* (Edited by K. D. Karlin and J. Jubieta). Adenine, Guilderland, New York (1985) and refs therein.
5. J. P. Costes, J. F. Serra, F. Dahon and J. P. Laurent, *Inorg. Chem.* 1986, **25**, 2790; H. Taube, *Electron Transfer Reactions of Complex Ions in Solutions.* Academic Press, New York (1970); A. Haim, *Accts Chem. Rev.* 1975, **8**, 264.
6. D. Wohrle and G. Manecke, *Angew. Chem. Int. Ed.* 1969, **8**, 928; V. G. Manecke and D. Wohrle, *Makromolec. Chem.* 1968, **116**, 36; Z. J. Zhong, H. Okawa, R. Aoki and S. Kida, *Inorg. Chim. Acta* 1988, **144**, 233.
7. J. A. McCleverty, *Prog. Inorg. Chem.* 1968, **10**, 49; R. Eisenberg, *Prog. Inorg. Chem.* 1970, **12**, 295; J. S. Miller and A. J. Epstein, *Prog. Inorg. Chem.* 1976, **20**, 1.
8. W. E. Hatfield (Ed.), *Molecular Metals.* Plenum Press, New York (1979); J. T. Devreese, R. P. Evrard and V. E. Van Doren (Eds), *Highly Conducting One-Dimensional Solids.* Plenum Press, New York (1979).
9. L. Valade, J. P. Legros, M. Bousseau, P. Cassoux, M. Garbauskas and L. V. Intemante, *J. Am. Chem. Soc.* 1986, **108**, 1908.
10. M. Kaneko and G. Maneck, *Macromolec. Chem.* 1974, **174**, 2795.
11. D. Coucouvanis, *Prog. Inorg. Chem.* 1970, **11**, 233; 1979, **26**, 301.
12. M. L. Caffery and D. D. Coucouvanis, *J. Inorg. Nucl. Chem.* 1975, **37**, 2081; D. Coucouvanis, N. C. Baenziger and S. M. Johnson, *Inorg. Chem.* 1974, **13**, 1191; D. Coucouvanis and D. Piltingsrud, *J. Am. Chem. Soc.* 1973, **95**, 5556 and refs therein; D. Coucouvanis, N. C. Baenziger and S. H. Johnson, *J. Am. Chem. Soc.* 1973, **95**, 3875.
13. R. C. Aggarwal, N. Singh and S. Singh, *Ind. J. Chem.* 1982, **21A**, 268; R. C. Aggarwal, N. Singh and S. Singh, *Polyhedron* 1985, **4**, 343; N. Singh, N. K. Singh and C. Kaw, *Bull. Chem. Soc. Jpn* 1989, **62**, 3328.
14. R. C. Aggarwal, B. Singh and M. K. Singh, *J. Ind. Chem. Soc.* 1982, **59**, 269; R. C. Aggarwal, B. Singh and M. K. Singh, *Ind. J. Chem.* 1983, **22A**, 533.
15. F. J. Hollander, R. Pedelty and D. Coucouvanis, *J. Am. Chem. Soc.* 1974, **96**, 4032; F. J. Hollander, R. Pedelty and D. Coucouvanis, *Inorg. Chem.* 1977, **16**, 2691.
16. D. Coucouvanis, F. J. Hollander and M. L. Caffery, *J. Am. Chem. Soc.* 1974, **96**, 4682; D. Coucouvanis, F. J. Hollander and M. L. Caffery, *Inorg. Chem.* 1976, **15**, 1853.
17. K. A. Jensen and L. Henriksen, *Acta Chem. Scand.* 1968, **22**, 1107.
18. A. I. Vogel, *A Textbook of Quantitative Inorganic Analysis*, 3rd edn. Longmans, London (1961).
19. W. J. Geary, *Coord. Chem. Rev.* 1971, **7**, 81.
20. A. R. Hendrickson, J. M. Hope and R. L. Martin, *Inorg. Chem.* 1976, **15**, 1118; O. Siiman and J. Frasco, *J. Am. Chem. Soc.* 1970, **92**, 2652.
21. F. L. Urbach, R. D. Bereman, J. A. Topich, M. Hriharan and B. J. Kalbacher, *J. Am. Chem. Soc.* 1974, **96**, 5063.
22. Y. Nishida and S. Kida, *Inorg. Nucl. Chem. Lett.* 1971, **7**, 325; Y. Nishida and S. Kida, *Coord. Chem. Rev.* 1979, **27**, 275; Y. Nishida, K. Hayashida, A. Sumita and S. Kida, *Inorg. Chim. Acta Lett.* 1978, **31**, 19.
23. M. F. Corrigna, K. S. Murray, B. O. West and J. R. Pilbrow, *Aust. J. Chem.* 1977, **30**, 2455; M. V. Rajasekharan, C. N. Sethulakshimi, P. T. Manoharan and H. Gudel, *Inorg. Chem.* 1976, **15**, 2657.
24. L. M. Engelhardt, P. C. Healy, R. M. Shephard, B. W. Skelton and A. H. White, *Inorg. Chem.* 1988, **27**, 2371.
25. J. P. Fackler and D. Coucouvanis, *J. Am. Chem. Soc.* 1966, **88**, 3913; A. R. Latham, V. C. Hascall and H. B. Gray, *Inorg. Chem.* 1965, **4**, 788.

Polyhedron Vol. 9, No. 12, pp. 1447–1451, 1990
Printed in Great Britain

0277–5387/90 $3.00+.00
© 1990 Pergamon Press plc

NEUTRAL AMINOCARBENE COMPLEXES OF NICKEL FROM THE REACTION OF [Ni{η^2-C(NBu^t)CH$_2$CMe$_3$}(NC$_4$H$_2$Me$_2$)(PMe$_3$)] WITH DIPROTONIC ACIDS

ERNESTO CARMONA,* PILAR PALMA and MANUEL L. POVEDA

Departamento de Química Inorgánica-Instituto de Ciencia de Materiales, Universidad de Sevilla-CSIC, Apartado 553, 41071-Sevilla, Spain

(*Received* 18 *September* 1989; *accepted* 29 *January* 1990)

Abstract—The dihaptoiminoacyl complex [Ni{η^2-C(NBu^t)CH$_2$CMe$_3$}(NC$_4$H$_2$Me$_2$)(PMe$_3$)] (**1**), containing the coordinated 2,5-dimethylpyrrolyl ligand, reacts with CO_2, in the presence of water, with protolytic cleavage of the Ni—N bond and protonation of the iminoacyl nitrogen atom, to furnish an η^2-carbonate aminocarbene complex of composition [Ni(η^2-CO$_3$){C(NHBu^t)CH$_2$CMe$_3$}(PMe$_3$)] (**2**). This transformation has been shown to be a general reaction of **1** with diprotonic acids, and compounds related to **2** have been obtained using oxalic, parabanic and salicylic acids. The new compounds have been fully characterized by analytical and spectroscopic methods.

A recent contribution from our laboratory has described the formation of various η^1-iminoacyl complexes of nickel(II) with the composition [Ni{η^1-C(NBu^t)R}Cl(PMe$_3$)$_2$]. Substitution of the chloride ligand by the bulkier 2,5-dimethylpyrrolyl group induces a change in the coordination mode of the iminoacyl ligand and provides the dihaptoiminoacyl compounds [Ni{η^2-C(NBu^t)R}(NC$_4$H$_2$Me$_2$)(PMe$_3$)].[1] A characteristic feature of the chemistry of the η^1-iminoacyls is the extreme facility with which the coordinated iminoacyl nitrogen can be protonated, even by water, to form the cationic aminocarbene species,[1] [Ni{C(NHBu^t)R}Cl(PMe$_3$)$_2$]$^+$.

During studies aimed at the investigation of the chemical properties of the η^2-iminoacyl complexes containing the 2,5-dimethylpyrrolyl ligand, we have found that these can also be readily protonated and that action of commercial, high purity CO_2 on solutions of a representative member, [Ni{η^2-C(NBu^t)CH$_2$CMe$_3$}(NC$_4$H$_2$Me$_2$)(PMe$_3$)] (**1**), causes both iminoacyl protonation and Ni—N bond heterolysis, with formation of the neutral aminocarbene [Ni(η^2-CO$_3$){C(NHBu^t)CH$_2$CMe$_3$}(PMe$_3$)] (**2**), which contains a bidentate carbonate ligand. Herein we describe the formation and spectroscopic characterization of **2** and of other related aminocarbene complexes resulting from the protonation of **1** with various diprotonic acids. Analytical and selected IR and ^{1}H NMR data for the new compounds are given in the Experimental, selected ^{13}C and ^{31}P NMR data are collected in Table 1.

RESULTS AND DISCUSSION

Compound **1** is fairly unreactive towards both H_2O and CO_2 as independent reagents. However, upon bubbling CO_2 through a solution of **1** in Et_2O, small amounts of a yellow, finely divided solid, identified as complex **2**, precipitate out of the solution. The addition of one or two drops of water induces further precipitation of this sparingly soluble solid, while if the above transformation is carried out using acetone as the solvent and the reaction mixture is allowed to stand overnight without stirring, complex **2** is obtained in the form of yellow, needle-shaped crystals in good yields. After the reaction is complete, an NMR analysis of the mother liquor reveals the presence of free 2,5-dimethylpyrrole, while IR and NMR studies of the yellow complex **2** show the presence of an aminocarbene and a carbonate ligands (see below). Accordingly, the reaction occurs with both hydrolytic cleavage of the Ni—N bond and protonation of the iminoacyl functionality, presumably by the

* Author to whom correspondence should be addressed.

Table 1. Selected NMR data for the new complexes

	$^{13}C\{^1H\}$								$^{31}P\{^1H\}$
		CH_2CMe_3			Ni—C—NHBu^t				
Compound	PMe_3	CH_2	C	Me	$C(Bu^t)$	$Me(Bu^t)$	Ni—C	Others	
2[a]	13.8d (33)	64.0s	35.1s	22.1s	61.6s	31.4s	243.1d (37)	170.2s (CO_3)	−2.2s
3	11.3d (33)	63.1s	35.0s	31.3s	61.0s	30.5s	240.5d (40)	169.2, 169.3 (s, C_2O_4)	4.0s
4	15.7d (33)	67.5s	38.6s	34.9s	65.0s	34.2s	[b]	C=O[b]	3.4s
5–6	[c] 11.5d (32)	62.9s	34.4s	30.5s	59.9s	29.9s	242.9d (44)	173.5s (COO)[e, g]	−4.9s
	[d] 11.5d (32)	63.1s	34.1s	30.8s	59.9s	29.9s	242.5d (42)	172.7s (COO)[f]	−3.9s

Coupling constants (Hz) in parentheses. In CD_3OD unless otherwise indicated.
[a] In D_2O.
[b] Non-observed resonances.
[c] Major isomer.
[d] Minor isomer.
[e] *C*—O—Ni: 168.3.
[f] *C*—O—Ni: 167.5.
[g] Aromatics at 114.0, 115.7, 122.1, 122.8, 122.9, 131.9, 132.6.

action of carbonic acid on complex **1**, as shown in eq. (1):

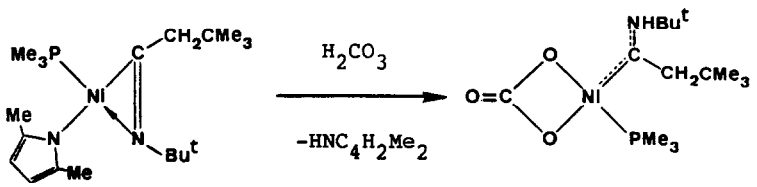

1 **2** (1)

Complex **2** is insoluble in most common organic solvents, but has appreciable solubility in polar solvents such as methanol or water. The presence of a carbonate ligand is indicated by the appearance of a strong IR absorption at *ca* 1580 cm^{-1}, whose frequency suggests bidentate coordination,[2,3] and by the observation of a ^{13}C resonance at *ca* 170 ppm (^{13}C enriched sample). On the other hand, the aminocarbene ligand gives a characteristic IR absorption at 3200 cm^{-1} due to the N—H stretching vibration, but the ν(C—N) band cannot be readily discerned since it overlaps with the strong carbonate absorption at 1580 cm^{-1}. Complex **2** crystallizes with one molecule of water of crystallization, and evidence for this and for the existence of a hydrogen-bonded network in the solid-state structure of **2** can be ascertained from IR data.[2]

The nickel-bound carbon atom of the aminocarbene ligand gives a ^{13}C resonance at 243 ppm, that is, in the range characteristic of aminocarbene functionalities,[4] and appears as a doublet due to its coupling to the ^{31}P nucleus. The value of 37 Hz found for the phosphorus-to-carbon coupling constant is indicative of a *cis* distribution of the aminocarbene and phosphine ligands. Interestingly, the methylene protons of the CH_2CMe_3 group appear as an AB quartet in the ^1H NMR spectrum. The inequivalence of these protons indicates that the aminocarbene ligand occupies a rigid position in a plane perpendicular to that containing the nickel centre and the donor atoms of the other ligands, as shown below (**A**). This, and the low-field chemical shift found for the aminocarbene carbon atom are clearly in accord with an important contribution of the carbene resonance structure **A** to the ground-state structure of this molecule.

Some brief comments seem appropriate at this point on the formation of the aminocarbene complex **2**. The first step probably involves the protolytic cleavage of the Ni—N bond by carbonic acid, with formation of an intermediate bicarbonate complex of possible structure **C**. This could then be followed by protonation of the iminoacyl nitrogen, in an

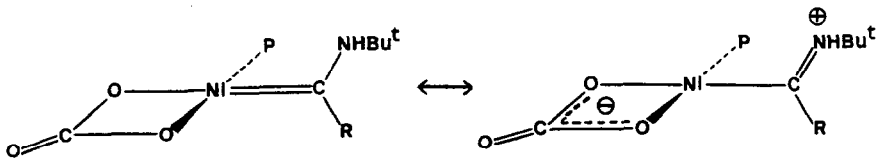

A B

intramolecular, concerted manner, as depicted in **D**.

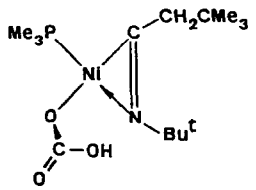

C

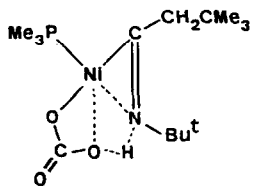

D

In an attempt to obtain aminocarbene complexes related to **2**, containing the larger, five-membered chelating O—C—C—O—Ni ring, the reactions of **1** with oxalic, $H_2C_2O_4$, and parabanic, $H_2C_3N_2O_3$, acids, have been investigated. Addition of oxalic acid to an acetone solution of **1** yields a yellow, microcrystalline precipitate of complex **3**, with solubility properties very similar to those of **2**. Microanalytical and spectroscopic data are in accord with bidentate oxalate coordination, as shown in eq. (2):

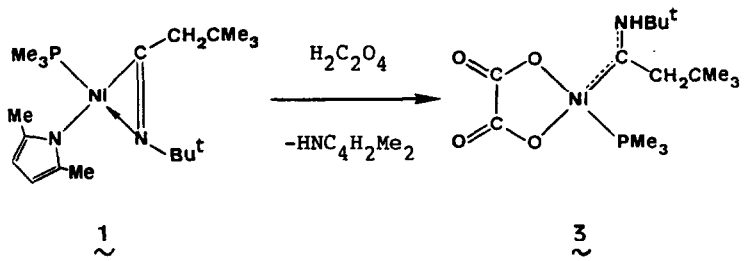

1 3 (2)

Thus, the IR spectrum of **3** displays several bands in the region 1700–1600 cm^{-1} which can be assigned to ν(C=O) of the bidentate oxalate ligand,[2,5] while the ^{13}C NMR spectrum of **3** exhibits two nearly coincident ^{13}C signals for the carbon atoms of the oxalate ligand in the proximity of 169 ppm. Other pertinent spectroscopic data for **3** are collected in the Experimental and in Table 1 and will not be discussed any further.

Parabanic acid, $H_2C_3N_2O_2$, provides an analogous species, **4**, for which the structure shown below can be proposed on the basis of analytical and spectroscopic data, and also by similarity with that assigned to the related compounds **2** and **3**. For complex **4**, however, its low solubility has prevented observation of the ^{13}C resonances of the parabanate ligand.

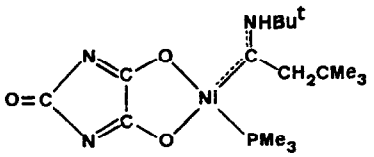

4

Finally, we have carried out the reaction of **1** with salicylic acid, to obtain a yellow, microcrystalline precipitate, which is shown by NMR to be composed of an isomeric mixture of compounds **5** and **6** [eq. (3)], in an approximate 3:2 ratio. The ^{13}C NMR spectrum of this isomeric mixture displays two doublets at 242.5 and 242.9 ppm ($^2J_{CP}$ = 42 and 44 Hz, respectively) that can be assigned to the nickel-bound aminocarbene carbon in both isomers, as well as two singlets at 173.5 and 172.7 ppm due to the carboxylate carbons. Similarly, the

$^{31}P\{^1H\}$ NMR shows two singlets at −4.9 and −3.9 ppm. The above data suggest that the isomerism is due to the geometric distribution of the salicylate group with respect to the other ligands, that is, to its positioning with the carboxylate functionality *trans* either to the phosphine or to the aminocarbene ligand, as indicated in eq. (3).

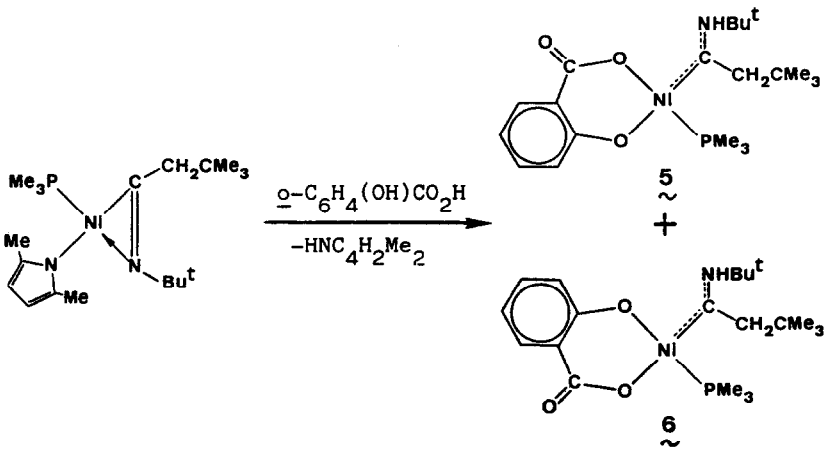

(3)

EXPERIMENTAL

Microanalyses were by Pascher Microanalytical Laboratory, Remagen (F.R.G.), and the Microanalytical Service of the University of Seville. The spectroscopic instruments used were Perkin–Elmer models 557 and 684 for IR spectra and Varian XL-200 for ^1H, ^{13}C and ^{31}P NMR spectra. All preparations and other operations were carried out under oyxgen-free nitrogen, following conventional Schlenk techniques. Solvents were dried and degassed before use. Complex **1** was prepared according to ref. 1 and parabanic acid following a literature method.[6]

Synthesis of [Ni(η^2-CO_3){C(NHBu^t)CH_2CMe_3}(PMe_3)]·H_2O (**2**)

A solution of [Ni{η^2-C(NBu^t)CH_2CMe_3}($NC_4H_2Me_2$)(PMe_3)] (**1**) (0.30 g, 1 mmol) in acetone (100 cm^3) was treated with a few drops of water and then transferred to a Fischer–Porter vessel. The N_2 atmosphere was replaced by CO_2, the CO_2 pressure increased to 3 atm and the solution was kept undisturbed overnight. The yellow, crystalline precipitate that formed was filtered off, washed with acetone and dried under vacuum. Yield: 90%. IR (Nujol mull): 3200 cm^{-1} (NH), 1580 cm^{-1} (br, CO_3 and C=N). Found: C, 45.4; H, 8.4; N, 3.7; O, 16.8. Calc. for $C_{14}H_{30}NO_3PNi \cdot H_2O$: C, 45.7; H, 8.7; N, 3.8; O, 17.4%. ^1H NMR (D_2O, 200 MHz): δ 1.12 (d, $^2J_{HP}$ = 11.4 Hz, PMe_3), 1.17 (s, CH_2CMe_3), 1.82 (s, CMe_3), 1.93, 2.65 (d, dd, $^2J_{HH}$ = 12.5, $^4J_{HP}$ = 2.8 Hz, diastereotopic CH_2 protons).

Preparation of [Ni(η^2-C_2O_4){C(NHBu^t)CH_2CMe_3}(PMe_3)]·H_2O (**3**)

Complex **1** (0.26 g, 0.7 mmol) was dissolved in acetone (40 cm^3) and treated with solid $H_2C_2O_4 \cdot 2H_2O$ (0.088 g, 0.7 mmol). The reaction mixture was stirred at room temperature for 4 h and the resulting yellow precipitate filtered off, washed with acetone and dried under vacuum. Yield: 60%. IR (Nujol mull): 3200 cm^{-1} (NH), 1700–1600 cm^{-1} (several bands, C_2O_4 and C=N). Found: C, 45.9; H, 7.5. Calc. for $C_{15}H_{30}NO_4PNi \cdot H_2O$: C, 45.5; H, 8.1%. ^1H NMR (CD_3OD, 200 MHz): δ 1.42 (d, $^2J_{HP}$ = 11.6 Hz, PMe_3), 1.50 (s, CH_2CMe_3), 2.12 (s, CMe_3), 2.35, 2.95 (d, dd, $^2J_{HH}$ = 12.3, $^4J_{HP}$ = 3.1 Hz, diastereotopic CH_2 protons).

Synthesis of [Ni(η^2-$C_3O_3N_2$){C(NHBu^t)CH_2CMe_3}(PMe_3)] (**4**)

A solution of parabanic acid (0.114 g, 1 mmol) in methanol (40 cm^3) was added via canula to a stirred solution of complex **1** (0.38 g, 1 mmol) in acetone (30 cm^3). After stirring overnight, the reaction mixture was taken to dryness and the residue triturated with Et_2O (30 cm^3). The resulting solid was filtered off and dried. Yield: 60%. IR (Nujol mull): 3200 cm^{-1} (NH), 1640 cm^{-1} (br, C=O and C=N). ^1H NMR (CD_3OD, 200 MHz): δ 1.43 (d, $^2J_{HP}$ = 11.4, PMe_3), 1.50 (s, CH_2CMe_3), 2.12 (s, CMe_3), 2.30, 2.94 (d, dd, $^2J_{HH}$ = 12.2, $^4J_{HP}$ = 3.2 Hz, diastereotopic CH_2 protons).

Synthesis of [Ni(η^2-$C_7H_4O_3$){C(NHBu^t)CH_2CMe_3}(PMe_3)] (**5**) *and* (**6**)

Complex **1** (0.18 g, 0.5 mmol) dissolved in acetone

($20\ cm^3$) was reacted with a solution of salicylic acid (0.05 g, 0.5 mmol) in acetone ($30\ cm^3$). A yellow solid started precipitating upon mixing of the reactants. The reaction mixture was allowed to stand overnight and the resulting microcrystalline solid filtered off, washed with acetone and dried. Yield: 60%. IR (Nujol mull): 3200 cm^{-1} (NH), 1600–1540 cm^{-1} (several bands, C=O and C=N). Found: C, 56.1; H, 7.9; N, 3.2. Calc. for $C_{20}H_{34}NO_3PNi$: C, 56.4; H, 8.0; N, 3.3%. ^1H NMR (CD_3OD, 200 MHz) major isomer: δ 1.37 (d, $^2J_{HP}$ = 11.1 Hz, PMe_3), 1.55 (s, CH_2CMe_3), 2.18 (s, CMe_3), 2.25, 2.93 (d, dd, $^2J_{HH}$ = 12.1, $^4J_{HP}$ = 3.0 Hz, diastereotopic CH_2 protons), 6.4–7.8 (m, aromatics); minor isomer: δ 1.37 (d, $^2J_{HP}$ = 11.1 Hz, PMe_3), 1.56 (s, CH_2CMe_3), 2.17 (s, CMe_3), 2.24, 2.90 (d, dd, $^2J_{HH}$ = 12.1, $^4J_{HP}$ = 3.0 Hz, diastereotopic CH_2 protons), 6.4–7.8 (m, aromatics).

Acknowledgement—We thank the Dirección General de Política Científica for financial support.

REFERENCES

1. E. Carmona, P. Palma, M. Paneque and M. L. Poveda, *Organometallics* 1990, **9**, 583.
2. K. Nakamoto, *Infrared and Raman Spectra of Inorganic and Coordination Compounds*, 4th edn. Wiley Interscience, New York (1986).
3. (a) H. H. Karsh, *Chem. Ber.* 1977, **210**, 2213; (b) D. A. Palmer and R. V. Eldik, *Chem. Rev.* 1983, **83**, 651.
4. B. E. Mann and B. F. Taylor, *^{13}C NMR Data for Organometallics Compounds*. Academic Press, London (1981).
5. R. C. Mehrotra and R. Bohra, *Metal Carboxylates*. Academic Press, London (1986).
6. J. I. Murray, *Organic Synthesis*, Vol. IV. Wiley Interscience, New York (1963).

Polyhedron Vol. 9, No. 12, pp. 1453–1455, 1990
Printed in Great Britain

0277–5387/90 $3.00+.00
Pergamon Press plc

SYNTHESES OF NEW ORGANO-LANTHANIDE COMPLEXES $[(CH_3OCH_2CH_2C_5H_4)_2LnCl]_2$ AND THEIR XPS

DAOLI DENG, BING LI and CHANGTAO QIAN*

Shanghai Institute of Organic Chemistry, Academia Sinica, 345 Lingling Lu, 200032 Shanghai, China

(*Received* 27 *October* 1989; *accepted* 29 *January* 1990)

Abstract—The substituted cyclopentadienyl sodium salt $CH_3OCH_2CH_2C_5H_4Na$ reacts with $LnCl_3$ (Ln = La, Nd, Gd, Ho, Er, Yb and Y) in THF at room temperature to give the new complexes $[(CH_3OCH_2CH_2C_5H_4)_2LnCl]_2$ in good yield. XPS (X-ray photoelectron spectroscopy) studies show that the metals in these complexes are coordinated through the oxygen atoms.

Since $[(C_5H_5)_2LnCl]_2$ complexes are important precursors to lanthanide alkyl and hydride species,[1–4] the syntheses of these complexes, especially, the syntheses of early organo-lanthanide complexes have attracted much attention. In order to stabilize bis-cyclopentadienyl early lanthanide chlorides and prevent their disproportionation, bulky pentamethylcyclopentadienyl,[5–10] bis(trimethylsilyl) cyclopentadienyl,[10,11] hexamethylindenyl[12] have been used as ligands. In another method, bridged cyclopentadienyl was used as the ligand. Previously, we have reported that the stabilization of early organo-lanthanide complexes has been achieved by using 1,1′-trimethylenebis-cyclopentadienyl,[13] 1,1′-(3-oxa-pentamethylene)bis-cyclopentadienyl,[14] 1,1′-(*m*-xylylene)bis-cyclopentadienyl, 1,1′-(*p*-xylylene)bis-cyclopentadienyl[15] and pyridine-2,6-di(methylenecyclopentadienyl)[16] as ligands. In this communication we wish to describe the synthesis of the new complexes $[(CH_3OCH_2CH_2C_5H_4)_2LnCl]_2$ (Ln = La, Nd, Gd, Ho, Er, Yb and Y) and XPS structural information of these complexes. The success of synthesizing bis(2-methoxyethylcyclopentadienyl) early lanthanide chlorides reveals 2-methoxyethylcyclopentadiene to be an efficient ligand to stabilize bis-cyclopentadienyl early lanthanide chlorides.

Two equivalents of $CH_3OCH_2CH_2C_5H_4Na$ and $LnCl_3$ (Ln = La, Nd, Gd, Ho, Er, Yb and Y) react in THF at room temperature to give the new complexes $[(CH_3OCH_2CH_2C_5H_4)_2LnCl]_2$ in good yields. The complexes have been fully characterized by elemental analyses (C, H and M), IR (Table 1), XPS (Table 2), MS, ^1H and ^{13}C NMR spectroscopy.[17]

The IR spectra of the complexes $[(CH_3OCH_2CH_2C_5H_4)_2LnCl]_2$ show two C—O—C bands at 1045 and 1060 cm^{-1}. Comparing the C—O—C bands of $CH_3OCH_2CH_2C_5H_4Na$ with the title complexes, the values of $\Delta\nu$ are about 50 and 60 cm^{-1}, respectively, which implies that an intramolecular coordination bond is present.[18]

The XPS data on the complexes given in Table 2 shows that the binding energies of O_{1s} increase in these complexes compared with that in $CH_3OCH_2CH_2C_5H_4Na$ and the binding energies of the lanthanide metal atoms all decrease on complexation, compared within the bis-cyclopentadienyl lanthanide chlorides. This obviously indicates that the lone pair of electrons of the oxygen atom in these complexes is partly transferred from the oxygen to the lanthanide metal centre and a O→M coordinate bond is formed. The decrease of charge densities around the oxygen atom causes the increase in the binding energies of the oxygen atom. Because of the increase of the charge densities around the lanthanide metal atom, the binding energies of the lanthanide metal atom decrease.

The binding energies of Cl_{2p} all decrease compared with those in the bis-cyclopentadienyl lanthanide chlorides. This demonstrates that the charge densities around the chlorine atom increase. This is due to the inductive effect, and the charge is partly transferred from lanthanide metal to the chlorine atom.[19] These results are similar to those

* Author to whom correspondence should be addressed.

Table 1. C, H and Ln[a] and IR[b] data of complexes

Complex	Yield (%)	C	H	Ln	(C—O—C) (cm^{-1})[c]
1 La	64	45.3(45.7)	5.2(5.3)	32.4(33.0)	1045s; 1080m
2 Nd	70	45.6(45.0)	5.3(5.2)	33.4(33.9)	1045s; 1060s
3 Gd	56	43.9(43.8)	5.1(5.1)	36.5(35.8)	1045s; 1060s
4 Ho	53	43.1(43.0)	4.9(5.0)	37.8(36.9)	1045s; 1060s
5 Er	60	42.6(42.8)	5.0(5.0)	37.9(37.3)	1048s; 1060s
6 Yb	51	42.1(42.3)	5.9(4.9)	38.6(38.0)	1045s; 1060s
7 Y	49	51.9(51.8)	6.0(6.0)	24.8(24.0)	1050s; 1060s

[a] Calculated values in parentheses.
[b] m: medium; s: strong.
[c] Absorption peaks of C—O—C in $CH_3OCH_2CH_2C_5H_4Na$ at 1095s and 1120s cm^{-1}.

Table 2. Binding energy data (eV) for complexes and Cp_2LnCl

Compound	O_{1s} E_b	O_{1s} E[a]	Ln_{4d} E_b	Ln_{4d} E[b]	Cl_{2p} E_b	Cl_{2p} E[c]	Cl_{2p}[f] E_b	Cl_{2p}[f] E
$CH_3OCH_2CH_2C_5H_4Na$	531.0							
(1) La	532.4	+1.4	836.6[d]		199.0			
(3) Gd	531.7	+0.7	144.1	−0.4	199.1	−1.6	199.8	0.0
Cp_2GdCl			144.5		200.7		199.8	
(4) Ho	532.2	+1.2	163.5	−0.8	199.0	−1.6	199.8	−0.6
Cp_2HoCl			164.3		200.6		200.4	
(5) Er	532.3	+1.3	170.0	−0.8	198.7	−1.4	199.6	−0.4
Cp_2ErCl			170.8		200.1		200.0	
(6) Yb	532.6	+1.6	186.6	−0.5	199.3	−1.1	200.1	−0.3
Cp_2YbCl			187.1		200.4		200.4	
(7) Y	532.5	+1.5	158.9[e]	−0.5	198.8	−1.6	199.9	−0.7
Cp_2YCl			159.4[e]		200.4		200.6	

[a] $E = E_b(O_{1s}) - 531.0$.
[b] $E = E_b(Ln_{4d}) - E_b[Ln_{4d}(Cp_2LnCl)]$.
[c] $E = E_b(Cl_{2p}) - E_b[Cl_{2p}(Cp_2LnCl)]$.
[d] $La_{3d^{5/2}}$.
[e] $Y_{3d^{5/2}}$.
[f] Cl_{2p} for $(C_5H_4CH_2CH_2OCH_2CH_2C_5H_4)LnCl$.

of 1,1′-(3-oxa-pentamethylene)bis-cyclopentadienyl lanthanide chlorides.[14] However, absolute values of ΔE in the title complexes are larger than that of 1,1′-(3-oxa-pentamethylene)biscyclopentadienyl lanthanide chlorides. Perhaps the good coordinative abilities and oxophilicity of the central lanthanide metals in the title complexes favour the formation of coordinate bonds, moreover, they strengthen the coordination bond and give greater stability. The XPS studies reveal that the metals in these complexes are coordinated through the oxygen atoms. There are two possible structures

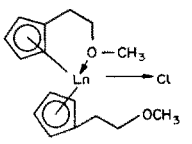

I

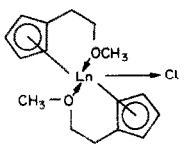

II

of the title complexes (**I** and **II**). Very recently, the preliminary results of an X-ray crystal structure analysis indicated that the title complexes are probably similar to structure (**II**).[17]

Acknowledgements—We gratefully acknowledge the financial assistance of the Natural Science Foundation of China and Academia Sinica. We also acknowledge Mr Jiquan Hu for performing the synthetic work.

REFERENCES

1. W. J. Evans, *Adv. Organomet. Chem.* 1985, **24**, 131.
2. T. J. Marks and R. D. Ernst, in *Comprehensive Organometallic Chemistry* (Edited by G. Wilkinson, F. G. A. Stone and E. W. Abel), Ch. 21. Pergamon Press, Oxford (1982).
3. H. Schumann and W. Genthe, in *Handbook on the Physics and Chemistry of Rare Earths* (Edited by K. A. Gschneidner Jr and L. Eyring), Vol. 7, Ch. 53. Elsevier, Amsterdam (1985) and refs therein.
4. W. J. Evans, in *The Chemistry of the Metal–Carbon Bond* (Edited by F. R. Hartley and S. Patai), Ch. 12. John Wiley, New York (1982).
5. A. L. Wayda and W. J. Evans, *Inorg. Chem.* 1980, **19**, 2190.
6. T. D. Tilley and R. A. Andersen, *Inorg. Chem.* 1981, **20**, 3267.
7. Q. Shen and P. Zhou, *Kexue Tongbao* 1985, **30**, 319.
8. G. Jeske, H. Lauke, H. Mauermann, P. N. Swepton, H. Schumann and T. J. Marks, *J. Am. Chem. Soc.* 1985, **107**, 8091.
9. Q. Shen, H. Tian, Z. Sun and R. Shi, *Youji Huaxue* 1985, 241.
10. M. D. Rausch, K. J. Moriarity, J. L. Atwood, J. A. Weeks, W. E. Hunter and H. G. Brittain, *Organometallics* 1986, **5**, 1281.
11. M. F. Lappert, A. Singh, J. L. Atwood and W. E. Hunter, *J. Chem. Soc., Chem. Commun.* 1981, 1190.
12. M. Tsutsui, L. Chen, D. E. Bergbreiter and T. K. Miyamoto, *J. Am. Chem. Soc.* 1982, **104**, 855.
13. C. Qian, C. Ye, H. Lu, Y. Li and Y. Huang, *J. Organomet. Chem.* 1984, **263**, 333.
14. C. Qian, Z. Xie and Y. Huang, *J. Organomet. Chem.* 1987, **323**, 285.
15. C. Qian, X. Wang, Y. Li and C. Ye, *Polyhedron* 1990, **9**, 479.
16. C. Ye, Y. Li, X. Yang, C. Qian and G. Paolucci, *Chinese Sci. Bull.* 1989, **34**, 1760.
17. D. Deng, J. Hu and C. Qian, to be published.
18. L. Jin, L. Ren, B. Chen and L. Huang, *Chem. J. Chinese* 1986, 7, 99.
19. C. Qian, B. Yao, S. Huang, C. Ye, Y. Li, H. Lu and Y. Huang, *Synth. React. Inorg. Met.-Org. Chem.* 1984, **14**, 663.

Polyhedron Vol. 9, No. 12, pp. 1457–1462, 1990
Printed in Great Britain

0277–5387/90 $3.00+.00
© 1990 Pergamon Press plc

COPPER COMPLEXES OF THE METHYL ESTER OF DITHIOCARBAZIC ACID AND ITS N(3)-SUBSTITUTED DERIVATIVES

LUCANTONIO PETRILLI and FRANCO TARLI*

Istituto di Teoria e Struttura Elettronica e Comportamento Spettrochimico dei Composti di Coordinazione del C.N.R., Area della Ricerca di Roma, C.P. 10, via Salaria km 29.500, 00016 Monterotondo Stazione, Rome, Italy

(*Received* 1 *September* 1989; *accepted* 8 *February* 1990)

Abstract—The ligand behaviour of the methyl esters of dithiocarbazic acids $NH_2NHC(S)SMe$ (L), NHPhNHC(S)SMe (PhL), $NHCH_2PhNHC(S)SMe$ ($PhCH_2L$) and $NMe_2NHC(S)SMe$ (Me_2L) in the copper complexes $CuLCl_2$, CuL_2Cl_2, $Cu(L-H)_2$, $Cu(PhCH_2L-H)_2$, $Cu(Me_2L-H)_2$, $Cu(PhL-2H)_2$, $Cu(PhL)_2Cl$, $Cu(Me_2L)_2Cl$ and $Cu(PhCH_2L)_2Cl$ have been investigated. The electronic and IR spectra have been obtained and magnetic moments calculated. Electrochemical measurements have been performed on $Cu(PhL-2H)_2$.

Derivatives of dithiocarbazic acid, $NH_2NHC(S)SH$, are the subject of many reports which confirm the interest in these multidentate ligands, whose ligating properties critically depend on the N- and S-substituents as we have already shown for the nickel and platinum complexes.[1,2]

Here we report a study of the ligating behaviour of N(3)-substituted derivatives of the methyl ester of dithiocarbazic acid in copper complexes.

The ligands considered are $NH_2NHC(S)SMe$ (L), NHPhNHC(S)SMe (PhL), $NHCH_2PhNHC(S)SMe$ ($PhCH_2L$) and $NMe_2NHC(S)SMe$ (Me_2L). Preliminary results have already been presented.[3] Previous literature reports on copper coordination compounds of esters of dithiocarbazic acids are limited to the X-ray structure of $Cu(Me_2L)_2Cl$[4] and to a study on the antifungal action of some copper complexes, whose complete characterization was not reported.[5] Copper complexes of the Schiff bases of esters of dithiocarbazic acid have been extensively studied.[6]

EXPERIMENTAL

Materials

The chemicals were commercial analytical grade reagents and used without further purification, except for the solvents employed for electrochemical measurements which were purified as described in ref. 8. Nitrogen gas was an ultra-high purity commercial product. All the compounds were dried *in vacuo* (1 torr) over P_4O_{10}, unless otherwise stated. Deuterated solvents were Aldrich Chem. Comp. or Merck UVASOL (99.9 atom % D).

Preparation of the ligands

The ligands L, PhL, $PhCH_2L$, Me_2L, L·HCl and PhCH=NNHC(S)SMe were prepared following the methods reported in ref. 1.

Preparation of the complexes

$CuLCl_2$. A solution of $CuCl_2 \cdot 2H_2O$ (2 mmol) in ethanol (15 cm^3) was added dropwise to a solution of L (4 mmol) in ethanol (15 cm^3). After a few minutes, the solution became pale green, and after 1.5 h of stirring the product was filtered off, washed with water–ethanol (1 : 2) and dried; yield 60%. IR bands; 3177s, 3175s, 3064s, 1597s, 1570sh, 1496s, 1177s, 1154s, 1075s, 1020m, 986s, 967s, 510m, 370m, 289s.

CuL_2Cl_2. A solution of $CuCl_2 \cdot 2H_2O$ (1.7 mmol) in ethanol (20 cm^3) containing 37% HCl (1 cm^3)

* Author to whom correspondence should be addressed.

was added to a solution of L (3.4 mmol) in ethanol (20 cm^3) containing 37% HCl (1 cm^3). The product separated immediately. After 2 h of stirring the product was filtered off, washed with benzene and dried; yield 80%. IR bands: 3210sh, 3196s, 3190sh, 3177s, 3069s, 2671s, 1619s, 1607s, 1598s, 1528w, 1501m, 1159s, 1084s, 986s, 969s, 538w, 320m.

$Cu(L-H)_2$ [L−H = NH_2N=C(S)SMe]. A solution of L (4 mmol) in ethanol (30 cm^3) was added to $Cu(CH_3COO)_2 \cdot H_2O$ (2 mmol) dissolved in ethanol (170 cm^3). After 3 h of stirring the product was filtered off, washed with water–ethanol (2:1) and dried; yield 90%. IR bands: 3213m, 3151m, 3108m, 3048w, 1559s, 1503w, 1190s, 989s, 964m, 924m, 529m, 354m.

$Cu(PhL)_2Cl$. A solution of $CuCl_2 \cdot 2H_2O$ (0.5 mmol) in ethanol (10 cm^3) was added to a solution of PhL (1 mmol) in ethanol (30 cm^3). The solution immediately turned dark green. After 2 h of stirring the product was filtered off, washed with ethanol and dried; yield 70%. IR bands: 3270sh, 3241s, 3150sh, 3124s, 3025sh, 1603s, 1523s, 1493m, 1353m, 1040s, 1030m, 1023m, 970sh, 962w, 247w.

$Cu(PhL-2H)_2$ [PhL−2H = NPhNC(S)SMe]. A solution of $Cu(CH_3COO)_2 \cdot H_2O$ (1.5 mmol) in ethanol (75 cm^3) was added to a solution of PhL (3 mmol) in ethanol (40 cm^3). After 1.5 h of stirring, in an open vessel in the dark, the green product was filtered off, washed with water and dried; yield 30%. IR bands: 3060m, 1586m, 1482s, 1450s, 1042m, 1031m, 985s, 950w, 466w, 372m.

$Cu(PhCH_2L)_2Cl$. A solution of $CuCl_2 \cdot 2H_2O$ (0.7 mmol) in ethanol (30 cm^3) was slowly added to a solution of $PhCH_2L$ (1.4 mmol) in 30 cm^3 of the same solvent. From the resulting green solution, a pale yellow product separated. After stirring (10 min) the product was filtered off, washed with water–ethanol (1:1, 5 cm^3) and dried; yield 50%. IR bands: 3248w, 3136s, 3086m, 3060w, 1600m, 1570w, 1534s, 1525s, 1493m, 1357sh, 1344s, 1030m, 1023m, 965m, 957m, 946m, 910w, 528w, 241w.

$Cu(PhCH_2L-H)_2$ [$PhCH_2L$−H = $NHCH_2$ PhN=C(S)SMe]. A solution of $Cu(CH_3COO)_2 \cdot H_2O$ (1 mmol) in a 1:1 water–ethanol mixture (20 cm^3) was added dropwise to a solution of $PhCH_2L$ (2 mmol) in ethanol (10 cm^3). After 1.5 h of stirring in the dark the product was filtered off, washed with ethanol and dried; yield 70%. IR bands: 3023s, 1598s, 1567w, 1518s, 1492m, 1030m, 1018m, 985w, 946s, 912sh, 455w, 371m.

$Cu(Me_2L)_2Cl$. A solution of $CuCl_2 \cdot 2H_2O$ (0.5 mmol) in ethanol (5 cm^3) was added slowly to a solution of Me_2L (1.5 mmol) in ethanol (5 cm^3). After 0.5 h stirring the product separated, and was filtered off, washed with ethanol and dried; yield 70%. IR bands: 3193m, 3155s, 3074s, 2791w, 2785w, 1525sh, 1516s, 1505sh, 1495m, 1091w, 1032s, 1017s, 961s, 376m, 284sh.

$Cu(Me_2L-H)_2$ [Me_2L−H = NMe_2N=C(S) SCH_3. A solution of $Cu(CH_3COO)_2 \cdot H_2O$ (0.8 mmol) in ethanol (40 cm^3) was added to a solution of Me_2L (1.6 mmol) in ethanol (5 cm^3). From the dark brown solution the product slowly separated. It was filtered off, washed with ethanol and dried; yield 70%. IR bands: 1516s, 1005sh, 982s, 923s, 452m, 353m.

$Cu(PhCH{=}NN{=}C(S)SMe)_2$. A solution of Cu $(CH_3COO)_2 \cdot H_2O$ (0.7 mmol) in water–ethanol (1:4, 100 cm^3) was added to a solution of PhCH=NNHC(S)SMe (1.4 mmol) in ethanol (40 cm^3). After 24 h of stirring a pale brown product was filtered off, washed with water–ethanol (1:4) and dried; yield 80%.

Analytical data are given in Table 1. Microanalyses were performed by the Microanalytical Service of the Area della Ricerca di Roma del C.N.R.

Physical measurements

The electronic solution spectra were recorded with a Perkin–Elmer 330 spectrophotometer. IR spectra were recorded in Nujol or poly(chlorotrifluoroethylene) mulls with a Perkin–Elmer 983 spectrophotometer. Reflectance spectra and room-temperature magnetic susceptibilities were measured as described in ref. 7.

Electrochemical measurements

D.C. and A.C. polarography and cyclovoltammetry were performed, as reported in ref. 8, with an Amel model 471 three-electrode multifunctional assembly. The working electrode was a standard Amel pulsing or stationary electrode and the counter electrode was a platinum wire. An Hg ‖ Hg_2Cl_2, NaCl (saturated, aq) ‖ agar–NaCl(aq) ‖ agar (1.5 %, w/v)–DMF–water (40%, v/v)–NEt_4ClO_4 (saturated) ‖ methyl cellulose (5%, w/v)–DMF–NEt_4ClO_4 (saturated) sintered glass-disk (DMF = dimethylformamide) served as reference electrode. Its potential was 40 mV vs an aqueous saturated calomel electrode (SCE), the liquid junction potential being included. All potentials reported in Table 2 are quoted with respect to the reference electrode with an accuracy of ±5 mV.

Conductivity measurements were carried out with a conductometer Metrohm model E 382.

Molecular weight determination was performed by the cryoscopic method as described in ref. 9.

Table 1. Analytical data for the complexes[a]

Compound	Colour	C	H	N	Cl	S
$[CuLCl_2]$	Dark green	9.5	2.3	10.7	27.4	25.2
		(9.4)	(2.3)	(10.9)	(27.6)	(25.0)
$[CuL_2Cl_2]$	Pale green	12.6	3.2	14.5	19.0	
		(12.7)	(3.2)	(14.8)	(18.7)	
$[Cu(L-H)_2]$	Brown	15.6	3.3	18.4		42.2
		(15.7)	(3.3)	(18.3)		(41.9)
$[Cu(PhL)_2Cl]$	Dark blue	39.0	3.9	11.1	7.3	
		(38.8)	(4.1)	(11.3)	(7.1)	
$[Cu(PhL-2H)_2]$	Dark green	42.4	3.4	12.5		27.8
		(42.1)	(3.5)	(12.3)		(28.1)
$[Cu(BzL-H)_2]$	Brown	44.2	4.4	11.5		
		(44.5)	(4.6)	(11.5)		
$[Cu(BzL)_2Cl]$	Yellow	41.1	4.4	10.5	6.9	24.2
		(41.3)	(4.6)	(10.7)	(6.8)	(24.5)
$[Cu(Me_2L)_2Cl]$	Yellow	23.8	4.9	13.8	8.9	
		(24.0)	(5.0)	(14.0)	(8.8)	
$[Cu(Me_2L-H)_2]$	Brown	26.2	4.9	15.2		
		(26.5)	(5.0)	(15.5)		

[a] Calculated values are in parentheses.

Table 2. Electrochemical data for the reduction of $Cu(PhL-2H)_2$ in CH_2Cl_2 (1×10^{-3} mol dm^{-3})[a]

Cyclic voltammetry[b]			D.C. voltammetry[c]		
E_{pc} (V)	$E_{pa}{}^c$ (V)	i(cat)/i(an)	$E_{1/2}$ (V)	i (μA)	Slope[d] (V)
−0.070	+0.02	0.9	+0.020	0.80	0.080

[a] Containing 0.1 mol dm^{-3} NBu_4BF_4.

[b] Measurements performed at different sweep rates (50, 100, 200 mV s^{-1}).

[c] At pulsing platinum electrode, pulsing time, $t_p = 2$ s, $T = 20$°C.

[d] Calculated using $E_{3/4} - E_{1/4}$.

RESULTS AND DISCUSSION

Preparation and properties of the copper complexes

All the ligands react readily with copper(II) salts in aqueous ethanol giving complexes whose constitution critically depends on the reaction conditions and on the substituents on N(3). L reacts with $CuCl_2 \cdot 2H_2O$ giving $CuLCl_2$, whereas the N(3)-substituted ligands give the compounds $Cu(PhL)_2Cl$, $Cu(PhCH_2L)_2Cl$ and $Cu(Me_2L)_2Cl$. Strong acidification of the reaction medium (HCl) influences the reaction of L and CuL_2Cl_2 is obtained. The same compound can be prepared starting from L·HCl. All the ligands react with $Cu(CH_3COO)_2 \cdot H_2O$ giving the complexes, containing the deprotonated ligands, $Cu(L-H)_2$, $Cu(PhCH_2L-H)_2$, $Cu(Me_2L-H)_2$, whereas Cu $(PhL-2H)_2$ contains the doubly-deprotonated ligand. Efforts to isolate the complexes containing the doubly-deprotonated ligands starting from $Cu(L-H)_2$ and $Cu(PhCH_2L-H)_2$, in strongly basic medium (NH_3), were unsuccessful. This differs from the reactions of similar compounds of nickel and platinum.[1,2] $Cu(PhCH{=}NN{=}C(S)SMe)_2$, containing the mono-deprotonated Schiff base of the dithiocarbazic ester as ligand, is obtained from the reaction of $Cu(PhCH_2L-H)_2$. Its formation suggests that the complex, containing the doubly-deprotonated ligand $Cu(PhCH_2L-2H)_2$ is formed as a labile intermediate, which rearranges, following the reaction pattern that we have reported for thermal disproportionation of $M(PhCH_2L-2H)_2$ (M = Pt, Ni), and leads to the accumulation of $M(PhCH{=}NNC(S)SMe)_2$.[10,11]

All the complexes decompose in organic solvents,

except $Cu(PhL-2H)_2$, $Cu(PhL)_2Cl$, $Cu(Me_2L)_2Cl$ and $Cu(PhCH_2L)_2Cl$. These complexes are non-electrolytes in CH_2Cl_2.

Infrared spectra

IR data are given in the Experimental and in Table 3. The IR spectra of ligands are reported in ref. 1 and references therein. In the spectrum of $CuLCl_2$, the bands attributable to ν(N—H) (at 3175, 3177 and 3064 cm^{-1}) and to δ(N—H)+ν(C⋯N) (at 1496 cm^{-1}) are shifted to lower frequencies with respect to the spectrum of the free ligand L, suggesting coordination of the NH_2 group and coordination of non-methylated sulphur. The appearance of new bands attributable to ν(Cu—N), ν(Cu—S) and ν(Cu—Cl) confirms that chelation of the ligand and coordination of chlorine occur.

In the spectrum of CuL_2Cl_2 several bands in the region 3210–2671 cm^{-1}, attributable to the quaternary ammonium group,[12] suggest that the ligand is coordinated in the form of an ammonium salt, as we have already found for PtL_2Cl_2.[1] A band at 1528 cm^{-1}, not shifted on deuteriation, is assigned to the ν(Cu⋯N) partial double bond of the ligand deprotonated at N(2). New bands attributable to ν(Cu—N) and ν(Cu—S) are found in the spectrum with respect to that of L·HCl, suggesting chelation of the ligand through N(2) and non-methylated sulphur, $Cu[NH_3N{=}C(S)SMe]_2Cl_2$.

$Cu(L-H)_2$ shows bands attributable to ν(N—H) (at 3213, 3151, 3108 and 3048 cm^{-1}) shifted to lower frequencies with respect to the spectrum of the free ligand and new bands, attributable to ν(Cu—N) and ν(Cu—S), suggesting chelation of the deprotonated ligand through N(3) and non-methylated sulphur. The band attributable to the ν(C⋯N) partial double bond is found at 1503 cm^{-1}.

The spectrum of $Cu(PhL)_2Cl$ shows bands attributable to ν(N—H) (at 3270, 3241, 3150 and 3124 cm^{-1}) shifted to higher frequencies with respect to the spectrum of the free ligand suggesting that NH groups are not coordinated. The shift of the δ(N—H)+ν(C⋯N) band (at 1523 cm^{-1}) to lower frequencies suggests coordination of non-methylated sulphur. New bands attributable to ν(Cu—S) and ν(Cu—Cl) confirm sulphur coordination and suggest chlorine coordination.

The spectrum of $Cu(PhL-2H)_2$ lacks all the bands attributable to ν(N—H), an indication that the ligand is doubly-deprotonated. ν(C⋯N) is found at 1450 cm^{-1}, in the same region as found previously for the ν(C⋯N) bands of platinum and nickel dithiolene-like complexes.[1,2] New bands attributable to ν(Cu—N) and ν(Cu—S) confirm N, S chelation of the ligand. In the spectrum of $Cu(PhCH_2L)_2Cl$, bands attributable to ν(N—H) (at 3248, 3136 and 3086 cm^{-1}) are not shifted to lower frequencies suggesting that NH groups are not coordinated. New bands attributable to ν(Cu—S) and ν(Cu—Cl) suggest coordination of non-methylated sulphur and chlorine.

In the spectrum of $Cu(PhCH_2L-H)_2$, the bands attributable to ν(N—H) (at 3032 cm^{-1}) are shifted to lower frequencies indicating that N(3) is coordinated. The new bands attributable to ν(Cu—N) and ν(Cu—S) suggest N,S chelation. In the spectrum of $Cu(Me_2L)_2Cl$, bands attributable to ν(N—H) (at 3193, 3115 and 3074 cm^{-1}) are not shifted to lower frequencies and the bands at 2790 and 2780 cm^{-1}, attributable to ν(C—H), which are characteristic of the NMe_2 group, are still present, suggesting that N(3) is not coordinated.[13] New bands attributable to ν(Cu—S) and ν(Cu—Cl) suggest coordination of non-methylated sulphur and chlorine, according to the X-ray structure, which shows the presence of bridges of thione sulphur between two copper atoms and coordination of chlorine.[4]

In the spectrum of $Cu(Me_2L-H)_2$, bands attributable to ν(N—H) are lacking, in agreement with deprotonation at N(2). The disappearance of ν(C—H) bands characteristic of NMe_2 groups indicates that the NMe_2 group is coordinated.[13] N,S chelation is confirmed by the presence of new bands attributable to ν(Cu—N) and ν(Cu—S).

Table 3. Selected IR bands

Compound	ν(Cu—N)	ν(Cu—S)	ν(Cu—Cl)
$[CuLCl_2]$	510m	370m	289s
$[CuL_2Cl_2]$	538w	320m	
$[Cu(L-H)_2]$	529m	354m	
$[Cu(PhL)_2Cl]$			247w
$[Cu(PhL-2H)_2]$	466w	372m	
$[Cu(BzL)_2Cl]$		528w	241w
$[Cu(BzL-H)_2]$	455w	371m	
$[Cu(Me_2L)_2Cl]$		376m	284sh
$[Cu(Me_2L-H)_2]$	452m	353m	

Magnetic moments and electronic spectra

The magnetic moments (Table 4) of $CuLCl_2$, CuL_2Cl_2, $Cu(L-H)_2$, $Cu(Me_2L-H)_2$ and $Cu(PhL-2H)_2$ range from 1.70 to 1.97 BM, as expected for a +2 oxidation state of copper. The magnetic moment of $Cu(BzL-H)_2$ is abnormally low but consistent with the +2 oxidation state.[14] $Cu(PhL)_2Cl$, $Cu(BzL)_2Cl$ and $Cu(Me_2L)_2Cl$ are diagmag-

Table 4. Room temperature magnetic moments (μ_{eff}) and electronic (reflectance) spectra of copper complexes

Compound	μ_{eff} (BM)	$10^{-3}\,\nu^a$ (cm^{-1})
$[CuLCl_2]$	1.82	13.7, 27.0, 30.8, 38.5
$[CuTscCl_2]^b$	1.70[b]	13.5, 15.0, [15.9], [19.4], [26.4], 30.9
$[CuL_2Cl_2]$	1.97	14.7, 25.6, 32.2, 39.2
$[CuTsc_2Cl_2]^b$	1.77[b]	15.6, 20.3, 23.0, 29.8, 34.9
$[Cu(L-H)_2]$	1.71	[15.3], 19.9, 26.2, 42.6
$[Cu(BzL-H)_2]$	1.27	15.6, 27.8, 30.1, [33.3], [40.0)
$[Cu(Me_2L-H)_2]$	1.70	[14.8], [17.8], 19.0, 24.7, [27.0]
$[Cu(PhL-2H)_2]$	1.93	12.8, [37.5]
		[12.8] (3.26), [16.0] (3.45), 19.0 (3.63),
		29.4 (4.02), 35.7 (4.14)
$[Cu(A)_2]^c$	1.70[c]	12.7 (3.73), 18.8 (3.81), [19.6] (3.80),
		27.6 (4.44), [30.3] (4.34)
$[Cu(PhL)_2Cl]$	Diamagnetic	16.1, 27.4
		15.0 (3.39), [27.0] (3.82), 32.1 (4.25)
$[Cu(BzL)_2Cl]$	Diamagnetic	28.6, 29.6, [34.6], [36.1]
$[Cu(Me_2L)_2Cl]$	Diamagnetic	23.8

[a] Shoulders are given in square brackets, $\log(\varepsilon/dm^3\ mol^{-1}\ cm^{-1})$ in parentheses, solution spectra in CH_2Cl_2.

[b] See ref. 15, Tsc = thiosemicarbazide.

[c] See ref. 16, in dichloromethane, A = $PhNNC(S)NEt_2$.

netic suggesting a +1 oxidation state of copper. The electronic spectra of Cu^{2+} complexes show broad bands which give little information. The spectrum of $CuLCl_2$ shows a broad band, which can be assigned simultaneously to the *d–d* transitions of a highly distorted octahedral chromophore. The close similarity of the spectrum with the spectrum of $CuTscCl_2$, for which a highly distorted octahedral polymeric structure was suggested,[15] the similarity of the ligands, and the high insolubility, also suggest a similar structure for our compound [Fig. 1(a)]. The spectra of CuL_2Cl_2, $Cu(L-H)_2$, $Cu(PhCH_2L-H)_2$ and $Cu(Me_2L-H)_2$ agree with the presence of quasi-planar structures

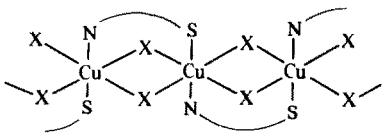

1a

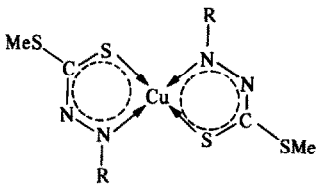

1c

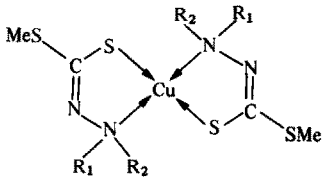

1b

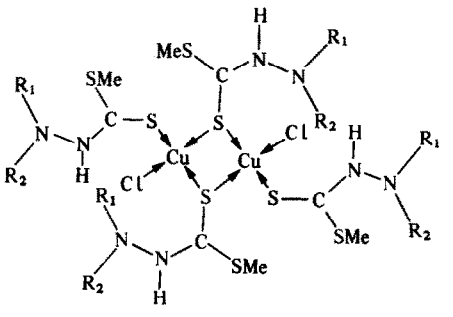

1d

Fig. 1. (a) $CuLCl_2$ (X = Cl); (b) $Cu(L-H)_2$ ($R_1 = R_2 = H$), $Cu(PhCH_2L-H)_2$ ($R_1 = H$, $R_2 = PhCH_2$), $Cu(Me_2L-H)_2$ ($R_1 = R_2 = Me$); (c) $Cu(PhL-2H)_2$ (R = Ph); (d) $Cu(PhL)_2Cl$ ($R_1 = H$, $R_2 = Ph$), $Cu(PhCH_2L)_2Cl$ ($R_1 = H$, $R_2 = PhCH_2$), $Cu(Me_2L)_2Cl$ ($R_1 = R_2 = Me$).

[Fig. 1(b)] containing N,S chelation of the ligands, as suggested by IR spectra. The spectrum of $Cu(PhL-2H)_2$ is characteristic of dithiolene-like complexes, which show very intense charge-transfer bands in the visible. A dithiolene-like complex, $Cu(NPhNC(S)NEt_2)_2$,[16] with a ligand similar to ours [Fig. 1(c)] has been described in the literature. Its structure was suggested to be tetrahedral and its spectrum is similar to that of our compound. The spectra of Cu^+ complexes do not show absorption bands in the visible, as expected, but $Cu(PhL)_2Cl$ [Fig. 1(d)], which is deeply coloured, shows a band at 15.0 kK which we assign to a L→M charge-transfer transition.

Electrochemical measurements

The electrochemical behaviour of $Cu(PhL-2H)_2$, in CH_2Cl_2 solution, shows electron-transfer properties as already found for other dithiolene-like copper complexes with a five-membered delocalized N—S ring.[16] It has been investigated by means of D.C. and cyclic voltammetry. Data are reported in Table 2. The voltage range +0.5 to −1.0 V was explored in reduction. The compound shows one well-defined polarographic wave corresponding to the one-step reduction process, which is electrochemically reversible and mono-electronic at the scan rates considered, as suggested by the cyclovoltammetric $i(cat)/i(an)$, by the ΔEp value ($\Delta Ep = Ep_c - Ep_a = 0.09$ V) and by the slope value in D.C. polarography. The coulometry in CH_2Cl_2 suggests a dimeric structure of the complex which was confirmed by the mol. wt determination in C_6H_6.[9] The reduction process is:

$$[Cu(PhL-2H)_2]_2^0 \underset{-1e}{\overset{+1e}{\rightleftharpoons}} [Cu(PhL-2H)_2]_2^-$$

Acknowledgements—We thank Mr F. Dianetti for microanalyses and Mr G. Chiozzini for help with the electrochemical measurements.

REFERENCES

1. V. Fares, A. M. Giuliani, P. Imperatori, L. Suber and F. Tarli, *J. Chem. Soc., Dalton Trans.* 1987, 1035 and refs therein.
2. D. Attanasio, V. Fares, P. Imperatori, G. Mattogno and F. Tarli, *J. Chem. Soc., Dalton Trans.* 1988, 1217.
3. L. Suber, F. Tarli and L. Petrilli, *Proc. 20th Nat. Conf. Inorg. Chem.*, Pavia, Italy A21, p. 129 (1987).
4. G. Dessy and V. Fares, *Cryst. Struct. Commun.* 1982, **11**, 1811.
5. F. Tarli, A. Monaci and A. Formigoni, C.N.R., Progetto Finalizzato "Fitofarmaci e Fitoregolatori" Convegno nuovi fitofarmaci e fitoregolatori, risultati del sottoprogetto 7, Milano, (14–15 October 1982).
6. M. Akbar Ali, M. Uddin and M. N. Uddin, *Ind. J. Chem.* 1985, **24A**, 758.
7. A. Monaci and F. Tarli, *J. Chem. Soc., Dalton Trans.* 1980, 499.
8. R. Andruzzi and A. Trazza, *J. Electroanal. Chem.* 1978, **86**, 201.
9. D. F. Shriver, *The Manipulation of Air-Sensitive Compounds*, p. 160. McGraw-Hill, New York (1969).
10. L. Suber, F. Tarli, G. Chiozzini and C. Riccucci, *J. Therm. Anal.* 1988, **34**, 1073.
11. L. Suber, F. Tarli, G. Chiozzini, M. Zugarini and C. Riccucci, *J. Therm. Anal.* 1989, **35**, 849.
12. U. Yayasooriya and D. P. Powell, *Inorg. Chem.* 1982, **21**, 1054.
13. J. F. Braunholtz, E. A. V. Ebsworth, F. G. Mann and N. Sheppard, *J. Chem. Soc.* 1958, 2780.
14. M. F. Iskander, L. El-Sayed and A. El-Toukhy, *J. Inorg. Nucl. Chem.* 1980, **42**, 1145.
15. M. J. Campbell and R. Grzeskowiak, *J. Chem. Soc. A* 1967, 396.
16. K. Bechgaard, *Acta Chem. Scand.* 1977, **31A**, 683.

Polyhedron Vol. 9, No. 12, pp. 1463–1467, 1990
Printed in Great Britain

0277–5387/90 $3.00+.00
© 1990 Pergamon Press plc

THE 4-CHLORO-2-OXO-1,3,5,5,8-PENTAMETHYL-1,3,8-TRIAZA-5-AZONIA-4λ⁵-PHOSPHASPIRO[3.4]OCTYL CATION: X-RAY CRYSTAL STRUCTURE DETERMINATION AND VARIABLE TEMPERATURE ^{1}H NMR SPECTRA

THOMAS KAUKORAT, LUDGER ERNST and REINHARD SCHMUTZLER*

Institut für Anorganische und Analytische Chemie der Technischen Universität, Hagenring 30, D-3300 Braunschweig, F.R.G.

and

DIETMAR SCHOMBURG

Gesellschaft für Biotechnologische Forschung (GBF), Mascheroder Weg 1, D-3300 Braunschweig-Stöckheim, F.R.G.

(*Received* 27 *October* 1989; *accepted* 8 *February* 1990)

Abstract—The ^{1}H NMR spectrum of the spirophosphorane **1** at room temperature indicates dynamic behaviour of the cation. From high and low temperature ^{1}H NMR spectra it is concluded that exchange between the $N(CH_3)_2$ groups and between the NCH_3 groups in the four-membered ring takes place. The free enthalpy of activation for this dynamic process was determined (62.4±2.5 kJ mol^{-1}). In the reaction of **1** with sodium tetraphenylborate the crystalline compound, **2**, involving the non-coordinating anion, $[B(C_6H_5)_4]^-$, was obtained. The X-ray crystal structure analysis of **2** reveals the presence of a five-membered ring, formally as a result of intramolecular donor–acceptor interaction between the nitrogen atom of the $N(CH_3)_2$ group and phosphorus.

We have recently reported[1] the unusual spirophosphorane **1**. The bicyclic structure of this compound is due to intramolecular donor–acceptor interaction between the nitrogen atom of the $(CH_3)_2N$ grouping and phosphorus which is accompanied by displacement of chloride ion [eq. (1)]:

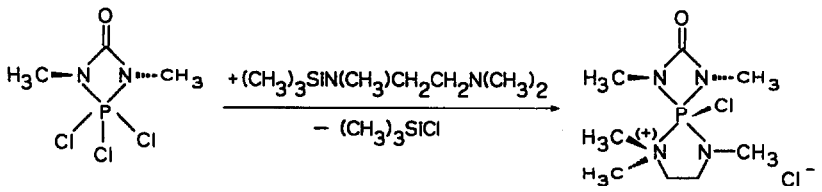

(1)

1

Similar monocyclic compounds, involving phosphorus(III) as a central atom, have been reported.[2,3]

RESULTS AND DISCUSSION

The NMR spectroscopic investigation of **1** indicates the fluxional character of the ion in solution. The ^{1}H NMR spectrum of **1**, recorded in $CDCl_3$ solution at room temperature, reveals a sharp doublet (coupling with ^{31}P) and two broad resonances which indicate a dynamic process of medium rate. At lower temperature (243 K) five CH_3 doublets of equal intensity are observed (Table 1). Signals a and

* Author to whom correspondence should be addressed.

Table 1. ^{1}H NMR signals for the methyl groups of **1** (in $CDCl_3$)

Signal	δ(H)	^3J(PH) (Hz)
a	3.527	9.9
b	3.397	10.2
c	3.216	17.2
d	3.045	14.9
e	2.731	14.1

b were observed to coalesce at $T_c = 296 \pm 8$ K, and signals c and e at $T_c = 312 \pm 7$ K, while the shape of signal d was not temperature dependent (Fig. 1). The coalescence temperatures cannot be determined more accurately because the CH_2 resonances interfere with the a/b coalescence while doublet d interferes with the c/e coalescence. The free enthalpy of activation for the dynamic process has been estimated from both coalescences, using the Eyring equation,[4] to be 62 ± 2.5 kJ mol^{-1}. The high temperature spectrum ($T \gg 312$ K) exhibits three doublets of intensity ratio 2:2:1, and it is concluded that the structurally equivalent methyl groups, i.e. of the $N(CH_3)_2$ groups and of the NCH_3 groups, are exchanging with each other. Such an exchange process proceeds via an (idealized) transition state (or the appropriate intermediate) with tetra-coordinate phosphorus. Both phosphorus-bonded ligands which are not part of the four-membered ring, are situated in a plane, perpendicular to this ring, through phosphorus and the carbon atom of the carbonyl group (Scheme 1). Such a transition state/

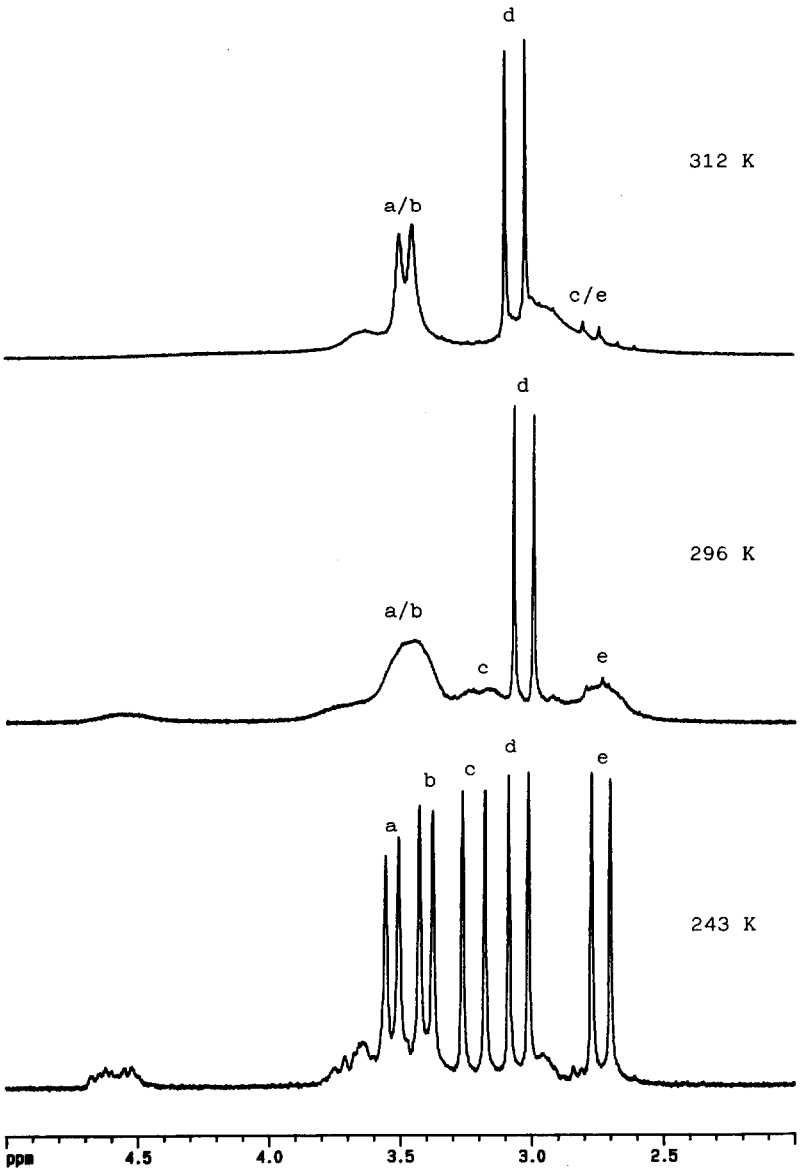

Fig. 1. Variable temperature ^{1}H NMR spectra of **1** (in $CDCl_3$).

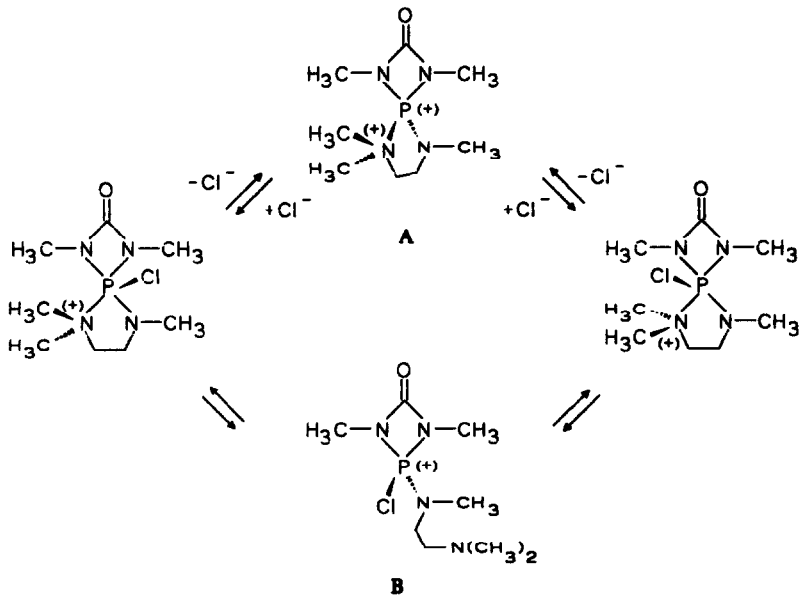

Scheme 1. Possible exchange mechanism of the N-methyl groups in **1**.

intermediate may be achieved either by the departure of chloride ion (with formation of the dication **A**) or by breaking the coordinative $PN(CH_3)_2$ bond (with formation of **B**). While these alternatives cannot be distinguished NMR-spectroscopically the pathway via **B** is considered energetically more favourable since it does not necessitate a species with positive charges on two neighbouring atoms. The structure of the cation of **1** was determined by a single crystal X-ray structure analysis. Because of the unsatisfactory quality of the crystals of **1** the chloride ion was replaced by the non-coordinating $[B(C_6H_5)_4]^-$ ion in a metathetical reaction with sodium tetraphenylborate [eq. (2)]:

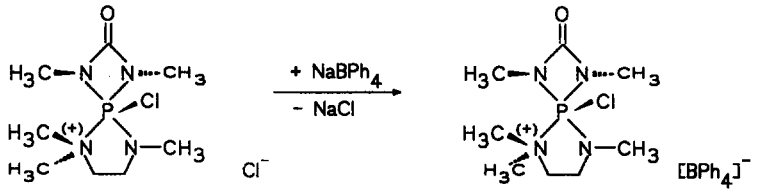

(2)

1 **2**

It was thus possible to obtain crystals of **2**, suitable for the X-ray structure determination.

Discussion of the structure of **2**

The X-ray crystal structure determination of **2** (see Figs 2 and 3) reveals that the phosphorus atom is five-coordinate (λ^5) and that there is strong acceptor–donor interaction between λ^5P and the nitrogen atom of the $N(CH_3)_2$ grouping. The λ^5 phosphorus atom is present in a distorted trigonal-bipyramidal (TBP) environment. A deviation from the ideal TBP geometry is caused, especially, by a decrease of the axial bond angle to 170.2° which is accompanied by an increase of the angle between the two equatorial P—N bonds to 131.9°. A similar geometry has also been observed for a chlorospiro-tetraazaphosphorane[5] (N_{ax}—P—N_{ax} 169.2°; N_{eq}—P—N_{eq} 129.8°). The observed P—Cl bond length (203.7 pm) is identical to that in this chlorospiro-tetraazaphosphorane.[5] It should be noted that the equatorial geometry at the central phosphorus atom is exactly planar (i.e. the sum of the three angles, X_{eq}—P—Y_{eq} = 360°). On the other hand the bond lengths between phosphorus and the nitrogen atom reflect the unusual bonding situation at the central phosphorus atom. All four bond lengths are markedly different. While the bond, P—N_{eq} (167.6 pm), is slightly longer than in the chlorospiro-tetraazaphosphorane mentioned above

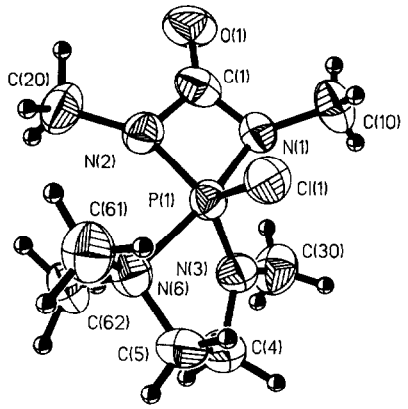

Fig. 2. Structure of the cation of **2** in the crystal.

(166.2 pm, ref. 5), the P—N_{ax} (N_{ax} belonging to N,N'-dimethylurea) bond length is decreased by *ca* 2 pm, compared to the axial P—N bond in the related chlorospiro-tetraazaphosphorane (mean value, 175.3 pm). The bond between phosphorus and the equatorially-bonded nitrogen atom, N(3) (161.5 pm), is remarkably short. Apparently the partial positive charge at phosphorus permits a particularly effective bond to the ideally planar nitrogen atom which may be rationalized in terms of $(d\text{–}p)_\pi$ interactions. A comparison of the distance between the nitrogen atom of the $(CH_3)_2N$ group, acting as an electron donor, and phosphorus (197.5 pm) with the sum of the van der Waals' radii (335 pm, ref. 6) suggests a strongly bonding interaction. It should be noted, though, that in the related intramolecular adduct, $[(CH_3)_2\overline{NCH_2}\,\overline{CH_2N(CH_3)}PCl]^+Cl^-$, a significantly shorter P—N distance (184.2 pm[7]) has been observed. No cation–anion interactions were observed. Other bond parameters which were not discussed here fell in the usually observed ranges.

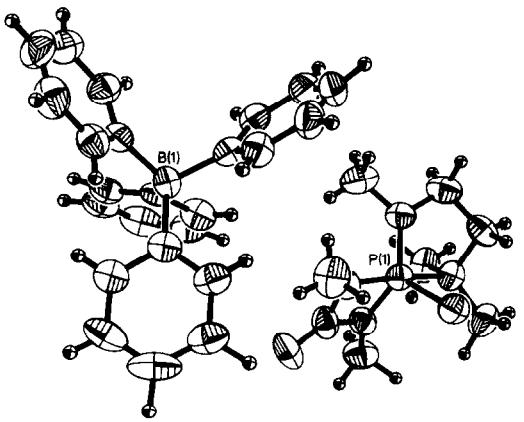

Fig. 3. Relative positions of the cation and anion of **2** in the crystal.

EXPERIMENTAL

The reaction, **1**→**2**, was conducted in conventional glass apparatus in an atmosphere of dry nitrogen. Solvents were dried by standard procedures,[8] and were stored over molecular sieves. NMR spectra were recorded on a Bruker AC 200 intrument at 200.1 (^{1}H) and 81.0 MHz (^{31}P). References: internal TMS and external 85% H_3PO_4. High-field shifts are defined as negative.

Reaction of **1** *with sodium tetraphenylborate: Synthesis of* 4-*chloro*-2-*oxo*-1,3,5,5,8-*pentamethyl*-1,3,8-*triaza*-5-*azonia*-4λ^5-*phosphaspiro*[3.4]*octyl tetraphenylborate* (**2**)

In a 50 cm^3 centrifuge flask a solution of sodium tetraphenylborate (1.62 g, 4.7 mmol) in 15 cm^3 of a mixture of CH_2Cl_2–CH_3CN (2:1) was added dropwise with magnetic stirring during 30 min to a solution of 1.37 g (4.7 mmol) of **1** in 10 cm^3 of CH_2Cl_2. Stirring at room temperature was continued for 1 h. Subsequently, the solid product was removed by centrifugation. The supernatant liquid was decanted, the solvents were stripped off *in vacuo* (0.1 mm), and the remaining solid was recrystallized from a CH_2Cl_2–CH_3CN (3:1) solvent mixture. Yield: 1.27 g (47%); m.p. 149°C.

^{1}H NMR (CD_3CN): δ = 7.33–7.22 (m, 8 H, *ortho*-H of $[B(C_6H_5)_4]^-$), 7.04–6.96 (m, 8 H, *meta*-H), 6.89–6.80 (m, 4 H, *para*-H), 3.64—*ca* 3.1 (m, 4H, CH_2CH_2), 3.05 [very broad d, J(PH) ≈ 17 Hz (partially hidden), NCH_3], 3.02 [broad d, J(PH) = 9.5 Hz, NCH_3], 2.96 [broad d, J(PH) = 9.4 Hz, NCH_3], 2.89 [d, J(PH) = 15.2 Hz, NCH_3], 2.69 [very broad d, J(PH) ≈ 14 Hz, NCH_3]. ^{31}P NMR (CD_3CN): δ = −38.5 (s). Found: C, 67.1; H, 7.0; N, 9.7. Calc. for $C_{32}H_{39}BClN_4OP$: C, 67.1; H, 6.9; N, 9.8%.

X-ray crystal structure determination

Compound **2** crystallized from CH_2Cl_2–CH_3CN (3:1) in the monoclinic space group C_c. Lattice constants [determined diffractometrically from 15 reflections ($\pm hkl$)]: a = 1584.8(2); b = 1016.1(1); c = 1940.6(2) pm; β = 99.387(9)°; Z = 4, d_{calc} = 1.234 g cm^{-3}. The diffraction intensities were measured at room temperature on a Syntex diffractometer (Type P3F), using monochromatic Cu-K_α radiation (λ = 154.18 pm) in the θ–2θ mode ($3° \leqslant 2\theta \leqslant 115°$). The scan speed varied between

Table 2. Selected bond lengths (pm) and bond angles (°) in **2**

Cl(1)—P(1)	203.7(3)	N(1)—P(1)	173.2(5)
N(3)—P(1)	161.5(4)	N(6)—P(1)	197.5(4)
N(2)—P(1)	167.6(5)	N(6)—C(5)	150.8(8)
C(10)—N(1)	145.0(8)	C(1)—N(1)	134.6(7)
O(1)—C(1)	120.9(7)	N(2)—C(1)	140.1(7)
C(20)—N(2)	147.3(8)	C(30)—N(3)	146.4(10)
C(4)—N(3)	146.0(8)	C(5)—C(4)	150.3(9)
C(61)—N(6)	148.4(8)	C(62)—N(6)	152.9(7)
C(111)—B(1)	163.4(8)	C(141)—B(1)	164.2(8)
C(121)—B(1)	163.5(7)	C(131)—B(1)	165.6(7)
N(1)—P(1)—Cl(1)	95.6(2)	N(2)—P(1)—Cl(1)	113.6(2)
N(2)—P(1)—N(1)	75.2(2)	N(3)—P(1)—N(2)	131.9(2)
N(3)—P(1)—Cl(1)	114.5(2)	N(3)—P(1)—N(1)	98.6(2)
N(6)—P(1)—Cl(1)	90.9(2)	N(6)—P(1)—N(1)	170.2(2)
N(6)—P(1)—N(2)	95.5(2)	N(6)—P(1)—N(3)	85.2(2)
C(1)—N(1)—P(1)	92.8(3)	C(1)—N(1)—C(10)	123.4(5)
C(10)—N(1)—P(1)	135.7(5)	O(1)—C(1)—N(1)	133.6(5)
N(2)—C(1)—N(1)	98.4(5)	N(2)—C(1)—O(1)	128.1(5)
C(1)—N(2)—P(1)	93.3(3)	C(20)—N(2)—P(1)	144.3(4)
C(20)—N(2)—C(1)	121.9(5)	C(30)—N(3)—P(1)	126.1(5)
C(4)—N(3)—P(1)	121.2(4)	C(4)—N(3)—C(30)	112.7(5)
C(5)—C(4)—N(3)	105.7(5)	N(6)—C(5)—C(4)	105.1(6)
C(5)—N(6)—P(1)	101.2(3)	C(61)—N(6)—P(1)	118.3(3)
C(61)—N(6)—C(5)	110.9(5)	C(62)—N(6)—P(1)	109.2(3)
C(62)—N(6)—C(5)	108.7(4)	C(62)—N(6)—C(61)	108.2(4)
C(121)—B(1)—C(111)	104.0(4)	C(131)—B(1)—C(111)	110.8(4)
C(131)—B(1)—C(121)	113.1(4)	C(141)—B(1)—C(111)	112.6(4)
C(141)—B(1)—C(121)	113.1(4)	C(141)—B(1)—C(131)	103.6(4)

2.93 and 29.3° min^{-1}, depending on the intensity of the reflection. The data were corrected for Lorentz, polarization and absorption effects ($\mu = 1.725$ mm^{-1}). For the refinement, 1859 out of 2207 measured reflections with $F \geqslant 4.0\sigma(F)$ were used. The structure was solved by direct methods and by difference Fourier synthesis. The hydrogen atom positions were determined from difference Fourier syntheses, and were refined, using isotropic temperature factors. The refinement converged at $R = 0.040$ ($R_w = 0.037$). In the final refinement cycle, the ratio of the change in the parameter, relative to the estimated standard deviation, was less than 1% for all parameters. A final difference map displayed no electron density higher than 0.17×10^6 e/pm³. The program SHELX-76[9] and our own programs were employed. Complex atom scattering factors[10] were used. Selected bond parameters are listed in Table 2, using the numbering scheme shown in Fig. 2.

REFERENCES

1. T. Kaukorat and R. Schmutzler, *Z. Naturf.* 1989, **44b**, 481.
2. W. Becker and R. Schmutzler, *Phosphorus and Sulfur* 1988, **37**, 231.
3. W. Becker and R. Schmutzler, *Phosphorus, Sulfur and Silicon*, 1989, **42**, 21.
4. H. Günther, *NMR-Spektroskopie*, p. 228f. Georg Thieme Verlag, Stuttgart (1983).
5. H. W. Roesky, H. Djarrah, D. Amirzadeh-Asl and W. S. Sheldrick, *Chem. Ber.* 1981, **114**, 1554.
6. A. Bondi, *J. Phys. Chem.* 1964, **68**, 441.
7. G. Bettermann, D. Schomburg and R. Schmutzler, *Phosphorus and Sulfur* 1986, **28**, 327.
8. D. D. Perrin, W. L. F. Armarego and D. R. Perrin, *Purification of Laboratory Chemicals*. Pergamon Press, Oxford (1966).
9. G. M. Sheldrick, unpublished.
10. D. T. Cromer and J. T. Waber, in *International Tables for Crystallography*, Vol. IV, pp. 99ff and 149. Kynoch Press, Birmingham (1974).

Polyhedron Vol. 9, No. 12, pp. 1469–1474, 1990
Printed in Great Britain

0277–5387/90 $3.00+.00
© 1990 Pergamon Press plc

COPPER(I) COMPLEXES WITH LIGAND SYSTEMS CONTAINING NITROGEN AND SULPHUR DONOR ATOMS. SPECTROSCOPY AND ELECTROCHEMISTRY OF THE COPPER(II)/COPPER(I) COUPLE

MICHELE GULLOTTI,† LUIGI CASELLA and GIANFRANCO PALLANZA

Dipartimento di Chimica Inorganica e Metallorganica, Centro CNR, Via Venezian 21, 20133 Milano, Italy

and

FRANCO LASCHI and PIERO ZANELLO

Dipartimento di Chimica Dell'Università, Pian dei Mantellini 44, 53100 Siena, Italy

(*Received* 7 *November* 1989; *accepted* 14 *February* 1990)

Abstract—A series of copper(I) complexes with imine ligands resulting from the condensation of 3-formyl-1-phenyl-2-(1*H*)-pyridinethione with aminoalkylthioalkylbenzimidazoles has been synthesized and spectroscopically characterized. The redox propensity of the present copper(I) complexes, investigated by electrochemical techniques, confirms the relatively difficult access to the corresponding copper(II) complexes, as expected on the basis of their previously reported electrochemistry. Structural reorganizations accompanying the copper(I)/copper(II) redox change are discussed.

In the attempt to synthesize model complexes with a ligand donor set of some relevance in the context of the biomimetic chemistry of blue copper active sites, we have recently reported the preparation and physicochemical characterization of a family of copper(II) complexes with CuN_2SS' cores **1**.[1] The change in the length of the alkyl chain R produces significant variations in the coordination geometry of the copper(II) centres. The electrochemical properties of these complexes provided evidence for the stability of the corresponding copper(I) derivatives. For copper(II) complexes with longer R chains, however, some difficulty arose because of their instability in solution. This prompted us to synthesize the copper(I) analogues **2**–**4** in order to gain further insight into the physicochemical properties of these systems. The zinc complex **5** and the free ligand **6** were also synthesized for comparison purposes. Very often the lack of structural information for both the copper(II) and copper(I) forms of the redox couple limits the discussion of the redox change in terms of the usual tetrahedral-to-planar or tetrahedral-to-tetrahedral conversions.[2,3] We now have the opportunity to correlate more precisely structural information with redox parameters.

RESULTS AND DISCUSSION

Synthesis and spectroscopic characterization

The imine complexes were prepared by metal-ion template condensation between the aminoalkylthioalkylbenzimidazole derivatives and 3-formyl-1-phenyl-2-(1*H*)-pyridinethione, as described previously for the synthesis of the copper(II) complexes.[1] The copper(I) compounds are reasonably stable in the solid state but undergo slow oxidation reactions in solution. In the IR spectra, bands typical of the imine groups occur in the usual range (1635–1645 cm^{-1}) (Table 1), well separated from

† Author to whom correspondence should be addressed.

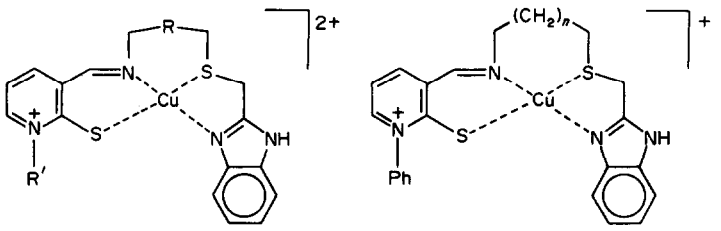

1: R=$(CH_2)_n$, n=2–4
R′=Ph,i-Pr

2: n = 2
3: n = 3
4: n = 4

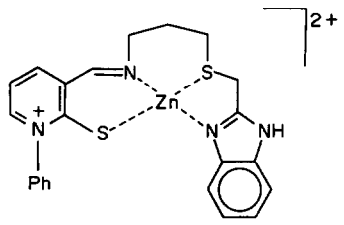

5

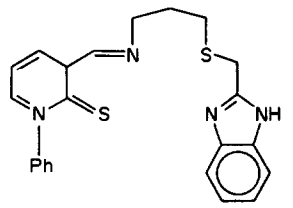

6

the aromatic ring vibration modes, while the broad, ill-defined perchlorate bands near 1100 cm^{-1} indicate that, as expected, these anions are not coordinated to the metal centres.

As discussed previously for the bis(imine) ligands **7** and their copper(I) (**8**) and zinc(II) (**9**) complexes,[4] binding of the pyridinethione–imine residue to a metal results in an increase of the pyridinium thiolate character that is clearly indicated by the electronic and NMR spectra of the complexes. The aromatization and increased positive charge of the pyridine nucleus in the complexes produces, for

Table 1. Elemental analyses,[a] imine stretching frequencies[b] and ^1H NMR spectral data in CD_3CN[c] for compounds **2–6**

Compound	C	H	N	ν(C=N) (cm^{-1})	CH=N	Py—H + Ph—H	Bim—CH_2—S	CH_2—N	CH_2—S	C—CH_2—C
2	46.9 (46.5)	3.7 (3.5)	10.0 (9.9)	1635	8.55 ~ s	7.0–7.8, 7.9–8.3 m	4.19 s	3.78 m	2.95 m	
3	47.3 (47.5)	4.0 (3.8)	9.6 (9.6)	1635	8.40 s	7.1–7.7, 7.9–8.2 m	4.06 s	3.83 m	2.85 m	~ 2.0[d] m
4	48.1 (48.4)	4.0 (4.1)	9.2 (9.4)	1636	8.65 s	7.1–7.9, 8.0–8.3 m	4.15 s	3.88 ~ t	2.78 ~ t	2.0–2.4[d]
5	40.3 (40.5)	3.5 (3.3)	8.3 (8.2)	1644	8.78 s	7.1–7.9, 8.1–8.5 m	4.21 s	4.09 m	2.96 m	~ 2.2[d] m
6	66.2 (66.0)	5.2 (5.3)	13.3 (13.4)	1635	9.00	7.1–8.0 m, 6.82 t	3.98 s	3.76 ~ t	2.76 m	~ 2.0[d] m

[a] Calculated values in parentheses.

[b] Obtained in Nujol mulls. All bands are of medium or strong intensity.

[c] All chemical shift data are referenced to $SiMe_4$. Abbreviations: Py = pyridine ring, Ph = phenyl ring, Bim = benzimidazole ring.

[d] Obscured by solvent absorption.

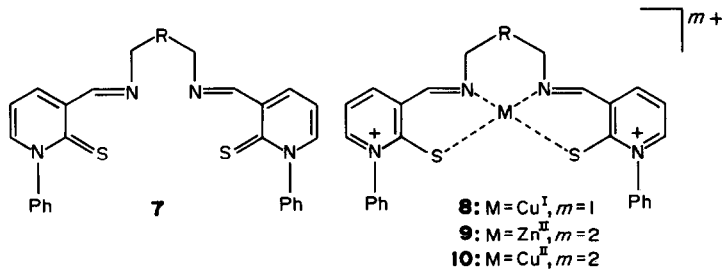

instance, downfield shifts of the ring proton NMR signals, while the azomethine signal is found at unusually low field in the ligand thione form (Table 1). Also, the signals of the methylene groups adjacent to the donor atoms of the ligands undergo downfield shifts on metal binding and it is interesting to note that in the series **2–4** the signal of the CH_2—N group moves progressively more downfield while that of the CH_2—S group undergoes the opposite effect. This probably reflects correspondingly stronger Cu—N interactions and weaker Cu—S interactions in the above series. The signals of the imine proton and the methylene group attached to the benzimidazole group do not appear to be similarly correlated but here the additional contributions to the shielding of the protons by the aromatic nuclei are difficult to rationalize. In general, the proton NMR signals of the zinc(II) complex occur at lower fields with respect to the corresponding signals of the copper(I) complexes because of the higher positive charge of the metal ion.

In the electronic spectra the absorption band of the aromatic $\pi \rightarrow \pi^*$ transition at lowest energy shifts from 408 nm in the free ligand **6** to 364 nm in the zinc(II) complex **5** (Table 2). This band probably occurs between 350 and 400 nm in the spectra of the copper(I) complexes **2–4**, but it is more difficult to locate because it overlaps with the charge-transfer transitions involving filled copper(I) *d* orbitals and the lowest π^* orbital of the conjugated imine ligands. These broad MLCT bands extend to above 500 nm in the visible region. For the series of copper(I) complexes **8** it was possible to relate the position of the MLCT bands to the degree of distortion of the metal chromophore from a flattened tetrahedral to a more regular tetrahedral geometry according to the length of the carbon chain R.[4] In the present case it is difficult to deduce any trend in the MLCT bands. Since the structure of the ligands is no longer symmetrical and the nature of the donor atoms is different in the two halves of the molecule, it is likely that the structures of the metal chromophores are of lower symmetry. Remarkable differences in the behaviour were actually found in the two series of copper(II) complexes **10**[5] and **1**[1] as a function of the R chain length. In the former case the change in copper(II) geometry on increasing R was rather regular from square-planar towards flattened tetrahedral, while for the series **1** a more complicated pattern was observed. The complexes, in fact, exhibited a tendency to assume five-coordinate structures with a solvent molecule in the coordination sphere, but the geometries varied from square-pyramidal ($n = 2$), to trigonal-bipyramidal ($n = 3$), to severely distorted ($n = 4$).

Table 2. Electronic spectral data of compounds **2–6** in acetonitrile solution[a]

Compound	UV–vis, λ_{max}, nm (ε, $M^{-1}\,cm^{-1}$)		
2	273 (14,500)	279 (13,700)	315 (6400)
	398 (4500)		
3	275 (14,600)	280 (13,900)	310 (8250)
	350 sh (5000)	410 (4300)	470 sh (2700)
4	275 (13,200)	280 (13,100)	308 (8000)
	345 sh (5700)	402 (4400)	
5	274 (9800)	280 (9700)	323 (8900)
		364 (4300)	
6	277 (10,200)	284 (9700)	318 (14,000)
		408 (4600)	

[a] Spectra recorded under an inert atmosphere.

Electrochemistry

In view of the relative redox instability of the copper(II) forms of the present copper(I) complexes in acetonitrile solution, cyclic voltammetric measurements were performed in the temperature range from −20 to +20°C. The voltammetric profiles of complexes **2** and **3** parallel those found for the corresponding copper(II) species.[1] In fact, as shown in Fig. 1 for **3**, they display an uncomplicated quasireversible copper(II) oxidation. Irreversible

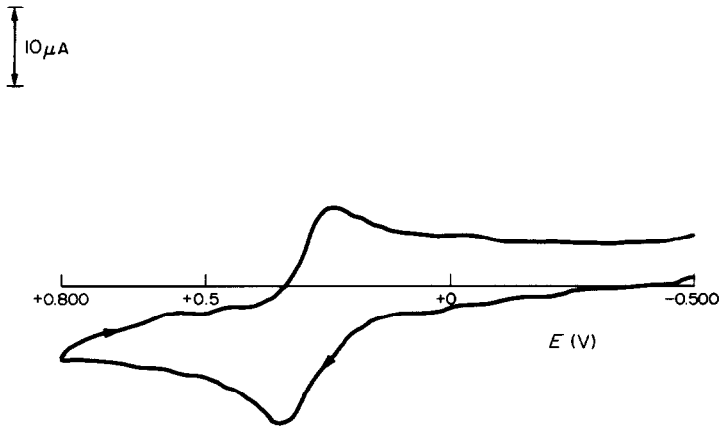

Fig. 1. Cyclic voltammogram recorded at a platinum electrode on an acetonitrile solution of **3** (2.0×10^{-3} mol dm^{-3}) and $[NEt_4]ClO_4$ (0.1 mol dm^{-3}). $T = -18°C$; scan rate 0.2 V s^{-1}.

processes also occur at more positive (Cu^{II}/Cu^{III}) and more negative (Cu^{I}/Cu^{0}) potential values, but these will not be further discussed here. As illustrated in Fig. 2, increasing the temperature makes the one-electron removal more difficult.

Less straightforward is the electrochemical behaviour of complex **4**, which is slightly soluble in acetonitrile at low temperatures. The cyclic voltammogram recorded at 13°C, Fig. 3, displays an ip_c/ip_a ratio significantly lower than unity (0.53), indicating the occurrence of a chemical reaction following the copper(II) electrogeneration.[6] Increasing the scan rate prevents such a chemical complication and at about 1 V s^{-1} the ip_c/ip_a ratio reaches unity, thus enabling a reliable computation of the formal electrode potential. Assuming the occurrence of a first-order reaction coupled with electron-transfer, a half-life of 1–2 s can be assigned[6] to the copper(II) complex analogue of **4**, which supports our previous difficulties in determining its redox behaviour.[1] Table 3 summarizes the most significant redox parameters for the copper(I) complexes studied.

Since the copper(II) complex corresponding to **4** is the most interesting among those of series **1**, we performed EPR measurements of the species electrogenerated by macroelectrolytic oxidation at −20°C of **4** in acetonitrile solution. The room-temperature EPR spectrum (Fig. 4) shows well-resolved hyperfine components with $g_{iso} = 2.087$ and $A_{iso} = 63.5 \times 10^{-4}$ cm^{-1}. The fourth hyperfine line ($I = +3/2$) additionally shows a superhyperfine structure of five equally spaced lines (relative intensity 1 : 2 : 3 : 2 : 1), attributable to coupling of the unpaired electron with two almost identical nitrogen nuclei in the coordination sphere. A coupling constant of 13.0 G was estimated by second derivative spectral analysis for the IS interaction. The frozen solution EPR spectrum displays a relatively

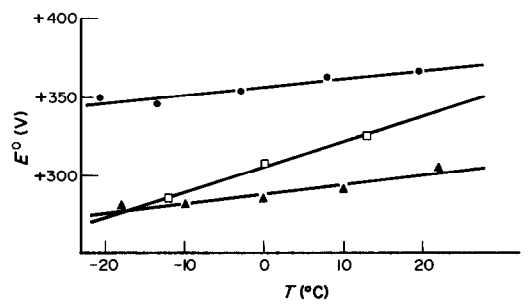

Fig. 2. Variation of the formal electrode potential for the Cu^{II}/Cu^{I} redox change with temperature. (●) complex **2**; (▲) complex **3**; (□) complex **4**.

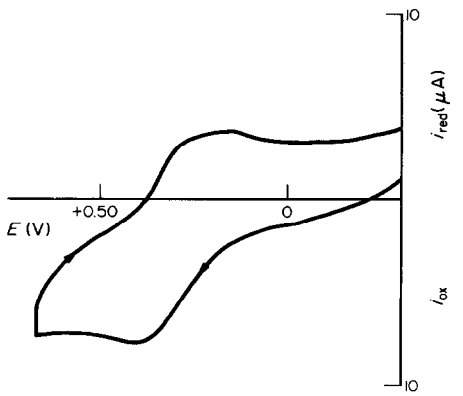

Fig. 3. Cyclic voltammogram recorded at a platinum electrode on an acetonitrile solution of **4** (1.42×10^{-3} mol dm^{-3}) and $[NEt_4]ClO_4$ (0.1 mol dm^{-3}). $T = 13°C$; scan rate 0.1 V s^{-1}.

Table 3. Redox potentials (in V vs SCE) and peak-to-peak separation (in mV, at 0.2 V s^{-1}) for the one-electron oxidation of complexes **2**–**4** in acetonitrile solution, at different temperatures (°C)

2			**3**			**4**		
T	$E^{0\prime}$	ΔE_p	T	$E^{0\prime}$	ΔE_p	T	$E^{0\prime}$	ΔE_p
19.5	+366	100	22	304	85	13	+325	130
8	+362	92	10	290	88	0	+308	185
−3	+354	108	0	284	104	−12	+285	110
−13.5	+346	148	−10	281	122			
−20.5	+350	196	−18	280	110			

broad absorption that probably results from a mixture of species. It is possible to calculate the following EPR parameters of the major species from the spectrum: $g_{\parallel}$ 2.173, $A_{\parallel}$ 152×10^{-4} cm^{-1} and $g_{\perp} \sim 2.07$. The broadness of the perpendicular component of the signal indicates that it is probably rhombic. The EPR parameters are slightly different from those obtained for the copper(II) complex **1** with $n = 4$ ($g_{\parallel}$ 2.236, $A_{\parallel}$ 145×10^{-4} cm^{-1}, $g_{\perp} \sim 2.06$)[1] and in particular the latter spectrum was more typical of the axial type. We attribute this difference to the different solvent mixture employed in the latter case; it is known that the flexibility of the alkyl chain of the ligand with $n = 4$ allows a range of isomeric structures for the corresponding copper(II) complexes.[1] Under these conditions the composition of the solvent mixture forming the glass for the EPR measurement may be important in determining the structural arrangement preferred by the complex in the frozen state. The EPR parameters obtained here for the electrogenerated copper(II) species are indicative of a distorted five-coordinate structure, while those obtained previously for the same copper(II) complex agreed with a distorted tetrahedral structure. These are also the most likely structures for complexes of this type deduced from the solution spectral behaviour.[1]

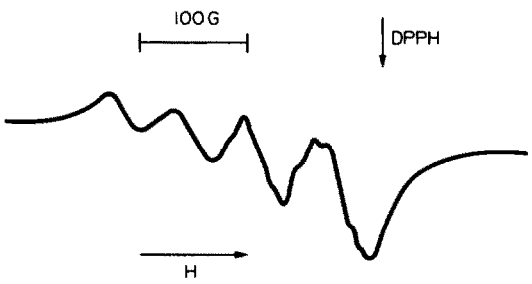

Fig. 4. X-band room temperature EPR spectrum recorded on an acetonitrile solution from exhaustive one-electron oxidation of **4** at −20°C.

A discussion of the structural reorganization accompanying the copper(I)/copper(II) electron-transfer on the basis of the relevant thermodynamic electrode potentials, implies the knowledge of the actual structures of the complexes in both oxidation states. In spite of the uncertainties mentioned above, the potential values for the couples extrapolated at 20°C:

$$E^{0\prime}_{n=2} = +0.366 \text{ V}$$

$$E^{0\prime}_{n=4} = +0.337 \text{ V}$$

$$E^{0\prime}_{n=3} = +0.299 \text{ V},$$

indicate an easier Cu^{I}/Cu^{II} redox change, and hence a lower structural reorganization,[7] in the system with $n = 3$. In this case the copper(II) species is trigonal-bipyramidal and the copper(I) species can be assumed as distorted tetrahedral. Although we expected an easier redox change for the system with $n = 4$, likely involving a similar structural reorganization, it may well be that other factors involving metal–solvent and ligand–solvent interactions play some role in determining the energy barrier to the one-electron removal. In any case, the highest energy barrier belongs to the system with $n = 2$ that involves a square-pyramidal copper(II) species and the least tetrahedral copper(I) complex in the series **2**–**4**, since it contains the shortest R chain and the least flexible ligand.

A final aspect of the Cu^{II}/Cu^{I} redox change that is of relevance in copper biomimetic chemistry, as we previously highlighted,[4] concerns the relevant electron-transfer entropy. Gray and co-workers pointed out that the Cu^{II}/Cu^{I} reduction of blue copper proteins in aqueous solutions (pH 6.5–7.0) is coupled to a negative entropy change.[8] In the present case, the variation of $E^{0\prime}$ values with temperature enables computation[9] of a ΔS_{tr} for the Cu^{II}/Cu^{I} reduction of 11.2 e.u. for the system with $n = 2$, 13.5 e.u. for the system with $n = 3$ and 36.8 e.u. for the system with $n = 4$. The opposite sign

with respect to the biological derivatives is indeed to be expected, because in low molecular weight model complexes the hydrophilic/hydrophobic environments responsible for solvent reordering effects upon charge variation are lacking.[8] The most straightforward explanation for the variation in ΔS_{tr} values observed throughout the series is that the longer alkyl chains can induce intrinsic disorder during the molecular reorganization.

EXPERIMENTAL

Elemental analyses were performed at the microanalytical laboratory of the University of Milano. IR spectra were recorded on a Nicolet MX-1E FT-IR instrument, electronic spectra on a Perkin–Elmer Lambda 5 spectrophotometer, and ^{1}H NMR spectra on a Bruker WP-80 spectrometer. The EPR spectra were obtained with a Bruker D-SRC instrument operating at 9.78 GHz (X-band), equipped with a Bruker variable-temperature ER 4111 VT unit. Both materials and apparatus for electrochemical measurements have been described previously.[1] Under the actual experimental conditions the ferrocenium/ferrocene couple which resulted was located at +0.38 V vs SCE.

The synthesis of the aminoalkylthioalkylbenzimidazole derivatives to be condensed with 3-formyl-1-phenyl-2-(1*H*)-pyridinethione[10] was reported previously.[1] The imine ligand **6** was prepared by refluxing equimolar amounts (1 mmol) of the formylpyridinethione and 3-(benzimidazol-2′-ylmethylthio)propylamine in ethanol for *ca* 1 h. The solution was evaporated to a small volume and chromatographed on silica gel (eluent: ethanol–chloroform, 1 : 1 v/v). The main yellow fraction was collected, evaporated to a small volume and precipitated with diethyl ether. The copper(I) complexes **2–4** were prepared according to the following procedure. A solution of the Schiff base was prepared under nitrogen by refluxing in ethanol for 2–3 h a mixture of equimolar amounts of formylpyridinethione and the appropriate aminoalkylthioalkylbenzimidazole (1 mmol) in Schlenk apparatus. Solid tetrakis(acetonitrile)copper(I) perchlorate (1 mmol) was then added and the mixture was allowed to reach room temperature. The brown precipitate thus formed was recovered by filtration under an inert atmosphere and dried *in vacuo*. The yellow zinc(II) complex **5** was prepared similarly in air using zinc(II) perchlorate hexahydrate. The elemental analyses of the compounds are reported in Table 1. All the complexes exhibited IR bands of medium or strong intensity near 1590, 1545 and 1490 cm^{-1} for the aromatic ring vibrations, and near 760, 750, 720 and 695 cm^{-1} for the aromatic C—H bending vibrations.

Acknowledgement—The authors thank the Italian Ministero Pubblica Istruzione for financial support.

REFERENCES

1. L. Casella, M. Gullotti, A. Pintar, F. Pinciroli, R. Viganò and P. Zanello, *J. Chem. Soc., Dalton Trans.* 1989, 1161.
2. P. Zanello, *Comm. Inorg. Chem.* 1988, **8**, 45.
3. P. Zanello, in *Stereochemistry of Organometallic and Inorganic Compounds* (Edited by I. Bernal), Vol. IV. Elsevier, Amsterdam, in press.
4. M. Gullotti, L. Casella, A. Pintar, E. Suardi, P. Zanello and S. Mangani, *J. Chem. Soc., Dalton Trans.* 1989, 1979.
5. L. Casella, M. Gullotti and R. Viganò, *Inorg. Chim. Acta* 1986, **124**, 121.
6. (a) E. R. Brown and J. R. Sandifer, in *Physical Methods of Chemistry. Electrochemical Methods* (Edited by B. W. Rossiter and J. F. Hamilton), Vol. 2, Ch. 4. John Wiley, New York (1982); (b) U. Sakaguchi and A. W. Addison, *J. Chem. Soc., Dalton Trans.* 1979, 600.
7. H. B. Gray and E. I. Solomon, in *Copper Proteins* (Edited by T. G. Spiro), p. 1. John Wiley, New York (1981).
8. N. Sailasuta, F. C. Anson and H. B. Gray, *J. Am. Chem. Soc.* 1979, **101**, 455.
9. E. L. Yee, R. J. Cave, K. J. Guyer, P. D. Tyma and M. J. Weaver, *J. Am. Chem. Soc.* 1979, **101**, 1131.
10. J. Becher and E. G. Frandsen, *Acta Chem. Scand.* 1976, **30B**, 863.

Polyhedron Vol. 9, No. 12, pp. 1475–1477, 1990
Printed in Great Britain

0277–5387/90 $3.00+.00
Pergamon Press plc

OPTICAL ABSORPTION SPECTRA OF COBALT(II) AND NICKEL(II) IONS IN LEAD ACETATE GLASSES

J. LAKSHMANA RAO,* G. L. NARENDRA and S. V. J. LAKSHMAN

Department of Physics, S.V. University, Tirupati 517 502, India

(*Received* 7 *November* 1989; *accepted* 14 *February* 1990)

Abstract—The optical absorption spectra of cobalt(II) and nickel(II) ions in lead acetate glasses have been studied both at room and liquid nitrogen temperatures. The absorption bands have been interpreted in terms of Ligand Field Theory. The crystal field-parameter (Dq) and Racah inter-electronic repulsion parameters (B and C) have been evaluated. From the spectral analysis it is found that cobalt(II) and nickel(II) ions substitute the lead(II) ions.

Ingram *et al.*[1] extensively studied the structural chemistry of a wide range of glass-forming molten acetates using cobalt(II) as a spectroscopic probe. From the observed features they concluded that acetate glasses vary considerably in ionic–covalent character. Cobalt(II) and nickel(II) ions are known to be good probes for optical absorption studies.[2–8] These ions can easily be dissolved in lead acetate glass systems. These probe ions may occupy sites both similar to and different from lead(II) sites in these glasses. The present study describes the detailed investigation of the optical absorption spectra of cobalt(II) and nickel(II) ions in lead acetate glasses.

EXPERIMENTAL

Glasses were prepared by taking the accurately weighed reagents of lead acetate mixed with cobalt acetate in the weight ratio Co/Pb 0.03. The mixture was melted in a crucible in an electric furnace at temperatures 50°C higher than the liquid temperatures. The melt was then quenched on porcelain plates. Similarly, lead acetate glasses doped with nickel acetate were also prepared in the weight ratio Ni/Pb 0.03.

Optical absorption spectra were recorded at room temperature (RT) and liquid nitrogen temperature (LNT) on Perkin–Elmer UV–vis and Carl-Zeiss NIR spectrophotometers. The optical measurements could be made with an accuracy of $\pm 5\ cm^{-1}$.

RESULTS AND DISCUSSION

Cobalt(II) : *lead acetate glass*

Cobalt usually occurs in glass as cobalt(II). The colour of the glasses containing cobalt(II) changes from pink to blue when the coordination number of cobalt decreases from six to four. In the present work, the glasses prepared were pink in colour and therefore the analysis of the spectrum has been carried out assuming that the cobalt(II) ion is in octahedral symmetry. The optical absorption spectra observed at RT and LNT are shown in Fig. 1. The spectrum observed at RT consists of two strong bands centred at 8000 and 18,865 cm^{-1}. These two broad, intense bands are assigned to the spin-allowed quartet–quartet transitions $^4T_{1g}(F) \rightarrow {}^4T_{2g}(F)$ and $^4T_{1g}(F) \rightarrow {}^4T_{1g}(P)$, respectively. The positions of these bands at LNT are 8100 and 19,225 cm^{-1}, respectively. In addition, a number of weak bands are also observed. These bands are identified with the spin-forbidden quartet–doublet transitions. On cooling the glass to LNT the intensity of the bands decreased and the bands became sharper. A small blue shift of the order 100–500 cm^{-1} was observed for the band maxima. The assignments of the transition for all the observed bands are given in Table 1.

By diagonalizing the energy matrices[9] for the d^7 Co^{2+} ion configuration, the crystal-field parameter

* Author to whom correspondence should be addressed.

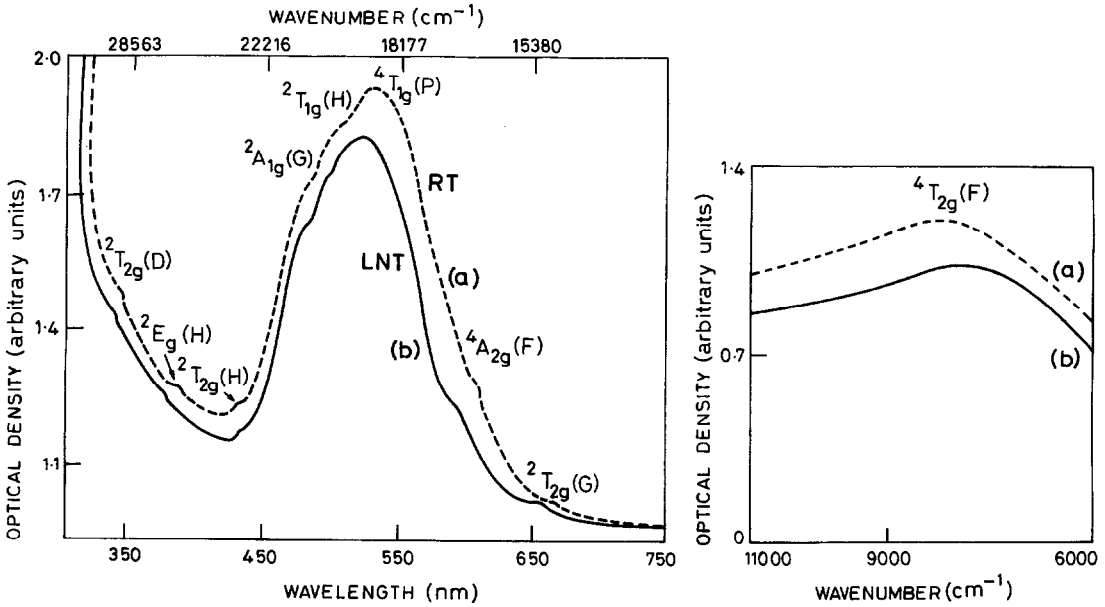

Fig. 1. Absorption spectra of cobalt(II) in lead acetate glass: (a) at room temperature; (b) at liquid nitrogen temperature.

(*Dq*) and the Racah inter-electronic repulsion parameters (*B* and *C*) have been evaluated. The *Dq* and *B* values obtained in the present work are as expected for cobalt(II) ions in octahedral symmetry.[4,8]

Nickel(II): *lead acetate glass*

Nickel occurs in glass as nickel(II) in octahedral, square-planar and tetrahedral symmetries depending upon the composition of the glass.[10] The colour of the high-spin octahedral nickel(II) glasses is olive green. In the present work the glasses were yellowish-green in colour and therefore the analysis of the spectrum has been carried out assuming the nickel(II) ion in octahedral symmetry. The spectra observed at RT and LNT are shown in Fig. 2. At room temperature three main bands are observed centred at 8300, 14,080 and 24,995 cm^{-1}. These three intense bands are assigned to the spin-allowed triplet–triplet transitions, $^3A_{2g}(F) \rightarrow {}^3T_{2g}(F)$, $^3A_{2g}(F) \rightarrow {}^3T_{1g}(F)$ and $^3A_{2g}(F) \rightarrow {}^3T_{1g}(P)$, respectively. These three bands observed at LNT are at 8400, 14,280 and 24,635 cm^{-1}, respectively. The remaining weak bands in the spectrum are identified with the spin-forbidden triplet–singlet transitions. On cooling the sample the bands became sharper and the intensities of the bands increased. The assignments of the transitions for all the observed bands are given in Table 2.

Table 1. The observed and calculated energies for the bands of cobalt(II) in lead acetate glasses; $Dq = 915$ cm^{-1}, $B = 820$ cm^{-1} and $C = 3444$ cm^{-1}

Transition $^4T_{1g}(F) \rightarrow$	Observed energy (cm^{-1}) RT	LNT	Calculated energy (cm^{-1})
$^4T_{2g}(F)$	8000	8100	8044
$^2T_{2g}(G)$	15,475	15,500	15,016
$^4A_{2g}(F)$	17,090	17,240	17,193
$^4T_{1g}(P)$	18,865	19,225	19,237
$^2T_{1g}(H)$	19,995	20,400	19,064
$^2A_{1g}(G)$	20,830	21,270	21,650
$^2T_{2g}(H)$	22,985	23,525	23,469
$^2E_g(H)$	26,310	26,800	26,561
$^2T_{2g}(D)$	29,840	29,405	29,450

By diagonalizing the energy matrices for the d^8 Ni^{2+} configuration[9] the crystal-field parameter (*Dq*) and the Racah inter-electronic repulsion parameters (*B* and *C*) have been evaluated. The *Dq* and *B* values obtained in the present work are as expected for nickel(II) ions in octahedral symmetry.[2]

The *Dq* values obtained in the present work for both cobalt(II) and nickel(II) ions follow the spectrochemical series.[11]

The inter-electronic repulsion parameter, *B*, for free cobalt(II) and nickel(II) ions is 1120 and 1080 cm^{-1}, respectively.[11] In the present work the *B* values obtained for cobalt(II) and nickel(II) are 820 and 980 cm^{-1}, respectively. This indicates that the

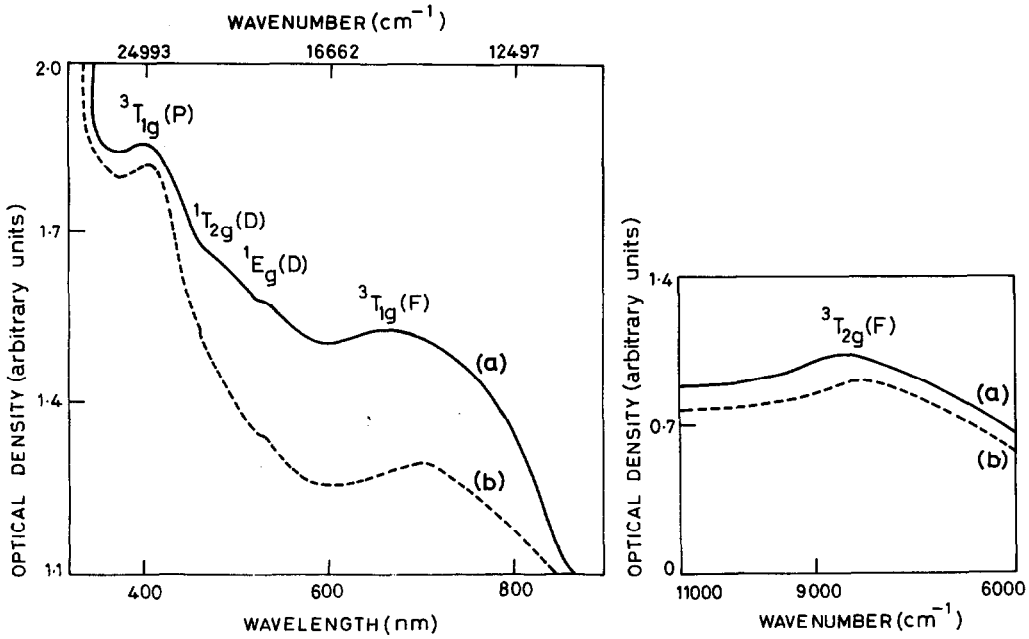

Fig. 2. Absorption spectra of nickel(II) in lead acetate glass: (a) at liquid nitrogen temperature; (b) at room temperature.

bonding between the metal ion and the ligand is more covalent for the cobalt(II) than for the nickel(II) ion, and in both the cases the site symmetry is octahedral.

CONCLUSION

In lead acetate glasses the ligand-field parameters for cobalt(II) were found to be $Dq = 915\ cm^{-1}$, $B = 820\ cm^{-1}$ and $C = 3444\ cm^{-1}$, and for nickel (II), $Dq = 840\ cm^{-1}$, $B = 980\ cm^{-1}$ and $C = 3920\ cm^{-1}$. The optical studies reveal that the cobalt(II) and nickel(II) ions go substitutionally into lead(II) ion sites and the site symmetry around these transition metal ions is octahedral.

Table 2. The observed and calculated energies for the bands of nickel(II) in lead acetate glasses, $Dq = 840\ cm^{-1}$, $B = 980\ cm^{-1}$ and $C = 3920\ cm^{-1}$

Transition $^3A_{2g}(F) \rightarrow$	Observed energy (cm^{-1}) RT	LNT	Calculated energy (cm^{-1})
$^3T_{2g}(F)$	8300	8400	8400
$^3T_{1g}(F)$	14,080	14,280	14,067
$^1E_g(D)$	18,515	18,865	18,780
$^1T_{2g}(D)$	21,775	22,215	22,980
$^3T_{1g}(P)$	24,995	25,635	25,833

Acknowledgement—The authors wish to express their sincere thanks to the UGC, New Delhi, for financial assistance.

REFERENCES

1. M. D. Ingram, G. G. Lewis and J. A. Duffy, *J. Phys. Chem.* 1972, **76**, 1035.
2. A. Paul and R. W. Douglas, *Phys. Chem. Glasses* 1969, **4**, 133.
3. A. Paul and A. N. Tiwari, *J. Mater. Sci.* 1974, **9**, 1057.
4. A. Paul and A. N. Tiwari, *Phys. Chem. Glasses* 1974, **15**, 81.
5. M. Beretz and S. L. Holt, *J. Inorg. Nucl. Chem.* 1974, **36**, 49.
6. Amit Sarkar, Ashok Dasgupta, Bharatt Basu and A. Paul, *J. Mater. Sci. Letts* 1983, **2**, 697.
7. M. Morsi, S. El-Konsol and M. I. El-Shahawy, *J. Non-Cryst. Solids* 1986, **83**, 241.
8. K. Kojima, J. Matsuda and T. Kimura, *Phys. Chem. Glasses* 1988, **29**, 154.
9. Y. Tanabe and S. Sugano, *J. Phys. Soc. Jpn* 1954, **9**, 753.
10. A. Paul and R. W. Douglas, *Phys. Chem. Glasses* 1967, **8**, 233.
11. B. N. Figgis, *Introduction to Ligand Fields*. Wiley Eastern, New Delhi (1976).

Polyhedron Vol. 9, No. 12, pp. 1479–1482, 1990
Printed in Great Britain

0277–5387/90 $3.00+.00
© 1990 Pergamon Press plc

COORDINATING PROPERTIES OF 2-PYRIDYLDIPHENYLPHOSPHINE WITH SOME METAL CARBONYLS

H. G. ANG,* W. L. KWIK and P. T. LAU

Department of Chemistry, National University of Singapore, Lower Kent Ridge Road, Singapore 0511, Republic of Singapore

(*Received* 21 *November* 1989; *accepted* 14 *February* 1990)

Abstract—The reaction of 2-pyridyldiphenylphosphine with iron carbonyl affords 2-$(C_5H_4N)P(C_6H_5)_2Fe(CO)_4$ in which the ligand is bonded through the phosphorus donor atom. Similar substitution reactions occur with $Mn_2(CO)_{10}$, $Re_2(CO)_{10}$, $Cr(CO)_6$ and $Mo(CO)_6$ to give 2-$C_5H_4NP(C_6H_5)_2Mn_2(CO)_8$, $[2\text{-}C_5H_4NP(C_6H_5)_2Re(CO)_4]_2$ and 2-$C_5H_4NP(C_6H_5)_2M(CO)_5$ (M = Cr, Mo), respectively.

2-Pyridyldiphenylphosphine (I) has attracted much interest as a ligand[1] especially in the synthesis of bridged heteroatomic transition metal complexes.[2–8] The present study sets out to investigate the coordinating properties of ligand I with various transition metal carbonyls under conditions similar to those reported in our earlier studies[9–13] involving the reactivities of (*o*-diphenylphosphinobenzyl)dimethylsilane and 2-pyridyldimethylsilane towards metal carbonyls. We report below the preparation and properties of complexes obtained from reactions of I with metal carbonyls of chromium, molybdenum, manganese, rhenium and iron.

RESULTS AND DISCUSSION

Iron complex

Ligand I was prepared in this study by the reaction between the Grignard reagent 2-C_5H_4NMgBr and chlorodiphenyl phosphine in ether:

$$2C_5H_4NMgBr + ClP(C_6H_5)_2 \longrightarrow 2C_5H_4NP(C_6H_5)_2 + MgBrCl.$$

Treatment of the distillate at 120–140°C/0.5 mm Hg gave I as a crystalline solid. The reactions of I with iron pentacarbonyl in benzene proceeded at 125°C to give a monosubstituted iron carbonyl derivative, $C_5H_4NP(C_6H_5)_2Fe(CO)_4$ (II), formulated on the basis of IR data and elemental analysis. The same product was also obtained from the reaction of diiron nonacarbonyl with I at 40°C. Prolonged reaction of more than 18 h did not yield the disubstituted derivative. This is to be contrasted with the reaction[13] of *o*-chlorophenyldiphenylphosphine with iron pentacarbonyl and diiron nonacarbonyl wherein a disubstituted complex $[o\text{-}ClC_6H_4P(C_6H_5)_2]_2Fe(CO)_3$ (**A**) was obtained in the former case, while both monosubstituted *o*-$ClC_6H_4P(C_6H_5)_2Fe(CO)_4$ (**B**) and the disubstituted **A** derivatives were isolated in the latter. The IR spectra of complexes **A** and **B** display carbonyl stretching vibrations at 1970, 1930, 1890, 1870 cm^{-1} and 2050, 1975, 1946 cm^{-1}, respectively. The carbonyl stretching vibrations of II are located at 2050, 1980, 1940 and 1890 cm^{-1}. This suggests that bonding of I to iron is most likely to occur through the phosphorus atom only, as shown in structure II.

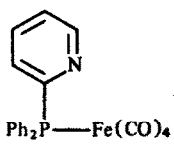

II

*Author to whom correspondence should be addressed.

This mode of bonding is consistent with the basic reaction pattern established by Balch and co-workers[3] for formation of bridged heteronuclear-transition metal complexes. The first step invariably led to the formation of the monosubstituted derivative with **I** being bonded to the metal by the phosphorus atom. Moreover, the low affinity[14] of iron(0) for the pyridine nitrogen has been further demonstrated by a reaction of $(C_5H_4N)_2Si(CH_3)_2$ and diiron noncarbonyl in benzene at 100°C, from which only triiron dodecacarbonyl and unreacted ligand were isolated.[13] It is also noted that the pyridine vibrations at 604 and 405 cm^{-1} have not been appreciably affected in compound **II**.[15]

Manganese and rhenium complexes

The reactions of **I** with $Mn_2(CO)_{10}$ and $Re_2(CO)_{10}$ proceeded in benzene at a much higher temperature of 160°C. The manganese derivative **III** is an orange solid characterized by seven CO stretching vibrations at 2060, 2000, 1982, 1960, 1940, 1930 and 1902 cm^{-1}. Its analytical data do not differentiate it between the formula $C_5H_4NP(C_6H_5)_2Mn_2(CO)_9$ (**IIIa**) and $C_5H_4NP(C_6H_5)_2Mn_2(CO)_8$ (**IIIb**). The IR data are not consistent with structure **IIIa** which normally gives five bands.[16] However, the presence of seven bands suggests that the most probable structure is **IIIb**.

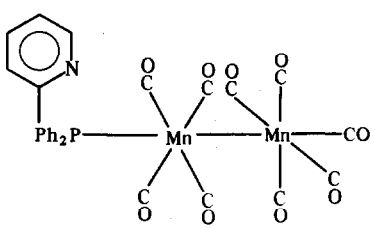

(IIIa)

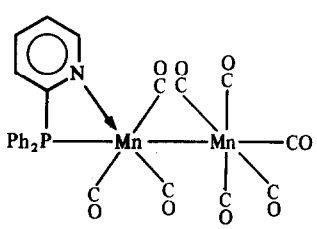

(IIIb)

The complex formed with the rhenium carbonyl can be formulated as $[2\text{-}C_5H_4NP(C_6H_5)_2Re(CO)_4]_2$ (**IV**) on the basis of elemental analysis and CO stretching vibrations which gave bands located at 2080, 1980, 1940 and 1902 cm^{-1}. Following from the above discussion, structure **IV** is proposed. The lower number of CO stretching vibrations observed in this case is consistent with the high symmetry of structure **IV** compared to the manganese analogue (**IIIb**).

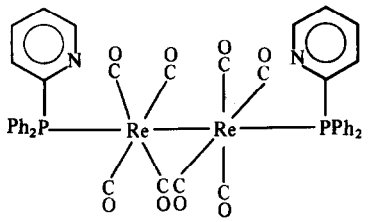

(IV)

Chromium and molybdenum complexes

The reactions between ligand **I** and chromium carbonyl proceeded in benzene at a temperature of 105°C to give a creamy crystalline solid which can be formulated as $C_5H_4NP(C_6H_5)_2Cr(CO)_5$ (**V**) on the basis of its IR data and elemental analysis. An analogous monosubstituted molybdenum(0) derivative (**VI**) was also obtained from a reaction with molybdenum hexacarbonyl at 125°C in benzene. As both chromium and molybdenum form monopyridine[17] as well as monotriphenylphosphine[18] complexes of the general formula $LM(CO)_5$ (L = pyridine/triphenylphosphine), attempts were made to ascertain the mode of coordination of **I** in **V** and **VI**. A careful comparison of the carbonyl stretching frequencies of several complexes (Table 1) reveals that synergic interactions of triphenylphosphine with chromium(0) and molybdenum(0) is apparently greater than with pyridine.

EXPERIMENTAL

The IR spectra of solids, as KBr pellets, were recorded on a Perkin–Elmer Model 337 IR spectrophotometer. The IR spectra of metal carbonyl complexes in the carbonyl region were recorded on chloroform solutions.

Synthesis of 2-pyridyldiphenylphosphine

A solution of ethyl bromide (2.2 g, 0.02 mol) in dry ether (50 cm^3) was added to dry magnesium turnings (15.0 g, 0.62 mol) placed in a three-necked flask. A few iodine crystals were added to initiate the reaction. A solution of 2-bromopyridine (76.9 g, 0.49 mol) and ethyl bromide (24.8 g, 0.23 mol) in ether (250 cm^3) was added over 75 min while keeping the reaction mixture under reflux. After a further reflux for another 2 h, the reaction mixture was cooled. A solution of diphenylchlorophosphine (70.6 g, 0.32 mol) in ether (275 cm^3) was added slowly and the resultant reaction mixture was

refluxed for a further 2 h. Upon cooling, the reaction mixture was treated with saturated ammonium chloride solution (275 cm^3). The ether layer was dried over anhydrous sodium sulphate overnight and fractional distillation at 180°C/1–2 mm Hg yielded 2-pyridyldiphenylphosphine (26.9 g), m.p. 84–85°C. (Found: C, 77.5; H, 5.3; N, 5.1. Calc. for $C_{17}H_{14}NP$: C, 77.6; H, 5.3; N, 5.3%.) IR (Nujol mull): 3050w, 2950s, 2920s, 2860s, 1565m, 1460s, 1435s, 1412s, 1090m, 1048m, 1025m, 998m, 772s, 746s, 716m, 695s, 620m.

Reaction of 2-pyridyldiphenylphosphine with chromium hexacarbonyl

A mixture of chromium hexacarbonyl (0.50 g, 2.27 mmol), 2-pyridyldiphenylphosphine (0.50 g, 1.90 mmol) and benzene (10 cm^3) was sealed in an evacuated tube and kept at 105°C for 20 h. The solution was then filtered and concentrated to yield a solid. Yellow crystals were obtained upon recrystallization from acetone, $C_5H_4NP(C_6H_5)_2Cr(CO)_5$, m.p. 107–109°C. (Found: C, 58.2; H, 3.3. Calc. for $C_{22}H_{14}CrO_5NP$: C; 58.0; H, 3.1%.) IR ($CHCl_3$ solution): 2060s, 1995m, 1920vs, 1660w, 1570s, 1480w, 1420m, 1320w, 1300w, 1090s, 990s, 630s.

Reaction of 2-pyridyldiphenylphosphine with molybdenum hexacarbonyl

A mixture of molybdenum hexacarbonyl (0.56 g, 2.12 mmol), 2-pyridyldiphenylphosphine (0.50 g, 1.90 mmol) and benzene (10 cm^3) was sealed in an evacuated tube at 126°C for 18 h. The solution was then filtered and concentrated to give a solid which upon recrystallization from acetone formed yellow crystals of $C_5H_4NP(C_6H_5)_2Mo(CO)_5$, m.p. 119–121°C. (Found: C, 53.5; H, 3.1. Calc. for $C_{22}H_{14}MoO_5NP$: C, 52.9; H, 2.8%.) IR: 2075s, 1995m, 1940vs, 1710w, 1580s, 1430m, 1329w, 1301w, 1151w, 1090s, 1000sh, 990s, 900m, 608s.

Reaction of 2-pyridyldiphenylphosphine with manganese carbonyl

A mixture of 2-pyridyldiphenylphosphine (0.59 g, 2.25 mmol), manganese carbonyl (0.899, 2.28 mmol) and benzene (15 cm^3) was sealed in a tube at 160°C for *ca* 10 min. The solution was filtered and the filtrate concentrated under nitrogen. The orange–brown solid obtained was subjected to vacuum sublimation at 50°C to remove the unreacted parent carbonyl. The residue was then recrystallized from hexane to yield bright orange crystals, m.p. 181–182°C. This compound was identified as 2-$C_5H_4NP(C_6H_5)_2Mn_2(CO)_8$. (Found: C, 50.1; H, 2.6; N, 2.2. Calc. for $C_{25}H_{14}PNMn_2O_8$: C, 49.9; H, 2.2; N, 2.2%.) IR ($CHCl_3$ solution): 2980m, 2060s, 2000m, 1985s, 1960s, 1940s, 1930s, 1902s, 1460m, 1430m, 1180w, 1160w, 1125w, 1095w, 1085w, 1020w, 1000w, 765m, 750m, 720m, 695m, 663s, 645s, 623s.

Reaction of 2-pyridyldiphenylphosphine with rhenium carbonyl

A mixture of 2-pyridyldiphenylphosphine (0.263 g, 0.89 mmol), rhenium carbonyl (0.695 g, 1.06 mmol) and benzene (10 cm^3) was sealed in an evacuated tube at 160°C for 2 h. The solvent was removed under vacuum and the residual was subjected to sublimation at 80°C to remove the unreacted rhenium carbonyl. The remaining solid was fractionally recrystallized from hexane to give white crystals, m.p. 219–220°C. This compound was identified as $[2\text{-}C_5H_4NP(C_6H_5)_2Re(CO)_4]_2$. (Found: C, 44.7; H, 2.0; N, 2.1. Calc. for $C_{42}H_{28}P_2N_2Re_2O_8$: C, 44.9; H, 2.5; N, 2.5%.) IR ($CHCl_3$ solution): 3050w, 2940s, 2845s, 2095w, 2060w, 2020sh, 2008m, 1980s, 1940vs, 1902s, 1565m, 1485m, 1420s, 1450s, 1418m, 1375m, 1185w, 1155w, 1095sh, 1078m, 1020w, 1000w, 988w, 765w, 743m, 720w, 698m, 625m, 615s.

Reaction of 2-pyridyldiphenylphosphine with iron pentacarbonyl

A mixture of 2-pyridyldiphenylphosphine (0.51 g, 1.92 mmol), iron pentacarbonyl (0.429 g, 2.51 mmol) and benzene (8 cm^3) was placed in a sealed tube at 125°C for 11 h. The resultant solution was filtered and the filtrate concentrated under nitrogen. The yellow crystals formed were recrystallized from acetone. The product (m.p. 155–157°C decomp.) was identified as $2\text{-}C_5H_4NP(C_6H_5)_2Fe(CO)_4$. (Found: C, 59.1; H, 3.5; N, 3.0. Calc. for $C_{21}H_{14}NPFeO_4$: C, 58.5; H, 3.2; N, 3.2%.) IR ($CHCl_3$ solution): 3060w, 3050w, 2940s, 2910s, 2850s, 1995w, 1970s, 1930m, 1890s, 1870s, 1570w, 1480m, 1465m, 1455m, 1435m, 1425s, 1375m, 1365w, 1270w, 1255m, 1180w, 1125w, 1108m, 1095m, 1038m, 995w, 873w, 758s, 738m, 715m, 708m, 695s, 638s.

REFERENCES

1. H. G. Ang, W. E. Kow and K. F. Mok, *Inorg. Nucl. Chem. Lett.* 1972, **8**, 829.
2. M. J. Auburn and F. A. Cotton, *J. Am. Chem. Soc.* 1984, **106**, 1323.

3. J. P. Farr, M. M. Olmstead and A. L. Balch, *J. Am. Chem. Soc.* 1980, **102**, 6654.
4. A. Maisonnet, J. P. Farr and A. L. Balch, *Inorg. Chem. Acta* 1981, **53**, L217.
5. J. P. Farr, M. M. Olmstead, C. H. Hunt and A. L. Balch, *Inorg. Chem.* 1981, **20**, 1182.
6. A. Maisonnet, J. P. Farr, M. M. Olmstead, C. T. Hunt and A. L. Balch, *Inorg. Chem.* 1982, **21**, 3961.
7. J. P. Farr, M. M. Olmstead and A. L. Balch, *Inorg. Chem.* 1983, **22**, 1229.
8. J. P. Farr, M. M. Olmstead, F. E. Wood and A. L. Balch, *J. Am. Chem. Soc.* 1983, **105**, 792.
9. H. G. Ang and P. T. Lau, *J. Organomet. Chem.* 1985, **291**, 285.
10. H. G. Ang and P. T. Lau, *J. Organomet. Chem.* 1972, **37**, C4.
11. H. G. Ang and P. T. Lau, *Organometallic Chem. Rev. A* 1972, **8**, 235.
12. H. G. Ang and W. L. Kwik, *J. Organomet. Chem.* 1989, **361**, 27.
13. H. G. Ang, unpublished results.
14. F. A. Cotton and G. Wilkinson, *Advanced Inorganic Chemistry*, 5th edn. John Wiley, New York (1988).
15. K. Nakamoto, *Infrared and Raman Spectra of Inorganic and Coordination Compounds*, 4th edn. John Wiley, New York (1986).
16. R. H. Reimann and E. Singleton, *J. Chem. Soc., Dalton Trans.* 1976, 2109.
17. C. S. Kraihanzel and F. A. Cotton, *Inorg. Chem.* 1963, **2**, 533.
18. T. A. Magel, C. N. Matthews, T. S. Wang and J. H. Wotiz, *J. Am. Chem. Soc.* 1961, **83**, 3200.

Polyhedron Vol. 9, No. 12, pp. 1483–1485, 1990
Printed in Great Britain

0277–5387/90 $3.00+.00
© 1990 Pergamon Press plc

THE PREPARATION AND CHARACTERIZATION OF BIS(2,2-DIMETHYLPROPYL)CADMIUM(II) AND ITS 2,2′-BIPYRIDYL ADDUCT

PAUL O'BRIEN* and JOHN R. WALSH

Department of Chemistry, Queen Mary and Westfield College, Mile End Road, London E1 4NS, U.K.

and

ANTHONY C. JONES* and SIMON A. RUSHWORTH

Epichem Ltd, Power Road, Bromborough, Wirral, Merseyside L62 3QF, U.K.

(*Received* 30 *January* 1990; *accepted* 19 *February* 1990)

Abstract—The synthesis and characterization of the compound bis(2,2-dimethylpropyl) cadmium(II), {bis(neopentyl)cadmium(II)} and its 1:1 adduct with 2,2′-bipyridyl are reported. The alkyl is moderately volatile (vapour pressure *ca* 3 torr, 52°C) and may find application as a precursor for the deposition of cadmium-containing films by MOCVD.

Dimethyl cadmium is used as a precursor for the deposition of a wide range of II/VI materials by metallo-organic chemical vapour deposition, MOCVD.[1,2] The properties of this compound as a precursor have been somewhat modified by the use of adducts such as the dioxan[3] and the bis-tetrahydrothiophene,[4] but the only other alkyl of cadmium to have been used for MOCVD is the bis-ethyl.[5] This fact may reflect the unstable nature of the higher alkyls of cadmium, which are particularly prone to photochemical decomposition.[6] In view of all these factors it is surprising that there appear to be no literature reports[6,7] concerning the synthesis and properties of bis(neopentyl)cadmium(II). The neopentyl group is well known for its ability to form stable metal alkyl complexes, presumably because β-elimination reactions are precluded; for example it has been successfully used to prepare manganese(II) alkyls.[8] Moreover, the mercury[9] and zinc[10] neopentyls are both known compounds. In this report we describe, for the first time, the synthesis and characterization of bis(neopentyl)cadmium(II).

RESULTS AND DISCUSSION

Bis(neopentyl)cadmium(II) is a waxy solid melting at *ca* 40°C, and distilling at 50°C, 10^{-2} torr. The compound has been characterized by its ^{1}H NMR, mass (*m/z*, ^{116}Cd 258.02 found, 258.08 calc), and IR spectra; the NMR results are summarized in Table 1. The alkyl is remarkably thermally stable and discolours only slightly, in daylight, over a period of hours at 90°C, behaviour which may be contrasted with that of diethyl cadmium which deposits cadmium metal in minutes (*ca* 30°C, daylight). The thermal stability of the compound allowed a preliminary assessment of its vapour pressure to be made in a closed glass system. Typical values for the vapour pressure were *ca* 11.7 torr at 90°C and *ca* 3 torr at 52°C.

The compound shows the typical behaviour[11,12] of a group 12 alkyl and forms a solid, yellow adduct of 1:1 stoichiometry with 2,2′-bipyridyl; the spectroscopic results for this compound are also included in Table 1. The stoichiometry of the compound is confirmed by integration of the ^{1}H NMR spectrum. The adduct is remarkably stable and it is difficult to remove the alkyl by distillation under reduced pressure, which is markedly different

* Authors to whom correspondence should be addressed.

Table 1. Analytical and spectroscopic results[a]

	%C	%H	δ (ppm) CH_2	δ (ppm) CH_3	δ (ppm) Bipy
$Cd(CH_2C(CH_3)_3)_2$[b]	45.4 (47.2)	8.8 (8.7)	0.20 (4H)[c]	0.60 (18H)	—
$Cd(CH_2C(CH_3)_3)_2 \cdot bipy$			1.50 (4H)	1.96 (18H)	9.3 (2H,m) 8.8 (2H,m) 8.1 (2H,m) 7.7 (2H,m)

[a] NMR spectra in D_8 toluene, referenced to toluene ($\delta = 7.1$ ppm).
[b] Calculated in parentheses.
[c] Cadmium satellites observed.

behaviour to that observed for similar adducts of dimethyl cadmium.[12,13]

CONCLUSIONS

Bis(neopentyl)cadmium(II) is a low-melting point solid (m.p., *ca* 40°C) which shows remarkable thermal and photolytic stability. It readily forms 1 : 1 adducts with bidentate nitrogen donors such as 2,2′-bipyridyl, but in contrast with the adducts of dimethyl[12] or diethyl cadmium[5] the neopentyl is not easily liberated on heating the adduct *in vacuo*. The compound is at present being evaluated* as a precursor for the growth of both wide and narrow band-gap compound semiconductors by MOCVD.

EXPERIMENTAL

Materials and methods

Neopentyl bromide was purchased from Fluka, all other chemicals were from BDH. Solvents were dried before use with molecular sieves. All manipulations were carried out using a vacuum line and standard Schlenk techniques.

Physical measurements. Electronic spectra were recorded with a Perkin–Elmer 330 spectrophotometer; IR spectra were recorded on a Mattson Polaris FT-IR spectrometer, as Nujol mulls or in a gas cell; NMR spectra were recorded using a Bruker WH 400, pulsed FT NMR instrument; and mass spectra were recorded with a Kratos MS50 TC instrument (only a weak spectrum was obtained but this showed a clear molecular ion). Microanalyses were performed by the University College, London, Service.

Preparation of compounds

Bis(neopentyl)cadmium(II). Neopentyl bromide (1-bromo-2,2-dimethylpropane, 300 g, 0.2 mol) was added dropwise to magnesium turnings (6 g, 0.2 mol) in 200 cm^3 of dry diethyl ether with stirring, to give a solution of the Grignard reagent (this reaction sometimes took some time to initiate, but was generally successful). The solution of the Grignard reagent in ether was then added dropwise to a suspension of cadmium iodide (33 g, 0.2 mol) in 100 cm^3 of diethyl ether. The resulting solution was stirred overnight to give a pale yellow solution and a white precipitate.

Approximately 80% of the ether was removed under reduced pressure leaving an off-white solid residue. The residue was distilled at 140–150°C giving an ethereal solution of bis(neopentyl)cadmium(II). The remaining ether was removed by pumping off the solution at −20°C and the alkyl was obtained as a waxy solid (m.p., 40°C). Major IR bands (cm^{-1}): 2925, 1260, 1096, 1036, 1007, 800, 682, 568.

2,2′-Bipyridyl adduct. 2,2′-Bipyridyl (6.1 g, 0.039 mol) was added to bis(neopentyl)cadmium (10 g, 0.04 mol) in 50 cm^3 of diethyl ether. Removal of the ether resulted in the precipitation of the adduct as a bright orange solid. Major IR bands (cm^{-1}):

* The alkyl has successfully been used in combination with H_2S to grow films of CdS on GaAs 111A at 350°C. The growth rate was low, *ca* 0.06 μm h^{-1}, and there was some homogeneous reaction between the alkyl and hydrogen sulphide; the films showed hexagonal features. The low growth rate obtained with the source at room temperature suggests that the alkyl is unsuitable for atmospheric pressure MOCVD. Bis(neopentyl)cadmium may have an application as a p-type dopant for InP and related III/V alloys.

3054, 2945, 2854, 1583, 1457, 1356, 1232, 1090, 1066, 1001, 757, 671, 620, 568.

Acknowledgements—This work has been supported by a SERC CASE Studentship to J.W.; P.O'B. and J.W. wish to thank Epichem Ltd for their support of work at Q.M.W. We are extremely grateful to P. J. Parbrook (R.S.R.E., Malvern) for details of preliminary growth experiments.

REFERENCES

1. B. Cockayne and P. J. Wright, *J. Cryst. Growth* 1984, **68**, 223.
2. A. C. Jones, *Chemtronics* 1989, **4**, 15.
3. P. J. Wright, B. Cockayne, A. C. Jones, E. D. Orrell, P. O'Brien and O. F. Z. Khan, *J. Cryst. Growth* 1989, **97**, 94.
4. A. C. Jones, S. A. Rushworth, P. J. Wright, B. Cockayne, P. O'Brien and J. Walsh, *J. Cryst. Growth* 1989, **97**, 573.
5. L. M. Smith, J. Thompson, A. C. Jones and P. R. Jacobs, *Mater. Lett.* 1988, **7**, 22.
6. J. Boersma, *Comprehensive Organometallic Chemistry* (Edited by G. Wilkinson, F. G. A. Stone and E. W. Abel), p. 823. Pergamon Press, Oxford (1982).
7. *Dictionary of Organometallic Compounds* and Supplements 1–4. Chapman and Hall, London and New York (1984, 1985, 1986, 1987 and 1988).
8. R. A. Andersen, E. Carmona-Guzman, J. F. Gibson and G. Wilkinson, *J. Chem. Soc., Dalton Trans.* 1976, 2204.
9. F. C. Whitmore and E. Rohrmann, *J. Am. Chem. Soc.* 1939, **61**, 1591.
10. S. Moorhouse and G. Wilkinson, *J. Chem. Soc., Dalton Trans.* 1974, 2187.
11. K. H. Thiele, *Z. Anorg. Allg. Chem.* 1964, **330**, 8.
12. G. E. Coates and S. I. E. Green, *J. Chem. Soc.* 1962, 3340.
13. P. R. Jacobs, E. D. Orrell, J. B. Mullin and D. J. Cole-Hamilton, *Chemtronics* 1986, **1**, 15.

Polyhedron Vol. 9, No. 12, pp. 1487–1489, 1990
Printed in Great Britain

0277-5387/90 $3.00+.00
© 1990 Pergamon Press plc

SYNTHESIS OF A μ_3-η^1 ISOCYANIDE TRIANGULAR NICKEL CLUSTER: X-RAY CRYSTAL STRUCTURE OF $[Ni_3(\mu_3\text{-CNMe})(\mu_3\text{-I})(dppm)_3][I]$

KEVIN S. RATLIFF, PHILLIP E. FANWICK and CLIFFORD P. KUBIAK*

Department of Chemistry, Purdue University, West Lafayette, IN 47907, U.S.A.

(*Received* 29 *December* 1989; *accepted* 21 *February* 1990)

Abstract—The reaction of the trinickel cluster $[Ni_3(\mu_3\text{-CNMe})(\mu_3\text{-I})(CNMe)_2(dppm)_2][I]$ (**1**), which contains the first example of a linear, symmetrically triply-bridging (μ_3-η^1) isocyanide, with one equivalent of dppm ($PPh_2CH_2PPh_2$) in acetonitrile under reflux conditions, results in the formation of a more stable trinickel cluster, $[Ni_3(\mu_3\text{-CNMe})(\mu_3\text{-I})(dppm)_3][I]$ (**2**), which also possesses a linear μ_3-η^1 isocyanide ligand. The structure of **2** was established by X-ray crystallography.

Molecular clusters provide the opportunity to study the interactions of small molecules with metal surfaces in a homogeneous environment. Recently, the novel trinickel complex $[Ni_3(\mu_3\text{-CNMe})(\mu_3\text{-I})(CNMe)_2(dppm)_2][I]$ (**1**) was synthesized in our laboratory.[1] The complex demonstrated the first example of a linear, symmetrically triply-bridging methyl isocyanide. The μ_3-η^1 mode of isocyanide binding was unprecedented in both cluster chemistry and on metal surfaces. Muetterties found that methyl isocyanide absorbs on nickel surfaces by binding in an η^2 fashion, with considerable interaction between the isocyanide nitrogen atom and the metal surface.[2] Several clusters of the type $M_3(\mu\text{-dppm})_3$ (M = Pd,[4] Pt,[5] Cu,[6] Ag[7]) with planar triangular frameworks are known. The coordination chemistry at the triply-bridging site of the complex $[Pd_3(\mu_3\text{-CO})(dppm)_3]^{2+}$ has been investigated.[3] Our studies of the reactivity of complex **1** were hampered by the instability of the trinickel core. Therefore, in an effort to further stabilize the trinickel core of **1**, an additional diphosphine (dppm) was used to bridge the third side of the Ni_3 triangle.

$$[Ni_3(\mu_3\text{-CNMe})(\mu_3\text{-I})(CNMe)_2(dppm)_2]^+ + dppm \quad (1)$$

$$\xrightarrow[\text{vacuum}]{} [Ni_3(\mu_3\text{-CNMe})(\mu_3\text{-I})(dppm)_3]^+ + 2\,CNMe. \quad (2)$$

EXPERIMENTAL

The ligand dppm (0.19 g, 0.496 mmol) was added to a stirred solution of **1** (0.5 g, 0.496 mmol) in 50 cm^3 of acetonitrile at ambient temperature. The resulting solution was refluxed for 36 h with occasional purging of the apparatus with N_2(g) to aid in the removal of volatile CNMe. The solvent and any remaining free CNMe were then removed *in vacuo* and the crude product was recrystallized from CH_2Cl_2–pentane. The resulting crystals were then washed with a small amount of CH_3CN (5 cm^3), Et_2O (30 cm^3), and dried *in vacuo*. Yield 0.71 g, 84%.

NMR (CD_2Cl_2): ^1H (300 MHz) 4.01 ppm, 4.08 ppm (doublets, 6H, $PPh_2PC\mathit{H}_2PPh_2$), 4.25 ppm (s, 3H, $CNC\mathit{H}_3$), 6.8–7.3 ppm (m, 60H, Ph); $^{31}P\{^1H\}$ (89 MHz) 0.02 ppm (s). IR(KBr) ν(CN) = 1922 cm^{-1}.

* Author to whom correspondence should be addressed. Research Fellow of the Alfred P. Sloan Foundation, 1987–1991.

Crystals of **2** were obtained from CH_2Cl_2–pentane and contained one molecule of CH_2Cl_2 per unit cell. $I_2Ni_3Cl_2P_6NC_{78}H_{71}$, F.W. = 1709.13, monoclinic, $C2/c$, $a = 35.602(7)$, $b = 19.991(3)$, $c = 23.665(7)$ Å, $\beta = 120.10(1)°$, $V = 14571(1)$ Å^3, $Z = 8$, $d_c = 1.558$ g cm^{-3}, $\mu = 18.56$ cm^{-1} for Mo-K_α radiation ($\lambda = 0.71073$ Å). Intensity data: Enraf–Nonius CAD4 diffractometer, 9861 unique reflections. The structure of **2** was solved using the structure solution program SHELX-86 and refined by full-matrix least-squares using 5627 reflections with $I \geqslant 3.0\sigma(I)$. The final residuals were $R = 0.038$ and $R_w = 0.044$.

RESULTS AND DISCUSSION

The reaction of **1** with dppm under refluxing conditions affords **2** in excellent yield. An ORTEP of **2** is shown in Fig. 1. The molecule consists of a strongly bonding triangular nickel core with d(Ni—Ni)$_{av}$ = 2.41(2) Å. Each side of the nickel triangle is bridged by one dppm to form a nearly planar $[Ni_3L_6]^{2+}$ core. The triangle is capped by an iodide on one face of the nickel triangle. The most significant feature of the structure is the linear, symmetrically triply-bridging methyl isocyanide on the other face of the nickel triangle. A skeletal view of the $[Ni_3(\mu_3\text{-CNMe})(\mu_3\text{-I})]^+$ core with selected bond distances and bond angles is shown in Fig. 2. Aside from our earlier report of **1**, only one other claim of a symmetrically-bridged μ_3-η^1 isocyanide exists. Fortune and co-workers have described the complex $Co_3(C_5H_5)_3(\mu_3\text{-CNC}_6H_{11})(\mu_3\text{-S})$ (**3**) which

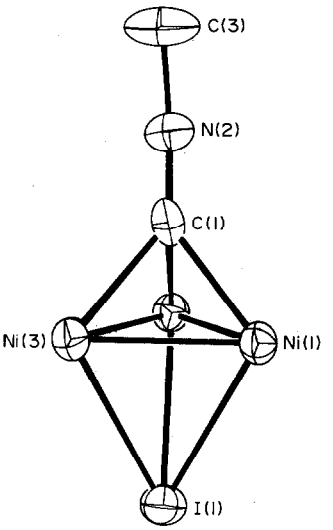

Fig. 2. Skeletal view of **2** with selected bond distances (Å) and bond angles (°): Ni(1)—Ni(2), 2.431(1); Ni(1)—Ni(3), 2.395(1); Ni(2)—Ni(3), 2.432(1); Ni(1)—C(1), 2.020(9); Ni(2)—C(1), 1.995(9); Ni(3)—C(1), 2.016(9); C(1)—N(2), 1.17(1); N(2)—C(3), 1.40(1); ∠C(1)—N(2)—C(3), 164.6(9).

was refined crystallographically to $R = 0.092$ and $R' = 0.120$. Complex **3** shows no apparent interaction between the nitrogen atom of the isocyanide and the triangular cobalt cluster.[7] However, the μ-isocyanide of **3** is significantly bent to angles of 141 and 129° for the two independent isomers refined. The π^* orbitals of a truly symmetric μ_3-η^1 iso-

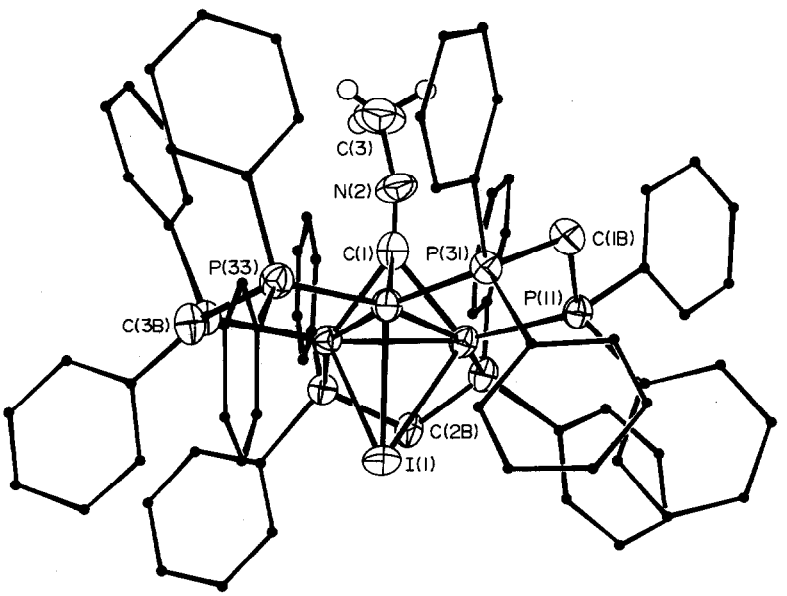

Fig. 1. ORTEP drawing of $[Ni_3(\mu_3\text{-CNMe})(\mu_3\text{-I})(dppm)_3]^+$ (**2**).

cyanide are degenerate and thus no bending should occur. The trinuclear nickel clusters, **1** and **2**, thus represent the only genuine examples of symmetric μ_3-η^1 isocyanide binding to metal clusters.[1] Complexes **1** and **2** are unique since there are no interactions between the nitrogen atom of the isocyanide and the metal clusters; and the bonding between the nickel triangles and the π^* orbitals of the isocyanides is sufficiently symmetric that no significant bending of the isocyanide occurs, $\angle$CNC = 164.6(9) for **2**. The IR spectrum of **2** reveals $\nu(\mu$-CN) = 1922 cm^{-1}, which is 20 cm^{-1} lower in energy than $\nu(\mu$-CN) = 1942 cm^{-1} for **1** and over 200 cm^{-1} higher than $\nu(\mu$-CN) = 1700 cm^{-1} for CNMe on the Ni(111) surface.[8] The unusually high energies of the CN stretching frequencies indicate that the out-of-plane *d* orbitals of the Ni_3 triangle do not interact extensively with the π^* orbitals of the isocyanide. Electrochemical studies reveal a reversible 1e$^-$ reduction of the Ni_3^{2+} core of complex **2** at $E = -1.07$ V vs Ag/AgCl. Chemical, electrochemical and theoretical studies of these unusual μ_3-η^1 isocyanide clusters are continuing.

Supplementary materials available: Atomic coordinates have been deposited with the Director, Cambridge Crystallographic Data Centre.

Acknowledgements—This work was supported by NSF (CHE-8707963). We are also grateful to NSF for support of the Chemical X-ray Diffraction Facility at Purdue.

REFERENCES

1. K. S. Ratliff, G. K. Broeker, P. E. Fanwick and C. P. Kubiak, *Angew. Chem. Int. Edn Engl.* 1990, **29**, 395.
2. E. L. Muetterties, *New Horizons in Catalysis: Proceedings of the 7th International Congress on Catalysis*, Tokyo, 30 June–4 July 1980, p. 36.
3. L. M. Muir, K. W. Muir, B. R. Lloyd and R. J. Puddephatt, *J. Chem. Soc., Chem. Commun.* 1983, 1336.
4. G. Ferguson, B. R. Lloyd and R. J. Puddephatt, *Organometallics* 1986, **5**, 344.
5. D. M. Ho and R. Bau, *Inorg. Chem.* 1983, **22**, 4079.
6. A. A. M. Aly, D. Neugebauer, O. Orama, U. Schubert and H. Schmidbaur, *Angew. Chem. Int. Edn Engl.* 1978, **17**, 125.
7. J. Fortune, A. R. Manning and F. S. Stephens, *J. Chem. Soc., Chem. Commun.* 1983, 1071.
8. C. M. Friend, E. L. Muetterties and J. L. Gland, *J. Phys. Chem.* 1981, **85**, 3256.

Polyhedron Vol. 9, No. 12, pp. 1491–1495, 1990
Printed in Great Britain

0277-5387/90 $3.00+.00
© 1990 Pergamon Press plc

SYNTHESIS AND CRYSTAL STRUCTURE OF A TETRANUCLEAR MIXED-METAL ALKYLIDENE COMPLEX $CpWOs_3(CO)_9(\mu\text{-}O)(\mu\text{-}H)(\mu\text{-}CHTol)$

SHIE-MING PENG*† and GENE-HSIANG LEE

Department of Chemistry, National Taiwan University, Taipei 10764, Taiwan, R.O.C.

and

YUN CHI*

Department of Chemistry, National Tsing Hua University, Hsinchu 30043, Taiwan, R.O.C.

(*Received* 21 *November* 1989; *accepted* 27 *February* 1990)

Abstract—The solid-state structure of a tetranuclear mixed-metal cluster $CpWOs_3(CO)_9(\mu\text{-}O)(\mu\text{-}H)(\mu\text{-}CHTol)$ (**2**) which possesses a bridging hydride, a bridging oxo and a bridging tolylalkylidene ligand is presented. Complex **2** crystallizes in the triclinic space group $P\bar{1}$, with $a = 9.763(5)$, $b = 10.759(4)$, $c = 13.336(3)$ Å, $\alpha = 88.00(3)$, $\beta = 108.56(3)$, $\gamma = 100.44(3)°$, $Z = 2$; 3463 observed reflections with $I > 3\sigma(I)$ were used in the refinement. The R values converged to $R_F = 0.057$, $R_w = 0.058$.

The reactivity of mixed-metal clusters has been of interest for many years.[1] Research in this area is stimulated by a belief that the combination of metals having very different chemical properties within one compound may induce unique chemical transformations. In seeking to develop a systematic way to prepare the mixed-metal clusters of higher nuclearity, Stone and co-workers have used $Cp(CO)_2W{\equiv}CR$ as a building block to prepare many mixed-metal clusters containing a bridging alkylidyne fragment.[2] As the number of the mixed-metal alkylidyne clusters has increased dramatically in the past few years, there is increasing interest in examining the chemistry of the alkylidyne clusters because of the possible roles of the alkylidynes as reaction intermediates in, and/or models of various catalytic processes.[3] In the present study we have explored the hydrogenation of a tetrahedral mixed-metal alkylidyne complex $CpWOs_3(CO)_9(\mu_3\text{-}CTol)_2(\mu\text{-}H)$ (**1**)[4] which produces an alkylidene complex $CpWOs_3(CO)_9(\mu\text{-}O)(\mu\text{-}H)(\mu\text{-}CHTol)$ (**2**) in low yield (Scheme 1). The single-crystal X-ray diffraction study on complex **2** suggests that its gross geometry and ligand configuration are complementary to those of the related, structurally characterized WOs_3 clusters $CpWOs_3(CO)_9(\mu\text{-}O)(\mu\text{-}H)(\mu\text{-}CHCH_2Tol)$ (**3**)[5] and $CpWOs_3(CO)_9(\mu\text{-}O)(\mu\text{-}Cl)(\mu\text{-}CHCH_2Tol)$ (**4**)[6] (Scheme 2).

RESULTS AND DISCUSSION

Hydrogenation of complex **1** in refluxing xylenes solution (1 atm, 6 h) produced an orange–brown solution. The solvent was removed *in vacuo* and the product purified by thin-layer chromatography (TLC), giving an orange product in low yield. The mass spectrum indicates a parent ion at m/z 1198, corresponding to a composition $C_{22}H_{14}O_{10}Os_3W$. The ^{13}C NMR spectrum ($CDCl_3$, 100.6 MHz, 213 K) exhibits nine Os—CO signals at δ 194.5, 184.4, 181.4, 180.9, 176.4, 173.2, 169.9, 169.7, 169.1 and the ^1H NMR spectrum ($CDCl_3$, 400 MHz, 294 K) shows two singlets at δ 5.52 and −18.05, in addition to signals corresponding to one Cp ligand and one tolyl fragment. The IR spectrum (C_6H_{12}) in the carbonyl region shows absorption bands at 2090(s), 2965(vs), 2028(vs), 2020(vs), 2014(s), 2007(m),

* Authors to whom correspondence should be addressed.
† To whom inquiries concerning the X-ray crystallographic work should be addressed.

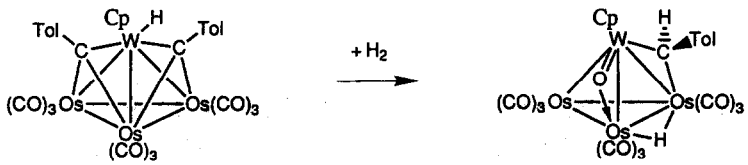

(1) (2)

Scheme 1.

1991(w), 1958(w), 1940(m) cm^{-1}, indicating that the molecule is analogous to the recently reported dioxo cluster $CpWOs_3(CO)_9(\mu\text{-}O)_2(\mu\text{-}H)$.[7] Based on these spectroscopic data, a formulation $CpWOs_3(CO)_9(\mu\text{-}O)(\mu\text{-}H)(\mu\text{-}CHTol)$ is proposed for this complex. The exact source of the oxo ligand in **2** and the fate of the second alkylidyne in **1** are unknown. However, based on reports in the literature, we speculate that the oxo ligand may be derived from a CO ligand by C—O bond scission or from other possible sources (O_2 or H_2O)[8] in the solution and that the alkylidyne may be eliminated as a *para*-xylene molecule.[9]

The molecular structure of **2** was determined by a single-crystal X-ray diffraction study. The ORTEP diagram and the scheme used for labelling the atoms are shown in Fig. 1. The bond distances and angles are listed in Tables 1 and 2, respectively. The molecule consists of one tungsten atom and three osmium atoms which define a tetrahedral core associated with the expected 60 outer valence electrons. The tungsten atom is coordinated to a Cp, a bridging oxo and a bridging alkylidene ligand, whereas each of the three basal osmium atoms is associated with three terminal CO ligands arranged in a pseudo-octahedral geometry.

The oxo ligand O(10) bridges the W—Os(2) edge and the W—O(10)—Os(2) interaction is characterized by the short tungsten–oxygen bond distance (W—O(1) = 1.77 Å), the comparatively long Os(2)—O(10) bond length (2.13 Å) and the small W—O(10)—Os(2) angle (94.6°). These data are compatible with the parameters for the typical W=O→Os bonding interaction as has been found previously in the related WOs_3 complexes.[10] In addition, there is also a doubly bridging alkylidene ligand (μ-CHTol) which is associated with the second W—Os edge of the triangular face defined by the atoms W, Os(1) and Os(2). The W—C(22) distance (2.08 Å) is slightly shorter than the Os(1)—C(22) distance (2.24 Å) and the tolyl substituent is oriented toward the bridging oxo ligand. Finally, the structurally undetermined bridging hydride ligand is proposed to be associated with the third Os—Os edge of this WOs_2 triangle. Consistent with our postulate, this metal–metal vector displays a relatively large Os(1)—Os(2) distance (2.997 Å) and possesses two enlarged Os—Os—CO angles (113–114°) and two regular Os—Os—CO angles (89–94°). The other two Os—Os distances within the molecule are slightly smaller, with Os(1)—Os(3) = 2.844(2) and Os(2)—Os(3) = 2.846(2) Å. After the position of the bridging hydride ligand is established, the formal electron counts for the W, Os(1), Os(2) and Os(3) atoms are calculated to be 17, 18.5, 19.5 and 17e^-, respectively.

The structure of **2** is different from those of the analogous hydrido-alkylidene complex **3** and the chloro-alkylidene complex **4** in terms of the location of the bridging hydride and the configuration of the bridging alkylidene ligand (Scheme 2). In complex **3**, the bridging hydride is located on the Os—Os edge eclipsed to the W—Os edge which is associated with the alkylidene fragment; therefore, the metal–metal edges supporting the bridging hydride, oxo and alkylidene ligands are aligned in a zigzag

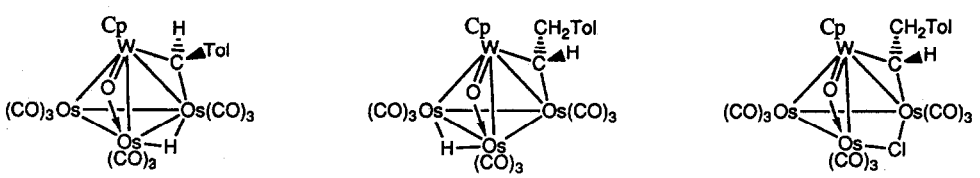

(2), anti (3), syn (4), syn

Scheme 2.

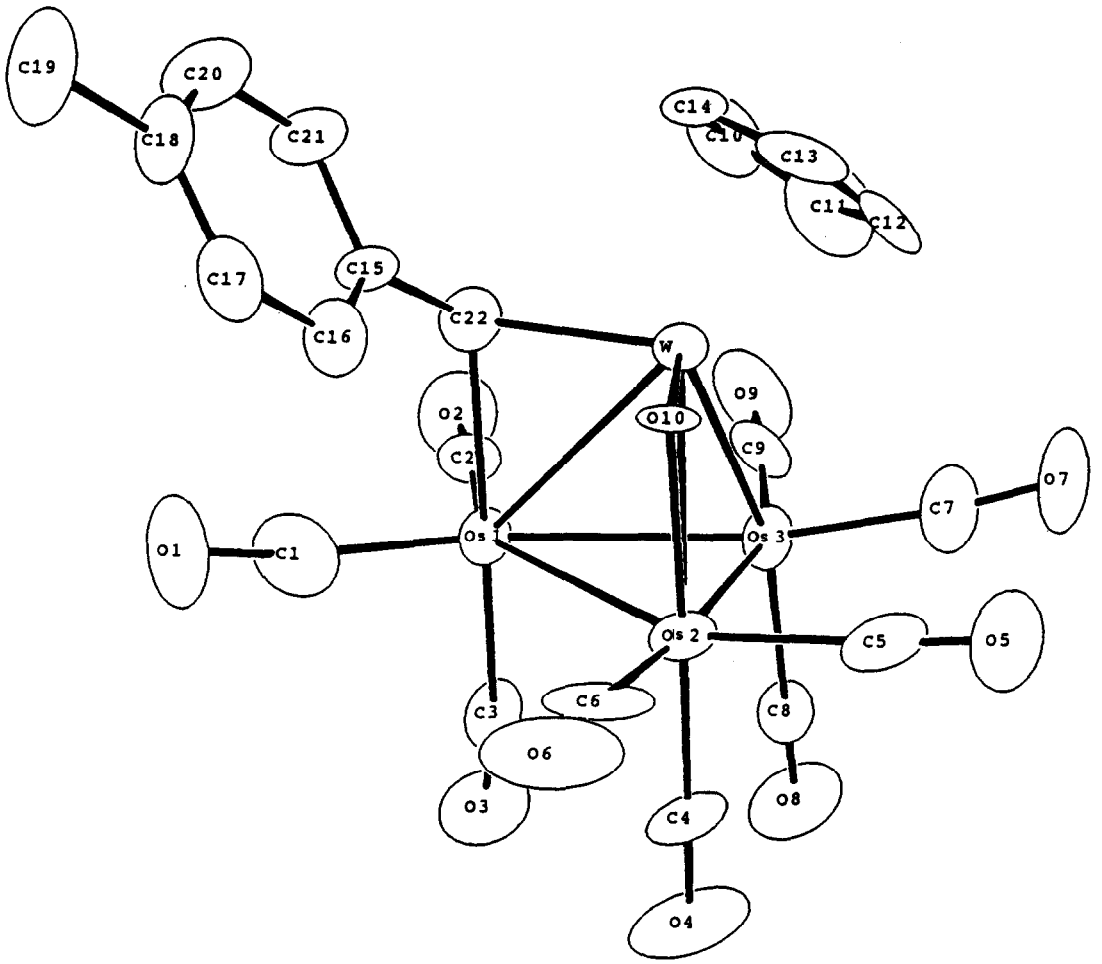

Fig. 1. The molecular structure of $CpWOs_3(CO)_9(\mu\text{-}O)(\mu\text{-}H)(\mu\text{-}CHTol)$ (**2**) showing the atomic numbering scheme.

Table 1. Selected interatomic distances (Å) of complex **2** (ESADs in parentheses)

Os(1)—Os(2)	2.977(2)	Os(1)—Os(3)	2.844(2)
Os(2)—Os(3)	2.846(2)	W—Os(1)	2.857(2)
W—Os(2)	2.874(2)	W—Os(3)	2.629(2)
W—O(10)	1.77(2)	Os(2)—O(10)	2.13(2)
W—C(22)	2.08(2)	Os(1)—C(22)	2.24(2)
Os(1)—C(1)	1.92(3)	Os(1)—C(2)	1.95(3)
Os(1)—C(3)	1.96(3)	Os(2)—C(4)	1.86(3)
Os(2)—C(5)	1.94(3)	Os(2)—C(6)	1.68(4)
Os(3)—C(7)	1.87(3)	Os(3)—C(8)	1.95(3)
Os(3)—C(9)	1.80(3)	C(1)—O(1)	1.13(3)
C(2)—O(2)	1.08(4)	C(3)—O(3)	1.10(4)
C(4)—O(4)	1.11(4)	C(5)—O(5)	1.15(3)
C(6)—O(6)	1.30(5)	C(7)—O(7)	1.17(3)
C(8)—O(8)	1.08(4)	C(9)—O(9)	1.19(4)
W—C(10)	2.34(4)	W—C(11)	2.39(4)
W—C(12)	2.35(2)	W—C(13)	2.37(3)
W—C(14)	2.31(3)	C(22)—C(15)	1.53(3)

arrangement. In contrast, the bridging chloro ligand of complex **4** is located at a position similar to that of the bridging hydride in complex **2**; therefore, the respective metal–metal edges are arranged in a triangular pattern. In addition, because the bridging chloro ligand is a three-electron-donor, the bond distance between the osmium atoms linked by chloro ligand is not in the range of a typical Os—Os single bond.

On the other hand, the α-hydrogen of the alkylidene ligand in both complexes **3** and **4** is oriented toward the bridging oxo ligand; therefore, the configuration of the bridging alkylidene (denoted as *syn*) is in contrast to that of complex **2** (denoted as *anti*). We propose that the formation of the *anti* configuration for complex **2** is due to its greater thermodynamic stability with respect to the unobserved *syn* configuration, and the latter is destabilized because of the unfavourable steric repulsion between the tolyl substituent and the Cp ligand.

Table 2. Selected bond angles (°) of complex **2** (ESADs in parentheses)

W—Os(1)—Os(2)	58.98(4)	W—Os(2)—Os(1)	58.43(4)
Os(1)—W—Os(2)	62.58(4)	W—Os(1)—Os(3)	54.91(4)
W—Os(3)—Os(1)	62.79(4)	Os(1)—W—Os(3)	62.29(4)
W—Os(2)—Os(3)	54.72(5)	W—Os(3)—Os(2)	63.17(5)
Os(2)—W—Os(3)	62.11(5)	Os(1)—Os(2)—Os(3)	58.42(4)
Os(2)—Os(3)—Os(1)	63.08(5)	Os(3)—Os(1)—Os(2)	58.49(4)
Os(1)—C(1)—O(1)	172(3)	Os(1)—C(2)—O(2)	178(2)
Os(1)—C(3)—O(3)	172(3)	Os(2)—C(4)—O(4)	177(4)
Os(2)—C(5)—O(5)	176(3)	Os(2)—C(6)—O(6)	169(3)
Os(3)—C(7)—O(7)	174(3)	Os(3)—C(8)—O(8)	175(4)
Os(3)—C(9)—O(9)	178(2)	Os(1)—C(22)—W	82.7(8)
W—Os(1)—C(22)	46.3(5)	Os(1)—W—C(22)	51.1(6)
Os(2)—O(10)—W	94.6(7)	Os(2)—W—O(10)	47.5(5)
W—Os(2)—O(10)	37.9(5)	W—C(22)—C(15)	119(2)
Os(1)—C(22)—C(15)	123(2)	Os(1)—Os(2)—C(4)	94.4(9)
Os(1)—Os(2)—C(6)	113(1)	Os(2)—Os(1)—C(1)	114(1)
Os(2)—Os(1)—C(3)	89(1)		

EXPERIMENTAL

IR spectra were recorded using a Perkin–Elmer 580 spectrometer calibrated using the absorption of cyclohexane at 2138.5 cm^{-1} and the absorption of polystyrene film at 1944.5 cm^{-1}. Both ^1H and ^{13}C NMR spectra were recorded using a Bruker AM-400 instrument. Mass spectra were obtained on a JEOL-HX110 instrument operating in electron impact, field desorption or fast atom bombardment modes. All reactions were performed under a nitrogen atmosphere using deoxygenated solvents dried with an appropriate reagent. The progress of reactions was monitored by analytical TLC (5735 Kieselgel 60 F_{254}, E. Merck) and the products were separated on the commercially available preparative TLC plates (Kieselgel 60 F_{254}, E. Merck). The mixed-metal complexes $CpWOs_3(CO)_9(\mu_3\text{-}CTol)_2(\mu\text{-}H)$ (**1**) were prepared according to the literature method.[4]

Preparation of $CpWOs_3(CO)_9(\mu\text{-}O)(\mu\text{-}H)(\mu\text{-}CHTol)$ (**2**)

A xylene solution (45 cm^3) of $CpWOs_3(CO)_9(\mu_3\text{-}CTol)_2(\mu\text{-}H)$ (**1**) (56 mg, 0.043 mmol) was heated at reflux under 1 atm of hydrogen. After refluxing for 6 h, the solvent was evaporated *in vacuo* and the residue was separated on a preparative TLC plate (hexane–dichloromethane, 3:2), giving the alkylidene complex **2** (6 mg, 0.005 mmol, 12%) as red–orange crystals after recrystallization from dichloromethane–methanol. In addition, some starting materials (10 mg, 0.008 mmol, 18%) were also recovered from the residue of the reaction mixture.

Spectroscopic data for complex **2**. MS (EI, ^{192}Os, ^{184}W), *m/z* 1198(M^+); IR(C_6H_{12}): ν(CO), 2090(s), 2065(vs), 2028(vs), 2020(vs), 2014(s), 2007(m), 1991(w), 1958(w), 1940(m) cm^{-1}; ^1H NMR (400 MHz, $CDCl_3$, 294 K): δ 7.05–6.45 (m, 4H), 5.94 (s, 5H), 5.52 (s, 1H), 2.39 (s, 3H), −18.05 (s, 1H); $^{13}C\{H\}$ NMR (100.4 MHz, $CDCl_3$, 213 K): Os—CO, δ 194.5, 184.4, 181.4, 180.9, 176.4, 173.2, 169.9, 169.7, 169.1.

Structural determination of complex **2**

Crystals suitable for diffraction analysis were obtained from a dichloromethane–methanol solution. A crystal was mounted on a glass fibre. Diffraction measurements were carried out on a Nonius CAD-4 fully automated four-circle diffractometer. The unit cell was determined and refined using setting angles of 25 randomly selected reflections, with 2θ angles in the range of 2.5–50°, obtained by using the CAD-4 automatic search, centre, index and least-squares routines. All data reduction and structure refinement were performed using the NRCC-SDP-VAX packages. The structure was solved by the Patterson method and refined by least-squares; all non-hydrogen atoms were refined with anisotropic thermal parameters. The data collection parameters are summarized in Table 3. Tables of atomic coordinates, anisotropic thermal parameters, structure factor amplitudes, and non-essential bond distance and angle parameters have been deposited as supplementary data and are available from the authors (S.M.P.).

Table 3. Experimental data for the X-ray diffraction study of complex **2**

(A) *Crystal data*	
a (Å)	9.763(5)
b (Å)	10.759(4)
c (Å)	13.336(3)
α (°)	88.00(3)
β (°)	108.56(3)
γ (°)	100.44(3)
$F(000)$	1056
Temperature (K)	297
Crystal system	Triclinic
Space group	$P\bar{1}$
Z	2
Formula	$C_{22}H_{14}O_{10}Os_3W_1$
V (Å^3)	1305.6(9)
Molecular weight	1192.8
Density (calc.) (g cm^{-3})	3.034
(B) *Data collection, reduction, solution and refinement*	
Data collection instrument	Nonius CAD-4
Radiation (monochromated in incident beam)	Mo-K_α (λ = 0.71073 Å)
Scan method	2θ–θ scan mode
Scan range	$0.65+0.35\tan\theta$
Scan speed	Variable; 1.10–8.24°/min
Crystal size (mm)	$0.25\times0.40\times0.40$
Linear absorption coefficient (mm^{-1})	19.10
Transmission factors: max, min.	0.99, 0.55
Number of unique data, total with $I > 3\sigma(I)$	4574, 3463
Number of atoms and parameters refined	36, 326
Largest and mean Δ/σ	0.228, 0.001
R; R_w[a] (%)	5.7; 5.8
G.O.F.[b]	3.71
Residual electron density (e Å^{-3}): max./min.	4.43/−2.88

[a] $w^{-1} = \sigma^2(F)$.

[b] $S = [\Sigma w|F_o - F_c|^2/(N_o - N_v)]^{1/2}$ (N_o = number of observations; N_v = number of variables).

REFERENCES

1. D. A. Roberts and G. L. Geoffroy, in *Comprehensive Organometallic Chemistry* (Edited by G. Wilkinson, F. G. A. Stone and E. W. Abel), Vol. 6, Ch. 40. Pergamon Press, Oxford (1982).
2. (a) F. G. A. Stone, in *Inorganic Chemistry: Toward the 21st Century* (Edited by M. H. Chisholm), ACS Symp. Ser. No. 211, p. 383. American Chemical Society, Washington, D.C. (1983); (b) S. J. Davies, J. A. K. Howard, R. J. Musgrove and F. G. A. Stone, *Angew. Chem. Int. Edn Engl.* 1989, **28**, 624 and refs cited therein.
3. (a) E. L. Muetterties and J. Stein, *Chem. Rev.* 1979, **79**, 479; (b) L. R. Beanan and J. B. Keister, *Organometallics* 1985, **4**, 1713.
4. (a) J. T. Park, J. R. Shapley, C. Bueno, J. W. Ziller and M. R. Churchill, *Organometallics* 1988, **7**, 2307; (b) J. T. Park, J. R. Shapley, M. R. Churchill and C. Bueno, *J. Am. Chem. Soc.* 1983, **105**, 6182.
5. M. R. Churchill and Y. J. Li, *J. Organomet. Chem.* 1985, **291**, 61.
6. Y. Chi, J. R. Shapley, J. W. Ziller and M. R. Churchill, *Organometallics* 1987, **6**, 301.
7. Y. Chi, L.-S. Hwang, G.-H. Lee and S.-M. Peng, *J. Chem. Soc., Chem. Commun.* 1988, 1456.
8. M. R. Churchill, C. Bueno, J. T. Park and J. R. Shapley, *Inorg. Chem.* 1984, **23**, 1017.
9. (a) J. B. Keister, *J. Chem. Soc., Chem. Commun.* 1979, 214; (b) G. Fachinetti, R. Lazzaroni and S. Pucci, *Angew. Chem. Int. Edn Engl.* 1981, **20**, 1063; (c) J. B. Keister, M. W. Payne and M. J. Muscatella, *Organometallics* 1983, **2**, 219.
10. M. R. Churchill and Y. J. Li, *J. Organomet. Chem.* 1985, **294**, 367.

Polyhedron Vol. 9, No. 12, pp. 1497–1502, 1990
Printed in Great Britain

0277–5387/90 $3.00+.00
Pergamon Press plc

COMMUNICATION

DEVELOPMENT OF NEW TECHNETIUM CORES CONTAINING TECHNETIUM–NITROGEN MULTIPLE BONDS. SYNTHESIS AND CHARACTERIZATION OF SOME DIAZENIDO-, HYDRAZIDO- AND IMIDO- COMPLEXES OF TECHNETIUM

C. M. ARCHER, J. R. DILWORTH,* P. JOBANPUTRA and R. M. THOMPSON

Department of Chemistry and Biological Chemistry, University of Essex, Wivenhoe Park, Colchester, Essex CO4 3SQ, U.K.

and

M. McPARTLIN

School of Chemistry, Polytechnic of North London, Holloway Road, London N7 8DB, U.K.

and

D. C. POVEY and G. W. SMITH

Department of Chemistry, University of Surrey, Guildford, Surrey GU2 5XH, U.K.

and

J. D. KELLY

Amersham International plc, White Lion Road, Amersham, Buckinghamshire HP7 9LL, U.K.

(*Received* 29 *March* 1990; *accepted* 26 *April* 1990)

Abstract—The syntheses of several novel diazenido-, hydrazido- and imido- complexes of technetium are described. These precursors which contain technetium–nitrogen multiple bonds are derived directly from the appropriate organohydrazine or amine in good yield. Some of the chemistry has been extended to the metastable isotope ^{99m}Tc (γ, $t_{1/2}$ = 6 h) in highly dilute aqueous media to give single species in high radiochemical purity. These preparations are applicable to the synthesis of new technetium radiopharmaceuticals and should provide for the development of a whole new range of technetium-based diagnostic agents in nuclear medicine.

The development of the basic coordination chemistry of the synthetic radioactive element technetium has undergone a revolution in recent years owing to its expanding application in the diagnostic imaging of internal organs by γ-scintillation detection.[1,2] The combination of reasonable cost, extensive availability and optimal nuclear properties makes technetium-99m the radionuclide of choice for many applications in nuclear medicine.[1,2] Typical requirements for technetium complexes to be clinically useful radiopharmaceuticals are ease of preparation (to give a single radiochemically-pure

* Author to whom correspondence should be addressed.

Abbreviations: dppe, 1,2-bis(diphenylphosphino)ethane; dmpe, 1,2-bis(dimethylphosphino)ethane; depe, 1,2-bis(diethylphosphino)ethane; Ar, generalized aryl substituent.

product), stability (under biological conditions), controllable overall charge (oxidation state) and redox properties, and useful biodistribution properties.[3] The biological targeting ability of such γ-emitting technetium species depends largely on the physical or metabolic properties of its coordinated ligands, which cause the complex to locate in a particular organ after intravenous injection.[1-4] The development of new technetium chemistry and subsequently the design of new or improved radiopharmaceutical reagents therefore depends crucially on the availability of both new ligand systems and new technetium central core moieties.

The chemistry of technetium in its higher and intermediate oxidation states is dominated by its tendency to form oxo-species. Indeed, several of the currently used clinical reagents are coordination compounds of the mono-oxo- $[Tc^{V}{=}O]^{3+}$ and dioxo- $[O{=}Tc^{V}{=}O]^{+}$ cores, and these are used to image all the major organs including kidney, liver, heart and brain.

Potential alternative cores for technetium are the nitrosyl moiety $[TcNO]^{4}$ and *trans*-$[Tc^{III}Cl_2]^{+}$,[3] but these are not currently utilized in any commercial radiopharmaceuticals. Baldas and Bonnyman[5] have reported the facile synthesis of the robust nitrido-moiety [Tc≡N], and demonstrated its ability to undergo various ligand substitution reactions. However, there have been few reports of derivatives of this core of potential use as imaging agents. We report here the synthesis of several novel ^{99}Tc precursors containing Tc—N multiple bonds (Fig. 1). These include mono- and bis-diazenido-, hydrazido(2−)- and imido- species. Some of this chemistry has been successfully extended to the metastable isotope ^{99m}Tc (γ emitter = 140 keV, $t_{1/2}$ = 6 h) in highly dilute (*ca* 10^{-8} M) aqueous media to give single compounds in high radiochemical purity. These novel technetium cores with their chemically robust metal–nitrogen bonds in combination with appropriate ancillary ligands to control biological targeting characteristics offer a whole new range of possibilities for the development of technetium-based diagnostic agents.

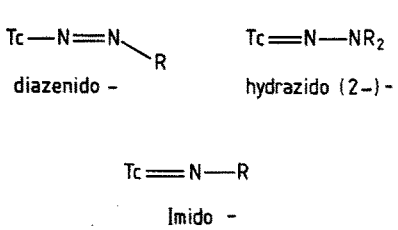

Fig. 1. New core moieties for technetium radiopharmaceuticals.

TECHNETIUM DIAZENIDO- COMPLEXES

Monosubstituted organodiazenido ligands, M—N=NR, may adopt several different bonding modes in transition metal complexes (Fig. 2).[6] The singly bent geometry (**I**) is the most common structure found. The doubly bent geometry (**II**) and bridging mode (**III**) are much less common. We have previously reported the synthesis and characteristics of the rhenium bis(diazenido)- complexes, $[ReCl(N_2Ar)_2(PPh_3)_2]$.[7] These rhenium(III) bis(diazenido)- complexes are easily protonated or alkylated at the β-nitrogen of one of the coordinated diazenido- ligands to give the rhenium(V) diazenido–hydrazido- complexes, $[ReCl_2(NNAr)(NNHAr)(PPh_3)_2]$, in quantitative yield. The complex with Ar = C_6H_5— was structurally characterized and shown to contain a linear (three-electron donor) diazenido- ligand and a bent (two-electron donor) hydrazido(2−)- ligand.[7]

Reaction of $[n\text{-}Bu_4N][TcOCl_4]$ with excess arylhydrazine and PPh_3 in alcohol gives air-stable, orange, crystalline $[TcCl(N_2Ar)_2(PPh_3)_2]$ complexes in 70–80% yield. These are entirely analogous to the rhenium complexes, $[ReCl(N_2Ar)_2(PPh_3)_2]$,[7] and HPLC analysis indicates that these technetium species form in > 95% yield in solution. They are diamagnetic five-coordinate technetium(III) d^4 compounds. The ^{31}P NMR spectrum exhibits a singlet consistent with a *trans*-arrangement of PPh_3 groups. A trigonal bipyramidal structure with *cis*-diazenido ligands in the equatorial plane is proposed by analogy with the known rhenium structure.[8] This has very recently been verified by the independent structural characterization of $[TcCl(NNC_6H_4Br)_2(PPh_3)_2]$.[9] These workers also investigated the facile protonation at N_β of these species,[9] which we demonstrated earlier for the $[ReCl(N_2Ar)_2(PPh_3)_2]$ complexes.[7] We have now shown that the chlorido and phosphine ligands may be displaced by a range

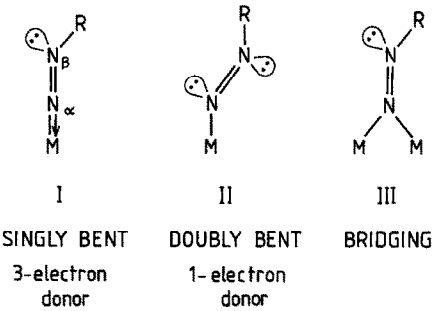

Fig. 2. Formal bonding modes for transition metal organodiazenido- complexes.

of other ligands to give new technetium(III) mono- and bis-diazenido- complexes. Indeed, subsequent reaction of $[TcCl(N_2Ar)_2(PPh_3)_2]$ with P—P (P—P = dppe, dmpe) under reflux in alcohol gives orange–yellow $[TcCl(N_2Ar)(P—P)_2]^+$ in high (70%) yield with loss of one $—N_2Ar$ ligand. HPLC analysis indicates that these species comprise > 95% of the reaction product in solution. These synthetic reactions can also be carried out directly from TcO_4^- in high yield and this chemistry has been extended to the ^{99m}Tc level. The monodiazenido- complex with Ar = C_6H_5— and P—P = dppe has been structurally characterized (Fig. 3) as its PF_6-salt.* This complex cation has slightly distorted *trans*-octahedral coordination geometry. Equatorial sites are occupied by phosphorus donor atoms of the two bidentate dppe ligands. The phenyldiazenido- and chlorido-ligands occupy the *trans*-axial sites. The diazenido-ligand is described as singly bent with an intermediate Tc—N_α—N_β angle of 162(2)° and is thus formally a three-electron donor.[6] The Tc—N bond length of 1.917(19) Å is much longer than that normally found for diazenido- complexes,[6] and may reflect the repulsive interaction with the four equatorial phosphorus atoms. This complex has the same overall structure as the isoelectronic technetium nitrosyl cation, $[TcCl(NO)(depe)_2]^+$.[10]

This behaviour of $[TcCl(N_2Ar)_2(PPh_3)_2]$ contrasts sharply with that of $[ReCl(N_2Ar)_2(PPh_3)_2]$ which reacts under similar conditions with bidentate phosphines to give the formally 20-electron rhenium(III) species $[Re(N_2Ar)_2(P—P)_2]^+$. The presence of two *trans*-diazenido-singly bent (formally three-electron donor) ligands bound to rhenium has been verified by the structural determination of the complex with Ar = $CH_3C_6H_4$— and P—P = dppe.[11]

TECHNETIUM HYDRAZIDO(2−)-COMPLEXES

1,1-Disubstituted organohydrazines (R_2NNH_2) may give rise to terminally bound hydrazido(2−)-ligands, M = NNR_2 (Fig. 4). These may also arise from the protonation or alkylation of N_β of organodiazenido- ligands.[6,12] Hydrazido(2−)- complexes are also proven intermediates in the protonation of coordinated dinitrogen to give ammonia.[13] The linear bonding mode (**IV**) M≡N—NR_2 is formally isoelectronic with the metal–oxo core, and there are

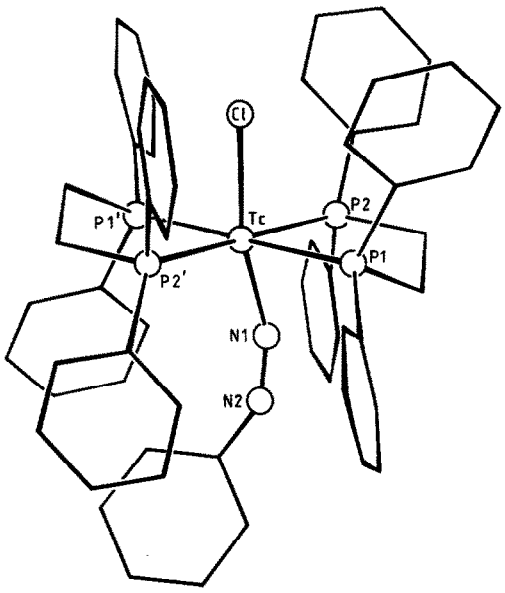

Fig. 3. Structural representation of the complex cation $[TcCl(NNC_6H_5)(dppe)_2]^+$.

many examples of essentially isostructural metal–oxo and metal–hydrazido(2−)- complexes.[14]

The addition of 1,1-disubstituted hydrazines to $[n\text{-}Bu_4N][TcOCl_4]$ in dry methanol gives a deep red solution which contains a single technetium-containing species (HPLC, β-detection). This species is tentatively presumed to be $[Tc(NNR_2)Cl_4]^-$. It is not easily characterized, but can be routinely generated *in situ* and further derivatized to give desired technetium hydrazido(2−)- products. Thus reaction of $[n\text{-}Bu_4N][TcOCl_4]$ with $MePhNNH_2$ in refluxing methanol with PPh_3 gives the technetium(V) species $[TcCl_3(NNMePh)(PPh_3)_2]$. Use of less bulky phosphines such as PMe_2Ph leads to the formation of the cationic species $[TcCl_2(NNMe$

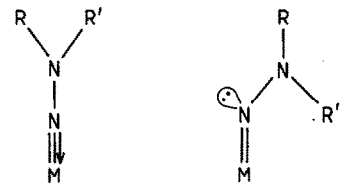

Fig. 4. Formal bonding modes of the terminally-bound hydrazido(2−)- moiety.

* Preliminary representations of all of the structures are given and full details will be reported at a later date.

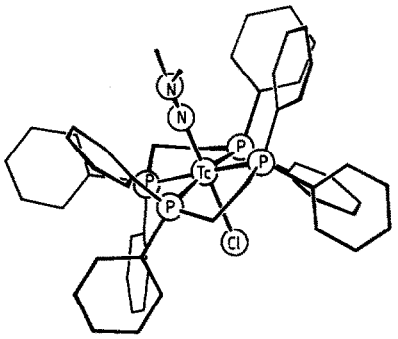

Fig. 5. Structural representation of the complex cation $[TcCl(NNMe_2)(dppe)_2]^+$.

Ph)$(PMePh)_3]^+$ in moderate yield. Excess hydrazine gives access to bis(hydrazido)- complexes believed to be analogous to the known rhenium complex $[ReCl_2(NNR_2)_2(PPh_3)]^+$.[15] Reaction of $[n\text{-}Bu_4N][TcOCl_4]$ with Me_2NNH_2 and dppe in methanol at room temperature gives good yields of the technetium(IV) cation $[TcCl(NNMe_2)(dppe)_2]^+$. This has been structurally characterized as its PF_6^- salt (Fig. 5). The synthetic chemistry is again easily extrapolated to ^{99m}Tc in high overall radiochemical purity.

Reactions of organohydrazines are notoriously dependent on reaction conditions,[6,12] and some unexpected products due to cleavage or loss of the hydrazido(2−)- moiety have been isolated. Thus, reaction of $[n\text{-}Bu_4N][TcOCl_4]$ with Me_2NNH_2 and dppe in methanol under reflux gives lower yields of the cationic $[TcCl(NNMe_2)(dppe)_2]^+$ together with a yellow neutral product, we believe to be

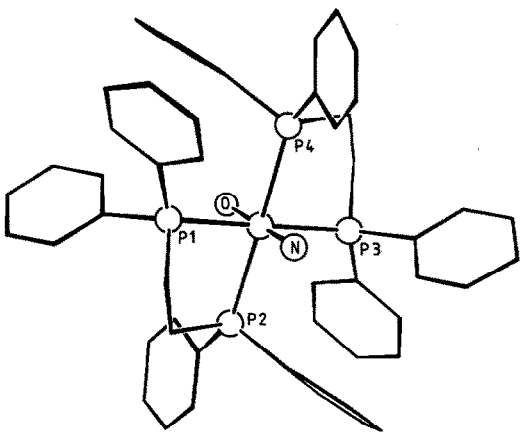

Fig. 6. Structural representation of the complex cation *trans*-$[TcO(NH)(dppe)_2]^+$.

$[TcCl(N_2)(dppe)_2]$, $\nu(N_2)$ 1980 cm^{-1}, which is not formed under argon. However, use of $MePhNNH_2$ and dppe in methanol under reflux yields *trans*-$[TcO(NH)(dppe)_2]^+$, which has the new oxo–imido-technetium(V) core moiety $[O{=}Tc^V{=}NH]^+$. This has also been confirmed by an X-ray structural analysis (Fig. 6). Although the structural data was better refined as a bis(imido)- complex $[Tc(=NH)_2]^+$, the marked asymmetry in the bonding of the two axial ligands and elemental analysis suggests that they should be assigned as oxo- and imido-, respectively.

TECHNETIUM IMIDO- COMPLEXES

The terminal imido(2−)- ligand is formally isoelectronic with the more common terminal oxo(2−)- group.[16] However, the imido- ligand is much more resistant to protic attack and rarely bridges between transition metal ions. The ligand may function formally as either a linear four-electron donor (**VI**) or as a bent two-electron donor (**VII**) where the M—N—C framework is generally about 140° and two electrons reside on the nitrogen (Fig. 7).[16] The R group is easily varied and derivatives with alkyl[12] and aryl[12] —COPh[17] and —SO_2Ph[18] are known. In the special case where R = NR_2' a dialkylamide, the ligand is more commonly named hydrazido(2−)-.

Reaction of $[n\text{-}Bu_4N][TcOX_4]$ (X = Cl, Br) with excess ArNCO in refluxing dry toluene under nitrogen gives $[Tc(NAr)X_4]^-$ as diamagnetic blue–black solids in virtually quantitative yield. These anionic technetium(V) complexes are quite sensitive to adventitious moisture but are useful starting materials for the preparation of a whole range of technetium(V) imido- species. The $[Tc(NAr)X_4]^-$ complexes contain the new core moiety $[Tc^V{=}NAr]^{3+}$, making $[Tc(NAr)X_4]^-$ a 16-electron species in which the imido- ligand functions as a linear four-electron donor.

In efforts to derive preparative routes more applicable for radiopharmaceutical synthesis, $[n\text{-}Bu_4N][TcOCl_4]$ was reacted with aromatic amines

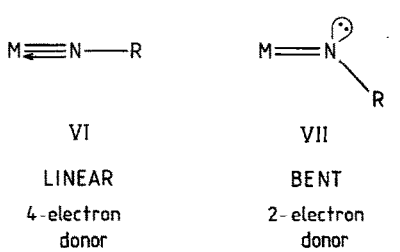

Fig. 7. Bonding modes of the imido(2−)- ligand

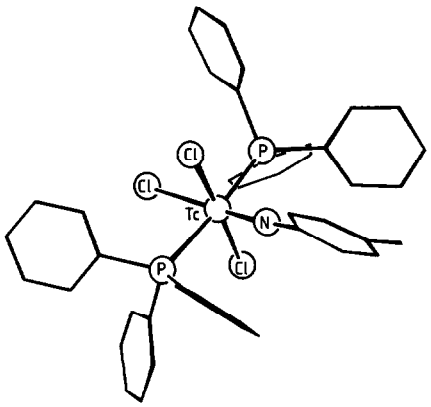

Fig. 8. Structural representation of $[TcCl_3(Ntol)(PPh_3)_2]$.

and PPh_3 in alcohols to give the neutral green–brown $[TcCl_3(NAr)(PPh_3)_2]$ complexes which are directly analogous to the known rhenium complexes $[ReCl_3(NAr)(PPh_3)_2]$.[19] These air-stable technetium(V) compounds are diamagnetic solids which exhibit a singlet in the ^{31}P NMR spectrum indicating two *trans*-PPh_3 groups. They are more stable than the $[Tc(NAr)X_4]^-$ species and consequently are superior starting materials for the preparation of a range of technetium imido- complexes. The derivative with $Ar = CH_3C_6H_4$— has been structurally characterized (Fig. 8), and is pseudo-octahedral with two *trans*-PPh_3 groups. The tolyl-imido- ligand is essentially linear with a Tc—N—C angle of 168° and a Tc—N distance of 1.7 Å, characteristic of a metal–nitrogen multiple bond. The imido- ligand is therefore functioning as a four-electron donor giving the technetium complex an overall 18-electron valence configuration. The analogous technetium oxo- complex is not known due to facile oxygen atom abstraction and reduction in the presence of monodentate tertiary phosphines.

Reaction of $[n\text{-}Bu_4N][TcOCl_4]$ with aromatic amines and dppe in refluxing alcohols gives cationic, purple technetium(IV) complexes, $[TcCl(NAr)(dppe)_2]^+$, in good yield. These air-stable complexes exhibit no ν(NH) and show broadened NMR spectra characteristic of paramagnetic metal centres. They are formally analogous to the structurally characterized technetium(IV) hydrazido (2−)- complex $[TcCl(NNMe_2)(dppe)_2]^+$ (Fig. 5).

Related technetium alkyl imido- complexes may be synthesized using phosphinimines,[17] alkylamines[20] and symmetrically substituted dialkyl hydrazines,[21] and these investigations will be reported at a later date.

CONCLUSION

We have described the synthesis and characterization of some novel technetium diazenido-, hydrazido- and imido- complexes derived directly from the appropriate organohydrazine or amine in good yield, and successfully extrapolatd the chemistry to the ^{99m}Tc level in some cases. These preparations are extremely applicable to the synthesis of new technetium radiopharmaceuticals.

Unlike previous core moieties these multiply-bonded nitrogenous ligands may carry a wide variety of different substituents attached to the nitrogen. This allows the coordination properties of these geometrically versatile ligands to be very effectively varied and also permits the complexes to be easily functionalized for suitable attachment to biological materials. We have as yet only directed the synthetic work of the new technetium cores to the generation of cationic species for possible use as potential myocardial imaging agents. However, the further substitution chemistry of these new cores will be reported at a later date. This work has been the subject of a recent patent application.[22]

Acknowledgements—We are indebted to Amersham International plc for financial support of this work and for provision of laboratory facilities for ^{99m}Tc chemistry and biodistribution studies. We thank the SERC for provision of a CASE Award (to P.J.).

REFERENCES

1. E. Deutsch, K. Libson, S. Jurisson and L. F. Lindoy, *Prog. Inorg. Chem.* 1983, **30**, 75.
2. E. Deutsch and K. Libson, *Comm. Inorg. Chem.* 1984, **3**, 83.
3. M. J. Clarke and L. Podbielski, *Coord. Chem. Rev.* 1987, **78**, 253; C. J. Jones, *Comprehensive Coordination Chemistry* (Edited by G. Wilkinson, R. D. Gillard and J. A. McCleverty), p. 881. Pergamon Press, Oxford (1988).
4. J. D. Eakins, D. G. Humphreys and C. E. Mellish, *J. Chem. Soc.* 1963, 6012; L. J. Radnovich and J. L. Hoard, *J. Phys. Chem.* 1984, **88**, 6713; R. A. Armstrong and H. Taube, *Inorg. Chem.* 1976, **15**, 1904.
5. J. Baldas and J. Bonnyman, *Int. J. Appl. Radiat. Isot.* 1985, **36**, 133.
6. B. F. G. Johnson, B. L. Haymore and J. R. Dilworth, *Comprehensive Coordination Chemistry* (Edited by G. Wilkinson, R. D. Gillard and J. A. McCleverty), Ch. 13.3, pp. 99–159. Pergamon Press, Oxford (1988).
7. J. R. Dilworth, S. A. Harrison, D. R. M. Walton and E. Schweda, *Inorg. Chem.* 1985, **24**, 2594.
8. T. Nicholson, P. Lombardi and J. Zubieta, *Polyhedron* 1987, **6**, 1577.

9. T. Nicholson, N. de Vries, A. Davison and A. G. Jones, *Inorg. Chem.* 1989, **28**, 3813.
10. I. A. Latham, J. R. Thornback and J. E. Newman, *Eur. Patent* 0291281-A1 (1988).
11. C. M. Archer, J. R. Dilworth, P. Jobanputra, R. M. Thompson, J. Strahle and S. Schmid, unpublished work.
12. W. A. Nugent and B. L. Haymore, *Coord. Chem. Rev.* 1980, **31**, 123.
13. J. R. Dilworth and R. L. Richards, *Comprehensive Organometallic Chemistry* (Edited by G. Wilkinson, F. G. A. Stone and E. W. Abel), p. 1017. Pergamon Press, Oxford (1982); J. Chatt, J. R. Dilworth and R. L. Richards, *Chem. Rev.* 1978, **78**, 589; R. A. Henderson, G. J. Leigh and C. J. Pickett, *Adv. Inorg. Chem. Radiochem.* 1983, **27**, 197.
14. R. Cotton, I. B. Tomkins and P. W. Wilson, *Aust. J. Chem.* 1964, **17**, 496; F. W. Moore and M. L. Larson, *Inorg. Chem.* 1967, **6**, 988; J. Chatt, B. A. Crichton, J. R. Dilworth, P. Dahlstrom, R. Gutkoska and J. Zubieta, *Inorg. Chem.* 1982, **21**, 2383; J. R. Dilworth and S. Morton, *Transition Met. Chem.* 1987, **12**, 41.
15. J. R. Dilworth, P. Jobanputra, S. J. Parrott and R. M. Thompson, unpublished work.
16. M. H. Chisholm and I. P. Rothwell, *Comprehensive Coordination Chemistry* (Edited by G. Wilkinson, R. D. Gillard and J. A. McCleverty). Pergamon Press, Oxford (1988).
17. J. Chatt and J. R. Dilworth, *Chem. Commun.* 1972, 519.
18. M. W. Bishop, J. Chatt, J. R. Dilworth, M. B. Hursthouse and M. Motevalli, *J. Less-Common Met.* 1977, **54**, 487.
19. D. Bright and J. A. Ibers, *Inorg. Chem.* 1968, **7**, 1099; D. Bright and J. A. Ibers, *Inorg. Chem.* 1969, **8**, 703; G. V. Goeden and B. L. Haymore, *Inorg. Chem.* 1983, **22**, 157.
20. J. Chatt, J. D. Garforth, N. P. Johnson and G. A. Rowe, *J. Chem. Soc.* 1964, 1012.
21. J. Chatt, J. R. Dilworth and G. J. Leigh, *J. Chem. Soc. A* 1970, 2239.
22. C. M. Archer, J. R. Dilworth, I. A. Latham and R. M. Thompson, *Brit. Pat. Applic.* 8919488.0 (filed 29 August 1989).

Polyhedron Vol. 9, No. 13, pp. 1503–1535, 1990
Printed in Great Britain

0277–5387/90 $3.00+.00
© 1990 Pergamon Press plc

POLYHEDRON REPORT NUMBER 32

KINETICS AND MECHANISMS OF CO SUBSTITUTION OF METAL CARBONYLS

FRED BASOLO

Department of Chemistry, Northwestern University, Evanston, IL 60208-3113, U.S.A.

CONTENTS

1. INTRODUCTION 1504

2. BINARY METAL CARBONYLS 1504
   2.1. Four-coordinate complexes 1504
   2.2. Five-coordinate complexes 1506
   2.3. Six-coordinate complexes 1507
   2.4. Metal carbonyl clusters 1509

3. METAL NITROSYL CARBONYLS 1512
   3.1. Four-coordinate complexes 1512
   3.2. Five-coordinate complexes 1513
   3.3. Six-coordinate complexes 1513

4. RING-SLIPPAGE ASSISTED REACTIONS 1515
   4.1. Cyclopentadienyl metal carbonyls 1515
   4.2. Heterocycle metal carbonyls 1517
   4.3. Indenyl ligand effect 1518
   4.4. Allyl metal carbonyls 1520

5. LIGAND SUBSTITUTION LABILITY OF 2ND ROW TRANSITION METAL CARBONYLS 1521
   5.1. Mononuclear complexes 1521
   5.2. Metal carbonyl clusters 1522

6. CATALYSIS OF CO SUBSTITUTION 1522
   6.1. Acid catalysis 1522
   6.2. Base catalysis 1522

7. MIGRATORY INSERTION REACTIONS 1524
   7.1. Methyl migration 1524
   7.2. Acid-induced reaction 1524

8. 17-ELECTRON METAL CARBONYLS 1525
   8.1. $V(CO)_6$ 1525
   8.2. $(\eta^5\text{-ligand})_2V(CO)$ 1526

9. OXYGEN ATOM TRANSFER TO METAL CARBONYLS 1528
   9.1. $M(CO)_6$ (M = Cr, Mo, W) 1528
   9.2. $M_3(CO)_{12}$ and $M(CO)_5$ (M = Fe, Ru, Os) 1530

1. INTRODUCTION

This article is not a comprehensive review of CO substitution of metal carbonyls, it is instead a report of research carried out in our laboratory on this topic during the past 34 years. However, reference will be made to articles that relate to our research. Furthermore, excellent review articles[1] and chapters in books[2] provide more detailed treatments of ligand substitution reactions of transition metal organometallic compounds.

When I arrived at Northwestern University, September 1946, I wanted to initiate a research programme on the kinetics and mechanisms of ligand substitution in octahedral and in square-planar metal complexes. The place to start seemed to be with Werner complexes of cobalt(III) and of platinum(II), respectively. At this time, physical organic chemists were investigating tetrahedral substitution, and they had arrived at the now well-known S_N1 and S_N2 mechanisms. It appeared that a similar kinetic and stereochemical approach could be used to obtain the mechanisms of octahedral and of square-planar substitutions.[3a] Thanks to the good work of our students and postdoctorates in inorganic chemistry, and to the collaboration with my colleague Ralph G. Pearson, some of the seminal research in this area was accomplished. Much of the work was discussed in 1958 in the book entitled *Mechanisms of Inorganic Reactions*.[3b]

In May 1955 at the *III International Conference on Coordination Chemistry*, a plenary lecture was given by the late Professor Walter Hieber, whom some of us consider to be the "father" of metal carbonyl chemistry. In response to a question as to the mechanisms of some of the reactions presented, he said almost nothing was known about the mechanisms. I immediately felt that the on-going research in our laboratory on the kinetics and mechanisms of ligand substitution reactions of metal amine complexes could be extended to metal carbonyls. This seemed like a golden opportunity for graduate students, because any kinetic study of CO substitution reactions of metal carbonyls would be new and readily lead to an acceptable doctorate thesis and to original scientific publications. In spite of this our students at first were somewhat hesitant to tackle a problem that involved compounds and experimental conditions foreign to our research group. Also recall that in the mid 50s there was little interest in the chemistry of metal carbonyls, and the designation of transition metal organometallic chemistry as an important area of chemistry had yet to be realized.

This article presents an overview of the saga of our investigations on CO substitution reactions of metal carbonyls.

2. BINARY METAL CARBONYLS

Research in our laboratory started with a study of the kinetics and mechanisms of CO exchange with well-known binary metal carbonyls. Initially it was decided to investigate metal carbonyls having different coordination numbers [$Ni(CO)_4$, $Fe(CO)_5$ and $Cr(CO)_6$], and systems with bridging and terminal COs [$Co_2(CO)_8$]. Since ^{13}C NMR was not then in use, it was decided to use ^{14}CO and follow the rates of CO exchange by monitoring changes in radioactivity of CO in the gas phase as it was being circulated through a solution of the metal carbonyl.[4a] This experimental method was later found[4b] to be flawed, particularly for studies on volatile metal carbonyls. Similar studies had been reported[5] earlier showing a wide range of rates of CO exchange with metal carbonyls, e.g. half-lives of exchange at room temperature are minutes for $Ni(CO)_4$ and years for $Fe(CO)_5$. However, this kinetic study did not investigate the mechanisms of CO exchange. Rates of CO exchange or replacement by a dissociative mechanism of some of the more common binary metal carbonyls are given in Table 1.

2.1. *Four-coordinate complexes*

Monomeric binary metal carbonyls are now known to generally react by a dissociative mechanism [eq. (1)]:

$$\underset{\text{18-electron}}{M(CO)_n} \xrightarrow[\text{Slow}]{-CO} \underset{\text{16-electron}}{M(CO)_{n-1}} \xrightarrow[\text{Fast}]{+L} \underset{\text{18-electron}}{M(CO)_{n-1}L}. \qquad (1)$$

Table 1. Dissociation rate constants (k_1) for CO substitution of some binary metal carbonyls

Carbonyl	Temperature (°C)	k (s^{-1})	Reference
$Ni(CO)_4$	10	1.2×10^{-3}	4b
$Fe(CO)_5$	50	6×10^{-11}	6
$Ru(CO)_5$	50	3.0×10^{-3}	7
$Os(CO)_5$	50	4.9×10^{-8}	6
$Cr(CO)_6$	131	1.4×10^{-4}	8
$Mo(CO)_6$	112	2.1×10^{-4}	8
$W(CO)_6$	166	1.1×10^{-4}	8
$Mn_2(CO)_{10}$	25	10 years[a]	5
$Fe_3(CO)_{12}$	50	9.8×10^{-4}	9
$Ru_3(CO)_{12}$	50	1.0×10^{-4}	9
$Os_3(CO)_{12}$	50	1.0×10^{-8}	9
$Co_2(CO)_8$	0	1.5×10^{-3}	4a
$V(CO)_6$	10	7 h[a]	10
$[V(CO)_6]^-$	80	N.R.[b]	11
$[Mn(CO)_5]^-$	40	N.R.[c]	12
$[Mn(CO)_6]^+$	30	N.R.[c]	12

[a] Values in h and years are for half-lives of CO exchange. $V(CO)_6$ (17-electron) reacts very fast with good nucleophiles by an associative mechanism.[13]

[b] No reaction in molten PPh_3.

[c] No CO exchange in one day.

This behaviour is readily understood in terms of the 16,18-electron rule,[14] which suggests that an associative mechanism is not involved because it requires the formation of a 20-electron transition state or intermediate instead of the more stable 16-electron system formed in a dissociative pathway. Yet a decade prior to the 16,18-electron rule the first study of ^{14}CO exchange with $Ni(CO)_4$ gave results that were not expected. Since $Ni(CO)_4$ has a low coordination number for nickel, it was felt that its coordination number could easily increase and allow for an associative mechanism. What was found[4a] is that the rate of exchange is first-order in $Ni(CO)_4$ and zero-order in CO concentrations, indicating a dissociative pathway. The result was explained in terms of the filled *d*, *s* and *p* orbitals of nickel leaving no empty low-energy metal orbital to accept a pair of electrons from the entering nucleophile (today expressed as an 18-electron system not adding a pair of electrons to form an unstable 20-electron species). It later became necessary to repeat these experiments in order to obtain correct kinetic data, but the rate law did not change. The later experiments[4b] involved monitoring the exchange of $C^{18}O$ with $Ni(CO)_4$ by following changes in the CO stretching region of the IR. Temperature dependence studies gave large values of $\Delta H^{\ddagger}$ (24 kcal mol^{-1}) and positive values of $\Delta S^{\ddagger}$ (+12 eu), both of which are indicative of a dissociative mechanism. This mechanism requires that in a competition experiment of different nucleophiles for the active intermediate "$Ni(CO)_3$", the sum of the rates of formation of the different products equals the rate of dissociation of $Ni(CO)_4$. This was tested[4b] by competing $C^{18}O$ against PPh_3, and it was found to be true [eq. (2)]:

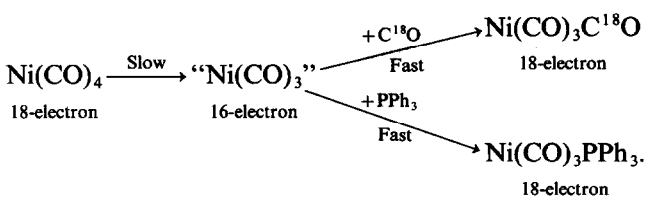

(2)

The results showed that PPh_3 is five times a better nucleophile towards "$Ni(CO)_3$" than is CO. In fact it is now recognized that CO is a poor nucleophile, compared to phosphines and phosphites often used in CO substitution reactions of metal carbonyls.

Gray and Wojcicki,[15] with assistance from Angelici, when graduate students in Pearson and my research group and without our knowledge, investigated the ligand exchange of all three of the ligands in $Rh(CO)Cl(PPh_3)_2$. They observed that in individual experiments all three of the ligands exchange rapidly with the free labelled ligands, presumably by an associative process [eq. (3)]:

$$\underset{\text{16-electron}}{Rh(CO)Cl(PPh_3)_2} \xrightarrow[k_2]{+{}^{14}CO} \text{“}\underset{\text{18-electron}}{Rh(CO)({}^{14}CO)Cl(PPh_3)_2}\text{”} \xrightarrow[\text{Fast}]{-CO} \underset{\text{16-electron}}{Rh({}^{14}CO)Cl(PPh_3)_2}. \qquad (3)$$

This result was expected because the filled dps^2 hybrid orbitals on rhodium(I) leave a vacant low-energy p orbital to accept a pair of electrons from the entering nucleophile, similar to the then well-known S_N2 reactions of platinum(II) complexes.[3b]

2.2. *Five-coordinate complexes*

Binary metal carbonyls of the iron triad of transition metals are five-coordinate $M(CO)_5$ (M = Fe, Ru, Os). Metal carbonyls [$Ni(CO)_4$ and $Fe(CO)_5$] were discovered a century ago this year by Mond and co-workers.[16] Kept in the dark at room temperature $Fe(CO)_5$ is stable and its many different reactions have been extensively investigated.[17] Yet there has not been a detailed kinetic study of CO substitution of $Fe(CO)_5$, because of its extremely slow thermal reaction which would require high temperatures where it is both volatile and unstable. One attempt made at such a study allows an estimate of a 4 year[5] half-life for CO exchange at 25°C with $Fe(CO)_5$. Another attempt[18] suggests that CO substitution with phosphines proceeds by a dissociation mechanism, as was shown for the reaction of $Fe(CO)_4PPh_3$ with PPh_3 to form $Fe(CO)_3(PPh_3)_2$. Assuming that the difference in rates of CO substitution between $Fe(CO)_5$ and $Fe(CO)_4PPh_3$ is about the same as that between $Ru(CO)_5$[7] and $Ru(CO)_4PPh_3$,[19] then one can approximate a rate for $Fe(CO)_5$[6] (Table 1). The anomalously slow rate of reaction of the iron compound compared to the other members of its triad is briefly discussed at the end of this section.

Wilkinson and co-workers[20] reported that strong acids protonate some metals of organometallic compounds, and for some metal carbonyls the C—O stretching frequency may increase by as much as 140 cm^{-1} on protonation. This increase in ν(CO) suggests a decrease in metal-to-carbon π-bonding, and a weaker M—CO bond. We immediately wanted to test this hypothesis by investigating the exchange of ^{14}CO with $Fe(CO)_5$ in the presence of a strong protonic acid. Much to our satisfaction it was found[21] that CO exchange is extremely fast in the presence of added CF_3COOH (at -21°C $t_{1/2} = 20$ min, compared with $t_{1/2} = 4$ years at 25°C without added acid[5]). The kinetic results were explained on the basis of a rapid acid–base pre-equilibrium followed by the rate-determining dissociation of the protonated substitution labile intermediate (a S_N1CA mechanism or an S_N1 reaction of the conjugate acid) [eq. (4)]:

$$Fe(CO)_5 \underset{\text{Fast}}{\overset{+H^+}{\rightleftharpoons}} [HFe(CO)_5]^+ \xrightarrow[k_1]{-CO} \text{“}[HFe(CO)_4]^+\text{”} \xrightarrow[\text{Fast}]{+CO} Fe(CO)_5 + H^+. \qquad (4)$$

Years later it was suggested[22] that the tremendous increase in rate of CO exchange may be caused by the formation of substitution labile iron carbonyl radicals. Further study is needed to clarify the supposition of a radical chain reaction. Also, it should be of interest to attempt the use of Lewis acids as catalysts for CO exchange with certain other metal carbonyls. For example, Lewis acids are known to interact with the CO oxygen,[23] M—CO—BF_3, of certain metal carbonyls, and to enhance rates of alkyl migration onto a carbonyl carbon[24] (see Section 7).

The pentacarbonyls of the other members of the iron triad, $M(CO)_5$ (M = Ru, Os), are not stable relative to their respective trimeric clusters, $M_3(CO)_{12}$ (M = Ru, Os). However, photolysis of solutions of the trimeric clusters does afford the pentacarbonyls,[25] and the CO substitution reactions of both have recently been studied [eq. (5)]:

$$M(CO)_5 + L \xrightarrow{k_1} M(CO)_4L + CO. \qquad (5)$$
$$[M = Ru, Os;\ L = PR_3, P(OR)_3]$$

In both cases, as with $Fe(CO)_5$, the reactions involve a dissociative mechanism. The rate of reaction of $Ru(CO)_5$[7] is 10^5 times faster than that of $Os(CO)_5$[6] (Table 1). It is generally expected that the 2nd row metal of a given transition metal triad will react faster than the corresponding 3rd row metal complex (see Section 5). What is anomalous is that $Fe(CO)_5$ reacts 10^8 times slower than $Ru(CO)_5$, resulting in relative estimated rates in the order Fe <<< Ru >> Os.

The extreme slowness of CO substitution of $Fe(CO)_5$ compared with the other members of its triad may be due to its transition state/active intermediate, "$Fe(CO)_4$", being high-spin[26] while the other tetracarbonyls are low-spin.[27] Thus a partial explanation of the very slow rate of CO substitution of $Fe(CO)_5$ may be the much less favourable crystal-field activation energy (CFAE)[28] in going from low-spin $Fe(CO)_5$ to high-spin "$Fe(CO)_4$" relative to the CFAE in going from low-spin $M(CO)_5$ (M = Ru, Os) to low-spin "$M(CO)_4$". The electron spin change for $Fe(CO)_5$ corresponds to a spin-forbidden process, whereas for $M(CO)_5$ with no spin change, reaction takes place by a spin-allowed process.

2.3. *Six-coordinate complexes*

Independent studies at the same time were under way by the Italians[29] on the gas-phase CO exchange with $M(CO)_6$ (M = Cr, Mo, W), which they found to proceed by a dissociative pathway. This result was expected because studies of ligand substitution of cobalt(III) complexes[3b] had taught us that six-coordinate metal complexes generally react by predominantly a dissociative pathway. Furthermore, since the low-energy metal orbitals (*d*, *s* and *p*) are filled with electrons, there is no energetically favourable way to accommodate a pair of electrons that must attack the metal in an associative process. Today the 16,18-electron rule[14] makes it easier to say the same thing, by stating that a more stable 16-electron transition state (S_N1) is favoured over a 20-electron transition state (S_N2).

Graham and Angelici[8] (Table 1) investigated the CO substitution reactions [eq. (6)]:

$$M(CO)_6 + L \longrightarrow M(CO)_5L + CO \tag{6}$$

of $M(CO)_6$ (Cr, Mo, W) with various nucleophiles and found the reactions involve a two-term rate law [eq. (7)]:

$$\text{Rate} = (k_1 + k_2[L])[M(CO)_6]. \tag{7}$$

This rate law suggests a competitive dual pathway reaction, that by k_1 which is zero-order in nucleophile is S_N1 and that by k_2 which depends on the nucleophile is S_N2. The parallel reactions are illustrated by eq. (8):

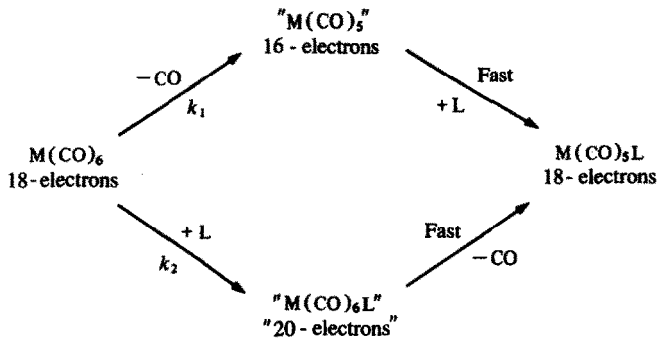

(8)

The dissociative pathway via a 16-electron intermediate is consistent with the 16,18-electron rule, but not so the associative pathway involving a 20-electron intermediate. However, it has been suggested[30] that the associative pathway can maintain an 18-electron count providing that a pair of electrons are localized on the carbonyl ligands in order to empty a low-energy metal orbital for attack by the entering nucleophile [eq. (9)] (see Section 3).

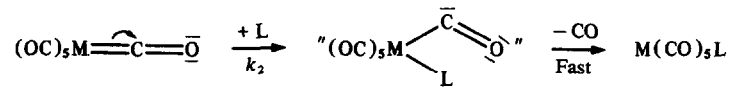

(9)

Investigations in our laboratory on six-coordinate metal carbonyls were carried out largely on CO substitution reactions of $Mn(CO)_5X$ (X = Cl, Br, I). Initial studies[31] involved rates of ^{14}CO exchange with $Mn(CO)_5X$, which showed the exchanges are S_N1 and the rates decrease in the order Cl > Br > I. It also appeared that the four radial COs exchange more readily than does the axial CO. This seemed reasonable at the time, because the axial Mn—CO bond is stronger than that with the radial COs. This difference in bond strength results from the axial CO being more strongly π-bonded due to its having to compete for such bonding with the poorer π-bonding *trans*-halogeno ligand, whereas the radial COs must compete with the strong π-acid CO in the *trans* positions. The result was further believable at the time, since the fluxional nature of organometallic compounds had not yet been discovered.[32] Had this been known, it would have suggested the five-coordinate intermediates "$Mn(CO)_4X$" are fluxional, thus rendering all COs equivalent in any slow ^{14}CO exchange process.

Unfortunately, as with our initial $Ni(CO)_4$ report,[4] the experiments of ^{14}CO exchanges with $Mn(CO)_5X$ were flawed. The saga of what followed is a long one and it will not be discussed in detail here, but relevant references are cited for the interested reader. This exchange was re-examined in three different laboratories using ^{13}CO or $C^{18}O$ and following the exchange with IR.[33] In all three cases, the IR studies show that the CO label is incorporated into both the axial and radial positions of $Mn(CO)_5X$. The most recent publications[34,35] on this subject deal with the principle of microscopic reversibility as applied to the kinetics and stereochemistry of the CO exchange. The challenge[34] that one of the proposed mechanisms could not be correct, because it was contrary to the law of microscopic reversibility, was based on our initial incorrect ^{14}CO exchange study. The reply by Brown[35] states "The application of ^{14}CO methods to the study of metal carbonyl reactions represented a pioneering foray into an important and previously unexplored area of organometallic chemistry.[36] However, the accuracy and degree of explicitness with which the incorporation of label can be discerned with use of IR methods that came later are far greater than can be achieved with the radiolabelling methods". Thus, hopefully ends the saga of CO exchange with $Mn(CO)_5X$.

Early kinetic studies[37] on the substitution of CO in $Mn(CO)_5X$ by various nucleophiles [eq. (10)]:

$$Mn(CO)_5X + L \longrightarrow \textit{cis}\text{-}Mn(CO)_4XL + CO \qquad (10)$$

(X = Cl, Br, I; L = phosphines and phosphites)

gave a first-order rate law, dependent only on the substrate concentration. It was suggested that the dissociative pathway involves the loss of a radial CO with the formation of a tetragonal pyramid intermediate, "$Mn(CO)_4X$", and addition of the entering nucleophile to afford *cis*-$Mn(CO)_4XL$. Now that we realize the intermediate is fluxional and could lead to either a *cis* or *trans* product or a mixture of the two, it appears the *cis*-isomer is formed because it permits the maximum amount of back π-bonding to the two COs *trans* to ligands X and L. It was further noted that the rates of substitution for $Mn(CO)_5X$ decrease in the order Cl > Br > I. This is also the order of decreasing C—O stretching frequency of the more intense IR band of the four radial COs, e.g. Cl, 2070; Br, 2064; I, 2056 cm^{-1}. The lowest frequency for the iodo compound suggests more π-bonding giving the strongest Mn—CO bond thus the slowest dissociation rate. This is understandable because the iodo ligand is the least electronegative and most polarizable, thus its manganese has the highest electron density and the greatest tendency to back π-bond to CO.

It was suggested[37] that the radial COs are more substitution labile than the axial CO in $Mn(CO)_5X$, because in the ground state the CO *trans* to X is more strongly π-bonded to Mn than are the COs *cis* to X. Later the difference in reactivity was explained in terms of *cis*-labilization[38] of COs in metal carbonyls *cis* to some other ligand. For example, CO substitution of $Mn(CO)_5X$ is faster than that of $[Mn(CO)_6]^+$, and $Cr(CO)_5L$ or $[Cr(CO)_5X]^-$ complexes react faster than $Cr(CO)_6$. The *cis*-labilization is attributed to a stabilization of the transition state for reaction, because in several cases X-ray structures show a shortening of the *cis*-M—CO bond in the ground state which then is less prone to M—CO bond rupture causing a slower rate of dissociation.

Rates of CO substitution of the monosubstituted compounds *cis*-$Mn(CO)_4LX$ were also found[39] to proceed by a dissociation mechanism, and for a given X the rates decrease with changes in L in the order: $PPh_3 > AsPh_3 > P(n\text{-}Bu)_3 \sim PPh_2Cl > P(OPh)_3 \sim SbPh_3 > PPhCl_2$ $P(O—n\text{-}Bu)_3 > P(OCH_2)_3CCH_3$. The results were interpreted loosely in terms of the well-known[3b] steric acceleration of dissociative reactions, where the driving force is a lowering of steric strain by decreasing the coordination number of the metal with the formation of the transition state. However, in this system there is, at best, only a rough qualitative correlation with the cone angle.[40] It was further observed[41] that *fac*-$Mn(CO)_3L_2X$ isomerizes to the *mer*-isomer [eq. (11)]:

Facial Meridional (11)

by an intermolecular mechanism involving the dissociation and re-entry of ligand L. The *fac*-isomer is expected to be electronically the more stable, because the three COs achieve their maximum π-bonding being *trans* to other less π-bonding ligands. Isomerization to the *mer*-isomer is driven by the bulkiness of L, as shown by steric acceleration of the rates of isomerization.

Finally, perhaps the first time a point was made of a correlation between the rates of dissociative CO exchange or substitution of metal carbonyls and their C—O stretching frequencies (Fig. 1) was in an article[42] dealing with ^{14}CO exchange with $Rh(PPh_3)_2COCl_3$. Ligand substitutions of all the six-coordinate complexes in Fig. 1 take place by M—CO bond rupture, and the one with the strongest bond is the slowest to react. This is also the one with the largest amount of π-bonding which means a lower C—O stretching frequency. One must note that this correlation does not apply if the mechanisms of CO substitution differ. For example, ^{14}CO exchange with $Rh(PPh_3)_2COCl$[15] is much faster than it is with $Rh(PPh_3)_2COCl_3$,[42] although the values of ν(CO) indicate that the bond of Rh^{I}—CO (ν(CO) = 1981 cm^{-1}) is stronger than that of Rh^{III}—CO (ν(CO) = 2108 cm^{-1}). This is understood, because the two substitution processes differ with bond breaking assisted by bond making (S_N2) involved for the rhodium(I) complex and only bond breaking (S_N1) for the rhodium(III) complex.

2.4. *Metal carbonyl clusters*

The earliest kinetic study of polymetal carbonyls was carried out on the dinuclear compounds $Co_2(CO)_8$ and on $Mn_2(CO)_{10}$. The two compounds represent two metal–metal bonded structures,

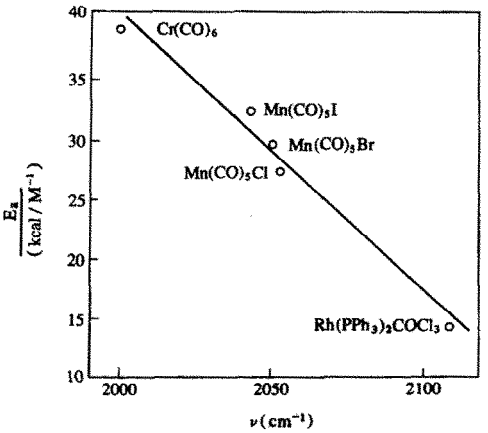

Fig. 1. The activation energies for the replacement of CO from metal carbonyls vs the C—O stretching frequencies.

one with (Co)[43] and one without (Mn)[44] bridging carbonyls. Early kinetic studies[4a] of ^{14}CO exchange with $Co_2(CO)_8$ was carried out with the specific goal of seeing if the two bridging COs exchange at a different rate from the six terminal COs. Much time and effort was spent in an attempt to detect a difference, but what was found is that exchange is rapid and all eight of the COs exchange at the same rate. The futility of these experiments was recognized 2 years later when it was reported[45] that in solution $Co_2(CO)_8$ rapidly equilibrates [eq. (12)]:

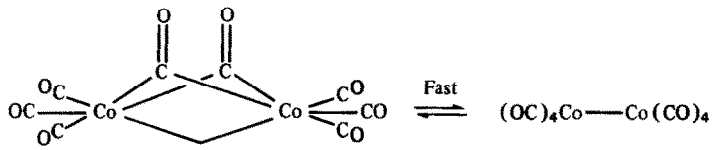

(12)

Soon afterwards the fluxional nature[32] of organometallic compounds was recognized, which further suggests that all eight COs rapidly scramble and are equivalent in solution on the time scale of exchange with ^{14}CO.

Somewhat related to the structure $(OC)_4Co—Co(CO)_4$ is the structure $(OC)_4Co—Hg—Co(CO)_4$,[46] and its exchange[47] with ^{14}CO is also rapid and proceeds by a first-order rate law dependent only on substrate concentration. One of the mechanisms suggested for CO exchange is represented by [eq. (13)]:

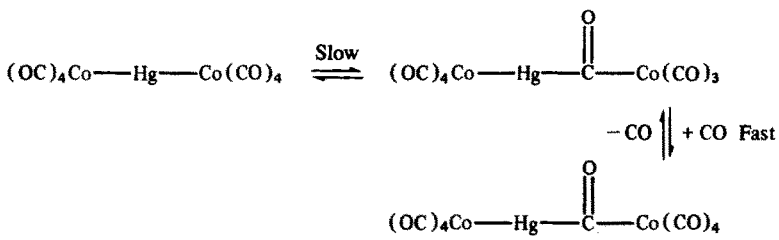

(13)

In this process, the rate-determining step involves CO insertion[48] (or ligand migration[49]) followed by the rapid addition and scrambling of CO. Studied[47] in less detail was the exchange of ^{14}CO with other heterometal–metal bonded carbonyls: $Cd[Co(CO)_4]_2$, $(CH_3)_3SnCo(CO)_4$, $(C_6H_5)_3SnCo(CO)_4$, $Ph_3PAuCo(CO)_4$ and $Ph_3PAuMn(CO)_5$. In all cases CO exchange was rapid at room temperature and below.

One other CO substitution of $Co_2(CO)_8$ was attempted in our laboratory, but unfortunately it did not work. The replacement of two COs by acetylenes had been reported[50] [eq. (14)]:

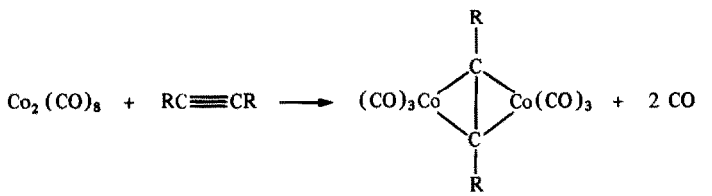

(14)

so it was decided to try using N_2 which is also triply bonded. This did not work [eq. (15)]:

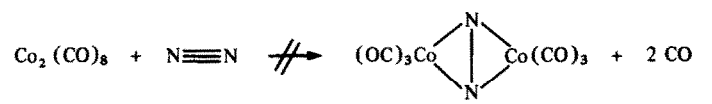

(15)

and the behaviour of N_2 as a ligand in $[Ru(NH_3)_5N_2]^{2+}$ was left for Allen and Senoff[51] to discover 5 years later.

Our early investigation[52] of the kinetics of CO replacement in $Mn_2(CO)_{10}$ by various nucleophiles

in *p*-xylene solutions at 100–120°C was interpreted in terms of a simple S_N1 process [eq. (16)]:

$$Mn_2(CO)_{10} \xrightarrow[-CO]{\text{Slow}} \text{“}Mn_2(CO)_9\text{”} \xrightarrow[+L]{\text{Fast}} Mn_2(CO)_9L. \tag{16}$$

The reactions were first-order in $Mn_2(CO)_{10}$ and zero-order in nucleophile concentrations. In further support of a dissociative mechanism was the large enthalpy ($\Delta H^{\ddagger} = 37$ kcal mol^{-1}) and positive entropy ($\Delta S^{\ddagger} = +20$ eu) of activation, along with a retardation of the reaction rate with added CO.

What followed was a series of articles[53] on the kinetics of the thermal CO substitution reactions of $Mn_2(CO)_{10}$, $Re_2(CO)_{10}$ and $MnRe(CO)_{10}$, which were interpreted to take place with the rate-determining step being metal–metal bond cleavage. The substitution labile metal carbonyl radicals, $^{\cdot}M(CO)_5$ formed, would then rapidly react to give $^{\cdot}M(CO)_4L$ and rapidly recouple to form the product $M_2(CO)_9L$. This mechanism was first challenged in a report[54] on the kinetic study of CO substitution of $MnRe(CO)_{10}$. The conclusion reached in this paper was that dissociation of a Mn—CO is rate-determining, although the monosubstituted product has the entering ligand on rhenium [eq. (17)]:

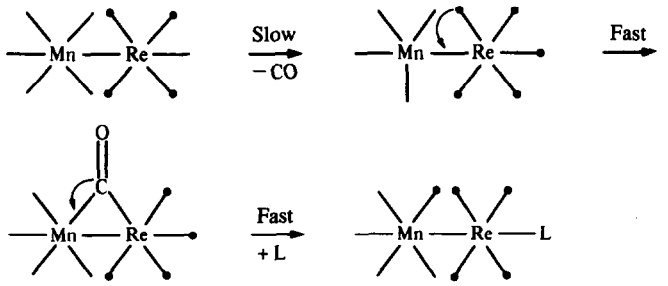

(17)

This mechanism suggests the metal–metal bond rupture mechanism is incorrect.

Although one can never prove a mechanism is correct, it is possible to prove a mechanism is wrong. For example, the metal–metal bond cleavage mechanism proposed for CO substitution of $M_2(CO)_{10}$ carbonyls requires the formation of metal carbonyl radicals, $^{\cdot}M(CO)_5$, and their recoupling to form crossover products [eq. (18)]:

$$Re_2(CO)_{10} + Mn_2(CO)_{10} \not\longrightarrow 2MnRe(CO)_{10}. \tag{18}$$

Crossover experiments,[55] at reaction conditions where six half-lives of the reaction of $Re_2(CO)_{10}$ with PPh_3 to form $Re_2(CO)_9PPh_3$, would take place, showed no heterodimetal product in solutions containing equivalent amounts of the homodimetal decacarbonyls. Since no crossover resulted, this proves that the metal–metal bond cleavage is not correct. This thermal process contrasts with the photochemical cross-coupling reaction between $Mn_2(CO)_{10}$ and $Re_2(CO)_{10}$, which produces metal–metal bond homolysis and generates $MnRe(CO)_{10}$ in high yield.[56]

Muetterties and co-workers,[57] a year later, reported the elegant experiments using isotopic labelling to determine if crossover takes place with $Re_2(CO)_{10}$ and with $Mn_2(CO)_{10}$ at conditions known to yield monosubstituted phosphine products. Their results showed no crossover [eqs (19) and (20)]:

$$^{185}Re_2(CO)_{10} + {}^{187}Re_2(CO)_{10} \not\longrightarrow 2\,^{185}Re\,^{187}Re(CO)_{10} \tag{19}$$

$$Mn_2(CO)_{10} + Mn(^{13}CO)_{10} \not\longrightarrow Mn_2(CO)_5(^{13}CO)_5, \tag{20}$$

and they state “our results confirm the original Wawersik and Basolo[52] mechanistic proposal for $Mn_2(CO)_{10}$ ligand-substitution reactions”. The dissociative mechanism may further involve the intermediate formation of a $\underset{M—C—M}{\overset{O}{\|}}$ bridged species.[54] That such a CO bridged intermediate may form is supported by the observation[58] that solutions of $(OC)_5Mn—Re(^{13}CO)_5$ undergo CO migration between metals to give initially $(OC)_4(O^{13}C)Mn—Re(^{13}CO)_4(CO)$.

The kinetics and mechanisms of thermal CO substitution of metal carbonyl clusters have been the subject of detailed studies, mostly by Poë and co-workers.[59] Such studies are more complicated

for metal clusters, which may fragment during substitution reactions, than with mononuclear or binuclear metal carbonyls. For this reason, it is also often not clear in using metal carbonyls as homogeneous catalysts[60] if the cluster or one of its fragmentation species is the catalyst. One attempt to avoid competing fragmentation reactions is to use the tripod ligand $HC(PPh_2)_3$ to stabilize clusters such as $M_4(CO)_9[HC(PPh_2)_3]$ (M = Co, Rh, Ir).[61] The initial study[62] of ^{13}CO exchange with $Co_4(CO)_9$(tripod) focused on the dissociative loss of CO in the cluster, our investigation[63a] extended this to CO substitution by phosphines and phosphites and to the corresponding rhodium and iridium clusters. Reactions of the clusters follow the two-term rate law [eq. (21)]:

$$\text{Rate} = (k_1 + k_2[\text{L}])[\text{M}_4(\text{CO})_9(\text{tripod})], \tag{21}$$

where k_1 and k_2 are dissociative and associative pathways, respectively. These assignments are further supported by the values of enthalpies and entropies of activation. Since the entering nucleophile is on the apical metal in the reaction products, it is possible to speculate as to the formations and structures of the dissociative [eq. (22)] and associative [eq. (23)] intermediates:

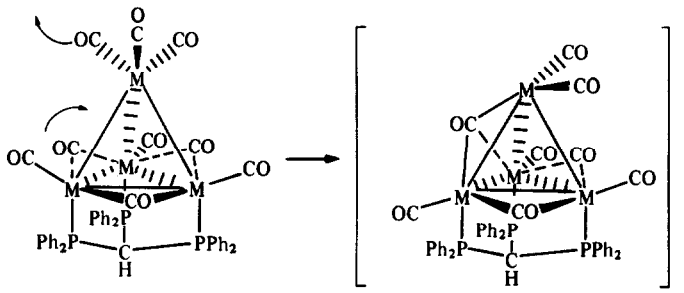

(22)

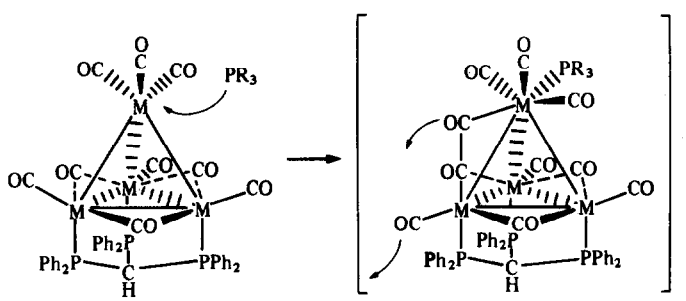

(23)

Perhaps the most notable chemical feature of this study is the exceptional reactivity of the rhodium cluster, whose substitution reactions proceed within seconds at room temperature (see Section 5). Similarly, studies on $M_4(CO)_{12}$ showed[63b] the rates of reaction vary in the order Co << Rh >>> Ir.

3. METAL NITROSYL CARBONYLS

3.1. *Four-coordinate complexes*

As discussed earlier, binary metal carbonyls (18-electron systems) undergo CO substitution by a dissociative process [eq. (1)]. Imagine the surprise when $Co(CO)_3(NO)$[64] and $Fe(CO)_2(NO)_2$,[68] isoelectronic and isostructural with $Ni(CO)_4$, which reacts by a dissociative mechanism, were found to react by an associative mechanism. This behaviour, prior to the X-ray structure of bent nitrosyls[65] and prior to the 16,18-electron rule,[14] was attributed to localizing a pair of electrons on the nitrogen in the transition state for reaction in order to vacate a metal orbital of low energy for nucleophilic attack [eq. (24)]:

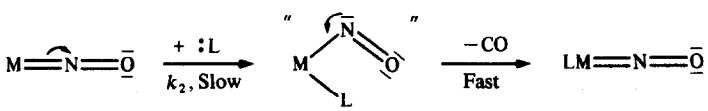

(24)

18 - electrons 18 - electrons 18 - electrons

This S_N2 mechanism for ligand substitution reactions is general for metal nitrosyl carbonyls, with only the poorest of nucleophiles (e.g. $AsPh_3$) permitting a contribution by an S_N1 pathway. The metal nitrosyl carbonyls investigated in our laboratory are shown in Table 2, and their mechanism of CO substitution is compared with that of related (isoelectronic or pseudo-isoelectronic) metal carbonyls.

Since the reactions of $Co(CO)_3(NO)$ and $Fe(CO)_2(NO)_2$ are associative, this permitted the first attempts[64,68] to quantify the nucleophilic strengths of different entering ligands towards a metal carbonyl. The results showed that for a given ligand atom (P or N) there is a reasonable linear correlation of the log of the rate constant, k_2, vs the protonic basicity of the ligand (Fig. 2). For a given basicity, it is seen that the more polarizable P ligands are better nucleophiles than the N ligands. This is readily explained in terms of formally Co(−I) and Fe(−II) being class b[73] or soft[74] metals preferring the class b or soft ligands of P over the class a or hard ligands of N. Note that this was done before the added influence of the steric factor of the nucleophiles was stressed in terms of their cone angles.[75] A considerable amount of data has since been gathered on the reactivity of various nucleophiles towards metal carbonyls, and some success has been reported[76,77] in the development of empirical equations that take care of the contributions of basicity and steric factors to the nucleophilic strengths of various ligands.

3.2. *Five-coordinate complexes*

Although the first kinetic studies of CO substitution of metal nitrosyl carbonyls were carried out on tetra-coordinate systems, $Co(CO)_3(NO)$[64] and $Fe(CO)_2(NO)_2$,[68] it should be noted that subsequent studies showed (Table 2) that five- and six-coordinate systems likewise react predominantly by an associative mechanism. It seems reasonable that the five-coordinate trigonal bipyramid $Mn(CO)_4(NO)$ could readily expand its coordination number to six by the addition of the entering ligand in the trigonal plane to form the octahedral intermediate "$Mn(CO)_4(NO)L$" with a bent Mn—NO and an 18-electron count.[67]

3.3. *Six-coordinate complexes*

Somewhat more difficult are the associative reactions of six-coordinate metal nitrosyl carbonyls through a seven-coordinate 18-electron intermediate with a bent nitrosyl. However, even this is possible, for seven-coordinate metal carbonyls are known.[78]

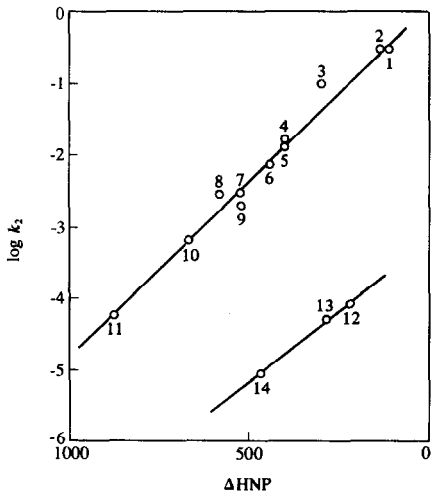

Fig. 2. The linear free-energy relationships of the rate of CO substitution with the basicity of P and of N nucleophiles for the reaction of $Co(CO)_3(NO)$. (1) PEt_3, (2) $P(n\text{-}Bu)_3$, (3) $PPhEt_2$, (4) PPh_2Et, (5) $PPh_2(n\text{-}Bu)$, (6) $P(p\text{-}CH_3OC_6H_4)_3$, (7) $P(O\text{-}n\text{-}Bu)_3$, (8) PPh_3, (9) $P(OCH_3)_3$, (10) $P(OCH_2)_3CCH_3$, (11) $P(OPh)_3$, (12) 4-picoline, (13) pyridine, (14) 3-chloropyridine. ΔHNP is the difference in half-neutralized potential between the nucleophile and N,N′-diphenylguanidine in nitromethane, so the smaller ΔHNP the more basic the nucleophile. C. A. Streuli, *Anal. Chem.* 1960, **32**, 985. R. C. Bush and R. J. Angelici, *Inorg. Chem.* 1988, **27**, 681.

Table 2. Mechanisms[a] of CO substitution of metal carbonyls compared with related metal nitrosyl carbonyls

Six-coordinate	Mechanism	Reference	Five-coordinate	Mechanism	Reference	Four-coordinate	Mechanism	Reference
$Cr(CO)_6$	S_N1	8	$Fe(CO)_5$	S_N1	6	$Ni(CO)_4$	S_N1	4
$V(CO)_5NO$	S_N2	66	$Mn(CO)_4(NO)$	S_N2	67	$Co(CO)_3(NO)$	S_N2	64
$Cr(CO)_5L$	S_N1	8				$Fe(CO)_2(NO)_2$	S_N2	68
trans-$V(CO)_4(NO)L$	S_N1[b]	66				$Mn(CO)(NO)_3$	S_N2	67
$Re(CO)_5X$	S_N1	69				$Ni(CO)_2L_2$	S_N1	70
$W(CO)_4(NO)X$	S_N2	71				$Co(CO)_2(NO)L$	S_N2	64
$PPh_3SnM(CO)_4(NO)$ (M = Cr, Mo, W)	S_N2	72						

[a] The predominate mechanism is indicated. For S_N1 some contribution of S_N2 may occur with strong nucleophiles, whereas for S_N2 some contribution of S_N1 may occur for poor nucleophiles.

[b] This dissociative process is attributed to the electron-rich $P(CH_3)_3$ *trans* to NO greatly reducing its ability in the transition state to accept a pair of electrons required for an associative pathway.

The nitrosyls $W(CO)_4(NO)X$ (X = Cl, Br, I) are pseudo-isoelectronic with $Mn(CO)_5X$ (X = Cl, Br, I) and isoelectronic with $Re(CO)_5X$ (X = Cl, Br, I). The CO substitution of the nitrosyl compound proceeds by a two-term rate law, with largely an S_N2 pathway for reactions with strong nucleophiles.[71] In comparison, the Mn (see Section 2) and the Re[69] carbonyls react by an S_N1 mechanism. One factor the three systems have in common is that for each compound the rates of reaction decrease in the order Cl > Br > I. This is explained in terms of the relative electronegativity and polarizabilities of the halogeno ligand. Since Cl is the most electronegative and the least polarizable, it puts the least electron density on the metal so there is less M—CO π-bonding resulting in the weakest and most substitution labile M—CO.

Finally, the most recent kinetic study[72] of CO substitution on metal nitrosyl carbonyls made in our laboratory was on the chromium triad of compounds $Ph_3SnM(CO)_4(NO)$ (M = Cr, Mo, W), which is believed to be the only transition metal triad reported to form the same corresponding metal nitrosyl carbonyls.[79] All of the reactions follow a two-term rate law, with the S_N2 pathway predominating for good nucleophiles. The most interesting result of this study was the finding that the rates of reaction vary in the order Cr << Mo >> W, which is the usual order of the 2nd row transition metal organometallic being the most substitution labile member of its triad of metals (see Section 5).

4. RING-SLIPPAGE ASSISTED REACTIONS

Our laboratory was the first to report[80] an associative ring-slippage mechanism for CO substitution of metal carbonyls. Ring-slippage has become an important fundamental part of certain organometallic reactions, and the extensive literature on this subject was recently reviewed by O'Connor and Casey.[81] Reported here are only the studies carried out in our laboratory, with some necessary literature references.

4.1. *Cyclopentadienyl metal carbonyls*

In the 1960s, Professor E. O. Fischer and I had a collaborative pre-doctoral exchange programme. One of his students, who had just prepared for the first time the compounds $(\eta^5\text{-}C_5H_5)M(CO)_2$ (M = Co, Rh, Ir), arrived to work in our research group. He knew these compounds readily react with phosphines to replace CO, which seemed strange at the time because if one considers an $\eta^5\text{-}C_5H_5$ ligand "equivalent" to three COs then these compounds are pseudo-isoelectronic with $Fe(CO)_5$ for which CO replacement is difficult. A kinetic study of the reactions of $(\eta^5\text{-}C_5H_5)M(CO)_2$ with phosphines and phosphites [eq. (25)]:

$$(\eta^5\text{-}C_5H_5)M(CO)_2 + L \longrightarrow (\eta^5\text{-}C_5H_5)M(CO)L + CO \qquad (25)$$

showed the reactions proceed by an associative mechanism. These results were obtained at a time when the associative reactions of metal nitrosyl carbonyls were being explained by localizing a pair of electrons on the nitrosyl in order to maintain an 18-electron count of the intermediate (see Section 3). An attempt was made to account for the associative reactions of $(\eta^5\text{-}C_5H_5)M(CO)_2$ by localizing a pair of electrons on the cyclopentadienyl ligand. Since there was no precedence for this and since the π-allyl-ene $\eta^3\text{-}C_5H_5$ metal bonding had yet to be discovered, the 18-electron intermediate was formulated[80] as a familiar diolefin metal complex with an $\eta^4\text{-}C_5H_5$ ligand and the pair of electrons localized on a ring carbon. This vacated a low-energy metal orbital for attack by the entering ligand, with the intermediate maintaining an 18-electron count. The intermediate was first formulated correctly several years later by Cramer and Seiwell[82] in this report on the replacement of C_2H_4 by phosphines and phosphites in $(\eta^5\text{-}C_5H_5)Rh(C_2H_4)_2$. Three years later, Brintzinger and co-workers[83] confirmed by means of an X-ray structural determination the presence of an $\eta^3\text{-}C_5H_5$ in the compound $(\eta^5\text{-}C_5H_5)(\eta^3\text{-}C_5H_5)W(CO)_2$. Today the associative reactions of $(\eta^5\text{-}C_5H_5)M(CO)_2$

(M = Co, Rh, Ir) are believed to proceed by an $\eta^5 \rightarrow \eta^3 \rightarrow \eta^5$ *slippage* mechanism [eq. (26)]:

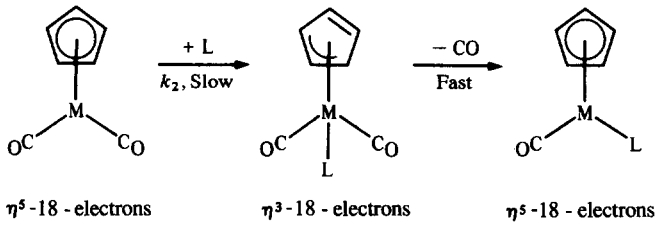

(26)

Casey and co-workers[84] have also observed $\eta^5 \rightarrow \eta^1$ slippage of the cyclopentadienyl ligand, which presumably involves an intermediate formation of the η^3 species. It is even possible for phosphines to displace the η^5-C_5H_5 ligand,[85] perhaps via the stepwise ring-slippage $\eta^5 \rightarrow \eta^3 \rightarrow \eta^1 \rightarrow \eta^0$.

More detailed kinetic studies were made in our laboratory of the $\eta^5 \rightarrow \eta^3 \rightarrow \eta^5$ ring-slippage mechanism [eq. (26)]. This mechanism predicts that electron-withdrawing substituents on the η^5-C_5H_5 ligand will enhance localization of electron density on the ring, and thus assist nucleophilic attack on the metal and increase the rate of ligand substitution. Just the opposite is predicted for electron-donating substituents, which are expected to retard nucleophilic attack and decrease the rate of reaction. In addition to this electronic effect of the substituents, steric factors may also become important and numerous, or bulky substituents on the ring may sterically hinder nucleophilic attack at the metal and retard the rate of reaction. These predictions were initially tested[86] using the compounds $(\eta^5\text{-}C_5H_5)Rh(CO)_2$, $(\eta^5\text{-}C_5H_4NO_2)Rh(CO)_2$ and $(\eta^5\text{-}C_5(CH_3)_5)Rh(CO)_2$ which gave the relative reaction rates of 1, 10^4 and 10^{-2}, respectively. This is as predicted, with the electron-withdrawing substituent NO_2 increasing the rate, and the electron-donating substituents CH_3 decreasing the rate. In the case of the η^5-$C_5(CH_3)_5$ system, it is not known how much of the 10^{-2} decrease in rate is due to electronic and how much to steric factors. In any case the results show it is possible to fine tune the rates of ligand substitution of organometallic compounds over a range of 10^6; this is important to note when considering the use of these compounds as homogeneous catalysts.[60]

A more recent investigation reports[87] results obtained on the rates of reaction of $(\eta^5\text{-}C_5H_4X)Rh(CO)_2$ [X = H, NO_2, CF_3, Cl, CH_3 or $N(CH_3)_2$] with PPh_3 to afford $(\eta^5\text{-}C_5H_4X)Rh(CO)PPh_3$. The monosubstituents on the ring are expected to have a negligible steric effect, so the rates of CO substitution are believed to be controlled by changes in electronic factors. Substituent effects on the reactivity of aromatic molecules have been studied by organic chemists for decades, and they have successfully found a linear free energy relationship between the log of the rate constants and the Hammett σ values of the substituents.[88] First, it was noted[87] that a good linear correlation exists between the values of CO stretching frequencies, ν(CO) and the Hammett σ values of the X ring substituents for the compounds $(\eta^5\text{-}C_5H_4X)Rh(CO)_2$ and their mono-PPh_3 derivatives. This is believed to mirror the electron density on Rh, which then results in greater or lesser π-backbonding from Rh → CO.

Solely on the basis of electron density on the metal, one expects the rates of associative CO substitution to show a similar linear correlation with changes in Hammett σ values of X (rates decreasing with increasing electron density on the metal). This is true for all the substituents used, except for Cl and $N(CH_3)_2$ which cause much more rapid reactions than expected on the basis of the linear correlation of the other substituents with Hammett σ. Beside the electron density on the metal affecting the rate of reaction, it is also affected by the stability of the slipped active intermediate "$(\eta^3\text{-}C_5H_4X)Rh(CO)_2L$". The substituents Cl and $N(CH_3)_2$ differ from the other substituents, being the only ones with one or more filled non-bonding p orbitals. It was suggested[87] that these two substituents can resonance stabilize the transition state [eq. (27)]:

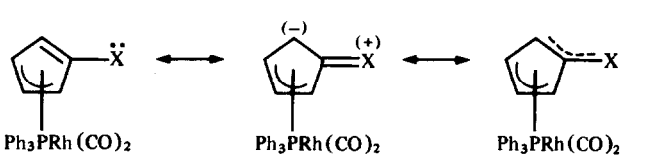

(27)

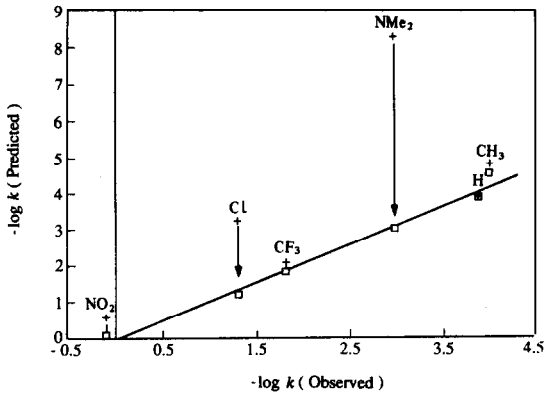

Fig. 3. □, correlation of observed rates of CO substitution to predicted rates from relative ionizations for the series of compounds $(\eta^5\text{-}C_5H_4X)Rh(CO)_2$. +, predicted rates with the σ term only, so the difference between the points + and □ represents the contribution of the π term to the predicted rates.

and enhance the reaction rate beyond that predicted by Hammett σ values. Lichtenberger *et al.*[89] have determined the photoelectron spectra of these $(\eta^5\text{-}C_5H_4X)Rh(CO)_2$ compounds, and they have obtained information on the extent of σ- and π-bonding in these systems. On the basis of this, a two parameter equation was used to estimate the rates of reaction for each substituent relative to the known value for the compound where X = H. The predicted rate constants, by this method of considering both σ- and π-bonding contributions, are in good agreement with the experimental values of k_2 (Fig. 3). If the π-contribution to bonding is not used, then the points for X = Cl and $N(CH_3)_2$ are far off the line. This supports the earlier suggestion[87] that Cl and $N(CH_3)_2$ are efficient in resonance stabilization of the slipped intermediates "$(\eta^3\text{-}C_5H_4X)Rh(CO)_2PPh_3$".

4.2. *Heterocycle metal carbonyls*

Other systems investigated in our laboratory relate to $(\eta^5\text{-}C_5H_5)Mn(CO)_3$. It had been shown earlier[90] that this compound does not react with PPh_3 at 140°C over a 3-day period. Based on the ring-slippage mechanism for CO substitution, it was felt that with a more electron-withdrawing ring the reaction rate would increase. Instead of putting electron-withdrawing substituents on the ring, it was decided to prepare and test some η^5-heterocyclic systems such as **I**. Unfortunately these compounds have been studied much less[91] than have their ubiquitous η^5-carbocyclic analogues, so several of the compounds investigated had to be prepared and characterized for the first time.[92] The results showed that only the N-heterocycle manganese compounds undergo CO substitution by phosphines and phosphites. These results were attributed to the greater electronegativity[93] of N (3.0) than that of C (2.5), P (2.1) and As (2.0). Since the latter three $(\eta^5\text{-ring})Mn(CO)_3$ compounds did not react, it was not possible to test the hypothesis that reactivity may correlate with the electronegativity of element E in the ring.

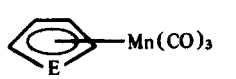

(E = N,P,As)

I

Knowing that $(\eta^5\text{-}C_5H_5)Rh(CO)_2$ reacts readily, it was decided to prepare and test the corresponding $(\eta^5$-heterocycle$)Rh(CO)_2$ compounds. A plausible approach to the syntheses of these compounds is that reported[94] for the preparation of $(\eta^5\text{-}C_5H_5)Rh(CO)_2$ by the reaction of $[Rh(CO)_2Cl]_2$ with $C_5H_5^-$. However, reaction with the pyrrole anion does not give the desired

product, but affords a unique bridged dimer[95] [eq. (28)]:

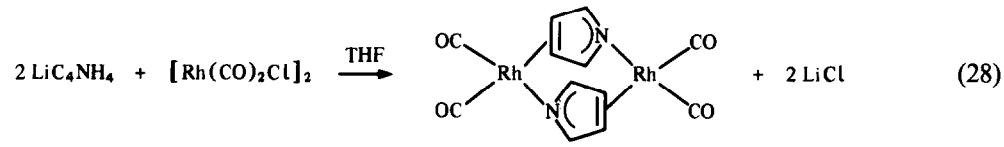

(28)

This leaves the hypothesis that the reaction rates of η^5-heterocycle metal carbonyls will correlate the electronegativity of the hetero-elements untested.

One question addressed for the $\eta^5 \rightarrow \eta^3 \rightarrow \eta^5$ ring-spillage mechanism of the associative reactions of the (η^5-pyrrolyl)$Mn(CO)_3$ compounds was the formulation of the η^3 intermediate. The question is does the N atom form part of the allyl, and if so is it an η^3-1-azaallyl or an η^3-2-azaallyl? In an attempt to obtain some information on this point the dimethylpyrrolyl manganese complexes **II** and **III** were prepared and examined.[92] The rate constants, k_2 (M^{-1} s^{-1}), of the reaction with $P(n\text{-}Bu)_3$ at 130°C of the parent compound **I** and of **II** and **III** are, respectively, 3.4×10^{-4}, 1.4×10^{-4} and 1.2×10^{-6}. The slower rates of the dimethyl derivatives, **II** and **III**, than the parent, **I**, is in accord with an $\eta^5 \rightarrow \eta^3 \rightarrow \eta^5$ mechanism where the methyl electron-donating substituents retard electron delocalization into the ring ligand. The slower rates are also consistent with an associative reaction where increased substitution on the η^5-ring leads to a more crowded transition state.

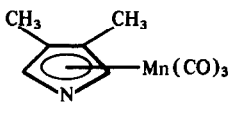

II

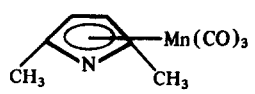

III

It is important to note that the position of the methyl substituents on the η^5-pyrrolyl ring has a marked effect on the rate of associative CO substitution. Thus, compound **II** reacts 10^2 times faster than does compound **III**, although both have two methyl groups on the η^5-cyclic ligand. This difference does not seem due to electronic factors because the C—O stretching frequencies of the two complexes are approximately equal in energy, suggesting the electron densities on the metals are about the same. Likewise, the pK_as of the two free pyrroles are almost identical, indicating comparable electronic characteristics of both rings. Therefore, it appears that steric factors are responsible for the reactivity differences of **II** > **III**. The more crowded transition state of **III** over **II** suggests an η^3-2-azaallyl bonding mode of the metal moiety to the pyrrolyl ring (**IV**). Further support for **IV** is provided[96] by the X-ray structure of **II**, which shows a "slip-distortion" of the $Mn(CO)_3$ moiety away from the ring centroid toward N. It appears this slippage is largely steric in origin, since no allylene type bonding is observed in the pyrrolyl ring of **II**.

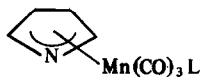

IV

4.3. *Indenyl ligand effect*

Mawby and co-workers[97] were the first to study the kinetics and mechanisms of reactions of η^5-indenyl metal carbonyls compared with the corresponding η^5-cyclopentadienyl compounds. They found[97a] that the methyl migration in $Mo(\eta^5\text{-}C_9H_7)(CO)_3CH_3$ was ligand assisted. The S_N2 nature of this reaction was attributed to the ability of indenyl ligand to undergo an η^5- to η^3-migration allowing associative attack on the metal centre. They believed that the benzene of the indenyl ring provided stabilization of the η^3-allyl intermediate; the cyclopentadienyl analogue reacted 10 times slower. They[97b] also compared CO substitution by phosphines for the compounds $Mo(\eta^5\text{-}C_5H_5)(CO)_3X$ and $Mo(\eta^5\text{-}C_9H_7)(CO)_3X$ (X = Cl, Br, I), and found that CO substitution for the

cyclopentadienyl compound proceeds by a purely dissociative (S_N1) pathway, whereas the indenyl compound is substituted by both an S_N1 and ligand association (S_N2) pathway. There is a rate enhancement of about 6000 for the S_N1 path for the indenyl compound, compared to the cyclopentadienyl compound, in addition to the previously observed creation of an S_N2 path by the indenyl ligand. In another study[97c] the rate of CO replacement by $P(OEt)_3$ for $Fe(\eta^5\text{-}C_5H_5)(CO)_2I$ and $Fe(\eta^5\text{-}C_9H_7)(CO)_2I$ was compared. In both cases the replacement of CO by $P(OEt)_3$ proceeds by an S_N1 pathway, with the indenyl compound reacting 575 times faster than the cyclopentadienyl compound. To show that the rate enhancement was due to the electronic nature of the indenyl ligand, the arene ring was hydrogenated and the rate of CO replacement for this compound was only half the rate observed for the cyclopentadienyl compound.

Our investigations[86,98] of the associative CO replacement reactions of the indenyl compound $(\eta^5\text{-}C_9H_7)Rh(CO)_2$ show it to react 10^8 times faster than does the corresponding cyclopentadienyl compound, so it was decided to refer to this large rate enhancement as the *kinetic indenyl ligand effect*. Since this rate effect for S_N2 ligand substitution is so large, it was felt that $(\eta^5\text{-}C_9H_7)Mn(CO)_3$ might react with phosphines and phosphites even though the cyclopentadienyl compound is inert[90] to thermal CO substitution at 140°C. This was found[99] to be correct, and it appears that the usual ring-slippage mechanism is involved [eq. (29)]:

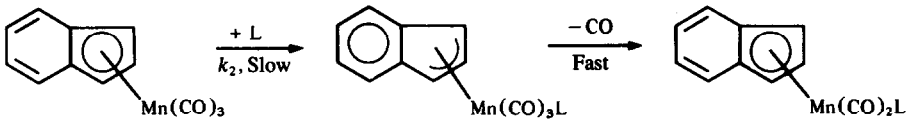

(29)

As suggested earlier,[97] the driving force for this indenyl rate effect is the aromatization of the fused six-membered ring in the transition state for reaction. Further rate enhancement in going to two fused six-membered rings, fluorenyl, is only 10^3 times instead of the 10^8 times for addition of the first six-membered ring. Relative rates of CO substitution for analogous metal carbonyls with different η^5-ring ligands increase in the order cyclopentadienyl <<< indenyl < fluorenyl. Recent studies[100] show that in addition to the monosubstitution of CO, strongly basic nucleophiles react further to displace the fluorenyl ligand and give as the final product $HMn(CO)_3L_2$.

Research is now in progress[101] on the kinetics of CO substitution of eight different methyl substituted indenyl complexes, $(\eta^5\text{-Ind})Rh(CO)_2$, with a variety of different nucleophiles. As the number of methyl groups on the ring increases, there is the expected decrease in rate of substitution. The rate decrease is caused by the electron-donating properties of the methyl groups, but steric factors predominate when there are several methyl substituents and particularly if these are on the five-membered ring. With these sterically hindered systems, the nucleophilic strength of the entering ligand is largely controlled by its cone angle. For example, compounds **V** and **VI** react with $P(n\text{-}Bu)_3$ and with PCy_3 to give the ratio of rate constants $k(n\text{-}Bu)_3/kPCy_3 = 100$ for **V** and 250 for **VI**. Since the two phosphines are of about the same basicity, their nucleophilic strengths are sterically controlled with the larger PCy_3 being the poorer nucleophile towards these two substrates. The application of empirical equations developed earlier[76,77] for the correlation of nucleophilic reactivity based on basicity and steric factors, supports the predominance of steric factors for reactions with these crowded substrates.

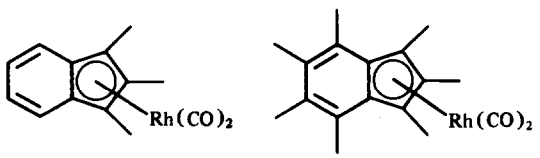

V **VI**

Another interesting series of compounds is currently under investigation. These are metal carbonyl derivatives of trindene (Td),[102] with isolobal groups of $M(CO)_3$ or $M(CO)_2$. Preliminary results[103] show that each of these three compounds react with $PPhMe_2$ to afford slippage of $\eta^5 \rightarrow \eta^1$

at one $Re(CO)_3$. At room temperature the relative rates of reaction are $(\eta^5\text{-Ind})Re(CO)_3$ > **VII** > **VIII** > **IX**, $(\eta^5\text{-Cp})Re(CO)_3$, where the latter two compounds do not react at these conditions. This result is consistent with the view that the step-wise reactions involve slippage of $\eta^5 \rightarrow \eta^3 \rightarrow \eta^1$, and that the fastest to react is the compound which allows the maximum amount of π-delocalization in the central six-membered ring.

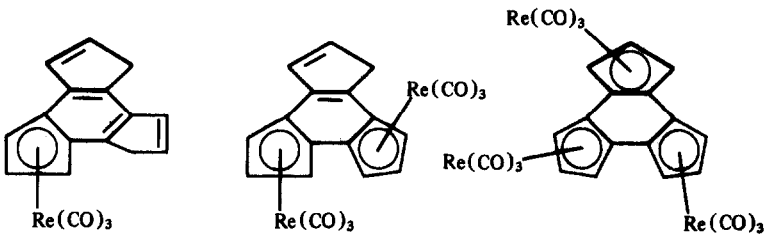

VII **VIII** **IX**

4.4. *Allyl metal carbonyls*

Finally, CO substitution reactions of π-allyl derivatives, $(\eta^3\text{-}C_3H_4X)Mn(CO)_4$, with different nucleophiles were investigated[104] [eq. (30)]:

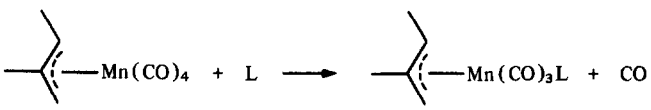

(30)

Earlier studies indicated that CO replacement in $(\eta^3\text{-}C_3H_4X)Co(CO)_3$ takes place by an S_N1 process,[105] whereas $(\eta^3\text{-}C_3H_4X)Fe(CO)_2(NO)$[106] reacts by an $\eta^3 \rightarrow \eta^1 \rightarrow \eta^3$ associative mechanism.

Our studies[104] of the kinetics and mechanism of CO substitution in $(\eta^3\text{-}C_3H_4X)Mn(CO)_4$ show the rates of reaction are first-order in substrate and zero-order in reagent concentrations. This suggests either an S_N1 process, or an $\eta^3 \xrightarrow{\text{slow}} \eta^1 \xrightarrow{\text{fast}} \eta^3$ mechanism. Unequivocal proof that the latter mechanism is not correct was obtained by starting with $(\eta^1\text{-}C_3H_4X)Mn(CO)_4$ L and finding that its rate of CO loss is much too slow to account for the overall CO substitution rate of the reaction [eq. (30)]. Considering the effect of substituents in the 1- or 2-positions (X) of $(\eta^3\text{-}C_3H_4X)Mn(CO)_4$ on its rate of reaction gave some interesting results. Alkyl groups, electron-donating, on the allyl are expected to enhance the electron density on the metal, promoting more π-backbonding and a slower rate of CO substitution. This is what was found for ligands of the 1-*syn*-allyl type, but corresponding 1-*anti*-allyl ligands enhance the rate of reaction. It seems reasonable this should happen, because in the *syn* structure the substituent group points away from the metal and offers no steric destabilization to the CO ligands. In contrast, the *anti* structure has the group in towards the metal and does sterically promote loss of CO. Substituents in the 2-position of the allyl all increase the rate of reaction. This seems to be a steric effect because the rate increase correlates the substituent size, and because the X-ray structure of **X** shows that the group in the 2-position eclipses one of the CO ligands. The result is in keeping with the general steric rate acceleration of S_N1 reactions.[3b]

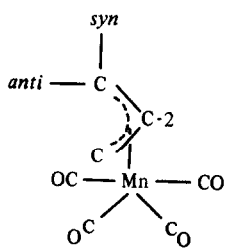

X

5. LIGAND SUBSTITUTION LABILITY OF 2ND ROW TRANSITION METAL CARBONYLS

Ligand substitution reactions of octahedral and of square-planar Werner metal complexes for a given transition metal triad generally decrease with increasing atomic number of the metal,[3,3b] for example, rates of Cl^- substitution of $[M(NH_3)_5Cl]^{2+}$ decrease in the order Co > Rh > Ir. As with most generalities, this one also has some exceptions with the 2nd row member of a given triad forming the most substitution labile metal complexes.[111]

5.1. *Mononuclear complexes*

However, it has now long been known[2] that for complexes of metals in low oxidation states, organometallic compounds, the 2nd row transition metal complex of a given triad is generally the most substitution labile, for example, rates of CO substitution of $CpM(CO)_2$ differ in the order Co < Rh > Ir. Table 3 gives specific examples, with appropriate references, which show that the rates of ligand substitution in these systems vary in the order *1st row < 2nd row > 3rd row*. To my knowledge, the only known exception to this general order of CO substitution in mononuclear metal carbonyls is for the vanadium triad of $CpM(CO)_4$[108,109] where the rates decrease in the order V > Nb > Ta.

Since rapid ligand substitution is essential in any use made of such compounds in homogeneous catalysis,[60] it is not surprising to find that most commercial processes make use of 2nd row transition metal (Mo, Ru, Rh or Pd) organometallics as homogeneous catalysts. This rate variation of 1st row < 2nd row > 3rd row seems to hold, regardless of mechanism. For example, the triads of $M(CO)_6$ and of $M[P(OEt)_3]_4$ react by a dissociative process, whereas the triad of $CpM(CO)_2$ reacts by an associative process. For the triad $Cp_2M(CO)_2$, the Ti compound reacts by an S_N1 mechanism but the Zr and Hf compounds react by an S_N2 process. Similarly, for $CpM(CO)_4$ an S_N1 reaction is involved with V, where Nb and Ta react by competing S_N1 and S_N2 pathways. In these two triads the associative reactions of the 2nd and 3rd row metal complexes are attributed to their larger size which permits nucleophilic attack at the metal, whereas this does not happen with the sterically more crowded 1st row metal complexes. The V triad of $CpM(CO)_4$ are anomalous[109] in that the rates decrease with increasing atomic number of the metal.

As to why 2nd row transition metal organometallic compounds are generally the most substitution labile for a given triad of metals remains somewhat of an open question. Early explanations were given in terms of σ- and π-bonding.[112] A similar explanation was given[113] in terms of the low electronegativity of 1st row metals as one factor, and a good matching of the orbital energy of 3rd row metals with the ligand as another factor. The latest word[114] on this is the detailed molecular orbital calculations based on density functional theory to estimate the first CO ligand dissociation energy ΔH of $M(CO)_n$ for the three binary metal carbonyl triads $M(CO)_6$ (M = Cr, Mo, W), $M(CO)_5$ (M = Fe, Ru, Os) and $M(CO)_4$ (M = Ni, Pd, Pt). For each triad of transition metals, the calculated ordering of the M—CO bond strengths (including relativistic effects) is $3d > 5d > 4d$. Whatever the reason, the fact remains that in general the 2nd row transition metal organometallic compounds react the fastest for a given triad.

Table 3. Relative CO substitution rates for corresponding metal carbonyls of a given transition metal triad

$Cp_2Ti(CO)_2$[107]	$CpV(CO)_4$[108]	$Cr(CO)_6$[8]	$Mn_2(CO)_{10}$[110]	$Fe(CO)_5$[6]	$CpCo(CO)_2$[80]	$Ni[P(OEt)_3]_4$[112]
∧	∨	∧	∧	⇈	∧	∧
$Cp_2Zr(CO)_2$[107]	$CpNb(CO)_4$[109]	$Mo(CO)_6$[8]	$Tc_2(CO)_{10}$[110]	$Ru(CO)_5$[7]	$CpRh(CO)_2$[80]	$Pd[P(OEt)_3]_4$[112]
∨	∨	∨	∨	⇊	∨	∨
$Cp_2Hf(CO)_2$[107]	$CpTa(CO)_4$[109]	$W(CO)_6$[8]	$Re_2(CO)_{10}$[110]	$Os(CO)_5$[6]	$CpIr(CO)_2$[80]	$Pt[P(OEt)_3]_4$[112]

5.2. *Metal carbonyl clusters*

Kinetic studies of CO substitution in metal carbonyl clusters have been largely limited to the clusters $M_3(CO)_{12}$ (M = Fe, Ru, Os)[9] and M_4CO_{12} (M = Co, Rh, Ir).[115] The rates of CO displacement by a dissociative process for $M_3(CO)_{12}$ decrease in the order Fe > Ru > Os (Table 1). It has been suggested[115] that bridging carbonyl groups may enhance cluster lability, because they withdraw more electron density from the metal than do terminal carbonyls.[116] Since $Fe_3(CO)_{12}$ is the only member of this triad to have bridging COs, it is expected to be the fastest to react. In accordance with this concept of bridging COs, the iron cluster reacts 10^8 times faster than does $Fe(CO)_5$. In contrast, the rates of reaction of the Ru and the Os clusters, without bridging COs, are about the same as the rates of the corresponding $Ru(CO)_5$ and $Os(CO)_5$ (Table 1). It should further be noted that the anomalously slow reaction of $Fe(CO)_5$ may result from a spin-forbidden dissociative process (see Section 2).

Extensive mechanistic studies[115,117] have been reported on $Ir_4(CO)_{12}$ where CO substitution occurs by a two-term rate law with a dominant second-order process for phosphorus and carbon nucleophiles. The mechanism of CO substitution in $Co_4(CO)_{12}$ and in $Rh_4(CO)_{12}$ is less well understood. The reaction of $Co_4(CO)_{12}$ with L to yield $Co_4(CO)_{11}L$ was too fast to measure, suggesting an associative mechanism.[118] Carbonyl substitution in $Rh_4(CO)_{12}$ occurs so rapidly that only a lower limit could be set on the rate of reaction.[115] We decided to investigate these systems, using stopped-flow spectrophotometry or a variable low temperature IR cell. The results[63] showed that both clusters react by two-term rate laws [eq. (7)]. Relative reactivities for the $M_4(CO)_{12}$ clusters by the dissociative pathway are Co < Rh > Ir, and by the associative pathway Co << Rh >> Ir. This is in accordance with the 2nd row transition metal cluster being the fastest to react, as is true of mononuclear metal complexes, but the differences in rate are larger for the clusters.

Similar results[62,63] were obtained by CO substitution of the more stable clusters $M_4(CO)_9[HC(PPh_2)_3]$ [see eqs (22) and (23) for structure]. Here relative reactivities for the k_1 pathways are Co (1), Rh (667), Ir (10^{-5}), and for the k_2 pathways are Co (1), Rh (10^6), Ir (10^{-3}). The most notable chemical feature is the exceptional reactivity of the rhodium cluster, whose substitutions proceed within seconds at room temperature. Also a unique aspect of substitution in cluster compounds compared to mononuclear metal carbonyls is the presence of rapid associative pathways for CO substitution. This may result from the presence of low-lying acceptor orbitals for nucleophilic attack derived from metal–metal antibonding orbitals of the cluster.

6. CATALYSIS OF CO SUBSTITUTION

6.1. *Acid catalysis*

As mentioned earlier [eq. (4)] the CO exchange of $Fe(CO)_5$ is acid catalysed. This is believed to involve protonation at the metal, to form $[HFe(CO)_5]^+$ which then is substitution labile. Albers, Coville and co-workers[119] have recently shown that a variety of transition metal salts catalyse CO substitution of $Fe(CO)_5$ and $Cr(CO)_6$ by different entering ligands. Catalysis perhaps involves attack of a CO oxygen by the metal ion to give M—CO---M^{2+}, which weakens the M—CO bond and enhances the rate of reaction. Lewis acids are known[23] to interact with certain metal carbonyls to form adducts of the type M—CO—BX_3 (see Section 7).

6.2. *Base catalysis*

The rate of CO substitution of $Fe(CO)_2(NO)_2$, with the poor nucleophile $AsPh_3$, was found[120] to markedly increase in the presence of added base [eq. (31)]:

$$Fe(CO)_2(NO)_2 + AsPh_3 \xrightarrow{B} Fe(CO)(NO)_2AsPh_3 + CO \qquad (31)$$

B = R_4NX (X = Cl, Br, I, N_3), $NaOCH_3$, pyrrolidine, imidazole.

The reactions followed the rate law given by eq. (32):

$$\text{Rate} = k_B[Fe(CO)_2(NO)_2][B]. \qquad (32)$$

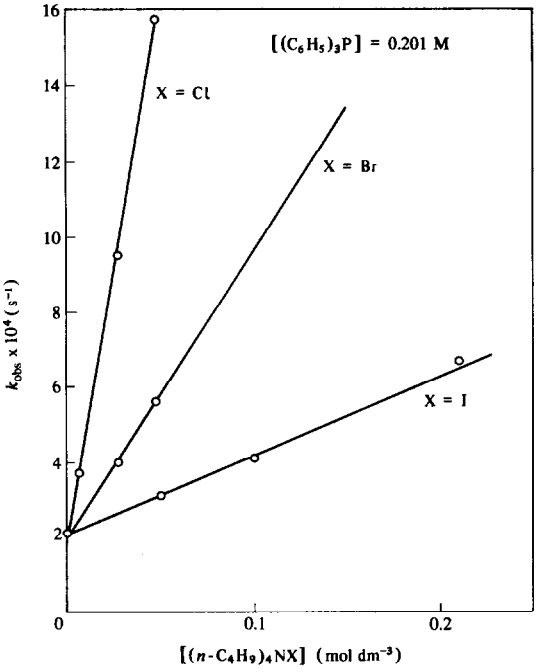

Fig. 4. Plot of k_{obs} vs $[(n\text{-}C_4H_9)_4NX]$ for the reaction of $Fe(NO)_2(CO)_2$ with $(C_6H_5)_3P$ in the presence of $(n\text{-}C_4H_9)_4NX$ in dichloromethane at 25°C.

A plot of the observed rate constants vs halide ion concentrations is shown in Fig. 4. The mechanism proposed for this catalytic pathway involves attack by the catalyst on the carbon of a CO ligand [eq. (33)]:

$$(ON)_2(OC)Fe{=}C{=}\bar{O} \xrightarrow[k_B]{+B} \text{“}(ON)_2(OC)Fe{-}\underset{\|}{\overset{O}{C}}{-}B\text{”} \xrightarrow[-B\ -CO]{+AsPh_3\ \text{Fast}} Fe(CO)(NO)_2AsPh_3. \tag{33}$$

This is believed to be the site of attack, because the rate decreases in the order $Cl^- > Br^- > I^-$. The hard base Cl^- is expected to preferentially attack the hard positive carbon site rather than the soft metal. Consistent with this is the observation that these same bases do not catalyse the reactions of $Co(CO)_3(NO)$, presumably because only one NO does not remove enough electron density from the metal to render the carbonyl carbons sufficiently positive for base attack. There are a large number of examples of base attack on the more positive carbons of metal carbonyls.[2]

For this base catalysis of CO substitution of $Fe(CO)_2(NO)_2$, it was suggested that the formation of $Fe{-}\underset{\|}{\overset{O}{C}}{-}B$ weakens the Fe—C bond and promotes the loss of the CO that was attacked by base. However, there is no evidence this is the CO that is replaced, and some years later it was suggested[121] that base catalysis results from the *cis*-labilization of a CO adjacent to the carbonyl attacked by base [eq. (34)]:

$$(OC)_{n-1}MCO \xrightarrow[k_B]{+B} (OC)_{n-1}M{-}\underset{B}{\overset{O}{C}} \xrightarrow[\text{Fast}]{-CO} (OC)_{n-2}M{-}\underset{B}{\overset{O}{C}} \xrightarrow[\text{Fast}]{+L} L(OC)_{n-2}M{-}\underset{B}{\overset{O}{C}} \xrightarrow[\text{Fast}]{-B} (OC)_{n-1}ML \tag{34}$$

It has also been found[122] that base catalysis may involve attack on the metal followed by *cis*-labilization of an adjacent CO. For example, $(n\text{-Bu})_3PO$ catalyses ^{13}CO exchange with $M(CO)_5L$ (M = Cr, Mo, W) but not with $M(CO)_6$. This happens only if L is a good leaving group, which can readily be replaced by the catalyst $(n\text{-Bu})_3PO$.

7. MIGRATORY INSERTION REACTIONS

7.1. *Methyl migration*

Migratory CO insertion into transition metal alkyl bonds is one of the most fundamental and extensively studied reactions in organometallic chemistry[2] and in homogeneous catalysis.[60] The early discoveries[123] of insertion reactions in organometallic chemistry were soon followed by the elegant experiment[124] showing that the labelled CO added to convert $CH_3Mn(CO)_5$ into $(CH_3CO)M(CO)_5$ is not the CO acetyl, but one of the five terminal COs. The term insertion describes the overall result, but we felt it was mechanistically misleading and that the reactions really involve ligand migration. An experiment was designed in an attempt to learn if the reaction is mechanistically insertion or methyl migration.[125] This was done by decarbonylating *trans*-$(CH_3CO)Mn(CO)_4PPh_3$ and determining the isomeric structure of the $CH_3Mn(CO)_4PPh_3$ product. The product was the *cis*-isomer which, applying the law of microscopic reversibility, requires the reverse process to proceed by methyl migration and not CO insertion that would give the *trans*-isomer. Unfortunately it was later shown[126] that although the conclusion reached was correct, the experiment was flawed because at the conditions used the starting *trans*-acetyl isomerizes to the *cis*-acetyl prior to decarbonylation. A similar experiment using ^{13}CO has shown this to be a methyl migration reaction, and these reactions are now best described as ligand migratory insertion reactions.

Kinetic studies were made[127] of the methyl migration reactions of $CH_3Mn(CO)_5$, $(\eta^5\text{-}C_5H_5)Fe(CO)_2CH_3$ and $(\eta^5\text{-}C_5H_5)Mo(CO)_3CH_3$ with a variety of entering ligands. In all cases, the rates of reaction were found to depend on ligand concentration with the same limiting rate being reached at high ligand concentrations. The results were explained in terms of a solvent and/or ligand assisted mechanism, eq. (35):

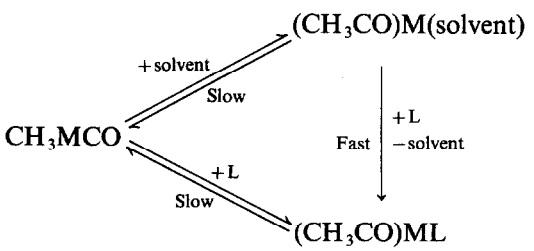

(35)

(other ligands not shown)

One of the more recent publications[128] on the mechanism of these reactions largely resembles that shown in eq. (35).

7.2. *Acid-induced reaction*

One final point is that CO migratory insertion reactions, like some CO substitution reactions, can be induced by Lewis acids. For example, the rate of methyl migration of $CH_3Mn(CO)_5$ in the presence of $AlCl_3$ or $AlBr_3$ is 10^8 times faster than in the absence of Lewis acid.[24] One possible mechanism for this rate enhancement is coordination of the Lewis acid to the oxygen atom of a

carbonyl in $CH_3Mn(CO)_5$, followed by methyl migration and coordination of one of the halide groups [eq. (36)].

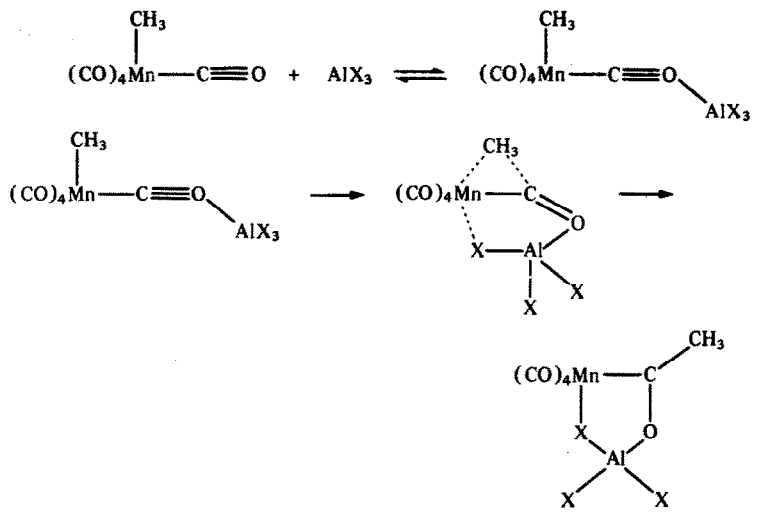

(36)

8. 17-ELECTRON METAL CARBONYLS

8.1. $V(CO)_6$

It is well known that for molecular transition metal organometallic compounds, 18-electrons is the magic number for maximum stability. A decade ago Brown and co-workers[129] reported that, unlike 18-electron substitution inert metal carbonyls, 17-electron metal carbonyl radicals such as $Mn(CO)_5$ and $Re(CO)_5$ are substitution labile. These metal carbonyl radicals are formed, and studied, *in situ* by the photochemical homolytic metal–metal bond cleavage of $M_2(CO)_{10}$. We decided to investigate the kinetics and mechanism of CO substitution of $V(CO)_6$, the only known[130] stable homoleptic metal carbonyl radical. At the time it was believed that $Mn(CO)_5$ reacts by a dissociative process,[129] whereas $Re(CO)_5$ involves an associative process.[131] It was later found[132] that $Mn(CO)_5$ reacts by an associative process, and it is now generally agreed[133] that the rapid reactions of metal carbonyl radicals are S_N2. The reaction of $V(CO)_6$ with a variety of ligands [eq. (37)]:

$$V(CO)_6 + L \longrightarrow V(CO)_5L + CO \tag{37}$$

is first-order in carbonyl and first-order in ligand concentrations.[134] The most significant result of this study was that it allowed, for the first time, a quantification of the rates of CO substitution for corresponding 17- and 18-electron metal carbonyls. The relative rates of associative CO substitution by $P(n\text{-}Bu)_3$ of analogous metal carbonyls is as follows:

	$Cr(CO)_6$ (18-electrons)[8]	$V(CO)_6$ (17-electron)[134].
Relative rates	1	10^{10}

That the associative rate of reaction for a 17-electron system is faster than for the analogous 18-electron system is readily understood, because it surely is easier for a nucleophile to attack a 17-electron than an 18-electron substrate. What is not yet understood is the extremely large magnitude of the rate enhancement. Furthermore, the reactions of $V(CO)_6$ show only slight sensitivity to the steric properties of an attacking nucleophile. This is puzzling, because a mechanism that involves a seven-coordinate transition state is expected to exhibit steric preferences. This observation suggests that the transition state occurs at a relatively long V—nucleophile distance. Such may be the case, since the electron pair of the nucleophile is expected to attack a half-filled $d(t_g)$ orbital of $V(CO)_6$ and form a two-centre three-electron bond. This bond would have a bond order of 1/2, so the transition state would have a long V—nucleophile distance in keeping with the low sensitivity to the cone angle of the entering nucleophile.

8.2. (η^5-*ligand*)$_2$V(CO)

Our investigation of reactions of 17-electron systems have been exended to different (η^5-ligand)$_2$V(CO) compounds (**XI, XII** and **XIII**). The vanadocene and decamethylvanadocene (**XI**) carbonyls are substitution labile and react by an associative mechanism. The pentadienyl compounds (**XII**) are more inert and react at elevated temperatures by a dissociative pathway.[135] The cyclohexadienyl compound (**XIII**) affords a rare example[136] of a slow associative substitution for a 17-electron metal carbonyl.

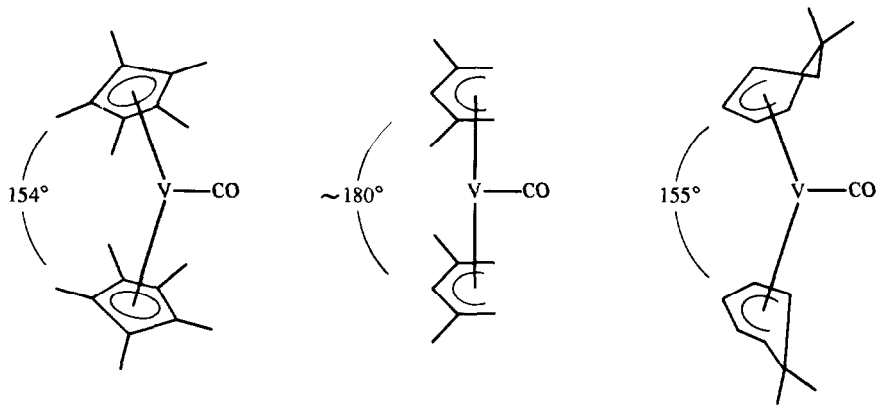

XI **XII** **XIII**

The more rigid structure and shorter M—C bond lengths of **XII** cause steric retardation of nucleophilic attack, so substitution takes place by a slow dissociation process. Further, a dihedral angle of about 150° for **XI** and **XIII** compared to 180° for **XII** indicates that the former two have a more sterically accessible binding site for nucleophilic attack.

The IR carbonyl stretching frequencies and EPR isotropic coupling constants are also informative (Table 4). The greater electron-withdrawing ability of the dimethyl cyclohexadienyl ligand compared to cyclopentadienyl is reflected in the CO frequencies of 1912 and 1881 cm^{-1}, respectively. One might expect that the more positively charged vanadium in **XIII** would be more susceptible to nucleophilic attack than in **XI**. However, the opposite is observed. The rate of substitution of **XIII** is 10^{-4} times that of **XI**. This is believed to reflect the position of the unpaired electron. If this electron occupies a largely metal-based singly occupied orbital, then a more positively charged vanadium will lead to reduced delocalization of this unpaired spin from the metal centre. EPR data in Table 4 are consistent with this argument. It would appear that nucleophilic attack on a metal orbital containing an electron may be retarded relative to the same system with that electron largely delocalized onto the ligands. Thus, **XI** is expected to have a more favourable electronic distribution of the unpaired electron for nucleophilic attack (represented in Table 4 as + for electronic, relative − for **XII** and **XIII**).

Table 4. Associative rates of CO exchange and EPR data for (η^5-L)$_2$VCO complexes

Complex	k_2[a] (M^{-1} s^{-1})	ν(CO) (cm^{-1})	A_{iso} (G)	Steric[b]	Electronic[b]
XI	*ca* 800	1881	28.8	+	+
XII	0.004	1959	79.1	−	−
XIII	0.073	1912	71	+	−

[a] At 60°C in decalin.

[b] Favourable for associative reaction represented by +, unfavourable represented by −.

Compound **XII** reacts almost exclusively by a dissociative pathway, in accordance with associative retardation by both steric and electronic factors. Complex **XIII** reacts entirely by an associative pathway, although its electronic retardation is expected to be similar to **XII**. This would suggest that the greater steric accessibility of **XIII** relative to **XII** permits **XIII** to react by an associative pathway. However, electronic factors are important, and in the case of **XIII** it gives us a rare example of a slow associative substitution reaction for a 17-electron metal carbonyl. The fastest to react is **XI** which experiences less steric and less electronic retardation than do compounds **XII** and **XIII** to associative substitution.

It appears[133] that the rapid S_N2 CO substitution reactions of 17-electron metal carbonyls take place via a 19-electron transition state (or intermediate). At one point it was believed that $(\eta^5\text{-}C_5H_5)_2VCO$ may react by a ring-slippage mechanism (see Section 4) in order to maintain an 18-electron count in the transition state. It was decided to prepare and investigate $(\eta^5\text{-indenyl})_2VCO$, thinking it would react more rapidly than the cyclopentadienyl compound due to the indenyl ligand effect. Much to our surprise, the indenyl compound rapidly reacts with CO to afford $(\eta^5\text{-indenyl})(\eta^3\text{-indenyl})V(CO)_2$ with the **XIV** structure determined by X-ray diffraction.[137] This shows the strong tendency towards $\eta^5 \rightarrow \eta^3$ slippage of the indenyl ligand in a 17-electron system, as is known in 18-electron systems.[81]

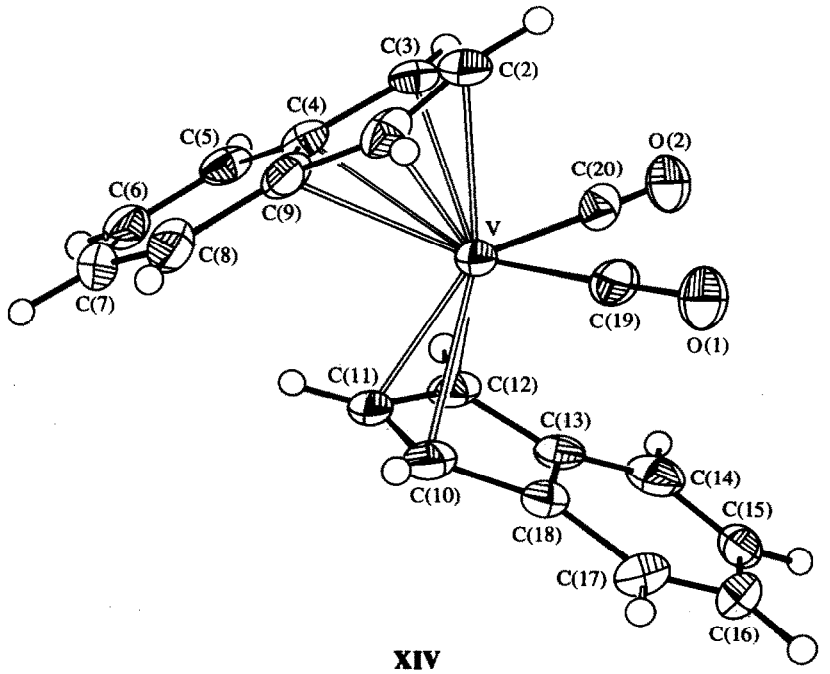

XIV

Although the rate of associative CO substitution of $V(CO)_6$(17e) is 10^{10} times faster than the corresponding reactions of $Cr(CO)_6$ (18e), we find[136] that the dissociative rates of $(\eta^5\text{-}C_5H_5)(\eta^5\text{-}C_5H_7)VCO$ (17e) and $(\eta^5\text{-}C_5H_5)(\eta^5\text{-}C_5H_7)CrCO$ (18e) are about the same. Qualitatively, the two contrasting results are readily understood on the basis of an energy/reaction coordinate diagram. For the rapid associative substitution of a 17- vs 18-electron system, it is clear that the less stable 17-electron substrate involves a 19-electron transition state which is more stable than the 20-electron transition state required by the more stable 18-electron substrate. The lower activation energy involved in the associative substitution reaction of the 17-electron system leads to a faster reaction rate compared to the 18-electron system [Fig. 5(a)]. Contrast this with the well-known fact that 16-electron compounds are generally more stable than their 15-electron counterparts, and it follows that the activation energies for dissociative substitution of 17- and 18-electron systems may be of similar magnitude [Fig. 5(b)]. Thus one expects differences in rates of dissociative ligand substitution of 17- and 18-electron systems to be smaller than for corresponding associative reactions.

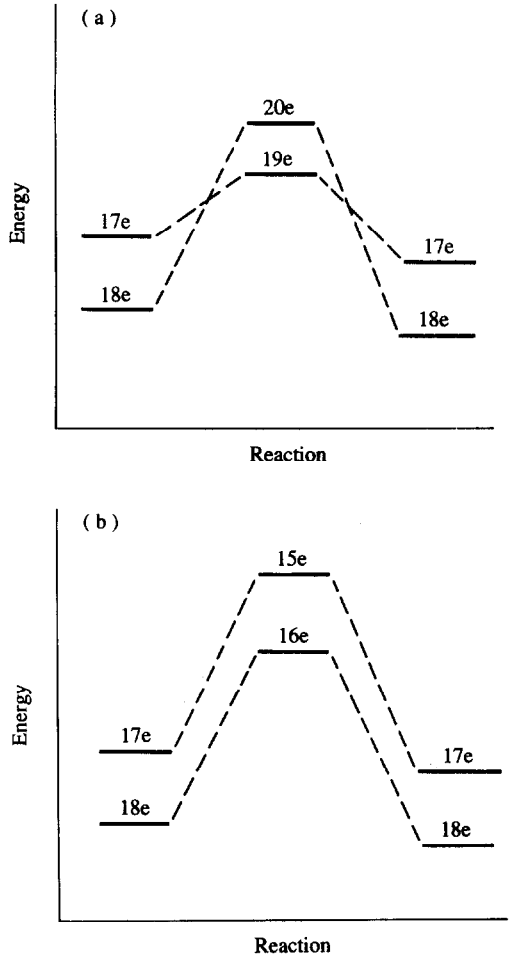

Fig. 5. (a) Energy/reaction coordinate diagram for an associative 18- and 17-electron ligand substitution reaction. (b) Energy/reaction coordinate diagram for a dissociative 18- and 17-electron ligand substitution reaction.

9. OXYGEN ATOM TRANSFER TO METAL CARBONYLS

9.1. $M(CO)_6$ (M = Cr, Mo, W)

Hieber and Lipp[138] first reported the use of pyridine N-oxide to facilitate CO release from $Fe(CO)_5$. A decade later, Alper and Edward[139] established the generality of the reaction and suggested a possible mechanism. Since that time the reaction has been extensively used for the syntheses of metal carbonyl derivatives.[119,140] In spite of this, ours was the first kinetic study[141] of the reaction.

The initial study was on the reactions of $M(CO)_6$ (M = Cr, Mo, W) with PPh_3 in the presence of $(CH_3)_3NO$ [eq. (38)]:

$$M(CO)_6 + PPh_3 + (CH_3)_3NO \longrightarrow M(CO)_5PPh_3 + CO_2 + (CH_3)_3N. \quad (38)$$

The reactions are extremely rapid compared with the rates[8] of thermal substitution in the absence of $(CH_3)_3NO$. The rapid substitution results from the efficient annihilation of one of the CO ligands by converting it into CO_2, which is a poor ligand and a good leaving group. The reactions [eq. (38)] have a second-order rate law [eq. (39)]:

$$-d[M(CO)_6]/dt = k[M(CO)_6][(CH_3)_3NO] \quad (39)$$

being first-order in carbonyl and in $(CH_3)_3NO$, but zero-order in entering ligand, PPh_3, concentration. The rate law is consistent with an associative process, where both bond-making by attack of the $(CH_3)_3NO$ nucleophile and bond-breaking of the M—C bond contribute to the energetics of the rate-determining step. This mechanism is supported by the low values of $\Delta H^{\ddagger}$ and negative values of $\Delta S^{\ddagger}$, which are typical of an associative reaction.

The nucleophilic attack of $(CH_3)_3NO$ is believed to be on C of a CO, because CO_2 is formed and there is ample precedence for such an attack by a variety of nucleophiles.[142] An oxygen atom transfer then forms CO_2, a good leaving group, and generates the very reactive coordinatively unsaturated "$M(CO)_5$" which readily adds the entering ligand [eq. (40)]:

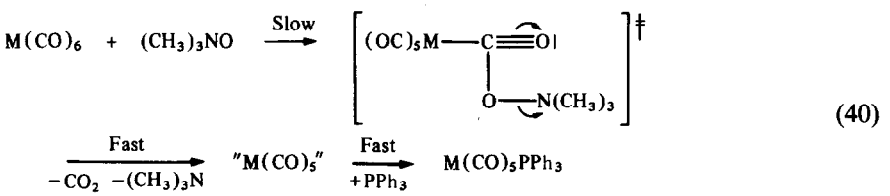

(40)

An alternative four-centre mechanism was easily proven incorrect because it requires the intermediate formation of $M(CO)_5N(CH_3)_3$, which reacts with PPh_3 much too slowly to permit such a pathway for the formation of $M(CO)_5PPh_3$.

The rates of reaction of $M(CO)_6$ decrease in the order W > Mo $\gtrsim$ Cr. Previous studies[143] suggest the ease of nucleophilic attack on C of a metal carbonyl correlates with the C—O stretching frequency of the carbonyl. The higher the value of ν(CO), the more positive is C and the more readily is it attacked by an entering nucleophile. On this basis the rates are expected to vary in the order Mo ~ Cr > W. This is not what is found, and the more rapid rate for $W(CO)_6$ is seen to be due to a more favourable $\Delta S^{\ddagger}$ term, which is perhaps due to a less restricted transition state for the largest member of the triad, tungsten. One other point of interest is the unexpected nucleophilic strength of $(CH_3)_3NO$.[141] The nucleophilic strengths for attack on C of metal carbonyls decrease[142] in the order $CH_3Li > (CH_3)_3NO > PhCH_2MgBr >> N_3^- > NCO^- > NCS^- > Cl^- > Br^- > I^-$. That $(CH_3)_3NO$ is such a strong nucleophile is perhaps because of the high negative charge[144] on O in $(CH_3)_3N^{\delta+} \rightarrow O^{\delta-}$. What is further anomalous is that $(CH_3)_3NO$ is both a good nucleophile and a good oxidizing reagent, since these reactions involve oxidation of CO to CO_2 with reduction of $(CH_3)_3NO$ to $(CH_3)_3N$. Usually a good nucleophile is a good reducing agent,[145] because both processes require the release of electrons by the reagent towards the substrate.

Similar studies were carried out[146] on the monosubstituted compounds $Mo(CO)_5L$ [L = P(*c*-H)$_3$, PPh_3, P(*n*-Bu)$_3$, $N(CH_3)_3$, py, $AsPh_3$, $P(OC_2H_5)_3$, $P(OCH_3)_3$]. Reactions with L in the presence of $(CH_3)_3NO$ follow the same rate law [eq. (39)], and the rates of reaction are slower ($\sim 10^{-3}$) than for the reaction of $Mo(CO)_6$. For ligands L with cone angles less than 135°, the rates of reaction increase with increasing C—O stretching frequencies. For ligands of larger cone angles the rates of reaction are faster than expected on the basis of ν(CO) values, and this is believed to be due to the steric weakening of adjacent M—CO bonds both in the ground and in the transition states for reaction.

Considerable attention[147] has been given to the use of iodosobenzene (PhIO) as an oxygen atom transfer reagent to organic compounds, particularly in the presence of transition metal porphyrins. An example of the use of PhIO in organometallic chemistry is provided by its use[148] in the synthesis of $[(\eta^5\text{-}C_5(CH_3)_5)Re(CO)(NO)PPh_3]BF_4$. It was therefore felt that we should study the oxygen atom transfer properties towards metal carbonyls.

Iodosobenzene is an insoluble polymer,[129] $(PhIO)_n$, but it reacts with and dissolves in methanol as the ester $PhI(OCH_3)_2$. Addition of $Cr(CO)_6$ and CH_3CN to such a solution of $PhI(OCH_3)_2$ results in no reaction, but addition of water catalyses the formation of $Cr(CO)_5(NCCH_3)$.[150] A kinetic study of the reaction in CH_3OH–THF solvent shows the rate is first-order in concentrations of $Cr(CO)_6$, PhIO and H_2O, but inversely proportional to the square of CH_3OH and zero-order in CH_3CN concentrations. These observations are consistent with the following step-wise reactions

[eqs (41), (42), (43) and (44)]:

$$PhI(OCH_3)_2 + H_2O \overset{Fast}{\rightleftharpoons} PhIO + 2CH_3OH \tag{41}$$

$$Cr(CO)_6 + PhIO \xrightarrow{Slow} [Cr(CO)_6—PhIO]^{\ddagger} \tag{42}$$

$$[Cr(CO)_6—PhIO]^{\ddagger} \xrightarrow{Fast} \text{“}Cr(CO)_5\text{”} + PhI + CO_2 \tag{43}$$

$$\text{“}Cr(CO)_5\text{”} + CH_3CN \xrightarrow{Fast} Cr(CO)_5(NCCH_3). \tag{44}$$

The mechanism of the rate-determining step [eq. (42)] for the reaction, is believed to be similar to that for $(CH_3)_3NO$ [eq. (40)] with attack on C by the O atom of PhIO [eq. (45)]:

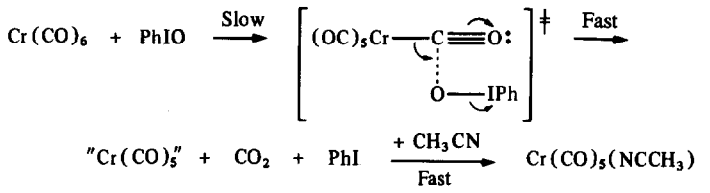

(45)

Not knowing the actual concentration of molecular PhIO in the reaction solutions, it was not possible to quantitatively compare the reactivity of PhIO with that of $(CH_3)_3NO$ towards $Cr(CO)_6$. However, qualitatively it is certain that PhIO is orders of magnitude more effective as an oxygen atom transfer reagent in this reaction than is $(CH_3)_3NO$.

9.2. $M_3(CO)_{12}$ *and* $M(CO)_5$ (M = Fe, Ru, Os)

Although kinetic studies of CO substitution of metal clusters have been extensive,[9,59] ours[151] is the only study of CO substitution in the presence of $(CH_3)_3NO$. In aprotic solvents the reactions [eq. (46)]:

$$M_3(CO)_{12} + L + (CH_3)_3NO \longrightarrow M_3(CO)_{11}L + CO_2 + (CH_3)_3N \tag{46}$$

$$[M = Fe, Ru, Os \text{ and } L = PPh_3, AsPh_3, P(OPh)_3]$$

are too fast to study by conventional spectroscopy, but the rates decrease with added protonic solvents. Reactions are readily monitored at room temperature in the mixed solvent $CHCl_3$–C_2H_5OH (v/v, 2:1), and the rates are inversely proportional to the concentration of C_2H_5OH. It appears this is caused by hydrogen bonding to give $(CH_3)_3NO—HOC_2H_5$, which is unreactive compared with the very reactive free $(CH_3)_3NO$.

The reactions [eq. (46)] follow a second-order rate law, with the rates being first-order in concentrations of metal cluster and of $(CH_3)_3NO$ but zero-order in entering ligand. This rate law is identical with that observed[141] for corresponding reactions of $M(CO)_6$, and it is believed the mechanisms of reaction are the same [eq. (40)]. One marked difference is that the rates of reaction of the clusters are orders of magnitude larger than for the mononuclear carbonyls. This is in agreement with previous studies[143] that show that rates of nucleophilic attack on carbon in metal carbonyls increase with increasing CO stretching frequencies.

In spite of the general correlation between increasing rates of nucleophilic attack on carbon in metal carbonyls with increasing values of ν(CO), just the opposite is observed for this cluster triad with relative rates of $Fe_3(CO)_{12} > Ru_3(CO)_{12} > Os_3(CO)_{12}$. Since the ground-state positive charge on carbon does not control the relative rates, it is necessary to consider factors that can affect the stabilities of the transition states. Gross and Ford[152] report the same rate order for the reactions of $M_3(CO)_{12}$ with CH_3O^- to form $[M_3(CO)_{11}C(O)CH_3]^-$. This reaction also involves attack of CH_3O^- on a C atom, and it was suggested that rates decrease in the order Fe > Ru > Os because the stability of the transition state for reaction decreases in this same order. The reason given for such an order of transition-state stability is that bridging carbonyls are more electron withdrawing[153] and can better accommodate the developing negative charge on the metal cluster as CH_3O^- attacks

a carbonyl carbon in the transition state. The ground-state structure of $Fe_3(CO)_{12}$ in solid and solution contains two bridging carbonyls, whereas $Ru_3(CO)_{12}$ and $Os_3(CO)_{12}$ contain only terminal carbonyls.[154] Because of the longer M—M bond distances going down the iron triad, it becomes increasingly difficult to form bridging carbonyls to delocalize negative charge accumulating in the transition state. For example, the mechanism proposed[155] for the intramolecular fluxional scrambling of COs in $M_3(CO)_{12}$ is believed to involve bridging carbonyls, and the rates of CO scramble decrease in the order Fe > Ru > Os. A more specific example[156] of a third-row transition metal carbonyl with only terminal carbonyls, which forms bridging carbonyls to accommodate negative charge, is provided by $Ir_4(CO)_{12}$ and $[Ir_4(CO)_{11}C(O)OCH_3]^-$, respectively.

Although the addition of Me_3NO to $M_3(CO)_{12}$ in the transition state does not develop a negative charge on the cluster, as does the addition of CH_3O^-, attack by the negative oxygen of $Me_3N^{\delta+}$—$O^{\delta-}$ does increase the electron density in the cluster. This may be sufficient to require carbonyl bridge formation in the transition state for reaction and to account for the relative rates observed. However, it should be noted that reaction of $M_3(CO)_{12}$ with Me_3NO requires breaking a M—C bond. Reactions that do require M—C bond cleavage are thermal CO substitution or exchange reactions of $M_3(CO)_{12}$, which also decrease in rate[9] in the order Fe > Ru > Os. These observations are consistent with the relative rates found for the reactions of $M_3(CO)_{12}$ with Me_3NO, which are believed to involve both O—C bond making and M—C bond breaking.

In an attempt to test the importance of bridging COs on the relative rates of reaction of $M_3(CO)_{12}$ with $(CH_3)_3NO$, it was decided to examine the corresponding reactions of $M(CO)_5$ (M = Fe, Ru, Os) where bridging COs can not be invoked. To begin with, the same second-order rate law [eq. (39)] and presumably the same mechanism [eq. (40)] was found[157] for the reactions of $M(CO)_5$ [eq. (47)]

$$M(CO)_5 + PPh_3 + (CH_3)_3NO \longrightarrow M(CO)_4PPh_3 + CO_2 + (CH_3)_3N. \quad (47)$$

The results show that for a given metal, except for osmium, the rates of reaction for $M_3(CO)_{12}$ are faster than for $M(CO)_5$. For iron the rate difference is about two orders of magnitude, whereas it is approximately one order of magnitude for ruthenium, and $Os_3(CO)_{12}$ reacts at about the same rate as does $Os(CO)_5$. This result is expected on the basis of the usual behaviour that rates of nucleophilic attack on carbon of metal carbonyls increase with increasing frequencies of C—O stretch.[143] The highest values of ν(CO) for $M_3(CO)_{12}$ are approximately 2055 cm^{-1}, compared with 2030 cm^{-1} for $M(CO)_5$.

That the largest rate difference between $M(CO)_5$ and $M_3(CO)_{12}$ is for iron and the smallest is for osmium can be rationalized in terms of formation of bridging carbonyls in the transition state for reaction of the metal carbonyl clusters.[151,152] Since it is known[154] that the degree of difficulty in forming bridging COs in $M_3(CO)_{12}$ clusters increases in the order Fe < Ru < Os, it follows that osmium would experience the greatest rate retardation. This then might explain why the osmium cluster reacts at about the same rate as does $Os(CO)_5$, whereas the largest difference in rate is for iron which has bridging COs in the cluster ground state, and ruthenium experiences an intermediate difference between that of iron and of osmium. Although the CO bridging concept in assisting to dissipate negative charge[153] brought to the transition state by nucleophilic attack is perhaps attractive, surely other factors affect differences in rate between corresponding monomeric and cluster metal carbonyls. Steric effects, symmetry requirements, coordination number and other factors can contribute to the stability of transition states for reactions.

Finally, the reactivities of $M(CO)_5$ with $(CH_3)_3NO$ increase in the order Fe < Ru < Os. This is in agreement with the general correlation[143] between increasing rates of nucleophilic attack on carbon in metal carbonyls with increasing values of ν(CO). The rate order is opposite to what was observed for similar reactions of $M_3(CO)_{12}$, where the rates decrease in the order Fe > Ru > Os. The difference in order of relative rates of reaction of $M(CO)_5$ and $M_3(CO)_{12}$ is consistent with the hypothesis that the ease of bridging COs in the transition state for reactions of clusters enhance their rates of reaction. It is further noteworthy that the mononuclear metal carbonyls $M(CO)_5$ (M = Fe, Ru, Os) and $M(CO)_6$ (M = Cr, Mo, W), respectively, have a similar order of reactivity with $(CH_3)_3NO$. Furthermore, for each triad the difference in rate is small (4 times for the iron triad and 2.5 times for the chromium triad), suggesting the metal plays an indirect role in these reactions where attack is on the carbonyl carbon. In contrast to these small differences, there are large differences[6–8] for rates of thermal CO substitution in the absence of $(CH_3)_3NO$ for each of the triads.

Acknowledgements—I wish to thank Professor M. H. Chisholm for inviting me to write this *Polyhedron Report*. More particularly, I want to thank all my co-workers over the years, without whose help with the experiments and the ideas this research would not have been possible. The research was thankfully supported by Northwestern University and by NSF, AEC, NIH, AFOSR, and PRF.

REFERENCES

1. J. A. S. Howell and P. M. Burkinshaw, *Chem. Rev.* 1983, **83**, 557.
2. (a) J. D. Atwood, *Inorganic and Organometallic Reaction Mechanisms*. Brooks/Cole, Monterey, California (1985); (b) J. P. Collman, L. S. Hegedus, J. R. Norton and R. G. Finke, *Principles and Applications of Organotransition Metal Chemistry*. University Science Books, Mill Valley, California (1987); (c) R. H. Crabtree, *The Organometallic Chemistry of the Transition Metals*. John Wiley, New York (1988).
3. (a) F. Basolo, *Chem. Rev.* 1953, **52**, 459; (b) F. Basolo and R. G. Pearson, *Mechanisms of Inorganic Reactions*. John Wiley, New York, 1st edn (1958); 2nd edn (1967).
4. (a) F. Basolo and A. Wojcicki, *J. Am. Chem. Soc.* 1961, **83**, 520; (b) J. P. Day, F. Basolo and R. G. Pearson, *J. Am. Chem. Soc.* 1968, **90**, 6927.
5. D. F. Keeley and R. E. Johnson, *J. Inorg. Nucl. Chem.* 1959, **11**, 33.
6. J. K. Shen, Y. C. Gao, Q. Z. Shi and F. Basolo, *Inorg. Chem.* 1989, **28**, 4304.
7. R. Huq, A. J. Poë and S. Chawla, *Inorg. Chim. Acta* 1980, **38**, 121.
8. J. R. Graham and R. J. Angelici, *Inorg. Chem.* 1967, **6**, 2082.
9. J. P. Candlin and A. C. Shortland, *J. Organomet. Chem.* 1969, **16**, 289; A. Shojaie and J. D. Atwood, *Organometallics* 1985, **4**, 187; A. J. Poë and V. C. Sekhar, *Inorg. Chem.* 1985, **24**, 4377.
10. G. Pajaro, F. Calderazzo and R. Ercoli, private communication.
11. A. Davison and J. E. Ellis, *J. Organomet. Chem.* 1971, **31**, 239.
12. W. Hieber and K. Wollmann, *Chem. Ber.* 1962, **95**, 1552; J. D. Atwood and T. L. Brown, *J. Am. Chem. Soc.* 1976, **98**, 3160.
13. Q. Z. Shi, T. G. Richmond, W. C. Trogler and F. Basolo, *J. Am. Chem. Soc.* 1984, **106**, 71.
14. C. A. Tolman, *Chem. Soc. Rev.* 1972, **1**, 337.
15. H. B. Gray and A. Wojcicki, *Proc. Chem. Soc.* 1960, 358.
16. L. Mond, C. Langer and F. Quincke, *J. Chem. Soc.* 1890, **57**, 749.
17. W. Hieber, in *Advances in Organometallic Chemistry* (Edited by F. G. A. Stone and R. West), pp. 1–28. Academic Press, New York (1970).
18. E. E. Siefert and R. J. Angelici, *J. Organomet. Chem.* 1967, **8**, 374.
19. B. F. G. Johnson, J. Lewis and M. V. Twigg, *J. Chem. Soc., Dalton Trans.* 1975, 1876.
20. A. Davidson, W. McFarlane, L. Pratt and G. Wilkinson, *J. Chem. Soc.* 1962, 3653.
21. F. Basolo, A. T. Brault and A. J. Poë, *J. Chem. Soc.* 1964, 676.
22. T. L. Brown, private communication.
23. P. Horwitz and D. F. Shriver, *Adv. Organomet. Chem.* 1984, **23**, 219.
24. S. B. Butts, S. H. Strauss, E. M. Holt, R. E. Stimson, N. W. Alcock and D. F. Shriver, *J. Am. Chem. Soc.* 1980, **102**, 5093; T. G. Richmond, F. Basolo and D. F. Shriver, *Inorg. Chem.* 1982, **21**, 1272.
25. F. Calderazzo and F. L'eplattenier, *Inorg. Chem.* 1967, **6**, 1220.
26. J. K. Burdett, *J. Chem. Soc., Faraday Trans. II* 1974, **70**, 1599; M. Poliakoff and J. J. Turner, *J. Chem. Soc., Dalton Trans.* 1974, 2276.
27. T. Ziegler, *Inorg. Chem.* 1986, **25**, 2721.
28. Reference 2(a), pp. 145–158; S. P. Modi and J. D. Atwood, *Inorg. Chem.* 1983, **22**, 26.
29. G. Pajaro, F. Calderazzo and R. Ercoli, *Gazz. Chim. Ital.* 1960, **90**, 1486; G. Cetini and O. Gambino, *Atti Accad. Sci. Torino* 1963, **97**, 757, 1189, 1197.
30. F. Basolo, *Inorg. Chim. Acta* 1985, **100**, 33.
31. A. Wojcicki and F. Basolo, *J. Am. Chem. Soc.* 1961, **83**, 525.
32. F. A. Cotton, *Accts Chem. Res.* 1968, **1**, 257; E. L. Muetterties, *Accts Chem. Res.* 1970, **3**, 266.
33. H. D. Kaesz, R. Bau, D. Hendrickson and J. M. Smith, *J. Am. Chem. Soc.* 1967, **89**, 2844; B. F. Johnson, J. Lewis, J. R. Miller, B. H. Robinson, P. W. Robinson and A. Wojcicki, *J. Chem. Soc. A* 1968, 522; J. D. Atwood and T. L. Brown, *J. Am. Chem. Soc.* 1975, **97**, 3380.
34. W. G. Jackson, *Inorg. Chem.* 1987, **26**, 3004.
35. T. L. Brown, *Inorg. Chem.* 1989, **28**, 3229.
36. F. Basolo, *Chem. Ber.* 1969, **5**, 505.
37. R. J. Angelici and F. Basolo, *J. Am. Chem. Soc.* 1962, **84**, 2495.
38. J. D. Atwood and T. L. Brown, *J. Am. Chem. Soc.* 1976, **98**, 3155, 3160.
39. R. J. Angelici and F. Basolo, *Inorg. Chem.* 1963, **2**, 728.
40. C. A. Tolman, *J. Am. Chem. Soc.* 1970, **92**, 2956.
41. R. J. Angelici, A. J. Poë and F. Basolo, *J. Am. Chem. Soc.* 1963, **85**, 2215.

42. A. T. Brault, E. M. Thorsteinson and F. Basolo, *Inorg. Chem.* 1964, **3**, 770.
43. G. G. Summer, H. P. Klug and L. E. Alexander, *Acta Cryst.* 1964, **17**, 732.
44. L. F. Dahl and R. E. Rundle, *Acta Cryst.* 1963, **16**, 419.
45. K. Noack, *Spectrochim. Acta* 1963, **19**, 1925; *Helv. Chim. Acta* 1964, **47**, 1064.
46. H. Stammreich, K. Kawai, O. Sala and P. Krumholz, *J. Chem. Phys.* 1961, **35**, 2175.
47. S. Breitschaft and F. Basolo, *J. Am. Chem. Soc.* 1966, **88**, 2702.
48. T. H. Coffield, R. D. Closson and J. Kozikowski, *J. Org. Chem.* 1957, **22**, 598.
49. R. J. Mawby, F. Basolo and R. G. Pearson, *J. Am. Chem. Soc.* 1964, **86**, 5043.
50. H. W. Sternberg, H. Greenfield, R. A. Friedel, J. H. Wotiz, R. Markby and I. Wender, *J. Am. Chem. Soc.* 1954, **76**, 1457; 1956, **78**, 120.
51. A. D. Allen and C. Senoff, *Chem. Commun.* 1965, 621.
52. H. Wawersik and F. Basolo, *Chem. Commun.* 1966, 366; *Inorg. Chim. Acta* 1969, **3**, 113.
53. A. J. Poë, *Inorg. Chem.* 1981, **20**, 4029 and refs therein.
54. J. D. Atwood, *Inorg. Chem.* 1981, **20**, 4031 and refs therein.
55. S. P. Schmidt, W. C. Trogler and F. Basolo, *Inorg. Chem.* 1982, **21**, 1699.
56. M. S. Wrighton and D. S. Ginley, *J. Am. Chem. Soc.* 1975, **97**, 2065.
57. A. M. Stolzenberg and E. L. Muetterties, *J. Am. Chem. Soc.* 1983, **105**, 822; N. J. Coville, A. M. Stolzenberg and E. L. Muetterties, *J. Am. Chem. Soc.* 1983, **105**, 2499.
58. S. P. Schmidt, F. Basolo, C. M. Jensen and W. C. Trogler, *J. Am. Chem. Soc.* 1986, **108**, 1894.
59. A. J. Poë, *Metal Clusters* (Edited by M. Moskovits), pp. 53–103. John Wiley, New York (1986); N. M. J. Brodie, L. Chen and A. J. Poë, *Int. J. Chem. Kinet.* 1988, **20**, 467 and refs therein.
60. G. W. Parshall, *Homogeneous Catalysis*. John Wiley, New York (1980); J. K. Kochi, *Organometallic Mechanisms and Catalysis*. Academic Press, New York (1978).
61. A. A. Arduini, A. A. Bahsoun, J. A. Osborn and C. Voelker, *Angew. Chem. Int. Ed. Engl.* 1980, **19**, 1024.
62. D. J. Darensbourg, D. J. Zalewski and T. J. Delord, *Organometallics* 1984, **3**, 1210; 1985, **4**, 92.
63. (a) J. R. Kennedy, P. Selz, A. L. Rheingold, W. C. Trogler and F. Basolo, *J. Am. Chem. Soc.* 1989, **111**, 3615; (b) J. R. Kennedy, F. Basolo and W. C. Trogler, *Inorg. Chim. Acta* 1988, **146**, 75.
64. E. M. Thorsteinson and F. Basolo, *J. Am. Chem. Soc.* 1966, **88**, 3929; *Inorg. Chem.* 1966, **5**, 1691.
65. D. J. Hodgson and J. Ibers, *Inorg. Chem.* 1969, **8**, 1282.
66. Q. Z. Shi, T. G. Richmond, W. C. Trogler and F. Basolo, *Inorg. Chem.* 1984, **23**, 957.
67. H. Wawersik and F. Basolo, *J. Am. Chem. Soc.* 1967, **89**, 4626.
68. D. E. Morris and F. Basolo, *J. Am. Chem. Soc.* 1968, **90**, 2531.
69. D. A. Brown and R. T. Sane, *J. Chem. Soc. A* 1971, 2088.
70. L. S. Meriwether and M. L. Fiene, *J. Am. Chem. Soc.* 1959, **81**, 3200.
71. Y. Sulfab, F. Basolo and A. L. Rheingold, *Organometallics* 1989, **8**, 2139.
72. F. Hoq, M. Cheong, J. K. Shen, M. Sabat and F. Basolo, *Gazz. Chim. Ital.*, in press.
73. S. Ahrland, J. Chatt and N. R. Davies, *Quart. Rev. (Lond.)* 1958, **12**, 265.
74. R. G. Pearson, *J. Am. Chem. Soc.* 1963, **85**, 3533.
75. C. A. Tolman, *J. Am. Chem. Soc.* 1970, **92**, 2956.
76. A. J. Poë, *Pure Appl. Chem.* 1988, **60**, 1209 and refs therein.
77. M. M. Rahman, H. Y. Liu and W. P. Giering, *Organometallics* 1987, **6**, 650.
78. R. B. King, *Inorg. Chem.* 1964, **3**, 1039.
79. W. L. Gladfelter, *Adv. Organomet. Chem.* 1985, **24**, 41.
80. H. G. Schuster-Woldan and F. Basolo, *J. Am. Chem. Soc.* 1966, **88**, 1657.
81. J. M. O'Connor and C. P. Casey, *Chem. Rev.* 1987, **87**, 307.
82. R. Cramer and L. P. Seiwell, *J. Organomet. Chem.* 1975, **92**, 245.
83. G. Huttner, H. H. Brintzinger, L. G. Bell, P. Friedlich, V. Bejenke and D. Neugebauer, *J. Organomet. Chem.* 1978, **145**, 329.
84. C. P. Casey, W. D. Jones and S. G. Harsey, *J. Organomet. Chem.* 1981, **206**, C38; C. P. Casey, J. M. O'Conner, W. D. Jones and K. Haller, *Organometallics* 1983, **2**, 535.
85. C. P. Casey, J. M. O'Conner and K. J. Haller, *J. Am. Chem. Soc.* 1985, **107**, 1241.
86. M. E. Rerek and F. Basolo, *Organometallics* 1983, **2**, 372; *J. Am. Chem. Soc.* 1984, **106**, 5908.
87. M. Cheong and F. Basolo, *Organometallics* 1988, **7**, 2041.
88. L. P. Hammett, *J. Am. Chem. Soc.* 1937, **59**, 96.
89. D. L. Lichtenberger, S. K. Renshaw, M. Cheong and F. Basolo, *Organometallics*, in press.
90. R. J. Angelici and W. Lowen, *Inorg. Chem.* 1967, **6**, 682.
91. M. Novi, G. Giuseppe and C. Dell'Erba, *J. Heterocycl. Chem.* 1975, **12**, 1055; D. L. Kershner and F. Basolo, *Coord. Chem. Rev.* 1989, **79**, 279.
92. L. N. Ji, D. L. Kershner, M. E. Rerek and F. Basolo, *J. Organomet. Chem.* 1985, **296**, 83; D. L. Kershner and F. Basolo, *J. Am. Chem. Soc.* 1987, **109**, 7396.
93. H. O. Pritchard and H. A. Skinner, *Chem. Rev.* 1955, **55**, 745.

94. E. O. Fischer and K. Bittler, *Z. Naturfor.* 1961, **166**, 225.
95. K. Yünlü and F. Basolo, *J. Organomet. Chem.* 1987, **330**, 221.
96. D. L. Kershner, A. Rheingold and F. Basolo, *Organometallics* 1987, **6**, 197.
97. (a) A. J. Hart-Davis and R. J. Mawby, *J. Chem. Soc. A* 1969, 2403; (b) C. White, R. J. Mawby and A. J. Hart-Davis, *Inorg. Chim. Acta* 1970, **4**, 261, 441; (c) D. J. Jones and R. J. Mawby, *Inorg. Chim. Acta* 1972, **6**, 157.
98. M. E. Rerek, L. N. Ji and F. Basolo, *J. Chem. Soc., Chem. Commun.* 1983, 1208.
99. L. N. Ji, M. E. Rerek and F. Basolo, *Organometallics* 1984, **3**, 740.
100. R. N. Biagioni, I. M. Lorkvic, J. Skelton and J. B. Hartung, *Organometallics* 1990, **9**, 547.
101. A. K. Kakkar, T. B. Marder, N. C. Hallinan, J. K. Shen and F. Basolo, unpublished results.
102. T. J. Katz and W. Slusorek, *J. Am. Chem. Soc.* 1980, **102**, 1058.
103. H. Bang, J. W. Freeman, T. J. Lynch and F. Basolo, unpublished results.
104. G. T. Palmer and F. Basolo, *J. Am. Chem. Soc.* 1985, **107**, 3122.
105. R. F. Heck, *J. Am. Chem. Soc.* 1963, **85**, 655.
106. G. Cardaci and S. M. Murgia, *J. Organomet. Chem.* 1970, **25**, 483.
107. G. T. Palmer, F. Basolo, L. B. Kool and M. D. Rausch, *J. Am. Chem. Soc.* 1986, **108**, 4417.
108. G. C. Faber and R. J. Angelici, *Inorg. Chem.* 1970, **9**, 1586; 1984, **23**, 4781.
109. J. W. Freeman and F. Basolo, *Organometallics*, in press.
110. L. I. B. Haines, D. Hopgood and A. J. Poë, *J. Am. Chem. Soc.* 1968, 421; L. I. B. Haines and A. J. Poë, *J. Am. Chem. Soc.* 1969, 2826; J. P. Fawcett and A. J. Poë, *J. Chem. Soc., Dalton Trans.* 1976, 2039.
111. H. Doine, K. Ishihara, H. R. Krouse and T. W. Swaddle, *Inorg. Chem.* 1987, **26**, 3240 and refs therein.
112. M. Meier, F. Basolo and R. G. Pearson, *Inorg. Chem.* 1969, **8**, 795.
113. N. A. Beach and H. B. Gray, *J. Am. Chem. Soc.* 1968, **90**, 5713.
114. T. Ziegler, V. Tschinke and B. Ursenbach, *J. Am. Chem. Soc.* 1987, **109**, 4825.
115. J. R. Norton and J. P. Collman, *Inorg. Chem.* 1973, **12**, 476; K. J. Karel and J. R. Norton, *J. Am. Chem. Soc.* 1974, **96**, 6812.
116. G. F. Holland, D. E. Ellis, D. R. Tyler, H. B. Gray and W. C. Trogler, *J. Am. Chem. Soc.* 1987, **109**, 4276; J. S. Kristoff and D. F. Shriver, *Inorg. Chem.* 1974, **13**, 499.
117. G. F. Stuntz and J. R. Shapley, *J. Organomet. Chem.* 1981, **213**, 389; D. C. Sonnenberger and J. D. Atwood, *Inorg. Chem.* 1981, **20**, 3243; K. Dahlinger, F. Falcone and A. J. Poë, *Inorg. Chem.* 1986, **25**, 2654.
118. D. J. Darensbourg and M. J. Incorvia, *Inorg. Chem.* 1980, **19**, 2585.
119. M. O. Albers and N. J. Coville, *Coord. Chem. Rev.* 1984, **53** and refs therein.
120. D. E. Morris and F. Basolo, *J. Am. Chem. Soc.* 1968, **90**, 2531.
121. J. D. Atwood and T. L. Brown, *J. Am. Chem. Soc.* 1976, **98**, 3160; T. L. Brown and P. A. Bellus, *Inorg. Chem.* 1978, **17**, 3726 and refs therein.
122. D. J. Darensbourg, N. Walker and M. Y. Darensbourg, *J. Am. Chem. Soc.* 1980, **102**, 1212; *Inorg. Chem.* 1981, **20**, 1918.
123. R. F. Heck, *Adv. Chem. Ser.* 1965, **49**, 181 and refs therein.
124. T. H. Coffeld, R. D. Closson and J. Kozikowski, *J. Org. Chem.* 1957, **22**, 598.
125. R. J. Mawby, F. Basolo and R. G. Pearson, *J. Am. Chem. Soc.* 1964, **86**, 5043.
126. F. Calderazzo, *Angew. Chem. Ind. Ed.* 1977, **16**, 299.
127. R. J. Mawby, F. Basolo and R. G. Pearson, *J. Am. Chem. Soc.* 1964, **86**, 3994; I. S. Butler, F. Basolo and R. G. Pearson, *Inorg. Chem.* 1967, **6**, 2074.
128. S. L. Webb, C. M. Giandomenico and J. Halpern, *J. Am. Chem. Soc.* 1986, **108**, 345.
129. D. R. Kidd and T. L. Brown, *J. Am. Chem. Soc.* 1978, **100**, 4095; T. L. Brown, *Ann. N.Y. Acad. Sci.* 1980, **333**, 80.
130. R. Ercoli, F. Calderazzo and A. Alberola, *J. Am. Chem. Soc.* 1960, **82**, 2966.
131. A. Fox, J. Malito and A. J. Poë, *J. Chem. Soc., Chem. Commun.* 1981, 1052 and refs therein.
132. T. R. Herrington and T. L. Brown, *J. Am. Chem. Soc.* 1985, **107**, 5700.
133. M. J. Therien and W. C. Trogler, *J. Am. Chem. Soc.* 1988, **110**, 4942 and refs therein.
134. Q. Z. Shi, T. G. Richmond, W. C. Trogler and F. Basolo, *J. Am. Chem. Soc.* 1984, **106**, 71.
135. R. M. Kowaleski, F. Basolo, W. C. Trogler, R. W. Gedridge, T. D. Newbound and R. D. Ernst, *J. Am. Chem. Soc.* 1987, **109**, 4860.
136. N. C. Hallinan, G. Morelli and F. Basolo, *J. Am. Chem. Soc.* 1988, **110**, 6585.
137. R. M. Kowaleski, A. L. Rheingold, W. C. Trogler and F. Basolo, *J. Am. Chem. Soc.* 1986, **108**, 2460.
138. W. Hieber and A. Lipp, *Chem. Ber.* 1959, **92**, 2085.
139. H. Alper and J. T. Edward, *Can. J. Chem.* 1970, **48**, 1543.
140. T. Y. Luh, *Coord. Chem. Rev.* 1984, **60**, 255.
141. Y. L. Shi, Y. C. Gao, Q. Z. Shi, D. L. Kershner and F. Basolo, *Organometallics* 1986, **6**, 1528.
142. R. J. Angelici and R. W. Brink, *Inorg. Chem.* 1973, **12**, 1067; K. J. Asali and G. R. Dobson, *J. Organomet.*

Chem. 1979, **179**, 169; H. Werner, W. Beck and H. Engelmann, *Inorg. Chim. Acta* 1969, **3**, 331; E. O. Fisher, K. Scherzer and R. Kreissl, *J. Organomet. Chem.* 1976, **118**, C33; R. B. King, *Inorg. Chem.* 1967, **6**, 25.
143. D. J. Darensbourg and M. Y. Darensbourg, *Inorg. Chem.* 1970, **9**, 1961.
144. S. D. Nelson, P. A. Kollman and W. F. Trager, *J. Med. Chem.* 1973, **16**, 1034.
145. J. O. Edwards, *J. Am. Chem. Soc.* 1954, **76**, 1540.
146. Y. C. Gao, Q. Z. Shi, D. L. Kershner and F. Basolo, *Inorg. Chem.* 1988, **27**, 188.
147. T. J. Groves, in *Metal Ion Activation of Dioxygen* (Edited by T. G. Spiro), p. 125. John Wiley, New York (1980).
148. A. T. Patton, C. E. Strouse, C. B. Knobler and J. A. Gladysz, *J. Am. Chem. Soc.* 1983, **105**, 5804.
149. B. C. Schardt and C. L. Hill, *Inorg. Chem.* 1983, **22**, 1563.
150. J. K. Shen, Y. K. Shi, Y. C. Gao, Q. Z. Shi and F. Basolo, *Organometallics* 1988, **7**, 531.
151. J. K. Shen, Y. L. Shi, Y. C. Gao, Q. Z. Shi and F. Basolo, *J. Am. Chem. Soc.* 1988, **110**, 2414.
152. D. C. Gross and P. C. Ford, *J. Am. Chem. Soc.* 1985, **107**, 585.
153. S. C. Avanzino and W. L. Jolly, *J. Am. Chem. Soc.* 1976, **98**, 6505.
154. L. F. Dahl and C. Blount, *Inorg. Chem.* 1965, **4**, 1373.
155. E. Band and E. L. Muetterties, *Chem. Rev.* 1978, **78**, 639; P. Chini, *Inorg. Chim. Acta* 1968, **2**, 31.
156. L. Garlaschelli, S. Martinengo, P. Chini, F. Canziani and R. Bau, *J. Organomet. Chem.* 1981, **213**, 397.
157. J. K. Shen, Y. C. Gao, Q. Z. Shi and F. Basolo, *Organometallics* 1989, **8**, 2144.

Polyhedron Vol. 9, No. 13, pp. 1537–1539, 1990
Printed in Great Britain

0277–5387/90 $3.00+.00
© 1990 Pergamon Press plc

A POTENTIOMETRIC STUDY ON THE COMPLEXATION BETWEEN MERCURY(II) AND PHENOLATE IONS

F. BEDIA ERIM

Department of Chemistry, Technical University of Istanbul, Maslak 80626, Istanbul, Turkey

(*Received* 22 *January* 1990; *accepted* 19 *February* 1990)

Abstract—The stepwise stabilities of the complexes formed by mercury(II) with the phenolate and *p*-nitrophenolate ions have been determined potentiometrically in an aqueous sodium perchlorate medium of unit ionic strength at 25.0°C. In both of the systems studied, only the strong, mononuclear complexes were formed in the range of concentrations used. No evidence has been found for the formation of polynuclear and/or acid complexes.

Mercury(II)–phenolate complexes have been studied by Veselinović and Malešev at 20°C and various ionic strengths.[1] The mercury(II)–*p*-nitrophenolate system, on the other hand, seems to have not been studied so far.

The present investigation has been performed at 25°C and in an aqueous sodium perchlorate medium of ionic strength 1 mol dm^{-3}. The potentiometric measurements have been carried out by means of a glass electrode. Thus, the free ligand concentrations, [L], have been determined via pH measurements in metal ion solutions containing phenol–phenolate buffers.

EXPERIMENTAL

Chemicals

Mercury(II) perchlorate, sodium perchlorate, perchloric acid and Ag, AgCl electrodes were prepared and analysed as before.[2,3] The free acid concentrations in the stock solutions were determined both potentiometrically and by passing aliquots through a column containing Dowex 50 W cation-exchange resin in the hydrogen form and titrating the eluate with standard sodium hydroxide. Phenol (Merck for synthesis) was freshly distilled in vacuum. Stock solutions were analysed by the bromate method. *p*-Nitrophenol (Merck for synthesis) was recrystallized from chloroform (m.p. 114°C). Stock solutions of *p*-nitrophenol were prepared from weighed portions of the substances. Phenol–sodium phenolate buffer solutions were prepared by mixing phenol solutions with standard sodium hydroxide and adjusting the ionic strength with sodium perchlorate to 1 mol dm^{-3}.

Apparatus and procedure

A Metrohm 654 Digital pH Meter equipped with a Metrohm EA 109 glass electrode was used for measurements. The EMFs of the following cell were measured:

$$-\mathrm{RE}//C_M\mathrm{M\ Hg(ClO_4)_2},\ C_H\mathrm{M\ HClO_4},\ C_L\mathrm{M\ NaOC_6H_4X},\ C_{L'}\mathrm{M\ HOC_6H_4X}\ (\mathrm{X = H\ or\ NO_2}),\ \mathrm{NaClO_4\ to}\ I = 1\ \mathrm{M/GE+},$$

where

$$\mathrm{RE//Ag,\ AgCl/0.025\ M\ NaCl,\ 0.975\ M\ NaClO_4/1.0\ M\ NaClO_4/}.$$

The measurements have been arranged as titrations at constant metal ion and acid concentrations, C_M and C_H, respectively. Equal volumes of the solutions T_1 and T_2 were added to V_0 cm^3 of solution S. Solutions S, T_1 and T_2 have the following compositions:

$$\mathrm{S}: C_M\mathrm{M\ Hg(ClO_4)_2},\ C_H\mathrm{M\ HClO_4},\ (1-C_H-3\,C_M)\mathrm{M\ NaClO_4}$$

$$T_1: C_L\mathrm{M\ NaOC_6H_4X},\ C_{L'}\mathrm{M\ HOC_6H_4X}\ (\mathrm{X = H\ or}\ p\text{-}\mathrm{NO_2}),\ (1-C_L)\mathrm{M\ NaClO_4}$$

T_2: $2C_M$M $Hg(ClO_4)_2$, $2C_H$M $HClO_4$,
$(1-2C_H-6C_M)$M $NaClO_4$.

The titrations were carried out in a Metrohm titration vessel at 25 ± 0.05°C. A magnetic stirrer was used for mixing. Every titration was repeated at least four times with a reproducibility within ±0.2 mV.

Calculations

By measuring the EMFs of the above cell, the free hydrogen ion concentration, h, can be determined. In order to evaluate the formation constants from these measurements, the free ligand concentration, [L], and the average ligand number, $\bar{n}$, must first be calculated from

$$[L] = K_a(C_H + C_{L'} - h)/h \quad (1)$$

and

$$\bar{n} = (C_L - C_H + h - [L])/C_M, \quad (2)$$

respectively. Where C_H is the total acid concentration and C_L and $C_{L'}$ are total phenolate and phenol concentrations, respectively, after the addition of equal volumes of T_1 and T_2 to V_0 cm^3 of solution S.

Once the corresponding values of $\bar{n}$ and [L] are known, the function $X = 1+\Sigma_{j=1}^{N}\beta_j[L]^j$ can be evaluated from a graphical integration of the $\bar{n}$/[L] vs [L] plot. The constants are then obtained graphically[4] by plotting the functions $X_j = (X_{j-1}-\beta_{j-1})/[L]$ vs [L], where $1 \leqslant j \leqslant N$, $X_0 = X$, $\beta_0 = 1$.

RESULTS AND DISCUSSION

The proton–phenolate system

The measurements were carried out as a series of titrations of a solution of phenol varying concentrations, i.e. 300, 400 and 500 mM with a 100 mM NaOH solution ($I = 1$ M). For the *p*-nitrophenol, the concentrations were 30, 40 and 50 mM and titrations were performed with a 10 mM NaOH solution. From these measurements, the acidity constants of phenols can be calculated by the relation

$$K_a = h(C_{NaOH}+h-OH^-)/(C_L - C_{NaOH} - h + OH^-), \quad (3)$$

where C_L is the total phenol concentration.

The values of $K_a = (1.44\pm0.02)\times10^{-10}$ M obtained for phenol and $K_a = (9.17\pm0.08)\times10^{-8}$ M for *p*-nitrophenol from these measurements agree excellently with those reported in the literature under the same conditions.[5]

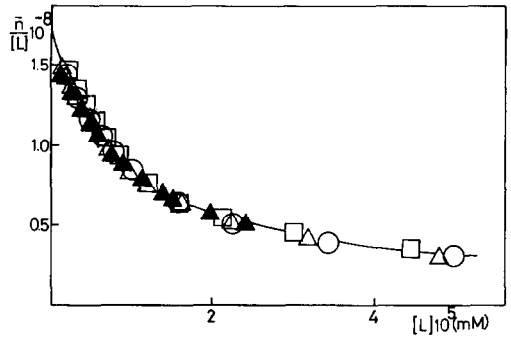

Fig. 1. Plot of $\bar{n}$/[L] vs [L] for the mercury(II)–phenolate system. (○) $C_M = 0.350$ mM, $C_H = 1.493$ mM; (□) $C_M = 0.461$ mM, $C_H = 1.540$ mM; (△) $C_M = 0.645$ mM, $C_H = 1.781$ mM; (▲) $C_M = 0.792$ mM, $C_H = 2.930$ mM.

The mercury(II)–phenolate system

The potentiometric titrations were performed with four different values for C_M. Various ratios of C_M/C_H have been used for each series. Experiments indicated that for values of C_M higher than 1 mM, the precipitation of $Hg(C_6H_5O)_2$ was formed. Therefore no high values of C_M could be used. Instead of using unbuffered sodium phenolate as a ligand solution, titrations were carried out by using phenolate–phenol buffers around pH ~ 8.5 in order to prevent the hydrolysis of mercury(II) ion.

The n/[L] vs [L] plot is shown in Fig. 1, and the complex formation function is presented in Fig. 2. No systematic deviations could be seen between the four titration series used, which shows that neither polynuclear nor acid complexes are formed in the range studied.

The variations of K_a within the limits of error have little effect on β_1, however, the uncertainties of the C_H values of solutions markedly influence the values of $\bar{n}$/[L] for small values of [L] making the

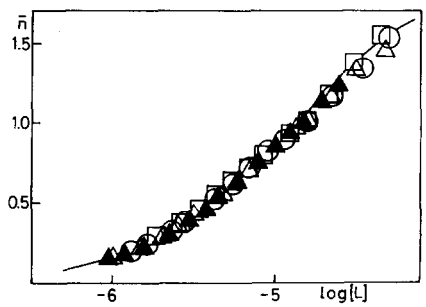

Fig. 2. The complex formation function of the mercury(II)–phenolate system. For symbols refer to Fig. 1 {[L] in mM}.

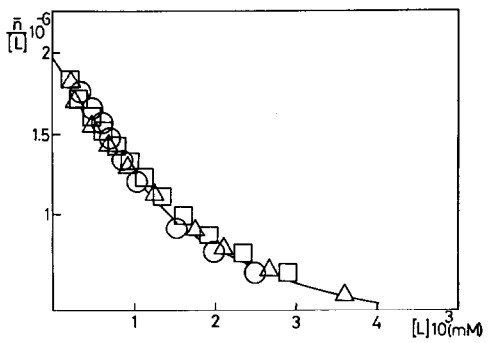

Fig. 3. Plot of $\bar{n}/[L]$ vs [L] for the mercury–*p*-nitrophenolate system. (○) $C_M = 0.739$ mM, $C_H = 2.982$ mM; (□) $C_M = 1.256$ mM, $C_H = 5.373$ mM; (△) $C_M = 1.497$ mM; $C_H = 5.436$ mM.

intercept rather uncertain. Though the C_H values of S solutions have been determined precisely, the uncertainty in β_1 is high. The value of β_2 is little affected by the value of β_1 and will therefore nevertheless be fairly precise.

The mercury(II)–p-*nitrophenolate system*

Three different mercury(II) solutions were employed. Different ratios of C_M/C_H have been used for each series. A buffered ligand solution having pH ~ 8 was used. The $\bar{n}/[L]$ vs [L] plot is shown in Fig. 3, and the complex formtion function, i.e. $\bar{n}$ vs log [L], is plotted in Fig. 4. The complex formation function is independent of both C_M and C_H, which indicates that no polynuclear or acid complexes exist.

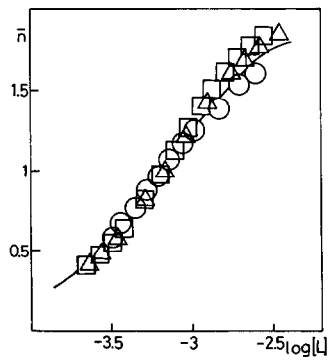

Fig. 4. The complex formation function of the mercury(II)–*p*-nitrophenolate system. For symbols refer to Fig. 3 {[L] in mM}.

Table 1. The overall formation constants for the consecutive steps of mercury(II)–phenolate and mercury(II)–*p*-nitrophenolate systems at 25.0°C and $I = 1$ M. The errors given correspond to estimated errors

System	j	β_j (M^{-j})
Mercury(II)–$C_6H_5O^-$	1	$(1.74 \pm 0.20) \times 10^8$
	2	$(5.60 \pm 0.15) \times 10^{15}$
Mercury(II)–$NO_2C_6H_4O^-$	1	$(1.96 \pm 0.10) \times 10^6$
	2	$(2.24 \pm 0.16) \times 10^{12}$

The constants obtained in this investigation are given in Table 1. The constants for mercury–phenolate complexes are considerably higher than the values found by Veselinović and Malešev, which is to be attributed to the different media used.

The β_1 value of $Hg(C_6H_5O)^+$ is approximately a hundred times larger than that of $Hg(NO_2C_6H_4O)^+$. With regard to the influence of the *p*-nitro group, the formation constants of complexes in general closely parallels that for the corresponding proton–phenolate association.

Acknowledgement—This paper is dedicated to Professor Efraim Avşar, whose stimulating advice and discussions led the Author to undertake the present research.

REFERENCES

1. D. S. Veselinović and D. Malešev, *Glas. Hem. Drus. Beograd.* 1984, **49**, 191.
2. E. Avşar and F. B. Erim, *Polyhedron* 1986, **5**, 1335.
3. F. B. Erim and E. Avşar, *Polyhedron* 1988, **7**, 213.
4. S. Fronaeous, in *Techniques of Inorganic Chemistry* (Edited by H. B. Jonassen and A. Weissberger), Vol. 1, Ch. 1. Interscience, New York (1963).
5. R. M. Smith and A. E. Martell, *Critical Stability Constants*, Vol. 4. Plenum Press, New York (1976).

Polyhedron Vol. 9, No. 13, pp. 1541–1553, 1990
Printed in Great Britain

0277–5387/90 $3.00+.00
© 1990 Pergamon Press plc

MOLYBDENUM(VI) COMPLEXES OF BRANCHED LIGANDS WITH [N,O,O,O] AND [O,O,O] DONOR SETS. THE CRYSTAL AND MOLECULAR STRUCTURES OF $[MoO_2\{HOC_2H_4N(C_2H_4O)_2\}]$, $[(n\text{-}C_4H_9)_4N]_2[Mo_2O_4\{O_2NC(CH_2O)_3\}_2]\cdot 2O_2NC(CH_2OH)_3$, $[(n\text{-}C_4H_9)_4N]_2[Mo_2O_5\{HO_2CCH_2N(CH_2CO_2)_2\}_2]\cdot H_2O$ AND $[(n\text{-}C_4H_9)_4N][Mo_3O_6(OCH_3)\{CH_3C(CH_2O)_3\}_2]$

SHUNCHENG LIU, LIDUN MA, DEBORAH McGOWTY and JON ZUBIETA*

Department of Chemistry, State University of New York at Albany, Albany, NY 12222, U.S.A.

(*Received* 1 *November* 1989; *accepted* 21 *February* 1990)

Abstract—Reactions in methanol of $[TBA]_2[Mo_2O_7]$ with the appropriate branched polyhydroxylic and polycarboxylic ligands yielded the complexes $[MoO_2\{HOC_2H_4N(C_2H_4O)_2\}]$ (**3**), $[TBA]_2[Mo_2O_4\{O_2NC(CH_2O)_3\}_2]\cdot 2O_2NC(CH_2OH)_3$ (**4**), $[TBA]_2[Mo_2O_5\{HO_2CCH_2N(CH_2CO_2)_2\}_2]\cdot H_2O$ (**5**) and $[TBA][Mo_3O_6(OCH_3)\{CH_3C(CH_2O)_3\}_2]$ (**6**) [where TBA = $(n\text{-}C_4H_9)_4N$]. The deprotonation of **3** yields $[Et_3NH][MoO_2\{N(C_2H_4O)_3\}]$ (**3a**), while **4** was found to aggregate with additional molybdate to give $[TBA][Mo_3O_6(OCH_3)\{O_2NC(CH_2O)_3\}_2]$ (**4a**) and $[Mo_4O_8(OCH_3)_2\{O_2NC(CH_2O)_3\}_2]$ (**4b**). The structural interrelationship of this series of polymolybdate coordination compounds is discussed in terms of simple aggregation processes. Crystal data: **3**, monoclinic $P2_1/n$, $a = 10.688(2)$, $b = 7.559(3)$, $c = 11.386(7)$ Å, $\beta = 99.62(1)°$, $V = 905.2(5)$ Å^3, $Z = 4$, $D_{calc} = 2.02$ g cm^{-3}; 1786 reflections, $R = 0.0406$. **4**, triclinic $P\bar{1}$, $a = 10.965(2)$, $b = 11.850(3)$, $c = 13.247(3)$ Å, $\alpha = 84.72(1)$, $\beta = 89.52(2)$, $\gamma = 66.95(2)°$, $V = 1576.4(7)$ Å^3, $Z = 1$, $D_{calc} = 1.40$ g cm^{-3}; 4718 reflections, $R = 0.0389$. **5**, monoclinic $P2_1$, $a = 10.735(2)$, $b = 13.404(6)$, $c = 19.257(6)$ Å, $\beta = 90.61(2)°$, $V = 2770.9(16)$ Å^3, $Z = 2$, $D_{calc} = 1.36$ g cm^{-3}; 3212 reflections, $R = 0.0380$. **6**, monoclinic $P2_1/n$, $a = 10.908(2)$, $b = 25.674(5)$, $c = 13.059(2)$ Å, $\beta = 96.35(2)°$, $V = 3635.6(12)$ Å^3, $Z = 4$, $D_{calc} = 1.62$ g cm^{-3}; 3143 reflections, $R = 0.0490$.

Coordination complexes of polyoxomolybdates with alkoxy and carbonyl oxygen donor ligands[1–6] have been discussed as models for surface-bound intermediates in heterogeneous catalysis employing solid molybdenum oxides.[7–12] Studies of oxomolybdate(VI) coordination to branched polydentate ligands with oxygen and oxygen and nitrogen donor sets reveal a variety of structural types with features such as pendant donor groups, varying protonation of donor groups, and bridging donor groups, resulting in diverse degrees of aggregation.

Thermally-induced condensation reactions using MoO_3 have been demonstrated to afford a general synthetic method for obtaining Mo^{VI}–oxo complexes from deprotonated di- or polyhydroxylic ligands.[13–16] On the other hand, reactions of branched polydentate $[O_3]$ and $[NO_3]$ donor ligands with molybdate precursors soluble in common organic solvents have not been systematically investigated, nor has the influence of reaction conditions on the degree of aggregation of the molybdate products been addressed. In this paper, we describe the chemistry of $[TBA]_2[Mo_2O_7]$† with the branched polydentate ligands triethanolamine (**1a**), nitrilotriacetic acid (**1b**), tris-hydroxymethylethane (**2a**) and tris-hydroxymethylnitromethane (**2b**). Under identical reaction conditions these ligands give four different structural types, all

* Author to whom correspondence should be addressed.
† (TBA) ≡ tetra-*n*-butylammonium.

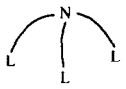

L = $-C_2H_4OH$ **(1a)**
L = $-CH_2CO_2H$ **(1b)**

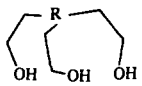

R = $-CCH_3$ **(2a)**
R = $-CNO_2$ **(2b)**

possessing the *cis*-dioxomolybdate(VI) core: the mononuclear $[MoO_2\{HOC_2H_4N(C_2H_4O)_2\}]$ **(3)**, the binuclear $[(n\text{-}C_4H_9)_4N]^+[TBA]_2[Mo_2O_4\{O_2NC(CH_2O)_3\}_2]\cdot 2O_2NC(CH_2OH)_3$ **(4)**, the binuclear $[TBA]_2[Mo_2O_5\{HO_2CCH_2N(CH_2CO_2)_2\}_2]\cdot H_2O$ **(5)** and the trinuclear $[TBA][Mo_3O_6(OCH_3)\{CH_3C(CH_2O)_3\}_2]$ **(6)**, whose structures are described herein.

RESULTS AND DISCUSSION

Synthesis and IR spectra

Studies of the coordination chemistry of molybdate with polyhydroxylic ligands and polycarboxylate ligands have generally employed MoO_3 as a synthetic precursor in the preparation of species of various nuclearities. Thus, the reaction of MoO_3 with **1b** in water affords $Na_2[Mo_2O_5\{HO_2CCH_2N(CH_2CO_2)_2\}_2]$[16] or $K_3[MoO_3\{N(CH_2CO_2)_3\}]\cdot H_2O$[17] depending on the base added. Likewise, the reaction of MoO_3 with **2a** in aqueous media yielded $[Mo_2O_2(OEt)_2\{CH_3C(CH_2O)_3\}_2]$[14] and $[Mo_4O_8(OEt)_2\{CH_3C(CH_2O)_3\}_2]$.[18] The chemistry exploits the tendency of molybdenum(VI) to develop distorted octahedral coordination with oxygen ligands through the use of combinations of terminal and bridging oxo groups and ligand oxygen donors. However, the core structure adopted by the complexes is determined by a subtle combination of ligand configurations and reaction conditions.

In an attempt to gain some insight into the influences of reaction conditions and ligand type on the core structures and degrees of aggregation of oxomolybdate complexes, we reacted the ligands **1a**, **1b**, **2a** and **2b** with $[TBA]_2[Mo_2O_7]$ under identical conditions. Thus, one equivalent of $[TBA]_2[Mo_2O_7]$ was reacted with two equivalents of the ligand in a minimum amount of refluxing methanol for 24 h. The products were isolated by carefully layering the resulting clear solutions with ether and allowing them to stand for periods of 3 days to a month. Complexes **3**–**6** were isolated as translucent colourless crystals.

As anticipated, the complexes themselves provided precursors for deprotonation and aggregation reactions. Complex **3** reacts with triethylamine to yield the anionic species $[MoO_2\{N(CH_2O)_3\}]^-$, isolated as the triethylammonium salt, $[Et_3NH][MoO_2\{N(CH_2O)_3\}]$ **(3a)**. However, attempts to deprotonate **5** by a similar route yielded intractable mixtures, and no further attempts were made to isolate products.

The binuclear species **4** was found to react with $[TBA]_2[Mo_2O_7]$ in methanol in the presence of excess $O_2NC(CH_2OH)_3$ to give the trinuclear species $[TBA][Mo_3O_6(OCH_3)\{O_2NC(CH_2O)_3\}_2]$ **(4a)**, which is structurally analogous to **6**. A by-product of this reaction is $[TBA]_2[Mo_3O_7\{O_2NC(CH_2O)_3\}_2]$ **(4b)**, which is presumably an analogue of the previously reported $[TBA]_2[Mo_3O_7\{CH_3C(CH_2O)_3\}_2]$.[19] In turn, reaction of **4a** with $[TBA]_2[Mo_2O_7]$ in methanol yielded a mixture of $[Mo_4O_8(OMe)_2\{O_2NC(CH_2O)_3\}_2]$ **(4b)** and the previously reported $[TBA]_2[Mo_4O_{10}(OCH_3)_6]$. Similarly, reaction of **6** with $[TBA]_2[Mo_2O_7]$ in methanol yielded $[Mo_4O_8(OCH_3)_2\{CH_3C(CH_2O)_3\}_2]$ **(6a)**, a species analogous to **4b** and to the structurally characterized $[Mo_4O_8(OEt)_2\{CH_3C(CH_2O)_3\}_2]$.[18]

The IR spectra of the complexes exhibit features characteristic of the *cis*-dioxomolybdate(VI) core common to the structures of these species. The spectrum of **3** displays strong bands at 920 and 940 cm^{-1}, characteristic of $\nu(Mo{=}O_t)$ for the *cis*-dioxomolybdate unit. Similar features at 923 and 908 cm^{-1} in the spectrum of **4** establish the presence of the *cis*-$[MoO_2]$ unit, while the absence of bands in the 700–800 cm^{-1} region precludes the presence of bridging oxo units. In contrast, the spectrum of **5** exhibits bands at 925 and 913 cm^{-1}, associated with the *cis*-$[MoO_2]$ unit, and an additional feature at 770 cm^{-1} assigned to $\nu(Mo{-}O{-}Mo)$, suggesting the presence of the common $[Mo_2O_5]^{2+}$ structural core. The spectrum of **6** displays a complicated pattern of bands associated with $\nu(Mo{=}O_t)$ in the 900–935 cm^{-1} range and no significant features in the 650–850 cm^{-1} region, consistent with the presence of chemically distinct $(Mo{-}O_t)$ moieties and the absence of $(Mo{-}O_b{-}Mo)$ units.

Structural studies

As illustrated in Fig. 1, the structure of **3** consists of discrete mononuclear $[MoO_2\{HOC_2H_4N(C_2H_4O)_2\}]$ units, with distorted octahedral geometry about the molybdenum centre. The metrical parameters tabulated in Table 1 are unexceptional for mononuclear *cis*-dioxomolybdenum(VI) species. The molybdenum–oxo distances are within the range of 1.66–1.76 Å commonly observed for structures with the *cis*-$[MoO_2]$ unit and the molybdenum–alkoxy oxygen distances, Mo—O(3) and Mo—O(4) are consistent for molybdenum(VI)–alkoxide interactions.[20] The long Mo—N distance is a consequence of the strong *trans* influence of

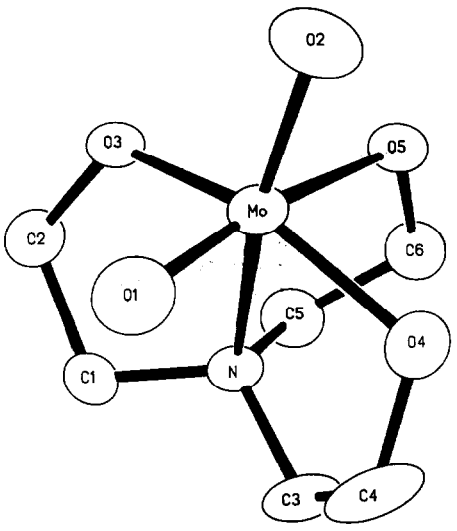

Fig. 1. ORTEP view of the structure of $[MOO_2\{HOC_2H_4N(C_2H_4O)_2\}]$ (3).

O(2) and in the range of other Mo—N distances for complexes with the *cis*-dioxomolybdenum core.

The most unusual feature of the structure is the long Mo—O(5) distance of 2.342(2) Å. Although O(5) is *trans* to the terminal oxo group, O(1), which should result in some lengthening from the normal Mo—O(alkoxide) distance of 1.92–1.96 Å to *ca* 2.10 Å, the significantly longer Mo—O(5) distance is attributed to the protonation of O(5). Since complex **5** is a neutral molybdenum(VI) species, charge requirements dictate that one of the ligand oxygen donors be protonated. Lengthening of the Mo—O distance is a well-documented consequence of the presence of the alcohol rather than the alkoxy form of the ligand.[21–25]

The structure of the molecular anion of **4** is shown in Fig. 2, and relevant bond lengths and angles are presented in Table 2. The molecular anion consists of discrete binuclear units $[Mo_2O_4\{O_2NC(CH_2O)_3\}_2]^{2-}$, with each molybdenum centre displaying $[MoO_6]$ distorted octahedral geometry. A centre symmetry located at the midpoint of the Mo(1)—Mo(1a) vector relates the symmetry equivalent halves of the molecule. The molybdenum centres again exhibit the *cis*-dioxomolybdate core with the polyhydroxyl ligand providing terminal and bridging alkoxy oxygen donors to complete the coordination geometry. The metrical parameters are not unusual, displaying the two short–two long–two intermediate pattern common to $[MoO_6]$ cores.[11] An unusual feature of the structure is the absence of bridging oxo groups; thus, the structure presents $[MoO_2]^{2+}$ moieties bridged by the alkoxy groups of the tridentate poly-

Table 1. Selected bond lengths (Å) and angles (°) for $[MoO_2\{HOC_2H_4N(C_2H_4O)_2\}]$ (3)

Mo—O(1)	1.697(3)	Mo—O(2)	1.721(3)
Mo—O(3)	1.969(3)	Mo—O(4)	1.916(3)
Mo—O(5)	2.342(3)	Mo—N	2.342(3)
O(3)—C(2)	1.431(5)	O(4)—C(4)	1.431(5)
O(5)—C(6)	1.439(5)	N—C(1)	1.484(5)
N—C(3)	1.493(6)	N—C(5)	1.475(4)
C(1)—C(2)	1.535(6)	C(3)—C(4)	1.509(6)
C(5)—C(6)	1.515(5)		
O(1)—Mo—O(2)	108.1(1)	O(1)—Mo—O(3)	95.0(1)
O(2)—Mo—O(3)	100.5(2)	O(1)—Mo—O(4)	96.3(1)
O(2)—Mo—O(4)	105.8(2)	O(3)—Mo—O(4)	146.4(1)
O(1)—Mo—O(5)	167.9(1)	O(2)—Mo—O(5)	84.1(1)
O(3)—Mo—O(5)	82.7(1)	O(4)—Mo—O(5)	79.7(1)
O(1)—Mo—N	95.1(1)	O(2)—Mo—N	156.5(1)
O(3)—Mo—N	73.0(1)	O(4)—Mo—N	74.6(1)
O(5)—Mo—N	72.8(1)	Mo—O(3)—C(2)	119.5(2)
Mo—O(4)—C(4)	114.0(3)	Mo—O(5)—C(6)	113.2(2)
Mo—N—C(1)	102.0(2)	Mo—N—C(3)	107.2(2)
C(1)—N—C(3)	114.1(3)	Mo—N—C(5)	112.1(2)
C(1)—N—C(5)	110.8(3)	C(3)—N—C(5)	110.4(3)
N—C(1)—C(2)	107.7(3)	O(3)—C(2)—C(1)	111.6(3)
N—C(3)—C(4)	109.8(3)	O(4)—C(4)—C(3)	110.1(4)
N—C(5)—C(6)	109.9(3)	O(5)—C(6)—C(5)	108.7(3)

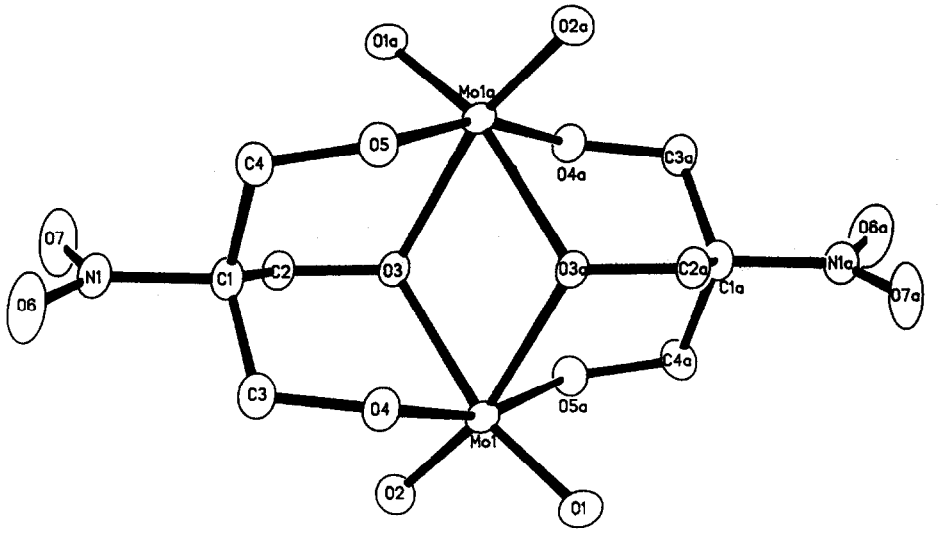

Fig. 2. ORTEP view of the structure of the molecular anion of (**4**), $[Mo_2O_4\{O_2NC(CH_2O)_3\}_2]^{2-}$.

alkoxide ligand. The ligands are disposed so as to bridge the molybdenum centres symmetrically; hence, each ligand spans the Mo(1)—Mo(1a) distance by providing a terminal alkoxy donor to each molybdenum centre, while the third alkoxy group assumes a bridging coordination mode between the molybdenum centres.

Complex **5** also exhibits a binuclear molecular core, as illustrated in Fig. 3, with bonding parameters presented in Table 3. The complex anion exhibits the common $[Mo_2O_5]^{2+}$ core, with the terminal oxo groups in an *anti* configuration. In order to satisfy the coordination requirements of the molybdenum centres, each ligand functions in a tridentate mode through coordination of the nitrogen and of an oxygen of each of two carboxylate groups. The third carboxylate unit of each ligand assumes a pendant geometry and is protonated to satisfy the charge requirements of the molecular anion. Pendant carboxylate units have been described for molybdenum complexes of both the fully deprotonated and the monoprotonated forms of the nitrilo-

Table 2. Selected bond lengths (Å) and bond angles (°) for $[TBA]_2[Mo_2O_4\{O_2NC(CH_2O)_3\}_2]$ (**4**)

Mo(1)—O(1)	1.705(3)	O(3)—C(2)	1.415(4)
Mo(1)—O(2)	1.699(3)	O(4)—C(3)	1.408(5)
Mo(1)—O(3)	2.166(2)	O(5)—C(4)	1.405(5)
Mo(1)—O(4)	1.987(2)	O(6)—N(1)	1.216(5)
Mo(1)—O(3a)	2.194(3)	O(7)—N(1)	1.198(6)
Mo(1)—O(5a)	1.983(2)	N(1)—C(1)	1.525(5)
		C(1)—C(2)	1.537(5)
		C(1)—C(3)	1.531(6)
		C(1)—C(4)	1.534(6)
O(1)—Mo(1)—O(2)	107.2(2)	O(3)—Mo(1)—O(4)	81.4(1)
O(1)—Mo(1)—O(3)	160.4(1)	O(3)—Mo(1)—O(3a)	70.4(1)
O(1)—Mo(1)—O(4)	94.1(1)	O(3)—Mo(1)—O(5a)	84.0(1)
O(1)—Mo(1)—O(3a)	90.2(1)	O(4)—Mo(1)—O(3a)	84.4(1)
O(1)—Mo(1)—O(5a)	96.3(1)	O(4)—Mo(1)—O(5a)	162.3(1)
O(2)—Mo(1)—O(3)	92.2(1)	O(3a)—Mo(1)—O(5a)	81.3(1)
O(2)—Mo(1)—O(4)	95.7(1)	Mo(1)—O(3)—Mo(1a)	109.6(1)
O(2)—Mo(1)—O(3a)	162.5(1)	Mo(1a)—O(3)—C(2)	118.0(2)
O(2)—Mo(1)—O(5a)	94.8(1)	Mo(1a)—O(5)—C(4)	124.3(2)
		Mo(1)—O(4)—C(3)	123.7(2)

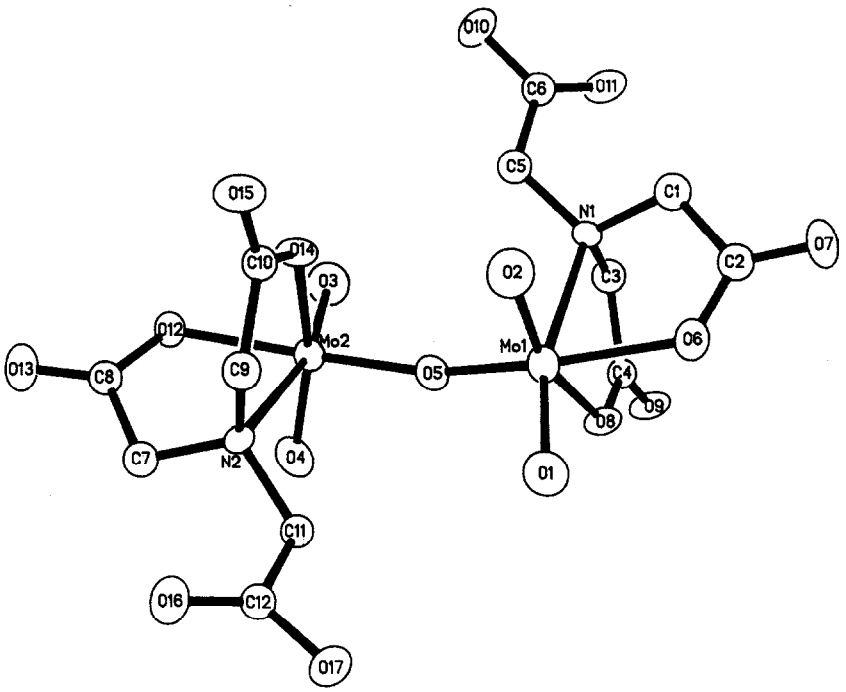

Fig. 3. ORTEP view of the structure of the molecular anion of (**5**), $[Mo_2O_5\{HO_2CCH_2N(CH_2CO_2)_2\}_2]^{2-}$.

triacetate ligands for the complexes $K_3[MoO_3\{N(CH_2CO_2)_3\}]\cdot H_2O$[17] and $Na_2[Mo_2O_5\{HO_2CCH_2N(CH_2CO_2)_2\}_2]\cdot 8H_2O$,[14] respectively. The latter possesses a molecular anion whose structure is essentially identical to that described for **5**.

The bonding parameters associated with the structure of **5** are unexceptional. The molybdenum–terminal oxo distances fall in the usual range, as do the Mo—O(5) distances. The strong *trans* influence of the terminal oxo groups is evident in the Mo(1)—N(1), Mo(2)—N(2), Mo(1)—O(8) and Mo(2)—O(14) distances (2.457(7), 2.488(6), 2.144(6) and 2.130(7) Å, respectively). The Mo—O distances for the alkoxy donors *trans* to the bridging oxo group are considerably shorter than those *trans* to the terminal oxo groups (2.077(7) and 2.060(7) Å vs 2.144(6) and 2.130(7) Å), but somewhat longer than molybdenum–alkoxy-oxygen distances observed for cases of co-ligands which exert no *trans* influence. The bond parameters for the pendant carboxylate groups establish O(10) and O(17) as the protonation sites.

Crystal structure analysis of **6** revealed the discrete trinuclear anion illustrated in Fig. 4. The molybdenum centres exhibit the usual $[MoO_6]$ distorted octahedral geometry with the bond parameters given in Table 4. There are two distinct molybdenum geometries: Mo(1) and Mo(2) each coordinate to two terminal oxo ligands and complete their coordination requirements through ligation to bridging and terminal alkoxy donors, while the Mo(3) centre bonds to two terminal oxo groups and to a terminal methoxy group while completing its coordination by ligating to three bridging alkoxy groups provided by the $\{CH_3C(CH_2O)_3\}^{3-}$ ligands. The ligands are inequivalent: one provides three doubly-bridging alkoxy donors O(1), O(2) and O(3), while the second exhibits a triply-bridging oxygen O(8), and two terminal alkoxy groups, O(6) and O(7).

These structural studies indicate that grossly different structural types result from minor variations in the ligand configuration, even under identical reaction conditions. The mononuclear nature of **3** is predicated by the tendency of the ligand to adopt a pyramidal tetradentate ligation mode. The protonation of one alkoxy group, resulting in a neutral complex, appears to be a function of the reaction conditions, since in the presence of triethylamine the anionic analogue $[MoO_2\{N(CH_2O)_3\}]^{2+}$ (**3a**) is obtained.

In contrast, the nitrilotriacetate ligand is known to function as tridentate, leaving one carboxylate function pendant. This type of coordination should favour the formation of binuclear oxo-bridged species, and the $[Mo_2O_5]^{2+}$ core is a predominant unit in the structural chemistry of binuclear molybdenum(VI) species.

Table 3. Selected bond lengths (Å) $(CH_2CO_2)_2$ and angles (°) for $[TBA]_2[Mo_2O_5\{HO_2CCH_2N(CH_2CO_2)_2\}_2]\cdot H_2O$ (**5**)

Mo(1)—O(1)	1.704(7)	Mo(1)—O(2)	1.716(8)
Mo(1)—O(5)	1.854(7)	Mo(1)—O(6)	1.077(7)
Mo(1)—O(8)	2.144(6)	Mo(1)—N(1)	2.457(7)
Mo(2)—O(3)	1.694(6)	Mo(2)—O(4)	1.689(7)
Mo(2)—O(5)	1.914(7)	Mo(2)—O(12)	2.060(7)
Mo(2)—O(14)	2.130(7)	Mo(2)—N(2)	2.488(6)
O(6)—C(2)	1.286(12)	O(7)—C(2)	1.211(13)
O(8)—C(4)	1.286(10)	O(9)—C(4)	1.232(11)
O(10)—C(6)	1.295(11)	O(11)—C(6)	1.189(12)
O(12)—C(8)	1.289(12)	O(13)—C(8)	1.209(13)
O(14)—C(10)	1.274(11)	O(15)—C(10)	1.226(12)
O(16)—C(12)	1.202(11)	O(17)—C(12)	1.296(12)
N(1)—C(1)	1.488(13)	N(1)—C(3)	1.471(12)
N(1)—C(5)	1.458(11)	N(2)—C(7)	1.476(12)
N(2)—C(9)	1.457(13)	N(2)—C(11)	1.489(11)
C(1)—C(2)	1.505(14)	C(3)—C(4)	1.489(13)
C(5)—C(6)	1.533(13)	C(7)—C(8)	1.526(14)
C(9)—C(10)	1.500(14)	C(11)—C(12)	1.527(12)
O(1)—Mo(1)—O(2)	105.9(3)	O(1)—Mo(1)—O(5)	102.8(4)
O(2)—Mo(1)—O(5)	99.4(3)	O(1)—Mo(1)—O(6)	92.6(4)
O(2)—Mo(1)—O(6)	92.3(3)	O(5)—Mo(1)—O(6)	157.1(3)
O(1)—Mo(1)—O(8)	95.0(3)	O(2)—Mo(1)—O(8)	157.2(3)
O(5)—Mo(1)—O(8)	84.3(3)	O(6)—Mo(1)—O(8)	77.6(3)
O(1)—Mo(1)—N(1)	162.8(3)	O(2)—Mo(1)—N(1)	84.5(3)
O(5)—Mo(1)—N(1)	88.5(3)	O(6)—Mo(1)—N(1)	73.1(3)
O(8)—Mo(1)—N(1)	73.1(2)	O(3)—Mo(2)—O(4)	106.6(4)
O(3)—Mo(2)—O(5)	102.0(3)	O(4)—Mo(2)—O(5)	99.0(3)
O(3)—Mo(2)—O(12)	93.5(3)	O(4)—Mo(2)—O(12)	92.2(3)
O(5)—Mo(2)—O(12)	157.4(3)	O(3)—Mo(2)—O(14)	97.8(3)
O(4)—Mo(2)—O(14)	154.3(3)	O(5)—Mo(2)—O(14)	83.7(3)
O(12)—Mo(2)—O(14)	78.0(3)	O(3)—Mo(2)—N(2)	163.7(3)
O(4)—Mo(2)—N(2)	82.6(3)	O(5)—Mo(2)—N(2)	89.6(2)
O(12)—Mo(2)—N(2)	72.4(2)	O(14)—Mo(2)—N(2)	71.8(2)
Mo(1)—O(5)—Mo(2)	161.2(4)	Mo(1)—O(6)—C(2)	125.0(7)
Mo(1)—O(8)—C(4)	124.1(5)	Mo(2)—O(12)—C(8)	125.1(6)
Mo(2)—O(14)—C(10)	126.6(6)	Mo(1)—N(1)—C(1)	102.7(5)
Mo(1)—N(1)—C(3)	107.0(5)	Mo(2)—N(2)—C(7)	101.8(5)
Mo(1)—N(1)—C(5)	112.3(5)		
Mo(2)—N(2)—C(9)	107.2(5)		
Mo(2)—N(2)—C(11)	109.4(4)		

Complexes **4** and **6** are perhaps the most unusual as examples of multinuclear molybdenum(IV)–oxo species with no bridging oxo ligands. In both instances, the cluster integrity is provided by alkoxy units which generate the framework bridging the $[MoO_2]^{2+}$ structural cores. The common feature of the four structures **3**–**6** is the presence of the *cis*-dioxomolybdate(VI) unit.

It is instructive to compare the structures of complexes **4** and **6**. Figure 5 illustrates the structures of **4**, **6** and the related $[Mo_4O_8(OEt)_2\{CH_3C(CH_2O)_3\}_2]$ viewed as the conventional ball and stick representations and the corresponding depiction as edge-sharing octahedra. Complex **4** is thus represented as two octahedra sharing an edge defined by the two bridging alkoxy oxygen donors. The structure of **6** is then constructed by condensing a $[MoO_2(OR)]^+$ unit onto the $[Mo_2O_4\{RC(CH_2O)_3\}_2]^{2-}$ core using three alkoxy groups so disposed as to provide facial tridentate coordination. Figure 5(a) and (b) illustrates the aggregation process, while Fig. 5(d) and (e) shows the simple relationship of edge-sharing otahedra which results. The structure shown in Fig. 5(b) may of

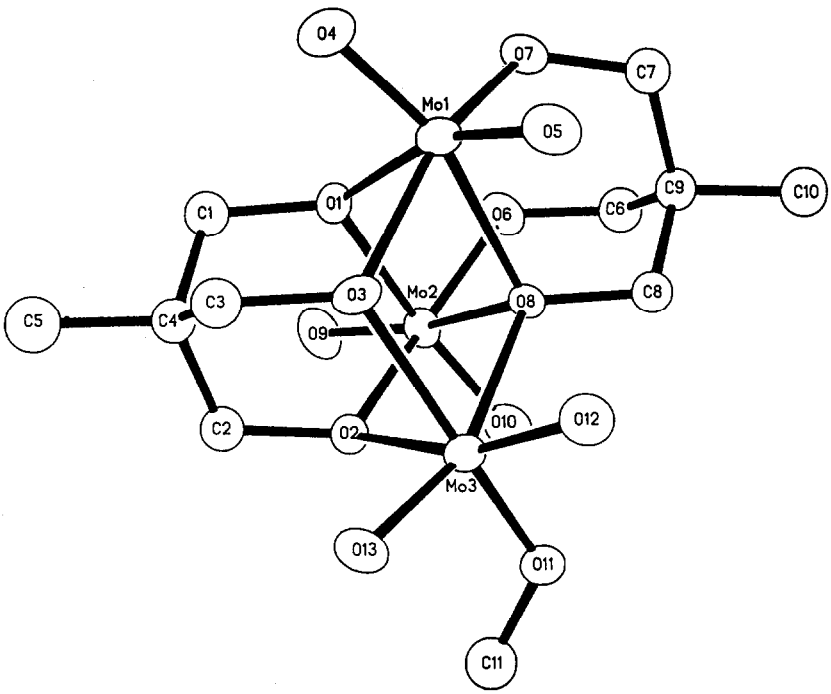

Fig. 4. ORTEP view of the structure of the molecular anion of **6**, $[Mo_3O_6(OCH_3)\{CH_3C(CH_2O)_3\}_2]^-$.

course accommodate an additional $[MoO_2(OR)]^+$ fragment on its opposite face by providing another set of alkoxy donors positioned in a vicinal tridentate grouping. The structure of $[Mo_4O_8(OEt)_2\{CH_3C(CH_2O)_3\}_2]$, shown in Fig. 5(c), may thus be viewed as a condensation product of **6** with an additional $[MoO_2(OR)]^+$ unit. The polyhedral model is illustrated in Fig. 5(f).

It is tempting to speculate on the mechanisms of aggregation processes of polyoxomolybdate coordination complexes based on these structural relationships between the binuclear, trinuclear and tetranuclear complexes of the tris-methoxyethane ligand. The principles underlying polyanion accretion are not understood in detail, although various condensation processes have been invoked.[26,27] In the present instance, the various aggregates may form according to the series of simple condensations outlined below, where H_3L is $CH_3C(CH_2OH)_3$:

$$[Mo_2O_7]^{2-} + 2H_3L \longrightarrow [Mo_2O_4L_2]^{2-} + 3H_2O$$

$$2[Mo_2O_4L_2]^{2-} + [Mo_2O_7]^{2-} + H_3L + MeOH \longrightarrow [Mo_3O_6(OMe)L_2]^{2-} + [Mo_3O_7L_2]^{2-} + 2H_2O + L^{3-}$$

$$2[Mo_3O_6(OMe)L_2]^{-} + [Mo_2O_7]^{2-} + 6MeOH \longrightarrow [Mo_4O_8(OMe)_2L_2] + [Mo_4O_{10}(OMe)_6]^{2-} + H_2O + 2H_2L^{-}.$$

The synthesis of $[TBA][Mo_3O_6(OMe)\{O_2NC(CH_2O)_3\}_2]$ from $[TBA]_2[Mo_2O_4\{O_2NC(CH_2O)_3\}_2]$ in a methanolic solution of $[Mo_2O_7]^{2-}$ and excess H_3L suggest that this sequence of condensation steps is not totally naive or a simple formalism. However, it is also apparent that, whatever the merit of this scheme in explaining the aggregation of the tris-methoxyethane type of clusters, it is specific to this set of complexes and cannot be applied to other ligand systems. Ligand geometry and donor groups appear to be dominant features in determining the structural type adopted. Hence, a general mechanistic description of aggregation in polyoxomolybdate coordination complexes remains elusive.

Although the tetranuclear core is a common feature of the chemistry of coordination complexes of polyoxomolybdates, the arrangement of octahedra in these species exhibits considerable variation, as shown in Fig. 6. The most common arrangement is that shown in Fig. 6(1); it may be significant that this is also the most compact structure[28] of the tetranuclear clusters described to date. The molybdenum(V) species $[Mo_4\{HB(pz)_3\}_2O_4(OCH_3)_2(CH_3OH)_2]$[21] exhibits the arrangement illustrated in Fig. 6(3), while the structure of Fig. 6(4) has been described for $[Me_3N(CH_2)_6NMe_3]_2[Mo_4O_{11}(citrate)_2]\cdot 12H_2O$.[29] Although corner-sharing of octahedra is unusual in polyoxometalate chemistry, several examples have been described in recent years in the course of the development of

Table 4. Selected bond lengths (Å) and angles (°) for [TBA][$Mo_3O_6(OCH_3)\{CH_3C(CH_2O)_3\}_2$] (**6**)

Mo(1)—O(1)	2.149(6)	Mo(1)—O(3)	2.088(6)
Mo(1)—O(4)	1.686(7)	Mo(1)—O(5)	1.696(7)
Mo(1)—O(7)	1.883(7)	Mo(1)—O(8)	2.297(5)
Mo(2)—O(1)	2.178(6)	Mo(2)—O(2)	2.068(6)
Mo(2)—O(6)	1.883(7)	Mo(2)—O(8)	2.261(6)
Mo(2)—O(9)	1.712(7)	Mo(2)—O(10)	1.697(7)
Mo(3)—O(2)	2.240(6)	Mo(3)—O(3)	2.127(6)
Mo(3)—O(8)	2.266(6)	Mo(3)—O(11)	1.874(7)
Mo(3)—O(12)	1.696(6)	Mo(3)—O(13)	1.695(7)
O(1)—C(1)	1.434(11)	O(2)—C(2)	1.446(11)
O(3)—C(3)	1.431(12)	O(6)—C(6)	1.403(12)
O(7)—C(7)	1.450(12)	O(8)—C(8)	1.445(10)
O(11)—C(11)	1.435(12)	C(1)—C(4)	1.508(13)
C(2)—C(4)	1.491(14)	C(3)—C(4)	1.552(15)
C(4)—C(5)	1.575(14)	C(6)—C(9)	1.553(15)
C(7)—C(9)	1.552(14)	C(8)—C(9)	1.514(13)
C(9)—C(10)	1.539(14)		

O(3)—Mo(1)—O(1)	78.5(2)	O(4)—Mo(1)—O(1)	91.3(3)
O(4)—Mo(1)—O(3)	94.9(3)	O(5)—Mo(1)—O(1)	159.3(3)
O(5)—Mo(1)—O(3)	89.8(3)	O(5)—Mo(1)—O(4)	106.8(4)
O(7)—Mo(1)—O(1)	87.1(3)	O(7)—Mo(1)—O(3)	155.8(3)
O(7)—Mo(1)—O(4)	104.8(3)	O(7)—Mo(1)—O(5)	97.6(3)
O(8)—Mo(1)—O(1)	70.9(2)	O(8)—Mo(1)—O(3)	72.5(2)
O(8)—Mo(1)—O(4)	159.7(3)	O(8)—Mo(1)—O(5)	89.4(3)
O(8)—Mo(1)—O(7)	84.5(2)	O(2)—Mo(2)—O(1)	78.8(2)
O(6)—Mo(2)—O(1)	85.4(3)	O(6)—Mo(2)—O(2)	155.4(3)
O(8)—Mo(2)—O(1)	71.1(2)	O(8)—Mo(2)—O(2)	73.3(2)
O(8)—Mo(2)—O(6)	83.8(2)	O(9)—Mo(2)—O(1)	91.3(3)
O(9)—Mo(2)—O(2)	96.1(3)	O(9)—Mo(2)—O(6)	103.1(3)
O(9)—Mo(2)—O(8)	160.7(3)	O(10)—Mo(2)—O(1)	160.4(3)
O(10)—Mo(2)—O(2)	91.9(3)	O(10)—Mo(2)—O(6)	97.0(3)
O(10)—Mo(2)—O(8)	89.7(3)	O(10)—Mo(2)—O(9)	107.0(4)
O(3)—Mo(3)—O(2)	78.0(2)	O(8)—Mo(3)—O(2)	70.1(2)
O(8)—Mo(3)—O(3)	72.4(2)	O(11)—Mo(3)—O(2)	84.0(3)
O(11)—Mo(3)—O(3)	159.5(3)	O(11)—Mo(3)—O(8)	92.3(3)
O(12)—Mo(3)—O(2)	158.6(3)	O(12)—Mo(3)—O(3)	94.3(3)
O(12)—Mo(3)—O(8)	88.5(3)	O(12)—Mo(3)—O(11)	99.1(3)
O(13)—Mo(3)—O(2)	93.3(3)	O(13)—Mo(3)—O(3)	90.7(3)
O(13)—Mo(3)—O(8)	158.2(3)	O(13)—Mo(3)—O(11)	100.2(3)
O(13)—Mo(3)—O(12)	106.9(4)	Mo(2)—O(1)—Mo(1)	112.3(3)
C(1)—O(1)—Mo(1)	118.5(6)	C(1)—O(1)—Mo(2)	117.6(6)
Mo(3)—O(2)—Mo(2)	111.1(3)	C(2)—O(2)—Mo(2)	120.0(5)
C(2)—O(2)—Mo(3)	116.4(6)	Mo(3)—O(3)—Mo(1)	111.7(3)
C(3)—O(3)—Mo(1)	119.8(6)	C(3)—O(3)—Mo(3)	118.4(6)
C(6)—O(6)—Mo(2)	124.8(6)	C(7)—O(7)—Mo(1)	122.6(6)
Mo(2)—O(8)—Mo(1)	104.1(2)	Mo(3)—O(8)—Mo(1)	99.7(2)
Mo(3)—O(8)—Mo(2)	103.4(2)	C(8)—O(8)—Mo(1)	114.3(5)
C(8)—O(8)—Mo(2)	114.9(5)		
C(11)—O(11)—Mo(3)	124.1(7)		

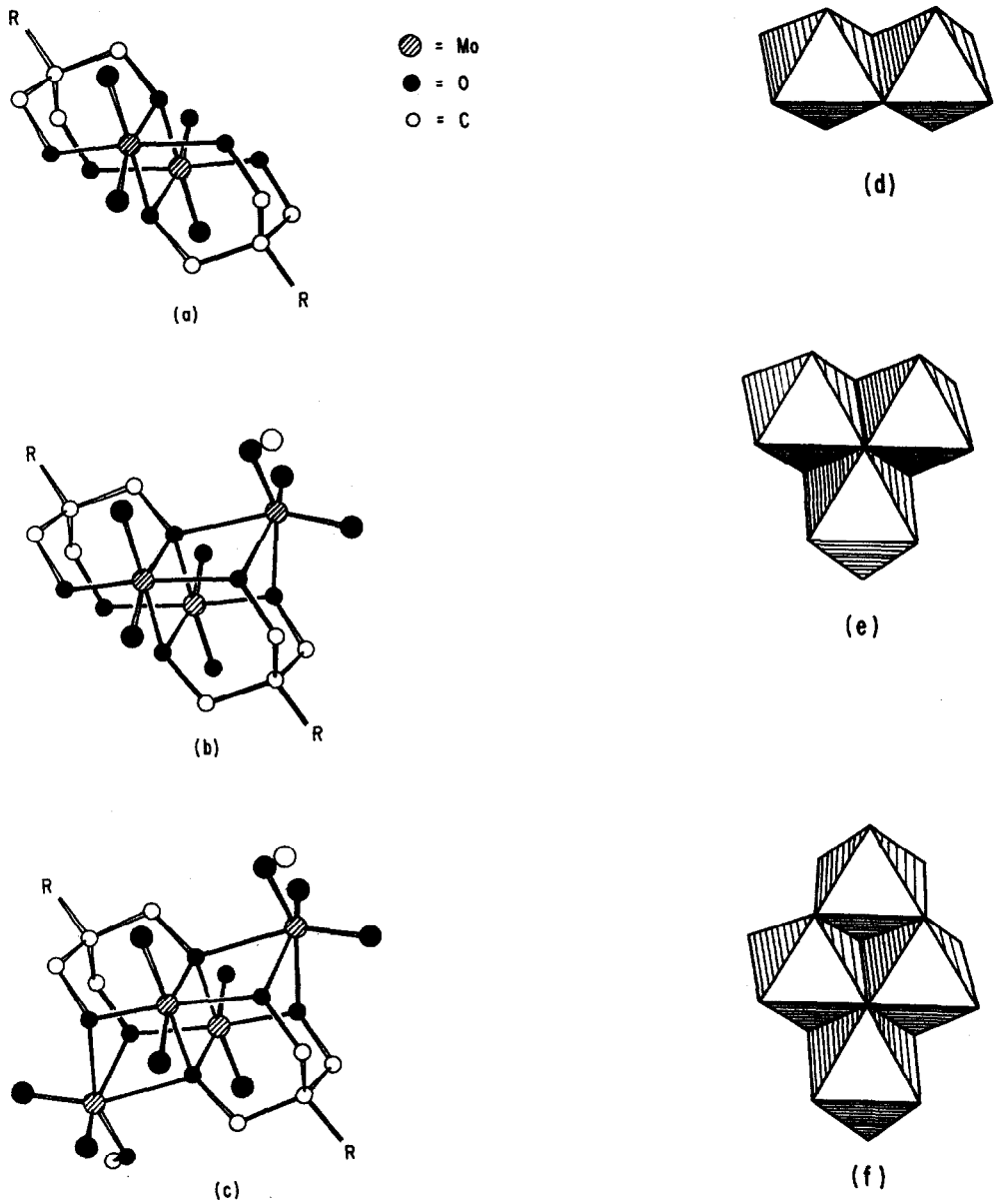

Fig. 5. Schematic ball and stick representations of the structures of (a) $[Mo_2O_4\{RC(CH_2O)_3\}_2]^{2-}$, (b) $[Mo_3O_6(OCH_3)\{RC(CH_2O)_3\}_2]^-$ and (c) $[Mo_4O_8(OCH_3)_2\{RC(CH_2O)_3\}_2]$. The corresponding polyhedral models (d) $[Mo_2O_4\{RC(CH_2O)_3\}_2]^{2-}$, (e) $[Mo_3O_6(OCH_3)\{RC(CH_2O)_3\}_2]^-$ and (f) $[Mo_4O_8(OCH_3)_2\{RC(CH_2O)_3\}_2]$.

the coordination chemistry of polyoxometalates. Other examples of corner-sharing interactions for tetranuclear species include $[Mo_4O_{12}\{CH_3C(NH)NO\}_2]^{2-}$ [30] and $[Mo_4O_{11}\{tolC(NH_2)NHO\}_2\{tolC(NH)NHO\}\{tolC(NH)NO\}]^-$ [31] shown diagrammatically in Fig. 6(5) and (6). This range of structural types for tetranuclear polyoxomolybdate coordination complexes emphasizes the dominant role played by the ligand donor set and geometrical constraints in determining the geometry of the complex.

CONCLUSIONS

Under identical reaction conditions, $[TBA]_2[Mo_2O_7]$ reacts with the branched polydentate ligands triethanolamine, tris-hydroxymethylnitromethane, nitrilotriacetic acid, and tris-hydroxymethylethane to give $[MoO_2\{HOC_2H_4N(C_2H_4O)_2\}]$ (**3**), $[TBA]_2[Mo_2O_4\{O_2NC(CH_2O)_3\}_2]\cdot 2O_2NC(CH_2OH)_3$ (**4**), $[TBA]_2[Mo_2O_5\{HO_2CCH_2N(CH_2CO_2)_2\}_2]\cdot H_2O$ (**5**) and $[TBA][Mo_3O_6(OCH_3)\{CH_3C(CH_2O)_3\}_2]$ (**6**). The type of molybdenum–

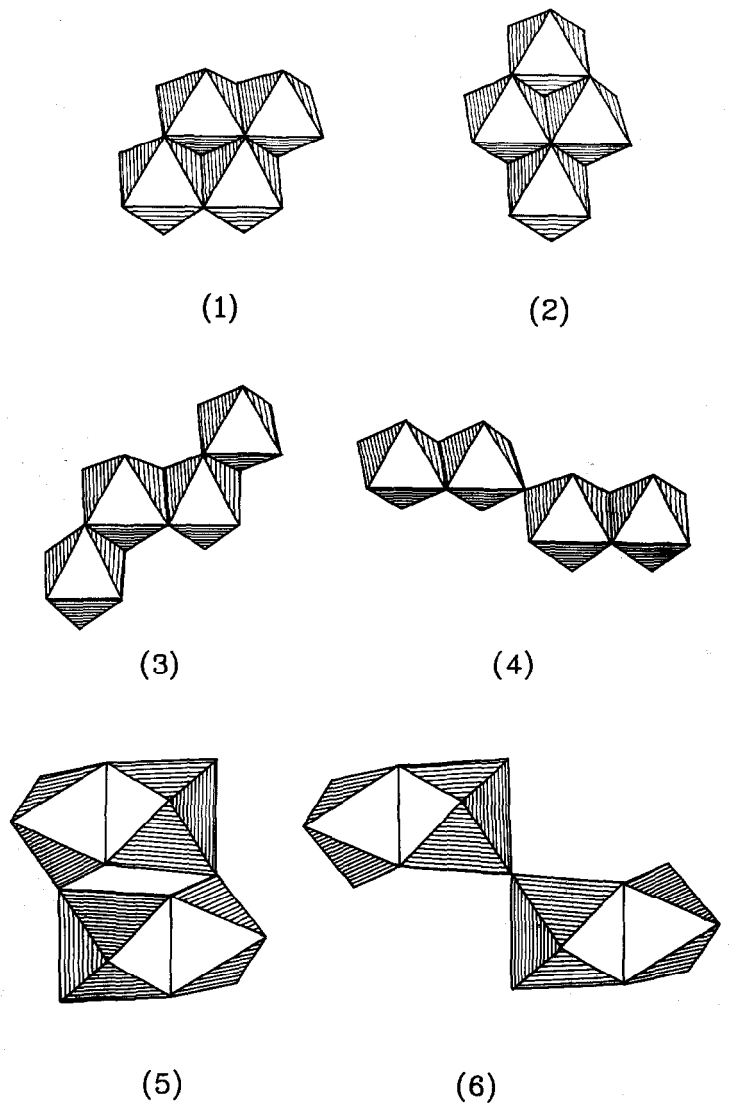

Fig. 6. Polyhedral representations of the structures of $[Mo_4O_{10}(OCH_3)_6]^{2-}$ (1), $[Mo_4O_8(OEt)_2\{CH_3C(CH_2O)_2\}_2]$ (2), $[Mo_4\{HB(pz)_3\}_2O_4(OCH_3)_2(HOCH_3)_2]$ (3), $[Mo_4O_{11}(citrate)_2]^{2-}$ (4), $[Mo_4O_{12}\{CH_3C(NH_2)NO\}_2]^{2-}$ (5) and $[Mo_4O_{11}\{tolC(NH_2)NHO\}_2\{tolC(NH)NHO\}\{tolC(NH)NO\}]^-$ (6).

oxo core isolated is determined in large part by the ligand donor set and configuration, although the $[MoO_2]^{2+}$ unit is a common feature of all the structures.

For the limited set of complexes **4**, **6** and $[Mo_4O_8(OR)_2\{R'C(CH_2O)_3\}_2]$, a common structural core is apparent, and aggregation appears to occur via a series of simple condensation-type processes. However, the detailed mechanisms of aggregation of polyoxomolybdate coordination complexes remain elusive, and general conclusions about interconversions of structural types cannot be drawn from the limited data available.

EXPERIMENTAL

Materials and methods

All reactions were performed in freshly dried and distilled solvents. Dichloromethane was technical grade and was redistilled from $CaCl_2$ and P_4O_{10}. All other solvents were reagent grade and were obtained from standard commercial sources without further purification. $[(n\text{-}C_4H_9)_4N]_2[Mo_2O_7]$ was prepared according to the published method.[32]

The following instruments were used in this work: IR, Perkin–Elmer 283B IR spectropho-

tometer; X-ray crystallography, Nicolet R3m/V diffractometer.

Preparation of compounds

$[MoO_2\{HOC_2H_4N(C_2H_4O)_2\}]$ (**3**). $[TBA][Mo_2O_7]$ (3.10 g, 5.7 mmol) was dissolved in methanol (20 cm^3) and added to a stirred solution of $N(C_2H_4OH)_3$ (**1a**) (1.70 g, 11.4 mmol) in methanol (5 cm^3). After refluxing for 24 h and filtering, the clear solution was layered with 30 cm^3 of diethyl ether and allowed to stand at room temperature for 5 days. Translucent, colourless crystals were collected in 42% yield. Found: C, 25.9; H, 4.6; N, 5.2. Calc. for $C_6H_{13}NO_5Mo$: C, 26.2; H, 4.7; N, 5.1%.

$[Et_3NH][MoO_2\{N(C_2H_4O)_3\}]$ (**3a**). Complex **3** (0.5 g, 1.8 mmol) was reacted with excess triethylamine (0.36 g, 3.6 mmol) in methanol (30 cm^3). After stirring for 3 h, the clear solution was layered with diethyl ether. After 2 weeks, a white powder was collected. Found: C, 38.5; H, 7.3; N, 7.2. Calc. for $C_{12}H_{28}N_2O_5Mo$: C, 38.3; H, 7.4; N, 7.4%.

$[TBA]_2[Mo_2O_4\{O_2NC(CH_2O)_3\}_2]\cdot 2O_2NC(CH_2OH)_3$ (**4**). $[TBA]_2[Mo_2O_7]$ (3.10 g, 5.7 mmol) was dissolved in methanol (20 cm^3) and added to a stirred solution of $O_2NC(CH_2OH)_3$ (**2b**) (1.72 g, 11.4 mmol) in methanol (5 cm^3). After refluxing for 24 h and filtering, the clear solution was layered with 30 cm^3 of diethyl ether. After standing for 2 weeks at room temperature, translucent, colourless crystals of **4** were obtained in 36% yield. Found: C, 43.6; H, 7.5; N, 5.9. Calc. for $C_{48}H_{102}N_6O_{24}Mo_2$: C, 43.0; H, 7.6; N, 6.3%.

$[TBA][Mo_3O_6(OCH_3)\{O_2NC(CH_2O)_3\}_2]$ (**4a**). Complex **4** (1.5 g, 1.1 mmol), dissolved in methanol (10 cm^3), was added to a solution of $[TBA]_2[Mo_2O_7]$ (0.60 g, 1.1 mmol) and **2b** (0.17 g) in methanol (20 cm^3). After refluxing for 3 h, the solution was cooled to room temperature and a white precipitate of $[Mo_4O_8(OMe)_2\{O_2NC(CH_2O)_3\}_2]$ was collected. The filtrate was treated with 30 cm^3 of diethyl ether and the solution was stored at −4°C for 2 days, whereupon a white microcrystalline precipitate of **4a** was collected. Found: C, 31.2; H, 5.4; N, 4.7. Calc. for $C_{25}H_{51}N_3O_{17}Mo_3$: C, 31.5; H, 5.3; N, 4.4%.

$[Mo_4O_8(OCH_3)_2\{O_2NC(CH_2O)_3\}_2]$ (**4b**). Complex **4a** (1.0 g, 1 mmol) was added to a solution of $[TBA]_2[Mo_2O_7]$ (0.54 g, 1 mmol) in methanol (20 cm^3). After refluxing for 4 h, the volume was reduced to 5 cm^3. Upon standing for 1 week at −4°C, the white powder of **4b** which precipitated was collected. Treatment of the filtrate with diethyl ether and standing at room temperature for 5 days yielded a small amount (10% yield) of $[TBA]_2[Mo_4O_{10}(OCH_3)_6]$. Found: C, 13.3; H, 1.9; N, 3.0. Calc. for $C_9H_{12}N_2O_{19}Mo_4$: C, 13.8; H, 2.1; N, 3.2%.

$[TBA]_2[Mo_2O_5\{HO_2CCH_2N(CH_2CO_2)_2\}_2]\cdot H_2O$ (**5**). The complex was synthesized using an identical procedure to that used for the synthesis of **3** and **4**. Thus, $[TBA]_2[Mo_2O_7]$ (3.10 g, 5.7 mmol) was reacted with $N(CH_2COOH)_3$ (**1b**) (2.18 g, 11.4 mmol) to give complex **5** in 40% yield as translucent, colourless needles. Found: C, 45.3; H, 7.3; N, 4.5. Calc. for $C_{44}H_{88}N_4O_{18}Mo_4$: C, 45.8; H, 7.6; N, 4.9%.

$[TBA][Mo_3O_6(OCH_3)\{CH_3C(CH_2O)_3\}_2]$ (**6**) The synthesis was identical to that employed for **3–5**, with the exception that $CH_3C(CH_2OH)_3$ (1.37 g, 11.4 mmol) was used as ligand. Complex **6** was isolated in 32% yield as translucent, colourless crystals. Found: C, 36.2; H, 6.3; N, 1.5. Calc. for $C_{27}H_{57}NO_{13}Mo_3$: C, 36.4; H, 6.4; N, 1.6%.

$[Mo_4O_8(OCH_3)_2\{CH_3C(CH_2O)_3\}_2$ (**6a**). Complex **6** (1.0 g, 1.1 mmol) was added to a solution of $[TBA]_2[Mo_2O_7]$ (0.60 g, 1.1 mmol) in methanol (20 cm^3). After refluxing for 24 h, the resulting clear solution was concentrated to 5 cm^3 and allowed to stand for 3 weeks at room temperature. Crystals of **6a** were collected in 23% yield. Found: C, 17.3; H, 2.6. Calc. for $C_{12}H_{24}O_{16}Mo_4$: C; 17.8; H, 3.0%.

X-ray crystallography

The details of the crystal data, data collection methods and refinement procedures are given in Table 5. (Supplementary Tables provide atomic positional parameters for the structures reported. Tables of bond lengths and angles, anisotropic thermal parameters and calculated and observed structure factors for all complexes are available.)* Full details of the crystallographic methodlologies may be found in ref. 33.

In no instance was an extinction correction applied for the data. Idealized hydrogen atom positions were used throughout the analysis, with the C—H and N—H distances set at 0.96 and 0.94 Å, respectively.

Acknowledgement—This research was supported by a grant from the National Science Foundation (CHE8815299).

* Supplementary materials available: Fractional coordinates have been deposited with the Director, Cambridge Crystallographic Centre. Complete listings of bond distances and angles are available from the Editor, Queen Mary and Westfield College, London.

Table 5. Summary of experimental details for the X-ray diffraction studies of $[MoO_2\{HOC_2H_4N(C_2H_4O)_2\}]$ (**3**), $[TBA]_2[Mo_2O_4\{O_2NC(CH_2O)_3\}_2]\cdot 2O_2NC(CH_2OH)_3$ (**4**), $[TBA]_2[Mo_2O_5\{HO_2CCH_2N(CH_2CO_2)_2\}_2]\cdot H_2O$ (**5**) and $[TBA][Mo_3O_6(OCH_3)\{CH_3C(CH_2O)_3\}_2]$ (**6**)

	3	**4**	**5**	**6**
(a) *Crystal parameters*[a]				
a (Å)	10.688(2)	10.965(2)	10.735(2)	10.908(2)
b (Å)	7.559(3)	11.850(3)	13.404(6)	25.674(5)
c (Å)	11.386(3)	13.247(3)	14.257(6)	13.059(2)
α (°)	90.00	84.72(1)	90.00	90.00
β (°)	99.62(1)	89.52(2)	90.61(2)	96.35(2)
γ (°)	90.00	66.95(2)	90.00	90.0
V (Å^3)	905.2(5)	1576.4(7)	2770.9(16)	3635.6(12)
Space group	$P2_1/n$	$P\bar{1}$	$P2_1$	$P2_1/n$
Z	4	1	2	4
D_{calc} (g cm^{-3})	2.02	1.40	1.36	1.62
(b) *Measurement of intensity data*				
Crystal colour and shape	Colourless parallelepiped	Colourless needle	Colourless block	Colourless needle
Crystal dimensions	0.26 × 0.30 × 0.29	0.21 × 0.40 × 0.26	0.34 × 0.30 × 0.32	0.34 × 0.47 × 0.29
Instrument	Nicolet R3m diffractometer			
Radiation	Mo-K_α (λ = 0.71073 Å)			
Scan mode	Coupled θ(crystal) − 2θ(counter)			
Scan rate	2–15° min^{-1}			
Scan range	$2.0° < 2\theta \leqslant 50°$			
Scan length	From $[2\theta(K\alpha_1)-1.0]$ to $[3\theta(K\alpha_2)+1.0]$°			
Background measurement	Stationary crystal, stationary counter, at the beginning and end of each 2θ scan, each for half the time taken for the scan			
Standards	Three collected every 197			
Number of reflections collected	2614	5313	3952	5129
Number of reflections used in solution $[F_o \geqslant 6\sigma(F_o)]$	1786	4718	3212	3143
(c) *Reduction of intensity data and summary of structure solution and refinement.*[b] *Data corrected for background, attenuators, Lorentz and polarization effects in the usual fashion*				
Absorption coefficient (cm^{-1})	14.1	4.60	5.10	10.24
Absorption correction	(Not applied)			
Structure solution	Patterson synthesis yielded the molybdenum positions; all remaining non-hydrogen atoms were located via standard Fourier techniques			
Atom scattering factors[c]	Neutral atomic scattering factors were used throughout the analysis			
Anomalous dispersion[d]	Applied to all non-hydrogen atoms			
Final discrepancy factors[e]				
R =	0.0406	0.0389	0.0380	0.0490
R_w =	0.0417	0.0389	0.0385	0.0526
Goodness-of-fit[f]	1.56	1.23	1.85	1.54

[a] From a least-squares fitting of the setting angle of 25 reflections.

[b] All calculations were performed on a Data General Nova 3 computer using local versions of the Nicolet SHELXTL interactive crystallographic software package as described in G. M. Sheldrick, Nicolet SHELXTL Operations Manual. Nicolet XRD Corp., Cupertino, CA (1979).

[c] D. T. Cromer and J. B. Mann, *Acta Cryst.* 1968, **A24**, 321.

[d] *International Tables for X-ray Crystallography*, Vol. III. Kynoch Press, Birmingham, U.K. (1962).

[e] $R = \Sigma[|F_o|-|F_c|/\Sigma|F_o|]$; $R_w = [\Sigma w(|F_o|-|F_c|)^2/\Sigma w|F_o|^2]^{1/2}$; $w = 1/\delta^2(F_o+g^*(F_o)$; $g = 0.001$.

[f] G-O-F $= [\Sigma w(|F_o|-|F_c|)^2/(NO-NV)]^{1/2}$, where NO is the number of observations and NV is the number of variables.

REFERENCES

1. E. M. McCarron III and R. L. Harlow, *J. Am. Chem. Soc.* 1983, **105**, 6179.
2. A. J. Wilson, W. T. Robinson and C. J. Wilkins, *Acta Cryst.* 1983, **C39**, 54.
3. S. Liu, S. N. Shaikh and J. Zubieta, *Inorg. Chem.* 1987, **26**, 4303.
4. L. Ma, S. Liu and J. Zubieta, *Polyhedron* 1989, **8**, 1571.
5. V. W. Day, M. R. Thompson, C. J. Day, W. G. Klemperer and R.-S. Liu, *J. Am. Chem. Soc.* 1980, **102**, 5973.
6. Q. Chen, S. Liu, H. Zhu and J. Zubieta, *Polyhedron* 1989, **8**, 2915.
7. R. K. Grasselli and J. D. Burrington, *Adv. Catal.* 1981, **30**, 133.
8. H.-F. Liu, R.-S. Liu, K. Y. Liew, R. E. Johnson and J. H. Lunsford, *J. Am. Chem. Soc.* 1984, **106**, 4117.
9. C. J. Machiels, U. Chrowdry, R. H. Staley, F. Ohuchi and A. W. Sleight, in *Catalytic Conversions of Synthetic Gas and Alcohols to Chemicals* (Edited by R. G. Herman). Plenum Press, New York (1984).
10. V. W. Day and W. G. Klemperer, *Science* 1985, **228**, 533.
11. M. T. Pope, *Heteropoly and Isopoly Oxometalates.* Springer, New York (1983).
12. V. W. Day, W. G. Klemperer, C. Schwart and R.-C. Wang, in *NATO ASI Series C*, Vol. 231: Surface organometallic chemistry: Molecular approaches to surface catalysis (Edited by J.-M. Bassett *et al.*), p. 173. Kluwer, Dordrecht (1988).
13. H. Schultheis, German Pat. 1,022,205/1958; 1,162,849/1964; *Chem. Abstr.* 1960, **54**, 4390; 1964, **60**, 15,909.
14. V. McKee and C. J. Wilkins, *J. Chem. Soc., Dalton Trans.* 1987, 523.
15. R. N. Hilder and C. J. Wilkins, *J. Chem. Soc., Dalton Trans.* 1984, 495.
16. C. B. Knobler, B. R. Penfold, W. T. Robinson, C. J. Wilkins and S. H. Yong, *J. Chem. Soc., Dalton Trans.* 1980, 284.
17. R. J. Butcher and B. R. Penfold, *Cryst. Molec. Struct.* 1976, **6**, 13.
18. A. J. Wilson, W. T. Robinson and C. J. Wilkins, *Acta Cryst.* 1983, **C39**, 54.
19. L. Ma, S. Liu and J. Zubieta, *Inorg. Chem.* 1989, **28**, 175.
20. H. Kang, S. N. Shaikh, T. Nicholson and J. Zubieta, *Inorg. Chem.* 1989, **28**, 980 and refs therein.
21. S. Lincoln and S. A. Koch, *Inorg. Chem.* 1986, **25**, 1594.
22. M. H. Chisholm, *Polyhedron* 1983, **2**, 681.
23. M. H. Chisholm, *Transition Met. Chem. (Weinheim, Ger.)* 1978, **3**, 321.
24. Q. Chen, S. Liu and J. Zubieta, *Inorg. Chim. Acta* 1990, **162**, 163.
25. V. Chilou, P. Gouzerh, T. C. Hsieh, Y. Jeannin, G. Olivares, F. Robert and J. Zubieta, *Polyhedron* 1989, **8**, 29.
26. D. C. Kepert, *Inorg. Chem.* 1969, **8**, 1556.
27. K. H. Tytko and O. Glemser, *Adv. Inorg. Chem. Radiochem.* 1976, **19**, 239.
28. A. Goiffen and B. Spinner, *Rev. Chim. Minér.* 1975, **12**, 316.
29. L. R. Nassimbeni, M. L. Niven, J. J. Cruywagen and J. B. B. Heyns, *J. Cryst. Spectrosc. Res.* 1987, **17**, 373.
30. V. Chilou, P. Gouzerh, Y. Jeannin and F. Robert, *J. Chem. Soc., Chem. Commun.* 1987, 1469.
31. V. Chilou, P. Gouzerh, Y. Jeannin and F. Robert, *J. Chem. Soc., Chem. Commun.* 1988.
32. V. W. Day, M. F. Fredrich, W. G. Klemperer and W. Shum, *J. Am. Chem. Soc.* 1977, **99**, 6146.
33. A. Bruce, J. L. Corbin, P. L. Dahlstrom, J. R. Hyde, M. Minelli, E. I. Stiefel, J. T. Spence and J. Zubieta, *Inorg. Chem.* 1982, **21**, 917.

Polyhedron Vol. 9, No. 13, pp. 1555–1559, 1990
Printed in Great Britain

0277–5387/90 $3.00+.00
© 1990 Pergamon Press plc

^{31}P NMR STUDY ON THE BINDING ISOMERS OF CHROMIUM(III) PHOSPHINATE COMPLEXES IN SOLUTION

QI FENG and HIROHIKO WAKI*

Department of Chemistry, Faculty of Science, Kyushu University, Hakozaki, Higashiku, Fukuoka, Japan

(*Received* 26 *September* 1989; *accepted* 22 *February* 1990)

Abstract—A ^{31}P NMR study on the structure of chromium(III) phosphinate complexes has been made. The formation of the outer-sphere complexes gave a downfield shift of the ^{31}P NMR signal, though the signal could not be separated from that of free phosphinate anion due to their great lability. On the other hand, the inner-sphere complexes gave an upfield shift of the signal separated from that of outer-sphere type. Furthermore, it was found that the signal for the inner-sphere complex has two peaks, one being due to non-chelate binding and the other being due to chelate binding. By distinguishing these binding modes, based on the experimental evidence, a large number of new isomers for chromium(III) phosphinate have been revealed.

For the complex formation between phosphorus oxo-anions and metal ions, a large number of stability constants have been reported.[1,2] However, it has not been clarified whether a monomeric phosphorus oxo-anion coordinates to a metal ion with a single oxygen atom (non-chelate binding) or with two or more oxygen atoms (chelate binding). Although chelation has been reported for phosphite in some crystalline compounds,[3–5] this is not the case for solution species. Recently we accomplished a complete equilibrium analysis on the chromium phosphinate complex system, $[Cr(PH_2O_2)_m(H_2O)_{6-m}\cdot(PH_2O_2)_x^{out}]^{(m+x-3)-}$, and evaluated a set of stability constants distinguishing inner-sphere and outer-sphere coordination;[6] but it was still unknown whether the phosphinate anion is bound as a monodentate (I) or as a bidentate (II) ligand. In the saturated inner-sphere complex $Cr(PH_2O_2)_6^{3-}$ all the ligands should be monodentate, but in the lower complexes the presence of other modes of binding can not be denied, considering the coordination number of chromium.

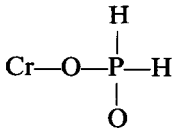

(I)

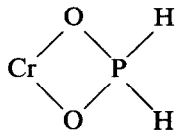

(II)

The purpose of this work is to clarify the binding mode of a phosphinate anion to a chromium ion and/or to prove the co-existence of non-chelate and chelate complexes. ^{31}P NMR spectrometry was employed in this study, since the NMR spectrum should be sensitive to different binding modes for the complexes in solutions. This information for the phosphinate ligand may lead to an understanding of the coordination for other phosphate ligands, for example orthophosphate and phosphite anions, and also for more general oxo-anion ligands.

EXPERIMENTAL

Chemicals

Chromium(III) perchlorate, sodium phosphinate and tetramethylammonium chloride were of commercially-available reagent grade. The chromium(III) phosphinate solution was prepared by passing a chromium perchlorate solution through a column of phosphinate form Dowex 1-4X (100–200 mesh).

^{31}P *NMR measurements*

^{31}P NMR spectra of the chromium(III) phosphinate complexes were recorded with a JEOL NMR spectrometer JNM-GX 400 operating at 161.86 MHz and 20°C in the pulsed mode. The

* Author to whom correspondence should be addressed.

chemical shifts were referred to standard 85% H_3PO_4. When necessary, integration was employed to increase the sensitivity of the NMR spectrometer.

Preparation of the sample solution of the inner-sphere chromium(III) phosphinate complexes for NMR measurements

The equilibrium mixture of the chromium(III) phosphinate complexes was prepared by leaving a solution containing chromium perchlorate or chromium phosphinate and sodium phosphinate in an appropriate ratio, at 100°C for 3 h to reach equilibrium. The sample solutions of individual inner-sphere complex species were obtained by separating the equilibrium mixture of the chromium phosphinate complexes by Donnan exclusion chromatography.[6-8] A column containing SP-Sephadex C-25 in the tetramethylammonium form (1.5 cm $\phi \times 90$ cm bed) was used. The chromium complex species in the effluent were automatically detected with an Atto variable-wavelength spectrophotometer LDC Model Spectromonitor III (420 nm), which was connected to the separating column. The purity of the NMR sample solution of a particular complex species was chromatographically checked by Donnan exclusion chromatography after the NMR measurements. These purities were above 95% in all cases. The average ligand number of the inner-sphere chromium phosphinate complex for the equilibrium mixture was determined in the same way as for the purity measurement.

Time-dependence measurement of the ^{31}P NMR spectra of chromium phosphinate complexes

The solutions of chromium perchlorate and sodium phosphinate were mixed to form a 0.02 M chromium perchlorate–0.5 M sodium phosphinate solution, which was kept at 100°C. The ^{31}P NMR spectrum of this solution was measured at appropriate time intervals. The spectrum of a 0.62 M sodium phosphinate solution was used as the standard spectrum of the free $PH_2O_2^-$ ion.

RESULTS AND DISCUSSION

Behaviour of the ^{31}P NMR spectra of chromium(III) phosphinate outer-sphere complexes

The NMR resonance of the chromium(III) phosphinate outer-sphere complex is not detected as a separate peak from free phosphinate ion, since outer-sphere complexes are very labile. Thus information on complexation could only be obtained from the shift of the ^{31}P NMR peak position. The chemical shift, δ_{obs}, for the one-to-one complexation is given by

$$\delta_{obs} = \alpha_0\delta_0 + \alpha_1{}^{out}\delta_1{}^{out},$$

where α_0 and $\alpha_1{}^{out}$ are mole fractions of free phosphinate anion and of phosphinate anion bound in the outer-sphere, respectively, and δ_0 and $\delta_1{}^{out}$ are their inherent chemical shifts.

Figure 1 shows the time dependence of the ^{31}P NMR chemical shift for the solution in which chromium perchlorate and sodium phosphinate were mixed at 100°C. The resonance first shifted downfield instantaneously after mixing and then returned to the free phosphinate resonance gradually. Clearly the downfield shift is due to outer-sphere complexation, and the subsequent upfield shift is due to decrease of α^{out} by its gradual conversion to inner-sphere complexation. This fact may support the results obtained from the absorption spectrum and equilibrium analysis in the previous report.[6]

^{31}P NMR spectra of the inner-sphere complexes

The inner-sphere chromium(III) phosphinate complexes are inert and the rate of ligand exchange is very low, different from the outer-sphere complexes, thus the NMR resonance can be observed as independent peaks separated from that of free phosphinate or its outer-sphere complexes. The ^{31}P NMR spectrum of the chromium phosphinate and sodium phosphinate solution, equilibrated at 100°C for 3 h, is shown in Fig. 2. The huge triplet peak, the centre signal being at 9.3 ppm, is due to free phosphinate anion present in large excess. Two smaller peaks also appeared and they were assigned to the inner-sphere complexes. The difference in chemical shift from the free anion was considerable, as in the case of other phosphate complexes,[9,10] and the shift was in the opposite direction to that of

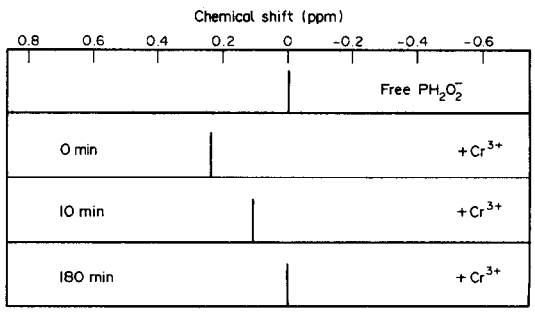

Fig. 1. Time dependence of the ^{31}P NMR chemical shift of a 0.02 M $Cr(ClO_4)_3$–0.5 M $NaPH_2O_2$ solution at 100°C, relative to free $PH_2O_2^-$ anion.

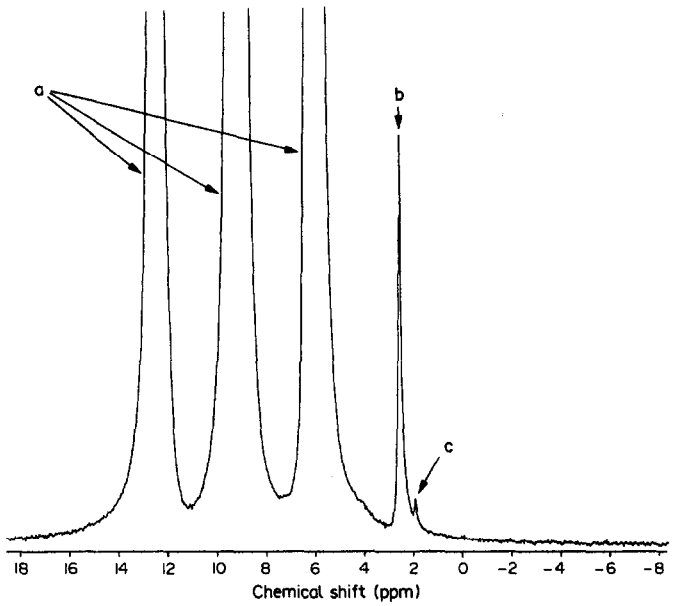

Fig. 2. ^{31}P NMR spectrum of a solution containing 0.05 M $Cr(PH_2O_2)_3$ and 1 M $NaPH_2O_2$ kept at 100°C for 3 h at pH 3.

the outer-sphere complexes, reflecting a different coordination sphere. It may be most important to clarify the assignment of the observed two inner-sphere peaks.

In order to obtain ^{31}P NMR spectra of the inner-sphere complex of a single composition, the mutual separation of inner-sphere complexes is necessary. The recently developed Donnan exclusion chromatography for separation of the inner-sphere complexes was employed.[6] The ^{31}P NMR spectrum of the $Cr(PH_2O_2)_4^-$ complex sample taken from the corresponding fraction of chromatographic effluent is shown in Fig. 3. The triplet, peak *a*, is due to the free phosphinate ion, and both peaks *b* and *c* are due to the $Cr(PH_2O_2)_4^-$ complex. The NMR spectra of other complexes were also recorded in the same way.

It was found that identification of the complexes

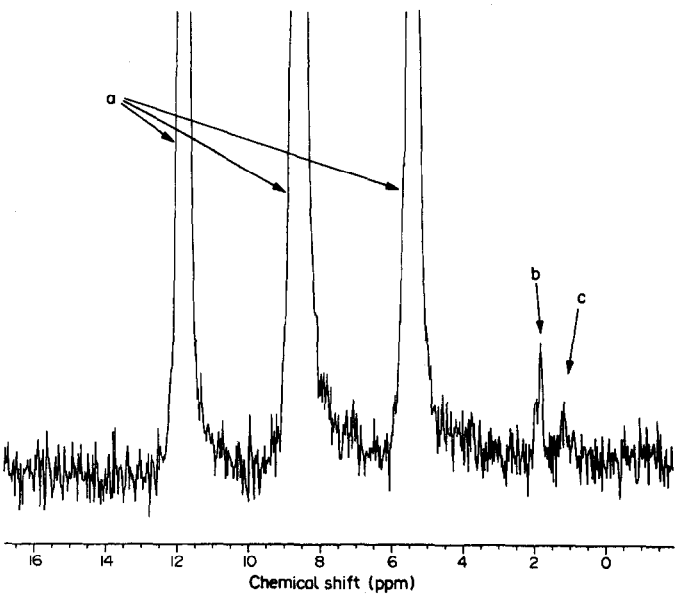

Fig. 3. ^{31}P NMR spectrum for the $Cr(PH_2O_2)_4^-$ fraction of chromatography.

using the NMR spectrum becomes more difficult with decreasing ligand number, due to broadening of the spectrum arising from the long electron-spin relaxation time associated with the paramagnetic chromium(III) ion.[11] Fortunately, the higher complexes such as $Cr(PH_2O_2)_4^-$, $Cr(PH_2O_2)_5^{2-}$ and $Cr(PH_2O_2)_6^{3-}$ studied here, are considered more important for our purpose due to the above reason.

The chemical shift data for these higher complexes are summarized in Fig. 4. The chemical shift data for the equilibrium mixture of mean ligand number $n = 5.3$, in which $[Cr(PH_2O_2)_6^{3-}]$: $[Cr(PH_2O_2)_5^{2-}]$: $[Cr(PH_2O_2)_4^-] = 1 : 0.65 : 0.39$, are also shown for comparison. A single peak for the $Cr(PH_2O_2)_6^{3-}$ complex and two peaks for the $Cr(PH_2O_2)_5^{2-}$ or $Cr(PH_2O_2)_4^-$ complexes were observed, respectively. This indicates that there are two different types of ligand in these complexes. These will be discussed in detail in the following section. Also, for the mixture only two peaks were observed which have the same chemical shift values as those of $Cr(PH_2O_2)_5^{2-}$ and $Cr(PH_2O_2)_4^-$ samples. This indicates that the chemical shifts for the complexes are almost independent of the ligand number, in the system studied.

Binding modes of the inner-sphere complexes

In the spectrum of $Cr(PH_2O_2)_6^{3-}$ only one peak was observed, whereas in the spectra of $Cr(PH_2O_2)_5^{2-}$ and $Cr(PH_2O_2)_4^-$, in addition to a peak which has the same chemical shift as $Cr(PH_2O_2)_6^{3-}$ other peaks were also observed at higher field (Fig. 4). Since the coordination number of the chromium(III) complex is six, in $Cr(PH_2O_2)_6^{3-}$ all phosphinate ligands coordinate to chromium(III) using a single oxygen atom to form non-chelate binding, giving only one peak in the spectrum. On the other hand, in $Cr(PH_2O_2)_5^{2-}$,

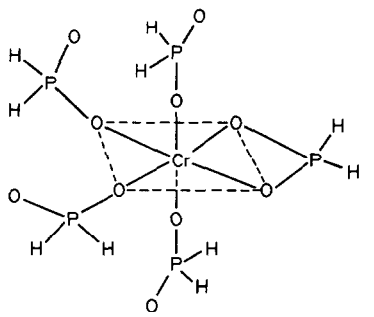

$Cr(O_2PH_2)(OPH_2O)_4^{2-}$

Fig. 5. Binding mode of inner-sphere chromium(III) phosphinate complex.

besides non-chelate binding, chelate binding, in which the phosphinate ligand coordinates to chromium(III) with two oxygen atoms, may occur (Fig. 5). The chelate and non-chelate binding ligands have different effects on the phosphorus atom, thus two peaks were observed. For the same reason, two peaks were observed also in the spectrum of $Cr(PH_2O_2)_4^-$. Peak *b*, which is a common peak for the complexes $Cr(PH_2O_2)_6^{3-}$, $Cr(PH_2O_2)_5^{2-}$ and $Cr(PH_2O_2)_4^-$, can be assigned to the non-chelate binding ligand, and peak *c* to the chelate binding ligand. Since chelate binding is stronger than non-chelate binding, the resonance for the chelate binding ligand should appear at a higher field than for the non-chelate one. Also for the lower complexes such as $Cr(PH_2O_2)_3$, $Cr(PH_2O_2)_2^+$ and $Cr(PH_2O_2)^{2+}$, it may be possible to consider the co-existence of non-chelate and chelate isomers, although experimental evidence was not obtained due to low sensitivity.

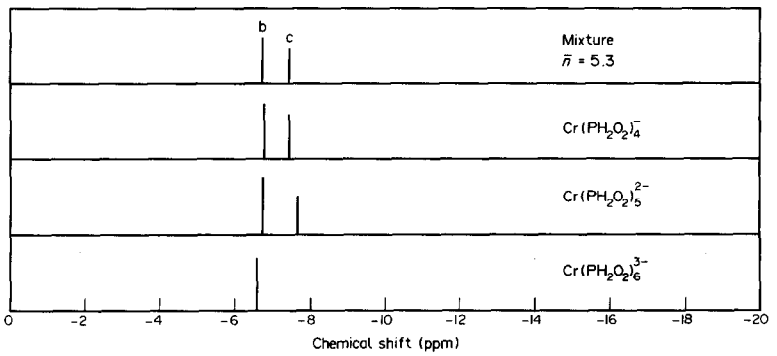

Fig. 4. ^{31}P NMR chemical shift for individual inner-sphere complexes and the mixture at pH 3, relative to free $PH_2O_2^-$ anion.

Table 1. Possible isomers of the inner-sphere complexes

$Cr:PH_2O_2^-$	Charge	Non-chelate	Mixed chelate–non-chelate	Chelate
1:1	+2	$Cr(OPH_2O)(H_2O)_5$		$Cr(O_2PH_2)(H_2O)_4$
1:2	+1	$Cr(OPH_2O)_2(H_2O)_4$	$Cr(O_2PH_2)(OPH_2O)(H_2O)_3$	$Cr(O_2PH_2)_2(H_2O)_2$
1:3	0	$Cr(OPH_2O)_3(H_2O)_3$	$Cr(O_2PH_2)(OPH_2O)_2(H_2O)_2$ $Cr(O_2PH_2)_2(OPH_2O)(H_2O)$	$Cr(O_2PH_2)_3$
1:4	−1	$Cr(OPH_2O)_4(H_2O)_2$	$Cr(O_2PH_2)(OPH_2O)_3(H_2O)$ $Cr(O_2PH_2)_2(OPH_2O)_2$	
1:5	−2	$Cr(OPH_2O)_5(H_2O)$	$Cr(O_2PH_2)(OPH_2O)_4$	
1:6	−3	$Cr(OPH_2O)_6$		

The presence of a variety of isomers for the inner-sphere complexes shown in Table 1 may theoretically be expected by distinguishing between chelate and non-chelate binding. Thus successful observation distinguishing these isomers is undoubtedly caused by a slow dehydration rate in the following steps

$$[Cr(OH_2)_6]^{3+} \xrightarrow[\text{fast}]{+PH_2O_2} [Cr(OH_2)_6 \cdot (PH_2O_2)]^{2+} \quad (1)$$

$$\xrightarrow[\text{slow}]{-H_2O} [Cr(OPH_2O)(OH_2)_5]^{2+} \quad (2)$$

$$\xrightarrow[\text{slow}]{-H_2O} [Cr(O_2PH_2)(OH_2)_4]^{2+}. \quad (3)$$

Equation (3), formation of the chelate binding complex from the non-chelate binding complex, is an intramolecular reaction, thus the concentration ratio of the chelate to non-chelate forms should be independent of the solution condition.

The presence of the same type of isomer could be possible in other moderately inert complex systems. Recently we found these isomers in the systems of aluminium phosphinate, phosphite and phosphate complexes, the details of which will be reported elsewhere.

REFERENCES

1. R. M. Smith and A. E. Martell (Eds), *Critical Stability Constants, Inorganic Complexes*, Vol. 4. Plenum Press, New York (1976).
2. E. Hogfeldt (Ed.), *Stability Constants of Metal-Ion Complexes*, Part A: Inorganic Ligands. Pergamon Press, Oxford (1982).
3. J. Podlaha and M. Ebert, *Nature* 1960, **188**, 657.
4. M. Ebert and L. Kavan, *Coll. Czech. Chem. Commun.* 1979, **44**, 2737.
5. R. N. Puri and R. O. Asplund, *Inorg. Chim. Acta* 1982, **57**, 57.
6. H. Waki, Q. Feng, K. Tsuruta and S. Ohashi, *Polyhedron* 1986, **5**, 1239.
7. H. Waki and Y. Tokunaga, *J. Chromatogr.* 1980, **201**, 259.
8. H. Waki and Y. Tokunaga, *J. Liq. Chromatogr.* 1982, **5**, 105.
9. R. D. Cornelius, P. A. Hart and W. W. Cleland, *Inorg. Chem.* 1977, **16**, 2799.
10. R. N. Bose, R. D. Cornelius and R. E. Viola, *Inorg. Chem.* 1985, **24**, 3989.
11. W. D. Wheeler, S. Kaizaki and J. I. Legg, *Inorg. Chem.* 1982, **21**, 3248.

Polyhedron Vol. 9, No. 13, pp. 1561–1565, 1990
Printed in Great Britain

0277–5387/90 $3.00+.00
© 1990 Pergamon Press plc

THE PREPARATION OF MIXED-LIGAND DITHIOLENE COMPLEXES: X-RAY STRUCTURE OF $Pt(PMe_2Ph)_2(mnt)$ AND $[Bu_4N][Au(mnt)_2]$

JONATHAN C. FITZMAURICE, ALEXANDRA M. Z. SLAWIN, DAVID J. WILLIAMS and J. DEREK WOOLLINS*

Department of Chemistry, Imperial College of Science and Technology, South Kensington, London SW7 2AY, U.K.

and

ALAN J. LINDSAY

Minnesota 3M Research Ltd, Harlow, Essex, U.K.

(*Received* 20 *October* 1989; *accepted* 21 *February* 1990)

Abstract—Reaction of $PtCl_2(PR_3)_2$ with sodium dithiolates gives mixed-ligand complexes such as $Pt(PR_3)_2(mnt)$ (**1**). Attempts to prepare mixed S—N/mnt complexes of gold were unsuccessful, $[Bu_4N][Au(mnt)_2]$ (**2**) being obtained. New compounds were characterized by IR and NMR spectroscopy and microanalyses, and in the case of **1** and **2** by X-ray crystallography. Both **1** and **2** are square planar. In **2**, one of the crystallographically independent anions lies over a symmetry related neighbour.

Transition-metal dithiolene complexes have been of interest for a number of years as they have potential for conductivity in the solid state.[1–5] In general, bis complexes have been most studied since they are planar and resemble compounds used in organic metals [e.g. if a metal replaces the central ethylene group atoms in tetrathiofulvalene (TTF), $M(dmit)_2$ complexes are formed. Complexes containing the ligand dmit (4,5-dimercapto-1,3-dithiole-2-thione) and dddt (4,5-dihydro-1,4-dithiin-2,3-dithiolate) have a high structural resemblance to the bis (ethylenedithio)tetrathiafulvalene molecule (ET)]. Recently, we have prepared complexes of the type $[Pt(S_2N_2H)(PR_3)_2]X$ and note that despite their lack of symmetry these materials stack in the solid state.[6,7] Here, we describe our investigations into the synthesis of mixed-ligand dithiolene complexes. The X-ray structures of $Pt(PMe_2Ph)_2(mnt)$ (**1**) and $[Bu_4N][Au(mnt)_2]$ (**2**) are also reported.

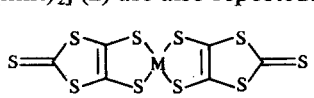

$M(dmit)_2$

* Author to whom correspondence should be addressed.

EXPERIMENTAL

General conditions and spectroscopic methods were as described previously.[8] Na_2mnt,[9] Na_2edt,[10] quinoxaline-2,3-dithiol (QDT),[11] $S_4N_4H_4$,[12] $[Me_2SnS_2N_2]_2$[13] and $[Bu_4N][Au(mnt)Br_2]$[14] were prepared as described in the literature. $PtCl_2(COD)$ was prepared from K_2PtCl_4 and COD in the presence of $SnCl_2 \cdot 2H_2O$.[15] Compounds of the type *cis*-$PtCl_2(PR_3)_2$ were made by adding stoichiometric amounts of the appropriate free phosphine to $PtCl_2(COD)$.

Electrochemical work was performed at ambient temperature and pressure using a Princeton Applied Research (PAR) Model 273 and peripheral equipment on solutions which were deoxygenated by purging with argon. $[Bu_4N][PF_6]$ was prepared by mixing hot aqueous solutions of $[Bu_4N]I$ and $[NH_4][PF_6]$; the precipitate was recrystallized twice from methanol and vacuum dried at 100°C for 24 h. CH_2Cl_2 (distilled from CaH_2) was transferred to a voltammetry cell containing sufficient $[Bu_4N][PF_6]$ and electroactive compound to make the solution *ca* 0.1 and 5×10^{-4} M in these compounds, respectively. All potentials are referred to the Ag/Ag^+ electrode.

Preparation of $Pt(PR_3)_2(mnt)$ ($PR_3 = PEt_3$, PMe_2Ph)

In a typical reaction, $PtCl_2(PMe_2Ph)_2$ (70 mg, 0.129 mmol) was mixed with an equimolar amount of Na_2mnt (24 mg, 0.129 mmol) and CH_2Cl_2–MeOH (20 cm^3, 3:1). After 2 h, the orange–red solution was filtered and evacuated to dryness. The resulting solid was dissolved in $CDCl_3$ (2–3 cm^3). The orange solid was recrystallized from hot ethanol to give shiny pink microcrystals of $Pt(PMe_2Ph)_2(mnt)$ (51 mg, 65%). Layering a CH_2Cl_2 solution of the compound with *n*-hexane gave crystals suitable for X-ray diffraction. Found: C, 39.2; H, 3.5; N, 4.3. Calc. for $Pt(PMe_2Ph)_2(mnt)$: C, 39.3; H, 3.6; N, 4.3%. $^{31}P\{^1H\}$ (ppm): δ −19.34(s) $^1J(^{195}Pt—^{31}P)$ 2778 Hz; ^1H (ppm): δ 1.71 (s, 12H, Me) $^2J(^{31}P—^1H)$ 10 Hz $^3J(^{195}Pt—^1H)$ 29 Hz, 7.38 (m, 10H, Ph) *o* 7.35, *p* 7.39, *m* 7.42. IR (cm^{-1}): 2222m, 2205vs, 1492vs, 1436vs, 1420vs, 1385s, 1287m, 1154s, 1107vs, 946vs, 924vs, 851m, 807w, 741vs, 719vs, 691vs, 508w, 482s, 445m, 434m, 372w.

Pale pink crystals were obtained for the PEt_3 derivative. Found: C, 33.6; H, 5.2; N, 4.8. Calc. for $Pt(PEt_3)_2(mnt)$: C, 33.6; H, 5.3; N, 4.9%. $^{31}P\{^1H\}$ (ppm): δ 4.82(s) $^1J(^{195}P—^{31}P)$ 2749 Hz, ^1H (ppm): δ 1.12 (t, 3H, Me) $^3J(CH_2—CH_3)$ 8 Hz $^3J(^{31}P—^1H)$ 16 Hz, 2.05 (m, CH_2) with Pt—H and P—H couplings. IR (cm^{-1}): 2221m, 2202vs, 1497vs, 1453s, 1416m, 1384m, 1260m, 1152s, 1110m, 1035vs, 1011m, 870w, 804w, 768s, 752vs, 745s, 726s, 701m, 629m, 508m, 441m, 426m, 387w, 310w.

Preparation of $Pt(PR_3)_2(edt)$ ($PR_3 = PEt_3$, PMe_2Ph)

Na_2edt (27 mg, 0.2 mmol) was added to a stirred solution of $PtCl_2(PEt_3)_2$ (100 mg, 0.2 mmol) in CH_2Cl_2 (10 cm^3). An immediate yellow coloration resulted. After 2 h, the solution was filtered and evacuated to dryness. The $^{31}P\{^1H\}$ NMR revealed two peaks with accompanying Pt—P splittings; that of the desired product and the starting phosphine (δ 9.13 ppm, ^1J 3513 Hz). Evaporation of the solvent to *ca* 0.5 cm^3 resulted in the formation of white needle-shaped crystals. Yield 55 mg (57%). Found: C, 32.1; H, 6.0. Calc. for $Pt(PEt_3)_2(edt)$: C, 32.2; H, 6.2%. $^{31}P\{^1H\}$ (ppm): δ 4.35(s), $^1J(^{195}Pt—^{31}P)$ 2732 Hz. IR (cm^{-1}): 1523m, 1453m, 1415m, 1384m, 1376m, 1103w, 1033vs, 811s, 767vs, 760vs, 725vs, 675vs, 634m, 417m, 354w, 325w, 292w.

Addition of diethyl ether was required to precipitate the PMe_2Ph derivative as a yellow solid (63 mg, 61%). Found: C, 37.9; H, 4.2. Calc. for $Pt(PMe_2Ph)_2(edt)$: C, 38.5; H, 4.3%. $^{31}P\{^1H\}$ (ppm): δ −19.00(s) $^1J(^{195}Pt—^{31}P)$ 2722 Hz. IR (cm^{-1}): 1519w, 1475w, 1434m, 1417m, 1400m, 1312w, 1262w, 1155w, 1103vs, 945s, 905vs, 853w, 839w, 808m, 758m, 748s, 734s, 716m, 697s, 667s, 482m, 447m, 432m, 374w, 366w, 337w, 328w.

Preparation of $Pt(PR_3)_2(QDT)$ ($PR_3 = PMe_2Ph$, PEt_3)

To a stirred solution of QDT (30 mg, 0.154 mmol) in MeOH (5 cm^3) was added sodium (10 mg, 0.435 mmol). After 10 min, $PtCl_2(PMe_2Ph)_2$ was added together with CH_2Cl_2 (5 cm^3) and the resulting solution was stirred for 2 h. Evaporation of the solvent to 5 cm^3 and addition of Et_2O resulted in precipitation of the orange complex. Found: C, 43.1; H, 3.9; N, 4.2. Calc. for $Pt(PMe_2Ph)_2(QDT)$: C, 43.4; H, 3.9; N, 4.2%. $^{31}P\{^1H\}$ (ppm): δ −17.9(s) $^1J(^{195}Pt—^{31}P)$ 2835 Hz. IR (cm^{-1}): 1547m, 1482w, 1434m, 1414m, 1387w, 1356m, 1328w, 1313w, 1259s, 1172vs, 1121vs, 1105s, 1049w, 1024w, 948s, 907vs, 843w, 805w, 762m, 743m, 717m, 689m, 599m, 489m, 445m, 428m. PEt_3 derivative: Found: C, 38.1; H, 5.4; N, 4.4. Calc. for $Pt(PEt_3)_2(QDT)$: C, 38.5; H, 5.5; N, 4.5%. $^{31}P\{^1H\}$ (ppm): δ 5.5(s) $^1J(^{195}Pt—^{31}P)$ 2817 Hz. IR (cm^{-1}): 1550m, 1480w, 1458m, 1453m, 1417m, 1370w, 1365m, 1254s, 1179vs, 1123vs, 1038vs, 1025s, 1004m, 802w, 768vs, 757vs, 726vs, 638m, 598m, 444m, 426m.

Reaction of $[Bu_4N][Au(mnt)Br_2]$ *with* $S_4H_4N_4$/dbu

$[Bu_4N][Au(mnt)Br_2]$ (59.2 mg, 8.01×10^{-5} mol) was dissolved in CH_2Cl_2 (10 cm^3) to which was added $S_4N_4H_4$ (7.5 mg, 4.0×10^{-5} mol) and an excess of dbu (~ 5 drops). The solution darkened to an orange–brown colour. After filtration, the solvent was reduced *in vacuo* to 0.5 cm^3. Dark red crystals were formed. Found: C, 39.5; H, 5.0; N, 9.6. Calc. for $[Bu_4N][Au(mnt)_2]$: C, 40.0; H, 5.0; N, 9.7%. Mass spectrometry: M^- (FAB): 477 $Au(mnt)_2^-$.

Reaction of $[Bu_4N][Au(mnt)Br_2]$ *with* $[Me_2SnS_2N_2]_2$

$[Bu_4N][Au(mnt)Br_2]$ (87 mg, 0.105 mmol) and $[Me_2SnS_2N_2]_2$ (28.3 mg, 5.25×10^{-5} mol) were combined in degassed CH_2Cl_2 (15 cm^3). After 24 h, the yellow–brown solution was filtered through celite and reduced to ~ 5 cm^3 *in vacuo*. Ether was added slowly until a dark brown, crystalline solid was deposited. Recrystallization from acetone–EtOH followed by slow hexane diffusion into a dichloromethane solution of the com-

pound gave dark red crystals which analysed as $[Bu_4N][Au(mnt)_2]$.

Crystal data

$C_{20}H_{22}N_2P_2PtS_2$ (**1**), $M = 611.6$, triclinic, $a = 9.22(5)$, $b = 11.318(6)$, $c = 11.552(7)$ Å, $\alpha = 84.02(4)$, $\beta = 84.64(4)$, $\gamma = 71.73(4)°$, $U = 1149$ Å^3, space group $P\bar{1}$, $Z = 2$, $D_c = 1.77$ g cm^{-3}. Pink, air-stable prisms, μ(Cu-K_α) = 146 cm^{-1}, $\lambda = 1.54178$ Å, $F(000) = 592$. $C_{24}H_{36}AuN_5S_4$ (**2**), $M = 719.8$, triclinic, $a = 13.405(5)$, $b = 13.533(5)$, $c = 17.612(5)$ Å, $\alpha = 75.98(3)$, $\beta = 79.92(3)$, $\gamma = 78.37(3)°$, $U = 3089$ Å^3, space group $P\bar{1}$, $Z = 4$ (two crystallographically independent molecules), $D_c = 1.59$ g cm^{-3}, μ(Cu-K_α) = 120 cm^{-1}, $\lambda = 1.54178$ Å, $F(000) = 1432$.

Data collection and processing

Nicolet R3m diffractometer, ω-scan method ($\theta \leqslant 50$ and 58°, respectively), graphite monochromated Cu-K_α radiation; for **1** 2662 and for **2** 8126 independent measured reflections, 2559 and 6883 observed ($|F_o| > 3\sigma(|F_o|)$), corrected for Lorentz and polarization factors; empirical absorption corrections based on 343 and 360 azimuthal measurements. Maximum and minimum transmission factors for **1** were 0.602 and 0.17, and for **2** 0.131 and 0.042, respectively.

Structure analysis and refinement

Complex **1** was solved by the heavy atom method and **2** by direct methods; in both cases all the non-hydrogen atoms were refined anisotropically. The hydrogen atoms were idealized (C—H = 0.96 Å), assigned isotropic thermal parameters $U(H) = 1.2\,U\text{eq}(C)$ and allowed to ride on their parent carbons. In **2** the methyl groups were refined as rigid bodies. Refinement was by block-cascade full-matrix least-squares to $R = 0.040$ ($R = \Sigma(|F_o| - |F_c|)/\Sigma|F_o|$), $R_w = 0.042$ ($w^{-1} = \sigma^2(F) + 0.0010F^2$) for **1**, and to $R = 0.050$, $R_w = 0.55$ ($w^{-1} = \sigma^2(F) + 0.00144F^2$) for **2**. The maximum and minimum residual electron densities in the final ΔF maps were 1.67, 1.25 and −1.07, −1.77 eÅ^{-3}, and the mean and maximum shifts/error in the final refinement cycle were 0.002, 0.008 and 0.018, 0.048, respectively. Computations were carried out on an Eclipse S140 computer using the SHELXTL program system.[16]

RESULTS AND DISCUSSION

In the light of the observed stacking properties in $[Pt(S_2N_2H)(PR_3)_2]X$, we have prepared mixed-ligand complexes containing dithiolenes and phosphines as well as studying methods for the preparation of complexes containing dithiolenes and SN ligands. Reaction of $PtCl_2(PR_3)_2$ with the sodium salt of the appropriate dithiolene ligand (mnt, edt, QDT) gives the desired mixed-ligand complex in fair yield. The new compounds gave satisfactory microanalyses and had the expected spectroscopic properties. Their ^{31}P NMR spectra consist of singlets with platinum satellites ($^1J(^{31}P—^{195}Pt)$ *ca* 2800 Hz).

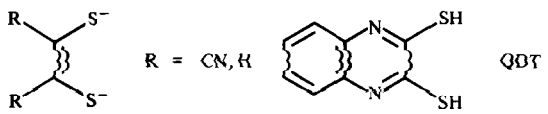

The IR spectra are as expected.[17] In the case of the mnt complexes the $\nu(C{\equiv}N)$ and $\nu(C{=}C)$ vibrations increase in frequency by *ca* 10 and 55 cm^{-1}, respectively, upon complexation indicating a decrease in bond length, whilst the $\nu(C{=}S)_{sym}$ vibration is reduced in frequency consistent with lengthening of the C—S bonds.

We have also attempted to prepare mixed dithiolene/SN complexes of gold. Thus reaction of $S_4N_4H_4$ or $[Me_2SnS_2N_2]_2$ with $[Bu_4N][Au(mnt)Br_2]$ was carried out by analogy with previous routes to $S_2N_2^{2-}$ complexes.[6-8] In both cases we observed formation of $[Bu_4N][Au(mnt)_2]$ (**2**) rather than the desired complex. Complex **2** has previously been obtained[18] from the reaction of auric acid and Na_2mnt.

A number of the compounds prepared have been studied by cyclic voltammetry. The cyclic voltammogram for $Au(mnt)_2^-/CH_2Cl_2$ was found to contain oxidative and reductive one electron reversible couples at $E_{1/2(oxid)} = +1.15$ V and $E_{1/2(red)} = -0.88$ V. This compares with the results obtained by Schlupp and Maki[19] for $Au(mnt)_2^-$/DMSO ($E_{1/2(red)} = -0.41$ V vs SCE).

Gold(III) is isoelectronic with platinum(II) (d^8) and it is probable that the gold and platinum mnt complexes have similar electronic structures. Schlupp and Maki have calculated that in the formal gold(III) complex $Au(mnt)_2^{3-}$ (d^8) the electron is largely based on the ligand orbital (80% A_g character). Geiger *et al.*[20] have noted the difficulty in assigning $Pt(mnt)_2^{3-}$ as platinum(I) (isoelectronic with $Au(mnt)_2^{2-}$) and have concluded that reduction of the platinum(II) complex could be either metal or ligand based. This is also likely for $Au(mnt)_2^-$.

The redox chemistry of $M[S_2C_2Ph_2]_2$ (M = Ni, Pd, Pt)[21] and $[M(S_2C_2Ph_2)(PPh_3)_2]$ (M = Pd, Pt) has been studied with the existence of the dithioketyl radical $C_2S_2Ph_2^-$ characterized by ESR.

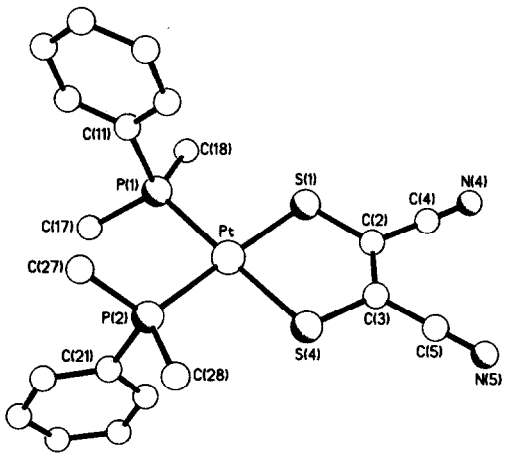

Fig. 1. The X-ray structure of **1**.

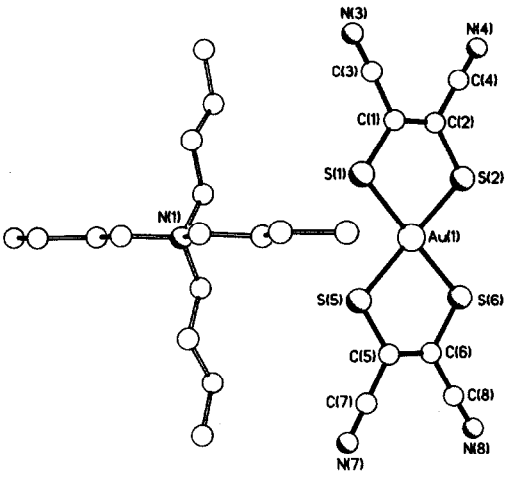

Fig. 2. The X-ray structure of **2**.

Reversible oxidation is found to occur on the dithiolene ligand and is relatively independent of the metal atom or phosphine. In the case of $Pt(PR_3)_2(mnt)$ studied here we observed irreversible oxidative peaks at +1.25 V indicating a secondary process (e.g. ligand dissociation).

The X-ray structures of $Pt(PMe_2Ph)_2(mnt)$ (**1**) and $[Bu_4N][Au(mnt)_2]$ (**2**) are shown in Figs 1 and 2, with selected bond lengths and angles in Tables 1 and 2. Complex **1** has the expected square-planar geometry with approximate non-crystallographic C_2 symmetry. There is a characteristic slight enlargement of the P—Pt—P angle (92.4(1)°) as a consequence of the bulk of the phosphine ligands. The Pt—P and Pt—S bond lengths are typical for platinum(II). The Pt—S bond length in **1** is slightly longer than in $Pt(mnt)_2^-$,[4] reflecting the difference in the *trans* effect of sulphur versus phosphorus rather than the difference in formal oxidation state. The transannular S···S distance is 3.23 Å. In **2** there are two crystallographicaly independent molecules. There are no significant differences in their geometries; both anions having approximate non-crystallographic D_{2h} symmetry. The bond lengths and angles are within statistical significance identical to those reported[22] for $[Au(S_2CNBu_2)_2][Au(mnt)_2]$. Replacement of platinum by gold does not appear to have any effect on the M—S distance in complexes of this type.[4,22] The transannular S···S distance in **2** (3.27 Å) is essentially identical to the *cis* inter-ring S···S distance (3.28 Å) underlining that mnt^{2-} is an almost optimum chelating ligand for the formation of undistorted bis complexes.

Table 1. Selected bond lengths (Å) and angles (°) in **1**

Pt—S(1)	2.309(2)	Pt—S(4)	2.301(2)
Pt—P(1)	2.278(2)	Pt—P(2)	2.289(2)
S(1)—C(2)	1.715(8)	P(1)—C(11)	1.828(7)
P(1)—C(17)	1.824(9)	P(1)—C(18)	1.818(13)
P(2)—C(21)	1.819(8)	P(2)—C(27)	1.809(8)
P(2)—C(28)	1.817(12)		
S(1)—Pt—S(4)	88.8(1)	S(1)—Pt—P(1)	89.5(1)
S(4)—Pt—P(1)	178.3(1)	S(1)—Pt—P(2)	178.1(1)
S(4)—Pt—P(2)	89.2(1)	P(1)—Pt—P(2)	92.4(1)
Pt—S(1)—C(2)	102.7(3)	S(1)—C(2)—C(3)	124.1(6)
S(1)—C(2)—C(4)	117.4(7)	C(3)—C(2)—C(4)	118.5(7)
C(2)—C(3)—S(4)	120.9(6)	C(2)—C(3)—C(5)	121.6(8)
S(4)—C(3)—C(5)	117.5(8)	Pt—S(4)—C(3)	103.5(3)
C(2)—C(4)—N(4)	178.6(10)	C(3)—C(5)—N(5)	179.1(9)

Table 2. Selected bond lengths (Å) and angles (°) for the two independent molecules in **2**

Au(1)—S(2)	2.308(3)	2.304(3)
Au(1)—S(6)	2.300(3)	2.312(2)
Au(1)—S(1)	2.307(3)	2.306(3)
Au(1)—S(5)	2.309(3)	2.309(3)
S(1)—C(1)	1.749(10)	1.731(10)
C(1)—C(3)	1.424(15)	1.453(13)
C(2)—C(4)	1.389(14)	1.421(16)
C(4)—N(4)	1.142(14)	1.162(18)
C(5)—C(6)	1.351(15)	1.336(13)
C(6)—S(6)	1.746(10)	1.707(9)
C(7)—N(7)	1.148(14)	1.160(14)
S(1)—Au(1)—S(2)	90.4(1)	90.6(1)
S(2)—Au(1)—S(5)	178.9(1)	179.6(1)
S(2)—Au(1)—S(6)	88.6(1)	90.1(1)
Au(1)—S(1)—C(1)	101.1(4)	100.1(3)
S(1)—C(1)—C(3)	115.3(9)	114.7(7)
C(1)—C(2)—S(2)	122.8(7)	122.7(8)
S(2)—C(2)—C(4)	114.8(9)	116.9(8)
C(1)—C(3)—N(3)	179.1(10)	177.2(12)
Au(1)—S(5)—C(5)	101.1(4)	100.5(3)
S(5)—C(5)—C(7)	116.6(8)	115.1(7)
C(5)—C(6)—S(6)	122.9(7)	124.2(7)
S(6)—C(6)—C(8)	114.4(8)	117.3(7)
S(1)—Au(1)—S(5)	90.6(1)	89.2(1)
S(1)—Au(1)—S(6)	178.9(1)	177.1(1)
S(5)—Au(1)—S(6)	90.4(1)	90.0(1)
S(1)—C(1)—C(2)	124.1(7)	125.6(7)
C(2)—C(1)—C(3)	120.5(9)	119.6(9)
C(1)—C(2)—C(4)	122.3(10)	120.3(9)
Au(1)—S(2)—C(2)	101.5(4)	100.8(3)
C(2)—C(4)—N(4)	176.4(12)	177.9(14)
S(5)—C(5)—C(6)	124.4(7)	124.1(7)
C(6)—C(5)—C(7)	119.0(9)	120.8(9)
C(5)—C(6)—C(8)	122.7(9)	118.5(8)
Au(1)—S(6)—C(6)	101.1(4)	101.1(3)

In **1** there are no close contacts and there is no evidence of any intermolecular stacking. In **2** there are no significant intermolecular interactions between the crystallographically independent anions (the planes of the anions are inclined *ca* 64°). However, centrosymmetrically related pairs of one of the anions pack parallel to each other (Fig. 3) with an interplanar separation of 3.7 Å; the C(5)—C(6) bond lying almost directly over, and parallel to, the S(5)″ ··· S(6)″ transannular vector of the symmetry related anion.

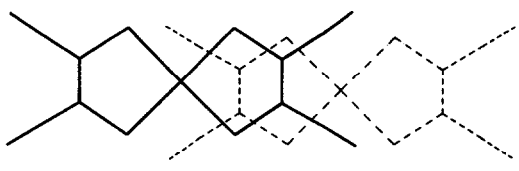

Fig. 3. Line drawing of the packing of centrosymmetrically related anions in **2**.

Acknowledgements—J.C.F. is grateful to Minnesota 3M Research Limited, Harlow and the SERC for support under the CASE scheme.

REFERENCES

1. J. S. Miller and A. J. Epstein, *Prog. Inorg. Chem.* 1976, **20**, 1.
2. J. M. Williams, H. H. Wang, T. J. Emge, U. Geiser, M. A. Beno, P. C. Leung, K. D. Carlson, R. J. Thorn and A. J. Schultz, *Prog. Inorg. Chem.* 1989, **35**, 51.
3. S. Alvarez, R. Vicente and R. Hoffmann, *J. Am. Chem. Soc.* 1985, **107**, 6253.
4. P. I. Clemenson, A. E. Underhill, M. B. Hursthouse and R. L. Short, *J. Chem. Soc., Dalton Trans.* 1989, 61.
5. M. B. Hursthouse, R. L. Short, P. I. Clemenson and A. E. Underhill, *J. Chem. Soc., Dalton Trans.* 1989, 67.
6. R. Jones, P. F. Kelly, C. P. Warrens, D. J. Williams and J. D. Woollins, *J. Chem. Soc., Chem. Commun.* 1986, 711.
7. R. Jones, P. F. Kelly, D. J. Williams and J. D. Woollins, *J. Chem. Soc., Dalton Trans.* 1988, 803.
8. R. Jones, C. P. Warrens, D. J. Williams and J. D. Woollins, *J. Chem. Soc., Dalton Trans.* 1987, 907.
9. E. I. Stiefel, L. E. Bennett, Z. Dori, T. H. Crawford, C. Simo and H. B. Gray, *Inorg. Chem.* 1970, **9**, 281.
10. W. Schrath and J. Peschel, *Chimia* 1964, **18**, 171.
11. L. J. Theriot, K. F. Ganguli, S. Kavanos and I. Bernal, *J. Inorg. Nucl. Chem.* **31**, 3133.
12. F. Feher, in *Handbook of Preparative Inorganic Chemistry* (Edited by G. Brauer), Vol. 1, p. 411. Academic Press, New York (1967).
13. H. W. Roesky and H. Weizer, *Angew. Chem. Int. Ed. Engl.* 1973, **12**, 674.
14. R. Uson, J. Vicente and J. Oro, *Inorg. Chim. Acta.* 1981, **52**, 29.
15. J. Chatt, L. M. Valerino and L. M. Venanzi, *J. Chem. Soc.* 1957, 2496.
16. G. M. Sheldrick, SHELXTL, An Integrated System for Solving, Refining and Displaying Crystal Structures from Diffraction Data. University of Göttingen, F.R.G. (1978); Revision 4.1 (August 1983).
17. C. W. Schlapfer and K. Nakamoto, *Inorg. Chem.* 1975, **14**, 1338.
18. A. Davison, N. Edelstein, R. H. Holm and A. H. Malik, *Inorg. Chem.* 1963, **2**, 1227.
19. R. L. Schlupp and A. H. Maki, *Inorg. Chem.* 1974, **13**, 44.
20. W. E. Geiger Jr, C. S. Allen, T. E. Miner and F. E. Senftleber, *Inorg. Chem.* 1980, **16**, 2003.
21. G. A. Bowmaker, P. D. W. Boyd and G. K. Campbell, *Inorg. Chem.* 1980, **19**, 2679.
22. J. H. Noordik and P. T. Beurskens, *J. Cryst. Molec. Struct.* 1971, **1**, 339.

Polyhedron Vol. 9, No. 13, pp. 1567–1571, 1990
Printed in Great Britain

0277–5387/90 $3.00 + .00
© 1990 Pergamon Press plc

REACTION OF Se_4N_4 WITH $Pt(PPh_3)_3$: THE PREPARATION AND X-RAY STRUCTURE OF $[Pt(Se_2N_2)(PPh_3)]_2 \cdot CH_2Cl_2$

PAUL F. KELLY, ALEXANDRA M. Z. SLAWIN, DAVID J. WILLIAMS and J. DEREK WOOLLINS*

Department of Chemistry, Imperial College of Science, Technology and Medicine, South Kensington, London SW7 2AY, U.K.

(*Received* 26 *January* 1990; *accepted* 1 *March* 1990)

Abstract—Reaction of $Pt(PPh_3)_3$ with Se_4N_4 in CH_2Cl_2 leads to a mixture of $Pt(Se_2N_2)(PPh_3)_2$ (**1**) and an intermediate species, which decomposes via loss of PPh_3 to give $[Pt(Se_2N_2)(PPh_3)]_2 \cdot CH_2Cl_2$ (**2**). X-ray crystallography reveals **2** to be dimeric, with $[Pt(Se_2N_2)(PPh_3)]$ units bridged by Pt—N bonds in a Pt_2N_2 ring. The central $[PtSe_2N_2]_2$ core is planar and the geometry of the individual $PtSe_2N_2$ rings is comparable to that in the only other example reported, $[Pt(Se_2N_2H)(PMe_2Ph)_2]Cl$.

In contrast to the chemistry of metalla–sulphur–nitrogen species, which has been extensively explored in the last 20 years, studies into analogous selenium–nitrogen complexes have only recently come to fruition, with the preparation of the first complexes of NSeCl, Se_3N^-, $Se_2N_2^{2-}$ and $Se_2N_2H^-$.[1-4] The most convenient of these preparations, which circumvents the praecidigitogenic Se_4N_4, involves the use of a solution of $SeCl_4$ in liquid ammonia, which acts as precursor to the $Se_2N_2^{2-}$ ligand.[4] Reaction of Se_4N_4 with $[PtCl_2(PMe_2Ph)]_2$ yields $Pt(Se_3N)Cl(PMe_2Ph)$ and $Pt(Se_2N_2H)Cl(PMe_2Ph)$, although the procedure is rendered somewhat unsatisfactory by the low yield and need for a high temperature (with consequent danger of Se_4N_4 detonation). Another drawback to this reaction is that it is not directly analogous to the equivalent S_4N_4 reaction, which proceeds via oxidative addition to give $Pt(S_4N_4)Cl_2(PMe_2Ph)$;[5] as a result, analysis of the reaction mechanism is difficult.

Here we report on the reaction of Se_4N_4 with the zerovalent platinum species $Pt(PPh_3)_3$, which proceeds at ambient temperature in a manner analogous to the same reaction of S_4N_4.[6,7] Reaction in CH_2Cl_2 results in the formation of a mixture of complexes, including the previously reported $Pt(Se_2N_2)(PPh_3)_2$ (**1**) and the dimeric species $[Pt(Se_2N_2)(PPh_3)]_2$, which we have characterized by X-ray crystallography [as the CH_2Cl_2 solvate (**2**)]. Compound **2** is the first example of a binuclear complex of the $Se_2N_2^{2-}$ ligand and only the second complex containing the $PtSe_2N_2$ ring to be crystallographically characterized.

EXPERIMENTAL

General reaction conditions were as described previously.[4] $Pt(PPh_3)_3$ was prepared from K_2PtCl_4 and PPh_3;[8] solutions in CH_2Cl_2 were made up immediately prior to reaction to avoid decomposition. Se_4N_4 was prepared by reaction of NH_3 with $(EtO)_2SeO$,[9] a method we have found to be less hazardous than the high pressure reaction of $SeCl_4$ with NH_3.

SAFETY NOTE: Se_4N_4 is substantially less stable than S_4N_4 and can explode on contact with a metal spatula. In contrast to the safety note in *Gmelin*,[10] which lists 100 mg as a safe amount, we have found that the destructive capacity of amounts as small as 20 mg is sufficient to warrant extreme care. Se_4N_4 residues are best destroyed by cautious addition of hypochlorite solution to a suspension in water.

In a typical reaction Se_4N_4 (40 mg, 0.11 mmol) was suspended in CH_2Cl_2 (30 cm^3) and stirred for $\approx$ 15 min to give a very fine dispersion which was

* Author to whom correspondence should be addressed.

then treated with a solution of $Pt(PPh_3)_3$ (106 mg, 0.11 mmol) in CH_2Cl_2 (30 cm^3). The resulting dark coloured mixture was stirred for 20 min then filtered (**NOTE**: filtrations were performed using sintered glass funnels with copious amounts of celite filter-aid, which must be present to trap unreacted Se_4N_4 and avoid its potentially explosive combination with the sintered glass), the volume of CH_2Cl_2 was reduced to 5 cm^3 *in vacuo*, and the products precipitated as a red–brown solid by addition of pentane (50 cm^3). At this point the ^{31}P NMR spectrum of a $CDCl_3$ solution of the products revealed the presence of $Pt(Se_2N_2)(PPh_3)_2$ (**1**) (AX spectrum δ_a 27.7 [$^1J\{^{195}Pt-^{31}P\}$ 2925], δ_b 6.4 [^1J 2757]; lit. δ_a 26.8 [^1J 2963], δ_b 6.2 ppm [^1J 2778 Hz]) together with a singlet at δ 26.2 ppm [^1J 3198 Hz] and another AX pattern δ_a 25.8 [^1J 2932], δ_b 3.3 ppm [^1J 2876 Hz].

The $CDCl_3$ solution was layered with pentane and slow diffusion resulted in a large crop of very dark green microcrystals (including some large enough to be suitable for X-ray crystallography) together with a smaller number of orange crystals. The solution was decanted from the product, which was washed with CH_2Cl_2 (3×30 cm^3) to remove any crystals of **1**. The remaining orange crystals were presumed to be Se_4N_4 and were carefully separated manually from the green crystals, which were shown by X-ray crystallography to be $[Pt(Se_2N_2)(PPh_3)]_2 \cdot CH_2Cl_2$ (**2**). Typical yield of **2** 20 mg ($\approx$ 30% based upon Pt). Found: C, 32.3; H, 2.1; N, 3.8. Calc. for $[Pt(Se_2N_2)(PPh_3)]_2 \cdot CH_2Cl_2$: C, 32.4; H, 2.4; N, 4.1%.

Crystal data

Compound **2**, $C_{36}H_{30}N_4P_2Se_4Pt_2 \cdot CH_2Cl_2$, M = 1371.6, monoclinic, $a = 9.336(2)$, $b = 14.982(4)$, $c = 14.744(4)$ Å, $\beta = 99.57(2)°$, $U = 2034$ Å^3, space group $P2_1/n$, $Z = 2$ (the molecule is disposed about a centre of symmetry), $D_c = 2.24$ g cm^{-3}. Crystal dimensions $0.07 \times 0.07 \times 0.40$ mm. μ(Cu-K_α) = 193 cm^{-1}, $\lambda = 1.54178$ Å, $F(000)$ = 1268.

Data collection and processing

Nicolet R3m diffractometer, ω-scan method, ($\theta \leqslant 58°$), graphite monochromated Cu-K_α radiation; 2733 independent measured reflections, 2530 observed [$|F_o| > 3\sigma(|F_o|)$], corrected for Lorentz and polarization factors; numerical absorption correction (face-indexed crystal). Maximum and minimum transmission factors: 0.390 and 0.153, respectively.

Structure analysis and refinement

The structure was solved by direct methods and all the non-hydrogen atoms refined anisotropically. A ΔF map revealed the presence of a disordered CH_2Cl_2 molecule; the hydrogen atoms of the solvent were not located. The positions of the remaining hydrogen atoms were idealized (C—H = 0.96 Å), assigned isotropic thermal parameters $U(H) = 1.2\ U\text{eq}(C)$ and allowed to ride on their parent carbons. Refinement was by block-cascade full-matrix least-squares to $R = 0.034$, ($R = \Sigma[|F_o| - |F_c|]/\Sigma|F_o|$), $R_w = 0.037$ ($w^{-1} = \sigma^2(F) + 0.00028F^2$). The maximum and minimum residual electron densities in the final ΔF map were 1.23 and -0.84 eÅ^{-3} and the mean and maximum shifts/error in the final refinement cycle were 0.003 and 0.086, respectively. Computations were carried out on an Eclipse S140 computer using the SHELXTL program system[11] and published scattering factors.[12]

RESULTS AND DISCUSSION

The zerovalent platinum complex $Pt(PPh_3)_3$ reacts with Se_4N_4 in a similar fashion to that previously reported for S_4N_4.[6,7] In the latter case reaction in CH_2Cl_2 results in the formation of $Pt(S_2N_2)(PPh_3)_2$ together with an intermediate which decomposes via loss of PPh_3 to give $[Pt(S_2N_2)(PPh_3)]_2 \cdot CH_2Cl_2$ (**3**), a binuclear complex bridged by Pt—N bonds. The intermediate has not been characterized by X-ray crystallography due to its instability; its ^{31}P NMR spectrum consists of a singlet and an AX pattern, both with ^{195}Pt satellites, and it analyses as $[\{Pt(S_2N_2)(PPh_3)_2\}\{Pt(S_2N_2)(PPh_3)\}]$. These observations have lead to suggestions that it may be a single dimeric complex, bridged by one platinum–nitrogen bond,[6] although work by us, using ^{15}N labelling techniques suggests that the structure may well be more complex than this. The above formulation is consistent with the observation that upon decomposition to **3** PPh_3 is lost from the intermediate (as shown by ^{31}P NMR), and that neither of the constituent NMR patterns have been observed separately.[13] The ^{31}P NMR spectrum of the products from the Se_4N_4 reaction, performed by addition of a solution of $Pt(PPh_3)_3$ in CH_2Cl_2 to a suspension of Se_4N_4 in the same solvent, shows the presence of both **1** and an intermediate of apparently similar structure to that formed in the S_4N_4 reaction. Again, the latter decomposes via loss of PPh_3 to give the dimeric species **2**. We have been unable to isolate a pure sample of the intermediate in the Se_4N_4 reaction, but its ^{31}P NMR spectrum is

so similar to that from the S_4N_4 case that we are confident that eq. (1) is a good description of the fate of the platinum-containing species in the reaction.

$$Pt(PPh_3)_3 + Se_4N_4 \longrightarrow Pt(Se_2N_2)(PPh_3)_2 + Pt_2(Se_2N_2)_2(PPh_3)_3$$
$$\text{(1)} \qquad \downarrow -PPh_3$$
$$[Pt(Se_2N_2)(PPh_3)]_2.$$

Compound **2** is a dark-green insoluble solid which can be obtained in crystalline form by slow pentane diffusion into a solution of the crude products of the reaction; also produced are a few small aggregations of orange crystals of Se_4N_4. In view of this, **2** is best prepared in crystalline form rather than as a powder, since otherwise it would prove impossible to separate from the Se_4N_4, and in consequence any manipulations, such as preparations of mulls etc., would be hazardous. Once pure **2** represents no explosive hazard and appears to be air-stable.

The colour of **2** provides an interesting correlation between the dimeric species, **2** and **3**, and the related species $Pt(S_3N)Cl(PMe_2Ph)$ and $Pt(Se_3N)Cl(PMe_2Ph)$. In the case of the sulphur species both are an intense red colour, while the selenium complexes are both dark green. The X-ray crystal structure of **2** (Fig. 1) shows the molecule to be isostructural with its sulphur analogue, **3**,[7] there being slight increases in each of the unit cell lengths but no change in the β angle. The molecule is dimeric with a central Pt_2N_2 ring. The $[PtSe_2N_2]_2$ core is planar to within 0.017 Å with the phosphorus atom lying 0.096 Å from this plane. Whereas in **3** in the Pt_2N_2 ring the Pt—N bonds are of the same length, in **2** the Pt—N(1) bond (2.005(8) Å, Table 1) is significantly shorter than that for Pt—N(1′) (2.062(7) Å). The N—Pt—N′ angle is slightly contracted in **2** (75.0(3)°, cf. 77.1(5)° in **3**) with a commensurate small increase in the Pt···Pt′ distance (3.23, cf. 3.21 Å in **3**) and decrease in the N···N′ separation (2.48, cf. 2.56 Å in **3**). It is surprising that the Pt—N bond *trans* to the chalcogen is unchanged on going from S to Se, whereas the Pt—P(1) and Pt—N(1) distances are both contracted. Within the $PtSe_2N_2$ ring the Pt—Se(2) bond is slightly shorter than in $[Pt(Se_2N_2H)(PMe_2Ph)_2]Cl$ (**4**)[3] (2.334(1) Å in **2** and 2.405(1) Å in **4**), reflecting the difference in the *trans* substituent (N vs PMe_2Ph). The remaining bond lengths within the ring do not differ significantly from those in **4**. The dimeric nature of the complex together with the presence of the bulky phosphine ligands and the solvated CH_2Cl_2 preclude any stacking of the $PtSe_2N_2$ rings.

Figure 2 shows the difference spectrum in which the IR spectrum of **2** has been subtracted from that of the sulphur analogue, **3**, in an attempt to distinguish the bands due to $S_2N_2^{2-}$ and $Se_2N_2^{2-}$ from those of the PPh_3 ligand. Although some peaks due to PPh_3 remain (dotted lines), the spectrum clearly shows the peaks due to $S_2N_2^{2-}$ (upper) and $Se_2N_2^{2-}$ (lower). The two most prominant in each case (Table 2) occur at 1034 and 724 cm^{-1} in **3** and at 815 and 550 cm^{-1} in **2**. Analogous bands are present in the IR spectra of the related complexes $Pt(E_2N_2)(PPh_3)_2$ (E = S, Se), although complexes **2** and **3** both show an extra peak, at 676 and 917 cm^{-1}, respectively, which is not present in the spectra of the bis-phosphine species. All these peaks can be assigned to S/Se—N stretches, with the

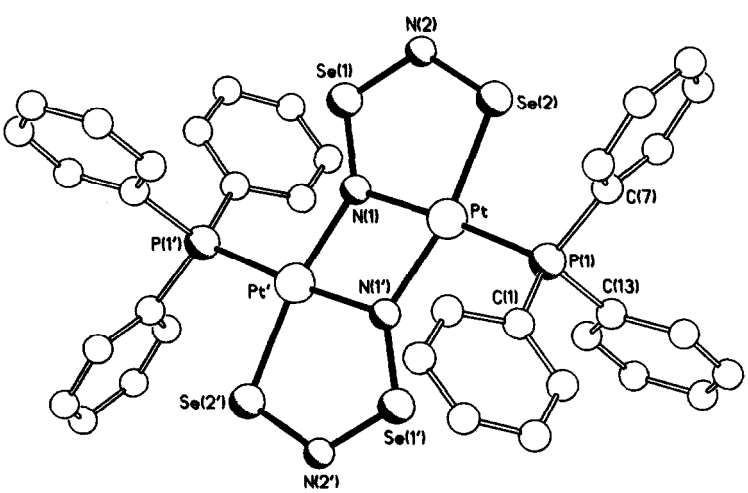

Fig. 1. The X-ray crystal structure of **2**.

Table 1. Selected bond lengths (Å) and angles (°) in **2**

Pt—N(1)	2.005(8)	Pt—Se(2)	2.334(1)
Pt—P(1)	2.244(2)	Pt—N(1′)	2.062(7)
Se(1)—N(2)	1.732(7)	N(2)—Se(2)	1.818(9)
N(1)—Se(1)	1.745(7)	P(1)—C(1)	1.832(7)
P(1)—C(7)	1.825(7)	P(1)—C(13)	1.817(8)
N(1)—Pt—Se(2)	91.3(2)	N(1)—Pt—N(1′)	75.0(3)
Pt—N(1)—Se(1)	120.1(4)	N(1)—Se(1)—N(2)	107.3(4)
Se(1)—N(2)—Se(2)	118.2(4)	Pt—Se(2)—N(2)	103.1(2)
Pt—N—Pt′	105.0(3)	P(1)—Pt—Se(2)	93.2(1)
P(1)—Pt—N(1′)	100.5(2)		

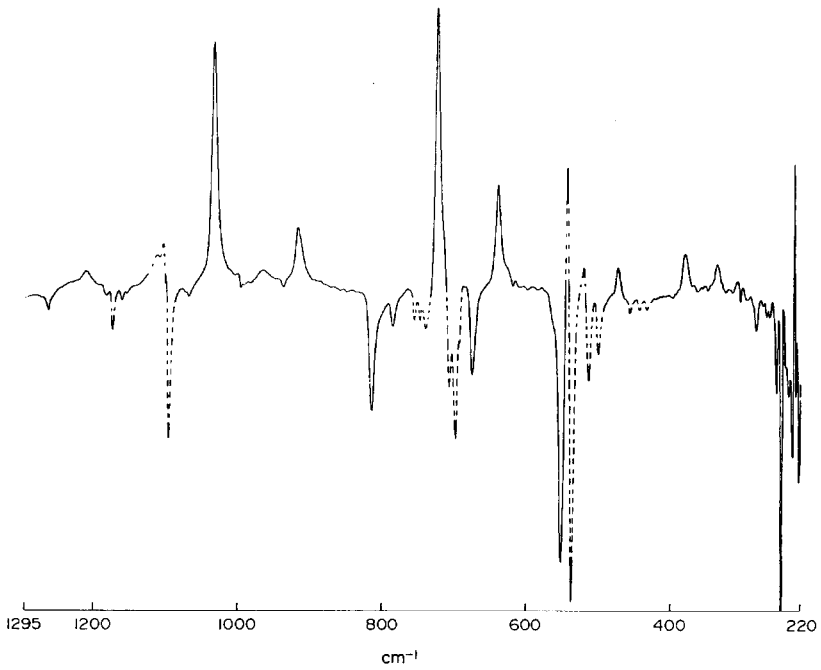

Fig. 2. Difference IR spectrum, **3**−**2**, showing residual peaks due to S—N (upper) and Se—N (lower) vibrations.

Table 2. Frequencies of S—N and Se—N vibrations in **2** and **3**

$[Pt(S_2N_2)(PPh_3)]_2$	$[Pt(Se_2N_2)(PPh_3)]_2$	Assignment
1034(vs)	815(s)	ν(N—S/Se)
917(m)	676(m)	ν(N—S/Se)
724(vs)	550(vs)	ν(N—S/Se)
640(m)	282(w)	δ(N—S/Se)
473(w)		ν(Pt—N)
379(w)		δ(N—S)
335(w)		ν(Pt—S)

expected decrease in frequency upon changing from S to the heavier Se, although it is not obvious why the dimeric species should show three such stretches and the monomers only two, especially as monomeric complexes of the type $M(S_2N_2H)_2$ show three (NS) stretches. By analogy with other systems the bands at 640, 473, 379 and 335 cm^{-1} in **3** can be assigned to δ(N—S), ν(Pt—N), δ(N—S) and ν(Pt—S), respectively; in conrast, the spectrum of **2** shows only a band at 282 cm^{-1} in this region, which is probably best assigned to δ(N—Se), and no obvious Pt—N stretch.

The reaction of Se_4N_4 with $Pt(PPh_3)_3$ is important since it shows that it is possible for Se_4N_4 to react via oxidative addition in a manner identical to S_4N_4. Although Se_4N_4 is undoubtedly much more inert than its sulphur counterpart, it would appear likely that its chemistry is substantially more diverse than has previously been imagined.

Acknowledgements—We are grateful to the Wolfson Foundation and Research Corporation Trust for financial support and to Johnson Matthey for loans of precious metals.

REFERENCES

1. J. Adel, A. El-Kholi, W. Willing, U. Muller and K. Dehnicke, *Chimia* 1988, **42**, 70.
2. P. F. Kelly, A. M. Z. Slawin, D. J. Williams and J. D. Woollins, *J. Chem. Soc., Chem. Commun.* 1989, 408.
3. P. F Kelly, I. P. Parkin, A. M. Z. Lawin, D. J. Williams and J. D. Woollins, *Angew. Chem. Int. Ed. Engl.* 1989, **28**, 1047.
4. I. P. Parkin and J. D. Woollins, *J. Chem. Soc., Dalton Trans.* 1990, 925.
5. M. B. Hursthouse, P. F. Kelly, M. Motevalli and J. D. Woollins, *Polyhedron* 1989, **8**, 997.
6. C. A. Ghilardi, S. Midollini, S. Moneti and A. Orlandini, *J. Organomet. Chem.* 1985, **286**, 419.
7. R. Jones, P. F. Kelly, D. J. Williams and J. D. Woollins, *J. Chem. Soc., Chem. Commun.* 1985, 1325.
8. R. Ugo, F. Cariati and G. LaMonica, *Inorg. Synth.* 1968, **11**, 105.
9. J. Adel, C. Ergezinger, R. Figge and K. Dehnicke, *Z. Naturfor.* 1988, **43b**, 639.
10. *Gmelin, Handbook of Inorganic Chemistry*, Se (Supplement, Vol. B1). Springer, Berlin (1981).
11. G. M. Sheldrick, SHELXTL, An Integrated System for Solving, Refining and Displaying Crystal Structures from Diffraction Data. University of Göttingen, Göttingen F.R.G. (1978), Revision 4.1 (August 1983).
12. *International Tables for X-Ray Crystallography*, Vol. 4, pp. 99–149. Kynoch Press, Birmingham (1974).
13. P. F. Kelly, Sulphur–nitrogen compounds of platinum and palladium, PhD thesis. University of London (Imperial College) (1987).

Polyhedron Vol. 9, No. 13, pp. 1573–1587, 1990
Printed in Great Britain

0277–5387/90 $3.00+.00
© 1990 Pergamon Press plc

SYNTHESIS AND STRUCTURES OF PHOSPHINE, PHOSPHIDO AND PHOSPHINIDENE DERIVATIVES OF TRIOSMIUM FROM REACTIONS OF R_2PH (R = *t*-Bu, CYCLOHEXYL) WITH $Os_3(CO)_{12}$

ATTA M. ARIF, THERESA A. BRIGHT, DUANE E. HEATON, RICHARD A. JONES* and CHRISTINE M. NUNN

Department of Chemistry, The University of Texas at Austin, Austin, TX 78712, U.S.A.

(*Received* 8 *December* 1989; *accepted* 27 *February* 1990)

Abstract—Photolysis of $Os_3(CO)_{12}$ and *t*-Bu_2PH in toluene yields the trisubstituted phosphine cluster $Os_3(CO)_9(t\text{-}Bu_2PH)_3$ (**1**) (63%). Reaction of *t*-Bu_2PH with $Os_3(CO)_{12}$ by heating in toluene (12 h) yields the disubstituted phosphine complex $Os_3(CO)_{10}(t\text{-}Bu_2PH)_2$ (**2**) (24%) and the bis-phosphido complex $Os_3(CO)_8(\mu\text{-}H)_2(\mu\text{-}t\text{-}Bu_2P)_2$ (**3**) (50%). Compound **3** may be converted into the 46-electron complex $Os_3(CO)_6(t\text{-}Bu_2PH)(\mu\text{-}H)_2(\mu\text{-}t\text{-}Bu_2P)_2$ (**4**) by further heating in refluxing toluene with *t*-Bu_2PH. Refluxing **1**, **2**, **3** or **4** in di-*n*-butylether (143°C) affords the phosphinidene complex $Os_3(CO)_7(t\text{-}Bu_2PH)_2(\mu_3\text{-}t\text{-}BuP)$ (**5**) (68%). The reaction of dicyclohexylphosphine (Cy_2PH) with $Os_3(CO)_{12}$ in refluxing toluene yields the tris-phosphido-bridged complex $Os_3(CO)_7(\mu\text{-}H)(Cy_2P)_3$ (**6**) (60%). The structures of **1**–**6** have been determined via single-crystal X-ray diffraction studies. The molecular structure of **1** is based on that of $Os_3(CO)_{12}$ with the three *t*-Bu_2PH ligands occupying equatorial sites on each osmium in order to minimize steric interactions. The structure of **2** has two *t*-Bu_2PH ligands in equatorial positions arranged *trans* to each other across an Os—Os bond. Complex **3** contains two bridging *t*-Bu_2P^- groups which lie above and below the Os_3 plane. Two bridging hydrides occupy positions *trans* to these groups. The coordination geometry of each metal is roughly octahedral if one ignores the Os—Os bonds. The structure of **4** is similar to that of **3** except that one CO groups has been replaced by an $Os(CO)_3$ unit and the adjacent $Os(CO)_3$ group now bears only two CO units. Complex **5** contains a μ_3-capping phosphinidene group (*t*-BuP^{2-}) in addition to two terminal phosphines (*t*-Bu_2PH) on adjacent metal atoms. The structure of **6** features three bridging Cy_2P^- groups which lie above, in and below the Os_3 plane.

There is presently considerable interest in the chemistry of ruthenium and osmium clusters.[1] Our interest was drawn to the chemistry of trinuclear species which feature phosphido, arsenido, phosphinidene and arsinidene ligands by the work of several groups.[2] In addition to unusual structural features in such complexes, interesting organometallic transformations have also been observed. These have included P—C or As—C bond cleavages as well as a variety of insertion reactions.[2]

A general observation is that both primary and secondary phosphines react with the trinuclear carbonyls of ruthenium and osmium [$M_3(CO)_{12}$] under mild conditions to give phosphido-bridged hydrido clusters such as $Ru_3(\mu\text{-}H)_2(\mu\text{-}PPh_2)(CO)_8$[3] and under more forcing conditions to give μ_3-PR (phosphinidene) species. These reactions no doubt involve an initial substitution of CO in $M_3(CO)_{12}$ to give phosphine adducts. This is followed by migration of hydrogen and further loss of CO molecules.

Huttner and co-workers have shown this sequence of reactions occurs with primary phosphines.[4] Thus RPH_2 (R = C_6H_5, *p*-$CH_3OC_6H_4$, C_6H_{11}) react with $Os_3(CO)_{12}$ in the presence of Me_3NO under mild conditions to give $Os_3(CO)_{11}(PRH_2)$ and $Os_3(CO)_{10}(\mu\text{-}H)(\mu\text{-}PRH)$. At higher

* Author to whom correspondence should be addressed.

temperatures $Os_3(CO)_9(\mu\text{-}H)_2(\mu_3\text{-}PR)$ is formed. Lewis and co-workers have shown that reacting $Os_3(CO)_{11}(MeCN)$ with PR_2H gives the corresponding phosphine-substituted clusters $Os_3(CO)_{11}(PR_2H)$ (R = C_6H_5, H).[5]

As part of a programme focused on the unusual behaviour of metal complexes containing bulky phosphido and arsenido ligands, we have studied the reactions of the ruthenium and osmium carbonyl clusters with *t*-Bu_2PH and *t*-Bu_2AsH. A preliminary report of our initial studies with $Ru_3(CO)_{12}$ has appeared.[6] We report here details of the reactions of $Os_3(CO)_{12}$ with *t*-Bu_2PH and Cy_2PH (Cy = cyclohexyl). These reactions produce a variety of new phosphine, phosphido and phosphinidene complexes (see Scheme 1). The tris-phosphine complex $Os_3(CO)_9(t\text{-}Bu_2PH)_3$ (**1**) is formed by photolysis of $Os_3(CO)_{12}$ with *t*-Bu_2PH in THF, while the disubstituted product $Os_3(CO)_{10}(t\text{-}Bu_2PH)_2$ (**2**) and the bis-phosphido complex $Os_3(CO)_8(\mu\text{-}H)_2(\mu\text{-}t\text{-}Bu_2P)_2$ (**3**) are formed by refluxing the mixture in toluene (12 h). More prolonged heating of the reaction mixture (24 h) affords **3** as well as the 46-electron cluster $Os_3(CO)_6(t\text{-}Bu_2PH)(\mu\text{-}H)_2(\mu\text{-}t\text{-}Bu_2P)_2$ (**4**). Interestingly, the 48-electron complex, **3**, may be converted into **4** by warming with excess *t*-Bu_2PH in THF. The reverse reaction occurs when **4** is reacted with CO (1 atm). The interconversions represent an unusual facile interconversion of 46- and 48-electron clusters.[7] The phosphinidene complex $Os_3(CO)_7(t\text{-}Bu_2PH)_2(\mu\text{-}H)_2(\mu_3\text{-}t\text{-}BuP)$ (**5**) is formed in good yields by heating either **1**, **2**, **3** or **4** in refluxing di-*n*-butylether (143°C) for 24 h. We have also investigated the possibility of using slightly less bulky phosphido groups. The use of dicyclohexyl phosphine (Cy_2PH) permits the isolation of $Os_3(CO)_7(\mu\text{-}H)(\mu\text{-}Cy_2P)_3$ (**6**) which contains three bridging phosphido units. The complexes have been characterized spectroscopically (IR, NMR) and their structures in the solid state determined by single-crystal X-ray diffraction studies.

RESULTS AND DISCUSSION

Synthesis of phosphine complexes: $Os_3(CO)_9(t\text{-}Bu_2PH)_3$ (**1**) *and* $Os_3(CO)_{10}(t\text{-}Bu_2PH)_2$ (**2**)

Complex **1** may be prepared in *ca* 63% yield by photolysis of a mixture of $Os_3(CO)_{12}$ and three equivalents of *t*-Bu_2PH in THF for 18 h. It may be crystallized as air-stable, red–orange crystals from hexane solutions at −30°C. In contrast, the thermal reaction of $Os_3(CO)_{12}$ with three equivalents of *t*-Bu_2PH in refluxing toluene (12 h) produces a mixture of the disubstituted phosphine complex **2** (24%) and the bis-phosphido species **3** (50%). The compounds may be separated by column chromatography (see Experimental). Both complexes may be recrystallized as orange (**2**) and yellow–orange (**3**), air-stable crystals from hexane (−30°C).

Spectroscopic data for both **1** and **2** are in accord with the solid-state structures as determined by X-ray crystallography. Thus the IR spectra contain terminal ν(CO) bands at 1973 (s), 1955 (s), 1918 (s) and 1873 (w) cm^{-1} for **1** and at 1990 (s), 1952 (s) and 1928 (s) cm^{-1} for **2**. Both **1** and **2** have P—H stretches in their IR spectra (2320 (w), 2300 (w) **1**; 2310 (w) **2**, cm^{-1}). The $^{31}P\{^1H\}$ NMR spectra of **1** and **2** consist of singlets at δ 17.93 and 21.46, respectively. These signals split into broad doublets in the ^{31}P spectra confirming the presence of phosphine (*t*-Bu_2PH) units.

X-ray structure of **1**

Table 1 gives pertinent X-ray data collection parameters for all the complexes. Figure 1 shows an ORTEP view of **1** with the atom numbering scheme. Key bond lengths and angles for **1** are given in Table 2. Complex **1** crystallizes in the orthorhombic space group *Pbca* with eight molecules in the unit cell. The molecular structure of **1** is similar to that of $Os_3(CO)_{12}$ with the three secondary phosphine ligands occupying equatorial sites on each metal so as to minimize the steric interactions between them. There is a distortion from the idealized D_{3h} symmetry found in $Os_3(CO)_{12}$ to D_3. This is achieved by a twisting of the "ML_4" [$Os(CO)_3(t\text{-}Bu_2PH)$] moieties about the Os—Os vectors. This is in agreement with the proposal by Lauer that the D_{3h} structure will be less stable than the D_3 structure from descriptions of surface force-fields applied to metal carbonyl clusters.[8] The Os—Os bond lengths are similar [2.920 Å (av.)] and may be compared with those found in $Os_3(CO)_{12}$ [2.877(3) Å].[9] The Os—P bond lengths are also similar and average 2.37 Å. The P-*H* hydrogen atoms of the *t*-Bu_2P-*H* units were not located in the X-ray structure, although their presence was confirmed by IR and NMR spectroscopic data.

X-ray structure of **2**

Figure 2 shows an ORTEP view of **2** with the atom numbering scheme. Table 3 contains selected bond lengths and angles for the molecule. Compound **2** crystallizes in the monoclinic space group $P2_1$ (No. 4) with two molecules in the unit cell. The molecular structure is based on the $Os_3(CO)_{12}$ framework as found for **1**. However, for **2** the two

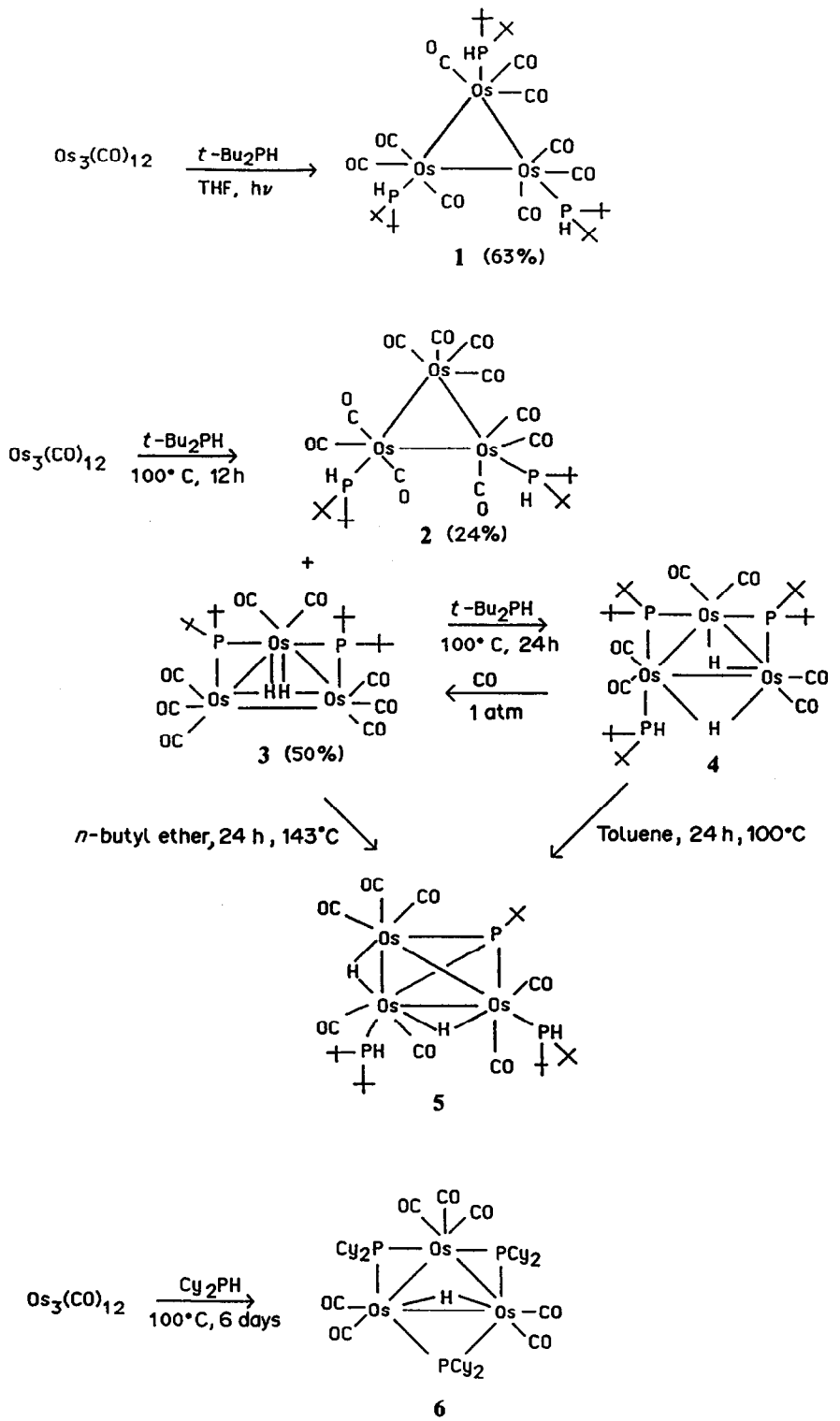
Os3(CO)12
t-Bu2PH
THF, hν
1 (63%)
Os3(CO)12
t-Bu2PH
100° C, 12h
2 (24%)
3 (50%)
t-Bu2PH
100° C, 24h
CO
1 atm
4
n-butyl ether, 24 h, 143°C
Toluene, 24 h, 100°C
5
Os3(CO)12
Cy2PH
100°C, 6 days
6

Scheme 1.

Table 1. Crystal data for compounds **1–6**

	1	**2**	**3**	**4**	**5**	**6**
Description of crystal						
Colour	Red–orange	Orange	Yellow–orange	Red	Yellow–orange	Orange
Habit	Prism	Hexagonal	Prism	Prism	Prism	Prism
Maximum crystal dimensions (mm)	$0.32 \times 0.30 \times 0.25$	$0.25 \times 0.40 \times 0.40$	$0.30 \times 0.25 \times 0.25$	$0.20 \times 0.20 \times 0.35$	$0.30 \times 0.15 \times 0.10$	$0.25 \times 0.15 \times 0.15$
Unit cell						
Crystal system	Orthorhombic	Monoclinic	Triclinic	Monoclinic	Triclinic	Triclinic
Space group	*Pbca*	$P2_1$	$P\bar{1}$	$P2_1/c$	$P\bar{1}$	$P\bar{1}$
Unit cell parameters						
a (Å)	12.911(5)	10.012(2)	10.993(3)	20.689(7)	12.211(3)	13.042(2)
b (Å)	16.595(4)	11.459(4)	17.565(5)	11.507(4)	18.047(5)	13.506(2)
c (Å)	40.346(2)	15.574(3)	8.774(5)	17.102(6)	18.412(5)	13.807(2)
α (°)	90	90	93.27(3)	90	96.97(2)	99.64(1)
β (°)	90	107.28(2)	105.74(2)	109.61(3)	105.78(2)	99.63(1)
γ (°)	90	90	106.93(2)	90	101.54(2)	93.72(1)
V (Å^3)	8644.67	1706.18	1542.91	3835.22	3758.71	2353.02
Molecules per unit cell	8	2	2	4	4	2
Formula	$C_{33}H_{57}Os_3P_3O_9$	$C_{26}H_{38}Os_3P_2O_{10}$	$C_{24}H_{38}Os_3P_2O$	$C_{30}H_{59}Os_3P_3O_6$	$C_{27}H_{47}Os_3P_3O_7$	$C_{43}H_{67}Os_3P_3O_7$
Molecular weight (g mol^{-1})	1261.3	1143.1	1087.11	1177.31	1145.2	1358.5
Calculated density (g cm^{-3})	1.938	2.225	2.340	2.039	2.024	1.917
μ_{calc} (cm^{-1})	89.63	113.00	124.846	100.89	102.93	82.37

Data collection						
Radiation (Å)	Mo-K_α (0.71073)	Mo-K_α (0.71073)	Mo-K_α (0.71073)	Mo-K_α (0.71073)	Mo-K_α (0.71073)	Mo-K_α (0.71073)
Scan technique	θ–2θ	θ–2θ	θ–2θ	θ–2θ	θ–2θ	θ–2θ
Scan width (°)	0.8+0.35 (tan θ)	0.8+0.35 (tan θ)	0.8+0.35 (tan θ)	0.8+0.35 (tan θ)	0.8+0.35 (tan θ)	0.8+0.35 (tan θ)
Range of indices (h,k,l)	+14, +19, +45	+9, +12, ±18	+12, ±19, ±10	±18, ±12, +22	11, ±12, ±19	+14, ±15, ±15
2θ Range (°)	3 to 48	3 to 50	3 to 48	3 to 46	3 to 44	3 to 48
Number of reflections measured	7494	3352	5183	4556	9714	7591
Standard reflections						
intensity	2 9 7, 5 6 6	$\bar{3}$ 0 6, $\bar{3}$ 1 5	1 $\bar{5}$ 5, 6 1 $\bar{1}$	$\bar{3}$ 3 3, 3 $\bar{3}$ $\bar{1}$	4 $\bar{7}$ 7, 2 $\bar{1}$ 10	2 6 2, 3 5 4
orientation	2 9 3, 6 3 10	5 1 $\bar{5}$, 5 2 0	5 3 1, 6 $\bar{4}$ 0	8 $\bar{4}$ 0, $\bar{5}$ 3 4	6 $\bar{1}$ $\bar{10}$, 6 $\bar{4}$ 4	2 5 3, 2 6 3
Decay of standards (%)	4	−3.6	−4.5	−3.5	−5.5	1
Minimum % transmission	59.3470	71.8803	28.77	56.20	57.8860	58.0685
Maximum % transmission	99.7661	99.7840	99.34	98.53	99.7816	99.9660
Average % transmission	82.0528	87.8975	73.72	80.47	82.0438	82.2100
Agreement factor for averaged reflections						
F(obs)		0.032	0.022	0.064	0.034	0.023
intensity	n/a	0.023	0.019	0.056	0.029	0.018
Structure determination						
Number of reflections used [$I > 3\sigma(I)$]	2296	2389	3141	2513	5299	3995
Number of parameters varied	223	360	334	334	716	505
Data/parameter ratio	10.296	6.636	9.404	7.524	7.401	7.911
Shift-to-error ratio	0.394	1.034	0.252	0.073	0.983	1.382
ESD of an observation of unit weight	2.1770	3.4263	5.5015	2.5832	3.5054	2.5093
R^a	0.0810	0.0402	0.0482	0.0422	0.0435	0.0412
$R_w{}^a$	0.0880	0.0550	0.0548	0.0498	0.0502	0.0495

[a] R and R_w are defined as $R = \Sigma||F_o| - |F_c||/\Sigma|F_o|$ and $R_w = [\Sigma w(|F_o| - |F_c|)^2/\Sigma w(|F_o|^2)]^{1/2}$.

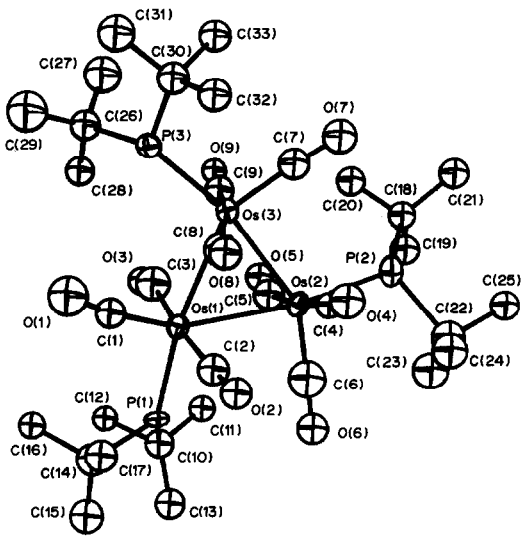

Fig. 1. ORTEP view of **1** showing the atom numbering scheme.

phosphine ligands occupy sites on adjacent metal atoms such that they are roughly *trans* to each other with respect to the Os—Os vector. The Os—Os bond lengths fall within normal limits [2.900(2)–2.925(1) Å] and the P—Os distances are similar to those found in **1** [Os(1)—P(1) = 2.335(9) Å, Os(2)—P(2) = 2.423(9) Å]. The *trans* arrangement of phosphines may again be in order to minimize steric interactions in the molecule.

Synthesis of phosphido complexes: $Os_3(CO)_8(\mu\text{-}H)_2(\mu\text{-}t\text{-}Bu_2P)_2$ (**3**) *and* $Os_3(CO)_6(t\text{-}Bu_2PH)(\mu\text{-}H)_2(\mu\text{-}t\text{-}Bu_2P)$ (**4**)

If the reaction of $Os_3(CO)_{12}$ with three equivalents of t-Bu_2PH in refluxing toluene is continued for 24 h, a dark red solution is obtained from which the bis-phosphido-bridged complex **3** (50%) as well as the 46-electron phosphido compound **4** (15%) may be isolated following column chromatography and recrystallization from hexane. The compound is a deep red, air-stable crystalline material. Interestingly yellow hexane solutions of **3** turn dark red when heated with excess t-Bu_2PH in THF and **4** may be isolated from this reaction in high yield by evaporation to dryness followed by recrystallization of the residue from hexane. The reverse transformation may be easily accomplished by simply bubbling CO (1 atm) through a hexane solution of **4**. Spectroscopic data for both **3** and **4** are in accord with the solid-state structures as determined by single-crystal X-ray diffraction studies.

The $^{31}P\{^1H\}$ NMR spectrum of **3** in C_6D_6 at 25°C is a sharp singlet at δ 147.0, indicating equivalent phosphido groups bridging metal–metal bonds.[10] The ^1H NMR shows a virtual triplet to high field (δ −17.50, apparent J_{P-H} = 11.5 Hz) which is assigned to the two hydride ligands. Similar resonances have been observed in the ^1H NMR spectra of $Os_3(CO)_8(\mu\text{-}H)_2(\mu\text{-}Ph_2P)_2$[11] and $Ru_3(CO)_8(\mu\text{-}H)_2(\mu\text{-}t\text{-}Bu_2P)_2$[7] and they have been attributed to an AA′XX′ type spectra. The $^{31}P\{^1H\}$ NMR spectrum of **4** contains two resonances to low field (δ 146.65, d d, $^2J_{P-P}$ = 91.6, 24.9 Hz and δ 183.04, d, $^2J_{P-P}$ = 91.6 Hz) and a doublet at δ 29.11 ($^2J_{P-P}$ = 24.2 Hz). The former two resonances are assigned to the two phosphido groups which are now inequivalent. In the ^{31}P NMR spectrum the latter resonance splits into a broad doublet ($^1J_{P-H}$ = 345.7 Hz), confirming its assignment to the terminal t-Bu_2PH ligand. The high-field region of the ^1H NMR spectrum of **4** contains two multiplets at δ −9.72 and −11.72 indicating that the μ-H ligands are also now non-equivalent.

Table 2. Selected bond lengths (Å) and angles (°) for **1**

Atom 1	Atom 2	Distance	Atom 1	Atom 2	Atom 3	Angle
Os(1)	Os(2)	2.910(4)	Os(2)	Os(1)	Os(3)	60.1(1)
Os(1)	Os(3)	2.927(4)	Os(2)	Os(1)	P(1)	108.4(5)
Os(2)	Os(3)	2.924(4)	Os(2)	Os(3)	P(3)	167.5(5)
Os(1)	P(1)	2.35(2)	Os(1)	Os(2)	Os(3)	60.2(1)
Os(2)	P(2)	2.38(2)	Os(1)	Os(2)	P(2)	170.7(5)
Os(3)	P(3)	2.37(2)	Os(3)	Os(2)	P(2)	110.5(5)
			Os(3)	Os(1)	P(1)	168.1(5)
			Os(1)	Os(3)	Os(2)	59.7(1)
			Os(1)	Os(3)	P(3)	108.1(5)
			Os(1)	Os(3)	C(7)	148(1)

Numbers in parentheses are ESDs in the least significant digits.

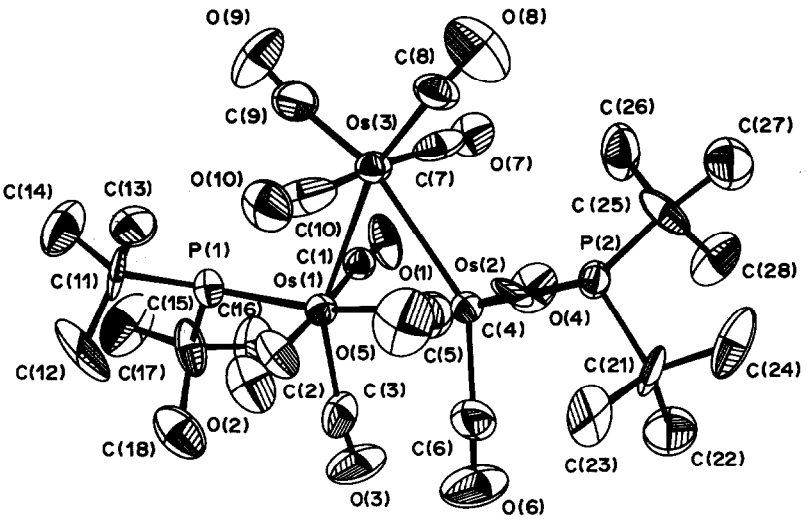

Fig. 2. ORTEP view of **2** showing the atom numbering scheme.

X-ray structures of $Os_3(CO)_8(\mu\text{-}H)_2(\mu\text{-}t\text{-}Bu_2P)_2$ **(3)** *and* $Os_3(CO)_6(t\text{-}Bu_2PH)(\mu\text{-}H)_2(\mu\text{-}t\text{-}Bu_2P)_2$ **(4)**

The molecular structures of **3** and **4** are shown as ORTEP views in Figs 3 and 4, respectively. Key bond lengths and angles for **3** and **4** are given in Tables 4 and 5, respectively. Complex **3** crystallizes in the triclinic space group $P\bar{1}$ with two molecules per unit cell. The molecular geometry of **3** consists of a closed 48-electron Os_3 cluster in which two of the Os—Os bonds are bridged by $\mu\text{-}t\text{-}Bu_2P^-$ units [Os(1)—Os(2) = 2.944(1) Å and Os(1)—Os(3) = 2.883(1) Å]. These groups lie above and below the Os_3 plane. The structure is similar to those of the diphenylphosphido and ruthenium analogues. The unique osmium atom [Os(1)] which is bonded to two phosphido groups also bears two *cis*-CO units. The other two osmium atoms each have three CO groups and are separated by a fairly long Os—Os bond of 3.010(1) Å. Although the hydrides were not located in the X-ray structure of **3**, it is reasonable to assume that they occupy the bridging sites across Os(1)—Os(2) and Os(1)—Os(3) and opposite to the $\mu\text{-}t\text{-}Bu_2P^-$ groups. Thus, the phosphido groups are roughly *trans* to each other [P(2)—Os(1)—P(1) = 151.15(9)°]. The coordination geometry of each metal is roughly octahedral if one ignores the metal–metal bonds for Os(2) but includes the Os(2)—Os(3) interaction for Os(2) and Os(3).

The striking difference between the structures of **3** and **4** is that in **4** one CO group on Os(2) has been replaced by a $t\text{-}Bu_2PH$ ligand and this is accompanied by the loss of a CO group on a *different* osmium atom [Os(3)]. Although formal electron counting procedures are sometimes misleading, one possible interpretation is that there are now two 18-electron osmium atoms [Os(1) and Os(2)] and a 16-electron atom [Os(3)], while the total electron count on the molecule is 46.

The Os—Os distances in **4** are, on the average, shorter than those in **3** (2.825 vs 2.962 Å). There is

Table 3. Selected bond lengths (Å) and angles (°) for **2**

Atom 1	Atom 2	Distance	Atom 1	Atom 2	Atom 3	Angle
Os(1)	Os(2)	2.900(2)	Os(3)	Os(1)	Os(3)	60.18(5)
Os(1)	Os(3)	2.925(1)	Os(2)	Os(1)	P(1)	168.5(2)
Os(2)	Os(3)	2.921(2)	Os(1)	Os(3)	Os(2)	59.49(4)
Os(1)	P(1)	2.335(9)	Os(3)	Os(2)	P(2)	109.6(2)
Os(2)	P(2)	2.423(9)	Os(1)	Os(2)	Os(3)	60.34(4)
			Os(1)	Os(2)	P(2)	169.8(2)
			Os(3)	Os(1)	P(1)	108.4(2)

Numbers in parentheses are ESDs in the least significant digits.

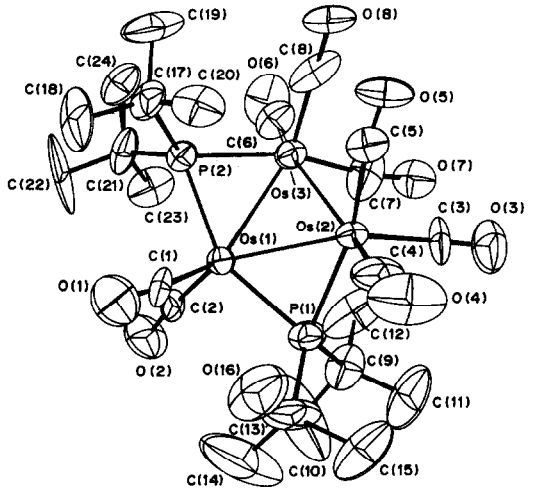

Fig. 3. ORTEP view of **3** showing the atom numbering scheme.

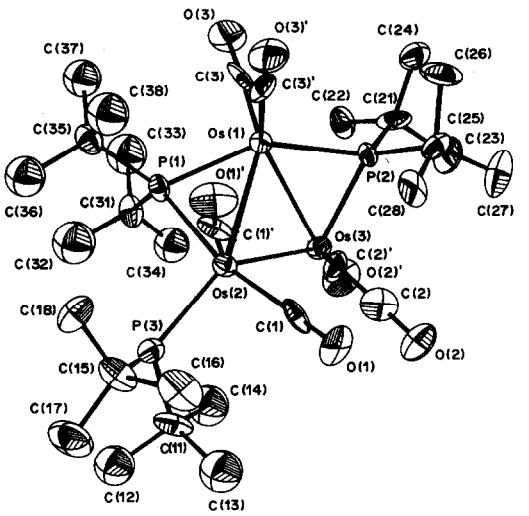

Fig. 4. ORTEP view of **4** showing the atom numbering scheme.

no particularly short Os—Os interaction, with the shortest now being Os(1)—Os(3) (2.706(1) Å). Os(2)—Os(3) which is not bridged by a phosphido group is now the second shortest (2.797(1) Å). The longest Os—Os bond is Os(1)—Os(2) at 2.971(1) Å. As for **3**, the coordination geometries of Os(1) and Os(2) may be described as roughly octahedral if one ignores the metal–metal interactions. The coordination geometry of Os(3) is roughly trigonal bipyramidal.

One question concerns the location of the two hydride ligands in **4**. Both spectroscopic and structural data do not permit unequivocal assignment of their positions. Consideration of space-filling

Table 4. Selected bond lengths (Å) and angles (°) for **3**

Atom 1	Atom 2	Distance	Atom 1	Atom 2	Distance
Os(2)	C(4)	1.84(1)	P(1)	Os(1)	2.368(3)
Os(2)	C(5)	1.95(1′)	P(1)	Os(2)	2.440(2)
Os(3)	P(2)	2.404(3)	P(1)	C(9)	1.93(1)
Os(1)	Os(2)	2.944(1)	P(1)	C(13)	1.98(1)
Os(1)	Os(3)	2.883(1)	P(2)	Os(1)	2.365(2)
Os(3)	C(6)	1.84(1)	Os(1)	C(1)	1.81(1)
Os(3)	C(7)	1.82(1)	Os(1)	C(2)	1.84(1)
Os(3)	C(8)	1.92(1)	Os(2)	Os(3)	3.010(1)
			O(1)	C(1)	1.20(2)

Atom 1	Atom 2	Atom 3	Angle	Atom 1	Atom 2	Atom 3	Angle
Os(2)	Os(1)	Os(3)	62.20(1)	Os(1)	Os(2)	C(3)	136.1(3)
Os(2)	Os(1)	P(1)	53.35(6)	Os(1)	Os(2)	C(4)	117.7(4)
Os(2)	Os(1)	P(2)	100.94(6)	Os(1)	Os(2)	C(5)	116.4(3)
Os(2)	Os(1)	O(1)	110.7(2)	Os(3)	Os(2)	P(1)	93.91(6)
Os(2)	Os(1)	O(2)	147.9(2)	Os(2)	Os(3)	C(6)	163.0(4)
Os(2)	Os(1)	C(1)	110.0(5)	Os(2)	Os(3)	C(7)	75.7(4)
Os(2)	Os(1)	C(2)	149.7(3)	Os(2)	Os(3)	C(8)	96.1(3)
Os(3)	Os(1)	P(1)	98.82(7)	Os(1)	Os(3)	C(6)	125.7(4)
Os(3)	Os(1)	P(2)	53.44(6)	Os(1)	Os(3)	C(7)	113.9(5)
Os(3)	Os(1)	C(1)	142.3(4)	Os(1)	Os(3)	C(8)	132.4(3)
Os(3)	Os(1)	C(2)	119.7(3)	Os(2)	Os(3)	P(2)	98.19(6)
Os(1)	Os(2)	Os(3)	57.91(1)	Os(1)	Os(3)	Os(2)	59.90(1)
Os(1)	Os(2)	P(1)	51.16(6)	Os(1)	Os(3)	P(2)	52.20(6)

Numbers in parentheses are ESDs in the least significant digits.

Table 5. Selected bond lengths (Å) and angles (°) for **4**

Atom 1	Atom 2	Distance	Atom 1	Atom 2	Distance
Os(2)	Os(3)	2.797(1)	Os(3)	C(2)′	1.82(4)
Os(2)	Os(1)	2.971(1)	Os(3)	C(2)	1.84(3)
Os(2)	P(3)	2.361(6)	Os(1)	P(2)	2.384(7)
Os(2)	P(1)	2.453(7)	Os(1)	P(1)	2.364(6)
Os(2)	C(1)	1.92(3)	Os(1)	C(3)	1.74(3)
Os(2)	C(1)′	1.86(3)	Os(1)	C(3)′	1.89(3)
Os(3)	Os(1)	2.706(2)	Os(1)	C(11)	1.92(3)
Os(3)	P(2)	2.327(7)			

Atom 1	Atom 2	Atom 3	Angle	Atom 1	Atom 2	Atom 3	Angle
Os(3)	Os(2)	Os(1)	55.84(3)	Os(2)	Os(1)	P(2)	103.4(2)
Os(3)	Os(2)	P(3)	131.4(2)	Os(2)	Os(1)	P(1)	53.3(2)
Os(3)	Os(2)	P(1)	90.3(1)	Os(2)	Os(1)	C(3)	151.5(9)
Os(3)	Os(2)	C(1)	78.8(7)	Os(2)	Os(1)	C(3)′	98.1(7)
Os(3)	Os(2)	C(1)′	129.3(7)	Os(3)	Os(1)	P(2)	54.0(2)
Os(1)	Os(2)	P(3)	152.7(2)	Os(3)	Os(1)	P(1)	94.5(2)
Os(1)	Os(2)	P(1)	50.6(1)	Os(3)	Os(1)	C(3)	133(1)
Os(1)	Os(2)	C(1)	115.9(7)	Os(3)	Os(1)	C(3)′	132.2(8)
Os(1)	Os(2)	C(1)′	91.3(6)	P(2)	Os(1)	P(1)	148.4(3)
P(3)	Os(2)	P(1)	102.4(2)	P(2)	Os(1)	C(3)	102.7(9)
P(3)	Os(2)	C(1)	91.0(7)	P(2)	Os(1)	C(3)′	100.9(8)
P(3)	Os(2)	C(1)′	96.2(7)	P(1)	Os(1)	C(3)	98.2(9)
P(1)	Os(2)	C(1)	166.4(6)	P(1)	Os(1)	C(3)′	103.3(8)
P(1)	Os(2)	C(1)′	96.2(9)	Os(3)	Os(1)	Os(3)	58.82(3)
C(1)	Os(2)	C(1)′	85(1)				
Os(2)	Os(3)	Os(1)	65.33(4)				

Numbers in parentheses are ESDs in the least significant digits.

models suggest that there is room for a hydride to bridge any of the three of the Os—Os bonds. Since Os(3) is now both coordinatively and (formally) electronically unsaturated, we very tentatively assign the μ-H atoms to the two bridging locations which span Os(1)—Os(3) and Os(2)—Os(3).

The replacement of one CO in Os(2) by the bulky phosphine ligand might be expected to result in further loss of CO from Os(2) from that metal on steric grounds. However, the increased electron density on Os(2), caused by the presence of the σ-donating t-Bu_2PH ligand, may increase the strength of the Os(2)—CO π-backbonding interaction and prevent the loss of the two remaining CO ligands on Os(2). The loss of a CO ligand from Os(3) may still be due to steric effects since there is considerable steric congestion around the molecule caused by the two bulky t-Bu_2P^- units as well as the phosphine (t-Bu_2PH).

Synthesis of the phosphinidene complex $Os_3(CO)_7(t\text{-}Bu_2PH)_2(\mu\text{-}H)_2(\mu_3\text{-}t\text{-}BuP)$ **(5)**

The reaction of $Os_3(CO)_{12}$ with t-Bu_2PH (3 equiv.) in refluxing di-n-butylether (143°C) for 24 h affords the orange phosphinidene complex **5** in 68% yield. This compound may also be obtained by heating **1**, **2**, **3** or **4** in di-n-butylether (24 h). Spectroscopic data for **5** are in accord with the structure as determined by X-ray crystallography. The IR spectrum contains ν(CO) absorptions in the terminal CO region in addition to peaks at 2351 (w) and 2313 (w) cm^{-1} assigned to ν(P—H) stretching vibrations. The $^{31}P\{^1H\}$ NMR spectrum consists of two doublets at δ 208.12 and 14.08 ($^2J_{P-P}$ = 89.0 Hz) assigned to the phospinidene (t-BuP) and phosphine (t-Bu_2PH) nuclei, respectively. The ^1H NMR spectrum exhibits resonances assigned to the t-Bu_2PH and t-BuP ligands in addition to a triplet at δ −21.17 ($^2J_{P-H}$ = 10.2 Hz) which is assigned to the two bridging hydrides in the complex.

X-ray structure of **5**

Molecules of **5** crystallize in the triclinic space group $P\bar{1}$ with two independent molecules in the asymmetric unit, four per unit cell. The molecules have similar geometric parameters. The molecular structure of one molecule is shown as an ORTEP view in Fig. 5. Key bond lengths and angles are

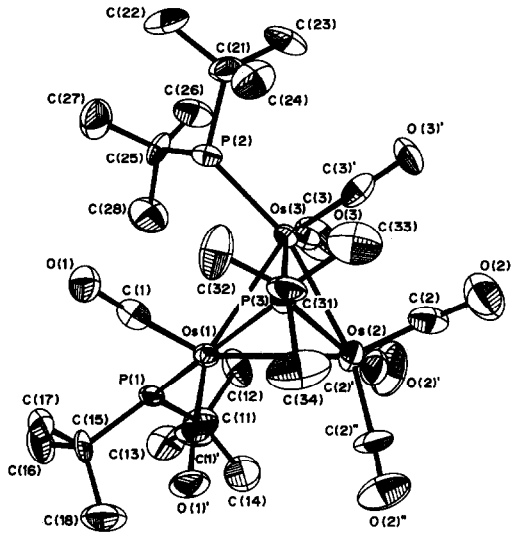

Fig. 5. ORTEP view of **5** showing the atom numbering scheme.

given in Table 6. The molecular structure of **5** consists of an Os_3 triangle (Os—Os = 2.954 Å, av.) capped by a μ_3-P(*t*-Bu) group. Two osmium atoms [Os(1), Os(3)] each bear two CO ligands as well as a terminal phosphine (t-Bu_2PH) ligand. The third osmium atom has three CO groups. There are several related analogues of this compound. They include $H_2Ru_3(CO)_9(\mu_3\text{-PPh})$,[12] $H_2Ru_3(CO)_9[\mu_3\text{-P}(p\text{-}CH_3OC_6H_4)]$[13] and $Ru_3(CO)_8(t\text{-}Bu_2PH)(\mu\text{-H})_2(\mu_3\text{-}t\text{-BuP})$.[6] The two hydride ligands were not located in the X-ray study although it seems reasonable to suggest that they occupy bridging positions between Os(1)—Os(2) (2.983(1) Å) and Os(2)—Os(3) (2.853(1) Å), below the Os_3 triangle opposite to the phosphinidene ligand. Both of these bonds are shorter than the remaining metal–metal bond [Os(1)—Os(3) = 3.025(1) Å]. The symmetrical triplet in the ^{1}H NMR spectrum for the hydrides is also consistent with their occupying chemically and magnetically equivalent positions. The Os—P(phosphinidene) distances for the osmium atoms which bear t-Bu_2PH ligands are slightly longer than those for the osmium atom which bears three CO units. Thus Os(1)—P(3) and Os(3)—P(3) are 2.330(4) and 2.329(4) Å, respectively, while Os(2)—P(3) is 2.306(4) Å. The second molecule of **5** exhibits a similar distortion. The Os—P(phosphine) distances are similar (Os(1)—P(1) = 2.411(4), Os(3)—P(2) = 2.364(4) Å) and fall within the normal limits for such bonds.

Table 6. Selected bond lengths (Å) and angles (°) for one molecule of **5**

Atom 1	Atom 2	Distance
Os(1)	Os(2)	2.983(1)
Os(1)	Os(3)	3.025(1)
Os(2)	Os(3)	2.853(1)
Os(1)	P(1)	2.411(4)
Os(1)	P(3)	2.330(4)
Os(3)	P(3)	2.329(4)
Os(2)	P(3)	2.306(4)
Os(3)	P(2)	2.364(4)

Atom 1	Atom 2	Atom 3	Angle	Atom 1	Atom 2	Atom 3	Angle
Os(2)	Os(1)	Os(3)	56.70(2)	Os(2)	Os(1)	P(1)	118.68(9)
Os(2)	Os(1)	P(3)	49.59(9)	Os(3)	Os(1)	P(1)	115.25(8)
Os(3)	Os(1)	P(3)	49.49(9)	Os(1)	Os(2)	Os(3)	62.39(2)
Os(1)	Os(2)	P(3)	50.30(9)	Os(1)	P(3)	Os(2)	80.1(1)
Os(1)	P(3)	Os(3)	81.0(1)	Os(2)	P(3)	Os(3)	76.0(1)
P(1)	Os(1)	P(3)	163.2(1)	Os(3)	Os(2)	P(3)	52.37(9)
P(1)	Os(1)	C(1)′	94.9(6)	P(1)	Os(1)	C(1)	93.8(5)
P(3)	Os(1)	C(1)′	98.4(6)	P(3)	Os(1)	C(1)′	98.4(6)
P(3)	Os(1)	C(1)	95.5(5)	C(1)′	Os(1)	C(1)	93.3(7)
P(3)	Os(2)	C(2)′	146.8(6)	P(3)	Os(2)	C(2)	97.4(6)
P(3)	Os(2)	C(2)″	108.9(6)	C(2)′	Os(2)	C(2)	94.4(8)
C(2)′	Os(2)	C(2)″	101.3(8)	C(2)	Os(2)	C(2)″	92.9(8)
P(2)	Os(3)	P(3)	108.0(1)	P(2)	Os(3)	C(3)	102.0(5)
P(2)	Os(3)	P(3)	108.0(1)	P(2)	Os(3)	C(3)	102.0(5)
P(2)	Os(3)	C(3)′	102.1(5)	P(2)	Os(3)	C(3)	146.4(5)
P(3)	Os(3)	C(3)′	96.9(5)	C(3)	Os(3)	C(3)′	91.2(7)

Numbers in parentheses are ESDs in the least significant digits.

Synthesis of $Os_3(CO)_7(\mu\text{-H})(Cy_2P)_3$ (**6**)

The interaction of $Os_3(CO)_{12}$ and dicyclohexylphosphine (Cy_2PH) in refluxing toluene (6 days) yields the tris-phosphido, 48-electron cluster $Os_3(CO)_7(\mu\text{-H})(Cy_2P)_3$ (**6**). Spectroscopic data for **6** are in accord with the structure as determined by X-ray crystallography. The IR spectrum exhibits ν(CO) absorptions in the terminal CO region at 2210, 1990, 1975, 1967 and 1932 cm^{-1}. The $^{31}P\{^1H\}$ NMR spectrum shows only a singlet at δ 112.75 at room temperature, indicating that the three phosphido bridges are equivalent in solution on the NMR time scale. The ^1H NMR shows only a simple quartet in the hydride region indicating that the hydride is fluxional and is equivalent to all three phosphides on the NMR time scale. The presence of three phosphido bridges, one across each Os—Os bond, contrasts with two phosphido bridges in **3** and **4** and with other Os_3 diphenylphosphido analogues.[2] The isolation of **6** further demonstrates that differences in steric bulk of phosphido ligands can result in major differences in stoichiometry and structure for the complexes they form.

X-ray structure of **6**

Figure 6 shows the molecular geometry and atom numbering scheme, while a view of the central core of **6** is shown in Fig. 7. Selected bond lengths and angles are given in Table 7. Complex **6** consists of a triangular core of osmium atoms with each edge of the triangle bridged by μ_2-P(Cy)$_2$ units and a μ_2-hydrido ligand bridging the Os(1)—Os(2) bond. One of the phosphido bridges [P(1)] is bent dramatically below the plane of the three osmium atoms, while the other two phosphido bridges, P(2) and P(3), are well above the Os_3 plane. To our knowledge, **6** is the first trinuclear osmium complex with a bridging phosphido group across each of the Os—Os vectors. In addition, Os(1) and Os(2) are each coordinated by two CO ligands, while Os(3) bears three carbonyl groups. Excluding metal–metal bonding, each osmium atom has a roughly

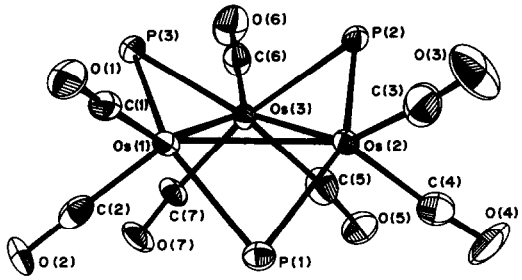

Fig. 7. View of the central core of **6** showing the arrangement of the phosphido ligands. Cyclohexyl groups have been omitted for clarity.

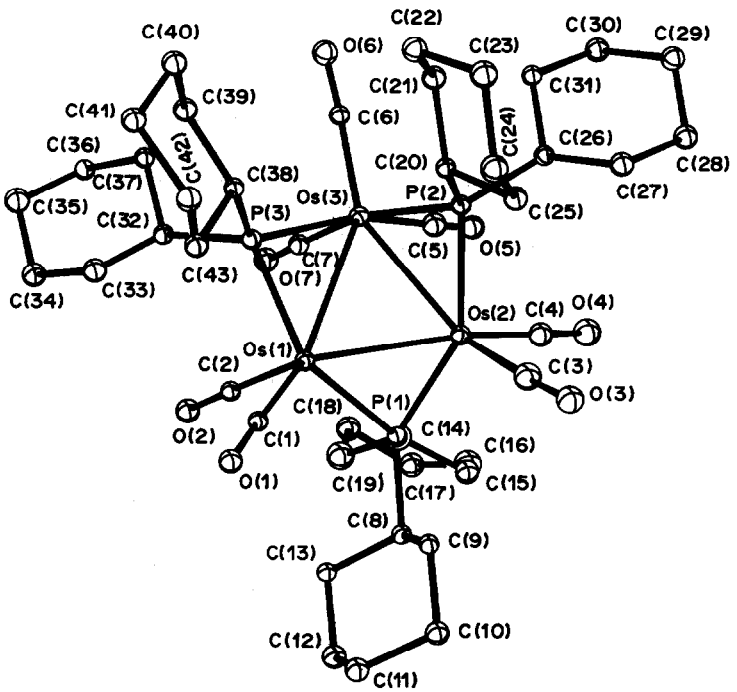

Fig. 6. ORTEP view of **6** showing the atom numbering scheme.

Table 7. Selected bond lengths (Å) and angles (°) for **6**[a]

Atom 1	Atom 2	Distance	Atom 1	Atom 2	Atom 3	Angle
Os(1)	Os(2)	2.817(1)	Os(2)	Os(1)	Os(3)	63.07(2)
Os(1)	Os(3)	3.022(1)	Os(2)	Os(1)	P(1)	53.53(8)
Os(1)	P(1)	2.365(3)	Os(2)	Os(1)	P(3)	103.94(8)
Os(1)	P(3)	2.345(3)	Os(3)	Os(1)	P(1)	97.22(8)
Os(2)	Os(3)	3.059(1)	Os(3)	Os(1)	P(3)	52.49(8)
Os(2)	P(1)	2.368(3)	P(1)	Os(1)	P(3)	149.7(1)
Os(2)	P(2)	2.338(3)	Os(1)	Os(2)	Os(3)	61.75(2)
Os(3)	P(2)	2.456(3)	Os(1)	Os(2)	P(1)	53.41(8)
Os(3)	P(3)	2.450(3)	Os(1)	Os(2)	P(2)	98.70(8)
			Os(3)	Os(2)	P(1)	96.17(8)
			Os(3)	Os(2)	P(2)	53.08(8)
			P(1)	Os(2)	P(2)	147.4(1)
			Os(1)	Os(3)	Os(2)	55.19(2)
			Os(1)	Os(3)	P(2)	90.87(8)
			Os(1)	Os(3)	P(3)	49.39(8)
			Os(2)	Os(3)	P(2)	48.67(8)
			Os(2)	Os(3)	P(3)	94.81(8)
			P(2)	Os(3)	P(3)	99.3(1)

Numbers in parentheses are ESDs in the least significant digits.
[a] A complete listing is available in the supplementary material.

square-pyramidal coordination geometry. Os(1) and Os(2) may be considered to have formal oxidation states of (+1), while Os(3) would formally be (+2) with all three metal atoms attaining an 18-electron count.

The key structural parameters of the molecule all fall within normal limits. The Os—Os bonds range from 3.059(1) to 2.817(1) Å with an average of 2.966 Å, while the Os—P bonds range from 2.456(3) to 2.338(3) Å with an average of 2.387 Å. These values are comparable to analagous ones found in other phosphido-bridged trinuclear osmium complexes.

The position of the hydride ligand, although not located in the X-ray structure, is tentatively assigned a bridging position across the shorter Os(1)—Os(2) bond since this is clearly an open site as shown in Fig. 7.

EXPERIMENTAL

All operations were performed under dry nitrogen or *in vacuo*. Hexane and THF were dried over sodium benzophenone under nitrogen and distilled under nitrogen before use. The di-*n*-butylether was refluxed over potassium hydroxide pellets and the fraction with a boiling point in the range 142–143°C was collected. Melting points were determined in sealed capillaries under nitrogen (1 atm) and are uncorrected. $Os_3(CO)_{12}$[13] and *t*-Bu_2PH[14] were prepared as previously described. Dicyclohexylphosphine was purchased from the Strem Chemical Company, Newburyport, MA, and was used as received. Instruments, IR: Perkin–Elmer 1330; NMR: Varian EM-390 (^1H, 90 MHz), G.E. QE 300 (^1H, ^{31}P).

Synthesis of $Os_3(CO)_9(t\text{-}Bu_2PH)_3$ (1)

Dodecacarbonyltriosmium (0.20 g, 0.22 mmol) and di-*tert*-butylphosphine (0.09 cm^3, 0.66 mmol) in THF were photolysed with a 550 W Hanovia mercury vapour lamp for 18 h in a quartz Schlenk tube. During this time the colour of the solution deepened continuously until it was bright orange. The reaction mixture was evaporated to dryness under reduced pressure and extracted with hexane. The solution was filtered and evaporated (10 cm^3). Cooling (−30°C) yielded orange crystals which were collected and dried *in vacuo*. Yield: 0.17 g, 63.0%; m.p.: 170–172°C. X-ray quality crystals were prepared by slow evaporation of benzene in air. NMR ^1H (C_6D_6, δ rel. Me_4Si 300 MHz): δ 5.39 (d, 1H, J_{P-H} = 344 Hz, *t*-Bu_2PH), δ 1.28 (d, 54H, J_{P-H} = 16 Hz, *t*-Bu_2PH); $^{31}P\{^1H\}$ [in C_6D_6, amb. temp., rel. 85% H_3PO_4 (aq.)]: δ 17.93 (s, *t*-Bu_2PH). IR (Nujol mull, NaCl): 2320 w, 2300 w, 2040 w, 1973 s, 1955 s, 1918 s, 1873 w, 1255 m, 1203 w, 1175 w, 1090 m, 1017 m, 930 w, 903 m, 860 m, 805 m, 719 w, 610 m, 565 m (cm^{-1}).

Synthesis of $Os_3(CO)_{10}(t\text{-}Bu_2PH)_2$ **(2)** *and* $Os_3(CO)_8(\mu\text{-}H)_2(\mu\text{-}t\text{-}Bu_2P)_2$ **(3)**

Dodecacarbonyltriosmium (0.2 g, 0.22 mmol) and three molar equiv. of t-Bu_2PH (0.09 cm^3, 0.66 mmol) were heated in toluene (50 cm^3) under reflux for 12 h. During this time the colour of the solution deepened continuously until it was deep orange. The reaction mixture was allowed to cool and evaporated to dryness under vacuum. The residue was extracted with hexane, concentrated (10 cm^3), and poured onto a silica gel column. The column was first eluted with hexane to give a yellow fraction. Subsequent elution with toluene gave an orange–red fraction. The yellow fraction was evaporated to dryness *in vacuo* to give yellow–orange crystals of **3** which were recrystallized from hexane. Yield: 0.12 g, 50.0%; m.p. 203–205°C. The orange–red fraction was evaporated to dryness under vacuum to give orange crystals of **2** which were recrystallized from hexane. Yield: 0.06 g, 24.0%; m.p. 162–165°C. For **2**: NMR ^1H (C_6D_6, δ rel. Me_4Si at 300 MHz): δ 4.89 (d, 2H, J_{P-H} = 381 Hz, t-Bu_2PH), δ 1.16 (d, 36H, J_{P-H} = 15 Hz, t-Bu_2PH); $^{31}P\{^1H\}$ [in C_6D_6, amb. temp., rel. 85%, H_3PO_4 (aq.)]: δ 21.46 (s, t-Bu_2PH). IR (Nujol mull, NaCl): 2310 w, 2080 w, 2020 s, 1990 s, 1952 s, 1928 s, 1258 w, 1175 m, 1022 m, 852 m, 810 m, 768 w (cm^{-1}).

Reaction of $Os_3(CO)_{12}$ *with* t-Bu_2PH: *Synthesis of* **3** *and* **4**

An excess of di-*tert*-butylphosphine (0.09 cm^3, 0.66 mmol) was added to a toluene solution (40 cm^3) of $Os_3(CO)_{12}$ (0.2 g, 0.22 mmol). This mixture was refluxed for 24 h and turned red during this time. After the mixture was cooled, the solvent was removed *in vacuo*, and the residue was extracted into a minimum of hexane and applied to an alumina-packed column under nitrogen. The products were separated using hexane as an eluant. Two products, $Os_3(CO)_8(\mu\text{-}H)_2(\mu\text{-}t\text{-}Bu_2P)_2$ **(3)** and $Os_3(CO)_6(t\text{-}Bu_2PH)(\mu\text{-}H)_2(\mu\text{-}t\text{-}Bu_2P)_2$ **(4)** were obtained. In order of elution they were **3** (0.12 g, 50.0%) and **4** (0.02 g, 15.4%; m.p. 178–182°C). For **3**: NMR, ^1H (C_6D_6, δ rel. Me_4Si at 300 MHz): δ 1.31 (m, 36H, t-Bu_2P, J_{P-H} = 14 Hz), δ −17.50 (t, 2H, μ-H, J_{P-H} = 11.5 Hz); $^{31}P\{^1H\}$ [C_6D_6, amb. temp., rel. 85% H_3PO_4 (aq.)]: δ 147.00 (s, t-Bu_2P). IR (Nujol mull, NaCl): 2040s, 2000s, 1990s, 1955s, 1941s, 1919s, 1242m, 1150, 1080w, 1000w, 782w, 700w, 650m, 580m (cm^{-1}). For **4**: NMR, ^1H (C_6D_6, δ rel. Me_4Si at 300 MHz) δ 5.65 (d of d, 1H, t-Bu_2PH, $^1J_{P-H}$ = 339.0 Hz, $^3J_{P-H}$ = 9.61 Hz), δ 1.61 (d, 18H, t-Bu_2PH, $^2J_{P-H}$ = 14.3 Hz), δ 1.36 (d, 18H, μ-t-Bu_2P, $^2J_{P-H}$ = 14.3 Hz), δ 1.09 (d, 18H, μ-t-Bu_2P, $^2J_{P-H}$ = 14.6 Hz), δ −9.76 (m, 2H, μ-H, $^2J_{P-H}$ = 10.5 Hz), δ −11.72 (m, 2H, μ-H, $^2J_{P-H}$ = 10.3 Hz); $^{31}P\{^1H\}$ [C_6D_6, amb. temp., rel. 85% H_3PO_4 (aq.)]; δ 183.07 (d, μ-t-Bu_2P, $^2J_{P-P}$ = 88.5 Hz); δ 146.67 (d of d, μ-t-Bu_2P, $^2J_{P-P}$ = 92.7); δ 29.10 (br.t, t-Bu_2PH, $^2J_{P-P}$ = 15.5 Hz); ^{31}P (C_6D_6, amb. temp.) the δ 29.10 peak splits into a doublet of triplets, $^1J_{P-H}$ = 333.8 Hz. IR (Nujol mull, NaCl): 2347w, 2010s, 1971s, 1938s, 1915s, 1391w, 1310m, 1261m, 1169m, 1096m, 1023m, 936w, 889w, 862w, 843w, 806m, 598m, 573m, 549m (cm^{-1}).

Synthesis of the complex $Os_3(CO)_7(\mu\text{-}H)_2(t\text{-}Bu_2PH)(\mu_3\text{-}t\text{-}BuP)$ **(5)**

Dodecacarbonyltriosmium (0.2 g, 0.22 mmol) and di-*tert*-butylphosphine (0.9 cm^3, 0.66 mmol) in 100 cm^3 di-*n*-butylether were heated for several hours. The colour of the solution turned bright orange after 2 h and dull orange after 24 h. The reaction mixture was cooled and evaporated to dryness *in vacuo*. The residue was extracted into hexane, concentrated to 5 cm^3, and cooled (−35°C), producing an orange, air-stable crystalline material which was collected and dried *in vacuo*. Yield: 0.17 g, 68%; m.p.: 158–160°C. NMR, ^1H (C_6D_6, δ rel. Me_4Si, 300 MHz): δ 4.594 (d, 2H, J_{P-H} = 342.5 Hz, t-Bu_2PH), δ 1.547 (d, 9H, J_{P-H} = 20.7 Hz, μ^3-t-BuP), δ 0.916 (d, 36H, J_{P-H} = 15.0 Hz, t-Bu_2PH), δ −21.17 (t, 2H, $^2J_{P-H}$ = 10.2 Hz, μ-H); $^{31}P\{^1H\}$ [in C_6D_6, amb. temp., rel. 85%, H_3PO_4 (aq.)]: δ 208.12 (d, $^2J_{P-P}$ = 89.0 Hz, μ^3-t-BuP), δ 14.08 (d, $^2J_{P-P}$ = 89.1 Hz, t-Bu_2PH). IR (Nujol mull, NaCl): 2351 w, 2313 w, 2066 s, 2043 s, 2008 s, 1989 s, 1948 s, 1921 s, 1913 s, 1261 m, 1170 m, 1066 m, 1026 s, 860 m, 851 m, 813 s, 675 m, 569 s, 528 m, 521 s (cm^{-1}).

Synthesis of the complex $Os_3(CO)_7(\mu\text{-}H)(Cy_2P)_3$ **(6)**

Cy_2PH (0.41 cm^3, 1.9 mmol) was added to a suspension of $Os_3(CO)_{12}$ (0.57 g, 0.63 mmol) in toluene (100 cm^3). The mixture was heated under reflux (6 days) during which time the $Os_3(CO)_{12}$ dissolved producing a red–orange solution. Volatile materials were removed *in vacuo*, and the residue extracted into toluene (3 × 40 cm^3). The filtered combined extracts were reduced in volume under vacuum and cooled (−35°C), producing **5** as an orange, air-stable microcrystalline powder. The material was collected and dried *in vacuo*. Yield: 60%; m.p. 290–293°C (dec). NMR, ^1H (C_6D_6, rel. to Me_4Si δ 0.0, 25°C, 360 MHz): δ 1.8 (br. mult., 66H, μ-P(Cy)$_2$), δ −17.18 (quartet, 1H, μ-H);

$^{31}P\{^1H\}$ (C_6D_6, rel. to 85% H_3PO_4 (δ 0.0), 25°C, 32.384 MHz); δ 112.75 (s, μ-PCy_2).

X-RAY EXPERIMENTAL

General

Data for all six compounds were collected on an Enraf–Nonius CAD-4 diffractometer using graphite-monochromated Mo-K_α radiation. Data for the unit cell determinations were collected by the θ–2θ scan technique at 23 ± 1°C. Details of the standard data collection methods were similar to those outlined previously.[15] All calculations were performed on a PDP 11/44 computer using the Enraf–Nonius software package "SDP-PLUS".[16] Supplementary material is available for all six compounds.*

Suitable crystals were obtained by slow cooling of hexane solutions (−10°C), mounted in thin-walled glass capillaries, and sealed under inert atmospheres. Unit cell parameters were obtained from 25 strong reflections (**1**: $22° < 2\theta < 26°$; **2**: $22° < 2\theta < 28°$; **3**: $22° < 2\theta < 27°$; **4**: $8° < 2\theta < 25°$; **5**: $26° < 2\theta < 28°$; **6**: $20° < 2\theta < 24°$). The data were then corrected for Lorentz and polarization effects, and an anisotropic decay correction was applied for **1**, **2** and **5**. An empirical absorption correction (program EAC) was applied for each compound. The structures were obtained by direct methods (MULTAN)[17] except for **5** which was solved by Patterson methods, and successive cycles of difference Fourier maps followed by least-squares refinement. Hydrogen atoms were not located in the structure determinations although their contributions were included in the refinements. Data with intensities less than $3\sigma(I)$† and $\sin\theta/\lambda$ less than 0.05 were excluded, and a non-Poisson contribution weighting scheme with an experimental instability factor P set at 0.07 (**1**, **2** and **6**) and 0.03 (**3** and **5**) and 0.05 (**4**) were used in the final stages of refinement.* Crystal data and collection parameters are given in Table 1. Scattering factors were taken from ref. 18.

For **1**, the highest peak in the final difference Fourier map had a height of 0.899 e/Å^3 and was located 1.043 Å from Os(1). For **2**, the highest peak in the final difference Fourier map had a height of 1.140 e/Å^3 and was located 1.14 Å from Os(2). For **5**, the highest peak in the final difference Fourier map had a height of 3.393 e/Å^{-3} and was located 1.15 Å from Os(6). For **6**, the highest peak in the final difference Fourier map had a height of 0.895 e/Å^{-3} and was locatd 0.995 Å from C(35).

Acknowledgements—We thank the Robert A. Welch Foundation (Grant F-816) and the National Science Foundation (CHE-8818984) for support. R.A.J. thanks the Alfred P. Sloan Foundation for a fellowship (1985–1989).

REFERENCES

1. A. J. Deeming, *Adv. Organomet. Chem.* 1986, **26**, 1; K. Burgess, *Polyhedron* 1984, **3**, 1175; F. A. Cotton and G. Wilkinson, *Advanced Inorganic Chemistry*, 5th edn, Ch. 19. John Wiley, New York (1988).
2. M. R. Churchill, F. J. Hollander and J. R. Hutchinson, *Inorg. Chem.* 1977, **16**, 2697; B. F. G. Johnson, D. A. Kaner, J. Lewis and P. R. Raithby, *J. Organomet. Chem.* 1981, **215**, C33; S. A. R. Knox, J. W. Koepke, M. A. Andrews and H. D. Kaesz, *J. Am. Chem. Soc.* 1975, **97**, 3942; J. A. Clucas, M. M. Harding and A. K. Smith, *J. Chem. Soc., Chem. Commun.* 1985, 1280; J. A. Clucas, D. F. Foster, M. M. Harding and A. K. Smith, *J. Chem. Soc., Chem. Commun.* 1984, 949.
3. V. D. Patel, A. A. Cherkas, D. Nucciarone, N. J. Taylor and A. J. Carty, *Organometallics* 1985, **4**, 1792; J. S. Field, R. J. Haines, M. H. Moore, D. N. Smit and L. M. Steer, *S. Afr. J. Chem.* 1984, **3**, 36.
4. K. Natarajan, L. Zsolnai and G. Huttner, *J. Organomet. Chem.* 1981, **220**, 365; F. Iwasaki, M. J. Mays, P. R. Raithby, P. I. Taylor and P. J. Wheatley, *J. Organomet. Chem.* 1981, **220**, 185.
5. S. B. Colbran, B. F. G. Johnson, J. Lewis and R. M. Sorrell, *J. Organomet. Chem.* 1985, **296**, C1.
6. A. M. Arif, T. A. Bright, R. A. Jones and C. M. Nunn, *J. Am. Chem. Soc.* 1988, **110**, 6894.
7. See for example: D. F. Rieck, R. A. Montag, T. S. McKechnie and L. F. Dahl, *J. Am. Chem. Soc.* 1986, **108**, 1330.
8. J. Lauer, *J. Am. Chem. Soc.* 1986, **108**, 1521.
9. M. R. Churchill and B. G. DeBoer, *Inorg. Chem.* 1977, **16**, 878.
10. See for example: A. J. Carty, *Adv. Chem. Ser.* 1982, **196**, 163 and refs therein; A. J. Carty, S. A. MacLaughlin and D. Nucciarone, in *Phosphorus-*

*Tables of complete bond lengths and angles, positional and thermal parameters, observed and calculated structure factors for **1**–**6** and a ORTEP view of the second independent molecule of **5** have been deposited as supplementary material with the Editor, from whom copies are available on request. Atomic coordinates have also been submitted to the Cambridge Crystallographic Data Centre.

†P is used in the calculation of $\sigma(I)$ to downweight intense reflections in the least-squares refinement. The function minimized was $\Sigma w(|F_o|-|F_c|)^2$, where $w = 4(F_o)^2/[\Sigma(F_o)^2]^2$, where $[\Sigma(F_o)^2]^2 = [S^2(C+R^2B)+\{P(F_o)^2\}^2]/Lp^2$, where S is the scan rate, C is the total integrated peak count, R is the ratio of scan time to background counting time, B is the total background count and Lp is the Lorentz-polarization factor.

31 *NMR Spectroscopy in Stereochemical Analysis* (Edited by J. G. Verkade and L. D. Quin), Ch. 16, p. 559. VCH (1987).
11. F. Iwasaki, M. J. Mays, P. R. Raithby, P. L. Taylor and P. J. Wheatley, *J. Organomet. Chem.* 1981, **213**, 185.
12. K. Natarajan, O. Scheidsteger and G. Huttner, *J. Organomet. Chem.* 1981, **221**, 301.
13. B. F. G. Johnson and J. Lewis, *Inorg. Synth.* 1972, **13**, 93.
14. H. Hoffman and P. Schellenbeck, *Chem. Ber.* 1966, **99**, 1134.
15. R. A. Jones and T. C. Wright, *Organometallics* 1983, **2**, 1842.
16. SDP Plus (4th edn, 1981), B. A. Frenz and Associates, College Station, TX 77840.
17. G. Germain, P. Main and M. M. Woolfson, *Acta Cryst.* 1971, **A27**, 368.
18. *International Tables for X-ray Crystallography*, Vol. IV. Kynoch Press, Birmingham (1974).

Polyhedron Vol. 9, No. 13, pp. 1589–1591, 1990
Printed in Great Britain

0277–5387/90 $3.00+.00
© 1990 Pergamon Press plc

TRANS-CHLOROACETATONITROSYLBIS(TRIPHENYLPHOSPHINE)RHODIUM

ROBIN B. ENGLISH

Department of Chemistry and Biochemistry, Rhodes University, P.O. Box 94, Grahamstown 6140, South Africa

(*Received* 3 *August* 1989; *accepted* 1 *March* 1990)

Abstract—The synthesis and structural characterization of the tetragonal pyramidal complex $[Rh(O_2CCH_3)Cl(NO)(PPh_3)_2]$ are reported. This complex has a *trans* arrangement of basal ligands with a bent apical nitrosyl group inclined towards the *acetato* ligand.

We are currently investigating the stereochemistry and reactivity of the tetragonal pyramidal complexes $[RhX_2(NO)(PR_3)_2]$ (X is an anionic ligand and PR_3 *a secondary or tertiary phosphine*).[1] In one experiment we set out to prepare crystals of $[Rh(O_2CCH_3)_2(NO)(PPh_3)_2]$ (**I**) of diffraction quality, with the aim of comparing its structure with that of the *trifluoroacetato* analogue $[Rh(O_2CCF_3)_2(NO)(PPh_3)_2]$.[2] The synthesis of **I** is described in *Inorganic Syntheses*[3] and is straightforward. To our surprise, recrystallization of **I** from chloroform yielded crystals which were *not*, on microanalytical evidence, composed of **I**. A single crystal X-ray diffraction study was performed and revealed that a reaction had taken place during the crystallization to give the *chloro*-substituted derivative $[Rh(O_2CCH_3)Cl(NO)(PPh_3)_2]$ (**II**), whose structure is described in this communication.

EXPERIMENTAL

Green microcrystalline **I** (100 mg, 0.13 mmol) was dissolved in warm (40°C) chloroform (10 cm^3). The rate of dissolution appeared to depend inversely on the crystallite size, and of several batches of **I**, some were almost insoluble; dissolution was also extremely slow in carefully purified chloroform. A bright green solution was obtained which slowly and inexorably darkened to olive-green over 2 h. The solution was filtered and cooled to 2°C; over 12 h large, green–brown solvated crystals of the *product* formed in 10% yield [ν(N—O) 1612 cm^{-1}]. Manipulations were carried out in an atmosphere of nitrogen.

X-ray crystallography

$[Rh(O_2CCH_3)Cl(NO)(PPh_3)_2]\cdot 2CHCl_3$, $C_{40}H_{35}Cl_7NO_3P_2Rh$, $M_r = 990.9$, $P2_1/c$ (No. 14), $a = 9.797(5)$, $b = 23.20(1)$, $c = 19.45(1)$ Å, $\beta = 91.38(5)°$, $F(000) = 2000$, $U = 4420(6)$ Å^3, $Z = 4$, $\mu = 8.3$ cm^{-1}, crystal size $0.2\times0.2\times0.15$ mm, $N_{reflections} = 8240$ ($-11 \leqslant h \leqslant 11$, $0 \leqslant k \leqslant 23$, $0 \leqslant l \leqslant 22$), N(observed, unique with $I \geqslant 2.5\sigma(I)$) = 3651, $R = 0.098$, $R_w = 0.103$, $w = k/[\sigma^2(F_o) + g(F_o)^2]$ with $k = 0.629$, $g = 0.0233$. Data collection, structure solution and refinement methods have been described previously;[4] phenyl carbons and the nitrosyl oxygen atom were refined with isotropic temperature factors, otherwise full anisotropic refinement was employed; chloroform molecules exhibited thermal and possible disorder effects and were therefore treated as rigid groups with C—Cl 1.75 Å and Cl—C—Cl 109.5°. The rather high final R reflects the poor definition in the region of the solvent chlorine atoms, which contribute 20.4% of the total electron count in the unit cell. Two peaks, ~ 1.5 eÅ^{-3}, in the final difference map were associated with the nitrosyl oxygen atom, whose final temperature factor was quite large, 0.2 Å^2. Three other peaks with heights > 1 eÅ^{-3} were close to the rhodium atom; otherwise the map was featureless. Some bond lengths (Å) and angles (°):* Rh—N 1.91(1), Rh—Cl 2.355(4), Rh—P(1)

* Atomic coordinates, derived parameters and F_o/F_c data have been deposited with the Editor as supplementary data: atomic coordinates are also available from the Cambridge Crystallographic Data Centre.

2.377(4), Rh—P(2) 2.368(4), Rh—O(*acetato*) 2.05(1), N—O(nitrosyl) 0.92(3); Rh—N—O 130(2), P(1)—Rh—P(2) 171.0(1), Cl—Rh—O(*acetato*) 169.5(3), P(1)—Rh—Cl 88.3(1), P(2)—Rh—Cl 90.4(1), P(1)—Rh—O(*acetato*) 89.5(3), P(2)—Rh—O(*acetato*) 90.2(3), N—Rh—basal ligand angles range from 92.7(6) to 97.7(5)

RESULTS AND DISCUSSION

The structure of **II** is shown in Fig. 1. Like other complexes in the $[RhX_2(NO)(PR_3)_2]$ series, **II** is tetragonal pyramidal with a bent apical nitrosyl group. The geometry of the metal—N—O system has been the subject of considerable discussion.[5] In **II** the Rh—N—O angle is close to that in $[RhCl_2(NO)(PPh_3)_2]$,[6] 125(2)°, and indeed corresponding bond lengths and angles in the two molecules are not significantly different. However, the *direction* of bending of the NO group is different; in **II** NO bands in the N—Rh—O(*acetato*) plane (torsion angle O(nitrosyl)—N—Rh—O(*acetato*) 3.8°), whereas in $[RhCl_2(NO)(PPh_3)_2]$ the Rh—P bond is eclipsed [O(nitrosyl)—N—Rh—P 10(3)°]. If one discounts crystal packing as a secondary influence, the substitution of an acetate for a chloride ligand can be the only cause of this difference.

A theoretical analysis of the electronic structure of five-coordinate nitrosyl complexes, by Hoffmann *et al.*, was published some years ago.[5] The relevant conclusions in this treatment are as follows:

(a) in compounds of the type $ML_2L'_2(NO)$, L *trans* to L, the NO group should bend in the plane containing the poorer donors or, alternatively, the better π-acceptors; and
(b) in a compound of the type $ML_2DA(NO)$, D = π-donor *trans* to A = π-acceptor, if the NO group bends in the DMA plane then it should incline towards A.

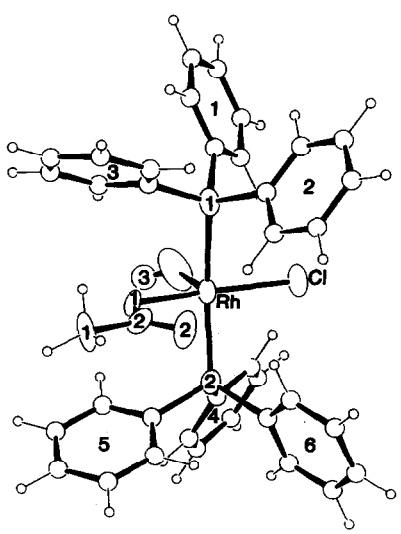

Fig. 1. Structure of $[Rh(O_2CCH_3)Cl(NO)(PPh_3)_2]$: numbers refer to the atomic coordinate list.

The structure of $[RhCl_2(NO)(PPh_3)_2]$ is then explained in terms of (a) by making the reasonable assumption that PPh_3 is a better π-acceptor than Cl.

Similarly, the Rh—N—O conformation in **II** follows if one makes the assumptions that the *acetato* ligand is a better π-acceptor and weaker donor than either PPh_3 or Cl^-, and that, taken together, Cl^- and $CH_3CO_2^-$ are weaker electron-donors than two PPh_3 groups. These statements are not quite so intuitively acceptable.

However, when both the Cl ligands are replaced by *trifluoroacetato* groups, which presumably are *better* π-acceptors and weaker donors than PPh_3 due to the powerful electron-withdrawing influence of the CF_3 substituents, the NO does not bend in the RhO_2 plane as expected: in $[Rh(O_2CCF_3)_2(NO)(PPh_3)_2]$ the torsion angle $O(CF_3CO_2)$—Rh—N—O(nitrosyl) is 43°, so the NO group bends in a plane bisecting a P—Rh—$O(CF_3CO_2)$ bond. The model fails to predict this geometry.

Hoffmann's conclusions are based on symmetry arguments combined with extended Hückel calculations carried out on the model compounds $[IrCl_4(NO)]^{2-}$, $[IrCl_2(NO)(PH_3)_2]$ and $Mn(CO)_4(NO)$, and do not take steric interactions into account. Certainly, the *bending* of the NO ligand must be due to electronic effects; however, the primary influence determining its *conformation* is probably steric in nature, while electrostatic interaction between the dipole of the NO and the resultant dipole of the rest of the molecule should also be considered. Orbital influences play a minor role.

Figure 2 depicts the molecules $[Rh(O_2CCH_3)Cl(NO)(PPh_3)_2]$, $[RhCl_2(NO)(PPh_3)_2]$ and $[Rh(O_2CCF_3)_2(NO)(PPh_3)_2]$ drawn with van der Waals' radii for the atoms, in "plan" and "elevation"; it is clearly apparent that rotation of the NO ligand round the Rh—N bond is hindered by the presence of the PPh_3 phenyl groups. It is also interesting to see how the conformational swivelling of the NO group becomes a very minor structural phenomenon when the molecules are depicted "realistically" rather than in the conventional ORTEP-style plots. In fact, such ball-and-stick plots can be quite misleading. For example, in ref. 5 the ". . . more sterically crowded Ph_3P—Ir—PPh_3 axes in $[IrCl_2(NO)(PPh_3)_2]$ . . ." are mentioned. Inspection of Fig. 2(b) shows that the

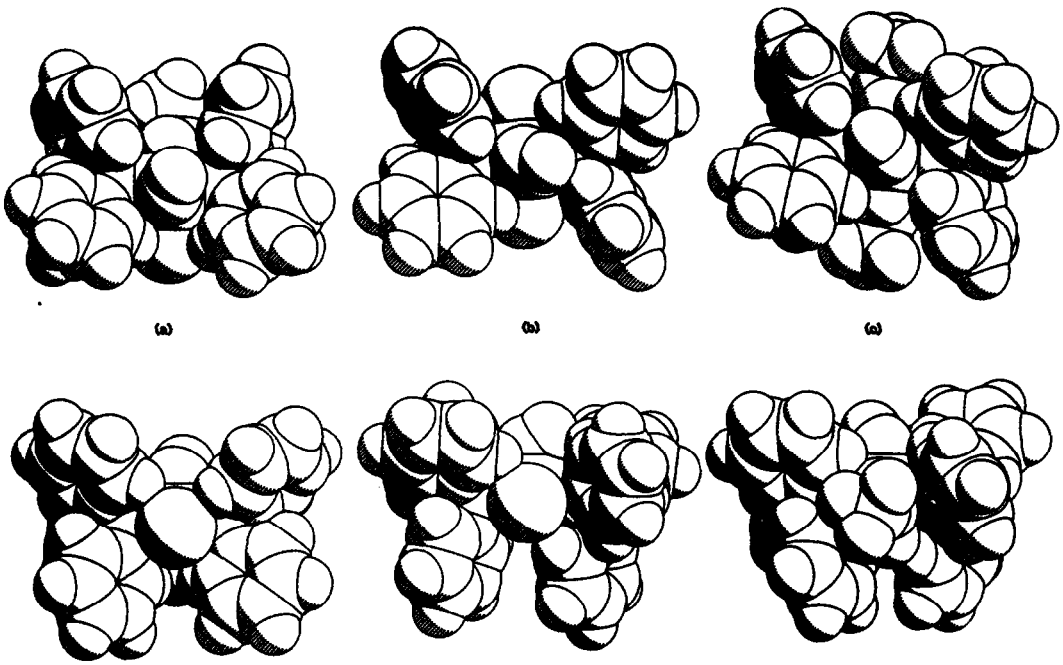

Fig. 2. The molecules **II** (a), $[RhCl_2(NO)(PPh_3)_3]$ (b) and $[Rh(O_2CCF_3)_2(NO)(PPh_3)_2]$ (c), drawn with van der Waals' radii for the atoms: top, viewed along the Rh—N vector, and bottom, viewed perpendicular to the Rh—N vector and parallel to the Rh—N—O plane.

Cl—Rh—Cl axes in $[RhCl_2(NO)(PPh_3)_2]$ (isostructural with the iridium analogue) are just as crowded by the phenyl groups, and in terms of steric hindrance there is little to choose between these two regions.

We feel that the structures observed in these complexes correspond to potential energy minima, that steric and electrostatic effects both play a part in determining NO conformation; the balance between the two effects obviously will vary with the nature of the basal ligands, and that orbital effects are minor in comparison.

The mechanism of formation of **II** from $[Rh(O_2CCH_3)_2(NO)(PPh_3)_2]$ is not obvious. Impurities *are* likely to be present in $CHCl_3$ which has been exposed to oxygen and light; these include HCl and Cl_2[7] and it is likely that **II** formed by dissociation of a $CH_3CO_2^-$ group and subsequent attack by Cl^-. In support of this suggestion we found that $[Rh(O_2CCH_3)_2(NO)(PPh_3)_2]$ was virtually insoluble in $CHCl_3$ which has been dried and stored away from light over K_2CO_3. We are currently examining the reactivity of $[Rh(O_2CCH_3)_2(NO)(PPh_3)_2]$ towards substitution of $CH_3CO_2^-$ by other weak nucleophiles including alkyls and metal-containing species.

Acknowledgements—My thanks are due to Mr D. da Costa for assistance, the University of Cape Town for the intensity data collection and the Foundation for Research Development and Rhodes University for financial and practical support.

REFERENCES

1. R. B. English, M. M. de V. Steyn and R. J. Haines, *Polyhedron* 1987, **6**, 1503; R. B. English, *Polyhedron* 1989, **8**, 2565.
2. A. Dobson, D. S. Moore, S. D. Robinson, A. M. R. Galas and M. B. Hursthouse, *J. Chem. Soc., Dalton Trans.* 1985, 611.
3. A. G. MacDiarmid (Ed.), *Inorganic Syntheses*. Vol. 17, pp. 124–132. McGraw-Hill, New York (1977).
4. R. B. English and M. M. de V. Steyn, *S. Afr. J. Chem.* 1984, **37**, 177.
5. R. Hoffmann, M. M. L. Chen. M. Elian, A. R. Rossi and D. M. P. Mingos, *Inorg. Chem.* 1974, **13**, 2666 and refs therein.
6. S. Z. Goldberg, C. Kubiak, C. D. Meyer and R. Eisenberg, *Inorg. Chem.* 1975, **14**, 1650.
7. D. P. Perrin and W. L. F. Armarego (Eds), *Purification of Laboratory Chemicals*, 3rd edn, pp. 121–122. Pergamon Press, Oxford (1988).

Polyhedron Vol. 9, No. 13, pp. 1593–1601, 1990
Printed in Great Britain

0277–5387/90 $3.00+.00
© 1990 Pergamon Press plc

COORDINATION CHEMISTRY OF N,N′-BIS (2-HYDROXYPHENYL)ETHYLENEDIAMINE-N,N′-DIACETIC ACID AND SOME RELATED LIGANDS

OWEN J. VAUGHAN and JOHN F. GIBSON*

Inorganic Chemistry Laboratories, Imperial College, London SW7 2AY, U.K.

(*Received* 7 *September* 1989; *accepted* 1 *March* 1990)

Abstract—Iron(III) complexes of new hexadentate phenolic aminocarboxylate ligands based upon N,N′-bis(2-hydroxyphenyl)ethylenediamine-N,N′-diacetic acid (HPED) have been synthesized. These iron(III) complexes have been characterized utilizing Raman, IR, Mössbauer and ESR spectroscopy. Copper(II)–HPED has been studied in solution, utilizing electronic and ESR spectroscopy.

The treatment of β-thalassaemia, a genetic disease originating from deficiencies in the biosynthesis of the β-chain of haemoglobin, requires indefinite transfusion therapy. However, this therapy leads to the toxic accumulation of iron in the tissues, which eventually results in the failure of vital organs, mortality being associated with cardiotoxicity, hepatic cirrhosis and pancreatic dysfunction.[1]

The current drug of choice for the treatment of this iron-overload condition is desferrioxamine (DFB).[2–4] However, the utility of this drug, a trihydroxamic acid, is limited by low oral activity, rapid metabolism and only moderate efficacy, as well as inconvenient and expensive modes of administration.

The symptoms of Wilson's disease, a condition associated with an excess of copper accumulated in the liver, brain and kidneys, include hepatic cirrhosis, lack of coordination, severe tremors and progressive mental deterioration.[5] The symptoms are dependent upon the amount of copper present, and may be reversed by the use of chelating agents, such as $Na_2CaEDTA$ and penicillamine, to remove excess amounts of copper from the body.

As a consequence of these and other metal-overload conditions, we have become involved in the search for more effective metal chelating agents; in particular, ones that are orally active. In this work we report the preliminary detailed investigation of the coordination chemistry of the iron(III) and copper(II) complexes of a series of hexadentate phenolic aminocarboxylate ligands, based upon N,N′-bis(2-hydroxyphenyl)ethylenediamine-N,N′-diacetic acid (HPED) (R = H, in **IV** of Scheme 1).

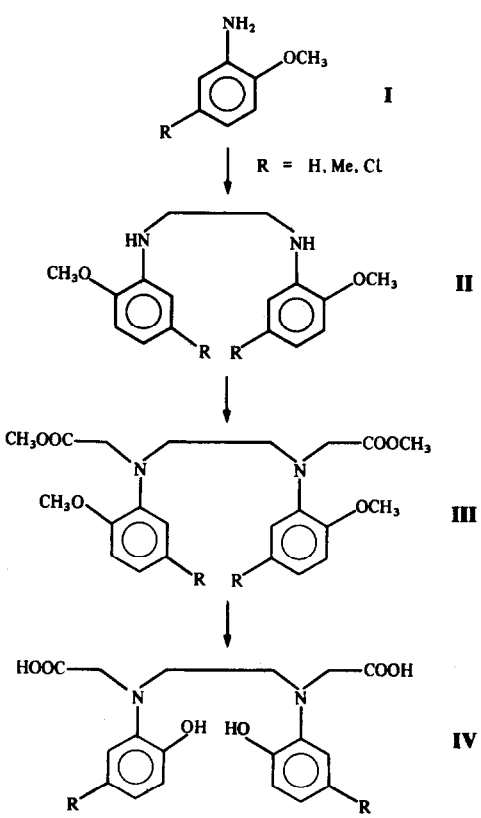

Scheme 1. Symmetric HPED ligands.

*Author to whom correspondence should be addressed.

EXPERIMENTAL

Symmetric ligands (*Scheme* 1, R = H, Cl, Me)

These were prepared using a substantially modified procedure to that described by Bao and coworkers,[6] and are shown in Scheme 1. All symmetric ligands were prepared in the same manner as described below for the formation of HPED (R = H).

Step 1. Using the procedure of Bennett *et al.*,[7] a solution of *o*-anisidine (**I**) (30.00 g, 0.24 mol) and 1,2-dibromoethane (11.44 g, 0.06 mol), in dimethylformamide (DMF) (100 cm^3), over calcium carbonate (10.00 g, 0.10 mol), was heated at 100°C for 2 h, under nitrogen and with vigorous stirring. After removal of the DMF by rotary evaporation, a solution of potassium hydroxide (100 cm^3, 5% w/w) was added and the mixture steam distilled for 2 h, before being extracted into dichloromethane (DCM). The DCM layer was separated off and dried. After removal of the DCM, the oil was recrystallized from ethanol–water to yield fine white crystals of N,N′-bis(2-methoxyphenyl)ethylenediamine (**II**) (11.36 g, 70%).

Step 2. A solution of **II** (8.00 g, 0.03 mol) and methyl bromoacetate (17.97 g, 0.12 mol), in DMF (100 cm^3), over calcium carbonate (6.00 g, 0.06 mol), was heated at 80°C for 2 h with vigorous stirring under nitrogen. After removal of the DMF by evaporation, the oil was taken up in DCM, washed with saturated sodium chloride solution and dried. After removal of the DCM, the semi-solid material was recrystallized from ethanol–water to yield white platelets of N,N′-bis (2-methoxyphenyl)N,N′ - bis(methylacetate)ethylenediamine (**III**) (11.44 g, 95%).

Step 3. At 0°C and under nitrogen, DMF (50 cm^3) was added dropwise to lithium powder (0.83 g, 0.12 mol) with stirring, followed by the dropwise addition of thioethanol (7.46 g, 0.12 mol) in DMF (25 cm^3). To the mixture, **III** (5.00 g, 0.012 mol), in DMF (25 cm^3), was added dropwise. The solution was then heated at 100°C for 8 h. After being cooled the solution was poured on to acetone (400 cm^3) with vigorous stirring, leading to the formation of a fine white precipitate. After filtration and drying, the solid was taken up in boiling water (15 cm^3). The solution was cooled to 4°C, and cold (0°C) concentrated hydrochloric acid (5 cm^3) added dropwise with stirring. Trituration of the solution yielded a fine white solid of N,N′-bis(2-hydroxyphenyl)ethylenediamine-N,N′-diacetic acid dihydrochloride (**IV**) (2.83 g, 54%). Microanalyses, IR and mass spectra were found to be satisfactory, see Tables 1 and 2.

Table 1. Physical properties of ligands

Ligand			Yield (%)	ν(C=O) (cm^{-1})	*m/z* (FAB)[a] MH^+
Symmetric ligands (Scheme 1)					
R = H			54	1712	361.04 (56)
Me			42	1716	389.03 (100)
Cl			33	1709	430.88 (22)
Asymmetric ligands (Scheme 2)					
R_1	R_2	R_3			
H	Me	H	79	1717	375.02 (100)
H	Cl	H	50	1713	396.96 (25)
H	MeO	H	35	1713	391.02 (36)
Me	Cl	H	38	1712	410.96 (33)
Me	H	Cl	46	1728	411.00 (5)
Cl	MeO	H	38	1711	426.96 (30)
Dilactones (Scheme 3)					*m/z* (EI)[b]
R = H			19	1767	329.99 (15)
Me			39	1768	352.04 (98)
Cl			5	1775	394.03 (10)[c]

[a] MH^+ refers to the parent molecular ion. In the case of chlorine substituents, MH^+ refers to the highest peak in the chlorine cluster. Values in parentheses are the relative intensities.

[b] Refers to the parent molecular ion. Values in parentheses are the relative intensities.

[c] Refers to the highest peak in the chlorine cluster.

Asymmetric ligands (*Scheme* 2, R_1 = H, Me, Cl, MeO; R_2 = H, Me, Cl; R_3 = H, Cl)

For the synthesis of these ligands (Scheme 2) a new procedure was developed. All asymmetric ligands were prepared in the same manner as described below for N-(2-hydroxy-5-methylphenyl) - N′ - (2 - hydroxyphenyl)ethylenediamine-N,N′-diacetic acid.

Step 1. To a stirred cold (0°C) solution of bromoacetic acid (14.59 g, 0.11 mol) in DCM (75 cm^3), dicyclohexylcarbodiimide (21.66 g, 0.11 mol) in DCM (25 cm^3) was slowly added. The mixture was stirred at 0°C for 30 min, and then 2-methoxy-5-methylaniline (**V**) (14.40 g, 0.11 mol), in DCM (100 cm^3), was added dropwise. Stirring was continued for a further 90 min, after which the mixture was warmed to room temperature. The mixture was filtered into 100 cm^3 of ice–water. The organic layer was washed successively with 2 M hydrochloric acid, saturated sodium bicarbonate, and saturated sodium chloride solutions, before being dried. Removal of the solvent and recrystallization of the material from ethanol–water yielded white

Table 2. Microanalysis data for ligands

Ligand	Calculated C	H	N	Cl	Found C	H	N	Cl
Symmetric ligands[a] (Scheme 1)								
R = H	49.9	5.1	6.5	16.4	49.7	5.2	6.5	16.2
Me	52.1	5.7	6.1	15.4	52.1	5.8	6.0	15.2
Cl	43.1	4.0	5.6	28.2	43.4	4.0	5.6	27.1
Asymmetric ligands[a] (Scheme 2)								
R_1 R_2 R_3								
H Me H	51.0	5.4	6.3	15.9	51.1	5.4	6.3	15.8
H Cl H	46.2	4.5	6.0	22.7	46.2	4.6	6.0	21.9
H MeO H	49.3	5.2	6.1	14.4	49.1	5.2	6.1	15.3
Me Cl H	47.4	4.8	5.8	22.1	47.2	4.8	5.8	21.0
Me H Cl	47.4	4.8	5.8	22.1	48.2	4.8	5.8	21.7
Cl MeO H	45.8	4.7	5.6	21.4	45.8	4.7	5.6	18.9
Dilactones (Scheme 3)								
R = H	66.7	5.0	8.6	—	66.5	5.0	8.6	—
Me	68.2	5.7	8.0	—	68.2	5.7	7.9	—
Cl	55.0	3.6	7.1	18.0	54.7	3.5	7.0	17.8

[a] Analysed as the dihydrochloride.

crystals of 2-methoxy-5-methyl-bromoacetanilide (**VI**) (14.40 g, 53%).

Step 2. A solution of *o*-anisidine (10.58 g, 0.09 mol), **VII** (11.10 g, 0.04 mol) and calcium carbonate (10.00 g, 0.10 mol), in DMF (100 cm^3), was heated at 80°C for 2 h, with stirring under nitrogen. After filtration and removal of the solvent, potassium hydroxide solution (40 cm^3, 10% w/w) was added to the oil. The mixture was steam distilled for 3 h. The remaining material was extracted into DCM, which was then washed with saturated sodium chloride solution, before being dried. The solvent was removed and the solid recrystallized from ethanol–water to yield white crystals of **VIII** (10.20 g, 79%).

Step 3. To a stirred cold (0°C) solution of lithium aluminium hydride (1.50 g, 0.04 mol) in tetrahydrofuran (THF) (50 cm^3) under nitrogen, a solution of **VIII** (3.55 g, 0.01 mol) in THF (50 cm^3) was added dropwise. The solution was refluxed for 2 h, before being cooled to 0°C. Ethyl acetate (50 cm^3) was added, followed by water (10 cm^3) and a further 50 cm^3 of ethyle acetate. Sodium sulphate (20.00 g) was added and the mixture was stirred for 60 min, before filtration and removal of the solvent. The solid was recrystallized from ethanol to yield fine white crystals of N-(2-methoxy-5-methylphenyl)-N′-(2-methoxyphenyl)ethylenediamine (**IX**) (3.01 g, 89%).

The synthesis was completed via **X** and **XI** utilizing steps 2 and 3 of Scheme 1. Analyses, IR and mass spectra were satisfactory, see Tables 1 and 2.

Dilactones (*Scheme* 3, R = H, Me, Cl)

Because esterification of the carboxylic acid groups is likely to aid oral activity,[6] three dilactones of the symmetric HPED ligands were synthesized. They were prepared in a manner similar to that described by Freedman and Frost,[8] and are shown in Scheme 3, although the dilactone of HPED (R = H) has previously been prepared by another route.[6]

A mixture of 2-hydroxy-5-methylaniline (**XII**) (10.00 g, 0.08 mol) and 1,2-dibromoethane (15.25 g, 0.08 mol), in water (200 cm^3), was refluxed under nitrogen with stirring for 2 h. The solvent was decanted and the remaining oily material converted to a white solid by washing with diethyl ether. The solid was recrystallized from ethanol (400 cm^3) to yield fine white needles of N,N′-bis(2-hydroxy-5-methylphenyl)ethylenediamine (**XIII**) (4.30 g, 39%).

To a solution of chloroacetic acid (1.88 g, 0.02 mol) and sodium hydroxide (1.59 g, 0.04 mol), in water (75 cm^3), **XIII** (1.00 g, 0.004 mol) was added with stirring. The solution was refluxed under nitrogen for 2 h, before being cooled and made acidic by the addition, with stirring, of cold concentrated hydrochloric acid (10 cm^3). Trituration yielded

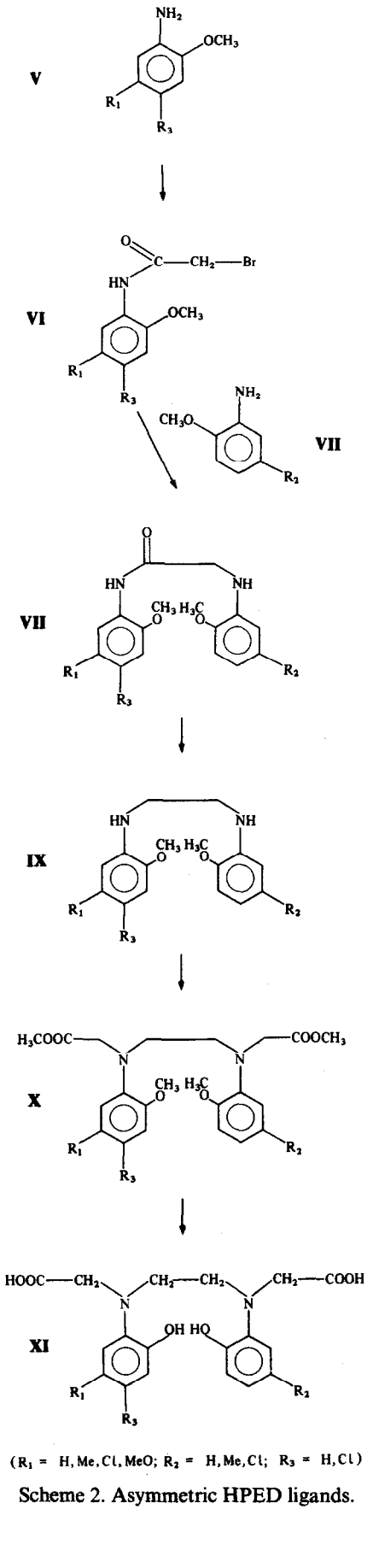

Scheme 2. Asymmetric HPED ligands.

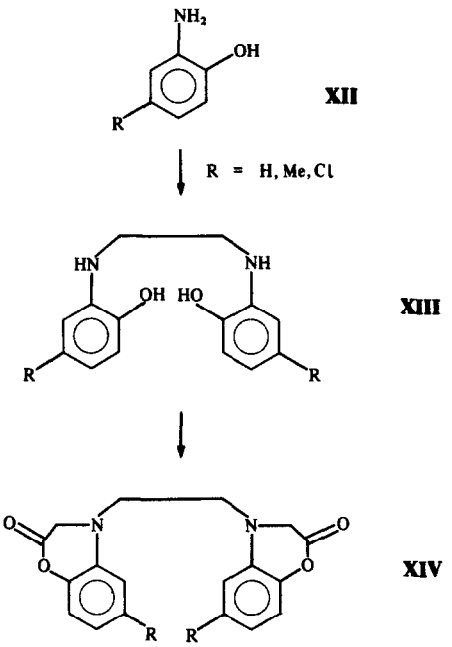

Scheme 3. HPED dilactones.

fine white crystals of the dilactone (**XIV**) (0.51 g, 39%). Analyses, IR and mass spectra were all satisfactory, see Tables 1 and 2.

Iron(III) *complexes*

All iron(III) complexes were prepared from the symmetric and asymmetric HPED ligands using a method similar to that described by Gaber *et al.*[9]

Equimolar quantities of the ligand dihydrochloride (0.577 mM), freshly precipitated ferric oxide (0.577 mM) and potassium hydrogen carbonate (0.058 g, 0.577 mM), were stirred in a 3 : 1 water–methanol (40 cm^3) solution, under nitrogen, for 3 days. The solution was filtered and the solvent removed by evaporation. The resultant solid was extracted into ethanol. The solution was reduced to 15 cm^3 and left to stand for 12 h. Deep purple–red crystals were filtered off and washed with diethyl ether. A second crop was obtained upon the addition of diethyl ether to the remaining filtrate. The product was dried over phosphorus pentoxide *in vacuo*. Analyses and other physical data may be found in Tables 3, 4 and 5.

General procedures and techniques

All the anilines were purified by distillation before use. N,N-dimethylformamide (HPLC grade) was dried over sodium.

Resonance Raman spectra were measured at

Table 3. Microanalysis data for iron(III) complexes

Ligand	Calculated C	H	N	Found C	H	N
Symmetric ligands (Scheme 1)						
R = H[a]	44.4	4.1	5.8	44.1	4.1	5.9
Me	46.6	4.7	5.4	46.3	4.6	5.5
Cl	38.9	3.3	5.0	39.4	3.2	5.1
Asymmetric ligands (Scheme 2)						
R_1 R_2 R_3						
H Me H	46.5	4.4	5.6	47.5	4.3	5.5
H Cl H	41.4	3.7	5.4	41.6	3.7	5.3
H MeO H	47.4	3.8	5.8	47.1	3.7	5.8
Me Cl H	42.6	4.0	5.2	42.3	4.0	5.2
Me H Cl	42.6	4.0	5.2	43.9	3.9	5.2
Cl MeO H	44.2	3.3	5.4	44.1	3.2	5.3

[a] Analysed as $K[Fe(L)] \cdot 2H_2O$.

200–400 mW using the 484 nm line of an Innova 70 CRL argon laser with a Spex Ramalog V instrument and Spex Datamate data acquisition unit. Samples were contained in 1 mm capillary tubes held perpendicular to the scattering plane. Raman shifts were determined relative to the ν_1 mode of SO_4^{2-} (981 cm^{-1}).

IR spectra were recorded with a Perkin–Elmer 1720 Fourier-transform spectrometer, using Nujol mulls or KBr discs.

UV–vis spectra were made with a Philips PU8700 spectrophotometer, using 10 mm quartz cuvettes.

X-band ESR spectra were recorded with a Varian E12 spectrometer operating at *ca* 9.2 GHz. Q-band

Table 4. Raman spectral data for iron(III) complexes

Iron(III) complex	In-plane C—O bending (cm^{-1})	Phenolate C—O stretch (cm^{-1})	Symmetric ring stretch (cm^{-1})	Ring "quadrant" stretch (cm^{-1})	Ring deformation modes (cm^{-1})	
Symmetric ligands (Scheme 1)						
R = H	1120	1285	1489	1596	—	613
Me	1118	1291	1499	1592	643	602
Cl	1112	1291	1487	1586	638	605
Asymmetric ligands (Scheme 2)						
R_1 R_2 R_3						
H Me H	1119	1290	1498	1595	—	613
H Cl H	1116	1290	1486	1588	—	608
H MeO H	1124	1288	1494	1593	—	624
Me Cl H	1117	1293	1495	1592	638	619
Me H Cl	1115	1286	1486	1592	—	615
Cl MeO H	1138	1301	1501	1553	—	616
EHPG[a]	1168	1286	1482	1600	637	610
Transferrin[a]	1174	1288	1508	1613	—	—
Lactoferrin[b]	1175	1275	1505	1605	—	—

[a] Reference 9.
[b] Reference 12.

Table 5. ESR and Mössbauer spectral data of iron(III) complexes

Ligand	δ_{Fe} (mm s^{-1})	ΔE_q (mm s^{-1})	g_{eff} values	References
HPED	0.57	1.19	9.63, 4.31 4.26, 4.24	—
L1[a]	0.55	1.15	9.63, 4.31 4.26, 4.24	—
L2[b]	0.56	1.15	9.63, 4.31 4.26, 4.24	—
EHPG[c]	0.37	0.77	4.47	14, 15
HBED[c]	0.38	0.75	4.26	14
Transferrin[c]	0.38	0.75	9.18, 4.42 4.16, 4.08	15, 16
Lactoferrin[c]	0.39	—	8.84, 4.39 4.29, 4.15	12, 15, 17

[a] L1 (R_1 = H, R_2 = Me, R_3 = H, see Scheme 2).
[b] L2 (R_1 = H, R_2 = Cl, R_3 = H, see Scheme 2).
[c] The data for these ligands is included for comparison only.

ESR spectra were measured using a Bruker ER200D-SRC spectrometer operating at *ca* 34.2 GHz.

Mass spectra were performed by the Organic Mass Spectroscopy Laboratory, Imperial College, on a VG Micromass 7070E mass spectrometer.

Microanalyses were carried out by Mr K. I. Jones of the Microanalytical Department, Imperial College.

RESULTS AND DISCUSSION

The HPED ligand anion provides six binding sites for iron(III): two tertiary amine nitrogen atoms; two carboxylate oxygen atoms; and two phenolate oxygen atoms. The electronic spectrum of the iron(III)–HPED complex in aqueous solution at pH 2.7 is shown in Fig. 1. Spectra taken over the pH range 2.5–12.0, like those of the analogous iron(III) complexes of ethylene-1,2-bis(2-hydroxyphenylglycine) (EHPG),[10] and N,N′-bis(2-hydroxybenzyl)ethylenediamine-N,N′-diacetic acid (HBED),[11] show that the pH-dependent band of the ligand is replaced by a single band at 277.5 nm which is independent of pH. This is indicative of complete dissociation of the phenol groups which must be bound to the iron(III) ion over the entire pH range 2.5–13.0. The visible absorption of iron(III)–phenolate complexes has long been known,[10,11] and the deep-red colour of the iron(III)–HPED complex (Fig. 1) can thus confidently be assigned to the interaction of the two phenolate groups with the iron(III) ion, the amine and carboxylic acid binding sites providing no basis for an intense visible absorption. The visible absorption band of the iron(III)–HPED complex, at 484.6 nm, is assigned to a charge-transfer transition from the oxygen $p\pi$ orbital of the bound phenolate to the iron(III) $d\pi^*$ orbitals. It is therefore reasonable to infer that the resonance-enhanced Raman bands of iron(III)–HPED (Fig. 2) arise from phenolate vibrations. All of these vibrations correlate with phenolate modes.

The four high energy bands of the resonance

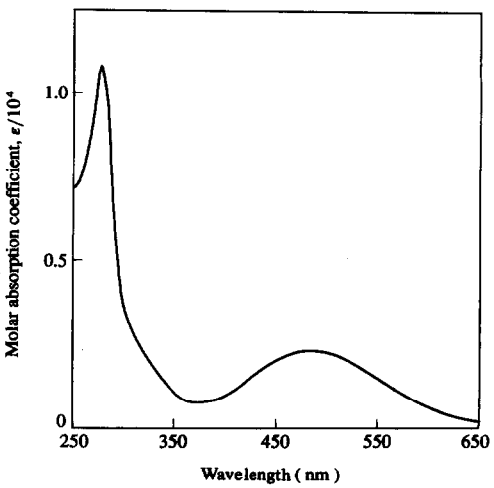

Fig. 1. UV–vis. spectrum of iron(III)–HPED. [Fe^{III}HPED] = 2×10^{-4} M, μ = 0.10 M (KNO_3), 25°C.

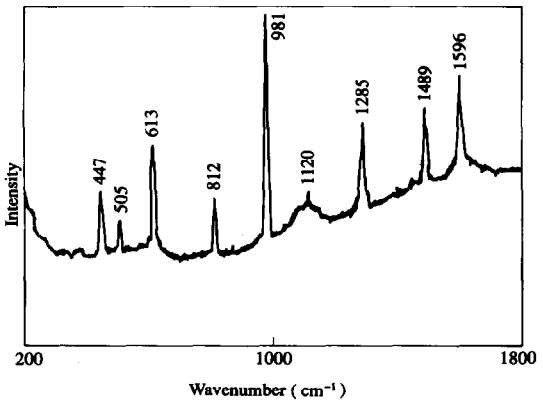

Fig. 2. Resonance Raman spectrum of K[Fe(HPED)]. Concentration = 2×10^{-4} M, in aqueous Na_2SO_4 (0.5 M) at 488 nm; spectral slit width, 8 cm^{-1}; scan rate, 1 cm^{-1} s^{-1}.

Raman spectrum of $[Fe(HPED)]^-$ (Fig. 2), which are also observed in both the iron(III)–EHPG and iron(III)–transferrin spectra, are assigned, by analogy,[9] as follows: 1120 cm^{-1}, in-plane C—O bending, with substantial ring character; 1285 cm^{-1} (phenol at 1281 cm^{-1}), phenolate C—O stretching; 1489 cm^{-1} (1502 cm^{-1} in phenol), symmetric ring stretch; and 1596 cm^{-1}, ring "quadrant" stretch (1614 cm^{-1} in *p*-cresol). The IR spectrum of iron(III)–HPED reveals associated bands at 1112, 1288, 1481 and 1590 cm^{-1}, as might be expected for a complex with no centre of symmetry. The resonance Raman bands for the related iron(III) complexes studied in this work are given in Table 4.

In iron(III)–EHPG, the ring deformation modes at 610 and 637 cm^{-1} are quite strong, but for the iron(III) complexes studied here, the deformation modes, in the regions 602–624 and 637–643 cm^{-1}, are mostly relatively weak. These modes are unobserved for iron(III)–transferrin, which, however, shows much greater relative intensity for the C—O in-plane bending mode at 1174 cm^{-1}. These differences probably arise from the fact that the phenolate groups in HPED and EHPG, are *ortho*-substituted, while those in transferrin and lactoferrin, in the form of tyrosine groups,[13] are *para*-substituted to the bulk of the molecule.

The ^{57}Fe Mössbauer spectra of K[Fe(HPED)], and of the two similar complexes with ligands L1 and L2 of Table 5, have isomer shifts of 0.57, 0.55 and 0.56 mm s^{-1}, respectively. These values are with respect to the iron metal, and clearly indicate the ionic nature of the bond between the ligand and the high-spin iron(III) in these complexes. For the analogous iron(III)–EHPG and iron(III)–HBED complexes the reported values are 0.37 and 0.38 mm s^{-1}, respectively, suggesting much more covalency in their bonding. These latter values lie close to those of iron(III)–transferrin, at 0.38 mm s^{-1}, and iron(III)–lactoferrin, at 0.39 mm s^{-1}. The higher isomer shift of the iron(III)–HPED complex is consistent with the higher ionic character expected with electron donation into the ring by the nitrogen *ortho* to the phenolic group; such a mechanism does not exist for EHPG, HBED or transferrin. All the complexes, listed in Table 5, have large quadrupole splittings, a characteristic of the unsymmetric ligand field around the iron(III) ion.

The ESR spectral data, also shown in Table 5, and the frozen solution ESR spectra, typified by that of iron(III)–HPED shown in Fig. 3, confirm the presence of high-spin iron(III) in these complexes. Effective g values in the region of 4.27 (Table 5) are quite typical of the resonance from the so-called rhombically distorted high-spin iron(III). In a situation with maximum rhombicity ($E/D = 1/3$), the large zero-field splitting (D) leaves the three Kramers doublets well separated, and an isotropic $g_{eff} = 4.27$ signal arises from the central doublet. The fact that the signals we observe in this region are anisotropic indicates a symmetry slightly more axial than fully rhombic ($E/D < 1/3$), and an approximation using the graphs of Dowsing and Gibson[18] yields $E/D = 0.325$ with a D value greater than about 0.60 cm^{-1}. The low-field feature

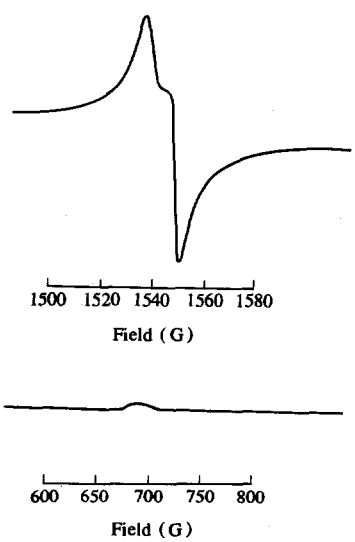

Fig. 3. X-band ESR spectrum of K[Fe(HPED)]. Concentration = 1×10^{-3} M, in a 5 : 1 glycerol–water matrix; temperature, 77 K; time constant, 0.3 s; modulation amplitude, 0.63×10^{-1} G; receiver gain, 2.5×10 (5×10^2 for low-field signal); microwave frequency, 9.233 GHz; microwave power, 200 mW; scan time, 4 min.

(g_{eff} = 9.63) arising from the other two doublets, is also nicely predicted by this procedure.

Copper(II)–HPED was also studied in solution by both electronic and ESR spectroscopy. At or below pH 5.5, the typical blue colour of a copper(II) complex was observed, and is characterized by a broad absorption band at 716 nm (14,000 cm^{-1}). The asymmetry of the observed absorption band indicates overlapping of at least two, probably three, absorption bands, since tetragonal distortion splits the e_g and t_{2g} levels of the d^9 copper(II) to give three possible *d–d* transitions.[10,11]. This band is likely to be associated with a two-proton displacement from the carboxylates of the HPED ligand by the copper(II) ion, to form the diprotonated complex $CuLH_2^0$ ($L = HPED^{4-}$). As compared with the hexaaquo ion,[19] the λ_{max} (716 nm) and the molar extinction coefficient, ε (80 M^{-1} cm^{-1}), of the complex are consistent with the increased ligand-field of lower symmetry at the copper(II) ion expected from nitrogen donation, as found in copper(II)–EHPG and copper(II)–HBED.[9,10] The coordination by LH_2^{2-} is therefore likely to be via the ethylenediamine nitrogen atoms and the carboxylate oxygen atoms, with possible loose coordination by water and/or protonated phenolic oxygens in the axial positions. However, as the pH is increased above 5.5, deprotonation of the phenol groups occurs allowing coordination to the copper(II) ion with the concomitant change in colour from blue to green. This colour change results from the added appearance of a new band at 361 nm, the intensity of which increases with pH, remaining constant above pH 10.5. It may be presumed to be associated with the conversion of $CuLH_2^0$ to CuL^{2-}, via the monoprotonated species $CuLH^-$.

For ESR spectroscopy aliquots of an equimolar solution of $Cu(NO_3)_2$ and HPED were adjusted in pH and frozen. Their X-band ESR spectra (Fig. 4), taken at 77 K, were found to be extremely sensitive to pH. Analysis of these spectra indicates the involvement of at least three copper(II) species in solution. At the low pH of 2.46, a relatively simple spectrum is obtained at both X- and Q-band frequencies, consistent with the copper(II) ion sited in an axial symmetric ligand field, where $g_\parallel = 2.28$, $A_\parallel = 0.016\ cm^{-1}$, and $g_\perp \sim 2.07$, $A_\perp < 0.007\ cm^{-1}$. The spectra are presumably associated with the $CuLH_2^0$ ($L = HPED^{4-}$) species, where the ethylenediamine bridging nitrogens and the carboxylate oxygens form a plane around the copper(II) ion. The weak features in the X-band spectrum of Fig. 4 are seen in $Cu(NO_3)_2$ solution alone, and indicate that only about 80% of the copper(II) is bound as $CuLH_2^0$ at this pH. As the pH is increased the ESR spectra become more complex. In the X-band spectrum recorded at pH 6.26 a second species is also observed. The formation of this new species is expected to involve the removal of a proton from one of the phenolic oxygens, which then binds to the copper(II) ion forming $CuLH^-$ and at the same time imparting some rhombicity to the observed ESR spectrum. At a pH of 10.90 a third species, presumably CuL^{2-}, is clearly seen; this would correspond to the removal of the second phenolic proton with consequent phenolate binding. The spectrum at pH 12.20 indicated the likely presence of primarily just this one species, and was further resolved using Q-band ESR. Our assignment provides evidence for a rhombic ligand-field, where $g_x = 2.31$, $A_x = 0.008\ cm^{-1}$; $g_y = 2.18$, $A_y = 0.004\ cm^{-1}$; $g_z = 2.01$, $A_z = 0.009\ cm^{-1}$.

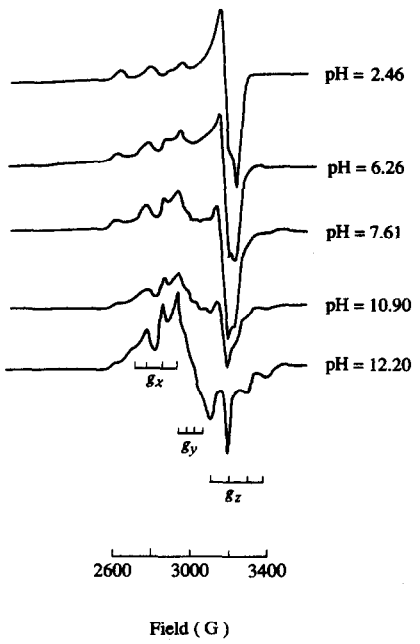

Fig. 4. X-band ESR spectra of copper(II)–HPED. Concentration = 2×10^{-4} M, in a 5:1 glycerol–water matrix; temperature, 77 K; time constant, 0.3 s; modulation amplitude, 0.63×10 G; receiver gain, 6.3×10^2; microwave frequency, 9.113 GHz; microwave power, 200 mW; scan time, 4 min.

The studies undertaken here indicate that HPED and its related ligands form well-defined stable complexes in aqueous solution, and thus merit further investigation of their potential in the treatment of metal-overload conditions, particularly iron.

Acknowledgements—We thank Mr J. N. Bilton for the mass spectra. We would also like to thank Dr B. W. Fitzsimmons and Mr C. M. Lawrence of Birkbeck

College for measuring the Mössbauer spectra. One of us (O.J.V) thanks the SERC for a grant.

REFERENCES

1. D. J. Weatherall and J. B. Clegg, *The Thalassaemia Syndromes*, 3rd edn. Blackwell Scientific Publications, Oxford (1981).
2. R. D. Propper, B. Cooper, R. R. Rufo, A. W. Nienhaus, W. F. Anderson, H. F. Bunn, A. Rosenthal and D. G. Nathan, *New Engl. J. Med.* 1977, **297**, 418.
3. M. A. M. Hussain, N. Green, D. M. Flynn, S. Hussein and A. V. Hoffbrand, *The Lancet* 1976, **2**, 1278.
4. W. F. Anderson, D. G. Badman and A. E. Martell (Eds), *Development of Iron Chelators for Clinical Use*. Elsevier/North Holland, New York (1981).
5. M. N. Hughes, *The Inorganic Chemistry of Biological Processes*, 2nd edn, pp. 298–299. Wiley, Chichester (1981).
6. C. G. Pitt, Y. Bao, J. Thompson, M. C. Wani, H. Rosenkrantz and J. J. Metterville, *J. Med. Chem.* 1986, **29**, 1231.
7. G. M. Bennett, A. N. Mosses and F. S. Statham, *J. Chem. Soc.* 1930, 1668.
8. H. H. Freedman and A. E. Frost, *J. Org. Chem.* 1958, **23**, 1292.
9. B. P. Gaber, V. Miskowski and T. G. Spiro, *J. Am. Chem. Soc.* 1974, **96**, 6868.
10. A. E. Frost, H. H. Freedman, S. J. Westerback and A. E. Martell, *J. Am. Chem. Soc.* 1958, **80**, 530.
11. F. L'Eplattenier, I. Murase and A. E. Martell, *J. Am. Chem. Soc.* 1967, **89**, 837.
12. E. W. Ainscough, A. M. Brodie, J. E. Plowman, S. J. Bloor, J. S. Loehr and T. M. Loehr, *Biochemistry* 1980, **19**, 4072.
13. B. F. Anderson, H. M. Baker, E. J. Dodson, G. E. Norris, S. V. Rumball, J. M. Waters and E. N. Baker, *Proc. Natl. Acad. Sci.* 1987, **84**, 1769.
14. E. W. Ainscough, A. M. Brodie, J. E. Plowman, K. L. Brown, A. W. Addison and A. R. Gainsford, *Inorg. Chem.* 1980, **19**, 3655.
15. P. Aisen and A. Leibman, *Biochim. Biophys. Acta* 1972, **257**, 314.
16. K. Spartalian and W. T. Oosterhuis, *J. Chem. Phys.* 1973, **59**, 617.
17. J. Laidriere, R. Coussement and B. Theuwissen, *J. Phys. (Paris), Colloq.* 1974, 351.
18. R. D. Dowsing and J. F. Gibson, *J. Chem. Phys.* 1969, **50**, 294.
19. F. A. Cotton and G. Wilkinson, *Advanced Inorganic Chemistry*, 5th edn, pp. 769–771. Wiley, Chichester (1988).

Polyhedron Vol. 9, No. 13, pp. 1603–1608, 1990
Printed in Great Britain

0277–5387/90 $3.00+.00
© 1990 Pergamon Press plc

AN ELECTRON DIFFRACTION STUDY OF GASEOUS BIS(PENTAN-2,4-DIONATO)OXOVANADIUM(IV), $VO(CH_3COCHCOCH_3)_2$

GEORGE A. FORSYTH and DAVID A. RICE*

The Department of Chemistry, University of Reading, Whiteknights, P.O. Box 224, Reading RG6 2AD, U.K.

and

KOLBJØRN HAGEN

The Department of Chemistry, The University of Trondheim, Trondheim N-7055, Norway

(*Received* 2 *November* 1989; *accepted* 21 *March* 1990)

Abstract—The structure of bis(pentan-2,4-dionato)oxovanadium(IV), $VO(CH_3COCHCOCH_3)_2$, has been determined by gas-phase electron diffraction. Gaseous $VO(CH_3COCHCOCH_3)_2$ has C_{2v} symmetry with the vanadium atom terminally bound to one oxygen atom along the two-fold axis $\{r_\alpha[V{=}O(5)] = 1.565(17)$ Å$\}$ and four further oxygen atoms $\{r_\alpha[V{-}O(1)] = 1.990(6)$ Å$\}$ from two chelating $CH_3COCHCOCH_3$ groups. The angle $\angle_\alpha$ O(5)=V—O(1) is 105.1(13)° while the bite angle subtended by the ligands [i.e. $\angle_\alpha$ O(1)—V—O(2)] is 87.2(15)°. The ligand distances in the VOCCHCO ring are $r_\alpha[C(1){-}O(1)] = 1.271(8)$ Å, and $r_\alpha[C(1){-}C(2)] = 1.410(10)$ Å. In contrast to results obtained in the solid state, no evidence was obtained to indicate that the plane of the chelating moiety of the ligand was not co-planar with its associated O(1)—V—O(2) plane. Errors quoted are 2σ including estimates of systematic errors and correlation in the experimental data.

β-Diketonate complexes of the transition metals have, for coordination complexes, quite remarkably high thermal stability and volatility. Thus it has proved possible to use these complexes to separate metals by gas-chromatography.[1]

Numerous single crystal X-ray studies of β-diketonate complexes have been published and $VO(CH_3COCHCOCH_3)_2$ is the subject of two of the reports.[2,3] The first study yielded[2] a value of 1.56(4) Å for the V—O multiple bond. This value is much shorter than that observed in $VO(PhCOCHCOCH_3)_2$ [1.605(10) Å],[4] which is surprising as the dimensions of the VOCCHCO ring are the same in both compounds. The difference between the two values prompted an anisotropic refinement of the original X-ray data for $VO(CH_3COCHCOCH_3)_2$:[3] the accuracy of the value for the V—O multiple bond increased but the value remained statistically the same [1.571(20) Å]. Bond length values for related V—O multiple bonds cover a wide range [e.g. 1.584(10) Å in $VOCl_2(OPPh_3)_2$[5] to 1.620(12) Å in $(NH_4)_2VO(NCS)_4 \cdot 5H_2O$[6]] with the majority of the values being towards the higher end of the range. It was decided to determine the gas-phase structure of $VO(CH_3COCHCOCH_3)_2$ and so obtain an accurate value for the V—O multiple bond to ascertain if the value from the X-ray studies was influened by crystal packing forces.

In a number of the structural studies of β-diketonate complexes a non-zero value has been reported for the angle between the plane formed by the atoms of the ligand that form part of the chelate ring (i.e. OCCHCO) and that formed by the O—M—O fragment (M = metal ion). While it is possible that in the solid state packing forces may

* Author to whom correspondence should be addressed.

cause an angle between the two planes, it is questionable if such a deviation can be detected in the gas phase. Such an interplanar angle has been included, as a parameter, in a number of gas-phase electron diffraction studies,[7,8] but in our recent structural studies of gaseous $Cu\{S_2CN(CH_3)_2\}_2$ and $Zn\{S_2CN(CH_3)_2\}_2$[9] we found no advantage accrued from the inclusion of the angle between the CS_2 and MS_2 planes as a variable. A study by gas-phase electron diffraction of $VO(CH_3COCHCOCH_3)_2$ provides an ideal case for judging the relevance of inclusion of the angle between the OCCHCO and MO_2 planes as a parameter. The presence of the V—O multiple bond is expected to produce an angle greater than 90° between the V—O multiple and other V—O bonds, and so it is probable that the two $CH_3COCHCOCH_3$ fragments will be brought closer together than in, for example, $Cu(CH_3COCHCOCH_3)_2$[8] and thus increases the chances of observing a non-zero angle between the OCCHCO and MO_2 planes in $VO(CH_3COCHCOCH_3)_2$.

EXPERIMENTAL

Preparation of $VO(CH_3COCHCOCH_3)_2$

A slurry of V_2O_5 (5.0 g) in a mixture of water (12.0 cm^3), ethanol (25.0 cm^3) and concentrated sulphuric acid (9.0 cm^3) was heated under reflux for 1 h. The resulting blue precipitate was isolated by filtration and treated with an excess of pentan-2,4-dione. To the mixture was added dropwise a solution, formed by dissolving anhydrous Na_2CO_3 (20.0 g) in water (125.0 cm^3). Blue crystals of $VO(CH_3COCHCOCH_3)_2$ formed and these were isolated by filtration and recrystallized from $CHCl_3$.

Electron diffraction photographs were obtained using the Reading University apparatus,[10] which is fitted with a rotating sector whose angular opening is proportional to r^3. The nozzle-to-plate distances were 494.11 and 244.52 mm and the data were obtained with the nozzle in the temperature range 222–239°C. The electron wavelength (0.061781 Å) was calibrated against diffraction pictures of benzene.[11] Three plates from the long and four from the short camera distance were selected for use in the final analysis and were traced on the Joyce–Loebel microdensitometer at the Chemistry Department of the University of Oslo. The usable data, interpolated at intervals of $\Delta s = 0.25$ Å^{-1}, spanned the ranges $2.50 \leqslant s \leqslant 13.50$ Å^{-1} and $8.00 \leqslant s \leqslant 29.00$ Å^{-1}. The experimental data were processed as described previously[12] with scattering factors being taken from refs 13 and 14. Average curves were produced for each camera distance, and these are depicted in Fig. 1. Root-mean-square vibrational amplitudes (l), perpendicular amplitude corrections (K) and centrifugal distortions (δr) were calculated[15] from an assumed valence force-field using values for the force constants obtained for related molecules.[16] As a complete analysis of the vibrational spectra of $VO(CH_3COCHCOCH_3)_2$ has not been published, the calculated values must be regarded as approximate.

Analysis of the structure

The refinements of the structure were based upon the molecule depicted in Fig. 1, which contains the atom numbering scheme.

In the analysis of the structure the following assumptions were made:

(1) The molecule possesses C_{2v} symmetry.
(2) All the carbon and oxygen atoms in each of the $CH_3COCHCOCH_3$ fragments lie in a plane that has C_{2v} symmetry.
(3) The methyl groups have C_{3v} symmetry with the axis of symmetry lying along the Me—C bond.
(4) The hydrogen atoms of one methyl group are eclipsed with respect to those on the other methyl group of the same ligand.

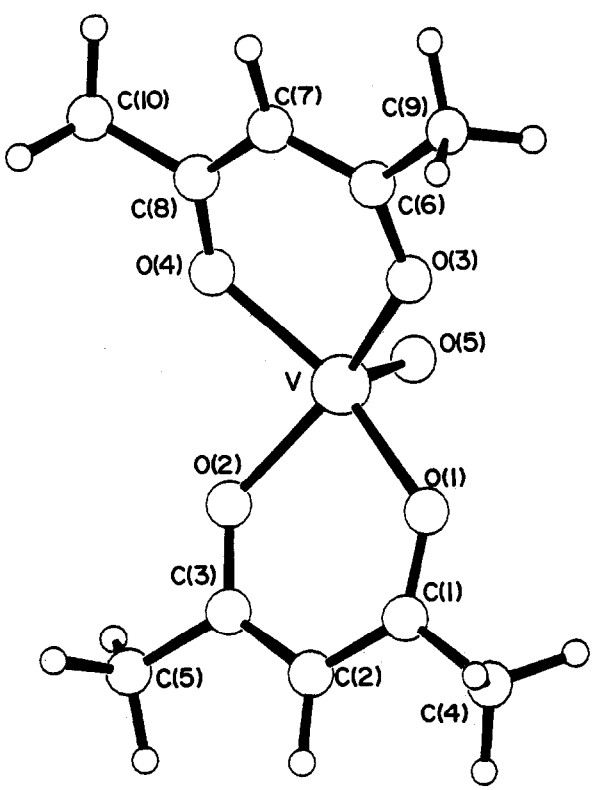

Fig. 1. The $VO(CH_3COCHCOCH_3)_2$ molecule with the atom numbering scheme.

(5) All the C—H bonds are of the same length.
(6) The hydrogen atom of the C(2)—H group lies in the plane of the O(1)C(1)C(2)C(3)O(2) moiety.

Using these assumptions a geometrical model was constructed which initially had 12 independent structural parameters that consisted of six distances {r[V—O(5)], r[V—O(1)], r[C(1)—O(1)], r[C(1)—C(2)], r[C(1)—C(4)] and r(C—H)}, five valence angles [$\angle$O(1)—V—O(2), $\angle$V—O(1)—C(1), $\angle$O(1)—C(1)—C(4), $\angle$C(1)—C(4)—H and $\angle$O(5)—V—C(2)] and a torsion angle, θ_1, to describe the position of the hydrogen atoms of the methyl groups with respect to the ligand skeleton. If $\theta_1 = 0°$, one of the hydrogen atoms on the methyl group bound to C(1) is eclipsed with respect to the C(1)—O(1) vector. At a later stage a further variable, θ_2, the angle between the VO(1)O(2) and O(1)C(1)C(2)C(3)O(2) planes was included as a variable. The model differs from that used by previous workers in that r(C—H) and $\angle$C(1)—C(4)—H were included as variables rather than being fixed at 1.10 Å and 110.0°, respectively.[7,8]

Refinements of the structure were carried out by the least-squares procedure based on the intensity curves by adjusting one theoretical curve to the two averaged experimental curves (one from each nozzle-to-plate distance) using a unit weight matrix. The average experimental and the theoretical curves are shown in Fig. 2. The radial distribution (RD) curve calculated in the usual manner by Fourier transformation of the $s[I_m(s)]$ values after multiplication by $(Z_V Z_O / f_V f_O)\exp(-0.0025s^2)$, is shown in Fig. 3, together with the appropriate difference curve.

In the early refinements θ_1 was set at zero, all the bonded distances and valence angles were refined, as were the vibrational amplitudes of all the bonded interactions. Of the non-bonded interactions only those thought to be most influential were refined, i.e. those involving the metal atom, l(C···C), l(C···O) and l(O···O) (see Table 1). In general all the amplitudes involving hydrogen atoms were held at calculated values. The results of these early refinements gave a good fit between the experimental and theoretical curves. After the initial study, in an effort to improve the fit, θ_1 was allowed to refine. The value it assumed was not significantly different from zero as the standard error was larger than the value of the parameter. Accordingly, further refinements were carried out in which all the variables, except θ_1, were allowed to refine, while θ_1 was varied in a stepwise manner over the interval $0 < \theta_1 < 120°$. The R factors for both short and long camera data were recorded as a function of θ_1. There was little variation in R factor with θ_1, however, such maximum value as there was occurred at 60° while the minimum was at 0°. Consequently θ_1 was kept at 0° in all further

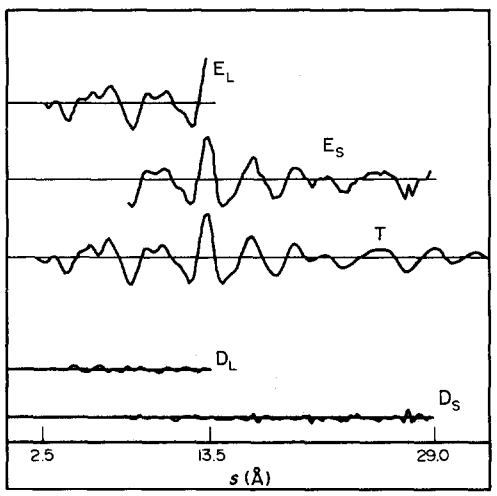

Fig. 2. Intensity curves $sI_m(s)$ for $VO(CH_3COCHCOCH_3)_2$. Experimental curves (E) are averages of all the data from the plates for the two camera distances. The theoretical curves (T) were calculated from the structural parameters shown in Table 1. The difference curves (D) result from subtracting the relevant part of the theory curve from the experimental curves.

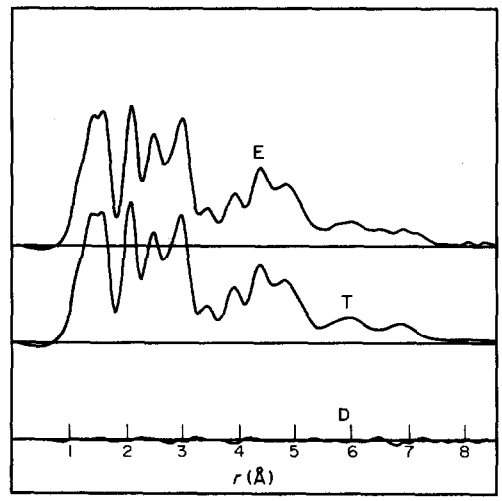

Fig. 3. Radial distribution curves for $VO(CH_3COCHCOCH_3)_2$ showing the experimental (E), and theoretical (T) and difference (D) curves. The radial distribution curves were calculated in the usual manner using the theoretical curves that yielded the data contained in Table 1. To obtain the radial distribution curves the theoretical curves were multiplied by $(Z_V Z_O / f_V f_O)\exp(-0.0025s^2)$ before carrying out the Fourier transformation. Theoretical data were used for the unobserved area $s \leqslant 2.50$ Å^{-1}.

Table 1. Final structural parameters for $VO(CH_3COCHCOCH_3)_2$[a]

Parameter	r_g	r_α	l_{ref}	l_{calc}	X-ray data[b]
		Independent variables			
r[V—O(5)]	1.586(17)	1.565(17)	0.0375(6)	0.0416	1.571(20)
r[V—O(1)]	2.005(6)	1.990(6)	0.0631(1)	0.0629	1.969(16)
r[C(1)—O(1)]	1.293(8)	1.273(8)	0.0504(2)	0.0437	1.280(28)
r[C(1)—C(2)]	1.425(10)	1.410(10)	0.0457(5)	0.0462	1.400(32)
r[C(1)—C(4)]	1.547(14)	1.518(14)	0.0498(5)	0.0483	1.515(32)
r(C—H)	1.100(18)	1.052(18)	0.0615(15)	0.0779	Not determined
∠O(1)—V—O(2)		87.2(15)			87.6(6)
∠O(1)—V—O(3)		85.0(16)			
∠O(5)—V—C(2)		111.5(24)			Not determined
∠V—O(1)—C(1)		129.6(14)			129.2(14)
∠O(1)—C(1)—C(4)		112.7(15)			115.7(20)
∠C(1)—C(4)—H		105.4(56)			Not determined
$\angle\theta_1$[c]		0.0			Not determined
$\angle\theta_2$[c]		0.0			10.9 (calc. mean)
		Selected dependent distances and angles			
∠O(5)—V—O(1)		105.1(13)			106.2(4)
r[O(1)···O(2)]	2.763(31)	2.746(31)	0.1208(40)	0.1407	
r[O(1)···O(3)]	2.703(31)	2.688(33)	0.1449(74)	0.2155	
r[C(1)···C(3)]	2.480(24)	2.462(24)	0.0885(42)	0.0722	
r[C(2)···C(4)]	2.558(21)	2.558(21)	0.1042(50)	0.0731	
r[V···C(1)]	2.983(13)	2.973(13)	0.0811(4)	0.0878	
r[V···C(2)]	3.393(18)	3.393(18)	0.0838(7)	0.1248	
r[V···C(4)]	4.314(12)	4.290(12)	0.0746(5)	0.0854	
		R value[d]			
		0.12			

[a] Distances (r_α and r_g) and amplitudes (l) in Ångstroms, and angles ($\angle_\alpha$) in degrees. Parenthesized uncertainties are 2σ and, for the electron diffraction data, include estimates of systematic errors and correlation in the experimental data.

[b] Data taken from ref. 3.

[c] θ_1 Describes the position of the hydrogen atoms of the methyl groups with respect to the ligand skeleton. If $\theta_1 = 0°$ one of the hydrogen atoms on the methyl group bound to C(1) is eclipsed with respect to the C(1)—O(1) vector. θ_2 Is the angle between the VO(1)O(2) and O(1)C(1)C(2)C(3)O(2) planes.

[d] $R = [\Sigma w_i\Delta_i^2/\Sigma w_i[s_iI_i(\text{obs.})]^2]^{1/2}$, where $\Delta_i = s_iI_i(\text{obs.}) - s_iI_i(\text{calc.})$.

refinements. With θ_1 fixed at 0°, θ_2, the angle between the VO(1)O(2) and O(1)C(1)C(2)C(3)O(2) planes, was included as a variable. Allowing it to refine led to a value of 4.9(11.2)° for θ_2, while the values for the remaining parameters were unchanged from the values obtained with θ_1 and θ_2 at 0°. Refinements were also carried out in which θ_2 was varied stepwise in a similar manner to that described above for θ_1. The range used for θ_2 was $-4 < \theta_2 < 10°$. The resulting R factors showed no significant change although there was an extremely shallow minimum in the region 0–5°. There was no significant change in the other variables with θ_2.

The results of the final refinement with θ_1 and θ_2 set at 0°, are recorded in Table 1. A correlation matrix (Table 2) which highlights the interdependence of distances and/or angles was obtained by fixing the vibrational amplitudes at the values obtained from the final refinement, having θ_1 and θ_2 set at 0° and allowing the other parameters to refine.

RESULTS AND DISCUSSION

The results of the present study are in accord with gaseous $VO(CH_3COCHCOCH_3)_2$ having C_{2v}

Table 2. Correlation matrix (×100) for $VO(CH_3COCHCOCH_3)_2$

Parameter	σ^a	r_1	r_2	r_3	r_4	r_5	r_6	$\angle_1$	$\angle_2$	$\angle_3$	$\angle_4$	$\angle_5$
r[V—O(5)]	0.44	100	4	5	47	−54	−7	10	4	16	14	−22
r[V—O(1)]	0.15		100	−6	−9	−12	−4	14	−32	0	26	−10
r[C(1)—O(1)]	0.19			100	21	−14	37	36	−19	−24	20	21
r[C(1)—C(2)]	0.25				100	−5	5	23	5	−10	26	−19
r[C(1)—C(4)]	0.35					100	−5	−11	4	−38	−6	19
r(C—H)	0.46						100	12	−5	0	−6	−6
∠O(1)—V—O(2)	38							100	−89	3	25	−40
∠V—O(1)—C(1)	35								100	10	−18	30
∠O(1)—C(1)—C(4)	37									100	−1	−24
∠C(1)—C(4)—H[b]	140										100	−27
∠O(5)—V—C(1)	35											100

[a] σ Taken from least-squares refinement.

[b] H is one of the three hydrogen atoms bound to C(4).

symmetry. Inspection of the correlation matrix (see Table 2) reveals that r[V—O(5)] and r [C(1)—C(4)] are highly correlated. Both distances occur under the same broad peak in the radial distribution curve (see Fig. 3) and since $Z_V Z_O / r_{VO(5)}$ has a very similar value to $4 \times Z_C Z_C / r_{C(1)C(4)}$ the errors associated with r[V—O(5)] and r[C(1)—C(4)] are quite large. Even so, the value determined for r[V—O(5)] (1.565(17) Å) is in good agreement with that obtained from the X-ray study (1.571(20) Å)[3] and should be compared with the V—O multiple bond distance found in $VO(PhCOCHCOCH_3)_2$ (1.605(10) Å).[4] The dimensions of the ligand part of the chelate rings, i.e. O(1)C(1)C(2)C(3)O(2), and the "bite" angles found in the present study are the same as those found from the X-ray studies of $VO(PhCOCHCOCH_3)_2$[4] and $VO(CH_3COCHCOCH_3)_2$[3] (see Table 1); however, the V—O distances in the chelate ring determined in the present structure {r[V—O(1)] = 1.990(6) Å} are longer than those found from the X-ray studies [1.969(16)].[3]

From the discussion given above it is clear that there is little change in the bonded distances with change in phase (see Table 1). An apparent difference appears to be in the value of the angle between the VO(1)O(2) and O(1)C(1)C(2)C(3)O(2) planes, i.e. θ_2, which was set at 0° in the present study (see section devoted to the analysis of the structure for the discussion relating to θ_2, where a value of 4.9(11.2)° was reported), while in the solid state a value of 10.9° was obtained but noticeably no error value was given (see Table 1). The failure to include an error value precludes a detailed comparison of the two values obtained for θ_2. These two values give rise to an apparent difference in the angles between the two ligand planes which is 145° in the present structure and 163° in the solid state. However, as we have shown that the analysis of the electron diffraction data is largely insensitive to small variations in the value of θ_2, we believe that the inclusion of θ_2 as an extra parameter is not justified as its inclusion only leads to a very slight improvement in the R factor. When values for θ_2 much greater than zero were included in refinement (e.g. 20°), noticeably large deviations between the experimental and theoretical RD curves occurred in the outer regions.

The carbon–carbon distance in the ring {r[C(1)—C(2)] = 1.410(10) Å} is comparable to the carbon–carbon distance in benzene[11] (1.395(2) Å) but longer than that in ethene[17] (1.335(4) Å). The carbon–oxygen distances {r[C(1)—O(1)] = 1.271(10) Å} are longer than those in propanone (1.210(4) Å)[18] and methanol (1.207(6) Å),[19] which are double bonds, but shorter than those in diethyl ether (1.415(1) Å)[20] and tetrahydrofuran (1.428(2) Å),[21,22] which are ordinary single bonds. The $CH_3COCHCOCH_3$ anion is usually depicted as having a delocalized charge over the OCCCO chain. However, in $VO(CH_3COCHCOCH_2)_2$ the possibility of further delocalization around the six-membered VOCCHCO rings can be envisaged as the rings are planar (i.e. $\theta_2 = 0°$), the metal ion has empty d orbitals of suitable symmetry to take part in π-bonding in the ring and there are six electrons available for π-bonding. The occurrence of this delocalization around the ring is in accord with the distances observed.

Acknowledgements—We thank Mrs Snefrid Gundersen of the University of Oslo for tracing the plates, the SERC

for support (G.A.F.), and NATO for the award of a travel grant No. 117/82 (K.H. and D.A.R.).

REFERENCES

1. W. R. Wolf, M. L. Taylor, B. M. Hughes, T. O. Tierman and R. E. Sievers, *Analyt. Chem.* 1972, **44**, 616.
2. R. P. Dodge, D. H. Templeton and A. Zalkin, *J. Chem. Phys.* 1961, **35**, 55.
3. P-K. Hon, R. L. Belford and C. E. Pfluger, *J. Chem. Phys.* 1965, **43**, 3111.
4. P-K. Hon, R. L. Belford and C. E. Pfluger, *J. Chem. Phys.* 1965, **43**, 1323.
5. M. R. Caira and B. J. Gellatly, *Acta Cryst.* 1980, **36B**, 1198.
6. A. C. Hazell, *J. Chem. Soc.* 1963, 5745.
7. S. Shibata and M. Ohta, *J. Molec. Struct.* 1981, **77**, 265.
8. S. Shibata, T. Sasase and M. Ohta, *J. Molec. Struct.* 1983, **96**, 347.
9. K. Hagen, C. J. Howill and D. A. Rice, *Inorg. Chem.* 1989, **28**, 3239.
10. C. J. Howill, PhD thesis, University of Reading, U.K. (1987).
11. K. Tamagawa, T. Iijima and M. Kimura, *J. Molec. Struct.* 1976, **30**, 243.
12. K. Hagen, R. J. Hobson, C. J. Howill and D. A. Rice, *Inorg. Chem.* 1986, **25**, 3659.
13. *International Tables for X-ray Crystallography.* Kynoch Press, Birmingham, U.K. (1974).
14. H. L. Sellers, L. Schäfer and R. A. Bonham, *J. Molec. Struct.* 1978, **49**, 125.
15. R. L. Hildebrandt and J. D. Weiser, *J. Chem. Phys.* 1971, **55**, 4648.
16. B. G. Thomas, M. L. Morris and R. L. Hilderbrandt, *J. Molec. Struct.* 1976, **35**, 241.
17. K. Kuchitsu, *J. Chem. Phys.* 1966, **44**, 906.
18. T. Iijima, *Bull. Chem. Soc. Jpn* 1972, **45**, 3526.
19. T. Iijima and S. Tsuchiya, *J. Molec. Struct.* 1972, **44**, 88.
20. K. Tamagawa, M. Takemura, S. Konaka and M. Kimura, *J. Molec. Struct.* 1984, **125**, 131.
21. H. J. Geise, W. J. Adams and L. S. Bartell, *Tetrahedron* 1969, **25**, 3045.
22. A. Almemingen, H. M. Seip and T. Willadsen, *Acta Chem. Scand.* 1969, **23**, 2748.

Polyhedron Vol. 9, No. 13, pp. 1609–1612, 1990
Printed in Great Britain

0277-5387/90 $3.00+.00
© 1990 Pergamon Press plc

SYNTHESIS AND COPPER-63 NMR STUDIES OF COPPER(I) STIBINE COMPLEXES

A. HETHERINGTON, W. LEVASON* and M. D. SPICER

Department of Chemistry, The University, Southampton SO9 5NH, U.K.

(*Received* 15 *December* 1989; *accepted* 26 *March* 1990)

Abstract—The copper(I) stibine complexes $[CuL_4]BF_4$ (L = $SbPh_3$, $SbEt_3$, $SbMe_3$; L_2 = $Me_2Sb(CH_2)_3SbMe_2$, $Ph_2Sb(CH_2)_3SbPh_2$) as well as $[Cu(PMe_3)_4]BF_4$ and $[Cu(AsMe_3)_4]BF_4$ have been prepared from $[Cu(MeCN)_4]BF_4$ and the appropriate ligand. They have been characterized by analysis and IR spectroscopy. ^{63}Cu and ^{31}P NMR data are reported.

Copper(I) complexes of phosphine and arsine ligands are well known and readily prepared from the appropriate copper(I) salt and the ligand, or by reduction of a copper(II) salt with excess ligand.[1,2] Complexes with Cu–ligand ratios varying from 1 : 1 to 1 : 4 can be isolated in many cases, and in solution complex equilibria are usually present due to the lability of the d^{10} ion.[3] Further interest attaches to copper(I) complexes in that they are diamagnetic and contain two relatively sensitive NMR nuclei, ^{63}Cu and ^{65}Cu. However, both are quadrupolar ($I = 3/2$) and only in a limited number of cases where the metal environment approaches cubic symmetry are the lines sharp enough to be observed.[4] Due to this fast relaxation and also to rapid ligand exchange in solution, few copper NMR resonances have been observed from group 15 donor ligand complexes. Examples include the phosphites, phosphonites and phosphinites $[Cu\{P(OR)_{3-n}R_n\}_4]^+$ ($n = 0$, 1, 2)[5,6] and $[Cu(Ph_2PCH_2CH_2PEt_2)_2]^+$.[7] Here we report a number of stibine complexes and their spectroscopic characterization including ^{63}Cu NMR data.

EXPERIMENTAL

Physical measurements were made as described previously.[8] ^{63}Cu NMR spectra were recorded on a Bruker AM 360 spectrometer operating at 95.5 MHz, and are referenced to a solution of $[Cu(MeCN)_4]BF_4$ in MeCN ($\delta = 0$), with shifts reported using the high frequency positive convention.

$[Cu(MeCN)_4]BF_4$ was prepared by an adaption of the method of Kubas.[9] A suspension of Cu_2O (4 g) in acetonitrile (80 cm^3) was treated with 40% aqueous HBF_4, with cooling to maintain the temperature at *ca* 20°C. The unreacted Cu_2O was filtered off, and the pale blue filtrate refrigerated for 48 h. The white, crystalline product was filtered off, washed with diethyl ether and dried *in vacuo*. Yield 65%.

All the complexes were made by the same general method, and all manipulations and reactions were carried out under a dinitrogen atmosphere. A typical preparation is described below.

Preparation of $[Cu(SbEt_3)_4]BF_4$

$[Cu(MeCN)_4]BF_4$ (0.21 g, 0.67 mmol) was dissolved in MeCN (5 cm^3) and the ligand (0.565 g, 2.7 mmol) added dropwise with vigorous stirring. The solvent was removed *in vacuo* and the resulting solid washed with diethyl ether and vacuum dried. Found: C, 33.1; H, 6.8. Calc. for $C_{24}H_{60}BCuF_4Sb_4$: C, 33.0; H, 6.9%.

$[Cu(SbMe_3)_4]BF_4$, Found: C, 17.4; H, 4.5. Calc. for $C_{12}H_{36}BCuF_4Sb_4$: C, 17.6; H, 4.4%.

$[Cu(SbPh_3)_4]BF_4$, Found: C; 56.5; H, 3.9. Calc. for $C_{72}H_{60}BCuF_4Sb_4$: C, 55.3; H, 3.9%.

$[Cu(Me_2Sb(CH_2)_3SbMe_2)_2]BF_4$, Found: C, 19.9; H, 4.4. Calc. for $C_{14}H_{36}BCuF_4Sb_4$: C, 20.0; H, 4.3%.

$[Cu(Ph_2Sb(CH_2)_3SbPh_2)_2]BF_4$, Found: C, 48.6; H, 4.0. Calc. for $C_{54}H_{52}BCuF_4Sb_4$: C, 48.4; H, 3.9%.

$[Cu(AsMe_3)_4]BF_4$, Found: C, 22.9; H, 6.0. Calc. for $C_{12}H_{36}As_4BCuF_4$: C, 22.9; H, 5.8%.

* Author to whom correspondence should be addressed.

$[Cu(PMe_3)_4]BF_4$, Found: C, 32.3; H, 8.1. Calc. for $C_{12}H_{36}BCuF_4P_4$: C, 31.7; H, 8.0%.

RESULTS AND DISCUSSION

The colourless or white $[Cu(SbR_3)_4]BF_4$ (R = Me, Et, or Ph) and $[Cu(R_2Sb(CH_2)_3SbR_2)_2]BF_4$ (R = Me or Ph) complexes were readily obtained by reaction of $[Cu(MeCN)_4]BF_4$ and the appropriate ligand in MeCN under nitrogen. The $SbPh_3$ complex has been reported previously[10] and $[Cu(SbPh_3)_4]ClO_4$ is also known.[11] Several attempts to prepare a $[Cu(L—L)_2]BF_4$ complex from o-$C_6H_4(SbPh_2)_2$ were unsuccessful, only greyish materials of approximate composition "$Cu_2(L—L)_3(BF_4)_2$" were obtained. The alkylstibine complexes decompose slowly in air, turning green over a few days, but the arylstibine complexes appear air-stable. The colourless $[Cu(PMe_3)_4]BF_4$ and $[Cu(AsMe_3)_4]BF_4$ complexes were made similarly, and like the alkylstibine complexes were unstable in air. All are 1:1 electrolytes in MeCN solution, and have IR spectra typical of complexes with ionic BF_4^- ions.[12]

Previous attempts to observe the ^{63}Cu NMR spectrum of $[Cu(PPh_3)_4]^+$ failed[5,6] and in this work no signals were observed from this complex nor from $[Cu(AsPh_3)_4]^+$ in CH_2Cl_2 either at room temperature or at 190 K. However, the ^{63}Cu NMR resonance of $[Cu(SbPh_3)_4]^+$ in CH_2Cl_2 solution is easily seen even at room temperature as a moderately sharp line at $\delta = -249$ ppm ($W_{1/2} = 250$ Hz). The resonance does not shift significantly on cooling the solution to 190 K and is unaffected by addition of $SbPh_3$. However, a mixture of this complex and $[Cu(MeCN)_4]^+$ in MeCN gave no resolvable resonances showing that exchange produced $[Cu(MeCN)_{4-x}(SbPh_3)_x]^+$, which undergo fast quadrupolar relaxation due to the lower symmetry environment. ^{63}Cu resonances were similarly readily recorded for $[Cu(SbMe_3)_4]^+$ and $[Cu(SbEt_3)_4]^+$ (Fig. 1). More surprisingly, the two complexes of the trimethylene backboned distibines, $[Cu(R_2Sb(CH_2)_3SbR_2)_2]BF_4$ (R = Me or Ph), also gave moderately sharp ^{63}Cu resonances. It is possible that the 3-carbon backbones of the ligands allow the donors to approach a "regular" tetrahedral arrangement, and slow the quadrupolar relaxation rate. It would be most interesting in this respect to know the Sb—Cu—Sb bond angle, but unfortunately attempts to grow crystals for an X-ray study have been unsuccessful. The crystals obtained have all been of poor quality, and deteriorated rapidly apparently due to loss of solvent when removed from the mother liquor.

Based upon these results we thought examination of the spectra of $[Cu(AsMe_3)_4]^+$, $[Cu(PMe_3)_4]^+$ and $[Cu(PEt_3)_4]^+$ worthwhile. The last showed no observable ^{63}Cu resonance, but the arsine shows a ^{63}Cu resonance at -42 ppm, whilst the ^{63}Cu and ^{31}P NMR spectra of the PMe_3 complex are shown in Fig. 2. Both clearly show well-resolved $^1J(^{63/65}Cu–^{31}P)$ coupling patterns consistent with a CuP_4 moiety, and the separate $^1J(^{63}Cu–^{31}P)$ and $^1J(^{65}Cu–^{31}P)$ couplings are just resolved upon the outer lines of the multiplet ($\gamma^{63}Cu/\gamma^{65}Cu = 0.934$).[4] Although such coupling has been observed in phosphite complexes, it is highly unusual in phosphines, indeed most copper(I) phosphines show very broad featureless ^{31}P NMR spectra, with the chemical shifts varying with concentration and the presence of free ligand, indicative of fast intermolecular

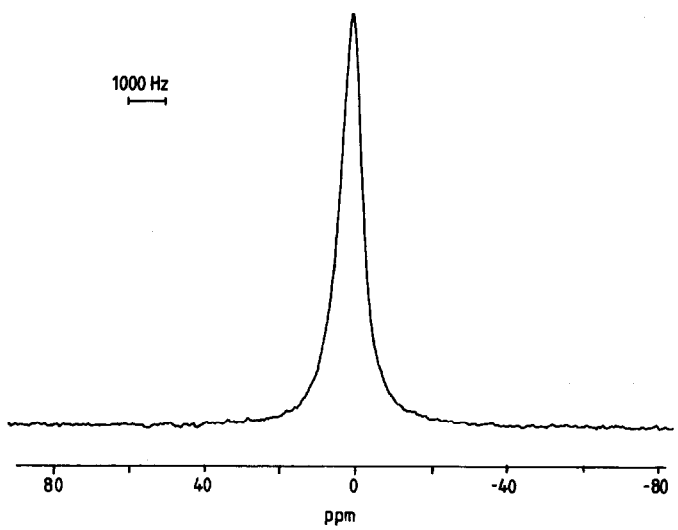

Fig. 1. ^{63}Cu NMR spectrum of $[Cu(SbEt_3)_4]BF_4$ in CH_2Cl_2/CD_2Cl_2.

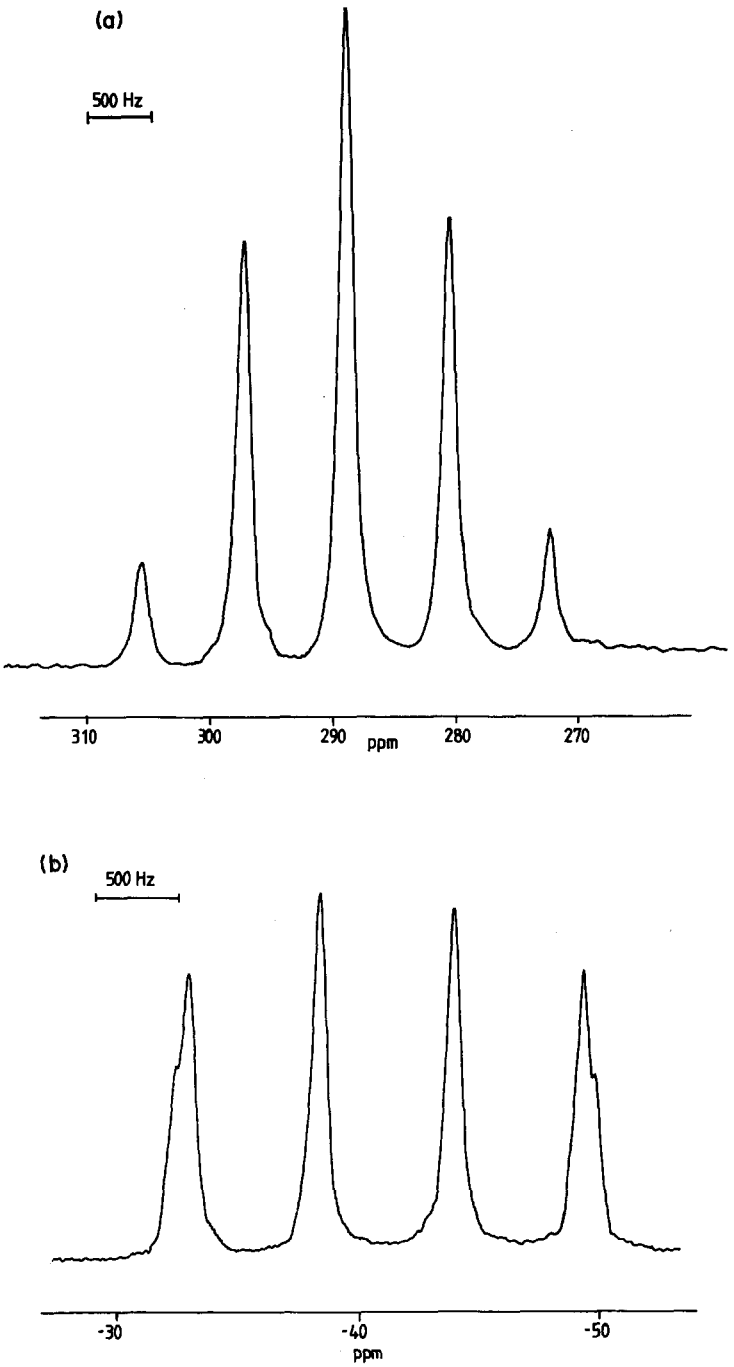

Fig. 2. (a) ^{63}Cu and (b) ^{31}P NMR spectrum of $[Cu(PMe_3)_4]BF_4$ in CH_2Cl_2/CD_2Cl_2.

exchange. Addition of PMe_3 to a solution of $[Cu(PMe_3)_4]^+$ had no effect on the resonance of the bound phosphines. The magnitude of the ^1J coupling in the phosphine complex is significantly smaller (790 Hz) than those reported for the phosphites[6] which range from *ca* 1100 to 1450 Hz. The NMR data are presented in Table 1.

Copper(I)–group 15 donor ligand bonds are believed to be of predominantly σ-type with any π-component small or absent,[13] and detailed studies both of the solid-state structures and of solution behaviour have been interpreted in terms of significant steric effects.

There is only one X-ray crystal structure of a copper(I) stibine, $[Cu(SbPh_3)_3Cl]$,[14] which shows a long Cu—Sb bond length of 2.554 Å. Based upon this structure we have calculated a cone angle for $SbPh_3$ of 127°. Comparable cone angles are PMe_3

Table 1. Selected NMR data

Complex	$\delta(^{63}Cu)$ (ppm)[a]	$W_{1/2}$ (Hz)	$\delta(^1H)$ (ppm)[b]
$[Cu(SbMe_3)_4]BF_4$	−6	180	2.1(s)
$[Cu(SbEt_3)_4]BF_4$	+1	680	2.1 (2H) 2.15 (3H)
$[Cu(SbPh_3)_4]BF_4$	−249	250	—
$[Cu(Me_2Sb(CH_2)_3SbMe_2)_2]BF_4$	−167	390	2.05 (12H) 2.6–3.1 (6H)
$[Cu(Ph_2Sb(CH_2)_3SbPh_2)_2]BF_4$	−197	1250	2.25 (6H) 7.2 (20H)
$[Cu(AsMe_3)_4]BF_4$	−42	6000	2.21(s)
$[Cu(PMe_3)_4]BF_4$	+286[c]	—	1.33(s)[d]
$[Cu\{P(OMe)_3\}_4]ClO_4$[e]	+82	166	
$[Cu\{P(OEt)_3\}_4]ClO_4$[e]	+88	137	
$[Cu(PMe_2Ph)_4]ClO_4$[e]	+247	2750	

[a] In CH_2Cl_2/CD_2Cl_2 solution, chemical shifts relative to $[Cu(MeCN)_4]^+$ in MeCN.

[b] In CD_2Cl_2 solution, chemical shifts relative to internal TMS.

[c] $^1J(^{63}Cu–^{31}P) = 790$ Hz, $^1J(^{65}Cu–^{31}P) = 830$ Hz.

[d] Broad singlet, see ref. 18 for an explanation of the lack of resolvable $^2J(PH)$ coupling.

[e] Data from ref. 6.

(118°), PPh_3 (145°) and PEt_3 (132°).[15] Using the interatomic distances from the electron diffraction data[16] on Me_3Sb and Me_3As and the Cu—Sb and Cu—As distances from $[Cu(SbPh_3)_3Cl]$ and $[\{CuCl(PhMe_2As)_2\}_2]$,[13] respectively, corresponding cone angles of 113 and 116° result. Extrapolation suggests that the cone angle of $SbEt_3$ will be $120 \pm 4°$.

It thus seems likely that one major factor in our ability to record ^{63}Cu NMR spectra for the tertiary stibine complexes could be the reduced steric interactions, and the resulting reduced tendency to dissociate ligand. The cone angles of PMe_3 and $AsMe_3$ compared with those of other phosphines which fail[6] to give ^{63}Cu resonances from their CuP_4^+ complexes support this interpretation. The X-ray structure of $[Cu(PPh_3)_4]ClO_4$ shows a crowded cation with little deviation from regular tetrahedral angles,[17] and hence the failure of this complex to give a ^{63}Cu NMR signal would seem to be more likely due to ligand dissociation in solution rather than to a distorted geometry.

Acknowledgement—We thank the SERC for support.

REFERENCES

1. C. A. McAuliffe and W. Levason, *Phosphine, Arsine and Stibine Complexes of the Transition Elements*. Elsevier, Amsterdam (1979).
2. F. H. Jardine, *Adv. Inorg. Chem. Radiochem.* 1975, **17**, 115.
3. D. J. Fife, W. M. Morse and K. W. Morse, *Inorg. Chem.* 1984, **23**, 1684, and refs therein.
4. J. Mason (Ed.), *Multinuclear NMR*. Plenum Press, New York (1987).
5. O. Lutz, H. Oehler and P. Kroneck, *Z. Naturfor.* 1978, **33A**, 1021.
6. P. Kroneck, O. Lutz, A. Nolle and H. Oehler, *Z. Naturfor.* 1980, **35A**, 221.
7. S. J. Berners-Price, C. Brevard, A. Pagelot and P. J. Sadler, *Inorg. Chem.* 1985, **24**, 596.
8. D. J. Gulliver, W. Levason, K. G. Smith, M. J. Selwood and S. G. Murray, *J. Chem. Soc., Dalton Trans.* 1980, 1872.
9. G. J. Kubas, *Inorg. Synth.* 1979, **19**, 90.
10. W. T. Reichle, *Inorg. Chim. Acta.* 1971, **5**, 325.
11. A. Bell, R. A. Walton, D. A. Edwards and M. A. Poulter, *Inorg. Chim. Acta* 1985, **104**, 171.
12. A. P. Gaughan, Z. Dori and J. A. Ibers, *Inorg. Chem.* 1974, **13**, 1657.
13. J. T. Gill, J. J. Mayerle, P. S. Welcker, D. F. Lewis, D. A. Ucko, D. J. Barton, D. Stowens and S. J. Lippard, *Inorg. Chem.* 1976, **15**, 1155.
14. A. L. Rheingold and M. E. Fountain, *J. Cryst. Molec. Struct.* 1984, **14**, 549.
15. C. A. Tolman, *Chem. Rev.* 1977, **77**, 313.
16. R. Blom, A. Haarland and R. Seip, *Acta Chem. Scand.* 1983, **A37**, 595.
17. L. M. Engelhardt, C. Pakawatchai, A. H. White and P. C. Healy, *J. Chem. Soc., Dalton Trans.* 1985, 125.
18. H. Schmidbaur, J. Adlkofer and K. Schwirten, *Chem. Ber.* 1972, **105**, 3382.

Polyhedron Vol. 9, No. 13, pp. 1613–1616, 1990
Printed in Great Britain

0277–5387/90 $3.00+.00
© 1990 Pergamon Press plc

COMMUNICATION

STRUCTURAL CHARACTERIZATION OF BIS(2,2′-BIPYRIDINE) [2-(2-PYRIDYL)PHENYL-*C,N*]RHODIUM(III) HEXAFLUOROPHOSPHATE; AN ANALOGUE OF A TRIS(2,2′-BIPYRIDINE) COMPLEX INCORPORATING A *C,N*-DONOR LIGAND

EDWIN C. CONSTABLE* and TROY A. LEESE

University Chemical Laboratory, Lensfield Road, Cambridge CB2 1EW, U.K.

and

DEREK A. TOCHER*

Department of Chemistry, University College London, 20 Gordon Street, London WC1H 0AJ, U.K.

(*Received* 15 *January* 1990; *accepted* 21 *March* 1990)

Abstract—The preparation, spectroscopic and electrochemical properties of the cyclometallated complex $[Rh(bipy)_2(ppy)][PF_6]_2$ are reported. The crystal and molecular structure of the complex are reported; the cation exhibits a six-fold disorder and closely resembles the $[Rh(bipy)_3]^{3+}$ cation.

Complexes containing 2,2′-bipyridine and related ligands have been of interest to coordination chemists for over a 100 years.[1,2] Recent interest has centred upon the redox, photochemical, photophysical and photoelectrochemical properties, with a particular view to incorporation into photoconversion and photocatalytic systems.[3] It has been found that the replacement of the N_2-donor ligand, 2,2′-bipyridine, by structurally analogous cyclometallated *C,N*-donors results in useful changes in the redox and photophysical properties of the complexes.[4] Remarkably few complexes containing a cyclometallated 2-phenylpyridine ligand have been structurally characterized,[5–7] and of these the majority refer to square-planar[5] or tellurium[6] species. In the octahedral complexes which have been characterized, substituents have been introduced onto the 2-phenylpyridine which perturb the metal–carbon interactions.[7] As part of our programme to develop synthetic methodology for the synthesis of cyclometallated compounds,[8] we have prepared and structurally characterized the complex $[Rh(bipy)_2(ppy)][PF_6]_2$ (Hppy = 2-phenylpyridine).

The reaction of $[Rh(bipy)_2(O_3SCF_3)_2][O_3SCF_3]$ with $[Hg_4(ppy)_4Cl_4]$ results in the deposition of metallic mercury and the formation of a pale pink solution from which $[Rh(bipy)_2(ppy)][PF_6]_2$ may be precipitated in 75–85% yield by the addition of $[NH_4][PF_6]$. Recrystallization from acetone resulted in the formation of X-ray quality pale pink crystals of the compound (λ_{max} 315, 304, 242 nm). The ^1H NMR spectrum of the complex in CD_3COCD_3 solution is shown in Fig. 1; assignments were made on the basis of double quantum filtered phase-sensitive COSY, TOCSY and CAMELSPIN spectra. The spectrum very closely resembles that of $[Ru(bipy)_2(ppy)]^+$ which we have reported previously,[8] although variations associated with the differences in formal charge are

* Authors to whom correspondence should be addressed.

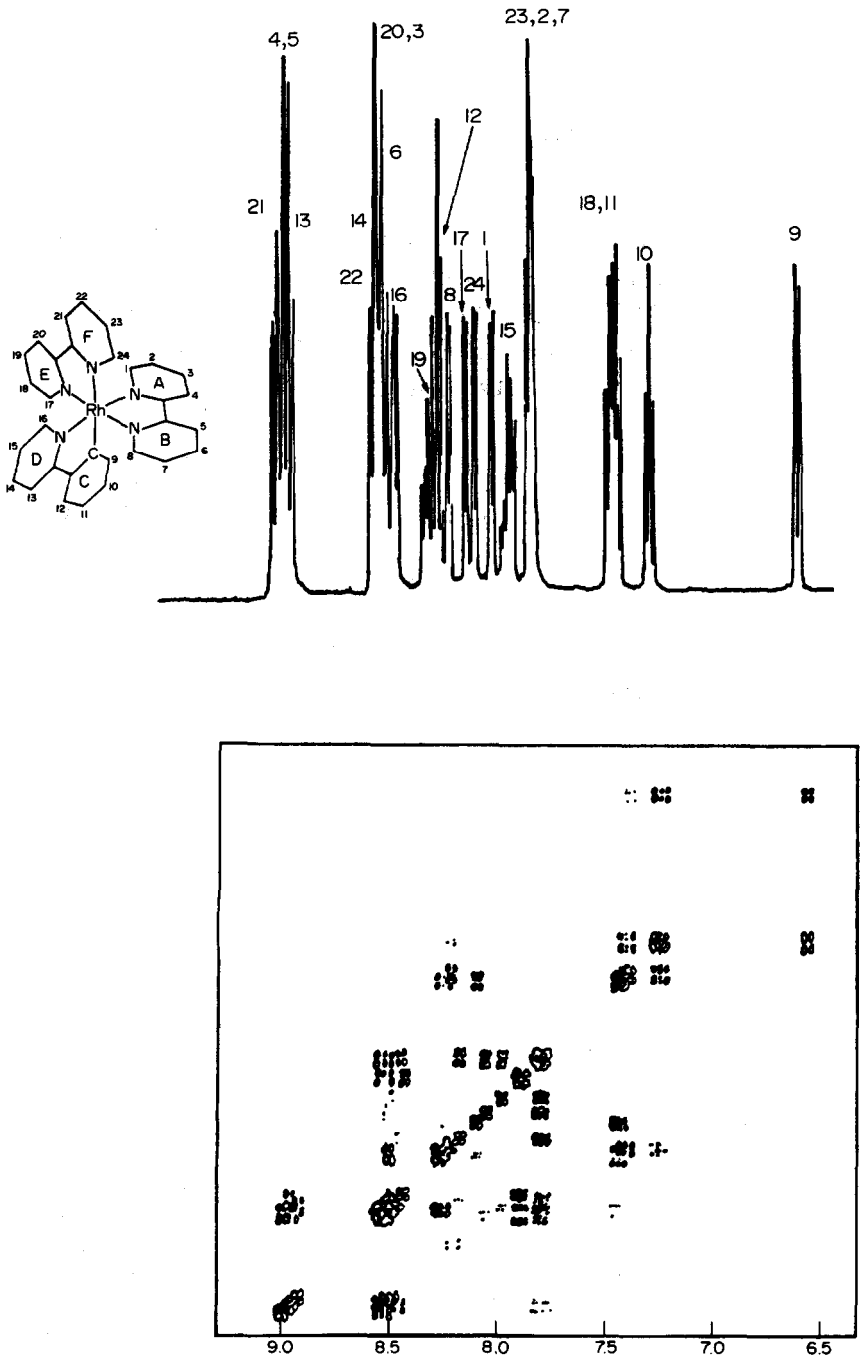

Fig. 1. 400 MHz ^{1}H NMR spectrum of $[Rh(bipy)_2(ppy)][PF_6]_2$ in CD_3COCD_3 solution showing assignments and the double quantum filtered phase-sensitive COSY spectrum used to derive connectivity.

observed.[9] The FAB mass spectrum (3-nitrobenzyl alcohol matrix) exhibited a peak at *m/z* 569 {(Rh (bipy)$_2$(ppy)]}. The complex is redox active, and the cyclic voltammogram (Fig. 2) exhibits a reversible one-electron reduction at -1.59 V (ΔE_p 70 mV, referenced to internal Fc/Fc$^+$) and a two-electron feature at -1.83 V; no variations in this feature were observed with variation of scan rate in the range 20–200 mV s^{-1}. This behaviour is in marked contrast to that of $[Rh(bipy)_3]^{3+}$ in which the first one-electron reduction occurs at -1.17 V,[10] and parallels the trend previously reported for $[Ru(bipy)_3]^{2+}$/$[Ru(bipy)_2(ppy)]^+$.[8]

The structure of the cation in $[Rh(bipy)_2$

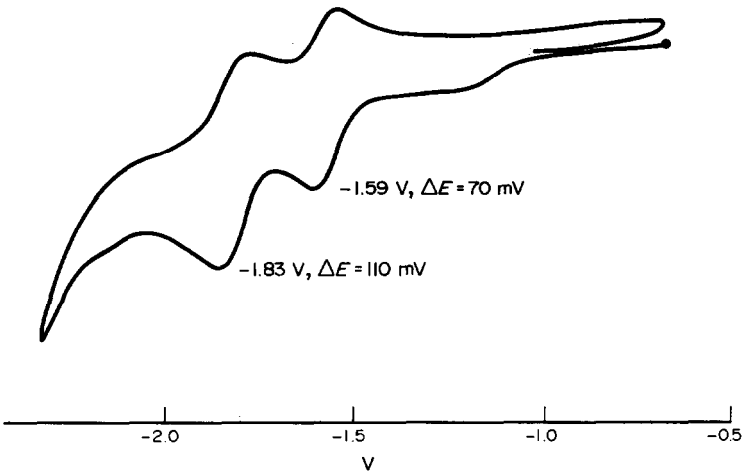

Fig. 2. Cyclic voltammogram of $[Rh(bipy)_2(ppy)][PF_6]_2$ (MeCN solution, 0.1 M[^{n}Bu$_4$N][BF_4] supporting electrolyte, referenced to internal ferrocene/ferrocinium added at the end of the experiment, scan rate 200 mV s^{-1}, room temperature).

(ppy)][PF_6]$_2$ is shown in Fig. 3, together with the numbering scheme adopted.* The cation exhibits apparent D_3 symmetry, with a six-fold crystallographic disorder associated with the phenyl and pyridyl rings. Examination of the thermal parameters associated with the donor atoms did not allow us to assign a single site to the metallated phenyl ring. However, only two $[PF_6]^-$ counterions are observed in the lattice, establishing unambiguously that the cation has a +2 charge, and hence contains the metallated ring. The final refinements were made with scattering factors for a 83.3 : 16.7 distribution of N : C for atom X. The Rh(1)—X(1) distance of 2.043(3) Å does not differ significantly from those of 2.031(8)–2.038(7),[11] 2.015[12] and 2.057 Å[12] reported in separate determinations of $[Rh(bipy)_3]^{3+}$ salts. The bite of 79.7° is typical for chelated 2,2′-bipyridine ligands.[1]

This structural determination is the first to be reported of a complex in which a 2,2′-bipyridine ligand has been replaced by a fully isostructural and isoelectronic cyclometallating ligand. The important conclusion is that such replacement has *no* significant effect upon the structure of the complex ion; in contrast, the observation of significantly different M—C and M—N distances in complexes of structurally developed ligands is an artefact introducted by their use. The useful and novel photophysical effects associated with cyclometallated 2-phenylpyridine complexes are thus a conse-

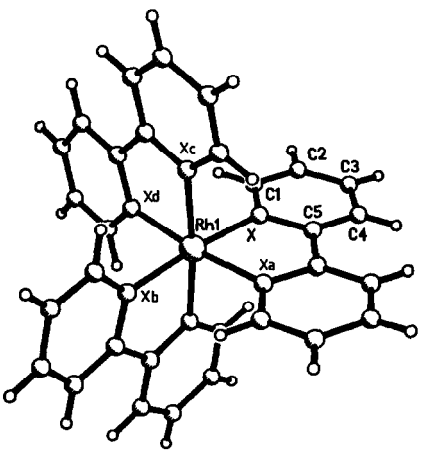

Fig. 3. The crystal and molecular structure of [Rh(bipy)$_2$(ppy)][PF_6]$_2$ showing the number scheme adopted. Selected bond lengths (Å): Rh(1)—X(1), 2.043(3); selected bond angles (°): X—Rh—Xa (chelate), 79.7(1); X—Rh—Xb (*trans*), 174.0(1); X—Rh—Xc (*cis* 1), 88.7(1); X—Rh—Xd (*cis* 2), 96.0(1).

*Crystal data: $C_{31}F_{12}H_{24}N_5P_2Rh$, pale pink blocks, crystal dimensions 0.26 × 0.26 × 0.50 mm^3, trigonal, space group $P\bar{3}c1$ (No. 165), a = 10.723(2), b = 10.723(2), c = 16.401(2) Å, γ = 120.0°, Z = 2, U = 1633.7(5) Å^3, D_c = 1.75 g cm^{-3}, D_m not measured, Mo-K_α radiation (λ = 0.71073 Å), μ(Mo-K_α) = 7.08 cm^{-1}, F(000) = 856. 11,440 reflections collected on a four-circle diffractometer to 2θ(max) 50°. The data were averaged and 907 unique reflections with $I > 3\sigma(I)$ were used in structure solution and refinement. The structure was solved by direct methods, and refined [Rh, P, F, C, N and O anisotropic; H isotropic in calculated positions] to R = 0.0378, R_w = 0.0387. Atomic coordinates, bond lengths and angles, and thermal parameters have been deposited at the Cambridge Crystallographic Data Centre.

quence of their *electronic* properties[13] rather than any gross structural change. We are currently studying the photophysical properties of $[Rh(bipy)_2(ppy)][PF_6]_2$.[14]

Acknowledgement—We should like to thank the SERC for the award of a studentship (T.A.L).

REFERENCES

1. W. R. McWhinnie and J. D. Miller, *Adv. Inorg. Chem. Radiochem.* 1969, **12**, 135; E. C. Constable, *Adv. Inorg. Chem. Radiochem.* 1989, **34**, 1.
2. E. C. Constable, *Adv. Inorg. Chem. Radiochem.* 1986, **30**, 69.
3. A. Juris, V. Balzani, F. Barigelletti, S. Campagna, P. Belser and A. von. Zelewsky, *Coord. Chem. Rev.* 1988, **84**, 85 and refs therein.
4. I. Omaw, *Organometallic Intramolecular-Coordination Compounds*, J. Organomet. Chem. Library 18, Elsevier, Amsterdam (1986) and refs cited therein; I. Omae, *Coord. Chem. Rev.* 1988, **83**, 137 and refs cited therein; E. C. Constable, *Polyhedron* 1984, **3**, 1037; E. C. Constable, *Polyhedron* 1983, **2**, 551.
5. A. Abboud, F. R. Fronczek and S. F. Watkins, *Am. Cryst. Assoc., Ser. 2* 1981, **9**, 21; L. Chassot, E. Muller and A. von Zelewsky, *Inorg. Chem.* 1984, **23**, 4249; E. C. Constable, T. A. Leese and D. A. Tocher, *J. Chem. Soc., Chem. Commun.* 1989, 570; C. Cornioley-Deuschel, T. Ward and A. von Zelewsky, *Helv. Chim. Acta* 1988, **71**, 130.
6. N. Al-Salim, A. A. West, W. R. McWhinnie and T. A. Hamor, *J. Chem. Soc., Dalton Trans.* 1988, 2363; A. A. West, W. R. McWhinnie and T. A. Hamor, *J. Organomet. Chem.* 1988, **356**, 159.
7. F. R. Fronczek, M. A. Guttierrez and J. Selbin, *Cryst. Struct. Commun.* 1982, **11**, 1119; J. M. Patrick, A. H. White, M. I. Bruce, M. J. Beatson, D. St. C. Black, G. B. Deacon and N. C. Thomas, *J. Chem. Soc., Dalton Trans.* 1983, 2121; P. Reveco, R. H. Schmehl, W. R. Cherry, F. R. Fronczek and J. Selbin, *Inorg. Chem.* 1985, **24**, 4078; M. Lavin, E. M. Holt and R. H. Crabtree, *Organometallics* 1989, **8**, 99.
8. E. C. Constable, *J. Chem. Soc., Dalton Trans.* 1985, 1719; E. C. Constable and J. M. Holmes, *J. Organomet. Chem.* 1986, **301**, 203; E. C. Constable and T. A. Leese, *J. Organomet. Chem.* 1987, **335**, 293; E. C. Constable, R. P. G. Henney and T. A. Leese, *J. Organomet. Chem.* 1989, **361**, 277; E. C. Constable, R. P. G. Henney and D. A. Tocher, *J. Chem. Soc., Chem. Commun.* 1989, 913; E. C. Constable, R. P. G. Henney, T. A. Leese and D. A. Tocher, *J. Chem. Soc., Dalton Trans.* 1990, 443; E. C. Constable, R. P. G. Henney, T. A. Leese and D. A. Tocher, *J. Chem. Soc., Chem. Commun.* 1990, 513.
9. E. C. Constable, *Polyhedron* 1989, **8**, 83.
10. M. Kirch, J-M. Lehn and J-P. Sauvage, *Helv. Chim. Acta* 1979, **62**, 1345.
11. B. Hubesch, B. Mahieu and J. Meunier-Piret, *Bull. Soc. Chim. Belg.* 1985, **94**, 685.
12. A. Hauser, K. Mader, W. T. Robinson, R. Murugesan and J. Ferguson, *Inorg. Chem.* 1987, **26**, 1331.
13. E. C. Constable and C. E. Housecroft, *Polyhedron*, in press.
14. E. C. Constable, T. A. Leese, H. Torres and R. J. Watts, unpublished results.

Polyhedron Vol. 9, No. 13, pp. 1617–1619, 1990
Printed in Great Britain

0277-5387/90 $3.00+.00
© 1990 Pergamon Press plc

COMMUNICATION

STRUCTURE AND SPECTROSCOPIC PROPERTIES OF $[(2,6\text{-}Ph_2C_6H_3O)_2Ti(\mu\text{-}Cl)_2Ti(OC_6H_3Ph_2\text{-}2,6)_2]$: EVIDENCE FOR A STRONG METAL–METAL INTERACTION

JOHN E. HILL, JOHN M. NASH, PHILLIP E. FANWICK and IAN P. ROTHWELL*

Department of Chemistry, Purdue University, West Lafayette, IN 47907, U.S.A.

(*Received* 19 *February* 1990; *accepted* 26 *April* 1990)

Abstract—The compound $[(2,6\text{-}Ph_2C_6H_3O)_2Ti(\mu\text{-}Cl)_2Ti(OC_6H_3Ph_2\text{-}2,6)_2]$ which is formed by sodium amalgam reduction of $Ti(OC_6H_3Ph_2\text{-}2,6)_2Cl_2$ ($OC_6H_3Ph_2$-2,6 = 2,6-diphenylphenoxide) contains a relatively short Ti—Ti distance of 2.9827(7) Å and acute Ti—(μ-Cl)—Ti angles of 77.79(3) and 78.05(3)°. Crystal data at −130°C: space group $P\bar{1}$; $a = 13.342(4)$, $b = 13.808(4)$, $c = 16.057(3)$ Å, $\alpha = 97.35(2)$, $\beta = 104.63(2)$, $\gamma = 91.64(2)°$, $Z = 2$; $\rho_{calc} = 1.346$ g cm^{-3}.

The last 10 years have seen dramatic developments in the chemistry of metal–metal bonded dinuclear complexes of the *d*-block elements.[1] Despite these advances there has been only limited success in the isolation and characterization of dinuclear Group 4 metal complexes containing metal–metal bonds and this area has been the focus of much recent attention.[2–4] During our studies of the low valent chemistry of titanium associated with aryloxide ligation[5] we have isolated an unusual di-titanium(III) complex which appears to contain a strong metal–metal interaction.

The reduction of the deep red dichloride $Ti(OC_6H_3Ph_2\text{-}2,6)_2Cl_2$ ($OC_6H_3Ph_2$-2,6 = 2,6-diphenylphenoxide)[6] with Na/Hg (1 Na per Ti) in toluene solution leads to the formation of a deep brown reaction mixture. Routine work-up allows the isolation of a deep purple crystalline product of composition $[(2,6\text{-}Ph_2C_6H_3O)_2Ti(\mu\text{-}Cl)_2Ti(OC_6H_3Ph_2\text{-}2,6)_2]$ (**1**).† A single crystal X-ray diffraction analysis of **1**† shows the compound to consist of a dinuclear unit with two bridging chloride atoms and four terminally bound aryloxide ligands (Fig. 1). The $Ti_2Cl_2O_4$ central core can best be described as a distorted edge-shared bis-tetrahedral structure. Several features of the structure of **1** are worthy of note. The Ti—Ti distance of 2.9827(7) Å is very short for two titanium atoms bridged by two chlorine atoms; cf. the Ti—Ti distances of 3.943(2) and 3.968(2) Å in the compound $Cp_2Ti(\mu\text{-}Cl_2)TiCp_2$.[7] Coupled with this surprisingly short distance are acute Ti—(μ-Cl)—Ti angles of 78.05(3) and 77.79(3)°. Both of these structural features indicate the presence of a strong interaction between the two d^1-metal centres. A survey of structurally characterized compounds containing a planar $Ti(\mu\text{-}Cl)_2Ti$ unit shows typical Ti—(μ-Cl)—Ti angles of 95–103° and Ti—Ti distances > 3.50 Å.[8–10] The bridging unit in compound **1** bears a striking resemblance to that found for the $[L_2Cl_2Zr(\mu\text{-}Cl)_2ZrL_2Cl_2]$ (L = phosphine) series of compounds, where Zr—Zr distances of 3.104–3.182 Å and Zr—(μ-Cl)—Zr angles of 75.4–77.4° have been taken as evidence for the presence of a zirconium–zirconium single bond.[4]

* Author to whom correspondence should be addressed.

† Found: C, 75.6; H, 4.7; Cl, 5.9. Calc. for $Ti_2Cl_2O_4C_{72}H_{52}$: C, 75.3; H, 4.6; Cl, 6.2%. Crystal data: Space group $P\bar{1}$; $a = 13.342(4)$; $b = 13.808(4)$; $c = 16.057(3)$ Å; $\alpha = 97.35(2)$; $\beta = 104.63(2)$; $\gamma = 91.64(2)°$; $Z = 2$; $\rho_{calc} = 1.346$ g cm^{-3}; 5634 unique data collected at −130°C with $I > 3\sigma(I)$ yielded $R = 0.039$, $R_w = 0.052$. Atomic coordinates, bond lengths and angles, and thermal parameters have been deposited at the Cambridge Crystallographic Data Centre.

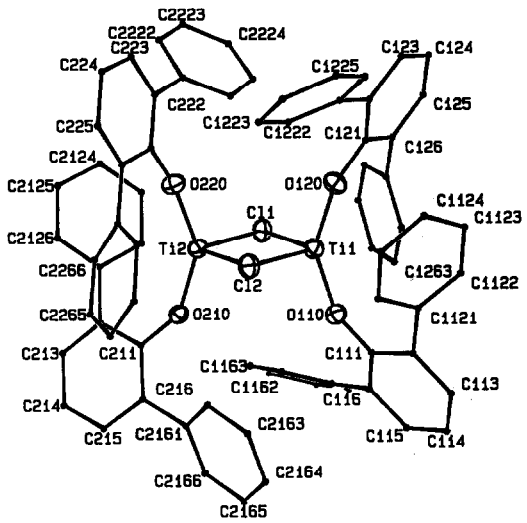

Fig. 1. ORTEP view of the molecular structure of **1** showing the numbering scheme used:

Distances (Å)

Ti(1)—Ti(2)	2.9827(7)	Ti(2)—Cl(1)	2.3712(9)
Ti(1)—Cl(1)	2.3660(9)	Ti(2)—Cl(2)	2.3743(9)
Ti(1)—Cl(2)	2.3761(9)	Ti(2)—O(210)	1.825(2)
Ti(1)—O(110)	1.820(2)	Ti(2)—O(220)	1.819(2)
Ti(1)—O(120)	1.805(2)		

Angles (°)

Cl(1)—Ti(1)—Cl(2)	102.13(3)
Cl(1)—Ti(2)—Cl(2)	102.02(3)
O(110)—Ti(1)—O(120)	144.27(9)
O(210)—Ti(2)—O(220)	144.17(9)
Ti(1)—Cl(1)—Ti(2)	78.05(3)
Ti(1)—Cl(2)—Ti(2)	77.79(3)
Ti(1)—O(110)—C(111)	153.4(2)
Ti(1)—O(120)—C(121)	152.0(2)
Ti(2)—O(210)—C(211)	146.9(2)
Ti(2)—O(220)—C(221)	155.3(2).

Further interesting features of the molecular structure of **1** are the large O—Ti—O angles of 144.17(9) and 144.27(8)° between the terminal aryloxide ligands. These large angles cannot be accounted for on steric grounds: cf. the O—Ti—O angle of 123.9(1)° in $(2,6\text{-}Ph_2C_6H_3O)_2Ti(C_6H_5)_2$.[11] A possible explanation of the opening up of this angle in **1** is based on the π-donor properties of aryloxide ligands when bound to early *d*-block metal centres.[12] The formation of a Ti—Ti σ-bond from overlap of the two d_{z^2} orbitals would be destabilized by the presence of terminal π-donor ligands in a regular edge-sharing bis-tetrahedral structure. Forcing the aryloxide ligands further out of the $Ti(\mu\text{-}Cl)_2Ti$ plane will reduce π-donation into this orbital and hence interfere less with the metal–metal interaction. An EHMO calculation on $(HO)_2Ti(\mu\text{-}Cl)_2Ti(OH)_2$ using O—Ti—O angles of 144 and 120° supports this bonding picture, clearly showing stabilization of the Ti—Ti σ-bond when this angle is increased. A further consequence of opening up the O—Ti—O angle is the presence of a considerable gap in the metal coordination sphere along the Ti—Ti axis. In compound **1** this space is occupied by two *ortho*-CH bonds of the aryloxide ligands. The distances to these groups are long, however, Ti(1)—C(1262) = 2.947(1) Å, Ti(1)—H(12621) = 2.83(1) Å and Ti(2)—C(2122) = 2.853(1) Å, Ti(2)—H(21221) = 2.84(1) Å, precluding the existence of an agostic interaction.[13] Similar close contacts have been observed for other metal derivatives of 2,6-diphenylphenoxide ligation.[14]

Solutions of **1** in hydrocarbon solvents exhibit an uninformative ^1H NMR spectrum with unresolvable resonances in the δ 6.5–7.5 ppm region. Studies using Evans' method[15] showed the solutions to be only weakly paramagnetic with $\mu_{obs} \simeq 0.5$ BM; a broad ESR signal was also observed at $g = 1.956$.

Acknowledgement—We thank the National Science Foundation for financial support of this research.

REFERENCES

1. F. A. Cotton and R. A. Walton, *Multiple Bonds Between Metal Atoms*. John Wiley, New York (1982).
2. (a) L. Messerle, *Chem. Rev.* 1988, **88**, 1229; (b) F. A. Cotton, *Polyhedron* 1987, **6**, 667.
3. (a) Y. Wielstra, S. Gambarotta, A. Meetsma and A. L. Spek, *Organometallics* 1989, **8**, 2948; (b) Y. Wielstra, S. Gambarotta, A. Meetsma and J. L. de Boer, *Organometallics* 1989, **8**, 250.
4. (a) J. H. Wengrovius, R. R. Schrock and C. S. Day, *Inorg. Chem.* 1981, **20**, 1844; (b) F. A. Cotton, M. P. Diebold and P. A. Kibala, *Inorg. Chem.* 1988, **27**, 799; (c) M. F. Lappert and A. R. Sanger, *J. Chem. Soc. A.* 1971, 874.
5. (a) L. D. Durfee, J. E. Hill, J. L. Kerschner, P. E. Fanwick and I. P. Rothwell, *Inorg. Chem.* 1989, **28**, 3095; (b) L. D. Durfee, P. E. Fanwick and I. P. Rothwell, *Angew. Chem. Int. Edn (Engl.)* 1988, **27**, 1181; (c) L. D. Durfee, P. E. Fanwick, I. P. Rothwell, K. Folting and J. C. Huffman, *J. Am. Chem. Soc.* 1987, **109**, 4720.
6. J. R. Dilworth, J. Hanich, M. Krestel, J. Beck and J. Strahle, *J. Organomet. Chem.* 1986, **315**, C9.
7. R. Jungst, D. Sekutowski, J. Davis, M. Luly and G. Stucky, *Inorg. Chem.* 1977, **16**, 1645.
8. (a) C. E. Davis, I. M. Gardiner, J. C. Green, M. L. H. Green, P. D. Grebenik, V. S. B. Mtetwa and K. Prout, *J. Chem. Soc., Dalton Trans.* 1985.

669; (b) G. J. Olthof, *J. Organomet. Chem.* 1977, **127**, 367 and refs therein.

9. The metal–metal distances in compounds containing a $M(\mu\text{-}X)_2M$ unit is highly sensitive to the nature of X and the possible presence of other bridging ligands. see: (a) L. F. Dahl, E. R. de Gil and R. D. Feltham, *J. Am. Chem. Soc.* 1969, **91**, 1653; (b) M. Mera, P. Royo, R. Serrano, M. H. Pellinghelli and A. Tirpicchio, *Organometallics* 1988, **7**, 258 and refs therein; (c) E. G. Perevalova, I. F. Urazowski, D. A. Lemonovskii, Y. L. Slovokhotos and Y. T. Struchkov, *J. Organomet. Chem.* 1985, **289**, 319; (d) L. J. Guggenberger and F. N. Tebbe, *J. Am. Chem. Soc.* 1976, **98**, 4137; (c) G. P. Pez, *J. Am. Chem. Soc.* 1976, **98**, 8072.
10. The compound $[TiCl_3(dippe)]_2$ has recently been reported to have a Ti—Ti distance of 3.438(2) Å, see A. R. Hermes and G. S. Girolani, *Inorg. Chem.* 1990, **29**, 313.
11. R. W. Chesnut, L. D. Durfee, P. E. Fanwick, I. P. Rothwell, K. Folting and J. C. Huffman, *Polyhedron* 1987, **6**, 2019.
12. (a) J. L. Kerschner, P. E. Fanwick, I. P. Rothwell and J. C. Huffman, *Inorg. Chem.* 1989, **28**, 780; (b) T. W. Coffindaffer, B. D. Steffey, I. P. Rothwell, K. Folting and J. C. Huffman, *J. Am. Chem. Soc.* 1989, **111**, 4742.
13. M. Brookhart and M. L. H. Green, *J. Organomet. Chem.* 1983, **250**, 395.
14. (a) G. D. Smith, P. E. Fanwick and I. P. Rothwell, *Inorg. Chem.* 1989, **28**, 618; (b) J. L. Kerschner, J. S. Yu, P. E. Fanwick, E. M. Torres, I. P. Rothwell and J. C. Huffman, *Organometallics* 1989, **8**, 1414.
15. D. F. Evans, *J. Chem. Soc.* 1959, 2003.

Polyhedron Vol. 9, No. 13, p. 1621, 1990
Pergamon Press plc. Printed in Great Britain

BOOK REVIEW

Reactions of Coordinated Ligands, Volume 2. Edited by P. S. Braterman, Plenum, New York, 1989, ISBN 0-306-43094-0, 414 pp., £79.20

This is the long-awaited second (and final) volume of this work describing the chemistry of coordinated ligands. The book contains five chapters discussing the reactivity of ligands which are bound to a metal through an atom other than carbon. The manuscript has been prepared in a camera-ready format, with the consequent inconsistencies between chapters by various authors. This is no real criticism, but the quality of structural diagrams varies very considerably between chapters.

The first chapter (Miller, 140 refs to 1983) discusses the chemistry of coordinated carbon dioxide. This is a well-written and interesting survey of an area of considerable interest and importance. The review is an excellent starting point for an entry into the chemistry of carbon dioxide, but the cut-off date of 1983 means that the reader will really have to look elsewhere for an up-to-date account.

The second chapter is concerned with the reaction of coordinated dinitrogen and related species (Hidai and Mizobe, 202 refs to 1985). The authors limit themselves to more recent progress and give adequate reference to previous reviews. I found this chapter particularly useful and informative, and recommend it strongly as providing a "taste" of an exciting and fast-moving area. Perhaps a small *caveat* should be issued; this review is concerned with the chemistry *not* the biochemistry of dinitrogen ligands.

The reactions of nitrosyl complexes are discussed in Chapter 3 (Bottomley, 518 refs to 1985). This is a truly excellent and useful article which must remain a key reference for anyone with a passing or all-consuming interest in nitrosyl chemistry. I was particularly impressed by the clear, readable and informative account of the plethora of reactions of nitroprusside ions, which is an area which has now been successfully demystified for me.

The penultimate chapter is an account of the hydrolysis and condensation reactions of oxygen- and nitrogen-bonded ligands (Hay, 543 refs to 1986). This is a superb discussion of the reactions of coordinated nitriles, amides and related compounds. To a newcomer to the area this is an excellent primer, whilst the comprehensive literature coverage (through 1986) provides a few gems for those who thought they knew the subject! The organization and content of this chapter is very similar to that by the same author in *Comprehensive Coordination Chemistry*. This is only to be expected, as the same material is covered, but I must confess to a preference for the typeset format of text and diagrams in *Comprehensive Coordination Chemistry*.

The final chapter concerns reactions of coordinated phosphorus and sulphur ligands (Minahan, Hill and McAuliffe, 150 refs to 1979). I found this to be the most disappointing chapter in the book. The coverage of the subject area is adequate, but the apparent cut-off at 1979 means that an entire decade's worth of extremely relevant chemistry has been omitted. The references to previous reviews are very comprehensive, but with the proviso that the literature later than 1979 is of no interest. I am sure that this is no fault of the editor or the authors, but I would have thought that the 1989 publication date would have merited an update of a chapter that was undoubtedly written much earlier. As it stands, the chapter is not a greatly helpful contribution to a very interesting area of ligand reactivity.

Overall, I liked this book. The omission of sections dealing with the reactions of heterocyclic ligands or the oxygenation and other metal-directed reactions of aromatic ligands somewhat reduce its utility in giving a general overview of the area. My main criticism concerns the cut-off dates of some of the literature coverage, but this is always unavoidable in a venture of this type. However, 10 years is a little extreme!

This book should be in all chemical libraries, and devotees of ligand reactivity will undoubtedly want their own copies. Well done to Paul Braterman and his team for a successful coverage of such a disparate area.

EDWIN C. CONSTABLE
University Chemical Laboratory
Lensfield Road
Cambridge CB2 1EW, U.K.

Polyhedron Vol. 9, No. 13, p. 1623, 1990
Pergamon Press plc. Printed in Great Britain

ANNOUNCEMENT

CALL FOR PAPERS

POLYHEDRON SYMPOSIUM-IN-PRINT

HOMOPOLYATOMIC SILICON, GERMANIUM AND TIN CHEMISTRY

Species containing bonds between Group 14 elements and their associated chemistry has been the subject of intense interest. In the last decade we have seen many exciting advances including the characterization of silenes, silaethenes, polyhedral polycyclic Group 14 compounds and network germanium polymers, new frontiers in the synthesis of strained cyclic Group 14 species and in the generation of heavy carbene analogues, and a better understanding of the properties of polysilane high polymers.

The purpose of this Symposium-in-Print is to bring together these recent advances in homopolyatomic and related chemistry of silicon, germanium and tin. Topics that are appropriate to this Symposium include synthesis, structure, reactivity, mechanistic studies, theoretical studies and properties of the title or related compounds.

The deadline for the submission of articles is 1 September 1990 and manuscripts should be mailed to Dr M. Hampden-Smith, Department of Chemistry, Clark Hall 103, University of New Mexico, Albuquerque, NM 87131, U.S.A. If you have any questions please call (505) 277-4713.

Polyhedron Vol. 9, No. 14, pp. 1625–1631, 1990
Printed in Great Britain

0277–5387/90 $3.00+.00
© 1990 Pergamon Press plc

A BONDING MODEL FOR M_3X_3 CLUSTER COMPOUNDS $M_3X_{4-n}Y_nL_9^c$ (M = Mo, W; X = O, S, Cl, Br; Y = O, S; L = TERMINAL LIGAND; $n = 0, 1$; c = CHARGE)

CHENG WENDAN,† ZHANG QIANER, HUANG JINSHUN and LU JIAXI

Fujian Institute of Research on the Structure of Matter, Chinese Academy of Sciences, Fuzhou, Fujian, 350002 China

(*Received* 30 *November* 1989; *accepted* 18 *January* 1990)

Abstract—A bonding model has been developed for *d–p* π-conjugate interactions over the M_3X_3 skeleton. The orbitals forming *d–p* π- and *d–d* interactions have been constructed, and it has been found that the *d–p* π-conjugate interaction is in competition with *d–d* interactions. The weaker the *d–d* interactions between M—M atoms, the stronger is the *d–p* π-conjugate interaction over M_3X_3 (X = O, S); the contrary relations are true over M_3X_3 (X = Cl, Br). It is believed that the *d–p* π-conjugate interaction over M_3X_3 increases on descending each of the two vertical groups, X = VIA and X = VIIA, and is stronger for a X = VIA than a X = VIIA element in the periodic table. The increase is correlated with a corresponding increase in the *d–p* π-overlap population over the M_3X_3 ring skeleton.

Incomplete transition metal cubane-type cluster compounds (ICTMCTC) having a non-planar ring skeleton, M_3X_3 (M = Mo, W; X = O, S, Cl, Br), have been an active subject[1–15] in the chemistry of molybdenum and tungsten. Some of the experimental and theoretical results in this area have been published in two recent reviews.[16,17] It has been shown that the $M_3X_4^{4+}$ (X = O, S) core is stable to substitution of the terminal ligands,[1,12] and that the charge-transfer bands of the sulphur ligand to molybdenum are observed only with the bridging sulphur ligand but not with the capping sulphur ligand in the electronic specra[16] of ICTMCTC compounds. Therefore, the bonding in M_3X_3 cluster compounds is of interest in ICTMCTC compounds. We have suggested that a *d–p* π-conjugate interaction exists over M_3X_3 (X = O, S) and that this interaction is stronger over M_3S_3 than M_3O_3, and explained some of the physicochemical properties for ICTMCTC compounds, such as the cooperative effect among the triply bridging ligand X (X = O, S) in chemical reactions[1] and the average of bond lengths[1,2] between M—X atoms over M_3X_3, in the preceding publications.[18] In this paper we give bonding details for a non-planar ring skeleton M_3X_3 and construct the orbitals which are formed for *d–p* π- and *d–d* interactions under the local coordinate system. Also, we describe the relationship between the *d–p* π- and *d–d* orbital interactions in terms of the mixing orbitals and find that the Hückel rule $(4n+2)$ fits for the π-electrons over M_3X_3 (X = O, S). The balance between the *d–p* π-conjugate and *d–d* direct interactions over M_3X_3 is discussed using the bonding model presented here for ICTMCTC compounds.

RESULTS AND DISCUSSION

Mixing orbital determination

ICTMCTC compounds of the type $M_3X_{4-n}Y_nL_9^c$ are presented here and are shown in Fig. 1. They belong to the classification M_3 used in ref. 15. Each metal atom is generally six-coordinate, if M—M bonds are not considered in the M_3 triangle in ICTMCTC compounds. Hence, each M atom needs six valence orbitals to form the σ-framework bonds with capping and bridging ligands, as well as terminal ligands. Three valence orbitals are left on each M atom, two of them form M—M interactions and one of them forms π-interactions with the *p*-orbital of the neighbourhood bridging ligands within the non-planar ring skeleton M_3X_3. The σ-

† Author to whom correspondence should be addressed.

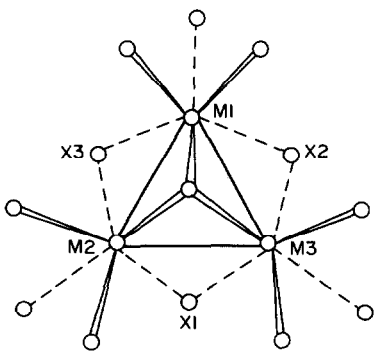

Fig. 1. $[M_3X_{4-n}Y_nL_9]^c$ cluster configuration.

bonds between metal and ligand atoms are generally stable in transition metal cluster compounds, so we only consider the M—M and *d–p* π-interactions within the M_3X_3 cluster. The question of how to pick out three valence orbitals on each metal atom is answered as follows.

Generally, the *d–p* π-interaction between the M and X bridging atoms is comparable in energy to the *d–d* interaction between M atoms. Therefore, three *d* typical mixing orbitals will be only considered to use *d–d* and *d–p* π-interactions within M_3X_3, and six d^2sp^3 hybrid orbitals are considered to form the σ-framework bonds with the ligand atoms. The local coordinate system, which is defined by a non-planar ring skeleton M_3X_3, is convenient in determining the three *d* typical mixing orbitals. As shown in Fig. 2, the M_3X_3 cluster consists of two parallel triangles (M_3 and X_3), all of the *y* axes are parallel to one another and perpendicular to the two triangles, the *z* axes on each M atom and on each X atom point towards the centre of the M_3 and X_3 triangle, respectively, and the tangential *x* axes on the two triangles are fixed by requiring a right-hand coordinate system. The expressions of the three mixing orbitals are as follows:

$$h_1^i = (2/3)^{1/2}(x^2-y^2)-(1/3)^{1/2}z^2 \qquad (1.1)$$

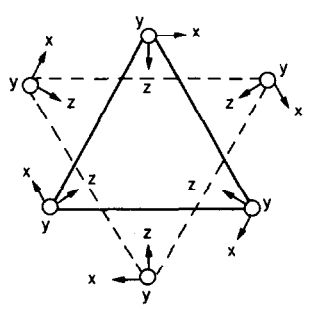

Fig. 2. Local atomic coordinate systems.

$$h_2^i = -(1/6)^{1/2}(x^2-y^2)-(1/3)^{1/2}z^2+(1/2)^{1/2}xz \qquad (1.2)$$

$$h_3^i = -(1/6)^{1/2}(x^2-y^2)-(1/3)^{1/2}z^2-(1/2)^{1/2}xz, \qquad (1.3)$$

and they are made up of three *d* orbitals (x^2-y^2, z^2 and xz). We find that the three *d* orbitals, centred on each M atom, have larger overlaps with both the *d* orbitals of the neighbourhood M atoms and the p_y orbitals of the neighbourhood bridging X ligand atoms. The p_y orbital on each *X* atom is perpendicular to the M_3X_3 non-planar ring skeleton, and the interactions between the p_y orbital on the X atom and x^2-y^2, z^2, as well as the *yz* orbital on the M atom, are homomorphic[19] (constant sign of overlap over M_3X_3); however, the interactions between the p_y and *xy*, *xz* orbital are heteromorphic[19] (alternating sign of overlap over M_3X_3), according to the definition of the local coordinate systems shown in Fig. 2. It is seen from Table 1, that the overlap integrals are smaller between the z^2 orbital on the M atom and the p_y orbital on the X atom than the *xy* orbital on the M atom and the p_y orbital on the X atom, however, the overlap integrals are larger between the z^2 orbitals than the *xy* orbitals on the two M atoms over M_3X_3. Moreover, it is found from Fig. 2, that the x^2-y^2, z^2 and *xz* orbitals on each M atom lie in the trimetal plane, and that the *xy* and *yz* orbitals on each M atom stand on the trimetal plane. The latter ones on each M atom have larger interactions with the capping or terminal ligands. Hence, the x^2-y^2, z^2 and *xz* orbitals are selected to construct three mixing orbitals, h_1^i, h_2^i and h_3^i on each metal atom. These mixing orbitals have larger overlaps between both the *d–d* orbitals on the M atoms and the *d* orbital on the M atom and p_y orbital on the X atom, and it is possible for the maximum binding energy among atoms within M_3X_3.

Qualitative analyses for the d–p *π-interaction between the* M_3 *and* X_3 *fragments*

From early qualitative analysis of the valence bond theory, we know that one of three *d* typical mixing orbitals is available for the π-interaction between the M and X atoms, and that two of them are available for direct M—M interactions. Now, the question will arise again; which is the mixing orbital available for the *d–p* π-interaction? The answer is provided by the overlap integrals: the mixing orbital h_1 on the M atom has the largest overlap with the p_y orbital on the neighbourhood X atoms, and the interactions amongst the h_1 and

Table 1. Overlap integrals between the atomic orbitals with the local coordinate for $[M_3X_{4-n}Y_n]^{4,5+}$ ($n = 0, 1$)

	$[Mo_3O_4]^{4+}$	$[Mo_3S_4]^{4+}$	$[Mo_3Cl_3O]^{5+}$	$[Mo_3Br_3O]^{5+}$
$\langle d_{x^2-y^2}\|d_{x^2-y^2}\rangle$	0.043	0.029	0.038	0.036
$\langle d_{x^2-y^2}\|d_{z^2}\rangle$	−0.015	−0.009	−0.013	−0.013
$\langle d_{x^2-y^2}\|d_{xz}\rangle$	0.028	0.023	0.026	0.027
$\langle d_{z^2}\|d_{z^2}\rangle$	0.096	0.073	0.088	0.087
$\langle d_{z^2}\|d_{xz}\rangle$	0.004	0.011	0.006	0.007
$\langle d_{xy}\|d_{xy}\rangle$	−0.045	−0.029	−0.039	−0.037
$\langle d_{xz}\|d_{xz}\rangle$	−0.083	−0.031	−0.078	−0.077
$\langle d_{z^2}\|p_y\rangle$	−0.021	−0.033	−0.041	−0.047
$\langle d_{xy}\|p_y\rangle$	0.037	0.061	0.084	0.093
$\langle h_1\|p_y\rangle$	0.086	0.105	0.069	0.068
$\langle h_2\|p_y\rangle$	−0.069	−0.067	−0.030	−0.023
$\langle h_3\|p_y\rangle$	0.019	0.009	0.032	0.032

$h_1 = \sqrt{2/3}d_{x^2-y^2} - \sqrt{1/3}d_{z^2}$.
$h_2 = -\sqrt{1/6}d_{x^2-y^2} - \sqrt{1/3}d_{z^2} + \sqrt{1/2}d_{xz}$.
$h_3 = -\sqrt{1/6}d_{x^2-y^2} - \sqrt{1/3}d_{z^2} - \sqrt{1/2}d_{xz}$.

p_y orbitals are homomorphic and available for d–p π-conjugate interaction over the M_3X_3 non-planar ring skeleton. Next, we will discuss the details of the d–p π-conjugate interaction over M_3X_3.

The h_1 mixing orbital is constructed from x^2-y^2 and z^2 atomic orbitals, and drawn in Fig. 3. According to the pictorial approach to molecular bonding developed by Verkade,[20] three MOs, $L^M{}_{\Gamma\gamma}$, symmetry-adapted linear combination of mixing atomic orbitals, are constructed in the trimetal atom skeleton under C_{3v} point group symmetry. It is necessary to declare that the choice of generator orbital (GO) is dependent on the coordinate orientation and some of the GOs presented here are different from those of Verkade.[20] Three MOs for the M_3 skeleton are drawn in Fig. 4 and written as

$$L^M{}_{a_1} = N_1/(3)^{1/2}(h_1{}^1 + h_1{}^2 + h_1{}^3) \quad (2.1)$$

$$L^M{}_{e1} = N_2/(6)^{1/2}[2h_1{}^1 - (h_1{}^2 + h_1{}^3)] \quad (2.2)$$

$$L^M{}_{e2} = N_3/(2)^{1/2}(h_1{}^2 - h_1{}^3), \quad (2.3)$$

where N_i is a normalization coefficient for MO in M_3 and dependent on d–d overlap integrals. It is found from Fig. 4, that $L^M{}_{a_1}$ is the d–d π-bonding MO and $L^M{}_{e1}$, $L^M{}_{e2}$ are the degenerate d–d π-antibonding MOs. The relative energy levels for π-MOs of the M_3 fragment are drawn on the left of Fig. 6, all of the π-MOs will be non-occupied orbitals if the M_3 skeleton has six electrons, and the $L^M{}_{a_1}$ MO will be the occupied orbital if the M_3 skeleton has eight electrons (the six electrons are considered to be d–d σ-sigma-bonds). The π-MOs are constructed for the X_3 fragment as for M_3, but the GO is the p_y orbital for $L^X{}_{a_1}$ MO, and the GO is, respectively, yz and xy for MOs $L^X{}_{e1}$ and $L^X{}_{e2}$. These MOs are drawn in Fig. 5 and written as

$$L^X{}_{a_1} = (1/3)^{1/2}(p_y{}^1 + p_y{}^2 + p_y{}^3) \quad (3.1)$$

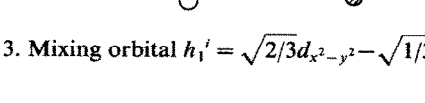

Fig. 3. Mixing orbital $h_1{}' = \sqrt{2/3}d_{x^2-y^2} - \sqrt{1/3}d_{z^2}$.

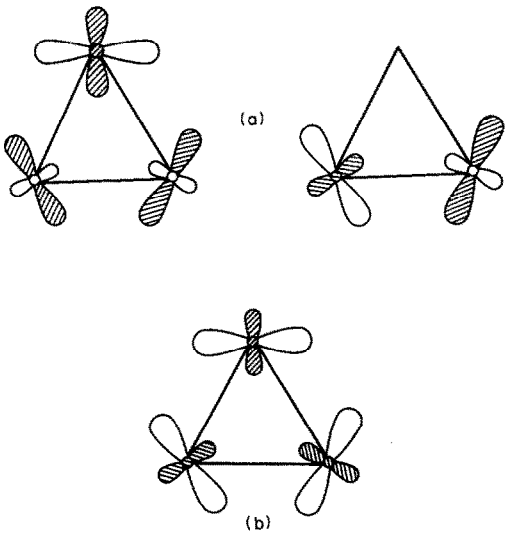

Fig. 4. (a) π-MO of e symmetry; (b) π-MO of a_1 symmetry ($3h_1 - e + a_1$).

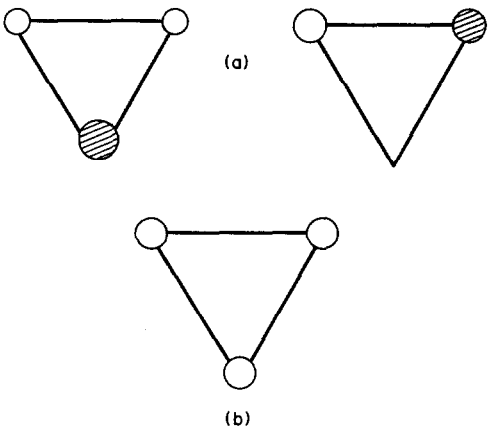

Fig. 5. (a) π-MO of e symmetry; (b) π-MO of a_1 symmetry ($3p_y - e + a_1$).

$$L^X_{e1} = (1/6)^{1/2}[2p_y^1 - (p_y^2 + p_y^3)] \quad (3.2)$$

$$L^X_{e2} = (1/2)^{1/2}(p_y^2 - p_y^3). \quad (3.3)$$

The relative energy levels for the π-MOs of the X_3 fragment are drawn on the right of Fig. 6, and the three lone-pair electrons will occupy three MOs. The normalization coefficients are not considered in Formula (3) because the interaction between X—X atoms is very weak. Now, the *d–p* π-conjugate interaction takes place between the two fragments, M_3 and X_3, under the symmetry rule for fragment interaction, and this interaction diagram is shown in Fig. 6. Because the M_3 and X_3 fragments are not co-planar, the interactions between the h_1 and p_y orbitals over M_3X_3 are not exact π-interactions due to the definition of the local coordinate of M_3X_3 as shown in Fig. 2, but we still call them π-interactions in our studies. The six π-MOs of the M_3X_3 non-planar ring skeleton are constructed from the π-MOs of M_3 and X_3 fragments, and the expressions of the MOs are written as

$$L^R_{a_1} = A_{1,2}L^M_{a_1} + - A_{2,1}L^X_{a_1} \quad (4.1)$$

$$L^R_{e1} = B_{1,2}L^M_{e1} + - B_{2,1}L^X_{e1} \quad (4.2)$$

$$L^R_{e2} = C_{1,2}L^M_{e1} + - C_{2,1}L^X_{e2}, \quad (4.3)$$

where the "$+-$" sign and the subscript "1,2" in turn correspond to the interaction of the bonding and antibonding MOs. The three bonding π-MOs only are drawn in Fig. 7. It is seen that the MO belonging to a_1 symmetry has no node and more stabilization for the bonding MO, and more destabilization for the antibonding MO. The relative energy levels are shown in the middle of Fig. 6. The three lone-pair electrons from the X_3 fragment will occupy three bonding π-MOs of the M_3X_3 cluster. Hence, the six π-electrons in the non-planar ring skeleton M_3X_3 (X = O, S) will fit the Hückel rule ($4n+2$). However, the order of the relative energy levels for antibonding π-MOs in the M_3X_3 (X = Cl, Br) cluster change between e and a_1 symmetry, and the eight π-electrons (two addtional π-electrons from M_3) in the M_3X_3 (X = Cl, Br) cluster will occupy four MOs and the Hückel rule will break down. The components of the occupied bonding π-MOs of the $[Mo_3X_3]^{6+}$, $[Mo_3X_4]^{4+}$ (X = O, S) and the $[Mo_3X_3]^{7+}$, $[Mo_3X_3O]^{5+}$ (X = Cl, Br) clusters are listed in Table 2.

Relation between the d–p *and* d–d *interactions*

It is believed that the principal bonding interaction between transition metal atoms in cluster

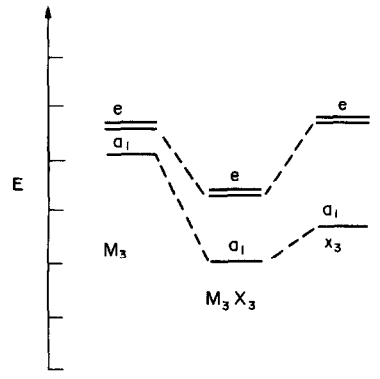

Fig. 6. The relative energy levels for the π-MOs.

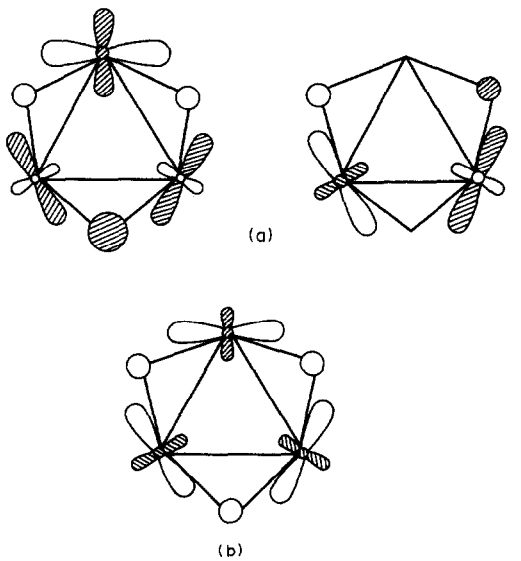

Fig. 7. (a) The bonding π-MO of e symmetry for M_3X_3; (b) the bonding π-MO of a_1 symmetry for M_3X_3.

Table 2. The π-components in the occupied MO of the near frontier for some species

Species	MO	Components h_1^1	h_1^2	h_1^3	p_y^1	p_y^2	p_y^3
$[Mo_3S_3]^{6+}$	e	0.348	−0.174	−0.174	−0.327	0.163	0.163
			−0.302	0.302		0.283	−0.283
	a_1	0.031	0.031	0.031	0.311	0.311	0.311
$[Mo_3O_3]^{6+}$	e	0.257	−0.129	−0.129	−0.358	0.178	0.178
			−0.223	0.223		0.310	−0.310
	a_1	0.021	0.021	0.021	0.280	0.280	0.280
$[Mo_3S_4]^{4+}$	e	0.394	−0.197	−0.197	−0.357	0.179	0.179
			−0.341	0.341		0.309	−0.309
	a_1	0.117	0.117	0.117	0.316	0.316	0.316
$[Mo_3O_4]^{4+}$	e	0.208	−0.104	−0.104	−0.284	0.142	0.142
			−0.182	0.182		0.248	−0.248
	a_1	0.127	0.127	0.127	0.302	0.302	0.302
$[Mo_3Cl_3O]^{5+}$	$2a_1$	−0.361	−0.361	−0.361	0.288	0.288	0.288
	e	0.302	−0.151	−0.151	−0.402	0.201	0.201
			−0.261	0.261		0.347	−0.347
	$1a_1$	0.151	0.151	0.151	0.235	0.235	0.235
$[Mo_3Br_3O]^{5+}$	$2a_1$	−0.370	−0.370	−0.370	0.271	0.271	0.271
	e	0.326	−0.163	−0.163	−0.398	0.199	0.199
			−0.265	0.265		0.344	0.344
	$1a_1$	0.094	0.094	0.094	0.392	0.392	0.392

compounds is due to the metal d-electrons and the d-orbital overlaps.[21,22] Thus, the direct interaction between the M—M atoms is mostly contributed from the typical d-mixing orbitals, h_2^i or h_3^i, in ICTMCTC compounds. The Mulliken overlap populations between $h_2^i-h_2^j$ or $h_3^i-h_3^j$ for some species are listed in Table 3, and the above mentioned conclusion is supported by these populations. For instance, the $h_2^i-h_2^j$ (or $h_3^i-h_3^j$) populations, acting as a M—M σ-interaction, are far larger than the $h_1^i-h_1^j$ populations in ICTMCTC compounds containing six valence electrons of the trimetal atomic skeleton $[Mo_3]^{12+}$. It is understood that the $h_1^i-h_1^j$ interaction, acting as a d–d π-role, gives some contribution to the d–d bonding interactions, especially in the species with strong M—M bonding, like $[Mo_3X_3O]^{5+}$ (X = Cl, Br), in which the Mulliken overlap populations between

Table 3. The overlap populations of d_M–d_M and d_π–p_π

	Populations (e) h_2-h_2 (or h_3-h_3)	h_1-h_1	h_1-p_y	Distances (Å) M—M	M—μ_2-X	Reference
$[Mo_3S_3]^{6+}$	0.023	0.005	0.089	2.765	2.312	5
$[Mo_3S_4]^{4+}$	0.024	0.004	0.088	2.765	2.312	5
$[Mo_3O_3]^{6+}$	0.025	0.010	0.068	2.493	1.915	2
$[Mo_3O_4]^{4+}$	0.027	0.007	0.063	2.493	1.915	2
$[Mo_3Cl_3]^{7+}$	0.028	0.013	0.049	2.577	2.419	8
$[Mo_3Cl_3O]^{5+}$	0.031	0.018	0.010	2.577	2.419	8
$[Mo_3Br_3]^{7+}$	0.028	0.013	0.049	2.594	2.548	8
$[Mo_3Br_3O]^{5+}$	0.030	0.020	0.014	2.594	2.548	8
$[W_3S_4]^{4+}$	0.028	0.004	0.089	2.765	2.308	6
$[W_3O_4]^{4+}$	0.026	0.008	0.064	2.534	1.910	7

$h_1^i-h_1^j$ (0.020) are comparable to $h_2^i-h_2^j$ (or $h_3^i-h_3^j$) (0.030), as shown in Table 3. It is seen that the *d–d* ($h_2^i-h_2^j$ plus $h_1^i-h_1^j$) overlap populations are, respectively, larger in $[Mo_3X_3O]^{5+}$ (X = Cl, 0.049; X = Br, 0.050) and $[Mo_3X_3]^{7+}$ (X = Cl, 0.041; X = Br, 0.041) than in $[Mo_3X_4]^{4+}$ (X = O, 0.028; X = S, 0.034) and $[Mo_3X_3]^{6+}$ (X = O, 0.028; X = S, 0.035), and that the *d–d* ($h_1^i-h_1^j$) π-interaction between the M—M atoms is an obvious contribution to the *d–d* interactions over M_3X_3 (X = Cl, Br); however, the *d–d* π-interaction between the M—M atoms is a negligible contribution to the *d–d* interactions over M_3X_3 (X = O, S), by virtue of the Mulliken population analyses. This means that the M—M transannular interactions[23] are greater in M_3X_3 (X = Cl, Br) than in M_3X_3 (X = O, S), and this is also one reason why the M—M bond is stronger in ICTMCTC compounds containing M_3X_3 (X = Cl, Br) than in those containing M_3X_3 (X = O, S) ring skeletons.

There are two cases which contain the *d–p* π-conjugate interaction over the M_3X_3 non-planar ring skeleton, one has six valence electrons in the trimetal atom $[M_3]^{12+}$ cluster and the π-electrons over M_3X_3 (X = O, S) are contributed by the three lone-pair electrons in the X_3 fragment, the other one has eight valence electrons in the trimetal $[M_3]^{10+}$ cluster and the π-electrons over M_3X_3 (X = Cl, Br) are contributed by both the three lone-pair electrons in the X_3 fragment and the two electrons in the trimetal atom skeleton. The earlier case has six π-electrons over the M_3X_3 (X = O, S) cluster and fits the Hückel rule, whilst the latter case has eight π-electrons over the M_3X_3 (X = Cl, Br) cluster and reduces the *d–p* π-conjugate interaction over M_3X_3. In the $[M_3]^{10+}$ system, the eight π-electrons over M_3X_3 will occupy four π-MOs. The highest occupied π-MO, $2a_1$ in $[Mo_3X_3O]^{5+}$ (X = Cl, Br), as shown in Table 2, mainly consists of the three h_1 orbitals of the Mo_3 fragment and the p_y orbitals of the X_3 (X = Cl, Br) fragment. The $h_1^i-h_1^j$ (*d–d* π) interactions between the M—M atoms over M_3X_3 (X = Cl, Br) are bonding and contribute to *d–d* stabilization interactions in the $2a_1$ π-MO, however, the h_1–p_y (*d–p* π) interactions are antibonding, according to the contributions of the π-orbital characters shown in Table 2. The $2a_1$ π-MO is important in balancing *d–p* π-conjugate and *d–d* direct interaction over M_3X_3 (X = Cl, Br). It is also found, from the overlap populations (index of bond strength[24]) listed in Table 3, that the *d–p* π-conjugate interaction over the $[Mo_3S_3]^{6+}$ or $[Mo_3S_4]^{4+}$ species is stronger than over the $[Mo_3O_3]^{6+}$ or $[Mo_3O_4]^{4+}$ species; however, the *d–d* interactions between the M—M atoms are weaker over $[Mo_3S_3]^{6+}$ or $[Mo_3S_4]^{4+}$. The π-MOs belonging to the *e* irreducible representation have an important role in the balance between the *d–p* π- and *d–d* π-interactions over M_3X_3 (X = O, S). As shown in Fig. 4(a) and Table 2, the interactions between the $h_1^i-h_1^j$ orbitals (*d–d* π) are antibonding over the cross ring M_3, and the interactions between the h_1–p_y orbitals are bonding over the non-planar ring skeleton M_3X_3 in the MOs of *e* symmetry. In other words, the more contribution from the h_1 and p_y orbitals, the more stable is the *d–p* π-conjugate interaction over the M_3X_3 (X = O, S) non-planar ring skeleton; however, the *d–d* π-interaction between the M—M atoms over M_3X_3 in the MOs of *e* symmetry is less stable according to the orbital components of Table 2.

Conclusions

There are two different interactions between M—M and M—μ_2-X atoms in ICTMCTC compounds. It is seen from the bonding model that one interaction is due to the fact that the highest occupied π-MOs (*e* symmetry) consist of the in-phase overlaps among *d–p* π-orbitals over M_3X_3 (X = O, S) and the out-of-phase overlaps among the *d–d* π-orbitals over M_3, and that another interaction is because the highest occupied π-MO (a_1 symmetry) consists of the in-phase overlaps among the *d–d* π-orbitals over M_3 and the out-of-phase overlaps among the *d–p* π-orbitals over M_3X_3 (X = Cl, Br). It has also been shown that the π-conjugate interaction among metal and bridging ligand atoms is in competition with the M—M interaction, and that either M—M bonds or M—μ_2-X bonds are broken down in the two limiting cases in ICTMCTC compounds.

COMPUTATIONAL DETAILS

The calculations were based on the SCCC–EH MO method with weighted H_{ij}'s developed by Hoffmann *et al.*[25,26] There are nine VSIE(Q) functions for valence orbitals in transition metal atom in the calculations. The standard of convergence is 0.002 on the iterative procedure. All the atom and charge iteration parameters used in the calculations were taken from the default values of the program ICON8,[26] except those of the Mo, W and Br atoms. All the geometric parameters were taken from the crystal structural data[2,5–8] and idealized to C_{3v} symmetry, the $[M_3X_{4-n}Y_n]^c$ core or $[M_3X_3]^c$ ring conformations in the calculations were the same as those of the core or ring in cluster compound $[M_3X_{4-n}Y_nL_9]^c$ (M = Mo, W; X = O, S, Cl, Br; Y = O, S; L = terminal ligand; n = 1,0; c =

charge). The atomic parameters of Mo and W were taken from ref. 27. The charge iteration parameters of W atom were the same as those of the Mo atom and taken from ref. 28. The parameters for the valence 4*s* and 4*p* orbitals in the Br atom are as follows: orbital exponents are both 2.127 and the Coulomb integral is −24.1 eV and −12.5 eV respectively; the iterative parameter A, B, C is individually 0.0, 9.86, 23.79 for the 4*s* orbital and is individually 0.0, 9.86 and 11.84 for the 4*p* orbital.

The data presented here under the local coordinate is transformed from the calculated results by the ICON8 program. The subset (x^2-y^2, z^2, xz) of the *d* orbital set of atom 2 (as shown in Fig. 1) is transformed under C_{3v} symmetry

$$\begin{pmatrix} x^2-y^2 \\ z^2 \\ xz \end{pmatrix} = \begin{pmatrix} 5/8 & (3)^{1/2}3/8 & (3)^{1/2}/4 \\ (3)^{1/2}3/8 & -1/8 & -3/4 \\ -(3)^{1/2}/4 & 3/4 & -1/2 \end{pmatrix} \begin{pmatrix} x^2-y^2 \\ z^2 \\ xz \end{pmatrix}'$$

where the prime indicates the orbitals used in the calculations by the ICON8 program. The overlap population between the atomic orbitals under the local coordinate is given

$$\begin{aligned} P_{\mu\lambda} &= 2\sum_i C_{\mu i}C^*_{\lambda i}S_{\mu\lambda} \\ &= 2\sum_{i,t} T_{\mu_t i}C_{\mu_t i}C^*_{\lambda_i}\sum_l T_{\mu_l i}S_{\mu_l\lambda} \\ &= \sum_t (T_{\mu_t})^2 P_{\mu_t\lambda} + \sum_t [(P_{\mu_t\lambda}T_{\mu_t})/S_{\mu_t\lambda}] \sum_{l\neq t} (T_{\mu_l\lambda}S_{\mu_l\lambda}), \end{aligned}$$

where T_{μ_t} is the transformation coefficient, and $P_{\mu_t\lambda}$ and $S_{\mu_t\lambda}$ are, respectively, the overlap population and overlap integral from the calculated results using the ICON8 program. It must be noted that the coordinate orientation of the λth atom is selected to be the same as that of the molecular coordinate system in this formula. The overlap population between the mixing orbitals are transformed from $P_{\mu\lambda}$ and listed in Table 3.

Acknowledgements—This investigation was supported by the Science Foundation of the Chinese Academy of Sciences and by Fuzhou Laboratory of Structural Chemistry, Fujian Institute of Research on the Structure of Matter. We thank Professor C.-W. Liu, X.-T. Wu, S.-F. Lu and J.-Q. Huang for the stimulating discussions.

REFERENCES

1. J.-Q. Huang, S.-F. Lu, M.-Y. Shang, X.-T. Lin, M.-D. Huang, Y.-H. Lin, D.-M. Wu, H.-H. Zhuang, J.-L. Huang and J.-X. Lu, *Jiegou Huaxue* (*J. Struct. Chem.*) 1987, **6**, 219.
2. K. R. Rodgers, R. K. Murmann, E. O. Schlemper and M. E. Shelton, *Inorg. Chem.* 1985, **24**, 1313.
3. X.-T. Lin, Y.-H. Lin, J.-L. Huang and J.-Q. Huang, *Kexue Tongbao* 1987, **32**, 810.
4. M.-D. Huang, S.-F. Lu, J.-Q. Huang and J.-L. Huang, *Jiegou Huaxue* (*J. Struct. Chem.*) 1987, **6**, 29.
5. N. C. Howlader, J. P. Haight Jr., T. W. Hambley, J. A. Lawrance, K. M. Rahmoeller and M. R. Snow, *Aust. J. Chem.* 1983, **36**, 377.
6. T. Shibahara, K. Kohda, A. Ohtsuji, K. Yasuda and H. Kuroya, *J. Am. Chem. Soc.* 1986, **108**, 2757.
7. M. Segawa and Y. Sasaki, *J. Am. Chem. Soc.* 1985, **107**, 5565.
8. D.-M. Wu, H.-H. Zhuang, J.-J. Zheng, J.-L. Huang, J.-X. Lu and J.-Q. Huang, *Scientia Sinica B* 1985, **10**, 875.
9. T. Shibahara, H. Miyke, K. Kobayashi and N. Kuroya, *Chem. Lett.* 1986, 139.
10. T. Shibahara, T. Yamada and H. Kyroya, *Inorg. Chem. Acta* 1986, **13**, L19.
11. B. E. Bursten, F. A. Cotton, M. B. Hall and R. C. Naiiar, *Inorg. Chem.* 1982, **21**, 302.
12. R. Jostes, A. Muller and F. A. Cotton, *Angew. Chem. Int. Edn Engl.* 1980, **19**, 875.
13. J.-L. Huang, J.-X. Lu, Y.-S. Jiang and R. Hoffmann, *Scientia Sinica B*(*Engl.*) 1985, **28**, 1036.
14. P. J. Vergamini, H. Vahrenkamp and L. F. Dahl, *J. Am. Chem. Soc.* 1971, **93**, 6327.
15. Y.-S. Jiang, A.-Q. Tang, R. Hoffmann, J.-L. Huang and J.-X. Lu, *Organometallics* 1985, **4**, 27.
16. A. Muller, *Polyhedron* 1986, **5**, 323.
17. F. A. Cotton, *Polyhedron* 1986, **5**, 3.
18. W.-D. Cheng, Q.-E. Zhang, J.-S. Huang and J.-X. Lu, *Polyhedron* 1989, **8**, 2785.
19. K. A. R. Mitchell, *Chem. Rev.* 1969, **69**, 157.
20. J. G. Verkade, *A Pictorial Approach to Molecular Bonding*. Springer, New York (1986).
21. R. G. Woolley, *Inorg. Chem.* 1985, **24**, 3519.
22. J.-Q. Li, *J. Molec. Struct.* (*Theochem.*) 1988, **181**, 185.
23. J. P. Faucher, J.-F. Labarre and R. A. Shaw, *Naturfor.* 1976, **B316**, 677.
24. J.-Q. Li and W.-D. Cheng, *J. Molec. Struct.* (*Theochem.*) 1987, **151**, 19.
25. R. Hoffmann, *J. Chem. Phys.* 1963, **39**, 1397; R. Hoffmann and W. W. Lipscomb, *J. Chem. Phys.* 1962, **36**, 2179.
26. R. Hoffmann *et al.*, ICON8 program descriptions.
27. R. H. Summervill and R. Hoffmann, *J. Am. Chem. Soc.* 1979, **101**, 3830.
28. R. Munitaj and R. Letelier, *Theoret. Chem. Acta* 1981, **58**, 167.

Polyhedron Vol. 9, No. 14, pp. 1633–1637, 1990
Printed in Great Britain

0277–5387/90 $3.00+.00
© 1990 Pergamon Press plc

REACTIONS OF SULPHUR DIOXIDE WITH PALLADIUM(II) COMPLEXES

FATIMA T. ESMADI* and MAHMOUD K. DOHAIDEL

Department of Chemistry, Yarmouk University, Irbid, Jordan

(*Received* 20 *November* 1989; *accepted* 14 *February* 1990)

Abstract—The reactions of sulphur dioxide with the salt K_2PdCl_4 and the anion $[HPd(CO)Cl_2]^-$ are described. The complexes were isolated either as salts of Ph_4As^+ and Ph_4P^+ cations or as complexes of neutral nitrogen donor ligands (L—L). The ligands used were bidentate or tridentate ligands such as 2,2′-bipyridine (bipy), 1,10-phenanthroline (phen), *o*-phenylenediamine (*o*-phen) and 2,2′ : 6,2″-terpyridine (terpy). Reaction of sulphur dioxide with K_2PdCl_4 in aqueous ethanol gave an ethoxysulphonyl dinuclear palladium anion, $[PdCl_2(SO_3C_2H_5)]_2^{2-}$, which reacted with nitrogen donor ligands giving the previously known palladium complexes, $Pd(L—L)Cl_2$. If sulphur dioxide was allowed to react with $Pd(L—L)Cl_2$ complexes suspended in aqueous ethanol, sulphato complexes of the formula $[Pd(L—L)SO_4]\cdot H_2O$ were obtained. Reaction of sulphur dioxide with a solution of the anion $[HPd(CO)Cl_2]^-$ and then addition of nitrogen donor ligands, led to the formation of sulphur dioxide complexes.

Due to the increased interest in sulphur dioxide as one of the major pollutants, many reports have appeared lately concerning its reactions with different species. It was found that SO_2 has variable coordination geometries and therefore the chemistry of SO_2 as a coordinating group became a fascinating topic worthy of study. Reviews[1,2] appeared that relate the coordination mode of SO_2 to the electronic characteristics of the parent molecule and correlate its bonding mode to its IR stretching frequencies.

Sulphur dioxide complexes are usually synthesized by reaction of SO_2 with metal salts, or by displacement of some labile groups from a complex or by addition to a coordinating unsaturated complex. Metal halocarbonyls were used as starting materials for preparation of many different complexes including SO_2 complexes. It is found that SO_2 can replace CO, as in the case of $(M(CO)_2Cl_2)^-$ (M = Rh, Ir), which reacts with SO_2 to produce SO_2 complexes.[3] Platinum carbonyl clusters were found to react with SO_2 to produce Pt—SO_2 clusters,[4] such as $[Pt_4(\mu\text{-}CO)_5(PMe_2Ph)_4]$, which produces $[Pt(\mu\text{-}SO_2)_3(PMe_2Ph)]$ upon reaction with SO_2, although in some reactions SO_2 can be replaced by CO.[5]

In spite of the large number of transition metal–SO_2 complexes which were synthesized and characterized, those of palladium and platinum are relatively few. The known Pd— and Pt—SO_2 complexes are mostly those of monodentate[3–5] or polydentate[6] phosphorus donor ligands and some are known that contain arsenic donor ligands.[7] $PdCl_2$ and $PtCl_2$ suspended in alcohol have been found to react with SO_2 to produce dinuclear complexes of the formula $[M_2Cl_4(SO_2OR)_2]^{2-}$ (M = Pd, Pt and R = Me, Et, *n*-Pr).[8] It is proposed that these dinuclear complexes are formed by insertion of SO_2 into a Pd—OR species present in solution. Pt— and Pd—SO_2 complexes containing nitrogen donor ligands are rare and we therefore tried to synthesize and characterize some of them. The complexes obtained depend upon reaction conditions. Pd–SO_2 complexes were obtained from reaction of SO_2 with the $[HPd(CO)Cl_2]^-$ anion, but sulphate complexes were obtained when SO_2 was reacted with $Pd(L—L)Cl_2$ complexes, and an ethoxysulphonyl complex was obtained upon reacting SO_2 with K_2PdCl_4 in aqueous ethanol.

* Author to whom correspondence should be addressed.

EXPERIMENTAL

Sulphur dioxide was purchased from Matheson Division, dried over sulphuric acid and used without further purification. All solvents used were analytical reagent grade and were used as purchased. K_2PdCl_4 (Aldrich), terpyridine, 2,2′-bipyridine (Lancaster) and 1,10-phenanthrolinre (Aldrich) were purchased commercially and used as received. *o*-Phenylenediamine was purchased from Aldrich and crystallized from benzene before use.

$[HPd(CO)Cl_2]^-$ and $(C_6H_5CN)_2PdCl_2$ were prepared according to the methods described in the literature.[9,10]

Analyses for carbon, hydrogen, nitrogen, chlorine and sulphur were carried out by M-H-W Laboratories, Phoenix, Arizona, U.S.A. The IR spectra were recorded over the range 4000–200 cm^{-1}, on a Pye Unicam SP3-300 IR spectrophotometer using KBr and CsI pellets. ^1H NMR spectra were recorded on a Brucker WP 80Y instrument using d_6-dimethylsulphoxide as solvent. Conductivity measurements were carried out using 10^{-3} (M solutions in dimethylsulphoxide with a Harris conductivity meter. Melting points were measured on an electrothermal melting point apparatus and were not corrected.

Preparation of complexes

$[Ph_4E]_2[Pd_2Cl_4(SO_3C_2H_5)_2]$ (E = As, P). The complexes were prepared by the following two methods:

(a) K_2PdCl_4 (1 mmol) was dissolved in 20 cm^3 of water–ethanol (1 : 1 v/v) and then SO_2 was passed through it for 4 h when the colour changed to orange–red. Ph_4AsCl or Ph_4PCl (2 mmol) in 5 cm^3 of ethanol was added to the solution with stirring and the mixture was allowed to stand at 5°C overnight; orange crystals were formed in the case of the Ph_4P^+ salt and orange–brown crystals in the case of the Ph_4As^+ salt. The crystals were isolated by filtration, washed with ethanol, then diethyl ether and dried *in vacuo* at room temperture. The yield was 60–65%.

(b) The same procedure as described in (a) except $Pd(C_6H_5CN)_2Cl_2$ (1 mmol) dissolved in 15 cm^3 ethanol was used instead of K_2PdCl_4.

$[Pd(L—L)SO_4]\cdot H_2O$ (L—L = *phen*, o-*phen*, *bipy*). K_2PdCl_4 (1 mmol) was dissolved in 20 cm^3 of ethanol–water (1 : 1 v/v) and then a solution of the ligand (L—L) (1 mmol) dissolved in 5 cm^3 of ethanol was added to it with stirring. A yellow precipitate was formed immediately. Sulphur dioxide was passed through the suspension which dissolved and its colour faded. The solution was left at 5°C overnight when a yellow precipitate was formed. This was filtered, washed with ethanol then diethyl ether and dried *in vacuo* at room temperature. The yield was 60–70%.

$[Pd(phen)(SO_2)Cl]Cl$ *and* $[Pd(terpy)(SO_2)]Cl_2$. Sulphur dioxide was passed through the yellow solution containing $[HPd(CO)Cl_2]^-$ (1 mmol), which was prepared as reported in the literature.[9] The colour changed immediately from yellow to dark red. A solution of the ligand (1 mmol) dissolved in ethanol (10 cm^3) was added to the dark red solution and immediate formation of a precipitate was observed. The precipitate was isolated by filtration, washed with ethanol and diethyl ether and finally dried *in vacuo* at room temperature. The yield was 55–60%.

The analytical data for the obtained complexes along with their colour, melting points and molar conductivity are listed in Table 1. The important IR absorption bands and ^1H NMR data for the alkoxysulphonyl complexes are listed in Table 2.

RESULTS AND DISCUSSION

Reaction of SO_2 *with* K_2PdCl_4

Upon bubbling SO_2 through a solution of K_2PdCl_4 in ethanol–water, a red solution containing the anion $[Pd_2Cl_4(SO_2OC_2H_5)_2]^{2-}$ is formed. This anion was precipitated by addition of Ph_4AsCl or Ph_4PCl. Dinuclear ethoxysulphonyl palladium complexes were formulated on the basis of their IR and NMR spectra. IR spectra exhibit the absorption bands characteristic of the ethoxysulphonyl group [$\nu(S{=}O)_{asym}$ falls in the range 1266–1270 cm^{-1}, $\delta(S{=}O)_{sym}$ in the range 1108–1110 cm^{-1}, $\nu(S—O)$ in the range 905–908 cm^{-1} and $\delta(O—S—O)$ in the range 598–600 cm^{-1}]. There are also IR bands that are attributed to both bridging and terminal Pd—Cl bonds [$\nu(Pd—Cl)$ in the range 285–287, 350 and 265–270 cm^{-1}]. The absorption band occurring at lowest frequency is due to the bridging chloride, whereas the other two absorption bands are due to the terminal chlorides.[11]

The ^1H NMR spectra of the ethoxysulphonyl complexes obtained show absorptions due to the $—SO_2OC_2H_5$ group in agreement with the reported values for organic sulphonates. The band which falls in the range 4.09–4.10(q) is due to $—CH_2$ protons and the band which falls in the range 1.14–1.15(t) is due to $—CH_3$ protons. The α-proton chemical shifts are moved to a higher field relative to the free alcohol.[12]

Table 1. Properties and analytical data of palladium(II) complexes

Complex	Analysis: Found (Calc.)% C	H	N	Cl	S	Colour	Melting point[a] (dec.)	Λ_m[b]
$[Ph_4As]_2[Pd_2Cl_4(SO_3Et)_2]$	47.1 (46.4)	4.1 (3.8)	—	10.7 (10.8)	4.8 (4.7)	Orange–brown	172[m]	105
$[Ph_4P]_2[Pd_2Cl_4(SO_3Et)_2]$	49.9 (50.1)	4.4 (4.0)	—	12.29 (11.9)	5.27 (5.23)	Orange	175[m]	109
$[Pd(bipy)SO_4]\cdot H_2O$	31.0 (31.9)	2.3 (2.7)	7.8 (7.4)	—	8.1 (8.5)	Yellow	200[d]	5
$[Pd(phen)SO_4]\cdot H_2O$	35.4 (36.0)	2.3 (2.5)	6.5 (7.0)	—	8.3 (8.0)	Yellow	225[d]	3
$[Pd(o\text{-phen})SO_4]\cdot H_2O$	22.1 (21.9)	3.2 (3.0)	9.2 (8.5)	—	10.2 (9.8)	Yellow	260[d]	4
$[Pd(SO_2)(terpy)]Cl_2$	37.3 (37.9)	2.2 (2.3)	8.0 (8.8)	15.3 (15.0)	6.7 (6.7)	Yellow–green	350[d]	106
$[Pd(SO_2)(phen)Cl]Cl$	34.3 (34.2)	1.8 (1.9)	7.3 (6.6)	15.8 (16.9)	7.8 (7.6)	Brown	340[d]	51

[a] m is melting point; d is decomposition point.
[b] Λ_m stands for molar conductance in Ω^{-1} mol^{-1} cm^2 of 10^{-3} M solutions in dimethylsulphoxide at 25°C.

Conductivity measurements in dimethylsulphoxide show that the salts obtained are 2:1 electrolytes (Λ_m falls in the range 104–109 Ω^{-1} cm^2 mol^{-1}).

Reaction of this dinuclear ethoxysulphonyl anion with neutral nitrogen donor ligands resulted in the formation of the known complexes of the general formula Pd(L—L)Cl_2, where L—L = *o*-phen, phen, bipy.[13–16] It seems that the ethoxysulphonyl group is easily displaced by other ligands.

The anion $[Pd_2Cl_4(SO_2OR)_2]^{2-}$, were R = Me, Et, *n*-Pr, was reported by Ros *et al.*[8] to be formed by reaction of SO_2 with a suspension of $PdCl_2$ in alcohol for a long period of time. The formation of this anion was explained mainly as a result of SO_2 insertion into a postulated palladium alkoxide intermediate (>Pd—OR). Another possibility for the formation of this dinuclear complex is by an attack of an alkoxide group at a coordinated SO_2. A third possibility could be the formation of a monoester of sulphurous acid (RSO_3H group) in

Table 2. Selected IR and ^{1}H NMR data of palladium(II) complexes

Complex	ν(—$SO_3C_2H_5$, SO_4, SO_2) (cm^{-1})	ν(Pd—Cl)	δ of ethoxy protons (ppm)
$[Ph_4As]_2[Pd_2Cl_4(SO_3Et)_2]$	1270(vs), 1110(vs), 905(s), 598(s)	350(s) 285(w) 265(m)	4.10(q) 1.14(t)
$[Ph_4P]_2[Pd_2Cl_4(SO_3Et)_2]$	1266(vs), 1108(s), 908(s), 600(s)	350(s) 287(w) 270(m)	4.09(q)
$[Pd(bipy)SO_4]\cdot H_2O$	1240(m), 1148(m), 946(m), 880, 820(m), 645(m)	—	—
$[Pd(o\text{-phen})SO_4]\cdot H_2O$	1215(s), 1110(s), 990(m), 870(m), 840(m), 640(m)	—	—
$[Pd(SO_2)(terpy))Cl_2$	1200(m), 1050(s), 595(s)	—	—
$[Pd(SO_2)(phen)Cl]Cl$	1210(m), 1060(s), 590(s)	340(s)	—

alcoholic solution by reaction of SO_2 with ROH ($SO_2 + ROH \rightleftharpoons RSO_3H$)[17] and then coordination of this group to palladium.

Stable complexes containing the —SO_2OR group bonded to the metal were reported previously to be formed by reaction of $(Ph_3P)_2M(NCO)_2$ (M = Pd, Pt) with SO_2 in methanol, and the products were of the formula $(Ph_3P)_2M(SO_3Me)$.[18]

Reaction of SO_2 *with* Pd(L—L)Cl_2 (L—L = *phen, bipy,* o-*phen*)

Addition of the ligand (L—L) to K_2PdCl_4 in a 1:1 molar ratio results in the formation of complexes of the formula Pd(L—L)Cl_2.[13–16] Pd(L—L)Cl_2 complexes were prepared and while still suspended in solvent, SO_2 was allowed to pass through them. The resulted compounds were of the formula $[Pd(L—L)SO_4] \cdot H_2O$.

IR spectra of these complexes show four strong bands which fall in the following ranges 1215–1240, 1110–1148, 946–990; 870–880; 820–840 and 640–654 cm^{-1} which are in accord with the symmetry of the SO_4 group acting as a bidentate ligand (C_{2v})[19] and is in reasonable agreement with the spectrum reported by Barraclough and Tobe[20] for the complex $[Co(en)_2SO_4]Br$. It is observed that the highest frequency band is split into three.[21] The IR spectra of the isolated sulphato complexes also exhibit absorption bands due to lattice water [ν(O—H) falls in the range 3430–3450 cm^{-1} and δ(H—O—H) in the range 1620–1630 cm^{-1}].

Conductivity measurements of the sulphato complexes indicated that they are non-electrolytes (Table 1).

Formation of sulphate by oxidation of SO_2 is known and many examples are reported where the molecular oxygen complexes have been found to react with SO_2 to form coordinated sulphate.[19,22] Some SO_2 complexes are also found to react with O_2 to give sulphato complexes. The complexes $M(SO_2)(PPh_3)_2$ (M = Pd, Pt) have been found to undergo oxidation forming $M(SO_4)(PPh_3)_2$.[6] Many other transition metal–SO_2 complexes were also found to form sulphato complexes upon exposure to air.[23–25]

Reaction of SO_2 *with* $[HPd(CO)Cl_2]^-$

As SO_2 was allowed to pass through the yellow solution of $[HPd(CO)Cl_2]^-$ an immediate colour change was observed. Addition of Ph_4AsCl to the resulting solution gave a solid which was not easy to characterize but the addition of neutral ligands such as phen or terpy resulted in the formation of SO_2 complexes which are formulated as $[Pd(SO_2)(terpy)]Cl_2$ and $[Pd(SO_2)(phen)Cl]Cl$. Both compounds are water-soluble and conductivity measurements prove that they are ionic (Table 1).

IR spectra of both compounds exhibit the characteristic bands of SO_2 [$\nu(SO_2)_{asym}$ falls in the range 1200–1210 cm^{-1}, $\nu(SO_2)_{sym}$ in the range 1050–1060 cm^{-1} and δ(O—S—O) in the range 590–595 cm^{-1}]. These values are shifted to lower frequencies relative to free SO_2.

From comparison with other Pd—SO_2 complexes,[2] it is concluded that SO_2 is bonded in the η^1-pyramidal mode. Most of the reported Pd— and Pt—SO_2 complexes have η^1-pyramidal SO_2 which is commonly associated with the more basic transition metals.[1,2]

Reaction of SO_2 with K_2PtCl_4 has been tried and the results are found to be different from the K_2PdCl_4 reactions. The results of the reactions of SO_2 with the K_2PtCl_4 system will be reported as soon as they are complete.

Acknowledgement—The authors gratefully acknowledge the support from Yarmouk University for this project.

REFERENCES

1. R. R. G. J. Kubas, D. C. Moody and P. G. Eller, *Struct. Bond. (Berlin)* 1981, **46**, 47.
2. D. M. P. Mingos, *Transition Met. Chem.* 1978, **3**, 1.
3. M. Fayyad, to be published.
4. C. E. Briant, P. G. Evans and D. M. Mingos, *J. Chem. Soc., Dalton Trans.* 1986, 1535.
5. A. C. Jesse, J. F. Van Baar, D. J. Stufkens and K. Vrieze, *Inorg. Chim. Acta* 1976, **17**, L13.
6. J. J. Levison and S. D. Robinson, *J. Chem. Soc., Chem. Commun.* 1967, 199.
7. C. D. Cook and G. S. Jauhal, *J. Am. Chem. Soc.* 1967, **89**, 3066.
8. R. Ros, G. Carturan and M. Graziani, *Transition Met. Chem.* 1976, **1**, 13.
9. J. V. Kingston and G. R. Scollary, *J. Chem. Soc., Chem. Commun.* 1969, 455.
10. F. R. Hartley, *Organomet. Chem. Rev.* 1970, **A6**, 123.
11. K. Nakamoto, *Infrared and Raman Spectra of Inorganic and Coordination Compounds*, 3rd edn, p. 239. John Wiley, New York (1978).
12. L. M. Jackman and S. Stenhell, *Applications of Nuclear Magnetic Resonance Spectroscopy in Organic Chemistry*. Pergamon Press, Oxford (1972).
13. J. R. Durig, B. R. Mitchell, D. W. Sink, J. N. Willis and A. S. Wilsh, *Spectrochim. Acta* 1967, **23A**, 1121.
14. G. T. Morgan and T. H. Burstall, *J. Chem. Soc.* 1934, 965.
15. K. Bowman and Z. Dori, *Inorg. Chem.* 1970, **9**, 395.
16. L. Rosenblatte and A. Schleedem, *Liebs Ann.* 1933, **51**, 505.
17. L. F. Audrieth and J. Kleinberg, *Non-Aqueous Solvents*. John Wiley, New York (1953).

18. K. Werner, W. Beck and U. Bohner, *Chem. Ber.* 1974, **107**, 2434.
19. R. W. Horn, E. Weissberger and J. P. Collman, *Inorg. Chem.* 1970, **9**, 2367.
20. C. G. Barraclough and M. L. Tobe, *J. Chem. Soc.* 1961, 1993.
21. K. Nakamoto, J. Fujita, S. Tanaka and M. Kobayashi, *J. Am. Chem. Soc.* 1957, **79**, 4904.
22. S. P. Mehandru and A. B. Anderson, *Inorg. Chem.* 1985, **24**, 2570.
23. M. H. B. Stiddard and R. E. Townsend, *J. Chem. Soc., Chem. Commun.* 1969, 1372.
24. J. Valentine, D. Valentine and J. P. Collman, *Inorg. Chem.* 1971, **10**, 219.
25. S. J. LaPlaca and J. A. Ibers, *Inorg. Chem.* 1969, **8**, 1921.

Polyhedron Vol. 9, No. 14, pp. 1639–1644, 1990
Printed in Great Britain

0277–5387/90 $3.00+.00
© 1990 Pergamon Press plc

STUDIES ON LANTHANIDE COMPLEXES WITH PYRONE LIGANDS—V.* TERBIUM(III) AND EUROPIUM(III) COMPLEXES WITH A NEW LIGAND DERIVED FROM THE CONDENSATION OF 4-OXO-4H-BENZOPYRAN-3-CARBOXYALDEHYDE AND 2-AMINO-4-CHLOROPHENOL

C. BISI CASTELLANI

Dipartimento di Chimica Generale dell'Università di Pavia, via Taramelli 12, I-27100 Pavia, Italy

and

O. CARUGO†

Dipartimento di Medicina Preventiva, Occupazionale e di Comunità dell'Università di Pavia, via Boezio 14, I-27100 Pavia, Italy

(*Received* 16 *January* 1990; *accepted* 19 *February* 1990)

Abstract—A novel ligand, 3-[(2-hydroxy-5-chlorophenylamino)methoxy]methylchromone, Hbpcap, was obtained by reacting 4-oxo-4H-benzopyran-3-carboxyaldehyde, bpa, and 2-amino-4-chlorophenol, cap, in methanol. Elemental analysis and vibrational and NMR spectra revealed that Hbpcap is a cathecolamine derivative of bpa. Complexes, of general formula $Ln(bpcap)_2X \cdot nH_2O$ ($Ln^{3+} = Eu^{3+}$ and $n = 2$; $Ln^{3+} = Tb^{3+}$ and $n = 1$; $X^- = NO_3^+$, Cl^-, ClO_4^-), were isolated and characterized. Unlike the bpa complexes with Eu^{3+} and Tb^{3+}, they did not exhibit ionic emission due to the excitation of the ligand. In order to explain this behaviour, the ligand excited states have been examined.

Luminescent lanthanide complexes are presently the focus of attention in many laboratories, mainly because of their possible applications in bioinorganic chemistry.[2] For this purpose, it is necessary to bind Eu^{3+} or Tb^{3+} with chromophoric ligands, i.e. ligands able to absorb energy by radiation and then to transfer it effectively to the cation. Recently, we observed that pyrone ligands often fulfil these requirements. A promising ligand seemed to be bpa;[1a] but its lanthanide(III) complexes are not stable enough to allow future biological applications. An easy way to increase the stability of this type of complex could be the use of Schiff base derivatives of bpa as ligands. In order to verify the reliability of this strategy, we investigated the complexing and chromophoric properties of the novel ligand Hbpcap (see Scheme 1), obtained by condensing bpa and cap in methanol.

EXPERIMENTAL

Physicochemical measurements

Electronic absorption spectra were recorded with a Varian Cary spectrophotometer; the solid-state spectra were obtained by pasting the samples with Nujol and spreading them on strips of filter paper. Electronic emission and excitation spectra were recorded with an Aminco-Bauman MPF spectrophotofluorimeter. IR spectra were obtained with a 1130 Perkin–Elmer spectrophotometer as Nujol mulls. Conductometric measurements were carried out at 25 ± 0.1°C, on 6×10^{-5}–2×10^{-4} M solutions, in DMF, using a Radiometer CDM 80 conductometer, equipped with a Radiometer CDC

* For previous parts, see ref. 1.

† Author to whom correspondence should be addressed.

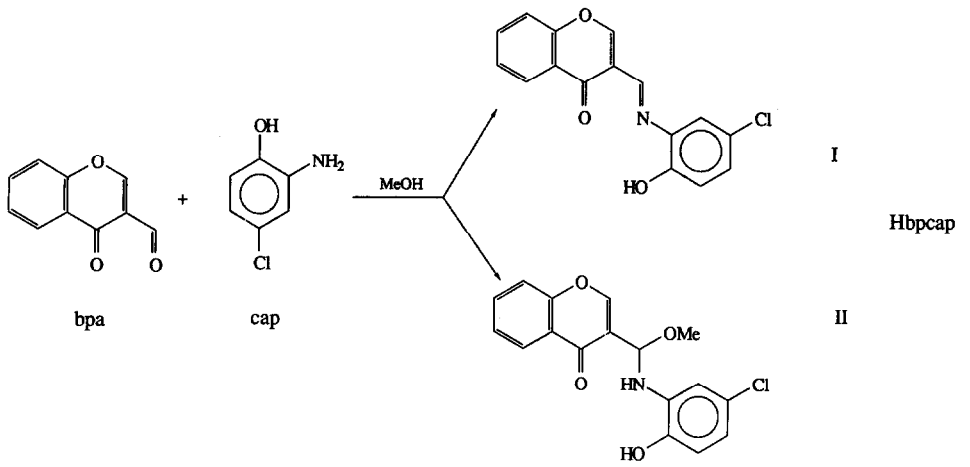

Scheme 1.

104 conductivity cell. NMR spectra were obtained with a Bruker WP80SY spectrometer.

Syntheses

The lanthanide salts were prepared as previously described;[3] bpa was prepared by literature methods;[4] cap was obtained from Fluka.

3-[(2-*Hydroxy*-5-*chlorophenylamino)methoxy*] *methylchromone*. 2-Amino-4-chlorophenol (6 mmol) was dissolved in 100 cm^3 of MeOH, and added to a solution of bpa (6 mmol) in 200 cm^3 of MeOH. This solution was stirred at room temperature, until a yellow solid began to separate; this mixture was filtered, after a period of 12 h, and Hbpcap was obtained in 70% yield. Decomposition point 215–218°C. Another less pure fraction of Hbpcap was obtained by evaporating the mother solution.

Complexes. 3-[(2-Hydroxy-5-chlorophenylamino) methoxy]methylchromone (3 mmol) and 3 mmol of LiOH were dissolved in 30 cm^3 of boiling MeOH. By adding a solution of 1.5 mmol of LnX_3 ($Ln^{3+} = Eu^{3+}$, Tb^{3+}; $X^- = NO_3^-$, Cl^-, ClO_4^-), an orange solid separated. The suspension thus obtained was refluxed for 1 h, stirred at room temperature for 12 h, and centrifuged. The solid product was washed with $CHCl_3$, MeOH and H_2O, and dried at room temperature and 0.5 mm Hg for 3 h.

Analytical and conductometric data are reported in Table 1.

RESULTS AND DISCUSSION

The bpa molecule has two electrophilic sites able to react with amino groups, i.e. the formyl function and the carbon in the two-position on the pyrone ring.[5] Aromatic 1,2-diamines are known to react with bpa, interacting first with the formyl group

Table 1. Elemental analyses and conductometric data

Compound	Found (calc.) (%)			Λ_M[a]
	C	H	N	
Hbpcap	61.0(61.5)	4.3(4.2)	4.3(4.2)	
$Eu(bpcap)_2NO_3 \cdot 2H_2O$	45.2(44.8)	3.5(3.3)	4.9(4.6)	68.3
$Eu(bpcap)_2Cl \cdot 2H_2O$	46.4(46.1)	3.3(3.4)	3.3(3.2)	79.2
$Eu(bpcap)_2ClO_4 \cdot 2H_2O$	43.4(43.0)	2.9(3.2)	3.2(2.9)	102.5
$Tb(bpcap)_2NO_3 \cdot H_2O$	45.4(45.3)	3.2(3.1)	4.9(4.7)	66.9
$Tb(bpcap)_2Cl \cdot H_2O$	46.8(46.7)	2.9(3.2)	3.3(3.2)	72.4
$Tb(bpcap)_2ClO_4 \cdot H_2O$	43.6(43.5)	3.1(3.0)	3.2(3.0)	90.4

[a] $\Omega^{-1}\,cm^2\,mol^{-1}$, in DMF.

and then with the two-position of the pyrone ring, to give benzodiazepines.[6] Only a few amines react with the formyl group of bpa without interacting with the two-position of the pyrone ring; examples of this include hydrazone, oxime, semicarbazone, etc.[7] In the present work, cap was selected as the reacting amine, because of the following properties: (i) its nucleophilicity is presumably low and (ii) the hydroxyl oxygen atom is a potentially good donor for lanthanide cations but interaction with bpa would not be probable. The expected product of the condensation between bpa and cap was molecule **I** (see Scheme 1). However, characterization of the isolated product indicates that it is better formulated as molecule **II** (see Scheme 1), which can be thought of as the methyl pseudo-hemiacetal of molecule **I**. Although this behaviour is uncommon in Schiff base compounds, a few similar cases have been reported.[8]

The formulation of Hbpcap as molecule **II** is based on the following experimental evidence. (i) The elemental analytical data indicate that the condensation product between bpa and cap implies a methanol molecule in the molecular formula. Of course this feature could be explained by the solvation of form **I**; however, form **II** is preferred, based on the spectroscopic evidence reported under points (ii) and (iii); moreover, ill-defined products are obtained by reacting bpa and cap in solvents other than methanol (acetonitrile, acetone, ethanol). (ii) In the ^{1}H NMR spectrum, in addition to the multiplets assignable to the aromatic and benzopyrone protons (6.96–7.25 and 7.45–8.25 ppm, respectively), which have no diagnostic value in discriminating between forms **I** and **II**, two signals at 5.8 and 3.3 ppm are present; these are not consistent with formulation **I**, while they can be assigned, respectively, to the pseudo-hemiacetal and the methoxyl protons of form **II**. Moreover, two other signals typical of acidic protons appear at 10.5 and 12.4 ppm; they can be assigned to the NH and OH protons of form **II**, while form **I** should show only one signal of an acidic proton strongly hydrogen bonded. (iii) Also, the IR spectral data may indicate that form **II** is preferred. The IR spectrum of bpa shows the following diagnostic stretchings: ν(CH=O) at 1700 cm^{-1}, ν(C=O, pyrone) at 1650 cm^{-1} and ν(C=C) at 1620 and 1560 cm^{-1}.[5] The IR spectrum of Hbpcap in addition to a broad OH and/or NH stretching band with transmission minimum at 3250 cm^{-1}, shows signals at 1640, 1600, 1580 and 1540 cm^{-1}; the first one is typical of a pyrone carbonyl stretching[9] and the other three should probably be assigned to C=C stretchings; an eventual C=N stretching, which should be present in the spectrum of compound **I** in the region 1613–1631 cm^{-1},[10] is absent, thus supporting formulation **II**.

Unfortunately, no Hbpcap crystals suitable for X-ray crystallographic studies were obtained, probably due to the instability of this molecule in solutions of the most common organic solvents (the initially yellow solution turns dark red after a few hours).

The complexes of Eu^{3+} and Tb^{3+} with Hbpcap were isolated as orange powders, and formulated as $Ln(bpcap)_2X \cdot nH_2O$ ($X^- = NO_3^-, Cl^-, ClO_4^-$; $n = 1$ for $Ln^{3+} = Tb^{3+}$; $n = 2$ for $Ln^{3+} = Eu^{3+}$; bpcap is the monodeprotonated form of the ligand Hbpcap), on the basis of the elemental analytical data. The water content, higher in the Eu^{3+} than in the Tb^{3+} complexes, could be indicative of the solution of continuity in the coordination number often observed in the lanthanide series at the Gd^{3+} level.[11]

All the complexes show very low solubility in the most common organic solvents (including DMSO and DMF). Their ionic conductivities in DMF indicate a 1:1 electrolyte behaviour.[12] (In effect, the ionic conductivities of the complexes containing ClO_4^- are slightly higher than the range commonly accepted for 1:1 electrolytes in DMF solution, 65–90 Ω^{-1} cm^2 mol^{-1}, but much lower than the range corresponding to 1:2 eletrolytes in the same solvent, 130–170 Ω^{-1} cm^2 mol^{-1}.)[12] From the ionic conductivity data, it can be seen that the freedom of the ionic pairs is higher for Eu^{3+} than for Tb^{3+} complexes (the inorganic anion being the same), according to the lower polarizing behaviour of Eu^{3+} compared with Tb^{3+}. Within each series of complexes (i.e. Eu^{3+} and Tb^{3+} complexes) the conductivity depends on the inorganic anion, being the highest in the case of ClO_4^- and the lowest for NO_3^-. This agrees with the observation that NO_3^- is a better ligand towards La^{3+} than Cl^-, which is a better ligand than ClO_4^-,[13] and appears more significant considering the different ionic equivalent conductivities of NO_3^-, Cl^- and ClO_4^- (71.5, 76.4 and 67.4 Ω^{-1} cm^2 mol^{-1}, respectively, in water at infinite dilution; it is probably not important to compare data from different solvents, because we are only interested in the differences between these values).

The IR spectra of all the complexes, superimposable in the double bond region, are similar to the Hbpcap spectrum. In addition to a ν(OH) band with two transmission minima at 3340 and 3190 cm^{-1}, they show signals at 1620, 1605, 1580 and 1545 cm^{-1}. The first of these bands can be assigned to the stretching of the pyrone carbonyl, shifted to lower frequencies with respect to the free ligand (1640 cm^{-1}) maybe because of a coordinative bond

with the cation. Similar shifts have been observed in other series of pyrone lanthanide complexes.[3] The frequencies of the other three signals are almost the same as those of the free ligand (1600, 1580 and 1540 cm^{-1}), as expected for bands due to vibration of bonds not directly involved in coordination to the metal. The complexes containing the ClO_4^- anion show the typical signals of the ionic perchlorate in *Td* symmetry (broad ν_3 at 1100 cm^{-1} and unsplit ν_4 at 620 cm^{-1},[14]) agreeing with the solution conductivity data. In the IR spectra of the nitrate-containing complexes, the expected NO_3^- bands are not clearly discernable from the other signals due to the organic moiety; therefore we cannot infer anything about the NO_3^- solid-state coordination to the metal.

In order to examine the chromophoric behaviour of Hbpcap towards Eu^{3+} and Tb^{3+}, we studied some of the excited state properties of the free ligand. Figure 1(a) shows the electronic absorption spectrum of Hbpcap in ethanol (λ_{max} at 209, 230(sh), 247, 267, 314(sh) and 397 nm, log ε 4.39, 3.96, 3.98, 3.88, 3.51 and 4.38, respectively). The high intensity of all the bands and the fact that they are red-shifted by the addition of water to the solution (and thus increasing the polarity of the solvent) indicate their π^*–π or charge-transfer character.[15] It is worthwhile to compare this spectrum with those of the parent compounds, bpa* (λ_{max} at 300, 294(sh) and 310(sh) nm, log ε 3.98, 3.96 and 3.89, respectively) and cap (λ_{max} at 206, 291 and 327(sh) nm, log ε 3.91, 3.50 and 3.16, respectively) which are shown in Figs 1(b) and (c). It can be seen that the intense band of Hbpcap at low energy is absent in the spectra of bpa and cap. This is probably indicative of the charge-transfer nature of this absorption.

The solid-state electronic absorption spectrum of Hbpcap [Fig. 2(a)] is different from that in solution, especially in the region at low energy, where a broad, very intense band with maximum at 432 nm and shoulders at 400 and 454 nm are present. This difference is difficult to explain with certainty, but if the charge-transfer nature of this transition is admitted, it may well be an effect due to the surroundings.

The electronic absorption spectra of all the complexes are identical, and those in DMF solution slightly differ from those in the solid state. In fact the main band at low energy is found at 412 nm in DMF solution and at 392 nm in the solid state. This

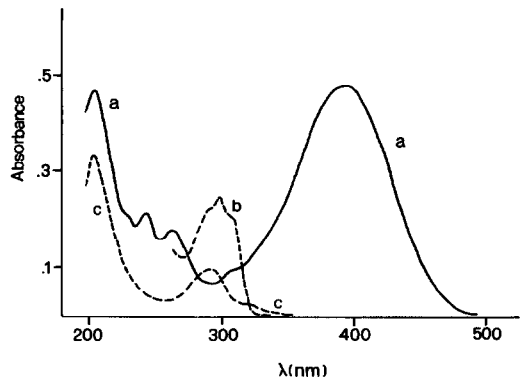

Fig. 1. Electronic absorption spectra of: (a) Hbpcap in EtOH; (b) bpa in CCl_4; (c) cap in EtOH.

indicates the instability of the complexes in solution and agrees with the conductometric data reported above. The solid-state spectrum of $Eu(bpcap)_2Cl \cdot 2H_2O$ [reported as an example in Fig. 2(b)] is different from that of solid Hbpcap: as a consequence of the deprotonation and/or the coordination of the ligand to the metal, in the spectra of the complexes all the bands at high frequencies which correlate with those of the free ligand are shifted to higher energies (from 217 to 216 nm, from 250 to 244 nm, and from 320 to 292 nm) and the shoulders at 268 and 284 nm disappear; moreover, the low energy charge-transfer band of the ligand changes its pattern considerably and appears less intense, with respect to the higher energy bands.

By exciting the complexes in the 350–450 region in DMF solution, no luminescence was observed. Although this may be due to many factors (non-radiative decay of the excited states of the cations via multiphonon-like processes,[16] dissociation of the complexes in solution,[17] etc.) there are two features that probably play the most important roles:

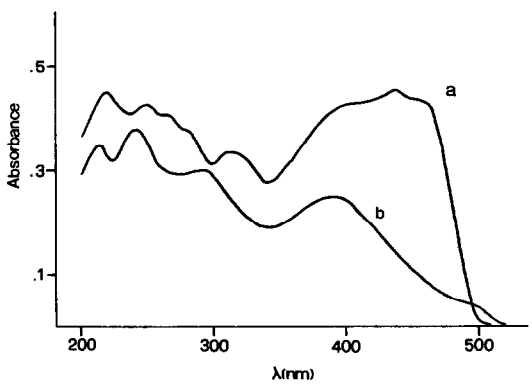

Fig. 2. Solid-state electronic absorption spectra of: (a) Hbpcap; (b) $Eu(bpcap)_2Cl \cdot 2H_2O$.

* The electron absorption spectrum of bpa is reported in CCl_4 instead of EtOH, because bpa in alcoholic solvents is in equilibrium with its hemiacetal and acetal (see ref. 1a).

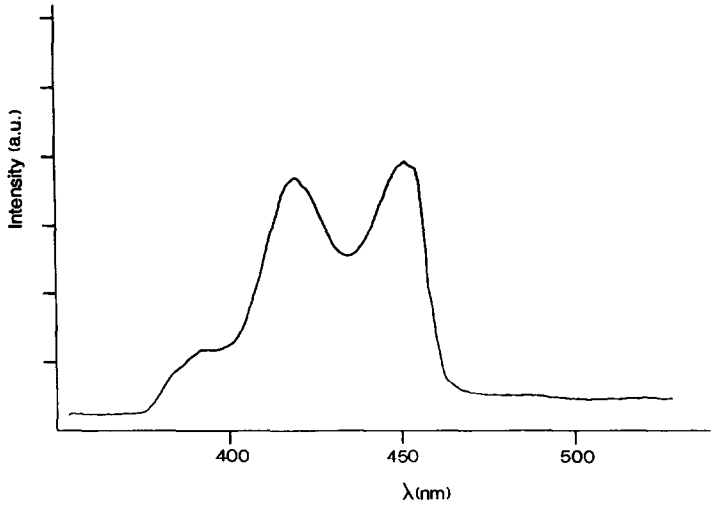

Fig. 3. Phosphorescence emission spectra of bpa in an epa mixture (ether, pentane, ethanol) at liquid nitrogen temperature (λ_{ex} = 300 nm).

(i) the energy of the ligand excited states, and (ii) the kinetics of their decays to the ground state.

(i) The phosphorescence emission spectrum of bpa in a glass of epa (ether, pentane, ethanol) at liquid nitrogen temperature is shown in Fig. 3. It shows a structured band with three maxima at 392, 420 and 452 nm. From this spectrum, it is possible to assign a value of about 26,700 cm^{-1} to the bpa triplet energy, which is high enough to populate the excited states of Eu^{3+} and Tb^{3+} (17,277 and 20,500 cm^{-1}, respectively[16]), which are not very much affected by the surrounding. Also as the coordinative bonds with lanthanide cations have been shown to be considerably covalent,[18] the electronic transitions observable in Tb^{3+} and Eu^{3+} ions involve only the 4*f* electrons which do not participate, in a first approximation, to coordinative bond formation. Contrary to bpa, the free Hbpcap does not show phosphorescence emission at liquid nitrogen temperature in a glass of epa; therefore, we do not know its triplet energy. Nevertheless, it is possible that the triplet energy of Hbpcap is too low to effectively populate the Eu^{3+} and Tb^{3+} excited states. In this regard, we can note that even the first singlet excited state of Hbpcap has too low an energy (20,400 cm^{-1}) to excite Tb^{3+}. Moreover, if the triplet-to-singlet stabilization energy of Hbpcap is of the same order as that of bpa (about 50 nm), it follows that the Hbpcap triplet energy probably drops to a value which is too low (about 18,500 cm^{-1}) to effectively excite Eu^{3+}.[1b]

(ii) Another less probable explanation for the lack of lanthanide emission in the Eu^{3+} and Tb^{3+} Hbpcap complexes could be the low yield of intersystem crossing between the first singlet excited state and the corresponding triplet state of Hbpcap. In fact, the lack of phosphorescence emission by Hbpcap, even at low temperatures, could indicate that the charge-transfer singlet excited state of this ligand is too short-lived to decay by intersystem crossing. Thus, also in the presence of a heavy atom, the yield of the ligand triplet population may be too low to give high populations of the Eu^{3+} and Tb^{3+} excited states.

CONCLUSIONS

As the chromophoric properties of bpa towards Eu^{3+} and Tb^{3+} are unavailable in the various fields of bioinorganic chemistry, because of the very low stability of the bpa complexes with these cations, we decided to transform bpa into its Schiff base. However, the Schiff base-like derivative reported here, Hbpcap, does not conserve the chromophoric behaviour of the parent aldehyde. This behaviour is probably a consequence of a low energy electronic charge-transfer absorption band, which is present in the Hbpcap spectrum, but which may not be present in other Schiff base derivatives of bpa. Thus, further studies are necessary, in order to establish if this type of functionalization can be effective in designing chromophoric ligands, based on the bpa structure, which could be of practical interest.

Acknowledgements—We gratefully acknowledge Professors A. Gamba Invernizzi and A. Albini, Dipartimento di Chimica Organica dell'Università di Pavia, for the NMR and the electronic emission spectra. Financial support by Consiglio Nazionale delle Ricerche is also acknowledged.

REFERENCES

1. (a) C. Bisi Castellani, O. Carugo, C. Tomba and A. Gamba Invernizzi, *Inorg. Chem.* 1988, **27**, 3965; (b) C. Bisi Castellani and O. Carugo, *Inorg. Chim. Acta* 1989, **159**, 157; (c) C. Bisi Castellani and O. Carugo, *Polyhedron* 1990, **9**, 939; (d) C. Bisi Castellani, O. Carugo, P. Ghigna and A. Invernizzi Gamba, submitted for publication.
2. E. P. Diamandis, *Clin. Chem.* 1988, **21**, 139; J.-C. Bünzli, *Inorg. Chim. Acta* 1987, **139**, 219.
3. C. Bisi Castellani, *J. Inorg. Nucl. Chem.* 1970, **32**, 2899.
4. A. Nohara, T. Umetani and Y. Sanno, *Tetrahedron* 1974, **30**, 3553.
5. C. K. Ghosh, *J. Heterocyclic Chem.* 1983, **20**, 1437.
6. C. K. Ghosh and S. Khan, *Synthesis* 1980, 701.
7. A. Nohara, *Tetrahedron Lett.* 1974, 1187; C. K. Ghosh and K. K. Mukhopadhyay, *J. Ind. Chem. Soc.* 1978, **55**, 52; C. K. Ghosh and K. K. Mukhopadhyay, *J. Ind. Chem. Soc.* 1978, **55**, 386.
8. D. E. Fenton, U. Casellato, P. A. Vigato and M. Vidali, *Inorg. Chim. Acta* 1984, **95**, 187; K. K. Abid and D. E. Fenton, *Inorg. Chim. Acta* 1984, **95**, 119.
9. P. J. Brogden, C. D. Gabbutt and J. D. Hepworth, in *Comprehensive Heterocyclic Chemistry* (Edited by A. R. Katritzky and C. W. Rees), Vol. 3, p. 573. Pergamon Press, Oxford (1984).
10. M. Calligaris and L. Randaccio, in *Comprehensive Coordination Chemistry* (Edited by G. Wilkinson, R. D. Gillard and J. A. McCleverty), Vol. 2, p. 715. Pergamon Press, Oxford (1987).
11. V. G. Vokhmin and G. V. Ionova, *Russ. J. Inorg. Chem.* 1987, **35**, 1552.
12. W. J. Geary, *Coord. Chem. Rev.* 1971, **7**, 81.
13. J.-C. Bünzli, A. E. Merbach and R. M. Nielson, *Inorg. Chim. Acta* 1987, **139**, 151.
14. J.-C. Bünzli and D. Wessner, *Coord. Chem. Rev.* 1984, **60**, 191.
15. C. A. Parker, *Photoluminescence of Solutions*. Elsevier, Amsterdam (1968).
16. W. T. Carnall, in *Handbook on the Physics and Chemistry of Rare Earths* (Edited by K. A. Gschneider and L. Eyring), Vol. 3, p. 171. North-Holland, Amsterdam (1979).
17. C. Bisi Castellani, M. Rizzi and O. Carugo, *Proceedings of the Interdisciplinary Meeting on Luminescence: Fundamentals and Applications*, p. 42. Bologna, Italy (1989).
18. G.-X. Xu, J. Ren, C.-H. Huang and J.-G. Wu, *Pure Appl. Chem.* 1988, **60**, 1145.

Polyhedron Vol. 9, No. 14, pp. 1645–1652, 1990
Printed in Great Britain

0277-5387/90 $3.00+.00
© 1990 Pergamon Press plc

BIS[HYDROTRIS(PYRAZOLYL)BORATO]DICHLOROACTINIDE(IV) COMPLEXES: X-RAY CRYSTAL STRUCTURES OF $ThCl_2(HBPz_3)_2$ AND $UCl_2(HBPz_3)_2$

ÂNGELA DOMINGOS,* JOAQUIM MARÇALO, ISABEL SANTOS and A. PIRES DE MATOS

Departamento de Química, ICEN, LNETI, 2686 Sacavém Codex, Portugal

(*Received* 30 *November* 1989; *accepted* 27 *February* 1990)

Abstract—The crystal and molecular structures of $ThCl_2(HBPz_3)_2$ (**1**) and $UCl_2(HBPz_3)_2$ (**2**) have been determined by single-crystal X-ray diffraction. The crystals of **1** are orthorhombic, *Pbca*, $a = 14.406(2)$, $b = 18.523(3)$, $c = 18.947(4)$ Å, $V = 5055.9$ Å^3 and $Z = 8$. The crystals of **2** are triclinic, $P\bar{1}$, $a = 13.134(2)$, $b = 14.481(3)$, $c = 17.030(2)$ Å, $\alpha = 75.72(2)$, $\beta = 75.08(2)$, $\gamma = 68.20(2)°$, $V = 2864.3$ Å^3 and $Z = 4$. The actinide centre in both compounds is eight-coordinate and displays square antiprismatic geometry, distorted towards bicapped trigonal prismatic, with the thorium compound presenting a higher distortion relative to the uranium compound.

The tripodal ligands $(HBPz_3)^-$ and $[HB(3,5\text{-}Me_2Pz_3)]^-$ have been used in our laboratories as stabilizing ligands in the synthesis of organo compounds of thorium and uranium, giving stability to complexes through steric saturation. Using $AnCl_2(HBPz_3)_2$ and $AnCl_3[HB(3,5\text{-}Me_2Pz)_3](THF)$ (An = Th^{IV}, U^{IV}) as precursors, a large variety of derivatives namely alkyls, alkoxides, aryloxides, thiolates, amides and carboxylates, have been prepared.[1–7] For actinide complexes involving the $(HBPz_3)^-$ ligand, two compounds have already been structurally characterized, $UCl(OR)(HBPz_3)_2$ (R = Ph, Bu^t).[8] In both compounds the uranium centre is eight-coordinate displaying square antiprismatic geometries (SAP).

For the lanthanides (Ln) several eight-coordinate compounds of the type $Ln(HBPz_3)_2X$ (where X is a uninegative bidentate ligand) and $Ln(HBPz_3)_2ClL$ (where L = H_2O or PzH) have been structurally characterized.[9–15] The coordination geometries found for these complexes are predominantly SAP, although in a few cases bicapped trigonal prismatic geometries (BCTP) have been observed. The sizes of the metal atom and of the X ligand seem to be responsible for the differences found in the coordination geometries.

In order to obtain structural information on the complexes based on the $An(HBPz_3)_2^{2+}$ moiety and to ascertain if the different sizes of thorium and uranium atoms influence the coordination geometries of the complexes $AnCl_2(HBPz_3)_2$, we have undertaken the X-ray structural analyses of these compounds.

EXPERIMENTAL

The syntheses and characterization of **1** and **2** have been reported earlier.[2,16,17] Crystals suitable for X-ray diffraction were obtained by slow diffusion of *n*-pentane into saturated solutions of the compounds in CH_2Cl_2. The crystals were mounted in thin-walled glass capillaries in a nitrogen-filled glove box.

Data were collected at room temperature on a Enraf–Nonius CAD4 diffractometer with graphite-monochromated Mo-K_α radiation, using the ω–2θ scan mode, in the range $3.0 < 2\theta < 50°$. Unit cell parameters were determined from 25 reflections with $26 < 2\theta < 34°$. A summary of the crystal data and data collection and refinement is given in Table 1. Data were corrected for Lorentz-polarization, for absorption by empirical corrections based on ψ scans, and for linear decay using the Enraf–Nonius program. The structures were solved by Patterson and Fourier methods.[18] For **1** all the non-hydrogen atoms were refined anisotropically by full-matrix least-squares. For **2** all but the carbon atoms were

* Author to whom correspondence should be addressed.

Table 1. Crystallographic data

Compound	$ThCl_2(HBPz_3)_2$ (1)	$UCl_2(HBPz_3)_2 \cdot 0.5CH_2Cl_2$ (2)
Formula	$C_{18}H_{20}B_2Cl_2N_{12}Th$	$C_{18}H_{20}B_2Cl_2N_{12}U \cdot 0.5CH_2Cl_2$
Formula weight	729.00	777.46
Crystal system	Orthorhombic	Triclinic
Space group	*Pbca*	$P\bar{1}$
a (Å)	14.406(2)	13.134(2)
b (Å)	18.523(3)	14.481(3)
c (Å)	18.947(4)	17.030(2)
α (°)	90	75.72(2)
β (°)	90	75.08(2)
γ (°)	90	68.20(2)
V (Å^3)	5056	2864
Z	8	4
D_{calc} (g cm^{-3})	1.915	1.803
Linear absorbance coefficient (cm^{-1}) (Mo-K_α)	58.6	57.0
Decay corrections: min., max.	1.00008, 1.11213 (−19.2% in 110.7 h)	1.00001, 1.02104 (−4.1% in 116.7 h)
Range in absorbance corrections factors	0.9206, 0.9996	0.8199, 0.9987
Number of unique data collected	3620	11 282
Number of unique data used	2846 [$F_o > 2\sigma(F_o)$]	9446 [$F_o > 5\sigma(F_o)$]
Number of parameters refined	323	456 (block refined)
Weighting scheme used, w = $(\sigma^2(F_o)+gF_o^2)^{-1}$, g	0.0007	0.0005
Final R, R_w	0.044, 0.046	0.046, 0.074

refined anisotropically by block full-matrix methods. The structural analysis of **2** revealed one CH_2Cl_2 molecule of crystallization in the unit cell, with high temperature factors and poorly localized. The contribution of the hydrogen atoms were included in calculated positions, constrained to ride on their carbon and boron atoms with group U_{iso} values assigned. Maximum and minimum heights in final difference Fourier maps were +1.99, −2.20 eÅ^{-3} and +2.43, −1.99 eÅ^{-3} for compounds **1** and **2**, respectively, close in both cases to the actinide atom.

Atomic scattering factors and anomalous dispersion terms were taken from *International Tables for X-ray Crystallography*.

Tables of final atomic positional and thermal parameters, full lists of bond lengths and angles, equations of mean-least-square planes, coordination polyhedron parameters and tables of F_o/F_c values have been deposited as supplementary material with the Editor.

DESCRIPTION OF THE STRUCTURES

In both compounds the crystal structures consist of discrete molecules in which the actinide atom is eight-coordinated by six nitrogens of the two tridentate ligands and by two chlorine atoms. The coordination geometries are described as SAP. The donor nitrogens of each pyrazolyl ligand occupy two triangular faces of the SAP while the chlorine atoms are in adjacent sites along a lateral edge.

The structure of the $ThCl_2(HBPz_3)_2$ is shown in Fig. 1, together with the atom numbering scheme. Figure 2 shows a view of the coordination polyhedron and Table 2 presents the normalized edge lengths. The values of the shape parameters for the normalized polyhedron,[19,20] namely the dihedral angles, δ, refered to the edges of the polyhedron and the ϕ values for the planarity of the two orthogonal trapezoids are presented in Table 3 along with the values for the three regular ML_8 polyhedra. Although these values compare satisfactorily with the values for the regular SAP geometry, there is a clear distortion. The face formed by Cl(1), N(3), N(1) and N(5) is approximately planar (root-mean-square deviation of 0.0021 Å) with δ values of 0.58° and diagonal distances of 1.69 Å, while the Cl(2) N(2) N(4) N(6) face is quite folded with δ values of 15.1 and 16.4° for the N(4)—Cl(2) and N(2)—N(6) diagonals, with lengths of 1.63 and 1.78 Å, respectively. The loss of the planarity of this face coupled

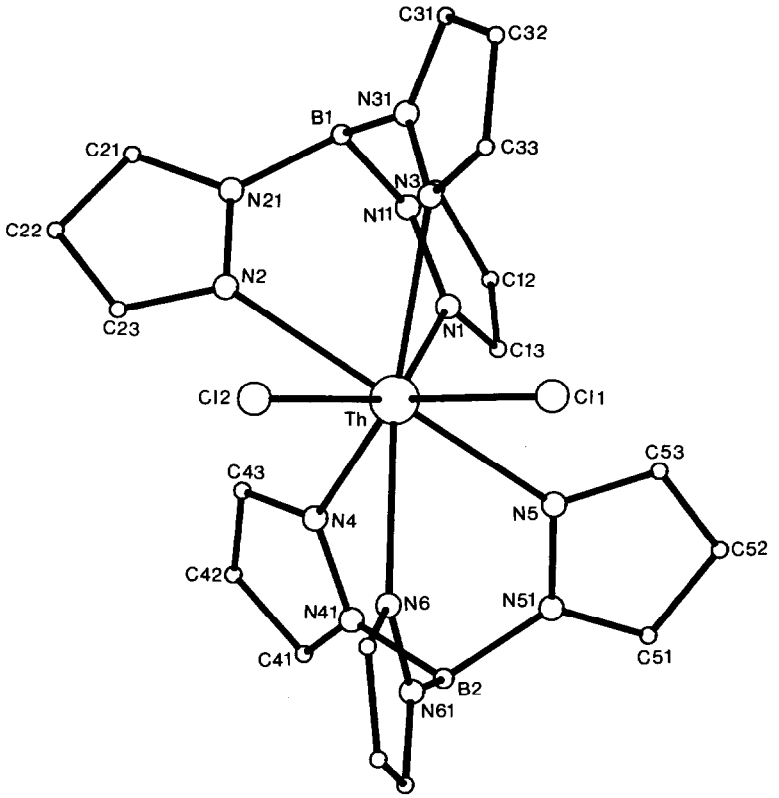

Fig. 1. PLUTO view of $ThCl_2(HBPz_3)_2$.

with the shortening of the N(4)—Cl(2) diagonal show that the distortion of the SAP is along the geometric pathway towards the BCTP.

Table 4 shows selected bond lengths and bond angles for **1**. The Th—N bond lengths range from 2.554(10) to 2.644(10) Å, with a mean value of 2.60(3) Å. The longest Th—N distance is the one opposite the chlorine atom on the planar square-face, while for the folded square-face the longest distances are those corresponding to the longer diagonal, which are, respectively, Th—N(2) and Th—N(6).

In the structure of $UCl_2(HBPz_3)_2 \cdot 0.5CH_2Cl_2$ there are two crystallographically independent mol-

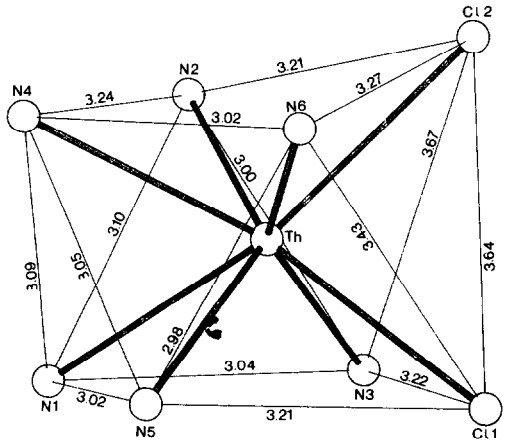

Fig. 2. PLUTO view of the SAP coordination polyhedron of $ThCl_2(HBPz_3)_2$. Edge lengths are in Å.

Table 2. Normalized polyhedral edges (Å) for $ThCl_2(HBPz_3)_2$

	(I) Square edges		
N(1)—N(5)	1.16	N(4)—N(6)	1.16
N(5)—Cl(1)	1.22	N(6)—Cl(2)	1.24
Cl(1)—N(3)	1.22	Cl(2)—N(2)	1.21
N(3)—N(1)	1.16	N(2)—N(4)	1.24
	(II) Triangular edges		
N(1)—N(4)	1.18	Cl(1)—Cl(2)	1.36
N(1)—N(2)	1.18	Cl(1)—N(6)	1.29
N(5)—N(4)	1.19	N(3)—Cl(2)	1.40
N(5)—N(6)	1.15	N(3)—N(2)	1.16
	(III) Square diagonals		
N(1)—Cl(1)	1.69	N(4)—Cl(2)	1.63
N(3)—N(5)	1.69	N(2)—N(6)	1.78

Table 3. Normalized shape parameters (°) for $ThCl_2(HBPz_3)_2$

			SAP	BCTP	DOD
δ_s	N(1)[N(3)N(5)]Cl(1)	0.58	0.0	0.0	29.5
δ_s	N(2)[N(4)Cl(2)]N(6)	15.1	0.0	21.8	29.5
δ_l	N(1)[N(4)N(5)]N(6)	47.5	52.5	48.2	29.5
δ_l	Cl(1)[Cl(2)N(3)]N(2)	44.7	52.5	48.2	29.5
ϕ	N(3)—Cl(1)—N(6)—N(4)	19.4	24.5	14.1	0.0
ϕ	N(5)—N(1)—N(2)—Cl(2)	15.8	24.5	14.1	0.0

ecules in the asymmetric unit. Figure 3 shows a view of the two molecules in the asymmetric unit, with the atom numbering scheme. The CH_2Cl_2 of crystallization does not interact with the uranium molecules and is not shown. In both molecules the coordination geometries around the uranium are best described as SAP as can be seen from the δ and ϕ values shown in Table 5. In molecule 1 (Fig. 4), one of the square-faces is nearly planar (root-mean-square deviation of 0.0064 Å) with a δ value of 1.8° and square diagonals of 1.67 and 1.68 Å, while the face Cl(2) N(3) N(4) N(5) with δ values of 5.9 and 6.1° is less planar (root-mean-square deviation of 0.0221 Å) and has diagonal distances of 1.67 and 1.72 Å. In molecule 2, one of the two square-faces is folded with δ values of 9.6 and 10.1° and diagonal distances of 1.63 and 1.72 Å, while the other remains planar (δ = 1.0° and diagonal distances of 1.69 Å). Both molecules are distorted SAP (Tables 5 and 6), giving the second molecule a greater distortion with considerable folding of one of its square-faces (δ = 10.1°).

Selected bond lengths and angles are presented in Table 7. Within three standard deviations, the two molecules have similar molecular dimensions. The U—N bond lengths range from 2.532(8) to 2.576(9) Å in molecule 1, and from 2.524(11) to 2.593(8) Å in molecule 2. The longest U—N distances are those opposite to the chlorine atoms in each square-face.

DISCUSSION

The An—Cl and An—N bond length differences between compounds **1** and **2** are consistent with the difference of 0.05 Å between the ionic radii of Th^{IV} and U^{IV} (av. Th—Cl and Th—N are 2.68(1) and 2.60(3) Å, compared with 2.63(1) and 2.55(2) Å for U—Cl and U—N distances).

A comparison of the bond lengths of **2** with

Table 4. Selected bond lengths (Å) and bond angles (°) for $ThCl_2(HBPz_3)_2$[a]

Th—Cl(1)	2.690(4)	Th—N(3)	2.578(10)
Th—Cl(2)	2.676(4)	Th—N(4)	2.599(10)
Th—N(1)	2.644(10)	Th—N(5)	2.554(10)
Th—N(2)	2.616(9)	Th—N(6)	2.622(9)
B—N	1.54(2)	N—C	1.35(2)
N—N	1.36(1)	C—C	1.37(1)
N—B—N	112(1)		

Cl(1)—Th—Cl(2)	85.4(2)	N(4)—Th—N(5)	72.7(4)
Cl(1)—Th—N(3)	75.3(3)	N(4)—Th—N(6)	70.8(4)
Cl(1)—Th—N(5)	75.4(3)	N(6)—Th—N(5)	70.2(4)
Cl(1)—Th—N(6)	80.5(3)	N(1)—Th—N(4)	72.2(4)
Cl(2)—Th—N(2)	74.6(3)	N(1)—Th—N(5)	71.0(4)
Cl(2)—Th—N(3)	88.7(3)	N(2)—Th—N(4)	76.8(4)
Cl(2)—Th—N(6)	76.3(3)	Cl(1)—Th—N(1)	114.8(3)
N(1)—Th—N(2)	72.2(4)	N(3)—Th—N(5)	115.1(4)
N(1)—Th—N(3)	71.1(4)	Cl(2)—Th—N(4)	109.5(3)
N(3)—Th—N(2)	70.6(4)	N(2)—Th—N(6)	125.3(4)

[a] The average B—N, N—N, N—C and C—C distances and the average N—B—N angle of the ligand $HBPz_3$ are given.

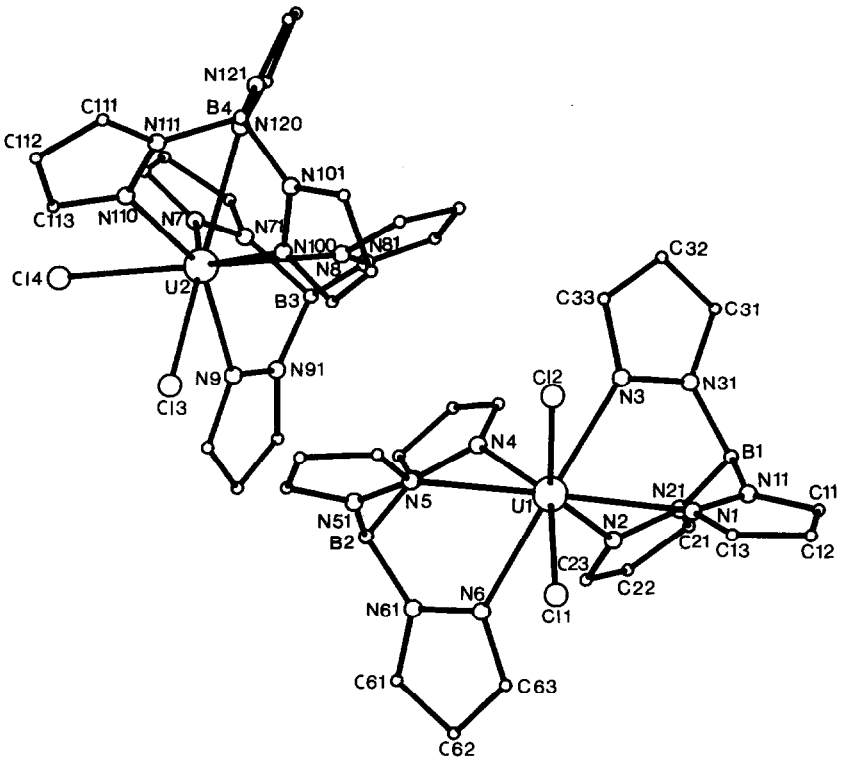

Fig. 3. PLUTO view of $UCl_2(HBPz_3)_2$, as they are in the asymmetric unit.

those of the related $UCl(OBu^t)(HBPz_3)_2$ and $UCl(OC_6H_5)(HBPz_3)_2$ complexes shows longer U—Cl bond distances in the latter compounds (2.697(2) and 2.682(6) Å, respectively) probably due to the larger size of the oxygen donor ligands. The U—N bond distances (av. 2.60(2) and 2.57(2) Å) fall within the range found for compound **2**.

The An—Cl bond distances in **1** and **2** can be compared with corresponding bond distances in the formally eight-coordinated compounds, $AnCl_2Cp''_2$ ($Cp'' = C_5H_3$-1,3-$(SiMe_3)_2$; An = Th^{IV}, 2.632(2) Å; An = U^{IV}, 2.579(2) Å).[21] The longer distances observed for the polypyrazolylborate complexes are certainly due to the larger size of the $(HBPz_3)^-$ ligand compared to the $(Cp'')^-$ ligand. Taking into account the recently introduced concept of the steric coordination number of a ligand,[22] the above formally eight-coordinate complexes have different steric coordination numbers of 7.80 for $AnCl_2(HBPz_3)_2$ and 7.20 for $AnCl_2Cp''_2$, which is in agreement with the longer An—Cl bond distances observed in the former complexes.

The referred analogy between the hydrotris(pyrazolyl)borate and the cyclopentadienyl ligands has sometimes led to a description of these types of compound in terms of a bent sandwich geometry. In MCp_2X_2 complexes the relevant angular parameters are the dihedral angle formed by the planes CpMCp (Cp = centre of gravity of cyclo-

Table 5. Normalized shape parameters (°) for $UCl_2(HBPz_3)_2$

	Molecule 1		Molecule 2	
δ_s	Cl(1)[N(1)N(6)]N(2)	1.8	Cl(3)[N(9)N(100)]N(8)	1.0
δ_s	N(3)[Cl(2)N(4)]N(5)	5.9	N(7)[Cl(4)N(120)]N(110)	9.6
δ_t	N(2)[N(4)N(6)]N(5)	43.5	Cl(3)[Cl(4)N(9)]N(7)	44.9
δ_t	Cl(1)[Cl(2)N(1)]N(3)	45.2	N(110)[N(100)N(120)]N(8)	44.4
ϕ	Cl(2)—N(3)—N(2)—N(6)	17.2	Cl(4)—N(7)—N(8)—N(100)	17.0
ϕ	N(4)—N(5)—Cl(1)—N(1)	20.2	N(9)—Cl(3)—N(110)—N(120)	19.1

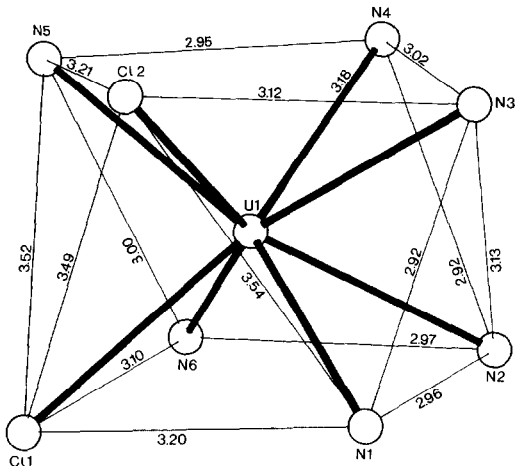

Fig. 4. PLUTO view of the SAP polyhedron of molecule 1 of $UCl_2(HBPz_3)_2$. Edge lengths are in Å.

pentadienyl) and XMX, which are found to be close to 90°, and the four Cp—M—X angles, which are identical. In the case of MCp_2XY complexes there are two sets of identical Cp—M—X and identical Cp—M—Y angles. For the hydrotris(pyrazolyl) borate complexes where structures are known, the corresponding parameters can be obtained by taking the boron atom as the centre of the tridentate ligand, and the values obtained are presented in Table 8.

It is apparent from the table that only for the BCTP complexes are the parameters considered in agreement with the bent sandwich geometry. For the majority of these complexes whose molecular structures are known, this type of description is inadequate, being, however, an easy way to distinguish SAP from BCTP complexes.

CONCLUSIONS

The structural analyses undertaken show that compounds **1** and **2** are not isomorphous. However, the coordination geometries are similar in the two compounds, SAP, distorted towards BCTP, with the thorium compound presenting a greater distorsion. This may be a consequence of the larger size of thorium which makes ligand–ligand repulsions in the coordination sphere of lesser importance (there are nine short intra-ligand contacts in **1** compared with 16 in **2**). Additionally, the thorium compound presents a few short intermolecular contacts,

Table 6. Normalized polyhedral edges (Å) for $UCl_2(HBPz_3)_2$

Molecule 1		Molecule 2	
	(I) Square edges		
Cl(1)—N(1)	1.23	Cl(3)—N(9)	1.24
N(1)—N(2)	1.15	N(9)—N(8)	1.16
N(2)—N(6)	1.16	N(8)—N(100)	1.17
N(6)—Cl(1)	1.20	N(100)—Cl(3)	1.22
Cl(2)—N(3)	1.21	Cl(4)—N(7)	1.17
N(3)—N(4)	1.18	N(7)—N(120)	1.16
N(4)—N(5)	1.16	N(120)—N(110)	1.18
N(5)—Cl(2)	1.25	N(110)—Cl(4)	1.24
	(II) Triangular edges		
Cl(1)—Cl(2)	1.33	Cl(3)—Cl(4)	1.35
Cl(2)—N(1)	1.37	Cl(4)—N(9)	1.38
N(1)—N(3)	1.16	N(9)—N(7)	1.16
N(3)—N(2)	1.22	N(7)—N(8)	1.21
N(2)—N(4)	1.14	N(8)—N(120)	1.14
N(4)—N(6)	1.24	N(120)—N(100)	1.25
N(6)—N(5)	1.18	N(100)—N(110)	1.17
N(5)—Cl(1)	1.37	N(110)—Cl(3)	1.34
	(III) Square diagonals		
N(1)—N(6)	1.68	Cl(3)—N(8)	1.69
Cl(1)—N(2)	1.67	N(9)—N(100)	1.69
Cl(2)—N(4)	1.67	Cl(4)—N(120)	1.63
N(3)—N(5)	1.72	N(7)—N(110)	1.72

Table 7. Selected bond lengths (Å) and bond angles (°) for $UCl_2(HBPz_3)_2$[a]

Molecule 1		Molecule 2	
U(1)—Cl(1)	2.626(4)	U(2)—Cl(3)	2.626(4)
U(1)—Cl(2)	2.621(5)	U(2)—Cl(4)	2.640(3)
U(1)—N(1)	2.534(8)	U(2)—N(7)	2.563(9)
U(1)—N(2)	2.576(9)	U(2)—N(8)	2.593(8)
U(1)—N(3)	2.541(11)	U(2)—N(9)	2.524(11)
U(1)—N(4)	2.563(9)	U(2)—N(100)	2.527(8)
U(1)—N(5)	2.532(8)	U(2)—N(110)	2.527(10)
U(1)—N(6)	2.554(11)	U(2)—N(120)	2.574(11)
B—N	1.53(3)	B—N	1.55(4)
N—N	1.36(2)	N—N	1.36(2)
N—C	1.35(4)	N—C	1.34(2)
C—C	1.38(5)	C—C	1.38(4)
N—B—N	109(2)	N—B—N	109(1)
Cl(1)—U(1)—Cl(2)	83.4(2)	Cl(3)—U(2)—Cl(4)	84.9(2)
Cl(1)—U(1)—N(1)	76.7(3)	Cl(3)—U(2)—N(9)	76.6(3)
Cl(1)—U(1)—N(5)	86.1(3)	Cl(3)—U(2)—N(100)	75.3(3)
Cl(1)—U(1)—N(6)	73.4(3)	Cl(3)—U(2)—N(110)	84.2(3)
Cl(2)—U(1)—N(1)	86.6(3)	Cl(4)—U(2)—N(7)	71.8(3)
Cl(2)—U(1)—N(3)	74.3(4)	Cl(4)—U(2)—N(9)	87.4(3)
Cl(2)—U(1)—N(5)	77.1(3)	Cl(4)—U(2)—N(110)	76.7(3)
N(2)—U(1)—N(4)	69.3(4)	N(7)—U(2)—N(120)	71.1(4)
N(2)—U(1)—N(6)	70.8(4)	N(8)—U(2)—N(100)	71.8(3)
N(3)—U(1)—N(4)	72.4(4)	N(8)—U(2)—N(120)	69.6(4)
Cl(1)—U(1)—N(2)	113.3(3)	Cl(3)—U(2)—N(8)	115.4(3)
N(1)—U(1)—N(6)	115.3(4)	N(9)—U(2)—N(100)	116.2(4)
Cl(2)—U(1)—N(4)	112.8(4)	Cl(4)—U(2)—N(120)	109.2(3)
N(3)—U(1)—N(5)	118.6(4)	N(7)—U(2)—N(110)	119.0(4)
N(1)—U(1)—N(2)	70.9(4)	N(7)—U(2)—N(8)	74.5(3)
N(1)—U(1)—N(3)	70.3(4)	N(7)—U(2)—N(9)	71.2(4)
N(3)—U(1)—N(2)	75.3(4)	N(9)—U(2)—N(8)	70.8(4)
N(4)—U(1)—N(5)	70.6(3)	N(100)—U(2)—N(110)	71.4(4)
N(4)—U(1)—N(6)	76.9(4)	N(100)—U(2)—N(120)	77.0(4)
N(6)—U(1)—N(5)	72.1(4)	N(120)—U(2)—N(110)	72.2(4)

[a] The average B—N, N—N, N—C and C—C distances and the average N—B—N angles of the ligand $HBPz_3$ are given.

Table 8. Angular parameters in the "bent-sandwich" description of $M(X)(Y)(HBPz_3)_2$ complexes

Compound		Coordination geometry	$[B_1MB_2][XMY]$	B_1MX	B_1MY	B_2MX	B_2MY	Reference
$ThCl_2(HBPz_3)_2$		SAP	100.0	115.7	104.2	100.2	114.3	
$UCl_2(HBPz_3)_2$	mol. 1	SAP	101.3	116.8	104.2	102.6	118.4	This work
	mol. 2		101.5	117.8	101.7	104.0	117.0	
$UCl(OBu^t)(HBPz_3)_2$		SAP	101.4	116.5	102.7	100.6	116.5	8
$UCl(OPh)(HBPz_3)_2$		SAP	102.4	115.6	99.7	100.9	117.2	
$UCl(OC_2H_5)(HBPz_3)_2$		SAP	98.4	114.7	105.5	101.5	114.0	23
$YCl(H_2O)(HBPz_3)_2$		SAP	105.2	120.9	98.8	103.6	117.7	14
$YCl(PzH)(HBPz_3)_2$		SAP	110.8	120.6	93.9	98.3	120.3	15
$Yb(acac)(HBPz_3)_2$	mol. 1	SAP	102.4	118.4	105.6	100.7	116.7	11
	mol. 2		104.0	118.3	102.4	102.7	119.3	
$Ce(acac)(HBPz_3)_2$		BCTP	91.4	108.6	111.7	111.7	111.7	
$Yb(HBPz_3)_3$		BCTP	90.6	104.1	103.9	113.8	115.3	9

namely between Cl···C(51) 3.45, C(51)···C(53) 3.24 and C(51)···C(52) 3.39 Å (there are no short intermolecular contacts in **2**). The differences found in the coordination geometries could also be due to the different packings observed.

REFERENCES

1. N. Marques, A. Pires de Matos, I. Santos and M. Silva, *19èmes Journées des Actinides*. Madonna de Campiglio, Italy (1989).
2. I. Santos, J. Marçalo, N. Marques and A. Pires de Matos, *Inorg. Chim. Acta* 1987, **134**, 315.
3. I. Santos, N. Marques and A. Pires de Matos, *Inorg. Chim. Acta* 1987, **139**, 89.
4. J. Marçalo and A. Pires de Matos, unpublished results.
5. I. Santos, Â. Domingos, J. Marçalo, N. Marques and A. Pires de Matos, *XXVI Int. Conf. Coord. Chem.* Porto, Portugal (1988).
6. I. Santos and A. Pires de Matos, *Actinides*-89. Tashkent, U.S.S.R. (1989).
7. N. Marques, PhD thesis. Technical University of Lisbon, Portugal (1989).
8. Â. Domingos, A. Pires de Matos and I. Santos, *J. Less-Common Met.* 1989, **149**, 279.
9. M. V. R. Stainer and J. Takats, *Inorg. Chem.* 1982, **21**, 4050.
10. W. D. Moffat, M. V. R. Stainer and J. Takats, *Inorg. Chim. Acta* 1987, **139**, 75.
11. M. A. J. Moss, C. J. Jones and A. J. Edwards, *J. Chem. Soc., Dalton Trans.* 1989, 1393.
12. M. A. J. Moss and C. J. Jones, *Polyhedron* 1989, **8**, 117.
13. M. A. J. Moss and C. J. Jones, *Polyhedron* 1989, **8**, 555.
14. D. L. Reger, J. A. Lindeman and L. Lebioda, *Inorg. Chim. Acta* 1987, **139**, 71.
15. D. L. Reger, J. A. Lindeman and L. Lebioda, *Inorg. Chem.* 1988, **27**, 3923.
16. K. W. Bagnall, J. Edwards, J. G. H. du Preez and R. F. Warren, *J. Chem. Soc., Dalton Trans.* 1975, 140.
17. K. W. Bagnall, A. Beheshti and F. Heatley, *J. Less-Common Met.* 1978, **61**, 171.
18. G. M. Sheldrick, *SHELX Crystallographic Program*. University of Cambridge (1976).
19. E. L. Muetterties and L. J. Guggenberger, *J. Am. Chem. Soc.* 1974, **96**, 1748.
20. M. G. B. Drew, *Coord. Chem. Rev.* 1977, **24**, 179.
21. P. C. Blake, M. F. Lappert, R. G. Taylor, J. L. Atwood and H. Zhang, *Inorg. Chim. Acta* 1987, **139**, 13.
22. J. Marçalo and A. Pires de Matos, *Polyhedron* 1989, **8**, 2431.
23. Â. Domingos, I. Santos and A. Pires de Matos, manuscript in preparation.

Polyhedron Vol. 9, No. 14, pp. 1653–1657, 1990
Printed in Great Britain

0277–5387/90 $3.00+.00
© 1990 Pergamon Press plc

PREPARATION AND REACTION OF SALTS OF $[ZrO(O_2)F_2]^{2-}$ AND $[ZrO(O_2)_2F]^{3-}$

CHIRA R. BHATTACHARJEE, MANISH BHATTACHARJEE, MIHIR K. CHAUDHURI* and SURAJIT CHOUDHURY

Department of Chemistry, North-Eastern Hill University, Shillong 793 003, India

(*Received* 23 *October* 1989; *accepted* 1 *March* 1990)

Abstract—Salts of oxoperoxofluorozirconates(IV), $[ZrO(O_2)F_2]^{2-}$ and $[ZrO(O_2)_2F]^{3-}$, have been prepared from the reaction of $ZrO_2 \cdot nH_2O$ with H_2O_2 and hydrofluoric acid at pH 6 and 12, respectively. No peroxozirconate could be obtained below pH 6. A μ-oxo species $[F_5Zr—O—ZrF_5]^{4-}$ has been isolated from a similar reaction at pH 5. The compounds have been characterized by chemical analyses, magnetic susceptibility and EPR measurements, IR and laser Raman spectroscopic studies. $(NH_4)_2[ZrO(O_2)F_2]$ in water reacts with SO_2(g) to produce a ternary complex $(NH_4)_2[ZrO(SO_4)F_2] \cdot 7H_2O$.

Investigation of various aspects of peroxo–metal systems[1–4] is of current interest. Synthesis and characterization, followed by studies of reactivity provide a systematic approach to this field. Some of our earlier papers dealt with this aspect of a few lighter transition metals[1,4,5] and as a sequel such studies have now been extended to zirconium. Information on peroxozirconates is scanty.[6] Complexes $[Zr(O_2)F_5]^{3-}$ and $[Zr_2(O_2)_2F_7]^{3-}$ are known and the structure of $(NH_4)_3[Zr(O_2)F_5]$ has been determined by X-ray crystallography.[8] There has been no report of solid diperoxozirconates(IV) except one in which diperoxo species were claimed[9] but not isolated. Our aim was to prepare newer peroxozirconates including diperoxozirconates(IV) from the reaction of ZrO_2 with H_2O_2 and F^-, and to rationalize the course of reactions through isolation of compounds at different stages of the reaction. It was also of interest to study the reaction of peroxozirconates with SO_2(g) in aqueous medium. This was important since the earlier reports[10] involved group VIII metal–peroxo species and the reactions were conducted in non-aqueous medium. This report presents an account of the preparation, characterization and reaction of salts of $[ZrO(O_2)F_2]^{2-}$ and $[ZrO(O_2)_2F]^{3-}$.

* Author to whom correspondence should be addressed.

EXPERIMENTAL

The chemicals used were all reagent grade products. IR and laser Raman (LR) spectra were recorded on the instruments described earlier.[11–13] LR spectra were recorded only on solids. Magnetic susceptibilities were measured by the Gouy method; $Hg[Co(NCS)_4]$ was the calibrant. The pH values were measured with a Systronics type 335 digital pH meter and also with pH indicator (BDH) paper. The reactions and other manipulations were conducted in polyethylene apparatus. The water used for reactivity studies was deoxygenated by first boiling for 30 min under N_2 atmosphere and then cooling to room temperature, followed by bubbling of N_2(g) for 15 min. The water was stored in an airtight container. A suspension of $(NH_4)_2[ZrO(O_2)F_2]$ was prepared under N_2.

Synthesis of alkali metal or ammonium oxomonoperoxodifluorozirconates(IV), $A_2[ZrO(O_2)F_2]$ (A = Na, K *or* NH_4)

An aqueous solution (20 cm^3) of $ZrO(NO_3)_2 \cdot H_2O$ (1.0 g, 4 mmol) was treated with aqueous ammonia (sp.gr. 0.9) until $ZrO_2 \cdot nH_2O$ was completely precipitated. This was filtered off and washed thoroughly. To a water suspension of $ZrO_2 \cdot nH_2O$ was added 15 cm^3 (132.36 mmol) of

30% H_2O_2 with stirring followed by 1 cm^3 (24 mmol) of 48% HF, when a clear solution resulted. The pH of the solution was increased to 6 by adding AOH solution (20%) or aqueous ammonia (sp. gr. 0.9), whereupon a small amount of white product appeared. To ensure complete precipitation, 50 cm^3 of ethanol was added. The compound was filtered, washed 4–5 times with ethanol, and finally dried *in vacuo* over P_4O_{10}. Yields of $Na_2[ZrO(O_2)F_2]$, $K_2[ZrO(O_2)F_2]$ and $(NH_4)_2[ZrO(O_2)F_2]$ were 0.73 g(82%), 0.81 g (79%) and 0.75 g (87%), respectively.

Synthesis of sodium or ammonium oxodiperoxomonofluorozirconate(IV) *dihydrates*, $A_3[ZrO(O_2)_2F]\cdot 2H_2O$ (A = Na *or* NH_4)

The $A_3[ZrO(O_2)_2F]\cdot 2H_2O$ compounds were prepared in a manner analogous to that described above for the synthesis of $A_2[ZrO(O_2)F_2]$ except that the pH of the reaction solution was increased to 12. Yields of $Na_3[ZrO(O_2)_2F]\cdot 2H_2O$ and $(NH_4)_3[ZrO(O_2)_2F]\cdot 2H_2O$ were 0.87 g (71%) and 0.78 g (75%), respectively.

Isolation of alkali metal or ammonium μ-oxodecafluorodizirconates(IV), $A_4[F_5Zr—O—ZrF_5]$ (A = Na, K *or* NH_4)

The $A_4[F_5Zr—O—ZrF_5]$ complexes were isolated from reaction solutions obtained in a similar way to those described under the synthesis of $A_2[ZrO(O_2)F_2]$. However, the pH of the reaction solution was held at 5 instead of increasing it to 6. The compound was precipitated out by the addition of ethanol. Yields of $Na_4[Zr_2OF_{10}]$, $K_4[Zr_2OF_{10}]$ and $(NH_4)_4[Zr_2OF_{10}]$ were 1.37 g (72%), 1.73 g (80%) and 1.38 g (74%), respectively.

Reaction of $(NH_4)_2[ZrO(O_2)F_2]$ *with* SO_2(g). *Isolation of* $(NH_4)_2[ZrO(SO_4)F_2]\cdot 7H_2O$

Through an aqueous (25 cm^3) suspension of $(NH_4)_2[ZrO(O_2)F_2]$ (1 g, 4.69 mmol), SO_2(g) was slowly bubbled until the solution registered a pH value of 2–1. This was filtered and ethanol was added to initiate precipitation. It was allowed to stand for 2 h and then filtered to isolate the white crystalline product. The compound was washed with water and ethanol, and finally dried *in vacuo* over conc. H_2SO_4. The yield of $(NH_4)_2[ZrO(SO_4)F_2]\cdot 7H_2O$ was 0.97 g (47%).

Elemental analyses

Zirconium was estimated gravimetrically as ZrO_2.[14a] The peroxide content was determined by redox titration with standard solutions of $KMnO_4$[14b] or Ce^{4+}.[14c] Fluoride was precipitated as PbClF and chloride estimated by Volhard's method, from which the fluoride content was calculated.[14d] Nitrogen, potassium, sodium and sulphate were estimated by methods described previously.[11,15] The analytical results are given in Table 1.

RESULTS AND DISCUSSION

Synthesis

Peroxo–metal systems can be stabilized in the presence of an appropriate heteroligand at a suitable pH.[1,5,11–13] The present strategy was to react ZrO_2 with H_2O_2 and F^- in the presence of each other and also to evaluate the appropriate pH for the desired synthesis. The pH values conducive to the preparation of $[ZrO(O_2)F_2]^{2-}$ and $[ZrO(O_2)_2F]^{3-}$ were ascertained to be 6 and 12, respectively. While the salts of the monoperoxo complex were anhydrous, those of the diperoxo species were dihydrates. $A_3[ZrO(O_2)_2F]\cdot 2H_2O$ (A = Na or NH_4) were obtained, for the first time, in the solid state. In order to gain an insight into the course of the reaction, the product at pH 5 was isolated and characterized as a μ-oxo species, $[F_5Zr—O—ZrF_5]^{4-}$. It is possible that a peroxozirconate might have formed at this pH but decomposed leading to the μ-oxo complex as obtained. Such a problem is encountered in peroxo–metal chemistry.[16]

Characterization

The compounds are diamagnetic, EPR silent and sparingly soluble. They dissolve in an acidified (dil. H_2SO_4) solution in which the peroxozirconates(IV) quantitatively liberate active oxygen. The results of chemical analyses are consistent with the formulae, $A_2[ZrO(O_2)F_2]$, $A_3[ZrO(O_2)_2F]$ and $A_4[Zr_2OF_{10}]$. LR spectra of $A_4[Zr_2OF_{10}]$ could not be recorded owing to extensive fluoroescence, however, the IR spectra (Table 1) provide clear evidence for the ν(Zr—F) and Zr—F deformation modes.[7] Absence of any absorption at *ca* 950 cm^{-1} and the consistent appearance of a band at *ca* 740m,br cm^{-1} attest to the occurrence of Zr—O—Zr vibrations[17] in accord with a μ-oxo dimer. The diagnostic IR and LR signatures for $A_2[ZrO(O_2)F_2]$ and $A_3[ZrO(O)_2F]\cdot 2H_2O$ comprise ν(Zr=O), ν(O—O) (ν_1), ν(Zr—O_2) (ν_2,ν_3), and ν(Zr—F) modes (Table 1). The peroxide ligand binds the metal centre, in each case, in a triangular bidentate manner. Two additional IR bands at *ca* 1640s and *ca* 3455s cm^{-1} for the

Table 1. Analytical data and structurally significant IR and Raman bands of $A_2[ZrO(O_2)F_2]$ (A = Na, K or NH_4), $A_3[ZrO(O_2)_2F]\cdot 2H_2O$ (A = Na or NH_4) and $A_4[F_5Zr—O—ZrF_5]$ (A = Na, K or NH_4)

Compound	Analysis[a] (%) A or N	Zr	O_A[b] or SO_4[c]	F	IR (cm^{-1})	Raman (cm^{-1})	Assignment
$(NH_4)_2[ZrO(O_2)F_2]$	13.0	42.1	15.3	18.1	981s	1020	ν(Zr=O)
	(13.1)	(42.8)	(15.0)	(17.8)	850s	847	ν(O—O) ν_1
					640s	650	ν(Zr—O_2) ν_2
					585m	590	ν(Zr—O_2) ν_3
					460s	480	ν(Zr—F)
					249		(Zr—F) def.
$Na_2[ZrO(O_2)F_2]$	20.2	41.1	14.5	17.3	980s	1015	ν(Zr=O)
	(20.6)	(40.9)	(14.3)	(17.0)	850s	850	ν(O—O) ν_1
					645s	650	ν(Zr—O_2) ν_2
					580m	595	ν(Zr—O_2) ν_3
					455s	480	ν(Zr—F)
					250		(Zr—F) def.
$K_2[ZrO(O_2)F_2]$	30.1	36.2	12.8	15.2	985s	1017	ν(Zr=O)
	(30.6)	(35.7)	(12.5)	(14.9)	850s	850	ν(O—O) ν_1
					640s	650	ν(Zr—O_2) ν_2
					585m	590	ν(Zr—O_2) ν_3
					440s	475	ν(Zr—F)
					250		(Zr—F) def.
$(NH_4)_3[ZrO(O_2)_2F]\cdot 2H_2O$	15.1	32.2	23.1	7.1	990s	1025	ν(Zr=O)
	(15.0)	(32.5)	(22.8)	(6.8)	860s	858	ν(O—O) ν_1
					640s	650	ν(Zr—O_2) ν_2
					580m	590	ν(Zr—O_2) ν_3
					455s	470	ν(Zr—F)
					250		(Zr—F) def.
					3455s		ν(O—H)
					1640s		δ(H—O—H)
$Na_3[ZrO(O_2)_2F]\cdot 2H_2O$	23.6	31.3	22.1	6.8	985s	1020	ν(Zr=O)
	(23.4)	(30.9)	(21.7)	(6.4)	860s	860	ν(O—O) ν_1
					650s	650	ν(Zr—O_2) ν_2
					578m	590	ν(Zr—O_2) ν_3
					450s	460	ν(Zr—F)
					250		(Zr—F) def.
					3460s		ν(O—H)
					1640s		δ(H—O—H)
$(NH_4)_4[F_5Zr—O—ZrF_5]$	12.3	40.1		41.6	741		ν(Zr—O—Zr)
	(12.2)	(39.6)		(41.2)	490		ν(Zr—F)
					246		(Zr—F) def.
$Na_4[F_5Zr—O—ZrF_5]$	19.5	38.0		40.3	749		ν(Zr—O—Zr)
	(19.1)	(38.2)		(39.5)	468		ν(Zr—F)
					248		(Zr—F) def.
$K_4[F_5Zr—O—ZrF_5]$	29.1	34.0		35.2	735		ν(Zr—O—Zr)
	(28.7)	(33.5)		(34.9)	460		ν(Zr—F)
					240		(Zr—F) def.
$(NH_4)_2[ZrO(SO_4)F_2]\cdot 7H_2O$	6.9	22.3	24.2[c]	9.2	980s	1010	ν(Zr=O)
	(6.9)	(22.6)	(23.8)	(9.4)	970m	990	ν_1
					470m	470	ν_2
					1220s	1215	ν_3
					1145s	1145	ν_3
					1030s	1020	ν_3
					685s	680	ν_4
					635s	640	ν_4
					605s	610	ν_4
					460m	460	ν(Zr—F)

SO_4 modes

[a] Calculated values are given in parentheses. [b] Active oxygen. [c] Sulphate.

diperoxo complexes are in agreement with the presence of lattice water.[18,19]

Reaction of $SO_2(g)$ *with* $(NH_4)_2[ZrO(O_2)F_2]$

The oxoperoxodifluorozirconate(IV) readily reacted with $SO_2(g)$ in an aqueous medium as evident from a near quantitative solubility of the complex species during the bubbling of $SO_2(g)$ (*vide* Experimental). The reaction solution registered a pH value of 2–1 at that stage and the product isolated was characterized to be $(NH_4)_2[ZrO(SO_4)F_2]\cdot 7H_2O$.

The compound is diamagnetic in nature and sparingly soluble. The IR and LR spectra of the compound produced evidence for the complete absence of peroxide, which was also ascertained by chemical analysis. The spectra provide clear evidence for the ν(Zr=O) and ν(Zr—F) vibrations in similar regions to those of the other compounds reported herein and the expected bands for the presence of NH_4^+ and lattice water. For sulphate, the appearance of medium intensity ν_1 and ν_2 modes and the splitting of ν_3 and ν_4 vibrations into three bands each (Table 1), in contrast to the absence of ν_1 and ν_2 and occurrence of unsplit ν_3 and ν_4, suggest the lowering of the symmetry of SO_4^{2-} from T_d to C_{2v},[20] and its presence as a chelated ligand in the complex. The formation of the sulphato complex is explained in terms of an insertion of SO_2 into the O—O bond of the coordinated peroxide, without causing any reduction of the metal centre. This is an interesting reaction because it not only provides access to a new ternary complex of zirconium(IV), but also this route prevents the formation of a binary fluorozirconate(IV) which is normally a problem in the synthesis of mixed-ligand fluorozirconates(IV).

Concluding remarks

As in the case of titanium, monoperoxo and diperoxofluoro complexes of zirconium(IV) are capable of being synthesized under the appropriate experimental conditions. The pH of the reaction medium plays a very important role; a pH > 7 is required for the successful synthesis of diperoxo complexes of both titanium and zirconium. The peroxo compounds of zirconium are obtained as oxoperoxozirconate(IV) species containing a zirconyl (ZrO^{2+}) centre, unlike those of titanium[5] which contain titanium(IV) centres. Isolation of a μ-oxo-dizirconate(IV) species, $[F_5Zr—O—ZrF_5]^{4-}$, at pH $\geqslant 5 < 6$ suggests that such a complex might be the precursor for the oxomonoperoxozirconate(IV), however, the chances of peroxozirconate(IV) formation at a pH of *ca* 5 which may have decomposed to the μ-oxo complex either in the solution or in the process of its isolation, so often encountered in peroxo–metal chemistry,[16] should not be discounted. The complex $[ZrO(O_2)F_2]^{2-}$ ion reacts with $SO_2(g)$ in aqueous medium to afford the ternary $[ZrO(SO_4)F_2]^{2-}$ complex through insertion of SO_2 into the O—O bond.

Acknowledgement—The authors thank the CSIR, New Delhi, for the award of fellowships to M.B. and C.R.B., and also for financial support (Grant. No. 1(1049)/86).

REFERENCES

1. M. K. Chaudhuri, *Proc. Ind. Nat. Sci. Acad.* 1986, **52A**, 996.
2. H. Mimoun, *The Chemistry of Functional Groups, Peroxides* (Edited by S. Patai), p. 463. John Wiley, New York (1983); H. Mimoun, L. Saussine, E. Daire, M. Postal, J. Fischer and R. Weiss, *J. Am. Chem. Soc.* 1983, **105**, 3101; H. Mimoun, M. Mignard, P. Brechot and L. Saussine, *J. Am. Chem. Soc.* 1986, **108**, 3711.
3. C. Djordjevic and G. L. Wampler, *J. Inorg. Biochem.* 1985, **25**, 51; M. Rau, M. S. Patole, S. Vijay, C. K. R. Kurup and T. Ramsarma, *Molec. Cell. Biochem.* 1987, **75**, 151; M. S. Patole, C. K. R. Kurup and T. Ramsarma, *Molec. Cell. Biochem.* 1987, **75**, 161.
4. M. K. Chaudhuri, *J. Molec. Catal.* 1988, **44**, 129 and refs cited therein.
5. M. K. Chaudhuri and B. Das, *Inorg. Chem.* 1986, **25**, 168.
6. R. J. H. Clark, D. C. Bradley and P. Thornton, The Chemistry of Titanium, Zirconium and Hafnium, in *Pergamon Texts in Inorganic Chemistry*, Vol. 19, p. 453. Pergamon Press, Oxford (1975); W. P. Griffith and T. D. Wickins, *J. Chem. Soc. A* 1968, 397; M. T. H. Tarafdar and M. A. L. Miah, *Inorg. Chem.* 1986, **25**, 2265.
7. P. W. Smith, R. Socssiger and A. G. Turnbell, *J. Chem. Soc.* 1968, 3013; G. V. Jere and M. T. Santhamma, *Inorg. Chim. Acta* 1977, **24**, 57.
8. R. Schmidt, G. Pauseway and W. Massa, *Z. Anorg. Chem.* 1986, **535**, 135.
9. A. K. Babko and N. V. Ul'ko, *Ukr. Khim. Zh.* 1961, **27**, 290.
10. A. R. Miksztal and J. S. Valentine, *Inorg. Chem.* 1984, **23**, 3548.
11. M. K. Chaudhuri and S. K. Ghosh, *Polyhedron* 1982, **1**, 553; *Inorg. Chem.* 1982, **21**, 4020; 1984, **23**, 534; *J. Chem. Soc., Dalton Trans.* 1984, 507.
12. M. K. Chaudhuri and B. Das, *Polyhedron* 1985, **4**, 1449; M. N. Bhattacharjee, M. K. Chaudhuri and R. N. Dutta Purkayastha, *J. Chem. Soc., Dalton Trans.* 1985, 409.
13. M. K. Chaudhuri, S. K. Ghosh and N. S. Islam, *Inorg. Chem.* 1985, **24**, 2706; J. K. Basumatary, M. K. Chaudhuri, R. N. Dutta Purkayastha and Z. Hiese, *J. Chem. Soc., Dalton Trans.* 1986, 709.

14. A. I. Vogel, *A Text Book of Quantitative Inorganic Analysis*. Longmans, Green, London (1962); (a) p. 548; (b) p. 295; (c) p. 325; (d) p. 269.
15. M. K. Chaudhuri and N. S. Islam, *Inorg. Chem.* 1986, **25**, 3749; C. R. Bhattacharjee, M. K. Chaudhuri and R. N. Dutta Purkayastha, *Inorg. Chim. Acta* 1989, **160**, 147.
16. E. McCandlish, A. R. Miksztal, M. Nappa, A. Q. Sprenger, J. S. Valentine, J. D. Strong and T. G. Spiro, *J. Am. Chem. Soc.* 1980, **102**, 4268.
17. D. J. Hewkin and W. P. Griffith, *J. Chem. Soc. A* 1966, 4772.
18. N. F. Curtis, *J. Chem. Soc. A* 1968, 1584.
19. M. N. Bhattacharjee, M. K. Chaudhuri, H. S. Dasgupta and D. T. Khathing, *J. Chem. Soc., Dalton Trans.* 1981, 2587.
20. K. Nakamoto, *Infrared and Raman Spectra of Inorganic and Coordination Compounds*, 4th edn, p. 249. Wiley-Interscience, New York (1986).

Polyhedron Vol. 9, No. 14, pp. 1659–1666, 1990
Printed in Great Britain

0277–5387/90 $3.00+.00
Pergamon Press plc

CONTRIBUTIONS TO THE CHEMISTRY OF SILICON–SULPHUR COMPOUNDS—LVII.* SYNTHESIS, MOLECULAR STRUCTURE AND PROPERTIES OF CYCLO-TETRAKIS-[TRI-*TERT*-BUTOXYSILANETHIOLATOCOPPER(I)], $[(t\text{-}C_4H_9O)_3SiSCu]_4$, THE FIRST EXAMPLE OF A SQUARE PLANAR Cu_4S_4 RING

BARBARA BECKER and WIESŁAW WOJNOWSKI

Department of Chemistry, Technical University of Gdańsk, PL-80-952 Gdańsk, Poland

and

KARL PETERS,† EVA-MARIA PETERS and HANS GEORG VON SCHNERING

Max-Planck-Institut für Festkörperforschung, D-7000 Stuttgart 80, F.R.G.

(*Received* 12 *December* 1989; *accepted* 1 *March* 1990)

Abstract—The preparation of cyclo-tetrakis[tri-*tert*-butoxysilanethiolatocopper(I)] from tri-*tert*-butoxysilanethiol and copper(II) acetate or CuCl or Cu_2O is described. The compound crystallizes as colourless monoclinic rods. The molecular structure is characterized by a nearly planar alternating Cu_4S_4-eight-membered ring with three-fold coordinated sulphur and two-fold coordinated copper atoms. According to the mass spectrum the tetrameric molecule is also preserved in the vapour phase. The compound was characterized spectroscopically by ^{29}Si, ^{13}C, ^1H NMR, IR and UV. Reactions with triphenylphosphine, 1,10-phenanthroline, and 2,2′-bipyridine afforded three adducts with formal stoichiometries $RSCu \cdot (PPh_3)_2$, $RSCu \cdot phen$ and $(RSCu)_2 \cdot bipy$, respectively.

Many of the recent developments in metal thiolate chemistry were stimulated by studies on metallothioneins, a unique class of metalloproteins which are polymetallic with exclusive coordination by the cysteine thiolate function.[2] As copper is one of the most abundant metallic elements in nature, copper–thiolate chemistry is of considerable current interest.

Complexes formed by copper(I) and alkyl or aryl thiolate ligands are numerous and their structures show a great variety. Insoluble compounds with RSCu stoichiometry are presumed to be non-molecular in structure.[3,4] On the other hand, the structures of monometallic linear $[Cu(SC_6HMe_4\text{-}2,3,5,6)_2]^-$[5] and trigonal planar $[Cu(SPh)_3]^{2-}$[6,7] anions, oligomeric copper(I) thiolate species such as tetrametallic $[Cu_4(SR)_6]^{2-}$ (R = Ph,[6,8] Me[8]), $\{Cu_4[(SCH_2)_2C_6H_4]_3\}^{2-}$[9] and pentametallic $[Cu_5(SPh)_7]^{2-}$,[10] $[Cu_5(SBu\text{-}t)_6]^-$[11,12] anions or octametallic neutral aggregates such as $[Cu(SC_6H_2Pr_3\text{-}i)]_8$[13] are known. Molecular structures were also determined for several copper thiolates bearing additional ligands such as triphenylphosphine in $Cu_2(SPh)_2(PPh_3)_4$,[14] $Cu_3(SPh)_3(PPh_3)_4$,[15] $Cu_4(SBu\text{-}t)_4(PPh_3)_2$,[3] $Cu_4(SPh)_4(PPh_3)_4$,[16] bis(diphenylphosphino)methane in $Cu_4[SC(CH_3)_2C_2H_5]_4[(PPh_2)_2CH_2]_2$,[17] thioxanthate in $Cu_8(SC_5H_{11})_4(S_2CSC_5H_{11})_4$,[18] pyridine nitrogen as in $Cu_6(SC_5H_3NSiMe_3)_6$[19] or tetrathiomolybdate group as in $[(PhS)CuS_2MoS_2]^{2-}$ and $[(PhS)CuS_2MoS_2Cu(SPh)]^{2-}$ anions.[20]

Some years ago we reported the preparation and molecular structure of the first silanethiolate, namely cyclotetrakis[tri-*tert*-butoxysilanethiolatosilver(I)], $[(t\text{-}C_4H_9O)_3SiSAg]_4$,[21] obtained by a reaction of tri-*tert*-butoxysilanethiol with silver nitrate in benzene–water. This was followed by syntheses and molecular structure determinations of

* For part LVI, see ref. 1.

† Author to whom correspondence should be addressed.

tri-*tert*-butoxysilanethiolates of thallium $[(t\text{-BuO})_3SiSTl]_2$,[22] mercury $[(t\text{-BuO})_3SiS]_2Hg$,[23] and lead $\{[(t\text{-BuO})_3SiS]_2Pb\}_2$.[24] All these silanethiolates were obtained with quantitative yields and in any case other products such as higher oligomers or polymers were found, suggesting that it is steric demand of the bulky $(t\text{-BuO})_3SiS$ ligand which probably reduces the tendency of thiolate sulphur to bridge metal centres and/or prevents close approach to thiolate units thus limiting the formation of oligomeric aggregates.

Copper complexes with silanethiolate ligands were never investigated. Herein, we report the preparation, molecular structure and some properties of cyclo-tetrakis[tri-*tert*-butoxysilanethiolatocopper(I)], $[(t\text{-}C_4H_9O)_3SiSCu]_4$ (**1**), the first structurally characterized copper silanethiolate complex.

EXPERIMENTAL

Syntheses

Tri-*tert*-butoxysilanethiol, $(t\text{-BuO})_3SiSH$, was prepared as described previously.[25] All other chemicals were commercial products. Solvents, if necessary, were dried according to common procedures.

Preparation of $[(t\text{-BuO})_3SiSCu]_4$ (1)

Three synthetic routes to the title complex were developed:

Method A. To a solution of $(t\text{-BuO})_3SiSH$ (7 g, 25 mmol) in 50 cm^3 of benzene, a solution of copper(II)acetate (5 g, 25 mmol) in 25 cm^3 of water was added and the resulting two-phase mixture shaken vigorously for *ca* 2 h until the silanethiol disappeared, as verified by TLC. The benzene layer was separated, washed twice with water, dried over magnesium sulphate and finally the benzene was removed *in vacuo*. The solid residue, containing in addition to **1** also bis(tri-*tert*-butoxysilyl)disulphide, was twice crystallized from isopropanol–benzene (3:1 v/v) yielding 2.12 g of pure colourless **1**; m.p. 222–223°C, yield 50%.

Method B. Copper(I) chloride (1.070 g, 10.7 mmol), $(t\text{-BuO})_3SiSH$ (2.772 g, 9.9 mmol), anhydrous Et_3N (1.05 g, 10.5 mmol) and 20 cm^3 of anhydrous benzene were mixed together under argon atmosphere and stirred for *ca* 30 min. Insoluble material was then removed by filtration and washed with a further 20 cm^3 portion of benzene. Both liquid phases were combined and evaporated to dryness *in vacuo*. The solid residue was recrystallized from *i*-PrOH–benzene, yielding 2.622 g of pure **1**; m.p. as above, yield 74%.

Method C. A solution of $(t\text{-BuO})_3SiSH$ (0.560 g, 2 mmol) in 2 cm^3 of anhydrous benzene was added to copper(I) oxide (0.144 g, 1 mmol) and the mixture refluxed with stirring under Ar for *ca* 7 h. Then 5 cm^3 of benzene was added and traces of the remaining Cu_2O were removed by filtration. Evaporation to dryness and subsequent recrystallization from *i*-PrOH–benzene afforded 0.585 g of pure **1**; m.p. as above, yield 84%. Found: C, 42.0; H, 7.9. Calc. for $Cu_4S_4Si_4O_{12}C_{48}H_{108}$: C, 42.0; H, 7.9%.

Reaction of **1** *with triphenylphosphine*

To a solution of **1** (1.370 g, 1 mmol) in 10 cm^3 of anhydrous benzene, Ph_3P (2.1 g, 8 mmol) was added, the mixture refluxed for 2.5 h under argon and then left overnight at room temperature. The deposited solid material was separated by filtration, washed with *n*-hexane and then recrystallized from hexane–ethanol (7:5 v/v) affording 3.366 g of colourless plates; m.p. 154–154.5°C. ^1H NMR spectrum: 7.20 ppm (m, 30H, C_6H_5), 1.35 and 1.15 ppm; (two broad poorly separated singlets, 27H, CH_3), and microanalytical data consistently indicated the composition $(t\text{-}C_4H_9O)_3SiSCu\cdot(PPh_3)_2$; yield 97%. When the **1** to Ph_3P molar ratio was only 1:4 the same product was obtained with a yield of *ca* 45%. Found: C, 66.6; H, 6.6. Calc. for $CuSSiO_3P_2C_{48}H_{57}$: C, 66.4; H, 6.6%.

Reaction of **1** *with* 1,10-*phenanthroline monohydrate* (phen·H_2O)

Phen·H_2O (0.396 g, 2 mmol) was added to 5 cm^3 of anhydrous benzene and refluxed until a clear solution was obtained. Then to the hot solution a solution of **1** (0.685 g, 0.5 mmol) in 3 cm^3 of anhydrous benzene was added. The mixture which rapidly turned deep red was left to stand for 1 day at room temperature. The dark red crystals which grew were collected, washed with hexane and dried *in vacuo*. 0.986 g of product was obtained; m.p. 164–166°C. Attempts to recrystallize the product from hot benzene resulted in partial decomposition. Microanalytical data suggested the composition $(t\text{-}C_4H_9O)_3SiSCu\cdot$phen; yield 94%. Found: C, 55.1; H, 6.7. Calc. for $CuSSiN_2O_3C_{24}H_{35}$: C, 55.1; H, 6.7%.

Reaction of **1** *with* 2,2′-*bipyridine* (bipy)

To a solution of **1** (0.785 g, 0.573 mmol) in 5 cm^3 of anhydrous hexane a solution of bipy (0.358 g, 2.292 mmol) in 10 cm^3 of anhydrous benzene was added. The mixture turned orange and after *ca* 1–2 min, fine pink–red crystals began to deposit. After 3 h, when the solution over the solid was colourless,

the crystals were collected, washed with hexane and dried *in vacuo*. 0.961 g of product was obtained, m.p. 186–188°C. From the hexane fraction, which analysed by TLC did not show the presence of starting **1**, the solvent was evaporated affording 0.175 g (~ 50%) of unreacted bipy, identified by a mixed melting point. According to the above result also microanalytical data pointed to the composition $[(t\text{-}C_4H_9O)_3SiSCu]_2 \cdot$ bipy. Yield quantitative. Found: C, 48.7; H, 7.5. Calc. for $Cu_2S_2Si_2N_2O_6C_{34}H_{62}$: C, 48.5; H, 7.4%.

ANALYTICAL PROCEDURES

Thin-layer chromatography

TLC was performed on Silufol 254 + 366 (Kavalier, CSSR) plates with hexane–benzene (4 : 1 v/v) as a mobile phase. The spots were visualized by UV (a pink–red spot of **1**, $R_F = 0.85$) and silver nitrate solution (in EtOH–H_2O 1 : 1) {black spot for **1** and brown spots for $(t\text{-BuO})_3SiSH$, $R_F = 0.66$ and $(t\text{-BuO})_3SiSH$, $R_F = 0.57$}.

Elemental analyses

Carbon and hydrogen contents were determined by the microcombustion method.[26] Melting points are uncorrected.

Spectral measurements

Spectral measurements were performed as follows: IR: 4000–400 cm^{-1}, Specord 75IR (C.Zeiss), solution in CCl_4; UV: 52,000–30,000 cm^{-1}, Specord UV–vis (C.Zeiss), 1.5×10^{-5} M solution in hexane, argon atmosphere; ^1H NMR: Varian 360A (60 MHz), solution in CCl_4 (TMS int.); ^{13}C NMR: Bruker AM 250 ($\nu_0 = 62.896$ MHz), solution in $CDCl_3$ (TMS int.); ^{29}Si NMR: Bruker AM 250 ($\nu_0 = 49.689$ MHz), solution in $CDCl_3$ (TMS int.), $Cr(acac)_3$ as a relaxation reagent at room temperature with inverse gated broad band proton noise decoupling; Mass spectrum: Varian Mat 8230 (E.I., 70 eV), direct inlet.

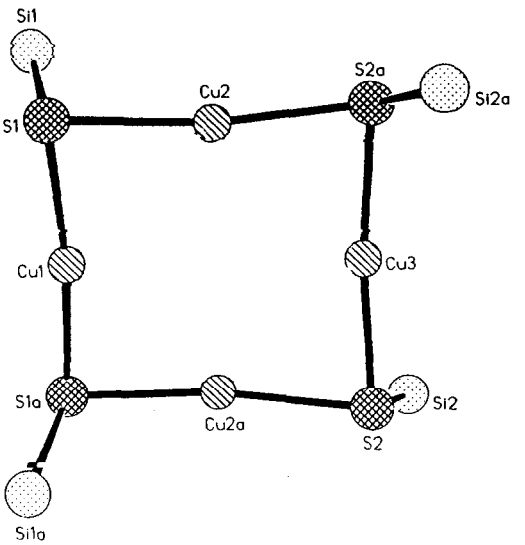

Fig. 1. Atom labelling for the central $Si_4S_4Cu_4$ part of the molecule of **1**.

Crystal and molecular structure determination of **1**

The crystal and molecular structure of **1** was determined by a single crystal diffraction study. Figure 1 shows a perspective drawing of the central $Si_4S_4Cu_4$ part of **1** with the atom labelling, and Fig. 2 a stereo pair of the whole molecule.

Atomic coordinates, displacement factor coefficients, full lists of bond lengths and angles and lists of F_o/F_c values have been deposited as supplementary data with the Editor, from whom copies are available on request. Atomic coordinates have also been deposited with the Cambridge Crystallographic Data Centre.

RESULTS AND DISCUSSION

Synthesis of **1**

The preparation of a new tetracopper(I) silanethiolate complex $[(t\text{-}C_4H_9O)_3SiSCu]_4$ (**1**) is readily achieved, commencing from either copper(II) or copper(I), however, the synthesis of **1** starting from

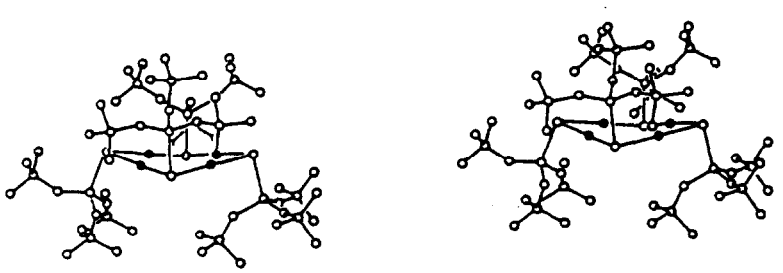

Fig. 2. Stereo pair of the molecule of **1**, hydrogen atoms are omitted for clarity.

Table 1. Summary of crystal data, intensity collection and structural refinement for **1**

Crystallographic section	
Compound	**1**
Empirical formula	$Cu_4S_4Si_4O_{12}C_{48}H_{108}$
Molecular mass	1372.25
a (pm)	2478.7(15)
b (pm)	2472.1(27)
c (pm)	1271.4(7)
β (°)	100.99(4)
V ($pm^3 \times 10^{-6}$)	7648(9)
Z	4
d(calc) [$g\ cm^{-3}$]	1.192
Crystal system	Monoclinic
Space group	$C2/c$
Data collection	
Diffractometer	Nicolet R3m/V
Radiation	Mo-K_α
Monochromator	Graphite
Crystal size (mm)	$0.35 \times 0.45 \times 4.0$
Data collection mode	Wyckoff-scan
θ range (°)	1.75–27.5
Recip. latt. segment	$h = 0$–32 $k = 0$–32 $l = -16$–16
Number of reflections measured	4091
Number of unique reflections	3889
Number of reflections $F > 3\sigma(F)$	3878
Linear abs. coefficient (mm^{-1})	1.31
Abs. Correction	ψ-scan
Structural analysis and refinement	
Solution by	Direct phase determination
Method of refinement	Full-matrix LSQ. Hydrogen positions were calculated and refined isotropically
Parameter/F_o ratio	0.084
R, R_w	0.059, 0.064
Program used	Nicolet SHELXTL PLUS

copper(II) substrate as in eq. (1):

$$4\ Cu(OAc)_2 + 8\ (t\text{-}BuO)_3SiSH \longrightarrow [(t\text{-}BuO)_3SiSCu]_4 + 2\ [(t\text{-}BuO)_3Si]_2 + 8\ AcOH \quad (1)$$

seems to be of minor preparative importance since the half amount of introduced silanethiol is converted to the appropriate disulphide, which must be subsequently separated from the desired copper(I) silanethiolate **1**. On the other hand, the easy oxidation of silanethiol by copper(II) salts, analogous to those known for organic thiols, may also serve as a source of bis(tri-*tert*-butoxysilyl)disulphide, prepared by us previously using the more convenient oxidation of sodium silanethiolate by iodine, and characterized structurally.[27]

Much better results were obtained starting from copper(I) compounds. The route from copper(I) chloride and silanethiol, in the presence of tertiary amine as the HCl acceptor [eq. (2)], can be regarded

$$4\ CuCl + 4\ (t\text{-}BuO)_3SiSH + 4\ Et_3N \longrightarrow [(t\text{-}BuO)_3SiSCu]_4 + 4\ Et_3N \cdot HCl \quad (2)$$

as a classical one and gives a good yield of **1**. The best results, however, were obtained for the simplest case where silanethiol reacts with copper(I) oxide forming **1** and water only as a byproduct [eq. (3)]:

$$2\ CuO + 4\ (t\text{-}BuO)_3SiSH \longrightarrow [(t\text{-}BuO)_3SiSCu]_4 + 2H_2O. \quad (3)$$

This route has never been used before for the synthesis of copper thiolate complexes, maybe because

organic thiols are far less acidic than silanethiols.[28] As we have shown previously, mercury[23] and lead[24] molecular tri-*tert*-butoxysilanethiolates can also be obtained by the same method with quantitative yields.

Crystal and molecular structure of **1**

Cyclo - tetrakis[tri - *tert* - butoxysilanethiolato-copper(I)] (**1**) crystallizes monoclinically as colourless rods, melting at 222–223°C without decomposition. The crystal lattice parameters are given in Table 1, and the molecular structure of **1** is illustrated in Figs 1 and 2.

The molecule consists of four $(t\text{-BuO})_3SiSCu$ units, where every sulphur atom is triply coordinated and thus serves as a bridge for two adjacent, doubly coordinated copper atoms. The Cu_4S_4 core is almost planar since the mean shift of sulphur atoms from the Cu_4 plane was found to be only 32 pm. Such a structure type has never been observed previously for copper(I) thiolates although similar Cu_4X_4 cores have been found in other homoleptic copper(I) complexes, namely $(t\text{-BuOCu})_4$,[29] $(Me_3SiCH_2Cu)_4$[30] and $[CuCo(CO)_4]_4$[31] (here the Cu_4Co_4 cycle is distinctly non-planar). The molecule of **1** is of 2-C_2 symmetry (the two-fold axis passes through Cu(1) and Cu(3) atoms) and isomorphous with tetrameric silver tri-*tert*-butoxysilanethiolate, $[(t\text{-BuO})_3SiSAg]_4$, whose preparation and molecular structure were described by us previously.[21]

For both copper and silver silanethiolates the discrete eight-membered cyclic molecular units of alternating metal and sulphur atoms exhibit no secondary metal ···S interactions. This reflects the steric demand of the bulky tri-*tert*-butoxysilanethiolate ligand which prevents any close approach of the molecules and precludes any secondary bridging interaction to form oligomeric aggregates. In this sense the above silanethiolate ligand can be compared with the thiolate ligands which originate from $(PhMe_2Si)_3CSH$ and $(Me_3Si)_3CSH$ which, as it was shown recently by their investors Block and Zubieta,[32] behave similarly affording silver thiolates with small Ag_3S_3 and Ag_4S_4 cores, respectively.

Table 2 lists the selected interatomic distances and interatomic angles determined for the molecule of **1**.

Table 2. Selected bond lengths (pm) and angles (°) for **1** (standard deviations in parentheses)

Bond lengths			
Cu(1)—Cu(2)	285.5(1)	Cu(2)—Cu(3)	284.6(1)
Cu(1)—Cu(2a)	285.4(1)	Cu(2)—S(1)	217.5(2)
Cu(1)—S(1)	217.2(2)	Cu(2)—S(2a)	217.0(2)
		Cu(3)—S(2)	216.1(2)

Si—S	212.7(3)–213.8(2);	mean 213.2(2)
Si—O	150.7(6)–161.6(8);	mean 155.0(3)
C—O	135.2(9)–142.6(12);	mean 138.7(5)
C—C	137.4(19)–150.5(20);	mean 143.3(4)

Bond angles			
Cu(2)—Cu(1)—S(1)	49.0(1)	Cu(2)—Cu(1)—Cu(2a)	89.3(1)
Cu(2)—Cu(1)—S(1a)	137.6(1)	S(1)—Cu(1)—S(1a)	173.4(1)
Cu(1)—Cu(2)—Cu(3)	90.5(1)	Cu(1)—Cu(2)—S(1)	48.9(1)
Cu(3)—Cu(2)—S(1)	138.7(1)	Cu(1)—Cu(2)—S(2a)	137.4(1)
Cu(3)—Cu(2)—S(2a)	48.8(1)	S(1)—Cu(2)—S(2a)	172.0(2)
Cu(2)—Cu(3)—S(2)	136.8(1)	Cu(2)—Cu(3)—Cu(2a)	89.7(1)
Cu(2)—Cu(3)—S(2a)	49.1(1)	S(2)—Cu(3)—S(2a)	174.0(1)
Cu(1)—S(1)—Cu(2)	82.1(1)	Cu(1)—S(1)—Si(1)	95.8(1)
Cu(2)—S(1)—Si(1)	94.5(1)	Cu(3)—S(2)—Si(2)	100.4(1)
Cu(3)—S(2)—Cu(2a)	82.1(1)	Si(2)—S(2)—Cu(2a)	100.9(1)

S—Si—O	104.8(3)–112.9(2);	mean 109.9(1)
O—Si—O	106.6(4)–111.6(5);	mean 109.0(2)
Si—O—C	144.6(6)–157.0(9);	mean 149.6(3)
O—C—C	103.2(9)–114.2(12);	mean 109.0(5)
C—C—C	101.2(13)–117.7(12);	mean 109.8(5)

As observed previously for the isomorphous silver silanethiolate,[21] for copper(I)silanethiolate (**1**) the displacement of copper atoms from linear coordination towards the centre of the Cu_4S_4 ring (S—Cu—S, average 172.8°) decreases the metal–metal distances. The *d*(Cu—Cu) value (285 pm), which is the same as determined for the closed $[Cu_{12}S_8]^{4-}$ cage,[33] is, however, substantially larger than the Cu—Cu single bond distance (234 pm). Significant deviations from co-linear S—Cu—S bonds were reported for the $[Cu_{12}S_8]^{4-}$ cage anion (S—Cu—S angle, 166.9–170.9°),[33] the neutral thiolate $[Cu(SC_6H_2Pr_3\text{-}i)]_8$, (S—Cu—S, average 177.5°),[13] and also for the anionic thiolate complexes containing not only triply but also doubly coordinated copper—$[Cu_5(SBu\text{-}t)_6]^-$ (S—Cu—S angles 169.2–173.4°)[12] and $[Cu_5(SPh)_7]^{2-}$ (S—Cu—S angle 175.2°).[10] These similarities are not restricted to the S—Cu—S angles since the Cu—S bonds forming these angles are also of comparable lengths. For **1** the Cu—S distances are 216.1 and 217.0 pm, and for the compounds mentioned above[10,12,13,33] the *d*(Cu—S) values are within the same limits.

It is remarkable that although in **1** sulphur is triply coordinated, the Si—S bond lengths, *d*(Si—S) 213.3 pm, are similar to those determined for two-fold bonded sulphur compounds (e.g. *d*(Si—S), 213.2 pm[27] in $[(t\text{-BuO})_3SiS]_2$).

Due to great similarities between the molecular structures of silver[21] and copper (this work) tri-*tert*-butoxysilanethiolates, a more detailed discussion about the latter is not necessary. The reader is asked to consult our previous paper[21] where all structural details are thoroughly discussed, since the general conclusions formulated there can be, in our opinion, applied also to the present case.

Properties of **1**

Cyclo - tetrakis[tri - *tert* - butoxysilanethiolato-copper(I)] (**1**) shows very good solubility in benzene, hexane and carbon tetrachloride. The solubility however falls with growing solvent polarity, so **1** is poorly soluble in acetonitrile and lower alcohols, and insoluble in water.

The IR spectrum of **1** (4000–400 cm^{-1}) contains only features typical for the $(t\text{-}C_4H_9O)_3SiS$ group (ν = 2970, 1470, 1385, 1360, 1235, 1200, 1185, 1060, 1015, 685, 635 and 530 cm^{-1}). This is consistent with previously reported[7,9] data for copper(I) thiolates pointing out that ν(Cu—S) stretching modes are at lower frequencies (350–300 cm^{-1}).

The UV absorption spectrum of **1** consists of a broad asymmetric band (λ_{max} 202 nm, $\varepsilon \sim 4600$) with a distinct shoulder (λ_{max} 225 nm, $\varepsilon \sim 2000$) and a second, well separated symmetric band (λ_{max} 285 nm, $\varepsilon \sim 1400$). The shortest wavelength maximum at *ca* 200 nm is attributed to the σ(Si—S) → σ^*(Si—S) transition, however, any detailed discussion on this interesting spectrum cannot be given without further investigations on the other silanethiolates. Such investigations are now in progress.

The ^1H, ^{13}C and ^{29}Si NMR spectra of **1** are very simple—only one singlet for CH_3 hydrogens at 1.35 ppm, two singlets for two different carbon atoms at 31.78 ppm (CH_3) and 74.46 ppm (CMe_3), and one singlet at −72.73 ppm for silicon atoms were detected, respectively. The above values are similar to those reported by us previously for Ag, Tl, Hg and Pb tri-*tert*-butoxysilanethiolates.[21–24]

The mass spectrum of **1** shows a group of peaks at *m/z* 1368–1379 (max. abundance 20%) which can be attributed to the ions originating from the parent molecule with four copper atoms, on the basis of identity of both experimental and calculated isotope patterns. In the region above *m/z* 1000, two other groups of peaks were found—the group centred at *m/z* 1090 (5%) $[M-(t\text{-BuO})_3SiS]$ and the group at *ca m/z* 1030 (10%), most probably corresponding to the ions with $[(t\text{-BuO})_3SiSCu]_3$ composition. Some other peaks with abundances greater than 5% were found at *m/z* 586 (8%), 265 (23%), 209 (12%), 153 (33%), 135 (40%), 95 (25%) and 79 (27%), and the base peak at *m/z* 58 (100%). No peaks which could be attributed to ions with the $[(t\text{-BuO})_3SiSCu]_n$ (n = 1 or 2) composition were detected. The mass spectrum indicates that not only in the solid but also in the vapour phase the molecule of **1** is quite stable. The existence of $[(t\text{-BuO})_3SiSCu]_3$ molecules also seems possible. Although a homoleptic copper thiolate with a cyclic Cu_3S_3 core has not yet been prepared, the six-membered cycle of alternating silver and sulphur atoms was found in the $[(PhMe_2Si)_3CSAg]_3$ molecule.[32]

Compound **1** is stable to water and does not hydrolyse even in the presence of acetic acid, as has been seen from method (A) of its synthesis. An attempt however to prepare **1** from CuCl and $(t\text{-BuO})_3SiSH$ in benzene, in the absence of a hydrogen chloride acceptor, failed. Although the transient formation of small amounts of **1** was observed on TLC, it was quickly destroyed by evolving HCl finally giving a mixture of black copper sulphides.

In **1** copper is only doubly coordinated and it was thus interesting to investigate if it can further react with compounds which are known to be the good donor ligands. Reaction of **1** with trimethylphosphine was performed producing a high yield of colourless crystals of a new complex for which the formula $[(t\text{-BuO})_3SiSCu(PPh_3)_2]_n$ could be attributed on the basis of elemental analysis and

^{1}H NMR spectrum, however, the value of n remains unknown. From steric considerations it is of very low probability that the Cu_4S_4 core of **1** is preserved in the phosphine adduct. Although three complexes containing the Cu_4S_4 core and phosphine as an additional ligand are known—$(t\text{-BuSCu})_4(PPh_3)_2$,[3] $(C_5H_{11}SCu)_4(Ph_2PCH_2PPh_2)_2$[17] and $(PhSCu)_4(PPh_3)_4$[16]—in all of them a maximum of one phosphorus atom is coordinated to the copper atom. The same $SCuP_2$ stoichiometry as our phosphine ligated copper silanethiolate was found by Dance *et al.*[14] for $(Ph_3P)_2Cu(SPh)_2Cu(PPh_3)_2$, whose molecular structure is characterized by pseudo-tetrahedral coordination on copper (P_2CuS_2) and the unique planar stereochemistry at the sulphur atoms which is enforced by crowding of the 12 phenyl rings on the surface of the molecule. A similar structure could also be expected for $[(t\text{-BuO})_3SiSCu(PPh_3)_2]_n$ ($n = 2$) but, taking into account the steric hindrance caused by the very bulky $(t\text{-BuO}_3)SiS$ ligand, much greater than that of benzenethiolate, it seems doubtful.

The ^{1}H NMR spectrum of $[(t\text{-BuO})_3SiSCu(PPh)_2]_n$ in the methyl region consists of two broad singlets (ratio *ca* 2:1) separated by only 0.2 ppm, suggesting that the methyls are in different environments. This could be easily realized in the monometallic structure depicted below, where steric requirements are also minimized.

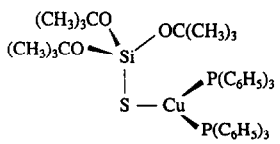

The structure has no precedents in the chemistry of neutral copper thiolate derivatives and requires further verification.

Compound **1** reacts also with 1,10-phenanthroline affording, almost quantitatively, dark red crystals of a new complex, poorly soluble in common organic solvents, with formal stoichiometry $(t\text{-BuO})_3SiSCu \cdot phen$, similar to that found for the phosphine complex if phosphorus atoms are substituted for the nitrogen atoms of phenanthroline.

Reaction of **1** with 2,2′-bipyridine gave, however, a different result, the formal stoichiometry of a pink–red complex, also formed quantitatively, was found to be $[(t\text{-BuO})_3SiSCu]_2 \cdot bipy$. Its solubility is even lower than that of the phenanthroline complex.

The most intriguing question arises from comparison of the stoichiometries of both amine complexes, which are completely different despite the great similarities exhibited by these ligands. Presently, the molecular structure of the phenanthroline and bipyridine derivatives of copper(I) silanethiolate are unknown, but the possibility that 2,2′-bipyridine does not act as a chelate ligand but forms a bridge between two metal centres cannot be excluded on consideration of recent results of Craven *et al.*[34] They reported a molecular structure of 4,4′-dimethyl-2,2′-bipyridylbis[pentacarbonylchromium(0)] where the orientation of the ligand pyridyl rings is mutually perpendicular and every nitrogen atom coordinates one chromium forming a bridged, binuclear structure. It is the first reported example of this type of coordination which, although possible for 2,2′-bipyridine, cannot be realized for 1,10-phenanthroline and, therefore, in particular cases can account for significant differences between complexes formed by both these ligands.

Acknowledgements—The authors are grateful to Professor A. Meller (University of Göttingen, F.R.G.) for determination of NMR and mass spectra. B.B. and W.W. acknowledge the Polish Academy of Sciences (CPBP 01.13.3.6) for financial support.

REFERENCES

1. J. Pikies and W. Wojnowski, *J. Organomet. Chem.*, in press.
2. J. H. R. Kagi and M. Nordberg, (Eds), *Metallothionein*. Birkhauser, Basel (1979).
3. I. G. Dance, *Polyhedron* 1986, **5**, 1037.
4. I. G. Dance, *Polyhedron* 1988, **7**, 2205.
5. S. A. Koch, R. Fikar, M. Millar and T. O'Sullivan, *Inorg. Chem.* 1984, **23**, 121.
6. D. Coucouvanis, C. N. Murphy and S. K. Kanodia, *Inorg. Chem.* 1980, **19**, 2993.
7. C. D. Garner, J. R. Nicholson and W. Clegg, *Inorg. Chem.* 1984, **23**, 2148.
8. I. G. Dance and J. C. Calabrese, *Inorg. Chim. Acta* 1976, **19**, L41; I. G. Dance, G. A. Bowmaker, C. R. Clark and J. K. Seadon, *Polyhedron* 1983, **2**, 1031.
9. J. R. Nicholson, I. L. Abrahams, W. Clegg and C. D. Garner, *Inorg. Chem.* 1985, **24**, 1092.
10. I. G. Dance, *Aust. J. Chem.* 1978, **31**, 2195.
11. I. G. Dance, *J. Chem. Soc., Chem. Commun.* 1976, 68.
12. G. A. Bowmaker, G. R. Clark, J. K. Seadon and I. G. Dance, *Polyhedron* 1984, **3**, 535.
13. Q. Yang, K. Tang, H. Liao, Y. Han, Z. Chen and Y. Tang, *J. Chem. Soc., Chem. Commun.* 1987, 1976.
14. I. G. Dance, P. J. Guerney, A. D. Rae and M. L. Scudder, *Inorg. Chem.* 1983, **22**, 2883.
15. I. G. Dance, L. J. Fitzpatrick and M. L. Scudder, *J. Chem. Soc., Chem. Commun.* 1983, 546.
16. I. G. Dance, M. L. Scudder and L. J. Fitzpatrick, *Inorg. Chem.* 1985, **24**, 2547.
17. M. A. Khan, R. Kumar and D. G. Tuck, *Polyhedron* 1988, **7**, 49.

18. R. K. Chadha, R. Kumar and D. G. Tuck, *Polyhedron* 1988, **7**, 1121.
19. E. Block, M. Gernon, H. Kang and J. Zubieta, *Angew. Chem.* 1988, **100**, 1389.
20. S. R. Acott, C. D. Garner, J. R. Nicholson and W. Clegg, *J. Chem. Soc., Dalton Trans.* 1983, 713.
21. W. Wojnowski, M. Wojnowski, K. Peters, E.-M. Peters and H. G. von Schnering, *Z. Anorg. Allg. Chem.* 1985, **530**, 79. In this paper $[(t\text{-}C_4H_9O)_3SiSAg]_4$ was erroneously reported triclinically. Transformation to the correct monoclinic unit cell is given by (111, −111, 00−1).
22. W. Wojnowski, K. Peters, E.-M. Peters and H. G. von Schnering, *Z. Anorg. Allg. Chem.* 1985, **531**, 147.
23. W. Wojnowski, M. Wojnowski, H. G. von Schnering and M. Noltemeyer, *Z. Anorg. Allg. Chem.* 1985, **531**, 153.
24. W. Wojnowski, M. Wojnowski, K. Peters, E.-M. Peters and H. G. von Schnering, *Z. Anorg. Allg. Chem.* 1986, **535**, 56.
25. R. Piękoś and W. Wojnowski, *Z. Anorg. Allg. Chem.* 1962, **318**, 212.
26. W. Wojnowski and A. Olszewska-Borkowska, *Chem. Anal.* 1975, **20**, 209.
27. W. Wojnowski, M. Wojnowski, B. Becker and M. Noltemeyer, *Z. Anorg. Allg. Chem.* 1988, **561**, 167.
28. B. Becker, E. W. Felcyn, A. Herman, J. Pikies and W. Wojnowski, *Z. Anorg. Allg. Chem.* 1982, **488**, 229.
29. T. Greiser and E. Weiss, *Chem. Ber.* 1976, **109**, 3142.
30. J. A. J. Jarvis, R. Pearce and M. F. Lappert, *J. Chem. Soc., Dalton Trans.* 1977, 999.
31. P. Klüfers, *Angew. Chem.* 1984, **96**, 288.
32. K. Tang, M. Aslam, E. Block, T. Nicholson and J. Zubieta, *Inorg. Chem.* 1987, **26**, 1488.
33. P. Betz, B. Krebs and G. Henkel, *Angew. Chem.* 1984, **96**, 293.
34. B. S. Craven, C. Long, R. A. Howie, G. P. McQuillan and J. Low, *Inorg. Chim. Acta* 1989, **157**, 151.

Polyhedron Vol. 9, No. 14, pp. 1667–1670, 1990
Printed in Great Britain

0277–5387/90 $3.00+.00
© 1990 Pergamon Press plc

COPPER(II) CARBOXYLATE–CARBOXYLIC ACID ADDUCTS: THE CRYSTAL AND MOLECULAR STRUCTURE OF TETRAKIS-[μ-(2-PHENOXYBENZOATO-*O,O'*)]BIS[(2-PHENOXYBENZOIC ACID)COPPER(II)]

THOMAS C. W. MAK and WAI-HING YIP

Department of Chemistry, The Chinese University of Hong Kong, Shatin, New Territories, Hong Kong

and

COLIN H. L. KENNARD

Department of Chemistry, University of Queensland, Brisbane, 4072 Australia

and

GRAHAM SMITH*

Department of Chemistry, Queensland University of Technology, Brisbane, 4000 Australia

(*Received* 8 *January* 1990; *accepted* 1 *March* 1990)

Abstract—The crystal structure of the carboxylic acid adduct of a tetracarboxylate-bridged dimeric species, $[Cu_2(RCO_2)_4(RCO_2H)_2]$, where RCO_2H = 2-phenoxybenzoic acid, has been determined by X-ray diffraction and refined to a residual $R = 0.037$ for 2827 observed reflections. The centrosymmetric dimer has a Cu—Cu separation of 2.602(1) Å, a mean Cu—O (plane) bond length of 1.960(3) Å and a Cu—O (axial) length of 2.182(3) Å, to the adducted acid molecule. The acid proton is hydrogen bonded to a cage carboxylate oxygen (O---O, 2.64(1) Å).

The number of copper(II) complexes of the type $[Cu_2(RCO_2)_4L_2]$ having tetra-(carboxylato-*O,O'*) bridges has increased since the first example (R = CH_3, L = H_2O) was reported by van Niekerk and Schoening,[1] so that the Cambridge Crystallographic Data Base now has more than 100 examples. These involve a diversity of carboxylic acid types and axially adducted (L) species, including nitrogen base as well as oxygen donor groups. Although the majority form discrete dimeric species (type 1), polymeric types may result from extension through the axial sites (types 2 and 3).

The type 2 (straight chain) polymer forms links through bifunctional L groups, e.g. L = pyrazine, R = CH_3;[2] L = hexamethylenetetramine, R = CH_3;[3] L = 1,4-dioxane, R = CH_3CH_2;[4] and L = 2-aminopyrimidine, R = (2-Cl·C_6H_4·OCH_2).[5]

The type 3 (step chain) motif involves a link between copper and the carboxylate oxygen of an adjacent dimer unit, as found in the anhydrous examples, R = CH_3CH_2;[6] R = $CH_3(CH_2)_2$;[7] R = (2-Cl·C_6H_4·OCH_2).[5]

The title compound, prepared from 2-phenoxybenzoic acid and having a stoichiometric formula $[Cu(RCO_2)_2(RCO_2H)]$, had the colour characteristics indicative of a dimeric copper species, which would suggest a rare acid adduct form of the type found for $[Cu_2(CH_3CO_2)_4](CH_3CO_2H)_2$.[8] However, a complex adduct of the type $[Cu(RCO_2)_2(H_2O)_2]\cdot 2[RCO_2H]\cdot 2H_2O$[9] (R =

* Author to whom correspondence should be addressed.

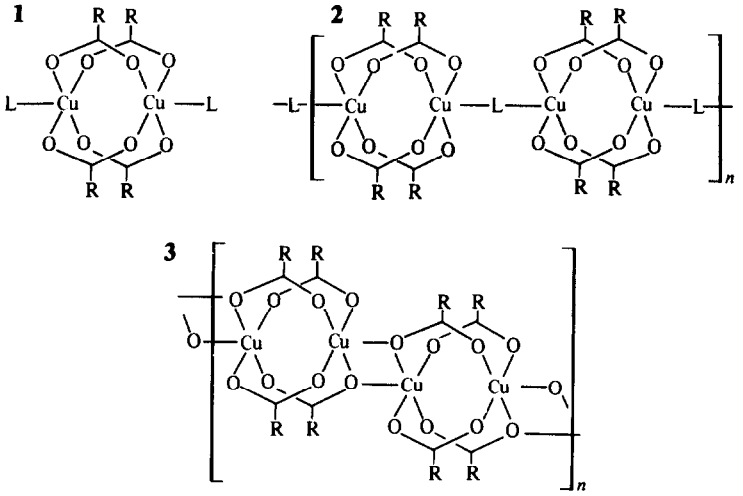

4-F·C_6H_4·OCH_2), also rare, could not be discounted.

EXPERIMENTAL

$[Cu_2(C_{12}H_{10}CO_2)_4(C_{12}H_{10}CO_2H)_2]$ was prepared by digesting an excess of $Cu(OH)_2 \cdot CuCO_3$ in hot (90°C) 50% aqueous ethanol. Dark green crystals grew from the filtered solution on standing for a period of several days at room temperature. An IR spectrum together with measured density and cell parameters indicated the presence of adducted acid molecules.

Crystal data

$C_{78}H_{56}Cu_2O_{18}$, $M_r = 1408.4$, monoclinic, space group $P2_1/c$, $a = 12.333(2)$, $b = 15.392(2)$, $c = 17.327(2)$ Å, $\beta = 98.55(1)°$, $V = 3252.6(7)$ Å^3, $F(000) = 1452$, $D_m = 1.47$ g cm^{-3}, D_c ($Z = 2$) = 1.437 g cm^{-3}, μ(Mo-K_α) = 7.6 cm^{-1}, max./min. transmission factors 0.847, 0.825, $T = 293$ K.

Data collection, structure solution and refinement

Intensity data were collected on a Nicolet R3m four-circle diffractometer (crystal monochromatized Mo-K_α radiation, $\lambda = 0.71073$ Å) from a crystal of dimensions $0.14 \times 0.16 \times 0.28$ mm. Of 4257 unique data collected up to $2\theta_{max} = 45°$, 2827 with $I > 2.5\sigma(I)$ were considered observed and used in structure refinement. Intensity variation of not greater than 1% in two standards monitored during the data collection period indicated negligible crystal decay. Data were corrected for absorption. The structure was solved by the automatic Patterson method of SHELXS-86[10] and refined by full-matrix least-squares (SHELX-76[11]) with anisotropic thermal parameters for all non-hydrogen atoms. Hydrogens were located in a difference Fourier synthesis and their positional and isotropic thermal parameters were refined. The final R [$= \Sigma||F_o|-|F_c||/\Sigma|F_o|$] and R_w [$= \Sigma w(||F_o|-|F_c||^2/|\Sigma w|F_o|^2)^{1/2}$] values were 0.037 and 0.038, respectively, using $w = 0.95/(\sigma^2 F_o + 6.4 \times 10^{-4} F_o^2)$. Neutral atom scattering factors were used.[12]

Table 1. Bond distances (Å) and angles (°) about the coordination polyhedron

(a) Distances			
Cu—O(8)A	1.987(3)	Cu—O(9)B′	1.949(3)
Cu—O(9)A′	1.950(3)	Cu—O(9)C	2.182(3)
Cu—O(8)B	1.955(3)	Cu—Cu′	2.602(1)
(b) Angles			
O(8)A—Cu—O(8)B	90.2(1)	O(8)B—Cu—O(9)B′	169.0(1)
O(8)A—Cu—O(9)A′	169.3(1)	O(8)B—Cu—O(9)C	90.9(1)
O(8)A—Cu—O(9)B′	89.8(1)	O(9)A′—Cu—O(9)B′	89.7(1)
O(8)A—Cu—O(9)C	89.1(1)	O(9)A′—Cu—O(9)C	101.5(1)
O(8)B—Cu—O(9)A′	88.3(1)	O(9)B′—Cu—O(9)C	100.1(1)

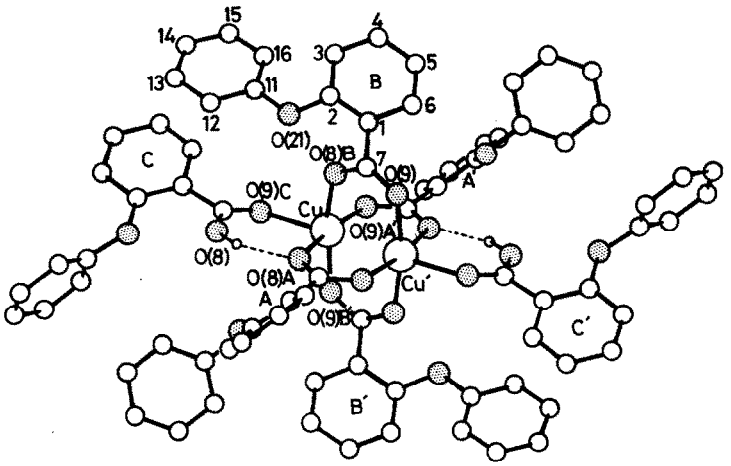

Fig. 1. Molecular configuration and atom naming scheme.

Atomic coordinates, thermal parameters, hydrogen atom coordinates, intraligand bond distances and angles, and observed and calculated structure factors have been deposited with the Editor as supplementary material, from whom copies are available on request. Atomic coordinates have also been deposited with the Cambridge Crystallographic Data Centre. Bond distances and angles about the coordination polyhedron are given in Table 1.

DISCUSSION

The complex forms discrete centrosymmetric tetracarboxylate bridged dimers of the copper(II) acetate hydrate type[1] (Fig. 1). The bond distances and angles about the dimer are considered normal for this system with Cu—O (equatorial) ranging from 1.949(3) to 1.987(3) Å [1.960(3) Å mean] and Cu—O (axial) 2.182(3) Å. The Cu—Cu separation is 2.602(1) Å. This value shows a much larger range throughout the series and is dependent upon a number of factors, including ligand and axial group types.[13] The most unusual feature of this structure is the presence of protonated acids, providing carboxyl oxygen atoms in the axial sites of the dimer. This represents only the second crystallographically described example of such a complex. The previous example was tetrakis-μ-[acetato-O,O']bis[acetic acid copper(II)],[8] prepared by treatment of dehydrated copper(II) acetate with acetic acid–acetic anhydride. The presence of water in this system results in the reversion to the conventional copper acetate hydrate structure, with water replacing acetic acid in the axial sites. The preparation of the

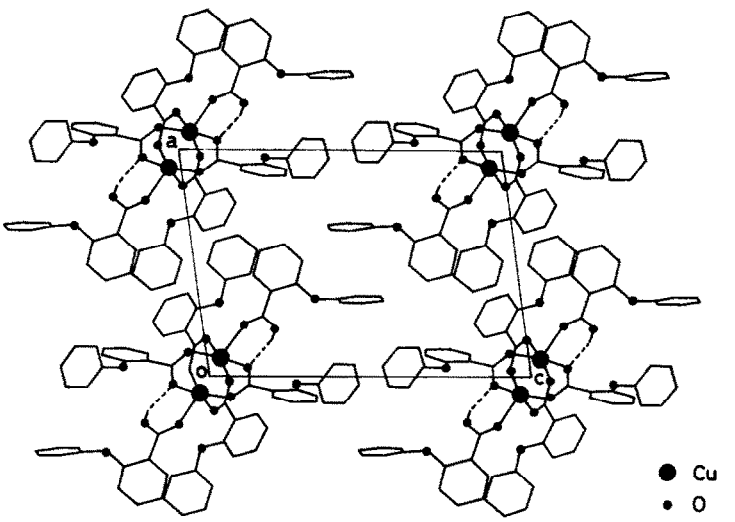

Fig. 2. Packing in the unit cell viewed down *b*.

title compound, however, involves a solution of the acid in aqueous ethanol so that the reason for incorporation of such sterically bulky groups in the axial sites is puzzling. A high concentration of unreacted acid in the crystallizing solution is normal with this method of preparation, but in no other examples has this type of incorporation of unprotonated acid been observed. Solvent molecules such as methanol,[8] ethanol,[14] 1,4-dioxane,[15] acetone,[16] dimethylformamide,[8,17] and dimethylsulphoxide[18] are common. Comparative bond lengths [Cu—O (axial) and Cu—Cu] for the acetic acid dimer are 2.197(2) and 2.581(1) Å, respectively.[8]

Packing of the dimers in the unit cell involves no significant inter-dimer associations (Fig. 2), a phenomenon not unusual with ligands having no typically associative peripheral groups. The stability of the axial group is enhanced by a strong O—H---O hydrogen bonding interaction [O---O, 2.64(1) Å], a feature in common with the acetic acid example where the comparative O---O distance is 2.62 Å.

Acknowledgements—The authors thank The Chinese University of Hong Kong, The University of Queensland and the Queensland University of Technology for financial support.

REFERENCES

1. J. N. van Niekerk and F. R. L. Schoening, *Acta Cryst.* 1953, **6**, 227.
2. B. Morosin, R. C. Hughes and Z. G. Soos, *Acta Cryst.* 1975, **31B**, 762.
3. J. Pickardt, *Acta Cryst.* 1981, **37B**, 1753.
4. M. M. Borel and A. Leclaire, *Acta Cryst.* 1976, **32B**, 1275.
5. G. Smith, E. J. O'Reilly, C. H. L. Kennard and A. H. White, *J. Chem. Soc., Dalton Trans.* 1985, 243.
6. A. V. Ablov, Yu. A. Siminov and T. I. Malinovskii, *Sov. Phys. Dokl.* 1967, **11**, 1029.
7. M. J. Bird and T. R. Lomer, *Acta Cryst.* 1972, **28B**, 242.
8. V. M. Rao and H. Manohar, *Inorg. Chim. Acta* 1979, **34**, L213; W. M. Rao, D. N. Sathanarayana and H. Manohar, *J. Chem. Soc., Dalton Trans.* 1983, 2167.
9. E. J. O'Reilly, G. Smith and C. H. L. Kennard, *Inorg. Chim. Acta* 1984, **90**, 63.
10. G. M. Sheldrick, SHELXS-86. Structure Solution Package. University of Göttingen, F.R.G. (1986).
11. G. M. Sheldrick, SHELX-76 Program for Crystal Structure Determination. University of Cambridge, U.K. (1976).
12. *International Tables for X-ray Crystallography*, Vol. 4. Kynoch Press, Birmingham (1974).
13. M. Melnik, *Coord. Chem. Rev.* 1982, **42**, 259.
14. W. Clegg, I. R. Little and B. P. Straughan, *Acta Cryst.* 1986, **42C**, 1489.
15. G. Reck and W. Jahnig, *J. Prakt. Chem.* 1979, **321**, 549.
16. G. Smith, E. J. O'Reilly, C. H. L. Kennard, T. C. W. Mak and W.-H. Yip, *Polyhedron* 1985, **4**, 451.
17. M. G. Mys'kiv, V. V. Olynik, E. E. Kriss, N. F. Konakhovich and A. S. Grigor'eva, *Koord. Khim.* 1982, **8**, 1415; A. S. Batsanov, Yu. T. Struchkov, A. S. Grigor'eva, E. E. Kriss, N. F. Konakhovich and Yu. A. Fialkov, *Koord. Khim.* 1981, **7**, 784.
18. M. Klinga, M. R. Sundberg, M. Melnik and J. Mrozinski, *Inorg. Chim. Acta* 1989, **162**, 39.

Polyhedron Vol. 9, No. 14, pp. 1671–1676, 1990
Printed in Great Britain

0277–5387/90 $3.00+.00
© 1990 Pergamon Press plc

ISOLATION AND X-RAY STRUCTURE DETERMINATION OF A SULPHUR-BRIDGED INCOMPLETE CUBANE-TYPE MOLYBDENUM(IV) AQUA CLUSTER, $[Mo_3S_4(H_2O)_9](CH_3 \cdot C_6H_4 \cdot SO_3)_4 \cdot 9H_2O$

HARUO AKASHI, TAKASHI SHIBAHARA* and HISAO KUROYA

Department of Chemistry, Okayama University of Science, 1-1 Ridai-cho, Okayama 700, Japan

(*Received* 9 *January* 1990; *accepted* 1 *March* 1990)

Abstract—The title compound was isolated in high yield (72%) from 4 M HPTS solution, and the X-ray crystal structure has been determined. The cluster cation has an approximate C_{3v} symmetry. The average Mo—Mo distance (2.735[8] Å) in the aqua complex is the shortest reported in complexes with Mo_3S_4 cores so far. Every SO_3^- moiety of the pts^- anion faces towards the complex cation.

The chemistry of the incomplete cubane-type sulphur-bridged molybdenum cluster with Mo_3S_4 cores has attracted much attention. Although the aqua ion, $Mo_3S_4(aq)^{4+}$, has been prepared and characterized in solution[1–3] and many X-ray structures of analogous complexes with Mo_3S_4 cores have been determined,[4,5] no X-ray structure of the aqua cluster itself has been reported as yet. Furthermore, cubane-type mixed-metal clusters with Mo_3MS_4 (M = Fe, Co, Ni, Cu, Sn, Hg) cores have been prepared from the aqua ion and corresponding metal and/or metal ions lately,[2,6] and the aqua ion, $Mo_3S_4(aq)^{4+}$, will be studied more actively.

We report here the preparation and X-ray structure analysis of an incomplete cubane-type molybdenum aqua cluster, $[Mo_3S_4(H_2O)_9](CH_3 \cdot C_6H_4 \cdot SO_3)_4 \cdot 9H_2O$ (**1**), which provides direct evidence for the existence of the incomplete cubane-type molybdenum(IV) aqua ion, $[Mo_3S_4(H_2O)_9]^{4+}$. As for the X-ray structure determination of metal cluster complex compounds with aqua ligands alone, only a few complex compounds are known and they all include *p*-toluenesulphonates as counteranions.[6,7] The role of the anion will also be discussed.

* Author to whom correspondence should be addressed.

EXPERIMENTAL

Preparation of $[Mo_3S_4(H_2O)_9](CH_3 \cdot C_6H_4 \cdot SO_3)_4 \cdot 9H_2O$ (**1**)

The aqua ion, $Mo_3S_4(aq)^{4+}$ in 2 M HCl, which was obtained by the published procedure[1] was diluted to 10 times its original volume with water and was absorbed on Dowex 50W-X2 cation exchanger. Washing of the resin with 0.1 M HPTS (*p*-toluenesulphonic acid) to remove Cl^- ion, and elution with 4 M HPTS gave a green solution. Cooling of the eluted solution in a refrigerator for a few days gave green plate crystals; yield *ca* 72% based on $Mo_3S_4(aq)^{4+}$ in 2 M HCl. Found (Calc.): C, 23.9 (23.6); H, 4.0 (4.5)%.

X-ray data collection and structure determination

A crystal of **1** was mounted in a glass capillary. The crystallographic parameters are given in Table 1. The intensities of three standard reflections did not show any appreciable decay. The data were corrected for Lorentz and polarization effects. No absorption correction was applied. The structure was solved by a direct method[8] and refined by a block-diagonal least-squares technique. Application of an anisotropic thermal parameter to the sulphur atom [Sp(4)] in one of the four pts^- anions

Table 1. Summary of crystal data, intensity collections, and structure refinement parameters for $[Mo_3S_4(H_2O)_9](CH_3C_6H_4SO_3)_4 \cdot 9H_2O$

Formula	$Mo_3S_8O_{30}C_{28}H_{64}$
Mol. wt	1425.10
Crystal system	Triclinic
Space group	$P\bar{1}$
a (Å)	15.361(4)
b (Å)	16.730(4)
c (Å)	12.084(5)
α (°)	95.32(3)
β (°)	108.85(3)
γ (°)	102.60(2)
V (Å^3)	2822.9(16)
Z	2
$d_{calc.}$ (g cm^{-3})	1.677
d_{obs} (g cm^{-3})	1.67
μ(Mo-K_α) (cm^{-1})	10.0
Crystal size (mm)	$0.32 \times 0.23 \times 0.25$
Radiation (λ) (Å)	Mo-K_α (0.71073)[a]
Data collection instrument	RIGAKU AFC-6A
Scan method	ω ($2 \leqslant 30°$), ω–2θ ($2\theta > 30°$)
Scan speed (° min^{-1})	2
Scan range (°)	$1.50+0.5 \tan\theta$
Background measurement (s)	5
Data collected	$\pm h, \pm k, +l$ ($2\theta \leqslant 50°$)
Total no. of reflections	10,680
Number of unique data[b]	4349
Number of variables	601
R (R_w) (%)[c]	6.01(7.77)

[a] Graphite-monochromatized.
[b] $|F_o| \geqslant 8\sigma(F_o)$.
[c] $R = \Sigma||F_o|-|F_c||/\Sigma|F_o|$;
$R_w = [\Sigma w(|F_o|-|F_c|)^2/\Sigma w|F_o|^2]^{1/2}$.
$w = 1/[\sigma^2(|F_o|)+g|F_o|^2]$; $g = 0.001$.

gave unreasonable O—S—O angles in the SO_3^- group, and we used isotropic thermal parameters for the sulphur atom and the three oxygen atoms [OP(41), OP(42) and OP(43)] attached to the sulphur atom. Isotropic thermal parameters were also used for the two disordered waters of crystallization [OW(8A), OW(8B), OW(9A) and OW(9B)]. Anisotropic thermal parameters were used for all other atoms. No attempt was made to locate hydrogen atoms. No chemically significant peaks were observed on the final difference Fourier map. Computations were performed on a FACOM M380 computer at Okayama University of Science. The programs in the UNICS[9] were employed. The figures were drawn by use of ORTEP.[10] The atomic scattering factors, with corrections for anomalous scattering of Mo and S, were taken from ref. 11.

RESULTS AND DISCUSSION

The structure of $[Mo_3S_4(H_2O)_9]^{4+}$ is shown in Fig. 1, and the interatomic distances and angles of the complex cation are collected in Table 2. The cation has an approximate symmetry of C_{3v}. The average Mo—Mo distance (2.735[8] Å) in the aqua complex is the shortest of the complexes with Mo_3S_4 cores so far reported. The complex with H_2O ligands as well as oxalato ones[5] has the second shortest Mo—Mo distance. No relevance can be found between Mo—Mo distances and charges of complexes with Mo_3S_4 cores.[4,5] The Mo—μ_2S and Mo—μ_3S distances are in the range of the values so far reported.

Every SO_3^- group, negatively charged moiety of the pts^- anion, faces towards the complex cluster cation as shown in Fig. 2. Some hydrogen bonds exist between coordinated water molecules and oxygens of SO_3^- groups: short contacts are collected in Table 3. Mean values of bond distances and angles in pts^- anions are listed in Table 4.

Isolation of the crystalline aqua compound from 4 M HPTS solution was achieved in a good yield by use of ion exchange techniques. Addition of solid HPTS to the aqua ion in 2 M HCl so as to make 4 M HPTS did not give any crystals. Hydrogen bonds between coordinated water molecules and pts^- anions (see below) stabilize crystalline products, but coordination of chloride ions to the Mo_3S_4 core prevents the aqua ion from being isolated in crystalline form: when the medium was changed from HPTS (1–4 M) to HCl (1–2 M), a shift (from 602 to 620 nm) of the absorption peak of the aqua ion was observed in the visible region of the electronic spectrum. To the best of our knowledge, all the aqua cluster compounds isolated as crystals include pts^- as counteranions and sulphur bridges between metal atoms within the cluster ions.[6,7] The X-ray

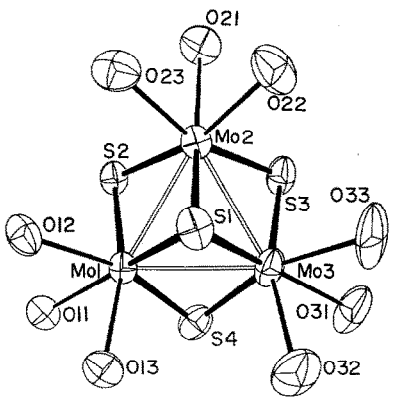

Fig. 1. Perspective view of $[Mo_3S_4(H_2O)_9]^{4+}$.

Table 2. Selected interatomic distances (Å) and angles (°) in $[Mo_3S_4(H_2O)_9]^{4+}$

Bond distances (Å)			
Mo(1)—Mo(2)	2.737(2)	Mo(1)—O(11)	2.191(11)
Mo(1)—Mo(3)	2.742(2)	Mo(1)—O(12)	2.174(10)
Mo(2)—Mo(3)	2.727(2)	Mo(1)—O(13)	2.178(8)
Mean	2.735[8]	Mo(2)—O(21)	2.183(9)
Mo(1)—S(1)	2.333(5)	Mo(2)—O(22)	2.159(13)
Mo(2)—S(1)	2.336(3)	Mo(2)—O(23)	2.174(12)
Mo(3)—S(1)	2.343(4)	Mo(3)—O(31)	2.194(13)
Mean	2.337[5]	Mo(3)—O(32)	2.199(11)
Mo(1)—S(2)	2.285(3)	Mo(3)—O(33)	2.182(13)
Mo(1)—S(4)	2.282(5)	Mean	2.182[12]
Mo(2)—S(2)	2.289(4)		
Mo(2)—S(3)	2.279(4)		
Mo(3)—S(3)	2.285(3)		
Mo(3)—S(4)	2.277(5)		
Mean	2.283[4]		
Bond angles (°)			
Mo(2)—Mo(1)—Mo(3)	59.69(5)	Mo(1)—Mo(2)—O(23)	97.9(3)
Mo(1)—Mo(2)—Mo(3)	60.24(5)	Mo(3)—Mo(2)—O(22)	98.4(3)
Mo(1)—Mo(3)—Mo(2)	60.07(5)	Mo(2)—Mo(3)—O(32)	100.2(3)
Mean	60.00[28]	Mo(2)—Mo(3)—O(33)	97.7(4)
Mo(2)—Mo(1)—S(1)	54.2(1)	Mean	98.1[11]
Mo(3)—Mo(1)—S(1)	54.3(1)	S(1)—Mo(1)—S(2)	106.3(1)
Mo(1)—Mo(2)—S(2)	54.1(1)	S(1)—Mo(1)—S(4)	105.7(2)
Mo(3)—Mo(2)—S(1)	54.5(1)	S(1)—Mo(2)—S(2)	106.1(1)
Mo(1)—Mo(3)—S(1)	53.9(1)	S(1)—Mo(2)—S(3)	106.6(1)
Mo(2)—Mo(3)—S(1)	54.2(1)	S(1)—Mo(3)—S(3)	106.2(2)
Mean	54.2[2]	S(1)—Mo(3)—S(4)	105.5(2)
Mo(2)—Mo(1)—S(2)	53.3(1)	Mean	106.1[4]
Mo(3)—Mo(1)—S(4)	52.9(1)	S(2)—Mo(1)—S(4)	95.3(1)
Mo(1)—Mo(2)—S(2)	53.2(1)	S(2)—Mo(2)—S(3)	94.6(2)
Mo(3)—Mo(2)—S(3)	53.4(1)	S(3)—Mo(3)—S(4)	96.5(2)
Mo(1)—Mo(3)—S(4)	53.1(1)	Mean	95.5[10]
Mo(2)—Mo(3)—S(3)	53.2(1)	S(1)—Mo(1)—O(12)	86.9(3)
Mean	53.2[2]	S(1)—Mo(1)—O(13)	84.6(3)
Mo(2)—Mo(1)—S(4)	98.3(1)	S(1)—Mo(2)—O(22)	85.5(3)
Mo(3)—Mo(1)—S(2)	97.3(1)	S(1)—Mo(2)—O(23)	87.6(3)
Mo(1)—Mo(2)—S(3)	98.5(1)	S(1)—Mo(3)—O(32)	88.4(4)
Mo(3)—Mo(2)—S(2)	97.6(1)	S(1)—Mo(3)—O(33)	85.7(4)
Mo(1)—Mo(3)—S(3)	98.2(1)	Mean	86.5[14]
Mo(2)—Mo(3)—S(4)	98.8(1)	S(2)—Mo(1)—O(11)	87.3(2)
Mean	98.1[6]	S(2)—Mo(1)—O(12)	91.1(3)
Mo(2)—Mo(1)—O(11)	140.5(2)	S(4)—Mo(1)—O(11)	87.5(3)
Mo(2)—Mo(1)—O(13)	138.7(3)	S(4)—Mo(1)—O(13)	90.6(3)
Mo(3)—Mo(1)—O(11)	140.4(3)	S(2)—Mo(2)—O(21)	88.7(3)
Mo(3)—Mo(1)—O(12)	141.0(3)	S(2)—Mo(2)—O(23)	90.8(3)
Mo(1)—Mo(2)—O(21)	141.8(3)	S(3)—Mo(2)—O(21)	85.5(3)
Mo(1)—Mo(2)—O(22)	139.6(2)	S(3)—Mo(2)—O(22)	92.8(3)
Mo(3)—Mo(2)—O(21)	138.7(3)	S(3)—Mo(3)—O(31)	84.7(3)
Mo(3)—Mo(2)—O(23)	142.0(2)	S(3)—Mo(3)—O(33)	91.9(3)
Mo(1)—Mo(3)—O(31)	141.0(4)	S(4)—Mo(3)—O(31)	87.9(4)
Mo(1)—Mo(3)—O(33)	139.6(3)	S(4)—Mo(3)—O(32)	90.9(4)
Mo(2)—Mo(3)—O(31)	137.8(3)	Mean	89.1[26]
Mo(2)—Mo(3)—O(32)	142.6(4)	S(1)—Mo(1)—O(11)	159.7(2)
Mean	140.3[15]	S(1)—Mo(2)—O(21)	159.7(4)
Mo(2)—Mo(1)—O(12)	97.6(3)	S(1)—Mo(3)—O(31)	161.3(3)
Mo(3)—Mo(1)—O(13)	96.9(3)	Mean	160.2[9]

Table 2—*continued*

S(2)—Mo(1)—O(13)	165.5(3)	O(31)—Mo(3)—O(32)	78.2(4)
S(4)—Mo(1)—O(12)	163.6(3)	O(31)—Mo(3)—O(33)	78.7(5)
S(2)—Mo(2)—O(22)	163.8(3)	O(32)—Mo(3)—O(33)	77.0(5)
S(3)—Mo(2)—O(23)	162.7(3)	Mean	78.3[10]
S(3)—Mo(3)—O(32)	161.1(3)	Mo(1)—S(1)—Mo(2)	71.8(1)
S(4)—Mo(3)—O(33)	163.4(4)	Mo(1)—S(1)—Mo(3)	71.8(1)
Mean	163.4[14]	Mo(2)—S(1)—Mo(3)	71.3(1)
O(11)—Mo(1)—O(12)	77.7(4)	Mean	71.6[3]
O(11)—Mo(1)—O(13)	79.8(3)	Mo(1)—S(2)—Mo(2)	73.5(1)
O(12)—Mo(1)—O(13)	79.8(4)	Mo(2)—S(3)—Mo(3)	73.4(1)
O(21)—Mo(2)—O(22)	77.5(4)	Mo(1)—S(4)—Mo(3)	73.9(2)
O(21)—Mo(2)—O(23)	78.1(4)	Mean	73.6[3]
O(22)—Mo(2)—O(23)	78.2(5)		

Table 3. Short contacts (Å) in $[Mo_3S_4(H_2O)_9](CH_3C_6H_4SO_3)_4 \cdot 9H_2O$

O(11)—OP(22)	2.63(2)	O(33)—OW(9A)	2.58(3)
O(11)—OP(11)[a]	2.73(2)	OP(12)—OW(4)[a]	2.79(3)
O(12)—OP(21)	2.62(2)	OP(13)—OW(7)	2.71(3)
O(12)—OP(32)	2.61(2)	OP(21)—OW(1)	2.68(2)
O(13)—OP(33)	2.73(2)	OP(31)—OW(9A)[b]	2.58(4)
O(13)—OW(4)	2.66(2)	OP(33)—OW(2)	2.72(2)
O(21)—OP(11)	2.68(2)	OP(33)—OW(6)[c]	2.95(3)
O(21)—OW(3)	2.65(2)	OP(41)—OW(2)[b]	2.83(3)
O(22)—OW(7)	2.53(3)	OP(41)—OW(4)[d]	2.77(3)
O(22)—OW(9A)	2.75(3)	OP(43)—OW(6)[e]	2.84(4)
O(22)—OW(9B)	2.71(4)	OW(1)—OW(3)	2.70(2)
O(23)—OW(1)	2.68(2)	OW(3)—OW(8B)[a]	2.82(5)
O(23)—OW(2)	2.66(2)	OW(5)—OW(6)[c]	2.71(4)
O(31)—OP(23)[a]	2.69(2)	OW(5)—OW(8A)[d]	2.68(3)
O(32)—OW(5)	2.63(3)	OW(5)—OW(9B)[b]	2.55(5)
O(32)—OW(8A)	2.66(3)	OW(6)—OW(7)[a]	2.87(4)
O(33)—OP(42)	2.58(3)		

Symmetry operations: [a] $1-x, -y, -z$; [b] $2-x, -y, -z$; [c] $x+1, y, z$; [d] $2-x, -y, 1-z$; [e] $1-x, -y, 1-z$.

Table 4. Mean values of bond distances (Å) and angles (°) in $CH_3C_6H_4SO_3^{-}$ [a,b]

S—O	1.45[3]
S—C	1.78[1]
C—C[a]	1.35[7]
C—C[b]	1.52[5]
O—S—O	111[10]
O—S—C	107[2]
S—C—C	121[2]
C—C—C[a]	120[4]
C—C—C[b]	123[3]

[a] Carbon atoms in a phenylene group.
[b] Carbon atoms in methyl and phenylene groups.

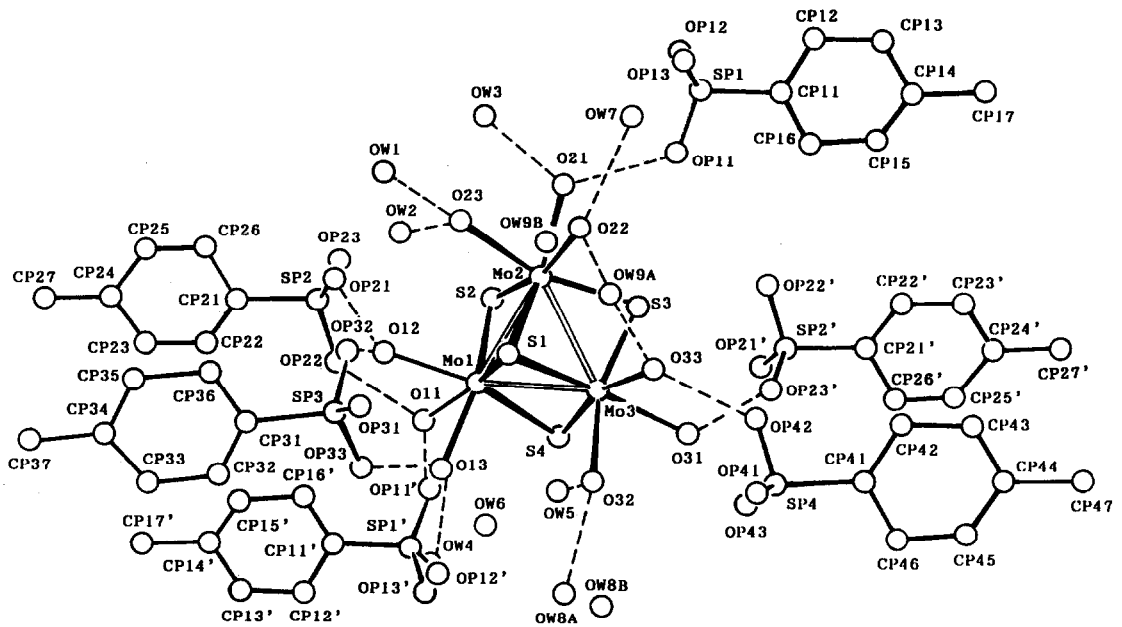

Fig. 2. Short contacts in $[Mo_3S_4(H_2O)_9](CH_3 \cdot C_6H_4 \cdot SO_3)_4 \cdot 9H_2O$[a,b]: (a) Hydrogen bonds are shown by broken lines. (b) The primed atoms are related to unprimed ones by a centre of symmetry.

structures of the derivatives of the aqua ions with oxygen and sulphur bridge(s), $Mo_3O_{4-n}S_n(aq)^{4+}$ ($n = 0$–3), had been determined,[12] and we have tried to isolate the crystalline incomplete cubane-type aqua ions from 4 M HPTS solution, but in vain. Furthermore, in the corresponding tungsten aqua ions of $W_3O_{4-n}S_n(aq)^{4+}$ ($n = 0$–4), the sulphur-bridged one alone, $[W_3S_4(H_2O)_9]^{4+}$,[6] has been isolated as crystals.[13] These indicate that the presence of hydrogen bonds between the coordinated water molecules and pts^- anions is not the only determining factor in the formation of crystalline aqua compounds, but sulphur bridges may be also useful. However, there is no short contact between sulphur bridges and other atoms including atoms in pts^-, and we can not explain the role of the sulphur bridges in the crystallization at present.

Acknowledgement—This work was supported by a Grant-in-Aid for Scientific Research (No. 62470043) from the Ministry of Education, Science and Culture.

Supplementary materials available. The atomic coordinates and anisotropic thermal parameters, and bond distances and angles for pts^- groups, and tables of F_o and F_c values are deposited.

REFERENCES

1. T. Shibahara and H. Kuroya, *Abstract of Papers*, 5th International Conference on the Chemistry and Uses of Molybdenum, Newcastle upon Tyne, U.K., Climax Molybdenum, Ann Arbor, MI, p. 59 (1985); T. Shibahara and H. Kuroya, *Polyhedron* 1986, **5**, 357.
2. B.-L. Ooi and A. G. Sykes, *Inorg. Chem.* 1989, **28**, 3799.
3. B.-L. Ooi, C. Sharp and A. G. Sykes, *J. Am. Chem. Soc.* 1989, **111**, 125; F. A. Cotton, Z. Dori, R. Llusar and W. Schwotzer, *J. Am. Chem. Soc.* 1985, **107**, 6734; P. Kathirgamanathan, M. Martinez and A. G. Sykes, *J. Chem. Soc., Chem. Commun.* 1985, 953; P. Kathirgamanathan, M. Martinez and A. G. Sykes, *J. Chem. Soc., Chem. Commun.* 1985, 1437; P. Kathirgamanathan, M. Martinez and A. G. Sykes, *Polyhedron* 1986, **5**, 505; M. Martinez, B.-L. Ooi and A. G. Sykes, *J. Am. Chem. Soc.* 1987, **109**, 4615.
4. $[Mo_3S_4Cl_3(dmpe)_3]^+$ (Mo—Mo = 2.766[4] Å): F. A. Cotton, R. Llusar and C. T. Eagle, *J. Am. Chem. Soc.* 1989, **111**, 4332; $[Mo_3S_4Cp_3]^+$ (Mo—Mo = 2.812[1] Å): P. J. Vergamini, H. Vahrenkamp and L. F. Dahl, *J. Am. Chem. Soc.* 1971, **93**, 6327; $[Mo_3S_4(CN)_9]^{5-}$ (Mo—Mo = 2.775[8] Å): A. Muller, R. Jostes, W. Eltzner, C.-S. Nie, E. Diemann, H. Bogge, M. Zimmermann, M. Dartmann, U. Reinsch-Vogell, S. Che, S. J. Cyvin and B. N. Cyvin, *Inorg. Chem.* 1985, **24**, 2872; $[Mo_3S_4(CN)_9]^{5-}$ (Mo—Mo = 2.765[7] Å): N. C. Howlader, G. P. Haight Jr, T. W. Hambley, G. A. Lawrance, K. M. Rahmoeller and M. R. Snow, *Aust. J. Chem.* 1983, **36**, 377; $[Mo_3S_4(ida)_3]^{2-}$ (Mo—Mo = 2.754[11] Å), ref. 1; $[Mo_3S_4(Hnta)_2(nta)]^{3-}$ (Mo—Mo = 2.761[1] Å): F. A. Cotton, R. Llusar, D. O. Marler and W. Schwotzer, *Inorg. Chim. Acta* 1985, **102**, L25; $[Mo_3S_3([9]aneN_3)_3]^{4+}$ (Mo—Mo = 2.773[7] Å): F. A. Cotton, Z. Dori, R.

Llusar and W. Schwotzer, *Inorg. Chem.* 1986, **25**, 3654; $[Mo_3S_4(SCH_2CH_2S)_3]^{2-}$ (Mo—Mo = 2.783[12] Å): T. R. Halbert, K. McGauley, W.-H. Pan, R. S. Czernuszewicz and E. I. Stiefel, *J. Am. Chem. Soc.* 1984, **106**, 1849; $[Mo_3S_4(S_2P(OEt)_2)_4(H_2O)]$ (Mo—Mo = 2.754[18] Å): X.-T. Lin, Y.-H. Lin, J.-L. Huang and J.-Q. Huang, *Kekue Tongbao* 1987, **32**, 810; $[Mo_3S_4(S_2P(OEt)_2)_4P(C_6H_5)_3]$ (Mo—Mo = 2.744[12] Å): J.-Q. Huang, S.-F. Lu, Y.-H. Lin, J.-L. Huang and J.-X. Lu, *Acta Chim. Sin.* 1987, **45**, 213; $[Mo_3S_4(S_2P(OEt)_2)_4(PhCH_2CN)]$ (Mo—Mo = 2.756 Å): S.-F. Lu, J.-Q. Huang, Y.-H. Lin and J.-L. Huang, *Jiegou Huaxue* 1987, **6**, 154; $[Mo_3S_4Cl_3(dmpe)_3]^+$ (Mo—Mo = 2.766[4] Å): F. A. Cotton and R. Llusar, *Polyhedron* 1987, **6**, 1741; $[Mo_3S_4Cl_4(PEt_3)_3(MeOH)_2]$ (Mo—Mo = 2.766[24] Å), $[Mo_3S_4Cl_4(PEt_3)_4(MeOH)]$ (Mo—Mo = 2.790[5] Å): T. Saito, N. Yamamoto, T. Yamagata and H. Imoto, *Chem. Lett.* 1987, 2025.

5. $[Mo_3S_4(ox)_3(H_2O)_3]^{2-}$ (Mo—Mo = 2.738(5) Å): F. A. Cotton, Z. Dori, Z. R. Llusar and W. Schwotzer, *J. Am. Chem. Soc.* 1985, **107**, 6734.
6. H. Akashi and T. Shibahara, *Inorg. Chem.* 1989, **28**, 2906 and refs cited therein.
7. T. Shibahara, A. Takeuchi, A. Ohtsuji, K. Khoda and H. Kuroya, *Inorg. Chim. Acta* 1987, **127**, L45.
8. G. Sheldrick, SHELXS-86, Institut für Anorganishe Chemie der Universität, Tammannstrasse 4, D-3400 Göttingen, F.R.G.
9. The Universal Crystallographic Program System. The Crystallographic Society of Japan, Tokyo (1969).
10. C. K. Johnson, ORTEP, Report ORNL-3794. Oak Ridge National Laboratory, Oak Ridge, TN (1965).
11. *International Tables for X-Ray Crystallography*, Vol. IV, pp. 71 and 148. Kynoch Press, Birmingham (1974).
12. For example, $[Mo_3O_4(C_2O_4)_3(H_2O)_3]^{2-}$: E. Benory, A. Bino, D. Gibson, F. A. Cotton and Z. Dori, *Inorg. Chim. Acta* 1985, **99**, 137; $[Mo_3O_3S(Hnta)_3]^{2-}$: T. Shibahara, H. Akashi, S. Nagahata, H. Hattori and H. Kuroya, *Inorg. Chem.* 1989, **28**, 362; $[Mo_3O_2S_2(NCS)_9]^{5-}$: T. Shibahara, T. Yamada, H. Kuroya, E. F. Hills, P. Kathirgamanathan and A. G. Sykes, *Inorg. Chim. Acta* 1986, **113**, L19; $[Mo_3OS_3(HN(CH_2CO_2)_2)_3]^{2-}$: T. Shibahara, H. Miyake, K. Kobayashi and H. Kuroya, *Chem. Lett.* 1986, 139; $[Mo_3(\mu_3\text{-}O)(\mu\text{-}S)_3(S_2P(OEt)_2)_4(C_3H_3N_2)]$: M.-D. Huang, S.-F. Lu, J.-Q. Huang and J.-L. Huang, *Jiegou Huaxue* 1987, **6**, 29.
13. X-ray structures of several incomplete cobane-type complexes with $W_3O_{4-n}S_n$ cores (n = 0–3) have been determined. For example, $[W_3O_4(NCS)_9]^{5-}$: M. Segawa and Y. Sasaki, *J. Am. Chem. Soc.* 1985, **107**, 5565; $[W_3O_3S(NCS)_9]^{5-}$: Z. Dori, F. A. Cotton, R. Llusar and W. Schwotzer, *Polyhedron* 1986, **5**, 907; $[W_3O_2S_2(N(CH_2CO_2)_2(CH_2CO_2H))_3]^{2-}$: T. Shibahara, A. Takeuchi, T. Kunimoto and H. Kuroya, *Chem. Lett.* 1987, 867; $[W_3OS_3\{N(CH_2CO_2)_2(CH_2CO_2H)\}_3]^{2-}$, T. Shibahara, A. Takeuchi and H. Kuroya, *Inorg. Chim. Acta* 1987, **127**, L39.

Polyhedron Vol. 9, No. 14, pp. 1677–1681, 1990
Printed in Great Britain

0277-5387/90 $3.00+.00
© 1990 Pergamon Press plc

SYNTHESIS AND REACTIVITY OF 1,2- AND 1,4-DIHYDROXYARENE COMPLEXES OF CHROMIUM TRICARBONYL

HANS SCHUMANN,* ATTA M. ARIF and THOMAS G. RICHMOND†

Department of Chemistry, University of Utah, Salt Lake City, UT 84112, U.S.A.

(*Received* 29 *December* 1989; *accepted* 7 *March* 1990)

Abstract—Direct reaction of Me_3Si protected 1,2- or 1,4-dihydroxyarenes with $Cr(CO)_6$ affords fair to good yields of the corresponding $Cr(CO)_3$ complexes (**1a–4a**) which were characterized by ^1H and ^{13}C NMR and IR spectroscopic measurements. Removal of the Me_3Si protecting groups with $KF \cdot 2H_2O$ or $HBF_4 \cdot Et_2O$ afforded the 1,2- or 1,4-dihydroxyarene complexes **1b–4b** which were characterized in solution but their instability and air-sensitivity precluded their isolation. Proton transfer reactions were monitored by IR spectroscopy. The crystal structure of $2,3\text{-}(Me_3Si)_2C_{10}H_6Cr(CO)_3$ was determined in the space group $P2_1/c$ with $a = 11.019(4)$, $b = 17.613(9)$, $c = 11.843(4)$ Å, $\beta = 105.11(3)°$, $V = 2219.0$ Å^3, $Z = 4$. This synthetic route provides access to the π-coordination chemistry of 1,2-dihydroxyarenes which cannot be prepared by direct interaction of the arene with $Cr(CO)_6$.

Arene complexes of chromium tricarbonyl have played a central role in the development of organometallic chemistry and these complexes have found extensive application in organic synthesis.[1] Although a myriad of substituted arenes have been coordinated to the $Cr(CO)_3$ fragment, a successful synthesis of hydroquinone chromium tricarbonyl (**1b**) has only recently been reported by Wright who reacted 1,4-hydroquinone with $Cr(CO)_3(CH_3CN)_3$ in refluxing tetrahydrofuran.[2] Complex **1b** could not be isolated and was reported to be unstable in the higher boiling ether solvents typically employed in direct preparations from $Cr(CO)_6$. The hydroxyarene chemistry of $Cr(CO)_3$ has been investigated in some detail since Fischer's preparation[3] of $(HOPh)Cr(CO)_3$ by direct reaction of $Cr(CO)_6$ with phenol at 190°C. Aside from the above note, the π-coordination chemistry of 1,2- and 1,4-dihydroxyaromatics at $Cr(CO)_3$ is unexplored. Note that direct reaction of 1,2-quinones or catechols with $Cr(CO)_6$ results in O-bound chelates and oxidative decarbonylation of the metal centre.[4]

Our interest in these compounds is based on the potentially unusual redox chemistry of the π-coordinated dihydroxyaromatic that might be expected based on the known behaviour of the O-bound complexes of these ligands.[4] Ligand-based oxidation may involve changes in the coordination mode of the arene.[5] Attempts to generate coordinated dihydroxyarenes by protonation of coordinated quinones bound to later transition metals have been reported.[6] We thus sought a general route to these materials by a protecting group strategy. In this work we report that trimethylsilyl protected dihydroxyarenes react directly with $Cr(CO)_6$ to afford the corresponding $Cr(CO)_3$ complexes and removal of the trimethylsilyl groups provides a method of generating the desired materials. Although the dihydroxyaromatic chromium tricarbonyl complexes were sufficiently stable to be spectroscopically characterized in solution, attempts to isolate samples in the solid state resulted in decomposition to unidentified chromium(III) complexes. The crystal structure of the naphthalene derivative $2,3\text{-}(Me_3SiO)_2C_{10}H_6Cr(CO)_3$ is also reported.[7]

EXPERIMENTAL

All reactions were carried out under a nitrogen atmosphere using standard Schlenk techniques.[8]

* Present address: Fakulät für Chemie der Universität Bielefeld, Postfach 8640, D-4800, Bielefeld, F.R.G.

† Author to whom correspondence should be addressed.

Solvents were purified by distillation from Na/benzophenone (ethers, alkanes) or P_2O_5 (CH_3CN, CH_2Cl_2). Other chemicals were reagent grade and used as received from commercial sources. Elemental microanalyses were performed by Desert Analytics, Tucson, AZ 85717, U.S.A. NMR spectra were recorded in 5 mm tubes on a Varian XL-300 spectrometer using solvent resonances for internal standards and reported in ppm from Me_4Si (δ). IR spectra were obtained in 1,2-$C_2Cl_2H_4$ using 0.1 mm pathlength CaF_2 cells on a Perkin–Elmer 298 spectrometer.

The ligands **1–4** were prepared according to the procedures outlined by Miller and co-workers[9] in approximately 80% yield after recrystallization from Et_2O–pentane. The following ligand NMR resonances were observed in addition to those contained in Table 1. **1**: ^1H, 0.22 ($SiMe_3$); ^{13}C, 0.14 ($SiMe_3$). **2**: ^1H, 0.32 ($SiMe_3$), 1.34 (CMe_3); ^{13}C, 0.14 ($SiMe_3$), 29.97, 34.67 (CMe_3). **3**: ^1H, 0.32, 0.38 ($SiMe_3$), 1.29, 1.38 (CMe_3); ^{13}C, 1.00, 2.29 ($SiMe_3$), 30.91, 31.81, 34.76, 35.61 (CMe_3). **4**: ^1H, 0.36 ($SiMe_3$); ^{13}C, 0.41 ($SiMe_3$).

The following general procedure[10] was used for the preparation of **1a–4a**. A suspension of 10 mmol of $Cr(CO)_6$ and 15 mmol of ligand **1–4** in 25 cm^3 5 : 1 (n-$Bu)_2O$–THF was heated in an oil bath at the reflux temperature for 1–3 days with periodic return of sublimed $Cr(CO)_6$ to the reaction mixture. The reaction was stopped when sublimation of $Cr(CO)_6$ ceased. Removal of solvent *in vacuo*, followed by recrystallization from CH_2Cl_2–pentane and drying *in vacuo*, afforded the desired products (see Scheme 1 for yields and IR data). Additional NMR data is collected below. **1a**: ^1H, 0.32 ($SiMe_3$); ^{13}C, 0.03 ($SiMe_3$). **2a**: ^1H, 0.41 ($SiMe_3$), 1.43 (CMe_3); ^{13}C, 0.42 ($SiMe_3$), 30.45, 34.93 (CMe_3). **3a**: ^1H, 0.40, 0.54 ($SiMe_3$), 1.29, 1.44 (CMe_3); ^{13}C, 0.97, 2.49 ($SiMe_3$), 30.80, 31.48, 34.34, 35.54 (CMe_3). **4a**: ^1H, 0.23 ($SiMe_3$); ^{13}C, 0.39 ($SiMe_3$). **2a**: Found; C, 54.7; H, 7.7. Calc. for $C_{23}H_{38}CrO_5Si_2$: C, 55.0; H, 7.6%. **3a**: Found: C, 54.5; H, 7.7. Calc. for $C_{23}H_{38}CrO_5Si_2$: C, 55.0; H, 7.6%. **4a**: Found: C,

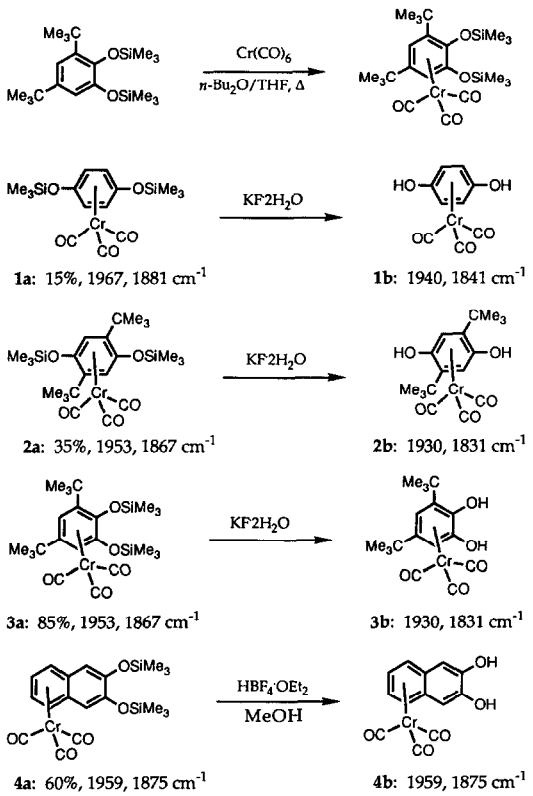

Scheme 1.

Table 1. Arene ^1H and ^{13}C NMR data for compounds **1–4** in acetone-d[6]

Complex	^1H	$^{13}C\{^1H\}$	Cr—CO
1	6.74	121.66 (CH); 150.29 (CO)	
1a	5.49	86.82 (CH); 133.63 (CO)	235.57
1b	5.37	83.82 (CH); 136.93 (CO)	236.82
2	6.71	118.15 (CH); 137.49 (CC); 148.20 (CO)	
2a	5.41	86.01 (CH); 113.77 (CC); 131.66 (CO)	236.42
2b	5.59	85.01 (CH); 111.48 (CC); 136.11 (CO)	238.23
3	6.96, 6.85	114.96, 116.62 (CH); 132.00, 133.00 (CC); 140.62, 142.84 (CO)	
3a	5.72, 5.85	89.84, 91.82 (CH); 112.12, 114.40 (CC); 112.90, 126.10 (CO)	236.60
3b	5.28, 5.63	83.58, 86.42 (CH); 108.22, 113.06 (CC); 136.45, 139.07 (CO)	239.49
4	7.32, 7.36, 7.73	117.02, 124.83, 127.00 (CH); 130.99 (CC); 147.83 (CO)	
4a	5.66, 6.44, 7.14	92.32, 93.35, 116.12 (CH); 105.55 (CC); 151.14 (CO)	234.69
4b	5.56, 6.30, 6.98	91.95, 92.43, 110.01 (CH); 105.12 (CC); 150.12 (CO)	234.58

51.8; H, 5.6. Calc. for $C_{19}H_{24}CrO_5Si_2$: C, 51.8; H, 5.4%.

Preparation of **4b**

To a solution of **4a** (1.76 g, 4.00 mmol) in 10 cm^3 of CH_3OH was added $HBF_4 \cdot Et_2O$ (3.7 g of a 52% solution in Et_2O, 10.0 mmol)[11] and the resulting solution stirred for 4 h, during which time the colour changed from red to orange. The solvent was removed under reduced pressure and the residue extracted with CH_2Cl_2. Addition of pentane and storage at −20°C afforded 0.47 g (40%) of orange powder which was isolated by filtration and dried *in vacuo*. Found: C, 49.7; H, 3.2. Calc. for $C_{13}H_8CrO_5 \cdot H_2O$: C, 49.7; H, 3.2%.

Crystallographic study of **4a**

A 0.47 × 0.35 × 0.35 mm red crystal was cleaved from a larger block obtained from CH_2Cl_2–pentane. The sample crystallizes in the space group $P2_1/c$ with $a = 11.019(4)$, $b = 17.613(9)$, $c = 11.843(4)$ Å, $\beta = 105.11(3)°$, $V = 2219.0$ Å^3, $Z = 4$. Of 3416 reflections measured (Syntex $P\bar{1}$, Mo-K_α) at ambient temperature, 2515 were unique and had $I > 3\sigma(I)$ and were used in the solution (Patterson) and refinement. Final refinement with all non-hydrogen atoms as anisotropic and hydrogen atoms as fixed isotropic contributions (244 variables) using an empirical absorption correction ($\mu = 6.319$ cm^{-1}) gave $R = 3.75$, $R_w = 3.95$, and GOF = 1.31. The highest peak in the final Fourier difference map was 0.260 e/Å^3 (Table 2).

RESULTS AND DISCUSSION

Trimethylsilyl protected hydroxyaromatics (**1–4**) were synthesized by a literature method.[9] Complexes **1a–4a** were prepared by extended reaction of $Cr(CO)_6$ and 1.5 equivalents of the ligand in 5 : 1 *n*-Bu_2O–THF at the reflux point in 15–85% isolated yields after recrystallization from CH_2Cl_2–pentane. Higher yields of the air-stable solids were obtained with the more highly substituted arenes. The complexes were characterized by elemental analysis (**2a–4a**) and exhibit the ν_{CO} bands expected for a C_{3v} $Cr(CO)_3$ group (see Scheme 1). Characteristic upfield shifts of the aromatic protons and carbons

Table 2. Summary of crystallographic data

Molecular formula	$CrSi_2O_5C_{19}H_{24}$
Molecular weight	440.57
Crystal system	Monoclinic
Space group	$P2(1)/c$
Cell dimensions	
a (Å)	11.019(4)
b (Å)	17.613(9)
c (Å)	11.843(4)
β (°)	105.11(3)
Volume (Å)	2219.0
z	4
d_{calc} (g cm^{-1})	1.319
T (°C)	15.0
Crystal dimensions (mm)	0.47 × 0.35 × 0.35
Diffractometer	Syntex $P\bar{1}$
Radiation (Å)	0.71073
Data collection method	2θ–θ
Scan speed (° min^{-1})	Variable (2.5–8.0)
Reflections measured	3416, h(0,12), k(0,19), l(−12,12)
Scan range	K_{α_1} − 1.0 to K_{α_2} + 1.0
2θ limits (°)	3.0–46.0
Total background time/scan time	0.5
Number of reflections between standards	98
Total unique data	3240
Observed data, $I > 3\sigma(I)$	2515
Abs. coeff (μ) (cm^{-1})	6.319
Number of variables	244
R (averaging)	0.025, 0.017

upon coordination to $Cr(CO)_3$ are also observed (Table 1).

In the case of the deep red 2,3-$(Me_3SiO)_2C_{10}H_6Cr(CO)_3$ complex (**4a**), ^{1}H and ^{13}C NMR measurements are indicative of coordination to the unsubstituted ring and no isomeric products were detected. This is confirmed by a single crystal X-ray diffraction study of **4a** as shown in Fig. 1. Bond distances (Table 3) and angles (Table 4) appear normal in comparison with other naphthalene $Cr(CO)_3$ complexes,[12] with the Cr—C(9) and Cr—C(4) distances (av. = 2.31 Å) elongated compared to the other coordinated arene carbon–Cr distances (av. = 2.22 Å). The chromium atom is 1.744 Å from the mean plane of the six coordinated carbons.

Deprotection of **4a** was achieved by treatment with $HBF_4 \cdot Et_2O$ in CH_3OH to afford **4b** which was isolated as an orange microcrystalline powder in 40% yield. Microanalytical data suggest that **4b** exists as a hydrate. As given in Table 1, ^{1}H and ^{13}C NMR data indicate that the $Cr(CO)_3$ group remains coordinated to the unsubstituted arene ring.

Removal of the Me_3Si groups of **1a–3a** was accomplished by stirring with excess $KF \cdot 2H_2O$ in CH_2Cl_2 to afford **1b–3b** which are partially deprotonated by excess fluoride in solution. This is not unexpected given the great increase in acidity for $(C_6H_5OH)Cr(CO)_3$ relative to C_6H_5OH.[13] More rapid cleavage of the protecting groups was effected by wet $[(n\text{-}Bu)_4N]F$. However, in both instances the hygroscopic nature of these fluorides coupled with the sensitivity of the products **1b–3b** prevented reliable control of the degree of protonation. Thus a solution of **1b** prepared with $KF \cdot 2H_2O$ exhibits ν_{CO} bands approximately 20 cm^{-1} lower in frequency compared with the fully protonated material reported by Wright.[2] For example, deprotection of **2a** with $KF \cdot 2H_2O$ afforded **2b** with ν_{CO} = 1930 and 1831 cm^{-1}, but ν_{CO} = 1938 and 1838 cm^{-1} for the complex obtained from wet $[(n\text{-}Bu)_4N]F$. Addition of excess aqueous HBF_4 afforded the fully protonated material with ν_{CO} = 1951 and 1862 cm^{-1}. Thus the donor ability of the arene is only slightly influenced by the replacement of a proton for the Me_3Si group. Reaction of **2b** with 2.5 equivalents of KOH in CH_3CN afforded a complex with ν_{CO} = 1898 and 1784 cm^{-1} which is probably fully deprotonated. These proton transfer reactions appear to be reversible, although solutions slowly decomposed at room temperature. Regardless of the degree of protonation, ^{1}H and ^{13}C NMR spectra (Table 1) of **1b–3b**, prepared by $KF \cdot 2H_2O$ deprotection, definitely show that the arene remains coordinated to the $Cr(CO)_3$ unit. Fluorine NMR spectroscopic examination of a sample of **2a** prepared by deprotection with $[(n\text{-}Bu)_4N]_4F$ did not indicate the presence of HF which could conceivably hydrogen bond to the dihydroxyarene ligand.

Table 3. Selected bond distances for **4a** (in Å)

Cr—C(1)	1.833(4)	O(4)—C(11)	1.353(4)
Cr—C(2)	1.827(4)	O(5)—C(12)	1.362(4)
Cr—C(3)	1.827(4)	C(4)—C(5)	1.432(5)
Cr—C(4)	2.312(3)	C(4)—C(9)	1.418(5)
Cr—C(5)	2.234(4)	C(4)—C(13)	1.425(5)
Cr—C(6)	2.218(4)	C(5)—C(6)	1.398(5)
Cr—C(7)	2.209(4)	C(6)—C(7)	1.414(6)
Cr—C(8)	2.207(4)	C(7)—C(8)	1.385(5)
Cr—C(9)	2.297(3)	C(8)—C(9)	1.442(5)
Si(1)—O(4)	1.667(2)	C(9)—C(10)	1.426(5)
Si(2)—O(5)	1.664(3)	C(10)—C(11)	1.357(5)
O(1)—C(1)	1.150(4)	C(11)—C(12)	1.434(5)
O(2)—C(2)	1.153(4)	C(12)—C(13)	1.355(5)
O(3)—C(3)	1.151(4)		

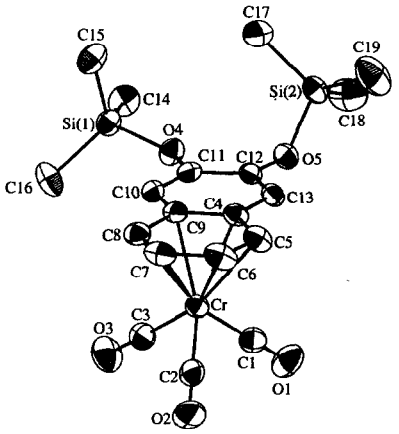

Fig. 1. ORTEP representation of **4a** showing the atom labelling scheme.

Unfortunately, all attempts to isolate the protonated complexes **1a–3a** or their deprotonated forms (as K^+, $[(n\text{-}Bu)_4N]^+$, $[PPh_3Me]^+$ or $[PPN]^+$ salts) proved fruitless. Concentration of these solutions resulted in green, intractable solids. Perhaps O-bound coordination of the ligand is occurring along with oxidation to chromium(III).[4] Thus, these materials may have potential as ligands for other metal centres as recently reported for (phenoxide)$Cr(CO)_3$ complexes.[14] Although hydroquinone complexes of $Cr(CO)_3$ could not be isolated as solids, solution spectroscopic characterization of these materials shows that they can be generated from Me_3Si protected precurcors. In particular, this route provides access to the π-coor-

Table 4. Selected bond angles for **4a** (in deg)

C(1)—Cr—C(2)	89.3(2)	C(6)—C(7)—C(8)	120.5(3)
C(1)—Cr—C(3)	89.4(2)	C(7)—C(8)—C(9)	120.4(4)
C(2)—Cr—C(3)	88.8(2)	C(4)—C(9)—C(8)	119.1(3)
Si(1)—O(4)—C(11)	131.7(2)	C(4)—C(9)—C(10)	119.1(3)
Si(2)—O(5)—C(12)	127.8(2)	C(8)—C(9)—C(10)	121.8(3)
Cr—C(1)—O(1)	178.9(4)	C(9)—C(10)—C(11)	120.8(3)
Cr—C(2)—O(2)	179.2(4)	O(4)—C(11)—C(10)	124.2(3)
Cr—C(3)—O(3)	179.2(1)	O(4)—C(11)—C(12)	115.9(3)
C(5)—C(4)—C(9)	119.3(3)	C(10)—C(11)—C(12)	119.9(3)
C(5)—C(4)—C(13)	121.8(3)	O(5)—C(12)—C(13)	121.1(3)
C(9)—C(4)—C(13)	118.9(3)	C(11)—C(12)—C(13)	120.5(3)
C(4)—C(5)—C(6)	120.3(4)	O(5)—C(12)—C(11)	118.3(3)
C(5)—C(6)—C(7)	120.2(3)	C(4)—C(13)—C(12)	120.7(3)

dination chemistry of 1,2-dihydroxyarenes which cannot be prepared by direct interaction of the arene with $Cr(CO)_6$.

Acknowledgements—This work was supported in part by the National Science Foundation in the form of a PYI Award to T.G.R. and by a Camille & Henry Dreyfus Foundation New Faculty Grant to T.G.R. H.S. thanks the Studienstiftung Des Deutschen Volkes, Bonn, F.R.G. for a scholarship.

REFERENCES

1. R. Davis and L. A. P. Maguire, *Comprehensive Organometallic Chemistry* (Edited by G. Wilkinson, F. G. A. Stone and E. W. Abel), Vol. 3, pp. 1001–1077. Pergamon Press, Oxford (1982).
2. M. E. Wright, *J. Organomet. Chem.* 1989, **376**, 353.
3. E. O. Fischer, K. Ofele, H. Essler, W. Frohlick, A. P. Mortensen and W. Semmlinger, *Chem. Ber.* 1958, **91**, 2763.
4. C. G. Pierpont and R. M. Buchanan, *Coord. Chem. Rev.* 1982, **38**, 45.
5. E. L. Muetterties, J. R. Bleeke and E. J. Wucherer, *Chem. Rev.* 1982, **82**, 499; S. P. Gubin and V. S. Khandkorova, *J. Organomet. Chem.* 1968, **12**, 523.
6. G. Fairhurst and C. White, *J. Organomet. Chem.* 1978, **160**, C17; G. N. Schrauzer and H. Thyret, *Angew. Chem. Int. Ed. Engl.* 1963, **2**, 478; G. M. Bodner and T. R. Englemann, *J. Organomet. Chem.* 1975, **88**, 391; M. J. Chetcuti, J. A. K. Howard, M. Pfeffer, J. L. Spencer and F. G. A. Stone, *J. Chem. Soc., Dalton Trans.* 1981, 276.
7. A preliminary account of this work was presented at the XIIIth International Conference on Organometallic Chemistry, Turino, Italy (1988); Abstract 313.
8. D. F. Shriver and M. A. Drezdon, *Manipulation of Air Sensitive Compounds*, 2nd edn. Wiley, New York (1986).
9. J. P. Willis, K. A. Z. Gogins and L. L. Miller, *J. Org. Chem.* 1981, **46**, 3125.
10. C. A. L. Mahaffy and P. L. Pauson, *Inorg. Synth.* 1979, **19**, 154.
11. H. Schumann, *Chemiker-Ztg* 1984, **108**, 289.
12. O. L. Carter, A. T. McPhail and G. A. Sim, *J. Chem. Soc. A* 1968, 1866; R. E. Davis and R. Pettit, *J. Am. Chem. Soc.* 1970, **92**, 716; A. V. Kunz and W. Nowacki, *Helv. Chim. Acta* 1967, **50**, 1052.
13. A. Wu, E. R. Biehl and P. C. Reeves, *J. Chem. Soc., Perkin Trans.* 1972, 449.
14. J. A. Heppert, T. J. Boyle and F. Takusagama, *Organometallics* 1989, **8**, 461.

Polyhedron Vol. 9, No. 14, pp. 1683–1688, 1990
Printed in Great Britain

0277–5387/90 $3.00+.00
© 1990 Pergamon Press plc

THE STRUCTURAL EFFECTS OF STERIC OVERCROWDING IN BIS(TRICYCLOHEXYLPHOSPHINE)PLATINUM(II) COMPLEXES: THE CRYSTAL AND MOLECULAR STRUCTURE OF *TRANS*-$PtBr_2(PCy_3)_2$

T. S. CAMERON, H. C. CLARK,* A. LINDEN and A. M. NICHOLAS

Department of Chemistry, Dalhousie University, Halifax, Nova Scotia, Canada B3H 4J3

(*Received* 31 *July* 1989; *accepted* 8 *March* 1990)

Abstract—The crystal and molecular structure of *trans*-$PtBr_2(PCy_3)_2$ has been determined. Crystals are triclinic, space group $P\bar{1}$, $a = 10.038(1)$, $b = 10.212(1)$, $c = 10.775(1)$ Å, $\alpha = 113.18(1)$, $\beta = 109.81(1)$, $\gamma = 91.51(1)°$, $V = 938.8$ Å^3, $Z = 1$ and $D_c = 1.620$ g cm^{-3}. Refinement, based on 4021 reflections with $I > 3\sigma(I)$ converged at $R = 0.032$. The structure consists of discrete *trans*-$PtBr_2(PCy_3)_2$ molecules in which steric overcrowding is indicated by a long Pt—P bond length of 2.345(1) Å and Br···C and Br···H non-bonded contact distances significantly smaller than the sum of the van der Waals' radii of the respective atoms. A comparison of structural parameters for *trans*-$PtXY(PR_3)_2$ (X, Y = H, Cl, Br or I; R = Me, Et or Cy) permits identification of the modes of the steric distortion in these complexes. For the symmetrical complexes (X = Y), Pt—P bond extension is found to be the principal type of distortion in response to unfavourably short intramolecular X···H and X···C non-bonded interactions that arise in these molecules on account of overcrowding.

Although many structure determinations have been made for phosphine complexes of platinum, only a few of the results permit a direct comparison to be made between the effects of tricyclohexylphosphine (PCy_3) and a less bulky triorganophosphine in a similar molecular environment.[1,2] Such comparisons are essential if one is to assess the effects of steric overcrowding on the geometry and reactivity of a platinum(II) phosphine complex. For example, the increase in the Pt—P bond distance by 0.055 Å when PMe_3 is replaced by PCy_3 in the complex *trans*-$PtI_2(PR_3)_2$, has been rationalized as a steric effect and significant non-bonded interactions have been identified in the PCy_3 complex.[3,4] However, it is difficult to determine the electronic component of this observed bond extension without further investigations of similar complexes.

In view of the importance of steric control in many reactions involving phosphine complexes it is desirable to have structural information which can be related to the bulk of the phosphine ligand. Accordingly, several PCy_3 complexes of platinum (II) containing additional bulky ligands have been prepared and structurally characterized.[1,5,6]

In this paper, the X-ray crystal structure analysis of *trans*-$PtBr_2(PCy_3)_2$ is reported and compared with the iodo[3] and chloro[7] analogues and with *trans*-$PtBr_2(PEt_3)_2$,[8] in an effort to determine the types of distortion which occur in response to non-bonded repulsive interactions in situations of varying steric demand by the ligands.[9]

EXPERIMENTAL

Yellow crystals of *trans*-$PtBr_2(PCy_3)_2$ [$^{31}P\{^1H\}$ NMR(CH_2Cl_2): δ 13.4 ($J_{P-Pt} = 2320$ Hz)][10] were obtained by slow crystallization from a dichloromethane solution of *cis*-$PtBr_2(PCy_3)_2$. The *cis* complex [$^{31}P\{^1H\}$ NMR(CH_2Cl_2): δ 16.9 ($J_{P-Pt} = 3585$ Hz)] was obtained either by the addition of stoichiometric amounts of 1 M $SnBr_4$ in CH_2Cl_2 to $PtO_2(PCy_3)_2$ in methanol[6] or tritylbromide to the dioxygen complex in dichloromethane.[11]

*Author to whom correspondence should be addressed.

X-ray crystallographic structure determination

A crystal suitable for X-ray studies was mounted on a glass fibre. The data collection and refinement parameters are given in Table 1. The unit cell constants were obtained by least-square analysis of the diffractometer setting angles of 25 well-centred reflections with $2\theta = 28$–$32°$. The intensities were reduced to a standard scale using routine procedures.[12] Corrections for Lorentz and polarization factors were applied. An empirical absorption correction was applied using DIFABS.[13] Scattering factors for neutral atoms were those recorded in *International Tables for X-ray Crystallography*[14] and were corrected for the real part of anomalous dispersion.

The positions of the platinum, phosphorus and bromine atoms were obtained by the Patterson method and the remaining non-hydrogen atoms were located in a subsequent difference-Fourier synthesis. Refinement was carried out by using the SHELX-76[15] system. The hydrogen atom positions were determined from a difference-Fourier synthesis, and allowed to refine. C—H bond length constraints (1.08 Å) were applied to four hydrogen atoms only. The final refinements were with anisotropic temperature factors on the non-hydrogen atoms and individual isotropic temperature factors on the hydrogen atoms. A four-block matrix least-squares method was employed, minimizing $\Sigma w(|F_o| - |F_c|)^2$. The largest peaks in the final difference maps were 1.7 e Å^{-3} within 1.1 Å of the platinum atom and 0.60 e Å^{-3} elsewhere. No correction was applied for extinction.

Selected interatomic distances and interbond angles for *trans*-$PtBr_2(PCy_3)_2$ are given in Table 2. A diagram of the molecular structure with the numbering scheme for the atoms is given in Fig.

Table 1. Physical properties and parameters for data collection and refinement

Formula	$C_{36}H_{66}Br_2P_2Pt$
Molecular weight	915.7
$F(000)$	460
Crystal class	Triclinic
Space group	$P\bar{1}$ (No. 2)
a (Å)	10.038(1)
b (Å)	10.212(1)
c (Å)	10.775(1)
α (°)	113.18(1)
β (°)	109.81(1)
γ (°)	91.51(1)
V (Å^3)	938.8
Z	1
d_{calc} (g cm^{-3})	1.620
μ (cm^{-1})	62.91
Crystal dimensions (mm)	$0.15 \times 0.17 \times 0.40$
Diffractometer	Enraf–Nonius CAD4
Radiation	Mo-K_α (graphite monochromator)
λ (Å)	0.70926
Temperature (K)	291
Scan type	ω–2θ
Scan speed (° min^{-1})	Variable: 1.6–3.3
hkl range	$\pm h, \pm k, +l$
2θ range (°)	2–56
Standards	3 (no variation)
Number of data collected	4768
Number of unique data	4529
Number of observed data [$I > 3\sigma(I)$] (N_O)	4021
Number of variables (N_V)	319
Maximum and minimum absorption coefficients	1.272, 0.738
Weighting scheme	$1.153/[\sigma^2(F_o) + 0.00118F_o^2]$
$R = (\Sigma \|\|F_o\| - \|F_c\|\|)/(\Sigma \|F_o\|)$	0.032
$R_w = [\Sigma w(\|F_o\| - \|F_c\|)^2/(\Sigma w\|F_o\|^2)]^{1/2}$	0.033
$S = [\Sigma (\|F_o\| - \|F_c\|)^2/(N_O - N_V)]^{1/2}$	0.986

Table 2. Selected interatomic distances (Å) and interbond angles (°) for *trans*-$PtBr_2(PCy_3)_2$

Distances (Å)		Angles (°)	
Pt—Br	2.435(1)	Br—Pt—P	90.97(3)
Pt—P	2.345(1)	Pt—P—C(1)	115.45(14)
P—C(1)	1.853(5)	Pt—P—C(7)	110.92(15)
P—C(7)	1.855(5)	Pt—P—C(13)	112.96(14)
P—C(13)	1.846(4)	C(1)—P—C(7)	102.4(2)
		C(1)—P—C(13)	109.6(2)
		C(7)—P—C(13)	104.4(2)

1(a) and a SPACEFILL[16] drawing is shown in Fig. 1(b).

RESULTS AND DISCUSSION

It has been suggested that a ligand X may affect Pt—P bond lengths *cis* to X via competition for the d_π electrons of platinum.[17] In order to study steric effects free from such interactions only *trans*-$PtXX'(PR_3)_2$ complexes, in which the π-interaction of X and X′ with platinum is negligible, have been considered. Furthermore, spherical monatomic

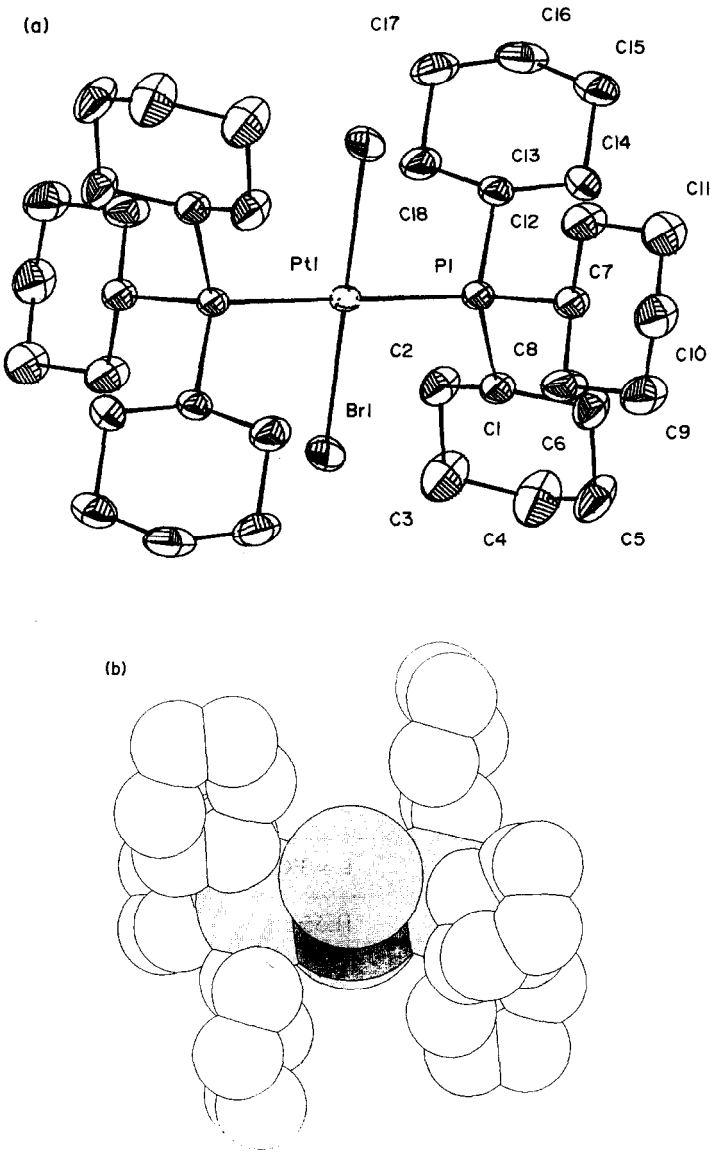

Fig. 1. (a) The molecular structure of *trans*-$PtBr_2(PCy_3)_2$ showing the atomic numbering system used in the analysis, and giving a perspective view of the molecule with thermal ellipsoids displaying 50% probability. (b) A SPACEFILL drawing of *trans*-$PtBr_2(PCy_3)_2$.

ligands (X) have been chosen so that their size can be described easily. Since the non-bonded interaction between X and the hydrogen and carbon atoms of the phosphine ligand that surrounds X is the feature of interest, the ligand size of X is described best by its van der Waals' radius.

The Pt—P and Pt—Y bond distances for a series of *trans*-$PtXY(PR_3)_2$ (R = Cy, Et or Me and X, Y = H, Cl, Br or I) are given in Table 3. The Pt—P bond lengths, for a chosen phosphine, increase progressively with increasing size of ligands X and Y. In addition, for any selection of X and Y, the Pt—P and Pt—Y bond distances in *trans*-$PtXY(PR_3)_2$ are significantly larger for R = Cy or *i*-Pr compared with R = Et or Me. These increases in Pt—P lengths are illustrated in Fig. 2 with a plot of r(Pt—P) vs r^*, the sum of the van der Waals' radii of X and Y [$r^* = r_{vw}(X) + r_{vw}(Y)$].

If steric effects control the variation in the Pt—P bond distance, the expected increase in Pt—P length with the progressive increase of the bulk of X and Y should be modulated in situations of less steric demand involving less bulky phosphines such as PMe_3 or PEt_3. Consequently, the observation that the magnitude of the increase of r(Pt—P) with r^* is larger for the bulkier phosphines is in agreement with steric modification of the Pt—P bond distance. Nevertheless, for the smaller phosphine ligands the increase in Pt—P distance could be due to a σ electronic effect as well because no significant non-bonded I···H or I···C interactions have been found, for example, in *trans*-$PtI_2(PMe_3)_2$. The non-linear larger variation in r(Pt—P) with r^* for L = PCy_3 warrants further investigation, presented below, of the structural parameters of the dihalo complexes, *trans*-$PtX_2(PCy_3)_2$, in an effort to understand how the bulk of X affects the bonding of these complexes.

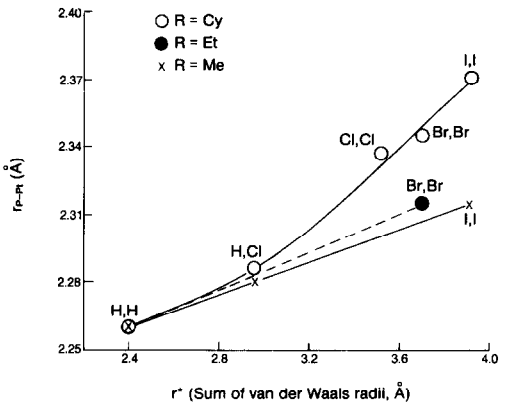

Fig. 2. A plot of the Pt—P bond distance, r(Pt—P) vs r^*, the sum of van der Waals' radii of X and Y, in *trans*-$PtXY(PR_3)_2$. The nature of X and Y is denoted by (X,Y) above the point corresponding to it. The van der Waals' radii of the atoms H, Cl, Br and I are 1.2, 1.75, 1.85 and 1.96 Å, respectively.

The unit cell volumes for the essentially isostructural complexes *trans*-$PtX_2(PCy_3)_2$, where X = Cl, Br and I, are V = 929.9, 938.8 and 988.8 $Å^3$, respectively, which demonstrates the effect of increase of the size of X.

In Table 4 the P—Pt—X angles listed in column 2 show a small deviation from the expected 90° value for an ideal square-planar geometry. This deviation decreases with an increase in the bulk of X. This is probably because ligand X has non-bonded interactions with both PCy_3 groups and for the very bulky X an opening of the P—Pt—X angle

Table 3. A comparison of the principal bond lengths (Å) in *trans*-$PtXYL_2$

		P—Pt		Pt—Y		References	
X	Y	L = PCy_3	L = PR_3[a]	L = PCy_3	L = PR_3[a]	L = PCy_3	L = PR_3
H	H	2.26(1)	2.259(3)[b]	[1.55(3)][c]	—	18	19
H	Cl	[2.286(1)][c]	2.280(6)[b]	[2.395(1)][c]	2.423(6)[b]	9	19
Cl	Cl	2.337(2)[d]	2.30(2)[e]	2.317(2)[f]	2.294(9)[e]	7	8
Br	Br	2.345(1)	2.315(4)[e]	2.435(1)	2.428(2)[e]	This work	8
I	I	2.371(2)	2.315(4)[b]	2.612(1)	2.599(2)[b]	3	4

[a] PR_3 is a relatively small ligand compared with PCy_3.
[b] R = Me.
[c] Value for L = P(*i*-Pr)$_3$; assumed to be equal to that of L = PCy_3.
[d] The corresponding value for L = P(*i*-Pr)$_3$ is 2.339(1) Å (see ref. 9).
[e] R = Et.
[f] The corresponding value for L = P(*i*-Pr)$_3$ is 2.303(1) Å (see ref. 9).

Table 4. A comparison of bond angle (°) data in *trans*-$PtX_2(PCy_3)_2$

X	P—Pt—X	Pt—P—C (mean)	β[a]
Cl[b]	91.2(1)	112.6(2)	6.7[c]
Br[d]	90.97(3)	113.1(2)	6.2
I[e]	90.63(5)	113.4(3)	5.5[c]

[a] The β value is defined in the text (see ref. 20).
[b] Reference 7.
[c] Estimated from Fig. 2 in ref. 20.
[d] This work.
[e] Reference 3.

to relieve strain due to one PCy_3 group is resisted by an increase in steric interactions of X with the other PCy_3 ligand. The absence of a significant increase in the mean Pt—P—C angles listed in column 3 of Table 4 with an increase in the size of X may be the result of steric repulsion between Cy groups of PCy_3 resisting further folding back of the phosphine ligand.

Recently, Powell[20] has shown that the Pt—P—C_T bending (where C_T is the centroid of the α-carbon atoms of the phosphine) is an important mode of distortion in phosphine complexes. For *trans* complexes Powell introduced a β value, where $\beta = 180° - \angle(PtPC_T)$, which has been correlated with electronic repulsion effects in the molecule. When X = Cl, only interactions between Cl and the most eclipsed Cy group are significant and the PCy_3 ligand can tilt away from that contact without necessitating much lengthening of the Pt—P bond and without causing severe interactions with other Cy groups. However, the decrease in β with an increase in ligand size may be a consequence of increased non-bonded interactions between all Cy groups and X.

Although there are several modes of distortion that are available in a square-planar complex for relief of steric strain, overcrowding is still present in molecules with very bulky ligands. To compare the extent of overcrowding in the halo complexes, significantly short non-bonded contact distances (r_{nb}) involving X···C and X···H are listed in Tables 5 and 6, respectively.

The r_{nb} values listed in Tables 5 and 6 indicate non-bonded interactions in all three complexes. There is a consistent decrease in Δ when Cl is replaced by Br, suggesting a significant increase in repulsive interactions in the bulkier bromo complex.

The repulsive force arising from a van der Waals' contact is very sensitive to a further decrease in the interatomic separation.[23] Consequently, if there is already a short, non-bonded contact between two atoms, even a small reduction in the contact distance will be precluded by a concomitant large increase in the repulsive force. Such a situation is present when Br is replaced by I. Here it would appear that the X···C(1) and X···C(13′) and the corresponding X···H interactions reach their limits and the large repulsive forces arising because of the additional bulk of I can no longer be accommodated. This results in significant lengthening of the Pt—P bond by 0.026(1) Å. On the other hand, when Cl is replaced by Br the overcrowding is not so severe as to require further lengthening of the Pt—P bond.

CONCLUSION

By considering structural parameters of *trans*-$PtXY(PR_3)_2$, the modes of steric distortion in these complexes have been identified. Pt—P bond length-

Table 5. Short non-bonded X···C distances (Å) (r_{nb}) in *trans*-$PtX_2(PCy_3)_2$. Primed atoms are related to unprimed ones by the inversion centre at the origin

Contact type[a]	r_{nb}			Δ[b]		
	X = I	Br	Cl	X = I	Br	Cl
X···C(1)	3.396(8)	3.317(4)	3.245(4)	−0.264	−0.233	−0.215
X···C(2)	3.725(9)	3.626(5)	3.556(4)	+0.065	+0.076	+0.096
X···C(13′)	3.483(8)	3.373(4)	3.307(4)	−0.177	−0.177	−0.153
X···C(18′)	3.719(9)	3.620(6)	3.586(4)	+0.059	+0.070	+0.126
X···C(12′)	3.716(9)	3.579(6)	3.525(4)	+0.056	+0.029	+0.065

[a] Carbon atom numbering corresponds to that used for X = Br in Fig. 1. The listed contacts for X = I, Cl involve C atoms in the same relative positions.
[b] $\Delta = r_{nb} - [r_{vw}(X) + r_{vw}(C)]$. The relevant van der Waals' radii sums are I···C = 3.66 Å, Br···C = 3.55 Å and Cl···C = 3.46 Å (see refs 21 and 22).

Table 6. Short non-bonded X···H distances (Å) (r_{nb}) in *trans*-$PtX_2(PCy_3)_2$. Primed atoms are related to unprimed ones by the inversion centre at the origin

Contact type	r_{nb}		Δ^a	
	X = I	Br	X = I	Br
X···H(011)[b]	2.63	2.63(4)	−0.53	−0.42
X···H(131′)	2.77	2.74(5)	−0.39	−0.31
X···H(122′)	3.06	2.84(6)	−0.10	−0.21
X···H(022)	3.20	3.08(6)	+0.04	+0.03
X···H(182′)	3.11	3.08(5)	−0.05	+0.03

[a] $\Delta = r_{nb} - [r_{vw}(X) + r_{vw}(H)]$. The relevant van der Waals' radii sums are I···H = 3.16 Å and Br···H = 3.05 Å.

[b] The hydrogen atoms are labelled so that the first two digits of the value in parentheses correspond to the label of the carbon atom (according to Fig. 1) to which it is attached.

ening is found to be the principal type of steric modification that occurs to overcome unfavourable X···H and X···C non-bonded intramolecular interactions that arise because of overcrowding. The extent of Pt—P bond lengthening increases with an increase in steric demand of all the ligands in the complex. An increase in the bulk of PR_3, X and Y is first accommodated mostly by a decrease in non-bonded contact distances, until further decreases cause severe steric strain that is then relaxed by Pt—P extension.

Acknowledgement—We are grateful to the Natural Sciences and Engineering Research Council of Canada for financial support.

REFERENCES

1. H. C. Clark and M. J. Hampden-Smith, *Coord. Chem. Rev.* 1987, **79**, 229.
2. C. A. Tolman, *Chem. Rev.* 1977, **77**, 313.
3. N. W. Alcock and P. G. Leviston, *J. Chem. Soc., Dalton Trans.* 1974, 1834.
4. P. B. Hitchcock, B. Jacobson and A. Pidcock, *J. Chem. Soc., Dalton Trans.* 1977, 2038.
5. H. C. Clark, G. Ferguson, M. J. Hampden-Smith, H. Reugger and B. L. Ruhl, *Can. J. Chem.* 1988, **66**, 3120.
6. T. S. Cameron, H. C. Clark, M. J. Hampden-Smith, A. Linden and A. M. Nicholas, *Inorg. Chim. Acta* 1989, **162**, 9.
7. A. Del Pra and G. Zanotti, *Inorg. Chim. Acta* 1980, **39**, 137.
8. G. G. Messmer and E. L. Amma, *Inorg. Chem.* 1966, **5**, 1775.
9. G. B. Robertson, P. A. Tucker and W. A. Wickramasinghe, *Aust. J. Chem.* 1986, **39**, 1495.
10. P. G. Leviston and M. G. H. Wallbridge, *J. Organomet. Chem.* 1976, **110**, 271.
11. Y. Tatsuno and S. Otsuka, *J. Am. Chem. Soc.* 1981, **103**, 5832.
12. T. S. Cameron and R. E. Cordes, *Acta Cryst.* 1979, **B35**, 748.
13. N. Walker and D. Stuart, *Acta Cryst.* 1983, **A39**, 158.
14. J. A. Ibers and W. C. Hamilton (Eds), *International Tables for X-Ray Crystallography*, Vol. 4. Kynoch Press, Birmingham, U.K. (1974).
15. G. M. Sheldrick, SHELX-76. Program for Crystal Structure Determination. University of Cambridge, Cambridge, U.K. (1976).
16. E. Dowty, ATOMS (1989). 521 Hidden Valley Road, Kingsport, TN 37663 U.S.A.
17. (a) P. H. Hitchcock, B. Jacobson and A. Pidcock, *J. Chem. Soc., Dalton Trans.* 1977, 2043; (b) L. Manojlovic-Muir, K. W. Muir and T. Solomun, *J. Organomet. Chem.* 1977, **142**, 265.
18. A. Immirzi, A. Musco, G. Carturan and U. Belluco, *Inorg. Chim. Acta* 1975, **12**, L23.
19. D. L. Packett, C. M. Jensen, R. L. Cowan, C. E. Strouse and W. C. Trogler, *Inorg. Chem.* 1985, **24**, 3578.
20. J. Powell, *J. Chem. Soc., Chem. Commun.* 1989, 200.
21. J. E. Huheey, *Inorganic Chemistry*, 2nd edn, pp. 232–233. Harper and Row, New York (1978).
22. A. Bondi, *J. Phys. Chem.* 1964, **68**, 441.
23. I. N. Levine, *Physical Chemistry*, 2nd edn, p. 778. McGraw-Hill, New York (1983).

Polyhedron Vol. 9, No. 14, pp. 1689–1694, 1990
Printed in Great Britain

0277–5387/90 $3.00+.00
© 1990 Pergamon Press plc

SQUARE, SULPHUR-BICAPPED TETRANIOBIUM CLUSTER COMPOUNDS

ELIZABETH BABAIAN-KIBALA, F. ALBERT COTTON* and PIOTR A. KIBALA

Department of Chemistry and Laboratory for Molecular Structure and Bonding, Texas A&M University, College Station, TX 77843, U.S.A.

(*Received* 5 *February* 1990; *accepted* 8 *March* 1990)

Abstract—By addition of first PhSSPh and then PMe_2R (R = Ph, Me) to a solution of $NbCl_5$ that has been reduced with Na/Hg, the orange, crystalline compounds $Nb_4S_2(SPh)_8(PMe_2Ph)_4 \cdot C_7H_8$ (**1**) and $Nb_4S_2(SPh)_8(PMe_3)_4 \cdot C_7H_8 \cdot C_4H_8O$ (**2**) are obtained. They are closely related to the $[Nb_4S_2(SPh)_{12}]^{4-}$ anion previously reported by Christou and co-workers (L. Seela, J. C. Huffman and G. Christou, *J. Chem. Soc., Chem. Commun.* 1987, 1258). In each compound four niobium and two sulphur atoms form a tetragonal bipyramid with sulphur atoms at the apices. The mean Nb—Nb and Nb—S_{ap} distances are, respectively, 2.816(8) and 2.491(3) Å, for **1** and 2.812(6) and 2.494(3) Å for **2**. Each Nb—Nb bond (postulated to be single) is bridged by two SPh groups (mean Nb—S_{br} distances for **1** and **2** are 2.624(8) and 2.626(3) Å, respectively) and there is a phosphine ligand coordinated to each niobium atom (mean Nb—P distances for **1** and **2** are 2.706(1) and 2.677(4) Å, respectively). Compound **1** crystallizes in triclinic space group $P\bar{1}$ with unit cell dimensions: $a = 13.411(6)$, $b = 14.588(4)$, $c = 13.058(5)$ Å, $\alpha = 98.05(3)$, $\beta = 114.95(3)$, $\gamma = 66.35(3)°$, $V = 2210(2)$ Å^3 and $d_{calc} = 1.530$ for $Z = 1$. The structure was refined to $R = 0.0439$ and $R_w = 0.0590$ for 4740 reflections with $I > 3\sigma(I)$. Compound **2** crystallizes in monoclinic space group $C2/m$ with unit cell dimensions: $a = 19.333(10)$, $b = 19.965(8)$, $c = 12.048(5)$ Å, $\beta = 120.00(4)°$, $V = 4027(7)$ Å^3, and $d_{calc} = 1.466$ for $Z = 2$. The structure was refined to $R = 0.0547$ and $R_w = 0.0674$ for 1480 reflections having $I > 3\sigma(I)$.

As part of an extensive effort to develop the chemistry of niobium and tantalum in their lower valence states (II–IV) without the use of η^5-C_5H_5 or related ligands,[1] we have studied the reactions of solutions containing the lower-valent metals with various sulphur-containing ligands. In this paper we report the preparation of compounds containing a tetragonal bipyramid of composition Nb_4S_2, namely, $Nb_4S_2(SPh)_8(PMe_2R)_4$, where R = Ph, Me. We shall describe the preparation and structure of these molecules, compare their structural features with those in other compounds, especially Christou's $[Nb_4S_2(SPh)_{12}]^{4-}$ ion,[2] and discuss the bonding in the cluster.

*Author to whom correspondence should be addressed.

EXPERIMENTAL

All solvents were dried over sodium–benzophenone ketyl and freshly distilled before use. $NbCl_5$ was purchased from Aesar Chemicals, PMe_2Ph and PMe_3 from Strem Chemicals.

Preparation of $Nb_4S_2(SPh)_8(PMe_2Ph)_4$ (1)

$NbCl_5$ (1.35 g, 4.97 mmol) was placed in a 100 cm^3 three-neck round-bottom flask. A side arm containing 1.91 g (8.76 mmol) of PhSSPh was connected to the flask. After addition of 50 cm^3 of toluene and 7.5 cm^3 of 4M Na/Hg, the mixture was stirred for 1.5 h. The PhSSPh was added to the flask and the mixture was stirred for 20 h. After a grey precipitate had formed the solution was heated to 60°C for 4 h then 10 cm^3 of THF was added. Upon

addition of 10 cm^3 of THF a brick-red solution formed, and was stirred for an additional 20 h. The solution was filtered and 0.70 cm^3 (5.24 mmol) of PMe_2Ph was added to the filtrate. This solution was gently heated at 40°C for 20 h and filtered again to separate a pale yellow precipitate from an orange solution. The filtered solution was transferred to a Schlenk tube and layered with 20 cm^3 of hexane. The crystalline product began depositing along the walls of the Schlenk tube after 10 days. Approximately 0.42 mg (21% yield based on $NbCl_5$) was obtained. Analysis, exp. (calc.) S: 16.91 (17.22).

Preparation of $Nb_4S_2(SPh)_8(PMe_3)_4$ **(2)**

$NbCl_5$ (0.5 g, 1.85 mmol) and 35 cm^3 of toluene were placed in a 100 cm^3 round-bottom flask equipped with a gas outlet. A side arm containing 0.70 g (3.21 mmol) of PhSSPh was connected to the flask. After addition of 3.7 cm^3 of 3M Na/Hg the mixture was stirred for 2 h. The PhSSPh and 5 cm^3 of THF were added to the flask. The resulting brick-orange solution was heated to 60°C and stirred for 2 h. The solution was then filtered and 0.20 cm^3 (1.96 mmol) of PMe_3 was added to the filtrate. This solution was gently heated at 50°C for 2 h and filtered again to separate a pale yellow precipitate from an orange solution. The filtered solution was transferred to a Schlenk tube and layered with 20 cm^3 of hexane. The red, rectangular crystals began to deposit along the walls of the Schlenk tube after 12 days.

X-ray crystallography

Both crystals were sealed with epoxy glue inside capillaries filled with degassed mineral oil to prevent decomposition in the air. Unit cell dimensions and Laue class were confirmed with oscillation photographs. For each crystal three control reflections monitored throughout the data collection showed no significant change in their intensities. Lorentz, polarization and empirical absorption correction were applied to the data. The general procedures, routine to this laboratory, are described elsewhere.[3] The data collection parameters are listed in Table 1.*

$Nb_4S_2(SPh)_8(PMe_2Ph)_4 \cdot C_7H_8$ **(1)**. The direct methods portion of the SHELXS-86 program revealed the positions of the heavy atoms. The tetramer was located around the inversion centre of the $P\bar{1}$ space group, making half of the tetramer the asymmetric unit. Consecutive least-squares cycles and difference Fourier maps completed the coordinated sphere about each metal atom. A toluene molecule was located around an inversion centre and successfully modelled and refined. In the final refinement all the atoms except the atoms of the solvent molecule were refined anisotropically. Hydrogen atoms were omitted.

$Nb_4S_2(SPh)_8(PMe_3)_4 \cdot C_7H_8 \cdot C_4H_8O$ **(2)**. Systematic absences indicated $C2/m$, Cm and $C2$ as possible space groups. The structure was initially solved in $C2/m$ space group and the failed attempts to refine the crystal in $C2$ and Cm space groups confirmed $C2/m$ as the correct choice. The direct methods portion of the SHELXS-86 program revealed the positions of the niobium, sulphur and phosphorus atoms. The tetramer was located around a $2/m$ symmetry site making a quarter of the molecule the asymmetric unit. The positions of the remaining atoms were derived through alternating use of least-squares refinements and Fourier maps. The phenyl rings of the SPh ligands were disordered in a way that could be described as resulting from rotation of the phenyl rings around the S—C bonds by 90°. This required refinement of the *ortho* and *meta* carbon atoms at half occupancy. The carbon atoms of the phosphine ligands were also disordered. The disorder of the two phosphine ligands in the asymmetric unit was modelled as resulting from rotation of the methyl groups around the Nb—P bonds by 180°. The two images of the first phosphine were refined at 50:50 occupancies while the two images of the second phosphine at 75:25 occupancies. A molecule of toluene and tetrahydrofuran were located around $2/m$ symmetry sites and were successfully modelled and refined. In the final refinement the niobium, sulphur and phosphorus atoms were refined anisotropically and the carbon atoms isotropically. Hydrogen atoms were not included in the refinement.

RESULTS

An ORTEP drawing of the $Nb_4S_2(SPh)_8(P)_4$ core is shown in Fig. 1, and the principal bond distances and angles are presented in Table 2.

The centre of each molecule is a tetragonal bipyramid formed by four niobium atoms in the equatorial plane and two sulphur atoms at the apical positions. Each Nb—Nb edge is bridged by two SPh groups, one above and one below the plane of the metal atoms. Each niobium atom is then

*Tables of atomic coordinates, structure factors, anisotropic thermal parameters and a complete list of bond distances and angles have been deposited with the Editor at Queen Mary and Westfield College and at the Cambridge Crystallographic Data Centre.

Table 1. Crystal data for $Nb_4S_2(SPh)_8(PMe_2Ph)_4 \cdot C_7H_8$ (1) and $Nb_4S_2(SPh)_8(PMe_3)_4 \cdot C_7H_8 \cdot C_4H_8O$ (2)

Formula	$C_{87}H_{92}Nb_4P_4S_{10}$	$C_{71}H_{92}Nb_4OP_4S_{10}$
Formula weight	1953.9	1777.9
Space group	$P\bar{1}$	$C2/m$
Systematic absences	None	$h, k, l; h+k = 2n+1$
a (Å)	13.411(6)	19.333(10)
b (Å)	14.588(4)	19.965(8)
c (Å)	13.058(5)	12.048(5)
α (°)	98.05(3)	90.0
β (°)	114.95(3)	120.00(4)
γ (°)	66.35(3)	90.0
V (Å^3)	2120(2)	4027(7)
Z	1	2
d_{calc} (g cm^{-3})	1.530	1.466
Crystal size (mm)	0.40 × 0.30 × 0.25	0.50 × 0.45 × 0.30
μ(Mo-K_α) (cm^{-1})	8.582	8.968
Data collection instrument	Rigaku AFC5R	Nicolet P3
Radiation (monochromated in incident beam)	Mo-K_α (λ = 0.71073 Å)	
Orientation reflections, number, range, 2θ (°)	25, 20 < 2θ < 30	25, 20 < 2θ < 30
Temperature (°C)	21	21
Scan method	ω–2θ	ω–2θ
Data collection range, 2θ (°)	4 ⩽ 2θ ⩽ 45	4 ⩽ 2θ ⩽ 45
Number of unique data, total with $F_o^2 > 3\sigma(F_o^2)$	6331 4740	2347 1480
Number of parameters refined	462	176
Transmission factors, max., min.	0.999, 0.922	0.999, 0.924
R^a	0.0439	0.0547
$R_w{}^b$	0.0590	0.0694
Quality-of-fit indicator^c	1.246	1.360
Largest shift/ESD, final cycle	0.01	0.05
Largest peak (e/Å^3)	1.019	0.856

[a] $R = \Sigma ||F_o| - |F_c|| / \Sigma |F_o|$.
[b] $R_w = [\Sigma w(|F_o| - |F_c|)^2 / \Sigma w|F_o|^2]^{1/2}$; $w = 1/\sigma^2(|F_o|)$.
[c] Quality-of-fit = $[\Sigma w(|F_o| - |F_c|)^2 / (N_{obs} - N_{parameters})]^{1/2}$.

coordinated by a phosphine molecule with the phosphorus atom lying along an axis passing through the centre of the bipyramid and the niobium atom. The SPh groups are oriented so that all four S—C bonds on each side of the central Nb_4 plane are parallel. Thus, the entire central group of atoms, $Nb_4S_2(SC)_8P_4$, have essentially D_{4h} symmetry.

DISCUSSION

The oxidation state of the niobium atoms in the $Nb_4S_2(SPh)_8(PMe_2R)_4$ (R = Me, Ph) molecules is III. This, together with the mean Nb—Nb distance, leads very naturally to the idea that in the square array of niobium atoms there is a set of Nb—Nb single bonds. In addition to these, each niobium atom forms two bonds to capping sulphur atoms, four bonds to the nearest bridging sulphur atoms and a bond to the outer phosphorus atom. In total, therefore, each metal atom forms nine bonds. This is reminiscent of the situation in the trinuclear molybdenum and tungsten compounds[4] of the type $M_3X_2(O_2CR)_6L_3$ with X = O or CCH_3. The major difference is that a μ_3-X group can supply a sufficient number of electrons in orbitals of appropriate symmetry to form three ordinary M—X two-electron bonds.

In the case of a $(\mu_4\text{-S})M_4$ group, the four M atoms may provide a set of four σ orbitals properly directed for bonding to the S atom, but the S atom cannot provide the necessary set of four atomic orbitals. The symmetry-adapted linear combi-

Table 2. Selected bond distances (Å) and angles (°) for $Nb_4S_2(PhS)_8(PMe_2Ph)_4 \cdot C_7H_8$ (1) and $Nb_4S_2(PhS)_8(PMe_3)_4 \cdot C_7H_8 \cdot C_4H_8O$ (2)

$Nb_4S_2(PhS)_8(PMe_2Ph)_4 \cdot C_7H_8$

Bond distances (Å)

Nb(1)—Nb(2)	2.810(1)	Nb(1)—P(1)	2.707(2)	S(0)—S(0)′	2.993(3)
Nb(1)—Nb(2)′	2.822(1)	Nb(2)—S(0)	2.490(2)	S(1)—S(1)′	2.808(3)
Nb(1)—S(0)	2.488(2)	Nb(2)—S(0)′	2.491(1)	S(1)—C(11)	1.786(8)
Nb(1)—S(0)′	2.495(2)	Nb(2)—S(1)	2.620(2)	S(1)′—C(11)′	1.786(8)
Nb(1)—S(1)	2.603(1)	Nb(2)—S(1)′	2.639(2)	S(2)—S(2)′	2.768(3)
Nb(1)—S(1)′	2.598(2)	Nb(2)—S(2)	2.601(2)	S(2)—C(21)	1.783(8)
Nb(1)—S(2)	2.652(2)	Nb(2)—S(2)′	2.624(2)	S(2)′—C(21)′	1.783(8)
Nb(1)—S(2)′	2.657(1)	Nb(2)—P(2)	2.705(2)		

Bond angles (°)

Nb(2)—Nb(1)—Nb(2)′	89.98(2)	S(2)—Nb(1)—P(1)	89.70(6)	S(1)′—Nb(2)—P(2)	84.73(6)
Nb(2)—Nb(1)—P(1)	131.34(5)	S(2)′—Nb(1)—P(1)	87.70(5)	S(2)—Nb(2)′—S(2)′	63.98(6)
Nb(2)′—Nb(1)—P(1)	138.65(4)	Nb(1)—Nb(2)—Nb(1)′	90.02(2)	S(2)—Nb(2)′—P(2)′	83.50(5)
S(0)—Nb(1)—S(0)′	73.84(6)	Nb(1)—Nb(2)—P(2)	134.63(4)	S(2)′—Nb(2)′—P(2)′	85.57(6)
S(0)—Nb(1)—S(1)	75.30(5)	Nb(1)′—Nb(2)—P(2)	135.28(4)	Nb(1)—S(0)—Nb(1)′	106.16(7)
S(0)—Nb(1)—S(1)′	113.58(5)	S(0)—Nb(2)—S(0)′	73.86(6)	Nb(1)—S(0)—Nb(2)	68.75(5)
S(0)—Nb(1)—S(2)	75.08(5)	S(0)—Nb(2)—S(1)	74.94(6)	Nb(1)—S(0)—Nb(2)′	69.05(4)
S(0)—Nb(1)—S(2)′	112.20(6)	S(0)—Nb(2)—S(1)′	112.11(5)	Nb(1)′—S(0)—Nb(2)	68.95(5)
S(0)—Nb(1)—P(1)	144.23(7)	S(0)′—Nb(2)′—S(2)	113.57(6)	Nb(1)′—S(0)—Nb(2)′	68.61(4)
S(0)′—Nb(1)—S(1)	113.03(5)	S(0)′—Nb(2)′—S(2)′	76.30(6)	Nb(2)—S(0)—Nb(2)′	106.14(7)
S(0)′—Nb(1)—S(1)′	75.40(6)	S(0)—Nb(2)—P(2)	145.02(6)	Nb(1)—S(1)—Nb(2)	65.11(4)
S(0)′—Nb(1)—S(2)	111.65(6)	S(0)′—Nb(2)—S(1)	112.55(4)	Nb(1)—S(1)—C(11)	123.0(2)
S(0)′—Nb(1)—S(2)′	75.62(4)	S(0)′—Nb(2)—S(1)′	74.73(5)	Nb(2)—S(1)—C(11)	120.7(2)
S(0)′—Nb(1)—P(1)	141.64(7)	S(0)—Nb(2)′—S(2)	75.95(4)	Nb(1)—S(1)′—Nb(2)	64.91(5)
S(1)—Nb(1)—S(1)′	65.34(6)	S(0)—Nb(2)′—S(2)′	113.20(5)	Nb(1)—S(1)′—C(11)′	121.1(2)
S(1)—Nb(1)—S(2)	115.33(6)	S(0)′—Nb(2)—P(2)	141.12(7)	Nb(2)—S(1)′—C(11)′	124.9(2)
S(1)—Nb(1)—S(2)′	170.36(5)	S(1)—Nb(2)—S(1)′	64.53(6)	Nb(1)—S(2)—Nb(2)′	64.98(5)
S(1)—Nb(1)—P(1)	82.79(5)	S(1)—Nb(2)—S(2)″	169.92(5)	Nb(1)—S(2)—C(21)	123.6(2)
S(1)′—Nb(1)—S(2)	170.58(5)	S(1)—Nb(2)—S(2)‴	115.00(6)	Nb(2)—S(2)—C(21)	122.0(2)
S(1)′—Nb(1)—S(2)′	114.76(6)	S(1)—Nb(2)—P(2)	86.43(5)	Nb(1)—S(2)′—Nb(2)′	64.59(4)
S(1)′—Nb(1)—P(1)	81.02(6)	S(1)′—Nb(2)—S(2)″	114.62(6)	Nb(1)—S(2)′—C(21)′	128.3(2)
S(2)—Nb(1)—S(2)′	62.85(6)	S(1)′—Nb(2)—S(2)‴	170.30(5)	Nb(2)—S(2)′—C(21)′	124.7(2)

$Nb_4S_2(PhS)_8(PMe_3)_4 \cdot C_7H_8 \cdot C_4H_8O$

Bond distances (Å)

Nb(1)—Nb(2)	2.806(3)	Nb(1)—P(1)	2.681(5)	S(0)—S(0)′	3.013(6)
Nb(1)—Nb(2)′	2.818(2)	Nb(2)—S(0)	2.492(3)	S(1)—S(1)	2.783(4)
Nb(1)—S(0)	2.497(3)	Nb(2)—S(1)	2.624(4)	S(1)—C(11)	1.778(13)
Nb(1)—S(1)	2.621(3)	Nb(2)—S(2)	2.633(4)	S(2)—S(2)	2.771(5)
Nb(1)—S(2)	2.625(3)	Nb(2)—P(2)	2.673(5)	S(2)—C(21)	1.781(13)

Bond angles (°)

Nb(2)—Nb(1)—Nb(2)′	89.81(6)	S(2)—Nb(1)—P(1)	84.9(1)	S(2)—Nb(2)′—S(2)′	63.5(1)
Nb(2)—Nb(1)—P(1)	135.1(1)	Nb(1)—Nb(2)—Nb(1)′	90.19(6)	S(2)—Nb(2)′—P(2)′	85.7(1)
Nb(2)′—Nb(1)—P(1)	135.1(1)	Nb(1)—Nb(2)—P(2)	134.1(1)	Nb(1)—S(0)—Nb(1)′	105.8(2)
S(0)—Nb(1)—S(0)′	74.2(1)	Nb(1)′—Nb(2)—P(2)	135.7(2)	Nb(1)—S(0)—Nb(2)	68.46(9)
S(0)′—Nb(1)—S(1)	113.0(1)	S(0)—Nb(2)—S(0)′	74.4(1)	Nb(1)—S(0)—Nb(2)′	68.77(9)
S(0)—Nb(1)—S(1)	75.51(8)	S(0)′—Nb(2)—S(1)	113.0(1)	Nb(2)—S(0)—Nb(2)′	105.6(2)
S(0)′—Nb(1)—S(2)	112.81(8)	S(0)—Nb(2)—S(1)	75.54(8)	Nb(1)—S(1)—Nb(2)	64.69(8)
S(0)—Nb(1)—S(2)	75.57(9)	S(0)′—Nb(2)′—S(2)	75.50(8)	Nb(1)—S(1)—C(11)	124.3(3)
S(0)—Nb(1)—P(1)	142.90(8)	S(0)—Nb(2)′—S(2)	112.68(8)	Nb(2)—S(1)—C(11)	123.1(4)
S(1)—Nb(1)—S(1)′	64.1(1)	S(0)—Nb(2)—P(2)	142.81(8)	Nb(1)—S(2)—Nb(2)′	64.81(9)
S(1)—Nb(1)—S(2)	115.1(1)	S(1)—Nb(2)—S(1)′	64.0(1)	Nb(1)—S(2)—C(21)	124.1(4)
S(1)—Nb(1)—S(2)′	170.0(1)	S(1)—Nb(2)—S(2)″	170.0(1)	Nb(2)′—S(2)—C(21)	123.8(5)
S(1)—Nb(1)—P(1)	85.0(1)	S(1)′—Nb(2)—S(2)″	115.3(1)		
S(2)—Nb(1)—S(2)′	63.7(1)	S(1)—Nb(2)—P(2)	84.3(1)		

Numbers in parentheses are ESDs in the least significant digits.

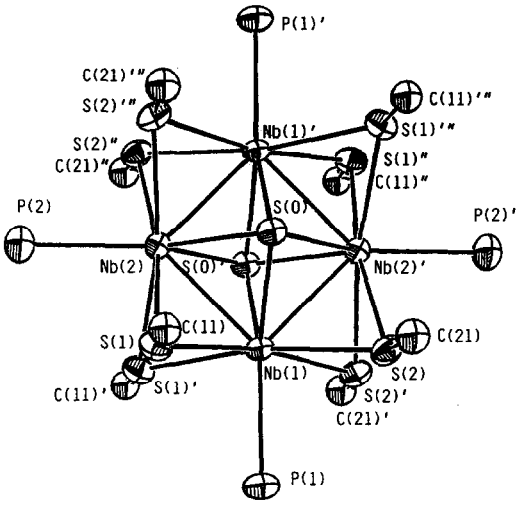

Fig. 1. An ORTEP drawing of the $Nb_4S_2(SPh)_8(PMe_2R)_4$ molecule. Some carbon atoms are omitted for clarity. Each atom is shown as its ellipsoid of thermal displacement contoured at the 50% probability level.

nations (SALCs) on the set of metal atoms will belong to *A*, *B* and *E* representations (for the set of eight in D_{4h} symmetry, A_{1g}, A_{2u}, B_{1g}, B_{2u} and E_g, E_u). The sulphur atom has only *s* (*A*), p_z (*A*) and p_x, p_y (*E*) orbitals available unless we assume that a d_{xy} (or $d_{x^2-y^2}$, depending on choice of *x* and *y* axis directions) also plays a role. If we restrict ourselves to only *s* and *p* orbitals, then the *B* SALCs must remain empty, non-bonding MOs, insofar as interaction with the capping sulphur atoms is concerned.

Nevertheless, the stability of the $Nb_4S_2(SPh)_8(PMe_2R)_4$ molecules can be attributed to the full utilization of all of the nine (five *d*, three *p*, and the *s*) orbitals of the metal atom valence shells and the occupation of all but two (B_{1g} and B_{2u}) of the molecular orbitals to which they contribute. One might, of course, wonder why niobium does not emulate molybdenum and tungsten in forming a trinuclear cluster with a central trigonal bipyramid in which all orbitals could be utilized. Probably the many bulky ligand side chains inhibit this sterically.

The occurrence of $(\mu_4\text{-S})M_4$ groups has a great many precedents. In recent years, for example, the work of Adams and co-workers[5] has produced a great many. In these compounds the M—S bond lengths are consistently in the range 2.4–2.5 Å, which may be compared with the mean value of 2.49 Å in the present case.

Christou and co-workers[2] have previously reported the compound $Li_4[Nb_4S_2(SPh)_{12}]\cdot 4THF$. The tetranuclear anion in this compound has practically the same structure as our $Nb_4S_2(SPh)_8(PMe_2R)_4$ molecules. The four PMe_2R molecules are replaced by terminal PhS^- ions and the arrangement of the bridging SPh groups is a little less regular. Two of the latter are oriented with their phenyl groups parallel to the Nb_4 plane instead of perpendicular. This difference may arise because of the packing requirements of the surrounding Li^+ ions and THF molecules, and it is certainly not of much importance. The principal dimensions of the cluster are practically the same as in the present case: Nb—Nb = 2.828(2) Å and Nb—S(cap) = 2.501(3) Å.

The synthetic chemistry in the two cases is, superficially at least, different. Christou used a dinuclear starting material, $Nb_2Cl_6(Me_2S)_3$, and his anion *may* have resulted from coupling of these without separation into mononuclear niobium intermediates. In our case, the starting material was $NbCl_5$ and we cannot say whether the overall reaction proceeds by initial formation of dinuclear intermediates or not. In both syntheses, there must be a step where the capping sulphur atoms are extracted from a species containing S—C bonds. In Christou's reaction this could be either Me_2S or PhS^-, while in our case it can only be PhS^-. This probably means that PhS^- was also the source in the other case as well.

In our synthesis we do not know whether the intermediate immediately preceding the final product is $[Nb_4S_2(SPh)_{12}]^{4-}$ (i.e. Christou's anion) or $[Nb_4S_2(SPh)_8Cl_4]^{4-}$, but these would seem to be the most likely. Some preference might be given to the former in view of its known existence. This can, of course, be tested by seeing if Christou's anion reacts directly with PMe_2Ph or other phosphines. We were able to prepare **1** and **2** using stoichiometries that were consistent with either of the two intermediates. We found that synthesis of **1** and **2** using stoichiometry that assumes $[Nb_4S_2(SPh)_8Cl_4]^{4-}$ as an intermediate takes less time and the products are obtained in better yields.

One final point concerns the possible existence of tantalum analogues in this type of M_4S_2 cluster compound. We have attempted to follow a similar procedure given in the experimental section substituting $TaCl_5$ for $NbCl_5$. However, the only product we have been able to isolate is $Ta_2S_2Cl_4(PMe_2Ph)_4$. We shall describe this compound and others related to it elsewhere.

Acknowledgement—We thank the Robert A. Welch Foundation (Grant No. A-494) for support.

REFERENCES

1. Representative recent publications from this laboratory: (a) F. A. Cotton and M. Shang, *J. Am.*

Chem. Soc. 1988, **110**, 7719; (b) F. A. Cotton, M. P. Diebold and W. J. Roth, *Inorg. Chem.* 1988, **27**, 2347; (c) F. A. Cotton, M. P. Diebold, X. Feng and W. J. Roth, *Inorg. Chem.* 1988, **27**, 3413; (d) J. A. M. Canich, F. A. Cotton, S. A. Duraj and L. R. Falvello, *Inorg. Chim. Acta* 1988, **143**, 185.

2. L. Seela, J. C. Huffman and G. Christou, *J. Chem. Soc., Chem. Commun.* 1987, 1258.
3. (a) A. Bino, F. A. Cotton and P. E. Fanwick, *Inorg. Chem.* 1979, **18**, 3558; (b) F. A. Cotton, B. A. Frenz, G. Deganello and A. J. Shaver, *J. Organomet. Chem.* 1973, **50**, 227; (c) A. C. T. North, D. C. Phillips and F. S. Mathews, *Acta Cryst.* 1968, **24A**, 351; (d) N. Walker and D. Stuart, *Acta Cryst.* 1983, **39A**, 158; (e) G. M. Sheldrick, SHELXS-86, Program for Crystal Structure Determination. University of Göttingen, F.R.G.; (f) The calculations were performed with the Enraf–Nonius Structure Determination Package on the Microvax II computer at the Laboratory for Molecular Structure and Bonding, Department of Chemistry, Texas A&M University, College Station, TX 77843, U.S.A.
4. F. A. Cotton, Z. Dori, D. O. Marler and W. Schwotzer, *Inorg. Chem.* 1984, **23**, 4033, 4738, and earlier refs therein.
5. See, for example, the following papers and earlier ones cited therein: (a) R. D. Adams, J. E. Babin, M. Tasi and T. A. Wolfe, *J. Am. Chem. Soc.* 1988, **110**, 7093; (b) R. D. Adams, J. E. Babin and M. Tasi, *Organometallics* 1988, **7**, 219, 503.

Polyhedron Vol. 9, No. 14, pp. 1695–1702, 1990
Printed in Great Britain

0277–5387/90 $3.00+.00
© 1990 Pergamon Press plc

SYNTHESIS AND CHARACTERIZATION OF $[\{2,4,6\text{-}(CH_3O)_3C_6H_2\}_3P{=}O]FeCl_3$: A FOUR-COORDINATE PHOSPHINE OXIDE ADDUCT OF $FeCl_3$

KIM R. DUNBAR,* STEVEN C. HAEFNER and ANNE QUILLEVÉRÉ

Department of Chemistry, Michigan State University, East Lansing, MI 48824, U.S.A.

(*Received* 18 *December* 1989; *accepted* 16 *March* 1990)

Abstract—The 1:1 reaction between anhydrous ferric chloride and tris(2,4,6-trimethoxyphenyl)phosphine (TMPP) in benzene produces a reactive complex, **1**, with the empirical formula $FeCl_3$(TMPP). This compound undergoes a facile reaction with molecular oxygen at room temperature and 1 atm to give a dark green intermediate and a final orange product, $FeCl_3[O{=}P\{C_6H_2(OMe)_3\}_3]$ (**3**). Crystal data for **3**: $P\bar{1}$, $a = 12.23(1)$, $b = 14.06(1)$, $c = 13.13(1)$ Å, $\alpha = 110.78(7)$, $\beta = 109.89(8)$, $\gamma = 72.58(8)°$, $V = 1648(3)$ Å^3, $Z = 2$, $d_{calc} = 1.432$ g cm^{-3}, μ(Mo-K_α) = 7.976 cm^{-1}, $R = 0.068$, $R_w = 0.078$ for 374 parameters and 1606 data with $F_o^2 > 3\sigma(F_o)^2$. The structure consists of a tetrahedrally coordinated iron(III) centre ligated by three chlorides and one phosphine oxide ligand. This is the first example of a four-coordinate phosphine oxide complex of $FeCl_3$ and one of only several known examples of a neutral tetrahedral iron(III) complex. The synthesis and properties of **3** are presented and discussed.

We are currently investigating the chemistry of an unusual bulky phosphine ligand, tris(2,4,6-trimethoxyphenyl)phosphine (TMPP), a highly basic derivative of triphenylphosphine.[1] In the broad study of the coordination chemistry of this ligand, we have recently synthesized several TMPP compounds, each exhibiting an entirely different binding mode for TMPP: monodentate, as in $[Ag(TMPP)_2]^+$ and in $[Rh(TMPP)_2(CO)]^+$ (**a**),[2] bidentate as in $[Rh(TMPP)_2(CO)]^+$ (**b**),[2] chelating tridentate as in $[Rh(TMPP)_2]^{2+}$ or $Mo(CO)_3$(TMPP) (**c**),[3,4] and the combination bridging and

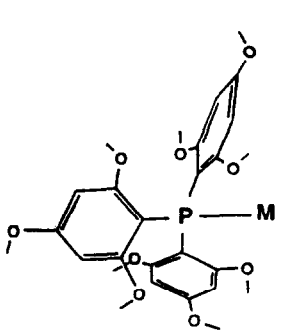

a

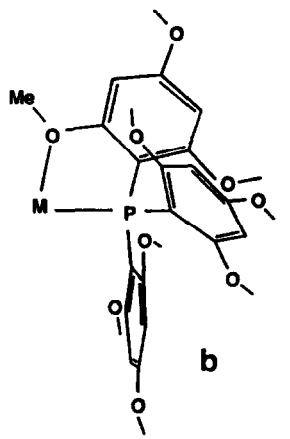

b

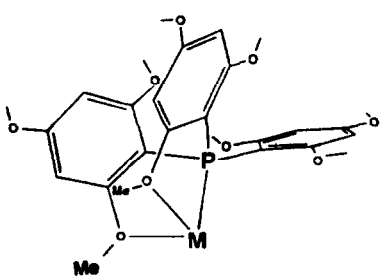

c

*Author to whom correspondence should be addressed.

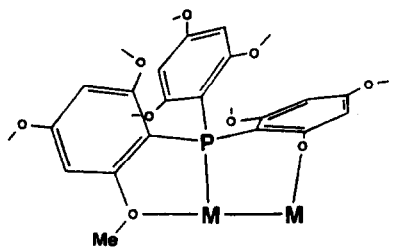

d

chelating tridentate mode as in our recently reported dimer $Rh_2(O_2CCH_3)_3[\{C_6H_2(OMe)_3\}_2\text{-}P\{C_6H_2(OMe)_2O\}](MeOH)$ (**d**).[5]

Our desire to elucidate the chemistry of TMPP with first-row transition metal halides prompted us to study its reactivity with iron(III) chloride. Our goal was to synthesize the neutral adduct $FeCl_3$(TMPP), stabilized by only one monodentate phosphine ligand, and to further study the interaction of this compound with small molecules. A perusal of the literature reveals that, to date, very few neutral $FeCl_3$ monophosphine adducts of a tetrahedral geometry have been fully characterized. Evidently the preferred formulation is the five-coordinate FeX_3L_2, where L is a phosphine or a phosphine oxide,[6] or FeX_3(L—L), where L—L is a bidentate diphosphine.[7] With regard to neutral four-coordinate iron(III) species, the syntheses of the complexes $FeCl_3(PPh_3)$,[8] $FeCl_3(PR_3)$ (R = Cy,[9] *t*-Bu[9b]), $FeCl_3(THF)$[10] and $FeCl_3(S_4N_4)$[11] have been reported. Crystal structures are known only for the last two examples.[10b,11] Recently the complex $FeI_3[SC(NMe_2)_2]$ was reported as the first example of a neutral FeI_3 derivative.[12]

In this paper we describe our efforts to understand an interesting series of reactions involving the 1:1 adduct of $FeCl_3$ and TMPP. The compound, which possesses the empirical formula $FeCl_3$(TMPP), reacts with molecular oxygen to form a moderately stable intermediate and a final stable phosphine oxide product. Herein we report the chemistry leading to the isolation and full characterization of $(R_3P{=}O)FeCl_3$, where R = 2,4,6-trimethoxyphenyl.

EXPERIMENTAL

Ferric chloride (anhydrous) was purchased from Strem Chemicals and was used without further purification. The phosphine ligand, TMPP, was prepared in our laboratories[13] according to a modification of a literature preparation[1a] and was recrystallized from EtOH. Solvents were dried and freshly distilled under nitrogen before use. Unless otherwise specified, all reactions were carried out under an argon atmosphere by using standard Schlenk-line techniques.

PHYSICAL MEASUREMENTS

IR spectra were recorded as Nujol mulls between CsI windows with a Nicolet 740 FT–IR spectrophotometer. Electronic absorption spectra were recorded on a Hitachi U-2000 or a Cary 17 spectrophotometer. SQUID susceptibility measurements were performed on a Quantum Design MPMS susceptometer housed in the Physics Department at Michigan State University.

Reaction of $FeCl_3$ *with* TMPP

Anhydrous $FeCl_3$ (150 mg, 0.90 mmol) was reacted with 1 equivalent of TMPP (500 mg, 0.90 mmol) in 10 cm^3 of carefully deoxygenated benzene. The reaction, which was stirred at room temperature for $\sim$ 5 h, produced a pale yellow solid over this period of time. The product was washed with copious amounts of fresh benzene and dried under a reduced pressure. After recrystallization from a mixture of CH_2Cl_2–benzene (10:1 v/v), the yield (relative to $FeCl_3$) was 70%. The product, **1**, is soluble in CH_2Cl_2, MeOH and EtOH, but is insoluble in other common solvents. Found: C, 46.0; H, 4.9; Cl, 15.3. Calc. for $C_{27}H_{33}Cl_3O_9PFe$: C, 46.6; H, 4.7; Cl, 15.3%. IR spectrum (CsI, Nujol mull), cm^{-1}: 1600 vs, 1580 vs, 1415 s, 1380 s, 1340 s, 1310 w, 1260 w, 1230 s, 1210 s, 1185 w, 1165 m, 1135 s, 1115 m, 1100 m, 1045 w, 1025 s, 950 m, 930 m, 920 m, 8910 w, 885 m, 820 s, 805 w, 790 w, 720 m, 690 w, 675 w, 665 w, 645 m, 520 w, 480 s, 430 m, 410 w, 400 w, 360 s, 300 m, 235 m. Electronic spectrum (Quartz, CH_2Cl_2), λ_{max}, nm (ε, M^{-1} cm^{-1}): 362 (8.59×10^3), 332 (1.23×10^4), 286 (sh), 260 (6.02×10^4).

Reaction of $FeCl_3$(TMPP) *with molecular oxygen*

An amount of $FeCl_3$(TMPP) (100 mg, 0.0864 mmol) was dissolved in CH_2Cl_2, with a constant stream of dry oxygen bubbling through the solution for 1 h. A colour change from yellow to dark green–black immediately ensued. A dark green residue was obtained by evaporation of the solvent. This intermediate, **2**, is tentatively formulated as $FeCl_3$(TMPP)O_2 (yield, relative to **1**: 90%). When the reaction solution was further exposed to oxygen (> 12 h), the solution slowly turned from green to orange. The solvent was removed *in vacuo* and a red–orange solid, $FeCl_3[O{=}P\{C_6H_2(OMe)_3\}_3]$ (**3**) was obtained (yield, relative to **1**: 89%). Suitable crystals of **3** were grown from a mixture of CH_2Cl_2–

MeOH (2 : 1 v/v). Found : C, 45.9; H, 4.7. Calc. for $C_{27}H_{33}Cl_3O_{10}PFe$: C, 45.6; H, 4.6%. IR spectrum (CsI, Nujol mull), cm^{-1}: 1600 vs, 1580 vs, 1410 s, 1380 s, 1340 s, 1300 w, 1230 s, 1210 s, 1185 w, 1165 m, 1125 s, 1105 s, 1070 m, 1025 w, 950 m, 920 m, 815 m, 740 w, 720 w, 700 w, 640 w, 525 w, 485 s, 450 m, 380 s, 340 w. Electronic spectrum (Quartz, CH_2Cl_2), λ_{max}, nm (ε, M^{-1} cm^{-1}): 375 (sh), 334 (8.08×10^3), 285 (sh), 258 (5.08×10^4).

X-ray crystallography

Data collection and reduction. Single crystals of $FeCl_3$(O=TMPP) suitable for X-ray crystallographic studies were grown from a CH_2Cl_2–MeOH solution of the compound at 0°C. An orange crystal with the approximate dimensions 0.28 mm × 0.20 mm × 0.13 mm was selected and mounted with epoxy cement on the tip of a glass fibre. Intensity and geometric measurements were performed on a Nicolet P3/F diffractometer at room temperature following general procedures described elsewhere.[14] A preliminary triclinic unit cell was determined by centring and indexing 14 reflections chosen from a rotational photograph. The cell was further refined by a least-squares determination of 12 reflections with $15 \leqslant 2\theta \leqslant 20$. Axial photographs and intensity data confirmed the choice of the triclinic cell.

Intensity data were collected at room temperature over the range 4–40° in 2θ, using a θ–2θ scan mode. In addition, three check reflections were measured at regular intervals during intensity data collection. A plot of the intensity of these reflections vs time showed that no decay in crystal quality had occurred. After averaging equivalent reflections, 2886 unique data remained of which 1606 were observed with $F_o^2 \geqslant 3\sigma(F_o)^2$.

Solution and refinement. All calculations were performed on a VAXSTATION 2000 computer by using the Structure Determination Package (SDP) programs from Enraf–Nonius. The position of the metal atom was obtained from a solution provided by the direct methods program in SHELXS-86. The positions of the remaining non-hydrogen atoms were located through a sequence of successive difference Fourier maps and least-squares cycles. All of the non-hydrogen atoms, except one carbon in the *meta*-position of a phenyl ring, were refined anisotropically. The final full-matrix refinement involved 374 parameters and 1606 data. The refinement converged with residuals, R and R_w of 0.068 and 0.078, respectively, and a quality-of-fit of 1.919. The final difference Fourier map showed a highest peak of 0.454 e/Å^3. A summary of crystallographic parameters is found in Table 1. A listing of selected bond angles and distances is given in Table 2. The complete listing of atomic and thermal parameters, bond angles and bond distances are available as supplementary material.

RESULTS AND DISCUSSION

From the reaction between equimolar amounts of $FeCl_3$ and $P[C_6H_2(OMe)_3]_3$, we isolated a yellow compound which is formulated as $FeCl_3$(TMPP) on the basis of spectroscopic and analytical data as well as similarities to the reported $FeCl_3(PPh_3)$[8] and $FeCl_3(PCy_3)$.[9] The broad and featureless ^1H NMR indicated that, as expected, the compound is paramagnetic. Magnetic susceptibility measurements revealed temperature-dependent paramagnetic behaviour which is either an indication of a chloride-bridged binuclear structure or a mixed spin-state six-coordinate iron(III) monomer.[15] Unfortunately, the fast atom bombardment mass spectrum shows only the presence of ($HTMPP^+$) (m/z = 533), so our attempts to assign a structure were not aided by this experiment. We do not favour an ionic formulation for **1** {i.e. $[FeCl_2(TMPP)_2][FeCl_4]$} due to the bulk of the TMPP ligands and because of the absence of characteristic ν(Fe—Cl) stretches for $[FeCl_4]^-$ (*vide infra*).

Upon exposure to dry oxygen, we initially obtain a green intermediate, **2**, which we have not as yet fully characterized. We are, of course, quite interested in this oxygen intermediate. It is under intense investigation by a variety of spectroscopic (IR, EPR, electronic) and magnetic methods. After further oxygen bubbling, the title compound, **3**, is formed in high yield. Production of phosphine oxide is known to occur with phosphines in the presence of $FeCl_3$ but the stabilization of intermediates in these reactions has not been noted to our knowledge.[6a,16] Evidently, the bis-phosphine oxide adducts, $FeCl_3(O{=}PR_3)_2$, are formed very quickly in this chemistry. No references to mono-phosphine oxide products, however, were ever made in this work. In the present case, the reaction to produce $O{=}PR_3$ occurs much more slowly. The formation of $FeCl_3[O{=}P\{C_6H_2(OMe)_3\}_3]$ by further reaction of the initial "$FeCl_3(TMPP)O_2$" complex, **2**, occurs slowly in pure dichloromethane but more rapidly in the presence of alcohols. It appears that protic solvents catalyse the transformation of **2** to **3**. We intend to fully investigate this chemistry and to elucidate the reaction mechanism. Interestingly, recent oxygen binding studies of nickel(II) complexes possessing the bulky tertiary phosphine P(*cyclo*-$C_6H_{11})_3$ have resulted in clean 1 : 1 nickel(II) : O_2 reactions that are sufficiently slow to allow for kinetic studies.[17]

Table 1. Crystal data for $FeCl_3[OP\{C_6H_2(OCMe)_3\}_3]$

Formula	$FeCl_3PO_{10}C_{27}H_{33}$
Formula weight	710.74
Space group	$P\bar{1}$
Systematic absences	None
a (Å)	12.23(1)
b (Å)	14.06(1)
c (Å)	13.13(1)
α (°)	110.78(7)
β (°)	109.88(8)
γ (°)	72.58(8)
V (Å^3)	1648(3)
Z	2
d_{calc} (g cm^{-3})	1.432
Crystal size (mm)	$0.28 \times 0.20 \times 0.13$
μ(Mo-K_α) (cm^{-1})	7.976
Data collection instrument	Nicolet P3/F
Radiation (monochromated in incident beam)	Mo-K_α ($\lambda_{\bar{\alpha}} = 0.71073$ Å); graphite monochromated
Orientations reflections number, range (2θ)	12; $15 \leqslant \theta \leqslant 20$
Temperature (°C)	22 ± 2
Scan method	θ–2θ
Data collection range, 2θ (°)	4–40
Number of unique data, total with $F_o^2 > 3\sigma(F_o^2)$	2886, 1606
Number of parameters refined	374
R^a	0.068
$R_w{}^b$	0.078
Quality-of-fit-indicator[c]	1.919
Largest shift/ESD, final cycle	0.01
Largest peak (e/Å^3)	0.454

[a] $R = \Sigma \| |F_o| - |F_c| \| / \Sigma |F_o|$.
[b] $R_w = [\Sigma w(|F_o| - |F_c|)^2 / \Sigma w|F_o|^2]^{1/2}$; $w = 1/\sigma^2(|F_o|)$.
[c] Quality-of-fit $= [\Sigma w(|F_o| - |F_c|)^2 / (N_{obs} - N_{parameters})]^{1/2}$.

Table 2. Selected bond distances (Å) and bond angles (°) for $FeCl_3[OP\{C_6H_2(OMe)_3\}_3]$

	Bond distances (Å)		
Fe(1)—Cl(1)	2.196(4)	O(10)—P(1)	1.550(7)
Fe(1)—Cl(2)	2.155(4)	P(1)—C(1)	1.76(1)
Fe(1)—Cl(3)	2.187(4)	P(1)—C(10)	1.79(1)
Fe(1)—O(10)	1.791(6)	P(1)—C(19)	1.80(1)
	Bond angles (°)		
Cl(1)—Fe(1)—Cl(2)	109.4(2)	O(10)—P(1)—C(1)	107.3(5)
Cl(1)—Fe(1)—Cl(3)	110.4(2)	O(10)—P(1)—C(10)	107.3(5)
Cl(1)—Fe(1)—O(10)	109.9(3)	O(10)—P(1)—C(19)	108.5(5)
Cl(2)—Fe(1)—Cl(3)	107.8(2)	C(1)—P(1)—C(10)	111.5(5)
Cl(2)—Fe(1)—O(10)	108.6(3)	C(1)—P(1)—C(19)	110.9(5)
Cl(3)—Fe(1)—O(10)	110.8(3)	C(10)—P(1)—C(19)	111.2(5)
Fe(1)—O(10)—P(1)	163.6(5)		

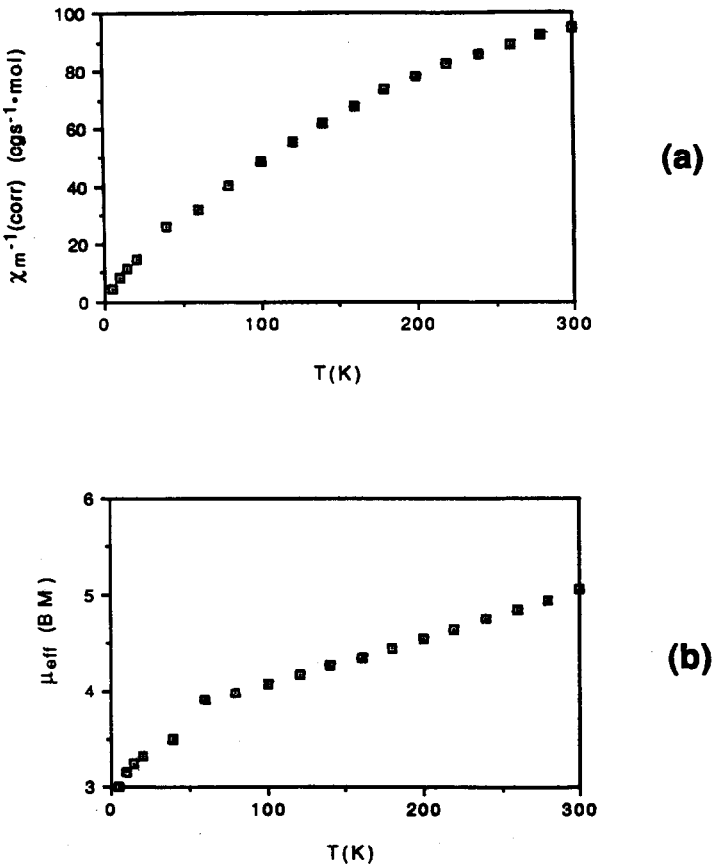

Fig. 1. Plots of (a) the reciprocal of the corrected molar magnetic susceptibility vs temperature and (b) the effective magnetic moment vs temperature for $FeCl_3$(TMPP).

Magnetic and EPR spectroscopic measurements

The room temperature magnetic moment (μ_{eff}) for $FeCl_3$(TMPP) is ~ 5.05 BM, which is much too low for a pure $S = 5/2$ Fe^{III} ground state. Spin equilibrium between $S = 1/2$ and $S = 5/2$ states for six-coordinate Fe^{III} is established in the literature[15] and may also account for the present observed magnetic behaviour. Plots of $1/\chi_m$(corr) vs T and μ_{eff} vs T for **1** are presented in Fig. 1(a) and (b). The compound $FeCl_3(OPR_3)$ exhibits magnetism that is indicative of isolated iron(III) ($S = 5/2$) metal centres. A plot of the corrected molar magnetic susceptibility vs $1/T$ follows the Curie–Weiss law: $\chi_m = C/T - \theta$ with a Weiss temperature $\theta = -1.6779$ K (Fig. 2).* The magnetic susceptibility at room temperature is 1.3050×10^{-2} emu/mol and $\mu_{eff} = 5.62$ BM ($\approx$ five unpaired electrons, tetrahedral Fe^{3+}, d^5). At low temperature

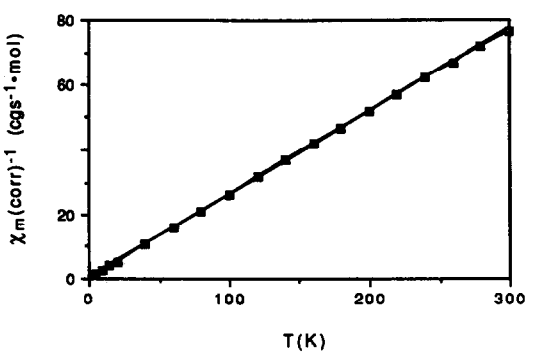

Fig. 2. Plot of the reciprocal of the corrected molar magnetic susceptibility vs temperature for $FeCl_3$(O=TMPP).

(−170°C), the EPR spectrum of $FeCl_3(O{=}PR_3)$ is characteristic of a pseudo-tetrahedral Fe^{3+} complex with a minor signal at $g = 7.44$ and a strong feature that appears at $g = 2.52$.

IR and electronic spectroscopy

IR spectra of **1** and **3** in the region 1700–400 cm^{-1} reveal the presence of the phosphine and phosphine

* A diamagnetic correction of -400.20×10^{-6} cgsu was applied based on -10×10^{-6} for Fe^{3+}, -70.2×10^{-6} for Cl^-, -320×10^{-6} for $OP[C_6H_2(OMe)_3]_3$.

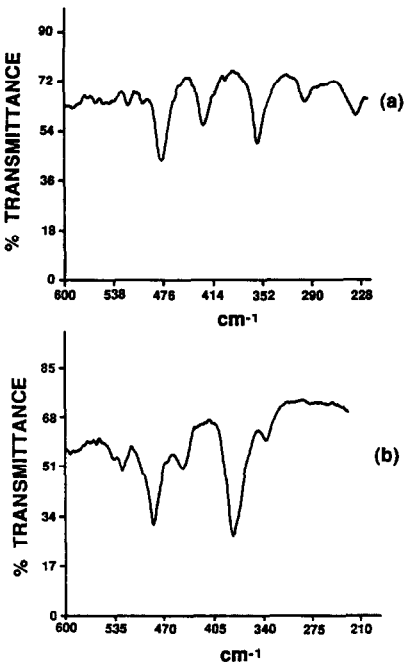

Fig. 3. Far-IR spectra of Nujol mull samples on CsI for (a) $FeCl_3$(TMPP) and (b) $FeCl_3$(O=TMPP).

oxide moiety, respectively. The far-IR spectra, presented in Fig. 3, are more useful in that they provide information about the local symmetry of the $FeCl_3$ group. Spectrum 3(b) for $FeCl_3(O{=}PR_3)$ is typical of that found for $FeCl_3$ adducts of C_{3v} symmetry. With two ν(Fe—Cl) stretches at 380 (s) and 340 (w), the far-IR spectrum of **3** is very similar to that reported for the tetrahedral anion $[FeCl_4]^-$ [378 (s), 330 (vw)][18] and the triphenylphosphine complex $FeCl_3(PPh_3)$ [370 (s), 320 (w)].[8] On the other hand, the phosphine derivative, **1**, exhibits three ν(Fe—Cl) modes at 360 (s), 300 (m) and 235 (m), indicative of a low molecular symmetry such as C_s. Consistent with this data is the interpretation of the structure as a six-coordinate monomer with an η^3-bonding mode for TMPP.

Electronic spectra are presented in Fig. 4. Compound **3** with λ_{max} values at 334 and 258 nm resembles that reported for NH_3FeCl_3 in the vapour phase (λ_{max}, 335 and 225).[19] The electronic absorption properties of $FeCl_3$(TMPP), displayed in Fig. 4(a), are similar to those of the aforementioned pyramidal $FeCl_3L$ species, although magnetic and IR data do not support such a structure for this molecule (*vide supra*).

X-ray crystal structure of $FeCl_3[OP\{C_6H_2(OMe)_3\}_3]$ (**3**)

An ORTEP drawing of $FeCl_3(O{=}TMPP)$ with the correct atom labelling scheme is shown in Fig. 5. Pertinent bond angles and distances are summarized in Table 2. The metal centre is surrounded by three chlorine atoms and the oxygen atom of a phosphine oxide ligand, resulting in an overall distorted tetrahedral coordination environment. The average Fe—Cl bond distance is 2.179[4] Å

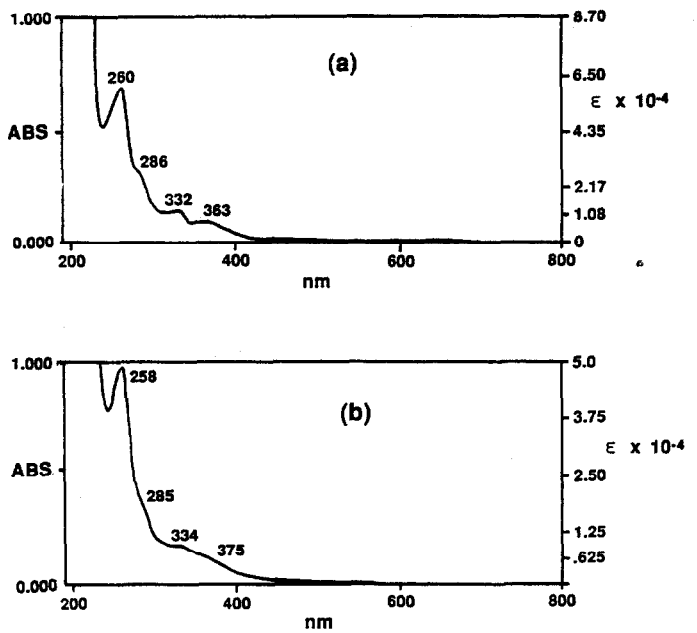

Fig. 4. UV–vis spectra performed in CH_2Cl_2 solution by using 1 cm quartz cells for (a) $FeCl_3$(TMPP) and (b) $FeCl_3$(O=TMPP).

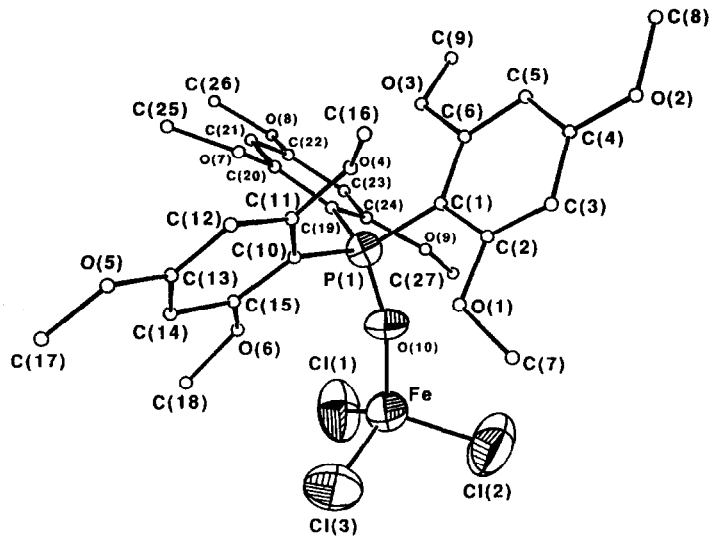

Fig. 5. ORTEP drawing of a single molecule of $FeCl_3[OP\{C_6H_2(OMe)_3\}_3]$ showing the atom labelling scheme. Phenyl group carbon and methoxy oxygen atoms are represented as small circles for clarity. All other atoms are represented by their 50% probability ellipsoids.

which is typical of the Fe—Cl distances found in salts of the anionic complex $\{FeCl_4\}^-$.[20] The angles ∠O—Fe—Cl vary from 108.6 to 110.8°, which is not a large difference, and may be due to a minor steric influence of the phosphine oxide which forms a bent interaction with the metal [∠Fe—O—P = 163.6(5)°]. As a result, the O—Fe—Cl bond angles are considerably distorted from an ideal tetrahedral geometry. The Fe—O bond distance of 1.791(6) Å in **3** is much shorter than the metal–oxygen distances found in similar tetrahedral phosphine oxide complexes such as $CoCl_2(O{=}PPh_3)_2$ for which the average Co—O distance is 1.999[9] Å.[21] Conversely, the P—O distance of 1.550(7) Å in the $FeCl_3(O{=}TMPP)$ case is much longer than the average corresponding distance in $CoCl_2(O{=}PPh_3)_2$ (P—$O_{(av)}$ = 1.499[9] Å).[21] These structural data are not to be interpreted strictly since a comparison of iron(III) and cobalt(II) chemistry must also take into consideration the oxidation state and size of the metal ion. It is, however, known that TMPP is much more donating than PPh_3,[7] thus phosphine oxide derivatives would be expected to follow the same trend in ligation properties. The average C—P—C bond angle for the $(O{=}PR_3$ group in **3** is 111.2(5)° which deviates considerably from the ideal tetrahedral geometry due to repulsions between the bulky trisubstituted phenyl rings. This results in a flattening out of the C—P—C angles.

In summary, few examples of neutral tetrahedral mono-adducts of $FeCl_3$ have been published. Singh and Rivest reported the existence of mono-tetrahedral adducts of $FeCl_3$ with triphenylarsine and triphenylphosphine in 1968.[8a] The formulation was confirmed by Mössbauer spectroscopy.[8b] In the early 1980's Von Thewalt reported the synthesis of two forms (α,β) of $FeCl_3(S_4N_4)$.[11] Recently Poli and Walker reported that mono-adducts of $FeCl_3$ can be prepared by using bulky tertiary phosphines such as tricyclohexylphosphine and tri-*t*-butylphosphine.[9b] Actually the synthesis of $FeCl_3(PCy_3)$ was reported as long ago as 1954 by Von Issleib and Brack.[9a] With the exception of $FeCl_3(THF)$[10b] and $FeCl_3(S_4N_4)$,[11] however, there are no crystallographically characterized examples of these complexes. As far as we are aware, the present study of $FeCl_3(O{=}TMPP)$ (**3**) represents the first example of a structurally characterized phosphine oxide adduct of $FeCl_3$.

Acknowledgements—The support of this research by Michigan State University is gratefully acknowledged. Mass spectral data were obtained at the Michigan State University Mass Spectrometry Facility, which is supported, in part, by a grant (DRR-00480) from the Biotechnology Resources Branch, Division of Research Resources, National Institutes of Health. SQUID magnetic measurements were obtained in the Physics Department on a Quantum Design MPMS susceptometer funded by the Center for Fundamental Materials Research, Michigan State University. X-ray equipment was supported by a grant from the National Science Foundation (CHE-8403823).

REFERENCES

1. (a) M. Wada and S. Higashizaki, *J. Chem. Soc., Chem. Commun.* 1984, 482; (b) M. Wada, S. Higa-

shizaki and A. Tsuboi, *J. Chem. Res. S* 1985, 38; (c) M. Wada, *J. Syn. Org. Chem. Jpn* 1986, 957; (d) M. Wada and A. Tsuboi, *J. Chem. Soc., Perkin Trans.* 1987, 151.
2. K. R. Dunbar and S. C. Haefner, *Inorg. Chem.*, in press.
3. K. R. Dunbar, S. C. Haefner and L. E. Pence, *J. Am. Chem. Soc.* 1989, **111**, 5504.
4. K. R. Dunbar, S. C. Haefner and D. J. Burzynski, *Organometallics* 1990, **9**, 1347.
5. S. J. Chen and K. R. Dunbar, *Inorg. Chem.* 1990, **29**, 588.
6. (a) M. J. Frazer, W. Gerrard and R. J. Twaits, *J. Inorg. Nucl. Chem.* 1963, **25**, 637; (b) J. D. Walker and R. Poli, *Inorg. Chem.* 1989, **28**, 1793; (c) J. D. Walker and R. Poli, *Polyhedron* 1989, **8**, 1293.
7. (a) S. A. Cotton and J. F. Gibson, *J. Chem. Soc. A* 1971, 859; (b) T. S. Lobana, H. S. Cheema and S. S. Sandhu, *J. Chem. Soc., Dalton Trans.* 1983, 2039.
8. (a) P. P. Singh and R. Rivest, *Can. J. Chem.* 1968, **46**, 1773; (b) T. Birchall, *Can. J. Chem.* 1969, **47**, 1351.
9. (a) K. Von Issleib and A. Brack, *Z. Anorg. Allg. Chem.* 1954, **277**, 258; (b) R. Poli and J. D. Walker, Paper INORG 125, 198th ACS National Meeting of the American Chemical Society, Miami, Florida, 10–15 September, 1989.
10. (a) L. S. Benner and C. A. Root, *Inorg. Chem.* 1972, **11**, 652; (b) F. A. Cotton, personal communication.
11. (a) U. Von Thewalt, *Z. Naturfor.* 1980, **35b**, 855; (b) U. Von Thewalt, *Z. Anorg. Allg. Chem.* 1981, **476**, 105.
12. S. Pohl, U. Bierbach and W. Saak, *Angew. Chem. Int. Edn Engl.* 1989, **28**, 776.
13. K. R. Dunbar and S. C. Haefner, unpublished results.
14. (a) A. Bino, F. A. Cotton and P. E. Fanwick, *Inorg. Chem.* 1979, **18**, 3558; (b) F. A. Cotton, B. A. Frenz, G. Deganello and A. Shaver, *J. Organomet. Chem.* 1973, **50**, 227.
15. See for example: (a) C. A. Tsipis, C. C. Hadjikostas and G. E. Manoussakis, *Inorg. Chim. Acta* 1977, **23**, 163 and refs therein; (b) M. Cox, J. Darken, B. W. Fitzsimmons, A. W. Smith, L. K. Larkworthy and K. A. Rodgers, *J. Chem. Soc., Dalton Trans.* 1972, 1192; (c) W. R. Scheidt and D. K. Geiger, *J. Chem. Soc., Chem. Commun.* 1979, 1154.
16. I. Ondrejkovicova, V. Vancova and G. Ondrejovic, *Coll. Czech. Chem. Commun.* 1983, **48**, 254.
17. G. Favero, S. I. Mohamud, A. Turco and U. Vettori, *Gazz. Chim. Ital.* 1989, **119**, 407.
18. J. S. Avery, C. D. Burbridge and D. M. L. Goodgame, *Spectrochim. Acta* 1968, **24A**, 1721.
19. N. W. Gregory, *Inorg. Chem.* 1981, **20**, 3667.
20. (a) F. A. Cotton and C. A. Murillo, *Inorg. Chem.* 1975, **10**, 2467; (b) R. Glowiak, E. Durcanska, I. Ondrejkovicova and G. Ondrejovic, *Acta Cryst.* 1986, **C42**, 1331; (c) G. Constant, J. C. Daran and Y. Jeannin, *J. Organomet. Chem.* 1972, **44**, 353.
21. M. M. Mangion, R. Smith and S. G. Shore, *Cryst. Struct. Commun.* 1976, **5**, 493.

Polyhedron Vol. 9, No. 14, pp. 1703–1708, 1990
Printed in Great Britain

0277–5387/90 $3.00+.00
© 1990 Pergamon Press plc

SYNTHESIS AND CHARACTERIZATION OF TETRANUCLEAR COPPER(II) COMPLEXES BY CONTINUED COMPLEXATION OF A NEW CLASS OF BINUCLEATING LIGAND 3,3′-DIMETHOXY-4,4′-BIS(1-ALKYL(R)TRIAZENE-1-OXIDE)BIPHENYL

A. RAMACHANDRAIAH,* T. SAROJINI and K. LAXMA REDDY

Department of Chemistry, Regional Engineering College, Warangal—506 004, Andhra Pradesh, India

and

P. S. ZACHARIAS*

School of Chemistry, University of Hyderabad, Hyderabad—500 134, Andhra Pradesh, India

(*Received* 11 *December* 1989; *accepted* 21 *March* 1990)

Abstract—A new class of binuclear copper(II) complexes, Cu_2L_2, yielded a series of tetranuclear copper(II) complexes, $Cu_2L_2(CuA_2)_2$, when mixed with CuA_2 in a 1 : 2 molar ratio (where LH_2 = 3,3′-dimethoxy-4,4′-bis(1-alkyl(R)triazene-1-oxide)biphenyl denoted as R-triaz-bp-OCH_3 and A = Cl, Br). No appreciable antiferromagnetic interaction was observed between any two sets of copper(II) centres as suggested by magnetochemical or ESR studies. The optical spectra suggest that the two sets of copper(II) centres have different geometries, the Cu_2L_2 based coppers are near square-planar while the CuA_2 based ones are near tetrahedral. The reason for the absence of magnetic interaction between any two copper(II) centres is discussed in the light of the structure of the complexes.

The unusual properties observed in the polynuclear metal complexes have maintained their interest over three decades. Recently, we reported the synthesis and studies of two novel series of binuclear copper(II) complexes, viz. bis-[3,3′-di(X)-substituted - 4,4′ - bis(3 - alkyl(R)triazene - 3 - oxide)-diphenyl]dicopper(II) denoted as $[Cu_2(R\text{-triaz-bp-}X)_2]$ (**1a**);[1,2] [3,3′-di(X)-substituted-4,4′-bis(salicylidinimino)diphenyl]dicopper(II) denoted as $[Cu_2(Sal\text{-bp-}X)_2]$ (**1b**).[3] Unlike the mononuclear analogues of these two series, which possess

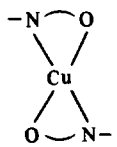

type *trans* chelate groups,[4–6] the binuclear complexes, $[Cu_2(R\text{-triaz-bp-}X)_2]$ and $[Cu_2(Sal\text{-bp-}X)_2]$ contain *cis* chelation to give

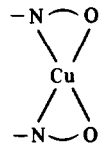

type chromophores. This *cis* positioning of the oxygen ligating atoms may facilitate further coordination to another metal centre so as to give

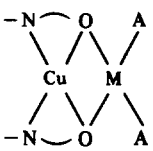

type centres (**1c**), where A can be any end ligand atom or group such as halide or thiocyanate, respec-

* Authors to whom correspondence should be addressed.

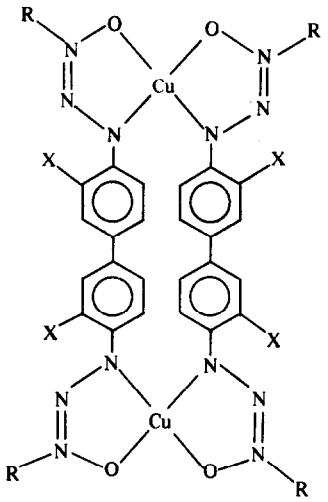

1a

Cu_2(R - triaz - bp - X)$_2$

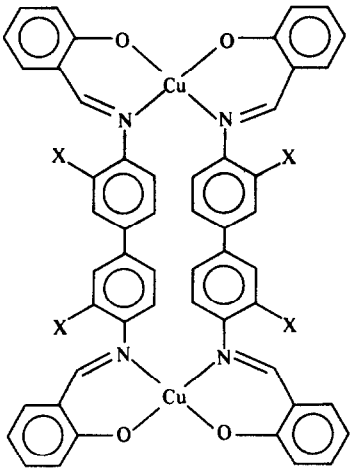

1b

Cu_2(Sal - bp - X)$_2$

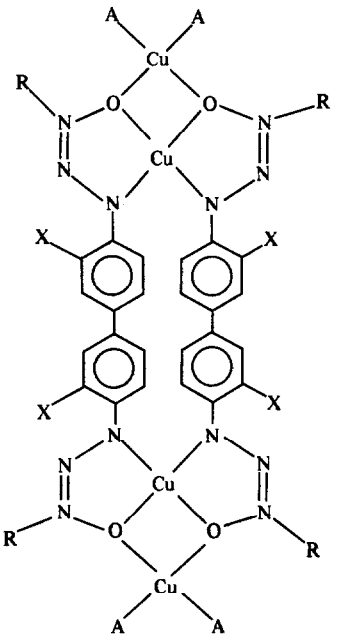

1c

Cu_2(R - triaz - bp - X)$_2$(CuA_2)$_2$

tively. This type of continued bridging is not unusual.[7-11] Here we report the synthesis and characterization of the complexes, [Cu_2(R-triaz-bp-OCH_3)$_2$(CuA_2)$_2$] (**1c**) generated from **1a**.

EXPERIMENTAL

The details of the synthesis of the binuclear complexes which act as ligands for the present tetranuclear complexes were previously reported.[1-3] Mixing ethanolic solutions of the anhydrous cupric halides with the concentrated solutions of the binuclear complexes in chloroform immediately yields the tetranuclear complexes. The green, shiny precipitates obtained from triazene-1-oxide-based complexes were filtered and air-dried.

In a typical experiment, 422 mg ($\sim$ 0.5 mM) of the binuclear complex, Cu_2(CH_3-triaz-bp-OCH_3)$_2$, were dissolved in 25 cm^3 of chloroform to which were added 130 mg ($\sim$ 1.0 mM) of anhydrous cupric chloride dissolved in 10 cm^3 of absolute ethanol. A shiny, green and silky precipitate, obtained immedi-

ately, was filtered and dried under nitrogen. The filtrate was nearly colourless indicating a quantitative reaction between the dark brown solution of the binuclear complex and the green solution of the cupric halide (yield ~ 98%).

The microanalytical data were obtained on a Hewlett–Packard CHN analyser and the metal content from either the thiocyanate method[12] or atomic absorption spectrophotometry.

The room and variable temperature susceptibility measurements, using Pascal constants[13] for diamagnetic correction, were obtained on a Sartorius microbalance with a liquid helium cryostat using Faraday's method. Cupric sulphate pentahydrate ($CuSO_4 \cdot 5H_2O$) was used as the reference.

IR spectra from 4000 to 200 cm^{-1} were recorded on a Perkin–Elmer Model 283 spectrophotometer. The solution electronic spectra were obtained on a Cary 17D spectrophotometer and the solid-state spectra on a PARC Photoacoustic spectrometer. The X-band ESR spectra were recorded on a JEOL FE 3X spectrometer.

RESULTS AND DISCUSSION

Infrared spectra

The C, H, N and metal analysis data are collected in Table 1 and are consistent with structure **1c**. The metal–halogen stretching frequencies and ν(M—Cl)/ν(M—Br) ratios are collected in Table 2. It is well known[14] that terminal metal–chloride stretches appear around 350 cm^{-1} and metal–bromide ones at 250 cm^{-1}, and also that the ratio ν(M—Cl)/ν(M—Br) (where M = Cu^{2+}, Zn^{2+}, Ni^{2+}, Co^{2+}) is in the order 1.30–1.35 for terminal metal–halogen bonds. The frequency ratios for the present complexes (~ 1.32) suggest that the halogen atoms are in terminal positions and not bridging.

Electronic spectra

The PAS spectra recorded for the tetranuclear copper(II) complexes exhibit well-resolved absorption bands at ~ 8000 and ~ 17,000 cm^{-1}. The solid-state electronic spectral data of the complexes are collected in Table 2, with that of the parent binuclear complexes given in parentheses. Representative spectra are given in Fig. 1.

In the case of the complexes shown in structure **2**, it is established that the square planarity of the

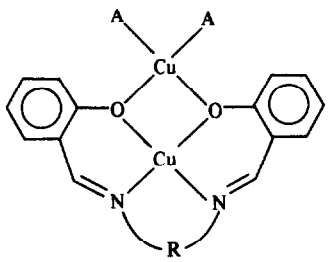

2

chelated inner coppers in the parent complex is enhanced upon further complexation with copper halides,[9,10,15] resulting in a hypsochromic (blue)

Table 1. Elemental analysis of tetranuclear copper(II) complexes, $Cu_2L_2(CuA_2)_2$[a]

Compound	Colour	% Cu	% C	% H	% N
$Cu_2(CH_3\text{-triaz-bp-}OCH_3)_2(CuCl_2)_2$	Olive green	23.1 (22.7)	34.6 (34.5)	3.5 (3.3)	15.2 (15.1)
$Cu_2(CH_3\text{-triaz-bp-}OCH_3)_2(CuBr_2)_2$	Pale green	19.8 (19.5)	29.6 (29.9)	2.8 (2.8)	13.0 (13.0)
$Cu_2(C_2H_5\text{-triaz-bp-}OCH_3)_2(CuCl_2)_2$	Green	22.0 (21.6)	36.8 (37.0)	3.8 (3.8)	14.4 (14.4)
$Cu_2(C_2H_5\text{-triaz-bp-}OCH_3)_2(CuBr_2)_2$	Pale green	19.1 (18.7)	32.2 (32.1)	3.3 (3.3)	12.5 (12.5)
$Cu_2(n\text{-}C_3H_7\text{-triaz-bp-}OCH_3)_2(CuCl_2)_2$	Green	21.2 (20.6)	32.2 (32.2)	4.2 (4.3)	13.7 (13.7)
$Cu_2(n\text{-}C_3H_7\text{-triaz-bp-}OCH_3)_2(CuBr_2)_2$	Green	18.2 (18.0)	34.2 (34.3)	3.7 (3.7)	11.8 (12.0)
$Cu_2(t\text{-}C_4H_9\text{-triaz-bp-}OCH_3)_2(CuCl_2)_2$	Green	17.8 (17.8)	47.2 (47.2)	4.2 (4.3)	11.9 (11.8)
$Cu_2(t\text{-}C_4H_9\text{-triaz-bp-}OCH_3)_2(CuBr_2)_2$	Pale green	15.7 (15.9)	41.9 (42.0)	3.7 (3.8)	10.4 (10.5)

[a] Calculated values are given in parentheses.

Table 2. Magnetic, IR and electronic spectral data of tetranuclear copper(II) complexes, $Cu_2L_2(CuA_2)_2$

Compound	μ_{eff} (BM)[a]	ν(Cu—A)[b]	ν(Cu—Cl)/ν(Cu—Br)	ν_{max}[c]
$Cu_2(CH_3$-triaz-bp-$OCH_3)_2(CuCl_2)_2$	1.78	325		7930 17,240
			1.300	(10,200)
$Cu_2(CH_3$-triaz-bp-$OCH_3)_2(CuBr_2)_2$	1.82	250		7810 17.850
$Cu_2(C_2H_5$-triaz-bp-$OCH_3)_2(CuCl_2)_2$	1.80	330		7690 16,600
			1.320	(9009)
$Cu_2(C_2H_5$-triaz-bp-$OCH_3)_2(CuBr_2)_2$	1.84	250		7690 17,240
$Cu_2(n$-C_3H_7-triaz-bp-$OCH_3)_2(CuCl_2)_2$	1.81	332		7140 16,700
			1.296	(10,400)
$Cu_2(n$-C_3H_7-triaz-bp-$OCH_3)_2(CuBr_2)_2$	1.85	256		6250 16,700
$Cu_2(t$-C_4H_9-triaz-bp-$OCH_3)_2(CuCl_2)_2$	1.79	338		7570 17,500
			1.305	(9700)
$Cu_2(t$-C_4H_9-triaz-bp-$OCH_3)_2(CuBr_2)_2$	1.83	259		6675 17,460

[a] Per copper centre.

[b] Stretching frequency in cm^{-1}.

[c] Recorded on a Photoacoustic spectrometer. The values in parentheses are the solid-state λ_{max} of the parent Cu_2(R-triaz-bp)$_2$ complexes (values in cm^{-1}).

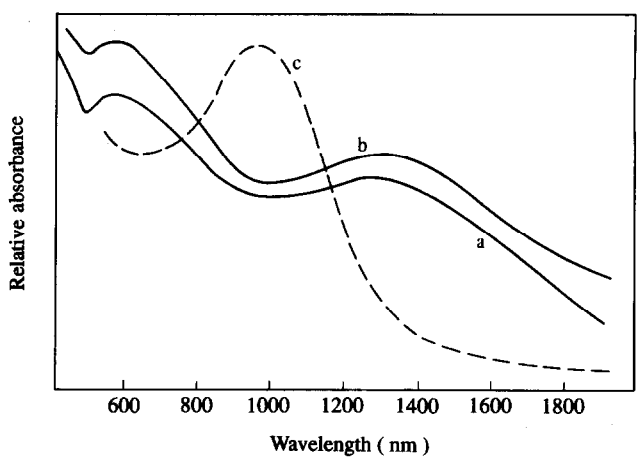

Fig. 1. Solid-state photoacoustic electronic spectra of (a) Cu_2(R-triaz-bp-$OCH_3)_2(CuCl_2)_2$, (b) Cu_2(R-triaz-bp-$OCH_3)_2(CuBr_2)_2$ and (c) Cu_2(R-triaz-bp-$OCH_3)_2$ in the near-IR and visible range.

shift, with respect to the parent complex. The low energy transition is attributed to the lower symmetric (C_2) outer copper.

It is also observed that the heavier the halogens on the outer coppers are, the greater is the tetrahedral nature for the outer coppers.[16] Tetrahedral coppers generally possess their crystal-field absorption in the range 14,000–7000 cm^{-1}, whereas the square-planar ones possess theirs in the range 19,000–14,000 cm^{-1}. The appearance of two λ_{max}

values for the present complexes indicates the presence of two structurally distinct copper pairs, one outer pair in near tetrahedral geometry absorbing at $\sim 8000\ cm^{-1}$, and the other at near square planarity absorbing at $\sim 17{,}000\ cm^{-1}$. The parent binuclear complexes, from which the inner coppers of the present tetranuclear complexes originate, have been observed to absorb at $\sim 11{,}000\ cm^{-1}$ and a distorted square-planar geometry was assigned to them.[2] The shift of this band to higher energy upon extended complexation in obtaining the present complexes means that planarity is enhanced at the inner coppers. The higher energy band at $\sim 17{,}000\ cm^{-1}$ is assigned to the $d_{z^2} \leftarrow d_{x^2-y^2}$ transition of the inner copper, and the lower one at $\sim 8000\ cm^{-1}$ is assigned to the $B_1 \leftarrow A_1$ transition of the outer copper.

Magnetic and ESR spectral data

The magnetic system in the present complex can be represented as

$$Cu(1)\overset{J}{\cdots}Cu(2)\overset{J'}{\cdots}Cu(3)\overset{J}{\cdots}Cu(4),$$

with J' as the interaction energy between the two inner copper centres, and J being the interaction energy between one outer copper and one inner copper. The other possible interaction between Cu(1) and C(3) or Cu(2) and Cu(4) is negligible. The magnetic moment data of all the complexes, collected in Table 2, are normal. It was already reported that the magnetic interaction between the two coppers in the parent binuclear complexes is negligibly small.[2] The observation of normal magnetic moment data for the present tetranuclear complexes is interesting, since there are copper centres bridged only by oxygen atoms. Even cryomagnetic studies from 4.2 K did not give any indication of the presence of measurable antiferromagnetic interaction.

In a planar CuO_2Cu type magnetosphere, the extent of magnetic interaction depends on the Cu—O—Cu bridging angle, ϕ. For hydroxo-bridged systems the interaction energy, $2J$, is given by[6,17]

$$2J = -74.53\phi + 7270\ cm^{-1}.$$

It is implied that the angle ϕ where J is nearly zero is around 98°. For bulky substitution on oxygen atoms, this angle comes close to 90°. X-ray crystallographic studies could not be undertaken on the present complexes as it was difficult to grow single crystals of them. However, the Cu—O—Cu angle was tentatively calculated from the X-ray crystallographic data available on their parent representative binuclear complex, $Cu_2(CH_3\text{-triaz-bp-}OCH_3)_2$ and that on comparable complexes having a site, CuO_2CuA_2, as in the present complexes assuming planarity to the CuO_2Cu core.[18–20] The angle thus calculated was $\sim 87°$, close to 90°, resulting in a negligible magnetic interaction.

The absence of magnetic interaction is further proved from the *X*-band ESR spectral analysis. All the copper complexes exhibit well-resolved parallel and perpendicular ESR transitions. The peak profiles are invariant throughout the temperature range 77–340 K. No solution ESR studies could be carried out as the complexes are highly insoluble in most of the solvents. The resolution of the parallel and perpendicular absorptions may be due to the negligible presence of dipolar interactions. A representative room-temperature polycrystalline ESR spectrum is provided in Fig. 2, and the relevant data in Table 3. The $\Delta M_s = \pm 2$ half-field transition was not observed even with improved instrumental parameters. The relative intensity of the $\Delta M_s = \pm 2$ transition with respect to that of the normal $\Delta M_s = \pm 1$ transition is given by

$$\text{relative intensity} = \frac{C}{r^6}\left(\frac{9.1}{\nu}\right)^2$$

for interacting binuclear systems[21] and is independent of the value of J. Here C is a constant (approximately 22 for bivalent copper systems), ν is the operating ESR frequency in GHz and r the interacting Cu—Cu distance. In the present tetra-

Table 3. ESR spectral data of tetranuclear copper(II) complexes, $Cu_2L_2(CuA_2)_2$

Compound	$g_\parallel$		$g_\perp$		g_0[a]	
	A = Cl	A = Br	A = Cl	A = Br	A = Cl	A = Br
$Cu_2(CH_3\text{-triaz-bp-}OCH_3)_2(CuA_2)_2$	2.259	2.252	2.095	2.1165	2.15	2.161
$Cu_2(C_2H_5\text{-triaz-bp-}OCH_3)_2(CuA_2)_2$	2.259	2.250	2.107	2.0815	2.158	2.14
$Cu_2(n\text{-}C_3H_7\text{-triaz-bp-}OCH_3)_2(CuA_2)_2$	2.259	2.250	2.1285	2.097	2.172	2.148
$Cu_2(i\text{-}C_3H_7\text{-triaz-bp-}OCH_3)_2(CuA_2)_2$	2.214	2.210	2.106	2.118	2.142	2.148

[a] $g_0 = 1/3[g_\parallel + 2g_\perp]$.

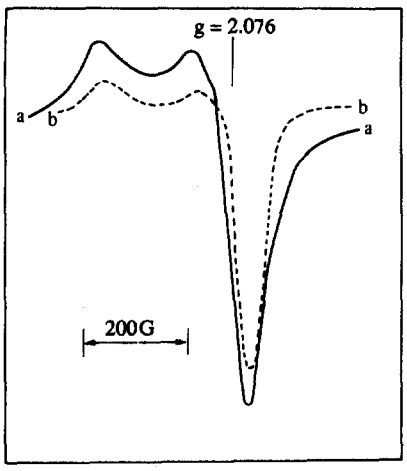

Fig. 2. *X*-band ESR spectra of (a) Cu_2(R-triaz-bp-OCH_3)$_2$ ($CuCl_2$)$_2$ and (b) Cu_2(R-triaz-bp-OCH_3)$_2$($CuBr_2$)$_2$ at room temperature.

nuclear complexes the distance between the closest copper atoms is *ca* 3 Å which gives $\sim 3.0 \times 10^{-2}$ as the relative intensity of the $\Delta M_s = \pm 2$ transition for an operating frequency of ~ 9.5 GHz. This very intense peak, could readily be observed by our instrument, but no $\Delta M_s = \pm 2$ transition was observed either at room temperature or 77 K implying the absence of antiferromagnetic interaction in the complexes.

Other indirect evidence for the absence of the magnetic interaction stems from the evident absence of zero-field splitting, D, given for the interacting binuclear complexes, by

$$D = \frac{1.39 \times 10^4 \times g}{r^3},$$

where g is the average g factor and r is the interacting Cu—Cu separation.[22,23] For $r = \sim 3$ Å and $g = \sim 2.15$, the value of D is calculated as ~ 1130 G implying the splitting of the normal $\Delta M_s = \pm 1$ transition separated by ~ 2260 G. No such split peaks were observed.

X-ray crystallographic molecular structure determinations would have provided interesting information but could not be undertaken due to the difficulty of generating a single crystal because of their insolubility in various solvents and thermal instability above 150°C.

Acknowledgements—The authors thank Professor S. Mitra, Tata Institute of Fundamental Research, Bombay, for extending the cryomagnetic facilities. One of the authors (T.S.) acknowledges with thanks the financial assistance provided by RECW through its CRT programme.

REFERENCES

1. A. Ramachandraiah and P. S. Zacharias, *Inorg. Nucl. Chem. Lett.* 1980, **16**, 433.
2. P. S. Zacharias and A. Ramachandraiah, *Polyhedron* 1985, **4**, 1013.
3. P. S. Zacharias, J. M. Elizabathe and A. Ramachandraiah, *Ind. J. Chem.* 1984, **23A**, 26.
4. A. Chakravorty, B. Behera and P. S. Zacharias, *Inorg. Chim. Acta* 1968, **2**, 85.
5. P. S. Zacharias, B. Behera and A. Chakravorty, *J. Am. Chem. Soc.* 1968, **90**, 7363.
6. R. H. Holm, G. W. Everett Jr and A. Chakravorty, *Progress in Inorganic Chemistry* (Edited by F. A. Cotton), Vol. 7, pp. 83–214, and refs therein. John Wiley, New York (1966).
7. W. E. Hatfield and J. A. Crisman, *Inorg. Nucl. Chem. Lett.* 1968, **4**, 731.
8. R. J. Butcher and E. Sinn, *Inorg. Chem.* 1976, **15**, 1604.
9. K. V. Patel and P. K. Bhattacharya, *Ind. J. Chem.* 1984, **23A**, 527.
10. M. Nakamura, H. Okawa and S. Kida, *Inorg. Chim. Acta* 1982, **62**, 201.
11. H. Okawa, Y. Kuwahara, M. Mikuriya and S. Kida, *Bull. Chem. Soc. Jpn* 1980, **53**, 549.
12. A. I. Vogel, *Text Book of Quantitative Inorganic Analysis*, 4th Edn. ELBS and Longman, London (1978).
13. S. F. A. Kettle, *Coordination Compounds*. ELBS and Nelson, (1973).
14. K. Nakamoto, *Infrared Spectra of Inorganic and Coordination Compounds*. John Wiley, New York (1970).
15. C. M. Harris, H. R. H. Patil and E. Sinn, *Inorg. Chem.* 1967, **6**, 1102.
16. S. J. Gruber, C. M. Harris and E. Sinn, *Inorg. Chem.* 1968, **7**, 268.
17. V. H. Crawford, H. W. Richerdson, J. R. Wasson, D. J. Hodgson and W. E. Hatfield, *Inorg. Chem.* 1976, **15**, 2107.
18. D. J. Hodgson, *Inorg. Chim. Acta* 1983, **75**, 225.
19. C. A. Bear, J. M. Waters and T. N. Waters, *J. Chem. Soc., Chem. Commun.* 1971, 703.
20. E. Sinn and W. F. Robinson, *J. Chem. Soc., Chem. Commun.* 1972, 359.
21. S. S. Eaton, K. N. More, B. M. Sawant and Eaton, *J. Am. Chem. Soc.* 1983, **105**, 6560.
22. T. D. Smith and J. R. Pilbrow, *Coord. Chem. Rev.* 1974, **13**, 173.
23. A. Buttafava, L. Fabbrizzi, A. Perotti and B. Seghi, *J. Chem. Soc., Chem. Commun.* 1982, 1166.

Polyhedron Vol. 9, No. 14, pp. 1709–1716, 1990
Printed in Great Britain

0277–5387/90 $3.00+.00
Pergamon Press plc

THE CHEMISTRY OF CERAMIC GLAZES—II. THE INFLUENCE OF THE PRESENCE OF THE OXIDES Na_2O, CaO OR Al_2O_3 ON THE THERMOLYSIS OF LAPONITE. ^{29}Si, ^{23}Na AND ^{27}Al MASNMR STUDIES

ARVIND-PAL S. MANDAIR and WILLIAM R. McWHINNIE*

Department of Chemical Engineering and Applied Chemistry, Aston University, Aston Triangle, Birmingham B4 7ET, U.K.

(*Received* 14 *December* 1989; *accepted* 21 *March* 1990)

Abstract—The influence of added oxides on the progress of the thermolysis of laponite at 1300°C was investigated. Calcium oxide promotes the depolymerization of the clay silicate lattice and, even at low CaO additions, mixed calcium/magnesium phases were identified; at higher additions akermanite was a dominant crystalline phase. Sodium oxide was even more effective as a depolymerizing agent; when the total molar proportion of Na_2O exceeded the total concentration of the other component oxides of laponite (Li_2O, MgO), a glass is formed and no crystalline phases were detected. By contrast, evidence was obtained that additions of Al_2O_3 could increase the degree of connectivity as evidenced by the formation of new alumino-silicate phases such as sillimanite; spinel, $MgAl_2O_4$, was a dominant crystalline phase at higher Al_2O_3 additions. The products of the reactions studied were examined using ^{29}Si, ^{23}Na and ^{27}Al MASNMR spectroscopy and this technique was shown to be particularly powerful for the study of systems in which glassy and crystalline phases co-exist.

Ceramic glazes are complex materials which are compounded from a variety of ingredients. These may include clay minerals, alkaline earth oxides (from carbonate precursors) together with feldspars, which function as a source of alkali metal oxides, alumina and extra silica; also silica itself is often an ingredient. Colouring oxides may also be present, e.g. transition metal oxides or perhaps materials such as SnO_2 or ZrO_2 which confer opacity to the glaze. We have made some attempts to follow chemical changes which occur when glazes are fired. Our approach has been to concentrate initially on one component and attempt to build up an understanding of the thermochemistry using a combination of resonance spectroscopies and XRD data. Thus we have investigated the thermolysis of the iron-containing minerals, montmorillonite and illite, using ^{57}Fe Mössbauer spectroscopy,[1] and have used the same technique to examine the chemical destination of iron in a simple feldspathic glaze maturing at 1280°C.[2] We have also investigated the thermochemistry (to 1300°C) of hectorite, a lithium–magnesium trioctahedral smectite clay, together with that of the synthetic counterpart laponite[3] using ^{29}Si MASNMR spectroscopy.

Laponite is attractive for NMR studies since it is virtually free of paramagnetic impurities which, if present in too great quantities,[3] may cause loss of resolution of the ^{29}Si MASNMR spectrum.[4] We therefore use laponite to pursue our studies and in this paper use a combination of ^{29}Si, ^{23}Na and, where appropriate ^{27}Al MASNMR spectroscopy, to investigate the influence of oxides such as CaO, Na_2O and Al_2O_3 on the thermolysis products of the clay at 1300°C.

EXPERIMENTAL

Materials

Laponite RD (laponite in this paper) in the sodium form was obtained from Laporte Industries Ltd [ideal formula: $Na_{0.67}(Mg_{5.33}Li_{0.67})Si_8O_{20}(OH)_4$]. Other materials were reagent grade.

* Author to whom correspondence should be addressed.

(a) *The effect of temperature on the reaction of a mixture of laponite and calcium oxide (constant composition).* Laponite (5 g) was mixed with calcium carbonate (to give a 1 : 1 CaO–SiO_2 molar ratio) until a homogeneous powder was obtained. The powder was transferred to a new porcelain crucible and fired in a Carbolyte furnace, under air, 400°C for 3 h. (Temperatures were monitored with a Pt/Rh thermocouple.) After firing, the crucible was removed from the furnace, covered with a lid, and allowed to cool completely in a desiccator overnight prior to grinding the product to a fine powder. (Material was selected from the centre of the mixture to eliminate problems arising from any surface reaction with the crucible.)

The procedure was repeated with identical mixtures of calcium carbonate and laponite at a range of temperatures to a mixture of 1300°C. This standard procedure was used for subsequent experiments.

(b) *The reaction of laponite at 1300°C with varying mole ratios (based on SiO_2) of calcium oxide.* Calcium carbonate was added to laponite (3 g) in increasing quantities (based on the mol % of CaO to the SiO_2 content) of laponite (see tables of data for details).

(c) *The influence of sodium oxide on the reaction of laponite–calcium oxide mixtures at 1300°C.* Laponite (3 g charges), calcium carbonate and sodium carbonate were mixed together in the molar proportions indicated in Table 3.

(d) *The influence of alumina (Al_2O_3) on the reaction of laponite–calcium oxide mixtures at 1300°C.* Mixtures of laponite (3 g charges) with calcium carbonate and alumina were prepared according to the proportions in Table 4.

Physical measurements

MASNMR spectra were obtained with a Bruker AC(E) 300 MHz spectrometer. The "magic angle" was set with KBr and Delrin rotor spinning rates were ~ 5 kHz. Frequencies were 59.580 MHz (^{29}Si), 79.392 MHz (^{23}Na) and 78.206 MHz (^{27}Al). IR spectra were recorded for KBr discs using a Perkin–Elmer 1710 FTIR instrument. XRD data were obtained with a Philips X-ray diffractometer using Co-K_α radiation with a typical scan speed of 1° 2θ min^{-1}. The d-spacings of the various phases present were calculated from 2θ values using standard Co-K_α charts.[5]

RESULTS

Table 1 gives the ^{29}Si chemical shifts (vs $(CH_3)_4Si$) for the laponite RD–CaO system (SiO_2–CaO = 1 : 1) fired to temperatures in the range 400–1300°C. Table 2 considers the influence on the ^{29}Si MASNMR data of varying quantities of CaO (all specimens fired to 1300°C). Table 3 gives ^{29}Si MASNMR data for the system laponite–Na_2O–CaO, together with the ^{23}Na MASNMR data. Tables 4 and 5 give the ^{29}Si and ^{27}Al MASNMR data, respectively, for the laponite–CaO–Al_2O_3 system. Figure 1 shows typical spectra. A complete tabulation of the IR data is available,[6] in this paper

Table 1. The reaction of laponite and calcium carbonate (SiO_2(clay)–CaO = 1 : 1) as a function of temperature monitored by ^{29}Si MASNMR spectroscopy

Firing temperature	Q^0		Q^1		Q^2		Q^3	
	δ[a]	I[b]	δ	I	δ	I	δ	I
400°C							−96.7	(100%)
500°C							−95.8	(100%)
600°C			−81.8	(11%)	−89.2	(20%)	−99.6	(10%)
			−79.6	(3%)	−85.3	(28%)	−93.8	(28%)
700°C			−79.6	(25%)			−93.8	(75%)
800°C			−79.4	(55%)				
			−76.9	(45%)				
900°C			−79.4	(55%)				
			−76.9	(45%)				
1000°C			−81.1	(31%)	−84.7	(23%)		
			−73.8	(8%)	−83.5	(38%)		
1300°C	−66.3	(7%)	−72.3	(86%)				
	−62.2	(7%)						

[a] Chemical shifts relative to TMS.

[b] Intensity as percentage of total spectral area.

Table 2. The reaction of laponite with calcium carbonate (mole per cent 20–200[a]) at 1300°C monitored by ^{29}Si MASNMR spectroscopy

Mole % CaO	Q^0 δ[b]	Q^0 I[c]	Q^1 δ	Q^1 I	Q^2 δ	Q^2 I	Q^3 δ	Q^3 I
20	−61.9	18			−84.6	82		
40	−61.9	13			−84.3	70	−91.9	17
50	−62.2	33			−84.7	67		
60	−61.8	21	−72.0	41	−84.3	38		
80	−61.8	7	−72.1	69	−84.5	6		
	−65.9	19						
100	−61.9	6	−72.1	74				
	−65.9	19						
200			−72.1	55				
			−73.6	45				

[a] Relative to "SiO_2" content of laponite.
[b] Chemical shifts relative to TMS.
[c] Intensity as percentage of total spectral area.

Table 3. ^{29}Si and ^{23}Na MASNMR data for the system laponite[a]–CaO–Na_2O = $1:x:1-x$ heated to 1300°C

		Q^0		Q^1		Q^2		^{23}Na shift	
$(1-x)$	Na–(Mg+Li+Ca)	δ[b]	I[c]	δ	I	δ	I	δ[d]	$\Gamma_{1/2}$ (Hz)[e]
0.1	0.28 : 1.65	−66.0	65	−72.0	28	−90.1	7	−8.81	2100
0.2	0.48: 1.55	−65.9	21						
		−61.9	7	−72.2	60	−85.6	12	−14.46	2100
0.3	0.68 : 1.45	−65.9	35						
		−61.8	5	−71.9	43	−85.0	17	−8.75	2550
0.4	0.88 : 1.35	−65.9	26						
		−61.8	18	−74.3	24	−85.0	32	−14.6	2250
0.6	1.28 : 1.15			−78.8	100			−10.24	2550
0.8	1.68 : 0.95			−79.9	100			−11.33	2500
1.0	2.08 : 0.75			−80.8	100			−12.24	2300

[a] Relative to "SiO_2" content of laponite.
[b] Chemical shifts relative to TMS.
[c] Intensity as percentage of total spectral area.
[d] Chemical shifts relative to aqueous sodium bromide.
[e] Width at half height (Hz).

Table 4. ^{29}Si MASNMR data for the system laponite[a]–CaO–Al_2O_3 = $1:x:1-x$ heated to 1300°C

			Q^3		
$(1-x)$	Q^0 $\delta(I)$[b]	Q^1 $\delta(I)$	3Al $\delta(I)$	2Al $\delta(I)$	0Al $\delta(I)$
0.1	−62.1(12%)	−72.3(54%)			
	−66.2(34%)				
0.2	−62.0(30%)	−72.2(65%)	−79.0 (5%)		
0.4	−61.9(30%)	−72.1(60%)	−80.4(10%)		
0.6	−61.9 (5%)		−80.4(95%)		
0.8	−61.9(38%)			−84.7(62%)	
1.0				−84.9(69%)	−95.5(31%)

[a] Relative to "SiO_2" content of laponite.
[b] Chemical shifts vs TMS (relative intensity).

Table 5. ^{27}Al MASNMR data for the system laponite[a]–CaO–Al_2O_3 = $1 : x : 1-x$ heated to 1300°C

$(1-x)$	δ (octahedral)[b]	δ (tetrahedral)[b]
0.2	0.6–6.5	60.2
0.4		64.8
0.6		55.8–59.6
0.8	7.6–9.1	55.8–58.0
1.0	10.6	68.2

[a] Relative to "SiO_2" content of laponite.
[b] Chemical shifts vs 0.1 M $[Al(H_2O)_6]^{3+}$.

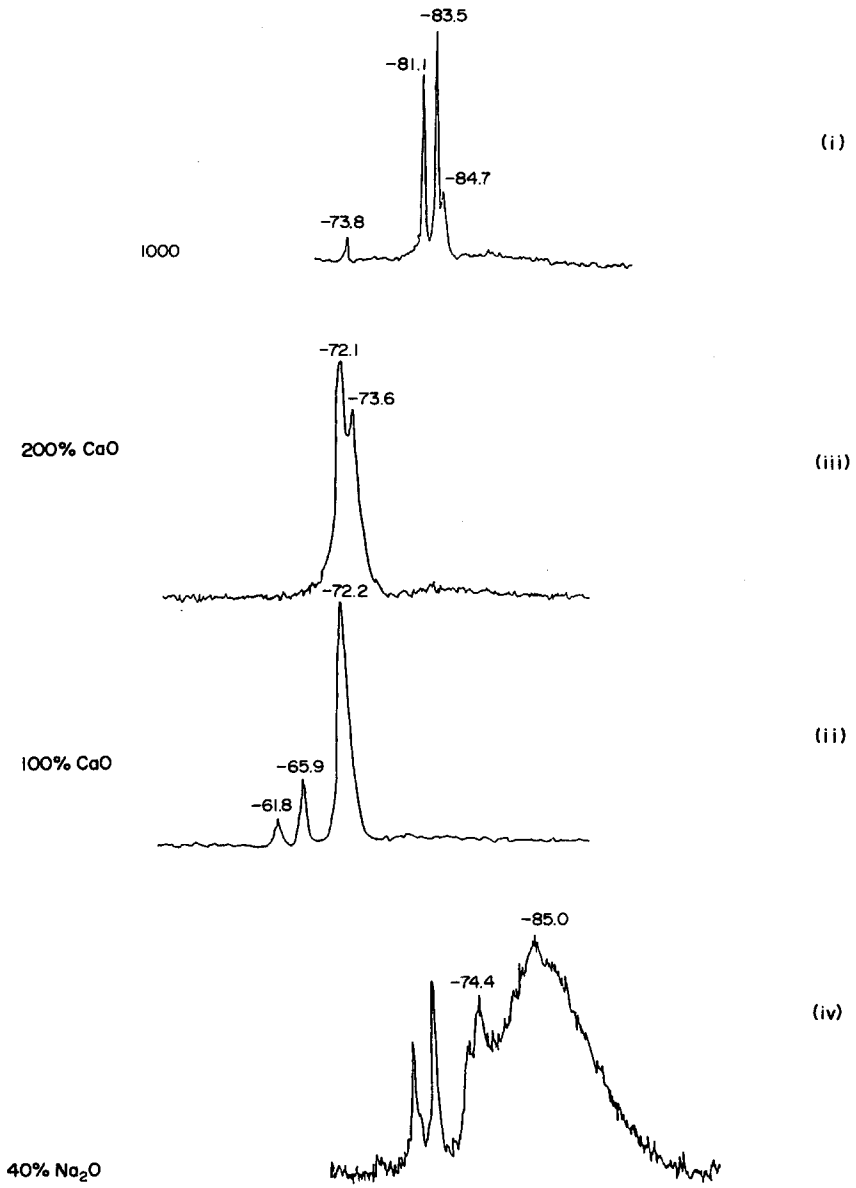

Fig. 1. Some selected ^{29}Si MASNMR spectra: (i) laponite + CaO fired to 1000°C; (ii) laponite + 100% CaO fired to 1300°C; (iii) laponite + 200% CaO fired to 1300°C; (iv) laponite + 40% Na_2O, $(1-x) = 0.4$, fired to 1300°C.

selected data will be referred to in the text as required.

DISCUSSION

Initially the reaction of calcium oxide (supplied as carbonate) with laponite in a 1:1 mole ratio (based on the "SiO_2" content of laponite) will be considered as a function of kiln temperature. Subsequently, the influence of varying the quantity of CaO on the reaction of CaO and laponite at 1300°C is discussed. Finally, the effect of gradually replacing CaO with either Na_2O or Al_2O_3 ["SiO_2" (from laponite)–CaO–$M_nO_m = 1:x:1-x$] is considered.

The reaction of laponite and CaO (SiO_2–CaO = 1:1)

In the NMR discussion the now standard "Q" notation developed[7] by Engelhardt *et al.* is used, thus Q^2 will denote a SiO_4 tetrahedron forming two siloxane linkages to two other such tetrahedra via apical oxygen atoms.

Although the materials fired to temperatures up to 700°C gave several XRD reflections, these could not be assigned with confidence to any crystalline phases. Mixtures fired to 800 and 900°C gave definite evidence for the presence of the crystalline phase rankinite ($Ca_3Si_2O_7$). The mixture fired to 1000°C gave XRD data which were difficult to interpret. Some reflections which matched those expected for γ-Ca_2SiO_4 were seen, but this assignment was not supported by the NMR data. No positive evidence for enstatite ($MgSiO_3$) was obtained, yet NMR evidence for the presence of the pyroxene was definite (see below). The material was possibly a microcrystalline dispersion. Firing to 1300°C gave a material in which the major phase present was akermanite ($Ca_2MgSi_2O_7$) and the minor phases monticellite ($CaMgSiO_4$) and forsterite (Mg_2SiO_4) were noted.

The ^{29}Si MASNMR data in Table 1 give a more detailed picture of the reactions than do the XRD data. Mixtures fired to 400 and 500°C show one broad Q^3 resonance. Laponite heated alone gave sharper lines and showed some evidence of Q^2 sites also;[3] it is likely that in the present case the weak Q^2 resonances were not resolved. The mixture heated to 600°C gave a complex spectrum of several overlapping broad lines with a total spectral width of 750 Hz. The broad band at $\delta = -99.6$ ppm may arise from the presence of an amorphous phase; alternatively it may be derived from laponite since it has earlier been suggested that the lithium ions may migrate from their trioctahedral positions to crystal edges thereby increasing the shielding of the lattice silicon atoms.[3] Despite the absence of crystalline phases, the presence of $CaCO_3$ has induced a significantly greater breakdown of the laponite Q^3 silicate lattice than occurred when the clay was heated to 600°C alone.[3] IR data showed clearly that $CaCO_3$ was still present in substantial quantities at 600°C.

The batch fired to 700°C showed two broad, resolved resonances indicating the essentially amorphous nature of this sample. The Q^1 site ($\delta = -79.6$ ppm) which was just discernible at 600°C is much more prominent in the 700°C spectrum. It was beyond 800°C that further distinctive changes occurred. The IR data showed the onset of thermal decomposition of $CaCO_3$ at 800°C and the availability of CaO induces further change and the formation of more crystalline phases. The ^{29}Si MASNMR spectrum showed sharp resonances at −79.6 and −76.4 ppm. Oldfield and Janes have calculated[8] that both ^{29}Si chemical shifts for rankinite should occur at −79.4 ppm, whereas Lippmaa *et al.*[9] have observed two resonances at −79.6 and −76.6 ppm for synthetic rankinite. Given the XRD support above, it is clear that rankinite is the major crystalline phase present in the batches heated to 800 and 900°C.

By 1000°C no trace of rankinite remained. The peaks at −81.1 and −84.7 ppm are assigned to the pyroxene enstatite ($MgSiO_3$),[3] an expected product from the thermolysis of laponite. However, it is interesting to note that between 800 and 900°C depolymerization of the laponite Q^3 lattice to the Q^1 species has occurred, but the formation of the pyroxene at 1000°C requires a re-polymerization to Q^2. Thus, although enstatite is an expected product, the mechanism of formation is likely to be different to that when laponite alone is thermolysed. A second Q^2 phase was also present with $\delta = -84.7$ ppm, this is assigned to a second pyroxene mineral diopside [$CaMg(SiO_3)_2$]. The pyrosilicate akermanite ($Ca_2MgSiO_2O_7$) was identified by the resonance at $\delta = -73.8$ ppm.[9,10] The 1300°C reaction product contained akermanite as the major crystalline product, a fact confirmed by ^{29}Si MASNMR and XRD data. The two Q^0 resonances are assigned to forsterite (Mg_2SiO_4, −62.2 ppm) and monticellite ($CaMgSiO_4$, −66.2 ppm), the observed chemical shifts being in good agreement with those obtained independently by Lippmaa *et al.*[9] and Smith *et al.*[10]

The reaction of laponite with CaO *at* 1300°C (SiO_2–CaO = 1:x *where* $0.2 < x < 2.0$)

The influence of differing proportions of CaO on the product ratios at 1300°C was investigated. ^{29}Si

MASNMR data are given in Table 2. The conclusions from a combined NMR and XRD study are tabulated below where Ca(20) denotes a 20% addition of CaO, ticks and crosses denote the presence or absence of XRD evidence for the particular phase, and where the indicated references give literature support for the NMR assignments.

Phase	(^{29}Si)	Ca(20)	Ca(40)	Ca(60)	Ca(80)	Ca(100)	Ca(200)
Forsterite	-61.9 (Q^0)[9,10]	√	√	√	√	×	×
Akermanite	-72.1 (Q^1)[9,10]	×	×	×	√	√	√
Monticellite	-65.9 (Q^0)[9,10]	×	×	×	√	√	×
Enstatite	-83.5 (Q^2)	√	×	×	×	×	×
Diopside	-84.3 (Q^2)[8,9]	√	√	√	√	×	×
γ-$Ca_2Si_2O_4$	-73.5 (Q^0)	×	×	×	×	×	√
CaO	—	×	×	×	×	×	√

The ternary system: laponite–calcium oxide–sodium oxide

A ceramic glaze will usually contain a quantity of an alkali metal oxide as a "fluxing" (glass forming) reagent. It is introduced to the raw glaze in a water insoluble form, e.g. as sodium or potassium feldspar. Laponite contains approximately 0.6% lithium and, given the choice of this clay as the silica source in these experiments, lithium which is a strong flux will contribute to glass formation;[3] also laponite was used as the sodium exchanged clay. Taking the silica content of laponite as unity, batches were made up with SiO_2–CaO–NaO = $1:x:1-x$, where $1-x$ is the *added* Na_2O. Table 3 details the ^{29}Si and ^{23}Na MASNMR shifts observed when these batches were fired to 1300°C; the table also details the actual Na–(Mg+Li+Ca) ratio taking account of the full constitution of the clay.

It is clear from Table 3 that at values of $(1-x)$ between 0.1 and 0.4 (where the total molar content of Li+Mg+Ca *exceeds* that of Na), sharp resonances assignable to the crystalline phases forsterite (−61.9 ppm), monticellite (−65.9 ppm) and akermanite (−72.2 ppm) are seen. In addition for $(1-x) = 0.2$ and above, a broad resonance to higher field is seen; beyond $(1-x) = 0.6$ (at which point the molar content of Na exceeds the combined molar content of Li+Mg+Ca) the spectrum is dominated by a broad resonance and no evidence of crystalline phases is seen.

For lower values of $(1-x)$, in addition to creating a glassy phase, the replacement of CaO by Na_2O alters the relative proportions of monticellite and akermanite. The broad resonance which ultimately dominates the spectrum beyond $(1-x) = 0.6$ is undoubtedly due to a glassy phase. Simple silicate glasses have been examined by Dupree *et al.*[11] and by Grimmer *et al.*,[12] and the ^{29}Si MASNMR data were shown to be consistent with a model based on a binary distribution. Laponite consists of Q^3 silicons, thus additions of Na_2O would initially promote the formation of Q^2 groups and, beyond a 33% addition, Q^1 groups will be formed. These simple arguments are complicated by the presence of MgO and CaO, however, in Fig. 2 the chemical shift of the broad resonance associated with the glassy phase is plotted against $(1-x)$. It is noted that a discontinuity occurs between $(1-x) = 0.4$ and 0.6; we believe this to represent the transition from an essentially Q^2 phase to a Q^1 phase. Also beyond $(1-x) = 0.6$ ions, Na^+, Li^+, Mg^{2+} and Ca^{2+} are incorporated in the glass structure. The observed chemical shifts of the Q^2 and Q^1 phases appear at higher field than would be expected for a simple Na_2O/SiO_2 glass,[11,12] however, the data are consistent with the incorporation of Mg^{2+} and Ca^{2+} which shift the resonances to more negative values.[13]

No attempt was made to deconvolute the broad resonance associated with the glass phase. The breath of the resonance may be attributed to a range of factors: variations in the Si—O—Si bond angles, variations in bond lengths, the co-existence of two Q^n types in some cases, and the combined presence of Na^+, Li^+, Mg^{2+} and Ca^{2+} as lattice modifiers.[14]

The ^{23}Na MASNMR spectra of these systems

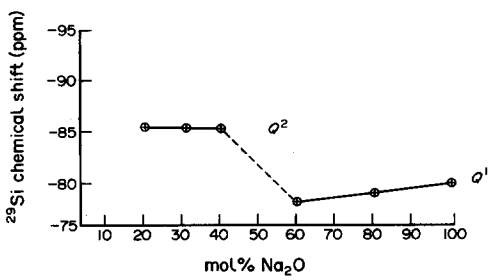

Fig. 2. ^{29}Si MASNMR chemical shift as a function of mol % Na_2O $(1-x)$ (SiO_2–CaO–Na_2O = $1:x:1-x$).

were featureless and showed signs of quadrupolar broadening, thus the "chemical shift" recorded in Table 3 cannot be assumed to represent the isotropic chemical shift. The resonance maximum is sensitive to the value of $(1-x)$ but not in an obviously consistent manner—at low values of $(1-x)$ when crystalline phases are present significant variation of the maximum was noted, however, once the glass phase dominated a more regular variation with $(1-x)$ was seen.

The ternary system: laponite–calcium oxide–aluminium oxide

The presence of alumina generated crystalline phases at all values of $(1-x)$ (Table 4). This is not surprising since it is known that the system $MgO[Al_2O_3]SiO_2$ may form the basis of a series of glass ceramics.[15] The phases identified by a combination of XRD and MASNMR are tabulated below.

For values of $(1-x)$ equal to and greater than 0.6, spinel ($MgAl_2O_4$) is clearly indicated in the XRD and the tetrahedral aluminium signals observed may be assigned to this phase. For $(1-x) = 0.8$ and 1.0, octahedral and tetrahedral signals are observed. Sillimanite contains aluminium in both octahedral and tetrahedral coordination, the ^{29}Si chemical shift and XRD evidence support the presence of this phase, but the combined presence of corundum and spinel (XRD) warn that at least part of the octahedral and tetrahedral signal intensity must arise from these sources. Thus it cannot be claimed that the ^{27}Al MASNMR data offer unambiguous support for the presence of sillimanite.

Acknowledgements—A-P.S.M. thanks Aston University for a studentship. We thank Dr M. C. Perry for assistance in obtaining MASNMR data.

	Percentage replacement of CaO by Al_2O_3				
Phase	Al(20)	Al(40)	Al(60)	Al(80)	Al(100)
Akermanite ($Ca_2MgSi_2O_7$)	√	√	×	×	×
Forsterite (Mg_2SiO_4)	√	√	×	×	×
Monticellite ($CaMgSiO_4$)	√	√	×	×	×
Calcium aluminate $[Ca(AlO_2)_2]$	×	√	×	×	×
Spinel ($MgAl_2O_4$)	×	×	√	√	√
Corundum	×	×	×	√	√
Sillimanite (Al_2SiO_5)	×	×	×	√	√

Table 5 lists some data for the quadrupolar ($I = 5/2$) ^{27}Al nucleus. It is possible to differentiate "octahedral" and "tetrahedral" sites since the six-coordinate aluminium will resonate close to the standard $[Al(H_2O)_6]^{3+}$ (i.e. $\delta \sim 0$), whereas the tetrahedral environment gives resonances at lower field ($\delta \sim 50$–80 ppm). Since second-order quadrupole effects are not averaged to zero by "magic angle" spinning, it is dangerous to relate the observed peak maxima to isotropic chemical shifts.

Tetrahedral sites are observed for aluminium for all values of $(1-x)$ considered. At low values of $(1-x)$, e.g. 0.2, 0.4, this band may be attributed to calcium aluminate which was detected by XRD in the $(1-x) = 0.4$ case. A similar origin for the octahedral resonance for $(1-x) = 0.2$ is suggested.

REFERENCES

1. P. J. Michael and W. R. McWhinnie, *Polyhedron* 1989, **8**, 2709.
2. N. J. Ali, P. A. Gillespie and W. R. McWhinnie, *Polyhedron* 1990, **9**, 999.
3. A-P. S. Mandair, P. J. Michael and W. R. McWhinnie, *Polyhedron* 1990, **9**, 517.
4. E. Oldfield, R. A. Kinsey, K. A. Smith, J. A. Nichols and R. J. Kirkpatrick, *J. Mag. Reson.* 1983, **51**, 325.
5. G. W. Brindley and G. Brown, in *Crystal Structure of Clay Minerals and their X-ray Identification*. Mineralogical Society, Monograph No. 5 (1951).
6. A-P. S. Mandair, PhD thesis, Aston University, Birmingham (1988).

7. G. Engelhardt, D. Zeigan, H. Jancke, D. Hoebbel and W. Wicker, *Z. Anorg. Allgem. Chem.* 1975, **418**, 17.
8. E. Oldfield and N. Janes, *J. Am. Chem. Soc.* 1985, **107**, 6769.
9. E. Lippmaa, M. Magi, A. Samoson, G. Engelhardt and A. R. Grimmer, *J. Phys. Chem.* 1984, **88**, 1518.
10. K. A. Smith, R. J. Kirkpatrick, E. Oldfield and D. M. Henderson, *Am. Miner.* 1983, **68**, 1206.
11. R. Dupree, D. Holland, P. W. McMillan and R. F. Pettifer, *J. Non-Cryst. Solids* 1984, **68**, 399.
12. A. R. Grimmer, M. Mägi, M. Hähnert, H. Stade, A. Samoson, W. Weiker and E. Lippmaa, *Phys. Chem. Glasses* 1984, **25**, 105.
13. J. B. Murdoch, J. F. Stebbins and I. S. E. Carmichael, *Am. Miner.* 1985, **70**, 332.
14. G. Engelhardt and D. Michel, *High Resolution Solid State NMR of Silicates and Zeolites*, pp. 194–205. John Wiley, Chichester (1987).
15. G. Partridge, C. A. Elyard and M. I. Budd, in *Glasses and Glass-Ceramics* (Edited by M. H. Lewis), p. 226. Chapman and Hall, London (1989).

Polyhedron Vol. 9, No. 14, pp. 1717–1721, 1990
Printed in Great Britain

0277–5387/90 $3.00+.00
© 1990 Pergamon Press plc

EXTRACTION OF MOLYBDENUM(VI) FROM AQUEOUS SOLUTION BY DONOR SOLVENTS

KATSUO MURATA* and SHINSUKE YAMASHITA

Naruto University of Education, Naruto, Tokushima, Japan 772

and

ETSUKO YAMAMOTO and SHIGERO IKEDA

Department of Chemistry, Faculty of Science, Osaka University, Toyonaka, Osaka, Japan 560

(*Received* 20 *December* 1989; *accepted* 21 *March* 1990)

Abstract—Molybdenum(VI) has been mainly extracted with chelating reagents by non-polar solvents due to difficulties with polar solvents such as alcohols, ethers and esters. However, the coordinative donor solvents propylene carbonate, cyclohexanone and tri-*n*-butyl phosphate did extract molybdate albeit slowly. Each of the extracted species was identified to be hexamolybdate by the use of Raman spectroscopy. The extraction equilibrium involving cyclohexanone indicated that the main extracted species is the ion pair $H_3O^+(HMo_6O_{19})^-$ in the lower concentration of 1.0×10^{-3} M [Mo]; but both the species $H_3O^+(HMo_6O_{19})^-$ and $(H_3O^+)_2Mo_6O_{19}^{2-}$ are extracted in the higher concentration of molybdate (1.0×10^{-2}–1.0×10^{-1} M).

The formation of 12-molybdoheteropoly acid is the well-known procedure for the determination of trace amounts of P, As, Si and Ge.[1,2] 12-Molybdoheteropoly acid is generally extracted into the mixed solvents in order to avoid the influence of excess molybdate. Excess molybdate does not usually interfere with the extraction of 12-molybdoheteropoly acid. We found, however, that molybdate was gradually extracted from the weak acidic solution by propylene carbonate[3] and cyclohexanone,[4] among several other solvents. The coordinative solvating solvents such as propylene carbonate, cyclohexanone and tri-*n*-butyl phosphate appeared to be much more effective in the extraction of molybdenum(VI). The purpose of this study is to clarify both the mechanism of extraction of molybdenum(VI) and the extracted species with those solvents using Raman spectroscopy.

EXPERIMENTAL

A solution of molybdate was prepared from sodium molybdate, $Na_2MoO_4\cdot2H_2O$ (analytical grade), and standardized as the gravimetric oxinate.[5] Propylene carbonate was distilled under reduced pressure: b.p. 92°C at 4.5 mm.[6] Cyclohexanone and tri-*n*-butyl phosphate were of analytical reagent grade.

The time needed for equilibration is much longer than that required for the usual extracting procedure. A stoppered centrifuge tube, containing 10 cm^3 of molybdate solution and the organic solvent, was ordinally shaken for 1 h at 25 ± 0.1°C. The molybdate content of the aqueous solution before and after extraction was determined by atomic absorption spectrometry. Raman spectra were measured with a JASCO R800 instrument, using 514.5 nm (Ar^+, laser) as the excitation source.

RESULTS AND DISCUSSION

There are many species of polynuclear molybdate in the weak acidic solutions, as seen in some of the literature surveying molybdate species.[7–10] Our results from the Raman study also indicate that the main species of polynuclear molybdate are $Mo_7O_{24}^{6-}$, $Mo_8O_{26}^{4-}$ and $Mo_{12}O_{37}^{2-}$.[11] The hexamolybdate of $Mo_6O_{19}^{2-}$, in small quantities,

* Author to whom correspondence should be addressed.

appears only in the acidic solution of pH 1. Hexamolybdate seems to be unstable in aqueous solution.

Concerning the extraction of molybdenum(VI), there are some recent papers involving quaternary ammonium salts,[12–14] high-molecular weight amines[15–17] and a neutral organophosphorus extractant.[18] Cruywagen and Rypstra studied the extraction of molybdenum(VI) by tri-*n*-butyl phosphate.[18] They concluded that the polynuclear molybdate extracted is hexamolybdate, $Mo_6O_{19}^{2-}$, by the use of a UV absorption spectrometer. This result is also supported by our Raman studies. Figure 1(a)–(c) shows Raman spectra of the tri-*n*-butyl phosphate layer. Figure 1(a) shows the Raman spectrum of the extracted layer which contains the extracted molybdate species, tri-*n*-butyl phosphate solvent and the distributed water. Figure 1(b) is the Raman spectrum of the tri-*n*-butyl phosphate equilibrated with water of the same pH value. Figure 1(c) shows the Raman spectrum of the extracted species, which is obtained by subtracting Fig. 1(b) from Fig. 1(a). The Raman spectrum of Fig. 1(c) resembles closely that of tetrabutylammonium hexamolybdate, $[(C_4H_9)_4N]_2Mo_6O_{19}$, which was prepared by precipitation from acidified aqueous solution and then recrystallization with acetone.[19] Therefore, the extracted species is considered to be hexamolybdate, $Mo_6O_{19}^{2-}$, in tri-*n*-butyl phosphate.

Figure 2(a)–(c) shows Raman spectra of the propylene carbonate layer which contains the extracted

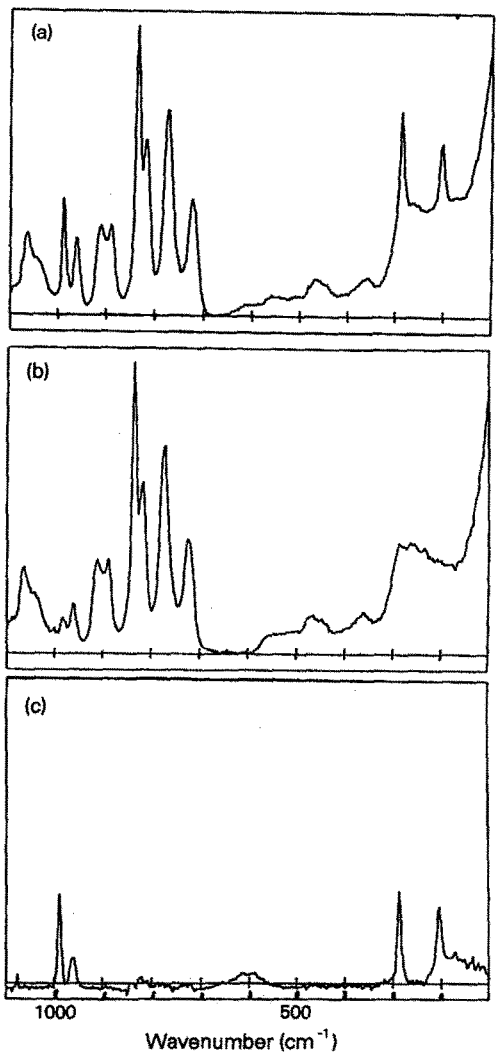

Fig. 1. Raman spectra of the extracted layer by tri-*n*-butyl phosphate: (a) the extracted layer, (b) tri-*n*-butyl phosphate equilibrated with water of pH 1 and (c) the extracted species.

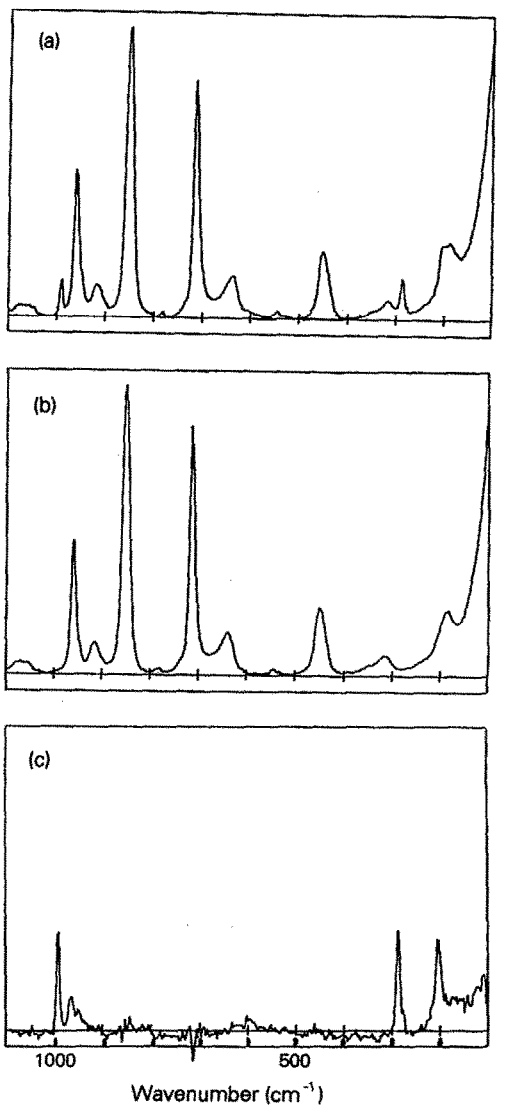

Fig. 2. Raman spectra of the extracted layer by propylene carbonate: (a) the extracted layer, (b) the propylene carbonate equilibrated with water of pH 1 and (c) the extracted species.

species, the distributed water and the solvent. Figure 2(b) shows the Raman spectrum of the propylene carbonate equilibrated with water of the same pH value. Figure 2(c) shows the Raman spectrum of the extracted species, which is obtained by subtracting Fig. 2(b) from Fig. 2(a). The Raman spectrum in Fig. 2(c) also resembles that of hexamolybdate. Hence the extracted species using propylene carbonate is hexamolybdate. We obtained the wrong conclusion concerning the extracted species in an earlier paper.[3] We must, therefore, correct our former conclusion that the main extracted species was the highly condensed polymer of c.a. 13.

Figure 3 shows the Raman spectra of both the cyclohexanone extract (solid line) and cyclohexanone (dotted line). Raman bands at 985, 958, 605, 287 and 206 cm^{-1} are closely related to those of hexamolybdate. Consequently, the extracted species is considered to be the hexamolybdate, $Mo_6O_{19}^{2-}$, in all the extractions using tri-*n*-butyl phosphate, propylene carbonate and cyclohexanone.

Next we investigated the extraction behaviour by cyclohexanone, since the extraction of molybdenum(VI) has been studied using tri-*n*-butyl phosphate[18] and propylene carbonate.[3] Figure 4 shows the extraction curves from the acidified molybdate solutions by cyclohexanone. As the concentration of molybdate increases, each curve shifts to the more acidic region, i.e. lower values of pH. But this does not imply that a different molybdate species is extracted from solutions of different concentrations. We obtain Fig. 5 when the data in Fig. 4 is replotted against the Z value, $Z = ([H^+]_{added} - [H^+]_{free})/[Mo]$, instead of pH, thus exhibiting approximately the polymerization degree of polynuclear molybdate.[10] Since three extraction curves

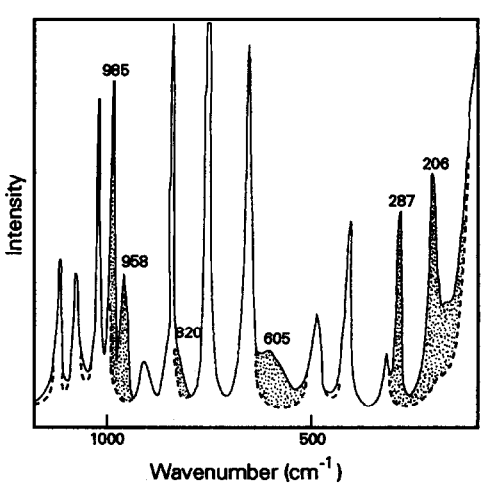

Fig. 3. Raman spectra of the extracted layer (solid line) and the blank solution of cyclohexanone (dotted line).

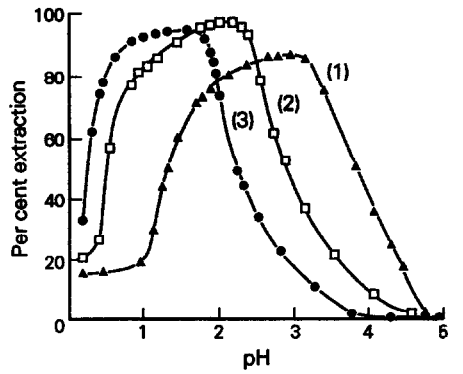

Fig. 4. Extraction curves of molybdenum(VI) by cyclohexanone: (1) 1.0×10^{-3} M, (2) 1.0×10^{-2} M and (3) 1.0×10^{-1} M.

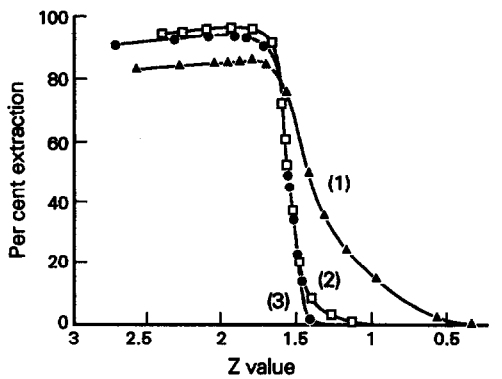

Fig. 5. Extraction curves plotted against the Z value of aqueous solutions: (1) 1.0×10^{-3} M, (2) 1.0×10^{-2} M and (3) 1.0×10^{-1} M.

almost coincide, it is expected that the same species are extracted in spite of the different molybdate concentrations. The extracted species should be hexamolybdate as both the Raman spectrum of the extract and the Z value of the molybdate solutions concur.

The distribution ratio of molybdic acid is plotted against the pH of the solutions in Fig. 6. The following equilibrium reaction is found for the extraction of hexamolybdate if the $(H_nMo_6O_{19})^{(2-n)-}$ species is considered to be mainly extracted as the ion pair with the oxonium ion, H_3O^+:

$$(H_nMo_6O_{19})^{(2-n)-} + (2-n)H_3O^+ \rightleftharpoons [(H_3O^+)_{2-n}(H_nMo_6O_{19})^{(2-n)-}]_{org.}$$

The extraction constant K_{ex} is given as follows:

$$K_{ex} = [(H_3O^+)_{2-n}(H_nMo_6O_{19})^{(2-n)-}]_{org}/([(H_nMo_6O_{19})^{(2-n)-}][H_3O^+]^{2-n}). \quad (1)$$

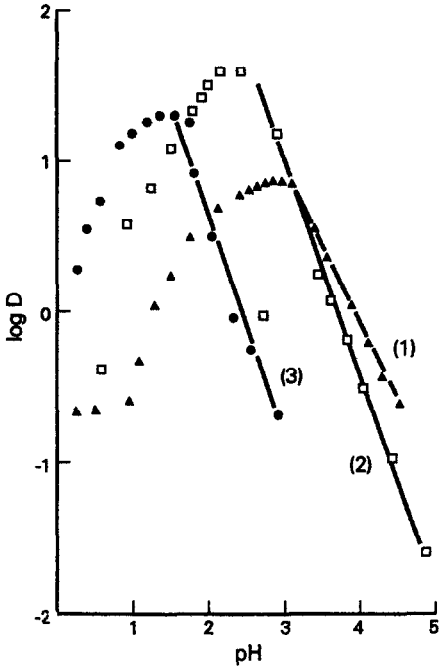

Fig. 6. Distribution equilibria of molybdenum(VI) by cyclohexanone: (1) 1.0×10^{-3} M, (2) 1.0×10^{-2} M and (3) 1.0×10^{-1} M.

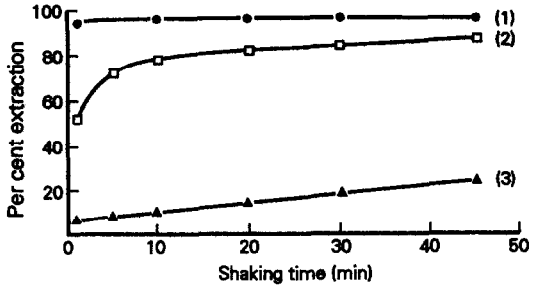

Fig. 7. The extraction rate of molybdenum(VI) by cyclohexanone: (1) 1.0×10^{-2} M, pH 2.0; (2) 1.0×10^{-2} M, pH 1.0; and (3) 1.0×10^{-3} M, pH 1.0.

The distribution ratio D is defined as

$$D = [(H_3O^+)_{2-n}(H_nMo_6O_{19})^{(2-n)-}]_{org}/[(H_nMo_6O_{19})^{(2-n)-}].$$

Equation (1) can be expressed as the logarithmic form:

$$\log D = (2-n)\log[H_3O^+] + \log K_{ex}. \quad (2)$$

When $\log D$ is plotted against the $\log[H_3O^+]$, the value of $2-n$ can be obtained from the slope of the straight line. Figure 6 shows that the values of $2-n$ are 1.0, 1.4 and 1.4 for the concentrations 1.0×10^{-3}, 1.0×10^{-2} and 1.0×10^{-1} M, respectively. This implies that the value of $n = 1$ is reasonable for the lower concentration of molybdate (1.0×10^{-3} M), but with the higher concentrations of molybdate (1.0×10^{-2} and 1.0×10^{-1} M) both species of $H_3O^+(HMo_6O_{19})^-$ for $n = 1$ and of $(H_3O^+)_2Mo_8O_{19}^{2-}$ for $n = 0$ should be extracted because the intermediate value of $2-n = 1.4$ can be obtained by mixing with the cases of $2-n = 1$ and $2-n = 2$.

Figure 7 shows the extraction rate for three different solutions of molybdate. The extraction rate is generally slow except in suitably acidic and concentrated molybdate solutions. This is attributable to the formation of hexamolybdate in quite small amounts in the weak acidic solutions.[11] The cyclohexanone molecule dissolved in aqueous molybdate solution can produce the extractable hexamolybdate during the mixing process of two phases in the extraction, as mentioned in an earlier paper.[11] This is the reason why the coordinative donor solvents such as cyclohexanone, propylene carbonate and tri-*n*-butyl phosphate are effective in the extraction of hexamolybdate. These solvents are able to produce the extractable species to some extent in aqueous solution due to their coordinative donor properties.

Acknowledgement—The authors thank Dr Ozeki for obtaining the Raman spectra.

REFERENCES

1. C. Wadelin and M. G. Mellon, *Analyt. Chem.* 1953, **25**, 1668.
2. F. Umland and G. Wunsch, *Z. Anal. Chem.* 1969, **225**, 362.
3. K. Murata and S. Ikeda, *J. Inorg. Nucl. Chem.* 1970, **32**, 267.
4. K. Murata, E. Yamamoto and S. Ikeda, *Bull. Chem. Soc. Jpn* 1983, **56**, 941.
5. H. R. Fleck and A. M. Ward, *Analyst* 1933, **58**, 388.
6. P. L. Kronick and R. M. Fuoss, *J. Am. Chem. Soc.* 1955, **77**, 6114.
7. J. Aveston, E. W. Anacker and J. S. Johanson, *Inorg. Chem.* 1964, **3**, 735.
8. Y. Sasaki and L. G. Sillen, *Ark. Kemi.* 1968, **29**, 253.
9. G. A. Tsigdinos, *Bulletin Cdb-12a.* Climax Molybdenum Company, Greenwich, Connecticut (1969).
10. K. Tytko and O. Glenser, *Adv. Inorg. Chem. Radiochem.* 1976, **19**, 239.
11. K. Murata and S. Ikeda, *Spectrochim. Acta* 1983, **39A**, 787.
12. D. Tao, W. Song, P. Zhao, P. Wu and C. Xie, *Youkuangye* 1988, 7, 8.
13. G. K. Kulmukhamedov, A. N. Zelikman, G. V. Verevkin, I. M. Ivanov, V. I. Bushmakina and V. P. Zaitsev, *Tsvetn. Met.* 1989, 90.

14. T. Hirai and I. Komasawa, *Proc. Symp. Solvent Extr.* 1988, 193.
15. S. Kikuchi, H. Hattori and T. Mosaka, *Shigen to Sozai* 1989, **130**, 111.
16. T. Lee, W. Wang and G. Ting, *Solvent Extr. Ion Exch.* 1984, **2**, 435.
17. A. S. Vieux, Kabwa-wa-Bibombe and N. Nesele, *Hydrometallurgy* 1980, **6**, 35.
18. J. J. Cruywagen and T. Rypstra, *Polyhedron* 1985, **4**, 545.
19. R. Mattes, H. Bierbusse and J. Fucks, *Z. Anorg. Allg. Chem.* 1971, **385**, 230.

Polyhedron Vol. 9, No. 14, pp. 1723–1728, 1990
Printed in Great Britain

0277–5387/90 $3.00+.00
© 1990 Pergamon Press plc

SYNTHESIS AND CHARACTERIZATION OF NEW CARBOXYLATE DIMERS OF RUTHENIUM

M. C. BARRAL, R. JIMÉNEZ-APARICIO,* C. RIAL, E. ROYER, M. J. SAUCEDO and F. A. URBANOS

Departamento de Química Inorgánica, Facultad de Ciencias Químicas, Universidad Complutense, Ciudad Universitaria, 28040 Madrid, Spain

(*Received* 2 *January* 1990; *accepted* 22 *March* 1990)

Abstract—A series of $Ru_2Cl(\mu\text{-}O_2CR)_4$ [R = C_2H_5 (**I**), cyclo-C_6H_{11} (**II**), C_6H_5 (**III**), *o*-ClC_6H_4 (**IV**), *o*-HOC_6H_4 (**V**)] complexes has been synthesized by reaction of $Ru_2Cl(\mu\text{-}O_2CCH_3)_4$ with the appropriate carboxylic acid. The reaction of these insoluble compounds with $AgBF_4$ in thf gives $[Ru_2(\mu\text{-}O_2CR)_4(thf)_2]BF_4$ (**VI**)–(**X**) which are soluble in polar organic solvents. The substitution in these complexes of the thf axial ligands in toluene by $OPPh_3$ or pyridine leads to new adducts of the type $[Ru_2(\mu\text{-}O_2CR)_4L_2]BF_4$ [L = $OPPh_3$ (**XI**)–(**XV**), L = py (**XVI**)–(**XIX**)] which are not easily accessible by other methods. The compounds have been characterized by elemental analysis, electrical conductance, magnetic susceptibility measurements and spectral data.

The influence of the axial and equatorial ligands on the chemistry of compounds with metal–metal bonds has been studied in some detail for several metals like rhodium[1–3] or molybdenum,[1,3–6] but is less known for ruthenium compounds. Thus, although several diruthenium(II, III) carboxylate compounds[1,7–11] have been described, and some of their physical properties have been reported,[12–18] the reactivity of these species has been little studied.

It has been proved in electrochemical studies[10,12,19–22] that the nature of the bridge ligand has an important influence on the electron density of the bimetallic centre. On the other hand, we have shown[23] that the triphenylphosphine oxide ligand reacts with the $[Ru_2(\mu\text{-}O_2CCH_3)_4]^+$ unit, giving $[Ru_2(\mu\text{-}O_2CCH_3)_4(OPPh_3)_2]^+$, whereas the triphenylphosphine ligand makes the $[Ru_2(\mu\text{-}O_2CCH_3)_4]^+$ core unstable. We are now studying the influence of the equatorial ligands on the reactivity of the $[Ru_2(\mu\text{-}O_2CR)_4]^+$ core towards axial ligands. In the present work we report the synthesis and characterization of the new species $Ru_2Cl(\mu\text{-}O_2CR)_4$ (R = cyclo-C_6H_{11}, *o*-ClC_6H_4, *o*-HOC_6H_4) and the adducts $[Ru_2(\mu\text{-}O_2CR)_4(thf)_2]BF_4$ (R = C_2H_5, cyclo-C_6H_{11}, C_6H_5, *o*-ClC_6H_4, *o*-HOC_6H_4). We have also studied the reactions of these thf adducts with triphenylphosphine oxide and pyridine.

RESULTS AND DISCUSSION

The reaction of $Ru_2Cl(\mu\text{-}O_2CCH_3)_4$ in a methanol–water (1 : 1) mixed solvent under reflux with alkyl or aryl carboxylic acids, for example CH_3CH_2COOH, cyclo-$C_6H_{11}COOH$, C_6H_5COOH, *o*-ClC_6H_4COOH or *o*-HOC_6H_4COOH, led to the substitution of the acetate groups giving the corresponding $Ru_2Cl(\mu\text{-}O_2CR)_4$ derivatives. The yields were high in the cases of R = C_6H_5, *o*-ClC_6H_4 and *o*-HOC_6H_4, which are insoluble in methanol–water. When R = C_2H_5 and cyclo-C_6H_{11}, the products are soluble in the reaction mixture and the yield is lower.

The reaction of these compounds with $AgBF_4$ in thf led to the formation of $[Ru_2(\mu\text{-}O_2CR)_4(thf)_2]BF_4$ in high yield. In all cases brown crystals have been isolated from brown–red solutions, except for the *o*-hydroxybenzoate and cyclo-hexylcarboxylate derivatives in which brown crystals of the adducts were isolated from a green solution of another uncharacterized compound.

The complexes $[Ru_2(\mu\text{-}O_2CR)_4(thf)_2]BF_4$ exchange the thf ligands readily in toluene by

*Author to whom correspondence should be addressed.

$OPPh_3$ giving the corresponding $[Ru_2(\mu\text{-}O_2CR)_4(OPPh_3)_2]BF_4$ compounds. The same reaction carried out in thf led to a mixture of the reaction product and the starting material indicating competition of the thf ligand with the $OPPh_3$ ligand to occupy the axial positions of the $[Ru_2(\mu\text{-}O_2CR)_4]^+$ unit.

Stephenson and Wilkinson[7] have observed that the reaction of pyridine with $Ru_2Cl(\mu\text{-}O_2CCH_3)_4$ in pure pyridine led to the rupture of the ruthenium–ruthenium bonds and the formation of $Ru(O_2CCH_3)_2(py)_2$ and $Ru(O_2CCH_3)_2(py)_4$ compounds; in contrast, the reaction of $[Ru_2(\mu\text{-}O_2CR)_4(thf)_2]BF_4$ with pyridine in toluene gave brown solids identified as $[Ru_2(\mu\text{-}O_2CR)_4(py)_2]BF_4$ which contain the Ru_2^{5+} unit. In addition to the brown solid, a green solution which presumably contains a $Ru(O_2CR)_2(py)_2$ compound was obtained when R = cyclo-C_6H_{11}. When R = *o*-HOC_6H_4, the solubilities of $[Ru_2(\mu\text{-}O_2C(o\text{-}HOC_6H_4))_4(py)_2]BF_4$ and the green product were very similar, so the pyridine adduct could not be obtained pure. A large excess of pyridine led to a decrease in the yield of the pyridine adducts and an increase in the green product.

A similar adduct, $[Ru_2(\mu\text{-}O_2CC_3H_7)_4(py)_2]Cl$, has been obtained by Drago *et al.*[24] by addition of an excess of pyridine to $Ru_2Cl(\mu\text{-}O_2CC_3H_7)_4$ in dichloromethane.

Table 1 contains yields, elemental analyses and some physical properties of the compounds obtained.

The IR spectra of the complexes in KBr discs contain strong absorption bands in the region 1500–1350 cm^{-1}, which are due to the antisymmetric and symmetric stretching vibrations of the RCOO bridged ligands. The absorption bands due to R and BF_4 groups are also observed.

In addition, the IR spectra of $[Ru_2(\mu\text{-}O_2CR)_4L_2]BF_4$ (L = py or $OPPh_3$) compounds show the characteristic absorptions of pyridine or triphenylphosphine oxide ligands.

The most characteristic absorption bands in the IR spectra are summarized in Table 2.

In the $[Ru_2(\mu\text{-}O_2CR)_4(thf)_2]BF_4$ derivatives no bands due to the thf ligand are observed. Similar behaviour showing the facile loss of the weakly coordinated axial thf ligand has been observed in the complexes $Ru_2(\mu\text{-}O_2CCH_3)_4(thf)_2$[25] and $[Ru_2(\mu\text{-}O_2CCH_3)_4(thf)_2]BF_4$.[23]

The presence of the thf ligand is shown in the ^1H NMR spectra in DMSO-d_6 solution; in these spectra two signals at 1.85 and 3.75 ppm due to free thf are observed in all cases. In these conditions the thf ligand is exchanged by molecules of DMSO solvent, and the free thf is observed.

Magnetic measurements were carried out from room temperature to 70 K and indicated that these compounds obey the Curie–Weiss law in this temperature range. The magnetic moments are in the range 4.6–3.7 BM per dimer (Table 2), which are in accordance with the values obtained by several authors for Ru^{II}–Ru^{III} compounds.[7,8] The values are consistent with species containing three unpaired electrons per dimer in accordance with the ground electronic configuration of $\sigma^2\pi^4\delta^2(\pi^*\delta^*)^3$.[16] Table 3 shows the variation of the magnetic susceptibilities with the temperature for the cyclohexylcarboxylate derivatives. The magnetic behaviour of the other compounds is very similar.

The electronic spectra (range 200–800 nm) of the complexes, in methanol solution, show two absorption bands. The band near 430 nm is assigned to $\pi(Ru\text{—}O, Ru_2) \rightarrow \pi^*(Ru_2)$, in agreement with Norman *et al.*[16] and Miskowski and Gray;[15] this transition is not sensitive to change of the carboxylate ligands, as has previously been observed in similar compounds.[15] The absorption near 280 nm is assigned to π(axial ligand) $\rightarrow \pi^*(Ru_2)$; usually this transition is sensitive to the axial ligands, but in these cases no change can be observed. This may be due to compounds such as $[Ru_2(\mu\text{-}O_2CR)_4(MeOH)_2]^+$ being formed in methanol and the electronic spectrum is the same in each case. Only, in the pyridine derivatives, are some shoulders observed, indicating that the substitution of the axial pyridine ligands by methanol is not complete. In the $[Ru_2(\mu\text{-}O_2C(o\text{-}HOC_6H_4))_4L_2]BF_4$ (L = thf, $OPPh_3$) compounds very intense bands are observed in the region 220–300 nm which probably include the π(axial ligand) $\rightarrow \pi^*(Ru_2)$ and intraligand transitions.

The conductivity measurements are in accordance in all cases with 1 : 1 electrolytes[26] (Table 1).

The elemental analyses and physical and spectroscopic properties of $[Ru_2(\mu\text{-}O_2CR)_4L_2]BF_4$ compounds are in accordance with a structure containing the $[Ru_2(\mu\text{-}O_2CR)_4]^+$ unit with L (L = thf, $OPPh_3$, py) occupying the axial positions, similar to that described for $[Ru_2(\mu\text{-}O_2CCH_3)_4(H_2O)_2]BF_4$[18] and $[Ru_2(\mu\text{-}O_2CCH_3)_4(OPPh_3)_2]BF_4$[27] whose crystal structures have been determined.

In conclusion, the variation in the nature of the equatorial carboxylate ligands does not cause a great change in the reactivity of these species. In fact, the reactivity is similar in all cases and only in the reaction with pyridine is the behaviour different; in this case when R = C_2H_5 the reaction is clean and only the adduct was obtained; in the other cases, particularly, when R = *o*-HOC_6H_4, the formation of the adduct was accompanied by the formation of a green uncharacterized compound, probably $Ru[O_2C(o\text{-}HOC_6H_4)]_2(py)_2$. Finally, in

Table 1. Physical properties and yields of the obtained compounds

	Compound	Yield (%)	Analysis (%) Found (calc.)	μ(BM) 260 K	Λ_M[b]
II	$Ru_2Cl(\mu\text{-}O_2CC_6H_{11})_4$	65	C 45.2 (45.1) H 6.3 (5.9)	3.4	79.5[c]
IV	$Ru_2Cl(\mu\text{-}O_2C(o\text{-}ClC_6H_4)_4$	80	C 38.3 (39.1) H 2.1 (1.9)	3.9	[d]
V	$Ru_2Cl(\mu\text{-}O_2C(o\text{-}HOC_6H_4)_4$	80	C 42.4 (42.8) H 2.8 (2.6)	4.2	[d]
VI	$[Ru_2(\mu\text{-}O_2CC_2H_5)_4(thf)_2]BF_4$	80	C 31.6 (33.1) H 5.0 (5.0)	3.9	139.0[e]
VII	$[Ru_2(\mu\text{-}O_2CC_6H_{11})_4(thf)_2]BF_4$	50	C 45.4 (45.9) H 6.9 (6.4)	4.6	118.6[e]
VIII	$[Ru_2(\mu\text{-}O_2CC_6H_5)_4(thf)_2]BF_4$	65	C 45.6 (47.1) H 4.4 (3.9)	4.1	140.3[e]
IX	$[Ru_2(\mu\text{-}O_2C(o\text{-}ClC_6H_4))_4(thf)_2]BF_4$	50	C 39.4 (40.9) H 3.4 (3.1)	4.7	142.9[e]
X	$[Ru_2(\mu\text{-}O_2C(o\text{-}HOC_6H_4))_4(thf)_2]BF_4$	40	C 42.4 (44.0) H 3.8 (3.7)	4.3	106.5[e]
XI	$[Ru_2(\mu\text{-}O_2CC_2H_5)_4(OPPh_3)_2]BF_4$[a]	70	C 49.7 (48.1) H 4.2 (4.3)	4.3	132.0[e]
XII	$[Ru_2(\mu\text{-}O_2CC_6H_{11})_4(OPPh_3)_2]BF_4$	50	C 56.8 (56.7) H 5.4 (5.5)	3.8	107.0[e]
XIII	$[Ru_2(\mu\text{-}O_2CC_6H_5)_4(OPPh_3)_2]BF_4$	70	C 57.2 (57.8) H 4.0 (3.8)	4.6	134.9[e]
XIV	$[Ru_2(\mu\text{-}O_2C(o\text{-}ClC_6H_4))_4(OPPh_3)_2]BF_4$	40	C 51.7 (52.4) H 3.3 (3.2)	3.7	135.6[e]
XV	$[Ru_2(\mu\text{-}O_2C(o\text{-}HOC_6H_4))_4(OPPh_3)_2]BF_4$	30	C 55.0 (55.1) H 3.5 (3.6)	4.6	108.0[e]
XVI	$[Ru_2(\mu\text{-}O_2CC_2H_5)_4(py)_2]BF_4$[a]	40	C 32.2 (33.5) H 4.0 (3.9) N 2.7 (3.4)	3.7	138.0[e]
XVII	$[Ru_2(\mu\text{-}O_2CC_6H_{11})_4(py)_2]BF_4$	40	C 47.7 (47.7) H 5.8 (5.7) N 3.0 (2.9)	3.8	131.4[e]
XVIII	$[Ru_2(\mu\text{-}O_2CC_6H_5)_4(py)_2]BF_4$[a]	40	C 46.5 (46.1) H 3.2 (3.2) N 2.9 (3.0)	4.4	128.1[e]
XIX	$[Ru_2(\mu\text{-}O_2C(o\text{-}ClC_6H_4))_4(py)_2]BF_4$	30	C 42.2 (42.7) H 2.6 (2.5) N 2.6 (2.6)	4.3	134.5[e]

[a] Crystallized with one molecule of CH_2Cl_2.
[b] $\Omega^{-1}\,cm^2\,mol^{-1}$.
[c] In methanol solution ($\sim 10^{-3}$ M).
[d] Insoluble.
[e] In acetone solution ($\sim 10^{-3}$ M).

the reaction with $AgBF_4$ a lower yield of the *o*-hydroxybenzoate derivative was observed.

EXPERIMENTAL

All reactions were carried out in an inert atmosphere, using standard Schlenk techniques. $Ru_2Cl(\mu\text{-}O_2CCH_3)_4$ was prepared by the literature procedure.[28] $RuCl_3 \cdot 3H_2O$ (Engelhard), C_2H_5COOH (Fluka), cyclo-$C_6H_{11}COOH$ (Merck), C_6H_5COOH (Probus), *o*-ClC_6H_4COOH (Fluka), *o*-HOC_6H_4COOH (Probus), $AgBF_4$ (Fluka), $OPPh_3$ (Probus) and pyridine (Probus) were obtained from commercial sources. Solvents were purified and distilled by standard methods except methanol which was used without previous purification.

Elemental microanalyses for C, N and H were

Table 2. Spectral data for the compounds obtained

Compound	IR data (cm^{-1})				UV–vis data	
	ν(COO)	$\nu(BF_4)$	ν(P=O)	ν(py)	λ (nm)	ε ($dm^3\ mol^{-1}\ cm^{-1}$)
II	1460–1420 s				430	707
					250	3415
IV	1500–1350 s				Insoluble	
V	1480–1350 s				Insoluble	
VI	1460–1425 s	1070 s br			426	968
					278	2051
VII	1450–1420 s	1070 s br			428	790
					250	3619
VIII	1480–1350 s	1070 s br			434	644
					318	3219
IX	1460–1400 s	1070 s br			434	636
					314	3074
X	1490–1370 s	1070 s br			422 sh	1122
					312	20,784
					240	26,926
XI	1465–1440 s	1070 s br	1155 s		426	658
					278	1700
XII	1480–1400 s	1070 s br	1150 s		426	416
					248	3722
XIII	1490–1390 s	1070 s br	1135 s		434	646
					316	3225
XIV	1480–1390 s	1070 s br	1150 s		436	618
					314	3087
XV	1490–1370 s	1070 s br	1140 s		422 sh	1980
					312	30,506
					282 sh	21,890
XVI	1465–1435 s	1070 s br		1450 s	426	752
					278	1934
XVII	1480–1380 s	1070 s br		1445 s	422 sh	2287
				1210 s	352 sh	3698
					300 sh	4752
					244	13,757
XVIII	1500–1360 s	1070 s br		1450 s	406 sh	1064
				1220 w	322	3341
XIX	1480–1360 s	1070 s br		1445 s	398 sh	2568
				1215 w	298	4061
					250	3988

s—strong; br—broad; w—weak; sh—shoulder.

performed with a Perkin–Elmer 240 B microanalyser. IR spectra in the region 4000–200 cm^{-1} were recorded as KBr discs on a Perkin–Elmer 1330 IR spectrophotometer. Magnetic measurements were made with a magnetometer DSM 5 in the range 290–70 K. ^1H NMR spectra were obtained on a Varian XL-300 spectrometer. Electronic spectra in the region 200–800 nm were recorded on a Hewlett–Packard Vectra spectrophotometer. Molar conductivities were measured with a Philips PW 9526 digital conductivity meter using a Philips PW 9512/60 conductivity measuring cell.

Synthesis of $Ru_2Cl(\mu\text{-}O_2C_2H_5)_4$ **(I)**

To $Ru_2Cl(\mu\text{-}O_2CCH_3)_4$ (2 g, 4.2 mmol) in methanol–water (60 cm^3) (1 : 1) was added an excess of C_2H_5COOH (1.9 cm^3, 25.2 mmol). The reaction mixture was heated under reflux for 3 h giving a red–orange solution. This solution was filtered and

Table 3. Magnetic data at various temperatures for the cyclohexylcarboxylate compounds

	$Ru_2Cl(\mu\text{-}O_2CC_6H_{11})_4$									
T	229.5	199.8	174.9	150.2	125.2	100.5	90.6	85.5	80.5	76.5
$\chi_M\ 10^3$	8.741	9.644	10.58	11.95	13.44	15.09	15.92	16.37	16.84	17.02
μ	4.022	3.942	3.863	3.805	3.684	3.497	3.411	3.360	3.307	3.241
	$[Ru_2(\mu\text{-}O_2CC_6H_{11})_4(thf)_2]BF_4$									
T	259.3	229.2	199.7	175.0	150.2	125.2	100.4	90.5	80.5	75.5
$\chi_M\ 10^3$	10.20	11.26	12.72	14.18	16.02	18.40	22.44	24.55	27.60	28.20
μ	4.619	4.562	4.526	4.474	4.405	4.311	4.263	4.233	4.233	4.144
	$[Ru_2(\mu\text{-}O_2CC_6H_{11})_4(OPPh_3)_2]BF_4$									
T	259.3	229.7	199.9	175.0	150.2	125.3	100.5	90.6	80.5	72.3
$\chi_M\ 10^3$	7.106	9.411	11.22	14.06	16.57	19.60	22.72	26.19	29.06	31.65
μ	3.855	4.176	4.253	4.455	4.480	4.451	4.291	4.375	4.344	4.296
	$[Ru_2(\mu\text{-}O_2CC_6H_{11})_4(py)_2]BF_4$									
T	259.8	229.9	199.8	175.0	150.2	125.1	100.5	90.5	80.5	78.2
$\chi_M\ 10^3$	7.019	7.763	8.874	10.26	11.84	14.00	17.04	18.59	20.58	20.91
μ	3.835	3.794	3.782	3.805	3.787	3.758	3.717	3.684	3.655	3.632

concentrated under reduced pressure. On standing at room temperature brown crystals of $Ru_2Cl(\mu\text{-}O_2CC_2H_5)_4$ were formed. The crystals were washed twice with methanol–diethyl ether (10 cm^3) (1 : 1) and dried *in vacuo*.

Synthesis of $Ru_2Cl(\mu\text{-}O_2CC_6H_{11})_4$ **(II)**

This compound was obtained by the method described above.

Synthesis of $Ru_2Cl(\mu\text{-}O_2CC_6H_5)_4$ **(III)**

This compound was prepared by the method described by Das and Chakravarty.[10]

To $Ru_2Cl(\mu\text{-}O_2CCH_3)_4$ (2 g, 4.2 mmol) in methanol–water (60 cm^3) (1 : 1) was added an excess of C_6H_5COOH (3.08 g, 25.2 mmol). The mixture was heated under reflux for 4 h, giving a brown solid and a red–brown solution. The mixture was cooled to room temperature. The solution was filtered out and the brown solid of $Ru_2Cl(\mu\text{-}O_2CC_6H_5)_4$ was washed twice with methanol–diethyl ether (10 cm^3) (1 : 1) and dried *in vacuo*.

Synthesis of $Ru_2Cl(\mu\text{-}O_2CR)_4$ [R = *o*-ClC_6H_4 **(IV)**, *o*-HOC_6H_4 **(V)**]

These compounds were obtained by the method described above.

Synthesis of $[Ru_2(\mu\text{-}O_2CC_2H_5)_4(thf)_2]BF_4$ **(VI)**

A suspension of $Ru_2Cl(\mu\text{-}O_2CC_2H_5)_4$ (1 g, 1.8 mmol) in 40 cm^3 of thf was treated with $AgBF_4$ (0.35 g, 1.8 mmol) and the mixture was stirred for 12 h. The precipitate of AgCl was removed by filtration over celite. The solution was concentrated under reduced pressure to one-third of its initial volume, and petroleum ether was added to give orange crystals of $[Ru_2(\mu\text{-}O_2CC_2H_5)_4(thf)_2]BF_4$.

The analogous $[Ru_2(\mu\text{-}O_2CR)_4(thf)_2]BF_4$ compounds [R = cyclo-C_6H_{11} **(VII)**, C_6H_5 **(VIII)**, *o*-ClC_6H_4 **(IX)**, *o*-HOC_6H_4 **(X)**] were obtained by the same method.

Synthesis of $[Ru_2(\mu\text{-}O_2CC_2H_5)_4(OPPh_3)_2]BF_4$ **(XI)**

To a suspension of $[Ru_2(\mu\text{-}O_2CC_2H_5)_4(thf)_2]BF_4$ (1 g, 1.3 mmol) in toluene (50 cm^3) was added $OPPh_3$ (0.72 g, 2.6 mmol). The reaction mixture was stirred at room temperature overnight. The solvent was removed by filtration and the yellow–brown solid was washed twice with diethyl ether (10 cm^3).

The solid was crystallized from CH_2Cl_2–petroleum ether giving brown crystals of $[Ru_2(\mu\text{-}O_2CC_2H_5)_4(OPPh_3)_2]BF_4 \cdot CH_2Cl_2$.

The analogous $[Ru_2(\mu\text{-}O_2CR)_4(OPPh_3)_2]BF_4$ compounds [R = cyclo-C_6H_{11} **(XII)**, C_6H_5 **(XIII)**, *o*-ClC_6H_4 **(XIV)**, *o*-HOC_6H_4 **(XV)**] were obtained by a similar method.

Synthesis of $[Ru_2(\mu\text{-}O_2CC_2H_5)_4(py)_2]BF_4$ **(XVI)**

Pyridine (0.2 cm^3, 2.6 mmol) was added to a suspension of $[Ru_2(\mu\text{-}O_2CC_2H_5)_4(thf)_2]BF_4$ (1 g, 1.3 mmol) in 40 cm^3 of toluene. The mixture was stirred for 12 h at room temperature, and the pre-

cipitate was collected by filtration, washed twice with diethyl ether and dried *in vacuo*.

The analogous $[Ru_2(\mu\text{-}O_2CR)_4(py)_2]BF_4$ compounds [R = cyclo-C_6H_{11} (**XVII**), C_6H_5 (**XVIII**), *o*-ClC_6H_4 (**XIX**)] were obtained by the same procedure.

Acknowledgements—We are grateful to the Dirección General de Investigación Científica y Técnica (DGICYT) (Spain) for financial support (project PS87-0028). Thanks are due to Mr Fernández and Mr Rojas for their help in obtaining the magnetic measurements.

REFERENCES

1. F. A. Cotton and R. A. Walton, *Multiple Bonds Between Metal Atoms*. Wiley-Interscience, New York (1982).
2. T. R. Felthouse, *Prog. Inorg. Chem.* 1982, **29**, 73.
3. R. S. Drago and C. J. Bilgrien, *Polyhedron* 1988, **7**, 1453.
4. F. A. Cotton and D. G. Lay, *Inorg. Chem.* 1981, **20**, 935.
5. G. S. Girolami and R. A. Andersen, *Inorg. Chem.* 1982, **21**, 1318.
6. D. J. Santure and P. A. Sattelberger, *Inorg. Chem.* 1985, **24**, 3477.
7. T. A. Stephenson and G. Wilkinson, *J. Inorg. Nucl. Chem.* 1966, **28**, 2285.
8. M. Mukaida, T. Nomura and T. Ishimori, *Bull. Chem. Soc. Jpn* 1972, **45**, 2143.
9. P. Higgins and G. M. McCaan, *J. Chem. Soc., Dalton Trans.* 1988, 661.
10. B. K. Das and A. R. Chakravarty, *Polyhedron* 1988, **7**, 685.
11. F. A. Cotton, M. Matusz and B. Zhong, *Inorg. Chem.* 1988, **27**, 4368.
12. F. A. Cotton and E. Pedersen, *Inorg. Chem.* 1975, **14**, 388.
13. R. J. H. Clark and L. T. H. Ferris, *Inorg. Chem.* 1981, **20**, 2759.
14. V. M. Miskowski, T. M. Loehr and H. B. Gray, *Inorg. Chem.* 1987, **26**, 1098.
15. V. M. Miskowski and H. B. Gray, *Inorg. Chem.* 1988, **27**, 2501.
16. J. G. Norman Jr, G. E. Renzoni and D. A. Case, *J. Am. Chem. Soc.* 1979, **101**, 5256.
17. R. J. H. Clark and M. L. Franks, *J. Chem. Soc., Dalton Trans.* 1976, 1825.
18. A. Bino, F. A. Cotton and T. R. Felthouse, *Inorg. Chem.* 1979, **18**, 2599.
19. D. A. Tocher, *Inorg. Chim. Acta* 1986, **115**, 51.
20. T. Malinsky, D. Chang, F. N. Feldmann, J. L. Bear and K. M. Kadish, *Inorg. Chem.* 1983, **22**, 3225.
21. A. R. Chakravarty, F. A. Cotton, D. A. Tocher and J. H. Tocher, *Polyhedron* 1985, **4**, 1475.
22. M. Y. Chavan, F. N. Feldmann, X. Q. Lin, J. L. Bear and K. M. Kadish, *Inorg. Chem.* 1984, **23**, 2373.
23. F. A. Urbanos, M. C. Barral and R. Jiménez-Aparicio, *Polyhedron* 1988, **7**, 2597.
24. R. S. Drago, R. Cosmano and J. Telser, *Inorg. Chem.* 1984, **23**, 4514.
25. A. J. Lindsay, G. Wilkinson, M. Motevalli and M. B. Hursthouse, *J. Chem. Soc., Dalton Trans.* 1985, 2321.
26. W. J. Geary, *Coord. Chem. Rev.* 1971, **7**, 81.
27. M. C. Barral, R. Jiménez-Aparicio, E. C. Royer, C. Ruiz-Valero, F. A. Urbanos, E. Gutierrez-Puebla and A. Monge, *Polyhedron* 1989, **8**, 2571.
28. R. W. Mitchell, A. Spencer and G. Wilkinson, *J. Chem. Soc., Dalton Trans.* 1973, 846.

Polyhedron Vol. 9, No. 14, pp. 1729–1735, 1990
Printed in Great Britain

0277–5387/90 $3.00+.00
© 1990 Pergamon Press plc

SYNTHESIS, STRUCTURE AND ELECTROCHEMICAL BEHAVIOUR OF OCTAHEDRAL NICKEL(II) COMPLEXES WITH ONE 1,1-DITHIO AND ONE MACROCYCLIC LIGAND

R. VICENTE,* A. ESCUER and J. RIBAS

Departament de Química Inorgànica, Universitat de Barcelona, Diagonal 647, 08028-Barcelona, Spain

and

A. DEI

Dipartimento di Chimica, Università degli Studi di Firenze, Via Maragliano 75-77, 50144-Firenze, Italy

and

X. SOLANS and T. CALVET

Departament de Cristal.lografia i Mineralogia, Universitat de Barcelona, C/Marti Franqués s/n 08028-Barcelona, Spain

(*Received* 8 *November* 1989; *accepted* 26 *March* 1990)

Abstract—The synthesis and electrochemical behaviour of [Ni(DL-CTH)L](ClO_4) and [Ni(Cy)L′](ClO_4), where DL-CTH is the racemic isomer of 5,5,7,12,12,14-hexamethyl-1,4,8,11-tetraazacyclotetradecane, Cy is 1,4,8,11-tetraazacyclotetradecane (Cyclam), L is dimethyldithiocarbamate (Me_2Dtc), diethyldithiocarbamate (Et_2Dtc), pyrrolidindithiocarbamate (PyrrDtc), ethylxanthogenate (Etxant), thioacetate (Tac) and acetate (Ac) and L′ are the same ligands except Tac and Ac, are described. The structure of [Ni(DL-CTH)(Et_2Dtc)](ClO_4) is also reported. This complex crystallizes in the monoclinic space group $P2_1/a$ with cell parameters $a = 19.551(4)$, $b = 13.446(3)$, $c = 11.428(3)$ Å, $\beta = 95.54(3)°$ and $Z = 4$. The isolated [Ni(DL-CTH)(Et_2Dtc)]$^+$ cation shows a distorted *cis*-octahedral coordination around the nickel(II) ion. The electrochemistry of these compounds indicates oxidation processes but with decomposition of the organic part, giving nickel(II) species with, probably, polymeric dithio derivatives.

The chemistry of derivatives derived from nickel(II) and 1,1-dithio ligands has been extensively studied.[1,2] All these compounds have two 1,1-dithio ligands, giving square-planar geometries with some rare octahedral exceptions.[3,4] They have interesting properties from industrial,[1,2] electrochemical[5] and magnetic[1,2,6] points of view. On the other hand, the properties of the macrocyclic cations [Ni(DL-CTH)]$^{2+}$, [Ni(Cy)]$^{2+}$ and their derivatives have been extensively studied.[7,8] These square-planar macrocyclic compounds have the possibility of folding, principally when they react with chelate ligands, to yield octahedral mixed-ligand compounds. Starting from this kind of reaction it would be interesting to synthesize new 1,1-dithio complexes in which the presence of the macrocyclic ligand allows the coordination of only one 1,1-dithio derivative. We report here two series of these new octahedral nickel(II) compounds with 1,1-dithio ligands and the above mentioned Cyclam and

* Author to whom correspondence should be addressed.

DL-CTH derivatives, being, consequently, the first rare octahedral complexes with only one 1,1-dithio ligand. Acetate and thioacetate derivatives with $[Ni(DL\text{-}CTH)]^+$ have been also prepared, with the aim of comparing the properties of sulphur derivatives with the oxygen ones. Electrochemistry of these new compounds has been studied to analyse the electrochemical behaviour of complexes with this unusual coordination with only one 1,1-dithio ligand and to compare with the most common square-planar bis(1,1-dithioligand)Ni^{II}. Starting from the electrochemical properties of these ligands, we studied the stabilization of the coupled nickel(II)–organic radical, related to $[Ni(DL\text{-}CTH)L]^+$, with L being an O-donor ligand, previously reported.[8]

EXPERIMENTAL

Synthesis

The complex $[Ni(DL\text{-}CTH)](ClO_4)_2$ was prepared by the method described by Tait and Busch.[9] The complex $[Ni(Cy)](ClO_4)_2$ was prepared by the method described by Bosnich *et al.*[7b] Acetate, thio and dithio ligands (alkaline salts, Fluka) were used without purification.

CTH *derivatives.* Equimolar amounts of $[Ni(DL\text{-}CTH)](ClO_4)_2$ and the corresponding acetate, thioacetate or 1,1-dithioalkaline salt, dissolved in the minimum amount of water, were mixed. The yellow colour of the solution immediately changed to blue–green, and the adduct compounds precipitated within a few minutes.

Cyclam *derivatives.* The same procedure was used, but some differences were observed. After mixing the reagents, no change in the colour of solution was observed and a violet precipitate was gradually formed in 5–6 h (Me_2Dtc and Et_2Dtc) or 2 days for PyrrDtc. For L = Etxant, after 1 day, an unidentified precipitate was removed by filtration. After a further day with constant stirring, a violet precipitate was formed. Recrystallization of this latter compound in acetonitrile gave the new complex as a microcrystalline powder. All the compounds are insoluble in water but very soluble in acetone, methanol and acetonitrile. Yield 20% for $[Ni(Cy)(Etxant)](ClO_4)$ and 80–90% for the remaining compounds. Attempts to prepare acetate and thioacetate derivatives under the same conditions were unsuccessful. Analytical data are summarized in Table 1.

Crystal structure determination

A prismatic crystal ($0.1 \times 0.1 \times 0.2$ mm) was selected and mounted on a Philips PW-1100 four-circle diffractometer. Unit cell parameters were determined from automatic centring of 25 reflections ($4 \leqslant \theta \leqslant 12°$) and refined by least-squares methods. Intensities were collected with graphite monochromatized Mo-K_α radiation, using the ω-scan technique, with scan width 0.8°, scan speed 0.03° s^{-1}. 2456 reflections were measured in the range $2 \leqslant \theta \leqslant 25°$; 1700 of which were assumed as observed when applying the condition $I \geqslant 2.5\sigma(I)$. Three reflections were measured every 2 h as orientation and intensity controls, and no significant intensity decay was observed. Lorentz–polarization but no absorption corrections were made.

The structure was solved by direct methods, using the MULTAN system of computer programs,[10] and refined by full-matrix least-squares, using the SHELX76 computer program.[11] The function minimized was $\Sigma w[[F_o]-[F_c]]^2$, where $w = (\sigma^2(F_o) + 0.0018[F_o]^2)^{-1}$; f, f' and f'' were taken from the *International Tables for X-ray Crystallography.*[12] Fifteen peaks were located around the chlorine atom, which could be assigned as oxygen positions

Table 1. Analytical data [Calc.(Found)]

Compound	C	N	H
$[Ni(CTH)(Ac)](ClO_4)$	43.1(43.2)	11.2(11.0)	7.8(7.4)
$[Ni(CTH)(Tac)](ClO_4)$	41.8(42.2)	10.8(10.9)	7.6(7.7)
$[Ni(CTH)(Me_2Dtc)](ClO_4)$	40.5(39.9)	12.4(12.1)	7.5(7.3)
$[Ni(CTH)(Et_2Dtc)](ClO_4)$	42.7(43.2)	11.8(11.6)	7.8(7.6)
$[Ni(CTH)(PyrrDtc)](ClO_4)$	44.0(42.9)	11.6(11.6)	7.4(7.2)
$[Ni(CTH)(Etxant)](ClO_4)$	40.5(40.3)	9.9(9.8)	7.3(7.2)
$[Ni(Cy)(Me_2Dtc)](ClO_4)$	32.6(33.5)	14.6(14.8)	6.3(6.5)
$[Ni(Cy)(Et_2Dtc)](ClO_4)$	35.5(36.2)	13.8(13.8)	6.8(6.8)
$[Ni(Cy)(PyrrDtc)](ClO_4)$	37.2(36.5)	13.5(13.8)	6.2(6.1)
$[Ni(Cy)(Etxant)](ClO_4)$	32.6(32.9)	11.7(11.5)	6.1(6.2)

of the perchlorate ion, according to bond lengths; six of them were assigned an occupancy factor of 1/3 according to peak heights and the remaining nine were assigned an occupancy factor of 2/9. The position of all hydrogen atoms were computed and refined with an overall isotropic temperature factor, using a riding model, while the oxygen atoms were refined only isotropically, and the remaining non-hydrogen atoms anisotropically. The final R factor was 0.059 ($wR = 0.062$) for all observed reflections. Number of refined parameters = 356. Maximum shift/ESD = 0.2 in y of O(11); maximum and minimum peaks in final difference synthesis were 0.4 and -0.3 e Å^{-3}, respectively.

Crystal data for [Ni(DL-CTH)(Et_2Dtc)](ClO_4). $C_{21}H_{44}N_5S_2NiClO_4$, formula weight = 590.88, monoclinic, $a = 19.551(4)$, $b = 13.446(3)$, $c = 11.428(3)$ Å, $\beta = 95.54(3)°$, $V = 2990(2)$ Å^3, $P2_1/a$, $D_x = 1.308$ g cm^{-3}, $Z = 4$, $F(000) = 1256$, (Mo-K_α) = 0.71069 Å, μ(Mo-K_α) = 9.05 cm^{-1}, 298 K.

Physical measurements

IR spectra (4000–200 cm^{-1}) were recorded as KBr pellets with a Beckman IR-20A spectrophotometer. UV–vis spectra were recorded in acetonitrile solutions with a Perkin–Elmer 550-S spectrophotometer.

Voltammetric measurements were performed with the use of DACFAMOV 05-03 microcomputer controlled instrumentation with ohmic resistance compensation.[13] Rigorously deareated acetonitrile (Carlo Erba) was used as a solvent and (n-Bu_4N)PF_6 (0.1 M) as supporting electrolyte. Solutions were deaerated by means of a stream of nitrogen for 10 min and a nitrogen blanket was maintained above the solutions during the electrochemical measurements. Potentials were referred vs an Ag/AgCl (0.1 M KCl) electrode separated from the bulk of the solution by a medium porosity disc. The potential for the one-electron oxidation of ferrocene is 420 and 460 mV vs the Ag/AgCl (0.1 M KCl) electrode with or without ohmic resistance compensation, respectively. A platinum wire auxiliary electrode was used in conjunction with a platinum discs working electrode (TACUSSEL EDI rotating electrode, area 3.14 mm^2). Electrochemical oxidations were performed in acetonitrile with a platinum electrode using the same DACFAMOV 05-03 instrumentation but working at 0.2 V above the $E_{1/2}$.

EPR measurements were recorded with a Brucker ER-200 spectrometer working at X-band frequency.

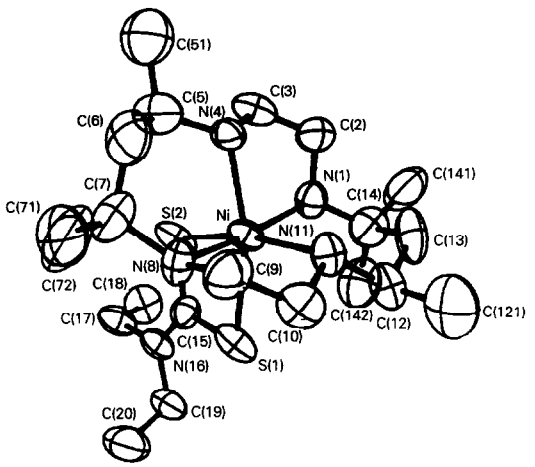

Fig. 1. Molecular structure of the [Ni(DL-CTH)(Et_2dtc)]$^+$ cation.

RESULTS AND DISCUSSION

Description of the structure

The crystal structure of [Ni(DL-CTH)(Et_2Dtc)](ClO_4) is formed from ClO_4^- and [Ni(DL-CTH)(Et_2Dtc)]$^+$ units, the latter showing a distorted *cis*-octahedral geometry around the nickel(II) ion. The structure of the cation is shown in Fig. 1, and the coordination environment of the nickel atom is shown in Fig. 2. Selected bond distances and angles are reported in Table 2.

The two sulphur atoms of the dithiocarbamate ligand occupy two *cis*-equatorial positions of the inner coordination sphere of the metal; the two Ni—S distances are 2.485(3) and 2.471(3) Å, which compare well with the values [2.449(3) and 2.448(2) Å] reported for the structure of the octahedral nickel–1,1-dithio compound bis(phenyldithioacetate)bis(pyridine)nickel(II).[3] These values are slightly longer than the same Ni—S distances

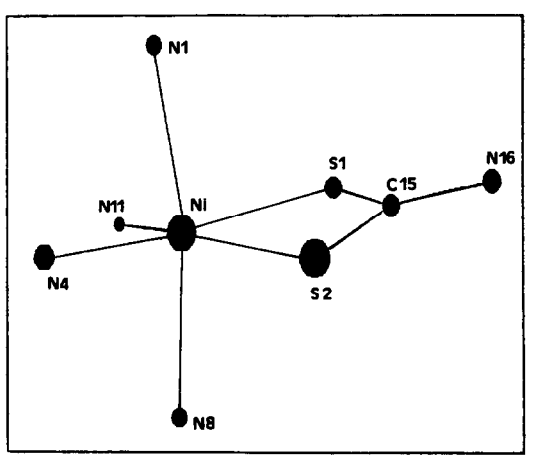

Fig. 2. Coordination environment of the nickel atom in the [Ni(DL-CTH)(Et_2dtc)]$^+$ cation.

Table 2. Bond lengths and angles for $C_{13}H_{26}N_5S_2Ni \cdot ClO_4$

S(1)—Ni	2.471(3)	C(72)—C(7)	1.599(20)
S(2)—Ni	2.485(3)	N(8)—C(7)	1.504(16)
N(1)—Ni	2.174(10)	C(9)—N(8)	1.511(15)
N(4)—Ni	2.142(8)	C(10)—C(9)	1.485(15)
N(8)—Ni	2.197(9)	N(11)—C(10)	1.509(14)
N(11)—Ni	2.134(9)	C(12)—N(11)	1.507(14)
C(15)—S(1)	1.705(11)	C(121)—C(12)	1.539(17)
C(15)—S(2)	1.724(11)	C(13)—C(12)	1.577(18)
C(2)—N(1)	1.475(14)	C(14)—C(13)	1.546(17)
C(14)—N(1)	1.478(15)	C(141)—C(14)	1.561(17)
C(3)—C(2)	1.472(16)	C(142)—C(14)	1.521(17)
N(4)—C(3)	1.474(15)	N(16)—C(15)	1.350(12)
C(5)—N(4)	1.486(15)	C(17)—N(16)	1.490(14)
C(51)—C(5)	1.504(17)	C(19)—N(16)	1.464(13)
C(6)—C(5)	1.483(17)	C(18)—C(17)	1.486(15)
C(7)—C(6)	1.507(20)	C(20)—C(19)	1.492(16)
C(71)—C(7)	1.548(18)		

S(2)—Ni—S(1)	71.8(1)	C(72)—C(7)—C(71)	105.4(13)
N(1)—Ni—S(1)	102.9(3)	N(8)—C(7)—C(6)	113.6(13)
N(1)—Ni—S(2)	87.1(3)	N(8)—C(7)—C(71)	110.7(13)
N(4)—Ni—S(1)	164.3(3)	N(8)—C(7)—C(72)	106.6(13)
N(4)—Ni—S(2)	94.7(3)	C(7)—N(8)—Ni	120.6(8)
N(4)—Ni—N(1)	83.7(4)	C(9)—N(8)—Ni	104.2(7)
N(8)—Ni—S(1)	86.5(3)	C(9)—N(8)—C(7)	112.7(11)
N(8)—Ni—S(2)	101.8(3)	C(10)—C(9)—N(8)	112.4(10)
N(8)—Ni—N(1)	168.8(4)	N(11)—C(10)—C(9)	107.9(10)
N(8)—Ni—N(4)	88.7(4)	C(10)—N(11)—Ni	105.0(7)
N(11)—Ni—S(1)	95.1(3)	C(12)—N(11)—Ni	116.5(7)
N(11)—Ni—S(2)	165.4(3)	C(12)—N(11)—C(10)	108.6(10)
N(11)—Ni—N(1)	89.6(4)	C(121)—C(12)—N(11)	110.3(11)
N(11)—Ni—N(4)	99.1(4)	C(13)—C(12)—N(11)	107.6(10)
N(11)—Ni—N(8)	83.4(4)	C(13)—C(12)—C(121)	109.2(11)
C(15)—S(1)—Ni	86.4(4)	C(14)—C(13)—C(12)	117.7(11)
C(15)—S(2)—Ni	85.5(4)	C(13)—C(14)—N(1)	112.1(11)
C(2)—N(1)—Ni	105.2(8)	C(141)—C(14)—N(1)	111.9(12)
C(14)—N(1)—Ni	120.9(8)	C(141)—C(14)—C(13)	105.3(12)
C(14)—N(1)—C(2)	112.0(10)	C(142)—C(14)—N(1)	108.9(11)
C(3)—C(2)—N(1)	109.7(11)	C(142)—C(14)—C(13)	111.5(13)
N(4)—C(3)—C(2)	112.4(11)	C(142)—C(14)—C(141)	107.1(12)
C(3)—N(4)—Ni	102.5(7)	S(2)—C(15)—S(1)	116.0(6)
C(5)—N(4)—Ni	115.9(7)	N(16)—C(15)—S(1)	122.4(8)
C(5)—N(4)—C(3)	114.7(10)	N(16)—C(15)—S(2)	121.6(8)
C(51)—C(5)—N(4)	112.2(13)	C(17)—N(16)—C(15)	122.9(9)
C(6)—C(5)—N(4)	110.7(11)	C(19)—N(16)—C(15)	120.7(10)
C(6)—C(5)—C(51)	107.7(13)	C(19)—N(16)—C(17)	116.5(9)
C(7)—C(6)—C(5)	118.9(13)	C(18)—C(17)—N(16)	112.3(11)
C(71)—C(7)—C(6)	109.7(13)	C(20)—C(19)—N(16)	110.8(10)

in the square-planar nickel–1,1-dithio derivatives (2.1–2.2 Å),[1,2] as a result of the high-spin nature of the nickel(II) ion.

The four nitrogen atoms of the CTH ligand occupy the two remaining equatorial and the two axial positions. The two axial bond distances, Ni—N(1) and Ni—N(8) are slightly longer than the equatorial ones, suggesting that the coordination polyhedron can be described as an elongated octahedron. The metal–nitrogen distances are in agreement with those of analogous *cis*-octahedral complexes of nickel(II) with CTH.[14–18]

Mean values for C—S bond distances, C(15)—S(1) = 1.705(11) Å and C(15)—S(2) = 1.724(11) Å, are slightly longer than in the case of bis(phenyldithiacetate)bis(pyridine)nickel(II)

(1.68(1) and 1.69(1) Å, respectively).[13] The C(15)—N(16) bond distance is equal to 1.350(12) Å, a value in the range of the C—N bond values found in the literature for analogous dithiocarbamate compounds.[1,2]

Finally, it is important to underline that the Ni—S(2)—S(1)—N(4)—N(11) plane is very distorted. For example, the N(8)—Ni—S(2) angle is 101.8(3)°, while N(8)—Ni—S(1) is 86.5(3)°; N(8)—Ni—N(4), 88.7(4)° and N(8)—Ni—N(11), 83.4(4)°. Moreover, the S(1)—Ni—S(2) angle is 77.8(1)°, much lower than the reported values for a square-planar environment in different bis(dithiocarbamato)nickel(II) complexes (between 78 and 79.5°)[1,9] but similar to the same angle in the other known octahedral complex (72°).[3]

IR and electronic spectra

IR spectra of the new complexes show the ν(N—H) bands at 2870 (m, sh), 2930 (s), 2970 (s) and 3230 (s) cm^{-1} for Ni(DL-CTH) derivatives and at 2860 (s), 2920 (s), 2960 (m, sh) and 3250 (s) cm^{-1} for Ni(Cyclam) derivatives. Additional bands centred at 1100 (s, broad) and 620 (s) cm^{-1} confirm the presence of the ClO_4^- anion. The ν(C—N) stretching band is observed at 1500 and 1485 cm^{-1} for the dimethyl and diethyl derivatives of Ni(CTH) and at 1500 and 1490 cm^{-1} for the same Ni(Cyclam) derivatives, respectively. These values indicate a certain amount of double bond character [ν(C=N) = 1690–1640 cm^{-1}; ν(C—N) = 1350–1250 cm^{-1}].[20] For the two [Ni(macrocycle)Etxant](ClO_4) complexes, bands at 1210 and 1050 cm^{-1}, characteristic of the C—O—C group[21] are observed.

Vis–UV spectra are summarized in Table 3. Visible spectra are all very similar, showing well defined *d–d* and metal to ligand charge-transfer bands. Bands at 550–600 nm and 364–368 nm may be assigned to *d–d* transitions of the octahedral nickel(II): $^3A_{2g} \rightarrow {}^3T_{1g}(F)$ and $^3A_{2g} \rightarrow {}^3T_{1g}(P)$. The intense absorptions in the UV region, are typical of charge-transfer bands, similar to those observed in the analogous square-planar nickel(II) compounds.[1,2] The similarity of the visible spectra allows us to assume that the geometry of all the complexes must be very similar to [Ni(DL-CTH)(Et$_2$Dtc)](ClO_4), whose molecular structure is known, i.e. distorted octahedral coordination around the nickel(II) ion.

Electrochemistry

The cyclic voltammogram for complexes with Me$_2$Dtc, Et$_2$Dtc and PyrrDtc show two oxidation couples in the range studied (0 → +2 V), the first being reversible and the second being irreversible. This second irreversible couple occurs at high potentials (over +1.2 V). The remaining complexes with Ac, Tac and Etxant show only one irreversible oxidation couple. Consequently, by replacing the sulphur donor atoms by more electronegative oxygen atoms or the replacement of the inner nitrogen atom linked to the carbon atom (dithiocarbamate) by oxygen (xanthogenate), produces a radical difference in their electrochemical behaviour. The positions of the first couples, peak width and the intensity ratio are shown in Table 4. All these new complexes do not present any couple in the reduction region (until −2 V). Instead, square-planar starting complexes [Ni(DL-CTH)](ClO_4)$_2$, [Ni(Cy)](ClO_4)$_2$ and [Ni(dithiocarbamate)$_2$] undergo both reduction and oxidation processes in acetonitrile.[11,13] In Fig. 3 one typical cyclic voltammogram for these kinds of complexes is shown.

After controlled oxidation of these complexes, the frozen acetonitrile solutions do not produce any signal in the EPR spectra. This feature may indicate that this oxidation does not affect the nickel(II) cation but only the organic part, which undergo a

Table 3. Electronic spectra of the new complexes in acetonitrile

Compound	λ (nm)			
[Ni(CTH)(Ac)](ClO_4)	576	364	304(sh)	212
[Ni(CTH)(Tac)](ClO_4)	582	368	260(sh)	220
[Ni(CTH)(Me$_2$Dtc)](ClO_4)	596	276	245	208
[Ni(CTH)(Et$_2$Dtc)](ClO_4)	595	278	248	210(sh)
[Ni(CTH)(PyrrDtc)](ClO_4)	598	273	246	208
[Ni(CTH)(Etxant)](ClO_4)	595	300		225
[Ni(Cy)(Me$_2$Dtc)](ClO_4)	558	276	242	208
[Ni(Cy)(Et$_2$Dtc)](ClO_4)	556	276	244	214
[Ni(Cy)(PyrrDtc)](ClO_4)	558	272	242	208
[Ni(Cy)(Etxant)](ClO_4)	552	300	238(sh)	220

Table 4. Cyclic voltammetry (acetonitrile)

Compound	Type	$E_{1/2}$	Width	Rel.
[Ni(CTH)(Ac)](ClO_4)	I	1.0		
[Ni(CTH)(Tac)](ClO_4)	I	1.0		
[Ni(CTH)(Me_2Dtc)](ClO_4)	R	0.686	0.076	1.04
[Ni(CTH)(Et_2Dtc)](ClO_4)	R	0.506	0.074	1.05
[Ni(CTH)(PyrrDtc)](ClO_4)	R	0.574	0.070	0.93
[Ni(CTH)(Etxant)](ClO_4)	I	0.900		
[Ni(Cy)(Me_2Dtc)](ClO_4)	R	0.507	0.067	1.13
[Ni(Cy)(Et_2Dtc)](ClO_4)	R	0.375	0.070	1.08
[Ni(Cy)(PyrrDtc)](ClO_4)	R	0.484	0.072	1.13
[Ni(Cy)(Etxant)](ClO_4)	I	0.805		

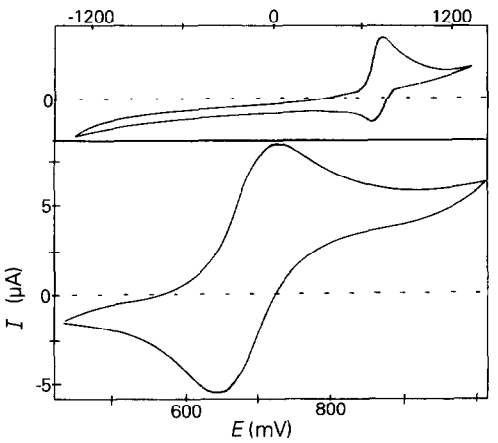

Fig. 3. Cyclic voltammogram of [Ni(DL-CTH)(Me_2dtc)](ClO_4) in acetonitrile solution (10^{-3} M) with 0.1 M (Bu_4N)PF_6 as electrolyte support (scan rate 0.1 V s^{-1}).

polymerization process, giving diamagnetic species. We can conclude, consequently, that if there is formation of organic radicals, these are unstable, even at low temperature.

CONCLUSIONS

New types of 1,1-dithio complex of nickel(II), with only one sulphur bidentate ligand and octahedral coordination, are synthesized and characterized by spectroscopic and X-ray measurements. These compounds show an unusual electrochemical behaviour: no reduction processes are present in the range 0 to −2 V, but one reversible couple appears between 0.375 and 0.686 V for the complexes with the R_2N–CS_2^- ligands. Attempts to obtain stable compounds by controlled oxidation were unsuccessful.

Acknowledgements—Financial assistance from the CICYT (Grant No. MAT88-0545) and from ACCION INTEGRADA HISPANO-ITALIANA No. 49, area 02 (1989), are acknowledged.

Supplementary Material Available. A listing of all bond distances and angles, final atomic coordinates, anisotropic thermal parameters, hydrogen atom coordinates and observed and calculated structure factors.

REFERENCES

1. D. Coucouvanis, *Prog. Inorg. Chem.* 1970, **11**, 233.
2. D. Coucouvanis, *Prog. Inorg. Chem.* 1979, **26**, 301.
3. M. Bonamico, G. Dessy, U. Fares, A. Flamini and L. Scaramuzza, *J. Chem. Soc., Dalton Trans.* 1976, 1743.
4. F. P. Emmenegger, *Inorg. Chem.* 1989, **28**, 2210 and refs therein.
5. A. M. Bond and R. L. Martin, *Coord. Chem. Rev.* 1984, **54**, 23.
6. R. P. Burns, F. P. McCullough and C. A. McAuliffe, *Adv. Inorg. Chem. Radiochem.* 1980, **23**, 211.
7. (a) F. Curtis, D. A. Swann and T. N. Water, *J. Chem. Soc.* 1973, 1963; (b) B. Bosnich, M. L. Tobe and G. A. Webb, *Inorg. Chem.* 1965, **4**, 1109; (c) L. G. Warner and D. H. Busch, *J. Am. Chem. Soc.* 1969, **91**, 4092.
8. C. Benelli, A. Dei, D. Gatteschi and L. Pardi, *Inorg. Chem.* 1988, **27**, 2831.
9. A. M. Tait and D. H. Busch, *Inorg. Synth.* 1976, **18**, 4.
10. P. Main, S. E. Fiske, S. L. Hull, L. Lessinger, G. Germain, J. P. Leclerc and M. M. Woolfson, MULTAN, An automatic system of computer programs for crystal sructure determination from X-ray diffraction data. University of York, U.K.; University of Lovain, Belgium (1984).
11. G. M. Sheldrick, SHELX, A computer program for crystal structure determination, University of Cambridge, U.K. (1976).
12. *International Tables for X-ray Crystallography*, Kynoch Press, Birmingham (1974).

13. P. Cassoux, R. Dartiguepeyron, P. L. Fabre and D. de Montauzon, *L'Actualité Chimique* 1985, 79; P. Cassoux, R. Dartiguepeyron, P. L. Fabre and D. de Montauzon, *Electrochim. Acta* 1985, **11**, 1485.
14. N. F. Curtis, D. A. Swann and T. N. Waters, *J. Chem. Soc., Dalton Trans.* 1973, 1408.
15. P. O. Whimp, M. F. Bailey and N. F. Curtis, *J. Chem. Soc. A*, 1970, 1956.
16. A. Bencini, A. Caneschi, A. Dei, D. Gatteschi, C. Zanchini and O. Kahn, *Inorg. Chem.* 1986, **25**, 1374.
17. H. Ito, J. Fujita, K. Toriumi and T. Ito, *Bull. Chem. Soc. Jpn* 1981, **54**, 2988.
18. H. Ito, K. Sugimoto and T. Ito, *Bull. Chem. Soc. Jpn* 1982, **55**, 1971.
19. P. W. G. Newman and A. H. White, *J. Chem. Soc., Dalton Trans.* 1979, 2239 and refs therein.
20. A. C. Fabetti, F. Forghieri, A. Giusti, C. Preti and G. Tosi, *Spectrochim. Acta* 1984, **40A**, 343.
21. M. L. Shankaranarayana and C. C. Patel, *Spectrochim. Acta* 1965, **21**, 95.
22. D. C. Olson and J. Vasilevskis, *Inorg. Chem.* 1969, **8**, 1611.
23. F. V. Lovecchio, E. S. Gore and D. H. Busch, *J. Am. Chem. Soc.* 1974, **96**, 3109.

Polyhedron Vol. 9, No. 14, pp. 1737–1740, 1990
Printed in Great Britain

0277–5387/90 $3.00+.00
© 1990 Pergamon Press plc

COMPLEXES OF THE PLATINUM METALS—XL.* HOMOLEPTIC TRIS(1,3-DIARYLTRIAZENIDO) COMPLEXES OF RUTHENIUM(III), OSMIUM(III), RHODIUM(III) AND IRIDIUM(III)

STEPHEN F. COLSON and STEPHEN D. ROBINSON†

Department of Chemistry, King's College London, Strand, London WC2R 2LS, U.K.

(*Received* 14 *March* 1990; *accepted* 2 *April* 1990)

Abstract—Homoleptic tris(triazenido) derivatives of ruthenium, osmium, rhodium and iridium, $M(ArNNNAr)_3$ (Ar = *p*-C_6H_4X; X = H, Me or Cl), have been prepared by treatment of the chlorides or chloro complexes—$RuCl_3$(aq.), $(NH_4)_2OsCl_6$(aq.), $RhCl_3$(aq.) and $(NH_4)_2IrCl_6$(aq.), respectively—with excess 1,3-diaryltriazene and triethylamine in boiling ethanol (M = Ru, Rh) or aqueous ethanol (M = Os, Ir). The sparingly soluble, air-stable, deep green (M = Ru, Os) or red–orange (M = Rh, Ir) complexes have been characterized by vibrational and NMR spectroscopy, and by magnetic measurements.

Since the discovery of 1,3-diaryltriazenes by Griess[2] in the mid-19th century the coordination chemistry of their conjugate bases, the 1,3-diaryltriazenide anions, has attracted sustained, albeit somewhat sporadic, interest.[3] Triazenide anions readily function as monodentate or bidentate—bridging or chelating—ligands in a wide range of complexes. However, work on simple homoleptic tris(triazenido) derivatives of the transition metals is remarkably sparse. Only four examples appear to be known, $Cr(PhNNNPh)_3$,[4,5] $Fe(PhNNNPh)_3$,[6] $Co(PhNNNPh)_3$,[7–9] and $Rh(p\text{-tolylNNNtolyl-}p)_3$,[10] and of these only the chromium(III) derivative has been fully characterized in the literature. The iron complex received only brief mention in a note on the general synthesis of transition metal triazenido complexes and, although the cobalt complex has been the subject of two independent X-ray diffraction studies,[8,9] details of its preparation and chemical or spectroscopic characterization do not appear to have been reported. The fourth member of the group $Rh(p\text{-tolylNNNtolyl-}p)_3$ received a passing mention some years ago in a paper from this laboratory, on the synthesis and characterization of some platinum group metal triazenido complexes containing phosphine and carbonyl ligands. Finally, while this paper was in preparation, tris(1,3-diphenyltriazenido) complexes of the p-block metals aluminium, gallium and indium analogous to the previously known indium(III) derivative[11] were reported.[12]

We now describe the synthesis and characterization of homoleptic 1,3-diaryltriazenido derivatives of ruthenium(III), osmium(III), rhodium(III) and iridium(III). Preliminary details of this work form part of the material disclosed in a recent note[13] on our current studies in the area of platinum metal triazene chemistry.

EXPERIMENTAL

General experimental techniques and conditions have been reported in an earlier paper.[14] Triazenes were prepared and purified by standard literature procedures.[15] Melting points and analytical data are given in Table 1 and spectroscopic data are collected in Table 2. Raman spectra were recorded using an argon ion laser source (5145 Å) for dark green samples and a krypton ion laser source (6471 Å) for red–orange samples.

Tris(1,3-*di*-p-*tolyltriazenido*)*ruthenium*(III)

A mixture of ruthenium trichloride trihydrate (0.2 g, 0.78 mmol), 1,3-di-*p*-tolyltriazene (1 g, 4.5 mmol) and triethylamine (1 g, 10 mmol) in ethanol (40 cm^3) was heated under reflux in a nitrogen atmo-

* For part XXXIX, see ref. 1.

† Author to whom correspondence should be addressed.

Table 1. Melting points[a] and analytical data[b]

Complex	Ar	Melting point (°C)	C	H	N
$Ru(ArNNNAr)_3$	p-C_6H_4Me	> 300	67.7 (65.1)[c]	5.6 (5.5)	15.8 (16.3)
$Ru(ArNNNAr)_3$	C_6H_5	219–221	65.1 (62.7)[c]	4.8 (4.4)	17.1 (18.2)
$Ru(ArNNNAr)_3$	p-C_6H_4Cl	> 300	49.4 (48.2)[c]	3.0 (2.7)	13.9 (14.0)
$Os(ArNNNAr)_3$	p-C_6H_4Me	> 300	60.1 (58.4)[c]	4.5 (4.9)	14.4 (14.6)
$Os(ArNNNAr)_3$	C_6H_5	250–253	55.5 (55.5)	4.0 (3.9)	16.2 (16.2)
$Os(ArNNNAr)_3$	p-C_6H_4Cl	> 300	44.6 (43.8)	2.6 (2.4)	12.9 (12.8)
$Rh(ArNNNAr)_3$	p-C_6H_4Me	> 300	64.5 (65.0)	5.4 (5.4)	16.3 (16.2)
$Rh(ArNNNAr)_3$	C_6H_5	244–245	62.6 (62.5)	4.3 (4.4)	18.0 (18.2)
$Rh(ArNNNAr)_3$	p-C_6H_4Cl	> 300	47.8 (48.1)	2.6 (2.7)	13.9 (14.0)
$Rh(ArNNNAr)_3$	p-C_6H_4OMe	245–247	57.6 (57.8)	4.7 (4.8)	13.8 (14.4)
$Ir(ArNNNAr)_3$	p-C_6H_4Me	> 300	57.7 (58.3)	4.6 (4.9)	13.9 (14.5)
$Ir(ArNNNAr)_3$	C_6H_5	274–277	55.3 (55.3)	3.6 (3.9)	15.6 (16.1)
$Ir(ArNNNAr)_3$	p-C_6H_4Cl	> 300	43.6 (43.8)	2.5 (2.4)	12.1 (12.7)

[a] Taken in sealed tubes under nitrogen.
[b] Calculated figures in parentheses.
[c] High carbon per cent thought to reflect up to 1 mol of benzene of solvation.

sphere for 3 h. After cooling, the solid product was filtered off, crystallized from benzene and washed successively with benzene, ethanol and diethyl ether, then dried *in vacuo* to afford dark green needle crystals (0.31 g, 51%).

The following were similarly prepared:

Tris(1,3-*diphenyltriazenido*)*ruthenium*(III) as dark green needle crystals (46.5%).
Tris(1,3-*di*-p-*chlorophenyltriazenido*)*ruthenium*(III) as dark green needle crystals (76.0%).

Tris(1,3-p-*tolyltriazenido*)*osmium*(III)

A mixture of ammonium hexachloro-osmate (0.2 g, 0.45 mmol), 1,3-di-*p*-tolyltriazene (0.6 g, 2.7 mmol) and triethylamine (4 g, 40 mmol) in ethanol (30 cm^3) and water (10 cm^3) was heated under reflux in a nitrogen atmosphere for 24 h. After cooling, the solid product was filtered off, crystallized from benzene and washed successively with benzene, ethanol and diethyl ether, then dried *in vacuo* to afford dark green needle crystals (0.15 g, 38%).

The following were similarly prepared:

Tris(1,3-*diphenyltriazenido*)*osmium*(III) as dark green needle crystals (37%).
Tris(1,3-*di*-p-*chlorophenyltriazenido*)*osmium*(III) as dark green needle crystals (31%).

Tris(1,3-*di*-p-*tolyltriazenido*)*rhodium*(III)

A mixture of rhodium trichloride trihydrate (0.2 g, 0.76 mmol), 1,3-di-*p*-tolyltriazene (0.75 g, 3.3 mmol) and triethylamine (2 g, 20 mmol) in ethanol (40 cm^3) was heated under reflux in a nitrogen atmosphere for 3 h. After cooling, the solid product was filtered off, crystallized from dichloromethane–ethanol and washed successively with ethanol and light petroleum, then dried *in vacuo* to afford orange microcrystals (0.27 g, 46%).

The following were similarly prepared:

Tris(1,3-*diphenyltriazenido*)*rhodium*(III) as maroon platelets (38%).
Tris(1,3-*di*-p-*chlorophenyltriazenido*)*rhodium*(III) as orange microcrystals (85%).
Tris(1,3-*di*-p-*methoxyphenyltriazenido*)*rhodium*(III) as red platelets (36.5%).

Tris(1,3-*di*-p-*tolyltriazenido*)*iridium*(III)

A mixture of ammonium hexachloro-iridate (0.2 g, 0.46 mmol), 1,3-di-*p*-tolyltriazene (0.6 g, 2.7 mmol) and triethylamine (4 g, 40 mmol) in ethanol (30 cm^3) and water (10 cm^3) was heated under reflux for 24 h in a nitrogen atmosphere. After cooling, the solid was filtered off, crystallized from dichloromethane–ethanol and washed successively with ethanol and light petroleum, then dried *in vacuo* to afford orange microcrystals (0.12 g, 31%).

The following were similarly prepared:

Tris(1,3-*diphenyltriazenido*)*iridium*(III) as orange microcrystals (33%).
Tris(1,3-*di*-p-*chlorophenyltriazenido*)*iridium*(III) as orange microcrystals (53%).

Table 2. Selected IR,[a] Raman[a] and ^{1}H NMR[b] spectroscopy data

Complex	Ar	IR data (cm^{-1})	Raman data (cm^{-1})	δ(aryl) (ppm)	δ(Me) (ppm)
$Ru(ArNNNAr)_3$	p-C_6H_4Me	1500(s) 1261(b,s)	1600(m) 1502(b,m) 1370(b,s)	Paramagnetic	
$Ru(ArNNNAr)_3$	C_6H_5	1478(s) 1256(b,s)	1589(m) 1490(b,m) 1358(b,s)	Paramagnetic	
$Ru(ArNNNAr)_3$	p-C_6H_4Cl	1481(s) 1257(b,s)	1582(m) 1485(m) 1362(b,s)	Paramagnetic	
$Os(ArNNNAr)_3$	p-C_6H_4Me	1500(s) 1265(b,s)	1600(m) 1500(b,m) 1368(b,s)	Paramagnetic	
$Os(ArNNNAr)_3$	C_6H_5	1480(s) 1259(b,s)	1589(m) 1488(b,m) 1360(b,s)	Paramagnetic	
$Os(ArNNNAr)_3$	p-C_6H_4Cl	1481(s) 1261(b,s)	1582(s) 1486(b,m) 1365(b,s)	Paramagnetic	
$Rh(ArNNNAr)_3$	p-C_6H_4Me	1500(s) 1280(b,s)	1602(m) 1504(b,m) 1370(b,s)	7.16(d) 6.97(d)	2.26(s)
$Rh(ArNNNAr)_3$	C_6H_5	1480(s) 1284(b,s)	1589(m) 1492(b,m) 1355(b,s)	7.29(d) 7.18(d of d) 7.6(t)	
$Rh(ArNNNAr)_3$	p-C_6H_4Cl	1481(s) 1288(b,s)	1584(s) 1486(b,m) 1371(b,s)		
$Rh(ArNNNAr)_3$	p-C_6H_4OMe			7.19(d) 6.73(d)	3.74(s)
$Ir(ArNNNAr)_3$	p-C_6H_4Me	1500(s) 1281(b,s)	1602(m) 1506(b,m) 1380(b,s)	7.12(d) 6.97(d)	2.25(s)
$Ir(ArNNNAr)_3$	C_6H_5	1481(s) 1283(b,s)	1590(m) 1495(b,m) 1370(b,s)	7.25(d) 7.17(d of d) 7.05(t)	
$Ir(ArNNNAr)_3$	p-C_6H_4Cl	1481(s) 1290(b,s)	1583(s) 1490(b,m) 1380(b,s)	7.19(d) 7.09(d)	

[a] s = strong, m = medium, b = broad.
[b] s = singlet, d = doublet, t = triplet.

RESULTS AND DISCUSSION

The ruthenium and rhodium tris(1,3-diaryltriazenido) complexes, $M(ArNNNAr)_3$, were obtained by heating a mixture of the free triazene, triethylamine and the appropriate hydrated metal chloride, $MCl_3 \cdot 3H_2O$, under reflux in ethanol for 3 h. The corresponding osmium and iridium complexes were similarly prepared from the hexachloro complex salts, $(NH_4)_2MCl_6 \cdot nH_2O$, in aqueous ethanol using a much longer reaction time (*ca* 24 h). The ruthenium and osmium products crystallized as dark green, paramagnetic needles from benzene. The rhodium and iridium complexes were obtained from dichloromethane–ethanol as red–orange (M = Rh) or orange (M = Ir) diamagnetic microcrystalline solids. All are stable and are sparingly soluble in benzene or chlorinated solvents (CH_2Cl_2, $CHCl_3$) but insoluble in water, ethanol, diethyl ether and light petroleum.

Triethylamine is added to the reaction mixtures to assist in deprotonation of the triazenes. However, by raising the pH of the reaction mixture it may also serve to inhibit the acidolysis reactions to which triazenes are susceptible. The rather modest yields obtained, particularly in the osmium and iridium based reactions which involved long reaction times, suggest that even in the presence of triethylamine degradation of the free triazene may be a problem.

The vibrational spectra—IR and Raman—for the complexes $M(ArNNNAr)_3$ are virtually identical for a given aryl group, and are consistent with the presence of chelate triazenido ligands.[16] Selected vibrations are listed in Table 2. Proton NMR data for the diagmagnetic rhodium and iridium complexes are also given in Table 2. Magnetic data for the paramagnetic ruthenium and osmium complexes (1.75–1.80 and 1.82–1.86 BM, respectively) are consistent with their formulations as low-spin d^5 ruthenium(III) and osmium(III) species.

Acknowledgements—We thank King's College for financial support given to S.F.C., Johnson Matthey plc for a generous loan of platinum metal salts, and the University of London Intercollegiate Research Service (ULIRS) Raman service at Imperial College for provision of Raman spectra.

REFERENCES

1. A. Sahajpal, S. D. Robinson, M. A. Mazid, M. Motevalli and M. B. Hursthouse, *J. Chem. Soc., Dalton Trans.* 1990, in press.
2. P. Griess, *Proc. R. Soc. (Lond.)* 1859, **9**, 594.
3. For a recent review of transition metal triazenido complexes see D. S. Moore and S. D. Robinson, *Adv. Inorg. Chem. Radiochem.* 1986, **30**, 1.
4. W. Seidel and H.-J. Mark, *Z. Anorg. Allg. Chem.* 1975, **416**, 83.
5. F. A. Cotton, G. W. Rice and J. C. Sekutowski, *Inorg. Chem.* 1979, **18**, 1143.
6. F.-E. Brinckman and H. S. Haiss, *Chem. Ind. (Lond.)* 1963, 1126.
7. M. Corbett and B. F. Hoskins, *Aust. J. Chem.* 1974, **27**, 665.
8. M. Corbett and B. F. Hoskins, *J. Am. Chem. Soc.* 1967, **89**, 1530.
9. W. R. Krigbaum and B. Rubin, *Acta Cryst.* 1973, **29B**, 749.
10. K. R. Laing, S. D. Robinson and M. F. Uttley, *J. Chem. Soc., Dalton Trans.* 1974, 1205.
11. D. St. C. Black, V. C. Davis, G. B. Deacon and R. J. Schultze, *Inorg. Chim. Acta* 1979, **37**, L528.
12. J. T. Leman, A. R. Barron, J. W. Ziller and R. M. Kren, *Polyhedron* 1989, **8**, 1909.
13. S. F. Colson and S. D. Robinson, *Polyhedron* 1988, **7**, 417.
14. P. A. Mura, B. G. Olby and S. D. Robinson, *J. Chem. Soc., Dalton Trans.* 1985, 2102.
15. A. J. Vogel, *Practical Organic Chemistry*, 3rd edn, p. 626. Longmans, London (1956).
16. S. D. Robinson and M. F. Uttley, *J. Chem. Soc., Chem. Commun.* 1971, 1315; 1972, 184.

Polyhedron Vol. 9, No. 14, pp. 1741–1746, 1990
Printed in Great Britain

0277–5387/90 $3.00+.00
© 1990 Pergamon Press plc

REDOX PROPERTIES OF IRON–SULPHUR–NITROSYL COMPLEXES: EXPLORATORY ELECTROCHEMISTRY OF MONONUCLEAR, DINUCLEAR AND TETRANUCLEAR COMPLEXES

JOSEPH A. CRAYSTON, CHRISTOPHER GLIDEWELL* and RONALD J. LAMBERT

Chemistry Department, University of St Andrews, St Andrews, Fife KY16 9ST, U.K.

(*Received* 9 *January* 1990; *accepted* 3 *April* 1990)

Abstract—Cyclic voltammetry shows two reversible, one-electron reductions for the neutral complexes $[Fe_2(SR)_2(NO)_4]$ (R = alkyl), to provide successively $[Fe_2(SR)_2(NO)_4]^-$ and $[Fe_2(SR)_2(NO)_4]^{2-}$. The paramagnetic complexes $[Fe_2(SR)_2(NO)_4]^-$, which can also be prepared by chemical reduction of neutral $[Fe_2(SR)_2(NO)_4]$, have been characterized by ESR spectroscopy: the complexes $[Fe_2(SR)_2(NO)_4]^{2-}$, which are isoelectronic with the substitution-labile cobalt complexes $[Co_2(SR)_2(NO)_4]$, undergo ready reaction with phosphorus ligands. The di-anion $[Fe_2S_2(NO)_4]^{2-}$ also exhibits two reversible, one-electron reductions, but for $[Fe_2(S_2O_3)_2(NO)_4]^{2-}$ only the first reduction is reversible. The tetranuclear complex $[Fe_4S_3(NO)_7]^-$ undergoes three reversible, one-electron reductions to yield $[Fe_4S_3(NO)_7]^{x-}$ (x = 2, 3 and 4). For all these complexes, the oxidation reactions are complex and irreversible. The neutral paramagnetic complexes $[Fe(NO)(S_2CNR_2)_2]$ (R = alkyl) all show a reversible one-electron reduction: the diamagnetic intermediates, which can also be prepared by chemical reduction, readily lose NO.

In recent work, we have described the reactions of iron–sulphur–nitrosyl complexes, such as $[Fe_2(SR)_2(NO)_4]$ and $[Fe_4S_3(NO)_7]^-$ with both nucleophiles[1] and electrophiles.[2] With the exception of the chemical and electrochemical reduction[3,4] of the related complex $[Fe_4S_4(NO)_4]$ to yield $[Fe_4S_4(NO)_4]^-$ and $[Fe_4S_4(NO)_4]^{2-}$ and of $[Fe_4S_2(NO)_4(NCMe_3)_2]$ to its mono-anion, the known[5] redox chemistry of such complexes is very sparse. Here we report the electrochemical properties of the neutral complexes $[Fe_2(SR)_2(NO)_4]$ (R = alkyl, C_1–C_4 and $[Fe(NO)(S_2CNR_2)_2]$ (R = alkyl, C_1–C_3) and of the anionic complexes $[Fe_2S_2(NO)_4]^{2-}$, $[Fe_2(S_2O_3)_2(NO)_4]^{2-}$ and $[Fe_4S_3(NO)_7]^-$.

EXPERIMENTAL

Previously described methods were used for the preparation of $[Fe_2(SR)_2(NO)_4]$,[6,7] $Na_2[Fe_2(S_2O_3)_2(NO)_4]$,[7] $(Bu_4N)_2[Fe_2(S_2O_3)_2(NO)_4]$,[7] $Na[Fe_4S_3(NO)_7]$,[8] $Me_3S[Fe_4S_3(NO)_7]$,[2] $Me_3SO[Fe_4S_3(NO)_7]$[2] and $[Fe(NO)(S_2CNR_2)_2]$.[2] $Na_2[Fe_2S_2(NO)_4]$[8] was prepared from $Na[Fe_4S_3(NO)_7]$ and converted to $(Et_4N)_2[Fe_2S_2(NO)_4]$ by metathesis (Found: C, 34.1; H, 7.3; N, 14.9. $C_{16}H_{40}Fe_2N_6O_4S_2$ requires: C, 34.5; H, 7.3; N, 15.1%). $(Et_4N)[Fe_4S_3(NO)_7]$ was prepared from $Na[Fe_4S_3(NO)_7]$ by metathesis (Found; C, 14.6; H, 2.7; N, 16.8. $C_8H_{20}Fe_4N_8O_7S_3$ requires: C, 14.6; H, 3.0; N, 17.0%). $(Bu_4N)[Fe_4S_3(NO)_7]$ was similarly obtained. Bu_4NPF_6 was recrystallized by addition of ethanol to a hot saturated aqueous solution: the product was dried at 110°C. $(MeO)_3P$, $(BuO)_3P$ and PPh_3 were purchased from Aldrich and were used as received. Solvents were dried and purified using standard methods.[9]

Cyclic voltammetry measurements were made at 25°C using a three-electrode cell equipped with either a platinum or glassy-carbon working electrode, a platinum counter electrode, and a silver reference electrode: an Amel model 553 potentiostat was coupled to an Amel model 567 wave function generator. The background electrolyte was 0.2 mol dm^{-3} $(C_4H_9)_4NPF_6$ and experimental solutions were 3×10^{-3} or 6×10^{-3} mol dm^{-3}. All EMF values are referred to the ferrocene/ferricinium

* Author to whom correspondence should be addressed.

couple;[10] in acetonitrile solution, the standard EMF of this couple, relative to the standard hydrogen electrode has been estimated[11] as +0.34 V. IR spectra were measured in THF solutions using a Perkin–Elmer model 1710 FTIR spectrometer. ESR spectra were measured in 1 mm quartz capillaries using a Bruker ER200D spectrometer, with di-*t*-butyl nitroxide as the standard for the measurement of line positions.

RESULTS AND DISCUSSION

Reduction of $[Fe_2(SR)_2(NO)_4]$

Solutions in tetrahydrofuran (THF) of the neutral complexes $[Fe_2(SR)_2(NO)_4]$ (R = Me, Et, *n*-Pr, *i*-Pr, *n*-Bu, *i*-Bu, *s*-Bu, *t*-Bu and CH_2COOCH_3) all undergo reversible reduction to mono- and di-anions. Cyclic voltammetry, using either glassy-carbon or oxidized platinum working electrodes at scan rates in the range 64–900 mV s^{-1}, showed two reversible, one-electron reductions, eq. (1):

$$[Fe_2(SR)_2(NO)_4] \rightleftharpoons [Fe_2(SR)_2(NO)_4]^- \rightleftharpoons [Fe_2(SR)_2(NO)_4]^{2-}. \quad (1)$$

Table 1 lists the corresponding $E^{\ominus}$ values, together with the mean diffusion coefficients. For the reduction to the mono-anion, the $E^{\ominus}$ values show a shift to more negative values as the electron donor properties of the R substituent increase: such behaviour was observed[12] with variation of the substitutent R in the tetranuclear clusters $[Fe_4S_4(SR)_4]^{2-}$. No such consistent trend was found for the rescond reduction, to the di-anions $[Fe_2(SR)_2(NO)_4]^{2-}$. A representative series of complexes, having R = Me, Et, *i*-Pr and *t*-Bu, were also studied in acetonitrile solution (Table 1): the variations in the $E^{\ominus}$ values closely follow the variations in THF solution, but the diffusion coefficients in THF are typically around one third the magnitude of those in acetonitrile. This attributed to the greater solvating capacity of THF.[13,14] From the $E^{\ominus}$ values, the equilibrium constants for the disproportionation equilibrium, eq. (2), were calculated (Table 1):

$$2[Fe_2(SR)_2(NO)_4]^- \overset{K_{disprop.}}{\rightleftharpoons} [Fe_2(SR)_2(NO)_4] + [Fe_2(SR)_2(NO)_4]^{2-}. \quad (2)$$

The values derived indicate that the mono-anions should be extremely stable to disproportionation, and indeed they were found to be long lived, in the absence of air. As expected from the very negative reduction potentials, the complexes $[Fe_2(SR)_2(NO)_4]^-$ are readily oxidized by air to the neutral species $[Fe_2(SR)_2(NO)_4]$.

Properties of $[Fe_2(SR)_2(NO)_4]^{x-}$

Reduction of THF solution of $[Fe_2(SMe)_2(NO)_4]$ with either sodium wire or $Li(BHEt_3)$ caused an immediate colour change from red–brown to deep green. Admission of air to the green solutions

Table 1. Redox properties of $[Fe_2(SR)_2(NO)_4]$

R	Solvent	$E^{\ominus}_{0\rightarrow -1}$ (V)[a]	$E^{\ominus}_{-1\rightarrow -2}$ (V)[a]	$D \times 10^6$ ($cm^2\ s^{-1}$)	$K_{disprop}$[b]
CH_3	THF	−1.050	−1.870	5.2	1.4×10^{-14}
	CH_3CN	−0.935	−1.595	17	6.9×10^{-12}
C_2H_5	THF	−1.074	−1.872	5.0	3.2×10^{-14}
	CH_3CN	−0.952	−1.610	21	7.5×10^{-12}
n-C_3H_7	THF	−1.075	−1.870	5.1	3.6×10^{-14}
n-C_4H_9	THF	−1.075	−1.877	3.8	2.7×10^{-14}
$CH_2CH(CH_3)_2$	THF	−1.085	−1.870	n.d.	5.3×10^{-14}
$CH(CH_3)_2$	THF	−1.095	−1.869	4.1	8.1×10^{-14}
	CH_3CN	−0.963	−1.625	16	6.4×10^{-12}
$CH(CH_3)C_2H_5$	THF	−1.088	−1.900	n.d.	1.9×10^{-14}
$C(CH_3)_3$	THF	−1.118	−1.825	3.6	1.1×10^{-12}
	CH_3CN	−0.975	−1.580	11	5.9×10^{-11}
CH_2COOCH_3	THF	−0.938	−1.718	3.3	6.4×10^{-14}

[a] Relative to ferrocene/ferricinium, at 25°C.
[b] See text, eq. (2).

allowed quantitative recovery of neutral $[Fe_2(SMe)_2(NO)_4]$. Bulk electrolysis in THF at −1.1 V relative to ferrocene/ferricinium, using Bu_4NPF_6 as background electrolyte, showed that the reduction was occurring with transfer of a single electron per $[Fe_2(SR)_2(NO)_4]$ unit and ESR examination of such an electrolysed solution, when R = Me, showed the presence of a single paramagnetic species having g at *ca* 1.99.

Reduction of a range of neutral complexes $[Fe_2(SR)_2(NO)_4]$ using excess $Li(BHEt_3)$ in THF gave in every case a green solution exhibiting a symmetric nine-line ESR spectrum (Table 2): for R = CMe_3, a second paramagnetic species was also present, having $g = 2.027$ and $A(^{14}N) = 2.7$ G, assigned as the known[1(a),5] complex $\{Fe(NO)_2(SCMe_3)_2\}^-$. The nine-line spectra showed no hyperfine coupling to α-hydrogen atoms in the R groups, and the relative intensities were consistent with hyperfine coupling to four equivalent $I = 1$ (^{14}N) nuclei: use of ^{15}N isotopic labelling caused the expected change to a five-line spectrum, with an increase of *ca* 40% in the $A(N)$ value. Consequently we assign the $g = 1.99$ species as $[Fe_2(SR)_2(NO)_4]^-$, in which the unpaired electron is delocalized such that the four nitrosyl ligands are equivalent. EHMO calculations on $\{Fe_2(SH)_2(NO)_4\}$ as a simple model for $[Fe_2(SR)_2(NO)_4]$ have shown[15] that the LUMO is concentrated primarily on the two irons, but also contains modest contributions from the nitrosyl ligands: the form of this orbital, which becomes the SOMO in $[Fe_2(SR)_2(NO)_4]^-$ can account[1(b),5] for the small $A(N)$ values observed in $\{Fe_2(SR)_2(NO)_4\}^-$.

The same reduced species, $[Fe_2(SR)_2(NO)_4]^-$, can be formed by reduction of neutral $[Fe_2(SR)_2(NO)_4]$ electrolytically, or with sodium or $Li(BHEt_3)$: the reduced species are long lived in the absence of air, and are quantitatively oxidized in air back to neutral $[Fe_2(SR)_2(NO)_4]$.

The behaviour of $[Fe_2(SR)_2(NO)_4]$ upon reduction may be contrasted with that of the closely analogous complex $[Fe_2(PPh_2)_2(NO)_4]$. This, upon reduction with sodium yields[16] $[Fe_2(PPh_2)_2(NO)_4]^{2-}$, the product of a two-electron transfer reaction; with $Li(BHEt_3)$, use of one equivalent provides the rearranged product $[(ON)_2Fe(\mu\text{-}PPh_2)(\mu\text{-}NO)Fe(NO)(PPh_2H)]^-$ in which hydride-transfer to phosphorus has occurred, while use of two equivalents converts this μ-NO complex to $[Fe_2(PPh_2)_2(NO)_4]^{2-}$. Thus under conditions in which chemical reduction of $[Fe_2(SR)_2(NO)_4]$ provides the mono-anion $[Fe_2(SR)_2(NO)_4]^-$, reduction of $[Fe_2(PPh_2)_2(NO)_4]$ provides the di-anion $[Fe_2(PPh_2)_2(NO)_4]^{2-}$.

The IR spectra of THF solutions of $[Fe_2(SR)_2(NO)_4]$ which had been reduced by excess $Li(BHEt_3)$ to form $\{Fe_2(SR)_2(NO)_4\}^-$ showed the characteristic pair of absorptions in the ν(NO) region to have been shifted by *ca* 100 cm^{-1} to lower energy, with the separation between the symmetric and asymmetric stretching frequencies of the $Fe(NO)_2$ fragments reduced from 25 to 20 cm^{-1} (Table 3). A similar shift was observed[16] upon reduction of $[Fe_2(PPh_2)_2(NO)_4]$ to $[Fe_2(PPh_2)_2(NO)_4]^{2-}$: in the neutral complex the ν(NO) absorptions occur at 1762 and 1748 cm^{-1} ($\Delta\nu = 14$ cm^{-1}), and for the di-anion there is a single, broad and presumably unresolved absorption at 1673 cm^{-1}. The ν-NO complex $[(ON)_2Fe(\mu\text{-}PPh_2)(\mu\text{-}NO)Fe(NO)(PPh_2H)]^-$ exhibits,[16] in addition to ν(NO) at 1420 cm^{-1} assigned to the bridging nitrosyl ligand, three absorptions assigned to terminal nitrosyl stretches at 1784, 1691 and 1651 cm^{-1}; it is probable, in view of the foregoing, that the 1670 and 1650 cm^{-1} absorptions arise from the terminal $Fe(NO)_2$ fragment.

When reduced solutions containing $[Fe_2(SR)_2(NO)_4]^-$ were aerated, in every case the low-frequency ν(NO) absorptions were cleanly and quantitatively replaced by the characteristic absorptions of the neutral complexes $[Fe_2(SR)_2(NO)_4]$.

The dinegative complexes $[Fe_2(SR)_2(NO)_4]^{2-}$ are 36-valence-electron species and are thus isoelectronic with the neutral cobalt complexes $[Co_2(SR)_2(NO)_4]$: these cobalt complexes have been shown[17] to be kinetically labile to ligand substitution. Thus $[Co_2(SPh)_2(NO)_4]$ undergoes rapid reaction at 25°C with two equivalents of PPh_3, to give the mononuclear complex $[Co(NO)_2(PPh_3)(SPh)]$ in almost quantitative yield. On the other hand, the neutral 34-valence-electron complex, $[Fe_2(SPh)_2(NO)_4]$, was found[17] to react only slowly with PPh_3, requiring forcing conditions, and providing $[Fe(NO)_2(PPh_3)_2]$ and Ph_2S_2 in a reduction involving both redox and substitution steps.

Table 2. ESR parameters for $[Fe_2(SR)_2(NO)_4]^-$ in THF solution at 250 K

R	g	$A(14N)$ (G)[a]
CH_3	1.994	1.4
C_2H_5	1.996	1.3
$n\text{-}C_3H_7$	1.996	1.0
$n\text{-}C_4H_9$	1.996	1.5
$CH(CH_3)C_2H_5$	1.996	1.5
$C(CH_3)_3$	1.995	1.5
CH_2COOCH_3	1.995	Not resolved

[a] $G = 10^{-4}$ T.

Table 3. Nitrosyl stretching frequencies for $[Fe_2(SR)_2(NO)_4]$ and $[Fe_2(SR)_2(NO)_4]^-$

R	$[Fe_2(SR)_2(NO)_4]$ ν(NO) (cm^{-1})	$[Fe_2(SR)_2(NO)_4]^-$ ν(NO) (cm^{-1})
CH_3	1776, 1751	1675, 1656
C_2H_5	1774, 1749	1674, 1655
n-C_3H_7	1774, 1749	1674, 1655
$CH_2CH(CH_3)_2$	1774, 1749	1674, 1655
$CH(CH_3)_2$	1773, 1748	1673, 1653
$C(CH_3)_3$	1771, 1745	1670, 1650

Lemoine[18] has recently introduced the concept of electron-induced nucleophilic substitution in reduced carbonyl clusters, and this suggested that substitution in $[Fe_2(SR)_2(NO)_4]$ by phosphorus nucleophiles could perhaps be accelerated by reduction of the iron complex to the 36-valence-electron di-anion: exploratory CV experiments appear to support this idea. For the couple $[Fe_2(SMe)_2(NO)_4]^-/[Fe_2(SMe)_2(NO)_4]^{2-}$ in THF, the ratio of i_A/i_c was reduced as aliquots of $P(OMe)_3$ were added: a linear relationship between i_a/i_c and added $P(OMe)_3$ was found throughout the region in which the ratio could be accurately measured ($1.0 \geqslant i_a/i_c > 0.4$). Extrapolation to $i_a/i_c = 0$ indicated a reaction stoichiometry $[Fe_2(SMe)_2(NO)_4]^{2-}$:$P(OMe)_3$ of 1:2. Similar stoichiometric ratios were found for the reactions between $[Fe_2(SEt)_2(NO)_4]^{2-}$ and $P(OMe)_3$ and between $[Fe_2(SCHMe_2)_2(NO)_4]^{2-}$ and $P(OBu)_3$. Further support for this concept may be derived from the preliminary report[19] that chemical reduction of $[Fe_2Cl_2(NO)_4]$ in the presence of either Ph_3P or $Ph_2PCH_2CH_2PPh_2$ yielded the neutral, d^{10} complexes, $Fe(NO)_2(phos)_2$ [phos = Ph_3P or $1/2(Ph_2PCH_2CH_2PPh_2)$].

Oxidation of $[Fe_2(SR)_2(NO)_4]$

For a range of complexes $[Fe_2(SR)_2(NO)_4]$ (R = Me, Et, *n*-Pr, *i*-Pr, *n*-Bu, *i*-Bu, *s*-Bu, *t*-Bu and CH_2COOCH_3), the oxidation is chemically irreversible, at both glassy-carbon and oxidized platinum electrodes, with E_p *ca*+1.1 V relative to ferrocene/ferricinium. In acetonitrile as solvent, a normal diffusion wave was observed with i_p proportional to $v^{1/2}$ for scan rates in the range 64–900 mV s^{-1}, but there was no reverse peak. A comparison of the i_p *vs* $v^{1/2}$ plots for the oxidation process with those for reduction of $[Fe_2(SR)_2(NO)_4]$ to $[Fe_2(SR)_2(NO)_4]^-$, for R = Me, Et, *i*-Pr and *t*-Bu, showed that in acetonitrile the number of electrons transferred, up to and including the rate limiting step of the irreversible process was 2.9. Further voltammetric scans showed no change from the initial scan, and no decomposition products were deposited on the electrode.

In dichloromethane as solvent, for all R studied, there was evidence for deposition of decomposition products on the electrode. If, after the oxidative step, the scan was repeated, the voltammogram collapsed: however, if the electrode was cleaned, or was taken to extreme negative potentials, and then scanned, the usual reduction waves were again observed. These observations indicate a deposit of decomposition product, removeable either mechanically or electrochemically. For the oxidation i_p was again proportional to $v^{1/2}$, showing that absorption occurs only after oxidation; the number of electrons transferred was determined as 2.8, similar to the value found in CH_3CN solutions.

The electron-transfer numbers above provide information only up to, and including, the rate limiting step, rather than providing a complete redox stoichiometry. The simplest oxidative decomposition which can be envisaged for $[Fe_2(SR)_2(NO)_4]$ would provide Fe^{2+}, RSSR and NO, corresponding to an overall four-electron oxidation.

Reduction of $[Fe_2(S_2O_3)(NO)_4]^{2-}$ *and* $[Fe_2(S_2O_3)_2(NO)_4]^{2-}$

Salts of Roussin's red anion, $[Fe_2S_2(NO)_4]^{2-}$, are cleanly and rapidly converted,[20,21] in CH_2Cl_2 solution, to salts of Roussin's black anion, $[Fe_4S_3(NO)_7]^-$: similar behaviour has now been observed in THF solutions. However, CH_3CN solutions are sufficiently stable to allow exploration of the redox properties of $[Fe_2S_2(NO)_4]^{2-}$. Two reversible, one-electron reductions were observed at a glassy-carbon electrode, eq. (3):

$$[Fe_2S_2(NO)_4]^{2-} \rightleftharpoons [Fe_2S_2(NO)_4]^{3-} \rightleftharpoons [Fe_2S_2(NO)_4]^{4-}. \quad (3)$$

The EMF values, relative to the ferrocene/ferricinium couple, are −1.08 and −1.68 V, respectively.

The μ-thiosulphato complex, $[Fe_2(S_2O_3)_2(NO)_4]^{2-}$, has recently been characterized,[7] in the solid state by X-ray crystallography, and in solution by ^{15}N NMR spectroscopy, using $[Fe_2(S_2O_3)_2(^{15}NO)_4]^{2-}$: the sodium salt is soluble in THF and the Bu_4N^+ salt in CH_2Cl_2. At a glassy-carbon elecrode, a THF solution of $Na_2[Fe_2(S_2O_3)_2(NO)_4]$ showed a reversible one-electron reduction at −1.310 V relative to ferrocene/ferricinium, corresponding to reduction to $[Fe_2(S_2O_3)_2(NO)_4]^{3-}$, but further reduction was only quasi-reversible for scan rates in the range 64–900 mV s^{-1}. In CH_2Cl_2 solution, at a platinum electrode, $(Bu_4N)_2[Fe_2(S_2O_3)_2(NO)_4]$ again showed a reversible one-electron reduction, at −1.276 V, but further reduction was wholly irreversible.

It is of interest that formation of a tetra-negative anion is reversible in the case of reduction of $[Fe_2S_2(NO)_4]^{2-}$ to $[Fe_2S_2(NO)_4]^{4-}$ [and of reduction of $[Fe_4S_3(NO)_7]^-$ to $[Fe_4S_3(NO)_7]^{4-}$ (see below)], but not for the reduction of $[Fe_2(S_2O_3)_2(NO)_4]^{2-}$, despite the apparently greater opportunity afforded for the delocalization of negative charge by the pendent S—SO_3 groups. Although the frontier orbitals calculated[7,15] for $[Fe_2S_2(NO)_4]^{2-}$ and for $[Fe_2(S_2O_3)_2(NO)_4]^{2-}$ are very similar, reduction of the thiosulphato complex to the tetra-negative anion could provide both an effective leaving group SO_3^{2-} and a stable residual cluster $[Fe_2S(S_2O_3)(NO)_4]^{2-}$.

Redox properties of $[Fe_4S_3(NO)_7]^-$

In THF solution, cyclic voltammetry of a range of salts $M^I[Fe_4S_3(NO)_7]$ ($M^I = Et_4N^+$, Bu_4N^+, Me_3S^+ or Me_3SO^+) at a glassy-carbon electrode showed reductive behaviour independent of the cation: for scan rates in the range 64–900 mV s^{-1}, three reversible, one-electron reductions were observed, with $E^\ominus$ values, relative to ferrocene/ferricinium of −1.31, −1.91 and −2.41 V, respectively, corresponding to eq. (4):

$$[Fe_4S_3(NO)_7]^- \rightleftharpoons [Fe_4S_3(NO)_7]^{2-} \rightleftharpoons [Fe_4S_3(NO)_7]^{3-} \rightleftharpoons [Fe_4S_3(NO)_7]^{4-}. \quad (4)$$

These EMF values show that, although very sensitive to aerial oxidation, the intermediate complexes, $[Fe_4S_3(NO)_7]^{2-}$ and $[Fe_4S_3(NO)_7]^{3-}$, are very stable to disproportionation: K values for the disproportionations described by eqs (5) and (6) are, respectively, 7.2×10^{-11} and 3.5×10^{-9}, implying considerable thermodynamic stability in the absence of oxygen.

$$2[Fe_4S_3(NO)_7]^{2-} \rightleftharpoons [Fe_4S_3(NO)_7]^- + [Fe_4S_3(NO)_7]^{3-} \quad (5)$$

$$2[Fe_4S_3(NO)_7]^{3-} \rightleftharpoons [Fe_4S_3(NO)_7]^{2-} + [Fe_4S_3(NO)_7]^{4-}. \quad (6)$$

For each of $Na[Fe_4S_3(NO)_7]$ in aqueous solution, $Et_4N[Fe_4S_3(NO)_7]$ in dichloromethane and $Me_3S[Fe_4S_3(NO)_7]$ in CH_3CN, the oxidation of the anion is a complex, multi-electron process which is chemically irreversible. From the peak current for the oxidation, when compared with the currents for the reductions described earlier, the number of electrons transferred was estimated as 8 ± 1: a value of 9 ± 1 was estimated for the analogous $Na[Fe_4Se_3(NO)_7]$ in acetonitrile. For the complete oxidative decomposition description by eq. (7), a total of nine electrons per anion are transferred:

$$[Fe_4X_3(NO)_7]^- \longrightarrow 7NO + 3X + 4Fe^{2+} + 9e^- \quad X = S, Se. \quad (7)$$

The overall waveform was indicative of the deposition of material on the electrode. Subsequent reduction of the absorbed material left the electrode clean, as judged by the subsequent repetition of the reduction to $[Fe_4S_3(NO)_7]^{x-}$ ($x = 2$, 3 and 4).

Redox properties of $[Fe(NO)(S_2CNR_2)_2]$

Solutions in THF of the neutral complexes $[Fe(NO)(S_2CNR_2)_2]$ (R = Me, Et, *n*-Pr) all exhibit a reversible, one-electron reduction, at platinum or glassy-carbon electrodes, eq. (8):

$$[Fe(NO)(S_2CNR_2)_2] \rightleftharpoons [Fe(NO)(S_2CNR_2)_2]^-. \quad (8)$$

The $E^\ominus$ values are −1.34, −1.39 and −1.38 V for R = Me, Et and *n*-Pr, respectively. Similar behaviour was observed in CH_2Cl_2, but in CH_3CN solutions, the ratio i_a/i_c was low at low scan rates, but approached unity as the scan rate increased. However, addition of free $[R_2NCS_2]^-$ to such solutions led to an increase in the i_a/i_c ratio, suggesting an equilibrium between the primary reduction product $[Fe(NO)(S_2CNR_2)_2]^-$ and its decomposition products, one of which is $[R_2NCS_2]^-$.

Chemical reduction of THF solutions of $[Fe(NO)(S_2CNR_2)_2]$ (R = Me or Et) using either sodium or $Li(BHEt_3)$ caused an immediate colour change from green to brown, accompanied by gas evolution. At the same time, the characteristic ESR spectrum disappeared: the diamagnetic nature of the reduction products was confirmed by the obser-

vation of clean ^{1}H NMR spectra. The IR spectra showed no trace of ν(NO).

These observations thus indicate that the neutral complexes $[Fe(NO)(S_2CNR_2)_2]$, in which the Fe—N—O group is linear,[1(b),22] undergo a one-electron reduction to give labile intermediates $[Fe(NO)(S_2CNR_2)_2]^-$ which are isoelectronic and thus presumably isostructural with neutral $[Co(NO)(S_2CNR_2)_2]$, where the Co—N—O group is non-linear[23] ($\angle$Co—N—O *ca* 135°). These intermediates readily lose NO to yield diamagnetic products.

Just as reduction of neutral $[Fe(NO)(S_2CNR_2)_2]$ yields a labile intermediate susceptible to NO loss, so too oxidation of neutral $[Co(NO)(S_2CNMe_2)_2]$,[24] by air, causes loss of NO, with formation of $[Co(S_2CNMe_2)_3]$. Despite the differing electron structures, $\{Co(NO)\}^8$ and $\{Fe(NO)\}$,[7] the complexes $[M(NO)(S_2CNMe_2)_2]$ (M = Co, Fe) show very similar electrochemical behaviour in THF, with a reversible, one-electron reduction, and an irreversible, one-electron oxidation.

Acknowledgements—We thank the Association for International Cancer Research for financial support, and Dr J. C. Walton for assistance in obtaining the ESR spectra.

REFERENCES

1. (a) A. R. Butler, C. Glidewell, A. R. Hyde and J. C. Walton, *Polyhedron* 1985, **4**, 797; (b) A. R. Butler, C. Glidewell, I. L. Johnson and J. C. Walton, *Polyhedron* 1987, **6**, 2085; (c) A. R. Butler, C. Glidewell and I. L. Johnson, *Polyhedron* 1987, **6**, 2091; (d) C. Glidewell and I. L. Johnson, *Polyhedron* 1988, **7**, 1371.
2. C. Glidewell, R. J. Lambert, M. E. Harman and M. B. Hursthouse, *J. Chem. Soc., Dalton Trans.*, 1990, in press.
3. C. T.-W. Chu, F. Y.-K. Lo and L. F. Dahl, *J. Am. Chem. Soc.* 1982, **104**, 3409.
4. C. T.-W. Chu, R. S. Gall and L. F. Dahl, *J. Am. Chem. Soc.* 1982, **104**, 737.
5. A. R. Butler, C. Glidewell and M.-H. Li, *Adv. Inorg. Chem.* 1988, **32**, 336.
6. A. R. Butler, C. Glidewell, A. R. Hyde, J. McGinnis and J. E. Seymour, *Polyhedron* 1983, **2**, 1045.
7. C. Glidewell, R. J. Lambert, M. B. Hursthouse and M. Motevalli, *J. Chem. Soc., Dalton Trans.* 1989, 2061.
8. G. Brauer (Ed.), *Handbuch der Präparativen Anorganische Chemie*, 2nd edn, Vol. 2. Enke, Stuttgart (1960).
9. D. D. Perrin, W. L. F. Armarego and D. R. Perrin, *Purification of Laboratory Chemicals*. Pergamon Press, Oxford (1966).
10. H. M. Koepp, H. Wendt and H. Strehlow, *Z. Elektrochem.* 1960, **64**, 483.
11. C. K. Mann and K. K. Barnes, *Electrochemical Reactions in Non-aqueous Systems*. Marcel Dekker, New York (1970).
12. V. DePamphilis, B. A. Averill, L. Que Jr and R. H. Holm, *J. Am. Chem. Soc.* 1974, **96**, 4159.
13. V. Gutmann, *Coordination Chemistry in Non-Aqueous Solvents*. Springer, New York (1968).
14. R. S. Drago, *Struct. Bond.* 1973, **15**, 75.
15. S.-S. Sung, C. Glidewell, A. R. Butler and R. Hoffmann, *Inorg. Chem.* 1985, **24**, 3856.
16. Y.-F. Yu, C.-N. Chau and A. Wojcicki, *Inorg. Chem.* 1986, **25**, 4098.
17. T. D. Weatherill, PhD thesis, University of Illinois at Urbana-Champaign, Urbana, Illinois (1985).
18. P. Lemoine, *Coord. Chem. Rev.* 1988, **83**, 169.
19. D. Ballivet, C. Billard and I. Tkatchenko, *Inorg. Chim. Acta* 1977, **25**, L58.
20. A. R. Butler, C. Glidewell, A. R. Hyde and J. McGinnis, *Inorg. Chem.* 1985, **24**, 2931.
21. C. Glidewell and I. L. Johnson, *Chem. Scripta* 1987, **27**, 441.
22. G. R. Davies, J. A. J. Jarvis, B. T. Kilbourn, R. H. B. Mais and P. G. Owston, *J. Chem. Soc. A* 1970, 1275.
23. J. H. Enemark and R. D. Feltham, *J. Chem. Soc., Dalton Trans.* 1972, 718.
24. O. A. Ileperuma and R. D. Feltham, *Inorg. Synth.* 1976, **16**, 7.

Polyhedron Vol. 9, No. 14, pp. 1747–1749, 1990
Printed in Great Britain

0277–5387/90 $3.00 + .00
© 1990 Pergamon Press plc

A NEW CHROMOPHORIC AND REDOX-RESPONSIVE IONOPHORE CONTAINING A TRICYANOVINYL MOIETY

PAUL D. BEER* and HARRISON SIKANYIKA

Department of Chemistry, University of Birmingham, P.O. Box. 363, Birmingham B15 2TT, U.K.

(*Received* 28 *February* 1990; *accepted* 3 *April* 1990)

Abstract—The treatment of tetracyanoethylene (**1**) with N-phenylaza-15-crown-5 (**3**) gives a new chromophoric and redox-responsive ionophore, **5**, containing a tricyanovinyl redox-active moiety. The electronic absorption spectrum of **5** exhibits hypochromic shifts on binding alkali and alkaline earth metal cations. Cyclic voltammetric electrochemical investigations reveal **5** to electrochemically recognize Na^+ and K^+ guest cations resulting in shifts of the tricyanovinyl reduction wave to more anodic potentials.

With regard to the future design and development of new molecular sensory devices considerable interest is being shown in the syntheses of redox-active macrocyclic receptor molecules that contain a redox centre in close proximity to a host binding site.[1] We[1–3] and others[4–7] have demonstrated that such systems can electrochemically recognize cationic (metal, ammonium[8]) and anionic[9] (bromide) guest species. Recently we reported the first example of *selective* electrochemical recognition of the potassium guest cation in the presence of equimolar amounts of sodium and magnesium ions by a novel ferrocenyl bis-benzo-crown ether ionophore.[10] This paper describes the synthesis, coordination and electrochemistry of a new type of redox-responsive ionophore which incorporates the redox-active and chromophoric tricyanovinyl group into a benzo-aza-crown ether macrocycle.

RESULTS AND DISCUSSION

Syntheses

Tetracyanoethylene (**1**) is known to react with both tertiary and secondary aromatic amines, to give 4-tricyanovinylamines.[11] These compounds have been shown to be brilliant red and blue dyes with strong affinity for hydrophobic fibres. Adaption of this simple synthetic methodology led to the preparation of the new chromophoric and redox-responsive ionophore, **5**.

The addition of N,N-dimethylaniline (**2**) or N-phenylaza-15-crown-5 (**3**) to **1** dissolved in dry dimethylformamide (DMF), instantly gave an intense blue-coloured solution, whereupon after gentle warming and work-up (see Experimental), dark blue crystals of **4** and **5**, respectively, were isolated in excellent yields (see Scheme 1).

The structures of **4** and **5** were characterized by elemental analysis, mass spectrometry, IR and ^1H NMR spectroscopy. Both tricyanovinylarylamines exhibited in their respective IR spectra, a band in the range 2240–2200 cm^{-1} characteristic of the —C≡N stretch.

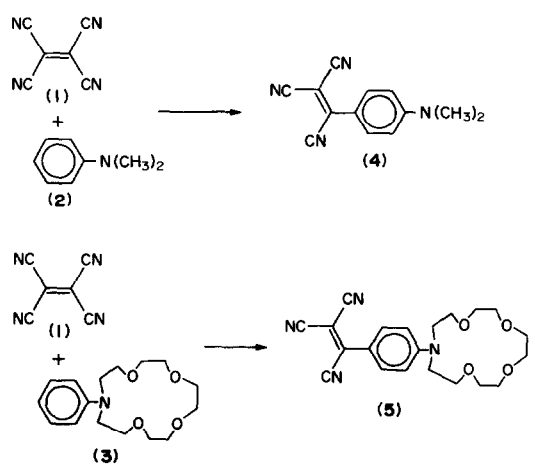

Scheme 1.

* Author to whom correspondence should be addressed.

Electronic studies

The UV–vis light absorption properties of **4** and **5** were investigated in acetonitrile, scanning from 700 to 190 nm. These 4-tricyanovinylarylamines absorb visible light very strongly, a property consistent with the highly conjugated structure assigned to them. For example, **4** dissolves in acetonitrile to give a deep red solution ($\lambda_{max} = 517$ nm; $\varepsilon = 40{,}000$). A similar intense red solution is produced with **5** ($\lambda_{max} = 515$ nm; $\varepsilon = 39{,}000$) and the spectrum for **5** was also recorded after addition of stoichiometric molar equivalents of Na^+, K^+ and Mg^{2+} cationic guests, Fig. 1. Significant hypochromic shifts of the intramolecular charge-transfer absorption of **5** occur upon addition of each metal cation. The magnitude of this shift increases in the order $K^+ < Na^+ < Mg^{2+}$. That a hypochromic shift is observed suggests binding of a metal cationic guest at the aza-crown ether receptor site inductively reduces the electron density at the tricyanovinyl moiety hence quenching the electronic $n \rightarrow \pi^*$ excitation. As pointed out by Vogtle and coworkers,[12] both the binding strength and the electrostatic effect of the particular metal cation are important factors in determining the magnitude of the spectral shift a cation induces upon complexation to a chromophoric crown ether. Of the two monocations studied, the Na^+ cation apparently features the optimum compromise between these factors and, therefore, induces a larger shift than the K^+ cation. As expected from electrostatic considerations, the shift induced by the Mg^{2+} dication exceeds those of the monocations.

Electrochemical studies

The electrochemical properties of **4** and **5** were investigated in acetonitrile using cyclic voltammetry with $[n\text{-}Bu_4N]BF_4$ as the supporting elecrolyte. The cyclic voltammograms were also recorded after progressive addition of stoichiometric equivalents of Na^+, K^+ and Mg^{2+} and the results obtained are presented in Table 1.

Both **4** and **5** undergo a reversible one-electron reduction process and on adding Na^+ or K^+ cationic guests to **5** the respective reduction wave shifts to more anodic potentials. With the same metal cation insignificant shifts ($\Delta E < 10$ mV) are observed with **4**. These observations suggest the binding of the metal cation at the aza-crown ether receptor site of **5** inductively withdraws electronic charge via the conjugated bond linkages from the tricyanovinyl redox-active moiety, thus making this redox centre easier to reduce. It is noteworthy that Na^+, having a larger charge/radius ratio than K^+, induces a larger magnitude of anodic shift. Surprisingly the addition of one equivalent of Mg^{2+} to **5**, although resulting in an anodic shift of the cathodic peak potential, the redox process becomes irreversible and the anodic wave is no longer seen.

Conclusions

A new redox-active and chromophoric ionophore, **5**, containing the tricyanovinyl group appended to a phenyl aza-crown ether has been prepared whose electronic absorption spectrum exhibits hypochromic shifts on binding Na^+, K^+ and Mg^{2+} guest cations. The electrochemical recognition of Na^+ and K^+ by this ionophore results in anodic shifts of the tricyanovinyl reduction wave.

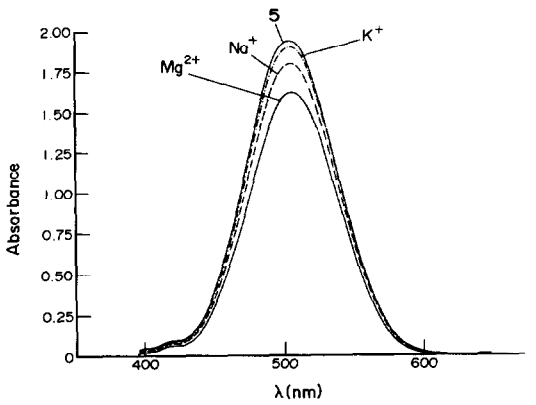

Fig. 1. The effect of Na^+, K^+ and Mg^{2+} (4 equiv.) on the visible absorption spectrum of **5** in acetonitrile at 21°C (concentration of **5** = 5.2×10^{-5} M).

Table 1. Electrochemical data

	4	**5**
$E_{1/2}$ (V)[a]	−0.64	−0.65
ΔE_p (mV)[b]	90	90
ΔE (Na^+) (mV)[c]	< 10	80
ΔE (K^+) (mV)[c]	< 10	20
ΔE (Mg^{2+}) (mV)	—	60[d]

[a] Obtained in acetonitrile solution containing 0.2 M $[n\text{-}Bu_4N]BF_4$ as supporting electrolyte. Potentials are quoted with reference to standard calomel electrode at 21 ± 1°C at 0.2 V s^{-1} scan rate.

[b] Separation between cathodic and anodic peak potentials of cyclic voltammograms; values for ferrocene under the same conditions ranged from 90 to 100 mV.

[c] Anodic shifts in reduction potential produced by presence of metal cation added as $MClO_4$ (4 equiv.).

[d] Anodic shift of the cathodic peak potential after addition of one equivalent of $Mg(ClO_4)_2$.

EXPERIMENTAL

Reactions were carried out under an atmosphere of dry nitrogen and solvents were distilled prior to use from an appropriate drying agent. ^{1}H NMR spectra were recorded at 400 and 270 MHz and ^{13}C NMR spectra at 100 and 67.8 MHz using tetramethylsilane (TMS) as internal standard. Microanalyses were performed by the Birmingham University Chemistry Department microanalytical service. Electrochemical measurements were performed using a PAR 174A polarographic analyser. Cyclic voltammetric measurements were carried out in acetonitrile solution containing 0.2 mol dm^{-3} [n-Bu_4N]BF_4 as supporting electrolyte using a platinum bead working electrode with ferrocene internal reference. Values are quoted relative to the saturated calomel reference electrode (SCE). Positive ion fast atom bombardment mass spectrometry was performed using a primary atom beam of argon (6 KeV) on a Kratos MS80 RF mass spectrometer coupled to a Kratos DS55 data system. UV and visible absorption spectra were recorded on a Schimadzu UV-240 spectrophotometer.

4-*Tricyanovinyl*-N,N′-*dimethylaniline* (**4**)

Tetracyanoethylene (TCNE) (**1**) (3.50 g, 0.027 mol) was added to a stirred solution of N,N-dimethylaniline (**2**) (12 cm^3, 0.095 mol) in dry DMF (15 cm^3) at 25–40°C. The mixture was stirred at 50–60°C for 20 min under N_2. The reaction mixture was poured on to ice-water (250 cm^3) and the precipitate was extracted with dichloromethane. After removal of the solvent, the residue was recrystallized twice from ethanol–pentane to yield **4** as deep blue crystals, 4.92 g (81%).

Melting point 172–174°C (lit.[11] 173–175°C), m/z 221. IR: 2220 cm^{-1} (—C≡N stretch). ^{1}H NMR ($CDCl_3$) δ: 3.23 (s, 6H, Me_2N), 6.75 (d, J = 9 Hz, 2H, ArH), 8.05 (d, J = 9 Hz, 2H, ArH). Found: C, 70.6; H, 4.2; N, 24.9. Calc. for $C_{14}H_{10}N_4$: C, 70.3; H, 4.5; N, 25.2%.

Compound **5** was prepared using the procedure described for **4** in 80% yield from TCNE (**1**) and N-phenylaza-15-crown-5 (**3**).

Melting point 130–132°C, m/z 369. IR: 2220 cm^{-1} (—C≡N stretch). ^{1}H NMR ($CDCl_3$) δ: 3.60–3.80 (m, 20H, crown-H), 6.70 (d, J = 9 Hz, 2H, ArH), 8.00 (d, J = 9 Hz, 2H, ArH). Found: C, 64.5; H, 6.4; N, 14.7. Calc. for $C_{21}H_{24}O_4N_4$: C, 63.6; H, 6.1; N, 14.1%.

Acknowledgements—We thank the British Council for financial support and the Research Corporation Trust, L. and D. Blond for additional equipment and consumable financial support.

REFERENCES

1. P. D. Beer, *Chem. Soc. Rev.* 1989, **18**, 409.
2. P. D. Beer, C. Blackburn, J. F. McAleer and H. Sikanyika, *Inorg. Chem.* 1990, **29**, 378.
3. P. D. Beer, H, Sikanyika, C. Blackburn, J. F. McAleer and M. G. B. Drew, *J. Organomet. Chem.* 1988, **350**, C15.
4. R. E. Wolf Jr. and S. R. Cooper, *J. Am. Chem. Soc.* 1984, **106**, 4646.
5. D. A. Gustowski, V. J. Gatto, L. Echegoyen and G. W. Gokel, *J. Am. Chem. Soc.* 1986, **108**, 7553.
6. T. Saji, *Chem. Lett.* 1986, 275.
7. E. Fu, J. Granell, M. L. H. Green, V. J. Lowe, S. R. Marder, G. C. Saunders and M. Tuddenham, *J. Organomet. Chem.* 1988, **355**, 205.
8. P. D. Beer, D. B. Crowe and B. Main, *J. Organomet. Chem.* 1989, **375**, C35.
9. P. D. Beer and A. D. Keefe, *J. Organomet. Chem.* 1989, **375**, C40.
10. P. D. Beer, H. Sikanyika, C. Blackburn and J. F. McAleer, *J. Chem. Soc., Chem. Commun.* 1989, 1831.
11. B. C. McKusick, R. E. Heckert, T. L. Cairns, D. D. Coffman and H. F. Mower, *J. Am. Chem. Soc.* 1958, **80**, 2806.
12. H. G. Lohr and F. Vogtle, *Accts Chem. Res.* 1985, 65.

Polyhedron Vol. 9, No. 14, pp. 1751–1756, 1990
Printed in Great Britain

0277–5387/90 $3.00 + .00
© 1990 Pergamon Press plc

HALODIOXORUTHENATE(VI) COMPLEXES AS CATALYSTS FOR THE OXIDATION OF ALCOHOLS

ANDREW C. DENGEL, WILLIAM P. GRIFFITH,* AHMED M. EL-HENDAWY† and JENNIFER M. JOLLIFFE

Inorganic Chemistry Laboratories, Imperial College of Science, Technology and Medicine, London SW7 2AY, U.K.

(*Received* 26 *March* 1990; *accepted* 3 *April* 1990)

Abstract—The new salts *trans*-(R-pyH)$_2$[RuO_2Cl_4] (R-py = pyridine and substituted pyridines), *trans*-R_2[RuO_2X_4] [X = Cl, Br; R = $Me_2NH(CH_2)_2NHMe_2$, $Me_2N(C_2H_4)_2NMe_2$]; (Ph_4P)[RuO_2Br_3], *trans*-(Ph_4P)$_2$[RuO_2Br_4] and *trans*-(Ph_4As)[$RuO_2Cl_3(OPPh_3)$] are reported. They function in dichloromethane or acetonitrile as two-electron catalysts for the oxidation of primary alcohols to aldehydes and of secondary alcohols to ketones, without competing olefinic bond cleavage, in the presence of N-methylmorpholine-N-oxide as co-oxidant. Vibrational spectra of the complexes are reported.

We have shown that oxo complexes of ruthenium(VI) are effective oxidants for alcohols, primary alcohols giving aldehydes[1–3] or carboxylic acids,[3,4] and secondary alcohols giving ketones,[1–4] often with good selectivity. In our earlier work on (Ph_4P)[RuO_2Cl_3] (prepared by the reaction of *trans*-[$RuO_3(OH)_2$]$^{2-}$ with excess HCl and Ph_4PCl) this was shown to be a mild and selective two-electron oxidant for alcohols;[3] the reagent was later used in a key step in the total synthesis of the natural product *iso*-drimeninol.[5] We were, however, unable to make the complex function catalytically at that time. We have shown recently that N-methylmorpholine-N-oxide (NMO) can be used as an efficient co-oxidant for [RuO_4]$^-$ [6] and for oxoruthenium(VI) complexes containing pyridine co-ligands,[1,2] and show here that [RuO_2Cl_3]$^-$, the new complexes [RuO_2Br_3]$^-$ and *trans*-[RuO_2Br_4]$^{2-}$, and also *trans*-[RuO_2Cl_4]$^{2-}$ (generated in solution[7] by adding excess Cl^- to [RuO_2Cl_3]$^-$) are efficient catalysts with NMO for the oxidation of alcohols with turnovers (turnover = mol product/mol catalyst) of up to 80 at room temperatures. New salts of *trans*-[RuO_2X_4]$^{2-}$ (X = Cl, Br), prepared by the passage of ruthenium tetraoxide vapour into a solution of a substituted pyridine or diamine in excess aqueous HX, can be used similarly as oxidation catalysts, as can the new triphenylphosphine oxide complex *trans*-(Ph_4As)[$RuO_2Cl_3(OPPh_3)$].

EXPERIMENTAL

Tetraphenylphosphonium dioxotrichlororuthenate (VI), (Ph_4P)[RuO_2Cl_3]

This was prepared by our earlier method[3] of adding excess Ph_4PCl and HCl to a basic solution of *trans*-[$RuO_3(OH)_2$]$^{2-}$ at 0°C.

Pyridinium and substituted pyridinium salts of trans-*dioxotetrachlororuthenate*(VI), trans-[RuO_2Cl_4]$^{2-}$

The preparation of *trans*-(4-^{t}BupyH)$_2$[RuO_2Cl_4] was typical. Ruthenium tetraoxide was generated as below from $RuO_2 \cdot nH_2O$ (0.75 g), $NaIO_4$ (2.75 g) and water (15 cm^3) and passed into an ice-cold solution of 4-^{t}butylpyridine (4-^{t}Bupy) (1.50 g, 11.1 mmol) in water (5 cm^3) and concentrated HCl (5 cm^3) until a dark red crystalline precipitate ceased to form. The solid was filtered off, washed with cold water (2 × 5 cm^3) and dried *in vacuo* immediately. The red salts *trans*-(R-pyH)$_2$[RuO_2Cl_4] [R-py = pyridine (py), 3-methylpyridine (3-Mepy), 3,4-dimethylpyridine (3,4-Me_2py), 8-hydroxyquinoline (8-

* Author to whom correspondence should be addressed.
† Present address: Department of Chemistry, Faculty of Science, Damietta, Egypt.

HQ) or 1,10-phenanthroline (phen)] were prepared similarly.

N,N,N′,N′-tetramethylpiperazonium dioxotetrahaloruthenate(VI), trans-$(Me_2N(C_2H_4)_2NMe_2)[RuO_2X_4]$ (X = Cl, Br)

The preparation of *trans*-$(Me_2N(C_2H_4)_2NMe_2)[RuO_2Cl_4]$ was typical. N,N,N′,N′-tetramethylpiperazonium dichloride was prepared from N,N,N′,N′-tetramethylethylenediamine and 1,2-dichloroethane by the method of Creighton and Taylor.[8] Ruthenium tetraoxide [generated as below from $RuO_2 \cdot nH_2O$ (0.50 g), $NaIO_4$ (1.80 g) and water (15 cm^3)] was passed into an ice-cold solution of $(Me_2N(C_2H_4)_2NMe_2)Cl_2$ (1.26 g, 3.0 mmol) in water (5 cm^3) and HCl (3 cm^3). The red crystalline product was filtered off, washed with cold water and dried *in vacuo*.

N,N,N′,N′-tetramethylethylenediammonium dioxotetrahaloruthenate(VI), trans-$(Me_2NH(CH_2)_2NHMe_2)[RuO_2X_4]$ (X = Cl, Br)

The preparation of *trans*-$(Me_2NH(CH_2)_2NHMe_2)[RuO_2Br_4]$ was typical. Ruthenium tetraoxide was generated as below [$RuO_2 \cdot nH_2O$ (0.50 g), $NaIO_4$ (1.8 g), water (15 cm^3)] and passed into an ice-cold solution of N,N,N′,N′-tetramethylethylenediamine (0.46 g, 4.0 mmol) in water (6 cm^3) and HBr (48%, 3.5 cm^3). The red crystalline product was filtered off, washed with cold water and dried *in vacuo*.

Tetraphenylphosphonium dioxotetrabromoruthenate(VI), trans-$(Ph_4P)_2[RuO_2Br_4]$

$(Ph_4P)[RuO_2Br_3]$ (0.20 g) was dissolved in dichloromethane (10 cm^3) and carbon tetrachloride (Analar grade; 1 cm^3). The green solution was reduced in volume until red in colour, and left at room temperature overnight. Red crystals of *trans*-$(Ph_4P)_2[RuO_2Br_4]$ appeared and were filtered off, washed with cold water and dried in a vacuum desiccator over silica gel.

Tetraphenylphosphonium dioxotribromoruthenate (VI), $(Ph_4P)[RuO_2Br_3]$

Ruthenium tetraoxide was generated by a method based on that of Nakata,[9] in which hydrated ruthenium dioxide ($RuO_2 \cdot nH_2O$; 1.5 g) was vigorously stirred with sodium periodate (5.5 g) in water (25 cm^3). It was passed into CCl_4 (Analar grade; 150 cm^3) using a stream of N_2 gas, and the resulting yellow solution was stirred overnight in a stoppered flask with 2.5 M NaOH solution. The red aqueous layer, containing the ruthenate ion, *trans*-$[RuO_3(OH)_2]^{2-}$, was separated and cooled to 0°C. To 10 cm^3 of this solution was added Ph_4PBr (1.05 g, 2.5 mmol) with stirring, followed by HBr (48%) dropwise until precipitation of an olive-green solid was complete. The solid was filtered off, washed with cold water (2 × 5 cm^3) and dried *in vacuo*.

Tetraphenylarsonium dioxotrichlorotriphenylphosphine oxide ruthenate(VI), trans-$(Ph_4As)[RuO_2Cl_3(OPPh_3)]$

Ruthenium tetraoxide was generated as above [$RuO_2 \cdot nH_2O$ (0.25 g), $NaIO_4$ (1.0 g) and water (15 cm^3)] and passed into a solution of triphenylphosphine (0.13 g, 0.05 mmol) and $Ph_4AsCl \cdot HCl \cdot H_2O$ (0.50 g, 0.10 mmol) in a minimum quantity of acetonitrile. After 3 h, the brown–green solution was reduced in volume, whereupon red–brown crystals appeared. These were filtered off, washed with diethyl ether and dried in a vacuum desiccator over silica gel.

Stoichiometric and catalytic oxidations

(i) *Stoichiometric.* The oxidation of *p*-methoxybenzyl alcohol by *trans*-$(4\text{-}^tBupyH)_2[RuO_2Cl_4]$ was typical. A stirred solution of *p*-methoxybenzyl alcohol (0.07 g, 0.51 mmol; a slight excess) in dichloromethane (5 cm^3) containing powdered 4 Å molecular sieves (0.25 g) was treated with *trans*-$(4\text{-}^tBupyH)_2[RuO_2Cl_4]$ (0.27 g, 0.50 mmol). After 2 h at room temperature the reaction solution was diluted with dichloromethane, filtered, washed with 1 M sodium thiosulphate solution (to remove the reduced ruthenium products), and dried over anhydrous $MgSO_4$. The solution was filtered, evaporated to dryness and the organic product either dissolved in minimum ethanol (for quantification as the 2,4-dinitrophenylhydrazone derivative), or in 10 : 1 petroleum ether (40–60°C) : ethyl acetate and purified by column chromatography (silica gel H) (for determination of yield by isolation and ^1H NMR study).

(ii) *Catalytic.* A similar procedure to that used in the stoichiometric oxidations was employed, except that a three-fold excess of NMO (with respect to the alcohol substrate) was added, and that a catalytic amount (10^{-2}–10^{-1} mmol) of the ruthenium oxidant was used. At the end of the 2 h reaction the dichloromethane solution was also washed with a saturated solution of copper(II) sulphate in order to remove NMO and its reduced products.

(iii) *Oxidations involving* $[RuO_2Cl_3]^-$ *and an excess of* Cl^-. The same procedure as in (ii) was used, with the addition of a 40-fold excess of tetra-

ethylammonium chloride, Et_4NCl. The green solution of $[RuO_2Cl_3]^-$ changed colour to red upon addition of the excess chloride, indicating formation in solution of the *trans*-$[RuO_2Cl_4]^{2-}$ species, as noted by Perrier and Kochi.[7] The alcohol was then added, along with excess NMO in the case of catalytic reactions.

General experimental

Carbon, hydrogen, nitrogen and halogen analyses were performed by Mr K. Jones of the Imperial College Microanalytical Department. Raman spectra were run as pressed discs with KBr supports on a Spex Ramalog V instrument with 5682 and 6471 Å krypton-ion excitation from a Coherent Radiation Innova 90 laser, and 5145 Å argon-ion excitation from a Coherent Radiation Innova 70 laser. IR spectra were recorded on a Perkin-Elmer 1720 (FT–IR) instrument as liquid paraffin mulls between KBr or CsI plates. ^1H NMR spectra were recorded on a Jeol 270 (FT) spectrometer, and UV–vis spectra on a Philips PU 8740 spectrometer using 10 mm quartz glass cells. In oxidation experiments the 2,4-dinitrophenylhydrazone derivatives were prepared using a saturated methanolic solution of 2,4-dinitrophenylhydrazine (acidified with sulphuric acid) and were compared with authentic samples.

RESULTS AND DISCUSSION

(a) *Oxidation studies*

In Table 1 we summarize our work on the oxidation of 11 alcohols, seven primary (of which four are unsaturated) and four secondary. Results are given for catalytic oxidations with $(Ph_4P)[RuO_2Cl_3]$; catalytic oxidations with $(Ph_4P)[RuO_2Cl_3]$ and an excess of chloride; stoichiometric and catalytic oxidations with *trans*-(4-^{t}BupyH)$_2$[RuO_2Cl_4] (the most organic soluble of the dioxotetrachlororuthenate(VI) salts); and catalytic oxidations with *trans*-$(Ph_4P)_2[RuO_2Br_4]$ and *trans*-$(Ph_4As)[RuO_2Cl_3(OPPh_3)]$. All oxidations were carried out at room temperature in dichloromethane solution, from which water was removed by using powdered molecular sieves; all catalytic oxidations were performed with NMO as the co-oxidant. In no case was there detectable oxidation of an alcohol in the presence of NMO but absence of ruthenium. There was no evidence of aerobic oxidation, as has been observed for several ruthenium oxidants, for example the oxoruthenium(VI) pyridine complexes $[Ru_2O_6(py)_4]$ and *trans*-$[RuO_2(py)_4]^{2+}$.[1]

Although it has been shown that $[RuO_2Cl_3]^-$ in acetonitrile as a stoichiometric oxidant attacks the olefinic double bond in *cyclo*hexene over a 2 h period giving a mixture of *cyclo*hexene oxide, 2-*cyclo*hexenone, 2-chloro*cyclo*hexenone and *cyclo*hexene chlorohydrin,[7] we find no competing double bond cleavage in the reaction of $[RuO_2Cl_3]^-$, *trans*-$[RuO_2X_4]^{2-}$ or *trans*-$[RuO_2Cl_3(OPPh_3)]^-$ over similar periods with unsaturated alcohols (cinnamyl alcohol, geraniol, chrysanthemyl alcohol, citronellol). In the catalytic reactions, turnovers are up to 70 for $(Ph_4P)[RuO_2Cl_3]$, 25 for *trans*-(4-^{t}BupyH)$_2$[RuO_2Cl_4] and 50 for *trans*-$(Ph_4P)_2[RuO_2Br_4]$ and *trans*-$(Ph_4As)[RuO_2Cl_3(OPPh_3)]$ over a 2 h period. By repeating the $[RuO_2Cl_3]^-$ stoichiometric and catalytic oxidations in the presence of a 40-fold excess of chloride (as Et_4NCl), the green trichloro species is converted to the red *trans*-$[RuO_2Cl_4]^{2-}$;[7] we find that the latter species is a more effective oxidant when prepared *in situ* than it is when used as its butylpyridinium salt. However, addition of excess chloride to oxidation reactions involving *trans*-(4-^{t}BupyH)$_2$[RuO_2Cl_4] decreases the yield and the catalytic turnover.

It is clear that *trans*-(4-^{t}BupyH)$_2$[RuO_2Cl_4] is a less effective oxidant than are $(Ph_4P)[RuO_2Cl_3]$ or *trans*-$(Ph_4P)_2[RuO_2Br_4]$. We believe that a possible reason for this is the potential coordinating ability of the butylpyridinium cation in its deprotonated form. We find that the electronic spectrum of *trans*-(4-^{t}BupyH)$_2$[RuO_2Cl_4] in dichloromethane solution is very similar to that of *trans*-(4-^{t}BupyH)[RuO_2Cl_3(4-^{t}Bu-py)] in the same solvent, suggesting that the following equilibrium is in operation (R = 4-^{t}Bupy):

$$(RH)_2[RuO_2Cl_4] \longleftrightarrow (RH)[RuO_2Cl_3(R)] + HCl.$$

Thus it seems likely that the *trans*-$[RuO_2Cl_3$(4-^{t}Bupy)$]^-$ species, isolated earlier in these laboratories,[1] is the predominant oxidizing species in solution in the latter system. Unlike $[RuO_2Cl_3]^-$, this species lacks a vacant coordination site, and this may be in some way responsible for its lower efficiency as an oxidant. It is interesting in this context to note that $[RuO_2Cl_3]^-$ and *trans*-$[RuO_2Cl_3(OPPh_3)]^-$ have comparable efficiencies as oxidants; this may arise from the lability of the weakly bound $OPPh_3$ ligand. It is also likely that salts of *trans*-$[RuO_2Br_4]^{2-}$ in solution dissociate to $[RuO_2Br_3]^-$.

It is clear that all of the species studied here are two-electron oxidants of alcohols to carbonyl compounds, and that they effect such reactions in a mild and selective manner. The best turnovers in catalytic systems are achieved using $(Ph_4P)[RuO_2Cl_3]$. Thus for example, 1.38 g (10 mmol) of *p*-methoxybenzyl alcohol is converted to 1.28 g (9.4

Table 1. Oxidation of alcohols with oxoruthenium(VI) complexes[a]

Alcohol	Product[b]	$(Ph_4P)[RuO_2Cl_3]$ Catalytic Yield (%), (Turnover[c])	$(4\text{-}^tBu\text{-}pyH)_2[RuO_2Cl_4]$ Stoichiometric Yield (%)	$(4\text{-}^tBu\text{-}pyH)_2[RuO_2Cl_4]$ Catalytic Yield (%), (Turnover[c])	$(Ph_4P)[RuO_2Cl_3(OPPh_3)]$ Catalytic Yield (%), (Turnover[c])	$(Ph_4P)_2[RuO_2Br_4]$ Catalytic Yield (%), (Turnover[c])
p-Methoxybenzyl alcohol	A	94(70)	90	87(23)	75(52)	87(44)
		87(70)	*45*	*60(18)*		
Piperonyl alcohol	A	93(65)	83	92(28)	47(29)	79(40)
		65(50)	*30*	*70(21)*		
Benzyl alcohol	A	93(65)	58	58(17)	41(30)	
		90(65)	*32*	*52(15)*		
Cinnamyl alcohol	A	84(50)	50	60(18)	39(28)	99(50)
		77(50)	*23*	*33(10)*		
Geraniol	A*	92(23)	20	34(14)	45(28)	
Chrysanthemyl alcohol	A*	93(24)	5	18(7)	42(26)	
Citronellol	A*	76(19)	32	47(19)	36(22)	
α-Tetralol	K	93(60)	89	79(24)	50(32)	
		94(50)	*54*	*59(18)*		
Benzhydrol	K	98(55)	88	42(13)	80(41)	70(35)
		92(50)	*30*	*48(14)*		
*cyclo*Hexanol	K	59(50)	44	53(16)	48(46)	
		58(50)	*28*	*55(17)*		
*cyclo*Pentanol	K	60(50)	20	30(9)	34(37)	
		46(50)	*15*	*32(10)*		

[a] All oxidations performed in CH_2Cl_2 at room temperature with 4 Å molecular sieves (catalytic oxidations using a three-fold excess of NMO). *Results in italics are for oxidations performed in the presence of a 40-fold excess of* Et_4NCl.

[b] A = aldehyde; K = ketone. Yields and turnovers quantified by formation of the 2,4-DNPH derivative, except for alcohols marked *, for which products were isolated.

[c] Catalytic turnover = mol product/mol catalyst.

mmol, 94% conversion) of *p*-methoxybenzaldehyde by 81 mg (0.14 mmol) of $(Ph_4P)[RuO_2Cl_3]$ in the presence of excess NMO over a period of 2 h.

In the case of the unsaturated alcohols cinnamyl alcohol, citronellol, geraniol and chrysanthemyl alcohol, ^1H NMR of the products was used to check that no competing epoxidation or cleavage of the olefinic double bonds was occurring. In no case was any such reaction observed to have taken place: resonances due to the unsaturated aldehyde product and due to unreacted alcohol substrate were the only ones seen. The relatively low yields of unsaturated aldehydes obtained in the oxidation of these alcohols are thus likely to be due to lack of activation of the alcohol group and definitely not to attack of the olefinic bond.

(b) *Vibrational spectra and structure of the complexes*

Perrier and Kochi[7] have recently shown that $\{(Ph_3P)_2N\}[RuO_2Cl_3]$ contains a trigonal bipyramidal anion with *cis*-dioxo ligands in the equatorial plane, though only one IR band at 881 cm^{-1}, rather than the two expected, was observed assignable to a Ru=O stretch, ν(Ru=O). In $(Ph_4P)[RuO_2Cl_3]$, which from X-ray studies[7] is shown to have a 6:4 occupancy of trigonal bipyramidal and square-based pyramidal anions, they report two strong IR bands at 891 and 878 cm^{-1}.

Vibrational spectroscopic data for all the oxoruthenium(VI) complexes prepared are presented in Table 2. All of the salts $[RuO_2Cl_4]^{2-}$ show a very

Table 2. Analytical and vibrational[a] data for oxoruthenium(VI) complexes

Complex	Analytical data: % Found[b] C	H	N	X[c]	$\nu(RuO_2)$ asym.	sym.	ν(RuX)[c]	Other bands
$(Ph_4P)[RuO_2Cl_3]$	49.4	3.2	5.2[d]	18.6	892s		310s	—
	(49.8)	(3.5)	(5.4)	(18.4)	879vs			
$(Ph_4P)[RuO_2Br_3]$	41.3	3.0	4.5[d]	34.1	888s			—
	(40.5)	(2.8)	(4.3)	(33.7)	876vs			
trans-$(pyH)_2[RuO_2Cl_4]$	27.2	2.7	6.3	32.1	824s	*840m*	306s	1052s[e]
	(27.6)	(2.8)	(6.4)	(32.1)				
trans-$(4^tBupyH)_2[RuO_2Cl_4]$	40.0	5.3	5.0	25.6	819s	*835m*	299s	1066s[e]
	(39.5)	(5.2)	(5.1)	(25.9)				
trans-$(3\text{-}MepyH)_2[RuO_2Cl_4]$	31.2	3.1	6.0	30.4	826vs	*852m*	298s	1044s[e]
	(31.1)	(3.5)	(6.1)	(30.6)				
trans-$(3,4\text{-}Me_2pyH)_2[RuO_2Cl_4]$	35.1	4.1	5.9	28.0	824s	*845m*	290s	1072s[e]
	(34.2)	(4.1)	(5.7)	(28.9)				
trans-$(8\text{-}HQH)_2[RuO_2Cl_4]$	37.0	2.7	4.7	25.1	825s	*847m*	290s	1096s[e]
	(38.1)	(2.8)	(4.9)	(25.0)				
trans-$(phenH)_2[RuO_2Cl_4]$	45.6	2.9	8.8	22.0	843s		304s	1076s[e]
	(45.2)	(2.8)	(8.8)	(22.3)	833s		284s	
trans-$(Me_2NH(CH_2)_2NHMe_2)[RuO_2Cl_4]$	18.7	4.6	7.4		834vs		293vs	—
	(18.3)	(4.6)	(7.1)					
trans-$(Me_2N(C_2H_4)_2NMe_2)[RuO_2Cl_4]$	23.0	4.8	6.6		829vs		295vs	—
	(22.9)	(4.8)	(6.7)					
trans-$(Ph_4P)_2[RuO_2Br_4]$	50.2	3.4	—		839vs		235s	—
	(50.9)	(3.6)						
trans-$(Me_2NH(CH_2)_2NHMe_2)[RuO_2Br_4]$	12.4	3.3	4.8		846m			—
	(12.6)	(3.2)	(4.9)					
trans-$(Me_2N(C_2H_4)_2NMe_2)[RuO_2Br_4]$	15.7	3.2	4.6		850m			—
	(16.1)	(3.4)	(4.7)					
trans-$(Ph_4As)[RuO_2Cl_3(OPPh_3)]$	53.9	3.7	—		824vs		290vs	1186s[f]
	(56.0)	(3.9)						1172s[f]

[a] cm^{-1}; s = strong, m = medium, v = very; Raman bands in italics; solution data in parentheses, otherwise solid state.

[b] Calculated values in parentheses.

[c] X = Cl or Br.

[d] Phosphorus analysis.

[e] ν(ring), band arising from the two A_1 ring-stretching modes of the pyridinium or substituted pyridinium cation.

[f] ν(P=O) of the coordinated $OPPh_3$ ligand.

strong IR band in the region 850–820 cm^{-1} due to the asymmetric stretch of the *trans*-O=Ru=O ("ruthenyl") unit, $\nu_{as}(RuO_2)$, and a Raman band in the same region due to the symmetric stretch, $\nu_s(RuO_2)$, of the same unit. From the centrosymmetric nature of the ruthenyl unit in these species $\nu_{as}(RuO_2)$ should be IR active but Raman inactive, and the reverse for $\nu_s(RuO_2)$. It is therefore clear that the *trans*-$[RuO_2Cl_4]^{2-}$ salts are all octahedral, as shown by the X-ray crystal structure of *trans*-$\{(Ph_3P)_2N\}_2[RuO_2Cl_4]$.[7] Their IR spectra also have a strong band in the region 310–290 cm^{-1} which is likely to arise from the ν_{as}(Ru—Cl) stretch of the coordinated chloro ligands. Similarly, the salts $[RuO_2Br_4]^{2-}$ show strong bands in the 840–820 cm^{-1} region, indicating presence of the *trans*-RuO_2 unit in an octahedral structure, and strong IR bands in the 250–220 cm^{-1} region due to ν_{as}(Ru—Br). The tribromo complex $(Ph_4P)[RuO_2Br_3]$ displays two bands in the IR spectrum at 888 and 876 cm^{-1}, consistent with a trigonal bipyramidal structure containing a *cis*-O=Ru=O unit.

The $(Ph_4As)[RuO_2Cl_3(OPPh_3)]$ species shows a strong, sharp IR band at 825 cm^{-1} due to the asymmetric Ru=O stretch of a ruthenyl unit. Strong bands at 1186 and 1172 cm^{-1} are likely[10] to arise from ν(P=O) stretches of the triphenylphosphine oxide ligand, and the strong IR band at 290 cm^{-1} is likely to be due to ν_{as}(Ru—Cl).

Acknowledgements—We thank the SERC for a postdoctoral grant (to A.C.D), the British Council and the University of Mansoura (A.M.E.), the SERC and BP Research for a CASE award (to J.M.J.). We also thank Dr M. J. Taylor for helpful discussions and Johnson, Matthey Ltd for loans of hydrated ruthenium trichloride.

REFERENCES

1. A. C. Dengel, A. M. El-Hendawy, W. P. Griffith, C. A. O'Mahoney and D. J. Williams, *J. Chem. Soc., Dalton Trans.* 1990, 737.
2. A. M. El-Hendawy, W. P. Griffith, F. I. Taha and M. N. Moussa, *J. Chem. Soc., Dalton Trans.* 1989, 901.
3. G. Green, W. P. Griffith, D. M. Hollinshead, S. V. Ley and M. Schröder, *J. Chem. Soc., Perkin Trans. I* 1984, 681.
4. A. M. El-Hendawy, W. P. Griffith, B. Piggott and D. J. Williams, *J. Chem. Soc., Dalton Trans.* 1988, 1983.
5. D. M. Hollinshead, S. C. Howell, S. V. Ley, M. Mahon and N. M. Ratcliffe, *J. Chem. Soc., Perkin Trans. I* 1983, 1579.
6. W. P. Griffith, S. V. Ley, G. P. Whitcombe and A. D. White, *J. Chem. Soc., Chem. Commun.* 1987, 1625.
7. S. Perrier and J. K. Kochi, *Inorg. Chem.* 1988, **27**, 4165.
8. J. A. Creighton and M. J. Taylor, *Can. J. Chem.* 1987, **65**, 2526.
9. H. Nakata, *Tetrahedron* 1963, **19**, 1959.
10. G. B. Deacon and J. H. S. Green, *Spectrochim. Acta* 1968, **24A**, 845.

Polyhedron Vol. 9, No. 14, pp. 1757–1764, 1990
Printed in Great Britain

0277–5387/90 $3.00+.00
© 1990 Pergamon Press plc

2,6-BIS(DIPHENYLPHOSPHINO)PYRIDINE: A CONVENIENT SYNTHESIS AND COMPLEXATION BEHAVIOUR

H. CHRISTINA E. McFARLANE, WILLIAM McFARLANE* and ALAN S. MUIR

Department of Chemistry, City of London Polytechnic, Jewry Street, London EC3N 2EY, U.K.

(*Received* 21 *February* 1990; *accepted* 2 *April* 1990)

Abstract—The reaction between sodium diphenylphosphide and 2,6-difluoropyridine in liquid ammonia gives the title compound in 40% yield. The reactions of this potentially polydentate ligand with simple substrates like MeI, chalcogen and $M(CO)_6$ proceed via attack on phosphorus in preference to nitrogen, and the ^{31}P NMR and vibrational spectra of some of the products are reported.

Polydentate ligands containing both hard and soft donor atoms (e.g. N and P) are important for their potential to form bi- and polymetallic complexes containing two different types of metal atom. Examples of such ligands include 2-methyl-6-bis (diphenylphosphino)methylpyridine,[1] tris(2-pyridyl)phosphine,[2] tris(diphenylphosphinoethyl)-amine[3] and 2-(diphenylphosphinomethyl)pyridine.[4] Of special interest in this connection are 2-(diphenylphosphino)pyridine (**I**) and 2,6-bis(diphenylphosphino)pyridine (**II**) because of the rigidity of their skeletons which leads to fixed relative positions of the nitrogen and phosphorus atoms, and also because the nitrogen atom in a pyridine ring can display a degree of softness. However, the reported synthesis of **II** is not especially convenient[5,6] and it has not been used extensively as a ligand, the bulk of the published work being by Balch and co-workers.[7–11] We report here that the reaction in liquid ammonia between sodium diphenylphosphide and the readily available 2,6-difluoropyridine provides a convenient one-pot route to **II**. Previously, this approach has been used for the synthesis of a series of polykis(diphenylphosphino)benzenes.[12,13]

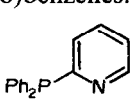

(I)

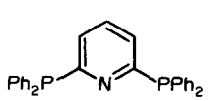

(II)

Transition metal complexes with four-membered chelate rings (e.g. for dppm) are well-known,[14–16] but calculations indicate that the degree of strain involved in monometallic bidentate coordination of **I** and **II** is considerable.[11] Only a few such complexes have been positively identified; e.g. $Ru(Ph_2Ppy)(CO)_2(Cl)_2$ with $\angle PRuN = 68.7°$, $\angle CPRu = 84.0°$[17] and $[Pt(Ph_2Ppy)_2Cl]^+$ with $\angle PPtN = 70.7°$, $\angle CPPt = 84.3°$.[18] Further reports of such chelation are not fully substantiated by spectroscopic or X-ray data,[19,20] although **I** may act as a tridentate ligand in reactions where orthometallation of one phenyl ring occurs.[21,22] The possibility of **II** acting in a monometallic tridentate mode can be discounted, although in the complex $[Rh_2\{(Ph_2P)_2py\}_2(CO)(I)]^+[BPh_4]^-$ it functions both as an NP chelator and as a phosphorus-bonded monodentate ligand.[11] Thus **I** and **II** have considerable potential for forming bi- and polymetallic systems with varying degrees of metal–metal interaction, and several studies of this have been undertaken.[7–11,17,18,23–26] In order to assess this type of behaviour it is desirable to have available data on the mono-coordinating abilities and we therefore present here reactions of **II** with methyl iodide, the chalcogens and the group VI metal hexacarbonyls, together with their NMR and some vibrational data. Some previous work is available on the analogous reacions of **I**.[6,27,28]

RESULTS AND DISCUSSION

The reaction between a liquid ammonia solution of sodium diphenylphosphide and 2,6-difluoro-

* Author to whom correspondence should be addressed. Address for correspondence: Department of Chemistry, University of Newcastle upon Tyne, Newcastle upon Tyne NE1 7RU, U.K.

pyridine gives **II** in *ca* 40% yield as air-stable white crystals. Attempts to prepare **I** by this method resulted in mixtures containing much of the desired product. Compound **II** reacts with neat methyl iodide to yield an off-white solid whose elemental composition approximates to $(Ph_2P)_2py \cdot 3MeI$ but which loses MeI on standing at room temperature and which yields $(Ph_2P)_2py \cdot 2MeI$ (**XV**) on heating to 80°C for 3 h *in vacuo*. Compound **XV** has a single ^{31}P NMR resonance indicating that both methyl groups are bound to phosphorus; this was confirmed by appropriate ^{1}H and ^{13}C NMR spectra. Compound **XV** can also be made by reaction of **II** with excess MeI, with CH_2Cl_2 as a solvent, and as an intermediate in this reaction, the adduct $(Ph_2P)_2py \cdot MeI$ [$\delta(^{31}P) = -1.2$ and 14.9 ppm, $J(PP) = 2.4$ Hz] in which a single methyl group is bound to phosphorus was detected. The related complex $Ph_2Ppy \cdot MeI$ has been reported[28] and NMR data indicated methyl attachment to the phosphorus atom. Reactions of **II** with MeI in either THF or diethyl ether solution gave products whose ^{13}C and ^{1}H NMR spectra were indicative of solvent complexation, probably with the pyridine nitrogen atom. This competitive reaction made the isolation of pure compounds impossible in these solvents.

The slow aerial oxidation (over weeks) of **II** in THF/methanol gave the dioxide **III**, and the reaction of **II** with either sulphur or selenium proceeded stepwise and smoothly via the monosulphide **IV** and monoselenide **VI**, respectively, to yield the disulphide **V** and diselenide **VII**.

One mole of carbon monoxide was displaced from $M(CO)_6$ (M = Cr, Mo, W) by refluxing with **II** in diglyme to finally yield the bimetallic species, **VIII**, **X** and **XI**: the monometallic derivatives with one uncoordinated phosphorus can be detected by ^{31}P NMR as intermediates and data are included in Table 2 for the $W(CO)_6$ intermediate, **XII**. In reactions with *cis*-$Mo(CO)_4pip_2$[29] there was still no evidence of any attack by the pyridine nitrogen upon the metal centre, the two products being **XIII** and **XIV** which lose piperidine upon standing at ambient temperature, making accurate elemental analyses impossible.

Reaction of **II** with other substrates such as $HgCl_2$, $SnCl_2$ and Me_2SnCl_2 in CH_2Cl_2 led to ill-defined materials with substantially unaltered phosphorus chemical shifts, from which it can be concluded that initial coordination was via nitrogen. Addition of a considerable excess of the metal halide did result in some larger changes in $\delta(^{31}P)$ but the products were still intractable.

Elemental analyses of isolated compounds are given in Table 1 and NMR data in Table 2. The ^{31}P

Table 1. Analytical and other data for derivatives of 2,6-bis(diphenylphosphino)pyridine

Number	Compound[c]	Melting point (°C)	% C		% H		% P		% N		RMM[d]		Colour
			Calc.	Found	Calc.	Found	Calc.	Found	Calc.	Found	Calc.	Found	
V	2,6-$[Ph_2P(S)]_2$py	206–208	68.1	67.8	4.5	4.5	12.1	11.8	2.7	2.3	511	511	White
VII	2,6-$[Ph_2P(Se)]_2$py	242–244	57.5	57.2	3.8	3.8	10.2	10.2	—	—	605	605	White
VIII	2,6-$(Ph_2P)_2$py$[Cr(CO)_5]_2$	d > 175	56.3	56.3	2.8	2.7	—	—	1.7	1.6	832	832	Light yellow
X	2,6-$(Ph_2P)_2$py$[Mo(CO)_5]_2$	d > 156	50.9	50.0	2.5	2.7	6.7	6.5	1.5	1.4	918	—[b]	Off-white
XI	2,6-$(Ph_2P)_2$py$[W(CO)_5]_2$	d 177	42.8	42.9	2.1	2.2	5.7	5.5	—	—	1095	1095	Off-white
XV	2,6-$(Ph_2P)_2$py$[MeI]_2$	d 232	50.9	50.1	4.0	3.9	—	—	1.9	1.8	730	—[b]	Light yellow

[a] Determined mass spectrometrically, molecular ion M^+.
[b] Molecular ion not observed.
[c] py = C_5H_3N.

chemical shifts of the chalcogen derivatives are in the expected regions and for the mono-derivatives **IV** and **VI** show that attack upon a remote site has little effect upon $\delta(^{31}P)$. The ^{31}P coordination chemical shifts[30] of **VIII**, **X** and **XI** are 62.5, 43.7 and 27.3 ppm, respectively, and as expected confirm the absence of chelate ring formation.

The chalcogen derivatives of **I** were observed in solution and are reported as **XVI**, **XVII** and **XVIII** in Table 2. Table 3 presents some IR and Raman data for **II**, **III** and **V** along with some general assignments. The IR spectra of **II** and **III** have been briefly reported[6] before but were not discussed, so reference was made to the documented spectra of Ph_3P[31,32] and 2,6-Me_2py.[33] The spectra are, as expected, dominated by the modes resulting from the phenyl moieties and various phosphorus/carbon vibrations; the modes solely from the pyridine function are obscured. In the case of **II**, the IR intense bands centred at 748 and 694 cm^{-1} are the C—H deformations and C—C ring modes typifying a mono-substituted aromatic compound, although

Table 2. ^{31}P and other NMR parameters of 2,6-bis(diphenylphosphino)pyridine and some derivatives

Number	Compound[a]	Spin system	$\delta(^{31}P)$ (ppm)[b]	$\delta(^{13}C)$ (ppm)[c]	J(PC) (Hz)	Notes
II	2,6-$(Ph_2P)_2$py	A_2	−4.2	C_q 136.9	11.6	[d]
				C_o 134.4	20.2	
				C_p 129.1	—	
				C_m 128.7	7.6	
III	2,6-$[Ph_2P(O)]_2$py	A_2	19.8	C_o 132.2	9.8	
				C_p 132.4	—	[d]
				C_m 128.9	13.5	
IV	2-Ph_2P,6-$[Ph_2P(S)]$py	AB	35.6, −2.6			[e]
V	2,6-$[Ph_2P(S)]_2$py	A_2	37.7	C_o 132.2	9.8	
				C_p 132.9	—	
				C_m 128.8	13.4	
VI	2-Ph_2P,6-$[Ph_2P(Se)]$py	AB	30.8, −2.8			[e,f,g]
VII	2,6-$[Ph_2P(Se)]_2$py	A_2	31.6	C_q 139.7	62.2	
				C_o 133.3	9.8	[h]
				C_p 132.2	—	
				C_m 128.9	13.4	
VIII	2,6-$(Ph_2P)_2$py$[Cr(CO)_5]_2$	A_2	57.5			
IX	2-$Ph_2P(O)$,6-$[Ph_2P(Cr(CO)_5)]$py	AB	58.3, 19.3			[e,f]
X	2,6-$(Ph_2P)_2$py$[Mo(CO)_5]_2$	A_2	39.5			
XI	2,6-$(Ph_2P)_2$py$[W(CO)_5]_2$	A_2	23.1			[i]
XII	2,6-$(Ph_2P)_2$py$[W(CO)_5]$	AB	21.7, −3.3			[e]
XIII	2,6-$(Ph_2P)_2$py$[Mo(CO)_4$pip$]$	AB	36.5, −4.8			[j]
XIV	2,6-$(Ph_2P)_2$py$[Mo(CO)_4$pip$]_2$	A_2	45.6			[j]
XV	2,6-$(Ph_2P)_2$py$[MeI]_2$	A_2	21.1	Me 8.4	54.7	
				C_o 135.2	32.3	
				C_p 134.4	—	
				C_m 130.9	13.7	

[a] py = C_5H_3N, pip = piperidine.
[b] In ppm to high frequency of 85% H_3PO_4.
[c] In ppm to high frequency of Me_4Si.
[d] Previously reported compound (refs 5 and 6).
[e] Observed in solution only.
[f] $^4J(^{31}P–^{31}P) = 2.4$ Hz.
[g] $^1J(^{31}P–^{77}Se) = 748$ Hz.
[h] $^1J(^{31}P–^{77}Se) = 741$ Hz.
[i] $^1J(^{31}–^{183}W) = 239$ Hz.
[j] Lime-coloured solid which loses piperidine on standing.

Table 3. IR and Raman spectra (cm^{-1}) of 2,6-bis(diphenylphosphino)pyridine and some chalcogen derivatives

II		III		V		
IR[a]	Raman[b]	IR[a]	Raman[b]	IR[a]	Raman[b]	General assignments
		3085(w,sh)		3090(w)	3100(w)	
3069(w,sh)	3070(w,sh)	3073(s)	3070(m)	3075(w)	3065(vs)	
3055(m)	3057(s)	3057(s)	(centre of broad, unresolved band)	3059(m)	3060(s)	ν(C—H) (aromatic)
3043(w,sh)	3043(w,sh)			3050(w,sh)	3051(s)	
3024(w)	3028(m/s)	3022(w,sh)		3022(w)		
3009(m)	3006(w)	3010(w,sh)		3011(w)	3009(w)	
		2991(w,sh)				
1982(w), 1963(w), 1892(w), 1826(w), 1812(w), 1777(w), 1703(w), 1670(w)		1967(w), 1773(w), 1686(w), 1656(w), (low quality spectrum in this area)		1962(w), 1898(w), 1819(w), 1774(w), 1734(w), 1672(w)		Combinations and overtones
1584(m)	1583(vs)	1589(w)	1591(vs)	1588(w)	1588(s)	ν(C—C), (C—N) (aromatic)
1569(w)	1571(w,sh)	1573(w,sh)		1574(m)	1576(w,sh)	
1556(w,sh)	1554(w,sh)	1562(m)		1560(w/m)		
1546(m/s)	1545(m)	1551(w)	1551(w)	1544(w/m)	1544(w)	
		1509(vw)		1510(w)		
1478(s)		1482(m)		1481(s)	1485(vw)	
1435(vs)		1436(vs)		1437(vs)	1426–1448(w,br)	
1422(vs)	1421(w)			1427(s,sh)		
1386(w)		1377(m/w)		1391(w)		
				1373(m)	1376(w)	
1357(w)	1357(w)					
	1334(w)	1329(w)		1335(w,br)	1325–1335(w,br)	
1324(w)	1323(w)					

1310(w)	1312(w)	1309(w)		1311(w/m)	1313(vw)
					1303(vw)
1276(w)		1281(w)		1263(w)	
		1211, 1202 (vs)	1209, 1199 (vs)		ν(P═O)
					1192(w)
				1188(w)	1185(w,br)
1180(w)		1179(m)	1182(w,br)	1178(w)	
1170(w/m)					1168(w)
1159(w/m)	1161(w)	1163(m/s)	1160(m,br)	1159(w)	1160(w)
		1154(m,sh)		1150(w/m)	1151(w,sh)
1134(m)	1136(m)				1140(vw)
	1127(w,sh)				
1120(w)		1120(vs)			
					1113(m,sh)
1094(s)	1094, 1083 (m,w,sh)	1099(m/s)	1101(m/w)	1104(vs)	1106, 1103 (m)
1068(w/m)		1076(m)		1071(m/s)	1073(w)
1026(m)	1026(m)	1026(w)	1029(m)	1029(m)	1032(m)
998(m)	997(vs)	997(w)	1002(vs)	1000(w/m)	1002(vs) —ρ(ring)
998(m/w)		988(m/w)	992(s,sh)	998(m)	992, 988 (m/s)
	981, 977 (m)				
974(w)			978(w)	976(w,br)	977, 974 (w,br)
937(w)					
		923(w)	925(vw)	924(w)	929(w,br) —δ(C—H)
		916(vw)			
910(w)	907(vw)				
856(m)	856(vw)	859(w)			853(vw)
846(w)		840(w)		841(w/m)	
		815, 805 (w,sh,m)		808, 801 (vs,s)	811, 800 (vw)
797(vs)	799(w)				
775(m/s)	776(m)				
748(vs)	753(vw)	746(vs)	751(vw)	744(vs)	
		722(vs)	725(vw)	721(vs)	723(w)
					717(w)
		709(vs)	711(w)		
	703				
694(vs,br)	698 (w/m)	696(vs)		693(vs)	696(w)
	690				

continued

Table 3—*continued.*

II		III		V		
IR[a]	Raman[b]	IR[a]	Raman[b]	IR[a]	Raman[b]	General assignments
				670(w,sh)	668(m)	
		658(w)	660(m)			
	651(w)					
				647(vs)	645(vs)	ν(P═S)
618(w)	617(m)	618(w)	619(m)	616(m)	620, 616 (m)	
590(m)	592(m)	593(vw)			594(w)	
				584(m)		
554(w)		556(vs)			555(vw)	
546(w)						
536(w)		535(vs)		522(vs)	524(vw)	
						δ(C—C), (C—P)
506(vs)	509(w)	510(m/s)		511(s,sh)	512(w)	
496(vs)	498(w)	498(w/m)				
				493(vs)		
486(vs)	485(m)			482(m/w)	483(w)	
		472(w)		471(m/w)	472(w)	
465(vs)	464(vw)					
				451(m/w)	450(vw,br)	
	443(vw)					
437(w)	438(w)					
	428(w)					
417(w/m)	423(w)	422(w)				
		411(w)		413(w)	415(w)	

s = strong, m = medium, w = weak, sh = shoulder, br = broad.

[a] Spectrum recorded as KBr disc.

[b] Sample sealed in glass capillary.

they are very broad. Bands at 1094 cm^{-1} (R,IR), 698 and 703 cm^{-1} (R), and 506, 496, 486 and 465 cm^{-1} (R,IR) are probably related to the various phosphorus/carbon motions. These correspond with the X-sensitive P—C stretches and deformations reported for $(Ph)_3P$.[31,32]

Substitution on the two phosphorus atoms of **II** with either oxygen or sulphur leads to changes in the spectra. For the dioxide **III**, ν(P=O) was assigned to a band at 1160 cm^{-1} by Newkome and Hager;[6] in the current study a band was observed at 1160 cm^{-1} as well as a noticeably stronger doublet at 1199–1211 cm^{-1} in both the IR and Raman. The latter was assigned to ν(P=O) and compares with values of 1190 and 1193 cm^{-1} attributed to the respective mode in $(Ph)_3P{=}O$.[34] In the disulphide **V**, ν(P=S) was confidently assigned as 647 cm^{-1} (IR) and 645 cm^{-1} (R), both bands being intense. This compares with values of 634 cm^{-1} (IR) and 633 cm^{-1} (R) reported for $Ph_3P{=}S$.[34] The skeletal modes of **II** appear less perturbed in the Raman spectra of **III** and **V** than they are in the IR, any shifts or intensity changes being quite small except in some of the low frequency modes (data not reported < 380 cm^{-1}), although the mode at 1583 cm^{-1} is shifted to high frequency by 5–8 cm^{-1} in the complexes. In the IR spectra of both **III** and **V**, the band at 1435 cm^{-1} is greatly enhanced at the expense of the shoulder at 1422 cm^{-1}. Also, the band at 1094 cm^{-1} is enhanced and shifted to higher frequency (+23 cm^{-1} in **III**; +13 cm^{-1} in **VI**). The medium/strong band at 797 cm^{-1} in **II** is shifted to high frequency by *ca* 10 cm^{-1} and is split in both cases. The strong broad absorptions at 748 and 694 cm^{-1} split and sharpen considerably on complexation at phosphorus, although their centres shift by no more than 4 cm^{-1}; this suggests some band overlap in the parent diphosphine **II**. The 450–550 cm^{-1} region of the spectrum changes quite markedly in both **III** and **V**. The parent compound **II** has four weak bands in the 525–555 cm^{-1} region and three more intense bands centred at 495 cm^{-1}, with another strong band at 465 cm^{-1}. In **III** there is a strong complex of bands from 500 to 556 cm^{-1}, whereas in **V** a similar arrangement occurs from 471 to 522 cm^{-1}. These are probably perturbations to modes principally involving P/C motion. No detailed study of the vibrational spectra of the Group VI metal carbonyl complexes **VII**, **X** and **XI** was undertaken, but carbonyl stretching modes are noted in the range 1930–2080 cm^{-1}.

EXPERIMENTAL

^1H and ^{13}C NMR spectra were recorded at 89.6 and 22.5 MHz on a Jeol FX90 Q multinuclear Fourier transform spectrometer. ^{31}P measurements were made at 36.2 MHz on this instrument and at 24.2 MHz on a Jeol FX60 Fourier transform spectrometer. Solutions were usually made in dichloromethane, THF or diglyme, occasionally with C_6D_6 or $CDCl_3$ added to provide a field/frequency lock, and spectra were recorded at 22°C.

Raman spectra were recorded on a Coderg PHO instrument with excitation provided at 488 nm by a Coherent Radiation argon laser and with samples in sealed glass capillaries. IR spectra were recorded as KBr discs using a Perkin–Elmer 1710 FT–IR spectrometer.

2,6-Difluoropyridine was obtained from Fluorochem Ltd and was used as supplied. Manipulations were performed under atmospheres of dry ammonia or dry nitrogen. Degassed and dried solvents were utilized where necessary. Syntheses were of three main classes and general details are given.

(a) 2,6-*Bis(diphenylphosphino)pyridine* (II)

This was prepared using the method described previously for 1,2,4,5-tetrakis(diphenylphosphino)benzene,[13] with crystallization of the product achieved by trituration of the oily residue with methanol at least three times (yield, 40%).

(b) *Reactions of* II *with sulphur or selenium*

Compounds **V** and **VII** were prepared by reaction of stoichiometric quantities of the chalcogen with **II** in dichloromethane. ^{31}P NMR indicated almost immediate formation of the monosubstituted species **IV** and **VI**; the reaction with sulphur was complete within 12 h and that with selenium within 48 h. Products were isolated and recrystallized from carbon disulphide and industrial methylated spirits to remove any retained colloidal chalcogen.

(c) (i) *Reactions of* II *with Group* VI *metal carbonyls*

Reactions to prepare **XIII**, **X** and **XI** were performed by refluxing **II** with a slight stoichiometric excess of the appropriate hexacarbonyl in diglyme for up to 30 min or until the solution started to darken. Reactions were monitored by ^{31}P NMR. The diglyme solution was separated from any precipitated hexacarbonyl, concentrated *in vacuo* with sublimation of any hexacarbonyl residue, and precipitation of the product followed methanol addition. Crystals were washed with methanol and were sometimes recrystallized from diethyl ether and meth-

anol. Reactions with $Cr(CO)_6$ were carried out away from direct sunlight because of the possible photosensitive nature of the products.

(ii) *Reactions of* **II** *with* cis-$Mo(CO)_4(pip)_2$

1:1 and 1:2 molar ratios of reactants were refluxed in dichloromethane with the products **XIII** and **XIV** precipitating out of solution. These crystals lost piperidine on standing at ambient temperature.

Acknowledgements—We thank Dr P. N. Gates and Mr S. Richards (RHBNC) for assistance with vibrational spectroscopy, Mr B. Saunderson for microanalyses and the SERC and the National Advisory Board for support.

REFERENCES

1. W. V. Dahloff, T. R. Dick, G. H. Ford, W. S. J. Kelly and S. M. Nelson, *J. Chem. Soc. A* 1971, 3495.
2. K. Wajda, F. Pruchnik and T. Lis, *Inorg. Chim. Acta* 1980, **40**, 207.
3. L. Sacconi and I. Bertini, *J. Am. Chem. Soc.* 1968, **90**, 5443.
4. W. Knebel and R. Angelici, *Inorg. Chem.* 1974, **13**, 632.
5. S. E. Cremer and R. J. Chorrat, *J. Org. Chem.* 1967, **32**, 4066.
6. G. R. Newkome and D. C. Hager, *J. Org. Chem.* 1978, **43**, 947.
7. F. E. Wood, M. M. Olmstead and A. L. Balch, *J. Am. Chem. Soc.* 1983, **105**, 6332.
8. F. E. Wood, J. Hvoslef and A. L. Balch, *J. Am. Chem. Soc.* 1983, **105**, 6986.
9. F. E. Wood, J. Hvoslef, H. Hope and A. L. Balch, *Inorg. Chem.* 1984, **23**, 4309.
10. A. L. Balch, H. Hope and F. E. Wood, *J. Am. Chem. Soc.* 1985, **107**, 6936.
11. A. L. Balch, L. A. Fossett and M. M. Olmstead, *Inorg. Chem.* 1986, **25**, 4526.
12. H. C. E. McFarlane and W. McFarlane, *Polyhedron* 1983, **2**, 303.
13. H. C. E. McFarlane and W. McFarlane, *Polyhedron* 1988, **7**, 1875.
14. S. O. Grim, W. L. Briggs, R. C. Barth, C. A. Tolman and J. P. Jesson, *Inorg. Chem.* 1975, **13**, 1095.
15. G. T. Andrews, I. J. Colquhoun, W. McFarlane and S. O. Grim, *J. Chem. Soc., Dalton Trans.* 1982, 2353.
16. G. T. Andrews, I. J. Colquhoun and W. McFarlane, *Polyhedron* 1983, **2**, 783.
17. M. M. Olmstead, A. Maisonnat, J. P. Farr and A. L. Balch, *Inorg. Chem.* 1981, **20**, 4060.
18. J. P. Farr, M. M. Olmstead, F. E. Wood and A. L. Balch, *J. Am. Chem. Soc.* 1983, **105**, 792.
19. H. G. Ang, W. E. Kow and K. F. Mok, *Inorg. Nucl. Chem. Letts* 1972, **8**, 829.
20. K. Kurtev, D. Ribola, R. A. Jones, D. J. Cole-Hamilton and G. Wilkinson, *J. Chem. Soc., Dalton Trans.* 1980, 55.
21. T. J. Barder, S. M. Tetrick, R. A. Walton, F. A. Cotton and G. L. Powell, *J. Am. Chem. Soc.* 1983, **105**, 4090.
22. T. J. Barder, F. A. Cotton, G. L. Powell, S. M. Tetrick and R. A. Walton, *J. Am. Chem. Soc.* 1984, **106**, 1323.
23. J. P. Farr, M. M. Olmstead and A. L. Balch, *J. Am. Chem. Soc.* 1980, **102**, 6654.
24. A. Maisonnat, J. P. Farr and A. L. Balch, *Inorg. Chim. Acta* 1981, **53**, L217.
25. J. P. Farr, M. M. Olmstead, C. H. Hunt and A. L. Balch, *Inorg. Chem.* 1981, **20**, 1182.
26. G. R. Newkome, D. W. Evans and F. R. Fronczek, *Inorg. Chem.* 1982, **26**, 3500.
27. F. G. Mann and J. Watson, *J. Org. Chem.* 1948, **13**, 502.
28. H. Schmidbaur and Y. Inoguchi, *Z. Naturfor.* 1980, **35b**, 1329.
29. D. J. Darensbourg and R. L. Kump, *Inorg. Chem.* 1978, **17**, 2680.
30. L. S. Meriwether and J. R. Leto, *J. Am. Chem. Soc.* 1961, **83**, 3182.
31. D. H. Whiffen, *J. Chem. Soc.* 1956, 1350.
32. G. B. Deacon and J. H. S. Green, *Spectrochim. Acta* 1968, **24A**, 845.
33. M. Goldstein, E. F. Mooney, A. Anderson and H. A. Gebbie, *Spectrochim. Acta* 1965, **21**, 105.
34. R. F. De Ketelaere and G. P. Van Der Keelen, *J. Molec. Struct.* 1974, **23**, 233.

Polyhedron Vol. 9, No. 14, pp. 1765–1767, 1990
Printed in Great Britain

0277–5387/90 $3.00+.00
© 1990 Pergamon Press plc

SYNTHESIS AND X-RAY CRYSTAL STRUCTURE OF A CHAIN POLYMER FORMED BY 1-METHYLHYDANTOIN WITH MERCURY(II)

DAVID M. L. GOODGAME,* ARWA M. KHALED, CAROLINE A. O'MAHONEY and DAVID J. WILLIAMS

Chemistry Department, Imperial College of Science, Technology and Medicine, London SW7 2AY, U.K.

(*Received* 1 *March* 1990; *accepted* 2 *April* 1990)

Abstract—Reaction of 1-methylhydantoin ($C_4H_6N_2O_2$) with mercury(II) acetate in water or methanol yields the compound $Hg(C_4H_5N_2O_2)_2$ (**1**). Compound **1** is monoclinic $C2/c$ with $a = 13.536(5)$, $b = 12.462(2)$, $c = 26.580(9)$ Å, $\beta = 104.62(3)°$, $Z = 8$. The structure was refined on 2836 reflections to $R = 0.042$. The deprotonated 1-methylhydantoin ligands bind to mercury via nitrogen with essentially linear N—Hg—N bonding and with a nearly co-planar, "head–tail" disposition of the rings. Dimeric $(HgL_2)_2$ units are formed by two additional Hg—O bonds, and these dimers are further linked to produce polymeric chains via interdimer Hg—O linkages.

We have recently demonstrated that relatively simple ambidentate (N,O donor) ligands, such as 2-pyrrolidone (**I**)[1] or 2-pyridone (**II**),[2] can produce a

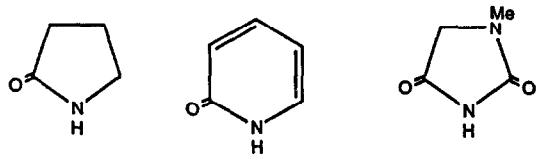

I II III

wide range of heterometallic, polynuclear complexes with unusual structures. An important, but not necessarily exclusive, component in such systems has been the use of mercury(II) to bind to a deprotonated ring nitrogen atom of the organic ligand, with consequent formation of an essentially linear N—Hg—N arrangement, leaving the exocyclic oxygen atoms free to bind to other metal ions.

In extending our work to include bridging ligands containing two carbonyl groups, each vicinal to the ring nitrogen, we have found it helpful to examine the geometry of the "parent" HgL_2 species. This information is available for some ligands of this type (1-methylthymine[3] and succinimide[4]) but for most potentially relevant bridging ligands of this class it is not. We report here the structure of HgL_2 (**1**), where L is the anion of 1-methylhydantoin (**III**).

EXPERIMENTAL

Preparations

Compound **1** precipitated as a white powder on mixing methanol solutions of **III** and mercury(II) acetate in a 2:1 mole ratio. Recrystallization from methanol gave colourless crystals. Found: C, 22.4; H, 2.2; N, 13.1. Calc. for **1**: C, 22.5; H, 2.4; N, 13.1%.

An analogous compound with 3-methyl-2-pyrrolidone (C_5H_8NO) was obtained by the same general procedure. $Hg(C_5H_7NO)_2 \cdot 0.5H_2O$: white solid, which separated over 2 days from MeOH–Et_2O solution, m.p. 190–192°C (dec.). Found: C, 29.6; H, 4.2; N, 6.8. Calc.: C, 29.6; H, 4.2; N, 6.9%.

X-ray studies

Crystal data for **1**: $C_{16}H_{20}Hg_2N_8O_8$, $M = 853.6$, monoclinic, $a = 13.536(5)$, $b = 12.462(2)$, $c = 26.580(9)$ Å, $\beta = 104.62(3)°$, $V = 4338$ Å^3, space group $C2/c$, $Z = 8$, $D_c = 2.61$ g cm^{-3}, Cu radiation, $\lambda = 1.54178$ Å, μ(Cu-K_α) = 275 cm^{-1},

* Author to whom correspondence should be addressed.

$F(000) = 3167$. Data were measured on a Nicolet R3m diffractometer with Cu-K_α radiation (graphite monochromator) using ω-scans. A crystal of dimensions $0.18 \times 0.18 \times 0.23$ mm was used. 2921 independent reflections ($2\theta \leqslant 116°$) were measured, of which 2836 had $|F_o| > 3\sigma(|F_o|)$ and were considered to be observed. The data were corrected for Lorentz and polarization factors; a numerical absorption correction (face-indexed crystal) was applied; maximum and minimum transmission factors were 0.112 and 0.007.

The structure was solved by direct methods. The non-hydrogen atoms were refined anisotropically. The positions of the hydrogen atoms were idealized, C—H = 0.96 Å, assigned isotropic thermal parameters, $U(H) = 1.2\ U_{eq}(C)$, and allowed to ride on their parent carbon atoms. The methyl groups were refined as rigid bodies. Refinement was by block-cascade full-matrix least-squares to $R = 0.042$, $R_w = 0.044$ $[w^{-1} = \sigma^2(F) + 0.00080F^2]$. The maximum and minimum residual electron densities in the final ΔF map were 1.63 and -1.98 eÅ^{-3}, respectively. The mean and maximum shift/error in the final refinement were 0.001 and 0.007, respectively. Computations were carried out on an Eclipse S140 computer using the SHELXTL system.[5]

Selected bond lengths and angles are listed in Table 1.

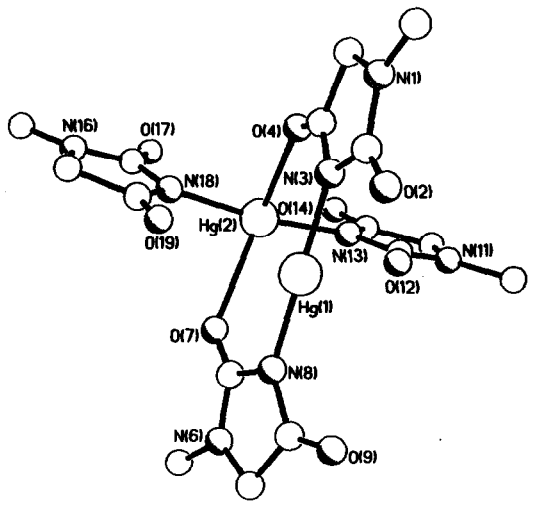

Fig. 1. Molecular structure of the $[HgL_2]_2$ dimer of compound **1**, with selected atom numbering.

RESULTS AND DISCUSSION

The X-ray analysis of **1** (Fig. 1) shows that the structure contains two crystallographically-independent HgL_2 units in which the deprotonated hydantoin anions bind to mercury via the nitrogen atom, so as to produce nearly linear N—Hg—N linkages [176.1(3)° at Hg(1) and 172.3(3)° at Hg(2)].

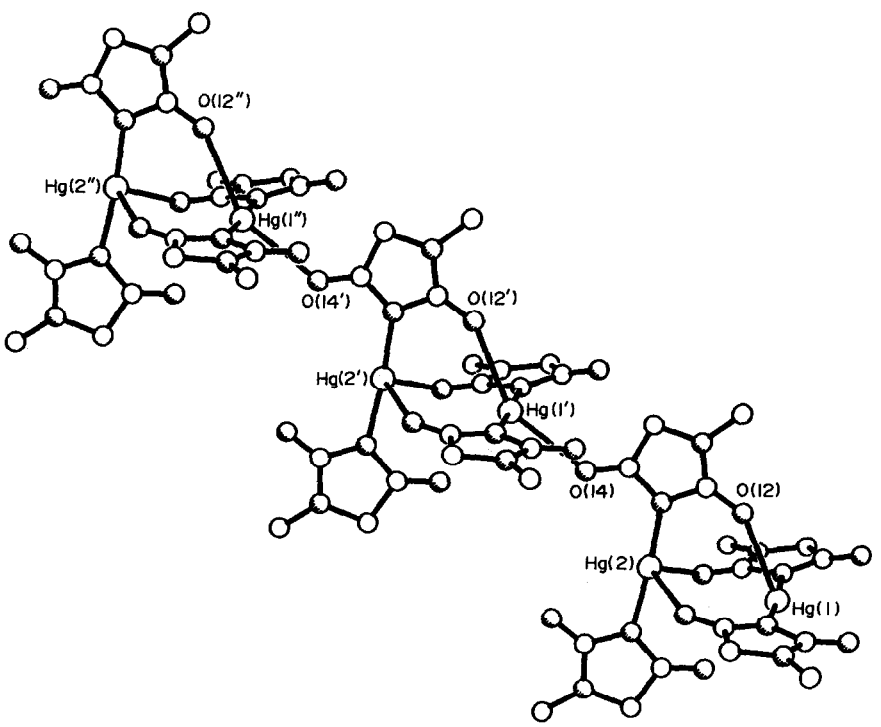

Fig. 2. Part of the Hg···O linked polymeric chain formed by **1** in the crystal.

Table 1. Selected bond lengths (Å) and angles (°) for **1**

Hg(1)—N(3)	2.007(7)	Hg(1)—N(8)	2.014(7)
Hg(2)—N(13)	2.018(8)	Hg(2)—N(18)	2.025(8)
Hg(2)—O(4)	2.730(7)	Hg(2)—O(7)	2.651(6)
N(3)—Hg(1)—N(8)	176.1(3)	N(13)—Hg(2)—N(18)	172.3(3)
O(4)—Hg(2)—O(7)	113.8(2)		

In both units the ligands adopt a near planar "head–tail" (*trans*-) geometry with respect to each other about N—Hg—N. The angles between the ligand mean planes about Hg(1) and Hg(2) are 13 and 10°, respectively. The Hg—N bonds are in the range 2.007(7)–2.025(8) Å and are similar to those we have observed[1] in the mercury complexes with 2-pyrrolidone.

Adjacent HgL_2 molecules lie with their planes nearly normal to each other and are weakly linked via two additional Hg–O bonds [2.651(6) and 2.730(7) Å, respectively] producing a dimeric $[HgL_2]_2$ unit. The O(4)Hg(2)O(7) angle is 113.8(2)°. The non-bonded Hg···Hg separation is 3.7 Å. There is an additional, weaker intradimer Hg···O linkage (2.83 Å) between Hg(1) and O(12). The complementary Hg(1)···O(19) distance is 3.0 Å.

In the crystal, the dimeric $[HgL_2]_2$ units are further linked via an additional Hg—O bond (2.75 Å) between Hg(1) and O(14′) to form a polymeric chain (Fig. 2). This arrangement is closely reminiscent of that observed[1] in the 2-pyrrolidone complex $[Hg_2(C_4H_6NO)_2Cl_2]_n$, but in **1** all the Hg···O interactions are weaker. There are no significant interchain contacts.

Acknowledgement—We thank the SERC for the X-ray diffractometer and for a Research Studentship (to C.A. O'M.).

REFERENCES

1. D. M. L. Goodgame, D. J. Williams and R. E. P. Winpenny, *Polyhedron* 1989, **8**, 1913 and refs therein.
2. D. M. L. Goodgame, D. J. Williams and R. E. P. Winpenny, *Polyhedron* 1989, **8**, 1531.
3. L. D. Kosturko, C. Folzer and R. F. Stewart, *Biochemistry* 1974, **13**, 3949.
4. D. Grdenic, B. Kamenar, M. Sikirica, T. Duplancic, S. Govedic, A. Hergold and P. Matkovic, *Acta Cryst.* 1975, **31A**, S132.
5. G. M. Sheldrick, SHELXTL, An integrated system for solving, refining and displaying crystal structures from diffraction data, Revision 4.1. University of Göttingen, F.R.G. (1983).

Polyhedron Vol. 9, No. 14, pp. 1769–1774, 1990
Printed in Great Britain

0277–5387/90 $3.00+.00
© 1990 Pergamon Press plc

GEOMETRICAL AND ORIENTATIONAL ISOMERS IN CLUSTERS

BRIAN F. G. JOHNSON,* ADRIAN W. BOTT and DEMELZA HUGH-JONES

University Chemical Laboratory, Lensfield Road, Cambridge CB2 1EW, U.K.

and

ALISON RODGER

Physical Chemistry Laboratory, South Parks Road, Oxford OX1 3QZ, U.K.

(*Received* 26 *January* 1990; *accepted* 5 *April* 1990)

Abstract—A new approach to the greater understanding of orientational and geometrical isomers in substituted carbonyl clusters is given with specific application to $Fe_3(CO)_{12-n}L_n$.

There is currently some considerable interest (see, for example, ref. 1) in the nature of $Fe_3(CO)_{12}$ and its substituted derivatives $Fe_3(CO)_{12-n}L_n$ in both solution and in the solid, but it is clear that a detailed appreciation of the complexities of the structures of these molecules is lacking. In this communication we wish to report a detailed analysis of the potential isomeric forms of these species. The method of analysis is general and the ideas presented herein may be applied to other cluster molecules and ions.

Little attention has been paid in the past to the ligand isomerism which can exist in cluster molecules and ions of the type M_mL_n, presumably because of the frequently complex relationship which exists between the central metal core and the peripheral ligating sphere.[2] Whereas isomerism in mononuclear molecules of type ML_n is, in general, relatively easily understood and described[3]—although even here the problem becomes increasingly difficult with increasing coordination number[4]—the higher coordination numbers and the lower symmetries quite often found for cluster molecules make for difficulty in any comprehensive and simple appreciation of the relationship between cluster isomers. In particular, problems have occurred due to failure to recognize the number of isomers that may exist for a given system, and also failure to understand the mechanisms by which interconversion between isomers may take place. For example, the apparently simple substituted molecule $Fe_3(CO)_{11}(PPh_3)$ can theoretically exist in (at least†) ten different isomeric forms, eight of which are energetically distinct as the ten isomers include two pairs of enantiomers. These are illustrated in Fig. 1. Failure to observe experimentally a given isomer in this and other cases is not unexpected and may be due either to differences in stability of the different isomers or to rapid interconversion in solution. Nevertheless, each isomer may be important for the chemistry of the molecule and consequently should not be ignored without justification.

It is convenient to describe cluster structures as consisting of two components: first the central metal core, and second, the surrounding ligand polyhedron.[2] These two parts of the molecule are frequently connected by essentially, non-directional bonds and the barrier to rotation of one polyhedron relative to the other is then small.[5] Thus, the iron triangle in $Fe_3(CO)_{12}$ may occupy three different orientations within the icosahedron of CO groups leading to three possible isomers (since the ligands are all the same), two with C_{2v} symmetry and one

* Author to whom correspondence should be addressed.

† This considers that the ligands adopt a *quasi*-icosahedral arrangement only, and that the Fe_3 triangle adopts either the C_{2v}-orientation shown in Fig. 2 or the D_3-form.[2] We have chosen to ignore the possibility of a C_{2v}-form with face-capping CO.[2] Clearly if account is taken of a possible cuboctahedral or anticuboctahedral arrangement then this number will be increased substantially. It is also assumed that L does not adopt a bridging position (but see text).

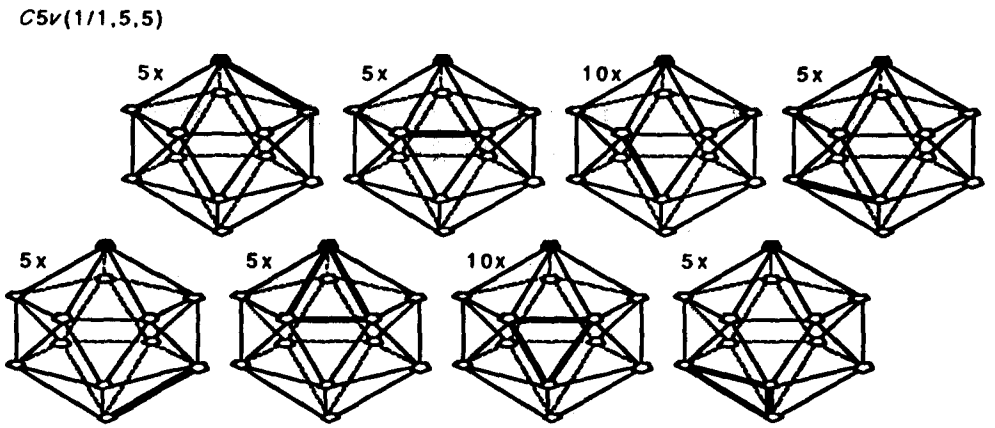

Fig. 1. Possible isomers of $Fe_3(CO)_{11}L$. The thick dark line indicates the position of M_3 within the ligand polyhedron. The single dark line is for a bridged structure. Thus each dark line defines a cluster geometry, and counting lines indicates numbers of isomers. Three thick dark lines indicate the geometry of the unbridged geometries. Thus each triangle defines a different unbridged geometry. 30 × etc., indicates the number of isomers which are indistinguishable from the one indicated (optical isomers are not separated).

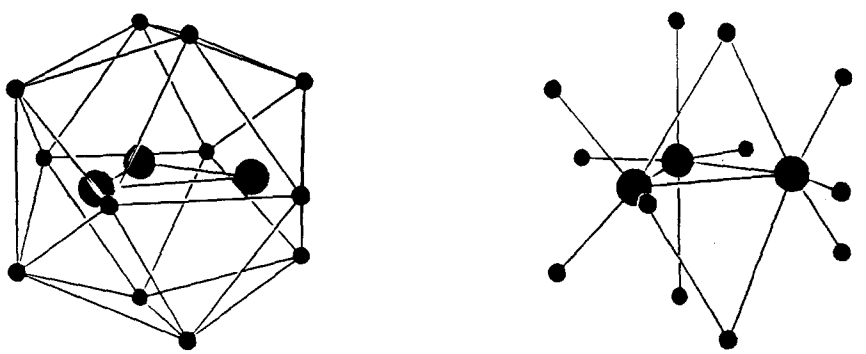

Fig. 2. Triangle in icosahedral (C_{2v}).

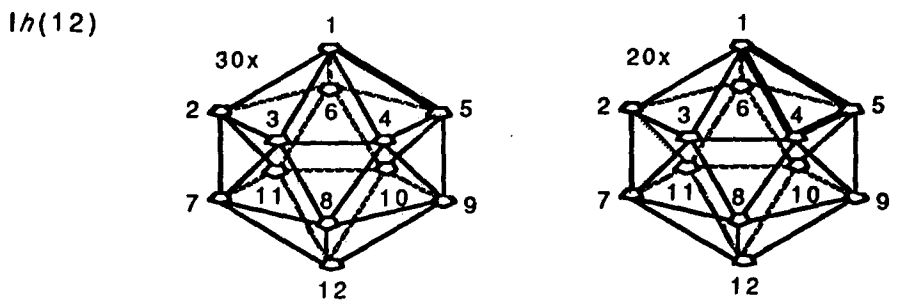

Fig. 3. The possible M_3 orientations within the $(CO)_{12}$ ligand polyhedron. Notation as in Figs 1 and 4.

* Strictly these arguments only apply to these molecules in solution. In the crystal, however, molecule packing may cause the molecules to adopt a lower symmetry, e.g. C_2 for $Fe_3(CO)_{12}$.

with D_3 symmetry (Fig. 2).* These form a class of isomers which we choose to call *orientational isomers*. The different isomers are schematically illustrated in Fig. 3, where the number of indis-

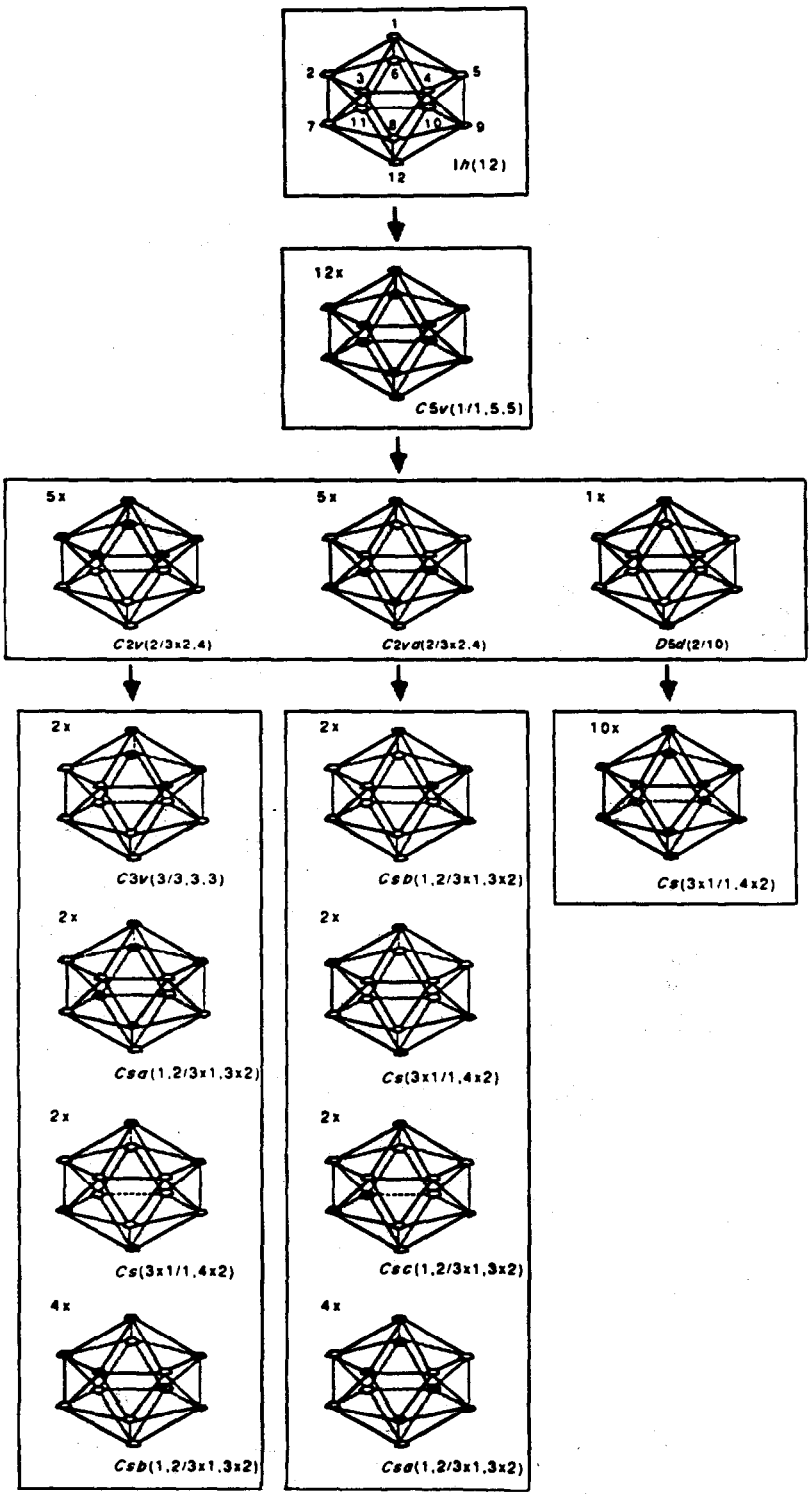

Fig. 4. The distinct ligand polyhedra for $(CO)_{12}$, $(CO)_{11}L$, $(CO)_{10}L_2$ and $(CO)_9L_3$. 12× etc., denotes the number of equivalent polyhedra in going from the previous step to the current one. C_{2v} (2/3 × 2,4) means the ligand polyhedron has C_{2v} symmetry, has two identical L, three pairs of identical COs, and one set of four identical COs. ● L; ○ CO; ● CO which is in an equivalent position to new L.

tinguishable (except in a labelled atom sense) isomers are also indicated. Orientational isomerism, the property of organizing one polygon or polyhedron (the metal cluster unit) within another (the ligand envelope), may be exhibited by a wide range of molecules in all states of aggregation. It is a particular property of carbonyl clusters but is also found in simpler systems such as $[Re_2Cl_8^{2-}]$.[7]

We now come to the second point concerning isomerism in clusters. An isolated ligand poly-

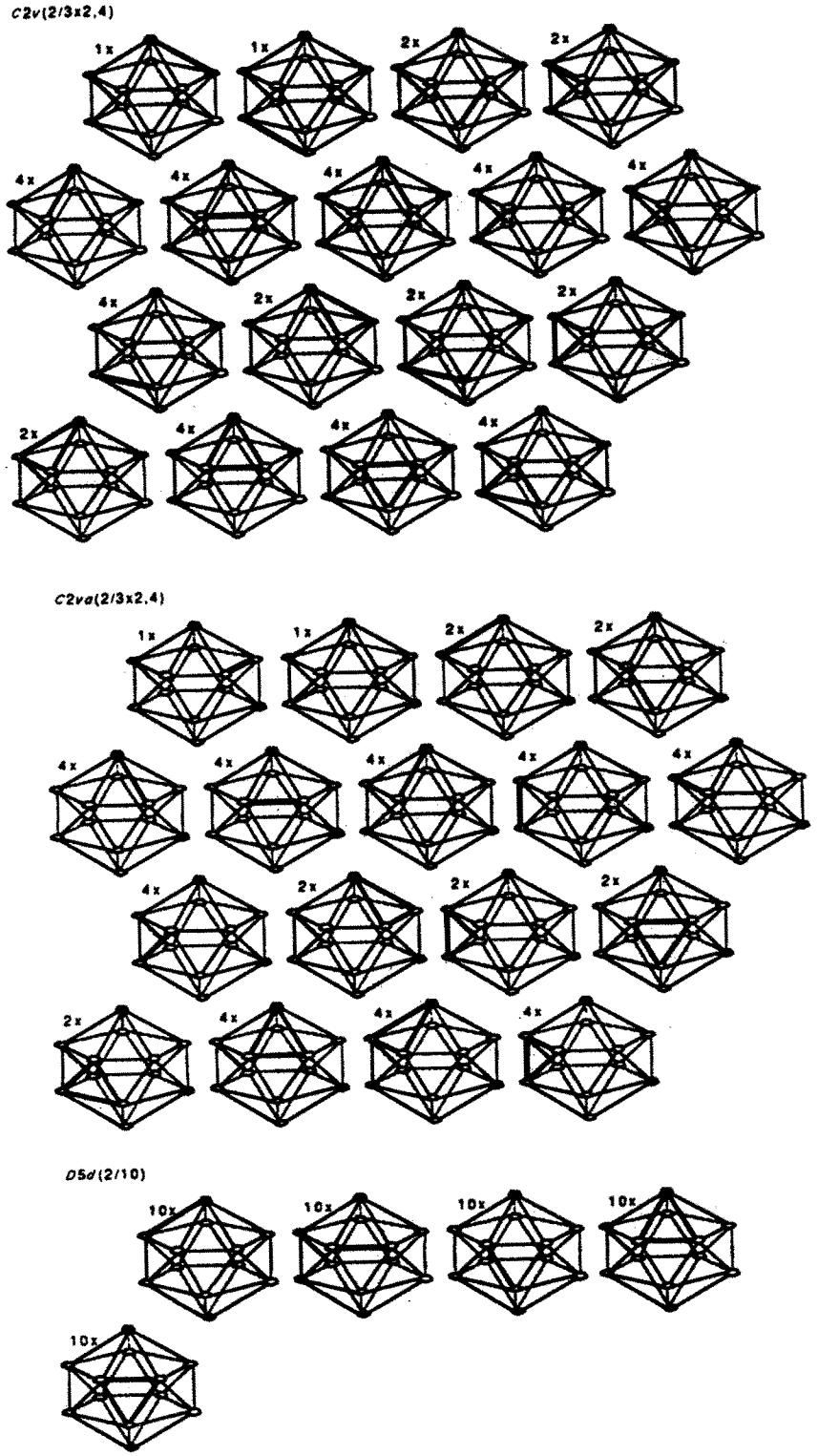

Fig. 5. Isomers for $Fe_3(CO)_{10}L_2$. Notation as in Figs 1 and 4.

hedron [for example the CO icosahedron in $Fe_3(CO)_{12}$] can undergo ligand substitution to produce new polyhedral forms such as $(CO)_{11}L$ or $(CO)_{10}L_2$. Because of the high symmetry of the parent polyhedron (all vertices are equivalent*), there is only one distinct monosubstituted ligand polyhedron (cf. Fig. 4). However, as mentioned above, when the metal polyhedron is inserted there are five distinguishable edge-bridged C_{2v} clusters (counting enantiomers as equivalent) and three distinguishable D_3 clusters. These are illustrated in Fig. 1, where the numbers of equivalent isomers of each kind are also indicated. If L can only be a terminal ligand then the second isomer illustrated in Fig. 1 will not occur.

The bis-substituted ligand polyhedron has three possible forms which we denote for simplicity the 1,2-form, the 1,7-form and the 1,12-form. Their relative weightings are 5:5:1. The more explicit labelling in the figures, e.g. $C2v(2/3 \times 2,4)$, indicates the symmetry of the ligand polyhedron in the absence of the metal triangle, the number of substituted ligands (in this case two), and the relationships between the remaining ligands (in this case there are three pairs of equivalent atoms and one set of four equivalent atoms). Now consider the consequence of inserting the Fe_3 triangle. As illustrated in Fig. 5 there are in total 23 distinct (once again counting enantiomers as indistinguishable)

* Incidentally, this is not general and only applies to the five platonic polyhedra.

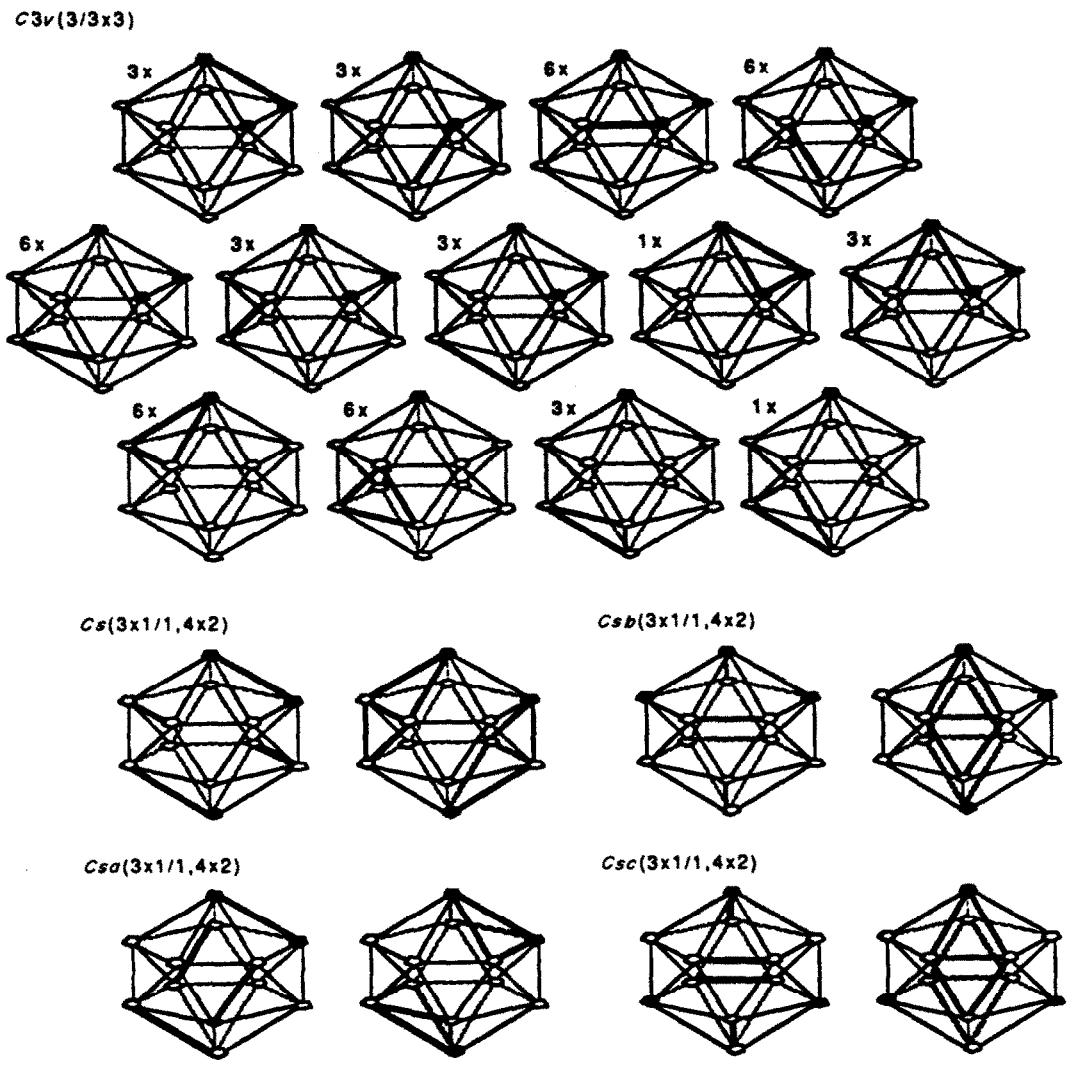

Fig. 6. Isomers of $M_3(CO)_9L_3$. Notation for C_{3v} geometry is as in Figs 1 and 4. Each C_s geometry has four unique edges and 13 sets of two equivalent edges and each edge correlates with a bridged cluster. The diagrams indicate the four unique edges. Each C_s geometry also has four unique faces and eight sets of two equivalent faces and each face correlates with an unbridged isomer. The diagrams indicate the unique faces.

edge-bridged isomers (seven of which involve bridge-site occupancy of the substituted ligand), and 16 distinct non-bridged isomers.

The number of isomers for $n > 2$ can be derived in the same manner. In general, the symmetry of these molecules is lower and the number of distinct isomers increases.

The mechanisms by which isomer interconversions may occur are moderately easy to visualize and understand within this model. They can be subdivided into two categories. (i) Those where interconversion between the various orientational isomers takes place by a simple librational motion (about the C_2-axis of the iron triangle) of the type recently described[6] for $Fe_3(CO)_{12}$ and other, related carbonyl clusters. Such a rearrangement leaves the ligand polyhedron essentially unchanged (though its metal–ligand bonding, and hence symmetry, may have changed). (ii) The second kind of rearrangement is when one ligand polyhedron is converted to another, e.g. when a 1,2-form changes to a 1,7-form in a bis-substituted cluster. This genuine ligand–polyhedron rearrangement is of a type described elsewhere, and more closely corresponds to the more traditional view of carbonyl fluxionality.

The factors which determine which isomers are observed are less easily defined. The relative statistical probabilities of the different isomers (cf. figures) influence the result, but the relative stabilities of the isomers and how much energy is required for rearrangement to occur are more significant. There is no doubt that a dominating contribution to the difference in energies between isomers is the steric constraints imposed by the ligand envelope. It is this which primarily governs the ligand polyhedron (i.e. icosahedral, or cuboctahedral or anti-cuboctahedral for 12 ligands) adopted in the ground state. The precise distribution of the ligands L within this polyhedron is, in our view, also governed mainly by steric arguments although undoubtedly electronic factors have a significant role to play. It is also important to note that although the idea of tertiary-phosphine bridges is somewhat alien to current views, this possibility should not be excluded from any mechanism of a high energy isomerization process. There is no intrinsic reason why this bonding mode should not exist, indeed we have recently observed it for the closely related ligand Ph_3Sb in the ground-state crystal structure of a cluster species. It simply represents a high(er) energy alternative.

In this communication we have attempted to reveal and unravel some of the complexities of cluster isomerism and to lay down some simple ground rules for a better appreciation of this widespread and frequently complicated phenomenon. We would again emphasize that the approach described here is not restricted to the trinuclear iron cluster carbonyls examined, but is general and may be applied to a wide range of cluster molecules and ions. The application of these ideas to a more comprehensive range of materials will be given in a subsequent, fuller report.

REFERENCES

1. See, for example, H. Adams, N. A. Bailey, G. W. Bentley and B. E. Mann, *J. Chem. Soc., Dalton Trans.* 1989, 1831.
2. B. F. G. Johnson, *J. Chem. Soc., Chem. Commun.* 1976, 211; 703.
3. See, for example, F. A. Cotton and G. Wilkinson, *Advanced Inorganic Chemistry*. John Wiley, New York (1980).
4. B. F. G. Johnson, to be published.
5. R. Benfield and B. F. G. Johnson, *J. Chem. Soc., Dalton Trans.* 1980, 1743.
6. C. E. Anson, R. E. Benfield, D. Braga, A. W. Bott, B. F. G. Johnson and E. A. Marseglia, *J. Chem. Soc., Chem. Commun.* 1988, 889.
7. F. A. Cotton and D. Walton, to be published.

Polyhedron Vol. 9, No. 14, pp. 1775–1778, 1990
Printed in Great Britain

0277–5387/90 $3.00+.00
© 1990 Pergamon Press plc

COMMUNICATION

COMPETITIVE ALKYL AND HALIDE METATHESIS IN THE REACTIONS OF GRIGNARD REAGENTS WITH Tl{η^3-HB(3-Bu^{t}pz)$_3$}

RUNYU HAN, MAX BACHRACH and GERARD PARKIN*

Department of Chemistry, Columbia University, New York, NY 10027, U.S.A.

(*Received* 12 *March* 1990; *accepted* 17 *May* 1990)

Abstract—The reactions of Grignard reagents RMgX [RMgX = CH_3MgCl, CH_3MgBr, CH_3MgI, CH_3CH_2MgCl, $(CH_3)_2CHMgCl$ and $(CH_3)_3CMgCl$] with Tl{η^3-HB(3-Bu^{t}pz)$_3$} (3-Bu^{t}pz = 3-$C_3N_2Bu^tH_2$) show that metathesis of the Mg—R bond is favoured for X = Cl, Br, whereas metathesis of the Mg—X bond is favoured for X = I.

The η^3-tris(pyrazolyl)hydroborato ligand has been used extensively to provide well-defined coordination environments for both the transition metals[1] and, more recently, the *s*- and *p*-block elements.[2,3] Conventional methods for the introduction of tris(pyrazolyl)hydroborato ligands generally involve the metathesis of a metal–halide bond with either the potassium or thallium salts of the tris(pyrazolyl)hydroborato ligand. We have recently reported that tris(pyrazolyl)hydroborato ligands may also be introduced by the metathesis of the metal-*alkyl* bonds of R_2Mg,[3] R_3Al[4] and R_2Zn,[5] and were particularly interested in investigating whether such metal-alkyl bond metathesis is more or less favoured than that of the corresponding metal–halide bonds. Here we describe the reactions between Grignard reagents and the complex Tl{η^3-HB(3-Bu^{t}pz)$_3$} (3-Bu^{t}pz = 3-$C_3N_2Bu^tH_2$) which demonstrate that for this system alkyl substitution is competitive with halide substitution, but is highly dependent upon the Grignard reagent.

The reactions of the chloro and bromo Grignard reagents RMgX [RMgX = CH_3MgCl, CH_3MgBr, CH_3CH_2MgCl, $(CH_3)_2CHMgCl$ and $(CH_3)_3CMgCl$] with Tl{η^3-HB(3-Bu^{t}pz)$_3$} in a 1:1 molar ratio in Et_2O at room temperature, result in metathesis of the Mg—R bond, in preference to the Mg—X bond, to give {η^3-HB(3-Bu^{t}pz)$_3$}MgX [eq. (1)]:[6]

$$RMgX + Tl\{\eta^3\text{-HB(3-Bu}^t\text{pz)}_3\} \xrightarrow{Et_2O} \{\eta^3\text{-HB(3-Bu}^t\text{pz)}_3\}MgX + [TlR]. \quad (1)$$

The molecular structure of {η^3-HB(3-Bu^{t}pz)$_3$}MgCl has been determined by single crystal X-ray diffraction (Fig. 1) which confirms both the monomeric nature of the complex and the η^3-coordination mode of the tris(pyrazolyl)hydroborato ligand.†

* Author to whom correspondence should be addressed.

† Crystal data for {η^3-HB(3-Bu^{t}pz)$_3$}MgCl: $C_{21}H_{34}N_6BMgCl$, $M = 441.18$, orthorhombic, space group *Pnma* (No. 62), $a = 16.048(7)$, $b = 16.006(3)$, $c = 9.840(1)$ Å, $U = 2527(1)$ Å^3, $Z = 4$, $D_c = 1.16$ g cm^{-3}, $F(000) = 944$ electrons, μ(Mo-K_α) = 20 cm^{-1}, $T = 295$ K, crystal dimensions $0.36 \times 0.60 \times 0.66$ mm^3. Intensity data were collected on a Nicolet R3M diffractometer using monochromated Mo-K_α radiation ($\lambda = 0.71073$ Å) and were corrected for Lorentz and polarization effects. A total of 3813 unique reflections were collected in the range $3 < 2\theta < 60°$, of which 1182 with $F_o > 6\sigma(F_o)$ were used in the structure determination. The structure was solved by direct methods and refined using standard difference map techniques. Most of the hydrogen atoms were located in the difference map after all the non-hydrogen atoms were located and refined anisotropically, but hydrogen atoms on carbon were allowed to refine in calculated positions [$d_{C-H} = 0.96$ Å; $U_{iso}(H) = 1.2U_{iso}(C)$]. Block-diagonal least-squares refinement converged to $R = 5.17$ ($R_w = 5.90$), with the maximum shift-to-σ ratio of 0.16 for the last cycle. The final difference map showed no significant features, with the highest final peak 0.2 e Å^{-3} near Mg. Atomic coordinates, bond lengths and angles, and thermal parameters have been deposited at the Cambridge Crystallographic Data Centre.

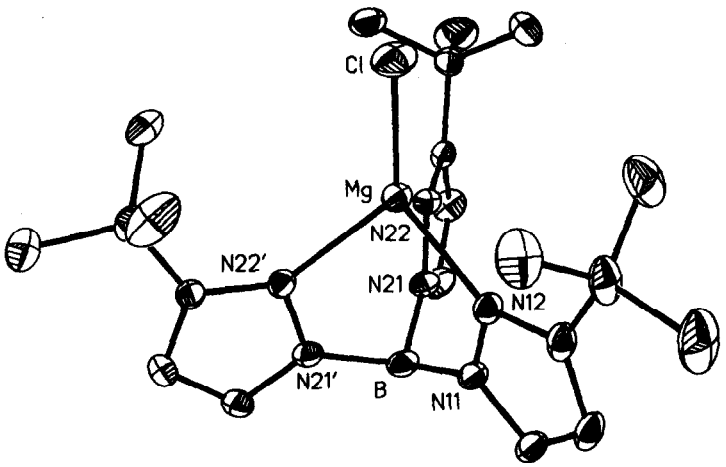

Fig. 1. ORTEP diagram of $\{\eta^3\text{-HB(3-Bu}^t\text{pz)}_3\}$MgCl. For clarity, thermal ellipsoids are shown at 20% probability. Selected bond distances (Å) and angles (°): Mg—Cl = 2.262(2), Mg—N(12) = 2.097(5), Mg—N(22) = 2.100(3), N(11)—N(12) = 1.379(6), N(21)—N(22) = 1.376(4), B—N(11) = 1.542(8), B—N(21) = 1.538(5); N(12)—Mg—N(22) = 93.7(1), N(22)—Mg—N(22)′ = 93.3(2), N(11)—B—N(21) = 110.0(3), N(21)—B—N(21)′ = 109.4(5), Cl—Mg—N(12) = 121.4(2), Cl—Mg—N(22) = 123.4(1).

In contrast to the sole formation of $\{\eta^3\text{-HB(3-Bu}^t\text{pz)}_3\}$MgX in the reaction of $Tl\{\eta^3\text{-HB(3-Bu}^t\text{pz)}_3\}$ with 1 equivalent of CH_3MgX (X = Cl, Br), the analogous reaction with CH_3MgI results in preferential metathesis of the Mg—I bond to give the methyl complex, $\{\eta^3\text{-HB(3-Bu}^t\text{pz)}_3\}MgCH_3$, as the major product [eq. (2)]:[6]

$$CH_3MgI + Tl\{\eta^3\text{-HB(3-Bu}^t\text{pz)}_3\} \xrightarrow{(80\%)} \{\eta^3\text{-HB(3-Bu}^t\text{pz)}_3\}MgCH_3 + TlI$$
$$\xrightarrow{(20\%)} \{\eta^3\text{-HB(3-Bu}^t\text{pz)}_3\}MgI + [TlCH_3]. \quad (2)$$

These results demonstrate that the order of metathesis for this system is Mg—I > Mg—CH_3 > Mg—X (X = Cl, Br). The preferential metathesis of the Mg—I bond versus the Mg—CH_3 bond is another illustration of the observation that reactions of transition metal halide derivatives with Grignard reagents often result in halide exchange rather than alkylation.[7]

In order to assess whether the trend Mg—I > Mg—CH_3 > Mg—X (X = Cl, Br) represents a kinetic or thermodynamic preference for this system, it is necessary to examine the pathways that may lead to the formation of both $\{\eta^3\text{-HB(3-Bu}^t\text{pz)}_3\}$MgR and $\{\eta^3\text{-HB(3-Bu}^t\text{pz)}_3\}$MgX. Alkyl and halide ligands in solutions of Grignard reagents are kinetically labile, as evidenced by the Schlenk equilibrium [eq. (3)]

$$3RMgX \rightleftharpoons R_2Mg + MgX_2 \quad (3)$$

and the position and rate of re-establishment of this equilibrium, for which relatively little quantitative information is available, may have a critical effect on the observed product distribution.[8] As a result of this complexity there exists a manifold of reaction pathways that may independently lead to the products $\{\eta^3\text{-HB(3-Bu}^t\text{pz)}_3\}$MgX and $\{\eta^3\text{-HB(3-Bu}^t\text{pz)}_3\}$MgR, of which the competitive metathesis of the Mg—R and Mg—X bonds of RMgX is the most direct, and simplest, pathway. Although the system is undoubtedly complicated and consequently the analysis subject to uncertainty, there is evidence that supports the view that the observed products are a result of direct metathesis between $Tl\{\eta^3\text{-HB(3-Bu}^t\text{pz)}_3\}$ and RMgX. For example, the formation of $\{\eta^3\text{-HB(3-Bu}^t\text{pz)}_3\}$MgCl by the independent reaction of $Tl\{\eta^3\text{-HB(3-Bu}^t\text{pz)}_3\}$ with $MgCl_2$ is notably slower than the reaction with

RMgCl, which thus suggests that the reaction between Tl{η^3-HB(3-Bu^{t}pz)$_3$} and RMgCl does not proceed via reaction with $MgCl_2$ that is generated by the Schlenk equilibrium.* Considering the pathway involving direct metathesis of Tl{η^3-HB(3-Bu^{t}pz)$_3$} with RMgX, the formation of the product {η^3-HB(3-Bu^{t}pz)$_3$}MgX does not, *per se*, indicate that Mg—R bond metathesis is kinetically favoured over Mg—X bond metathesis. For example, if Mg—R bond metathesis was rapidly reversible [eq. (4)], i.e.

$$RMgX + Tl\{\eta^3\text{-HB(3-Bu}^t\text{pz)}_3\} \rightleftharpoons \{\eta^3\text{-HB(3-Bu}^t\text{pz)}_3\}MgR + TlX, \quad (4)$$

then the product {η^3-HB(3-Bu^{t}pz)$_3$}MgX could be formed as a result of the driving force of the irreversible decomposition of unstable [TlR] [eq. (5)]:[6]

$$RMgX + Tl\{\eta^3\text{-HB(3-Bu}^t\text{pz)}_3\} \longrightarrow \{\eta^3\text{-HB(3-Bu}^t\text{pz)}_3\}MgX + Tl + \text{dec.} \quad (5)$$

If the above hypothesis was correct, then it would be necessary for {η^3-HB(3-Bu^{t}pz)$_3$}MgR to react with TlCl to give {η^3-HB(3-Bu^{t}pz)$_3$}MgCl [eq. (6)]:

$$\{\eta^3\text{-HB(3-Bu}^t\text{pz)}_3\}MgR + TlCl \rightleftharpoons RMgCl + Tl\{\eta^3\text{-HB(3-Bu}^t\text{pz)}_3\} \longrightarrow \{\eta^3\text{-HB(3-Bu}^t\text{pz)}_3\}MgCl + Tl + \text{dec.} \quad (6)$$

However, TlCl does not react with {η^3-HB(3-Bu^{t}pz)$_3$}MgR to give {η^3-HB(3-Bu^{t}pz)$_3$}MgCl, and thus the formation of {η^3-HB(3-Bu^{t}pz)$_3$}MgX in the reactions of Tl{HB(3-Bu^{t}pz)$_3$} with RMgX are a result of kinetically favoured Mg—R bond metathesis. Other evidence mitigating against preferential Mg—X (X = Cl, Br) bond metathesis is that the product {η^3-HB(3-Bu^{t}pz)$_3$}MgCl is not formed by the reaction of {η^3-HB(3-Bu^{t}pz)$_3$}MgR with excess RMgCl [eq. (7)]:

$$\{\eta^3\text{-HB(3-Bu}^t\text{pz)}_3\}MgR + RMgCl \not\rightarrow \{\eta^3\text{-HB(3-Bu}^t\text{pz)}_3\}MgCl + R_2Mg. \quad (7)$$

In contrast, {η^3-HB(3-Bu^{t}pz)$_3$}MgCl reacts with excess RMgX to give {η^3-HB(3-Bu^{t}pz)$_3$}MgR [eq. (8)]:

$$\{\eta^3\text{-HB(3-Bu}^t\text{pz)}_3\}MgX + RMgX \longrightarrow \{\eta^3\text{-HB(3-Bu}^t\text{pz)}_3\}MgR + MgX_2. \quad (8)$$

Thus, for the chloro and bromo Grignard reagents, RMgX (X = Cl, Br), the observed results are most consistent with the formation of {η^3-HB(3-Bu^{t}pz)$_3$}MgX as a result of kinetically favoured Mg—R bond metathesis. Furthermore, the irreversible decomposition of [TlR] that accompanies the formation of {η^3-HB(3-Bu^{t}pz)$_3$}MgI in the reaction of Tl{η^3-HB(3-Bu^{t}pz)$_3$} with CH_3MgI [eq. (2)] implies that the formation of {η^3-HB(3-Bu^{t}pz)$_3$}$MgCH_3$ as the major product must be a result of more facile Mg—I bond over Mg—CH_3 bond metathesis. Although {η^3-HB(3-Bu^{t}pyz)$_3$}$MgCH_3$ would also be obtained from the reaction of Tl{η^3-HB(3-Bu^{t}pz)$_3$} with $(CH_3)_2Mg$[3a] generated by the Schlenk equilibrium, this sequence would result in the deposition of Tl metal, in contrast to the observed TlI. As such, it is unlikely that this pathway is responsible for the formation of {η^3-HB(3-Bu^{t}pyz)$_3$}$MgCH_3$ from CH_3MgI.

In conclusion, the reactions of Tl{η^3-HB(3-Bu^{t}pz)$_3$} with Grignard reagents may result in substitution of either the alkyl ligand to give {η^3-HB(3-Bu^{t}pz)$_3$}MgX, or the halide ligand to give {η^3-HB(3-Bu^{t}pz)$_3$}MgR. Chloro and bromo Grignard reagents give products arising from alkyl metathesis, whereas the iodo Grignard reagent CH_3MgI favours halide metathesis. The data suggest that these observations reflect a kinetic preference for Mg—X bond metathesis in the sequence Mg—I > Mg—CH_3 > Mg—X (X = Cl, Br) for the reactions of Grignard reagents with Tl{η^3-HB(3-Bu^{t}pz)$_3$}.

Acknowledgement—We thank the donors of the Petroleum Research Fund, administered by the ACS, for partial support of this research.

REFERENCES

1. (a) S. Trofimenko, *Accts Chem. Res.* 1971, **4**, 17; (b) S. Trofimenko, *Chem. Rev.* 1972, **72**, 497; (c) S. Trofimenko, *Prog. Inorg. Chem.* 1986, **34**, 115; (d) A. Shaver, *Comprehensive Coordination Chemistry* (Edited by G. Wilkinson, R. D. Gillard and J. A. McCleverty), Vol. 2, pp. 245–259. Pergamon Press, Oxford (1987); (e) A. Shaver, *J. Organomet. Chem. Library* 1977, **3**, 157.
2. (a) S. Trofimenko, *J. Am. Chem. Soc.* 1967, **89**, 3170; (b) B. K. Nicholson, *J. Organomet. Chem.* 1984, **265**, 153; (c) S. K. Lee and B. K. Nicholson, *J. Organomet. Chem.* 1986, **309**, 257; (d) A. H. Cowley, C. J. Carrano, R. L. Geerts, R. A. Jones and C. M. Nunn, *Angew. Chem. Int. Ed. Engl.* 1988, **27**, 277; (e) A. H. Cowley, R. L. Geerts, C. M. Nunn and C. J. Carrano, *J. Organomet. Chem.* 1988, **341**, C27.
3. (a) R. Han, A. Looney and G. Parkin, *J. Am. Chem. Soc.* 1989, **111**, 7276; (b) R. Han and G. Parkin, *J. Am. Chem. Soc.* 1990, **112**, 3662.

*$MgCl_2$ was stirred in Et_2O overnight in order to obtain a saturated solution before addition of Tl{η^3-HB(3-Bu^{t}pz)$_3$}. However, we can not exclude the possibility that the solvated form of $MgCl_2$ generated as a result of the Schlenk equilibrium may lead to higher concentrations of "$MgCl_2$" being present under the reaction conditions using RMgCl as the reagent.

4. A. Looney and G. Parkin, *Polyhedron* 1990, **9**, 265.
5. I. B. Gorrell, A. Looney and G. Parkin, *J. Chem. Soc., Chem. Commun.* 1990, 220.
6. The reactions were typically carried out by addition of the appropriate Grignard reagent to solution of $Tl\{\eta^3\text{-}HB(3\text{-}Bu^tpz)_3\}$ (50 mg) in Et_2O (15 cm^3) at room temperature, and the products analysed by ^1H NMR spectroscopy after work-up. The products $\{\eta^3\text{-}HB(3\text{-}Bu^tpz)_3\}MgR$ [R = CH_3, CH_2CH_3, $CH(CH_3)_2$] and $\{\eta^3\text{-}HB(3\text{-}Bu^tpz)_3\}MgX$ (X = Cl, Br, I) have been reported previously (ref. 3). The reactions were also accompanied by the deposition of Tl metal, consistent with the proposed decomposition pathway for $[TlCH_3]$ (H. Gilman and R. G. Jones, *J. Am. Chem. Soc.* 1946, **68**, 517), while the reaction with CH_3MgI was also accompanied by the deposition of TlI. Product distributions are not markedly affected by prolonged reaction times.
7. See for example, B. Hessen, T. H. Lemmen, H. J. G. Luttikhedde, J. H. Teuben, J. L. Petersen, J. C. Huffman, S. Jagner and K. G. Caulton, *Organometallics* 1987, **6**, 2354.
8. (a) E. C. Ashby, *Pure Appl. Chem.* 1980, **52**, 545; (b) B. J. Wakefield, *Pure Appl. Chem.* 1966, **1**, 131; (c) M. S. Kharasch and O. Reinmuth, *Grignard Reactions of Nonmetallic Substances.* Prentice-Hall, New York (1954); (d) J. Toney and G. D. Stucky, *J. Organomet. Chem.* 1971, **28**, 5; (e) E. C. Ashby and M. B. Smith, *J. Am. Chem. Soc.* 1964, **86**, 4363; (f) E. C. Ashby and W. E. Becker, *J. Am. Chem. Soc.* 1963, **85**, 118.

Polyhedron Vol. 9, No. 14, p. 1779, 1990
Pergamon Press plc. Printed in Great Britain

BOOK REVIEW

Gmelin Handbook of Inorganic Chemistry. Ge–Germanium. (Organogermanium Compounds. Part 2.) Published by the Gmelin Institute for Inorganic Chemistry of the Max Planck Society for the Advancement of Science, 8th Edn. Springer, Berlin, 1989, ISBN 3-540-93585-1, 398 pp.

This is the second volume on organogermanium compounds in the excellent series of Gmelin Handbooks. Part 1 dealt with the tetraorganyls and Me_3GeR compounds with R = substituted methyl, higher alkyls or cyclic alkyls; Part 2 continues in this theme with R = unsaturated or heterocyclic groups, although its majority is devoted to compounds of the type Et_3GeR. The literature has been covered up to 1985.

The Me_3GeR compounds covered include the following R: linear and branched-chain alkenyls in which the longest carbon chain is C_8, cyclic and polycyclic alkenyls; alkynyls; aryls; and heterocyclics. Systems are included in which all the above ligands are substituted with various combinations of *p*-block or transition metal moieties. The remainder of the volume then deals with Et_3GeR, for which R is similar to those mentioned above, but in addition includes the following: unsubstituted alkyls up to C_{12}; alkyls up to C_8 (mainly C_1 and C_2) substituted with aryls and/or a variety of functional groups involving *p*-block elements, as well as one transition metal; and cycloalkyls, both simple and substituted.

This series is renowned for its very high quality in both presentation and comprehensiveness, and this text is no exception. Most data are presented in tabular form supplemented by notes on the more important compounds; it includes details on preparation, physical properties, structure and spectroscopic data. The empirical formula and ligand formula indexes prove most useful for the location of specific compounds.

In conclusion, the book can be recommended unreservedly for those who require ready availability of detailed information on this subject.

DARIO M. FRIGO

Billiton Research B.V.
Postbox 40
6800 AA Arnhem
The Netherlands

Polyhedron Vol. 9, No. 15/16, p. 1781, 1990
Pergamon Press plc. Printed in Great Britain

FOREWORD

I am delighted to have the opportunity to serve as Guest Editor for a Polyhedron Symposium-in-Print on The Interplay of Theory and Experiment in Inorganic Chemistry. This special issue contains contributions on a variety of topics in inorganic chemistry, most of which highlight the synergy between theoretical and experimental studies in inorganic and organometallic chemistry. I wish to thank all the contributors to this issue for the high quality of the science reported, and for their patience during the process of putting the issue together. I also want to thank the capable professionals at Pergamon Press, especially Miss Sheryl Fellows, for seeing this project through to fruition.

Current research aside, there is another, more compelling reason for the publication of this Symposium-in-Print: To honour Professor Richard F. Fenske on his retirement from the University of Wisconsin-Madison after nearly 30 years of service to that institution. Dick Fenske has been one of the pioneers in the application of molecular orbital theory to large inorganic systems. He has been one of the strongest proponents, and one of the most careful practitioners, of the interplay between theory and experiment in inorganic chemistry. His research has always been characterized by careful, incisive analysis, from his seminal studies of the bonding in metal hexacarbonyls, to the development of the very popular Fenske–Hall molecular orbital method, to his most recent work on the theoretical understanding of NMR chemical shifts. Dick's lectures at scientific meetings were legendary exhibitions of the power of the spoken word; his proselytising "sermons" on inorganic theory did much to increase the interest in theoretical studies among experimental inorganic chemists.

Dick Fenske's contributions to our craft extend far past his published scientific contributions. He served as Chairman of his Department for six years and as Associate Dean for five years. He has been honoured for his teaching excellence by the University of Wisconsin. He has left a sizable legacy to universities throughout the United States as more than half of his PhD students have chosen academic careers.

The contributors to this Symposium-in-Print include Dick's friends, colleagues, and former students. I think I speak for all of us in thanking Dick for his contributions to science, his insight, his counsel, and his good humour and colleagiality. While we will miss his active involvement in inorganic chemistry, we wish him well in his retirement.

BRUCE E. BURSTEN

Polyhedron Vol. 9, No. 15/16, pp. 1783–1797, 1990
Printed in Great Britain

0277–5387/90 $3.00+.00
© 1990 Pergamon Press plc

THE ELECTRONIC STRUCTURE OF NITROSYL AND CARBONYL SUPPORTED METAL–METAL INTERACTIONS. THE PHOTOELECTRON SPECTRA OF $[\eta^5\text{-}(C_5H_5)Fe(\mu\text{-}NO)]_2$, $[\eta^5\text{-}(C_5(CH_3)_5)Fe(\mu\text{-}NO)]_2$, $[\eta^5\text{-}(C_5H_5)Ru(\mu\text{-}NO)]_2$ AND $[\eta^5\text{-}(C_5(CH_3)_5)Co(\mu\text{-}CO)]_2$†

DENNIS L. LICHTENBERGER‡ and ANN S. COPENHAVER

Laboratory for Electron Spectroscopy and Surface Analysis, Department of Chemistry, University of Arizona, Tucson, AZ 85721, U.S.A.

and

JOHN L. HUBBARD

Department of Chemistry and Biochemistry, Utah State University, Logan, UT 84322-0300, U.S.A.

Abstract—The valence photoelectron ionizations of $[CpFe(\mu\text{-}NO)]_2$, $[Cp^*Fe(\mu\text{-}NO)]_2$, $[CpRu(\mu\text{-}NO)]_2$ and $[Cp^*Co(\mu\text{-}CO)]_2$ ($Cp = \eta^5\text{-}C_5H_5$ and $Cp^* = \eta^5\text{-}C_5(CH_3)_5$) are examined in comparison to several theoretical calculations of the electronic structure and bonding in these complexes. The photoelectron spectra of this group of complexes, when collected together, allow identification of the eight valence metal-based ionizations. There is considerable disparity among the various calculations on the predicted order of these ionizations. The combination of Fenske–Hall calculations with experimental observations of ionization *trends* between isoelectronic first row complexes [Fe(NO) vs Co(CO)], between first and second row complexes (Fe vs Ru), and between complexes with ring methylation (Cp vs Cp*) allows a consistent assignment of the valence ionizations. The interplay of theory and experiment gives unique insight into the nature of bridging ligand coordination and clarifies the relative strengths of metal–ligand and metal–metal interactions, in each complex. It is found that as many metal–metal antibonding orbitals are occupied as metal–metal bonding orbitals, so that the formal metal–metal bond order is zero. The interactions are important in defining the bonding and stability of the complexes. These interactions lead to large ligand character in two of the valence ionizations.

The understanding of electronic interactions between two metal centres and their coordinated ligands has been of fundamental experimental and theoretical interest.[1–8] One class of seemingly simple complexes which exhibit these interactions is represented by the following four complexes: $[CpFe(\mu\text{-}NO)]_2$, $[Cp^*Fe(\mu\text{-}NO)]_2$, $[CpRu(\mu\text{-}NO)]_2$ and $[Cp^*Co(\mu\text{-}CO)]_2$, where Cp is cyclopentadienyl and Cp* is pentamethylcyclopentadienyl. These complexes are isoelectronic and basically isostructural with one another. These metal dimers are bridged by either a carbonyl or nitrosyl and, with d^8 metal centres, formally possess a metal–metal double bond (see Fig. 1). Because of the relatively simple

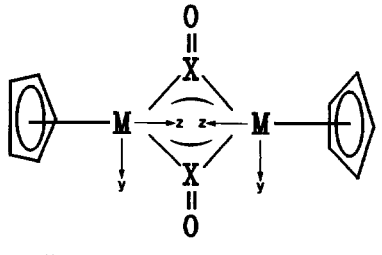

Fig. 1. Coordinate system for the planar D_{2h} $[CpM(\mu\text{-}XO)]_2$ dimers. The local coordinate system about each metal is right handed, so the x axis points above the plane for the left metal and below the plane for the right metal.

† Dedicated to Professor Richard F. Fenske, in appreciation of his pioneering contributions to theoretical and inorganic chemistry and, in particular for his sharing the excitement and joy of chemistry as my PhD mentor (D. L. L.).

‡ Author to whom correspondence should be addressed.

ligands and high symmetry, these complexes offer a unique opportunity to study and understand supported metal–metal interactions. Study of the interplay between metal–metal bonding and antibonding combinations and the interaction of the cyclopentadienyl coordination to the metal valence levels, as well as the stabilization due to bridging ligand backbonding with both metal centres, is addressed through these complexes.

In this paper we examine the electronic structure and bonding of these systems through photoelectron spectroscopy. The evaluation of these spectra is difficult because of the large number and the extensive overlap of these valence ionizations. Photoelectron spectra have been reported previously for a few of these complexes.[3,4,8] However, the earlier assignments of the ionizations of these complexes are highly uncertain because of low resolution in the spectra and a lack of correlation with the ionizations of similar complexes. Fenske–Hall and *ab initio* calculations have been used to assist in the evaluation and understanding of these isolated photoelectron spectra, but a survey of these calculations shows a wide variety of possible interpretations even between similar calculational methods.

Comparison of HeI and HeII relative ionization intensities aids in the assignment of metal versus ligand based ionizations. We are also able to resolve vibrational fine structure in several ionization features. This provides direct information on the character and bonding nature associated with the ionization. The most extensive information on the bonding characteristics is obtained by observing the effects of chemical substitutions which perturb the electronic structure and ionization features. For example, the π donating ability of the cyclopentadienyl ligand is changed by substituting pentamethylcyclopentadienyl for standard cyclopentadienyl. This perturbation preferentially shifts the cyclopentadienyl and mixed cyclopentadienyl–metal ionizations to lower binding energy, allowing the identification of mixed cyclopentadienyl–metal ionizations from the other metal and metal-bridging ligand ionizations.[9] The comparison of $[Cp^*Fe(\mu\text{-}NO)]_2$ and $[Cp^*Co(\mu\text{-}CO)]_2$ represents a net proton shift from each of the bridging ligands to the metals. The ionization energy shifts (or lack of shifts) are used to identify bridging ligand interactions with the metal.[10] The metal-based ionizations of the ruthenium analogue are stabilized with respect to iron, and are used to identify strong metal–metal interactions. The spectra of these complexes are presented here and a discussion on the spectral assignment is given based on comparisons between this series of related complexes.

EXPERIMENTAL

Compounds

The $[(\eta^5\text{-}C_5H_5)Fe(\mu\text{-}NO)]_2$, $[(\eta^5\text{-}C_5H_5)Ru(\mu\text{-}NO)]_2$ and $[(\eta^5\text{-}C_5Me_5)Co(\mu\text{-}CO)]_2$ complexes were prepared and purified according to published procedures.[11–13] Useful quantities of the $[(\eta^5\text{-}C_5Me_5)Fe(\mu\text{-}NO)]_2$ complex could not be obtained by published procedures,[14] so an alternate (and more facile) synthetic route is reported here.[15] Specifically, it was found that $(\eta^5\text{-}C_5Me_5)Fe(NO)Br_2$ is easily reduced to $[(\eta^5\text{-}C_5Me_5)Fe(\mu\text{-}NO)]_2$ by zinc dust in THF. The novel $(\eta^5\text{-}C_5Me_5)Fe(NO)Br_2$ complex is prepared by treating $(\eta^5\text{-}C_5Me_5)Fe(CO)_2Br$ with NOBr in CH_2Cl_2.

Synthesis of $(\eta^5\text{-}C_5Me_5)Fe(NO)Br_2$

A Schlenk flask was charged with $(\eta^5\text{-}C_5Me_5)Fe(CO)_2Br$[16] (5.0 g, 15.3 mmol) and 100 cm^3 of CH_2Cl_2 and cooled to 0°C. A solution of NOBr[17] (prepared by dissolving 2 cm^3 of $NOBr_{(l)}$ in 50 cm^3 of CH_2Cl_2 at 0°C) was added dropwise over a period of 30 min until gas evolution had largely ceased and IR indicated the complete disappearance of $(\eta^5\text{-}C_5Me_5)Fe(CO)_2Br$. The reaction mixture was concentrated *in vacuo* to approximately 25 cm^3 and transferred to the top of a 3×20 cm column of SiO_2 prepared in CH_2Cl_2. Elution of the column with pure CH_2Cl_2 produced a brownish-green zone, which after solvent removal *in vacuo* yielded 4.3 g of brown, microcrystalline $(\eta^5\text{-}C_5Me_5)Fe(NO)Br_2$. Crystallization at room temperature by layering 50 cm^3 of ether over the crude product dissolved in 30 cm^3 of CH_2Cl_2 produced 4.0 g (10.5 mmol, 67%) of analytically pure material. ^1H NMR ($CDCl_3$): δ 1.82 (s) 15H ($\eta^5\text{-}C_5\mathit{Me}_5$); IR (KBr): ν(NO) 1816 cm^{-1}; Found: C, 31.61; H, 3.79; N, 3.49. Calc. for $C_{10}H_{15}NOBr_2Fe$: C, 31.53; H, 3.94; N, 3.67%.

Synthesis of $[(\eta^5\text{-}C_5Me_5)Fe(\mu\text{-}NO)]_2$

A Schlenk flask was charged with $(\eta^5\text{-}C_5Me_5)Fe(NO)Br_2$ (0.56 g, 1.47 mmol), zinc dust (5 g, 76 mmol), and a magnetic stir bar and was capped with a new septum. The flask was then subjected to several vacuum/purge cycles to ensure a rigorously pure nitrogen atmosphere. THF (80 cm^3) was carefully added via syringe. The mixture was vigorously stirred for 1 h, during which time the starting brownish-green reaction colour changed to a deep chocolate-brown and the solution IR of the mixture showed the complete disappearance of the starting material. The reaction mixture was transferred to

the top of a 2 × 10 cm column of Al_2O_3 (I) slurry-packed in THF; elution with pure THF produced a dark-brown zone. Dark-brown, microcrystalline $[(\eta^5\text{-}C_5Me_5)Fe(\mu\text{-}NO)]_2$ (0.30 g, 0.68 mmol, 93% yield) was isolated upon removal of solvent *in vacuo*. The spectral and analytical data for this material was completely consistent with that reported by Diel for $[(\eta^5\text{-}C_5Me_5)Fe(\mu\text{-}NO)]_2$.[14]

HeI photoelectron spectra

Photoelectron spectra were measured on a spectrometer with specially designed photon sources, ionization cells, 36 cm radius hemispherical analyser (McPherson), power supplies, counter interface, and collection methods that have been described elsewhere.[18–22] The argon ionization at 15.759 eV (±0.002 eV) was used as an internal calibration lock of the energy scale. The moderately air-sensitive samples were handled in the dry-box to minimize exposure to air and were loaded into the instrument by established procedures.[23] Instrument pressure during sublimation was between 10^{-6} and 10^{-5} torr and the complexes were sublimed at 120°C for $[CpFe(\mu\text{-}NO)]_2$, 93°C for $[Cp^*Fe(\mu\text{-}NO)]_2$, 136°C for $[CpRu(\mu\text{-}NO)]_2$ and 103°C for $[Cp^*Co(\mu\text{-}CO)]_2$, with an uncertainty of ±3°C. The only abnormality observed was in the spectrum of $[CpFe(\mu\text{-}NO)]_2$. The low intensity ionization at 8.5 eV in this spectrum is due to decomposition impurity and is found in the background before and after compound sublimation.

Because high signal-to-noise is required for the vibrational analysis, spectra were obtained over a series of days. Individual data scans were collected by scanning a region for anywhere from 0.1 to 1.0 s per data point. The individual data scans were then summed together resulting in total collect times of 10–80 s per data point for the metal and ligand regions. At no time did any of the ionization features in earlier scans differ from those in later scans. Shifts of the internal calibrant between scans were at all times less than half the energy separation between data points of the respective region during collection.

HeII photoelectron spectra

Samples were handled similarly in the HeII study. The HeII radiation source was a differentially pumped, charged particle oscillator type lamp based on designs previously described[24] except for HeII spectra of $[CpFe(\mu\text{-}NO)]_2$ and $[Cp^*Fe(\mu\text{-}NO)]_2$. For these samples a capillary discharge was used with the HeI lamp set-up. For comparison of HeI/HeII ionization band cross sections, spectra have been corrected for the experimentally-determined variation of electron transmission with kinetic energy of the spectrometer analyser.[25] The HeII (40.81 eV) spectra have also been corrected for ionizations from the HeIIβ (48.4 eV, 12%) source excitation.

Molecular orbital calculations

Molecular orbital calculations were performed using the Fenske–Hall method.[26] Fenske–Hall calculations were performed on $[CpFe(\mu\text{-}NO)]_2$ and $[CpCo(\mu\text{-}CO)]_2$. Basis functions 1*s* through 3*d* for iron and cobalt were taken from the tables of Richardson *et al.*[27] Exponents for the single ζ 4*s* and 4*p* orbitals were set at 2.0 and 1.6 for iron and cobalt. The carbon, nitrogen and oxygen atoms had double ζ 2*p* functions, while hydrogen possessed a single ζ function with an exponent of 1.2. The bond distances and angles used for the $[CpFe(\mu\text{-}NO)]_2$ system[28,29] and $[CpCo(\mu\text{-}CO)]_2$ system[30] were obtained from crystal structures and were idealized to C_{2h} symmetry. The C—H distances used in the calculations of each complex were taken as 1.1 Å.

ELECTRONIC STRUCTURE CALCULATIONS

Previous calculations

Ab initio and Fenske–Hall calculations have been performed previously on $[CpFe(\mu\text{-}NO)]_2$[3,5,7] and $[CpCo(\mu\text{-}CO)]_2$.[4–6] The ionization energies are estimated from the *ab initio* calculations by an analysis that partially accounts for the effects of electron relaxation and configuration interaction. The ionization energies are estimated from the Fenske–Hall calculations by Koopmans' approximation, as is customary with this method.[31] The complete description of each orbital is not always presented in the previous publications. Therefore we have also carried out a Fenske–Hall calculation on these complexes for more detailed analysis. Table 1 compares the results of various calculations. There is little agreement to be found between these calculations as to the predicted order of the ionizations.

The calculated molecular orbitals are discussed here in terms of local D_{2h} point group symmetry, where the overall five-fold symmetry of the cyclopentadienyl groups is simplified to cylindrical symmetry. The notation throughout uses σ, π and δ to refer to the symmetry interactions between metals, while the superscripted a or s refers to the antisymmetric and symmetric combination of orbitals with respect to the mirror plane between the two

Table 1. Relative order of molecular orbitals and ionization energies (in eV) from several calculations

Fenske–Hall[a]		Fenske–Hall[b]		*Ab initio*		Experimental	
Label	Energy	Label	Energy	Label	Energy	Label	Energy
			[CpFe(μ-NO)]$_2$				
B_{3u} σ^a	10.74	B_{2u} $\pi^s_\perp$	10.4	B_{2u} $\pi^s_\perp$	6.03[c]	B_{3u} σ^a	6.92
A_g $\delta^s_\parallel$	11.02	B_{3u} σ^a	10.7	A_g $\delta^s_\parallel$	6.18	B_{2g} $\pi^a_\parallel$	7.14
B_{2g} $\pi^a_\parallel$	11.39	A_g $\delta^s_\parallel$	10.8	B_{3g} $\delta^s_\perp$	6.68	A_g $\delta^s_\parallel$	7.24
A_u $\delta^a_\perp$	11.48	B_{2g} $\pi^a_\parallel$	11.1	A_u $\delta^a_\perp$	6.70	A_u $\delta^a_\perp$	7.42
B_{2u} $\pi^s_\perp$	11.50	A_u $\delta^a_\perp$	11.3	B_{3u} σ^a	6.84	B_{3u} $\delta^a_\parallel$[f]	7.80
B_{3g} $\delta^s_\perp$	12.25	B_{3g} $\delta^s_\perp$	12.1	B_{2g} $\pi^a_\parallel$	7.60	B_{2u} $\pi^s_\perp$	7.88
A_g σ^s	12.38	A_g σ^s	12.3	B_{3u} $\delta^a_\parallel$	8.06	B_{3g} $\delta^s_\perp$[f]	7.95
B_{3u} $\delta^a_\parallel$	12.42	B_{3u} $\delta^a_\parallel$	12.4	A_g σ^s	8.08	A_g σ^s	8.13
			[CpCo(μ-CO)]$_2$				
B_{2g} $\pi^a_\parallel$	10.32	B_{2u} $\pi^s_\perp$	9.9	B_{2g} $\pi^a_\parallel$	3.82[d]	B_{2g} $\pi^a_\parallel$	6.22[e]
B_{2u} $\pi^s_\perp$	11.54	B_{2g} $\pi^a_\parallel$	10.0	A_u $\delta^a_\perp$	4.81	B_{3u} σ^a	6.61
B_{3u} σ^a	11.84	B_{3u} σ^a	11.3	A_g $\delta^s_\parallel$	5.05	A_g $\delta^s_\parallel$	6.79
A_g $\delta^s_\parallel$	12.31	A_g $\delta^s_\parallel$	11.4	B_{3g} $\delta^s_\perp$	5.13	B_{2u} $\pi^s_\perp$	6.92
B_{3u} $\delta^a_\parallel$	12.74	A_u $\delta^a_\perp$	12.0	B_{2u} $\pi^s_\perp$	5.14	A_u $\delta^a_\perp$	7.04
A_u $\delta^a_\perp$	12.80	B_{3g} $\delta^s_\perp$	12.4	B_{3u} $\delta^a_\parallel$	5.19	B_{3u} $\delta^a_\parallel$[f]	7.33
B_{3g} $\delta^s_\perp$	13.03	B_{3u} $\delta^a_\parallel$	12.5	B_{3u} σ^a	5.97	B_{3g} $\delta^s_\perp$[f]	7.33
A_g σ^s	13.71	A_g σ^s	12.9	A_g σ^s	6.92	A_g σ^s	7.51

[a] This work. The coordinate system is as seen in Fig. 1.
[b] Energies from ref. 5, with our labels for best correlation.
[c] Energies from ref. 3, with our labels for best correlation.
[d] Energies from ref. 6, with our labels for best correlation.
[e] The experimental assignments are for [Cp*Co(μ-CO)]$_2$.
[f] The order of B_{3u} $\delta^a_\parallel$ and B_{3g} $\delta^a_\perp$ assignment may be reversed.

metals. The subscripted $\parallel$ or $\perp$ indicates whether the orbital interactions are oriented within the plane of the metals and bridging ligands ($\parallel$) or whether the orbital interactions are oriented perpendicular to the plane of the metal and bridging ligands ($\perp$).

While most methods predict that the predominantly metal σ combination is the most stable metal-based orbital, the other seven metal–metal combinations shift relative positions depending upon the calculational method used. Note that even the two Fenske–Hall calculations do not produce the same order of the molecular orbitals, as a consequence of subtle differences in the metal 4*s* and 4*p* exponents and the exact bond distances used in the calculations.

Certain trends are observed between complexes and calculational methods. Fenske–Hall calculations suggest that the nitrosyl's backbonding capabilities are greater than the carbonyl's. The metal–metal π^* and π orbitals (involved with the bridging ligand backbonding) are found deeper down the stack for the nitrosyl versus carbonyl complexes.[5] However, this same expected trend is not reflected between the *ab initio* calculations of iron nitrosyl and cobalt carbonyl. The *ab initio* calculations tend to emphasize the importance of metal–ligand interaction over interactions between the two metals. This can be seen in the relatively narrow σ–σ^* separation versus the wider π–π^* separations in each *ab initio* calculation. The σ and σ^* interactions are predominantly metal-based interactions while the π and π^* interactions are supported through backbonding to the bridging ligands. The Fenske–Hall calculations tend to separate the σ and σ^* molecular levels more than the *ab initio* calculations.

As seen above, slight differences in geometries or basis functions can result in different molecular orbital order. This emphasizes the sensitivity of calculations on this molecular system to slight perturbations. Assignments of photoelectron spectra based solely on calculational results are, therefore, greatly suspect. However, a clearly delineated representation of the molecular orbital interactions for these complexes provides an understanding of the trends in ionization energy shifts with chemical substitutions. In the next section a qualitative description of the primary orbital interactions is given.

Molecular orbital analysis

The orbitals in these complexes are most clearly understood in terms of a fragment analysis. The metal, cyclopentadienyl and bridging ligand fragments may be combined in any order to obtain the same final result. For the purposes of understanding the ionizations of these complexes and the perturbations with ligand substitutions, we find it most useful to first combine a cyclopentadienyl and a metal, then form the CpM=MCp dimer, and finally add the bridging ligands. The qualitative interactions between these fragments are shown in Fig. 2.

Generally, the calculations on these d^8 metal dimers suggest an initial t_{2g} and e_g arrangement of metal orbitals. The e_g set of orbitals are metal orbitals situated for direct metal–cyclopentadienyl bonding (see Fig. 2, column A). These are composed of the d_{xz} and d_{yz} atomic orbitals of each metal, which mix with the filled e_1'' π orbitals of each cyclopentadienyl. The metal–metal interaction between these orbitals forms the metal–metal bonding and antibonding π combinations. The more stable t_{2g} set is composed of the $d_{x^2-y^2}$ and d_{xy} (δ interactions between metals) and the d_{z^2} (σ interactions between metals).

Once the bridging ligands are allowed to interact with the metal–metal dimer, four of the metal–metal molecular interactions (two of π type symmetry and two of δ type symmetry) are significantly stabilized through backbonding into the four π^* orbitals of the bridging ligands. Of these four metal-bridging ligand molecular orbitals (see Fig. 2, column C), the metal–metal π^* and π orbitals interact with the filled cyclopentadienyl e_1'' set, which is a destabilizing effect. A destabilization of 1.2 eV was found for a similar orbital of the monomer $Cp^*Co(CO)_2$[35] due to filled–filled interaction of the metal levels with the cyclopentadienyl ring levels. Therefore, the relative ordering between just these four metal–metal bridging ligand supported orbitals is clear. The most stable combinations are of δ symmetry. The π symmetry combinations of the metal, while stabilized by nitrosyl or carbonyl backbonding, are destabilized by filled–filled interactions with the cyclopentadienyl ligand.

The remaining four occupied orbitals are derived

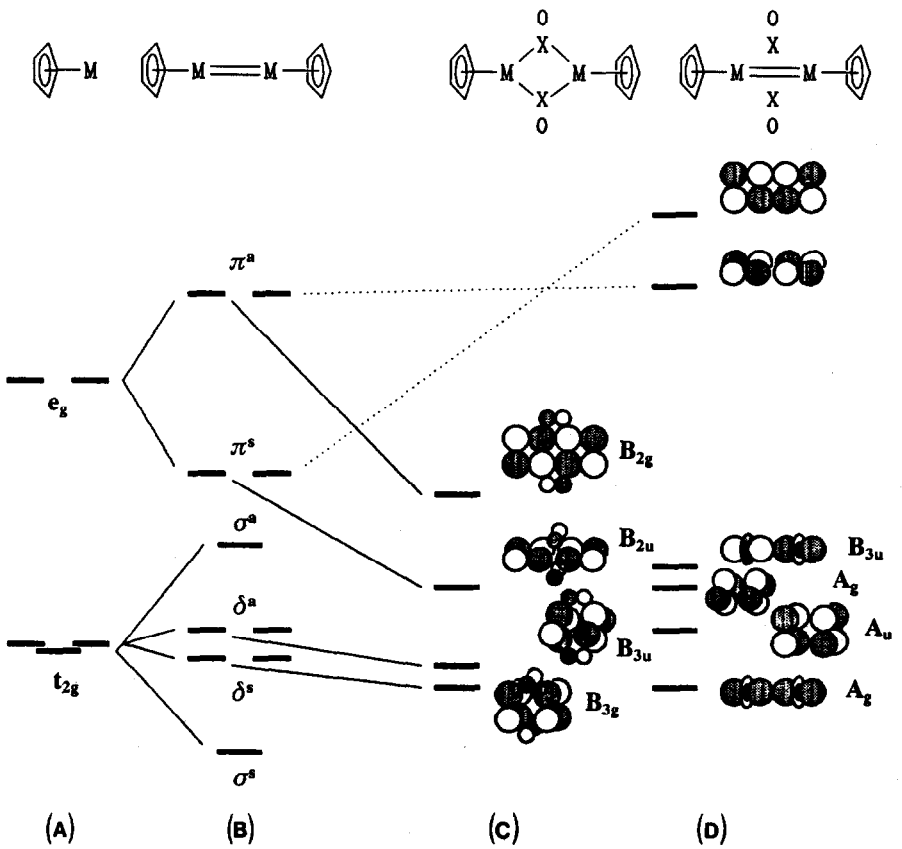

Fig. 2. Molecular orbital diagram of the metal–metal and metal–ligand interactions. (A) Metal–Cp interactions; (B) two metal–Cp interactions; (C) bridging ligand π^* backbonding interactions; (D) the remaining relative pure metal–metal interactions.

from the remaining metal–metal σ and δ interactions. These tend to be relatively unaffected by the bridging ligands. Of these four "pure" metal–metal interactions, only the $\delta^a{}_\perp$ antibonding orbital combination has a symmetry (A_u) which does not interact in any way with the bridging ligands. The other three "pure" metal–metal combinations may interact, by symmetry, with either the empty bridging ligand π^* orbitals (B_{3u} σ^a metal–metal combination) or the bridging ligands' σ donor orbitals (A_g σ^s and A_g $\delta^s{}_\parallel$ metal–metal combinations).

The remaining two empty orbitals have π and π^* symmetry and are unaffected by the bridging ligands' π^* backbonding capabilities. These are mainly required to accept electron density from the π donating cyclopentadienyl rings. The $\pi^s{}_\parallel$ combination is also set up to accept electron density from the bridging ligands' donor σ orbitals and is further destabilized.

The eight occupied combinations may be divided into three different subsets. One set contains two "e_g" metal–metal interactions which are destabilized by interaction with the cyclopentadienyl rings and stabilized by the bridging ligands. These will be labelled simply as $M^\ddagger$ in the figures and tables to designate that they are metal-based but contain substantial cyclopentadienyl and bridging ligand interactions. The second set contains two "t_{2g}" type metal–metal interactions which are stabilized by the bridging ligand's π^* backbonding interactions. These are labelled $M^\dagger$ in the figures and tables to designate metal-based interactions with substantial bridging ligand interactions. The third set contains four relatively "pure" σ and δ "t_{2g}" type metal–metal interactions and will be labelled M in the figures and tables.

The total ordering of the entire set of eight filled metal–metal interactions is highly uncertain at this point, depending on the electron-withdrawing power of the bridging ligands, the electron-donating ability of the cyclopentadienyl π system, the electron-donating ability of the bridging ligand σ interaction and the strength of interactions between metal orbitals.

PHOTOELECTRON RESULTS

Before discussing the complete assignments of the photoelectron ionizations, it is important to recognize several general features of the photoelectron spectra. Each spectral ionization profile will be discussed beginning at low ionization energy and proceeding to the higher energy ionizations. A total of eight metal ionizations should be present in each spectrum followed by four cyclopentadienyl ionizations separated to higher energy. The labelling of the photoelectron bands in the figures and tables reflect the predominant character of the ionization as either cyclopentadienyl or pentamethylcyclopentadienyl (labelled Cp) or metal (labelled M). As specified in the previous section, the label $M^\dagger$ is used to flag those ionizations which are found to contain metal and bridging ligand π^* backbonding character, while the label $M^\ddagger$ is used to flag those ionizations with metal, bridging ligand π^* backbonding and cyclopentadienyl ligand character.

The photoelectron data are modelled with analytical band shapes in order to obtain well-defined values for positions and band areas. Consistent values for the positions and areas, with known confidence limits, are important for comparisons of ionization band shifts between spectra. The data are represented analytically in terms of asymmetric Gaussian peaks. These are defined by parameters representing the position of the peak, the half-widths on the high (W_h) and low (W_l) binding energy sides of the peak and the amplitude of the peak as determined by program GFIT.[32,33] Vibrational fine structure is observed in several ionizations in these spectra. Vibrational progressions are modelled by symmetric Gaussians, where the high (W_h) and low (W_l) energy half-widths are constrained to be equal throughout an entire vibrational progression. The relative band areas are also evaluated in program GFIT to determine the relative ionization cross-section of the photoelectron band. The uncertainty in relative band area can be on the order of 15% for overlapping peaks or poorly defined baselines. For well-separated ionization bands that go to baseline between the peaks, the uncertainty is on the order of 5%.

Vibrational fine structure

A close-up of the low energy ionization region was collected for several of these complexes and vibrational fine structure was observed for [CpFe(μ-NO)]$_2$ and [Cp*Co(μ-CO)]$_2$. The frequencies are reported in Table 2 along with the vibrational frequencies found by IR for the neutral and anionic complexes.[11,14,29]

The vibrational progressions observed for [CpFe(μ-NO)]$_2$ are seen in Fig. 3. Two separate progressions are clearly observed in the ionization at 7.42 eV: a large separation, labelled ν(NO), with a frequency of 0.202(2) eV or 1632 ± 16 cm^{-1}, and a smaller progression with a frequency of 0.0516(5) eV (416 ± 4 cm^{-1}). The larger separation corresponds to the nitrosyl stretching frequency and is completely consistent with the known photoelectron behaviour of other nitrosyl or carbonyl[34,35]

Table 2. Vibrational frequencies of various dimers

	ν(XO) (cm^{-1}) Molecular charge			ν(M—X_2—M) (cm^{-1}) Ionization band	
	−1	0	+1	$A_u\ \delta^a{}_\perp$	$B_{3u}\ \sigma^a$
[Cp*Co(μ-CO)]$_2$	1719(1)	1752(1)	1742(160)	—	—
[CpFe(μ-NO)]$_2$	1395(1)	1510(1)	1632(16)	416(4)	430(4)
[Cp*Fe(μ-NO)]$_2$	1355(1)	1472(1)	—	—	—

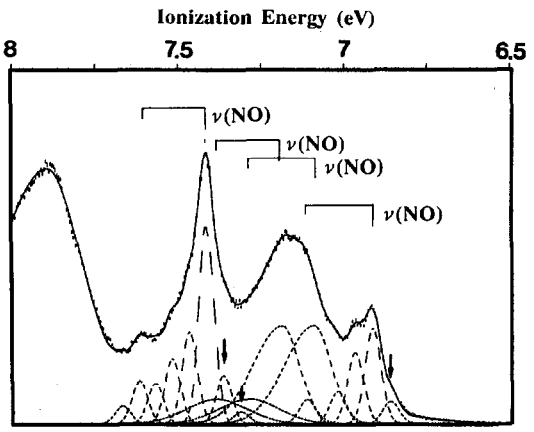

Fig. 3. Nitrosyl and ring breathing vibrational fine structure in the photoelectron spectrum of [CpFe(μ-NO)]$_2$. The arrows indicate the hot bands.

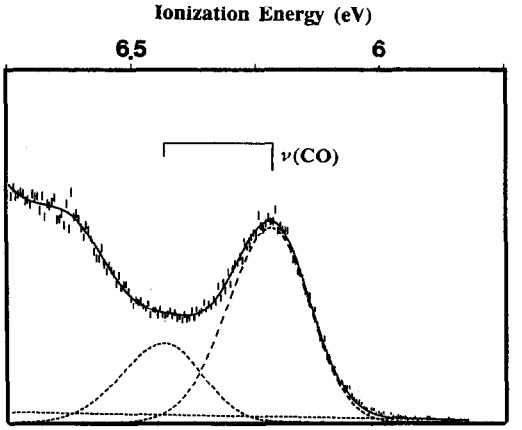

Fig. 4. Carbonyl vibrational fine structure in the photoelectron spectrum of [Cp*Co(μ-CO)]$_2$.

containing complexes. The ionization at lowest ionization energy (6.92 eV) also shows a vibrational progression with a 0.0533 eV energy separation or a 430 cm^{-1} frequency. These smaller frequencies are assigned to the M—X_2—M symmetric ring breathing mode. Vibrational structure observed in the photoelectron spectra generally corresponds to symmetric stretches.[36,37]

Ionizations which are weakly antibonding or non-bonding exhibit short vibrational progressions, in which the adiabatic and vertical ionization normally coincide. For these two ionizations, the leading narrow components at low intensity (indicated by the arrows) are attributed to hot bands. Results from Boltzmann's distribution supports the intensity pattern found for these leading components for spectra obtained at 120°C. This means that the adiabatic ionization is the most intense (vertical) for each of these ionizations and these two ionizations are relatively non-bonding. They will be assigned to reflect this observation.

In Fig. 4, the leading ionization of [Cp*Co(μ-CO)]$_2$, at 6.22 eV is observed to possess an ionization separated 0.216(20) eV to higher ionization energy or 1742 ± 160 cm^{-1}, a carbonyl vibrational stretching frequency. Although only barely resolved, the ionization intensity between the leading ionization and the next intense band at 6.61 eV clearly indicates the presence of the additional vibrational band. For neutral [Cp*Co(μ-CO)]$_2$, a single IR band at 1752 cm^{-1} is reported[38] and these values correspond well. The observation of the carbonyl stretching frequency in this leading ionization of the photoelectron spectrum supports the contention that the leading ionization in [Cp*Co(μ-CO)]$_2$ has carbonyl backbonding character, which is also indicated by previously published HeI/HeII comparisons.[4]

Modelling band shapes with vibrational progressions

The presence of the nitrosyl vibrational progression in [CpFe(μ-NO)]$_2$ leads to a pronounced asymmetric ionization profile with an additional intensity component at higher ionization energy. The ionization at 7.42 eV will be correlated in the next section to an orbital that is predominantly metal in character and which does not have any direct symmetry interaction with the π^* of the nitrosyls. This ionization is actually the least likely of the metal-based ionizations to possess vibrational

fine structure associated with the bridging nitrosyls. This metal-based ionization presumably activates the vibrational progression, because of its association with the M—X_2—M ring core, and it follows that the other metal-based ionizations will activate this progression as well. Therefore, the relative intensity and relative energy separation found for the nitrosyl vibrational structure on the ionization at 7.42 eV is used to define the model band profiles for other metal-based ionizations. This is illustrated in Fig. 3, where the NO vibrational components are indicated. The analytical model of this single ionization is expressed in the following equation:

$$C = A\,e^{-k(X-P/W_i)^2} + (0.26)A\,e^{-k(X-P-0.202/W_i)^2} \quad (1)$$

where C is the calculated counts, k is a constant $4\ln(2)$, A is the amplitude, P is the peak position and W_i is the half-width to low binding energy (W_l; $X < P$) or the half-width to high binding energy (W_h; $X > P$). Note that this function still only has four variable parameters. It does not use additional parameters, but merely alters the model band shape. With the use of this model, the photoelectron spectrum is represented accurately with the fewest number of variable parameters.

The example given in Fig. 5 illustrates the consequences of including and excluding the nitrosyl vibrational fine structure in the individual band contour model. In section A of Fig. 5, each ionization profile retains a vibrational component corresponding to nitrosyl vibrational fine structure. The overall spectral fit is good and the individual Gaussian bands have reasonable shapes and relative areas. Section B shows the overall spectral fit when the corresponding vibrationally excited nitrosyl bands are removed. When these eight Gaussian bands are allowed to converge to the data, as seen in section C, several of the individual Gaussian bands are found to shift into valleys previously occupied by the vibrationally excited nitrosyl band. The others increase in intensity and half-width to account for the area previously occupied by the shifting Gaussians. These Gaussian band positions and areas are clearly unreasonable representations of the eight ionizations in the spectrum.

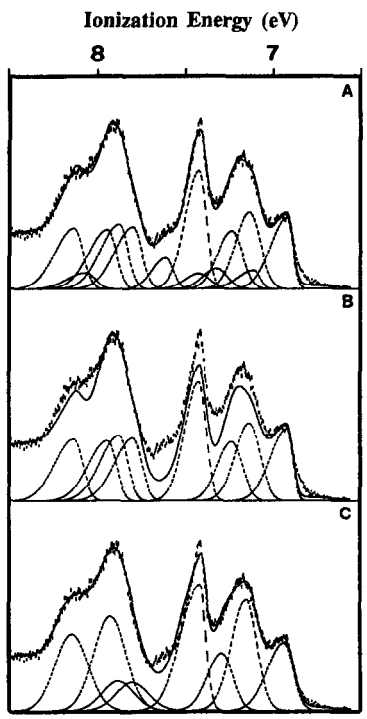

Fig. 5. Comparisons between photoelectron spectra (A) with nitrosyl vibrational fine structure included in the Gaussian band definition; (B) without fine structure (unconverged); (C) without fine structure (converged).

The spectra of both [CpFe(μ-NO)]$_2$ and [Cp*Fe(μ-NO)]$_2$ require the addition of the vibrationally excited band in order to reasonably account for the spectral features. However, these additional small bands are not plotted in the figures, as they visually complicate the illustration, while suggesting no additional insight. The ionizations in the HeII spectra are represented by the same peaks and positions as in the HeI spectra, allowing only the intensities to vary. The vertical ionization energies and relative areas of these complexes are reported in Table 3.

General photoelectron features

The HeI and HeII photoelectron spectra of [CpFe(μ-NO)]$_2$ are shown in Fig. 6. The leading ionization is observed at 6.92 eV and separated 0.22 eV from the next ionizations. The second band profile at 7.2 eV can not be fitted adequately with a single asymmetric Gaussian band, and the profile is well accounted for by two ionization bands. As further support of the presence of two ionizations under this band envelope, the band profile changes between HeI and HeII source energies, indicative of different HeI/HeII cross-section changes between the two ionizations under the one profile.

The distinct sharp ionization at 7.42 eV possesses a set of very narrow half-widths. Note that the overall half-width for this ionization is only 0.27 eV. All other ionization half-widths are of the order of $\sim$ 0.4 eV. This single ionization is expected to be relatively non-bonding because of the narrowness of the ionization. The vibrational fine structure analysis of this band in the previous section also showed that the adiabatic and vertical ionization energies coincide. This ionization is primarily metal in

Table 3. Vertical ionization energies (±0.02 eV), and HeI and HeII relative areas

$[Cp^*Co(\mu\text{-}CO)]_2$			$[Cp^*Fe(\mu\text{-}NO)]_2$			$[CpFe(\mu\text{-}NO)]_2$			$[CpRu(\mu\text{-}NO)]_2$		
	IE	HeI		IE	HeI	HeII		IE	HeI	HeII		IE	HeI	HeII
$M^{\ddagger}_1$	6.22	1.62	M_1	6.19	1.20	1.25	M_1	6.92	1.21	1.03	$M^{\ddagger}_1$	7.12	2.17	1.65
M_1	6.61	1.13	$M^{\ddagger}_1$	6.38	1.19	0.82	$M^{\ddagger}_1$	7.14	1.45	1.00	M_1	7.25	2.03	1.93
M_2	6.79	1.11	M_2	6.49	0.97	0.97	M_2	7.24	1.10	1.11	M_2	7.58	1.98	1.65
$M^{\ddagger}_2$	6.92	1.33	M_3	6.77	1.91	1.74	M_3	7.42	1.90	1.70	M_3	7.78	2.06	1.86
M_3	7.04	1.03	$M^{\ddagger}_2$	7.04	1.44	0.99	$M^{\dagger}_1$	7.80	1.02	0.80	$M^{\ddagger}_2$	7.86	1.87	1.51
$M^{\dagger}_1$	7.33	2.11	$M^{\dagger}_1$	7.12	1.16	0.91	$M^{\ddagger}_2$	7.88	1.33	0.66	$M^{\dagger}_1$	8.42	3.82	3.48
$M^{\dagger}_2$			$M^{\dagger}_2$	7.23	0.82	0.79	$M^{\dagger}_2$	7.95	0.97	0.95	$M^{\dagger}_2$			
M_4	7.51	1.0	M_4	7.40	1.0	1.0	M_4	8.13	1.0	1.0	M_4	9.19	1.0	1.0
Cp	8.28	12.	Cp	8.37	18.	12.	Cp	9.60	13.	4.	Cp_1	9.64	4.55	2.21
											Cp_2	10.2	3.94	2.10

character, as the HeI/HeII relative area increases relative to the ionization profile at 7.8 eV.

The ionization envelope starting at 7.8 eV obviously contains overlapping ionizations. The intense ionization at 7.88 eV in the HeI spectrum substantially decreases in the HeII spectrum, indicative of ligand contribution to this ionization. Also, the presence of other ionizations are needed to account for the area under the profile. The HeI/HeII behaviour of the shoulder at highest ionization energy (8.13 eV) suggests an ionization of predominantly metal character. This entire profile should account for a total of four overlapping ionization bands.

The ionization band at 9.6 eV correlates with the four characteristic cyclopentadienyl ionizations. This relative band intensity decreases substantially when viewed with HeII ionization source energy, as expected for predominantly cyclopentadienyl ligand character. This ionization is also very broad.

The general photoelectron features of $[Cp^*Fe(\mu\text{-}NO)]_2$ (see Fig. 7) are the same as those for $[CpFe(\mu\text{-}NO)]_2$. The major difference is a shift of all ionizations to lower ionization energy due to the presence of the electron donating pentamethylcyclopentadienyl rings. Some ionizations have shifted to a greater extent than others and those ionizations with the greater cyclopentadienyl character are expected to shift to a greater degree. Examina-

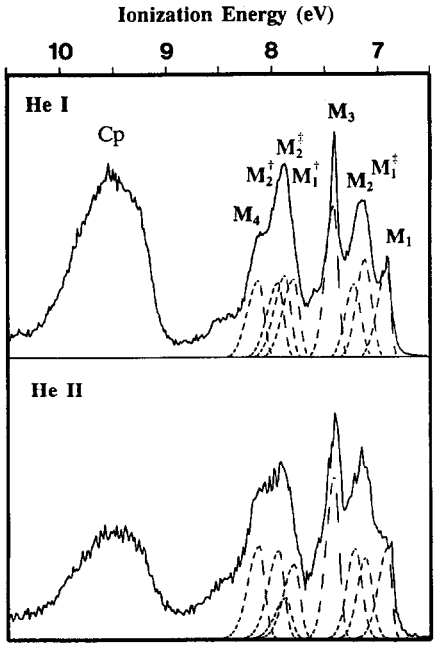

Fig. 6. HeI and HeII photoelectron specra of $[CpFe(\mu\text{-}NO)]_2$. The dashed Gaussian bands indicate the position of the eight predominantly metal ionizations. See text for further discussion.

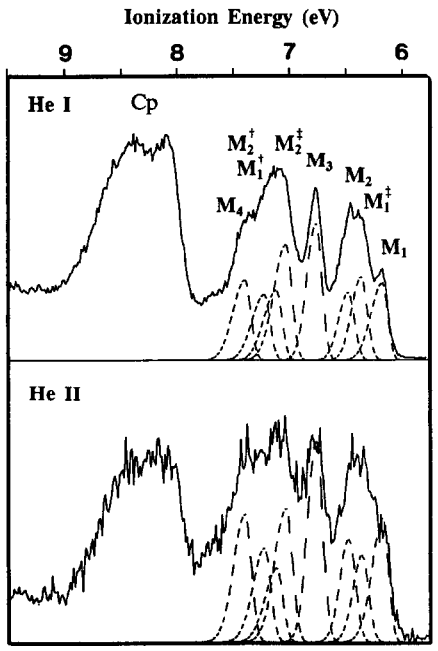

Fig. 7. HeI and HeII photoelectron spectra of $[Cp^*Fe(\mu\text{-}NO)]_2$. The dashed Gaussian bands indicate the position of the eight predominantly metal ionizations. See text for further discussion.

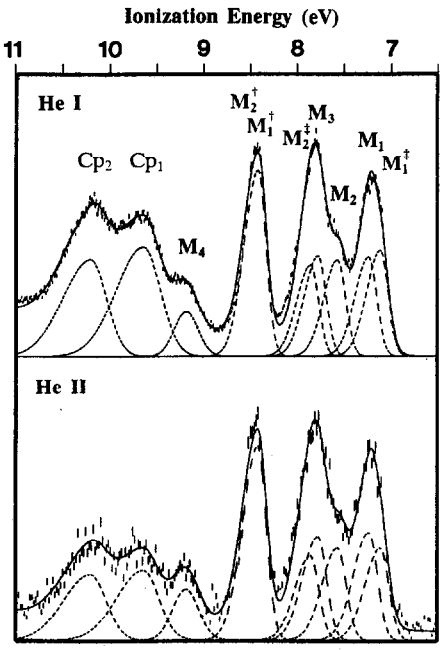

Fig. 8. HeI and HeII photoelectron spectra of [CpRu(μ-NO)]$_2$. The dashed Gaussian bands indicate the position of the eight predominantly metal ionizations and the two split cyclopentadienyl ionizations. The overall fit is given by the solid line through the photoelectron data.

tion of this effect and its usefulness in assigning these spectra will be discussed in greater detail in the next section.

The HeI/HeII photoelectron spectra of [CpRu(μ-NO)]$_2$, the second row counterpart to [CpFe(μ-NO)]$_2$, are given in Fig. 8. The leading intense ionization at 7.2 eV is nearly double the intensity of the ionization appearing as a shoulder at 7.58 eV. This suggests the presence of two narrow ionizations under the leading ionization profile. Two metal-based ionizations are assigned to the band profiles at 7.80 and at 8.42 eV. These bands are generally double the area and amplitude of the single ionization appearing as a shoulder at 7.58 eV. Both these intense ionizations will accommodate two ionizations, giving a total of seven ionizations between the energies of 7.10 and 8.50 eV. The eighth metal ionization is found at 9.20 eV. This broad ionization increases its relative intensity upon comparison between HeI and HeII data.

The broad ionizations at 9.6 and 10.2 eV significantly decrease in relative ionization intensity between HeI and HeII spectra, indicating ligand character. The ionization at 9.6 eV corresponds with the ionization energy found for the cyclopentadienyl ring ionizations of [CpFe(μ-NO)]$_2$. Since the second row ruthenium metal forms stronger interactions with the cyclopentadienyl rings as compared to the first row iron,[35,39] the ionizations at 10.2 eV (separated 0.6 eV to higher binding energy from the cyclopentadienyl ionizations at 9.6 eV) are also cyclopentadienyl ionizations. These are stabilized by interaction with the ruthenium metal e_g set. This metal–ring interaction is only hinted at in the broadness of the cyclopentadienyl ionization regions of [Cp*Fe(μ-NO)]$_2$ and [CpFe(μ-NO)]$_2$.

The overall spectrum of [Cp*Co(μ-CO)]$_2$ (see Fig. 9) is dissimilar in appearance to the ionization profile of [Cp*Fe(μ-NO)]$_2$. The spectrum of [Cp*Co(μ-CO)]$_2$ presents an ionization at 6.22 eV which is well-separated from the rest of the metal ionizations and has a profile typical in shape to that of a single ionization. The second ionization at 6.61 eV is the first of four overlapping ionizations found in the region from 6.61 to 7.04 eV. The precise locations and relative intensities of these overlapping ionizations are uncertain. The ionization found at 8.25 eV is due to the four cyclopentadienyl ionizations, at a similar energy to those found in [Cp*Fe(μ-NO)]$_2$. HeII ionization data as published by Green and others[4] indicate that the leading ionization at 6.22 eV decreases in relative ionization area, indicating a substantial percentage of ligand character in this ionization.

ASSIGNMENT OF PHOTOELECTRON SPECTRA

All the information available from the HeI/HeII comparisons, shifts between Co(CO) and Fe(NO) complexes, shifts between Cp and Cp* complexes, and between Fe and Ru metals is evaluated to determine the assignment of the photoelectron spectra

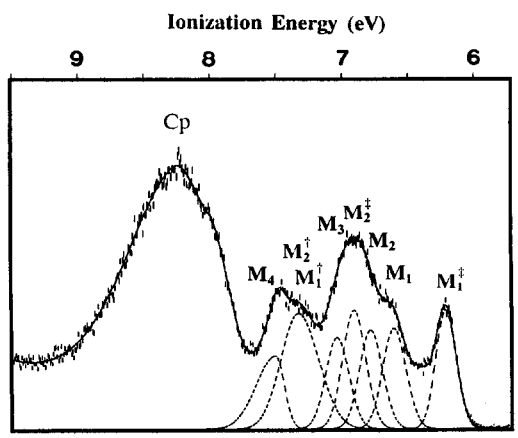

Fig. 9. HeI photoelectron spectrum of [Cp*Co(μ-CO)]$_2$. The dashed Gaussian bands indicate the position of the eight predominantly metal ionizations and the pentamethylcyclopentadienyl ionizations. The overall fit is given by the solid line through the photoelectron data.

of these compounds. Based on the confidence limits of the analysis of overlapping ionizations, any individual change in a band area or an ionization shift does not provide absolute proof of a band assignment. However, the collection of supporting changes leads to consistent band assignments. By using the trends associated with the chemical changes in these complexes, which are understood from previous studies of related cyclopentadienyl, carbonyl, and nitrosyl complexes, the eight predominantly metal ionizations may be confidently assigned without invoking calculations as the requisite of assignment. Listed below is a set of understood ionization trends applied to the spectra of these complexes.

(1) Pentamethylcyclopentadienyl (Cp*) ionizations are shifted $\approx$ 1.2 eV to lower ionization energy from cyclopentadienyl (Cp) ionizations.[9]
(2) Mixed Cp*–metal ionizations are shifted $\approx$ 0.8 eV to lower ionization energy from Cp–metal ionizations.[35]
(3) Metal-based ionizations are shifted $\approx$ 0.65–0.75 eV to lower ionization energy when Cp* is substituted for Cp.[35]
(4) The area of ligand-based ionizations relative to first row metal-based ionizations is less with HeII excitation than with HeI excitation.[40]
(5) Mixed ligand–metal ionizations will decrease proportionally in ionization area relative to more "pure" metal ionizations and increase proportionally in ionization area relative to more "pure" ligand ionizations.[41]
(6) The metal-based ionizations of $CpMn(CO)_3$ are $\approx$ 0.3 eV more stable than the metal-based ionization of $CpCr(CO)_2(NO)$ provided they were not involved in backbonding to the nitrosyl.[10] These complexes are related by the same proton shift from the metal to the ligand as the cobalt and iron complexes in this study.
(7) The metal ionizations stabilized by backbonding into the π^* of the bridging ligands are expected to be similar in energy between cobalt–carbonyl and iron–nitrosyl.[10] These ionizations experience a stabilization in the cobalt complex due to the metal's influence (trend 6) and a comparable destabilization due to the less effective backbonding to the carbonyl as compared to the nitrosyl. The net effect is little change in ionization energy.
(8) When comparing iron to ruthenium, all second row metal ionizations are stabilized with respect to the first row ionizations.[35]
(9) A sharp band profile with resolvable vibrational fine structure suggests relatively non-bonding molecular orbital character.

The shifts between the energies of corresponding ionizations of the four complexes {$[Cp^*Co(\mu\text{-}CO)]_2$, $[Cp^*Fe(\mu\text{-}NO)]_2$, $[CpFe(\mu\text{-}NO)]_2$ and $[CpRu(\mu\text{-}NO)]_2$} are given in Table 4, along with the assignments. The differences or shifts in ionization

Table 4. Shifts in photoelectron ionization bands between complexes[a]

Labels[b]			$[Cp^*Co(\mu\text{-}CO)]_2$ Shift (±0.04 eV)	$[Cp^*Fe(\mu\text{-}NO)]_2$ Shift (±0.04 eV)	$[CpFe(\mu\text{-}NO)]_2$ $[CpRu(\mu\text{-}NO)]_2$ Shift (±0.04 eV)
M_1	B_{3u}	σ^a	−0.42	+0.73	+0.32
M_2	A_g	$\delta^s_{\parallel}$	−0.23	+0.75	+0.34
M_3	A_u	$\delta^a_{\perp}$	−0.27	+0.65	+0.36
M_4	A_g	σ^s	−0.11	+0.73	+1.05
$M^{\dagger}_1$	B_{3u}	$\delta^a_{\parallel}$	−0.21	+0.68	+0.62
$M^{\dagger}_2$	B_{3g}	$\delta^s_{\perp}$	−0.10	+0.72	+0.48
$M^{\ddagger}_1$	B_{2g}	$\pi^a_{\parallel}$	+0.16	+0.76	−0.01
$M^{\ddagger}_2$	B_{2u}	$\pi^s_{\perp}$	+0.12	+0.84	−0.01
Cp			+0.09	+1.23	+0.04[c]

[a] The sign convention is defined so that the value, when added to the energy of an ionization of the molecule on the left, gives the energy of the corresponding ionization of the molecule on the right.

[b] The labels are grouped according to their mixed metal–ligand character. For the relative ionization order of each complex see Table 3 or Fig. 10.

[c] The shift in cyclopentadienyl ionizations between $[CpFe(\mu\text{-}NO)]_2$ and $[CpRu(\mu\text{-}NO)]_2$ is derived from the cyclopentadienyl ionization at lowest ionization energy in $[CpRu(\mu\text{-}NO)]_2$.

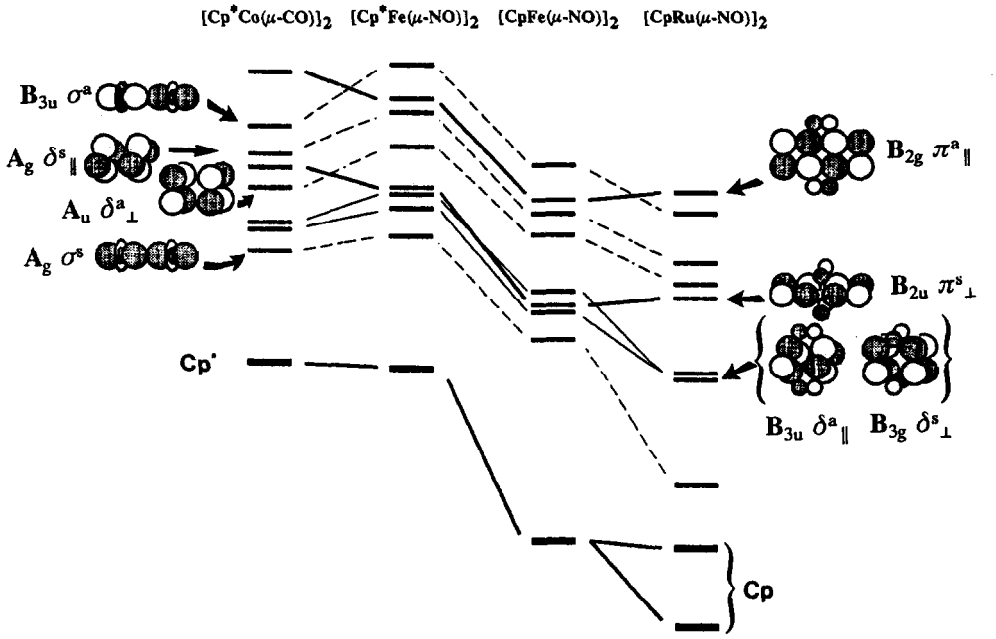

Fig. 10. Experimental energy correlation diagram. The four "pure" metal ionizations are depicted on the left of the figure and correlated between complexes with dashed lines. The two δ ionizations which are stabilized by backbonding to the bridging ligands are depicted on the right of the figure and correlated between complexes with solid lines. The two π ionizations which are stabilized by backbonding to the bridging ligands and destabilized by filled interactions with the cyclopentadienyl e_1'' orbitals are depicted on the right of the figure and correlated between complexes with dark solid lines.

energy between complexes are defined from the left to the right, in the table. Since the relative order of the closely spaced individual ionizations changes from complex to complex, the three general classes of ionizations with their assignments have been grouped together. The shifts of the "pure" metal ionizations (M_{1-4}) along with the metal and bridging ligand ionizations ($M^{\dagger}{}_{1,2}$) and the metal–ligand and cyclopentadienyl ionizations ($M^{\ddagger}{}_{1,2}$) are listed together in Table 4. The experimental ionization order is illustrated in the Fig. 10 and listed in Table 3. The assignment of the ionization bands with the symmetry designations in Table 3 can be easily correlated to the other figures and tables.

Analysis of these assignments will begin with the bands labelled $M^{\ddagger}{}_1$ and $M^{\ddagger}{}_2$ of the complexes [Cp*Fe(μ-NO)]$_2$ and [CpFe(μ-NO)]$_2$. $M^{\ddagger}{}_1$ and $M^{\ddagger}{}_2$ are assigned to the B_{2g} $\pi^a{}_{\|}$ and B_{2u} $\pi^s{}_{\perp}$ orbital symmetries, respectively. These two orbitals are unique in possessing cyclopentadienyl ligand character, nitrosyl backbonding character and metal–metal antisymmetric and symmetric π symmetry. In comparison to the more "pure" metal-based ionizations, $M^{\ddagger}{}_1$ and $M^{\ddagger}{}_2$ decrease in relative area from HeI to HeII excitation (trend 5). These same two ionizations shift position 0.76 and 0.84 eV to higher binding energy between the spectra of [Cp*Fe(μ-NO)]$_2$ and [CpFe(μ-NO)]$_2$, as expected for the partial cyclopentadienyl contribution to the character (trend 2). All the other metal-based ionizations shift an average of only 0.71 eV (trend 3).

Experimentally, the relative order of the B_{2g} $\pi^a{}_{\|}$ versus the B_{2u} $\pi^s{}_{\perp}$ is indeterminable. However, it is reasonable to expect the antisymmetric metal–metal combination, B_{2g} $\pi^a{}_{\|}$, to be the least stable of the pair. Since both combinations suffer to an equal degree from the filled cyclopentadienyl ring orbital donations into the filled metal π orbitals and assuming the stabilization gained from the bridging ligand backbonding with the metals is comparable between B_{2g} and B_{2u} combinations, then the only difference between the two combinations is the antibonding metal–metal destabilization of the B_{2g} versus the metal–metal bonding stabilization of the B_{2u} combination.[42]

When the spectrum of [CpRu(μ-NO)]$_2$ is compared to the spectrum of [CpFe(μ-NO)]$_2$, we expect the second row metal-based ionizations to be stabilized with respect to the first row metal ionizations (trend 9). All metal ionizations other than the $M^{\ddagger}{}_1$ and $M^{\ddagger}{}_2$ ionizations of [CpRu(μ-NO)]$_2$ are stabilized with respect to [CpFe(μ-NO)]$_2$ an average 0.53 eV. The greatest stabilization is found between

$[CpFe(\mu\text{-}NO)]_2$ and $[CpRu(\mu\text{-}NO)]_2$ for peak M_4 (1.05 eV). Because the ruthenium metal–metal bonding interactions should be progressively more important than first row iron metal–metal interactions, M_4 is assigned to the metal–metal $A_g\ \sigma^s$ interaction. The HeI/HeII comparison of $[CpRu(\mu\text{-}NO)]_2$ spectra suggests that ionizations $M^{\ddagger}_1$ and $M^{\ddagger}_2$ decrease in ionization area, indicative of cyclopentadienyl ligand character (trend 5). The ionization energies of bands $M^{\ddagger}_1$ and $M^{\ddagger}_2$ are destabilized 0.01 eV between $[CpFe(\mu\text{-}NO)]_2$ and $[CpRu(\mu\text{-}NO)]_2$.

HeI/HeII comparisons also identify the cyclopentadienyl ionization unquestionably in $[CpRu(\mu\text{-}NO)]_2$. The ionizations at 9.6 and 10.2 eV decrease markedly between the HeI and HeII spectra (trend 4). Also note that the splitting in the cyclopentadienyl ionizations indicates the importance of the second row metal ruthenium–cyclopentadienyl interactions.[35] The cyclopentadienyl–metal interactions are found at 10.2 eV, while the more "pure" cyclopentadienyl ionizations are found at 9.6 eV. This is reflected in a relative increase for HeII ionization area in the ionizations at 10.2 eV as compared to the more "pure" cyclopentadienyl ionizations at 9.6 eV. The cyclopentadienyl ionizations for the iron complex are also found at 9.6 eV, indicative of minimal first row cyclopentadienyl–metal interaction and of a nearly "pure" cyclopentadienyl ionization potential.

Two of the metal-based ionizations are labelled $M_1^{\dagger}$ and $M_2^{\dagger}$, because of evidence for significant interaction with the bridging ligands. These two bands are assigned to the $B_{3u}\ \delta^a_{\parallel}$ and $B_{3g}\ \delta^s_{\perp}$ ionizations. These are allowed by symmetry to strongly interact with the bridging ligands (see Fig. 2, column C). Since the $B_{3u}\ \delta^a_{\parallel}$ and $B_{3g}\ \delta^s_{\perp}$ are derived from the initially more stable metal "t_{2g}" set, these two are expected to be more stable than the corresponding $B_{2g}\ \pi^a_{\parallel}$ ($M^{\ddagger}_1$) and $B_{2u}\ \pi^s_{\perp}$ ($M^{\ddagger}_2$) nitrosyl backbonding interactions (derived from the less stable metal "e_g" set). Therefore, ionizations $M^{\dagger}_1$ and $M^{\dagger}_2$ of the $[CpRu(\mu\text{-}NO)]_2$ spectrum are assigned to be the two accidentally degenerate $B_{3u}\ \delta^a_{\parallel}$ and $B_{3g}\ \delta^s_{\perp}$ orbitals, sandwiched in energy between the most stable $A_g\ \sigma^s$ metal–metal ionization and the lowest lying metal–metal π symmetry ionization.

Of the remaining three unassigned "pure" metal–metal interactions, the ionization band M_3 of $[CpFe(\mu\text{-}NO)]_2$ and $[Cp^*Fe(\mu\text{-}NO)]_2$, clearly has a very sharp band profile and is expected to be relatively non-bonding in character. Figure 3 illustrates the vibrational progressions observed for $[CpFe(\mu\text{-}NO)]_2$ under the leading ionization at 6.92 eV and this sharp fourth ionization, at 7.42 eV. The very sharp and intense ionization at 7.42 eV, M_3, is assigned to the $A_u\ \delta^a_{\perp}$ molecular combinations. The $A_u\ \delta^a_{\perp}$ is the only molecular orbital of A_u symmetry. The Fenske–Hall calculation finds this orbital to be $\approx 100\%$ metal d_{xy} antibonding in character, with no possible stabilization factors due to the backbonding ligands and only weak interaction with the empty cyclopentadienyl e_2'' orbitals. The $\delta^a_{\perp}$ is best described as metal-based lone pairs with very little metal–metal interaction. The leading ionization of $[CpFe(\mu\text{-}NO)]_2$, M_1, is assigned to the $B_{3u}\ \sigma^a$, which is the only other orbital which is antibonding between the metals.

The last unassigned molecular orbital is the $A_g\ \delta^s_{\parallel}$ combination. This combination is assigned to the last remaining unassigned metal ionization, in $[CpFe(\mu\text{-}NO)]_2$ at 7.24 eV, M_2.

The assignment of the photoelectron spectrum of $[Cp^*Co(\mu\text{-}CO)]_2$ is obtained by applying a predicted ≈ 0.3 eV stabilization on all the metal "t_{2g}" ionizations of $[Cp^*Fe(\mu\text{-}NO)]_2$, (trend 6). If the four "pure" metal "t_{2g}" ionization shifts are evaluated between iron and cobalt (namely the $B_{3u}\ \sigma^a$, $A_g\ \delta^s_{\parallel}$, $A_u\ \delta^a_{\perp}$ and $A_g\ \sigma^s$), an average 0.27 eV stabilization is observed. This is in excellent agreement with the expected ≈ 0.3 eV stabilization. The $B_{3u}\ \delta^a_{\parallel}$ and $B_{3g}\ \delta^s_{\perp}$ ($M^{\dagger}_{1,2}$), which are metal combinations uninvolved with the cyclopentadienyl but involved with the backbonding bridging ligands, are stabilized only an average 0.16 eV. The metal π "e_g" ($M^{\ddagger}_{1,2}$) ionizations are then found to be destabilized an average 0.14 eV. These shifts between Fe(NO) and Co(CO) ionizations support the general assignment of "pure" metal ionizations (M_{1-4}), metal mixed bridging ligand ionizations ($M^{\dagger}_{1,2}$) and cyclopentadienyl–bridging ligand ionizations ($M^{\ddagger}_{1,2}$).

DISCUSSION

The trends in ionization features between the complexes allow assignment of the general characters of the ionizations without recourse to calculations. The analysis is based solely on the trends in the experimental data, but the assignments which emerge are also intuitively satisfying. The fourth ionization, $A_u\ \delta^a_{\perp}$, is relatively sharp and non-bonding. The three ionizations to lower ionization energy from the $A_u\ \delta^a_{\perp}$ contain substantial antibonding interactions, while the four ionizations to higher ionization energy contain substantial bonding interactions. For the iron complexes, the first ionization ($B_{3u}\ \sigma^a$) is σ antibonding between the metals and has little interaction with the ligands, the second ionization ($B_{2g}\ \pi^a_{\parallel}$) is π antibonding between the metals and antibonding with the cyclopentadienyl ring, but stabilized by backbonding to the nitrosyls. The stabilization by backbonding to the bridging

ligands is relatively less important for the ruthenium–nitrosyl and cobalt–carbonyl complexes, and this ionization becomes the first ionization. The third ionization ($A_g\ \delta^s_{\parallel}$) is weakly bonding between the metals but antibonding with the σ donor orbitals of the bridging ligands. On the other side of the non-bonding $A_u\ \delta^a$ ionization, the $B_{3u}\ \pi^s_{\perp}$, $B_{3u}\ \delta^a_{\parallel}$ and $B_{3g}\ \delta^s_{\perp}$ are stabilized by back-bonding to the bridging ligands, and the $A_g\ \sigma^s$ is stabilized by the metal–metal interaction.

All these complexes possess two d^8 metals and traditional electron counting leads to a metal–metal double bond. However, the occupied metal orbitals are:

$$(\sigma)^2(\delta_{\perp})^2(\delta_{\parallel}{}^*)^2(\pi_{\perp})^2(\delta_{\perp}{}^*)^2(\delta_{\parallel})^2(\pi_{\parallel}{}^*)^2(\sigma^*)^2.$$

In terms of symmetry interactions between the metals, as many antibonding orbitals as bonding orbitals are occupied, and a net zero formal metal–metal bond order is found. Although the formal metal–metal bond *order* is zero, the metal–metal bond *energy* is not zero. For instance, the $A_g\ \sigma^s$ ionization is broad, indicative of substantial bonding character in the metal–metal σ bonding symmetry orbital. The $B_{3u}\ \sigma^a$ ionization of $[Cp(Fe(\mu\text{-}NO)]_2$ is relatively narrow with resolved ligand vibrational structure. Thus the metal–metal σ antibonding symmetry orbital is more non-bonding between the two metals. The metal–metal bond energy in the σ bonding interaction is not completely cancelled by the σ antibonding interaction, and a net metal–metal σ bond results. The conclusion from these ionization characteristics of some net σ bonding between the metals is supported by the calculations of Hall.[8,43]

The bonding in the M—X_2—M ring looks more like a dimetallocyclobutadiene moiety. The molecular bonding may be perceived as two π bonding interactions which are formed through the bridging ligands' π^* backbonding orbitals. Further, the σ interactions between the bonding lone pairs of the bridging ligand into the empty metal acceptor levels accounts for bonding orbitals in the σ framework. The double bonds are not located directly between the two metals, but are coupled through the bridging ligand system. One, the $B_{2u}\ \pi^s_{\perp}$, is a π orbital delocalized around the ring with a node in the plane of the ring, somewhat like the totally symmetric $p\pi$ orbital in cyclobutadiene. The other is the $B_{2g}\ \pi^a_{\parallel}$, which is in the plane of the M—X_2—M ring. These dimetallocyclobutadiene orbitals stabilize the filled–filled interactions between the metals and cyclopentadienyl ligands.

This metal–metal π and π^* ionization pair is unique in that the separation between the π and π^* ionizations remains constant over all the complexes examined. The general separation between π and π^* is found to be 0.71 ± 0.03 eV for each complex. In contrast, the σ to σ^* separation for each complex varies from 1.94 eV separation for $[CpRu(\mu\text{-}NO)]_2$ to 1.21 eV separation for both iron complexes to 0.90 eV for $[Cp^*Co(\mu\text{-}CO)]_2$. The variable energy separation found between the metal–metal σ–σ^* ionizations is understood by simple periodic trends, where the second row metal ruthenium is expected to have the greatest orbital overlap and hence the largest metal–metal interaction. The iron centres (with formal 0 oxidation states) will have greater orbital overlap than the corresponding cobalt centres (with formal +1 oxidation states).

Earlier, when the assignment of the $[CpRu(\mu\text{-}NO)]_2$ complex was made, all metal-based ionizations were expected to stabilize from the corresponding iron complex. The π and π^* were found to be slightly destabilized (0.01 eV, see Table 4). This is one indication of the substantial ligand character in these ionizations. The leading ionizations of the $CpCo(CO)_2$ and $CpRh(CO)_2$ monomers[19] are similar in having a filled interaction with the cyclopentadienyl e_1'' orbitals and backbonding to the ligands. They were also found to be substantially ligand in character, without significant shifts of these ionizations between the first and second row analogues. The largest shifts in energy of the π and π^* pair between complexes is obtained with substitution of pentamethylcyclopentadienyl for cyclopentadienyl (0.80 eV). Otherwise, the substitution of second row metal for first row metal leaves the π/π^* system relatively unchanged in energy.

The substitution of cobalt carbonyl for iron nitrosyl also leaves the relative energy position of the π and π^* pair unaffected. For the cobalt system, the less effective backbonding capabilities of the bridging carbonyls are nearly countered by the more stable cobalt metal centres. However, the slight destabilization of the π/π^* pair (0.14 eV) illustrates the weaker carbonyl backbonding capabilities as compared to the nitrosyl.

CONCLUSIONS

The evaluation of these complicated photoelectron spectra strongly emphasizes the importance of comparing the ionizations of similar complexes. Through these comparisons, the complex spectra are assigned and the nature of individual ionizations of interest may be closely studied. The ionizations are sensitive to the interactions between the filled orbitals on the two metals, between the filled π orbitals on the metals and the filled cyclopentadienyl e_1'' orbitals, and between the filled π

and δ orbitals on the metals and the empty π^* orbitals on the bridging ligands. The relative dependence of the ionizations to these interactions vary from complex to complex. We observe that the direct metal–metal interactions are formally nonbonding according to the occupation of the bonding and antibonding levels. The bonding interactions are found through the bridging ligand–metal ring system, which compensates for individual antibonding orbital combinations between the metals and the cyclopentadienyls.

Acknowledgements—D.L.L. acknowledges support by the U.S. Department of Energy (Division of Chemical Sciences, Office of Basic Energy Sciences, Office of Energy Research, DE-FG02-86ER13501), the National Science Foundation (CHE8519560), and the Materials Characterization Program, Department of Chemistry, University of Arizona.

REFERENCES

1. A. R. Pinhas and R. Hoffmann, *Inorg. Chem.* 1979, **18**, 654.
2. F. Bottomley, *Inorg. Chem.* 1983, **22**, 2656.
3. G. Granozzi, P. Mougenot, J. Demuynck and M. Bénard, *Inorg. Chem.* 1987, **26**, 2588.
4. N. Dudeney, J. C. Green, O. N. Kirchner and F. St. J. Smallwood, *J. Chem. Soc., Dalton Trans.* 1984, 1883.
5. K. A. Schugart and R. F. Fenske, *J. Am. Chem. Soc.* 1986, **108**, 5094.
6. G. E. Quelch and I. H. Hillier, *Chem. Phys. Lett.* 1988, **144**, 153.
7. P. Mougenot, J. Demuynck and M. Bénard, *J. Phys. Chem.* 1988, **92**, 571.
8. G. L. Griewe and M. B. Hall, *Organometallics* 1988, **7**, 1923.
9. D. C. Calabro, J. L. Hubbard, C. H. Blevins II, A. C. Campbell and D. L. Lichtenberger, *J. Am. Chem. Soc.* 1981, **103**, 6839.
10. D. L. Lichtenberger and J. L. Hubbard, *Inorg. Chem.* 1985, **24**, 3835.
11. H. Brunner, *J. Organomet. Chem.* 1968, **14**, 173.
12. W. A. Herrmann and J. L. Hubbard, *J. Organomet. Chem.* 1984, **262**, C46.
13. W. J. Bailey, D. M. Collins, F. A. Cotton, J. C. Baldwin and W. C. Kaska, *J. Organomet. Chem.* 1979, **165**, 373.
14. B. N. Diel, *J. Organomet. Chem.* 1985, **284**, 257.
15. A full report of this chemistry will appear elsewhere.
16. R. B. King, W. M. Douglas and A. Efraty, *J. Organomet. Chem.* 1974, **69**, 131.
17. Prepared from the direct reaction of $NOHSO_{4(s)}$ and $NaBr_{(s)}$.
18. D. C. Calabro, J. L. Hubbard, C. H. Blevins II, A. C. Campbell and D. L. Lichtenberger, *J. Am. Chem. Soc.* 1981, **103**, 6839.
19. D. L. Lichtenberger, D. C. Calabro and G. E. Kellogg, *Organometallics* 1984, **3**, 1623.
20. J. L. Hubbard, *Diss. Abstr. Int. B.* 1983, **43**, 2203.
21. G. E. Kellogg, *Diss. Abstr. Int. B.* 1986, **46**, 3838.
22. D. L. Lichtenberger, G. E. Kellogg, J. G. Kristofzski, D. Page, S. Turner, G. Klinger and J. Lorenzen, *Rev. Sci. Instrum.* 1986, **57**, 2366.
23. C. H. Blevins II, *Diss. Abstr. Int. B.* 1984, **45**, 1186.
24. G. M. Lancaster, J. A. Taylor, A. Ignatiev and J. W. Rabalais, *J. Electr. Spectrosc. Relat. Phenom.* 1978, **14**, 143.
25. J. L. Hubbard and D. L. Lichtenberger, *J. Chem. Phys.* 1981, **75**, 2560.
26. M. B. Hall and R. F. Fenske, *Inorg. Chem.* 1972, **11**, 768.
27. J. W. Richardson, W. C. Nieuwport, R. R. Powell and W. F. Edgell, *J. Chem. Phys.* 1962, **36**, 1057.
28. J. L. Calderon, S. Fontana, E. Frauendorfer, V. W. Day and S. D. A. Iske, *J. Organomet. Chem.* 1974, **64**, C14.
29. K. A. Kubat-Martin, M. E. Barr, B. Spencer and L. F. Dahl, *Organometallics* 1987, **6**, 2570.
30. L. M. Cirjak, R. E. Ginsburg and L. F. Dahl, *Inorg. Chem.* 1982, **21**, 940.
31. T. Koopmans, *Physica* 1934, **1**, 104.
32. D. L. Lichtenberger and R. F. Fenske, *J. Am. Chem. Soc.* 1976, **98**, 50.
33. D. L. Lichtenberger and A. S. Copenhaver, *J. Electron. Spectrosc. Relat. Phenom.* (1990), in press.
34. J. L. Hubbard and D. L. Lichtenberger, *J. Am. Chem. Soc.* 1982, **104**, 2132.
35. D. L. Lichtenberger, D. C. Calabro and G. E. Kellogg, *Organometallics* 1984, **3**, 1623.
36. D. L. Lichtenberger and C. B. Blevins II, *J. Am. Chem. Soc.* 1984, **106**, 1636.
37. S.-Y. Lee, *J. Chem. Educ.* 1985, **62**, 561.
38. N. E. Schore, *J. Organomet. Chem.* 1979, **173**, 301.
39. S. Evans, M. L. H. Green, B. Jewitt, A. F. Orchard and C. F. Pygall, *J. Chem. Soc., Faraday Trans II* 1972, **68**, 1847.
40. J. C. Green, *Struct. Bond. (Berlin)* 1981, **43**, 37.
41. U. Gelius, *J. Electr. Spectrosc. Related Phenom.* 1974, **5**, 985.
42. Support for this order is provided by D. L. Lichtenberger, A. S. Copenhaver and J. L. Hubbard, *Am. Chem. Soc. Abstr.* 1986, **192**, INOR 230. Photoelectron spectroscopic work on $[CpFe(CO)]_2$-$\mu(CO)_2$ and $[CpFe(CO)]_2$-$\mu(CH_2)$-$\mu(CO)$, which has shown that the substitution of a bridging methylene for a bridging carbonyl, significantly stabilized the leading ionization in $[CpFe(CO)]_2$-$\mu(CO)_2$. Since the better backbonding μ-CH_2 possesses only one π orbital (oriented parallel to the metal and bridging ligand plane) able to backbond with the complex, the leading ionization of $[CpFe(CO)]_2$-$\mu(CO)_2$ was confidently assigned to the parallel oriented metal–metal $\pi^a_{\parallel}$ interaction with substantial bridging ligand backbonding contribution.
43. M. B. Hall, in *Metal–Metal Bonds and Clusters in Chemistry and Catalysis* (Edited by J. P. Fackler Jr), Plenum Press, New York (1990), in press.

Polyhedron Vol. 9, No. 15/16, pp. 1799–1808, 1990
Printed in Great Britain

0277–5387/90 $3.00+.00
© 1990 Pergamon Press plc

LINEAR SEMIBRIDGING CARBONYLS—III. CARBONYL AND THIOCARBONYL LIGANDS AS FOUR-ELECTRON DONORS†

ANDREW L. SARGENT and MICHAEL B. HALL‡

Department of Chemistry, Texas A&M University, College Station, TX 77843-3255, U.S.A.

Abstract—Parameter-free Fenske–Hall molecular orbital calculations predict the electronic structure and bonding of several heterobimetallic complexes containing linear semibridging carbonyl and thiocarbonyl ligands. The results suggest that the linear semibridging ligand acts as a four-electron donor only when the secondary metal centre is an electron-deficient early transition metal atom. When the secondary centre is a late transition metal atom, the linear semibridging ligand acts as a π-acceptor of electron density, even if the late metal has less than 18 electrons. Holes in the *d* shell of the early metal atoms are more prominent than those in the late metal atoms where the higher nuclear charge pulls the *d* electrons closer to the nucleus. The role of the semibridging ligand is to fill in the prominent holes in the *d* shell when they exist by donating electron density from an occupied π orbital. When there are no holes in the *d* shell, or when the holes are very small, the semibridging ligands accept electron density from the secondary metal centre into a π^* orbital.

Angelici and co-workers have recently reported the first semibridging thiocarbonyl complexes.[1,2] Experimental and theoretical evidence suggests that the thiocarbonyl (CS) ligand is not only a better π-donor than the carbonyl (CO) ligand, but is also a better π-acceptor.[3,4] This raises an interesting question: is the direction of electron density flow between a secondary metal centre and the semibridging CS ligand similar to that in analogous semibridging CO compounds? The direction of electron density flow between semibridging carbonyl ligands and secondary metal centres has been a point of controversy among chemists for several years. In the four-electron donor, or π-donor, model electron density flows from a π orbital of the semibridging carbonyl ligand to the secondary metal centre, M′, shown in **1**, whereas in the π-acceptor model, electron density flows from M′ to a π^* orbital of the semibridging ligand, as in **2**.

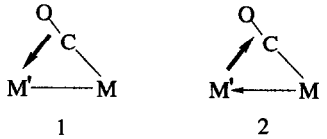

1 2

Crabtree has classified the different semibridging carbonyl complexes into three different types[5] that can be distinguished by the kind of metal atom in the secondary metal centre. Type I complexes typically contain early transition metal atoms, type II complexes contain atoms from the middle of the series, and type III contain late transition or main group atoms. Theoretical studies have been performed on examples of type II and type III complexes and have suggested that the π-acceptor model, **2**, most accurately represents the bonding in these two types of complexes.[6–9] The bonding in type I complexes, however, has not been analysed theoretically, but is thought to follow the π-donor model.[5]

We report the electronic structures of the following two semibridging thiocarbonyl complexes: $[HB(pz)_3](CO)_2W(\mu\text{-}CS)Mo(CO)_2(In)^2$ (**3**: In = η^5-$C_9H_7^-$, indenyl; $HB(pz)_3^- = HB(N_2C_3H_3)_3^-$,

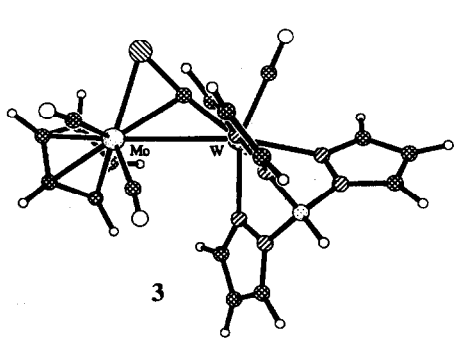

3

† Dedicated to Professor Richard F. Fenske in appreciation for his contagious enthusiasm and insightful leadership in theoretical inorganic chemistry. I especially want to thank him for his caring mentorship of my own formative scientific years.

‡ Author to whom correspondence should be addressed.

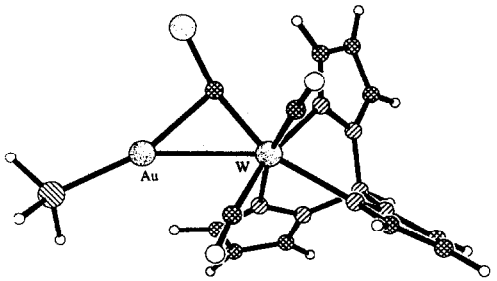

4

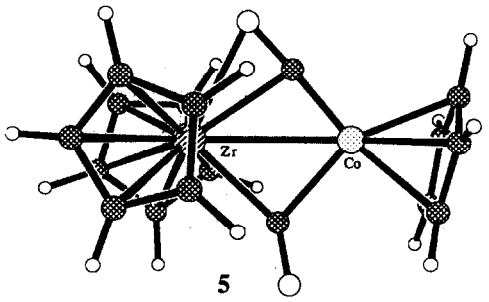

5

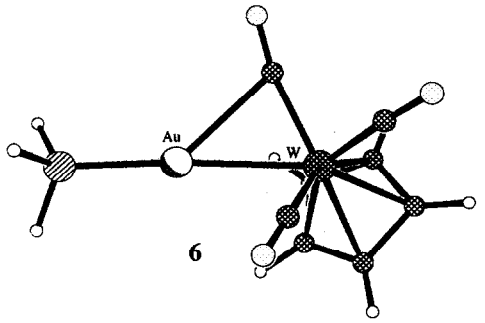

6

hydrotris(1-pyrazolyl)borate), and $[HB(pz)_3](CO)_2(CS)WAu(PPh_3)$[1] (**4**). We also examine the electronic structures of a type I semibridging carbonyl complex, $CpCo(\mu\text{-}CO)_2ZrCp_2$[10] (**5**: Cp = η^5-C_5H_5), and a type III semibridging carbonyl complex, $Cp(CO)_3WAu(PPh_3)$[11] (**6**). The In group has been abbreviated to a Cp group in **3** and the PPh_3 ligands represented as PH_3 ligands in **4** and **6** for simplicity.

METHODS

Unparameterized Fenske–Hall[12] molecular orbital (MO) calculations were performed on the Department of Chemistry's VAX 11/780 computer. The atomic positions were taken directly from the crystal data. The molecular symmetry of each complex was C_1. To reduce the size of the calculations, the In ligand was replaced by a Cp ligand in **3**, and the phenyl groups of the PPh_3 ligands in **4** and **6** were replaced by hydrogen atoms at a P—H distance of 1.42 Å.

The basis functions for all non-hydrogen atoms were generated by the numerical Xα atomic orbital program of Herman and Skillman[13] used in conjunction with the Xα-to-Slater basis program of Bursten and Fenske.[14] Ground-state atomic configurations were used for all non-transition metal atoms. The transition metal atoms assumed $d^{n+1}s^0$ cationic configurations. The exponents for the valence s and p orbitals of the transition metal atoms were determined by minimizing the energy difference between the valence eigenvalues obtained from molecular calculations and the experimental ionization potentials of $M(CO)_6$ and $M'(PF_3)_4$ (M = Cr, Mo, W; M′ = Ni, Pd, Pt). The numerical Xα-atomic orbitals were fit to double-ζ analytical Slater type orbitals for the valence d orbitals of the transition metal atoms and for the valence p orbitals of non-transition metal atoms. All other orbitals were represented as single-ζ functions. The orbital exponent for hydrogen was 1.20. The population analysis of Mulliken[15] was used in the calculations to determine gross and overlap populations, in addition to individual atomic charges.

RESULTS AND DISCUSSION

Figure 1 shows the results of a Fenske–Hall MO calculation on our model of **3**, where the results in the atomic basis have been transformed into the results of the molecular orbitals of the fragments, $CpMo(CO)_2^+$ (**3a**), and $W(CS)(CO)_2HB(pz)_3^-$ (**3b**). The molybdenum fragment is represented as a d^4 cationic species with 25 fragment molecular orbitals (FMOs) doubly occupied. The tungsten fragment is represented as a d^6 anionic species and FMO 58 is the doubly-occupied HOMO.

The Mulliken gross populations indicate that there is substantial interaction between FMOs 26 and 58, the LUMO of **3a** and the HOMO of **3b**, respectively. Nearly 0.9 e^- is transferred to the "electron-poor" (14 e^-) fragment, **3a**, from the "electron-rich" (16 e^-) fragment, **3b**, to form a dative metal–metal single bond. The contour plot in Fig. 2(b) illustrates how the CS π^* component of FMO 58 contributes to the overlap of the two fragment molecular orbitals in forming the M—M bonding MO 79. This type of interaction is a pervasive feature in heterobimetallic semibridging carbonyl complexes and has been discussed previously.[8,9]

The unusual interaction in Fig. 1 is between the CS π (bonding) orbital (FMO 55) and an unoccupied Mo d orbital (FMO 27). A significant amount of electron density flows from the CS π orbital into the vacant Mo orbital, while an almost

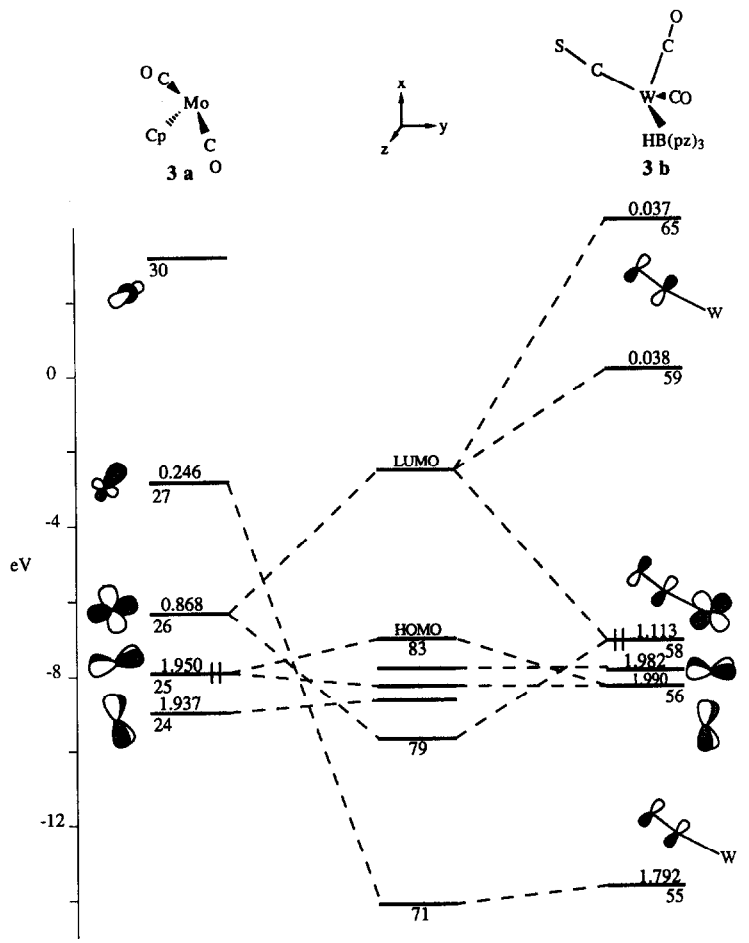

Fig. 1. Molecular orbital diagram of $[HB(pz)_3](CO)_2W(\mu\text{-}CS)Mo(CO)_2(Cp)$ constructed from $[HB(pz)_3](CO)_2W(\mu\text{-}CS)^-$ and $Mo(CO)_2(Cp)^+$ fragments. The principal components of the fragment molecular orbitals are drawn next to the corresponding energy levels. Significant Mulliken gross populations are listed with the fragment orbitals.

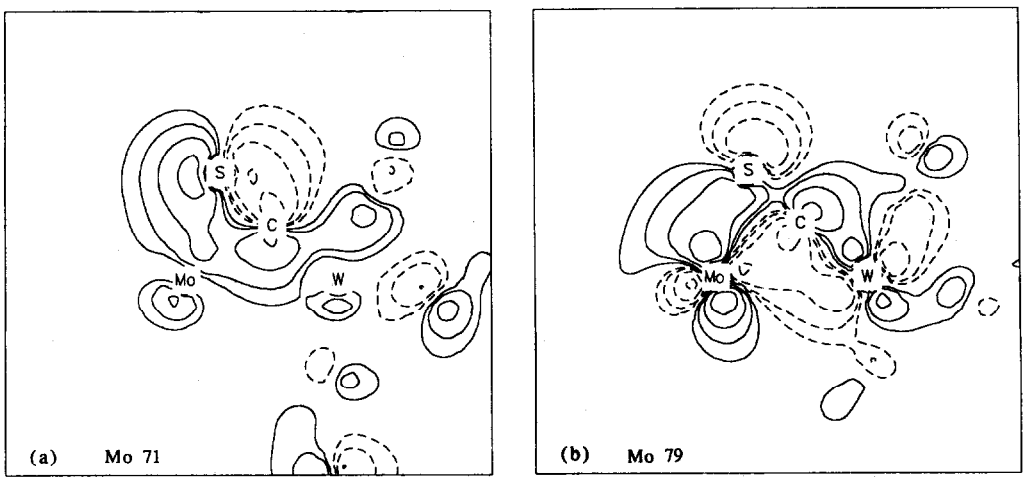

Fig. 2. Contour plots for selected valence orbitals of $[HB(pz)_3](CO)_2W(\mu\text{-}CS)Mo(CO)_2(Cp)$. Contours are geometric, differing by a factor of two, with the lowest contour of 0.01563 (e a.u.$^{-3}$)$^{1/2}$.

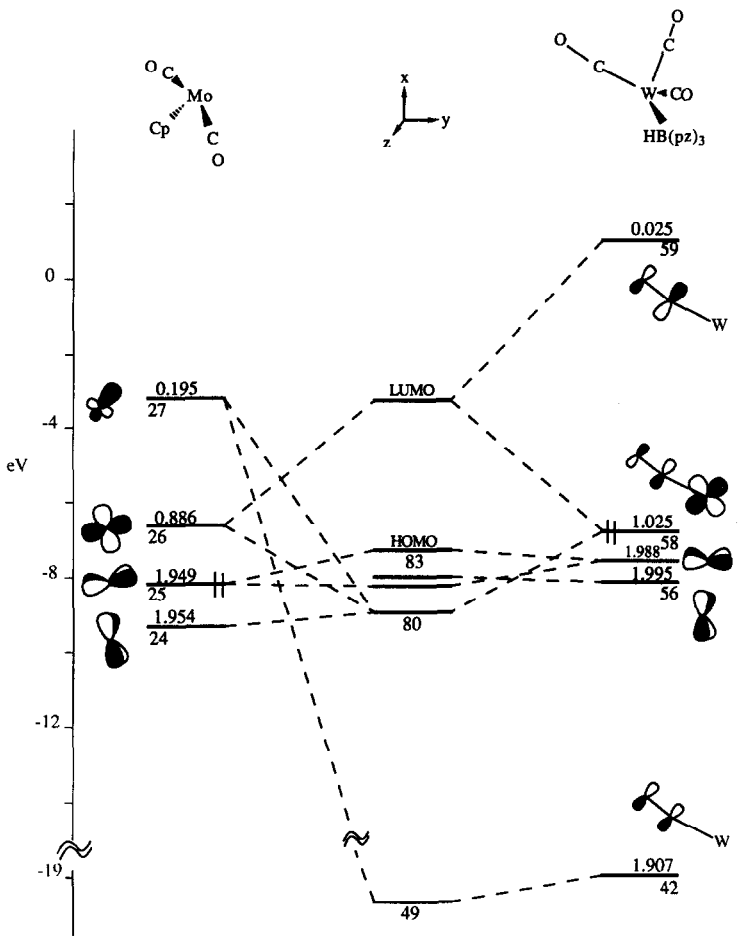

Fig. 3. Molecular orbital diagram of $[HB(pz)_3](CO)_2W(\mu\text{-}CO)Mo(CO)_2(Cp)$, the CO analogue of **3**.

negligible amount flows from the occupied orbitals of **3a** back to the CS π^* orbital of **3b** (the π^* component is roughly equally distributed between FMOs 59 and 65). The CS ligand therefore acts as a π-donor. The contour plot, shown in Fig. 2(a), illustrates the importance of the S—Mo overlap in the interaction. To our knowledge, this is the first time that quantum chemical calculations have supported the four-electron donor model[17] for complexes with semibridging ligands.

To better understand the differences between CO and CS that give rise to the four-electron bonding mode in **3**, calculations were performed on the semibridging CO analogue of **3**. In these calculations, CO replaces the CS ligand and is positioned at sensible M—C and C—O distances (W—C distance = 1.954 Å; C—O distance = 1.167 Å). The results are shown in Fig. 3. The most obvious difference between the two calculations is that the CO π orbitals are more than 4 eV lower in energy than the corresponding CS π orbitals. Energetically, these CO orbitals are much less able to interact with the unoccupied Mo *d* orbital (FMO 27), and less density is transferred as a result.† Less density is also transferred back to the CO π orbital, reflecting the poorer π-accepting ability of CO compared to CS. The theory predicts that the CO analogue of **3** is less stable than **3** due to the reduced interaction between the semibridging ligand and the Mo fragment. This prediction is consistent with the experimental results: the CO analogue of **3** is stable in solution but decomposes in the solid state over a period of several hours.[2]

Since CS is a better π-acceptor as well as a better π-donor than CO,[3,4] some additional factor must influence whether the ligand donates electron density to, or accepts electron density from, the secondary metal centre. That the secondary metal centre is electron deficient is a tempting but incomplete answer. A previous report was devoted to describ-

† Notice that while the Mulliken gross population of the Mo FMO 27 is nearly 0.2 e^-, less than 0.1 e^- comes from the semibridging CO 1π orbital. The remainder of the density comes from the W FMO 58, which is allowed to mix due to the low symmetry of the complex.

ing how semibridging CO ligands readily accept electron density from electron-deficient metal centres.[9] The key difference is that the secondary metal centres described in that report are all late transition metal centres that are formally either d^8 or d^{10} species. The secondary metal atom in **3** is d^4 Mo, an early transition metal. The *d* functions of early transition metal atoms are more diffuse than those of later atoms of the series. Holes in the *d* shell are not only more prevalent for the early atoms in the transition series, but they are also more prominent in these atoms than they are in the late transition metal atoms where the higher nuclear charge pulls the *d* electrons closer to the nucleus. This contraction decreases the relative size of the holes. Early metals typically have larger holes in the *d* shell due to a combination of simply having fewer *d* electrons and holding these electrons in diffuse orbits. Therefore, they more readily accept density from semibridging ligands that are able to donate to help fill in the holes.

Substituting the electron-deficient, early transition metal fragment **3a** with an electron-deficient, late transition metal, $Au(PPh_3)$ (**4a**), yields $[HB(pz)_3](CO)_2(CS)WAu(PPh_3)$ (**4**).[1] One might expect that since there are no holes in the *d* shell on the Au fragment (represented as a d^{10} cationic species) the CS ligand would act as a π-acceptor and pick up density from one of the filled Au *d* orbitals. As the MO diagram in Fig. 4 shows, very little density flows into or out of the CS π orbitals. The principal interaction between the two fragments is between the HOMO of **4b** (FMO 58) and the LUMO of **4a** (FMO 9). Here we see the donation of a substantial amount of density from the former to the latter to form a dative M—M bond in MO 65. The only significant interaction that the CS ligand has with the Au fragment appears in MO 64, which is principally antibonding between a Au *d* orbital (FMO 9) and the CS carbon-centred σ lone pair orbital (FMO 55). Orbital 64 is stabilized by the Au sp_z hybrid (FMO 10) and a small amount of density flows from the CS ligand into the hybrid. The CS π^* orbital (FMO 59) gains only 0.077 e^- from the Au fragment, which is small compared to what has been found in some semibridging CO

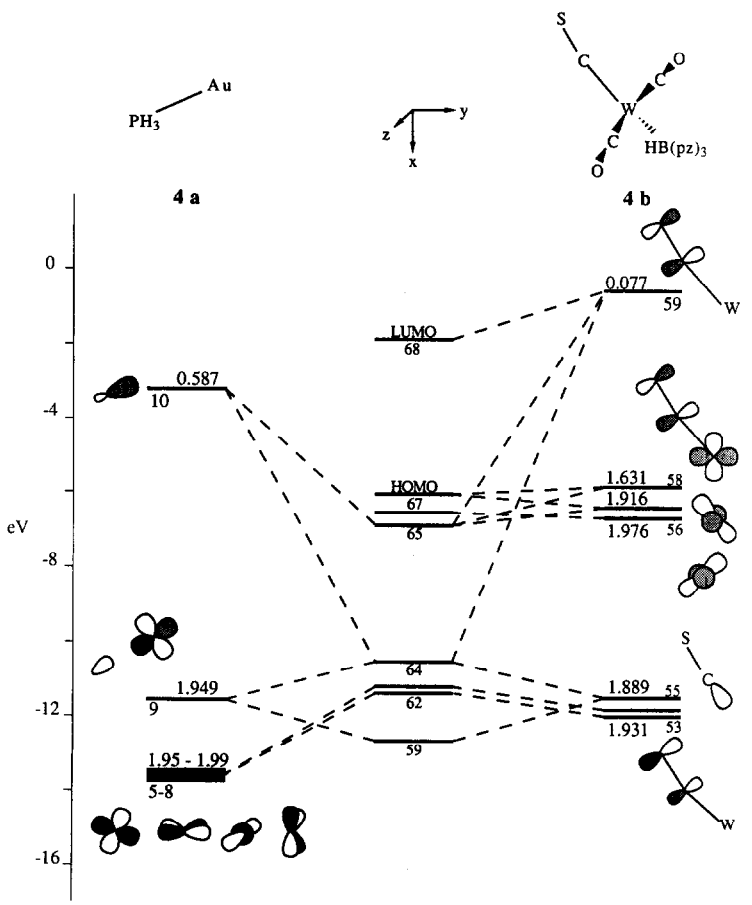

Fig. 4. Molecular orbital diagram of $[HB(pz)_3](CO)_2(CS)WAu(PH_3)$, constructed from $[HB(pz)_3](CO)_2(CS)W^-$ and $Au(PH_3)^+$ fragments.

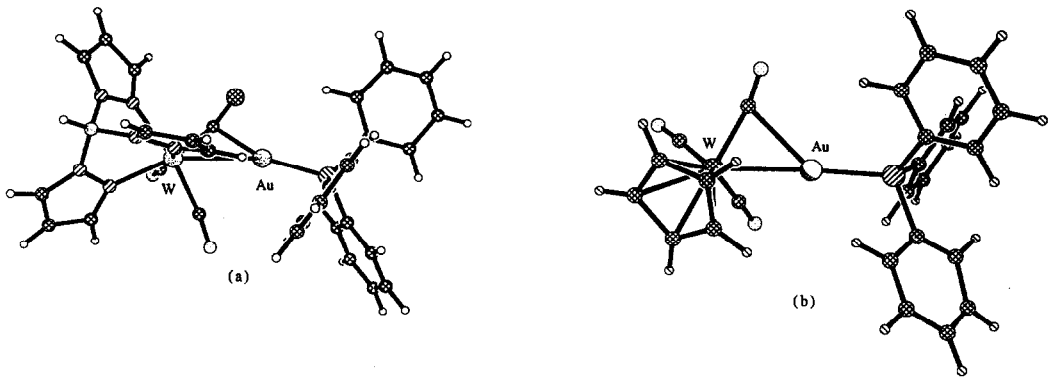

Fig. 5. (a) Full molecular structure of $[HB(pz)_3](CO)_2(CS)WAu(PPh_3)$. The reverse view is shown to highlight the close proximity of the pyrazole and phenyl rings. (b) Full molecular structure of $Cp(CO)_3WAu(PPh_3)$.

complexes,[9] especially considering that the CS ligand is a better π-acceptor than the CO ligand. One contributing factor might be that the long Au—W bond, at 2.825 Å, restricts the overlap between the Au d_{xy} and the CS π^* orbital, which is only 0.053.† Figure 5(a) indicates that the long bond may be due to steric interactions between the phenyl groups of PPh_3 and the $HB(pz)_3$ ligand. A smaller ligand in place of $HB(pz)_3$ might allow the M—M bond length to adjust to maximize the Au d_{xy}–CS π^* overlap and thereby allow more electron density to flow between them.

The semibridging CO analogue of **4** in which a Cp ligand replaces the $HB(pz)_3$ ligand coordinated to the W fragment, $Cp(CO)_3WAu(PPh_3)$[11] (**6**), is shown in Fig. 5(b). Comparing Figs 5(a) and (b) reveals that the steric interactions of the former are not present in the latter. While the Au—W bond length in **6** at 2.698 Å is shorter than that in **4**, the MO diagram in Fig. 6 suggests that no significant interaction exists between the Au fragment and the CO π orbitals. A contributing factor to this lack of interaction is the orientation of the phosphine ligand. That the Au—P axis in **6** is nearly linear to the Au—W axis hinders the interaction between the Au fragment and the CO π^* orbital for the following reason. The Au *d* orbital that is destabilized as a result of the ligand field splitting is the $d_{x^2-y^2}$, whereas the d_{xy} is the orbital that interacts with the semibridging CO ligand. Without this destabilization, the energy differerence between the d_{xy} and the CO π^* orbitals is too large to permit significant interaction.

This point is easily illustrated if we rotate the Au—P axis in **4** such that it is linear to the Au—W axis, shown in **7** and in Fig. 7. Comparison of the

† Typical values for metal *d*–semibridging CO overlap from previous calculations[8] are in the range of 0.1–0.2.

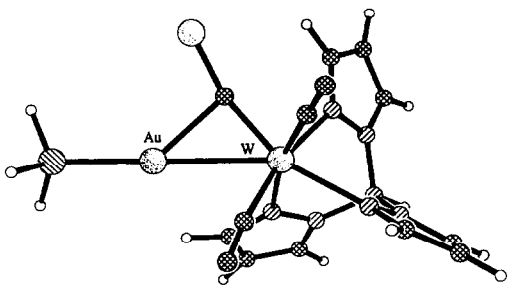

7

MO diagrams in Figs 4 and 7 show that the Au d_{xy} and $d_{x^2-y^2}$ orbitals switch positions as the ligand field changes. Note that the amount of electron density transferred in the dative M—M interaction increases as the phosphine group is rotated. The unoccupied Au sp_z hybrid (FMO 10) is directed along the M—M axis in **7** which increases the overlap with the W FMOs 58 and 57 (10–57 + 10–58 overlap = 0.379 in **4** and 0.431 in **7**) and allows for the greater transfer of charge. The bottom line concerning the bonding in **4** and **6** is that there is a minimal interaction between the secondary metal centre and the semibridging ligand. The lack of holes in the *d* shell precludes any π-donation from the semibridging ligand. A combination of factors prevents back donation to the semibridging ligand's π^* orbital to the extent that has been found for other, similar complexes.[9]

The final complex we wish to discuss is $CpCo(\mu\text{-}CO)_2ZrCp_2$[10] (**5**), a so-called type I semibridging carbonyl complex[5] in which the semibridging ligand is thought to act as a four-electron donor. The theoretical support for the four-electron donor model in the semibridging thiocarbonyl complex, **3**, raised our interest in whether theory would support this model in a known semibridging carbonyl complex involving an early metal centre. As in **3**, the secondary metal centre in **5** is an electron-deficient,

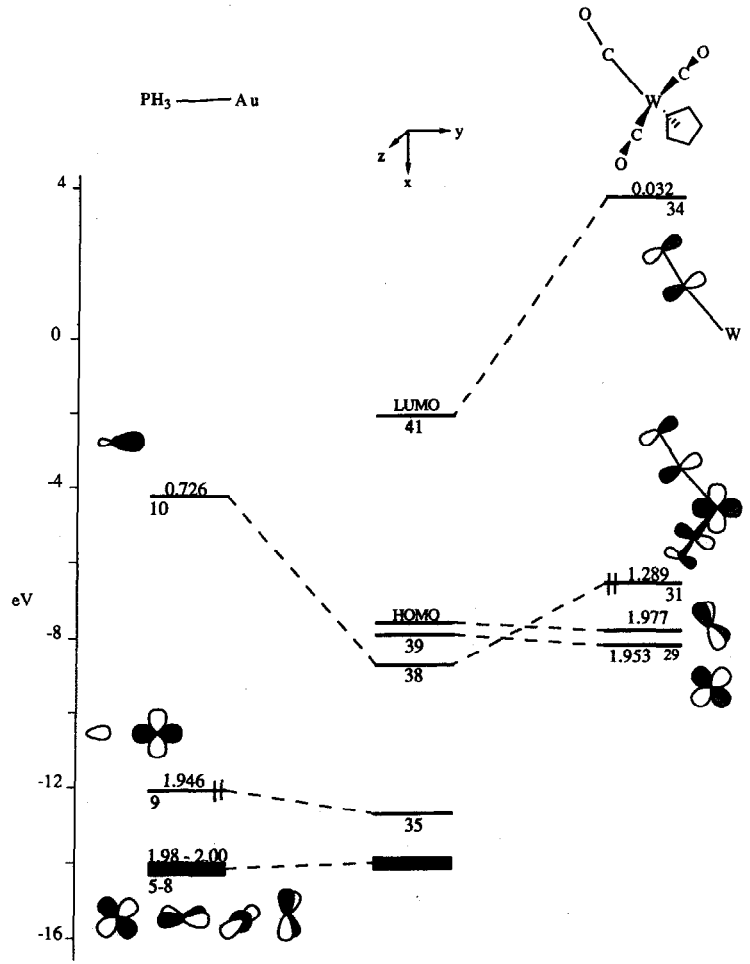

Fig. 6. Molecular orbital diagram of $Cp(CO)_3WAu(PPh_3)$, constructed from $Cp(CO)_3W^-$ and $Au(PPh_3)^+$ fragments.

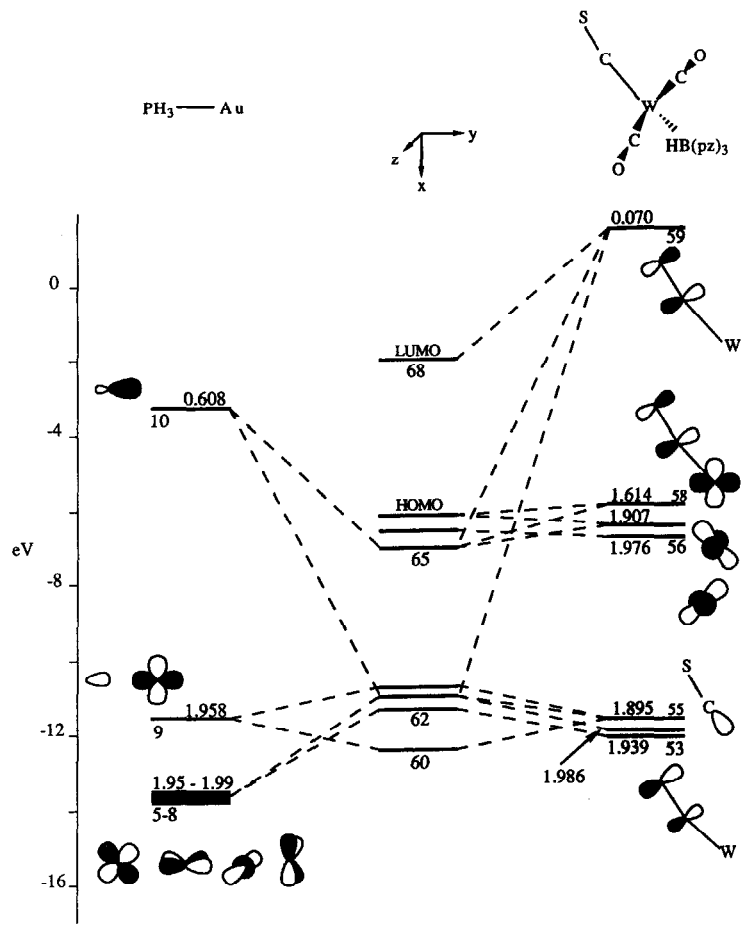

Fig. 7. Molecular orbital diagram of a hypothetical structural isomer of $[HB(pz)_3](CO)_2(CS)WAu(PH_3)$ in which the Au—PH_3 axis is co-linear with the Au—W axis.

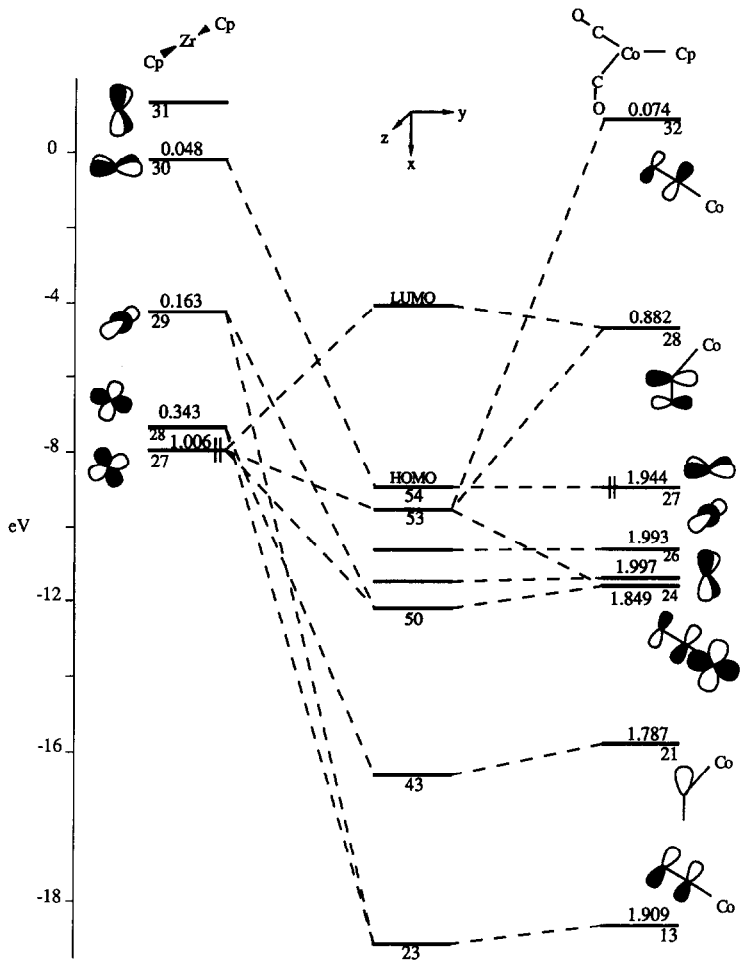

Fig. 8. Molecular orbital diagram of $CpCo(\mu\text{-}CO)_2ZrCp_2$ showing the interaction between the neutral $CpCo(\mu\text{-}CO)_2$ and $ZrCp_2$ fragments.

early transition metal atom. The results of the MO calculation are shown in Fig. 8. Both fragments are represented as closed-shell neutral species, where the d^2, 14 e^- Zr fragment as well as the d^8, 18 e^- Co fragment have 27 doubly-occupied orbitals prior to interaction. The most noteworthy interaction is that seen in MO 23 between Co FMO 13, the linear semibridging carbonyl π orbital, and Zr FMO 29, an unoccupied Zr d orbital. The Mulliken gross populations indicate that the CO π orbital donates roughly 0.1 e^- to a combination of unoccupied Zr d orbitals, FMOs 28 and 29. Despite the large energy gap between the interacting fragments, the diffuse d orbitals of the early transition metal Zr provide sufficient overlap with the CO π orbitals to yield significant interaction, as shown in the contour plot of Fig. 9(a). The semibridging CO ligand clearly acts as an electron donor to the secondary metal centre.

Note, however, that a significant, though not large, quantity of density is transferred back to the semibridging ligand's π^* orbital (FMO 32) from an occupied Zr orbital (FMO 27) in MO 53. Not only does the semibridging CO ligand donate electron density to the Zr fragment to help fill in holes in the d shell, but it also acts as an acceptor of density to a limited extent even with this very early metal.

Other features of the bonding in **5** that are worthy of note include the role of the symmetrically-bridging CO ligand. The 5σ orbital (FMO 21) donates a large amount of density (0.21 e^-) to one of the unoccupied Zr d orbitals. The contour plot of MO 43, shown in Fig. 9(b), shows how the CO σ (C lone pair) contributes to the Co—Zr σ overlap. The M—M bonding interaction in MO 50 is cancelled by the corresponding antibonding interaction in MO 53. The antibonding MO, however, gains significant stabilization from the symmetrically bridging ligand's π orbital (FMO 28) and as a result forms a three-centre, two-electron bond, shown in Fig. 9(c). This type of interaction has been discussed previously in detail.[8]

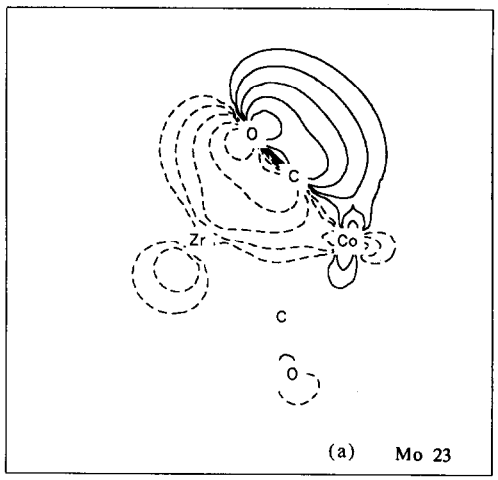

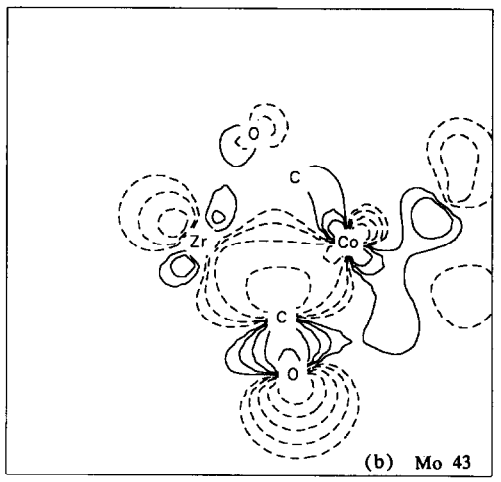

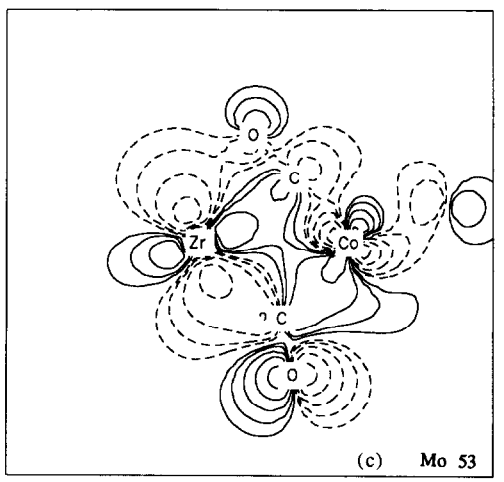

Fig. 9. Contour plots for selected valence orbitals of $CpCo(\mu\text{-}CO)_2ZrCp_2$. See Fig. 2 for contour information.

CONCLUSION

Theoretical support for the four-electron donor model of semibridging carbonyl and thiocarbonyl ligands has been presented. These linear semibridging ligands will act as four-electron donors only when the secondary metal centre is electron deficient and contains an early transition metal atom. The role of the semibridging ligand in this case is to help fill the large holes that are present in the *d* shell of the metal centre. Such holes are not only more prevalent in early transition metal centres, but are also more prominent than holes in the *d* shell of late transition metal centres where a higher nuclear charge contracts the orbits of the electrons and effectively reduces the size of the holes. Late transition metal centres are therefore more content to have fewer than 18 electrons in the valence shell and more readily form stable 14- and 16-electrons species. When secondary metal centres have fewer than 18 electrons and contain a late transition metal atom, the predominant role for the semibridging ligand is to function as a π-acceptor.

Acknowledgements—The authors thank the Robert A. Welch Foundation (Grant No. A-648) and the National Science Foundation (Grant No. CHE 86-19420) for their support. A.L.S. thanks the Shell Foundation for a predoctoral fellowship. The authors also thank R. J. Angelici for a preprint of ref. 2.

REFERENCES

1. H. P. Kim, S. Kim, R. A. Jacobson and R. J. Angelici, *J. Am. Chem. Soc.* 1986, **108**, 5154.
2. R. A. Doyle, L. M. Daniels, R. J. Angelici and F. G. A. Stone, *J. Am. Chem. Soc.* 1989, **111**, 4995.
3. D. L. Lichtenberger and R. F. Fenske, *Inorg. Chem.* 1976, **15**, 2015.
4. J. L. Hubbard and D. L. Lichtenberger, *Inorg. Chem.* 1980, **19**, 3965.
5. R. H. Crabtree and M. Lavin, *Inorg. Chem.* 1986, **25**, 805.
6. E. D. Jemmis, A. R. Pinhas and R. Hoffmann, *J. Am. Chem. Soc.* 1980, **102**, 2576.
7. M. Bénard, A. Dedieu and S. Nakamura, *Nouv. J. Chim.* 1984, **8**, 149.
8. Part I of Linear Semibridging Carbonyls: B. J. Morris-Sherwood, C. B. Powell and M. B. Hall, *J. Am. Chem. Soc.* 1984, **106**, 5079.
9. Part II of Linear Semibridging Carbonyls: A. L. Sargent and M. B. Hall, *J. Am. Chem. Soc.* 1989, **111**, 1563.
10. P. T. Barger and J. E. Bercaw, *J. Organomet. Chem.* 1980, **201**, C39.
11. J. B. Wilford and H. M. Powell, *J. Chem. Soc. A* 1969, 8.
12. M. B. Hall and R. F. Fenske, *Inorg. Chem.* 1972, **11**, 768.

13. F. Herman and S. Skillman, *Atomic Structure Calculations*. Prentice–Hall, Englewood Cliffs, New Jersey (1963).
14. (a) B. E. Bursten and R. F. Fenske, *J. Chem. Phys.* 1977, **67**, 3138; (b) B. E. Bursten, R. J. Jensen and R. F. Fenske, *J. Chem. Phys.* 1978, **68**, 3320.
15. R. S. Mulliken, *J. Chem. Phys.* 1955, **23**, 1833, 1841.
16. All contour plots were generated with the program MOPLOT. D. L. Lichtenberger, PhD Dissertation, University of Wisconsin, Madison, WI (1974). The program is available from the Quantum Chemistry Program Exchange, Indiana University, Bloomington, IN 47401, U.S.A., Program 284.
17. (a) R. J. Klingler, W. M. Butler and M. D. Curtis, *J. Am. Chem. Soc.* 1978, **100**, 5034; (b) M. D. Curtis and W. M. Butler, *J. Organomet. Chem.* 1978, **155**, 131.

Polyhedron Vol. 9, No. 15/16, pp. 1809–1819, 1990
Printed in Great Britain

0277–5387/90 $3.00+.00
© 1990 Pergamon Press plc

THE SYNTHESES, MOLECULAR AND ELECTRONIC STRUCTURES OF TWO μ^4-VINYLIDENE TETRAIRON CLUSTERS*

JOHN S. BRADLEY,† SUZANNE HARRIS,† ERNESTINE W. HILL and MICHELLE A. MODRICK

Exxon Research and Engineering Company, Route 22 East, Clinton Township, Annandale, NJ 08801, U.S.A.

Abstract—The syntheses, crystal structures and electronic structures of the new μ^4-vinylidene clusters, $Fe_4(CO)_{12}(C{=}C(OCH_3)_2)$ and $Fe_4(CO)_{12}(C{=}C(OCH_3)CH_3)$, are reported. $Fe_4(CO)_{12}(C{=}C(OCH_3)_2)$ was prepared by the methylation of $[Fe_4(CO)_{12}(CCO_2CH_3)]^-$ with trimethyloxonium fluoroborate in methylene chloride at 25°C. $Fe_4(CO)_{12}(C{=}C(OCH_3)CH_3)$ was prepared in an analogous manner from $[Fe_4(CO)_{12}(CC(O)CH_3)]^-$. $Fe_4(CO)_{12}(C{=}C(OCH_3)_2)$ crystallizes in the monoclinic space group $P2_1/c$ (C_{2h}^5 No. 14) with $a = 13.900(2)$, $b = 8.909(2)$, $c = 17.116(4)$ Å, $\beta = 94.59(2)°$; $\rho_{calc} = 2.03$ g cm^{-3} for mol. wt 645.6 and $Z = 4$. $Fe_4(CO)_{12}(C{=}C(OCH_3)CH_3)$ crystallizes in the monoclinic space group $P2_1/c$ (C_{2h}^5 No. 14) with $a = 28.441(6)$, $b = 9.204(2)$, $c = 17.466(4)$ Å, $\beta = 108.51(2)°$; $\rho_{calc} = 1.93$ g cm^{-3} for mol. wt = 629.6 and $Z = 8$. Both clusters have an open butterfly core of four iron atoms with the vinylidene ligand bound to all four metal atoms. Molecular orbital calculations using the Fenske–Hall method were carried out for the two clusters. The molecular and electronic structures of the molecules are compared with each other and with those of μ^4-methylidyne clusters. Although both of these clusters contain a formal C—C double bond in the vinylidene ligand, the presence of oxygen atoms in these ligands leads to a delocalized π system and only partial double bond character in this C—C bond. Changes in the structure of the cluster framework can be correlated with the oxygen content and thus double bond character in the vinylidene ligand.

The chemistry of transition metal clusters with an open butterfly geometry, bearing a μ^4-carbide ligand, and of their μ^4-methylidyne analogues, is of continuing interest. These compounds exhibit unique chemistry by virtue of the geometry of the binding site of the carbon ligand atom.[1] This family of molecules also has an additional attraction in that it may provide structural parallels to the chemisorbed state of organic molecules in four-fold sites on metal surfaces, parallels not provided by the higher symmetry molecular clusters most often found in organometallic cluster chemistry.

Some homometallic tetrairon clusters of this type which have been characterized by X-ray diffraction are shown in the Scheme 1. $Fe_4(CO)_{13}C$ (**1**),[2] $[Fe_4(CO)_{12}C]^{2-}$ (**2**)[3] and $[HFe_4(CO)_{12}C]^-$ (**3**)[4] all contain a μ^4-carbide ligand. $HFe_4(CO)_{12}CH$ (**4**)[5] is derived from **2** or **3** by protonation,[4,6] from **2** by oxidation under hydrogen,[6] or from **1** by treatment with hydrogen.[7] $[Fe_4(CO)_{12}(CCO_2CH_3)]^-$ (**5**) is derived from **1** by reaction with methanol,[2] and $[Fe_4(CO)_{12}(CC(O)CH_3)]^-$ (**6**) results from the reaction of methyl iodide with **2**.[3] The corresponding dianion of **6**, which has a similar structure, has also been reported.[8] $HFe_4(CO)_{12}(COCH_3)$ (**7**) is derived from the non-carbide cluster $[Fe_4(CO)_{12}]^{2-}$ by sequential methylation and protonation.[4] We have extended the range of μ^4-organic ligands in this cluster group by preparing two new μ^4-vinylidene clusters, $Fe_4(CO)_{12}(C{=}C(OCH_3)_2)$ (**8**) and $Fe_4(CO)_{12}(C{=}C(OCH_3)CH_3)$ (**9**) [eq. (1)].

* Dedicated to Professor Richard F. Fenske in appreciation of both his contributions to theoretical inorganic chemistry and his truly inspiring teaching which led me (S. H.) into this field.

† Authors to whom correspondence should be addressed.

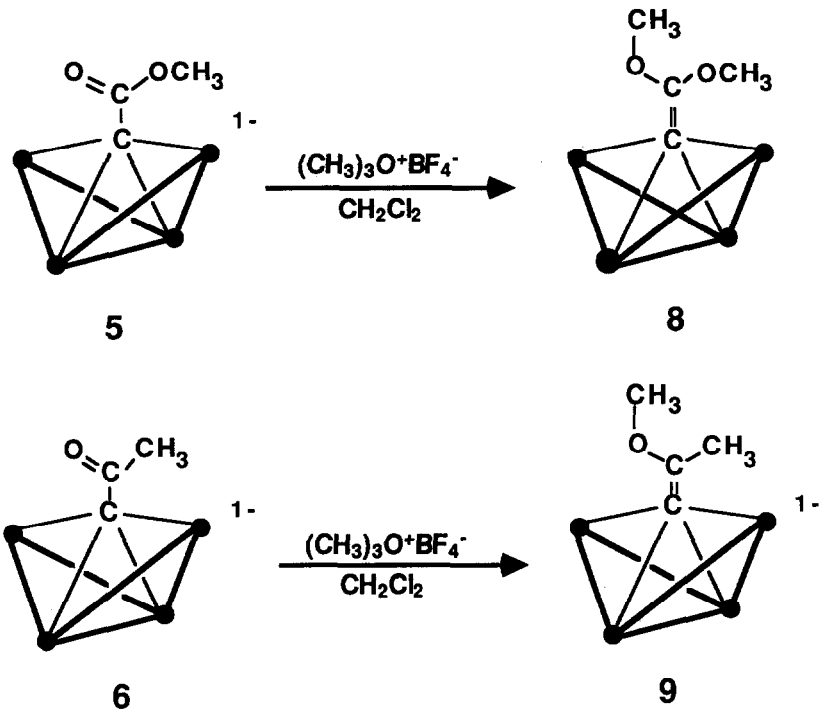
O=C-OCH3
C
1-
(CH3)3O+BF4-
CH2Cl2
CH3
O
C-OCH3
C
5
8
O=C-CH3
C
1-
(CH3)3O+BF4-
CH2Cl2
CH3
O
C-CH3
C
1-
6
9

(1)

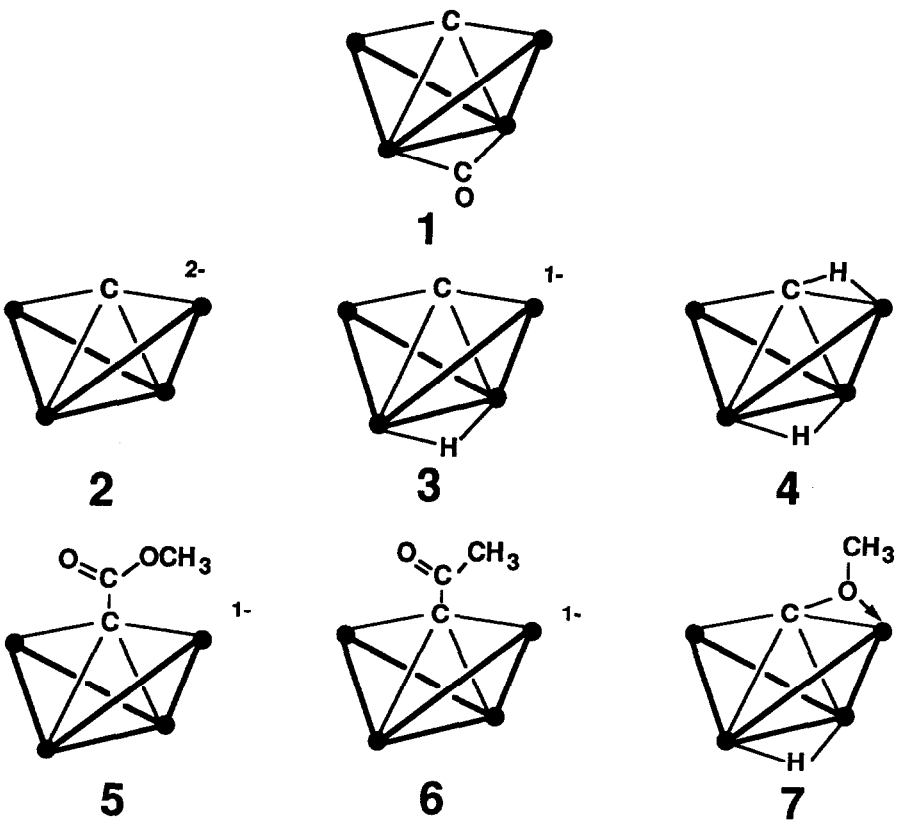
C
C
O
1
C
2-
2
C
1-
H
3
C
H
H
4
O=C-OCH3
C
1-
5
O=C-CH3
C
1-
6
CH3
O
C
H
7

Scheme 1.

In this paper we describe the synthesis and crystal structures of these clusters and compare the geometries and electronic structures of the molecules with each other and with those of μ^4-methylidyne clusters. A brief report of the preparation of **8** and **9** and the structure of **8** has appeared previously.[7]

EXPERIMENTAL

(1) *Syntheses*

All preparative procedures were performed in standard Schlenk glassware on a double manifold vacuum–nitrogen line. $Fe_4(CO)_{12}(C{=}C(OCH_3)_2)$ (**8**) was prepared by the methylation of $[Fe_4(CO)_{12}(CCO_2CH_3)]^-$ (**5**) with trimethyloxonium fluoroborate in methylene chloride at 25°C. $Fe_4(CO)_{12}(C{=}C(OCH_3)CH_3)$ (**9**) was prepared in an analogous manner from $[Fe_4(CO)_{12}(CC(O)CH_3)]^-$ (**6**). The starting materials for **8** and **9** were prepared by published procedures.[9]

$Fe_4(CO)_{12}(C{=}C(OCH_3)_2)$ (**8**). To a solution of $(C_2H_5)_4N[Fe_4(CO)_{12}(CCO_2CH_3)]$ (**5**) (1.50 g, 1.95 mmol) in methylene chloride (100 cm^3) was added trimethyloxonium tetrafluoroborate (0.291 g, 1.95 mmol) and the green–black mixture was stirred for 24 h. During this time the solution became a paler green, and the IR absorbances of the starting material were replaced by new bands at 2080, 2040, 2010, 1992 and 1950 cm^{-1}. The reaction mixture was evaporated to dryness under reduced pressure, and the residue extracted into boiling hexane (4 × 50 cm^3). The product, **8**, crystallizes on cooling the filtrate to room temperature. A second crop may be obtained by cooling the filtrate to −40°C. Combined yield of **8** = 0.800 g (1.24 mmol, 64%). Found: C, 29.19; H, 1.02; Fe, 33.79. Calc. for $C_{16}H_6O_{14}Fe_4$: C, 29.77; H, 0.94; Fe, 34.69%. IR (CH_2Cl_2): 2080, 2040, 2010, 1992, 1950 cm^{-1}. ^1H NMR (60 MHz, CD_2Cl_2, 25°C): 3.70 δ (OCH_3).

$Fe_4(CO)_{12}(C{=}C(OCH_3)CH_3)$ (**9**). To a solution of $(C_2H_5)_4N[Fe_4(CO)_{12}(CC(O)CH_3)]$ (5.0 g, 6.7 mmol) in methylene chloride (350 cm^3) was added trimethyloxonium tetrafluoroborate (1.0 g, 6.7 mmol) in an identical manner to the preparation of **8**. The colour of the solution changed from dark green to red–brown, and the progress of the reaction was monitored by the replacement of the IR absorbances of the starting material with those of the vinylidene product. After completion of the methylation reaction the solution was filtered and evaporated to dryness. Extraction into hexane followed by cooling to −50°C yielded black crystals of **9** (3.0 g, 4.8 mmol, 71%). Found: C, 30.40; H, 0.95; Fe, 35.12. Calc. for $C_{15}H_6O_{12}Fe_4$: C, 30.52; H, 0.96; Fe, 35.48%. ^1H NMR (60 MHz, CD_2Cl_2, 25°C): 2.21 δ ($=CCH_3$), 3.78 δ ($=COCH_3$).

(2) *X-ray crystallography*

The crystal structure of **8** was determined in the Analytical Sciences Laboratory, Exxon Research and Engineering Company. The crystal structure of **9** was determined at Crystalitics Inc., Lincoln, Nebraska.

The structure of $Fe_4(CO)_{12}(C{=}C(OCH_3)_2)$ (**8**). Crystals of **8** were grown from hexane at −40°C. Data were collected on an approximately cubic crystal, 0.44 mm on an edge, sealed under nitrogen in a glass capillary, on an Enraf–Nonius CAD-4 diffractometer using Mo-K_α radiation (λ = 0.7107 Å). The cluster crystallizes in the monoclinic space group $P2_1/c$ (C_{2h}^5 No. 14) with a = 13.900(2), b = 8.909(2), c = 17.116(4) Å, β = 94.59(2)°; ρ_{calc} = 2.03 g cm^{-3} for mol. wt 645.6 and Z = 4. Of 3696 reflections examined (scan range $0 < 2\theta < 50°$, ω–2θ scans, 2–7° min^{-1}), 1528 with $I > 2\sigma I$ were used in structure solution, using a combination of direct methods (MULTAN) and Fourier techniques, and refinement by full-matrix least-squares. No decay in intensity of three check reflections was observed during data collection. Data were corrected for absorption (μ = 27.6 cm^{-1}, psi scan, max/min 0.83–1.00) and for Lorentz and polarization factors. All non-hydrogen atoms were refined with anisotropic thermal parameters. Least-squares refinement converged to final residuals of R_1 = 0.054, R_2 = 0.044.[10] Interatomic distances and bond angles are given in Tables 1 and 2, respectively. The atom numbering scheme is shown in the ORTEP drawing of the molecule, Fig. 1, in which thermal ellipsoids are drawn to include 30% of the electron density.

The structure of $Fe_4(CO)_{12}(C{=}C(OCH_3)CH_3)$ (**9**). Crystals of **9** were grown from hexane at −40°C. Data were collected on a crystal measuring 0.42 × 0.42 × 0.70 mm, sealed under nitrogen in a glass capillary, on a four circle Nicolet Autodiffractometer. The molecule crystallizes in the monoclinic space group $P2_1/c$ (C_{2h}^5 No. 14) with a = 28.441(6), b = 9.204(2), c = 17.466(4) Å, β = 108.51(2)°; ρ_{calc} = 1.93 g cm^{-3} for mol. wt = 629.6 and Z = 8. The intensities of six check reflections were monitored over the period of data collection and no decay was observed. Of 5951 independent reflections collected ($0 < 2\theta < 45°$) 3364 with $I > 3\sigma(I)$ were used in the structure solution (SHELXTL direct methods) and refinement (cascade block-diagonal least-squares). Non-hydrogen atoms were refined with anisotropic thermal parameters. Hydrogen atoms were not located. Least-

Table 1. Interatomic distances (Å) for $Fe_4(CO)_{12}(C{=}C(OCH_3)_2)$ (**8**) and $Fe_4(CO)_{12}(C{=}C(OCH_3)CH_3)$ (**9**)

	8	9 (a)	9 (b)
Iron–iron			
Fe(1)—Fe(2)	2.489(2)	2.593(3)	2.587(3)
Fe(1)—Fe(3)	2.497(2)	2.587(3)	2.587(3)
Fe(1)—Fe(4)	2.532(2)	2.556(3)	2.548(3)
Fe(2)—Fe(4)	2.522(2)	2.525(3)	2.532(3)
Fe(3)—Fe(4)	2.555(2)	2.537(3)	2.546(3)
Iron–carbon			
Fe(1)—C(1)	1.77(1)	1.72(2)	1.74(2)
Fe(1)—C(2)	1.76(1)	1.75(1)	1.77(2)
Fe(1)—C(3)	1.76(1)	1.78(2)	1.77(2)
Fe(2)—C(4)	1.80(1)	1.81(2)	1.78(1)
Fe(2)—C(5)	1.78(1)	1.74(2)	1.74(2)
Fe(2)—C(6)	1.79(1)	1.76(2)	1.82(2)
Fe(3)—C(7)	1.76(1)	1.74(2)	1.77(2)
Fe(3)—C(8)	1.78(1)	1.77(2)	1.76(1)
Fe(3)—C(9)	1.79(1)	1.79(1)	1.79(2)
Fe(4)—C(10)	1.78(1)	1.75(2)	1.76(2)
Fe(4)—C(11)	1.78(1)	1.74(1)	1.75(2)
Fe(4)—C(12)	1.75(1)	1.80(2)	1.76(2)
Fe(1)—C(13)	1.97(1)	1.93(2)	1.96(1)
Fe(2)—C(13)	2.03(1)	1.97(1)	1.97(2)
Fe(3)—C(13)	2.02(1)	1.98(1)	2.00(2)
Fe(4)—C(13)	1.95(1)	1.93(2)	1.93(1)
Carbon–oxygen (carbonyl)			
C(1)—O(1)	1.16(1)	1.21(2)	1.16(2)
C(2)—O(2)	1.15(1)	1.15(2)	1.17(2)
C(3)—O(3)	1.16(1)	1.15(2)	1.17(2)
C(4)—O(4)	1.14(1)	1.14(2)	1.11(1)
C(5)—O(5)	1.13(1)	1.17(2)	1.17(2)
C(6)—O(6)	1.12(1)	1.16(2)	1.10(2)
C(7)—O(7)	1.15(1)	1.18(2)	1.13(2)
C(8)—O(8)	1.13(1)	1.14(2)	1.17(2)
C(9)—O(9)	1.13(1)	1.15(2)	1.13(2)
C(10)—O(10)	1.14(1)	1.20(2)	1.12(2)
C(11)—O(11)	1.14(1)	1.15(2)	1.16(2)
C(12)—O(13)	1.17(1)	1.12(3)	1.19(2)
Vinylidene			
C(13)—C(14)	1.44(1)	1.44(2)	1.44(2)
C(14)—O(13)	1.33(1)	1.44(2)	1.37(2)
C(14)—O(14)	1.28(1)		
C(15)—O(13)	1.47(1)	1.45(2)	1.44(2)
C(16)—O(14)	1.45(1)		
C(14)—C(16)		1.46(2)	1.46(2)

squares refinement[10] converged to final residuals of $R_1 = 0.068$, $R_2 = 0.068$ (defined as above). Anomalous dispersion factors for the four iron atoms were taken from ref. 11. Data were corrected for Lorentz and polarization factors. No absorption correction was applied.

Bond lengths and angles for the two cry-

Table 2. Bond angles (°) for $Fe_4(CO)_{12}(C{=}C(OCH_3)_2)$ (**8**) and $Fe_4(CO)_{12}(C{=}C(OCH_3)CH_3)$ (**9**)

	8	9 (a)	9 (b)
Fe(2)—Fe(2)—Fe(3)	103.2(1)	97.0(1)	97.6(1)
Fe(2)—Fe(1)—Fe(4)	61.1(1)	58.7(1)	59.1(1)
Fe(3)—Fe(1)—Fe(4)	61.1(1)	59.1(1)	59.4(1)
Fe(1)—Fe(2)—Fe(4)	60.3(1)	59.9(1)	59.7(1)
Fe(1)—Fe(3)—Fe(4)	60.2(1)	59.8(1)	59.5(1)
Fe(1)—Fe(4)—Fe(2)	58.6(1)	61.4(1)	61.2(1)
Fe(1)—Fe(4)—Fe(3)	58.8(1)	61.0(1)	61.0(1)
Fe(2)—Fe(4)—Fe(3)	99.8(1)	100.1(1)	100.1(1)
C(1)—Fe(1)—C(2)	93.7(5)	90.6(8)	93.2(8)
C(1)—Fe(1)—C(3)	98.0(5)	101.4(7)	98.4(7)
C(2)—Fe(1)—C(3)	93.0(6)	93.3(7)	93.4(7)
C(4)—Fe(2)—C(5)	96.4(5)	95.7(7)	91.5(8)
C(4)—Fe(2)—C(6)	92.4(5)	100.3(8)	97.4(7)
C(5)—Fe(2)—C(6)	91.6(6)	93.5(8)	93.9(8)
C(7)—Fe(3)—C(8)	92.4(5)	99.4(8)	96.8(7)
C(7)—Fe(3)—C(9)	92.4(5)	92.3(7)	92.0(8)
C(8)—Fe(3)—C(9)	97.2(6)	95.4(7)	94.9(7)
C(10)—Fe(4)—C(11)	91.4(6)	92.1(8)	92.3(8)
C(10)—Fe(4)—C(12)	92.9(6)	95.2(8)	92.0(8)
C(11)—Fe(4)—C(12)	98.8(5)	101.6(8)	98.4(8)
Fe(1)—C(1)—O(1)	178(1)	176(1)	177(1)
Fe(1)—C(2)—O(2)	170(1)	171(2)	170(2)
Fe(1)—C(3)—O(3)	172(1)	178(1)	175(2)
Fe(2)—C(4)—O(4)	178(1)	177(1)	173(2)
Fe(2)—C(5)—O(5)	179(1)	176(1)	175(1)
Fe(2)—C(6)—O(6)	178(1)	177(2)	173(2)
Fe(3)—C(7)—O(7)	175(1)	175(2)	176(2)
Fe(3)—C(8)—O(8)	176(1)	177(1)	178(1)
Fe(3)—C(9)—O(9)	176(1)	177(2)	179(2)
Fe(4)—C(10)—O(10)	169(1)	171(1)	175(2)
Fe(4)—C(11)—O(11)	178(1)	176(2)	172(2)
Fe(4)—C(12)—O(12)	176(1)	177(2)	179(2)
Fe(1)—C(13)—Fe(2)	77.0(3)	83.4(6)	82.4(6)
Fe(1)—C(13)—Fe(3)	77.3(3)	82.7(3)	81.8(3)
Fe(1)—C(13)—Fe(4)	80.4(3)	82.9(3)	82.1(3)
Fe(2)—C(13)—Fe(3)	149.5(3)	158.0(3)	157.4(3)
Fe(2)—C(13)—Fe(4)	79.8(3)	80.7(3)	81.0(3)
Fe(3)—C(13)—Fe(4)	80.1(3)	80.8(3)	80.9(3)
Fe(1)—C(13)—C(14)	148.0(3)	140.1(3)	137.1(3)
Fe(2)—C(13)—C(14)	105.0(3)	98.1(3)	101.3(3)
Fe(3)—C(13)—C(14)	105.5(3)	103.5(3)	101.3(3)
Fe(4)—C(13)—C(14)	131.6(3)	136.9(3)	140.8(3)
C(13)—C(14)—O(13)	117(1)		
C(13)—C(14)—O(14)	130(1)		
C(14)—O(13)—C(15)	121.1(9)		
C(14)—O(14)—C(16)	122.8(9)		
C(13)—C(14)—O(13)		113(1)	115(1)
C(13)—C(14)—C(15)		128(2)	124(1)
C(14)—O(13)—C(16)		123(1)	120(1)

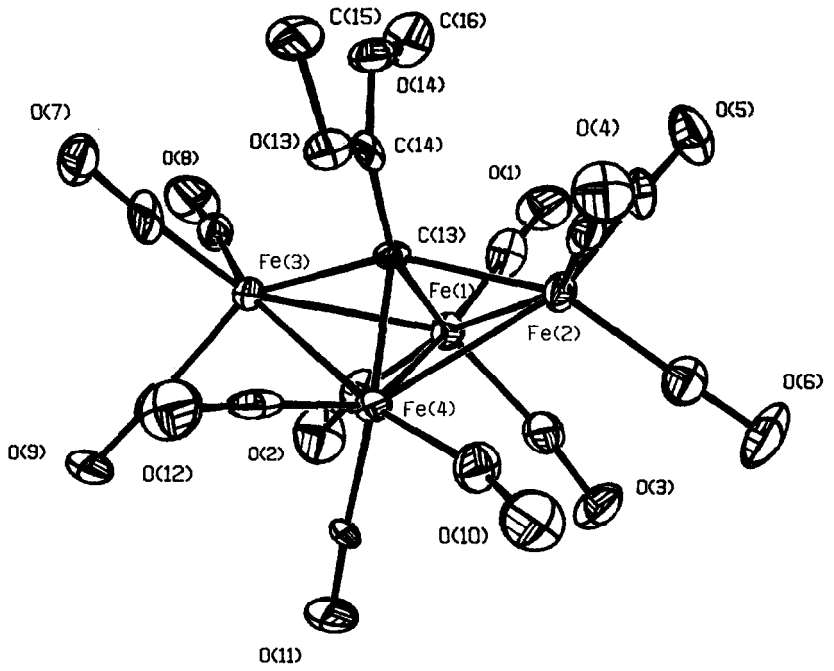

Fig. 1. ORTEP drawing of $Fe_4(CO)_{12}(C{=}C(OCH_3)_2)$ (**8**) showing 30% probability thermal ellipsoids. Only oxygen atoms for the carbonyls are numbered, and these define the carbon atom numbering scheme.

stallographically independent molecules of **9** present in the crystal are listed in Tables 1 and 2. The atom numbering scheme used is shown in the ORTEP drawing of one of the two molecules (Fig. 2), in which thermal vibration ellipsoids are drawn to include 30% of the electron density.

(3) *Molecular orbital calculations*

Molecular orbital calculations using the Fenske–Hall method[12] were carried out for **8** and **9**. Calculations for **2**, **5** and **6** have been reported previously,[13,14] and the results of those calculations

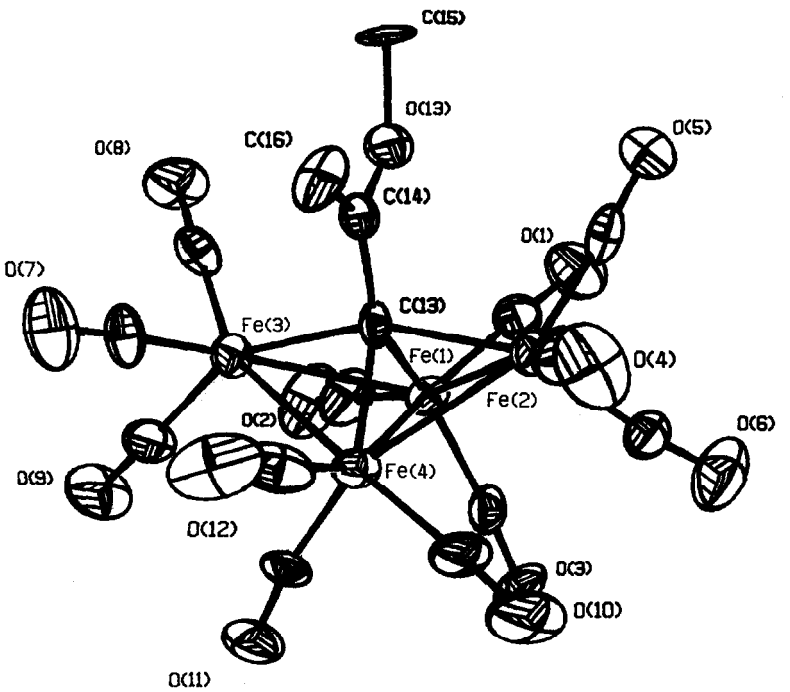

Fig. 2. ORTEP drawing of $Fe_4(CO)_{12}(C{=}C(OCH_3)CH_3)$ (**9**) showing 30% probability thermal ellipsoids.

are used for comparison here. Atomic positions used in the calculations for **8** and **9** were taken from the crystal structures reported here. The 1*s* through 3*d* functions for iron were taken from Richardson *et al.*,[15] while the 4*s* and 4*p* functions were chosen to have exponents of 2.0. The carbon and oxygen functions were taken from the double-ζ functions of Clementi.[16] The valence 2*p* functions were retained as the double-ζ functions, while the 1*s* and 2*s* functions were reduced to the single-ζ form. An exponent of 1.2 was used for hydrogen. In all of the calculations the local coordinate system on the vinylidene carbon was oriented with the *x*-axis parallel to a line connecting the two hinge iron atoms, Fe_1 and Fe_4, the *y*-axis parallel to a line connecting the two wingtip iron atoms, Fe_2 and Fe_3, and the *z* axis pointing out of the cluster.

RESULTS AND DISCUSSION

Structural parameters for **8** and **9** are listed in Tables 1 and 2. In making comparisons between the clusters we will use for **9** structural parameters which are the mean of those found for the two crystallographically independent molecules in the unit cell. The structures of the vinylidene clusters **8** and **9** are nominally similar in that the four iron atoms are arranged in an open butterfly configuration, each bearing three essentially linear terminal carbonyl ligands coordinated in the usual mutually orthogonal fashion to the iron atoms. The two clusters are also similar in that in each a vinylidene ligand $\rangle C{=}C(R_1)(R_2)$ is bonded in a μ^4-fashion through the vinylidene carbon to the four iron atoms which make up the core of the butterfly clusters.

Examination of the geometries of the Fe_4 units in the two clusters reveals subtle but significant differences between them. These differences can be most easily expressed by comparing the cluster structures of **8** and **9** with the structures of their anionic precursors **5** and **6**[14] (see Fig. 3). The dihedral angles between the wings of the butterfly in **8** (127°) and **9** (122°) are slightly smaller

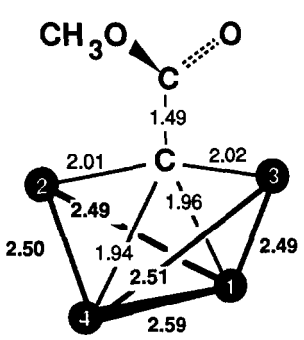

Dihedral = 130°

5

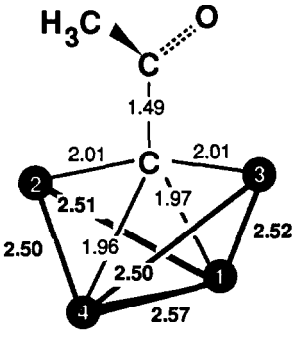

Dihedral = 128°

6

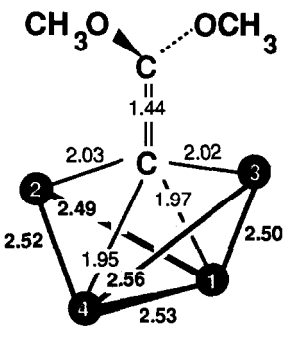

Dihedral = 127°

8

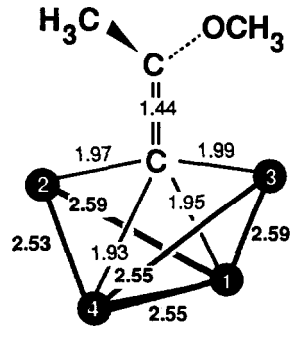

Dihedral = 122°

9

Fig. 3. Comparison of the structures of $Fe_4(CO)_{12}(C{=}C(OCH_3)_2)$ (**8**) and $Fe_4(CO)_{12}(C{=}C(OCH_3)CH_3)$ (**9**) with the structures of their precursors $[Fe_4(CO)_{12}(CCO_2CH_3)]^-$ (**5**) and $[Fe_4(CO)_{12}(CC(O)CH_3)]^-$ (**6**).

than those in **5** (130°) and **6** (128°). The two vinylidene clusters also differ slightly in their Fe—Fe bond lengths; for **8** the Fe(1)—Fe(2,3) and Fe(4)—Fe(2,3) distances are 2.50 and 2.55 Å (compared with 2.51 ± 0.01 Å for **5**), and for **9**, 2.59 and 2.54 Å (compared with 2.50 ± 0.01 Å for **6**). These differences are also reflected in the Fe—C(13) distances: for **8** the Fe(2,3)—C(13) distances are 2.02 ± 0.01 Å (2.01 Å in **5**) and the Fe(1,4)—C(13) distances are 1.96 Å (1.95 Å in **5**); for **9** the corresponding distances are 1.98 and 1.93 Å (2.01 and 1.96 Å for **6**). Finally, these differences can also be expressed in terms of the Fe(2)C(13)Fe(3) angles in the vinylidene clusters. In **8** and **9** the angles are 149.5° (147.9° in **5**) and 157.7° (148.6° in **6**). In short, while the geometry of **8** shows only small changes from the geometry of **5**, somewhat larger changes in geometry are observed in **9** in comparison with **6**. Most noticeable is the closing up of the Fe_4 butterfly framework which is observed in **9**. It should also be noted that the C(13)—C(14) distance in both **8** and **9** is 1.44 Å (compared to 1.49 Å in both **5** and **6**). The small change in this bond length between the methylidyne and vinylidene clusters is somewhat surprising, since the C(13)—C(14) bond in both **8** and **9** can be viewed formally as a double bond, while in both **5** and **6** this bond is viewed as a single bond. Examination of the structures of **8** and **9** also reveals substantial reorientations of the $Fe(CO)_3$ groups in both of these clusters. These reorientations, which can be viewed as rotations of the $(CO)_3$ groups, result in much less symmetric dispositions of the CO groups than are found in **5** and **6**.

In order to understand these changes in structure it is useful to compare the electronic, as well as the molecular structures, of these clusters with the same features of other members of the iron butterfly group of clusters. We have previously shown how the structures of carbido clusters such as **1**, **2** and **3**, which contain a μ^4-carbon atom, and those of methylidyne clusters such as **5** and **6**, which contain a μ^4-methylidyne ligand, reflect the electronic structures of both the $Fe_4(CO)_{12}$ core and the carbido carbon atom or methylidyne group.[13,14] In order to make an instructive comparison between all three classes of cluster, it is useful to review briefly the relationship between the electronic and geometric structures of the μ^4-carbon and μ^4-methylidyne clusters. In the μ^4-carbon clusters, **1**, **2** and **3**, the cluster geometry optimizes the interactions between the carbido carbon atom and the four iron atoms. The important Fe—C interactions are shown in Fig. 4. The near colinearity of the two wingtip iron atoms (Fe_w) and the μ^4-carbon atom leads to very strong C—Fe_w interactions. These include a σ overlap involving the C $2p_y$ orbital [Fig. 4(a)], and π overlaps involving the C $2p_x$ and $2p_z$ orbitals [Fig. 4(b,c)]. The C $2p_y$ orbital does not overlap with the hinge iron atoms (Fe_h), but both the p_x and p_z orbitals form σ bonds with the hinge iron atoms [Fig. 4(b,c)].

The geometries of the methylidyne clusters, **5** and **6**, reflect the formation of the C—C σ bond between

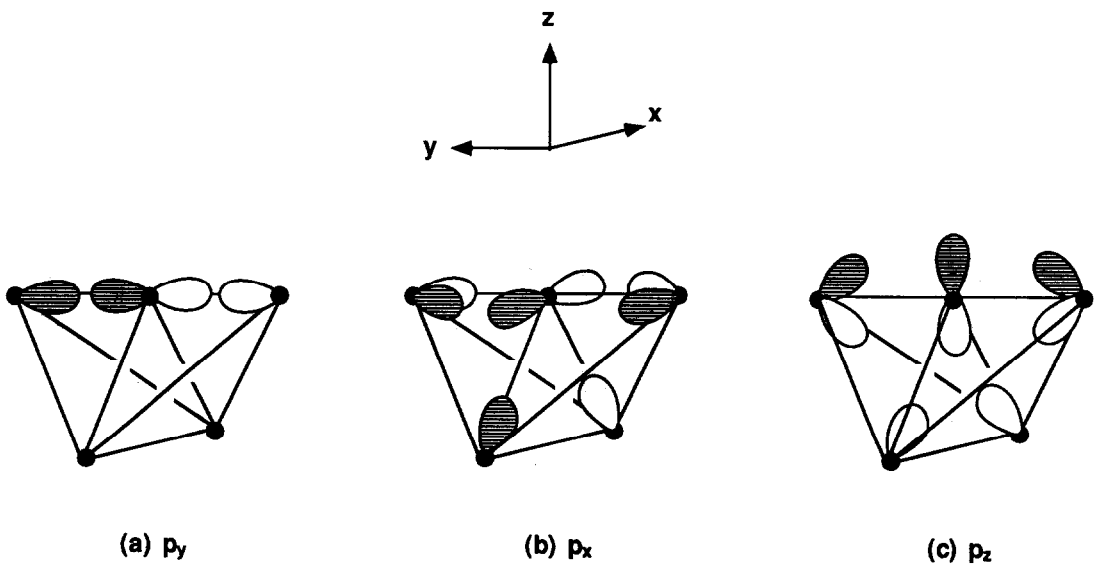

Fig. 4. Schematic representations of the bonding interactions between the carbido C p_y (a), p_x (b) and p_z (c) orbitals and the iron framework orbitals in $[Fe_4(CO)_{12}C]^{2-}$ (ref. 13). The local coordinate system on the carbon atom is defined as shown.

the μ^4-carbon atom and the carbomethoxy and acetyl groups.[14] The bond formation is accompanied by a folding back of the wings of the butterfly (the dihedral angle increases from 102 ± 2 to $129\pm1°$), a lengthening of the C—Fe_w distances (from 1.79 ± 0.01 to 2.02 ± 0.01 Å) and a shortening of the Fe_h—Fe_w distances (from 2.63 ± 0.01 to 2.51 ± 0.02 Å). In these derivatized clusters nearly all of the π bonding between the carbon atom and the wingtip iron atoms is lost and the σ bond between the carbon atom and the wingtip iron atoms is considerably weakened. This is illustrated in Fig. 5. The C $2p_z$ orbital, hybridized with the C $2s$ orbital, is used in bonding to the adjacent carbon atom. This leaves a C *sp* lone pair type orbital to bond with the hinge iron atoms [Fig. 5(c)], but no orbital for π bonding with the wingtip iron atoms. The C $2p_x$ orbital is unaffected by the formation of the C—C bond, but the much longer C—Fe_w distance results in the loss of most of the π bonding with the wingtip iron atoms. Finally, the σ bond between the C p_y orbital and the wingtip iron atoms is also weakened as a result of the longer C—Fe_w distance. The loss of bonding between the carbon atom and the Fe_w is compensated by the strengthening of the Fe_w—Fe_h bonds. At the same time, the C $2p_y$ orbital is somewhat stabilized by bonding to the adjacent carbon atom. Since the carbomethoxy and acetyl carbonyl groups in **5** and **6** lie in the xz plane, this allows the development of a small amount of double bond character between the methylidyne carbon and the adjacent sp^2 carbon.

In the methyilidyne clusters, **5** and **6**, the C—C bond can be viewed formally as a single bond. In the vinylidene clusters, **8** and **9**, on the other hand, the C—C bond can be viewed formally as a double bond, and we might expect both the interaction between the vinylidene group and the $Fe_4(CO)_{12}$ cluster core and the resulting cluster geometry itself to be somewhat different in **8** and **9** from that found in **5** and **6**. Instead, with only the small variations noted above, the cluster framework geometries of the vinylidene clusters **8** and **9** resemble those of their precursors **5** and **6**. The results of Fenske–Hall electronic structure calculations for the vinylidene clusters show that it is in fact not appropriate to view these ligands as having a localized double bond between the two carbons. At most, the C(13)—C(14) bond in these ligands is intermediate between single and double bond in character, and the small differences in geometry reflect the gradual appearance of partial double bond character in this C—C bond. The degree to which this occurs depends on the substituents on the vinyl carbon atom, C(14).

In the methylidyne clusters, **5** and **6**, the interaction between the methylidyne C $2p_y$ orbital and the cluster framework is illustrated as the interaction between a lone pair $2p_y$ orbital and the cluster framework [Fig. 5(a)]. That this is an appropriate picture can be seen by viewing the bonding in the methylidyne clusters in terms of the $Fe_4(CO)_{12}$ framework and the CC(O)R ($R = OCH_3$, CH_3) fragment. The CC(O)R fragment orbital which interacts with the wingtip metal framework orbitals is localized primarily on the methylidyne carbon and is C $2p_y$ in character. This is illustrated in Fig. 6(a) and (b), where schematic diagrams of this fragment molecular orbital (m.o.) in $[—CC(O)OCH_3]^-$ (6a) and $[—CC(O)CH_3]^-$ (6b) are shown. The coefficients of the atomic orbitals in each fragment molecular orbital are also indicated in Fig. 6. The methylidyne carbon $2p_y$ orbital makes a small contribution to two other lower lying

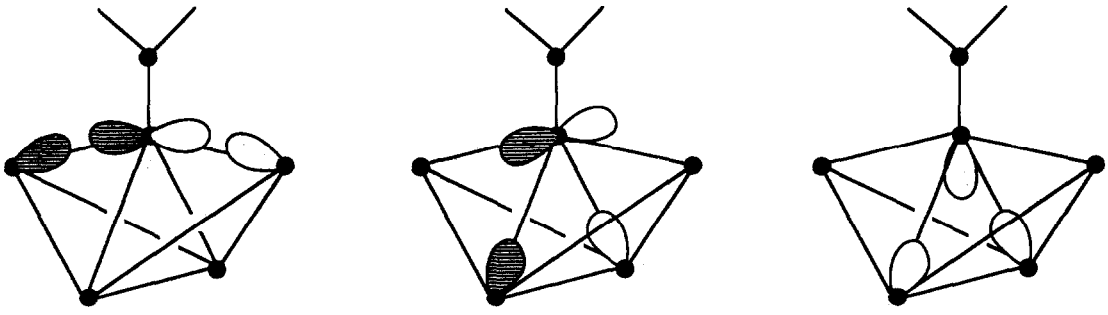

(a) (b) (c)

Fig. 5. Schematic representations of the bonding interactions between the μ^4-methylidyne carbon orbitals and the iron framework orbitals in the methylidyne clusters $[Fe_4(CO)_{12}(CCO_2CH_3)]^-$ (**5**) and $[Fe_4(CO)_{12}(CC(O)CH_3)]^-$ (**6**) (ref. 14). The coordinate system on the carbon atom is defined as in Fig. 4.

fragment π orbitals, but these lower lying orbitals are primarily localized on the oxygen end of the fragment and are bonding between oxygen and the sp^2-carbon. It is the π lone pair type orbital shown in Fig. 6(a) and (b) which participates in the bonding interaction shown in Fig. 5(a).

If the vinylidene fragments in clusters **8** and **9** actually incorporated a C—C double bond, we might expect the interaction between the vinylidene carbon and the wingtip iron atoms to be somewhat different from that shown in Fig. 5(a). A localized double bond between the two adjacent carbon atoms would preclude the presence of a C p_y non-bonding orbital. Instead, we would expect to observe an orbital with contributions from the p_y orbitals of both carbon atoms and a concentration of electron density in a region between the two carbons. This is not observed in the two vinylidene fragments, $—CC(OCH_3)_2$ and $—CC(OCH_3)CH_3$. Instead, the bonding within these two fragments more closely resembles the bonding in the methylidyne fragments in **5** and **6** described above. Both fragments have an orbital which is primarily C $2p_y$ in character [Fig. 6(c) and (d)], and once again it is this fragment orbital which participates in the cluster bonding interaction illustrated in Fig. 5(a). It is notable that this orbital is more localized on the vinylidene carbon in $—CC(OCH_3)_2$ than in $—CC(OCH_3)CH_3$, and we will discuss this difference below. In each fragment the vinylidene C $2p_y$ orbital also makes a smaller contribution to one or more lower energy π orbitals, but these lower energy orbitals are primarily bonding between the oxygen(s) and the sp^2 hybridized carbon.

When the electronic structure of the ligands is viewed in this light, we can understand the observed similarities and small differences in cluster geometry. As described above and illustrated in Fig. 5, the formation of a C—C bond in the methylidyne clusters **5** and **6** leads to the loss of nearly all C—Fe_w π bonding, so that the only remaining strong C—Fe_w interaction involves the non-bonding π type orbital localized on the methylidyne carbon atom [Fig. 5(a)]. In the vinylidene cluster **8**, bonding between the vinylidene group and the $Fe_4(CO)_{12}$ cluster is almost identical to that observed in clusters **5** and **6**. That is, the π lone pair orbital illustrated in Fig. 6(c) interacts with the metal framework in the manner illustrated in Fig. 5(a). This bonding mode and the consequent structure indicates that in **8** it is appropriate to view the C—C bond in the "vinylidene" ligand $—CC(OCH_3)_2$ as closer to a single bond than a double bond. In the vinylidene cluster **9** the interaction between the vinylidene group and the metal framework still resembles the interaction shown in Fig. 5(a), but, as shown in Fig. 6(d), the vinylidene π orbital involved in this interaction is not as strongly localized on the vinylidene carbon in **9** as it is in **8**. That is, we see a small shift in electron density away from the vinylidene carbon atom. The smaller dihedral angle in **9** can be correlated to the change in charac-

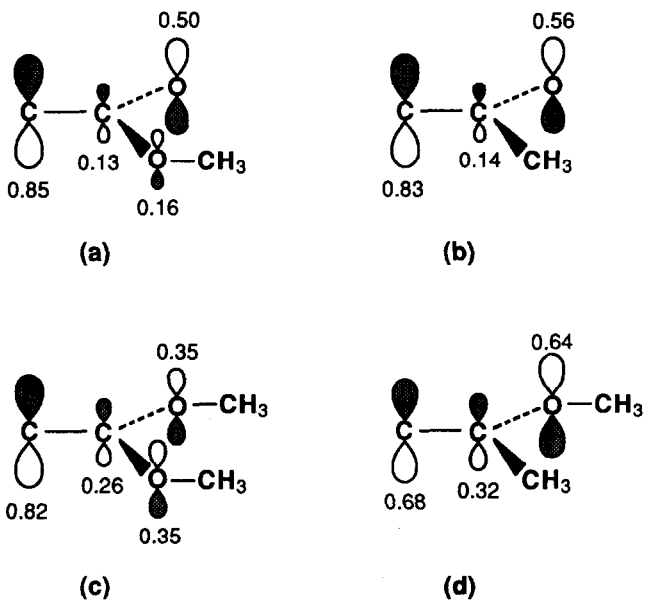

Fig. 6. Schematic representations of the orbitals on the methylidyne and vinylidene fragments, (a) $[CC(O)OCH_3]^-$, (b) $[CC(O)CH_3]^-$, (c) $CC(OCH_3)_2$ and (d) $CC(OCH_3)CH_3$, which interact with the wingtip iron atoms in each of the corresponding clusters. The coefficients of the atomic orbitals are indicated in each diagram.

ter of this vinylidene orbital. Since the only interaction between the wingtip iron atoms and the vinylidene carbon atom requires the participation of the electrons which occupy this orbital, the metal framework of the cluster closes up around the vinylidene group in order to gain access to these electrons. Both the character of the vinylidene π orbital and the cluster geometry itself suggest that in **9** it is appropriate to view the C—C bond in the "vinylidene" ligand —$CC(OCH_3)(CH_3)$ as something intermediate between a single and a double bond.

It follows from these observations that in a vinylidene cluster containing a truly localized double bond an even smaller dihedral angle would be expected. Since the electrons needed for bonding between the vinylidene ligand and the wingtip iron atoms would now be localized between the two carbon atoms, it would be necessary for the metal framework of the cluster to close up even further than in **8** and **9** in order to gain access to these electrons. An example of a butterfly cluster containing a localized vinylidene ligand is found in $Fe_4(CO)_{12}(C{=}CHCH_3)$, which has also been synthesized in this laboratory. The structure of this cluster, which will be reported in a subsequent paper, demonstrates precisely this phenomenon.[17] The dihedral angle in this cluster is 104°. It is interesting to note that the analogous cluster $HFe_4(CO)_{12}(CBH_2)$, recently reported by Fehlner and co-workers[18] which should have a similar electronic structure, has a dihedral angle of 105°.

Appropriate depictions of clusters **8** and **9** are shown below. As discussed above the C—C double bond character in the vinylidene ligands is greater in **9** than in **8**. This increase in double bond character is accompanied by a shortening of the Fe—C bonds and a decrease in the dihedral angle between the two wings of the butterfly as shown in Fig. 3. This double bond character can be directly related to the number of oxygen atoms in the vinylidene group, since as the number of oxygen atoms decreases, the number of electrons available to participate in the π framework of the vinylidene group decreases, and

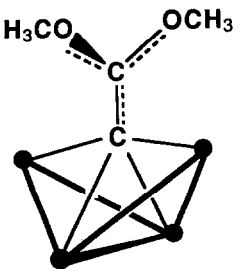

8

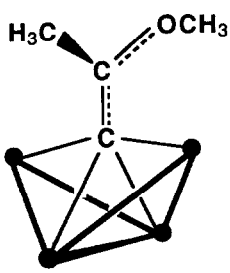

9

the C(13)—C(14) double bond character increases. The small amount of double bond character in the C(13)—C(14) bond is consistent with the relatively slight shortening of this bond which is observed in going from **5** or **6** to **8** or **9**. At the same time, we might have expected this bond to be shorter in **9** than in **8**. We must remember, however, that in the cluster, electrons which in the vinylidene fragment would occupy only the fragment orbital illustrated in Fig. 6(d) now occupy a delocalized cluster orbital which incorporates contributions from both that fragment orbital and the wingtip iron atoms. This delocalization of the electrons onto the metal cluster, which decreases any localized electron density between the two carbon atoms, is consistent with the absence of any shortening of the C—C bond.

Detailed comparisons between the CO coordination geometries in the pairs of molecules **5** and **8**, **6** and **9**, and **8** and **9** reveal marked distortions in the relative orientations of all four of the $Fe(CO)_3$ groups in **8** and **9**. For example, in going from **5** to **8** the two hinge $Fe(CO)_3$ groups rotate with respect to each other by $\sim 60°$, going from an almost perfectly eclipsed configuration to a staggered configuration. A similar relative rotation has been observed in the structure of the dianion of the acetylmethylidyne cluster **6**.[8] In **8** and **9**, rotations of the wingtip $(CO)_3$ groups are also observed. Just as for the dianion of **6**, the results of the molecular orbital calculations for **8** and **9** reveal no ready electronic explanation for these changes in CO orientation, and the reorientation of the $(CO)_3$ groups in **8** and **9** appears to be dictated by steric effects. Although we cannot give a full explanation of the relative magnitudes of these distortions, it is clear that in order to optimize the bonding interactions between the wingtip iron atoms and the vinylidene fragment, and at the same time accommodate the bulkiness of the substituents on the vinylidene ligand, the geometry of the $Fe(CO)_3$ units must severely distort.

Finally, it should be noted that the structures of the vinylidene clusters discussed here differ from the structures of other butterfly clusters such as $(\mu\text{-H})(\eta^5\text{-CpNi})Ru_3(CO)_9(\mu_4\text{-}\eta^2\text{-C}{=}CH\text{-}i\text{-Pr})$[19] and $(\eta^5\text{-CpFe})Co_3(CO)_7(\mu\text{-CO})_2(\mu_4\text{-}\eta^2\text{-C}{=}CH_2)$,[20] which also contain vinylidene ligands. In these latter clusters the vinylidene ligand does not lie in the plane of the two hinge atoms but instead leans over and binds in an η^2-manner to one of the wingtip metal atoms. At the same time, however, these latter clusters contain not only a localized vinylidene ligand, but also a heterometal and two extra cluster electrons. Comparisons between the electronic and

molecular structures of the simpler Fe_4 vinylidene clusters and the more complex heterometallic vinylidene clusters indicate that these are probably best viewed as two related but distinct groups of clusters. These comparisons will be described in a subsequent paper.[17]

SUMMARY

The syntheses, molecular and electronic structures of two μ^4-vinylidene tetrairon butterfly clusters, $Fe_4(CO)_{12}(C{=}C(OCH_3)_2)$ (**8**) and $Fe_4(CO)_{12}(C{=}C(OCH_3)CH_3)$ (**9**) have been described. The clusters have an open butterfly framework of four iron atoms with a vinylidene ligand bound to all four metal atoms, and in both clusters the vinylidene ligand is approximately co-planar with the two hinge iron atoms. The Fe_4C cores of the two clusters are similar in structure to the Fe_4C cores of their precursor methylidyne clusters, with the most noticeable differences being slightly smaller dihedral angles in the vinylidene clusters. The disposition of the CO ligands is much less symmetric in the vinylidene clusters than in their methylidyne precursors. This reorientation of the CO ligands appears to be dictated by steric crowding which results from the bulkiness of the substituents on the vinylidene ligand combined with the smaller dihedral angle between the two wings of the butterfly.

The small changes in core geometry can be attributed to the electronic structure of the vinylidene ligands. Although both clusters formally contain a C—C double bond in the vinylidene ligand, the presence of oxygen atoms in this ligand leads to a delocalized π system and only partial double bond character in the C—C bond. The double bond character increases as the number of oxygen atoms incorporated into the ligand decreases. The results of molecular orbital calculations show that changes in the structure of the cluster framework can be correlated with the double bond character in the vinylidene ligand, since an increase in double bond character leads to a shift in electron density away from the vinylidene carbon atom and a closing up of the butterfly framework around the vinylidene ligand.

REFERENCES

1. J. S. Bradley, *Adv. Organomet. Chem.* 1984, **22**, 1.
2. J. S. Bradley, G. B. Ansell, M. E. Leonowicz and E. W. Hill, *J. Am. Chem. Soc.* 1981, **103**, 4968.
3. J. H. Davis, M. A. Beno, J. M. Williams, J. Zimmie, M. Tachikawa and E. L. Muetterties, *Proc. Natl. Acad. Sci. USA* 1981, **78**, 668.
4. E. M. Holt, K. H. Whitmire and D. F. Shriver, *J. Organomet. Chem.* 1981, **213**, 125.
5. M. A. Beno, J. M. Williams, M. Tachikawa and E. L. Muetterties, *J. Am. Chem. Soc.* 1981, **103**, 1485.
6. M. Tachikawa and E. L. Muetterties, *J. Am. Chem. Soc.* 1980, **102**, 4541.
7. J. S. Bradley, *Philos. Trans. R. Soc., Lond.* 1982, **A308**, 103.
8. J. Wang, A. M. Crespi, M. Sabat, S. Harris, C. Woodcock and D. W. Shriver, *Inorg. Chem.* 1989, **28**, 697.
9. E. W. Hill and J. S. Bradley, *Inorg. Synth.* 1990, **27**, 182.
10. $R_1 = \Sigma||F_o|-|F_c||/\Sigma|F_o|$, $R_2 = \{\Sigma w(|F_o|-|F_c|)^2/\Sigma w|F_o|^2\}^{1/2}$. The weighting scheme used in the least-squares minimization of the function $\Sigma w(|F_o|-|F_c|)^2$ is defined as $w = 1/\sigma_{F^2}$. Here $\sigma_F = \{[\sigma(F_o)]^2 + 0.01|F_o|)^2\}^{-1/2}$.
11. *International Tables for X-Ray Crystallography*, Vol. IV, pp. 149–150. Kynoch Press, Birmingham (1974).
12. M. B. Hall and R. F. Fenske, *Inorg. Chem.* 1972, **11**, 768.
13. S. Harris and J. S. Bradley, *Organometallics* 1984, **3**, 1086.
14. J. S. Bradley, S. Harris, J. M. Newsam, E. W. Hill, S. Leta and M. Modrick, *Organometallics* 1987, **6**, 2060.
15. J. W. Richardson, W. C. Nieupoort, R. R. Powell and W. F. J. Edgell, *Chem. Phys.* 1962, **36**, 1057.
16. E. Clementi, *Chem. Phys.* 1964, **40**, 1944.
17. J. S. Bradley, S. Harris, E. W. Hill and M. A. Modrick, manuscript in preparation.
18. X. Meng, N. P. Rath and T. P. Fehlner, *J. Am. Chem. Soc.* 1989, **111**, 3422.
19. A. J. Carty, N. J. Taylor, E. Sappa and A. Tiripicchio, *Inorg. Chem.* 1983, **22**, 1871.
20. P. Brun, G. M. Dawkins, M. Green, R. M. Mills, J.-Y. Salaün, F. G. A. Stone and P. Woodward, *J. Chem. Soc., Dalton Trans.* 1983, 1357.

Polyhedron Vol. 9, No. 15/16, pp. 1821–1827, 1990
Printed in Great Britain

0277–5387/90 $3.00+.00
© 1990 Pergamon Press plc

MULTIPLY-BONDED DIMETAL FLUOROALKOXIDES—II. THE DISORDERED STRUCTURE OF $Mo_2(OC(CF_3)_3)_4(NMe_2)_2$ AND ITS IMPLICATIONS AS TO REARRANGEMENT BY AN INTERNAL FLIP*

RONALD G. ABBOTT, F. ALBERT COTTON† and LARRY R. FALVELLO

Department of Chemistry and Laboratory for Molecular Structure and Bonding, Texas A&M University, College Station, TX 77843, U.S.A.

Abstract—The existence of the title compound, which was tentatively reported in 1977, has been confirmed and its structure studied crystallographically. It crystallizes in space group $P2_1/n$ with $a = 10.571(3)$, $b = 14.927(3)$, $c = 12.099(3)$ Å, $\beta = 103.21(3)°$, $V = 1859(2)$ Å^3, $Z = 2$. The centrosymmetric molecules have an anti, staggered rotational conformation, with the C_2N—Mo≡Mo—NC_2 group of atoms being essentially planar. There is a disorder such that 69% of the Mo_2 units lie in one direction and 31% in a nearly perpendicular direction. This is presumed to indicate that there are entire molecules that adopt these two different orientations. Although no more than one of each ligand atom could be discerned, all of them, especially those in the $(CF_3)_3C$ groups refined with unusually high thermal displacement parameters. The two Mo—Mo distances, 2.216(2) Å (69%) and 2.201(3) Å (31%), while different in a statistical sense (0.015(4) Å) are nearly equal and of the appropriate magnitude for a triple bond between the molybdenum atoms. The observed disorder leads to the concept that the Mo_2 unit might undergo internal flips from one orientation to the other within a ligand cage that need relax only slightly from one orientation to the other. This would provide a simple unimolecular mechanism for interchanging proximal and distal R groups on NR_2 ligands in this and related molecules.

As noted elsewhere,[1] an exploratory study of the reactions of fluorinated alcohols, specifically $(CF_3)_3COH$, C_6F_5OH and $(CF_3)_2CHOH$, with $Mo_2(NMe_2)_6$ and $W_2(NMe_2)_6$, as well as the characterization of the reaction products, is in progress in this laboratory. The only earlier mention of such chemistry in the literature was a brief report[2] of the reaction of $(CF_3)_3COH$ with $Mo_2(NMe_2)_6$. This afforded an orange solid which was considered to be possibly a mixture of compounds, although the mass spectrum had a multiplet corresponding to $Mo_2(OC(CF_3)_3)_4(NMe_2)_2^+$. We have now re-examined the reaction, shown that it does indeed afford $Mo_2(OC(CF_3)_3)_4(NMe_2)_2$, and carried out an X-ray crystallographic study of this compound. The crystal structure displays a discrete disorder of the Mo_2 unit (i.e. two such units can be recognized) within a ligand shell consisting of an unresolvable superposition of two nearly coincident sets of ligand atoms. The occurrence of this disorder can be rationalized and leads to a consideration, for the first time, of the possibility of internal flips of the M_2 unit within M_2X_6 molecules.

EXPERIMENTAL

$Mo_2(NMe_2)_6$ was prepared by a standard method,[3] and $(CF_3)_3COH$ was purchased from P.C.R. Incorporated, Jacksonville, Florida. X-ray crystallographic methods for data collection and processing were standard in this laboratory and have been described elsewhere.[4]‡

Preparation

$Mo_2(NMe_2)_6$ (100 mg, 0.22 mmol) was dissolved in 10 cm^3 of hexane and this solution was mixed with a solution of $(CF_3)_3COH$ (0.270 cm^3, 1.8 mmol) in 10 cm^3 of benzene. The resulting orange–red reaction mixture was stirred overnight. The

* Dedicated to Dick Fenske, the best post-doc I never had, on the occasion of his retirement.

† Author to whom correspondence should be addressed.

‡ Calculations were carried out on a Micro VAXII with the SDP package software.

reaction mixture was then taken to dryness under vacuum, which removed essentially all of the $[NH_2Me_2][(CF_3)_3CO]$ as well as the solvents. The solid residue was washed with benzene (10 cm^3) and then hexane (10 cm^3). The yield of bright orange microcrystals was *ca* 70%. It can be sublimed in a working vacuum (*ca* 10^{-3} mm) at 100°C without decomposition.

The ^1H NMR spectrum (CD_2Cl_2) shows two peaks, singlets of equal intensity, at δ 4.82 and 3.15, assignable to the distal and proximal methyl groups. IR peaks (cm^{-1}, KBr or mineral oil): 1310 (w), 1260 (m,br), 1170 (m,br), 980 (m), 950 (s), 800 (w), 790 (w), 735 (s), 550 (w).

Structure determination

The crystallographic characteristics of the compound and the usual information pertaining to the collection of data and refinement of the structure are summarized in Table 1. The crystal used to collect data was grown from benzene solution. The actual course of the solution and refinement procedure were not straightforward and will be explained in detail shortly.

RESULTS AND DISCUSSION

Preparation

The preparative reaction can be represented by the following chemical equation:

$$Mo_2(NMe_2)_6 + 8(CF_3)_3COH \longrightarrow Mo_2(OC(CF_3)_3)_4(NMe_2)_2 + 4[NH_2Me_2][(CF_3)_3CO].$$

It appears to proceed fairly cleanly and the product is obtained in relatively high (*ca* 70%) yield. The previous uncertainties[2] as to the course of the reac-

Table 1. Crystal data for $Mo_2(OC(CF_3)_3)_4(NMe_2)_2$

Formula	$Mo_2O_4N_2C_{20}H_{12}F_{36}$
Formula weight	1220.15
Space group	$P2_1/n$
Systematic absences	$0k0$; $k \neq 2n$; $h0l$; $h+l \neq 2n$
a (Å)	10.571(3)
b (Å)	14.927(3)
c (Å)	12.099(3)
β (°)	103.21(3)
V (Å^3)	1859(2)
Z	2
d_{calc} (g cm^{-3})	2.180
Crystal size (mm)	0.70 × 0.50 × 0.70
μ(Mo-K_α) (cm^{-1})	8.982
Data collection instrument	CAD 4S
Radiation (monochromated in incident beam)	Mo-K_α
Orientation reflections, number, range (2θ)	25, $30° \leqslant 2\theta \leqslant 34.0°$
Temperature (°C)	20±2
Scan method	2θ–ω
Data collection range, 2θ (°)	$4° \leqslant 2\theta \leqslant 54°$
Number of unique data, total with $F_o^2 > 3\sigma(F_o^2)$	2530
Number of parameters refined	298
Trans. factors, max., min.	1.000, 0.903
R^a	0.0880
R_w^b	0.1132
Quality-of-fit indicator[c]	3.028
Largest shift/ESD, final cycle	0.01
Largest peak (e/Å^3)	0.874

[a] $R = \Sigma||F_o|-|F_c||/\Sigma|F_o|$.
[b] $R_w = [\Sigma w(|F_o|-|F_c|)^2/\Sigma w|F_o|^2]^{1/2}$; $w = 1/\sigma^2(|F_o|)$.
[c] Quality-of-fit = $[\Sigma w(|F_o|-|F_c|)^2/(N_{obs}-N_{parameters})]^{1/2}$.

Table 2. Bond distances (in Å)

Mo(1)—Mo(1)	2.216(2)	O(2)—C(2)	1.33(2)
Mo(1)—O(1)	1.923(7)	N(3)—C(31)	1.58(2)
Mo(1)—O(2)	1.909(10)	N(3)—C(32)	1.40(3)
Mo(1)—N(3)	1.952(14)	C(1)—C(11)	1.47(3)
Mo(2)—Mo(2)	2.201(3)	C(1)—C(12)	1.44(3)
Mo(2)—O(1)	1.907(7)	C(1)—C(13)	1.62(4)
Mo(2)—O(2)	1.925(9)	C(2)—C(21)	1.47(3)
Mo(2)—N(3)	2.135(12)	C(2)—C(22)	1.44(3)
O(1)—C(1)	1.401(12)	C(2)—C(23)	1.54(3)

Numbers in parentheses are ESDs in the least significant digits.

tion and the purity and identity of the orange product are thus removed. It may be noted that when a much larger mole ratio of $(CF_3)_3COH$ to $Mo_2(NMe_2)_6$ is used (as in ref. 2 where a 12:1 ratio was used) the homoleptic $Mo_2(OC(CF_3)_3)_6$ is still not obtained, but it becomes more difficult to purify the $Mo_2(O_2C(CF_3)_3)_4(NMe_2)_2$ because of the presence of excess alcohol and side products.

Structure

By using the direct methods routine embodied in the SHELXS-86 program a solution was obtained but it showed two high peaks about 1.0 Å apart. The higher of these was selected to be the unique molybdenum atom (the asymmetric unit should be half of the formula unit for $P2_1/n$ with $Z = 2$) and the usual procedure of searching for and refining the lighter atoms was carried out. It became clear rather quickly that this was not a viable approach, as the value of R remained around 0.35 and much of the rest of the molecule failed to appear.

Both high peaks found in the direct methods solution were then assigned as partially occupied molybdenum positions and their fractional occupancies were refined subject to the requirement that the fractions have a sum of unity. This led to a 0.69:0.31 ratio and R dropped to 0.20. All of the remaining non-hydrogen atoms were then found and no resolved disorder in any of the ligands was seen. It was necessary to apply bond length restraints to the $(CF_3)_3C$ groups to avoid false minima (SHELX-76), but at the end these were released and the refinement converged with the figures of merit stated in Table 1.

These figures of merit are not as good as those ordinarily expected and we attribute this to the fact that the ligand atoms (or some of them) are really two closely positioned partial atoms from the two differently oriented molecules. While they cannot be resolved and treated separately, treating them as single spherical atoms is only an approximation (albeit an unavoidable one) and denies us the precision to be expected when the atoms truly are single vibrating spheres. In addition, there may also be some small amount of the usual sort of disordering of CF_3 groups. The displacement parameters for all ligand atoms are unusually high (i.e. 6–8 $Å^2$ for O(1), O(2), N(3) and 16–26 $Å^2$ for the F atoms).

With due allowance for the disorder, the X-ray structure shows that the molecule has a centrosymmetric conformation arising from an *anti* rotational relationship of the two $Mo(OR)_2NMe_2$ halves. Tables 2 and 3 give bond lengths and bond angles, respectively, and Fig. 1 shows the major molecule. Additional crystallographic results are available.* The $C_2NMoMoNC_2$ set of atoms is practically planar and the two methyl groups of each NMe_2 ligand thus show a large chemical shift difference because of their proximal and distal relationship to the highly anisotropic Mo≡Mo bond. Figure 2 shows the two sets of metal atoms and how they are related to the single set of averaged ligand atom positions. Note that there is a centre of inversion.

The principal molecule (P, 69%) naturally contributes most to defining the average ligand positions and thus its internal dimensions are more reliable and realistic than those for the secondary molecule (S, 31%). This is shown in Fig. 3, where the important inner angles and distances for each are displayed. It must be emphasized that *in neither case* are the dimensions as reliable as the calculated ESDs would imply, because in neither case are the oxygen and nitrogen atoms exactly where they should be for that molecule.

* Atomic positional and displacement parameters, full lists of bond lengths and angles and F_o/F_c values have been deposited as supplementary material with the Editor, from whom copies are available on request. Atomic coordinates have also been deposited with the Cambridge Crystallographic Data Centre.

Table 3. Bond angles (in degrees)

Mo(1)—Mo(1)—O(1)	101.9(3)	Mo(1)—N(3)—C(32)	142(1)
Mo(1)—Mo(1)—O(2)	106.7(2)	Mo(2)—N(3)—C(31)	163(1)
Mo(1)—Mo(1)—N(3)	93.2(4)	Mo(2)—N(3)—C(32)	85.3(8)
O(1)—Mo(1)—O(2)	121.0(4)	C(31)—N(3)—C(32)	112(1)
O(1)—Mo(1)—N(3)	114.7(4)	O(1)—C(1)—C(11)	110(1)
O(2)—Mo(1)—N(3)	113.9(4)	O(1)—C(1)—C(12)	111(2)
Mo(2)—Mo(2)—O(1)	103.1(3)	O(1)—C(1)—C(13)	105(1)
Mo(2)—Mo(2)—O(2)	106.1(3)	C(11)—C(1)—C(12)	113(3)
Mo(2)—Mo(2)—N(3)	84.0(4)	C(11)—C(1)—C(13)	109(2)
O(1)—Mo(2)—O(2)	121.0(4)	C(12)—C(1)—C(13)	107(3)
O(1)—Mo(2)—N(3)	114.0(4)	O(2)—C(2)—C(21)	111(2)
O(2)—Mo(2)—N(3)	119.1(5)	O(2)—C(2)—C(22)	108(2)
Mo(1)—O(1)—C(1)	147.2(8)	O(2)—C(2)—C(23)	112(1)
Mo(2)—O(1)—C(1)	150.9(8)	C(21)—C(2)—C(22)	104(2)
Mo(1)—O(2)—C(2)	164.2(8)	C(21)—C(2)—C(23)	109(2)
Mo(2)—O(2)—C(2)	164.9(8)	C(22)—C(2)—C(23)	112(2)
Mo(1)—N(3)—C(31)	106(1)		

Numbers in parentheses are ESDs in the least significant digits.

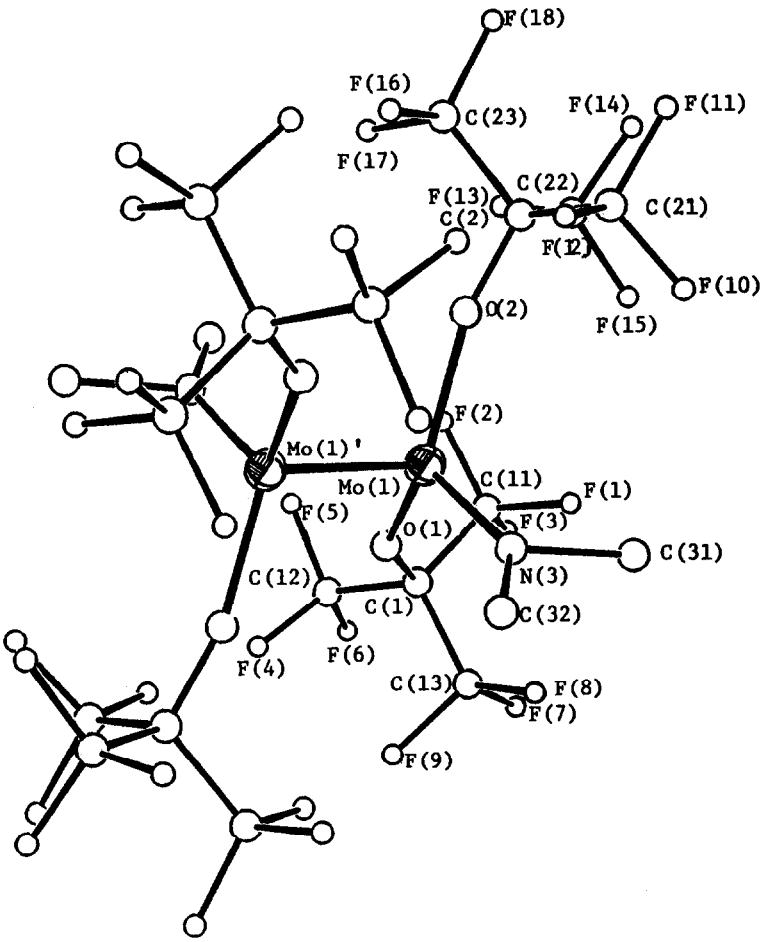

Fig. 1. An ORTEP drawing showing the ligand atoms and the two principal molybdenum atoms.

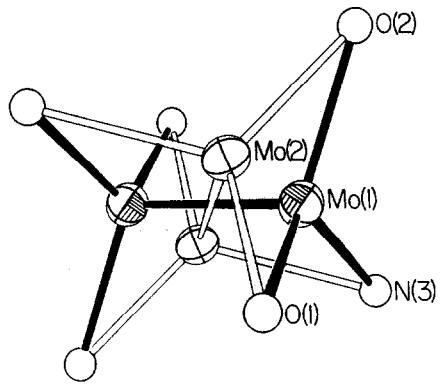

Fig. 2. A drawing of the average set of positions for the coordinated ligand atoms and the two orientations of the Mo_2 unit within it.

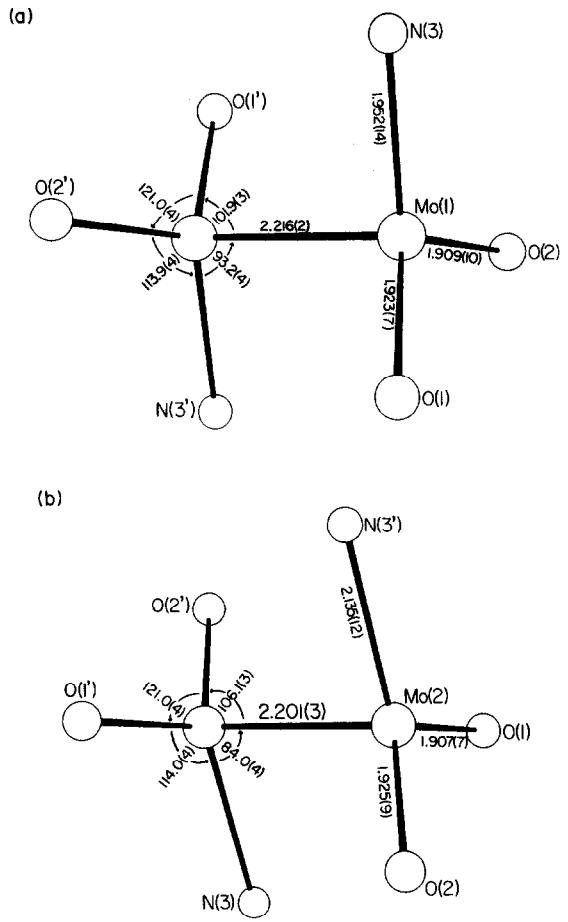

Fig. 3. Drawings showing key inner structural parameters for the principal and secondary molecules. Additional angles are:

O(2)—Mo(1)—Mo(1)′ = 106.7(2)°
O(1)—Mo(1)—N(3) = 114.7(4)°
O(1)—Mo(2)—Mo(2)′ = 103.1(3)°
O(2)—Mo(2)—N(3)′ = 119.1(5)°.

For the principal molecule, the Mo—O and Mo—N distances as well as the Mo—Mo—O and Mo—Mo—N angles are similar to those previously found in undisordered structures,[5] whereas those in the secondary molecule appear somewhat different, but, of course, are not to be taken seriously, as describing a true, single molecule.

Can internal flips occurs in M_2X_6 type molecules?

It has been recognized[6,7] that in M_2X_8 type species rearrangement (particularly isomerization) can occur by means of an internal flip of the M_2 unit from one axis to another within the nearly cubic array of eight X ligands. This is illustrated in Fig. 4(a). The idea that such a process might take place arose from the much earlier observations on the occurrence of disordering of the dimetal unit within the quasi-cubic cage of ligands in a number of cases, of which $[N(C_4H_9)_4]_2[Re_2I_8]$ provides the most spectacular example.[8]

Now that we have observed the first example of a similar type of disorder in an M_2X_6 molecule, the possibility of a comparable internal flip mechanism in M_2X_6 molecules comes into consideration. If the trigonal antiprism is idealized to an octahedron, just as in the M_2X_8 case the square parallelopiped can be idealized to a cube, there are four orientations for the M_2 unit, along the four lines between centres of opposite faces. Figure 4(b) shows two of these M_2 units.

The idealization of the set of six ligands to an octahedron in this case is well justified. By treating the centre of inversion at the midpoints of the Mo—Mo bonds as the centre, *C*, of the imagined octahedron, we have calculated the "bond" distances to the ligand atoms and the angles between the "bonds". These are listed in Table 4. It is clear that this octahedron is no more distorted than those found in many complexes that are normally described as octahedral. In addition, we have calculated the angles between the faces of the approximate octahedron, and these too are listed in Table 4. It is seen that all of them are close to the ideal angle of 109.5°.

While we are not asserting that in any real case the M_2 unit necessarily visits all orientations within the quasi-octahedron over a period of time, we do not rule that out. Nor do we argue that more than one orientation is necessarily accessible in reality, but it is worth pointing out the consequences in the present case of passing from one of the two observed orientations to the other. This can be appreciated by referring to Fig. 5, which shows the plane occupied by the principal pair of metal atoms, Mo(1)—Mo(1)′, the secondary pair,

Table 4. Dimensions of the O_4N_2 "octahedron" about the inversion centre of the $Mo_2(OC(CF_3)_3)_4(NMe_2)_2$ molecule

"Bond" distances to centre, *C* (Å)	
C—O(1)	2.42
C—O(2)	2.46
C—N(3)	2.31
"Bond" angles about centre, *C* (°)	
N(3)—*C*—N(3)′	180
O(1)—*C*—O(1)′	180
O(2)—*C*—O(2)′	180
N(3)—*C*—O(1)	87.5
N(3)—*C*—O(1)′	92.5
N(3)—*C*—O(2)	85.8
N(3)—*C*—O(2)′	94.2
O(1)—*C*—O(2)	87.1
O(1)—*C*—O(2)′	92.3

Angles between face planes (°)[a]

plane 1/plane 2,	105.1	plane 2/plane 7,	112.7
plane 1/plane 3,	110.6	plane 2/plane 8,	112.2
plane 1/plane 4,	108.4	plane 3/plane 7,	107.7

[a] O(1), O(2), N(3) define plane 1; O(1), O(2) N(3)′ define plane 2; O(1)′, O(2), N(3) define plane 4; O(1), O(2)′, N(3)′ define plane 7; O(1)′, O(2), N(3)′ define plane 8.

Mo(2)—Mo(2)′, and the two NR_2 ligands, whose average positions and orientations are seen to be symmetrically related to both M_2 units.

When the dimetal unit is in the Mo(1)—Mo(1)′ orientation, C(31)/C(31)′ are the distal groups and C(32)/C(32)′ are the proximal ones. It has been known for a long time[9,10] that proximal and distal R groups exchange roles with a moderate activation energy (*ca* 12–14 kcal mol^{-1}) and it has been considered that the barrier arises mainly from a combination of steric interactions between ligands and some degree of M—N π-bonding (consistent with the planarity of the M—NR_2 unit). However, it may be seen in Fig. 5 that if the Mo_2 unit simply flips from the Mo(1)—Mo(1)′ to the Mo(2)—Mo(2)′ orientation, a concerted distal–proximal exchange for both NR_2 ligands is accomplished. Bonding of the metal atoms to the pairs of OR groups would also be maintained as Mo(1)→Mo(2) and Mo(1)′→Mo(2)′.

A similar kind of flip process could successively exchange all proximal and distal R groups in $M_2(NR_2)_6$ molecules. Experimental data presently available do not allow us to decide between this possibility and the more conventional and previously proposed processes of rotation (singly or, more probably, in some concerted fashion) about the M—N bonds. It is interesting to note that the

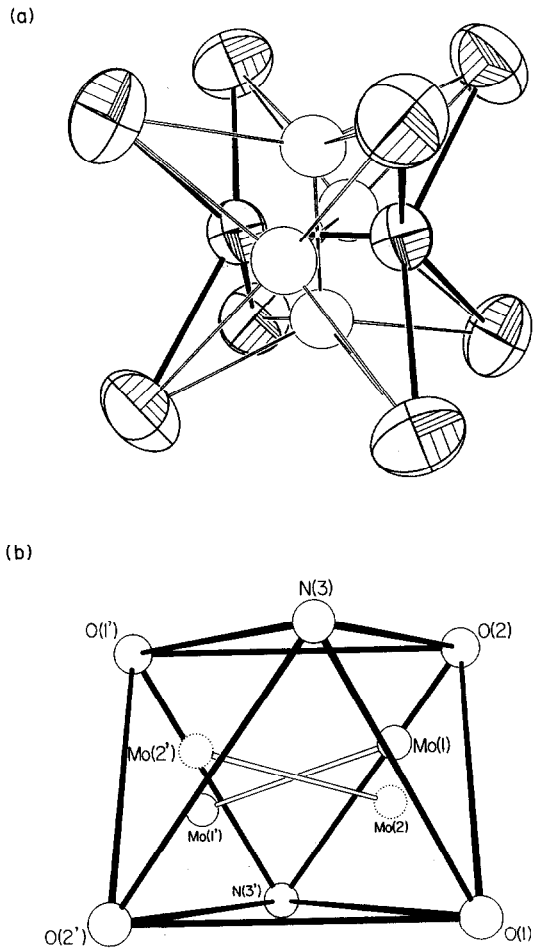

Fig. 4. (a) A quasi-cube of eight ligands with the M_2 unit in its three possible orientations; (b) a quasi-octahedron of six ligands with two of the four possible orientations of an M_2 unit within it.

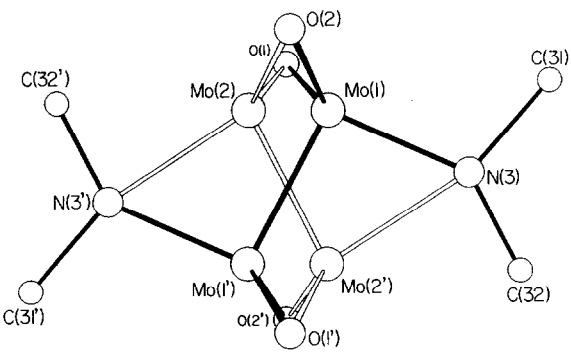

Fig. 5. A drawing showing how the distal and proximal character of the amido carbon atoms can be changed by flipping the Mo_2 unit within a fixed set of ligand atoms, while simultaneously preserving four properly oriented Mo—O bonds.

two processes should respond differently to increasing the size of the R groups, and that this may afford a means of choosing the correct one. As the R groups become bulkier, the rotational processes (even if concerted rotations about several bonds are invoked) would seem likely to show a significant increase in activation energy, since R groups on different NR_2 ligands would have to *pass* each other. On the other hand, the flip process can occur without any actual *passing* being required, although some bumping might occur. Therefore, the activation energy for the flip mechanism should be relatively insensitive to the bulk of the R groups. The only data available now that bear on this point are the $\Delta G^{\ddagger}$ values for $Mo_2(NMe_2)_6$ and $Mo_2(NEt_2)_6$, which are 11.5(2) and 13.6(5) kcal mol^{-1}, respectively. This rather small change is consistent with the operation of the flip process, but is not necessarily inconsistent with a concerted rotational process. Clearly, a more conclusive test can be devised, and we are pursuing that.

Acknowledgement—We thank the National Science Foundation for support.

REFERENCES

1. R. G. Abbott, F. A. Cotton and L. R. Falvello, *Inorg. Chem.* 1990, **29**, 514.
2. M. H. Chisholm, F. A. Cotton, C. A. Murillo and W. W. Reichert, *Inorg. Chem.* 1977, **16**, 1801.
3. M. H. Chisholm, D. A. Haitko, C. A. Murillo and F. A. Cotton, *Inorg. Synth.* 1982, **21**, 54.
4. See, for example, refs cited in F. A. Cotton and M. Matusz, *Inorg. Chem.* 1988, **27**, 2127.
5. F. A. Cotton and R. A. Walton, *Multiple Bonds Between Metal Atoms*, Section 5.3. John Wiley, New York (1982).
6. P. A. Agaskar, F. A. Cotton, D. R. Derringer, G. L. Powell, D. R. Root and T. J. Smith, *Inorg. Chem.* 1985, **24**, 2786.
7. F. A. Cotton and S. Kitagawa, *Polyhedron* 1988, **7**, 463.
8. F. A. Cotton, L. M. Daniels and K. Vidyasagar, *Polyhedron* 1988, **7**, 1667.
9. M. H. Chisholm, F. A. Cotton, B. A. Frenz, W. W. Reichert, L. W. Shive and B. R. Stults, *J. Am. Chem. Soc.* 1976, **98**, 4469.
10. M. H. Chisholm, F. A. Cotton, M. Extine and B. R. Stults, *J. Am. Chem. Soc.* 1976, **98**, 4477.

Polyhedron Vol. 9, No. 15/16, pp. 1829–1841, 1990
Printed in Great Britain

0277–5387/90 $3.00+.00
© 1990 Pergamon Press plc

TWELVE-ELECTRON TETRANUCLEAR TUNGSTEN ALKOXIDE CLUSTERS ARE NOT TETRAHEDRAL. PREPARATION, STRUCTURE AND BONDING IN $W_4(O)(OPr^i)_{10}$ AND $W_4(O)(Cl)(OPr^i)_9$. COMPARISONS WITH THE BONDING IN CARBONYL CLUSTERS*

MALCOLM H. CHISHOLM,† CHARLES E. HAMMOND, JOHN C. HUFFMAN and JAMES D. MARTIN

Department of Chemistry and Molecular Structure Center, Indiana University, Bloomington, IN 47405, U.S.A.

Abstract—Addition of H_2O (0.5 equiv) to a hexane/Pr^iOH solution of $W_4(OPr^i)_{12}$ yields $W_4(O)(OPr^i)_{10}$ (**II**) which reacts further with NH_4Cl to give $W_4(O)(Cl)(OPr^i)_9$ (**I**). The NMR data for **I** and **II** are indicative of common structural features and the molecular structure of **I** has been determined in the solid state by a single crystal X-ray diffraction study. At −146°C: $a = 41.172(18)$, $b = 9.185(2)$, $c = 22.718(8)$ Å, $\beta = 97.15(2)°$, $Z = 4$ and $d_{calc} = 2.113$ g cm^{-3}. A $WCl(OPr^i)$ moiety caps a basal $W_3(\mu\text{-}O)(\mu\text{-}OPr^i)_2(OPr^i)_6$ moiety. The local WO_4 geometry for the tungsten atoms in the basal plane is square planar. Of particular note are the short W—W distances involving the capping $WCl(OPr^i)$ moiety (*ca* 2.45 Å) relative to those W—W distances in the basal plane (*ca* 2.90 Å). The bonding in compounds **I** and **II**, modelled as $W_4(O)(Cl)(OH)_9$ and $W_4(O)(OH)_{10}$, respectively, has been investigated by MO calculations employing the method of Fenske and Hall. The combination of the d^4-WCl(OH) fragment with the d^8-$W_3(O)(OH)_8$ fragment yields multiple M—M bond character between the capping tungsten atom and the three W—W atoms in the basal plane. Interesting analogies are seen between carbonyl and alkoxide clusters based on the isolobal principle d^3-$W(OR)_3 \leftrightarrow d^9$-$Co(CO)_3 \leftrightarrow d^9$-$Os(CO)_3^-$ and d^4-$WX_2 \leftrightarrow d^{10}$-$PtL_2$. Specific comments are made with respect to the bonding in $M_4(OR)_{12}$ (M = Mo, W), $M_4(CO)_{12}$ (M = Co, Rh, Ir) (**I**, **II**) and $Os_3Pt(H)_2(CO)(PR_3)$.

Of long standing interest to us has been the structure and bonding in 12-electron M_4 alkoxide supported clusters (M = Mo, W) formed by the coupling of two $(M{\equiv}M)^{6+}$ units. In the original report[1] on the preparation and characterization of $Mo_2(OR)_6$ compounds (R = Bu^t, Pr^i, CH_2Bu^t, CMe_2Ph) we speculated that reduction in steric bulk of the alkoxy ligands might lead to tetrahedral M_4 clusters, an electron-precise structure for a 12-electron M_4 unit having six M—M electron pairs.

Substitution of OR by halides led to a series of $Mo_4X_4(OPr^i)_8$ clusters[2,3] based on a square (X = Cl) or a butterfly (an opened tetrahedron) of metal atoms (X = Br and I), while the fluoride $Mo_4F_4(OBu^t)_8$[4,5] and the mixed alkoxide $Mo_4(OMe)_2(OPr^i)_{10}$[6] were found to contain bisphenoids and rectangles of metal atoms, respectively. The bridging ligands (F or OMe and OPr^i) united two localized $(M{\equiv}M)^{6+}$ units. For tungsten we found that $W_2(OPr^i)_6$ existed in solution equilibrium with $W_4(OPr^i)_{12}$ and that the latter contained a distorted rhombus of metal atoms, an inorganic analogue of cyclobutadiene.[7,8] With a further decrease in the bulk of the attendant alkoxide ligands (R = CH_2Pr^i, CH_2Hex^c, CH_2Pen^c and CH_2Bu^c) both molybdenum and tungsten gave $M_4(OR)_{12}$ compounds having a common structure based on a highly asymmetrical M_4 butterfly with three short M—M distances, *ca* 2.5 Å, two long M—M bonded distances, *ca* 2.8 Å, and one nonbonding M—M distance.[9]

These structures reveal the desire of the metal atoms to maximize M—M and M—L (L = ligand) bonding. However, it seems that M—M bonding

* Dedicated to Professor R. Fenske on the occasion of his retirement and in appreciation of his former students from whom we have learned much

† Author to whom correspondence should be addressed.

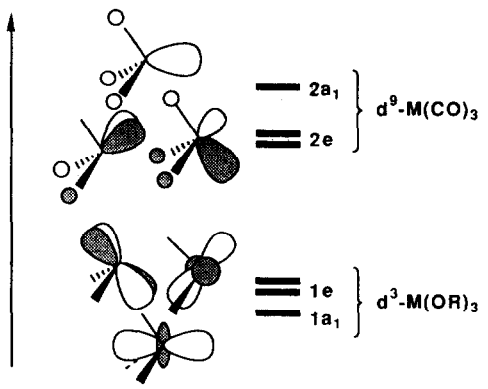

Scheme 1.

and M—L bonding are often in competition. For example, in the $M_2(OR)_6(M{\equiv}M)$ compounds the ethane-like structure indicates that M—M bonding wins at the expense of M—O bonding which would favour the Al_2X_6 fused tetrahedral structure.

We have previously noted the complementary nature of RO and CO ligands as π-buffers in early and late transition metal chemistry.[10] Furthermore, the frontier orbital relationship between d^3-$M(OR)_3$ (M = Mo, W) and d^9-$M(CO)_3$ fragments (M = Co, Rh, Ir), as shown in Scheme 1, provides the foundation for many similarities between di-, tri- and tetranuclear alkoxide and carbonyl clusters that coordinate common fragments, for example, as in $M_2(\mu\text{-X})$ compounds where X = alkyne or P_2, $M_3(\mu\text{-X})$ compounds where X = CR or P and $M_4(\mu_4\text{-C})$ compounds.[11,12] The tetranuclear carbonyl clusters $M_4(CO)_{12}$, where M = Co, Rh and Ir, have a tetrahedral M_4 core supported (M = Co, Rh)[13,14] or unsupported (M = Ir)[15] by carbonyl bridges. The tetrahedral alkoxide analogues $M_4(OR)_{12}$ (M = Mo, W) are conspicuous by their absence.

In this paper we describe the synthesis and characterization of tetranuclear 12-electron alkoxide clusters of tungsten, $W_4(O)(Cl)(OPr^i)_9$ and $W_4(O)(OPr^i)_{10}$, that adopt a novel structure based on a distorted tetrahedron of metal atoms having three short and three long bonds. This leads us to question whether or not any 12-electron M_4 cluster supported principally by alkoxide ligands would contain a tetrahedral M_4 unit. A preliminary aspect of this work has appeared.[16]

RESULTS AND DISCUSSION

Synthesis

The compound $W(O)(Cl)(OPr^i)_9$ (**I**) was discovered as a minor product formed in the preparation of $W_4(H)_2(OPr^i)_{14}$[17] from the reactants $W_2(O\text{-}Bu^t)_6$, $NaOPr^i/Pr^iOH$ (with adventitious H_2O) and $Me_2NH_2^+Cl^-$. Compound **I** is very soluble in hexane and is obtainable as orange crystals from Et_2O, forming above the solution on the walls of the flask. This allows for its isolation in analytically pure form, $[W_4Cl(O)(OPr^i)_9]\cdot 1/2Et_2O$, and easy separation from $W_4(H)_2(OPr^i)_{14}$ and $W_4(OPr^i)_{12}$ which are present in the reaction mixture.

In an attempt to elucidate how $W_4(O)(Cl)(OPr^i)_9$ was formed, $W_2(O\text{-}Bu^t)_6$ in hexanes was allowed to react with H_2O/Pr^iOH (1/2 equiv of H_2O in 10 equivalents of Pr^iOH). The ^1H NMR spectrum indicated a plethora of products. However, when addition of H_2O/Pr^iOH was preceded by addition of $HOPr^i$ forming $W_2(OPr^i)_6$, the reaction yielded $W_4(O)(OPr^i)_{10}$ (**II**) according to eq. (1) below. Crystals of $W_4(O)(OPr^i)_{10}$ were obtained from Et_2O, analytically pure for $[W_4(O)(OPr^i)_{10}]\cdot 1/2Et_2O$, but were unsuitable for X-ray analysis.

$$2''W_2(OPr^i)_6'' + H_2O \longrightarrow W_4(O)(OPr^i)_{10} + 2\,HOPr^i \quad (1)$$

Alternatively, $W_4(OPr^i)_{12}$ was dissolved in toluene-d_8 at room temperature [allowing for an equilibration with $W_2(OPr^i)_6$] and was allowed to react with $1/2H_2O$. ^1H NMR spectroscopy indicated the clean conversion to $W_4(O)(OPr^i)_{10}$. It is unclear whether the hydrolysis involves $W_2(OPr^i)_6$ or $W_4(OPr^i)_{12}$.

Spectroscopic characterization

The oxo ligand is confirmed as being derived from H_2O by carrying out the experiment using $H_2{}^{18}O$ and identifying the W—O—W stretching frequency in the IR spectrum. In **II**, $\nu = 667$ cm^{-1} and ^{18}**II**, $\nu = 635$ cm^{-1}, following closely to the harmonic oscillator model,[18] $\nu_{iso}/\nu_{ref} = (\mu_{ref}/\mu_{iso})^{1/2} \rightarrow \nu_{iso} = 0.9472 \times \nu_{ref}$. This knowledge permitted recognition of the W—O—W stretch $\nu = 678$ cm^{-1} in **I**. These W—O—W stretches are in the region expected for the symmetric stretch of bent M—O—M linkages.[19] In **I** there are two bands, $\nu = 515$ cm^{-1} and $\nu = 503$ cm^{-1} (Nujol mull). These diagnostic bands are at higher wave numbers than previously observed W—Cl bands by about 150 cm^{-1}. Their derivation is unclear at present but they may be due to the W—Cl coupling to other vibronic modes.

The ^1H NMR spectra of **I** and **II** indicate that the two compounds are structurally related, each having five different types of Pr^iO ligands as shown in Fig. 1. In both cases the unique non-dia-

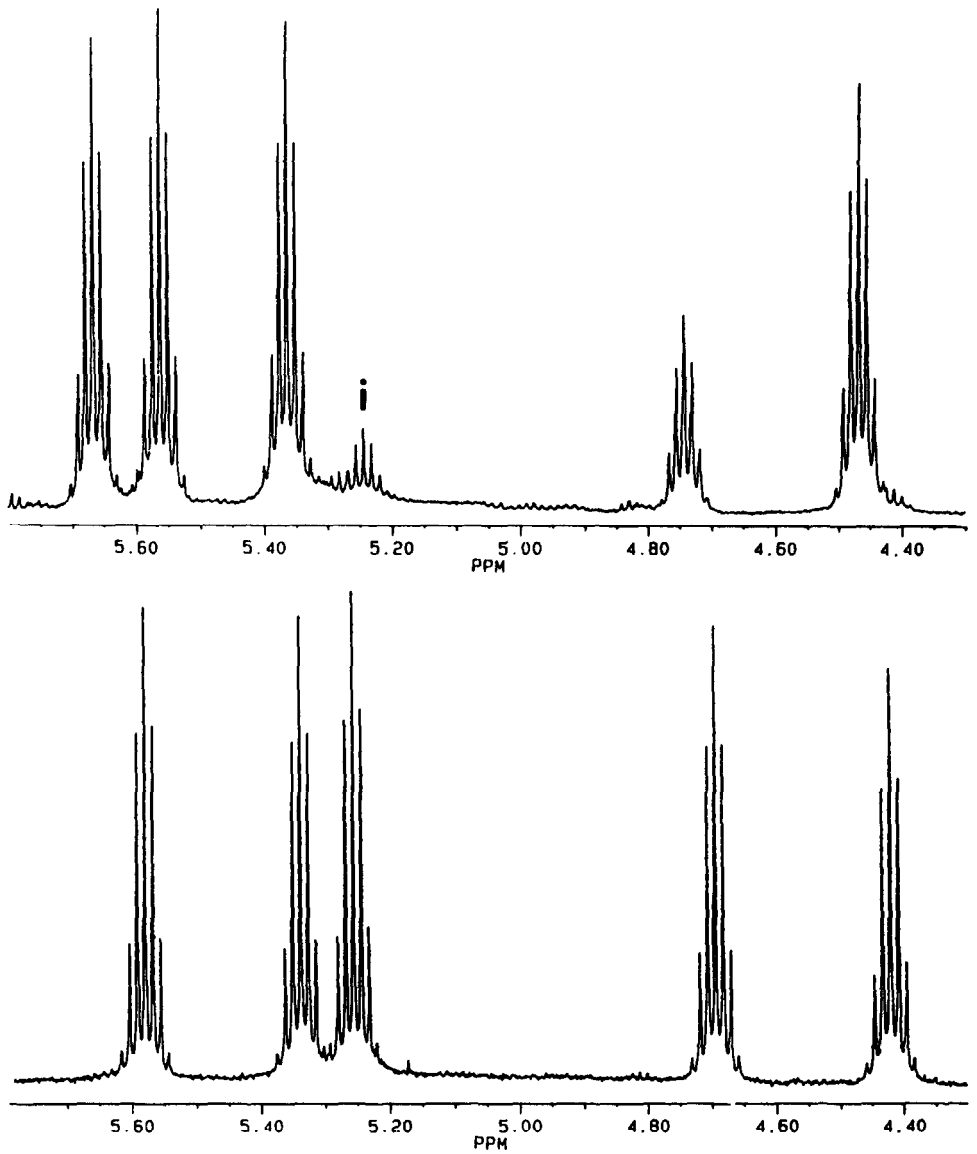

Fig. 1. ^1H NMR of the methine regions of $W_4(O)(Cl)(OPr^i)_9$ (top) and $W_4(O)(OPr^i)_{10}$ (bottom). The letter i denotes an impurity.

stereotopic methyl group is coupled to the methine at *ca* 4.7 ppm. Addition of excess $Me_2NH_2^+Cl^-$ to **II** causes the resonance at *ca* 4.7 ppm in the ^1H NMR spectrum to disappear, presumably, because $W_4Cl_2(O)(OPr^i)_8$ is formed. This suggests both ease and site selectivity for alkoxide ligand substitution by chloride ligands. The compound $W_4Cl_2(O)(OPr^i)_8$ has not, however, been isolated and fully characterized.

Solid-state and molecular structure

The molecular structure of **I** has been deduced from a single crystal X-ray study. Two ball-and-stick drawings that emphasize the W_4 pseudo-tetrahedron are shown in Fig. 2. A summary of crystallographic data is given in Table 1, and pertinent bond distances and angles are located in Tables 2 and 3, respectively.

The molecule consists of a $WCl(OPr^i)$ fragment, W(4), capping a triangle of tungsten atoms, W(1), W(2) and W(3), that is supported by two bridging Pr^iO ligands and one μ-oxo group together with two terminal OPr^i ligands per tungsten. The geometry of the WO_4 units in the basal W_3 unit is approximately square planar. Each terminal alkoxide is *trans* to a bridging oxygen atom of a μ-OPr^i or μ-oxo ligand. The oxo ligand, O(6), that is bonded to W(1) and

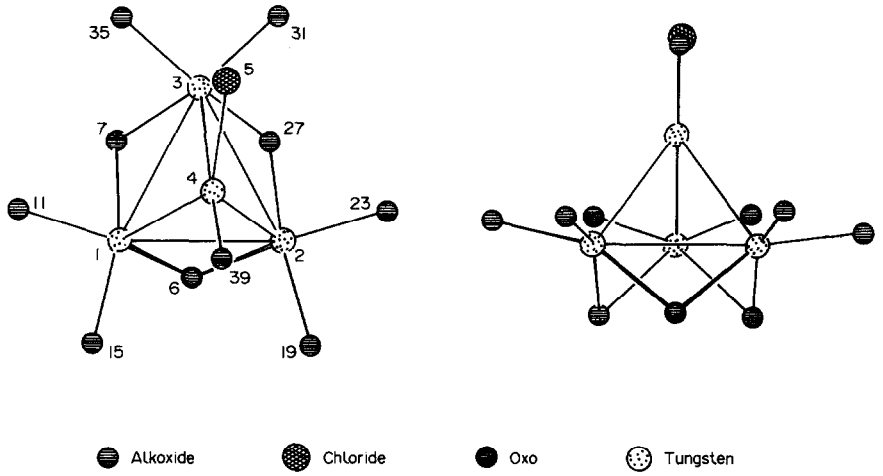

Fig. 2. Two views of the central $W_4Cl(O)_{10}$ skeleton of $W_4(O)(Cl)(OPr)_9$.

Table 1. Summary of crystal data

Empirical formula	$C_{27}H_{63}ClO_{10}W_8$; $1/2C_4H_{10}$
Colour of crystal	Redish-brown
Crystal dimensions (mm)	$0.16 \times 0.16 \times 0.18$
Space group	$C2/c$
Cell dimensions	
Temperature (°C)	−146
a (Å)	41.172(18)
b (Å)	9.185(2)
c (Å)	22.718(8)
β	97.15(2)
Z (Molecules/cell)	8
Volume (Å^3)	8524.28
Calculated density (g cm^{-3})	2.113
Wavelength (Å)	0.71069
Molecular weight	1355.71
Linear absorption coefficient (cm^{-1})	111.023
Detector to sample distance (cm)	22.5
Sample to source distance (cm)	23.5
Average omega scan width at half height	0.25
Scan speed (deg min^{-1})	6.0
Scan width (deg+dispersion)	1.6
Individual background (s)	6
Aperture size (mm)	3.0×4.0
2θ Range (deg)	6–45
Total number of reflections collected	6513
Number of unique intensities	5394
Number of $F > 0.0$	5304
Number of $F > 3.0\sigma(F)$	4851
R(F)	0.0505
$R_w(F)$	0.0498
Goodness-of-fit for the last cycle	1.215
Maximum δ/σ for last cycle	0.05

Table 2. Selected bond distances (Å) for $W_4(O)(Cl)(OPr^i)_9$

A	B	Distance
W(1)	W(2)	2.8473(15)
W(1)	W(3)	2.9584(14)
W(1)	W(4)	2.4836(11)
W(1)	O(6)	1.921(10)
W(1)	O(7)	2.071(10)
W(1)	O(11)	1.873(11)
W(1)	O(15)	1.874(11)
W(2)	W(3)	2.9646(14)
W(2)	W(4)	2.4703(11)
W(2)	O(6)	1.924(1)
W(2)	O(19)	1.861(11)
W(2)	O(23)	1.894(12)
W(2)	O(27)	2.062(1)
W(3)	W(4)	2.5467(11)
W(3)	O(7)	2.011(1)
W(3)	O(27)	2.026(11)
W(3)	O(31)	1.858(11)
W(3)	O(35)	1.896(11)
W(4)	O(39)	1.898(12)
W(4)	Cl(5)	2.462(4)

W(2) is contained in a virtual mirror plane together with W(3), W(4), Cl(5) and O(39).

The most striking feature of the molecular structure is the presence of a two-coordinate tungsten atom capping a triangle of four-coordinate tungsten atoms such that the unbridged W—W distances are roughly 0.5 Å shorter than the bridged W—W distances.

Empirical bond strength–bond length relationships have been used to determine or assign oxidation states in oxides of molybdenum.[20] We have shown that this can be extended to alkoxide clusters of both molybdenum and tungsten if the assumption is made that W—O and Mo—O bond distances are equivalent.[9] This assumption is valid to within one or two hundredths of an Angstrom. The chloride ligand is considered a uninegative ligand and is solely bonded to W(4). This gives the oxidation states W(1) = W(2) = +3.5, W(3) = +3.3, and W(4) = +1.9 for a total charge of +12.2, in close agreement with the formal charge of +12 for the 12-electron W_4 cluster in which Cl and OR are counted as uninegative ligands.

The ^{1}H NMR spectrum of **I** is entirely consistent with the structure observed in the solid state. The structure of **II** can most reasonably be formulated as being related to that of **I** by the replacement of Cl by OPr^i. However, the spectroscopic equivalence of the two terminal alkoxide ligands of the $W(OPr^i)_2$ cap raises some question as to the orientation of this WX_2 fragment. If the alkoxide ligands of **II** lie within the mirror plane, as in the solid-state structure of **I**, then two methyne chemical shifts are expected unless they are accidentally degenerate or there is facile rotation of the WX_2 cap. Alternatively, the WX_2 fragment could lie perpendicular to the virtual mirror plane.

It is unlikely, given their orientation with respect to the rest of the molecule, that the alkoxide ligands of the $W(OPr^i)_2$ cap would be accidentally degenerate. Variable temperature ^{1}H NMR studies in d_8-toluene give no evidence of freezing out any rotation of the $W(OPr^i)_2$ cap even at −90°C. Assuming that in the frozen-out spectrum the methyne protons of these alkoxides would show a separation of chemical shifts similar to those from the various environments of the terminal alkoxide ligands in the trianglar base (0.1–0.4 ppm), no rotational barrier less than 10 kcal mol^{-1} would be frozen out, on the NMR time scale, even at −90°C. Molecular orbital calculations (see later) by both the Extended Huckel and Fenske–Hall methods support a low barrier to a rotation of this WX_2 (X = Cl or OR) cap above the triangular basal plane.

BONDING CONSIDERATIONS

The bonding in these clusters is best understood from a fragment molecular orbital FMO analysis.[21,22] We consider the clusters to be formed from the fragments W(Cl)(OR) or $W(OR)_2$ and $W_3(O)(OR)_8$ and have investigated the bonding by using the method of Fenske and Hall[23] for the model compounds $W_4(O)(Cl)(OH)_9$ and $W_4(O)(OH)_{10}$.

$W_4(O)(Cl)(OPr^i)_9$ (I)

The molecular orbitals of the $W_3(O)(OH)_8$ fragment are similar to those previously described[11,12] for the $W_3(OR)_9$ fragment of $W_3(OR)_9(\mu_3\text{-CMe})$, though the presence of the bridging oxo group results in a reduction of symmetry from C_{3v} to C_s and a loss of one electron from the M_3 cluster fragment. The orbitals of the WCl(OH) fragment are reminiscent of those expected for a WX_2 fragment except for the notable mixing of the $1a''$ and $2a''$ orbitals so as to minimize the π-antibonding between the tungsten d_π and oxygen p_π electrons. A simplified interaction diagram of these two fragments is given in Fig. 3.

On combining the fragments the filled $1a'$ and $1a''$ orbitals of WCl(OH) find their match with unoccupied $4a'$ and $2a''$ non-bonding orbitals of the tri-tungsten fragment. Similarly the $1a'$, $2a'$ and $1a''$

Table 3. Selected bond angles (deg) for $W_4(O)(Cl)(OPr^i)_9$

A	B	C	Angle	A	B	C	Angle
W(2)	W(1)	W(3)	61.38(3)	W(1)	W(3)	O(7)	44.4(3)
W(2)	W(1)	W(4)	54.698(27)	W(1)	W(3)	O(27)	85.4(3)
W(2)	W(1)	O(6)	42.3(3)	W(1)	W(3)	O(31)	155.7(4)
W(2)	W(1)	O(7)	88.1(3)	W(1)	W(3)	O(35)	100.9(4)
W(2)	W(1)	O(11)	159.3(3)	W(2)	W(3)	W(4)	52.60(4)
W(2)	W(1)	O(15)	105.1(4)	W(2)	W(3)	O(7)	86.0(3)
W(3)	W(1)	W(4)	54.971(26)	W(2)	W(3)	O(27)	44.0(3)
W(3)	W(1)	O(6)	85.9(3)	W(2)	W(3)	O(31)	103.9(3)
W(3)	W(1)	O(7)	42.8(3)	W(2)	W(3)	O(35)	154.7(4)
W(3)	W(1)	O(11)	101.4(3)	W(4)	W(3)	O(7)	97.1(3)
W(3)	W(1)	O(15)	160.7(4)	W(4)	W(3)	O(27)	96.3(3)
W(4)	W(1)	O(6)	96.9(3)	W(4)	W(3)	O(31)	104.0(4)
W(4)	W(1)	O(7)	97.5(3)	W(4)	W(3)	O(35)	105.0(4)
W(4)	W(1)	O(11)	106.7(3)	O(7)	W(3)	O(27)	83.9(4)
W(4)	W(1)	O(15)	106.4(4)	O(7)	W(3)	O(31)	158.6(5)
O(6)	W(1)	O(7)	84.3(4)	O(7)	W(3)	O(35)	85.5(5)
O(6)	W(1)	O(11)	155.2(4)	O(27)	W(3)	O(31)	90.3(5)
O(6)	W(1)	O(15)	92.3(4)	O(27)	W(3)	O(35)	157.1(5)
O(7)	W(1)	O(11)	85.4(4)	O(31)	W(3)	O(35)	92.3(5)
O(7)	W(1)	O(15)	156.2(5)	W(1)	W(4)	W(2)	70.17(4)
O(11)	W(1)	O(15)	88.2(5)	W(1)	W(4)	W(3)	72.04(4)
W(1)	W(2)	W(3)	61.16(4)	W(1)	W(4)	Cl(5)	139.54(12)
W(1)	W(2)	W(4)	55.14(3)	W(1)	W(4)	O(39)	112.9(3)
W(1)	W(2)	O(6)	42.2(3)	W(2)	W(4)	W(3)	72.43(4)
W(1)	W(2)	O(19)	103.8(3)	W(2)	W(4)	Cl(5)	136.87(12)
W(1)	W(2)	O(23)	163.3(4)	W(2)	W(4)	O(39)	113.2(3)
W(1)	W(2)	O(27)	87.7(3)	W(3)	W(4)	Cl(5)	87.57(11)
W(3)	W(2)	W(4)	54.98(3)	W(3)	W(4)	O(39)	173.3(3)
W(3)	W(2)	O(6)	85.6(3)	Cl(5)	W(4)	O(39)	85.8(4)
W(3)	W(2)	O(19)	157.6(4)	W(1)	O(6)	W(2)	95.6(4)
W(3)	W(2)	O(23)	103.3(4)	W(1)	O(7)	W(3)	92.9(4)
W(3)	W(2)	O(27)	43.0(3)	W(1)	O(7)	C(8)	126.2(10)
W(4)	W(2)	O(6)	97.2(3)	W(3)	O(7)	C(8)	132.8(10)
W(4)	W(2)	O(19)	103.1(4)	W(1)	O(11)	C(12)	142.5(10)
W(4)	W(2)	O(23)	111.9(4)	W(1)	O(15)	C(16)	136.8(11)
W(4)	W(2)	O(27)	97.8(3)	W(2)	O(19)	C(20)	143.3(10)
O(6)	W(2)	O(19)	93.3(5)	W(2)	O(23)	C(24)	132.4(11)
O(6)	W(2)	O(23)	149.5(5)	W(2)	O(27)	W(3)	93.0(4)
O(6)	W(2)	O(27)	83.6(4)	W(2)	O(27)	C(28)	127.2(9)
O(19)	W(2)	O(23)	88.9(5)	W(3)	O(27)	C(28)	129.0(10)
O(19)	W(2)	O(27)	159.1(5)	W(3)	O(31)	C(32)	147.1(10)
O(23)	W(2)	O(27)	83.6(5)	W(3)	O(35)	C(36)	133.2(11)
W(1)	W(3)	W(2)	57.47(3)	W(4)	O(39)	C(40)	145.6(11)
W(1)	W(3)	W(4)	52.99(3)				

M—M bonding orbitals and the $3a'$ occupied non-bonding orbital of the W_3 fragment, made up of the in-phase combinations of tungsten z^2 orbitals, interact strongly with the respective $2a'$, $2a''$, $3a'$ and $4a'$ unoccupied orbitals of the WX_2 cap. The overlap populations corresponding to these interactions are given in Table 4. Placing electrons into M_3-non-bonding (or weakly antibonding) orbitals and withdrawing electrons from the M_3 bonding orbitals causes the Mulliken atomic charges of the tungsten atoms to be -0.631 for the capping atom and 1.407, 1.407 and 1.343 for those in the basal plane. This results in a severe weakening of the M—M bonding in the basal plane and M—M multiple bonding to the capping tungsten atom. The importance of the valence bond description

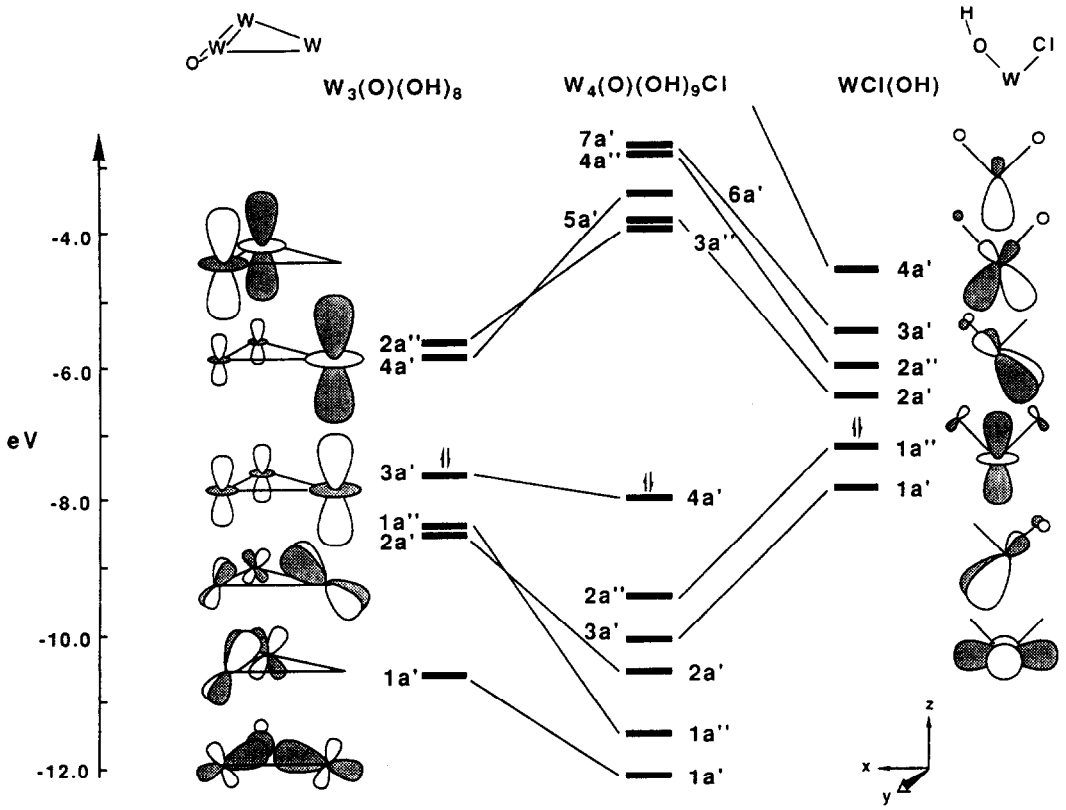

Fig. 3. A simplified interaction diagram showing the formation of $W_4(O)(Cl)(OH)_9$ from the combination of W(Cl)(OH) and $W_3(O)(OH)_8$ fragments.

depicted by the resonance structure **A**, relative to that of **B**, is apparent, where M_a represents the apical metal atom, i.e. the $WCl(OPr^i)$ unit.

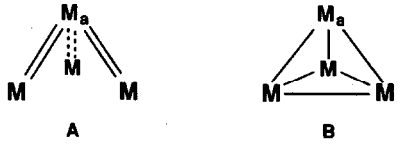

A slightly weaker interaction would be obtained were the W(Cl)(OH) fragment rotated by 180° such that the Cl bond was situated over the oxo bridge, **C**, rather than over the unique basal tungsten atom, **D**.

A discussion of the bonding in **I** would be incomplete without describing the orientational preference of the tungsten–alkoxide–chloride cap. The

Table 4. Overlap populations corresponding to the interaction of the W(Cl)(OH) fragment with the $W_3(O)(OH)_8$ fragment. The WX_2 cap is oriented parallel to the virtual mirror plane of the molecule as in the X-ray structure of **I**

	W(OH)(Cl)					
$W_3(O)(OH)_8$	1*a'*	1*a''*	2*a'*	2*a''*	3*a'*	4*a'*
1*a'*	−0.016	0.000	0.314	0.000	−0.012	0.167
2*a'*	0.087	0.000	0.005	0.000	0.313	0.026
1*a''*	0.000	−0.012	0.000	0.345	0.000	0.000
3*a'*	0.176	0.000	−0.020	0.000	0.001	0.368
4*a'*	0.082	0.000	0.060	0.000	0.270	0.006
2*a''*	0.000	0.370	0.000	−0.008	0.000	0.000
	0.329	0.358	0.359	0.337	0.572	0.567 = 2.522

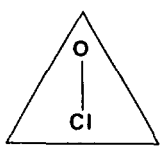

C

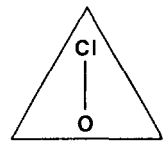

D

metal-based orbitals of the W(Cl)(OH) fragment are polarized away from the OH ligand slightly more than from the weaker donor Cl. Similarly the FMOs of the cluster fragment are polarized away from the oxo bridge toward the unique tungsten atom. This allows a maximum a' or σ-type overlap when oriented in configuration **D**, as found in the X-ray crystal structure, apparent from comparison of the overlap population tabulated in Tables 4 and 5. This same reasoning accounts for the slightly increased a'' or π-type overlap when the W(Cl)(OH) cap is rotated to orientation **C**. However, this better cap to cluster fragment a'' overlap in orientation **C** is at the expense of significantly increased M_a—Op_π antibonding (see Tables 6 and 7).

Table 6. Overlap populations corresponding to the interaction between W(4) and the Cl and OH ligands in orientation **C**[a]

	W(4)	
O *s*	0.288	$\sigma = 0.510$
pz	0.222	
px	0.262	$\pi = 0.344$
py	0.082	
Cl *s*	0.180	$\sigma = 0.588$
pz	0.408	
px	0.154	$\pi = 0.120$
py	−0.034	

[a] σ Interactions come from the valence *s* and *pz* orbitals of Cl and O, whereas π-interactions are derived from overlap with the *px* and *py* orbitals.

$W_4(O)(OR)_{10}$ (II)

The bonding in **II** is very similar to that previously described for **I**. We have examined the bonding in **II** by examining the hypothetical molecule $W_4(O)(OH)_{10}$ with the $W(OH)_2$ fragment both parallel and perpendicular to the virtual mirror plane of the molecule, as in **E** and **F** below.

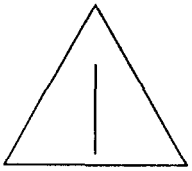

E

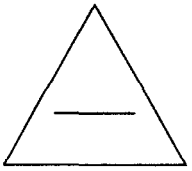

F

Minor differences arise in the bonding description of **I** and **II** because no significant stabilization of the $W(OH)_2$ fragment is achieved by mixing the $1a''$ and $2a''$ fragment orbitals. The substitution of an alkoxide for chloride makes the WX_2 cap a slightly poorer acceptor as seen by the reduced, compared with **I**, Mulliken atomic charges on each of the tungsten atoms. These are W(4) = −0.565, W(1) = W(2) = 1.375, and W(3) = 1.267 for **II** with the $W(OH)_2$ cap parallel to the molecular mirror plane. Nonetheless, to minimize antibonding with the stronger donor alkoxide ligands, the orbitals of the capping tungsten are polarized toward the rest of the cluster resulting in similar overlap populations to those seen in **I** (see Table 8). Rotation of the $W(OH)_2$ cap by 90° such that the fragment is perpendicular to the virtual mirror plane results in a slight decrease in the overlap population of the capping and basal fragments as seen in Table 9. The Walsh diagram, shown in Fig. 4, describes the destabilization of the metal-based molecular orbitals and reduction of the HOMO–

Table 5. Overlap populations corresponding to the interaction of the W(Cl)(OH) fragment with the $W_3(O)(OH)_8$ fragment. The WX_2 cap is rotated by 180°, configuration **C**

	W(OH)Cl					
$W_3(O)(OH)_8$	$1a'$	$1a''$	$2a'$	$2a''$	$3a'$	$4a'$
$1a'$	−0.001	0.000	0.302	0.000	−0.014	0.118
$2a'$	−0.003	0.000	0.029	0.000	0.202	0.155
$1a''$	0.000	0.357	0.000	−0.014	0.000	0.000
$3a'$	0.124	0.000	−0.011	0.000	0.193	0.254
$4a'$	0.224	0.000	0.035	0.000	0.161	−0.012
$2a''$	0.000	0.000	0.000	0.360	0.000	0.000
	0.344	0.357	0.355	0.346	0.542	0.515 = 2.459

Table 7. Overlap populations corresponding to the interaction between W(4) and the Cl and OH ligands in orientation **D**

	W(4)	
O *s*	0.293	$\sigma = 0.520$
pz	0.227	
px	0.262	$\pi = 0.328$
py	0.066	
Cl *s*	0.185	$\sigma = 0.597$
pz	0.412	
px	0.123	$\pi = 0.155$
py	0.032	

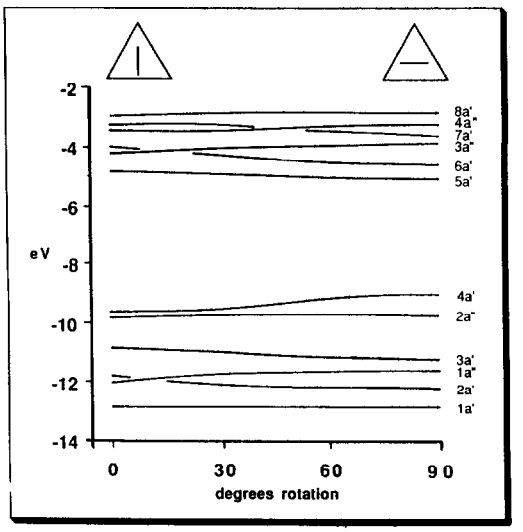

Fig. 4. Walsh diagram describing the destabilization of the metal based molecular orbitals of $W_4(O)(OH)_{10}$ upon rotation of the $W(OH)_2$ cap about the principal *z* axis.

LUMO gap upon rotation. This is consistent with the proposal that **I** and **II** adopt a similar ground-state structure, but exhibit a low barrier to rotation of the WX_2 cap in solution.

Comparisons with carbonyl clusters

As we have pursued the structure and bonding in early transition metal alkoxide clusters we have found many to have a complement among the later-transition metal carbonyl supported clusters. We have previously discussed the relationships between the d^3-$W(OR)_3$ and d^9-$Co(CO)_3$ fragments and their respective clusters of formula M_4X_{12} and $M_3X_9(\mu_3\text{-}Y)$ where M = Co and X = CO, M = W and X = OR and Y = CR or P.[11,12] We here describe aspects of the bonding in $W_4(O)(Cl)(OPr^i)_9$ which are reminiscent of the hypothetical cluster $[Os_3(CO)_9(\mu_3\text{-}PtL_2)]^{2-}$ discussed by Hoffmann,[24] where the hydrides of $Os_3Pt(H)_2(CO)_{10}(PR_3)$[25] are treated as protons. The frontier molecular orbitals of the $Os_3(CO)_9^{2-}$ fragment are essentially equivalent to those of the $Co_3(CO)_9$ fragment, but formally have one less electron. Thus the $Os_3(CO)_9^{2-}$ fragment is related to the $Co_3(CO)_9$ fragment in a similar fashion to the $W_3(O)(OR)_8$ and $W_3(OR)_9$ fragments. Furthermore, an internal isolobal analogy of ML_2 fragments described in Scheme 2 relates the $1b_1$ and $2a_1$ orbitals of the d^4-WX_2 fragment to the b_2 and $3a_1$ orbitals of the d^{10}-PtL_2 fragment. Because of the respective orientation of their "π-type" orbitals, the b_1 or b_2, one might predict orthogonal orientation of the WX_2 and PtL_2 caps above the tri-tungsten or tri-osmium cluster fragments in the ground state. In both cases, however, low barriers to rotation are expected due to orthogonal sets of orbitals, and to the a_1 orbitals

Table 8. Overlap populations corresponding to the interaction of the $W(OH)_2$ fragment with the $W_3(O)(OH)_8$ fragment. The WX_2 cap is oriented parallel to the virtual mirror plane of the molecule, **E**

	$W(OH)_2$					
$W_3(O)(OH)_8$	1*a'*	1*a"*	2*a"*	2*a'*	3*a'*	4*a'*
1*a'*	−0.027	0.000	0.000	0.240	0.001	0.182
2*a'*	0.013	0.000	0.000	0.029	0.295	0.091
1*a"*	0.000	0.144	0.195	0.000	0.000	0.000
3*a'*	0.215	0.000	0.000	0.002	0.047	0.331
4*a'*	0.150	0.000	0.000	0.045	0.253	−0.012
2*a"*	0.000	0.122	0.257	0.000	0.000	0.000
	0.351	0.266	0.452	0.316	0.596	0.592 = 2.573

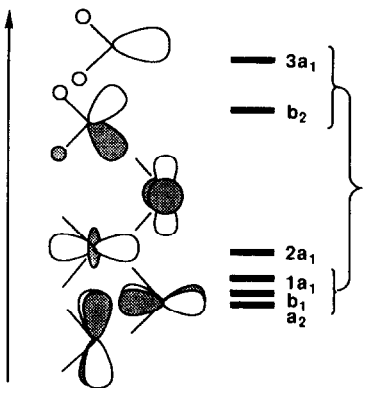

Scheme 2.

which are approximately invariant under rotation.

Though the WX_2 frontier orbitals are similar for d^4-WX_2 and d^{10}-PtL_2 they differ most notably in electron occupation, with the net result that the d^4-WX_2 fragment acts as an acceptor from M—M bonding orbitals of the basal $W_3(O)(OH)_8$ fragment. Such an interaction is not possible for a d^{10}-PtL_2 fragment. This then produces the obvious differences in the M—M distances within the alkoxide and carbonyl M_4 clusters under consideration.

Concluding remarks

The discovery of a new class of 12-electron W_4 alkoxide supported clusters $W_4(O)(OPr^i)_{10}$, $W_4(O)(Cl)(OPr^i)_9$ and $W_4(O)(Cl)_2(OPr^i)_8$ having the common structural feature of a d^4-WX_2 unit capping a $W_4(\mu\text{-}O)(\mu\text{-}OPr^i)_2(OPr^i)_6$ moiety, leads us once again to ponder whether or not the coupling of two $(W{\equiv}W)^{6+}$ units could yield a tetrahedral W_4^{12+} core. Given the several types of M_4^{12+} clusters supported by alkoxide ligands, the lack of the tetrahedral unit is quite striking. We now speculate why this is the case.

(1) Whenever coupling of two $(M{\equiv}M)^{6+}$ units occurs this is accompanied by ligand bridge formation—even when the $(M{\equiv}M)^{6+}$ units are retained as in $Mo_4F_4(OBu^t)_8$[2,3] and $Mo_4(OMe)_2(OPr^i)_{10}$.[6] Therefore, an unbridged $M_4(OR)_{12}$ molecule, an analogue of $Ir_4(CO)_{12}$, would seem unlikely based on considerations of optimizing metal–ligand bonding.

(2) We can think of building a pseudo-tetrahedral $M_4(OR)_{12}$ molecule by coupling a d^3-$M(OR)_3$ fragment with a nine-electron $M_3(\mu\text{-}OR)_3(OR)_6$ unit. This would be an analogue of the $M_3(\mu_3\text{-}X)(OR)_9$ compounds where X = CR′[26] or P.[27] From the present work, we see that this would not lead to a tetrahedral M_4 moiety because the MX_3 cap would act as an electron acceptor. However, the placing of the three alkoxides on the capping WX_3 unit would decrease the acceptor properties of the WX_3 unit relative to that seen for $W(Cl)(OPr^i)$.

(3) Finally, if we assume a tetrahedral M_4 moiety, we can ask the question—how may we dispose of 12 ligands so as to preserve this symmetry? The introduction of six edge-bridging ligands would leave six OR ligands for terminal and μ_3 sites—a situation that could not preserve tetrahedral symmetry. The only possible *pseudo*-tetrahedral geometry is based on a cubane-like structure having a central $M_4(\mu_3\text{-}OR)_4$ core. In a rigorous sense, a T_d-$M_4(OR)_{12}$ molecule could not be observed because the introduction of two terminal OR groups per metal atom would remove the C_3 element of symmetry. This not withstanding, there are known $M_4(\mu_3\text{-}L)_4L_8$ compounds and the bond-

Table 9. Overlap populations corresponding to the interaction of the $W(OH)_2$ fragment with the $W_3(O)(OH)_8$ fragment. The WX_2 cap is oriented perpendicular to the virtual mirror plane, F[a]

	$W(OH)_2$					
$W_3(O)(OH)_8$	1a′	1a″	2a′	3a′	2a″	4a′
1a′	−0.028	0.000	0.001	0.225	0.000	0.200
2a′	0.124	0.000	0.250	0.040	0.000	−0.007
1a″	0.000	0.138	0.000	0.000	0.234	0.000
3a′	0.196	0.000	0.024	0.005	0.000	0.355
4a′	0.038	0.000	0.193	0.051	0.000	0.071
2a″	0.000	0.125	0.000	0.000	0.334	0.000
	0.300	0.263	0.468	0.321	0.568	0.619 = 2.569

[a] This requires two orbitals of the MX_2 cap to change symmetry.

ing in these has been the subject of a recent theoretical analysis by Harris.[28] The local $X_2M(\mu_3\text{-}X)_3$ geometry may approximate either a trigonal bipyramid or a square-based pyramid. In both cases 12 electrons can be accommodated in M—M bonding molecular orbitals. Though we cannot discount the possibility that this type of structure may be eventually found it seems that this would be unlikely because the terminal OR groups would exert a *radial cluster influence*[29] thereby weakening the M—M bonding in the central M_4^{12+} core.

The alternative to a symmetrical disposition of ligands is one in which in one part of the molecule metal–ligand bonding is maximized and in another part metal–metal bonding is maximized. This is clearly seen in the structures of $M_4(OR)_{12}$ compounds (M = Mo, W; R = CH_2Pr^i, CH_2Hex^c, CH_2Pen^c, CH_2Bu^c) where one metal atom is coordinated to six OR groups and the other three metal atoms are coordinated to only four. Similarly in the present compounds a WX_2 group caps a W_4 $(\mu\text{-}O)(\mu\text{-}OPr^i)_2(OPr^i)_8$ unit. This disparity in coordination number leads to inequivalent oxidation states amongst the metal atoms within the cluster. It is interesting to note that the binary oxides M_2O_3 are not known for M = Mo and W. They are unstable with respect to MO_2 and the bulk metal, M. We propose that a symmetrical $M_4(OR)_{12}$ molecule (M = Mo, W) is similarly unstable with respect to a cluster of lower symmetry that favours local maximization of metal–ligand and metal–metal bonding.

EXPERIMENTAL

General

All reactions were carried out under an atmosphere of dry, oxygen-free nitrogen using standard Schlenk and glovebox techniques. Starting materials, $W_2(OBu^t)_6$[30] and $W_2(OPr^i)_6$,[8] were prepared by literature methods. All solvents were distilled from sodium benzophenone ketyl and stored over 4 Å molecular sieves. Isopropanol was dried over molecular sieves, but not distilled prior to use.

NMR spectra were recorded on Varian XL-300 and Bruker AM-500 spectrometers. IR spectra were recorded on a Perkin–Elmer 283 spectrometer. Elemental analyses were performed by Oneida Research Services Inc., Whitesboro, New York.

$W_4(O)(OPr^i)_{10}$

To a red solution of $W_2(OBu^t)_6$ (272 mg, 0.338 mmol) in hexane (10 cm^3), $HOPr^i$ (1 cm^3) was added while stirring to give a yellow solution. To this was added 1 equivalent of H_2O in $HOPr^i$ dropwise via a syringe and the solution darkened in colour with each drop. The solution was stirred for 4 h. The volatile components were removed and the sample was crystallized out of Et_2O (110 mg) to give $W_4(O)(OPr^i)_{10}(1/2Et_2O)$ in a moderate yield of 23.7%. The alkoxides are arbitrarily labelled a, b, c, etc. as a subscript in front of the three-bond coupling constant.

^1H NMR (500 MHz, 25°C, toluene-d_8): δ methines (2H, p) 5.58 ($^3_aJ_{HH}$ = 6.1 Hz), 5.37 ($^3_bJ_{HH}$ = 6.1 Hz), 5.25 ($^3_cJ_{HH}$ = 6.1 Hz), 4.69 ($^3_dJ_{HH}$ = 6.0 Hz), 4.42 ($^3_eJ_{HH}$ = 6.3 Hz); methyls (d); 1.57 (6H, $^3_bJ_{HH}$ = 6.1 Hz), 1.54 (6H, $^3_aJ_{HH}$ = 6.1 Hz), 1.54 (6H, $^3_bJ_{HH}$ = 6.1 Hz), 1.52 (6H, $^3_cJ_{HH}$ = 6.1 Hz), 1.49 (6H, $^3_cJ_{HH}$ = 6.1 Hz), 1.49 (6H, $^3_aJ_{HH}$ = 6.1 Hz), 1.39 (12H, $^3_dJ_{HH}$ = 6.0 Hz), 1.38 (6H, $^3_eJ_{HH}$ = 6.3 Hz), 1.26 (6H, $^3_eJ_{HH}$ = 6.2 Hz).

^{13}C NMR (125 MHz, 25°C, toluene-d_8): δ methines (1C, s), 83.0, 78.6, 77.8, 75.4, 71.5, methyls (s); 28.3 (1C), 28.2 (2C = 2), 27.8 (1C), 27.7 (1C), 27.4 (1C), 27.2 (1C), 26.8 (1C), 26.6 (1C), 26.5 (1C).

IR (Nujol mull, burnt orange, cm^{-1}): 1320 m, 1260 w, 1160 sh/m, 1118 s, 994 s, 943 sh/m, 841 m, 795 w, 667 w(ν_{W-O-W}), 595 m, 575 m, 456 w, 298 w.

Elemental analysis: Found: C, 26.43; H, 5.34. Calc. for $W_8C_{64}H_{50}O_{23}$ ($W_4(OPr^i)_{10}(O)\cdot 1/2Et_2O$): C, 27.86; H, 5.48%.

$W_4(^{18}O)(OPr^i)_{10}$

The same procedure was followed for synthesizing $W_4(^{18}O)(OPr^i)_{10}$ only $H_2{}^{18}O$ was used. The IR spectrum shows the W—^{18}O—W stretch at 635 cm^{-1}.

$W_4(O)(Cl)(OPr^i)_9$

Hexanes (15 cm^3) and isopropanol (12 cm^3) with presumably adventitious water were added at 23°C to 1.044 g (1.295 mmol) of $W_2(OBu^t)_6$ and 104 mg (1.267 mmol) of $Na(OPr^i)$. The solution was stirred for 12 h and the volatile components were removed *in vacuo*. To the solid residue was added 104 mg of $H_2NMe_2{}^+Cl^-$ as well as 25 cm^3 of hexanes and 5 cm^3 of isopropanol. The volatile components were removed *in vacuo*. The residue was dissolved in hexanes and filtered. From the hexane solution $H_2W_4(OPr^i)_{14}$ was isolated. The volatiles from the filtrate were removed *in vacuo* and Et_2O was added to try to crystallize more $H_2W_4(OPr^i)_{14}$. The previously unknown compound $W_4(O)(Cl)(OPr^i)_9\cdot 1/2Et_2O$ (mol. wt = 2722.41) crystallized, 20 mg isolated (0.58% yield).

^1H NMR (500 MHz, 25°C, C_6D_6): δ methines

(p); 5.67 (2H, ${}_{a}^{3}J_{HH}$ = 6.1 Hz), 5.56 (2H, ${}_{b}^{3}J_{HH}$ = 6.1 Hz), 5.36 (2H, ${}_{c}^{3}J_{HH}$ = 6.1 Hz), 4.74 (2H, ${}_{d}^{3}J_{HH}$ = 6.2 Hz), 4.47 (2H, ${}_{e}^{3}J_{HH}$ = 6.1 Hz); methyls (12H, d); 1.59 (${}_{a}^{3}J_{HH}$ = 6.1 Hz), 1.56 (${}_{a}^{3}J_{HH}$ = 6.1 Hz), 1.54 (${}_{b}^{3}J_{HH}$ = 6.2 Hz), 1.50 (${}_{b}^{3}J_{HH}$ = 6.1 Hz), 1.52 (${}_{c}^{3}J_{HH}$ = 6.1 Hz), 1.46 (${}_{c}^{3}J_{HH}$ = 6.1 Hz), 1.42 (${}_{d}^{3}J_{HH}$ = 6.1 Hz), 1.30 (${}_{e}^{3}J_{HH}$ = 6.2 Hz), 1.24 (${}_{e}^{3}J_{HH}$ = 6.3 Hz).

^{13}C NMR (125 MHz, 25°C, C_6D_6): δ methines (s); 82.38 (2C), 80.62 (2C), 78.77 (2C), 76.33 (2C), 70.81 (1C); methyls (s); 27.91 (2C), 27.42 (2C), 27.36 (2C), 27.14 (4C), 26.83 (2C), 26.67 (2C), 26.43 (2C), 26.38 (2C).

IR (Nujol mull, orange, cm^{-1}): 1365 s, 1328 s, 1261 w, 1167 w, 1112 vs, 990 vs, 940 s, 855 s, 675 m(ν_{W-O-W}), 602 s, 587 sh, 515 w(ν_{W-Cl}), 503 w(ν_{W-Cl}), 452 m, 303 m.

Elemental analysis: Found: C, 25.55; H, 4.98. Calc. for $W_8C_{58}H_{136}Cl_2O_{21}$: C, 25.64; H, 5.06%.

$W_4(O)(Cl)_2(OPr^i)_8$

Toluene-d_8 (0.4 cm^3) at 25°C in a dry box was added to $W_4(O)(OPr^i)_{10}$ (34 mg, 0.0253 mmol) and $H_2NMe_2^+Cl^-$ (6 mg, 0.0735 mmol). The reaction solution was stirred for 18 h and then transferred to an NMR tube. The main product was identified by ^{1}H and ^{13}C NMR as $W_4(O)(Cl)_2(OPr^i)_8$.

^{1}H NMR (500 MHz, 25°C, toluene-d_8): δ methines (2H, p); 5.58, 5.53, 5.32, 4.45; methyls (d); 1.57 (6H), 1.52 (6H), 1.51 (12H), 1.48 (6H), 1.47 (6H), 1.33 (H), 1.27 (6H).

^{13}C NMR (125 MHz, 25°C, toluene-d_8): δ methines (s), 82.48, 80.29, 78.55, 76.20; methyls (s), 27.97, 27.48, 27.44, 27.23, 26.97, 26.78, 26.51, 26.48.

Computational procedures

The coordinates for the model compounds $W_4(O)(Cl)(OH)_9$ (I) and $W_4(O)(OH)_{10}$ (II) were taken from the X-ray crystal structure of $W_4(O)(Cl)(OPr^i)_9 \cdot 1/2Et_2O$ and idealized C_s symmetry. An O—H bond distance of 0.96 Å was used. All rotations of the WX_2 cap were about the axis perpendicular to the W(1)—W(2)—W(3) plane and passing through W(4). Rotations of 0–180° were examined for **I** and 0–90° for **II**.

Molecular orbital calculations were performed using the Extended Huckel method and the method of Fenske and Hall. Fragment molecular orbital calculations were performed using the Fenske–Hall method[23] on the fragments $W_3(O)(OH)_8$, W(Cl)(OH) and $W(OH)_2$. Atomic wave functions for the Fenske–Hall calculations were generated by a best fit to Herman–Skillman atomic calculations using the method of Bursten, Jensen and Fenske.[31] Contracted double-ζ representations were used for the tungsten 5*d* atomic orbitals, as well as the chlorine 3*p* and oxygen 2*p* atomic orbitals. Basis functions for the metal atoms were generated for a +1 oxidation state with valence tungsten 6*s* and tungsten 6*p* exponents fixed at 1.80. An exponent of 1.16 was used for the hydrogen 1*s* atomic orbital since it minimized the energy of methane.

Crystallographic studies

General operating procedures have been previously reported.[32]

$W_4(O)(Cl)(OPr^i)_9$. A small, almost equidimensional, piece was cleaved from a larger mass of crystals. The crystal was cooled to −146°C for characterization and data collection. An automated search of a limited hemisphere of reciprocal space yielded a set of reflections which exhibited monoclinic symmetry (2/*m*). The systematic extinction of *hkl* for $h-k = 2n+1$, and of *h0l* for $l = 2n+1$ lead to the possible space groups: *Cc* or *C*2/*c*. The choice of the centrosymmetric space group *C*2/*c* was confirmed by the successful solution and refinement of the structure. Data collection was undertaken as noted in Table 1. A total of 6513 reflections was collected within the given range. This number includes the standard reflections as well as the space group extinctions that were not due to the carbon-centring. Following the usual data reduction and averaging of redundant data, a unique set of 5594 reflections was obtained. 4851 reflections were considered observed by the criterion $F > 3.0\sigma(F)$. A plot of the standard reflections showed no systematic trends. No absorption correction was carried out as the crystal was lost before it could be measured.

The structure was solved after some difficulty using direct methods and Fourier techniques. Some of the difficulty was attributed to the larger than expected number of heavy atoms, as well as the large *a*-axis dimension. When the four tungsten atoms were located in an *E*-map, the remainder of the non-hyrogen atoms were located in a difference Fourier phased with the tungsten atoms. The asymmetric unit contains one W_4 complex and one half molecule of ether solvent located at a two-fold axis. All hydrogen atoms, except for those on the solvent, were introduced in fixed calculated positions. The full-matrix least-squares refinement was completed using anisotropic thermal parameters on the solvent atoms [O(43) through C(45)] and fixed hydrogen atoms. The final *R* was 0.051, *Rw*(*F*) was 0.050. The number of parameters varied was 390, including the scale factor and the isotropic extinction parameter.

The final difference map was essentially feature-

less; there were a few peaks of about 2 e/Å^3 in the close proximity of the tungsten atoms.

Acknowledgements—We would like to thank the National Science Foundation for support and Dr Odile Eisenstein for helpful and enjoyable discussions.

REFERENCES

1. M. H. Chisholm, F. A. Cotton, C. A. Murillo and W. W. Reichert, *Inorg. Chem.* 1977, **16**, 1801.
2. M. H. Chisholm, R. J. Errington, K. Folting and J. C. Huffman, *J. Am. Chem. Soc.* 1982, **104**, 2025.
3. M. H. Chisholm, D. L. Clark, R. J. Errington, K. Folting and J. C. Huffman, *Inorg. Chem.* 1988, **27**, 2071.
4. M. H. Chisholm, J. C. Huffman and R. L. Kelly, *J. Am. Chem. Soc.* 1979, **101**, 7615.
5. M. H. Chisholm, D. L. Clark and J. C. Huffman, *Polyhedron* 1985, **4**, 1205.
6. M. H. Chisholm, C. E. Hammond, M. J. Hampden-Smith, J. C. Huffman and W. G. Van Der Sluys, *Angew. Chem. Intl. Edn Engl.* 1987, **26**, 904 [*Angew. Chem.* 1987, **99**, 937].
7. M. H. Chisholm, D. L. Clark, K. Folting, J. C. Huffman and M. J. Hampden-Smith, *J. Am. Chem. Soc.* 1987, **109**, 7750.
8. M. H. Chisholm, D. L. Clark and M. J. Hampden-Smith, *J. Am. Chem. Soc.* 1989, **111**, 574.
9. M. H. Chisholm, K. Folting, C. E. Hammond, M. J. Hampden-Smith and K. G. Moodley, *J. Am. Chem. Soc.* 1989, **111**, 5300.
10. W. E. Buhro and M. H. Chisholm, *Adv. Organomet. Chem.* 1987, **27**, 311.
11. M. H. Chisholm, D. L. Clark, M. J. Hampden-Smith and D. M. Hoffman, *Angew. Chem. Intl. Edn Engl.* 1989, **28**, 432 [*Angew. Chem.* 1989, **101**, 446].
12. M. H. Chisholm, B. K. Conroy and J. D. Martin, manuscript in preparation.
13. F. H. Carre, F. A. Cotton and B. A. Fenz, *Inorg. Chem.* 1976, **15**, 380.
14. C. H. Wei, *Inorg. Chem.* 1969, **8**, 2384.
15. M. R. Churchill and J. P. Hutchinson, *Inorg. Chem.* 1978, **17**, 3528.
16. M. H. Chisholm, K. Folting, C. E. Hammond, J. C. Huffman and J. D. Martin, *Angew. Chem. Intl. Edn Engl.* 1989, **28**, 1368 [*Angew. Chem.* 1989, **101**, 1399].
17. M. H. Chisholm, J. C. Huffman and C. A. Smith, *J. Am. Chem. Soc.* 1986, **108**, 222.
18. S. Pinchas and I. Laulicht, *Infrared Spectrum of Labelled Compounds*, p. 26. Academic Press, London, New York (1971).
19. G. J. J. Chen, J. W. McDonald, D. C. Bravard and W. E. Newton, *Inorg. Chem.* 1985, **24**, 2327.
20. R. E. McCarley, *Polyhedron* 1986, **5**, 51 and refs therein.
21. R. Hoffmann, *Angew. Chem. Intl. Edn Engl.* 1982, **21**, 711.
22. T. A. Albright, J. K. Burdett and M. H. Whangbo, in *Orbital Interactions in Chemistry*. John Wiley, New York (1985).
23. M. B. Hall and R. F. Fenske, *Inorg. Chem.* 1972, **11**, 768.
24. B. E. R. Schilling and R. Hoffmann, *J. Am. Chem. Soc.* 1979, **101**, 3456.
25. L. J. Farragia, J. A. K. Howard, P. Mitrprachachon, J. L. Spenser, F. G. A. Stone and P. Woodward, *J. Chem. Soc., Chem. Commun.* 1978, 260.
26. M. H. Chisholm, K. Folting, J. A. Heppert, D. M. Hoffman and J. C. Huffman, *J. Am. Chem. Soc.* 1985, **107**, 1234.
27. M. H. Chisholm, K. Folting and J. W. Pasterczyk, *Inorg. Chem.* 1988, **27**, 3057.
28. S. Harris, *Polyhedron* 1989, **8**, 2843.
29. B. Bursten, M. H. Chisholm and D. L. Clark, *Inorg. Chem.* 1988, **27**, 2084.
30. M. Akiyama, M. H. Chisholm, F. A. Cotton, M. W. Extine, D. A. Haitko, D. Little and P. E. Fanwick, *Inorg. Chem.* 1979, **18**, 2266.
31. B. E. Bursten, J. R. Jensen and R. F. Fenske, *J. Chem. Phys.* 1978, **68**, 3320.
32. M. H. Chisholm, K. Folting, J. C. Huffman and C. C. Kirkpatrick, *Inorg. Chem.* 1984, **23**, 1021.

Polyhedron Vol. 9, No. 15/16, pp. 1843–1848, 1990
Printed in Great Britain

0277–5387/90 $3.00+.00
© 1990 Pergamon Press plc

URANIUM ALKOXIDE CHEMISTRY—V.* SYNTHESIS, CHARACTERIZATION AND INTERCONVERSION OF URANIUM(IV) TERT-BUTOXIDE COMPLEXES†

WILLIAM G. VAN DER SLUYS and ALFRED P. SATTELBERGER‡

Inorganic and Structural Chemistry Group (INC-4), Isotope and Nuclear Chemistry Division, Los Alamos National Laboratory, Los Alamos, NM 87545, U.S.A.

and

MICHAEL W. McELFRESH

IBM T. J. Watson Research Center, P.O. Box 218, Yorktown Heights, NY 10598, U.S.A.

Abstract—The reaction of $[(Me_3Si)_2N]_2\overline{UN(SiMe_3)SiMe_2CH_2}$ with $\geqslant 4.5$ equivalents of t-butanol in toluene provides a green crystalline solid formulated as $U_2(OBu^t)_8(HOBu^t)$ on the basis of elemental analysis, ^1H NMR, IR and UV–vis spectroscopy. $U_2(OBu^t)_8(HOBu^t)$ reacts with $KOBu^t$ (or KH) to give the potassium salt $KU_2(OBu^t)_9$, with dry dioxygen to give $U_2(OBu^t)_9$, and with H_2O to give $U_3O(OBu^t)_{10}$. Temperature-dependent magnetic susceptibility measurements (2–250 K) on solid $U_3O(OBu^t)_{10}$ show Curie–Weiss behaviour from 90 to 250 K. Below 90 K the susceptibility becomes temperature independent with no evidence of magnetic ordering.

Early in the development of uranium(IV) chemistry, Gilman and co-workers reported the preparation of uranium(IV) alkoxides, $U(OR)_4$. These were obtained by alcoholysis of $[U(NEt_2)_4]_2$, or via the reaction of UCl_4 with LiOR in alcohol solution (R = Me, Et).[2] In the case of $U(OBu^t)_4$, a third procedure was advocated. Uranium tetrachloride and four equivalents of potassium amide were allowed to react in liquid ammonia, and the product, formulated as $U(NH_2)_4$ (not isolated), was treated with excess t-butanol [eq. (1)]:

$$UCl_4 + 4KNH_2 \xrightarrow{NH_3} \text{“}U(NH_2)_4\text{”} \xrightarrow{\text{excess } Bu^tOH} U(OBu^t)_4. \quad (1)$$

After removal of NH_3, a green solid was extracted into hexane and isolated by evaporation of the solvent. The identity of the final product as $U(OBu^t)_4$ was established solely on the basis of a uranium analysis. Six years later, Bradley *et al.* reported that they were unable to reproduce the synthesis of $U(OBu^t)_4$. Following Gilman's procedure, they isolated a grey–brown crystalline uranium(V) product, which was formulated as $UO(OBu^t)_3(Bu^tOH)$ on the basis of a uranium analysis and a valency determination.[3]

In 1979, Perego and co-workers claimed that they were able to prepare Gilman's $U(OBu^t)_4$ by a different route. They isolated a green solid by treatment of tetra(π-allyl)uranium(IV), $U(C_3H_5)_4$, with excess t-butanol in diethyl ether.[4] Characterization of the product as $U(OBu^t)_4$ was based on acceptable uranium analyses. Characteristic IR bands were also reported for $U(OBu^t)_4$, but no ^1H NMR data were presented. In view of subsequent work, however, it would appear that Perego's $U(OBu^t)_4$ is distinct from the compound reported by Gilman.

In 1984, Cotton and co-workers once again repeated Gilman's original procedure [eq. (1)] and, unlike Bradley *et al.*, they were able to isolate a green, hexane-soluble product. The latter was shown to be $KU_2(OBu^t)_9$ by X-ray crystallography.[5] The Cotton group indicated that rigorous exclusion of oxygen and water, and the maintenance of low temperatures ($\leqslant -10°C$) during work-up, were required to obtain this product pure and in reasonable yield. They also reported that, in

* For part IV, see ref. 1.

† This paper is dedicated to Professor Dick Fenske, friend and teacher, on the occasion of his retirement from the University of Wisconsin.

‡ Author to whom correspondence should be addressed.

solution, $KU_2(OBu^t)_9$ was slowly and spontaneously transformed into the mixed-valent diuranium(IV,V) compound $U_2(OBu^t)_9$. The same authors also found that another green uranium(IV) complex, viz. trinuclear $U_3O(OBu^t)_{10}$, could, in at least one instance, be isolated from the same reaction mixture.[6a] In a subsequent paper on $U_3O(OBu^t)_{10}$,[6b] the authors mentioned that their procedure for isolating the trimer differed from later preparations of $KU_2(OBu^t)_9$ in that the green hexane extract was kept at room temperature for an extended period of time.

Dormond *et al.*[7] have found that alcoholysis of the mononuclear uranium(IV) metallocycle complex, $[(Me_3Si)_2N]_2U\overline{N(SiMe_3)SiMe_2CH_2}$,[8] with either HO-2,6-$Me_2C_6H_3$ or Bu^tOH proceeds via initial rapid protonation of the U—C bond to form $[(Me_3Si)_2N]_3UOR$ complexes. It was also noted that, in the presence of an excess of either alcohol, substitution of amide ligands occurred. These multiply substituted products were not characterized further. We have recently shown that Dormond's procedure can be used to prepare $U(O\text{-}2,6\text{-}Bu^t_2C_6H_3)_4$, which is the first structurally characterized example of a monomeric $U(OAr)_4$ complex.[1] In this report, we describe the product obtained from the reaction of excess t-butanol with $[(Me_3Si)_2N]_2U\overline{N(SiMe_3)SiMe_2CH_2}$, some of its reaction chemistry, and its relationship to the compounds reported by Perego[4] and Cotton.[5,6]

RESULTS AND DISCUSSION

Synthesis and characterization

Reaction of $[(Me_3Si)_2N]_2U\overline{N(SiMe_3)SiMe_2CH_2}$ with $\geqslant 4.5$ equivalents of Bu^tOH in toluene [eq. (2)], results in complete substitution of amides for alkoxides, but the resulting complex does not have the empirical formula of $U(OBu^t)_4$. We formulate the green, hydrocarbon-soluble product as $U_2(OBu^t)_8(HOBu^t)$ on the basis of elemental analyses, ^1H NMR, IR and UV–vis spectroscopies, and chemical studies. The same compound can be prepared in an analogous fashion from $[U(NEt_2)_4]_2$ [eq. (3)]:[2,9]

$$[(Me_3Si)_2N]_2U\overline{N(SiMe_3)SiMe_2CH_2} + \geqslant 4.5Bu^tOH \xrightarrow[25°C]{\text{toluene}} 0.5\,U_2(OBu^t)_8(HOBu^t) + 3(Me_3Si)_2NH \quad (2)$$

$$[U(NEt_2)_4]_2 + \geqslant 9.0Bu^tOH \xrightarrow[25°C]{\text{toluene}} U_2(OBu^t)_8(HOBu^t) + 8Et_2NH. \quad (3)$$

The room temperature ^1H NMR spectrum of $U_2(OBu^t)_8(HOBu^t)$ in benzene-d_6 shows only one broad Bu^t signal (δ 1.5) and a broad signal at δ 13.0, which we assign as the OH proton. The intensity ratio of these two signals is *ca* 80 : 1. We were unable to "freeze out" a static structure in toluene-d_8 in the temperature range +25 to −90°C. A ν(O—H) stretch in the IR spectrum of $U_2(OBu^t)_8(HOBu^t)$ was not readily apparent. We tentatively assign it as the very weak band located at 3537 cm^{-1}. Other IR features are similar, but not identical, to those reported by Perego and co-workers[4] for their sample of $U(OBu^t)_4$.

$U_2(OBu^t)_8(HOBu^t)$ is stable in toluene at room temperature. It reacts readily with potassium t-butoxide or potassium hydride in toluene or hexane to generate $KU_2(OBu^t)_9$ [eqs (4)–(5)]:

$$U_2(OBu^t)_8(HOBu^t) + KOBu^t \xrightarrow{\text{toluene}} KU_2(OBu^t)_9 + HOBu^t \quad (4)$$

$$U_2(OBu^t)_8(HOBu^t) + KH \xrightarrow{\text{hexane}} KU_2(OBu^t)_9 + 0.5H_2. \quad (5)$$

Upon exposure to dry air, green solutions of $U_2(OBu^t)_8(HOBu^t)$ rapidly turn orange–red. The UV–vis spectrum of the latter is essentially identical to that reported by Cotton and co-workers for a sample of the crystallographically characterized mixed-valent compound $U_2(OBu^t)_9$ (Fig. 1).[5] These results, coupled with the fact that the UV–vis spectra of $U_2(OBu^t)_8(HOBu^t)$ and $KU_2(OBu^t)_9$ are very

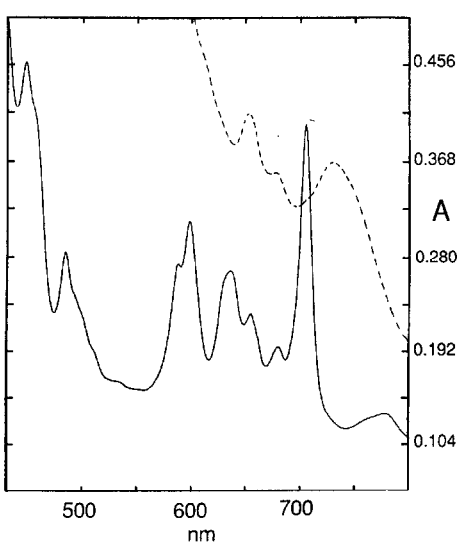

Fig. 1. Electronic absorption spectra of a 5.5×10^{-3} M hexane solution of $U_2(OBu^t)_8(HOBu^t)$ before (——) and after (– – –) exposure to dry air.

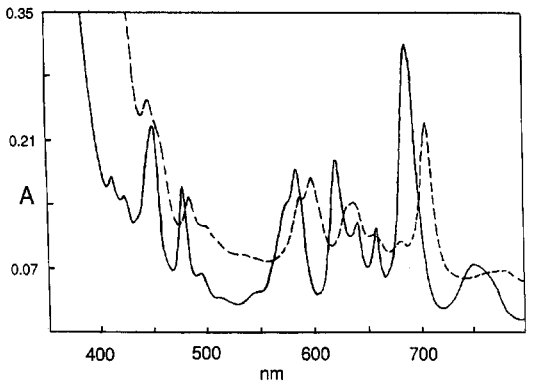

Fig. 2. Electronic absorption spectra of $U_2(OBu^t)_8(HOBu^t)$ (---) and $KU_2(OBu^t)_9$ (——), 3.1×10^{-3} M hexane solutions.

similar (Fig. 2), suggests that the compounds have similar structures. *Chem3D* representations of $KU_2(OBu^t)_9$ and the proposed structure of $U_2(OBu^t)_8(HOBu^t)$ are shown in Fig. 3.

We have also found that when toluene solutions of $U_2(OBu^t)_8(HOBu^t)$ are treated with oxygen-free H_2O, another green compound is reproducibly isolated in good yield [eq. (6)]:

$$3U_2(OBu^t)_8(HOBu^t)+2H_2O \xrightarrow{\text{toluene}} 2U_3O(OBu^t)_{10}+7HOBu^t. \quad (6)$$

The identity of the latter as $U_3O(OBu^t)_{10}$ was confirmed by comparison of the unit cell dimensions of a single crystal with those reported in the literature.[6] The ^1H NMR spectrum of $U_3O(OBu^t)_{10}$, which has not been reported previously is shown in Fig. 4. The 3:3:3:1 pattern is consistent with the solid state C_{3v} structure.[6] A *Chem3D* representation of $U_3O(OBu^t)_{10}$ is also shown in Fig. 3.

The $KU_2(OBu^t)_9$ used to record the spectrum shown in Fig. 2 was prepared in good yield directly from UCl_4 by the addition of 4.5 equiv. of $KOBu^t$ in THF [eq. (7)]. This method is more convenient than the original liquid ammonia synthesis. $KU_2(OBu^t)_9$ is thermally stable at room temperature under *rigorously* dry and anaerobic conditions.

$$UCl_4+4.5\text{eq. }KOBu^t \xrightarrow{\text{toluene}} 0.5\,KU_2(OBu^t)_9+4KCl. \quad (7)$$

When exposed to dry air, solutions of $KU_2(OBu^t)_9$ turn orange–red much more slowly (days) than do solutions of $U_2(OBu^t)_8(HOBu^t)$. This is consistent

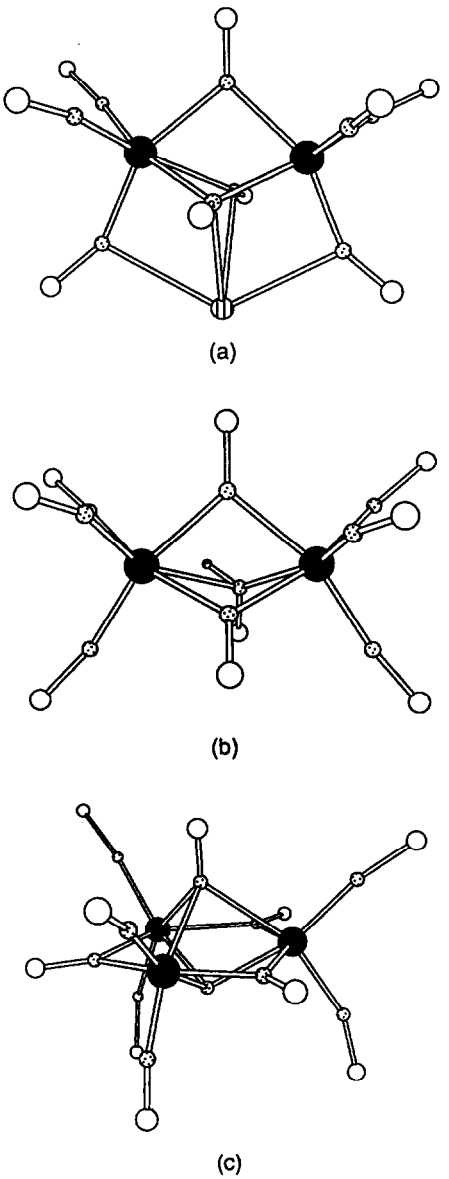

Fig. 3. *Chem3D*[18] representations of (a) $KU_2(OBu^t)_9$,[5] (b) $U_2(OBu^t)_8(HOBu^t)$ (proposed) and (c) $U_3O(OBu^t)_{10}$.[6] Uranium, oxygen, carbon and potassium atoms are indicated with black, speckled, open and hashed circles, respectively; the t-butyl methyl groups have been omitted from the drawings for clarity.

with Gilman's observations on the air-sensitivity of "$U(OBu^t)_4$".[2] $KU_2(OBu^t)_9$, like $U_2(OBu^t)_8(HOBu^t)$, also reacts with H_2O to produce $U_3O(OBu^t)_{10}$.* Thus, the reaction properties of both $KU_2(OBu^t)_9$ and $U_2(OBu^t)_8(HOBu^t)$ are complementary. A summary of all of this chemistry is given in Scheme 1.

Magnetic properties of $U_3O(OBu^t)_{10}$

As noted by Cotton,[6b] $U_3O(OBu^t)_{10}$ is structurally similar, in a qualitative sense, to the

* The presence or absence of small amounts of adventitious water in the synthesis of $KU_2(OBu^t)_9$ might account for the irreproducibility of the trimer synthesis.[6b]

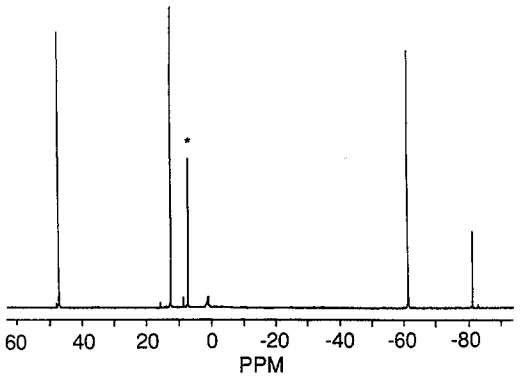

Fig. 4. ^{1}H NMR spectrum of $U_3O(OBu^t)_{10}$ in benzene-d_6 (*) at 22°C and 250 MHz.

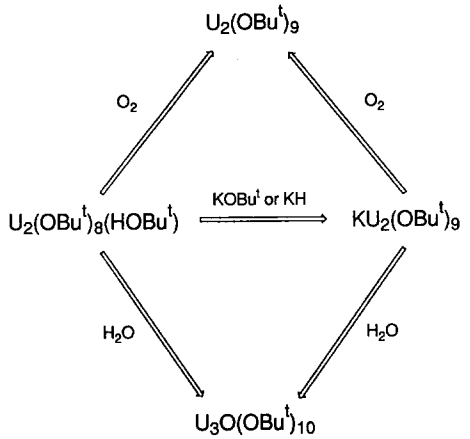

Scheme 1.

$M_3O(OR)_{10}$ cluster compounds (M = Mo or W; R = Pr^i) reported by Chisholm *et al.*[10] However, while the molybdenum(IV) and tungsten(IV) compounds contain M—M single bonds (d_{M-M} *ca* 2.5 Å), the U—U distance reported for the uranium trimer (3.573(1) Å) indicates that no U—U bonds are formed.[6] Uranium(IV), like molybdenum(IV) and tungsten(IV), has two electrons available for M—M bonding, but evidently the 5*f*–5*f* overlap is insufficient to stabilize U—U bonds.

The absence of metal–metal bonding in $U_3O(OBu^t)_{10}$ requires that the complex be paramagnetic. One indication of the latter is the isotropically shifted ^{1}H NMR spectrum shown in Fig.

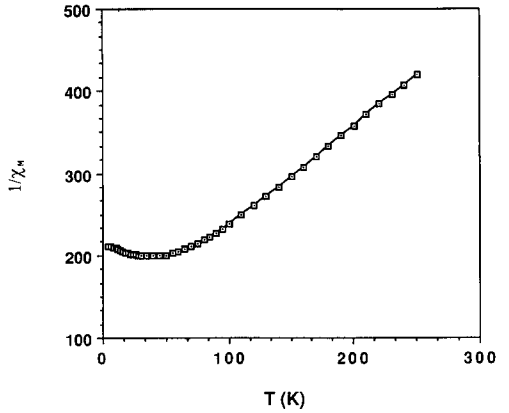

Fig. 5. Inverse susceptibility of $U_3O(OBu^t)_{10}$ vs temperature. The linear portion from 90 to 250 K was used to obtain the parameters given in the text.

4. The inverse of the molar magnetic susceptibility of $U_3O(OBu^t)_{10}$ in the temperature range 2–250 K is shown in Fig. 5. Above 90 K, the susceptibility follows the Curie–Weiss law

$$\chi_M = C/(T-\theta),$$

with $C = 0.78$, μ_{eff} (per uranium atom) $= 2.5\,\mu_B$ and $\theta = -88$ K.*

Below 90 K, the susceptibility deviates markedly from Curie–Weiss behaviour. One possibility to consider is magnetic ordering (i.e. antiferromagnetic coupling) in the trinuclear complex. Magnetic exchange phenomena have been claimed previously for two amide adducts of UCl_4, viz. $UCl_4 \cdot 3DMBA$ and $UCl_4 \cdot 3MAA$ (DMBA = N, N′-dimethylbenzamide; MAA = N-methylacetanalide).[12] The X-ray structures of these adducts are not known, but the authors assumed they were dimers and interpreted their susceptibility data, at least that portion from *ca* 70 to 280 K, in terms of a Heisenberg spin–spin interaction ($-2J\mathbf{s}_1 \cdot \mathbf{s}_2$) between the uranium centres. Assuming a Heisenberg coupling model, the Van Vleck equation for three interacting $S = 1$ ions arranged in an equilateral triangle is[13,14]

$$\chi_M = Ng^2\mu_B^2/kT \cdot [28e^{12J/kT} + 20e^{6J/kT} + 6e^{2J/kT}] \cdot [7e^{12J/kT} + 10e^{6J/kT} + 9e^{2J/kT} + 1]^{-1},$$

where J is the exchange energy and the other symbols have their usual meaning. Attempts to fit the molar susceptibility data to this equation, with J as the only variable, were unsatisfactory.†

The failure of the Heisenberg model prompts another explanation for the magnetic behaviour below 90 K. As noted above, uranium(IV) has a [Rn]$5f^2$ electron configuration. The ground *L*–*S* state of uranium(IV) is $^3H_4$. In an octahedral crystal-field, the $J = 4$ term splits into one singlet state,

* The values of C and μ_{eff} are comparable to those found for $[U(NEt_2)_4]_2$ and $[U(CH_3NCH_2CH_2NCH_3]_3$.[9,11]

† The susceptibility equation requires that χ_M decrease rapidly toward zero as $T \rightarrow 0$ K, which is clearly not the case with our data. We note that the expression for χ_M was derived assuming $g_x = g_y = g_z$, which need not be the case in the uranium(IV) cluster.

one doublet state and two triplet states.[15] In the trimer, the local symmetry about each uranium(IV) centre is only C_s. Lowering the symmetry to this level lifts all of the octahedral degeneracies. We propose that the empirical magnetic susceptibility is the sum of the susceptibilities of the three isolated uranium(IV) ions. The inverse susceptibility is nearly temperature independent in the region below 90 K and the measured results are consistent with a singlet ground state with a second singlet state (or states) located approximately 60 cm^{-1} above the former.*

SUMMARY

The history of "$U(OBu^t)_4$" dates back over 30 years. Early reports on the synthesis of this compound failed to provide conclusive proof for its existence.[2–4] In our opinion, Cotton and co-workers have established beyond reasonable doubt that the compound originally prepared in Gilman's laboratory was actually the potassium salt, $KU_2(OBu^t)_9$.[5] We have shown here that the alcohol adduct, $U_2(OBu^t)_8(HOBu^t)$, can be synthesized from well characterized starting materials, and have obtained spectroscopic data which support its formulation. We suggest that this is the same compound prepared by Perego and co-workers from $U(C_3H_5)_4$ and excess t-butanol.[4] We have also shown that Cotton's $KU_2(OBu^t)_9$ can be prepared from $U_2(OBu^t)_8(HOBu^t)$, or directly from UCl_4 and potassium t-butoxide. $KU_2(OBu^t)_9$ and $U_2(OBu^t)_8(HOBu^t)$ exhibit similar reactivity toward oxygen and water, and their UV–vis spectroscopic signatures indicate that they have similar structures.† Finally, we have developed a reproducible route to the previously reported trinuclear uranium(IV) complex, $U_3O(OBu^t)_{10}$, via hydrolysis of either $U_2(OBu^t)_8(HOBu^t)$ or $KU_2(OBu^t)_9$. $U_3O(OBu^t)_{10}$ is a promising starting material for further explorations of uranium(IV) cluster chemistry. Magnetic susceptibility data obtained on $U_3O(OBu^t)_{10}$ indicate that there is no magnetic ordering of its uranium(IV) centres down to 2 K.

It seems clear to us that $U(OBu^t)_4$ has not yet been reported in the literature. Since uranium(IV) compounds with sterically non-demanding ligands favour high coordination numbers (≥ 6), $U(OBu^t)_4$, assuming it can be isolated, will surely adopt an oligomeric structure, $[U(OBu^t)_4]_n$. Efforts to prepare this compound and related analogues are continuing in our laboratory.[17]

EXPERIMENTAL

General procedures

All reactions were carried out using standard techniques for the manipulation of air-sensitive materials. $[(Me_3Si)_2N]_2\overline{UN(SiMe_3)SiMe_2CH_2}$ was prepared and purified as described in the literature.[8] ^1H NMR spectra were recorded on an IBM AF250 spectrometer at 250 MHz. Chemical shifts are reported in ppm relative to the solvent ^1H impurity of benzene-d_6 (7.15 ppm).‡ IR spectra were recorded as Nujol mulls between KBr salt plates using a Digilab FTS-40 spectrophotometer. Electronic absorption spectra were recorded as hexane solutions using 1.0 and 0.10 cm matched quartz cells and a Perkin–Elmer Lambda 9 spectrophotometer. The X-ray powder pattern of $KU_2(OBu^t)_9$ was collected using a Siemens D-500 diffractometer with a θ–θ configuration. Low temperature (−90°C) single crystal X-ray data on $U_3O(OBu^t)_{10}$ were collected using a CAD-4 diffractometer. Elemental analyses were performed at Los Alamos using a Perkin–Elmer 2400 CHN Elemental Analyser and standard air-sensitive techniques. Samples were dried under high vacuum (10^{-4} torr) for 12 h. Hexane, toluene and THF were distilled under argon from sodium–potassium alloy and stored in a helium-filled dry-box operating at $\leq$ 1 ppm oxygen. Bu^tOH was dried by refluxing a benzene solution over magnesium, distilling the azeotrope and storing the solution in the dry-box. $KOBu^t$ was purchased from Aldrich and resublimed before use to remove non-volatile impurities.

Magnetic susceptibility data on $U_3O(OBu^t)_{10}$ were collected at the IBM T. J. Watson Research Center on a Quantum Design Superconducting Quantum Interference Device (SQUID) Magnetometer for temperatures ranging from 2 to 250 K at fields of 1 kOe and 10 kOe. Plots of magnetization vs field were linear at all temperatures. Data were background corrected for the sample tube (a 5 mm Pyrex NMR tube) and the ligands. The weight of the sample was 90 mg.

* The inverse molar susceptibilities of $[U(NEt_2)_4]_2$[9] and $U(SO_4)_2 \cdot 4H_2O$[16] also exhibit temperature independent behaviour at low temperature. Similar interpretations have been advanced to explain these observations.

† The latter point remains to be confirmed by X-ray crystallography. Structural characterization of $U_2(OBu^t)_8(HOBu^t)$ is in progress.

‡ The ^1H NMR spectra of the uranium complexes described in this paper are temperature *dependent*. The chemical shifts reported are for spectra collected at approximately 22°C.

$U_2(OBu^t)_8(HOBu^t)$

Excess Bu^tOH in benzene was slowly added to $[(Me_3Si)_2N]_2\overline{UN(SiMe_3)SiMe_2CH_2}$ (1.00 g, 1.39 mmol) in 20 cm^3 of toluene. The orange solution immediately turned green. The latter was stirred for 12 h at room temperature. The solution was evaporated to dryness *in vacuo* and the resulting green solid was recrystallized from hexane at −40°C and dried under high vacuum. Yield: 0.67 g, 85%. ^1H NMR (benzene-d_6, 22°C): δ 1.4 (br s, $C(CH_3)_3$); δ 13.0 (br s, O*H*). IR (cm^{-1}): 3537 (vw, OH); 1600 (w); 1352 (s), 1217 (ms), 1185 (s); 959 (vs); 903 (ms); 761 (m); 747 (mw); 726 (mw); 498 (ms); 474 (m). Found: C, 36.37, 36.26; H, 6.89, 6.84. Calc. for $C_{36}H_{82}O_9U_2$: C, 38.09; H, 7.29%.

$KU_2(OBu^t)_9$

UCl_4 (1.00 g, 2.63 mmol) was dissolved in 20 cm^3 of THF to give a green solution. 1.33 g (11.84 mmol) of $KOBu^t$ was added, in one portion, resulting in a colour change to purple–red and the formation of a white precipitate (KCl). Within a few minutes, the colour of the solution changed to green. After 12 h of stirring the solution was evaporated to dryness *in vacuo*. The green product was extracted into hexane and filtered through Celite. The volume was reduced and the solution cooled to −40°C, yielding 1.00 g of large green crystals, 65%. ^1H NMR (benzene-d_6, 22°C): δ 3.1 (s, 36H), 2.7 (s, 18H), −0.5 (s, 9H), −1.1 (s, 18H). IR (cm^{-1}): 1360 (s); 1350 (s); 1220 (s); 1197 (s); 1177 (vs); 1050 (mw); 1022 (w); 980 (s); 950 (vs); 921 (ms); 904 (s); 765 (ms); 755 (m); 665 (w); 523 (m); 494 (vs); 475 (s). Found: C, 36.61; H, 6.52. Calc. for $C_{36}H_{81}O_9KU_2$: C; 36.85; H, 6.97%. An X-ray powder pattern was in good agreement with the pattern calculated based on the single crystal data of Cotton *et al.*[5]

$U_3O(OBu^t)_{10}$

10 cm^3 of distilled H_2O were added to 500 cm^3 of toluene, and the resulting mixture was degassed by bubbling with HP argon for several hours. Addition of 50 cm^3 of this wet toluene to 1.0 g of either $KU_2(OBu^t)_9$ or $U_2(OBu^t)_8(HOBu^t)$ produced a slight colour change and the precipitation of a small amount of a solid. The solvent was immediately removed *in vacuo*. The green solid was extracted with hexane, the extracts were filtered and the green solution was stripped to dryness. At this point, a small amount of an unidentified impurity could be detected by ^1H NMR spectroscopy (δ 47.3, 46.0, 15.5, 8.8, −59.8, −60.8, −81.0; 1:2:1:2:1:2:1). The compound was recrystallized several times from hexane by slow cooling of a concentrated solution. The yields of $U_3O(OBu^t)_{10}$ from these reactions range from 50 to 80%. ^1H NMR (benzene-d_6, 22°C): δ 46.2 (s, 27H), 12.3 (s, 27H), −60.1 (s, 27H), −79.2 (s, 9H). Found: C, 32.63; H, 5.98. Calc. for $C_{40}H_{90}O_{11}U_3$: C, 32.87; H, 6.22%.

Acknowledgements—We wish to thank Drs C. J. Burns, J. Weinrach and E. Garcia for helpful discussion, and Dr D. Bish for obtaining the X-ray powder diffraction data on $KU_2(OBu^t)_9$. Generous financial support for this work was provided by the Office of Energy Research, Dvision of Chemical Sciences, U.S. Department of Energy.

REFERENCES

1. W. G. Van Der Sluys, A. P. Sattelberger, W. E. Streib and J. C. Huffman, *Polyhedron* 1989, **8**, 1247.
2. R. G. Jones, G. A. Martin and H. Gilman, *J. Am. Chem. Soc.* 1956, **78**, 4285.
3. D. C. Bradley, R. N. Kapoor and B. D. Smith, *J. Inorg. Nucl. Chem.* 1962, **24**, 863.
4. M. Brunelli, G. Perego, G. Lugli and A. Mazzei, *J. Chem. Soc., Dalton Trans.* 1979, 861.
5. F. A. Cotton, D. O. Marler and W. Schwotzer, *Inorg. Chem.* 1984, **23**, 4211.
6. (a) F. A. Cotton, D. O. Marler and W. Schwotzer, *Inorg. Chim. Acta* 1984, **85**, L31; (b) F. A. Cotton, D. O. Marler and W. Schwotzer, *Inorg. Chim. Acta* 1984, **95**, 207.
7. A. Dormond, A. A. E. Bouadili and C. Moise, *J. Chem. Soc., Chem. Commun.* 1985, 914.
8. (a) S. J. Simpson, H. W. Turner and R. A. Andersen, *Inorg. Chem.* 1981, **20**, 2991; (b) S. J. Simpson and R. A. Andersen, *J. Am. Chem. Soc.* 1981, **103**, 4063.
9. J. G. Reynolds, A. Zalkin, D. H. Templeton, N. M. Edelstein and l. K. Templeton, *Inorg. Chem.* 1976, **15**, 2498.
10. (a) M. H. Chisholm, K. Folting, J. C. Huffman and E. M. Kober, *Inorg. Chem.* 1985, **24**, 241; (b) M. H. Chisholm, K. Folting, J. C. Huffman and C. C. Kirkpatrick, *Inorg. Chem.* 1984, **23**, 1021.
11. J. G. Reynolds, A. Zalkin, D. H. Templeton and N. M. Edelstein, *Inorg. Chem.* 1977, **16**, 599.
12. C. Miyake, Y. Hinatsu and S. Imoto, *Chem. Phys. Lett.* 1979, **63**, 529.
13. E. Sinn, *Coordination Chem. Rev.* 1970, **5**, 313.
14. C. J. O'Connor, *Prog. Inorg. Chem.* 1982, **29**, 203.
15. C. A. Hutchinson Jr and G. A. Candela, *J. Chem. Phys.* 1957, **27**, 707.
16. J. Maluk, *J. Solid State Chem.* 1978, **25**, 355.
17. A dinuclear siloxide complex of uranium(IV), $[U(OSiMe_2Bu^t)_4]_2$, has recently been isolated and structurally characterized. W. G. Van Der Sluys, J. C. Huffman, W. E. Strieb and A. P. Sattelberger, in preparation.
18. *Chem3D* is a registered trademark of Cambridge Scientific Computing, Inc., Cambridge, MA 02139, U.S.A.

Polyhedron Vol. 9, No. 15/16, pp. 1849–1854, 1990
Printed in Great Britain

0277–5387/90 $3.00+.00
Pergamon Press plc

INDO/GIAO CALCULATIONS OF THE NMR SHIELDING CONSTANT INCLUDING *d* ORBITALS*

WEI-XIONG WU

Shanghai Institute of Computer Technology, Shanghai, China

and

XIAO-ZENG YOU† and AN-BANG DAI

Coordination Chemistry Institute, Nanjing University, China

and

SHOU-PING JING

Shanghai Institute of Biochemistry, Academia Sinica, China

Abstract—Application of the INDO calculation of NMR chemical shift has been extended. Firstly, it is applied to the calculations of ^{13}C, ^{15}N and ^{17}O shieldings for a series of representative nitrogen- and oxygen-containing compounds. Then several ^{13}C shieldings of the three iron complexes $(C_5H_5)Fe(CO)_2CN$, $(C_5H_4)_2Fe(COH)_2$ and $(C_5H_4)Fe(CH_2OH)_2$ have been evaluated. The theoretical results are in good agreement with the experimental. In addition, it is found that the calculated diamagnetic contributions, $\sigma^d(M)$, of ^{13}C, ^{15}N and ^{17}O atoms exhibit a good linear relationship with the net charge, $\rho(M)$, on these atoms.

The rapid development of the NMR pulsed technique and its applications have aroused increasing interest in the analysis and explanation of ^{13}C, ^{15}N and ^{17}O shieldings. Therefore, it is hoped that there may be a theory and method of calculation which can not only be used to accurately elucidate experimental facts, but which are also rather simple. From this point of view, the semi-empirical scheme seems to be attractive.[1]

On the basis of the Sum-Over-States (SOS) perturbation theory, a semi-empirical molecular orbital theory of diamagnetism and shielding, and its simplified "average excitation energy" approximation have been proposed by Pople and coworkers. Thence many theoretical studies, based on EHMO,[2] INDO,[3] X_α-Scattered Wave,[4] MNDO,[5] approximations or *ab initio*[6,7] have been carried out, including authors' calculations of NMR chemical shifts of transition metal and lanthanum compounds.[8,9] These calculations can give experimentally observed trends in the chemical shifts and provide some useful qualitative results. However, there are some difficulties involved in this theory. First the working formulae with average ΔE^{-1} (the reciprocal of energy level difference) may cause considerable error. A more serious problem arises from the dependence of theoretical results upon the origin of coordinates.

In 1972, Ditchfield presented an *ab initio* SCF–MO perturbation theory of ^{13}C shielding employing gauge-invariant atomic orbitals (GIAO), which has marked an important breakthrough in NMR shielding theory.[10] Soon after this, Ellis *et al.* proposed an INDO perturbation theory of ^{13}C shieldings[11] which retains considerable *ab initio* computational accuracy, and at the same time, the CUP calculation time is greatly reduced. This approach marks the beginning of a new semi-empirical method of NMR shielding calculation. On the basis of INDO, a modified set of hydrogen, carbon and fluorine[12] INDO parameters lead to semi-quantitative agreement of the theoretical results with the experimental results.

* Dedicated to Professor R. F. Fenske, in appreciation of his inspiring guidance as my adviser during my stay as a visiting scholar (X. Z. You) at Wisconsin University in 1981.

† Author to whom correspondence should be addressed.

The present paper is concerned with extending the INDO/GIAO perturbation theory to include shielding calculations of transition metal complexes: so INDO parameters of the nitrogen and oxygen are modified by minimizing ^{13}C, ^{15}N and ^{17}O shielding differences between theoretical and experimental data for a series of representative nitrogen and oxygen-containing compounds; and some ^{13}C chemical shifts of several iron-containing complexes are evaluated by optimizing some iron INDO parameters.

Considering the level of approximation, the good agreement of the calculated values with the experimental data encouraged us to extend the theory to cover shielding calculations of other metal compounds.

METHOD OF CALCULATION

By assuming a homogeneous external perturbation field to be **B**, then gauge-invariant atomic orbitals can be represented as:

$$\chi_v = \{\exp[-(i/C)\mathbf{A}_v \cdot \mathbf{r}]\}\chi_v^0 = f_v\chi_v^0, \quad (1)$$

where $\mathbf{A}_v$ is a vector potential at nucleus v, $\mathbf{A}_v = \frac{1}{2}\mathbf{B}\times\mathbf{R}$, with $\mathbf{R}_v$ as the position vector of the atom upon which the unperturbed atomic orbital is centred.

Then the molecular orbitals are expanded as linear combinations of GIAO with complex coefficients C_{vi}:

$$\phi_i = \sum_v \chi_v C_{vi}. \quad (2)$$

Here, the density matrix is defined as

$$R_{\eta\sigma} = \sum_j^{\text{occ}} C_{\eta j}^* C_{\sigma j} = R_{\eta\sigma}^r + iR_{\eta\sigma}^i, \quad (3)$$

where superscripts r and i stand for the real and imaginary parts, respectively.

The Fock matrix F is represented as

$$F = H+G = (H^r+G^r)+i(H^i+G^i), \quad (4)$$

then the G matrix is generated to include shielding calculations of the transition metal complex in the case where p and q are centred on the same atom by the following:

$$\overset{r}{G}pp = \sum_{B\neq A} 2R_{BB}^r v_{AB} + \sum_\lambda^A 2R_{\lambda\lambda}^r[(pp\|\lambda\lambda) - 1/2(p\lambda|p\lambda)] \quad (5)$$

$$\overset{i}{G}pp = 0$$

$$\overset{r}{G}pq = \overset{r}{R}pq[3(pq|pq) - (pp|qq)]$$

$$\overset{i}{G}pq = -\overset{i}{R}pq[(pq|pq) - (pp|qq)]. \quad (6)$$

When p and q refer to different atoms A and B, the formulae for G and H are the same as in ref. 11. The one-centre Coulomb integrals $(pp|qq)$ and exchange integrals $(pq|pq)$ of s, p and d orbitals in eqs (5) and (6) can be evaluated by Condon–Shortley integration.[12,13]

By substituting the equation in refs 12 and 13 into eqs (5) and (6), we obtain the integral formulae adopted by Ellis *et al.*,[11] which show that eqs (5) and (6) are, indeed, extended formulae.

The shielding tensor, $\sigma_{\alpha\beta}(M)$, can be obtained from the definition using eqs (7)–(9):

$$\sigma_{\alpha\beta}(M) = \sigma_{\alpha\beta}^d(M,M) + \sigma_{\alpha\beta}^p(M,M) + \sum_{K\neq M}[\sigma_{\alpha\beta}^d(M,K) + \sigma_{\alpha\beta}^p(M,K)] \quad (7)$$

$$\sigma_{\alpha\beta}^d(M,K) = 2\sum_\mu^K\sum_\nu^K R_{\mu\nu}(0)\langle\chi_\mu^0|h''_{\alpha\beta}(M)|\chi_\nu^0\rangle \quad (8)$$

$$\sigma_{\alpha\beta}^p(M,K) = 2\sum_\mu^K\sum_\nu^K (\partial R_{\mu\nu}/\partial B_\alpha)_0\langle\chi_\mu^0|h_\beta^{10}(M)|\chi_\nu^0\rangle, \quad (9)$$

where $\sigma_{\alpha\beta}^d(M,K)$ and $\sigma_{\alpha\beta}^p(M,K)$ are the diamagnetic and paramagnetic contributions of nuclear screening, respectively, and $R_{\mu\nu}(0)$ are the unperturbated density matrix elements. The derivative of $R_{\mu\nu}$ with respect to a component B_α of **B** is numerically approximated using a different method

$$(\partial R_{\mu\nu}/\partial B_\alpha)_0 \approx iR_{\mu\nu}^i/B_\alpha. \quad (10)$$

In order to consider the different molecular environments of non-equivalent atoms, as in previous work, Slater's screening rules are used to modify the "old" exponents in the calculation of integrals of $\langle r^{-3}\rangle$ and $\langle r^{-1}\rangle$ types. The following modified expression can be used

$$\xi'_N = \xi_N + 0.175Q_N, \quad (11)$$

where ξ_N stands for the pre-modified "old" Slater's exponent[14] and ξ'_N the modified "new" exponent for atom N which may be carbon, nitrogen, oxygen or fluorine; Q_N is the net charge on atom N.

CHOICE OF PARAMETERS

Firstly, we used the INDO/GIAO calculation of ^{13}C, ^{15}N and ^{17}O chemical shifts for a representative set of nitrogen and oxygen compounds by modifying nitrogen and oxygen INDO $(I+A)/2$ and β parameters so as to minimize the average difference between theoretical and experimental data. Table 1 gives the "new" parameters of nitrogen and oxygen together with those of hydrogen and carbon from ref. 11.

Then we further modified some iron INDO parameters in order to reduce the error of shielding of

Table 1. Standard and "new" H, C, N and O INDO parameters

		Standard	"New"
Hydrogen	$(I+A)_s/2$	7.176	7.176
	β_0	−9.0	−12.0
Carbon	$(I+A)_s/2$	14.051	17.051
	$(I+A)_p/2$	5.572	8.572
	β_0	−21.0	−17.0
Nitrogen	$(I+A)_s/2$	19.316	23.5
	$(I+A)_p/2$	7.275	10.5
	β_0	−25.0	−22.5
Oxygen	$(I+A)_s/2$	25.390	29.5
	$(I+A)_p/2$	9.111	15.75
	β_0	−31.0	−27.8

carbon atoms C^1, C^2 and C^3 in the iron complex $(C_5'H_5)Fe(C^2O)_2C^3N$. The iron Slater exponents[15] are fixed during the modification process. In the course of reparameterization, we noticed that the $(I+A)_{4s}/2$ and $(I+A)_{4p}/2$ INDO parameters do not have much influence upon the calculated results, so hitherto we have kept them fixed and only altered $(I+A)_{3d}/2$, $\beta_{4s}(\beta_{4p}=\beta_{4s})$ and β_{3d} parameters. The final iron INDO parameters are listed in Table 2. The Slater–Condon parameters[16] used to evaluate one-centre Coulomb and exchange integrals of iron are listed in Table 3.

From Table 1, by comparing "new" parameters with "old" ones for all carbon, nitrogen and oxygen atoms, we find an obvious trend of increasing $(I+A)/2$'s, with decreasing β's. Moreover, the δ^p and σ^d data listed in Tables 4 and 9 show that the change of chemical shifts is mainly determined by paramagnetic terms, σ^p, that is to say, σ^p terms change considerably for different molecules, while σ^d terms do not.

Table 2. Iron INDO parameters

Exponents[15]	Electronegative	Bonded parameters
$\xi_{4s}=1.3585$	$(I+A)_{4s}/2=4.120$[16]	$\beta^0_{4s}=-12.0$
$\xi_{4p}=1.1601$	$(I+A)_{4p}/2=1.062$[16]	$\beta^0_{4p}=-12.0$
$\xi_{3d}=3.7266$	$(I+A)_{3d}/2=9.50$	$\beta^0_{3d}=-45.0$

RESULTS AND DISCUSSION

Fortran language has been used to code the computer program INDO/GIAO for the above-mentioned INDO/GIAO theory using a Burroughs-6933 computer. Using the INDO/GIAO program with the parameters presented in Tables 1 and 2, we have carried out the ^{13}C, ^{15}N and ^{17}O chemical shift calculations for four groups of compounds, including H, C, N, O and Fe atoms. Moreover, geometries are quoted from refs 17–19 and the one-centre integration including *d* orbitals in eqs (7)–(9) from ref. 9. The calculated results are given in Tables 4–7. The shift data are relative to reference molecules with low-field shifts being positive.

Tables 5 and 6 show that the ranges of ^{15}N and ^{17}O shieldings of the two selected groups of nitrogen- and oxygen-containing compounds are about 380 and 600 ppm, respectively. Moreover, the average differences between theoretical and experimental values are 16.79 and 30.34 ppm, respectively.

In order to check the availability of new nitrogen and oxygen INDO parameters for the ^{13}C chemical shift calculation, we have chosen some compounds containing hydrogen, carbon, nitrogen and oxygen atoms, and evaluated their ^{13}C shifts. The data listed in Table 4 give an average absolute error of about 28.71 ppm. The data in Tables 4–9 show a good semi-quantitative agreement between calculated and experimental values, not only for ^{15}N and ^{17}O, but also for the ^{13}C shifts.

A number of important effects are revealed. The observed low-field ^{13}C shift of C^aH_3CN relative to CH_3C^aN in Table 4 is ascribed to the multiple bonds. Marked effects of the nature of substituents on carbon and the type of bonding are also shown.

Nitrogen has some features that distinguish it from carbon because of the presence of unshared electron pairs. The data in Table 5 also show the overall agreement between the calculated and the observed shifts. The nitrogen shifts are greatly dominated by paramagnetic contributions.

Although the medium effects caused by the electron pair on the oxygen atom occurred, the ^{17}O data in Table 6 show an overall satisfactory agreement between the calculated and experimental results. Moreover, our results also show the trend of singly-bonded ^{17}O shift of about 200 ppm downfield from

Table 3. Experimental iron data of *G* and *F*

^{2}*Fpp*	^{2}*Fpd*	^{2}*Fdd*	^{4}*Fdd*	^{1}*Gpd*	^{3}*Gpd*	^{1}*Gsp*	^{2}*Gsd*
0.0743	0.0342	0.0303	0.0112	0.0229	0.0160	0.2779	0.1750

Table 4. Calculated ^{13}C chemical shifts (ppm)

Compound	Net charge ρ(M)	σ^d(M)	σ^p(M)	σ(M)	$\delta_{calc.}$	$\delta_{exp.}$
CH_4	−0.4893	60.73	−54.68	6.05	0.0	0.0
C^aH_3CN	−0.3404	59.90	−60.91	−1.01	7.06	3.0
CH_3OH	−0.0412	57.97	−70.09	−12.11	18.16	50.0
HCN	−0.0148	57.79	−180.36	−122.57	128.62	120.0
CH_3C^aN	0.1634	56.51	−185.86	−129.34	135.39	120.0
CO_2	0.9849	49.21	−216.37	−167.16	173.21	126.0
CO	0.2787	55.83	−286.50	−230.67	236.72	184.0
HCHO	0.2695	55.70	−231.18	−175.48	181.53	197.0

[a] Calculated ^{13}C chemical shifts relative to CH_4.

Table 5. Calculated ^{15}N chemical shifts (ppm)

Compound	Net charge	σ^d(M)	σ^p(M)	σ(M)	$\delta_{calc.}$	$\delta_{exp.}$
NH_3	−0.5974	90.68	−151.28	−60.60	0.0	0.0
CH_3NH_2	−0.4496	89.78	−184.40	−94.62	34.02	5.0
N_2H_4	−0.3680	89.22	−204.12	−114.90	54.30	51.0
C_4H_4NH	−0.1907	88.02	−283.79	−195.77	135.18	148.0
C_2H_5CN	−0.2608	88.41	−382.19	−293.79	233.19	246.0
$C_3H_3N_3$	−0.2841	88.61	−426.68	−338.07	277.47	285.0
C_2H_5N	−0.2182	88.15	−479.89	−391.73	331.14	320.0
$C_4H_4N_2$	−0.1739	87.84	−478.57	−390.73	330.14	335.0
N_2	0.0	86.53	−535.96	−449.43	388.83	369.0
$C_2H_2N_4$	−0.0965	87.26	−508.35	−421.08	360.49	388.0

[a] Calculated chemical shifts with respect to NH_3.

Table 6. ^{17}O chemical shifts (ppm)

Compound	Net charge	σ^d(M)	σ^p(M)	σ(M)	$\delta_{calc.}$	$\delta_{exp.}$
H_2O	−0.7163	126.79	−184.83	−56.04	0.0	0.0
$CH_3COO^aCH_3$	−0.4968	125.24	−328.89	−203.65	145.61	137.3
$HCOO^aCH_3$	−0.4688	125.03	−360.15	−235.13	177.09	140.8
H_2O_2	−0.3867	124.35	−381.30	−256.95	198.91	187.0
CO	−0.2656	123.41	−518.59	−395.17	337.13	350.0
$CH_3CO^aOCH_3$	−0.6142	126.02	−529.29	−403.26	345.22	360.6
HCO^aOCH_3	−0.5506	125.57	−585.12	−459.54	401.50	364.9
$(CH_3CO^a)_2O$	−0.5567	125.62	−545.82	−420.20	362.16	393.0
H_2CO	−0.4343	124.72	−737.01	−612.28	554.24	580–600

[a] Calculated chemical shifts with respect to H_2O.

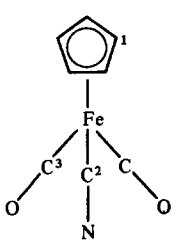

Table 7. ^{13}C chemical shifts[a] of $(C_5H_5)Fe(CO)_2CN$ (ppm)

	Net charge	σ^d(M)	σ^p(M)	σ(M)	$\sigma_{exp.}$	$\sigma_{x\alpha}$
C^1(CP)	0.1050	56.93	−121.19	−64.26	−85.9	168.69
C^2(CN)	0.2596	55.78	−213.83	−158.05	−154.7	158.58
C^3(CO)	0.7484	51.69	−286.79	−235.10	−211.1	145.26

[a] σ_{exp} and $\sigma_{x\alpha}$ are taken from ref. 20.

Table 8. ^{13}C chemical shifts of $(C_5H_4)_2Fe(CH_2OH)_2$ (ppm)[a]

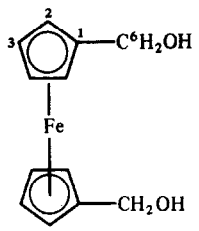

	Net charge ρ(M)	σ^d(M)	σ^p(M)	σ(M)	$\sigma_{exp.}$
C^1	0.1593	56.52	−128.89	−72.37	−89.26
C^2	0.0527	57.31	−118.72	−61.41	−66.91
C^3	0.0377	57.42	−119.29	−61.87	−67.90
C^6	0.1515	56.59	−76.55	−19.96	−60.17

[a] Molecular geometry and experimental data from ref. 20.

Table 9. ^{13}C chemical shifts of $(C_5H_4)_2Fe(CHO)_2$ (ppm)[a]

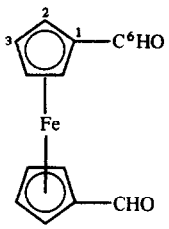

	Net charge	σ^d(M)	σ^p(M)	σ(M)	$\sigma_{exp.}$
C^1	0.1053	56.93	−120.22	−63.30	−80.10
C^2	0.0707	57.18	−120.31	−63.13	−74.05
C^3	0.0539	57.30	−119.06	−61.76	−70.75
C^6	0.3598	54.98	−231.66	−176.68	−192.71

[a] Molecular geometry and experimental data from ref. 20.

water and the doubly-bonded shift at still lower field, which agree well with the *ab initio* level.

The chemical shift calculations of organometallic compounds are rather complicated. ^{13}C shifts of compound $(C_5H_5)Fe(CO)_2CN$ have already been calculated. It is seen from Table 7 that the present calculations seem to reflect the experimental trends more succinctly.

It must be emphasized that Figs 1–3 show a good linear relationship between the calculated diamagnetic terms, σ^d(M), of ^{13}C, ^{15}N and ^{17}O shifts,

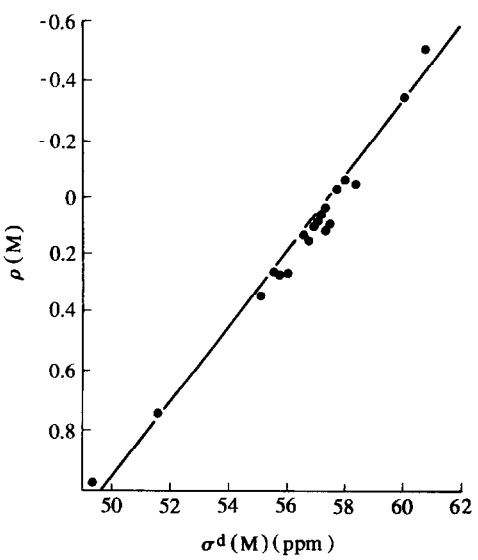

Fig. 1. ρ(M) of ^{13}C vs σ^d(M).

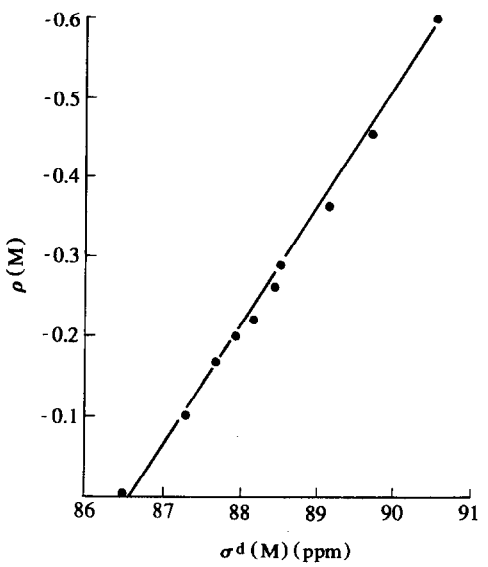

Fig. 2. ρ(M) of ^{15}N vs σ^d(M).

and the corresponding atomic net charge, β(M), on atom M.

The above-mentioned method has also been used to calculate the shieldings for more complicated organometallic compounds including *f* orbitals.[21]

SUMMARY AND CONCLUSIONS

The finite perturbation INDO method of ^{13}C shifts for hydrocarbons due to Ellis *et al.* has been extended to ^{13}C, ^{15}N and ^{17}O chemical shift cal-

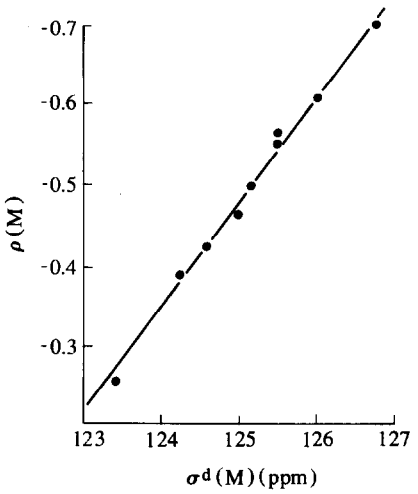

Fig. 3. ρ(M) of ^{17}O vs σ^d(M).

culations for a series of molecules including some organometallic compounds. The molecules treated cover a wide range of chemical environments and consequently a wide range of shieldings. A modified set of nitrogen, oxygen and carbon INDO parameters together with the careful selection of iron $(I+A)_{3d}/2$, β^0_{4s} and β^0_{3d} parameters lead to a reasonable agreement between calculated and experimental shifts. The computational scheme discussed in this paper is even better than the relevant X_α-Scattered Wave method for some shift calculations of organometallic compounds. Moreover, a close linear relationship between the diamagnetic terms σ^d(M) of ^{13}C, ^{15}N and ^{17}O shift, and the corresponding net atomic charge ρ(M) on atom M have been revealed.

Our calculation experiments showed high computational speed and good convergency even for rather complicated organometallic compounds including those having more than 100 molecular orbitals. It may therefore provide a suitable semiempirical method of chemical shift calculations for complicated metal complexes.

Acknowledgement—This work is supported by the National Natural Science Foundation of China as An Item of Major Project.

REFERENCES

1. G. A. Segal, *Semiempirical Method of Electronic Structure Calculation*, Part B. Plenum Press, New York (1977).
2. A. Velenik and R. M. Lynden-Bell, *Molec. Phys.* 1973, **19**, 371.
3. A. B. Strong, D. Ikenberry and D. M. Grant, *J. Magn. Reson.* 1973, **9**, 145.
4. D. G. Freier, R. F. Fenske and You Xiaozeng, *J. Chem. Phys.* 1985, **83**, 3525.
5. You Xiaozeng and Wu Weixiong, *Magn. Chem.* 1987, **25**, 860.
6. R. Ditchfield, D. D. Miller and J. A. Pople, *J. Chem. Phys.* 1971, **54**, 4861.
7. Wu Weixiong, You Xiaozeng and Dai Anbang, *Sci. Bull.* 1985, **16**, 1224.
8. Wu Weixiong, Hong Xinhong, You Xiaozeng and Dai Anbang, *Scientia Sin. B* 1987, **5**, 351.
9. Wu Weixiong, Hong Xinhong, You Xiaozeng, Zhu Lunggan and Dai Anbang, *Chem. J. Chinese Univ.* 1986, **7**, 725.
10. R. Ditchfield, *Chem. Phys. Lett.* 1972, **15**, 203.
11. P. D. Ellis, G. E. Maciel and J. W. McIver Jr, *J. Am. Chem. Soc.* 1972, **94**, 4069.
12. G. E. Maciel, J. L. Dallas, R. L. Elliot and H. C. Dorn, *J. Am. Chem. Soc.* 1973, **95**, 5857.
13. E. U. Condon and G. H. Shortley, *The Theory of Atomic Spectra.* The University Press, Cambridge (1957).
14. J. C. Slater, *The Quantum Theory of Atomic Structure*, Vol. 1. McGraw-Hill, New York (1960).
15. E. Clementi and D. L. Raimondi, *J. Chem. Phys.* 1963, **38**, 2686.
16. A. D. Bacon and M. C. Zener, *Theor. Chim. Acta.* 1979, **53**, 21.
17. *Tables of Interatomic Distances and Configurations in Molecules and Ions.* The Chemical Society, London (1965).
18. J. A. Pople and D. L. Beveridge, *Approximate Molecular Orbital Theory.* McGraw-Hill, New York (1970).
19. Li Cun, Wu Weixiong, Pen Xin, Chao Qirong, You Xiaozeng and Dai Anbang, *Acta Phys.-Chim. Sin.* 1986, **2**, 73.
20. You Xiaozeng, R. F. Fenske and D. G. Freier, *J. Molec. Sci (China)* 1983, **1**, 43.
21. You Xiaozeng, Wu Weixiong, Li Cun and Dai Anbang, *Sci. Bull. (China)* 1988, **33**, 265.

Polyhedron Vol. 9, No. 15/16, pp. 1855–1866, 1990
Printed in Great Britain

0277–5387/90 $3.00+.00
Pergamon Press plc

AN INVESTIGATION OF THE ELECTRONIC FACTORS THAT INFLUENCE STRUCTURAL DIFFERENCES BETWEEN *CIS*-$(CpMoCl)_2(\mu,\eta^4\text{-}Ar_4C_4)$ (Ar = *p*-TOLYL OR PHENYL) AND *TRANS*-$(CpNbCO)_2(Ph_2C_2)_2$†

MARIA CLELIA MILLETTI‡ and M. DAVID CURTIS

Department of Chemistry, The University of Michigan, Ann Arbor, MI 48109-1055, U.S.A.

Abstract—The influence of geometric factors, such as *cis*/*trans* isomerism, and electronic factors, such as π donor vs π acceptor ligands and coupled and uncoupled acetylene ligands, on the stability of *cis*-$(CpMoCl)_2(\mu,\eta^4\text{-}Ar_4C_4)$ and *trans*-$(CpNbCO)_2(Ph_2C_2)_2$ is investigated through patterns in molecular orbital diagrams, size of HOMO/LUMO gap and total energies. The comparison between the two dimers involves rationalization of why the observed structures appear so different, when in fact both clusters have the same number of valence electrons. In the course of the investigation, other stable niobium chlorine complexes are discussed and the kinetic vs thermodynamic stability of *trans*-$(CpNbCO)_2(Ph_2C_2)_2$ is analysed.

An interesting series of new organometallic dimers has been synthesized as part of an ongoing investigation of metal–metal multiple bonds.[1] This paper will focus on two of these dimers: they are of the type $Cp_2M_2L_2R$, where M = Mo or Nb, L = CO or Cl, and R = μ,η^4-Ar_4C_4 or $(Ar_2C_2)_2$ (Ar = *p*-tolyl or phenyl).

More specifically, it is of interest to compare the structures of *cis*-$(CpMoCl)_2(\mu,\eta^4\text{-}Ar_4C_4)$ (**1**) and *trans*-$(CpNbCO)_2(Ph_2C_2)_2$ (**2**).[2] These two complexes have identical electron counts: niobium has one less valence electron than molybdenum, but the carbonyl ligand is considered a two-electron donor, while chlorine is a one-electron donor [both $(\mu,\eta^4\text{-}Ar_4C_4)^{2-}$ and $(Ph_2C_2)_2$ are eight-electron donors].[3] Despite sharing the same number of valence electrons these two dimers have very different structures:[4]§

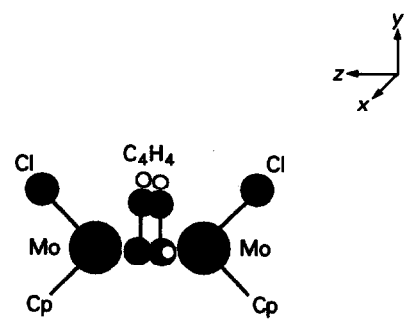

1

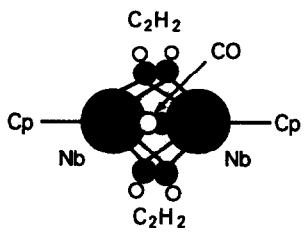

2

The two molecules differ in their conformation (one is *cis* and the other *trans*) and in the molybdenum dimer the two alkyne ligands have coupled to form a $(\mu,\eta^4\text{-}Ar_4C_4)$ ligand, while in the niobium complex two separate acetylene groups are present.

† Dedicated to Professor Richard F. Fenske in recognition of his contribution to theoretical organometallic chemistry and in appreciation of his guidance as my PhD adviser (M.C.M).

‡ Author to whom correspondence should be addressed.

§ The aryl and phenyl groups present in the dimers have been substituted by hydrogen atoms in order to simplify the molecular orbital calculations (see text).

The structural and electronic features that distinguish the molybdenum from the niobium dimer can be grouped into three categories: *cis* or *trans* arrangement, Cl or CO ligands, coupled C_4H_4 or uncoupled $(C_2H_2)_2$ alkyne ligands. This paper will attempt to explain why the molybdenum dimer prefers one set of features and the niobium dimer the other by using non-empirical molecular orbital calculations. The three aspects will first be studied separately, and then taken into consideration simultaneously in order to justify the observed structures. The results of the calculations will be analysed in terms of the nature and energy of the valence molecular orbitals, as well as the relative total energies of the complexes.

COMPUTATIONAL PROCEDURE

Calculations have been carried out by using the Fenske–Hall non-empirical method[5] on an IBM 3090-600 computer.[6] Atomic basis functions were employed; for oxygen, carbon and chlorine Clementi's double-ξ functions were used,[7] except for 1*s* and 2*s* functions, which were curve-fit to single-ξ by using the maximum overlap criterion.[8] The hydrogen exponent was set to 1.16. Molybdenum(I) and niobium(I) functions were obtained by performing an atomic X-α calculation on a set of optimized, orthonormal Slater-type orbitals.[9] In order to avoid working with metal outer functions that are too diffuse, the molybdenum 5*s* and 5*p* exponents were set to 1.85. The niobium 5*s* exponent was set to 1.602 and the 5*p* exponent to 1.259. The total energy for each molecule was calculated using the Hartree–Fock expression.[10,11]

The geometrical parameters used for the experimentally observed compounds [*cis*-$(CpMoCl)_2(\mu,\eta^4\text{-}Ar_4C_4)$,[3] *trans*-$(CpNbCO)_2(Ph_2C_2)_2$[2b] and *trans*-$(MeCp)_2Nb_2(Ar_2C_2)_2(\mu\text{-}Cl)_2$[12]] were taken from the actual X-ray structures, but, for simplicity of interpretation and greater ease in the calculations, the phenyl and *p*-tolyl substituents on the R ligands have been substituted by a hydrogen atom. Table 1 shows selected bond distances for the two basic dimer frames considered in this work: that of *cis*-$(CpMoCl)_2(C_4H_4)$ and that of *trans*-$(CpNbCO)_2(C_2H_2)_2$. These two geometries are also used for the structures of *cis*-$(CpNbCl)_2(C_4H_4)$ and *trans*-$(CpMoCO)_2(C_2H_2)_2$. For *cis*-$(CpMoCO)_2(C_4H_4)$, the Mo—C_{CO} bond distance was taken to be 1.99 Å, which is the value found in a series of $CpMo(CO)_3R$ complexes.[13] In *trans*-$(CpNbCl)_2(C_2H_2)_2$, the Nb—Cl bond distance was set to 2.25 Å.[14]

The geometry of *trans*-$(CpMoCl)_2(C_4H_4)$ cannot be made to match that of *trans*-$(CpNbCO)_2(C_2H_2)_2$ because the C_4H_4 ligand would be too close to the chlorine centres. Therefore, to obtain the geometry of the molybdenum dimer, half of the *cis*-$(CpMoCl)_2(C_4H_4)$ dimer was rotated by 180° along the Mo—Mo axis, leaving the C_4H_4 ligand in place. On the other hand, the arrangement in *cis*-$(CpNbCl)_2(C_2H_2)_2$ can be made to resemble that of the experimentally observed molybdenum dimer by rotating half of *trans*-$(CpNbCO)_2(C_2H_2)_2$ by 180° along the Nb—Nb axis and leaving the C_2H_2 ligands in place. Furthermore, the two cyclopentadienyl rings are moved closer together at a 45° angle to the M—M axis and the two carbonyl ligands are pointed away from, rather than at, each other. Bond lengths and angles for the other dimers were extrapolated from the known geometries.

RESULTS AND DISCUSSION

The two experimentally observed dimers

In order to study the influence of the three geometrical factors on the electronic structure of the title compounds, it is best to start from an analysis of the MO diagram for each of the two molecules. Figure 1 shows the MO diagram for *cis*-$(CpMoCl)_2(C_4H_4)$ (**1**). The HOMO/LUMO gap is fairly large (2.87 eV), pointing to the stability of the com-

Table 1. Selected bond distances for **1**, **2**, **11** and **12**[3,2b]

	cis-$(CpMCl)_2(C_4H_4)$[a]	*trans*-$(CpMCO)_2(C_2H_2)_2$[a]
M—M	2.933	2.731
M—C_{Cp}	2.3	2.3
M—C_{CO}	—	2.107
M—Cl	2.4	—
M—$C_{C_2H_2}$	—	2.0
M—$C_{C_4H_4}$	2.0, 2.2[b]	—

[a] All distances in Å.
[b] Distances for end and internal carbons.

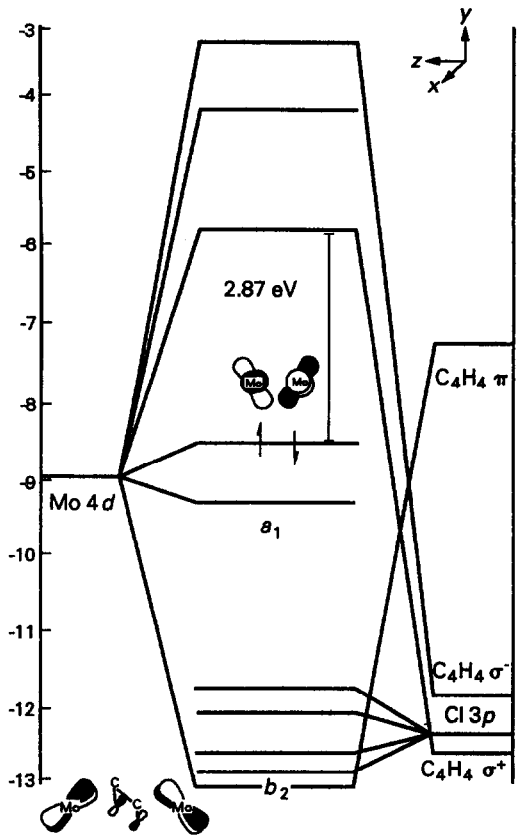

Fig. 1. Molecular orbital diagram for *cis*-$(CpMoCl)_2(C_4H_4)$ (**1**).

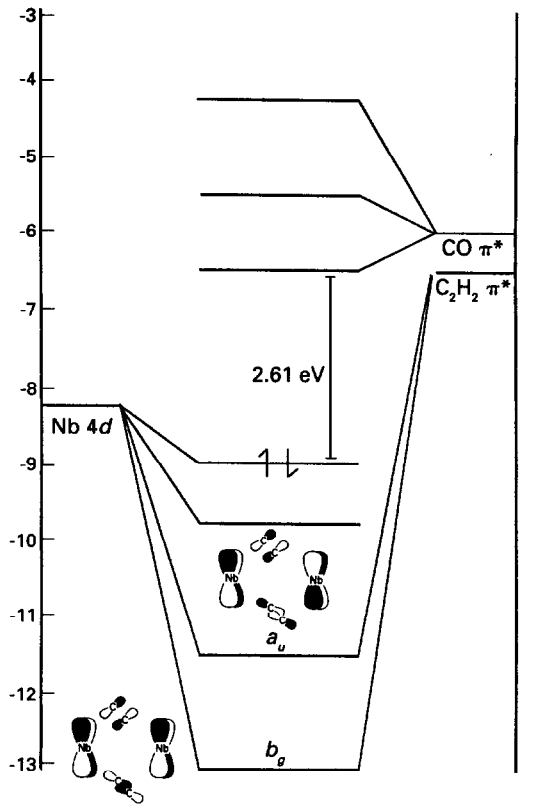

Fig. 2. Molecular orbital diagram for *trans*-$(CpNbCO)_2(C_2H_2)_2$ (**2**).

plex.[15] The five valence molecular orbitals (two occupied and three unoccupied) are in an e+t pattern and are largely metal-based. A fairly large gap separates the SHOMO (Second Highest Occupied Molecular Orbital) from the next set of occupied orbitals, which is comprised of in-phase and out-of-phase combinations of Cl 3*p* orbitals. The lowest-energy molecular orbital shown (b_2) is part of the atomic Mo—C_4H_4 bonding interaction: only the end carbons of the C_4H_4 ligand are participating in the bond via a hybrid orbital that is pointing toward one of the metal centres† [see Fig. 5(c)]. The metal centres are bonding with a combination of their d_{xy} and d_{xz} orbitals.

Figure 2 shows the MO diagram for the other dimer, *trans*-$(CpNbCO)_2(C_2H_2)_2$ (**2**). The HOMO/LUMO gap is not as large as the one in the molybdenum complex, but it still indicates that **2** is a stable molecule. The valence molecular orbitals do not show the e+t pattern present in **1** and they receive larger contributions from the ligand orbitals. The first three unoccupied molecular orbitals are mainly CO π* in character, as usual for molecules with carbonyl ligands.[11] The HOMO and the SHOMO are metal–metal bonding, which is consistent with the experimental observation of a Nb—Nb bond length characteristic of a double bond between the centres.[2b,16] The two lowest levels shown in Fig. 2, b_g and a_u, contribute to the bonding between the metals and the acetylene ligands. This interaction can be compared to that between Mos and C_4H_4 in **1**, which was observed in the b_2 orbital of that molecule. In both molecular orbitals, the π* orbital on the acetylene ligand [see Fig. 6(c)] bonds with the d_{xy} orbital on niobium. In the b_g orbital, each of the acetylene ligands has an in-phase interaction with only one of the metals, while in the a_u level the ligands bond with both metal centres at the same time, forming a true bridge between them.

If the metal to R ligand interactions in the valence molecular orbitals of **1** and **2** are compared, a number of similarities become apparent. In both cases the bond occurs between one or more metal *d* orbitals of appropriate symmetry and the first empty level on the ligand. In the dimer, the resulting

† The C_4H_4 ligand also contributes some small amount of electron density from the internal carbons, but the contribution is too small to be shown. The *p* orbitals on the internal carbons form out-of-phase combinations with the *p* orbitals on the end carbons shown in Fig. 1.

bonding level or levels are filled, so that the net result is metal-to-ligand electron density donation. Furthermore, the ligand orbital participating in the interaction is a linear combination of two *p* orbitals on each of the carbon centres involved. This mixing of atomic orbitals is necessary in order to redirect the ligand orbitals toward the metal centres, since in neither **1** or **2** are the carbon atoms along the metal–metal axis.

Since the ligand orbitals that are on the accepting side of this backbonding interaction have varying degrees of antibonding character between carbon centres,† the metal-to-ligand interaction effectively weakens the C—C bond in the R ligand. Further weakening of such bonds occurs when the low-lying, filled, *s* and *p* orbitals of the R ligand (see Figs 5 and 6) donate electron density to the metal centres through additional bonding molecular orbitals. These molecular levels are at lower energies, buried in the group of M—L and L—L bonding orbitals below the valence sets shown in Figs 1 and 2. This hypothesis of a net weakening of ligand C—C bonds is verified by experimental observations of C—C bond lengths in the coordinated ligands, which are longer than the C—C bond lengths in the isolated alkenes and alkynes.[2b]

C_4H_4 *vs* $(C_2H_2)_2$

The approach initially chosen to determine the role of the two different types of R ligand in the structure of the dimers was to consider a molybdenum complex with two acetylene ligands, *cis*-$(CpMoCl)_2(C_2H_2)_2$ (**3**) and a niobium complex with one C_4H_4 ligand, *trans*-$(CpNbCO)_2(C_4H_4)$ (**4**). Unfortunately, it is not possible to place a ligand such as C_4H_4, which wraps around the dimer in the plane perpendicular to the one containing the metals, on a *trans* frame such as that of the niobium complex. There is no orientation of the ligand that would prevent it from coming in too close proximity to the carbonyl ligands. This in part explains why the niobium dimer bonds to two distinct acetylene units, rather than one C_4H_4 ligand. To bond to the latter, the frame would have to adopt a *cis* configuration.

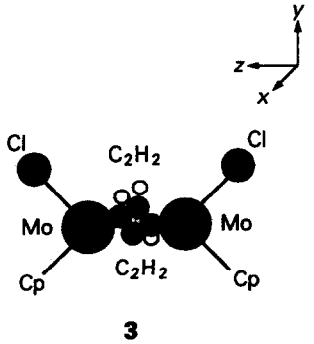

3

On the other hand, there are no difficulties in placing two acetylene units on the molybdenum *cis*-frame.

The molecular orbital diagram for **3** is shown in Fig. 3: the most striking feature of the diagram is the very small HOMO/LUMO gap (0.76 eV), combined with the comparatively large HOMO/SHOMO gap (1.32 eV). This suggests not only that **3** is an unstable complex, but also that oxidizing the molecule by two electrons might produce a more stable system. The fact that **3** is not stable is also confirmed by its total energy, which is higher than the total energy of **1** (see Table 2). Let us now investigate the electronic reasons why the *cis* molybdenum frame prefers one C_4H_4 to two C_2H_2 ligands.

Figures 1 and 3 show the same pattern of valence molecular orbitals consisting of five metal-based levels, two occupied and three unoccupied levels. The large gap that separates the metal-based orbitals from the Cl 3*p* orbitals in **1**, though, shrinks considerably in **3**. This is mostly due to the out-of-phase interaction of some of the chlorine *p* orbitals

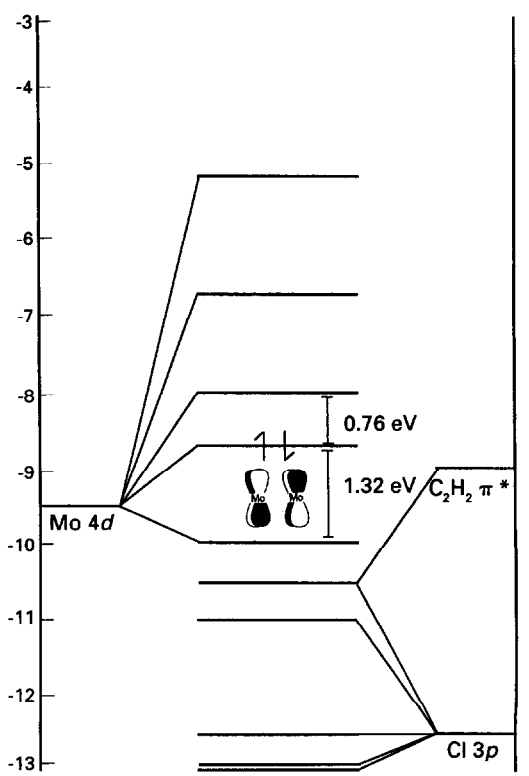

Fig. 3. Molecular orbital diagram for *cis*-$(CpMoCl)_2(C_2H_2)_2$ (**3**).

† See footnote † on p. 1857.

Table 2. Summary of energy considerations

	Total energy[a,b]	HOMO/LUMO gap[a]
cis-(CpMoCl)$_2$(C$_4$H$_4$) (**1**)	−256,219	2.87
cis-(CpMoCl)$_2$(C$_2$H$_2$)$_2$ (**3**)	−256,201	0.76
cis-(CpMoCO)$_2$(C$_4$H$_4$) (**5**)	−237,507	1.9
cis-(CpMoCO)$_2$(C$_2$H$_2$)$_2$ (**7**)	−237,472	1.69
trans-(CpMoCl)$_2$(C$_4$H$_4$) (**9**)	−256,153	1.05
cis-(CpNbCl)$_2$(C$_4$H$_4$) (**12**)	−244,162	0.96
trans-(CpNbCO)$_2$(C$_2$H$_2$)$_2$ (**2**)	−225,407	2.61
trans-(CpNbCl)$_2$(C$_2$H$_2$)$_2$ (**6**)	−244,115	3.43
trans-Cp$_2$Nb$_2$(C$_2$H$_2$)$_2$(μ-Cl)$_2$ (**8**)	−244,187	3.98
cis-(CpNbCO)$_2$(C$_2$H$_2$)$_2$ (**10**)	−225,438	1.61
cis-(CpNbCO)$_2$(C$_4$H$_4$) (**11**)	−225,398	0.49
trans-(CpMoCO)$_2$(C$_2$H$_2$)$_2$ (**13**)	−237,467	1.50

[a] Values in units of eV.

[b] The total energy values for the molecules being analysed should not be taken literally but used for comparison with the other complexes.[17]

with the C_2H_2 π^* level, which causes them to rise in energy, closer to the five valence orbitals.

The difference in the size of the HOMO/LUMO gap between **1** and **3** is due to two factors working together: a lowering in energy of the LUMO and a destabilization of the HOMO. In **1**, the LUMO is mostly metal–metal antibonding, but its energy is raised further by an out-of-phase interaction between the metals and the σ_- orbital on C_4H_4. This interaction disappears in **3**, where there is no C_4H_4 ligand, and the LUMO is consequently lowered in energy. In both molecules, the HOMO contains an antibonding combination of metal-based orbitals. In **1**, it is a bent π interaction between $d_{x^2-y^2}$ and d_{yz} orbitals on both centres, and as such it does not involve a large amount of overlap between the two metals. In fact, only one of the lobes on each centre actually participates in the interaction, and the orbital is not greatly destabilized with respect to the metal *d* atomic orbitals. In **3**, the interaction has δ symmetry and it is between d_{xy} orbitals. Even though δ-type overlap is usually not large, it is still greater than the bent π-type overlap just mentioned. Therefore, the HOMO in **3** is more destabilized than the HOMO in **1**, which contributes to closing the HOMO/LUMO gap.

CO *vs* Cl

In order to determine the influence of the carbonyl and chlorine ligands on the structure of the dimers, two complexes are considered: *cis*-(CpMoCO)$_2$(C$_4$H$_4$) (**5**) and *trans*-(CpNbCl)$_2$(C$_2$H$_2$)$_2$ (**6**). The dimers are identical to the experimentally observed ones, except for having exchanged chlorine and carbonyl ligands.

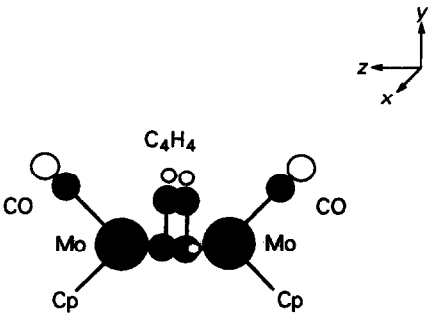

5

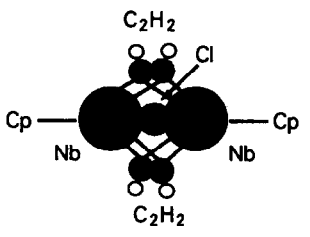

6

Figure 4 shows the influence of the carbonyl ligands on the molecular orbitals of the molybdenum dimer. It is immediately apparent that the empty CO π^* orbitals participate in most of the valence molecular orbitals, both occupied and unoccupied. In particular, the low-lying empty orbitals in **1** are pushed to higher energies by an antibonding interaction between the metals and filled orbitals on the C_4H_4 ligand [σ_+ and σ_-; see

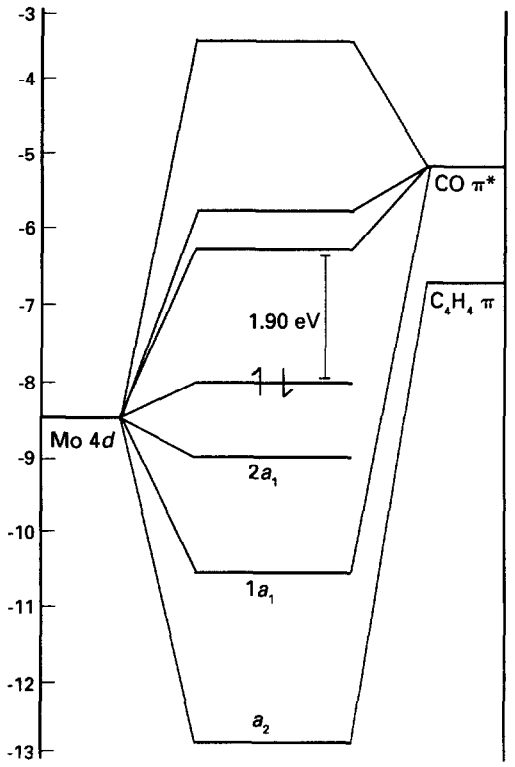

Fig. 4. Molecular orbital diagram for *cis*-$(CpMoCO)_2(C_4H_4)$ (**5**).

Fig. 5(a) and (b)]. In **5** these unoccupied orbitals are lowered in energy because of the participation of CO π^* levels, which substitute the C_4H_4 orbitals in the interaction with the metals. The C_4H_4 σ_+ and σ_- orbitals are instead greatly stabilized by ligand–ligand interaction with cyclopentadienyl π levels and they are found among the low-lying occupied orbitals of **5**. The lowering of unoccupied molecular orbitals in **5** becomes most important in the LUMO, where it contributes to the decrease in the HOMO/LUMO gap. The decreased size of the gap points to the fact that the molybdenum dimer is more stable with chlorine than with carbonyl ligands.

Despite these differences between these two molybdenum dimers, some of the features of their molecular orbital diagrams are similar. Two of the valence orbitals in **5** are analogous to two orbitals in the diagram for **1**: the M—C_4H_4, a_2 bonding orbital (b_2 in **1**), and the SHOMO of the molecule ($2a_1$ in **5** and a_1 in **1**), which is a Mo—Mo bonding interaction. The HOMO of **1**, which has contributions from Mo $d_{x^2-y^2}$ orbitals, is greatly stabilized in **5** (a_1 level) by a bonding interaction with CO π^* levels.

To investigate the effect of coupling and decoupling the R ligand on the *cis*-$(CpMoCO)_2$ frame, an additional calculation was performed on the molecule *cis*-$(CpMoCO)_2(C_2H_2)_2$ (**7**).

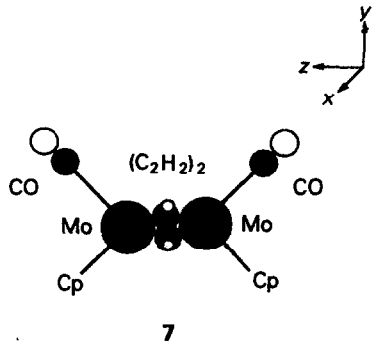

7

Table 2 shows that the dimer with the decoupled ligands (two C_2H_2 moieties) is less stable than its counterpart with the C_4H_4 ligand, both in terms of

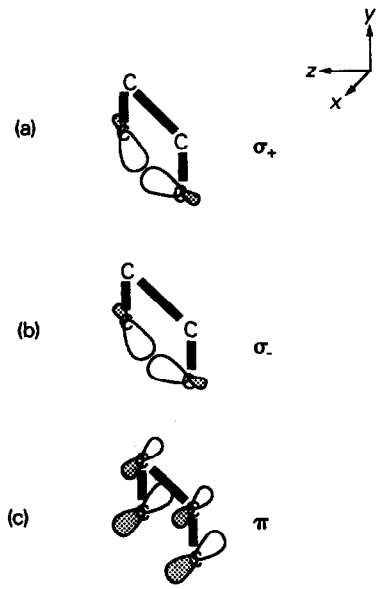

Fig. 5. Valence molecular orbitals of the $(C_4H_4)^{2-}$ ligand which participate in bonding with the metal centres. Orbitals *a* and *b* are filled, orbital *c* is unoccupied.

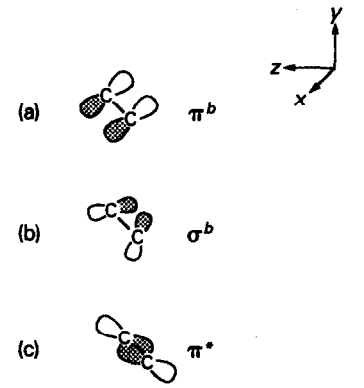

Fig. 6. Valence molecular orbitals of the C_2H_2 ligand which participate in bonding with the metal centres. Orbitals *a* and *b* are filled, orbital *c* is unoccupied.

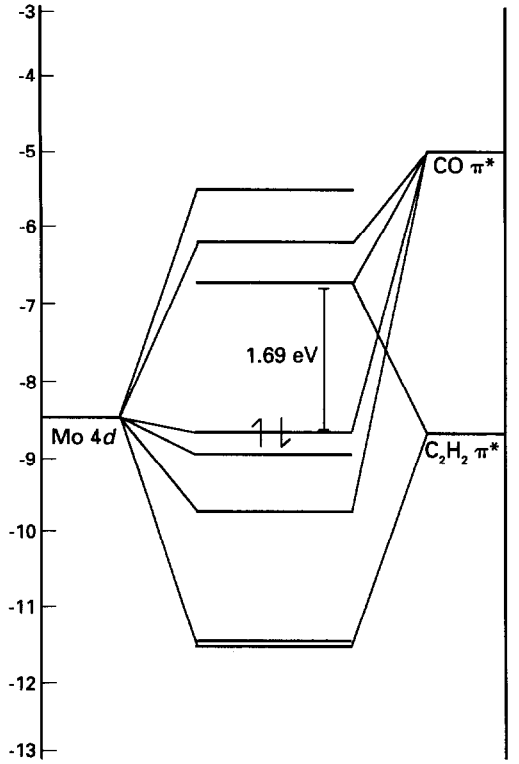

Fig. 7. Molecular orbital diagram for *cis*-(CpMoCO)$_2$ (C_2H_2)$_2$ (**7**).

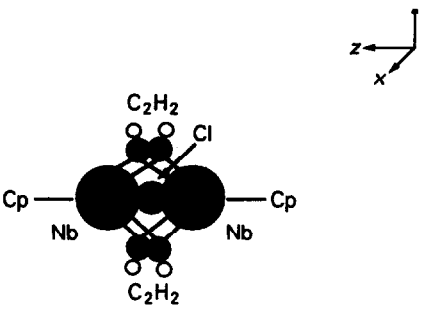

6

of CO π^* levels, which tend to push all low-lying unoccupied orbitals, including the LUMO, to lower energies. Also peculiarly absent in Fig. 8 is the participation of the empty C_2H_2 π^* level in bonding with the metals. In **2**, this bonding interaction is responsible for the stabilization of two valence molecular orbitals (a_u and b_g in Fig. 2); the lack of it causes the occupied valence orbitals of **6** ($1a_g$ and $2a_g$ in Fig. 8) to remain at higher energies. The C_2H_2 π^* levels in **6** contribute instead to a high energy virtual orbital, in which they combine in an antibonding fashion with Nb $d_{x^2-y^2}$ orbitals. In **2** this is not possible, since the $d_{x^2-y^2}$ orbitals form an out-of-phase combination with the CO π^* levels. There-

total energy and of HOMO/LUMO gap. Figure 7 is the molecular orbital diagram for **7**, which explains the stability trend just mentioned. Similarly to what is observed in Fig. 4, the diagram is dominated by the influence of the carbonyl π^* levels on most of the valence molecular orbitals. This pushes the virtual orbitals to lower energies, contributing to the relatively small HOMO/LUMO gap. Also common to both Figs 4 and 7 is the presence of one or more M—R ligand bonding orbitals (involving C_4H_4 π in Fig. 4 and C_2H_2 π^* in Fig. 7). In conclusion, then, the presence of a coupled or decoupled R ligand does not affect the electronic structure of dimers with frame *cis*-(CpMoCO)$_2$ as much as the presence of CO π^* levels does: complexes **5** and **7** show more similarities than differences in their molecular orbital diagrams.

The effect of substituting Cl for CO ligands was also studied for the *trans*-(CpNbCO)$_2$(C_2H_2)$_2$ dimer.

The molecular orbital diagram of **6** is shown in Fig. 8. As indicated on the diagram, the HOMO/LUMO gap for this molecule is quite large, actually larger than the one found in **2**. This is not an entirely surprising result, since some preliminary experiments indicate that **6** might also be an observed structure.[18] Again, the primary reason for the widening of the HOMO/LUMO gap is the absence

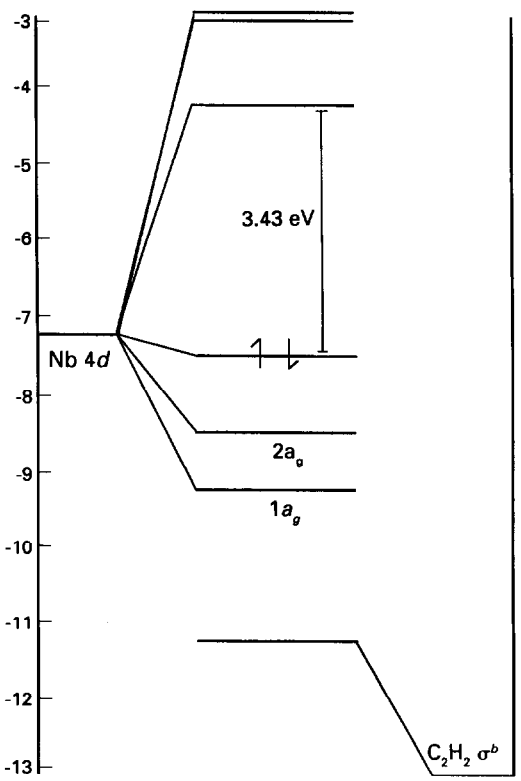

Fig. 8. Molecular orbital diagram for *trans*-(CpNbCl)$_2$(C_2H_2)$_2$ (**6**).

fore, the C_2H_2 π^* levels in **2** are free to combine with other metal orbitals in a bonding fashion, as they do in levels a_u and b_g.

There is one other niobium dimer related to **6** that has been observed experimentally:[12] *trans*-$Cp_2Nb_2(C_2H_2)_2(\mu\text{-}Cl)_2$ (**8**).

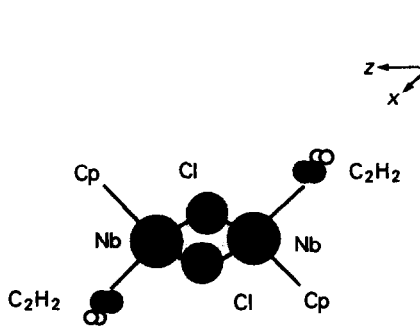

8

In this complex, which is otherwise identical to **6**, the acetylene ligands are terminal and it is the chlorine ligands that are bridging the metals. Figure 9 illustrates the fact that **8** is a stable compound with a large HOMO/LUMO gap (see Table 2 for the total energy value). Figures 8 and 9 show general agreement between the molecular orbitals of these two acetylene chlorine niobium dimers. In both cases there are six valence molecular orbitals, three occupied and three unoccupied. In **8**, all three occupied orbitals are more stabilized with respect to those in **6**. In particular, the two lowest levels are stabilized by a bonding interaction between the metals and the π^* orbitals on the C_2H_2 ligands, since the Nb d_{xy} orbitals have the appropriate symmetry to bond with the π^* levels of the acetylenes in terminal positions. But the principal factor that contributes to the widening of the HOMO/LUMO gap is the stabilization of the HOMO in **8** with respect to that in **6**. The lowering of this molecular orbital is also caused, even though indirectly, by the fact that the acetylenes in their new terminal positions are ideally suited to interact with the Nb d_{xy} orbitals. In **6**, the HOMO is a bonding combination of metal d_{z^2} and d_{xy} orbitals; while in **8**, because the d_{xy} orbitals participate in levels $1a_2$ and $2a_2$, the HOMO is just d_{z^2} in character. Therefore, the HOMO in the dimer with the bridging acetylenes has bent-π symmetry with a small overlap between centres and little stabilization; while the HOMO in the dimer with the bridging chlorines has σ symmetry, which leads to a larger stabilization of the molecular orbital.

† For details on the geometries of these two complexes, see the Computational Procedure section of this paper.

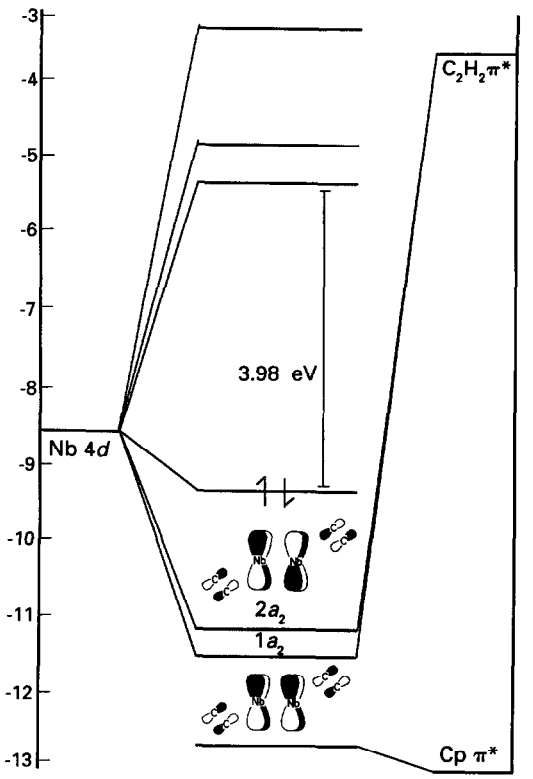

Fig. 9. Molecular orbital diagram for *trans*-$Cp_2Nb_2(C_2H_2)_2(\mu\text{-}Cl)_2$ (**8**).

Cis *vs* trans

The last factor to be considered is the *cis* vs *trans* comformation of the dimers. To this purpose, calculations on two additional complexes were carried out: *trans*-$(CpMoCl)_2(C_4H_4)$ (**9**) and *cis*-$(CpNbCO)_2(C_2H_2)_2$ (**10**).†

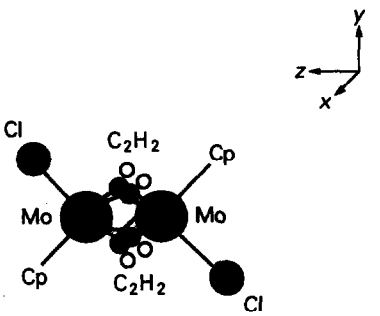

9

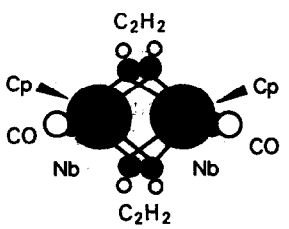

10

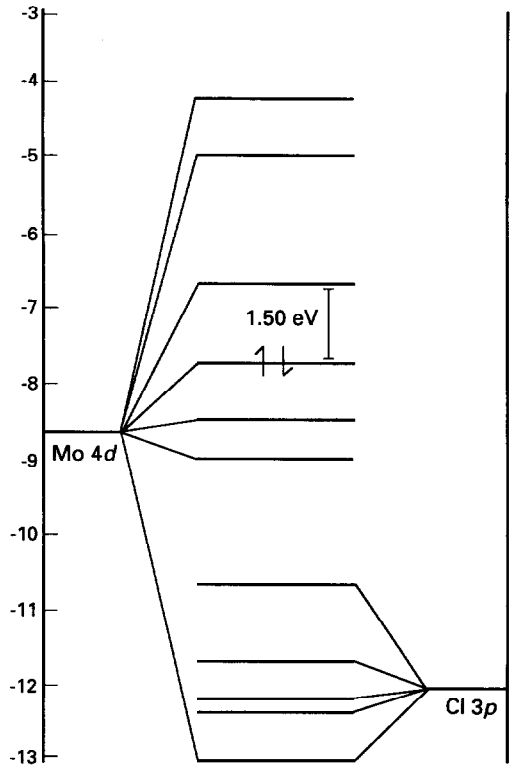

Fig. 10. Molecular orbital diagram for *trans*-(CpMoCl)$_2$ (C$_4$H$_4$) (**9**).

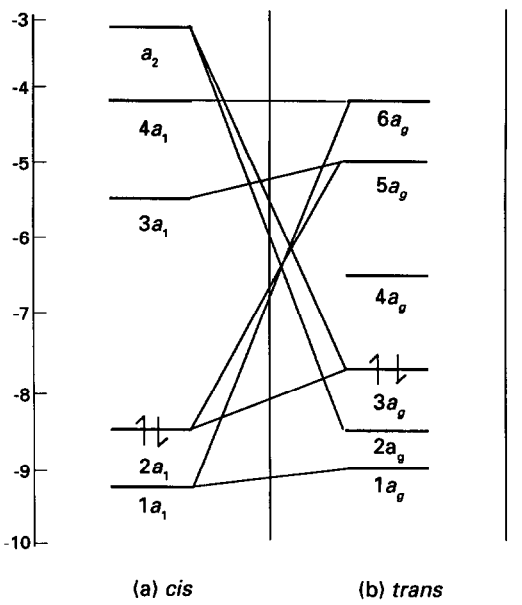

Fig. 11. Comparison of the valence molecular orbitals of **1** from Fig. 1(a) and those of **9** in Fig. 10(b). The lines between orbitals indicate how the orbitals in **a** mix give rise to the orbitals in **b**.

Figure 10 shows the molecular orbital diagram for **9**: when it is compared to the diagram in Fig. 1, it becomes apparent that the gross features in the two diagrams are roughly the same. There is a series of low-lying, ligand-based orbitals separated by a gap from metal-based, occupied and unoccupied valence orbitals. Because of the change in symmetry from *cis* to *trans*, though, much mixing of the molecular orbitals occurs and it becomes difficult to follow how each level changes in going from Fig. 1 to 10. Figure 11 gives some indication of the mixing that is occurring: the HOMO and SHOMO of the *cis* complex loosely translate into levels $1a_g$ and $3a_g$ of the *trans* complex. Similarly, the two lowest unoccupied orbitals of the *cis* dimer are related to $5a_g$ and $6a_g$ levels in the *trans* dimer; level $2a_g$ in part (b) of the figure, the SHOMO of the complex, most resembles the highest unoccupied level shown for the *cis* complex. The LUMO of the *trans* dimer is the only level that seems to have no counterpart in the *cis* dimer: it is a mixture of d_{yz} orbitals on both metal centres. Actually, this orbital plays a big role in making the *trans* molecule less stable than the *cis* one: its position between the HOMO and LUMO of part (a) of the figure is responsible for the markedly decreased size of the HOMO/LUMO gap (see Table 2). In summary, then, the *trans* conformation of the molybdenum dimer is less stable, according to both the total energy and the HOMO/LUMO gap, than the *cis* conformation. This arises from the presence of a new, metal-based level positioned between the HOMO and the LUMO. This orbital, which becomes the LUMO of the *trans* dimer, is mostly metal d_{yz} in character, but it is difficult to trace it back to the **1** dimer because of the extensive mixing occurring among the valence molecular orbitals.

Figure 12 shows the molecular orbital diagram for **10**, *cis*-(CpNbCO)$_2$(C$_2$H$_2$)$_2$. The overall pattern of orbitals in Figs 2 and 12 is similar: two, low-lying, metal-to-C$_2$H$_2$ π^* bonding orbitals (one for each metal centre); HOMO and SHOMO orbitals that are close in energy, are stabilized with respect to the niobium *d* atomic levels only to a small extent, and are Nb—CO π^* bonding in character; and three unoccupied orbitals that are mostly CO π^* in character. Despite these similarities, the HOMO/LUMO gap in **10** is significantly smaller than that in **2** (see Table 2), pointing to the fact that the *cis* dimer is not as stable as the *trans* conformation. This happens mostly because in **10** the first two virtual orbitals are significantly lower in energy. Unfortunately, an in depth examination of the atomic orbital contributions to these molecular levels gives no indication of why the lowering in energy occurs. Again, the transformation from *trans* to *cis* involves a change in symmetry for the

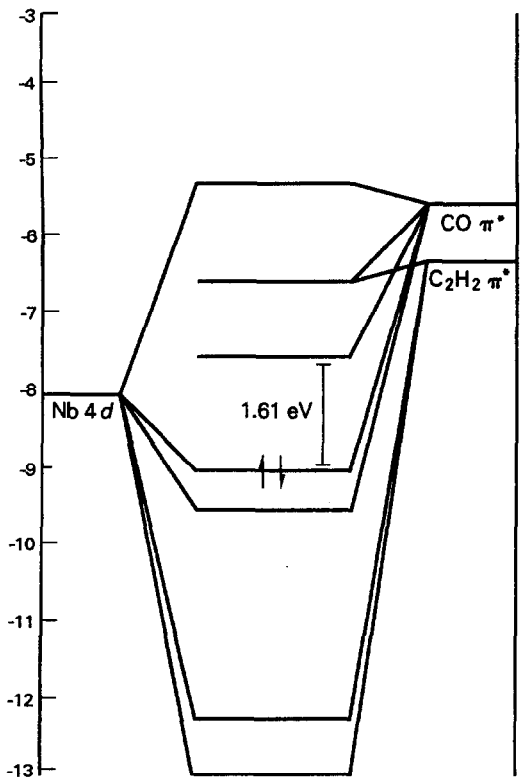

Fig. 12. Molecular orbital diagram for *cis*-$(CpNbCO)_2(C_2H_2)_2$ (**10**).

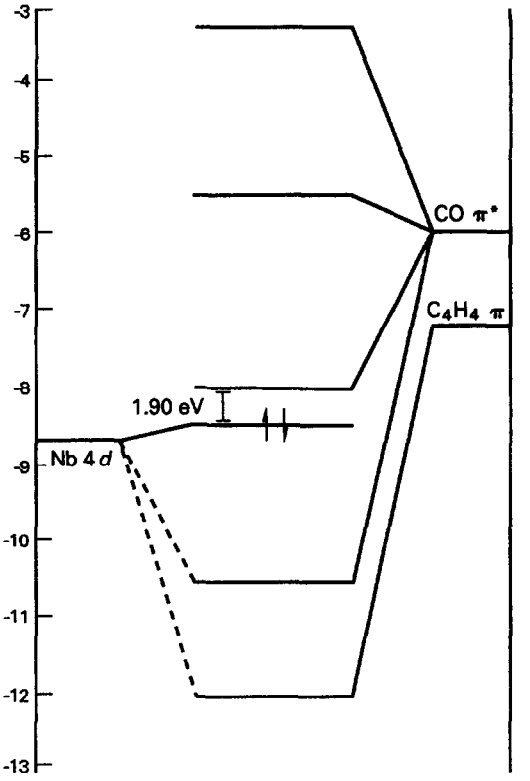

Fig. 13. Molecular orbital diagram for *cis*-$(CpNbCO)_2(C_4H_4)$ (**11**). (Dotted lines indicate minor contributions.)

molecule and extensive mixing of the orbitals, which makes it difficult to trace changes in the composition of the levels. In addition, Table 2 shows that **10** has a lower total energy value than **2**, which is contrary to the trend in HOMO/LUMO gap mentioned above. This suggests that **2** might be a kinetically, but not thermodynamically, stable product.

One possible thermodynamic product would be *cis*-$(CpNbCO)_2(C_4H_4)$ (**11**), where the acetylene ligands in **2** have been coupled.

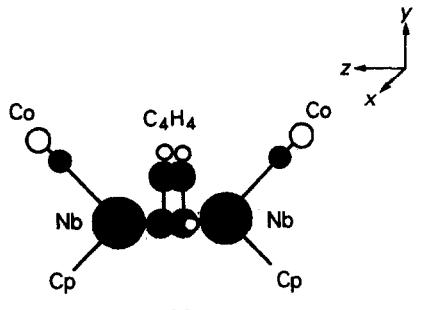

11

As previously mentioned, because of steric hindrance, which makes it impossible for the C_4H_4 ligand to exist in a *trans* dimer, **11** has also been made *cis*. Figure 13 shows the molecular orbital diagram of this complex. Both the HOMO/LUMO gap and total energy of the compound (see Table 2) indicate that **11** is in fact very unstable, with the smallest gap and highest energy of all the niobium dimers in the table. This is mostly due to the low-lying LUMO, which is mainly CO π^* in character. The carbonyl contribution pushes the molecular orbital particularly low in this complex because of the lack of metal *d* orbitals participation that usually destabilizes the virtual levels. It is a general trend, however, that the presence of carbonyl ligands in the dimers investigated in this work always causes the first few virtual orbitals to be low in energy because of contributions from CO π^* levels. This lies at the root of the instability of such complexes. If the thermodynamically stable complex related to **2** contains one or more carbonyl ligands, then it is possible that its structure be radically different from that of the dimer, in order for the complex to remain stable.

Overall influence of the three geometric factors

The last set of calculations involves substituting molybdenum atoms in the frame of **2** and niobium atoms in the frame of **1**. Analysing the results of calculations on *cis*-$(CpNbCl)_2(C_2H_4)$ (**12**) and *trans*-$(CpMoCO)_2(C_2H_2)_2$ (**13**) should help sum-

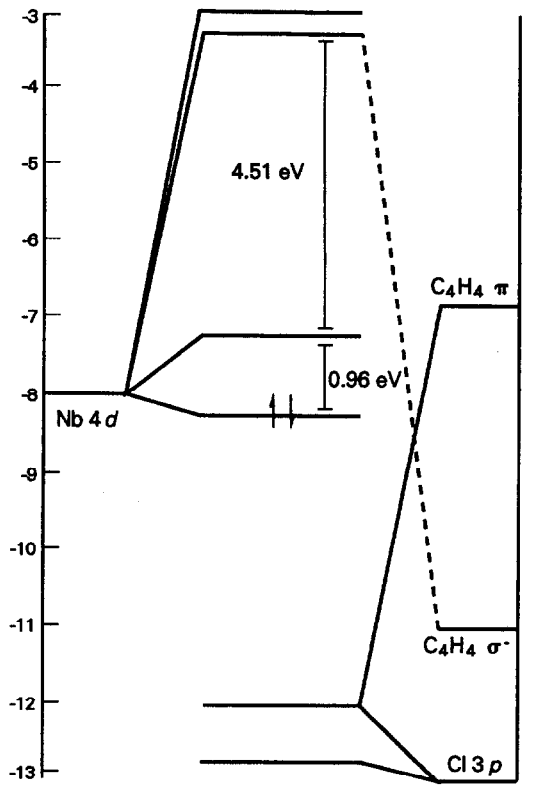

Fig. 14. Molecular orbital diagram for *cis*-(CpNbCl)$_2$(C$_4$H$_4$) (**12**).

marize the influence of all three geometric factors on the preferred geometry of the dimers and shed light on the reasons why molybdenum metals prefer a geometry like that in **1** and niobium metals prefer a **2**-type frame. The geometries of **12** and **13** are identical to those of **1** and **2**, except for the fact that the metals have been exchanged.†

Figure 14 is the molecular orbital diagram for **12**: the pattern of two, closely spaced orbitals that are almost degenerate with the metal *d* levels, plus two (or three) high-lying orbitals is the same in the diagrams of both **1** and **12** (compare Figs 1 and 14). In the case of **12**, though, the number of valence electrons is two less than that of **1**, since the metal centres are niobium and not molybdenum. Therefore, in **12** the HOMO and LUMO are closely-spaced levels around the metal *d* orbitals and consequently the gap between them is only 0.96 eV. This leads to the conclusion that **12** would be a very unstable complex. In fact, the gap between the first- and second-lowest virtual orbitals is so large (4.51 eV) as to suggest that a reduced form of the complex might be stable.

When molybdenum centres are substituted into the frame of dimer **2**, some changes occur in the character of the valence molecular orbitals. Figure 15 shows the diagram for **13**, which can be compared to that of **2**, in Fig. 2. They both show two, low-lying, metal-to-C$_2$H$_2$ π^* bonding orbitals and two, metal-based, moderately bonding orbitals. These last two levels are the HOMO and SHOMO of **2**, but in **13**, because of the extra valence electron in molybdenum with respect to niobium, there is an additional occupied level (a_g in Fig. 15). This orbital contributes to the bonding between the molybdenum centres and receives contributions from three molybdenum atomic orbitals. Since the a_g orbital comes between the HOMO and LUMO of Fig. 2, it substantially decreases the HOMO/LUMO gap of **13**, which in turn results in an unstable system.

CONCLUSIONS

From this series of calculations, a number of conclusions about the title compounds and related dimers can be drawn. Patterns of orbital symmetries and energies become apparent and it can be determined how they are influenced by the geometric structure and the type of ligands on the dimers. The principal question asked in this paper is why the two dimers assume different geometric configurations,

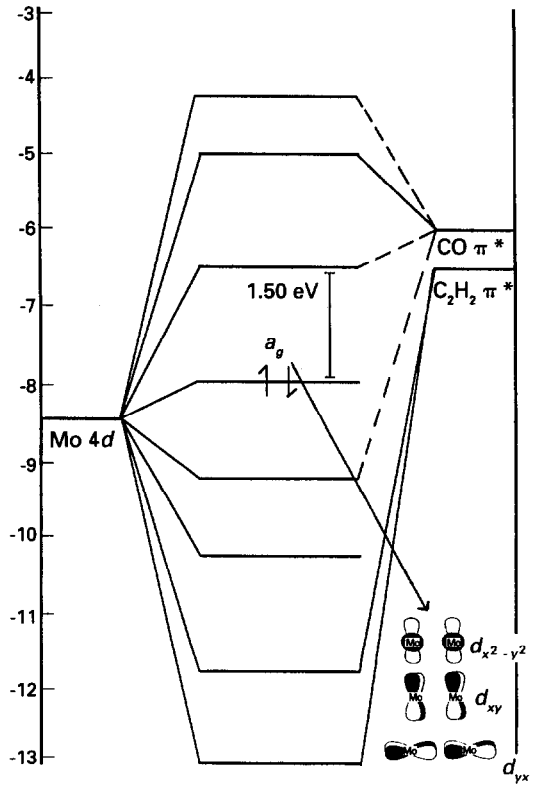

Fig. 15. Molecular orbital diagram for *trans*-(CpMoCO)$_2$(C$_2$H$_2$)$_2$ (**13**). (Dotted lines indicate minor contributions.)

† See footnote † on p. 1862.

when both clusters have the same number of valence electrons. The question is best answered by looking at Figs 14 and 15 and contrasting them with Figs 1 and 2. Such a comparison shows that each metal assumes the configuration that yields the largest HOMO/LUMO gap and therefore the most stable complex. If the metal is placed in the frame of the other complex, the difference in the number of metal valence electrons reduces the HOMO/LUMO gap drastically, which in turn diminishes the stability of the complex. Both the niobium and the molybdenum centres, therefore, assume the geometry that is appropriate to their number of valence electrons and type of ligands.

In examining the role of chlorine and carbonyl ligands in the dimers, it is also apparent that the π donor (Cl^-) has little influence on the valence molecular orbitals of the complex, since its p orbitals are found among the low-lying, filled levels of the molecule. On the other hand, the π acceptor ligand (CO) has a very strong influence on the molecular orbital composition of the complex, since its π^* virtual levels make up the majority of the low-energy, unoccupied orbitals of the molecule. The CO π^* influence usually leads to a lowering in the energy of such orbitals, and therefore it can potentially decrease the stability of the dimer.

When the coupled and decoupled forms of the R ligand (C_4H_4 and two C_2H_2) are compared, no dramatic differences are found. Both contribute to the bonding in the molecule with two, low-lying, filled levels that donate σ or π electron density to the metals and one virtual, π-type level that is used for metal-to-ligand backbonding (see Figs 5 and 6). The latter interaction gives rise to one (in the case of C_4H_4) or two (in the case of C_2H_2) markedly bonding molecular orbitals that have energies between those of the valence levels and those of the low-lying M—L and L—L levels.

The series of related compounds that has been investigated in this work could be augmented by additional, experimentally observed dimers which are variations on the basic geometries included in this paper.[19] In addition, more could be predicted based on the electronic factors influencing stability which are discussed above.[2b,12] Furthermore, there are other unanswered questions regarding these geometries, such as the relationship between substituent groups on the R ligands, their electron-withdrawing capabilities and bond angles and lengths in the complex.

REFERENCES

1. (a) M. D. Curtis, L. Messerle, N. A. Fotinos and N. F. Gerlach, *Am. Chem. Soc. Symps. Ser.* 1981, No. **155**, 221–257; (b) J. J. D'Errico and M. D. Curtis, *J. Am. Chem. Soc.* 1983, **105**, 4479.
2. (a) A. N. Nesmeyanov, A. I. Gusev, A. A. Pasynskii, K. N. Amisimov, N. E. Kolobova and Yu. T. Struchkov, *J. Chem. Soc., Chem. Commun.* 1969, 277; (b) A. N. Nesmeyanov, A. I. Gusev, A. A. Pasynskii, K. N. Amisimov, N. E. Kolobova and Yu. T. Struchkov, *J. Chem. Soc., Chem. Commun.* 1968, 1365.
3. W. Hirpo and M. D. Curtis, *J. Am. Chem. Soc.* 1988, **110**, 5218.
4. These diagrams were generated with the program Molecular Editor for the Apple Macintosh system, which was developed by Allan L. Smith, Drexel University.
5. M. B. Hall and R. F. Fenske, *Inorg. Chem.* 1972, **11**, 768.
6. The IBM 3090-600 computer is part of the Michigan Terminal System (MTS) at the University of Michigan.
7. E. Clementi, *J. Chem. Phys.* 1964, **40**, 1944.
8. D. D. Radtke, PhD thesis. University of Wisconsin, Madison, Wisconsin (1966).
9. S. Herman and S. Skillman, *Atomic Structure Calculations*. Prentice Hall, Englewood Cliffs, New Jersey (1963).
10. I. N. Levine, *Quantum Chemistry*, p. 375. Allyn and Bacon, Boston (1983).
11. M. C. Milletti, PhD thesis. University of Wisconsin, Madison, Wisconsin (1987).
12. M. D. Curtis and J. Real, *Organometallics* 1985, **4**, 940.
13. C. M. Lukehart, *Fundamental Transition Metal Organometallic Chemistry*, p. 58. Brooks/Cole Publishing, Monterey, California (1985).
14. F. A. Cotton and G. Wilkinson, *Advanced Inorganic Chemistry*, p. 835. John Wiley, New York (1980).
15. R. L. De Kock, PhD thesis. University of Wisconsin, Madison, Wisconsin (1970).
16. A. I. Gusev, N. I. Kirillova and Yu. T. Struchkov, *Zh. Strukt. Khim.* 1970, **11**, 62.
17. M. C. Milletti and R. F. Fenske, *Organometallics* 1989, **8**, 420.
18. Unpublished results.
19. (a) S. A. Knox, R. F. Stansfield, F. G. A. Stone, M. J. Winter and P. Woodward, *J. Chem. Soc., Dalton Trans.* 1982, 173; (b) G. Dettlaf and E. Weiss, *J. Organomet. Chem.* 1976, **108**, 213; (c) M. H. Chisholm, D. M. Hoffman and J. C. Huffman, *J. Am. Chem. Soc.* 1984, **106**, 6806.

Polyhedron Vol. 9, No. 15/16, pp. 1867–1881, 1990
Printed in Great Britain

0277–5387/90 $3.00+.00
© 1990 Pergamon Press plc

THE ORIGIN OF STRUCTURAL VARIETY OF ALKYNE COMPLEXES OF d^8 METALS. AN EXAMPLE OF STRUCTURAL ISOMERISM†

GREGORY MARINELLI, WILLIAM E. STREIB, JOHN C. HUFFMAN and KENNETH G. CAULTON‡

Department of Chemistry and Molecular Structure Center, Indiana University, Bloomington, IN 47405, U.S.A.

and

MICHEL R. GAGNÉ and JOSEF TAKATS

Department of Chemistry, University of Alberta, Edmonton, Alberta, Canada T6G 2G2

and

MICHÈLE DARTIGUENAVE

Laboratoire de Chimie de Coordination, CNRS, 205 Route de Narbonne, 31077 Toulouse, France

and

CATHERINE CHARDON, SARAH A. JACKSON and ODILE EISENSTEIN‡

Laboratoire de Chimie Théorique, Centre de Paris-Sud, 91405 Orsay, France

Abstract—The X-ray structures of three metal alkyne complexes are presented: $Ir(PMe_2Ph)_3(MeC_2Me)^+$, $M(CO)_4(F_3CC_2CF_3)$ (M = Ru, Os). The iridium(I) complex adopts an unusual structure ("CS") which differs notably from that expected for four-coordinate d^8 ML_4 square-planar complexes. The structure resembles that of a square pyramid, with essentially C_s symmetry, with a short apical M—P bond (2.236 vs 2.31 Å for the basal M—P bonds), short M—C (2.01 Å) and long C—C bonds (1.306 Å), which indicate a strong metal–alkyne interaction. The ruthenium(0) and osmium(0) complexes adopt the expected pseudo-octahedral structure. The unusual CS structures, previously reported for cobalt(I) and iron(0) complexes, contrast with the square-planar structure of platinum(II) alkyne complexes. Fluxionality is present in the iridium complex, as well as in those of cobalt, and is attributed to a rapid intramolecular site exchange among inequivalent phosphorus ligands. The iridium complex reacts with additional ligands like alkynes and H_2. Extended Hückel calculations are presented to rationalize the structural and reactivity aspects of the whole family of d^8 ML_3(alkyne) species (M = Pt^{II}, Ir^{I}, Co^{I}, Fe^{0}). It is shown that the four-electron donation of an alkyne ligand is responsible for the unusual CS structure of certain of these ML_3(alkyne) species. The alkyne moieties induce a four-electron destabilization in the square-planar structure which is large for diffuse *d* orbitals such as those of iridium(I), cobalt(I), iron(0), but not of platinum(II). The fluxionality of the complexes is shown to be associated with an easy rotation of the alkyne about the metal–alkyne midpoint,

† This paper is dedicated to Richard Fenske for the advice and stimulus he provided to his student, K.G.C.

‡ Authors to whom correspondence should be addressed.

accompanied by a breathing motion of the M—L bonds of the ML_3 metal fragment. It is shown that unsymmetrical alkynes stabilize a conformation of the complex in which the ligand is turned by 90° with respect to the one presented here. The reactivity towards additional ligands is shown to be associated with the presence of a low-lying LUMO pointing away from the apical bond. Effects of substituents at the alkyne and of ligands at the metal are discussed. It is shown that it is the residual four-electron destabilization in $M(CO)_4$(alkyne) complexes which is responsible for the lability of CO ligands and thus for the ligand exchange process.

A number of ligands have the ability to exist in structurally isomeric forms (e.g. acyl, NO, CO_2, SO_2, alkyl, **1**). Such isomerism is associated with a change in the number of ligand electrons shared with the metal valence orbitals. Most often the isomeric bonding forms are identifiable by clearly defined structural changes, but there are a few cases where the structural changes are quite subtle and thus difficult to perceive even when accurate structural parameters are known. One such example is the alkyne ligand. Here, in the absence of clearly diagnostic structural changes with change in electron donor number, molecular stoichiometry is used to evaluate the donor number of the alkyne moieties. Thus, it is conventional to perform a valence electron count on the fragment ML_n to which the alkyne is attached. If it is a 16-electron fragment, alkyne→M donation from only one of the two orthogonal alkyne π orbitals is assumed ("two-electron donor alkyne"). If it is a 14-electron fragment, donation from both alkyne π orbitals *may* take place. The reason for the qualification on this latter conclusion is that, for certain early and late metals, a 16-valence electron count is found in many isolable compounds. For example, in the case to be considered here, iridium(I) and platinum(II) are frequently "content" with a 16-valence electron count, and thus the above method does not lead to a clear deduction about the alkyne–metal bonding in such ML_3(alkyne) complexes.

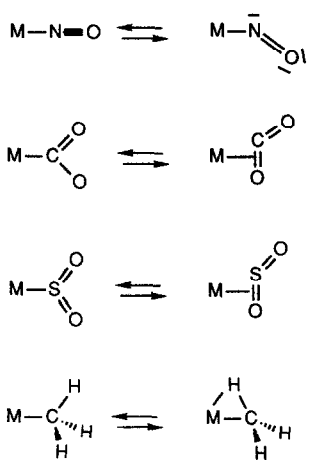

1

Scheme 1.

An interesting question that immediately arises concerns the consequences of having a ligand able to donate more electrons to the metal than this centre may accept. For instance, the well-known tendency of two-electron donor terminal alkynes to rearrange to vinylidene ligands [eq. (1)] may be rationalized by noting that such rearrangement diminishes the repulsion between the unused alkyne π-system and the filled metal *d* orbitals.[1] Internal alkynes in two-electron donor situations do not have this outlet, however.

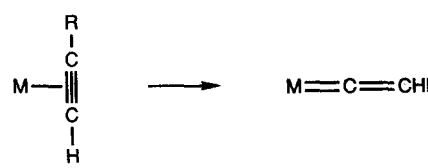

(1)

The present work offers structural results on some relevant compounds, an analysis of the bonding in several of the problematic situations identified above, and a rationalization of the observed chemical reactivity for each.[2]

EXPERIMENTAL

General procedures

All manipulations were performed under purified N_2 or Ar using standard Schlenk techniques or a Vacuum Atmospheres glove box. Solvents were dried and deoxygenated by distillation over Na/K-benzophenone ketyl under N_2. Methylene chloride was distilled over P_2O_5 under N_2, then subjected to a minimum of three freeze–pump–thaw degassing cycles to remove residual O_2.

Proton and phosphorus NMR spectra were

obtained on a Nicolet NT-360 at 360 and 146 MHz, respectively. Carbon NMR spectra were recorded on either a Nicolet NT-360 (91 MHz) or Bruker AM-500 (125 MHz). Proton chemical shifts are reported in units of δ (ppm downfield from tetramethylsilane) and were measured relative to residual solvent protons. Carbon shifts are reported in units of δ (ppm downfield from tetramethylsilane) and were measured relative to solvent absorption. Phosphorus shifts are reported in units of δ (ppm downfield from external 85% H_3PO_4).

Preparation of $[Ir(PMe_2Ph)_3(MeO_2CC_2CO_2Me)_2]BF_4$

(1) *Reaction of* $[Ir(PMe_2Ph)_3(C_2Me_2)]BF_4$ *with* $MeO_2CC_2CO_2Me$. $[Ir(PMe_2Ph)_3(C_2Me_2)]BF_4$ (51 mg, 0.084 mmol) was placed in a Schlenk flask under N_2. THe solid was then dissolved in CH_2Cl_2 (10 cm^3), after which $MeO_2CC_2CO_2Me$ (0.042 cm^3, 0.34 mmol) was added by syringe. The solution was stirred for 10 h, resulting in no apparent colour change. Solvent and excess $MeO_2CC_2CO_2Me$ was removed *in vacuo*, quantitatively giving $[Ir(PMe_2Ph)_3(MeO_2CC_2CO_2Me)_2]BF_4$ as a red oil.

(2) *By reaction of* $[IrH_4(PMe_2Ph)_3]BF_4$ *with* $MeO_2CC_2CO_2Me$. To a CH_2Cl_2 solution containing $[IrH_4(PMe_2Ph)_3]BF_4$ (0.085 mmol) was added $MeO_2CC_2CO_2Me$ (0.05 cm^3, 0.41 mmol, 5 equiv) by syringe. After 30 min of stirring, the originally pale yellow solution had changed to dark orange. The solvent was removed *in vacuo*, and THF (4 cm^3) was added to precipitate a red solid. The solution was concentrated to half its original volume to promote further precipitation, and the product was filtered.

^1H NMR (CD_2Cl_2): 7.4–7.1 (m, 15H), 3.91 (s, 6H), 3.78 (s, 6H), 1.87 (d, $J = 11$ Hz, 6H), 1.39 (vt, $J = 6$, 12H); ^{31}P NMR (CD_2Cl_2) −41.9 (d, $J = 16$), −57.3 (t, $J = 16$); ^{13}C {^1H} NMR (CD_2Cl_2, 125 MHz): 160.1 (s), 160.0 (s), 128–131 (phenyl), 81.9 (d, $J = 9$ Hz), 79.4 [d ($J = 24$) of t ($J = 36$)], 54.24 (s), 53.36 (s), 17.98 (d, $J = 36$), 11.71 (vt, $J = 37$).

X-ray structure determination of $[Ir(MeC_2Me)(PMe_2Ph)_3]BF_4$

A suitable crystal was cleaved from a larger piece grown by layering Et_2O onto a 1,2-dimethoxyethane solution of the compound. The crystal was mounted using silicone grease and transferred to a goniostat where it was cooled to −139°C for characterization and data collection

Table 1. Selected bond distances (Å) and angles (°) for $[Ir(MeC_2Me)(PMe_2Ph)_3]BF_4$

Bond distances (Å)			
Ir1—P2	2.3090(15)	P11—C12	1.824(7)
Ir1—P11	2.3119(15)	P11—C13	1.817(7)
Ir1—P20	2.2355(15)	P11—C14	1.826(6)
Ir1—C30	2.016(5)	P20—C21	1.809(6)
Ir1—C31	2.014(6)	P20—C22	1.809(6)
C29—C30	1.487(8)	P20—C23	1.813(6)
C30—C31	1.306(8)	F34—B33	1.377(8)
C31—C32	1.485(8)	F35—B33	1.390(8)
P2—C3	1.826(6)	F36—B33	1.391(10)
P2—C4	1.826(6)	F37—B33	1.393(10)
P2—C5	1.828(6)		

Bond angles (°)			
P2—Ir1—P11	106.14(5)	Ir1—C30—C31	71.0(3)
P2—Ir1—P20	90.62(5)	C29—C30—C31	143.7(6)
P2—Ir1—C30	137.35(16)	Ir1—C31—C30	71.2(3)
P2—Ir1—C31	104.37(16)	Ir1—C31—C32	149.8(4)
P11—Ir1—P20	94.07(5)	C30—C31—C32	138.9(6)
P11—Ir1—C30	99.37(17)	F34—B33—F35	110.4(5)
P11—Ir1—C31	135.07(16)	F34—B33—F36	109.2(6)
P20—Ir1—C30	121.34(15)	F34—B33—F37	108.8(7)
P20—Ir1—C31	117.80(16)	F35—B33—F36	109.3(7)
C30—Ir1—C31	37.82(22)	F35—B33—F37	109.5(6)
Ir1—C30—C29	145.1(4)	F36—B33—F37	109.7(6)

($6° \leqslant 2\theta \leqslant 45°$).[3] A systematic search of a limited hemisphere of reciprocal space revealed intensities with Laue symmetry and systematic absences consistent with space group $P2_1/n$. After correction for absorption, data processing gave a residual of 0.027 for 529 unique intensities which had been measured more than once. Four standards measured every 300 data showed no systematic trends.

The structure was solved using a combination of direct methods (MULTAN78) and Fourier techniques. After the non-hydrogen atoms had been located and refined, a difference Fourier map revealed most of the hydrogen atoms. All hydrogen atoms are placed in calculated positions prior to the final cycles of least-squares in which the non-hydrogen atoms were refined with anisotropic thermal parameters and the hydrogen atoms were refined with isotropic thermal parameters.

The final difference map had a residual near iridium of 2 e/Å^3. All other residual peaks were well under 1 e/Å^3. The results† of the X-ray study are shown in Table 1 and Figs 1 and 2. Additional details are available as supplementary material. Refined C—H distances range from 0.84(7) to 1.18(8) Å.

X-ray diffraction study of $M(CO)_4(F_3CC_2CF_3)$ (M = Ru, Os)

A suitable crystal of the osmium compound was located and transferred to the goniostat using inert atmosphere handling techniques and cooled to −155°C for characterization and data collection.[3]

A systemetic search of a limited hemisphere of reciprocal space located a set of diffraction maxima with symmetry and systematic absences corresponding to the unique monoclinic cell $P2_1/n$. Subsequent solution and refinement of the structure confirmed this choice. Data were reduced to a unique set of intensities and associated sigmas in the usual manner. There was not significant decomposition at −155°C, based on the intensities of four standards monitored every 2 h.

The structure was solved by a combination of direct methods (MULTAN78) and Fourier techniques. Data were corrected for absorption before the final anisotropic refinement. A final difference Fourier indicated several other peaks of intensity 1.8–2.2 e/Å^3 in the vicinity of the osmium atom and no other features. The large "ripples" near the osmium are probably due to an inaccurate absorption correction. The results† of the structural study are shown in Table 2 and Fig. 3.

The ruthenium compound is isomorphous and the data collection proceeded as for M = Os. No absorption correction was necessary. A final different Fourier was featureless, the largest peak being 0.7 e/Å^3. The atom numbering is identical to that of the osmium analogue.

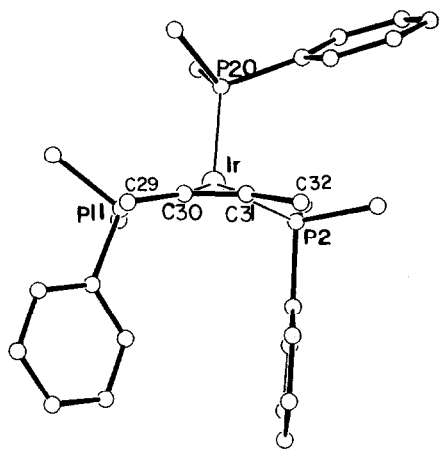

Fig. 1. ORTEP view of the cation $Ir(MeC_2Me)(PMe_2Ph)_3^+$, omitting hydrogens and showing selected atom labelling. This view emphasizes the approach to square-pyramidal geometry, with iridium lying above the approximate planar array of P11, P2, C30 and C31.

RESULTS

Structure of $Ir(MeC_2Me)(PMe_2Ph)_3BF_4$

$Ir(MeC_2Me)(PMe_2Ph)_3BF_4$ exists in the solid state as non-interacting $Ir(MeC_2Me)(PMe_2Ph)_3^+$ and BF_4^- ions. The closest approach of fluorine to iridium is 5.54 Å. The coordination geometry about iridium in the cation (Fig. 1) is clearly not planar or even distorted planar. Because of the large disparity in P—Ir—P angles (90.6, 94.0 and 106.1°) and Ir—P distances (2.309, 2.312 and 2.236 Å), it is equally inappropriate to characterize the coordination geometry as distorted tetrahedral. The one (idealized, non-crystallographic) symmetry element of the cation is a mirror plane containing P20, Ir and the C30—C31 midpoint. The phosphorus in this mirror plane has a dramatically shorter Ir—P distance than those involving the pair of "symmetry related" phosphines. To this "mirror symmetry" description can be added the observation that P2,

† Supplementary material available, anisotropic thermal parameters, parameters of the crystal and data collection, and all distances and angles have been deposited with the Cambridge Crystallographic Data Centre, University Chemical Laboratory, Lensfield Road, Cambridge CB2 1EW, U.K.

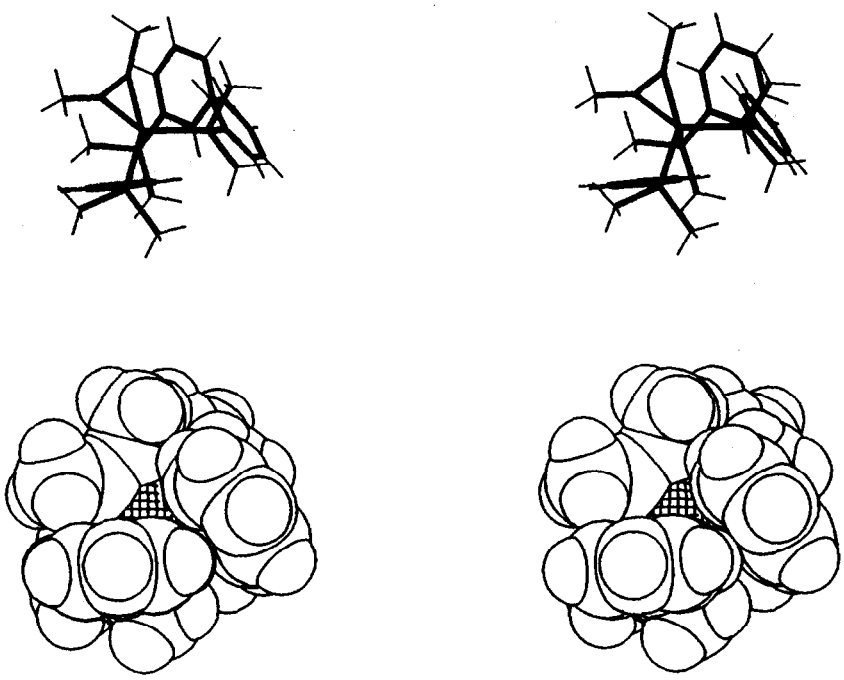

Fig. 2. Stereo stick figure and space-filling drawings of $Ir(MeC_2Me)(PMe_2Ph)_3^+$ from the direction opposite P20. The hatched atom is iridium. All C—H distances have been drawn at 1.08 Å.

P11 and alkyne carbons C30 and C31 are nearly planar (to ±0.04 Å), with iridium 0.49 Å above this plane (Fig. 1). Thus, because of the unique position of P20, the coordination geometry might be called quasi-trigonal planar (alkyne midpoint considered as one site) to which has been added a tightly bound P20 on the *pseudo*-three-fold axis. Alternatively (alkyne carbons considered as individual ligands), it might be described as square pyramidal. Consistent with both descriptions is the fact that the coordination sphere is fairly open (but shielded by *two* phenyl groups) *trans* to P20 (Fig. 2). There are no Ir···*ortho*-H distances short enough to suggest agostic donation; the shortest distance is 3.24 Å.

The Ir—P2 and Ir—P11 distances are indistinguishable from the Rh—P distances in $Rh(PMe_2Ph)_4^+$,[4] so it is the Ir—P20 distance which is unusually short. While the alkyne C30—C31 distance (1.306(8) Å) is lengthened from that in the free alkyne (1.213(1) Å),[5] such lengthening is not dramatically greater than in other coordinated alkynes.[6,7] Likewise, the $H_3C—C{\equiv}C$ angles here (138.9 and 145.7°) are quite unexceptional for coordinated alkynes. The Ir—C distances, however (2.01 Å), are remarkably shorter than the single bond Ir—C distances in *fac*-$IrMe_3(PMe_2Ph)_3$ (2.159 Å).[8] Both the unusual coordination geometry and the very short Ir—C and Ir—P20 distances require explanation.

$MeO_2CC_2CO_2Me$ *as a ligand on the* $Ir(PMe_2Ph)_3^+$ *fragment*

Reaction of $Ir(H_2)(H)_2(PMe_2Ph)_3^+$ with dimethyl acetylenediacarboxylate, under conditions used for the synthesis of $Ir(MeC_2Me)(PMe_2Ph)_3^+$, gives a bis-alkyne adduct $Ir(MeO_2CC_2CO_2Me)_2(PMe_2Ph)_3^+$ as the BF_4 salt. This molecule shows ^1H, ^{13}C and ^{31}P NMR spectra consistent with the following trigonal bipyramidal structure. The molecule is stereochemically rigid both with respect to phosphorus site exchanges and alkyne rotation. We have reported the analogous molecule $Ir(C_2H_4)_2(PMe_2Ph)_3^+$,[9] and have commented there on its rigidity. This analogy of $MeO_2CC_2CO_2Me$ to ethylene shows clearly that $MeO_2CC_2CO_2Me$ *can* serve as a formal two-electron donor. Finally, this same complex can be synthesized by displacement of MeC_2Me from $Ir(MeC_2Me)(PMe_2Ph)_3^+$, thus demonstrating that the butyne complex undergoes attack by nucleophiles.

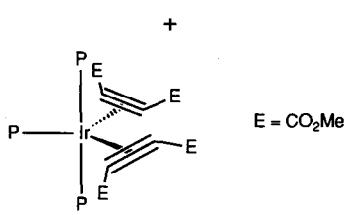

Table 2. Bond distances (Å) and angles (°) for $M(CO)_4(F_3CC_2CF_3)$ (M = Ru, Os)

M = Ru		M = Os	
Bond distances (Å)			
Ru1—C2	1.961(5)	Os1—C2	1.976(17)
Ru1—C4	1.967(5)	Os1—C4	1.974(15)
Ru1—C6	1.967(5)	Os1—C6	1.964(13)
Ru1—C8	1.971(5)	Os1—C8	1.964(14)
Ru1—C14	2.128(4)	Os1—C14	2.149(12)
Ru1—C15	2.121(4)	Os1—C15	2.135(12)
F10—C13	1.323(5)	F10—C13	1.346(17)
F11—C13	1.328(6)	F11—C13	1.335(19)
F12—C13	1.333(5)	F12—C13	1.317(17)
F17—C16	1.319(5)	F17—C16	1.322(17)
F18—C16	1.329(5)	F18—C16	1.317(17)
F19—C16	1.312(6)	F19—C16	1.312(19)
O3—C2	1.131(6)	O3—C2	1.113(20)
O5—C4	1.130(6)	O5—C4	1.125(19)
O7—C6	1.129(6)	O7—C6	1.130(17)
O9—C8	1.126(6)	O9—C8	1.117(17)
C13—C14	1.473(6)	C13—C14	1.475(18)
C14—C15	1.276(6)	C14—C15	1.276(19)
C15—C16	1.464(6)	C15—C16	1.460(19)
Bond angles (°)			
C2—Ru1—C4	93.66(22)	C2—Os1—C4	92.5(8)
C2—Ru1—C6	91.10(19)	C2—Os1—C6	92.2(8)
C2—Ru1—C8	98.68(18)	C2—Os1—C8	95.2(7)
C2—Ru1—C14	148.17(17)	C2—Os1—C14	150.6(7)
C2—Ru1—C15	113.22(17)	C2—Os1—C15	116.0(7)
C4—Ru1—C6	172.74(19)	C4—Os1—C6	172.6(6)
C4—Ru1—C8	93.18(19)	C4—Os1—C8	93.0(6)
C4—Ru1—C14	84.56(19)	C4—Os1—C14	84.7(6)
C4—Ru1—C15	85.39(17)	C4—Os1—C15	84.8(6)
C6—Ru1—C8	91.52(20)	C6—Os1—C8	92.1(6)
C6—Ru1—C14	88.51(17)	C6—Os1—C14	88.4(5)
C6—Ru1—C15	87.69(18)	C6—Os1—C15	88.0(5)
C8—Ru1—C14	113.15(17)	C8—Os1—C14	114.2(5)
C8—Ru1—C15	148.10(17)	C8—Os1—C15	148.8(5)
C14—Ru1—C15	34.96(16)	C14—Os1—C15	34.7(5)
Ru1—C2—O3	177.6(4)	Os1—C2—O3	173.6(19)
Ru1—C4—O5	175.9(4)	Os1—C4—O5	175.8(14)
Ru1—C6—O7	178.6(4)	Os1—C6—O7	179.3(13)
Ru1—C8—O9	177.6(4)	Os1—C8—O9	175.8(14)
F10—C13—F11	106.0(4)	F10—C13—F11	106.4(13)
F10—C13—F12	106.0(4)	F10—C13—F12	105.8(12)
F10—C13—C14	111.9(4)	F10—C13—C14	111.0(12)
F11—C13—F12	107.5(4)	F11—C13—F12	108.2(13)
F11—C13—C14	112.2(4)	F11—C13—C14	112.0(13)
F12—C13—C14	112.8(4)	F12—C13—C14	113.1(12)
Ru1—C14—C13	145.4(3)	Os1—C14—C13	146.2(11)
Ru1—C14—C15	72.21(26)	Os1—C14—C15	72.1(8)
C13—C14—C15	142.3(4)	C13—C14—C15	141.7(13)
Ru1—C15—C14	72.83(25)	Os1—C15—C14	73.3(8)
Ru1—C15—C16	145.3(3)	Os1—C15—C16	146.2(10)
C14—C15—C16	141.8(4)	C14—C15—C16	140.6(13)
F17—C16—F18	104.8(4)	F17—C16—F18	105.3(12)
F17—C16—F19	105.6(5)	F17—C16—F19	105.3(15)
F17—C16—C15	112.2(4)	F17—C16—C15	112.5(12)
F18—C16—F19	107.2(4)	F18—C16—F19	107.0(14)
F18—C16—C15	113.9(4)	F18—C16—C15	114.1(12)
F19—C16—C15	112.5(4)	F19—C16—C15	112.0(12)

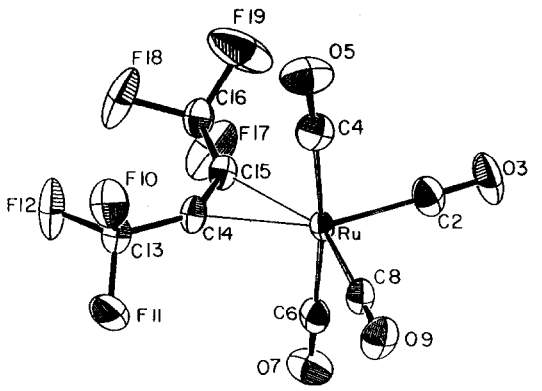

Fig. 3. ORTEP drawing of $Ru(CO)_4(F_3CC_2CF_3)$, showing atom labelling. The isomorphous osmium analogue is labelled identically.

Structure of $M(CO)_4(F_3CC_2CF_3)$ (M = Ru, Os)

The ruthenium and osmium complexes, $M(CO)_4(F_3CC_2CF_3)$, form isomorphous crystals from pentane at −78°C. The structure (Fig. 3) of the ruthenium compound has the greater precision, due to the large influence of absorption for osmium, but the molecular dimensions of the two are indistinguishable within a 3σ criterion. The axial and equatorial M—C distances are equal, as are the M—C(alkyne) distances and the alkyne C≡C distances. The molecules have a faithful approach to C_{2v} symmetry. A distortion from the idealized angles of a trigonal bipyramid is the reduction of the equatorial/equatorial intercarbonyl angle (C2—M—C8) to 95.2(7)° (Os) and 98.68(18)° (Ru) and indicates that these molecules are perhaps better regarded as six-coordinate octahedral species with the $M(F_3CC_2CF_3)$ fragments approaching the metallacyclopropene bonding extreme. This view is reinforced by the solution "rigidity" of these compounds at ambient temperature and above as evidenced by their ^{13}C NMR spectra.[10] The corresponding angle in the analogous $Os(CO)_4(Me_3SiC_2SiMe_3)$ complex is larger (108.8(3)°) in accord with the weaker Os—$Me_3SiC_2SiMe_3$ interaction. This observation is further corroborated by the larger C—C—R angle of the coordinated alkyne in the latter (av. 156(2) vs 142(1)°) and longer M—C(alkyne) distances (av. 2.26(1) vs 2.13(2) Å). Also noteworthy is the bending of the axial carbonyls towards the alkyne: C4—M—C6 = 172.74(19)° for ruthenium and 172.6(6)° for osmium, as previously observed in $Os(CO)_4(Me_3SiC_2SiMe_3)$.[11]

Two points bear mention in comparison to the bond lengths in $Ir(MeC_2Me)(PMe_2Ph)_3^+$. In the iridium complex, the C≡C distance is longer by 0.030 Å (five ESDs) and the M—C(alkyne) distances are shorter by 0.12 Å (20 ESDs). The alkyne is thus more tightly bound to the $Ir(PMe_2Ph)_3^+$ fragment that it is to $M(CO)_4$ (M = Os, Ru).

Analysis of the orbital interactions

For conventional ligands all $4d^8$ and $5d^8$ ML_4 complexes are square-planar. The introduction of an alkyne as a ligand induces a major change in the structure. More interestingly, the change of structure depends also on the nature of the metal. The known iridium(I) (**2**, **4**[12]), cobalt(I) (**3**)[13] and iron(0) (**5**)[14] alkyne complexes uniformly adopt a structure with approximate *Cs* symmetry ("CS"). They are distorted away from T_d symmetry and resemble a

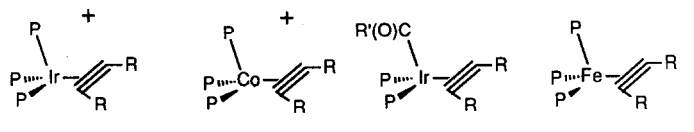

2 **3** **4** **5**

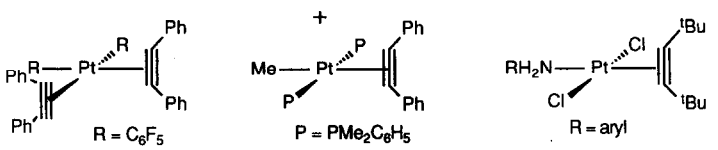

6

square pyramid. The metal-to-apical ligand bond length is especially short. In all these complexes, the metal–alkyne distance is very short, and the C—C bond is notably stretched which indicates a strong metal–alkyne interaction. In contrast, the platinum(II)[15] (e.g. **6**) alkyne complexes are all square-planar ("SP") with the axis of the alkyne perpendicular to the PtL_3 plane. Why should *isoelectronic* compounds have different structures and different reactivity? These are the points we will address here.

Our analysis is based on extended Hückel calculations. Atomic and structural parameters are given in the Appendix. The results of the calculations of the SP and CS structures for model complexes MP_3(acetylene) ($M = Pt^{II}$, Ir^{I}, Co^{I}, Fe^{0}, $P = PH_3$) are given in Table 3. Only platinum prefers the square-planar structure; all other metals favour the CS geometry, in good agreement with the experimental result.

As a background for understanding the reason for the trends in Table 3, we must consider the energy difference between a SP and a CS structure with purely σ ligands. We start the analysis with a study of the simplest model of an ML_4 d^8 complex in which all ligands are H^-. In the CS structure the M—H bonds (1.7 Å) were aligned with the M—P and M—acetylene midpoint vectors of the title iridium structure.

Calculations on IrH_4^{3-} and PtH_4^{2-} show the square-planar structure to be strongly favoured by about 67 kcal mol^{-1} over the CS for both metals. This large preference is easily accounted for by the consideration of the d splitting, since the energy of the occupied d block faithfully reflects the total energies. In a square-planar structure, three non-bonding orbitals are below a weakly antibonding z^2 (z axis perpendicular to the molecular plane). Above this set is the highly destabilized x^2-y^2 which is pointing toward the four ligands. In a CS structure the d splitting is close to that of a T_d complex:[16] two non-bonding orbitals are below a set of three destabilized ones which are not degenerate, due to the absence of a C_3 axis. Assuming a closed shell electronic configuration, the square-planar structure has six electrons in non-bonding orbitals and two in a weakly antibonding one. In contrast, housing eight electrons in the CS structure results in a significant destabilization for four of them. *Thus four σ ligands prefer a square-planar arrangement for any metal.* The occurrence of another structure is then undoubtedly due to π-effects.

Table 3. Relative total energies (kcal mol^{-1}) of $M(PH_3)_3$(acetylene) for SP and CS structures. Bond lengths were taken from the stable isomer and were kept equal in the other isomer. For the CS structure the experimental angles were chosen. The angles at the metal for the CS structure for platinum(II) were chosen identical to that of iridium(I)

Metal	SP	CS
Pt^{II}	0.0	0.3
Ir^{I}	1.9	0.0
Co^{I}	11.3	0.0
Fe^{0}	19.6	0.0

Square-planar and CS alkyne complexes

To understand the factors that favour each structure we will compare the complexes of the two atoms of the third period, platinum(II) and iridium(I) in which variations of bond lengths are expected to be minimal. The interaction diagrams for the acetylene ligand in the square-planar (left-hand side) and CS (right-hand side) geometries are presented in Fig. 4. Since the diagrams for platinum and iridium look similar and differ by only small changes in energy, we have shown the interaction diagrams for iridium only. Comparison between the two metals relies on numerical evaluations and will be discussed in the text. Note that from now on the z axis is along the metal-to-acetylene midpoint direction.

We will start the discussion with the square-planar geometry. This structure has been considered numerous times.[17] However, in order to discuss the bonding in both SP and CS structures, it is necessary to describe the bonding in SP that is germane to our analysis. In a T shape ML_3,[17] three non-bonding (xz, yz, xy) orbitals are just below a weakly antibonding orbital which is essentially oriented perpendicular to the fragment plane (y^2 in our coordinated system). Higher above is an empty σ hybrid which is mostly extended toward the empty site. Bending the alkyne lifts the degeneracy of the π orbitals ($\pi_\perp$, $\pi_\parallel$, $\pi^*_\parallel$, $\pi^*_\perp$). Due to the high symmetry (C_{2v}) of the complex, the interaction diagram is very simple to build. The $\pi_\parallel$ orbital interacts very weakly with y^2 and strongly with the empty σ hybrid. This last interaction is responsible for the metal–acetylene σ bond. The empty acetylene $\pi^*_\parallel$ interacts with the occupied yz orbital. This interaction is responsible for the metal–ligand backbonding and is stabilizing. The actylene $\pi_\perp$ has only the symmetry of the occupied xz orbital (**7**). This interaction between two occupied orbitals induces a four-electron destabilizing interaction. No bond results from the interaction and it actually contributes to a decrease of

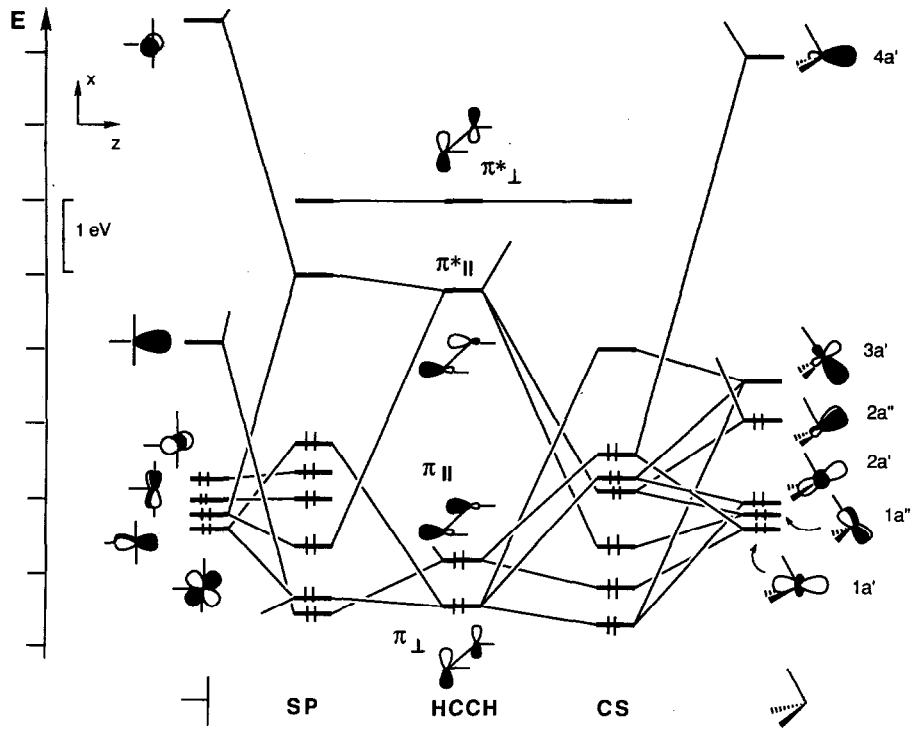

Fig. 4. Interaction diagram for a square-planar (SP) structure (left-hand side) and for the experimental (CS) structure for $IrP_3(HC_2H)^+$.

the total bonding between the two fragments. The higher empty orbital of acetylene, $\pi^*_\perp$, has the proper symmetry to stabilize the occupied metal xy orbital. However the interaction is very small since it is based on a δ type overlap. It will not be considered further.

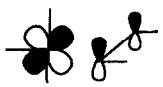

7

The analysis for the CS structure begins with the orbitals of the CS MP_3 fragment which resembles that of a ML_3 piece of an octahedron with C_{3v} symmetry. The symmetry labels that will be used are those of the C_s symmetry point group. Three low-lying ($1a'$, $2a'$, $1a''$), essentially non-bonding orbitals close in energy, are below a set of three hybrids which are made of a well-known mixture of d, s and p metal orbitals.[18] These three orbitals separate into a set of two ($2a''$, $3a'$), which would have been degenerate in C_{3v} symmetry, and a high-lying $4a'$. In the present geometry of the CS MP_3 fragment, $2a''$ is below $3a'$ and can be considered as the HOMO of the fragment. As will be evident later, the relative order of these two orbitals will play a central role in the rotational orientation of the acetylene ligand. These three orbitals, which are M—P antibonding, are strongly hybridized away from these ligands and are thus perfectly suited for a strong interaction with the incoming acetylene ligand. In C_s symmetry, the four acetylene orbitals are $1a'$ ($\pi_\perp$), $2a'$ ($\pi_\parallel$), $1a''$ ($\pi^*_\parallel$) and $2a''$ ($\pi^*_\perp$). The low symmetry of the complex might have resulted in a complicated interaction diagram. However, the analysis remains relatively simple due to consideration of local symmetry.

The $\pi_\parallel$ ($2a'$) orbital overlaps essentially with the occupied metal $1a'$ and the empty $4a'$ orbitals while it encounters the nodal plane of the filled $2a'$ and empty $3a'$. The interaction between $\pi_\parallel$ and the metal $1a'$ orbital is destabilizing but it is fully compensated by the strong stabilization caused by $4a'$. This last interaction is responsible for the metal–acetylene σ bond. The empty $\pi^*_\parallel$ orbital ($1a''$) overlaps with the occupied metal $1a''$ and $2a''$ orbitals giving rise to the metal–acetylene backbonding (the later interaction is represented in **8**). Both of these interactions are stabilizing but $2a''$ plays a preferential role since it is closer in energy to $\pi^*_\parallel$. We will see later the consequences of this privileged role. The occupied $\pi_\perp$ ($1a'$) acetylene orbital is in fact well suited to overlap with the occupied metal $2a'$ and the empty metal $3a'$ orbitals, since all of these orbitals have a spatially close nodal plane. In

contrast, the metal $1a'$ and $4a'$ orbitals are essentially pointing toward the nodal lane of $\pi_\perp$ and therefore do not interact with it. The interaction between $\pi_\perp$ and metal $2a'$ is destabilizing, while that with the empty $3a'$ is stabilizing. This last interaction, represented in **9**, produces electron-transfer from $\pi_\perp$ into the empty metal orbital and forms a second type of π bond between the acetylene and the metal. Therefore in the CS geometry, the four-electron destabilization between $\pi_\perp$ and a metal d lone pair, is in part compensated by a two-electron stabilization. Finally, the last orbital to consider is $\pi^*_\perp$. In CS geometry, as in the square-planar structure, this orbital plays essentially no role since it is only involved in a δ type overlap with the occupied $2a''$ orbital.

8

9

The metal is thus bonded to the acetylene via three bonds, one σ and two π. This accounts for the short Ir—C distance (2.01 Å) when compared to other Ir—C bond lengths (e.g. 2.159 Å in *fac*-$IrMe_3(PMe_2Ph)_3$).[8] The acetylene tends to give electrons to the metal via both its $\pi_\parallel$ and $\pi_\perp$ orbitals. As nicely discussed in a recent review[19] this is usually described as a four-electron donation, although no such complete electron-transfer is ever at work. In the square-planar geometry, the acetylene cannot behave like a four-electron donor and is at most a two-electron donor via $\pi_\parallel$ since there is no empty metal orbital available to receive electrons from $\pi_\perp$. In the CS structure, the four-electron donating capability can be fully used since the metal has the proper number of empty orbitals to receive the electrons.

Now that we have built both interaction diagrams, we need to discuss why some metals prefer the square-planar structure and others the CS one. Recall that the σ effect strongly favours the square-planar geometry and that the preference for CS can only be due to π bonding. For this reason, the interaction of the acetylene $\pi_\parallel$ orbital with the metal fragment cannot make the difference between the two structures since it participates only in the formation of the metal σ bonds. Calculations do indeed indicate that the interaction energy involving $\pi_\parallel$ equally favours the square-planar geometry for both metals. In consequence, $\pi_\perp$ and $\pi^*_\parallel$ are the only orbitals of the acetylene that need to be considered.

Let us then first compare the interactions that give rise to π systems in both geometries. Since we are mostly interested in the unusual iridium structure, numerical values in the following section will be given for iridium(I).

The $\pi_\perp$ orbital is only participating in four-electron destabilization in SP while in CS it is able to find an empty orbital ($3a'$, **9**), into which to donate electrons (0.29 e^- are transferred), thus relieving a part of the four-electron destabilization. This effect favours CS.

Metal-to-acetylene backbonding occurs from a non-bonding d orbital in the SP geometry, whereas in the CS structure it utilizes a high-lying hybrid orbital (1.1. eV higher in energy than the non-bonding d) pointing toward the acetylene ligand (**8**). Therefore for both energy and overlap (0.20 in SP, 0.26 in CS) reasons, the backbonding is stronger in CS. Larger electron-transfer (0.53 e^- in SP, 0.76 in CS) into $\pi^*_\parallel$ in the CS structure confirms this analysis.

Both of these effects oppose the σ interactions, which favours SP. The outcome of these competitive effects can only be established by numerical calculations. In agreement with experiments, the calculations show that the iridium complex is more stable for a CS structure, while the platinum complex prefers a SP geometry (Table 3). Why is that so?

The main difference between the two metals relevant to our study is that the d orbitals of iridium(I) are at a higher energy and more diffuse than those of platinum(II). As a consequence, the backbonding from $2a''$ into $\pi^*_\parallel$ is larger for iridium than for platinum due to a smaller energy gap and a better overlap.† The situation is difficult for the case of $\pi_\perp$. The four-electron destabilization is exclusively controlled by overlap[20] and thus influences the diffuse iridium orbitals more than the contracted platinum orbitals. Consequently there is larger built in destabilization in the SP structure for iridium than for platinum. In the CS structure, the electron-transfer from $\pi_\perp$ into $3a'$ is similar for both metals because the larger energy gap between the two orbitals in the iridium case is compensated by the larger overlap (0.14 for Pt, 0.16 for Ir).

It appears then that, in order to overcome the large preference for the square-planar structure resulting from the σ interactions, both of the above factors must be present for the CS structure to be preferred. It requires first of all a large four-electron destabilization in the square-planar geometry and

† Note that the interaction with $1a''$ follows the same trend but we will consider only $2a''$ since, being higher in energy and hybridized towards acetylene, it is responsible for the main interaction.

a large ability for back donation to stabilize CS. It is clear that the absence of a four-electron destabilization for *olefin* complexes leads to a square-planar geometry independent of the metal and the extent of back donation into the π^* orbital. Numerical calculations do indeed confirm this point. In summary, it is the *four-electron donation of an alkyne ligand which is responsible for the "unusual" CS structure of* ML_3*(alkyne) complexes* and any effect (e.g. increasing metal oxidation state or lowering the principal quantum number) which acts to quantitatively diminish the overlap between $\pi_\perp$ and the occupied metal *d* orbital will return the structure to the classical square-planar one.

The decrease in principal quantum number from iridium to cobalt might alter the ground-state structure, but the numerical calculations show that the CoP_3(acetylene)$^+$ (**3**) remains CS. This is because the shorter metal–carbon distances have maintained sufficient overlap with $\pi_\perp$. It follows that the isoelectronic iron(0) (**5**) complex is also CS.

Alkyne rotation: Ground-state structure and fluxionality

The structure observed for cobalt necessitates consideration of another structural parameter: rotation of the alkyne about its midpoint. Both $Ir(MeC_2Me)(PMe_2Ph)_3^+$ and $Co(PhC_2Ph)(PMe_3)_3^+$ (**10**)[13] have the alkyne oriented perpendicular to the mirror plane of ML_3 ("horizontal"). Remarkably $Co[PhC_2(n\text{-pentyl})](PMe_3)_3^+$ (**11**)[21] has the alkyne eclipsing one Co—P bond ("vertical"). However, interconversion between the horizontal and vertical isomers is facile since these cobalt complexes were reported to be highly fluxional. Fluxionality is also present in the iridium complex described in this work. The ^{31}P, ^1H and ^{13}C NMR spectra of $Ir(MeC_2Me)(PMe_2Ph)_3^+$ at 25°C all indicate that there is rapid intramolecular site exchange among inequivalent phosphorus ligands. The data exclude dissociation of phosphine or butyne as the mechanism for such fluxionality. The barrier for this process is small, since the $^{31}P\{^1H\}$ NMR spectrum remains a singlet even at −95°C.

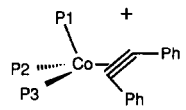

Co-P1 = 2.127Å
Co-P2(3) = 2.2081Å
P1-Co-P2 = 96°
P2-Co-P3 = 104°

10

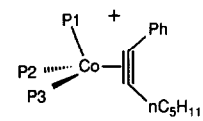

Co-P1 = 2.168Å
Co-P2(3) = 2.131, 2.183Å
P1-Co-P2 = 103° av.
P2-Co-P3 = 95°

11

First let us point out that the P—M—P angles are significantly different in the horizontal and vertical structure. Comparing the cobalt complexes, the P1—Co—P2(3) angle is about 96° (90° for Ir) and the P2—M—P3 angle is 104° (106° for Ir) in the

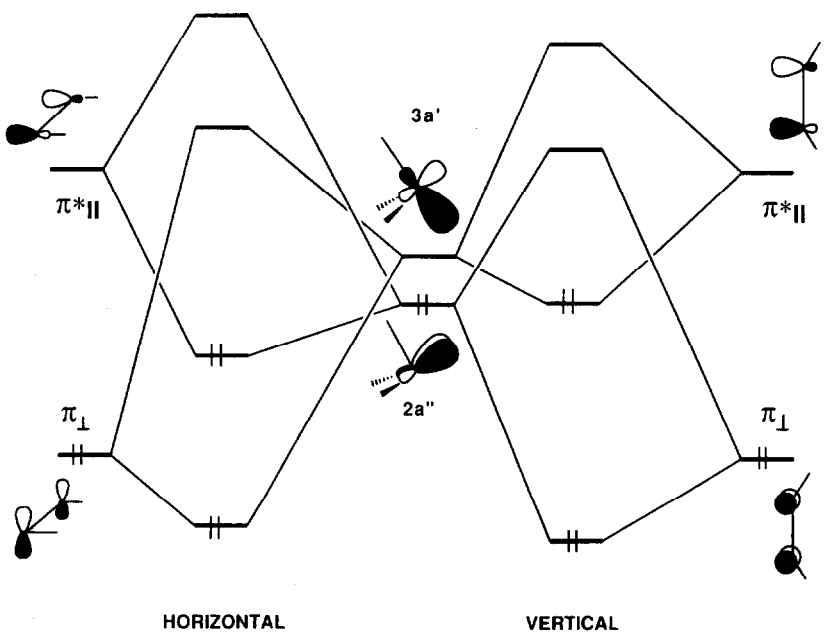

Fig. 5. Interaction diagram limited to the most relevant MOs for the horizontal (left-hand side) and the vertical (right-hand side) complex. In this diagram the structure of ML_3 corresponds to that observed in the horizontal isomer.

horizontal structure and, respectively, 103 and 95° in the vertical structure. As we will see there is, in fact, a pair of P—M—P angles best adapted to each conformer.

As a first step, we rotate the acetylene about its midpoint from the horizontal to the vertical orientation keeping the MP_3 angles at the values of the *horizontal structure*. Figure 5 shows that, during this rotation, $\pi_\perp$ and $\pi^*_\parallel$ have interchanged their partners on the metal. In the vertical conformation $3a'$ and $2a''$ interact with $\pi^*_\parallel$ and $\pi_\perp$, respectively. The rotation is energetically unfavourable since the stabilization of $2a''$ or $3a'$ by $\pi^*_\parallel$ is equivalent and thus $(3a^\circ + \varepsilon\pi^*_\parallel)$ is always higher in energy than $(2a'' + \varepsilon\pi^*_\parallel)$. The increased stabilization of $\pi_\perp$ in the vertical structure is too small to compensate the above effect. The vertical conformation would thus be more stable if $3a'$ were below $2a''$ in the ML_3 fragment. The angles between the phosphines determine the relative energies of these two orbitals. Since the $2a''$ and $3a'$ are composed to a large extent of *d* orbitals, the maximum of destabilization by the ligands occurs when the angle between the ligands is close to 90°. Thus a 90° angle between P2 and P3 destabilizes mostly $2a''$, while a 90° angle between P1 and P2(3) destabilizes mostly $3a'$ (we maintain a mirror plane through the Ir—P1 bond). In case the angles between the phosphines depart from this ideal 90° value, the higher destabilization is associated with the P—Ir—P angle that is closer to 90° as summarized in Fig. 6. Therefore the *angular relaxation of the* MP_3 *fragment is a determining factor for the stability of the vertical conformation.* It appears from the calculations that the vertical conformation becomes more stable when the geometry of MP_3 is relaxed to that observed in the experimental structure.

The rotation between horizontal and vertical conformers also alters M—P bond lengths. In the horizontal conformation, the M—P1 bond is significantly shorter than M—P2(3) while this is not so in the vertical conformer as shown in **10** and **11**. The unequal electron occupation of $2a''$ and $3a'$ in the acetylene complex in the two conformations is responsible for this fact. The $2a''$ orbital is equally antibonding with P2 and P3 while $3a'$ is much more antibonding with P1 than with P2(3) as represented in Fig. 6. In the horizontal conformation the electrons which are involved in the acetylene–Ir π bonds go into $(\pi_\perp + \varepsilon 3a')$ which is mostly centred on the acetylene part and in $(2a'' + \varepsilon\pi^*_\parallel)$ which is mostly centred onto $2a''$. Going to the vertical conformation, the electron occupation is reversed since the two MOs are now made up of $(\pi_\perp + \varepsilon 2a'')$, mostly on the acetylene and of $(3a' + \varepsilon\pi^*_\parallel)$, mostly on the metal $3a'$ orbital. Consequently turning the acetylene by 90° weakens mostly M—P1 and makes the three M—P bond lengths more equivalent. Although a better estimation of the structure of the MP_3 fragment accompanying the rotation of the acetylene is beyond the validity of the EHT method, the trend in the bond angle and bond length relaxation is well reproduced.

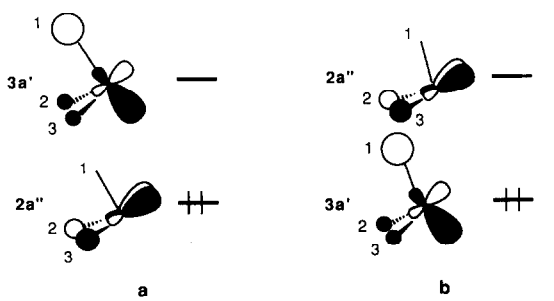

Fig. 6. Relative energy of the $(2a'', 3a')$ pair for (a) [P1—Ir—P2(3) = 90°, P2—Ir—P3 > 90°] and (b) [P1—Ir—P2(3) > 90°, P(2)—Ir—P3 = 90°].

This conclusion provides an unusually detailed view of the occurrence and the energetic importance of ML_3 "breathing" during acetylene rotation. Note however that the difference in energy between $2a''$ and $3a'$ is small since the MP_3 geometry is not far from C_{3v} symmetry, where the two orbitals would be rigorously degenerate thus allowing free rotation of the acetylene. The consequence is a small activation energy for alkyne rotation in all situations, in full agreeement with observed rapid fluxionality of all molecules discussed here.

Since there is a strong correlation between the angles within the MP_3 substructure and the orientation of acetylene, what is the factor which will eventually determine the preferred structure? Since symmetrical alkynes prefer to be horizontal while the asymmetrical one prefers the vertical position, the influence of alkyne asymmetry was next investigated.

The phenyl substituent destroys the symmetry of the π orbitals of alkyne and increases the coefficient of the carbon which is far from the phenyl ring in the frontier orbitals.[22] Recall at this point that the most important interaction between MP_3 and acetylene is that of the back donation into $\pi^*_\parallel$. The interaction is thus optimal when the large lobe of $3a'$ (i.e. opposite the M—P1 bond) overlaps with the large lobe of $\pi^*_\parallel$ as shown in **12**. This is achieved in the vertical conformation when the phenyl ring is *syn* to P1.

Changes within the ML_3 fragment also influence the preferred structure. Consider the horizontal structure of the IrP2(acyl)(alkyne) complex (**4**) where the acyl ligand replaces P1. Since the acyl

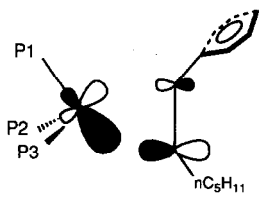

12

group is a stronger σ donor than a phosphine, the $3a'$ orbital is always higher than $2a''$ (the $2a''$–$3a'$ energy gap in the fragment $Ir(acyl)P_2^+$ is considerably larger than in IrP_3^+). The lowering of $2a''$ with respect to $3a'$ is even increased by the angles between the ligands (105° between the two phosphines and 92 and 95° between the acyl and the two phosphines, i.e. a structure similar to the IrP_3^+ horizontal complex). The horizontal conformation with the acyl group occupying the site of P1 is thus observed. Although steric bulk might also influence these two angles (in particular in opening the angles between the phosphines and contracting those between the acyl and the phosphine), in this case also there is a nice correlation between the intimate structure of the metal fragment and the orientation of the acetylene.

Reactivity

The $Ir(PMe_2Ph)_3(MeC_2Me)^+$ complex reacts easily with another alkyne or with H_2. The related cobalt complex **3** adds MeCN to give $Co(PMe_3)_3(MeCN)(PhC_2Ph)^+$.[13] All of these Lewis bases will seek out the LUMO of the metal complex, yet facile nucleophilic attack on an 18-electron complex might be viewed as unexpected. Therefore we now analyse the energy and spatial orientation of the LUMO of $IrP_3(acetylene)^+$ in the experimental (horizontal) conformation.

The LUMO, **13** of the complex is made of the

13

† It might be asked why this complex is not planar since $MeO_2CC_2CO_2Me$ is more adequately considered as a two-electron donor. However, the effect of $\pi_\perp$ is not offset totally and it is clear that it is not possible to determine in a reliable manner the limit between the SP and CS structures. The presence of iridium by itself substituted by strong σ donating ligand may have made the *d* block sufficiently diffuse to create a significant four-electron destabilization.

antibonding combination of $3a'$ and $\pi_\perp$ and is mostly centred on the $3a'$ orbital. This interaction is of moderate strength so that the LUMO remains at low energy and is also strongly developed *trans* to P1. Since the molecule approximates a square-pyramidal geometry the region *trans* to P1 is also the most sterically accessible. But why is the structure a square pyramid, that is why are P2 and P3 nearly in the Ir–acetylene plane? The dominant interaction between the metal fragment and the acetylene ligand is that between the high-lying occupied $2a''$ and $\pi^*_\parallel$, the one between the deeper $1a''$ and $\pi^*_\parallel$ being much smaller due to the larger energy gap. In order to maximize the dominant interaction, $2a''$ should point towards $\pi^*_\parallel$ as illustrated in **14**. This is achieved by putting P2 and P3 in the Ir–acetylene plane. Attendant diminution of the interaction between $2a''$ and $\pi^*_\parallel$ is of less importance. The LUMO in the square-pyramid type complex is at a particularly low energy since the overlap between $3a'$ and $\pi_\perp$ is smaller than in a more Td type structure.

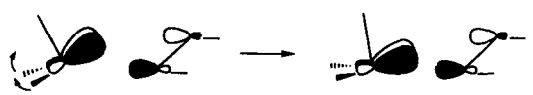

14

Tuning the four-electron destabilization by an alkyne substituent and by ligand effects

The above discussion of d^8 $ML_3(alkyne)^q$ species calls into question the related family of compounds $M(CO)_4(alkyne)$ (M = Fe, Ru, Os), several of whose structures are reported here. Are these 20-valence electron species? In particular, what are the factors which control the thermodynamics of eq. (2)? There is a clearly defined preference for L =

$$ML_4(alkyne) \rightleftharpoons ML_3(alkyne) + L \qquad (2)$$

phosphine to favour the right-hand side of eq. (2), while L = CO favours the left-hand side. What electronic factors are at work? In addition, how is it possible to diminish the four-electron repulsion expected in compounds such as $Os(CO)_4(alkyne)$.

The introduction of acceptor ligands such as CO_2Me on the alkyne in the plane of the bent alkyne delocalizes the $\pi_\perp$ orbital. Its overlap with metal orbitals in both the SP and CS structures is thereby significantly diminished. Thus the four-electron destabilization is considerably decreased (it is mostly controlled by the overlap) and it could behave as a two-electron donor.† This explains the otherwise curious production of $Ir(MeO_2CC_2CO_2Me)_2(PMe_2Ph)_3^+$, a bis-alkyne complex, under

conditions which produce monoalkyne complexes for phenyl and alkyl substituted alkynes. We can now see that the undetected intermediate $Ir(MeO_2CC_2CO_2Me)(PMe_2Ph)_3^+$, of CS structure, has a very low-lying LUMO since $3a'$ is not significantly destabilized by $\pi_\perp$. It thus easily adds an additional alkyne ligand. Interestingly the neutral mono dicarbomethoxy complex of IrP2(acyl) complex whose structure has been discussed above, is stable.[12] Its lack of reactivity relative to the present cationic IrP_3 fragment may be due to the strong σ donating effect of the acyl that takes the place of P1. The corresponding $3a'$ and consequently the LUMO of the monoalkyne complex is higher, which diminishes its affinity for an additional ligand.

Alternatively one can diminish the four-electron destabilization by delocalizing the "offending" metal orbital. This can be achieved by introducing CO ligands on the metal. The *xz* lone pair is delocalized into the four π^*_{CO} orbitals and thus its overlap with the alkyne $\pi_\perp$ orbital is only weakly destablizing. However, the molecule shows reactivity characteristics which can be attributed to the residual four-electron destabilization. While the $M(CO)_4$(alkyne) species (M = Ru, Os; alkyne = HC_2H,[23] $Me_3SiC_2SiMe_3$,[11] $F_3CC_2CF_3$[10]) have been characterized by the full range of modern techniques, it is important to recall that, with the exception of the $F_3CC_2CF_3$ derivatives, the compounds are thermally unstable and indeed more so than the related $M(CO)_4L$ complexes (L being the classical two-electron donor CO or $H_2C{=}CH_2$[11,23]). They thus show evidence of the four-electron repulsion predicted by simple electron counting rules. The observation that $Ru(CO)_4(Me_3SiC_2SiMe_3)$ readily deposits $Ru_3(CO)_{12}$ and that the decomposition is slowed down by added free $Me_3SiC_2SiMe_3$[11] reveals that alkyne dissociation is one way in which the instability is manifested. In addition, however, the unit $M(CO)_3$(alkyne) represented an intermediate with special stability due to the availability of the four-electron donor alkyne unit. This can account for the rapid incorporation of ^{13}CO into $M(CO)_4$(alkyne) (alkyne = HC_2H, $F_3CC_2CF_3$)[10,23] and, at least in part for the unusual facile condensation reactions of these compounds with other 18-electron species.[10,23]

Equilibrium (2) can thus be easily displaced towards one or the other side by a fine tuning of the four-electron destabilization.

CONCLUSION

It is well accepted that isomeric forms of certain ligands can furnish different numbers of electrons to the metal. From this work it is now clear that the mirror-image situation can be observed on the metal: isomeric fragments can accept a different number of electrons. Thus a T shape ML_3 d^8 fragment is a two-electron acceptor while a pyramidal ML_3 d^8 fragment is a four-electron acceptor (this is why butadiene and other four-electron conjugated dienes coordinate to a pyramidal d^8 ML_3 fragment). An encounter between a ligand and a metal fragment may thus induce structural changes in both partners to optimize the bonding/accepting capability of each. A search for other examples of adaptation of ML_n fragment geometry to the active partner ligand should be fruitful.

Acknowledgements—This work was supported by the U.S. NSF, the French CNRS, and the European Economic Community. The Laboratoire de Chimie Théorique is associated with the CNRS (URA 506) and is a member of ICMO and IPCM. The Laboratoire de Chimie de Coordination is associated with Université Paul Sabatier. We thank Scott Horn for skilled technical assistance.

REFERENCES

1. K. R. Birdwhistell, T. L. Tonker and J. L. Templeton, *J. Am. Chem. Soc.* 1987, **109**, 1401.
2. Preliminary results have been reported: G. Marinelli, I. El-Idrissi Rachidi, W. E. Streib, O. Eisenstein and K. G. Caulton, *J. Am. Chem. Soc.* 1989, **111**, 2347.
3. J. C. Huffman, L. N. Lewis and K. G. Caulton, *Inorg. Chem.* 1980, **19**, 2755.
4. E. G. Lundquist, W. E. Streib and K. G. Caulton, *Inorg. Chim. Acta* 1989, **159**, 23.
5. M. Tanimoto, K. Kichitsu and Y. Morino, *Bull. Chem. Soc. Jpn* 1969, **42**, 2519.
6. S. D. Ittel and J. A. Ibers, *Adv. Organomet. Chem.* 1976, **14**, 33.
7. S. Otsuka and A. Nakamura, *Adv. Organomet. Chem.* 1976, **14**, 245.
8. E. G. Lundquist, K. Folting, J. C. Huffman and K. G. Caulton, *Polyhedron* 1988, **7**, 2171.
9. E. G. Lundquist, K. Folting, W. E. Streib, J. C. Huffman, I. Eisenstein and K. G. Caulton, *J. Am. Chem. Soc.*, in press.
10. M. R. Gagné and J. Takats, *Organometallics* 1988, **7**, 561.
11. R. G. Ball, M. R. Burke and J. Takats, *Organometallics* 1987, **6**, 1918.
12. B. J. Rappoli, M. R. Churchill, T. S. Janik, W. M. Rees and J. D. Atwood, *J. Am. Chem. Soc.* 1987, **109**, 5145. We cannot agree with the conclusions of these authors that the alkyne is a two-electron donor.
13. B. Capelle, M. Dartiguenave, Y. Dartiguenave and A. L. Beauchamp, *J. Am. Chem. Soc.* 1983, **105**, 4662.
14. T. V. Harris, J. W. Rathke and E. L. Muetterties, *J. Am. Chem. Soc.* 1978, **100**, 6966.
15. (a) R. Uson, J. Fornies, M. Tomas, B. Menjon and

A. J. Welch, *J. Organomet. Chem.* 1986, **304**, C24; (b) B. W. Davies and N. C. Payne, *Can. J. Chem.* 1973, **51**, 3477; (c) B. W. Davies and N. C. Payne, *J. Organomet. Chem.* 1975, **102**, 245; (d) G. R. Davies, W. H. Hewertson, R. H. B. Maise, P. G. Owston and C. G. Patel, *J. Chem. Soc.* 1970, 1873; (e) A. L. Beauchamp, F. R. Rochon and T. Theophanides, *Can. J. Chem.* 1973, **51**, 126.

16. T. A. Albright, J. K. Burdett and M.-H. Whangbo, *Orbital Interactions in Chemistry*, p. 305. John Wiley, New York (1985).
17. T. A. Albright, R. Hoffmann, J. C. Thibeault and D. L. Thorn, *J. Am. Chem. Soc.* 1979, **101**, 3801; O. Eisenstein and R. Hoffmann, *J. Am. Chem. Soc.* 1981, **103**, 4308.
18. M. Elian, M. M. Chen, D. M. P. Mingos and R. Hoffmann, *Inorg. Chem.* 1976, **15**, 1148; T. A. Albright, P. Hofmann and R. Hoffmann, *J. Am. Chem. Soc.* 1977, **99**, 7546.
19. J. L. Templeton, *Adv. Organomet. Chem.* 1989, **29**, 1.
20. L. Salem, *J. Am. Chem. Soc.* 1968, **90**, 543.
21. A. Bouayad, M. Dartiguenave, M.-J. Menu, Y. Dartinguenave, F. Bélanger-Gariépy and A. L. Beauchamp, *Organometallics* 1989, **8**, 629.
22. O. Eisenstein, J.-M. Lefour, N. T. Anh and R. F. Hudson, *Tetrahedron* 1977, **33**, 523.
23. M. J. Burn, G.-Y. Kiel, F. Seils, J. Takats and J. Washington, *J. Am. Chem. Soc.* 1989, **111**, 6850.
24. J. H. Ammeter, H.-B. Bürgi, J. C. Thibeault and R. Hoffmann, *J. Am. Chem. Soc.* 1978, **100**, 3686.

APPENDIX

The extended Hückel calculations were carried out by using the weighted H_{ij} formula.[24] The atomic parameters are given in Table 4. The geometries of the calculated complexes were adapted from the experimental structures.

Table 4. Atomic parameters. A double expansion (coefficients C) is used for the d orbitals

Atom	Orbital	H_{ii} (eV)	ζ_1	ζ_2	C_1	C_2
Ir	6*s*	−8.600	2.500			
	6*p*	−4.900	2.200			
	5*d*	−12.17	5.796	2.557	0.63506	0.5556
Co	4*s*	−9.210	2.000			
	4*p*	−5.290	2.000			
	3*d*	−13/18	5.550	2.1	0.56786	0.60586
Pt	6*s*	−9.077	2.554			
	6*p*	−5.475	2.554			
	5*d*	−12.59	6.013	2.696	0.63338	0.55128
Fe	4*s*	−9.100	1.900			
	4*p*	−5.320	1.900			
	3*d*	−12.60	5.350	2.000	0.55052	0.6260
P	3*s*	−18.60	1.600			
	3*p*	−14.00	1.600			

Polyhedron Vol. 9, No. 15/16, pp. 1883–1891, 1990
Printed in Great Britain

0277–5387/90 $3.00+.00
Pergamon Press plc

REACTIONS OF THE η^2- AND η^4-ISOMERS OF Cp*Ir(2,5-DIMETHYLTHIOPHENE) WITH PHOSPHINES, CO AND H_2†

JIABI CHEN, LEE M. DANIELS‡ and ROBERT J. ANGELICI§

Department of Chemistry and Ames Laboratory, Iowa State University, Ames, IA 50011, U.S.A.

Abstract—The iridathiabenzene complex, Cp*Ir(η^2-2,5-Me_2T) (**2**), which may be formulated with a 16e$^-$ iridium centre, reacts with 2e$^-$ donor ligands (L = PMe_3, PMe_2Ph, $PMePh_2$, PPh_3, $P(OPh)_3$ and CO) to give adducts **3–8**; the structures of two of these

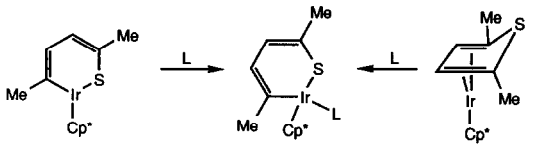

derivatives were determined by X-ray crystallography, and the bonding in their six-membered ring is contrasted with that in **2**. The η^4-thiophene complex Cp*Ir(η^4-2,5-Me_2T) (**1**) also reacts with L to give the same adducts, **3–8**; this reaction presumably involves **2** as an intermediate. Both **2** and **1** also undergo oxidative-addition with H_2 to give Cp*Ir(η^2-2,5-Me_2T)$(H)_2$ (**9**) which exists as the dihydride as determined by T_1 measurements.

As part of our general interests in the mechanisms of the heterogeneously-catalysed hydrodesulphurization (HDS) of organosulphur compounds in petroleum feedstocks, we have explored various modes of thiophene coordination and reactivity in metal complexes as models for the reactions of thiophenes on HDS catalysts.[1] Based on preliminary studies,[2] we recently found[3] that a 2e$^-$ reduction of Cp*Ir(η^5-2,5-Me_2T)$^{2+}$ (where 2,5-Me_2T is 2,5-dimethylthiophene) produces Cp*Ir(η^4-2,5-Me_2T) (**1**) in which the thiophene is coordinated through only the four carbon atoms [eq. (1)]:

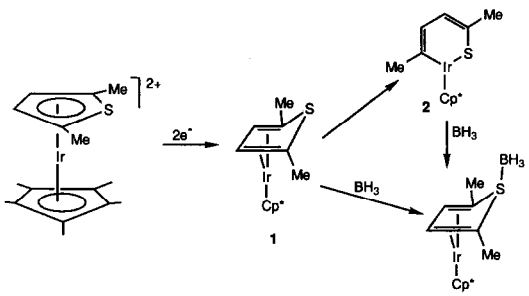

(1)

This isomer of Cp*Ir(2,5-Me_2T) is thermodynamically unstable with respect to the ring-opened isomer Cp*Ir(η^2-2,5-Me_2T) (**2**) to which it converts in the presence of basic alumina or amines as catalysts[4] [eq. (1)]. The sulphur of the thiophene in the η^4-complex (**1**) is an unusually good donor and readily forms a BH_3 adduct.[3,5] Surprisingly, the η^2-isomer (**2**) also reacts with BH_3 to undergo ring closure forming the same BH_3 adduct [eq. (1)].

The structure[4] of **2**, as determined by X-ray diffraction, contains an essentially planar six-membered ring which incorporates the four carbons, the iridium and the sulphur atoms. (The Cp* plane is perpendicular to the six-membered ring.) The structure and NMR studies of **2** strongly indicate that the π-system of the six-membered ring is delocalized and is best represented by two resonance forms, **A** and **B** [eq. (2)]:

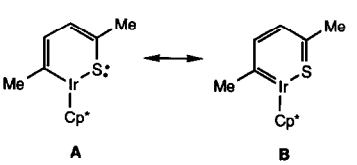

(2)

In form **A**, the iridium is a 16e$^-$ centre and might be expected to add 2e$^-$-donating ligands. In form **B**, the iridium has 18e$^-$ but the carbene carbon is expected to be electrophilic and susceptible to attack by 2e$^-$-donating nucleophiles. In this study,

† Dedicated to Professor Richard F. Fenske, a theoretical chemist whose results actually had an impact on synthetic organometallic chemistry.

‡ Iowa State University Molecular Structure Laboratory.

§ Author to whom correspondence should be addressed.

we examine the reactions of **2** with phosphines, CO and H_2, in order to determine whether the iridium or the carbene carbon is the centre of reactivity. Unexpectedly, the other isomer, **1**, an $18e^-$-complex, also reacts with the $2e^-$-donors to give the same products but at a slower rate.

EXPERIMENTAL

All reactions and product isolations were carried out under a N_2 atmosphere using Schlenk techniques. Reagent grade solvents were dried by refluxing over appropriate drying agents and stored over 4 Å molecular sieves under a N_2 atmosphere. Tetrahydrofuran (THF) and diethyl ether (Et_2O) were distilled over sodium benzophenone ketyl, while hexane and CH_2Cl_2 were distilled from CaH_2. The neutral Al_2O_3 (Brockmann, Activity I) used for chromatography was deoxygenated under high vacuum at room temperature for 16 h, deactivated with 5% (w/w) N_2-saturated water, and stored under N_2. PMe_3, PMe_2Ph, $PMePh_2$, PPh_3, $P(OPh)_3$ and $Ph_2PCH_2CH_2PPh_2$ (dppe) were purchased from Aldrich Chemical Co., and the gases CO and H_2 were used as purchased. Cp*Ir(η^4-2,5-Me_2T) (**1**) and Cp*Ir(η^2-2,5-Me_2T) (**2**) were prepared as previously reported.[4] Elemental analyses were performed by Galbraith Laboratory, Inc. The ^1H (Table 1) and ^{13}C NMR spectra were recorded on a Nicolet NT-300 spectrometer using deuteriated solvents as internal locks and references with respect to TMS. Electron ionization mass spectra (EIMS) were run on a Finnigan 4000 spectrometer. The melting points were determined in sealed N_2-filled capillaries and were not corrected.

Reaction of Cp*Ir(η^4-2,5-Me_2T) (**1**) *with* PMe_3 *to give* Cp*Ir(η^2-2,5-Me_2T)(PMe_3) (**3**)

Compound **1** (0.034 g, 0.077 mmol) was dissolved in 30 cm^3 of hexane at room temperature. To this solution was added PMe_3 (0.050 g, 0.657 mmol). The reaction solution was stirred at room temperature. The light yellow solution gradually turned a deeper yellow. After stirring for 48 h, the solvent was evaporated under vacuum, and the residue was chromatographed on Al_2O_3 (neutral) with hexane first and then hexane–Et_2O (20 : 1) as eluant. The yellow band was collected. After removal of solvent under vacuum, the crude product was recrystallized from hexane at −80°C to give 0.036 g (78%) of orange–yellow crystals of **3** (m.p. 141–142°C, decomp). MS: *m/e* 516 (M^+), 440 ($M^+ - PMe_3$), 404 ($M^+ - Me_2T$). Found: C, 44.53; H, 6.41. Calc. for $C_{19}H_{32}SPIr$: C, 44.25; H, 6.25%.

Table 1. ^1H NMR spectra of the complexes (ppm, relative to TMS)

Complex	Solvent	δ (2,5-Me_2T)	δ(C_5Me_5)[a]	δ(PR_3) or other
1	$CDCl_3$	4.53(s,2H), 1.11(s,6H)	1.92	
2	$CDCl_3$	7.47(d,1H), 7.34(d,1H), 3.10(s,3H), 2.79(s,3H)	1.93	
3	$CDCl_3$	5.82(d,1H), 5.38(d,1H), 2.15(s,3H), 1.90(s,3H)	1.75	1.50(d,9H)
	Acetone-d_6	5.76(d,1H), 5.24(d,1H), 2.16(s,3H), 1.98(s,3H)	1.76	1.51(d,9H)
4	$CDCl_3$	5.90(d,1H), 5.42(d,1H), 1.96(s,3H), 1.91(s,3H)	1.61	7.54(m,2H), 7.34(m,3H), 1.60(d,6H)
	Benzene-d_6	6.47(d,1H), 5.93(d,1H), 2.43(s,3H), 2.32(s,3H)	1.49	7.51(m,2H), 7.09(m,3H), 1.75(d,3H), 1.53(d,3H)
	Acetone-d_6	5.85(d,1H), 5.31(d,1H), 2.80(s,3H), 2.27(s,3H)	1.63	7.43(m,2H), 7.40(m,3H), 1.95(d,3H), 1.81(d,3H)
5	$CDCl_3$	5.83(d,1H), 5.40(d,1H), 2.14(s,3H), 2.11(s,3H)	1.58	7.40–7.29(m,10H), 1.91(d,3H)
	Acetone-d_6	5.75(d,1H), 5.29(d,1H), 2.15(s,3H), 2.11(s,3H)	1.61	7.46–7.37(m,10H), 1.94(d,3H)
6	$CDCl_3$	5.53(d,1H), 5.30(d,1H), 1.92(s,3H), 1.85(s,3H)	1.51	7.89–7.29(m,15H)
7	$CDCl_3$	5.71(d,1H), 5.30(d,1H), 2.34(s,3H), 1.90(s,3H)	1.62	7.31–7.07(m,15H)
8	$CDCl_3$	5.73(d,1H), 5.39(d,1H), 2.24(s,3H), 1.92(s,3H)	1.84	
9	$CDCl_3$	7.63(d,1H), 7.42(d,1H), 3.05(s,3H), 2.79(s,3H)	1.87	−16.27(s,2H), (Ir—H)

[a] All singlets with intensities of 15H.

Reaction of Cp*Ir(η^2-2,5-Me_2T) (**2**) *with* PMe_3 *to give* **3**

To a solution of **2** (0.040 g, 0.091 mmol) in hexane (30 cm^3) was added PMe_3 (0.060 g, 0.789 mmol) at −60°C with stirring. The red solution rapidly turned yellow. After being stirred at −60 to −40°C for 1 h, the resulting solution was evaporated to dryness under vacuum. Further treatment of the yellow residue was similar to that described for reaction of **1** with PMe_3 to give orange–yellow crystals of **3**, yield 0.043 g (91%) (m.p. 142°C, decomp). MS: *m/e* 516 (M^+), 440 ($M^+ - PMe_3$), 404 ($M^+ - Me_2T$). Found: C, 44.21; H, 6.18. Calc. for $C_{19}H_{32}SPIr$: C; 44.25; H, 6.25%.

Reaction of **1** *with* PMe_2Ph *to give* Cp*Ir(η^2-2,5-Me_2T)(PMe_2Ph) (**4**)

Compound **1** (0.026 g, 0.059 mmol) was dissolved in 30 cm^3 of hexane at room temperature. To this solution was added PMe_2Ph (0.050 g, 0.362 mmol). The solution was stirred for 52 h at room temperature. The colour of the solution changed gradually from light yellow to orange–yellow. Further treatment of the resulting mixture as described above for **3** gave 0.020 g (59%) of orange crystals of **4** (m.p. 115–117°C, decomp). MS: *m/e* 578 (M^+), 466 ($M^+ - Me_2T$), 440 ($M^+ - PMe_2Ph$). Found: C, 49.95; H, 6.12. Calc. for $C_{24}H_{34}SPIr$: C, 49.89; H, 5.93%.

Reaction of **2** *with* PMe_2Ph *to give* **4**

To a solution of **2** (0.030 g, 0.068 mmol) in 30 cm^3 of hexane was added PMe_2Ph (0.090 g, 0.651 mmol) at −60°C. The red solution rapidly turned yellow. The reaction solution was stirred for 2 h at −60 to −40°C. Further treatment of the resulting mixture as described in the reaction with PMe_3 gave 0.036 g (92%) of **4** as orange crystals (m.p. 115–116°C, decomp). ^{13}C NMR ($CDCl_3$): δ 136.21, 135.54, 131.50, 129.63, 127.83, 124.42, 123.81, 121.17, 94.92, 38.65, 27.30, 15.50, 14.96, 8.52. MS: *m/e* 578 (M^+), 466 ($M^+ - Me_2T$), 440 ($M^+ - PMe_2Ph$).

Reaction of **1** *with* $PMePh_2$ *to give* Cp*Ir(η^2-2,5-Me_2T)($PMePh_2$) (**5**)

Compound **1** (0.030 g, 0.068 mmol) reacted, in a similar manner as described in the reaction with PMe_3, with $PMePh_2$ (0.140 g, 0.699 mmol) for 60 h at room temperature. Subsequent treatment as described for **3** gave 0.025 g (57%) of orange–red crystals of **5** (m.p. 146–147°C, decomp). MS: *m/e* 640 (M^+), 528 ($M^+ - Me_2T$), 440 ($M^+ - PMePh_2$). Found: C, 54.21; H, 5.81. Calc. for $C_{29}H_{36}SPIr$: C, 54.44; H, 5.67%.

Reaction of **2** *with* $PMePh_2$ *to give* **5**

Similar to the procedure described in the reaction of **2** with PMe_3, **2** (0.027 g, 0.061 mmol) reacted with $PMePh_2$ (0.120 g, 0.600 mmol) for 2 h at −60 to −40°C. Subsequent treatment of the reaction mixture in a manner similar to that described for **3** gave orange–red crystals of **5** (m.p. 146–148°C, decomp); yield 0.035 g (90%). MS: *m/e* 640 (M^+), 528 ($M^+ - Me_2T$), 440 ($M^+ - PMePh_2$). Found: C, 54.03; H, 5.76. Calc. for $C_{29}H_{36}SPIr$: C, 54.44; H, 5.67%.

Reaction of **1** *with* PPh_3 *to give* Cp*Ir(η^2-2,5-Me_2T)(PPh_3) (**6**)

The reaction of **1** (0.025 g, 0.057 mmol) with PPh_3 (0.045 g, 0.167 mmol) was performed in a manner similar to that described for the reaction of **1** with PMe_3 for 68 h at room temperature. Further treatment of the reaction mixture as described above for **3** gave 0.022 g (55%) of orange–red crystals of **6** (m.p. 197–198°C, decomp). MS: *m/e* 702 (M^+), 625 ($M^+ - Ph$), 590 ($M^+ - Me_2T$), 440 ($M^+ - PPh_3$). Found: C, 57.85; H, 5.82. Calc. for $C_{34}H_{38}SPIr$: C, 58.18; H, 5.46%.

Reaction of **2** *with* PPh_3 *to give* **6**

Similar to that described in the reaction of **2** with PMe_3, **2** (0.020 g, 0.045 mmol) was reacted with 0.040 g (0.153 mmol) of PPh_3 at −40 to −30°C for 2 h. Subsequent treatment of the resulting mixture in a similar manner as described for **3** yielded 0.028 g (88%) of orange–red crystals of **6** (m.p. 198–199°C, decomp). MS: *m/e* 702 (M^+), 625 ($M^+ - Ph$), 590 ($M^+ - Me_2T$), 440 ($M^+ - PPh_3$).

Reaction of **1** *with* $P(OPh)_3$ *to give* Cp*Ir(η^2-2,5-Me_2T)[$P(OPh)_3$] (**7**)

Compound **1** (0.020 g, 0.045 mmol) was dissolved in 30 cm^3 of hexane at room temperature. To this solution was added $P(OPh)_3$ (0.140 g, 0.450 mmol). The solution was stirred for 48 h, during which time the light yellow solution gradually turned orange. After evaporating the solution *in vacuo*, the residue was chromatographed on Al_2O_3 (neutral) with hexane first and then hexane–Et_2O (10 : 1) as the eluant. The solvent was removed from the yellow fraction under vacuum, and the crude product was recrystallized from hexane at −80°C to give 0.019 g

(56%) of orange crystals of **7** (m.p. 20–21°C, orange oil). MS: *m/e* 750 (M^+), 638 ($M^+ - Me_2T$), 440 ($M^+ - P(OPh)_3$). Found: C; 54.05; H, 4.91. Calc. for $C_{34}H_{38}O_3SPIr$: C, 54.45; H, 5.11%.

Reaction of **2** *with* $P(OPh)_3$ *to give* **7**

To a solution containing **2** (0.030 g, 0.068 mmol) in 30 cm^3 of hexane was added $P(OPh)_3$ (0.200 g, 0.645 mmol) at −60°C. The colour of the solution changed immediately from red to yellow. After being stirred for 1 h at −60 to −40°C, the resulting mixture was then treated in a similar manner as described above for **3** to give 0.044 g (86%) of orange crystals of **7** (m.p. 20–21°C, orange oil). MS: *m/e* 750 (M^+), 638 ($M^+ - Me_2T$), 440 ($M^+ - P(OPh)_3$).

Reaction of **1** *with* CO *to give* Cp*Ir(η^2-2,5-Me_2T)(CO) (**8**)

Compound **1** (0.035 g, 0.080 mmol) was dissolved in 50 cm^3 of hexane at room temperature; CO gas was bubbled through the solution over a period of 10 h during which time the light yellow solution gradually turned orange. After evaporating the solution, the residue was chromatographed on Al_2O_3 (neutral) with hexane as the eluant, and the yellow band was collected. After removal of the solvent *in vacuo*, the crude orange powdery product was recrystallized from hexane at −80°C to afford 0.027 g (73%) of orange–yellow needles of **8** (m.p. 121°C, decomp). IR (hexane) ν(CO): 2020 s cm^{-1}. MS: *m/e* 468 (M^+), 440 ($M^+ - CO$), 356 ($M^+ - Me_2T$). Found: C, 43.30; H, 5.00. Calc. for $C_{17}H_{23}OSIr$: C, 43.66; H, 4.96%.

Reaction of **2** *with* CO *to give* **8**

Compound **2** (0.053 g, 0.120 mmol) was dissolved in 50 cm^3 of hexane at −30°C; CO was bubbled through the solution over a period of 2 h during which time the colour of the solution changed from red to yellow. Further treatment of the resulting solution in a similar manner as described above for the reaction of **1** with CO afforded 0.050 g (89%) of orange–yellow needles of **8** (m.p. 121–122°C, decomp). IR (hexane) ν(CO): 2020 s cm^{-1}. MS: *m/e* 468 (M^+), 440 ($M^+ - CO$), 356 ($M^+ - Me_2T$). Found: C, 43.20; H, 5.09. Calc. for $C_{17}H_{23}OSIr$: C, 43.66; H, 4.96.

Reaction of **1** *with* H_2 *to give* Cp*Ir(η^2-2,5-Me_2T)$(H)_2$ (**9**)

Compound **1** (0.036 g, 0.082 mmol) was dissolved in 50 cm^3 of hexane at room temperature; H_2 was bubbled through the solution over a period of 24 h; during that time the light yellow solution gradually turned orange–red. After evaporating the solution *in vacuo*, the red residue was chromatographed on Al_2O_3 (neutral) with hexane as the eluant. The red band was collected. The solvent was removed under vacuum and the crude product was recrystallized from hexane at −80°C to yield 0.017 g (47%) of red crystals of **9** (m.p. 148–149°C, decomp). MS: *m/e* 442 (M^+), 441 ($M^+ - H$), 440 ($M^+ - 2H$). Found: C, 43.62; H, 5.48. Calc. for $C_{16}H_{25}SIr$: C, 43.51; H, 5.71%. The mother liquor from the recrystallization was again chromatographed in the same manner as described above to give a red fraction. The solvent was removed under vacuum and the dark-red residue was recrystallized from hexane at −80°C to afford 0.008 g (22%) of dark-red crystals of **2** (m.p. 147°C, decomp). ^1H NMR ($CDCl_3$): δ 7.47 (d, 1H), 7.34 (d, 1H), 3.10 (s, 3H), 2.79 (s, 3H), 1.93 (s, 15H).

Reaction of **2** *with* H_2 *to give* **9**

Compound **2** (0.050 g, 0.114 mmol) was dissolved in 50 cm^3 of hexane at room temperature; H_2 was bubbled through the solution over a period of 24 h during which time no obvious colour change was observed. Subsequent treatment of the resulting red solution in the same manner as described above for the reaction of **1** with H_2 gave 0.034 g (68%) of red crystals of **9** (m.p. 148–149°C, decomp). MS: *m/e* 442 (M^+), 441 ($M^+ - H$), 440 ($M^+ - 2H$).

X-ray crystal structure determinations of **4** *and* **5**

The crystals of complexes **4** and **5** suitable for X-ray diffraction were obtained by recrystallization from hexane–CH_2Cl_2 solution at −80°C. Single crystals of approximate dimensions $0.20 \times 0.50 \times 0.55$ mm for **4** and $0.13 \times 0.17 \times 0.11$ mm for **5** were mounted on the ends of glass fibres and coated with a thin layer of epoxy cement. The cell constants were determined from lists of reflections found by an automated search routine. Relevant crystallographic information for **4** and **5** appear in Table 2.

The structure of **4** was solved by the Patterson method. All of the non-hydrogen atoms appeared in a difference map produced after the successful placement of the iridium atom. Hydrogen atoms were not included in the model. Because of the large absorption correction applied based on the psi-scan data, a numerical absorption correction was applied to the unaveraged data set following isotropic least-squares refinement of all the non-hydrogen atoms.[6] After this correction, the new averaging agreement

Table 2. Crystallographic data for Cp*Ir(η^2-2,5-Me_2T)(PMe_2Ph) (**4**) and Cp*Ir(η^2-2,5-Me_2T)($PMePh_2$) (**5**)

	4	**5**
Formula	$IrSPC_{24}H_{34}$	$IrSPC_{29}H_{36}$
Formula weight	577.78	639.85
Space group	$P2_1/c$ (No. 14)	$P2_1/n$ (No. 14)
a (Å)	9.373(2)	11.542(2)
b (Å)	27.287(2)	16.781(1)
c (Å)	9.668(2)	13.782(2)
β (°)	109.04(1)	97.00(1)
V (Å^3)	2337(1)	2649.3(6)
Z	4	4
d_{calc} (g cm^{-3})	1.642	1.604
Crystal size (mm)	0.20 × 0.50 × 0.55	0.13 × 0.17 × 0.11
μ(Mo-K_α) (cm^{-1})	58.50	51.69
Data collection instrument	Enraf–Nonius CAD4	Enraf–Nonius CAD4
Radiation (monochromated in incident beam)	Mo-K_α (λ = 0.71073 Å)	Mo-K_α (λ = 0.71073 Å)
Orientation reflections, number, range (2θ)	25, 21° < 2θ < 30°	18, 25° < 2θ < 32°
Temperature (°C)	−90	−70
Scan method	θ–2θ	ω-scans
Data collection range, 2θ (°)	4–50	4–45
Number of unique data, total:	4118	3451
with $F_o^2 > 3\sigma(F_o^2)$:	3511	2389
Number of parameters refined	244	174
Trans. factors, max., min. (psi scans)	1.00, 0.304	1.00, 0.641
Correction factors, max., min. (numerical)	1.16, 0.866	1.101, 0.910
R^a	0.0272	0.0381
$R_w{}^b$	0.0468	0.0479
Quality-of-fit indicator^c	1.04	1.20
Largest shift/ESD, final cycle	0.01	< 0.01
Largest peak (e/Å^3)	0.955	0.796

^{a} $R = \Sigma ||F_o| - |F_c|| / \Sigma |F_o|$.
^{b} $R_w = [\Sigma w(|F_o| - |F_c|)^2 / \Sigma w|F_o|^2]^{1/2}$; $w = 1/\sigma^2(|F_o|)$.
^{c} Quality-of-fit = $[\Sigma w(|F_o| - |F_c|)^2 / (N_{obs} - N_{parameters})]^{1/2}$.

factor was 1.9% based on F_{obs}. In the final cycles of refinement, all of the atoms were given anisotropic temperature factors; the refinement included 244 variable parameters and converged with unweighted and weighted agreement factors[7] of $R = 0.0272$ and $R_w = 0.0468$.

For **5**, the structure was also solved by the Patterson method. Refinement was carried out with full-matrix least-squares calculations. In the final stages of refinement the iridium, phosphorus, sulphur and carbon atoms of the chelating ligand were given anisotropic thermal parameters. Hydrogen atoms were placed in calculated positions on the phenyl rings and on the trigonal carbon atoms of the chelating ligand, then used to calculate structure factors only. The final cycle of refinement included 174 variable parameters and converged with unweighted and weighted agreement factors[7] of $R = 0.0381$ and $R_w = 0.0479$. Bond distances and selected angles are presented in Tables 3 and 4 and ORTEP drawings of **4** and **5** are given in Figs 1 and 2, respectively.

RESULTS AND DISCUSSION

Reactions of Cp*Ir(η^2-2,5-Me_2T) (**2**) *and* Cp*Ir(η^4-2,5-Me_2T) (**1**) *with phosphorus ligands and* CO

Complex **2**, which can be formulated as having a 16 e$^-$-resonance form [A in eq. (2)], reacts readily, even at −60 to −40°C, with phosphorus-donor ligands to give the corresponding orange-coloured

Table 3. Selected bond distances (Å)[a,b] for Cp*Ir(η^2-2,5-Me_2T)(PMe_2Ph) (**4**) and Cp*Ir(η^2-2,5-Me_2T)($PMePh_2$) (**5**)

	4	**5**
Ir—S	2.348(1)	2.346(3)
Ir—P	2.252(1)	2.255(3)
Ir—C(5)	2.074(5)	2.06(1)
Ir—C(11)	2.235(5)	2.25(1)
Ir—C(12)	2.250(4)	2.26(1)
Ir—C(13)	2.265(5)	2.25(1)
Ir—C(14)	2.266(5)	2.25(1)
Ir—C(15)	2.257(5)	2.27(1)
S—C(2)	1.741(5)	1.74(1)
P—C(7)	1.836(5)	1.84(1)
P—C(8)	1.837(6)	
P—C(26)	1.841(6)	1.83(1)
P—C(32)		1.83(1)
C(1)—C(2)	1.501(7)	1.54(2)
C(2)—C(3)	1.347(8)	1.34(2)
C(3)—C(4)	1.458(8)	1.42(2)
C(4)—C(5)	1.330(6)	1.36(2)
C(5)—C(6)	1.501(9)	1.52(2)

[a] Numbers in parentheses are ESDs in the least significant digits.

[b] Average C—C distances in the Cp* ring and average C—CH_3 distances are 1.435 and 1.51 Å, respectively, in **4** and 1.43 and 1.52 Å, respectively, in **5**.

18 e^--adducts Cp*Ir(η^2-2,5-Me_2T)(PR_3) [Eq. (3a)] in high isolated yields (> 86%). Complexes **3**–**7** are soluble in both polar and non-polar organic solvents and moderately air-sensitive in both the solid state and in solution. The complexes are characterized by their elemental analyses, mass spectra and ^{1}H NMR spectra (Table 1). The structures of **4** and **5** (see next section) were established by X-ray crystallography.

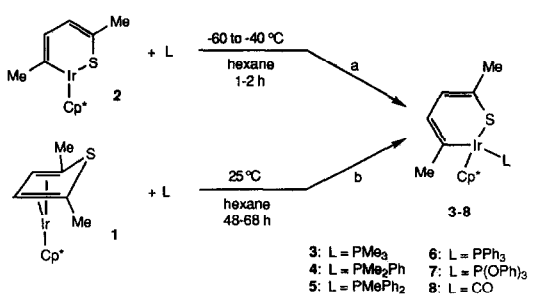

(3)

Although excesses of the phosphorus donor ligands were used in the reactions [eq. (3)], there was no evidence for further reaction of complexes **3**–**7** under these conditions. In an NMR tube reaction of **2** (or **1**) (10.0 mg, 0.023 mmol) with dppe (10.0 mg, 0.025 mmol) in 0.5 cm^3 of $CDCl_3$, the ^{1}H

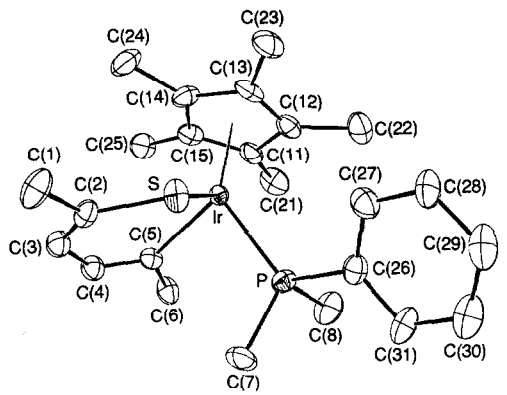

Fig. 1. ORTEP drawing of Cp*Ir(η^2-2,5-Me_2T)(PMe_2Ph) (**4**).

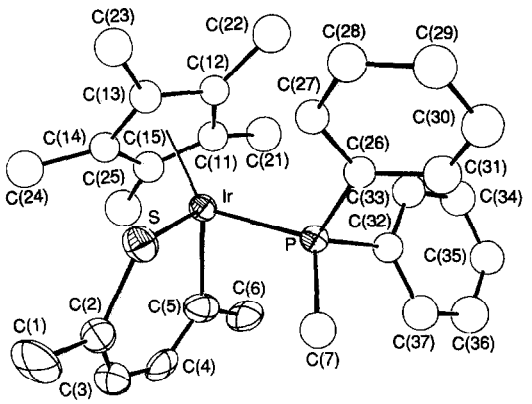

Fig. 2. ORTEP drawing of Cp*Ir(η^2-2,5-Me_2T)($PMePh_2$) (**5**).

NMR spectrum indicated that **2** had completely reacted in 0.5 h (4 h for **1**) at room temperature. The product, Cp*Ir(dppe), of the reaction [eq. (4)] was identified by its Cp* (δ 1.91, 15H), methylene (δ 2.32–2.48 and 2.07–2.16, m, 4H), and Ph (δ 7.30–7.85, m, 10H) resonances and mass spectrum [*m/e* 726 (M^+) and 328 ($M^+ - dppe$)]; however, since it was quite unstable and dissociated to give free dppe during recrystallization from hexane or hexane–CH_2Cl_2, it could not be purified for elemental analysis. Neither 2,5-Me_2T nor other recognizable organic products were identified as products of the reaction [eq. (4)].

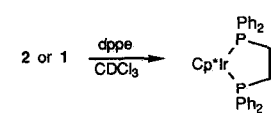

(4)

Although one might have expected the 18e^- complex Cp*Ir(η^4-2,5-Me_2T) (**1**) to react with phosphorus donors to give 2,5-Me_2T and Cp*IrL_2, this

Table 4. Selected bond angles (°)[a] for Cp*Ir(η^2-2,5-Me_2T)(PMe_2Ph) (**4**) and Cp*Ir(η^2-2,5-Me_2T)($PMePh_2$) (**5**)

	4	**5**
S—Ir—P	87.39(5)	87.9(1)
S—Ir—C(5)	91.5(1)	93.0(3)
P—Ir—C(5)	88.5(1)	86.1(3)
Ir—S—C(2)	110.0(2)	111.6(4)
Ir—P—C(7)	116.1(2)	115.1(5)
Ir—P—C(8)	115.3(2)	
Ir—P—C(26)	116.8(2)	116.2(4)
Ir—P—C(32)		117.9(4)
C(7)—P—C(8)	102.7(3)	
C(7)—P—C(26)	103.1(2)	100.1(5)
C(7)—P—C(32)		103.7(5)
C(8)—P—C(26)	100.5(3)	
C(26)—P—C(32)		101.3(5)
S—C(2)—C(1)	114.7(4)	111.2(9)
S—C(2)—C(3)	124.3(4)	126(1)
C(1)—C(2)—C(3)	121.0(4)	123(1)
C(2)—C(3)—C(4)	128.7(4)	129(1)
C(3)—C(4)—C(5)	130.3(5)	131(1)
Ir—C(5)—C(4)	125.6(5)	126.5(9)
Ir—C(5)—C(6)	116.1(3)	116.3(8)
C(4)—C(5)—C(6)	118.1(5)	117(1)
C(12)—C(11)—C(15)	106.8(5)	107.7(9)
C(11)—C(12)—C(13)	108.5(4)	108(1)
C(12)—C(13)—C(14)	108.2(2)	107.3(8)
C(13)—C(14)—C(15)	107.7(4)	108(1)
C(11)—C(15)—C(14)	108.8(5)	109.5(9)

[a] Numbers in parentheses are ESDs in the least significant digits.

reaction gives [eq. (3)] the same adducts **3**–**7** as were obtained from the reactions of **2**. However, **1** is much less reactive than **2**, requiring a higher reaction temperature (25°C) and longer reaction times (48–68 h), and the yields (55–78%) are somewhat lower. Qualitatively, the rates of reaction (3b) decrease as PMe_3 > PMe_2Ph > $PMePh_2$ > PPh_3 with PMe_3 requiring only 48 h and PPh_3 68 h. Somewhat surprisingly, $P(OPh_3)$ reacts faster than PMe_2Ph, $PMePh_2$ and PPh_3; which suggests that the small cone angle (128°) of $P(OPh)_3$ is important for its reactivity even though it is a weak base.[8]

The mechanism for the reaction of **1** with phosphorus-donors is likely to involve initial isomerization of **1** to **2**, catalysed by the phorphorus-donor ligand. Other bases, e.g. Et_3N, are known[4] to catalyse this isomerization. Since **2** would react rapidly [eq. (3a)] with phosphine, one would not expect to detect **2** as an intermediate in this reaction, and no intermediates were observed.

Like the phosphorus-donors, CO also reacts [eq. (3a)] with **2** under mild conditions (−30°C, 2 h) to give the orange–yellow adduct Cp*Ir(η^2-2,5-Me_2T)(CO) (**8**) in 89% yield [eq. (3a)]. Complex **1** also reacts [eq. (3b)] with CO to give **8** but more vigorous conditions (25°C, 10 h) are required. In this latter reaction, complex **2** was detected in the ^{1}H NMR ($CDCl_3$) spectrum of a sample taken during the reaction, which suggests that **2** is an intermediate in the reaction of **1** with CO. There is no evidence for products in which CO has inserted into the Ir—C bond.

Complex **8** is characterized by its elemental analysis, its IR spectrum showing a ν(CO) absorption at 2020 cm^{-1}, and its ^{1}H NMR spectrum (Table 1), which is very similar to those of the phosphorus-donor adducts, **3**–**7**. While **8** is soluble in both polar and non-polar organic solvents, these solutions are quite air-sensitive.

Structures of Cp*Ir(η^2-2,5-Me_2T)(PMe_2Ph) (**4**) *and* Cp*Ir(η^2-2,5-Me_2T)($PMePh_2$) (**5**)

The structures (Figs 1 and 2) of **4** and **5** are that of a piano stool with the P, S and C(5) "legs" at roughly right angles (86–93°) to each other. The cyclopentadienyl carbons, C(11)–C(15), of the Cp* rings lie in a plane (±0.008 Å in **4** and ±0.01 Å in **5**) and the five CH_3 carbons are an average of 0.13 Å (for **4**) and 0.17 Å (for **5**) out of this plane away from the iridium. The Ir—P bond distances, 2.252(1) and 2.255(3) Å, in **4** and **5**, respectively, are very similar to that (2.237(2) Å) in CpIr(CO)(PPh_3).[9]

The most interesting structural feature of these complexes is the η^2-2,5-Me_2T ligand. In complex **2**, the six-membered ring is planar and aromatic as determined from bond distances (Scheme 1) and NMR data.[4] The C—C bond distances in this ring are nearly equal suggesting a delocalized π-system, which may be described by resonance forms **A** and **B** [in eq. (2)] and we have termed an "iridathiabenzene". In the phosphine adducts, **4** and **5**, the six-membered ring is no longer planar and the bond distances have changed such that the ring is most appropriately represented by resonance form

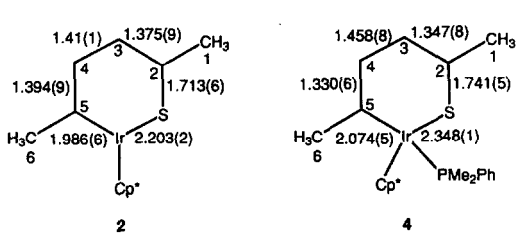

2 **4**

Scheme 1. Comparison of the six-membered rings in Cp*Ir(η^2-2,5-Me_2T) (**2**) and Cp*Ir(η^2-2,5-Me_2T)(PMe_2Ph) (**4**).

A which makes the η^2-2,5-Me_2T ligand a formal $2e^-$-donor and the two electrons from the phosphine ligand brings the iridium to an $18e^-$ count.

For a detailed structural comparison of **2** and the phosphine adducts, we have chosen adduct **4** because its structure refined better than **5**; however, the bond distances and angles in **5** are within experimental error the same as those in **4**. In contrast to the planar six-membered ring in **2**, only S, C(2), C(3), C(4) and C(5) are in a plane (± 0.06 Å) in **4**; the Ir is out of this plane by 0.69 Å; C(1) is 0.12 Å out of the plane toward the Ir and C(6) is 0.20 Å out of the plane away from Ir. Another measure of the non-planarity of the ring is the 148.8 (± 0.4)° dihedral angle between the S, Ir, C(5) and C(2), C(3), C(4) planes. The non-planarity of the rings in **4** and **5** suggests that the π-system is not delocalized in these complexes as it is in **2**.

Another indication is the change in bond distances in **4** as compared to **2**. In contrast to the nearly equal bond distances in the C(2)—C(3)—C(4)—C(5) part of the six-membered ring in **2**, in **4** the C(2)—C(3) (1.347(8) Å) and C(4)—C(5) (1.330(6) Å) bonds are considerably shorter than C(3)—C(4) (1.458(8) Å). The short distances are typical of $C(sp^2)$=$C(sp^2)$ double bonds (1.34 Å), while the longer distance (1.458(8) Å) is very close to that (1.48 Å) of a $C(sp^2)$—$C(sp^2)$ single bond. The C(2)—S distance (1.741(5) Å) is primarily a single bond since it is close to that (1.77 Å) of normal $C(sp^2)$—S single bonds[10,11] and substantially longer than $C(sp^2)$=S double bonds (1.61 Å).[12] Especially interesting is the Ir—C(5) distance (2.074(5) Å) which is 0.088 Å longer than in **2** and corresponds to an Ir—$C(sp^2)$ single bond as in compound **C**, where the Ir—C bond length[13] is

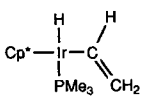

C

2.054(4) Å. Considering all of the bond distances, the bonding in **4** fits very well to the localized bonding represented by resonance form **A**.

Further support for this bonding comes from a comparison of the NMR spectra of **2** and **4**. In the ^{1}H NMR spectrum of **2**, the protons on C(3) and C(4) occur far downfield (δ 7.47 and 7.34, Table 1) consistent with a delocalized, aromatic ring. In **4** (and the other adducts), these protons are substantially upfield (δ 5.90 and 5.42) characteristic of olefinic protons. In the ^{13}C NMR spectrum of **2**, C(5) occurs at low field (δ 180.99)[4] indicating significant carbene character contributed by resonance form **B**. In contrast, there is no ^{13}C resonance in the δ 180 ppm region in the spectrum of **4**; thus, C(5) in **4** must be one of the eight signals in the range δ 121–136 (four for the Ph and four for the carbons in the six-membered ring). This upfield position means that C(5) does not have much carbene character but is in the region expected for a vinyl carbon as in compound **C**, in which the vinyl carbon signal occurs at δ 129.18.[13] Thus, the ^{1}H and ^{13}C NMR spectra of **4** are also consistent with its being best represented by resonance form **A**.

Reactions of Cp*Ir(η^2-2,5-Me_2T) (**2**) *and* Cp*Ir(η^4-2,5-Me_2T) (**1**) *with* H_2

As complex **2** is able to add $2e^-$-donor ligands [eq. (3a)], it can also undergo oxidative-addition with H_2 [eq. (5)] to give the red dihydride **9** in 68% yield. This product is characterized by elemental analyses, mass and ^{1}H NMR spectra. The singlet hydride resonance at δ −16.27 ppm integrates for 2H. A T_1 measurement on the hydride signal in **9**, in CD_2Cl_2 at −80°C, by the inversion–recovery method (180°-τ-90°, τ = variable) at 300 MHz on a Bruker WM 300 NMR instrument gave a value of 890 ms; this relatively long T_1 is consistent[14] with the formulation of **9** as a dihydride rather than as an η^2-H_2 complex.

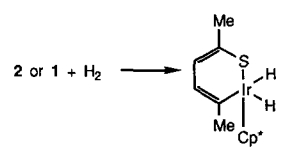

(5)

9

Complex **9** is also prepared in 47% yield from the reaction of **1** with H_2. A by-product of this reaction is **2** which is isolated in 22% yield; the isolation of **2** suggests that it may be an intermediate in the reaction of **1** since **2** reacts with H_2 to give **9** under the same conditions. It appears that H_2 catalyses the isomerization of **1** to **2**, which does not occur under these conditions in the absence of H_2.

Refluxing a hexane solution of **9** under N_2 did not give any isolable products; neither complex **2** nor **1** was identified; only slow decomposition to uncharacterized products was observed.

CONCLUSION

Although the iridathiabenzene portion of **2** is best represented by a combination of resonance forms **A** and **B** in which the iridium is a $16e^-$- or $18e^-$-centre, respectively, complex **2** reacts very much like a $16e^-$-system by adding $2e^-$-donor ligands such as phosphines and CO and by undergoing oxidative-addition with H_2. The other

isomer, **1**, undergoes the same reactions as **2** but generally they are slower; there is evidence to suggest that these reactions proceed by initial isomerization of **1** to **2**; then **2** combines with the $2e^-$-donor ligands or H_2 to form the final products.

Acknowledgements—This work was supported by U.S. Department of Energy under contract No. W-7405-Eng-82, Office of Basic Energy Sciences, Chemical Sciences Division. We appreciate the loan of $IrCl_3$ from Johnson Matthey, Inc.

REFERENCES

1. R. J. Angelici, *Accts Chem. Res.* 1988, **21**, 387.
2. S. C. Huckett and R. J. Angelici, *Organometallics* 1988, **7**, 1491.
3. J. Chen and R. J. Angelici, *Organometallics* 1989, **8**, 2277.
4. J. Chen, L. M. Daniels and R. J. Angelici, *J. Am. Chem. Soc.* 1990, **112**, 199.
5. J. Chen and R. J. Angelici, *Organometallics* 1990, **9**, 849.
6. D. N. Walker and D. Stuart, *Acta Cryst.* 1983, **A39**, 159.
7. Neutral-atom scattering factors and anomalous scattering corrections were taken from the *International Tables for X-ray Crystallography*, Vol. IV. Kynoch Press, Birmingham, U.K. (1974).
8. M. M. Rahman, H. Y. Liu, A. Prock and W. P. Giering, *Organometallics* 1987, **6**, 650.
9. M. J. Bennett, J. L. Pratt and R. M. Tuggle, *Inorg. Chem.* 1974, **13**, 2408.
10. B. Rozsondai, G. Schultz and I. Hargittai, *J. Molec. Struct.* 1981, **70**, 309.
11. S. Samdal, H. M. Seip and T. Torgrimsen, *J. Molec. Struct.* 1979, **57**, 105.
12. (a) A. P. Cox, S. B. Hubbard and H. Kato, *J. Molec. Spectrosc.* 1982, **93**, 196; (b) H. W. Kroto and B. H. Landsberg, *J. Molec. Spectroc.* 1976, **62**, 346.
13. (a) P. O. Stoutland and R. G. Bergman, *J. Am. Chem. Soc.* 1985, **107**, 4580; (b) P. O. Stoutland and R. G. Bergman, *J. Am. Chem. Soc.* 1988, **110**, 5732.
14. (a) R. H. Crabtree and D. G. Hamilton, *Adv. Organomet. Chem.* 1988, **28**, 299; (b) D. C. Hamilton and R. H. Crabtree, *J. Am. Chem. Soc.* 1988, **110**, 4126; (c) R. H. Crabtree, D. Hamilton and M. Lavin, in *Experimental Organometallic Chemistry* (Edited by A. L. Wayda and M. Y. Darensbourg), pp. 223–226. American Chemical Society, Washington, D.C. (1987).

Polyhedron Vol. 9, No. 15/16, pp. 1893–1899, 1990
Printed in Great Britain

0277–5387/90 $3.00+.00
© 1990 Pergamon Press plc

SYNTHESIS AND CRYSTAL STRUCTURES OF TWO DIRUTHENIUM POLYSULPHIDE COMPLEXES*

PAUL M. TREICHEL,† RICHARD A. CRANE and K. J. HALLER

Department of Chemistry, University of Wisconsin-Madison, Madison, WI 53706, U.S.A.

Abstract—The reaction between $Ru(SPh)(PPh_3)\{P(OMe)_3\}(\eta\text{-}C_5H_5)$ and sulphur, in acetonitrile, affords two diruthenium polysulphide complexes, $Ru_2\{P(OMe)_3\}_2(\eta\text{-}C_5H_5)_2S_4$ (**I**) and $Ru_2\{P(OMe)_3\}_2(\eta\text{-}C_5H_5)_2S_6$ (**II**). The latter could be converted to the former by reaction with PPh_3. Structures of both blue–black, crystalline species were determined by single crystal X-ray diffraction methods. The former contained a six-membered, non-planar ring (cyclohexane chair structure) consisting of the two metal atoms and four sulphurs with the metals in the 1- and 4-positions, while the latter contained a Ru_2S_6 eight-membered ring, with metal atoms in the 1- and 5-positions and a long bond between two sulphurs across this ring, a structure not unlike that of $[S_8]^{2+}$. Comments are presented on the unusual bonding in the Ru_2S_n rings in these two species.

The synergism between synthesis and theory has been much in evidence over the last two decades. In our laboratories, perhaps the most notable example of this arose with the collaboration that grew up between our group and the Fenske group involving studies on oxidative electrochemistry of metal complexes with isonitrile ligands. Theory established[1] that a linear relationship exists between ease of oxidation, as measured by an $E_{1/2}$ value, and the energy of the HOMO, the latter calculated by Fenske–Hall[2] methods. This work was later extended to rationalize the different $E_{1/2}$ values for isomeric species.[3] This research has taken on larger proportions as further experimental and theoretical studies were completed.[4,5]

A similar recent story is related here. Work in our group, part of a larger programme on organosulphur complexes of metals, resulted in the synthesis and characterization of the two compounds that are the subject of this paper; in turn, this led to investigations into the theory needed to understand these species.

Frequently, a well conceived reaction produces unexpected results and opens up a new area of even greater proportions than had been contemplated in the original study. We carried out a reaction between $Ru(SPh)(PPh_3)\{P(OMe)_3\}(\eta\text{-}C_5H_5)$ and sulphur; our expectation was that PPh_3 would dissociate and then be captured by reaction with sulphur. In this compound, as in a number of other ruthenium complexes, triphenylphosphine is quite easily displaced.[6] Sulphur had been used successfully as an agent to capture this phosphine in other situations.[7] Our initial goal was to prepare a dinuclear complex, $Ru_2(\mu\text{-}SPh)_2\{P(OMe)_3\}_2(\eta\text{-}C_5H_5)_2$, which we predicted would have striking oxidative chemistry by analogy to the behaviour of similar iron complexes.[8]

Instead, this reaction produced two diruthenium polysulphide complexes. We have characterized both by single crystal X-ray diffraction studies and found that they have unexpected molecular structures. To rationalize these structures and to explain the bonding in these species, a collaboration was set up with David Kanis, at the time a student in the Fenske group. The theoretical study that followed became a major part of Kanis' PhD thesis; two papers, one for each compound, describing the theoretical calculations and their interpretations have since been written.[9]

During the course of our work a communication was published by Rauchfuss and co-workers[10] describing the synthesis and structures of two similar compounds. These species, differing from ours by the nature of the phosphorus ligand, were obtained by a different route.

RESULTS AND DISCUSSION

The ruthenium complex that is the precursor in this synthesis was obtained in a two-step sequence

* Dedicated to our faculty colleague and friend, Professor Richard F. Fenske, upon his retirement.

† Author to whom correspondence should be addressed.

portrayed by the equations below:

$$RuCl(PPh_3)_2(\eta\text{-}C_5H_5) + P(OMe)_3 \longrightarrow RuCl(PPh_3)\{P(OMe)_3\}(\eta\text{-}C_5H_5) + PPh_3$$

$$RuCl(PPh_3)\{P(OMe)_3\}(\eta\text{-}C_5H_5) + n\text{-}Bu_3SnSPh \longrightarrow Ru(SPh)(PPh_3)\{P(OMe)_3\}(\eta\text{-}C_5H_5) + n\text{-}Bu_3SnCl.$$

There are analogous procedures in the literature for both the replacement of triphenylphosphine[6] and the use of tributyltin thiolate as a source of PhS^-.[11]

The reaction between $Ru(SPh)(PPh_3)\{P(OMe)_3\}(\eta\text{-}C_5H_5)$ and elemental sulphur (in small excess) was carried out in refluxing acetonitrile and resulted in formation of the two compounds, $Ru_2\{P(OMe)_3\}_2(\eta\text{-}C_5H_5)_2S_4$ (**I**) and $Ru_2\{P(OMe)_3\}_2(\eta\text{-}C_5H_5)_2S_6$ (**II**). As anticipated, the PPh_3 turned up as $S{=}PPh_3$. The disulphide, PhSSPh, was also found among the products of this reaction, making known the fate of the thiolate group and strongly suggesting that this group was not the source of sulphur in these two species.

Product **I** was most easily separated based on its much lower solubility in CH_2Cl_2 and it also crystallized well from $CHCl_3$. The second product, **II**, was then separated from small amounts of **I** using column chromatography.

It is possible to convert **II** to **I** by reaction with PPh_3. This type of desulphurization reaction has been used previously.[12] The reaction appears to be clean and specific, according to data obtained when the reaction was monitored by NMR. No intermediate products were seen and there was no indication that **I** will lose further sulphur.

$$\underset{(\mathbf{II})}{Ru_2\{P(OMe)_3\}_2(\eta\text{-}C_5H_5)_2S_6} + 2PPh_3 \longrightarrow \underset{(\mathbf{I})}{Ru_2\{P(OMe)_3\}_2(\eta\text{-}C_5H_5)_2S_4} + 2S{=}PPh_3.$$

The relatively mild conditions are noteworthy. The reaction occurs at reflux temperature of acetonitrile (80°C); no starting material remained after a reaction time of 50 min. A reaction between the rather similar complex $Ru(SH)(PPh_3)_2(\eta\text{-}C_5H_4Me)$ and sulphur, in refluxing toluene (b.p. 110°C) is reported to yield only a single species, the cubane-like tetramer, $Ru_4S_4(\eta\text{-}C_5H_4Me)_4$;[13] the fact that there is only a single product may be related to the lengthy reaction time, 18 h. In preliminary studies, we had also used toluene as a solvent and found a more complicated mixture of products which did, however, include both **I** and **II**.

Similar compounds, $Ru_2(PPh_3)_2(\eta\text{-}C_5H_5)_2S_x$ ($x = 4$, 6), were reported via a communication in the course of our work.[10] They were made by a different procedure that involved coupling of S_6^{2-} and the dication, $[(\eta\text{-}C_5H_5)Ru(PPh_3)_2\text{-}\mu\text{-}S_2\text{-}Ru(PPh_3)_2(\eta\text{-}C_5H_5)]^{2+}$, the latter having been made first from $RuCl(PPh_3)_2(\eta\text{-}C_5H_5)$, $AgSbF_6$ and S_8. Also, there is a recent reference to $Ru_2(CO)_2(\eta\text{-}C_5H_5)_2S_6$, a compound formed from photolysis of sulphur and $Ru_2(CO)_4(\eta\text{-}C_5H_5)_2$. This compound is possibly a carbonyl analogue of **II**, although confirming structural information was not presented.[14]

The structures of **I** and **II** were determined by single crystal X-ray diffraction and are shown in Figs 1 and 2. Selected bond lengths and angles for these compounds are given in Tables 1 and 2. In **I**, the two metals and four sulphurs form a six-membered non-planar ring (the chain form, as in cyclohexane). The metal atoms in the 1- and 4-positions contain the phosphite and cyclopentadienyl with axial and equatorial orientation, respectively. Sulphur–sulphur bond lengths in the ring are 2.04 Å, comparable with the single bond length value in S_8 of 2.05 Å. The ruthenium–sulphur bond lengths are 2.29 Å, shorter than a single bond between these elements which is generally assumed to be around 2.38 Å.[15] The structure of **II** may be viewed as an eight-membered ring with metal atoms in the 1- and 5-positions and a *trans*-ring interaction (bond) between the sulphur atoms in positions 4 and 8. [In the ORTEP drawing in Fig. 2, these atoms are labelled as S(1) and S(4).] There is a long distance between these sulphurs across the ring,

Table 1. Selected bond lengths and bond angles in **I**

Bond lengths (Å)		Bond angles (deg)	
Ru(1)—S(1)	2.290(1)	S(1)—Ru(1)—S(2)	101.3(0)
Ru(1)—S(2)	2.292(1)	S(2)—Ru(1)—P(1)	90.2(0)
Ru(1)—P(1)	2.209(1)	S(1)—Ru(1)—P(1)	91.4(0)
S(1)—S(2)+	2.042(1)		
av. Ru(1)—C(ring)	2.268(2)		

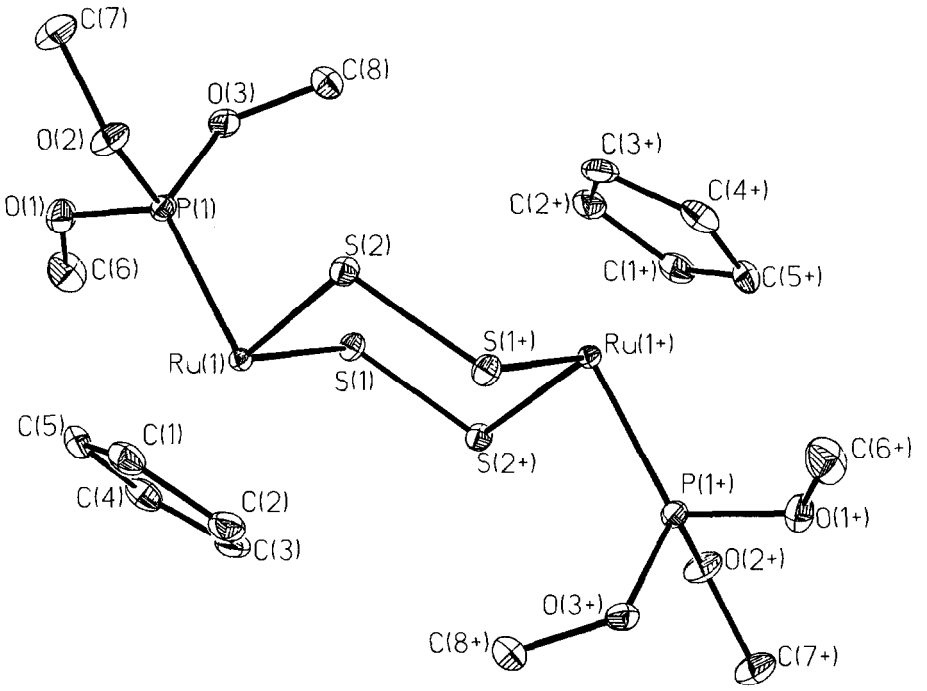

Fig. 1. ORTEP drawing of $Ru_2\{P(OMe)_3\}_2(\eta\text{-}C_5H_5)_2S_4$ (**I**); hydrogen atoms are omitted for clarity.

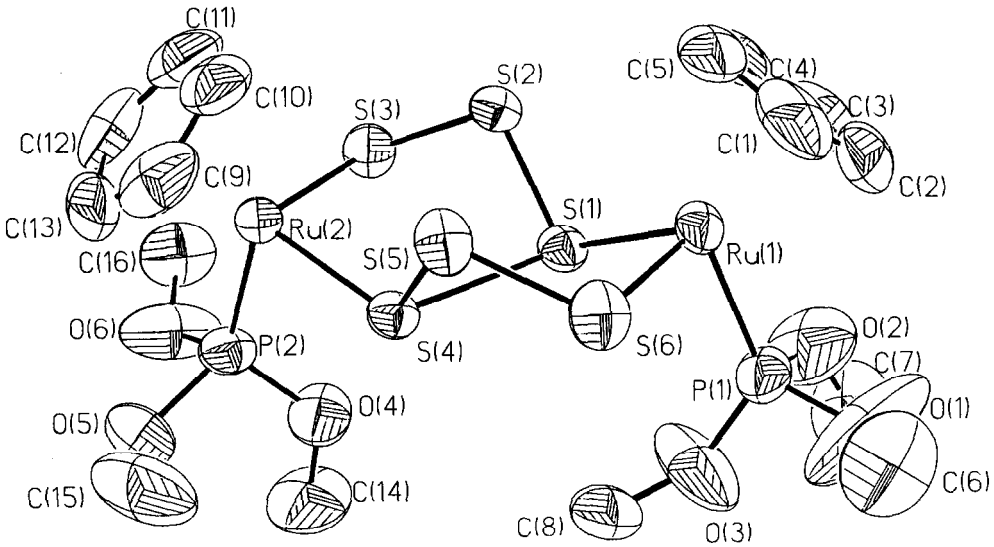

Fig. 2. ORTEP drawing of one of the two independent molecules of $Ru_2\{P(OMe)_3\}_2(\eta\text{-}C_5H_5)_2S_6$ (**II**); hydrogen atoms are omitted for clarity.

2.609(2) Å; this is shorter than the 2.77 Å measured for this bond in the triphenylphosphine analogue. Folding of the ring across this bond is consequent to these sulphurs being pyramidal; a further small distortion from planarity for each of the two halves of this molecule is seen to simply allow the atoms to bond with normal bond angles. Other sulphur–sulphur bond lengths in **II** are close to the single bond value. The two ruthenium–sulphur bonds are approximately 2.36 and 2.26 Å; the former is a typical single bond length[15] while the latter is like the ruthenium–sulphur bond length in **I**, the shortening presumed to be due to partial multiple bond character (*vide infra*).

A notable structural difference between **I** and its analogue is that the phosphorus and cyclo-

Table 2. Selected bond lengths and bond angles in **II**

Bond lengths (Å)		Bond angles (deg)	
Ru(1)—S(1)	2.261(1)	S(1)—Ru(1)—S(6)	92.0(1)
Ru(1)—S(6)	2.369(2)	S(1)—Ru(1)—P(1)	87.1(1)
Ru(1)—P(1)	2.216(1)	S(6)—Ru(1)—P(1)	95.7(1)
av. Ru(1)—C(ring)	2.225(10)	S(3)—Ru(2)—S(4)	92.5(1)
Ru(2)—S(3)	2.364(2)	S(3)—Ru(2)—P(2)	91.8(1)
Ru(2)—S(4)	2.260(1)	S(4)—Ru(2)—P(2)	88.6(1)
Ru(2)—P(2)	2.215(2)	Ru(1)—S(1)—S(2)	107.1(1)
av. Ru(2)—C(ring)	2.225(10)	S(1)—S(2)—S(3)	101.1(1)
S(1)—S(2)	2.049(2)	Ru(2)—S(3)—S(2)	102.2(1)
S(2)—S(3)	2.026(2)	Ru(2)—S(4)—S(5)	108.2(1)
S(4)—S(5)	2.051(2)	S(4)—S(5)—S(6)	101.7(1)
S(5)—S(6)	2.032(2)	Ru(1)—S(6)—S(5)	102.6(1)
S(1)—S(4)	2.610(2)		

pentadienyl groups have the opposite axial–equatorial orientation. This seems most likely to be a result of the sizes of these groups, with the largest group in each compound taking the least sterically-hindered equatorial site. Other than the difference in the *trans*-ring distance, noted above, bond lengths are similar to those reported for the analogous compounds.[10] Bond angles for **I** and **II** are also similar to the bond angles in the triphenylphosphine compound.

Our initial approach to rationalize these structures was based on simple valence bond representations. Noting that **I** is diamagnetic, we conceived a valence bond model with two resonance forms, shown below, to account for the fact that structural parameters showed equivalence of the two disulphur ligands:

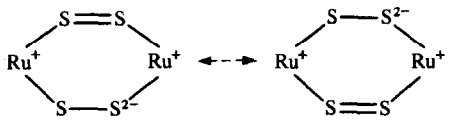

Formally, this picture portrays one of the bridging disulphur units as a neutral species (S_2) while the other unit is a dianion (S_2^{2-}). Each can donate a pair of electrons; in conjunction with the other ligands an 18-electron configuration is conveyed to each metal.

Given that a rather interesting and unusual type of delocalization is postulated, this compound seemed a logical candidate for a more detailed theoretical study.

In **II**, a rather more simple valence bond picture is possible, with a chain of sulphur atoms wrapped in a way that permits bidentate coordination of the sulphurs to the two metals.

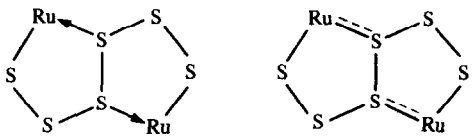

The problem with this representation of the structure is, of course, that the long bond across the ring between the two sulphurs is not explained. It is possible to overcome this obstacle by postulating delocalization, as shown, which involves hypervalent sulphur atoms. This bonding representation makes **II** also a likely candidate for further theoretical study. The fact that the structure is actually more like that for S_8^{2+}, with similarities including the long sulphur–sulphur bond, makes a theoretical study even more attractive.

Thus, as noted above, we set about interesting the experts in this problem. The detailed molecular orbital calculations (**I**) showed alignment of the energies of the metal orbitals and the π-symmetry orbitals of the S_4 unit to favour delocalization between these groups. A significant σ-bonding interaction between sulphurs on opposite sides of the ring was indicated by theory, even though the bond distance was long. Theory also points to multiple ruthenium–sulphur bonding, as postulated from bond length data. In the case of **II**, it was apparent from calculations that there is delocalization of charge in the molecular LUMO which involves multiple metal–sulphur bonding and antibonding character between sulphurs in the ring. The details of the calculations and the relationship of these species to analogous species like S_8^{2+} and S_6^{2+} may be found in the literature.[9]

EXPERIMENTAL

All experiments were carried out under nitrogen; this was largely a precautionary measure since reactants and products are not noticeably air-sensitive. Solvents were dried before use, following standard methodology (acetonitrile distilled from CaH_2; acetone distilled from K_2CO_3; CH_2Cl_2 distilled from P_4O_{10}; toluene distilled from Na; hexane distilled from $CaSO_4$). Alumina, weakly acidic, was purchased from Aldrich Chemical Co. and was used without pretreatment. Samples of n-Bu_3SnSPh[11] and $RuCl(PPh_3)_2(\eta\text{-}C_5H_5)$[16] were prepared by literature methods.

The precursor to the synthesis of the diruthenium polysulphide compounds, $Ru(SPh)(PPh_3)\{P(OMe)_3\}(\eta\text{-}C_5H_5)$, was prepared in a two-step process as described below.

Synthesis of $RuCl(PPh_3)\{P(OMe)_3\}(\eta\text{-}C_5H_5)$

A solution of $RuCl(PPh_3)_2(\eta\text{-}C_5H_5)$ (0.999 g, 1.38 mmol) and $P(OMe)_3$ (0.18 cm^3, 1.5 mmol) in 50 cm^3 of toluene was heated at reflux for 12 h. The resulting red–orange solution was allowed to cool and then concentrated to a volume of about 2 cm^3 on a rotary evaporator. Chromatography of the red oily substance was performed on an alumina column packed with CH_2Cl_2; a single orange band eluted with this solvent. After evaporation of solvent the material was dissolved in about 3 cm^3 of CH_2Cl_2; addition of 20 cm^3 of hexane caused the product to precipitate as orange crystals, m.p. 180–181°C (0.44 g, 55%).

Found: C, 52.69; H, 5.02. $C_{26}H_{29}ClO_3P_2Ru$ requires: C, 53.1; H, 4.97%. ^1H NMR ($CDCl_3$): 3.45 d, J(P—H) = 11 Hz, $P(OMe)_3$; 4.46 s, C_5H_5; 7.30 m, 9H and 7.57 m, 6H, PPh_3.

Synthesis of $Ru(SPh)(PPh_3)\{P(OMe)_3\}(\eta\text{-}C_5H_5)$

A solution of n-Bu_3SnSPh (0.15 cm^3, 0.42 mmol) and $RuCl(PPh_3)\{P(OMe)_3\}(\eta\text{-}C_5H_5)$ (0.192 g, 0.327 mmol) in 15 cm^3 of methanol was heated at reflux for 4 h. After being allowed to cool, the solvent was removed *in vacuo* to give an oily residue. This was chromatographed on an alumina column packed with acetone; acetone eluted a small colourless fraction containing the tin compound followed by a second orange fraction. The latter was concentrated to about 2 cm^3 and 20 cm^3 of hexane was layered on the top of this concentrated solution. On cooling the solution overnight at −25°C, the product precipitated as orange crystals, m.p. 161–163°C (0.134 g, 62%).

Found: C, 57.39; H, 5.34. $C_{32}H_{34}O_3P_2RuS$ requires: C, 58.1; H, 5.20%. ^1H NMR ($CDCl_3$): 3.34 d, J = 10 Hz, $P(OMe)_3$; 4.59 s, C_5H_5; 6.71 t, 1H, 6.90 t, 2H, 7.31 m, 9H, and 7.49 m, 8H, SPh and PPh_3.

Synthesis of $Ru_2\{P(OMe)_3\}_2(\eta\text{-}C_5H_5)_2S_x$ (x = 4, 6)

A three-necked flask with a water cooled condenser and magnetic stirring was charged with $Ru(SPh)(PPh_3)\{P(OMe)_3\}(\eta\text{-}C_5H_5)$ (0.436 g, 0.659 mmol), S_8 (0.51 g, 0.20 mmol) and 25 cm^3 of CH_3CN. The mixture was heated at reflux for 50 min, changing from red to blue during this time. After being allowed to cool, the solution was evaporated to dryness using a rotary evaporator. The black residue was extracted with CH_2Cl_2 until the extraction no longer gave blue solutions. The residue was dissolved in $CHCl_3$ and this solution was filtered. Slow evaporation of the solvent gave crystals of $Ru_2\{P(OMe)_3\}_2(\eta\text{-}C_5H_5)_2S_4$ as black platelets that did not melt up to 300°C (0.071 g, 31%).

^1H NMR ($CDCl_3$): 3.65 d, J = 11.8 Hz, $P(OMe)_3$; 4.40 s, C_5H_5. UV–vis ($CDCl_3$): λ(max) = 525 nm, ε = 6600.

The CH_2Cl_2 extracts from above were concentrated and then placed on an alumina chromatographic column packed with CH_2Cl_2. Elution with this solvent gave a colourless solution which on evaporation yielded a mixture of PhSSPh and S=PPh_3. Further elution using 5% acetone/95% CH_2Cl_2 eluted a blue band followed closely by a smaller purple band. The second band was shown to contain $Ru_2\{P(OMe)_3\}_2(\eta\text{-}C_5H_5)_2S_4$, isolated earlier. The blue band was collected and the solvent removed by evaporation *in vacuo*. The sticky residue was dissolved in a minimal quantity of CH_2Cl_2 and hexane was added. On standing, the second product, $Ru_2\{P(OMe)_3\}_2(\eta\text{-}C_5H_5)_2S_6$, crystallized as a black powder that did not melt up to 300°C (0.020 g, 8%).

^1H NMR ($CDCl_3$): 3.50 d, J = 11.9 Hz, $P(OMe)_3$; 4.95 s, C_5H_5. UV–vis ($CHCl_3$): λ(max) = 587 nm, ε = 4700.

Various other procedures for synthesis and separation were attempted; the procedure described here seemed to work the best.

Reaction of $Ru_2\{P(OMe)_3\}_2(\eta\text{-}C_5H_5)_2S_6$ *and* PPh_3

Equimolar samples of these reagents were placed in an NMR tube and C_6D_6 was distilled into the tube under vacuum. After the solution had warmed to room temperature and the solids were dissolved, the NMR tube was maintained at room temperature while ^1H NMR spectra were run period-

ically. Over several hours, new resonances associated with $Ru_2\{P(OMe)_3\}_2(\eta\text{-}C_5H_5)_2S_4$ were seen to grow into the spectrum while resonances for the starting material diminished accordingly. No cyclopentadienyl resonances indicating possible intermediates were seen and the product appeared to undergo no further reaction; this latter fact was confirmed by a similar study with a known sample of that species.

It was quite easy to obtain a clean sample of **I** from reaction mixtures by making use of this reaction to convert crude mixtures of **I** and **II** to this species.

X-ray diffraction study of $Ru_2\{P(OMe)_3\}_2(\eta\text{-}C_5H_5)_2S_6$ **(II)**

A dark blue crystal suitable for X-ray diffraction was grown by vapour diffusion of hexane into a 1 : 1 CH_2Cl_2–acetone solution of this compound at ambient temperature. Two crystal morphologies, feathery needles and parallelepipeds, were observed, a crystal of the latter being used for this study. Data (12,493 reflections, with 11,355 having $F_o > 3\sigma F_o$) were collected with a Syntex P3/F diffractometer and corrected for Lorentz and polarization factors.

Crystal data. $C_{16}H_{28}O_6P_2Ru_2S_6$, $M = 773$, triclinic, $a = 13.923(3)$, $b = 17.488(3)$, $c = 12.779(2)$ Å; $\alpha = 107.62(1)$, $\beta = 93.27(2)$, $\gamma = 93.27(1)°$, $U = 2719.1(2)$ Å^3, $Z = 4$, $D_c = 1.89$ g cm^{-3}, space group $P\bar{1}$, Mo-K X-radiation 0.71069 Å, graphite monochromator, $\mu = 16.80$ cm^{-1}.

The solution of the structure and subsequent refinement were carried out by heavy atom and differential Fourier methods. Interestingly, there were two independent molecules with opposite chirality in the unit cell; except for small differences in the orientation of the phosphite ligand these were mirror images (Fig. 2 shows only one of these molecules.) Anisotropic thermal parameters were used for all non-hydrogen atoms and hydrogen atoms were inserted in standard positions. Final refinement was by least-squares methods minimizing $w(F_o - F_c)^2$ in cascaded large blocks using appropriate atomic scattering factors* [17] to a final R value of 0.0633 ($R_w = 0.0867$).

X-ray diffraction study of $Ru_2\{P(OMe)_3\}_2(\eta\text{-}C_5H_5)_2S_4$ **(I)**

Dark blue crystals suitable for X-ray diffraction were grown by vapour diffusion of hexane into a chloroform solution of this compound. Data collection at −167°C yielded 3558 reflections with 3396 having $F_o > 3\sigma F_o$. Data collection and the solution and refinement of the structure were carried out with procedures described above.* Since the molecule was centrosymmetric, only half of the molecule was refined and the other half was generated by projection through the centre of symmetry. In the figure, these atoms are denoted by the symbol (+).

Crystal data. $C_{16}H_{28}O_6P_2Ru_2S_4$, $M = 708.7$, triclinic, $a = 7.636(2)$, $b = 7.644(1)$, $c = 11.001(1)$ Å, $\alpha = 84.37(1)$, $\beta = 77.20(1)$, $\gamma = 73.38(1)°$, $U = 599.6$ Å^3, $Z = 1$, $D_c = 1.96$ g cm^{-3}, space group $P\bar{1}$, Mo-K X-radiation, 0.71069 Å, graphite monochromator, $\mu = 17.33$ cm^{-1}.

Refinement of the structure was carried out to a final R value of 0.0227 ($R_w = 0.0371$).

*Atomic positional parameters, complete tables of bond lengths and angles, and structure factor tables have been deposited as supplementary material with the Editor. Atomic coordinates have also been submitted to the Cambridge Crystallographic Data Centre.

REFERENCES

1. A. C. Sarapu and R. F. Fenske, *Inorg. Chem.* 1975, **14**, 247.
2. M. B. Hall and R. F. Fenske, *Inorg. Chem.* 1972, **11**, 768.
3. P. M. Treichel, H. J. Mueh and B. E. Bursten, *Isr. J. Chem.* 1976/7. **15**, 253.
4. B. E. Bursten and M. R. Green, *Prog. Inorg. Chem.* 1988, **36**, 393.
5. Our most recent paper on organometallic electrochemistry: P. M. Treichel, M. H. Tegen, K. J. Haller, L. J. Lyons and D. H. Evans, *Organometallics* 1988, **7**, 357.
6. P. M. Treichel, D. A. Komar and P. J. Vincenti, *Synth. React. Inorg. Met.-Org. Chem.* 1984, **14**, 383.
7. S. G. Davies and S. Simpson, *J. Chem. Soc., Dalton Trans.* 1984, 993.
8. J. A. deBeer, R. J. Haines, R. Greatrex and J. A. Van Wyk, *J. Chem. Soc., Dalton Trans.* 1973, 2341.
9. D. R. Kanis, PhD thesis, University of Wisconsin-Madison (1989); D. R. Kanis and R. F. Fenske, *J. Am. Chem. Soc.*, in press. (We thank Dr Kanis for preprints of these papers.)
10. J. Amarasekera, T. B. Rauchfuss and A. L. Reingold, *Inorg. Chem.* 1987, **26**, 2017.
11. P. M. Treichel and M. H. Tegen, *Inorg. Synth.* 1988, **25**, 114.
12. M. A. El-Hinnawi, A. A. Santarsiero, D. R. McAlister and V. Shomaker, *Inorg. Chem.* 1983, **22**, 1585.
13. J. Amarasekera, S. R. Wilson and T. B. Rauchfuss, *J. Chem. Soc., Chem. Commun.* 1989, 14.
14. H. Brunner, N. Janietz, J. Wachter and B. Nuber, *J. Organomet. Chem.* 1988, **356**, 85.

15. Two examples: single ruthenium–sulphur bonds are assumed in $Ru(Pr^iSH)(PPh_3)_2(\eta\text{-}C_5H_5)$ (in the sulphide-to-metal bond, Ru—S = 2.38 Å) and in $Ru_2(\mu\text{-}S)_2(\mu\text{-}S_2)(\eta\text{-}C_5H_4Et)_2$ (the Ru—S bond distances in the Ru—S—Ru unit = 2.38 Å). See: T. B. Rauchfuss, D. P. S. Rodgers and S. R. Wilson, *J. Am. Chem. Soc.* 1986, **108**, 3114; and M. Draganjac, C. J. Ruffing and T. B. Rauchfuss, *Organometallics* 1985, **4**, 1909.
16. M. I. Bruce and N. J. Windsor, *Aust. J. Chem.* 1977, **30**, 1601.
17. *International Tables for X-ray Crystallography*, Vol. 4. Kynoch Press, Birmingham (1974).

Polyhedron Vol. 9, No. 15/16, pp. 1901–1911, 1990
Printed in Great Britain

0277–5387/90 $3.00+.00
© 1990 Pergamon Press plc

THE KAGOMÉ NET: BAND THEORETICAL AND TOPOLOGICAL ASPECTS*

ROY L. JOHNSTON† and ROALD HOFFMANN‡

Department of Chemistry and Materials Science Center, Cornell University, Ithaca, NY 14853, U.S.A.

Abstract—The Kagomé net (a two-dimensional hexagonal network comprising triangles and hexagons) is a building block of a number of intermetallic compounds. In order to understand the electronic characteristics of such an array of atoms, extended Hückel tight binding calculations have been performed on a Kagomé net of boron atoms. Comparisons have been drawn with other hexagonal nets, namely the graphite net and the close packed triangular net, and topological relationships between these nets are used to explain similarities in their band spectra. It is shown that simple Hückel theory can be used to obtain a rough estimate for the energies of the bands at specific high symmetry *k*-points, and a way of representing and evaluating energies of crystal orbitals with complex coefficients is discussed. A moments-based analysis of the relative energies of the three nets as a function of electron count is also presented. The effect on its band structure of trigonally distorting the Kagomé net is investigated. Finally, substituted ABC and AB_2 derivatives of the Kagomé net are discussed.

A particularly useful way of describing complex solids is via a conceptual decomposition of the structure into layers and nets.[1] This paper deals with a planar net (the so-called Kagomé net)[1a] which is found in a number of complex intermetallic compounds, most notably the Laves phases ($MgCu_2$, $MgZn_2$ and $MgNi_2$ types).[2] The Laves phases, which possess interesting electronic and magnetic properties[3] as well as being of great interest from a structural point of view,[2a,4] are the subject of a separate publication.[5]

The Kagomé net (**1**) is four-connected (each vertex has four neighbours) and is described by the indices (3636), meaning that if we start counting the rings around any vertex from one of the triangles we encounter in order (independent of the direction of motion) a triangle followed by a hexagon, then another triangle and finally another hexagon.[1a] It is a hexagonal net, belonging to the plane group *p6mm*.[6] The dashed line in **1** denotes the primitive unit cell of the net.

More familiar two-dimensional hexagonal nets are the graphitic (6^3) net (**2**), and the triangular or close packed (3^6) net (**3**).

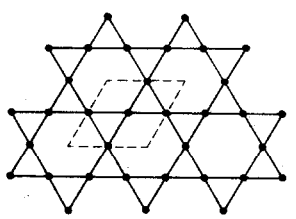

1

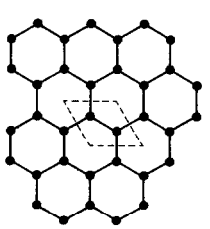

2

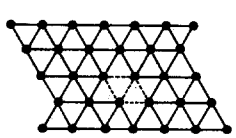

3

In the following sections we shall investigate the electronic band spectrum characteristic of a Kagomé net of main group atoms (boron), making comparisons with alternative graphitic and close packed layer structures. Calculations of the extended Hückel[7a] tight binding [7b,c] type were performed. Standard parameters for boron were chosen ($H_{ii}(2s) = -15.2$ eV, $H_{ii}(2p) = -8.5$ eV, $\zeta(2s) = \zeta(2p) = 1.30$).[7d] Average properties were

* This paper is dedicated to Dick Fenske, a scientist who always tries to understand, deeply.

† SERC/NATO Postdoctoral Fellow 1987–1989.

‡ Author to whom correspondence should be addressed.

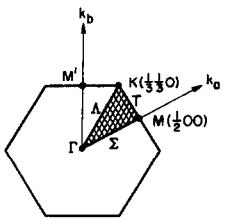

4

calculated using the irreducible wedge of the Brillouin zone shown in **4** (hashed area), with *k*-points chosen according to the geometrical method of Ramirez and Böhm.[7e]

While there are hundreds of Laves phases, only one of them contains boron. Many more do contain aluminium. And there is no phase in which the Kagomé net forms a separate bonded entity (we are using here the words of a perceptive reviewer of this paper). Why then study this net, for a main group element that does not form it?

The reason is that the net is simple and symmetrical. Stackings of it are plausible. It deserves to be studied; the question, one which will be approached in this paper, is why does it not occur, or, optimistically, what electron counts might favour its materialization.

COMPARISON OF THE BAND STRUCTURES OF KAGOMÉ, GRAPHITIC AND CLOSE PACKED NETS OF BORON ATOMS

In the solid state, boron is known to form icosahedral clusters which are bonded together in a three-dimensional lattice.[8] The connectivity of the boron atoms is six. This should be contrasted with the three-dimensional allotropes of carbon (e.g. diamond) where the carbon atoms are four-connected. It is also well known that boron forms molecular clusters with atom connectivities of five or more,[9] while carbon maintains an approximately tetrahedral local environment.[10] Electron-deficient atoms such as boron (with fewer electrons than valence orbitals) adopt highly-connected structures (with more nearest neighbours than valence orbitals) because such structures are known to stabilize the small number of occupied orbitals to a greater extent.[11] If this idea of increasing connectivity in order to mitigate electron deficiency is carried over into two-dimensions (think of three-connected layers of carbon atoms in graphite) then a layer structure based on Kagomé or close packed nets of boron atoms becomes an interesting possibility. We do not imply that two-dimensional elemental boron nets are likely—boron clearly likes icosahedra. But perhaps formally charged boron sheets of this type might occur in binary AB_x structures.

If we assume constant distances between connected vertices (bearing in mind that for nets of atoms the bond lengths generally increase with connectivity) then the relative densities of the three hexagonal nets (**1–3**) discussed above increase in the order graphite (1.0) < Kagomé (1.125) < close packed (1.5). Figure 1 depicts the partial band structures for nets of boron atoms (with B—B bonds of 1.8 Å) with these structures. Unit cells were chosen with one (close packed), two (graphite) and three (Kagomé) atoms (see **1–3**).

The Brillouin zone (BZ) has the same symmetry for all three nets (see **4**). Rather than using the plane group *p6mm*, it is convenient to assign these structures to the three-dimensional space group *P6mmm* (D^1_{6h}),[6] since the horizontal mirror plane is a good

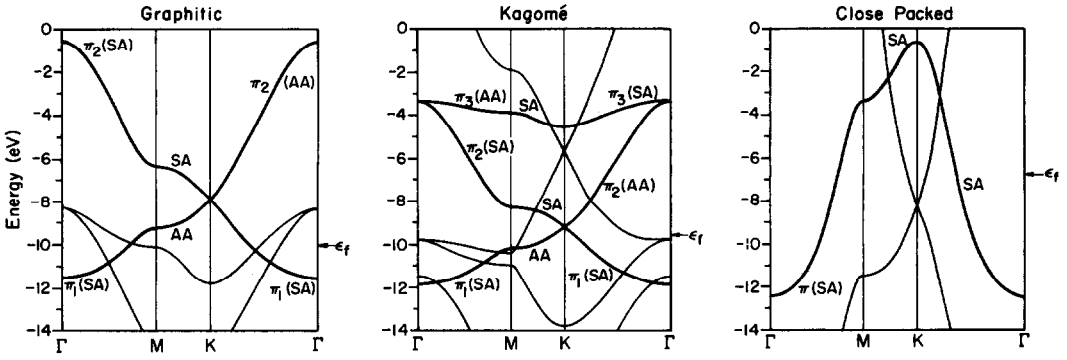

Fig. 1. Band structures of boron with the graphite, Kagomé and close packed (2-d) structures. The π-bands are highlighted and their symmetries with respect to vertical and horizontal mirror planes are indicated.

symmetry element, distinguishing between σ- and π-bands. The symmetries of the special points in the BZ (**4**) (i.e. the "group of k", G_k) for the space group *P6mmm* are as follows: $G_\Gamma = D_{6h}$; $G_M = D_{2h}$; $G_K = D_{3h}$, while the symmetries of the symmetry lines in the BZ are: $G_\Sigma = G_T = G_\Lambda = C_{2v}$.[12] We expect, therefore, to observe degeneracies at Γ and K, but not M. This is indeed the case, as can be seen in Fig. 1. We are only here interested in the π-bands. The labels of the bands (SA and AA) refer to the symmetries of the π bands (S = symmetric, A = antisymmetric) with respect to the two mirror planes containing each of the specified symmetry lines (where the first refers to the vertical plane and the second to the horizontal plane).

From the Figure, it is evident that, for boron, with three valence electrons per atom, all three structures are metallic due to overlap of the σ- and π-bands (the latter have been highlighted). Other interesting features of Fig. 1 include, for Kagomé boron [Fig. 1(b)], the small dispersion of the top π-band (π_3), the non-bonding nature of the middle π-band (π_2) at M (the energy of the atomic boron $2p$ orbitals is -8.5 eV) and the non-bonding nature of the degenerate π-bands at K in the graphite structure [Fig. 1(a)]. We shall endeavour to explain these features in the following paragraphs.

Each of these three planar sheet geometries presents interesting features, which are more or less familiar. The graphite network is best known, the Kagomé net least known. So we will concentrate on the latter.

The π-symmetry crystal orbitals of Kagomé boron (at the high symmetry points Γ, M and K) are sketched in Fig. 2, where the constituent atomic p-orbitals are shown in projection). To understand the figure, however, it will first be necessary to talk a little about the shading conventions used and the problem of the phase angle.

COMPLEX CRYSTAL ORBITALS: PHASE ANGLES AND OVERLAP

We are used to discussing bonding in terms of linear combinations of real atomic orbital functions. In the case of a simple diatomic, such as H_2, the orbital overlap (as a function of internuclear separation, r) is equal to $\pm S(r)$. The overlap is positive (stabilizing) when the orbitals are "in-phase" (**5a**) and negative (destabilizing) when the

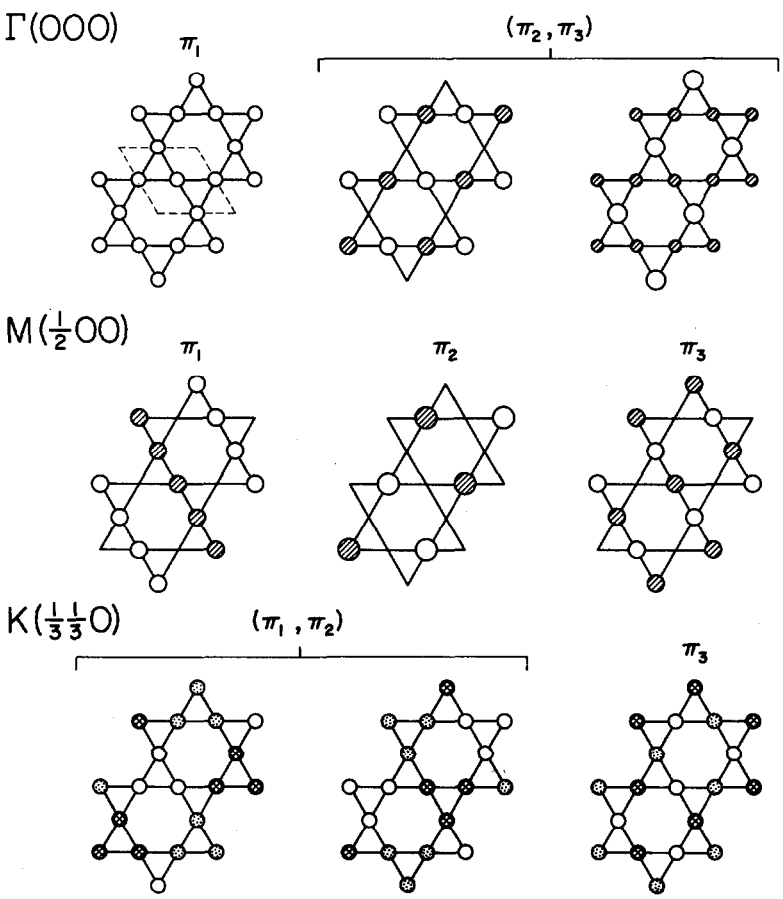

Fig. 2. Representation of the crystal orbitals of Kagomé boron at points Γ, M and K in the BZ.

5a 5b

orbitals are "out-of-phase" (**5b**). In the solid state, however, in most regions of the BZ (including some high symmetry points, such as K in the space group $P6mmm$) the crystal orbitals have coefficients which are complex (of the form $a+ib$, where $i=\sqrt{-1}$) rather than real. By depicting the coefficients of orbitals on neighbouring atoms as vectors on an Argand diagram we can calculate the angles made between these vectors and the (real) positive x-axis. These angles are the absolute "phase angles" (θ) of the orbital. However, in order to determine the size and sign of the overlap between neighbouring orbitals, it is the difference in "phase angle" ($\Delta\theta$) which is important. These concepts are illustrated in **6**, for an example where the coefficients have the same magnitude (i.e. the vectors have the same length, $a^2+b^2=c^2+d^2$).

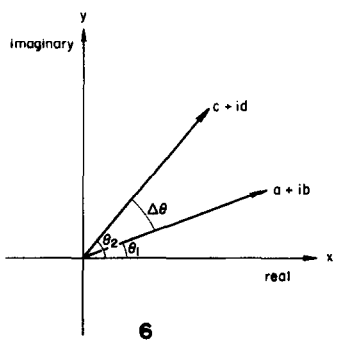

6

As a convention, we generally make one of the coefficients arbitrarily positive and real (i.e. lying along the positive x-axis of the Argand diagram), since only the relative phase angles (i.e. the differences) are important. Classical "in-phase" and "out-of-phase" combinations have phase angle differences ($\Delta\theta$) of 0 and 180°, respectively. The general expression for overlap between a pair of orbitals at separation r, with a phase angle difference of $\Delta\theta°$ between them, is:

$$S_{\Delta\theta}(r) = S_0(r)\cdot\cos(\Delta\theta),$$

where $S_0(r)$ is the overlap integral for $\Delta\theta = 0°$. From this formula, it can readily be seen that, when a pair of complex orbitals are orthogonal ($\Delta\theta = \pm 90°$) the overlap between them is zero.

The crystal orbitals in Fig. 2 have atomic orbital contributions related by factors $e^{2\pi i/3}$, $e^{\pi i}$, $e^{4\pi i/3}$, $e^{2\pi i}$, i.e. relative phase angles of 120, 180, 240 and 360° (≡0°). The shading conventions used to represent these phase angles are shown in **7**. The $\Delta\theta$

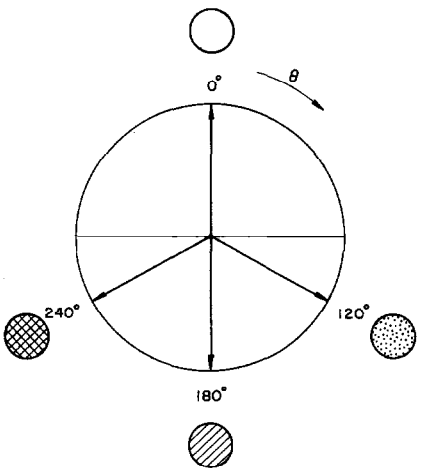

7

values which are present in the crystal orbitals shown in Fig. 2 are: 0 and 180° at Γ and M; and 0, 120 and 240° (−120°) at K. The corresponding overlaps are as follows:

S_0 ("in-phase") at a constant (arbitrary) separation

$S_{180} = -S_0$ ("out-of-phase")

$S_{120} = S_{240} = -0.5S_0$ ("half-out-of-phase").

The ideas developed above can be extended from the calculations of the overlap between complex orbitals to an estimation of their energies by means of simple Hückel theory.[13] Thus, the Hückel resonance energy (β) can be given a phase angle (difference) dependence:

$$\beta_{\Delta\theta} = \beta_0\cdot\cos(\Delta\theta)$$

while the Coulomb energy (α) is independent of phase angle.

It should be noted that the three orbital shadings shown in the representations of the crystal orbitals at K are equally out-of-phase (or in-phase) with respect to each other. This has an important effect which is related to the theory of alternancy.[14] An alternant (two- or three-dimensional) network or graph is one in which all rings or cycles (connected subgraphs) are even-membered. These networks (such as the square lattice shown in **8**) have the

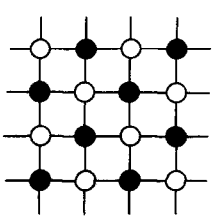

8

property that the vertices can be coloured in one of two ways such that no two adjacent vertices are coloured the same. In terms of atomic lattices, this means that there is always one crystal orbital in which all of the nearest-neighbour interactions are antibonding ($\Delta\theta = 180°$).[15] If we have three different colours (or types of shading) we can extend this principle to (some) systems containing odd-membered rings, such as the Kagomé net, which we shall describe as three-alternant. In three-alternant atomic lattices there will always be a crystal orbital (e.g. π_3 at K in the Kagomé net) in which all nearest-neighbour interactions are equally antibonding, though the phase angle difference ($\Delta\theta$) is now $\pm 120°$.

The small dispersion of the π_3-band in Kagomé boron [Fig. 1(b)] can be explained by examining the crystal orbitals in Fig. 2. At M the π_3-orbital is antibonding along chains of connected boron atoms. In a simple Hückel sense,[13] the energy of this band would be $\alpha-2\beta$. At Γ the π_3-orbital is one of a degenerate pair, one component of which can also be represented as antibonding chains of borons, with a Hückel energy of $\alpha-2\beta$. The energies of the bands in our extended Hückel calculation (and in reality) depart from the simple Hückel model through the inclusion of small non-nearest-neighbour interactions. The next-nearest-neighbour interactions at M are overall bonding while those at Γ are net antibonding, so the π_3-band lies at lower energy at M than the π_2/π_3 pair at Γ [see Fig. 1(b)]. At point K in the BZ, as mentioned above, the π_3-band describes a three-alternant pattern. In simple Hückel terms the energy of this crystal orbital would be $\alpha+4(-0.5\beta) = \alpha-2\beta$, once more. This time the next-nearest-neighbour interactions are more bonding (each atomic orbital has four next-nearest-neighbour orbitals which are in-phase) than at Γ or M, so the π_3-band shows a minimum at K. Thus, the bonding character of the π_3-band changes very little throughout the BZ. In the density of states (DOS) diagram for this net (not shown here), the flat π_3-band leads to a sharp spike. Because this band is so high above any realistic Fermi level, it is unlikely to have any consequence.

The π_2-band in the Kagomé structure is interesting in that it is antibonding at Γ (where it is degenerate with π_3), non-bonding at M (Hückel energy $= \alpha$), as there are no non-zero coefficients on adjacent sites and bonding at K, where it is degenerate with π_1 (Hückel energy $= \alpha+2\beta+2(-0.5\beta) = \alpha+\beta$). From Fig. 1 it can be seen that the π_1-band of graphite at M lies at almost exactly the same energy as the Kagomé π_2-band at K. Indeed the Hückel energy of this orbital (**9a**) is also $\alpha+\beta$. Incidentally, the upper π-band (π_2) of graphite at M (**9b**) is antibonding by the same amount (Hückel energy $= \alpha-\beta$) as π_1 is bonding.[16] As for the Kagomé π_2-band at M, the non-bonding nature of the two degenerate π-bands at K for the graphite structure [Fig. 1(c)] can also be rationalized in terms of complex linear combinations which have nodes at every second atom (**9c**).

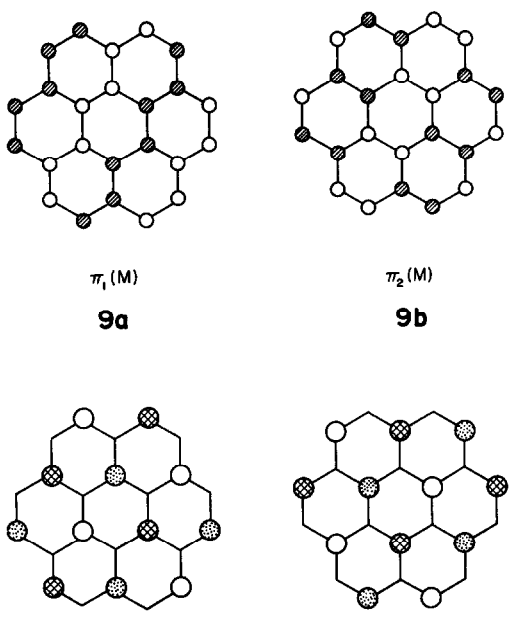

9a **9b** **9c**

From Fig. 1 (a and b), it is apparent that the π_1- and π_2-bands of the Kagomé net exhibit the same pattern as the two π-bands of the graphite net. Figure 3 shows the spectra of crystal orbitals at Γ, M and K for the two structures, with simple Hückel energies given, together with the spectrum of π-MO's obtained for the unit cell contents. It can be seen that at all the high symmetry points of the BZ the Kagomé π_1- and π_2-orbitals are stabilized with respect to those of graphite by β. The reason for this similarity can be traced to the topological relationship which exists between the two nets. Thus, the loci of the centroids of the triangles in the Kagomé net define the graphite net (similarly the centroids of the Kagomé hexagons define the close packed triangular net). The degenerate π-bands of graphite at K (**9c**) can be generated from those of the Kagomé net (Fig. 2) by replacing a triangle (in which all the atomic orbital contributions are in-phase) by a single atomic orbital, with the same phase. Triangles where there are three out-of-phase ($\Delta\theta = 120°$) coefficients are replaced by single atoms with zero atomic orbital coefficients (i.e. nodes).

The single π-band in the close packed structure [Fig. 1(c)] is highly dispersed, due to the high connectivity (six) of the lattice. The minimum energy

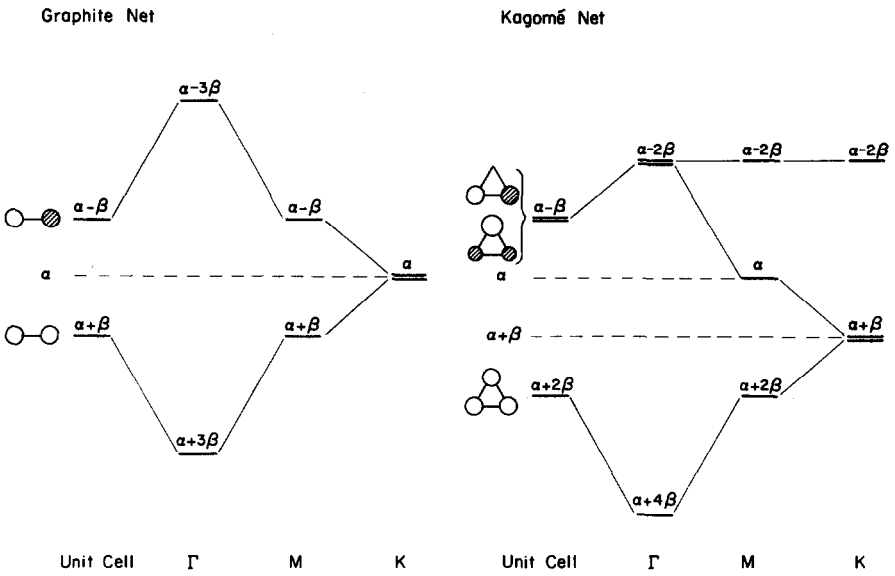

Fig. 3. Comparison of the spectra of crystal orbitals at the high symmetry BZ points for the graphite and Kagomé structures.

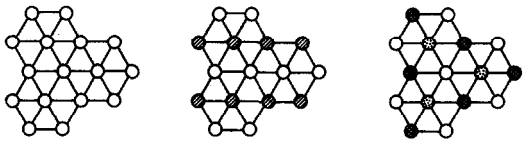

10a **10b** **10c**

occurs at Γ, where each atom experiences a bonding interaction with its six nearest neighbours (**10a**). At *M*, the π-band (**10b**) has a simple Hückel energy of $\alpha-2\beta$ and, indeed from Fig. 1 it can be seen that the energy of the π-band at *M* is close to that of the π_3-band of the Kagomé structure. At *K*, the π-band of the close packed structure has complex coefficients, again with phase angle differences of 0 and $\pm 120°$, and the crystal orbital may once more be represented by a three-alternant colouring (**10c**). The simple Hückel energy of the crystal orbital depicted in **10c** is $\alpha+6(-0.5\beta)=\alpha-3\beta$, which is the same energy as that of the π_2-band of graphite at Γ (**11**), where the connectivity is only three but the neighbouring orbitals are completely (180°) out-of-phase (since graphite is an alternant net).

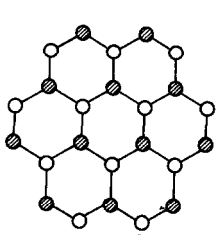

11

Of the two-dimensional structures studied for boron, the graphitic structure is calculated to be the most stable (by 0.47 eV/atom over Kagomé boron and by 1.46 eV/atom over the close packed layer structure). This order of relative stability is also reflected in the Fermi energies: −9.89 eV (graphitic); −9.53 eV (Kagomé); −6.73 eV (close packed), as well as in the B—B Mulliken reduced overlap populations,[17] which decrease with increasing connectivity: 0.84 (graphitic, three-connected); 0.67 (Kagomé, four-connected); 0.48 (close packed, six-connected).

As they have odd numbers of electrons in their unit cells, the Kagomé and close packed boron structures would be paramagnetic. In the case of Kagomé boron, a more likely structure would be composed of anionic $(B_3^-)_n$ sheets with intercalated alkali metal cations, leading to metallic solids with the composition MB_3.

COMPARISON OF THE RELATIVE STABILITIES OF THE GRAPHITE, KAGOMÉ AND CLOSE PACKED STRUCTURES BY THE MOMENTS METHOD

The moments method[18] has been applied to Hückel-based tight binding theory very successfully by Burdett and Lee, to establish relationships between geometric and electronic structures in a variety of solids.[19] The application of the moments method to the construction of the DOS of a given structure and to the calculation of the difference in

energy between two topologically distinct structures has proved particularly useful.

In mathematical terms, the nth moment is defined as the trace of the Hückel hamiltonian matrix (**H**) to the nth power:[18]

$$Tr(\mathbf{H})^n = \Sigma_i E_i^n$$

where the summation is over all the eigenvalues (E_i) generated by **H**. In geometric terms, the nth moment (μ_n) is equivalent to the weighted sum over all closed paths of length n amongst all the orbitals of the system.[19] Moments can also be split into σ and π components if the topology of the solid permits such separation, as in, for example planar nets.

Clusters containing all walks of length 2, 3 and 4 for the graphite, Kagomé and close packed nets are depicted in Fig. 4, together with the calculated π-only 2nd, 3rd and 4th moments. Burdett and Lee have stated that the same qualitative trends are seen for $\sigma+\pi$ occupation as for π alone, except at very low and very high orbital occupations where σ-orbitals alone are being filled. A moments-based comparison of the energies of these three nets as a function of electron count is complicated by the fact that the connectivities are different. This leads directly to the calculated differences in μ_2. One-electron models can lead to wrong conclusions by overestimating the μ_2's, thereby leading to the (incorrect) prediction that the highest-coordinate net is the most stable at all electron counts.

In the cases of the Kagomé and close packed nets, there are a large number of three-rings and the inherent instability of the three-rings at high electron counts (due to the nature of μ_3) can overcome the discrepancy in μ_2 and thus give a qualitatively correct difference curve. The large difference in μ_3 for all three structures leads to the prediction of a

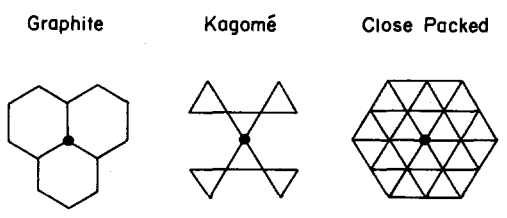

μ_2^π	$3\beta^2$	$4\beta^2$	$6\beta^2$
μ_3^π	0	$4\beta^3$	$12\beta^3$
μ_4^π	$15\beta^4$	$28\beta^4$	$90\beta^4$

Fig. 4. Clusters used to evaluate the 2nd, 3rd and 4th moments of the graphite, Kagomé and closed packed structures.

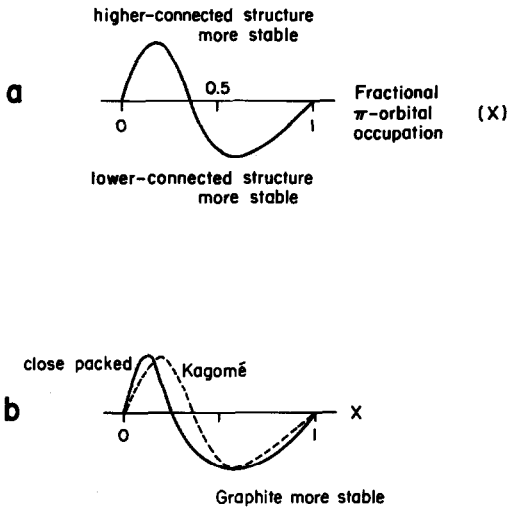

Fig. 5. Qualitative difference in energy curves as a function of the fractional occupation of the π-orbitals: (a) comparing any two of the three planar structures; (b) comparing all three structures together.

double peaked ΔE curve [see Fig. 5(a)] for graphite/Kagomé, Kagomé/close packed and close packed/graphite comparisons, with the more highly connected structure more stable until a certain band filling below the half-filled mark after which the less highly connected structure is more stable. Taken together, the close packed structure will be the most stable at very low counts, followed by the Kagomé structure and finally the graphite net is most stable, as shown schematically in Fig. 5(b). The stability of graphite for the half-filled shell is not surprising, since this is the situation for carbon. The large differences in μ_4 for the three structures may lead to extra nodes in the ΔE curves or may just create ripples on the μ_3 curve. As mentioned above, the differences in μ_2 will extend the range of stability of the more highly connected Kagomé and (especially) close packed structures to somewhat higher electron counts.

ELECTRONIC STRUCTURE OF A TRIGONALLY DISTORTED KAGOMÉ NET

In the hexagonal Laves phases ($MgZn_2$ type) the Kagomé nets of atoms (e.g. Zn) are often distorted such that the triangles alternate in size, as shown in **12**.[20] Such distortions are due to the capping of every second triangle above and below the Kagomé plane by zinc atoms, so that the capped triangles expand and the uncapped ones contract. It was decided to establish the effect of such a distortion on the π-bands of the boron Kagomé net.

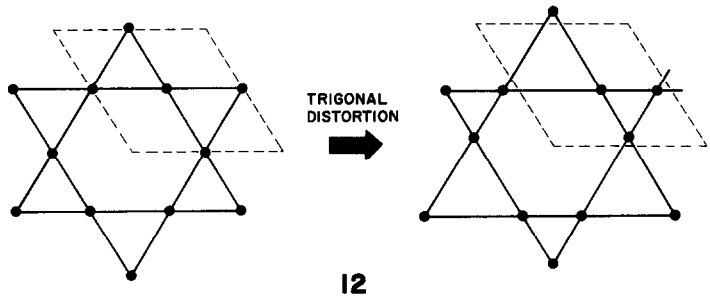

12

The B—B distances in the distorted Kagomé net are 1.70 and 1.90 Å, respectively. Since the average is 1.80 Å, the unit cell is the same size as in the undistorted case. The partial (π-only) band diagram for distorted Kagomé boron is shown in Fig. 6. The distorted Kagomé net possesses the same Bravais lattice as the undistorted net so the BZ has the same shape (**4**), though, as will be discussed below the symmetries of the special k points are different.

Comparing Fig. 6 with Fig. 1(b) reveals one very noticeable feature, namely that the lowest π-bands at $K(\pi_1/\pi_2)$ are no longer degenerate in the distorted structure (the splitting is approximately 1 eV for the distortion indicated above). In the following paragraphs, this loss of degeneracy will be rationalized using two different, though related explanations. The first makes use of symmetry arguments while the second, more empirical but more apparent explanation, uses simple ideas related to the changing of bonding and antibonding interactions as the structure is distorted.

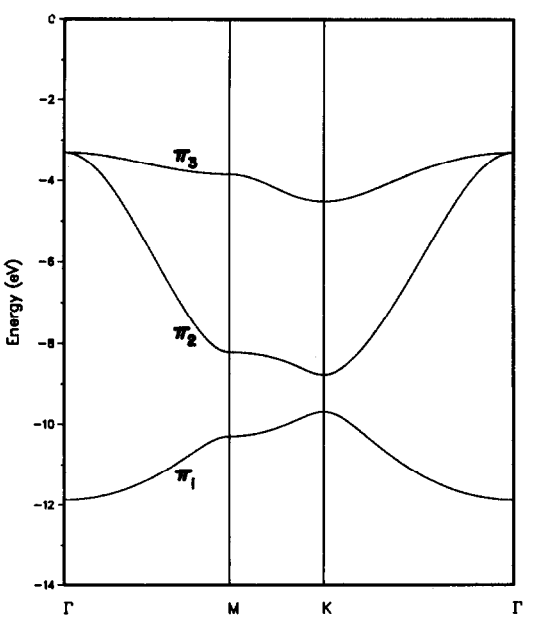

Fig. 6. π-Band diagram for boron with the trigonally distorted Kagomé structure.

The distorted Kagomé structure no longer has a six-fold axis and belongs to the plane group $p3m1$. If we include the horizontal mirror plane the distorted Kagomé net belongs to the three-dimensional space group $P\bar{6}m2$ (D^1_{3h}).[6] The symmetries of the special points in the BZ are as follows: $G_\Gamma = D_{3h}$; $G_M = C_{2v}$; $G_K = C_{3h}$ (the symmetries of the symmetry lines are: $G_\Sigma = C_{2v}$; $G_T = G_\Lambda = C_s$).[12] Thus, we expect to see some degenerate bands at Γ, but not at M. The point K is less straightforward, however. Although the point group C_{3h} does have degenerate representations (e' and e''), these representations are complex. The effect of this is that there are no degeneracies at K, but rather those bands of e' or e'' symmetry at K have their degenerate counterparts at $-K$. The character of the two components of the e (i.e. e' or e'') representations with respect to the three-fold rotation axis are ε and ε^*, where $\varepsilon = \exp(2\pi i/3)$ and, therefore $\varepsilon^* = \exp(-2\pi i/3)$. These represent phase angle changes upon C_3 rotation of 120 and 240° (−120°), respectively. Such a reversal does in fact occur as a consequence of time inversion (which is what interrelates $\pm K$).

The same lowering of symmetry and consequent loss of degeneracy at K is observed on going from graphite ($P6mmm$) to the boron nitride net ($P\bar{6}m2$) by replacing alternating carbons in the graphite structure by boron and nitrogen atoms.[21] As mentioned earlier, the Kagomé lattice is topologically related to that of graphite by the fact that the centroids of the triangles in the Kagomé net define the vertices of the graphite net. Thus the distorted Kagomé net, where alternate triangles are distinguishable, is topologically (and symmetry) related to the boron nitride structure. The loss of degeneracy between π_1 and π_2 at K on going from graphite to boron nitride can simply be explained by looking at the functional form of the crystal orbitals at this point. As shown in **9c**, π_1 and π_2 can be expressed as crystal orbitals with non-zero coefficients on either the starred or the unstarred (but not both) sets of atoms of the alternant graphite net. (The terms starred and unstarred refer to the convention of labelling every second atom of an alternant hydro-

carbon with a star, so that no two starred atoms are bonded.)[14] Upon substituting the carbon atoms by borons at the starred positions and by nitrogens at the unstarred positions the Hückel energies of the π-orbitals are simply α(B) and α(N). There is a loss of degeneracy simply because nitrogen is more electronegative than boron [i.e. α(N) is more negative than α(B)].

A similar analysis can be applied to the distortion of the Kagomé net. The π-symmetry crystal orbitals of the undistorted net, at the point K, are shown in Fig. 7. In this case the lowering in symmetry does not come about due to atom substitution (i.e. the loss of degeneracy is not due to changing α's) but rather arises out of the fact that the bond lengths are no longer constant. The Hückel β's are smaller for the longer bonds. If the central triangles of the crystal orbitals shown in Fig. 7 are contracted and the outer ones expanded, one component (labelled π_a in the figure) rises in energy because the antibonding interactions increase and the bonding ones decrease. The reverse is true for the second component (π_b) which, therefore descends in energy. Thus, the degeneracy is lifted. The π_3 crystal orbital is, however, essentially unaffected by the trigonal distortion because the increased antibonding interactions within the smaller triangles are approximately compensated by the decreased antibonding interactions within the larger triangles. To determine which of these two changes wins out it is necessary to know the change in interaction energy (whether as a Hückel β or some complex function of the overlap integral S) as a function of internuclear separation.

STRUCTURES OBTAINED BY MAKING SUBSTITUTIONS IN THE KAGOMÉ NET

As in the case of the graphite to BN "transformation", the symmetry of the Kagomé net can be lowered by substituting some of the sites.

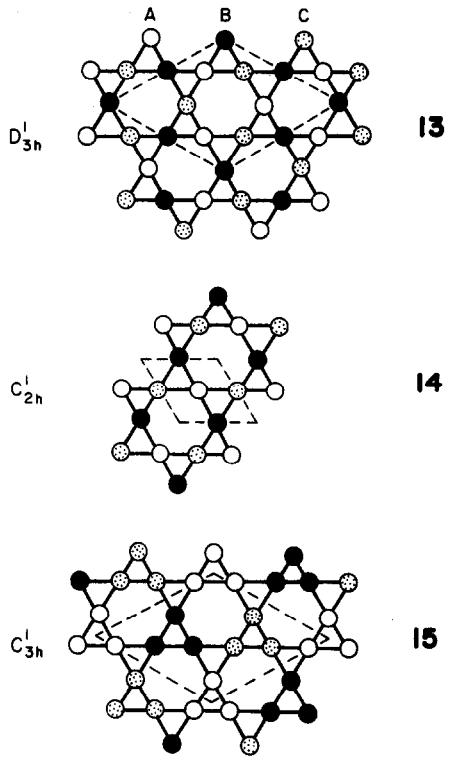

(i) *ABC substitutions*

In **13–15** are shown three derivatives of the Kagomé net, all with the stoichiometry ABC. The substitution patterns shown in **13** and **14** are three-alternant. The pattern in **13** has D^1_{3h} symmetry (as in BN) as half of the mirror planes of the Kagomé net have been lost, as well as the C_3 axes at the centre of the triangles. In contrast to the graphite/BN case, however, the substitution results in a unit cell which is three times as large as the original (i.e. nine atoms). This means that the loss of degeneracy due to lowering space group symmetry is countered by increased degeneracies due to band folding.[7c] It should be noted that this pattern is that observed for crystal orbital π_3 at K (see Fig. 2).

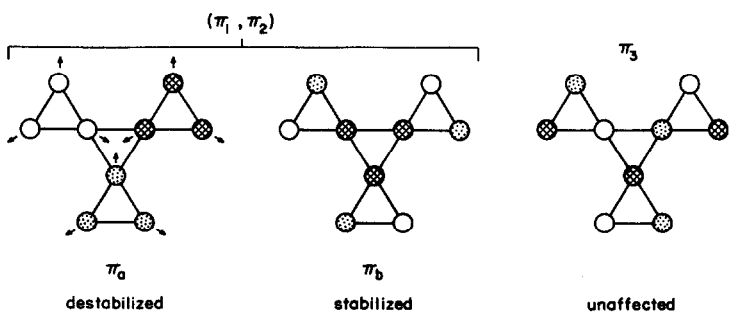

Fig. 7. Representation of the π-bands at K for the Kagomé structure, including the effect of the trigonal distortion (indicated by arrows at left) on their energies.

The substitution pattern shown in **14**, while also being three-alternant, is distinct from the first as going along straight lines of atoms in the structure the pattern is –A–B–A–B–A–; –B–C–B–C–B– and –A–C–A–C–A–, rather than –A–B–C–A–B–C– etc. This second pattern has much lower symmetry (C^1_{2h}), possessing C_2 axes (perpendicular to the net) at the atom sites and at the centres of the hexagons, with three atoms in the non-hexagonal unit cell (assuming all bond lengths are unequal). In terms of crystal orbitals, the shading of **14** is equivalent to a complex representation of one of the π_2, π_3 pair at Γ.

The substitution pattern shown in **15** is non-alternant, consisting of A_3, B_3 and C_3 triangles. Even with unequal bond lengths, three-fold symmetry is maintained at the centres of the hexagons and half of the triangles, though all vertical mirror planes and the C_6 axis have been lost. As for the first shading, the unit cell is three times the size of the Kagomé cell. This shading has the same symmetry (C^1_{3h}) as the complex representations of π_1 and π_2 at K (see Fig. 2).

(ii) *AB_2 substitutions*

Replacing atom type C by B in the pattern shown in **13** yields the AB_2 structure shown in **16**. The

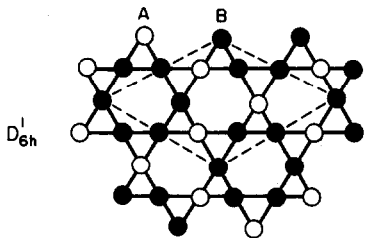

16

symmetry is D^1_{6h} once more, but with a nine-atom (A_3B_6) unit cell. It is intriguing to think of this pattern as representing a possible MC_2 solid, with planar C_6 rings having each edge coordinated to a metal atom (see **17**). The possibility of metal–metal bonding also exists.

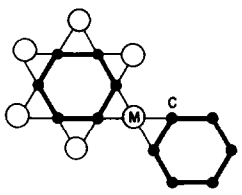

17

A similar substitution in the ABC net of **14** leads to an AB_2 net with parallel chains of B atoms coordinated to A atoms, as shown in **18**. A possible realization of this pattern is the metal–poly-

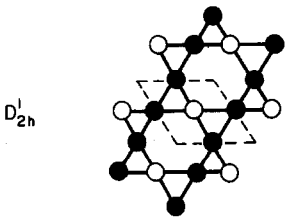

18

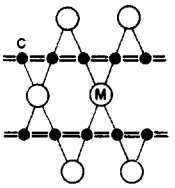

19

cumulene MC_2 structure shown in **19**. The symmetry is once again increased on going from ABC to AB_2, with the generation of vertical mirror planes leading to D^1_{2h} symmetry.

SUMMARY

The electronic band structure characteristic of a Kagomé net of boron atoms has been determined and compared with topologically related graphite and close packed (triangular) nets. The dispersion of the bands in these structures has been rationalized from a simple Hückel viewpoint and a method for determining the interaction between atomic orbitals with complex coefficients has been developed. This, together with an analysis of the topological relationships between the three nets has facilitated their comparison and enabled explanations to be constructed. The application of a moments analysis has shown how the relative stabilities of the three structures may vary with electron count. The symmetry reasons for the loss of band degeneracy at K upon trigonally distorting the Kagomé net, have also been rationalized. Finally, ABC and AB_2 substitution patterns have been presented and the effect of substitution on the symmetries of the net discussed.

Acknowledgements—The initial impetus for this work came from correspondence with Dr A. K. Cheetham concerning the bonding in Laves phase intermetallics (see ref. 5). The authors also wish to thank Dr P. A. Cox for helpful discussions, Jane Jorgensen and Elizabeth Fields for their expert drawings and Edith Chan for help in plotting one of the band pictures. R.L.J. is grateful to

the Science and Engineering Council of Great Britain for the award of a NATO postdoctoral fellowship. The research was supported by the National Science Foundation through research grants CHE84064119 and DMR84722702.

REFERENCES

1. (a) A. F. Wells, *Three-dimensional Nets and Polyhedra*. John Wiley, New York (1977); (b) W. B. Pearson, *The Crystal Chemistry and Physics of Metals and Alloys*, Ch. 2. John Wiley, New York (1972).
2. (a) W. B. Pearson, *The Crystal Chemistry and Physics of Metals and Alloys*, Ch. 12. John Wiley, New York (1972); (b) F. Laves, in *Intermetallic Compounds* (Edited by J. H. Westbrook), p. 129. Wiley, New York (1967); (c) J. H. Wernick, *ibid.*, p. 197.
3. For a discussion of physical properties and further references see: B. M. Klein, W. E. Pickett, D. A. Papaconstantopolous and L. L. Boyer, *Phys. Rev. B* 1983, **27**, 6721.
4. (a) S. Samson, in *Structural Chemistry and Molecular Biology* (Edited by A. Rich and N. Davidson), p. 687. Freeman, San Francisco (1968); (b) K. Girgis, in *Physical Metallurgy* (Edited by R. W. Cahn and P. Haasen), 3rd edn, Ch. 5. Elsevier, Amsterdam (1983).
5. R. L. Johnston and R. Hoffmann, manuscript in preparation.
6 *International Tables for Crystallography. Vol. A: Space-group Symmetry* (Edited by T. Hahn). Reidel, Dordrecht, Netherlands (1983).
7. (a) R. Hoffmann, *J. Chem. Phys.* 1963, **64**, 1397; (b) M.-H. Whangbo and R. Hoffmann, *J. Am. Chem. Soc.* 1978, **100**, 6093; (c) R. Hoffmann, *Angew. Chem. Int. Edn Engl.* 1987, **26**, 846; *Angew. Chem.* 1987, **99**, 871; (d) A. B. Anderson and R. Hoffmann, *J. Chem. Phys.* 1974, **60**, 4271; (e) R. Ramirez and M. C. Böhm, *Int. J. Quantum Chem.* 1986, **30**, 391.
8. J. Donohue, *The Structure of the Elements*, 2nd edn. John Wiley, New York (1974).
9. (a) W. N. Lipscomb, *Boron Hydrides*. Benjamin, New York (1963); (b) E. L. Muetterties (Ed.), *Boron Hydride Chemistry*. Academic Press, New York (1975).
10. (a) L. A. Paquette, *Accts Chem. Res.* 1971, **4**, 280; (b) R. J. Ternansky, D. W. Balogh and L. A. Paquette, *J. Am. Chem. Soc.* 1982, **104**, 4503.
11. (a) K. Wade, *Adv. Inorg. Chem. Radiochem.* 1976, **18**, 1; (b) R. B. King and D. H. Rouvray, *J. Am. Chem. Soc.* 1977, **99**, 7834.
12. C. J. Bradley and A. P. Cracknell, *The Mathematical Theory of Symmetry in Solids*. Clarendon Press, Oxford, U.K. (1972).
13. E. Heilbronner and H. Bock, *The HMO-model and its Application*. John Wiley, New York (1976).
14. See, for example: D. M. P. Mingos and Z. Lin, *New J. Chem.* 1988, **12**, 787.
15. R. L. Johnston, Z. Lin and D. M. P. Mingos, *New J. Chem.* 1989, **13**, 33.
16. P. A. Cox, *The Electronic Structure and Chemistry of Solids*, Ch. 4. Oxford University Press, Oxford, U.K. (1987).
17. T. A. Albright, J. K. Burdett and M.-H. Whangbo, *Orbital Interactions in Chemistry*, Ch. 2. John Wiley, New York (1985).
18. J. P. Gaspard and F. Cyrot-Lackmann, *J. Phys. C* 1973, **6**, 3077 and refs therein.
19. (a) J. K. Burdett and S. Lee, *J. Am. Chem. Soc.* 1985, **107**, 3050; (b) J. K. Burdett and S. Lee, *J. Am. Chem. Soc.* 1985, **107**, 3063.
20. (a) T. Ohba, Y. Kitano and Y. Komura, *Acta Cryst. (C)* 1980, **40**, 1; (b) M. M. J. de Almeida, M. M. R. Costa, L. Alte da Veiga, L. R. Andrade and A. Matos Beja, *Portg. Phys.* 1980, **11**, 219; (c) M. M. R. Costa and M. J. M. de Almeida, *Portg. Phys.* 1986, **17**, 173.
21. (a) E. Doni and G. Pastori Parravicini, *Nuevo Cimento* 1969, **64B**, 117; (b) J. Zupan, *Phys. Rev. B* 1972, **6**, 2477; (c) A. Zungar, A. Katzir and A. Halperin, *Phys. Rev. B* 1976, **13**, 5560.

Polyhedron Vol. 9, No. 15/16, pp. 1913–1918, 1990
Printed in Great Britain

0277–5387/90 $3.00+.00
© 1990 Pergamon Press plc

THE COORDINATION OF MONO- AND DIPHOSPHINES TO THE SURFACE OF CADMIUM SELENIDE*

CATHERINE J. MURPHY and ARTHUR B. ELLIS†

Department of Chemistry, University of Wisconsin-Madison, Madison, WI 53706, U.S.A.

Abstract—Band edge photoluminescence (PL) of single-crystal *n*-CdSe provides evidence for adduct formation between the solid's surface and various mono- and diphosphines present in toluene solution. Relative to a toluene ambient, solutions of triphenylphosphine (PPh_3), ethyldiphenylphosphine ($PEtPh_2$), bis(diphenylphosphino)methane (dppm) and bis(diphenylphosphino)ethane (dppe) in toluene enhance the semiconductor's PL intensity. For all of the phosphines, the increases in PL intensity can be fit to a dead-layer model, allowing the estimation of the reduction in depletion width resulting from phosphine exposure; reductions in dead-layer widths are about 300–400 Å for all phosphines except $PEtPh_2$, which yields a reduction roughly twice as large. Fits of the PL changes to the Langmuir adsorption isotherm model yield formation constants for the phosphine/CdSe adducts of $30 \pm 7\ M^{-1}$ for PPh_3 and $220 \pm 30\ M^{-1}$ for $PEtPh_2$; the diphosphines, which do not fit this simple model as well, give adsorption equilibrium constants of ~ 100–$200\ M^{-1}$. The results suggest that the diphosphines do not coordinate to the surface in a chelating fashion, but in some combination of bridging and monodentate bonding modes at lower effective surface coverages than the monophosphines.

Semiconductor-derived interfaces continue to be of fundamental and technological significance.[1] We have shown by PL measurements that the surfaces of the II–VI semiconductors CdS and CdSe [CdS(e)] can engage in adduct formation with a variety of Lewis acids and bases.[2–6] These studies have identified a "luminescent litmus test": relative to a reference nitrogen or solvent ambient for gas- and liquid-phase studies, respectively, Lewis bases increase the PL intensity of CdS(e), and Lewis acids decrease it. For Lewis bases, our working hypothesis has been that coordinatively unsaturated surface Cd^{2+} sites serve as the principal binding sites. In the systems studied to date, the surface-bound base (a monoamine, for example) has had a single functionality, making it a simple monodentate ligand.

In principle, other surface coordination modes should be achievable by use of multifunctional Lewis bases. Diphosphines are particularly attractive candidates for study: they are soft bases that should be capable of interacting with soft, acidic Cd^{2+} surface sites, based on the existence of molecular phosphine/Cd^{2+} complexes;[7] they are sterically and electronically tunable; and, based on molecular chemistry, they could exhibit monodentate, bidentate chelate, and bidentate bridging bonding modes, as illustrated for the 0001 face of CdSe in Scheme 1.[8,9]

In this paper, we demonstrate that the mono- and diphosphines whose structures are shown below, viz. PPh_3, $PEtPh_2$, dppm and dppe, form adducts from toluene solution with single-crystal *n*-CdSe surfaces, as revealed by changes in PL intensity. The PL changes can be used to estimate adduct-induced reductions in depletion width as well as equilibrium constants for adduct formation. These results are interpreted in terms of the steric and electronic properties of the phosphines, and suggest that the particular diphosphines of this study function as monodentate or bridging ligands with lower effective surface coverages than the monophosphines.

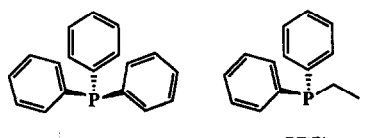

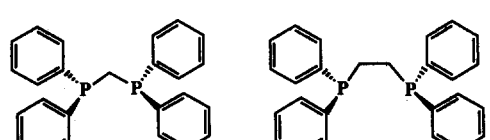

* Dedicated to Professor Richard F. Fenske on his retirement.

† Author to whom correspondence should be addressed.

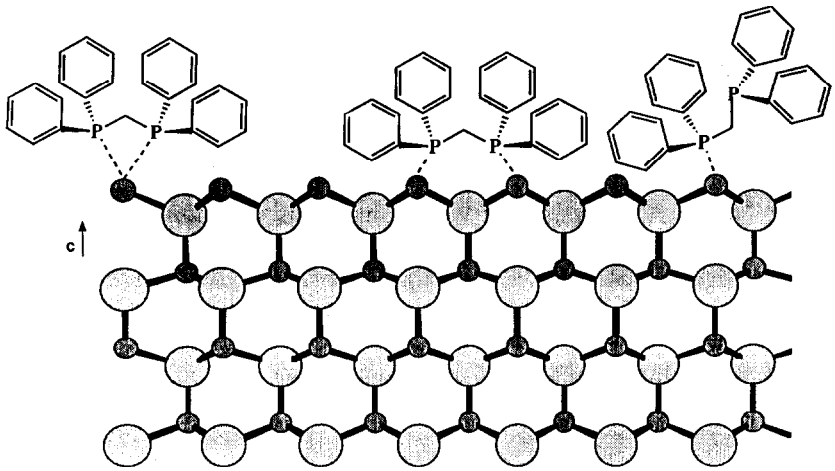

Scheme 1. Possible modes of diphosphine bonding (from left to right, chelating, bridging and monodentate) to the idealized 0001 face of CdSe, which is perpendicular to the plane of the figure. The smaller circles represent Cd^{2+} sites; the larger circles, Se^{2-} sites. Orientation of the crystallographic *c*-axis is indicated.

EXPERIMENTAL

Materials and methods

Triphenylphosphine (M & T) and bis(diphenylphosphino)ethane (Aldrich) were recrystallized from ether before use. Ethyldiphenylphosphine and bis(diphenylphosphino)methane were obtained from Strem Chemicals and used as received. Toluene was distilled over Na/benzophenone in an inert atmosphere. Stock 0.1 M solutions of each phosphine in toluene were prepared in oven-dried glassware in a dry, N_2-filled glovebag. Single-crystal, vapour-grown *c*-plates ($10 \times 10 \times 1$ mm) of *n*-CdSe with resistivity of $\sim 2\ \Omega$ cm were obtained from Cleveland Crystals, Inc., Cleveland, Ohio. Samples, scored and broken to $\sim 4 \times 4 \times 1$ mm, were etched in 1:30 (v/v) Br_2/MeOH for 5 s (or until the 0001, Cd-rich face was observed), sonicated and rinsed with methanol, and soaked in toluene at least 1 h prior to use. Samples were mounted with Duco cement and black epoxy as previously described.[3]

Apparatus

An all-glass cell was constructed for exposing *n*-CdSe to various solutions under a N_2 atmosphere and static conditions. The mounted crystal was placed in a Teflon adapter that served as a stopper for a 20-mm diameter tube that surrounded the sample. The bottom of the tube was equipped with a Teflon stopcock to drain the cell; during experiments involving repeated drainings, some air may enter the cell. Aliquots of N_2-saturated stock solutions were introduced via syringe through a sidearm equipped with a rubber septum. The entire cell was stored under N_2 when not in use.

Optical measurements

Irradiation sources included a Coherent Innova 90-5 Ar^+ laser (457.9 and 514.5 nm) and a Melles-Griot Model 80 He–Ne laser (632.8 nm). Laser plasma lines were eliminated by passing the beam through Oriel interference filters (fwhm of 10 nm, centred at the laser line). The beams from both lasers were passed through a $10\times$ beam expander and masked to illuminate only the semiconductor surface. Uncorrected, low resolution ($\sim$ 3 nm) PL spectra were obtained with a McPherson Model 270, 0.35-m monochromator, equipped with a grating blazed at 500 nm, and an R928 PMT. Laser excitation was filtered by placing a Corning 2-58 filter at the entrance slit to the emission monochromator. The PL signal was brought to the spectrometer by a 3-mm diameter optical fiber. Spectra were displayed on a Houston Model 2000 *X–Y* recorder. Typically, PL intensity was monitored by setting at the band maximum ($\sim$ 720 nm), with the recorder operated in time-base mode as the solution was varied. The detection optics were positioned between the incident and the reflected light beams.

RESULTS AND DISCUSSION

Upon irradiation with ultra-bandgap light, single-crystal *c*-plates of *n*-CdSe emit red band edge light ($E_g \sim 1.7$ eV; $\lambda_{max} \sim 720$ nm). For this study, the crystal was exposed to toluene solutions of several mono- and diphosphines, viz. PPh_3, $PEtPh_2$, dppm and dppe. The phosphines cause a reversible

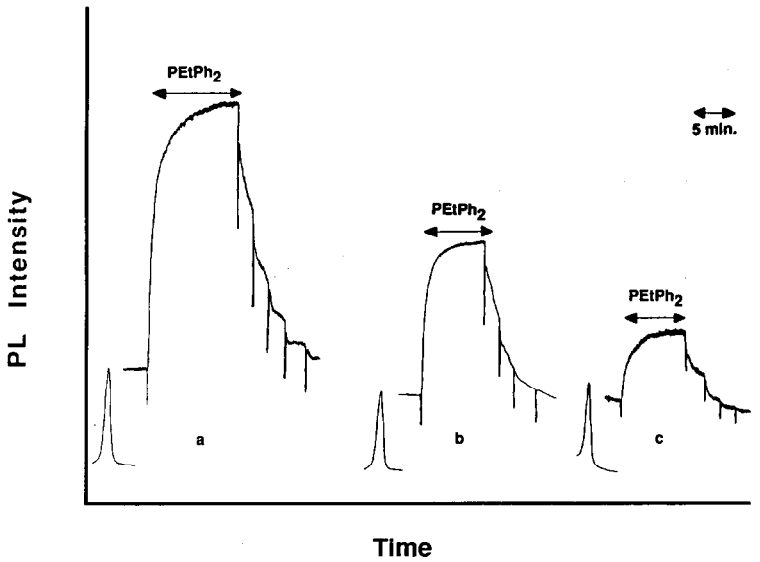

Fig. 1. Temporal changes in PL intensity at 720 nm for a single, etched CdSe crystal, in alternate contact with toluene and 0.1 M $PEtPh_2$ in toluene. Arrows indicate the duration of exposure to $PEtPh_2$. Downward spikes in the intensity are caused by the draining of the cell. Excitation wavelengths were (a) 457.9 nm, (b) 514.5 nm and (c) 632.8 nm. Superimposed on each plot is the initial PL spectrum in toluene.

increase in PL intensity relative to a pure toluene ambient. Because the spectral distribution of the emission does not change, we simply monitor PL intensity at the band maximum as a function of time. Figure 1 illustrates the modulation in intensity found with $PEtPh_2$ and the increase in this effect with shorter wavelength.

Electronic interactions

To quantify these changes in PL intensity, we have used a dead-layer model.[10] This model assumes that electron-hole pairs formed within a distance of the order of the depletion width do not contribute to PL. Ignoring changes in surface recombination velocity,[1]

$$PL_1/PL_2 = \exp(-\alpha'\Delta D), \qquad (1)$$

where PL_1 is the PL intensity in toluene; PL_2 is the PL intensity in phosphine solution; $\alpha' = (\alpha+\beta)$ is the sum of the CdSe absorptivities for the exciting and emitted light;[11] and ΔD is the contraction in dead-layer width that occurs upon passing from toluene to phosphine solution. The derivation of eq. (1) is illustrated in Fig. 2. An operational test of the dead-layer model involves excitation with several different interrogating wavelengths: α' and the corresponding PL ratios will vary (Fig. 1), but calculated values of ΔD should remain constant.

Figure 3 displays results for the phosphines employed. All of the phosphines gave excellent

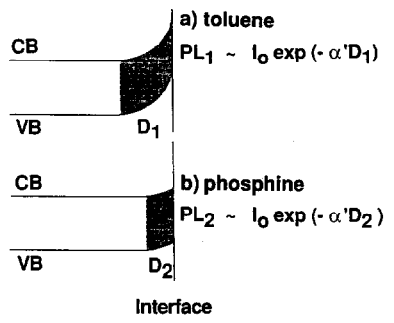

Fig. 2. The dead-layer model for analysing changes in PL intensity for two states, (a) and (b). As indicated in the figure, state (a) corresponds to the PL intensity in a toluene ambient, and state (b) corresponds to the PL intensity in the presence of toluene solutions of phosphines. CB and VB represent the solid's conduction and valence band edges, respectively. For each state, the PL intensity is proportional to the amount of incident light (intensity I_0; absorptivity α') absorbed beyond the non-emissive layer whose thickness is D. The ratio of the two PL intensities leads to eq. (1).

agreement with the dead-layer model. Looking first at the monophosphines, ΔD values of ~ 400 and 700 Å are found for PPh_3 and $PEtPh_2$, respectively. Qualitatively, we expect (and have found with amines and butenes[3,4]) that stronger bases provide

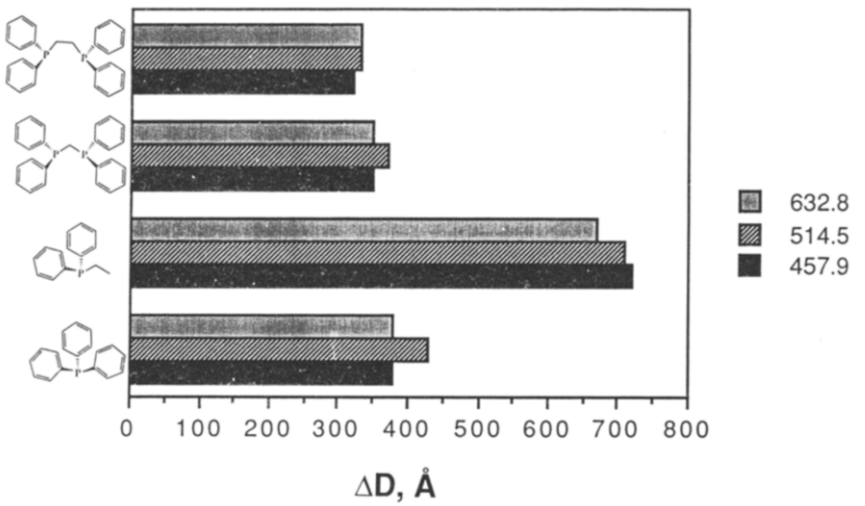

Fig. 3. Calculated values of ΔD ($\pm 20\%$) for each of the phosphines examined, using eq. (1) of the text. Excitation wavelengths (in nm) are shown in the legend.

larger dead-layer width reductions.[12] The substitution of an alkyl group for an aryl group of a tertiary phosphine is known to increase basicity in solution studies, implying that $PEtPh_2$ should yield a larger ΔD value, as observed.[13] The larger ΔD value for $PEtPh_2$ may also reflect its more compact dimensions (cone angle of 140° for $PEtPh_2$ vs 145° for PPh_3), permitting it to occupy more surface sites.[14]

Although the basicity of the diphosphines should be comparable and similar to $PEtPh_2$, their ΔD values, while being nearly equivalent within experimental error, more closely match the low value found for PPh_3 (Fig. 3). The diphosphine ΔD results by themselves are consistent with any of the bonding modes of Scheme 1: for monodentate binding, lower coverage by diphosphines relative to $PEtPh_2$ could occur because of steric bulk, thereby reducing ΔD; bidentate chelation could diminish ΔD if the different electronic structure that characterizes the individual Cd^{2+} sites yields a smaller electronic effect, or if relatively few sites of double coordinative unsaturation exist; and bidentate bridging could reduce ΔD through low coverage, resulting from ligand blockage of some fraction of the Cd^{2+} sites that are utilized in monodentate binding. In the last case we note that the smaller dppm can span metal centres approximately 6.5 Å apart.[15a] This distance would permit adjacent Cd^{2+} lattice sites ($\sim$ 4.3 Å separation on the idealized 0001 face of CdSe), or even next-nearest-neighbour Cd^{2+} lattice sites (separation distance of $\sim$ 6.1 Å) to be bridged.[15,16] We should note two other simplifications in our analysis: we are assuming a single binding mode when, in fact, a mixture of Cd^{2+} surface sites could result in the use of several binding modes simultaneously; and water, oxygen or species derived therefrom that are likely present on these ambiently-prepared surfaces could influence our results. We also cannot rule out phosphorus–selenium coordination.[17]

Adduct formation constants

The strength of the bonding interaction between the CdSe surface and the phosphines may be treated with the Langmuir adsorption isotherm model.[18] Experimentally, PL changes as a function of phosphine concentration, C_p, are determined. For either exclusively monodentate coordination or exclusively bidentate chelate coordination, the quantitative form of the model is

$$(1-\theta)/\theta = 1/(KC_p). \quad (2)$$

Here θ represents the fractional surface coverage, assumed equal to the fractional PL change, and K is the adsorption equilibrium constant. A plot of $(1-\theta)/\theta$ vs $1/C_p$ should be linear with a slope of $1/K$ and an intercept of zero. For simple bidentate bridging coordination, we would expect the multisite adsorption isotherm expression of eq. (3) to apply:[19]

$$(1-\theta)^2/\theta = 1/(2KC_p). \quad (3)$$

In this case, a plot of $(1-\theta)^2/\theta$ vs $1/C_p$ should give a straight line with a slope of $1/(2K)$ and an intercept of zero.

We have attempted to fit our data to both of these models and find that the one-site model of eq. (2) gives excellent fits for PPh_3[6] and $PEtPh_2$ (Fig. 4). Consistent with its greater basicity, $PEtPh_2$ exhibits a larger formation constant (220 ± 30 M^{-1})

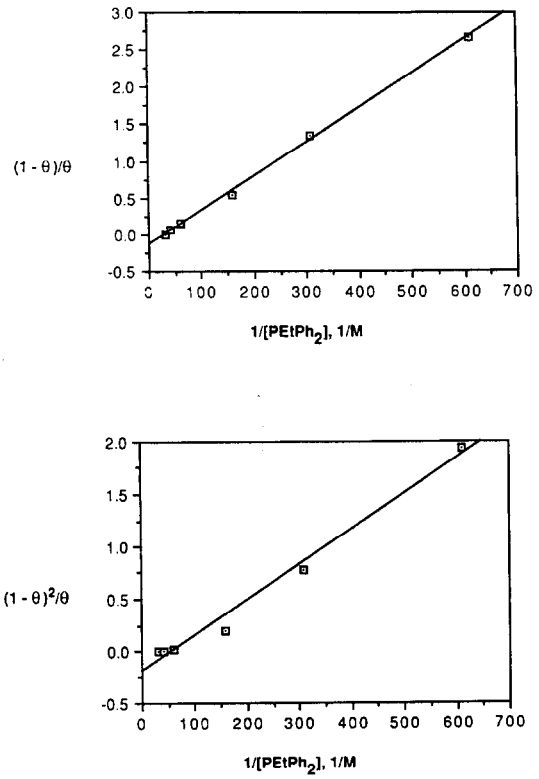

Fig. 4. Upper panel: Plot of $(1-\theta)/\theta$, where θ is the fractional surface coverage (equated to fractional PL change) vs $1/[PEtPh_2]$, using eq. (2) of the text. Lower panel: Plot of $(1-\theta)^2/\theta$ vs $1/[PEtPh_2]$, using eq. (3) of the text.

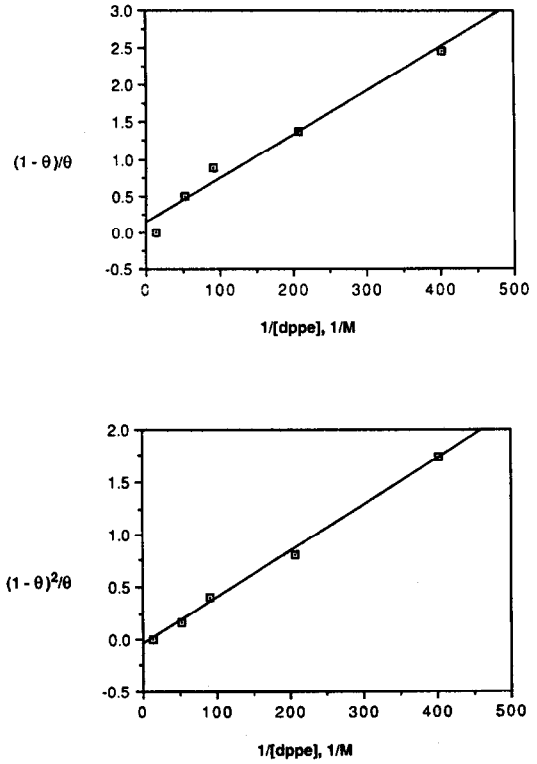

Fig. 5. Upper panel: Plot of $(1-\theta)/\theta$ vs 1/[dppe], using eq. (2) of the text. Lower panel: Plot of $(1-\theta)^2/\theta$ vs 1/[dppe], using eq. (3) of the text.

than PPh_3 (30 ± 7 M^{-1}). The diphosphine data are more ambiguous. For dppe, the two-site model of eq. (3) gives a better fit than the one-site case (Fig. 5). For dppm, neither model fits particularly well (Fig. 6). Despite the poorer fits, it is still possible to extract estimates of K from these plots for comparative purposes; the results are displayed in Table 1. In general, values of K for the diphosphines are intermediate between those of PPh_3 and $PEtPh_2$.

Table 1. Comparison of equilibrium constants for diphosphine/CdSe adducts[a]

Diphosphine	One-site[b] K (M^{-1})	Two-site[c] K (M^{-1})
dppm	140	80
dppe	170	110

[a] Equilibrium constants (±25%) for the indicated diphosphine/CdSe adducts in toluene solution.

[b] Calculated with eq. (2), using the data shown in Figs 5 and 6.

[c] Calculated with eq. (3), using the data shown in Figs 5 and 6.

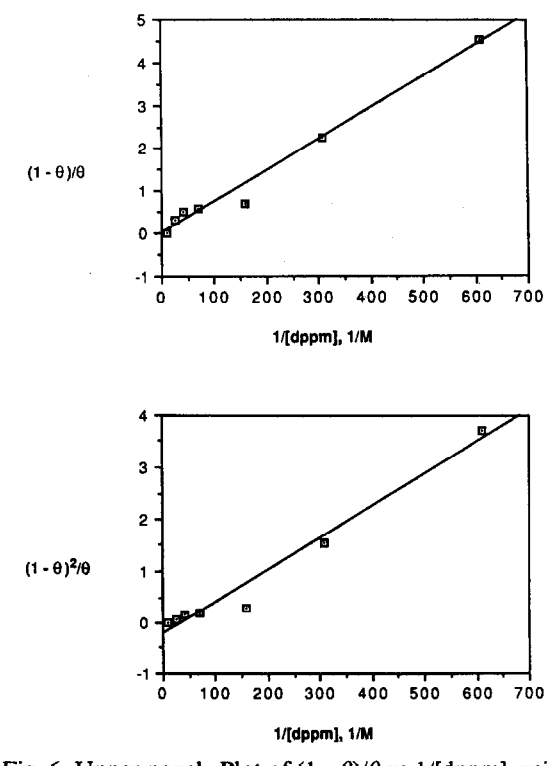

Fig. 6. Upper panel: Plot of $(1-\theta)/\theta$ vs 1/[dppm], using eq. (2) of the text. Lower panel: Plot of $(1-\theta)^2/\theta$ vs 1/[dppm], using eq. (3) of the text.

One explanation for the ambiguity of our results is that multiple binding modes exist simultaneously for the diphosphines, and the preponderance of one mode over another may be a function of concentration. For example, at low coverages the bridging mode may dominate, but at higher coverages monodentate binding is preferred. Another possibility is that assumptions inherent in eqs (2) and (3) are no longer valid for the diphosphines: we are assuming that there are no adsorbate–adsorbate interactions. Moreover, we are treating the two phosphine moieties of a bridging ligand as independent units, which may not be a good assumption given the short chain lengths involved.

In assessing the possibility of bidentate chelation, we note that chelating ligands generally impart greater stability to complexes than analogous monodentate ones and that five-membered chelate rings are generally more stable than four-membered rings.[8] Therefore, we would have anticipated clearly superior fits to eq. (2) and much larger values of K for the diphosphines, compared to $PEtPh_2$, as well as a significant difference between dppm and dppe, were chelation occurring. Based on our data, we feel that the primary mode of binding of the diphosphines to the CdSe surface does not involve chelation. Moreover, the lower ΔD values for the diphosphines compared to $PEtPh_2$ suggest that less effective coverage is present (*vide supra*), consistent with the more sterically demanding bridging or monodentate binding modes. Other diphosphines may, of course, employ different coordination modes and are being investigated.

Acknowledgements—C.J.M. thanks the Electrochemical Society, Inc., for a Summer Energy Research Fellowship Award. Both authors gratefully acknowledge financial support from 3M and the Office of Naval Research. Professors G. C. Lisensky, F. F. Crim, L. F. Dahl, S. H. Langer and P. M. Treichel, Jr, are thanked for helpful discussions.

REFERENCES

1. A. B. Ellis, in *Chemistry and Structure at Interfaces: New Laser and Optical Techniques* (Edited by R. B. Hall and A. B. Ellis), Ch. 6. VCH, Deerfield Beach, Florida (1986).
2. G. J. Meyer, G. C. Lisensky and A. B. Ellis, *Proc. Electrochem. Soc.* 1987, **87–9**, 438.
3. G. J. Meyer, G. C. Lisensky and A. B. Ellis, *J. Am. Chem. Soc.* 1988, **110**, 4914.
4. G. J. Meyer, L. K. Leung, J. C. Yu, G. C. Lisensky and A. B. Ellis, *J. Am. Chem. Soc.* 1989, **111**, 5146.
5. C. J. Murphy and A. B. Ellis, *J. Phys. Chem.*, in press.
6. C. J. Murphy, *J. Electrochem. Soc.*, in press.
7. (a) S. S. Sandhu, R. Dass and M. P. Gupta, *Ind. J. Chem.* 1970, **8**, 458; (b) R. G. Goel and N. K. Jha, *Can. J. Chem.* 1981, **59**, 3267; (c) D. Dakternieks, *Aust. J. Chem.* 1982, **35**, 469; (d) R. G. Goel, W. P. Henry and N. K. Jha, *Inorg. Chem.* 1982, **21**, 2551; (e) G. E. Coates and D. Ridley, *J. Chem. Soc.* 1964, 166; (f) N. A. Bell, T. D. Dee, M. Goldstein and I. W. Nowell, *Inorg. Chim. Acta* 1980, **38**, 191.
8. R. J. Puddephatt, *Chem. Soc. Rev.* 1983, **12**, 99 and refs therein.
9. (a) P. E. Fanwick, D. R. Root and R. A. Walton, *Inorg. Chem.* 1989, **28**, 2239; (b) A. J. Deeming, D. Nuel, N. P. Randle and C. Whittaker, *Polyhedron* 1989, **8**, 1537.
10. R. E. Hollingsworth and J. R. Sites, *J. Appl. Phys.* 1982, **53**, 5357 and refs therein.
11. R. B. Parsons, W. Wardzynski and A. D. Yoffe, *Proc. R. Soc. Lond., A* 1961, **262**, 120.
12. P. C. Stair, *J. Am. Chem. Soc.* 1982, **104**, 4045.
13. (a) W. A. Henderson Jr and C. A. Streuli, *J. Am. Chem. Soc.* 1960, **82**, 5791; (b) S. Ahrland and E. Avsar, *J. Organomet. Chem.* 1979, **181**, 17.
14. C. A. Tolman, *Chem. Rev.* 1977, **77**, 313.
15. (a) A. W. Coleman, H. Zhang, S. G. Bott, J. L. Atwood and P. H. Dixneuf, *J. Coord. Chem.* 1987, **16**, 9; (b) For other examples of long M---M interactions with bridging dppm ligands, see N. Van Order Jr, W. E. Geiger, T. E. Bitterwolf and A. L. Rheingold, *J. Am. Chem. Soc.* 1987, **109**, 5680; (c) A. T. Hutton, P. G. Pringle and B. L. Shaw, *J. Chem. Soc., Dalton Trans.* 1985, 1677; (d) L. Manojlovic-Muir, K. W. Muir, A. A. Frew, S. S. M. Ling, M. A. Thomson and R. J. Puddephatt, *Organometallics* 1984, **3**, 1637; (e) M. A. Albers, D. C. Liles, D. J. Robinson and E. Singleton, *Organometallics* 1987, **6**, 2179.
16. We have calculated the distance based on the wurtzite structure of CdSe: W. Zachariasen, *Z. Phys. Chem.* 1926, **124**, 436.
17. S. I. A. El Sheikh, M. S. Patel, B. C. Smith and C. B. Waller, *J. Chem. Soc., Dalton Trans.* 1977, 641.
18. K. J. Laidler, *Chemical Kinetics*, 3rd edn, pp. 230–232. Harper & Row, New York (1987).
19. T. Nitta, T. Shigetomi, M. Kuro-Oka and T. Katayama, *J. Chem. Engng Jpn* 1984, **17**, 39.

Polyhedron Vol. 9, No. 15/16, pp. 1919–1934, 1990
Printed in Great Britain

0277-5387/90 $3.00+.00
© 1990 Pergamon Press plc

A THEORETICAL STUDY OF THE LINEAR VERSUS BENT GEOMETRY FOR SEVERAL MX_2 MOLECULES: MgF_2, CaH_2, CaF_2, CeO_2 AND $YbCl_2$*

ROGER L. DeKOCK,† MICHAEL A. PETERSON and LINDA K. TIMMER

Department of Chemistry, Calvin College, Grand Rapids, MI 49546, U.S.A.

and

EVERT JAN BAERENDS and PIETER VERNOOIJS

Department of Chemistry, Free University, De Boelelaan 1083, 1081HV Amsterdam, The Netherlands

Abstract—We have completed Hartree–Fock–Slater theoretical studies on the title molecules. The minimum energy configuration corresponds to a linear geometry for MgF_2, whereas the remainder of the molecules are bent with a bond angle in the range 120–132°. These results are in agreement with experimental evidence where it exists. The bent geometries are more stable than the linear by only 1–3 kcal mol^{-1}. The simplest rationalization for the (anomalous) bent geometries is that the central metal $(n-1)d$ orbitals are more important to the bonding than are the *np* orbitals. In valence bond language we can summarize this as *sd* (bent) vs *sp* (linear) hybridization. The 4*f* orbitals of cerium and ytterbium also do not contribute enough for the molecules to become linear as a result of *f* orbital involvement. This analysis is borne out by close scrutiny of the eigenvalues and changes in Mulliken atomic populations for the linear and bent structures. There is no need to invoke a "reverse" polarization argument to rationalize the geometry of the bent molecules, as has been done in the classical multipole expansion model. We show that this model is very sensitive to the polarizability value chosen for the metal. Furthermore, in the multipole expansion the dipole–dipole term is of equal importance to the charge–dipole term, although in qualitative discussions only the latter is emphasized.

Early in 1989 Beattie and co-workers[1] published a short communication with the provocative title "Do Any AB_n Molecules Have Anomalous Shapes?". The paper predominantly dealt with a careful look at the experimental evidence relating to TiF_2, but called into question the gamut of evidence related to AB_n molecules. According to Beattie *et al.*, TiF_2 and CaF_2 are "key molecules" in the answer to their question. It is not our purpose here to review their discussion. Rather, this question sets the tone for the present manuscript.[2]

The molecular geometry of the gas-phase alkaline earth dihalides has been of interest ever since Skinner examined the comparative valence-state excitation energies of the alkaline earth metals.[3] In the closing paragraph of his paper he discusses the (then) unknown geometrical structures of the MX_2 molecules. He did not outright predict that they would be bent, but the possibility is definitely brought up for consideration. Some 8 years later Klemperer and co-workers reported electric deflection experiments on these molecules.[4] If the molecules deflected in the electric field it was assumed that they must possess a permanent dipole moment and hence be bent. Other experimental methods that have been applied to the determination of molecular structure for these species are gas-phase electron diffraction, matrix isolation IR spectroscopy and matrix isolation Raman spectroscopy.

There is extensive literature on the molecular

* Dedicated to Professor Richard F. Fenske upon the occasion of his retirement, with many thanks for introducing R.D.K. to the world of electronic structure and chemical bonding.

† Author to whom correspondence should be addressed.

Table 1. Structures of Group 2 dihalides, MX_2

	F	Cl	Br	I
Be	l	l	l	l
Mg	l	l	l	l
Ca	140°	l	l	l
Sr	108°	142°	l	l
Ba	100°	127°	—	148°

l = linear.

structure of these compounds; we refer to review articles only.[5] A brief summary of these results is given in Table 1, as found in ref. 5b. Where more than one bond angle is reported, from different experimental methods, we have arbitrarily presented the bond angle from the latest reference only. Although estimated uncertainties are not given for many of these numbers, those that are reported are in the order of $\pm 10°$. A recent matrix isolation IR spectrum[6] of CaF_2 reported results for both $^{40}CaF_2$ and $^{44}CaF_2$, and the bond angle was calculated to be $142 \pm 1°$.† The lightest dihalide of any alkaline-earth metal to be bent is CaF_2. The heavy-metal fluorides are all bent, but the tendency again returns to linear for heavier halides. For example, all of the di-iodides are linear except BaI_2. Turning to the title molecules other than those of Group 2, there are a number of references on CeO_2;[7] the bond angle is stated to be $146 \pm 2°$.[7c] A matrix isolation IR spectrum of $YbCl_2$ has been interpreted to give a bond angle of $126 \pm 5°$.[8] Among the title molecules, there are no experimental reports for CaH_2. It is included in our study to provide a model compound with a simple ligand.

It is not only the alkaline-earth dihalides, CeO_2 and $YbCl_2$, that provide examples of anomalous shapes for AB_2 type molecules. There are a number of Cp_2M molecules that are bent about the angle formed by the metal atom and the two ring centroids ("centroid" angle). For example, Andersen *et al.*[9] completed electron diffraction studies on Cp^*_2M where M = Mg, Ca and Yb and Cp* refers to the pentamethylcyclopentadienyl ligand. The rings were found to be parallel for M = Mg, but the centroid angle was 154° for the Ca compound and 158° for the Yb compound. Evans *et al.*[10] observed an angle of 140.1° in an X-ray structure of Cp^*_2Sm, and 140.1° for Cp^*_2Eu. Since the Cp ligand is isolobal[11] with F and Cl, these results are pertinent to the present study.

To round out this introduction on the matter of anomalous shapes of AB_2 molecules we note that ThO_2 has an angle of 122.5°,[7a,c] this molecule is isovalent with CeO_2. Also, ScH_2^+, which is isoelectronic with CaH_2, has a theoretical bond angle near 107°.[12]

A glance at the periodic table reveals that all of the title molecules have, in the ionic formulation, a metal valence configuration that is $s^0p^0d^0$, f^0 for Ce^{4+}, and f^{14} for Yb^{2+}. That is, all these molecules will be closed-shell with four valence σ electrons around the central metal atom in a covalent bond formulation. Hence, the bent molecules represent exceptions to the valence-shall-electron-pair-repulsion model (VSEPR), simple hybrid orbital, simple Walsh digram,[13] or simple second-order Jahn–Teller models.[13] The word "simple" in this context means that the metal atom employs predominantly its *s* and *p* orbitals in chemical bonding to the ligands. If we utilize *d* orbitals then all of the models just mentioned are capable of rationalizing the bent structures, except for the VSEPR model. The contention that the *d* orbitals do provide an Occam's razor understanding of the bent structures forms a major part of this paper.

We now introduce both the orbital model and the classical multipole expansion model that can be used to rationalize the bent structures. The orbital model may be cast either in valence bond language with the attendant use of localized (hybrid) orbitals, or in molecular orbital language with emphasis on the delocalized molecular orbitals. In valence bond language, the fact that many of the experimental structures are bent suggests that *sp* hybrid orbitals are incorrect and that one should instead invoke an *sd* set of hybrid orbitals.[14] We will not make more use of valence bond language, but refer to Scheme 1 in passing.

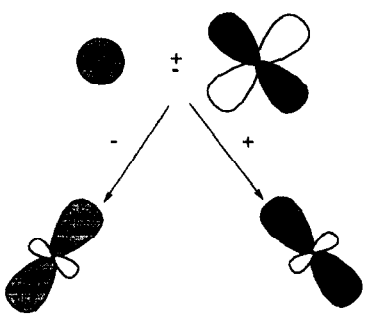

1

Scheme 1.

† Such reported uncertainties are within the framework of the assumptions used to calculate the bond angle. For example, most such calculations assume a harmonic force field. Interaction between stretching and bending frequencies are often neglected. If these effects are factored in, the reported uncertainty should be much larger.

We now turn to a qualitative molecular orbital scheme. Skinner[3] and later Hayes[15] introduced the idea that the $(n-1)d$ orbitals might be more important than the np orbitals in bonding to the ligands. This idea is introduced in Scheme 2 where the MOs that hold the four valence electrons of CaH_2 are depicted. This scheme summarizes the countering effects that the d and p valence orbitals exert regarding structure. In the HOMO the d orbital favours a bent structure and the p orbital a linear structure. In the penultimate MO it is just reversed. The sizeable energy splitting of the HOMO and the penultimate MO is caused mainly by the strong contribution of the metal s orbital to the penultimate MO (symmetric, S). This energy splitting results in a lesser interaction of either the d or the p metal orbitals in the penultimate MO as compared to the HOMO. Furthermore, these high-lying metal orbitals must compete with the metal s orbital for per cent character in the penultimate MO. Both of these effects serve to make mixing of d and/or p character into the HOMO more important than into the penultimate MO. Hence, the HOMO controls the geometry of these systems. (It is interesting to observe that it is the valence s orbital on the metal atom that indirectly exerts stereochemical activity.[16]) As seen in Scheme 2, the result is a linear geometry if p orbitals are important but a bent geometry if the d orbitals are involved. An example of the former might be BeH_2 and of the latter ScH_2^+. (We have purposely chosen the z axis to be perpendicular to the plane of the bent molecule. This will facilitate the population analysis and the angular overlap analysis to be presented later.)

But this is all by way of qualitative introduction. If life were as simple as presented in Scheme 2 there would be no need for this manuscript. Hence we present a brief review of the quantum chemical history of CaF_2. Hayes not only examined the neutral atom valence-state excitation energies but also those of the cation.[15] In a later paper Gole *et al.* completed an *ab initio* theoretical study and found indeed that if a basis set without d orbitals was employed the molecule was linear, but with d orbitals it was bent.[17] This would have been the end of the matter except that in the same year Yarkony *et al.*[18] also completed an *ab initio* study on the same molecule with a much larger d basis set and found the molecule to be linear! Other calculations of CaF_2 have appeared;[19] they predict a linear geometry or obtain a bent geometry only by choosing a d orbital exponent to provide the desired answer.

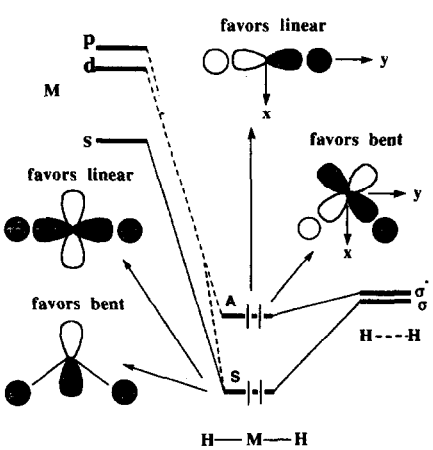

2

Scheme 2.

One of us has completed further *ab initio* theoretical studies[20] on both CaF_2 and CaH_2 using a larger basis set than used heretofore. Even though correlation effects were included at the CISD level the results still predicted a linear structure for both of these molecules. After our work was completed we learned that Marsden[21] had also carried out an *ab initio* study on CaF_2 in which the d basis set was enlarged even further and attention was paid to choosing "optimum" d exponents; he finds the most stable configuration to be bent at the SCF level.

We turn now to the multipole expansion model that was mentioned before. This model suggests that one should forget about orbital arguments and employ a classical multipole expansion, starting from the completely ionic formulation. This method was first used quantitatively by Rittner[22] to rationalize the vibration frequencies, dipole moments and dissociation energies of the alkali halides. It has subsequently been used extensively for the alkali halides, for which we provide a pair of more recent references.[23] In the multipole expansion the first-order term is the Coulombic interaction of the ions (charge–charge interaction). Higher-order terms involve the charge on one ion inducing a dipole on another, and the interaction of the induced dipoles with each other. We refer to these as simply charge–dipole (c–d) and dipole–dipole (d–d) interactions. See Scheme 3 for a pictorial introduction. The magnitude of these higher order interactions depends directly upon the (dipole) polarizability of the ion; in order to apply the model these values must be chosen from empirical data for both the cation and the anion.

The multipole expansion method also has been applied to the alkaline-earth dihalides. The most rigorous application has been that of Guido and Gigli.[24] Hildenbrand[25] employed a truncated version (charge–charge and charge–dipole terms only)

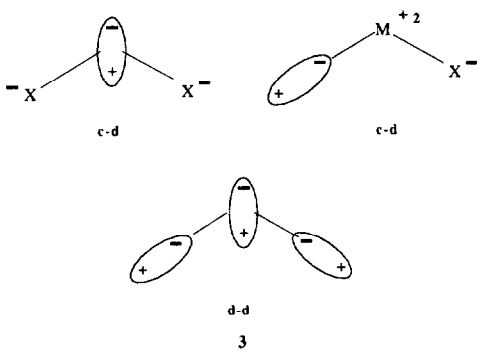

3

Scheme 3.

which he used to rationalize the bond dissociation energies but not to predict the molecular structure. There also are two papers[5a,26] which review the structures of the dihalides and qualitatively rationalize them in terms of polarizability arguments. In the inorganic chemistry literature this model is sometimes referred to as "reverse" polarizability, because it is stated that the term in which the anions polarize the cation is most important for causing the molecule to bend. The feature of this model which is difficult to accept is that the "core" electrons of the metal cation must be distorted in order to bring about this stabilization. For Ca^{2+} this means that the 3*s* and 3*p* electrons must be distorted. On the face of it this model sounds implausible, but because it has gained such widespread use in the literature we scrutinize it. The same model has been used to rationalize the structures of the bent Cp_2M molecules that were introduced above.[9,10]

The present study was undertaken with the desire to employ a single theoretical method to study the diverse molecules listed in the title. We have employed the Hartree–Fock–Slater (HFS) theoretical method;[27] once we had ascertained that the model reproduced the experimental results we set out to determine if we could trace the origin of the bending within an SCF (orbital-based) model. This method has been employed for a number of geometrical studies on small molecules[28] and on transition metal molecules.[29] We include relativistic effects for CeO_2 and $YbCl_2$ as described below.

THEORETICAL METHOD

Important background papers for the theoretical method have been referenced above. The basis set consists of uncontracted Slater-type atomic orbitals.[30] The method utilizes the frozen core approximation; valence orbitals are orthogonalized onto the core by employing a single ζ exponent in the valence set for each core type orbital. The following orbitals were kept in the core: O, F and Mg (1*s*); Cl and Ca (1*s*, 2*s*, 2*p*); Ce and Yb (1*s*, 2*s*, 2*p*, 3*s*, 3*p*, 3*d*, 4*s*, 4*p*, 4*d*). Notice that eight electrons more than "necessary" have been kept in the valence shell, except for O, F and Mg.

We used a flexible valence basis set which is briefly described as follows: H (double ζ, 1*s*; single ζ, 2*p*); O and F (double ζ, 2*s*; double ζ, 2*p*; single ζ, 3*d*); Mg (double ζ, 2*s*; double ζ, 2*p*; double ζ, 3*s*; double ζ, 3*p*; triple ζ, 3*d*); Ca (double ζ, 3*s*; double ζ, 3*p*; double ζ, 4*s*; double ζ, 4*p*; triple ζ, 3*d*); Ce and Yb (double ζ, 5*s*; double ζ, 5*p*; double ζ, 6*s*; double ζ, 6*p*; triple ζ, 5*d*; triple ζ, 4*f*).* Atomic calculations were performed and these eigenvectors were used as fragments for the molecular calculations. This feature facilitates the interpretation of the Mulliken population analysis for an uncontracted basis set.

The bond lengths and angles of the magnesium and calcium compounds were optimized using the recently developed analytical gradient method for the HFS model.[28] Since we knew that the difference in energy between the linear and bent structures would be small, we chose to employ a new, more accurate method for numerical integration in this work.[31] For the cerium and ytterbium molecules a manual procedure involving parabolic fits was employed to optimize the structure.

The atomization energies have been calculated for each of the compounds,[32] including Becke's non-local exchange correction.[33,34] For the purpose of incorporating relativistic effects, the quasi-relativistic theoretical method has recently gained attention.[35] With this approach bond dissociation energies can be calculated accurately for any element in the periodic table. Briefly, the quasi-relativistic method incorporates the major effects of relativity on the kinetic (mass–velocity term) and potential (Darwin term) energies of the electrons, but effects due to spin–orbit coupling are neglected. Since the ground states of the title molecules are closed-shell, the spin–orbit effects are of no consequence to us.

* We employed the neutral atom wave function in the molecular calculation and used the experimental atomic electron configuration in all cases, except for Yb where the configuration [core] $4f^{13}\ 5d^{1}\ 6s^{2}$ was used rather than the experimental configuration [core] $4f^{14}\ 5d^{0}\ 6s^{2}$. Since the population analysis for $YbCl_2$ showed that there was about one 5*d* electron, the basis set we have chosen is appropriate for the molecular study. We have corrected this reference state to that of the ground state Yb atom in reporting the theoretical atomization energy of $YbCl_2$.

RESULTS AND DISCUSSION

We divide the results and discussion into six sections. In the first we present an overview. In the second and third we examine the general population analysis and the *d* orbital population analysis. In the fourth section we look at the angular overlap model. The fifth section exhibits a decomposition of the bonding in CaH_2 in terms of Ca and H_2 fragments for both the linear and bent geometries. The last section examines the electrostatic multipole expansion method.

Overview

In Table 2 we present the theoretical geometries, a summary of the atomic charges as obtained from the Mulliken population analysis, energy differences between bent and linear structures, dipole moments, and the theoretical atomization energies.

The ground state of each molecule is bent, except for MgF_2. These results are in agreement with the electric deflection and IR spectral experiments, as was outlined in the introduction. The bond angle is calculated to be near 130° for CaH_2, CaF_2 and CeO_2, whereas it is 120° for $YbCl_2$. The bent structure is only about 1–3 kcal mol^{-1} more stable than the linear structure. This is indicative of a small bending potential, as is also evident from the small bending force constants that have been derived from the IR stretching frequencies. In contrast to the bent geometry of the Ca, Ce and Yb compounds, the MgF_2 molecule is predicted to be linear and strongly so. The difference in energy between the linear geometry and one at 120° is 13.4 kcal mol^{-1}. We will return to a detailed analysis of the linear vs bent structure later in the discussion.

Our theoretical bond lengths are about 0.05 Å shorter than the Hartree–Fock lengths for (linear) CaH_2 (2.10 Å) and CaF_2 (2.05 Å).[20] The Ce—O bond length of CeO_2 (1.82 Å) is close to the experimental bond length of the diatomic molecule CeO (1.84 Å).[36] The MgF_2 bond length is nearly identical to that reported from electron diffraction studies (1.77 Å).[5b,37] The optimized Yb—Cl bond distance of 2.40 Å is identical to that used by Culberson *et al.*[38] in their INDO study on this molecule. All in all, the bond lengths that we obtained are very reasonable.

In each case the difference in optimized bond length between the linear and the bent molecule is only a few hundredths of an Å. This also is an indication of the flatness of the potential energy surface for bending these molecules. This result is in contrast to the work of Baird[39] on simple molecules such as H_2O; he found large variations in bond length with angle, but he was looking at the range 90–120° where the energy varies strongly with angle. It is interesting to note that for CaH_2, CaF_2 and $YbCl_2$ there is a bond length *shortening* as the molecule is bent, whereas for MgF_2 there is a slight *lengthening* (Table 2). This is exactly what one would predict based upon the most stable geometry in each case. The minor variation in bond length with angle is in agreement with our *ab initio* results for CaF_2.[20]

Table 2. Theoretical results for the title molecules

Molecule	r (Å)	ϕ (degrees)	q (M)	ΔE^a (kcal mol^{-1})	Dipole moment[b]	Atomization energy[c]
MgF_2	1.75	180	1.32	0.0	—	243
MgF_2	1.76	120[d]	1.30	−13.4	—	—
CaH_2	2.06	180	0.90	—	—	—
CaH_2	2.01	127	1.00	2.0	4.77	76
CaF_2	1.99	180	1.38	—	—	—
CaF_2	1.96	130	1.35	1.5	5.23	265
CeO_2	1.82	180	1.39	—	—	—
CeO_2	1.82	132	1.37	3.1	4.59	346
$YbCl_2$	2.49	180	1.01	—	—	—
$YbCl_2$	2.40	120	0.89	1.8	5.86	154

[a] Difference in energy, linear minus bent. A positive number indicates that the bent form is more stable.

[b] In Debye units.

[c] In kcal mol^{-1}, for $MX_2 \rightarrow M + 2X$.

[d] This is an arbitrary point on the energy surface. No bent structures for MgF_2 were found to be stable.

The charge polarization is quite large based upon the Mulliken population analysis; the positive charge on the metal atom is in the range 0.9–1.4. The charge polarization in CeO_2 is no greater than in CaF_2; in the ionic formulation the charge on the cerium atom is two units larger than that on calcium. This is an example of Pauling's electroneutrality principle at work. The theoretical dipole moments also indicate significant charge polarization, although as Rittner warned us 40 years ago we should be careful about deducing partial charges from dipole moments.[22]

The atomization energies ($D_0°$) have been reported for MgF_2,[40] CaF_2[40] and CeO_2;[41] the values are 246, 266 and 344 kcal mol^{-1}, respectively. The theoretical results that we report in Table 2 are very close to these values. The theoretical value for CaH_2 is only 76 kcal mol^{-1}. Since the bond dissociation energy of H_2 is over 100 kcal mol^{-1},[42] it is evident that CaH_2 could exist only as a metastable molecule. However, this is not unusual for MH_2 molecules.[43]

The bond dissociation energy of CeO is reported as 192 kcal mol^{-1}.[44] With this value and the experimental atomization energy of CeO_2, we have enough information to obtain the stepwise bond dissociations of CeO_2:

$CeO_2 \rightarrow CeO + O$	152 kcal mol^{-1}
$CeO \rightarrow Ce + O$	192 kcal mol^{-1}
$CeO_2 \rightarrow Ce + 2O$	344 kcal mol^{-1}.

This contrasts with the corresponding values[45] for CO_2 which has the same valence electron count:

$CO_2 \rightarrow CO + O$	127 kcal mol^{-1}
$CO \rightarrow C + O$	257 kcal mol^{-1}
$CO_2 \rightarrow C + 2O$	384 kcal mol^{-1}.

Notice that the carbon atom in CO_2 is able to take "advantage" of the loss of the first O atom so as to considerably strengthen the bond with the remaining O atom. In classical Lewis electron dot structures (or more precisely GVB structures) we can see that there is a net loss of one σ bond for the first bond dissociation of CO_2, whereas the loss of the second O atom requires breaking one σ bond and two π bonds.

For CeO_2 the increase in bond dissociation for the loss of the second oxygen is not nearly so large as for CO_2. The most likely explanation for this difference is that the bonding is controlled more by electrostatic effects for CeO_2 than it is for CO_2. Hildenbrand[25,40] has tabulated the bond dissociation energies of MX and the atomization energies for MX_2, where M is an alkaline earth metal atom. The first bond dissociation energy is about 50% of the atomization energy for the alkaline earth dihalides, for CeO_2 it is 44%, and for CO_2 33%. From these values it is clear that CeO_2 behaves more like MX_2 than like CO_2.

We briefly examine the behaviour of the HOMO as a function of bond angle. For MgF_2 the HOMO is a degenerate π^* orbital which is destabilized by 0.7 eV as the molecule is bent to 120°. The σ_u orbital lies slightly lower in energy; it is destabilized by 0.4 eV upon bending the molecule. For each of the other title molecules the HOMO in the linear molecule is σ_u. As the molecule is bent this HOMO is *stabilized*, exactly as would be expected if the *xy* orbital on the metal takes an active role in the bonding (Scheme 2). The amount of stabilization (in eV) experienced by the HOMO is 0.05 (CaH_2), 0.19 (CaF_2), 0.66 (CeO_2) and 0.43 ($YbCl_2$). The idea that one can correlate molecular shape with the behaviour of the HOMO as a function of angular variation is well documented.[46] We turn to the population analysis in order to examine further the conjecture that the *xy* orbital is involved in causing the molecule to bend. First we look at the general population analysis and later focus explicitly on the *d* orbitals.

Angular geometry—General population analysis

In Table 3 we present the Mulliken population analysis for these molecules. First, we notice that the metal atom $(n-1)s$ and $(n-1)p$ orbitals that were included in the valence basis set have full occupation in all cases except for CeO_2. Even in that case the population of these orbitals changes little upon going from the linear to the bent geometry. Second, the populations of the ligand orbitals also change very little upon going from the linear to the bent configuration. The largest change is 0.05 electrons for the σ bonding (p_z) orbital of the Cl atom in $YbCl_2$. Third, the situation for the valence orbitals of the metal atom is quite different. In Table 2 we saw that the overall charge on the metal atom was relatively unchanged upon bending. Table 3 shows, however, that except for MgF_2 there is a dramatic rearrangement of electrons on the metal as bending occurs. We now look at the orbital occupancies in more detail.

The occupancy of the halogen p_π type orbitals is roughly 1.9 electrons, whereas there are only about 1.6 electrons in the corresponding orbitals on the oxygen atoms in CeO_2. This is evidence of π bonding in CeO_2. Turning to the metals, the population of the $(n-1)d$ orbitals shows a significant increase in each case, ranging from 0.06 electrons for CaF_2 to 0.26 for CeO_2. Meanwhile, the *np* population suffers a decrease ranging from 0.03 to 0.28 elec-

Table 3. Mulliken population analysis for the title molecules[a]

Molecule	Metal orbitals						Ligand orbitals[b]			
	$(n-1)s$	$(n-1)p$	$(n-1)d$	ns	np	$4f$	ns	np_x	np_y	np_z
MgF_2 (lin.)	2.0	6.0	0.19	0.18	0.31	—	2.05	1.90	1.90	1.82
MgF_2 (120°)	2.0	6.0	0.20	0.21	0.30	—	2.02	1.86	1.90	1.86
CaH_2 (lin.)	2.0	6.0	0.18	0.45	0.47	—	1.44	—	—	—
CaH_2 (127°)	2.0	6.0	0.30	0.52	0.19	—	1.49	—	—	—
CaF_2 (lin.)	2.0	6.0	0.44	0.03	0.15	—	2.01	1.90	1.90	1.87
CaF_2 (130°)	2.0	6.0	0.50	0.04	0.12	—	2.01	1.91	1.90	1.85
CeO_2 (lin.)	1.93	5.77	1.27	0.02	0.08	1.53	2.03	1.61	1.61	1.40
CeO_2 (132°)	1.93	5.78	1.53	0.01	0.05	1.31	2.04	1.59	1.59	1.43
$YbCl_2$ (lin.)	2.01	6.0	0.56	0.21	0.24	13.96	1.95	1.88	1.88	1.78
$YbCl_2$ (120°)	2.01	6.0	0.70	0.39	0.18	13.82	1.95	1.88	1.87	1.73

[a] There are some minor differences between this table and the charges reported in Table 2. Some of this is due to round-off, and some is due to that fact that we do not tabulate the (small) d orbital populations on the ligands.

[b] The coordinate system on the ligands has the p_z orbital pointing at the metal. The p_y orbital is perpendicular to the plane of the bent molecule.

trons. For CeO_2 and $YbCl_2$, there is a decrease in the $4f$ population of 0.22 and 0.14 electrons, respectively.

What do we conclude from these variations? The simplest conclusion is that the $(n-1)d$ orbitals provide the driving force for bending these molecules (except MgF_2). In other words we come to the same conclusion that Hayes came to more than 20 years ago.[15] In hybrid orbital language the sd hybridization (Scheme 1) which favours a bent molecule is more important than either sp or sf hybridization which favour the linear geometry.[47] The implication of the valence d orbitals is in agreement with the interpretation of the bonding in ScH_2^+,[12,*] and the conclusion that Wadt[48] and Pyykkö *et al.*[49] reached in their theoretical studies on ThO_2. (We do not agree with Culberson *et al.*[38] who ascribe the bent geometry of $YbCl_2$ to "a small amount of p orbital hybridization".) The use of "outer" d orbitals in chemical bonding has been a topic of ongoing discussion for many years. We provide but a few references to that literature here.[50]

Why do the d orbitals attain an importance that surpasses that of the p and f orbitals for the title molecules? Consider calcium; the relative energy of the $3d$ and $4p$ orbitals undergoes a dramatic change upon going from Ca to Ca^+.[15] The s–p promotion energy[51] of Ca is roughly 1.9 eV, whereas the s–d is 2.5 eV. The situation is more or less reversed for the cation, 3.2 and only 1.7 eV, respectively. The ordering of our theoretical excitation energies is the same as that found experimentally.† Hence the most accessible valence orbital (beyond $4s$) is the $3d$ orbital for Ca^+; see Scheme 2. This effect is seen for all of the Group 2 elements except for Be and Mg, the very elements that invariably exhibit a linear MX_2 geometry. The formation of the anions of Group 2 also shows how Mg is decidedly different from Ca, Sr and Ba; the states with an occupied d orbital are relatively high in energy for Mg.[52]

The $5d$ orbital also has a preferential position in the lanthanoid elements Ce and Yb.[53,54] For example the ground state of Ce is [core] $4f^15d^16s^2$, so that the d orbital already is occupied. The ground state of Yb is [core] $4f^{14}6s^2$, but there are low-lying states with the $5d$ orbital occupied. The latter statement applies also to cations of Ce and Yb.

But what about the $4f$ orbitals? If they were sufficiently involved in the bonding, the molecules would be linear. The $4f$ orbitals of Ce have a total population of 1.3 electrons in CeO_2, and those of Yb have 13.8 electrons in $YbCl_2$. The latter indicates that a full occupancy of 14 electrons is very nearly achieved for Yb, which would render the stereochemical activity of the $4f$ orbitals nil. But what about the 1.3 electrons of Ce? Might they tend to make the CeO_2 molecule linear? We believe that the answer is a decided no. The reason is that

* As part of the present study we also have determined the optimized geometrical structure of ScH_2^+; we find the bond length to be 1.74 Å and the bond angle to be 107°. These results are in excellent agreement with those reported in ref. 12.

† Energies are reported here for unrestricted calculations in "spherical" symmetry. That is, fractional electron occupancies are employed as needed. The four values, reported in the same order as the experimental numbers given in the text are: 1.4, 3.1, 3.0 and 2.4 eV.

although in energy terms the $4f$ orbitals function as valence orbitals, in terms of radial extent they behave as core orbitals.[54-56] In fact, this is true to such a large extent that electronic structure studies have been successful on atomic and molecular lanthanoids with partially occupied $4f$ orbitals treated as part of the core via pseudo-potentials.[54,57] The compact nature of the $4f$ orbitals compared to the $5d$ is borne out by the overlap integrals with the symmetry adapted linear combination of p_z orbitals on the ligands with the $f(z^3)$ and $d(z^2)$ orbitals for linear CeO_2 and $YbCl_2$.* Ortiz and Hoffmann have affirmed the lack of stereochemical activity of f orbitals in their Extended Hückel study of Cp_2Sm.[58]

Before leaving the CeO_2 and $YbCl_2$ molecules we point out that our theoretical study has employed the quasirelativistic method; we have not done the corresponding non-relativistic study. Results in the literature[59] suggest that relativity affects the lanthanoids much less than the actinoids, and that the effect is to stabilize s and p orbitals on the metal atom and to destabilize d and f orbitals. Such being the case, we expected that a non-relativistic study also will produce bent molecules since the $6p$ orbital will be destabilized and the $5d$ will be stabilized in relation to the relativistic results.

*Angular geometry—*d *orbital population analysis*

In the previous section we pointed out that the theoretical results implicate d orbital involvement as the important feature which causes the molecules to bend. In this section we examine the population of each of the five d orbitals in both the linear and bent geometries.

We employ a coordinate system in which the local z axis on the metal atom is perpendicular to the plane of the molecule. The local x axis is chosen to bisect the molecular bond (Scheme 2). This coordinate system has the advantage of producing a z^2 orbital which is isotropic to changes in bond angle with ligand σ bonding orbitals, and is unable to π bond with ligand orbitals either in-plane (π_{ip}) or out-of-plane ($\pi_\perp$). The metal x^2-y^2 orbital is purely σ bonding for the linear molecule and σ non-bonding at a bond angle of 90°; it is purely in-plane π bonding at 90°. The situation for the xy orbital is just the reverse of that for the x^2-y^2 orbital. The xz and yz orbitals are either non-bonding or purely π bonding, depending upon whether the molecule is linear or bent. This coordinate system has many advantages for understanding changes in population of the d orbitals as a function of angle. For example, other things being equal we expect no change in the z^2 orbital population as the angle is varied. In Scheme 4 we show some interactions of d orbitals with ligand orbitals. Some of the orbital interactions are shown for the linear configuration and others for the bent. The reader easily can envision the interactions that are not shown.

The results in Table 4 show that the z^2 orbital population changes only slightly as the molecule is bent.† This was expected in our coordinate system. The x^2-y^2 and xy orbitals are involved in σ and π_{ip} bonding. For both Ca molecules the former orbital loses population, while for the Ce and Yb molecules it gains population. The xy orbital gains in population in all cases, as expected, since the ligand σ bonding orbitals come into better alignment with it as the molecule is bent (see Scheme 2 or 4). Among the xz and yz orbitals ($\pi_\perp$), the changes also are as expected. For example, the former cannot participate in the bonding in the linear molecule since it is of δ symmetry. Upon bending the molecule it gains in $\pi_\perp$ bonding whereas yz loses because of less effective overlap with the ligand orbitals.

The really intriguing thing about these results can be garnered already by looking at the populations

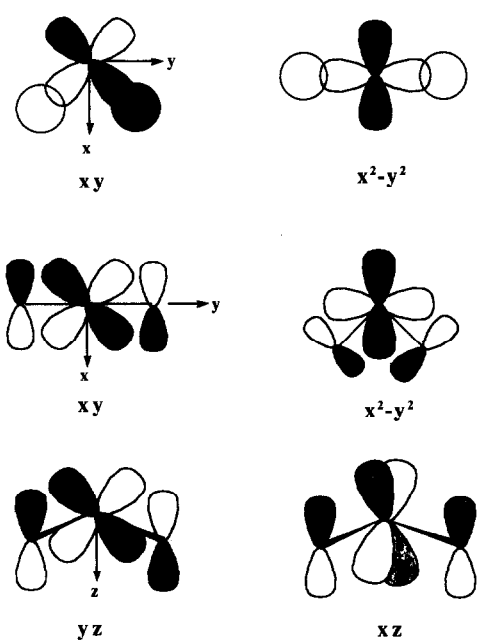

4

Scheme 4.

* For these overlap integrals we take the z axis as the molecular axis. The overlap integrals with the appropriate symmetry adapted linear combination [$p_z = (1/\sqrt{2})(z_1 \pm z_2)$] are as follows: CeO_2, $S(z^2,p_z) = 0.131$ and $S(z^3,p_z) = 0.080$; $YbCl_2$, $S(z^2,p_z) = 0.215$ and $S(z^3,p_z) = 0.026$.

† We do not present results for MgF_2 since the d orbitals were of no consequence for this molecule.

Table 4. Mulliken population analysis of the *d* orbitals[a]

Molecule	ϕ (degrees)	z^2	x^2-y^2	xy	xz	yz
CaH_2	180	0.046	0.138	0.0	0.0	0.0
CaH_2	127	0.051	0.053	0.196	0.0	0.0
CaF_2	180	0.047	0.134	0.127	0.0	0.127
CaF_2	130	0.059	0.131	0.177	0.026	0.110
CeO_2	180	0.099	0.297	0.438	0.0	0.438
CeO_2	132	0.164	0.389	0.483	0.370	0.128
$YbCl_2$	180	0.052	0.156	0.177	0.0	0.177
$YbCl_2$	120	0.058	0.179	0.256	0.048	0.159

[a] Molecule lies in the *xy* plane; the *x* axis is the two-fold axis for the bent molecule.

of the x^2-y^2 and xy orbitals of CaH_2. In the linear molecule the former is σ bonding and the latter nonbonding. If the molecule were bent to 90° their roles would just be reversed. Why then already at 127° do we find that the xy orbital gains in population more than the x^2-y^2 loses? The answer is easily seen in Scheme 2 and it was alluded to already in the introduction: the former is energetically closer in energy to the ligand bonding combination than is the latter. This effect is brought about by the metal *s* orbital involvement with the penultimate MO. We can quantify this idea by relating changes in population to changes in $S^2/\Delta e^0$, where S is the overlap integral of the ligand function with the designated *d* orbital and Δe^0 is the energy difference between the metal and ligand orbitals of the same symmetry. In the section on the angular overlap model presented next, we develop more fully the reason for choosing the function $S^2/\Delta e^0$. It should be clear to the reader that this function comes from second-order perturbation theory.

In Table 5 we present changes in *d* orbital population for the valence atomic orbital of our triple ζd basis set. For example, for Ca we tabulate the 3*d*

Table 5. Mulliken population analysis of the $(n-1)d$ orbitals, tabulated as changes upon going from the linear to the bent molecules[a,b]

Molecule	z^2	x^2-y^2	xy	xz	yz
$\Delta[S^2]$, σ	0.001	−0.026	0.030	—	—
CaH_2	**0.005**	**−0.087**	**0.198**	**0.0**	**0.0**
$\Delta[S^2/\Delta e^0]$, σ	−0.001	−0.116	0.158	—	—
$\Delta[S^2]$, σ	0.001	−0.020	0.021	—	—
$\Delta[S^2]$, π	—	0.016	−0.014	0.005	−0.003
CaF_2	**0.012**	**−0.018**	**0.059**	**0.024**	**−0.015**
$\Delta[S^2/\Delta e^0]$, σ	−0.001	−0.064	0.062	—	—
$\Delta[S^2/\Delta e^0]$, π	—	0.050	−0.037	0.014	−0.009
$\Delta[S^2]$, σ	0.0001	−0.007	0.007	—	—
$\Delta[S^2]$, π	—	0.100	−0.101	0.030	−0.031
CeO_2	**0.062**	**0.141**	**−0.019**	**0.128**	**−0.068**
$\Delta[S^2/\Delta e^0]$, σ	−0.0001	−0.043	0.043	—	—
$\Delta[S^2/\Delta e^0]$, π	—	0.801	0.237	0.112	−0.157
$\Delta[S^2]$, σ	−0.001	−0.027	0.025	—	—
$\Delta[S^2]$, π	—	0.094	−0.120	0.134	−0.076
$YbCl_2$	**0.006**	**0.060**	**0.037**	**0.054**	**−0.014**
$\Delta[S^2/\Delta e^0]$, σ	−0.006	−0.214	0.228	—	—
$\Delta[S^2/\Delta e^0]$, π	—	0.554	−0.064	0.134	−0.076

[a] Molecule lies in the *xy* plane; the *x* axis is the two-fold axis for the bent molecule.

[b] A positive number indicates an increase in population upon bending.

values and neglect the higher energy 4*d*-like and 5*d*-like orbitals. (The population changes in Table 5 cannot be gleaned directly from Table 4 since the latter included populations in all three *d* orbitals of the triple ζd basis set). It is clear that there is a rough correlation between change in population of a metal *d* orbital and $\Delta[S^2/\Delta e^0]$ but not with $\Delta[S^2]$. For example, in the case of CaH_2 the $\Delta[S^2]$ value decreases for the x^2-y^2 orbital by about the same amount that the xy increases. Yet the latter gains in population almost twice what the former loses. The inability of $\Delta[S^2]$ to track such trends in population changes is immediately obvious when one recalls the sum rule that is familiar in the angular overlap model (see below). For our situation, this sum rule states that the sum of $\Delta[S^2]$ must add to zero for the set of *d* orbitals. The reason they do not sum to exactly zero in Table 5 is that the Ca—H bond length is slightly different in the two geometries.

We next examine the xz and yz orbital changes, those orbitals that are $\pi_\perp$. (Here there can be no metal *s* orbital participation in either the linear or bent geometry and so there is no competitition between different types of metal orbitals.) These changes also are readily interpreted in terms of the function $\Delta[S^2/\Delta e^0]$. There is one exception (CeO_2) in that $\Delta[S^2/\Delta e^0]$ predicts the xz orbital should gain less than the yz loses, whereas the opposite occurs. We already knew that something was drastically amiss for CeO_2 in that the z^2 orbital experienced a large change in population contrary to what we would expect based upon its isotropic nature.

The correlation of population changes for the x^2-y^2 and xy orbitals is not so straightforward as it was for CaH_2. Perhaps the gain in population for the x^2-y^2 orbital of CeO_2 and $YbCl_2$ is due to a π_{ip} bonding interaction for these molecules. The population changes in the x^2-y^2 and xy orbitals of CaF_2 compared to CaH_2 are readily comprehended based on the contribution of π_{ip}.

In summary, the results of Table 5 indicate that the function $\Delta[S^2/\Delta e^0]$ provides a ready understanding of the population changes in the *d* orbitals on the metal atoms, except for CeO_2 where only about one-half of the changes can be understood in this fashion.

Angular overlap model

Under the assumption that the ligand levels are considerably more stable than the metal levels and/or the overlap between the metal and ligand orbitals is small, one can introduce perturbation approaches to determine if they provide an understanding of the angular geometry. There are two approaches. One is to use a perturbational molecular orbital (PMO) theory and the second is to use the angular overlap model (AOM).

Albright *et al.* show how PMO theory can be used to rationalize Walsh's rules.[60] We do not have available the necessary perturbation matrices which would allow us to employ this method. The first order terms involve changes in overlap and since the HOMO has a nodal plane (Scheme 2) it is clear[60] that the first-order perturbation terms would predict it to be *destabilized* upon bending. But our theoretical results show that the HOMO is stabilized (*vide supra*). Hence, we turn to the second-order terms which essentially leads us to AOM.[61]

Within AOM the energy of stabilization as a result of interaction between two orbitals is βS^2, where S is the overlap integral and β is given by $(e_M{}^0)^2/(e_X{}^0-e_M{}^0) = (e_M{}^0)^2/\Delta e^0$. This term for stabilization energy is very familiar in that it also appears in a second-order perturbation treatment within Extended Hückel Theory.[62] For purposes of our discussion, $e_X{}^0$ is the diagonal element of the **H** matrix for the symmetry adapted linear combination of ligand orbitals and $e_M{}^0$ is the corresponding term for a metal *d* orbital. The angular overlap model generally ignores changes that might occur in β and concentrates on changes in the values of the overlap integrals. (If our computational method is non-iterative EHT, there will be no change in β.) It is interesting to note that the electron population (Mulliken method) of the metal orbital in EHT is proportional to $[(e_M{}^0)S^2/\Delta e^0 + (e_M{}^0)^2S^4/(\Delta e^0)^2]$.[63] The leading term in this expression is closely related to the angular overlap term. In the application of AOM, if changes in S^2 do not distinguish one geometry over another the method is sometimes extended[62] to include the next higher power term in the expansion, namely $(-)\gamma S^4$, where γ is given by $(e_M{}^0)^4/(e_X{}^0-e_M{}^0)^3 = (e_M{}^0)^4/(\Delta e^0)^3$.

At the quadratic level there is a sum rule that can be invoked in AOM.[62,64] Consider CaH_2; the ligand combinations s_1+s_2 and s_1-s_2 are both occupied in this four-valence electron system, so that the sum of the squares of the overlap integrals between the metal and ligand orbitals will be constant with variation in bond angle. Hence, we cannot use "constant β" AOM to explain why CaH_2 is bent. This is the approach which Burdett used in his application of AOM.[61,62,65] We need to delve deeper into the problem in order to understand why the *d* orbitals gain in population as the molecule is bent; AOM predicts that there would be no change in population and no tendency to bend. (We neglect any contribution from the metal *s* orbital to the

bonding in the symmetric orbital in the previous statement.) Consideration of the fourth-order terms would provide a rationale for the bent structures. What we showed in the previous section is that there is no need to invoke a fourth-order perturbation approach, but that a detailed analysis of changes in metal orbital populations is provided by the function $S^2/\Delta e^0$.*

In summary, our work shows that AOM treatments which ignore changes in Δe^0 may be flawed. Treatments which pursue a fourth-order perturbation may be unnecessary if second-order terms are covered properly. Explanations that involve only overlap arguments to explain geometry also may be flawed if there is no cognizance of the sum rule. For example, Myers *et al.*[66] claim that the lanthanoid trihalides are pyramidal based on an overlap argument. The sum rule shows clearly that, while the square of one particular overlap is increasing, others are decreasing by a like amount. Jolly and Marynick[2d] have rationalized the pyramidal structure of ScH_3 with statements such as "all five *d* orbitals are of the correct symmetry" for bonding to the ligand orbitals in the pyramidal structure but not in the trigonal planar structure. Once again, such arguments essentially boil down to overlap considerations which do not take account of the sum rule mentioned above. Explanations might rather be sought that involve a function such as we have used: $\Delta[S^2/\Delta e^0]$. On the other hand, one could argue that the interactions between metal and ligand orbitals are so large for these molecules that an AOM approach should never be attempted. Then there is no validity to the sum rule, since one needs to solve the secular equations, and a back-of-the-envelope interpretation is not possible. In that case, the above authors cannot be criticized for their approach. The "rule of thumb" that a central atom seeks to use as many orbitals as possible in bonding to the ligands[62] cannot be rationalized at the quadratic level of AOM treatment.

Bond energy analysis of CaH_2 *from* Ca *and* H_2 *fragments*

The bond energy analysis of the wavefunction can be referenced to molecular fragments rather than to atomic fragments (atomization energies).[32,67] It can be broken down further into *steric* and *electronic* components; the latter can be subdivided into components due to each irreducible representation of the molecular point group. For CaH_2 we have completed such a fragment study in C_{2v} symmetry for both the linear and the bent molecule. The fragments that we have employed are the ground state Ca atom and the H_2 fragment in its "prepared" state. The latter is at the bond length appropriate for "insertion" of the Ca and with electron occupation $(\sigma_u)^2$. This choice of electron occupation for the two fragments ensures that we will not have an avoided crossing of energy states as the two fragments come together. That is, the reaction is symmetry allowed for the Ca atom approaching the "prepared" H_2 in a side-on fashion.

We are interested only in the relative values of the terms mentioned in the previous paragraph; that is, the bent geometry relative to the linear geometry. In Table 6 we present these values. Notice that the relative preparation energy is destabilizing for the bent geometry. This is as expected since we are forming the H_2 fragment with the electrons in the antibonding orbital. In the bent molecule the two protons are nearer each other so that this geometry is less stable than it is in the linear molecule. The steric term favours the bent geometry slightly. The major relative energy changes are in the electronic terms. As expected, the term involving the representation that includes the z^2 and x^2-y^2 orbitals shows a destabilization due to the decrease in effective overlap with the latter orbital. However, this destabilization is more than compensated by the stabilization afforded by the representation that contains the xy orbital. These energy numbers demonstrate very clearly effects that are used often in Walsh-rule explanations. For example, the importance of the antisymmetric representation to the bond (xy) which results in the molecule becoming bent. The sum of all these effects is the 2 kcal mol^{-1} stabilization for the bent

* As seen in the discussion, the leading term in the expression for population of metal orbital is $(e_M{}^0)S^2/\Delta e^0$. We ignore the $e_M{}^0$ term. The resultant term in $(-)S^2/\Delta e^0$ is familiar in second-order perturbation theory. Now, the eigenvalues in HFS take on a different meaning than in the Hartree–Fock theory. (L. Noodleman, D. Post and E. J. Baerends, *Chem. Phys.* 1982, **64**, 159.) This has little effect upon Δe^0 but it has a drastic effect upon $e_M{}^0$. The latter should be stabilized by several electron volts if it is going to take on the values found in the Hartree–Fock theory. Our values of $e_M{}^0$ are near zero for the metal *d* orbitals. Hence, shifts of only a few tenths of an electron volt can have a dramatic effect upon the expression $(e_M{}^0)S^2/\Delta e^0$. On the other hand, if $e_M{}^0$ values were at about -5 eV, shifts of a few tenths of an electron volt would have little influence upon $(e_M{}^0)S^2/\Delta e^0$. In principle, since $e_M{}^0$ values do not shift much for a given molecular system as the geometry is changed, we should be able to ignore it and garner trends from $(-)S^2/\Delta e^0$. Finally, we point out that the values of Δe^0 that we have available are not from the original **H** matrix, but rather from the transition state matrix.[32]

Table 6. Relative energetics for insertion of a ground-state calcium atom into "prepared" H_2

Term	Relative energy[a] (kcal mol^{-1})
Preparation of H_2 fragment	−3.4
Steric effect	0.5
Electronic effect	
symmetric representation (e.g. s, z^2, x^2-y^2)	−8.2
antisymmetric representation (e.g. xy)	13.0
Total	1.9

[a] A positive number indicates that the bent geometry is favoured.

geometry that we mentioned at the outset of our discussion on relative energies.

Angular geometry—Electric multipole expansion model

As mentioned in the introduction, the electric multipole expansion method[68] was first applied by Rittner[22] to the alkali halides and later by Guido and Gigli,[24] and Hildenbrand[25] to the alkaline earth dihalides. Guido and Gigli used the method to interpret both the geometry and the atomization energies. Hildenbrand used a truncated version (charge–charge and charge–dipole terms only) to rationalize the atomization energies. Both methods gave good results in comparison to experiment. Since we already have discussed the theoretical and experimental atomization energies, and since the published literature has established that the atomization energies can be understood well within the framework of the multipole expansion method, we focus our attention in this section on the ability of the multipole expansion to rationalize the *angular* geometry of the alkaline earth dihalides.

Following the approach of Hildenbrand, the variation in energy as a function of angle θ is given by the following expression for a metal cation (+2) and ligand anions (−1):

$$E(\theta) = -\frac{e^2}{r}\left(4-\frac{1}{2\cos\theta}\right) \quad \text{c–c}$$

$$-\frac{e^2}{r^4}\left[(2\sin^2\theta)\alpha_M+\left(4+\frac{1}{16\cos^4\theta}-\frac{1}{\cos\theta}\right)\alpha_X\right] \quad \text{c–d}$$

$$-\frac{6\alpha_M\alpha_X e^2}{r^7}\left[\sin^2\theta\left(2+\cos^2\theta-\frac{1}{2\cos\theta}\right)\right] \quad \text{d–d.}$$

The angle θ is related to the X—M—X bond angle, ϕ, by the relation $\theta = 90° - (1/2)\phi$. The M—X bond length is r, the dipole polarizability of the metal cation is α_M and that of the ligand anion is α_X. The first, second and third lines refer to the charge–charge, charge–dipole and dipole–dipole terms, respectively. The sign of the equation is such as to provide the energy *lowering* that results upon bringing the ions together to form the neutral molecule. We have not included dipole–dipole terms between the two ligands as this term is negligible for non-bonded atoms.[24] We also have neglected the (Born–Mayer) repulsive and (London) attractive terms that arise between the non-bonded ligands, since for the bond angles that we are interested in the distance between these two atoms is so large as to again make these terms unimportant.[23,24] Our expression is the same[69] as that given by Hildenbrand[25] except we have added the third term (d–d) in the multipole expansion. As we shall see this term is important if we are to make sense of the angular geometry of these molecules. In Scheme 3 we presented typical pictures that can be associated with the c–d and d–d terms. The first c–d picture on the left is associated with the "reverse" polarizability effect that was mentioned in the introduction. It is related to the $(2\sin^2\theta)\alpha_M$ term in the equation for $E(\theta)$.

Figure 1 shows the variation of each of the three terms as a function of angle for CaF_2, scaled

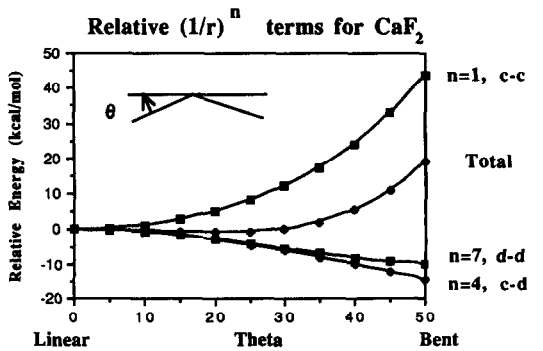

Fig. 1. Multipole expansion for CaF_2. See text for details.

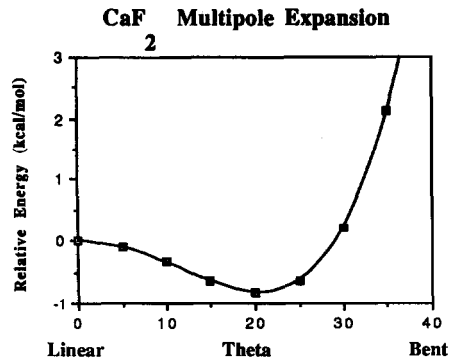

Fig. 2. Blow-up of the "total" energy term for the multipole expansion results of Fig. 1, for CaF_2.

relative to the value of the term for the linear molecule. The sum of these three terms is given also. The parameters that we have employed for this plot are: $r = 2.10$ Å, $\alpha_M = 0.95$ Å^3 and $\alpha_X = 1.0$ Å^3. The bond length is the same as that assumed by Hildenbrand and by Guido and Gigli. The α_M value corresponds to that chosen by Guido and Gigli and α_X to that used by Hildenbrand. (At this stage we take these values as representative. Other values could have been chosen for any of the three parameters but they would be close to these three. For example, Hildenbrand assumed a value for α_M of 0.70 Å^3; Guido and Gigli assumed a value of 1.05 Å^3 for α_X.)

Notice that the c–c term becomes *less* negative as the molecule is bent, exactly as expected due to the ligand–ligand repulsion. Meanwhile each of the higher order terms becomes *more* negative and are of about equal importance. The sum of the three gives the total energy $E(\theta)$, which on the scale of Fig. 1 seems not to show any energy lowering as a function of bond angle. However, a detailed blow-up as shown in Fig. 2 reveals that the energy drops by about 1 kcal mol^{-1} and reaches a minimum at a bond angle of about 140° before again increasing. This result is about the same as that provided by our quantum chemical results both for the depth of the well and the angle.

But how worthwhile is such a result for explanation of the bond angle? We contend that it is not worth much. For example, if we decrease the value of α_M from 0.95 to 0.70 Å^3 we find that no potential well is exhibited whatsoever! Guido and Gigli have argued that the model is fairly robust with respect to its ability to predict bond angles for different values of α_M. They used as their examples BaF_2 and $BaCl_2$. These are molecules that have a relatively deep potential well and so the effect of variation in one of the parameters is less important. For the case of CaF_2 we find that a slight variation in α_M is very important. Our point in presenting Figs 1 and 2 is simply to show the competing effects of the various terms in the multipole expansion, and to comment upon how sensitive the method is to changes in the parameters that are employed. We do not claim to have carried out a complete multipole expansion, but the terms that we have neglected are an order of magnitude less important than the ones we have included, as far as their angular dependence is concerned.*

We attempted to apply the multipole expansion method also to CeO_2.† The value of α_M was taken from Pauling (0.73 Å^3);[70] two values of α_X were employed: 2.75 and 3.88 Å^3.[49] A small value of α_X (1.93 Å^3) is suggested by the work of Duffy.[71] We also used a value of α_M that was 1.46 Å^3; in none of the six combinations of these parameters could we obtain an energy lowering upon bending the molecule.

In summary, we do not put much faith in the multipole expansion method as a reliable model to rationalize the angular geometry of the title molecules. This conclusion agrees with that of Coulson.[72] Furthermore, while it is true that the reverse polarization term $[(2\sin^2\theta)\alpha_M]$ is important in lowering the energy, the d–d effect is equally important as seen from Fig. 1. This also is clear from the detailed work of Guido and Gigli as shown in Fig. 4 of their paper.

Before leaving the electric multipole expansion model we note that the method is by no means outdated. Two areas in which it seems to be useful are in understanding the nature of weak *intermolecular* interactions[73a] and the bonding in singly charged metal clusters.[73b]

SUMMARY AND CONCLUSIONS

This work has shown that the simplest way to interpret the bent geometry of the title molecules is through *sd* hybridization (Scheme 1). The electric multipole expansion method is shown to be suspect for all the molecules, and unable to obtain the correct answer for CeO_2. Our results are in agreement

* Not only are the terms that we have neglected small, but they also tend to cancel one another. The Born–Mayer and negative dipole–negative dipole terms become more repulsive as the molecule is bent. The London term becomes more attractive.

† The form of the equations for the multipole expansion is exactly the same for CeO_2 as it is for MX_2, except that a factor of four is introduced into each term. Since we are interested only in change in energy with angle this has no effect in our treatment. The bond length that we used was 1.82 Å.

with the work of Schilling *et al.*[74] who obtain for CaH^+ a metal contribution to the bond which is 60.0% 4*s*, 16.3% 4*p* and 23.7% 3*d*. Their work further shows that, for CaH^+, the *intrinsic* bond strength of the 3*d* orbital is very high compared to that of the 4*s*, so that the 3*d* contribution to the bond strength is greater than indicated simply by the per cent composition of the orbital.

It is of interest to relate the present work to that of Group 12 divalent metal molecules such as $ZnCl_2$ or $Hg(CH_3)_2$ which are always linear about the metal atom.[5b,75] Our work[76] on such molecules emphasized that neither the unoccupied valence *p* orbital nor the fully occupied valence *d* orbital contribute much to the bonding, and so these molecules are best thought of in terms of three-centre four-electron bonds involving the metal *ns* orbital. A combination of *sp* hybridization and ligand–ligand repulsion effects work together to bring about the linear geometry for these molecules. The effect of the valence *d* orbitals on the bonding is minimal because these orbitals are fully occupied in the free atom. This conclusion is consistent with the work of Schilling *et al.*[74] who obtain for ZnH^+ a metal contribution to the bond which is 90.7% 4*s*, 8.9% 4*p* and 0.4% 3*d*. Finally, we point out that the "rule of thumb" that a central atom seeks to use as many orbitals as possible in bonding to the ligands cannot be rationalized on AOM grounds.

Acknowledgements—The authors thank Calvin College for a Calvin Research Fellowship to R.D.K. Financial support for this work also was provided by the Petroleum Research Fund, administered by the American Chemical Society, and by NATO through a Collaborative Research Grant. Appreciation also is expressed to A. J. Krominga and to D. L. Hildenbrand for assistance with the multipole expansion work. Thanks are also due to C. J. Marsden for communicating his results on CaF_2.

REFERENCES

1. I. R. Beattie, P. J. Jones and N. A. Young, *Angew. Chem. Int. Edn Engl.* 1989, **28**, 313.
2. It is interesting to note here that the geometry of d^0 ML_6 complexes has been the subject of discussion: (a) A. D. Cameron, G. Fitzgerald and M. C. Zerner, *Inorg. Chem.* 1988, **27**, 3439; (b) S. K. Kang, T. A. Albright and O. Eisenstein, *Inorg. Chem.* 1989, **28**, 1613; (c) P. M. Morse and G. S. Girolami, *J. Am. Chem. Soc.* 1989, **111**, 4114. There are some simple MX_3 molecules that also exhibit anomalous shapes (e.g. ScH_3): (d) C. A. Jolly and D. S. Marynick, *Inorg. Chem.* 1989, **28**, 2893.
3. H. A. Skinner, *Trans. Faraday Soc.* 1955, **51**, 1036.
4. (a) L. Wharton, R. A. Berg and W. Klemperer, *J. Chem. Phys.* 1963, **39**, 2023; (b) A. Buchler, J. L. Stauffer, W. Klemperer and L. Wharton, *J. Chem. Phys.* 1963, **39**, 2299; (c) A. Buchler, J. L. Stauffer and W. Klemperer, *J. Chem. Phys.* 1964, **40**, 3471; (d) A. Buchler, J. L. Stauffer and W. Klemperer, *J. Am. Chem. Soc.* 1964, **86**, 4544.
5. (a) M. C. Drake and G. M. Rosenblatt, *J. Electrochem. Soc.* 1979, **126**, 1387; (b) M. Hargittai, *Coord. Chem. Rev.* 1988, **91**, 35.
6. F. Ramondo, V. Rossi and L. Bencivenni, *Molec. Phys.* 1988, **64**, 513.
7. (a) M. Kaufmann, J. Muenter and W. Klemperer, *J. Chem. Phys.* 1967, **47**, 3365; (b) R. L. DeKock and W. Weltner, *J. Phys. Chem.* 1971, **75**, 514; (c) S. D. Gabelnick, G. T. Reedy and M. G. Chasanov, *J. Chem. Phys.* 1974, **60**, 1167.
8. I. R. Beattie, J. S. Ogden and R. S. Wyatt, *J. Chem. Soc., Dalton Trans.* 1983, 2343.
9. R. A. Andersen, R. Blom, J. M. Boncella, C. J. Burns and H. V. Volden, *Acta Chem. Scand.* 1987, **A41**, 24.
10. W. J. Evans, L. S. Hughes and T. P. Hanusa, *Organometallics* 1986, **5**, 1285.
11. (a) M. Elian and R. Hoffmann, *Inorg. Chem.* 1975, **14**, 1058; (b) M. Elian and M. M. L. Chen, *Inorg. Chem.* 1976, **15**, 1148; (c) M. Mancini, P. Bougeard, R. C. Burns, M. Mlekuz, B. G. Sayer, J. I. A. Thompson and M. J. McGlinchey, *Inorg. Chem.* 1984, **23**, 1072.
12. A. E. Alvarado-Swaisgood and J. F. Harrison, *J. Phys. Chem.* 1985, **89**, 5198.
13. T. A. Albright, J. K. Burdett and M.-H. Whangbo, *Orbital Interactions in Chemistry*, pp. 93–97. Wiley-Interscience, New York (1985).
14. R. L. DeKock and H. B. Gray, *Chemical Structure and Bonding*, pp. 180 and 476. University Science Books, Mill Valley, California (1989).
15. E. F. Hayes, *J. Phys. Chem.* 1966, **70**, 3740.
16. M. B. Hall, *Inorg. Chem.* 1978, **17**, 2261.
17. J. L. Gole, A. K. Q. Siu and E. F. Hayes, *J. Chem. Phys.* 1973, **58**, 857.
18. D. R. Yarkony, W. J. Hunt and H. F. Schaefer, *Molec. Phys.* 1973, **26**, 941.
19. (a) W. J. Pietro, B. A. Levi, W. J. Hehre and R. F. Stewart, *Inorg. Chem.* 1980, **19**, 2225; (b) K. E. Gottschalk, R. G. Hiskey, L. G. Pedersen and K. A. Koehler, *J. Molec. Struct.* 1982, **87**, 155.
20. Unpublished manuscript dated August, 1987. The authors are R. L. DeKock, R. B. Remington and H. F. Schaefer.
21. Private communication, Colin J. Marsden, University of Melbourne (January 1989); D. M. Hassett and C. J. Marsden, *J. Chem. Soc., Chem. Commun.* 1990, 667.
22. E. S. Rittner, *J. Chem. Phys.* 1951, **19**, 1030. In a footnote Rittner states that K. Fajans had been using polarization arguments qualitatively for a number of years.
23. (a) B. T. Gowda and S. W. Benson, *J. Phys. Chem.* 1982, **86**, 847; (b) B. T. Gowda, B. S. Sherigara and S. W. Benson, *J. Comp. Chem.* 1985, **6**, 93.
24. M. Guido and G. Gigli, *J. Chem. Phys.* 1976, **65**, 1307.
25. D. L. Hildenbrand, *J. Electrochem. Soc.* 1979, **126**, 1396.

26. M. Spoliti, G. De Maria, L. D'Alessio and M. Maltese, *J. Molec. Struct.* 1980, **67**, 159.
27. E. J. Baerends, D. E. Ellis and P. Ros, *Chem. Phys.* 1973, **2**, 41; E. J. Baerends and P. Ros, *Int. J. Quantum Chem. Symp.* 1978, **12**, 169.
28. L. Versluis and T. Ziegler, *J. Chem. Phys.* 1988, **88**, 322.
29. (a) T. Ziegler, W. Cheng, E. J. Baerends and W. Ravenek, *Inorg. Chem.* 1988, **27**, 3458; (b) T. Ziegler, V. Tschinke, L. Versluis, E. J. Baerends and W. Ravenek, *Polyhedron* 1988, **7**, 1625; (c) L. Versluis, T. Ziegler, E. J. Baerends and W. Ravenek, *J. Am. Chem. Soc.* 1989, **111**, 2018.
30. J. G. Snijders, E. J. Baerends and P. Vernooijs, Slater type basis functions for the whole periodic system, Internal Reports; Free University, Amsterdam, The Netherlands (1981); J. G. Snijders, E. J. Baerends and P. Vernooijs, *At. Nucl. Data Tables* 1982, **26**, 483.
31. P. M. Boerrigter, G. Te Velde and E. J. Baerends, *Int. J. Quantum Chem.* 1988, **33**, 87.
32. T. Ziegler and A. Rauk, *Theor. Chim. Acta* 1977, **46**, 1; T. Ziegler and A. Rauk, *Inorg. Chem.* 1979, **18**, 1558; T. Ziegler, J. G. Snijders and E. J. Baerends, *J. Chem. Phys.* 1981, **74**, 1271.
33. A. Becke, *J. Chem. Phys.* 1986, **84**, 4524.
34. V. Tschinke and T. Ziegler, *Density Matrices and Density Functionals* (Edited by R. M. Erdahl and V. H. Smith Jr). Reidel, Dordrecht, The Netherlands (1987).
35. T. Ziegler, V. Tschinke, E. J. Baerends, J. G. Snijders and W. Ravenek, *J. Phys. Chem.* 1989, **93**, 3050.
36. C. Linton, M. Dulick, R. W. Field, P. Carette and R. F. Barrow, *J. Chem. Phys.* 1981, **74**, 189.
37. V. V. Kasparov, Yu. S. Ezhov and N. G. Rambini, *Zh. Strukt. Khim.* 1980, **21**, 41.
38. J. C. Culberson, P. Knappe, N. Rosch and M. C. Zerner, *Theor. Chim. Acta* 1987, **71**, 21.
39. N. C. Baird, *Inorg. Chem.* 1989, **28**, 1224.
40. D. L. Hildenbrand, *J. Chem. Phys.* 1968, **48**, 3657.
41. J. Kordis and K. A. Gingerich, *J. Chem. Phys.* 1977, **66**, 483.
42. K. P. Huber and G. Herzberg, *Molecular Spectra and Molecular Structure IV. Constants of Diatomic Molecules*. Van Nostrand Reinhold, New York (1979).
43. P. E. M. Siegbahn, M. R. A. Blomberg and C. W. Bauschlicher, *J. Chem. Phys.* 1984, **81**, 1373; A. K. Rappe and T. H. Upton, *J. Chem. Phys.* 1986, **85**, 4400; K. Balasubramanian and M. Z. Liao, *J. Phys. Chem.* 1989, **93**, 89; K. Balasubramanian and Ch. Ravimohan, *J. Phys. Chem.* 1989, **93**, 4490; O. Novaro, J. Garcia-Prieto, E. Poulain and M. E. Ruiz, *J. Molec. Struct. (Theochem)* 1986, **135**, 79.
44. R. J. Ackermann and E. G. Rauh, *J. Chem. Phys.* 1974, **60**, 2266.
45. *Handbook of Chemistry and Physics*, 67th edn. CRC Press, Boca Raton, Florida (1986). These values are for D_{298}°.
46. B. M. Deb, *J. Chem. Ed.* 1975, **52**, 314.
47. The most comprehensive early treatment of hybrid orbitals is that given by Kimball: G. E. Kimball, *J. Chem. Phys.* 1940, **8**, 188. For *f* orbitals see: J. C. Eisenstein, *J. Chem. Phys.* 1956, **25**, 142. More recent treatments of the hybrid orbital concept may be found in the following three references: D. B. Cook and P. W. Fowler, *Am. J. Phys.* 1981, **49**, 857; W. Kutzelnigg, *J. Molec. Struct. (Theochem)* 1988, **169**, 403; C. Yang, *J. Molec. Struct. (Theochem.)* 1988, **169**, 1.
48. W. R. Wadt, *J. Am. Chem. Soc.* 1981, **103**, 6053.
49. P. Pyykkö, L. J. Laakkonen and K. Tatsumi, *Inorg. Chem.* 1989, **28**, 1801.
50. K. A. R. Mitchell, *Chem. Rev.* 1969, **69**, 157; T. B. Brill, *J. Chem. Educ.* 1973, **50**, 392; E. Magnusson and H. F. Schaefer, *J. Chem. Phys.* 1985, **83**, 5721; A. E. Reed and F. Weinhold, *J. Am. Chem. Soc.* 1986, **108**, 3586; C. Patterson and R. P. Messmer, *J. Am. Chem. Soc.* 1989, **111**, 8059.
51. C. E. Moore, *Atomic Energy Levels*, National Bureau of Standards, Circular 467, U.S. Government Printing Office, Washington, D.C., Vol. I, 1949; Vol. II, 1952; Vol. III, 1958. We have averaged the various levels of the lowest term that are derived from the specified configuration to obtain the numbers quoted in the text. Hayes[15] has averaged terms in his quoted numbers.
52. C. Froese Fischer, *Phys. Rev. A.* 1989, **39**, 963.
53. W. C. Martin, R. Zalubas and L. Hagan, *Atomic Energy Levels—The Rare Earth Elements*, NSRDS-NBS, No. 60, National Bureau of Standards, U.S. Department of Commerce, Washington, DC (1978).
54. M. Dolg, H. Stoll, A. Savin and H. Preuss, *Theor. Chim. Acta* 1989, **75**, 173.
55. R.W. Field, *Ber. Bunsenges. Phys. Chem.* 1982, **86**, 771.
56. D. R. Lloyd, *J. Chem. Ed.* 1986, **63**, 1986.
57. M. Dolg, H. Stoll and H. Preuss, *J. Chem. Phys.* 1989, **90**, 1730.
58. J. V. Ortiz and R. Hoffmann, *Inorg. Chem.* 1985, **24**, 2095.
59. P. Pyykkö and J.-P. Desclaux, *Accts Chem. Res.* 1979, **12**, 276; K. S. Pitzer, *Accts Chem. Res.* 1979, **12**, 271; D. R. McKelvey, *J. Chem. Ed.* 1983, **60**, 112; P. Pyykkö, *Chem. Rev.* 1988, **88**, 563.
60. T. A. Albright, J. K. Burdett and M.-H. Whangbo, *Orbital Interactions in Chemistry*, pp. 91–93. Wiley-Interscience, New York (1985).
61. J. K. Burdett, *Molecular Shapes*. Wiley-Interscience, New York (1980).
62. J. K. Burdett and T. A. Albright, *Inorg. Chem.* 1979, **18**, 2112.
63. T. A. Albright, J. K. Burdett and M.-H. Whangbo, *Orbital Interactions in Chemistry*, pp. 18–25. Wiley-Interscience, New York (1985). To obtain this expression we take the value of t from eq. (2.36) and apply the expression for EHT ($K = 2.0$) to Δ_{12}. Use this result in the expression for q_2 on p. 24.
64. J. K. Burdett, *Molecular Shapes*, p. 33. Wiley-Interscience, New York (1980).
65. J. K. Burdett, *Inorg. Chem.* 1975, **14**, 375.
66. C. E. Myers, L. J. Norman and L. M. Loew, *Inorg. Chem.* 1978, **17**, 1581.

67. E. J. Baerends and A. Rozendaal, *Quantum Chemistry: The Challenge of Transition Metals and Coordination Chemistry* (Edited by A. Veillard), p. 159. D. Reidel, Dordrecht, The Netherlands (1986).
68. A. Hinchcliffe, *Computational. Quantum Chemistry*, p. 68. John Wiley, New York (1988); A. D. Buckingham, *Adv. Chem. Phys.* 1967, **12**, 107.
69. Since we have neglected the Born–Mayer repulsion term this amounts to setting $\rho = 0.0$ in the equations of Hildenbrand. A useful reference to the Born–Mayer expression is: W. E. Dasent, *Inorganic Energetics*, p. 76. Penguin books, Middlesex, U.K. (1970); the 2nd edition of this book published by Cambridge University Press in 1982 provides slightly less detail.
70. L. Pauling, *Proc. R. Soc.* (*Lond.*) 1927, **A114**, 191; see also, J. R. Tessman, A. H. Kahn and W. Schockley, *Phys. Rev.* 1953, **92**, 890.
71. J. A. Duffy, *J. Solid State Chem.* 1986, **62**, 145. Using eq. (2) of Duffy's paper, we obtain a value of 1.93 $Å^3$ for the polarizability of the oxygen atom in CeO_2.
72. C. A. Coulson, in *Proc. of the Robert A. Welch Foundation, XVI., Theoretical Chemistry* (Edited by W. O. Milligan), pp. 61–117. Robert A. Welch Foundation, Houston, Texas (1973); C. A. Coulson, *Isr. J. Chem.* 1973, **11**, 683. Coulson did not allow for large polarizabilities of the metal cations, nor did he examine the dipole–dipole terms that we have included in our treatment. He dismissed the multipole expansion method out of hand as a method to understand the bent geometry of the MX_2 molecules.
73. (a) C. E. Dykstra, *Accts Chem. Res.* 1988, **21**, 355; C. E. Dykstra, *J. Am. Chem. Soc.* 1989, **111**, 6168; (b) G. Durand, *J. Chem. Phys.* 1989, **91**, 6225.
74. J. B. Schilling, W. A. Goddard III and J. L. Beauchamp, *J. Phys. Chem.* 1987, **91**, 5616.
75. M. Hargittai, J. Tremmel and I. Hargittai, *Inorg. Chem.* 1986, **25**, 3163.
76. R. L. DeKock, E. J. Baerends, P. M. Boerrigter and R. Hengelmolen, *J. Am. Chem. Soc.* 1984, **106**, 3387 and 6119.

Polyhedron Vol. 9, No. 15/16, pp. 1935–1937, 1990
Printed in Great Britain

0277–5387/90 $3.00+.00
Pergamon Press plc

ATOM SITE PREFERENCE IN S_4N_4*

KIMBERLY A. SCHUGART

Department of Chemistry and Biochemistry, California State University, Long Beach, CA 90840, U.S.A.

Abstract—The question of atom site preference as it pertains to the observed and inverse (not observed) structures of S_4N_4 is investigated from the standpoint of electronic structure theory. An analysis is made through an understanding of geometric constraints in simplified systems and extrapolation to the larger question of factors controlling structure is discussed.

The most fundamental issue of structural inorganic chemistry is the question of atom site preference. For a given structural framework of a molecule, polymer or solid, different arrangements of different types of atoms or atomic groupings can be imagined. In the case of S_4N_4 two sites exist. One is two-fold (a two-coordinate site) while the other is three-fold (a three-coordinate site). This experimentally observed form of the structure is shown in Fig. 1(a). In observed S_4N_4, sulphur occupies the three-fold positions while nitrogen occupies the two-fold sites. However, there is no obvious reason why the inverse structure (nitrogen in the three-fold position and sulphur in the two-fold position) could not exist, though its existence has not been detected. This inverse arrangement is shown in Fig. 1(b). In one sense the inverse structure is more plausible as the ground state of nitrogen is ^4S, making it a likely candidate for the three-fold position, and the ground state of sulphur is ^3P, placing it as a likely possibility for the two-fold site.

THEORETICAL APPROACH

The Gaussian 88[1] electronic structure methodology run on a Multiflow Trace 14 supercomputer generated the wavefunctions used in this study from a 6-31G basis set. All species considered were geometry optimized at the single determinant level. Constraints to maintain D_{2d} symmetry for observed and inverse structures of S_4N_4 and mirror plane symmetry in the fragment systems were the only restrictions to the optimizations.

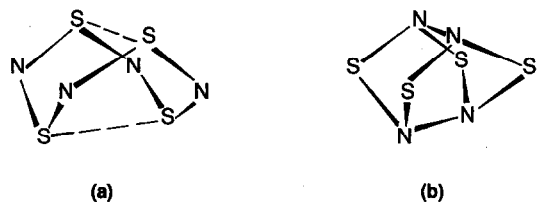

Fig. 1. Observed (a) and inverse (b) structures of S_4N_4.

RESULTS AND DISCUSSION

The atom site preference question has been treated through semi-empirical[2] and non-rigorous *ab initio*[3] approaches, as well as through topological[4] and group theoretical[5] methods. (Traditionally, the terms "delocalized bond" and "free electron model" categorize the computational and mathematical approaches, respectively.[6]) Here, the question is examined through a rigorous *ab initio* approach.

Table 1 compares the experimental structure with a geometry optimized single determinant wavefunction structure. The angles about nitrogen and sulphur are in close agreement with the theoretical

Table 1. Data for observed (experimentally determined) and inverse (theoretically determined) S_4N_4

	Experimental	Theoretical
Angles (in deg)		
S—N—S	115[8] and 113[9]	113.8
N—S—N	102[8] and 105[9]	104.3
Distances (in Å)		
N—S	1.62[8,9]	1.60
S—S	2.58[8,9]	2.58

* Dedicated to Professor Richard F. Fenske in appreciation of his fundamental contributions to molecular orbital theory and his inspiration as my PhD advisor.

results (roughly 114° for S—N—S and 104° for N—S—N) lie between the two sets of experimentally determined results (113 and 115° for S—N—S and 105 and 102° for N—S—N). Likewise, the results for the intramolecular distances show a good match between experimental (1.62 Å for N—S and 2.58 Å for S—S) and theoretical (1.60 Å for N—S and 2.58 Å for S—S) data. Table 2 lists the calculated results for the hypothetical inverse structure, the structure that is not observed experimentally. The S—N distance is lengthened considerably and the angles about sulphur and nitrogen are much smaller than in the observed structure. Both of these structural changes are expected.

The structural results of the calculations can be deduced from a comparison of Lewis dot structures for S_4N_4 and its inverse. The dot structures are shown in Figs 2 and 3. The extensive electron delocalization and concomitant N—S multiple bond character in the observed structure is clear through the type and number of resonance structures that must be used to describe the bonding as shown in Fig. 2. The observed and calculated angles in the observed structure correspond to the hybridization that is expected as well. While four structures are shown, many more might be drawn as well. Contrastingly, the inverse structure, with single S—N bonds is adequately represented by one diagram, shown in Fig. 3. The angles about sulphur and nitrogen in the inverse arrangement point to the 90.0° arrangements that characterize angles about atoms which bond to other atoms primarily through *p* orbitals. Interestingly, the total energy of the inverse, unobserved structure, −1807.1691 hartrees, is lower than the total energy of the observed structure, −1807.0737 hartrees. The 95 millihartree difference between these two values can be understood as the inadequacy of the single determinant wavefunction to truly represent the many resonance structures that are involved in a complete description of the molecule's electronic structure. As the data for both the observed and inverse structures appear reasonable in terms of molecular geometries, and the energies of the two are close in the limit of the single determinant wavefunction, the question of atom site preference must be addressed by breaking the compound into smaller fragments, to assess more simply the forces involved in the larger structure.

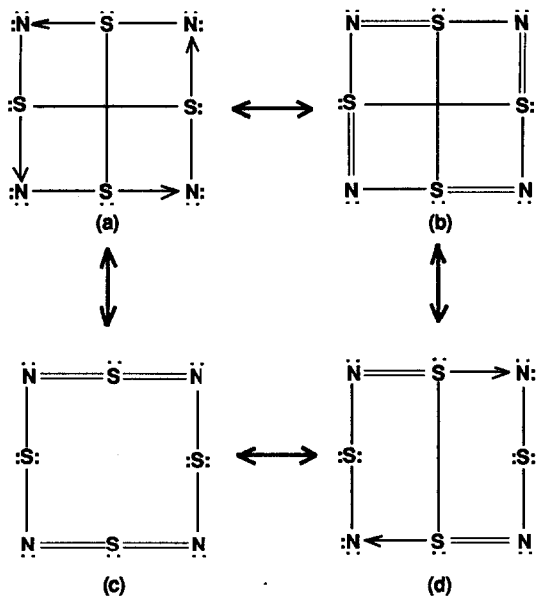

Fig. 2. Lewis dot representations of electronic structure of observed S_4N_4.

A pivotal difference that can be analysed easily lies in the bonding at the two-fold sites in the observed and inverse structures. The two-fold position is occupied by nitrogen in the observed structure and by sulphur in the inverse one. The angle at nitrogen in the observed structure is stretched somewhat with respect to a tetrahedral angle (113.8 vs 109.5°), while the angle at sulphur in the inverse structure of S_4N_4 is compressed to 83° relative to the 90° angles for *p* orbital bonding orientations. Two artificial fragment structures can be constructed to mimic the environments of the sulphur and nitrogen in the two-fold positions they occupy in the inverse and observed structures respectively, and these are shown in Fig. 4. Figure 4(a) shows the fragment used to analyse the two-fold position for the nitrogen in the observed structure and Fig. 4(b) shows the one used to mimic the two-fold position for sulphur in the inverse structure. Both frag-

Table 2. Data for inverse (theoretically determined) S_4N_4

Angles (in deg)	
S—N—S	95.0
N—S—N	83.0
Distances (in Å)	
N—S	1.86
S—S	2.75

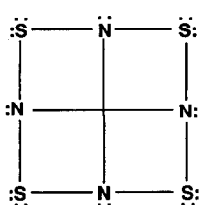

Fig. 3. Lewis dot representation of inverse S_4N_4.

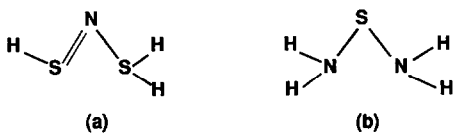

Fig. 4. Fragment structures for two-fold sites: (a) two-fold site for observed S_4N_4 and (b) two-fold site for inverse S_4N_4.

ments are described as ground-state singlet wavefunctions with hydrogen atoms tying-off electrons that would otherwise serve to connect the fragment to the rest of the structure. By optimizing the angles for these two systems and then comparing the energies of the optimized angle wavefunctions to the energies for the angles as they are constrained for these two systems in the larger parent molecules, an assessment of the energetic costs to form the entire molecule is derived.

The data for the angle optimization and cost to achieve the geometry of the actual molecular structure is presented in Table 3. For the observed structure, the optimum angle about the two-fold nitrogen site is 105.2°. Stretching this angle to the 113.8° of the observed molecule costs 0.002 hartree. The potential for the angle opening is soft and little energy is required to achieve it. For the inverse structure, the optimum angle about the two-fold sulphur site is 106.1°. A difference of 23° exists between it and the 83° angle of the optimized structure. The energetic costs to compress the fragment angle is substantial; it requires 33 millihartrees to do so. All told then, while virtually no energy input is required to alter the two-fold site fragment for the observed structure to its parent molecular geometry, more than 30 millihartrees is required to alter the two-fold site fragment for the inverse structure to its parent molecular geometry. By this analysis, although the total energies of the observed and inverse strucures are close, the actual energetic cost to building the molecule in the inverse structure will be substantially higher. The conclusion that can be drawn is not that the inverse structure will never be observed, but rather that a markedly different set of conditions is required to synthesize it.

Table 3. Data for optimized angles of fragment structures and costs to achieve geometry of parent structures

Species	Optimum angle (deg)	Parent structure angle (deg)	Difference (hartrees)
Fragment of observed	105.2	113.8	+0.002
Fragment of inverse	106.1	83.0	+0.033

CONCLUSION

Based upon the analysis of the two-fold sites in S_4N_4 and its inverse, the reason for the site preference of the observed over the inverse structure is the much greater energetic cost encountered in meeting the geometric requirements of the inverse structure. This argument, in its most abstract sense suggesting that an investiture of energy to overcome a barrier will yield an alternative result, can be seen as reducing the question of atom site preference to one of kinetic control. It is important to recognize, though, that kinetic control is not exclusive of thermodynamic control and only through further study of S_4N_4 can a more complete determination of the reasons for site preference in this molecule be made.

Acknowledgement—The author gratefully acknowledges travel support from California State University, Long Beach.

REFERENCES

1. M. J. Frisch, M. Head-Gordon, H. B. Schlegel, K. Raghavachari, J. S. Binkley, C. Gonzales, D. J. Defrees, D. J. Fox, R. A. Whiteside, R. Seeger, C. F. Melius, J. Baker, R. Martin, L. R. Kahn, J. J. P. Stewart, E. M. Fluder, S. Topiol and J. A. Pople, Gaussian 88. Gaussian Inc., Pittsburgh, PA (1988).
2. Main group and transition metal cluster bonding have been investigated semi-empirically in: (a) R. Hoffmann, B. E. R. Schilling, R. Kau, H. D. Keasz and D. M. P. Mingos, *J. Am. Chem. Soc.* 1978, **100**, 6088 ; (b) B. E. R. Schilling and R. Hoffmann, *J. Am. Chem. Soc.* 1979, **101**, 3546.
3. Non-rigorous *ab initio* approaches have been used to address the problems of bonding in bare metal and ligated cluster structures: (a) B. K. Teo, M. B. Hall, R. F. Fenske and L. F. Dahl, *J. Organomet. Chem.* 1974, **70**, 413; (b) P. T. Cheskey and M. B. Hall, *Inorg. Chem.* 1981, **20**, 4419; (c) D. E. Sherwood Jr and M. B. Hall, *Inorg. Chem.* 1982, **21**, 3458.
4. Graph theoretical approach and applications: (a) R. B. King and D. H. Rouvray, *J. Am. Chem. Soc.* 1977, **99**, 7834; (b) R. B. King, *Inorg. Chim. Acta* 1981, **49**, 237; (c) R. B. King, *Polyhedron* 1982, **1**, 132.
5. D. B. Redmond, C. M. Quinn and J. G. R. McKiernan, *J. Chem. Soc., Dalton Trans. II* 1983, **79**, 1791.
6. D. M. P. Mingos and R. L. Johnston, *Struct. Bond.* 1987, **68**, 29.
7. J. K. Burdett and S. K. Lee, *J. Am. Chem. Soc.* 1985, **107**, 3050; (b) *op. cit.* 3063; (c) J. K. Burdett, S. J. Lee and T. J. McLarnan, *J. Am. Chem. Soc.* 1985, **107**, 3083.
8. D. Clark, *J. Chem. Soc.* 1952, 1615.
9. B. D. Sharma and J. Donahue, *Acta Cryst.* 1963, **16**, 891.

Polyhedron Vol. 9, No. 15/16, pp. 1939–1947, 1990
Printed in Great Britain

0277–5387/90 $3.00+.00
© 1990 Pergamon Press plc

THE ELECTRONIC STRUCTURE OF SOME RUTHENIUM(II) COMPLEXES RELATED TO $[Ru(bipy)_3]^{2+}$: AN INVESTIGATION OF THE STEPWISE REPLACEMENT OF *N,N*-DONORS BY *C,N*-DONORS*

EDWIN C. CONSTABLE and CATHERINE E. HOUSECROFT

University Chemical Laboratory, Lensfield Road, Cambridge CB2 1EW, U.K.

Abstract—An analysis of the electronic structures of members of the series of complexes $[Ru(bipy)_{3-n}(ppy)_n]^{(2-n)+}$ (bipy = 2,2′-bipyridine and Hppy = 2-phenylpyridine) is presented. The cyclometallated complexes (i.e. those in which one or more $[ppy]^-$ replace bipy ligands) exhibit a distinct separation of Ru—C and Ru—N σ-bonding character, and in *cis*-$[Ru(bipy)(ppy)_2]$, further separation of bonding character occurs to give MO's which possess *either* Ru—C, Ru—$N_{[ppy]^-}$, *or* Ru—N_{bipy} components. Comparisons of the *cis*- and *trans*-isomers of $[Ru(bipy)(ppy)_2]$ and of the *fac*- and *mer*-isomers of $[Ru(ppy)_3]^-$ suggest that the observed experimental preference for *cis*- over *trans*- and *fac*- over *mer*-structures may be due to the enhanced σ-donating ability of the carbon atom when it resides *trans* to a nitrogen rather than carbon donor.

The photolysis and photochemical properties of the complex cation $[Ru(bipy)_3]^{2+}$ have been the subject of intensive investigation in the past decade.[1] Particular interest has centred upon the possibilities of using this species as a primary photocatalyst in solar energy photoconversion systems, and numerous chemical modifications involving variation of the metal centre and/or the ligand set have been described. Other transition metal tris(2,2-bipyridine) complexes have been studied, and iridium(III) complexes have proved to possess novel chemical and useful photophysical properties.[2] Complexes nominally formulated as $[Ir(bipy)_3]^{3+}$ have been known since 1959, but have been shown to possess anomalous properties. The anomalies are associated with the formation of cyclometallated complexes in which a bipy ligand is bonded to the metal in a *C,N*-mode. The cyclometallated complex exhibits long luminescence lifetimes in fluid solution and has led us and others to investigate the properties of transition metal complexes incorporating cyclometallated ligands. The ligand Hppy forms cyclometallated complexes in which the $[ppy]^-$ anion may be formally regarded as a *C,N*-donor analogue of bipy (Fig. 1).[3] The introduction of the *C,N*-donor ligand has a dramatic effect upon both the ground- and excited-state redox and electronic properties of the complexes.[4–6] In order to probe the origins of the ground-state effects and to investigate the electronic consequences of the sequential introduction of the cyclometallated ligands we have performed Fenske–Hall quantum chemical calculations upon the series of ruthenium(II) complexes $[Ru(bipy)_{3-n}(ppy)_n]^{(2-n)+}$ (n = 3, 2, 1, 0). A particular interest was to determine whether the spatial arrangement of the cyclometallated ligands in the complexes with n = 2 and 3 greatly perturbed the electronic properties. This is of considerable importance as frequently only one isomer is available from the synthetic routes adopted. The results determined here for the ruthenium(II) complexes (not all of which are known experimentally) are expected to be applicable by analogy to other isoelectronic and isostructural series incorporating $[ppy]^-$ and bipy ligands.

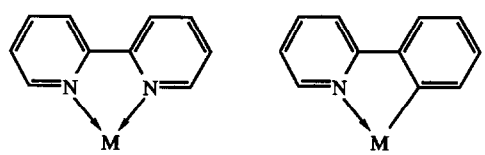

Fig. 1. *N,N*-coordination mode of bipy compared to *C,N*-mode of coordination of the 2-pyridylphenyl ligand, $[ppy]^-$.

* This paper is dedicated to Professor Dick Fenske on the occasion of his retirement.

EXPERIMENTAL

The Fenske–Hall[7,8] quantum chemical technique was used to examine the bonding in $[Ru(bipy)_3]^{2+}$ (**I**), $[Ru(bipy)_2(ppy)]^+$ (**II**), *cis*-$[Ru(bipy)(ppy)_2]$* (**III**), *trans*-$[Ru(bipy)(ppy)_2]$ (**IV**), *fac*-$[Ru(ppy)_3]^-$ (**V**) and *mer*-$[Ru(ppy)_3]^-$ (**VI**). In each case, a four fragment transformed orbital basis set was generated such that the interaction of each ligand with the metal ion could be examined. Positional coordinates for the complexes were taken from those previously reported in structural determinations of salts of the $[Ru(bipy)_3]^{2+}$[9] and isomorphous $[Os(bipy)_3]^{2+}$[10] complex cations. The introduction of the cyclometallated $[ppy]^-$ ligand is known to have no effect upon the overall crystallographic symmetry or individual M—N distances in the $[Rh(bipy)_2(ppy)]^{2+}$ dication[11] which exhibits a six-fold disorder.

The Fenske–Hall calculations employed single-ζ Slater functions for the 1*s* and 2*s* functions of carbon and nitrogen. The exponents were obtained by curve-fitting the double-ζ functions of Clementi[12] while maintaining orthogonal functions; the double-ζ functions were used directly for the 2*p* orbitals. An exponent of 1.16 was used for hydrogen. The ruthenium basis functions were augmented by 5*s* and 5*p* functions with exponents of 2.20;[13] ruthenium functions were chosen for the (+1) oxidation state since these provided a more reasonable charge distribution in line with the Pauling Electroneutrality Principle than results for those using the (+2) oxidation state.

RESULTS AND DISCUSSION

Ligand frontier orbitals

An appreciation of the differences in the bonding capabilities of the bipy and $[ppy]^-$ ligands is fundamental to an investigation of the bonding in compounds **I**–**VI**. Energies and orbital characteristics of the frontier MO's of the two ligands are depicted in Fig. 2. In bipy, MO's 28 and 29 (HOMO) are the in- and out-of-phase combinations of nitrogen atom lone pairs; for each MO, molecular symmetry dictates that there is a 50% contribution from each nitrogen-based orbital. The introduction of carbon in place of nitrogen reduces the symmetry of the ligand, and the effect upon the frontier MO's is quite dramatic. The HOMO of $[ppy]^-$ possesses

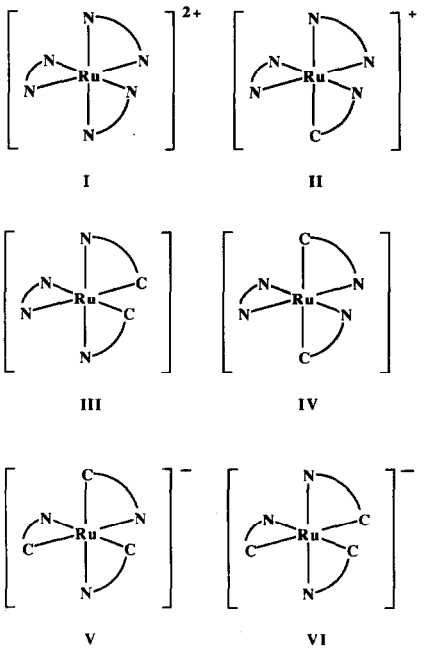

> 95% carbon character while the nitrogen lone pair character is localized in MO 28. Figure 2 illustrates that the energy separation of the donor orbitals 28 and 29 is far greater in $[ppy]^-$ than in

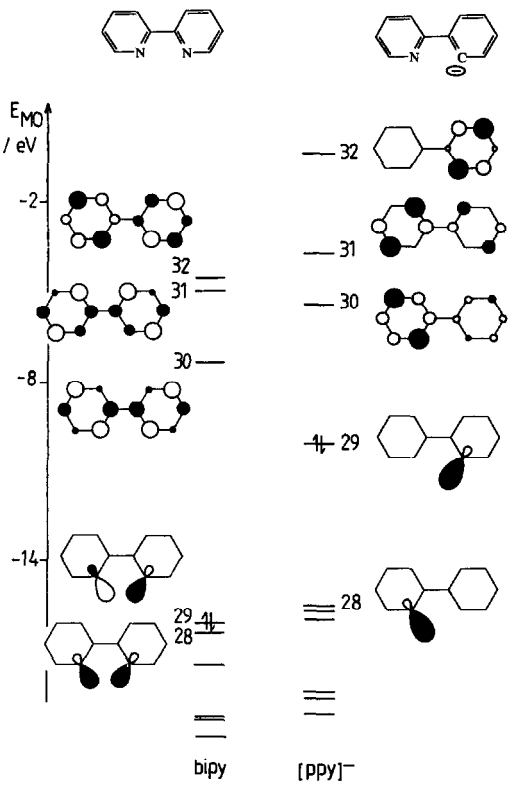

Fig. 2. Comparison of the frontier MO's of bipy and $[ppy]^-$. The MO energies are taken from the Fock matrix of complex **II**.[14] The π-systems of the vacant MO's are represented as a projection down onto the bipy and $[ppy]^-$ rings.

* There are 2 possible isomers of $[Ru(bipy)(ppy)_2]$ in which the C atoms are *cis* with respect to one another, **III** and **VII**. Experimental data are consistent only with structure **III**; see ref. 5.

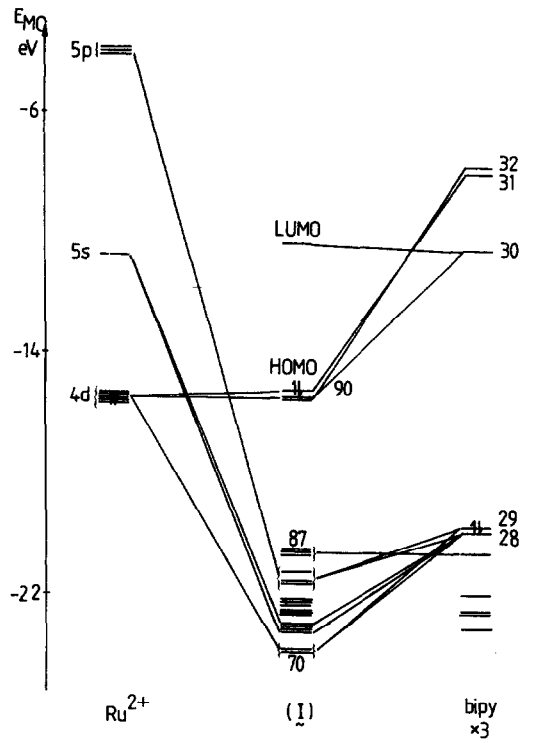

Fig. 3. Orbital correlation diagram for the interaction of three bipy ligands with Ru^{2+} in **I**. Since the three ligands are all chemically equivalent, the MO's of only one bipy is shown. The fragment orbital energies are taken from the Fock matrix of complex **I**.[14] Contributions made by each of MO's 30–32 to MO's 88–90 $\leqslant$ 6%.

bipy and this observation is critical to the discussion which follows. A similar partitioning of orbital character for the nitrogen and carbon donor rings occurs for the unoccupied ligand MO's represented in Fig. 2, where the relative sizes of the 2*p* lobes correspond to atomic orbital coefficients.

The calculated atomic charge distribution for the free ligands results in each nitrogen atom of bipy carrying a charge of −0.295. This remains essentially the same in $[ppy]^-$ (−0.297), leaving the carbon donor site to carry most of the overall negative charge (−0.748).

Bonding in $[Ru(bipy)_3]^{2+}$ (I)

The interaction of the three bipy ligands with the ruthenium centre follows the classical pattern of bonding for an approximately octahedral set of six donor atoms as illustrated in Figs 3 and 4. Linear combinations of bipy MO's 28 and 29 from the three ligands interact with the metal $4d_{x^2-y^2}$, $4d_{z^2}$, 5*s* and 5*p* orbitals to provide the Ru—N σ-bonds; 92% of the total metal–ligand Mulliken overlap population involves these interactions. The molecular symmetry of **I** is D_3 rather than O_h, and hence the interaction of the metal $5p_x$, p_y and p_z orbitals with the bipy frontier orbitals gives rise to a_2 (MO 84) and *e* (MO 82/83) bonding MO's rather

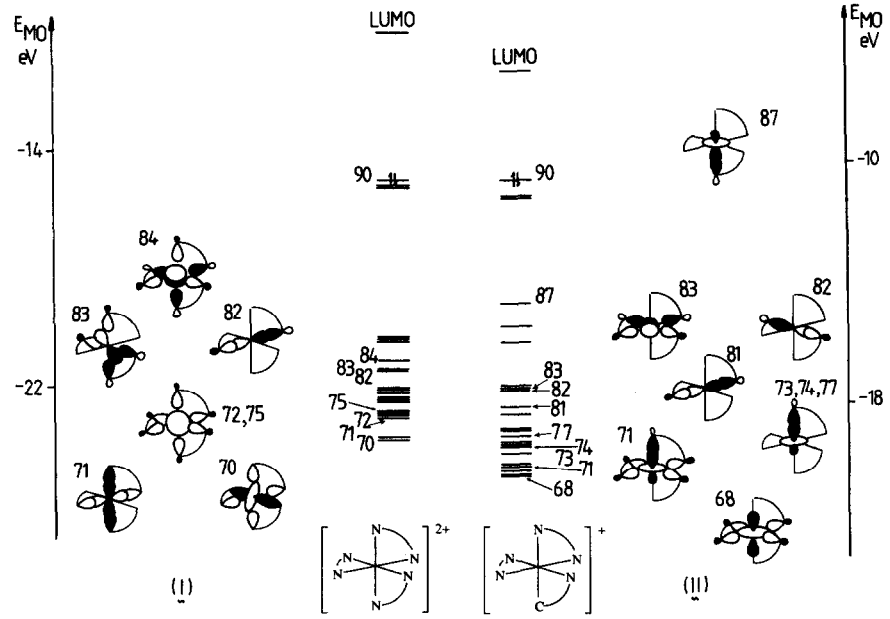

Fig. 4. Perturbation of the MO's of **I** upon substitution of one bipy for the $[ppy]^-$ ligand, i.e. generation of **II**. The energy scales of **I** and **II** have been shifted linearly with respect to each other to facilitate easy comparison of the MO's. MO's 88–90 possess π-backbonding character. Where one diagrammatic representation is assigned to more than one MO, the character is spread through the stated MO's and mixes with the other (Ru—L non-bonding) ligand, L, MO's.

than a t_{1u} set; similarly, MO's 88–90 have a_1 and e symmetries rather than t_{2g}.[15] Within the framework of the Fenske–Hall method, the character of the bonding interaction between the metal 5*s* orbital and in-phase ligand MO's 28 appears both in MO's 72 and 75 of **I** (Fig. 4).

Metal-to-ligand backbonding accounts for 8% of the total Ru–bipy Mulliken overlap population and the lowest unoccupied ligand MO's (30–32) together gain 0.223 electrons per bipy ligand, 67% of this being accepted by the original LUMO.

Comparison of $[Ru(bipy)_2(ppy)]^+$ **(II)** *with* **I**

The degree to which the molecular orbitals of **I** are perturbed upon the substitution of $[ppy]^-$ for one bipy ligand is illustrated in Fig. 4. Firstly, with respect to the HOMO, the lowest unoccupied MO's of **II** tend to be lower in energy than those in **I**. This trend is consistent with the experimental observation that there is a shift to lower energy for transitions in the absorption spectrum in going from **I** to **II**.[16]

The second important feature is that the $Ru—C_{[ppy]^-}$ character is essentially localized in one orbital, MO 87. In **I**, MO's 85–87 comprise a set of ligand based orbitals derived from MO 27 (the highest occupied π-orbital) of each bipy ligand (Fig. 3); this set is identified as MO's 84 through 86 in **II**. Lying above these, but below the Ru—L π-backbonding MO's, is MO 87, the character of which is 90% $Ru—C_{[ppy]^-}$ bonding (Fig. 4). On the other hand, $Ru—N_{[ppy]^-}$ bonding character appears in orbitals which are also $Ru—N_{bipy}$ bonding as shown schematically in Fig. 4. The partitioning of $Ru—C_{[ppy]^-}$ and $Ru—N_{[ppy]^-}$ character in **II** reflects the separation of carbon and nitrogen donor atom character in the free $[ppy]^-$ ligand. The HOMO of $[ppy]^-$, comprising wholly carbon rather than nitrogen σ-donor character and being significantly higher in energy than the nitrogen σ-donor MO 28 (Fig. 2), will interact with the ruthenium AO's to generate $Ru—C_{[ppy]^-}$ bonding orbitals which are higher in energy than the $Ru—N_{[ppy]^-}$ containing MO's.

A third effect resulting from the substitution of one ligand in **I** is, naturally, a change in the σ-donating and π-accepting abilities of the ligands. These trends are shown in Figs 5 and 6, respectively. The occupancies of ligand MO's 28 and 29 after complex formation are a measure of the σ-donating ability of the ligand. Conversely, the occupancies of ligand MO's 30–32 indicate the degree to which ruthenium → ligand π-backbonding occurs. Figure 5 illustrates that the introduction of a $[ppy]^-$ ligand, **I** to **II**, reduces the donor capacity of each remaining bipy ligand. However, the change is slight. Looking now at the right-hand side of Fig. 5, we observe that charge transferred from $[ppy]^-$ MO 29 greatly exceeds that lost by $[ppy]^-$ MO 28. This is expected on the grounds of electronegativities; the carbon

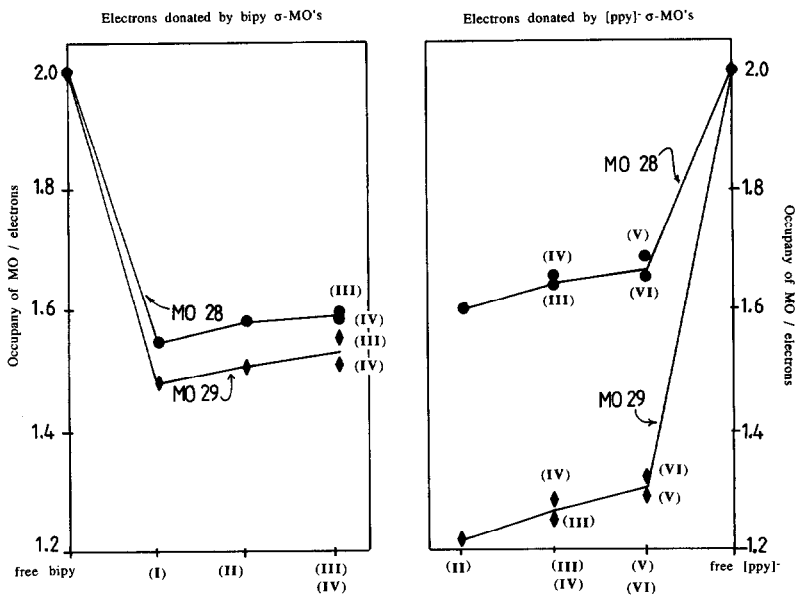

Fig. 5. Donor abilities of bipy and $[ppy]^-$ ligands in complexes **I**–**VI**. Reading from left to right, the diminishing ability of the bipy ligands is observed as increasing substitution occurs. From right to left, the increasing ability of the $[ppy]^-$ ligand to donate σ-electron density as a function of complex composition is seen. Where like donor sites are geometrically distinct, average values are given unless significant variation is seen.

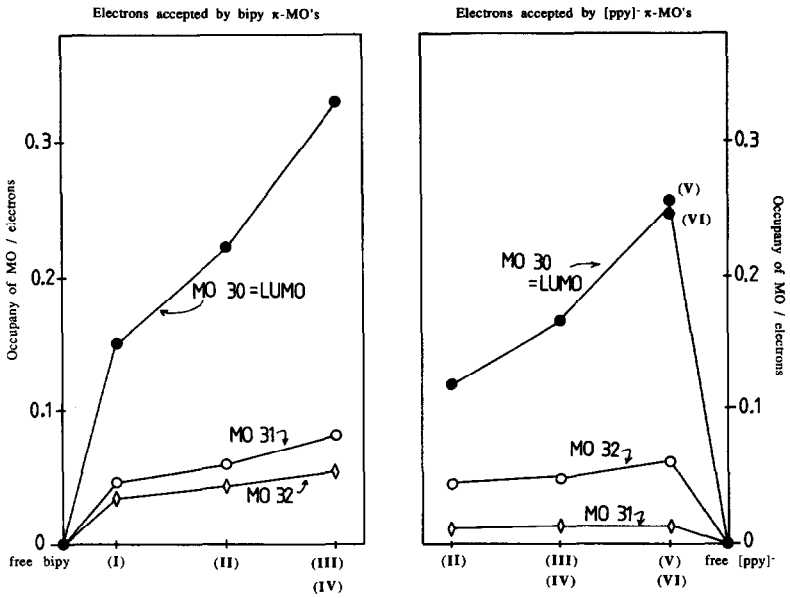

Fig. 6. Acceptor ability of bipy and $[ppy]^-$ ligands as a function of substitution in $[Ru(bipy)_{3-n}(ppy)_n]^{(2-n)+}$ ($n = 0, 1, 2, 3$).

(localized in MO 29) is a better σ-donor than the nitrogen atom (localized in MO 28). The σ-donating ability of $[ppy]^-$ MO 29 greatly exceeds either of bipy MO's 28 and 29. However, the final atomic charge on the ruthenium atom does not change significantly in going from complex **I** to **II** (Table 1).* The reason for this is apparent on inspection of Fig. 6; the π-accepting ability of the bipy ligand is quite dramatically enhanced upon the introduction of the $[ppy]^-$ ligand, and together, the two bipy ligands in **II** remove the excess electron density pumped on to the metal centre by the $[ppy]^-$ ligand.

General trends accompanying stepwise substitution of $[ppy]^-$ *for* bipy *ligands*

The trends in orbital energies, composition and charge distribution discussed above continue

Table 1. Atomic charges for atoms in the coordination sphere in complexes **I–VI**

	Net atomic charge/electrons			
Complex	Ru	N_{bipy}	$N_{[ppy]^-}$	$C_{[ppy]^-}$
I	+0.169	−0.079		
II	+0.162	−0.101[a] −0.073[b]	−0.085	−0.266
III	+0.161	−0.104	−0.083	−0.264
IV	+0.159	−0.070	−0.080	−0.302
V	+0.154		−0.103	−0.273
VI	+0.154		−0.080 (2N)[c] −0.107 (1N)[a]	−0.308 (2C)[d] −0.269 (1C)[e]

[a] N *trans* to C.
[b] N *cis* to C.
[c] N *trans* to N.
[d] C *trans* to C.
[e] C *trans* to N.

*Absolute atomic charges and related properties are dependent on the ruthenium basis functions chosen, but the trends are independent.

smoothly as bipy ligands are sequentially replaced by $[ppy]^-$ ligands. (A detailed analysis of the bonding in isomers **III** vs **IV** and in **V** vs **VI** is given below.) Consider first the charge distributions. Figure 5 illustrates two important features: (i) the donor ability of the nitrogen atom of the $[ppy]^-$ ligand is always less than that of the nitrogen atoms of bipy, and (ii) the σ-electron donating capacity of the carbon site in $[ppy]^-$ always exceeds that of nitrogen. Corresponding to these differences is a differential in the π-acceptor properties of the two ligands (Fig. 6), controlled largely by the availability of the LUMO. As shown in Fig. 1, the LUMO for $[ppy]^-$ is essentially localized on the nitrogen-containing ring, thus making the nitrogen atom of this ligand a more effective site for π-acceptance than the metal associated carbon atom. The occupancies of MO's 30–32 are represented in Fig. 6 as a function of ligand substitution in $[Ru(bipy)_{3-n}(ppy)_n)]^{(2-n)+}$ ($n = 0, 1, 2, 3$). The π-accepting ability of the bipy ligand (dominated by the rôle of the LUMO) *increases* with the degree of substitution, n, and this increase compensates for the lower π-accepting and for the increased σ-donating capability of the $[ppy]^-$ ligand. Compared to its rôle in the mixed ligand complexes, each $[ppy]^-$ ligand in the tris(2-pyridylphenyl) complex functions more efficiently as a π-acceptor. This state arises from the fact that $[ppy]^-$ ligands *alone* must now satisfy the need of the metal ion to offload residual negative charge and hence satisfy the Electroneutrality Principle.

Trends in orbital energies are influenced by the variation in overall charge of the complexes, and, as expected, the energy of the HOMO becomes less negative as $[ppy]^-$ ligands replace bipy ligands. The observed trend of higher energy HOMO's across the series $[Ru(bipy)_{3-n}(ppy)_n]^{(2-n)+}$ ($n = 0, 1, 2, 3$), is consistent with the increasing ease with which the complexes are oxidized.*

From **I** to **II**, we noted that $Ru—C_{[ppy]^-}$ and $Ru—N_{[ppy]^-}$ bonding character is partitioned, the former being localized in MO 87 of **II** (Fig. 4), while $Ru—N_{[ppy]^-}$ and $Ru—N_{bipy}$ characters mix together. This pattern continues as further ligand substitution occurs. The $Ru—C_{[ppy]^-}$ bonding orbital(s) is(are) always distinct from and lie(s) at higher energy with respect to those containing $Ru—N_{[ppy]^-}$ and $Ru—N_{bipy}$ bonding character. The C/N separation is most noticeable in *fac*-$[Ru(ppy)_3]^-$ (**V**) (see below).

Comparison of cis- *and* trans-$[Ru(bipy)(ppy)_2]$ (**III**) *vs* **IV**

The stereochemistries of $[M(bipy)(ppy)_2]^{n+}$ complexes have not been assigned unambiguously by crystallographic methods. $[M(bipy)(ppy)_2]^{n+}$ complexes are derived from chloro-compounds such as $[M(ppy)_2(\mu\text{-}Cl)_2M(ppy)_2]$ or $[M(ppy)_2Cl_2]^{n-}$, which are known to possess a *cis*-arrangement of the carbon donor atoms, with the chlorine ligands *trans* to carbon (structure **VII**).[17] There are three possible isomers for $[M(bipy)(ppy)_2]^{n+}$ (structures **III**, **IV** and **VIII**), and NMR spectroscopic data are consistent with either **III** and **IV**, each of which possesses C_2 symmetry, although the results of NOE experiments indicate that isomer **III** persists in solution.[5] This structure is also assigned by analogy with the chloro-bridged dimers from which they are prepared. One of the aims of our present study is to attempt to quantify the preference for the *cis*-arrangement of the carbon donor atoms, i.e. the apparent preference for structure **III** over **IV**.

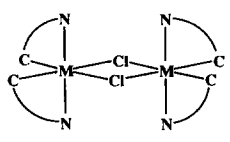

VII

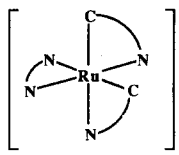

VIII

The diagram in Fig. 7 illustrates the ruthenium–ligand bonding orbitals in complexes **III** and **IV**. As in **II**, we observe partitioning of the $Ru—C_{[ppy]^-}$ and Ru—N σ-bonding character, with $Ru—C_{[ppy]^-}$ lying at the higher energy. One additional feature which is peculiar to the *cis*-isomer of $[Ru(bipy)(ppy)_2]^+$ (**III**) is a separation within the Ru—N σ-manifold into $Ru—N_{bipy}$ and $Ru—N_{[ppy]^-}$ bonding MO's. This may be explained in terms of the *local* symmetry of each N_4-donor set.† Each of isomers **III** and **IV** possesses molecular C_2 symmetry, but the separation of Ru—C and Ru—N character and the fact that the ligand frontier orbitals which are involved in σ-bonding are localized on the donor atoms (see Fig. 2) mean that the interaction of the ruthenium and nitrogen orbitals may be considered in terms of the local symmetry of the set of four nitrogen atoms rather than the molecular symmetry as a whole.‡ The N_4-donor set in **III** possesses C_{2v}

*Although the ruthenium complexes $[Ru(bipy)_{3-n}(ppy)_n]^{(2-n)+}$ are not known for $n = 2$ or 3, the corresponding rhodium and iridium complexes have been characterized. The *trends* within the isostructural series may thus be determined.

† Since atomic positions in **III** and **IV** are based upon the experimental coordinates for **I**, the symmetry is approximate, although deviation from C_{2v} or D_{4h} is not significant.

‡ The Ru—N bonding MO's, although constructed initially under local symmetry will obviously be perturbed by entry into a C_2 regime.

symmetry, and mixing of the two N_4-ligand group orbitals with a_1 symmetry is therefore allowed. Linear combinations of these orbitals provide the observed localization of N_{bipy} and $N_{[ppy]^-}$ character. The b_1 and b_2 orbitals are already localized on either bipy of $[ppy]^-$ nitrogen donors. In contrast, the local D_{4h} symmetry of the N_4-donor set in **IV** produces ligand group orbitals between which mixing is disallowed by symmetry. Hence, each Ru—N bonding MO in **IV** contains contributions from all four nitrogen atoms (i.e. independent of ligand) while in **III**, the Ru—N bonding MO's may be identified as being either Ru—N_{bipy} *or* Ru—$N_{[ppy]^-}$ in nature. Although the present analysis of electronic structure addresses a ground-state species, the localization of Ru—bipy or Ru—$[ppy]^-$ character should be paralleled in the excited state. This offers a possible origin for the differing emitive properties of complexes incorporating cyclometallated ligands as compared to $[M(bipy)_3]^{n+}$.

The separation of Ru—C, Ru—N_{bipy} and Ru—$N_{[ppy]^-}$ character in **III** described above may be consistent with the presence of the *cis*- rather than *trans*-isomer of $[Ru(bipy)(ppy)_2]$, but it does *not* provide a satisfactory explanation for the structural preference of **III** over **IV**. In Fig. 7, on going from **III** to **IV** the highest-lying Ru—C bonding orbital, MO 87, is destabilized by $\approx$ 1 eV. However, concomitant stabilization of other Ru—C bonding MO's appears to more than sufficiently compensate for the change in energy of MO 87. Similarly for the Ru—N bonding MO's, there is no obvious net orbital destabilization on going to **IV**. The HOMO–LUMO separations for the two isomers are similar, and using this energy difference as a means of estimating the relative stabilities of **III** and **IV**, then **IV** appears to be marginally more stable (2.92 vs 3.44 eV). However, this distinction is far from convincing. In terms of the ruthenium–ligand Mulliken overlap populations, there is only a marginal difference between the two isomers, again in favour of **IV**; in each complex, there is negligible difference between the overlap populations for ruthenium interacting with bipy or with $[ppy]^-$. The most significant difference between **III** and **IV** is in the atomic charge distribution (Table 1). We noted in complex **II** that a nitrogen atom *trans* to carbon is a poorer σ-donor than one *trans* to another nitrogen atom. This N—Ru—C *trans*-effect benefits the carbon atom in that it is able to reduce its net atomic charge from -0.748 electrons in free $[ppy]^-$ to -0.264 electrons in **III**. In isomer **IV** where the carbon donors lie *trans* to one another, the charge must be symmetrically distributed across the C—Ru—C bonding interaction and a higher negative charge results on carbon. Electronegativities would suggest that the nitrogen rather than the carbon atom can tolerate the extra negative charge and hence we suggest that the *cis*-isomer (**III**) is favoured on electronic grounds over the *trans*-isomer (**IV**). This result agrees with the related and experimentally based proposal of von Zelewsky and

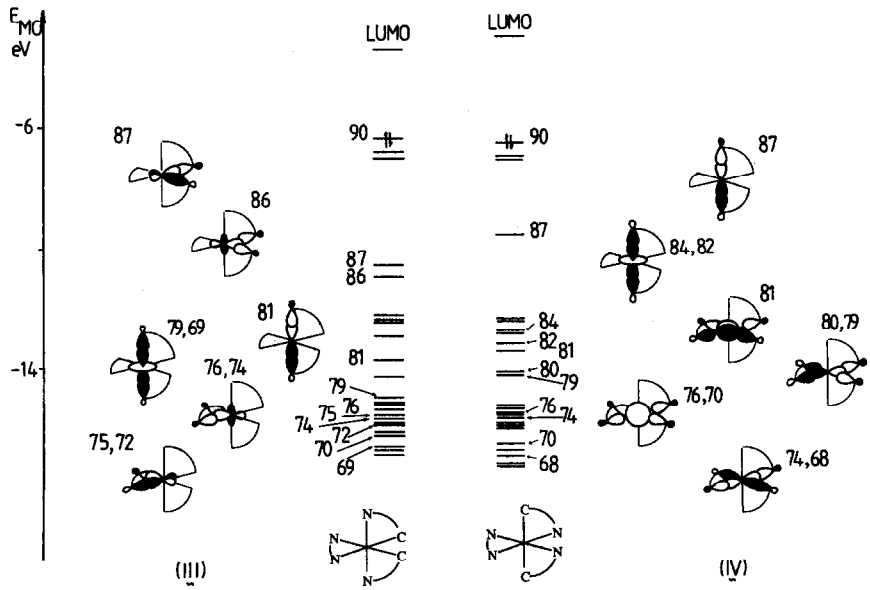

Fig. 7. Comparison of the ruthenium–ligand σ-bonding MO's in **III** and **IV**; MO's 88–90 possess π-backbonding character. Where one diagrammatic representation is assigned to more than one MO, the character is spread through the stated MO's and mixes with other (Ru—L non-bonding) ligand, L, MO's.

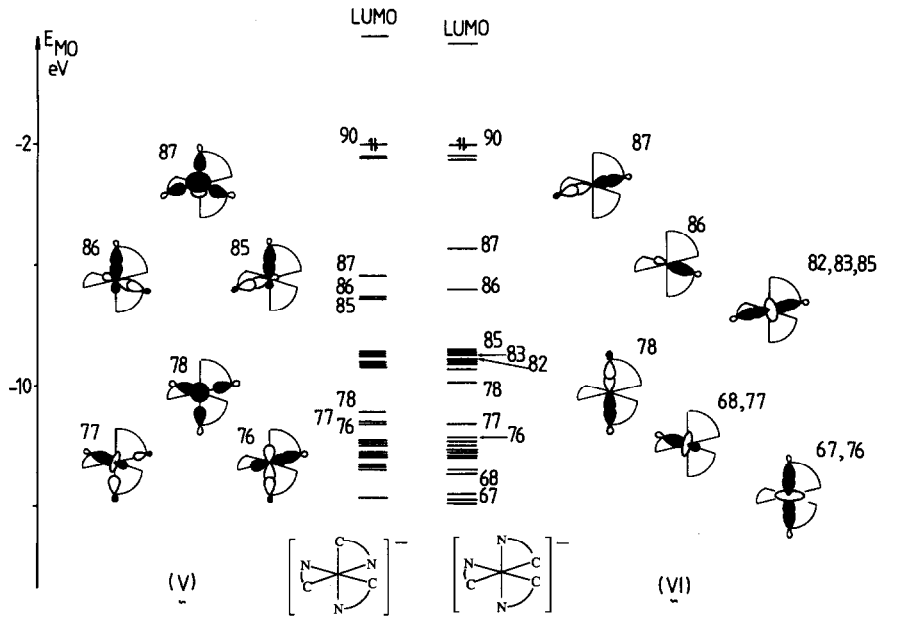

Fig. 8. Comparison of the ruthenium–ligand σ-bonding MO's in V and VI; MO's 88–90 possess π-backbonding character. Where one diagrammatic representation is assigned to more than one MO, the character is spread through the stated MO's and mixes with other (Ru—L non-bonding) ligand, L, MO's.

co-workers.[5] However, our results indicate that the isomer preference dictated by small differences in electronic structure between **III** and **IV** might well be altered if the steric requirements of the ligands are changed.[18]

Comparison of fac- *and* mer-$[Ru(ppy)_3]^-$ (V) *vs* VI

There are two possible isomers of a pseudo-octahedral $[M(ppy)_3]^{n+}$ complex; to date, two such complexes, $[Ir(ppy)_3]$ and $[Rh(ppy)_3]$, have been characterized and only the *fac*-isomer, **V**, has been obtained.[6] By way of rationalizing this observation, the same arguments regarding charge separation across the N—M—C bonds applies to $[M(ppy)_3]^{n+}$ as to $[M(bipy)(ppy)_2]^{m+}$, and atomic charges for isomers **V** and **VI** are listed in Table 1. The carbon donor atoms can reduce their negative charge most effectively when sited *trans* to nitrogen and this, we consider, is the major driving force behind the preference for *fac*- over *mer*-isomer formation.

An analysis of the electronic structures of **V** and **VI** reveals the now familiar separation of Ru—C and Ru—N bonding character (Fig. 8). In **V**, the Ru—C σ-bonding character is localized in MO's 85–87 and a second set of three MO's (76–78) constitute the Ru—N σ-bonding orbitals. On going to **VI**, each three atom donor set, N_3- or C_3-, lowers in local symmetry from C_3 to C_{2v} and, while maintaining their mutual separation, Ru—C and Ru—N σ-bonding character becomes delocalized over a larger number of MO's in **V** than in **VI**, with mixing of the N_3- or C_3-ligand group a_1 orbitals giving rise to MO's containing contributions from only one or two donor atoms rather than from all three. The highest-lying Ru—C σ-bonding MO 87 in **VI** is destabilized with respect to the degenerate set of MO's 85–86 in **V** from which it is derived and rises to a higher energy than the highest-lying Ru—C bonding MO in **V**. However, interpreting this in terms of relative complex stability is ambiguous since significant stabilization of Ru—C σ-bonding character also occurs in going from **V** to **VI**; similarly with the Ru—N σ-bonding character.

Acknowledgements—C.E.H. thanks the Royal Society for a 1983 University Research Fellowship. We are also grateful to Professor F. A. Cotton, and Drs Malcolm Gerloch and Anthony Stone for fruitful discussions.

REFERENCES

1. A. Juris, V. Balzani, F. Barigelletti, S. Campagna, P. Belser and A. von Zelewsky, *Coord. Chem. Rev.* 1988, **84**, 85; E. A. Seddon and K. R. Seddon, *The Chemistry of Ruthenium*. Elsevier, Amsterdam (1984); V. Balzani, F. Bolletta, M. T. Gandolfi and M. Maestri, *Top. Curr. Chem.* 1978, **75**, 1; V. Balzani, F. Bolletta, F. Scandola and R. Balardini, *Pure Appl. Chem.* 1979, **51**, 299; V. Balzani, L. Moggi, M. F.

Manfrini, F. Bolletta and G. S. Lawrence, *Coord. Chem. Rev.* 1975, **15**, 321; G. DeArmond, K. W. Hanck and D. W. Wertz, *Coord. Chem. Rev.* 1981, **64**, 65; T. J. Meyer, *Prog. Inorg. Chem.* 1983, **30**, 389; T. J. Meyer, *Accts Chem. Res.* 1978, **11**, 94; N. Sutin and C. Creutz, *Pure Appl. Chem.* 1980, **52**, 2717; R. J. Watts, *J. Chem. Educ.* 1983, **60**, 834.

2. R. J. Watts, J. S. Harrington and J. van Houten, *J. Am. Chem. Soc.* 1977, **99**, 2179; W. A. Wickramasinghe, P. H. Bird and N. Serpone, *J. Chem. Soc., Chem. Commun.* 1981, 1284; G. Nord, A. C. Hazell, R. G. Hazell and O. Farver, *Inorg. Chem.* 1983, **22**, 3429; P. J. Spellane, R. J. Watts and C. J. Curtis, *Inorg. Chem.* 1983, **22**, 4060; A. Slama-Schwok, S. Gershuni, J. Rabani, H. Cohen and D. Meyerstein, *J. Phys. Chem.* 1985, **89**, 2460; R. J. Watts and S. F. Bergeron, *J. Phys. Chem.* 1979, **83**, 425; J. L. Kahl, K. DeArmond and K. W. Hanck, *J. Phys. Chem.* 1978, **82**, 540; H. Cohen, A. Slama-Schwok, J. Rabani, R. J. Watts and D. Meyerstein, *J. Phys. Chem.* 1985, **89**, 2465; S. F. Bergeron and R. J. Watts, *J. Am. Chem. Soc.* 1979, **101**, 3151; P. J. Spellane and R. J. Watts, *Inorg. Chem.* 1981, **20**, 3561; J. L. Kahl, K. DeArmond and K. W. Hanck, *J. Inorg. Nucl. Chem.* 1979, **41**, 495; P. S. Braterman, G. A. Heath, A. J. McKenzie, B. C. Noble, R. D. Peacock and L. J. Yellowlees, *Inorg. Chem.* 1984, **23**, 3425; A. C. Hazell and R. G. Hazell, *Acta Cryst.* 1984, **C40**, 806.
3. E. C. Constable, *Polyhedron* 1984, **3**, 1037; I. Omae, *Organometallic Intramolecular Coordination Compounds*. Elsevier, Amsterdam (1986); I. Omae, *Coord. Chem. Rev.* 1988, **83**, 137.
4. D. Sandrini, M. Maestri, V. Balzani, U. Maeder and A. von Zelewsky, *Inorg. Chem.* 1988, **27**, 2640; F. D. Garces, K. A. King and R. J. Watts, *Inorg. Chem.* 1988, **27**, 3464; V. Balzani, M. Maestri, A. Melandri, D. Sandrini, L. Chassot, C. Cornioley-Deuschel, P. Jolliet, U. Maeder and A. von Zelewsky, *Photochem. Photophys. Coord. Compd.* [*Proc. Int. Symp.*] 7th, 1987, 71–77; F. Barigelletti, D. Sandrini, M. Maestri, V. Balzani, A. von Zelewsky, L. Chassot, P. Jolliet and U. Maeder, *Inorg. Chem.* 1988, **27**, 3644; M. Maestri, D. Sandrini, V. Balzani, U. Maeder and A. von Zelewsky, *Inorg. Chem.* 1987, **26**, 1323; K. A. King and R. J. Watts, *J. Am. Chem. Soc.* 1987, **109**, 1589; Y. Ohsawa, S. Sprouse, K. A. King, M. K. DeArmond, K. W. Hanck and R. J. Watts, *J. Phys. Chem.* 1987, **91**, 1047; A. Vogler and H. Kunkley, *Am. Chem. Soc., Symp. Ser.* 1987, 333 (*High Energy Processes Organomet. Chem*) 155; M. Maestrin, D. Sandrini, V. Balzani, L. Chassot, P. Jolliet and A. von Zelewsky, *Chem. Phys. Lett.* 1985, **122**, 375; P. Reveco, W. R. Cherry, J. Medley, A. Garber, R. J. Gale and J. Selbin, *Inorg. Chem.* 1986, **25**, 1842; P. Reveco, R. H. Schmehl, W. R. Cherry, F. R. Fronczek and J. Selbin, *Inorg. Chem.* 1988, **24**, 4078; S. Sprouse, K. A. King, P. J. Spellane and R. J. Watts, *J. Am. Chem. Soc.* 1984, **106**, 6647.
5. U. Mäder, T. Jenny and A. von Zelewsky, *Helv. Chem. Acta* 1986, **69**, 1085.
6. K. A. King, M. F. Finlayson, P. J. Spellane and R. J. Watts, *Sci. Pap. Inst. Phys. Chem. Res.* (*Jpn*) 1984, **78**, 97; K. A. King, P. J. Spellane and R. J. Watts, *J. Am. Chem. Soc.* 1985, **107**, 1431; K. Ichimura, T. Kobayashi, K. A. King and R. J. Watts, *J. Phys. Chem.* 1987, **91**, 6104.
7. M. B. Hall and R. F. Fenske, *Inorg. Chem.* 1972, **11**, 768.
8. The Fenske–Hall method has been used previously for mononuclear metal complexes in which the metal is in a formal (+1) or (+2) oxidation state. See for example: A. C. Sarapu and R. F. Fenske, *Inorg. Chem.* 1975, **14**, 247; A. C. Sarapu and R. F. Fenske, *Inorg. Chem.* 1972, **11**, 3021; B. E. Bursten and R. F. Fenske, *Inorg. Chem.* 1977, **16**, 963; E. C. Constable and C. E. Housecroft, *Transition Met. Chem.* (*Weinheim Ger.*) 1988, **13**, 19.
9. T. Tada, *J. Sci. Hiroshima Univ.* 1982, **46**, 73; D. P. Rillema, D. S. Jones and H. A. Levy, *J. Chem. Soc., Chem. Commun.* 1979, 849.
10. E. C. Constable, P. R. Raithby and D. N. Smit, *Polyhedron* 1989, **8**, 367.
11. E. C. Constable, T. A. Leese and D. A. Tocher, *J. Chem. Soc., Chem. Commun.*, submitted.
12. E. Clementi, *J. Chem. Phys.* 1964, **40**, 1944.
13. J. W. Richardson, M. J. Blackman and J. F. Ranochak, *J. Chem. Phys.* 1973, **58**, 3010.
14. See for example: K. M. Kostic and R. F. Fenske, *Inorg. Chem.* 1983, **22**, 666.
15. N. Sanders, *J. Chem. Soc. A* 1971, 1563; N. Sanders and P. Day, *J. Chem. Soc. A* 1970, 1190; N. Sanders, *J. Chem. Soc., Dalton Trans.* 1972, 345; D. W. Clack and R. D. Gillard, *Transition Met. Chem.* (*Weinheim Ger.*) 1985, **10**, 419; D. W. Clack, L. A. P. Kane-Maguire, D. W. Knight and P. A. Williams, *Transition Met. Chem.* (*Weinheim Ger.*) 1980, **5**, 376.
16. E. C. Constable and J. M. Holmes, *J. Organomet. Chem.* 1986, **301**, 203.
17. $[(ppy)_2Rh(\mu\text{-}Cl)_2Rh(ppy)_2]$: D. Sandrini, M. Maestri, V. Balzani, U. Maeder and A. von Zelewsky, *Inorg. Chem.* 1988, **27**, 2640.
18. F. R. Fronczek, M. A. Gutierrez and J. Selbin, *Cryst. Struct. Commun.* 1982, **11**, 1119.

Polyhedron Vol. 9, No. 15/16, pp. 1949–1953, 1990
Printed in Great Britain

0277–5387/90 $3.00+.00
© 1990 Pergamon Press plc

EMISSION LIFETIMES OF BINUCLEAR (d^{10}–d^{10}) PALLADIUM AND PLATINUM COMPLEXES*

PIERRE D. HARVEY and HARRY B. GRAY†

Arthur Amos Noyes Laboratory, California Institute of Technology, Pasadena, CA 91125, U.S.A.

Abstract—The emission lifetimes of binuclear (d^{10}–d^{10}) palladium and platinum dibenzylideneacetone complexes and certain derivatives have been measured as a function of emission wavelength and temperature in 2-methyltetrahydrofuran solutions. An unusual wavelength dependence of the emission lifetimes at 77 K is observed. The magnitude of this wavelength dependence is significantly smaller when the substitution occurs at the two-position of the aryl groups of the ligands, suggesting that steric effects play an important role in these excited-state deactivation processes.

Organometallic complexes containing metal–olefin bonds that exhibit luminescence in solution are rare.[1] However, emission from d^{10}–d^{10} $M_2(dba)_3$ complexes (M = Pd, Pt; dba = dibenzylideneacetone) has recently been reported.[2,3] Based on the energy gap between the lowest energy MLCT absorption and emission bands, and on the relatively long lifetime of the excited state, the observed emission has been assigned to a triplet → singlet MLCT transition.[2,3] In the course of our work, we found unusual emission behaviour for the $M_2(dba)_3$ complexes and their substituted derivatives in 77 K glasses. The principal findings of this more detailed investigation are presented here.

EXPERIMENTAL

Materials

The compounds investigated in this work are listed in Table 1; the compounds were synthesized‡ according to standard procedures.[4,5] The complexes were purified by triple recrystallization in dry toluene/hexane or toluene/propanol. There was no change in emission lifetimes when changing the solvent of recrystallization. Purity was checked by elemental analysis and ^{1}H NMR spectroscopy (500 MHz; 1000 scans). The ligands employed in the preparation of complexes were synthesized§ according to Conrad and Dolliver.[6] 2-Methyltetrahydrofuran (2-MeTHF; Aldrich) was purified by a standard procedure.[7] Toluene (B&J) was used without further purification. All spectroscopic measurements were performed immediately after freeze–pump–thaw degassing of the solutions.

Measurements

The UV–vis absorption spectra were recorded on Cary 17 (measurements at 77 K) and Hewlett Packard 8450A Diode Array (measurements at room temperature) spectrophotometers. The emission and excitation spectra were obtained using a Perkin–Elmer MPF-66 spectrofluorometer. The emission lifetime measurements were made on a Quanta Ray Nd–YAG (8 ns FWHM; 532 nm excitation) laser system.[8] Conditions: slit widths, 300 μm, 200 pulses, ~40 mJ/pulse, solute concentrations, 10^{-6}–10^{-3} M.

* Dedicated to Dick Fenske, whose work on the electronic structures of metal complexes has greatly enriched inorganic chemistry.

† Author to whom correspondence should be addressed; this is contribution No. 8038 from the Arthur Amos Noyes Laboratory.

‡ Attempts to synthesize the 2,2′,6,6′-tetrasubstituted binuclear dibenzylideneacetone complexes failed (X = Cl, CH_3, OCH_3).

§ A 2:1 aldehyde–acetone mixture was added dropwise (~1 drop/s) to the 10% NaOH water–ethanol (1:1) solution. For solid aldehyde, a saturated ethanol solution was made prior to addition. After stirring for 2 h, an equivalent portion of water was slowly added to complete precipitation of the yellow product. After filtration, the filtrate was dried *in vacuo* (10^{-6} torr; 24 h) and recrystallized in acetylacetate. The compounds were characterized by ^{1}H NMR, UV, IR and elemental analysis.

Table 1. Binuclear complexes

Compound	Abbreviation
1-Tris(dibenzylideneacetone)dipalladium(0)[a]	$Pd_2(dba)_3$
2-Tris(dibenzylideneacetone)diplatinum(0)[a]	$Pt_2(dba)_3$
3-Tris(4,4′-dimethoxydibenzylideneacetone)dipalladium(0)	$Pd_2(4,4'\text{-dmdba})_3$
4-Tris(2,2′-dimethoxydibenzylideneacetone)dipalladium(0)	$Pd_2(2,2'\text{-dmdba})_3$
5-Tris(2,2′-dimethyldibenzylideneacetone)dipalladium(0)	$Pd_2(2,2'\text{-dMdba})_3$
6-Tris(α-dinaphthalideneacetone)dipalladium(0)	$Pd_2(\alpha\text{-dnapha})_3$
7-Tris(β-dinaphthalideneacetone)dipalladium(0)	$Pd_2(\beta\text{-dnapha})_3$

[a] Isolated solid contains one toluene molecule of crystallization.

RESULTS AND DISCUSSION

Single-crystal X-ray diffraction[9,10] and ^1H NMR spectroscopic studies[11,12] have shown that the molecular structures of the $M_2(dba)_3$ complexes are the same in solution and in the solid state. The two trigonal planar M(olefin)$_3$ units are held face-to-face by the three bridging ligands. For $Pd_2(dba)_3$, r(Pd—Pd) = 3.24 Å. In mono- and binuclear complexes, the dba ligands generally adopt an s-*cis*,*trans* conformation,[10,11,13–15] as shown in Fig. 1. Interestingly, a study of ^1H and ^{13}C NMR spectra of the tris(4,4′ - diisopropyldibenzylideneacetone)dipalladium(0) and -diplatinum(0) complexes (M_2(4,4′-dipba)$_3$) has confirmed[16] that the molecular framework is stereochemically rigid on the NMR time scale over the temperature range −90 to 60°C. The ^1H NMR spectra show that the aryl groups are rotating at 25°C, but are frozen out at low temperature.[16]

At room temperature, the luminescence of $M_2(dba)_3$ is very weak in solution and of medium intensity in a rigid medium such as polymethylmethacrylate. The λ_e(max) values are ~ 755 and 815 nm for M = Pd and Pt at 295 K, respectively; they are ~ 15 nm blue-shifted at 77 K. The τ_e(295K) values show that the exicted states are relatively long-lived ($\tau_e(Pd_2) = 0.22$, $\tau_e(Pt_2) = 0.23$ μs),[3] thereby suggesting that the emissions originate from an MLCT triplet state.[2,3] The finding that d^{10}–d^{10} $Pd_2(dppm)_3$ [dppm = diphenylphosphino(methane)] exhibits a longer τ_e[17,18] and larger emission quantum yield (Φe)[18] than $Pd_2(dba)_3$ in solution at 295 and 77 K is not surprising, because the dppm complex is not as flexible as the binuclear dba species.

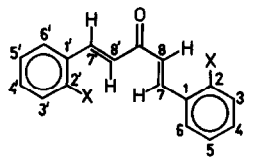

Fig. 1. Structure of s-*cis*,*trans*-2,2′-disubstituted dibenzylideneacetone. With X = H, bridging ligand = dba. (The benzene protons are omitted for the sake of clarity.)

The emission spectra of $M_2(dba)_3$ and the variation of τ_e with λ at 77 K in 2-MeTHF are shown in Fig. 2. Lifetime ranges are $7.5 < \tau_e < 13.5$ (M = Pd) and $0.90 < \tau_e < 1.60$ μs (M = Pt).* The measurements were performed using small slit widths and all decay curves were rigorously monoexponential. The τ_e measurements also were repeated at different solute concentrations (10^{-6}–10^{-3} M) and different toluene–isopentane mixtures at 77 K (1, 3, 5 and 10%).† The τ_e results are

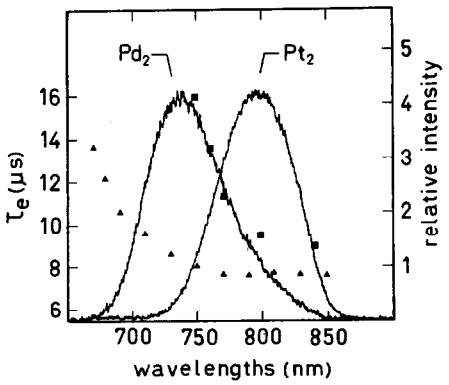

Fig. 2. Emission spectra of $M_2(dba)_3$ complexes in 2-MeTHF at 77 K and λ-dependence of τ_e (M = Pd, ▲; M = Pt, ■). The y-scale has been multiplied by a factor of 10 for M = Pt. Emission intensity has not been corrected for PM tube detection below 750 nm.

* The order $\tau_e(Pd_2) > \tau_e(Pt_2)$ also has been observed[17] for $M_2(dppm)_3$ complexes.

† The $M_2(dba)_3$ complexes are not soluble in saturated hydrocarbons. A mixture of toluene and saturated hydrocarbons at 77 K causes precipitation of the complexes if the quantity of toluene is not sufficient.

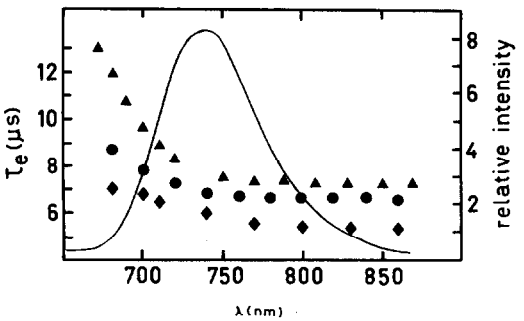

Fig. 3. Emission spectra of Pd_2(4,4′-dmdba)$_3$ in 2-MeTHF at 77 K, and λ-dependence of τ_e for Pd_2(4,4′-dmdba)$_3$ (▲), Pd_2(2,2′-dMdba)$_3$ (◆), and Pd_2(2,2′-dmdba)$_3$ (●). Emission intensity has not been corrected for PM tube detection below 750 nm.

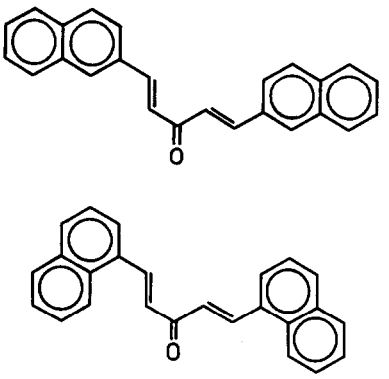

Fig. 4. Structures of β- (top) and α-dinaphthalidine-acetone (bottom) (s-*cis*,*trans*-conformation).

reproducible for both complexes, and the possibility of aggregation as an explanation of this unusual emission behaviour is ruled out.

In attempts to interpret these results, a number of substituted derivatives of Pd_2(dba)$_3$ were investigated. The λ-dependences of τ_e for Pd_2(4,4′-dmdba)$_3$, Pd_2(2,2′dmdba)$_3$ and Pd_2(2,2′-dMdba)$_3$ in 2-MeTHF at 77 K are shown in Fig. 3. There is no spectroscopic difference nor change in τ_e behaviour as a function of λ between Pd_2(4,4′-dmdba)$_3$ and Pd_2(dba)$_3$. On the other hand, substitution at the 2,2′-positions of dba lowers the gap (Δ) significantly between τ_e(min) and τ_e(max); Pd_2(2,2′-dmdba)$_3$, $6.8 < \tau_e < 8.8$ ($\Delta \sim 2.0$); Pd_2(2,2′-dMdba)$_3$, $5.3 < \tau_e < 8.8$ μs ($\Delta \sim 1.6$ μs). Moreover, as for the M_2(dba)$_3$ complexes, τ_e is λ-independent for Pd_2(4,4-dmdba)$_3$ and Pd_2(2,2′-dmdba)$_3$ in 2-MeTHF at room temperature. These results strongly suggest that a dynamic process involving interactions between atom H(8) and substituent X(2) [as well as H(8′) and X(2′)] via rotations of the aryl groups along the C(1)—C(4) axis (see Fig. 1) is the origin of this phenomenon at 77 K.

The postulated role of steric interactions has been tested by investigating complexes with larger aryl groups, such as naphthalene. The two possible structural forms of the dinaphthalideneacetone ligand are the α- and β-isomers (Fig. 4). Figure 5 shows the excitation and emission spectra of these complexes and the τ_e variation with λ. The λ(max) values of the MLCT absorption and emission bands, are, respectively, 585 and 773 (Pd_2(α-dnapha)$_3$) and 570 and 745 nm (Pd_2(β-dnapha)$_3$). The τ_e behaviour with λ at 77 K should be similar for both Pd_2(dba)$_3$ and Pd_2(β-dnapha)$_3$ based on

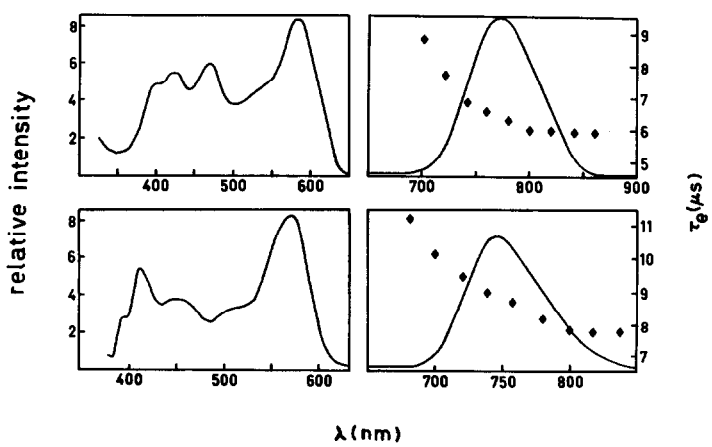

Fig. 5. Emission (right) and excitation (left) spectra of Pd_2(α-dnapha)$_3$ (top) and Pd_2(β-dnapha)$_3$ (bottom) in 2-MeTHF at 77 K, and the λ-dependence of τ_e (◆) in each case. Emission intensity has not been corrected for PM tube detection below 750 nm.

Table 2. Band positions and emission lifetimes

Compound	λ(MLCT) 77 K (nm)	τ_e(295 K) (μs)	λ(max) (nm)	τ_e(77 K) (μs)	λ(max) (nm)	Δ[a] (μs)
$Pd_2(dba)_3$	552	0.22[b]	755	7.5–13.5	740	~ 6.0
$Pt_2(dba)_3$	578	0.23[b]	810	0.9–1.6	800	~ 0.70
$Pd_2(4,4'\text{-dmdba})_3$	556	0.23	760	7.3–13.3	742	~ 6.0
$Pd_2(2,2'\text{-dmdba})_3$	552	—[c]	—	6.8–8.8	748	~ 2.0
$Pd_2(2,2'\text{-dMdba})_3$	566	0.039	765	5.3–6.9	757	~ 1.6
$Pd_2(\alpha\text{-dnapha})_3$	585	—[c]	—	6.0–8.7	773	~ 2.7
$Pd_2(\beta\text{-dnapha})_3$	570	—[c]	—	7.7–11.3	745	~ 3.6

[a] Δ is the difference between the minimum and maximum values for τ_e(77 K).
[b] Data taken from ref. 3.
[c] Due to extensive dissociation of the complexes in fluid solution, room temperature measurements were not made.

H(8)—H(2) steric arguments. Owing to the fact that the barrier to rotation around the C(1)—C(7) bond is larger in the β-dnapha and α-dnapha compounds, the τ_e changes should be smaller, as is the case (Table 2). For $Pd_2(\alpha\text{-dnapha})_3$, the substituent X is a rigid H—C≡ group (Fig. 4), and the steric interactions are larger than that in $Pd_2(\beta\text{-dnapha})_3$. Based on this argument, the Δ values should vary as dba = 4,4′-dmdba > β-dnapha > α-dnapha > 2,2′-dmdba > 2,2′-dMdba, as observed.

The variation of τ_e with temperature for each of the complexes in solution also has been investigated. Figure 6 shows plots of $\ln(k_e)$ ($k_e = 1/\tau_e$) vs $1/T$ for the $M_2(dba)_3$ complexes in 2-MeTHF. At room temperature, the τ_e values for both complexes are the same, and it can be seen from Fig. 6 that this equality is a coincidence. Figure 7 shows the variation of $\ln(k_e)$ with $1/T$ for $Pd_2(4,4'\text{-dmdba})_3$ and $Pd_2(2,2'\text{-dMdba})_3$ in 2-MeTHF. The τ_e behaviour for $Pd_2(4,4'\text{-dmdba})_3$ is virtually the same as that for $Pd_2(dba)_3$, indicating that substitution at the 4,4′-positions of the dba ligand does not influence excited-state deactivation.

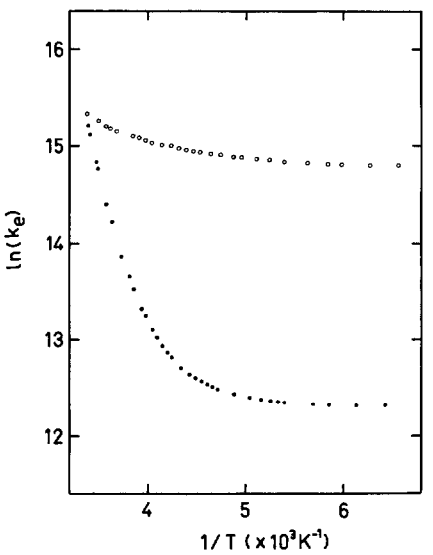

Fig. 6. Plots of $\ln(k_e)$ vs $1/T$ for $M_2(dba)_3$ (M = Pd, ●; M = Pt, O) in 2-MeTHF.

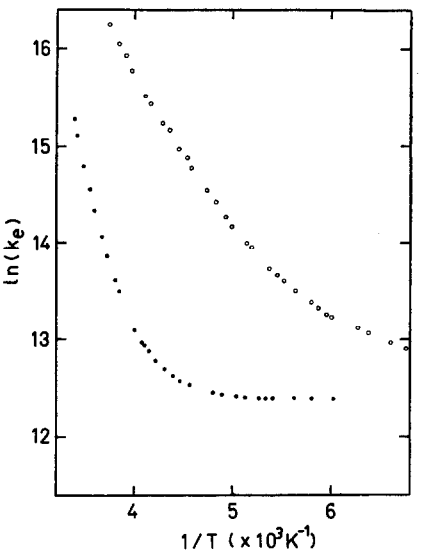

Fig. 7. Plots of $\ln(k_e)$ vs $1/T$ for $Pd_2(4,4'\text{-dmdba})_3$ (●) and $Pd_2(2,2'\text{-dMdba})_3$ (○) in 2-MeTHF.

Acknowledgements—This research was supported by National Science Foundation Grant CHE84-19828. P.D.H. acknowledges the National Research Council of Canada for an NSERC-NATO postdoctoral fellowship.

REFERENCES

1. A. J. Lees, *Chem. Rev.* 1987, **87**, 711.
2. N. A. P. Kane-Maguire, L. L. Wright, J. A. Guckert and W. S. Tweet, *Inorg. Chem.* 1988, **27**, 2905.
3. P. D. Harvey, F. Adar and H. B. Gray, *J. Am. Chem. Soc.* 1989, **111**, 1312.
4. Y. Takahashi, T. Ito and Y. Ishii, *J. Chem. Soc., Chem. Commun.* 1970, 1065.
5. K. Moseley and P. M. Maitlis, *J. Chem. Soc., Chem. Commun.* 1971, 982.
6. C. R. Conrad and M. A. Dolliver, *Organic Synthesis, Collection*, Vol. 2, p. 167. John Wiley, New York (1943).
7. A. J. Gordon and R. A. Ford, *The Chemist's Companion. A Handbook of Practical Data, Techniques and References*, p. 436. John Wiley, New York (1972).
8. D. G. Nocera, J. R. Winkler, K. M. Yocom, E. Bordignon and H. B. Gray, *J. Am. Chem. Soc.* 1984, **106**, 5145.
9. (a) M. C. Mazza and C. G. Pierpont, *J. Chem. Soc., Chem. Commun.* 1973, 207; (b) C. G. Pierpont and M. C. Mazza, *Inorg. Chem.* 1974, **13**, 1891.
10. T. Urai, H. Kawazura, Y. Ishii, J.-J. Bonnet and J. A. Ibers, *J. Organomet. Chem.* 1974, **65**, 253.
11. H. Kawazura, H. Tanaka, K. Yamada, T. Takahashi and Y. Ishii, *Bull. Chem. Soc. Jpn* 1978, **51**, 3466.
12. H. Tanaka and H. Kawazura, *Bull. Chem. Soc. Jpn* 1979, **52**, 2815.
13. M. C. Mazza and C. G. Pierpont, *Inorg. Chem.* 1973, **12**, 2955.
14. C. G. Pierpont, R. M. Buchanan and H. H. Downs, *J. Organomet. Chem.* 1977, **124**, 103.
15. H. Tanaka and H. Kawazura, *Bull. Chem. Soc. Jpn* 1980, **53**, 1743.
16. A. Keasey, B. E. Mann, A. Yates and P. M. Maitlis, *J. Organomet. Chem.* 1978, **152**, 117.
17. P. D. Harvey and H. B. Gray, *J. Am. Chem. Soc.* 1988, **110**, 2145.
18. J. V. Caspar, *J. Am. Chem. Soc.* 1985, **107**, 6718.

Polyhedron Vol. 9, No. 15/16, pp. 1955–1963, 1990
Printed in Great Britain

0277-5387/90 $3.00+.00
© 1990 Pergamon Press plc

ON THE ENERGETICS OF THE FORMATION OF E—H—M FROM M—H—M INTERACTIONS ON TRANSITION METAL CLUSTERS

THOMAS P. FEHLNER

Department of Chemistry, University of Notre Dame, Notre Dame, IN 46556, U.S.A.

Abstract—Experimental studies from several laboratories have demonstrated that, when a main group–transition metal atom cluster contains endo-cluster hydrogens, equilibria between tautomers which differ in the placement of one or more endo-hydrogens between M—H—M and E—H—M (E = main group atom, M = transition metal) bridging sites can exist. In this study we show that the preference for E—H—M versus M—H—M sites can be simply described in terms of the difference in electronegativities of the E and M atoms. This model allows a correlation of observed site preferences with calculated enthalpy change and allows predictions of site preference in presently unknown compounds. Further, as the model is independent of exo-cluster structure, it can be used to explain some aspects of the relative reactivity of main group atoms when bound to transition metal atoms at the surface or grain boundaries of a bulk metal.

The body of research created by Richard F. Fenske and his students is distinguished by constant attention to the explanation of inorganic chemistry at the synthetic frontier via approximate, but parameter-free, theory. An essential element of his philosophy has been the development of approaches that not only explain known chemistry but also point to the next logical question to be addressed experimentally. It is an approach that I have admired for many years and one which is difficult to emulate. But it is in this spirit that the following analysis of the placement of endo-cluster hydrogens on transition metal–main group atom clusters is offered. It presents a straightforward way of understanding observed hydrogen site preferences and suggests that characterization of tautomeric equilibria of the type discussed can provide a body of data useful for exploring not only discrete molecules but also solid state systems.

INTRODUCTION

The participation of formally monovalent moieties such as H and CH_3 in bridging interactions constitutes a structural feature that distinguishes inorganic chemistry from classical organic chemistry.[1] Although still occasionally viewed with surprise, examples of the E—H—M interactions, E = main group atom, M = transition metal, for E = C are well established in many mononuclear as well as cluster systems.[2] As this structural feature constitutes a real connection between main group and organic chemistry, the relationship of the natures of atoms and M to the relative stability of the E—H—M interaction deserves to be understood. On metal surfaces, the connection between M—H—M and E—H—M interactions is very important to understanding the hydrogenation and dehydrogenation of main group fragments.[3] In bulk metals the same connection is a crucial part of the explanation of the role of main group species in stabilizing or destabilizing a metal towards hydrogen embrittlement.[4]

The factors important for the formation of C—H—M interactions in mononuclear complexes have been clearly developed.[2] A metal-based empty orbital is a requirement and the CH bond of a ligand acts primarily as a σ donor to the metal, i.e. the σ-CH orbital is depopulated but the σ^* orbital is not significantly populated in forming the C—H—M interaction.[5] This contrasts with C—H—M interactions on metal surfaces[6] or in clusters[7] where no formal metal unsaturation is required and significant population of the σ^* orbital of the organic fragment is important. Even though the various factors important in forming a C—H—M interaction have been discussed, the intimate connection with E—H—M interactions involving other main atoms is often neglected and systematic trends in the formation of E—H—M interactions as a func-

tion of main group atom and transition metal have not been documented previously. A sufficient number of closely related examples of compounds with E—H—M interactions now exist such that a correlation of fundamental significance can be constructed.

Previously, we have compared the properties of isoelectronic clusters containing E—H—M, E = C, B; M = Fe, utilizing Fenske–Hall calculations in an attempt to define factors favouring E—H—M over M—H—M interactions.[7,8] On the basis of these results, we suggested that in these tri- and tetrametal clusters the electronic charge available to an endo-hydrogen at a given site was important. However, geometrical factors associated with the spatial distribution of CO and H ligands were also found to be important, i.e. there is a relationship between the geometric positions of the exo-ligands on the cluster core atoms and the distribution of electron density in the molecular orbital (MO).[9] Hence, steric interactions between exo-cluster ligands can be coupled to the endo-cluster bonding thereby affecting endo-hydrogen site stabilities. The importance of steric repulsion between a substituent on the E atom with the equatorial CO ligands of a capped trimetal cluster in promoting M—H—M over C—H—M interactions was subsequently defined experimentally for $Co_2Fe(CO)_9(HCR)$.[10]

Both the experimental and theoretical studies emphasize the subtlety of the structural problem in that significant electronic structural change is accompanied by small energy changes.[11] Despite this fundamental complexity, the MO calculations on capped trimetal clusters do suggest that the interaction of the orbitals of the capping atom, possessing π symmetry with respect to an axis perpendicular to the trimetal plane, with the appropriate orbitals of the trimetal fragment is particularly crucial in understanding the electronic structure. This suggests that the interaction will be sensitive to the effective nuclear charge of the capping atom as well as the number and location of bridging hydrogens.

Considering the foregoing, one might assume that only with much more sophisticated calculations will the observed structure/energy relationships between tautomers containing E—H—M vs M—H—M interactions be reproduced. Even if such calculations are forthcoming, it is not clear that any more understanding of the fundamental driving forces leading to these kinds of interactions will be produced. On the other hand, the existing experimental characterizations of tautomeric equilibria involving the interconversion of E—H—M and M—H—M interactions in cluster systems provides a set of unambiguous thermodynamic data suitable for exploring general trends. That is, the measured equilibrium constants provide a sensitive measure of E—H—M vs M—H—M preference and, because of the exponential relationship between equilibrium constant and energy, also precisely define energy differences between the two structural forms. The following correlation of observed relative abundances of tautomers with M—H—M vs E—H—M interactions with atom electronegativities verifies earlier observations derived from calculations and allows trends for unknown systems to be easily predicted in a qualitative fashion. Further, selected examples show that because the model is independent of nonlocal structure the conclusions extend beyond discrete cluster chemistry.

RESULTS

The principal data upon which the arguments are based are the observed preferences for reaction (1)

$$[M—H—M] = [E—H—M] \qquad (1)$$

which are given in Table 1, where [M—H—M] refers to a tautomeric cluster structure containing one more M—H—M and one less E—H—M interaction than the tautomer [E—H—M]. These data illustrate trends in the balance of reaction (1) as a function of E and M for tri- and tetranuclear transition meal clusters. Of crucial importance are those systems for which the existence of a tautomeric equilibrium has been established. These systems constitute E,M combinations where the stability of the E—H—M tautomer approaches that of the M—H—M tautomer and define a dividing line of relative stability as E and M are varied. For the trinuclear clusters, note the diagonal relationship (Scheme 1), i.e. the clusters E = B, M = Ru and E = C, M = Fe exhibit tautomeric equilibria, while those for E = B, M = Fe and E = C, M = Ru do not. Further, for the BFe system [E—H—M] is favoured over [M—H—M] while the reverse is true

E = B M = Fe EHM > MHM	E = C M = Fe EHM ≈ MHM
E = B M = Ru EHM ≈ MHM	E = C M = Ru EHM < MHM

Scheme 1.

Table 1. Observed preferences for E—H—M versus M—H—M interactions on selected cluster systems

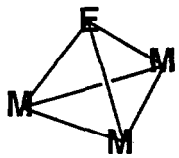

Compound[a]	Number of endo-H	Predominant form[b]	ΔH_R[c]		Reference
$HFe_3(CO)_9(H_3BH)$	4	$(E—H—M)^3$, $M—H—M$	3.6	3.8	33
$HFe_3(CO)_{10}(HBH)$	2	(E—H—M), (M—H—M)	3.6	3.8	34
$Ru_3(CO)_9(BH_5)$	4	$(E—H—M)^3$, M—H—M ≈ $(E—H—M)^2$, $(M—H—M)^2$	7.0	8.6	35
$H_3Os_3(CO)_9BCO$	3	$(M—H—M)^3$	9.6	6.3	36
$Fe_3(CO)_9(CH_4)$	3	$(M—H—M)^3$ ≈ E—H—M, $(M—H—M)^2$	10.3	7.8	37
$H_3Fe_3(CO)_9CCH_3$	3	$(M—H—M)^3$	10.3	7.8	38
$HFe_3(CO)_{10}CCH_3$	1	M—H—M	10.3	7.8	31
$H_2Fe_3(CO)_9NR$	2	$(M—H—M)^2$	14.2	11.6	39
$H_3Ru_3(CO)_9CH$	3	$(M—H—M)^3$	15.3	14.8	40
$H_3Os_3(CO)_9CH$	3	$(M—H—M)^3$	18.8	11.9	41
$H_2Ru_3(CO)_9NPh$	2	$(M—H—M)^2$	19.4	18.6	42

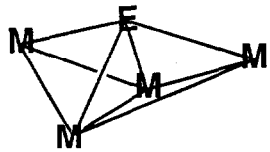

Compound	Number of endo-H	Predominant form	ΔH_R[d]	Reference
$HFe_4(CO)_{12}(H_2B)$	3	M—H—M, $(E—H—M)^2$	3.6	43
$[HFe_4(CO)_{12}(HB)]^-$	2	M—H—M, E—H—M	3.6	44
$[Fe_4(CO)_{12}(HB)]^{2-}$	1	E—H—M	3.6	45
$HFe_4(CO)_{12}(HC)$	2	M—H—M, E—H—M	7.8	46
$[HFe_4(CO)_{12}C]^-$	1	M—H—M	7.8	47
$Fe_3Mn(CO)_{13}(HC)$	1	E—H—M	8.8	48
$[Fe_3Cr(CO)_{13}(HC)]^-$	1	E—H—M	9.2	41
$Fe_3Rh(CO)_{12}(HC)$	1	E—H—M	10.3	41
$[Fe_3W(CO)_{13}(HC)]^-$	1	E—H—M ≈ M—H—M	10.7	41
$HFe_4(CO)_{12}N$	1	M—H—M	11.6	49
$Ru_4(CO)_{12}(CH_2)$	2	E—H—M, M—H—M ≈ $(M—H—M)^2$	14.8	50

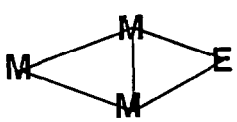

Compound	Number of endo-H	Predominant form	ΔH_R[e]	Reference
$Os_3(CO)_{10}CH_4$	2	$(M—H—M)^2$ ≈ E—H—M, M—H—M	18.8	51
$HOs_3(CO)_{10}(HSnR_2)$	2	M—H—M, E—H—M	8.4	52

[a] For compounds that exist in solution as equilibria between two tautomeric forms only the molecular, rather than structural formula is given.

[b] When E—H—M ≈ M—H—M is indicated, an equilibrium between structures containing these types of endo-hydrogen bridges has been observed.

[c] The first column contains ΔH_R calculated using Mullay's electronegativities and the second column ΔH_R from Allred/Rochow's electronegativities.

[d] Calculated from Allred/Rochow's electronegativities.

[e] Calculated using Mullay's electronegativities.

for the CRu system. The experimental evidence shows that the observed trends are due in significant part to enthalpic differences.[10] Thus our approach is based on a consideration of changes in bond energy term values or average bond energies with E and M.

The overall enthalpy change for reaction (1) may be written as:

$$\Delta H = D(\mathrm{MHM}) + D(\mathrm{ME}) - D(\mathrm{EHM}) - D(\mathrm{MM}), \quad (2)$$

where D(X—H—M) and D(XX) refer to average bond energies for three- and two-centre interactions, respectively. The three-centre interaction can be written as a sum of two-centre interactions, i.e. $D(\mathrm{XHM}) = \alpha[D(\mathrm{XH}) + D(\mathrm{MH}) + D(\mathrm{MM})]$ where α is a constant between 0 and 1. Equation (2) then becomes:

$$\Delta H = \alpha[D(\mathrm{MH}) - D(\mathrm{EH})] + (1-\alpha)[D(\mathrm{ME}) - D(\mathrm{MM})]. \quad (3)$$

If the enthalpy is expressed in terms of metal and main group atom electronegativities by using a modified Pauling expression for the two-centre bond energy, i.e. $D(\mathrm{AB}) = 1/2[D(\mathrm{AA}) + D(\mathrm{BB})] + X_{\mathrm{AB}}$, where X_{AB} is a function of the electronegativity difference between atoms A and B,[12] eq. (3) becomes:

$$\Delta H = (\alpha - 1/2)[D(\mathrm{MM}) - D(\mathrm{EE})] + \alpha(X_{\mathrm{MH}} - X_{\mathrm{EH}}) + (1-\alpha)X_{\mathrm{ME}}. \quad (4)$$

The magnitude of α can be obtained from bond energy data, however, thermochemical data on the bond energetics of main group–transition metal compounds is very sparse. Thus the approximate value of α is obtained from data on B—H—B and Fe—H—Fe interactions. D(BHB), D(BH) and D(BB) ae 108, 90 and 74 kcal mol^{-1}, respectively,[13] while D(FeHFe), D(FeH) and D(FeFe) are 83, 55 and 20 kcal mol^{-1}, respectively.[14]. Thus, writing the three-centre interaction as a fraction, α, of the sum of the two-centre interactions leads to values of α of 0.43 and 0.64 for boron and iron, respectively. For convenience in the mixed system we have taken α to be 0.5 and, thus, eq. (4) reduces to:

$$\Delta H \approx 0.5[X_{\mathrm{MH}} - X_{\mathrm{EH}} + X_{\mathrm{ME}}], \quad (5)$$

which expresses the enthalpy of reaction (1) as a function of the electronegativity differences between M, H and E atoms. The electronegativity difference is given by $X_{\mathrm{AB}} = 105\{1 - \exp[-0.219(X_{\mathrm{A}} - X_{\mathrm{B}})^2]\}$ which reduces to $23(X_{\mathrm{A}} - X_{\mathrm{B}})^2$ in the limit of small ΔX.[15]

There are several scales of electronegativity and selected values for the elements of interest here are gathered in Table 2. Clearly, eq. (5) requires electronegativities[16] that reflect the real differences in transition metals and, thus, Pauling's original values[17] are too imprecise to be of use. The Allred/Rochow[18] and the recent scale of Mullay[19] are suitably fine grained. As will be seen below, the qualitative results do not depend on the choice of electronegativity scale and even the Pauling values for different main group atoms and a fixed metal yield the same qualitative conclusions. Pearson's approach utilizing electronegativity and hardness[20] gives essentially the same results as that using electronegativity alone. Thus, the additional complexity of his approach is not justified. It would, or course, be more appropriate to use group electronegativities for the fragments that make up the cluster, i.e. the effective electronegativity of a metal carbonyl fragment can be much higher than that of the metal atom itself. However, until a self-consistent set of such values are available we must be satisfied with atom values. As long as the metal (and main group atom) ligands remain constant, these values should give the correct trends. In addition, if they do so, then the results are not restricted to discrete clusters.

With the electronegativities contained in Table 2, eq. (5) is used to calculate the enthalpies for reaction (1) for a variety of three and four metal cluster systems. The results are given in Table 1 with the

Table 2. Selected electronegativities of the elements

Element	Mullay[a]	Allred/Rochow[b]	Pauling[c]
H	2.08 (*s*)	2.10	2.1
B	1.85 (sp^2)	2.01	2.0
C	2.47 (sp^3)	2.50	2.5
N	3.41 (sp^3)	3.07	3.0
Si	1.91 (sp^3)	1.74	1.8
P	1.99 (*p*)	2.06	2.1
Ti	1.26 (*d*)	1.32	1.5
Cr		1.56	1.6
Mn		1.60	1.5
Fe	1.55 (*d*)	1.64	1.8
Co	1.62 (*d*)	1.7	1.9
Ni	1.70 (*d*)	1.75	1.9
Ru	1.39 (*d*)	1.42	2.2
Rh	1.45 (*d*)	1.45	2.2
Sn	1.78 (sp^3)	1.72	1.8
W		1.40	1.7
Os	1.29 (*d*)	1.52	2.2

[a] Reference 19.
[b] Reference 18.
[c] Reference 17.

cluster systems ordered according to the magnitude of ΔH. One notes immediately that all the enthalpy values are positive. The free energy change for reaction (1) also includes an entropy term. The overall entropy change for reaction (1) will be generated in large part by the conversion of M—H—M and E—M to M—M and E—H—M interactions. The hydrogen-bridged interactions have relatively high vibrational frequencies (> 1600 cm^{-1}) while the E—M and M—M frequencies are much lower. At room temperature, the latter will be dominant contributors to the entropy and, hence, ignoring any steric interactions which should be small for a hydrogen ligand on E, the overall entropy change should be > 0. Further, for the $Co_2Fe(CO)_9(HCR)$ system[10] we have demonstrated that ΔH is small and < 0 for reaction (1). Thus, the positive values in Table 1 reflect a systematic error in the calculation. This is not surprising as one could hardly hope that such an approximate method would give correct absolute enthalpies. The source of the error may be the neglect of the $(\alpha - 1/2)[D(MM) - D(EE)]$ term in eq. (4), i.e. the choice of $\alpha = 0.5$. As $D(EE)$ is always significantly larger than $D(MM)$ and α does not exactly equal $(1-\alpha)$, this could account for the discrepancy. Likewise the use of atom rather than group electronegativities could be the source of the problem. Thus, we focus discussion on trends as atom type in the cluster framework is varied.

Considering first the ΔHs for the capped trinuclear clusters one notes a crossover from an endo-hydrogen site preference for E—H—M to that for M—H—M at $\Delta H \approx 7$–10 kcal mol^{-1}. The trends in site stability defined by the observed equilibria correlate well with the calculated energetics with the borderline exception of $H_3Os_3(CO)_9BCO$. Most likely the CO ligand when directly bound to boron significantly changes the electronegativity of boron relative to boron in the B—H fragment. But even in this case, the direction of rearrangement of the endo-hydrogens in going from $HFe_3(CO)_{10}(HBH)$ to $H_3Os_3(CO)_9BCO$ is correctly predicted by the ΔH values. Hence, eq. (5) constitutes a quantitative statement of our earlier empirical observation that, for a fixed metal atom type, as the electronegativity of the main group atom increases, M—H—M is favoured over E—H—M and for a constant main group atom, as the electronegativity of the metal is increased, E—H—M is favoured over M—H—M. Thus, with E = B or C going from Fe to Ru promotes the M—H—M interaction while for M = Fe, going from C to B promotes the E—H—M interaction. Note that the difference in ΔHs for E = C and M = Fe, Ru is 4–5 kcal mol^{-1}, which is consistent with the fact that although the C—H—Ru tautomer is not observed directly it is energetically accessible and has been identified as an important intermediate.[21] The situation is similar for osmium.[22] As mentioned above, the modulation of electronegativity by hardness in the manner of Pearson does not change the sign of the enthalpy nor does it particularly improve the correlation with K(eq).[20]

In our approach, the ΔH values are independent of the substituents on metal or main group atoms. However, replacing H with Me on the $Fe_3(CO)_9(H_3CR)$ system leads to a promotion of the M—H—M interaction in that only the tautomer with M—H—M interactions is observed in solution. As the group electronegativity of Me is larger than that of H,[16] the electronegativity of CMe should be larger than that of CH. Hence, ΔH for CMe should be somewhat more positive than that for a CH capping fragment and methyl substitution on the capping carbon leads to promotion of M—H—M site stability over C—H—M.[23] This approach allows one to predict that for the presently unknown compounds $M_3(CO)_9(SiH)_4$, that for M = Fe a form with Si—H—Fe interactions should be prominent ($\Delta H = 4.2$ and 1.4 kcal mol^{-1} using Mullay and Allred/Rochow electronegativities, respectively), while for M = Ru there is a chance to observe an equilibrium between forms containing Si—H—Ru and Ru—H—Ru interactions ($\Delta H = 7.9$ and 4.5 kcal mol^{-1} using Mullay and Allred/Rochow electronegativities, respectively). Although the trimetal capped clusters containing silicon and endo-hydrogens are not known, the Si—H—M interaction has been characterized in mononuclear compounds containing chromium and manganese.[24]

For the $M_4(CO)_{12}CH_2$ cluster system one tautomer is observed for M = Fe (one Fe—H—Fe and one Fe—H—C interaction) but two for M = Ru (a tautomer like the iron analogue and one with two Ru—H—Ru interactions.). In the latter case the tautomer with two M—H—M interactions is seven times more abundant. Again, decreasing the electronegativity of the metal for the same E atom, promotes M—H—M interactions relative to E—H—M. However, one notes that with E = C, M = Fe, tautomeric species are observed in equilibrium in the trinuclear system but with M = Ru only the tautomer with Ru—H—Ru interactions is observed. On the other hand, in the tetranuclear system a similar tautomeric equilibrium is observed for E = C, M = Ru but not for M = Fe. Thus, as might have been anticipated, there is a cluster structural factor in addition to cluster fragment electronegativity involved in determining the absolute tautomer stabilities. The correlation with electronegativity only shows trends and is not sufficient

to predict in an absolute sense when tautomeric equilibria will be observed.

An inspection of the ΔH values in Table 1 shows that this structural dependence is of equal importance to the electronegativity differences. For the clusters with two endo-hydrogens the crossover is at $\Delta H \approx 15$ kcal mol^{-1}, for the homonuclear clusters with one endo-hydrogen the crossover is between 4 and 8 kcal mol^{-1} while for the heteronuclear clusters of Shriver with one endo-hydrogen the crossover is ≈ 10.7 kcal mol^{-1}. Still, even though the electronegativity differences are not as dominating as they appear to be in the trinuclear cluster systems, the trends in the magnitudes of the calculated ΔH values clearly identify one factor of importance in determining endo-hydrogen site stability.

The final two compounds in Table 1 involve a comparison of the first experimentally characterized example of an E—H—M, M—H—M equilibrium, with E = C, with a more recently described tin compound. The $Os_3(CO)_{10}(CH_4)$ cluster in solution exists as an equilibrium mixture of a form with two Os—H—Os bridges plus a bridging CH_2 and a form with one Os—H—Os bridge plus a bridging CH_3 with a single Os—H—C interaction. The tin analogue, $Os_3(CO)_{10}(SnH_2R_2)$, is found as a single species with one Os—H—Os bridge and a bridging $SnHR_2$ fragment with an Os—H—Sn interaction. As predicted by the ΔH calculation, the tin compound is observed exclusively as the Sn—H—Os tautomer. Again the fact that the tautomeric equilibrium is observed for a $\Delta H \approx 19$ rather than ≈ 10 kcal mol^{-1} shows that there is a structure factor differentiating the capped versus uncapped trimetal clusters.

The data in Table 1 constitute a closely related set of equilibrium constants but there are other individual observations of equilibria equivalent to (1) that allow further testing and, ultimately, justification of the correlation with electronegativity. The cluster of composition $Co_2Fe(CO)_9(CHR)$ has a C—H—M/M—H—M ratio greater than one. The calculated ΔHs for all possible hydrogen edge-bridging combinations in reaction (1) are given in Table 3. Note that eq. (5) cannot be applied directly but taking into account the different metals leads to eq. (6) which is applicable to the first entry in Table 3. Two of the four calculated ΔH are in the 7–10 kcal mol^{-1} range for which a tautomeric equilibrium is observed in the homonuclear cases in Table 1. Based on an analysis of the IR spectra of a mixture of the two tautomers, we have suggested[10] that reaction (1) involves Fe—H—Co and C—H—Fe sites and, indeed, this combination is one of the two with low calculated ΔH values.

Table 3. Calculated ΔH for the various possible sites of the $Fe_2Co(CO)_9HCCH_3$ mixed metal cluster

Reaction (1)	ΔH (M)[a]	ΔH (A/R)[b]
Co—H—Co → Co—H—C	8.4	6.8
Fe—H—Co → Fe—H—C	9.5	7.8
Fe—H—Co → Co—H—C	11.4	9.4
Co—H—Co → Fe—H—C	12.6	10.0

[a] Mullay's electronegativities.
[b] Allred/Rochow's electronegativities.

$$\Delta H \approx 0.5[X_{M'H} - X_{EH} + X_{M'E} - X_{MM'}] \quad (6)$$

Finally, the two compounds shown in Scheme 2 provide a more stringent test of the model. The bridging methyl group can form a C—H—M bridge with either titanium or rhodium. Experimentally only the C—H—Ti bridge has been observed.[25] For the change as shown in Scheme 2, the model gives $\Delta H = 0.9$ and 0.6 kcal mol^{-1} using the Mullay and Allred/Rochow electronegativities, respectively. If we assume the crossover is 7–10 kcal mol^{-1}, as it is in the trinuclear cluster systems, then the C—H—Ti bridge is favoured by 6–10 kcal mol^{-1}. In any case, the qualitative result is the same, i.e. bridging to the metal with the lower electronegativity is favoured.

DISCUSSION

The formation and rupture of E—H—M interactions are of fundamental importance to understanding the ease of oxidation and reduction of main group fragments by the action of transition metals. The source and sink of hydrogen is M—H

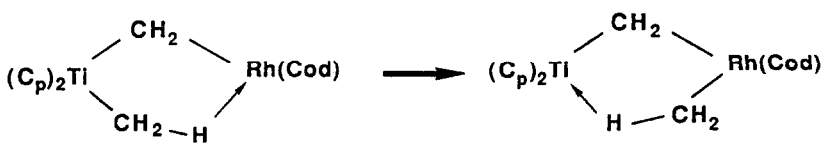

Scheme 2.

bonds of some type and M—H—M bridges can certainly play a role. If terminal M—H bonds are solely involved, the value of the enthalpy of the equivalent of reaction (1) will be changed but the relative direction of the "driving" force will remain the same. This view of metal versus main group interactions with hydrogen can be applied to significant chemical problems outside of discrete cluster chemistry *per se*. Two relevant examples follow.

The hydrogenation of carbon monoxide in the presence of heterogeneous catalysts involves the rupture of C—O bonds and the formation of C—H and C—C bonds.[26] This chemistry, known as the Fischer–Tropsch process, is very complex and the products observed are a complex function of catalyst and condition. The model developed here has some relevance to understanding the distribution of hydrocarbon products formed. A crucial point in the Fischer–Tropsch mechanism for hydrocarbon production is the partitioning of the products between CH_4 and those containing C—C bonds.[27] That is, chain growth by C—C bond formation at a metal site competes with chain termination via hydrogenation. If hydrogenation is very fast then chain growth is not competitive and CH_4 will be the primary product of CO reduction. It is reasonable to assume that hydrogenation of a CR_n fragment proceeds via a R_nC—H—M interaction by movement of a hydrogen atom from a M—H—M site on the catalyst surface. If barriers are low such that equilibria determine branching ratios then the greater the stability of the C—H—M site relative to the M—H—M site the more predominant will be the methanation reaction and the shorter will be the C—C chain products. Equation (5) allows one to estimate the effect of metal on the stabilization of C—H—M over M—H—M interactions in reaction (1) and in Table 4 ΔHs for M_3CH systems are calculated as a function of metal atom. One sees that on going from iron to cobalt to nickel the C—H—M interaction becomes more favoured relative to the M—H—M interaction. It is a well known fact that nickel is exclusively a methanation catalyst while iron yields both methane as well as higher hydrocarbons.[28] Going from iron to ruthenium favours the M—H—M interaction and should result in longer chain products. Indeed at high pressures with a ruthenium catalyst, linear polymethylene is the principal product.[29] Further, potassium promotes an increase in average chain length in the Fischer–Tropsch process. We expect potassium to donate electron density to the metal thereby reducing its effective electronegativity, promoting the M—H—M interaction and increasing the C—C chain length of the products. Of course by focusing entirely on the hydrogen transfer process we ignore other important factors, e.g. heats of adsorption of hydrogen, that change with the metal. Our point is not to explain the mechanism in any complete sense but merely to demonstrate that the model developed here can be effectively incorporated into an overall description of the Fischer–Tropsch process.

Table 4. Variation in preferences for E—H—M versus M—H—M interactions on main group atom capped trimetal sites

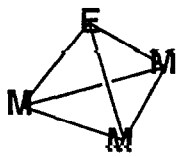

	Metal	ΔH_R[a]
E = C	Fe	10.3
	Co	8.4
	Ni	6.3
	Ru	15.3
E = B	Fe	3.6
E = P	Fe	5.2

[a] Calculated using Mullay's electronegativities.

The embrittlement of steel by hydrogen is an important practical problem.[30] It is known that hydrogen embrittlement of steel is inhibited by the presence of boron,[31] that carbides and nitrides are inert and that phosphorus and arsenic promote brittle failure in iron-based materials.[32] Again in Table 4 we compare Fe_3E clusters for E = B, C and P. Based on the ΔH values, the tendency for E—H—Fe interactions to form decreases in the order B > P > C. The main group atom tends to be segregated at grain boundaries and we have suggested previously that the size of the E—H fragment relative to the metal is important.[4] Hence, when boron is located at grain boundaries, there will be a tendency for it to sequester hydrogen in the form of B—H—Fe interactions which, because of the small size of boron, does not result in decohesion. Phosphorus also will have a significant tendency to form P—H—Fe interactions at grain boundaries but now the large size leads to destabilization at the grain boundary. Carbon has less tendency to form C—H—M interactions and, further, has a small size. Hence, carbon neither promotes nor inhibits hydrogen embrittelement. Again our point here is that the understanding of the distribution of hydrogen atoms between E—M and M—M sites provided

by our model can be readily applied to aspects of complex problems.

Although the overall picture is clear, this approach suffers from its simplicity and the fact that electronegativities are not well enough defined to give precise answers. Still, there is sufficient correlation with observed chemistry to show that conclusions based on an analysis of discrete cluster systems do carry over to reactions on surfaces. This suggests that more precise predictions would be both useful and enlightening. The use of electronegativities could be avoided if more equilibria were known. This would allow one to sort out the effects of structure as well as number and types of ligands on the metal and main cluster atoms. Hence, the characterization of more cluster systems with observable tauromeric equilibria, particularly those involving different main group atoms and metals, would constitute a valuable addition to our understanding of hydrogen transfer between main group and transition metal atoms. When combined with an appropriately more sophisticated model than the one presented here, these data will provide predictive insight on the distribution of hydrogen atoms between metal and main group atoms in a variety of structural environments.

Acknowledgement—The support of our work by the National Science Foundation is gratefully acknowledged.

REFERENCES

1. N. N. Greenwood and A. Earnshaw, *Chemistry of the Elements*. Pergamon Press, Oxford (1984).
2. M. Brookhart and M. L. H. Green, *J. Organomet. Chem.* 1983, **250**, 395; R. H. Crabtree, *Chem. Rev.* 1985, **85**, 245; M. Brookhart, M. L. H. Green and L.-L. Wong, *Prog. Inorg. Chem.* 1988, **36**, 1.
3. E. L. Muetterties, *Chem. Rev.* 1982, **82**, 283.
4. M. A. Cavanaugh, T. P. Fehlner, J. A. Kargol and N. F. Fiore, *Scripta Metalug.* 1982, **16**, 709.
5. J.-Y. Saillard and R. Hoffmann, *J. Am. Chem. Soc.* 1984, **106**, 2006; A. Demolliens, Y. Jean and O. Eisenstein, *Organometallics* 1986, **5**, 1457.
6. R. Baetzold, *J. Am. Chem. Soc.* 1983, **105**, 4271.
7. M. M. Lynam, D. M. Chipman, R. D. Barreto and T. P. Fehlner, *Organometallics* 1987, **6**, 2405.
8. C. H. Housecroft, M. L. Buhl, G. J. Long and T. P. Fehlner, *J. Am. Chem. Soc.* 1987, **109**, 3323.
9. C. E. Housecroft and A. L. Rheingold, *Organometallics* 1987, **6**, 1332.
10. R. D. Barreto and T. P. Fehlner, *J. Am. Chem. Soc.* 1988, **110**, 4471; R. D. Barreto, J. Puga and T. P. Fehlner, *Organometallics* 1990, **9**, 662.
11. A related study on tetrametal clusters has appeared. S. Harris, M. L. Blohm and W. L. Gladfelter, *Inorg. Chem.* 1989, **28**, 2290.
12. There have been a number of recent applications of this equation to the energetics of organometallic reactions. J. A. Labinger and J. E. Bercaw, *Organometallics* 1988, **78**, 926; L. E. Schock and T. J. Marks, *J. Am. Chem. Soc.* 1988, **110**, 7701.
13. T. P. Fehlner and C. E. Housecroft, in *Molecular Structure and Energetics* (Edited by J. F. Liebman and A. Greenberg), Vol. 1, p. 149. VCH, Deerfield Beach, Florida (1986).
14. J. Vites and T. P. Fehlner, *Organometallics* 1984, **3**, 491.
15. R. L. Matcha, *J. Am. Chem. Soc.* 1983, **105**, 4859.
16. J. Mullay, *Struct. Bond.* 1985, **66**, 1.
17. L. Pauling, *The Nature of the Chemical Bond*, 3rd edn. Cornell University Press, Ithaca, New York (1960).
18. A. L. Allred and E. G. Rochow, *J. Inorg. Chem. Nucl. Chem.* 1958, **5**, 264; E. J. Little and M. M. Jones, *J. Chem. Educ.* 1960, **37**, 231.
19. J. Mullay, *J. Am. Chem. Soc.* 1984, **106**, 5842.
20. R. G. Pearson, *Inorg. Chem.* 1988, **27**, 734; R. G. Pearson, *Inorg. Chem.* 1984, **23**, 4675; R. G. Pearson, *J. Am. Chem. Soc.* 1988, **110**, 7684.
21. T. P. Duggan, D. J. Barnett, M. J. Muscatella and J. B. Keister, *J. Am. Chem. Soc.* 1986, **108**, 6076.
22. D. G. Van der Velde, J. S. Holmgren and J. R. Shapley, *Inorg. Chem.* 1987, **26**, 3077.
23. This ignores the larger steric effect of the methyl group which will also favour the M—H—M site. See ref. 10.
24. U. Schubert, J. Müller and H. G. Alt, *Organometallics* 1987, **6**, 469.
25. J. W. Park, P. B. Mackenzie, W. P. Schafer and R. H. Grubbs, *J. Am. Chem. Soc.* 1986, **108**, 6402.
26. C. M. Lukehard, *Fundamentals of Transition Metal Organometallic Chemistry*. Brooks-Cole, Monterey, California (1985); C. Masters, *Adv. Organomet. Chem.* 1979, **17**, 61.
27. C. K. Rofer-DePoorter, *Chem. Rev.* 1981, **81**, 447; G. Henrici-Olive and S. Olive, *Angew. Chem. Int. Edn Engl.* 1976, **15**, 136; E. L. Muetterties and J. Stein, *Chem. Rev.* 1979, **79**, 479.
28. P. Biloen and W. M. H. Sachtler, *Adv. Catal.* 1981, **30**, 165.
29. H. Pichler, *Brennst.-Chem.* 1938, **19**, 226.
30. K. Yoshino and C. J. McMahon Jr, *Met. Trans.* 1974, **5**, 363.
31. Y. Ogino and T. Yamasaki, *Scripta Met.* 1981, **15**, 821.
32. C. J. McMahon Jr, V. Vitek and G. R. Belton, *Scripta Met.* 1978, **12**, 785.
33. J. Vites, C. E. Housecroft, C. Eigenbrot, M. L. Buhl, G. J. Long and T. P. Fehlner, *J. Am. Chem. Soc.* 1986, **108**, 3304.
34. J. C. Vites, C. E. Housecroft, G. B. Jacobsen and T. P. Fehlner, *Organometallics* 1984, **3**, 1591.
35. A. K. Chipperfield and C. E. Housecroft, *J. Organomet. Chem.* 1988, **349**, C17.
36. S. G. Shore, D.-Y. Jan, L.-Y. Hsu and W.-L. Hsu, *J. Am. Chem. Soc.* 1983, **105**, 5923.
37. T. K. Dutta, J. C. Vites, G. B. Jacobsen and T. P. Fehlner, *Organometallics* 1987, **6**, 842.
38. T. K. Dutta, X. Meng, J. C. Vites and T. P. Fehlner, *Organometallics* 1987, **6**, 2191.

39. M. A. Andrews and H. D. Kaesz, *J. Am. Chem. Soc.* 1979, **101**, 7255.
40. C. R. Eady, B. F. G. Johnson and J. Lewis, *J. Chem. Soc., Dalton Trans.* 1977, 477.
41. A. J. Deeming and M. Underhill, *J. Chem. Soc., Chem. Commun.* 1973, 277.
42. S. Bhaduri, K. S. Gopalkrishnan, W. Clegg, P. G. Jones, G. M. Sheldrick and D. Stalke, *J. Chem. Soc., Dalton Trans.* 1984, 1765.
43. K. S. Wong, W. R. Scheidt and T. P. Fehlner, *J. Am. Chem. Soc.* 1982, **104**, 1111.
44. C. E. Housecroft and T. P. Fehlner, *Organometallics* 1986, **5**, 379.
45. N. P. Rath and T. P. Fehlner, *J. Am. Chem. Soc.* 1987, **109**, 5273.
46. M. A. Beno, J. M. Williams, M. Tachikawa and E. L. Muetterties, *J. Am. Chem. Soc.* 1981, **103**, 1485.
47. J. H. Davis, M. A. Beno, J. M. Williams, J. Zimmie, M. Tachikawa and E. L. Muetterties, *Proc. Natl. Acad. Sci. USA* 1981, **78**, 668.
48. J. A. Hriljac, S. Harris and D. F. Shriver, *Inorg. Chem.* 1988, **27**, 816.
49. D. E. Fjare and W. L. Gladfelter, *Inorg. Chem.* 1981, **20**, 3533.
50. A. G. Cowie, B. F. G. Johnson, J. Lewis and P. R. Raithby, *J. Organomet. Chem.* 1986, **306**, C63.
51. R. B. Calvert and J. R. Shapley, *J. Am. Chem. Soc.* 1977, **99**, 5225.
52. C. J. Cardin, D. J. Cardin, H. E. Parge and J. M. Power, *J. Chem. Soc., Chem. Commun.* 1984, 609.

Polyhedron Vol. 9, No. 15/16, pp. 1965–1973, 1990
Printed in Great Britain

0277–5387/90 $3.00+.00
© 1990 Pergamon Press plc

He I VALENCE PHOTOELECTRON SPECTRA OF OXOMOLYBDENUM(V) COMPLEXES CONTAINING DIOLATO OR ALKOXIDE LIGANDS*

C. S. J. CHANG, A. RAI-CHAUDHURI, D. L. LICHTENBERGER and J. H. ENEMARK†

Department of Chemistry, University of Arizona, Tucson, AZ 85721, U.S.A.

Abstract—The He I valence photoelectron spectra (PES) are reported for several monooxomolybdenum(V) compounds with the general formula of $LMoO[O—(CH_2)_n—O]$ and $LMoO(OR)_2$ (L = hydrotris(3,5-dimethyl-1-pyrazolyl)borate; $n = 2$–4; R = Me, Et, ^{n}Pr). The spectra show that the size of the metal–chelate ring in these diolato complexes has a substantial effect on the HOMO ionization. As the chelate ring size in the diolato complexes increases, the HOMO shifts (*ca* 0.21–0.24 eV) to lower ionization energy. The diolato complexes have their HOMO's at a higher ionization energy than analogous open chain bis-alkoxide complexes possessing the same number of carbon atoms. The unconstrained bis-alkoxide complexes show much smaller shifts ($\leqslant 0.11$ eV) in the ionization potential associated with the HOMO upon the addition of a CH_2 unit to each alkoxide group. These gas-phase results are similar to the results observed by electrochemistry in acetonitrile solution, where both the diolato and bis-alkoxide complexes become easier to oxidize upon increasing the number of CH_2 groups, as indicated by their half-wave potentials. The $p\pi$ orbital ionizations of the oxygen atoms in the alkoxide functions are also shifted (*ca* 0.12 eV) to lower ionization energy upon adding CH_2 residues to the alkoxide chain.

The study of models for the molybdenum cofactor (Mo-co) remains an intriguing topic.[1–5] Previous studies of model compounds for Mo-co of "oxo-type" molybdoenzymes[6] have mainly focused on mimicking the enzyme's catalytic reactions,[7,8] or duplicating parameters of the EPR (electron paramagnetic resonance) spectra,[9] the EXAFS (Extended X-Ray Absorption Fine Structure) spectra,[5,10] and electrochemical behaviour.[9d,11,12] To date, however, little attention has been given to the role of the backbone and side chain of the metal–chelate ring and how it can affect the electrochemical and spectroscopic properties of the molybdenum centre. Some systematic investigations of the effect of the backbone of the metal–chelate ring on the spectroscopic properties of a metal centre have been reported,[13] but only a few studies of the spectroscopic properties of monooxo–metal complexes with chelated ligands have been published.[14]

We have recently reported solution electrochemical and spectroscopic measurements of a series of diolato and bis-alkoxide oxomolybdenum(V) complexes with the general structure shown below in **1**–**6**,[15] where compounds **1**–**3**, and **4**–**6** are diolato and bis-alkoxide complexes, respectively.

The reduction potentials of both the Mo^{VI}/Mo^{V} and the Mo^{V}/Mo^{IV} pairs and the lowest energy electronic absorption bands (λ_{max}) for these complexes are a function of the backbone of the diolato or alkoxide ligands. The shifts of the half-wave potentials of the Mo^{VI}/Mo^{V} pair for compounds **2** and **3**, **4** and **5**, and **5** and **6** are 0.217, 0.030 and 0.019 V, respectively. Clearly, the shifts are significant in the diolato compound series, but not in the bis-alkoxide compound series. A similar situation is also observed for the half-wave potentials of the Mo^{V}/Mo^{IV} pair, where the shift is 0.168 and 0.218 V between compounds **1** and **2**, **2** and **3**, individually, and the shift for compounds **4** and **5**, and **5** and **6** is 0.066 and 0.042 V, respectively. We have

* Dedicated to Professor Richard F. Fenske for his contributions to theoretical inorganic chemistry and for his inspiration to others.

† Author to whom correspondence should be addressed.

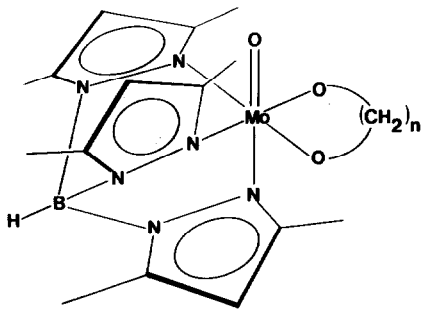

(1) n = 2
(2) n = 3
(3) n = 4

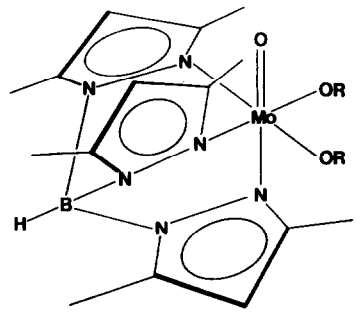

(4) R = Me
(5) R = Et
(6) R = ^{n}Pr

suggested that a steric effect, especially ring strain, could be primarily responsible for this observed pattern of electrochemical behaviour because unconstrained bis-alkoxide complexes show no significant changes in their electrochemical properties.

Photoelectron spectroscopy provides primary information about the orbital ionization energies of electrons and about electron distribution in the complexes. In addition, comparison of results obtained from PES of a series of related families of compounds is considered to be highly useful for obtaining secondary information relating to the geometries of compounds.[16] The relative shifts of the valence ionizations in a series of similar compounds are not only sensitive to charge distributions and relaxation energies, but also to the orbital overlap interactions. The result of the He I valence photoelectron spectroscopy measurements and their significance for these complexes form the basis of this report.

EXPERIMENTAL

Preparation

Compounds **1–7** were prepared by previously reported methods,[3,15] and characterized by elemental analysis, mass spectrometry, cyclic voltammetry, IR, UV–vis spectroscopy and EPR. The neutral ligand, tris(3,5-dimethylpyrazolyl)methane [compound (**8**)] was prepared by a modification of the method of Trofimenko[17] and showed a satisfactory C, H, and N analysis.

Photoelectron spectra

All PES were measured with use of a spectrometer which features a 36-cm radius hemispherical analyser (10-cm gap), and customized sample cells, excitation sources, detection and control electronics, and data collection methods that have been described previously.[18] The Ar $^{2}P_{3/2}$ ionization at 15.759 eV was used as an internal spectral lock for the energy scale. The spectrum of each compound was taken at least twice with no discernable differences between replicate spectra; no decomposition was observed either before or after the compound sublimed. Data were collected at different sample cell temperatures for different compounds (130°C for **1**, 141°C for **2**, 158°C for **3**, 130°C for **4**, 121°C for **5**, 120°C for **6**, 173°C for **7** and 45°C for **8**). The mass spectra recorded at temperatures used in the collection of the spectra indicated that the samples do not decompose. The collected data are represented analytically with the best fit of asymmetric Gaussian peaks by using the program GFIT.[19] The asymmetric Gaussian peaks are defined with the position, the amplitude, the half-width indicated by the high binding energy side of the peak (W_h), and the half-width indicated by the low binding energy side of the peak (W_l). The confidence limits of the peak positions and deviation for widths are generally ± 0.02 eV. The confidence limit of the area of a band envelope is about $\pm 5\%$, with uncertainties introduced in the baseline subtraction and fitting in the tails of the peaks. The parameters of overlapping peaks are not independent and therefore are more uncertain.

RESULTS AND DISCUSSION

Photoelectron spectra

The He I valence PES of the complexes studied in this work are recorded over the range 5.5–15.5 eV, as shown in Fig. 1. The ionization energy region above 11.0 eV displays broad and unresolved overlapping ionizations which mainly result from ionization of σ-bonding electrons in ligand moieties, C—C, C—H etc., and will not be discussed further.

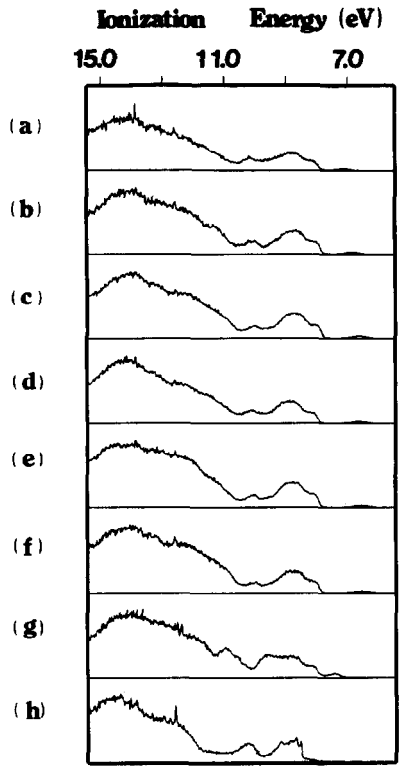

Fig. 1. Photoelectron spectra from 5.5 to 15.5 eV of compounds (a) LMoO[O—$(CH_2)_2$—O]; (b) LMoO[O—$(CH_2)_3$—O]; (c) LMoO[O—$(CH_2)_4$—O]; (d) $LMoO(OMe)_2$; (e) $LMoO(OEt)_2$; (f) $LMoO(^nPr)_2$; (g) $LMoOCl_2$; (h) $HC\{(3,5\text{-}Me)_2Pz\}_3$.

The close-up PES are shown in Figs 2–4. For Figs 2 and 4, the region of 5.5–11.0 eV was analytically represented with six and seven asymmetric Gaussian peaks (labelled 1–6 and 1–7), respectively, whereas only three peaks (labelled 1–3) were used to fit Fig. 3 which is the PES of compound **8**. The overall band shapes for the metal and ring π-ionization bands of compounds **1–6** remain the same throughout the series and are obviously different from those of $LMoOCl_2$ [compound (**7**)], which is the starting material.

In Figs 2 and 4, three distinct regions of ionizations can be observed in the close-up spectra of the diolato and bis-alkoxide compounds. The first region comprises the lowest ionization energy band (band 1), which is always broad and well isolated from other ionizations, except for that of the ethanediolato compound (**1**). The second region is a broad, unshifted set of bands (*ca* 7.75–9.5 eV) with one distinct shoulder on the low ionization energy side (band 2) and one partially resolved shoulder on the high ionization energy side (band 4 in Fig. 2 and bands 4 and 5 in Fig. 4). The last region (band 5 in Fig. 2 and band 6 in Fig. 4) is a broad band with similar position as observed in compound **8** (band 3 in Fig. 3). The vertical ionization energies of the bands are given in Table 1.

Diolato complexes **1–3**

From Fig. 2 and Table 1, it is very clear that band 1 shifts toward lower ionization energy with the increase in the size of the metal–chelate ring. Band 1 (HOMO) represents the contribution from the unpaired electron in the 4*d* orbital of the molybdenum atom. This assumption is based on the fact that this ionization is not observed in the PES of diols,[20] alcohols[20,21] and tris(3,5-dimethylpyrazolyl)methane [compound (**8**)]. The ranges of W_h and W_l for this ionization envelope are 0.62–0.70 eV and 0.37–0.51 eV, respectively. Such a broad feature reflects the bonding property for this band, and shows that the electron is not absolutely localized in the molybdenum *d* orbital.

Band 2 (SHOMO) in Fig. 2 also has a pronounced asymmetric feature not observed in the spectrum of compound **8**. Band 2 is primarily comprised of the $2p_x$ and $2p_y$ orbital ionizations of the terminal oxo ligand, which are oriented to interact with the empty $4d_{xz}$ and $4d_{yz}$ orbitals of the mol-

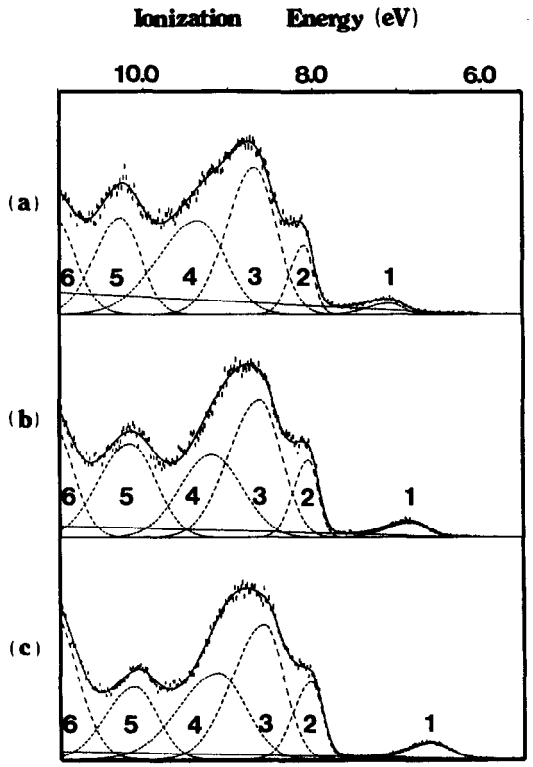

Fig. 2. Close-up PES in the range of 5.5–11.0 eV of (a) LMoO[O—$(CH_2)_2$—O]; (b) LMoO[O—$(CH_2)_3$—O]; (c) LMoO[O—$(CH_2)_4$—O].

Table 1. Ionization data for compounds **1–6** and **8**[a]

Compound	Ionization	Binding energy (eV)	Relative amplitude	W_h (eV)	W_l (eV)	Normalized area
	1	7.09	1.00	0.62	0.37	0.06
	2	8.11	6.15	0.37	0.27	0.22
1	3	8.69	12.97	0.77	0.61	1.00
	4	9.36	8.32	1.10	0.77	0.87
	5	10.27	9.13	0.72	0.57	0.61
	1	6.85	1.00	0.70	0.43	0.08
	2	8.06	5.08	0.42	0.27	0.26
2	3	8.60	9.09	0.88	0.59	1.00
	4	9.21	5.45	0.88	0.59	0.71
	5	10.16	6.18	0.87	0.71	0.73
	1	6.64	1.00	0.64	0.51	0.10
	2	8.04	4.74	0.50	0.30	0.32
3	3	8.59	8.19	0.92	0.53	1.00
	4	9.14	5.28	1.10	0.76	0.83
	5	10.12	4.42	0.82	0.61	0.54
	1	6.69	1.00	0.60	0.55	0.08
	2	8.11	4.92	0.49	0.23	0.24
	3	8.72	10.99	0.76	0.59	1.00
4	4	9.24	6.99	0.72	0.60	0.62
	5	9.85	3.62	0.48	0.43	0.22
	6	10.18	5.33	0.85	0.35	0.43
	1	6.58	1.00	0.68	0.52	0.09
	2	8.09	5.91	0.73	0.25	0.43
	3	8.70	10.41	0.77	0.52	1.00
5	4	9.15	6.08	0.77	0.51	0.58
	5	9.73	2.44	0.66	0.37	0.19
	6	10.10	4.07	0.86	0.33	0.36
	1	6.58	1.00	0.65	0.52	0.07
	2	8.09	6.54	0.57	0.25	0.33
	3	8.65	11.22	0.96	0.50	1.00
6	4	9.11	5.69	0.66	0.58	0.43
	5	9.61	3.46	0.40	0.40	0.17
	6	10.06	5.72	0.77	0.40	0.40
	1	8.74	1.40	0.60	0.44	1.00
8	2	9.26	1.00	0.60	0.44	0.71
	3	10.24	1.17	1.37	0.61	1.59

[a] For the first ionization, the error bar in the fit analysis is ± 0.02 eV for peak position, 0.05–0.2 eV in half-widths, 5–10% in relative amplitudes.

ybdenum atom. This ionization envelope is also observed in compound **7** [Fig. 1(g)], with a similar position to that shown in the spectra of compounds **1–3** [Fig. 1(a)–(c)]. Since the only oxygen atom involved in compound **7** is the terminal oxo ligand, we assign band 2 to ionizations from this oxygen atom. In addition, the lone-pair electrons of chlorine ligands in compound **7** should be well separated from the ionization envelope of lone-pair electrons of the oxygen atom. The Fenske–Hall molecular orbital calculations on compound **7** showed that the ionization energies of the lone-pair electrons of chlorine differ by at least 0.6 eV from those of the oxygen atom. The experimental result shows that the lone-pair electrons on the chlorine atoms in compound **7** have much higher ionization energy (IP $\approx$ 11 eV) compared with the lone-pair electrons of the terminal oxygen atom. Similar behaviour is found for many organic compounds[20] containing both a chlorine atom and carbonyl oxygen atom

and which exhibit ionization energies for the lone-pair electrons of the oxygen atom that are lower than the lone-pair electrons of the chlorine atom. Band 2 shows almost no shift with change of the number of methylene units in diolato or alkoxide groups (8.04–8.11 eV and 8.09–8.11 eV for diolato and bis-alkoxide compounds, respectively). The small range of ionization energies is also consistent with the narrow range of molybdenum–oxygen bond lengths in most monooxo complexes.[22] Thus, the bonding between the molybdenum atom and the terminal oxo ligand is quite insensitive to the nature of the ligands which occupy the remaining coordination sites.

Comparison of the spectra obtained from 1H-pyrazole,[23] 1H-3,5-dimethylpyrazole[24] and tris(3,5-dimethylpyrazolyl)methane (Figs 1(h) and 3) indicate that bands 3 and 4 are probably derived from the $p\pi$ orbital electron ionizations of the pyrazole rings. The energies of these orbitals will not be significantly affected by a change of the local environment around the metal centre of the complexes. However, comparison of the band widths of the $p\pi$ ionizations (bands 1 and 2) of compound **8** with bands 3 and 4 of the complexes shows that the band 4 is significantly more broadened than band 3. This result indicates that either the bonding character has increased or that overlapping with other ionizations occurs (as is observed in bands 4 and 5 of compounds **4–6**, *vide infra*). These $p\pi$ orbitals do not interact with the *d* orbitals of molybdenum and show no disturbance of their electronic environment by other ligands around the metal centre, and the first possibility can be ruled out. The broadening of band 4 is assigned to overlapping $p\pi$ ionizations from oxygen atoms in the diolato ligands that might be buried under band 4.

The last band (band 5) for compounds **1–3**, is assigned to the lone-pair electrons of nitrogen atoms in the pyrazole rings and has a similar feature to band 3 in compound **8**. Ionizations of the oxygen

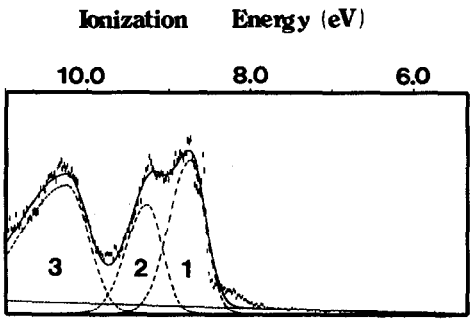

Fig. 3. Close-up PES in the range of 5.5–11.0 eV of compound **8**, $HC\{(3,5\text{-}CH_3)Pz\}_3$.

$p\pi$ electrons might also have some overlap with this band; however, it is very difficult to confirm this. The ionization energy of this band shifts from 10.27 to 10.12 eV from compound **1** to **3**, suggesting that the ionization energy of band 5 is still quite close to that of compound **8**, probably also indicating that the interaction with the *d* orbitals of the metal centre is not as important as that between $p\pi$ electrons of the diolato oxygen atoms and $d\pi$ electrons of the molybdenum atom mentioned above. The symmetry of these molecules is no higher than C_s, and these compounds contain at least four kinds of chemically different nitrogen atoms. Nevertheless, no splitting of this ionization is observed, in contrast to the case of $[Ir(\mu\text{-dimethylpyrazolyl})(CO)_2]_2$.[24]

For the ionization energies within the range of 9–10 eV, compounds **1–3** can be represented by one asymmetric Gaussian peak (band 5), whereas compounds **4–6** are represented by two asymmetric Gaussian peaks (bands 5 and 6). In complexes **4–6**, the ionizations of $p\pi$ electrons of the alkoxide oxygen atoms are observed separately as band 5 which is at lower IP than band 6 which is the nitrogen lone pair ionization. The oxygen $p\pi$ ionizations are not resolved in complexes **1–3** because they are shifted due to the stabilization of the diolato oxygen $p\pi$ ionizations in these complexes as a result of $O(p\pi)$–$Mo(d\pi)$ bonding interactions.

Bis-alkoxide complexes **4–6**

The vertical ionization energies of each band for these complexes are listed in Table 1 (spectra in Fig. 4). Bands 2, 3, 4 and 6 for all these compounds maintain similar positions throughout the entire compound series and they are also located in similar positions to those in the diolato complexes. Therefore, they probably arise from those orbitals mentioned in the case of the diolato complexes. The only difference is that the ionizations from $p\pi$ electrons of the orbitals of the oxygen atoms (band 5) of the alkoxide ligands are resolved in these compounds, whereas the ionizations from $p\pi$ electrons of the diolato oxygen atoms are not.

The PES of alkyl alcohol, ROH (R = Me, Et and ^{n}Pr), have been published.[21] The leading vertical ionization potentials decrease from 10.94 to 10.49 eV from R = Me to R = ^{n}Pr due to association with the inductive effect of alkyl groups and reduced oxygen 2*p* character in the HOMO. The ionization energies of the oxygen $p\pi$ electrons are initially lowered by forming the alkoxide anion (RO^-) from the alcohol molecule due to increase of the electron density of the oxygen atom in the alkoxide ligand.

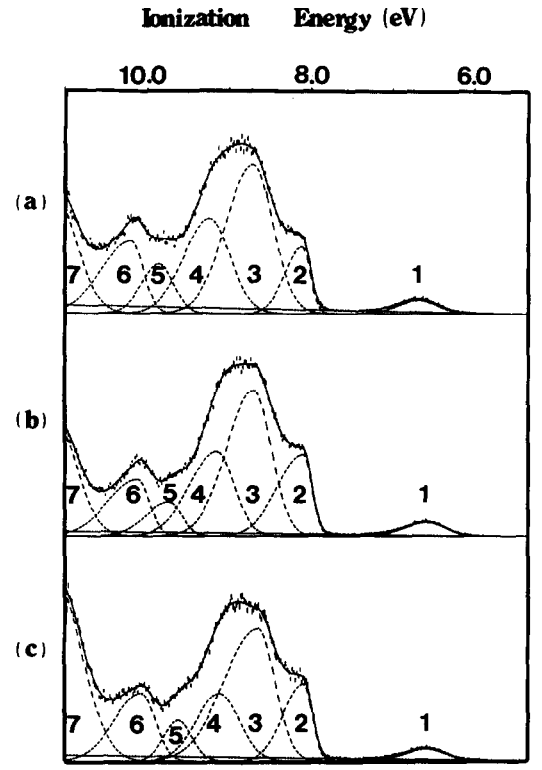

Fig. 4. Close-up PES in the range of 5.5–11.0 eV of (a) $LMoO(OMe)_2$; (b) $LMoO(OEt)_2$; (c) $LMoO(O^nPr)_2$.

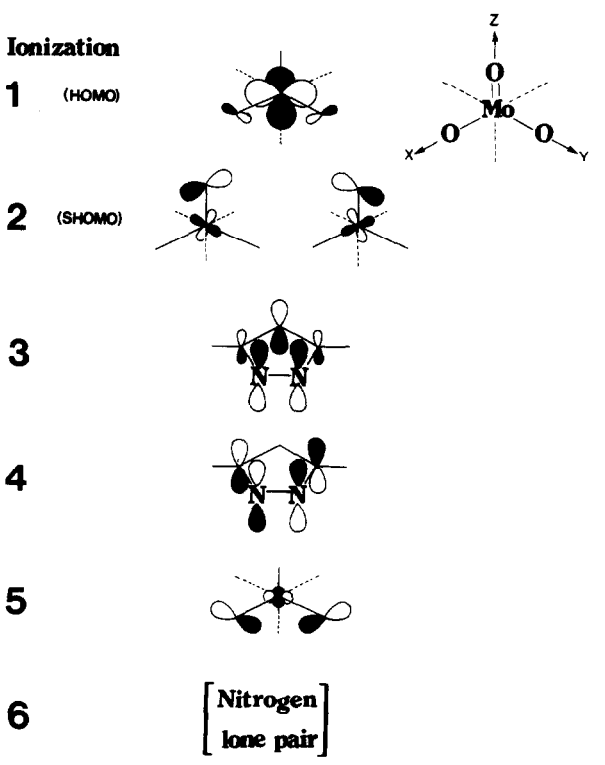

Scheme 1.

The σ-bonding between the oxygen atom in the alkoxide ligand and the molybdenum atom slightly stabilizes this $p\pi$ ionization, but there is no additional stabilization from π-bonding interactions between the alkoxide oxygen atoms and the molybdenum d electron, as occurs in the diolato complexes (*vide supra*).

In bis-alkoxide complexes, both bands 1 and 5 exhibit shifts to lower ionization energy with the introduction of more methylene units to the linear alkyl groups. For band 1, the maximum shift is only 0.11 eV. The error in the fit analysis is ± 0.02 eV for peak position, so the shift in band 1 among the bis-alkoxide compound series is barely significant. Briefly, according to these two facts, in the bis-alkoxide complexes, the interaction between $p\pi$ electrons of the oxygen atoms, in the alkoxide groups and the $d\pi$ electron of the molybdenum atom is a purely electrostatic repulsion. Consequently, the HOMO is only destabilized by a small degree upon increasing the number of methylene units in the alkyl moieties. This is different from the case in the diolato complex series. Since the HOMO in the diolato complexes is destablized by an overlap interaction between $p\pi$ electrons of the diolato oxygen atoms and the $d\pi$ electron of the molybdenum atom, a significant variation of the ionization energy of the HOMO is observed upon changing the number of methylene units in the ring (*vide ante*).

Summary of PES spectra

Both the diolato and bis-alkoxide compound series exhibit similar He I PES. Consequently, comparing with the PES of 1H-3,5-dimethylpyrazole and tris(3,5-dimethylpyrazolyl)methane, a purely qualitative molecular orbital diagram can be used to assign each band discussed in compounds **1**–**6**, as shown in Scheme 1 (for compounds **4**–**6**) and Scheme 2 (for compounds **1**–**3**).

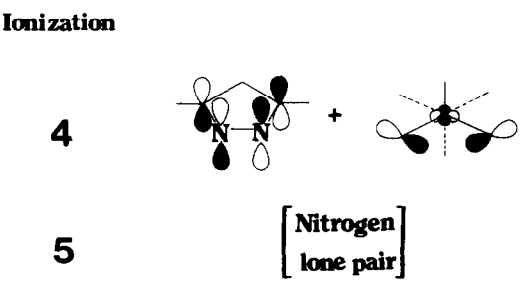

Scheme 2.

Correlation with electrochemistry

The detailed results of solution electrochemistry have been reported earlier.[15] Within the diolato compound series, the complexes become easier to oxidize with increasing chelate ring size. In the bis-alkoxide compound series, complexes become easier to oxidize with extension of alkyl chains in alkoxide ligands.

The oxidation potential recorded from solution electrochemistry is the energy difference between the positively charged molecular ion (oxidized species) in its electronic ground state and the neutral molecule and some other energy terms, like solvation energy. The ionization potential for the HOMO is the energy necessary to generate the positive ion in its electronic ground state in the gas phase and can be thought of as a difference of the heat of formation between the molecule and its molecular ion, neglecting vibrational energy. Nevertheless, since we measure a series of similar complexes under similar experimental conditions, the $E_{1/2}$ value from solution electrochemistry should be directly proportional to the HOMO energy from gas-phase PES, as suggested by Bursten:[25]

$$E_{1/2} = k_1(-\varepsilon_{\mathrm{HOMO}}) + k_2.$$

The equation for the least-squares line of compounds **2**–**6** is shown in Fig. 5, where IP(eV) = $0.685(E_{1/2},\mathrm{V}) + 6.25$ with a correlation coefficient of 0.919.

The half-wave potentials ($E_{1/2}$) for oxidation obtained from solution phase by electrochemical methods can be thought of as a "solution ionization potential" of the highest occupied orbital.[25] Studies on the linear correlation between the HOMO energy and $E_{1/2}$ for oxidation have been reported for many systems.[25,26] In the present oxidation–reduction reactions, the participating orbital is mainly the Mo($4d_{xy}$) orbital, which has the lowest ionization energy. Consequently, the less stable the HOMO of a complex, the easier it is to oxidize, as shown in Fig. 5. The oxidation potentials from solution electrochemistry follow the order **6** < **5** < **4** < **3** < **2**; however, this trend is altered somewhat in the gas phase, **6** ≃ **5** < **3** < **4** < **2** < **1**. In the solution electrochemistry measurement, the redox process is not a Frank–Condon type instantaneous electronic excitation. However, the photoionization of a molecule in the gas phase obeys the Frank–Condon principle. Consequently, the difference between these trends from two different phases might reflect a contribution from the solvation energy of various molecular ions.

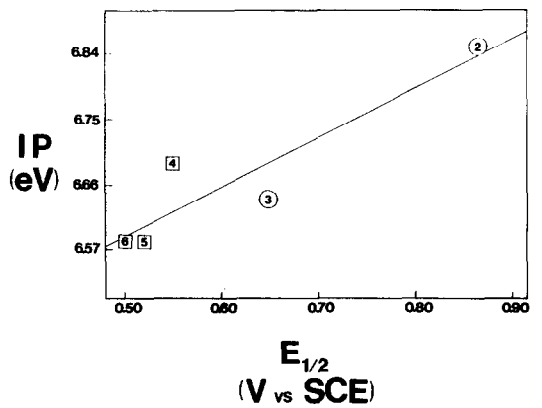

Fig. 5. Correlation of half-wave oxidation potential ($E_{1/2}$), in V vs SCE, with lowest energy ionization potential (IP), in eV, for compounds **2**–**6**.

On the basis of arguments mentioned earlier, the ionizations 1, 2, 4 (for compounds **1**–**3**), or 5 (for compounds **4**–**6**) contain some *p* character from oxygen atoms in the diolato and alkoxide ligands. Therefore, the *strength* of the interaction between $d\pi$ electron of the molybdenum atom and $p\pi$ electrons of the ligand group orbitals of diolato or alkoxide moieties primarily determines whether or not the HOMO will be destabilized. The larger the interaction between the half-filled $d\pi$ and filled oxygen $p\pi$ orbitals, the more the HOMO will be destabilized, and the easier it is to oxidize the complex. In the diolato compound series, this interaction becomes significant in a compound with larger ring size because better overlap is possible between $4d_{xy}$(Mo) and $p\pi$(O) with such a flexible ring conformation. This phenomenon is reflected by increasing the ionization energy difference between band 4 and band 1 from 2.27 to 2.50 eV for compounds **1** to **3**. The seven-membered ring diolato compound (**3**) has the lowest ionization energy for a HOMO in a diolato series, and it also exhibits the lowest half-wave potential and becomes the easiest to oxidize in that series. The unconstrained bis-alkoxide compounds show only minor or no shift of the HOMO to lower ionization energy with longer chain alkyl groups, suggesting that the interaction between $4d_{xy}$(Mo) and the alkoxide $p\pi$(O) orbitals is quite similar in all bis-alkoxide compounds because of similar electronic and steric effects among those alkoxide ligands. However, for the diolato complex series, the steric constraints of the chelate ring will alter the $4d_{xy}$(Mo) and $p\pi$(O) interaction for different complexes.

CONCLUSION

This work has shown that a series of structurally similar diolato and bis-alkoxide complexes exhibit

similar PES. However, there are three differences between these two complex series. (1) The ionization energies of the HOMO of the diolato complexes show significant shifts, but those for the bis-alkoxide complexes do not. (2) The ionization from the $p\pi$ electrons of the alkoxide oxygen atoms is resolved as band 5 in the bis-alkoxide complexes, but that from analogous diolato oxygen atoms in the diolato complexes is not. (3) The main source of the shifts of the ionization energies of the HOMO of the diolato complexes is the bonding interaction between the $p\pi$(O) and $d\pi$(Mo) orbitals which depends on the steric constraints of the metal–chelate ring. Such steric constraints are absent in the bis-alkoxide complexes and the slight destabilization of the HOMO is mainly due to electrostatic repulsion between the $p\pi$(O) and $d\pi$(Mo) electrons which varies little among the compounds.

The electronic effect for diolato and alkoxide ligands having the same number of carbon atoms in their backbones should be similar to one another (as ethanediolato and butanediolato are similar to that of bis-methoxide and bis-ethoxide, respectively), but their steric effects can be considerably different. This work shows that the diolato compound series exhibits a significant shift of the ionization energy of the HOMO, but only a small shift is found among the bis-alkoxide compounds. This result implies that the steric effect resulting from the strain in the diolato chelated ring is primarily responsible for the strength of the interaction between $4d_{xy}$(Mo) and $2p\pi$(O).

Acknowledgements—Support by the National Institutes of Health (Grant GM37773) to J.H.E. is gratefully acknowledged. D.L.L. acknowledges support by the U.S. Department of Energy (Division of Chemical Sciences, Office of Basic Energy Sciences, Office of Energy Research, DE-FG02-86ER13501), and the Materials Characterization Program, Department of Chemistry, University of Arizona. We also thank Michael D. Carducci for providing tris(3,5-dimethylpyrazolyl)methane, and Roy Hogan for helpful discussions.

REFERENCES

1. K. Yamanouchi, J. T. Huneke and J. H. Enemark, in *Molybdenum Chemistry of Biological Significance* (Edited by W. E. Newton). Plenum Press, New York (1979).
2. E. I. Steifel, in *Progress in Inorganic Chemistry* (Edited by S. J. Lippard), Vol. 22, pp. 1–223. John Wiley, New York (1977).
3. W. E. Cleland, K. M. Barnhart, K. Yamanouchi, D. Collison, F. E. Mabbs, R. B. Ortega and J. H. Enemark, *Inorg. Chem.* 1987, **26**, 1017.
4. U. Küsthardt and J. H. Enemark, *J. Am. Chem. Soc.* 1987, **109**, 7926.
5. R. Singh, J. T. Spence, G. N. George and S. P. Cramer, *Inorg. Chem.* 1989, **28**, 8.
6. (a) T. D. Tullius, D. M. Kurtz, Jr., S. D. Conradson and K. D. Hodgson, *J. Am. Chem. Soc.* 1979, **101**, 2776; (b) J. Bordas, R. C. Bray, C. D. Garner, S. Gutteridge and S. S. Hasnain, *J. Inorg. Biochem.* 1979, **11**, 181; (c) J. Bordas, R. C. Bray, C. D. Garner, S. Gutteridge and S. S. Hasnain, *Biochem. J.* 1980, **191**, 499; (d) S. P. Cramer, H. B. Gray and K. V. Rajagopalan, *J. Am. Chem. Soc.* 1979, **101**, 2772.
7. (a) C. D. Garner, M. R. Hyde, F. E. Mabbs and V. I. Routledge, *J. Chem. Soc., Dalton Trans.* 1975, 1180; (b) M. R. Hyde and C. D. Garner, *J. Chem. Soc., Dalton Trans.* 1975, 1186.
8. R. D. Taylor, P. G. Todd, N. D. Chasteen and J. T. Spence, *Inorg. Chem.* 1979, **18**, 44.
9. (a) M. I. Scullane, R. D. Taylor, M. Minelli, J. T. Spence, K. Yamanouchi, J. H. Enemark and N. D. Chasteen, *Inorg. Chem.* 1979, **18**, 3213; (b) G. R. Hanson, G. L. Wilson, T. D. Bailey, J. R. Pilbrow and A. G. Wedd, *J. Am. Chem. Soc.* 1987, **109**, 2609; (c) D. Dowerah, J. T. Spence, R. Singh, A. G. Wedd, G. L. Wilson, F. Farchione, J. H. Enemark, J. Kristofzski and M. J. Bruck, *J. Am. Chem. Soc.* 1987, **109**, 5655; (d) J. R. Bradbury, G. R. Hanson, I. W. Boyd, S. F. Gheller, A. G. Wedd, K. S. Murry and A. M. Bond, in *Proceedings of the Climax Third International Conference on the Chemistry and Uses of Molybdenum* (Edited by H. F. Barry and P. C. H. Mitchell), pp. 300–309. Climax Molybdenum Co. Ltd, Ann Arbor, Michigan (1979).
10. S. P. Cramer, H. B. Gray, N. S. Scott, M. Barber and K. V. Rajagopalan, in *Molybdenum Chemistry of Biological Significance* (Edited by W. E. Newton), pp. 157–168. Plenum Press, New York (1979).
11. J. K. Howie and D. T. Sawyer, *Inorg. Chem.* 1976, **15**, 1892.
12. J. Topic and N. Berger, *Inorg. Chim. Acta.* 1982, **65**, L131.
13. (a) A. J. Panighianti, D. J. Minn, W. C. Fultz and J. L. Burmeister, *Inorg. Chim. Acta.* 1989, **1591**, 65; (b) A. Zanardo, R. A. Michelin, F. Pinna and G. Struku, *Inorg. Chem.* 1989, **28**, 1648; (c) W. E. Hill, L. A. McAuliffe, I. E. Niven and R. V. Parish, *Inorg. Chim. Acta.* 1980, **38**, 273; (d) A. Pryde, B. Shaw and B. Weeks, *J. Chem. Soc., Dalton Trans.* 1976, 322; (e) R. Romeo, D. Minniti, S. Lanza and M. L. Tobe, *Inorg. Chim. Acta.* 1977, **22**, 87; (f) W. Levason and L. A. McAuliffe, *Adv. Inorg. Chem. Radiochem.* 1972, **14**, 173.
14. (a) R. W. Wiggins, J. C. Huffman and G. J. Christun, *J. Chem. Soc., Chem. Commun.* 1983, 1313; (b) J. K. Money, J. C. Huffman and G. Christun, *Inorg. Chem.* 1985, **24**, 3297; (c) A. Davison, B. V. Depamphillis, R. Faggiani, A. G. Jones, C. J. L. Lock and C. Orvig, *Can. J. Chem.* 1985, **63**, 319; (d) J. E. Smith, F. E. Byrnl, F. A. Cotton and J. C. Sekutowski, *J. Am. Chem. Soc.* 1978, **100**, 5571;

(e) P. T. Bishop, J. R. Dilworth, J. Hutchinson and J. A. Zubieta, *J. Chem. Soc., Chem. Commun.* 1982, 1052; (f) F. L. Phillips and A. C. Skapski, *Acta Cryst.* 1975, **B31**, 1814.
15. C. S. J. Chang, D. Collison, F. E. Mabbs and J. H. Enemark, *Inorg. Chem.*, in press.
16. A. D. Baker and C. R. Brundle, in *Electron Spectrocopy: Theory, Techniques and Applications* (Edited by C. D. Brundle and A. D. Baker), Vol. 1, pp. 1–73. Academic Press, New York (1977).
17. S. Trofimenko, *J. Am. Chem. Soc.* 1970, **92**, 5118.
18. (a) D. C. Calabro, J. L. Hubbard, C. H. Blevins II, A. C. Campbell and D. L. Lichtenberger, *J. Am. Chem. Soc.* 1981, **103**, 6839; (b) D. L. Lichtenberger, D. C. Calabro, G. E. Kellogg, J. G. Kristofzski, D. Page, S. Turner, G. Klinger and J. Lorenzen, *Rev. Sci. Instrum.* 1986, **57**, 2366.
19. D. L. Lichtenberger and R. F. Fenske, *J. Am. Chem. Soc.* 1976, **98**, 50.
20. K. Kimura, S. Katsumata, Y. Achiba, T. Yamazaki and S. Iwata, in *Handbook of* He I *Photoelectron Spectra of Fundamental Organic Molecules*, pp. 149–161. Japan Scientific Societies, Tokyo (1981).
21. (a) A. D. Baker, D. Betteridge, N. R. Kemp and R. E. Kirby, *Analyt. Chem.* 1971, **43**, 375; (b) S. Katsmata, T. Iwai and K. Kimura, *Bull. Chem. Soc. Jpn* 1973, **46**, 3391.
22. J. M. Mayer, *Inorg. Chem.* 1988, **27**, 3899.
23. S. Cradock, R. H. Findlay and M. H. Palmer, *Tetrahedron* 1973, **29**, 2173.
24. D. L. Lichtenberger, A. S. Copenhaver, H. B. Gray, J. L. Marshall and M. D. Hopkins, *Inorg. Chem.* 1988, **27**, 4488.
25. B. E. Bursten, *J. Am. Chem. Soc.* 1982, **104**, 1299.
26. (a) M. E. Peover, in *Electroanalytical Chemistry* (Edited by A. J. Bard), Vol. 2, pp. 1–51. Marcel Dekker, New York (1967); (b) R. S. Glass, S. W. Andruski, J. L. Broeker, H. Firouzabadi, L. Steffen and G. S. Wilson, *J. Am. Chem. Soc.* 1989, **111**, 4036; (c) D. L. Lingtenberger, R. L. Johnston, K. Hinkelmann, T. Susuki and F. Wudl, unpublished result.

Polyhedron Vol. 9, No. 15/16, pp. 1975–1983, 1990
Printed in Great Britain

0277–5387/90 $3.00+.00
© 1990 Pergamon Press plc

STERIC EFFECTS ON THE SELECTIVITY OF PROTEIN LABELLING WITH CHELATE COMPLEXES OF PLATINUM(II)*

XIA YING ZHOU and NENAD M. KOSTIĆ†

Department of Chemistry, Iowa State University, Ames, IA 50011, U.S.A.

Abstract—The Cl^- ligand in complexes of the type [Pt(tridentate)Cl] can be displaced by amino-acid side chains in proteins so that the Pt(tridentate) tag becomes covalently attached to the protein. The selectivity in this displacement can be controlled by adjusting the steric properties of the tridentate ligand. In the complex $[Pt(dipic)Cl]^-$, in which dipic represents 2,6-pyridinedicarboxylate, the Cl^- ligand is accessible. This complex reacts with methionine and histidine and their derivatives and with the side chain of methionine 65 in cytochrome *c*. The reactivity of amino-acid side chains toward $[Pt(trpy)Cl]^-$ depends mainly on their nucleophilicity; the soft thio-ether ligand in methionine is more reactive than the hard imidazole ligand in histidine. In the complex $[Pt(dpes)Cl]^+$, in which dpes represents di(2-pyridyl-β-ethyl)sulphide, the Cl^- ligand is partially shielded. This complex reacts with N-acetylmethionine, N-acetylhistidine, and the side chains of both methionine 65 and histidine 33 in cytochrome *c*. The reactivity of amino-acid side chains toward $[Pt(dpes)Cl]^+$ depends on their steric bulk as well as on their nucleophilicity; the thio-ether ligand in methionine is less reactive than the imidazole ligand in histidine. Principles of stereochemistry can be used in designing metal complexes for selective covalent modification of proteins.

Covalent modification of proteins is an important and frequent procedure in biochemical work. As many organic reagents have been used for this purpose,[1] the potential of inorganic reagents is becoming recognized. The amino-acid side chains contain heteroatoms that can bind metal atoms. Because substitution reactions of transition-metal complexes can be controlled by the choice of the metal and the ligands, and because these complexes have convenient spectroscopic and other properties, they are well-suited for selective labelling of proteins.[2] The complex chloro(2,2′:6′,2″-terpyridine)platinum(II) or $[Pt(trpy)Cl]^+$, designated **1**, contains a tridentate trpy ligand, so that only the chloride ion is displaced under ordinary conditions. Because complexes of platinum(II) are kinetically inert, the $Pt(trpy)^{2+}$ tag is stable on the protein. Because the tag is a UV–vis chromophore, it is easily detected and quantitated. Our studies with various cytochromes *c*,[2–4] α-chymotrypsin,[2,5] α-lytic protease,[5] papain,[6] peptides[2–4] and amino acids[2–4] showed that $[Pt(trpy)Cl]^+$ reacts mainly with cysteine and histidine side chains, i.e. with thiolate and imidazole (Im) functional groups. Arginine side chain (the guanidine group) can also react if its basicity, i.e. the pK_a value of the guanidinium ion, is lower than usual.[7,8]

The unreactivity of methionine and reactivity of histidine toward $[Pt(trpy)Cl]^+$ was surprising since a thio-ether should be much more nucleophilic than imidazole toward the soft platinum(II) atom. Our molecular orbital calculations on $[Pt(trpy)SMe_2]^{2+}$ and on $[Pt(trpy)Im]^{2+}$ showed that this unusual reactivity is caused by the ancillary terpyridine ligand.[3] The *ortho*-H atoms repel the thio-ether, but not the imidazole.[3] The strain in the N—Pt—N bond angles,[9–11] and perhaps also the aromatic character of terpyridine,[12] facilitate the displacement of the chloride ligand by the imidazole. A comparison between the complexes $[Pt(trpy)Cl]^+$ and $[PtCl_4]^{2-}$ shows the decisive effect of the ancillary ligands on the selectivity of protein labelling. Although both of them are platinum(II) chloro complexes, the former does not react with methionine even under forcing conditions,[3] whereas the latter is used as a methion-

* Dedicated to Professor Richard F. Fenske on the occasion of his retirement.

† Author to whom correspondence should be addressed.

ine-specific heavy-atom tag in protein crystallography.[13] Indeed, our molecular orbital calculations revealed no steric crowding in $[PtCl_3(SMe_2)]^-$ and $[PtCl_3Im]^-$ because the chloride ligands are small.[14] In the absence of steric effects, evidently, the displacement reactivity depends on the nucleophilicity of the competing functional groups in the protein that act as entering ligands.

In this study we show how the selectivity of platinum(II) toward the protein can be controlled by adjusting the steric properties of ancillary ligands attached to the metal. These ligands are 2,6-pyridinedicarboxylate (dipicolinate) in the complex designated **2** and di(2-pyridyl-β-ethyl)sulphide in the complex designated **3**.

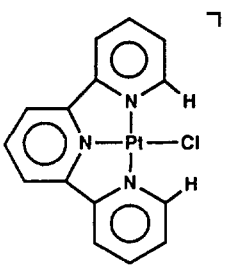

1

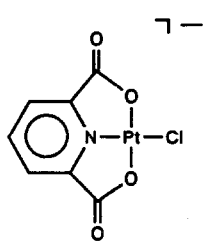

2

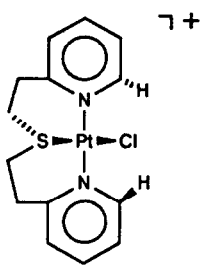

3

EXPERIMENTAL

Materials and methods

Amino acids, horse-heart cytochrome *c* (of type VI), tuna-heart cytochrome *c* (of type XI), and cation exchanger CM 52 were obtained from Sigma. The horse protein was purified chromatographically,[15] and the tuna protein was used as received. Piperidine was obtained from Fisher; 2-vinylpyridine, $K_2[PtCl_4]$ and D_2O, from Aldrich; and CD_3OD, from Cambridge Isotope Laboratories. Water was distilled and demineralized. Ultrafiltration was carried out with Amicon YM 5 membranes under nitrogen at 4°C.

The UV–vis spectra were recorded with an IBM 9430 spectrophotometer. The difference spectra of the labels were obtained by subtracting the spectrum of the native cytochrome *c* from the spectra of the different labelled derivatives. The IR spectra were recorded with an IBM IR 98 spectrophotometer. The ^1H NMR spectra were recorded at 300 MHz with a Nicolet NT 300 spectrometer, with DSS as an internal reference. The proteins for NMR measurements were ultrafiltered into D_2O and lyophilized repeatedly with it. The ^{195}Pt NMR spectra were recorded with a Bruker WM 200 spectrometer; the chemical shifts are expressed with respect to $K_2[PtCl_4]$. Differential-pulse voltammograms were obtained with an IBM EC 225 analyser in the standard way.

Synthetic procedures

Horse-heart cytochrome *c* was carboxymethylated by the published procedure.[16,17] Potassium (2,6 - pyridinedicarboxylato)chloroplatinate(II), K[Pt(dipic)Cl], was prepared by our published procedure.[18] The aromatic protons, H^3 and H^4, are in *meta* and *para* positions with respect to the nitrogen atom.

Di(2-pyridyl-β-ethyl)sulphide was prepared by the published method.[19] The aromatic protons are designated H^3, H^4, H^5 and H^6, with H^6 being the *ortho*-H highlighted in the complex **3**; the CH_2 protons adjacent to the ring and those adjacent to the sulphur atom are designated H^7 and H^8, respectively. ^1H NMR (δ values) in CD_3OD: 8.47 d (H^6, 2H), 7.77 t of d (H^4, 2H), 7.35 d (H^3, 2H), 7.27 t of d (H^5, 2H), $^3J(H—H) = 6.3$ Hz, $^4J(H—H) = 1.5$ Hz; 3.07 t of d (H^7, 4H), 2.92 t of d (H^8, 4H), $^3J(H—H) = 7.8$ Hz, $^2J(H—H) = 1.4$ Hz.

Di(2-pyridyl-β-ethyl)sulphidochloroplatinum(II) chloride, [Pt(dpes)Cl]Cl, was prepared by the published method.[20] M.p.: 205°C. ^1H NMR (δ values) in D_2O: 9.02 d, 8.03 t of d, 7.60 d, 7.45 t of d, $^3J(Pt—H^6) = 30$ Hz, $^3J(H—H) = 7.2$ Hz, $^4J(H—H) = 1.5$ Hz; 3.94 t of d, 3.55 d of t, 3.26 d of t, 3.11 t of d, $^3J(Pt—H^8) = 42$ Hz, $^2J(H—H) = 14.6$ and 2.9 Hz, $^3J(H—H) = 13.7$ and 3.4 Hz. IR in Nujol: 358, 326 and 243 cm^{-1}. UV–vis in water: $\lambda = 265$ nm, $\varepsilon = 12{,}000$ M^{-1} cm^{-1}.

Reactions with amino acids

The following amino acids and their N-acetyl derivatives were incubated, one at a time, with K[Pt(dipic)Cl] and with [Pt(dpes)Cl]Cl: Met, Cys, His, Trp, Tyr, Asp, Asn, Glu, Gln, Lys, Arg, Pro, Thr and Gly. The reaction mixture was 5–10 mM in each reactant, the solvent was either 85 mM phosphate buffer at pH 7.0 or D_2O adjusted to the desired pH value with NaOD or DCl. The incubation lasted for several days at room temperature,

and the reaction mixtures were examined periodically by UV–vis and ^{1}H NMR spectroscopy. When the substitution reactions took place they were complete or nearly complete, except that substitution of AcMet for Cl^- in $[Pt(dpes)Cl]^+$ was only partial. The reactivity of His, Trp, Tyr and Arg was compared with the reactivity of imidazole, indole, phenol and guanidine, respectively. Salts for the IR spectroscopic measurements were prepared by precipitation with common counterions.

Labelling of cytochrome c *with* $[Pt(dipic)Cl]^-$

An equimolar mixture (2 mM each) of ferricytochrome *c* and K[Pt(dipic)Cl] in 85 mM phosphate buffer at pH 7.0 or in 100 mM acetate buffer at pH 5.0 was left for 24 h at room temperature. The reaction was ended by ultrafiltration into the phosphate buffer. The reaction mixture was oxidized by $[Co(phen)_3](ClO_4)_3$, and the excess of the oxidizing agent was removed by ultrafiltration into the phosphate buffer. The chromatographic separation on a CM 52 column was achieved easily by elution with 60 mM phosphate buffer at pH 7.0. The horse cytochrome *c* yielded 16% of the labelled protein and 84% of the native protein, in this elution order. The incubation of ferrocytochrome *c* with an excess of K[Pt(dipic)Cl], up to the molar ratio of 1:4, followed by oxidation and chromatography as before, gave a greater yield of the modified protein, up to 56%. The two fractions were identified by comparison of their mobilities with the mobility of the native protein on a parallel column, and by spiking each fraction with the known amount of the native protein. The mixture of the first fraction and the native protein gave two bands, whereas the mixture of the second fraction and the native protein gave only one band on the CM 52 column. The tuna protein reacted like the horse protein and gave similar chromatographic results.

Labelling of cytochrome c *with* $[Pt(dpes)Cl]^+$

Ferricytochrome *c* (2 mM) was incubated with [Pt(dpes)Cl]Cl (6 mM) in 85 mM phosphate buffer at pH 7.0 or in 100 mM acetate buffer at pH 4.0 for 4 days at 25°C. The reaction was ended, and the reaction mixture chromatographed, as described above. The horse cytochrome *c* at pH 7.0 yielded 18% of the native protein (N) and the following derivatives: 16% of the singly-labelled (S1), 49% of the singly-labelled (S2), 10% of the singly-labelled (S3), 3% of the doubly-labelled (D1), 3% of the doubly-labelled (D2) and 1% of the triply-labelled (T), in this elution order. The horse protein at pH 4.0 yielded only the derivative S3. The tuna protein at pH 7.0 yielded the derivatives S1 and S3, but at pH 4.0 it yielded only S3. The number of the platinum labels was determined by subtracting the spectrum of the native protein from the spectra of the protein derivatives. The band of the $Pt(dpes)^{2+}$ chromophore at *ca* 261 nm was seen clearly in the spectra of the protein derivatives and in the difference spectra. The number of the chromophores was estimated using the assumption that the $Pt(dpes)^{2+}$ chromophore has the same extinction coefficient when attached to an amino acid and to such an amino-acid residue in cytochrome *c*.

RESULTS AND DISCUSSION

Properties of the complexes $[Pt(dipic)Cl]^-$ *and* $[Pt(dpes)Cl]^+$

The chemical and physical properties of the various $[Pt(dipic)Cl]^-$ salts were described in our previous publication.[18] The presence of the ^{195}Pt satellites around both the aromatic and aliphatic ^{1}H resonances in the NMR spectrum of [Pt(dpes)Cl]Cl proves the tridentate coordination of the dpes ligand. The ^3J(Pt—H) values are consistent with the analogous coupling constants in bipyridyl[21] and thio-ether[22,23] complexes of platinum(II). The aromatic ^{1}H resonances of the free dpes ligand are not significantly affected by coordination, but the aliphatic resonances are. In particular, the geminal methylene protons in the complex are inequivalent. Even without a detailed analysis it is evident that the two chelate rings in the tridentate complex $[Pt(dpes)Cl]^+$ are puckered. The IR bands at 358, 326 and 243 cm^{-1} can be assigned to the Pt—S,[24] Pt—Cl[25] and Pt—N[26] stretching vibrations. The UV band at 265 nm can be assigned to the pyridine $\pi \rightarrow \pi^*$ transition.

Reactions of $[Pt(dipic)Cl]^-$ *with amino acids*

Every amino acid containing heteroatoms in the side chain was tested, and glycine was tested in order to check the (un)reactivity of the α-NH_2 and α-COO^- groups. The compounds (e.g. imidazole) that are contained in the side chains of important amino acids (e.g. His) were tested separately. Only the side chains of Cys, Met and His proved reactive under the general conditions of protein labelling. Since the horse and tuna cytochromes *c* do not contain free Cys, the reactions of this amino acid were not investigated further. In order to make the model reactions more relevant to the protein reactions, N-acetyl derivatives, esters and amides

Table 1. ^{1}H NMR chemical shifts (in ppm) of platinum(II) dipicolinate complexes containing methionine and its derivatives as ligands

Ligand	Complex[a] 4	5	6	7	Assignment
Met[b]	8.51 t	8.26 t	8.25 t	8.27 t	dipic H^4
		7.94 d	7.85 d	7.90 d	dipic $H^{3,5}$
		7.76 d	7.74 d	7.68 d	
2.06 s		2.47 s			CH_3S
AcMet[c]	8.51 t	8.35 t	8.32 t	8.34 t	dipic H^4
	8.00 d	7.92 d	8.03 d	8.01 d	dipic $H^{3,5}$
		7.75 d	7.80 d	7.84 d	
2.04 s	2.54 s	2.55 s			CH_3S
1.97 s	2.02 s	2.07 s			CH_3CO
$AcMetNH_2$[d]	8.52 t	8.35 t	8.33 t		dipic H^4
	8.02 d	7.92 d	8.03 d		dipic $H^{3,5}$
		7.74 d	7.81 d		
2.04 s		2.55 s			CH_3S
1.98 s		2.03 s			CH_3CO
$MetCH_3$[e]		8.34 t	8.34 t		dipic H^4
	8.51 t	8.01 d	8.03 d		dipic $H^{3,5}$
	8.03 d	7.85 d	7.83 d		
2.07 s		2.55 s			CH_3S

[a] See the text for formulae.
[b] Methionine. Complex **4** is present only early in the reaction.
[c] N-Acetylmethionine.
[d] N-Acetylmethionine amide.
[e] Methionine methyl ester. Complex **4** is present only early in the reaction.

were used instead of the free amino acids in most of the experiments.

Immediately upon addition of Met or its derivatives to the yellow complex $[Pt(dipic)Cl]^-$, the solution becomes pale yellow or colourless, and the UV absorption band at 328 nm disappears. The reactions are best followed by ^{1}H NMR spectroscopy because the aromatic resonances due to dipic and the aliphatic ones due to the incoming ligand do not overlap; see Table 1. The downfield shift of the CH_3S resonance is characteristic of thioether coordination to platinum(II). The products, designated **4**–**7**, are shown below. In neutral and weakly-acidic solutions the amino group is pro-

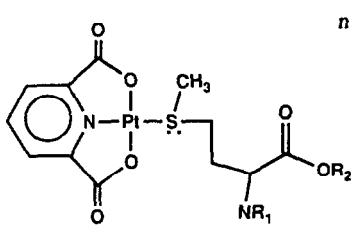

4

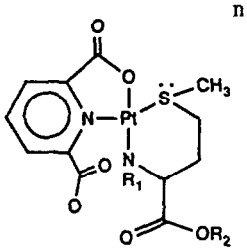

5

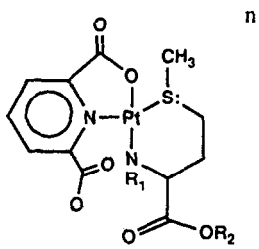

6

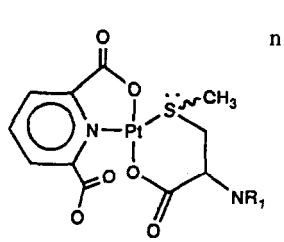

7

Ligand	Met	AcMet	$AcMetNH_2$	$MetCH_3$
R_1	H_3	CH_3CO	CH_3CO	H_3
R_2	None	None	NH_2	CH_3
n in **4**	0	–	0	+
n in **5**	–	2–	–	0
n in **6**	–	2–	–	0
n in **7**	0	–	None	None

tonated, and the carboxylate group is deprotonated. The ligands $AcMetNH_2$ and $MetCH_3$ cannot form the chelate complex **7**. The complexes **4** show only one doublet in the aromatic region, evidence of tridentate (symmetrical) coordination of the dipicolinate ligand. The complexes **5**, **6** and **7** show two such doublets, evidence of bidentate (unsymmetrical) coordination of this ligand. The easy displacement of one of the two carboxylate groups from the platinum(II) atom is probably a consequence of the steric strain in the tridentate Pt(dipic) unit.[18] The yields of the products **4**–**7** after 1 day are as follows: with Met, 0, 52, 26 and 13%; with AcMet, 31, 36, 9 and 9%; with $AcMetNH_2$, 35, 56, 3 and 0%; and with $MetCH_3$, 0, 56, 44 and 0%. The total yields are less than 100% because small amounts of the reactants remain. The ligands Met and $MetCH_3$ form the product **4** initially, but this product is no longer evident after 1 day. The products **4** and **7** convert into the products **5** and **6** with time. The ligands $AcMetNH_2$ and $MetCH_3$ cannot form the product **7** because the carboxylate group in them is blocked. The coordination of methionine as an S-unidentate and an S,O-bidentate ligand has been observed in other platinum(II) complexes as well.[27] The products **5** and **6** are diastereomers, having different configurations at the chiral sulphur atom. The S,N-bidentate coordination of Met (as in the complexes **5** and **6**) and coordination of the peptide nitrogen atom in such chelates also are known.[28–30]

The reaction between $[Pt(dipic)Cl]^-$ and AcMet was followed by ^{195}Pt NMR spectroscopy at 21°C. The resonance at 43 ppm is assigned to the tridentate $[Pt(dipic)AcMet]^-$ complex, **4**. The resonances at −574 and −580 ppm differ little in chemical shift, as is expected of the diastereomeric platinum(II) thio-ether complexes;[22,23] they are assigned to the complexes **5** and **6**. Indeed, these two resonances coalesce at *ca* 80°, as expected of the diastereomers.[22,23]

When His and $[Pt(dipic)Cl]^-$ are mixed at pH 7.0 an orange precipitate forms immediately, but when they are mixed at pH 5.0 the precipitate appears only after some time. Imidazole behaves exactly like His. Evidently the amino acid coordinates via the pyridine-like nitrogen atom (N^3), whose pK_a value is *ca* 6.2.[31] The Pt—Cl stretching band disappears when $[Pt(dipic)Cl]^-$ is converted into [Pt(dipic)Im]. The conversion of $[Pt(dipic)Cl]^-$ into [Pt(dipic)AcHis]$^-$ does not affect the UV–vis spectrum significantly, but the reaction is easily followed by ^1H NMR spectroscopy. Only one product, designated **8**, is formed. ^1H NMR (δ values) in D_2O: 8.44 t dipic H^4, 7.88 d dipic $H^{3,5}$, 7.63 s Im H^2, 7.07 s Im H^4, 4.70 t CH, 2.90 d CH_2 and 1.98 s CH_3CO.

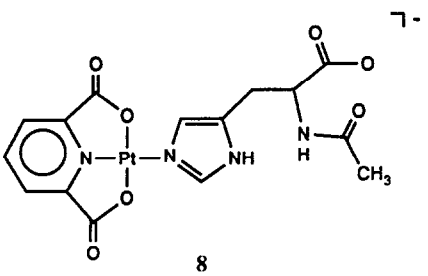

8

Reactions of $[Pt(dpes)Cl]^+$ *with amino acids*

Only the side chains of His and Met react with this complex under the general conditions of protein modification. The reactions were studied with the N-acetyl derivatives of these amino acids, and the ^1H NMR properties of the products, designated **9** and **10**, are summarized in Table 2. The resonances

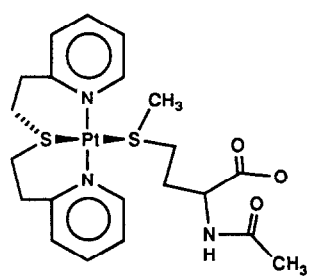

9

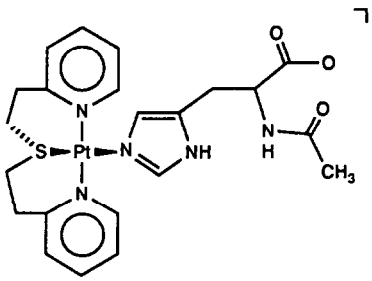

10

of the pyridine protons move downfield by 0.15–0.19 ppm upon the displacement of the Cl^- ligand by AcMet, except the resonance of H^6, which moves upfield by 0.03 ppm. Both this anomaly and the small downfield movement (by 0.09 ppm) of the CH_3S resonance upon coordination may be due to the spatial proximity of the CH_3S and H^6 protons and to the anisotropic effects of the Pt—S bond on H^6.[9] The upfield movement by 0.10 ppm of the CH_3CO resonance may be an indication of non-covalent, probably hydrophobic, interactions between the AcMet and dpes ligands.[32,33] A band at 317 cm^{-1} in the IR spectrum of [Pt(dpes)AcMet]PF_6 can be assigned to the Pt—S stretching vibration.

Table 2. ^{1}H NMR chemical shifts (in ppm) of di(2-pyridyl-β-ethyl)sulphidoplatinum(II) complexes containing aminoacid ligands

[Pt(dpes)Cl]$^+$ (3)[a]	AcMet	[Pt(dpes)(AcMet)]$^+$ (9)[a]	AcHis	[Pt(dpes)(AcHis)]$^+$ (10)[a] major	minor	Assignment[b]
9.02 d		8.99 d		8.72 d	8.49 d	H^6
8.03 t		8.18 t		8.04 t	8.70 t	H^4
7.60 d		7.79 d		7.65 d	7.68 d	H^3
7.45 t		7.6 t		7.38 t	7.32 t	H^5
3.94 t of d		3.86 t		3.9–4.4	3.9–4.4	H^7
3.55 d of t		3.70 d		3.5–3.7	3.5–3.7	H^7
3.26 d of t		3.40 d		3.0–3.4	3.0–3.4	H^8
3.11 t of d		3.1–3.3		3.0–3.4	3.0–3.4	H^8
	2.03 s	2.12 s				CH_3S
	1.95 s	1.85 s				CH_3CO
			8.55 s	8.92 s	8.22 s	Im-CH^2
			7.23 s	6.95 s	7.22 s	Im-CH^4
			1.97 s	1.69 s	1.77 s	CH_3CO

[a] See the text for formulae.
[b] The protons designated only by numbers belong to the dpes ligand.

The reaction between [Pt(dpes)Cl]$^+$ and AcHis gives two products in a ratio of 1 : 0.6. Since only the Cl^- ligand in [Pt(dpes)Cl]$^+$ is displaced by AcHis, the two products probably are stereoisomers of [Pt(dpes)AcHis]$^+$, designated **10**, with different configurations of the non-planar dpes chelate, the AcHis ligand, or both. The UV–vis spectrum of [Pt(dpes)Cl]$^+$ does not change significantly as the Cl^- ligand is replaced by AcMet or AcHis.

Binding sites in cytochrome c

Cytochrome *c* is an electron-transporting haem protein. In the schematic representations **11**, **12** and **13**, the haem group and the polypeptide backbone are shown in a simplified way, and only the binding amino-acid residues are shown in detail. Since the cytochrome *c* from neither horse nor tuna contains free Cys residues, the possible binding sites for the platinum(II) reagents are Met and His residues. They are His 18, His 26, His 33, Met 65 and Met 80 in the horse protein and His 18, His 26, Met 65 and Met 80 in the tuna protein. The position 33 in the tuna protein is occupied by Trp, an amino acid unreactive toward the platinum(II) complexes. In the identification of the binding sites we benefitted from our thorough previous studies, including peptide-mapping experiments, of labelling of different proteins with the [Pt(trpy) Cl]$^+$ complex.[2–7]

Protein derivatives having the same number of identical, charged labels in different locations are separated efficiently by cation-exchange chromatography.[3,4] Since [Pt(dipic)Cl]$^-$ yields only one protein derivative, this complex probably binds to a single site. Binding to His 18 and Met 80, which are axial ligands to the iron atom, can be ruled out. As Table 3 shows, labelling does not perturb the UV–vis spectrum and the reduction potential of the protein. These properties, especially the band at 695 nm, are very sensitive to the changes in the axial ligation of the iron atom. The ^{1}H NMR hyperfine chemical shifts are sensitive to the tertiary structure of the protein in the vicinity of the haem.[34,35] Since these shifts in the labelled protein [Pt(dipic)cyt] are not perturbed appreciably, the protein structure is probably not significantly altered. Histidine 26 is barely accessible,[36] and even the highly reactive [Pt(trpy)Cl]$^+$ labels it with a very low yield.[3] The labelling yields of 16–56%, achieved with [Pt(dipic)Cl]$^-$, are inconsistent with His 26 as the binding site. Carboxymethylation, which blocks only His 33 and Met 65,[16,17] practically suppresses the reaction of the protein with [Pt(dipic)Cl]$^-$. Histidine 33 is ruled out by two different experiments. Firstly, the labelling yield is the same at pH 5.0 and 7.0; because the pK_a value of His 33 is 6.4,[36] its imidazole group should be almost fully protonated and thus unreactive at pH 5.0. Secondly, the tuna protein, although it lacks His 33, reacts with [Pt(dipic)Cl]$^-$ like the horse protein.

Since the yield is independent of pH, the binding site must be Met 65, which has a thio-ether in its side

Table 3. Spectroscopic and electrochemical properties of native and Pt(dipic)-labelled horse cytochrome *c*

Property		Cyt	[Pt(dipic)cyt]
UV–vis abs. max. (nm)		410 530 695	410 530 695
E^0 (mV) vs NHE		260±5	257±5
Hyperfine-shifted ^{1}H NMR, δ (ppm)[a]	CH_3 in ring IV	35.7	35.4
	CH_3 in ring II	32.5	32.5
	β-CH_2 of His 18	14.6	14.5
	β-CH_2 of propionate in ring IV	11.4	11.4
	CH_3 in ring III	9.9	10.0
	CH_3 in ring I	6.8	6.8
	SCH-CH_3 in ring II	−2.5	−2.4
	SCH-CH_3 in ring I	−2.8	−2.7
IR bands (cm^{-1})		No band below 400	340 and 321

[a] For the ring numbering, see ref. 3.

Table 4. Spectroscopic properties of native and $Pt(dpes)^{2+}$-labelled horse cytochrome *c*

Property	Native	Modified at His 33	His 26	Met 65
UV–vis abs. max. (nm)	410 530	410 530	410 530	410 530
Difference UV max (nm)		262	260	262
^{1}H NMR (ppm)[a]				
CH_3 in ring IV	35.81	35.29		
CH_3 in ring II	32.72	32.62		
SCH in ring II	24.7	24.2		
βCH_2 of propionate in ring IV	19.30	18.77		
βCH_2 of His 18	14.73	14.31		
Unassigned	12.85	12.81		
βCH_2 of propionate in ring IV	11.40	11.39		
CH_3 in ring III	9.87	10.13		
CH_3 in ring I	6.82	6.80		
SCHCH_3 in ring II	−2.54	−2.48		
SCHCH_3 in ring I	−2.81	−2.80		
meso-CH of haem	−4.39	−4.36		
meso-CH of haem	−6.57	−6.48		
CH_3 of Met 80	−24.58	−24.72		
γCH_2 of Met 80	−28.4	−28.0		
Im-CH^2 in His 33	8.87	8.54		
Im-CH^4 in His 33	7.87	7.81		
Im-CH^2 in His 26	7.63	7.66		
Im-CH^4 in His 26	6.96	6.98		
CH_3 of Met 65	1.91	1.92		

[a] For ring numbering, see ref. 3.

chain. Indeed, this residue is exposed on the protein surface.[37,38] Because the [Pt(dipic)AcMet]$^-$ complex has a featureless absorption band (a sloping tail) in the UV region, in which the protein absorbs strongly, the label is not evident in the UV–vis difference spectrum.

The number of the Pt(dpes)$^{2+}$ chromophores in the protein derivatives—one, two or three—was determined on the basis of the UV–vis difference spectra, all of which contain the characteristic absorption band in the region 260–263 nm. The lack of significant perturbations of the protein derivatives, evident in Table 4, rules out the labelling of His 18 and Met 85. The binding sites are deduced by comparing the yields of the horse-protein derivatives obtained at pH 7.0 and at pH 4.0 and by comparing the derivatives of the two proteins obtained at the same pH (4.0 and 7.0), keeping in mind that His 33 (in the horse protein) and Met 65 (in both proteins) are exposed on the surface, whereas His 26 (in both proteins) is unexposed. Derivatives designated S1, S2, S3, D1, D2 and T contain the Pt(dpes)$^{2+}$ labels at His 26, at His 33, at Met 65, at His 26 and His 33, at His 33 and Met 65, and at His 26, His 33, and Met 65, respectively. The most abundant derivative, S2, was also examined by ^{1}H NMR spectroscopy. The labelling of His 33 causes a movement upfield of the imidazole H^2 and H^4 resonances by 0.33 and 0.06 ppm, respectively. The corresponding movements in the minor form of the model complex [Pt(dpes)AcHis]$^-$ are 0.33 and 0.01 ppm.

Selectivity in protein labelling

Because platinum(II) is a soft metal, it has a greater affinity, in both a kinetic and a thermodynamic sense, for the soft thio-ether ligand (the Met side chain) than for the hard imidazole ligand (the His side chain). The trpy ligand, however, sterically shields the Cl$^-$ ligand in [Pt(trpy)Cl]$^+$ and prevents its displacement by the Met side chain, which is rather bulky. Displacement by the His side chain, which is less bulky, occurs readily.[3–5]

Because the dipic ligand does not shield the Cl$^-$ ligand, the complex [Pt(dipic)Cl]$^-$ reacts with both Met and His (and their derivatives), but faster with the former than with the latter. In cytochrome *c*, however, only Met 65 is labelled (as shown schematically in **11**), whereas His 33 is not. Perhaps His 33 is unreactive toward this anionic complex because the environment of this residue is negatively charged, whereas the environment of Met 65 is approximately electroneutral. Indeed, His 33 reacts only slightly with the anionic reagent [Pt(sbpaphy)Cl]$^-$.[39]

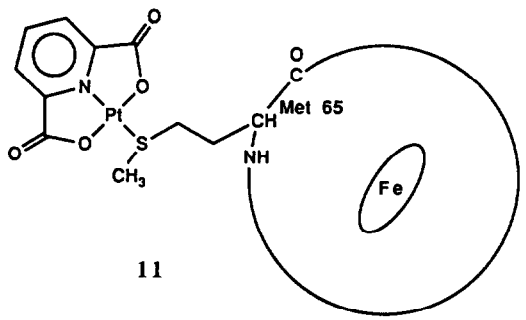

11

The steric properties of [Pt(dpes)Cl]$^+$ (**3**) are intermediate between those of [Pt(trpy)Cl]$^+$ (**1**) and of [Pt(dipic)Cl]$^-$ (**2**). Molecular models of **3** show that the puckering of the chelate rings tilts the S—Pt—Cl axis away from the pyridine planes and that the Cl$^-$ ligand therefore is incompletely shielded by the *ortho*-H atoms of the pyridine rings. Moreover, the Cl$^-$ ligand is labilized owing to the pronounced *trans* effect of the thio-ether ligand.

The reactivity of the complex **3** likewise is intermediate between those of the complexes **1** and **2**. It reacts with both Met and His (and their derivatives) and with both Met 65 and His 33 in cytochrome *c*, as shown schematically in **12** and **13**. But the Cl$^-$ atoms must still be considerably shielded because the yield of the His 33 derivative is greater than the yield of the Met 65 derivative.

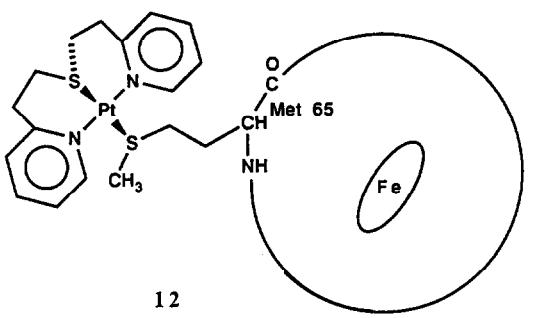

12

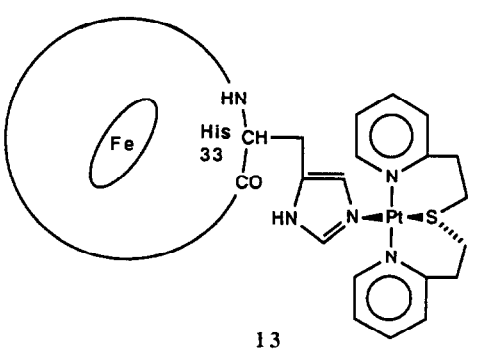

13

CONCLUSION

Principles of coordination chemistry and stereochemistry can be used in designing inorganic reagents for selective covalent modification of proteins.

Acknowledgement—This research was supported by the National Science Foundation through a Presidential Young Investigator Award (CHE-8858387) to N.M.K.

REFERENCES

1. R. L. Lundblad and C. M. Noyes, *Chemical Reagents for Protein Modification*, Vols I and II. CRC Press, Boca Raton, Florida (1984).
2. N. M. Kostić, *Comm. Inorg. Chem.* 1988, **8**, 137 and refs cited therein.
3. E. M. A. Ratilla, H. M. Brother II and N. M. Kostić, *J. Am. Chem. Soc.* 1987, **109**, 4592.
4. H. M. Brothers II and N. M. Kostić, *Inorg. Chem.* 1988, **27**, 1761.
5. H. M. Brothers II and N. M. Kostić, *Biochemistry* 1990, in press.
6. H. M. Brothers II and N. M. Kostić, unpublished work.
7. E. M. A. Ratilla and N. M. Kostić, *J. Am. Chem. Soc.* 1988, **110**, 4427.
8. E. M. A. Ratilla, B. K. Scott, M. S. Moxness and N. M. Kostić, *Inorg. Chem.* 1990, **29**, 918.
9. K. W. Jennette, J. T. Gill, J. A. Sadownick and S. J. Lippard, *J. Am. Chem. Soc.* 1976, **98**, 6159.
10. Y. Wong and S. J. Lippard, *J. Chem. Soc., Chem. Commun.* 1977, 824.
11. J. C. Dewan, S. J. Lippard and W. R. Bauer, *J. Am. Chem. Soc.* 1980, **102**, 858.
12. R. J. Mureinik and M. Bidani, *Inorg. Chim. Acta* 1978, **29**, 37.
13. G. A. Petsko, D. C. Phillips, R. J. P. Williams and I. A. Wilson, *J. Molec. Biol.* 1978, **120**, 345.
14. L. Zhu and N. M. Kostić, unpublished work.
15. D. L. Brautigan, S. Ferguson-Miller and E. Margoliash, *Methods Enzymol.* 1978, **53**, 129.
16. K. Ando, H. Matsubara and K. Okunuki, *Biochim. Biophys. Acta* 1966, **118**, 240.
17. K. Ando, H. Matsubara and K. Okunuki, *Biochim. Biophys. Acta* 1966, **118**, 256.
18. X. Y. Zhou and N. M. Kostić, *Inorg. Chem.* 1988, **27**, 4402.
19. S. M. Nelson and J. Rodgers, *Inorg. Chem.* 1967, **6**, 1390.
20. V. E. Uhlig, B. Borek and L. M. Ngu, *Z. Anorg. Allg. Chem.* 1977, **432**, 33.
21. E. Bielli, P. M. Gidney, R. D. Gillard and B. T. Heaton, *J. Chem. Soc., Dalton Trans.* 1974, 2133.
22. D. D. Gummin, E. M. A. Ratilla and N. M. Kostić, *Inorg. Chem.* 1986, **23**, 2429 and refs cited therein.
23. J. A. Galbraith, K. A. Menzel, E. M. A. Ratilla and N. M. Kostić, *Inorg. Chem.* 1987, **26**, 2073.
24. K. Nakamoto, *Infrared Spectra of Inorganic and Coordination Compounds*. John Wiley, New York (1970).
25. K. Nakamoto, *Infrared Spectra of Inorganic and Coordination Compounds*, 2nd edn, pp. 215 and 265. John Wiley, New York (1970).
26. D. M. Adams, *Metal–Ligand and Related Vibrations*. St Martin's Press, New York (1968).
27. T. G. Appleton, J. W. Connor and J. R. Hall, *Inorg. Chem.* 1988, **27**, 130.
28. L. M. Volshtein, *Sov. J. Coord. Chem.* (*Engl. Transl.*) 1976, **1**, 483 and refs cited therein.
29. C. A. McAuliffe and S. G. Murray, *Inorg. Chem. Acta Rev.* 1972, **6**, 103; 111.
30. H. Sigel and R. B. Martin, *Chem. Rev.* 1982, **82**, 385.
31. D. D. Perrin, *Dissociation Constants of Organic Bases in Aqueous Solution*. Butterworth, London (1965).
32. H. Ōkawa, *Coord. Chem. Rev.* 1988, **92**, 1.
33. H. Sigel, *Pure Appl. Chem.* 1989, **61**, 923.
34. H. Toi, G. N. LaMar, R. Margalit, C.-M. Che and H. B. Gray, *J. Am. Chem. Soc.* 1984, **106**, 6213.
35. G. R. Moore and G. Williams, *Biochim. Biophys. Acta* 1984, **788**, 147.
36. J. S. Cohen and M. B. Hayes, *J. Biol. Chem.* 1974, **249**, 5472.
37. T. Takano, O. B. Kallai, R. Swanson and R. E. Dickerson, *J. Biol. Chem.* 1973, **248**, 5234.
38. S.-C. Tam and R. J. P. Williams, *Struct. Bond.* 1985, **63**, 103.
39. S. C. Shah, J. S. Johnson, H. M. Brothers II and N. M. Kostić, *J. Serb. Chem. Soc.* 1988, **53**, 139.

Polyhedron Vol. 9, No. 15/16, pp. 1985–1999, 1990
Printed in Great Britain

0277–5387/90 $3.00+.00
Pergamon Press plc

COUNTING ELECTRONS AND RATIONALIZING STRUCTURES OF CLUSTERS AND CLUSTERS OF CLUSTERS*

BOON K. TEO† and HONG ZHANG

Department of Chemistry, University of Illinois at Chicago, Chicago, IL 60680, U.S.A.

Abstract—The investigation of the electronic structures of high nuclearity metal clusters constitutes an important prerequisite for the basic understanding of the relationship between discrete metal clusters and the extended bulk metal. Simple electron counting principles are particularly useful in this regard. It not only allows a systematization or rationalization of the observed structures of these clusters, but also can lead to prediction of clusters of yet unknown molecular architectures and/or formulations. In this review, electron counting principles for the metal clusters of varying nuclearity (magic numbers), size, shape and packing arrangements will be discussed. Emphasis will be focused upon: (1) the topological electron counting (*TEC*) rule; (2) the C^2 model for clusters of clusters; (3) the *Shell* model for v_n polytopal close-packed metal clusters; and (4) the *Extended Hume–Rothery* rule for metal clusters of close-packed arrangements.

A cluster is an aggregate of atoms or molecules. Current interest in clusters stems from the fact that the collective behaviour of a cluster often differs significantly from that of its constituents.

Chemists have been able to prepare and/or observe a wide variety of clusters in gas, liquid, solution or solid phases. Some clusters are *naked* (for example, Bi_8^{2+} [1a] and Ge_9^{2-} [1b]) while others are *ligated* with ligands such as phosphines {e.g. $[Au_{13}Cl_2(PMe_2Ph)_{10}]^{2+}$ [2]} and carbonyls {e.g. $[Pt_{19}(CO)_{22}]^{4-}$ [3]}. They can either be discrete clusters in solution or extended clusters in solid states. Finally, atoms (or molecules) within a cluster can be held together by ionic, covalent, metallic or hydrogen bonding, as well as weak van der Waals' interactions.

A metal cluster, as defined by Cotton and Wilkinson,[4] is "a group of two or more metal atoms in which there are substantial and direct *bonds* between the metal atoms". Large metal clusters[5,6] (containing, say, dozens of metal atoms) are of particular interest in that they lie in the region of aggregation between individual atoms and bulk metal. Investigations of the chemical and physical properties of these clusters will therefore shed light on how, where and when metallic behaviour begins or ends. In other words, how many metal atoms must a cluster have before it begins to behave as a metal? Conversely, how small must metal particles become before they lose their metallic character? In the region between one and a large number of associated atoms, there is, evidently, some intermediate number or numbers that determine the presence or absence of metallic or other bulk properties.

A crucial first step toward such a goal is the understanding of the structure and bonding of large, structurally well-defined metal clusters with discrete *size* and *shape* approaching that of small metal particles. Recent developments in cluster synthesis[7–9] have produced high nuclearity metal clusters with metal arrangements resembling (or related to) fragments of the bulk metal.

The investigation of the electronic structures of these high nuclearity metal clusters constitutes an important prerequisite for the basic understanding of the relationship between discrete metal clusters and the extended bulk metal. Simple electron counting principles[10–17] are particularly useful in this regard. It not only allows a systematization or rationalization of the observed structures of these clusters, but also can lead to predictions of clusters of yet unknown molecular architectures and/or formulations.

In this review, we shall give a brief account of the electron counting principles we helped develop over the years for metal cluster systems.

We shall categorize metal clusters into three broad classes. The *primary* clusters are the simplest *polytopal* clusters such as a triangular or a tetra-

* Dedicated to Professor Richard F. Fenske on his retirement.

† Author to whom correspondence should be addressed.

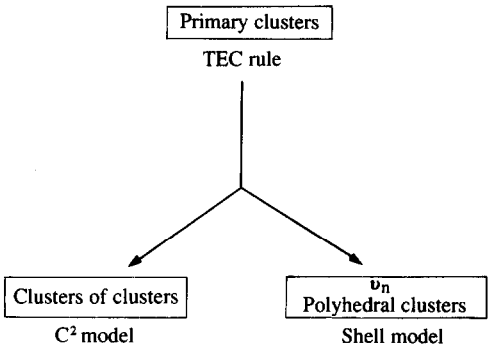

Chart 1. Three classes of clusters and applicable electron counting rules.

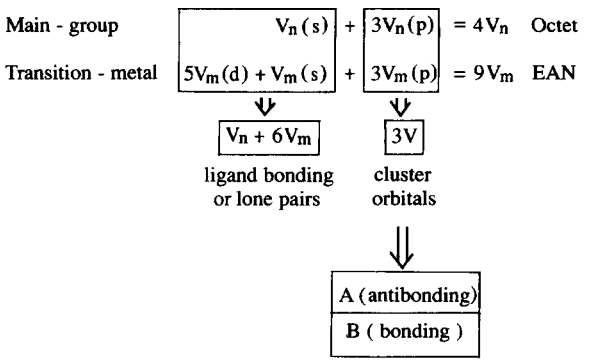

Chart 2. Basic assumptions of the TEC rule: Partition of valence orbitals of a cluster containing V_n main-group and V_m transition metal atoms ($V = V_n + V_m$).

hedral cluster. Mathematically, a *polytope*[18] is the general term for point, line, polygon and polyhedron in 0-, 1-, 2- and 3-dimensions, respectively. A polytopal cluster therefore constitutes a cluster framework which comprises isolated, chain-like, polygonal or polyhedral atomic arrangements in the respective dimensions. These clusters, generally of low nuclearity, are of prime importance in that they can be used as "*building blocks*" or "*nucleation core*" for the *secondary* clusters which may be categorized into two broad classes: the "*clusters of clusters*"[19]; and the "v_n *polytopal clusters*",[5-9] respectively, as depicted schematically in Chart 1. We shall first briefly describe electron counting principles for the primary clusters, followed by similar discussions on the two categories of secondary clusters. Emphasis will be placed upon: (1) the topological electron counting (*TEC*) rule;[13,14] (2) the C^2 model for clusters of clusters;[16] (3) the *Shell* model[15] for v_n polytopal close-packed metal clusters; and (4) the *Extended Hume–Rothery* role[17] for metal clusters of close-packed arrangements. Readers are referred to the literature[10-12] for other elegant alternative electron counting schemes which may or may not be equivalent to those discussed in this review.

TOPOLOGICAL ELECTRON COUNTING (TEC) RULE

Basic assumptions

The TEC scheme assumes that (1) each vertex atom contributes three orbitals for cluster interaction of which only the bonding contributions (B) are filled; and (2) the remaining valence orbitals (one for main-group and six for transition metal vertex atoms) are "filled" as a result of ligand bondings or as lone pairs, as represented schematically in Chart 2. For a cluster with V_n main-group and V_m transition metal vertices, there will therefore be $3V$ orbitals for cluster interaction (where $V = V_n + V_m$). [These orbitals can be visualized as hybrid orbitals based on the three valence p orbitals. The remaining valence orbitals (one s for main-group elements; five d and one s for transition metals) as "atomic" orbitals are used for ligand bonding or lone pairs. In reality, of course, extensive mixing of s and p orbitals and of d, s and p orbitals can occur for main-group elements and transition metals, respectively.]

If B is the number of (filled) *bonding* orbitals formed by the 3V *cluster orbitals*, the total number of topological electron pairs is given by[14]

$$T = V_n + 6V_m + B. \quad (1)$$

Equation (1) in effect separates the total number of electron pairs into two parts: viz. those occupying the energetically low-lying valence orbitals (V_n s orbitals for main-group elements, $5V_m$ d orbitals and V_m s orbitals for transition metals) and those (B) primarily responsible for "holding the cluster together".

Physical significance of B *and* T

We shall illustrate the utility of the TEC[14a] theory with an example, $As_3Co(CO)_3$, shown in Chart 3(a). Here we have $V_n = 3$, $V_m = 1$. The observed electron count is $N = 3 \times 5(As) + 1 \times 9(Co) + 3 \times 2(CO) = 30$, or a total of $T = N/2 = 15$ electron pairs. Note that the Co atom contributes nine atomic orbitals and nine electrons while each As atom contributes four atomic orbitals and five electrons to cluster bonding. The disposition of 15 topological electron pairs, T (outer circle), is shown pictorially in Chart 3(b): three bonding electron pairs donated by the three carbonyls (dotted), six lone pairs (crossed), three on the Co atom and one

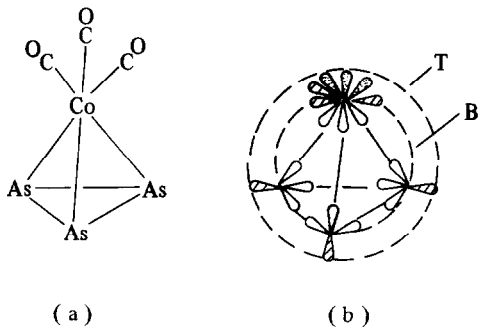

(a) (b)

Chart 3. (a) Structure of $As_3Co(CO)_3$, a tetrahedral cluster. (b) Pictorial representation of the topological electron pairs, T (outer circle), and the skeletal electron pairs, B (inner circle).

on each of the three As atoms, and six bonding electron pairs ($B = 6$) that occupy the bonding combinations of the 12 cluster orbitals (open), three from each vertex atom.

If the electron pairs "exo" to the cluster [cf. dotted or crossed orbitals in Chart 3(b)] are removed, one obtains a quantity B [cf. inner circle, Chart 3(b)]:

$$B = T-(V_n+6V_m) = 15-(3+6\times 1) = 6. \quad (2)$$

For this particular cluster, the value of $B = 6$ corresponds exactly to the number of the edges of a tetrahedron (this is not always the case as we shall see). Hence, the parameter B can be interpreted as the number of *bonding cluster orbitals/electron pairs*. As we shall see later, for primary clusters, parameter B also corresponds to the number of *skeletal electron pairs* in the context of the skeletal electron pairs (SEP) theory.[10c] It is interesting to note that B depends on the total number of vertices, V, regardless of its make-up (V_n or V_m).†

COUNTING ELECTRONS AND RATIONALIZING STRUCTURES OF PRIMARY CLUSTERS

Three-dimensional polyhedral clusters

Two types of polyhedra are of particular importance in cluster chemistry: three-connected polyhedra and deltahedra, which we shall discuss next.

Three-connected polyhedral clusters. It is of interest to consider a particular type of polyhedra in which each vertex is connected to three other vertices. Some examples of three-connected polyhedra are shown in Chart 4. Polyhedral C_nH_n belongs to this class of clusters. Other examples of main-group or metal clusters are listed in refs 13 and 14. Since each vertex is connected to three other vertices via three cluster orbitals, these clusters (with a total of V vertices) can be considered as electron precise in that one half of the $3V$ orbitals will be bonding:

$$B = 3V/2 \text{ for three-connected polyhedral clusters.} \quad (3)$$

The other half, of course, will be antibonding ($A = 3V/2$) as tabulated in Table 1. As it turns out (Euler's theorem), for three-connected polyhedra, the number of edges, E, is also given by $3V/2$. Hence, the B value for a three-connected polyhedron is equal to the number of edges ($B = E$). The B values for other important three-connected polyhedral clusters are given in Chart 4.

Deltahedral clusters. A deltahedron is a polyhedron with triangular faces only. Important examples are also shown in Chart 4. Boron hydrides of general formula $B_nH_n^{2-}$ are prime examples of this class of clusters. Other representative main-group or transition metal clusters can be found in refs 13 and 14.

SEP theory[10c] predicts that the number of skeletal electron pairs, $B = V+1$ for this class of clusters (except tetrahedron). The B values for the common deltahedra are given in Chart 4. For example, an icosahedron has $V = 12$ vertices and a B value of 13, thereby satisfying the

$$B = V+1 \quad \text{for deltahedral clusters} \quad (4)$$

rule of the SEP theory.

It turns out that the SEP theory applies not only to deltahedral clusters (excluding tetrahedron) but also to polyhedra which can be visualized as derivable from a deltahedron with one, two or three missing vertices. Equation (4) is appropriately modified to $B = V+2$, $V+3$, $V+4$ for these latter polyhedra, commonly called *nido-*, *arachno-* or *hypho*-clusters. For example, a square pyramid ($V = 5$) can be considered as an octahedron ($V = 6$) with a missing vertex (a *nido*-cluster) as shown below, hence $B = V+2 = 5+2 = 7$. We may call this the *debor* principle.

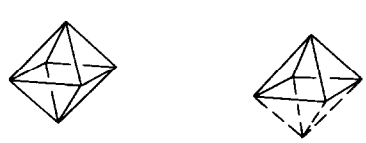

† It is apparent that eq. (1) allows a direct comparison between TEC and the SEP rules. As pointed out in ref. 14(a), both theories can be derived from molecular orbital calculations.

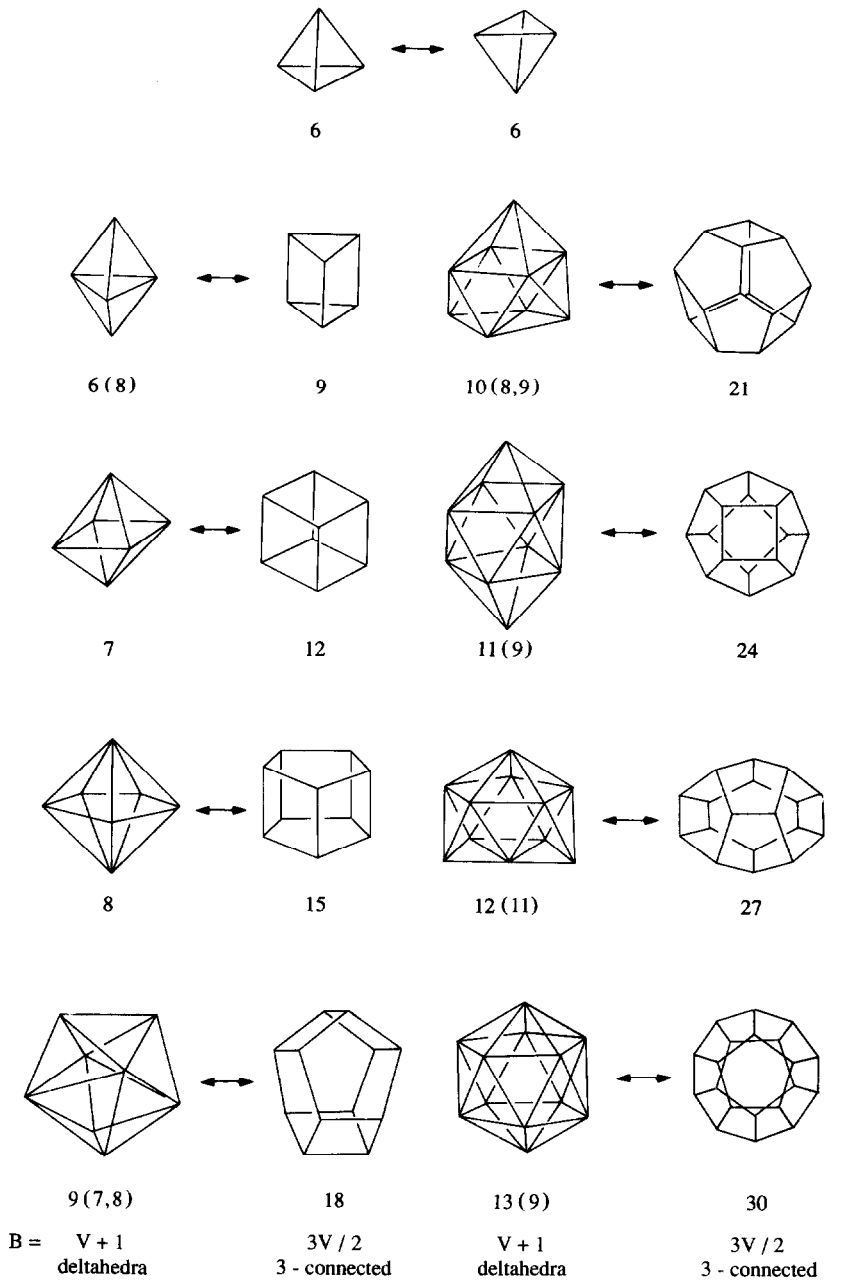

Chart 4. The B values for some 3-D polyhedral clusters and their duality: the three-connected (left) and the deltahedra (right).

Table 1. Numbers of antibonding (A) and bonding (B) cluster orbitals for a cluster with V vertices (Sum: $A+B=3V$)

Dimensions	3-D 3-Connected	3-D Deltahedron	2-D Ring	1-D Chain	0-D Isolated
A (empty)	$3V/2$	$2V-1$	V	$V-1$	0
B (filled)	$3V/2$	$V+1$	$2V$	$2V+1$	$3V$

The opposite of the *debor* principle is the *capping* principle,[20] which states that capping does not alter the number of skeletal electron pairs of the parent polyhedron. For example, tetracapped tetrahedron is a deltahedron with eight vertices, yet there are only six skeletal electron pairs ($B = 6$) within the central tetrahedron.

One important feature of the pairs of polyhedra shown in Chart 4 is their *duality* or *conjugation*. The dual of a polyhedron is defined as the polyhedron formed by interchanging the vertices and the faces. *Dual polyhedra have exactly the same number of edges.* (Note that tetrahedron is self-dual.)

Zero-, one- and two-dimensional clusters

Since the TEC rule assumes that each vertex atom contributes three orbitals for cluster bonding, the B value for zero-, one- or two-dimensional (D) clusters can be given by[14b]

$$B = 3V - E \quad \text{for 0-, 1-, 2-D clusters,} \qquad (5)$$

where E is the number of edges (or bonds). The B values for some representative zero-, one- and two-dimensional clusters are given in Chart 5. For example, the n-membered ring clusters will have n sides (bonds) and therefore $B = 3n - n = 2n$ via eq. (5). Other more complex polyhedral two-dimensional clusters can likewise be determined.

We can now summarize the number of anti-bonding (A) and bonding (B) cluster orbitals for clusters of various dimensions in Table 1. Since each vertex atom contributes three orbitals for cluster orbitals, we have $A + B = 3V$. The utility of Table 1 will be illustrated later in this review.

Counting electrons and rationalizing structures

Two ways of selecting cluster framework. For a metal cluster with bridging ligands, electron counting principles can be applied to either the metal framework or the metal-(bridging ligand) cluster framework. For example, the framework of the $Ni_8(\mu_4\text{-}PPh)_6(CO)_8$ cluster[21] can either be considered as a cube (Ni_8) [Chart 6(a)] or a hexa-capped cube (Ni_8P_6) [Chart 6(b)].

From formula to structure. For the $Ni_8(\mu_4\text{-}PPh)_6(CO)_8$ cluster, we may consider

(a) (b)

Chart 6. The (a) Ni_8 and (b) Ni_8P_6 core of $Ni_8(\mu_4\text{-}PPh)_6(CO)_8$.

(a) Ni_8 as cluster framework, then from the formula, we obtain,

$$N_{obs} = 8 \times 10(Ni) + 6 \times 4(\mu_4\text{-}PPh) + 8 \times 2(CO) = 120$$

$$T = N/2 = 120/2 = 60$$

$$B = T - 6V_m = 60 - 6 \times 8 = 12$$

via eq. (1). We therefore conclude that Ni_8 has a cubic structure ($B = 12$) which is a three-connected polyhedron (cf. Chart 4).

(b) Ni_8P_6 as cluster framework, again, from formula,

$$N_{obs} = 8 \times 10(Ni) + 6 \times 5(P) + 6 \times 1(Ph) + 8 \times 2(CO) = 132$$

$$T = N/2 = 132/2 = 66$$

$$B = T - V_n - 6V_m = 66 - 6 - 6 \times 8 = 12$$

via eq. (1). We conclude, in this case, that Ni_8P_6 is a hexa-capped cube ($B = 12$ since capping does not change the B value of the parent polyhedron).

From structure to formula. Given a particular cluster geometry, electron counting allows reasonable predictions to be made concerning the electronic requirements of the cluster. This is highly valuable in the design and synthesis of clusters. It may also be helpful in cases where the exact formulation (e.g. the number of disordered ligands, the interstitial hydrides or the overall charges) is difficult to ascertain.

For example, suppose one wishes to synthesize an octahedral and bicapped tetrahedral cluster of the general formula $[Os_6(CO)_{18}]^{q-}$, what should the charge q be? From Chart 4, an octahedral cluster has a B value of 7, eq. (1) gives

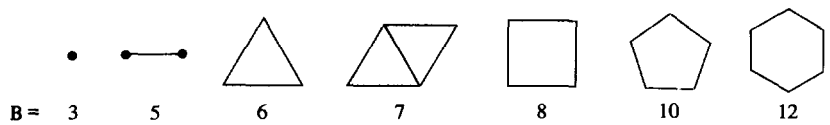

Chart 5. The B values for some 0-, 1- and 2-D cluster systems.

$T = 6V_m + B = 6 \times 6 + 7 = 43$ or $N = 2T = 86$. The overall charge can be calculated as follows: $q = 86 - (6 \times 8 + 18 \times 2) = 2$. So the formula for the octahedral cluster should be $[Os_6(CO)_{18}]^{2-}$. Similarly, for the bicapped tetrahedral cluster, $B = 6$ (since the capping does not change the B value), $T = 6 \times 6 + 6 = 42$, $N = 84$, $q = 84 - (6 \times 8 + 18 \times 2) = 0$, and hence the formula $Os_6(CO)_{18}$. These formulae are indeed observed by Lewis, Johnson and co-workers.[22]

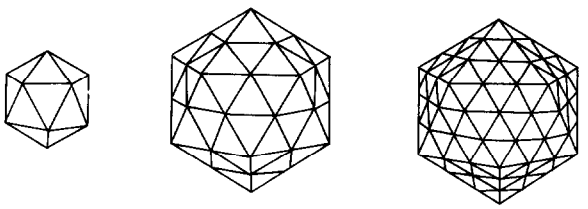

Chart 8. The v_n polyhedral clusters.

COUNTING ELECTRONS AND RATIONALIZING STRUCTURES OF HIGH NUCLEARITY CLUSTERS

As discussed earlier, the *primary* clusters can either be used as building blocks to form cluster of clusters, or, act as nucleation/core for further layer-by-layer (LBL) growth. Here we shall distinguish between two broad categories of highly symmetrical high-nuclearity metal clusters: the s_n supraclusters and the v_n polyhedral clusters.

A s_n supracluster is defined as a cluster of n smaller cluster units fused together via vertex-, edge- or face-sharing.[16] Chart 7 illustrates the early members of supraclusters based on vertex-sharing centred icosahedral cluster units of 13 atoms. Since these supraclusters, s_n, are made up of smaller cluster units, they are also referred to as clusters of clusters (COC).[19] One common characteristic of cluster of clusters is that the interactions of the metal atoms within the cluster units are stronger than those between the units.

A v_n polyhedral cluster[15] is defined as a cluster with $(n+1)$ atoms on each edge of the polyhedron and built by LBL growth on a cluster surface.[5-9] Chart 8 portrays the early members of the v_n icosahedral clusters (Mackay[23] Sequence). The magic numbers, defined as the nuclearity (number of atoms) of a cluster, are given in parentheses. These magic numbers represent structurally stable, often closed-shell, configurations of atoms in a cluster and can be observed experimentally. For example, adiabatic jet expansion of inert gas (e.g. Xe)[24] produces van der Waals' clusters following the sequence of magic numbers: 1, 13, 55, 147, ...

The C^2 *model for cluster of clusters*

According to the C^2 model,[16] for a supracluster which can be regarded as a cluster formed by n polyhedral clusters fused together, the B value is given by the sum of the B_j values (j = 1–n) of the n individual cluster *units* (building blocks) minus the sum of the B_k values (k = 1–s) of the s *shared* vertice(s), edge(s) or face(s). The B values for the commonly observed cluster units and shared moieties can be found in Chart 5. In other words, in order to obtain the overall number of skeletal electron pairs (B) of a supracluster, we simply sum up the skeletal electron pairs (B_j) of the individual cluster units (building blocks) followed by subtracting the overcounting of the skeletal electron pairs (B_k) of the shared vertices, edges or faces. Some interesting examples of vertex-, edge- and face-sharing supraclusters in 2-D, 3-D, or mixed 2-D and 3-D systems can be found in ref. 16. The total number of electron pairs (T) can be calculated from eq. (1) and the total electron counts is given by $N = 2T$.

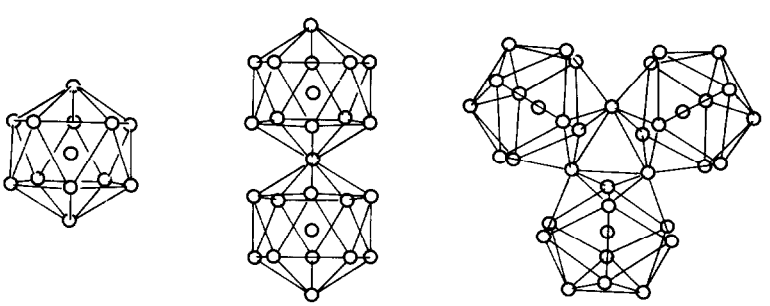

Chart 7. The s_n supraclusters: (a) s_1 (13); (b) s_2 (25); (c) s_3 (36).

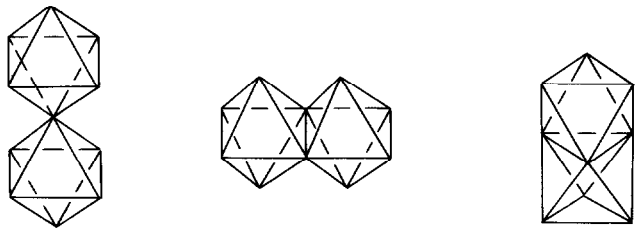

B = 2 x 7 − 3 = 11 2 x 7 − 5 = 9 2 x 7 − 6 = 8

Chart 9. Two octahedra sharing a vertex (left), an edge (middle) and a face (right).

Take, for example, two octahedra sharing a vertex, an edge, or a face as depicted in Chart 9. Since each octahedron (O_h) contributes a B value of 7 [cf. eq. (4)], two octahedra sharing a vertex (Chart 9, left), an edge (middle) and a face (right) will give rise to the predicted B values of $B = 2\times7(O_h)-3(\text{atom}) = 11$, $2\times7(O_h)-5(\text{edge}) = 9$, and $2\times7(O_h)-6(\Delta) = 8$, respectively (cf. Chart 5). The latter two structures are exemplified by clusters $Ru_{10}C_2(CO)_{24}^{2-}$[5f] and $Rh_9(CO)_{19}^{3-}$[25] with $N_{obs} = 10\times8+2\times4+24\times2+2 = 138$ and $9\times9+19\times2+3 = 122$, which agree reasonably well with the predicted electron counts of $N = 2T = 2(6V_m+B) = 2\times(6\times10+9) = 2\times69 = 138$, $2\times(6\times9+8) = 124$, respectively.

For the 25-atom cluster formed by two centred-icosahedra sharing one vertex [cf. Fig. 1 and Chart 7(b)], the C^2 model predicts that $B = 2\times13$ (icosahedron) $-(1\times3)$(sharing one vertex) $= 23$, and the TEC rule [eq. (1)] predicts $T = 6V_m+B = 6\times(25-2)+23 = 161$ skeletal electron pairs or a total valence electron count of $N = 2\times161 = 322$. One known example is the structurally characterized $[(p\text{-Tol}_3P)_{10}Au_{13}Ag_{12}Br_2(\mu\text{-Br})_2(\mu_3\text{-Br})_4]^+$ cluster[26] for which the N_{obs} of $(10\times2+25\times11+2\times1+2\times3+4\times5-1) = 322$ electrons is in accordance with the calculated value. Likewise, three 13-atom centred-icosahedra [Chart 7(c)] sharing three vertices in a cyclic manner result in $B = (3\times13)-(3\times3) = 30$. For such a 36-atom cluster, $T = 6V_m+B = 6\times(36-3)+30 = 228$ and $N = 2\times228 = 456$. This cluster is presently unknown. However, the closely related structurally characterized 38-atom cluster $[(p\text{-Tol}_3P)_{12}Au_{18}Ag_{20}Cl_2(\mu\text{-Cl})_6(\mu_3\text{-Cl})_6]$[19b,27] depicted in Fig. 2, is predicted to have $456+2\times18 = 492$ valence electrons, since the two exopolyhedral Ag atoms do not form metal–metal bonds with the 36-atom polyhedral framework, as is indeed observed: $N_{obs} = 12\times2+38\times11+2\times1+6\times3+6\times5 = 492$. [If six metal–metal bonds (three on each side) are formed between the two exopolyhedral Ag atoms and the 36-atom polyhedral framework, the electron count would reduce to $492-12 = 480$.]

Other highly symmetrical higher members of this series of vertex-sharing centred-icosahedral clusters are shown in Fig. 1 of ref 16(a), in analogy to $B_nH_n^{2-}$ clusters. The electron counting principles based on the C^2 model had also been discussed. We shall discuss here one member of this series, $s_4(46)$, and its capped derivatives.

The superpolyhedron of $s_4(46)$ is a supertetrahedron based on four vertex-sharing centred-icosahedra. The capped derivatives (designated by the asterisk), s_5, s_6*, s_7* and s_8*, correspond to the mono-, bi-, tri- and tetracapped supertetrahedra as shown in Fig. 3. Here each sphere represents a 13-atom centred icosahedron. The corresponding

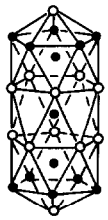

$Au_{13}Ag_{12}$

Fig. 1. The metal framework of the 25-atom cluster: $[Au_{13}Ag_{12}Br_8(p\text{-Tol}_3P)_{10}]^+$.

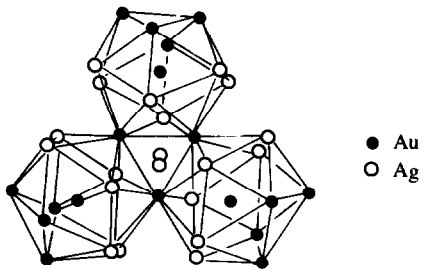

Fig. 2. The metal framework of the 38-atom cluster: $[Au_{18}Ag_{20}Cl_{14}(p\text{-Tol}_3P)_{12}]$.

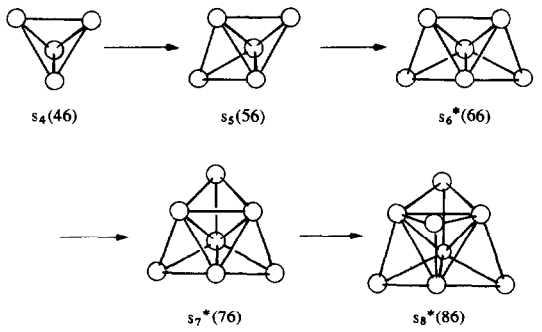

Fig. 3. Successive cappings of the super-tetrahedron to form mono-, bi-, tri- and tetracapped supertetrahedra, corresponding to the vertex-sharing icosahedral supraclusters $s_4(46)$, $s_5(56)$, s_6*(66), s_7*(76), and s_8*(86), respectively. The nuclearities are in parentheses. Here each sphere represents a 13-atom centred icosahedron.

nuclearities are 56, 66, 76 and 86, respectively, which follow the $(10n+6)$ rule. In fact, the general formulae given by us in ref. 16(a) for super-deltahedral supraclusters also apply here. In other words, since each cap of the superpolyhedron implies the addition of one icosahedron to the parent cluster via sharing of three vertices, the C^2 model predicts that the B value should increment by 13(icosahedron) -3×3(sharing three vertices) $= 4$. The general formula for B would still be†

$$B = 4n+18 \qquad (6)$$

for $n \geqslant 3$ [see eq. (8) of ref. 16(a)]. Similarly, since the addition of each icosahedron increases the number of "surface" atoms by 9 [13 − 3(shared vertices) − 1(central atom of icosahedron)] and B by 4, the general formula for T remains as‡

$$T_n = 58n+54 \qquad (7)$$

[see eq. (9) of ref. 16(a)]. The total electron count should be

$$N_n = 2T_n = 116n+108. \qquad (8)$$

We can use eqs (6) and (7) to predict the electron counts for the *stellated* supraclusters s_n*$(10n+6)$, where $N = 4$–8 as depicted in Fig. 3. For example, one possible formulation for $s_5(56)$ may be $(Ph_3P)_{12}M_{56}(\mu\text{-X})_6(\mu_3\text{X})_6$ [$N = 12\times2+56\times11+6\times3+6\times5 = 688$ which agrees with $116\times5+108 = 688$ via eq. (8)] and that for s_6*(66) may be $[(Ph_3P)_{12}M_{66}(\mu\text{-X})_7(\mu_3\text{-X})_6(\mu_4\text{-X})]^{2+}$ [$N = 12\times2+66\times11+7\times3+6\times5+1\times5-2 = 804$ which agrees with $116\times6+108 = 804$ via eq. (8)], where M = Au, Ag; X = Cl, Br.

† Note that $B_{n+1} = B_n + B_{cap} = (4n+18)+4 = 4(n+1)+18$.

‡ Note that $T_{n+1} = T_n + T_{cap} = (58n+54)+(6\times9+4) = 58(n+1)+54$.

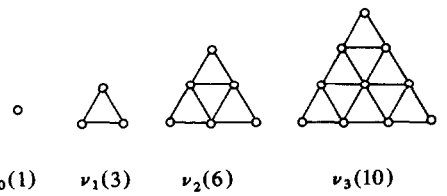

Chart 10. ν_n Triangular clusters of frequency (n) 0, 1, 2 and 3.

The Shell model for ν_n polytopal metal clusters

A ν_n polytopal cluster is a polygonal or a polyhedral cluster in two- or three-dimensions, respectively, as exemplified by ν_n triangles (Chart 10), ν_n tetrahedra (Chart 11), and ν_n octahedra (Chart 12).

Concepts of "peeling onion" and "slicing cheese" for atom counting. In order to understand the packing of spheres (or atoms) in a ν_n polyhedron, Teo and Sloane[15a] introduced the concepts of "peeling an onion" and "slicing a cheese".

"Peeling an onion" refers to the removal of the S_n surface atoms (the "skin") to reveal the I_n interior atoms (the "core") of a ν_n polyhedral cluster. There are, in fact, three classes of ν_n polyhedral clusters. In the *first* class, exemplified by the icosahedron, the cuboctahedron and twinned cuboctahedron, the removal of the surface atoms produces a ν_{n-1} polyhedron of the same shape. In this case the whole "onion" can be built up from layers of the same shape. The *second* class is exemplified by a ν_n octahedron which has the property that removal of the outer shell produces a ν_{n-2}, not a ν_{n-1} octahedron. The "onion" is now composed of layers of the same shape, but the size of the layers decreases by two each time, viz. step size of $s = 2$. Similarly, for a ν_n

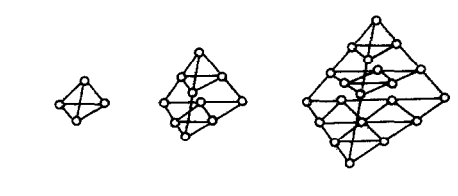

Chart 11. ν_n Tetrahedral clusters of frequency (n) 0, 1, 2 and 3.

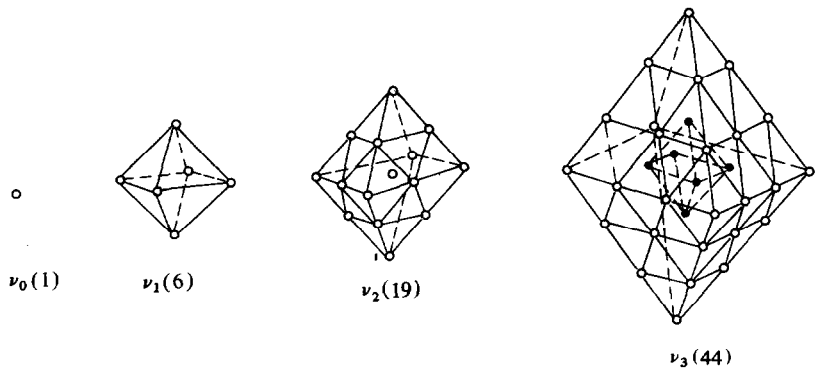

Chart 12. ν_n Octahedral clusters of frequency (n) 0, 1, 2 and 3.

tetrahedron the interior is a ν_{n-4} tetrahedron, in steps (s) of 4. A *third* class comprises those in which the interior polyhedron has a shape different from the original. For example, removing the outer shell from a truncated ν_3 octahedron does not produce a similar polyhedron of a smaller size. The core of a truncated ν_3 octahedron [cf. Chart 13(a)], in fact, is a ν_1 octahedron.

The concept of "slicing a cheese" involves removing the atoms layer by layer, i.e. in planar layers, each layer being parallel to the next, as illustrated in Chart 13 for the truncated ν_3 octahedron along the three-fold [13(b)] and the four-fold [13(c)] symmetry axes. Here we assume close-packing arrangements between adjacent layers of metal atoms. The most common types of close packing are; icosahedral (icp), face-centred cubic (fcc), hexagonal close packing (hcp), cubic, and body-centred cubic (bcc) as we shall discuss in the next section.

Electron counting of close-packed ν_n *polytopal metal clusters.* From eq. (1), a ν_n polytopal (polygonal or polyhedral) metal cluster is required to have a total of T_n topological electron pairs (TEC rule):[14]

$$T_n = 6S_n + B_n, \tag{9}$$

where S_n is the number of "surface" atoms and B_n is the number of *shell electron pairs*.† For a *close-packed* high nuclearity metal cluster, T_n can be rewritten (Shell model)[15a] as

$$T_n = 6G_n + K, \tag{10}$$

where G_n is the total number of atoms (nuclearity) and K is related to the B value of the centre of the cluster. One of two possibilities arises. First, if the cluster is centred at a *primary* cluster such as a triangle, a tetrahedron or an octahedron, $K = B_1$, where B_1 corresponds to the primary cluster (or hole) at the centre. The commonly observed polytopes/holes and the corresponding B_1 values are tabulated in Table 2. Second, if the cluster is centred at an atom, then the $K = B_0$ which depends on the coordination sphere (geometry and symmetry) of the central atom. For example, $K = B_0 = 7$ if the central atom is surrounded by 12 neighbouring atoms in a cuboctahedral arrangement of fcc packing. Note that in this case $T_0 = 6 \times 1 + 7 = 13$ which is exactly equal to the B_1 value of the 13-atom centred cuboctahedral cluster. Other commonly observed coordinations can be found in Table 2. Note the similarities between Table 2 and Charts 4 and 5.

We can now use eq. (10) and the K values listed in Table 2 to predict the electron counts of ν_n polygonal or polyhedral close-packed metal clusters. We shall consider three series: (a) ν_n triangular clusters (Chart 10); (b) ν_n tetrahedral clusters (Chart 11); and (c) ν_n octahedral clusters. The K, B and T values for the first few members of the series are

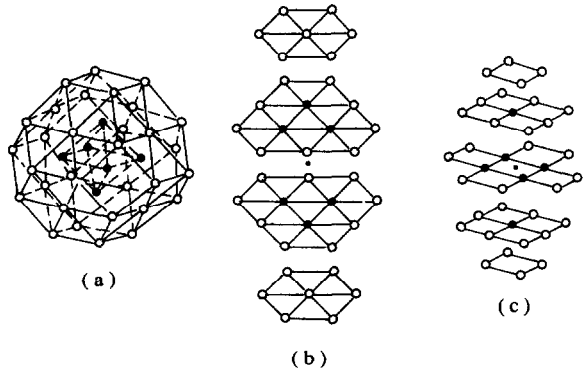

Chart 13. Three views of the truncated ν_3 octahedral cluster: Peeling onion (a); slicing cheese along the three-fold (b) and the four-fold (c) axes.

† As pointed out in ref. 15(a), T_n, B_n and S_n correspond to T, B and V_m, in eq. (1) only for the primary clusters. For large clusters of close-packed metal atoms, this connection is lost.

Table 2. The K, B and T values for various cluster centres[a]

Number	Centre	$K = B_0$ (Atom)	$K = B_1$ (Hole)	T_1
1	Monomer (see below)		3	7
2	Dimer		5	17
3	Trimer		7	25
4	Triangle		6	24
5	Butterfly		7	31
6	Square		8	32
7	Pentagon		10	40
8	Tetrahedron (T_d)		6	30
9	Trigonal bipyramid (tbp)		6	36
10	Octahedron (O_h)		7	43
11	Icosahedron (I_h)	3	9	81
12	Icosahedron (I_h)	7	13	85
13	Bicapped pentagonal prism (bpp)	9	15	87
14	Cuboctahedron (fcc)	7	13	85
15	Twinned cuboctahedron (hcp)	7	13	85
16	Cubic	6	12	60
17	Body-centred cubic (bcc)	6	12	96
18	Rhombic dodecahedron (rdd)	9	15	99

[a] $K = B_0$ or B_1 for metal clusters centred at an atom or a hole, respectively. $T_1 = 6S_1 + B_1$ and $T_0 = 6 \times 1 + B_0$ (since $S_0 = 1$) follow directly from the TEC rule [cf. eq. (9)]. $B_1 = T_0$ for polyhedra 11–18 follows from inclusion principle (see text).

tabulated in Tables 3–5, respectively. General formulae for atom and electron countings are also given in the Tables. Some known clusters are discussed below.

v_n *Triangular metal clusters.* An examination of Chart 10 revealed that a v_n triangle repeats itself in steps of three. In other words, removal of the peripheral atoms of a v_n triangle produces a v_{n-3} triangle. Hence we have the following three situations: (1) for v_0, v_3, v_6, ..., v_{3n} triangles centring at an atom, $K = 7$; (2) for v_1, v_4, v_7, ..., v_{3n+1} triangles centring at a triangle, $K = 6$; and (3) for v_2, v_5, v_8, ..., v_{3n+2} triangles centring at a triangle, $K = 6$. Only the first two structures are known in metal clusters:

(i) The v_1 triangular metal cluster (cf. Chart 10 and Table 2):

Table 3. Electron counting of the v_n triangular metal clusters via the Shell model[a]

	v_0	v_1	v_2	v_3	v_4	v_5	...	v_{10}
S_n	1	3	6	9	12	15		30
I_n	0	0	0	1	3	6		36
G_n	1	3	6	10	15	21		66
K	7	6	6	7	6	6		6
B	7	6	6	13	24	42		222
T	13	24	42	67	96	132		402

[a] The general formulae[15a] are: $S_n = 3n$; $I_n = n^2/2 - 3n/2 + 1$; $G_n = n^2/2 + 3n/2 + 1$; $K = 7$ for v_{3n}; $K = 6$ for v_{3n+1} or v_{3n+2}; $B_n = T_n - 6S_n$ or $B_n = 6I_n + K$; $T_n = 6G_n + K$.

Table 4. Electron counting of the v_n tetrahedral metal clusters via the Shell model[a]

	v_0	v_1	v_2	v_3	v_4	v_5	...	v_{10}
S_n	1	4	10	20	34	52		202
I_n	0	0	0	0	1	4		84
G_n	1	4	10	20	35	56		286
K	7	6	7	6	7	6		7
B	7	6	7	6	13	30		511
T	13	30	67	126	217	342		1723

[a] General formulae[15a] are: $S_n = 2n^2 + 2$; $I_n = (n-1)(n-2)(n-3)/6$; $G_n = (n+1)(n+2)(n+3)/6$; $K = 7$ for v_{4n} (atom) or v_{4n+2} (O_h); $K = 6$ for v_{4n+1} (T_d) or v_{4n+3} (T_d); $B_n = 6I_n + K$; $T_n = 6G_n + K$.

Table 5. Electron counting of the v_n octahedral metal clusters via the Shell model[a]

	v_0	v_1	v_2	v_3	v_4	v_5	...	v_{10}
S_n	1	6	18	38	66	102		402
I_n	0	0	1	6	19	44		489
G_n	1	6	19	44	85	146		891
K	7	7	7	7	7	7		7
B	7	7	13	43	121	271		2941
T	13	43	121	271	517	883		5353

[a] General formulae are: $S_n = 4n^2+2$; $I_n = (n-1)(2n^2-4n+3)/3$; $G_n = (n+1)(2n^2+4n+3)/3$; $K = 7$; $B_n = 6I_n+K$; $T_n = 6G_n+K$.

$K = 6$

$T_1 = 6G_1+K = 6\times3+6 = 24$

$N_1 = 2T_1 = 48$

e.g. $N_{obs} = 3\times8+12\times2 = 48$ in $Os_3(CO)_{12}$.[28]

(ii) The v_2 triangular metal cluster centring at a triangle structure (cf. Chart 10 and Table 2):

$K = 6$

$T_2 = 6G_2+K = 6\times6+6 = 42$

$N_2 = 2T_2 = 84$

e.g. $N_{obs} = 3\times11+3\times8+12\times2+3 = 84$ in $[Cu_3Fe_3(CO)_{12}]^{3-}$.[29]

v_n *Tetrahedral metal clusters.* As mentioned earlier, a v_n tetrahedron repeats itself in steps of four (cf. Chart 11). We have the following four situations: (1) since v_1, v_5, v_9, ... tetrahedra all centre at a tetrahedral hole, $K = 6$; (2) since v_2, v_6, v_{10}, ... tetrahedra all centre at an octahedral hole, $K = 7$; (3) since v_3, v_7, v_{11}, ... tetrahedra all centre at a tetrahedral hole, $K = 6$; (4) since v_4, v_8, v_{12}, ... tetrahedra all centre at an atom, $K = 7$. Only the first two structures are characterized in metal clusters:

(i) The v_1 tetrahedral metal cluster (cf. Chart 11 and Table 2):

$K = 6$

$T_1 = 6G_1+K = 6\times4+6 = 30$

$N_1 = 2T_1 = 60$

e.g. $N_{obs} = 4\times9+12\times2 = 60$ in $Co_4(CO)_{12}$.[30a]

(ii) The v_2 tetrahedral metal cluster centred on an octahedron hole framework (cf. Chart 11 and Table 2):

$K = 7$

$T_2 = 6G_2+K = 6\times10+7 = 67$

$N_2 = 2T_2 = 134$

e.g. $N_{obs} = 10\times8+4+24\times2+2 = 134$ in $[Os_{10}C(CO)_{24}]^{2-}$.[5e]

v_n *Octahedral metal clusters.* As discussed earlier, a v_n octahedron repeats itself in steps of two (cf. Chart 12). For v_0. v_2, v_4, ..., v_{2n} octahedra centring at an atom with a cuboctahedral coordination, $K = 7$ (cf. Table 2). For v_1, v_3, v_5, ..., v_{2n+1} octahedra centring at an atom with octahedral hole, $K = 7$ (cf. Table 2). Hence, $K = 7$ for all v_n octahedral metal clusters. Only the following examples are known:

(i) The v_1 octahedral metal cluster (cf. Chart 12 and Table 2):

$K = 7$

$T_1 = 6G_1+K = 6\times6+7 = 43$

$N_1 = 2T_1 = 86$

e.g. $N_{obs} = 6\times9+16\times2 = 86$ in $Rh_6(CO)_{16}$.[30b]

(ii) The v_3 octahedral metal cluster (cf. Chart 12 and Table 2):

$K = 7$

$T_3 = 6G_3+K = 6\times44+7 = 271$

$N_3 = 2T_3 = 542$

e.g. $N_{obs} = 38\times10+6\times10+48\times2+1+5$

$= 542$ $[Ni_{38}Pt_6(CO)_{48}H]^{5-}$.[6a]

If we now apply the TEC rule [eq. (9)] to the v_3 octahedral metal cluster we just discussed, we obtain $B_3 = T_3-6S_3 = 271-6\times38 = 43$. This turns out to be exactly equal to the T_1 value of the v_1 octahedral metal cluster described previously. Since a v_3 octahedron can completely encapsulate a v_1 octahedron (cf. Chart 12), this electron counting characteristic (viz. $B_3 = T_1$) signifies a sort of *inclusion principle* which deserves further comments in the next section.

The electron counting results, via the Shell model, of other representative examples of close-packed metal clusters are tabulated in Table 6.

Inclusion principle. A natural consequence of the Shell model in the electron counting of high nuclearity close-packed metal clusters is the *inclusion principle.* This follows directly from the "peeling onion" concept (atom counting) we described in a previous section. As is evident from Charts 10–13 and Tables 3–5, for close-packed v_n polygonal or polyhedral

Table 6. Electron counting of close-packed metal clusters via the Shell model

Cluster[a]	Packing[b]	G^c	K^d	T^e	$N_{Shell}{}^f$	N_{obs}
$[Pt_{19}(CO)_{22}]^{4-}$	bpp	19	5	119	238	238
$[Rh_{22}(CO)_{35}H_{5-q+x}]^{q-}$	fcc/bcc	22	5	137	274	$273+x$
$[Au_{13}Ag_{12}Cl_8(PPh_3)_{10}]^+$	icp	25	7	157	314	314
$[Pt_{26}(CO)_{32}]^{2-}$	hcp	26	6	162	324	326
$[Ni_{38}Pt_6(CO)_{48}H_{6-n}]^{n-}$	fcc	44	7	271	542	542
$[Pt_{38}(CO)_{44}]^{2-}$	fcc	38	7	235	470	470
$[Au_{13}Cl_2(PMe_2Ph)_{10}]^{3+}$	icp	13	3	81	162	162
$[Rh_{12}Sb(CO)_{27}]^{3-}$	icp	12	13	85	170	170
$[Rh_{13}(CO)_{24}H_{5-q}]^{q-}$	hcp	13	7	85	170	170
$[Pt_{24}(CO)_{30}]^{2-}$	fcc	24	7	151	302	302
$[Rh_{14}(CO)_{25}H_{4-q}]^{q-}$	bcc	14	6	90	180	180
$[Rh_{14}(CO)_{26}]^{2-}$	bcc	14	6	90	180	180
$[Rh_{15}(CO)_{27}]^{3-}$	bcc/hcp	15	6	96	192	192
$[Rh_{15}(CO)_{30}]^{3-}$	rdd	15	9	99	198	198

[a] See ref. 17 for additional literature references to these clusters.
[b] See Table 2 for abbreviations.
[c] The total number of atoms.
[d] From Table 2.
[e] $T = 6G+K$.
[f] $N_{Shell} = 2T$.

metal clusters, $B_n = T_{n-s}$. For example, for v_n octahedral metal clusters, $T_0 = B_2$, $T_1 = B_3$, $T_2 = B_4$, ..., $B_n = T_{n-2}$ (Table 5). In other words, the number of shell electron pairs of a v_n polytopal cluster is exactly equal to the number of topological electron pairs of a (smaller) polytopal v_{n-s} cluster. This is actually not too surprising because in previous sections we have shown that the clusters can be built up in step size of s. In other words, a v_{n-s} polyhedral can be completely encapsulated within a v_n polyhedral cluster of the same shape (the "onion" concept). In fact, we can generalize this principle by combining eqs (9) and (10) to give

$$B_n = 6I_n + K, \tag{11}$$

since $G_n = S_n + I_n$, where I_n is the number of "interior" atoms. Now if there is a smaller cluster (denoted by n') containing $G_{n'} = I_n$ atoms, we have [via eq. (10)]

$$B_n = 6G_{n'} + K = T_{n'}. \tag{12}$$

Again, using the v_3 octahedron ($n = 3$) as an example, we have a total of $G_3 = 44$ atoms, of which $S_3 = 38$ are surface atoms and $I_3 = 6$ are interior atoms (cf. Chart 12). The latter constitutes a v_1 octahedron ($n' = 1$) with $G_1 = I_3 = 6$. Equation (12) therefore predicts that $B_3 = T_1$. In other words, in order for a cluster (denoted by n) to completely encapsulate a smaller cluster (denoted by n'), $B_n = T_{n'}$. This is the essence of the *inclusion principle*. (Incomplete encapsulation can occur if $T_{n'} > B_{n'}$.) For example, a v_3 octahedron and truncated v_3 octahedron both have $B = 43$ shell electron pairs, which satisfy the $T = 43$ total electron pairs of a v_1 octahedron. Indeed, both $[Ni_{38}Pt_6(CO)_{48}H]^{5-}$ [6a] and $[Pt_{38}(CO)_{44}]^{2-}$ [5a] (Chart 13) contain a completely encapsulated Pt_6 octahedron. The electron counting procedures for these two clusters, highlighting the inclusion principle, are given in Chart 14.

In fact, this inclusion principle holds for any *close-packed metal cluster* with encapsulants which may be an atom, a primary cluster, or a smaller close-packed cluster. Some representative examples are listed in Table 7. The inclusion principle, in combination with the TEC rule, allows electron counting of these high nuclearity metal clusters without the assignment of the "degrees of radial vs tangential bonding contributions".[31]

For example, the cluster $[Pt_{19}(CO)_{22}]^{4-}$ (**1**)[3] has a dimer as its core. Applying the Shell model [eq. (10)], we obtain $T = 6G+K = 6\times 19+5 = 119$, since $K = 5$ for a dimer (cf. Chart 5 or Table 2). The predicted electron count of $N = 2T = 2\times 119 = 238$ agrees with the observed value of $N_{obs} = 19\times 10+22\times 2+4 = 238$. On the other hand, the inclusion principle is also operative in cluster **1**. Here the TEC rule gives $B = 5$ (Chart 5) and

(a) $[Ni_{38}Pt_6(CO)_{48}H_{6-n}]^{n-}$

For the v_1 octahedral core:

$B_1 = 7$ (v_1 O_h core)

$T_1 = 6S_1 + B_1 = 6\times6+7 = 43.$ (TEC on v_1 O_h core)

For the v_3 octahedron:

$B_3 = T_1$ (inclusion principle)

$T_3 = 6S_3 + B_3 = 6\times(44-6)+43 = 271$ (TEC on v_3 O_h)

$N = 2T = 542$

$N_{obs} = 38\times10+6\times10+48\times2+6 = 542.$

(b) $[Pt_{38}(CO)_{44}]^{2-}$

For the v_1 octahedral core:

$B_1 = 7$ (v_1 O_h core)

$T_1 = 6S_1 + B_1 = 6\times6+7 = 43.$ (TEC on v_1 O_h core)

For the truncated v_3 octahedron:

$B_3 = T_1$ (inclusion principle)

$T_3 = 6S_3 + B_3 = 6\times(38-6)+43 = 235$ (TEC on truncated v_3 O_h)

$N = 2T = 470$

$N_{obs} = 38\times10+44\times2+2 = 470.$

Chart 14. Inclusion principle for clusters $[Ni_{38}Pt_6(CO)_{48}H_{6-n}]^{n-}$ and $[Pt_{38}(CO)_{44}]^{2-}$.

$T_i = 6\times S_i + B_i = 6\times2+5 = 17$ for the encapsulated dimer (designed by the subscript i). The inclusion principle then predicts $B = T_i = 17$ and $T = 6S+B = 6\times(19-2)+17 = 6\times17+17 = 119$ or $N = 238$.

Other close-packed metal clusters listed in Table 6 can likewise be treated; the results are tabulated in Table 7.

A detailed examination of Tables 6 and 7 shows that the Shell model and the inclusion principle, in combination with the TEC rule, give essentially the same results, as expected from the earlier discussions. However, for a very large metal cluster, it is more convenient to apply the *one-step* Shell model [cf. eq. (10)] than to invoke the *multi-step* inclusion principle [eq. (12)]. For example, a v_5 octahedral metal cluster is predicted to have $T_5 = 6G_5+K = 6\times146+7 = 883$ by the Shell model [eq. (10)]. The same result can also be obtained by applying the inclusion principle successively to v_5, v_3, v_1 octahedral clusters (via the "peeling onion" concept) as follows (cf. Table 5)

Table 7. Electron counting of close-packed metal clusters via the inclusion principle and extended Hume–Rothery rule

Cluster[a]	S_i[b,c]	S[c]	B_i[d]	$T_i = B$[e]	T[f]	N_{Inc}[g]	N_{obs}	N_{EHR}[h]
$[Pt_{19}(CO)_{22}]^{4-}$	2(dimer)	17	5	17	119	238	238	235.9
$[Rh_{22}(CO)_{35}H_{5-q+x}]^{q-}$	2(dimer)	20	5	17	137	274	273+x	275.3
$[Au_{13}Ag_{12}Cl_8(PPh_3)_{10}]^{+}$	3(trimer)	22	7	25	157	314	314	310.0
$[Pt_{26}(CO)_{32}]^{2-}$	3(triangle)	23	6	24	162	324	326	339.3
$[Ni_{38}Pt_6(CO)_{48}H_{6-n}]^{n-}$	6(O_h)	38	7	43	271	542	542	548.0
$[Pt_{38}(CO)_{44}]^{2-}$	6(O_h)	32	7	43	235	470	470	471.9
$[Au_{13}Cl_2(PMe_2Ph)_{10}]^{3+}$	1(icp)	12	3	9	81	162	162	161.9
$[Rh_{12}Sb(CO)_{27}]^{3-}$	0(icp)	12	13	13	85	170	170	—
$[Rh_{13}(CO)_{24}H_{5-q}]^{q-}$	1(hcp)	12	7	13	85	170	170	170.4
$[Pt_{24}(CO)_{30}]^{2-}$	1(fcc)	23	7	13	151	302	302	301.9
$[Rh_{14}(CO)_{25}H_{4-q}]^{q-}$	1(bcc)	13	6	12	90	180	180	179.7
$[Rh_{14}(CO)_{26}]^{2-}$	1(bcc)	13	6	12	90	180	180	179.7
$[Rh_{15}(CO)_{27}]^{3-}$	1(bcc)	14	6	12	96	192	192	192.6
$[Rh_{15}(CO)_{30}]^{3-}$	1(rdd)	14	9	15	99	198	198	192.6

[a] See ref. 17 for additional literature references to these clusters.

[b] See Table 2 for abbreviations.

[c] $S_i = m_b$ and $S = m_s$ in ref. 17.

[d] From Table 2.

[e] $B = T_i$ (inclusion principle); $T_i = 6S_i + B_i$ (TEC rule). See Table 2.

[f] $T = 6S+B$.

[g] $N_{Inc} = 2T$.

[h] From ref. 17. See text.

$$
\begin{aligned}
T_5 &= 6S_5+B_5 && \text{(TEC rule on } v_5\text{)}\\
&= 6S_5+T_3 && (v_5 \text{ encapsulates } v_3)\\
&= 6S_5+(6S_3+B_3) && \text{(TEC rule on } v_3\text{)}\\
&= 6(S_5+S_3)+T_1 && (v_3 \text{ encapsulates } v_1)\\
&= 6(S_5+S_3)+(6S_1+B_1) && \text{(TEC rule on } v_1\text{)}\\
&= 6(S_5+S_3+S_1)+B_1 = 6\times(102+38+6)+7\\
&= 883.
\end{aligned}
$$

Hume–Rothery rule—the bulk connection

A simple electron counting rule based on the extended Hume–Rothery rule has been suggested in ref. 17 for correlating and/or predicting the metal packing arrangements in high nuclearity metal clusters. For a metal cluster with m_b "*bulk*" atoms and m_s "*surface*" atoms (the nuclearity is $m = m_b+m_s$), the total number of electrons N (including valence electrons from the metals and electrons donated by the ligands) is given by $N = m_bn_b+m_sn_s = (m_b+rm_s)n_b$, where n_b and n_s are the numbers of electrons per bulk and surface atoms, respectively, and $r = n_s/n_b$, which is basically an empirical constant given by $18/16 = 1.125$. Including the d electrons, the n_b values for the commonly observed close-packed structures are: 11.17 for pentagonal close-packing; 11.24 for fcc; 11.50 for bcc; 11.62 for γ-phase; and 11.75 for hcp.† The electron counts predicted by the extended Hume–Rothery rule are also given in Table 7. They compare favourably with the observed values.

It is striking to find that the electronic requirements predicted by the Hume–Rothery rule or band structure theory for bulk metals or metallic alloys, which are characterized by long-range order, can be extended to discrete metal clusters where only short-range order is important. Nevertheless, the electron counting rule proposed here is consistent with the recent theoretical results that the density of states of a metal cluster rapidly converges to that of the bulk metal even at the aggregation of 13 (fcc) to 15 (bcc) atoms.[33] As the cluster size increases, this approximation should improve. This is, in essence, the *bulk connection* of large metal clusters.

Acknowledgements—Acknowledgement is made to the National Science Foundation (CHE-8722339) for financial support of this research. B.K.T. would also like to acknowledge the important contributions of his present and past co-workers whose names appear in the references.

† The Hume–Rothery rule (see ref. 32) states that certain alloy structures occur at a definite electron/atom ratio (viz., sum of valence electrons/sum of ionic atoms). For example, the β (body-centred cubic, bcc), γ (complicated cubic structure) and ε (hexagonal close packed, hcp) phases inevitably occur at ratios 21/14, 21/13 and 21/12, as exemplified by CuZn, Cu_5Zn_8 and $CuZn_3$, respectively. Also observed is the α (face-centred cubic, fcc) phase of Cu_3Zn at the ratio of 5/4. If we include d shell electrons, the number of valence electrons per bulk atom can be approximated by $n = 10+21/18 = 11.17$ for pentagonal; $10+21/17 = 11.24$ for fcc; $10+21/14 = 11.50$ for bcc; $10+21/13 = 11.62$ for γ phase; and $10+21/12 = 11.75$ for hcp structures.

REFERENCES

1. (a) B. Krebs, M. Hucke and C. S. Brendel, *Angew. Chem. Int. Ed. Engl.* 1982, **21**, 445; (b) C. H. E. Belin, J. D. Corbett and A. Cisar, *J. Am. Chem. Soc.* 1977, **99**, 7163.
2. C. E. Briant, B. R. C. Theobald, J. W. White, L. K. Bell, D. M. P. Mingos and A. J. Welch, *J. Chem. Soc., Chem. Commun.* 1981, 201.
3. D. M. Washecheck, E. J. Wucherer, L. F. Dahl, A. Ceriotti, G. Longoni, M. Manassero, M. Sansoni and P. Chini, *J. Am. Chem. Soc.* 1979, **101**, 6110.
4. F. A. Cotton and G. Wilkinson, *Advanced Inorganic Chemistry*, 4th edn. John Wiley, New York (1980).
5. (a) G. Longoni and L. Dahl, unpublished results; (b) S. Martinengo, A. Fumagalli, R. Bonfichi, G. Ciani and A. Sironi, *J. Chem. Soc., Chem. Commun.* 1982, 825; (c) J. L. Vidal, R. C. Schoening and J. M. Troup, *Inorg. Chem.* 1981, **20**, 227; (d) R. W. Broach, L. F. Dahl, G. Longoni, P. Chini, A. J. Schultz and J. M. Williams, *Adv. Chem. Ser.* 1978, **167**, 93; (e) P. F. Jackson, B. F. G. Johnson, J. Lewis, W. J. H. Nelson and M. McPartlin, *J. Chem. Soc., Dalton Trans.* 1982, 2099; (f) C. M. T. Hayward, J. R. Shapley, M. R. Churchill, C. Bueno and A. L. Rheingold, *J. Am. Chem. Soc.* 1982, **104**, 7347.
6. (a) A. Ceriotti, F. Demartin, G. Longoni, M. Manassero, M. Marchionna, G. Piva and M. Sansoni, *Angew. Chem. Int. Ed. Engl.* 1985, **24**, 697; (b) G. Longoni, M. Manassero and M. Sansoni, *J. Chem. Soc.* 1980, **102**, 3242; (c) A. Fumagalli, S. Martinengo, G. Ciani and A. Sironi, *J. Chem. Soc., Chem. Commun.* 1983, 453; (d) P. D. Boyle, B. J. Johnson, A. Buehler and L. H. Pignolet, *Inorg. Chem.* 1986, **25**, 5; (e) B. D. Alexander, P. D. Boyle, B. J. Johnson, A. L. Casalnuovo, S. M. John, A. M. Mueting and L. H. Pignolet, *Inorg. Chem.* 1987, **26**, 2547; (f) J. J. Steggerda, J. J. Bour and J. W. A. van der Velden, *Recl. J. R. Neth. Chem. Soc.* 1982, **101**, 164.
7. K. Kharas and L. Dahl, *Adv. Chem. Phys.* 1988, **70**, 1.
8. (a) P. Chini, *Gazz. Chim. Ital.* 1979, **109**, 225; (b) P. Chini, *J. Organomet. Chem.* 1980, **200**, 37; (c) P. Chini, G. Longoni and V. G. Albano, *Adv. Organomet. Chem.* 1976, **14**, 285.

9. B. F. G. Johnson (Ed.), *Transition Metal Clusters*. Wiley-Interscience, Chichester (1980).
10. (a) R. Hoffmann and W. N. Lipscomb, *J. Chem. Phys.* 1962, **36**, 2179; (b) R. E. Williams, *Inorg. Chem.* 1971, **10**, 210; (c) K. Wade, *J. Chem. Soc., Chem. Commun.* 1971, 792; *Adv. Inorg. Chem. Radiochem.* 1976, **18**, 1; (d) D. M. P. Mingos, *Accts Chem. Res.* 1984, **17**, 311; (e) A. Stone, *Inorg. Chem.* 1981, **20**, 563.
11. J. W. Lauher, *J. Am. Chem. Soc.* 1978, **100**, 5305; 1979, **101**, 2604; *J. Organomet. Chem.* 1981, **213**, 25.
12. (a) R. B. King, *Inorg. Chim. Acta* 1986, **116**, 99; 109; 119; 125; (b) R. B. King and D. H. Rouvray, *J. Am. Chem. Soc.* 1977, **99**, 7834.
13. (a) B. K. Teo, *Inorg. Chem.* 1984, **23**, 1251; (b) B. K. Teo, G. Longoni and F. R. K. Chung, *Inorg. Chem.* 1984, **23**, 1257.
14. (a) B. K. Teo, *Inorg. Chem.* 1985, **24**, 1627; (b) B. K. Teo, *Inorg. Chem.* 1985, **24**, 4209.
15. (a) B. K. Teo and N. J. A. Sloane, *Inorg. Chem.* 1985, **24**, 4545; (b) N. J. A. Sloane and B. K. Teo, *J. Chem. Phys.* 1985, **83**, 6520; (c) B. K. Teo and N. J. A. Sloane, *Inorg. Chem.* 1986, **25**, 2315.
16. (a) B. K. Teo and H. Zhang, *Inorg. Chem.* 1988, **27**, 414; (b) B. K. Teo and H. Zhang, *Inorg. Chim. Acta* 1988, **144**, 173.
17. B. K. Teo, *J. Chem. Soc., Chem. Commun.* 1983, 1362.
18. H. S. M. Coxeter, *Regular Polytopes*, 3rd edn. Dover, New York (1973).
19. (a) B. K. Teo, M. C. Hong, H. Zhang and D. B. Huang, *Angew. Chem. Int. Ed. Engl.* 1987, **26**, 897; (b) B. K. Teo, M. Hong, H. Zhang, D. Huang and X. Shi, *J. Chem. Soc., Chem. Commun.* 1988, 204; (c) B. K. Teo, *Polyhedron* 1988, **7**, 2317.
20. (a) M. I. Forsyth and D. M. P. Mingos, *J. Chem. Soc., Dalton Trans.* 1977, 610; (b) D. M. P. Mingos, *Nature* 1972, **236**, 99.
21. L. D. Lower and L. F. Dahl, *J. Am. Chem. Soc.* 1976, **98**, 5046.
22. M. McPartlin, C. R. Eady, B. F. G. Johnson and J. Lewis, *J. Chem. Soc., Chem. Commun.* 1976, 883.
23. A. L. Mackay, *Acta Cryst.* 1962, **15**, 916.
24. O. Echt, K. Sattler and E. Recknagel, *Phys. Rev. Lett.* 1981, **47**, 1121.
25. S. Martinengo, A. Fumagalli, R. Bonfichi, G. Ciani and A. Sironi, *J. Chem. Soc., Chem. Commun.* 1982, 825.
26. B. K. Teo, H. Zhang and X. Shi, *Inorg. Chem.* 1990, **29**, 2083.
27. B. K. Teo, H. Zhang and X. Shi, *J. Am. Chem. Soc.*, accepted.
28. (a) E. R. Corey and L. F. Dahl, *Inorg. Chem.* 1962, **1**, 521; (b) M. R. Churchill and B. G. DeBoer, *Inorg. Chem.* 1977, **16**, 878.
29. G. Doyle, K. A. Eriksen and D. Van Engan, *J. Am. Chem. Soc.* 1985, **107**, 7914.
30. (a) C. H. Wei and L. F. Dahl, *J. Am. Chem. Soc.* 1966, **88**, 1821; (b) E. R. Corey, L. F. Dahl and W. Beck, *J. Am. Chem. Soc.* 1963, **85**, 1202.
31. D. M. P. Mingos, *J. Chem. Soc., Chem. Commun.* 1985, 1352.
32. W. Hume-Rothery, *The Metallic State*, p. 328. Oxford University Press, New York (1931).
33. (a) R. P. Messmer, S. K. Knudson, K. H. Johnson, J. B. Diamond and C. Y. Yang, *Phys. Rev. B* 1976, **13**, 1396; (b) C. Y. Yang, K. H. Johnson, D. R. Salahub, J. Kaspar and R. P. Messmer, *Phys. Rev. B*. 1981, **24**, 5637.

Polyhedron Vol. 9, No. 15/16, pp. 2001–2011, 1990
Printed in Great Britain

0277–5387/90 $3.00+.00
© 1990 Pergamon Press plc

VALENCE ORBITAL ENERGETICS AS A TOOL FOR ORGANOMETALLIC SYNTHESIS: ON THE SCARCITY OF TWO-LEGGED PIANO-STOOL COMPLEXES*

BRUCE E. BURSTEN† and MICHAEL G. GATTER

Department of Chemistry, The Ohio State University, Columbus, OH 43210, U.S.A.

and

KAREN I. GOLDBERG

Department of Chemistry, Illinois State University, Normal, IL 61761, U.S.A.

Abstract—The stability of 18-electron two-legged piano-stool complexes of the type (η^n-C_nH_n)ML_2 (n = 4, 5 or 6; L = CO or NO; M = first-row transition metal) is correlated to the energetic separation of the HOMO from both the LUMO and the SHOMO (second-highest occupied molecular orbital) of the complexes calculated by using the Fenske–Hall molecular orbital method. Complex stability is observed to increase with increasing HOMO/LUMO and decreasing HOMO/SHOMO separations. This correlation is reflected in an examination of known stable complexes and unsuccessful synthetic attempts at others. On the basis of these findings, predictions are made as to the stability of a number of unknown 18-electron two-legged piano-stool complexes for which syntheses have not yet been attempted.

The synthesis of 18e two-legged piano-stool organometallic complexes containing carbonyl and/or nitrosyl ligands (**1**) appears to have lagged behind that of their three-legged analogues (**2**); in contrast to the dozens of known three-legged species, only a

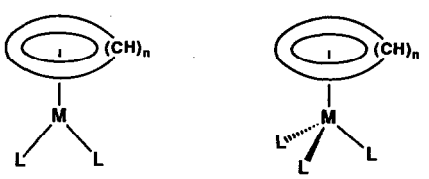

1 2

very limited number of two-legged complexes have been isolated. We believe that the relative dearth of compounds **1** likely results from electronic differences between the coordination environments **1** and **2**. In the course of our earlier investigations of the comparative orbital energetics of two- and three-legged piano-stool complexes resulting from deprotonation of three- and four-legged piano-stool hydride species, we observed that the HOMO of 18e two-legged piano-stools is metal-localized and non-bonding, whereas the HOMO in three-legged complexes is involved in extensive metal-to-ligand π-backbonding.[1,2] Furthermore, the stability of the two-legged piano-stool complexes was noted to depend upon two energetic differences, viz. the HOMO/LUMO separation (HOMO = highest occupied molecular orbital; LUMO = lowest unoccupied molecular orbital) and the HOMO/SHOMO separation (SHOMO = second-highest occupied molecular orbital).

In this paper we report the use of these two orbital energetic quantities as a means of predicting the stability of various systems **1**. It will be demonstrated that, kinetic arguments notwithstanding, the isolability of two-legged piano-stool complexes is highly dependent on the *relative* orbital energies, even for an isoelectronic series. Inasmuch as all the compounds studied obey the effective atomic number rule, we propose that there are electronic

* Dedicated to Professor Richard F. Fenske on the occasion of his retirement. His insight, counsel, friendship and good humour have inspired us all, particularly B.E.B., who received his PhD degree under Dick's supervision.

† Author to whom correspondence should be addressed.

constraints beyond the 18e rule that govern the successful synthesis of these systems. Finally, we will use these arguments to predict some new complexes that should be electronically stable.

COMPUTATIONAL SECTION

Molecular orbital calculations were carried out on an Amdahl 470/V8 computer system or an IBM 3081D computer system using the Fenske–Hall approximate MO method.[3]

In all of the calculations, the cyclobutadiene, cyclopentadienyl and benzene rings are assumed to have local D_{4h}, D_{5h} and D_{6h} symmetry with C—C bond lengths of 1.46, 1.38 and 1.42 Å, respectively. All C—H bond lengths were chosen to be 1.08 Å. The geometry assumed for all of the $(\eta^n\text{-}C_nH_n)ML_2$ piano-stool complexes has the ML_2 plane orthogonal to the plane of the C_nH_n ring, with the L—M—L angle equal to 90°; this geometry is adopted by the structurally characterized species $(\eta^5\text{-}C_5Me_5)Co(CO)_2$,[4] $(\eta^5\text{-}C_5Me_5)Rh(CO)_2$[5] and $[(\eta^5\text{-}C_5H_5)Fe(CO)_2][Bu_4N]$,[6] and our previous calculations indicate that it is the optimum geometry for two-legged piano-stool complexes.[1] All C—O and N—O bond lengths were set equal to 1.13 Å, and the assumed metal–ligand distances are listed in Table 1.

The atomic orbital basis was generated by a least-squares fit of Slater-type orbitals to the atomic orbitals from neutral (C, N, O) or +1 (transition metal atoms) Herman–Skillman atomic calculations.[7] Contracted double-ζ minimal basis representations were used for the metal 3*d* AOs and for the C, N and O 2*p* AOs; single-ζ representations were used for the remainder of the AOs. The 4*s* exponent was fixed at 2.0 for Cr, Mn, Fe and Co, with the 4*p* exponents for these being set to 1.6, 1.8, 2.0 and 2.2, respectively. The 4*s* and 4*p* exponents for Ni were both fixed at 2.2. An exponent of 1.16 was used for the H 1*s* AO.[8] In all calculations, the 3σ and the 6σ MOs of CO and NO, and the first three occupied and all virtual orbitals above the LUMO of the C_nH_n ligands, were deleted from the basis transformation set.[9]

Table 1. Bond lengths used in the $(\eta^n\text{-}C_nH_n)ML_2$ calculations

M—L bond lengths (Å)		Metal-to-ring[a] centroid distance (Å)	
Cr—C	1.90	Cr—Cp	1.85
Cr—N	1.72	Cr—Bz	1.65
Mn—C	1.72	Mn—Cp	1.80
Mn—N	1.72	Mn—Bz	1.65
Fe—C	1.76	Fe—Cb	1.79
Fe—N	1.76	Fe—Cp	1.72
		Fe—Bz	1.54
Co—C	1.73	Co—Cp	1.70
Co—N	1.73	Co—Bz	1.53
Ni—C	1.80	Ni—Cb	1.75
		Ni—Cp	1.74

[a] Cb denotes $\eta^4\text{-}C_4H_4$; Cp denotes $\eta^5\text{-}C_5H_5$; Bz denotes $\eta^6\text{-}C_6H_6$.

RESULTS AND DISCUSSION

The molecular orbitals of the ML_2 fragment and (polyene)ML_2 complexes have been discussed previously by several authors.[10] We will briefly reiterate these so that the effects of changing ML_2 fragments upon the electronic structure of two-legged piano-stool molecules will be more apparent.

The frontier orbitals of a typical C_{2v} d^8 ML_2 fragment, $Co(CO)_2^+$, are shown in Fig. 1. The results are very similar to those of Lichtenberger, *et al.*[10a] We consider the ML_2 fragment to lie in the *xy* plane. At lowest energy, we find an orbital of a_1 symmetry, which can roughly be described as a $d_{x^2-y^2}$ orbital on the metal that is stabilized by interaction with the in-plane π^* orbitals of the ligands L. At slightly higher energy are orbitals of b_1 and a_2 symmetries, corresponding to the metal d_{yz} and d_{xz} orbitals, respectively. Each of these can be stabilized by donation to the out-of-plane L π^* orbitals. The HOMO of the fragment is another orbital of a_1 symmetry, which is best described as a d_{z^2} orbital on M. This orbital is non-bonding with respect to the ligands L and is essentially localized on the metal atom, a fact that has been used by us to explain the seemingly anomalous differences in carbonyl stretching frequencies in 16- and 18e $CpM(CO)_2$ complexes.[11] The LUMO of the frag-

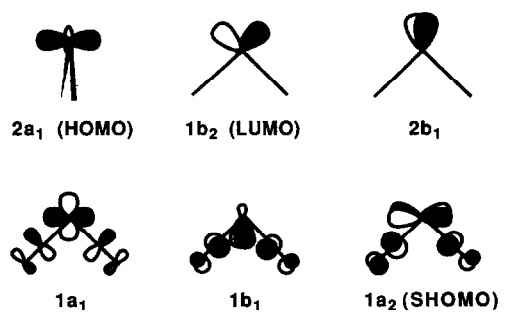

Fig. 1. Metal-based frontier orbitals of a d^8 ML_2 fragment.

ment is an orbital of b_2 symmetry corresponding to the M d_{xy} orbital. This orbital is at higher energy as it is the antibonding counterpart of one of the M—L σ bonding orbitals.

The interaction of a Cp^- ligand with the d^8 ML_2 fragment is shown in Fig. 2. The important frontier orbitals of the Cp ligand to consider are the doubly-degenerate, occupied e_1'' orbitals; the occupied a_2'' and unoccupied e_2'' are too low and too high in energy, respectively, to perturb the ML_2 orbitals significantly. The two e_1'' orbitals are of appropriate symmetry to interact with the ML_2 b_1 and b_2 orbitals. For a d^8 ML_2 fragment, the b_2 frontier orbital is empty and hence the corresponding Cp e_1'' orbital is stabilized while the LUMO is raised in energy. The other e_1'' interacts with the filled orbital of b_1 symmetry on the ML_2 fragment. This "filled–filled" interaction results in two occupied orbitals of b_1 symmetry, the lower one bonding and the higher one antibonding between the ML_2 fragment and the Cp ring. In the case of $CpCo(CO)_2$, the higher of these two is pushed above the non-bonding a_1 orbital and becomes the HOMO of the complex, an ordering that has been determined unequivocally from photoelectron spectroscopic studies.[10a]

The energies of the $1a_1$, $1b_1$, $1a_2$ and $1b_2$ orbitals of the ML_2 fragment are substantially dependent on both the nature of M and the relative energies of the interacting orbitals on M and L. The $2a_1$ orbital, by comparison, is non-bonding with respect to L and will be comparatively unaffected by the choice of L. The right-side of Fig. 2 shows the effect of replacing the $Co(CO)_2^+$ fragment with the isoelectronic $Mn(NO)_2^+$ fragment. In making this change, M has become more electropositive and L has become a stronger π-acid. The $1a_1$, $1a_2$ and $1b_1$ orbitals of $Mn(NO)_2^+$ are at nearly the same energy as those of $Co(CO)_2^+$. This is a result of the compromise between the higher energy 3*d* orbitals of the manganese compared to cobalt and the greater stabilization conferred by the nitrosyl ligands as compared to the carbonyl ligands. However, because the $2a_1$ orbital of $Mn(NO)_2^+$ is not affected by the change in L, it is significantly higher in energy than that of $Co(CO)_2^+$.

As can be seen in Fig. 2, the influence of these changes on the electronic structure of the resulting $CpML_2$ molecule is quite profound. The energetic separation of the $2a_1$ and $1b_1$ orbitals of $Mn(NO)_2^+$ is now great enough that the former comprises the HOMO of $CpMn(NO)_2$, and the HOMO is at a higher energy than the HOMO in $CpCo(CO)_2$. In addition, because NO^+ is a weaker σ donor than CO, the $1b_2$ orbital of $Mn(NO)_2^+$ is less polarized toward the Cp ligand than that of $Co(CO)_2^+$; hence the antibonding b_2 interaction is weaker in $CpMn(NO)_2$ than in $CpCo(CO)_2$. This results in a lower-lying LUMO in $CpMn(NO)_2$ than in $CpCo(CO)_2$. The combination of these two effects leads to a much smaller HOMO/LUMO gap in $CpMn(NO)_2$ than in $CpCo(CO)_2$. It is also noted that the HOMO is energetically quite separated from the SHOMO in $CpMn(NO)_2$, whereas the HOMO and SHOMO are nearly degenerate in $CpCo(CO)_2$. We believe that the small HOMO/

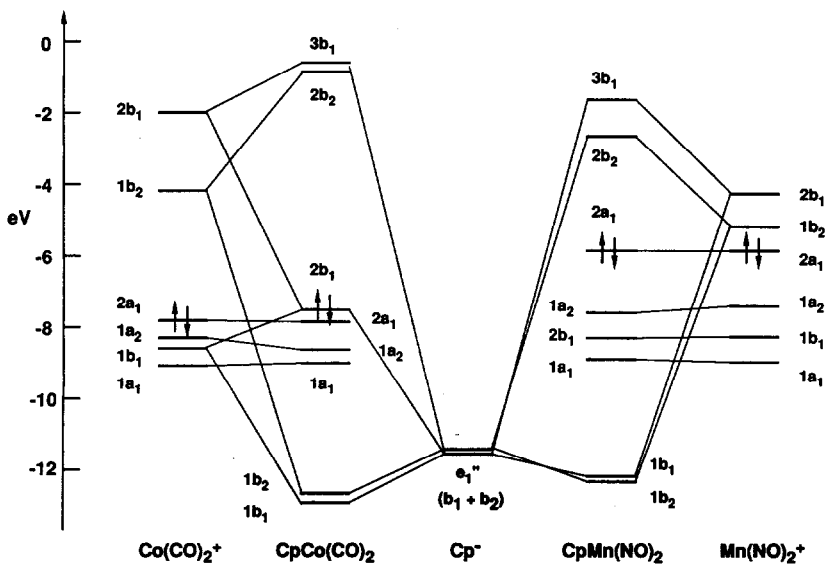

Fig. 2. Molecular orbital interaction diagram comparing the orbitals of $CpCo(CO)_2$ and $CpMn(NO)_2$.

LUMO and large HOMO/SHOMO gap in $CpMn(NO)_2$ contribute to its electronic instability relative to $CpCo(CO)_2$, as will be discussed below.

The effect on the molecular orbitals of changing the ligand L in $CpML_2$ is evident in Table 2, in which the Mulliken per cent characters of the valence orbitals of $CpCo(CO)_2$ and $CpMn(NO)_2$ are compared. It is seen that the stronger π-acidity of nitrosyl relative to carbonyl manifests itself in greater π^* L contributions in the $1a_1$, $2b_1$ and $1a_2$ orbitals of $CpMn(NO)_2$ than in $CpCo(CO)_2$. It is also seen that the character of the $2a_1$ MO is virtually invariant to the changes in M and L.

On comparing $CpCo(CO)_2$ and $CpMn(CO)_2$, we can see several trends that govern the comparative orbital energetics of these isoelectronic d^8 two-legged piano-stool complexes. First, a more electropositive metal atom (i.e. earlier or in a lower formal oxidation state) will lead to an overall rise in the energies of the metal-based MOs. Second, as the π-accepting ability of the ligand L increases, the stabilization of the $1a_1$, $1b_1$ and $1a_2$ orbitals of the ML_2 fragment increases. By contrast, the nonbonding $2a_1$ orbital of ML_2 is unaffected by the π-acidity of the ligand. Third, as the σ-donating ability of L decreases, the HOMO/LUMO separation in the ML_2 fragment decreases, and the $1b_2$ LUMO of ML_2 becomes less polarized toward the cyclic hydrocarbon "bench" of the piano stool. Because the relative π-acidity and σ-basicity of isoelectronic ligands are usually inversely related (as they are for CO and NO^+), the HOMO/LUMO separation in the ML_2 fragments generally will decrease and the HOMO/SHOMO separation will increase as the ligand becomes a stronger π-acid. Finally, we note that the HOMO/LUMO separation in the $CpML_2$ complexes is proportional to the HOMO/LUMO separation in the ML_2 fragments; the Cp cap serves to "amplify" the HOMO/LUMO gap in the fragment.

What influence will the HOMO/LUMO and HOMO/SHOMO separations have on the stability of the two-legged piano-stool complexes? A difficult aspect of any such discussion is to define what is meant by *stable*, and whether this stability is thermodynamic or kinetic. Inasmuch as we are interested in addressing the synthesis of the complexes by standard synthetic organometallic methods, we must consider the means by which such complexes demonstrate their instability. As we will see, most failed attempts to synthesize two-legged piano-stool complexes lead to (a) coordination of a third leg to

Table 2. Valence orbital energies and Mulliken per cent characters for $CpCo(CO)_2$ and $CpMn(NO)_2$

$CpCo(CO)_2$						
Orbital	ε (eV)	Co 3*d*	Co 4*s*	Co 4*p*	Cp e_1''	CO 2π
$3b_1$	−0.63	23	0	4	7	64
$2b_2$	−0.75	43	0	14	18	16
$2b_1$[a]	−7.57	54	0	5	13	26
$2a_1$	−7.88	91	5	1	1	1
$1a_2$	−8.77	89	0	0	2	8
$1a_1$	−9.15	79	0	0	0	20
$1b_2$	−12.67	9	0	2	83	2
$1b_1$	−12.75	20	0	0	77	0
$CpMn(NO)_2$						
Orbital	ε(eV)	Mn 3*d*	Mn 4*s*	Mn 4*p*	Cp e_1''	NO 2π
$3b_1$	−1.63	56	0	3	11	28
$2b_2$	−2.68	15	0	4	10	67
$2a_1$[a]	−5.87	91	6	0	1	0
$1a_2$	−7.59	67	0	0	1	32
$2b_1$	−8.27	32	0	10	0	55
$1a_1$	−8.84	47	0	10	0	48
$1b_1$	−12.20	10	0	4	85	0
$1b_2$	−12.25	11	0	4	83	0

[a] Highest occupied molecular orbital (HOMO).

the piano stool, (b) oxidation of the metal atom, (c) both increased coordination and oxidation, or (d) ill-defined products. The ease with which an additional ligand can be coordinated depends in some way on the σ-acidity of the complex, i.e. the energy of its LUMO in a molecular orbital picture. Likewise, the ease of oxidation of a complex depends on the energy of its HOMO. These are, of course, not new notions. As a complement to Mulliken electronegativities,[12] Pearson has recently advanced the concept of "formal hardness", a parameter that, in an orbital picture, is equal to one-half the HOMO/LUMO separation.[13] Pearson ties his definition to the long-accepted but poorly-understood correlation between HOMO/LUMO separation and molecular stability: "There seems to be a rule of nature that molecules arrange themselves so as to be as hard as possible. A large HOMO/LUMO gap increases stability".[14]

With regard to the HOMO/SHOMO gap, we believe this to be tied to the ease with which the two-electron oxidation of a two-legged piano stool can be accomplished. Within the constraints of Koopmans' theorem,[15] the HOMO/SHOMO gap of an 18e $(\eta^n\text{-}C_nH_n)ML_2$ complex will be related to the HOMO/LUMO gap of the 16e doubly-oxidized complex $(\eta^n\text{-}C_nH_n)ML_2^{2+}$. Because the two electrons in the HOMO of most two-legged piano stools are non-bonding, their removal should not significantly perturb the metal–ligand bonding. Thus, the HOMO/SHOMO gap could be related to the stability of a hypothetical electronically-unsaturated decomposition product, which presumably could react further to form an 18e three-legged piano stool. While the above rationalization may strike the reader as specious, the main reason for including the HOMO/SHOMO gap is a pragmatic one: the correlation between stability and orbital energetics that we will describe shortly does not exist unless we include the HOMO/SHOMO separation.

The HOMO/LUMO separation, ΔE^{HL}, and HOMO/SHOMO separation, ΔE^{HS}, for the two-legged piano-stool complexes are defined in Fig. 3.* If the relative stability of a complex depends on both ΔE^{HL} and ΔE^{HS}, it is convenient to define a single energetic quantity that incorporates both of these energetic differences. The simplest means of combining these in proper functional relationship is to define a new quantity, $\Delta\Delta E$, as

$$\Delta\Delta E = \Delta E^{HL} - \Delta E^{HS}.$$

It is seen that a complex with a large ΔE^{HL} and a small ΔE^{HS} will lead to a large positive value for $\Delta\Delta E$, whereas a small ΔE^{HL} and a large ΔE^{HS} can lead to a negative value for $\Delta\Delta E$. It is proposed, therefore, that electronic stability should increase as $\Delta\Delta E$ increases.

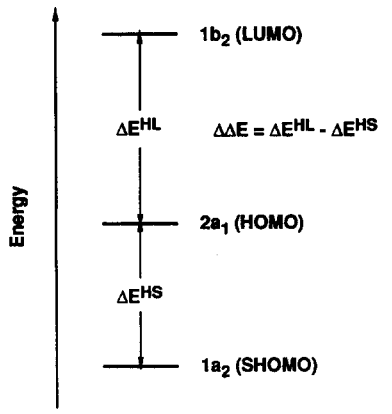

Fig. 3. Definitions of the HOMO/LUMO separation, ΔE^{HL}, the HOMO/SHOMO separation, ΔE^{HS}, and $\Delta\Delta E$ for most d^8 two-legged piano-stool complexes.

Fenske–Hall molecular orbital calculations have been used to calculate $\Delta\Delta E$ for a variety of known and unknown $(\eta^n\text{-}C_nH_n)ML_2$ complexes. Qualitatively, the orbital energetics of all such d^8 complexes with $n = 5$ or 6 are described by the bonding schemes discussed above for $CpCo(CO)_2$ and $CpMn(NO)_2$. However, as we have seen for these two isoelectronic Cp derivatives, there are quantitative differences in the compositions of the frontier orbitals, and hence in ΔE^{HL} and ΔE^{HS}, and, ultimately, in the value of $\Delta\Delta E$. In Table 3, we report the $\Delta\Delta E$ values for a large number of 18e $(\eta^n\text{-}C_nH_n)ML_2$ piano-stools. In the discussion to follow, we will examine the correlation of experimentally observed stability with $\Delta\Delta E$ values. To understand better the electronic effects influencing the stability of two-legged piano-stool systems, we examine both the isolability of known compounds as well as the results of reactions that might be expected to lead to as yet unknown derivatives.

Dicarbonyl complexes

Given the number of such compounds that are known, the dicarbonyl derivatives appear to be the

* In most d^8 two-legged piano stools, the non-bonding $2a_1$ orbital is the HOMO of the complex, as shown in Fig. 3. In rare instances, such as $CpCo(CO)_2$ (Fig. 2), the $2a_1$ orbital is the SHOMO of the complex. While in principle this would change the significance of ΔE^{HL} and ΔE^{HS}, in practice the HOMO and SHOMO of such systems are very close in energy,[10a] and the conclusions drawn here will be unaffected.

Table 3. ΔE^{HL}, ΔE^{HS} and $\Delta\Delta E$ values and predicted stabilities of some known and unknown $(\eta^n\text{-}C_nH_n)ML_2$ complexes

Complex	ΔE^{HL} (eV)	ΔE^{HS} (eV)	$\Delta\Delta E$ (eV)	Predicted stability[a]	Reference
Known complexes					
$CpCo(CO)_2$	6.06	0.18	5.88	Stable	37
$CpFe(CO)_2^-$	5.10	0.72	4.38	Stable	32
$CpMn(CO)_2^{2-}$	3.91	1.30	2.61	Reactive	20
$BzFe(CO)_2$	5.64	0.44	5.20	Stable	16
$BzMn(CO)_2^-$	4.75	1.16	3.59	Reactive	22
$BzCr(CO)_2^{2-}$	4.12	1.23	2.90	Reactive	21
$CpCo(CO)(NO)^+$	5.04	0.03	5.01	Stable	26
Unknown complexes					
$CpNi(CO)_2^+$	5.39	1.70	3.69	Reactive	
$CpCr(CO)_2^{3-}$	2.58	1.19	1.39	Unstable	24
$BzCo(CO)_2^+$	6.10	0.12	5.98	Stable	
$CpFe(CO)(NO)$	3.99	0.54	3.45	Reactive	27
$CpMn(CO)(NO)^-$	3.25	1.26	1.99	Unstable	28, 30
$BzFe(CO)(NO)^+$	5.85	0.48	5.37	Stable	
$BzMn(CO)(NO)$	3.82	1.15	2.67	Reactive	
$BzCr(CO)(NO)^-$	2.77	1.56	1.21	Unstable	
$CpFe(NO)_2^+$	4.63	0.86	3.77	Reactive	
$CpMn(NO)_2$	3.18	1.72	1.46	Unstable	18, 36
$CpCr(NO)_2^-$	1.70	2.42	−0.72	Unstable	31
$BzMn(NO)_2^+$	3.99	1.73	2.26	Unstable	
$BzCr(NO)_2$	2.83	2.21	0.62	Unstable	35
$BzV(NO)_2^-$	1.55	2.61	−1.06	Unstable	

[a] Predicted stabilities are from the criteria discussed in the text.

most stable $(\eta^n\text{-}C_nH_n)ML_2$ piano-stool complexes. This is also the conclusion reached by examination of the calculated $\Delta\Delta E$ values in Table 3. Three complexes in the table, $CpFe(CO)_2^-$, $CpCo(CO)_2$ and $(\eta^6\text{-}C_6Me_6)Fe(CO)_2$[16] (modelled with an unsubstituted benzene ring) are among the small group of known two-legged piano-stool complexes. All three are considered quite stable and reasonably straightforward to synthesize. These complexes all have large $\Delta\Delta E$ values, greater than 4 eV, resulting from large HOMO/LUMO gaps and small HOMO/SHOMO gaps.

The synthesis of other two-legged piano-stool complexes has not been as simple as for those above. For example, consider $CpMn(CO)_2^{2-}$, which is isoelectronic to $CpCo(CO)_2$ and $CpFe(CO)_2^-$. Ellis *et al.* attempted the synthesis of this dianion[17] by a reductive route similar to the one Fischer used to prepare $CpV(CO)_3^{2-}$ from $CpV(CO)_4$.[18] Quite unexpectedly, sodium reduction of $CpMn(CO)_3$ led to the formation of the trianion $Mn(CO)_4^{3-}$, which is isoelectronic to $Ni(CO)_4$. Similarly, the attempted synthesis of $CpRe(CO)_2^{2-}$ by the double deprotonation of $CpRe(CO)_2H_2$ was unsuccessful; the parent dihydride could only be singly deprotonated, yielding the three-legged piano-stool hydride anion, $CpRe(CO)_2H^-$.[19] Leong and Cooper have recently synthesized $CpMn(CO)_2^{2-}$ via the sodium naphthalenide reduction of $CpMn(CO)_2(py)$,[20] a synthetic route that is arguably less obvious than the previous ones attempted.

In addition to $CpMn(CO)_2^{2-}$, there are many other $(\eta^n\text{-}C_nH_n)M(CO)_2$ complexes that have been reported as having marginal stability; for some of these, only partial characterization has been obtained. These include $BzCr(CO)_2^{2-}$ $(Bz = \eta^6\text{-}C_6H_6)$,[21] $BzMn(CO)_2^-$,[22] and $Bz^*Mn(CO)_2^-$ $(Bz^* = \eta^6\text{-}C_6Me_6)$,[23] all of which have $\Delta\Delta E$ values between 2.5 and 4 eV. While these complexes can be generated in synthetically useful quantities, they are generally harder to make, far more reactive, and less stable than the cobalt and iron complexes. We believe this inherent reactivity is reflected in the smaller values of $\Delta\Delta E$ relative to the more stable complexes such as $CpCo(CO)_2$.

The trianion $CpCr(CO)_2^{3-}$, while isoelectronic

with $CpCo(CO)_2$, is as yet unknown. MO calculations on this trianion give a $\Delta\Delta E$ value of 1.39 eV. We believe this small value is indicative of an inherent electronic instability and will prevent even detection of such a species. As shown below, the synthesis of $Cp^*Cr(CO)_2^{3-}$ ($Cp^* = \eta^5$-C_5Me_5) has been attempted by Na/Hg reduction of the Cr—Cr triply-bonded dimer $[Cp^*Cr(CO)_2]_2$:[24]

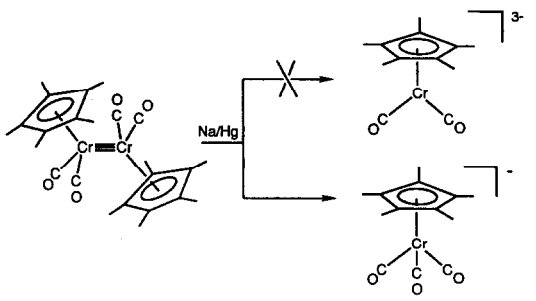

(1)

This reaction might have been expected to proceed in an analogous fashion to the facile reductive cleavage of $[CpCr(CO)_3]_2$ to $CpCr(CO)_3^-$.[25] Rather, $[Cp^*Cr(CO)_2]_2$ undergoes reductive disproportionation to yield the d^6 three-legged piano-stool anion $CpCr(CO)_3^-$, a remarkable example of the desire of the chromium atom to avoid a two-legged, d^8 configuration. The d^6 three-legged piano-stool $CpCr(CO)_3^-$ complex enjoys stabilized filled orbitals very similar to those of d^6 octahedral complexes, whereas the d^8 two-legged piano-stool trianion is burdened with a destabilized HOMO.

Mononitrosylmonocarbonyl complexes

To our knowledge, the only reasonably well-characterized examples of a $(\eta^n$-$C_nH_n)M(CO)(NO)$ derivative are $CpCo(CO)(NO)^+$ and $(\eta^5$-$C_5Me_5)Co(CO)(NO)^+$, isolated as PF_6^- salts in 33 and 80% yields, respectively, from the reaction of the dicarbonyl with $[NO][PF_6]$.[26] Care must be taken to add the dicarbonyl slowly to a well-stirred $[NO][PF_6]$ suspension as the dicarbonyl can add in a nucleophilic fashion to the carbonylnitrosyl product (possibly through a bent NO) to give the μ-NO dicarbonyl dimer:

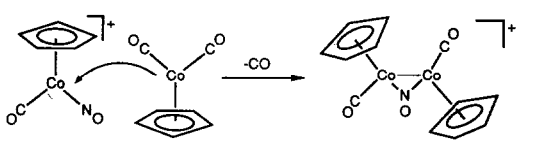

(2)

It should be noted that although these $(\eta^5$-$C_5R_5)Co(CO)(NO)^+$ derivatives are described as reactive and highly air- and water-sensitive, they were prepared and isolated at room temperature. Our MO calculations indicate that $CpCo(CO)(NO)^+$ has a $\Delta\Delta E$ value of 5.01 eV. On the basis of this high value we would predict this complex to be electronically stable. This is in agreement with the experimental results as the reactivity described can probably be attributed to low kinetic barriers for nucleophilic reaction.

The synthesis of CpFe(NO)(CO) has been attempted with indeterminate success.[27] We note that the $\Delta\Delta E$ value of this complex is smaller than that of the cobalt cation, but is larger than some other $(\eta^n$-$C_nH_n)ML_2$ species that have been detected. Other mononitrosyl complexes with considerably smaller $\Delta\Delta E$ values have not yet been isolated, even though reactions have been attempted that could reasonably be expected to lead to their synthesis. For example, the attempted synthesis of $CpMn(CO)(NO)^-$ via Na/Hg reduction of $[CpMn(CO)(NO)]_2$ leads to intractable products;[28] likewise, a study of the electrochemistry of $[CpMn(CO)(NO)]_2$ indicates a very complicated series of reduction steps.[29] Synthesis of the third-row analogue, $CpRe(CO)(NO)^-$, has been attempted by the treatment of CpRe(CO)(NO)H with base.[30] Even with extremely strong bases such as $NaN(SiMe_3)_2$ or KO(*t*-Bu), the hydride complex cannot be deprotonated to give the two-legged anion.

Dinitrosyl complexes

Although isoelectronic to various CO derivatives, there are no known examples of $(\eta^n$-$C_nH_n)M(NO)_2$ piano-stool complexes. Our MO calculations indicate that most of these dinitrosyl complexes suffer from small $\Delta\Delta E$ values. This unfavourable orbital energetic arrangement as compared to carbonyl piano-stool complexes results from the electronic differences between CO and NO, as discussed earlier in the comparison of $CpCo(CO)_2$ and $CpMn(NO)_2$.

Many reactions, however, have been carried out that might have been expected to lead to dinitrosyl complexes, and it is instructive to examine the results of these reactions. Early attempts to prepare $CpCr(NO)_2^-$, involved the reduction of $[CpCr(NO)_2]_2$ by sodium amalgam.[31] In contrast to the reduction of $[CpFe(CO)_2]_2$, which readily leads to quantitative yields of the stable $CpFe(CO)_2^-$ anion,[32] the attempted reduction of $[CpCr(NO)_2]_2$ under identical conditions resulted in only the rapid and complete decomposition of

the chromium dimer:

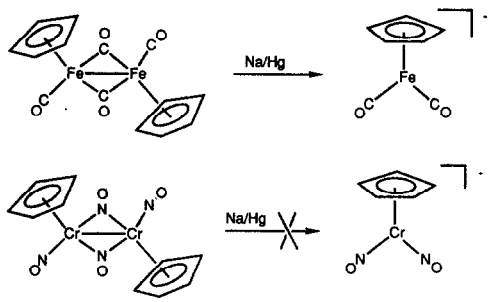

(3)

Subsequent attempts to prepare the tungsten analogue of $CpCr(NO)_2^-$ by deprotonation of $CpW(NO)_2H$ have also failed.[33] The electrochemical reduction of $[CpCr(NO)_2]_2$ was reported to form the dinuclear radical anion $[CpCr(NO)_2]_2^-$ rather than $CpCr(NO)_2^-$, unlike the electrochemical reduction of $[CpFe(CO)_2]_2$, which yields $CpFe(CO)_2^-$.[34] As we saw for $CpMn(NO)_2$, the inherent instability of $CpCr(NO)_2^-$ vis-à-vis the stability of $CpFe(CO)_2^-$ reflects the greater ability of the nitrosyl ligands to stabilize the LUMO and the orbitals below the HOMO, leading to a small HOMO/LUMO gap and a large HOMO/SHOMO gap. Similarly, $BzCr(NO)_2$ ($\Delta\Delta E = 0.62$ eV) does not exist, whereas the carbonyl analogue, $Bz^*Fe(CO)_2$ ($\Delta\Delta E = 5.20$ eV for the Bz analogue) is known.

The proposed inherent instability of some of the nitrosyl complexes appears to be supported experimentally. For example, in contrast to the successful metal atom synthesis of $BzCr(PF_3)_3$, an attempt to prepare $BzCr(NO)_2$ from chromium, benzene and nitric oxide in a metal atom reactor resulted instead in a violent explosion:[35]

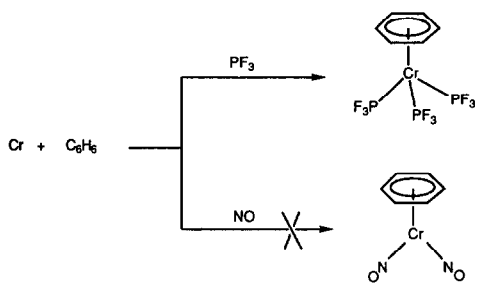

(4)

It is not surprising that $BzCr(PF_3)_3$ could be isolated while $BzCr(NO)_2$ could not; the former is a d^6 three-legged piano-stool complex with stabilized filled orbitals very similar to those of d^6 octahedral complexes, whereas the latter is a d^8 two-legged piano-stool complex with a destabilized HOMO.

* It has been suggested to us that a one-legged piano stool would be better referred to as a barstool.

An attempted synthesis of $CpMn(NO)_2$ by treatment of $CpMn(NO)(CO)_2^-$ with nitrite ion yielded instead polymeric $[CpMn(NO)_2]_n$ ($n \geqslant 2$).[18] The structures proposed for the dimer (**3**) and the trimer (**4**) both allow the manganese atom to adopt a three-legged piano-stool configuration via bridging NO groups. In essence, the coordination sphere about each manganese atom consists of the Cp ligand, one linear nitrosyl (usually formulated as NO^+) and two bent nitrosyls (usually formulated as NO^-), allowing the metal to achieve a d^6 configuration. Thus, the oligomerization of $CpMn(NO)_2$ appears to be one further example of how the unfavourable orbital energetics imposed by a two-legged structure can be avoided through the formation of a d^6 three-legged piano-stool complex.

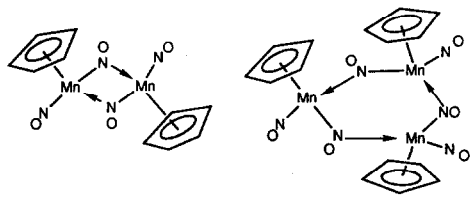

3 4

Another reaction that might have been expected to yield $CpMn(NO)_2$ is the addition of nitric oxide to manganocene.[36] Whereas the reaction of Cp_2Ni with NO leads to the monomeric one-legged piano-stool $CpNiNO$,[37]* treatment of Cp_2Mn with NO yields the dimeric product $Cp_3Mn_2(NO)_3$, another compound that contains local three-legged piano-stool fragments (excluding the dative metal–metal bond):[32,38,39]

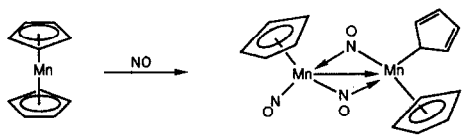

(5)

Cyclobutadiene complexes

We consider cyclobutadiene piano-stool complexes, such as $CbNi(CO)_2$ ($Cb = \eta^4$-C_4H_4), separately as these species are formally d^{10} and their electronic structure does not strictly parallel that of the d^8 complexes discussed above. We have previously advanced a rationale for the inherent instability of $CbNi(CO)_2$,[40] an explanation that depended on the large HOMO/SHOMO gap of the complex. This separation was offered as an explanation of the preferential formation of the d^8 dimeric complex $[Cb^*NiCl_2]_2$ ($Cb^* = \eta^4$-C_4Me_4) from the reaction of $Ni(CO)_4$ with 1,2,3,4-tetra-

methyl-3,4-dichlorobutene:[41]

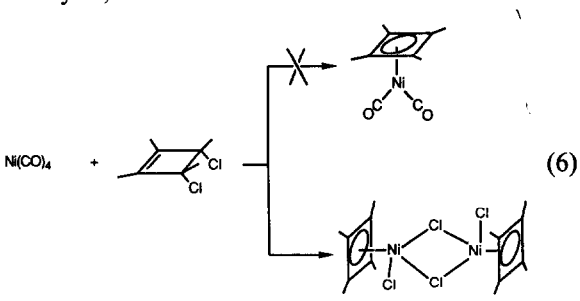

(6)

As was the case for the $[CpMn(NO)_2]_n$ derivatives, the nickel atoms in this dimer achieve a local three-legged geometry.[42] In view of our finding large $\Delta\Delta E$ values for the stable d^8 three-legged cyclobutadiene complexes $(\eta^4\text{-}C_4Ph_4)Mn(CO)_2NO$[43] ($\Delta\Delta E = 5.10$ eV), $CbFe(CO)_2(NO)^+$[44] ($\Delta\Delta E = 7.33$ eV), and $CbFe(CO)_3$[45] ($\Delta\Delta E = 5.10$ eV), we are encouraged that the $\Delta\Delta E$ values seem to be applicable to systems other than the aforementioned d^6 three-legged and d^8 two-legged piano-stool complexes. It is also clear, however, that the relationships between d^8 three-legged and d^{10} two-legged complexes will depend strongly on the nature of the ligands. Thus, although $CbNi(CO)_2$ is still unknown despite numerous attempts at its synthesis, Eisch *et al.* have successfully made and structurally characterized $(\eta^4\text{-}C_4Ph_4)Ni(PEt_3)_2$.[46] We find it rather surprising that the electron-rich nickel centre apparently prefers alkyl phosphine ligands to carbonyl ligands.

Predictions using $\Delta\Delta E$

After examining the data in Table 3, it appears that we can use the value of $\Delta\Delta E$ as a stability criterion for two-legged piano-stool complexes. Stable and isolable complexes such as $CpCo(CO)_2$, $CpFe(CO)_2^-$, $BzFe(CO)_2$ and $CpCo(CO)(NO)^+$ all have $\Delta\Delta E$ values greater than 4 eV. In contrast, those complexes with $\Delta\Delta E$ values less than 2.5 eV appear to be intrinsically unstable, escaping isolation or even detection. In the middle range of $\Delta\Delta E$ values between 2.5 and 4 eV, we observe "reactive" complexes, such as $CpMn(CO)_2^{2-}$. These are complexes that exist but are likely to be extremely reactive and difficult to isolate.

It should thus be possible to use these $\Delta\Delta E$ values to predict the electronic stability or instability of two-legged piano-stool complexes that are not as yet known. We have therefore performed Fenske–Hall MO calculations and found $\Delta\Delta E$ values for various $CpML_2$ and $BzML_2$ complexes, the syntheses of which, to our knowledge, have not yet been attempted. The ΔE^{HL}, ΔE^{HS} and $\Delta\Delta E$ values can be found in Table 3, along with predictions of their stabilities according to the criteria noted above. Thus, we expect the cationic complexes, $BzCo(CO)_2^+$ and $BzFe(CO)(NO)^+$ to be stable, isolable complexes, while two other cationic species $CpNi(CO)_2^+$ and $CpFe(NO)_2^+$ and the neutral $BzMn(CO)(NO)$ fall into the "reactive" range. $BzMn(NO)_2^+$, $BzCr(CO)(NO)^-$ and $BzV(NO)_2^-$ are predicted to be so unstable as to escape detection. In light of our above discussions, it is not surprising that the cationic complexes of this group should be the most stable, and that stability should decrease within an isoelectronic series as CO is replaced by NO.

It is interesting to note that different trends seem to hold for d^{10} cyclobutadiene two-legged piano-stool complexes. As mentioned earlier, $CbNi(CO)_2$ is not a known molecule; not surprisingly, it has a small $\Delta\Delta E$ value (1.67 eV). We do not yet know whether the quantitative values of $\Delta\Delta E$ for d^{10} systems follow the same stability scale as those for the d^8 systems. Nevertheless, the isoelectronic molecule $CbFe(NO)_2$, which is also unknown, has a significantly higher $\Delta\Delta E$ value (3.09 eV). We would therefore expect $CbFe(NO)_2$ to be less unstable than $CbNi(CO)_2$. By analogy to the synthesis of $(\eta^4\text{-}C_4H_4)Mn(NO)(CO)_2$,[43] we have attempted the synthesis of the tetraphenyl derivative of $CbFe(NO)_2$ via the direct reaction of PhC≡CPh and $Fe(CO)_2(NO)_2$:

$$Fe(CO)_2(NO)_2 + 2PhC{\equiv}CPh \longrightarrow (\eta^4\text{-}C_4H_4)Fe(NO)_2.$$

Although the IR and ^{13}C NMR spectra of the product of this reaction are consistent with its formulation as the cyclobutadiene derivative, we have been unable to isolate it as a pure compound.[47]

CONCLUSIONS

It is nearly certain that the scarcity of d^8 two-legged piano-stool complexes as compared to d^6 three-legged ones is due to the electronic demands of each geometry. As has been pointed out previously, d^6 three-legged piano-stool complexes of π-acid ligands achieve an electronic structure quite similar to that of d^6 octahedral complexes with π-acid ligands.[48] On the other hand, the two-legged piano-stool geometry in consort with the 18e rule dictates that the HOMO of such complexes cannot be stabilized by the π-acid ligands, and it is the relative energy of this HOMO in relation to both the LUMO and the SHOMO that will govern the existence of the complexes.

The empirical observation that a large HOMO/LUMO gap is an indication of stability has traditionally been accepted. Rationalizations for this

observation include the notion that promotion to excited electronic states as well as the ease of reduction of the complex have an inverse dependence on the magnitude of the energy difference between the HOMO and the LUMO. That the stability of a complex should be related to the value of ΔE^{HS} is also an empirical observation and also can be rationalized. If a complex possesses a large HOMO/SHOMO difference and the HOMO is non-bonding, oxidation should have a significant stabilizing effect. Thus, just as a small HOMO/LUMO gap might be an indication that a complex is prone to reduction, a large HOMO/SHOMO gap may be a sign that a complex is likely to undergo oxidation easily.

The use of orbital energy differences to predict the stability or instability of piano-stool complexes appears to be quite promising. There are some unresolved questions with regard to the utilization of $\Delta\Delta E$ values, most notably: (1) Although we can rationalize the observations of stability with increasing ΔE^{HL} and decreasing ΔE^{HS}, a theoretical basis for this analysis is still lacking. (2) The definition of $\Delta\Delta E$ was chosen empirically and is the simplest means of combining ΔE^{HL} and ΔE^{HS} into a single parameter. Lacking a firm theoretical understanding of the significance of ΔE^{HL} and ΔE^{HS} separately, it is not clear that they should be weighted equally in arriving at $\Delta\Delta E$. (3) The electronic stability predicted by $\Delta\Delta E$ is entirely thermodynamic; there is no consideration made for kinetic stability or instability. It does not seem likely, however, that kinetic arguments could explain the correlations found. (4) The values of ΔE^{HL} and ΔE^{HS} are highly dependent on the choice of atomic orbital basis sets, and, it seems likely, computational method. The use of $\Delta\Delta E$ as a stability criterion in the future will thus require both a systematic method of basis set choice (such as that used here) and suitable benchmark calculations to establish the ranges for $\Delta\Delta E$ values.

In spite of the above questions, we believe that orbital energetics will prove to be important in the prediction of new molecules that should be amenable to synthesis. However, we emphasize that our observations are empirical in nature and to generalize these ideas, we are directing further efforts toward a firmer theoretical understanding of the significance of ΔE^{HL} and ΔE^{HS}.

Acknowledgements—We thank Dr Melanie Pepper for verification of some of the calculations and for helpful discussions. K.I.G. acknowledges support from the National Cancer Institute, National Institutes of Health, as a postdoctoral fellow.

REFERENCES

1. B. E. Bursten and M. G. Gatter, *J. Am. Chem. Soc.* 1984, **106**, 2554.
2. B. E. Bursten and M. G. Gatter, *Organometallics* 1984, **3**, 941.
3. M. B. Hall and R. F. Fenske, *Inorg. Chem.* 1972, **11**, 768.
4. L. R. Byers and L. F. Dahl, *Inorg. Chem.* 1980, **19**, 277.
5. D. L. Lichtenberger, C. H. Blevins and R. B. Ortega, *Organometallics* 1984, **3**, 1614.
6. J. P. Selegue, personal communication.
7. B. E. Bursten, J. R. Jensen and R. F. Fenske, *J. Chem. Phys.* 1978, **68**, 3320.
8. W. J. Hehre, R. F. Stewart and J. A. Pople, *J. Chem. Phys.* 1969, **51**, 2657.
9. D. L. Lichtenberger and R. F. Fenske, *J. Chem. Phys.* 1976, **64**, 4247.
10. See for example: (a) D. L. Lichtenberger, D. C. Calabro and G. E. Kellogg, *Organometallics* 1984, **3**, 1623; (b) P. Hofmann, *Angew. Chem. Int. Edn Engl.* 1977, **16**, 536; (c) J. Silvestre and T. A. Albright, *J. Am. Chem. Soc.* 1985, **107**, 6829; (d) T. A. Albright, R. Hoffmann, Y.-C. Tse and T. D'Ottavio, *J. Am. Chem. Soc.* 1979, **101**, 3812.
11. P. Legzdins, S. J. Rettig, L. Sanchez, B. E. Bursten and M. G. Gatter, *J. Am. Chem. Soc.* 1985, **107**, 1411.
12. R. S. Mulliken, *J. Chem. Phys.* 1932, **2**, 782.
13. R. G. Pearson, *J. Am. Chem. Soc.* 1985, **107**, 6801.
14. R. G. Pearson, *J. Chem. Ed.* 1987, **64**, 561.
15. T. Koopmans, *Physica (Utrecht)* 1933, **1**, 104.
16. S. R. Weber and H. H. Brintzinger, *J. Organomet. Chem.* 1977, **127**, 45.
17. J. E. Ellis, R. A. Flatynek and S. G. Hentges, *J. Organomet. Chem.* 1976, **120**, 389.
18. E. O. Fischer and S. Vigoureaux, *Chem. Ber.* 1958, **91**, 2205.
19. G. K. Yang and R. G. Bergman, *J. Am. Chem. Soc.* 1983, **105**, 1500.
20. V. S. Leong and N. J. Cooper, *Organometallics* 1988, 7, 2080.
21. V. S. Leong and N. J. Cooper, *Organometallics* 1987, **6**, 2000.
22. P. K. Rush, S. K. Noh and M. Brookhart, *Organometallics* 1986, **5**, 1745.
23. R. J. Bernhardt, M. A. Wilmoth, J. J. Weers, D. M. LaBrush, D. P. Eynman and J. C. Huffman, *Organometallics* 1986, **5**, 883.
24. R. B. King, A. Efraty and W. M. Douglas, *J. Organomet. Chem.* 1973, **60**, 125.
25. J. E. Ellis and E. A. Flom, *J. Organomet. Chem.* 1975, **99**, 263.
26. (a) S. Clamp, N. G. Connelly and J. D. Payne, *J. Chem. Soc., Chem. Commun.* 1981, 897; (b) S. Clamp, N. G. Connelly, J. A. K. Howard, I. Manners, J. D. Payne and W. E. Geiger, *J. Chem. Soc., Dalton Trans.* 1984, 1659.

27. R. B. King, *Inorg. Chem.* 1967, **6**, 30.
28. B. W. S. Kolthammer, PhD dissertation. University of British Columbia, Vancouver, B.C. (1979).
29. P. Legzdins and B. Wassink, unpublished results.
30. J. R. Sweet and W. A. G. Graham, *Organometallics* 1982, **1**, 982.
31. B. W. S. Kolthammer and P. Legzdins, *J. Chem. Soc., Dalton Trans.* 1978, 31.
32. T. S. Piper and G. Wilkinson, *J. Inorg. Nucl. Chem.* 1956, **3**, 104.
33. P. Legzdins and D. T. Martin, *Inorg. Chem.* 1979, **18**, 1250.
34. P. Legzdins and B. Wassink, *Organometallics* 1984, **3**, 1811.
35. R. Middleton, J. R. Hull, S. R. Simpson and P. L. Timms, *J. Chem. Soc., Dalton Trans.* 1973, 120.
36. T. S. Piper and G. Wilkinson, *J. Inorg. Nucl. Chem.* 1956, **2**, 38.
37. T. S. Piper, F. A. Cotton and G. Wilkinson, *J. Inorg. Nucl. Chem.* 1955, **1**, 165.
38. R. B. King and M. B. Bisnette, *Inorg. Chem.* 1964, **6**, 791.
39. J. L. Calderon, S. Fontana, E. Frauendorfer, V. W. Day and B. R. Stults, *Inorg. Chim. Acta* 1976, **17**, L31.
40. B. E. Bursten and R. F. Fenske, *Inorg. Chem.* 1979, **18**, 1760.
41. R. Criegee and G. Schröder, *Just. Lieb. Ann. Chem.* 1954, **623**, 1.
42. U. Thewalt, R. Hemmer and H. A. Brune, *Z. Naturf.* 1979, **34b**, 859.
43. M. D. Rausch, B. H. Edwards, J. L. Atwood and R. D. Rogers, *Organometallics* 1982, **1**, 1567.
44. A. Efraty, R. Bystrek, J. A. Geaman, S. S. Sandhu, M. H. A. Haung and R. H. Herber, *Inorg. Chem.* 1974, **13**, 1269.
45. G. F. Emerson, L. Watts and R. Pettit, *J. Am. Chem. Soc.* 1965, **87**, 131.
46. J. J. Eisch, A. M. Piotrowski, A. A. Aradi, C. Krüger and M. J. Romao, *Z. Naturfor.* 1985, **40b**, 624.
47. M. G. Gatter, PhD dissertation. The Ohio State University (1985).
48. (a) M. Elian and R. Hoffmann, *Inorg. Chem.* 1975, **14**, 1058; (b) D. L. Lichtenberger and R. F. Fenske, *J. Am. Chem. Soc.* 1976, **98**, 50; (c) B. E. R. Schilling, R. Hoffmann and D. L. Lichtenberger, *J. Am. Chem. Soc.* 1979, **101**, 585; (d) D. C. Calabro, J. L. Hubbard, C. H. Blevins, A. C. Campbell and D. L. Lichtenberger, *J. Am. Chem. Soc.* 1981, **103**, 6839; (e) B. E. Bursten, D. J. Darensbourg, G. E. Kellogg and D. L. Lichtenberger, *Inorg. Chem.* 1984, **23**, 4361; (f) D. S. Yang, G. M. Bancroft, R. J. Puddephatt, B. E. Bursten and S. D. McKee, *Inorg. Chem.* 1989, **28**, 872.

Polyhedron Vol. 9, No. 17, pp. 2013–2018, 1990
Printed in Great Britain

0277–5387/90 $3.00+.00
© 1990 Pergamon Press plc

SQUARE PLANAR AND SQUARE PYRAMIDAL COMPLEXES OF RHODIUM(II)

KRISHNA K. PANDEY,† DELEEP T. NEHETE and RAM B. SHARMA

Department of Chemistry, Devi Ahilya University of Indore, Khandwa Road, Indore 452001, India

(*Received* 16 *May* 1989; *accepted after revision* 21 *March* 1990)

Abstract—The rhodium nitrosyl complex $Rh(NO)Cl_2(PPh_3)_2$ reacts with $Na(S_2CNR_2)$ (R = Et or Me), in benzene under reflux, to give the square planar complexes $Rh(S_2CNR_2)_2$. A similar reaction, on stirring the reaction mixture affords the square pyramidal complexes $Rh(S_2CNR_2)_2(PPh_3)$. The products have been characterized by elemental analysis, IR, UV–vis, magnetic measurements, ESR and ^1H NMR studies.

Coordination compounds of platinum metal d^7 ions have as yet attracted less attention than those of d^5 and d^6 metal ions of ruthenium and osmium, and d^6 and d^8 metal ions of rhodium, iridium, palladium and platinum. There is a very marked contrast in the coordination compounds of d^7 metal ions between iron, cobalt and nickel on the one hand and platinum metals on the other. Only a few substantiated examples of mononuclear complexes of ruthenium(I),[1–7] osmium(I),[8,9] rhodium(II),[10–30] iridium(II),[31–36] palladium(III)[37–39] and platinum(III),[40–42] have been reported in the literature.

We have previously described the synthesis of ruthenium(I) and osmium(I) complexes,[7,9] and in this paper we wish to report the synthesis of mononuclear square planar and square pyramidal complexes of rhodium(II). So far there is no report of the penta-coordinated monomeric rhodium(II) complex.

EXPERIMENTAL

All the reagents used were AnalaR or of chemically pure grade. All the solvents were dried by standard procedures and were freshly distilled before use. Dichloronitrosylbis(triphenylphosphine)rhodium(I) was prepared by a literature method.[43] Dithiocarbamate ligands were used as purchased from Fluka.

Sulphur estimation in the complexes was carried out by the standard method.[44] Carbon, hydrogen and nitrogen analyses were performed by the Microanalytical Section of the Central Drug Research Institute, Lucknow. For the estimation of phosphorus, samples were decomposed with sodium peroxide, sugar and sodium nitrate in the ratio 20 : 1 : 3 in a Parr bomb crucible and extracted with water. The solution was then neutralized with dil. H_2SO_4 and an excess of conc. H_2SO_4 (0.5 cm^3) added. This was heated until the evolution of SO_3 fumes ceased, then cooled and diluted with water. From the filtrate of the solution, phosphorus was estimated as phosphoammonium molybdate. The IR spectra of the samples were recorded with a Perkin–Elmer Model 580 spectrophotometer in the range 4000–300 cm^{-1}. The electronic spectra were recorded in benzene solution on a Simadzu 160 spectrophotometer. ESR spectra of the powdered samples were recorded on a Varian Associates E-line ESRCentury Series Model E-104 A spectrometer at X-band frequencies. The spectra were calibrated by using a sample of DPPH ($g = 2.0036 \pm 0.0003$). The magnetic measurements were made on a Gouy balance at room temperature (25°C) and mercury tetrathiocyanatocobaltate(II) was used as calibrant. A varian CFT-20 spectrometer was used to obtain ^1H NMR spectra. All the results are given in Tables 1–4.

(a) *Preparation of* $Rh(S_2CNEt_2)_2$

$Rh(NO)Cl_2(PPh_3)_2$ (0.2 g) and $Na(S_2CNEt_2)\cdot 3H_2O$ (0.4 g) were refluxed in benzene (30 cm^3) for 4 h. The resulting orange solution was filtered and reduced in vacuum to *ca* 5 cm^3, and on addition

† Author to whom correspondence should be addressed.

Table 1. Colour, melting point and elemental analyses for rhodium(II) complexes

Compounds	Colour	Melting point (°C)	Found (calc.) %C	%H	%N	%S	%P
$Rh(S_2CNEt_2)_2$	Orange	237	30.2 (30.1)	5.1 (5.0)	7.2 (7.0)	32.2 (32.1)	—
$Rh(S_2CNMe_2)_2$	Yellowish-orange	210	20.7 (21.0)	3.6 (3.5)	8.2 (8.2)	37.5 (37.3)	—
$Rh(S_2CNEt_2)_2(PPh_3)$	Yellow	120	50.9 (50.8)	5.5 (5.3)	4.1 (4.2)	19.2 (19.4)	4.8 (4.7)
$Rh(S_2CNMe_2)_2(PPh_3)$	Yellow	110	47.5 (47.6)	4.4 (4.5)	4.7 (4.6)	21.3 (21.2)	5.2 (5.1)

Table 2. Important IR frequencies (cm^{-1}) and electronic spectral data for rhodium(II) complexes

Compound	IR bands ν(CN)	ν(Rh—S)	Electronic absorption bands $\bar{\nu}_{max}$ (cm^{-1})	ε (mol^{-1} dm^3 cm^{-1})	Assignment
$Rh(S_2CNEt_2)_2$	1552	355, 340	23,260	2060	$e_g \rightarrow b_{1g}$
			31,850	45,090	CT
			35,710	26,370	CT
$Rh(S_2CNMe_2)_2$	1540	355, 330	23,260	2320	$e_g \rightarrow b_{1g}$
			32,050	44,080	CT
			35,590	29,190	CT
$Rh(S_2CNEt_2)_2(PPh_3)$	1530	330	23,460	1830	$e_g \rightarrow b_{1g}$
			31,750	36,360	CT
			35,710	20,860	CT
$Rh(S_2CNMe_2)_2(PPh_3)$	1545	340	23,260	1930	$e_g \rightarrow b_{1g}$
			32,680	31,430	CT
			35,710	32,860	CT

CT = charge transfer.

Table 3. ^1H NMR spectra of rhodium(II) complexes[a]

Compounds	—CH_3	—CH_2	—C_6H_5	Integration
$Rh(S_2CNEt_2)_2$	1.31, 1.23, 1.14	3.56, 3.64, 3.74, 3.83		CH_3–CH_2 = 1.7:1
$Rh(S_2CNMe_2)_2$	3.2			
$Rh(S_2CNEt_2)_2(PPh_3)$	1.33, 1.25, 1.15	3.81, 3.74, 3.65, 3.57	Complex multiplet broadened, 7.36	C_6H_5–CH_3–CH_2 = 2.1:1.6:1
$Rh(S_2CNMe_2)_2(PPh_3)$	3.21		Complex multiplet broadened, 7.44	C_6H_5–CH_3 = 1.5:1

[a] All the bands are relative to TMS.

Table 4. ESR data and magnetic moment for rhodium(II) complexes

Compounds	g_1	g_2	g_3	$\langle g \rangle^a$	Magnetic moment μ (BM)
$Rh(S_2CNEt_2)_2$	2.0529	2.0148	1.9816	2.0166	2.12
$Rh(S_2CNMe_2)_2$	2.0523	2.0135	1.9828	2.0164	2.08
$Rh(S_2CNEt_2)_2(PPh_3)$	2.0516	2.0073	1.9858	2.0151	2.02
$Rh(S_2CNMe_2)_2(PPh_3)$	2.0503	2.0085	1.9858	2.0156	2.10
$(Bu_4N)_2RhC_4S_4(CN)_4$[b]	2.447	2.019	1.936	2.146	1.91
Rh(TPP)[c]	2.089	2.029	1.990	2.036	1.2

[a] $\langle g \rangle = [1/3g_1^2 + 1/3g_2^2 + 1/3g_3^2]^{1/2}$.
[b] Taken from ref. 11.
[c] Taken from ref. 26.

of *n*-hexane, orange crystals of $Rh(S_2CNEt_2)_2$ separated. These were centrifuged, then washed with water and cold ethanol, and dried *in vacuo* (yield 90 mg, 83%); m.p. 237°C.

(b) *Preparation of* $Rh(S_2CNMe_2)_2$

$Rh(NO)Cl_2(PPh_3)_2$ (0.2 g) and $Na(S_2CNMe_2)\cdot 2H_2O$ (0.3 g) were refluxed in benzene (30 cm^3) for 4 h. The yellowish-orange crystals of $Rh(S_2CNMe_2)_2$ were isolated by a procedure similar to that given in part (a) (yield 70 mg, 74%); m.p. 210°C.

(c) *Preparation of* $Rh(S_2CNEt_2)_2(PPh_3)$

$Rh(NO)Cl_2(PPh_3)_2$ (0.2 g) and $Na(S_2CNEt_2)\cdot 3H_2O$ (0.1 g) were stirred in benzene (30 cm^3) for 6 h. The resulting solution was filtered and reduced *in vacuo* to *ca* 5 cm^3. Addition of *n*-hexane precipitated the yellow complex $Rh(S_2CNEt_2)_2(PPh_3)$, which was filtered off, washed with water and dried *in vacuo* (yield 124 mg, 75%); m.p. 120°C.

(d) *Preparation of* $Rh(S_2CNMe_2)_2(PPh_3)$

$Rh(NO)Cl_2(PPh_3)_2$ (0.2 g) and $Na(S_2CNMe_2)\cdot 2H_2O$ (0.1 g) were stirred in benzene (30 cm^3) for 6 h. The yellow complex $Rh(S_2CNMe_2)_2(PPh_3)$ was isolated by a procedure similar to that given in part (c) (yield 141 mg, 78%); m.p. 110°C.

RESULTS AND DISCUSSION

Reaction of the rhodium nitrosyl complex, $Rh(NO)Cl_2(PPh_3)_2$, with $Na(S_2CNR_2)$ (R = Et or Me), in benzene under reflux, gives the square planar complexes $Rh(S_2CNR_2)_2$. A similar reaction, on stirring the reaction mixture for 6 h without reflux, affords square pyramidal complexes, $Rh(S_2CNR_2)_2(PPh_3)$. The IR spectra of these complexes show no bands due to ν(NO), indicating the absence of the NO group in the complexes. The IR spectra exhibit bands due to the S_2CNR_2 ligands in $Rh(S_2CNR_2)_2$ complexes and due to S_2CNR_2 and PPh_3 ligands in $Rh(S_2CNR_2)_2(PPh_3)$. The ν(CN) frequency of these complexes at *ca* 1540 cm^{-1} is nearly independent of the substituent. It is shifted to higher energy compared with the free ligand as a result of increased double bond character upon coordination to the metal centre.[45,46]

The electronic spectra of $Rh(S_2CNR_2)_2$ and $Rh(S_2CNR_2)_2(PPh_3)$ complexes (Table 2) show intense absorption bands in the UV region in the vicinity of 315–280 nm ($\varepsilon = 10^4$ mol^{-1} dm^3 cm^{-1}). A very weak absorption band was also seen in the 425 nm region (Fig. 1). A study of dithiolic acids assigned the high energy absorption to π–π^* transitions.[47] The ground state of low-spin rhodium(II) complexes in square planar and square pyramidal environments is probably $^2A_{1g}$ with the configuration $e_g^4 b_{2g}^2 a_{1g}^1$. The band in the region 425 nm is probably a transition from the lower filled orbitals $e_g(d_{xz},d_{yz})$ to the empty $b_{1g}(d_{x^2-y^2})$ antibonding orbital. The four coordinated complexes are more intensely coloured. The shoulders at *ca* 425 nm in the visible region were stronger for the four coordinated complexes.

The ^{1}H NMR spectrum of $Rh(S_2CNEt_2)_2$ produced a triplet and quartet due to the $-CH_3$ and $-CH_2$ groups, respectively (Table 3). A singlet was observed for $Rh(S_2CNMe_2)_2$, indicating the equivalence of the methyl group. The complex $Rh(S_2CNEt_2)_2(PPh_3)$ showed a triplet, quartet and a complex multiplet due to the $-CH_3$, $-CH_2$ and $-C_6H_5$ groups, respectively. The spectrum of $Rh(S_2CNMe_2)_2(PPh_3)$ produced a sharp singlet and

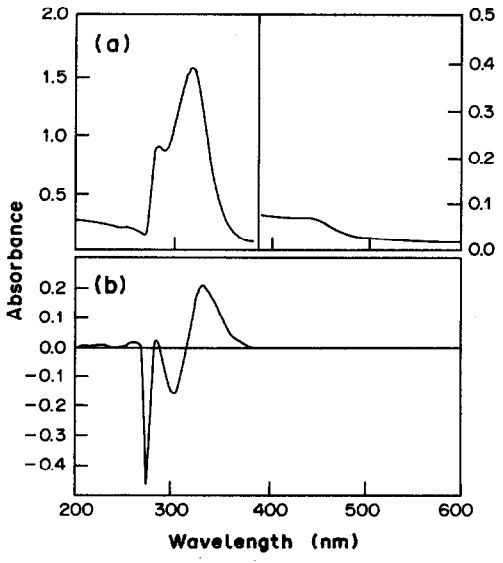

Fig. 1. Absorption spectrum of $Rh(S_2CNEt_2)_2$: (a) absorption curve; (b) first derivative curve.

a complex multiplet due to the $-CH_3$ and $-C_6H_5$ groups. The ^1H NMR spectra indicate that the chemical shifts are the same for $Rh(S_2CNR_2)_2$ and $Rh(S_2CNR_2)_2(PPh_3)$ despite the differences in coordination number and symmetry. This constancy suggests that the total rhodium–sulphur π-bonding in these complexes is invariant.

The complexes $Rh(S_2CNR_2)_2$ and $Rh(S_2CNR_2)_2(PPh_3)$ are paramagnetic with magnetic moment $\mu = 2.0$–2.1 at 298 K. The first derivative X-band ESR powder spectra of the undiluted rhodium(II) complexes (Fig. 2) show three g values ($g_1 > g_2 > g_3$) near two (Table 4). The ESR spectra are similar to the previously reported ESR spectrum for rhodium(II) complexes with sulphur ligands.[11,30] The following g values have been reported for $[Rh(S_2C_2(CN)_2)_2]^{2-}$, $g = 2.447$, 2.019 and 1.936, and for $[Rh(o\text{-Me-Cys}^-)_2]$, $g = 2.035$, 2.020 and 1.955. Hyperfine splitting could not be observed on the broad lines. To interpret the EPR data, we use the theory described by various authors[48–51] to determine the sign of g_1 components and the correspondence between the experimental g values and g_x, g_y and g_z components of the g tensor. The g_1, g_2 and g_3 values are derived as g_x, g_y and g_z, respectively. If the axis of the square planar molecules $Rh(S_2CNR_2)_2$ are as defined in Fig. 3, one would expect energy level ordering as in Fig. 4. The ground state electronic configuration is then $(e_g)^4(b_{2g})^2(a_{1g})^1$, leading to a $^2A_{1g}$ ground term for which the g values, $g_\parallel$ (approximately equal to g_3) and $g_\perp$ (approximately equal to g_1) are

$$g_\parallel = 2.0023$$

$$g_\perp = 2.0023 - \frac{6K^2\lambda}{\Delta E(E_{d_{xz,yz}} - E_{d_{z^2}})},$$

where K is the orbital angular momentum reduction factor[52,53] and λ is the spin–orbit coupling constant, equal to -1235. The $g_\parallel$ value which is smaller than two may be justified by higher order perturbation terms. Using the values of ΔE from the electronic spectra of the complexes, K is found from $g_\perp$ to be approximately 0.4. For the penta-coordinated d^7 system, the unpaired electron could be either in d_{z^2} in the case of square pyramidal geometry, the normal g value pattern being $g_\perp > g_\parallel = 2.00$, or the

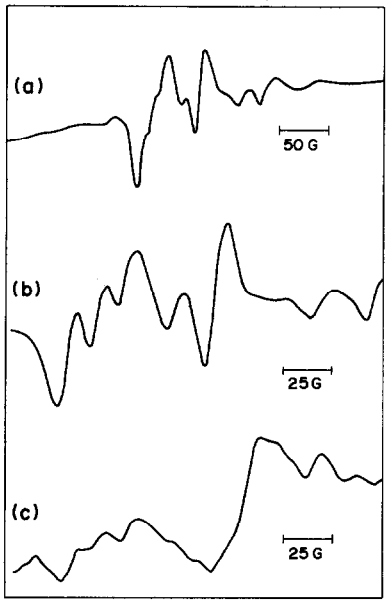

Fig. 2. ESR spectrum of (a, b) $Rh(S_2CNEt_2)_2$ and (c) $Rh(S_2CNEt_2)_2(PPh_3)$ at 295 K.

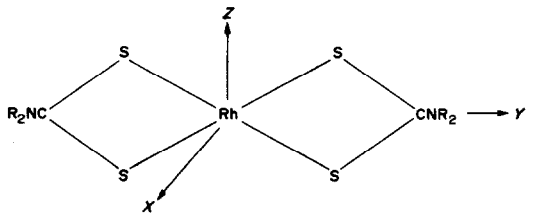

Fig. 3. Stereochemistry of $Rh(S_2CNR_2)_2$.

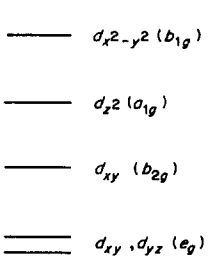

Fig. 4. Energy level ordering of a square planar complex.

unpaired electron may be in a $d_{(x^2-y^2)}$ or $d_{(xy)}$ orbital in the case of trigonal bipyramidal geometry, yielding $g_\parallel > g_\perp > 2.00$.[53,54] The g value patterns for the complexes $Rh(S_2CNR_2)_2(PPh_3)$ (R = Et or Me) are those of a square pyramidal structure.

Acknowledgements—This research was supported by the Council of Scientific and Industrial Research, New Delhi, under Project No. 1(998)/84-EMR-II. We thank Professor U. C. Agarwala, Department of Chemistry, Indian Institute of Technology, Kanpur, for his help and stimulating discussions.

REFERENCES

1. W. Manchot and H. Schmid, *Chem. Ber.* 1931, **64**, 2673.
2. R. J. Irving and P. G. Laye, *J. Chem. Soc. A* 1966, 161.
3. R. S. Eachus and F. G. Herring, *Can. J. Chem.* 1972, **50**, 162.
4. M. C. R. Symons and J. G. Wilkinson, *J. Chem. Soc., Dalton Trans.* 1973, 965.
5. R. W. Callahan, G. M. Brown and T. J. Meyer, *J. Am. Chem. Soc.* 1975, **97**, 894.
6. R. W. Callahan and T. J. Meyer, *Inorg. Chem.* 1977, **16**, 574.
7. K. K. Pandey, S. R. Ahuja, N. S. Poonia and S. Bharti, *J. Chem. Soc., Chem. Commun.* 1982, 1268.
8. G. W. Watt, E. M. Potrafke and D. S. Klett, *Inorg. Chem.* 1963, **2**, 868.
9. K. K. Pandey and S. R. Ahuja, *Inorg. Chem.* 1985, **24**, 2855.
10. B. Martin, W. R. McWhinne and G. M. Waind, *J. Inorg. Nucl. Chem.* 1961, **23**, 207.
11. A. H. Maki, N. Edelstein, A. Davision and R. H. Holm, *J. Am. Chem. Soc.* 1964, **86**, 4580.
12. E. O. Fisher and H. H. Linder, *Organomet. Chem.* 1964, **1**, 307.
13. S. E. Livingstone, *Quart. Rev.* 1965, **19**, 386.
14. H. P. Fritz and C. G. Kreiter, *J. Organomet. Chem.* 1965, **4**, 198.
15. J. A. Osborn, F. H. Jardine and G. Wilkinson, *J. Chem. Soc. A* 1966, 1711.
16. M. A. Bennett, A. Bramney and P. A. Longstaff, *J. Chem. Soc., Chem. Commun.* 1966, 806.
17. E. O. Fischer and H. Wawersik, *J. Organomet. Chem.* 1966, **5**, 559.
18. S. McVey and P. M. Maitlis, *Can. J. Chem.* 1966, **44**, 2429.
19. H. J. Keller and H. Wawersik, *J. Organomet. Chem.* 1967, **8**, 185.
20. M. A. Bennett and P. A. Longstaff, *J. Am. Chem. Soc.* 1969, **91**, 6266.
21. R. P. A. Muniz, N. V. Vngman and J. Danon, *J. Chem. Phys.* 1971, **54**, 1284.
22. M. C. Baird, *Inorg. Chim. Acta* 1971, **5**, 46.
23. C. Masters, W. S. McDonald, G. Raper and B. L. Shaw, *J. Chem. Soc., Chem. Commun.* 1971, 210.
24. C. Masters and B. L. Shaw, *J. Chem. Soc. A* 1971, 3679.
25. *B. R. James, F. T. T. Ng and E. Ochiai, Can. J. Chem.* 1972, **50**, 590.
26. B. R. James and D. V. Styres, *J. Am. Chem. Soc.* 1972, **94**, 6225.
27. F. G. Moers, J. A. M. de Jong and P. M. H. Beaumont, *J. Inorg. Nucl. Chem.* 1973, **35**, 1915.
28. H. D. Empsall, E. M. Hyde, C. E. Jones and B. L. Shaw, *J. Chem. Soc., Dalton Trans.* 1974, 1980.
29. H. L. M. Van Gall, J. M. J. Verlaak and T. Posno, *Inorg. Chim. Acta* 1977, **23**, 43.
30. G. Pneumatikakis and P. Psaroulis, *Inorg. Chem. Acta* 1980, **46**, 97.
31. L. Malatesta, M. Angoletta and G. Caglia, *Angew. Chem. Int. Edn.* 1963, **2**, 739.
32. L. Malatesta, L. Naldini and F. Cariati, *J. Chem. Soc.* 1964, 961.
33. R. Mason, K. M. Thomas, H. D. Empsall, S. R. Fletcher, E. M. Hyde, C. E. Jones and B. L. Shaw, *J. Chem. Soc., Chem. Commun.* 1974, 612.
34. A. Araneo, F. Morazzoni and T. Napoletano, *J. Chem. Soc., Dalton Trans.* 1975, 2039.
35. G. Mercati and F. Morazzoni, *J. Chem. Soc., Dalton Trans.* 1979, 569.
36. S. Zecchin, G. Zotti and G. Pilloni, *J. Organomet. Chem.* 1985, **294**, 379.
37. A. J. Blake, A. J. Holder, T. I. Hyde, Y. V. Roberts, A. J. Lavery and M. Schroder, *J. Organomet. Chem.* 1987, **323**, 261.
38. A. J. Blake, A. J. Holder, T. I. Hyde and M. Schroder, *J. Chem. Soc., Chem. Commun.* 1987, 987.
39. A. J. Blake, L. M. Gordon, A. J. Holder, T. I. Hyde, G. Reid and M. Schroder, *J. Chem. Soc., Chem. Commun.* 1988, 1452.
40. R. Uson, J. Fornies, M. Tomas, B. Menjon, K. Sunkel and R. Bau, *J. Chem. Soc., Chem. Commun.* 1984, 751.
41. R. Uson, J. Fornies, M. Tomas, M. Menjon, R. Bau, K. Sunkel and E. Kuwabara, *Organometallics* 1986, **5**, 1576.
42. A. J. Blake, R. O. Gould, A. J. Holder, T. I. Hyde, M. O. Odulate, A. J. Lavery and M. Schroder, *J. Chem. Soc., Chem. Commun.* 1987, 118.
43. G. R. Crooke and B. F. G. Johnson, *J. Chem. Soc. A* 1970, 1662.
44. A. I. Vogel, *A Textbook of Quantitative Inorganic Analysis*, 3rd Edn. Longmans, London (1961).
45. C. O'Connor, J. D. Gilbert and G. Wilkinson, *J. Chem. Soc. A* 1969, 84.
46. J. Chatt, L. A. Dunn, L. A. Duncanson and L. M. Venanzi, *Nature* 1966, **177**, 1042.
47. M. L. Shankaranaryana and C. C. Patel, *Acta Chem. Scand.* 1965, **19**, 1113.
48. K. W. H. Stevens, *Proc. R. Soc. Lond. Ser. A* 1953, **219**, 542.
49. B. Bleaney and M. C. M. O'Brien, *Proc. Phys. Soc. Lond* 1056, B59.
50. J. S. Griffith, in *The Theory of Transition Metal Ions*. Cambridge University Press, Cambridge (1961).
51. A. Abragam and B. Bleaney, in *Electron Para-*

magnetic Resonance of Transition Metal Ions, pp. 15, 138 and 422. Oxford University Press, London (1970).
52. M. Gerloch and J. R. Miller, *Prog. Inorg. Chem.* 1968, **10**, 1.
53. B. A. Goodman and J. B. Raynor, *Adv. Inorg. Radiochem.* 1970, **13**, 135.
54. H. A. Kushaka and M. T. Rogers, *Coordination Chemistry* (Edited by A. E. Martell), Vol. I, p. 186. Van Nostrand, New York (1971).

Polyhedron Vol. 9, No. 17, pp. 2019–2022, 1990
Printed in Great Britain

0277–5387/90 $3.00+.00
Pergamon Press plc

COMPLEXES OF LANTHANIDE NITRATES WITH A SCHIFF BASE DERIVED FROM *o*-VANILLIN AND *p*-TOLUIDINE

LIU GUOFA,* NA CHONGWU, LI BIN and MAO KUNYUAN

Institute of Material Science, Jilin University, Changchun, China

(*Received* 27 *July* 1989; *accepted* 21 *March* 1990)

Abstract—New complexes of lanthanide nitrates with a Schiff base derived from *o*-vanillin (2-hydroxy-3-methoxy-benzaldehyde) and *p*-toluidine having the general formula $[LnL_2(NO_3)_2]NO_3$ (where Ln = Pr–Lu except Pm, L = Schiff base) have been prepared and characterized. Molar conductance studies indicate 1 : 1 electrolyte behaviour for these complexes. The IR spectra show that two Schiff base ligands and two nitrate groups are bound to the lanthanide ion in a bidentate fashion. Another nitrate group is in the outer coordination sphere. TG and DTA studies indicate that these complexes are stable up to 235°C and do not contain water or alcohol molecules.

There have been a number of reports about lanthanide ion complexes with Schiff bases derived from acetylacetone and ethylenediamine,[1] bis-acetylacetone and ethylenediamine,[2] bis-acetylacetone and benzidine,[3] salicylaldehyde and anthranilic acid,[4] bis-salicylaldehyde and ethylenediamine,[5] bis-salicylaldehyde and *o*-phenylenediamine,[5] *p*-dimethylaminobenzaldehyde and benzidine,[6] 2,6-pyridinedicarboxaldehyde and *o*-aminophenol,[7] vanillin and triethylenetetraamine,[8] bis-vanillin and *o*-phenylenediamine,[9] bis-vanillin and benzidine,[10] 2-hydroxybenzaldehyde and 4-aminoantipyrine.[11] In this paper the lanthanide complexes of a Schiff base derived from *o*-vanillin (2-hydroxy-3-methoxy-benzaldehyde) and *p*-toluidine, $[LnL_2(NO_3)_2]NO_3$ (where Ln = Pr–Lu except Pm, L = Schiff base), have been prepared and characterized.

EXPERIMENTAL

Preparation of the Schiff base

The Schiff base was prepared by reaction of *o*-vanillin (3.04 g) with an equimolar amount of *p*-toluidine (2.14 g) in absolute alcohol (50 cm^3). The reaction solution was heated and brought to reflux for 1 h. The precipitate was filtered, washed with absolute alcohol, and recrystallized from absolute alcohol. Yield 4.34 g, 90%.

Preparation of Schiff base complexes

The absolute alcohol solution (10 cm^3) of lanthanide nitrate $Ln(NO_3)_3 \cdot 6H_2O$ (1.0×10^{-3} mol, 0.31–0.35 g, Pr–Lu) was added in drops to the absolute alcohol solution (10 cm^3) of Schiff base (2.0×10^{-3} mol, 0.48 g) for 5 min with vigorous stirring. The solution was then allowed to stand for 1 week at room temperature. The precipitate was filtered, washed with absolute alcohol and dried *in vacuo*. The crude product was recrystallized from absolute methanol. Yields 0.63–0.69 g, 75–85% (Table 1).

Measurements

Elemental analyses were obtained with a 240C auto elmentary analyser. IR spectra were recorded on a 5DX-FT spectrometer in the region 400–4000 cm^{-1} using KBr pellets. Molar conductances of 10^{-3} mol dm^{-3} methanol solutions at 25°C were measured on a DDX-111A conductometer. TG and DTA were carried out using a 4.1 mode thermobalance (sample: 20 mg, heating rate: 10°C min^{-1}, atmosphere: static air).

RESULTS AND DISCUSSION

Composition of the complexes

Analytical results (Table 1) show that the composition of all these complexes is $LnC_{30}H_{30}N_5O_{13}$

* Author to whom correspondence should be addressed.

Table 1. Analyses, yields and molar conductance measurements

Complexes	C (%)[a]	H (%)[a]	N (%)[a]	Yield (g)	Yield (%)	Λ_M (Ω^{-1} cm^2 mol^{-1})
Pr	45.1	3.8	8.6	0.69	85	80
	(44.5)	(3.7)	(8.6)			
Nd	44.3	3.6	8.3	0.68	84	84
	(44.3)	(3.7)	(8.6)			
Sm	44.2	3.7	8.6	0.67	82	83
	(44.0)	(3.7)	(8.6)			
Eu	43.3	3.6	8.7	0.66	80	81
	(43.9)	(3.7)	(8.5)			
Gd	43.9	3.4	8.3	0.64	78	80
	(43.6)	(3.7)	(8.5)			
Tb	43.3	3.6	8.6	0.62	75	84
	(43.5)	(3.6)	(8.5)			
Dy	42.9	3.6	8.7	0.64	78	81
	(43.4)	(3.6)	(8.4)			
Ho	43.0	3.5	8.6	0.64	77	86
	(43.2)	(3.6)	(8.4)			
Er	43.3	3.4	8.4	0.63	75	87
	(43.1)	(3.6)	(8.3)			
Tm	42.9	3.5	8.6	0.65	77	83
	(43.0)	(3.6)	(8.4)			
Yb	42.7	3.7	8.5	0.64	76	86
	(42.8)	(3.6)	(8.3)			
Lu	42.7	3.4	8.7	0.63	75	85
	(42.7)	(3.6)	(8.3)			

[a] Calculated values are given in parentheses.

Table 2. Important IR frequencies (cm^{-1}) of the Schiff base and its complexes

Complexes	$\nu_{C=N}$	ν_{OH}	ν_{C-O}	NO_3^- ν_4	ν_1	ν_2	ν_6	ν_3	ν_5
Pr	1640s	3402w	1383s	1501s	1293s	1021m	818m	749m	703m
Nd	1641s	3402w	1380s	1507s	1297s	1029m	817m	748m	703m
Sm	1640s	3409w	1384m	1502s	1300s	1029m	817m	746m	703m
Eu	1640s	3418w	1382m	1501s	1300s	1019m	816m	750m	703m
Gd	1640s	3418w	1383m	1504s	1301s	1028m	816m	746m	703m
Tb	1641s	3409w	1383m	1502s	1294s	1023m	816m	747m	703m
Dy	1643s	3409w	1384m	1501s	1294s	1025m	817m	749m	702w
Ho	1642s	3402w	1384m	1503s	1293s	1028m	816m	749m	701w
Er	1642s	3402w	1383m	1503s	1295s	1028m	817m	748m	702w
Tm	1642s	3409w	1385m	1503s	1299s	1028m	816m	748m	703w
Yb	1642s	3402w	1383m	1504s	1298s	1028m	815m	748m	702w
Lu	1642s	3403w	1381m	1503s	1295s	1030m	816m	749m	705w
L	1618s	3452w	1420m						

s: strong, m: medium, w: weak.

and they have the general formula $[LnL_2(NO_3)_2]NO_3$.

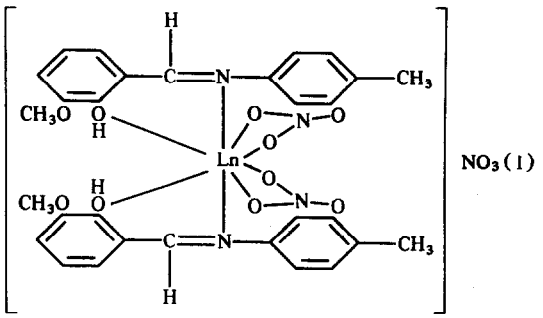

IR spectra

The important IR frequencies of the Schiff base ligand and the complexes are presented in Table 2. The IR spectrum of the Schiff base shows a strong band at 1618 cm^{-1} attributable to the C=N stretching vibration. On complexation this band shifts to the region 1635–1652 cm^{-1} showing that nitrogen of the azomethine group is coordinated to the lanthanide ions.[12,13] A broad band at 3452 cm^{-1} is due to the phenolic OH stretching vibration in the Schiff base. On complexation this band shifts to the region 3402–3409 cm^{-1}. A medium intensity band at 1420 cm^{-1} is due to the phenolic C—O stretching vibration in the Schiff base. In complexes this band shifts to the region 1380–1385 cm^{-1}. Since the phenolic OH and C—O stretching vibrations shift to lower wavenumbers, this indicates that the oxygen of the phenolic OH is also coordinated to the lanthanide ion.[12,13]

The complexes show six absorption bands near 1501, 1295, 1025, 817, 749 and 702 cm^{-1} which are assigned, respectively, to ν_4, ν_1, ν_2, ν_6 ν_3 and ν_5 vibrations of the coordinated (C_{2v}) nitrate group.[14,15] The magnitudes of ν_4–ν_1 and ν_3–ν_5 are in the range 201–210 and 43–47 cm^{-1}, respectively, indicating that the nitrate groups are coordinated in bidentate fashion.

Molar conductance

The molar conductance data of the complexes are presented in Table 1. From these data it is clear that all the complexes show 1 : 1 electrolytic behaviour in absolute methanol.[16]

Thermal behaviour

The thermal analytical results of some complexes (Table 3 and Fig. 1) show that the complexes are stable up to 235°C. The TG and DTA curves do not have stages or peaks up to 235°C, therefore the complexes do not contain small molecules (water or alcohol). The complexes undergo complete decomposition in the region 660–690°C.

Table 3. Thermal analysis data for some of the complexes

Complexes	Decomposition ranges in TG (°C)	Peaks in DTA (°C)
Pr	262–684	283, 366, 482, 654
Sm	258–680	276, 353, 418, 641
Gd	249–682	277, 327, 476, 653
Ho	247–660	268, 347, 477, 621
Lu	235–690	260, 350, 496, 672

On the basis of elemental analysis, IR spectra, molar conductance and thermal analysis, it is concluded that two Schiff base ligands and two nitrate groups are bound to the lanthanide ion, and another nitrate group is in the outer coordination sphere. Hence the present complexes may be formulated as $[LnL_2(NO_3)_2]NO_3$ (I). The lanthanide ions in the complexes exhibit eight coordination numbers.

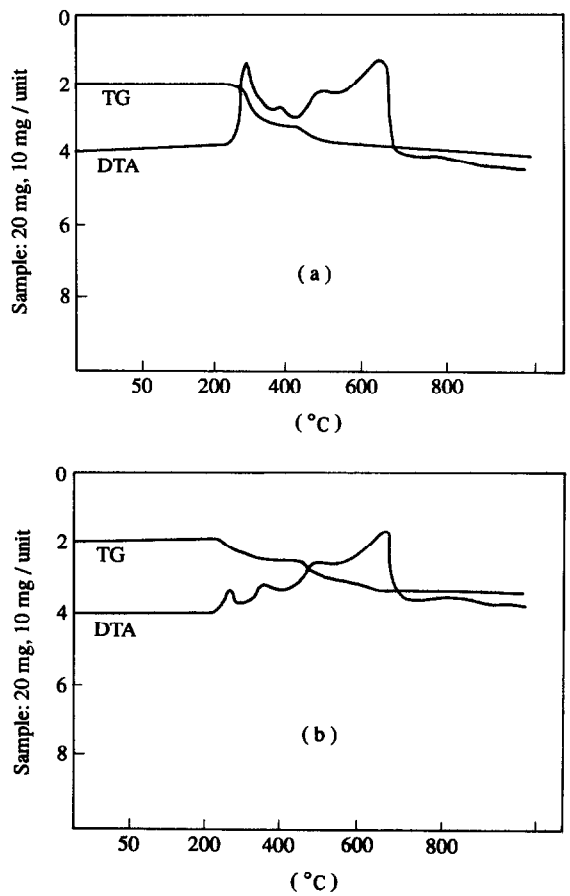

Fig. 1. TG and DTA of (a) Pr and (b) Lu complexes.

Acknowledgement—We thank the National Natural Science Foundation of China for financial support of this work.

REFERENCES

1. A. M. Sayeed, K. Inftikhar, A. V. Malic and N. Ahmad, *Synth. React. Inorg. Met. Chem.* 1983, **13**, 735.
2. N. K. Dutt and K. Nag, *J. Inorg. Nucl. Chem.* 1968, **30**, 3273.
3. A. L. Sharma, K. R. R. Arvind and N. Ahmad, *J. Phy. Soc. Jpn* 1983, **52**, 81.
4. G. F. De Sa and E. Giesbrecht, *J. Inorg. Nucl. Chem.* 1975, **37**, 109.
5. N. K. Dutt and K. Nag, *J. Inorg. Nucl. Chem.* 1968, **30**, 2499.
6. K. Iftikhar, A. M. Sayeed and N. Ahmad, *Ind. J. Chem.* 1968, **25A**, 589.
7. H. A. Tayim, M. Absi, A. Darwish and S. K. Thabet, *Inorg. Nucl. Chem. Lett.* 1975, **11**, 395.
8. A. Shahma, M. Athar and N. Ahmad, *Ind. J. Chem.* 1982, **21A**, 185.
9. M. S. Ansary and N. Ahmad, *Acta Chim. Acad. Scient. Hungaricae* 1977, **92**, 27.
10. M. S. Ansary and N. Ahmad, *J. Inorg. Nucl. Chem.* 1976, **38**, 1232.
11. P. K. Radhakrisnan, P. Indrasenan and C. G. R. Nair, *Polyhedron* 1984, **3**, 67.
12. J. I. Bullock and Heider-Ali Tajmir-Riachi, *J. Chem. Soc., Dalton Trans.* 1978, 36.
13. G. K. Joshi, M. P. Bhutra and S. N. Misra, *J. Inorg. Nucl. Chem.* 1981, **43**, 525.
14. B. M. Gatehouse, S. E. Livingstone and R. S. Nyholm, *J. Chem. Soc.* 1957, 4222.
15. N. F. Curtis and Y. M. Curtis, *Inorg. Chem.* 1965, **4**, 804.
16. W. J. Geary, *Coord. Chem. Rev.* 1971, **7**, 81.

Polyhedron Vol. 9, No. 17, pp. 2023–2028, 1990
Printed in Great Britain

0277–5387/90 $3.00+.00
© 1990 Pergamon Press plc

X-RAY CRYSTAL STRUCTURE OF GUANIDINIUM HEXAMOLYBDOBIS(*o*-NITROPHENYLARSONATE)MONOHYDRATE, $(CN_3H_6)_5[(o\text{-}NO_2C_6H_4As)_2Mo_6O_{25}H]\cdot H_2O$

BEN-YAO LIU,* GAO-YANG XIE and YIH-TONG KU

Department of Chemistry, Fudan University, Shanghai, China

and

XIN WANG

Center of Analysis and Measurement, Lanzhou University, Lanzhou, China

(*Received* 1 *August* 1989; *accepted* 21 *March* 1990)

Abstract—The structure of guanidinium hexamolybdobis(*o*-nitrophenylarsonate)monohydrate was determined by single-crystal X-ray diffraction analysis. Each molecule contains one $[(o\text{-}NO_2C_6H_4As)_2Mo_6O_{25}H]^{5-}$ anion, five $CN_3H_6^+$ cations and one water molecule. The structure of the anion is similar to $[(C_6H_5As)_2Mo_6O_{25}H]^{5-}$, $[(C_6H_5As)_2W_6O_{25}H]^{5-}$ and $[(p\text{-}NH_3C_6H_4As)_2W_6O_{25}]^{4-}$ except for one molybdenum atom which is considered as five-coordinated. Five MoO_6 octahedra and one MoO_5 square-pyramid are connected with edge- or corner-sharings to form a ring. Two *o*-nitrophenylarsenic groups join the ring above and below. Although the two arsenic atoms are not equivalent in their bonding manner, both dihedral angles between the phenyl plane and the corresponding nitro plane are 28.8°. It may be noted that the two phenyl planes are almost perpendicular to each other. It is indicated that a special oxygen atom may be bonded to a proton.

The organo-phosphorus and organo-arsenic polymolybdates have been synthesized by Pope and co-workers.[1,2] The compounds consist of a ring of linked MoO_6 octahedra with two organic handles above and below the molybdenum ring.[3] It was stated by Pope and co-workers that only one type of organo-arsenic polymolybdate $[(RAs)_2Mo_6O_{24}]^{4-}$ is formed at pH = 3–5 independent of whether R is an alkyl or aryl group.[2] They only reported the crystal structural data for a double salt of the methyl derivative $[(CH_3)_4N]_2Na_2[(CH_3As)_2Mo_6O_{24}]\cdot 6H_2O$[2] and took it for granted that all alkyl- or aryl-arsenic polymolybdates are of the same type. Matsumoto reported, however, the crystal and molecular structure of a guanidinium salt of the phenyl derivative $(CN_3H_6)_4[(C_6H_5As)_2Mo_6O_{25}H_2]\cdot 4H_2O$.[4]

When *n*-propylarsenic polymolybdates were prepared in our laboratory, we found a unique phenomenon that two types of crystal, containing different numbers of ring molybdenum atoms, are formed under the same pH conditions from the same solution.[5] The six-molybdenum compound $(CN_3H_6)_4[(n\text{-}C_3H_7As)_2Mo_6O_{24}]$[6] is consistent with Pope's prediction, whereas the five-molybdenum compound $(CN_3H_6)_4[(n\text{-}C_3H_7As)_2Mo_5O_{21}]\cdot 2H_2O$[7] is isostructural with organo-phosphorus polymolybdates.[8] In the case of allyl arsonic acid, however, only a five-molybdenum compound $(CN_3H_6)_4[(n\text{-}C_3H_5As)_2Mo_5O_{21}]\cdot 2H_2O$ can be isolated.[9] When phenylarsenic polymolybdates were prepared in our laboratory, only $(CN_3H_6)_5[(C_6H_5As)_2Mo_6O_{25}H]\cdot H_2O$ was isolated from the solution at pH = 3–5.[10] Single-crystal X-ray diffraction studies and elemental analyses show that this compound is different from that reported by Matsumoto, but is isostructural with its tungsten

* Author to whom correspondence should be addressed.

congener $(CN_3H_6)_5[(C_6H_5As)_2W_6O_{25}H]\cdot 2H_2O$ reported by Wasfi *et al.*[11] In order to investigate the types of compound of arylarsenic polymolybdates, we have prepared *ortho*-, *meta*- and *para*-nitrophenylarsonic acid and tested the reactions of these acids with sodium molybdate at pH = 3–5. Five new salts of arylarsenic polymolybdates have been synthesized and characterized.[12] Here we wish to report the X-ray crystal structure of one of these five new salts: the *o*-nitrophenyl derivative. It is demonstrated that the $[(RAs)_2Mo_6O_{25}H]^{5-}$ type of complex and not the $[(RAs)_2Mo_6O_{24}]^{4-}$ type as stated by Pope and co-workers, is formed.

EXPERIMENTAL

The starting material, *o*-nitrophenylarsonic acid, was prepared by the improved Bart reaction.[13] The title compound was prepared by mixing an aqueous solution of sodium molybdate with a hot aqueous solution of *o*-nitrophenylarsonic acid in the molar ratio Mo/As = 3, adjusting the pH value to 3–5 with hydrochloric acid, followed by adding guanidinium hydrochloride solution. The light yellow crystals can be obtained by recrystallization from water. A selected single crystal with $0.1\times0.1\times0.2$ mm approximate dimensions was mounted on a glass fibre. All the intensity data were collected on an Enraf–Nonius CAD4 diffractometer using graphite-monochromated Mo-K_α radiation ($\lambda = 0.7107$ Å). The scan mode was ω–2θ. 4973 independent reflections were collected in the range $2° < 2\theta < 50°$, and 4612 independent reflections with $I > 3\sigma(I)$ were used for further computation.

The title compound is orthorhombic, space group $P2_12_12_1$, mol. wt 1689.09, cell dimensions $a = 12.826(1)$, $b = 18.386(1)$, $c = 21.701(3)$ Å, $V = 5117.3$ Å^3, $Z = 4$, $D_{calc} = 2.192$ g cm^{-3}, $F(000) = 3280$, $\mu = 27.725$ cm^{-1}.

The structure analysis was performed on a PDP11/44 computer with the SDP program. The positions of all the molybdenum and arsenic atoms were determined by direct methods. The positions of the other non-hydrogen atoms were revealed by difference Fourier synthesis. The structure was refined by full-matrix least-squares to a final $R = 0.044$.

DESCRIPTION OF THE STRUCTURE AND DISCUSSION

The selected bond distances and bond angles are listed in Tables 1 and 2, respectively. The final atomic coordinates and the thermal parameters, together with bond distances and bond angles relating to the aromatic rings and the cations, have been deposited as Supplementary Material with the Editor, from whom copies are available on request. The structure of the anion $[(o\text{-}NO_2C_6H_4As)_2Mo_6O_{25}H]^{5-}$ and its atomic numbering is shown in Fig. 1, while Fig. 2 shows the crystal structure. It can be seen that each molecule has one $[(o\text{-}NO_2C_6H_4As)_2Mo_6O_{25}H]^{5-}$ anion, five $CN_3H_6^+$ cations and one water molecule. In the anion, each molybdenum atom is bonded to six oxygen atoms and is located in the centre of a distorted octahedron, except for the Mo(5) atom which is bonded to only five oxygen atoms and is located in the centre of a distorted square-pyramid. Four MoO_6 octahedra are connected by edge-sharing [Mo(1) and Mo(2) by O(3)O(5) edge-sharing, Mo(2) and Mo(3) by O(9)O(10), Mo(3) and Mo(4) by O(12)O(14), respectively], while the other Mo(6) octahedron is connected to Mo(1) by corner-sharing [O(4)]. The Mo(5) square-pyramid is connected to Mo(4) and Mo(6) by corner-sharing [O(18)] and edge-sharing [O(21)O(22)], respectively. All of these molybdenum polyhedra are connected to form a ring. Each arsenic atom is tetrahedrally coordinated by three oxygen atoms from these molybdenum polyhedra and an *o*-nitrophenyl group, and each joins the ring by sharing the three oxygen atoms with the molybdenum atoms. It is notable that these

Table 1. Selected bond distances (Å) with ESDs in parentheses

Mo(1)—O(1)	1.738(5)	Mo(5)—O(19)	1.714(5)
Mo(1)—O(2)	1.683(4)	Mo(5)—O(20)	1.726(5)
Mo(1)—O(3)	1.983(4)	Mo(5)—O(21)	1.971(4)
Mo(1)—O(4)	1.915(4)	Mo(5)—O(22)	2.135(4)
Mo(1)—O(5)	2.258(4)	Mo(6)—O(4)	1.876(4)
Mo(1)—O(6)	2.175(4)	Mo(6)—O(21)	1.909(4)
Mo(2)—O(3)	1.877(4)	Mo(6)—O(22)	2.175(4)
Mo(2)—O(5)	2.408(4)	Mo(6)—O(23)	1.737(5)
Mo(2)—O(7)	1.706(4)	Mo(6)—O(24)	1.720(5)
Mo(2)—O(8)	1.713(4)	Mo(6)—O(25)	2.298(4)
Mo(2)—O(9)	1.927(4)	As(1)—O(5)	1.697(4)
Mo(2)—O(10)	2.228(4)	As(1)—O(14)	1.671(4)
Mo(3)—O(9)	1.950(4)	As(1)—O(25)	1.676(4)
Mo(3)—O(10)	2.261(4)	As(1)—C(1)	1.949(6)
Mo(3)—O(11)	1.722(4)	As(2)—O(6)	1.671(4)
Mo(3)—O(12)	1.883(4)	As(2)—O(10)	1.721(4)
Mo(3)—O(13)	1.718(5)	As(2)—O(17)	1.660(4)
Mo(3)—O(14)	2.258(4)	As(2)—C(7)	1.921(6)
Mo(4)—O(12)	1.965(4)	O(26)—N(1)	1.177(10)
Mo(4)—O(14)	2.379(4)	O(27)—N(1)	1.184(10)
Mo(4)—O(15)	1.711(4)	O(28)—N(2)	1.216(8)
Mo(4)—O(16)	1.715(5)	O(29)—N(2)	1.225(9)
Mo(4)—O(17)	2.234(4)	N(1)—C(6)	1.452(11)
Mo(4)—O(18)	1.891(4)	N(2)—C(12)	1.435(12)
Mo(5)—O(18)	1.871(4)		

Table 2. Selected bond angles (°) with ESDs in parentheses

O(1)—Mo(1)—O(2)	104.0(2)	O(10)—Mo(3)—O(11)	91.7(2)	O(21)—Mo(5)—O(22)	72.0(2)
O(1)—Mo(1)—O(3)	96.3(2)	O(10)—Mo(3)—O(12)	86.6(2)	O(4)—Mo(6)—O(21)	150.6(2)
O(1)—Mo(1)—O(4)	96.2(2)	O(10)—Mo(3)—O(13)	160.6(2)	O(4)—Mo(6)—O(22)	82.6(2)
O(1)—Mo(1)—O(5)	87.1(2)	O(10)—Mo(3)—O(14)	73.8(1)	O(4)—Mo(6)—O(23)	100.2(2)
O(1)—Mo(1)—O(6)	162.2(2)	O(11)—Mo(3)—O(12)	96.9(2)	O(4)—Mo(6)—O(24)	100.1(2)
O(2)—Mo(1)—O(3)	95.6(2)	O(11)—Mo(3)—O(13)	104.4(2)	O(4)—Mo(6)—O(25)	85.5(2)
O(2)—Mo(1)—O(4)	100.1(2)	O(11)—Mo(3)—O(14)	163.4(2)	O(21)—Mo(6)—O(22)	72.3(2)
O(2)—Mo(1)—O(5)	166.2(2)	O(12)—Mo(3)—O(13)	101.8(2)	O(21)—Mo(6)—O(23)	97.6(2)
O(2)—Mo(1)—O(6)	93.9(2)	O(12)—Mo(3)—O(14)	74.8(2)	O(21)—Mo(6)—O(24)	98.8(2)
O(3)—Mo(1)—O(4)	156.9(2)	O(13)—Mo(3)—O(14)	91.4(2)	O(21)—Mo(6)—O(25)	72.8(2)
O(3)—Mo(1)—O(5)	74.8(1)	O(12)—Mo(4)—O(14)	70.6(2)	O(22)—Mo(6)—O(23)	96.3(2)
O(3)—Mo(1)—O(6)	81.2(2)	O(12)—Mo(4)—O(15)	99.6(2)	O(22)—Mo(6)—O(24)	160.3(2)
O(4)—Mo(1)—O(5)	86.6(2)	O(12)—Mo(4)—O(16)	98.0(2)	O(22)—Mo(6)—O(25)	72.7(2)
O(4)—Mo(1)—O(6)	80.9(2)	O(12)—Mo(4)—O(17)	79.7(2)	O(23)—Mo(6)—O(24)	102.4(3)
O(5)—Mo(1)—O(6)	75.2(2)	O(12)—Mo(4)—O(18)	148.0(2)	O(23)—Mo(6)—O(25)	166.9(2)
O(3)—Mo(2)—O(5)	73.0(1)	O(14)—Mo(4)—O(15)	168.1(2)	O(24)—Mo(6)—O(25)	88.1(2)
O(3)—Mo(2)—O(7)	102.3(2)	O(14)—Mo(4)—O(16)	86.4(2)	O(5)—As(1)—O(14)	110.0(2)
O(3)—Mo(2)—O(8)	99.7(2)	O(14)—Mo(4)—O(17)	86.1(1)	O(5)—As(1)—O(25)	112.9(2)
O(3)—Mo(2)—O(9)	145.7(2)	O(14)—Mo(4)—O(18)	83.6(2)	O(5)—As(1)—C(1)	102.1(2)
O(3)—Mo(2)—O(10)	82.2(2)	O(15)—Mo(4)—O(16)	101.8(2)	O(14)—As(1)—O(25)	110.2(2)
O(5)—Mo(2)—O(7)	86.5(2)	O(15)—Mo(4)—O(17)	85.6(2)	O(14)—As(1)—C(1)	112.6(2)
O(5)—Mo(2)—O(8)	168.5(2)	O(15)—Mo(4)—O(18)	103.3(2)	O(25)—As(1)—C(1)	108.9(2)
O(5)—Mo(2)—O(9)	80.2(2)	O(16)—Mo(4)—O(17)	172.6(2)	O(6)—As(2)—O(10)	112.1(2)
O(5)—Mo(2)—O(10)	81.0(1)	O(16)—Mo(4)—O(18)	98.7(2)	O(6)—As(2)—O(17)	110.7(2)
O(7)—Mo(2)—O(8)	104.0(2)	O(17)—Mo(4)—O(18)	80.2(2)	O(6)—As(2)—C(7)	113.5(3)
O(7)—Mo(2)—O(9)	96.8(2)	O(18)—Mo(5)—O(19)	103.1(2)	O(10)—As(2)—O(17)	106.9(2)
O(7)—Mo(2)—O(10)	164.8(2)	O(18)—Mo(5)—O(20)	99.3(2)	O(10)—As(2)—C(7)	102.3(2)
O(8)—Mo(2)—O(9)	102.9(2)	O(18)—Mo(5)—O(21)	148.0(2)	O(17)—As(2)—C(7)	110.8(2)
O(8)—Mo(2)—O(10)	89.3(2)	O(18)—Mo(5)—O(22)	86.5(2)	O(26)—N(1)—O(27)	123.7(9)
O(9)—Mo(2)—O(10)	72.7(2)	O(19)—Mo(5)—O(20)	104.9(3)	O(26)—N(1)—C(6)	115.1(8)
O(9)—Mo(3)—O(10)	71.6(2)	O(19)—Mo(5)—O(21)	102.0(2)	O(27)—N(1)—C(6)	121.0(9)
O(9)—Mo(3)—O(11)	98.6(2)	O(19)—Mo(5)—O(22)	94.6(2)	O(28)—N(2)—C(29)	125.0(1)
O(9)—Mo(3)—O(12)	153.5(2)	O(20)—Mo(5)—O(21)	93.1(2)	O(28)—N(2)—C(12)	116.0(1)
O(9)—Mo(3)—O(13)	95.0(2)	O(20)—Mo(5)—O(22)	157.7(2)	O(29)—N(2)—C(12)	119.6(6)
O(9)—Mo(3)—O(14)	84.5(2)				

two arsenic atoms are not equivalent in their bonding manner. As(1) is bonded to one molybdenum-unshared oxygen atom and two edge-shared oxygen atoms, and so it is connected to five MoO_6 octahedra. As(2) is bonded to one edge-shared oxygen atom and two molybdenum-unshared oxygen atoms, and so it is connected to four MoO_6 octahedra. It is interesting to note that each *o*-nitro group is not co-planar with its corresponding phenyl group, see Table 3. Although the two arsenic atoms are not equivalent in their bonding manner, both dihedral angles between the phenyl plane and the corresponding *o*-nitro plane are 28.8°. It is also noticed that the two phenyl planes are almost perpendicular to each other, the dihedral angle between them is 86°.

Each molybdenum atom has two terminal oxygen atoms, which are connected to neither the other molybdenum atom nor to the arsenic atom. This type of Mo—O_t bond length is the shortest one. As shown in Table 2, the 12 Mo—O_t bond lengths range from 1.683 to 1.738 Å, and the average is 1.717 Å. There are four Mo—O_c bond lengths between the corner-shared polyhedra. They range from 1.871 to 1.915 Å, and the average is 1.888 Å. In the case of edge-shared polyhedra, the 10 Mo—O_e bond lengths range from 1.877 to 2.175 Å, and the average is 1.978 Å, if the oxygen atoms are doubly shared by two molybdenum atoms; whereas the six Mo—O_{ea} bond lengths range from 2.228 to 2.408 Å, and the average is 2.299 Å, if the oxygen atoms are triply shared by two molybdenum atoms and one arsenic atom. The Mo—O_{ea} bond length is the longest one. When the oxygen atom is only shared by one molybdenum atom and one arsenic atom, the Mo—O_{ma} bond lengths range from 2.175 to 2.234 Å, and the average is 2.205 Å. The average Mo—O bond lengths of the various types follow

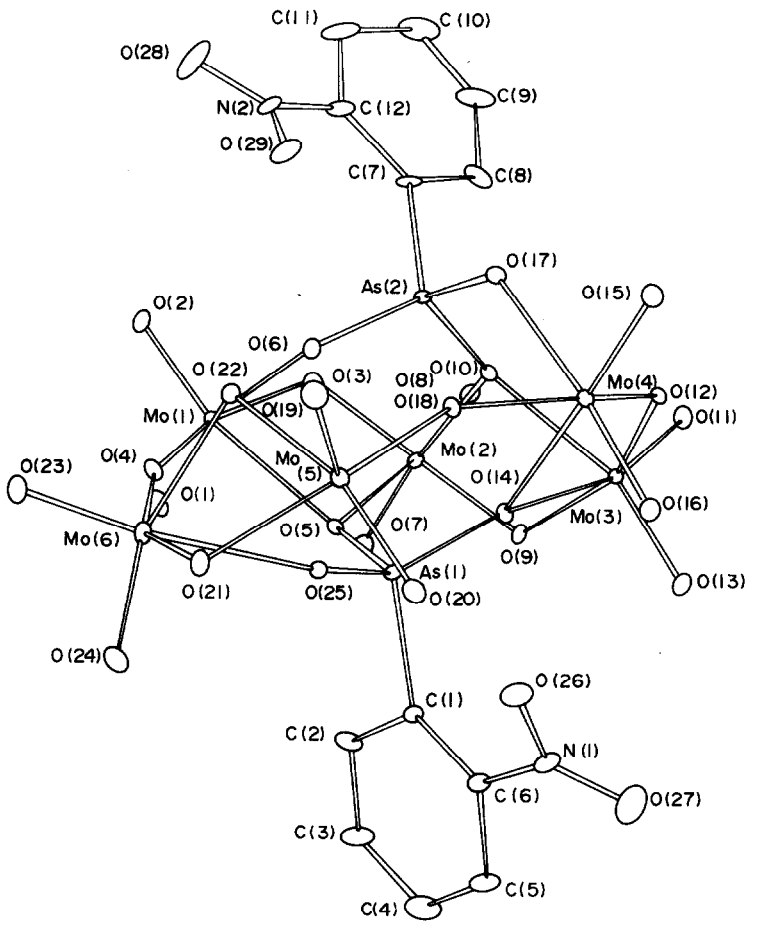

Fig. 1. Structure of the anion $[(o\text{-}NO_2C_6H_4As)_2Mo_6O_{25}H]^{5-}$.

Table 3. Equations of some planes and distance from atom to plane

Equation of plane 1:	$0.5425x-0.8255y-0.1559z = 2.1152$									
Atoms in plane and others atoms:	O(18)	O(20)	O(21)	O(22)	Mo(5)	O(19)				
Distance from atom to plane:	−0.053	0.055	−0.062	0.061	0.381	2.091				
Equation of plane 2:	$0.8595x+0.0346y-0.5100z = -6.2547$									
Atoms in plane and other atoms:	C(1)	C(2)	C(3)	C(4)	C(5)	C(6)	As(1)	N(1)	O(26)	O(27)
Distance from atom to plane:	−0.004	0.002	−0.004	0.009	−0.011	0.009	0.034	0.117	0.624	−0.367
Equation of plane 3:	$-0.2804x+0.7816y-0.5572z = -14.9638$									
Atoms in plane and other atoms:	C(7)	C(8)	C(9)	C(10)	C(11)	C(12)	As(2)	N(2)	O(28)	O(29)
Distance from atom to plane:	−0.014	0.002	0.024	−0.035	0.022	0.001	−0.096	−0.128	0.310	−0.637

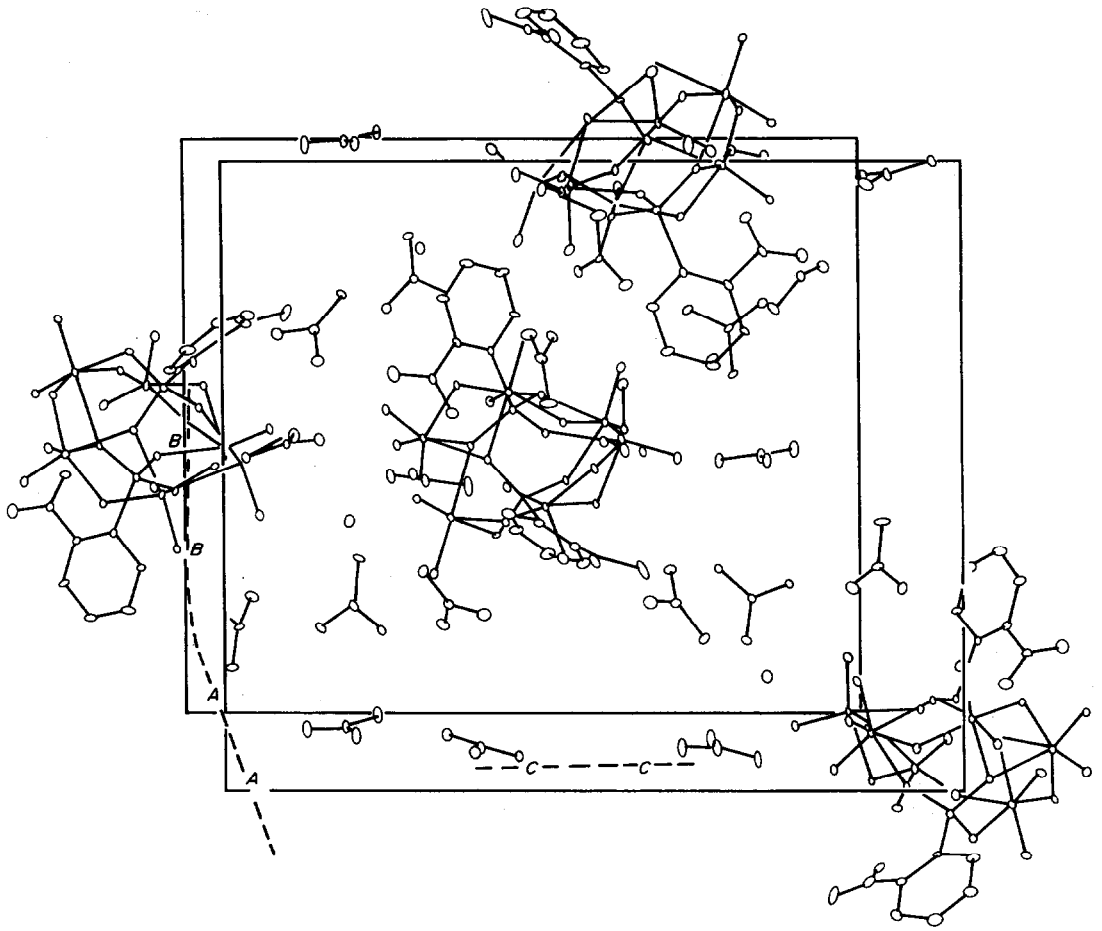

Fig. 2. A view of the unit cell.

the sequence:

$$\underset{1.717}{Mo—O_t} < \underset{1.888}{Mo—O_c} < \underset{1.978}{Mo—O_e} < \underset{2.205}{Mo—O_{ma}} < \underset{2.299}{Mo—O_{ea}}$$

It is obvious that the Mo—O_{ma} bond lengths are much longer than Mo—O_c and Mo—O_e bond lengths. This phenomenon is due to the large electronegativity of the arsenic atom.

The As—O bond lengths range from 1.660 to 1.721 Å, and the average is 1.683 Å. The bonding environments of the oxygen atoms have little influence on the As—O bond lengths. The average As—C bond length is 1.935 Å. In the *o*-nitrophenyl group, the 12 C—C bond lengths range from 1.338 to 1.53 Å, and the average is 1.393 Å, the average C—N bond length is 1.444 Å, the four N—O bond lengths range from 1.177 to 1.225 Å, and the average is 1.201 Å.

From Table 2 it can be seen that the angles O—Mo—O vary regularly with the coordination properties of the oxygen atoms. The O—Mo—O angles are larger than 145.7° if two oxygen atoms are in the *trans* position. When the Mo—O bond lengths increase, the O—Mo—O angles decrease, so that the distances of neighbouring oxygen atoms in the same polyhedron are staying in the similar level. The O—As—O angles range from 106.9 to 112.9°, and the average is 110.5°; while the O—As—C angles range from 102.1 to 113.5°, and the average is 108.4°.

The structure of the anion is similar to that of the known anions $[(C_6H_5As)_2Mo_6O_{25}H]^{5-}$,[10] $[(C_6H_5As)_2W_6O_{25}H]^{5-}$[11] and $[(p\text{-}NH_3C_6H_4As)_2W_6O_{25}]^{4-}$.[14] In all these known anions, all molybdenum atoms are six-coordinated. This Mo(5) is five-coordinated. As shown in Table 3, the oxygen atoms O(18), O(20), O(21) and O(22) are almost co-planar, they constitute the bottom of a square pyramid. The distance from the Mo(5) atom to the plane is 0.381 Å. The calculated distance between Mo(5) and O(25), 2.497(5) Å, is so large that these atoms cannot be considered as bonding to each other. It is emphasized that the O(25) atom is a special one. The bond length Mo(6)O(25), 2.298 Å,

is much longer than the average Mo—O_{ma} bond length of 2.205 Å where the oxygen atom is doubly shared, and almost equal to the average Mo—O_{ea} bond length of 2.299 Å where the oxygen atom is triply shared. From the fact that the Mo(6)O(25) bond length is unusually large, it may be deduced that the O(25) atom should be bonded to an X-ray-undetected hydrogen atom.

In five $CN_3H_6^+$ cations, the C—N bond lengths range from 1.279 to 1.402 Å. The average, 1.337 Å, is between single and double bonds. The angles N—C—N are all close to 120°. Each $CN_3H_6^+$ cation adopts a planar structure, and the multiple-electron delocalized π bond Π_4^6 is thus formed. From the fact that each molecule contains five $CN_3H_6^+$ cations, not four, it may be concluded that the $[(RAs)_2Mo_6O_{25}H]^{5-}$ type of compounds is formed and there must be a proton attached somewhere in the anion to balance the electrical charge.

There is one water molecule in the lattice. Together with the five $CN_3H_6^+$ cations, they provide many hydrogen atoms to form a large number of hydrogen bonds with oxygen atoms in the large anion. These hydrogen bonds between the cations and anions throughout the whole crystal play an important role in stabilizing the crystal. As a matter of fact, the crystals of the title compound remain transparent for a long time.

REFERENCES

1. W. Kwak, M. T. Pope and T. F. Scully, *J. Am. Chem. Soc.* 1975, **97**, 5735.
2. W. Kwak, L. M. Rajkovic, J. K. Stalick, M. T. Pope and C. O. Quicksall, *Inorg. Chem.* 1976, **15**, 2778.
3. F. A. Cotton and G. Wilkinson, *Advanced Inorganic Chemistry*, 4th edn, p. 859. John Wiley, New York (1980).
4. K. Y. Matsumoto, *Bull. Chem. Soc. Jpn* 1978, **51**, 492.
5. B. Y. Liu, Y. T. Ku, M. Wang and P. J. Zheng, *Inorg. Chem.* 1988, **27**, 3868.
6. M. Wang, P. J. Zheng, B. Y. Liu and Y. T. Ku, *Acta Phys.-Chim. Sin.* 1987, **3**, 485.
7. M. Wang, P. J. Zheng, B. Y. Liu and Y. T. Ku, *Acta Cryst.* 1988, **C44**, 1503.
8. J. K. Stalick and C. O. Quicksall, *Inorg. Chem.* 1976, **15**, 1577.
9. B. Y. Liu, Y. T. Ku and X. Wang, *Inorg. Chim. Acta* 1989, **161**, 233.
10. B. Y. Liu, Y. T. Ku, M. Wang and P. J. Zheng, *Acta Chim. Sin.* (*English edn*) 1990, **2**, 121.
11. S. H. Wasfi, W. Kwak, M. T. Pope, K. M. Barkigia, R. J. Butcher and C. O. Quicksall, *J. Am. Chem. Soc.* 1978, **100**, 7786.
12. B. Y. Liu and Y. T. Ku, *Chem. J. Chinese Univ.* 1989, **10**, 453.
13. H. Bart, *Ger. Pat.* 250264 (1910); G. O. Doak, *J. Am. Chem. Soc.* 1923, **45**, 1311; 1940, **62**, 167.
14. B. Y. Liu, Y. T. Ku and X. Wang, *Acta Chim. Sin.* (*English edn*) 1990, **1**, 37.

Polyhedron Vol. 9, No. 17, pp. 2029–2034, 1990
Printed in Great Britain

0277–5387/90 $3.00+.00
© 1990 Pergamon Press plc

SPECTRAL, MAGNETIC AND ELECTRICAL PROPERTIES OF 1-SUCCINYL BIS(4-PHENYLTHIOSEMICARBAZIDE) COMPLEXES

A. A. EL-ASMY,* T. Y. AL-ANSI, R. R. AMIN and M. MOUNIR†

Chemistry Department, Faculty of Science, Sana'a University, Sana'a, P.O. Box 11503, Yemen AR

(*Received* 20 *October* 1989; *accepted* 21 *March* 1990)

Abstract—The preparation and properties of a series of transition metal complexes $M(SPTS)\cdot nH_2O$ [where SPTS is the deprotonated form of 1-succinyl bis(4-phenylthiosemicarbazide), H_2SPTS; M = Co^{II}, Ni^{II}, Cu^{II}, Zn^{II} and Cd^{II} and $n = 0$–2] are described. Analytical, spectral (IR, ^1H NMR), conductometric, magnetic and electronic spectral data show that the cobalt(II) and copper(II) complexes have tetrahedral and octahedral structures, respectively, while the nickel(II) complex shows a mixed stereochemistry of tetrahedral and square-planar isomers. In its complexes, the ligand behaves as a dibasic quadridentate (NSSN) donor. The stoichiometry and stability constants of cobalt(II), nickel(II) and copper(II) complexes have been determined spectrophotometrically. Also, the electrical properties of H_2SPTS and its cobalt(II), nickel(II), copper(II) and zinc(II) complexes were investigated and their activation energies calculated. The values obtained for the nickel(II), cobalt(II) and copper(II) complexes are similar to narrow band semiconductor materials.

Metal ion interaction with ligands containing the thiosemicarbazide moiety plays a vital role in a vast number of widely differing biological processes. They are well known for their anticarcinogenic,[1,2] antibacterial[3] and antifungal[4] properties, as well as certain types of tumour.[5] In our previous work, the antimicrobial activities of some thiosemicarbazides were investigated.[6] In addition, transition metal complexes of these compounds have assumed new importance due to their medicinal properties.[7] In the last three decades, complexes of many thiosemicarbazides have been prepared and characterized.[8–11] In view of the biological significance and diverse coordinating behaviour of these compounds, it was considered worthwhile to study the interaction of some thiosemicarbazide and bis(thiosemicarbazide) derivatives with transition metal ions. In the present investigation, complexes of cobalt(II), nickel(II), copper(II), zinc(II) and cadmium(II) with 1-succinyl bis(4-phenylthiosemicarbazide) are discussed with the aim of investigating the possibility of applying these compounds as semiconductors.

EXPERIMENTAL

All the chemicals used are BDH quality.

Preparation of H_2SPTS

Phenylisothiocyanate (13.5 cm^3, 0.1 mol) was added dropwise with constant stirring to a solution of succinic acid hydrazide (7.8 g, 0.05 mol) in absolute ethanol in a 2 : 1 ratio. The mixture was refluxed for 1/2 h. A white precipitate appeared after cooling in a refrigerator and on scratching the mixture with a glass rod in the presence of diethyl ether. The precipitate was removed by filtration, washed with EtOH and recrystallized, dried and preserved *in vacuo* over anhydrous $CaCl_2$.

Preparation of the metal complexes

A hot, ethanolic solution of metal chloride (0.01 mol) was mixed with an aqueous–ethanol solution

* Author to whom correspondence should be addressed.
† Physics Department, Faculty of Science, Sana'a University, Sana'a, P.O. Box 11503, Yemen AR.

of H_2SPTS (0.01 mol). The mixture was refluxed on a water bath for 3–5 h depending on the metal salt and concentrated to half volume. The product thus formed was filtered, washed with ethanol and dried in an electric oven at ~ 60°C and preserved in a desiccator over anhydrous $CaCl_2$.

Physical measurements

Magnetic measurements were carried out by the Gouy method using mercury tetrathiocyanatocobaltate(II) ($\chi_g = 16.44 \times 10^{-6}$ cgs unit) as a calibrating agent. Electronic and spectral studies in solution were carried out on a Pye Unicam SP 8800 spectrophotometer. IR spectra were recorded on a Perkin–Elmer 1430 model with samples in KBr pellets. The ^1H NMR spectrum of H_2SPTS was recorded on a EM-390 (90 μHz) NMR spectrometer using d_6-DMSO. The molar conductance values were measured with a Leitfahigkeitsme PHYWE bridge. Elemental analyses were carried out in Egypt at the Microanalytical Unit of Cairo University. The analyses of sulphur and the metal ions were carried out according to standard methods.[12] For electrical conductivity measurements in the solid state, compressed pellets, 1 cm^2 area and 0.3–0.5 cm thickness, were moulded at a pressure of 8 tons cm^{-2}. Two thin copper wires of 0.2 mm diameter were attached to the major surface of the pellet after carefully painting them with conducting silver paste. The conduction current was measured using a Keithly 610 C electrometer. The minimum current which can be measured by this method is 10^{-4} A with an accuracy of 2–4%. All measurements were carried out in the 20–180°C temperature range; an electric oven was used to control the ambient temperature. The cell used in the measurements was as described previously.[13]

RESULTS AND DISCUSSION

The reaction of H_2SPTS with the chloride and/or the sulphate salts of cobalt(II), nickel(II), copper(II) or zinc(II) and $CdCl_2$ gives only one type of complex having the formula $M(SPTS)\cdot nH_2O$; the reaction with $CdSO_4$ affords $Cd(H_2SPTS)SO_4\cdot 2H_2O$. The first type is isolated in the presence of CH_3COONa and accompanied by the replacement of two hydrogen atoms, the reaction being exothermic. All the complexes have melting points $\geqslant$ 244°C and are insoluble in most available organic solvents. The cadmium(II) complexes are readily soluble in dimethylsulphoxide (DMSO) and their molar conductivity values (Table 1) lie in the range of non-electrolyte complexes.[14] The presence of the sulphate group in the $CdSO_4$ complex was confirmed quantitatively and supported by IR spectra.

The ligand IR spectrum exhibits three intense bands at 3080, 3230 and 3310 cm^{-1} assigned to $\nu(N^1H)$, $\nu(N^2H)$ and $\nu(N^4H)$ vibrations,[15] respectively, while the band at 1000 cm^{-1} is due to the ν(N—N) vibration.[16] The ν(C=C) vibration of the benzene ring is observed as a strong band at 1595 cm^{-1}. The two bands at 1720 (strong) and 1690 (weak) cm^{-1} are assigned to the stretching vibrations of free and bonded carbonyl groups. The other amide bands (II–IV) are observed at 1510, 1210 and 720 cm^{-1} as reported earlier.[17] The existence of these bands at lower wavenumbers proves hydrogen bonding (Structure I). The ligand spectrum also shows two bands at 770 and 1270 cm^{-1} assignable to ν(C=S) (IV) and a combination of ν(C=S)+ν(N—C—N) (II) vibrations. The other thioamide bands, [δ(C—H)+δ(N—H)] (I) and [ν(C—N)+ν(C=S)] (III), are observed at 1540 and 930 cm^{-1}, respectively. The keto : thioketo form (**I**) is one of the four tautomeric forms of H_2SPTS and

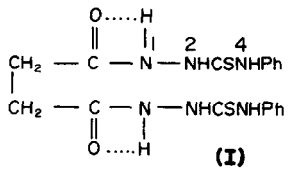

(I)

Table 1. Elemental analysis with some physical properties of H_2SPTS and its metal complexes

Compound	Λ_m	μ_{eff} (μ_B)	% Calc. C	H	N	S	M	H_2O	% Found C	H	N	S	M	H_2O
H_2SPTS	—	—	51.9	4.8	—	15.4	—	—	52.2	5.1	—	16.1	—	—
$[Cu(SPTS)]\cdot 2H_2O$	—	2.11	42.0	4.3	—	12.5	13.3	7.0	42.1	4.5	—	12.6	13.5	7.7
$[Co(SPTS)]\cdot 2H_2O$	—	1.54	42.4	4.0	16.5	12.6	11.6	7.1	42.4	4.0	16.1	12.4	11.3	8.1
[Ni(SPTS)]	—	2.25	45.6	3.7	17.8	13.5	12.4	—	45.5	3.5	18.0	12.3	12.2	—
[Zn(SPTS)]	—	Diam.	45.0	3.8	16.9	13.4	13.6	—	44.5	4.0	16.5	13.1	13.7	—
$[Cd(H_2SPTS)SO_4\cdot H_2O]\cdot H_2O$	12.4	Diam.	32.7	3.7	12.7	14.5	17.0	2.7	32.3	4.0	12.4	14.1	16.1	2.8
$[Cd(SPTS)2H_2O]$	6.2	Diam.	38.4	3.9	—	11.4	20.0	—	38.4	4.1	—	12.1	20.5	—

is supported by the absence of ν(SH) in the 2600–2400 cm^{-1} region. There is also a broad band centred at 3500 cm^{-1} which may be due to the ν(O···H—N) vibration of the intramolecular hydrogen bond.[18]

Two strong signals are observed at 9.5 and 10.1 ppm in the ^{1}H NMR spectrum of H_2SPTS which are attributed to N^4H and N^2H protons, while the weak signal at 9.7 ppm is due to the N^1H proton. The weakness is due to hydrogen bonding.

In the complexes, M(SPTS)·nH_2O, the ligand acts as a quadridentate dibasic (NSSN) donor forming two five-membered rings, as well as a seven-membered ring as shown in structure **II** for the copper(II) complex and **III** for the cobalt(II), zinc(II) and Cd(SPTS)·$2H_2O$ complexes. In their IR spectra, the $\nu(N^2H)$ vibration completely disappears, $\nu(N^1H)$ shifts to lower wavenumbers, the ν(N—N) vibration is slightly shifted to higher wavenumbers and two new bands at ~ 1570 and ~ 430 cm^{-1} due to ν(C=N) and ν(M←N)[19] appear. This evidence suggests nitrogen coordination. Also, the thioamide band I suffers a negative shift upon coordination of nitrogen. Strong evidence for enethiolization is the disappearance of thioamide II and IV bands; this indicates that the —NH—C(S)— moiety converts to —N=C(SH)— by enethiolization. Also, the appearance of a new band at ~ 580 cm^{-1}, due to ν(C—S),[20] is strong evidence for the enethiolization process as well as the coordination through sulphur; this phenomenon is also confirmed by the appearance of the ν(M—S) vibration[21] at ~ 495 cm^{-1}. Finally, the existence of amide bands, which are more or less invariant, indicates that the C=O group is not taking part in coordination.

The reflectance spectrum of Co(SPTS)·$2H_2O$, in Nujol mull, shows a band centred at 16,400 cm^{-1} due to a *d–d* transition; the absence of any bands at ~ 20,000 and ~ 12,000 cm^{-1}, which are characteristic for the square-planar geometry, excludes this structure. The observed broad band is due to the ν_3 [$^4A_2 \rightarrow {}^4T_1$(P)] transition in a tetrahedral structure.[22] Unfortunately, the other bands for the suggested structure are not observed when using our instrument due to its limited range (up to 850 nm). The anomalous moment (1.54 BM) determined for this complex may be due to lower symmetry; the only evidence for this phenomenon is the broadening of the ν_3 transition. Knowing the magnetic moment of the complex, $10Dq$ is generally calculated by the equation: $\mu_{eff} = 3.87(1 - 4\lambda/10Dq)$. Moreover, the anomalous moment of our complex precluded the calculation of $10Dq$ and also B and β values.

The magnetic and spectroscopic studies of Ni(SPTS) suggest a structure with nickel atoms in two different stereochemistries. Its magnetic value is 2.25 BM which is lower than that reported for both tetrahedral and octahedral values; the lowering may be due to mixed geometries of tetrahedral and planar isomers (structure **IV**). The calculation may suggest equal proportions. The reflectance spectrum shows two bands at 14,184 and 23,258 cm^{-1} which are due to the $^3T_1 \rightarrow {}^3A_2$ and $^3T_1 \rightarrow {}^3T_1(F)$ transitions in tetrahedral geometry. Also, the spectrum shows a band at 18,518 cm^{-1} assigned

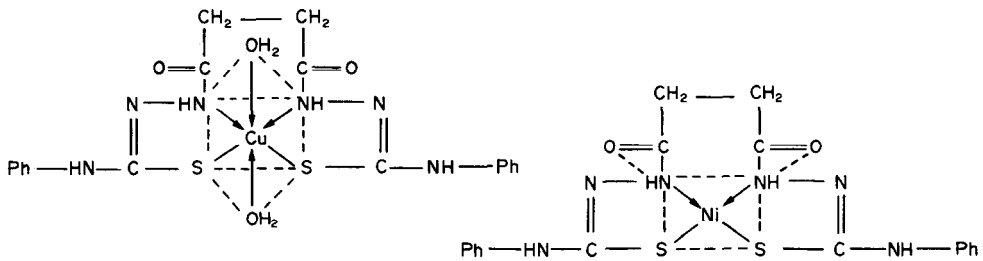

(II)

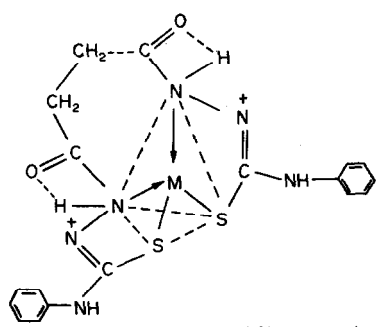

M = Co(II), Zn(II) or Cd(II)

(III)

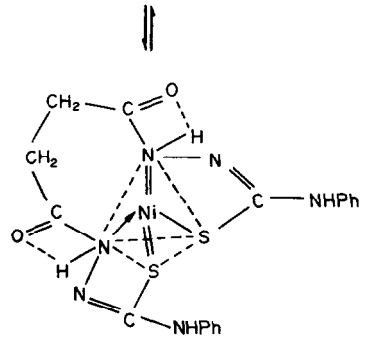

(IV)

to the $^1A_{1g} \rightarrow {}^1A_{2g}$ transition in the square-planar environment. It is concluded that the position and assignments of the reflectance spectral bands reveal the existence of mixed stereochemistries for the nickel(II) complex.

The magnetic moment value (2.11 BM) for the copper(II) complex lies within the permissible range recorded for one unpaired electron. This value excludes the copper–copper interaction and is measured only for compounds with strong covalent bonds. The reflectance spectrum shows one broad band centred at 20,408 cm^{-1} which is characteristic for the existence of the copper(II) ion in an octahedral configuration.[23] The broadening may be due to a lower symmetry resulting from the Jahn–Teller effect. The water molecules complete the octahedral configuration (**II**) and its characteristic bands are observed in the IR spectra at 3460 [ν(OH)], 1630 [$\delta(H_2O)$], 915 [$\rho_r(H_2O)$] and 715 [$\rho_w(H_2O)$] cm^{-1}.

Spectral studies in solution

The spectrum of H_2SPTS was recorded in EtOH and buffer solutions with pHs ranging from 3.15 to 11.86. The UV spectrum recorded in EtOH shows three bands at 202, 228 and 266 nm due to π–π^* and n–π^* transitions. The absorption spectra measured in a series of aqueous Thiel–Coch buffer solutions exhibit two bands at 220 and 248 nm in solutions of the pH range 3.15–8.0 with a slight increase in absorbance. These bands are mainly due to absorption of the non-ionic form of H_2SPTS (**I**). On increasing the pH, a blue shift is observed in the band at 220 nm while its absorbance decreases; this shift reaches a maximum at pH > 10. However, the band at 248 nm is still present at higher pH but its absorbance decreases. The ligand pK values are calculated using the method of half-height of the absorbance–pH curve and are found to be 9.5 and 10.5.

By comparing the metal–ligand spectrum with that of the ligand it has been shown that a new band is formed, indicating the formation of a new species in solution. The new band is found at 290, 306 and 300 nm for the cobalt(II), nickel(II) and copper(II) complexes, respectively.

The widely used Job's method of continuous variation[24] was applied to determine the composition of the complexes formed in EtOH and/or buffer media. The results indicate that the overall ratios of M–L are 1 : 1 and 1 : 2. The stoichiometry of the complexes was also confirmed by the molar ratio method.[25] The apparent formation constant (K_f) for the investigated complexes is calculated using the results obtained from the continuous variation method. The $\log\beta$ values for the cobalt(II), nickel(II) and copper(II) species are listed in Table 2.

Table 2. Apparent formation constants for H_2SPTS complexes

Metal chloride	Cobalt(II)	Nickel(II)	Copper(II)
Type of complex	1 : 1 1 : 2	1 : 1 1 : 2	1 : 1 —
Concentration	4.15×10^{-5} 6.25×10^{-5}	7.7×10^{-6} 1.4×10^{-5}	4.6×10^{-5} —
A/Am	0.9625 0.9478	0.9416 0.9645	0.9714 —
λ_{max} (nm)	290	300	300
K_f	1.65×10^{7} 4.34×10^{11}	3.5×10^{7} 2.77×10^{13}	2.16×10^{7} —
$\log\beta$	7.22 11.64	7.55 13.44	7.33 —

Beer's law is not valid for these systems, so the ligand could not be used in the microdetermination of these metal ions.

Electrical conductivity measurements

The conductivity (σ) and the activation energy (ΔE) of the studied compounds were calculated by applying the Arrhenius equation:

$$\sigma = \sigma_0 \exp -\Delta E/KT.$$

Since this equation is obeyed by inorganic semiconductors, it may also be used to describe the electrical properties of organic and complex compounds.

Figure 1 shows the temperature dependence of the dc electrical conductivity of H_2SPTS and of its cobalt(II), nickel(II) and zinc(II) complexes. The plot of $\ln\sigma$ vs $1/T$ is nearly linear for the cobalt(II) complex but an inflection is observed in the case of H_2SPTS and its nickel(II) complex; this may be attributed to a change in conduction mechanism. The activation energies of cobalt(II) and nickel(II) complexes are calculated to be 0.54 and 0.71 eV, respectively. The conductivity of H_2SPTS and its zinc(II) complex decreases slightly with temperature, i.e. $d\sigma/dT$ is negative. This decrease may be due to the rearrangement of molecules or to the accidental impurities on the surface.

Figure 2 shows the relationship between the electrical conductivity of the copper(II) complex and the applied electric field measured at 50 and 100°C. It is clear that the conductivity sharply increases; the increase becomes more pronounced at $T =$

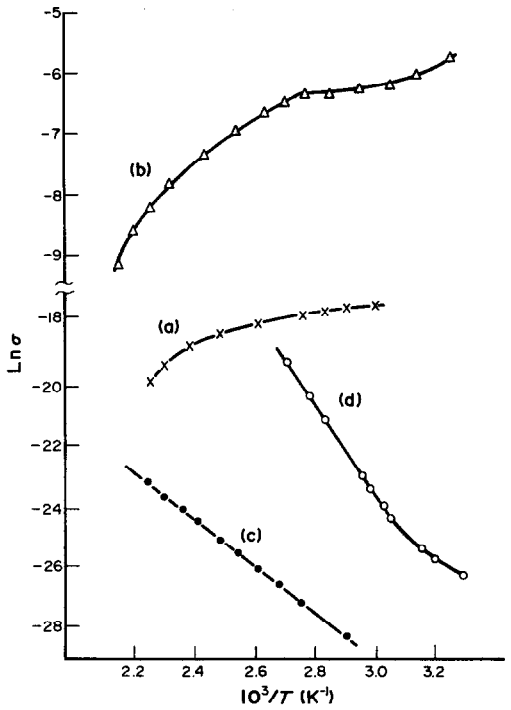

Fig. 1. Plot of ln σ vs $1/T$ for: (a) ligand; (b) Zn^{II} complex; (c) Co^{II} complex; (d) Ni^{II} complex.

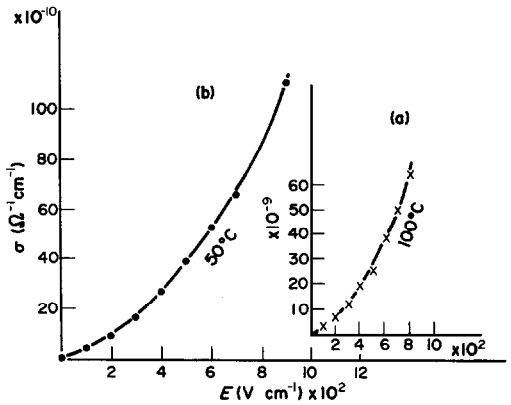

Fig. 2. Dependence of the electrical conductivity (σ) of the copper(II) complex on the applied electric field (E) at (a) 100°C and (b) 50°C.

100°C (see inset a). At room temperature ($\sim$ 22°C), the current is independent of the applied voltage.

The temperature dependence of the electrical conductivity for the annealed and unannealed copper(II) complex is shown in Fig. 3. The error in the measurements, due to the dependence of conductivity on time, is very small. The conductivity of annealed and unannealed samples increases with temperature, i.e. $d\sigma/dT$ is positive and the activation energy is 0.72 eV. This increase may be due to the loss of water molecules at 120°C which are

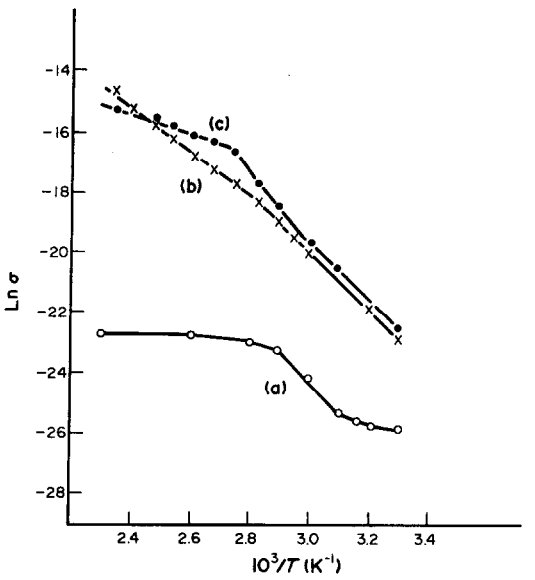

Fig. 3. Plot of ln σ vs $1/T$ for the copper(II) complex: (a) unannealed sample; (b) annealed at 120°C for 1 h; (c) annealed at 120°C for 2 h.

present in the unannealed sample (Table 1). The annealed sample has a large value of conductivity which increases with increasing annealing time.

In conclusion, the activation energy values for the cobalt(II), nickel(II) and copper(II) complexes are similar to those reported for narrow band semiconductor materials.[26]

REFERENCES

1. M. J. M. Campbell, *Coord. Chem. Rev.* 1975, **15**, 279.
2. B. L. Feedlander and A. Fraust, *J. Am. Chem. Soc.* 1952, **64**, 367.
3. N. P. Bauu-Hoi, T. B. Voc and N. D. Xuong, *Bull. Chem. Soc. Fr.* 1955, 694.
4. M. A. Ali and S. E. Livingston, *Coord. Chem. Rev.* 1974, **13**, 101.
5. H. G. Petering, H. H. Buskik and G. E. Underwood, *Cancer Res.* 1964, **64**, 367.
6. A. A. El-Asmy, A. S. Babaqi and A. A. Al-Hubaishi, *Transition Met. Chem.* 1987, **12**, 248.
7. J. P. Scovill, D. L. Kalyman and C. E. Franchino, *J. Med. Chem.* 1982, **25**, 126.
8. A. A. El-Asmy and M. M. Mostafa, *Polyhedron* 1983, **2**, 591.
9. A. A. El-Asmy, *Bull. Chem. Soc. Fr.* 1989, **2**, 171.
10. A. A. El-Asmy, *J. Chin. Chem. Soc.* 1988, **35**, 29.
11. A. A. El-Asmy, T. Y. Al-Ansi, R. R. Amin and M. F. Al-Shahat, *Transition Met. Chem.*, in press.
12. A. I. Vogel, *Text Book of Quantitative Inorganic Analysis*. Longmans, London (1961).
13. A. A. El-Asmy, T. Y. Al-Ansi, M. Mounir and S. A. Ashour, *Synth. React. Inorg. Met-Org. Chem.* 1989, **19**, 309.

14. W. J. Geary, *Coord. Chem. Rev.* 1971, 7, 81.
15. M. M. Mostafa, A. M. Shallaby and A. A. El-Asmy, *J. Inorg. Nucl. Chem.* 1981, **43**, 2992.
16. K. M. Ibrahim, M. M. Bekheit, G. M. Ibrahim and M. M. Mostafa, *Polyhedron* 1986, **5**, 1635.
17. M. Mashima, *Bull. Chem. Soc. Jpn* 1974, **37**, 974.
18. D. Hall, *Acta Cryst.* 1965, **18**, 955.
19. O. Noboru and K. Nakamoto, *Inorg. Chem.* 1971, **10**, 798.
20. K. M. Purohit and D. V. Romana Rao, *Ind. J. Chem.* 1983, **22**, 520.
21. J. R. Ferraro, *Low Frequency Vibrations of Inorganic and Coordination Compounds*. Plenum Press, New York (1971).
22. A. B. P. Lever, *Inorganic Electronic Spectroscopy*. Elsevier, Amsterdam (1968).
23. M. J. M. Campbell and R. Grzeskowiak, *J. Chem. Soc.* 1967, 396.
24. P. Job and A. R. Hebo, *Scand. Acad. Sci.* 1925, **108**, 928.
25. J. H. Yoe and A. L. Jones, *Ind. Engng Chem. Anal.* 1944, **66**, 111.
26. P. D. Ankrum, *Semiconductor Electronics*. Prentice Hall, India (1981).

Polyhedron Vol. 9, No. 17, pp. 2035–2040, 1990
Printed in Great Britain

0277–5387/90 $3.00+.00
© 1990 Pergamon Press plc

COPPER(II) COMPLEXES WITH 1-(2-CARBAMYLETHYL)-2-ALKYLIMIDAZOLES AND OXYANIONS

M. CLARA R. M. P. BASTO,* M. JOSÉ P. FERREIRA, EULÁLIA F. A. C. PEREIRA and ADÉLIO A. S. C. MACHADO

Department of Chemistry, Faculty of Science, University of Oporto, P4000 Oporto, Portugal

(*Received* 1 *December* 1989; *accepted* 21 *March* 1990)

Abstract—Complexes of copper(II) acetate, oxalate and sulphate and 1-(2-carbamylethyl)-2-alkylimidazoles (alkyl = H, CIm; = CH_3, CMIm; = CH_2CH_3, CEIm) have been studied. The following compounds have been prepared and characterized by spectral (IR, UV–vis and EPR) and variable temperature magnetic susceptibility determinations: $Cu(CH_3COO)_2L_n$ (L = CIm, $n = 2$ and 4; L = CMIm or CEIm, $n = 2$), $Cu(C_2O_4)(CIm)_2 \cdot H_2O$, $Cu(SO_4)L_n \cdot xH_2O$ (L = CIm, $n = 1.5$, 3 and 4, $x = 1$ or 3; L = CMIm, $n = 1$ and 2, $x = 2$). Only for $Cu(SO_4)(CIm)_{1.5} \cdot H_2O$ and $Cu(SO_4)(CMIm)_n \cdot 2H_2O$ ($n = 1$ and 2) has evidence of magnetic interactions been found.

Complexes of imidazole and its derivatives have been thoroughly studied and are very important due to their application as analytical, industrial and biochemical reagents[1,2] (and see refs in ref. 3). For instance, the complex bis(acetato)bis(imidazole) copper(II) was recently found to have antitumour activity.[2]

There has also been great interest in dimeric copper(II) carboxylate complexes with bridged structures of the copper(II) acetate monohydrate or similar types, many of which have nitrogen-donor ligands in the terminal positions.[4–6] Oxalate and similar ligands have also been found to form bridges between copper atoms.[7,8] Sulphate can also act as a bridge between metal ions forming, for example, copper(II) compounds with sulphate-bridged chain polymeric structures[9,10] and magnetic interactions have been found in compounds where sulphate bridges alone[9] or with other bridges are present.[11]

In 1-(2-carbamylethyl)-2-alkylimidazoles another biologically important coordinating moiety, the amide group, co-exists with the imidazole group. We have been investigating the coordinating properties of these ligands[3,12] and recently reported halide or pseudo-halide copper(II) complexes with three ligands of this type (alkyl = H, CIm; = CH_3, CMIm; = CH_2CH_3, CEIm).[3] Considering the interest in copper(II) complexes with oxyanions in which polyatomic bridges support magnetic interaction between paramagnetic metal centres, it was decided to extend the study to compounds with acetate, oxalate and sulphate, which is reported in this paper.

EXPERIMENTAL

Chemicals

All the reagents used were commercially available and were used without further purification. 1-(2-Carbamylethyl)imidazole was prepared according to a reported procedure[13] and the other two ligands by a similar procedure, using 2-methylimidazole or 2-ethylimidazole instead of imidazole.[3]

Synthesis and analysis of the complexes

Metal complexes were obtained by the following general procedure. A solution of the organic ligand in methanol (*ca* 1 M) was mixed with 0.25 M copper(II) sulphate or 0.08 M copper(II) acetate solution in methanol previously dehydrated with 2,2′-dimethoxypropane. Acetate complexes were

* Author to whom correspondence should be addressed.

obtained using stoichiometric amounts of metal salt and organic ligand, except for $Cu(CH_3COO)_2(CIm)_4$ which was obtained from a 1 : 6 molar ratio mixture. $Cu(SO_4)(CIm)_n \cdot xH_2O$ (n = 1.5, 3 and 4) compounds were isolated, respectively, from mixtures with 1 : 2, 1 : 4 and 1 : 5 molar ratios. Very often, no solid separated immediately and to obtain a precipitate, the solution was concentrated by slow evaporation (IR lamp) and left standing overnight at room temperature. The solids were filtered off, washed with acetone and dried *in vacuo* (over P_4O_{10}). The following two compounds were prepared by different procedures:

$Cu(SO_4)(CMIm)_2 \cdot 2H_2O$. By adding a 0.25 M solution of the metal salt to a 0.5 M solution of the organic ligand, both in methanol (1 : 2 molar ratio), a light green product was formed (this solid decomposes on standing). After filtering off this powder, acetone was added to the solution and a light blue compound precipitated. This was filtered, washed with methanol and dried over P_4O_{10}.

$Cu(C_2O_4)(CIm)_2 \cdot H_2O$. By heating a mixture of aqueous solutions (all *ca* 1 M) of copper(II) nitrate, potassium oxalate and the organic ligand (1 : 1 : 2), a light blue product precipitated. After cooling, the solid was filtered off and discarded. Acetone and propanol were added to the filtrate, the resulting solution was allowed to stand for a few days, and eventually a flocculent product suspended in the solution and a blue crystalline precipitate formed. The latter was separated by decantation, washed with acetone and dried as before.

The compounds are hygroscopic and were handled under nitrogen atmosphere.

Carbon, nitrogen and hydrogen microanalyses were performed by the Microanalytical Laboratory of the University of Manchester or by the Laboratório Nacional de Engenharia e Tecnologia Industrial (Queluz, Portugal). The copper contents of the complexes were determined by titration with EDTA.

Physical measurements

The following equipment was used: Varian–Cary 17DX spectrophotometer for electronic spectra (Nujol mulls and solutions, 30–8.0 × 10^3 cm^{-1}); Perkin–Elmer 457 spectrophotometer for IR spectra (KBr pellets or Nujol mulls, 4000–250 cm^{-1}); Varian E-109 spectrometer for X-band EPR spectra (operated at ~ 9 GHz and 100 kHz field modulation); Metrohm E518 conductivity meter for measurements on *ca* 10^{-3} M methanolic solutions of the complexes (at 25°C). Magnetic susceptibilities were measured as before.[3]

RESULTS AND DISCUSSION

Synthesis

Yields, analytical and some physical data for the compounds are presented in Table 1.

Tetrakis-complexes were obtained only with 1-(2-carbamylethyl)imidazole. For the other ligands, in contrast with what was found for copper(II) halides, where tetrakis-complexes were also obtained with 1-(2-carbamylethyl)-2-methylimidazole,[3] we were unable to prepare compounds with a ligand-to-metal molar ratio higher than 2 : 1.

Attempts to prepare copper(II) acetate complexes with the metal ion and organic ligands in a 1 : 1 molar ratio were unsuccessful. In attempts to synthesize oxalate compounds of the type $Cu(C_2O_4)L_2$ (where L = CMIm or CEIm), impure products were always obtained.

All the sulphate compounds contain water molecules. These were probably absorbed from the atmosphere during handling of the solutions from which they were isolated.

Copper(II) acetate complexes

The electronic spectra (Table 2) of the compounds with acetate are of the general type found for square- or tetragonally-distorted octahedral copper(II) complexes. They show a broad *d–d* band in the visible region (15–19 × 10^3 cm^{-1}), with a shoulder on the lower energy side [except for $Cu(CH_3COO)_2(CMIm)_2$]. The molar conductivity values (Table 1) for methanolic solutions of the compounds (*ca* 10^{-3} M) indicate a non-electrolyte type of behaviour,[14] but electronic spectra show that the compounds undergo some structural changes in solution.

It seems reasonable to assign to $Cu(CH_3COO)_2(CIm)_4$ a structure with the four coordinating atoms of the organic ligands in the equatorial plane and very weak axially-coordinated or even uncoordinated acetate anions. The IR spectrum of the compound exhibits a multiple and very broad band in the region 1600–1500 cm^{-1} and another band at about 1400 cm^{-1}. These involve bands assignable to acetate vibrations, and suggest that this anion may be ionic or semi-coordinated.[15,16] Assuming D_{4h} symmetry, the observed broad band in the electronic spectrum is assigned to the $^2B_{1g} \rightarrow {}^2B_{2g}, {}^2E_g$ transition. The EPR data (Table 2) for this compound also support tetragonal symmetry and nitrogen coordination of 1-(2-carbamylethyl)imidazole. The EPR spectrum of the powdered compound is of the axial type with $g_\parallel > g_\perp$ ($d_{x^2-y^2}$ ground state). Observed g values are

Table 1. Analytical data and some properties of the compounds

Compound	Colour	Yield (%)	Melting point (°C)	Analysis (%): Found (Calc.) Cu	C	N	H	Λ_M (S cm^2 mol^{-1})
$Cu(CH_3COO)_2(CIm)_4$	Lilac	49	133–136	8.7 (8.6)	45.4 (45.5)	23.4 (22.8)	5.8 (5.7)	49.0
$Cu(CH_3COO)_2(CIm)_2$	Lilac	43	188–191	13.8 (13.8)	41.7 (41.8)	18.2 (18.3)	5.4 (5.3)	34.9
$Cu(CH_3COO)_2(CMIm)_2$	Blue	44	194–196	13.0 (13.0)	44.1 (44.3)	17.3 (17.2)	5.8 (5.8)	50.2
$Cu(CH_3COO)_2(CEIm)_2$	Bluish-lilac	46	184–186	12.2 (12.3)	46.6 (46.5)	16.4 (16.3)	6.4 (6.3)	26.2
$Cu(C_2O_4)(CIm)_2 \cdot H_2O$[a]	Light blue	33	162–164	14.1 (14.2)	37.8 (37.5)	18.7 (18.8)	4.3 (4.5)	[b]
$Cu(SO_4)(CIm)_4 \cdot 3H_2O$	Violet	64	85	8.1 (8.2)	36.4 (37.4)	21.5 (21.8)	5.6 (5.5)	6.89
$Cu(SO_4)(CIm)_3 \cdot 3H_2O$	Blue	54	82–85	9.3 (10.1)	34.9 (34.3)	20.6 (20.0)	5.4 (5.3)	5.61
$Cu(SO_4)(CIm)_{1.5} \cdot H_2O$	Light blue	42	138–140	16.2 (16.4)	28.2 (28.0)	15.7 (16.3)	4.0 (4.0)	≈ 0
$Cu(SO_4)(CMIm)_2 \cdot 2H_2O$	Light blue	34	118–120	12.6 (12.7)	34.2 (33.5)	16.7 (16.7)	5.1 (5.2)	15.6
$Cu(SO_4)(CMIm) \cdot 2H_2O$	Light green	49	218–220	18.3 (18.2)	23.8 (24.1)	11.8 (12.0)	3.7 (4.3)	0.46

[a] Per cent $C_2O_4^{2-}$: 20.1 (19.7).
[b] Insoluble in common organic solvents.

Table 2. Electronic spectra, EPR data and magnetic moments of the compounds

Compound	Electronic spectra $\nu(\varepsilon)$ 10^3 cm^{-1} (M^{-1} cm^{-1})	EPR data T (K)	g values $g_\parallel$	$g_\perp$ or g_m	$A_\parallel$ (G)	A_N (G)	μ^a (BM)
$Cu(CH_3COO)_2(CIm)_4$	Solid 15.4(sh) 18.7	133	2.24	2.06			1.89
	Solution 15.4(57)	103	2.27	2.06	180	15	
$Cu(CH_3COO)_2(CIm)_2$	Solid 15.4(sh) 18.8	103	2.25	2.07			1.84
	Solution 14.8(57)	103	2.31	2.08	161	16	
$Cu(CH_3COO)_2(CMIm)_2$	Solid 15.3	133[b]		2.07[c]			1.91
	Solution 14.8(47)	103	2.32	2.07	162	15	
$Cu(CH_3COO)_2(CEIm)_2$	Solid 14.7(sh) 17.6	103[b]		2.07[c]			1.88
	Solution 14.6(59)						
$Cu(C_2O_4)(CIm)_2 \cdot H_2O$	Solid 14.0	133	2.26	2.15 2.05			1.87
$Cu(SO_4)(CIm)_4 \cdot 3H_2O$	Solid 17.7	113	2.25	2.07	178		1.78
	Solution 14.7(64)	113	2.27	2.06	180	15	
$Cu(SO_4)(CIm)_3 \cdot 3H_2O$	Solid 17.6	133[b]		2.10[c]			1.79
	Solution 14.5(48)	103	2.28	2.05	170	15	
$Cu(SO_4)(CIm)_{1.5} \cdot H_2O$	Solid 13.0	113[b]		2.12[c]			1.82
	Solution 14.0(39)						
$Cu(SO_4)(CMIm)_2 \cdot 2H_2O$	Solid 13.5	113		2.10[c]			1.86
	Solution 13.9(60)	113	2.30	2.07	160	≈ 15	
$Cu(SO_4)(CMIm) \cdot 2H_2O$	Solid 13.1	113	2.30	2.08	155		1.86
	Solution 13.6(42)						

[a] At 298 K.
[b] EPR spectrum of this compound shows a very weak feature at half-field region.
[c] g value obtained from the magnetic field value corresponding to the interception point of the high-field derivative line with the horizontal base line.

in the ranges usually found for tetragonally-distorted copper(II) compounds with four monodentate nitrogen donor ligands.[17] Unlike what was observed for $CuX_2(CIm)_4$ compounds, with $X = Cl^-$, Br^-, ClO_4^-,[3] no hyperfine structure due to copper is observed in the parallel signal (probably due to an increase in dipole–dipole or exchange interactions). Although the compound undergoes structural changes in methanol, its axial EPR spectrum in frozen solution shows, beyond copper hyperfine structure in the $g_\parallel$ signal, superhyperfine structure in the $g_\perp$ region due to nitrogen coordinated atoms of the imidazolic group of the ligand (the amide group nitrogen only coordinates when the amide group is deprotonated[18]).

The complexes $Cu(CH_3COO)_2L_2$ (L = CIm, CMIm or CEIm) exhibit IR spectra that confirm the presence of acetate groups. However, in the region of 1400 cm^{-1} (where the $\nu_s(CO_2)$ band, sensitive to the acetate coordination mode, is expected), the organic ligands also absorb and therefore no conclusions about the coordination mode of the anion are possible (anyway, limitations to the usefulness of IR spectroscopy for the diagnosis of carboxylate coordination have been noted[19]).

Spectral data for $Cu(CH_3COO)_2(CIm)_2$ show that its structure is either monomeric square-distorted involving a CuN_2O_2 chromophore or tetragonally-distorted octahedral, depending whether the terminal acetate oxygen atoms are or are not weakly bonded in (or close to) the axial positions. The compound of the same type with imidazole has an almost *trans*-square planar arrangement of CuN_2O_2, with the second oxygen atoms of the two carboxylate groups interacting weakly with the copper atom, and forming a distorted octahedron.[20] However, steric requirements and different hydrogen bonding possibilities due to the replacement of the hydrogen atom at the N(1) atom of the imidazole ring in 1-(2-carbamylethyl)imidazole by the carbamylethyl group, may provoke a different spacial distribution of atoms in the inner coordination sphere of $Cu(CH_3COO)_2(CIm)_2$. The observation of axial EPR spectra (Table 2) agree with the above proposed geometries.

EPR spectra for powdered $Cu(CH_3COO)_2L_2$ (L = CMIm or CEIm) compounds exhibit an unsymmetrical signal (Fig. 1) and a very weak intensity feature at the half-field region, but are not typical of dimeric copper(II) compounds. The axial spectrum of $Cu(CH_3COO)_2(CMIm)_2$ in frozen solution exhibits poorly resolved superhyperfine structure in the $g_\perp$ region, due to nitrogen coordinated atoms of the organic ligand.

Room temperature magnetic moments (Table 2) for powdered samples of the $Cu(CH_3COO)_2L_2$ compounds are all above the spin-only value expected for a copper(II) ion. The molar magnetic susceptibilities at different temperatures follow the Curie–Weiss law (Table 3) and, since θ values are small and only very slight variations of magnetic moments with temperature are observed, provide no evidence of significant magnetic interactions between copper atoms.

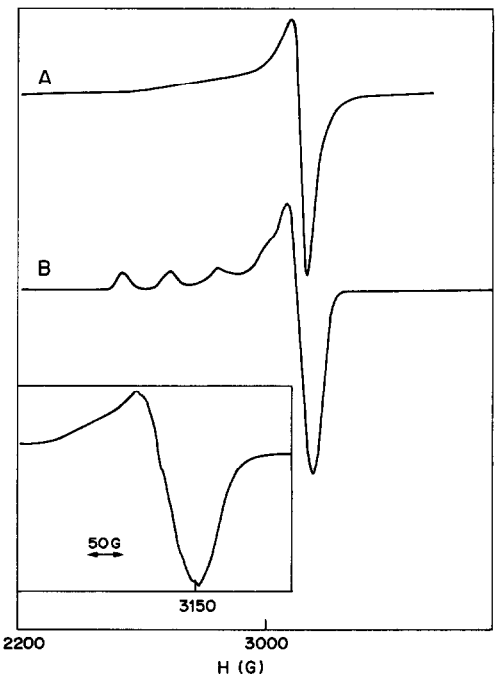

Fig. 1. EPR spectra of: (A) $Cu(CH_3COO)_2(CMIm)_2$, powder, at 133 K; (B) $Cu(CH_3COO)_2(CMIm)_2$ in methanol, at 103 K; insert: *ibidem*, in the $g_\perp$ region.

Copper(II) *oxalate complexes*

The electronic spectrum (Table 2) of the compound $Cu(C_2O_4)(CIm)_2 \cdot H_2O$ consists of an unsymmetrical broad band whose maximum position is consistent with a pentacoordinated copper(II) complex or a rhombic octahedral stereochemistry. An EPR spectrum with three g values is observed, which agrees with low symmetry for the compound. Magnetic data for this complex (Table 3) provide no clear evidence for the existence of significant magnetic interaction. In conclusion, these results do not rule out a monomeric structure for the compound but, as for bis(2-methylimidazole)(oxalato)copper(II),[8] which exhibits weak ferromagnetic coupling, it may have a chain structure.

Table 3. Magnetic data for some of the compounds

Compound	μ (BM)							Curie–Weiss law[a]	
	T (K) 298.4	250.2	206.2	175.7	155.9	126.5	97.0	$10^5 C$ (m^3 mol^{-1} K)	θ
$Cu(CH_3COO)_2(CIm)_2$	1.84	1.85	1.85	1.84	1.85	1.87	1.86	0.5273	4
$Cu(CH_3COO)_2(CMIm)_2$	1.91	1.90	1.91	1.90	1.90	1.90	1.89	0.5800	−3
$Cu(CH_3COO)_2(CEIm)_2$	1.88	1.88	1.90	1.91	1.92	1.92	1.92	0.5447	7
$Cu(C_2O_4)(CIm)_2 \cdot H_2O$	1.87	1.89	1.90	1.90	1.91	1.92	1.97	0.5330	10
$Cu(SO_4)(CIm)_{1.5} \cdot H_2O$	1.82	1.80	1.80	1.76	1.74	1.72	1.67	0.5705	−29
$Cu(SO_4)(CMIm)_2 \cdot 2H_2O$	1.86	1.86	1.85	1.80	1.78	1.77	1.73	0.5896	−24
$Cu(SO_4)(CMIm) \cdot 2H_2O$	1.86	1.83	1.77	1.74	1.72	1.64	1.54	0.6896	−81

[a] Values of C and θ were obtained by least-squares adjustment of magnetic susceptibility data to the Curie–Weiss law, $\chi = C/(T-\theta)$. Values of the correlation coefficients were always greater than 0.999.

Copper(II) sulphate complexes

The organic ligands exhibit bands in the IR regions where sulphate groups are expected to absorb and therefore the IR spectra provide no useful information about coordination modes of sulphate in the compounds.

Electric conductance data in methanol (*ca* 10^{-3} M) (Table 1) indicate that the compounds behave as non-electrolytes in solution, but their electronic spectra in the same solvent (Table 2) show that they undergo structural changes, especially the 1-(2-carbamylethyl)imidazole compounds (the EPR spectrum for $Cu(SO_4)(CIm)_{1.5} \cdot H_2O$ seems to indicate the presence of more than one species in solution). The electronic spectra of all the compounds in Nujol mulls exhibit one broad unsymmetrical *d–d* band, although this occurs in different regions (Table 2). For the compounds $Cu(SO_4)(CIm)_n \cdot 3H_2O$ ($n = 3$, 4) the band appears at higher energy and the spectra are consistent with a tetragonal arrangement of coordinated atoms around copper. In $Cu(SO_4)(imidazole)_4$, distorted octahedral coordination occurs, with the four nitrogen atoms from the imidazoles in the equatorial plane and the two oxygens from the two shared sulphate groups completing the octahedron.[21] On the other hand, $Cu(NH_3)_4(H_2O)(SO_4)$ shows square-based pyramidal symmetry with non-coordinated sulphate.[22] The observed high energy for the *d–d* band in the spectrum of $Cu(SO_4)(CIm)_4 \cdot 3H_2O$ is consistent with very weak coordination of the sulphate group in the axial position. The axial EPR spectrum of this compound (Fig. 2) is characterized by the resolution of copper ion hyperfine structure in the $g_\parallel$ region. In the spectrum in frozen solution, superhyperfine structure is observed in the $g_\perp$ region, due to coordinated nitrogen atoms.

The EPR spectrum of $Cu(SO_4)(CIm)_3 \cdot 3H_2O$ consists of a broad unsymmetrical signal in the high field region, and provides no information about the stereochemistry of the compound.

Solution and Nujol mull spectra (Table 2) for $Cu(SO_4)L_n \cdot xH_2O$ ($n = 1$, 1.5 or 2 and L = CIm or CMIm) are similar, with the maxima positions in the solution spectra slightly shifted to higher energies, which could be due to substitution of coordinated species by methanol molecules or even to structural change.

The EPR spectrum for $Cu(SO_4)(CIm)_{1.5} \cdot H_2O$ shows an apparently axial signal with a perpendicular component at $g = 2.12$ and a shoulder derivative around $g = 2.45$. In addition to this large signal, the spectrum exhibits a very weak feature in the half-field region which corresponds to the $\Delta M_s = 2$ forbidden transition in a dimeric copper(II) compound.

With respect to the 1-(2-carbamylethyl)-2-methylimidazole compounds, the EPR spectrum of $Cu(SO_4)(CMIm) \cdot 2H_2O$ is of the axial type and exhibits copper hyperfine structure resolution in the parallel signal (three of the four lines are clearly seen). $Cu(SO_4)(CMIm)_2 \cdot 2H_2O$ exhibits a broad spectrum (Fig. 2) with apparently only partially resolved hyperfine structure in the parallel signal (no data can be extracted from this spectrum but the g value measured at the point with a derivative value of zero).

Magnetic moments for the sulphate compounds, at room temperature, are all above the spin-only value for single copper(II) ions. Magnetic susceptibility data in the range 90–300 K for $Cu(SO_4)(CMIm)_n \cdot 2H_2O$ ($n = 1$ or 2) and $Cu(SO_4)(CIm)_{1.5} \cdot H_2O$ show that their magnetic moments decrease with decreasing temperature (Table 3). When molar magnetic susceptibilities are fitted to $1/\chi = f(T)$, negative values of θ are obtained (Table

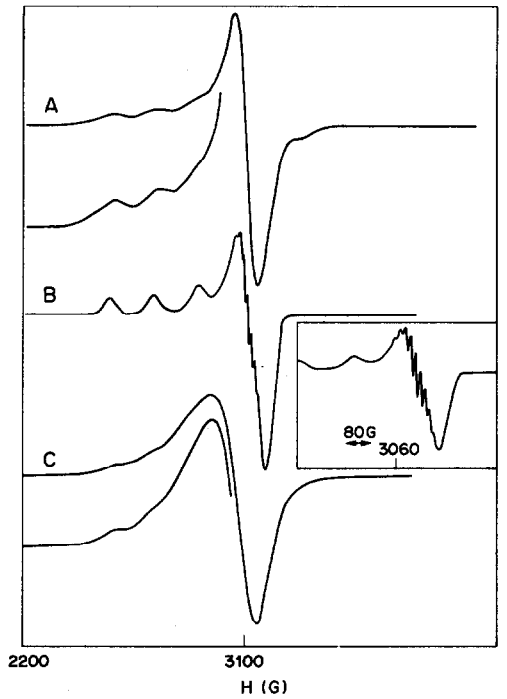

Fig. 2. EPR spectra of: (A) $Cu(SO_4)(CIm)_4 \cdot 3H_2O$, powder, at 113 K; (B) $Cu(SO_4)(CIm)_4 \cdot 3H_2O$ in methanol, at 113 K; insert: *ibidem*, in the $g_\perp$ region; (C) $Cu(SO_4)(CMIm)_2 \cdot 2H_2O$, powder, at 113 K.

3). These results indicate that antiferromagnetic interactions may operate between copper(II) atoms in these compounds. Nevertheless, the EPR spectra of $Cu(SO_4)(CMIm)_n \cdot 2H_2O$ ($n = 1$ or 2) exhibit hyperfine structure which is usually absent for magnetically concentrated compounds.[23] However, signals due to small amounts of impurities not detected by elemental analysis may be responsible for these features in the spectra.

The stoichiometry of the compound $Cu(SO_4)(CIm)_{1.5} \cdot H_2O$ would be consistent with a dimeric structure with a bridged 1-(2-carbamylethyl) imidazole molecule. If this is the case, as magnetic properties for the compound indicate magnetic exchange interaction, and this molecule is not effective to transmit intramolecular exchange, this exchange may be also of the intermolecular type.

CONCLUSIONS

In view of the measured properties, it is not possible to assign unequivocal structures to some of the synthesized complexes.

With reference to magnetic interactions, these were not clearly detected in the $Cu(CH_3COO)_2L_2$ compounds, which leads to the exclusion of acetate bridges in these complexes. For some sulphate compounds, variable temperature magnetic susceptibility results show evidence of magnetic interactions. The results for $Cu(SO_4)CMIm)_n \cdot 2H_2O$ compounds do not rule out polymeric structures with bridged sulphate groups but the magnetic exchange pathway may also involve the water molecules.

Acknowledgements—We thank M. Teresa Domingues for preliminary work on solid $Cu(SO_4)(CIm)_3 \cdot 3H_2O$ and acetate complexes. Financial support from INIC, Lisbon, received through Research Line 4 of CIQ(UP), is acknowledged.

REFERENCES

1. R. J. Sundberg and R. B. Martin, *Chem. Rev.* 1974, **74**, 471.
2. H. Tamura, H. Imai, J. Kuwahara and Y. Sugiura, *J. Am. Chem. Soc.* 1987, **109**, 6870.
3. M. C. R. M. P. Basto and A. A. S. C. Machado, *Polyhedron* 1990, **9**, 713.
4. M. Melník, L. Macásková and J. Mrozinski, *Polyhedron* 1988, **7**, 1745.
5. M. Melník, *Coord. Chem. Rev.* 1981, **36**, 1.
6. M. Melník, *Coord. Chem. Rev.* 1982, **42**, 259.
7. A. Bencini, C. Benelli, D. Gatteschi, C. Zanchini, A. C. Fabretti and G. C. Franchini, *Inorg. Chim. Acta* 1984, **86**, 169.
8. U. Geiser, B. L. Ramakrishna, R. D. Willett, F. B. Hulsbergen and J. Reedijk, *Inorg. Chem.* 1987, **26**, 3750.
9. W. M. Reiff, H. Wong, B. Dockum, T. Brennan and C. Cheng, *Inorg. Chim. Acta* 1978, **30**, 69.
10. J. C. Tedenac, N. D. Phung, C. Avinens and M. Maurin, *J. Inorg. Nucl. Chem.* 1976, **38**, 85.
11. C. K. Thompson, A. W. Hanson and B. S. Ramaswamy, *Inorg. Chem.* 1984, **23**, 2459.
12. M. T. S. D. Vasconcelos and A. A. S. C. Machado, *Talanta* 1987, **34**, 525.
13. R. Dowbenko, C. C. Anderson and W. H. Chang, *Ind. Eng. Chem. Prod. Res. Develop.* 1971, **10**, 344.
14. W. J. Geary, *Coord. Chem. Rev.* 1971, **7**, 81.
15. K. Nakamoto, *Infrared and Raman Spectra of Inorganic and Coordination Compounds*, 3rd edn. Wiley, New York (1978).
16. L. S. Gelfand, L. L. Pytlewski, A. N. Speca, C. M. Mikulski and N. M. Karayannis, *J. Inorg. Nucl. Chem.* 1980, **42**, 209 and refs therein.
17. J. Reedijk, *Transition Met. Chem.* 1981, **6**, 195.
18. T. A. Kabanos and J. M. Tsangaris, *J. Coord. Chem.* 1984, **13**, 89.
19. G. B. Deacon, F. Huber and R. J. Phillips, *Inorg. Chim. Acta* 1985, **104**, 41.
20. H. A. Henriksson, *Acta Cryst.* 1977, **B33**, 1947.
21. G. Fransson and B. K. S. Lundberg, *Acta Chem. Scand.* 1972, **26**, 3969.
22. B. Morosin, *Acta Cryst.* 1969, **24**, 19.
23. A. Abragam and B. Bleaney, *EPR of Transition Ions*. Clarendon Press, Oxford (1970).

Polyhedron Vol. 9, No. 17, pp. 2041–2045, 1990
Printed in Great Britain

0277–5387/90 $3.00+.00
© 1990 Pergamon Press plc

SYNTHESIS AND X-RAY CRYSTAL STRUCTURE OF A MERCURY(II)–TELLUROAMINE COMPLEX. MONODENTATE BEHAVIOUR BY A POTENTIALLY BIDENTATE HYBRID TELLURIDE LIGAND, 1-(NMe_2)-2-(TeC_6H_4-4-OEt)-4-MeC_6H_3

B. L. KHANDELWAL,* A. K. SINGH and V. SRIVASTAVA

Department of Chemistry, Indian Institute of Technology, New Delhi-110 016, India

and

D. C. POVEY and G. W. SMITH

Department of Chemistry, University of Surrey, Surrey GU2 5XH, U.K.

(*Received* 22 *January* 1990; *accepted* 22 *March* 1990)

Abstract—The telluroamines 1-(NMe_2)-2-(TeAr)-4-MeC_6H_3 (**1**) (Ar = 4-$MeOC_6H_4$ or 4-$EtOC_6H_4$) react with mercury(II) halides forming adducts of composition $HgX_2 \cdot$ **1** (X = Cl or Br). The IR, far-IR (up to 50 cm^{-1}), ^1H and ^{13}C NMR spectra of the mercury(II) complexes indicate that the ligands (**1**) behave as monodentate donors, coordinating through tellurium only. The complexes seem to be dimers of the composition [**1** · $XHg(\mu\text{-}X)_2HgX \cdot$ **1**]. The crystal structure of the adduct obtained from mercury(II) bromide has been determined. It reveals that the NMe_2 group does not coordinate with mercury(II) and the complex is a dimer in which two somewhat asymmetrical bromine bridges are present between the mercury atoms. The coordination environment of each mercury is almost tetrahedral [91.25(3)–118.40(4)°]. The Hg—Br bridging bond lengths are 2.755(1) and 2.710(1) Å.

Considerable interest has been devoted to the ligand chemistry of tellurium during the last 15 years,[1–4] but very few hybrid bidentate or polydentate ligands containing the element are known.[5–7] We are interested in the synthesis of potentially polydentate ligands containing "hard" donor atoms, viz. nitrogen and oxygen along with tellurium, and we have recently synthesized telluroamines, 1-(NMe_2)-2-(TeAr)-4-MeC_6H_3[8] and $RN(CH_2CH_2TeAr)_2$[9] (where Ar = C_6H_5, 4-$MeOC_6H_4$ or 4-$EtOC_6H_4$ and R = Me or H) and investigated their complexation behaviour with palladium(II) and platinum(II). They ligate as bi- and tridentate donors, respectively. The potentially bidentate (Te, N) donors 1-(NMe_2)-2-(TeAr)-4-MeC_6H_3 (**1**), however, coordinate with mercury(II) through tellurium only, resulting in a halo-bridged dimer of composition $[Hg_2X_4(\mathbf{1})_2]$ (X = Cl or Br). The monodentate behaviour of a potentially bidentate ligand,

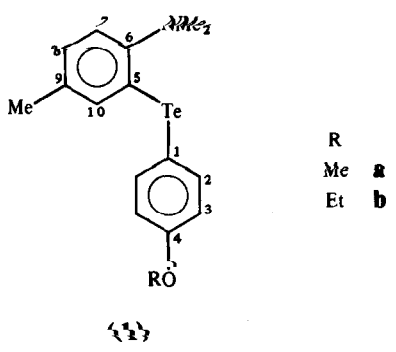

(**1**)

1b, has been demonstrated by the crystal structure of $[Hg_2Br_4(\mathbf{1b})_2]$. The synthesis of mercury complexes of **1**, their IR, far-IR and ^1H and ^{13}C NMR spectra and X-ray crystal structure of one such derivative mentioned above are the subject of the present paper. The complexes described here are the first examples in which a potentially bidentate hybrid organotellurium ligand has been shown to behave as a monodentate donor.

* Author to whom correspondence should be addressed.

EXPERIMENTAL

The ligands, 1-(NMe_2)-2-(TeAr)-4-MeC_6H_3 (Ar = 4-$MeOC_6H_4$ or 4-$EtOC_6H_4$), were synthesized by the method reported earlier.[8] Chloride, bromide, mercury and tellurium were estimated by standard methods.[10] Carbon, hydrogen and nitrogen analyses were carried out with a Perkin–Elmer elemental analyser 240C. ^1H and $^{13}C\{^1H\}$ NMR spectra were recorded in $CDCl_3$ on a JEOL FX-100 FT–NMR spectrometer at 99.55 and 25 MHz, respectively. IR spectra (of Nujol mulls between CsI windows or KBr/CsI discs) in the range 4000–200 cm^{-1} were recorded on a Nicolet 5DX FT–IR spectrometer. Far-IR spectra (400–50 cm^{-1}) were recorded on a Perkin–Elmer Far-FT–IR spectrometer model 1700X on the sample between polyethylene films. The conductance measurements were made on *ca* 1 mM solutions in acetonitrile with a Pye conductivity bridge. Molecular weights (5–20 mM solutions) in chloroform were determined using a Knauer vapour pressure osmometer.

Synthesis of $HgX_2 \cdot$ **1** (X = Br *or* Cl)

$HgCl_2$ or $HgBr_2$ (1 mmol) was dissolved in methanol (~ 5 cm^3). The solution of the ligand **1a** or **1b** (1 mmol in ~ 5 cm^3 benzene) was added dropwise with stirring at room temperature to a solution of the mercuric halide. The white to pale yellow crystalline solid which precipitated instantaneously, was filtered and then successively washed with methanol (~ 10 cm^3) and benzene (~ 5 cm^3). The mercury complexes were recrystallized from a chloroform–benzene mixture (80 : 20 and 60 : 40 for the adducts of $HgCl_2$ and $HgBr_2$, respectively). The yield, melting point, results of elemental analyses, ^1H and $^{13}C\{^1H\}$ (25°C) spectral data are recorded below.

$HgCl_2 \cdot$ **1a**. Yield 82%; m.p. ~ 150°C (dec.). Found: C, 29.5; H, 2.9; N, 2.5; Te, 19.4; Hg, 30.9; Cl, 10.5. Calc. for $C_{16}H_{19}NOCl_2TeHg$: C, 30.0; H, 3.0; N, 2.2; Te, 19.9; Hg, 31.3; Cl, 11.1%. NMR [^1H]: δ, 2.20 (s, 3H, Me); 2.74 (s, 6H, NMe_2); 3.82 (s, 3H, OMe); 6.90–7.89 (m, 7H, aryl); [$^{13}C\{^1H\}$]: δ 20.8 (Me); 47.5 (NMe_2); 55.4 (OMe); 105.0 (C_1); 116.6 (C_3); 121.0 (C_{10}); 132.0 (C_7); 135.0 (C_8); 137.0 (C_5); 140.0 (C_2); 151.0 (C_6); 161.0 (C_4). The signal for C_9 was not observed.

$HgCl_2 \cdot$ **1b**. Yield 85%; m.p. ~ 160°C (dec.). Found: C, 30.9; H, 3.2; N, 2.4; Te, 18.8; Hg, 30.0; Cl, 10.2. Calc. for $C_{17}H_{21}NOCl_2TeHg$: C, 31.2; H, 3.2; N, 2.1; Te, 19.5; Hg, 30.7; Cl, 10.8%. NMR [^1H]: δ, 1.35–1.48 (t, 3H, CH_3 of OEt); 2.19 (s, 3H, Me); 2.74 (s, 6H, NMe_2); 3.94–4.15 (q, 2H, CH_2 of OEt); 6.88–7.87 (m, 7H, aryl); [$^{13}C\{^1H\}$]: δ, 14.7 (CH_3 of OEt); 20.8 (Me); 47.4 (NMe_2); 63.8 (CH_2 of OEt); 105.1 (C_1); 117.1 (C_3); 121.1 (C_{10}); 121.3 (C_9); 132.1 (C_7); 135.3 (C_8); 137.6 (C_5); 140.5 (C_2); 152.1 (C_6); 161.6 (C_4).

$HgBr_2 \cdot$ **1a**. Yield 62%; m.p. ~ 155°C (dec.). Found: C, 25.9; H, 2.7; N, 1.6; Te, 16.2; Hg, 26.7; Br, 20.6. Calc. for $C_{16}H_{19}NOBr_2TeHg$: C, 26.3; H, 2.6; N, 1.9; Te, 17.5; Hg, 27.5; Br, 21.9%. NMR [^1H]: δ 2.19 (s, 3H, Me); 2.74 (s, 6H, NMe_2); 3.82 (s, 3H, OMe); 6.90–7.87 (m, 7H, aryl).

$HgBr_2 \cdot$ **1b**. Yield 68%; m.p. ~ 165°C (dec.). Found: C, 26.9; H, 2.7; N, 1.7; Te, 16.1; Hg, 25.2; Br, 20.1. Calc. for $C_{17}H_{21}NOBr_2TeHg$: C, 27.4; H, 2.8; N, 1.9; Te, 17.2; Hg, 27.0; Br, 21.5%. NMR [^1H]: δ, 1.34–1.48 (t, 3H, CH_3 of OEt); 2.18 (s, 3H, Me); 2.74 (s, 6H, NMe_2); 3.93–4.14 (q, 2H, CH_2 of OEt); 6.88–7.86 (m, 7H, aryl).

Determination of crystal structure

Crystals of $HgBr_2 \cdot$ **1b** suitable for X-ray analysis were grown from a chloroform–benzene (60 : 40) solvent as pale yellow prisms.

Crystal data. $C_{17}H_{21}NOBr_2HgTe$, $M = 743.37$, monoclinic, $a = 15.417(2)$, $b = 14.693(3)$, $c = 19.252(4)$ Å, $\beta = 104.96(2)°$, $U = 4213.2$ Å^3, space group C_2/c, $Z = 8$, $D_c = 2.344$ g cm^{-3}, $F(000) = 2720$, μ(Mo-K_α) = 124.3 cm^{-1}.

Data collection and processing. Intensity data from a crystal of dimensions $0.3 \times 0.4 \times 0.3$ mm were collected on an Enraf–Nonius CAD4 diffractometer in the ω–2θ scan mode with scan width = $0.7 + 0.35 \tan\theta$ (scan speed 3.33° min^{-1} to a maximum of 90 s for weak reflections) using graphite-monochromated Mo-K_α radiation. 4462 reflections were measured (h, k, $\pm l$; $l \leqslant \theta \leqslant 26.0°$) yielding 4120 unique reflections after averaging and rejection of systematic absences. During the course of the data collection (89 h) a standard reflection monitored hourly showed a 3% decay for which a correction was applied. The unfavourable orientation of the crystal did not enable a set of ψ-reflections to be collected and hence, no empirical absorption correction could be applied.

Structure analysis and refinement. The structure was solved by the heavy atom method, the coordinates of both the mercury and tellurium atoms being derived. Subsequent Fourier maps determined the positions of all the remaining non-hydrogen atoms. Full-matrix anisotropic refinement of the metal and bromine atoms, isotropic refinement of the remaining atoms converged at $R = 0.102$. An absorption correction using "DIFABS",[11] followed by subsequent full-matrix anisotropic refinement of all non-hydrogen atoms converged at $R = 0.036$, $R_w = 0.042$. Hydrogen atoms positions were deter-

mined from geometric criteria and were included but not refined. The weighting scheme $\omega = 1/[\sigma(F^2)+(0.02F)^2+2.0]$ gave a satisfactory agreement analysis with the ESD of an observation of unit weight = 1.1. All calculations were performed on a DEC Microvax II computer using the SDP Plus V. 3.0 system of crystallographic programs.[12]

Table 1. Selected bond distances (Å)[a]

Hg—Te	2.728(1)	O—C(24)	1.406(12)
Hg—Br(1)	2.755(1)	O—C(27)	1.360(14)
Hg—Br(2)	2.710(1)	N—C(16)	1.411(13)
Hg—Br(3)	2.500(1)	N—C(17)	1.457(13)
C(11)—Te	2.097(9)	N—C(18)	1.468(15)
C(21)—Te	2.100(9)	C(27)—C(28)	1.55(2)
		C(13)—C(19)	1.52(2)

[a] Detailed bond lengths for the phenyl rings have been deposited as supplementary data. [C—C(phenyl) distances range from 1.348(14) to 1.398(14) Å.]

Important bond lengths and angles are given in Tables 1 and 2, respectively. Atomic coordinates, anisotropic thermal parameters, observed and calculated structure factors and a full list of bond lengths and angles have been deposited as supplementary data with the Editor.

RESULTS AND DISCUSSION

The telluroamines, **1a** and **1b**, synthesized by us recently by mercuration of 1-(NMe_2)-4-MeC_6H_4, followed by transmetallation with a suitable aryltellurium(IV) chloride in good yield (Scheme 1), have been shown to behave as bidentate ligands[8] with palladium(II) and platinum(II). The mercury(II) halides, HgX_2 (X = Cl or Br), react with **1a** and **1b** resulting in adducts of composition $HgX_2 \cdot$ **1a**/**1b**, which behave as non-electrolytes in acetonitrile at millimolar concentration levels. In the ^1H NMR spectra of the mercury complexes the NMe_2 protons appear as a singlet, marginally

Table 2. Selected bond angles (°)[a]

Te—Hg—Br(1)	115.26(2)	C(21)—Te—C(11)	98.50(3)
Te—Hg—Br(2)	110.98(2)	C(24)—O—C(27)	116.00(1)
Te—Hg—Br(3)	118.40(4)	C(16)—N—C(17)	114.00(1)
Br(1)—Hg—Br(2)	91.25(3)	C(16)—N—C(18)	113.10(9)
Br(1)—Hg—Br(3)	105.92(3)	C(17)—N—C(18)	109.80(9)
Br(2)—Hg—Br(3)	111.75(3)	N—C(16)—C(11)	117.00(9)
Hg—Br(1)—Hg	87.84(4)	N—C(16)—C(15)	125.00(1)
Hg—Br(2)—Hg	89.65(4)	O—C(24)—C(23)	127.00(1)
Te—C(11)—C(12)	126.30(7)	O—C(24)—C(25)	114.00(1)
Te—C(11)—C(16)	113.00(7)	O—C(27)—C(28)	106.00(1)
Te—C(21)—C(22)	119.20(7)	Hg—Te—C(21)	100.90(3)
Te—C(21)—C(26)	122.40(6)	Hg—Te—C(11)	91.60(3)

[a] Detailed bond angles for the phenyl rings have been deposited as supplementary data. [C—C—C phenyl angles range from 117.0(1) to 123.0(1)°.]

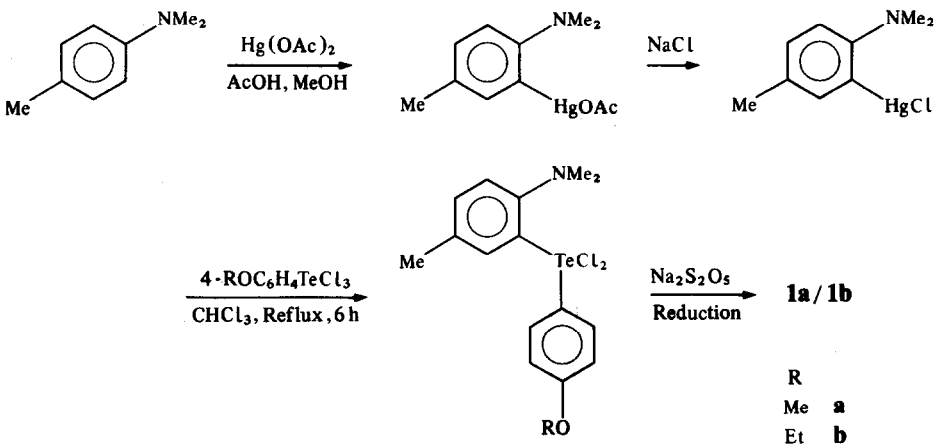

Scheme 1.

deshielded ($\sim$ 0.06 ppm) in comparison to similar protons of the ligands. This suggests that these ligands (**1a/1b**), in solution, probably do not coordinate with mercury through nitrogen, otherwise a doublet for these protons would have appeared. The small deshielding of these protons may arise due to the effect of the Te---Hg interaction on the ring current. The two ν(C—N) bands undergo a blue shift (10–15 cm^{-1}) on the formation of mercury complexes in comparison to their positions around 1280 cm^{-1} (Ar—N) and 1200–1250 cm^{-1} (NMe_2) in the spectra of ligands **1a** or **1b**. There probably exists a Te$\cdots$N interaction[6] in the ligands and its breakdown results in the observed blue shift. The $^{13}C\{^1H\}$ NMR spectra of $HgCl_2\cdot$**1a** and $HgCl_2\cdot$**1b** are consistent with the conclusion drawn above about the dormant NMe_2 group, as the signal of C_6 remains unaffected on complexation of **1a/1b** with mercury(II). The C_1 signal of **1a/1b**, appearing around 103.4 ppm, has been found to be deshielded by $\sim$ 2 ppm on the formation of mercury(II) complexes. Similarly, the C_5 signals appearing around 136.3 ppm for the ligands, undergo a downfield shift ($\sim$ 0.6–1.0 ppm) on complexation with mercury(II). The deshielding of the signals of carbon atoms linked to tellurium is not very high but favours the coordination of mercury(II) through tellurium. The small magnitude of the deshielding of these carbon signals is consistent with the fact that the mercury–tellurium bond strength, particularly in the complexes of the neutral Te-donors, is considered somewhat weak. Thus ligands **1a** and **1b** probably behave as a monodentate Te-donor in the mercury complexes. Mercury(II) generally adopts a tetrahedral geometry in its complexes, therefore the moiety $HgX_2\cdot$**1a/b** having a three-coordinate mercury(II) may be expected to dimerize and result in [**1a/b**$\cdot XHg(\mu\text{-}X)_2HgX\cdot$**1a/1b**], which has the usual four-coordinate mercury. Such a speculation has been substantiated by the far-IR spectrum of $HgBr_2\cdot$**1a** and the crystal structure of $HgBr_2\cdot$**1b**. The far-IR spectrum of $HgBr_2\cdot$**1a** contains bands at 119(s), 156(w) and 189(s) cm^{-1} which may be assigned to ν(Te—Hg), ν(Hg—Br_b) and ν(Hg—Br_t), respectively. The occurrence of a band in the region of the Hg—Br(bridging) vibration supports the possibility of dimerization. The bands appearing at 256, 272, 286 and 300 cm^{-1} in the far-IR spectrum of this complex may be attributed to various Te—Ph vibrations, whereas ν'(phenyl)[13] appears at 232 cm^{-1}.

The mercury complex ($HgCl_2\cdot$**1a/1b**) on refluxing for 35 h in toluene results in the mercurated aniline derivatives [eq. (1)] and a yellow-coloured polymeric material almost insoluble in all organic solvents. The ratio of mercury and tellurium suggests that it has composition **2** shown in eq. (1). The molecular weights of the mercury complexes have been found in chloroform to be almost half of the dimer. Therefore, either the reaction shown in eq. (1) or dissociation of one ligand molecule (or both) due to heating of the solution in the course of osmometric molecular weight measurements seem to be responsible for obtaining the lower values for molecular weights.

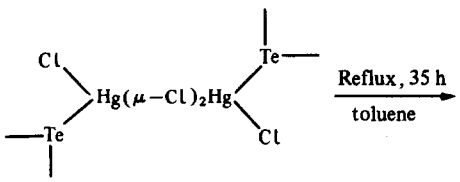

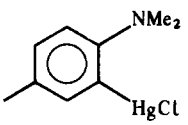

$+ \quad [ArTeHg(TeArAr')Cl]_n \qquad (1)$

(2)

Crystal structure of [**1b**$\cdot BrHg(\mu\text{-}Br)_2HgBr\cdot$**1b**]

The structure in the solid state consists of discrete dimeric molecules. The molecular structure and numbering scheme are shown in Fig. 1, while important bond lengths and bond angles are given in Tables 1 and 2. The geometries of the phenyl rings appear normal and their bond information has been deposited as supplementary material. The dimer has a two-fold rotation axis. Each mercury atom is situated in a roughly tetrahedral coordination environment [91.25(3)–118.40(4)°], bonding to two bridging bromine atoms at distances of 2.710(1) and 2.755(1) Å, one terminal bromine at 2.500(1) Å and one terminal tellurium at 2.728(1) Å. The Hg—Te bond length is consistent with the earlier report.[14] The asymmetry in the bromine bridges is of the order reported for the chloro-bridge in $(PPh_3)ClHg(\mu\text{-}Cl)_2HgClPPh_3$[15] ($\sim$ 0.04 Å). On adding the difference between the covalent radii of bromine and chlorine to the Hg—Cl(bridge) bond lengths,[15] the expected values for the present Hg—Br(bridge) bond lengths are calculated as 2.77 and 2.81 Å, which are of the order of the observed Hg—Br(bridge) bond lengths and consequently support our results. The distance between the nitrogen of the NMe_2 group and mercury is 3.56 Å, which rules out any interaction between them. Thus the potentially bidentate telluroamines ligate with mercury(II) only through tellurium behaving as a monodentate ligand. The distance between two mercury atoms is 3.82 Å, ruling out the possibility of any interaction between them.

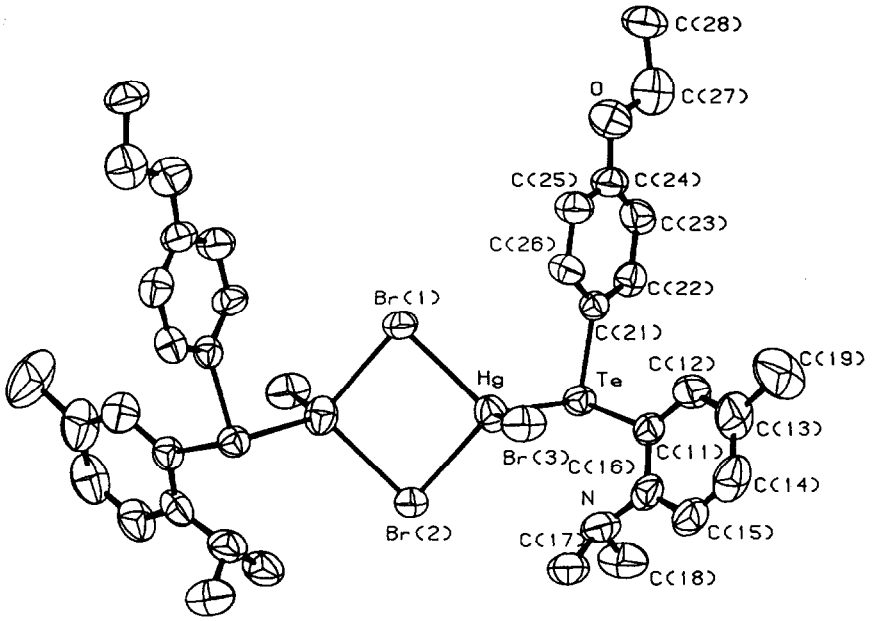

Fig. 1. Molecular structure and labelling scheme for [**1b** · $BrHg(\mu\text{-}Br)_2HgBr$ · **1b**] (ORTEP diagram).

Acknowledgement—The authors thank CSIR (India) for financial support.

REFERENCES

1. H. J. Gysling, *Coord. Chem. Rev.* 1982, **42**, 133.
2. H. J. Gysling, in *The Chemistry of Organic Selenium and Tellurium Compounds* (Edited by S. Patai and Z. Rappoport), Vol. 1, pp. 679–855. Wiley, New York (1986).
3. H. J. Gysling, in *The Proceedings of the Fourth International Conference on the Organic Chemistry of Selenium and Tellurium* (Edited by W. R. McWhinnie and F. J. Berry), p. 32. The University of Aston, Birmingham (1983).
4. F. J. Berry, in *The Comprehensive Coordination Chemistry* (Edited by G. Wilkinson, R. D. Gillard and J. A. McCleverty), Vol. 2, Ch. 17, p. 668. Pergamon Press, London (1987).
5. H. J. Gysling and H. R. Luss, *Organometallics* 1984, **3**, 596.
6. N. I. Al-Salim, T. A. Hamor and W. R. McWhinnie, *J. Chem. Soc., Chem. Commun.* 1986, 453.
7. T. Kemmit and W. Levason, *Organometallics* 1989, **8**, 1303.
8. A. K. Singh, V. Srivastava and B. L. Khandelwal, *Polyhedron* 1990, **9**, 495.
9. A. K. Singh, V. Srivastava and B. L. Khandelwal, *Polyhedron* 1990, **9**, 851.
10. F. H. Kruse, R. E. Sanftner and J. F. Suttle, *Anal. Chem.* 1953, **25**, 500; A. I. Vogel, *A Text Book of Quantitative Inorganic Analysis*, 3rd edn, p. 324. Longmans, London (1961).
11. N. Walker and D. Stuart, *Acta Cryst.* 1983, **A39**, 158.
12. B. A. Frenz, *Enraf Nonius Structure Determination Package SDP Users Guide*, Version 3.0; Enraf Nonius, Delft, The Netherlands (1985).
13. C. H. W. Jones and N. G. Dance, *J. Organomet. Chem.* 1978, **152**, 175.
14. F. W. B. Einstein, C. H. W. Jones and R. D. Sharma, *Inorg. Chem.* 1983, **22**, 3924.
15. N. A. Bell, M. Goldstein, T. Jones and I. W. Nowell, *J. Chem. Soc., Chem. Commun.* 1976, 1039; *Inorg. Chim. Acta* 1981, **48**, 185.

Polyhedron Vol. 9, No. 17, pp. 2047–2051, 1990
Printed in Great Britain

0277–5387/90 $3.00+.00
© 1990 Pergamon Press plc

KINETICS AND MECHANISM OF LIGAND EXCHANGE REACTIONS OF THE METHYLBIS(DIMETHYLGLYOXIMATO)RHODIUM(III) COMPLEX IN NON-COORDINATING SOLVENT

R. DREOS GARLATTI* and G. TAUZHER

Dipartimento di Scienze Chimiche, Università degli Studi di Trieste, P. le Europa 1, 34127 Trieste, Italy

(*Received* 17 *January* 1990; *accepted* 22 *March* 1990)

Abstract—Axial ligand exchange reactions of the methylbis(dimethylglyoximato) rhodium(III) complex were studied in dichloromethane. When exchanging ligands have similar dissociation rate constants, reactions do not go to completion in the presence of an excess of added leaving ligand. Kinetic results for the examined reactions are fully consistent with a *D* mechanism, where the five-coordinate intermediate reacts at approximately the same rate with all the incoming ligands.

We have previously studied both the anation and the hydrolysis reactions of alkylbis(dimethylglyoximato)rhodium(III) complexes (organorhodoximes) in aqueous solution.[1–3]

A first indication that a dissociative activation process is operative for these reactions comes from the relative independence of the anation rate constants of the nature of the entering ligand.[1] This suggestion is further supported by the parallel lability trend in the anation reactions of organorhodoximes and organocobaloximes,[3] the latter being known to undergo substitution through a dissociative mechanism.[4] As no kinetic evidence has been found for a five-coordinate intermediate, the mechanism was classified as I_d.[3]

On the other hand, it has been recognized for some time that establishing the stoichiometric mechanism of substitution reactions of octahedral complexes in aqueous solution, or more generally in coordinating solvents, is very difficult owing to the competition of the coordinating solvent itself.[5,6] In non-coordinating solvents this difficulty is removed, but some ambiguities still persist. If reactions proceed to completion both a *D* mechanism and an outer-sphere complexation mechanism, including pre-association with both entering and leaving ligand, lead to equivalent expressions of k_{obs}.[7–9]

In spite of this ambiguity, Marzilli *et al.* were able to prove that the axial substitution reactions of organocobaloximes in CH_2Cl_2 occur through a *D* mechanism[4,9]

$$\text{X—M—L} \underset{k_{-1}}{\overset{k_1}{\rightleftharpoons}} \text{X—M} + \text{L} \qquad \text{Step 1}$$

$$\text{X—M} + \text{L}' \underset{k_{-2}}{\overset{k_2}{\rightleftharpoons}} \text{X—M—L}' \qquad \text{Step 2}$$

Scheme 1.

where M represents the central metal ion with the equatorial ligands and X is the non-labile axial group.

The steady-state treatment for X—M leads to the relationship

$$k_{obs} = \frac{k_1 + k_{-2}k_{-1}[L]/k_2[L']}{1 + k_{-1}[L]/k_2[L']}, \qquad (1)$$

which reduces to

$$k_{obs} = \frac{k_1}{1 + k_{-1}[L]/k_2[L']} \qquad (2)$$

if the reaction proceeds to completion, that is if the reverse reaction of Step 2 is neglected.

In the present work we report a kinetic study

* Author to whom correspondence should be addressed.

of the substitution reactions of the methyl-bis(dimethylglyoximato)rhodium(III) complex in dichloromethane and show that a *D* mechanism is fully consistent with the kinetic results.

EXPERIMENTAL

Preparation of complexes

The $CH_3Rh(DH)_2L$ complexes, where L = pyridine (py), tetramethylthiourea (tmtu), triphenylphosphine (PPh_3), N-methylimidazole (NCH_3im), were prepared from $CH_3Rh(DH)(DH_2)I$, whose synthesis has been previously described.[3] 0.2 g of this complex were dissolved in the least volume of methanol and a stoichiometric amount of $AgNO_3$ was added. The resulting precipitate of AgI was filtered off and a slight excess of the appropriate ligand or of its methanolic solution, if solid, was added to the clear solution. The volume was reduced in a rotary evaporator until precipitation began. Crystals of the desired products were obtained by allowing the solution to stand. $CH_3Rh(DH)_2py$: Found: C, 38.1; H, 5.0; N, 16.2. Calc. for $C_{14}H_{22}N_5O_4Rh$: C, 39.3; H, 5.2; N, 16.4%. $CH_3Rh(DH)_2tmtu$: Found: C, 36.5; H, 6.5; N, 18.2. Calc. for $C_{14}H_{19}N_5O_4RhS$: C, 34.9; H, 6.1; N, 17.5%. $CH_3Rh(DH)_2PPh_3$: Found: C, 50.3; H, 4.6; N, 9.1. Calc. for $C_{27}H_{32}N_4O_4PRh$: C, 53.1; H, 5.3; N, 9.2%. $CH_3Rh(DH)_2NCH_3im$: Found: C, 36.1; H, 5.4; N, 19.6. Calc. for $C_{15}H_{23}N_6O_4Rh$: C, 36.2; H, 5.6; N, 19.5%.

If ligand L was added directly to a methanolic solution of $CH_3Rh(DH)(DH_2)I$, without previous treatment with $AgNO_3$, compounds were obtained whose analytical composition corresponds to $CH_3Rh(DH)(DH_2)L^+I^-$. $CH_3Rh(DH)(DH_2)py^+I^-$: Found: C, 29.0; H, 4.2; N, 12.4. Calc. for $C_{14}H_{23}N_5O_4IRh$: C, 30.3; H, 4.2; N, 12.6%. $CH_3Rh(DH)(DH_2)tmtu^+I^-$: Found: C, 26.0; H, 4.6; N, 13.2. Calc. for $C_{14}H_{20}N_6O_4IRhS$: C, 27.6; H, 5.0; N, 13.8%. $CH_3Rh(DH)(DH_2)PPh_3^+I^-$: Found: C, 41.8; H, 4.4; N, 7.3. Calc. for $C_{27}H_{33}N_4O_4IPRh$: C, 43.9; H, 4.5; N, 7.6%.

As the yields of the above reported syntheses were rather poor and the products very soluble, no recrystallization has been attempted. The discrepancies between the calculated and found elemental analyses are likely to be due to the presence of absorbed impurities.

Reagents

Triphenylphosphine was recrystallized from diethyl ether. All other materials were reagent grade and used without further purification.

Kinetic measurements

Ligand substitution reactions were followed spectrophotometrically in the range 350–450 nm using a Perkin–Elmer Lambda 5 spectrophotometer for the slower reactions and a Hi Tech SF3 series stopped-flow apparatus for the faster reactions.

Kinetic runs were carried out under a pseudo-first-order excess of entering ligand, with L′ concentrations ranging from 4×10^{-3} to 5×10^{-1} M. Generally, $2\text{–}4\times10^{-4}$ M solutions of complex were used.

The same concentration range was used in competition experiments, where a pseudo-first-order excess of both incoming and leaving ligand was present. The highest accessible [L]/[L′] ratio was determined by the requirement that reactions remain within a conveniently observable range of velocities and that spectral variation, which decreases at high [L]/[L′] for equilibrium reactions, does not become too small.

Data analysis

The computer program used for the non-linear least-squares analysis was the Statistical Package for Social Sciences, Version 9.0 (Vogelback Computing Center, Northwestern University, U.S.A.).

RESULTS

The axial ligand exchange reactions

$$CH_3Rh(DH)_2L+L' \rightleftharpoons CH_3Rh(DH)_2L'+L \quad (3)$$

were studied at 25°C, in a non-coordinating solvent (CH_2Cl_2) under a pseudo-first-order excess of entering ligand (L′). The observed rate constants were obtained from the linear plots of $\log(A_t-A_\infty)$ vs time.

In a first series of experiments, carried out without added leaving ligand, the k_{obs} values were independent of the concentration of the incoming ligand

$$k_{obs} = a. \quad (4)$$

The values of a so obtained are reported in Table 1. It can be noted that the k_{obs} values for the dissociation of py in reactions with PPh_3 and NCH_3im are very similar.

In a second series of experiments, performed in the presence of an excess of both entering and leaving ligand, at various [L]/[L′] ratios, different results were obtained depending on the chemical identity of the exchanging ligands.

Table 1. Kinetic parameters for exchange reactions of $CH_3Rh(DH)_2L$ with L′ in CH_2Cl_2 at 25°C

L	L′	$a = k_1$ (s^{-1})	$b = k_{-1}k_{-2}/k_2$ (s^{-1})	$c = k_{-1}/k_2$	$b/c = k_{-2}$ (s^{-1})
tmtu	PPh_3	$(4.6\pm0.2)\ 10^{-1}$ [a] $4.7\ 10^{-1}$ [b]		0.9 ± 0.1	
py	PPh_3	$(3.3\pm0.1)\ 10^{-2}$ [a] $2.9\ 10^{-2}$ [b]		1.1 ± 0.1	
py	NCH_3im	$(3.10\pm0.05)\ 10^{-2}$ [a] $3.07\ 10^{-2}$ [b]		0.8 ± 0.1	
NCH_3im	PPh_3	$(3.07\pm0.05)\ 10^{-3}$ [a] $3.07\ 10^{-3}$ [b]	$(1.5\pm0.4)\ 10^{-3}$	1.8 ± 0.3	$(8\pm3)\ 10^{-4}$ [c]
PPh_3	NCH_3im	$(6.34\pm0.05)\ 10^{-4}$ [a] $6.7\ 10^{-4}$ [b]	$(2.1\pm0.6)\ 10^{-3}$	0.6 ± 0.3	$(3.5\pm2.0)\ 10^{-3}$ [c]

[a] Extrapolated from plot of k_{obs} vs [L]/[L′].

[b] Measured in experiments without added leaving ligand. The values reported are the mean of at least three independent determinations performed at various concentrations of entering ligand.

[c] The relatively high uncertainty of this value arises from propagation of errors of b and c, which are inherently large.

(i) For L = py or tmtu and L′ = Ph_3P, and for L = py and L′ = NCH_3im an inverse dependence of k_{obs} on [L]/[L′] is observed (Fig. 1), which is consistent with the expression

$$k_{obs} = \frac{a}{1+c[L]/[L']}. \qquad (5)$$

A plot of $1/k_{obs}$ vs [L]/[L′] is linear and allows calculation of a and c. The values reported in Table 1 have been calculated by a non-linear least-squares analysis on the basis of these preliminary estimates.

(ii) For L = NCH_3im and L′ = PPh_3, k_{obs} still decreases with [L]/[L′]. The kinetic data are consistent with a rate law for which k_{obs} can be expressed as

$$k_{obs} = \frac{a+b[L]/[L']}{1+c[L]/[L']}. \qquad (6)$$

A linear relationship was found between $1/(a-k_{obs})$ and [L′]/[L] from which a, b and c can be calculated. These values were used as preliminary estimates in the calculation of a, b and c performed by a non-linear least-squares analysis.

(iii) For L = PPh_3 and L′ = NCH_3im, k_{obs} increases almost linearly over the range of examined [L]/[L′], but some deviations are evident at the highest [L]/[L′] ratios (Fig. 2). The kinetic data are still in accord with eq. (6). Preliminary estimates of a, b and c were obtained from the linear plots of $1/(k_{obs}-a)$ vs [L′]/[L].

Values of a, b and c are summarized in Table 1.

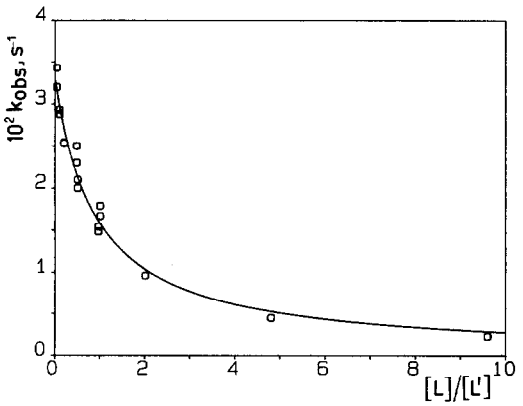

Fig. 1. Dependence of k_{obs} on [L]/[L′] for the reaction between $CH_3Rh(DH)_2py$ and PPh_3. The solid line is calculated from eq. (1) and the parameters contained in Table 1.

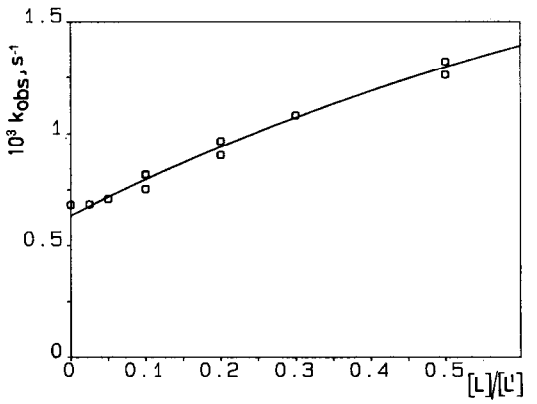

Fig. 2. Dependence of k_{obs} on [L]/[L′] for the reaction between $CH_3Rh(DH)_2PPh_3$ and NCH_3im. The solid line is calculated from eq. (4) and the parameters contained in Table 1.

DISCUSSION

In the present case, Scheme 1 and the related expression of k_{obs} [eq. (1)] are consistent with all the above kinetic results, with $a = k_1$, $b = k_{-2}k_{-1}/k_2$ and $c = k_{-1}/k_2$.

When the experiments are performed without addition of leaving ligand, [L]/[L'] is about zero, so that kinetics follow a pseudo-first-order rate law until near completion, when the release of L by the complex could cause deviations. In these conditions k_{obs} reduces to k_1, according to the experimentally found expression (4).

When the reactions are carried out in the presence of an excess of both entering and leaving ligand, the reverse reaction of Step 2 may become relevant. It can be predicted that the term $k_{-2}k_{-1}$[L]/k_2[L'] in the numerator of eq. (1) will not be negligible at high [L]/[L'] values or, even at relatively low [L]/[L'], when the exchanging ligands are of comparable strength ($k_{-1}k_{-2}/k_1k_2$ is not very different from 1). For the ligands reported in Table 1 k_{-1}/k_2 is never far from 1, which implies that the five-coordinate intermediate reacts at approximately the same rate with all the examined incoming ligands. As the reactions were performed at relatively low [L]/[L'] ratios the reverse reaction will not be negligible only when k_1 and k_{-2}, that is the dissociation rates of L and L' from the complex have comparable values. It appears from the data of Table 1 that NCH_3im dissociates from the complex only about five times faster than PPh_3, so that the reverse reaction should become relevant even at low [L]/[L']. Actually, for the exchange reaction between L = NCH_3im and L' = PPh_3 the experimental expression of k_{obs} [eq. (6)] agrees completely with the expression of k_{obs} calculated by taking into account the reverse reaction of Step 2 [eq. (1)].

It should be noted that, if the reaction does not proceed to completion, addition of an excess of leaving ligand may cause either a deceleration or an acceleration in the substitution rate. More quantitatively, eq. (1) indicates that if k_{-2}/k_1 is less than 1, as in the exchange between L = NCH_3im and L' = PPh_3, a rate retardation will be observed when an excess of leaving ligand is present in solution. When k_{-2}/k_1 is greater than 1 an acceleration will be observed if an excess of leaving ligand is present in solution. This actually occurs in the reaction between $CH_3Rh(DH)_2PPh_3$ and NCH_3im. The almost linear dependence of k_{obs} on [L]/[L'] (Fig. 2) is in accord with the fact that at a sufficiently low [L]/[L'] ratio the term k_{-1}[L]/k_2[L'] in the denominator of eq. (1) becomes negligible.

If the reverse reaction of Step 2 can be neglected, as occurs if $k_1 \gg k_{-2}$, k_{obs} reduces to eq. (2), which is in complete agreement with the empirical rate expression found for L = py or tmtu and L' = PPh_3, and for L = py and L' = NCH_3im [eq. (5)]. For these ligands the dissociation rate constant of L is at least ten times that of L' (Table 1).

The consistency of the proposed scheme can be verified in several ways by the agreement between the values of kinetic constants relative to the same process calculated from data obtained in different exchange reactions.

First of all, the dissociation rate constants experimentally measured in the reactions carried out without added leaving ligand agree very well with those extrapolated from the plots of k_{obs} vs [L]/[L'] (Table 1).

Furthermore, when the reactions do not go to completion, the dissociation rate constant of L' can be calculated as $k_{-2} = b/c$ and compared with that directly measured. For the examined complexes, the dissociation rate constant of PPh_3 may be calculated as k_{-2} from data relative to the reaction between $CH_3Rh(DH)_2NCH_3im$ and PPh_3 and that of NCH_3im from data relative to the reaction between $CH_3Rh(DH)_2PPh_3$ and NCH_3im. The calculated values are in reasonable accord with the k_1 values measured in the dissociation reactions of $CH_3Rh(DH)_2PPh_3$ and $CH_3Rh(DH)_2NCH_3im$, respectively (Table 1).

Internal checks are also possible for the k_{-1}/k_2 values, as the value for the reaction between $CH_3Rh(DH)_2L$ and L' should be the inverse of that for the reaction between $CH_3Rh(DH)_2L'$ and L. This relationship is satisfactorily verified when the exchanging ligands are NCH_3im and PPh_3.

Finally, a sufficient agreement, in the limits of experimental errors, is obtained between the k_{-1}/k_2 value directly obtained from the reaction between $CH_3Rh(DH)_2py$ and NCH_3im (1.8 ± 0.3) and that calculated as the ratio of the k_{-1}/k_2 values obtained for the exchange reactions between L = py and L' = PPh_3 and between L = NCH_3im and L' = PPh_3 (1.4 ± 0.2).

On the basis of the above considerations it seems quite reasonable to assume that ligand exchange reactions of $CH_3Rh(DH)_2L$ in non-coordinating solvent occur via a *D* mechanism. The independence of k_1 of both concentration and nature of the entering ligand, indicating that dissociation of L is the rate-determining step, and the k_{-1}/k_2 ratios being very close to 1, suggesting the formation of a five-coordinate intermediate, are both in accordance with a *D* process.

An interchange mechanism including pre-association with both entering and leaving ligand has been ruled out because the related k_{obs} expression[7-9] becomes independent of entering

ligand only when virtually all the substrate or the product are present in the associated form, and no evidence has been found for such extensive aggregation.

Previous extensive studies on the analogous $RCo(DH)_2L$ complexes led to the conclusion that the ligand exchange process in non-coordinating solvents is dissociative.[4,9] Furthermore, for these complexes it was evidenced that the dissociation rate increases with decreasing basicity and with increasing steric bulk of the leaving ligand.[4] The relatively small number of data in Table 1 does not allow us to draw similar conclusions for $CH_3Rh(DH)_2L$; however, the low dissociation rate of PPh_3 appears somewhat surprising, as in the analogous cobalt complexes PPh_3 dissociates about five times faster than py,[4] due to its lower basicity and greater steric bulk. The remarkable inertness of the phosphorus ligand in the rhodium complex could suggest that the electronic and steric properties of L may affect the dissociation rate in cobalt and rhodium complexes in different ways. Further studies are in progress to elucidate this point.

REFERENCES

1. R. Dreos Garlatti, G. Tauzher, M. Blaschich and G. Costa, *Inorg. Chim. Acta* 1984, **86**, L63.
2. R. Dreos Garlatti, G. Tauzher, M. Blaschich and G. Costa, *Inorg. Chim. Acta* 1985, **105**, 129.
3. R. Dreos Garlatti, G. Tauzher and G. Costa, *Inorg. Chim. Acta* 1986, **121**, 27.
4. N. Bresciani Pahor, M. Forcolin, L. G. Marzilli, L. Randaccio, M. F. Summers and P. J. Toscano, *Coord. Chem. Rev.* 1985, **63**, 1 and refs therein.
5. C. H. Langford and H. B. Gray, *Ligand Substitution Reactions*. Benjamin, New York (1965).
6. J. H. Espenson and R. Russell, *Inorg. Chem.* 1974, **13**, 7.
7. F. R. Jensen and R. C. Kiskis, *J. Am. Chem. Soc.* 1975, **97**, 5820.
8. J. A. Ewen and D. J. Darensbourg, *J. Am. Chem. Soc.* 1976, **98**, 4317.
9. R. C. Stewart and L. G. Marzilli, *J. Am. Chem. Soc.* 1978, **100**, 818.

Polyhedron Vol. 9, No. 17, pp. 2053–2059, 1990
Printed in Great Britain

0277–5387/90 $3.00+.00
© 1990 Pergamon Press plc

THE SYNTHESIS AND SOLID-STATE PROPERTIES OF THE SALTS OF $[M(S_2C_2(CN)_2)_2]^{2-}$ (WHERE M = Ni, Pd OR Pt) WITH SMALL GROUP I AND GROUP II CATIONS, INCLUDING THE CRYSTAL STRUCTURE OF $Rb_2[Ni(S_2C_2(CN)_2)_2]\cdot H_2O$

P. I. CLEMENSON and A. E. UNDERHILL*

Department of Chemistry and Institute of Molecular and Biomolecular Electronics, University College of North Wales, Bangor, Gwynedd LL57 2UW, U.K.

and

A. KOBAYASHI

Department of Chemistry, Faculty of Science, The University of Tokyo, Hongo, Tokyo 113, Japan

and

H. KOBAYASHI

Department of Chemistry, Faculty of Science, Toho University, Funabashi, Chiba 274, Japan

(*Received* 8 *November* 1989; *accepted* 26 *March* 1990)

Abstract—The synthesis and characterization of the salts of $[M(S_2C_2(CN)_2)_2]^{2-}$ (where M = Ni, Pd and Pt) with small counter cations is described. The solid-state electronic spectra of the salts indicate some degree of interaction which is cation dependent. The crystal structure of $Rb_2[Ni(S_2C_2(CN)_2)_2]\cdot H_2O$ shows the anions to be well separated with no S···S contacts of less than 4 Å.

Recent studies on the structures and properties of metal dithiolene monoanions have revealed important differences between compounds containing bulky cations such as Et_4N^+ and those containing the relatively small Group 1 cations.[1] In the latter compounds extensive cooperative phenomena may be observed but in the former compounds the presence of the bulky counter ions prevents long range interactions between the anions and only intradimer interactions are observed. Previous structural studies on $[M(S_2C_2(CN)_2)_2]^{2-}$ (where M = Ni, Pd or Pt) dianion salts have been restricted to the salts of the bulky cations $[N(CH_3)_4]^+$ and $[N(C_4H_9)_4]^+$.[2,3] We now report an extensive series of studies of the dianion salts of $[M(S_2C_2(CN)_2)_2]$ (where M = Ni, Pd or Pt) containing the relatively small cations of Group I and Group II.

EXPERIMENTAL

Preparation of the bis(1,2-dicyanoethylene-1,2-dithiolato)nickelate(2−) dianion salts

Preparation of $(NH_4)_2[Ni(S_2C_2(CN)_2)_2]\cdot 2H_2O$. An aqueous solution of $NiCl_2\cdot 6H_2O$ (2.40 g, 20 cm^3) was added to an aqueous solution of $Na_2S_2C_2(CN)_2$ (3.72 g, 20 cm^3). The solution was stirred for 5 min and filtered. To the filtrate was added NH_4Cl (4.0 g) to yield, on agitation, a red crystalline product (4.14 g, 100%).[4] The product was filtered off, washed with distilled water (1–2 cm^3) and dried *in vacuo* at 30°C. ^1H NMR (acetone

* Author to whom correspondence should be addressed.

d_6): 8.02 (N—*H*, very broad) also a shoulder ≈ 5 (O—*H*). Found: C, 23.2; H, 3.2; N, 20.0. Calc. for $C_8H_{12}N_6NiO_2S_4$: C, 23.4; H, 2.9; N, 20.4%.

Preparation of $Rb_2[Ni(S_2C_2(CN)_2)_2]\cdot 1.5H_2O$. An aqueous solution of $(NH_4)_2[Ni(S_2C_2(CN)_2)_2]\cdot 2H_2O$ (1.0 g, 15 cm^3) was filtered and to the filtrate was added a saturated solution of RbCl (0.96 g, 5 cm^3). The red precipitate which formed immediately was filtered off, washed with distilled water (1 cm^3) and dried *in vacuo* at 42°C. The product was collected and recrystallized from hot water to yield large red single crystals of $Rb_2[Ni(S_2C_2(CN)_2)_2]\cdot 1.5H_2O$, one of which was selected for a crystal structure determination. Found: C, 17.8; H, 0.49; N, 10.7. Calc. for $C_8H_3N_4NiO_{1.5}Rb_2S_4$: C, 17.9; H, 0.56; N, 10.4%.

Preparation of $Mg[Ni(S_2C_2(CN)_2)_2]\cdot 6H_2O$. A solution of $[N(C_2H_5)_4]_2[Ni(S_2C_2(CN)_2)_2]$ (1.0 g, 250 cm^3) in 70% acetone–water was eluted through a cationic exchange column Dowex 50W-X8 in the acid form. The elutant was passed into a suspension of MgO (0.11 g) under a nitrogen atmosphere. The mixture was filtered and the filtrate rotary evaporated to dryness. The product was dried *in vacuo* overnight at 52°C to give the red product $Mg(Ni(S_2C_2(CN)_2)_2]\cdot 6H_2O$. Found: C, 20.5; H, 2.1; N, 10.6. Calc. for $C_8H_{12}MgN_4NiO_6S_4$: C, 20.4; H, 2.6; N, 11.9%.

Preparation of $K_2[Ni(S_2C_2(CN)_2)_2]\cdot 2.5H_2O$. $K_2[Ni(S_2C_2(CN)_2)_2]\cdot 2.5H_2O$ was prepared using KCl in a similar manner to that used to prepare $Rb_2[Ni(S_2C_2(CN)_2)_2]\cdot 1.5H_2O$. Found: C, 21.0; H, 1.1; N, 11.9. Calc. for $C_8H_5K_2N_4NiO_{2.5}S_4$: C, 20.8; H, 1.2; N, 12.1%.

Preparation of $Cs_2[Ni(S_2C_2(CN)_2)_2]\cdot 2H_2O$. $Cs_2[Ni(S_2C_2(CN)_2)_2]\cdot 2H_2O$ was prepared using CsCl in a similar manner to that used to prepare $Rb_2[Ni(S_2C_2(CN)_2)_2]\cdot 1.5H_2O$. Found: C, 14.7; H, 0.30; N, 8.6. Calc. for $C_8H_4Cs_2N_4NiO_2S_4$: C, 15.0; H, 0.63; N, 8.7%.

Preparation of the bis(1,2-*dicyanoethylene*-1,2-*dithiolato*)*palladate*(2−) *dianion salts*

Preparation of $(NH_4)_2[Pd(S_2C_2(CN)_2)_2]\cdot 0.5H_2O$. An aqueous suspension of $PdCl_2$ (0.59 g, 50 cm^3) in deaerated water was stirred under nitrogen for 72 h. To this suspension was added $Na_2S_2C_2(CN)_2$ (1.86 g) under nitrogen and the solution was stirred for a further period of 24 h. The solution was filtered and a deaerated aqueous solution of NH_4Cl (2.0 g, 20 cm^3) was added to the filtrate. After stirring for 5–10 min the product was filtered off and washed with chilled water (5 cm^3). The product was obtained in high yields and purity after drying *in vacuo* overnight at 42°C. The yields can be increased to near 100% by stirring for longer periods prior to the addition of $Na_2S_2C_2(CN)_2$. ^1H NMR (acetone d_6): s, 7.31 and 3.76, N—*H* and O—*H*, respectively. Found: C, 23.1; H, 2.5; N, 20.1. Calc. for $C_8H_9N_6O_{0.5}PdS_4$: C, 22.2; H, 2.1; N, 19.5%.

Preparation of $Li_2[Pd(S_2C_2(CN)_2)_2]\cdot 3H_2O$. A deaerated aqueous solution of $(NH_4)_2[Pd(S_2C_2(CN)_2)_2]\cdot 0.5H_2O$ (0.70 g, 100 cm^3) was passed down a column of Dowex 50W-X8 cationic exchange resin (in acid form) under nitrogen. The acid, $H_2[Pd(S_2C_2(CN)_2)_2]$, was neutralized with an aqueous solution of $LiOH\cdot H_2O$ (0.14 g, 5 cm^3), filtered and evaporated to dryness, to yield a dark green product after drying *in vacuo* for 24 h. Found: C, 21.0; H, 1.4; N, 11.9. Calc. for $C_8H_6Li_2N_4O_3PdS_4$: C, 21.0; H, 1.3; N, 12.3%.

Preparation of $Na_2[Pd(S_2C_2(CN)_2)_2]\cdot 2H_2O$. $Na_2[Pd(S_2C_2(CN)_2)_2]\cdot 2H_2O$ was prepared according to the following procedure of Haller.[5] $PdCl_2$ (1.0 g) was added to an aqueous solution of $Na_2S_2C_2(CN)_2$ (2.15 g, 100 cm^3) in deaerated water under nitrogen. The product was obtained in high purity by rotary evaporation at 35°C and drying *in vacuo* at 46°C for 48 h. Found: C, 20.6; H, 0.70; N, 12.2. Calc. for $C_8H_4N_4Na_2O_2PdS_4$: C, 20.5; H, 0.86; N, 11.9%.

Preparation of $K_2[Pd(S_2C_2(CN)_2)_2]\cdot H_2O$. KCl (1.0 g) was added to a filtered aqueous solution of $(NH_4)_2[Pd(S_2C_2(CN)_2)_2]\cdot 0.5H_2O$ (1.0 g, 45 cm^3) producing a light green precipitate of $K_2[Pd(S_2C_2(CN)_2)_2]\cdot H_2O$. The product was collected by filtration and washed with chilled water (5 cm^3) and dried *in vacuo* for 24 h. Found: C, 20.0; H, 0.64; N, 12.3. Calc. for $C_8H_2K_2N_4O_2PdS_4$: C, 19.9; H, 0.42; N, 11.6%.

Preparation of $Rb_2[Pd(S_2C_2(CN)_2)_2]\cdot 2H_2O$. $Rb_2[Pd(S_2C_2(CN)_2)_2]\cdot 2H_2O$ was prepared using RbCl in a similar manner to that used to prepare $K_2[Pd(S_2C_2(CN)_2)_2]\cdot H_2O$. Found: C, 15.9; H, 0.74; N, 8.7. Calc. for $C_8H_4N_4O_2PdRb_2S_4$: C, 16.2; H, 0.68; N, 9.4%.

Preparation of $Cs_2[Pd(S_2C_2(CN)_2)_2]\cdot H_2O$. $Cs_2[Pd(S_2C_2(CN)_2)_2]\cdot H_2O$ was prepared using CsCl in a similar manner to that used to prepare $K_2[Pd(S_2C_2(CN)_2)_2]\cdot H_2O$. Found: C, 14.6; H, 0.20; N, 8.4. Calc. for $C_8H_2Cs_2N_4OPdS_4$: C, 14.3; H, 0.30; N, 8.3%.

Preparation of the bis(1,2-*dicyanoethylene*-1,2-*dithiolato*)*palladate*(2−) *dianion salts with the alkaline earth counter cations* $M = Ca^{2+}$, Sr^{2+} *and* Ba^{2+}

The Ca^{2+}, Sr^{2+} and Ba^{2+} dianion salts were prepared in a similar manner to that used to prepare

$Li_2[Pd(S_2C_2(CN)_2)_2]\cdot 3H_2O$ by neutralizing the acid $H_2[Pd(S_2C_2(CN)_2)_2]$ with either the appropriate metal hydroxide or carbonate.

M = Ca^{2+}; Found: C, 21.7; H, 1.2; N, 12.0. Calc. for $C_8H_2CaN_4OPdS_4$: C, 21.6; H, 0.45; N, 12.6%.

M = Sr^{2+}; Found: C, 18.4; H, 1.7; N, 10.8. Calc. for $C_8H_6N_4O_3PdS_4Sr$: C, 18.4; H, 1.1; N, 10.6%.

M = Ba^{2+}; Found: C, 18.1; H, 0.37; N, 10.6. Calc. for $C_8H_2BaN_4OPdS_4$: C, 17.7; H, 0.37; N, 10.3%.

Preparation of the bis(1,2-dicyanoethylene-1,2-dithiolato)platinate(2−) dianion salts

Preparation of $(NH_4)_2[Pt(S_2C_2(CN)_2)_2]\cdot 2H_2O$. A filtered, aqueous solution of $K_2[PtCl_4]$ (4.15 g, 40 cm^3) was added dropwise to an aqueous solution of $Na_2S_2C_2(CN)_2$ (3.72 g, 20 cm^3) and the solution stirred for 5 min and then filtered. To the filtrate was added NH_4Cl (4.0 g) and the $(NH_4)_2[Pt(S_2C_2(CN)_2)_2]\cdot 2H_2O$ precipitated as dark red crystals which were filtered off and washed with a little chilled water (3 cm^3). The product was dried *in vacuo* at 40°C (yield 85%). ^1H NMR (acetone d_6): 7.46 (N—*H*, very broad) and 4.36 (O—*H*, very broad). Found: C, 17.4; H, 2.1; N, 14.4. Calc. for $C_8H_{12}N_6O_2PtS_4$: C, 17.5; H, 2.2; N, 15.3%.

Preparation of $K_2[Pt(S_2C_2(CN)_2)_2]\cdot 2H_2O$ *and* $Rb_2[Pt(S_2C_2(CN)_2)_2]\cdot H_2O$. $K_2[Pt(S_2C_2(CN)_2)_2]\cdot 2H_2O$ and $Rb_2[Pt(S_2C_2(CN)_2)_2]\cdot H_2O$ were prepared using KCl or RbCl, respectively, in a similar manner to that used to prepare $Rb_2[Ni(S_2C_2(CN)_2)_2]\cdot 1.5H_2O$ as described earlier.

M = K^+; Found: C; 16.1; H, 0.90; N, 9.3. Calc. for $C_8H_4K_2N_4O_2PtS_4$: C, 16.3; H, 0.69; N, 9.2%.

M = Rb^+; Found: C, 14.6; H, 0.80; N, 8.1. Calc. for $C_8H_2N_4OPtRb_2S_4$: C, 14.5; H, 0.30; N, 8.4%.

Chemical analyses of the dianion salts suggest that these compounds have a variable degree of water of crystallization. Microanalysis was performed by Mr E. Lewis, using a Carlo Erba Strumentazione elemental analyser, Model 1106.

Reflectance spectra were recorded on powdered samples using a Beckman DK-2A ratio recording spectrophotometer fitted with a standard reflectance attachment. The reference material in all cases was Al_2O_3 and where necessary samples were diluted with Al_2O_3.

The solution spectra of the dianions were recorded on a Beckman DK-2A ratio recording spectrometer.

Electrical conduction measurements of single crystals of the ammonium salts were carried out as previously described.[6] Aquadag (colloidal graphite in water) was used as the contact material between the crystal and the 0.001 in. diameter gold wires. Unfortunately the small crystal size only permitted two probe conduction measurements to be made.

X-ray data collection and analysis of the structure of $Rb_2[Ni(S_2C_2(CN)_2)_2]\cdot H_2O$

A crystal for X-ray structure determination was cut from a large red crystal, $0.15\times 0.2\times 0.25$ mm.

Crystal data

$Rb_2[Ni(S_2C_2(CN)_2)_2]\cdot H_2O$, $M = 528.016$, orthorhombic, space group *Pbcn*, $a = 13.513(2)$, $b = 6.810(1)$, $c = 16.651(2)$ Å, $Z = 4$, $V = 1541.3$ Å^3, density: calc. 2.275 g cm^{-3}, found 2.270 g cm^{-3}.

All the X-ray diffraction intensities were measured on a Rigaku automatic four circle diffractometer, ω–2θ scan mode, using a graphite-monochromator, Mo-K_α radiation.*

RESULTS AND DISCUSSION

(1) *Crystal structure of* $Rb_2[Ni(S_2C_2(CN)_2)_2]\cdot H_2O$

The $[Ni(S_2C_2(CN)_2)_2]^{2-}$ anion is almost planar with average bond lengths of Ni—S 2.175 Å, S—C 1.738 Å and C—C 1.380 Å. The bond lengths and angles are in good agreement with those found for the dianion in the $[N(C_4H_9)_4]^+$ salt.[3] Selected intramolecular bond lengths and angles for $Rb_2[Ni(S_2C_2(CN)_2)_2]\cdot H_2O$ are given in Table 1.

The projection of the crystal structure down the *b*-axis is given in Fig. 1. It can be seen that the anions are arranged in columns along the *b*-direction of the unit cell. The equidistant intramolecular separation of ≈ 6.8 Å is almost twice the intra-stack separation found in the monoanion salt $NH_4[Ni$

* The total number of measured reflections was 3059 and independent reflections ($|F_o| > 3\sigma|F_o|$) 1183. The structure was solved by the usual heavy-atom method and refined by a block-diagonal least-squares method. Anisotropic thermal parameters were applied to all the atoms. Atomic scattering factors and anomalous scattering corrections were taken from *International Tables for X-ray Crystallography*.[7] The final *R* value was 0.077 and *R*w was 0.091. The weighting formula was $w = 1/(\sigma^2+0.01|F_o|)$, $|F_o| \geq 15.0$, $w = 1/(1.0+0.01|F_o|^2)$, $|F_o| < 15.0$. The absorption correction was not made due to the crystal's irregular shape. The fractional atomic coordinates are deposited. Calculations were carried out on a HITAC M680H computer at the Computer Centre of the University of Tokyo with a local version of UNICS.[8]

Table 1. Selected intramolecular bond lengths (Å) and angles (°)

Lengths		Angles	
Ni—S(1)	2.172(2)	S(1)—Ni—S(2)	92.19(10)
Ni—S(2)	2.178(3)	Ni—S(1)—C(1)	103.2(3)
S(1)—C(1)	1.728(10)	Ni—S(2)—C(2)	103.8(3)
S(2)—C(2)	1.748(10)	S(1)—C(1)—C(2)	121.9(7)
C(1)—C(2)	1.379(14)	S(2)—C(2)—C(1)	118.8(7)
C(3)—N(1)	1.148(13)	C(2)—C(1)—C(3)	119.8(9)
C(1)—C(3)	1.416(12)	C(1)—C(2)—C(4)	122.0(9)
C(2)—C(4)	1.403(14)	C(1)—C(3)—N(1)	174.7(1.1)
C(4)—N(2)	1.141(14)	C(2)—C(4)—N(2)	179.2(1.2)
		S(1)—C(1)—C(3)	118.3(8)
		S(2)—C(2)—C(4)	119.0(8)

$(S_2C_2(CN)_2)_2]\cdot H_2O$.[9] The dianion centred at $(\frac{1}{2}\,\frac{1}{2}\,0)$ penetrates between the anions forming these columns. Clearly there can be no interaction between the anions at these distances.

In a number of metal dithiolene complexes the columns of anions have been shown to pack together in an arrangement similar to that shown along *c* in Fig. 1 and this results in S—S contacts slightly shorter than the sum of the van der Waals' radii, thus allowing interactions between the columns of anions. Hoffmann and co-workers have discussed this arrangement in terms of minimizing the steric interaction of the lone pair of electrons on the sulphur atoms.[10] However, the separation of the columns in the *c*-direction in $Rb_2[Ni(S_2C_2(CN)_2)_2]\cdot H_2O$, is 8.4 Å, which is much greater than that commonly found in compounds of this type ($\approx$ 6.7 Å).[9]

In $Rb_2[Ni(S_2C_2(CN)_2)_2]\cdot H_2O$, therefore, there are no short S···S contacts and all intra-anion S···S contacts are greater than 4 Å. Thus clearly in the $Rb_2[Ni(S_2C_2(CN)_2)_2]\cdot H_2O$ salt the anions are completely isolated from one another. It was observed that the presence of small Group I cations in the monoanion series of salts of $[Ni(S_2C_2(CN)_2)_2]^-$ facilitated inter-anion interactions. The absence of any interaction between anions in the $[Ni(S_2C_2(CN)_2)_2]^{2-}$ salts is therefore not dependent upon the size of the cation but probably results from the absence of free spins in the HOMO in contrast to the one unpaired electron in the HOMO of the monoanion.

(2) *The reflectance spectra of the dianion salts*

The reflectance spectra of the bis(1,2-dicyanoethylene-1,2-dithiolato)nickelate(2−), palladate(2−) and platinate(2−) dianion salts were

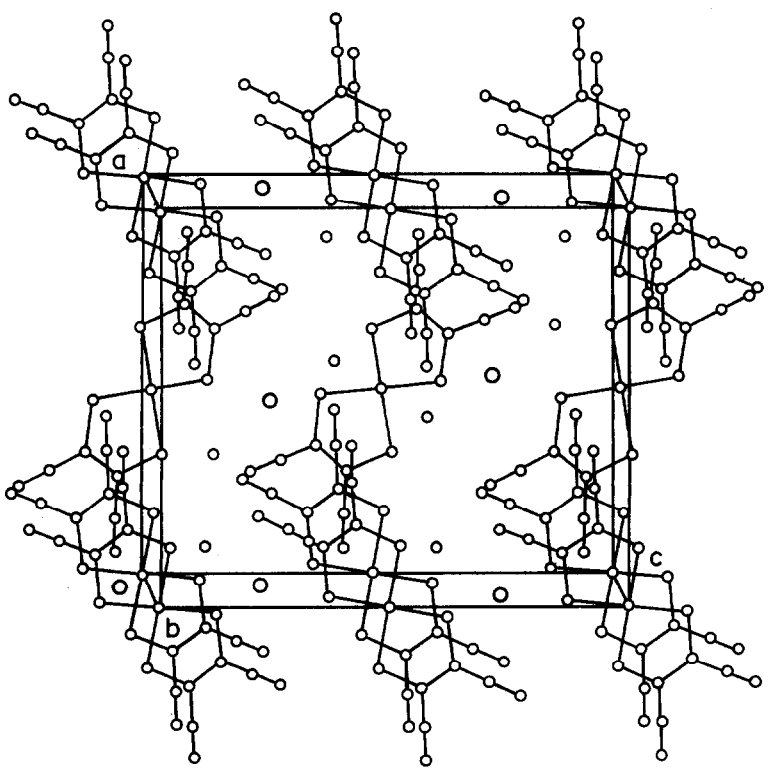

Fig. 1. The *b*-axis projection of $Rb_2[Ni(S_2C_2(CN)_2)_2]\cdot H_2O$.

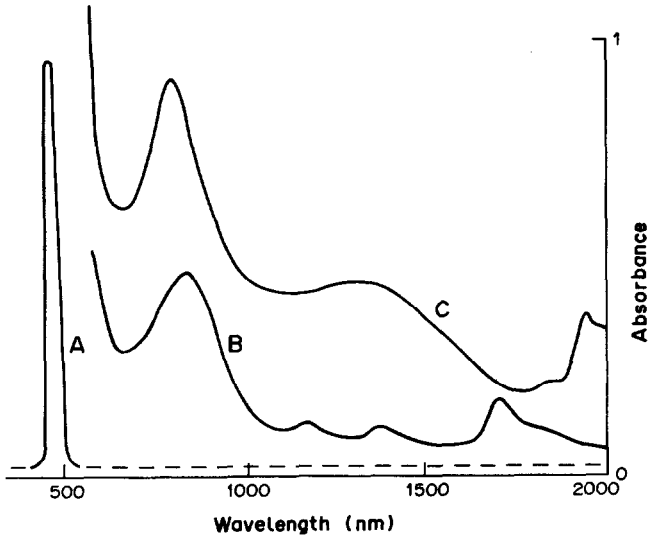

Fig. 2. (A) The UV–vis spectra in acetone of $(NH_4)_2[Ni(S_2C_2(CN)_2)_2]\cdot 2H_2O$ and reflectance spectra of (B) $[N(C_4H_9)_2]_2[Ni(S_2C_2(CN)_2)_2]$ and (C) $(NH_4)_2[Ni(S_2C_2(CN)_2)_2]\cdot 2H_2O$.

determined in order to establish whether or not the salts show evidence of interactions between the dianions in the solid state.

The UV–vis spectrum of an acetone solution of $(NH_4)_2[Ni(S_2C_2(CN)_2)_2]\cdot 2H_2O$ (A) is given together with the reflectance spectra $[N(C_4H_9)_4]_2[Ni(S_2C_2(CN)_2)_2]$ (B) and $(NH_4)_2[Ni(S_2C_2(CN)_2)_2]\cdot 2H_2O$ (C) in Fig. 2. The observed solution spectrum (λ_{max} 478 nm) is similar to that observed for an acetonitrile solution of $[N(C_2H_5)_4]_2[Ni(S_2C_2(CN)_2)_2]$ (λ_{max} 476 nm).[11] The solution spectrum of $[N(C_4H_9)_4]_2[Pd(S_2C_2(CN)_2)_2]$ (A) is compared with the reflectance spectra of $[N(C_4H_9)_4]_2[Pd(S_2C_2(CN)_2)_2]$ (B) and $(NH_4)_2[Pd(S_2C_2(CN)_2)_2]\cdot 0.5H_2O$ (C) in Fig. 3. Finally, the solution spectrum of $(NH_4)_2[Pt(S_2C_2(CN)_2)_2]\cdot 2H_2O$ (A) is compared with the reflectance spectra of $[N(C_2H_5)_4]_2[Pt(S_2C_2(CN)_2)_2]$ (B) and $Mg[Pt(S_2C_2(CN)_2)_2]\cdot xH_2O$ (C) in Fig. 4.

The overall intensity of the reflectance spectra of the dianion salts decreases in the approximate order $NH_4^+ > Rb^+ > K^+ > Cs^+ > [N(C_4H_9)_4]^+$ for

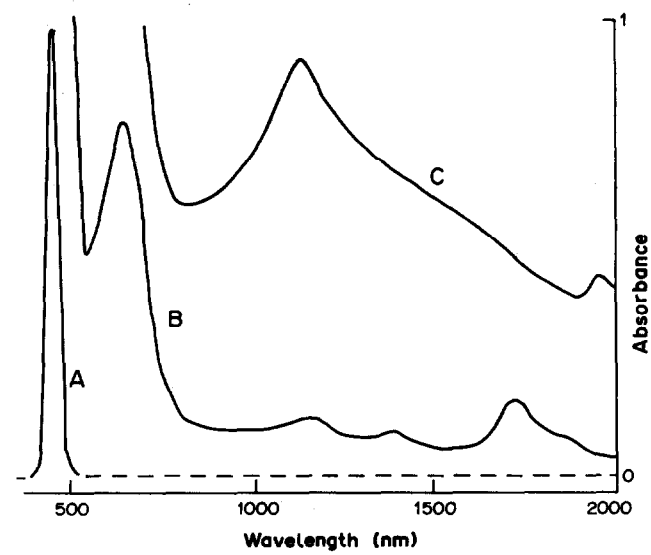

Fig. 3. The solution spectra of $[Pd(S_2C_2(CN)_2)_2]^{2-}$ (A) is compared with the reflectance spectra of $[N(C_4H_9)_4]_2[Pd(S_2C_2(CN)_2)_2]$ (B) and $(NH_4)_2[Pd(S_2C_2(CN)_2)_2]\cdot 0.5\ H_2O$ (C).

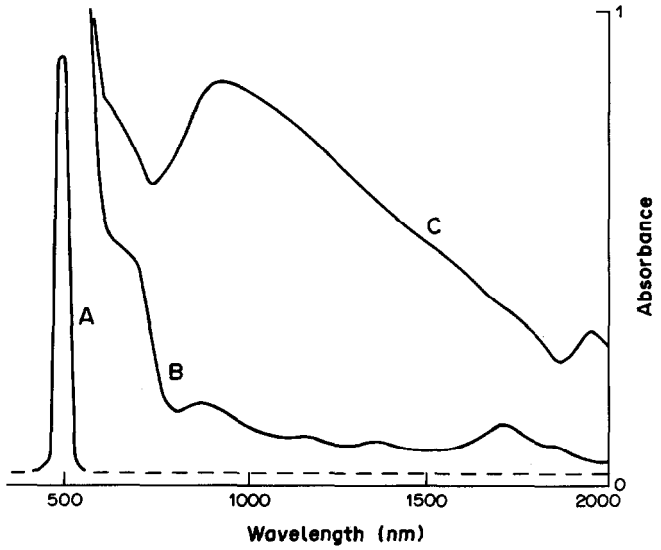

Fig. 4. The acetone solution spectra (A) and reflectance spectra of the $[Pt(S_2C_2(CN)_2)_2]^{2-}$ salts (B) = $[N(C_2H_5)_4]_2[Pt(S_2C_2(CN)_2)_2]$ and (C) = $Mg[Pt(S_2C_2(CN)_2)_2]\cdot xH_2O$.

the nickelate(2−) salts, $NH_4^+ > Ca^{2+} > Rb^+ > Cs^+ > [N(C_4H_9)_4]^+$ for the palladate(2−) salts and $Mg^{2+} > NH_4^+ > K^+ > Rb^+ > [N(C_2H_5)_4]^+$ for the platinate(2−) salts. The increased intensity of the reflectance spectra compared to the solution spectrum indicates that there is some degree of solid-state interactions in many of the dianion salts and that the extent of this effect is dependent on the cation. The salts of the large cation $[NR_4]^+$ always exhibit much lower intensities than those of the smaller cations with the NH_4^+ salts often being the most intense. It has been shown that $[Ni(S_2C_2(CN)_2)_2]^{2-}$ salts exhibit adsorptions at higher energies than most square-planar nickel complexes.[12] More recently Vogler and Kunkely[13] reported the reflectance spectra of $[Ni(tim)]^{2+}[M(S_2C_2(CN)_2)_2]^{2-}$ (tim = 2,3,9,10-tetramethyl-1,4,8,11-tetraazocyclotetradeca-1,3,8,10-tetracene, M = Ni^{2+}, Pd^{2+} and Pt^{2+}) and considered that the intense absorption band at 840 nm for the nickel complex was due to an outer-sphere ligand-to-ligand charge-transfer transition from the anion to the cation. However, the reflectance spectra of all the $[Ni(S_2C_2(CN)_2)_2]^{2-}$ dianion salts of small cations discussed here exhibit an intense broad band around 820–860 nm. The $[Pd(S_2C_2(CN)_2)_2]^{2-}$ and $[Pt(S_2C_2(CN)_2)_2]^{2-}$ salts exhibit a similar band from around 900 to 1500 nm. Since anion-to-cation charge-transfer would not be expected in this region for the cations present in these compounds it seems that the absorption must arise from some other source.

The electrical conductivity of single crystals of $(NH_4)_2[Pd(S_2C_2(CN)_2)_2]\cdot 0.5H_2O$ and $(NH_4)_2[Pt(S_2C_2(CN)_2)_2]\cdot 2H_2O$ salts at room temperature (see Table 2) are higher than those observed previously for compressed pellets of the dianion salts $[N(C_2H_5)_4]_2[Ni(S_2C_2(CN)_2)_2]$ ($< 10^{-12}\ \Omega^{-1}\ cm^{-1}$) and $[N(C_2H_5)_4]_2[Pt(S_2C_2(CN)_2)_2]$ ($< 10^{-10}\ \Omega^{-1}\ cm^{-1}$).[14] This observation is consistent, however, with the increased intensity of the reflectance spectra for the dianion salts with small counter cations,

Table 2. Electrical conductivity of single crystals

	σ_{RT} ($\Omega^{-1}\ cm^{-1}$)	Activation energy of the semiconductor (meV)
$(NH_4)_2[Pd(S_2C_2(CN)_2)_2]\cdot 0.5H_2O$	8×10^{-6}	280 (310–210 K)
$(NH_4)_2[Pt(S_2C_2(CN)_2)_2]\cdot 2H_2O$	7×10^{-8}	360 (310–210 K)

when compared to salts containing bulky counter cations.

Acknowledgements—We thank the SERC for their support and Johnson Matthey plc for the loan of precious metal salts.

REFERENCES

1. A. E. Underhill and P. I. Clemenson, *Physica B* 1986, **143**, 316.
2. R. Eisenberg and J. A. Ibers, *Inorg. Chem.* 1965, **4**, 605.
3. A. Kobayashi and Y. Sasaki, *Bull. Chem. Soc. Jpn* 1977, **50**, 2650.
4. L. C. Isett, Personal communication to A. E. Underhill (1986).
5. R. K. Haller, *Fr. Patent* 2,084,997 (1971).
6. A. E. Underhill and D. J. Wood, in *Molecular Metals* (Edited by W. E. Hatfield), p. 377. Plenum Press, New York and London (1979).
7. *International Tables for X-ray Crystallography*, Vol. 4. Kynoch Press, Birmingham (1974).
8. T. Sakurai, UNICS, Universal Crystallographic Computation Program System. The Crystallographic Society of Japan, Tokyo (1967).
9. P. I. Clemenson, A. E. Underhill, M. B. Hursthouse and R. L. Short, *J. Chem. Soc., Dalton Trans.* 1988, 1689.
10. S. Alvarez, R. Vincente and R. Hoffmann, *J. Am. Chem. Soc.* 1985, **107**, 6253.
11. L. Persaud and C. H. Langford, *Inorg. Chem.* 1985, **24**, 3562.
12. A. R. Latham, V. C. Hascall and H. B. Gray, *Inorg. Chem.* 1965, **4**, 788.
13. A. Vogler and H. Kunkely, *J. Chem. Soc., Chem. Commun.* 1986, 1616.
14. M. M. Ahmad and A. E. Underhill, *J. Chem. Soc., Dalton Trans.* 1983, 165.

Polyhedron Vol. 9, No. 17, pp. 2061–2069, 1990
Printed in Great Britain

0277–5387/90 $3.00+.00
© 1990 Pergamon Press plc

INFLUENCE OF THE COMPLEXATION OF COPPER(II) ON THE STRUCTURE AND REACTIVITY OF 4-HYDROXY-6-METHYL-3-[3-DIMETHYLAMINOACRYLOYL]-2H-PYRAN-2-ONE

O. CARUGO*

Dipartimento di Medicina Preventiva, Occupazionale e di Comunità dell'Università di Pavia, via Boezio 24, I-27100 Pavia, Italy

and

C. BISI CASTELLANI and M. RIZZI

Dipartimento di Chimica Generale dell'Università di Pavia, via Taramelli 12, I-27100 Pavia, Italy

(*Received* 29 *January* 1990; *accepted* 26 *March* 1990)

Abstract—Four novel copper(II) complexes of 4-hydroxy-6-methyl-3-[dimethylamino-acryloyl]-2H-pyran-2-one (Hacrp) have been isolated: $Cu(acrp)_2 \cdot 1/2KCl$, $Cu(acrp)_2(py) \cdot H_2O$, $Cu(acrp)(bipy)Cl \cdot H_2O$ and $Cu(acrp)(phen)Cl \cdot 2H_2O$ (acrp = monodeprotonated form of Hacrp; py = pyridine; bipy = 2,2′-bipyridine; phen = 1,10-phenanthroline). The crystal structures of Hacrp and $Cu(acrp)_2(py) \cdot H_2O$ have been determined. Hacrp is clearly a pyran-2-one molecule. The copper(II) ion is pentacoordinated, in a square-pyramidal stereochemistry, with py in the apical position; the acrp ligand is intermediate between the pyran-2-one form and the pyran-2,4-dione one. Both Hacrp and $Cu(acrp)_2(py) \cdot H_2O$ react with hydroxylamine hydrochloride in ethanol to give the novel molecule 8-hydroxy-5-oxo-7-methyl-5,8-dihydro-4H-pyrano[2,3-b]pyridin-4-one. Hacrp, in aqueous hydrochloric acid, transforms into 2,4-dihydroxyacetophenone. The same product has been obtained by reacting Hacrp and $CuCl_2 \cdot 2H_2O$ in water. Mechanisms for these reactions are proposed.

In the course of our studies on the structure and reactivity of pyrone derivatives and their complexes with metal ions,[1] we turned our attention to the 4-hydroxy-6-methyl-3-[3-dimethylaminoacryloyl]-2H-pyran-2-one (referred to as Hacrp). This molecule appears to be very promising because it presents a complicated set of tautomeric equilibria (see Scheme 1) and a presumably high reactivity (as well as most enamines) both of which could be influenced by interaction with metal ions.

Among the metal ions we choose copper(II) because many naturally occurring pyrone derivatives (i.e. flavonoids) are known to interact strongly, although in a still unknown way, with Cu^{2+} in several biological systems;[2] the study of the complexes between Cu^{2+} and pyrone derivatives could therefore provide useful information for understanding the biological interaction between flavonoids and copper ions. In the present paper we describe the synthesis and characterization of four novel copper(II) complexes of Hacrp: $Cu(acrp)_2 \cdot 1/2KCl$, $Cu(acrp)_2(py) \cdot H_2O$, $Cu(acrp)(bipy)Cl \cdot H_2O$ and $Cu(acrp)(phen)Cl \cdot 2H_2O$ (acrp = monodeprotonated form of Hacrp; py = pyridine; bipy = 2,2′-bipyridine; phen = 1,10-phenanthroline). The molecular structures of Hacrp and of $Cu(acrp)_2(py) \cdot H_2O$ have been determined in order to examine the effects of copper coordination to the ligand. Moreover, the hydrolysis of Hacrp

*Author to whom correspondence should be addressed.

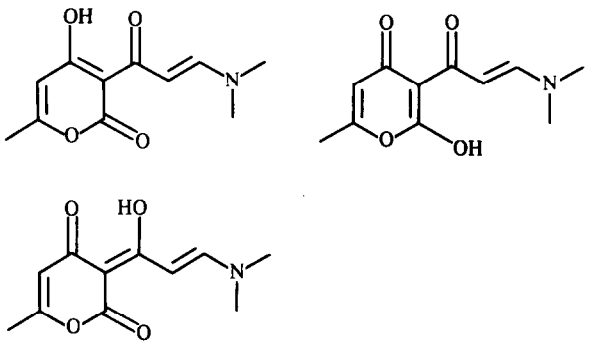

Scheme 1.

and its reaction with hydroxylamine, both in the absence and in the presence of copper(II), have been studied. The 2,4-dihydroxyacetophenone has been recovered by hydrolysing Hacrp in the presence of hydrochloric acid or $CuCl_2 \cdot 2H_2O$. A novel molecule, 8-hydroxy-5-oxo-7-methyl-5,8-dihydro-4H-pyrano[2,3-b]pyridin-4-one, has been obtained by reacting Hacrp or $Cu(acrp)_2(py) \cdot H_2O$ with hydroxylamine.

EXPERIMENTAL

Physicochemical measurements

IR spectra were recorded with a 1130 Perkin–Elmer spectrophotometer; electronic absorption spectra were obtained with a Varian Cary spectrophotometer; NMR spectra were recorded on a Bruker WP80SY spectrometer; and mass spectra were obtained with a Finnigan-MAT 8222 spectrometer. The deprotonation constant of Hacrp was determined using the Calvin–Wilson pH-titration technique,[3] in ethanol–water (1 : 1 v/v). An E366 Metrohm pH-meter equipped with a Metrohm glass electrode was used for pH measurements; the concentration of Hacrp was 1×10^{-4} M, temperature 25 ± 0.1°C and $I = 0.1$ M $NaClO_4$. The deprotonation constant of Hacrp in its first singlet excited state was calculated using the appropriate equation,[4] by observing that in ethanol–water (1 : 1 v/v) λ_{0-0} is 433 nm (in $HClO_4$ 0.1 M) and 480 nm (in KOH 0.05 M).

Synthesis of Hacrp

Hacrp was synthesized by literature methods.[5]

Synthesis of $Cu(acrp)_2 \cdot 1/2KCl$

$CuCl_2 \cdot 2H_2O$ (0.1 g) in 6 cm^3 of ethanol was added to an aqueous boiling solution of Hacrp (0.26 g) and KOH (0.065 g), and the mixture was refluxed for about 1 h. The dark green solid which separated at room temperature was filtered off, washed with ethanol and dried for 3 h at room temperature and 0.5 mm Hg. M.p. 260°C. Found: C, 48.7; H, 4.5; N, 5.1. Calc. for $C_{22}H_{24}Cl_{0.5}CuK_{0.5}N_2O_8$: C, 48.5; H, 4.4; N, 5.1%.

Synthesis of $Cu(acrp)_2(py) \cdot H_2O$

$Cu(acrp)_2 \cdot 1/2KCl$ (0.2 g) in 60 cm^3 of a mixture of pyridine and ethanol (1 : 1 v/v) were refluxed for about 1 h. By slowly concentrating the obtained solution, small dark green crystals precipitated in a few days. They were filtered, washed with ethanol, and dried for 3 h at room temperature and 0.5 mm Hg. M.p. 135–140°C. Found: C, 55.0; H, 5.1; N, 7.1. Calc. for $C_{27}H_{29}CuN_3O_8$: C, 55.2; H, 5.0; N, 7.2%.

Synthesis of $Cu(acrp)(bipy)Cl \cdot H_2O$

2,2′-Bipyridine (0.06 g) in 5 cm^3 of ethanol were added to a suspension of $Cu(acrp)_2 \cdot 1/2KCl$ (0.2 g) in 40 cm^3 of ethanol and refluxed for about 2 h, thus obtaining the dissolution of all the solid residue. By slowly evaporating the solvent, a green product was precipitated, filtered off and washed with ethanol and dried for 3 h at room temperature and 0.5 mm Hg. M.p. 240–250°C. Found: C, 51.2; H, 4.3; N, 8.5. Calc. for $C_{21}H_{22}ClCuN_3O_5$: C, 50.9; H, 4.5; N, 8.5%.

Synthesis of $Cu(acrp)(phen)Cl \cdot 2H_2O$

In the synthesis of $Cu(acrp)(phen)Cl \cdot 2H_2O$, the same procedure as described for Cu(acrp)(bipy) $Cl \cdot H_2O$ was used, using 1,10-phenanthroline instead of 2,2′-bipyridine. M.p. 190°C. Found: C, 51.3; H, 4.4; N, 7.6. Calc. for $C_{23}H_{24}ClCuN_3O_6$: C, 51.4; H, 4.5; N, 7.8%.

Synthesis of 8-*hydroxy*-5-*oxo*-7-*methyl*-5,8-*dihydro*-4H-*pyrano*[2,3-b]*pyridin*-4-*one*

(a) Hydroxylamine hydrochloride (0.03 g) and Hacrp (0.10 g) were dissolved in 50 cm^3 of ethanol, stirred at room temperature for 12 h. By slowly concentrating this solution, a yellow solid precipitated which was filtered off and dried at room temperature and 0.5 mm Hg for 3 h. Dec. point 245–248°C. Found: C, 55.8; H, 3.6; N, 7.2. Calc. for $C_9H_7NO_4$: C, 55.9; H, 3.6; N, 7.2%. Mass spectrum: M^+ 193. ^1H NMR (^6D-DMSO): 2.25 (d, 3H, $J = 0.5$ Hz, CH_3), 6.20 (d, 1H, $J = 0.5$ Hz,

6-H), 6.75 (d, 1H, $J = 5$ Hz) and 8.50 ppm (d, 1H, $J = 5$ Hz, CH=CH).

(b) By adding hydroxylamine hydrochloride (0.076 g) to a boiling suspension of $Cu(acrp)_2 \cdot 1/2KCl$ (0.15 g) in 30 cm^3 of ethanol, a clear solution was obtained and refluxed for about 1 h. By slowly evaporating the solvent, a yellow solid precipitated. This was collected and dried as described above and identified as 8-hydroxy-5-oxo-7-methyl-5,8-dihydro-4H-pyrano[2,3-b]pyridin-4-one.

Synthesis of (2,4-dihydroxyacetophenonato) copper(II)

$CuCl_2 \cdot 2H_2O$ (0.075 g) in 6 cm^3 of water was added to a boiling solution of Hacrp (0.20 g) in 20 cm^3 of water. The mixture was refluxed for 1 h and the green product obtained was filtered and dried at room temperature and 0.5 mm Hg for 3 h. Dec. point 240–250°C. Found: C, 44.7; H, 2.8. Calc. for $C_8H_6CuO_3$: C, 44.8; H, 2.8%.

Synthesis of 2,4-*dihydroxyacetophenone*

(a) Hacrp (0.5 g) in 20 cm^3 of water and 1 cm^3 of hydrochloric acid (37%), was refluxed for 1 h. The resulting solution was chromatographed on silica gel (70–230 mesh) with cyclohexane–ethyl acetate (7 : 3 v/v). 2,4-Dihydroxyacetophenone was obtained as a first fraction.

(b) A suspension of (2,4-dihydroxyacetophenonato)copper(II) (0.2 g) and KCN (0.14 g) in 40 cm^3 of ethanol was refluxed for 5 h and then filtered. By slowly concentrating the so obtained solution, crude 2,4-dihydroxyacetophenone was obtained, which was purified by chromatography as described above.

X-ray analysis of Hacrp

The specimen size was $0.10 \times 0.15 \times 0.25$ mm. All measurements were made at 18 ± 2°C with Cu-K_α radiation (1.5418 Å) using a CAD 4 diffractometer equipped with a graphite monochromator. All the calculations were performed with SDP software.[6]

Crystal data: $C_{11}H_{13}NO_4$; $M_r = 223.23$; orthorhombic; space group *Pnma*; $a = 12.652(1)$, $b = 6.775(1)$, $c = 12.907(1)$ Å; $U = 1106.3$ Å^3; $Z = 4$; $D_c = 1.340$ g cm^{-3}; $F(000) = 118$; μ(Cu-K_α) = 8.2 cm^{-1}.

The cell was determined by refining the angular parameters of 25 reflections with $50 < \theta < 55°$ automatically centred. The space group was determined from systematic absences and intensity statistics, and confirmed by the structure analysis. 1252 *hkl* reflections were measured for $2 < \theta < 70°$, with scan mode 3ω–2θ, scan speed 4.12° min^{-1} and scan width $(1.05 + 0.142 \operatorname{tg}\theta)°$; their intensities were corrected for Lorentz–polarization, decay (three standard reflections, maximum correction 17.8%) and absorption effects[7] (transmission minimum 90.28%; maximum 99.59%).

The structure was solved with MULTAN, by considering 1048 unique reflections (systematic absences rejected), and Fourier methods, by considering only 704 reflections [$I > 3\sigma(I)$]. The positions of the hydrogen atoms were calculated (C—H = 1.0 Å; the methylic ones were considered disordered), and their thermal parameters were taken proportionally ($\times 1.3$) to those of the bonded non-hydrogen atoms. All the non-hydrogen atoms were refined anisotropically with full-matrix least-squares, minimizing the function $[\Sigma w(F_o - F_c)^2 / \Sigma F_o^2]^{1/2}$, with $w = 959/F_o$ (for $F_o < 959$) and $w = F_o/959$ (for $F_o > 959$) being 959 one third of the largest F_o. The structure converged to a final $R = 7.6\%$ ($R_w = 8.2\%$).

An ORTEP view of the structure of Hacrp is reported in Fig. 1; bond distances and angles are reported in Tables 1 and 2.

X-ray analysis of $Cu(acrp)_2(py) \cdot H_2O$

The procedure was analogous to that above described for the X-ray analysis of Hacrp, with the following differences.

The specimen size was $0.06 \times 0.06 \times 0.08$ mm.

Crystal data: $C_{27}H_{29}CuN_3O_8$; $M_r = 587.09$; orthorhombic; space group *Pnna*; $a = 14.275(2)$, $b = 13.095(2)$, $c = 14.904(2)$ Å; $U = 2786.1$ Å^3; $Z = 4$; $D_c = 1.400$ g cm^{-3}; $F(000) = 305$; μ(Cu-K_α) = 15.2 cm^{-1}.

The cell was determined by refining the angular parameters of 22 reflections with $39 < \theta < 40°$. 2954 *hkl* reflections were measured for $2 < \theta < 70°$, with scan mode 3ω–4θ, scan speed 2.75° min^{-1}, scan width $(1.10 + 0.142 \operatorname{tg}\theta)°$. Maximum decay correction 3.5%. Transmission minimum 93.02%; maximum 99.97%

The structure was solved with MULTAN, by

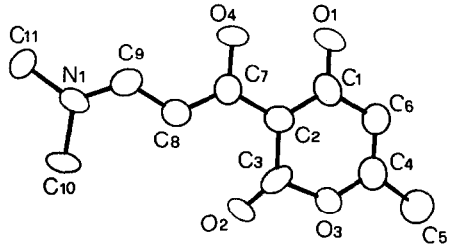

Fig. 1. ORTEP view of the Hacrp molecule.

Table 1. Bond distances (Å) for Hacrp and $Cu(acrp)_2(py)\cdot H_2O$, with their estimated standard deviations

Cu—O(1)		1.911(5)
Cu—O(4)		1.907(4)
Cu—N(2)		2.310(8)
O(1)—C(1)	1.281(16)	1.293(7)
O(2)—C(3)	1.179(16)	1.209(8)
O(3)—C(3)	1.422(16)	1.393(8)
O(3)—C(4)	1.351(16)	1.365(8)
O(4)—C(7)	1.318(14)	1.297(7)
N(1)—C(9)	1.327(17)	1.322(9)
N(1)—C(10)	1.453(17)	1.460(12)
N(1)—C(11)	1.489(16)	1.500(15)
C(1)—C(2)	1.382(18)	1.414(8)
C(1)—C(6)	1.470(20)	1.442(9)
C(2)—C(3)	1.457(17)	1.458(9)
C(2)—C(7)	1.442(18)	1.437(8)
C(4)—C(5)	1.530(21)	1.480(12)
C(4)—C(6)	1.350(20)	1.333(12)
C(7)—C(8)	1.400(19)	1.429(9)
C(8)—C(9)	1.391(19)	1.372(13)
N(2)—C(12)		1.336(8)
C(12)—C(13)		1.360(12)
C(13)—C(14)		1.391(12)

Table 2. Bond angles (°) for Hacrp and $Cu(acrp)_2(py)\cdot H_2O$, with their estimated standard deviations. The atoms marked with a prime are transformed as x, $1/2-y$, $1/2-z$

O(1)—Cu—O(1)′		166.2(2)
O(1)—Cu—O(4)		90.0(2)
O(1)—Cu—O(4)′		88.6(2)
O(1)—Cu—N(2)		96.9(2)
O(1)′—Cu—O(4)		88.6(2)
O(1)′—Cu—O(4)′		90.0(2)
O(1)′—Cu—N(2)		96.9(2)
O(4)—Cu—O(4)′		168.5(2)
O(4)—Cu—N(2)		95.8(2)
O(4)′—Cu—N(2)		95.8(2)
Cu—O(1)—C(1)		127.7(4)
Cu—O(4)—C(7)		130.7(4)
Cu—N(2)—C(12)		122.1(4)
C(3)—O(3)—C(4)	124.7(1.0)	123.0(6)
C(9)—N(1)—C(10)	121.6(1.0)	124.3(6)
C(9)—N(1)—C(11)	120.9(1.0)	119.6(7)
C(10)—N(1)—C(11)	117.4(1.0)	116.1(6)
O(1)—C(1)—C(2)	123.0(1.2)	125.1(6)
O(1)—C(1)—C(6)	117.1(1.2)	114.8(5)
C(2)—C(1)—C(6)	119.9(1.2)	120.1(5)
C(1)—C(2)—C(3)	121.3(1.1)	117.0(6)
C(1)—C(2)—C(7)	119.1(1.1)	123.0(5)
C(3)—C(2)—C(7)	119.5(1.1)	119.8(5)
O(2)—C(3)—O(3)	115.0(1.1)	113.3(6)
O(2)—C(3)—C(2)	130.9(1.2)	128.0(7)
O(3)—C(3)—C(2)	114.1(1.0)	118.6(6)
O(3)—C(4)—C(5)	111.1(1.2)	113.0(7)
O(3)—C(4)—C(6)	121.9(1.2)	120.4(6)
C(5)—C(4)—C(6)	127.0(1.3)	126.6(7)
C(1)—C(6)—C(4)	118.1(1.2)	120.9(7)
O(4)—C(7)—C(2)	115.6(1.1)	120.2(5)
O(4)—C(7)—C(8)	118.9(1.2)	115.8(5)
C(2)—C(7)—C(8)	125.6(1.1)	124.1(5)
C(7)—C(8)—C(9)	121.0(1.2)	118.5(6)
N(1)—C(9)—C(8)	124.4(1.2)	127.5(6)
C(12)—N(2)—C(12)′		115.7(7)
N(2)—C(12)—C(13)		124.7(7)
C(12)—C(13)—C(14)		118.0(8)
C(13)—C(14)—C(13)′		118.9(9)

using 2112 unique reflections [$I > 0.01\sigma(I)$], and Fourier methods, by using 1324 reflections [$I > 3\sigma(I)$]. Form factors with anomalous dispersion components were used.[8] The function minimized in full-matrix least-squares was $[\Sigma w(F_o - F_c)^2/\Sigma w F_o^2]^{1/2}$, with $w = \sigma^2 + 0.01F_o + 1.0$. The structure converged to a final $R = 6.5\%$ ($R_w = 7.5\%$).

An ORTEP view of the structure of the $Cu(acrp)_2(py)$ complex is reported in Fig. 2; bond distances and angles are reported in Tables 1 and 2.

RESULTS AND DISCUSSION

The aim of the present work was to study the influence of the complexation to copper(II) on the structure and the reactivity of Hacrp. The preliminary step was the synthesis of copper(II) complexes of Hacrp. By reacting this ligand and $CuCl_2\cdot 2H_2O$ in the presence of KOH, the complex $Cu(acrp)_2\cdot 1/2KCl$ was obtained, but it was impossible to grow crystals suitable for crystallographic studies. In order to overcome this problem, we reacted $Cu(acrp)_2\cdot 1/2KCl$ with some nitrogen heterocyclic bases [pyridine (py), 2,2′-bipyridine (bipy) and 1,10-phenanthroline (phen)], and three new complexes, formulated as $Cu(acrp)_2(py)\cdot H_2O$, $Cu(acrp)(bipy)Cl\cdot H_2O$ and $Cu(acrp)(phen)Cl\cdot 2H_2O$ on the basis of the analytical data, were obtained. A crystallographic study was possible only on the first complex (see below); in it, the pyridine ligand, although present in large excess during the synthesis (i.e. as solvent), does not replace any of the pyrone ligands. On the contrary, 2,2′-bypyridine and 1,10-phenanthroline, although used in stoichiometric amounts, replace one of the two pyrone ligands bonded to the metal.

In the IR spectra of the molecules here described the stretching of the pyrone carbonyl is the only band of sound diagnostic value. In the case of Hacrp, this band is found at 1705 cm^{-1}, indicating

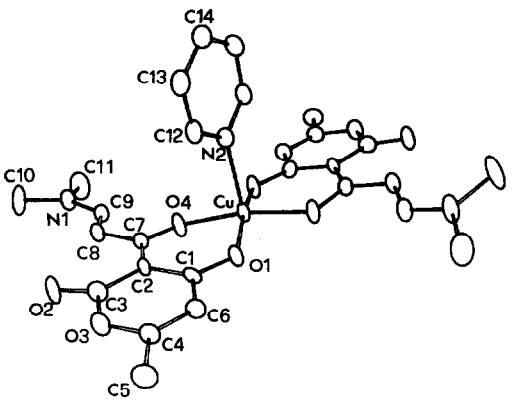

Fig. 2. ORTEP view of the $Cu(acrp)_2(py)$ complex.

that the heterocyclic ring is probably a pyran-2-one.[9] In the complexes $Cu(acrp)_2 \cdot 1/2KCl$ and $Cu(acrp)_2(py) \cdot H_2O$, the ν(C=O, pyrone) is slightly shifted to lower energy (1695 cm^{-1}) with respect to the free ligand. Such a small shift could easily depend on packing effects, and it agrees with the crystallographic data (see below) which show a lengthening of the pyrone carbonyl bond on passing from Hacrp [1.179(16) Å] to $Cu(acrp)_2(py) \cdot H_2O$ [1.209(8) Å]. In the complexes $Cu(acrp)(bipy)Cl \cdot H_2O$ and $Cu(acrp)(phen)Cl \cdot 2H_2O$, the ν(C=O, pyrone) is found at 1675 and 1670 cm^{-1}, respectively, thus quite greatly shifted to lower energy. A shift as large as 30–35 cm^{-1} could be justified by coordination of the pyrone carbonyl oxygen to the metal, or by isomerization of the heterocyclic ring from pyran-2-one to pyran-4-one; in fact, in pyran-4-ones, the carbonyl stretching is generally found at 1665–1670 cm^{-1}, and it is not greatly affected by the substituents on the ring.[9]

Also, the electronic absorption spectra show a significant difference between $Cu(acrp)_2 \cdot 1/2KCl$ and $Cu(acrp)_2(py) \cdot H_2O$ on one side, and $Cu(acrp)(bipy)Cl \cdot H_2O$ and $Cu(acrp)(phen)Cl \cdot 2H_2O$ on the other side. All the spectra are dominated by the intense bands of the ligands, whose tail probably hides the *d–d* copper(II) transitions at lower energy (the lower energy band of Hacrp in ethanol shows two maxima at 368.5 and 380.5 nm, with $\log \varepsilon$ 4.68 and 4.69, respectively). The spectra of the adducts $Cu(acrp)_2 \cdot 1/2KCl$ and $Cu(acrp)_2(py) \cdot H_2O$ are different in the solid state (λ_{max}: 242, 314, 375, and 270, 318, 396 nm, respectively), but almost superimposable in ethanol solution (λ_{max}: 228, 258, 298, 366 nm). This indicates their instability in solution, where they probably decompose to give a molecule with the formula $Cu(acrp)_2$. This behaviour is frequently observed in hexa- and pentacoordinated adducts of neutral copper(II) bis-chelated.[10] However, no attempt to isolate a complex of formula $Cu(acrp)_2$ was successful. The spectra of the complexes $Cu(acrp)(bipy)Cl \cdot H_2O$ and $Cu(acrp)(phen)Cl \cdot 2H_2O$ are different both in the solid state (λ_{max}: 246, 314, 376, 398, and 205, 280, 400 nm respectively) and in ethanol solution (λ_{max}: 231, 308, 370, 380, and 223, 260, 292, 370 nm, respectively); they also differ significantly from the spectra of $Cu(acrp)_2 \cdot 1/2KCl$ and $Cu(acrp)_2(py) \cdot H_2O$.

However, in the absence of crystallographic data, it is impossible to infer any conclusion about the actual structures of the 2,2′-bipyridine and 1,10-phenanthroline adducts, thus it is not clear what the influence of bipy and phen is on the molecular structure and the coordinative properties of Hacrp.

Structural studies

The Hacrp molecule is planar and located on the crystallographic plane at $y_0 = 1/4$. The ring is clearly a pyran-2-one and not a 4-one nor a 2,4-dione (see Scheme 1). In fact, the distance C(3)—O(2) [1.179(16) Å] is shorter than C(1)—O(1) [1.281(16) Å], and the carbon–carbon bonds of the ring are alternatively short and long as expected for such a structure. This diagnosis is supported also by an analysis of the ring aromaticity, which considers all the bond distances in the whole ring. For Hacrp we obtain an HOMAS of −0.593,[11] and an I_6 of 32.9,[12] which are closer to the values of pyran-2-one (HOMAS = −0.341 and I_6 = 32.9) than to those of pyran-4-one (HOMAS = −0.146 and I_6 = 37.2).[11]

Another interesting feature arising from the structural data of Hacrp is the charge separation existing in the acryloyl chain, which can be represented as reported in Scheme 2. In fact the dis-

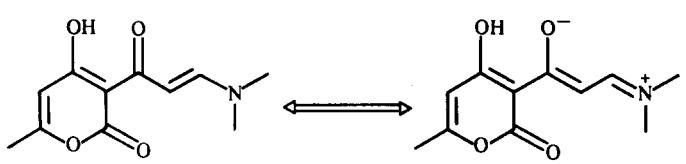

Scheme 2.

tance C(9)—N(1) [1.327(17) Å] is considerably shorter than the expected one for a carbon–nitrogen single bond [1.474 Å];[11] moreover, the bond distances C(7)—C(8) [1.400(19) Å] and C(8)—C(9) [1.391(19) Å] are not significantly different; eventually the bond distance C(7)—O(4) [1.318(14) Å] is longer than the enolic one C(1)—O(1) [1.281(16) Å]. The negative charge localized on the O(4) atom could be stabilized by strong hydrogen bonding to the hydroxyl group on the 4-position of the pyrone ring; the hydrogen atom of this OH group was not found even in the last difference-Fourier map; thus with no evidence for its actual position in the molecule, we do not know if it is nearer to O(1) than to O(4). The existence of a charge separation in the acryloyl chain is also supported by the following observations. (i) The projection of the packing of the Hacrp crystal structure down axis *a* (Fig. 3) shows that the molecules are packed in layers; each enaminic nitrogen atom of a molecule is surrounded by the O(1) atoms of two other molecules belonging to different layers (related to N(1) by the symmetry transformations $1/2-x$, $-y$, $1/2+z$ and $1/2-x$, $1-y$, $1/2+z$), and the O(1) atom of each molecule is surrounded by the N(1) atoms of two other molecules belonging to different layers (related to O(1) by the symmetry transformations $1/2-x$, $-y$, $-1/2+z$ and $1/2-x$, $1-y$, $-1/2+z$); the intramolecular distance O(1)—N(1) [3.426(2) Å] is not much higher than the sum of the van der Waals' radii (2.9 Å),[13] indicating a certain ionic interaction. (ii) The deprotonation constant of Hacrp in its electronic ground state ($\log K_a = -9.37 \pm 0.01$) is very low (see for comparison the value of dehydroacetic acid: $\log K_a = -5.12$[14]), consistently with an excess of negative charge on the atoms O(1) and/or O(4). By means of appropriate relations,[4] it is possible to estimate the acidity of Hacrp in its first singlet excited state as $\log K_a = -4.63$; therefore, it is probable that the lowest energy electronic absorption band of Hacrp is an intramolecular charge-transfer one, that undergoes the charge separation between O(1)/O(4) and N(1); this interpretation agrees with the high intensity of this band ($\log \varepsilon = 4.69$) and with the red-shift of its maxima induced by increasing the solvent polarity (from 368.5 and 380.5 nm in ethanol, to 370.5 and 383.0 nm in 70% aqueous ethanol).

In the complex $Cu(acrp)_2(py)\cdot H_2O$, the copper(II) chromophore is clearly a square-pyramid, with the two pyrone ligands bonded to the metal through the oxygen atoms O(1) and O(4) at the vertices of the square base, and the pyridine nitrogen atom N(2) in the apical position. The Zemann *R* factor is only 0.037, quite a low value for pentacoordinated copper(II) complexes, which are normally very distorted.[15] The four basal oxygen atoms are in a plane of equation $x-1.8870=0$, with the copper(II) atom shifted by 0.212(2) Å out of this plane towards the pyridine nitrogen atom. The mean Cu—O basal distance [1.909(5) Å] is 0.397 Å shorter than the Cu—N(2) distance [2.306(8) Å], agreeing with the axial distortions generally observed in square-pyramidal copper(II) complexes.[16] The plane of the pyridine forms dihedral angles of 62.3° with the plane containing the atoms O(4), Cu and N(2), and of 26.5° with the plane containing the atoms O(1), Cu and N(2). As a consequence of this asymmetric orientation of the pyridine plane with respect to the direction of the basal coordinative bonds, a strong π-interaction between the copper(II) atom and the pyridine seems unlikely, in agreement with the observations of Menabue *et al.*[17] The copper(II) centre, the nitrogen atom N(2) and the carbon atom C(14) are situated along the two-fold axis at $x_0 = y_0 = 1/4$. Thus, the whole complex results from two asymmetric units related by the symmetry transformation x, $1/2-y$, $1/2-z$. Also the oxygen atom of the water molecule, O(5), is in a special position, on the two-fold axis

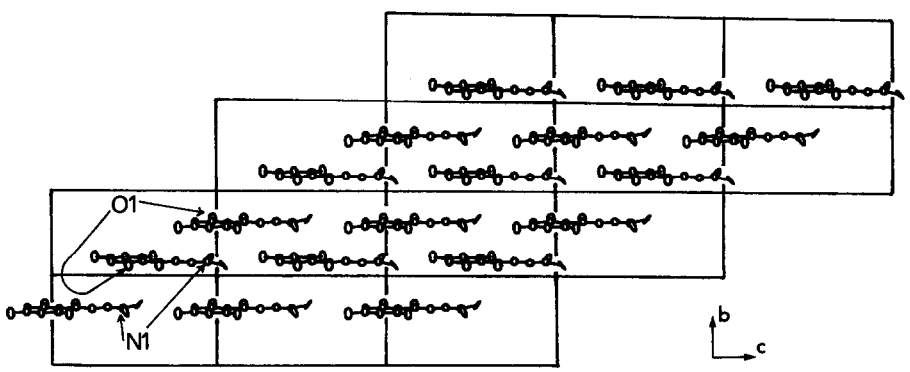

Fig. 3. Projection down the *a* axis of the crystal structure of Hacrp.

at $x_0 = 1/4$ and $y_0 = 0$, and it is at the centre of a cluster of hydrogen bonds. In fact it is bonded to four other oxygen atoms, O(1) (with symmetry transformation x, y, z), O(4)^{i} (with symmetry transformation $x, 1/2-y, 1/2-z$), O(4)^{ii} (with symmetry transformation $1/2-x, -1/2+y, 1/2-z$) and O(1)^{iii} (with symmetry transformation $1/2-x, -y, z$), at distances O(5)—O(1) = 2.999(8) Å, O(5)—O(4)^{i} = 3.290(5) Å, O(5)—O(4)^{ii} = 3.290(5) Å and O(5)—O(1)^{iii} = 2.999(8) Å. The two hydrogen atoms of the water molecule are considered disordered with occupancy 0.5 (for obvious symmetry reasons); they are considered located in the direction of O(1) and O(1)^{iii}, because the contacts O(5)—O(1) and O(5)—O(1)^{iii} are the shortest ones and the angle O(1)—O(5)—O(1)^{iii} [94.1(3)°] is not far from the theoretical H—O—H bond angle.

The ligand acrp coordinated to the copper(II) atom is intermediate between the two limit formulae depicted in Scheme 3. In fact, the C(3)—O(2) bond distance [1.209(8) Å] is still shorter than the C(1)—O(1) one [1.293(7) Å] and the HOMAS aromaticity index (−0.334)[11] is nearer to that of pyran-2-one (−0.341) than to that of pyran-4-one (−0.146). However, the I_6 aromaticity index (35.5)[12] is intermediate between that of pyran-2-one (32.9) and that of pyran-4-one (37.2) and the alternance between short and long carbon–carbon bonds within the heterocyclic ring is not as pronounced as expected. In particular, the C(1)—C(2) bond distance [1.414(8) Å] is greater than the corresponding one in the free ligand [1.382(18) Å]. Moreover, the Cu—O(1) and Cu—O(4) bond distances [1.911(5) and 1.907(4) Å] are not significantly different, indicating that the two oxygen atoms O(1) and O(4) are electronically similar. As a consequence of the resonance shown in Scheme 3, the charge separation in the acryloyl chain, clearly present in the free ligand, is inhibited in the ligand coordinated to the metal. In fact, although the enaminic group is still planar and the C(9)—N(1) bond distance is short [1.322(9) Å], the bond distances C(7)—C(8) and C(8)—C(9) [1.429(9) and 1.370(10) Å] are significantly different, contrary to the corresponding ones in the free ligand [1.400(19) and 1.392(19) Å].

Study of the reactivity

We studied the reaction of Hacrp with hydroxylamine and hydrolysis in acid medium, in order to compare its reactivity in the presence and in the absence of copper(II).

It is well known that Hacrp reacts with an excess of hydroxylamine in alkaline aqueous solution to give 8-hydroxy-5-oximino-7-methyl-5,8-dihydro-4H-pyrano[2,3-b]pyridin-4-one (referred to as Hppyox).[5] The same procedure cannot be followed with the Hacrp copper(II) complexes, because of the hydrolysis of the metal cation. Thus, this reaction was performed in ethanol using hydroxylamine hydrochloride (molar ratio Hacrp–hydroxylamine in the range from 1:1 to 1:4). Under these conditions, both Hacrp and Cu(acrp)$_2$·1/2KCl reacted to give the novel molecule 8-hydroxy-5-oxo-7-methyl-5,8-dihydro-4H-pyrano[2,3-b]pyridin-4-one (referred to as Hppy). By analogy with the mechanism proposed for Hppyox formation, we suppose that Hppy is formed as shown in Scheme 4. Hydroxylamine opens the pyran-2-one ring, by interacting with the carbon in the 2-position; then, in acid medium, two new rings are formed with elimination of dimethylamine. The novel molecule Hppy has been characterized by its analytical, mass and ^{1}H NMR spectral data. From these data it is not clear which is the isolated tautomer but some more information is obtained from its IR spectrum. In the latter one, three significant absorption bands are present at 1660, 1705 and 3200 cm^{-1}. They can be assigned to a pyran-4-one carbonyl stretching,[9] to a pyridone carbonyl stretching, and to a ν(OH), respectively; therefore, the most probable Hppy structure seems to be the tautomer I (see Scheme 4).

It is noteworthy that the formation of Hppy instead of Hppyox is merely determined by the acidity of the reaction medium. A possible explanation of this behaviour may be the protonation of the acryloyl carbonyl which stabilizes the charge separation in the acryloyl chain, thus inhibiting the acquisition of double bond character by the C(1)—O(1) bond and its consequent oximation. This interpretation apparently diagrees with the fact

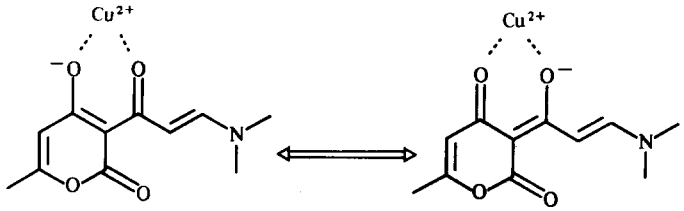

Scheme 3.

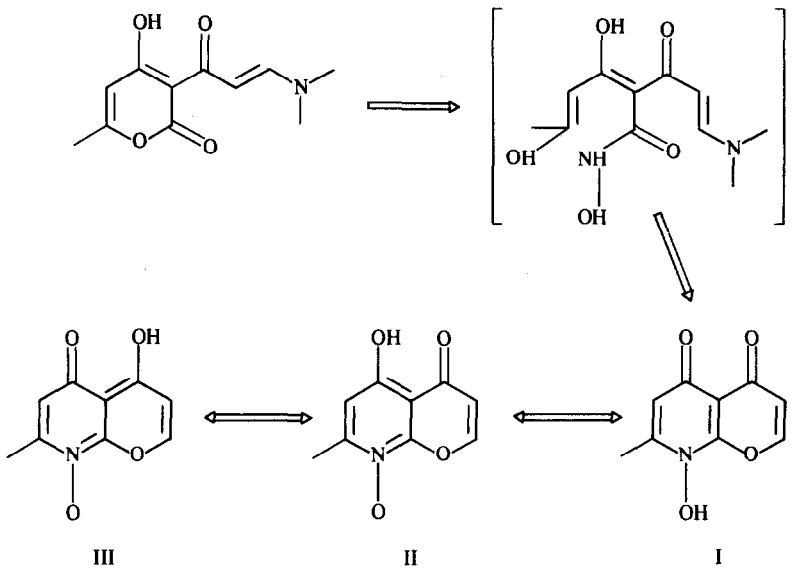

Scheme 4.

that Hppy is also obtained by reacting hydroxylamine hydrochloride with $Cu(acrp)_2 \cdot 1/2KCl$; in fact, it seems probable that in this complex the C(1)—O(1) bond acquires double bond character (as observed in the adduct $Cu(acrp)_2(py) \cdot H_2O$), thus becoming more easily oximable. However, it is possible that in the case of $Cu(acrp)_2 \cdot 1/2KCl$, the reaction proceeds only after the dissociation of the copper(II) complex and the subsequent protonation of acrp.

By reacting Hacrp with aqueous hydrochloric acid, 2,4-dihydroxoacetophenone was obtained instead of the expected β-diketone. A mechanism for this reaction is proposed in Scheme 5. The

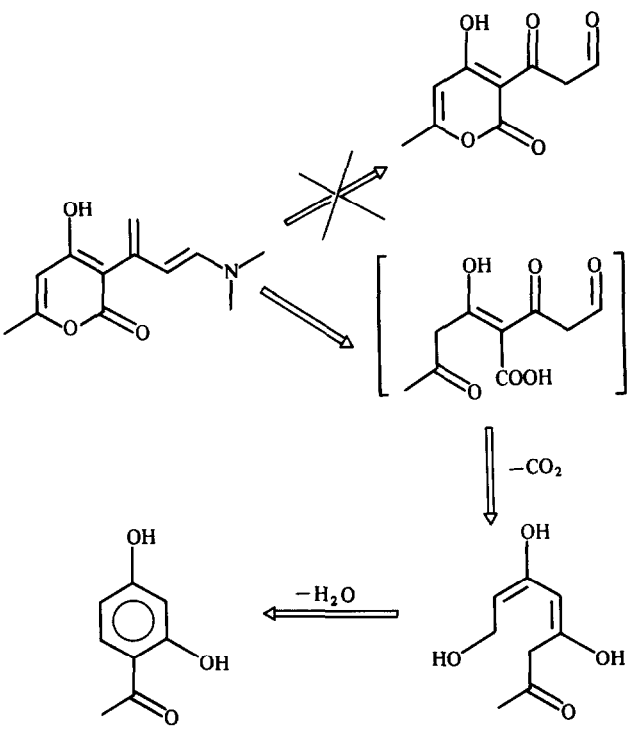

Scheme 5.

β-diketone is perhaps an intermediate of the reaction, but the pyrone ring opens, eventually giving the 2,4-dihydroxoacetophenone by elimination of carbon dioxide and water. In fact, carbon dioxide has been evidenced by stripping in a $Ba(OH)_2$ solution. 2,4-Dihydroxyacetophenone has been identified by comparing its IR, ^1H NMR and mass spectra and melting point with those of an authentic sample. By reacting the copper(II) complexes of Hacrp described here, with aqueous hydrochloric acid, only ill-defined products were isolated. However, the 2,4-dihydroxyacetophenone was also formed by reacting Hacrp with an aqueous solution of $CuCl_2 \cdot 2H_2O$. In this case the (2,4-dihydroxyacetophenonato)copper(II) was isolated at first, and then the 2,4-dihydroxyacetophenone was recovered by precipitating the metal as cyanide, thus proving considerable hard Lewis acid character of the copper(II) ion.

Acknowledgements—We are grateful to Professor A. Coda, Sezione di Cristallografia del Dipartimento di Genetica e Microbiologia dell'Università di Pavia, for helpful discussions. We also gratefully acknowledge Professor A. Gamba Ivernizzi and Dr G. Mellerio, Dipartimento di Chimica Organica dell'Università di Pavia, for the NMR and the mass spectra.

REFERENCES

1. C. Bisi Castellani, O. Carugo, C. Tomba and A. Gamba Invernizzi, *Inorg. Chem.* 1988, **27**, 3965; C, Bisi Castellani and O. Carugo, *Inorg. Chim. Acta* 1989, **159**, 157; C. Bisi Castellani and O. Carugo, *Polyhedron* 1990, **9**, 939; C. Bisi Castellani, O. Carugo, P. Ghigna and A. Invernizzi Gamba, submitted for publication; C. Bisi Catellani and O. Carugo, *Polyhedron* 1990, **9**, 1639.
2. M.-C. Ronzière, D. Herbage, R. Garrone and J. Frey, *Biochem. Pharm.* 1981, **30**, 1771; G. Cetta, G. Pallavicini, R. Tenni and C. Bisi, *Ital. J. Biochem.* 1977, **26**, 317.
3. F. J. C. Rossotti and H. Rossotti, *The Determination of Stability Constants*. McGraw-Hill, New York (1961).
4. J. A. Barltrop and J. D. Coyle, *Excited States in Organic Chemistry*, p. 49. John Wiley, London (1975).
5. W. Lowe, *J. Heterocycl. Chem.* 1977, **14**, 931.
6. B. A. Frenz and Associated Inc., College Station, TX 77840 and Enraf–Nonius, Delft, Holland (1985).
7. A. C. T. North, D. C. Phillips and F. S. Mathews, *Acta Cryst.* 1968, **A24**, 351.
8. *International Tables for X-ray Crystallography*, Vol. IV. Kynoch Press, Birmingham (1974).
9. P. J. Brogden, C. D. Gabbutt and J. D. Hepworth, in *Comprehensive Heterocyclic Chemistry* (Edited by A. R. Katritzky and C. W. Rees), Vol. 3, p. 573. Pergamon Press, Oxford (1984).
10. C. Bisi Castellani and O. Carugo, *Inorg. Chim. Acta* 1988, **150**, 119.
11. M. Gdaniec, I. Turowska-Tyrk and T. M. Krygowski, *J. Chem. Soc., Perkin Trans. II* 1989, 613.
12. C. W. Bird, *Tetrahedron* 1985, **41**, 1409; 1986, **42**, 89.
13. L. Pauling, *The Chemical Bond*. Cornell University Press, Ithaca, New York (1967).
14. G. C. S. Manku, *Aust. J. Chem.* 1971, **24**, 925.
15. W. Zemann, *Z. Anorg. Allg. Chem.* 1963, **324**, 241.
16. B. J. Hathaway, *Struct. Bond. (Berlin)* 1984, **57**, 55.
17. L. Menabue, M. Saladini, L. P. Battaglia and A. Bonamartini Corradi, *Inorg. Chim. Acta* 1987, **138**, 127.

Polyhedron Vol. 9, No. 17, pp. 2071–2080, 1990
Printed in Great Britain

0277–5387/90 $3.00+.00
© 1990 Pergamon Press plc

SYNTHESIS AND REACTIONS OF TRIS(TETRAMETHYLETHYLENEDIAMINELITHIUM)HEXAMETHYLMETALLATES OF RHODIUM, IRIDIUM AND RUTHENIUM(III) AND OF HEXAKIS(NEOPENTYL)(μ-OXO)DIRHODIUM(IV). X-RAY CRYSTAL STRUCTURES OF *FAC*-$RhMe_3(CO)(Me_2NCH_2CH_2NMe_2)$, *FAC*-$RhMe_3(C_4H_8S)(Me_2NCH_2CH_2NMe_2)$, *FAC*-$RhMe_3(PMe_3)_3$ AND $[(Me_3CCH_2)_3Rh]_2O$

ROBYN S. HAY-MOTHERWELL and GEOFFREY WILKINSON*

Johnson Matthey Laboratory, Chemistry Department, Imperial College, London SW7 2AY, U.K.

and

BILQUIS HUSSAIN-BATES and MICHAEL B. HURSTHOUSE*

Chemistry Department, Queen Mary and Westfield College, Mile End Road, London E1 4NS, U.K.

(*Received* 8 *March* 1990; *accepted* 2 *April* 1990)

Abstract—The interaction of methyllithium and the tetrahydrothiophen (THT) complexes, $MCl_3(THT)_3$ (M = Ru, Rh and Ir), in diethyl ether in the presence of tetramethylethylenediamine (TMED) gives the air- and thermally-sensitive compounds $[Li(TMED)]_3[MMe_6]$. The rhodium compound is the starting material for the synthesis of the *fac*-trimethyl compounds, $RhMe_3(THT)(TMED)$, $RhMe_3(CO)(TMED)$ and $RhMe_3(PMe_3)_3$; the iridium compound *fac*-$IrMe_3(CO)(TMED)$ is also described. Interaction of neopentyllithium or neopentylmagnesium bromide with $RhCl_3(THT)_3$ in the presence of a source of oxygen atoms (O_2 or Me_3NO) gives the diamagnetic compound, $[(Me_3CCH_2)_3Rh]_2\mu$-O, which contains rhodium in the IV oxidation state and a linear Rh—O—Rh bond. X-ray structures of the compounds listed in the title have been determined.

As noted in a preliminary communication,[1] the first homoleptic compounds of the platinum group metals to be described were the anionic species $[PtMe_6]^{2-}$ and $[PtMe_4]^{2-}$, that were characterized in solution by spectroscopic methods.[2] Subsequently, pentahalogeno anions for both palladium and platinum in oxidation states II and III have been characterized;[3] during the course of this work, the compound $[Ph_3P(CH_2Ph)][Rh(C_6F_5)_5]$, where the anion had a square-pyramidal structure according to X-ray study, was reported.[4] Neutral homoleptic alkyls[5,6] such as $Ru_2(CH_2SiMe_3)_6$ and $Ru(C_6H_{11})_4$ and aryls[6,7] such as $Ru(2\text{-}MeC_6H_4)_4$ and $Os(C_6H_5)_4$ have been described and some of the reactions of $Os(o\text{-}tol_4)$[8] and the electrochemistry[9] of the tetra-*o*-tolyls of Mo, Re, Ru and Os studied; the X-ray structure of the osmium(V) cation in the salt $[Os(2\text{-}MeC_6H_4)_4]CF_3SO_3$ was also determined by X-ray diffraction.[10]

This paper gives details of the synthesis and reactions of the compounds $[Li(TMED)]_3[MMe_6]$ (M = Ru, Rh and Ir); the X-ray structures of the rhodium and iridium compounds are described.[1] We describe also the synthesis and structure of the neopentyl compound $[(Me_3CCH_2)_3Rh]_2\mu$-O, which

* Authors to whom correspondence should be addressed.

contains rhodium, formally in the IV oxidation state.

RESULTS AND DISCUSSION

(1) *Lithium hexamethylmetallates of rhodium*(III), *iridium*(III) *and ruthenium*(III)

The compounds $[Li(TMED)]_3[MMe_6]$ (M = Rh, Ir, Ru) were made by interaction of the tetrahydrothiophen compounds, $MCl_3(THT)_3$, with six equivalents of methyllithium in diethyl ether at −78°C, with subsequent addition of TMED and crystallization from ether at *ca* −30°C.

All three compounds are very air-sensitive and thermally unstable; the rhodium and iridium compounds are stable to about 20°C but the ruthenium analogue decomposes above about 0°C. Although X-ray studies on the rhodium and iridium compounds were successful,[1] we have been able to show only that $[Li(TMED)]_3[RuMe_6]$ is isomorphous with the other two since decomposition under X-radiation occurs quite rapidly even at low temperature.

The hexamethylruthenate compound and $RuCl_3(THT)_3$ gave good X-band EPR spectra. For the latter in toluene at 77 K there are three distinct g values (2.61, 2.31 and 1.73); this is consistent with the *mer* structure of C_{2v} symmetry found in various ruthenium(III) tertiary phosphine and dialkyl and aryl sulphide complexes.[11] The EPR spectrum of $[Li(TMED)]_3[RuMe_6]$ in THF at 77 K indicated that it was consistent with that of an octahedral species of higher symmetry, with $g = 2.53$ and 1.56. A small band in the spectrum at $g = 2.08$ was shown to be a decomposition product as it increased in size at the expense of the other bands on re-recording the spectrum after storage at −30°C. The interaction of the $MCl_3(THT)_3$ compounds with a variety of lithium alkyls and aryls, e.g. $LiCH_2SiMe_3$, $Li(2\text{-}MeC_6H_5)$ and $LiCH_2CMePh_2$, gave solutions from which no clearly defined products could be isolated. However, the use of neopentyllithium or neopentyl Grignard reagent in the presence of an oxygen source led to the compound $[(Me_3CCH_2)_3Rh]_2O$ discussed below.

Reactions of the hexamethylmetallates. The rhodium compound has been most studied since it is easier to obtain than its iridium analogue and is somewhat more reactive. No clean reactions of the ruthenium compound have been discovered.

$[Li(TMED)]_3[RhMe_6]$ is stable for long periods in solution in petroleum, diethyl ether and aromatic hydrocarbons at −30°C. When the C_6D_6 solution stands at room temperature, decomposition occurs giving a black deposit and a colourless solution; successive ^1H NMR spectra showed that there is an unstable, unisolable intermediate containing equivalent methyl groups different from those in the hexamethyl with δ −0.36 ppm, $J_{Rh-H} = 1.0$ Hz, while the TMED resonances collapsed to a broad singlet at 2.06 ppm. When a concentrated diethyl ether solution of the initial reaction products from $RhCl_3(THT)_3$ and MeLi, containing $[Li(TMED)]_3[RhMe_6]$ and tetrahydrothiophen, is allowed to stand for a long period (*ca* 7 days at −30°C) a different product, namely $RhMe_3(TMED)(THT)$, can be isolated; the crystal structure is described later. An alternative, faster route to this compound is the interaction of ethylene with the filtered initial solution from the reaction of $RhCl_3(THT)_3$ and MeLi to which TMED was added. The hexamethyliridate is more stable in solution at −30°C but no isolable product has been obtained after decomposition. Interaction of $[Li(TMED)]_3[RhMe_6]$ with many reagents causes only decomposition and formation of rhodium metal or rhodium-containing solutions from which no clean products could be isolated. Molecular hydrogen with all three hexamethylates rapidly gives metal and methane.

Interaction of the rhodium and iridium compounds with carbon monoxide at atmospheric pressure gives the compounds *fac*-$MMe_3(CO)(TMED)$. The reaction presumably removes MeLi as an intermediate acylate,[12] for example

$$[LiTMED]_3[RhMe_6] \xrightarrow{CO} RhMe_3(CO)(TMED) + 3\text{ "Li(MeCO)"} + 2TMED.$$

The rhodium compound can also be made by action of carbon monoxide on $RhMe_3(TMED)(THT)$. Trimethylphosphine with the ruthenium compound gives only a black insoluble material; the iridium compound is unreactive up to the point where decomposition occurs but the rhodium compound and $RhMe_3(THT)(TMED)$ give *fac*-$RhMe_3(PMe_3)_3$ [m.p. (decomp.) 135°C]. A compound of this stoichiometry (m.p. 106–108°C) was made previously[13] by interaction of $Rh_2(CO_2Me)_4$, PMe_3 and $MgMe_2$, and was formulated as the *fac*-compound; however, in view of the X-ray structure of the present compound (below), its NMR spectra and difference in melting points, we now consider the earlier product to be the *mer*-isomer.

Cyclic voltammetric studies on the three lithium compounds in THF gave only irreversible waves for ruthenium, no oxidation or reduction waves for iridium, and only an irreversible oxidation wave for rhodium.

X-ray structures of the fac-*trimethyl compounds.* Diagrams of the three trimethylrhodium complexes are given in Figs 1 $RhMe_3(CO)(TMED)$, 2 $RhMe_3(THT)(TMED)$ and 3 $RhMe_3(PMe_3)_3$. Bond lengths and angles are given in Tables 1–3, respectively. For the carbonyl complex, the Rh—C(methyl) bond *trans* to the CO ligand is slightly longer than those *trans* to the nitrogen atoms, as expected. The ethylene bridge carbons of TMED are disordered, but this does not seem to have affected the positioning of the TMED methyl groups, which are probably locked into position via the rhodium-bonded methyl groups. Similarly, for the THT complex, the longest Rh—C bond is *trans* to the THT ligand.

For the phosphine complex the three Rh—C and the three Rh—P bonds are very similar, with the Rh—C(methyl) bonds longer than any of those in the first two complexes, indicating perhaps both greater steric crowding and *trans* influence from the trimethylphosphine ligands.

(2) *The compound* $[(Me_3CCH_2)_3Rh]_2\mu$-O

On one occasion, the interaction of neopentyllithium with $RhCl_3(THT)_3$ in diethyl ether gave a solution from which, after evaporation and extraction of the residue with hexane, green black crystals were obtained. This compound, as discussed below, has been shown to be the oxo-bridged rhodium(IV) species. It has turned out that, as in the discovery of hexamethyltungsten,[14] fortuitous interaction with oxygen dissolved in hexane was involved. The solubility of dioxygen in *n*-hexane at ambient temperature and pressure is *ca* 0.015 mol dm^3;[15] dioxygen reacts with alkyllithiums [ref. 11(a) p. 129 and (b) p. 192] to yield *ca* 36% of a peroxo species which could be the source of oxygen in the rhodium complex. Thus, for *ca* 0.3 g $RhCl_3(THT)_3$ used, a six-fold excess of neopentyllithium in degassed hexane needed to be treated with 28.4 cm^3 of dioxygen. In the absence of oxygen no compound could be isolated. Instead of dioxygen, we have found trimethylamine-N-oxide can be used. The addition of Li_2O, to thoroughly de-oxygenated reaction systems did not give the oxo complex. Even in the presence of oxygen sources, other lithium or magnesium alkylating agents, such as $LiCH_2SiMe_3$, $LiCH_2CMePh_2$, etc. do not give isolable products. The only exceptions are the aryls (mesityl and 2,6-xylyl) that will be described separately. Similar reactions using the ruthenium and iridium tetrahydrothiophen complexes gave no evidence for similar compounds.

As discussed below, the X-ray structural data on the compound initially suggested that it was a

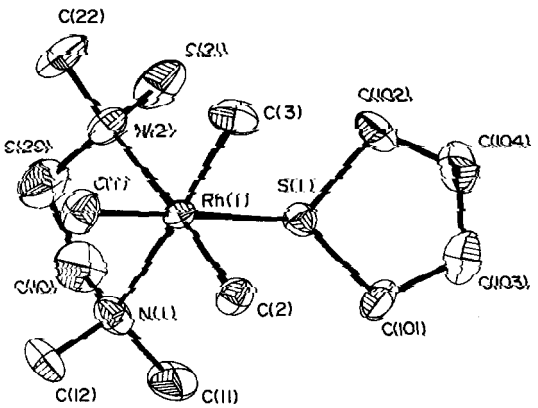

Fig. 2. The structure of *fac*-$RhMe_3(THT)(TMED)$.

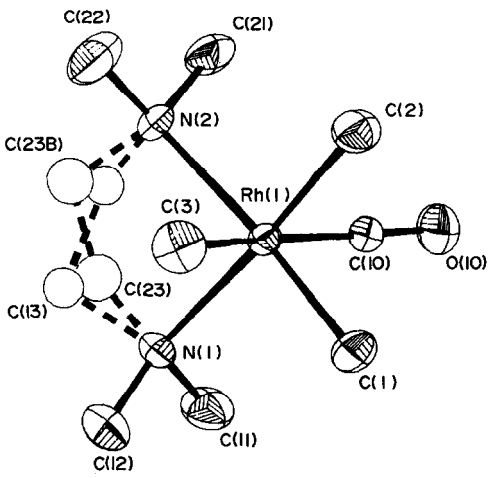

Fig. 1. The structure of *fac*-$RhMe_3(CO)(TMED)$.

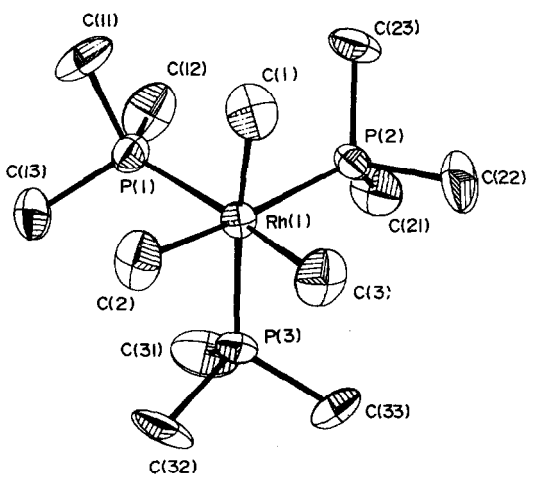

Fig. 3. The structure of *fac*-$RhMe_3(PMe_3)_3$.

Table 1. Selected bond lengths and bond angles for $C_{10}H_{25}N_2ORh$

Bond lengths (Å)			
N(1)—Rh(1)	2.266(7)	N(2)—Rh(1)	2.281(6)
C(1)—Rh(1)	2.065(8)	C(2)—Rh(1)	2.073(8)
C(3)—Rh(1)	2.096(8)	C(10)—Rh(1)	1.896(7)
Bond angles (°)			
N(2)—Rh(1)—N(1)	81.2(3)	C(2)—Rh(1)—C(1)	88.0(4)
C(10)—Rh(1)—N(1)	96.6(3)	C(10)—Rh(1)—N(2)	95.3(3)
C(1)—Rh(1)—N(1)	94.4(3)	C(1)—Rh(1)—N(2)	175.2(2)
C(1)—Rh(1)—C(10)	87.2(4)	C(2)—Rh(1)—N(1)	177.0(2)
C(2)—Rh(1)—N(2)	96.3(3)	C(2)—Rh(1)—C(10)	85.3(4)
C(3)—Rh(1)—N(1)	91.1(3)	C(3)—Rh(1)—N(2)	92.5(3)
C(3)—Rh(1)—C(10)	169.7(3)	C(3)—Rh(1)—C(1)	85.6(4)
C(3)—Rh(1)—C(2)	87.2(4)	C(11)—N(1)—Rh(1)	112.3(5)
C(12)—N(1)—Rh(1)	116.5(5)	C(13)—N(1)—Rh(1)	104.5(6)
C(13B)—N(1)—Rh(1)	103.0(7)	C(21)—N(2)—Rh(1)	113.0(5)
C(22)—N(2)—Rh(1)	116.7(5)	C(23)—N(2)—Rh(1)	103.9(5)
C(23B)—N(2)—Rh(1)	105.0(7)	O(10)—C(10)—Rh(1)	169.5(5)

lithium salt, so that it was necessary therefore to rigorously exclude this possibility:

(a) No lithium was found by flame test or by direct analysis.
(b) The identical compound, as shown by X-ray powder diffraction study and by NMR spectra, was obtained using neopentylmagnesium bromide again in the presence of dioxygen.
(c) Since X-ray photoelectron spectroscopic data is available for rhodium compounds in different oxidation states[16] we compared, under identical conditions, $Rh_2^{II}(O_2CMe)_4$, $Rh^{III}Cl_3(THT)_3$ and the μ-oxo compound. The observed binding energy for Rh $3d_{5/2}$ in each was 315.25, 316.3 and 317.0 eV (vs C1*s* of 291.3 eV), respectively, confirming the oxo species as having Rh^{IV}.

The molecular structure of $[(Me_3CCH_2)_3Rh]_2\mu$-O found by the X-ray study is shown in Fig. 4; diagrams of the crystal packing are shown in Figs 5 and 6. Selected bond lengths and angles are given in Table 4. The Rh—O—Rh bridge is linear by symmetry and the two Rh—O distances are equal within experimental error. Similarly, the Rh—C distances at the two independent rhodium atoms are equal within error, indicating equivalence of the

Table 2. Selected bond lengths and bond angles for $C_{13}H_{33}N_2RhS$

Bond lengths (Å)			
N(1)—Rh(1)	2.322(8)	N(2)—Rh(1)	2.295(8)
S(1)—Rh(1)	2.460(4)	C(1)—Rh(1)	2.073(10)
C(2)—Rh(1)	2.047(9)	C(3)—Rh(1)	2.061(9)
Bond angles (°)			
N(2)—Rh(1)—N(1)	81.2(3)	S(1)—Rh(1)—N(1)	88.1(3)
S(1)—Rh(1)—N(2)	91.0(3)	C(1)—Rh(1)—N(1)	92.6(4)
C(1)—Rh(1)—N(2)	91.4(4)	C(1)—Rh(1)—S(1)	177.6(2)
C(2)—Rh(1)—N(1)	96.5(4)	C(2)—Rh(1)—N(2)	176.0(3)
C(2)—Rh(1)—S(1)	92.3(3)	C(2)—Rh(1)—C(1)	85.3(4)
C(3)—Rh(1)—N(1)	175.6(3)	C(3)—Rh(1)—N(2)	94.4(4)
C(3)—Rh(1)—S(1)	91.8(4)	C(3)—Rh(1)—C(1)	87.7(5)
C(3)—Rh(1)—C(2)	87.9(4)	C(10)—N(1)—Rh(1)	104.1(6)
C(11)—N(1)—Rh(1)	114.0(6)	C(12)—N(1)—Rh(1)	114.2(7)
C(20)—N(2)—Rh(1)	102.7(6)	C(21)—N(2)—Rh(1)	114.8(6)
C(22)—N(2)—Rh(1)	113.7(6)	C(101)—S(1)—Rh(1)	114.8(4)
C(102)—S(1)—Rh(1)	115.8(4)		

Table 3. Selected bond lengths and bond angles for $C_{12}H_{36}P_3Rh$

Bond lengths (Å)			
P(1)—Rh(1)	2.321(5)	P(2)—Rh(1)	2.325(5)
P(3)—Rh(1)	2.322(6)	C(1)—Rh(1)	2.150(16)
C(2)—Rh(1)	2.162(15)	C(3)—Rh(1)	2.131(15)
Bond angles (°)			
P(2)—Rh(1)—P(1)	97.6(2)	P(3)—Rh(1)—P(1)	97.3(2)
P(3)—Rh(1)—P(2)	96.6(2)	C(1)—Rh(1)—P(1)	91.6(6)
C(1)—Rh(1)—P(2)	85.1(5)	C(1)—Rh(1)—P(3)	170.7(5)
C(2)—Rh(1)—P(1)	85.0(5)	C(2)—Rh(1)—P(2)	171.1(5)
C(2)—Rh(1)—P(3)	91.5(6)	C(2)—Rh(1)—C(1)	86.4(7)
C(3)—Rh(1)—P(1)	168.4(5)	C(3)—Rh(1)—P(2)	92.1(6)
C(3)—Rh(1)—P(3)	87.8(6)	C(3)—Rh(1)—C(1)	83.0(7)
C(3)—Rh(1)—C(2)	84.5(7)	C(11)—P(1)—Rh(1)	116.5(7)
C(12)—P(1)—Rh(1)	121.1(6)	C(13)—P(1)—Rh(1)	116.7(6)
C(21)—P(2)—Rh(1)	122.2(6)	C(22)—P(2)—Rh(1)	116.3(7)
C(23)—P(2)—Rh(1)	115.8(6)	C(31)—P(3)—Rh(1)	121.3(6)
C(32)—P(3)—Rh(1)	116.8(7)	C(33)—P(3)—Rh(1)	117.4(7)

two rhodium atoms, which are thus assigned as rhodium(IV). This is significant since the complex could be formulated as a mixed-valence species $R_3Rh^V{=}O \rightarrow Rh^{III}R_3$ with donor oxygen, but this seems less satisfactory. On the basis of the Dunitz and Orgel model for the linear M—O—M bonding[17] ion, the Rh—O—Rh bonding could be represented as $(e^6)^4[(b_{2g})^2(b_{1u})^2(e_g)^4](e_4{*})^2$, and the length of the Rh—O bonds at *ca* 1.90 Å perhaps reflect the occupancy of the antibonding orbitals.

The diamagnetism of the compound is thus associated with electron pairing of rhodium(IV) and Rh d_π–O p_π bonding. Other species[18a,b] with linear MOM groups include ions such as $[M_2(\mu\text{-O})X_{10}]^{4-}$ (M = Ru, Os, X = halogen) and $[Mo_2(\mu\text{-O})(MeCN)_{10}]^{4+}$.[18c]

The ^1H and ^{13}C NMR spectra of the compound show only neopentyl group resonances while IR spectra show neopentyl bands plus a band at 802 cm^{-1} that is assigned to the Rh—O—Rh stretch. We were unable to detect a RhORh band in the Raman spectrum, probably due to the intense

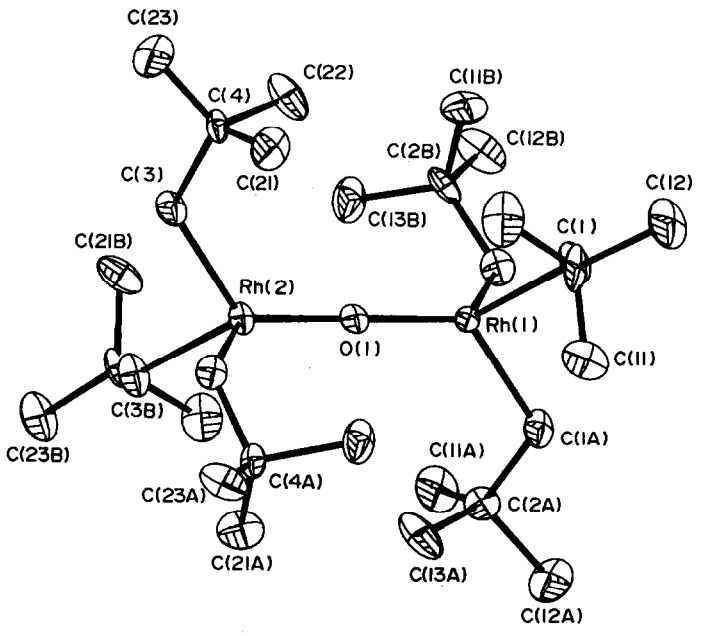

Fig. 4. The structure of $[(Me_3CCH_2)_3Rh]_2\mu$-O.

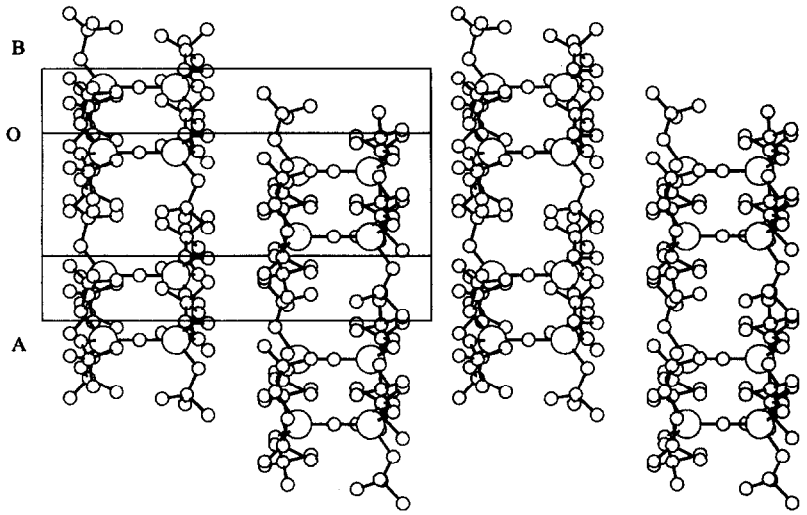

Fig. 5. Crystal packing in $[(Me_3CCH_2)_3Rh]_2\mu$-O.

colour of the solution. No oxo species of this type have been described for rhodium; μ_3-oxo groups in compounds of the type $[Rh_3(\mu_3O)(CO_2R)_6L_3]^+$ (L = neutral ligand) are known [18a,19] and an oxo-bridged species $[ONpORh^{III}(H_2O)_5]^{4+}$ has been characterized in solution.[20a] Well-characterized rhodium(IV) species are also rare.[20b,c] The only known organometallic compounds of rhodium in oxidation states IV and V are those having η^5-pentamethylcyclopentadienyl groups such as $[*CpRh^{IV}Me(\mu\text{-}CH_2)]_2$.[21]

The compound reacts with CO and Bu^{t}NC but several products are formed in both cases and we have not succeeded in isolating well-defined compounds. There was no reaction with O_2 nor with PhNCO at room temperature.

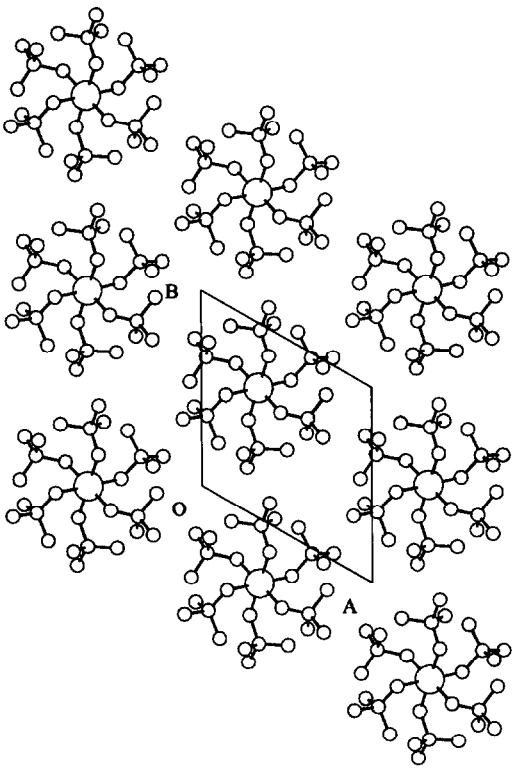

Fig. 6. Crystal packing along the *C* axis.

EXPERIMENTAL

Microanalyses were carried out by Imperial College Laboratories and Pascher, F.R.G. Spectrometers used were, IR, Perkin–Elmer 1720 (spectra in Nujol mulls in cm^{-1}); NMR, Bruker AM-500 and Bruker W-M 250 (data in ppm relative to $SiMe_4$ for ^1H in C_6D_6 unless otherwise stated and relative to external 85% H_3PO_4 for ^{31}P); EPR, X-band, Varian E-12.

X-ray powder spectra were recorded on a Siemens D-500 diffractometer with Cu-K_α, 40 kV, 30 mA source, using the following conditions: slit, 1°–1°–1°–0.15 mm; stepwidth, 0.02°; time, 0.5 s, and scan range, 2–60° (2θ). The rhodium compounds were finely ground and sealed in plastic bags, 25 × 10 mm, under argon.

X-ray photoelectron spectroscopic studies used a VG ESCALAB Mark II spectrometer with Al-K_α X-ray radiation. The analyser was set at 0.4 eV and the base pressure in the analysis chamber was 5×10^{-11} torr. The sample discs were prepared under argon with a layer of firmly ground compound pressed onto the surface of KBr.

Table 4. Selected bond lengths and bond angles for $C_{30}H_{66}ORh_2$

Bond lengths (Å)			
O(1)—Rh(1)	1.882(44)	O(1)—Rh(2)	1.900(44)
C(1)—Rh(1)	2.047(18)	C(3)—Rh(2)	2.037(18)
Bond angles (°)			
C(1)—Rh(1)—O(1)	124.5(5)	C(3)—Rh(2)—O(1)	124.9(6)
Rh(2)—O(1)—Rh(1)	180.0	C(2)—C(1)—Rh(1)	120.3(12)
C(1)—Rh(1)—C(1A)	91.2(7)	C(4)—C(3)—Rh(2)	112.7(12)
C(3)—Rh(2)—C(3A)	90.6(8)		

Melting points were determined in sealed capillaries and are uncorrected. Solvents were purified by standard methods and all manipulations were carried out *in vacuo* or under purified argon or nitrogen. Methyllithium was prepared by standard methods from lithium metal and CH_3Cl in diethyl ether, while neopentyllithium was prepared by sonication as described previously.[22] Me_3NO was dried using literature methods.[23]

(1) *Tris(tetramethylethylenediaminelithium)hexamethylmetallates of rhodium, iridium and ruthenium*(III)

Rhodium. To a stirred solution of $RhCl_3(C_4H_8S)_3$[24] (0.6 g, 1.3 mmol) in diethyl ether (*ca* 50 cm^3), at −78°C, was added a cooled six-fold excess of methyllithium (29.2 cm^3 of 0.26 M solution in Et_2O), and the solution allowed to warm to 0°C with vigorous stirring. After disappearance of $RhCl_3(THT)_3$ (*ca* 1 h) the colourless solution was filtered and $Me_2NCH_2CH_2NMe_2$ (4 cm^3) added. After 5 min the solution was reduced to about a third of its volume at 0°C under vacuum, then cooling to −30°C gave the hexamethylrhodate salt as colourless crystals. Yield: *ca* 92%. Recrystallization from Et_2O gave crystals of X-ray quality. The compound is very air-sensitive and decomposes above *ca* 20°C turning black.

^{1}H NMR: −0.52, 18H, d (J_{Rh-H} = 1.1 Hz), Rh—CH_3; 2.0, 12H, s, CH_2 (TMED); 2.04, 36H, s, NCH_3(TMED).

Iridium. The preparation was similar to that above but using $IrCl_3(THT)_3$[24] and allowing the reaction mixture to stir for a longer time (2–3 h) to completion. Yield: *ca* 90%. X-ray quality crystals were obtained from Et_2O at −30°C.

^{1}H NMR: 2.14, 54H, br, s, IrCH_3 plus N—CH_3(TMED); 2.18, 12H, br, s, CH_2(TMED). In concentrated solutions only a broad singlet at *ca* 2.0 ppm is observed and lowering the temperature gives no improved resolution.

Ruthenium. The previously unreported $RuCl_3(THT)_3$ was obtained as follows. To "$RuCl_3$(aq.)" (4.0 g, 19.3 mmol) in ethanol (300 cm^3) was added tetrahydrothiophen (10 cm^3) and the solution refluxed for 30 min. After filtering hot, the solution was cooled (−10°C) and the red crystalline product collected and dried *in vacuo*. Yield: 55%; m.p. 161–163°C. (Found: C, 30.6; H, 5.1. $C_{12}H_{24}Cl_3RuS_3$ requires: C, 30.6; H, 5.1%.)

The synthesis of [Li(TMED)]$_3$[RuMe$_6$] followed that for the rhodium compound. The yield is high, *ca* 90%, but the compound is very difficult to handle due to its low thermal stability and high air-sensitivity, but crystals can be obtained from ether and mounted in a capillary provided the temperature is kept at as low temperature as feasible.

(2) fac-*Trimethylrhodium and -iridium compounds*

fac - *Trimethyl(tetrahydrothiophen)(tetramethylethylenediamine)rhodium*(III). As noted in the discussion, this compound was first isolated from aged solutions of the reaction solution of $RhCl_3(THT)_3$ and MeLi in Et_2O. It is best obtained as follows. Through a diethyl ether solution of $RhCl_3(THT)_3$ (0.4 g, 0.8 mmol) and six equivalents of MeLi in Et_2O, to which TMED had been added at −78°C as above, was bubbled ethylene while the solution was allowed to warm to 0°C. After removal of volatiles *in vacuo*, the residue was extracted with hexane (*ca* 50 cm^3), which on cooling at −30°C gave the product. Yield: *ca* 75%; m.p. 83–84°C decomp. X-ray quality crystals were obtained from hexane. (Found: C, 45.0; H, 9.5; N, 8.1. $C_{13}H_{33}N_2RhS$ requires: C, 44.3; H, 9.4; N, 7.95%.)

^{1}H NMR: 0.5, 9H, d (J_{Rh-H} = 2.5 Hz), Rh—CH_3; 1.5, 4H, m, CH_2CH_2CH_2CH_2S; 1.87, 4H, s, CH_2(TMED); 2.01, 12H, s, CH_3(TMED); 2.61, 4H, br, s, CH_2CH$_2$CH$_2$CH_2S. ^{13}C-{^{1}H} NMR: −2.08, d (J_{Rh-C} = 36 Hz), Rh—CH_3; 30.65, $CH_2CH_2CH_2CH_2S$; 31.33, br, CH_2CH_2

CH_2CH_2S; 48.33, CH_3(TMED); 59.6, CH_2 (TMED).

fac - *Trimethyl(carbonyl)(tetramethylethylenediamine)rhodium*(III). Through a tetrahydrofuran solution of $[Li(TMED)]_3[RhMe_6]$ (0.7 g 1.25 mmol) and TMED (0.19 cm^3, 1.26 mmol) at −78°C was slowly bubbled CO for 0.75 h; after warming to room temperature and removing volatiles *in vacuo* the residue was extracted with hexane (50 cm^3), which was filtered, reduced in volume (15 cm^3) and cooled at −30° to give cream crystals. Yield: 0.12 g, 50%; m.p. 104–106°C decomp. X-ray quality crystals were obtained from hexane at −30°C. (Found: C, 40.2; H, 8.6; N, 8.9. $C_{10}H_{25}N_2ORh$ requires: C, 41.1; H, 8.6; N, 9.6%.)

IR (Nujol): 1978 [ν(CO)]. ^{1}H NMR: 0.32, 3H, d (J_{Rh-H} = 1.8 Hz), Rh—CH_3; 0.71, 6H, d (J_{Rh-H} = 2.4 Hz), Rh(CH_3)$_2$; 1.64, 4H approx. AB system ($J_{a-b/2}$ = 2.1 Hz), CH_2 (TMED); 1.8, 6H, s, NCH_3; 2.1, 6H, s, NCH_3. ^{13}C-{^{1}H} NMR: −4.6, d (J_{Rh-C} = 28.8 Hz), Rh(CH_3)$_2$; 25.7, d (J_{Rh-C} = 25.2 Hz), Rh—CH_3; 47.0, NCH_3; 54.1, NCH_3 60.0 CH_2(TMED); 190.75, d (J_{Rh-C} = 50.2 Hz), Rh—CO.

There was no further reaction of the compound with CO at 100°C and no reaction with Me_3NO, but Bu^{t}NC (at low temperature) gave a cream-coloured crystalline material which rapidly turned black–red at room temperature; no clean product could be isolated.

fac - *Trimethyltris(trimethylphosphine)rhodium*(III). Although this compound can be made from $[Li(TMED)]_3[RhMe_6]$ it is more convenient to use $RhMe_3$(THT)(TMED) (*ca* 1g) in Et_2O at 0°C and excess PMe_3. After *ca* 15 min the solution was evaporated, and the residue extracted with hexane (*ca* 10 cm^3); cooling at −30°C gave yellow crystals. Yield; *ca* 95%; dec. >135°C. (Found: C, 38.0; H, 9.7. $C_{12}H_{36}P_3Rh$ requires: C, 38.3; H, 9.6%.)

^{1}H NMR: 0.94, 27H, m (J = 5.6 Hz) P—CH_3; this resonance has a broad central line flanked by the 1:1 doublet; the J value corresponds to the separation of the outer peaks; 0.20, 9H, complex m, Rh—CH_3. ^{13}C-{^{1}H} NMR: 6.5 d, d, d, d, ($J_{P_{ax}-C}$ = 114 Hz, J_{Rh-C} = 22.5 Hz, J_{P-C} = 13.8 Hz, J_{P-C} = 9 Hz) Rh—CH_3; 17.9, complex m, P—CH_3. ^{31}P-{^{1}H} NMR: −32.4, *d* (J_{Rh-P} = 83.5 Hz).

fac - *Trimethyl(carbonyl)tetramethylethylenediamine)iridium*(III). A THF solution of $[Li(TMED)]_3$ $[IrMe_6]$ (*ca* 0.5 g) was treated with CO as for the rhodium analogue above to give a cream solid. Yield: *ca* 40%.

IR (Nujol): 1962 [ν(CO)]. ^{1}H NMR: 0.24, 3H, s, Ir—CH_3; 1.02, 6H, s, Ir—CH_3; 1.69, 4H, complex m, CH_2 (TMED); 1.87, 6H, s, NCH_3; 2.38, 6H, s, NCH_3. The complex multiplet for the CH_2 groups in $Me_2NCH_2CH_2NMe_2$ showed increased inequivalence of these CH_2 ring protons compared to those in the rhodium analogue.[25]

(3) *Bis[tris(neopentyl)rhodium*(IV)]μ-oxo

To a six-fold excess of neopentyllithium (7.8 cm^3 of a 0.49 M solution in Et_2O) in Et_2O (30 cm^3) at −78°C was added, via syringe, 28.4 cm^3 of dry dioxygen. The solution was allowed to warm slowly to room temperature, then re-cooled to −78°C when it was added to a suspension of $RhCl_3(THT)_3$ (0.3 g, 0.6 mmol) in Et_2O (30 cm^3) at −78°C. The vigorously stirred solution was allowed to warm to room temperature and after *ca* 1 h, the volatiles were removed *in vacuo* and the residue extracted with hexane (3 × 30 cm^3). Reduction in volume of the filtered solution to 40 cm^3 and cooling at −30°C gave dark green–black crystals. Yield: *ca* 30%; m.p. 167–168°C decomp. Crystals of X-ray quality were obtained by repeated crystallization from hexane. (Found: C, 55.5; H, 10.2; O, 2.5; Li, 0.0. $C_{30}H_{66}ORh_2$ requires: C, 55.5; H, 10.3; O, 2.5; Li 0.0%.)

IR: 802, Rh—O—Rh, and neopentyl bands. ^{1}H NMR: 1.29, 54H, s, CCH_3; 2.9, 12H, s, CH_2. Pulse studies gave no evidence of ^{103}Rh coupling with the CH_2 groups bound to Rh. ^{13}C-{^{1}H} NMR: 32.9 (CH_3)$_3$C; 34.8 Me_3C; 52.8 d (J_{Rh-C} = 39 Hz), RhCH_2.

The compound is also obtained in similar yield by addition to $RhCl_3(THT)_3$, as above, of a four-fold excess of neopentyllithium plus a two-fold excess of trimethylamineoxide in Et_2O. An alternative procedure uses the Grignard reagent: a mixture of a four-fold excess of neopentylmagnesium bromide (0.25 M) and Me_3NO (0.064 g, 0.85 mmol) in Et_2O (27 cm^3) was added to $RhCl_3(THT)_3$ (0.8 g, 1.69 mmol) in Et_2O (60 cm^3) at −78°C. After warming to room temperature the mixture was stirred for *ca* 12 h after which it was evaporated *in vacuo*. Extraction of the residue with hexane and work-up gave the compound in *ca* 36% yield.

X-ray crystallography

Crystals of the three trimethylrhodium compounds were sealed under argon in thin-walled glass capillaries. Following preliminary photography, orientation matrices and associated cell dimensions were obtained using standard procedures on a CAD4 diffractometer with graphite monochromated Mo-K_α radiation (λ = 0.71069 Å). In the case of the oxo-bridged dimer, many crystals had to be tried before an acceptable one was found.

Table 5. Crystal data, details of intensity measurements and structure refinement

Molecular formula	$C_{10}H_{25}N_2ORh$	$C_{13}H_{33}N_2RhS$	$C_{12}H_{36}P_3Rh$	$C_{30}H_{66}ORh_2$
Molecular weight	292.220	352.374	376.22	648.664
Crystal system	Monoclinic	Monoclinic	Monoclinic	Trigonal
a (Å)	8.163(3)	12.689(3)	15.318(3)	9.898(3)
b (Å)	13.321(3)	15.855(5)	13.657(8)	9.898(3)
c (Å)	13.385(4)	8.421(3)	9.402(1)	20.172(4)
α (°)	90	90	90	90
β (°)	101.10(2)	90.1(3)	93.90(1)	90
γ (°)	90	90	90	120
V (Å^3)	1428.30	1706.47	1962.32	1716.84
Space group	$P2_1/n$	$P2_1/n$	$P2_1/n$	$P\bar{3}1c$
Z	4	4	4	2
D_c (g cm^{-3})	1.302	1.371	1.273	1.258
μ (cm^{-1})	10.60	10.889	8.43	8.92
F(000)	608	744	792	688
h, k, l range	$0 \rightarrow 9$	$-15 \rightarrow 15$	$-16 \rightarrow 16$	$0 \rightarrow 10$
	$0 \rightarrow 15$	$0 \rightarrow 18$	$0 \rightarrow 15$	$0 \rightarrow 10$
	$-15 \rightarrow 15$	$0 \rightarrow 10$	$0 \rightarrow 10$	$-22 \rightarrow 22$
Total number of reflections	2831	3295	3066	1920
Number of unique reflections	2513	2949	2725	802
Number of reflections used ($F > 3\sigma(F)$	2115	2485	1510	609
Number of parameters	167	154	145	119
Weighting scheme parameter g in $w = 1/[\sigma^2(F_o + gF_o^2)]$	0.0003	0.0011	0.0005	0.0016
Final R	0.0391	0.0583	0.0460	0.0407
Final R_w	0.0453	0.0551	0.0483	0.0422

Intensity data were recorded using the ω–2θ scan mode and empirical absorption corrections were applied. The structures were solved and developed via the Patterson and heavy atom method, and refined by full-matrix least-squares. Non-hydrogen atoms were assigned anisotropic displacement factor coefficients and hydrogens were included in idealized positions, with individual U_{iso} values only in the carbonyl structure and then not on the TMED CH_2 groups which were disordered over two sites (occupancies 0.56 and 0.44).

For the oxo-bridged compound, a difference map computed after all atoms in the [(Me$_3$CCH$_2$)$_3$Rh]$_2$O unit had been included showed four residual peaks of significant density, all on three-fold axes. At first these were believed to be lithium ions with the occupancies summing to give an overall complex formula $Li_2\{[(Me_3CCH_2)_3Rh]_2O\}$, and thus a rhodium(III) complex, moreover, the lithium ions were co-ordinated, albeit with a very distorted geometry, to neopentylmethyl groups. After comprehensive chemical and spectroscopic studies (see above) showed quite clearly that there was no lithium present, we realized that the four peaks, which occurred in two pairs were images of the Rh—Rh pair—the interatomic distances were closely similar. The origin of this "ghosting" we believe to be stacking faults. Examination of the molecular packing shows that the dimers, aligned along the C axis, occur on sheets—see Fig. 6—and it is easy to see how slippage could occur in the stacking of the layers. Although the occupancy of the ghost sites corresponds to only *ca* 0.07 Rh, inclusion in the structure factor calculation made a very significant difference to the R value—0.041 vs 0.064 and led to stable refinement. The geometry parameters for the dimer molecule were essentially unaffected. Accordingly, these fractional rhodium atoms have been retained in the atom list and for the final R value calculation. Details of the crystal data, data collection and structure refinements are given in Table 5. Tables of atom parameters and F_o/F_c values have been deposited as supplementary material with the Editor. Atomic coordinates have also been deposited with the Cambridge Crystallographic Data Centre.

Acknowledgements—We thank Johnson Matthey plc for loan of platinum group metals, Dr R. G. Egdell and Mr M. Golden for X-ray photoelectron spectra, Mr Heyeng He for X-ray powder diffraction studies, and Mr R. Shep-

pard and Dr J. F. Gibson for helpful discussions on NMR and EPR spectra.

REFERENCES

1. R. S. Hay-Motherwell, G. Wilkinson, B. Hussain and M. B. Hursthouse, *J. Chem. Soc., Chem. Commun.* 1989, 1436.
2. G. W. Rice and R. S. Tobias, *J. Am. Chem. Soc.* 1977, **99**, 2141; C. S. Creaser and J. A. Creighton, *J. Organomet. Chem.* 1978, **157**, 243.
3. R. Usón and J. Fornies, *Adv. Organomet. Chem.* 1988, **28**, 219.
4. M. P. Garcia, L. A. Oro and F. J. Lahoz, *Angew. Chem. Int. Edn Engl.* 1988, **27**, 1700.
5. R. P. Tooze, G. Wilkinson, M. Motevalli and M. B. Hursthouse, *J. Chem. Soc., Dalton Trans.* 1986, 2711.
6. P. Stavropoulos, P. D. Savage, R. P. Tooze, G. Wilkinson, B. Hussain, M. Motevalli and M. B. Hursthouse, *J. Chem. Soc., Dalton Trans.* 1987, 557.
7. P. D. Savage, G. Wilkinson, M. Motevalli and M. B. Hursthouse, *J. Chem. Soc., Dalton Trans.* 1988, 669.
8. J. Arnold, G. Wilkinson, B. Hussain and M. B. Hursthouse, *Organometallics* 1989, **8**, 1362.
9. J. Arnold, G. Wilkinson, B. Hussain and M. B. Hursthouse, *J. Chem. Soc., Dalton Trans.* 1989, 2149.
10. J. Arnold, G. Wilkinson, B. Hussain and M. B. Hursthouse, *J. Chem. Soc., Chem. Commun.* 1988, 1349.
11. A. Hudson and M. J. Kennedy, *J. Chem. Soc. A* 1969, 1116; J. Chatt, G. J. Leigh and A. P. Storace, *J. Chem. Soc. A* 1971, 1380.
12. B. J. Wakefield (a) *Organolithium Methods*, p. 95. Academic Press, London (1988); (b) *The Chemistry of Organolithium Compounds*, p. 122. Pergamon Press, Oxford (1974).
13. R. A. Anderson, R. A. Jones and G. Wilkinson, *J. Chem. Soc., Dalton Trans.* 1978, 446.
14. A. L. Galyer and G. Wilkinson, *J. Chem. Soc., Dalton Trans.* 1976, 2235.
15. E. Wilhelm and R. Battino, *Chem. Rev.* 1973, **73**, 1; R. Battino and H. L. Clever, *Chem. Rev.* 1966, **66**, 395.
16. H. E. Fisher and J. Schwartz, *J. Am. Chem. Soc.* 1989, **111**, 7644 and refs quoted therein.
17. J. D. Dunitz and L. E. Orgel, *J. Chem. Soc.* 1953, 2594.
18. (a) B. O. West, *Polyhedron* 1989, **8**, 219 (Review on oxo complexes); (b) F. A. Cotton and G. Wilkinson, *Advanced Inorganic Chemistry*, 5th edn, p. 466. John Wiley, New York (1988); (c) B. S. McGilligan, T. C. Wright, G. Wilkinson, M. Motevalli and M. B. Hursthouse, *J. Chem. Soc., Dalton Trans.* 1988, 1737.
19. A. Spencer, S. Uemura and G. Wilkinson, *J. Chem. Soc., Dalton Trans.* 1973, 2565.
20. (a) F. H. Jardine and P. S. Sheridan, *Comprehensive Coordination Chemistry* (Edited by G. Wilkinson, R. D. Gillard and J. A. McCleverty), Vol. 4, Sect. 48.6.65. Pergamon Press, Oxford (1987); (b) *ibid.*, Sect. 48.7; (c) ref. 18 (b), p. 914.
21. I. M. Saez, N. J. Meanwell, A. Nutton, K. Isobe, V. Vazquez de Miguel, D. W. Bruce, S. Okeya, D. G. Andrews, P. R. Ashton, I. R. Johnstone and P. M. Maitlis, *J. Chem. Soc., Dalton Trans.* 1986, 1565.
22. R. S. Hay-Motherwell, G. Wilkinson, B. Hussain-Bates and M. B. Hursthouse, *Polyhderon* 1990, **9**, 931.
23. V. Franzen, *Org. Synth.* 1967, **47**, 96.
24. E. A. Allen and W. Wilkinson, *J. Chem. Soc., Dalton Trans.* 1972, 613.
25. For a discussion of diamine complex spectra, see T. W. Hambley, C. J. Hawkins, J. Martin, J. A. Palmer and M. L. Snow, *Aust. J. Chem.* 1981, **34**, 2505.

Polyhedron Vol. 9, No. 17, pp. 2081–2096, 1990
Printed in Great Britain

0277–5387/90 $3.00+.00
© 1990 Pergamon Press plc

t-BUTYLIMIDO AND *t*-BUTYLIMIDO OXO ARYLS OF RHENIUM. X-RAY CRYSTAL STRUCTURES OF $Re(NBu^t)_2(2,6\text{-}Me_2C_6H_3)_2$, $Re(NBu^t)(2,4,6\text{-}Me_3C_6H_2)(C_{27}H_{32})$, $Re(NBu^t)_3(2,4,6\text{-}Me_3C_6H_2)$, $[(Bu^tN)Br(2,4,6\text{-}Me_3C_6H_2)Re(\mu\text{-}NBu^t)(\mu\text{-}O)Re(OC_6H_2Me_2CH_2)(NBu^t)]$, $[Re(NBu^t)(O)Ar(\mu\text{-}O)]_2$, Ar = 2,6-$C_6H_3$ AND 2,4,6-C_6H_2

ANGEL GUTIERREZ and GEOFFREY WILKINSON*

Johnson Matthey Laboratory, Chemistry Department, Imperial College, London SW7 2AY, U.K.

and

BILQUIS HUSSAIN-BATES and MICHAEL B. HURSTHOUSE*

Chemistry Department, Queen Mary and Westfield College, Mile End Road, London E1 4NS, U.K.

(*Received* 14 *March* 1990; *accepted* 2 *April* 1990)

Abstract—The interaction of $Re(NBu^t)_2Cl_3$ with 2,6-xylyl magnesium bromide gives rise to the paramagnetic rhenium(VI) compound, $Re(NBu^t)_2(xyl)_2$, which is readily oxidized to the cation $[Re(NBu^t)_2(xyl)_2]^+$, isolated as its PF_6^- salt; the latter with Bu^tNC gives the iminoacyl cation $[Re(NBu^t)_2(xyl)(Bu^tN{=}Cxyl)]^+$. An unstable rhenium(V) anion, $[Re(NBu^t)_2(xyl)_2]^-$, has been characterized. Interaction of $Re(NBu^t)_2Cl_3$ with excess mesityl Grignard gives a compound of stoichiometry $Re(NBu^t)(mes)(C_{27}H_{32})$ in which three aromatic rings are coupled, the central one comprising a η^5-cyclohexadienyl ring bearing an *exo*-mesityl group in the 1-position and in the 3-position linked by a CH_2 group to an aryl group σ-bonded to the metal, which is formally in the V oxidation state. The compound $Re(NBu^t)_2Cl(o\text{-}tol)_2$ has been synthesized; treatment with $AgPF_6$ produces the salt $[Re(NBu^t)_2(o\text{-}tol)_2]PF_6$. Hydrolysis of $Re(NBu^t)_2ReCl_3$ with LiOH gives $Re(NBu^t)_2Cl(OH)_2$, which on arylation, gives the oxo imido species $Re(NBu^t)_2(O)mes$ and $[(Bu^tN)Br(mes)Re(\mu\text{-}NBu^t)(\mu\text{-}O)Re(OC_6H_2Me_2CH_2)(NBu^t)_2]$. Interaction of excess NO with $Re(NBu^t)_2Ar_2$, Ar = 2,6-xylyl and mesityl, gives the compounds $[Re(NBu^t)(O)(\mu\text{-}O)Ar]_2$; the reaction involves a unique N—N bond formation to give $Bu^tN{=}NAr$. Stoichiometric reactions of $Re(NBu^t)_2(xyl)_2$ and NO lead to the complexes $Re(NBu^t)_2(xyl)_2NO$ and $Re(NBu^t)_2(O)(xyl)$. Mechanisms for the NO reactions are proposed. X-ray structures of the compounds listed in the title have been determined; the compounds $[Re(NBu^t)(O)(\mu\text{-}O)Ar]_2$ have asymmetric oxo bridges.

In previous papers we have described the synthesis and X-ray crystal structures of a number of oxo[1,2] and *t*-butylimido[2,3] aryls of rhenium(V), (VI) and (VII). Extensions of these studies are now reported; Table 1 summarizes present knowledge of the aryl compounds. Table 2 gives analytical and physical data for the new compounds described in this paper.

RESULTS AND DISCUSSION

(1) t-*Butylimido aryls*

(a) 2,6-*Dimethylphenyl compounds*. Although the interaction of $Re(NBu^t)_2Cl_3$ with *o*-tolyl Grignard reagent gives the triaryl,[3] the mesityl Grignard

* Authors to whom correspondence should be addressed.

Abbreviations used: *o*-tol = 2-MeC_6H_4, xyl = 2,6-$Me_2C_6H_3$, mes = 2,4,6-$Me_3C_6H_2$.

Table 1. *t*-Butylimido, *t*-butylimidoxo and oxo aryls of rhenium[a]

Oxidation state	Compound	X-ray structure
V	$[O_2ReAr_2]_2Mg(THF)_2$; xyl,[b] mes,[c]	
	$(Bu^tN)Re(mes)(\sigma,\eta^5\text{-}C_{27}H_{32})$[d]	[d]
	$(Bu^tN)_2Re(NO)(xyl)_2$[d]	
	$[(Bu^tN)_2Re(xyl)_2]^-$[d]	
VI	$OReAr_4$; mes,[c] *o*-tol,[c] *o*-$MeOC_6H_4$[c]	mes[c]
	$(O)_2ReAr_2$; mes,[c] xyl[b]	mes,[c] xyl[b]
	$Re_2(NBu^t)_2(\mu\text{-}NBu^t)(\mu\text{-}O)Br(mes)(OC_6H_2Me_2CH_2)$[d]	[d]
	$(Bu^tN)_2ReAr_2$; xyl,[d] mes[e]	xyl[d]
VII	O_3ReAr; mes[f,g] and others[g]	mes[g]
	$(Bu^tN)_2(O)ReAr$; xyl,[d] mes[d]	
	$[(Bu^tN)(O)_2ReAr]_2$; xyl,[d] mes[d]	xyl,[d] mes[d]
	$(Bu^tN)_2Re(o\text{-tol})_3$[e]	
	$(Bu^tN)_2ReCl(o\text{-tol})_2$[d]	
	$(Bu^tN)_2ReCl_2Ar$; Ph,[e] *o*-tol,[b] xyl,[b] mes[b]	Ph,[e] *o*-tol[b]
	$[(Bu^tN)_2ReAr_2]^+$; *o*-tol,[d] xyl,[d] mes[e]	
	$\{(Bu^tN)_2ReAr[\eta^2\text{-}RN{=}CAr]\}^+$; xyl,[d] mes[e]	
	$(Bu^tN)_3ReAr$; *o*-tol,[b] xyl,[b] mes[b]	mes[d]

[a] *o*-tol = 2-MeC_6H_4, xyl = 2,6-$Me_2C_6H_3$, mes = 2,4,6-$Me_3C_6H_2$.
[b] Reference 2.
[c] Reference 1.
[d] This paper.
[e] Reference 3.
[f] Reference 11.
[g] W. A. Herrmann *et al.*, *J. Organomet. Chem.* 1989, **371**, C13.

produced the rhenium(VI) compound, $Re(NBu^t)_2(mes)_2$, which was paramagnetic with one unpaired electron and which was readily oxidized to the rhenium(VII) cation $[Re(NBu^t)_2(mes)_2]^+$. The latter gave an iminoacyl cation with Bu^tNC.

The 2,6-dimethylphenyl analogue has now been made in a similar way; it is also oxidized by Ag^+ salts to give the cation $[Re(NBu^t)_2(xyl)_2]^+$ which was isolated as orange PF_6^- or $CF_3SO_3^-$ salts. The ^1H NMR spectrum of the salts in solution shows equivalent *t*-butyl and xylyl groups. This cation, like the mesityl analogue, undergoes insertion with *t*-butylisocyanide to give the iminoacyl cation which was isolated as a white, air-stable PF_6^- salt.

Although a cyclic voltammetry study showed[3] that $Re(NBu^t)_2(mes)_2$ underwent a reversible one-electron reduction, the rhenium(V) anion could not be isolated. Reduction of the xylyl by Na/Hg or Mg in THF gives purple solutions of a very air-sensitive diamagnetic species that is evidently $[Re^V(NBu^t)_2(xyl)_2]^-$. Dark purple, crystalline solids can be isolated from the solution but they are difficult to handle being very readily re-oxidized to the rhenium(VI) precursor. The ^1H NMR spectrum of the anion has signals at 7.24–7.06 (*m*, *p*-$C_6H_3Me_2$), 2.41 (*o*-Me) and 1.49 (Bu^t) ppm that are shifted relative to those in the cation (cf. 7.42–7.21, 2.46, 1.80 ppm); this shift is consistent with the anionic formulation.

The X-ray crystal structure of $Re(NBu^t)_2(xyl)_2$ has been determined and a diagram of the structure is shown in Fig. 1; bond lengths and angles are given in Table 3. The coordination geometry of rhenium is, as expected, very similar to that found for the analogous dioxo complex.[2] The Re—C (xylyl) distances in the imido complex are just slightly larger [*ca* 0.03(1) Å] than those in the oxo complex. The C—Re—C angles are equal within experimental error. The Re=NBu^t distances are *ca* 0.05(1) Å longer than the Re=O distances, consistent with the large covalent radius of N, but the N—Re—N angle at 121.7(6)° is equal, within error, to the O—Re—O angle of 121.3(4)°.

$Re(NBu^t)_2(xyl)_2$ in solution at 295 K has an electron paramagnetic resonance spectrum similar to that for the mesityl analogue;[3] there is again

Table 2. Analytical[a] and physical data for rhenium compounds

Compound	Colour	Melting point (°C)	Analysis (%)[b] C	H	N
$Re(NBu^t)_2(xyl)_2$	Red	117	54.1 (53.4)	6.7 (6.7)	5.2 (5.1)
$[Re(NBu^t)_2(xyl)_2]PF_6$	Orange	161	40.4 (42.1)	5.2 (5.3)	4.2 (4.1)
$Re(NBu^t)_2(xyl)(Bu^tN{=}Cxyl)PF_6$	Colourless	167	43.4 (45.4)	5.7 (5.9)	5.8 (5.5)
$Re(NBu^t)(mes)(C_{27}H_{32})$	Red	205	65.4 (65.6)	7.1 (7.1)	1.8 (1.9)
$Re(NBu^t)_2Cl(o\text{-tol})_2$	Yellow	120	48.1 (48.4)	5.7 (5.8)	5.1 (5.1)
$[Re(NBu^t)_2(o\text{-tol})_2]PF_6$	Yellow	141	40.8 (40.3)	4.6 (4.9)	4.2 (4.3)
$Re(NBu^t)_2Cl(OH)_2$	Yellow	[c]	22.0 (24.1)	5.1 (5.1)	6.8 (7.0)
$Re(NBu^t)_2(O)(mes)$	Yellow	106	45.0 (44.1)	6.1 (6.2)	5.0 (6.0)
$Re_2(NBu^t)_3Br(O)(mes)(CH_2Me_2C_6H_2O)$	Red	d 205	38.6 (38.5)	5.2 (5.2)	4.5 (4.5)
$[Re(NBu^t)(O)_2(xyl)]_2$	Yellow	99	36.2 (36.4)	4.6 (4.6)	3.5 (3.5)
$[Re(NBu^t)(O)_2(mes)]_2$	Orange	97	38.2 (38.1)	5.0 (5.0)	3.4 (3.4)
$Re(NBu^t)_2(xyl)_2NO$	Orange	141	45.8 (50.6)	6.4 (6.3)	7.3 (7.4)
$Re(NBu^t)_2(O)(xyl)$	Dark yellow	144	43.0 (42.6)	6.0 (6.0)	6.2 (6.2)

[a] For mass spectra see Experimental.
[b] Required in parentheses.
[c] Melting point, 134°C, is probably that of $Re(NBu^t)_2Cl(O)$ formed on loss of H_2O.

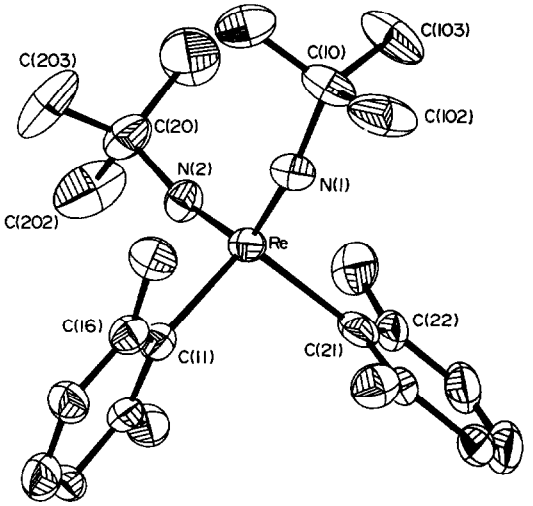

Fig. 1. The structure of $Re(NBu^t)_2(xyl)_2$.

a six-line hyperfine structure with $g_{iso} = 1.934$, $A = 0.0141\ cm^{-1}$. On lowering the temperature the spectrum changes giving a complicated pattern comprising three sets of six rhenium hyperfine lines with uneven spacing. Similar patterns for the mesityl[3] and the related oxo aryls, $Re(O)_2(Ar)_2$,[1,2] were attributed to restriction of rotation of the aryl groups about the Re—C bonds and the same explanation probably holds in the present case.

(b) *The compound* $Re(NBu^t)(mes)(C_{27}H_{32})$. As noted above, interaction of $Re(NBu^t)_3Cl_3$ with mesityl Grignard, in diethyl ether gave $Re(NBu^t)_2(mes)_2$.[3] When this reaction is carried out in THF using a large excess of Grignard reagent (1:5 or more), about 15% of the rhenium can be recovered as a new complex with the structure shown in structure **1** together with $Re(NBu^t)_2(mes)_2$

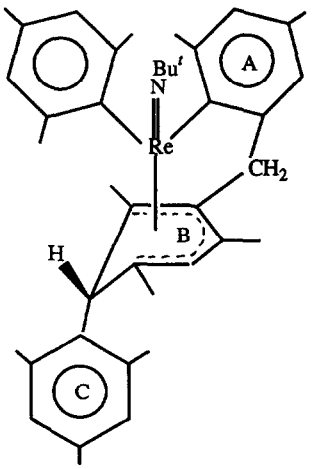

(1)

and small amounts of bimesityl. The structure was determined by X-ray diffraction and a diagram of the molecule is shown in Fig. 2; selected bond lengths and angles are given in Table 4.

The formulation shown above as **1** was confirmed by experimental location and successful refinement of one hydrogen on each of C(31) and C(33). The bonding of the rhenium atom to the cyclohexadienyl ring is unsymmetrical with the Re—C(31) and Re—C(32) distances of 2.19 and 2.25(1) Å being considerably shorter than Re—C(34), Re—C(35) and Re—C(36) distances, 2.45, 2.44 and 2.39(1) Å, respectively. The shortest C—C distances in the ring are C(34)—C(35) and C(35)—C(36), each at 1.40(1) Å. The five-atom fragment C(31), C(32), C(34), C(35) and C(36) is planar to within 0.05 Å and the envelope fold up to C(33) is 36.7°. The two Re—C(aryl) distances are slightly different with Re—C(21) being the shortest at 2.159(7)°. Interestingly, the Re—C(11) distance, 2.191(8) Å, is very similar to the shortest Re—(dienyl) distance Re—C(31), 2.194(7) Å. The Re≡N distance to the *t*-butylimido ligand lies in the range found for the same interaction in other complexes. The compound is diamagnetic having rhenium formally in the V oxidation state. The ^{1}H NMR spectrum shows numerous bands for CH_3, CH_2 and aryl hydrogens and we have not attempted detailed assignment.

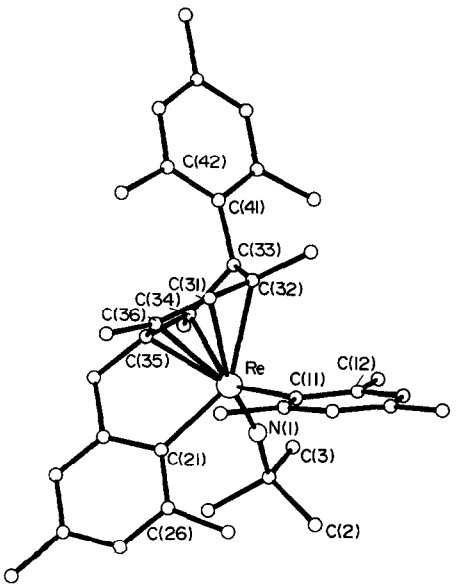

Fig. 2. The structure of the compound Re(Bu^{t}N)(mes) ($C_{27}H_{32}$).

The formation of the main product in the reaction, $Re(NBu^t)_2(mes)_2$, is presumably an independent reaction involving one-electron reduction by the Grignard of unisolated $Re(NBu^t)_2(mes)_2Cl$ or of $[Re(NBu^t)_2(mes)_2]^+$.

The generation of the moiety with rhenium bound to rings **A**, **B** and **C** in structure **1** may be accounted for by the established reactions of cyclometallation[4a] and reductive coupling,[4b,5] followed by nucleophilic attack[4c] by mesitylmagnesium bromide (i.e. by mes$^-$) on a cationic species.

Table 3. Selected bond lengths and bond angles for $C_{24}H_{36}N_2Re$

Bond lengths (Å)			
N(1)—Re(1)	1.737(11)	N(2)—Re(1)	1.738(11)
C(11)—Re(1)	2.105(13)	C(21)—Re(1)	2.096(14)
Bond angles (°)			
N(2)—Re(1)—N(1)	121.7(6)	C(11)—Re(1)—N(1)	110.4(5)
C(11)—Re(1)—N(2)	103.8(5)	C(21)—Re(1)—N(1)	104.8(6)
C(21)—Re(1)—N(2)	112.9(6)	C(21)—Re(1)—C(11)	101.5(5)
C(10)—N(1)—Re(1)	157.7(8)	C(20)—N(2)—Re(1)	160.3(9)
C(12)—C(11)—Re(1)	118.8(10)	C(16)—C(11)—Re(1)	122.4(9)
C(22)—C(21)—Re(1)	123.7(11)	C(26)—C(21)—Re(1)	118.1(10)

Table 4. Selected bond lengths and bond angles for $C_{40}H_{51}NRe$

Bond lengths (Å)			
N(1)—Re(1)	1.715(7)	C(11)—Re(1)	2.191(8)
C(21)—Re(1)	2.159(7)	C(31)—Re(1)	2.194(7)
C(32)—Re(1)	2.253(7)	C(33)—Re(1)	2.864(8)
C(34)—Re(1)	2.451(6)	C(35)—Re(1)	2.443(7)
C(36)—Re(1)	2.389(8)	C(32)—C(31)	1.435(9)
C(36)—C(31)	1.463(10)	C(33)—C(32)	1.530(9)
C(35)—C(34)	1.401(10)	C(36)—C(35)	1.401(9)
C(34)—C(33)	1.503(10)	C(33)—C(41)	1.535(9)
Bond angles (°)			
C(11)—Re(1)—N(1)	100.7(3)	C(21)—Re(1)—N(1)	89.8(3)
C(21)—Re(1)—C(11)	103.1(3)	C(31)—Re(1)—N(1)	119.3(3)
C(31)—Re(1)—C(11)	139.9(2)	C(31)—Re(1)—C(21)	76.6(3)
C(32)—Re(1)—N(1)	99.9(3)	C(32)—Re(1)—C(11)	141.9(2)
C(32)—Re(1)—C(21)	108.7(3)	C(32)—Re(1)—C(31)	37.6(2)
C(33)—Re(1)—N(1)	109.9(3)	C(33)—Re(1)—C(11)	110.2(3)
C(33)—Re(1)—C(21)	136.6(2)	C(33)—Re(1)—C(31)	60.1(3)
C(33)—Re(1)—C(32)	32.0(2)	C(34)—Re(1)—N(1)	130.3(2)
C(34)—Re(1)—C(11)	81.5(3)	C(34)—Re(1)—C(21)	138.7(2)
C(34)—Re(1)—C(31)	74.7(3)	C(34)—Re(1)—C(32)	60.8(3)
C(34)—Re(1)—C(33)	31.6(2)	C(35)—Re(1)—N(1)	163.5(2)
C(35)—Re(1)—C(11)	79.3(3)	C(35)—Re(1)—C(21)	106.4(3)
C(35)—Re(1)—C(31)	63.1(3)	C(35)—Re(1)—C(32)	72.1(3)
C(35)—Re(1)—C(33)	55.8(3)	C(35)—Re(1)—C(34)	33.3(2)
C(36)—Re(1)—N(1)	155.1(2)	C(36)—Re(1)—C(11)	103.2(3)
C(36)—Re(1)—C(21)	78.0(3)	C(36)—Re(1)—C(31)	36.9(2)
C(36)—Re(1)—C(32)	64.7(3)	C(36)—Re(1)—C(33)	68.1(3)
C(36)—Re(1)—C(34)	61.2(3)	C(36)—Re(1)—C(35)	33.7(2)
C(12)—C(11)—Re(1)	117.0(6)	C(16)—C(11)—Re(1)	126.9(5)
C(22)—C(21)—Re(1)	115.7(4)	C(26)—C(21)—Re(1)	128.6(5)
C(33)—C(34)—Re(1)	89.5(4)	C(35)—C(34)—Re(1)	73.1(4)
C(32)—C(31)—Re(1)	73.4(4)	C(36)—C(31)—Re(1)	78.8(4)
C(31)—C(32)—Re(1)	69.0(4)	C(33)—C(32)—Re(1)	96.6(4)
C(41)—C(33)—Re(1)	165.1(4)	C(32)—C(33)—Re(1)	51.4(3)
C(34)—C(33)—Re(1)	58.8(3)	C(34)—C(35)—Re(1)	73.7(4)
C(36)—C(35)—Re(1)	71.0(4)	C(31)—C(36)—Re(1)	64.3(4)
C(35)—C(36)—Re(1)	75.3(4)	C(36)—C(31)—C(32)	118.1(6)
C(33)—C(32)—C(31)	122.3(6)	C(32)—C(33)—C(41)	119.3(6)
C(34)—C(33)—C(41)	120.4(5)	C(34)—C(33)—C(32)	103.8(5)
C(35)—C(34)—C(33)	119.6(6)	C(36)—C(35)—C(34)	123.2(7)
C(35)—C(36)—C(31)	116.4(6)	C(361)—C(36)—Re(1)	135.7(3)
C(221)—C(31)—Re(1)	114.1(4)	C(341)—C(34)—Re(1)	129.8(5)
C(321)—C(32)—Re(1)	119.5(4)		

Thus, assuming an initial rhenium(V) species (**A**), a reasonable sequence for the synthesis of the compound can be envisaged as in Scheme 1. A problem arises in the formation of species **A** from the reaction of $Re(NBu^t)_2Cl_3$ with the Grignard reagent and in the loss of the NBu^t group, as well as in the fate of the hydride ion removed in Scheme 1. In the reaction products we have not been able to identify Bu^tNH_2 or Bu^t(mes)NH, which should arise from attack on the imido group by mes^-. There are precedents for removal of imido groups, e.g. by the attack of H^- on Re≡NPh in reductions of $Re(NPh)Cl_3(PR_3)_2$ by Na in THF.[6a] Interaction of this rhenium compound with excess $Mg(CH_2SiMe_3)_2$ also led to removal of the phenylimido group.[6b] The interaction of $Cr(OR)_2(NBu^t)_2$ with $ZnPh_2$ gave rise to Bu^tNHPh, biphenyl and other products,[7] while another elimination of an NBu^t

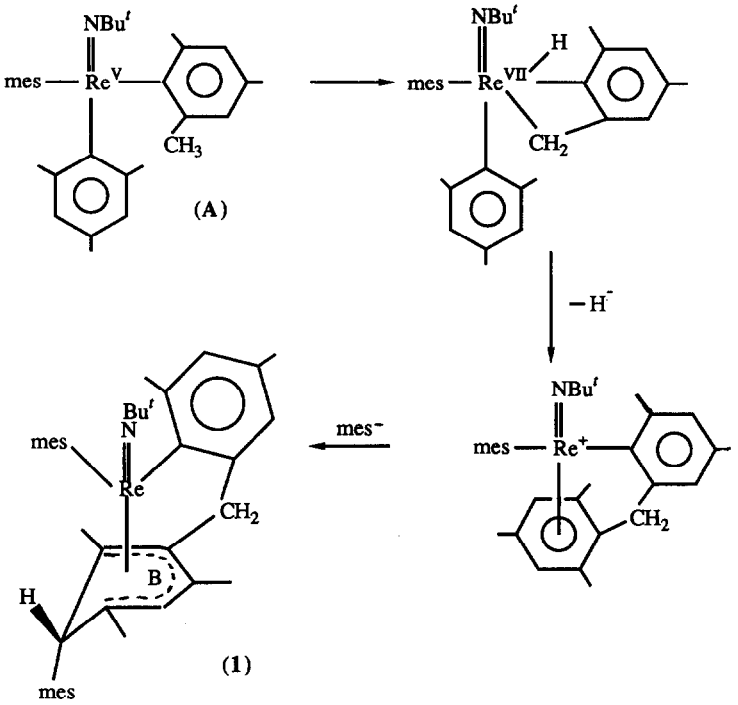

Scheme 1. Possible route for linking of mesityl groups with starting compound **A**.

group is that from $Cr(NBu^t)_2(COmes)_2$ to give *t*-butylmesitylamide, probably via acyl transfer to the imido nitrogen atom followed by another hydride transfer, probably from a mesityl group.[8]

(c) *Other aryl compounds.* The interaction of one equivalent of (*o*-tol)MgBr with $Re(NBu^t)_2Cl_3$ gave $Re(NBu^t)_2Cl_2(o\text{-tol})$[2] and three equivalents of $Re(NBu^t)_2(o\text{-tol})_3$.[3] Using two equivalents we obtained $Re(NBu^t)_2Cl(o\text{-tol})_2$ whose NMR spectrum suggests a *tbp* structure with equatorial imido and chlorine ligands (cf. refs 2 and 3). The IR spectrum has a band at 322 cm^{-1} assignable as ν(Re—Cl). The compound reacts with $AgPF_6$ in THF and the salt $[Re(NBu^t)_2(o\text{-tol})_2]PF_6$, which is a 1 : 1 electrolyte in MeCN, can be isolated. The ^1H NMR spectrum of the cation is similar to that of $Mo(NBu^t)_2(xyl)_2$[8] and of the mesityl and xylyl analogues discussed above.

For the molecule $Re(NBu^t)_3mes$, the crystals that could be obtained were not of good quality and this has reduced the precision of the structural determination. A diagram of the molecule is given in Fig. 3, selected bond lengths and angles in Table 5. The geometry is distorted tetrahedral with angles ranging from 95 to 123(1)°. The Re—N—C angles in the imido ligands vary from 142 to

Table 5. Selected bond lengths and bond angles for $C_{21}H_{38}N_3Re$

Bond lengths (Å)			
N(1)—Re(1)	1.738(29)	N(2)—Re(1)	1.657(30)
N(3)—Re(1)	1.769(29)	C(10)—Re(1)	2.097(36)
Bond angles (°)			
N(2)—Re(1)—N(1)	123.1(14)	N(3)—Re(1)—N(1)	109.2(13)
N(3)—Re(1)—N(2)	109.3(14)	C(10)—Re(1)—N(1)	94.8(14)
C(10)—Re(1)—N(2)	113.3(14)	C(10)—Re(1)—N(3)	105.3(14)
C(1)—N(1)—Re(1)	142.4(22)	C(2)—N(2)—Re(1)	161.3(25)
C(3)—N(3)—Re(1)	157.1(27)	C(20)—C(10)—Re(1)	121.7(28)
C(60)—C(10)—Re(1)	126.2(23)		

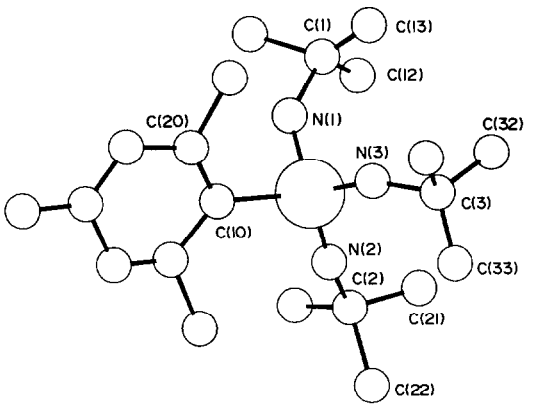

Fig. 3. The structure of $Re(NBu^t)_3(mes)$.

161(1)° and the large deviations from 180° are consistent with the metal electron count exceeding 18 if all three imido groups were to act as 4e ligands.

(2) t-*Butylimido oxo compounds*

A number of compounds having both Bu^tN and oxo groups were obtained either from the hydrolysis product of $(Bu^tN)_2ReCl_3$ or by interaction of nitric oxide with the aryls $(Bu^tN)_2Re(Ar)_2$, Ar = xyl and mes. A bis-imido oxo compound, $ReO[N(2,6\text{-}C_6H_3{}^iPr_2)]_2CH_2Bu^t$, was made[9] by interaction of $Re(NAr)_2(CHBu^t)Cl$ with Me_4NOH in MeOH and characterized spectroscopically; the reaction was proposed to proceed via a hydroxo intermediate; an osmium(VI) compound, $Os(NBu^t)(O)(mes)_2$, has been structurally characterized by X-ray diffraction.[10]

(a) *From hydroxo species.* In a reaction of mesMgBr with a sample of $Re(NBu^t)_2Cl_3$ that had been inadvertently exposed to air for several weeks, work-up gave the two imido oxo aryls described below. In order to obtain a more rational synthesis, the hydroxo compound $Re(NBu^t)_2Cl(OH)_2$ was made by interaction of the trichloride with two equivalents of LiOH. The NMR and IR spectra are consistent with this formula; on heating, loss of water occurs to give $Re(NBu^t)_2Cl(O)$ as shown by the disappearance of OH bands and the appearance of an Re=O band in the IR spectrum. Interaction of the hydroxide in THF with mesMgBr gave products similar to the ones obtained from the aged sample of $Re(NBu^t)_2Cl_3$. These were separated by fractional crystallization and identified as $Re(NBu^t)_2(O)(mes)$, $[(Bu^tN)Br(mes)Re(\mu\text{-}NBu^t)(\mu\text{-}O)\overline{Re(OC_6H_2Me_2CH_2)(NBu^t)}]$, Bu^tNH_3Cl and a magnesium-containing solid. The compound $Re(NBu^t)_2(O)(mes)$ has also been obtained as the sole rhenium-containing product by the reaction

$$Re(NBu^t)_2ReCl_2(mes) \xrightarrow{Ag_2O,\ Et_2O} Re(NBu^t)_2(O)(mes) + 2AgCl.$$

This monomeric compound has a Re=O stretch at 908 cm^{-1} in the IR spectrum, while the mass spectrum shows the parent ion and peaks due to loss of oxygen and NBu^t groups.

The more complicated bridged dimer has been characterized by X-ray diffraction and the structure is shown in Fig. 4; selected bond lengths and angles are given in Table 6.

Neglecting the proposed metal–metal interaction, the coordination geometry at each metal is very distorted trigonal bipyramidal. Thus, for Re(1), O(1) and O(2) define the axis [angle = 149.9(4)°] and for Re(2), N(1) and Br(1) [angle = 158.0(3)°]. The Re—O(1)—Re bridge is close to symmetrical, whereas the two Re—N distances

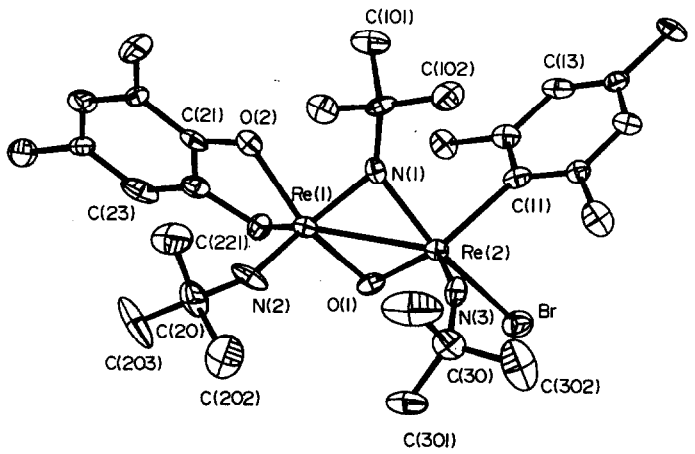

Fig. 4. The structure of $[(Bu^tN)Br(mes)Re(\mu\text{-}NBu^t)(\mu\text{-}O)\overline{Re(OC_6H_2Me_2CH_2)(NBu^t)}]$.

Table 6. Selected bond lengths and bond angles for $C_{30}H_{48}BrN_3O_2Re_2$

Bond lengths (Å)			
O(1)—Re(1)	1.909(11)	N(1)—Re(1)	1.922(13)
O(2)—Re(1)	1.964(12)	C(21)—Re(1)	2.856(19)
C(221)—Re(1)	2.139(17)	N(2)—Re(1)	1.708(14)
Br(1)—Re(2)	2.552(5)	O(1)—Re(2)	1.886(12)
N(1)—Re(2)	1.990(14)	C(11)—Re(2)	2.149(16)
N(3)—Re(2)	1.695(14)		
Bond angles (°)			
N(1)—Re(1)—O(1)	92.5(6)	O(2)—Re(1)—O(1)	149.9(4)
O(2)—Re(1)—N(1)	85.0(5)	C(21)—Re(1)—O(1)	135.9(4)
C(21)—Re(1)—N(1)	108.7(5)	C(21)—Re(1)—O(2)	25.4(4)
C(221)—Re(1)—O(1)	82.2(6)	C(221)—Re(1)—N(1)	131.8(5)
C(221)—Re(1)—O(2)	77.4(6)	C(221)—Re(1)—C(21)	54.7(6)
N(2)—Re(1)—O(1)	108.6(7)	N(2)—Re(1)—N(1)	125.0(6)
N(2)—Re(1)—O(2)	97.2(7)	N(2)—Re(1)—C(21)	90.7(7)
N(2)—Re(1)—C(221)	101.8(7)	N(1)—Re(2)—Br(1)	158.0(3)
N(1)—Re(2)—O(1)	91.1(5)	O(1)—Re(2)—Br(1)	82.0(4)
C(11)—Re(2)—Br(1)	79.6(4)	C(11)—Re(2)—O(1)	127.3(6)
C(11)—Re(2)—N(1)	88.4(6)	N(3)—Re(2)—Br(1)	93.0(5)
N(3)—Re(2)—O(1)	120.9(6)	N(3)—Re(2)—N(1)	108.3(6)
N(3)—Re(2)—C(11)	109.0(7)	Re(2)—O(1)—Re(1)	87.0(5)
Re(2)—N(1)—Re(1)	83.8(6)	C(10)—N(1)—Re(1)	138.1(9)
C(10)—N(1)—Re(2)	137.0(9)	C(16)—C(11)—Re(2)	125.3(11)
C(21)—O(2)—Re(1)	116.7(10)	O(2)—C(21)—Re(1)	37.9(6)
C(22)—C(21)—Re(1)	79.9(10)	C(26)—C(21)—Re(1)	152.7(12)
C(22)—C(221)—Re(1)	109.4(12)	C(30)—N(3)—Re(2)	157.8(11)
C(20)—N(2)—Re(1)	161.9(13)		

in the Re—N(1)—Re bridge differ by *ca* 0.07 Å, with Re(2)—N(1) being the longer. This may be a reflection of N(1) occupying an axial site in the Re(2) coordination. The two imino functions show some bending [Re(1)—$\widehat{N(2)}$—C(20) = 162(1)°, Re(2)—$\widehat{N(3)}$—C(30) = 158(1)°] but both can be considered to act as normal 4e ligands, Re≡N—R.

The rhenium atoms that are bridged by μ-O and μ-NBu^t have formal oxidation state VI; since the compound is diamagnetic there is probably a metal–metal bond as in the homoleptic rhenium(VI) dimer,[3] $Re_2(NBu^t)_4(\mu\text{-}NBu^t)_2$, and the bond distances in the two compounds are 2.61 and 2.70 Å, respectively.

The ^{1}H NMR and IR spectra of the compound can be interpreted in terms of the above structure; the ^{1}H resonance of the *t*-butyl group of μ-NBu^t is at lower field than the terminal ones and the latter appear equivalent.

There must be a complex series of reactions leading to this product probably comprising condensation of Re(OH) groups to give ReORe, and hydrolysis of one imido group, probably via an amido intermediate; the phenolic moiety could arise by a cyclometallation reaction of an *o*-CH_3 group on a mesityl followed by an oxygen atom "insertion" into the Re—C bond.

(b) *From nitric oxide.* When NO is bubbled rapidly through hexane solutions of $Re(NBu^t)_2(Ar)_2$, Ar = xylyl or mesityl, the colour changes almost instantaneously and from the solutions yellow (xyl) or orange (mes) crystals of the dioxoimido compounds, $[Re(NBu^t)(O)_2Ar]_2$, can be isolated in high yield.

The X-ray crystallographic structure determinations of these two complexes have showed them to be dimeric with two oxo bridges. Diagrams of the structures are given in Figs 5 and 6, with selected bond lengths and angles in Table 7. In both cases the geometry about the metal is trigonal bipyramidal with the terminal imido group and a bridging oxygen atom occupying the axial sites. The bridging thus involves one axial and one equatorial site and both dimers are centrosymmetric.

In the mesityl the bridges are quite unsymmetrical, with equatorial and axial Re—O distances of 1.791(7) and 2.364(7) Å, respectively. This is not unexpected and can be ascribed to lengthening of the axial Re—O bond through the *trans* influence of the imido group. It was, therefore, surprising to

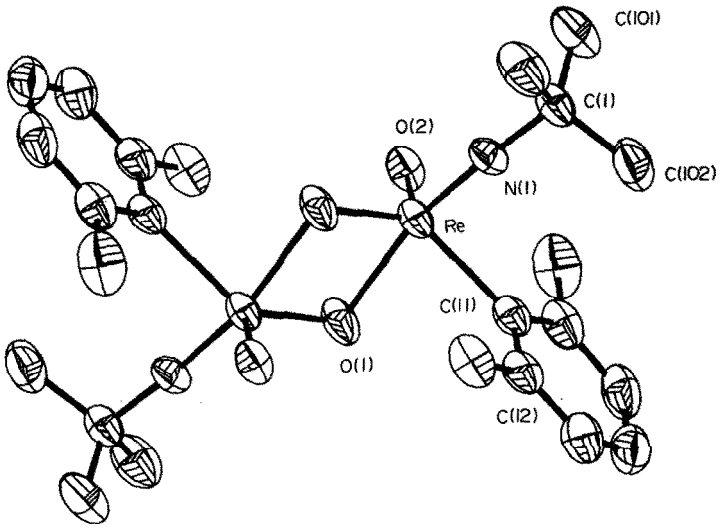

Fig. 5. The structure of $[Re(NBu^t)(O)(\mu\text{-}O)(xyl)]_2$.

find that in the xylyl, the bridge is more symmetrical, with equatorial and axial Re—O distances of 1.867(8) and 2.081(8) Å—a difference of only 0.21 Å compared to 0.57 Å in the mesityl. In all other respects, the geometries of the two compounds are very similar. We find it difficult to explain this major difference. The two compounds differ only in the presence of the extra methyl group in the mesityl complex, and this is most unlikely to affect the geometry of ligands around the metal. It does, however, affect the packing of the molecules in the unit cell, as evidenced by the choice of two quite different unit cells and crystal systems.

Asymmetric M_2O_2 rings have also been found in $Ru_2(\mu\text{-}O)_2(CH_2SiMe_3)_6$,[10a] which has a metal–metal bond and Ru—O distances of 2.208 and 1.733 Å, while $[OsO(o\text{-}OC_6H_{10}O)(quin)]_2$,[10b] quin = quinuclidene, has Os—O distances of 2.22 and 1.78 Å. An unsymmetrical single bridge has been found in a tungsten compound.[10c] For general information on MO and MOM distances see ref. 7(b) Table 5.2, p. 159 and West;[10d] in other compounds with Re_2O_2 rings such as $Re_2O_2(\mu\text{-}O)_2(CH_2CMe_3)_4$,[10e] the Re($\mu$-O) distances are essentially the same (1.967, 1.946 Å) but there is also a Re—Re bond (2.606 Å).

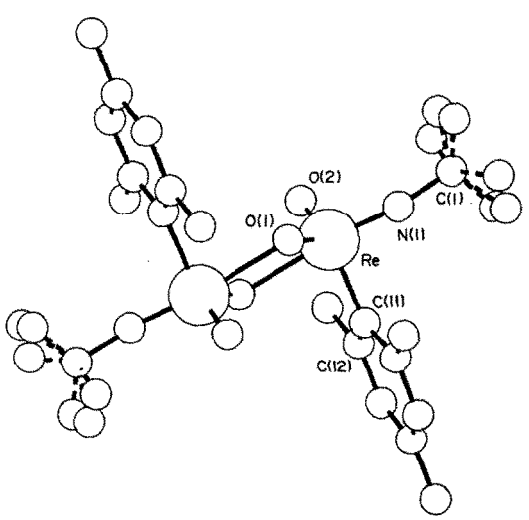

Fig. 6. The structure $[Re(NBu^t)(O)(\mu\text{-}O)(mes)]_2$.

The mass spectra do not show peaks of mass greater than the monomeric parent ions, $Re(NBu^t)_2(O)_2Ar^+$, so that the dimers must dissociate in the gas phase; there are other peaks to lower mass indicating loss of oxo and NBu^t groups.

The IR spectra of these and similar aryls (see Table 1 and ref. 11) show strong aromatic bands in the region associated with metal–oxygen stretching frequencies, and consequently it is not always easy to identify the Re=O or Re—O—Re stretch, and indeed some of these could be obscured. The IR of the xylyl compound shows two Re=O stretches at 952 and 925 cm^{-1} both in the solid state and in hexane solution. The mesityl differs in that only bands at 939 and 830 cm^{-1} in the solid-state spectrum can be identified, while in solution in hexane there are, as in the xylyl, two bands at 956 and 932 cm^{-1}. Oxygen exchange with $^{18}OH_2$ which would have helped identification of ReO bands cannot be done due to hydrolysis of the imido groups. For discussion of IR spectra of MO compounds see refs 7(b) and 10(d) and for compounds with Re_2O_2 (μ-O)$_2$ groups, ref. 10(e).

The other products of the NO reactions were identified as N_2O (by MS) and the unsymmetrical

Table 7. Selected bond lengths and bond angles for $[C_{13}H_{20}NO_2Re]_2$ and $[C_{12}H_{18}NO_2Re]_2$

	$[C_{13}H_{20}NO_2Re]_2$	$[C_{12}H_{18}NO_2Re]_2$
Bond lengths (Å)		
O(1)—Re(1)	1.791(7)	2.081(8)
O(2)—Re(1)	1.704(8)	1.708(9)
O(1a')—Re(1)	2.364(7)	1.867(8)
C(11)—Re(1)	2.090(10)	2.147(10)
N(1)—Re(1)	1.741(8)	1.722(9)
Re(1)—Re(1a)	3.332(4)	3.118(2)
Bond angles (°)		
O(2)—Re(1)—O(1)	119.4(4)	94.2(4)
C(11)—Re(1)—O(1)	115.3(4)	79.4(4)
C(11)—Re(1)—O(2)	112.0(4)	108.7(4)
N(1)—Re(1)—O(1)	105.5(4)	161.0(4)
N(1)—Re(1)—O(2)	105.3(4)	103.9(5)
N(1)—Re(1)—C(11)	95.6(4)	89.4(4)
O(1)—Re(1)—O(1a)	74.2(4)	75.8(4)
O(2)—Re(1)—O(1a)	79.9(4)	113.4(4)
C(11)—Re(1)—O(1a)	79.2(4)	132.1(3)
N(1)—Re(1)—O(1a)	173.8(4)	101.4(5)
Re(1)—O(1)—Re(1a)	105.8(4)	107.7(4)
C(12)—C(11)—Re(1)	121.4(8)	116.9(7)
C(16)—C(11)—Re(1)	116.7(7)	121.9(8)
C(1)—N(1)—Re(1)	153.7(7)	173.8(7)

Key to symmetry operations relating designated atoms to reference atoms at (x, y, z); (a) $-x, 1.0-y, 2.0-z$.

azo compounds, Bu^{t}N=NAr, so that the stoichiometry is that of eq. (1):

$$Re(NBu^t)_2(Ar)_2 + 3\,NO \longrightarrow Re(NBu^t)(O)_2Ar + N_2O + Bu^tN{=}NAr. \quad (1)$$

The reaction of $Re(NBu^t)_2(xyl)_2$ with one equivalent of NO was much slower than when excess NO was bubbled through the solution (*ca* 1 h vs a few seconds) and from the solution the nitrosyl compound, $Re(NBu^t)_2(xyl)_2(NO)$, could be isolated. This compound, formally having rhenium(V), is diamagnetic and the ^{1}H NMR spectrum shows that the NBu^t and aryl groups have a 1:1 ratio and that the equivalence is maintained to 223 K as there is no broadening or splitting of the peaks. The IR spectrum has a new band at 1639 cm^{-1} assignable as ν(ReNO). The spectra are thus consistent with a *tbp* structure with equatorial NBu^t and axial aryl groups. The mass spectrum shows the parent ion at $m/z = 569$ (Re^{187}) with other peaks due to loss of NO, O, Bu^t, N(xyl) and xylyl. Crystals suitable for X-ray study could not be obtained. The only similar nitrosyl derived by addition to a rhenium(VI) compound is the diamagnetic $ReMe_6(NO)$ which has ν(NO) at 1710 cm^{-1}.[12] The low NO stretches suggest that both species have bent MNO groups.

Treatment of the nitrosyl with slightly less than one equivalent of NO gives, as the final product, the complex $Re(NBu^t)_2(O)(xyl)$, which is the analogue of the tetrahedral $Re(NBu^t)_2(O)(mes)$ obtained by arylation of $Re(NBu^t)_2Cl(OH)_2$ as described above. Hence, there appears to be a substantial difference, presumably due to kinetic factors, between the reactions of the diaryls with stoichiometric amounts of NO and the very rapid reaction found when NO is bubbled through the solution. The final product in both cases has rhenium(VII) and does not react further with NO.

Considering first the stoichiometric reaction, this can be accounted for by well established chemistry as in Scheme 2. The five-coordinate diamagnetic nitrosyl **A** reacts with more NO to give a six-coordinate, paramagnetic dinitrosyl **B**, which would then undergo the well established aryl (or alkyl) transfer reaction[13] (also ref. 4, p. 1210) via an η^2-RNO intermediate leading to an M=O group and RN=NR as found for other paramagnetic compounds[12,13] such as $ReOMe_4$[13c] and

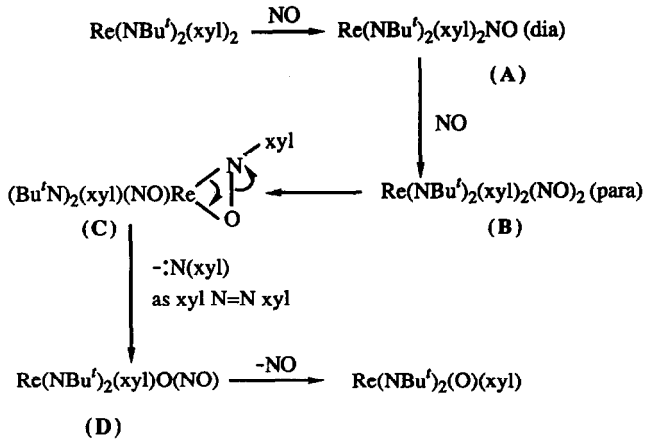

Scheme 2. Stoichiometric reaction of $Re(NBu^t)_2(xyl)_2$ with NO leading to $Re(NBu^t)_2(O)(xyl)_2$ and xylN=Nxyl.

$(C_5H_5)_2NbMe_2$.[13d] The oxo species **D** would doubtless readily lose NO to give the final stable product; the overall reaction is that of eq. (2):

$$Re(NBu^t)_2(xyl)_2 + NO \longrightarrow Re(NBu^t)_2(O)(xyl) + \tfrac{1}{2}(xyl)N{=}N(xyl). \quad (2)$$

The fast reaction presents a different problem since the mixed azo compounds, $Bu^tN{=}NAr$, were isolated. Although mixed azo compounds have been prepared by other methods,[14] these particular ones appear to be new. In Scheme 3 we propose that the ArNO species first formed by aryl migration to

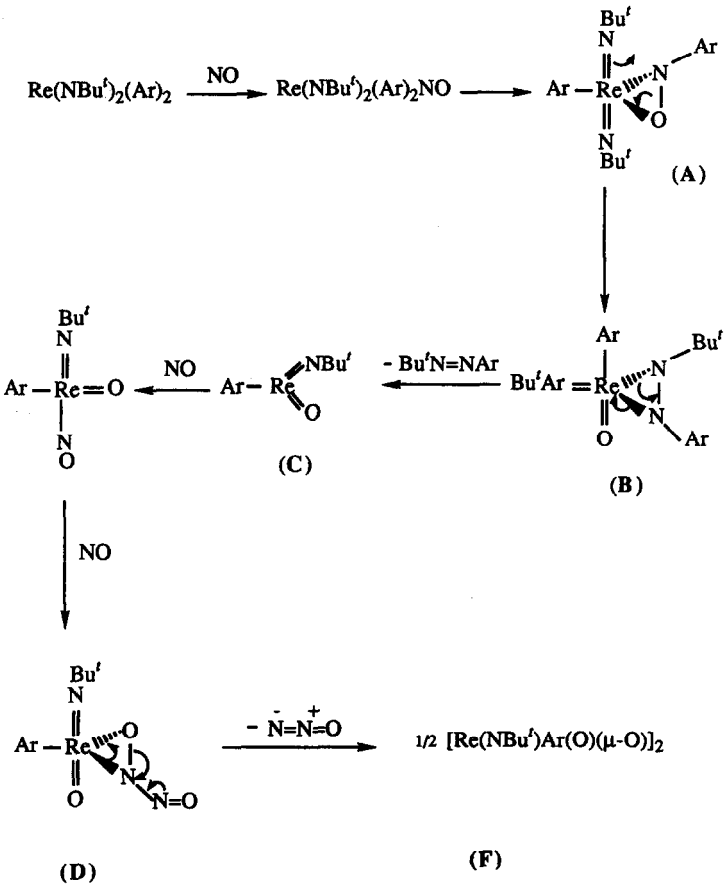

Scheme 3. Interaction of $Re(NBu^t)_2(Ar)_2$, Ar = xyl, mes, with excess NO.

NO (either η^2 as in **A** of Scheme 2, or η^1), instead of giving ArN=NAr, either in an intermolecular reaction or by dimerization of eliminated :NAr, undergoes N—N bond formation to give species **B**. This intermediate could be regarded as an η^2-azo compound of rhenium(V) or more likely as a rhenium(VII) compound with a hydrazido (2−) ligand as drawn in Scheme 3. Examples of metal azo and hydrazido (2−) complexes are well established;[15] the distinction between azo and hydrazido (2−) is a somewhat formal one (cf. alkene and alkyne complexes, ref. 4, p. 71). This species, **B**, then undergoes a cheletropic[16] elimination of the azo compound leaving the coordinately unsaturated species **C** to react successively with two molecules of NO, probably via a dinitrosyl,[17a] to form the hyponitrite **D** which finally eliminates N_2O giving the isolated products **F**. The initial formation of a dinitrosyl as in **B** (Scheme 2) and elimination of N_2O at this point can be ruled out as this would give $Re(NBu^t)_2(Ar)_2O$ with rhenium in the impossible oxidation state of VIII.

While hyponitrites such as **D** have been proposed as intermediates and some examples characterized spectroscopically,[12a,b,17] recent calculations[17b] comparing $Re(NS)_2$ coupling with $Re(NO)_2$ coupling suggest[17b] that the latter "is disfavoured but might occur via N—N bonding". It can be noted regarding the formation of the azo compound that no examples of coupling of $M(NR)_2$ appear to be known (see ref. 7b, p. 273).

Finally, a question arises why in its reactions with NO, $Re(NBu^t)_2(mes)_2$ differs from $Re(O)_2(mes)_2$ which reacts quantitatively[10] as in eq. (3) to give dimesitylamido trioxorhenium(VII) via an η^2-ON(mes) intermediate,

$$Re(O)_2(mes)_2 + NO \longrightarrow O_3Re{=}N(mes)_2. \quad (3)$$

There would seem to be no reason *a priori* why the present reaction should not give $Re(NBu^t)_2O(Nmes_2)$ by the same route, but in order for a second aryl transfer to NAr to occur, the second aryl group would have to be in a position *cis* to the N atom of the η^2-ONAr group. Species **A** hence presumably has a NBu^t group in this position as shown in Scheme 3; *cis* geometry would be preserved even if the molecule is fluxional.

EXPERIMENTAL

Microanalyses were carried out by Imperial College and Pascher, Remagen, Laboratories. The spectrometers and general techniques used have been described.[3] The compounds $Re(NBu^t)_2Cl_3$[18] and $Re(NBu^t)_3Cl$[3] were prepared as described. Nitrogen oxide (British Oxygen Company) was passed through a tube of solid KOH and a copper spiral cooled at −78°C. In mass spectra, the rhenium compounds showed the correct $Re^{185,187}$ patterns for parent ions and fragments. NMR spectra were referenced to Me_4Si and are in ppm; IR spectra in cm^{-1} are in Nujol mulls unless otherwise specified.

(1) *Di*(t-*butylimido*)*di*(2,6-*dimethylphenyl*)*rhenium* (VI)

To $Re(NBu^t)_2Cl_3$ (0.43 g, 1 mmol) in Et_2O (20 cm^3) at −20°C was added 13 cm^3 of a 0.38 M solution of xylylmagnesium bromide in Et_2O. The resulting red solution was then stirred for 15 h at room temperature. After filtration and evaporation of the solution, the residue was extracted with hexane (3×15 cm^3) and the solution filtered through celite; concentration to 20 cm^3 and cooling at −20°C gave large red crystals. Yield: 0.45 g (83%). MS(FAB): 539 (100%), $^{187}M^+$; 537 (58%), $^{185}M^+$; 483 (8%), $M^+ - Bu^t$; 434 (10%), $M^+ - xylyl$; 427 (7%), $M^+ - 2Bu^t$. IR: 3047m, 2969s, 2926s, 1594m, 1456s, 1360s, 1261s, 1210m, 1091w, 1022m, 911vs, 801s, 766s, 716m, 525w. EPR: see text.

(2) *Di*(t-*butylimido*)*di*(2,6-*dimethylphenyl*)*rhenium* (VII) *hexafluorophosphate*

The solids $Re(Bu^tN)_2(xyl)_2$ (0.54 g, 1 mmol) and $AgPF_6$ (0.25 g, 1 mmol) were mixed under nitrogen and 25 cm^3 of THF added. On vigorous stirring the solution became bright orange and a grey precipitate of Ag appeared. After 2 h the solution was filtered and Et_2O (15 cm^3) added; cooling at −20°C gave crystals of the salt. Yield: 0.6 g (88%). MS(FAB): 539 (100%), $^{187}M^+$; 483 (5%), $M^+ - Bu^t$; 434 (6%), $M^+ - xyl$; 427 (5%), $M^+ - 2Bu^t$. IR: 1572w, 1365s, 1302w, 1261m, 1227m, 1173m, 1140w, 1099w, 1026w, 914s, 876w, 840vs, 786m, 739m, 704w, 557s, 471w. NMR: ^1H ($CDCl_3$): 7.42 (1H, m, *p*-$C_6H_3Me_2$); 7.21 (2H, d, *m*-$C_6H_3Me_2$); 2.46 (6H, s, *o*-$C_6H_3Me_2$); 1.80 (9H, s, NBu^t).

The *trifluoromethanesulphonate* was obtained similarly using AgO_3SCF_3 (0.26 g, 1 mmol). Yield: 0.55 g (81%); m.p. 131°C dec. The IR spectrum is the same as for PF_6^- except for anion bands.

(3) *Interaction of* $[Re(NBu^t)_2(xyl)_2]PF_6$ *and* Bu^tNC

To the PF_6^- salt (0.2 g, 0.3 mmol) in THF (15 cm^3) was added Bu^tNC (0.04 cm^3, 0.35 mmol). The solution became pale yellow and after stirring for 1 h, hexane (10 cm^3) was added to precipitate a white solid. Recrystallization from THF gave crystals of

$[Re(NBu^t)_2(xyl)(\eta^2\text{-}Bu^tNC{=}Cxyl)]PF_6$. MS(EI): 513 (1%), $^{187}M^+$, and a variety of peaks from 435 to 131. IR: 2981s, 2935s, 1713s, 1639w, 1459s, 1365m, 1246m, 1215m, 1188s, 1173s, 1093w, 1030w, 911m, 816w, 842vs, 785m, 737w, 710w, 558s, 472w, 360w. NMR: ^1H ($CDCl_3$): 7.34 (2H, m, *p*-$C_6H_3Me_2$); 7.21 (4H, m, *m*-$C_6H_3Me_2$); 2.44 (6H, s, *o*-$C_6H_3Me_2$); 2.32 (6H, s, *o*-$C_6H_3Me_2C{=}NBu^t$); 1.61 (18H, s, NBu^t); 1.14 (9H, s, $C{=}NBu^t$).

(4) $(Bu^tN)(2,4,6\text{-}Me_3C_6H_2)(C_{27}H_{32})Re^V$

To $(Bu^tN)_2ReCl_3$ (0.7 g, 1.6 mmol) in THF at −40°C was added mesMgBr (8 cm^3 of a 1 M solution in THF) and the red solution stirred for 12 h, while warming to room temperature. The solvent was removed, the residue extracted with Et_2O and this solution evaporated and the residue extracted with hexane. The filtered solution on cooling at −20°C yields $Re(NBu^t)_2(mes)_2$[1] in *ca* 65% yield. Dissolution of the residue from the hexane extraction in THF–hexane (2 : 1) and cooling the solution at −20°C gave red crystals. Yield: *ca* 13%. The compound was recrystallized from THF–hexane to give X-ray quality crystals. IR: 2973s, 1638s, 1618, 1505w, 1456w, 1403w, 1385w, 1372w, 1357s, 1256s, 1211s, 1134s, 1010m, 949w, 922w, 844s, 805w, 710m, 669m, 602w, 554w, 511w, 464w. NMR: ^1H (C_6D_6): 6.94 (2H, s, *m*-H); 6.71 (2H, s, *m*-H); 3.98 (1H, s, cyclohexadienyl-H); 2.80 (1H, s, *endo*cyclic H); 2.27 (3H, s, Me); 2.18 (2H, s, CH_2); 2.15 (3H, s, Me); 2.11 (3H, s, Me); 2.06 (3H, s, Me); 2.04 (9H, s, 3Me); 1.98 (12H, s, 4Me); 1.26 (9H, s, Bu^t). Some bimesityl[19] was also isolated from the solution after removal of $Re(NBu^t)_2(mes)_2$.

(5) *Bis*(t-*butylimido*)*chlorobis*(2-*methylphenyl*)*rhenium*(VII)

To $Re(NBu^t)_2Cl_3$ (1.0 g, 2.3 mmol) in Et_2O (10 cm^3) at −25°C was added *o*-tolMgBr (1.5 cm^3 of a 3.3 M solution in Et_2O) and the mixture slowly warmed to room temperature and stirred for 5 h. Removal of solvent, extraction of the residue with hexane (*ca* 10 cm^3) and cooling (−20°C, 3 days) gave crystals. Yield: 0.86 g (68%). MS(FAB): 511 (100%), $^{187}M^+ - Cl$; 437 (53%), $^{187}Re(NBu^t)(o\text{-tol})_2^+$; 420 (16%), $^{187}Re(NBu^t)_2(o\text{-tol})^+$.

(6) *Bis*(t-*butylimido*)(2-*methylphenyl*)*rhenium*(VII) *hexafluorophosphate*

The interaction of equimolar quantities of $Re(NBu^t)_2(o\text{-tol})_2Cl$ (0.464 g) and $AgPF_6$ (0.225 g), each in THF (*ca* 5 cm^3), at room temperature gives a precipitate of AgCl and a yellow solution. After 2 h stirring, the solution was filtered, concentrated (5 cm^3) and hexane (*ca* 3 cm^3) added; cooling at −20°C gave crystals. Yield: 0.43 g (78%). MS(FAB): 511 (85%), $^{187}Re(NBu^t)_2(o\text{-tol})_2^+$; 420 (19%), $^{187}Re(NBu^t)_2(o\text{-tol})^+$; 57 (100%), Bu^{t+}.

(7) *Bis*-t-*butylimido*(*chloro*)(*dihydroxo*)*rhenium*(VII)

To a mixture of $(Bu^tN)_2ReCl_3$ (0.435 g, 1 mmol) and LiOH (0.06 g, 1.5 mmol) was added THF (50 cm^3). The dark red solution slowly turns yellow with a white precipitate (LiCl). After stirring for 1 h the solution was filtered, concentrated (3 cm^3) and hexane (5 cm^3) added to precipitate the yellow solid which was washed with Et_2O (3 × 10 cm^3). Yield: 81%. MS(FAB): 399, (35%) $^{187}M^+$; 74 (100%), $Bu^tNH_3^+$; 57 (100%), Bu^{t+}. MS(EI): 310 (1%), $^{187}Re(NBu^t)OH^{35}Cl^+$; 270 (2%), $^{187}Re(N)(OH)_2{}^{35}Cl^+$; 58 (100%), Bu^tH^+. IR: 3417s(OH), 2966m, 2925w, 1634m, 1455w, 1359w, 1261s, 1219w, 1093s, 1019s, 914s, 879w, 858m, 800m, 454m, 397m, 321m. NMR: ^1H ($CDCl_3$): 5.62 (2H, br, OH); 1.32 (18H, s, Bu^t).

(8) *Reaction of* $Re(NBu^t)_2Cl(OH)_2$ *with mesityl magnesium bromide*

(a) *Bis*(t-*butylimido*)*oxomesitylrhenium*(VII). *Method A*: To $Re(NBu^t)_2Cl(OH)_2$ (0.6 g) in THF (10 cm^3) at −20°C was added mesMgBr (6 cm^3, 1 M solution in Et_2O) and the solution stirred for 12 h at room temperature. Removal of solvent, extraction of the residue into hexane (3 × 15 cm^3), filtration and concentration (5 cm^3) of the dark yellow solution followed by cooling at −20°C gave yellow crystals of $Re(NBu^t)_2(O)(mes)$. Yield: 0.48 g (68%). MS(EI): 464 (29%), $^{187}M^+$; 448 (25%), $^{187}M^+ - O$; 393 (80%), $^{187}M^+ - NBu^t$; 336 (24%), $^{187}Re(N)(O)(mes)^+$; 329 (3%), $^{187}Re(NBu^t)_2^+$; 306 (9%), $^{187}Re(mes)^+$; 58 (100%), Bu^tH^+. IR: 2970s, 2924s, 1597w, 1453m, 1376w, 1359m, 1261s, 1209s, 1094s, 1025s, 908s, 849m, 805s, 706w, 596w, 511w, 462w, 387m.

Method B: A solution of $Re(Bu^tN)_2Cl_2(mes)$[1] (0.26 g) in THF (10 cm^3) was stirred with 0.15 g of moist Ag_2O for 2 h. After filtration the solution was evaporated and the residue extracted into hexane (15 cm^3); concentration (to 3 cm^3), followed by cooling at −20°C gave yellow crystals of $Re(NBu^t)_2(O)mes$. Yield: 0.18 g (73%).

(b) *The bridge species* $(Bu^tN)(Br)(mes)Re(\mu\text{-}NBu^t)(\mu\text{-}O)\overline{ReOC_6H_2Me_2CH_2}(NBu^t)$. The mother liquor from above in method A after removal of $Re(NB^t)_2(O)(mes)$ was evaporated and the residual dark yellow oil allowed to stand at −20°C for *ca* 3

days. The red crystals were collected, washed with Et_2O and dried. Yield: 0.25 g (19%). IR: 2974s, 2924s, 2856m, 1456s, 1385s, 1357s, 1259s, 1200s, 1133m, 1099m, 1018s, 912w, 844s, 805s, 710s, 669s, 513m. NMR: $^1H(C_6D_6)$: 6.87 (1H, s, *m*-H); 6.83 (1H, s, *m*-H); 6.49 (2H, s, *m*-H); 3.01 (3H, s, Me); 1.68 (6H, s, 2Me); 1.07 (9H, s, μ-NBu^t); 0.88 (18H, s, NBu^t).

(9) *Reactions with nitrogen monoxide*

(a) t-*Butylimido(dioxo)(2,6-dimethylphenyl)rhenium*(VII). Nitrogen monoxide was bubbled through a hexane solution of $Re(NBu^t)_2(xyl)_2$ (0.54 g, 1 mmol) until the colour changed to light orange. The solvent was removed and the residue was dissolved in hexamethyldisiloxane (5 cm^3); the solution was filtered, concentrated to 2 cm^3 and cooled to -20°C to give yellow crystals. Yield 0.35 g (90%). MS(EI): 395 (35%), $^{187}M^+$; 393 (21%), $^{185}M^+$; 379 (71%), M^+-O; 339 (85%), M^+-Bu^t; 323 (62%), $^{187}Re(NH)(O)(xyl)^+$; 105 (100%), xyl. IR: 2966s, 1652w, 1575w, 1447m, 1404w, 1379m, 1362m, 1261s, 1130w, 1023m, 952s, 925s, 829s, 805m, 770m, 752w, 707w, 558m, 483w, 391m. NMR: ^1H ($CDCl_3$): 7.31–7.19 (3H, m, *m*, *p*-$C_6H_3Me_2$); 2.55 (6H, s, *o*-$C_6H_3Me_2$) 1.58 (9H, s, Bu^{t}N).

(b) t-*Butylimido(dioxo)(2,4,6-trimethylphenyl) rhenium*(VII). Nitrogen monoxide was bubbled through $(Bu^tN)_2Re(mes)_2$ (0.283 g) in hexane (10 cm^3) at room temperature until the dark red solution became light orange with the appearance of a faint precipitate. The solution was filtered, evaporated and the residue extracted into hexamethyldisiloxane (*ca* 8 cm^3). After concentration (3 cm^3) and cooling (-20°C) the orange crystals were collected. Yield: 0.29 (84%). MS(EI): 409 (40%), $^{187}M^+$; 393 (71%), $^{187}M^+-O$; 377 (4%), M^+-O_2; 353 (73%), $^{187}M^+-Bu^t$; 306 (13%), $^{187}Re(mes)^+$; 119 (90%), $C_9H_{11}^+$. IR: 3016w, 2975s, 2920m, 1589s, 1541w, 1467w, 1448s, 1398w, 1379m, 1362m, 1286m, 1230s, 1033m, 984w, 939s, 857m, 830s, 803m, 706w, 599m, 582m, 565w, 541w, 387w, 329m. NMR: ^1H ($CDCl_3$): 7.14 (2H, s, *m*-H); 2.52 (6H, s, *o*-Me), 2.32 (3H, s, *p*-Me); 1.58 (9H, s, Bu^t).

The hexamethyldisiloxane mother liquor from above was evaporated, the residue dissolved in Et_2O (5 cm^3), the solution filtered, concentrated to 2 cm^3 and cooled at -20°C to give orange crystals of the azo compound Bu^{t}N=Nmes, which were recrystallized from Et_2O. Yield: 0.05 g (70%), m.p. 116°C. [Found (required): C, 74.2 (74.5); H, 9.5 (9.8); N, 13.9 (13.7)%.] NMR: ^1H ($CDCl_3$): 6.98 (2H, s, *m*-$C_6H_2Me_3$); 2.80 (6H, s, *o*-$C_6H_2Me_3$); 2.18 (3H, s, *p*-$C_6H_2Me_3$); 1.60 (9H, s, N*Bu^t*). IR: 2966s, 2921m, 2861m, 1652w, 1610w, 1597w, 1550w, 1465s, 1376w, 1360m, 1261m, 1208w, 910w, 882w, 853m, 801s, 709w.

(c) *Di*(t-*butylimido)di*(2,6-*dimethylphenyl)nitrosylrhenium*(V). To a solution of $Re(NBu^t)_2(xyl)_2$ (0.3 g, 0.55 mmol) in hexane (10 cm^3) at -78°C, in a small flask with septum, was injected via a gas syringe NO (11 cm^3, 0.5 mmol). The solution was allowed to warm and was stirred at room temperature until the initial deep red colour changed to light yellow (*ca* 1 h). Evaporation in vacuum, extraction of the residue into $(Me_3Si)_2O$ (2×3 cm^3) and cooling of the solution (-30°C) gave orange crystals. Yield: 0.14 g (45%). MS(EI): 569 (44%), $^{187}M^+$; 567 (26%), $^{185}M^+$; 553 (14%), M^+-O; 539 (10%), M^+-NO; 513 (8%), M^+-Bu^t; 450 (30%), $Re(NBu^t)_2(xyl)O^+$; 434 (51%), $Re(NBu^t)_2(xyl)^+$; 379 (72%), $Re(NBu^t)NH(xyl)^+$; 322 (33%), $Re(NH)_2(xyl)^+$; 105 (100%), xyl^+. IR: 1639m, 1616m, 1575w, 1564w, 1533m, 1439s, 1384w, 1360s, 1286w, 1250m, 1230s. NMR: $^1H(CDCl_3)$: 7.21–7.11 (3H, m, *m*, *p*-$C_6H_3Me_2$); 2.85 (6H, s, *o*-$C_6H_3Me_2$); 1.61 (9H, *s*, NBu^t).

(d) *Interaction of nitrosyl compound with* NO. To a solution of $Re(NBu^t)_2(xyl)_2NO$ (0.1 g, 0.17 mmol) in Et_2O (15 cm^3) was injected slightly less than one equivalent of NO and the solution stirred for *ca* 12 h. No change in colour takes place. Evaporation of the solution, extraction of the residue with $(Me_3Si)_2O$ (5 cm^3) and cooling of the filtered solution (-30°C) affords dark yellow crystals of $Re(NBu^t)_2(O)(xyl)$. Yield: 0.06 g (68%). MS(EI): 450 (30%), $^{187}M^+$; 448 (18%), $^{185}M^+$; other peaks due to M^+-Bu^t and M^+-NBu^t; 338 (21%), $Re(NH)_2(O)(xyl)^+$; 323 (17%), $ReNH(O)(xyl)^+$; 105 (61%), xyl^+; 58 (100%), $C_4H_{10}^+$. IR: Re=O, 912 cm^{-1} and other Bu^{t}N and xylyl bands. NMR: ^1H ($CDCl_3$): 7.37–7.15 (3H, m, *m*, *p*-$C_6H_3Me_2$); 2.78 (6H, s, *o*-$C_6H_3Me_2$); 1.62 (18H, s, *Bu^t*N).

X-ray crystallography

Crystals of all six compounds were sealed under argon in thin-walled glass capillaries for X-ray work. Following preliminary photography, orientation matrices and associated cell dimensions were obtained using a CAD4 diffractometer and standard procedures. Intensity data were recorded[20] using ω–2θ scans and graphite monochromated Mo-K_α radiation ($\lambda = 0.71069$ Å), and corrected for Lp effects and for absorption using psi-scan information. Further corrections for absorption were made during the refinement process, using the DIFABS method.[21]

Table 8. Crystal data, details of intensity measurements and structure refinement

Molecular formula	$C_{24}H_{36}N_2Re$	$C_{40}H_{52}NRe$	$C_{21}H_{38}N_3Re$	$C_{30}H_{48}BrN_3O_2Re_2$	$C_{26}H_{40}N_2O_4Re_2$	$C_{24}H_{36}N_2O_4Re_2$
Molecular weight	442.518	732.02	518.74	935.04	816.984	788.926
Crystal system	Monoclinic	Triclinic	Triclinic	Triclinic	Orthorhombic	Triclinic
a (Å)	17.576(3)	10.924(1)	9.965(8)	8.952(1)	10.536(3)	8.379(2)
b (Å)	14.342(2)	11.049(3)	11.568(7)	10.685(2)	12.428(1)	12.373(3)
c (Å)	9.946(2)	15.478(3)	11.960(9)	17.785(4)	21.310(4)	6.947(1)
α (°)	90	99.84(3)	75.49(6)	95.93(2)	90	97.23(2)
β (°)	95.21(2)	95.80(4)	106.32(8)	95.02(3)	90	103.49(2)
γ (°)	90	108.80(5)	77.32(6)	99.38(6)	90	93.71(2)
Volume (Å)	2421.47	1717.91	1216.26	1659.92	2790.36	671.07
Space group	$P21/n$	$P\bar{1}$	$P\bar{1}$	$P\bar{1}$	$Pbca$	$P\bar{1}$
Z	4	2	2	2	4	1
D_c (g cm^{-3})	1.477	1.415	1.416	1.873	1.944	1.952
μ (cm^{-1})	48.04	39.09	50.68	85.70	44.17	91.38
$F(000)$	1064	746	460	876	1268	372
h, k, l range	$-19 \rightarrow 19$	$0 \rightarrow 13$	$0 \rightarrow 10$	$0 \rightarrow 9$	$0 \rightarrow 12$	$-9 \rightarrow 9$
	$0 \rightarrow 15$	$-13 \rightarrow 13$	$-12 \rightarrow 12$	$-11 \rightarrow 11$	$0 \rightarrow 14$	$-14 \rightarrow 14$
	$0 \rightarrow 10$	$-18 \rightarrow 18$	$-13 \rightarrow 13$	$-19 \rightarrow 19$	$0 \rightarrow 25$	$0 \rightarrow 8$
Total number of reflections	3758	6383	3607	4947	3457	2573
Number of unique reflections	3356	6036	2346	4597	2453	2359
Number of reflections	2219	5069	2346	3537	1308	2182
Significance test	$[F > 3\sigma(F)]$	$[F > 3\sigma(F)]$	$[F > 6\sigma(F)]$	$[F > 3\sigma(F)]$	$[F > 6\sigma(F)]$	$[F > 3\sigma(F)]$
Number of parameters	244	380	196	347	154	145
Weighting scheme parameter g in $w = 1/[\sigma^2(F_o)+gF_o^2]$	0.0008	0.0009	0.00009	0.000002	0.09	0.002
Final R	0.0393	0.0309	0.0885	0.0432	0.0512	0.0474
Final R_w	0.0374	0.0327	0.0885	0.0393	0.0550	0.0469

The structures were solved and developed via the heavy atom method and refined by full-matrix least-squares. The usual difficulties were encountered with disorder of *t*-butyl groups generally, and the crystal quality for $Re(NBu^t)_3(xyl)$ was poor. Otherwise all atoms were refined in the anisotropic displacement mode and no hydrogens were included except for $Re(NBu^t)(mes)(C_{27}H_{32})$.

Details of the crystal data, intensity measurements and refinement are given in Table 8.

Tables of final atomic positional parameters and displacement factor coefficients, bond lengths and angles and F_o/F_c values have been deposited with the Editor, from whom copies are available on request. Atomic coordinates have also been deposited with the Cambridge Crystallographic Data Centre.

Acknowledgements—We thank the Universidad Complutense, Madrid, for support and study leave (A.G.) and the SERC for provision of X-ray facilities.

REFERENCES

1. P. Stavropoulos, P. G. Edwards, T. Behling, G. Wilkinson, M. Motevalli and M. B. Hursthouse, *J. Chem. Soc., Dalton Trans.* 1987, 169.
2. C. J. Longley, P. D. Savage, G. Wilkinson, B. Hussain and M. B. Hursthouse, *Polyhedron* 1988, **7**, 1079.
3. A. A. Danopoulos, C. J. Longley, G. Wilkinson, B. Hussain and M. B. Hursthouse, *Polyhedron* 1989, **8**, 2657.
4. F. A. Cotton and G. Wilkinson, *Advanced Inorganic Chemistry*, 5th edn, pp. (a) 1217, (b) 1136, (c) 1182. John Wiley, New York (1988).
5. J. Arnold, G. Wilkinson, B. Hussain and M. B. Hursthouse, *Organometallics* 1989, **8**, 1362.
6. K. W. Chiu, W-K. Wong, G. Wilkinson, A. M. R. Galas and M. B. Hursthouse, *Polyhedron* 1982, **1**, (a) 37, (b) 31.
7. (a) W. A. Nugent and R. L. Harlow, *J. Am. Chem. Soc.* 1980, **102**, 1759; (b) W. A. Nugent and J. M. Mayer, *Metal–Ligand Multiple Bonds*, p. 246. John Wiley, New York (1988).
8. A. C. Sullivan, G. Wilkinson, M. Motevalli and M. B. Hursthouse, *J. Chem. Soc., Dalton Trans.* 1988, 53.
9. A. D. Horton and R. R. Schrock, *Polyhedron* 1988, **7**, 1841.
10. (a) R. P. Tooze, G. Wilkinson, M. Motevalli and M. B. Hursthouse, *J. Chem. Soc., Dalton Trans.* 1986, 2711; (b) W. P. Griffith, N. T. McManus and A. D. White, *J. Chem. Soc., Dalton Trans.* 1986, 1035; (c) M. R. Churchill, C. Bueno, J. T. Park and J. R. Shapley, *Inorg. Chem.* 1984, **23**, 1017; (d) B. O. West, *Polyhedron* 1989, **8**, 219; (e) S. Cai, D. M. Hoffman, J. C. Huffman, D. A. Wierda and H. G. Woo, *Inorg. Chem.* 1987, **26**, 3693.
11. B. S. McGilligan, J. Arnold, G. Wilkinson, B. Hussain-Bates and M. B. Hursthouse, *J. Chem. Soc., Dalton Trans.* 1990, in press.
12. A. R. Middleton and G. Wilkinson, *J. Chem. Soc., Dalton Trans.* 1981, 1898.
13. (a) J. A. McCleverty, *Chem. Rev.* 1979, **79**, 53; (b) F. Bottomley, in *Reactions of Coordinated Ligands* (Edited by P. S. Braterman). Plenum Press, New York (1989); (c) K. Mertis and G. Wilkinson, *J. Chem. Soc., Dalton Trans.* 1976, 1488; (d) A. R. Middleton and G. Wilkinson, *J. Chem. Soc., Dalton Trans.* 1980, 1888.
14. J. W. Timberlake and J. C. Stowell, in *The Chemistry of Hydrazo, Azo and Azoxy Groups* (Edited by S. Patai), Pt 1, p. 69. John Wiley, New York (1975).
15. (a) For references and discussion see F. W. B. Einstein, D. Sutton and K. G. Tyers, *Inorg. Chem.* 1987, **26**, 111; M. R. Smith III, R. L. Keys, G. L. Hillhouse and A. L. Rheingold, *J. Am. Chem. Soc.* 1989, **111**, 8312; (b) For recent examples of diphenylhydrazido(2−) species of the type $Cp_2Zr(L)(Ph_2N_2)$, L = THF, PMe_3, etc., see P. J. Walsh, F. J. Hollander and R. G. Bergman, *J. Am. Chem. Soc.* 1990, **112**, 896.
16. W. Mock, in *Pericyclic Reactions* (Edited by A. P. Marchand and R. E. Lehr), Vol. 2, p. 141. Academic Press, New York (1977); T. L. Gilchrist and R. C. Storr, *Organic Reactions and Orbital Symmetry*. Cambridge University Press, Cambridge (1972).
17. (a) D. Muccigrosso, F. Mares, S. E. Diamond and J. P. Solar, *Inorg. Chem.* 1983, **22**, 960; (b) M. Kersting and R. Hoffman, *Inorg. Chem.* 1990, **29**, 278, and refs quoted.
18. D. S. Edwards, L. V. Biondi, Z. W. Ziller, M. B. Churchill and R. R. Schrock, *Organometallics* 1983, **2**, 1505.
19. P. Kovacic and C. Wu, *J. Org. Chem.* 1961, **26**, 759.
20. M. B. Hursthouse, R. A. Jones, K. M. A. Malik and G. Wilkinson, *J. Am. Chem. Soc.* 1979, **101**, 4128.
21. N. P. C. Walker and D. Stuart, *Acta Cryst.* 1983, **A39**, 1580.

Polyhedron Vol. 9, No. 17, pp. 2097–2100, 1990
Printed in Great Britain

0277–5387/90 $3.00+.00
© 1990 Pergamon Press plc

CATIONIC BIS(CYCLOPENTADIENYL)TITANIUM COMPLEXES. THE SYNTHESIS AND STRUCTURE OF $[Cp^*_2Ti(OH)(HN{=}CPh_2)]BPh_4 \cdot Et_2O$

MANFRED BOCHMANN† and ANDREW J. JAGGAR

School of Chemical Sciences, University of East Anglia, Norwich NR4 7TJ, U.K.

and

MICHAEL B. HURSTHOUSE and MOHAMMED MAZID

Department of Chemistry, Queen Mary and Westfield College, Mile End Road, London E1 4NS, U.K.

(*Received* 14 *February* 1990; *accepted* 2 *April* 1990)

Abstract—The oxidation of the titanium(III) ketimido complex, $Cp^*_2Ti{-}N{=}CPh_2$ ($Cp^* = C_5Me_5$), with $AgBPh_4$ in the presence of traces of moisture gives the cationic ketimine complex $[Cp^*_2Ti(OH)(HNCPh_2)]BPh_4 \cdot Et_2O$ (**1**). The structure of the complex has been determined by X-ray diffraction. The cation has a pseudo-tetrahedral structure. The Ti—OH distance is short [1.853(7) Å], indicating Ti—O double bond character, while the diphenylketimine ligand acts as an N-donor, with a bent Ti—N—C arrangement [145.1(5)°].

Cationic titanium complexes of the type $[Cp_2Ti{-}X]^+$ are highly reactive, coordinately unsaturated organometallic Lewis acids. If X = alkyl they readily undergo insertion reactions with unsaturated organic substrates,[1,2] including the polymerization of alkenes.[3] As we have shown recently,[4] the one-electron oxidation of titanium(III) complexes by $AgBPh_4$ provides a convenient synthetic route to such complexes under very mild conditions. We have explored the usefulness of this method for the synthesis of a number of compounds with different ligands X and report here the synthesis and crystal structure of a complex obtained by the oxidation of a titanium(III) ketimido complex.

EXPERIMENTAL

All operations were carried out under dry argon using standard vacuum-line techniques. Solvents were distilled under nitrogen from sodium benzophenone (THF, diethyl ether, petrol), sodium (toluene) or calcium hydride (dichloromethane). Perkin–Elmer 684 and 1720X (IR) and Jeol PMX-60 spectrometers were used. Cp^*_2TiCl[5] and $AgBPh_4$[4] were prepared as described. $LiN{=}CPh_2$ was prepared from PhCN and LiPh in diethyl ether.[6]

Preparation of $[Cp^*_2Ti(OH)(HNCPh_2)]BPh_4 \cdot Et_2O$ (1)

To a solution of Cp^*_2TiCl (0.5 g, 1.4 mmol) in 30 cm^3 of diethyl ether at −70°C were added dropwise 6 cm^3 of a 0.25 M solution in $LiNCPh_2$ in Et_2O–THF 10:1 (1.5 mmol). The mixture was allowed to warm to room temperature, during which time the colour changed from blue to brown. The solvent was removed *in vacuo*, the residue was extracted with petrol and filtered. Removal of the solvent left $Cp^*_2Ti{-}NCPh_2$ as an air-sensitive brown oil. IR (neat film, cm^{-1}): 1630 [ν(C=N)]. The product was not characterized further but was immediately used for the subsequent reaction.

The crude product was taken up in 20 cm^3 of THF and the solution cooled to −78°C. After addition of solid $AgBPh_4$ (0.5 g, 1.1 mmol) in small portions the solution turned orange and was allowed to warm to room temperature. Removal of the solvent gave a deep orange oil which solidified

† Author to whom correspondence should be addressed.

on treatment with diethyl ether. The product was recrystallized from THF–Et_2O to give **1** as orange plates (0.3 g, 0.34 mmol, 31%). IR (Nujol mull, cm^{-1}): 3630 [m, sharp, ν(OH)], 3275 [m, sharp, ν(NH)], 1648 [m, ν(C=N)]. Found: C, 80.5; H, 8.3; N, 1.5. Calc. for $C_{61}H_{70}BNTiO$: C, 82.1; H, 7.9; N, 1.6.

X-ray crystallography

All measurements were made on a crystal sealed under argon in a glass capillary, using a CAD4 diffractometer and graphite monochromated Mo-K_α radiation (λ = 0.071069 Å). Unit cell and intensity data were obtained following standard procedures previously described.[7]

The structure was solved using the heavy-atom procedure and refined via full-matrix least-squares methods. Non-hydrogen atoms were refined anisotropically, hydrogen atoms with idealized positions and group U_{iso} values. The ketimine hydrogen was located on a difference map and included, but the hydroxyl hydrogen was not. A molecule of diethyl ether of solvation was identified towards the end of the structure determination.

Crystal data. $C_{61}H_{72}BNO_2Ti$, M_r = 1066.44, triclinic, a = 10.321(5), b = 14.774(2), c = 17.151(3) Å, α = 86.01(1), β = 85.63(3), γ = 89.55(3)°, V = 2601.36 Å^3, Z = 2, D_{calc} = 1.36 g cm^{-3}, $F(000)$ = 977, μ(Mo-K_α) = 1.62 cm^{-1}, space group $P\bar{1}$. 5715 intensities measured ($1.5 \leqslant \theta \leqslant 25.0°$), 5571 unique, 3348 observed [$F_o > 3\sigma(F_o)$], corrected for absorption via azimuthal scan data. 241 parameters in least squares, R = 0.070, R_w = 0.070, g = 0.001188.

Atomic coordinates, displacement factor coefficients, full lists of bond lengths and angles and F_o/F_c lists have been deposited with the Editor, from whom copies are available on request. Atomic coordinates have also been deposited with the Cambridge Crystallographic Data Centre.

RESULTS AND DISCUSSION

While there is evidence for 16-electron cationic titanium azavinylidene complexes as intermediates of nitrile insertion reactions of $[Cp_2TiMe(L)]^+$, such compounds could not be isolated.[2] By contrast, analogous isoelectronic (and presumably isostructural) neutral compounds of scandium exist.[8] Work was therefore aimed at exploiting increased steric hindrance as a means of stabilizing coordinately unsaturated azavinylidene complexes of titanium(IV).

Treatment of the blue titanium(III) complex Cp^*_2TiCl with $LiC{=}NPh_2$ gives brown solutions of a petrol-soluble oily product, assumed to be $Cp^*_2TiNCPh_2$, which could not be crystallized. Oxidation of this compound with $AgBPh_4$ in THF is facile, producing metallic silver and an orange product, **1**, which is obtained as orange plates on recrystallization from THF–diethyl ether. The IR spectrum of **1** indicates the presence of C=N double bonds and also exhibits two sharp bands at 3630 and 3275 cm^{-1}. While the first of these is the typical stretching frequency of an OH ligand free of hydrogen bonding,[4] the second is reminiscent of ν(N—H) in ketimine complexes; in the Lewis adduct $(4\text{-}MeC_6H_4)_2C{=}NH \cdot BF_3$, for example, this band appears at 3280 cm^{-1}.[6] Apparently, traces of moisture† were present during the oxidation reaction, leading to the formation of a titanium hydroxo complex and the protonation of the azavinylidene ligand [eq. (1)]:

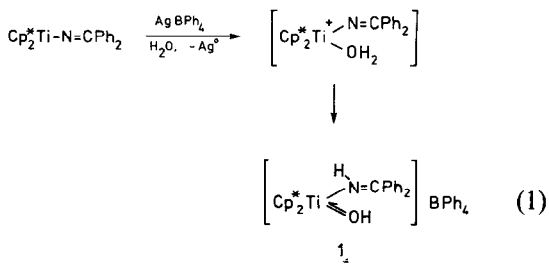

(1)

1

The structure of **1** has been determined by X-ray crystallography. A diagram of the cation is shown in Fig. 1, selected bond lengths and angles are given in Table 1. The coordination geometry of the titanium centre in the cation is pseudo tetrahedral. The Ti—OH distance is remarkably short [1.853(7) Å], suggesting double bond character via d_π–p_π interactions for the Ti—O bond. The neutral diphenylketimine ligand forms a Ti—N single bond of 2.170(9) Å, similar to the Ti—nitrile bond in $[(Indenyl)_2Ti(N{=}CMePh)(NCPh)]^+$ [2.175(7) Å][2] but significantly less than the Ti—pyridine distance in the sterically crowded complex $Ti(OC_6H_3Bu^tCMe_2CH_2)(OC_6H_3Bu^t_2)(CH_2SiMe_3)(py)$ [2.293(5) Å].[9] Comparison with the pyridine complex points to an absence of significant steric hindrance in the case of **1**. The Ti—N—C(21) linkage forms an angle of 145.1(5)°, rather wider than required for sp^2-hybridized nitrogen, and is tilted 18.1° out of the O—Ti—N plane. The two phenyl substituents of C(21) are twisted out of the

† Examination of the $AgBPh_4$ used by FT-IR suggested minute traces of coordinated water [ν(OH) 3670, 3610 cm^{-1}] which could not be removed by vacuum drying at 60°C for 6–8 h. Complete removal of water is hampered by the temperature sensitivity of the silver salt.

Table 1. Bond lengths and bond angles for **1**

(a) Bond lengths (Å)

O(1)—Ti	1.853(7)	N—Ti	2.170(9)
C(1)—Ti	2.455(9)	C(2)—Ti	2.428(9)
C(3)—Ti	2.454(8)	C(4)—Ti	2.398(9)
C(5)—Ti	2.404(9)	C(11)—Ti	2.441(7)
C(12)—Ti	2.451(7)	C(13)—Ti	2.430(6)
C(14)—Ti	2.456(7)	C(15)—Ti	2.411(7)
C(21)—N	1.268(11)	C(5)—C(1)	1.423(12)
C(2)—C(1)	1.391(11)	C(3)—C(2)	1.410(11)
C(6)—C(1)	1.484(12)	C(4)—C(3)	1.413(10)
C(7)—C(2)	1.517(12)	C(5)—C(4)	1.401(12)
C(8)—C(3)	1.489(11)	C(12)—C(11)	1.410(8)
C(3)—C(1)	1.413(10)	C(16)—C(11)	1.504(10)
C(9)—C(4)	1.512(14)	C(17)—C(12)	1.505(11)
C(10)—C(5)	1.536(13)	C(18)—C(13)	1.529(11)
C(2)—C(7)	1.517(12)	C(19)—C(14)	1.486(10)
C(15)—C(11)	1.412(8)	C(20)—C(15)	1.475(10)
C(13)—C(12)	1.404(6)	C(21)—C(28)	1.487(9)
C(14)—C(13)	1.400(8)		
C(15)—C(14)	1.439(6)		
C(21)—C(22)	1.492(10)		

(b) Bond angles (°)

N—Ti—O(1)	98.7(3)	C(1)—Ti—O(1)	106.8(3)
C(21)—N—Ti	145.1(5)	C(2)—Ti—O(1)	133.3(2)
C(1)—Ti—N	74.3(3)	C(2)—Ti—C(1)	33.1(2)
C(2)—Ti—N	90.9(3)	C(3)—Ti—N	124.3(3)
C(3)—Ti—O(1)	116.5(3)	C(3)—Ti—C(2)	33.6(2)
C(3)—Ti—C(1)	55.6(3)	C(4)—Ti—N	128.1(3)
C(4)—Ti—O(1)	83.5(3)	C(4)—Ti—C(2)	55.9(3)
C(4)—Ti—C(1)	56.1(3)	C(5)—Ti—O(1)	77.6(3)
C(4)—Ti—C(3)	33.8(2)	C(5)—Ti—C(1)	34.0(3)
C(5)—Ti—N	95.5(3)	C(5)—Ti—C(3)	56.2(3)
C(5)—Ti—C(2)	55.9(3)	C(2)—C(1)—Ti	72.4(5)
C(5)—Ti—C(4)	33.9(3)	C(5)—C(1)—C(2)	107.2(7)
C(5)—C(1)—Ti	71.0(5)	C(6)—C(1)—C(2)	126.9(8)
C(6)—C(1)—Ti	130.4(5)	C(1)—C(2)—Ti	74.5(5)
C(6)—C(1)—C(5)	125.0(8)	C(3)—C(2)—C(1)	109.6(7)
C(3)—C(2)—Ti	74.2(5)	C(7)—C(2)—C(1)	124.5(8)
C(7)—C(2)—Ti	128.4(6)	C(2)—C(3)—Ti	72.2(5)
C(7)—C(2)—C(3)	124.5(7)	C(4)—C(3)—C(2)	106.5(7)
C(4)—C(3)—Ti	70.9(5)	C(8)—C(3)—C(2)	127.6(7)
C(8)—C(3)—Ti	135.1(5)	C(3)—C(4)—Ti	75.3(5)
C(8)—C(3)—C(4)	123.6(7)	C(5)—C(4)—C(3)	108.7(7)
C(5)—C(4)—Ti	73.3(5)	C(9)—C(4)—C(3)	125.6(8)
C(9)—C(4)—Ti	122.0(6)	C(1)—C(5)—Ti	75.0(5)
C(9)—C(4)—C(5)	125.4(7)	C(4)—C(5)—C(1)	107.8(7)
C(4)—C(5)—Ti	72.8(5)	C(10)—C(5)—C(1)	125.6(8)
C(10)—C(5)—Ti	124.9(6)	C(22)—C(21)—N	123.4(7)
C(10)—C(5)—C(4)	126.1(8)	C(28)—C(21)—C(22)	116.1(7)
C(28)—C(21)—N	120.5(7)	C(27)—C(22)—C(21)	120.3(6)
C(23)—C(22)—C(21)	119.7(6)	C(33)—C(28)—C(21)	120.6(6)
C(29)—C(28)—C(21)	119.4(6)		

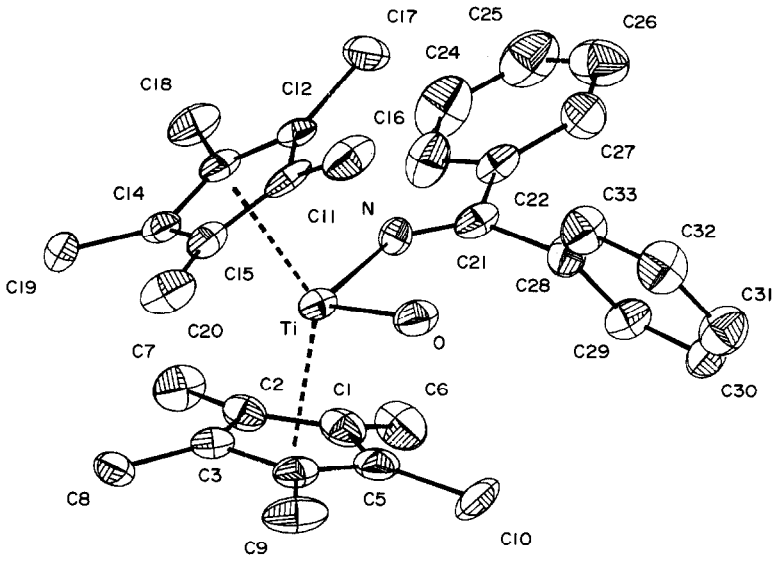

Fig. 1.

Ti—N—C(21) plane by 25.9 and 120.1°, respectively.

The coordination geometry of **1** and the bond lengths distribution resembles a pattern previously observed for $[Cp^*_2Ti(OH)(OH_2)]^+$, with a tightly bonded OH ligand free of hydrogen bonds, and a more loosely coordinated neutral donor ligand.[4] The formation of the hydroxo-ketimine complex **1** in preference to the isomeric azavinylidene-aquo complex $[Cp^*_2Ti(N{=}CPh_2)(OH_2)]^+$ reflects the different acidities of the two ligands and is evidence for the more effective Ti—O d_π–p_π interaction compared to Ti—N.

REFERENCES

1. M. Bochmann and L. M. Wilson, *J. Chem. Soc., Chem. Commun.* 1986, 1610; M. Bochmann, L. M. Wilson, M. B. Hursthouse and R. L. Short, *Organometallics* 1987, **6**, 2556.
2. M. Bochmann, L. M. Wilson, M. B. Hursthouse and M. Motevalli, *Organometallics* 1988, **7**, 1148.
3. M. Bochmann, A. J. Jaggar and J. N. Nicholls, *Angewandte Chem.*, in press.
4. M. Bochmann, A. J. Jaggar, L. M. Wilson, M. B. Hursthouse and M. Motevalli, *Polyhedron* 1989, **8**, 1838.
5. J. W. Pattiasina, H. J. Heeres, F. van Bolhuis, A. Meetsma and J. H. Teuben, *Organometallics* 1987, **6**, 1004.
6. B. Samuel, R. Snaith, C. Summerford and K. Wade, *J. Chem. Soc. A* 1970, 2019.
7. M. B. Hursthouse, R. A. Jones, K. M. A. Malik and G. Wilkinson, *J. Am. Chem. Soc.* 1979, **101**, 4128.
8. J. E. Bercaw, D. L. Davies and P. T. Wolczanski, *Organometallics* 1986, **5**, 443.
9. S. L. Latesky, A. K. McMullen, I. P. Rothwell and J. C. Huffman, *J. Am. Chem. Soc.* 1985, **107**, 5981.

Polyhedron Vol. 9, No. 17, pp. 2101–2125, 1990
Printed in Great Britain

0277–5387/90 $3.00+.00
© 1990 Pergamon Press plc

OXOVANADIUM(IV) AND AMINO ACIDS—IV.† THE SYSTEMS L-CYSTEINE OR D-PENICILLAMINE+VO^{2+}; A POTENTIOMETRIC AND SPECTROSCOPIC STUDY

J. COSTA PESSOA and L. F. VILAS BOAS

Centro di Química Estrutural, Complexo I, Instituto Superior Técnico, 1096 Lisboa, Portugal

and

R. D. GILLARD‡

School of Chemistry and Applied Chemistry, University of Wales, College of Cardiff, P.O. Box 912, Cardiff CF1 3TB, Wales, U.K.

(*Received* 24 *January* 1990; *accepted* 3 *April* 1990)

Abstract—The aqueous equilibria in the systems L-cysteine or D-penicillamine + VO^{2+} have been studied by a combination of pH-potentiometric and spectroscopic methods [electron paramagnetic resonance (EPR), visible absorption and circular dichroism (CD)] in the pH range 1.8–13.5. For pH > 4, high ligand-to-metal ratios were used. The results of the various methods are made self-consistent, then rationalized assuming an equilibrium model including species ML_2H_2, ML_2H_4, ML_2H_3, ML_2H_2, ML_2H, ML_2, ML_2H_{-1} and M_2L_2 (where H_2L denotes either L-cysteine or D-penicillamine) and several hydrolysis products; their formation constants and individual electronic spectra (isotropic and CD) are given. Isomeric structures are discussed for each stoichiometry.

The first part of this series[1] introduced our work and gave detailed results for the system L-AlaH + VO^{2+} in the pH range 2–12. Part II concerned complexing of oxovanadium(IV) by L-serine or L-threonine,[2] and Part III the L-aspartic acid + VO^{2+} system.[3] The present paper describes our potentiometric and spectroscopic study of the complexation of oxovanadium(IV) by the sulphur-containing amino acids L-cysteine and D-penicillamine. Part of this work has been presented in a preliminary form.[4]

The inherent interest of such vanadium sulphur systems exemplified by studies of their localization in blood components from cells of ascidians (e.g. *A. mentula* and *A. aspersa*)[5] is reinforced by the discovery that the vanadium nitrogenase of *Azotobacter* is apparently a vanadium–sulphur–iron complex.[6] Further, the well-known vanadium impurities in some crude oils, arising from vanadyl porphyrins and elsewhere, are converted under hydrorefining to sulphido–vanadium complexes. These deactivate hydrotreating catalysts, rendering the treatment of Western crudes problematic.[7]

Some work has been published on systems involving cysteine and its derivatives.[8–17] Johnson and Shepherd[8] recorded EPR spectra at room temperature of solutions at pH = 7 with total oxovanadium(IV) and L-cysteine concentrations of 6.8×10^{-3} and 1.0 M, respectively, and calculated $A_0 = 85$ gauss. The corresponding visible spectra show maxima at 535 and 730 nm. Comparing these results with those for several other systems, Johnson and Shepherd concluded that, under their conditions, coordination of cysteine to VO^{2+} involves in-plane binding of sulphhydryl S and glycinate N.[8]

Cysteine reduces vanadate(V) to oxovanadium(IV): kinetics and products depend on the pH

† For Parts I–III, see refs 1–3.

‡ Author to whom correspondence should be addressed.

and on the concentrations of cysteine and vanadium.[9] With excess of cysteine, cystine is produced.[9,11-13]

In solutions containing an excess of cysteine at pH ~ 7, a stable, purple complex forms with a structure probably similar to that of the complex of cysteine methyl ester (CysOMe) prepared and characterized by X-ray diffraction by Sakurai and co-workers.[13-15] This contained S_2N_2 coordination in the equatorial plane.

The EPR spectra of the CysOMe–VO^{2+} complex in borate buffer (pH 10.5) at 77 K show the presence of two species, the more important having $g_\parallel = 1.964$, $g_\perp = 2.003$, $A_\parallel = 143.6$ and $A_\perp = 47.0 \times 10^{-4}$ cm^{-1}.[14] The minor component was detected not only in the EPR but in the IR and Raman spectra and Sakurai and co-workers concluded that *cis*- and *trans*-isomers were present.[13,14] Sifri and Riechel studied the electrochemistry in DMSO of 2:1 complexes of cysteine, CysOMe and CysOEt.[16]

A Chinese publication mentions the preparation of $K[VO(CysH)(H_2O)_2]SO_4$ and *cis*- and *trans*-$K_2[VO(Cys)_2]$ ($CysH_2$ = cysteine).[17] Further, for $VOSO_4$ and cysteine in 1:1 ethylene glycol–water, when increasing the pH from 1 to 14, the EPR spectra were said to suggest stepwise formation of $[VO(OH_2)_5]^{2+}$, $[VO(H_2O)_3(CysH_2)]^{2+}$, $[VO(H_2O)_2(CysH)]^{+}$, *cis*- and *trans*-$[VO(Cys)_2]^{2-}$ and $[VO(OCH_2CH_2O)_2]^{2-}$.

The results of our work with L-$CysH_2$ and D-$PenH_2$ differ from those for the L-AlaH,[1] L-SerH, L-ThrH,[2] L-aspartic acid[3] and L-glutamic acid[18] systems for much of the pH range studied (1.8–13.5). This difference stems from coordination of the thiol group at quite low pH (~ 4).

Experimental difficulties in work involving oxovanadium(IV) and amino acids were discussed in Part I.[1] Between pH 4 and 8, relatively high ligand-to-metal ratios (L/M) must be used to avoid extensive hydrolysis and eventual precipitation of $VO(OH)_2$. However, such precipitation and/or the presence of a soluble product of oxovanadium(IV) hydrolysis for pH $\gtrsim$ 5 is clearly less important for L-$CysH_2$ and especially for D-$PenH_2$ as compared to L-AlaH, L-SerH and L-ThrH systems, and lower L/M ratios may be used.

Both ligands contain three dissociable protons, with macroscopic dissociation constants: $pK_{a1} \sim 2$, $pK_{a2} \sim 8$ and $pK_{a3} \sim 10.5$. The value of pK_{a1} can be ascribed unambiguously to deprotonation of the carboxyl group, but the values of pK_{a2} and pK_{a3} arise from a combination of microprocesses corresponding to (i) dissociation of the thiol group followed by the amino group, or (ii) dissociation of the amino group followed by the thiol group. For the present study of formation constants the microconstants are not required, so we have not measured them.

Since pK_{a1}, pK_{a2} and pK_{a3} can easily be determined, the calculated formation constants correspond to the general reaction:

$$xM^{2+} + yL^{2-} + zH^{+} \rightleftharpoons M_xL_yH_z. \qquad (1)$$

We abbreviate L-cysteine as H_2C and the cysteinate dianion is then C^{2-}. D-Penicillamine is abbreviated as H_2P and the penicillaminate dianion as P^{2-}. For the formulations $(VO)_x(Cys)_y(H)_z$ and $(VO)_x(Pen)_y(H)_z$ we normally use the abbreviations $M_xC_yH_z$ and $M_xP_yH_z$, respectively, or $M_xL_yH_z$ to denote both. When needed, we abbreviate L-alanine and L-serine as HA and HS, and alaninate and serinate as A^- and S^-, respectively.

For each $M_xL_yH_z$ in our final equilibrium model, the isotropic visible absorption spectrum (ε_{xyz}) and CD spectrum ($\Delta\varepsilon_{xyz}$) are calculated and possible structures are discussed.

EXPERIMENTAL

Materials and methods

The MINIQUAD,[19] SUPERQUAD[20] and the SQUAD[21] programs were used to refine formation constants and calculate spectra of individual species.

All solutions were prepared in an inert atmosphere (high purity dinitrogen passed through soda-lime and glass wool). All measurements were performed at 25°C with solutions containing 2.25 M $NaNO_3$.

The instruments used and the calibration procedure for pH measurements were described in Part I.[1] The maximum pH value for the titration curves of solutions containing L-$CysH_2$ or D-$PenH_2 + VO^{2+}$ was ~ 6.7.

D-Penicillamine (Sigma) for stock solutions was dried for 2 days (in a vacuum desiccator over silica gel). For the more concentrated solutions, HNO_3 (2.00 M) was added. For cysteine stock solutions, L-$CysH_2 \cdot HCl \cdot xH_2O$ ($x \sim 1$) (Merck) was always used. The value of x was determined by thermogravimetry. Such stock solutions were used within a maximum of ~ 36 h and exact concentrations were checked by titration with strong base (graphic representation and the Gran procedure[22] were used). Refinement of total H^+ and/or amino acid, in the calculations with SUPERQUAD, always gave final values for these "dangerous parameters" very close to the initial values supplied.

Several titration curves with $0.04 \lesssim C_{Cys}$ or

$C_{Pen} \lesssim 0.07$ M (C_{Cys}, C_{Pen}—total cysteine and penicillamine concentrations, respectively) were obtained to determine the protonation constants in 2.25 M $NaNO_3$; NaOH (2.2 M) was used. As $J_H \sim 20$ [eq. (2)], the corrections in the acid range are significant only for pH < 2.0.

$$E = E^{\ominus} + S \times \log[H^+] + J_H \times [H^+] + J_{OH} \times [OH^-]. \quad (2)$$

As for previous systems,[1-3] two types of titration curves were obtained: those involving measurements in the range $2.2 \lesssim pH \lesssim 4.3$ (with $1 \lesssim L/M \lesssim 4$ and $0.005 \lesssim C_{VO} \lesssim 0.017$ M) and those involving pH measurements in the range $4.0 \lesssim pH \lesssim 6.7$ ($20 \lesssim L/M \lesssim 79$ and $0.0025 \lesssim C_{VO} \lesssim 0.0063$ M).

Unusually, for D-$PenH_2$, in the titration with L/M = 4 ($C_{VO} = 0.016$ M), no precipitation or unstable EMF readings were found in the pH range 4–7. This notwithstanding, EMF readings for pH > 4.3 were not used in the calculations with MINIQUAD and SUPERQUAD, because the properties of the soluble hydrolysed vanadium species which forms in this pH range (presumably $[(VO)_2(OH)_5^-]_n$) are not accurately known.[23,24]

Totals of 75 and 100 CD spectra were recorded for the L-cysteine and the D-penicillamine systems, respectively; a total of about 50 isotropic visible absorption spectra was recorded for each system. Calculations with the SQUAD program were made only for D-Pen: 40 visible spectra and 95 CD spectra (visible region) were used for the calculation of spectra of individual species, with total concentrations in the range $0.0017 \lesssim C_{VO} \lesssim 0.03$ M and $0.036 \lesssim C_{Pen} \lesssim 0.26$ M, respectively. Ligand-to-metal ratios were in the range 1.9–73.

Several spectra were recorded with solutions containing S-methyl-L-cysteine (Sigma) or L-cysteine ethyl ester (Aldrich). For these, a solution of pH = 2.0 and $C_{VO} = 0.0088$ M was prepared and its CD spectrum recorded. NaOH (4 M) was added and CD was measured for each ~0.6 pH increment. At pH ~ 4.2, vanadyl hydroxide precipitated. An excess of base was then added to pH ~ 9.2, and the CD spectrum taken of the resulting clear greenish-blue solution. HNO_3 (2 M) was added and CD spectra were recorded for each decrement of ~0.6 pH units. For pH < 5.0, vanadyl hydroxide again precipitated.

For $pH \gtrsim 10$, the pH reading of solutions containing L-CysOEt: VO^{2+} = 45.1 slowly decreased. For $pH \gtrsim 11.3$, this decrease was fairly rapid (the $|\Delta\varepsilon_m|$ values simultaneously increased). This is probably due to hydrolysis of the ester group, producing L-cysteine. This may also be the origin of the slight pH modifications in solutions containing L-CysOEt + VO^{2+} at pH < 3.0.

For $pH \lesssim 10$, L-CysOEt hydrolyses slowly: the production of any appreciable concentration of L-Cys would have prevented precipitation of vanadyl hydroxide at pH 4–5. However, this was in fact observed both on addition of base to solutions with pH < 4, or of acid to solutions with pH > 8. Consequently, the measured spectra involve L-CysOEt as ligand.

RESULTS

(1) *Preliminary comments*

The spectroscopic results permit, on cursory inspection, some deductions useful in defining the detailed method of treating the potentiometric results. We therefore present our results in two sections, viz. these preliminary deductions from spectra followed by the calculations of speciation.

EPR spectra

The EPR spectra for frozen "solutions" containing L-cysteine or D-penicillamine and VO^{2+} at 77 K are typical VO^{2+} axial spectra. The field region that corresponds to $A_\parallel$ and $M_I = 5/2$ and 7/2 gives more information about the type and number of species present.

Figure 1 includes the high-field region of the spectra of frozen "solutions" containing D-penicillamine with L/M 18.5 at several values of pH. Results for L-cysteine are similar. PI to PVII (CI to CVII for the L-cysteine system) represent distinct components. Each corresponds to a set of g and A values ($\parallel$ and $\perp$): there may of course be more than one vanadium complex with these approximately the same, so there is not necessarily a 1:1 correlation of observed component with a single chemical species.

Analysing Fig. 1, and comparing it with results for L-cysteine and other systems, we make the general observations:

(i) Components PIII, PIV and PV are detected at values of pH lower by 0.3–0.8, than are CIII–CV.

(ii) For $pH \lesssim 4.7$ (for L-Cys) or $\lesssim 3.9$ (for D-Pen) one can distinguish at least two components, PI (or CI) and PII (or CII). Their g and A parameters indicate that the species responsible are of the same type as those we earlier associated with components LI and LII in the L-AlaH, L-SerH and L-ThrH + VO^{2+} systems.

(iii) The g and A parameters for CIII and PIII

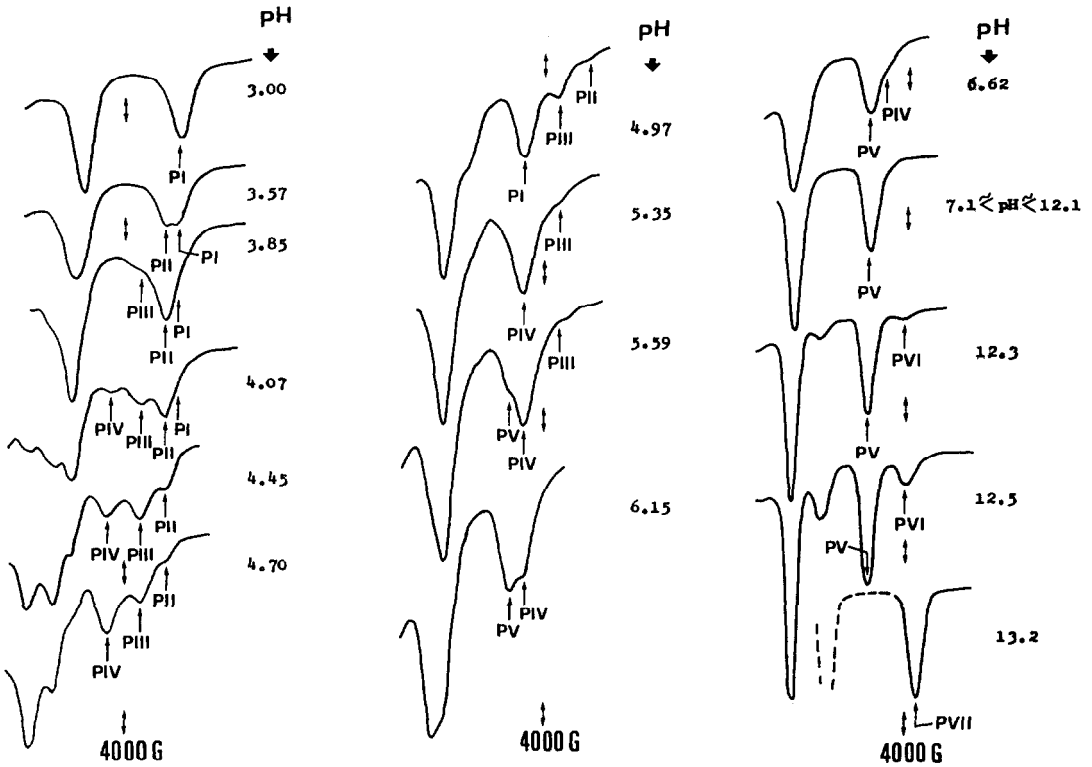

Fig. 1. High-field range (3600–4200 gauss) of the first derivative EPR spectra at 77 K of frozen "solutions" containing D-Pen and VO^{2+} with L/M = 18.5. The total vanadium concentration is ~ 0.004 M. pH values are indicated.

correspond to those for LIII in the L-AlaH, L-SerH and L-ThrH + VO^{2+} systems.[1,2] However, while in those systems, LIII is the sole component detected at pH ~ 6, CIII and PIII are always detected simultaneously with other signals, and they predominate at lower pH values (~ 4.1–7 for CIII and ~ 3.8–5.7 for PIII). Further, the stepwise spectral changes CIII → CIV → CV and PIII → PIV → PV occur in a much narrower range of pH than for the "same type" of components in the L-serine or L-threonine systems.

(iv) While the transformations SIV → SIV′ (L-serine system) and TIV → TIV′ (L-threonine system) occur with no detectable differences in the g and A parameters,[2] in the "corresponding" transformations CIV → CV and PIV → PV, $A_{\parallel}$(CIV,PIV) > $A_{\parallel}$(CV,PV).

(v) The range of pH where CIV + CV or PIV + PV can be detected, ~ 5–12.2 and 4–13, respectively, is much broader than for SIV + SIV′ or TIV + TIV′.

(vi) In the L-Cys and D-Pen systems, PV, PVI and PVII (or CV, CVI and CVII) are clearly distinct. This was not the case for the "corresponding" components in the L-SerH and L-ThrH + VO^{2+} systems.[2]

(vii) Hydrolysis at high pH of the cysteinate and penicillaminate complexes ($[VO(OH)_3]^-$ being formed?) occurs at slightly lower pH than for the "corresponding" serinate and threoninate complexes.

Components CV and PV correspond to $g_{\perp} = 1.976$, $g_{\parallel} = 1.962$, $A_{\perp} = 45$ and $A_{\parallel} = 143 \times 10^{-4}$ cm^{-1}; the following approximate values are estimated from spectra with two or more components:[25]

PIII and CIII → $g_{\parallel} \sim 1.945$ and $A_{\parallel} \sim 164 \times 10^{-4}\,cm^{-1}$

PIV and CIV → $g_{\parallel} \sim 1.956$ and $A_{\parallel} \sim 151 \times 10^{-4}\,cm^{-1}$

PVI and CVI → $g_{\parallel} \sim 1.942$ and $A_{\parallel} \sim 156 \times 10^{-4}\,cm^{-1}$.

The EPR parameters estimated for PVII (and CVII) approximately correspond to those reported for $[VO(OH)_3]^-$.[26]

CD and visible absorption spectra

As for EPR, these electronic absorption spectra and their changes with pH are similar for the present systems. We ascribe minor differences to the fact that the stepwise transformations as pH increases: PI, PII → PIII → PIV → PV occur in a narrower pH range than for the L-cysteine case. We shall, in the main, present results (and calculations) for D-penicillamine. L-Cysteine is, *mutatis mutandis*, similar.

(a) *Fixed* L/M, *variable pH*. Figures 2 and 3 include visible spectra of D-PenH_2 solutions with L/M 23.7 (ε_m and $\Delta\varepsilon_m$ are measured ε and $\Delta\varepsilon$ per mole of vanadium). The changes in the pH range 2–4.5 resemble those for L-serine and L-threonine[2] in the pH range 2–6. In the pH range 4.5–7.4, bands I and II shift further to lower wavelengths, but while band II weakens, band I increases.

In the pH range 8.3–10.3, the visible spectra are invariant with maxima at 526 and 729 nm and $\varepsilon_m = 18.3$ and 42.1. This and the EPR spectra suggest that in these conditions only one species exists: its visible spectrum is therefore known. For pH $\gtrsim$ 12.6, as in the other systems studied, the general increase in ε_m (especially for 450–600 nm) suggests extensive hydrolysis of VO^{2+}; the characteristic bands I and II are no longer distinct.

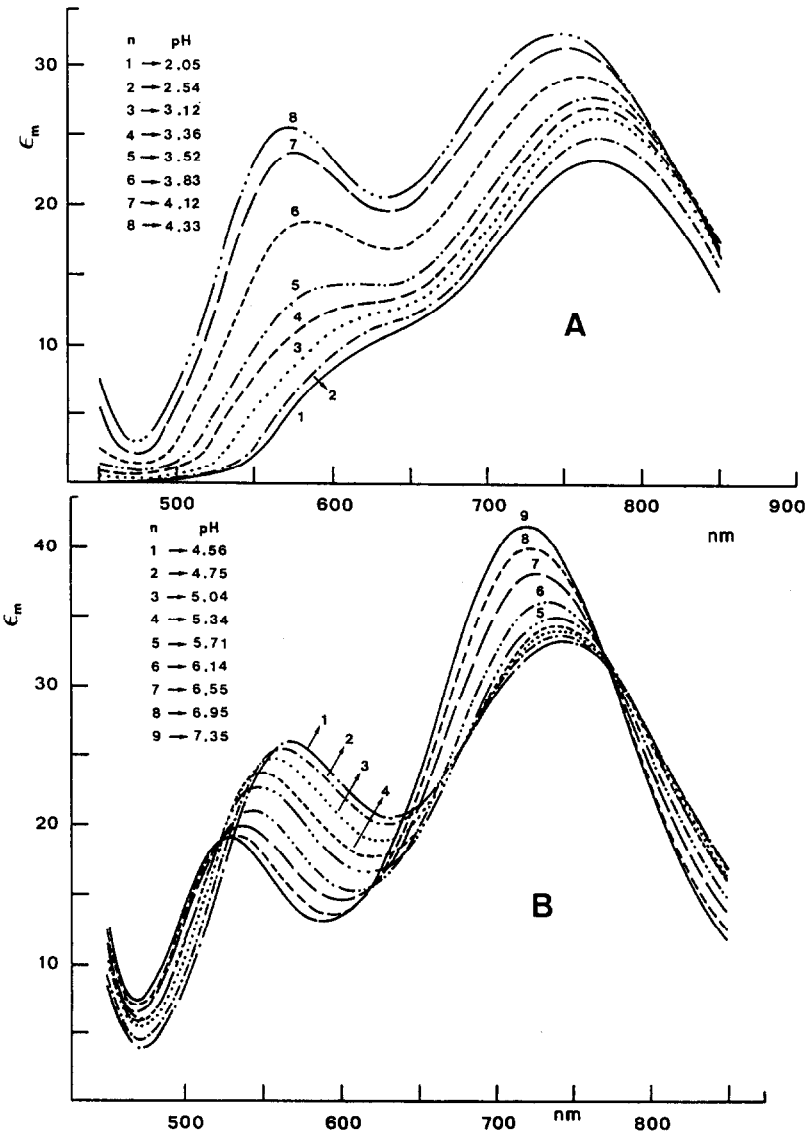

Fig. 2. Visible spectra of solutions containing D-Pen+VO^{2+} with L/M = 23.7 and $C_{VO} = 9.8$–10.6×10^{-3} M. The pH corresponding to each spectrum is indicated. The CD spectra of some of these solutions are given in Figs 4 and 5.

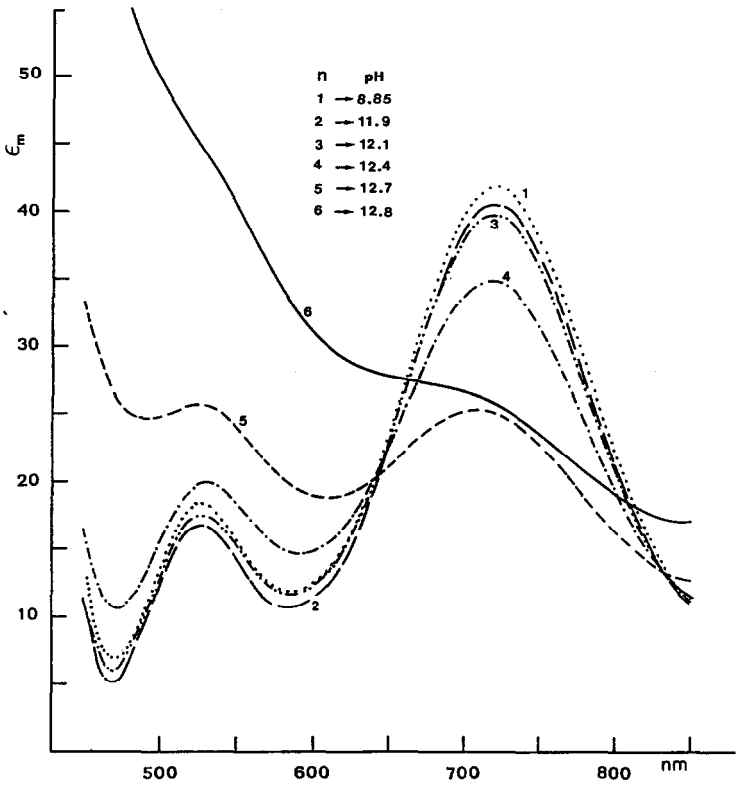

Fig. 3. Visible spectra of solutions containing D-Pen+VO^{2+} for pH > 8.8 with L/M = 23.7 and $C_{VO} = 8.9–9.8 \times 10^{-3}$ M. The pH corresponding to each spectrum is indicated and the CD spectra for the same solutions are given in Fig. 6.

As for other systems,[1-3,18] the visible CD spectra for D-penicillamine or L-cysteine+VO^{2+} vary enormously in the pH range 1–14. For them, this occurs especially for $2 \lesssim pH \lesssim 7.5$ and $10.5 \lesssim pH \lesssim 13.5$. Figures 4–6 include CD spectra for D-penicillamine with L/M = 23.7, all inverted [$\Delta\varepsilon_m \times (-1)$] to facilitate comparison with other L-amino acids. The CD spectra and their changes with pH have some similarities with those in the L-serine and L-threonine systems.[2]

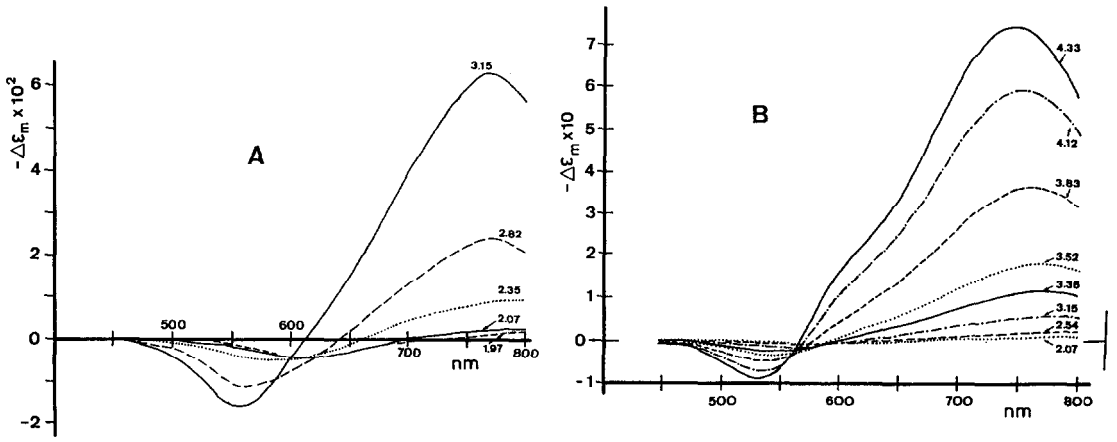

Fig. 4. CD spectra of solutions containing D-Pen+VO^{2+} with L/M = 23.7 and $C_{VO} \sim 0.01$ M. The pH corresponding to each spectrum is indicated. The visible spectra of some of these solutions are given in Fig. 2.

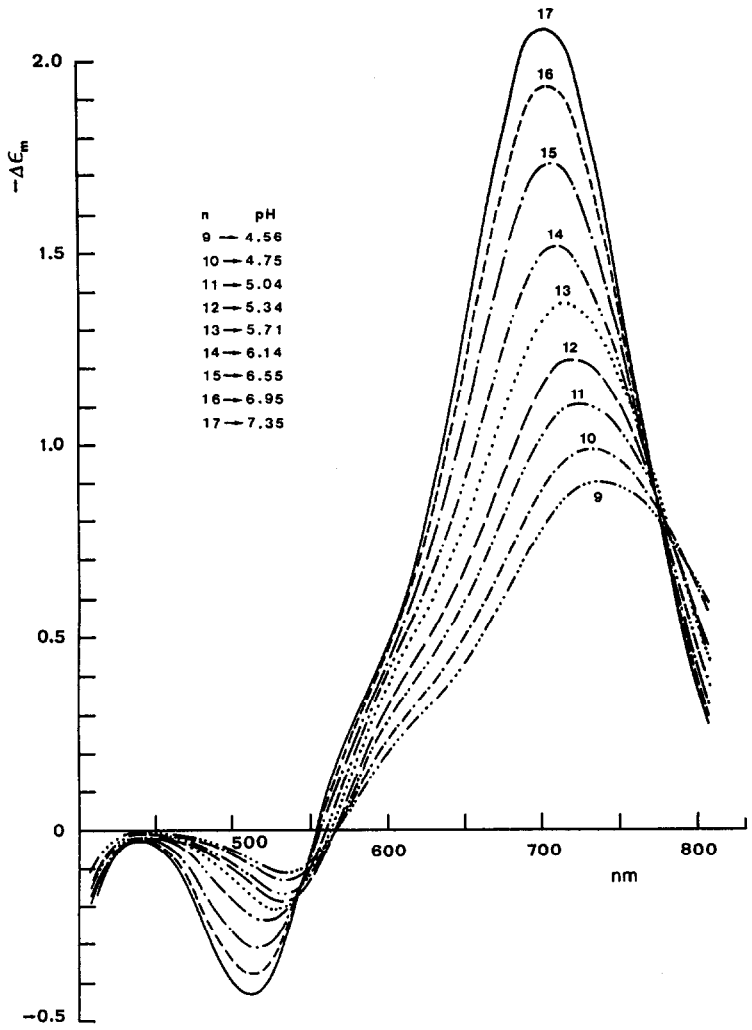

Fig. 5. CD spectra of solutions containing D-Pen+VO^{2+} with L/M = 23.7 and $C_{VO} \sim 0.01$ M. The isotropic absorption spectra of these solutions are given in Fig. 2.

Analysing Figs 2–6, and comparing them with L-cysteine and other systems, we can make the general observations:

(i) The CD spectra of Fig. 4 show that—for very low pH—$\Delta\varepsilon_m$ for $\lambda > 600$ nm are approximately zero. Depending on C_{VO} and C_{Pen}, $\Delta\varepsilon_m$ are always very small but may be of either sign. This, clearer in the glutamic acid system,[18] suggests the existence of two (or more) complexes with differing signs of $\Delta\varepsilon$ for $\lambda > 600$ nm. Their relative importance may differ slightly in the L-cysteine system. This (L/M = 35.0 and $C_{VO} = 0.01$ M, pH $\sim$ 1.2 and 1.8) manifests two CD bands at $\sim$ 680 and 780 nm and $\Delta\varepsilon_m > 0$, as for L-Ala at low pH.[1]

(ii) For pH < 3.5, $|\Delta\varepsilon_m|^{Pen}$, and—to an extent—$|\Delta\varepsilon_m|^{Cys}$ ($400 < \lambda < 800$ nm), are much greater than $|\Delta\varepsilon_m|^{Ser,Thr}$, notably for $\lambda > 600$ nm. The species are akin (as concluded from the EPR spectra), but complexes with high $|\Delta\varepsilon_{xyz}|$ values form at lower pHs with L-cysteine or D-penicillamine.

(iii) As pH increases, the differences between $|\Delta\varepsilon_m|^{Pen,Cys}$ and $|\Delta\varepsilon_m|^{Ser,Thr}$ diminish and $|\Delta\varepsilon_m|^{Pen,Cys}$ of band I increase much more than those of band II.

(iv) As for the visible spectra, CD spectra of solutions containing D-penicillamine with L/M = 23.7 coincide in the range $8.3 \lesssim$ pH $\lesssim 10.3$. Spectra in the same range with L/M = 72.7 still coincide.

(v) For L-cysteine/VO^{2+} = 35.0, the visible and CD spectra in the pH range 8.8–10.3 do not quite coincide. This means that—besides

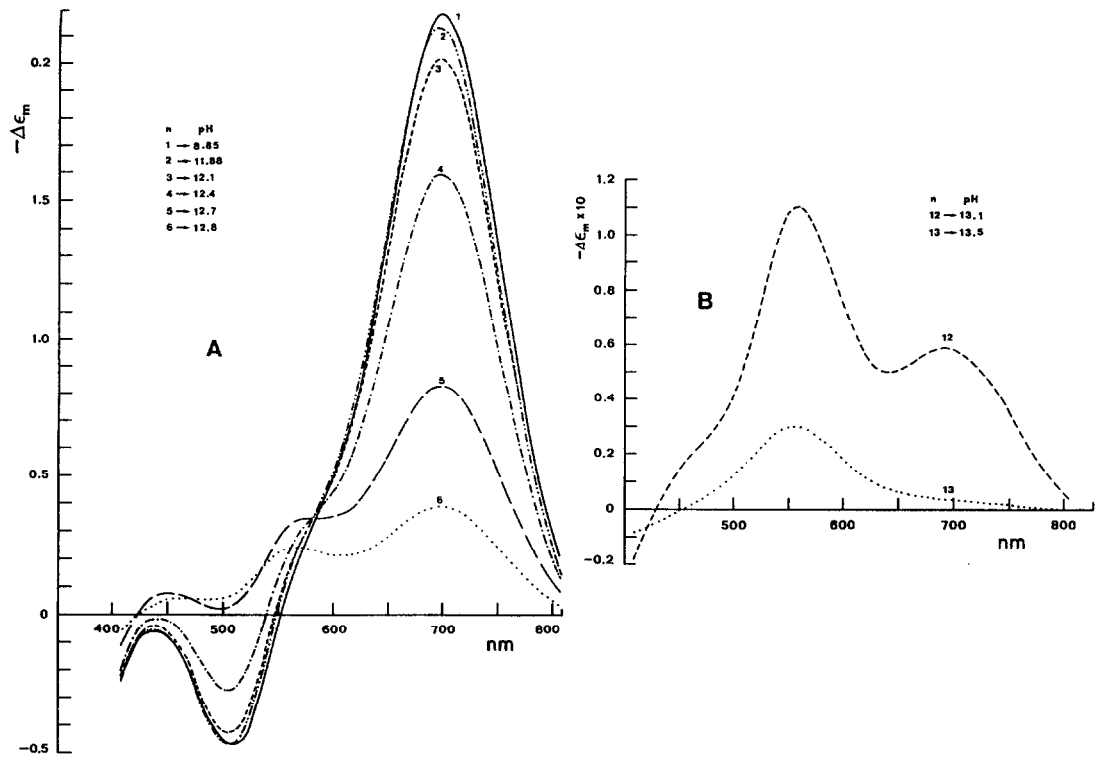

Fig. 6. CD spectra of solutions containing D-Pen + VO^{2+} with L/M = 23.7 and $C_{VO} = 8.4–9.6 \times 10^{-3}$ M. The isotropic absorption spectra of the solutions with pH < 12.8 are given in Fig. 3. Note the different scales for (A) and (B).

species CIII, CIV and CV forming at pH higher than the corresponding PIII, PIV and PV—CV never (unlike PV) gets to ~ 100%.

(vi) For pH > 10.3, $|\Delta\varepsilon_m|$ for $600 < \lambda < 800$ nm decrease [Fig. 6(A)] and for pH ~ 12.7 a band at ~ 500 ($\Delta\varepsilon < 0$) is clear. The complex responsible probably gives component PVI in the EPR (Fig. 1). At pH ~ 13.5, the CD spectrum [13 in Fig. 6(B)] of D-Pen : VO^{2+} = 23.7 gives only one band for $\lambda > 500$ nm. For L-Cys with L/M = 35.0, the spectra at pH ~ 12.8 and 13.2 (C1 and C2 in Fig. 15) clearly show this band ($\lambda \sim 550$ nm; $\Delta\varepsilon_m > 0$) and another ($\lambda \sim 660$ nm; $\Delta\varepsilon_m < 0$). The species responsible (CVI?) is probably a product from hydrolysis of CV. A similar CD spectrum is *not* seen for pH ~ 13.5 for D-penicillamine, probably because PV hydrolyses at significantly higher pH than CV does.

(b) *Fixed pH, variable* L/M. Figures 7–9 show CD spectra for D-penicillamine (Fig. 9(A) is for L-cysteine) at fixed pH and variable L/M. Analysing and comparing them with L-cysteine, we can make the following general observations:

(i) At pH = 4.04 [Fig. 7(A)], the CD spectra show only minor changes for L/M in the range 72.7–38.8. For L/M $\lesssim$ 30 the $|\Delta\varepsilon_m|$ decrease substantially.

(ii) At pH = 4.54 [Fig. 7(B)], as L/M decreases from 72.7 to 14.5, $|\Delta\varepsilon_m|$ (600–800 nm) clearly increase and band I shifts hypsochromically. For L/M < 14, all $|\Delta\varepsilon_m|$ (400–600 nm) decrease.

(iii) At pH = 5.54 [Fig. 8(A)], the CD spectra show no important changes, but as L/M decreases from 72.8 to 4.8, $|\Delta\varepsilon_m|$ (600–800 nm) clearly fall and band I shifts to higher wavelengths. To a lesser extent, the same happens at pH 5.74 (spectra not shown).

(iv) At pH ~ 7.2, for both L-cysteine and D-penicillamine, the CD spectra show minor changes as L/M decreases (spectra not shown). For L-cysteine, $\Delta\varepsilon_m$ ($\lambda \sim 710$ nm) decreases only by 10% as L/M varies from 97.0 to 9.7.

(v) At pH ~ 12.8 [Fig. 8(B)], the visible $|\Delta\varepsilon_m|$ substantially decrease as L/M varies from 23.7 to 7.8; an isodichroic point is observed ($\lambda \sim 420$ nm, $\Delta\varepsilon_m \sim 0$). For L-cysteine at pH ~ 12.8 with L/M between 35 and 13, the CD spectra all resemble C1 (Fig. 15) and the $|\Delta\varepsilon_m|$ values decrease with L/M. For pH ~ 12.5 and

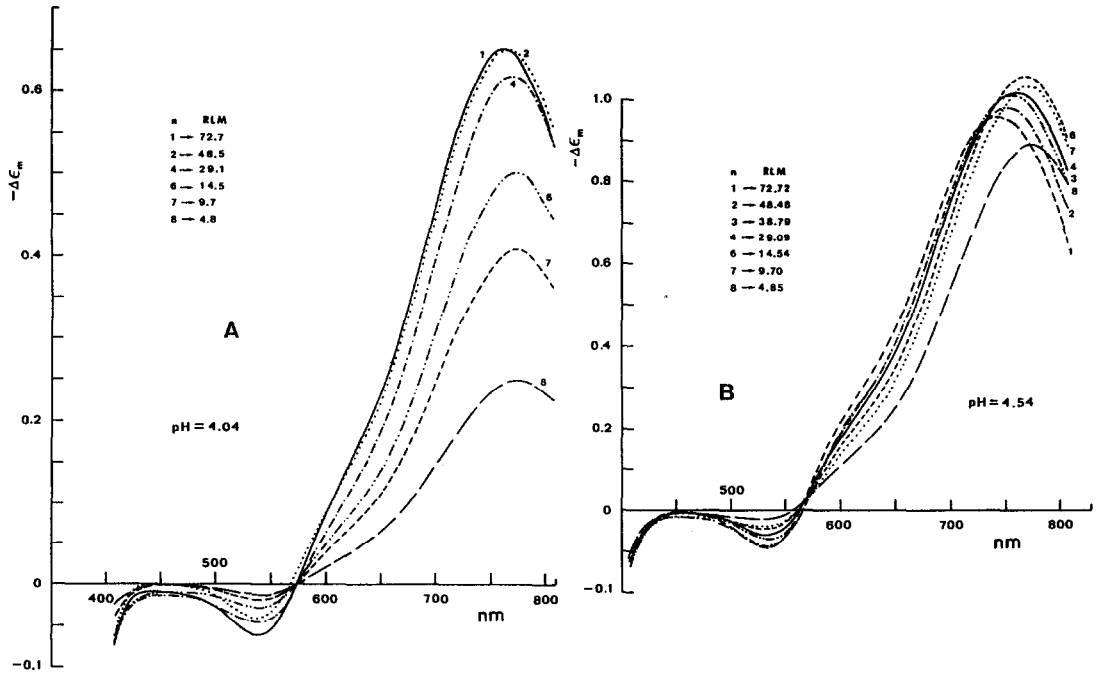

Fig. 7. CD spectra of solutions containing D-Pen and oxovanadium(IV) with varying L/M (denoted by RLM) at fixed pH.

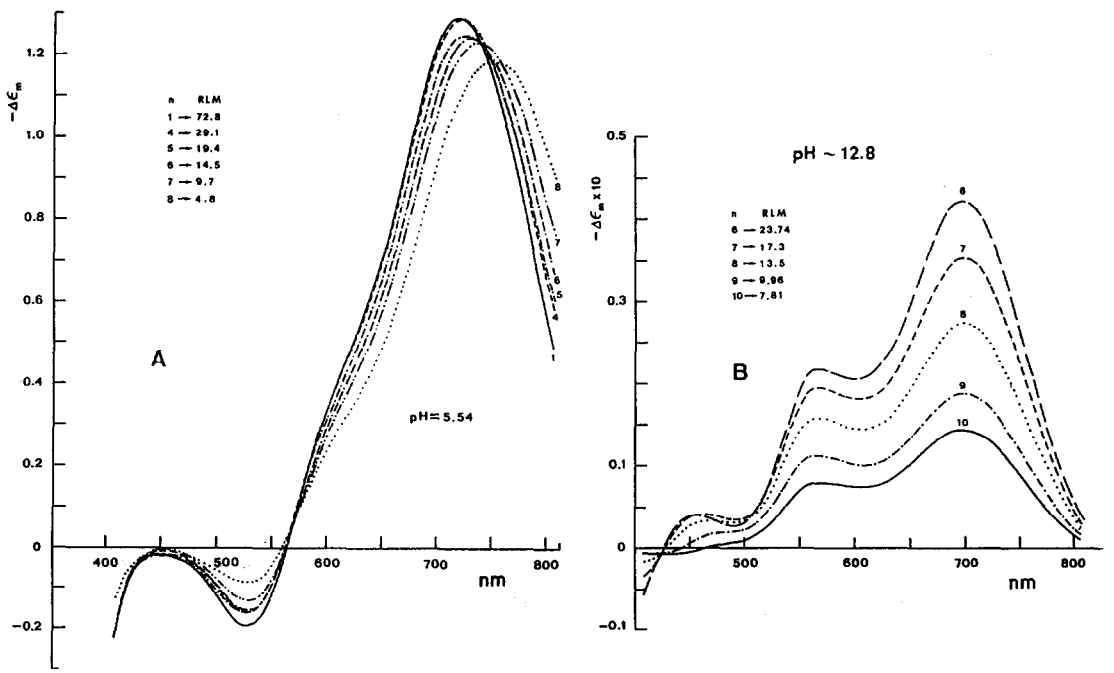

Fig. 8. CD spectra of solutions containing D-Pen and oxovanadium(IV) with varying L/M (denoted by RLM) at fixed pH.

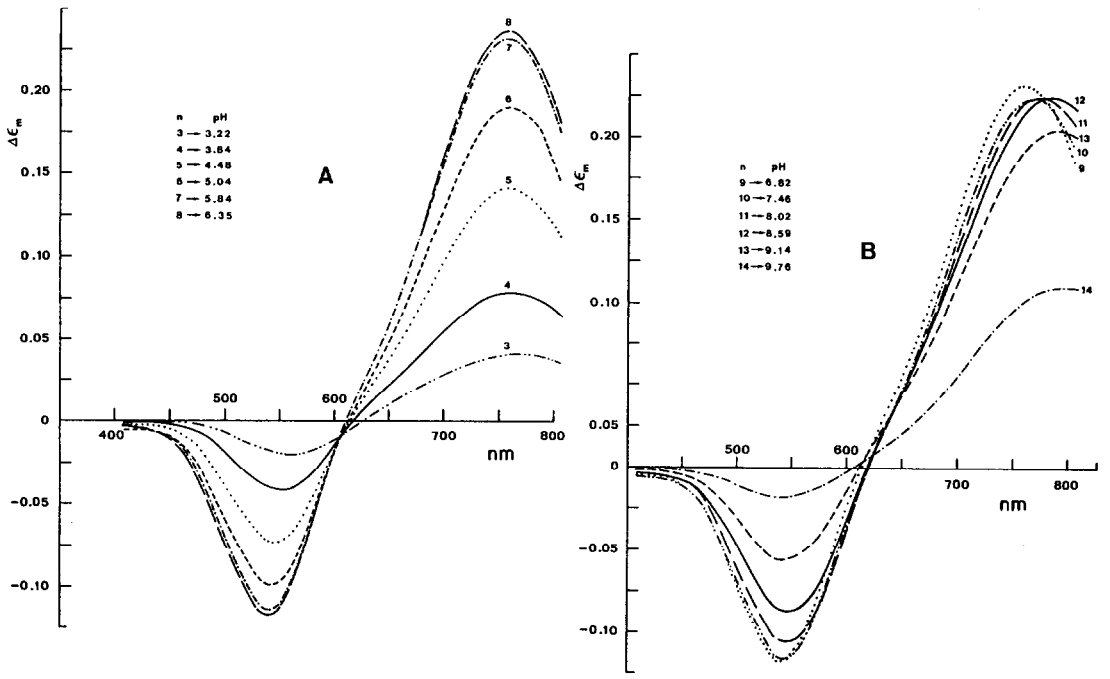

Fig. 9. CD spectra of solutions containing S-methyl-L-cysteine+VO^{2+} with L/M = 41.0 and $C_{VO} \sim 0.01$ M. The pH corresponding to each spectrum is indicated.

L/M = 35, the CD spectra of L-Cys solutions are like those in Fig. 8(B).

The spectroscopic results show that, for pH < 12, polymeric species are relatively much more important with L-alanine[1] than for L-cysteine or D-penicillamine. Here polymers are more important for $3.3 \lesssim$ pH $\lesssim 6.0$ and for pH $\gtrsim 12$. For L/M $\gtrsim 20$, hydrolysis {of $[(VO)_2(OH)_5^-]_n$} hardly happens (at least for pH < 12). Potentiometric results confirm this.

(c) *Substituted derivatives of* L-*cysteine*. The CD spectra (Fig. 9) of solutions containing S-methyl-L-cysteine (S—Me—Cys) with L/M = 41.0 resemble those for L-alanine[1] showing that sulphur is not coordinated. They differ completely from those for cysteine and penicillamine, confirming that, for them, sulphur does coordinate to vanadium for pH $\gtrsim 4$.

Figure 10 includes CD spectra for L-cysteine ethyl ester (L-CysOEt) with L/M = 45.1. These practically coincide in the pH range 8.9–9.2 (see spectrum 7 in Fig. 10).

One can make the following comments:

(i) In the pH range 2–3.5, the spectra resemble those for L-cysteine (or D-penicillamine), but the $\Delta\varepsilon_m$ values are much lower.

(ii) For pH > 3.5, CD spectra for L-CysOEt do not differ much from the L-cysteine (and D-penicillamine) systems. The main difference is for 400–580 nm, where $|\Delta\varepsilon_m|$ are much lower than for $\lambda > 580$ nm as compared to L-cysteine (or D-penicillamine).

(iii) The $|\Delta\varepsilon_m|$ values for 550–800 nm in the pH range 8.3–9.2 are $\sim 20\%$ lower than for the corresponding L-cysteine solutions with L/M = 35.0.

From these differences, the carboxylate group of at least one L-cysteine is coordinated to vanadium in the pH range 4–10 (at least).

The CD spectra for L-CysOEt (Fig. 10) are relatively similar to those for L-cysteine in similar conditions, suggesting that CV and PV involve equatorial coordination of N_2S_2.

(2) *Calculations of speciation from observations*

Potentiometry

Protonation constants calculated by the MINIQUAD[19] and SUPERQUAD[20] programs almost coincide. From SUPERQUAD, for L-cysteine in solutions containing 2.25 M $NaNO_3$ (at 25°C): $pK_{a1} = 2.092 \pm 0.006$, $pK_{a2} = 8.367 \pm 0.003$ and $pK_{a3} = 10.358 \pm 0.007$, and for D-penicillamine: $pK_{a1} = 2.128 \pm 0.005$, $pK_{a2} = 8.151 \pm 0.003$ and $pK_{a3} = 10.637 \pm 0.008$.

As we had found for L-alanine,[1] L-serine and L-

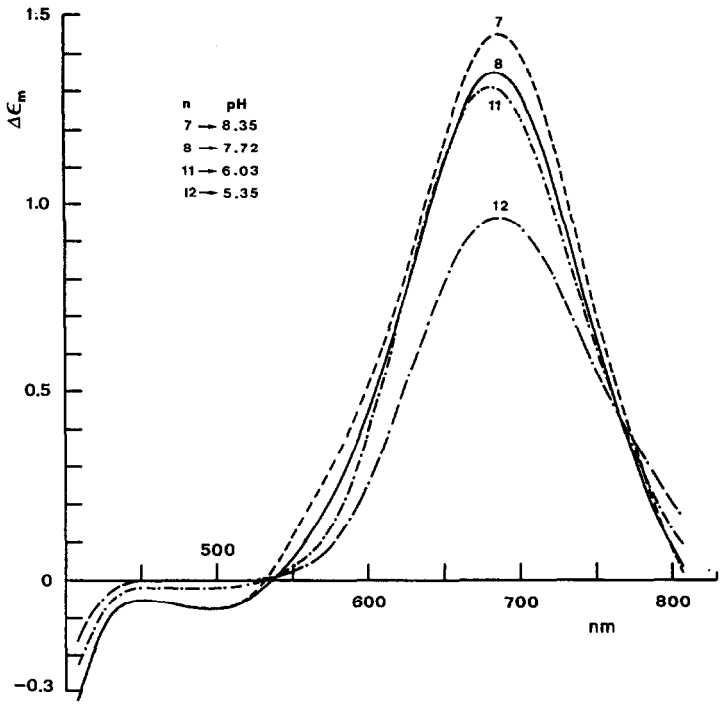

Fig. 10. CD spectra of solutions containing L-cysteine ethyl ester and VO^{2+} with L/M = 45.1 and $C_{VO} = 5.5–6.7 \times 10^{-3}$ M. The pH corresponding to each spectrum is indicated. Spectra of similar solutions at pH 4.5 and 5.9 were recorded every 10 min. At least till 60 min after the preparation of the solutions the CD spectra showed no evolution with time.

threonine,[2] the titration curves with high L/M show a progressive increase of pH as base is added in the pH range 3.5–7. The formation curves calculated for these conditions have $\bar{n} \sim 1.5$ in the pH range 5.8–6.7, so ML_2H complexes make an important contribution.

As in previous cases,[1-3] refinements of β_{xyz} values for all possible species (i.e. $M_xL_yH_z$ with x, y, z quite general) were meaningless. For L-alanine,[1] L-serine and L-threonine,[2] our strategy determined formation constants of species predominant at low pH using selected "titration points" from curves with low L/M. This was impossible for the present systems, because MLH_2, ML_2H_4, MLH and/or ML_2H_3 and ML_2H_2 become important at quite low pH. Therefore β_{122} and β_{124} were determined after a critical examination of results: (i) from titration curves of solutions of "low" L/M, (ii) from all titration curves and (iii) from visible and CD spectra recorded for pH < 5.

Taking β_{122} and β_{124} as known, the programs MINIQUAD and SUPERQUAD were used to calculate the β_{xyz} of the other species, including the full set of the "complete" titration curves.

Our best model (model I) from this procedure is in Table 1. For each value $\log \beta_{xyz}$, plausible ranges are also given, established by a critical examination of all calculations, including those based on the spectroscopic results (model II).

Using SUPERQUAD, attempts to refine both β_{111} and β_{123}, simultaneously, failed; normally β_{111} was rejected. If a fixed value for either constant was included, eventually the other would refine but with unacceptable statistical parameters.

For some of the earlier models tested for Ala, Ser and Thr, we also had some similar difficulties in refining the corresponding pair of constants β_{110} and β_{121},[1,2] but in our final models their simultaneous refinement was possible (and necessary). Here for the pair β_{111} and β_{123}, this never happened.

A major problem in all calculations for L-alanine[1] was hydrolysis in the pH range 5–8.[2,3] Hydrolysis is much less important in the L-serine and L-threonine systems[2] and scarcely exists in the L-aspartic acid system[3] for pH < 8 and relatively high L/M ratios. The same occurs in the present study; consequently, the calculations are more reliable and the χ^2 values (10–30) of the models contributing to Table 1 are reasonable, considering the complexity of the systems, the many titration curves included, the several NaOH concentrations used and the two pH ranges included (2.2–4.3 and 4.0–6.7).

Table 1. Composition and formation constants of the species in the system L-cysteine or D-penicillamine + VO^{2+} assuming various equilibrium models. Values for $\log \beta_{xyz}$ of eq. (1) are given[a,b]

Species[c]	D-Pen + VO^{2+} Model IA	D-Pen + VO^{2+} Model IIA	L-Cys + VO^{2+} Model IB and IIB
MLH_2	20.09 (0.2)	20.09 (0.2)	19.9 (0.2)
MLH[d]	16.3 (0.3)	16.3 (0.3)	16.1 (0.3)
ML_2H_4	39.4 (0.4)	39.4 (0.4)	39.1 (0.4)
ML_2H_3	36.1 (0.3)	36.1 (0.3)	35.8 (0.3)
ML_2H_2	32.2 (0.3)	32.2 (0.3)	31.4 (0.3)
ML_2H	27.5 (0.3)	27.5 (0.3)	26.4 (0.3)
ML_2	21.0 (0.2)	21.0 (0.2)	19.6 (0.3)
M_2L_2	26.7 (0.3)	26.7 (0.3)	25.3 (0.3)
ML_2H_{-1}	—	7.9 (0.4)	[e]
MH_{-3}	—	−18.5 (0.4)	[e]
MLH_{-2}[d]	—	−5.2 (0.4)	[e]
H_3L	20.915	20.915	20.817
H_2L	18.787	18.787	18.725
HL	10.637	10.637	10.358

[a] Some constants here differ slightly from the preliminary results presented in Table 1 of ref. 4(c).

[b] The products of hydrolysis of vanadium(IV) considered with their formation constants are given in Table 1 of ref. 1.

[c] In the calculations performed with MINIQUAD, SUPERQUAD and SQUAD, it was possible to refine formation "constants" for such stoichiometries as M_2L_2H and $M_2L_2H_{-1}$. However, the values differed substantially depending on the other formation constants included; further, at least for $M_2L_2H_{-1}$, the β values obtained were such that it was impossible to rationalize them with the experimental visible and CD spectra.

[d] MLH and MLH_{-2} are not needed to explain the potentiometric and spectroscopic results for solutions with high L/M. If they exist, their formation constants will have the indicated order of magnitude.

[e] Model IIA resulted from calculations with SQUAD but these were not performed for solutions containing L-Cys + VO^{2+} for pH > 7.

Spectrometry

In solutions of VO^{2+} and L-cysteine or D-penicillamine, only the species containing vanadium contribute to ε_m or $\Delta\varepsilon_m$ in the visible. This by-passes the limitation of potentiometry to those regions of pH where the ligand has no significant buffer effect. Consequently, calculations of formation constants based on visible or CD spectra do better for species like MLH_2 and ML_2H_4, which predominate in the pH range 1.5–4.0. Further, solutions with pH > 7 may be used.

As in previous work,[1-3] the SQUAD program was used to check that the visible and CD measurements were consistent with the potentiometric results in the pH range 2–7. Calculations were performed on results for 450–830 nm (visible) and 445–800 nm (CD), respectively. ε (or $\Delta\varepsilon$) corresponding to the stoichiometries MPH_2, MPH, MP_2H_4, MP_2H_3, MP_2H_2, MP_2H, MP_2 and M_2P_2 are considered as parameters to be refined: β_{xyz} were calculated either individually or in sets (2, 3, 4 or even 5 $\log \beta_{xyz}$ values).

Either MLH or ML_2H_3 must be excluded from the equilibrium model, because no meaningful calculations using both could be achieved, for either spectrophotometric or potentiometric results. Since results were better when ML_2H_3 is included, we exclude MLH.

The β_{xyz} values calculated are within the range obtained with MINIQUAD and SUPERQUAD, so those given in model IA may be accepted as correct. Taking these as known, the visible and CD spectra of the corresponding species were calculated

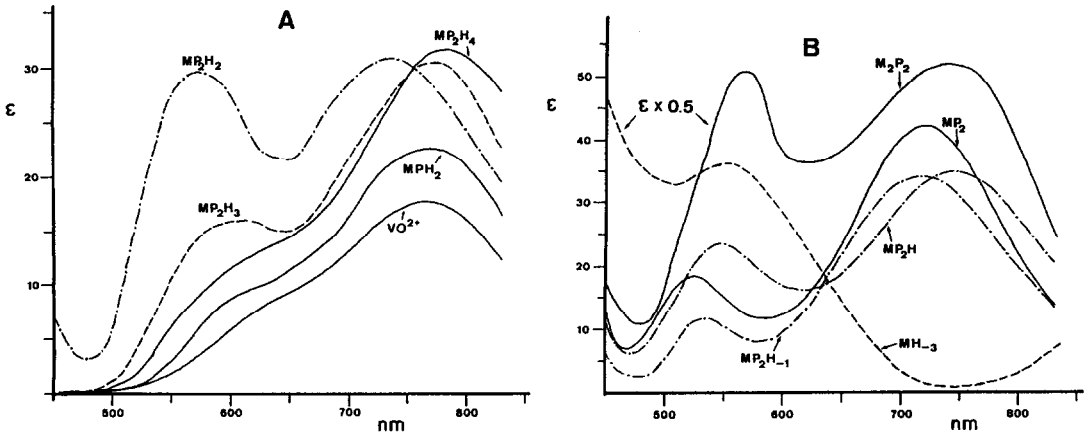

Fig. 11. Visible absorption spectra of the species in solutions containing D-Pen and oxovanadium(IV) with high L/M, calculated using the SQUAD[18] program (see text for details). (A) Species that predominate for pH < 5. (B) Species that predominate for pH > 5 (except M_2P_2).

using SQUAD based on experimental spectra in the pH range 2–8.3. As for previous systems,[1,2] we went step-by-step, but now following the order:

Visible spectra:

(i) MP_2H and MP_2,

(ii) MPH_2 and MP_2H_4,

(iii) MP_2H_3, MP_2H_2 and M_2P_2.

CD spectra:

(i) MP_2H and MP_2,

(ii) MPH_2, MP_2H_4, MP_2H_3, MP_2H_2 and M_2P_2.

The calculated spectra are included in Figs 11 and 12.

Once spectra of the species important for pH < 8 are known, calculations may be performed for the high pH range. In solutions containing D-penicillamine with high L/M, between pH 8.3 and 10.3, almost 100% of vanadium(IV) exists as MP_2. For calculations involving solutions with pH > 10, only the spectrum of MP_2 needs to be included in SQUAD. Tables 2 and 3 summarize the results.

Besides the inherent uncertainties of pH measurements in alkaline solutions containing high Na^+ concentrations, the unknown nature of hydrolysis products at high pH introduces several inaccuracies.[23] For the models tested in Tables 2 and 3, the sole hydrolysed species important for pH > 10–11 is $[(VO)_2(OH)_5^-]$ ($\log\beta = -22.22$).[1,23] Species of the type $[(VO)_2(OH)_6^{2-}]_n$ (or with other stoichiometries) are not included.

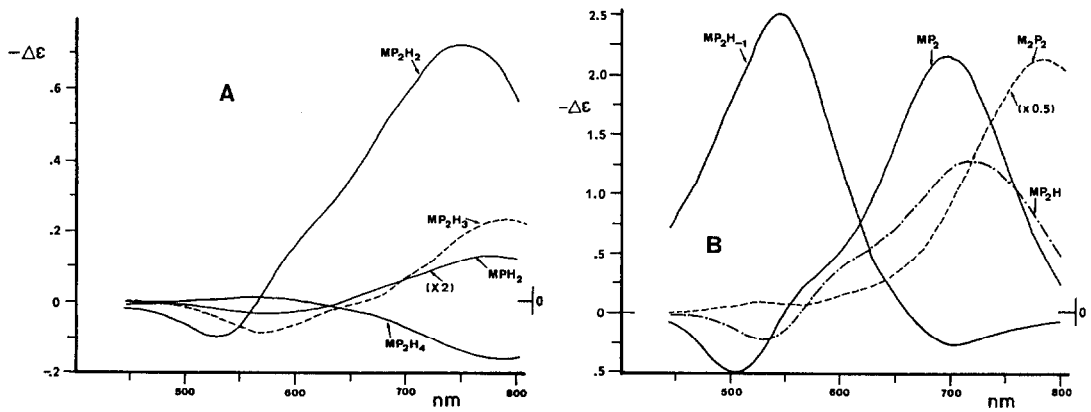

Fig. 12. CD spectra of the species in solutions containing D-Pen and oxovanadium(IV) with high L/M, calculated using the SQUAD[18] program (see text for details). (A) Species that predominate for pH < 5. (B) Species that predominate for pH > 5 (except M_2P_2). The spectra for MPH_2 and MP_2H_4 have opposite signs in the range 600–800 nm. This explains why $\Delta\varepsilon_m \sim 0$ values were found in some of the experimental CD spectra at low pH.

Table 2. Calculations of visible spectra and/or formation constants using the SQUAD program,[18] based on experimental visible spectra (450–830 nm) of D-Pen + VO^{2+} solutions (high L/M) in the pH range 8.3–12.4[a,b,c]

Calculation number	Refinement of		
	$\log\beta_{12-1}$	$\log\beta_{11-2}$	$\log\beta_{10-3}$
VIS1	8.3±0.1	−5.1±0.3[d]	−18.2±0.2[d]
VIS2	8.7±0.1	—	−18.1±0.1
VIS3	8.16±0.04	—	−18.7 (Fixed)
VIS4	—	−4.5±0.1	−18.7 (Fixed)
VIS5	8.4±0.1	−5.3±0.15	−18.7 (Fixed

[a] In all calculations the ε_{xyz} of the complexes included are also refined. Where β_{10-3} is assumed to have a fixed value, the ε_{10-3} values are considered as parameters to be refined.

[b] According to the order of magnitude obtained for the formation constants of MP_2H_{-1}, MPH_{-2} and MH_{-3}, the concentration of M_2H_{-5} is significant only for pH $\gtrsim$ 12.5.

[c] All calculations involving MPH_{-3} diverged.

[d] The visible spectrum calculated for this species makes no sense.

Despite these problems, the results using SQUAD based on experimental visible and CD spectra are self-consistent and satisfactory. For both spectroscopic techniques, β_{12-1} and β_{10-3} are consistently refined, but while for CD spectra, their log values are ~ 7.8±0.3 and ~ −18.6±0.2, respectively, from visible spectra, they are ~ 8.4±0.3 and ~ −18.2±0.2.

For basic solutions containing D-Pen + VO^{2+}, the spectrophotometric results are consistent with the

Table 3. Calculations of CD spectra and/or formation constants using the SQUAD program,[18] based on experimental CD spectra (445–800 nm) of D-Pen and VO^{2+} solutions (high L/M) in the pH range 8.3–13.5[a,b]

Calculation number	Refinement of			
	$\log\beta_{12-1}$	$\log\beta_{11-2}$	$\log\beta_{11-3}$	$\log\beta_{10-3}$
CD1	—	−5.21±0.04[c]	—	18.7±0.1
CD2	—	—	[d]	[d]
CD3	—	[d]	[d]	−18.6 (Fixed)
CD4	[d]	—	[d]	[d]
CD5	[d]	[d]	[d]	[d]
CD6	[e]	[e]	[e]	−18.7 (Fixed)
CD7	[d]	—	[d]	−18.7 (Fixed)
CD8	7.5±0.5[c]	−5.3±0.2[c]	—	−18.6±0.2
CD9	7.7±0.05	—	—	−18.7 (Fixed)

[a] In all calculations involving β_{10-3}, $\Delta\varepsilon_{10-3} = 0$ (fixed values). For the other species, which do contain coordinated penicillamine, the corresponding $\Delta\varepsilon_{xyz}$ are considered as parameters to be refined.

[b] All calculations involving MP_2H_{-2} diverged.

[c] The calculated spectrum is not appropriate to explain the experimental CD spectra obtained at high pH.

[d] The calculation diverged; main problem in β_{11-3}.

[e] The calculation diverged; main problem in β_{11-2}.

existence of MH_{-3} with $\log\beta_{10-3}$ being -18 to -19 (as for the L-Ser+VO^{2+} system[2]), and of MP_2H_{-1} with $\log\beta_{12-1}$ in the range 7.5–8.7.

DISCUSSION

The equilibrium model—the set of species (with values for their formation constants) proposed to explain all the experimental potentiometric and spectroscopic results—is shown in Table 1 (model II). For low L/M, other complex species might be important.

Figure 13 gives the concentration distribution of components in the EPR spectra (Fig. 1 and spectra obtained for the L-cysteine system). Comparing Fig. 13(B) with the concentration distribution of species presented in Fig. 14, calculated using the program COMICS[27] for $C_{Pen}/C_{VO} = 23.7$ and with the total vanadyl concentration close to those corresponding to the EPR, visible and CD spectra of Figs 1–6, one may remark that:

(i) Signals PI+PII correspond to several stoichiometries: M, MPH_2, MP_2H_4 and MP_2H_3 (and MPH). The L-Ala, L-Ser and L-Thr+VO^{2+} systems[1,2] presented a similar situation. The EPR peaks show only gradual (but clear) changes in positions as H_2O in $[VO(OH_2)_5]^{2+}$ is substituted by the first and second R—COO^- group or by a R—NH_2 group.

(ii) Component PIII corresponds to the species of stoichiometry MP_2H_2 (M_2P_2 is probably EPR silent). Its crossing point with EPR signals PI+PII at pH 4.2 in Fig. 13(B) approximately coincides with the crossing point of $\{MP_2H_4+MPH_2+MP_2H_3\}$ and MP_2H in Fig. 14.

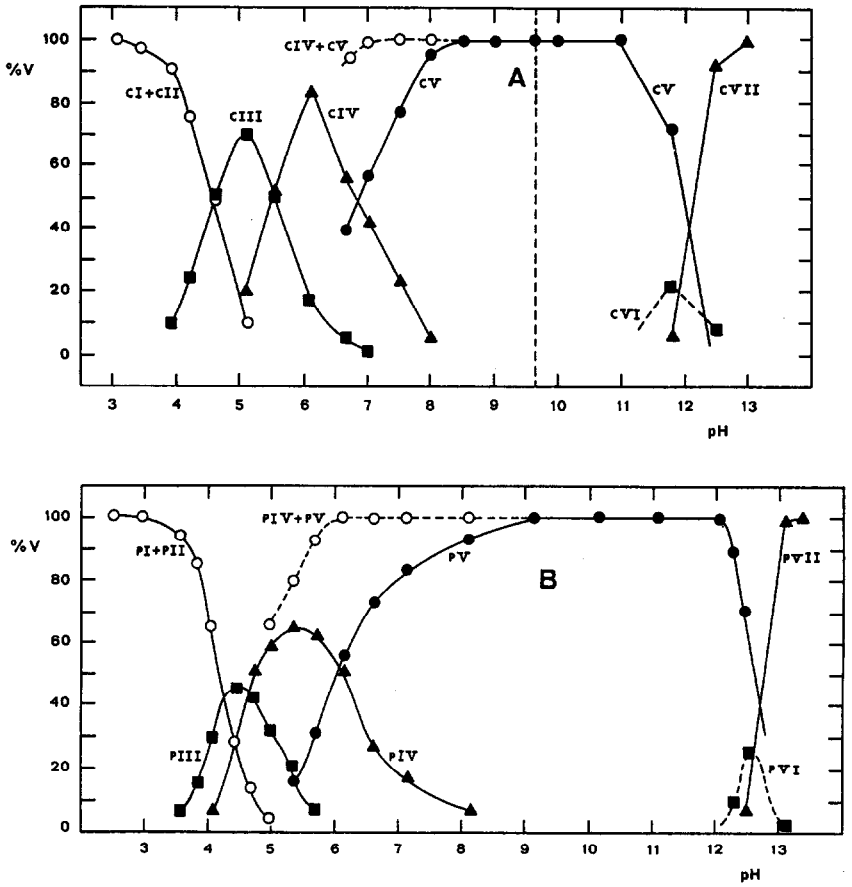

Fig. 13. Concentration distribution of the components CI–CVII (A) and PI–PVII (B), detected in the EPR spectra. These distributions should be considered approximate. EPR silent species are obviously not included. (A) L-Cysteine+VO^{2+} system: pH < 9.8, concentrations were estimated from EPR spectra with L/M = 26.2 and $C_{VO} \sim 0.01$ M; for pH > 9.8, from spectra with L/M = 20.0 and $C_{VO} \sim 0.004$ M. (B) D-Penicillamine+VO^{2+} system: the species concentrations were estimated from EPR spectra with L/M = 18.5 and $C_{VO} \sim 0.004$ M (Fig. 1).

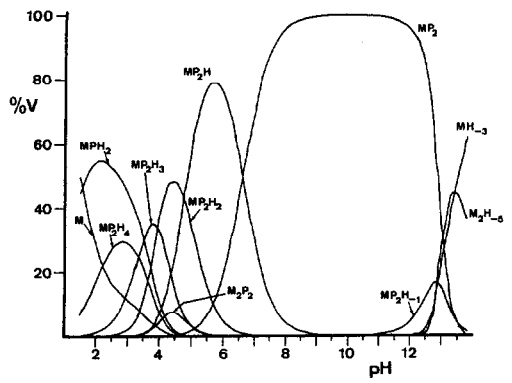

Fig. 14. Concentration distribution of the complexes formed in the D-Pen+VO^{2+} system with $C_{VO} = 0.01$ M and L/M = 23.7, calculated using the β_{xyz} of model IIA in Table 1 (MPH not included), $\log\beta_{20-5} = -22.22$ and $\log\beta_{10-3} = -18.7$. Because no other hydrolysed species was included in the equilibrium model, the only polymeric species indicated for pH > 12 is M_2H_{-5}. If the formation constant of any species with such a stoichiometry as $[VO(OH)_3^-]_n$ ($n > 2$) were included in the model, the calculated concentration for M_2H_{-5} would become small. This speciation is on a molar basis, while the concentration distribution of Fig. 11 in Part I[1] was calculated on an atomic basis. On recalculating this concentration distribution but now including MPH with $\log\beta = 16.3$, the ratio of the concentrations: $MP_2H_3/MPH \sim 2$.

(iii) Signals PIV and PV correspond to species of stoichiometry MP_2H and MP_2, respectively.
(iv) Components PVI and PVII arise from species with stoichiometry MP_2H_{-1} and MH_{-3}, respectively.

Our model differs from an earlier proposal:[17] it has more species but no evidence for *cis*- and *trans*-isomers of $[VO(L)_2]^{2-}$ complexes.

Under the conditions used by Johnson and Shepherd for EPR spectra ($C_{VO} = 6.8 \times 10^{-3}$ M, $C_{Cys} = 1.0$ M and pH = 7),[8] our model would predict approximately 60% of MC_2 and 40% of MC_2H. One component only is detected (although in Fig. 1 of ref. 1 the higher field EPR signal is rather broad). The g and A parameters corresponding to MC_2H and MC_2 are similar (see PIV and PV in Fig. 1). The visible spectra (maxima at 535 and 730 nm) presented by Johnson and Shepherd also suggest that MC_2 is not the only species present[8] (compare with results for MP_2H and MP_2 in Table 4).

According to Fig. 14, the sole polymer of importance in the pH range 2–12 is M_2P_2, which is significant in the pH range 3.8–5.3. In solutions with high L/M at fixed pH no great change should occur in the experimental $\Delta\varepsilon_m$ as C_{VO} varies, if (at that pH) there is no equilibrium between species with different degrees of polymerization.[1,2] In fact, such $\Delta\varepsilon_m$ change significantly at pH 4.04 and 4.54 (Fig. 7), and much less at pH 5.54 [Fig. 8(A)], 5.74 and 7.1 (not shown). In Fig. 7(B) (pH 4.54), as L/M decreases to ~ 10, λ and $\Delta\varepsilon_m$ of band I both clearly increase. This can be easily understood from the spectra for MP_2H_2, MP_2H and M_2P_2 and the equilibrium:

$$\begin{bmatrix} MP_2H_2 \\ \text{and} \\ MP_2H \end{bmatrix} \underset{\text{L/M increases}}{\overset{\text{L/M decreases}}{\rightleftharpoons}} M_2P_2.$$

Correlation of formation constants

Representation of $\log\beta^{Pen}$ vs $\log\beta^{Cys}$ does not obey a single linear correlation.

To compare the present β_{xyz} values with those for the L-alanine, L-serine and L-threonine+VO^{2+} systems,[1,2] it is convenient to consider constants β^*_{xyz} defined according to eq. (3) instead of eq. (1).

$$xM^{2+} + yHL^- + zH^+ \overset{\beta^*_{xyz}}{\rightleftharpoons} M_xL_yH_z \qquad (3)$$

$$\beta^*_{xyz} = \beta_{xyz}/(\beta_{013})^y. \qquad (4)$$

A linear correlation of $\log\beta^{*Pen}$ (or $\log\beta^{*Cys}$) vs $\log\beta^{Ser}$, is observed only for pK_{a1}, MLH_2, MLH, ML_2H_4 and ML_2H_3 (L = P, C) against the corresponding stoichiometries in the L-serine system. Therefore, for other stoichiometries, the structure and/or the donor atoms of the complexes containing D-penicillamine (or L-cysteine) and VO^{2+} differ from those in the L-serine system.

The formation constants calculated for MP_2H_2, MP_2H, MP_2 and M_2P_2 are substantially greater than for corresponding stoichiometries in the L-Cys+VO^{2+} system. The differences seem too large to be explained solely by the slightly higher basicity of D-penicillamine than L-cysteine.

No major differences were detected between the CD spectra of the L-cysteine and D-penicillamine systems, which indicates that the donor atoms and their coordination positions are the same in both systems.

Formation constants for complexes of vanadyl often correlate well with those of nickel,[28] at least for ligands containing nitrogen and oxygen donor atoms. Indeed, as we find for vanadyl, the β(NiL) and $\beta(NiL_2)$ formation constants for penicillamine are substantially greater than for cysteine, in both the distinct equilibrium models which have been assumed for Pen or Cys and nickel(II). Lenz and Martell,[29] assuming that only NiL and

Table 4. Spectroscopic properties for each $[(VO)_x(P)_y(H^+)_z]$ species

Species	Band II[a]				Band I[a]			
	λ	ε	$\Delta\varepsilon$	$\lvert\Delta\varepsilon/\varepsilon\rvert$ ($\times 10^2$)	λ	ε	$\Delta\varepsilon$	$\lvert\Delta\varepsilon/\varepsilon\rvert$ ($\times 10^2$)
MPH_2	~ 610	~ 9	—	0.15	770	22.7	—	0.30
	585	—	0.0138		770	—	−0.068	
MP_2H_4	~ 605	~ 12	—	0.14	780	31.6	—	0.49
	~ 565	—	−0.015		785	—	0.155	
MP_2H_3	600	16.0	—	0.51	775	30.5	—	0.79
	570	—	0.082		780	—	−0.240	
MP_2H_2	570	29.6	—	0.34	735	30.8	—	2.3
	530	—	0.102		740	—	−0.722	
MP_2H	545	23.5	—	0.86	745	34.8	—	3.7
	535	—	0.202		725	—	−1.29	
MP_2	525	18.3	—	0.27	720	42.1	—	5.1
	507	—	0.500		715	—	−2.14	
MP_2H_{-1}	540	11.7	—	2.1	720	34.1	—	1.5
	543	—	−2.5		700	—	0.50	
M_2P_2	~ 565	~ 100	—	0.18	~ 740	~ 102	—	4.2
	~ 530	—	−0.18		775	—	−4.3[b]	
$M_2A_2H_{-2}^1$	~ 515	—	0.1		~ 740	—	−0.31[b]	—
$M_2S_2H_{-2}^2$	585	51.9	—	0.96	778	59.3	—	1.2
	542	—	0.5		730	—	−0.736[b]	

[a] The ε and $\Delta\varepsilon$ are the extinction coefficients—at λ—of the visible and CD spectra, respectively, calculated for each of the $M_xL_yH_z$ species included in model IIa (Table 1). $|\Delta\varepsilon/\varepsilon|$ is the asymmetry factor (so called g-factor) for each band, according to: [$|\Delta\varepsilon|$ (at its λ)]/[ε (at its λ)]: values of $10^2 g$ greater than one prove that the transition is magnetic-dipole in character.

[b] The CD spectra for $M_2A_2H_{-2}^1$ and $M_2S_2H_{-2}^2$ are rather similar, but differ completely from the one obtained for the corresponding stoichiometry M_2P_2, where band I at ~ 775 nm is extremely intense.

NiL_2^{2-} are present, obtained: $\log\beta(NiC) = 9.6$, $\log\beta(NiC_2) = 19.0$, $\log\beta(NiP) = 11.1$ and $\log\beta(NiP_2) = 21.8$. Perrin and Sayce[30] later obtained: $\log\beta(NiP) = 10.75$ and $\log\beta(NiP_2) = 22.89$ (no other complexes in solution), and $\log\beta(NiC) = 8.98$ and $\log\beta(NiC_2) = 20.16$ (other complexes in solution).

While it is often considered that the methyl groups in penicillamine might sterically hinder, or even prevent, the bridging of metal ions by sulphur atoms, inhibiting formation of polynuclear species, the observed preference of vanadyl and nickel for penicillamine may also reflect geometric differences in the coordination sphere of VO^{2+} in order to accommodate the steric demands of the $—(Me)_2S^-$ donor unit, some sort of interligand interaction (e.g. hydrophobic interaction involving the β,β-dimethyl substituents) or an entropic origin.

Structures

Because the vanadyl ion is lop-sided, many of its chelates may form more isomers than do apparently analogous monoatomic metal centres; refs 1 and 23 briefly discuss this. Even in the absence of this extra isomerism, i.e. for monodentate ligands, such as amino acid bonded via carboxylate, the common geometric isomers may both be present.

Table 5 includes structures for each stoichiometry of Table 1. Estimated values of EPR parameters $g_\parallel$ and $A_\parallel$ for each structure using those contributions of $R—COO^-$, $R—NH_2$, RS^-, OH^- and H_2O to $g_\parallel$ and $A_\parallel$ proposed by Chasteen are also included.[25] Such estimates consider only groups coordinated equatorially. They imply that the axial ligand is H_2O: when this is not the case, no safe estimates can be made for $g_\parallel$ and $A_\parallel$.

Table 5. Schematic representations of possible structures for complexes in solutions containing L-Cys or D-Pen and oxovanadium(IV). The corresponding estimated $g_{\|}$ and $A_{\|}$ EPR parameters[25] are also included (see text for details)

	Structure[a]	Stoichiometry[b]	$g_{\|}$	$A_{\|}$
I	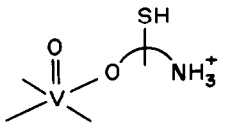	ML*H or ML_2	1.935	179.7
II	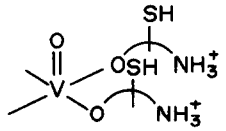	ML_2*H_2 or ML_2H_4	1.937	176.8
III	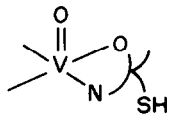	ML* or MLH	1.941	174.1
IV	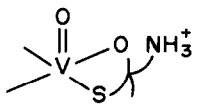		1.948	166.0
V	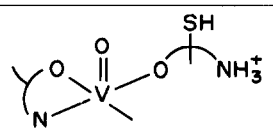	ML_2*H or ML_2H_3	1.942	171.2
VI	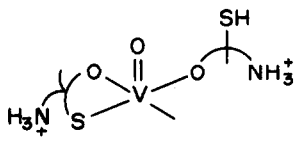		1.950	163.0
VII	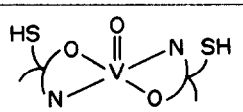	ML_2* or ML_2H_2	1.948	165.6
VIII	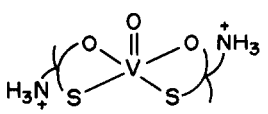		1.964	149.3
IX	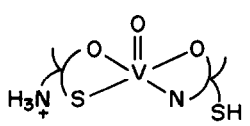		1.956	157.4
X	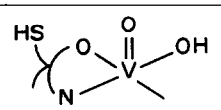	ML*H_{-1} or ML	1.948	167.1
XI	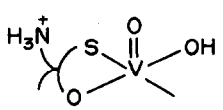		1.956	160.4
XII	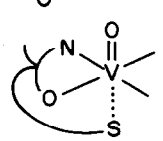		1.948	167.1
XIII	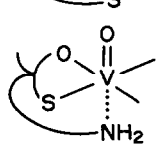		1.956	160.4

Table 5—*continued*

	Structure[a]	Stoichiometry[b]	$g_{\parallel}$	$A_{\parallel}$
XIV	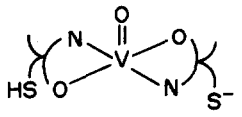		1.948	165.6
XV	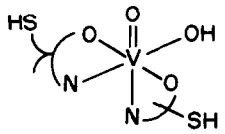		1.950	164.2
XVI	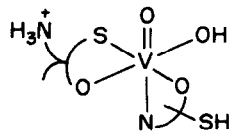		1.958	156.0
XVII	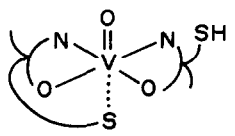		1.948	165.6
XVIII	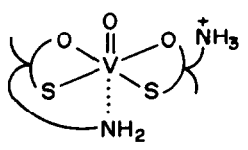	$ML_2{*}H_{-1}$ or ML_2H	1.964	149.3
XIX	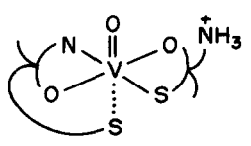		1.956	157.4
XX	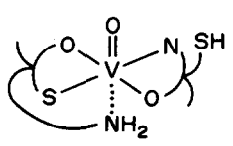		1.956	157.4
XXI	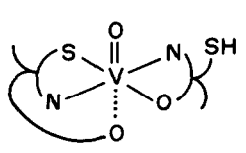		1.959	154.8
XXII	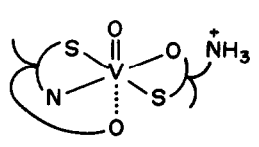		1.967	146.6

continued overleaf

Table 5—*continued*

	Structure[a]	Stoichiometry[b]	$g_{\parallel}$	$A_{\parallel}$
XXIII	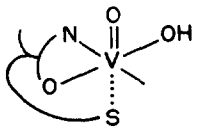		1.948	167.1
XXIV	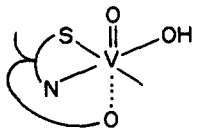	ML* or MLH_{-1}	1.959	156.3
XXV	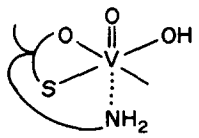 etc.		1.956	159.0
XXVI	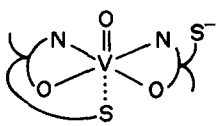		1.948	165.6
XXVII	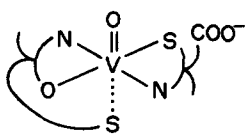	ML_2*H_{-2} or ML_2	1.959	154.8
XXVIII	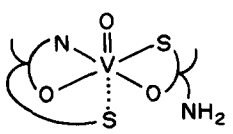		1.956	157.4
XXIX	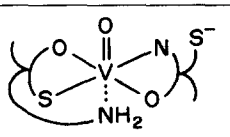		1.956	157.4
XXX	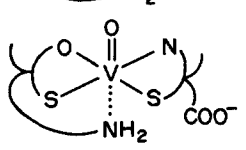		1.967	146.6
XXXI	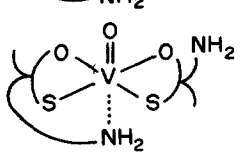	ML_2*H_{-2} or ML_2	1.964	149.3
XXXII	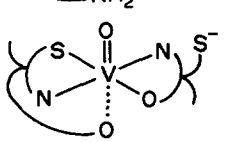		1.959	154.8
XXXIII	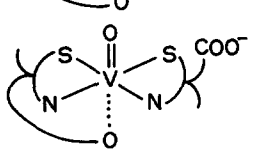		1.971	144.0
XXXIV	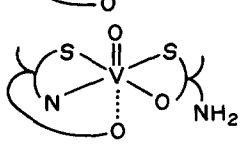		1.967	146.6

Table 5—*continued*

	Structure[a]	Stoichiometry[b]	$g_{\parallel}$	$A_{\parallel}$
XXXV	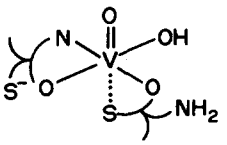		1.950	164.2
XXXVI	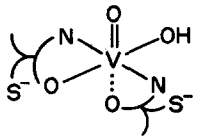	$ML_2{}^*H_{-3}$ or ML_2H_{-1}	1.953	161.6
XXXVII	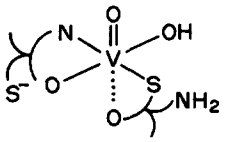		1.956	159.0
XXXVIII	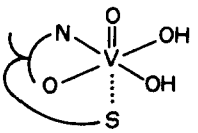		1.955	160.1
XXXIX	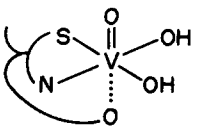		1.966	149.4
		ML^*H_{-3} or MLH_{-2}		
XL	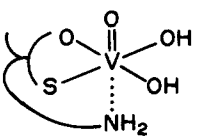		1.963	152.0
XLI	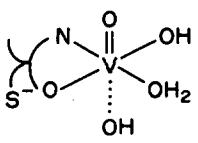		1.948	167.1

(c)

[a] In the schematic representation of the structures, when no group is included in any of the coordination positions, it is assumed that H_2O is coordinated. When (...) is included opposite to the V=O bond, this means that coordination in the axial position may occur (or not).

[b] $M_xL_yH_z \rightarrow$ stoichiometries according to eq. (1). $M_xL^*_yH_z \rightarrow$ stoichiometries according to eq. (3).

MLH_2 *stoichiometry*

This corresponds to complexes with the R—COO^- group equatorial, as in (I)—Table 5. Writing their formation as ($n = 1$):

$$VO^{2+} + nH_2L \overset{K_n}{\rightleftharpoons} [VO(H_2L)_n]^{2+}, \qquad (5)$$

K_1(D-Pen) = 20.0 and K_1(L-Cys) = 15.0, to be compared with K_1(L-Ala) = 15.6,[1] K_1(Gly) = 14.8[30] (in a different medium, 1 M $NaClO_4$), K_1(L-Ser) = 12.5, K_1(L-Thr) = 12.9[2] and K_1(L-Asp) = 78.[3]

The visible spectrum for MPH_2 is, as expected, similar to those for the corresponding stoichiometries: MAH, MSH and MDH_2 (L-alanine, L-serine and L-aspartic acid systems, respectively), with amino acids monodentate via carboxylate.

ML_2H_4 *stoichiometry*

This probably corresponds to complexes with two monodentate carboxylate groups coordinated equatorially, as in (II)—Table 5. From Table 1, K_1K_2(D-Pen) ~ 70 and K_1K_2(L-Cys) ~ 45. The corresponding values for L-Ser and L-Ala are ~ 24[1] and ~ 30,[2] respectively.

At this point, we re-emphasize that the particular stoichiometry for each "species" $M_xL_yH_z$ corresponds to more than one isomer. Relative isomeric concentrations are independent of concentrations of metal, ligand and H^+, so our experimental techniques do not discriminate (in some cases, detailed study of the EPR spectra may ultimately help do this). Therefore not only each formation constant, but also the visible and CD spectra reflect the features of each isomer in proportion to its relative importance. For example, for stoichiometry ML_2H_4, the value for β_{124} is the weighted sum of $\beta_{124}(cis)+\beta_{124}(trans)$ and the visible and CD spectra may involve contributions from both geometric isomers.

The visible spectrum calculated for MP_2H_4 is very similar to that for MS_2H_2.[2] However, the CD spectra calculated for MP_2H_4 and MS_2H_2 differ. In particular, $|\Delta\varepsilon_{124}$(D-Pen)$| \gg |\Delta\varepsilon_{122}$(L-Ser)$|$, $|\Delta\varepsilon_{122}$(LAla)$|$ [Fig. 12(A)].

This striking difference in the size of CD spectra for the corresponding stoichiometries: MP_2H_4 as against MS_2H_2 (or MA_2H_2) is real. The spectra of Fig. 12(A) are based on many experimental CD spectra, with a very broad range of amino acid and vanadyl concentrations and the results of several types of calculation were always consistent. However, despite this difference in magnitude, the signs for the CD absorptions at *ca* 750 nm are positive both for M(L—S)$_2H_2$ and for M(D—P)$_2H_4$. (Note that in Fig. 12, the ordinate, $\Delta\varepsilon$, has been inverted, by -1.) The configurational shorthand attached to penicillamine, based upon the same rules as those for serine and the like, shows that D-penicillamine is a derivative of D-cysteine. As an α-amino acid (i.e. unidentate via carboxylate, or chelated bidentate via O and N) D-penicillamine is opposite to L-serine or L-alanine in the chirality it induces at the metal centre.

In general, for complex molecules $[(VO)L_n(OH_2)_m(OH)_y]^{2\pm}$ of related structures, differing only in the nature of the amino acid (say for L-alaninate as against L-serinate), we expect and find related CD spectra. Similarly, where the overall structures of two such species differ only in the hand of the ligated amino acids, we expected similar but essentially enantiomeric CD spectra, as, for example, found for MP_2H_2 [Fig. 12(A)] and MS_2 (Fig. 12 of ref 2) or for the pair MP_2H_3 [Fig. 12(A)] and MS_2H [Fig. 10(b) of ref. 2].

Conversely, the similarity of sign, in this one case, between the CD of stoichiometric analogues containing D-Pen and L-Ser speaks strongly for the D-Pen species, MP_2H_4 (containing two coordinated unidentate α-amino acids) having a structure different from these of MS_2H_2.

It may be that the ratio of *cis*- to *trans*-isomers present in MP_2H_4 differs from that for MS_2H_2 and that this would help to account for the much greater $\Delta\varepsilon$ at longer wavelengths in the D-Pen case. This could also underlie two other differences between MS_2H_2 (or MA_2H_2) and MP_2H_4, namely the presence of two obvious positive CD components for the former, at ~ 640 and 780 nm (640 and 740 nm for L-alaninate) as opposed to the single Cotton effect (at 780 nm) for the penicillamine complex, and the anomaly in stepwise formation constants. Values of K_1 and K_1K_2 of eq. (5) are comparable between L-serine (12.5 and 24) and L-alanine (15.6 and 30) but are distinct for D-penicillamine (K_1 = 20.0 but K_1K_2 = 70) and L-cysteine (K_1 = 15.0, but K_1K_2 = 45).

ML_2H_3 *stoichiometry*

This corresponds to complexes with one amino acid bidentate (probably equatorial) and the other coordinated by the carboxylate group (probably also equatorial), as shown for V and VI in Table 5.

The visible spectrum for MP_2H_3 is quite similar to those for the "corresponding" stoichiometries MA_2H[1] and MS_2H;[2] bands I and II are slightly less separated (by ~ 20 nm) in MP_2H_3. The CD spectra for MP_2H_3, MA_2H and MS_2H are likewise similar except that:

(i) in MP_2H_3, bands I and II are slightly more separated (by 10 nm);
(ii) $|\Delta\varepsilon(MP_2H_3)| \sim 2.5 \times |\Delta\varepsilon(MA_2H$ or $MS_2H)|$.

As MP_2H_3 (and MPH) is important only for pH $\lesssim$ 4.5, it corresponds approximately to the component PII in Figs 1 and 13(B). The values of $g_\parallel$ and $A_\parallel$ are inconsistent with RS^- being coordinated, but structures like V (Table 5) seem adequate.

Therefore, EPR, visible and CD spectra all suggest that the geometries of the species corresponding to MP_2H_3, MS_2H and MA_2H are very alike. For each, more than one isomer may be important and their relative concentrations may differ. This, the different nature of the ligands and the possibility that the visible and CD spectra calculated for MP_2H_3 may incorporate part of the spectra of MPH, may account for the differences in their spectra.

ML_2H_2 *stoichiometry*

Several structures (e.g. VII–IX in Table 5) can be envisaged for this stoichiometry. Despite minor differences in band II, the visible spectrum for MP_2H_2 is similar to those of the corresponding stoichiometries MA_2[1] and MS_2.[2] Further, the CD spectrum calculated for MP_2H_2 is also quite similar to those of MA_2 and MS_2.

The stoichiometry corresponds to PIII (or CIII) in Fig. 1. Their estimated $g_\parallel$ and $A_\parallel$ parameters suggest, as do the two electronic spectra, that both ligands are coordinated through their carboxylate and amino groups. Only two *d–d* bands are found for MA_2, MS_2 and MP_2H_2 rather than the three for many complexes with *trans*-geometries.[23] Assuming equatorial coodination of N_2O_2, this suggests that the *cis*-isomeric geometry predominates: $\beta_{122}(\text{Pen}) \sim \{\beta_{122}(\text{Pen})\}^{cis}$.

M_2L_2 *stoichiometry*

Here, several structures are plausible (e.g. XLII and XLIII, where the $-z$ means that the corresponding non-coordinated group of the ligand is antiparallel to the V=O group). These representations are merely schematic: both ligands are, of course, the same enantiomer.

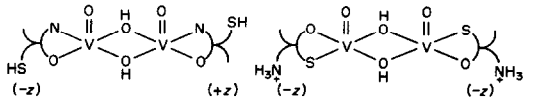

(XLII) (XLIII)

The electronic spectra of M_2P_2 differ (Table 4) from those of $M_2A_2H_{-2}$ and $M_2S_2H_{-2}$, therefore the structures differ. Further, $\log\beta_{220}$ is higher—the corresponding $\log\beta^*$ [from eq. (3)] does not correlate with $\log\beta_{22-2}$(L-Ser). The differences could arise from the same isomers being present but in different proportions, though this alone would not suffice to explain the different properties for M_2P_2 and $M_2A_2H_{-2}$ (or $M_2S_2H_{-2}$). More likely, the range of isomers (geometric and/or linkage —RS^-) differs from M_2P_2 to $M_2A_2H_{-2}$.

ML_2H *stoichiometry*

This, the most important stoichiometry in the pH range 5–7, corresponds to PIV (and CIV) in the EPR spectra (Figs 1 and 13). Many structures can be envisaged (e.g. XIV–XXII in Table 5).

The visible and CD spectra for MP_2H, and the order of magnitude of the corresponding $\log\beta^*$ are quite different from those of the corresponding MA_2H_{-1}[1] and MS_2H_{-1}.[2] Therefore the structures are not alike here. As $A_\parallel(ML_2H) \sim 151 \times 10^{-4}$ cm^{-1}, at least one RS^- group is coordinated equatorial (Table 5). Only two *d–d* bands are present in the electronic spectrum of MP_2H, so structure XVIII (Table 5) is reasonable and consistent with the high value of β_{121}.

ML_2 *stoichiometry*

This, the most important in the pH range 7–13, corresponds to PV (and CV) EPR (Figs 1 and 13). Structures XXVI–XXXIV in Table 5 may be envisaged. As mentioned above, the calculated $A_\parallel = 143 \times 10^{-4}$ cm^{-1} and the CD spectra for L-cysteine+VO^{2+} (pH range 8–12) and L-Cys OEt+VO^{2+} (pH range 6–9.5), are consistent with the coordination of the thiol and amino groups. Further, the results suggested that a carboxylate group is coordinated: g and A parameters and λ (bands I and II) for MP_2 agree with a much stronger ligand-field strength than in MP_2H.

In the L-cysteine methyl ester–vanadyl complex, (from X-ray diffraction[15]) the nitrogen and sulphur atoms are *trans*. Sakurai *et al.*[14] detected two EPR components in solutions at pH 10.5 containing L-CysOMe (10 mM) and VO^{2+} (2 mM). One had g and A parameters corresponding to the present PV and CV (only $g_\perp$ differs): a minor component corresponded to higher $A_\parallel$. The conclusion was that the two components correspond to *cis*- and *trans*-isomers. The EPR spectra of *cis*- and *trans*-VO(Cys OMe)$_2$ differ much and more likely correspond to VO(CysOMe)$_2$ and its hydrolysis product. In the EPR spectra for L-cysteine+VO^{2+} solutions (with higher L/M ratios), we detect only one component.

For the present cases of MP_2 and MC_2 only two *d–d* bands are detected, suggesting *cis*-geometry.

ML_2H_{-1} *stoichiometry*

This (MP_2H_{-1} is never an important species) probably corresponds to PVI (and CVI) in the EPR spectra (Figs 1 and 13). Some of the many possible structures are in Table 5 (XXXV–XXXVII).

Comments on the equilibria at high pH

As found in the L-Ser and L-Thr+VO^{2+} systems, when increasing the pH equilibration is reversible and very fast, except when the complexes hydrolyse extensively and the solutions become brown.

The pH at which solutions become brown depends at least on the nature of the amino acid, on L/M, and on C_{VO}. When adding acid to the "very basic" brown solutions to pH 10–11, they remain brown for some time, then become green and finally the original colour at the corresponding pH is

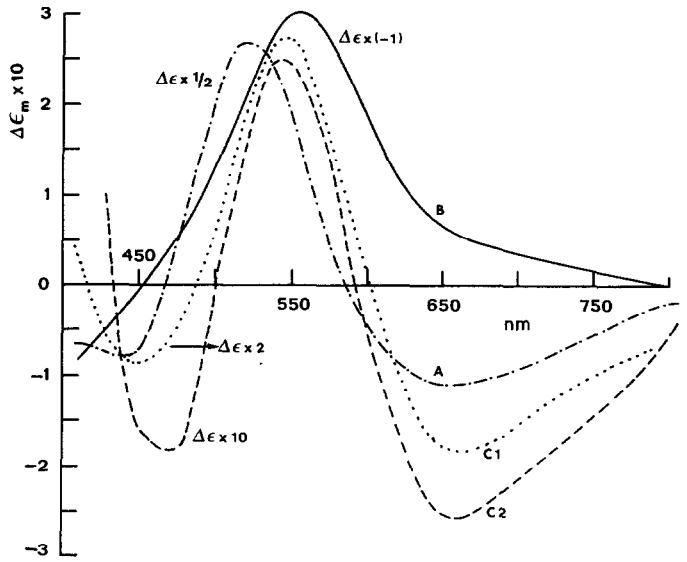

Fig. 15. CD spectra of solutions containing VO^{2+} and amino acids at high pH: (A) L-Ser+VO^{2+} solution with L/M = 38 and C_{VO} = 0.0068 M at pH ~ 13.6. (B) D-Pen+VO^{2+} solution with L/M = 23.7 and C_{VO} = 0.0084 M at pH ~ 13.5. (C) L-Cys+VO^{2+} solutions with L/M = 35 and C_{VO} = 0.0078 M at pH ~ 12.8 (C1) and ~ 13.2 (C2). The similarity between (A) the L-Ser+VO^{2+} and (C) L-Cys+VO^{2+} is quite clear. For (B) D-Pen+VO^{2+} at pH 13.6, MP_2 is still important: its spectrum masks that of the species that forms at high pH. This species would have the same −, +, − pattern (×(−1) as it involves a D-amino acid), as for L-Cys: MC_2 hydrolyses at approximately one unit lower in pH. In the calculations with SQUAD, the stoichiometry MP_2H_{-1} alone of those tested gave such a −, +, − pattern, a main reason for including it in the final equilibrium.

recovered. At pH 8–10 the equilibrium is established much faster and for pH < 8 fast equilibration occurs.

Figure 8(B) includes spectra of D-penicillamine +VO^{2+} solutions with variable total vanadium concentration at pH ~ 12.8. Similar experiments were performed for L-cysteine+VO^{2+} solutions at pH ~ 12.9 with L/M varying from 35.0 to 13.9. The type of spectra differ (in passing, the latter are similar to spectra C1 in Fig. 15) and the $|\Delta\varepsilon_m|$ also decrease as C_{VO} is increased.

For both sets of spectra, as C_{VO} is increased, $|\Delta A|$ decreases. The opposite was observed for L-serine and L-threonine+VO^{2+} solutions (Fig. 17(a) in ref. 2). This indicates that VO^{2+} complexes of amino acids containing ROH as side groups are more "resistant" to hydrolysis than those of penicillamine and cysteine. As in the systems involving L-serine and L-threonine, a fair description at high pH is of optically active monomeric complexes in equilibrium with dimeric (or oligomeric) non-optically active hydrolysis products of vanadium(IV).

Acknowledgements—The authors thank the British Council for grants; J.C.P. and L.F.V.B. thank the Instituto Nacional de Investigação Científica and Fundação Calouste Gulbenkian for financial support; R.D.G. acknowledges the award of study leave which has been valuable in this project.

REFERENCES

1. Part I: J. Costa Pessoa, L. F. Vilas Boas, R. D. Gillard and R. J. Lancashire, *Polyhedron* 1988, **7**, 1245.
2. Part II: J. Costa Pessoa, L. F. Vilas Boas and R. D. Gillard, *Polyhedron* 1989, **8**, 1173.
3. Part III: J. Costa Pessoa, R. L. Marques, L. F. Vilas Boas and R. D. Gillard, *Polyhedron* 1990, **9**, 81.
4. (a) R. D. Gillard, R. J. Lancashire, J. Costa Pessoa and L. F. Vilas Boas, Comunicação 3All, 2° Encontro Nacional de Química, Porto (1979); (b) J. Costa Pessoa and L. Vilas Boas, 1980 Autumn Meeting—Chemical Society, University College, Cardiff (1980); (c) J. Costa Pessoa, L. F. Vilas Boas and R. D. Gillard, *Polyhedron* 1989, **8**, 1745.
5. B. J. S. Pirie and M. V. Bell, *J. Exp. Mar. Biol. Ecol.* 1984, **74**, 187.
6. R. Eady, *Polyhedron* 1989, **8**, 1695.
7. J. N. Brauthaver, *A.C.S. Symposium series 334*. American Chemical Society, Washington D.C. (1987).
8. C. R. Johnson and R. E. Shepherd, *Bioinorg. Chem.* 1978, **8**, 115.

9. J. P. Paumard and M. Cadiot, *Bull. Soc. Chim. Fr. I* 1981, 441.
10. A. P. Payasi, K. Sharma and V. K. Sharma, *J. Ind. Chem. Soc.* 1987, **64**, 186.
11. J. Costa Pessoa, MSc thesis. Universidade Nova de Lisboa (1979).
12. F. Bergel, K. R. Harrap and A. M. Scott, *J. Chem. Soc.* 1962, 1101.
13. H. Sakurai, S. Shimomura and I. Ishizu, *Inorg. Chim. Acta* 1981, **55**, L67.
14. H. Sakurai, Y. Hamada, S. Shimomura and S. Yamashita, *Inorg. Chim. Acta* 1980, **46**, L119.
15. H. Sakurai, Z. Taira and N. Sakai, *Inorg. Chim. Acta* 1988, **151**, 85.
16. M. D. Sifri and T. L. Riechel, *Inorg. Chim. Acta* 1988, **142**, 229.
17. Y. Xu, X. Li, L. Yu, C. Liu, J. Lu and W. C. Liu, *Jeigon Huaxue* 1982, **1**, 55; *Chem. Abstr.* 98 : 136555r.
18. J. L. Antunes, J. Costa Pessoa, L. F. Vilas Boas and R. D. Gillard, to be published.
19. A. Sabatini, A. Vacca and P. Gans, *Talanta* 1974, **21**, 53; P. Gans, A. Sabatini and A. Vacca, *Inorg. Chim. Acta* 1976, **18**, 237.
20. P. Gans, A. Sabatini and A. Vacca, *Inorg. Chim. Acta* 1983, **79**, 219; P. Gans, A. Sabatini and A. Vacca, *J. Chem. Soc., Dalton Trans.* 1985, 1195.
21. D. J. Leggett and W. A. E. McBryde, *Analyt. Chem.* 1975, **47**, 1065; D. J. Leggett, *Analyt. Chem.* 1977, **49**, 276; D. J. Leggett, S. L. Kelly, L. R. Shine, Y. T. Wu, D. Chang and K. M. Kadish, *Talanta* 1983, **30**, 579.
22. G. Gran, *Acta Chem. Scand.* 1950, **4**, 559; G. Gran, *Analyst* 1952, **77**, 661.
23. L. F. Vilas Boas and J. Costa Pessoa, Chapter on *Vanadium* in *Comprehensive Coordination Chemistry* (Edited by G. Wilkinson, R. D. Gillard and J. A. McCleverty), Vol. 3, pp. 453–583. Pergamon Press, Oxford (1987).
24. D. Labonnette, *J. Chem. Res. (S)* 1988, 250.
25. N. D. Chasteen, in *Biological Magnetic Resonance* (Edited by J. J. Berliner and H. Reuben), Vol. 3, p. 53. Plenum Press, New York (1981).
26. M. M. Iannuzzi and P. H. Rieger, *Inorg. Chem.* 1975, **14**, 2895.
27. D. D. Perrin and I. G. Sayce, *Talanta* 1967, **14**, 833.
28. J. Felcman and J. J. R. Fraústo da Silva, *Talanta* 1983, **30**, 565.
29. G. R. Lenz and A. E. Martell, *Biochemistry* 1964, **3**, 745.
30. D. D. Perrin and I. G. Sayce, *J. Chem. Soc. A* 1968, 53 and refs therein.
31. I. Fábián and I. Nagypál, *Inorg. Chim. Acta* 1982, **62**, 193.

Polyhedron Vol. 9, No. 17, pp. 2127–2133, 1990
Printed in Great Britain

0277–5387/90 $3.00+.00
© 1990 Pergamon Press plc

ADDUCTS OF COORDINATION COMPOUNDS—XV.* THE STRUCTURE OF *TRANS*-$[Rh(py)_4Cl_2][Ag(ONO_2)_2]$, A SALT OF THE DINITRATO-ARGENTATE(I) ION, $[Ag(ONO_2)_2]^-$

R. D. GILLARD†

Department of Chemistry and Applied Chemistry, University of Wales, College of Cardiff, P.O. Box 912, Cardiff CF1 3TB, Wales, U.K.

and

LYALL R. HANTON **and** SIMON H. MITCHELL

Department of Chemistry, University of Otago, Dunedin, New Zealand

(*Received* 23 *February* 1990; *accepted* 2 *April* 1990)

Abstract—The compound originally reported by Poulenc in 1935 as *trans*-$[Rh(py)_4Cl_2]NO_3 \cdot AgNO_3$ is the salt *trans*-$[Rh(py)_4Cl_2][Ag(ONO_2)_2]$ (py = pyridine). Its crystal structure consists of discrete silver dinitrate anions $[Ag(ONO_2)_2]^-$ and the complex cation $[Rh(py)_4Cl_2]^+$, each with C_2 symmetry. The silver atom is disordered between two neighbouring sites [0.30(2); 0.20(2)]. There are two pairs of Ag—O distances (given in pm); Ag(1): 224.8(3) (almost linear on silver) and 259.7(5), Ag(2): 231.3(7) and 241.3(10).

There are many solid adducts of coordination (and other) salts, formula A, with silver salts, AgX, B, of formula A_xB_y. These include[2] AB and AB_2 with B = silver perchlorate, for A = $[M(acac)_n]$, where $n = 3$ and M = Cr, Co, etc., and where $n = 2$ and M = Ni, Pd (acac indicating the monoanion of pentane-2,4-dione). Similarly, adducts of the silver salt $Ag[Ni(acac)_3]$ are known with 1 and 2 moles of "extra" silver nitrate.

Such adducts ($A \cdot nAgNO_3$, where A is a known compound capable of independent existence) formally involving silver nitrate are occasionally described. Their structures, whether they involve one ($n = 1$) or more ($n > 1$) moles of silver nitrate, have not yet been found to contain discrete anions $[E(NO_3)_2]^-$, with $E = Ag^+$. Rather, silver is variously coordinated by four to six atoms or molecules giving an irregular geometry and forming chains or sheets in the lattice. Silver nitrate itself has a peculiar structure.

Poulenc's compound[3] (an adduct of silver bromide) was recently characterized[1] as *trans*-$[Rh(py)_4Br_2][AgBr_2]$ and we synthesized[4] a number of new adducts AB_n, where A was *trans*-$[ML_4X_2](NO_3)$ (M = Rh, Ir; L is a pyridine; X = Cl or Br) and B was $AgNO_3$. For the 1:1 adducts, *trans*-$[M(L)_4X_2](NO_3) \cdot ENO_3$ (with $E = Ag^+$), the properties suggested[4] a close analogy to the hydrogen dinitrates ($E = H^+$), and consequently formulation as salts of the silver dinitrate ion $[Ag(ONO_2)_2]^-$. The structure of the hydrogen dinitrate is well known[5] from X-ray and neutron diffraction.

We now report the crystal and molecular structure, determined by X-ray diffraction, of *trans*-$[Rh(py)_4Cl_2]NO_3 \cdot AgNO_3$. This confirms our earlier deductions.[4] The compound is indeed a salt of the novel dinitrato(O-)argentate(I) ion, remarkably similar to the $[H(ONO_2)_2]^-$ salt, in that the silver ion is linearly coordinated by two oxygen atoms from the two nitrate groups. Other features of the present structure are described, including the propeller conformation of the N-heterocyclic ligand blades about the Cl—Rh—Cl spindle.

* For Part XIV, see ref. 1.

† Author to whom correspondence should be addressed.

EXPERIMENTAL

Crystals were grown in methanol (2–3 cm^3) in the dark by allowing dissolved material to diffuse together from silver nitrate (excess) and *trans*-$[Rh(py)_4Cl_2]NO_3 \cdot 5H_2O$ (*ca* 30 mg) solids separated in a vial. Suitably large crystals grew over 7–10 days.

Cell: $C_{20}H_{20}AgCl_2N_6O_6Rh$, $M = 722.09$; orthorhombic $a = 7.658(2)$, $b = 21.486(3)$, $c = 14.953(3)$ Å; $U = 2460.36(88)$ $Å^3$, space group *Pbcn* (no. 60), $Z = 4$, $D_c = 1.95$, $D_m = 1.91$ g cm^{-3} (by flotation in $ZnBr_2$ solution). A crystal, $0.16 \times 0.16 \times 0.70$ mm, was used. Results were collected at low temperature (boil-off gas from liquid N_2) using an ω-scan method and Mo-K_α radiation. This acquisition of results was carried out by Dr W. T. Robinson at the University of Canterbury, Christchurch, New Zealand. An empirical absorption correction was applied to the reflection results. There were originally 4480 unique reflections, 391 of which were rejected from the analysis ($F_o > 3\sigma F_o$).

SHELX programs[6] were used for the structure determination. Atomic scattering factors for rhodium and silver were taken from the *International Tables for X-ray Crystallography*.[7]

All non-hydrogen atoms were located from Patterson and difference Fourier maps; hydrogen atoms were introduced by calculation of their positions (C—H bond length 108 pm, coordinates riding with the appropriate carbon atom). The structure was refined using the full-matrix least-squares method, with the weighting scheme $w = 1/sF_o$.

A good R factor ($R = 0.057$, $R_w = 0.0438$) was obtained from a structure containing all the necessary atoms. However, difference Fourier maps showed residual electron density on a C_2 site close to the silver, but too close to be part of the "existing" anion.

Alternative models (2) and (3) were investigated in which the residual electron density is explained by the presence of an alternative silver position/site. Model (2) has two distinct but disordered anions. In (3), the silver atom alone is disordered between two sites.

Model (2): the site occupancy of both silver atoms was refined, with the already known nitrate atoms assigned to the major silver atom. The result of refining this structure was that the major silver gained strength while the minor silver moved away along the C_2 axis, leaving the original electron density by the major silver.

Model (3): from the same starting point, the occupancy of the silver atoms was refined. This refinement progressed satisfactorily and gave $R = 0.0434$, $R_w = 0.0327$ and occupancies of 0.299(19) [Ag(1)] and 0.201(19) [Ag(2)].

The program PARST[8] was used to calculate structural dimensions, with ESDs where appropriate.

RESULTS AND DISCUSSION

The crystal structure consists of discrete silver dinitrate anions and *trans*-$[Rh(py)_4Cl_2]^+$ cations, each with C_2 symmetry. The general features of the entire structure are shown in Fig. 1. The structure

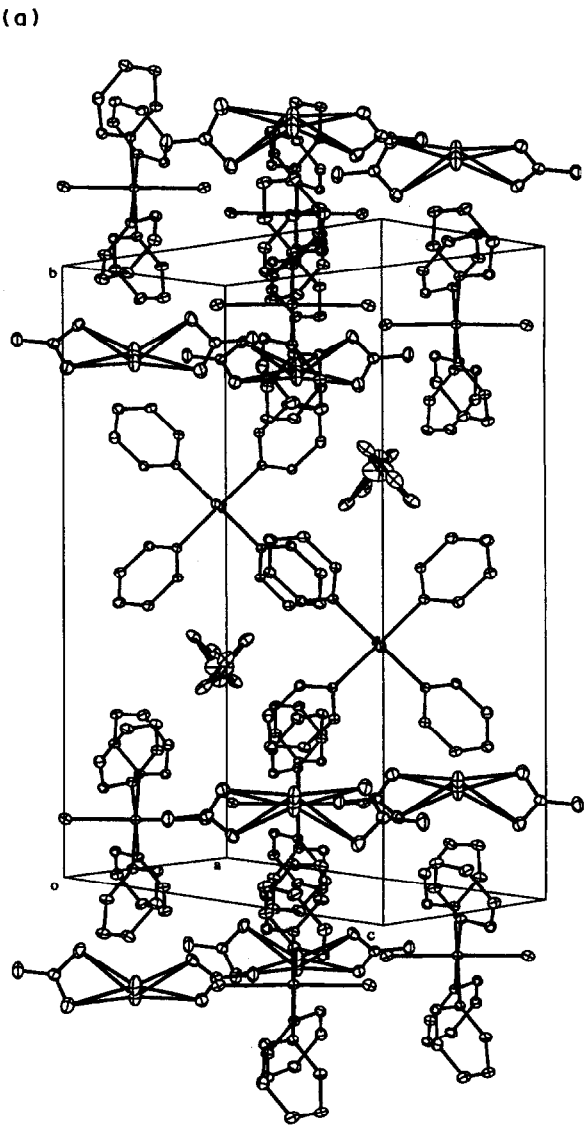

Fig. 1. ORTEP views of the cell of *trans*-$[Rh(C_5H_5N)_4Cl_2][Ag(ONO_2)_2]$: (a) down *a*-axis; (b) down *c*-axis; (c) down *b*-axis; (d) Perspective view. Ellipsoids of probability 50% for *a*, *b* and *c*, but 30% for *d*.

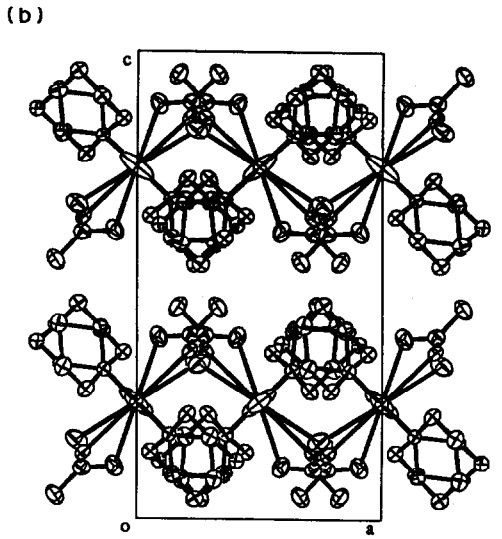

Fig. 1(b).

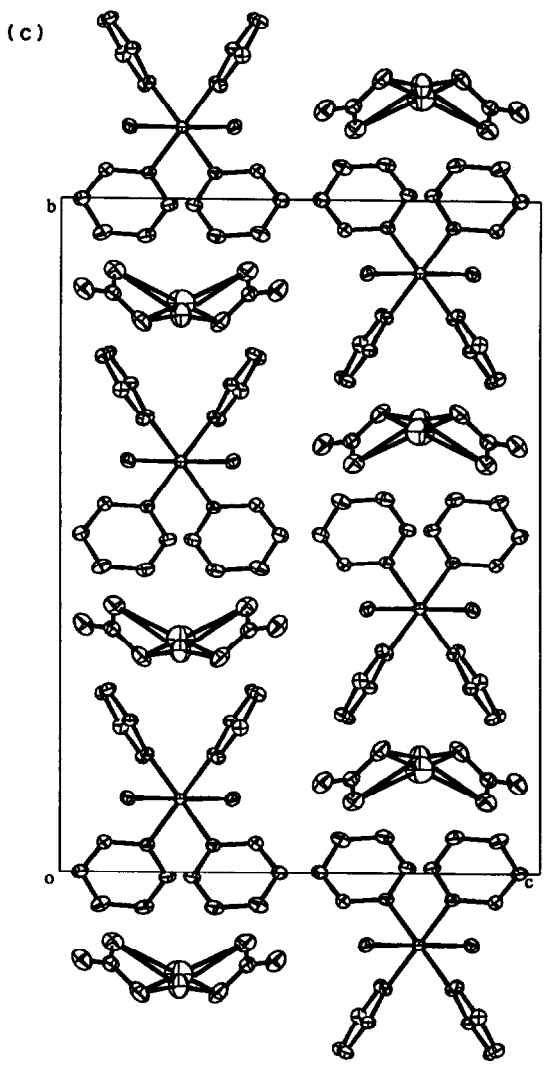

Fig. 1(c).

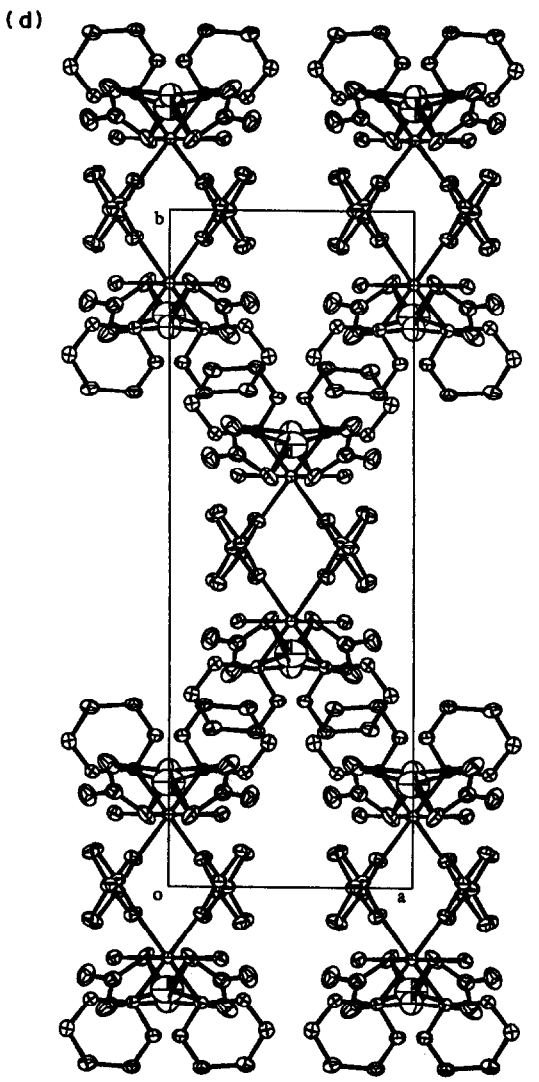

Fig. 1(d).

of the anions is shown in Fig. 2, and relevant dimensions and angles are given in Tables 1 and 2.

The anion containing Ag(1) has an O(1)—Ag—O(1) sequence that approaches linearity. The Ag—O distances around this silver ion are very different. The Ag(1)—O(2) bond is longer by 34.9 pm than the Ag(1)—O(1) bond, while the silver in the other site is less linear and its Ag—O bonds differ only by 10.0 pm. The nitrate–nitrate interplanar angle is 81.8(1)°.

Comparison with the hydrogen dinitrate analogue studied by Roziere and others[9] confirms our earlier conclusion[4] that the two structures are isomorphous.

The complex cations in both structures have similar coordinates and geometry (see Table 1).

The main distinction is for the anions. It results largely from the differing H—O and Ag—O bond lengths. Apart from this difference and the con-

sequential effect on angles O(1)—Ag—O(2), Ag—O(2)—N and inter-nitrate separations, the anions are remarkably similar (see Table 3).

The present salt increases the already significant number of known structures involving species with four flat moieties disposed around a spindle, such as *trans*-$[ML_4X_2]^{n+}$, where M = a metal ion of charge m^+ like platinum(II), rhodium(III) or iridium(III), L = an N-heterocycle—such as pyridine—attached to the metal via N, X is a unidentate ligand, charge x^-, and $n = (m-2x)$. L is not restricted to uncharged N-heterocycles, and may for example be a positively-charged species, like S-nicotine in[10] *trans*-$[Rh(S\text{-}nicH)_4Cl_2](PF_6)_5$ or indeed any planar unit, like NO_2 in Erdmann's salt[11] K-{*trans*-Co$(NH_3)_2(NO_2)_4$]}.

The possible conformations for essentially tetra-

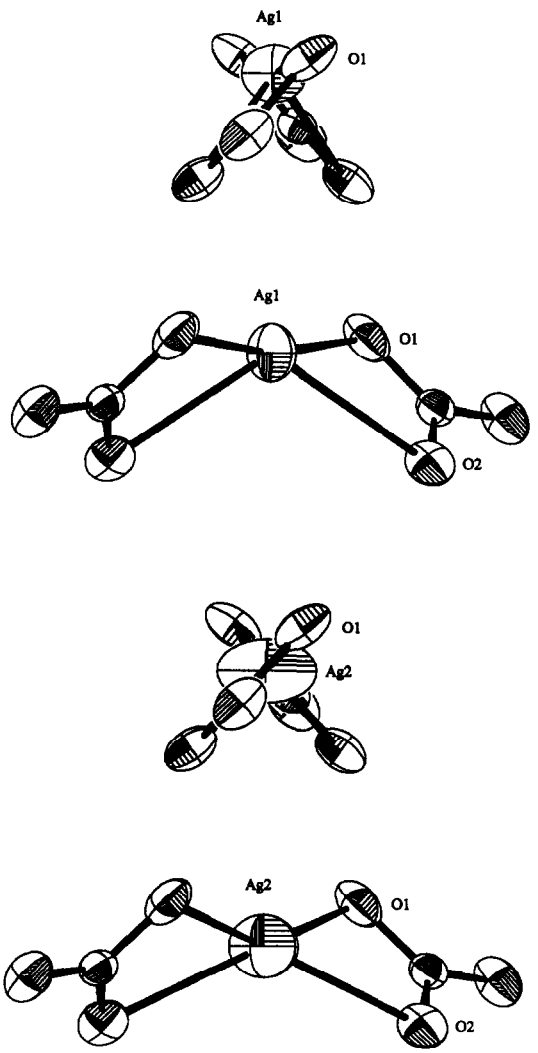

Fig. 2. ORTEP plots of the two distinct silver dinitrate anions.

Table 1. Dimensions of cells and ions for *trans*-$[Rh(C_5H_2N)_4Cl_2][E(ONO_2)_2]$

	E = Ag^{+a}	E = H^{+b}
a	7.6580 (0.002)	7.5290 (0.005)
b	21.4860 (0.003)	21.7170 (0.006)
c	14.9530 (0.003)	14.7170 (0.007)
U (Å^3)	2460.36 (0.88)	2406.34 (2.08)
Rh—N(11)	207.0(3)	206.6(2)
Rh—N(21)	205.6(2)	205.0(2)
Rh—Cl	233.8(1)	232.9(2)
O—E(1)—O	169.3(2)	167.3(12)
E(1)—O(1)	224.8(3)	123.7(12)
E(1)—O(2)	259.7(5)	231.0(19)
O—E(2)—O	150.7(1)	167.4(11)
E(2)—O(1)	231.3(7)	124.5(11)
E(2)—O(2)	241.3(10)	219.4(20)
N—O(1)	128.1(4)	
N—O(2)	124.7(4)	
N—O(3)	122.9(4)	
N(11)—C(12)	134.0(4)	
N(11)—C(16)	135.9(4)	
C(12)—C(13)	138.2(4)	
C(13)—C(14)	138.1(4)	
C(14)—C(15)	138.6(5)	
C(15)—C(16)	137.3(4)	
N(21)—C(22)	134.4(4)	
N(21)—C(26)	134.4(4)	
C(22)—C(23)	138.3(4)	
C(23)—C(24)	137.6(5)	
C(24)—C(25)	138.0(5)	
C(25)—C(26)	139.9(4)	

[a] Bond lengths and angles from this study.

[b] These values are recalculated, using PARST, from earlier results.[4,9]

We transformed the *z*-coordinates (by $0.5-z$) to compare directly.

gonal arrangements of four such planar units around a common central point are many, but the four-bladed propeller is quite common and is again found here.

The present observation of two forms of the anion may result from the low temperature of this diffraction study. All our previous measurements[4] were made at room temperature and hence may refer to one form of dinitrato-argentate only. The IR spectrum is consistent with (though it does not prove) one structure only for the anion.

We analysed[4] the IR spectrum in terms of the bands of free monomeric NO_3^- becoming split on bonding in pairs to the silver ion. One band only (ν(NO) at 1281 cm^{-1}) showed fine structure, attributed to coupling. A number of bands remained unobserved.

Coordination of the nitrate

Nitrate groups serving as essentially unidentate ligands are not yet particularly common. The few isoleptic examples include (a) $K_2[Pt(ONO_2)_4]H_2O$ (with a strange lop-sided structure[12] for the complex anion, all four nitrate groups lying to one side of the PtO_4 ligand plane); (b) $K[Au(ONO_2)_4]$;[13] and (c) $K_2[Pd(ONO_2)_4]H_2O$, rather similar[14] to its platinous analogue. Unidentate nitrate groups on silver(I) seem uncommon:[15] typically, in $[Ag(Pcy_3)_2]NO_3$, where cy denotes cyclohexyl, the nitrate ligand is bidentate,[16] though the Ag—O distances differ (245 and 273 pm). In (μ-1-methyluracilato-N^3,O^4) (μ-1-methylcytosine-N^3,O^2)-*cis*-diammineplatinum(II)·silver dinitrate·silver nitrate·$2\frac{1}{2}$ water, some nitrate ions (others are ionic) bridge four-coordinated silver ions, some of which also carry unidentate nitrate ions.[17]

Among oxo-anion environments, a number (like the present) have two stronger bonds (or, at least, shorter distances) almost linear, from oxygen to silver and between one and four rather longer interactions, the $2+n$ arrangement, here in Ag(2) 2+2. This is found in $[Co(PO_4)(NH_3)_5]3AgNO_3 \cdot H_2O$, where two of the crystallographically-independent silver ions have the properties: O—Ag(1)—O, 157.7°; Ag(1)—O, 219.0, 216.5 and 267.5, 270.1 pm; O—Ag(3)—O, 163.3°; Ag(3)—O, 214.6, 216.0 and 271.1, 280.6 pm.[18]

One virtue of the present cation is that it is relatively non-polar and—in its unsolvated salts— complications from hydrogen-bonding to or from it are unlikely. The properties of the two silver ions here possibly reflect this. In substances involving stoi-

Table 2. Bond angles (°)

Cl(1)—Rh—N(11)	88.7(1)	
Cl(1)—Rh—N(21)	90.3(1)	
N(11)—Rh—N(21)	89.2(1)	
	$n=1$	$n=2$
C(*n*2)—N(*n*1)—C(*n*6)	118.6(3)	119.4(3)
N(*n*1)—C(*n*2)—C(*n*3)	121.9(3)	122.2(3)
C(*n*2)—C(*n*3)—C(*n*4)	119.7(3)	119.3(3)
C(*n*3)—C(*n*4)—C(*n*5)	118.4(3)	118.4(3)
C(*n*4)—C(*n*5)—C(*n*6)	119.6(3)	120.4(3)
N(*n*1)—C(*n*6)—C(*n*5)	121.8(3)	120.2(3)
O(1)—Ag(*n*)—O(2)	52.7(1)	54.7(1)
Ag(*n*)—O(1)—Ni	102.2(2)	95.3(2)
Ag(*n*)—O(2)—Ni	86.6(2)	91.5(2)
O(1)—N(1)—O(2)	118.4(3)	
O(1)—N(1)—O(3)	119.8(3)	
O(2)—N(1)—O(3)	121.8(3)	
O(1)—Ag(*n*)—O(1a)	169.3	150.8
O(2)—Ag(*n*)—O(2a)	114.0	128.9
O(1)—Ag(*n*)—O(2a)	135.1(1)	142.8(1)
N—O(1)—Ag(*n*)—O(1a)	177.6	138.6
N—O(2)—Ag(*n*)—O(2a)	131.2	131.3
N—O(2)—Ag(*n*)—O(1a)	−168.4(3)	−148.3(10)

O(*n*a) related to O(*n*) by the symmetry operation $1-x$, y, $0.5-z$.

Table 3. A comparison of anion geometries for *trans*-$[Rh(py)_4Cl_2][E(ONO_2)_2]$

			E	
	Ag(1)	Ag(2)	H(1)	H(2)
Angles[a]				
O(1a)—E—O(1)	169.3(2)	150.7(1)	167.3(12)	167.4(11)
E—O(1)—N(1)	102.2(2)	95.3(2)	111.6(13)	105.8(13)
O(2)—E—O(1)	52.7(1)	54.6(1)	114.74	110.29
Torsion angles				
O(2)—N(1)—O(1)—E	−2.8(3)	−3.0(5)	4.0(29)	15.3(26)
N(1)—O(1)—E—O(1a)	177.6	138.6	135.2	127.2
Distances[b]				
O(1)—O(1a)	447.7		246.0	247.0
N(*n*)—N(*n*a)	545.6		394.0	384.0
Interplanar angle				
NO_3—NO_3(a)	81.8(1)		83.6	89.1

[a] Atoms denoted by (a) are related to the corresponding atom in the asymmetric unit by symmetry operation $1-x$, y, $0.5-z$.

[b] Bond lengths (O—Ag(1)—O, etc.) are compared in Table 1.

chiometric dinitrato-argentate(I) ions, the only examples so far known of homoleptic monomeric silver–nitrate systems, $MAg(NO_3)_2$—for $M = K^+$, NH_4^+ or Rb^+—contain $[Ag_2(NO_3)_4]^{2-}$ chains:[19] the resulting structure seems to represent a compromise between the small bite of the nitrate acting as a bidentate ligand and the range of silver–oxygen bond lengths for varied coordination numbers of the silver ion. Approximately speaking, the four-membered chelate ring is strained, and the compromise situation is adopted.

Coordination numbers at silver(I)

The description of coordination numbers and bonding in these Ag—O systems depends on the prediction of Gagnon and Beauchamp[20] that a silver–oxygen distance shorter than 300 pm indicates an interaction between a silver ion and an oxygen. A strong (or covalent) interaction is (based on the Pauling sum of covalent radii[21]) around 210 pm. The close similarity between the $[H(ONO_2)_2]^-$ ion and the $[Ag(ONO_2)_2]^-$ ion here may raise some question as to the nature of (secondary) Ag—O interactions larger than about 260 pm.

We would describe the hydrogen dinitrate ions in Table 3 as containing two coordinated protons, essentially linear, and it seems illogical to alter that description when we refer to the equally linear silver ions of $[Ag(ONO_2)_2]^-$. Indeed, the angle at the silver(I) ion is actually closer to linearity than at H^+.

As a further encouragement to reconsider the meaning of the secondary Ag—O contacts, we may take the known isoleptic complexes of unidentate nitrate. These are three, the tetrakis-nitrato-metallates of palladium(II), platinum(II) and gold(III). The former pair are eutropic, the latter isoelectronic. In each case, we accept the description as of four unidentate nitrates, all disposed to the same side of the M—O_4 plane. However, the distance to the secondary oxygens for Pt is 299 pm, and to the primary oxygens is 201 pm. The platinum ion is slightly above its PtO_4 plane.

The silver dinitrate ion studied here (certainly that containing Ag(1), with bond angle 169.7°) could reasonably be described in the same vein as a linear complex with two unidentate nitrate groups on silver, with both nitrate ligands situated on the same side of the line through silver, parallel to the O—O direction.

Such non-linear, two-coordinated silver ions are known elsewhere. For example, in silver thiocyanate, AgSCN, in proustite (Ag_3AsS_3) and in pyrargyrite (Ag_3SbS_3), the angles S—Ag—S are also about 165°.

The salts $[M(py)_4Cl_2]E(ONO_2)_2$ are all isomorphous,[4] with $M = Rh^{III}$, Ir^{III}; $E = H^+$, Ag^+. The member with $M = Rh^{III}$, $E = Ag^+$ is the subject of the present paper so—*mutatis mutandis*—the present findings apply equally to the other members.

The importance of the complex anion

Aqueous solutions of silver nitrate have great practical importance as analytical reagents, as oxidants often in syntheses, and as progenitors of controlled values of *p*Ag in producing photographic emulsions. This lends particular interest to observations of new species in them. The aqueous equilibria (1)

$$Ag(OH_2)_n^+ + RXO_2^- \rightleftharpoons [Ag(RXO_2)]^0 + (y-1)RXO_2^- \rightleftharpoons [Ag(RXO_2)_y]^{(y-1)-} \quad (1)$$

are known[22] for carboxylates (X = C, R = alkyl, $y > 1$) but seem not to have been previously observed for nitrate, X = N, R = O, $y = 2$. Clearly, from the existence of solid salts of the anion $[Ag(ONO_2)_2]^-$, it has a finite concentration in solution. Ethanoate (acetate: $R = CH_3$) is a 24-electronic system, isoelectronic with nitrate. For equilibrium (1), with $y = 2$, Vartak and Shetiya recorded[22a] (for $\mu = 1.0$, $T = 30°C$) a value of $\log K$ of 0.62 for the benzoate ion as the carboxylate, while MacDougall and Topol had earlier helped[22b] to explain the lack of precipitation of silver ion at neutral pH in the presence of ethanoate by measuring the stability constant for

$$Ag^+ + 2CH_3COO^- \rightleftharpoons Ag(CH_3COO)_2^-$$

as $\log K = 0.64$.

Quantitative values for the equilibria in (2)

$$Ag^+ + 2ONO_2^- \rightleftharpoons [Ag(ONO_2)_2] + (n-2)NO_3^- \rightleftharpoons [Ag(ONO_2)_n]^{(n-1)-} \quad (2)$$

and in particular for β_{120} are not yet known. In concentrated aqueous silver nitrate, the Raman spectrum shows[23] no identified Ag—O bands, though the nitrato-argentates of (2) were described as "inner-sphere complex".

Monomeric complex anions $[AgY_2]^-$, where Y is itself a singly-charged anionic ligand, are not so common as would be expected. In adducts, environments for silver are extremely varied, but rarely include the quasi-linear. Thus, in the adduct of bis-1,2-benzenequinonedioximatoplatinum(II) with silver perchlorate $Pt(C_6N_2O_2H_5)_2 \cdot 0.5AgClO_4$, the $Ag^+ClO_4^-$ ion pairs are intact as such within the parent lattice.[24] In a similar way, crystalline $NH_4Ag(SCN)_2$ was made up of intact AgSCN mol-

ecules and of thiocyanate and ammonium ions.[25] Coordination numbers in the related systems of stoichiometry HgX_2 and $[CuX_2]^-$ are discussed by Sandström and Persson;[26] here too, deviation from two is common.

Among the complex anions of silver(I), a cation of the type *trans*-$[M(py)_4X_2]^+$ ($X = Br^-$ or Cl^-; M = Rh or Ir) has again served to crystallize an unusual ion.

The following supplementary material has been deposited with the editor: (a) Table A. Observed and calculated structure factors. (b) Table B, list of atomic coordinates. (c) Table C, thermal parameters. (d) PARST output (for silver compound only: A similar one is available for the hydrogen dinitrate if that should be required).

REFERENCES

1. R. D. Gillard, S. H. Mitchell and D. Thomas, *Polyhedron* 1989, **8**, 211.
2. J. P. Fackler, *Prog. Inorg. Chem.* 1966, **7**, 412.
3. P. Poulenc, *Ann. Chim.* 1935, **4**, 567.
4. R. D. Gillard and S. H. Mitchell, *Polyhedron* 1987, **6**, 1885.
5. N. Al-Zamil, E. H. M. Evans, R. D. Gillard, D. W. James, T. E. Jenkins, R. J. Lancashire and P. A. Williams, *Polyhedron* 1982, **1**, 525 and refs therein.
6. G. M. Sheldrick, SHELX-76, Program for Crystal Structure Determination. University of Cambridge (1976); SHELX86, Program for Crystal Structure Solution. University of Göttingen (1986).
7. *International Tables for X-ray Crystallography*, Vol. IV. Kynoch Press, Birmingham (1974).
8. M. Nardelli, *Computers and Chemistry*, 1983, **7**, 95; PARST; a system of computer routines for calculating molecular parameters from results of crystal structure analyses.
9. J. Roziere, M. S. Lehmann and J. Potier, *Acta Cryst.* 1979, **B35**, 1099 and refs therein.
10. R. D. Gillard and J. P. D. L. Jesus, *Croat. Chem. Acta* 1989, **62**, 151.
11. I. Bernal, *Inorg. Chim. Acta* 1986, **121**, 1.
12. L. I. Elding and A. Oskarsson, *Inorg. Chim. Acta* 1985, **103**, 127.
13. R. Countryman and W. J. Macdonald, *Acta Cryst.* 1977, **B33**, 3580.
14. L. I. Elding, B. Noren and A. Oskarsson, *Inorg. Chim. Acta* 1986, **114**, 71.
15. R. J. Lancashire, Silver, in *Comprehensive Coordination Chemistry* (Edited by G. Wilkinson, R. D. Gillard and J. A. McCleverty), Vol. 5, p. 800. Pergamon Press, Oxford (1987).
16. M. Camalli and F. Caruso, *Inorg. Chim. Acta* 1988, **144**, 205.
17. H. Schollhorn, U. Thewalt and B. Lippert, *Inorg. Chim. Acta* 1987, **135**, 155.
18. D. Mentzatos, H. A. Tazmir-Riahi and A. Terzis, *Acta Cryst.* 1988, **C44**, 784.
19. E. Zobetz, *Monatsh. Chem.* 1980, **11**, 1253.
20. C. Gagnon and A. Beauchamp, *Acta Cryst.* 1977, **B33**, 1448; the general question of the restriction on chelation imposed by limited bite of oxo-anions is discussed by B. L. Hathaway, in *Comprehensive Coordination Chemistry* (Edited by G. Wilkinson, R. D. Gillard and J. A. McCleverty), Vol. 2, p. 414. Pergamon Press, Oxford (1987).
21. L. Pauling, *The Nature of the Chemical Bond*, pp. 224 and 256. Cornell University Press, New York (1960).
22. (a) D. G. Vartak and R. S. Shetiya, *J. Inorg. Nucl. Chem.* 1967, **29**, 1261; (b) F. H. MacDougall and L. E. Topol, *J. Phys. Chem.* 1952, **56**, 1090; (c) The (few) available quantities are summarized in the present ref. 15, p. 808.
23. R. L. Frost and D. W. James, *J. Chem. Soc., Faraday Trans.* 1982, **78**, 3263.
24. H. Endres, M. Megnamisi-Belombe, H. J. Keller and J. Weiss, *Acta Cryst.* 1976, **B32**, 457.
25. I. Lindqvist and B. Strandberg, *Acta Cryst.* 1957, **10**, 173.
26. M. Sandström and I. Persson, ICCC, Brisbane, Australia (1989); Abstract W112 and refs therein.

Polyhedron Vol. 9, No. 17, pp. 2135–2138, 1990
Printed in Great Britain

0277–5387/90 $3.00+.00
© 1990 Pergamon Press plc

THE SYNTHESIS AND BRIDGE-CLEAVAGE REACTIONS OF THE NOVEL DICATIONIC IODO-BRIDGED DIMER $[\{W(\mu\text{-}I)(CO)\{Ph_2P(CH_2)PPh_2\}(\eta^2\text{-}MeC_2Me)\}_2][BF_4]_2$

PAUL K. BAKER* and KEVIN R. FLOWER

Department of Chemistry, University of Wales, Bangor, Gwynedd LL57 2UW, U.K.

(*Received* 21 *December* 1989; *accepted* 2 *April* 1990)

Abstract—The monobut-2-yne tungsten complex $[WI_2(CO)(dppm)(\eta^2\text{-}MeC_2Me)]$ [dppm = $Ph_2P(CH_2)PPh_2$] reacts in CH_2Cl_2 at room temperature with $Ag[BF_4]$ to slowly afford the iodo-bridged dimer $[\{W(\mu\text{-}I)(CO)(dppm)(\eta^2\text{-}MeC_2Me)\}_2][BF_4]_2$ (**1**) in good yield. ^{13}C NMR spectroscopy suggests that each but-2-yne ligand is donating four electrons to each tungsten centre in **1**. Compound **1** reacts with two equivalents of L [L = CN^tBu, $P(O^iPr)_3$ and $SC(NH_2)_2$] in CH_2Cl_2 to give the iodo-bridge cleaved products $[WI(CO)L(dppm)(\eta^2\text{-}MeC_2Me)][BF_4]$ (**2–4**) in high yield. ^{13}C NMR spectroscopy of **2–4** indicates that the but-2-yne ligand is donating four electrons to the tungsten in these compounds.

Cationic alkyne complexes of molybdenum(II) and tungsten(II) have received considerable attention in recent years. In particular, the cationic cyclopentadienyl or indenyl bis-alkyne complexes of the type $[Mo(CO)(\eta^2\text{-}RC_2R')_2(\eta^5\text{-}C_5H_5$ or $C_9H_7)][BF_4]$[1] have been found to be extremely useful precursors for a wide range of novel chemistry.[2–8] However, very few cationic halo-alkyne complexes of molybdenum(II) and tungsten(II) have been reported. Some examples include the cationic isonitrile complexes of the type $[MI(CNR)_4(\eta^2\text{-}RC_2R')]I$ and closely related derivatives reported by Lippard and co-workers.[9–14]

Recently we have reported the synthesis of the cationic alkyne complexes $[WI(CO)(NCMe)\{Ph_2P(CH_2)_nPPh_2\}(\eta^2\text{-}RC_2R)][BF_4]$ (n = 1–6; R = Me or Ph).[15] These complexes are prepared by reaction of the neutral complexes $[WI_2(CO)\{Ph_2P(CH_2)_nPPh_2\}(\eta^2\text{-}RC_2R)]$ (n = 1–6; R = Me or Ph) with one equivalent of $Ag[BF_4]$ in acetonitrile to give $[WI(CO)(NCMe)\{Ph_2P(CH_2)_nPPh_2\}(\eta^2\text{-}RC_2R)][BF_4]$. In this paper we describe the reaction of $[WI_2(CO)(dppm)(\eta^2\text{-}MeC_2Me)]$ [dppm = $Ph_2P(CH_2)PPh_2$] with an equimolar quantity of $Ag[BF_4]$ in CH_2Cl_2 to give the novel dicationic dimeric complex $[\{W(\mu\text{-}I)(CO)(dppm)(\eta^2\text{-}MeC_2Me)\}_2][BF_4]_2$ (**1**), and several bridge-cleavage reactions of this complex.

* Author to whom correspondence should be addressed.

EXPERIMENTAL

The complex $[WI_2(CO)(dppm)(\eta^2\text{-}MeC_2Me)]$ was prepared according to the published method.[16] All chemicals were purchased from commercial sources except for dppm which was prepared according to the literature method.[17]

Elemental analyses for carbon, hydrogen and nitrogen were determined using a Carlo Erba elemental analyser MOD 1106 (using helium as a carrier gas). IR spectra were recorded on a Perkin–Elmer 1430 ratio recording IR spectrophotometer in $CHCl_3$ as thin films between NaCl plates. ^1H and ^{13}C NMR spectra were recorded on a Bruker AC 250 CP/MAS NMR spectrometer (all spectra were calibrated against tetramethylsilane).

$[\{W(\mu\text{-}I)(CO)(dppm)(\eta^2\text{-}MeC_2Me)\}_2][BF_4]_2$ (1)

To $[WI_2(CO)(dppm)(\eta^2\text{-}MeC_2Me)]$ (1 g, 1.106 mmol) dissolved in CH_2Cl_2 (25 cm^3), with continuous stirring under a stream of dry nitrogen, was added $Ag[BF_4]$ (0.2153 g, 1.106 mmol). After 72 h the solution was filtered and the solvent volume reduced to 4 cm^3. Dropwise addition of Et_2O precipitated the brown cationic complex $[\{W(\mu\text{-}I)(CO)(dppm)(\eta^2\text{-}MeC_2Me)\}_2][BF_4]_2$ (**1**). The supernatant was then syringed off and the crude product washed with Et_2O (15 cm^3) twice and dried *in vacuo*. The product was then recrystallized from CH_2Cl_2–Et_2O

to afford brown crystals of **1**, yield of pure product = 0.54 g, 57%.

[WI(CO)(CN^{t}Bu)(dppm)(η^2-MeC$_2$Me)][BF$_4$] (**2**)

To **1** (0.5 g, 0.29 mmol) dissolved in CH_2Cl_2 (10 cm^3) was added ^{t}BuNC (0.0488 g, 0.58 mmol). After stirring for 2 h the solution was filtered and the solvent volume reduced to 3 cm^3. Dropwise addition of Et_2O precipitated the brown cationic complex [WI(CO)(CN^{t}Bu)(dppm)(η^2-MeC$_2$Me)][BF$_4$] (**2**), which was washed with Et_2O (15 cm^3) twice and dried *in vacuo*. Recrystallization of **2** from CH_2Cl_2–Et_2O afforded brown crystals of **2**, yield of pure product = 0.3 g, 54%.

Similar reactions of **1** with two equivalents of L [L = P(O^{i}Pr)$_3$ and SC(NH$_2$)$_2$] in CH_2Cl_2 at room temperature for 2 h gave the bridge-cleaved products [WI(CO)L(dppm)(η^2-MeC$_2$Me)][BF$_4$] (**3** and **4**) (see Table 1 for physical and analytical data).

Table 2. IR data[a] for the compounds [{W(μ-I)(CO)(dppm)(η^2-MeC$_2$Me)}$_2$][BF$_4$]$_2$ and [WI(CO)L(dppm)(η^2-MeC$_2$Me)][BF$_4$]

Compound	ν(C≡O) cm^{-1}	ν(C≡N) cm^{-1}	ν(C≡C) cm^{-1}
1[b]	1940 (b,s)	—	—[c]
2[b]	1995 (s)	2200 (m) 2150 (m)	—[c]
3[b]	1965 (s)	—	1640 (vw)
4[b]	1925 (s)	—	—[c]

s, strong; m, medium; vw, very weak; b, broad.

[a] Spectra recorded in $CHCl_3$ as thin films between NaCl plates.

[b] A broad strong band at ~1020 cm^{-1} [ν(BF)] is observed for all the complexes **1**–**4**.

[c] ν(C≡C) was not observed for these complexes.

RESULTS AND DISCUSSION

Equimolar quantities of the complex [WI$_2$(CO)(dppm)(η^2-MeC$_2$Me)] and Ag[BF$_4$] react in CH_2Cl_2 at room temperature to afford eventually a good yield of the novel dicationic iodo-bridged dimer **1**. Compound **1** reacts with two equivalents of L [L = CN^{t}Bu, P(O^{i}Pr)$_3$ and SC(NH$_2$)$_2$] in CH_2Cl_2 at room temperature to give the bridge-cleaved products **2**–**4** in high yield. Complexes **1**–**4** have been fully characterized by elemental analysis (C, H and N) (Table 1), IR (Table 2), ^{1}H and ^{13}C NMR spectroscopy (Tables 3 and 4). Complexes **1**–**4** are stable when stored under nitrogen, however they are air-sensitive when exposed to air, particularly in solution. The dinuclear complex, **1**, is only slightly soluble in CH_2Cl_2 and $CHCl_3$ and insoluble in diethyl ether and hydrocarbon solvents, whereas the mononuclear compounds, **2**–**4**, are much more soluble in CH_2Cl_2 and $CHCl_3$, but as expected since they are salts they are insoluble in diethyl ether and hydrocarbon solvents.

Reaction of [WI$_2$(CO)(dppm)(η^2-MeC$_2$Me)] and an equimolar quantity of Ag[BF$_4$] in CH_2Cl_2 must initially involve iodide abstraction by Ag^+ to give AgI leaving a vacant coordination site. Two equivalents of [WI(CO)(dppm)(η^2-MeC$_2$Me)]$^+$ combine by forming two dative bonds with the lone

Table 1. Physical and analytical data[a] for the complexes [{W(μ-I)(CO)(dppm)(η^2-MeC$_2$Me)}$_2$][BF$_4$]$_2$ and [WI(CO)L(dppm)(η^2-MeC$_2$Me)][BF$_4$]

Compound	Colour	Yield (%)	Analysis
[{W(μ-I)(CO)(dppm)(η^2-MeC$_2$Me)}$_2$][BF$_4$]$_2$ (**1**)	Brown	57	C: 41.6(41.7) H: 3.4(3.3)
[WI(CO)(CN^{t}Bu)(dppm)(η^2-MeC$_2$Me)][BF$_4$] (**2**)	Brown	54	C: 44.1(44.5) H: 4.2(3.7) N: 1.5(1.6)
[WI(CO){P(O^{i}Pr)$_3$}(dppm)(η^2-MeC$_2$Me)][BF$_4$] (**3**)	Red	53	C: 43.4(43.7) H: 4.7(4.6)
[WI(CO){SC(NH$_2$)$_2$}(dppm)(η^2-MeC$_2$Me)][BF$_4$] (**4**)	Pink	58	C: 39.3(39.6) H: 3.5(3.4) N: 2.7(2.9)

[a] Calculated values in parentheses.

Table 3. ^{1}H NMR data[a] for the compounds [{W(μ-I)(CO)(dppm)(η^2-MeC_2Me)}$_2$][BF_4]$_2$ and [WI(CO)L(dppm)(η^2-MeC_2Me)][BF_4]

Compound	^{1}H (δ) ppm
1	7.28 (bm, 40H, *Ph*); 4.9 (bm, 4H, PCH_2P); 2.96 (s, 12H, ≡C*Me*)
2	7.35 (bm, 20H, *Ph*); 4.52 (bm, 2H, PCH_2P); 3.30 (s, 6H, ≡C*Me*); 2.2 (bs, 9H, CH_3)
3	7.26 (bm, 20H, *Ph*); 5.72 (m, 3H, OC*H*); 4.58 (bm, 2H, PCH_2P); 2.3 (s, 6H, ≡C*Me*); 1.3 (d, 18H, $CHCH_3$, J_{H-H} = 6.03 Hz)
4	7.36 (bs, 20H, *Ph*); 6.36 (s, 4H, NH_2); 4.5 (bm, 2H, PCH_2P); 3.11 (s, 6H, ≡C*Me*)

[a] Spectra recorded in $CDCl_3$ (+25°C) and referenced to Me_4Si.

s = singlet, d = doublet, m = multiplet, bm = broad multiplet.

Table 4. ^{13}C NMR data[a] for the compounds [{W(μ-I)(CO)(dppm)(η^2-MeC_2Me)}$_2$][BF_4]$_2$ and [WI(CO)L(dppm)(η^2-MeC_2Me)][BF_4]

Compound	^{13}C (δ) ppm
1	222.62 (s, *C*≡*C*); 207.6 (s, *C*≡O); 134.04 → 128.5 (m, *Ph*); 31.54 (bs, PCH_2P); 21.57 (s, ≡C*Me*)
2	221.99 (s, *C*≡*C*); 205.27 (s, *C*≡O); 180.4 (s, *C*≡N); 133.59 → 129.75 (m, Ph); 59.8 (s, C≡N*C*); 32.15 (t, PCH_2P, J_{P-C} = 12.9 Hz); 30.12 (t, C*Me*); 20.58 (s, ≡C*Me*)
3	221.56 (s, *C*≡*C*); 216.17 (s, C≡O); 132.2 → 128.13 (m, *Ph*); 72.39 (d, OCH, J_{P-C} = 4.1 Hz); 32.1 (bs, PCH_2P) 23.91 (s, CH_3); 22.09 (s, ≡C*Me*)
4	221.43 (s, *C*≡*C*); 205.9 (s, *C*≡O); 181.93 (s, *C*=S); 133.07 → 128.78 (bm, *Ph*); 31.23 (bs, PCH_2P); 21.31 (s, ≡C*Me*)

[a] Spectra recorded in $CDCl_3$ (+25°C) and referenced to Me_4Si.

s = singlet, d = doublet, m = multiplet, t = triplet, b = broad.

pairs on the iodide ions to give **1**. The structure of **1** is likely to have but-2-yne ligands *trans*- to iodide which has often been observed for other halo-alkyne complexes of molybdenum(II) and tungsten(II),[15,18-21] which leaves the bidentate phosphine and carbon monoxide ligands to occupy the other sites, as shown in Fig. 1. Unfortunately we were unable to grow suitable single crystals of **1** for X-ray crystallography, however the IR and NMR data conforms with the proposed structure shown in Fig. 1. The IR spectrum of **1** shows a broad, single carbonyl band at 1940 cm^{-1} which suggests the *trans*-arrangement of carbonyl ligands, and the ^{1}H NMR shows a single resonance for the but-2-yne ligands which indicates rapid rotation of the but-2-yne ligands (faster than the NMR time scale) at room temperature. This rapid rotation of a but-2-yne ligand attached to molybdenum(II) and tungsten(II) has been observed previously.[2,15,16,18,20-22] The ^{13}C NMR spectrum of **1** shows a single alkyne contact carbon resonance at δ = 222.62 ppm and a single carbonyl resonance at δ = 207.6 ppm, which again agrees with the structure shown in Fig. 1. The alkyne contact carbon resonance at δ = 222.62 ppm indicates[23] that each but-2-yne ligand on **1** is donating four electrons to each tungsten atom in **1**.

The dicationic iodo-bridged dimer [{W(μ-I)(CO)(dppm)(η^2-MeC_2Me)}$_2$][BF_4]$_2$ (**1**) reacts with two equivalents of L [L = CN^tBu, $P(O^iPr)_3$ and $SC(NH_2)_2$] in CH_2Cl_2 at room temperature to afford the bridge-cleaved products [WI(CO)L(dppm)(η^2-MeC_2Me)][BF_4] (**2–4**). These complexes have been previously prepared from reaction of the mono-acetonitrile complex [WI(CO)(NCMe)(dppm)(η^2-MeC_2Me)][BF_4] with an equimolar quantity of L in CH_2Cl_2.[15,21,24] The X-ray crystal structures of the cations [WI(CO)L(dppm)(η^2-MeC_2Me)]$^+$ [L = $P(O^iPr)_3$[15] and $SC(NH_2)_2$[21]] have been determined and the disposition of ligands around the tungsten is the same for both complexes and is shown in Fig. 2. Reaction of **1** (shown in Fig. 1) with two equivalents of L afford, after symmetric cleavage of the iodo-bridges, the structure shown in Fig. 2 with iodide *trans*- to

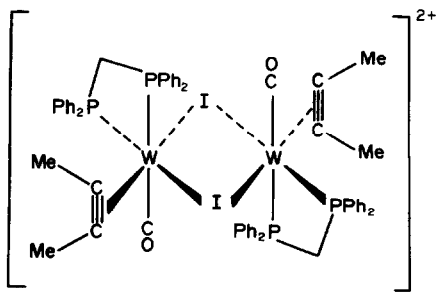

Fig. 1. Proposed structure of [{W(μ-I)(CO)(dppm)(η^2-MeC_2Me)}$_2$][BF_4]$_2$

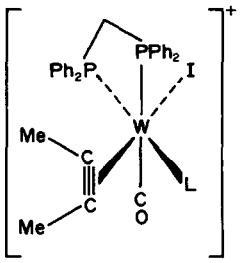

Fig. 2. Proposed structure of [WI(CO)L(dppm)(η^2-Me C_2Me)][BF_4].

but-2-yne, which also helps to confirm the structure of **1** shown in Fig. 1. ^{13}C NMR studies again show[23] the but-2-yne ligand in **2**–**4** is utilizing both of its filled $p\pi$-orbitals to donate four electrons to the metal in **2**–**4**. Refluxing the dicationic iodo-bridged dimer **1** in acetonitrile or acetone for 24 h did not afford mononuclear complexes of the type [WI(CO)L(dppm)(η^2-MeC_2Me)][BF_4] (L = NCMe or $OCMe_2$); only starting material **1** was recovered from these reactions. Also no reaction occurred when carbon monoxide was bubbled through a CH_2Cl_2 solution of **1** for 24 h.

Acknowledgement—K.R.F. thanks the SERC for a studentship.

REFERENCES

1. M. Bottrill and M. Green, *J. Chem. Soc., Dalton Trans.* 1977, 2365.
2. S. R. Allen, P. K. Baker, S. G. Barnes, M. Green, L. Trollope, L. M. Muir and K. W. Muir, *J. Chem. Soc., Dalton Trans.* 1981, 873.
3. M. Green, N. C. Norman and A. G. Orpen, *J. Am. Chem. Soc.* 1981, **103**, 1267.
4. S. R. Allen, P. K. Baker, S. G. Barnes, M. Bottrill, M. Green, A. G. Orpen, I. D. Williams and A. J. Welch, *J. Chem. Soc., Dalton Trans.* 1983, 927.
5. R. G. Beevor, M. Green, A. G. Orpen and I. D. Williams, *J. Chem. Soc., Chem. Commun.* 1983, 673.
6. S. R. Allen, R. G. Beevor, M. Green, N. C. Norman, A. G. Orpen and I. D. Williams, *J. Chem. Soc., Dalton Trans.* 1985, 435.
7. M. Green, *Polyhedron* 1986, **5**, 427 and refs cited therein.
8. M. Green, *J. Organomet. Chem.* 1986, **300**, 93 and refs cited therein.
9. C. T. Lam, P. W. R. Corfield and S. J. Lippard, *J. Am. Chem. Soc.* 1977, **99**, 617.
10. P. W. R. Corfield, L. M. Baltusis and S. J. Lippard, *Inorg. Chem.* 1981, **20**, 922.
11. C. Casavana, C. M. Giandomenico and S. J. Lippard, *Inorg. Chem.* 1982, **21**, 1860.
12. C. M. Giandomenico, C. T. Lam and S. J. Lippard, *J. Am. Chem. Soc.* 1982, **104**, 1263.
13. R. Hoffmann, C. N. Wilker, S. J. Lippard, J. L. Templeton and D. C. Brower, *J. Am. Chem. Soc.* 1983, **105**, 146.
14. S. Warner and S. J. Lippard, *Organometallics* 1986, **5**, 1716.
15. P. K. Baker, K. R. Flower, M. G. B. Drew and G. Forsyth, *J. Chem. Soc., Dalton Trans.* 1989, 1903.
16. E. M. Armstrong, P. K. Baker, M. E. Harman and M. B. Hursthouse, *J. Chem. Soc., Dalton Trans.* 1989, 295.
17. K. Sommer, *Z. Anorg. Allg. Chem.* 1970, **376**, 37.
18. P. B. Winston, S. J. N. Burgmayer, T. L. Tonker and J. L. Templeton, *Organometallics* 1986, **5**, 1707.
19. E. M. Armstrong, P. K. Baker and M. G. B. Drew, *Organometallics* 1988, **7**, 319.
20. P. K. Baker, E. M. Armstrong and M. G. B. Drew, *Inorg. Chem.* 1989, **28**, 2406.
21. P. K. Baker, K. R. Flower, P. A. Bates and M. B. Hursthouse, *J. Organomet. Chem.* 1989, **372**, 263.
22. J. L. Davidson and G. Vasapollo, *J. Chem. Soc., Dalton Trans.* 1985, 2239.
23. J. L. Templeton and B. C. Ward, *J. Am. Chem. Soc.* 1980, **102**, 3288.
24. P. K. Baker and K. R. Flower, *Inorg. Chim. Acta* 1989, **165**, 241.

Polyhedron Vol. 9, No. 17, pp. 2139–2141, 1990
Printed in Great Britain

0277–5387/90 $3.00+.00
© 1990 Pergamon Press plc

SYNTHESIS AND STRUCTURE OF DICHLORODI-[1,2-BIS(DIMETHYLPHOSPHINO)ETHANE]IRON(III) TETRACHLOROFERRATE(III), $[Fe(DMPE)_2Cl_2]^+[FeCl_4]^-$

LESLIE D. FIELD* and ADRIAN V. GEORGE

Department of Organic Chemistry, University of Sydney, N.S.W., 2006, Australia

and

TREVOR W. HAMBLEY

Department of Inorganic Chemistry, University of Sydney, N.S.W., 2006, Australia

(*Received* 19 *February* 1990; *accepted* 2 *April* 1990)

Abstract—$[Fe(DMPE)_2Cl_2]^+[FeCl_4]^-$ was formed in high yield by the photochemical oxidation of $Fe(DMPE)_2Cl_2$ with chlorinated organic solvents CH_2Cl_2, $CHCl_3$ or CCl_4. Crystals of $[Fe(DMPE)_2Cl_2]^+[FeCl_4]^-$ are orthorhombic, space group *Pcab*, $a = 16.250(3)$, $b = 19.392(3)$, $c = 34.451(7)$ Å, $Z = 16$, $R = 0.058$ (3597 F). This represents the first structural characterization of an iron(III) complex with a P_4Cl_2 donor set and saturated phosphine ligands.

Iron(II) bis(diphosphine)dihalide complexes of the type $[Fe(PP)_2X_2]$ [PP = 1,2-bis(dialkyl- or diarylphosphino)ethane, X = halide] have been intensively studied and the crystal structures of a number of such compounds have been determined.[1] By contrast, little work on the iron(III) analogues has been reported, although the *ortho*-phenylenebis(dimethyl)arsine complexes of iron(III) halides were synthesized and characterized in the 1950s.[2] $[Fe(DMPE)_2Cl_2]^+$ [DMPE = 1,2-bis(dimethylphosphino)ethane] has been employed in metal exchange experiments to produce $[^{99}Tc(DMPE)_2Cl_2]^+$, used as a myocardial imaging agent.[3,4] Exposure of methanol solutions of $Fe(DMPE)_2Cl_2$ or $Fe(DEPE)_2Cl_2$ [DEPE = 1,2-bis(diethylphosphino)ethane] to oxygen results in the formation of red iron(III) cationic complexes[5] and the redox chemistry of the iron(II)–iron(III)–iron(IV) dihalide complexes with bisphosphine and bisarsine ligands has been investigated in some depth.[6,7] Iron(III) complexes containing neutral ligands have been employed as precursors for reactive iron(IV) species.[7]

We report here, the facile photochemical synthesis of $[Fe(DMPE)_2Cl_2]^+[FeCl_4]^-$ (**1**), and the crystal structure of this iron(III) complex. Previously reported syntheses of $[Fe(DMPE)_2Cl_2]^+$ include the ferric chloride oxidation of the iron(II) complex, $Fe(DMPE)_2Cl_2$,[5] and a direct route involving the reaction of ferric chloride and DMPE in refluxing anhydrous methanol.[3]

EXPERIMENTAL

NMR spectra were recorded on a Bruker WM400 NMR spectrometer operating at 400.1 MHz for ^1H observation and 162.0 MHz for ^{31}P observation. ^1H NMR spectra were referenced to residual solvent resonances; ^{31}P NMR spectra were referenced to external neat trimethyl phosphite (taken to be 140.85 ppm at the temperature quoted).

Synthesis of $[Fe(DMPE)_2Cl_2]^+[FeCl_4]^-$ (1)

Dichloromethane, chloroform and carbon tetrachloride were of reagent grade and were degassed before use. Dichloromethane was shaken with concentrated H_2SO_4, washed with water, aqueous

* Author to whom correspondence should be addressed.

Na_2CO_3, water, then dried over $CaCl_2$ and distilled from P_4O_{10}.[8] $Fe(DMPE)_2Cl_2$ was prepared using the method of Chatt and Hayter.[9]

A stirred solution of $Fe(DMPE)_2Cl_2$ in dichloromethane (Pyrex flask) was irradiated with a 125 W mercury vapour lamp at 30°C. The initially green solution darkened and after 3 h the solution had attained a magenta colour and the irradiation was stopped. The solvent was removed under reduced pressure and the crude solid recrystallized from chloroform/carbon tetrachloride to yield $[Fe(DMPE)_2Cl_2]^+[FeCl_4]^-$ (**1**) as a magenta crystalline solid in 68% isolated yield, m.p. >160°C (dec.). The complex is insoluble in carbon tetrachloride, toluene and pentane, but soluble in dichloromethane, chloroform, acetone and isopropanol. ^{31}P NMR (CH_2Cl_2, 220 K) δ59 (very broad singlet $W_{1/2}$ 153 Hz at 200 K; 723 Hz at 220 K; 2900 Hz at 250 K); ^1H NMR (acetone-d_6, 220 K) δ2.1 (very broad singlet, 8H, 4× —CH_2—), 1.4 (very broad singlet, 24H, 8× —CH_3). λ_{max} (CH_3CN, log ε) 556 (3.35), 360 (3.72), 283 (4.29), 237 (4.35), 207 (3.28) nm.

X-ray crystallography

Cell constants were determined by a least-squares fit to the θ values of 25 independent reflections, measured and refined on an Enraf–Nonius CAD4-F diffractometer with a graphite monochromator. Data were reduced and Lorentz, polarization, absorption and decomposition corrections were applied using the Enraf–Nonius Structure Determination Package.[10] The structure was solved by direct methods and was refined by full-matrix least-squares analysis with SHELX-76.[11] Hydrogen atoms were included at sites calculated assuming tetrahedral geometry (C—H, 0.97 Å) with group isotropic thermal parameters, all other atoms were refined anisotropically. Conformational disorder in one of the chelate rings is evidenced by very high thermal parameters. Attempts to locate alternative sites for C(9) and C(10) were unsuccessful and the electron density appears as a smear, particularly for the former atom. Scattering factors and anomalous dispersion corrections for iron were taken from the *International Tables for X-ray Crystallography*,[12] and for all others the values supplied in SHELX-76 were used. The atomic nomenclature is defined in Fig. 1.[13]

Crystal data. $C_{12}H_{32}Cl_6Fe_2P_4$, $M = 624.70$, orthorhombic, space group *Pcab*, $a = 16.250(3)$, $b = 19.392(3)$, $c = 34.451(7)$ Å, $U = 10856(3)$ Å^3, D_c ($Z = 16$) = 1.529 g cm^{-3}, $F(000) = 5088$, μ(Mo-K_α) = 18.33 cm^{-1}. Specimen: magenta prisms, 0.12 × 0.26 × 0.15 mm. $N = 7733$, $N_o = 3597$, range of *hkl*: 0 → 17, 0 → 21, 0 → 37, $R = 0.058$, $R_w = 0.058$, residual extrema ±0.50 eÅ^{-3}.

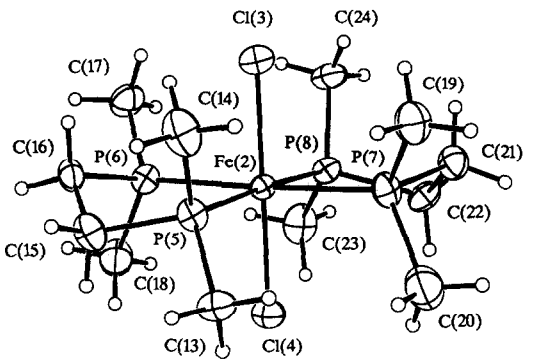

Fig. 1. ORTEP plot of cation 2 of $[Fe(DMPE)_2Cl_2]^+$ $[FeCl_4]^-$ (**1**).

RESULTS AND DISCUSSION

Photolysis of $Fe(DMPE)_2Cl_2$ in a halogenated solvent in a Pyrex vessel, under an atmosphere of argon, resulted in the effectively quantitative production of a magenta-coloured complex, identified by X-ray crystallography as the tetrachloroferrate salt of $[Fe^{III}(DMPE)_2Cl_2]^+$ (**1**) (Fig. 1).

The complex, **1**, is formed equally well if dichloromethane or chloroform is used as the reaction solvent; in carbon tetrachloride, the complex precipitates directly from solution. The reaction probably involves a light-stimulated electron transfer from iron(II) to the alkyl halide, resulting in a chain reaction which exhaustively oxidizes iron(II) to iron(III) and forms organic radicals. After the irradiation is complete, the reaction solution contains a mixture of various condensed chloroalkanes whose formation can be rationalized by reductive radical coupling.

The electronic spectrum of the complex is in accord with that reported previously for $[Fe(DMPE)_2Cl_2]^+[BF_4]^-$.[7] The complex is paramagnetic and the ^{31}P NMR spectrum is observable as a single broad resonance only at low temperatures.

Description of the structure

The asymmetric unit is made up of two $[Fe(DMPE)_2Cl_2]^+$ cations and two $[FeCl_4]^-$ anions, packed with no unusual contacts between them. The cations have geometries which are close to octahedral with the Cl^- ligands *trans* to one another. The largest deviations from octahedral geometry are the chelate ring bite angles of 83.9(1)–84.8(1)°. The average Fe—Cl and Fe—P bond lengths are 2.240 and 2.304 Å, similar to, but marginally longer

Table 1. Comparison of average Fe—Cl and Fe—P bond lengths (Å) in $[Fe(diphosphine)_2Cl_2]^{x+}$ and $[FeCl_4]^-$ complexes

Complex	Fe—Cl	Fe—P	Reference
$[Fe(DMPE)_2Cl_2]^+$	2.240	2.304	This work
$[Fe\{o\text{-}C_6F_4(PMe_2)_2\}_2Cl_2]^+$	2.234	2.294	6(c), 7
$Fe(DMPE)_2Cl_2$	2.352	2.235	1(e)
$Fe(DEPE)_2Cl_2$	2.344	2.260	1(a)
$Fe(DPrPE)_2Cl_2$	2.345	2.268	1(a)
$[FeCl_4]^-$	2.179		This work
$[FeCl_4]^-$	2.182		7, 15

than those in the only other structurally characterized iron(III) complex with four phosphine and two chloride ligands, $[Fe\{o\text{-}C_6F_4(PMe_2)_2\}_2Cl_2]^+[BF_4]^-$ (2.234(1) and 2.292–2.295(1) Å).[14] The similarity of the Fe—P bond lengths in these structures shows that they are not significantly affected by the steric or electronic properties of the diphosphine ligands. The Fe—Cl bonds are shorter than those in comparable iron(II) complexes $[Fe(PP)_2Cl_2$, PP = DMPE, DPPE, DPrPE; DPrPE = 1,2-bis (di-*n*-propylphosphino)ethane] which range from 2.344(1) to 2.352(1) Å, but the Fe—P bonds are significantly longer than those in the iron(II) complexes (2.230(1)–2.275(2) Å, Table 1).[1a,e]

The anions have nearly tetrahedral geometries with the Cl—Fe—Cl angles ranging from 107.0(2) to 114.2(3)°. The Fe—Cl bond lengths range from 2.165(7) to 2.199(5) Å and average 2.179 Å, which is indistinguishable from that found in $[As(C_6H_5)_4]^+[FeCl_4]^-$ (2.182(1) Å).[15] A tetragonal distortion was observed in that structure which is similar to that in one of the anions in the present structure. However, since the distortion of the other anions in the present structure is significantly lower (108.4(2)–112.1(2)°) we suggest that these distortions are the result of crystal packing forces.

Acknowledgement—We gratefully acknowledge financial support from the Australian Research Council.

REFERENCES

1. (a) M. V. Baker, L. D. Field and T. W. Hambley, *Inorg. Chem.* 1988, **27**, 2872; (b) J. E. Barclay, G. J. Leigh, A. Houlton and J. Silver, *J. Chem. Soc., Dalton Trans.* 1988, 2865; (c) J. E. Barclay, A. Hills, D. L. Hughes and G. J. Leigh, *J. Chem. Soc., Dalton Trans.* 1988, 2871; (d) G. S. Girolami, G. Wilkinson, A. M. R. Galas, M. Thornton-Pett and M. B. Hursthouse, *J. Chem. Soc., Dalton Trans.* 1985, 1339; (e) M. Di Vaira, S. Midollini and L. Sacconi, *Inorg. Chem.* 1981, **20**, 3430; (f) M. Antberg and L. Dahlenburg, *Inorg. Chim. Acta* 1985, **104**, 51; (g) F. Cecconi, M. Di Vaira and L. Sacconi, *Cryst. Struct. Commun.* 1981, **10**, 1523; (h) L. Horner and E. Mueller, *Phosphorus* 1972, **2**, 117.
2. (a) R. S. Nyholm, *J. Chem. Soc.* 1950, 851; (b) R. S. Nyholm and R. V. Parish, *Chem. Ind.* 1956, 470.
3. R. D. Neirinckx, E. R. Squibb and Sons Inc. US 4419339 A, CA100(10): 73987.
4. R. Berger, R. Syhre, S. Seifert, D. Kloetzer, P. Maeding and R. Muenze, *Appl. Radiat. Isot.* 1986, **37**, 197.
5. J. M. Bellerby, M. J. Mays and P. L. Sears, *J. Chem. Soc., Dalton Trans.* 1976, 1232.
6. (a) L. F. Warren and M. A. Bennett, *J. Am. Chem. Soc.* 1974, **96**, 3340; (b) L. F. Warren and M. A. Bennett, *Inorg. Chem.* 1976, **15**, 3130; (c) S. J. Higgins and W. Levason, *Inorg. Chem.* 1985, **24**, 1105.
7. (a) S. K. Harborn, S. J. Higgins, W. Levason, M. C. Feiters and A. T. Steel, *Inorg. Chem.* 1986, **25**, 1789.
8. D. D. Perrin and W. L. F. Armarego, *The Purification of Laboratory Chemicals*, 3rd edn, p. 145. Pergamon Press, Oxford (1988).
9. J. Chatt and R. G. Hayter, *J. Chem. Soc.* 1961, 5507.
10. Enraf–Nonius Structure Determination Package (SDP). Enraf–Nonius, Delft, Holland (1985).
11. G. M. Sheldrick, SHELX-76, A Program for X-Ray Crystal Structure Determination. University of Cambridge, U.K. (1976).
12. D. T. Cromer and J. T. Waber, *International Tables for X-Ray Crystallography*, Vol. IV. Kynoch Press, Birmingham, U.K.
13. Figures were drawn with ORTEP, C. K. Johnson, ORTEP, A Thermal Ellipsoid Plotting Program. Oak Ridge National Laboratories, Oak Ridge, Tennessee (1965).
14. S. J. Higgins, H. C. Jewiss, W. Levason and M. Webster, *Acta Cryst.* 1985, **C41**, 695.
15. F. A. Cotton and C. A. Murillo, *Inorg. Chem.* 1975, **14**, 2467.

Polyhedron Vol. 9, No. 17, pp. 2143–2148, 1990
Printed in Great Britain

0277–5387/90 $3.00+.00
© 1990 Pergamon Press plc

SYNTHESIS AND THERMAL STABILITY OF MIXED-LIGAND LANTHANIDE COMPLEXES INVOLVING BOTH CYCLOPENTADIENYL AND TWO DIFFERENT CHELATE LIGANDS—TRIFLUOROACETATO AND EITHER 8-QUINOLINOLATO OR *o*-AMINOPHENOLATO LIGANDS

ZHONGZHI WU,* FEIMING ZHAO and ZHENNAN ZHOU

Institute of Organic Chemistry, Anhui Normal University, Wuhu, Anhui 241000, P.R.C.

(*Received* 21 *December* 1989; *accepted* 2 *April* 1990)

Abstract—Eight new mixed-ligand lanthanide complexes of the general formula CpLnLL′ [Ln = Sm, Dy, Ho, Yb; Cp = C_5H_5; L = CF_3COOO; L′ = 8-OC_6H_3N:CHCH:CH, OC_6H_4(*o*-NH_2)] have been synthesized. All the complexes were characterized by elemental analysis, IR, XPS and MS spectra, showing that they are dimers with carboxylate ions as bridging groups, and the donor atom nitrogen in each complex coordinates with the metal. Their thermal stability has been studied and discussed. All these complexes are thermally unstable, and at moderately high temperatures they tend to disproportionate into a mixture of Cp_2LnL, Cp_2LnL', LnL_3 and LnL'_3.

Recently, we have reported studies on the thermal stability of some mixed-ligand lanthanide (Nd, Yb) complexes involving both cyclopentadienyl (Cp) and classical chelate ligands (8-quinolinolato, *o*-aminophenolato, *o*-aldehydophenolato, furfuralcoholato ligand), and found that they are susceptible to heat and tend to disproportionate at moderately high temperatures.[1,2] However, the mixed-ligand lanthanide complexes involving both Cp and two different classical chelate ligands have not hitherto been reported and studied. In continuation of our previous work,[1,2] we have now carried out the synthesis and studies on the thermal stability of eight new mixed-ligand lanthanide (Sm, Dy, Ho, Yb) complexes involving three ligands including the Cp ligand and two different classical chelate ligands—trifluoroacetato and either 8-quinolinolato or *o*-aminophenolato ligands, and the results are reported in this paper.

RESULTS AND DISCUSSION

By the reaction of Cp_2LnCl (Ln = Sm, Dy, Ho, Yb) first with sodium trifluoroacetate and then with 8-hydroxyquinoline or *o*-aminophenol (mole ratio, 1:1:1) in THF (tetrahydrofuran) at room temperature, eight new mixed-ligand lanthanide complexes involving the Cp ligand and two classical chelate ligands—trifluoroacetato and either 8-quinolinolato or *o*-aminophenolato ligands have been synthesized, as shown in the following equation:

$$Cp_2LnCl + NaL + HL' \xrightarrow[RT]{THF} CpLnLL' + C_5H_6 + NaCl$$

Ln = Sm, Dy, Ho, Yb; L = CF_3COO;

L′ = 8-OC_6H_3N:CHCH:CH, OC_6H_4(*o*-NH_2).

All these complexes were characterized by elemental analysis, IR, XPS and MS spectra.

The elemental analyses (Table 1) for all the complexes are in compliance with the general formula CpLnLL′. All the complexes are soluble in THF, but only partially soluble in benzene and toluene. All of them are insoluble in pentane and n-hexane. They have no melting points; decomposition is observed in a sealed capillary above 200°C.

The IR spectra (Table 2) of all the complexes show absorptions at about 250, 780, 1010, 1400 and 3080 cm^{-1}, characteristic of the η^5-Cp ligand.[3] All

* Author to whom correspondence should be addressed.

Table 1. Physical properties and elemental analyses for complexes

Complex	Colour	Yield (%)	Decomposition temperature (°C)	Found (calc.) (%) Ln	C	H	N
$CpSm(CF_3COO)(8\text{-}OC_6H_3N:CHCH:CH)$ (**1**)	Pale red	46	210	31.5 (31.8)	40.4 (40.6)	2.3 (2.4)	3.0 (2.9)
$CpDy(CF_3COO)(8\text{-}OC_6H_3N:CHCH:CH)$ (**2**)	Yellow	57	240	33.4 (33.5)	39.7 (39.6)	2.4 (2.3)	2.9 (2.9)
$CpHo(CF_3COO)(8\text{-}OC_6H_3N:CHCH:CH)$ (**3**)	Yellow	61	265	33.7 (33.8)	39.4 (39.4)	2.6 (2.3)	3.3 (2.8)
$CpYb(CF_3COO)(8\text{-}OC_6H_3N:CHCH:CH)$ (**4**)	Yellow	52	280	34.8 (34.9)	38.7 (38.8)	2.3 (2.2)	2.9 (2.8)
$CpSm(CF_3COO)[OC_6H_4(o\text{-}NH_2)]$ (**5**)	Yellow	35	200	34.2 (34.4)	35.2 (35.8)	2.5 (2.5)	3.0 (3.2)
$CpDy(CF_3COO)[OC_6H_4(o\text{-}NH_2)]$ (**6**)	Pale yellow	42	220	36.1 (36.2)	34.6 (34.8)	2.4 (2.5)	3.1 (3.1)
$CpHo(CF_3COO)[OC_6H_4(o\text{-}NH_2)]$ (**7**)	Pale yellow	40	243	36.5 (36.6)	34.3 (34.6)	2.5 (2.5)	3.2 (3.1)
$CpYb(CF_3COO)[OC_6H_4(o\text{-}NH_2)]$ (**8**)	Yellow	40	260	37.6 (37.7)	33.4 (34.0)	2.3 (2.4)	2.9 (3.1)

four 8-quinolinolato complexes exhibit two bands characteristic of the 8-quinolinolato ligand at about 1495 and 1570 cm^{-1}.[4] Moreover, a band appearing in the 390 cm^{-1} region may be assigned to the chelate ring deformation vibration of 8-quinolinolato complexes.[5] The IR spectra of four *o*-aminophenolato complexes show the bands of the 1,2-disubstituted benzene ring at about 750, 1500, 1600 and 3030 cm^{-1}.[6] In addition, two ν(OH) bands for the free ligand *o*-aminophenol at 3527 and 3628

Table 2. IR spectral data for complexes **1**–**8** (4000–200 cm^{-1})

Complex	Main absorptions (cm^{-1})
$CpSm(CF_3COO)(8\text{-}OC_6H_3N:CHCH:CH)$ (**1**)	3075w, 3025w, 1665s, 1571m, 1498s, 1455s, 1435sh, 1209s, 1114m, 1106m, 1018m, 780m, 726s, 642w, 490w, 384w, 275w, 252w.
$CpDy(CF_3COO)(8\text{-}OC_6H_3N:CHCH:CH)$ (**2**)	3080w, 3035w, 1666s, 1574m, 1500s, 1454s, 1435sh, 1206s, 1115m, 1104m, 1017m, 791s, 755m, 642w, 495w, 389w, 280w, 250w.
$CpHo(CF_3COO)(8\text{-}OC_6H_3N:CHCH:CH)$ (**3**)	3078w, 3050w, 1659s, 1571m, 1501s, 1450s, 1442sh, 1208m, 1112m, 1103m, 1019m, 786s, 725s, 647w, 495w, 572m, 393w, 280w, 258w.
$CpYb(CF_3COO)(8\text{-}OC_6H_3N:CHCH:CH)$ (**4**)	3082w, 3045w, 1667s, 1575m, 1501s, 1455s, 1430sh, 1208s, 1116m, 1106s, 1015m, 788s, 752s, 647w, 577m, 520w, 494m, 392w, 270w, 248w.
$CpSm(CF_3COO)[OC_6H_4(o\text{-}NH_2)]$ (**5**)	3355m, 3240m, 3081w, 3028w, 1663s, 1602m, 1488s, 1455s, 1430m, 1210s, 1113m, 1102m, 1025m, 780s, 752s, 480w, 273w, 245w.
$CpDy(CF_3COO)[OC_6H_4(o\text{-}NH_2)]$ (**6**)	3351m, 3233m, 3080w, 3030w, 1667s, 1603m, 1489s, 1454s, 1435m, 1210s, 1115m, 1101s, 1020s, 775m, 751m, 486m, 274w, 250w.
$CpHo\ (CF_3COO)[OC_6H_4(o\text{-}NH_2)]$ (**7**)	3356m, 3246w, 3065w, 3025w, 1660s, 1603m, 1489s, 1454s, 1440sh, 1205s, 1114m, 1102m, 1030m, 774m, 749s, 484w, 275w, 246w.
$CpYb(CF_3COO)[OC_6H_4(o\text{-}NH_2)]$ (**8**)	3335m, 3225m, 3075w, 3040w, 1667s, 1603m, 1492s, 1455s, 1432m, 1206s, 1116m, 1106m, 1013m, 775m, 752s, 490w, 271w, 252w.

cm^{-1} are absent in the complexes, and the two $\nu(NH_2)$ bands for the free ligand at about 3390 and 3478 cm^{-1} are shifted to lower frequencies, about 3230 and 3360 cm^{-1}, on complexation. This indicates coordination of the nitrogen atoms of the NH_2 groups.[7] All the complexes also exhibit two bands in the IR spectra in the regions 270 and 1115 cm^{-1}. We tentatively attribute the first one to a Ln—N vibration mode and the second one to Ln—O—C bond stretching.[5,8,9] A band appearing near 490 cm^{-1} may be assigned to the ν(Ln—O) mode.[8]

In the IR spectra of all the complexes, the absorptions associated with the antisymmetric and symmetric stretches of carboxylate ions appear near 1455 and 1660 cm^{-1}, respectively. Deacon pointed out that three useful correlations between $\nu(CO_2)$ frequencies and carboxylate coordination can be justified for trifluoroacetato complexes, viz. (a) separations between $\nu(CO_2)$ frequencies (Δ) substantially greater than ionic are indicative of unidentate carboxylate coordination; (b) separations significantly less than ionic values are indicative of chelating and/or bridging carboxylate groups; (c) very low separations generally indicate chelation or a combination of chelation and bridging.[10] The $\nu(CO_2)$ separations of the eight new complexes are lower than the ionic values (Table 3). Therefore, we assume that all these complexes may be dimers with carboxylate ions as bridging groups.

These complexes were also verified by X-ray photoelectron spectroscopy. From the XPS data (Table 4), it was revealed that in each complex the binding energy of the nitrogen atom of the 8-quinolinolato or *o*-aminophenolato ligand was increased, as compared with corresponding reference substances. This further proves coordination through the nitrogen atom of the 8-quinolinolato or *o*-aminophenolato ligand.

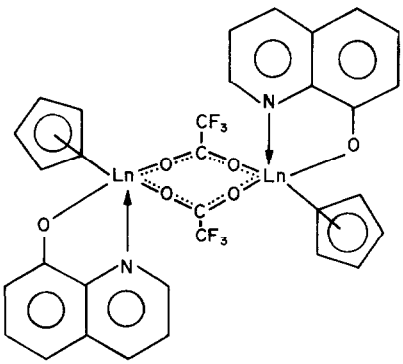

Fig. 1.

The molecular ions and main fragments of these complexes are clearly observed in their mass spectra (Table 5). All the molecular ions are characterized by the ready loss of the Cp group with the $(M—Cp)^+$ ion as base peak in the mass spectra, but the peaks corresponding to the fragments of dimers of greater mass than the molecular ions are observed as well. So, on the basis of elemental and spectral analyses, it can be concluded that all the complexes are dimers with carboxylate ions as bridging groups and the intramolecular five-membered chelating ring, produced by chelation coordination of the 8-quinolinolato or *o*-aminophenolato ligand, in each complex. Thus, the structures shown in Figs 1 and 2 for the complexes may be proposed.

For the purpose of studying the thermal stability of these complexes, their mass spectra were recorded at different evaporation temperatures. It is interesting to note that when the evaporation temperature of a sample reaches a certain value for each complex, not only are the molecular ion $CpLnLL'^+$

Table 3. IR frequencies of $\nu(CO_2)$ for complexes

Complex[a]	$\nu_{as}(COO^-)$ (cm^{-1})	$\nu_s(COO^-)$ (cm^{-1})	$\Delta[\nu_{as}(COO^-)-\nu_s(COO^-)]$ (cm^{-1})
$CpSm(CF_3COO)(Q)$ (**1**)	1665	1455	210
$CpDy(CF_3COO)(Q)$ (**2**)	1666	1454	212
$CpHo(CF_3COO)(Q)$ (**3**)	1659	1450	209
$CpYb(CF_3COO)(Q)$ (**4**)	1667	1455	212
$CpSm(CF_3COO)(A)$ (**5**)	1663	1455	208
$CpDy(CF_3COO)(A)$ (**6**)	1667	1454	213
$CpHo(CF_3COO)(A)$ (**7**)	1660	1454	206
$CpYb(CF_3COO)(A)$ (**8**)	1667	1455	212
CF_3COONa[16]	1680	1457	223

[a] Q = 8-OC_6H_3N:CHCH:CH; A = (*o*-NH_2)C_6H_4O.

Table 4. XPS data of complexes and complexes for references

Complex[a]	XPS (eV) $E_b(N_{1s})$	ΔE^b
CpSm(L)(8-OC_6H_3N:CHCH:CH) (**1**)	401.2	
Na(8-OC_6H_3N:CHCH:CH)	399.5	1.7
CpDy(L)(8-OC_6H_3N:CHCH:CH) (**2**)	401.0	
Na(8-OC_6H_3N:CHCH:CH)	399.5	1.5
CpHo(L)(8-OC_6H_3N:CHCH:CH) (**3**)	401.0	
Na(8-OC_6H_3N:CHCH:CH)	399.5	1.5
CpYb(L)(8-OC_6H_3N:CHCH:CH) (**4**)	400.6	
Na(8-OC_6H_3N:CHCH:CH)	399.5	1.1
CpSm(L)[OC_6H_4(*o*-NH_2)] (**5**)	401.0	
Na[OC_6H_4(*o*-NH_2)]	400.2	0.8
CpDy(L)[OC_6H_4(*o*-NH_2)] (**6**)	400.8	
Na[OC_6H_4(*o*-NH_2)]	400.2	0.6
CpHo (L)[OC_6H_4(*o*-NH_2)] (**7**)	400.7	
Na[OC_6H_4(*o*-NH_2)]	400.2	0.5
CpYb(L)[OC_6H_4(*o*-NH_2)] (**8**)	400.7	
Na[OC_6H_4(*o*-NH_2)]	400.2	0.5

[a] L = CF_3COO.
[b] ΔE is the binding energy difference.

peaks observed in the spectra, but the peaks corresponding to Cp_2LnL^+, $Cp_2LnL'^+$, LnL_3^+ and their fragments are observed also. Furthermore, with increasing evaporation temperature, the molecular ion $CpLnLL'^+$ peaks gradually disappear and the ion peaks of Cp_2LnL^+, $Cp_2LnL'^+$, LnL_3^+ and their fragments are enhanced. According to the results reported in our previous reports,[1,2] we predict that the following disproportionation reaction may take place:

$$4CpLnLL' \rightarrow Cp_2LnL + Cp_2LnL' + LnL_3 + LnL'_3.$$

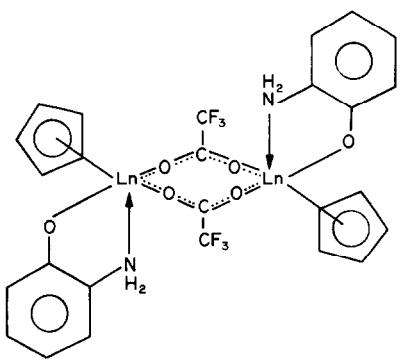

Fig. 2.

The ion peaks of the disproportionation product LnL'_3 were not observed in the mass spectra.

As the η^5-Cp ligands in both lanthanide and actinide complexes are quite labile,[11] it may be assumed that the lability of Cp ligands causes the above disproportionation reaction. It is also possible that the disproportionation reaction takes place via an intermediate bimolecular complex in which the Cp ligands are bonded in an η^5-fashion to one molecule, and in an η^1-fashion to the second molecule of the complex. The transfer of one Cp ligand from one molecule to another may initiate the disproportionation reaction.

Since no $CpLnL_2^+$ and $CpLnL'^+_2$ ion peaks were observed in the mass spectra recorded at different evaporation temperatures, we predict that all the complexes do not undergo the following rearrangement reaction:

$$2CpLnLL' \rightarrow CpLnL_2 + CpLnL'_2$$

but directly disproportionate into a mixture of Cp_2LnL, Cp_2LnL', LnL_3 and LnL'_3 during the course of raising the temperature.

In view of decomposition temperatures and MS data, we also found that the order of relative thermal stability of the complexes is CpYbLL' > CpHoLL' > CpDyLL' > CpSmLL', which may be due to the lanthanide contraction. The attraction of the Ln–ligand bond formed by

Table 5. MS data for complexes **1–8** at different evaporation temperatures

Complex	Evaporation temperature (°C)	Main ion peaks (m/z)[a]
(**1**) L = CF_3COO; L′ = 8-OC_6H_3N:CHCH:CH.	100, 120, 150	883 (M_2-Cp), 818 (M_2-2Cp), 474 (M), 409 (M−Cp), 361 (M−L), 296 (M−Cp−L), 184 (SmO_2), 152 (Sm).
M = CpSmLL′; M′ = Cp_2SmL; M″ = Cp_2SmL'; M‴ = SmL_3.	160, 200, 250	491 (M‴), 426 (M″), 395 (M′), 361 (M″−Cp), 330 (M′−Cp), 296 (M″−2Cp), 217 (M′−Cp−L), 152 (Sm).
(**2**) L = CF_3COO; L′ = 8-OC_6H_3N:CHCH:CH.	100, 120, 150	842 (M_2-2Cp), 729 (M_2-Cp-L), 421 (M−Cp), 373 (M−L), 308 (M−Cp−L), 164 (Dy).
M = CpDyLL′; M′ = Cp_2DYL; M″ = Cp_2DyL'; M‴ = DyL_3.	170, 200, 250	503 (M‴), 438 (M″), 407 (M′), 373 (M″−Cp), 342 (M′−Cp), 308 (M″−2Cp), 294 (M′−L), 164 (Dy).
(**3**) L = CF_3COO; L′ = 8-OC_6H_3N:CHCH:CH.	120, 140, 160	905 (M_2-CF_3), 844 (M_2-2Cp), 487 (M), 422 (M−Cp), 374 (M−L), 309 (M−Cp−L), 165 (Ho).
M = CpHoLL′; M′ = Cp_2HoL; M″ = Cp_2HoL'; M‴ = HoL_3.	180, 220, 250	504 (M‴), 439 (M″), 408 (M′), 374 (M″−Cp), 343 (M′−Cp), 343 (M′−Cp), 309 (M″−2Cp), 295 (M′−L), 165 (Ho).
(**4**) L = CF_3COO; L′ = 8-OC_6H_3N:CHCH:CH.	140, 160, 180	862 (M_2-2Cp), 749 ($M_2-2Cp-L$), 496 (M), 431 (M−Cp), 318 (M−Cp−L), 174 (Yb).
M = CpYbLL′; M′ = Cp_2YbL; M″ = Cp_2YbL'; M‴ = YbL_3.	200, 250, 300	513 (M‴), 448 (M″), 417 (M′), 383 (M″−Cp), 352 (M′−Cp), 318 (M″−2Cp), 174 (Yb).
(**5**) L = CF_3COO; L′ = OC_6H_4(*o*-NH_2).	80, 100, 130	876 (M_2), 746 (M_2-2Cp), 677 ($M_2-Cp-CF_3$), 438 (M), 373 (M−Cp), 325 (M−L), 281 (M−Cp−$C_6H_4NH_2$), 260 (M−Cp−L).
M = CpSmLL′; M′ = Cp_2SmL; M″ = Cp_2SmL'; M‴ = SmL_3.	140, 200, 250	491 (M‴), 395 (M′), 390 (M″), 330 (M′−Cp), 325 (M″−Cp), 282 (M′−L), 260 (M″−2Cp), 152 (Sm).
(**6**) L = CF_3COO; L′ = OC_6H_4(*o*-NH_2).	100, 120, 150	835 (M_2-Cp), 770 (M_2-2Cp), 751 ($M_2-F-2Cp$), 450 (M), 385 (M−Cp), 337 (M−L), 272 (M−Cp−L), 164 (Dy).
M = CpDyLL′; M′ = Cp_2DyL; M″ = Cp_2DyL'; M‴ = DyL_3.	160, 200, 250	503 (M‴), 407 (M′), 402 (M″), 342 (M′−Cp), 337 (M″−Cp), 294 (M′−L), 272 (M″−2Cp), 164 (Dy).
(**7**) L = CF_3COO; L′ = OC_6H_4(*o*-NH_2).	100, 120, 150	837 (M_2-Cp), 833 (M_2-CF_3), 772 (M_2-2Cp), 659 ($M_2-2Cp-L$), 451 (M), 386 (M−Cp), 338 (M−L), 273 (M−Cp−L), 165 (Ho).
M = CpHoLL′; M′ = Cp_2HoL; M″ = Cp_2HoL'; M‴ = HoL_3.	180, 200, 250	504 (M‴), 408 (M′), 403 (M″), 343 (M′−Cp), 338 (M″−Cp), 273 (M″−2Cp), 165 (Ho).
(**8**) L = CF_3COO; L′ = OC_6H_4(*o*-NH_2).	100, 150, 170	790 (M_2-2Cp), 677 (M_2-Cp-L), 460 (M), 395 (M−Cp), 347 (M−L), 287 (M−Cp−L), 174 (Yb).
M = CpYbLL′; M′ = Cp_2YbL; M″ = Cp_2YbL'; M‴ = YbL_3.	200, 250, 300	513 (M‴), 417 (M′), 412 (M″), 352 (M′−Cp), 347 (M″−Cp), 304 (M″−L′), 282 (M″−2Cp), 174 (Yb).

[a] MS data are given for the isotopes ^{152}Sm, ^{164}Dy, ^{165}Ho, ^{174}Yb, ^{14}N, ^{16}O and ^{19}F, the peak patterns correspon to theoretical values based on the natural abundance of isotopes.

Ln^{3+} and an anionic ligand increases with decreasing Ln^{3+} radius. According to the concept of correlation of stability with steric saturation,[12,13] the above order also may be a consequence of the greater steric saturation present around the smaller metal centre. In addition, the four 8-quinolinolato complexes have relatively higher decomposition and disproportionation temperatures than the corresponding *o*-aminophenolato complexes. This can be attributed to the following. Firstly, probably due to the stronger complexing ability of the 8-quinolinolato ligand compared with the *o*-aminophenolato ligand. The Ln–ligand bond formed by Ln^{3+} and the 8-quinolinolato ligand is stronger than that of the *o*-aminophenolato ligand. Secondly, the large steric volume of the 8-quinolinolato ligand relative to the *o*-aminophenolato ligand is favourable for the stabilization of the coordinated unsaturated organolanthanide complexes.

EXPERIMENTAL

All operations were carried out in an atmosphere of dry oxygen-free argon using standard Schlenk techniques or in a glovebox. All the reagents are of analytical or chemically pure grade. All solvents were dried over sodium, refluxed over sodium benzophenone or finely divided $LiAlH_4$ and distilled immediately before use. Cp_2LnCl (Ln = Sm, Dy, Ho, Yb) were prepared by literature methods.[14]

The analyses for C, H and N were performed using a Yanaco MT- 2 CHN analyser. Metal analyses for lanthanides were accomplished by a literature method.[15] The IR spectra were recorded in the range 4000–200 cm^{-1} with a Perkin–Elmer 983G spectrometer. Samples were prepared as Nujol and Fluorolube mulls between CsI plates. The X-ray photoelectron spectra were obtained on a VG ESCALAB MKII spectrometer with Mg-K_α exciting irradiation. All the mass spectrometric measurements were performed on a VG ZAB-HS spectrometer operating in EI mode at a resolving power of 1000 (electron energy, 70 eV; emission current, 1 mA; ion acceleration, 3 kV). The samples were protected under argon and introduced by direct inlet techniques with a source temperature of 110°C and sample evaporation temperature in the range of 50–300°C.

General procedure for the synthesis of complexes

The appropriate CF_3COONa (2 mmol) was added to a 50 cm^3 THF solution of Cp_2LnCl (Ln = Sm, Dy, Ho, Yb) (2 mmol). The reaction mixture was allowed to stir for 24 h at room temperature. Then, equimolor 8-hydroxyquinoline or *o*-aminophenol was added to the reaction mixture. After the resulting mixture was stirred for 24 h at room temperature, the volume was reduced *in vacuo* to about 20 cm^3. The NaCl precipitate was removed from the reaction mixture by centrifugation. By the addition of 40 cm^3 of n-hexane to the resulting solution, a solid precipitated out which was recrystallized twice from THF–n-hexane and dried *in vacuo* to afford the product. Yields, analyses and physical properties of all the complexes are given in Table 1.

Acknowledgements—This work was financially supported by the National Science Foundation. We would like to thank the Instrument Centre of the University of Science and Technology of China for recording the X-ray photoelectron and mass spectra. We also thank Mr Baohui Du and Ms Jipin Hu for assistance.

REFERENCES

1. Zhongwen Ye and Zhongzhi Wu, *Synth. React. Inorg. Met.-Org. Chem.* 1989, **19**, 157.
2. Zhongzhi Wu, Zhongwen Ye and Zhennan Zhou, *Polyhedron* 1989, **8**, 2109.
3. Changtao Qian, Changqin Ye, Hanzhang Lu, Yuqin Li, Jialie Zhou, Yuanwen Ge and M. Tsutsui, *J. Organomet. Chem.* 1983, **247**, 161.
4. L. J. Bellamy, *The Infrared Spectra of Complex Molecules*, 2nd edn. John Wiley, New York (1958).
5. N. Ohkaku and K. Nakamoto, *Inorg. Chem.* 1971, **10**, 798.
6. C. J. Pouchert, *The Aldrich Library of Infrared Spectra*, p. 418. Aldrich Chemical Co., Inc. (1970).
7. I. S. Maslennikova, *Zh. Fic. Khim.* 1974, **48**, 1510.
8. K. Nakamoto, *Infrared and Raman Spectra of Inorganic and Coordination Compounds*, 3rd edn, pp. 199 and 228. Wiley Interscience, New York (1978).
9. R. Lozano, J. Roman and F. D. Jesus, *Polyhedron* 1989, **8**, 947.
10. G. B. Deacon and R. J. Phillips, *Coord. Chem. Rev.* 1980, **33**, 242 and refs cited therein.
11. K. W. Bagnall, in *Organometallics of the* f-*Elements* (Edited by T. J. Marks and R. D. Fischer), pp. 221–247. Riedel, Dordrecht (1979).
12. W. J. Evans, *Polyhedron* 1987, **6**, 803.
13. R. D. Fischer and L. Xing-Fu, *J. Less-Common Met.* 1985, **112**, 404.
14. R. E. Maginn, S. Manastyrskj and M. Dubeck, *J. Am. Chem. Soc.* 1963, **85**, 672.
15. Changqin Ye and Yuqin Li, *J. Org. Chem.* (*Chinese*) 1981, 210.
16. W. Klemperer and G. C. Pimentel, *J. Chem. Phys.* 1954, **22**, 1399.

Polyhedron Vol. 9, No. 17, pp. 2149–2152, 1990
Printed in Great Britain

0277-5387/90 $3.00+.00
© 1990 Pergamon Press plc

AMINOCARBOXYLATO CHELATE LIGAND CONFORMATION INFLUENCE ON THE OPTICAL ACTIVITY OF COBALT(III) COMPLEXES—III.* *S*-VALINATO LIGAND CONFORMATION IN THE CRYSTAL STRUCTURE OF Δ-*cis*(NO_2),*trans*(NH_2)-SILVER(I)–DINITROBIS(*S*-VALINATO)COBALTATE(III)

B. V. PRELESNIK, R. HERAK and Z. TOMIĆ

"Boris Kidrič" Institute of Nuclear Sciences, 11001 Beograd, P.O. Box 522, Yugoslavia

and

K. ANDJELKOVIĆ, M. J. MALINAR and N. JURANIĆ†

Institute of Chemistry, Faculty of Sciences, University of Beograd, 11001 Beograd, P.O. Box 550, Yugoslavia

(*Received* 5 *February* 1990; *accepted* 2 *April* 1990)

Abstract—In the crystal structure of Δ-*cis*(NO_2),*trans*(NH_2)-silver(I)–dinitrobis(*S*-valinato) cobaltate(III) the *S*-valinato ligand is found to form the chelate ring of a strained envelope conformation with one methyl group of the ring side chain completely axially oriented and in the proximity of the cobalt atom. The conformation supports the basic idea that an axial positioning of an aminocarboxylato chelate ring side chain induces a large contribution to the optical activity of a complex.

In the investigation of the optical activity of *cis*(NO_2),*trans*(NH_2)-bis(*S*-aminocarboxylato)dinitrocobaltate(III) diastereomers we have observed the effect of the conformation of the aminocarboxylato chelate ligand on the optical activity.[1] On the basis of the crystal structures of two complexes [Δ-*cis*(NO_2),*trans*(NH_2)-silver(I)–bis(*S*-alaninato)dinitrocobaltate(III)[2] and Λ-*cis*(NO_2),*trans*(NH_2)-bis(*S*-arginine)dinitrocobalt(III) nitrate[3]] and the solution NMR data for the aminocarboxylato ligands in all complexes from the series, it has been inferred that a more axially oriented ring side chain of an *S*-aminocarboxylato ligand induces a larger negative contribution to the circular dichroism of a complex.[1] The largest contribution has been observed for the Δ-diastereomers of the investigated complexes containing *S*-valinato and *S*-isoleucinato ligands. Hence, the ligand conformation in these complexes is of special importance for the explanation of the effect.

Therefore, we undertook a crystal structure analysis of Δ-*cis*(NO_2),*trans*(NH_2)-silver(I)–dinitrobis(*S*-valinato)cobaltate(III) and the investigation of the ligand conformation in relation to the solution optical activity of the complex.

EXPERIMENTAL

Crystal preparation

About 0.5 g of the optically pure Δ-*cis*(NO_2), *trans*(NH_2)-potassium–dinitrobis(*S*-valinato)cobaltate(III)[1] was dissolved in 10 cm^3 of water and 1.2 cm^3 of silver nitrate solution (1 mol dm^{-3}) added. The solution was kept overnight in a refrigerator and dark brown prismatic crystals of the corresponding silver salt were obtained.

* Part II: N. Juranić, M. J. Malinar, K. Andjelković, M.B. Ćelap, R. Herak, Lj. Manojlović-Muir, D. Vučelić and M. Vučić, *Polyhedron* 1989, **8**, 1227.

† Author to whom correspondence should be addressed.

X-ray analysis

Crystal data: $Ag[Co(C_5H_{10}NO_2)_2(NO_2)_2]$; M_r = 496.8, monoclinic, space group $C2$, a = 18.851(2), b = 7.019(1), c = 6.2788(7) Å, β = 102.01(4)°, V = 812.6(1) Å^3, Z = 2, D_o = 2.070 g cm^{-3}, D_x = 2.088 g cm^{-3}, μ(Mo-K_α) = 22.5 cm^{-1}.

The dark brown prismatic crystal having the dimensions 0.48 × 0.20 × 0.34 mm was mounted with the b axis approximately parallel to the ϕ axis of an ENRAF–NONIUS CAD 4 automatic diffractometer equipped with a graphite monochromator. Unit cell dimensions were determined from a least-squares fit of the setting angles of 25 reflections with $15 < \theta < 18°$. Intensity data were collected with graphite monochromatized Mo-K_α, radiation (λ = 0.71069 Å) at room temperature (20°C). The θ–2θ scanning mode was used with $\Delta\theta = 0.80 + 0.35 \tan\theta$, and the background was estimated by extending the scans of both ends by 25%. The scan speeds were adjusted to give $\delta I/I > 0.03$ subject to a time limit of 90 s. Of the 1310 independent intensities measured with $2 < \theta < 36°$, 976 were considered to be observed [$I > 3\sigma(I)$]. Two standard reflections measured every 120 min showed no sign of decay over the period of data collection. The data were corrected for Lorentz and polarization effects, but not for absorption.

The structure was solved by heavy-atom and difference Fourier methods and refined by full-matrix least-squares, minimizing the function $\Sigma w(|F_o| - |F_c|)^2$, where $w = 1/\sigma^2(F_o)$. At a later stage of isotropic refinement of non-hydrogen atoms, the absolute configuration was established by carrying out the refinement with the two alternative configurations for values of polarity factor, η, 1 and −1 giving R factors of 0.076 and 0.072, respectively. The model of the lower R value which was in accordance with the configuration deducted from the configuration of *S*-valine, was further anisotropically refined. All hydrogen atoms were included in the structural model at calculated positions at C—H and N—H distances of 0.95 Å and were allowed to ride on the atom to which they are bonded with $U(H) = 1.2 \times U$ of the corresponding atom. The final least-squares refinement of the accepted enantiomorph included an extinction coefficient, g (defined by Stout and Jensen[4]), converged at R = 0.025 and R_w = 0.031. Scattering factors for neutral atoms and anomalous dispersion terms were taken from ref. 5. All calculations were performed on a PDP 11/73 computer using the SDP program,[6] version 4.2.

RESULTS AND DISCUSSION

Crystal structure

The crystal structure of Δ-*cis*(NO_2),*trans*(NH_2)-silver(I)–dinitrobis(*S*-valinato)cobaltate(III) consists of the complex molecule anions and silver cations joined by Coulombic forces. An ORTEP drawing of the complex molecule with the numbering scheme of the atoms is given in Fig. 1. The cobalt atoms lie on two-fold axes and are six-coordinated

Table 1. Bond distances and bond angles

Bond distances (Å)			
Co—O(1)	1.930(4)	O(4)—N(2)	1.228(8)
Co—N(1)	1.950(4)	N(1)—C(1)	1.483(7)
Co—N(2)	1.890(5)	C(1)—C(2)	1.541(6)
O(1)—C(2)	1.294(6)	C(1)—C(3)	1.548(8)
O(2)—C(2)	1.234(7)	C(3)—C(4)	1.523(11)
O(3)—N(2)	1.224(9)	C(3)—C(5)	1.541(7)
Bond angles (°)			
O(1)—Co—N(1)	83.6(2)	N(1)—C(1)—C(3)	114.3(4)
O(1)—Co—N(2)	90.7(2)	C(2)—C(1)—C(3)	110.0(5)
N(1)—Co—N(2)	95.6(3)	O(1)—C(2)—O(2)	123.8(4)
Co—O(1)—C(2)	114.2(3)	O(1)—C(2)—C(1)	116.7(4)
Co—N(1)—C(1)	111.5(2)	O(2)—C(2)—C(1)	119.6(5)
Co—N(2)—O(3)	123.6(5)	C(1)—C(3)—C(4)	112.5(5)
Co—N(2)—O(4)	117.7(5)	C(1)—C(3)—C(5)	110.4(5)
O(3)—N(2)—O(4)	118.6(6)	C(4)—C(3)—C(5)	111.3(4)
N(1)—C(1)—C(2)	107.8(4)		

Numbers is parentheses are ESDs in the least significant digit.

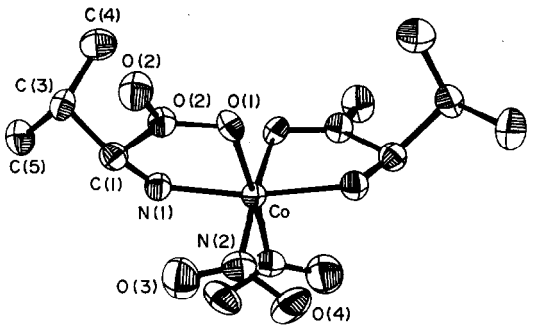

Fig. 1. An ORTEP drawing of the complex molecule with the numbering scheme of the atoms.

by two carboxylato oxygen atoms and two amino nitrogen atoms belonging to different valinato ligands and two nitro nitrogen atoms, respectively.

Bond lengths and angles in the anion are listed in Table 1. The Co—O and Co—N bond distances and angles are in agreement with values previously observed in the cobalt(III) amino acidato complexes. The largest deviation from octahedral geometry occurs for the O(1)—Co—N(1) angle of the five-membered aminocarboxylato chelate ring. The bond distances and angles in the valinato ligand are unexceptional; the same holds for the nitro group.

The conformation of the five-membered chelates and the positions of the ring side chain methyl groups are expressed by the relevant parameters, as given in Table 2. The chelate rings adopt the strained λ-envelope conformation, with one of the side chain methyl groups in the axial position relative to the mean least-square plane defined by the five-membered ring. In addition, the side chain methyl groups are in positions which correspond to almost ideal staggered conformations relative to the amino and carboxylato groups of the ligand.

The cation resides on a crystallographic two-fold axis. Each Ag^+ ion is surrounded in an irregular arrangement by the eight oxygen atoms belonging to the four complex anions. The independent $Ag\cdots O$ distances are 2.529 and 2.616 Å for the carboxylato groups and 2.456 and 2.999 Å for the nitro groups.

Ligand conformation in relation to optical activity

It has been suggested by us that the λ-twist conformation of an *S*-aminocarboxylato chelate ring is typical for the Δ-*cis*(NO_2),*trans*(NH_2)-bis(aminocarboxylato)dinitrocobaltate(III) diastereomers.[1] However, in the present case, the strained envelope conformation of the *S*-valinato ligand is established in the solid complex. This seems to be caused mainly by a mutual repulsion of the ring side chains of two *S*-valinato ligands in the complex molecule. If so, *S*-valinato ligand conformations could be considered fixed by intramolecular interactions. Indeed, the proton NMR spectrum of the complex in solution shows that the *S*-valinato chelate ring side chains do not rotate. Furthermore, in the H_α proton signal, observed as a quartet of lines in the spectrum, the spin–spin coupling constant with H_β proton ($J_{\alpha\beta} = 3.6$ Hz) corresponds very well[7] with the conformation of the *S*-valinato ligand observed in the solid complex. On this bases the ligand conformation observed in

Table 2. Conformational parameters of the chelate ring in the crystal structure of Δ-*cis*(NO_2),*trans*(NH_2)-silver(I)–dinitrobis(*S*-valinato)cobaltate(III)

(a) Displacements (Å) of the atoms from their least-squares mean planes

Atoms in the ring:							
Co	−0.140	O(1)	0.152	C(2)	−0.076		
C(1)	−0.081			N(1)	0.145		
Atoms out of the ring:							
O(2)	−0.254	C(5)	0.981	C(4)	2.345	C(3)	0.956

(b) Torsional angles (°)

N(1)—Co—O(1)—C(2)	22.9	N(1)—C(1)—C(2)—O(2)	−179.7
O(1)—Co—N(1)—C(1)	−21.0	C(3)—C(1)—C(2)—O(1)	−122.8
Co—O(1)—C(2)—C(1)	−19.4	C(3)—C(1)—C(2)—O(2)	55.6
Co—N(1)—C(1)—C(2)	15.9	N(1)—C(1)—C(3)—C(4)	−67.8
N(1)—C(1)—C(2)—O(1)	1.9	N(1)—C(1)—C(3)—C(5)	57.5
Co—O(1)—C(2)—O(2)	162.4	C(2)—C(1)—C(3)—C(4)	53.0
Co—N(1)—C(1)—C(3)	138.6	C(2)—C(1)—C(3)—C(5)	178.4

the solid complex may be considered relevant for the solution optical activity of the complex. This gives an opportunity of checking whether the proposed explanation of the aminocarboxylato ligand conformation influence on the optical activity is supported by the experimentally observed ligand conformation.

The effect of the *S*-valinato ligand conformation on the optical activity of the complex, according to the Quadrant rule for ligand contribution to the optical activity of the octahedral complexes,[8] is presented in Fig. 2. It is seen that there is a strong negative contribution to the optical activity, in accordance with the experimental result.[1] Since a completely axial positioning of one CH_3-group of the ring side chain is displayed, the basic idea that an axial positioning of a side chain atom induces a large contribution to the optical activity is fully supported. Moreover, it is evident that early branching of the ring side chain is important for the axial positioning of a CH_3-group in the proximity of the cobalt atom. This then explains the largest contribution of the *S*-valinato and *S*-isoleucinato ligands to the optical activity of Δ-*cis*(NO_2), *trans*(NH_2)-bis(aminocarboxylato)dinitrocobaltate(III) complexes.

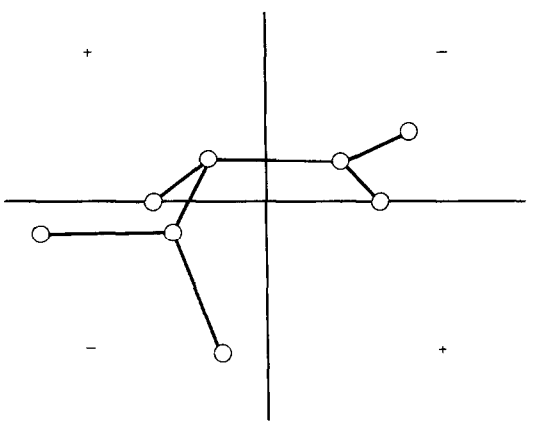

Fig. 2. The *S*-valinato ligand skeletal atom projection according to the Quadrant rule for ligand contribution to the optical activity of a complex.

Acknowledgement—We are grateful to Dr S. Niketić for providing the ORTEP drawing.

REFERENCES

1. N. Juranić, M. J. Malinar, P. N. Radivojša, S. Zarić, D. Vučelić, M. Vučić and M. B. Ćelap, *Polyhedron* 1988, **7**, 1153.
2. R. Herak, B. Prelesnik, Lj. Manojlović-Muir and K. W. Muir, *Acta Cryst.* 1974, **B30**, 229.
3. W. H. Watson, O. R. Johnson, M. B. Ćelap and B. Kamberi, *Inorg. Chim. Acta* 1972, **8**, 591.
4. G. H. Stout and L. H. Jensen, *X-ray Structure Determination*, p. 412. The Macmillan Company Collier Macmillan Ltd, London (1968).
5. *International Tables for X-ray Crystallography*, Vol. IV, p. 149. Kynoch Press, Birmingham (1974).
6. B. A. Frenz, Enraf–Nonius Structure Determination Package for the CAD-4 Diffractometer (1974).
7. U. Sakaguchi, K. Morito and H. Yoneda, *Inorg. Chim. Acta* 1979, **37**, 209.
8. B. Bosnich and J. McB. Harrowfield, *J. Am. Chem. Soc.* 1972, **94**, 3425.

Polyhedron Vol. 9, No. 17, pp. 2153–2162, 1990
Printed in Great Britain

0277–5387/90 $3.00+.00
© 1990 Pergamon Press plc

REACTIONS OF [RuH(CO)Cl(EPh$_3$)$_3$] (E = P, As) AND [Ru(η^5-C$_5$H$_5$)ClL$_2$] [L$_2$ = (PPh$_3$)$_2$, (AsPh$_3$)$_2$, dppe, dppm] WITH 4-CYANOPYRIDINE, 1,4-DICYANOBENZENE AND 1,4-DICYANOBUTENE

D. S. PANDEY, R. L. MISHRA,* A. MISHRA and U. C. AGARWALA†

Department of Chemistry, Indian Institute of Technology, Kanpur 208016, India

(*Received* 5 *February* 1990; *accepted* 2 *April* 1990)

Abstract—Reactions of [RuH(CO)Cl(EPh$_3$)$_3$] (E = P, As) with 4-cyanopyridine, 1,4-dicyanobenzene, 1,4-dicyanobutene and of [Ru(η^5-C$_5$H$_5$)ClL$_2$] [L$_2$ = (PPh$_3$)$_2$, (AsPh$_3$)$_2$, dppe, dppm] with 1,4-dicyanobenzene in the presence of anions like BF$_4^-$, PF$_6^-$, BPh$_4^-$, ClO$_4^-$, have been carried out. Cyanopyridine containing hydridocarbonyl complexes showed a marked tendency to react with halogenated solvents yielding complexes containing no hydride ions. The cationic mononuclear, binuclear and neutral complexes have been characterized by elemental analyses and spectral (IR, UV–vis, ^{1}H and ^{13}C NMR) studies.

We describe and discuss herein the structural properties of the complexes resulting from the reactions of [RuH(CO)Cl(EPh$_3$)$_3$] (E = P, As) with 4-cyanopyridine (4-CNPy), 1,4-dicyanobenzene (DCB) and 1,4-dicyanobutene (DCBT). Although the ligational behaviour of 4-CNPy has been the subject of several previous publications[1] those of DCB and DCBT have little studied.[2] Our interest in these ligands stems from the presence of two donor sites which raises the possibility of formation of mononuclear and bi/or polynuclear complexes. The latter systems are of interest in various fields, for example, in understanding the mechanism of biological redox processes, and in the conversion of solar to chemical energy. An additional feature of this study was to investigate the effect on the bonding properties of a second functional group, remote from the coordinated site in the mononuclear complexes (if formed). In addition to this, we have been concerned for the past few years with the coordination properties of organonitriles, which prompted us to extend our studies in a similar direction.

EXPERIMENTAL

The chemicals used for reactions were Analar or chemically pure grade. Solvents were dried prior to use. [RuH(CO)Cl(EPh$_3$)$_3$] (E = P or As) and [Ru(η^5-C$_5$H$_5$)ClL$_2$] (L = PPh$_3$, AsPh$_3$ or SbPh$_3$; L$_2$ = dppe, dppm) were prepared by the literature procedures.[3–5] 4-Cyanopyridine (Aldrich), 1,4-dicyanobenzene (Aldrich) and *trans*-1,4-dicyanobutene (Fluka) were used as received. Physicochemical measurements were made as described elsewhere.[6] The results are given in Table 1.

(A) *Reactions of* [RuH(CO)Cl(EPh$_3$)$_3$] (E = P, As) *with* 4-CNPy *in the presence of a suitable anion* (BF$_4^-$, BPh$_4^-$, PF$_6^-$, ClO$_4^-$)

A solution of 4-CNPy (0.3 mmol) and [RuH(Co)Cl(EPh$_3$)$_3$] (0.16 mmol) in benzene (30 cm^3) was heated under reflux for 4.5 h. After cooling the resultant solution to room temperature it was filtered to remove any solid impurity and the filtrate was concentrated to about 5 cm^3 under reduced pressure. A solution of the suitable anion (NaBF$_4$, NaBPh$_4$, NH$_4$PF$_6$ or LiClO$_4$) in methanol (30 cm^3) was added and it was then left for slow crystallization. After about 10 h, a brown microcrystalline complex separated out, which was centrifuged, washed with methanol, water, methanol, diethyl ether and dried *in vacuo*. Its analyses corresponded to [RuH(CO)(NCpy)$_2$(EPh$_3$)$_2$]X (X = BF$_4^-$, PF$_6^-$, BPh$_4^-$, ClO$_4^-$) (hereafter referred to as **I**; yield, *ca* 55%).

Reactions of [RuH(CO)Cl(EPh$_3$)$_3$] with DCB and *trans*-DCBT in the presence of anions were

* Present address: St. Aloysiu's High School, 36 Cantt, Kanpur-4, India.

† Author to whom correspondence should be addressed.

Table 1. Analytical and spectral data of complexes

Complexes (Colour, melting point, synthetic process)	Analyses, Found (Calc.)			Major IR bands (cm^{-1})			^1H NMR (ppm)	^{13}C NMR (ppm)	
	C	H	N	$\nu(C{\equiv}N)$	$\nu(C{\equiv}O)$	$\nu(Ru{-}H)$	(η^5-C_5H_5)	(η^5-C_5H_5)	λ_{max}
$[RuH(CO)(CNPy)_2(PPh_3)_2]PF_6$ (I) (RB, 182°C, A)	58.9 (58.4)	4.3 (3.9)	5.4 (5.6)	2240	1940	1995			
$[RuH(CO)(CNPy)_2(PPh_3)_2]BF_4$ (I) (RB, 188°C, A)	62.0 (61.9)	4.7 (4.1)	5.1 (5.9)	2245	1945	2000			
$[RuH(CO)(CNPy)_2(PPh_3)_2]BPh_4$ (I) (YB, 195°C, A)	72.9 (74.1)	5.4 (5.0)	4.5 (4.7)	2230	1940	1995			
$[RuH(CO)(CNPy)_2(PPh_3)_2]ClO_4$ (I) (RB, 230°C, A)	62.0 (60.1)	4.2 (4.0)	5.4 (5.8)						
$[RuH(CO)(CNPy)_2(AsPh_3)_2]BF_4$ (I) (B, 185°C, A)	57.1 (56.5)	4.2 (3.7)	4.1 (5.4)						
$[Ru(CO)(CNPy)_2(AsPh_3)_2]PF_6$ (I) (RB, 210°C, A)	54.1 (53.7)	4.1 (3.6)	4.8 (5.1)	2215	1960	1995			
$[RuH(CO)(CNPy)_2(AsPh_3)_2]BPh_4$ (I) (YB, 175–178°C, A)	70.1 (69.0)	4.2 (3.7)	4.1 (5.4)						
$[RuH(CO)(CNPy)_2(AsPh_3)_2]ClO_4$ (I) (RB, 190°C, A)	56.2 (56.5)	4.5 (3.7)	5.1 (5.3)						
$[RuH(CO)(PPh_3)_2(CNPy)$-μ-$CNPy$-$Ru(\eta^5$-$C_5H_5)(PPh_3)_2](BF_4)_2$ (IV) (OB, 149°C, B)	62.9 (62.5)	4.6 (4.3)	3.0 (3.2)	2220	1940	1990			
$[RuH(CO)(PPh_3)_2(CNPy)$-μ-$CNPy$-$Ru(\eta^5$-$C_5H_5)(PPh_3)_2](PF_6)_2$ (IV) (OB, 145°C, B)	56.6 (58.6)	4.8 (4.0)	2.8 (3.0)	2240	1940	2000			
$[RuH(CO)(PPh_3)_2(CNPy)$-μ-$CNPy$-$Ru(\eta^5$-$C_5H_5)(PPh_3)_2](BPh_4)_2$ (IV) (OB, 165°C, B)	76.0 (75.6)	5.6 (5.2)	2.1 (2.5)	2230	1960	2010			
$[RuH(CO)(PPh_3)_2(CNPy)$-μ-$CNPy$-$Ru(\eta^5$-$C_5H_5)(AsPh_3)_2](BF_4)_2$ (IV) (OB, 148°C, B)	60.1 (59.5)	4.7 (4.1)	2.9 (3.1)	2220	1965	1990			
$[RuH(CO)(PPh_3)_2(CNPy)$-μ-$CNPy$-$Ru(\eta^5$-$C_5H_5)(AsPh_3)_2](PF_6)_2$ (IV) (B, 145°C, B)	56.2 (55.9)	4.1 (3.8)	2.9 (2.1)	2240	1940	2000			
$[RuH(CO)(PPh_3)_2(CNPy)$-μ-$CNPy$-$Ru(\eta^5C_5H_5)(AsPh_3)_2](BPh_4)_2$ (IV) (B, 150°C, B)	73.1 (72.6)	5.4 (5.0)	2.3 (2.4)	2235	1965	2000			
$[RuH(CO)(PPh_3)_2DCB]_2(BF_4)_2$ (II) (YB, 240°C, A)	62.4 (62.2)	4.5 (4.0)	3.0 (3.2)	2230	1940 1965	2000			
$[RuH(CO)(PPh_3)_2DCB]_2(PF_6)_2$ (II) (YB, 210°C, A)	58.8 (58.2)	4.0 (3.8)	2.8 (3.0)	2225	1950	1990			
$[RuH(CO)(PPh_3)_2DCB]_2(BPhy)_2$ (II) (B, 194°C, A)	75.2 (75.1)	5.4 (5.0)	2.3 (2.5)	2220	1960	2000			

[RuH(CO)(PPh$_3$)$_2$DCB]$_2$(ClO$_4$)$_2$ (II)	62.5	4.4	3.1	2220	1940	1990				
(OB, 225 dec, A)	(61.2)	(4.0)	(3.2)							
[RuH(CO)(AsPh$_3$)$_2$DCB]$_2$(BF$_4$)$_2$ (II)	57.1	4.5	2.7	2230	1955	1995				
(Y, 212°C, A)	(56.4)	(3.6)	(2.9)							
[RuH(CO)(AsPh$_3$)$_2$DCB]$_2$(PF$_6$)$_2$ (II)	54.5	4.3	2.1	2225	1960	1995				
(YB, 195°C, A)	(53.2)	(3.4)	(2.7)							
[RuH(CO)(AsPh$_3$)$_2$DCB]$_2$(BPh$_4$)$_2$ (II)	71.2	4.9	2.6	2230	1965	2000				
(YB, 185°C, A)	(69.6)	(4.6)	(2.3)							
[RuH(CO)(AsPh$_3$)$_2$DCB]$_2$(ClO$_4$)$_2$ (II)	56.1	4.1	2.5	2225	1950	1995				
(YB, 220°C, A)	(55.6)	(3.6)	(2.9)							
[(η^5-C$_5$H$_5$)(PPh$_3$)$_2$-Ru-DCB-Ru-(PPh$_3$)$_2$(η^5-C$_5$H$_5$)](BF$_4$)$_2$ (V)	63.8	4.6	2.1	2218			4.6(s)	84.6(s)		
(Y, 125°C, C)	(64.2)	(4.4)	(1.7)							
[(η^5-C$_5$H$_5$)(PPh$_3$)$_2$Ru-DCB-Ru-(PPh$_3$)$_2$(η^5-C$_5$H$_5$)](PF$_6$)$_2$ (V)	59.6	4.2	1.3	2225			4.58	83.3		
(Y, 170–173°C, C)	(60.0)	(4.1)	(1.6)					84.3(s)		
[(η^5-C$_5$H$_5$)(PPh$_3$)$_2$Ru-DCB-Ru-(η^5-C$_5$H$_5$)(AsPh$_3$)$_2$](BF$_4$)$_2$ (V)	58.6	4.2	1.9	2225			4.7	83.6		
(Y, 130°C, C)	(58.1)	(3.9)	(1.5)							
[(η^5-C$_5$H$_5$)(AsPh$_3$)$_2$Ru-μ-DCB-Ru-(AsPh$_3$)$_2$(η^5-C$_5$H$_5$)](PF$_6$)$_2$ (V)	54.0	4.4	1.2	2220			4.57–4.68	83.3	404.4	
(Y, 168–170°C, C)	(54.7)	(3.7)	(1.4)							
[(η^5-C$_5$H$_5$)(SbPh$_3$)$_2$Ru-DCB-Ru-(SbPh$_3$)(η^5-C$_5$H$_5$)](BF$_4$)$_2$ (V)	52.0	4.3	1.7	2230			4.72	83.9		
(Y, 170°C, C)	(52.8)	(3.6)	(1.4)							
[(η^5-C$_5$H$_5$)(SbPh$_3$)$_2$Ru-DCB-Ru-(SbPh$_3$)$_2$(η^5-C$_5$H$_5$)](PF$_6$)$_2$ (V)	50.3	3.9	1.9	2220			4.78	78.9		
(Y, 155°C, C)	(49.9)	(3.4)	(1.3)							
[(η^5-C$_5$H$_5$)(dppm)Ru-DCB-Ru(dppm)(η^5-C$_5$H$_5$)](BF$_4$)$_2$ (V)	58.8	4.6	2.7	2220			—			
(Y, 100°C, C)	(58.2)	(4.1)	(2.0)							
[(η^5-C$_5$H$_5$)(dppm)Ru-DCB-Ru(dppm)(η^5-C$_5$H$_5$)](PF$_6$) (V)	53.2	4.2	2.1	2225			4.5–5.0(m)	80.18		
(Y, 105°C, C)	(53.7)	(3.8)	(1.8)							
[(η^5-C$_5$H$_5$)(dppe)Ru-DCB-Ru(dppe)(η^5-C$_5$H$_5$)](BF$_4$) (V)	59.0	4.8	2.3	2220			4.94(s)	80.3(s)	436.2	
(Y, 102°C, C)	(58.7)	(4.3)	(1.9)							
[(η^5-C$_5$H$_5$)(dppe)Ru-DCB-Ru(dppe)(η^5-C$_5$H$_5$)](PF$_6$)$_2$ (V)	54.6	4.4	2.2	2218			4.9(s)	80.6		
(Y, 105–108°C, C)	(53.9)	(4.0)	(1.8)							
[RuH(CO)(DCBT)(PPh$_3$)$_2$]$_2$(BF$_4$)$_2$ (III)	61.5	5.2	2.9	2255	1960	1990				
	(60.9)	(4.3)	(3.3)							
[RuH(CO)(DCBT)(PPh$_3$)$_2$]$_2$(PF$_6$)$_2$ (III)	58.4	4.9	3.2	2250	1965	1990				
	(57.0)	(4.1)	(3.1)							
[RuH(CO)(DCBT)(PPh$_3$)$_2$]$_2$(BPh$_4$)$_2$ (III)	75.2	5.6	2.4	2260	1945	1995				
	(74.5)	(5.3)	(2.6)							
[RuH(CO)(DCBT)(PPh$_3$)$_2$]$_2$(ClO$_4$)$_2$ (III)	61.2	4.9	2.9	2255	1960	1990				
	(60.0)	(4.3)	(3.2)							
[RuH(CO)(DCBT)(AsPh$_3$)$_2$]$_2$(BF$_4$)$_2$ (III)	56.2	4.7	2.7	2260	1945	1990				
	(55.2)	(3.9)	(3.0)							

continued overleaf

Table 1—*continued*

Complexes (Colour, melting point, synthetic process)	Analyses, Found (Calc.) C	H	N	Major IR bands (cm^{-1}) ν(C≡N)	ν(C≡O)	ν(Ru—H)	^{1}H NMR (ppm) (η^5-C_5H_5)	^{13}C NMR (ppm) (η^5-C_5H_5)	λ_{max}
$[RuH(CO)(DCBT)(AsPh_3)_2]_2(PF_6)_2$ **(III)**	52.6	4.6	2.5	2250	1955	1995			
	(51.9)	(3.7)	(2.8)						
$[RuH(CO)(DCBT)(AsPh_3)_2]_2(BPh_4)_2$ **(III)**	69.2	5.2	2.3	2260	1935	1980			268
	(68.9)	(4.9)	(1.9)						
$[RuH(CO)(DCBT)(AsPh_3)_2]_2(ClO_4)_2$ **(III)**	54.9	4.6	2.5	2265	1940	1995			
	(54.4)	(3.9)	(2.9)						
$[Ru(CO)Cl_2(PPh_3)CNPy]_2$ **(VI)**	53.2	3.9	4.5	2250	1960	—			
(YO, 145°C, D)	(52.9)	(3.3)	(4.9)						
$[Ru(CO)_2Cl_2(PPh_3)MeOH]$ **(VII)**	49.4	4.3	—	—	1960	—			
(YO, 195°C, D)	(48.1)	(3.6)			2065				

RB = red–brown; YB = yellowish-brown; B = brown; OB = orange–brown; CNPy = 4-cyanopyridine; DCB = 1,4-dicyanobenzene; DCBT = 1,4-dicyanobutene.

carried out using a similar procedure to that described in (A) except that DCB or DCBT was used in place of 4-CNPy. Their analyses corresponded to a dinuclear formula $[RuH(CO)(EPh_3)_2\text{-}\mu\text{-}\{DCB \text{ or } DCBT\}_2,\mu\text{-}RuH(CO)(EOh_3)_2]X_2$ (hereafter referred to as **II** (DCB) and **III** (DCBT); yield, *ca* 55%).

(B) *Reactions of* $[Ru(\eta^5\text{-}C_5H_5)Cl(E'Ph_3)_2]$ (E' = P, As) *with* $[RuH(CO)(NCPy)_2(PPh_3)_2]X$ *in the presence of a suitable anion* (BF_4^-, PF_6^-, BPh_4^-, ClO_4^-)

A suspension of $[RuH(CO)(NCPy)_2(EPh_3)_2]X$ (0.15 mmol) and $[Ru(\eta^5\text{-}C_5H_5)Cl(E'Ph_3)_2]$ (0.21 mmol) in methanol (30 cm^3) was heated under reflux for *ca* 5 h, whereupon the suspended material went into a reddish-brown solution. This was cooled to room temperature and filtered to remove any solid residue. The filtrate was concentrated to about 5 cm^3 under reduced pressure and a solution of the suitable anion (BF_4^-, PF_6^-, BPh_4^-, ClO_4^-) in methanol (25 cm^3) was added. This was then left for slow crystallization whereby a red–brown microcrystalline compound was obtained, which was separated by filtration, washed with methanol, water, methanol, diethyl ether and dried *in vacuo*. The analyses corresponded to a dinuclear complex, $[H(CO)(PPh_3)_2(NCPy)Ru\text{-}\mu\text{-}NCPy\text{-}Ru(\eta^5\text{-}C_5H_5)(E'Ph_3)_2]X_2$ (hereafter referred to as **IV**; yield, *ca* 50%).

(C) *Reactions of* 1,4-*dicyanobenzene with* $[Ru(\eta^5\text{-}C_5H_5)ClL_2]$ (L = PPh_3, $AsPh_3$, $SbPh_3$; L_2 = dppe or dppm) *in the presence of a suitable anion* (BF_4^-, PF_6^-)

The complex $[Ru(\eta^5\text{-}C_5H_5)ClL_2]$ (0.13 mmol) was suspended in dry methanol (25 cm^3) containing a salt of a suitable anion ($NaBF_4$, NH_4PF_6) (0.25 mmol) and DCB (0.31 mmol). The contents were refluxed for *ca* 2 h, whereupon $[Ru(\eta^5\text{-}C_5H_5)ClL_2]$ slowly dissolved and bright yellow shiny crystals appeared. These were separated by filtration, washed with methanol, diethyl ether, light petroleum ether and dried *in vacuo*. In the cases of the complexes of dppe or dppm, crystals did not separate out. In those cases the bright yellow filtrate was evaporated to dryness and the residue was extracted with 5 cm^3 of CH_2Cl_2. Addition of about 40 cm^3 of petroleum ether to the extract precipitated a bright yellow compound which was filtered, washed several times with petroleum ether and dried *in vacuo* (yield, *ca* 40%). Analyses corresponded to a dinuclear formula $[Ru_2(\eta^5\text{-}C_5H_5)_2(L_2)_2(\mu\text{-}C_8H_4N_2)]X_2$ (L = PPh_3, $AsPh_3$, $SbPh_3$; L_2 = dppe or dppm; X = BF_4^-, PF_6^-) (hereafter referred to as **V**; yield, 50%).

(D) *Reactions of* $[RuH(CO)(EPh_3)_2(NCPy)_2]X$ (E = P, As) *with* CH_2Cl_2 *or* $CHCl_3$

$[RuH(CO)(EPh_3)_2(NCPy)_2]X$ (0.2 mmol) was refluxed in 30 cm^3 of $CHCl_3$–CH_2Cl_2 for *ca* 4 h, which resulted in an orange–brown solution. After cooling to room temperature it was filtered to remove any remaining solid and evaporated to dryness under reduced pressure. The residue thus obtained was dissolved in CH_2Cl_2 (5 cm^3) and filtered. To the filtrate, light petroleum ether (*ca* 40 cm^3) was added, whereupon a yellowish-brown precipitate formed. This was separated by filtration, washed with methanol, light petroleum ether and dried *in vacuo*.

Reactions of $[RuH(CO)Cl(EPh_3)_3]$ with 4-CNPy in a 1 : 2 molar ratio in CH_2Cl_2–$CHCl_3$ yielded the same product as in reaction (D)

Purification of the reaction products of reaction (D)

The product obtained in reaction (D) was dissolved in the minimum volume of CH_2Cl_2 and passed through a neutral alumina column (25 × 1.5 cm). It was eluted by CH_2Cl_2. The first major yellow band was collected and evaporated to dryness. The residue was extracted with CH_2Cl_2 and precipitated with light petroleum ether. This was washed several times with petroleum ether and dried *in vacuo*; it was analysed for $[Ru(CO)Cl_2(EPh_3)NCPy]_2$ (hereafter referred to as **VI**; yield, 25%).

The second brownish band was eluted with methanol and the complex was obtained by evaporating the eluent to dryness, extracting it with dichloromethane and precipitating it using light petroleum ether. This was separated by filtration, washed several times with light petroleum ether and dried *in vacuo*. It was analysed for $[Ru(CO)_2Cl_2(EPh_3)MeOH]$ (hereafter referred to as **VI**; yield 25%).

RESULTS AND DISCUSSION

The reddish-brown to yellow cationic complexes (Table 1) resulting from the reactions of $[RuH(CO)Cl(EPh_3)_3]$ (E = P, As) with CNPy, DCB or DCBT were found to be non-hygroscopic, air-stable, high melting, crystalline solids. The reactions with CNPy yielded the mononuclear cationic species (**I**), while those with DCB and DCBT yielded dinuclear complexes (**II** DCB, **III** DCBT). Mononuclear complexes did not react any further with the $[RuH(CO)Cl(EPh_3)_3]$. These were then allowed to react with

$[Ru(\eta^5\text{-}C_5H_5)Cl(EPh_3)_2]$, whereupon dinuclear cyano-bridged complexes (**IV**) (Table 1) were formed. These were slightly soluble in methanol, benzene; soluble in chloroform, dichloromethane, DMF, DMSO; and insoluble in light petroleum ether and diethyl ether. The solutions of cyanopyridine complexes in halogenated solvents CH_3CN, DMSO, or in other coordinating solvents changed their colours slowly, from which yellowish-brown complexes (**VI** and **VII**), having different melting points, were obtained. Presumably complexes **I** reacted with the solvents, and because of this their NMR and electronic spectra in these solvents could not be obtained. In other solvents the complexes were practically insoluble.

The products **VI** and **VII** obtained from the solutions of cyanopyridine complexes in halogenated solvents were found to be neutral, highly soluble in most of the common solvents except hydrocarbons or ether. Neither there IR or NMR spectra exhibited any band characteristic of the Ru—H bond. Their analytical data and the fact that the Ru—H bond is absent in both the products suggested their formulae as $[Ru(CO)Cl_2(PPh_3)(NCPy)]_2$ (**VI**) and $[Ru(CO)_2Cl_2(PPh_3)MeOH]$ (**VII**). Attempts are being made to identify other products. It is interesting that a dicarbonyl complex (**VII**) is one of the products in the latter reactions but it is not unexpected because a number of ruthenium(II) hydride monocarbonyl complexes on reacting with $CHCl_3$ yield dicarbonyl products.[7]

The bonding modes in the complexes and their tentative structures have been deduced following the spectral studies.

IR spectra

The IR spectra of mononuclear cyanopyridine complexes (**I**) exhibited a fairly strong broad band for the cyanide stretching vibration around 2240 cm^{-1} compared to 2243 cm^{-1} in the corresponding free ligand. The broadness of the band indicated the presence of two CN groups in *cis* positions. The position of ν(CN) is essentially unaffected, implying the non-involvement of the CN group in coordination. A slight change ($+3$ cm^{-1}) in the ν(C≡N) position may be due to the resonance and the electronic effects arising from coordination with the metal ion. It is therefore presumed that the ligand binds the metal ion through its pyridine nitrogen atom. The bonding through the pyridine nitrogen is also evidenced from the blue shifts of the band arising from those having contributions from ν(C=C) and ν(C=N) of the pyridine molecule in the 1400–1600 cm^{-1} region.

Since our attempts to bind another molecule of $[RuH(CO)Cl(EPh_3)_3]$ with mononuclear complexes (**I**) through uncoordinated nitrogen of the nitrile failed, presumably because of the low basicity of the bonded 4-CNPy groups, these complexes were allowed to react with $[Ru(\eta^5\text{-}C_5H_5)Cl(EPh_3)_2]$. The purpose of doing this was to investigate the basicity of the nitrile nitrogen towards the cationic species $[Ru(\eta^5\text{-}C_5H_5)(EPh_3)_2]^+$ formed in their methanol solutions. These reactions yielded the dinuclear complexes $[(EPh_3)_2H(CO)CNPy\text{-}Ru\text{-}\mu\text{-}NCPy\text{-}Ru(\eta^5\text{-}C_5H_5)(EPh_3)_2]X_2$ ($X = BF_4^-$, PF_6^-, BPh_4^-) (**IV**). Their IR spectra exhibited a weak and a broad band corresponding to ν(C≡N) around 2230 cm^{-1} ($\nu_{1/2} = 15$ cm^{-1}). The broadness and shape of the band suggested the overlap of two ν(C≡N) bands of coordinated and uncoordinated CN groups. The analysis of the broad band indicated that it is composed of two bands, one having a maximum around 2240 cm^{-1} and the other at around 2230 cm^{-1}. This suggests that the reactions lead to binding of one of the two free C≡N groups of bonded cyanopyridine molecules in the mononuclear species (**I**) to the $[Ru(\eta^5\text{-}C_5H_5)(EPh_3)_2]^+$ ion, yielding dinuclear species (**IV**). The red shift of ν(C≡N) of the bridged 4-CNPy (2230 cm^{-1}) may be attributed to metal-to-ligand back-bonding. This is due to the drift of *d* π-electron density from the metal to the π^*-orbitals of the CN group, thus leading to a reduction in the CN bond order. The position of ν(CN) of the unbonded CN group in **IV** remained unchanged (2240 cm^{-1}). The band structure in the 1450–1600 cm^{-1} region is a little too complicated to make any definite assignments. It, however, suggests the presence of two non-equivalent pyridine rings.

The IR spectra of the free 4-dicyanobenzene molecule displayed one intense, sharp band around 2232 cm^{-1} assigned to ν(C≡N). In the spectra of the binuclear products resulting from the reactions of $[RuH(CO)Cl(EPh_3)_3]$ with DCB (**II** DCB), the band moved to 2225 cm^{-1}, while in those of the products obtained from the reactions with $[Ru(\eta^5\text{-}C_5H_5)L_2X]$ (**V**), it appeared around 2230 cm^{-1} [ν(C≡N)]. The presence of a single sharp band in the spectra of these complexes suggested the coordination of both nitrile groups to two separate ruthenium(II) centres forming a symmetrical bridge between them and the absence of any inter–intramolecular interactions.

The IR spectrum of the free 1,4-dicyanobutene displayed an intense, sharp band at 2280 cm^{-1} [ν(C≡N)]. The spectra of the binuclear cationic complexes obtained from the reactions between $[RuH(CO)Cl(EPh_3)_3]$ with DCBT (**II** DCBT) showed a shift of the sharp band which appeared around 2260 cm^{-1}. The ν(C≡N) bands of the com-

plexes of both ligands (**II** DCB, **III** DCBT) occurred at lower frequency compared with in the free ligands, indicating π-back donation from ruthenium to the π^*-orbitals of the CN group.

Interestingly, the order of the negative shift of the 1,4-dicyanobenzene, 4-cyanopyridine and 1,4-dicyanobutene complexes is DCBT > CNPy > DCB. This is consistent with the literature cited order of back-bonding ability of these ligands (DCBT > CNPy > DCB).[8] Attempts to prepare mononuclear complexes of DCB and DCBT failed and the reactions under various conditions yielded only binuclear complexes.

The positions of $\nu(C{\equiv}O)$ and $\nu(Ru{-}H)$ in the spectra of all the complexes were also shifted towards higher and lower frequency, respectively, leading to a decrease in the metal-to-carbon interaction and a decrease in the Ru—H bond order. All the bands of the "spectator" ligands and the anions, in addition to the bands assigned to $\nu(C{\equiv}N)$, $\nu(C{\equiv}O)$ and $\nu(Ru{-}H)$, were present in the spectra of these complexes at their characteristic positions.

The IR spectra [Fig. 1(a)] of the product, $[Ru(CO)Cl_2(PPh_3)(NCPy)]_2$ (**VI**), resulting from the reactions of mononuclear complexes of $[RuH(CO)(PPh_3)_2(NCPy)_2]$ with halogenated solvents showed a band due to $\nu(C{\equiv}N)$ at 2250 cm^{-1} and bands at 1592, 1541, 1495 and 1414 cm^{-1} due to the pyridine moiety of 4-CNPy. The bands of CNPy and PPh_3 appeared at the same positions as they did in the mononuclear complexes. The band due to $\nu(Ru{-}H)$ was absent in the spectrum and that due to $\nu(C{\equiv}O)$ became relatively sharper and appeared at 1960 cm^{-1}. The slight shift of the $\nu(C{\equiv}N)$ band towards higher wavenumbers suggested linkage of the CN group to the metal atom with practically no π-bonding from the metal centre. This observation seems to indicate that the CNPy molecule forms a bridge between two ruthenium centres. Thus in the spectrum of the complex, two CN bands will appear at the same position because of the equivalence of the two CN groups. In addition, the two ruthenium atoms compete to donate their electron densities from the *d*-orbitals to the π^*-orbitals of CNPy. This will result in a relatively small shift of the $\nu(CN)$ band.

In the spectrum [Fig. 1(b)] of the second product $[Ru(CO)_2Cl_2(EPh_3)MeOH]$ (**VII**) bands characteristic of (1) two *cis* (CO) stretching bands and (2) EPh_3 appeared at 2070, 1965 cm^{-1} and 1485, 1440, 1088, 840, 747, 698 cm^{-1}, respectively. The presence of two $\nu(C{\equiv}O)$ bands characteristic of the *cis* positions supports the evidence for the formation of the *cis*-dicarbonyl complex in the reactions with the halogenated hydrocarbons. In addition, the presence of CH_3OH bands in the spectrum suggested that one molecule of CH_3OH is either coordinated or is present as a lattice molecule in the complex. We prefer it to be acting as a lattice CH_3OH rather than a coordinated one. We further assume that the $[Ru(CO)_2Cl_2EPh_3]$ moiety is dimerizing via chloro-bridges, due to the broadness of the OH band indicating hydrogen bonding.

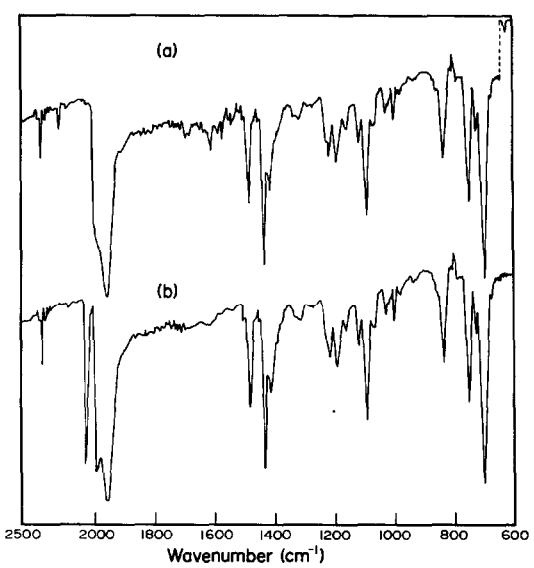

Fig. 1.

^1H *NMR spectra*

Because of poor solubility in some solvents or their tendency to react with halogenated solvents, we could not obtain good ^1H or ^{13}C NMR spectra of hydridocarbonyl complexes of cyanopyridine (**I**).

^1H NMR spectra of DCB complexes with $[Ru(\eta^5\text{-}C_5H_5)X(EPh_3)_2]$ (E = P, As, Sb; X = Cl) (**V**) displayed signals around δ 4.58–4.68 (η^5-C_5H_5); δ 7.1–7.8 (multiplets EPh_3 and DCB). In the spectra of the dppe and dppm complexes, the η^5-C_5H_5 protons were shifted downfield (δ 4.90) compared to that in the parent complexes $[Ru(\eta^5\text{-}C_5H_5)(EPh_3)_2Cl]$. These positions are comparable with those of $[Ru(\eta^5\text{-}C_5H_5)(EPh_3)_2(CN)]$. This suggests that the CN moiety in DCB affects the environment of the (η^5-C_5H_5) protons in a similar way to the NC group. The phenyl carbon atoms attached to the CN groups of DCB do not have much effect on the (η^5-C_5H_5) protons through their other contributing resonance structures like $N^+{\equiv}C\langle$ which are rather insignificant.

The signals of the phenyl protons of DCB should appear around δ7.8 ppm in the complexes (**V**).

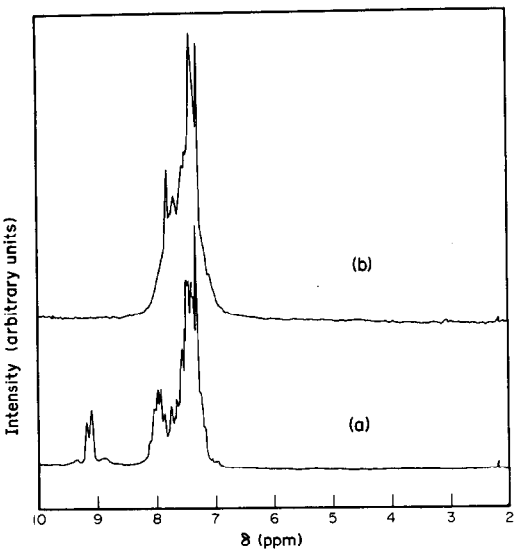

Fig. 2.

Although it was difficult for us to distinguish these from those of EPh_3, dppe or dppm protons, in a few of their PF_6 salts a single, sharp band appeared at δ7.8 which could be assigned to the phenyl protons of DCB. It appears that in these cases the interaction between $d\pi$-orbitals of the two ruthenium(II) centres with the lowest unoccupied π^*-orbitals of DCB seems to be simultaneously producing shielding and deshielding effects on the benzene protons of DCB, resulting in a very small net effect with the protons of DCB resonating at the same positions (δ7.2–7.81) as in the free ligand.

The ^{1}H NMR spectra [Fig. 2(b)] of the complex $[Ru(CO)Cl_2(PPh_3)CNPy]_2$ (**VI**) contained signals at δ9.1–9.3 (br multiplet; CNPy, protons); δ7.8–8.1 (br multiplet; CNPy, protons) and δ7.2–7.65 (EPh_3). The positions of the bands at δ9.1–9.3 and δ8.1 support the presence of cyanopyridine in the complex. The proton ratio of CNPy and PPh_3 (1 : 4) further suggested the presence of equal numbers of CNPy and PPh_3 molecules.

The ^{1}H NMR spectra [Fig. 2(a)] of the second product $[Ru(CO)_2Cl_2(EPh_3)MeOH]$ (**VII**) exhibited peaks around δ7.2–7.5 (EPh_3), δ2.2 (OH of CH_3OH) and δ 3.5 (CH_3). No signals appeared downfield of δ7.5 indicating the absence of CNPy.

^{13}C *NMR spectra*

The (η^5-C_5H_5) carbons of 1,4-dicyanobenzene complexes of $[Ru(\eta^5\text{-}C_5H_5)Cl(EPh_3)_2]$ (**II** DCB) in their ^{13}C NMR spectra appeared as a single band around δ84.6, while in dppe or dppm complexes the band appeared around δ80.2. In a few hexafluorophosphate salts of EPh_3 complexes the (η^5-C_5H_5) ^{13}C signal appeared as a doublet at δ83.3 and 84.3, indicating two different environments of the ring carbon. This may possibly be due to the interaction of the (η^5-C_5H_5) carbons with the other co-ligands or with phosphorus of PF_6^- anion.

The nitrile (C≡N) carbon in **II** DCB resonates at δ116.6 and shows a slight shift upfield (0.52 ppm) compared to that in the free ligand (*ca* δ117.1). Although the shift is not very large, it may be that on complexation of ruthenium with nitrile nitrogens, the electron density on the carbon atom of the C≡N group is polarized towards the nitrogen, resulting in the deshielding of the carbon atom through the σ-bond, but the back-donation of the electron density from the ruthenium to the π^*-orbitals of CN more than compensates the deshielding effect, so that only a small amount of net shielding of the carbon nucleus occurs. This supports the back-donation of π-electrons from ruthenium to the π^*-orbitals of DCB (cf. IR spectra). The carbon atoms of the benzene ring of DCB underwent deshielding due to the strong electron attracting inductive effect of the CN groups. This occurred at around δ122.9 in the complexes compared to the value reported for the free ligand. The *ortho-* and *meta*-carbon atoms of the benzene ring appeared in the region characteristic for phenyl carbon resonances of other co-ligands present in the complexes (δ128.0–136.0) as multiplets.

Electronic absorption spectra

The electronic spectra of DCB complexes with $[Ru(\eta^5\text{-}C_5H_5)XL_2]$ (**IV**) (Table 1) exhibited bands in the visible and UV region (420 and 348–360 nm). The broad, medium intensity band centred at 420 nm has been assigned to an MLCT transition arising due to transfer of charge density from the filled $d\pi(t_{2g})$ orbitals of ruthenium(II) to low-lying unoccupied π^*-orbitals of the CN group of DCB. The position of this band is comparable to those obtained in other organonitrile complexes. It also exhibited a negative solvatochromic effect which is strong evidence in support of the charge-transfer assignment. A metal-to-ligand charge-transfer leads to the separation of charge in the excited state. The energy required for this type of transition is generally sensitive to the environment of the complex ion. The band around 350 nm has been assigned to an MLCT transition [$Ru^{II} \rightarrow$ antibonding orbitals on (η^5-C_5H_5)]. It was also found to overlap with the broad band observed in this region in the UV spectra of these complexes. We have not made any assignments to the band. It could, however, be an intraligand transition.

In $[RuH(CO)(EPh_3)_2(CNPy)_2]$ complexes, two

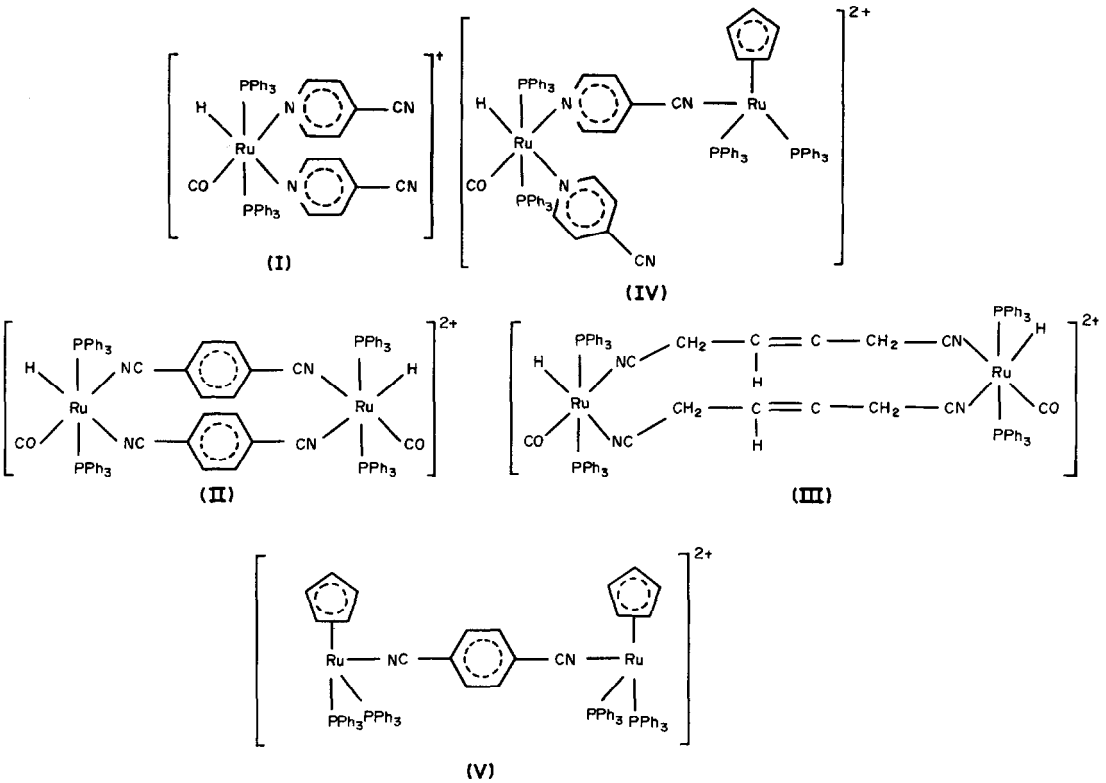

EPh_3 molecules have been shown to be *trans* to each other. This is based on the crystal structures of similar molecules determined previously.[9] On reacting these complexes with halogenated solvents like $CHCl_3$ or CH_2Cl_2 it appears that in the first product, viz. $[Ru(CO)Cl(EPh_3)(CNPy)]_2$, one of the two EPh_3 molecules and the hydride ion are substituted by Cl^- ions, and the two CNPy molecules form bridges with the two $[Ru(CO)Cl_2(EPh_3)]$ moieties. EPh_3, being strongly *trans* directing,[10] prefers to coordinate to the metal ion *trans* to a ligand having the weakest *trans* effect. Therefore in the presence of excess Cl^- ions (from $CHCl_3$ or CH_2Cl_2) one of the EPh_3 molecules (strong *trans*-directing) is labilized and is substituted by the chloride ion. In addition, it is generally observed that the hydride ion in many ruthenium hydride complexes is easily substituted by the chloride ion.[11] Thus the $[Ru(CO)Cl_2EPh_3]$ moiety could possibly be formed in the solution of the halogenated solvents, but we do not speculate any further on the mechanism of the reaction.

Based on the above spectral and analytical data it appears that the metal is coordinated in cyanopyridine mononuclear complexes (**I**) through the pyridine nitrogen, while in other complexes the coordination takes place through the CN groups. The above structures are therefore tentatively proposed for the reaction products.

REFERENCES

1. (a) R. A. Walton, *J. Inorg. Nucl. Chem.* 1966, **28**, 2229; (b) L. Elsayed and R. O. Ragsdale, *J. Inorg. Nucl. Chem.* 1961, **30**, 651; (c) I. Piljac and R. T. Iwamoto, *Inorg. Chem. Acta* 1969, **3**, 49; (d) F. Farha Jr and R. T. Iwamoto, *Inorg. Chem.* 1965, **4**, 844; (e) P. T. T. Wong and D. G. Brewer, *Can. J. Chem.* 1968, **46**, 131; (f) J. Nelson and S. M. Nelson, *J. Chem. Soc. A* 1969, 1597.
2. (a) G. S. Ashby, M. I. Bruce, I. B. Tomkins and R. C. Wallis, *Aust. J. Chem.* 1979, **32**, 1003; (b) W. C. Fultz, J. L. Burmeister, J. J. Macdougall and J. H. Nelson, *Inorg. Chem.* 1980, **19**, 1085, (c) N. G. Del V. Moreno, N. E. Katz, J. A. Olabe and P. J. Aymonino, *Inorg. Chim. Acta* 1979, **35**, 183.
3. N. Ahmad, J. J. Levison, S. D. Robinson and M. F. Uttley, *Inorganic Syntheses*, Vol. 15, p. 45. McGraw-Hill, New York (1974).
4. M. I. Bruce and N. J. Winsor, *Aust. J. Chem.* 1977, **30**, 1601.
5. (a) K. M. Rao, L. Mishra and U. C. Agarwala, *Polyhedron* 1986, **5**, 791; (b) K. M. Rao, L. Mishra and U. C. Agarwala, *Ind. J. Chem. A* 1987, **27**, 755.
6. A. Mishra and U. C. Agarwala, *J. Chem. Soc., Dalton Trans.* 1988, 2897.

7. D. S. Pandey and U. C. Agarwala, *Inorg. Chim. Acta* 1989, **159**, 197.
8. D. E. Richardson and H. Taube, *J. Am. Chem. Soc.* 1983, **105**, 51.
9. D. Mall and A. A. Taggart, *J. Chem. Soc.* 1965, 1359.
10. D. A. Snyder and W. L. Weaver, *J. Chem. Soc., Chem. Commun.* 1969, 1425.
11. (a) A. P. Humphries and S. A. R. Knox, *J. Chem. Soc., Dalton Trans.* 1975, 1710; (b) M. I. Bruce, M. G. Humphry, A. G. Swincer and R. G. Wallis, *Aust. J. Chem.* 1984, **37**, 1747.

Polyhedron Vol. 9, No. 17, pp. 2163–2169, 1990
Printed in Great Britain

0277-5387/90 $3.00+.00
© 1990 Pergamon Press plc

CYCLOPENTADIENYLRUTHENIUM COMPLEXES WITH SULPHUR DONOR LIGANDS–III.* COORDINATIVE ABILITY OF P,S-DONOR LIGANDS. X-RAY STRUCTURE OF $Ru(\eta\text{-}CH_3C_5H_4)(Ph_2PCSNPh)(PPh_3)$

ANGEL GUTIERREZ-ALONSO and LORETO BALLESTER-REVENTOS†

Departamento di Quimica Inorganica I, Facultad de Ciencias Quimicas, Universidad Complutense, 28040-Madrid, Spain

and

VIRGINIA PEREZ-GARCIA and CARIDAD RUIZ-VALERO

Laboratorio de Difracción de Rayos X, Facultad de Ciencias Quimicas, Universidad Complutense, 28040-Madrid, Spain

(*Received* 6 *March* 1990; *accepted* 2 *April* 1990)

Abstract—The phosphinothioformate ligands, $Ph_2PCS_2^-$ and $Ph_2PCSNPh^-$, react with $Ru(\eta^5\text{-}CH_3C_5H_4)ClL_2$ (L = PPh_3, dppe/2) and involve substitution of chlorine and bidentate coordination of the P,S-donor ligand to the metal in the triphenylphosphine complex. In the reaction of the dppe derivative only monodentate coordination has been observed. The crystal structure of $Ru(\eta^5\text{-}CH_3C_5H_4)(Ph_2PCSNPh)(PPh_3)$ has been determined.

In previous work[1,2] we have studied the interactions of 1,1-dithiolato ligands with the complexes $Ru(RCp)Cl(L)_2$‡ (R = H, CH_3, CH_3CO; L = PPh_3, dppe/2, CO). These reactions were characterized by the easy substitution of the chloride ligand, due to a labile Ru—Cl bond as has previously been reported.[3] In those reactions we found a competition between the donor character of the dithiolate, leading to bidentate S,S-complexes, and that of the phosphine that gives monodentate dithiolate complexes. We now report the reactions of $Ru(RCp)Cl(L)_2$ (L = PPh_3, dppe/2) with phosphinothiolate ligands that could be seen as intermediates between phosphines and dithiolates; in fact the ligands employed, $Ph_2PCS_2^-$ and $Ph_2PCSNPh^-$, usually have been found to be bonded bidentately to a metal via P and S in Ni[4] and Ir[5] complexes, respectively. The latter ligand, when neutral, i.e. $Ph_2PC(S)NHPh$, can also act as a typical phosphine, as in the complex $[Mo(Cp)Cl(CO)_2(Ph_2PCSNHPh)]$, with chelation by addition of base to form $[Mo(Cp)(Ph_2PCSNPh)(CO)_2]$.[6]

RESULTS AND DISCUSSION

The reaction of $Ru(RCp)Cl(PPh_3)_2$ (R = H, Me) with KPh_2PCS_2 or with $Ph_2PCSNHPh$ in the presence of excess NEt_3, affords the complexes $Ru(RCp)(P—S)(PPh_3)$ (**I–III**).

The IR spectra of these compounds show strong bands at 1130–1180 cm^{-1} for the $Ph_2PCS_2^-$ complexes and at 1585 cm^{-1} for the $Ph_2PCSNPh^-$ complex, attributed to the exocyclic $\nu(C{=}E)$, which indicates coordination via P—S to the metal[4] and formation of the cycle

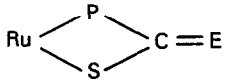

This coordination mode was confirmed by the ^{31}P NMR spectrum of **III**, which shows two doublets with a coupling constant of 36.5 Hz, indicating

* For Part II, see ref. 2.
† Author to whom correspondence should be addressed.
‡ RCp = $\eta^5\text{-}RC_5H_4$.

coordination by the phosphorus of the phosphinothioformamide ligand. The crystal structure of this complex (Fig. 1) also confirms this coordination.

The ^{1}H NMR spectrum of **I** shows one single resonance for the equivalent cyclopentadienyl protons, while that of **II** shows two resonances shifted to higher field, protons 2 and 5,[1] and lower field, protons 3 and 4, relative to **I**. On the other hand, complex **III** shows a set of four resonances for the non-equivalent cyclopentadienyl protons, as is expected for a chiral molecule.[7,8] The assignment of these resonances is not straightforward, but has been achieved in carbonylmethylcyclopentadienyliron complexes using NOE experiments,[7] determining protons 2 and 5, the *ortho* protons, as being responsible for the signals at the lowest and higher fields, with the peaks of 3 and 4 lying between them. This assignment is not a general one and there are many exceptions, even found by the same authors,[8,9] mainly with H(4) being more shielded than H(5); nevertheless it has always been observed that the separation between H(2) and H(5) is greater than that between H(3) and H(4), and the average of H(2) and H(5) lies at lower field than that of H(3) and H(4), as is observed in the M(RCp)(A)$_2$(B) type of complexes.[10]

We have not been able to obtain any conclusive data from the NOE spectra of compound **III**, where only small and inconclusive differences were observed, probably by consequence of the very small coupling between the protons which makes the signals appear as pseudo singlets. However, the ^{13}C NMR spectrum shows different signals for carbons 2–5. The first and the third resonances appear as doublets, probably by coupling with phosphorus. These two resonances can be assigned to C(2) and C(5), respectively, which lie over the two phosphorus atoms of the molecule, Fig. 2, and thus the other singlets correspond to C(3) and C(4). Assuming the same order for the proton resonances, the signals should correspond to H(2), 4.49 ppm; H(3), 4.14 ppm, H(5), 3.86 ppm; and H(4), 3.52 ppm. A similar pattern of signals for carbon and proton resonances has been found for Fe(MeCp)I(CO)(PR$_3$) using the same method of assignment as ours.[11]

The Ru(MeCp)Cl(dppe) complex reacts with $Ph_2PCS_2^-$ leading to unstable compounds which

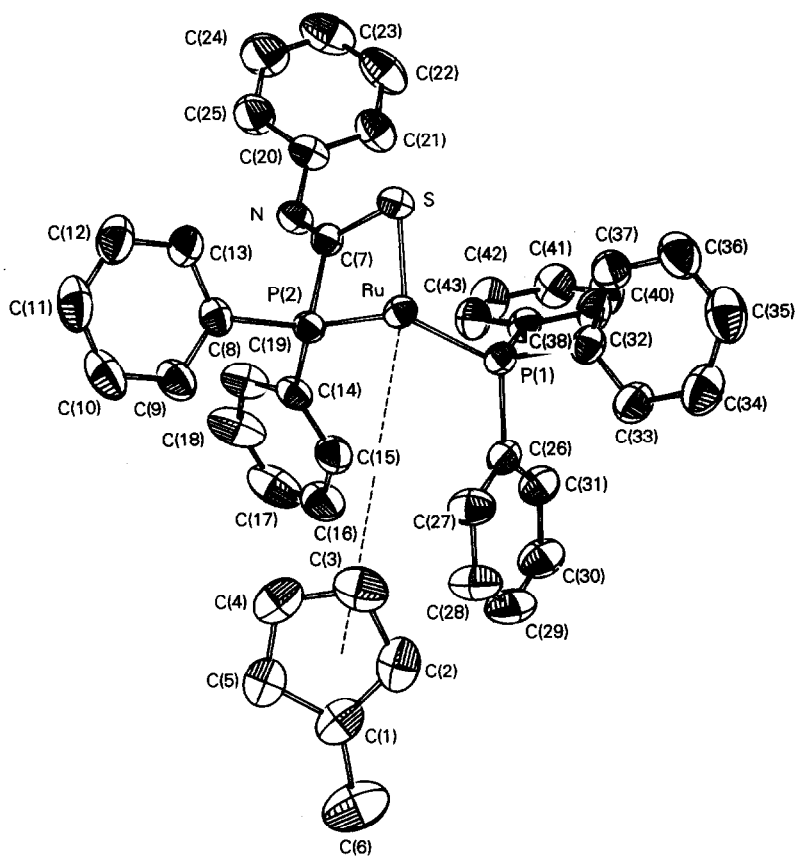

Fig. 1. ORTEP view of the structure of **III**.

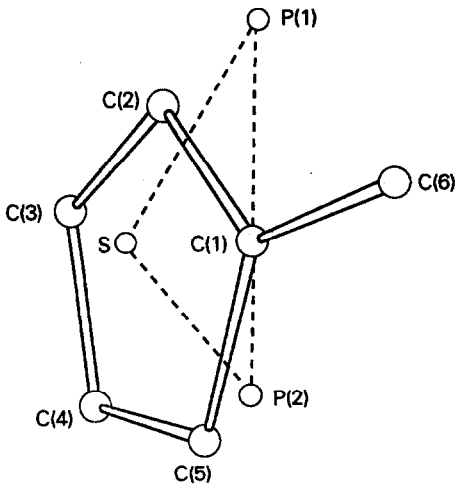

Fig. 2. Projection of the ring and the P(1)—P(2)—S planes of the molecule of **III**.

decompose before they can be isolated. However, the reaction with $Ph_2PCSNPh^-$ gives Ru(MeCp)($Ph_2PCSNPh$)(dppe) (**IV**) as an air-stable yellow solid, whose IR spectrum shows a ν(C=N) band shifted 60 cm^{-1} towards lower frequencies relative to that of complex **III**. There is also an additional band at 1185 cm^{-1}, which may be attributed to ν(C=S) for a phosphinothioformamide only bonded through the phosphorus and with a partial double C=S bond. This coordination mode is similar to that found for xanthates in their reaction with Ru(MeCp)Cl(dppe).[2] The ^{31}P NMR spectrum at 208 K seems to confirm the proposed coordination with a broad doublet at 92.2 ppm for the bidentate dppe and a triplet at 21.3 ppm (J = 76 Hz) for the coordinated phosphorus of $Ph_2PCSNPh^-$. The spectrum at room temperature shows only broad bands suggesting a kind of interchange in the molecule.

When the reaction between Ru(MeCp)Cl(PPh_3)$_2$ and $Ph_2PCSNHPh$ is carried out in toluene in the absence of base, the neutral ligand acts as a phosphine giving the complex Ru(MeCp)Cl(PPh_3)($Ph_2PCSHNPh$) (**V**), whose IR spectrum shows the ν(C=N) stretch at 1587 cm^{-1} and ν(C—S) at 934 cm^{-1}, with values similar to those found for the anionic bidentate phosphinothioformate, e.g. complex **III**. In addition to these bands which indicate a double C=N and a single C—S bond, also ν(Ru—Cl) = 286 cm^{-1} and a strong band at 2320 cm^{-1}, which should be attributed to a ν(S—H) stretch, appear, suggesting the displacement of the proton from the amido nitrogen to the sulphur:

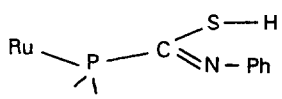

The proton bonded to the sulphur appears as a peak at 4.35 ppm in the ^1H NMR spectrum. This signal also diminishes in intensity when the sample is shaken with deuterated methanol, by interchange of the acidic thiol proton. As a chiral molecule, complex **V** also shows four signals for the cyclopentadienyl protons.

The ^{31}P NMR spectrum shows two doublets at 46.95 and 39.27 ppm (J = 46.4 Hz) for the two phosphorus atoms bonded to the metal. Physical data for all of these compounds are given in Table 1.

Crystal structure

Bond lengths and angles are given in Table 2; a view of the molecule is shown in Fig. 1.

The ruthenium atom is bonded to one sulphur atom, two phosphorus atoms and the cyclopentadienyl ring in the typical piano tool disposition. The five Ru—C bond lengths fall within the range found for individual Ru—C distances (2.16–2.26 Å)[12,13] in cyclopentadienyl ruthenium complexes. The five C—C distances in the ring are approximately equal, suggesting symmetrical coordination of the cyclopentadienyl ring. Both Ru—P distances are equal and fall in the usual range (2.2–2.4 Å).[14] The plane formed by P(1), P(2) and S is parallel to the cyclopentadienyl ring within an error of ±3°,[15] the phosphorus atom lying, respectively, below C(2) and C(5) (Fig. 2) and this fact may be responsible for the coupling observed in the ^{13}C NMR.

The phosphinothioformate ligand is coordinated to the ruthenium via P and S. Similar coordination has been observed for the closely related ligand (cyclo-C_6H_{11})$_2PCS_2$ in Ni(P—S)$_2$.[4]

The C—S distance is slightly shorter (0.05 Å) than that found for a single C—S bond[16] and the C—N distance is 0.15 Å shorter than N—Ph, reflecting a considerable double bond character in the C=N bond, partially delocalized over the C—S bond.

EXPERIMENTAL

All reactions were carried out under oxygen-free nitrogen. KPh_2PCS_2,[4] $Ph_2PCSNPh$,[17] Ru(Cp)Cl(PPh_3)$_2$,[18] Ru(MeCp)Cl(PPh_3)$_2$[1] and Ru(MeCp)Cl(dppe)[2] were prepared according to the published methods. Analyses were carried out by Elemental Microanalysis Ltd, Devon. IR spectra were taken on KBr pellets using a Perkin–Elmer 1330 spectrophotometer. ^1H, ^{13}C and ^{31}P NMR spectra were recorded on a Bruker WP80SY instru-

Table 1. Spectroscopic data for the complexes

	IR (cm^{-1})			^1H NMR (ppm)							^{31}P NMR	
					RC_5H_4							
	ν(C—S)	ν(C=X)	Others	Ph	H(2)	H(3)	H(4)	H(5)	*Me*Cp	Others	δ (ppm)	J_{PP} (Hz)
Ru(Cp)(Ph_2PCS)(PPh_3) (**I**)	1050s	1180s		7.4–7.0m	4.80	4.80	4.80	4.80				
Ru(MeCp)(Ph_2PCS_2)(PPh_3) (**II**)	1030s	1135s		7.3–7.0m	5.05	3.88	3.88	5.05	1.86s			
Ru(MeCp)($Ph_2PCSNPh$)(PPh_3) (**III**)	925m	1585s		7.9–7.0m	4.49	4.14	3.52	3.86	1.74s		54.06d 20.34d	36.5
Ru(MeCp)($Ph_2PCSNPh$)(dppe) (**IV**)	915w	1525s	1185m ν(C=S)	7.4–7.1m	4.65	3.40	3.40	4.65	1.83s	2.2sPC*H*$_2$	92.2d 21.3t	73
Ru(MeCp)Cl($Ph_2PCSNHPh$)(PPh_3) (**V**)	934m	1587s	2320 ν(S—H) 286m ν(Ru—Cl)	7.4–7.0m	4.54	4.23	3.05	3.88	1.93s	4.35s S*H*	46.95d 39.27d	46.4

ment in $CDCl_3$ solutions using TMS and 85% H_3PO_4 as standards.

Preparation of Ru(Cp)(Ph_2PCS_2)(PPh_3) (**I**)

To a refluxed suspension of Ru(Cp)Cl(PPh_3)$_2$ (0.74 g, 1 mmol) in 25 cm^3 of methanol, KPh_2PCS_2 (0.36 g) was added and the mixture was refluxed for 20 min. The solution was filtered and the solvent reduced to 5 cm^3 by concentration *in vacuo*. Addition of 2 cm^3 of Et_2O and cooling to $-20°C$ afforded a brown solid, recrystallized from chloroform–hexane. Yield 54%. Found: C, 62.4; H, 4.2. Required: C, 62.7; H, 4.4%.

Preparation of Ru(MeCp)(Ph_2PCS_2)(PPh_3) (**II**)

This complex was obtained using the same method as for **I**. Yield 68%. Found: C, 63.2; H, 4.5. Required: C, 63.1; H, 4.6%.

Preparation of Ru(MeCp)($Ph_2PCSNPh$)(PPh_3) (**III**)

A suspension of Ru(MeCp)Cl(PPh_3)$_2$ (0.75 g), $Ph_2PCSNHPh$ (0.38 g) and NEt_3 (0.1 cm^3) in 25 cm^3 of methanol was refluxed for 15 min. After cooling to room temperature, the solvent was removed *in vacuo* and the solid was recrystallized from chloroform–hexane to give orange crystals of **III**. Yield 84%. Found: C, 68.0; H, 4.9; N, 2.0. Required: C, 67.7; H, 4.9; N, 1.8%.

Preparation of Ru(MeCp)($Ph_2PCSNPh$)(dppe) (**IV**)

A suspension of Ru(MeCp)Cl(PPh_3)$_2$ (0.62 g), $Ph_2PCSNPh$ (0.38 g) and NEt_3 (0.1 cm^3) in 30 cm^3 of methanol was refluxed for 5 h. The resulting solution was concentrated *in vacuo* to 10 cm^3 and 5 cm^3 of Et_2O were added. The white precipitate that appears was filtered off and the solution was concentrated to 5 cm^3 and 2 cm^3 of degassed water were added. The yellow solid was recrystallized from dichloromethane–hexane. Yield 64%. Found: C, 68.2; H, 5.3; N, 1.7. Required: C, 68.1; H, 5.2; N, 1.6%.

Preparation of Ru(MeCp)Cl($Ph_2PCSHNPh$)(PPh_3) (**V**)

A solution of Ru(MeCp)Cl(PPh_3)$_2$ (0.74 g) and $Ph_2PCSNHPh$ (0.76 g) in 30 cm^3 of toluene was refluxed for 2 h. The solution was then concentrated *in vacuo* to one third of the volume and 10 cm^3 of Et_2O were added. The solid that appeared was filtered off and the clear solution was evaporated to dryness. Extraction with dichloromethane (10 cm^3)

and addition of 15 cm^3 of Et_2O–hexane (1:2 in volume) afforded orange microcrystals of **V**. Yield 71%. Found: C, 63.7; H, 4.7; N, 1.8. Required: C, 64.6; H, 4.7; N, 1.7%.

X-ray crystal structure

The crystal data and the parameters used during the collection and refinement of the diffraction data are summarized in Table 3. A red crystal was mounted on the diffractometer and the cell dimensions were refined by a least-squares fit of the θ values of 25 reflections. The intensities were corrected for Lorentz and polarization dispersion.

Scattering factors for neutral atoms and anomalous dispersion corrections for ruthenium and phosphorus were taken from the *International Tables for X-ray Crystallography*.[19]

The structure was solved by Patterson and Fourier methods, and an empirical absorption correction[20] was applied at the end of the isotropic refinement.

The final refinement was made with anisotropic thermal motion for the non-hydrogen atoms and

Table 2. Bond distances (Å) and angles (°) with ESDs in parentheses

Ru—C(1)	2.244(6)	C(14)—C(15)	1.380(7)
Ru—C(2)	2.231(6)	C(14)—C(19)	1.384(7)
Ru—C(3)	2.197(6)	C(15)—C(16)	1.401(9)
Ru—C(4)	2.203(5)	C(16)—C(17)	1.368(10)
Ru—C(5)	2.231(5)	C(17)—C(18)	1.369(9)
Ru—P(1)	2.299(1)	C(18)—C(19)	1.390(9)
Ru—P(2)	2.295(1)	C(20)—C(21)	1.384(8)
Ru—S	2.401(2)	C(20)—C(25)	1.366(8)
P(1)—C(26)	1.840(5)	C(21)—C(22)	1.386(8)
P(1)—C(32)	1.832(5)	C(22)—C(23)	1.365(9)
P(1)—C(38)	1.837(5)	C(23)—C(24)	1.342(11)
P(2)—C(7)	1.841(4)	C(24)—C(25)	1.384(9)
P(2)—C(8)	1.828(5)	C(26)—C(27)	1.386(7)
P(2)—C(14)	1.831(5)	C(26)—C(31)	1.386(7)
S—C(7)	1.762(5)	C(27)—C(28)	1.385(7)
N—C(7)	1.263(6)	C(28)—C(29)	1.370(9)
N—C(20)	1.413(6)	C(29)—C(30)	1.369(9)
C(1)—C(2)	1.397(8)	C(30)—C(31)	1.385(7)
C(1)—C(5)	1.429(7)	C(32)—C(33)	1.376(7)
C(1)—C(6)	1.483(8)	C(32)—C(37)	1.406(7)
C(2)—C(3)	1.424(8)	C(33)—C(34)	1.386(9)
C(3)—C(4)	1.411(9)	C(34)—C(35)	1.380(10)
C(4)—C(5)	1.420(8)	C(35)—C(36)	1.368(8)
C(8)—C(9)	1.381(7)	C(36)—C(37)	1.378(9)
C(8)—C(13)	1.393(7)	C(38)—C(39)	1.391(7)
C(9)—C(10)	1.390(8)	C(38)—C(43)	1.383(7)
C(10)—C(11)	1.374(9)	C(39)—C(40)	1.381(8)
C(11)—C(12)	1.371(9)	C(40)—C(41)	1.363(9)
C(12)—C(13)	1.378(7)	C(41)—C(42)	1.369(8)
		C(42)—C(43)	1.382(8)

P(2)—Ru—S	72.14(6)	C(14)—C(15)—C(16)	119.4(6)
P(1)—Ru—S	93.11(6)	C(15)—C(16)—C(17)	120.3(6)
P(1)—Ru—P(2)	101.5(6)	C(16)—C(17)—C(18)	120.3(7)
Ru—P(1)—C(38)	122.9(2)	C(17)—C(18)—C(19)	120.2(6)
Ru—P(1)—C(32)	109.9(2)	C(14)—C(19)—C(18)	119.9(5)
Ru—P(1)—C(26)	117.9(2)	N—C(20)—C(25)	117.6(5)
C(32)—P(1)—C(38)	101.6(2)	N—C(20)—C(21)	123.1(5)
C(26)—P(1)—C(38)	100.8(3)	C(21)—C(20)—C(25)	119.1(5)
C(26)—P(1)—C(32)	100.5(2)	C(20)—C(21)—C(22)	119.0(5)
Ru—P(2)—C(14)	133.4(2)	C(21)—C(22)—C(23)	121.2(7)
Ru—P(2)—C(8)	112.4(2)	C(22)—C(23)—C(24)	119.4(6)
Ru—P(2)—C(7)	94.4(2)	C(23)—C(24)—C(25)	120.9(7)
C(8)—P(2)—C(14)	101.1(2)	C(20)—C(25)—C(24)	120.4(6)

continued

Table 2—*continued*

C(7)—P(2)—C(14)	108.1(2)	P(1)—C(26)—C(31)	122.7(4)
C(7)—P(2)—C(8)	104.1(2)	P(1)—C(26)—C(27)	119.1(4)
Ru—S—C(7)	93.0(2)	C(27)—C(26)—C(31)	118.2(5)
C(7)—N—C(20)	123.6(4)	C(26)—C(27)—C(28)	121.2(5)
C(5)—C(1)—C(6)	126.9(5)	C(27)—C(28)—C(29)	119.5(6)
C(2)—C(1)—C(6)	124.8(5)	C(28)—C(29)—C(30)	120.4(6)
C(2)—C(1)—C(5)	108.3(5)	C(29)—C(30)—C(31)	120.2(6)
C(1)—C(2)—C(3)	108.5(5)	C(26)—C(31)—C(30)	120.5(5)
C(2)—C(3)—C(4)	107.6(5)	P(1)—C(32)—C(37)	118.4(4)
C(3)—C(4)—C(5)	108.4(5)	P(1)—C(32)—C(33)	123.5(4)
C(1)—C(5)—C(4)	107.2(5)	C(33)—C(32)—C(37)	118.1(5)
S—C(7)—N	134.1(4)	C(32)—C(33)—C(34)	121.1(6)
P(2)—C(7)—N	125.5(4)	C(33)—C(34)—C(35)	120.0(6)
P(2)—C(7)—S	100.3(2)	C(34)—C(35)—C(36)	119.9(6)
P(2)—C(8)—C(13)	121.3(4)	C(35)—C(36)—C(37)	120.5(6)
P(2)—C(8)—C(9)	118.8(4)	C(32)—C(37)—C(36)	120.5(5)
C(9)—C(8)—C(13)	119.6(5)	P(1)—C(38)—C(43)	119.3(4)
C(8)—C(9)—C(10)	120.0(6)	P(1)—C(38)—C(39)	122.7(4)
C(9)—C(10)—C(11)	119.8(6)	C(39)—C(38)—C(43)	117.8(4)
C(10)—C(11)—C(12)	120.5(6)	C(38)—C(39)—C(40)	120.2(5)
C(11)—C(12)—C(13)	120.2(6)	C(39)—C(40)—C(41)	121.2(5)
C(8)—C(13)—C(12)	119.9(5)	C(40)—C(41)—C(42)	119.5(5)
P(2)—C(14)—C(19)	120.3(4)	C(41)—C(42)—C(43)	120.0(5)
P(2)—C(14)—C(15)	119.7(4)	C(38)—C(43)—C(42)	121.4(5)
C(15)—C(14)—C(19)	120.0(5)		

Table 3. Crystal and refinement data

Formula	$RuP_2SNC_{43}H_{38}$
Crystal system	Monoclinic
Space group	$P2_1/c$
a (Å)	10.274(3)
b (Å)	17.887(4)
c (Å)	20.489(4)
β (°)	103.21(5)
V (Å^3)	3666(2)
ρ (calc.) (g cm^{-3})	1.38
Temperature (°C)	22
μ (cm^{-1})	5.90
Crystal dimensions (mm)	$0.35 \times 0.44 \times 0.30$
Diffractometer	Enraf-Nonius CAD4
Radiation	Graphite-monochromated Mo-K_α ($\lambda = 0.71096$ Å)
Scan technique	ω–2θ
Data collected	$(-13, 0, 0)$ (13, 22, 26)
Reflections collected	8234
Unique data	7961
Unique data (I) $\geqslant 2\sigma(I)$	5237
R(int) (%)	1.2
Standard reflections	3/135 reflections
Decay	$\leqslant$ 3% variation
R_F (%)	3.0
Rw_F (%)	4.4
Average shift/error	0.007
Average absorption correction	0.971

fixed isotropic temperature factors and calculated coordinates for hydrogen atoms.†

Most of the calculations were carried out with the XRAY80 system.[21]

Acknowledgement—We thank the Comisión Interministerial de Ciencia y Tecnología (Project PS87-0028) for financial support.

REFERENCES

1. L. Ballester and A. Gutierrez, *J. Organomet. Chem.* 1986, **309**, 179.
2. A. Gutierrez and L. Ballester, *J. Organomet. Chem.* 1988, **339**, 249.
3. R. J. Haines and A. L. du Preez, *J. Organomet. Chem.* 1975, **84**, 357.
4. J. Kopf, R. Lenck, S. N. Olafsson and R. Krsmolowsky, *Angew. Chem. Int. Edn Engl.* 1976, **15**, 12; 768.
5. D. H. M. W. Thewissen, H. P. M. M. Ambrosius, H. L. M. Van Gaal and J. J. Steggerda, *J. Organomet. Chem.* 1980, **192**, 101.
6. H. P. M. M. Ambrosius, A. H. I. M. Van der Linden and J. J. Steggerda, *J. Organomet. Chem.* 1980, **204**, 211.
7. P. Johnston, M. S. Loonat, W. L. Ingham, L. Carlton and N. J. Coville, *Organometallics* 1987, **6**, 2121.
8. J. du Toit, D. C. Levendis, J. C. A. Boeyens, M. S. Loonat, L. Carlton, W. Pickl and N. J. Coville, *J. Organomet. Chem.* 1989, **368**, 339.
9. M. S. Loonat, L. Carlton, J. C. A. Boeyens and N. J. Coville, *J. Chem. Soc., Dalton Trans.* 1989, 2407.
10. A. Eisenberg, A. Shaver and T. Tsutsui, *J. Am. Chem. Soc.* 1980, **102**, 1416.
11. L. Carlton, P. Johnston and N. J. Coville, *J. Organomet. Chem.* 1988, **339**, 339.
12. M. I. Bruce, F. S. Wong, B. W. Skelton and A. H. White, *J. Chem. Soc., Dalton Trans.* 1981, 1398.
13. H. Adams, N. A. Bayley and C. White, *Inorg. Chem.* 1983, **22**, 1155.
14. L. J. Guggenberger, *Inorg. Chem.* 1973, **12**, 1317.
15. M. Nardelli, A. Musatti, P. Domiano and G. D. Andreetti, *Ric. Sci. Parte 2: Sez. A* 1965, **8**, 807.
16. G. Bandoli, G. Bartolozzo, D. A. Clemente, U. Croatto and C. Panattoni, *J. Chem. Soc. A* 1970, 2778.
17. K. Issleib and G. H. Harzfeld, *Chem. Ber.* 1964, **97**, 3430.
18. M. I. Bruce and N. J. Windsor, *Aust. J. Chem.* 1977, **30**, 1601.
19. *International Tables for X-ray Crystallography*, Vol. IV, pp. 72–98. Kynoch Press, Birmingham (1974).
20. N. Walker and D. Stuart, *Acta Cryst.* 1983, **A39**, 158.
21. J. M. Stewart, The XRAY80 System. Computer Science Center, University of Maryland, College Park (1985).

† *Supplementary material available.* Tables of fractional coordinates, thermal parameters and observed and calculated structure factors have been deposited with the Editor and with the Cambridge Crystallograhic Data Centre.

Polyhedron Vol. 9, No. 17, pp. 2171–2173, 1990
Printed in Great Britain

0277-5387/90 $3.00+.00
© 1990 Pergamon Press plc

A STUDY OF THE INTERACTION OF DI-μ-PHENOXOBIS(DICHLOROPHENOXO)MOLYBDENUM(V) WITH ALIPHATIC AMINES

K. C. MALHOTRA, S. C. CHAUDHRY, A. V. S. RAJA RAO and NEERAJ SHARMA*

Department of Chemistry, Himachal Pradesh University, Summer Hill, Shimla-171005, India

(*Received* 4 *October* 1989; *accepted* 2 *April* 1990)

Abstract—The compound $[MoCl_2(OC_6H_5)_3]_2$ reacts with various aliphatic amines such as *n*-propylamine, *n*-butylamine, *sec*-butylamine, *t*-butylamine, diethylamine, di-isopropylamine and triethylamine under different experimental conditions to give complexes of 1 : 1 stoichiometry. The complexes have been characterized by elemental analysis, conductance measurements, molecular weight determinations and IR spectral studies. An octahedral configuration is proposed for all the complexes.

Transition metal halides are known to react with amines giving solvolytic, aminolysed or simple addition compounds depending upon experimental conditions such as temperature, concentration and the nature of the solvent used.[1-3] Edwards and Fowles[4] have reported the aminolysis of the Mo—Cl bond in the reactions of $MoCl_5$ with primary and secondary amines, while simple addition compounds are formed with tertiary amines. It was therefore of interest to investigate the reactions of $[MoCl_2(OC_6H_5)_3]_2$ (**I**) with amines under different experimental conditions.

EXPERIMENTAL

Compound **I** was prepared by the reported method.[5] The molybdenum content in the complexes was determined as bis(8-hydroxyquinolinol)dioxomolybdenum(VI). Chloride was estimated by Volhard's method and amines by steam distillation with alkali and titration of the distillate with sulphuric acid using Bromophenol blue.

IR spectra were recorded as KBr discs as well as in Nujol mulls on Perkin–Elmer 337 and 621 spectrophotometers. Molecular weights were determined cryoscopically in benzene.

The different conditions under which compound **I** was reacted with amines are:

(i) Compound **I** suspended in CCl_4 was reacted with amines in a 1 : 2 molar ratio with continuous stirring at room temperature for about 8 h. The compounds were isolated by the addition of petroleum ether.
(ii) An excess of amine was added to **I** suspended in CCl_4 and a clear solution was immediately obtained at room temperature. After about 8 h stirring, excess base was distilled off and the residue was extracted with petroleum ether.
(iii) Compound **I** in CCl_4 was refluxed with amine in a 1 : 2 molar ratio for about 8 h. Solvent was distilled off and the residue was extracted with petroleum ether.
(iv) Lastly, compound **I** was reacted directly with excess amine without using any solvent and refluxed. Excess base was distilled off, followed by addition of petroleum ether to obtain the product.

RESULTS AND DISCUSSION

The complexes of **I** isolated with different amines are given in Table 1. They are hygroscopic in character, non-electrolytes and monomers in nitrobenzene as is evident from the data in Table 1, which shows that an increase in amine concentration causes no base-catalysed elimination of

* Author to whom correspondence should be addressed.

Table 1. Analytical data and IR spectral data (cm^{-1}) for the complexes of $[MoCl_2(OC_6H_5)_2]_2$ with amines

Complex	% Found(Calc.) Mo	Cl	Λ_M in nitrobenzene (Ω^{-1} cm^2 mol^{-1})	Molecular weight Found (Calc.)	ν(N—H)	ν(C—N)	ν(Mo—O)	ν(Mo—Cl)	ν(Mo—N)
$MoCl_2(OC_6H_5)_3 \cdot n$-propylamine	18.9 (19.0)	13.8 (14.0)	2.2	492 (505)	3390	1040	515	340 336	308
$MoCl_2(OC_6H_5)_3 \cdot n$-butylamine	18.4 (18.4)	13.6 (13.6)	2.6	498 (520)	3382	1038	508	332	310
$MoCl_2(OC_6H_5)_3 \cdot sec$-butylamine	18.5 (18.4)	13.7 (13.6)	1.2	—	3370	1030	510	318 (324)	305
$MoCl_2(OC_6H_5)_3 \cdot t$-butylamine	18.4 (18.4)	13.5 (13.6)	2.1	—	3460	1130	502	342	302
$MoCl_2(OC_6H_5)_3 \cdot$diethylamine	18.5 (18.4)	13.5 (13.6)	2.5	490 (520)	3445	1125	506	345	300
$MoCl_2(OC_6H_5)_3 \cdot$di-isopropylamine	17.4 (17.5)	13.0 (12.9)	1.7	535 (547)	—	1160	512	350	308
$MoCl_2(OC_6H_5)_3 \cdot$triethylamine	17.4 (17.5)	12.8 (12.9)	3.1	525 (548)	3385	1035	505	325	315

hydrogen chloride and forms only 1:1 addition compounds. Even heating the reactants in the presence or absence of any solvent under reflux did not change the nature of the product formed. These observations are in contrast to those of Edwards and Fowles[4] and others, but in agreement with those of Colclough and co-workers[6,7] who have prepared a variety of addition compounds of aryloxides of boron(III) with different amines.

In the IR spectra of the complexes, sharp bands at *ca* 510–520 cm^{-1} have been assigned to terminal ν(Mo—O) modes. No band that could be assigned to bridging Mo<O>Mo modes has been observed in the IR spectra which suggests a breakdown of the dimeric structure of the title compound (**I**) on adduct formation. Splitting of the bands in the region 340–350 cm^{-1} assigned to the ν(Mo—Cl) modes[8] suggests that chlorine atoms in the adducts are in the *cis*-position in an octahedral environment. Coordination of amines to the metal has been further confirmed by the appearance of new bands around 300–310 cm^{-1} assigned to ν(Mo ← N) modes.[9] All the important bands are given in Table 1.

The most significant changes which have been observed in the IR spectra of the different amines on adduct formation with **I** concern the ν(N—H), ν(C—N) and H—N—C deformation modes. The trends in shifts of these bands on coordination with metal are in agreement with those earlier reported.[10–13] A significant positive shift of the H—N—C deformation mode in primary and secondary amines has been attributed to additional hydrogen bonds between the hydrogen of the N—H group and the chlorine of **I**. Similar observations have been made in the complexes of diaryl tin dihalides with diethylamine.[14] Thus, based upon limited analytical and spectroscopic data, it is proposed that the complexes of **I** with amines are mononuclear 1:1 adducts with an octahedral arrangement around molybdenum and no evidence for aminolysis has been obtained.

REFERENCES

1. M. Antler and A. W. Laubengayer, *J. Am. Chem. Soc.* 1955, **77**, 5250.
2. W. R. Trost, *Can. J. Chem.* 1952, **30**, 835.
3. G. W. A. Fowles and C. M. Pleass, *J. Chem. Soc.* 1957, 1674.
4. D. A. Edwards and G. W. A. Fowles, *J. Chem. Soc.* 1961, 24.
5. A. Rosenheim and C. Nernst, *Z. Anorg. Chem.* 1933, **214**, 209.
6. T. Colclough, W. Gerrad and M. F. Lappert, *J. Chem. Soc.* 1955, 907.

7. T. Colclough, W. Gerrad and M. F. Lappert, *J. Chem. Soc.* 1966, 3006.
8. A. Sabitini and I. Bertini, *Inorg. Chem.* 1966, **5**, 204.
9. K. S. Nagaraja and M. R. Udupa, *Ind. J. Chem.* 1983, **22A**, 531.
10. H. J. Bernstein, *Spectrochim. Acta* 1962, **18**, 161.
11. J. E. Stewart, *J. Chem. Phys.* 1959, **30**, 1259.
12. L. K. Dyall and J. E. Kemp, *Spectrochim. Acta* 1966, **22**, 467.
13. A. J. Moritz, *Spectrochim. Acta* 1960, **16**, 1176.
14. T. Tanaka, M. Komura, Y. Kawasaki and Okawara, *J. Organomet. Chem.* 1964, **1**, 484.

Polyhedron Vol. 9, No. 17, pp. 2175–2176, 1990
Printed in Great Britain

0277–5387/90 $3.00+.00
© 1990 Pergamon Press plc

COMMUNICATION

PREPARATION OF URANIUM TRIBROMIDE BY THERMAL VACUUM DECOMPOSITION OF $NH_4UBr_4 \cdot 1.5CH_3CN \cdot 6H_2O$

E. ZYCH and J. DROŻDŻYŃSKI*

Institute of Chemistry, University of Wrocław, 50-383 Wrocław, Poland

(*Received* 29 *March* 1990; *accepted* 26 *April* 1990)

Abstract—Pure uranium tribromide may be prepared by applying an effective non-static high vacuum of 10^{-5}–10^{-6} hPa over the temperature range 20 to 350°C to $NH_4UBr_4 \cdot 1.5CH_3CN \cdot 6H_2O$.

The most frequently recommended procedure for the preparation of UBr_3 involves the action of gaseous hydrogen bromide on finely powdered uranium or uranium hydride at 300°C.[1,2] This method is suitable also for large scale preparation but requires a somewhat complex apparatus. Other convenient methods are based on reduction of UBr_4 with metallic zinc or finally divided uranium at *ca* 600°C.[2] Since uranium tribromide is very sensitive to oxidation and hydrolysis and at higher temperatures reacts with silica, the preparative procedures need to be performed in tantalum or molybdenum installations under strict moisture- and oxygen-free conditions. All methods also involve very pure starting materials.

This paper describes a convenient method for the preparation of uranium tribromide by thermal vacuum decomposition of $NH_4UBr_4 \cdot 1.5CH_3CN \cdot 6H_2O$. The procedure does not require pure preparative materials and seems to be very suitable in cases where only gram amounts of the compound are needed.

For the preparation of the complex bromide uranium tetrabromide (4–4.4 g) was added on shaking to a mixture of 100 cm^3 of methyl cyanide with an excess of ammonium bromide and left standing for 10–15 h. Subsequently, 0.5 cm^3 of propionic acid, 0.4 cm^3 of water and after 0.5 h 15 cm^3 of freshly distilled ether, were added. Next, the filtered solution was reduced in an inert atmosphere by gently shaking with liquid zinc amalgam. The reduction resulted in a colour change of the solution from green to dark brown followed by the immediate formation of a fine, crystalline, greyish-green precipitate of the formula $NH_4UBr_4 \cdot 1.5CH_3CN \cdot 6H_2O$. The precipitate was filtered off, washed under an inert atmosphere with a deoxygenated 7:1:0.05 mixture of acetonitrile, ether and propionic acid, and afterwards, with ethyl ether. Finally, the compound was dried under reduced pressure for about 5 min and stored in sealed tubes at temperatures below 15°C. As for most uranium(III) compounds it must be handled under anhydrous and oxygen-free conditions.

The synthesis was performed in a relatively simple all-glass apparatus with provisions for precipitation, filtration and drying in an inert atmosphere.[3] The inert atmosphere was obtained by vacuum evaporation of the solution and wash-liquids for 1–2 min. The synthesis may also be performed in an inert atmosphere glove-box as well as by using a set of Schlenk tubes.

The preparation of uranium tetrabromide was based on the procedure given in ref. 4. Since the required compound could be of technical grade the method was significantly simplified. The product was obtained by passing bromine vapour in dry, oxygen-free nitrogen over a carbon–uranium oxide mixture placed in a quartz tube, at 700–800°C. Other reagents were of analytical grade. The physical and chemical properties of $NH_4UBr_4 \cdot 1.5CH_3CN \cdot 6H_2O$ will be given elsewhere.[5]

The complex bromide obtained in the above

* Author to whom correspondence should be addressed.

manner was converted into UBr_3 by a thermal high vacuum decomposition. For this purpose $NH_4UBr_4 \cdot 1.5CH_3CN \cdot 6H_2O$ (1–4 g) was placed in the bottom of the sealed-off end of a quartz tube, 40 cm long and 2 cm in diameter. The other end of the tube was fitted with a stopcock and connected to a high vacuum system. A small furnace was slipped over the tube and the system was pumped off to *ca* 10^{-6} hPa. The decomposition was first accomplished between 25 and 80°C for at least 2–3 h and then, the temperature was slowly raised to *ca* 350°C. The pressure should never be higher than *ca* 5×10^{-4} hPa. Samples of UBr_3 prepared in this manner are pale brown in colour. In order to obtain larger crystals, the section of the tube containing the product was sealed off and heated at 400°C for a couple of days. The pycnometrically determined density of the compound approaches 6.20 g cm^{-3} and is somewhat better than those reported in the literature.[2] From X-ray data[2] a value of 6.4 g cm^{-3} was obtained. Found: U, 50.1; Br, 50.3. Calc. for UBr_3: U, 49.8; Br, 50.2%.

REFERENCES

1. F. H. Spedding, A. S. Newton, R. Nottorf, J. Powell and V. Calkins, U.S. At. Energy Comm. TID-5290, Book 1, pp. 91–119 (1958).
2. D. Brown, Compounds of Uranium with Chlorine, Bromine and Iodine, in *Gmelin Handbook of Inorganic Chemistry*, Uran Suppl. Vol. C9, p. 1. Springer, Berlin (1981).
3. J. Drożdżyński, *Inorg. Chim. Acta* 1979, **32**, L83.
4. F. Hein and S. Herzog, in *Handbook of Preparative Inorganic Chemistry* (Edited by G. Brauer), p. 1440. Academic Press, New York (1965).
5. E. Zych and J. Drożdżyński, *J. Less-Common Met.* **161** (1990).

Polyhedron Vol. 9, No. 17, pp. 2177–2179, 1990
Printed in Great Britain

0277–5387/90 $3.00+.00
© 1990 Pergamon Press plc

COMMUNICATION

ALKALINE HYDROLYSIS OF LINEAR TETRA-, HEXA- AND OCTAPHOSPHATE

GENICHIRO KURA

Department of Chemistry, Fukuoka University of Education, Akama, Munakata, Fukuoka 811-41, Japan

(*Received* 5 *April* 1990; *accepted* 7 *June* 1990)

Abstract—The hydrolysis rates for the linear tetra-, hexa- and octaphosphate in several alkaline solutions have been determined. The hydrolysis reaction takes place most rapidly in LiOH solution. Activation energies of the linear polyphosphates in 1 M $(CH_3)_4NOH$ were higher than those for the cyclic oligomers with a similar polymerization degree.

Inorganic condensed phosphate polymers are one of the most commonly used materials in solution and solid-state chemistry.[1] These polymers consist mainly of the linear and cyclic phosphates. The structures of cyclo-octaphosphate and linear octaphosphate are shown in Fig. 1. We have studied the chemistry of oligomers with a polymerization degree smaller than about eight.[2–4] In this paper, the hydrolysis reaction of linear tetra-, hexa- and octaphosphates in alkaline solutions were investigated. These linear oligomers are very interesting materials for solution chemistry and their stability in aqueous solutions against hydrolysis must be known.

Since the preparative methods of the hexa- and octaphosphate in macro quantity have not been reported, the sample solutions to be hydrolysed were prepared by the partial hydrolysis of cyclo-hexa- and cyclo-octaphosphate. To prepare sample solutions which contain adequate quantities of linear hexamer or octamer, cyclo-hexa- or cyclo-octaphosphate were hydrolysed in 0.5 M LiOH at 40°C for about 7–9 h and the reactions were stopped by neutralization with HCl. The Li^+ ions contained in the sample solutions in the quantities prepared by the above procedure have been known to affect strongly the hydrolysis rates.[5] Thus, the Li^+ ions in the hydrolysis samples were converted to $(CH_3)_4N^+$ ions by the use of ion-exchange resins. The linear tetraphosphate was prepared as the ammonium salt by the method of Griffith.[6] Analyses of the parent phosphates and the hydrolysis products were performed using automated liquid chromatography.[7] In the analysis of the hydrolysis rates of hexa- and octaphosphates, the concentration of the corresponding cyclo-polyphosphates and the linear

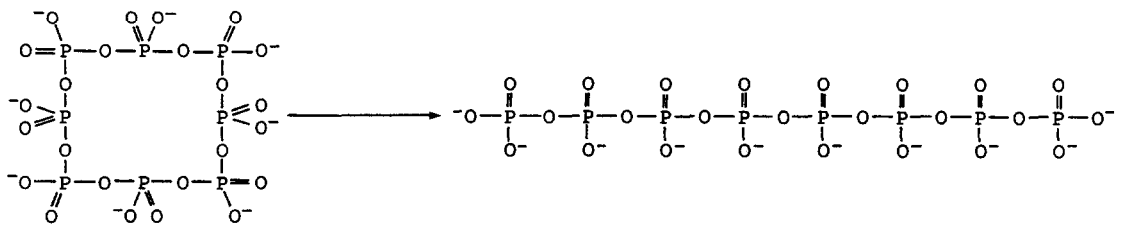

$P_8O_{24}^{8-}$ (P_{8m}) $P_8O_{25}^{10-}$ (P_8)

Fig. 1. The structures of cyclo-octaphosphate and linear octaphosphate.

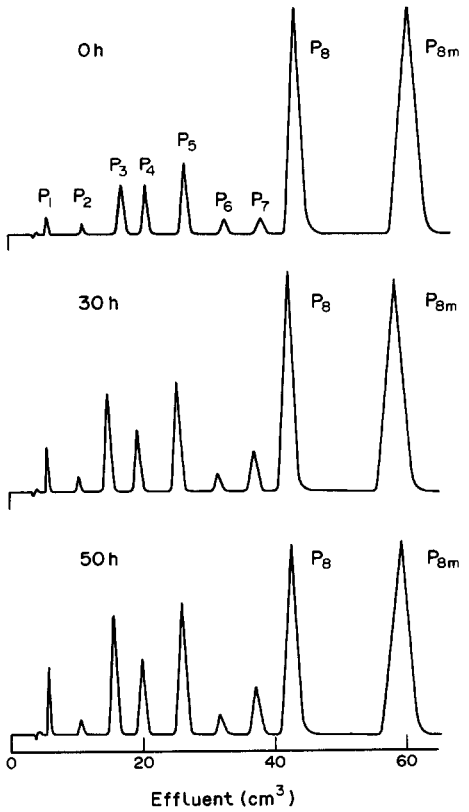

Fig. 2. Chromatograms of the hydrolysis samples in 0.5 M KOH at 50°C.

polyphosphates as the first hydrolysis product at time t are defined as x and y, respectively, and also their first-order rate constants are designated as k_m and k_n, respectively. The hydrolysis rate constant of hexa- or octaphosphates, k_n, can be obtained by solving the following differential equations:[7]

$$-dx/dt = k_m x \quad (1)$$

$$-dy/dt = k_n y - k_m x. \quad (2)$$

The chromatograms of the hydrolysis samples of octaphosphate in 0.5 M KOH at 50°C are shown in Fig. 2. In this paper, cyclic and linear oligomers are abbreviated as P_n and P_{nm}, in which n is the polymerization degree. The rate constant, k_n, was estimated by successive approximation involving substitution of the initial value of x and y, and k_m which had been already determined by the separate experiments in eq. (2). In Fig. 3, the time dependence of the concentration of octaphosphate is shown, where the curved line was drawn by substituting k_m and k_n into eq. (2) and the experimental points are indicated by black circles. The coincidence of both values is satisfactory. The hydrolysis rates in alkaline solutions have been known to be markedly affected not only by OH^- concentration

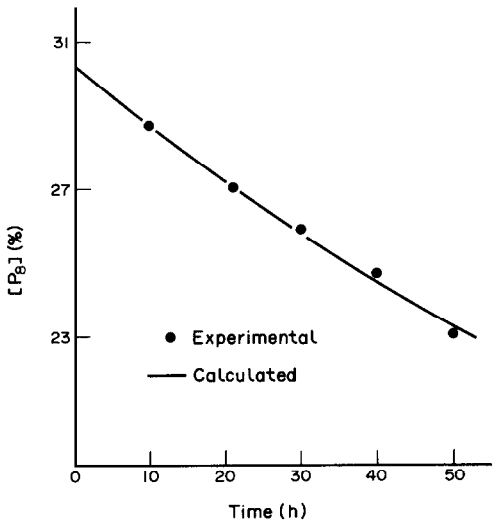

Fig. 3. Variation of the concentration of octaphosphate with time in 0.5 M KOH at 50°C.

but by the counter ion of OH^-.[8] The effect of the counter ions, Li^+, Na^+ and K^+, on the hydrolysis rates of linear tetra-, hexa- and octaphosphates at $[OH^-] = 0.5$ M were also examined. In Table 1, rate constants in each alkaline solution at 50°C are shown. For every linear phosphate, the hydrolysis reaction takes place most rapidly in 0.5 M LiOH and the reaction rate decreases in the order, LiOH > NaOH > KOH. In every alkaline solution, the hydrolysis rate decreases with decreasing polymerization degree, i.e. $P_8 > P_6 > P_4$. The Li^+ ions accelerate the hydrolysis rates the most and thus interact most strongly with linear phosphate anions. Next, the hydrolysis rates in $(CH_3)_4NOH$ were measured, where the $(CH_3)_4N^+$ ion is known to be an inert cation which does not interact with many anions. In this solution, the hydrolysis reactions of linear oligomers were very slow, thus the rates in 1.00 M $(CH_3)_4NOH$ and at relatively higher temperatures, i.e. 70, 80 and 90°C were determined. However, since the rates for tetraphosphate were very slow, taking into account the experimental error, only the rate at 90°C was measured. The rate constants obtained are shown in Table 2. Tetra-

Table 1. Hydrolysis rate constants of linear phosphates at 50°C

	k_n (h^{-1})		
	P_4	P_6	P_8
0.5 M LiOH	6.19×10^{-3}	4.92×10^{-2}	0.128
0.5 M NaOH	3.01×10^{-3}	1.42×10^{-2}	2.19×10^{-2}
0.5 M KOH	2.02×10^{-3}	9.34×10^{-3}	1.38×10^{-2}

Table 2. Hydrolysis rate constants of linear phosphates in 1 M $(CH_3)_4NOH$

	k_n (h^{-1})		
	P_4	P_6	P_8
70°C		4.25×10^{-3}	5.55×10^{-3}
80°C		1.31×10^{-2}	1.72×10^{-2}
90°C	1.33×10^{-2}	7.07×10^{-2}	5.72×10^{-2}
E_a (kcal mol^{-1})		34.7	28.8

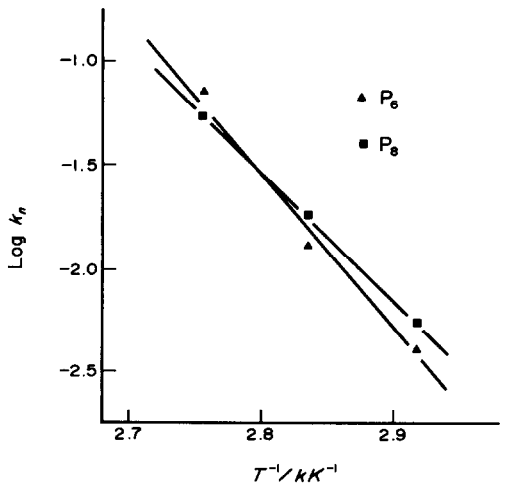

Fig. 4. Arrhenius plots of hexa- and octaphosphate in 1 M $(CH_3)_4NOH$.

phosphate is most stable and the half-life even at 90°C is 52 h. The large difference between the rates of hexa- and octaphosphates was not observed. The Arrhenius plots for hexa- and octaphosphates are shown in Fig. 4; linear relations were obtained. The rate constants of hexa- and octaphosphates at 50°C were estimated by the linear extrapolation of the Arrhenius plots as 1.64×10^{-4} and 4.04×10^{-4}, respectively. Although the concentration of OH^- is twice that of other alkalis, the hydrolysis reaction is very slow. The hydrolysis rates of linear phosphates in alkaline solution are markedly influenced by the cations present. Arrhenius activation energy of cyclo-hexa- and cyclo-octaphosphate in 1.00 M $(CH_3)_4NOH$ solution were 19.4 and 21.7 kcal mol^{-1}, respectively. The activation energies of linear hexa- and octaphosphates in Table 2 are about 10–15 kcal mol^{-1} larger. For the cleavage of the P—O—P bond due to the attack of OH^- ion on the P atoms, the electrostatic repulsion between OH^- and the anionic atmosphere near the P atoms is enhanced for the linear oligomer structure, and thus the activation energies are larger for the hydrolysis of the linear oligomers. When the hydrolysis rates, at 50°C, of the cyclic and linear oligomers are compared with each other, linear tetraphosphate is extremely stable relative to cyclo-tetraphosphate but the rate constants for the hexamer or octamer are comparable.

REFERENCES

1. J. R. Van Wazer, *Phosphorus and its Compounds*. Interscience, New York (1958).
2. G. Kura and S. Ohashi, *J. Inorg. Nucl. Chem.* 1976, **38**, 1151.
3. S. Ohashi, G. Kura, Y. Shimada and M. Hara, *J. Inorg. Nucl. Chem.* 1977, **39**, 1513.
4. G. Kura, *Polyhedron* 1986, **5**, 2097.
5. G. Kura, *Polyhedron* 1987, **6**, 1863.
6. E. J. Griffith, *J. Inorg. Nucl. Chem.* 1964, **26**, 1381.
7. G. Kura, *J. Chromatogr.* 1988, **447**, 91.
8. G. Kura, *Bull. Chem. Soc. Jpn* 1987, **60**, 2857.

Polyhedron Vol. 9, No. 17, pp. 2181–2183, 1990
Printed in Great Britain

0277-5387/90 $3.00+.00
© 1990 Pergamon Press plc

COMMUNICATION

SYNTHESIS AND X-RAY CRYSTAL STRUCTURE OF $[Pd(C_6F_5)(\eta^2\text{-}\{(Ph_2P)_3C\})(PPh_3)]$, A MONONUCLEAR COMPOUND CONTAINING η^2-TRIS(DIPHENYLPHOSPHINE)METHANIDE

J. FORNIÉS,* F. MARTÍNEZ, R. NAVARRO and E. P. URRIOLABEITIA

Departamento de Química Inorgánica, Instituto de Ciencia de Materiales de Aragón, Universidad de Zaragoza, C.S.I.C., 50009 Zaragoza, Spain

(*Received* 18 *May* 1990; *accepted* 20 *June* 1990)

Abstract—The reaction between $[Pd(C_6F_5)(acac)(PPh_3)]$ and $(Ph_2P)_3CH$ in CH_2Cl_2 affords $[Pd(C_6F_5)(\eta^2\text{-}\{(Ph_2P)_3C\})(PPh_3)]$ (**1**) which can be protonated by HBF_4 to yield $[Pd(C_6F_5)(\eta^2\text{-}\{(Ph_2P)_3CH\})(PPh_3)](BF_4)$ (**2**). The X-ray structure determination of complex **1** reveals a distorted square-planar environment for the metal centre with an η^2-coordination of the tris(diphenylphosphino)methanide, the skeletal P_3C group of this ligand is moderately distorted from a $C(sp^2)$ arrangement.

1,1,1-Tris(diphenylphosphino)methane, $(Ph_2P)_3CH$ (tdppm),[1] has received considerable attention because of its variety of coordination modes. Complexes in which $(Ph_2P)_3CH$ acts as an η^1-monodentate,[2] η^2- or η^3-chelating,[2,3] η^2-μ_2-bridging,[2] η^3-μ_2-bridging–chelating[2,3b,4] and η^3-μ_3-bridging ligand[3a,5] have been characterized. By contrast, as far as we know, no complexes containing the anionic methanide $[(Ph_2P)_3C^-]$ group have been described and only a few derivatives of main group elements with the similar $[(Me_2P)_3C^-]$ group have been characterized: $[Sn\{(Me_2P)_3C\}_2]$,[6] $[Al\{(Me_2P)_3C\}_3]$[7] and $[Ge\{(Me_2P)_3C\}_2]$.[8]

Here we present a preliminary report on the synthesis and structural characterization of $[Pd(C_6F_5)\{(Ph_2P)_3C\}(PPh_3)]$ (**1**) which contains an η^2-$[(Ph_2P)_3C^-]$ chelating group. The reaction of **1** with HBF_4 results in the protonation of the methanide ligand and formation of $[Pd(C_6F_5)\{(Ph_2P)_3CH\}(PPh_3)]^+$ (**2**), a cationic complex containing an η^2-$[(Ph_2P)_3CH]$ as neutral ligand.

Addition of tris(diphenylphosphino)methane, $(Ph_2P)_3CH$, to a colourless dichloromethane solution of $[Pd(C_6F_5)(acac)(PPh_3)]$[9] (1:1 molar ratio, room temperature) gives a yellow solution from which, after evaporation almost to dryness and addition of n-hexane, $[Pd(C_6F_5)\{(Ph_2P)_3C\}(PPh_3)]$ (**1**) is obtained, the triphosphine being deprotonated by $acac^-$ [eq. (1)]:

$$[Pd(C_6F_5)(acac)(PPh_3)]+(Ph_2P)_3CH \longrightarrow [Pd(C_6F_5)\{(Ph_2P)_3C\}(PPh_3)]+acacH. \quad (1)$$

On the other hand, the methanide $[(Ph_2P)_3C^-]$ ligand in **1** can be protonated by HBF_4, so that addition of HBF_4 (HBF_4/Et_2O, 54%) to a diethyl ether solution of **1** (molar ratio 1:1, room temperature) renders $[Pd(C_6F_5)\{(Ph_2P)_3CH\}(PPh_3)](BF_4)$ (**2**) (57% yield), which reacts with NaH in Et_2O yielding **1** (45% yield) [eq. (2)]:

$$[Pd(C_6F_5)\{(Ph_2P)_3C\}(PPh_3)] \underset{+NaH,\,-NaBF_4,\,-H_2}{\overset{+HBF_4}{\rightleftharpoons}} [Pd(C_6F_5)\{(Ph_2P)_3CH\}(PPh_3)](BF_4). \quad (2)$$

The cationic species $[Pd(C_6F_5)\{(Ph_2P)_3CH\}(PPh_3)]^+$ can also be obtained by reacting $[Pd(C_6F_5)(OClO_3)(PPh_3)_2]$ with $(Ph_2P)_3CH$ (molar ratio 1:1) in benzene [eq. (3)], although $[Pd(C_6F_5)(PPh_3)_3](ClO_4)$ is also formed:

$$[Pd(C_6F_5)(OClO_3)(PPh_3)_2]+(Ph_2P)_3CH \longrightarrow [Pd(C_6F_5)\{(Ph_2P)_3CH\}(PPh_3)](ClO_4) + [Pd(C_6F_5)(PPh_3)_3](ClO_4). \quad (3)$$

Complexes **1** and **2** give microanalytical data and IR, ^{19}F and $^{31}P\{^1H\}$ spectroscopic data which are in

* Author to whom correspondence should be addressed.

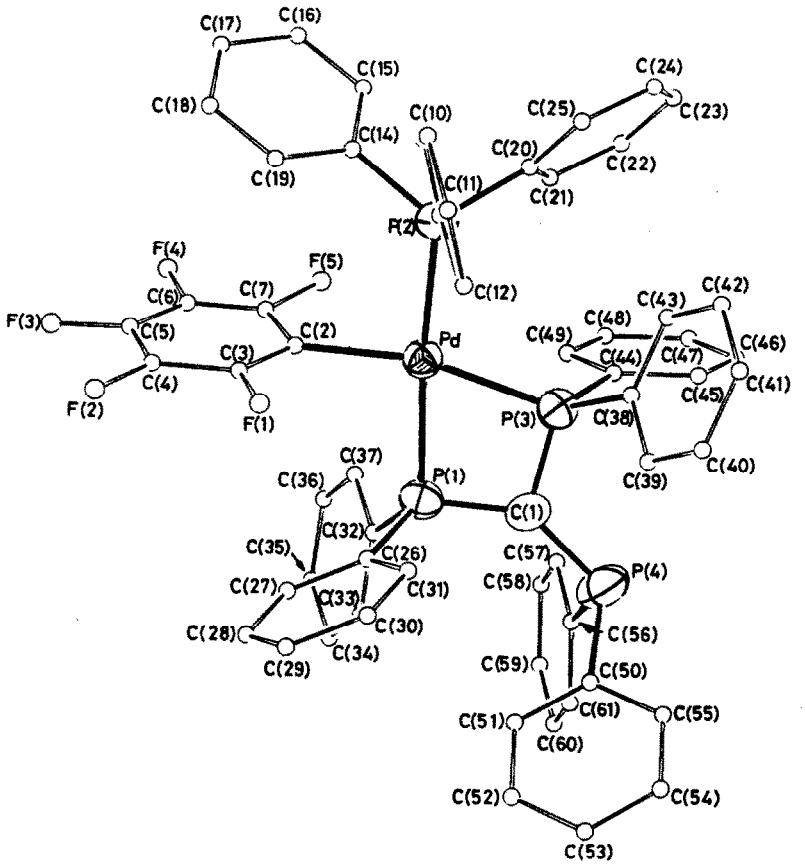

Fig. 1. An ORTEP of $[Pd(C_6F_5)\{(Ph_2P)_3C\}(PPh_3)]$ (1).

Distances (Å):

Pd—C(2)	2.079(12)	C(1)—P(1)	1.738(11)				
Pd—P(1)	2.313(3)	C(1)—P(3)	1.751(10)				
Pd—P(2)	2.366(3)	C(1)—P(4)	1.786(11)				
Pd—P(3)	2.329(3)						

Angles (°):

P(3)—Pd—P(1)	69.9(1)	P(3)—C(1)—P(1)	99.3(5)
P(3)—Pd—P(2)	105.0(1)	P(4)—C(1)—P(1)	138.7(6)
C(2)—Pd—P(2)	91.0(3)	P(4)—C(1)—P(3)	120.0(6)
C(2)—Pd—P(1)	94.7(3)		

accordance with the proposed formulae.* A strong absorption at 905 cm^{-1} in the IR spectrum of **1** is probably characteristic of the η^2-$[(Ph_2P)_3C^-]$ group. The different types of P atoms can be observed in the $^{31}P\{^1H\}$ NMR spectra of **1** and **2**.*

Suitable crystals of complex **1** for X-ray study were obtained by slow diffusion at −5°C of n-hexane into a solution of **1** in CH_2Cl_2.† The structure of **1** is shown in Fig. 1. The main distances and angles in **1** are given in the caption to Fig. 1.

*Analytical data: Found (Calc.), %. Complex **1**: C: 66.2(66.4); H: 4.7(4.1). Complex **2**: C: 61.0(61.5); H: 4.6(3.9). IR data (Nujol, cm^{-1}): Complex **1**, C_6F_5, 1500, 950, 775 (X-sensitive); $[(Ph_2P)_3C]^-$, 905. Complex **2**, C_6F_5, 1500, 950, 775 (X-sensitive); $[(Ph_2P)_3CH]$, 525, 510, 495; BF_4^-, 1100. ^{19}F NMR ($CDCl_3$, $CFCl_3$ reference, δ ppm): Complex **1**, F_o −116.34; F_m −164.50; F_p −163.15. Complex **2**, F_o −117.07; F_m −162.44; F_p −159.77; BF_4^- −153.11. $^{31}P\{^1H\}$ NMR ($CDCl_3$, PO_4H_3 85% reference, δ ppm, J Hz): Complex **1**, P_A 21.5 (dd); P_B −20.2 (dt); P_C −30.1 (t); P_D 7.5 (ddd); $^2J_{AB}$ 378; $^2J_{BC} \cong {}^2J_{BD} \cong {}^2J_{CD} \cong 54$; $^4J_{AD}$ 10. Complex **2**, P_A 21.4 (d); $P_{B'}$ −17.3 (ddd); $P_{C'}$ −26.5 (d,br); $P_{D'}$ −18.6 (t); $^2J_{AB'}$ 400; $^2J_{B'C'}$ 89; $^2J_{B'D'} \cong {}^2J_{C'D'} \cong 15$.

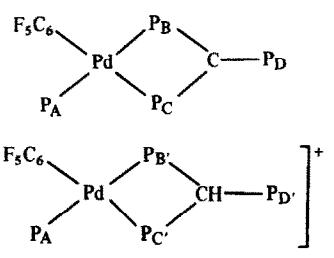

†Crystal data for **1**: $PdC_{60}H_{45}P_4F_5$, monoclinic, space group $P2_1/c$, $a = 15.1564(9)$, $b = 14.5591(8)$, $c = 23.7302(17)$ Å, $\alpha = 90.0$, $\beta = 91.81$, $\gamma = 90.0°$, $V = 5233$ Å^3, $Z = 4$, 3134 unique reflections with $F \leqslant 5\sigma(F)^2$. Refinement converged at $R = 0.0547$, $R_w = 0.0561$.

The palladium atom has a distorted square-planar environment formed by the C_6F_5 group, the P atom of the PPh_3 and two P atoms of the $[(Ph_2P)_3C^-]$ anion, which is acting as a chelating ligand. The four-membered chelate ring shows considerable distortion as evidenced by a P(3)—Pd—P(1) chelate bite angle of 69.9(1)° (90° for a regular square-planar coordination) and a P(3)—C(1)—P(1) angle of 99.3(5)° (120° for a C(1) sp^2 hybridization). The P(3)—Pd—P(1) angle is similar to those reported previously in bis(diphenylphosphino)methanide complexes, η^2-$[(Ph_2P)_2CH^-]$,[10] and larger than the ones reported in the complexes $[M\{(Me_2P)_3C\}_2]$[6,7] [M = Ge, 68.0(1) and 63.8(1)°; M = Sn, 62.9(1) and 62.8(1)°].

The four-membered ring Pd—P(3)—C(1)—P(1) is basically planar, the dihedral angle between the P(1)—Pd—P(3) and P(3)—C(1)—P(1) planes is 3.37°.[11]

The P—C(1)—P angles of the η^2-$[(Ph_2P)_3C^-]$ ligand average 119.3°, close to 120°, although the three P—C(1)—P angles are very different.

This situation is similar to the corresponding complexes $[M\{(Me_2P)_3C\}_2]$[6,7] (the P—C—P angles average: 119.9 and 120.0°, M = Sn and Ge, respectively), and logically different to the corresponding $(Ph_2P)_3CH$ derivatives; for instance in the case of $[Pt\{\eta^2\text{-}(Ph_2P)_3CH\}_2]^{2+}$ the P—C(1)—P angles average 110.7°, close to the tetrahedral value of 109.5°.[3c] The P—C—P angle of the chelate ring is smaller than the other two P—C—P angles, which involve the non-coordinated P atom. However, the P_3C skeleton is moderately distorted from planarity, the dihedral angles between the planes P(1)—C(1)—P(4) and P(4)—C(1)—P(3), P(1)—C(1)—P(4) and P(1)—C(1)—P(3), P(1)—C(1)—P(3) and P(3)—C(1)—P(4) are 19.88, 17.36 and 13.13°, respectively, and the distance from C(1) to the P(1)—P(3)—P(4) plane is 0.137 Å.

Deprotonation of the neutral group $(Ph_2P)_3CH$ leads to a delocalized system as shown in Fig. 2; the P—C(1) bond lengths (1.738(11), 1.751(10) and 1.786(11) Å) indicate some component of a double bond and are shorter than the single P—C(phenyl) distances (1.818(7)–1.850(7) Å) in complex **1**, and also shorter than the single P—CH distances in the $[Pt\{\eta^2\text{-}(Ph_2P)_3CH\}_2]^{2+}$ derivative (1.830(12), 1.878(10) and 1.891(11) Å).[3c]

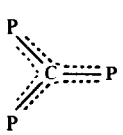

Fig. 2.

Acknowledgements—Financial support from the CICYT (Spain) is gratefully acknowledged. E.P.U. thanks DGA for a grant.

REFERENCES

1. K. Issleib and H. P. Abicht, *J. Prakt. Chem.* 1970, **312**, 456.
2. J. T. Magne and S. E. Dessens, *J. Organomet. Chem.* 1984, **262**, 347.
3. (a) J. A. Osborn and G. G. Stanley, *Angew. Chem. Int. Ed.* 1980, **19**, 1025; (b) A. A. Bahsoun, J. A. Osborn, P. H. Bird, D. Nucciarone and A. V. Peters, *J. Chem. Soc., Chem. Commun.* 1984, 72; (c) K. J. Beckett and S. J. Loeb, *Can. J. Chem.* 1988, **66**, 1073; (d) J. D. Goodrich and J. P. Selegne, *Organometallics* 1985, **4**, 798.
4. H. El-Amouri, A. A. Bahsoun, J. Fischer and J. A. Osborn, *Angew. Chem. Int. Ed.* 1987, **26**, 1169.
5. (a) A. A. Arduini, A. A. Bahsoun, J. A. Osborn and C. Voelker, *Angew. Chem. Int. Ed.* 1980, **19**, 1024; (b) A. F. M. J. van der Ploeg and G. van Koten, *Inorg. Chim. Acta* 1981, **51**, 225; (c) M. M. Harding, B. S. Nicholls and A. K. Smith, *J. Organomet. Chem.* 1982, **226**, C17; (d) A. A. Bahsoun, J. A. Osborn, C. Voelker, J. J. Bonnet and G. Lavigne, *Organometallics* 1982, **1**, 1114; (e) A. A. Bahsoun, J. A. Osborn, J. P. Kintzinger, P. H. Bird and U. Siriwardane, *Nouv. J. Chem.* 1984, **8**, 125; (f) D. J. Darensbourg, D. J. Zalewski and T. Delord, *Organometallics* 1984, **3**, 1210; (g) J. A. Clucas, M. M. Harding, B. S. Nicholls and A. K. Smith, *J. Chem. Soc., Chem. Commun.* 1984, 319; (h) D. J. Darensbourg and D. J. Zalewski, *Organometallics* 1985, **4**, 92; (i) M. Lusser and P. Peringer, *J. Organomet. Chem.* 1986, **301**, 269; (j) D. J. Darensbourg, D. J. Zalewski, A. L. Rheingold and R. L. Durney, *Inorg. Chem.* 1986, **25**, 3281.
6. H. H. Karsch, A. Appelt and G. Muller, *Organometallics* 1986, **5**, 1664.
7. H. H. Karsch, A. Appelt, J. Riede and G. Muller, *Organometallics* 1987, **6**, 316.
8. H. H. Karsch, B. Deubelly, G. Hanika, J. Riede and G. Muller, *J. Organomet. Chem.* 1988, **344**, 153.
9. J. Fornies, R. Navarro and E. P. Urriolabeitia, *J. Organomet. Chem.*, in press.
10. (a) M. P. Brown, A. Yavari, B. Manojlovic-Muir, K. W. Muir, R. P. Moulding and K. R. Seddon, *J. Organomet. Chem.* 1982, **286**, C32; (b) J. Browning, G. W. Bushnell and K. R. Dixon, *J. Organomet. Chem.* 1980, **198**, C11.
11. M. Nardelli, *Comput. Chem.* 1983, 7, 95.

Polyhedron Vol. 9, No. 17, pp. 2185–2187, 1990
Printed in Great Britain

0277–5387/90 $3.00+.00
Pergamon Press plc

COMMUNICATION

CYCLOPENTADIENYL REPLACEMENT BY TRISPYRAZOLYLBORATE AND THE SYNTHESES OF $M(\eta^5\text{-}C_5H_5)\{HB(C_3H_3N_2)_3\}X_2$ (M = Hf, X = Cl; M = Zr, X = Cl, OPh, OC_6H_4-4-NO_2, OC_6H_4-4-OMe, OC_6H_4-2-Ph)

ROMAN A. KRESINSKI, CHRISTOPHER J. JONES* and JON A. McCLEVERTY*

School of Chemistry, University of Birmingham, PO Box 363, Birmingham B15 2TT, U.K.

(*Received* 5 *June* 1990; *accepted* 25 *June* 1990)

Abstract—The reactions between $M\{C_5H_5\}_2Cl_2$ (M = Zr, Hf) and $HB(C_3H_3N_2)_3H$ afford $M(\eta^5\text{-}C_5H_5)\{HB(C_3H_3N_2)_3\}Cl_2$. These compounds undergo halide substitution reactions with phenols and the new complexes $Zr(\eta^5\text{-}C_5H_5)\{HB(C_3H_3N_2)_3\}X_2$ (X = Cl, OC_6H_4Z; Z = H, 4-NO_2, 4-OMe, 2-Ph) have been isolated and characterized.

An extensive chemistry has been developed[1] for the $\{Zr(\eta^5\text{-}C_5H_5)_2\}^{2+}$ moiety, much of which has been stimulated by the prospect of potential applications in homogeneous catalysis. In view of the parallel chemistries which may be developed for complexes containing the $C_5H_5^-$ and $HB(C_3H_3N_2)_3^-$ (L^-) ligands,[2,3] others[4] and ourselves have been interested in developing the chemistry of the $\{ZrL_2\}^{2+}$ moiety. Furthermore, although there are several reports describing polypyrazolylborate complexes of zirconium, to our knowledge there are no reports of such complexes containing hafnium. Zirconium complexes containing the hydrotris(pyrazol-1-yl) borate (L^-),[3,5] hydrotris(3,5-dimethylpyrazolyl) borate,[6] tetrakis(pyrazolyl)borate[7] and *i*-propyltris(pyrazolyl)borate[8] ligands have been reported. There is only one report of a zirconium complex containing two polyprazolylborate ligands.[7] This describes the synthesis of $\{B(C_3H_3N_2)_4\}_2ZrCl_2$ and $\{B(C_3H_3N_2)_4\}_2ZrBr_2$ by the reaction of the appropriate zirconium tetrahalide with $K^+B(C_3H_3N_2)_4^-$. Since this report, attempts to repeat the synthesis of the former complex in our laboratory, and that of others,[8] have failed. Similarly, our attempts to prepare ZrL_2Cl_2 directly from the reaction of $ZrCl_4$ with KL resulted only in the formation of insoluble intractable precipitates. As an alternative approach the reaction between $M(\eta^5\text{-}C_5H_5)_2Cl_2$ (M = Ti, Zr, Hf) and the free acid of the hydrotris(pyrazolyl)borate anion (HL)[9] was investigated in the hope that proton exchange between HL and $C_5H_5^-$ would provide a means of replacing C_5H_5 with L to give ML_2Cl_2.

The formation of HL was first reported[9] by Trofimenko, who found that the acidification of aqueous solutions containing L^- gave a precipitate which is tentatively formulated herein as $HB(C_3H_3N_2)_2(C_3H_4N_2)$ or HL. This material is unstable in solution, and also decomposes at its melting point of *ca* 95°C liberating pyrazole. In view of the instability of HL in solution it was considered best to melt an intimate mixture of solid $Zr(\eta^5\text{-}C_5H_5)_2Cl_2$ and HL together. Cyclopentadiene is evolved during this reaction but, irrespective of the amount of HL present in excess, only one of the two cyclopentadienyl ligands can be replaced affording the known[5] complex $Zr(\eta^5\text{-}C_5H_5)LCl_2$. Similar results were obtained using HL with $Hf(\eta^5\text{-}C_5H_5)_2Cl_2$ and the new compound $Hf(\eta^5\text{-}C_5H_5)LCl_2$ was isolated from the reaction mixture.† However, the reaction of $Ti(\eta^5\text{-}C_5H_5)_2Cl_2$ with HL did not afford any tractable products.

The reactions of HL with $Zr(\eta^5\text{-}C_5H_5)_2ClH$ and

* Authors to whom correspondence should be addressed.

† All of the new compounds have been characterized by IR, ^1H NMR and mass spectroscopy and all give satisfactory elemental analyses.

$ZrCl_4$ were also investigated but the only identifiable products were the two isomers of 1,4-dipyrazolylpyrazabole.[10] The stereochemistries of these two isomers were not determined and they are simply described here as isomers **A** and **B**. Whilst HL is known[10] to produce 1,4-dipyrazolylpyrazabole under certain conditions, the possibility exists that 1,4-dipyrazolylpyrazabole formation is stimulated by the association of two L ligands bound to a zirconium atom. If the $\{ZrL_2\}$ moiety were unstable with respect to decomposition to 1,4-dipyrazolylpyrazabole, this would account for our inability to obtain derivatives of $\{ZrL_2\}^{2+}$. The observation of decomposition products of tris(pyrazolyl)borate ligands is not unprecedented. Quite apart from examples of "complex dissociations" documented in the literature and resulting in the liberation of pyrazole,[11,12] the compounds $HB(C_3HN_2\text{-}3,5\text{-}Me_2)_3BH^+TaCl_6^-$ and $(C_3HN_2\text{-}3,5\text{-}Me_2)_3B(C_3H_2N_2\text{-}3,5\text{-}Me_2)$ have been isolated from the reaction of $K^+HB(C_3HN_2\text{-}3,5\text{-}Me_2)_3^-$ and $TaCl_5$.[13] The formation of both these products requires the cleavage of B—N bonds, as would the formation of 1,4-dipyrazolylpyrazabole.

Although the melting of HL alone afforded 1,4-dipyrazolylpyrazabole the reproducibility of this reaction was poor. However, it is clear that the behaviour of zirconium toward HL is not always totally passive. When HL was combined with $ZrO(NO_3)_2$ and heated, the zirconium salt acted purely as a diluent, reducing the yield of 1,4-dipyrazolylpyrazabole. When the procedure was repeated using $Zr(\eta^5\text{-}C_5H_5)_2ClH$ or $ZrCl_4$ in place of $ZrO(NO_3)_2$ a different isomer of 1,4-dipyrazolylpyrazabole was favoured depending upon the zirconium complex used. ^1H NMR studies[14] have shown that the reaction between HL and $Zr(\eta^5\text{-}C_5H_5)_2ClH$ gives a varying ratio of isomer **A** to isomer **B**. This ratio is strongly dependent on the concentration of $Zr(\eta^5\text{-}C_5H_5)_2ClH$, falling from 4.5:1 for 1:1 HL to $Zr(\eta_5\text{-}C_5H_5)_2ClH$ stoichiometry, to 2.5:1 for an 8.6:1 HL to $Zr(\eta^5\text{-}C_5H_5)_2ClH$ stoichiometry. Furthermore, the fractional yield of 1,4-dipyrazolylpyrazabole based on HL rises with the concentration of $Zr(\eta^5\text{-}C_5H_5)_2ClH$. The reaction between HL and $ZrCl_4$ afforded almost exclusively isomer **B**. Thus it seems possible that two L ligands may simultaneously associate with a zirconium centre, ultimately giving pyrazaboles as some of the products. The lack of reproducibility in the behaviour of HL has precluded any quantitative investigation of this system. However, the results obtained do indicate that the zirconium centre can play a role in the pyrazabole formation process.

The chloride substitution reactions of $Zr(\eta^5\text{-}C_5H_5)LCl_2$ have been investigated using phenols. The reactions of $Zr(\eta^5\text{-}C_5H_5)LCl_2$ with two molar equivalents of HOC_6H_4Z (Z = H, 4-OMe, 4-NO_2 and 2-Ph) in solutions containing triethylamine afforded the corresponding bis-phenoxides in yields of approximately 70%. In the case of $Zr(\eta^5\text{-}C_5H_5)_2(OC_6H_4\text{-}2\text{-}Ph)_2$ this formulation has been confirmed by an X-ray crystal structure[14,15] which shows the presence of an η^5-cyclopentadienyl ligand and a κ^3 hydrotrispyrazolylborate ligand as illustrated schematically in Fig. 1. ^1H NMR evidence indicates that similar reactions take place with $Hf(\eta^5\text{-}C_5H_5)_2Cl^2$ when using HOC_6H_4-4-OMe or HOC_6H_5-4-F, but the products could not be isolated in a sufficiently pure state to give satisfactory elemental analyses.

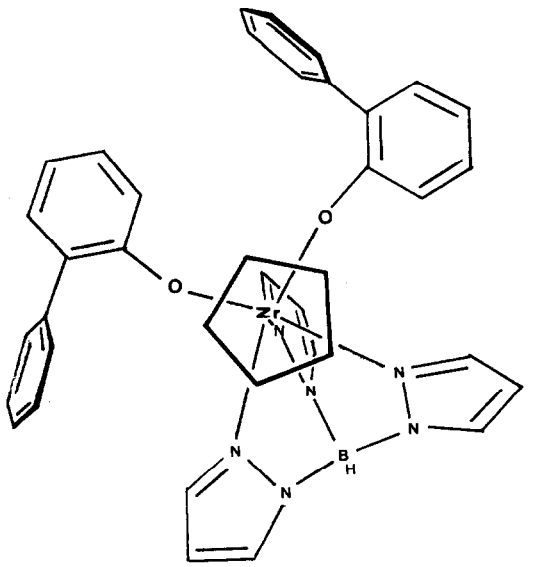

Fig. 1. A schematic view of the structure of $Zr(\eta^5\text{-}C_5H_5)_2(OC_6H_4\text{-}2\text{-}Ph)_2$ viewed along the Zr–C_5H_5 (ring centriod) vector. The third pyrazolyl ring of the ligand L is seen edge-on and lies behind, and is partly obscured by, the zirconium atom.

Acknowledgements—We are grateful to Professor W. J. Evans for helpful discussions and to the SERC and to BP Chemicals International for financial support (to R.A.K.).

REFERENCES

1. D. J. Cardin, M. F. Lappert, C. L. Raston and P. I. Riley, *Comprehensive Organometallic Chemistry* (Edited by G. Wilkinson, F. G. A. Stone and E. Abel), Vol. 3, pp. 559–634. Pergamon Press, Oxford (1982).
2. S. Trofimenko, *Prog. Inorg. Chem.* 1986, **34**, 115.
3. A. Shaver, *Comprehensive Organometallic Chemistry* (Edited by G. Wilkinson, R. D. Gillard and J. A.

McCleverty), Vol. 2, pp. 245–260. Pergamon Press, Oxford (1987).
4. D. L. Reger and M. E. Tarquini, *Inorg. Chem.* 1982, 840.
5. D. L. Reger, R. Mahtab, J. C. Baxter and L. Lebioda, *Inorg. Chem.* 1986, **25**, 2046.
6. D. L. Reger, M. E. Tarquini and L. Lebioda, *Organometallics* 1983, **2**, 1763.
7. S. Asslani, R. Rahbarnoohi and B. L. Wilson, *Inorg. Nucl. Chem. Lett.* 1979, **15**, 59.
8. D. L. Reger, M. E. Tarquini and L. Lebioda, *Inorg. Chem.* 1983, **22**, 1064.
9. S. Trofimenko, *J. Am. Chem. Soc.* 1967, **89**, 3170.
10. S. Trofimenko, *J. Am. Chem. Soc.* 1967, **89**, 3165.
11. A. Bond and M. Green, *J. Chem. Soc. A* 1971, 682.
12. N. F. Borkett and M. I. Bruce, *J. Organomet. Chem.* 1974, **65**, C51.
13. D. C. Bradley, M. B. Hursthouse, J. Newton and N. P. C. Walker, *J. Chem. Soc., Chem. Commun.* 1984, 188.
14. R. A. Kresinski, PhD thesis, University of Birmingham (1990).
15. R. A. Kresinski and T. A. Hamor, unpublished results.

Polyhedron Vol. 9, No. 17, pp. 2189–2190, 1990
Printed in Great Britain

0277–5387/90 $3.00+.00
© 1990 Pergamon Press plc

COMMUNICATION

SYNTHESIS AND PROPERTIES OF POLYFLUOROALKOXYGERMANES

H. G. ANG* and C. H. KOH

Chemistry Department, National University of Singapore, Kent Ridge Road, Singapore 0511, Republic of Singapore

(*Received* 24 *May* 1990; *accepted* 28 *June* 1990)

Abstract—Two new polyfluoroalkoxygermanes, $(CF_3)_2C(H)OGeH_3$ (**A**) and $[(CF_3)_2C(H)O]_2GeH_2$ (**B**), were synthesized from the reactions of $(CF_3)_2C{=}O$ and GeH_4. The Ge—O bond in **A** was cleaved by HCl to give $(CF_3)_2C(H)OH$ and GeH_3Cl. Pyrolysis of both the alkoxygermanes also resulted in the formation of the alcohol, with concomitant deposition of germanium metal.

Hexafluoroacetone has been known to add to hydrides of Group 14 elements to give polyfluoroalkoxide derivatives. A variety of hexafluoroisopropoxysilanes have been produced from the reactions of hexafluoroacetone with various substituted silanes.[1–3] However, the addition of hexafluoroacetone to germane has not received much attention. Until now, only one hexafluoroacetone derivative of germanium, namely, hexafluoroisopropoxytrimethylgermane, has been prepared from the reaction of hexafluoroacetone with trimethylgermane;[4] but its properties have not been investigated. We now report the isolation of two new alkoxygermanes from the reactions of hexafluoroacetone with germane, and also their properties.

When an equimolar mixture of hexafluoroacetone and germane was heated at 120°C for $2\frac{1}{2}$ days in an evacuated glass ampoule, hexafluoroisopropoxygermane and bis(hexafluoroisopropoxy)germane were obtained:

$$3(CF_3)_2C{=}O + 2GeH_4 \longrightarrow (CF_3)_2C(H)OGeH_3 + [(CF_3)_2C(H)O]_2GeH_2.$$
(**A**) (**B**)

The products were not formed at temperatures below 120°C. On the other hand, reactions at higher temperatures afforded decomposition products. Both products **A** and **B** are stable at room temperature.

Hexafluoroisopropoxygermane (**A**) was trapped as a white solid at −86°C under vacuum fractionation, and melted to a colourless liquid on warming to room temperature. Its IR spectrum showed the following absorptions: 2905 cm^{-1}, ν(C—H); 1376 cm^{-1}, δ(C—H); 2134, 2099 cm^{-1}, ν(Ge—H); 902, 859 cm^{-1}, δ(Ge—H); 1303, 1276, 1224, 1155, 1111 cm^{-1}, ν(C—F); 691 cm^{-1}, δ(C—F); 768 cm^{-1}, ν(Ge—O). Molecular weight determination by Regnault's method gave 242 g mol^{-1} ($C_3H_4F_6OGe$ requires 243 g mol^{-1}). Found: C, 15.1; H, 1.5; F, 47.9. $C_3H_4F_6OGe$ requires: C, 14.8; H, 1.6; F, 47.0%.

The EI–MS of **A** did not exhibit the parent ion. However, clusters of peaks due to the following fragmentation ions were observed: 241 $\{[C_3F_6{}^{72}GeH_3O]^{+\cdot}, [C_3F_6{}^{74}GeHO]^{+\cdot}\}$, 239 $\{[C_3F_6{}^{70}GeH_3O]^{+\cdot}, [C_3F_6{}^{72}GeHO]^{+\cdot}\}$, 237 $\{[C_3F_6{}^{70}GeHO]^{+\cdot}\}$, 175 $\{[C_2F_3{}^{74}GeH_4O]^{+\cdot}\}$, 173 $\{[C_2F_3{}^{72}GeH_4O]^{+\cdot}, [C_2F_3{}^{74}GeH_2O]^{+\cdot}\}$, 171 $\{[C_2F_3{}^{70}GeH_4O]^{+\cdot}, [C_2F_3{}^{72}GeH_2O]^{+\cdot}, [C_2F_3{}^{74}GeO]^{+\cdot}\}$, 93 $\{[{}^{74}GeH_3O]^{+\cdot}\}$, 91 $\{[{}^{72}GeH_3O]^{+\cdot}, [{}^{74}GeHO]^{+\cdot}\}$, 89 $\{[{}^{70}GeH_3O]^{+\cdot}, [{}^{72}GeHO]^{+\cdot}\}$, 77 $\{[{}^{74}GeH_3]^{+\cdot}\}$, 75 $\{[{}^{72}GeH_3]^{+\cdot}, [{}^{74}GeH]^{+\cdot}\}$, 73 $\{[{}^{70}GeH_3]^{+\cdot}, [{}^{72}GeH]^{+\cdot}\}$. Fragmentation ions of the hexafluoroisopropoxyl group were also found in the mass spectrum.

Bis(hexafluoroisopropoxy)germane (**B**) was isolated as a colourless liquid at a −30°C trap under fractionation. It remained as a colourless liquid at

* Author to whom correspondence should be addressed.

room temperature. The following peaks were observed in its IR spectrum: 2916 cm^{-1}, ν(C—H); 1377 cm^{-1}, δ(C—H); 2175 cm^{-1}, ν(Ge—H); 904, 866 cm^{-1}, δ(Ge—H); 1304, 1276, 1228, 1135, 1111 cm^{-1}, ν(C—F); 690 cm^{-1}, δ(C—F); 807, 763 cm^{-1}, ν(Ge—O). Found: C, 17.7; H, 0.98; F, 55.9. $C_6H_4F_{12}GeO_2$ requires: C, 17.6; H, 0.98; F, 55.8%.

The mass spectrum of **B** was very similar to that of **A**. Again, the parent ion was not observed, but clusters of peaks due to the isotopes of germanium were obtained. The highest *m/z* observed was 241, which was assigned to the fragmentation ions $[C_3F_6{}^{72}GeH_3O]^{+\cdot}$ and $[C_3F_6{}^{74}GeHO]^{+\cdot}$. An additional cluster of peaks with *m/z* 193 $\{[C_2F_4{}^{74}GeH_3O]^{+\cdot}\}$, 191 $\{[C_2F_4{}^{72}GeH_3O]^{+\cdot}, [C_2F_4{}^{74}GeHO]^{+\cdot}\}$, 189 $\{[C_2F_4{}^{70}GeH_3O]^{+\cdot}, [C_2F_4{}^{72}GeHO]^{+\cdot}\}$ was observed as compared to the mass spectrum of **A**.

The Ge—O bond in **A** was found to be completely cleaved by an equimolar quantity of anhydrous hydrogen chloride at 80°C to afford 2H-hexafluoro-2-propanol (**C**) and chlorogermane:

$$(CF_3)_2C(H)OGeH_3 + HCl \longrightarrow (CF_3)_2C(H)OH + GeH_3Cl.$$
(**C**)

Metal deposition was obtained upon pyrolysis of both alkoxygermanes, **A** and **B**. When **A** was pyrolysed at 180°C for 7 days, it underwent about 70% decomposition to give the alcohol (**C**), germanium metal and hydrogen gas. A trace of germane was also isolated:

$$(CF_3)_2C(H)OGeH_3 \longrightarrow (CF_3)_2C(H)OH + GeH_4 + H_2 + Ge.$$

However, pyrolysis of **B** at 150°C for 2 days afforded a quantitative yield of **C** and germanium metal, with the elimination of hydrogen, as shown below:

$$[(CF_3)_2C(H)O]_2GeH_2 \longrightarrow 2(CF_3)_2C(H)OH + H_2 + Ge.$$

In both cases germanium, confirmed by chemical analysis, was formed as a uniform mirror on the wall of the reaction ampoule.

Acknowledgements—We thank the National University of Singapore for a research grant and one of us (K.C.H.) is grateful to the university for a research scholarship.

REFERENCES

1. A. F. Janzen and C. J. Willis, *Can. J. Chem.* 1965, **43**, 3063.
2. A. F. Janzen and C. J. Willis, *Inorg. Chem.* 1967, **6**, 1900.
3. E. G. Howard, P. B. Sargeant and C. G. Krespan, *J. Am. Chem. Soc.* 1967, **89**, 1422.
4. W. R. Cullen and G. E. Styan, *Inorg. Chem.* 1965, **4**, 1437.

Polyhedron Vol. 9, No. 17, p. 2191, 1990
Pergamon Press plc. Printed in Great Britain

BOOK REVIEW

Gmelin Handbook of Inorganic Chemistry. Sn—Organotin Compounds, Part 17. By H. Schumann and I. Schumann. Organotin–Oxygen Compounds of the Types $RSn(OR')_3$ and $RSn(OR')_2OR''$; $R_2Sn(X)OR'$, $RSnX(OR')_2$ and $RSnX_2(OR')$. Published by Gmelin Institute for Inorganic Chemistry of the Max Planck Society for the Advancement of Science, 8th edn. Springer, Berlin, 1989, ISBN 3-540-93596-7, XIV + 245 pp., DM 1133.

This is the 17th volume on organotin compounds to be written by Herbert and Ingeborg Schumann (Berlin Technical University), and covers compounds of the type $RSn(OR')_3$, $RSn(OR')_2OR''$, $R_2Sn(X)OR'$, $RSnX(OR')_2$ and $RSnX_2(OR')$, where X = hydrogen, halogen or pseudohalogen. The principal examples are the alkoxides, phenoxides and carboxylates, and compounds such as the oxinates, β-diketones and triethanolamine (stannatrane) derivatives are included. The literature closing date is 1987.

The monoorganotin compounds have a significant patent literature relating to p.v.c. stabilization, pesticides and bactericides, transesterification catalysts, waterproofing and flame-proofing, and vulcanizing agents for polysiloxane elastomers, but they have not found the extensive and varied applications that the tri- and di-alkyltin compounds have.

In the usual Gmelin style, the compounds are collected in 175 pages of tables which list structure, preparative methods, properties and remarks, and references. Further information on special compounds is given in extensive footnotes. The book includes 55 pages of indexes of empirical formulae and ligand formulae.

The presentation of the information and the printing are of the usual high standard of this series. The publishers and authors are providing a valuable service to chemistry in making this information available.

Department of Chemistry
University College London
20 Gordon Street
London WC1H 0AJ, U.K.

A. G. DAVIES

Polyhedron Vol. 9, No. 18, pp. 2193-2197, 1990
Printed in Great Britain

0277-5387/90 $3.00+.00
© 1990 Pergamon Press plc

STEPWISE CONVERSION OF A FIVE- INTO A NINE-MEMBERED PHOSPHAMETALLACYCLE VIA TWO INSERTIONS OF ALKYNE INTO A CHROMIUM–CARBON DOUBLE BOND

NGOC HOA TRAN HUY, LOUIS RICARD and FRANÇOIS MATHEY*

Laboratoire de Chimie du Phosphore et des Métaux de Transition, DCPH, Ecole Polytechnique, 91128 Palaiseau Cedex, France

(*Received* 16 *February* 1990; *accepted* 2 *April* 1990)

Abstract—The reaction of a five-membered (η^1-P,η^1-C-phosphinocarbene)tetracarbonylchromium chelate with several electron-rich triple bonds including an ynamine, a cyanamide and an ethoxyacetylene gives stable seven-membered phosphametallacycles via the insertion of the triple bond into the chromium–carbene bond. With an excess of ethoxyacetylene, a double insertion also takes place leading to a nine-membered phosphametallacycle whose structure has been established by X-ray analysis. A C=C double bond of this cycle is loosely coordinated to the $Cr(CO)_3$ group: C—Cr = 2.384(4) and 2.619(4) Å. This first example of a stable double insertion product of a C≡C triple bond into a metal–carbene bond probably owes its stability to its phosphinocarbene chelate structure.

The insertion of triple bonds into metal–carbene bonds is a well documented process.[1] In many cases, a complicated series of events takes place which ultimately leads to carbocycles after extrusion of the transition metals. In some other cases the initial insertion products can be isolated. In such a way, aminovinylcarbene,[2,3] methyleneaminocarbene[4] and alkoxyvinylcarbene[5] complexes have been obtained, respectively, by insertion of ynamines,[2,3] cyanamides[4] and ethoxyacetylene[5] into carbene complexes. The reactivity of electrophilic carbene complexes toward these electron-rich triple bonds is highly dependent on the structural features of the carbene unit. For example, as far as we know, no ring expansion has been observed upon reaction of cyclic carbene complexes with these alkynes. In particular, the formation of the expected seven- or nine-membered rings does not occur during the reaction of the cyclic carbene, **1**, with ynamines; An insertion into the carbon–oxygen bond takes place instead[6] [eq. (1)]:

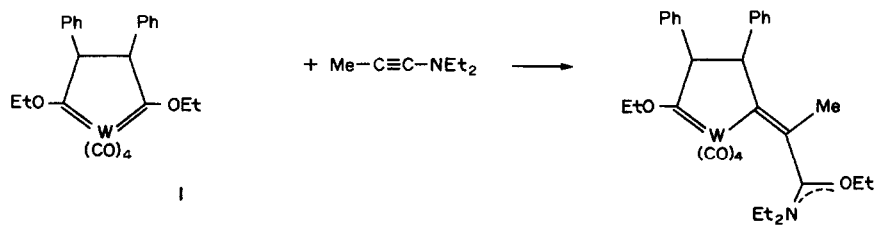

I (1)

In such a context, it was tempting to investigate the reaction of electron-rich triple bonds with a recently discovered phosphinocarbene chelate, **2**.[7] In so doing, we discovered an unprecedented double insertion of ethoxyacetylene converting a five- into a nine-membered phosphametallacycle.

RESULTS AND DISCUSSION

The reaction of **2** with a slight excess of 1-diethylaminopropyne leads cleanly and rapidly to the

* Author to whom correspondence should be addressed.

mono-insertion product **3** [eq. (2)]:

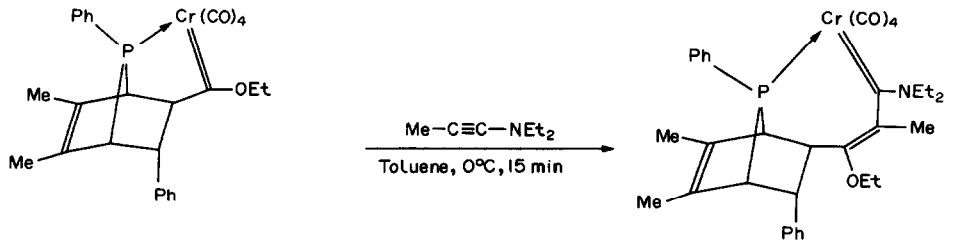

2 **3** (65%) (2)

The experimental formula of **3** was established by carbon and hydrogen elemental analyses and mass spectrometry (EI, 70 eV): *m/z* 595 ($M^+ - CO$, 27%), 511 ($M^+ - 4CO$, 100%). Its IR spectrum indicated a tetracarbonylchromium structure. The corresponding bands are shifted to lower frequencies by comparison with those of **2**, in agreement with the good σ-donor/weak π-acceptor properties of aminocarbene ligands.[8] Its ^1H, ^{13}C and ^{31}P spectra confirmed the proposed structure. The carbenic carbon resonates at 285.4 ppm, i.e. at much higher fields than in the starting product (356.4 ppm), supporting the aminocarbene formulation, and the ^{31}P resonance at low field (+161.4) is characteristic of the 7-phosphanorbornene skeleton.

A similar reaction takes place between complex **2** and dimethylcyanamide [eq. (3)]:

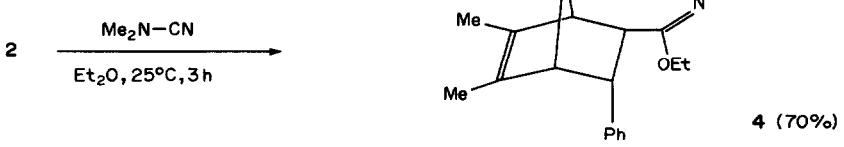

4 (70%) (3)

The presence of the amino–imino–carbene functionality and of the 7-phosphanorbornene skeleton was established as for compound **3**: δ (Cr=*C*) +245 ppm; $\delta^{31}P$ +162.1 ppm.

The case of ethoxyacetylene is more interesting. The reaction of a huge excess (8 equiv.) of this alkyne with complex **2** affords the mono-insertion product **5** and another complex **6**, the structure of which was more difficult to establish [eq. (4)]:

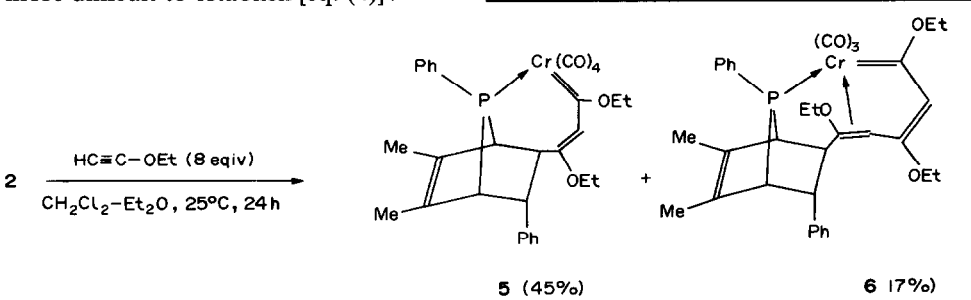

5 (45%) **6** 17%) (4)

The mass spectrum of **6** indicated that two molecules of ethoxyacetylene had reacted with **2**: *m/z* 624 (*M*(**2**)+2 EtO—C≡CH −CO, 100%). The IR spectrum clearly showed the disappearance of the $Cr(CO)_4$ complexing group, **5**: ν(CO), 2005 (s), 1900 (vs) cm^{-1} (in CH_2Cl_2); **6**: ν(CO), 1925 (vs), 1850 (s), 1815 (s) cm^{-1} (in CH_2Cl_2).

We thus decided to perform the X-ray crystal structure analysis of **6** (Fig. 1). A double insertion of ethoxyacetylene into the chromium–carbene bond of **2** had occurred to give a new nine-membered phosphametallacycle. Rather unexpectedly, one carbonyl has been lost in the process and one of the double bonds of the heterocycle is now coordinated to chromium. The coordination appears to be loose as indicated by the very long Cr—C(4) and Cr—C(5) bonds, respectively, 2.384(4) and 2.619(4) Å. The easy formation of chromium carbene–alkene chelates from the corresponding open-chain alkenylcarbene–chromium complexes has recently been described by Rudler and co-workers.[9] In the cases of both Rudler and ours, a six-membered cyclic structure is thus obtained. However, in our

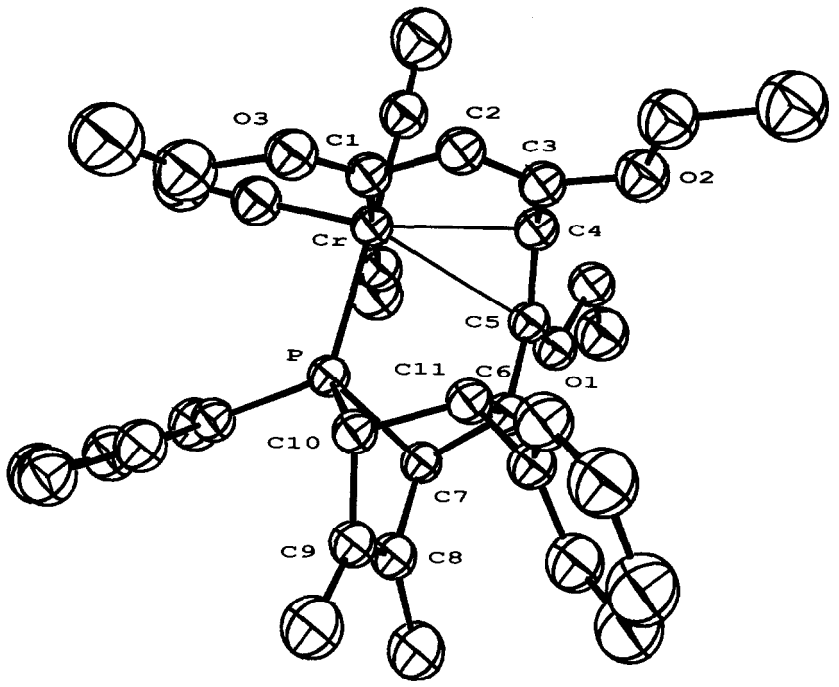

Fig. 1. ORTEP drawing of one molecule of **6**. Vibrational ellipsoids are scaled to enclose 50% of the electron density. Hydrogen atoms are omitted for clarity.Principal bond distances (Å): Cr—P, 2.327(1); Cr—C(1), 2.016(5); Cr—C(4), 2.384(4); Cr—C(5), 2.619(4); P—C(7), 1.839(5); P—C(10), 1.858(4); O(3)—C(1), 1.337(5); O(2)—C(3), 1.342(5); O(1)—C(5), 1.360(5); C(1)—C(2), 1.442(6); C(2)—C(3), 1.341(6); C(3)—C(4), 1.480(7); C(4)—C(5), 1.369(6); C(5)—C(6), 1.514(6); C(6)—C(7), 1.580(6); C(6)—C(11), 1.531(6); C(7)—C(8), 1.506(6); C(8)—C(9), 1.323(6); C(9)—C(10), 1.502(7); C(10)—C(11), 1.578(6). Selected bond angles (°): P—Cr—C(1) 90.4(1); P—Cr—C(4), 98.5(1); P—Cr—C(5), 72.9(1); C(1)—Cr—C(4), 77.5(2); C(1)—Cr—C(5), 95.5(2); C(4)—Cr—C(5), 31.3(1); Cr—P—C(7), 111.8(1); Cr—P—C(10), 123.7(1); C(7)—P—C(10), 79.7(2); Cr—C(1)—C(2), 120.1(3); C(1)—C(2)—C(3), 115.0(4); C(2)—C(3)—C(4), 123.3(4); C(3)—C(4)—C(5), 128.7(4); C(4)—C(5)—C(6), 132.1(4); C(5)—C(6)—C(7), 109.2(3), C(5)—C(6)—C(11), 116.6(4); P—C(10)—C(9), 103.4(3); P—C(10)—C(11), 98.4(3); P—C(7)—C(6), 94.1(3); P—C(7)—C(8), 104.9(3).

case, the strain which results from the distortion of the initial nine-membered metallacycle destabilizes the chromium–alkene bond.

From another standpoint, the stepwise insertion of two alkyne units into a chromium–carbene bond is already known.[10] However, the products resulting from this double insertion are always unstable and extrude chromium to give cyclohexadienones or phenols in low yields.[10] In our case, the double insertion product **6** probably owes its stability to its chelated phosphino carbene structure.

EXPERIMENTAL

All the reactions were performed under argon. NMR spectra were recorded on Multinuclear WP 80 and AC 200 SY Bruker spectrometers operating at 80.13 and 200.13 (^{1}H), 20.15 and 50.32 (^{13}C), and 32.44 (^{31}P) MHz. Chemical shifts are in ppm downfield from internal TMS (^{1}H and ^{13}C) and external 85% H_3PO_4 (^{31}P). Mass spectra were recorded on a Shimadzu GC-MS QP 1000 instrument at 70 eV under electronic impact. Elemental analyses were performed by the Service Central de Microanalyse du CNRS, France. Silica gel (70–230 mesh) was used for the chromatographic separations. All commercially available reagents were used as received from the suppliers.

Complex **3**

The ynamine, Me—C≡C—NEt_2 (0.3 cm^3, 2.6×10^{-3} mol, 5 equiv.), was added at 0°C to a solution of **2** (0.25 g, 5×10^{-4} mol) in toluene (5 cm^3). The reaction was monitored by TLC. After stirring for 15 min, the solvent was evaporated and the residual oil was chromatographed with pentane–CH_2Cl_2 (3:7) as the eluent. Complex **3** was obtained as yellow crystals in 65% yield (0.2 g).

^{31}P NMR ($CDCl_3$): δ+161.4; ^{1}H NMR

($CDCl_3$): δ 1.03 (s, 3H, CH_3—C), 1.19 (t, 3H, CH_3—CH_2), 1.29 (t, 3H, CH_3—CH_2), 1.57 (t, 3H, CH_3—CH_2), 1.62 (s, 3H, CH_3—C), 1.78 (s, 3H, CH_3—C=), 3.0 (m, 2H, CH—P), 3.4 (m, 1H, CH_2), 3.78 (m, 4H, CH_2+CH junction), 4.15 (m, 1H, CH_2), 4.75 (m, 1H, CH_2), 7.07–7.30 (m, 10H, Ph); ^{13}C NMR ($CDCl_3$): δ 13.76 (d, CH_3), 14.24 (d, CH_3), 15.96 (s, CH_3), 16.28 (d, CH_3), 22.74 (s, CH_3), 31.68 (s, CH_3, 46.81 (s, NCH_2), 47.91 (d, J(C—P) = 7.5 Hz, CH), 48.31 (s, CH), 51.43 (s, NCH_2), 52.27 (d, J(C—P) = 17.6 Hz, CH), 56.35 (d, J(C—P) = 17.1 Hz, CH), 65.43 (s, OCH_2), 219.46 (d, J(C—P) = 17.8 Hz, CO), 222.59 (d, J(C—P) = 16 Hz, CO), 228.14 (d, J(C—P) = 7.9 Hz, CO), 228.79 (s, CO), 285.38 (d, ^2J(C—P) = 12.07 Hz, *C*=Cr); IR (CH_2Cl_2): ν(CO) 1990 (s), 1900 (s), 1870 (vs) cm^{-1}; Found: C, 65.7; H, 6.9. Calc. for $C_{34}H_{38}NO_5PCr$: C, 65.5; H, 6.1%.

Complex **4**

An excess of Me_2N—CN (1 cm^3) was added to a solution of **2** (0.5 g) in ether (20 cm^3). After stirring for 3 h, the solution became yellow. The solvent was evaporated and the residual oil was chromatographed with pentane–CH_2Cl_2 (7:3) as the eluent. Yield of **4**: 0.4 g (70%) of yellow crystals; m.p. 158°C (dec.).

^{31}P NMR (Et_2O): δ +162.1; ^{1}H NMR ($CDCl_3$): δ 1.16 (s, 3H, CH_3), 1.34 (t, 3H, CH_3—CH_2), 1.69 (s, 3H, CH_3), 3.02 (s, 3H, CH_3—N), 3.07 (m, 3H, 3C*H*), 3.82 (s, 3H, CH_3N), 4.0 (m, 1H, C*H*), 4.16 (q, 2H, OCH_2), 7.0–7.3 (m, 10H, Ph); ^{13}C NMR ($CDCl_3$): δ 14.36 (s, Me), 14.59 (s, Me), 16.68 (s, Me), 40.54 (s, NMe), 47.05 (s, NMe), 47.18 (d, J(C—P) = 24.3 Hz, CH), 51.75 (d, J(C—P) = 13.1 Hz, CH), 53.57 (d, J(C—P) = 14.6 Hz, CH), 56.85 (d, J(C—P) = 16.8 Hz, CH), 62.96 (s, OCH_2), 150.67 (s, N=*C*—OEt), 220.72 (d, ^2J(C—P) = 17.1 Hz, CO), 222.61 (d, ^2J(C—P) = 16.8 Hz, CO), 226.46 (d, ^2J(C—P) = 8.8 Hz, CO); 229.48 (s, CO), 244.99 (d, ^2J(C—P) = 11.2 Hz, *C*=Cr); IR (CH_2Cl_2): ν(CO) 1995 (s), 1900 (shoulder), 1875 (vs) cm^{-1}; mass spectrum (EI, 70 eV): m/z 582 (M^+, 6%), 470 (M^+ −4CO, 100%).

Complex **5**

An excess of ethoxyacetylene (2 cm^3, 60% in Et_2O) was added to a solution of **2** (0.75 g) in dichloromethane (10 cm^3). The reaction was monitored by TLC. After stirring for 24 h, the solvent was evaporated and the residual oil was chromatographed with pentane–CH_2Cl_2 (4:1) as the eluent. Complex **5** was obtained in 45% yield (0.38 g) as red crystals; m.p. 103°C (dec.).

^{31}P NMR ($CDCl_3$): δ +163.8; ^{1}H NMR ($CDCl_3$): δ 1.16 (s, 3H, CH_3), 1.32 (t, 3H, CH_3—CH_2), 1.59 (t, 3H, CH_3—CH_2), 1.68 (s, 3H, CH_3), 3.0 (m, 2H, CH—P), 3.46 (m, 1H, CH), 3.79 (q, 2H, OCH_2); 3.97 (m, 1H, CH); 5.86 (s, 1H, =CH); 7.0–7.3 (m, 10H, Ph); ^{13}C NMR ($CDCl_3$): δ 14.36 (d, Me), 15.47 (s, Me), 16.55 (s, Me), 17.37 (s, Me); 51.53 (d, J(C—P) = 26.1 Hz, CH), 52.48 (d, J(C—P) = 7.2 Hz, CH), 56.32 (d, J(C—P) = 18.9 Hz, CH), 59.78 (d, J(C—P) = 20.7 Hz, CH), 64.42 (s, OCH_2), 72.30 (s, OCH_2), 119.69 (s, =CH), 164.42 (s, *C*—OEt), 342.95 (d, ^2J(C—P) = 10.6 Hz, *C*=Cr); IR (CH_2Cl_2): ν(CO) 2005 (s), 1900 (vs) cm^{-1}; mass spectrum (EI, 70 eV): m/z 554 (M^+ −CO, 7%), 470 (M^+ −4CO, 66%), 428 (100%).

Complex **6**

Complex **6** was eluted after complex **5** and isolated as black–red crystals in 17% yield (0.1 g); m.p. 158°C (dec).

^{31}P NMR ($CDCl_3$): +166.4; ^{1}H NMR ($CDCl_3$): δ 1.02 (s, 3H, CH_3); 1.14 (t, 3H, CH_3—CH_2), 1.42 (t, 3H, CH_3—CH_2), 1.50 (t, 3H, CH_3—CH_2), 1.68 (s, 3H, CH_3), 2.87 (m, 1H, CH—P?), 3.40 (dm, ^3J(H—P) = 40 Hz, HC_6 endo), 3.70–3.98 (m, 4H, OCH_2), 4.25 (s broad, 1H, CH—P?), 4.47–4.56 (m, 1H, OCH), 4.61 (d, 1H, HC_{11} *exo*), 4.73–4.62 (m, 1H, OCH), 4.96 (s, 1H, HC(4)=), 6.06 (s, 1H, HC(2)=, 6.79–7.48 (m, 10H, Ph); ^{13}C NMR ($CDCl_3$): δ 14.03, 14.33, 14.94, 15.61, 16.46 (5s, CH_3), 40.50 (d, J(C—P) = 11.1 Hz, CH), 50.77 (d, J(C—P) = 26.2 Hz, CH), 61.80 (d, J(C—P) = 13.1 Hz, CH), 62.88 (s, =C_4H), 67.62, 71.99, 74.62 (3s, OCH_2), 76.08 (s, =*C*(5)—OEt), 231.6 (s, CO), 233.15 (d, ^2J(C—P) = 13.4 Hz, CO), 236.92 (d, ^2J(C—P) = 13 Hz, CO), 327.94 (d, ^2J(C—P) = 14.8 Hz, *C*=Cr).

X-ray structure determination for **6**. Crystals of **6**, $C_{34}H_{36}CrO_6P \cdot CH_2Cl_2$, were grown at −18°C from a CH_2Cl_2–pentane solution of the compound. Data were collected at 18 ± 1° on an Enraf–Nonius CAD4 diffractometer. The crystal structure was solved and refined using the Enraf–Nonius supplied SDP package. The compound crystallizes in space group $P2_1/N$, a = 12.849(1), b = 19.226(2), c = 15.250(1) Å, β = 110.77(1)°; V = 3522.5(1.1) Å^3; Z = 4; d_{calc} = 1.336 g cm^{-3}; Mo-K_α radiation (l = 0.71073 Å) graphite monochromator; μ = 5.5 cm^{-1}; $F(000)$ = 1476. A total of 3277 unique reflections were recorded in the range 2° ≤ 2θ ≤ 40.0° of which 738 were considered as unobserved [$F^2 < 3.0\ \sigma(F^2)$], leaving 2539 for solution and refinement. The structure was solved by Patterson methods, yielding a solution for the chromium and

phosphorus atoms. The hydrogen atoms were included as fixed contributions in the final stages of least-squares refinement, while using anisotropic temperature factors for all other atoms. A non-poisson weighting scheme was applied with a p factor equal to 0.08. The final R factors were $R = 0.045$, $R\omega = 0.065$, G.O.F. = 1.46.

REFERENCES

1. J. P. Collman, L. S. Hegedus, J. R. Norton and R. G. Finke, *Principles and Applications of Organotransition Metal Chemistry* pp. 785–793. University Science Books, Mill Valley, California (1987).
2. K. H. Dötz and C. G. Kreiter, *J. Organomet. Chem.* 1975, **99**, 309.
3. N. H. Tran Huy, P. Le Floch, F. Robert and Y. Jeannin, *J. Organomet. Chem.* 1987, **327**, 211.
4. H. Fischer and U. Schubert, *Angew. Chem. Int. Edn. Engl.* 1981, **20**, 461.
5. C. P. Casey, S. W. Polichnowski, A. J. Shusterman and C. R. Jones, *J. Am. Chem. Soc.* 1979, **101**, 7282.
6. N. H. Tran Huy, E. O. Fischer, J. Riede, U. Thewalt and K. H. Dötz, *J. Organomet. Chem.* 1984, **273**, C29.
7. N. H. Tran Huy and F. Mathey, *Organometallics* 1988, **7**, 2233
8. N. H. Tran Huy and E. O. Fischer, *Nouveau J. Chim.* 1985, **9**, 257.
9. C. Alvarez, A. Parlier, H. Rudler, R. Yefsah, J. C. Daran and C. Knobler, *Organometallics* 1989, **8**, 2253.
10. W. D. Wulff, R. W. Kaesler, G. A. Peterson and P.-C. Tang, *J. Am. Chem. Soc.* 1985, **107**, 1060.

Polyhedron Vol. 9, No. 18, pp. 2199–2204, 1990
Printed in Great Britain

0277–5387/90 $3.00+.00
© 1990 Pergamon Press plc

ALKALI–NUCLEOBASE INTERACTIONS: INVOLVEMENT OF EXOCYCLIC OXYGENS OF 1-METHYLURACIL AND 1-METHYLTHYMINE IN Na^+ BINDING

BIRGIT FISCHER, HANS PREUT and BERNHARD LIPPERT*

Fachbereich Chemie, Universität Dortmund, D-4600 Dortmund, F.R.G.

and

HELMUT SCHÖLLHORN and ULF THEWALT

Sektion für Röntgen und Elektronenbeugung, Universität Ulm, D-7900 Ulm, F.R.G.

(*Received* 16 *February* 1990; *accepted* 2 *April* 1990)

Abstract—Co-crystallization of $Na[AuCl_4]$ with 1-methyluracil, $C_5H_6N_2O_2$ (1-MeUH), and 1-methylthymine, $C_6H_8N_2O_2$ (1-MeTH), at pH 0.8 yields predominently salts of composition $[Na(1\text{-MeUH})_4][AuCl_4]$ (**1**) and $[Na(1\text{-MeTH})(H_2O)_4][AuCl_4]\cdot 1\text{-MeTH}\cdot 2H_2O$ (**2**). Both **1** and **2** crystallize in space group $P\bar{1}$ with cell dimensions $a = 10.531(3)$, **1**, 8.436(5), **2**; $b = 9.194(3)$, **1**, 10.521(7), **2**; $c = 7.924(2)$, **1**, 15.917(11) Å, **2**; $\alpha = 96.68(3)$, **1**, 102.61(5), **2**; $\beta = 85.09(3)$, **1**, 90.45(5), **2**; $\gamma = 103.88(3)$, **1**, 108.10(5)°, **2**; $U = 738.4$, **1**, 1306(2) Å^3, **2**; $Z = 1$, **1**, 2, **2**. Na^+ binding to 1-MeUH is through O(4) in **1** and O(2) in **2**. The packing of cations and anions in **1** is special in that infinite stacks of alternating $[Na(1\text{-MeUH})_4]^+$ and $[AuCl_4]^-$ are formed with the metals 3.962(1) Å apart.

The neutralization of the negative charges of the nucleotides in nucleic acids is mainly accomplished by alkali cations.[1] With DNA, the cations appear to form a highly mobile cylinder of positive charges around the polynucleotide strands.[2] Interactions are thought to take place preferentially though the phosphate oxygens,[3] but it is feasible that donor atoms of the bases in the grooves are involved as well. In several X-ray structures of mono- and dinucleotides containing uracil or thymine bases, alkali cations are found to directly interact with O(2) oxygen atoms.[4] The O(4) sites usually are involved in hydrogen bonding. Theoretical calculations of charge density distributions in nucleobases,[5] as well as electrostatic potentials[6] in the unsubstituted bases, have suggested O(2) and O(4) of these bases to be intrinsic metal binding sites. According to an *ab initio* computation, Na^+ binding to neutral uracil is expected to take place via both O(2) and O(4).[7]

Reports on metal binding to the exocyclic oxygens of neutral uracil and thymine nucleobases are relatively scarce.[8–11] To our knowledge, only four X-ray structures of such compounds are available, including that of a potassium complex: $HgCl_2$(uracil-O^4)$_2$,[9] $HgCl_2$(dihydrouracil-O^4)$_2$,[9] $CuCl_2$(1,3-dimethyluracil-O^4)$_2$,[10] and $[K_2$(1-propylthymine-O^2,O^4)$_4][Pd_2Cl_6]$.[11] Na^+ binding to O(2) and O(4) of 1-methylthymine has also been observed in CH_3Hg(1-methylthyminate) $0.5NaNO_3$,[12] but the situation is different in that mercury binding to the deprotonated N(3) position increases the basicity of the exocyclic oxygens, generating a situation intermediate between an anionic and a neutral ligand. A similar situation also applies to the $NaNO_3$ adducts of *cis*-$(NH_3)_2$Pt(1-methyluracilate)$_2$.[13] Finally, K^+ binding to O(2) in potassium thyminate[14] is not unexpected and not to be compared with the situation described in this paper.

EXPERIMENTAL

Preparation

$[Na(C_5H_6N_2O_2)_4][AuCl_4]$ (**1**) and $[Na(C_6H_8N_2O_2)(H_2O_4)][AuCl_4]\cdot C_6H_8N_2O_2\cdot 2H_2O$ (**2**) were isolated from aqueous, HCl acidic solutions (pH ~ 0.8)

* Author to whom correspondence should be addressed.

containing 1-methyluracil (1-MeUH, $C_5H_6N_2O_2$) (**1**), 1-methylthymine (1-MeTH, $C_6H_8N_2O_2$) and $NaAuCl_4$ in a 1 : 1 ratio upon slow evaporation at 3°C. Yields were 65% (**1**) and 58% (**2**). Compound **1** crystallizes as yellow cubes while **2** forms orange–yellow needles. Found (**1**): C, 27.3; H, 2.6; N, 12.4. Calc. for $C_{20}H_{24}N_8O_8Cl_4AuNa$: C, 27.7; H, 2.7; N, 12.9%. Found (**2**): C, 19.2; H, 3.1; N, 7.4; O, 19.7; Cl, 18.8, Au, 26.3; Na, 3.1. Calc. for $C_{12}H_{28}N_4O_{10}Cl_4AuNa$: C, 19.2; H, 3.8; N, 7.5; O, 21.3; Cl, 18.9; Au, 26.2; Na, 3.0%. The poor analysis of H and O in **2** is probably due to partial loss of H_2O, as confirmed by thermogravimetry.

Spectroscopy

IR spectra were recorded as KBr pellets on a Perkin–Elmer 580 B spectrometer. No reliable spectra were obtained with Nujol mulls and CsI windows due to reaction of $[AuCl_4]^-$ with CsI, leading to Au^0 formation. Raman spectra (solid state) were obtained on a Coderg T 800 instrument with 647.1 nm excitation, ^1H NMR spectra on Bruker AM 300 and AC 200 spectrometers in D_2O. pD values were determined by use of a glass electrode and addition of 0.4 units to the meter reading.

Crystal data for **1** *and* **2**

$C_{20}H_{24}N_8O_8Cl_4AuNa$ (**1**), $M = 866.23$, triclinic, $a = 10.531(3)$, $b = 9.194(3)$, $c = 7.924(2)$ Å, $\alpha = 96.68(3)$, $\beta = 85.09(3)$, $\gamma = 103.88(3)°$, $U = 738.4$ Å^3, $F(000) = 422$, space group $P\bar{1}$, $Z = 1$, $D_c = 1.948$ g cm^{-3}, Mo-K_α radiation ($\lambda = 0.71069$ Å), μ(Mo-K_α) = 51.8 cm^{-1}.

$C_{12}H_{28}N_4O_{10}Cl_4AuNa$ (**2**), $M = 750.14$, triclinic, $a = 8.436(5)$, $b = 10.521(17)$, $c = 15.917(11)$ Å, $\alpha = 102.61(5)$, $\beta = 90.45(5)$, $\gamma = 108.10(5)°$, $U = 1306(2)$ Å^3, $F(000) = 732$, space group $P\bar{1}$, $Z = 2$, $D_c = 1.908$ g cm^{-3}, Mo-K_α radiation ($\lambda = 0.71073$ Å), μ(Mo-K_α) = 61.0 cm^{-1}, $T = 291(1)$ K.

Data collection and processing

Phillips PW-1100 (**1**) and Nicolet R3m/V diffractometer (**2**); θ–2θ technique ($\theta_{max} = 25°$) for **1**, ω—2θ scan, scan speed 2.00–14.65° min^{-1} in θ, scan width (1.2 + dispersion)° for **2**, graphite-monochromated Mo-K_α radiation; 2609 (**1**), 7083 (**2**) reflections measured, 2558 (**1**), 3104 (**2**) used [$F_o > 2F_o$ (**1**), $F_o > 3F_o$ (**2**)]; correction for Lorentz and polarization factors, empirical absorption correction.

Structure analysis and refinement

The structures were solved by the heavy-atom method. All non-hydrogen atoms were refined anisotropically. With **2**, hydrogen atoms were placed in geometrically calculated positions (C—H, N—H 0.96 Å). Refinement was by full-matrix least-squares method for **1** to $R = 0.064$, $R_w = 0.065$ ($w^{-1} = \sigma^2(F) + 0.0026\ F^2$) and for **2** to $R = 0.047$, $R_w = 0.046$ ($w^{-1} = \sigma^2(F) + 0.001157\ F^2$). Calculations were performed using SHELX 76 (**1**) and PARST, SHELXTL PLUS; PCK83, PLATON and MISSYM (**2**).*

RESULTS AND DISCUSSION

1-MeUH and $Na[AuCl_4]$ interact in moderately acidic solution (pH 1–2, HCl) mainly with formation of **1**. In the ^1H NMR spectra, resonances due to four minor products are observed in addition to the signals due to averaging between 1-MeUH and **1**. Only one of these, 5-chloro-1-methyluracil [δ(ppm) H(δ), 7.94, s], has unambiguously been identified. A second one, which amounts to *ca* 20% of **1** at 1-MeUH : $[AuCl_4]^- = 1$, is probably a species containing coordinated 1-MeU [δ(ppm) H6, 7.55, d, 7.7 Hz; H5, 5.80, d; CH_3, 3.41 s]. There is no indication of addition of HOCl to the 5,6-double bond of 1-MeUH after several days at 22°C, analogous to reactions of $[AuBr_4]^-$ with uridine[15] and uracil.[16] As the pH of the mixture of 1-MeUH and $Na[AuCl_4]$ is raised, reactions become very complex, leading to reduction to Au(1-MeU), elemental gold and other unidentified products.

Figure 1 provides a view of $[Na(1\text{-MeUH})_4][AuCl_4]$ (**1**) with the atom numbering as indicated. Selected bond lengths and angles are listed in Table 1. The compound consists of discrete $[Na(1\text{-MeUH})_4]^+$ cations and $[AuCl_4]^-$ anions. Within the centrosymmetric cation, the four 1-MeUH rings are bound via their exocyclic O(4) oxygens to a single Na^+, distances being 2.336(7) Å (rings *a*) and 2.301(8) Å (rings *b*). Rings *a* and *b* are almost coplanar (dihedral angle 5.3°). The geometry of the 1-MeUH rings do not display significant differences as compared to 1-MeUH in the absence of Na^+.[17] The geometry of the $[AuCl_4]^-$ is also normal.[18] Anions and cations are arranged in a co-linear fashion with gold and sodium lined up like pearls on a string (Fig. 2). Cations are parallel to each

* Additional details of the X-ray work, atomic coordinates, displacement factors coefficients, lists of bond lengths and angles and F_o, F_c values have been deposited as supplementary data with the Editor, from whom copies are available on request. Atomic coordinates have also been deposited with the Cambridge Crystallographic Data Centre.

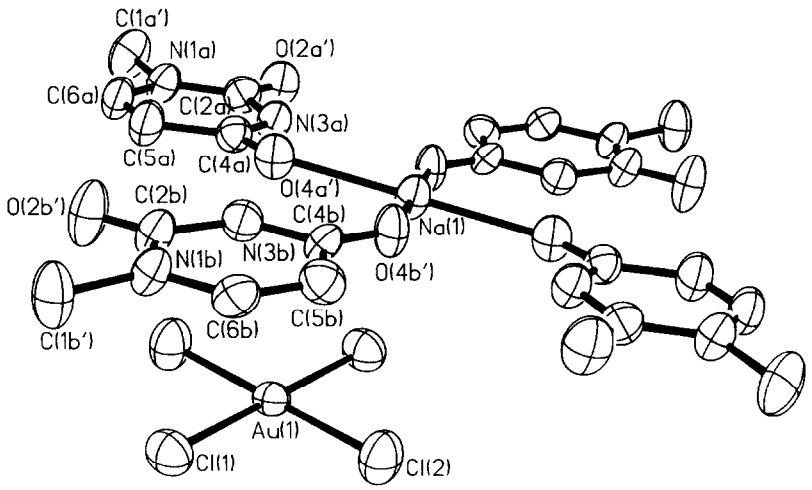

Fig. 1. Presentation of $[Na(1\text{-MeUH})_4]^+$ and $[AuCl_4]^-$ ions of **1** with the atom numbering scheme.

other and in an eclipsed arrangement, as are the anions, but there is a 14.6° angle between the $NaO(4)_4$ and $AuCl_4$ planes. Since the Au—Na separations of 3.962 Å are much too long for any significant interaction, the Na^+ may be regarded as being present in a square-planar coordination sphere. This situation appears to be unusual for sodium.

Figure 3 gives a view of the contents of the unit cell of $[Na(C_6H_8N_2O_2)(H_2O)_4][AuCl_4]\cdot C_6H_8N_2O_2 \cdot 2H_2O$ (**2**). Selected interatomic distances and angles are summarized in Table 2. The compound consists of a centrosymmetric $[Na_2(1\text{-MeTH})_2(H_2O)_8]^{2+}$ entity, two discrete $[AuCl_4]^-$ anions, two extra 1-MeTH rings and four molecules of water of crystallization. Binding of Na^+ to the 1-MeTH rings is through the exocyclic O(2) oxygens, designated O(12) and O(12a) in the figure. Refinement with O(4) as the assumed binding site [O(14), O(14a) in Fig. 3] gave somewhat poorer R values. The Na—O(12) distance [2.286(8) Å] in **2** is slightly shorter than Na—O(4a) in **1**. The octahedrally distorted coordination sphere of Na^+ is completed by three terminal and two bridging water molecules. The coordination pattern of the two Na^+ ions with two bridging aqua groups thus has similarities with those observed in alkali salt hydrates.[19] Geometries

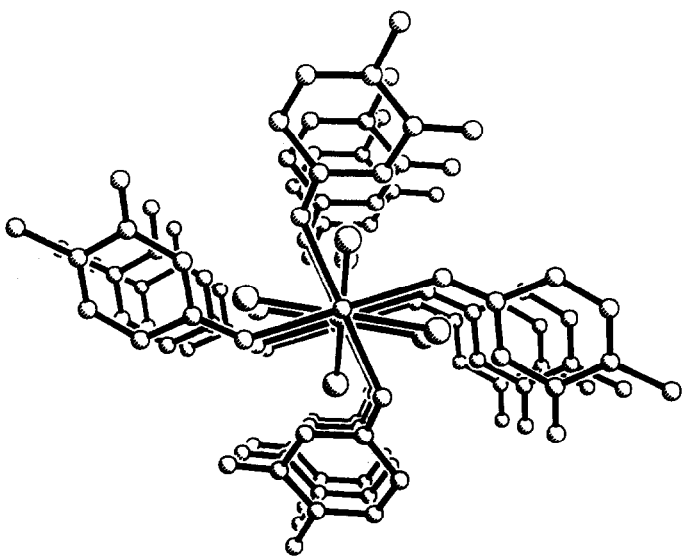

Fig. 2. A section of the stack of alternating $[Na(1\text{-MeUH})_4]^+$ and $[AuCl_4]^-$ ions in **1**.

Table 1. Selected bond lengths (Å) and bond angles for $[Na(1\text{-}MeUH)_4][AuCl_4]$ (1)

Na—O(4a)′	2.336(7)	O(4a)′—Na—O(4b)′	90.1(3)
Na—O(4b)′	2.301(8)		
Au—Cl(1)	2.280(3)	Cl(1)—Au—Cl(2)	89.9(1)
Au—Cl(2)	2.271(4)		
Na—Au	3.962(1)		
N(1a)—C(1a)′	1.49(2)	C(1a)′—N(1a)—C(6a)	120.2(8)
N(1a)—C(2a)	1.41(1)	C(1a)′—N(1a)—C(2a)	118.4(9)
C(2a)—O(2a)′	1.23(1)	C(6a)—N(1a)—C(2a)	121.3(8)
C(2a)—N(3a)	1.37(2)	O(2a)′—C(2a)—N(1a)	122.0(8)
N(3a)—C(4a)	1.37(1)	O(2a)′—C(2a)—N(3a)	123.0(9)
C(4a)—O(4a)′	1.24(1)	N(1a)—C(2a)—N(3a)	115.0(9)
C(4a)—C(5a)	1.46(1)	C(2a)—N(3a)—C(4a)	126.0(9)
C(5a)—C(6a)	1.34(2)	O(4a)′—C(4a)—N(3a)	118.0(9)
C(6a)—N(1a)	1.36(2)	O(4a)′—C(4a)—C(5a)	126(1)
		N(3a)—C(4a)—C(5a)	115.9(9)
		C(4a)—C(5a)—C(6a)	118(1)
		C(5a)—C(6a)—N(1a)	123(1)
N(1b)—C(1b)′	1.47(2)	C(1b)′—N(1b)—C(6b)	120.5(8)
N(1b)—C(2b)	1.38(2)	C(1b)′—N(1b)—C(2b)	118.9(8)
C(2b)—O(2b)′	1.22(1)	C(6b)—N(1b)—C(2b)	120.5(9)
C(2b)—N(3b)	1.40(1)	O(2b)′—C(2b)—N(1b)	124(1)
N(3b)—C(4b)	1.37(1)	O(2b)′—C(2b)—N(3b)	121(1)
C(4b)—O(4b)′	1.24(1)	N(1b)—C(2b)—N(3b)	115(1)
C(4b)—C(5b)	1.44(2)	C(2b)—N(3b)—C(4b)	124.9(9)
C(5b)—C(6b)	1.33(1)	O(4b)′—C(4b)—N(3b)	117.6(8)
C(6b)—N(1b)	1.38(1)	O(4b)′—C(4b)—C(5b)	125.3(9)
		N(3b)—C(4b)—C(5b)	117.2(9)
		C(4b)—C(5b)—C(6b)	188(1)
		C(5b)—C(6b)—N(1b)	124(1)

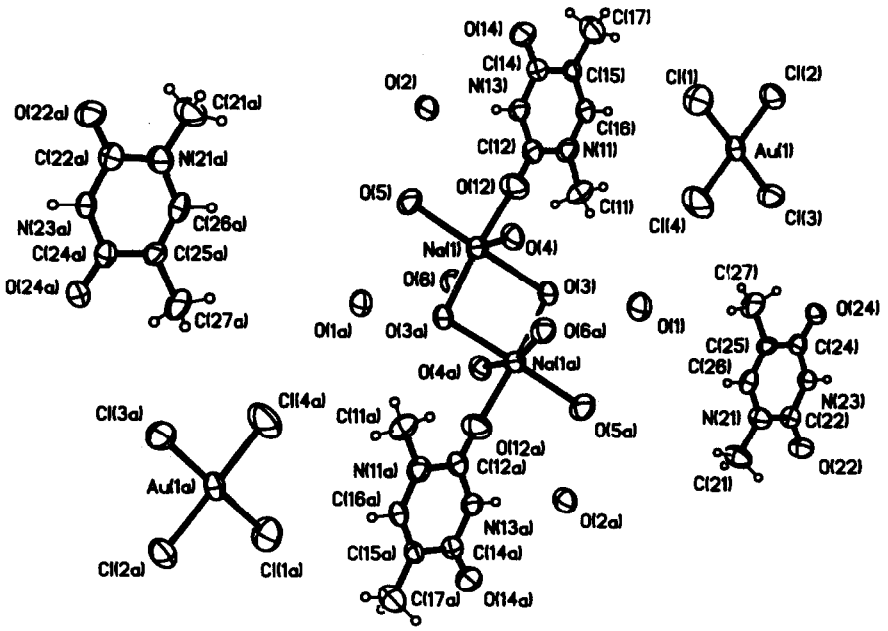

Fig. 3. View of $[Na(1\text{-}MeTH)(H_2O)_4][AuCl_4]\cdot 1\text{-}MeTH\cdot 2H_2O$ (2) with the atom numbering scheme.

Table 2. Selected bond lengths (Å) and bond angles for $[Na(1\text{-MeTH})(H_2O)_4][AuCl_4] \cdot 1\text{-MeTH} \cdot 2H_2O$ (**2**)

Na(1)—O(3)	2.474(8)	O(6)—Au(1)—O(12)	99.6(3)
Na(1)—O(3a)	2.465(6)	O(5)—Na(1)—O(12)	89.2(3)
Na(1)—O(4)	2.547(9)	O(5)—Na(1)—O(6)	93.5(3)
Na(1)—O(5)	2.378(8)	O(4)—Na(1)—O(12)	93.3(3)
Na(1)—O(6)	2.397(9)	O(4)—Na(1)—O(6)	161.7(4)
Na(1)—O(12)	2.286(8)	O(4)—Na(1)—O(5)	99.6(3)
		O(3)—Na(1)—O(12)	89.7(3)
		O(3)—Na(1)—O(6)	87.9(3)
		O(3)—Na(1)—O(5)	178.3(4)
		O(3)—Na(1)—O(4)	79.2(3)
		O(12)—Na(1)—O(3a)	173.2(3)
		O(6)—Na(1)—O(3a)	85.6(3)
		O(5)—Na(1)—O(3a)	94.9(3)
		O(4)—Na(1)—O(3a)	80.6(3)
		O(3)—Na(1)—O(3a)	86.1(3)
		Na(1)—O(3)—Na(1a)	93.9(2)
		Na(1)—O(12)—C(12)	172.4(8)
Au(1)—Cl(1)	2.269(4)	Cl(3)—Au(1)—Cl(4)	90.7(2)
Au(1)—Cl(2)	2.276(3)	Cl(2)—Au(1)—Cl(4)	179.6(3)
Au(1)—Cl(3)	2.280(3)	Cl(2)—Au(1)—Cl(3)	89.1(2)
Au(1)—Cl(4)	2.269(4)	Cl(1)—Au(1)—Cl(4)	89.3(2)
		Cl(1)—Au(1)—Cl(3)	179.9(3)
		Cl(1)—Au(1)—Cl(2)	90.9(2)
N(11)—C(11)	1.49(1)	C(12)—N(11)—C(16)	120.2(9)
N(11)—C(12)	1.39(1)	C(11)—N(11)—C(16)	121.6(9)
N(11)—C(16)	1.38(1)	C(11)—N(11)—C(12)	117.9(9)
C(12)—O(12)	1.21(1)	N(11)—C(12)—N(13)	114.3(9)
C(12)—N(13)	1.38(1)	N(11)—C(12)—O(12)	123(1)
N(13)—C(14)	1.36(1)	O(12)—C(12)—N(13)	122.4(9)
C(14)—O(14)	1.25(1)	C(12)—N(13)—C(14)	126.5(8)
C(14)—C(15)	1.39(1)	N(13)—C(14)—C(15)	117(1)
C(15)—C(16)	1.35(1)	N(13)—C(14)—O(14)	119.1(9)
C(15)—C(17)	1.46(1)	O(14)—C(14)—C(15)	123(1)
		C(14)—C(15)—C(17)	120(1)
		C(14)—C(15)—C(16)	118.4(9)
		C(16)—C(15)—C(17)	121.9(9)
		N(11)—C(16)—C(15)	123.2(9)
N(21)—C(21)	1.48(1)	C(22)—N(21)—C(26)	119.2(9)
N(21)—C(22)	1.39(1)	C(21)—N(21)—C(26)	121.0(9)
N(21)—C(26)	1.38(1)	C(21)—N(21)—C(22)	119.7(9)
C(22)—O(22)	1.24(1)	N(21)—C(22)—N(23)	115.3(9)
C(22)—N(23)	1.38(1)	N(21)—C(22)—O(22)	121.8(9)
N(23)—C(24)	1.36(1)	O(22)—C(22)—N(23)	122.8(9)
C(24)—O(24)	1.24(1)	C(22)—N(23)—C(24)	127.5(8)
C(24)—C(25)	1.42(1)	N(23)—C(24)—C(25)	115.4(9)
C(25)—C(26)	1.35(1)	N(23)—C(24)—O(24)	120.1(9)
C(25)—C(27)	1.51(1)	O(24)—C(24)—C(25)	125(1)
		C(24)—C(25)—C(27)	118.2(9)
		C(24)—C(25)—C(26)	119(1)
		C(26)—C(25)—C(27)	123.1(9)
		N(21)—C(26)—C(25)	123.8(9)

of the anion and of both types of 1-MeTH rings[20] are normal. Free and coordinated 1-MeTH stack along the *Y* axis (dihedral angle 2.9°). The $[AuCl_4]^-$ anion is virtually parallel with the two 1-MeTH rings (dihedral angles with bound and free ligand 2.0 and 2.1°, respectively) but does not participate in stacking with the two 1-methylthymines. Both N(3)H protons of the two rings are hydrogen bonded to water molecules [N(13)···O(2), 2.88(1) Å; N(23)···O(4) intermol., 2.90(1) Å].

Vibrational spectra of **1** and **2** differ from their respective starting components, 1-MeUH and 1-MeTH, in a number of details which refer, for example, to the CO stretching region of the IR (split into two intense components at 1705 and 1655 cm^{-1} in **1**, structured single band at 1660 cm^{-1} in 1-MeUH), to positions of the most intense ring modes[21] in the Raman [ring-stretch 1235 cm^{-1} (**1**), 1225 cm^{-1} (1-MeUH); ring-breathing 760 cm^{-1} (**1**), 770 cm^{-1} (1-MeUH)] or to the position of the δ_{oop} NH in the IR (860 cm^{-1} in **2**, 900 cm^{-1} in MeTH). It is not possible to attribute these difference exclusively to Na^+ binding, since the hydrogen bonding patterns are completely different in the free bases[17,20] and the Na^+ adducts **1** and **2**. It actually appears that the effects of Na^+ binding and hydrogen bonding are comparable since the Raman spectrum of **2** (solid state), albeit different from that of 1-MeTH, does not permit a differentation of modes due to 1-MeTH bound to Na^+ and free 1-MeTH. In both compounds **1** and **2**, the three Raman active Au—Cl vibrations are clearly identified at *ca* 350 (vs), 327 (s) and 169 (s) cm^{-1}.

Acknowledgement—This work was supported by the Fonds der Chemischen Industrie.

REFERENCES

1. W. Saenger, *Principles of Nucleic Acid Structures*. Springer, Berlin (1984).
2. M. LeBret and B. H. Zimm, *Biopolymers* 1984, **23**, 271.
3. B. Pullman, N. Gresh and H. Berthod, *Theoret. Chim. Acta* 1975, **40**, 71.
4. For example, M. A. Viswamitra, M. L. Post and O. Kennard, *Acta Cryst.* 1979, **B35**, 1089; N. C. Seeman, J. M. Rosenberg, F. L. Suddath, J. J. P. Kim and A. Rich, *J. Molec. Biol.* 1976, **104**, 109; N. Camerman, J. K. Fawcett and A. Camerman, *J. Molec. Biol.* 1976, **107**, 601.
5. A. V. Renugopalakrishnan, A. V. Laskshminarayanan and V. Sasisekharan, *Biopolymers* 1971, **10**, 1159.
6. R. Bonaccorsi, A. Pullman, E. Scrocco and J. Tomasi, *Theoret. Chim. Acta* 1972, **24**, 51.
7. D. Perahia, A. Pullman and B. Pullman, *Theoret. Chim. Acta* 1977, **43**, 207.
8. M. Goodgame and K. W. Johns, *J. Chem. Soc., Dalton Trans.* 1977, **2**, 1680; A. R. Sarkar and P. Ghosh, *Inorg. Chim. Acta* 1983, **78**, L39; S. Mansy and R. S. Tobias, *Inorg. Chem.* 1975, **14**, 287.
9. J. A. Carrabine and M. Sundaralingam, *Biochemistry* 1971, **10**, 292.
10. B. A. Cartwright, M. Goodgame, K. W. Johns and A. C. Skapski, *Biochem. J.* 1978, **175**, 337.
11. B. L. Kindberg, E. H. Griffith and E. L. Amma, *J. Chem. Soc., Chem. Commun.* 1975, 195.
12. F. Guay and A. Beauchamp, *Inorg. Chim. Acta* 1982, **66**, 57.
13. D. Neugebauer and B. Lippert, *J. Am. Chem. Soc.* 1982, **104**, 6596.
14. C. J. L. Lock, P. Pilon and B. Lippert, *Acta Cryst.* 1979, **B35**, 2533.
15. R. Ettore, *J. Chem. Soc., Dalton Trans.* 1983, 2329.
16. R. Ettore and M. Martelli, *Inorg. Chim. Acta* 1985, **108**, 73.
17. W. Micklitz, B. Lippert, H. Schöllhorn and U. Thewalt, *J. Heterocyclic Chem.* 1989, **26**, 1499; D. W. Green, F. S. Mathews and A. Rich, *J. Biol. Chem.* 1962, **237**, 3573.
18. J. C., Bowles and D. Hall, *Acta Cryst.* 1975, **B31**, 2149.
19. A. F. Wells, in *Structural Inorganic Chemistry*, pp. 675–677. Clarendon Press, Oxford (1984).
20. K. Hoogsteen, *Acta Cryst.* 1963, **16**, 28; A. Kvick, T. F. Koetzle and R. Thomas, *J. Chem. Phys.* 1974, **61**, 2711.
21. L. Colombo and D. Kirin, *Spectrochim. Acta* 1986, **42A**, 557; H. Susi and J. S. Ard, *Spectrochim. Acta* 1974, **30A**, 1843.

Polyhedron Vol. 9, No. 18, pp. 2205–2210, 1990
Printed in Great Britain

0277–5387/90 $3.00+.00
© 1990 Pergamon Press plc

ALKYLSILAZALANES. REACTION OF TRIMETHYLALUMINIUM WITH SILAZANES: SYNTHESIS AND MOLECULAR STRUCTURE OF $[Al(CH_3)_2]_2[C_{12}H_{32}N_2Si_4]$ AND $[Al(CH_3)_2]_2[C_8H_{28}N_2Si_4]$

JAMEICA J. BYERS, WILLIAM T. PENNINGTON
and GREGORY H. ROBINSON*

Department of Chemistry, Clemson University, Clemson, SC 29634-1905, U.S.A.

and

DUANE C. HRNCIR*

Department of Chemistry, University of Texas at Dallas, Richardson, TX 75083-0688, U.S.A.

(*Received* 23 *February* 1990; *accepted* 26 *April* 1990)

Abstract—The crystalline product $[Al(CH_3)_2]_2[C_{12}H_{32}N_2Si_4]$ (**I**), obtained from reaction of 2,2,5,5-tetramethyl-2,5-disila-1-azacyclopentane with trimethylaluminium in a heptane–chlorobenzene mixture, crystallizes in the orthorhombic space group *Pbca* (No. 61) with unit-cell parameters $a = 15.393(3)$, $b = 12.987(2)$, $c = 13.189(4)$ Å, $V = 2637.4(2)$ Å^3 and $D_c = 1.06$ g cm^{-3} for $Z = 4$. Full-matrix least-squares refinement based on 1549 observed reflections with intensities in the range $4.00 < 2\theta < 50.0°$ converged at $R = 0.048$ ($R_w = 0.064$). Compound **I** resides about a crystallographic centre of symmetry and contains a planar Al_2N_2 four-membered ring with an Al···Al contact of 2.790(3) Å. Reaction of trimethylaluminium with 1,1,3,3-tetramethyldisilazane in heptane affords the crystalline product $[Al(CH_3)_2]_2[C_8H_{28}N_2Si_4]$ (**II**). Compound **II** crystallizes in the triclinic space group $P\bar{1}$ (No. 2) with unit-cell parameters $a = 9.354(2)$, $b = 14.670(3)$, $c = 17.536(4)$ Å, $\alpha = 91.24(2)$, $\beta = 90.63(2)$, $\gamma = 99.46(2)°$, $V = 2372.7(9)$ Å^3 and $D_c = 1.06$ g cm^{-3} for $Z = 4$. Full-matrix least-squares refinement based upon 5033 observed reflections with intensities in the range $3.50 < 2\theta < 45.0°$ converged at $R = 0.035$ ($R_w = 0.048$). The mean Al···Al contact across the Al_2N_2 four-membered ring in **II** is 2.813(1) Å. The mean Al—N bond distance in **I** is 2.005(3) Å while the mean Al—N bond distance in **II** is 1.992(3) Å.

The interaction of aluminium species with amine moieties, particularly primary and secondary amines, has been extensively investigated. Seminal investigations may be traced to the condensation reactions involving aluminium alkyls and monodentate amines reported by Smith and coworkers.[1,2] These systems, demonstrated to eliminate alkane, were shown to result in interesting oligomeric reaction products possessing extensive Al—N association. The voluminous number of studies on the organoaluminium chemistry of primary and secondary amines notwithstanding, it is particularly interesting to note that the literature reveals a paucity of studies concerning the corresponding chemistry of silazanes. Silazanes represent a particularly intriguing class of compounds in this regard. Herein, we report the synthesis and molecular structure of $[Al(CH_3)_2]_2[C_{12}H_{32}N_2Si_4]$ (**I**) and $[Al(CH_3)_2]_2[C_8H_{28}N_2Si_4]$ (**II**). Compounds **I** and **II**, isolated from reactions of trimethylaluminium with 2,2,5,5-tetramethyl-2,5-disila-1-azacyclopentane and 1,1,3,3-tetramethyldisilazane, respectively, represent the first silazalanes characterized by single-crystal X-ray diffraction techniques.

* Authors to whom correspondence should be addressed.

EXPERIMENTAL

General comments

Standard Schlenk techniques were employed in conjunction with an inert-atmosphere glove-box (Vacuum Atmospheres HE-43 Dri-Lab). Heptane and chlorobenzene were distilled under prepurified argon prior to use. 1,1,3,3-Tetramethyldisilazane and 2,2,5,5-tetramethyl-2,5-disila-1-azacyclopentane were purchased from Petrarch Systems, Inc. Both silazanes were used as received. Single-crystal X-ray diffraction data for **I** were collected on an Enraf–Nonius CAD-4 diffractometer, while single crystal data for **II** were collected on a Nicolet R3m/V diffractometer. NMR data were recorded on an IBM 200 MHz NMR spectrometer. IR spectra were recorded on a Nicolet DX5 FT–IR spectrometer.

Synthesis of $[Al(CH_3)_2]_2[C_{12}H_{32}N_2Si_4]$ (I)

A reaction vessel was charged with a heptane–chlorobenzene mixture (20 and 5 cm^3, respectively) and 2,2,5,5-tetramethyl-2,5-disila-1-azacyclopentane (5.3 mmol) in the dry-box. Trimethylaluminium (5.2 mmol) was slowly added via syringe. Reaction was immediate and vigorous. The reaction vessel was removed from the dry-box and heated (120°C) in a sand bath for 24 h. The reaction vessel was vented periodically over the course of the reaction. The reaction system was allowed to slowly cool to room temperature at which point the solution was filtered via cannula and concentrated *in vacuo*. Colourless, extremely water-sensitive, X-ray quality crystals were isolated: 80% yield; m.p. 129–132°C. ^{1}H NMR ($CDCl_3$): δ −0.59 (s, 12H, $AlCH_3$), 0.41 (s, 24H, $SiCH_3$), 0.78 (s, 8H, $SiCH_2$). ^{29}Si NMR ($CDCl_3$): δ −0.44 (s). IR (Nujol): cm^{-1} 1255 (m, Si—CH_3).

Synthesis of $[Al(CH_3)_2]_2[C_8H_{28}N_2Si_4]$ (II)

A reaction vessel was charged with heptane (20 cm^3) and 1,1,3,3-tetramethyldisilazane (5.2 mmol) in the dry-box. Trimethylaluminium (5.2 mmol) was slowly added via syringe. Reaction was immediate and vigorous. The reaction vessel was removed from the dry-box and heated (90°C) in an oil bath for 24 h. The reaction vessel was vented periodically. After heating, the system was allowed to stand undisturbed for several hours at room temperature. A multitude of colourless, X-ray quality crystals were isolated: 75% yield; m.p. 163–66°C. ^{1}H NMR ($CDCl_3$): δ −0.45 (s, 12H, $AlCH_3$), 0.36–0.31 (m, 24H, $SiCH_3$), 4.80 (m, 4H, Si*H*). ^{29}Si NMR ($CDCl_3$): δ −2.25 (d). IR (Nujol): cm^{-1} 1270 (s, Si—CH_3), 2180 (m, Si—H).

Structural solution and refinement of I

A colourless parallelepiped crystal of **I** was mounted in a thin-walled glass capillary under an inert atmosphere of argon. Cell parameters and an orientation matrix for data collection, obtained from least-squares refinement using the setting angles of 25 reflections measured by the computer controlled diagonal slit method of centering, corresponded to an orthorhombic cell. The space group was determined to be *Pbca* (No. 61). The structure was solved by direct methods. The scan rate varied from 5 to 20° min^{-1} in omega. Hydrogen atoms were located from difference maps. The positional parameters of the hydrogen atoms were refined for several cycles and then fixed for the remainder of the refinement. The data were collected using the ω–2θ scan technique. Refinement based on 1549 observed reflections converged at $R = 0.048$, $R_w = 0.064$. Relevant crystallographic data for **I** are provided in Table 1, while selected bond distances and angles are given in Table 2.

Structural solution and refinement of II

A colourless parallelepiped crystal of **II** was mounted in a thin-walled glass capillary under an inert atmosphere of argon. Cell parameters and an orientation matrix for data collection, obtained from a least-squares refinement of the setting angles of 32 carefully centred reflections, corresponded to a triclinic cell. The space group was determined to be $P\bar{1}$ (No. 2). The structure was solved by direct methods and refined using SHELXTL PLUS.[3] Non-hydrogen atoms were refined by using anisotropic thermal parameters. Hydrogen atoms were located by standard difference Fourier techniques. Hydrogen atoms bound to silicon atoms were refined using isotropic thermal parameters. An isotropic group thermal parameter [$U_{iso} = 0.135(2)$] and positional parameters were refined for the methyl hydrogen atoms. The final cycle of full-matrix least-squares refinement, based on 5033 observed reflections, converged at $R = 0.035$, $R_w = 0.048$. Compound **II** crystallized with four molecules per unit cell.[4] Relevant crystallographic data are given in Table 1 while selected bond distances and angles are given in Table 3.

RESULTS AND DISCUSSION

Wiberg reported the reaction of trimethylaluminium with ammonia in 1948.[5] Smith and co-workers later studied the reactions of aluminium alkyls with primary and secondary amines

Table 1. Summary of the crystallographic data for $[Al(CH_3)_2]_2[C_{12}H_{32}N_2Si_4]$ (I) and $[Al(CH_3)_2]_2[C_8H_{28}N_2Si_4]$ (II)

	I	II
Empirical formula	$C_{16}H_{44}N_2Al_2Si_4$	$C_{12}H_{40}N_2Al_2Si_4$
Colour; habit	Colourless; parallelepiped	
Space group	Orthorhombic, *Pbca*	Triclinic, $P\bar{1}$
Unit-cell dimensions		
a (Å)	15.393(3)	9.354(2)
b (Å)	12.987(2)	14.670(3)
c (Å)	13.189(4)	17.536(4)
α (°)		91.24(2)
β (°)		90.63(2)
γ (°)		99.46(2)
V (Å^3)	2637.4(2)	2372.7(9)
Molecules/cell	4	4
Molecular weight	430.94	378.86
D_c (g cm^{-3})	1.06	1.06
Diffractometer	Enraf–Nonius CAD-4	Nicolet R3m/V
Radiation	Mo-K_α (λ = 0.71073 Å)	
Temperature (°C)	21	21
2θ range (°)	4.00–50.0	3.50–45.0
Reflections collected	5101	6524
Reflections observed	1549	5033
GOF	1.70	1.37
R	0.048	0.035
R_w	0.064	0.048

Table 2. Selected bond distances (Å) and angles (°) for $[Al(CH_3)_2]_2[C_{12}H_{32}N_2Si_4]$ (I)

Bond distances (Å)			
Si(1)—N(1)	1.810(3)	Si(2)—C(7)	1.844(6)
Si(1)—C(3)	1.880(5)	Si(2)—C(8)	1.836(5)
Si(1)—C(5)	1.847(5)	Al(1)—N(1)	2.005(3)
Si(1)—C(6)	1.847(5)	Al(1)—C(1)	1.949(4)
Si(2)—N(1)	1.806(3)	Al(1)—C(2)	1.969(4)
Si(2)—C(4)	1.860(5)	C(3)—C(4)	1.488(6)
Al(1)—Al(1a)	2.790(1)	Si(1)—Si(2)	2.786(1)

Bond angles (°)			
N(1)—Si(1)—C(3)	99.7(2)	C(4)—Si(2)—C(8)	114.6(2)
N(1)—Si(1)—C(5)	118.4(2)	C(7)—Si(2)—C(8)	104.8(2)
N(1)—Si(1)—C(6)	113.3(2)	N(1)—Al(1)—C(1)	117.9(2)
C(3)—Si(1)—C(5)	112.2(2)	N(1)—Al(1)—C(2)	115.3(1)
C(3)—Si(1)—C(6)	110.2(2)	C(1)—Al(1)—C(2)	104.9(2)
C(5)—Si(1)—C(6)	103.1(2)	Si(1)—N(1)—Si(2)	101.0(1)
N(1)—Si(2)—C(4)	98.9(2)	Si(1)—N(1)—Al(1)	116.4(1)
N(1)—Si(2)—C(7)	112.6(2)	Si(2)—N(1)—Al(1)	114.4(1)
N(1)—Si(2)—C(8)	118.5(2)	Si(1)—C(3)—C(4)	111.1(3)
C(4)—Si(2)—C(7)	107.1(2)	Si(2)—C(4)—C(3)	108.9(3)

Table 3. Selected bond distances (Å) and angles (°) for $[Al(CH_3)_2]_2[C_8H_{28}N_2Si_4]$ (II)

Bond distances (Å)			
Si(1)—N(1)	1.785(2)	Si(1)—C(1)	1.858(4)
Si(1)—C(2)	1.860(4)	Si(2)—N(1)	1.776(2)
Si(2)—C(3)	1.857(4)	Si(2)—C(4)	1.850(4)
Si(3)—N(2)	1.781(2)	Si(3)—C(5)	1.858(3)
Si(3)—C(6)	1.857(4)	Si(4)—N(2)	1.790(2)
Si(4)—C(7)	1.856(4)	Si(4)—C(8)	1.851(4)
Al(1)—Al(2)	2.813(1)	Al(1)—N(1)	1.999(2)
Al(1)—N(2)	1.990(2)	Al(2)—C(9)	1.960(4)
Al(1)—C(10)	1.960(4)	Al(2)—N(1)	1.992(2)
Al(2)—N(2)	1.994(2)	Al(2)—C(11)	1.954(3)
Al(2)—C(12)	1.963(4)		
Bond angles (°)			
N(1)—Si(1)—C(1)	112.9(2)	N(1)—Si(1)—C(2)	113.1(2)
C(1)—Si(1)—C(2)	108.2(2)	N(1)—Si(2)—C(3)	113.4(2)
N(1)—Si(2)—C(4)	113.6(2)	C(3)—Si(2)—C(4)	107.0(2)
N(2)—Si(3)—C(5)	113.4(2)	N(2)—Si(3)—C(6)	113.0(2)
C(5)—Si(3)—C(6)	107.7(2)	N(2)—Si(4)—C(7)	113.1(2)
N(2)—Si(4)—C(8)	113.4(2)	C(7)—Si(4)—C(8)	107.5(2)
N(1)—Al(1)—N(2)	90.2(1)	Al(2)—Al(1)—C(9)	125.1(1)
Al(2)—Al(1)—C(10)	125.3(1)	N(2)—Al(1)—C(9)	114.3(1)
N(1)—Al(2)—N(2)	90.3(1)	N(1)—Al(1)—C(10)	114.1(1)
Si(1)—N(1)—Si(2)	117.6(1)	C(9)—Al(1)—C(10)	109.6(2)
Si(2)—N(1)—Al(1)	111.4(1)	Al(1)—Al(2)—C(11)	125.3(1)
Si(2)—N(1)—Al(2)	112.1(1)	N(2)—Al(2)—C(11)	114.4(1)
Si(3)—N(2)—Si(4)	117.3(1)	N(1)—Al(2)—C(12)	113.1(1)
Si(4)—N(2)—Al(1)	111.4(1)	C(11)—Al(2)—C(12)	110.1(1)
Si(4)—N(2)—Al(2)	111.6(1)	Si(1)—N(1)—Al(1)	111.2(1)
Si(1)—N(1)—Al(2)	111.5(1)	Al(1)—N(1)—Al(2)	89.6(1)
Si(3)—N(2)—Al(1)	111.8(1)	Si(3)—N(2)—Al(2)	111.7(1)
Al(1)—N(2)—Al(2)	89.8(1)		

and reported that these systems would readily eliminate alkane and result in reaction products possessing Al_2N_2 fragments.[6] This laboratory has recently investigated the reaction of aluminium species with macrocyclic and multidentate open-chain amines and found that the coordination of core aluminium atoms could be extended beyond four-coordinate tetrahedral to five- and six-coordinate environments.[7,8] As silazalanes are relatively rare we endeavoured to examine the organo-aluminium chemistry of silazanes.

As shown in Fig. 1, **I** contains two tetramethyldisilaazacyclopentane moieties bridged by a pair of dimethylaluminium units. Compound **I** resides about a crystallographic centre of symmetry. The core of the dimer contains a four-membered Al_2N_2 ring. The independent Al—N bond distance of 2.005(3) Å may be considered rather long and may be regarded as a consequence of the crowding about the bridgehead nitrogen atom of the silazane imposed by the two bulky tetramethyldisila units. The Al—N—Al bond angle in the Al_2N_2 ring is 89.5(3)° while the N—Al—N bond angle is 90.5(2)°. The Al···Al contact in **I** is 2.790(1) Å. The preparation of **I** prompted us to consider the reaction of trimethylaluminium with silazanes possessing Si—H bonds. 1,1,3,3-Tetramethyldisilazane was examined in this regard.

The X-ray crystal structure of **II** is provided in Fig. 2. Several points are worthy of note regarding structure and bonding. Similar to **I**, compound **II** is a dimer as two tetramethyldisilazane units are bridged by a pair of dimethylaluminium units, thereby constituting an Al_2N_2 four-membered ring. The bond angles of the Al_2N_2 ring are determined to be 89.7(1) and 90.3(1)° for Al—N—Al and N—Al—N, respectively. The mean Al—N bond distance in **II** of 1.992(3) Å is certainly a

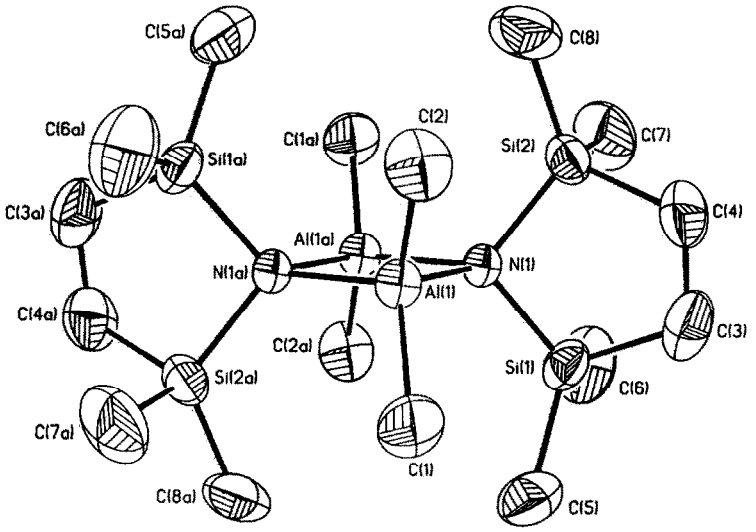

Fig. 1. A view of the $[Al(CH_3)_2]_2[C_{12}H_{32}N_2Si_4]$ (I) molecule showing the atom labelling scheme. Thermal ellipsoids show 50% probability levels; hydrogen atoms have been omitted.

result of less severe steric constraints than those found in **I**. The mean Al···Al contact of 2.813(1) Å in **II** is noticeably longer than the corresponding contact of 2.790(3) Å observed for **I**. It is also interesting that, regardless of the severity of the reaction conditions or the molar ratio of trimethylaluminium, the sila-hydrogen atoms remained inert with regard to reaction with the aluminium alkyl.

The literature reveals only a few studies concerning silazalanes. Based on cryoscopic molecular weight determinations, IR and NMR, Schmidbaur and Schmidt[9] reported the synthesis of $[(CH_3)_3SiNHAlCl_2]_2$ (**III**) and $[(CH_3)_3SiNHAl(CH_3)_2]_2$ (**IV**). These workers reported that **III** could be alkylated by methyllithium in a facile manner to provide **IV**. Both **III** and **IV** were predicted to contain Al_2N_2 four-membered rings. Even though **IV** has one remaining hydrogen atom on each nitrogen atom, condensation did not take place. More recently Sonnek *et al.*[10] reported the synthesis of some interesting Si—N—Al compounds.

The organoaluminium chemistry of silazalanes represents a potentially intriguing, and largely

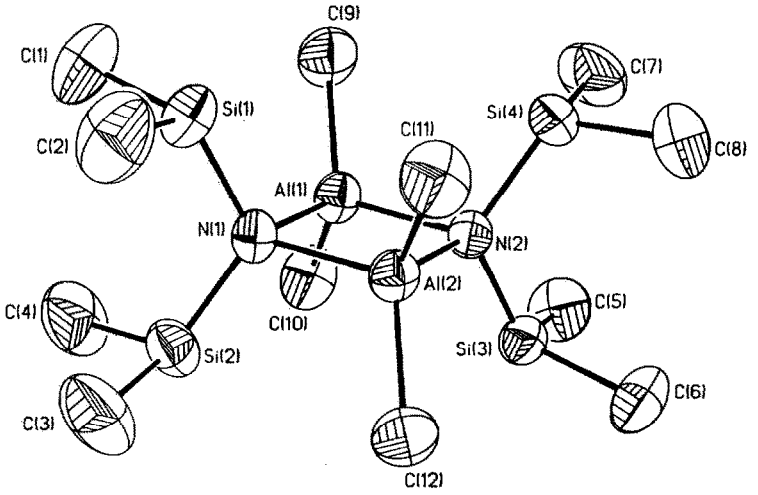

Fig. 2. A view of the $[Al(CH_3)_2]_2[C_8H_{28}N_2Si_4]$ (II) molecule showing the atom labelling scheme. Thermal ellipsoids show 50% probability levels; hydrogen atoms have been omitted.

unexplored, region of study. Future studies will continue to address the hydridic reactivity of the Si—H bond relative to organoaluminium moieties.

Acknowledgements—G.H.R. is grateful to the National Science Foundation for support of this work (RII-8520554). D.C.H. wishes to thank the donors of the Petroleum Research Fund, administered by the American Chemical Society.

Supplementary material available. A summary of data collection and refinement (5 pages), tables of crystal data, bond distances and angles, final fractional coordinates, thermal parameters (19 pages), and a listing of observed and calculated structure factors (23 pages) have been deposited with the Editor and are available upon request.

REFERENCES

1. A. W. Laubengayer, J. D. Smith and G. G. Ehrlich, *J. Am. Chem. Soc.* 1961, **83**, 542.
2. M. Cohen, J. K. Gilbert and J. D. Smith, *J. Chem. Soc.* 1965, 1092.
3. G. M. Sheldrick, SHELXTL, Crystallographic Computing System Revision 5.1; Nicolet Instruments Division: Madison, WI (1986).
4. The two independent molecules in the asymmetric unit are experimentally identical. As no higher symmetry could be recognized by analysis of the Niggli values of the reduced cell or by observation of a graphic representation of the intensity weighted reciprocal lattice, the presence of two independent molecules in the asymmetric unit appears to be the result of packing interactions.
5. E. Wiberg, in G. Bahr: Fiat Review of German Science, *Inorganic Chemistry* (Edited by W. Klemm), Part 2, Vol. 24, p. 155 (1948).
6. S. Amirkhalili, P. B. Hitchcock, A. D. Jenkins, J. Z. Nyathi and J. D. Smith, *J. Chem. Soc., Dalton Trans.* 1981, 1206.
7. G. H. Robinson and S. A. Sangokoya, *J. Am. Chem. Soc.* 1987, **109**, 6852.
8. G. H. Robinson, M. F. Self, S. A. Sangokoya and W. T. Pennington, *J. Am. Chem. Soc.* 1989, **111**, 1520.
9. H. Schmidbaur and M. Schmidt, *Angew. Chem. Int. Ed.* 1962, **1**, 327.
10. G. Sonnek, M. Pach, H. Bredereck and L. Oswald, *J. Organomet. Chem.* 1987, **329**, 31.

Polyhedron Vol. 9, No. 18, pp. 2211–2220, 1990
Printed in Great Britain

0277–5387/90 $3.00+.00
© 1990 Pergamon Press plc

MULTIPLE BONDS BETWEEN MAIN GROUP ELEMENTS AND TRANSITION METALS—LXXXI.* CONDENSATION REACTIONS OF HIGH-VALENT PENTAMETHYLCYCLOPENTADIENYL RHENIUM COMPLEXES WITH THIOPHENOL AND DERIVATIVES: SYNTHETIC AND STRUCTURAL ASPECTS

JANOS TAKACS,† PAUL KIPROF and WOLFGANG A. HERRMANN‡

Anorganisch-chemisches Institut der Technischen Universität München, Lichtenbergstraße 4, D-8046 Garching (Germany)

(*Received* 12 *March* 1990; *accepted* 26 *April* 1990)

Abstract—The half-sandwich rhenium(VII) complex $(\eta^5\text{-}C_5Me_5)ReO_3$ (**1**; Me = CH_3) undergoes reduction with thiophenol giving the rhenium(V) condensation product $(\eta^5\text{-}C_5Me_5)Re(O)(SC_6H_5)_2$ (**2a**) in high yield. However, toluene-3,4-dithiol reacts only slowly with **1**, with traces of the fully substituted rhenium(V) species $(\eta^5\text{-}C_5Me_5)Re(1,2\text{-}S_2C_6H_3\text{-}4\text{-}CH_3)_2$ (**3a**) being formed. The related *N,S*-chelating ligand 2-aminothiophenol forms the amido derivative $(\eta^5\text{-}C_5Me_5)Re[1,2\text{-}S(HN)C_6H_4]_2$ (**3b**) in good yield. Compounds **3a** and **3b** are also accessible by two alternative routes: (i) from $(\eta^5\text{-}C_5Me_5)Re(O)Cl_2$ (**4**) and the corresponding thiols in the course of two-step substitution/condensation reactions via the intermediates $(\eta^5\text{-}C_5Me_5)Re(O)(1,2\text{-}S_2C_6H_3\text{-}4\text{-}CH_3)$ (**2b**) and $(\eta^5\text{-}C_5Me_5)Re(O)[1,2\text{-}S(HN)C_6H_4]$ (**2c**), respectively; (ii) from the tetrachloro complex $(\eta^5\text{-}C_5Me_5)ReCl_4$ (**5**) and two equivalents of the respective ligands. Employing a 1:1 stoichiometry, reaction of $(\eta^5\text{-}C_5Me_4Et)ReCl_4$ (**5′**; Et = C_2H_5) with 2-aminothiophenol yields the amidothiophenolato(*N,S*) complex of formula $(\eta^5\text{-}C_5Me_4Et)Re[1,2\text{-}S(HN)C_6H_4]Cl_2$ (**6′**). The solid-state structure of the bis(dithiolato)rhenium(V) complex **3a** was determined by means of X-ray diffraction techniques. The core geometry around the rhenium is almost perfectly square pyramidal, with the five-membered ring ligand occupying the apical position (centroid π-coordination), while the four sulphur atoms define the basal plane. The relatively short distances between the interligand sulphur atoms (297–301 pm) are compatible with possible bonding interactions, e.g. partial disulphide character.

High oxidation state half-sandwich organometallic compounds have received considerable attention in recent years. Thiolato transition metal complexes in medium to high oxidation states are also the focus of interest, not least because of their special relationship to biochemically relevant systems.[1,2] Finally, some emphasis on rhenium stems from the properties of the ^{186}Re and ^{188}Re isotopes that are candidates for certain radiopharmaceuticals for therapeutic applications.[3]

It was recently determined in our laboratory that condensation reactions of methyltrioxorhenium(VII), CH_3ReO_3, with catechols and similar *aromatic* bifunctional ligands of type HX···Y (X = O, S, Y = N, NH_2, OH) provide a convenient route to novel hexacoordinate *cis*-dioxo(methyl) rhenium derivatives of d^0 configuration.[4,5] In order to find out as to whether replacement of the σ-bonded methyl group in CH_3ReO_3 by the much bulkier pentamethylcyclopentadienyl π-ligand in $(\eta^5\text{-}C_5Me_5)ReO_3$ would entail a different reactivity pattern, $(\eta^5\text{-}C_5Me_5)ReO_3$ (**1**), $(\eta^5\text{-}C_5Me_5)Re(O)Cl_2$

* Preceding communication in this series (No. LXXX): W. A. Herrmann, J. G. Kuchler, P. Kiprof and J. Riede, *J. Organomet. Chem.*, in press.

† Currently Alexander von Humboldt Fellow on leave from the Research Group for Petrochemistry of the Hungarian Academy of Sciences, Veszprem, Hungary.

‡ Author to whom correspondence should be addressed.

(**4**), $(\eta^5\text{-}C_5Me_5)ReCl_4$ (**5**) and $(\eta^5\text{-}C_5Me_4Et)ReCl_4$ (**5′**) were investigated in their reactions with mono- and bifunctional thiophenols. The synthetic results as well as the crystal structure of the bis (dithiolato) complex $(\eta^5\text{-}C_5Me_5)Re(1,2\text{-}S_2C_6H_3\text{-}4\text{-}CH_3)_2$ (**3a**) are reported in the present publication.

RESULTS AND DISCUSSION

(1) *Rhenium*(V) *complexes derived from aromatic thiols*

The reaction of $(\eta^5\text{-}C_5Me_5)ReO_3$ (**1**) with thiophenol is slow at room temperature as compared to the fast condensation reaction of this ligand with CH_3ReO_3.[6] Addition of mineral acids (that promote the protonation of the oxo ligand, presumed to be the first step in the condensation) or of 2,2-dimethoxypropane (as water scavenger) somewhat increase the rate but not sufficiently. However, temperatures around 110°C (boiling toluene) effect high-yield formation of the half-sandwich oxo complex of formula $(\eta^5\text{-}C_5Me_5)Re(O)(SC_6H_5)_2$ (**2a**) according to eq. (1). This compound is also formed from $(\eta^5\text{-}C_5Me_5)Re(O)Cl_2$ and thiophenolate,[7] but the new route reported here is more straightforward.

The process involves both *condensation* and *reduction* reactions as the heptavalent rhenium is reduced to oxidation state +V, with the thiol serving as reductant. Diphenyl disulphide [eq. (1)] was isolated and identified. Formation of the hypothetical rhenium(VII) condensation products such as $(\eta^5\text{-}C_5Me_5)Re(O)(SC_6H_5)_4$ (in analogy to the stable $CH_3Re(O)(SC_6H_5)_4$[6] formed from CH_3ReO_3) or $(\eta^5\text{-}C_5Me_5)Re(O)_2(SC_6H_5)_2$ does not occur. Due to the bulk of the pentamethylcyclopentadienyl and thiophenolate ligands, these complexes would sterically be more crowded than **2a**. Further condensation of **2a** to $(\eta^5\text{-}C_5Me_5)Re(SC_6H_5)_4$ was not observed even upon prolonged reflux with thiophenol.

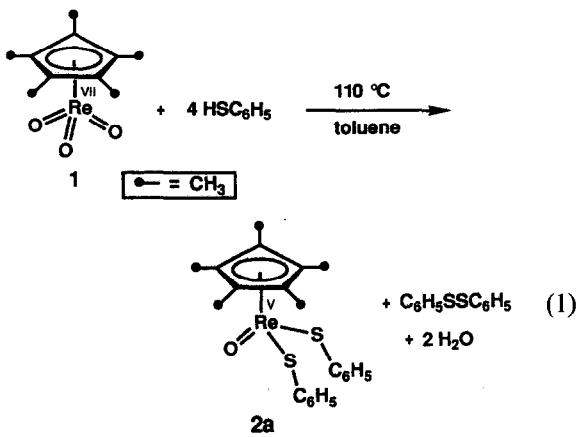

(1)

(2) *Rhenium*(V) *complexes of toluene*-3,4-*dithiol*

By way of contrast, reaction between **1** and toluene-3,4-dithiol under similar conditions is very slow. The starting compound **1** is recovered almost quantitatively after 2 h in refluxing toluene. This is surprising since both aromatic *mono-* and 1,2-*di*thiols react with CH_3ReO_3 cleanly with condensation.[6] This different reactivity is also puzzling, considering that the expected products $(\eta^5\text{-}C_5Me_5)Re(O)(1,2\text{-}S_2C_6H_3\text{-}4\text{-}CH_3)$ (**2b**) or $(\eta^5\text{-}C_5Me_5)Re(1,2\text{-}S_2C_6H_3\text{-}4\text{-}CH_3)_2$ (**3a**) are thermodynamically stable (*vide infra*). The difference in acidity of the dithiol does not impose a barrier on the condensation reaction (*vide infra*), and aromatic 1,2-dithiols are known to be stronger reductants than thiophenol.[8] On the other hand, they do not form simple disulphides but rather eight-membered $(C_2S_2S_2C_2)$ ring systems.

The above-mentioned monosubstituted rhenium (V) compound **2b** was synthesized from **4** and stoichiometric amounts of thiolate generated from thiol/triethylamine (Scheme 1). *Aliphatic* congeners of **2b,c** with *O,O*-, *O,S*-, *S,S*-, and *O,N*-chelating ligands have been reported from analogous reactions.[9] The substitution reaction shown in Scheme 1 is fast. If one employs an *excess* of dithiol, however, a subsequent slow condensation with high-yield formation of the reddish bis(dithiolato) derivative **3a** takes place.

(3) *Rhenium*(V) *complexes of* 2-*aminothiophenol*

Counting the oxo ligand as a two- or a four-electron donor, the half-sandwich rhenium(V) derivatives **2a,b** are formally *16e-* or *18e-*species, respectively. Although they did not form adducts with Lewis base amine ligands, it seemed interesting to study the reaction of **1** and **4** with the bifunctional ligand 2-aminophenol, since formation of a five-membered chelate ring with a N → Re dative bond or, more common in high oxidation state oxo complexes,[5,10] deprotonation of the amino group could not be excluded. If a toluene solution of **1** in the presence of an *excess* of 2-aminothiophenol is boiled under reflux, the colour quickly turns green. A dark green compound was isolated and characterized as the novel rhenium(V) complex **3b** of formula $(\eta^5\text{-}C_5Me_5)Re[1,2\text{-}S(HN)C_6H_4]_2$ (Scheme 2).

The same condensation product **3b** can be obtained in good yields at room temperature starting from **4** and *two equivalents* of 2-aminothiophenol in the presence of a base such as triethylamine to deprotonate the aminothiol (Scheme 2). Consecutive colour changes in this particular case

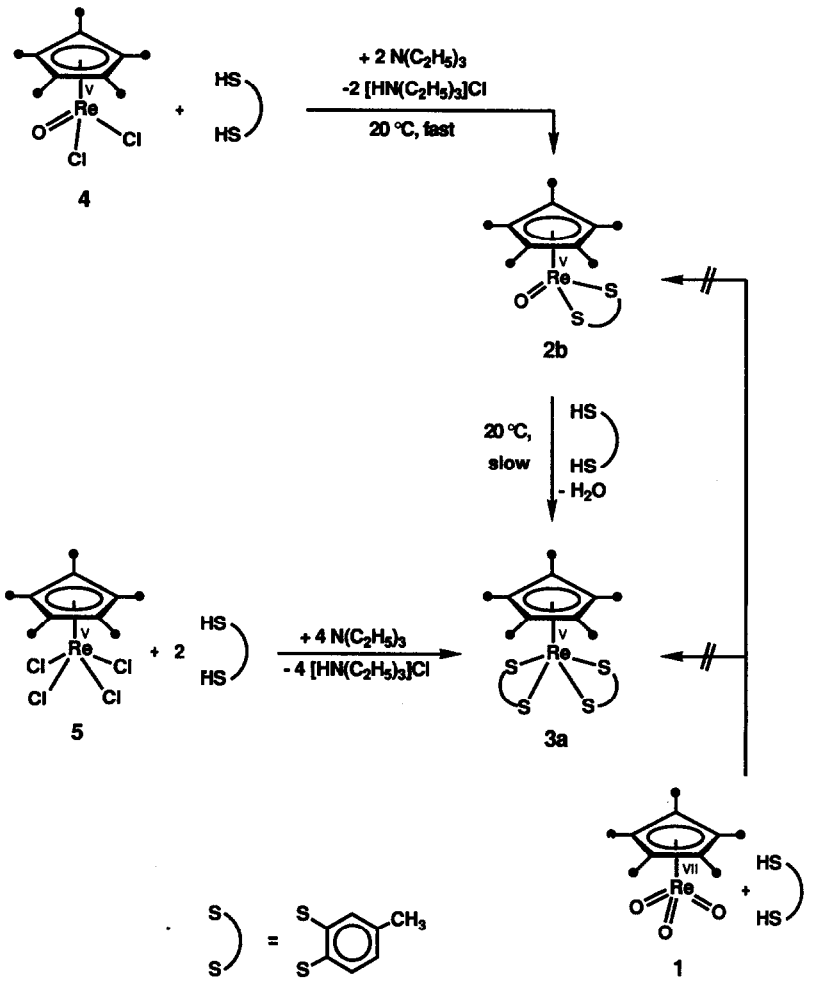

Scheme 1.

indicated that the formation of the fully substituted product **3b** proceeds in two steps: the first step is fast (HCl elimination), while the second step (condensation) is slow. The yellow intermediate **2c** of formula $(\eta^5\text{-}C_5Me_5)Re(O)[1,2\text{-}S(HN)C_6H_4]$ was isolated in high yields (Scheme 2).

Another convenient route to the bis(dithiolato-*S*,*S*) and bis(amidothiophenolato-*S*,*N*) compounds **3a** and **3b**, respectively, commences from the tetrachloro complex $(\eta^5\text{-}C_5Me_5)ReCl_4$ (**5**): treatment with two equivalents of toluene-3,4-dithiol and 2-aminothiophenol in the presence of a base according to Schemes 1 and 2, respectively, gives **3a** and **3b** in greater than 85% isolated yield.

A yellow complex, **6**, is formed when **5** and 2-aminothiophenol react in equimolar amounts. The formula $(\eta^5\text{-}C_5Me_5)ReCl_2[1,2\text{-}S(HN)C_6H_4]$ is tentatively assigned on the basis of the spectroscopic data. Complex **6** was also obtained by treatment of compound **2c** with chlorotrimethylsilane, a reagent widely used to replace an oxo ligand by two chloro ligands. However, the isolation of analytically pure **6** was rendered impossible due to its low solubility in organic solvents. In order to gain increased solubility, $(\eta^5\text{-}C_5Me_4Et)ReCl_4$ (**5'**) was used in a similar reaction, and the yellow dichloro complex of formula $(\eta^5\text{-}C_5Me_4Et)ReCl_2[1,2\text{-}S(HN)C_6H_4]$ (**6'**) was in fact isolated in high yields and analytically pure [eq. (2)].

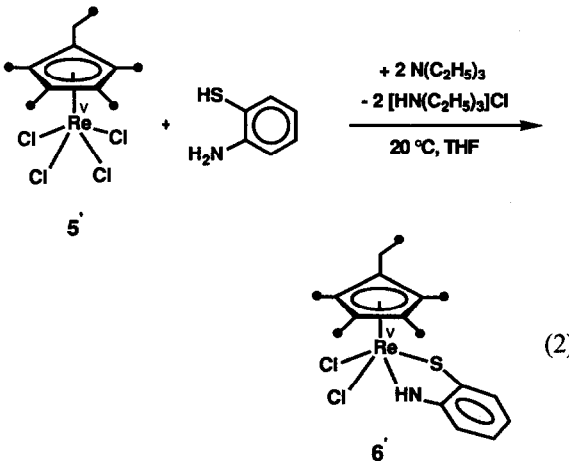

(2)

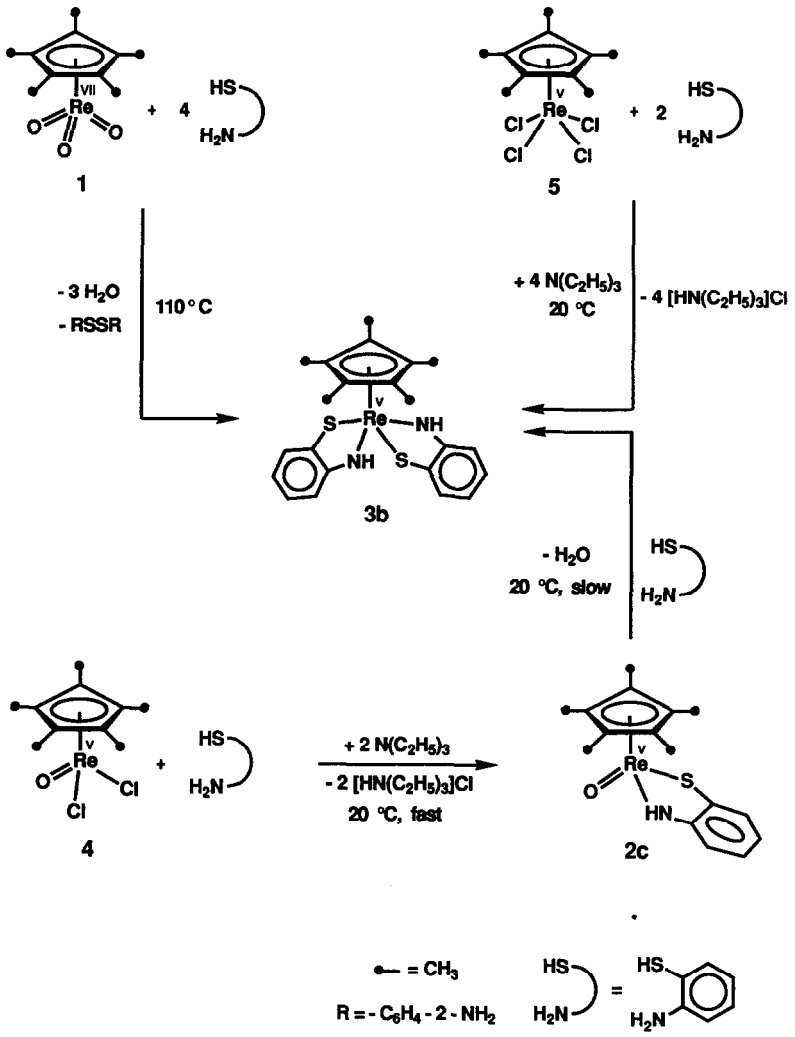

Scheme 2.

Attempted synthesis of $(\eta^5\text{-}C_5Me_5)Re(SC_6H_5)_4$ starting from **5** and an excess of thiophenolate lead to an intractable, moisture-sensitive oil which yielded **2a** upon hydrolysis.

(4) *Spectroscopic data*

All new compounds are thermally stable, and the condensation products **2a**, **3a** and **3b** are stable against water. The ^{1}H NMR spectra of compounds **2c** and **3b** show that the amido protons resonate at 8.89 and 9.23 ppm, respectively. The chemical shifts of the NH protons in compounds **6** and **6′**, are 12.67 and 12.68 ppm, respectively. As an explanation of this strong low-field shift, one is tempted to invoke an interaction (hydrogen bridge) between the NH proton and the chloride ligands.

CRYSTAL AND MOLECULAR STRUCTURE OF THE BIS(DITHIOLATE) RHENIUM(V) COMPLEX (3a)

Due to the asymmetry in the ligand toluene-3,4-dithiol, the synthesis of **3a** (Scheme 1) gives rise to formation of *cis*- and *trans*-isomers. Crystallographic investigations of **3a** have shown that the crystal chosen for this study contained both isomers (Fig. 1). As a result, disorder of one methyl group in the 4-position [(C(57) and C(57′)] occurs. The disorder at only one side of the molecule may arise from packing effects. Both methyl groups [C(57) and C(57′)] were nevertheless refined with anisotropic displacement parameters and a site occupation factor of 0.5.

The core geometry around the rhenium atom can

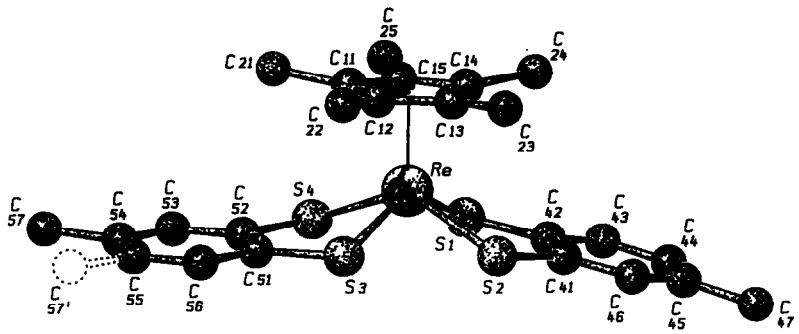

Fig. 1. SCHAKAL drawing of compound **3a**. Hydrogen atoms are omitted for clarity. The disordered methyl group C(57)′ is shown by dotted lines.

be described as square pyramidal, with the centre of the aromatic π-ligand located in the apical position and the four sulphur atoms forming the basal plane (Fig. 1). The rhenium atom lies 92 pm above this plane. All rhenium-to-sulphur distances are almost equal [231.8(1)–234.6(1) pm; Table 1] and are in the normal range for single bonds found in rhenium(V) thiolato complexes such as $[Re(O)(SR)_4]^-$ [11] and $[Re\{(SCH_2)_3CCH_3\}_2]^-$.[12] The angles S—Re—S′ are *all* close to 80°, and the sulphur–sulphur distances are almost the same within the ligands and between the two ligands, respectively. These distances cover the range between 298.5(3) and 307.4(3) pm (Table 1) so they hardly deviate from the data of the previously published bis(μ-sulphido) dinuclear compound $[(\eta^5\text{-}C_5Me_5)Re(O)(\mu\text{-}S)]_2$.[13] It is also remarkable that the sulphur contacts between two different ligands are significantly smaller [298.5(3) and 300.5(3) pm] as compared to the contacts of two sulphur atoms of the same ligand [305.4(3) and 307.4(3) pm]. For comparison, the sum of the van der Waals' radii is 360 pm; the S—S distance in the (monoclinic) elemental sulphur is 204 pm.[14] The relatively short interligand sulphur distances, e.g. the partial disulphide character of the toluene-3,4-dithiolate ligand is in our opinion due to both a repulsion effect of the sterically demanding C_5Me_5 ligand and an electronic effect originating from the oxidation state of the metal. Disulphide complexes M(RSSR) of transition metals are relatively rare as compared to the large number of thiolate compounds $M(SR)_2$.[15] Complexes with thiolate ligands showing *partial* disulphide character are usually found for the high metal oxidation states, examples being $[Re\{(SCH_2)_3CCH_3\}_2]^-$ [*d*(S—S): 283 pm[12]], $MoO_2[(R)_2NC(R)_2C(R)_2S]_2$ [*d*(S—S): 273–282 pm[16]], and/or have a sterically crowded environment around the metal atom such as in $(\eta^5\text{-}C_5H_5)_2Mo(SR)_2$.[17] *It is obvious that these two factors play an important role in the reductive elimination of organic disulphides from transition metal thiolato*

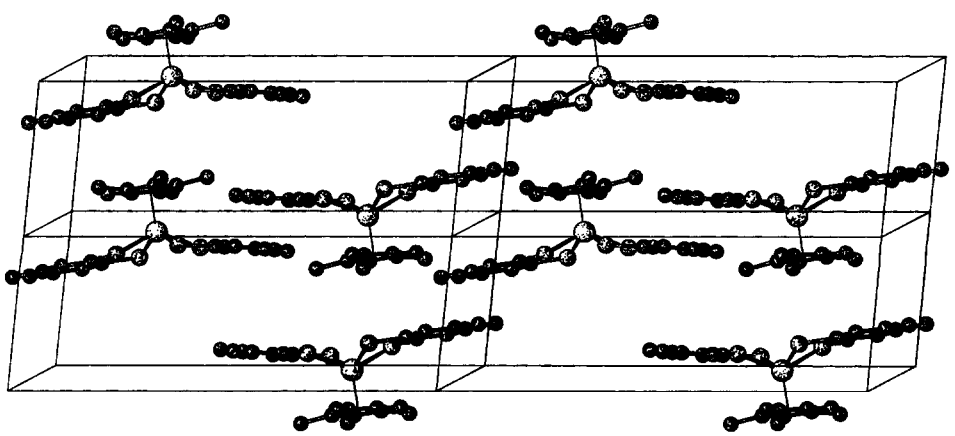

Fig. 2. Packing of compound **3a** (SCHAKAL).

Table 1. Selected bond lengths (pm), non-bonding distances (pm) and bond angles (°) for compound **3a**[a]

Re—S(1)	232.0(2)	S(1)—Re—S(2)	82.35(5)
Re—S(2)	231.8(1)	S(1)—Re—S(3)	134.08(5)
Re—S(3)	234.6(1)	S(1)—Re—S(4)	79.69(5)
Re—S(4)	234.0(1)	S(2)—Re—S(3)	80.25(6)
S(1)—C(42)	171.4(6)	S(2)—Re—S(4)	133.16(6)
S(2)—C(41)	174.7(6)	S(3)—Re—S(4)	82.02(5)
S(3)—C(51)	177.4(6)	Cp—Re—S(1)	114.0
S(4)—C(52)	175.7(6)	Cp—Re—S(2)	114.8
S(1)···S(4)	298.5(3)	Cp—Re—S(3)	111.9
S(2)···S(3)	300.5(3)	Cp—Re—S(4)	112.0
S(1)···S(2)	305.4(3)		
S(3)···S(4)	307.4(3)		
Re—Cp	198.1		

[a]Cp denotes the centre of the aromatic π-ligand [η^5-$C_5(CH_3)_5$].

complexes according to eq. (3).

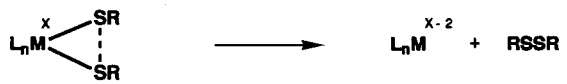

(3)

An interesting feature of the structure is the *folding* of the toluene-3,4-dithiolate ligands along the S—S axis by 22.6(2) and 36.5(1)° off planarity yielding the envelope form of the five-membered ring Re—S—C—C—S. The related rhenium(V) complex (η^5-C_5Me_5)Re(1,2-$O_2C_6Cl_4$)$_2$ contains practically *planar* catecholate ligands.[23] This difference may be attributed to the stronger π-donor properties of the oxygen atoms (catecholates have been shown to be good π-donor ligands) as compared to sulphur atoms, although packing effects as well as the inter-ligand sulphur–sulphur interaction may also effect the observed ligand folding. It seems likely that the difference in the folding angles of the two toluene-3,4-dithiolate ligands is the result of packing effects (Fig. 2).

CONCLUSIONS

Condensation reactions of the half-sandwich oxo rhenium(VII) complex (η^5-C_5Me_5)ReO_3 (**1**) with thiophenols proceed in a different manner than the analogous reactions of CH_3ReO_3. Reduction of the heptavalent rhenium to oxidation state V prevales, in spite of the fact that the electron-rich pentamethylcyclopentadienyl ligand is expected to make the rhenium less susceptible towards reduction as compared with CH_3ReO_3.* We believe that reduction is facilitated by the bulkiness of the pentamethylcyclopentadienyl ligand which prevents the accomodation of the same number of thiolate and oxo ligands at rhenium as in the case of $CH_3Re(O)(SR)_4$. This steric requirement could also induce the observed reductive elimination of disulphides [eq. (3)]. 1,2-Aminothiophenol leads to a similar deprotonation of the amine function as in the case of CH_3ReO_3; an amido group attached to rhenium thus forms. The crystal structure of the half-sandwich compound (η^5-C_5Me_5)Re(1,2-$S_2C_6H_3$-4-CH_3)$_2$ (**3a**) shows interaction between sulphur atoms of different toluene-3,4-dithiolate ligands, indicating some disulphide contribution to the overall structure. The chelate effect of the *S,S*-ligand is likely to prevent disulphide elimination in this particular case.

* Studies on the electrochemistry of CH_3ReO_3 and (η^5-C_5Me_5)ReO_3 support this view (W. A. Herrmann and R. Albach, unpublished results).

EXPERIMENTAL

All reactions were carried out in a dry nitrogen atmosphere employing conventional Schlenk techniques. The starting compounds **1**, **5**, **5′** and **4** were synthesized as described in the literature.[22] The thiols and 2-aminothiophenol were used as received from Aldrich Chemicals. The ^{1}H NMR spectra were recorded at 25°C and 400 MHz (JEOL JNM GX-400), electron-impact mass spectra at 70 eV (Finnigan MAT 311-A). The mass spectra are based on the ^{187}Re and ^{35}Cl isotopes (*m/z* values).

(1) *Synthesis of oxo(η^5-pentamethylcyclopentadienyl)bis(thiophenolato)rhenium*(V) (**2a**)

To **1** (73.8 mg, 0.2 mmol) in 10 cm^3 of toluene, thiophenol (81×10^{-3} cm^3, 0.8 mmol) was added.

The solution was refluxed for 2–3 h, then cooled down to room temperature. After filtration and concentration of the solution to 2–3 cm^3 *in vacuo*, n-hexane was added to precipitate the product as a yellowish-brown solid. Recrystallization from toluene–n-hexane at −30°C yielded analytically pure **2a**. Yield 79 mg (71%). Found (Calc.): C, 47.1 (47.5); H, 4.9 (4.5); Re, 33.3 (33.5); S, 11.3 (11.5)%.

IR (KBr; cm^{-1}): 923 vs [ν(Re═O)], 2962 m, 2915 m, 1577 s, 1465 s, 1381 s. ^1H NMR ($CDCl_3$; ppm): δ(C_5Me_5) 1.64 (s, 15H), δ(C_6H_5) 7.15–7.72 (m, 10H). EI–MS (*m/z*; rel. int. %): 556 ($[M]^+$), 447 ($[M-SC_6H_5]^+$, 65%), 370 ($[C_5Me_5ReOS]^+$, 100%).

(2) *Synthesis of oxo(η⁵-pentamethylcyclopentadienyl)(toluene-3,4-dithiolato-S,S′)rhenium*(V) (**2b**)

To **4** (81.6 mg, 0.2 mmol) dissolved in 10 cm^3 of toluene and 4 cm^3 of n-hexane, toluene-3,4-dithiol (26×10^{-3} cm^3, 0.2 mmol), and triethylamine (56×10^{-3} cm^3, 0.44 mmol) were added under vigorous stirring. The green solution turned yellow and triethylammonium chloride precipitated. After 3–4 min the solution was filtered through 2 cm of silylated silica (Merck No. 7719, 70–230 mesh), then the volume was reduced to 2–3 cm, and finally n-hexane was added. A yellowish-brown microcrystalline solid precipitated. The mother liquor was decanted and the product was washed twice with n-hexane and dried *in vacuo*. Recrystallization from toluene–n-hexane at −30°C afforded analytically pure **2b**. Yield 89 mg (90%). Found (Calc.): C, 41.8 (41.5); H, 4.1 (4.3)%.

IR (KBr; cm^{-1}): 920 sh, 912 s [ν(Re═O)], 2917 w, 1456 m, 1376 m, 1026 w, 808 s, 548 m. ^1H NMR ($CDCl_3$; ppm): δ(C_5Me_5) 2.04 (s, 15H); δ(1,2-$S_2C_6H_3$-4-CH_3) 2.35 (s, 3H); δ(5-$S_2C_6H_3CH_3$) 6.77 (d, 1H, $^3J = 7.7$ Hz); δ(3-$S_2C_6H_3CH_3$) 7.63 (s, 1H); δ(6-$S_2C_6H_3CH_3$) 7.70 (d, 1H, $^3J = 7.7$ Hz). EI–MS (*m/z*; rel. int. %): 492 ($[M]^+$, 100); 135 ($[C_{10}H_{15}]^+$, 10).

(3) *Synthesis of oxo(η⁵-pentamethylcyclopentadienyl)(1,2-amidothiophenolato-S,N)rhenium*(V) (**2c**)

A procedure similar to the synthesis of **2b** was used starting from **4** (81.6 mg, 0.2 mmol), 2-aminothiophenol (24×10^{-3} cm^3, 0.22 mmol) and triethylamine (61×10^{-3} cm^3, 0.44 mmol). Yield 72 mg (78%). Found (Calc.): C, 41.8 (41.7); H, 4.7 (4.4); N, 3.0 (3.0)%.

IR (KBr; cm^{-1}): 3321 m [ν(N—H)], 906 s [ν(Re═O)], 3055 w, 2920 w, 1467 m, 1444 m, 1376 m, 1297 m, 1022 w, 851 m, 754 s, 709 m. ^1H NMR ($CDCl_3$; ppm): δ(C_5Me_5) 1.98 (s, 15H); δ(HNC_6H_4S) 6.63–7.57 (m, 4H); δ(HNC_6H_4S) 8.89 (br, 1H). EI–MS (*m/z*; rel. int. %): 461 ($[M]^+$, 100).

(4) *Synthesis of (η⁵-pentamethylcyclopentadienyl) bis(toluene-3,4-dithiolato-S,S′)rhenium* (V) (**3a**)

Method (a), *from* **4**. To **4** (81.6 mg, 0.2 mmol) dissolved in toluene (8 cm^3), toluene-3,4-dithiol (58×10^{-3} cm^3, 0.44 mmol) and triethylamine (56×10^{-3} cm^3, 0.4 mmol) in 2 cm^3 methanol were added. The stirring was continued for 48 h at room temperature, then the dark brown–red precipitate was filtered, washed with small amounts of water and then cold methanol and finally dried *in vacuo*. Recrystallization from CH_2Cl_2–n-hexane at −30°C yielded 97 mg (89%) of **3a**.

Method (b), *from* **5**. A similar procedure as above starting from **5** (93 mg, 0.2 mmol) in toluene (5 cm^3), and toluene-3,4-dithiol (58×10^{-3} cm^3, 0.44 mmol) as well as triethylamine (122×10^{-3} cm^3, 0.88 mmol) in methanol (5 cm^3) yielded **3a** in 86% yield. Found (Calc.): C, 45.9 (45.8); H, 4.3 (4.3); Re, 29.9 (29.6)%.

IR (KBr; cm^{-1}): 2912 w, 1578 m, 1373 s, 1285 m, 1206 m, 1094 m, 1022 m, 813 sh, 798 s, 692 s, 545 m, 436 m. ^1H NMR ($CDCl_3$; ppm): δ(C_5Me_5) 1.71 (s, 15H), δ(1,2-$S_2C_6H_3$-4-CH_3) 2.34 (s, 6H), δ(5-$S_2C_6H_3CH_3$) 6.79 (d, 2H, $^3J = 7.9$ Hz), δ(3-$S_2C_6H_3CH_3$) 7.51 (S, 2H); δ(6-$S_2C_6H_3CH_3$) 7.57 (d, 2H, $^3J = 7.9$ Hz). EI–MS (*m/z*; rel. int. %): 630 ($[M]^+$, 100), 135 ($[C_{10}H_{15}]^+$, 33).

(5) *Synthesis of (η⁵-pentamethylcyclopentadienyl) bis(1,2-amidothiophenolato-S,N)rhenium* (**3b**)

Method (a), *from* **1**. To **1** (73.8 mg, 0.2 mmol) dissolved in toluene (10 cm^3), 2-aminothiophenol (86×10^{-3} cm^3, 0.8 mmol) was added and the mixture was refluxed for 1.5 h. After cooling to 25°C, the solution was filtered and concentrated to 3 cm^3 *in vacuo*. Upon addition of n-hexane (15 cm^3), an olive-green precipitate formed which was filtered and dried *in vacuo*. The product was recrystallized from THF–n-hexane at −30°C. The dark olive-green crystals contain 0.5 mol of the solvent THF per mol of **3b**. Yielded 91 mg (75%).

Method (**b**), *from* **4**. To **4** (81.6 mg, 0.2 mmol) dissolved in 10 cm^3 of toluene, 2-aminothiophenol (47×10^{-3} cm^3, 0.44 mmol) and triethylamine (70×10^{-3} cm^3, 0.5 mmol) were added under stirring. The colour turned yellow, while triethyl-

Table 2. Crystallographic data, parameters of data collection and structure refinement for **3a**

(a)	*Crystal parameters*	
	Empirical formula	$C_{24}H_{27}S_4Re$
	Formula weight	631.9
	Crystal colour and shape	Red, thin plates
	Crystal dimensions (mm)	0.72 · 0.34 · 0.03
	Radiation	Mo-K_α (λ = 71.073 pm)
	Temperature (°C)	22 ± 2
	Space group	$P\bar{1}$ (Int. Tab. No. 2)
	a (pm)	744.5(4)
	b (pm)	839.7(5)
	c (pm)	2090(2)
	α (°)	85.03(4)
	β (°)	89.49(4)
	γ (°)	64.72(6)
	V (pm^3)	1177×10^6
	Z	2
	ρ(calc.) (g cm^{-3})	1.784
	μ(Mo-K_α) (cm^{-1})	55.9
(b)	*Data collection*	
	Diffractometer	CAD4 Enraf–Nonius
	Monochromator	Graphite, incident beam
	Scan type	ω-Scan
	Scan time (s)	Maximum 60
	Scan width (°)	(1.40 + 0.30 · tgθ) ± 25% for corrections
	Maximum 2θ (°)	50
	Number of reflections measured	8227 (−8/8; −10/10, −24/24)
	Number of independent reflections	3951
	Corrections	Lorentz-polarization, (F_c(corr) = F_c/(1 + $\varepsilon \cdot F_c^2 \cdot$ LP)] numerical absorption corr. (6 Faces, transmission range: 0.219–0.835)
	Standard reflections	3 every 3600 s intensity check 3 every 200 orientation check
(c)	*Refinement*	
	Solution	Patterson method
	Hydrogen atoms	All calculated, not refined
	Refinement	Full-matrix least-squares
	Minimization function	$\Sigma w(\|F_o\| - \|F_c\|)^2$
	Weighting scheme	$1/\sigma(F_o)^2$
	Anomalous dispersion	All non-hydrogen atoms
	Number of reflections included, NO	3950 $I \geqslant 0.0$
	Number of parameters refined, NV	271
	R	0.049[a]
	R_w	0.039[b]
	Goodness-of-fit	2.886[c]
	Residual $\Delta\rho$ ($e^-/Å^3$)	+1.43 near Re −1.84
	Shift/error	0.00

[a] $R = \Sigma(||F_o| - |F_c||)/\Sigma|F_o|$.
[b] $R_w = [\Sigma w(|F_o| - |F_c|)^2/\Sigma w F_o^2]^{1/2}$.
[c] GOF = $[\Sigma w(|F_o| - |F_c|)^2/(NO - NV)]^{1/2}$.

ammonium chloride precipitated. After *ca* 5–10 min, the colour slowly started to turn green. The stirring was continued for 3 days. The volatiles were then removed *in vacuo*. The residue was extracted with toluene, the green solution was filtered and concentrated to *ca* 2–3 cm^3. Upon addition of n-hexane, a green precipitate of **3b** formed which was recrystallized from THF–n-hexane at −30°C. Yield 96 mg (87%).

Method (**c**), *from* **5**. A procedure similar to (b) starting from **5** (93 mg, 0.2 mmol), 2-aminothiophenol (47×10^{-3} cm^3, 0.44 mmol) and triethylamine (140×10^{-3} cm^3, 1.0 mmol) yielded **3b** in 87% yielded. Found (Calc. for **3b** · 0.5 THF): C, 47.6 (47.7); H, 4.7 (4.8); N, 4.7 (4.6); Re, 30.6 (30.8)%.

IR (KBr; cm^{-1}): 3294 m [ν(N—H)], 3053 w, 2908 w, 1569 m, 1442 m, 1375 m, 1301 s, 1023 m, 746 s, 726 m, 704 m, 459 m, 436 m. ^1H NMR ($CDCl_3$; ppm): $\delta(C_5Me_5)$ 1.66 (s, 15H), $\delta(HNC_6H_4S)$ 6.64–7.47 (m, 8H); $\delta(HNC_6H_4S)$ 9.23 (br, 2H). EI–MS (*m/z*; rel. int. %): 568 ($[M]^+$, 90): 135 ($[C_5Me_5]^+$, 10); 124 ($[SC_6H_4NH_2]^+$, 100).

(6) *Synthesis of dichloro*(η^5-*tetramethylethylcyclopentadienyl*)(1,2-*amidothiophenolato*-S,N)*rhenium* (V) (**6′**)

To **5′** (119.2 mg, 0.25 mmol) dissolved in 20 cm^3 of THF, 2-aminothiophenol (27.0×10^{-3} cm^3, 0.25 mmol) and anhydrous sodium carbonate (1–2 g powder) were added under vigorous stirring. The colour immediately turned to intense yellow. After 5 min, the solution was filtered, and the Na_2CO_3 was washed with THF. The combined THF fractions were evaporated to dryness. The residue was taken up in methylenechloride and was filtered through silylated silica (*ca* 3 cm). The filtrate was then concentrated *in vacuo*. Upon addition of n-hexane, a bright yellow microcrystalline solid separated, which was filtered and washed with n-hexane. Recrystallization from methylenechloride–n-hexane yielded 104 mg (79%) of analytically pure **6′**. Found (Calc.): C, 38.0 (38.5); H, 4.2 (4.2); N, 2.6 (2.6); Re, 35.0 (35.2)%.

IR (KBr; cm^{-1}): 3224 s [ν(N—H)], 2965 m, 2927 m, 1477 m, 1454 m, 1376 m, 1263 w, 1031 m, 1019 m, 821 w, 761 s. ^1H NMR ($CDCl_3$; ppm): $\delta(C_5Me_4CH_2CH_3)$ 0.96 (t, 3H, $^3J = 7.4$ Hz); $\delta(C_5Me_4CH_2CH_3)$ 1.62 (q, 2H, $^3J = 7.4$ Hz); $\delta(C_5[CH_3]_4CH_2CH_3)$ 1.71, 1.74, 1.77, 1.81 (4S, 12H); δ(1,2-S(NH)C_6H_4) 7.14–7.93 (m, 4H); δ(1,2-S(N*H*)C_6H_4) 12.68 (br, 1H). EI–MS (*m/z*; rel. int. %): 529 ($[M]^+$, 2); 493 ($[M - HCl]^+$, 3); 125 ($[H_2NC_6H_4S]^+$, 100).

(7) *X-ray diffraction study of* (η^5-*pentamethylcyclopentadienyl*)*bis*(*toluene* - 3,4 - *dithiolato* - S,S′) *rhenium*(V) (**3a**)[18–21]

Details of the data collection and structure refinement are listed in Table 2. The data were collected on a CAD4 (Enraf–Nonius). All computations were carried out on VAX 8200 and VAX 11/730 computers with the computer programs SDP[18] and SCHAKAL,[19] in the STRUX-II[21] system. Scattering factors were taken from ref. 20.

Acknowledgements—One of authors (J.T.) is grateful to the *Alexander von Humboldt Foundation* for the award of a research fellowship. We thank Dr M. Cook for helpful discussions. This work was supported by the *Deutsche Forschungsgemeinschaft* (Leibniz award to W. A. Herrmann) as well as *Degussa AG*.

REFERENCES

1. T. G. Spiro, *Metal Ions in Biology*. John Wiley, New York (1980).
2. H. Siegel, *Metal Ions in Biological Systems*. Dekker, New York (1974).
3. E. Deutsch, K. Libson, J. L. Vanderheyden, A. R. Ketring and H. R. Maxon, *Nucl. Med. Biol.* 1986, **13**, 465.
4. J. Takacs, P. Kiprof, J. G. Kuchler and W. A. Herrmann, *J. Organomet. Chem.* 1989, **369**, C1.
5. J. Takacs, P. Kiprof, J. Riede and W. A. Herrmann, *Organometallics* 1990, **9**, 782.
6. J. Takacs, W. A. Herrmann, P. Kiprof, J. G. Kuchler and M. Cook, *Organometallics* 1990, in press.
7. J. Takacs, P. Kiprof, G. Weichselbaumer and W. A. Herrmann, *Organometallics* 1989, **8**, 2394.
8. J. Houk and G. M. Whitesides, *J. Am. Chem. Soc.* 1987, **109**, 6825.
9. (a) W. A. Herrmann, D. Marz, E. Herdtweck, A. Schafer, W. Wagner and H.-J. Kneuper, *Angew. Chem.* 1987, **99**, 462; *Angew. Chem. Int. Ed. Engl.* 1987, **26**, 462; (b) W. A. Herrmann, D. W. Marz and E. Herdtweck, *J. Organomet. Chem.*, in press.
10. J. K. Gardner, N. Pariyadath, J. L. Corbin and E. I. Stiefel, *Inorg. Chem.* 1978, **17**, 897.
11. (a) A. C. McDonell, T. W. Hambley, M. R. Snow and A. G. Wedd, *Aust. J. Chem.* 1983, **36**, 253; (b) P. J. Blower, J. R. Dilworth, J. Hutchinson, T. Nicholson and J. Zubieta, *Inorg. Chim. Acta.* 1984, L27; (c) E. Block, H. Kang, G. Ofori-Okai and J. Zubieta, *Inorg. Chim. Acta* 1989, **156**, 27.
12. P. J. Blower, J. R. Dilworth, J. P. Hutchinson and J. Zubieta, *Transition Met. Chem.* 1982, **7**, 353.
13. W. A. Herrmann, K. A. Jung and E. Herdtweck, *Chem. Ber.* 1989, **122**, 2041.
14. A. F. Wells, *Structural Inorganic Chemistry*, p. 286. Clarendon Press, Oxford (1984).
15. I. G. Dance, *Polyhedron* 1986, **5**, 1037.
16. J. M. Berg, D. J. Spira, K. O. Hodgson, A. E. Bruce,

K. F. Miller, J. L. Corbin and E. I. Stiefel, *Inorg. Chem.* 1984, **23**, 3412.
17. M. A. A. F. De C. T. Carrondo, P. M. Matias and G. A. Jeffrey, *Acta Cryst.* 1984, **C40**, 932.
18. B. A. Frenz, The ENRAF Nonius CAD4 SDP SYSTEM, Computing in Crystallography, pp. 64–71. Delft University Press, Delft, Holland (1978).
19. E. Keller, SCHAKAL, Ein Program für die graphische Darstellung von Molekülmodellen. Kristallographisches Institut der Universität Freiburg (1988).
20. D. T. Cromer und J. T. Waber, *International Tables of Crystallography*, Vol. IV, Table 2.28. Kynoch Press, Birmingham, U.K. (1974).
21. R. E. Schmidt, M. Birkhahn, W. Massa, P. Kiprof and E. Herdtweck, STRUX-II, Programmsystem zur Verarbeitung von Röntgendaten. Universität Marburg (1980) and Technische Universität München (1985/87).
22. (a) W. A. Herrmann, E. Herdtweck, M. Flöel, J. Kulpe, U. Küsthardt and J. Okuda, *Polyhedron* 1987, **6**, 1165; (b) W. A. Herrmann, E. Voss and M. Flöel, *J. Organomet. Chem.* 1985, **297**, C5; (c) W. A. Herrmann, M. Flöel, J. Kulpe, J. K. Felixberger and E. Herdtweck, *J. Organomet. Chem.* 1988, **355**, 297.
23. W. A. Herrmann, U. Küsthardt and E. Herdtweck, *J. Organomet. Chem.* 1985, **294**, C33.

Polyhedron Vol. 9, No. 18, pp. 2221–2226, 1990
Printed in Great Britain

0277–5387/90 $3.00+.00
© 1990 Pergamon Press plc

MECHANISTIC FEATURES OF MOLECULAR REARRANGEMENTS

BRIAN F. G. JOHNSON*

University Chemical Laboratory, Lensfield Road, Cambridge CB2 1EW, U.K.

and

JONATHAN COOK, DANIEL ELLIS, SIMON HEFFORD and AUDREY WHITTAKER

Department of Chemistry, Long Road School, Cambridge, U.K.

(*Received* 27 *February* 1990; *accepted* 26 *April* 1990)

Abstract—A new scheme, which considers the sequential edge cleavage of ligand polyhedra, has been employed to explain the phenomenon of pseudorotation in simple homoleptic coordination complexes.

The stereochemical changes—fluxionality and isomerization—that many coordination compounds exhibit have become amongst the most widely studied phenomena in inorganic chemistry and although the mechanisms of some, for example, five- and six-coordination, may be simply explained, apart from simple ideas of diamond–square–diamond rearrangements no simple, coherent approach applicable to *all* examples appears to have evolved. In this paper we wish to discuss such an approach which we believe offers a unified view of these fascinating phenomena.

It is reasonable to claim that reactions in this category have become one of the most fascinating areas of study during the past decade. Although the phenomenon had been appreciated for some time the detailed examination of pseudorotation had to wait until the advent of a suitable analytical tool, and NMR proved ideal for this purpose. There were also early indications that X-ray analysis would provide support and complementary data for molecular rearrangements along well-defined pathways. In this case evidence derived for one molecular state (the solid) was initially employed to explain a phenomenon in another (solution). More recently magic-angle spinning (MAS) NMR spectrometry has been used to make detailed studies of molecular motions in the solid, and in an earlier communication, we commented[1] on the way in which information derived by this method could be used in conjunction with information from the X-ray experiment to explain motion in the solid. In this paper we shall examine possible complementary geometries for mononuclear coordination compounds ML_n and offer a new, more convenient method of understanding these phenomena.

MOLECULAR POLYHEDRA

Before we consider some of the problems associated with coordination geometry it is essential that we recall some of the more important aspects of polyhedral geometries. The most symmetric of all polyhedra are the regular polyhedra of Plato. These are the tetrahedron (a), the octahedron (b), the hexahedron (or cube) (c), the icosahedron (d), and the dodecahedron (e) which are illustrated in Fig. 1. These are the only convex polyhedra that are bound by identical regular polygonal faces in which all vertices are equivalent. Of these polyhedra only three, viz. the tetrahedron, the octahedron and the icosahedron, are fully triangulated and therefore stable. In contrast, the cube which has all square faces and 12 edges is unstable and will collapse (or contract) to the stable fully triangulated dodecahedron with 18 edges. Similarly, the dodecahedron

* Author to whom correspondence should be addressed.

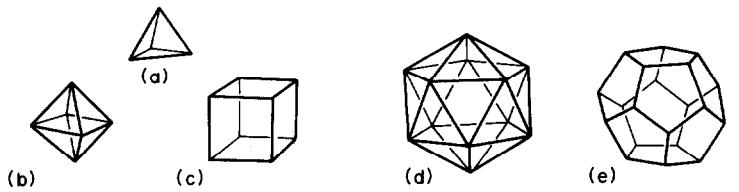

Fig. 1. The platonic solids.

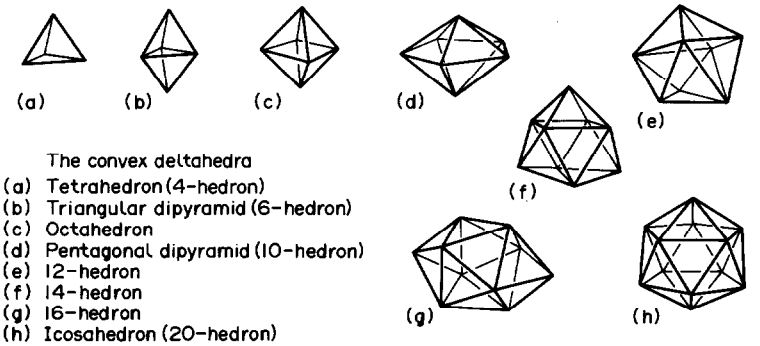

Fig. 2. Stable triangulated polyhedra.

with all pentagonal faces and 30 edges is also unstable and will collapse to the stable fully triangulated 36-hedron with 54 edges. Polyhedral stability does not therefore necessarily correlate with high symmetry. Rather, stability is associated with triangulation; the most stable polyhedra being those with all triangular faces. According to this view the most stable polyhedra for four- to 12-hedra are those given in Fig. 2. These are the polyhedra often observed in coordination chemistry and in the boranes and carboranes. We shall refer to them by their number of vertices, e.g. {4}, {5}, {6}, etc.

These polyhedra provide us with a prototypical array of geometric structures that reveals a useful and fascinating insight into chemical polyhedra. However, it is useful for our purposes to examine the relationship these polyhedra bear one to another. Consider the tetrahedron, {4}. Breakage of any one edge leads to a butterfly arrangement which, provided the extension is sufficiently large, corresponds to a trigonal bipyramid with one equatorial vertex removed—we shall therefore refer to this as {5−1}. Hence, if we cap this butterfly we produce the trigonal bipyramid {5} (see Fig. 3). Similarly, removal of one edge from the octahedron leads to the {7−1} polyhedron, and if we cap this polyhedral form the bicapped pentagonal bipyramid {7} (Fig. 4) will result. In the same vein we may progress from {7} through {8−1} to {8}, from {8} to {9−1} to {9}, and so on until we reach {10} (see Figs 3–5). If we consider these polyhedra to be

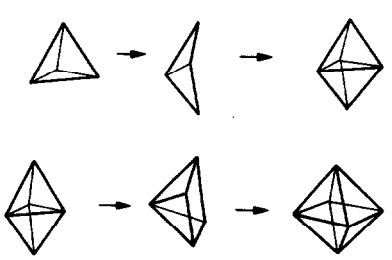

Fig. 3. Polyhedral growth sequence 1.

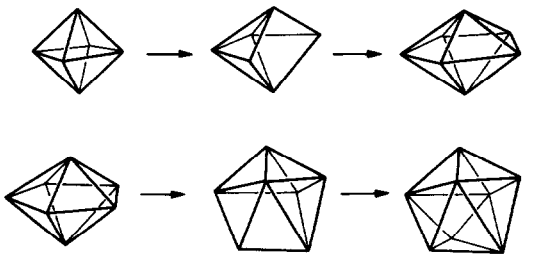

Fig. 4. Polyhedral growth sequence 2.

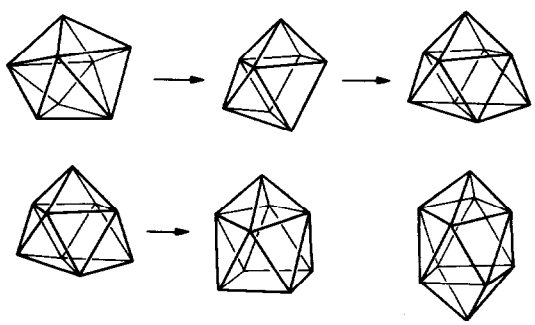

Fig. 5. Polyhedral growth sequence 3.

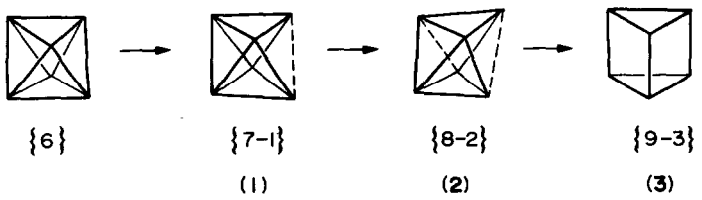

Fig. 6. Multi-edge cleavage for six-coordination.

constructed of equal spheres (or ligands) then progress from say {4} to {5−1} to {5} corresponds to an increase in size of the interstitial site. The site in the square-based pyramid, {6−1}, is larger than that in the trigonal bipyramid, {5}. For coordination polyhedra the same progression would require a steady and systematic increase in the metal–ligand bond lengths.

It is important to recognize that of the polyhedra given in Fig. 2 only the tetrahedron, the octahedron and the icosahedron are such that their vertices are constrained to lie on the surface of a sphere. Putting this in chemical terms, in coordination polyhedra all M—L bond lengths are equal only in these three arrangements in Fig. 2; all other polyhedra produce unequal bond lengths. For this reason alternative polyhedra for {5}, {7}, {8}, {9} and {10} in which all M—L bond lengths are equivalent have been sought. We shall not consider this aspect in detail but it is worth noting that a complete range of polyhedral forms in which the vertices lie on the surface of a sphere have been derived. Thus, if we consider eight-coordination the square antiprism {10−2} is an example of a polyhedron in which all M—L bonds are equal but which is not the most stable form. In coordination geometry we are frequently presented with the question of whether or not the coordination geometry approximates to one in which all L—L contacts are equal but the M—L bonds are not, or an alternative in which all M—L contacts are equal but longer. There is apparently no hard and fast answer to this question and examples of both occur.

It should also be noted that there is a discontinuity in this polyhedral growth sequence (Figs 3–5) at 11 and 12. According to the sequence developed above the polyhedron with 12 vertices corresponds to the omni-capped cuneane arrangement and not the icosahedron, although the two polyhedra are related by a simple edge transfer. The sequence of polyhedra for higher vertex numbers will be discussed in a subsequent paper.[2]

We shall consider now the effect of breaking two or more edges. Edge cleavage with retention of the maximum number of edges, will lead to the results shown in Fig. 6 for the octahedron, and in Fig. 7 for the triangulated dodecahedron. For {6}, the successive cleavage of appropriate edges leads first to {7−1}, then to {8−2}, and finally to {9−3}—the trigonal prism:

$$\{6\} \rightarrow \{7-1\} \rightarrow \{8-2\} \rightarrow \{9-3\}.$$

The corresponding treatment of {8} (Fig. 7) leads to the sequence:

$$\{8\} \rightarrow \{9-1\} \rightarrow \{10-2\} \rightarrow \{11-3\} \rightarrow \{12-4\} \rightarrow \{13-5\} \rightarrow \{14-6\}.$$

In this sequence, {9−1} is the bicapped trigonal prism, {10−2} the square antiprism and {14−6} the cube. There are no such simple names for the other members of this series.

For {9} we find:

$$\{9\} \rightarrow \{10-1\} \rightarrow \{11-2\} \rightarrow \{12-3\} \rightarrow \{13-4\} \rightarrow \{14-5\}$$

and for {10}:

$$\{10\} \rightarrow \{11-1\} \rightarrow \{12-2\} \rightarrow \{13-3\} \rightarrow \{14-4\}.$$

In each case the systematic and steady progression across the series leads to increasingly open polyhedra (i.e. with some square rather than all triangular faces) and a controlled increase in the M—L bond length. A decrease in stability will also follow the same progression. This will be important to our consideration of pseudorotation of coordination compounds.

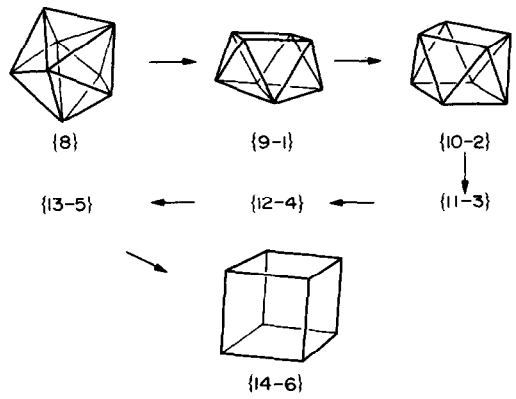

Fig. 7. Multi-edge cleavage for eight-coordination.

PSEUDOROTATION

The act of pseudorotation as it relates to simple coordination compounds ML_n requires that certain bond angles and bond distances in the parent compound change until the coordination shell of ligands, L, assumes its complementary geometry in what would constitute either the transition state or the intermediate. The ease with which these processes can occur will depend upon the energy difference between the complementary geometries (the ground state or the transition state) which constitutes the barrier to the process. These in turn depend on the relative movements of atoms or groups of atoms within the parent. When the complementary geometries are energetically close, either because of the nature of the ligands or because of the inherent properties of certain coordination numbers, the barrier to pseudorotation will be small. In many cases the barrier will be increased by the need of the system to traverse an intermediate in which the ligand distribution or unfavourable bond angles and/or unfavourable bond distances lead to instability. The best examples of pseudorotation and stereochemical non-rigidity will be found for those complexes in which the barrier between complementary geometries is significantly smaller than the free energy of activation for bond fission. The problem usually is on deciding upon the appropriate, accessible, complementary geometry.

For five-coordination the complementary geometries—the trigonal bipyramid, $\{5\}$, and the square pyramid, $\{6-1\}$, are energetically close to one another. Their relationship is clear to see. Expansion of one of the three *equatorial* edges of the trigonal bipyramid leads directly to the square pyramidal complementary geometry, and on further expansion along the same vector to the new trigonal bipyramid, $\{5\}'$ (Fig. 8). This expansion corresponds to a low energy or soft vibrational mode of the trigonal bipyramid and does not depend on excessive extension of the M—L bonds. As a consequence, the tendency to undergo pseudorotation via the Berry Twist Mechanism is quite considerable as is observed for $Fe(CO)_5$. This mechanism also provides an example of the simple, single diamond–square–diamond rearrangement process.

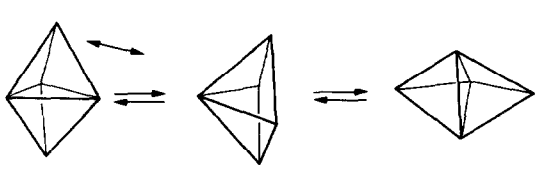

Fig. 8. Berry Pseudorotation Mechanism for five-coordination.

In contrast, the octahedron is stereochemically extremely rigid. According to the Bailar Twist Mechanism the most likely complementary geometry for pseudorotation is the trigonal prism and a trigonal twist of 60° about one of the octahedral three-fold axes will convert an octahedron into a trigonal prism and vice versa. The barrier to this pseudorotation is generally regarded as being similar to or greater than the activation energy for bond fission. The high barrier to pseudorotation in octahedral systems is thus easy to understand. First, it requires a considerable movement of ligands L, second, there is a significant decrease in the number of L—L contacts, finally, and most importantly, the conversion to the trigonal prismatic intermediate requires a substantial increase in the M—L bond lengths.

In the trigonal bipyramidal case we have an example of a relatively small movement of atoms or ligands leading to pseudorotation, and in the octahedron an example of a large movement leading to a relatively major reorganization of the molecular geometry. Clearly, the extent of these motions is dependent on the magnitude of the M—L bond strength (and to a much less extent on the L—L interactions), but most importantly on the physical state of the sample. First and foremost the complementary geometry must, obviously, be available by a low-energy procss corresponding to a soft normal mode of the molecule. Secondly, and very importantly, the route to the proposed complementary geometry must not involve any unreasonable extension of the M—L bond length. Finally, the process should sustain as many L—L contacts as possible. It is important to recognize that although two polyhedra may be easily converted one to another, the need to maintain reasonable M—L bond distances throughout the process is of paramount importance. It is also clear that, given the different constraints imposed on the molecule in either the solid or solution, barriers will vary widely from phase to phase.

In the past it has proved to be relatively more difficult to derive satisfactory complementary geometries for coordination numbers other than four, five and six. For larger coordination numbers, e.g. seven or eight, the availability of several closely related polyhedral forms has usually been taken as sufficient to explain the generally observed low barriers to fluxionality and no general scheme appears to exist. In this paper we wish to present such a general scheme which we believe offers a convenient approach to these fascinating phenomena and permits a simple view of suitable complementary geometries.

As we described above for five-coordination the

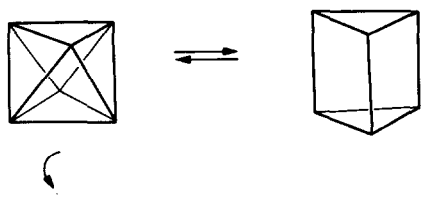

Fig. 9. Bailar Twist Mechanism.

complementary geometries—the trigonal bipyramid, {5}, and the square pyramid, {6−1}, are energetically close to one another, and so the essential, low-energy pseudorotation process may be viewed as involving two steps:

$$\{5\} \rightarrow \{6-1\} \rightarrow \{5\}'.$$

Of course we must not forget that there are three, equivalent, equatorial edges within the trigonal bipyramid and that the soft mode under consideration will lead to cleavage of any one of them. Hence, at any given moment three "different" {6−1} polyhedra may be produced from a given sample of ML_5 in the ground state, although of course for a homoleptic ML_5 complex they are indistinguishable.

For the octahedron which is stereochemically extremely rigid, the Bailar Twist is usually considered to occur in a one-step process as outlined in Fig. 9. However, here we will choose, for convenience, to consider the process as occurring in three distinct steps according to Fig. 6. Cleavage of one octahedral edge, which corresponds to a soft vibrational mode, generates intermediate (1), of two edges intermediate (2) and of three edges intermediate (3). Examination of these three species (1), (2) and (3) reveals that (1) corresponds to a *nido*-pentadonal bipyramid, {7−1}; that (2) corresponds to an *arachno*-dodecahedron, {8−2}; and finally (3) to a *hypho*-tricapped trigonal prism, {9−3}. Thus, the Bailar Twist Mechanism *could be viewed* as a six-step process:

$$\{6\} \rightarrow \{7-1\} \rightarrow \{8-2\} \rightarrow \{9-3\} \rightarrow \{8-2\}' \rightarrow \{7-1\}' \rightarrow \{6\}'.$$

The high barrier to pseudorotation in octahedral systems is thus more easily understood. It is interesting to observe that the formation of {7−1} from {6} corresponds to an opening of one polyhedral edge and is closely related to the process {5} → {6−1}. Hence, the energies for the two processes might be expected to be similar. However, the intermediate {7−1} does not collapse to a new {6} and ligand exchange does occur. It is also worth noting that any compound possessing a {7−1} geometry might be expected to show a lower barrier to interconversion since it has only two steps to the {9−3} complementary geometry. This is found to be the case for XeF_6. In this case rearrangement presumably occurs via the reaction sequence:

$$\{7-1\} \rightarrow \{8-2\} \rightarrow \{9\} \rightarrow \{8-2\}' \rightarrow \{7-1\}'.$$

This illustrates what we believe to be a general phenomenon, viz. pseudorotation always proceeds via polyhedral expansion, i.e. M—L stretching. Thus, for a compound with a square pyramidal, {6−1}, ground state, pseudorotation is expected to take place via a {7−2} intermediate and for a compound with a {9−1} ground state through a {10−2} intermediate, etc.

For seven-coordination there is no single-step suitable, complementary geometry available. Single edge cleavage, as illustrated in Fig. 4, will lead to a *nido*-dodecahedron {7−1} which cannot serve as a complementary geometry since operation of the diamond–square–diamond process in this instance will not return us to the parent polyhedral form {7}. Instead the capped-octahedron will be produced. This may be regarded as unfavourable for a homoleptic ML_7 complex since one M—L bond (viz. that involving a bond to the capping ligand) is required to undergo a relatively large extension. A further edge cleavage is required to give the more favourable *arachno*-tricapped trigonal prism, {9−2}, which can serve as an appropriate complementary geometry. Hence, ligand rearrangement in this case may be viewed as the five-step process:

$$\{7\} \rightarrow \{8-1\} \rightarrow \{9-2\} \rightarrow \{8-1\}' \rightarrow \{7\}'.$$

Again the edge cleavage corresponds to a soft vibrational mode, and it is important to remember that although we are *choosing* to consider the process as occurring in two independent steps it will in reality occur in one concerted motion. This may be visualized as taking place via the simultaneous opening of two edges (joining two vertices of connectivity four and five, and there are 10 such edges).

For eight-coordination we have a situation similar to that found for coordination number five. The parent polyhedron is the dodecahedron {8}. Single edge cleavage takes us to the bicapped trigonal prism or {9−1} which can clearly serve as a suitable complementary geometry since further extension along the same vector leads to a new dodecahedron {8}'. In this case, therefore, the rearrangement process may be viewed as:

$$\{8\} \rightarrow \{9-1\} \rightarrow \{8\}'.$$

Coordination number nine is somewhat similar. Here again single edge cleavage leads us directly to a suitable complementary geometry, in this instance

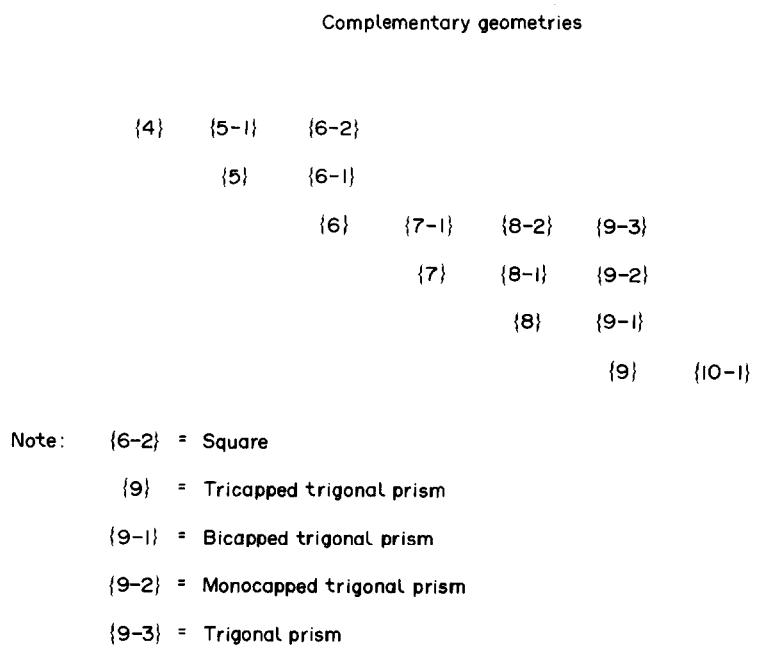

Fig. 10. General scheme for pseudorotation.

a *nido*-bicapped square antiprism—{10−1} (Fig. 5) and pseudorotation may occur via the process:

$$\{9\} \rightarrow \{10-1\} \rightarrow \{9\}'.$$

The general scheme shown in Fig. 10 for pseudorotation in coordination compounds thus emerges. It may be extended to higher (> 9) or lower (< 5) coordination numbers although care must be exercised when dealing with numbers > 11. This aspect will be the subject of a further publication.[2]

CONCLUSIONS

We have shown that the observed or postulated pseudorotation in simple coordination compounds may be understood in terms of a simple, polyhedral edge cleavage mechanism. The main advantage of this mechanism is the ease with which the complementary geometries for a range of coordination numbers may be derived and the wide range of energy barriers to rearrangement processes understood. Of particular importance is the need to limit the extent of M—L bond extension and sustain as many as possible L—L contacts.

REFERENCES

1. C. E. Ansell, R. E. Benfield, A. W. Bott, D. Braga, B. F. G. Johnson and E. A. Marseglia, *J. Chem. Soc., Chem. Commun.* 1988, 889.
2. B. F. G. Johnson, manuscript in preparation.

Polyhedron Vol. 9, No. 18, pp. 2227–2231, 1990
Printed in Great Britain

0277-5387/90 $3.00+.00
© 1990 Pergamon Press plc

MACROMONOCYCLE FORMATION FROM COPPER(II)- OR NICKEL(II)-DIRECTED CONDENSATION OF LINEAR TETRAAMINES AND FORMALDEHYDE WITH VARIOUS NITRO-CARBON ACIDS

GEOFFREY A. LAWRANCE,* MARCEL MAEDER, MARGARET A. O'LEARY and FONG-HA WOON

Department of Chemistry, The University of Newcastle, New South Wales 2308, Australia

(*Received* 14 *March* 1990; *accepted* 26 *April* 1990)

Abstract—Reaction of (4,7-diazadecane-1,10-diamine)copper(II) or (3,6-diazaoctane-1,8-diamine)nickel(II) ions in alcoholic base with formaldehyde and a variety of carbon acids with nitro-substituents has been studied. The R—CH_2—NO_2 carbon acids 1-nitrododecane, 12-nitrododecanoic acid, 3-nitropropanoic acid, tetrahydro-2-(2′-nitroethoxy)-2H-pyran and nitromethane undergo facile Mannich-type reactions to yield new pendant-arm macrocycles with a —NH—CH_2—C(R)NO_2—CH_2—NH— link built between the two primary amines of the precursor compound. In the case of nitromethane, R in the major product is —CH_2—OH rather than —H, due to further condensation of the residual acidic proton with formaldehyde; otherwise, R is the expected substituent carried through from reaction of the R—CH_2—NO_2 unit. Zinc/acid reduction of the copper(II) complex of the long-chain pendant macrocycle formed by condensation involving 12-nitrododecanoic acid permitted isolation of 1,4,8,12-cyclopentadecane-10-amine-10-undecanoic acid as the hydrochloride salt.

Reaction of copper(II) or nickel(II) complexes of polyamines which contain *cis*-disposed primary amines with formaldehyde and the carbon acid nitroethane have been shown to produce new substituted macrocycles in a facile reaction, eq. (1).[1–4] The generality of this type of reaction for nitro-carbon acids has not been investigated, with only nitropropane employed in addition to nitroethane previously.[4] We are aware that other types of carbon acids except nitro-carbon acids may be employed; for example, diethyl malonate reacts to yield a carboxylate-substituted macrocycle, but often with substantially lower yield.[5] Factors which influence the Mannich-type condensation reaction with formaldehyde and a carbon acid around the metal template are not fully understood, hence it was of interest to see how reaction with a range of nitro-substituted molecules which are strong carbon acids would proceed. The synthesis and characterization of a number of new pendant-arm macrocycles as the copper(II) or nickel(II) complexes are reported herein.

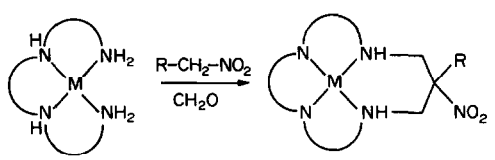

(1)

EXPERIMENTAL

Syntheses

Commercial samples of all precursor organic compounds were employed generally, as supplied. Analytical reagent grade metal salts were used as supplied, as well as laboratory reagent grade organic solvents.

(10-(Ethanoic acid)-10-nitro-1,4,8,12-tetraazacyclopentadecane)copper(II) perchlorate hydrate, [Cu(1)]$(ClO_4)_2 \cdot H_2O$

To a solution of copper(II) nitrate trihydrate (3.65 g) in methanol (200 cm^3) was added 4,7-diaz-

* Author to whom correspondence should be addressed.

adecane-1,10-diamine (2.75 g) in methanol (40 cm^3) and triethylamine (6 cm^3), and the solution was warmed. To the warm solution was added 3-nitropropionic acid (2.1 g) and formaldehyde (6 cm^3, 36% aq.), and the solution was heated and stirred at *ca* 60°C for 2 h, then stirred at room temperature overnight. The reaction was quenched with acetic acid and allowed to stand for 2 days. A blue solid formed and was collected, redissolved in water, treated with *ca* 10 cm^3 of 5 M $HClO_4$ and set aside to crystallize. Slow evaporation produced crystals, which were collected, washed with ethanol and then diethyl ether, and air dried (3.5 g).

Chromatography of the initial filtrate on SP-Sephadex C-25 resin using 0.2 M $NaClO_4$ as eluate separated a blue–purple band of the required product from small amounts of precursor complex and other products; however, only a small additional amount of the required product was isolated from this procedure, and minor bands did not contain sufficient compound to yield solid products for identification. Found: C, 25.9; H, 5.05; N, 11.5. Calc. for $C_{13}H_{27}Cl_2CuN_5O_{12}\cdot H_2O$: C, 26.1; H, 4.9; N, 11.7%. Electronic spectrum (water): λ_{max} 569 nm (ε 93 M^{-1} cm^{-1}). IR spectrum (KBr disc): 1588 cm^{-1} (—COO^-), 1545, 1350 cm^{-1} (—NO_2).

(12-(*Ethanoic acid*)-12-*nitro*-1,4,7,10-*tetraazacyclotridecane*)*nickel*(II) *perchlorate dihydrate ethanolate*, [Ni(**1A**)]$(ClO_4)_2\cdot 2H_2O\cdot C_2H_5OH$

To a warm solution of nickel(II) perchlorate hexahydrate (3.05 g, 8.3 mmol) in methanol (70 cm^3) was added dropwise a solution of 3,6-diazaoctane-1,8-diamine (1.2 g, 8.2 mmol) in methanol (*ca* 5 cm^3). The initial flocculent precipitate redissolved to give a deep green solution and a purple gum. Formaldehyde (3 cm^3, 36% aq., 36 mmol), 2-nitropropanoic acid (1.1 g, 9 mmol) and triethylamine (0.5 cm^3) were added and the mixture was heated and stirred for 4 h. Filtration gave a green fluffy solid (5 g). This was treated with conc. HCl and the green soluble material discarded. The residual yellow gum was again washed with HCl, then ethanol and diethyl ether, to give a yellow granular solid (3.5 g). This could be purified if required by chromatography on SP-Sephadex C-25 resin as above, and crystallized from water–ethanol. Found: C, 24.5; H, 5.2; N, 10.8. Calc. for $C_{11}H_{23}Cl_2CuN_5O_{12}\cdot 2H_2O\cdot C_2H_5OH$: C, 24.8; H, 5.3; N, 11.1%. Electronic spectrum (water): λ_{max} 365 nm (sh, ε 45 M^{-1} cm^{-1}). IR spectrum (KBr disc): 1730 cm^{-1} (—COOH), 1560, 1355 cm^{-1} (—NO_2). ^{13}C NMR spectrum (D_2O): δ 20.0 (CH_3CH_2OH), 38.0 (—CH_2—COOH), 46.1, 46.3, 47.5, 52.0 (—CH_2—NH), 60.0 (CH_3CH_2OH), 93.0, (C—NO_2), 174.0 (—COOH).

(10-*Nitro*-10-*undecyl*-1,4,8,12-*tetraazacyclopentadecane*)*copper*(II) *perchlorate ethanolate*, [Cu(**2**)]$(ClO_4)_2\cdot C_2H_5OH$

To a solution of copper(II) nitrate (3.7 g, 15.3 mmol) in methanol (80 cm^3) was added 4,7-diazadecane-1,10-diamine (2.7 g, 15.5 mmol), triethylamine (1 cm^3), 1-nitrododecane (3 g, 14 mmol) and aqueous formaldehyde (3 cm^3, 36 mmol). The mixture was stirred and warmed for 3 h, then filtered through Celite and sorbed onto a column of SP-Sephadex C-25 resin (6 × 3.5 cm). Elution with 0.2 M aqueous $NaClO_4$ removed some unreacted precursor complex, then elution with 0.2 M $NaClO_4$ as a 50% propanol solution removed an intense blue band. This separated into two layers on concentration on a rotary evaporator. The blue oil was washed well with water then taken up in methanol and evaporated to dryness. The residual gum (4 g) solidified on standing in the refrigerator. Trituration with ethanol–ether gave the product as a fine pearly blue solid. Found: C, 40.1; H, 7.3; N, 9.7. Calc. for $C_{22}H_{47}Cl_2CuN_5O_{10}\cdot C_2H_5OH$: C, 39.9; H, 7.4; N, 9.7%. Electronic spectrum (1:1 ethanol–water): λ_{max} 572 nm (ε 148 M^{-1} cm^{-1}), 268 (ε 9600). IR spectrum (KBr disc): 1550, 1350 cm^{-1} (—NO_2), 1470 cm^{-1} (—CH_2—).

Reduction of the nitro group to a pendant amino group can be achieved conveniently, and recomplexation to copper(II) performed. Dissolution of the above complex (*ca* 1 g) in aqueous methanol (75%, 200 cm^3) and addition of a half-volume of 1 M HCl and zinc powder (*ca* 4 g) afford reduction of the nitro group and the metal ion. The warmed solution was reacted until a colourless solution was obtained, then it was filtered through cellulose to remove excess zinc and copper, and excess copper(II) nitrate trihydrate was added, and the pH adjusted to *ca* 7 with 1 M NaOH. Filtration removed metal hydroxides, after which the filtrate was diluted with 1:1 EtOH–H_2O to *ca* 600 cm^3 and sorbed onto a column (25 × 3.5 cm) of SP-Sephadex C-25 resin, and the complex eluted with 0.2 M $NaClO_4$. Following reduction by rotary evaporation, a blue powder precipitated on standing, and was collected, washed with acetone, then diethyl ether, and air dried (0.3 g, 30%). Addition of ethanol and diethyl ether produced a second crop. The product analysed as the ethanol solvate of the protonated pendant amine complex. Found: C, 31.8; H, 5.8; N, 7.8. Calc. for $C_{24}H_{55}Cl_4CuN_5NaO_{17}$: C, 31.55; H, 6.05; N, 7.65%. Electronic

spectrum (MeOH): λ_{max} 585 nm (ε 112 M^{-1} cm^{-1}), 271 (2800). IR Spectrum (KBr disc): 2923 , 1465 cm^{-1} (—CH_2—), 1635 cm^{-1} (—NH_3^+).

(10-*Nitro*-10-(11′-*undecanoic acid*)-1,4,8,12-*tetraazacyclopentadecane*)*copper*(II) *perchlorate*, [Cu(**3**)]$(ClO_4)_2$

A methanolic solution (40 cm^3) of copper(II) nitrate trihydrate (0.4 g) and 4,7-diazadecane-1,10-diamine (0.3 g) was stirred, warmed (*ca* 40°C) and triethylamine (0.3 g), 1-nitrododecanoic acid (1.0 g) added, followed by aqueous formaldehyde (37%; 1 cm^3) added dropwise. After stirring for 1 h, the solution was stirred at room temperature overnight. The solution was made just acid with 1 M HCl, filtered, diluted with 1 : 1 ethanol–water (400 cm^3), and sorbed onto a column of SP-Sephadex C-25 resin. Following washing with 1 : 1 ethanol–water (200 cm^3), elution was performed with 0.2 M $NaClO_4$ in 1 : 1 ethanol–water, yielding a single purple band. Following concentration on a rotary evaporator, blue crystals formed on standing. These were collected, washed with ethanol, then diethyl ether, and dried (0.45 g, 35%). Further crops formed on extended standing. Found: C, 36.5; H, 6.5; N, 9.7. Calc. for $C_{22}H_{47}Cl_2CuN_5O_{13}$: C, 36.5; H, 6.5; N, 9.7%. Electronic spectrum (1 : 1 EtOH–H_2O): λ_{max} 572 nm (ε 110 M^{-1} cm^{-1}), 268 (ε 7800). IR spectrum (KBr disc): 2930, 2855 cm^{-1} (—CH_2—), 1720 cm^{-1} (—COOH), 1547, 1350 cm^{-1} (—NO_2).

(12-*Nitro*-12(11′-*undecanoic acid*)-1,4,7,10-*tetraazacyclotridecane*)*nickel*(II) *chloride dihydrate diethanolate*, [Ni(**3A**)]$Cl_2 \cdot 2H_2O \cdot 2C_2H_5OH$

A methanolic solution (*ca* 10 cm^3) of 3,6-diazaoctane-1,8-diamine (1.2 g, 8.2 mmol) was added dropwise to a warm solution of nickel(II) perchlorate hexahydrate (3.0 g, 8.2 mmol) in methanol (70 cm^3), to give a green solution and purple gum. Aqueous formaldehyde (3 cm^3, 36%, 39 mmol), 12-nitrododecanoic acid (1.8 g, 7.3 mmol) and triethylamine (1 cm^3) were then added. The mixture was warmed and stirred for 3 h, then filtered to give a pale green powder. This material was triturated with 1 M HCl to give a yellow gum. The gum was ground under ethanol–diethyl ether and dried to give a hygroscopic yellow granular powder (2.2 g, 50%). Found: C, 43.2; H, 9.0; N, 10.6. Calc. for $C_{20}H_{41}Cl_2N_5NiO_4 \cdot 2H_2O \cdot 2C_2H_5OH$: C, 42.8; H, 8.5; N, 10.4%. Electronic spectrum (water): λ_{max} 345 nm (sh, ε 750). ^{13}C NMR (D_2O–dioxan): δ 25.4, 29.7, 34.7, 36.2 (acid side-chain; cf. free acid), 44.1, 45.2 (—*C*—NH—), 73.3 (*C*—NO_2), 165.4 (—COOH); 14.5, 61.3 (EtOH). IR spectrum (KBr disc): 1738 cm^{-1} (—COOH), 1553, 1368 cm^{-1} (—NO_2), 1470 cm^{-1} (—CH_2—).

(10-*Nitro*-10-(2″-*tetrahydropyranyl*-2′-*oxaethyl*)-1,4,8,12-*tetraazacyclopentadecane*)*copper*(II) *perchlorate hydrate*, [Cu(**4**)]$(ClO_4)_2 \cdot H_2O$

A methanolic solution (70 cm^3) of copper(II) nitrate trihydrate (1.4 g, 5.8 mmol), 4,7-diazadecane-1,10-diamine (1.0 g, 5.7 mmol), formaldehyde (2 cm^3 of 36% aq., 25 mmol), triethylamine (1 cm^3) and tetrahydro-2-(2′-nitroethoxy)-2H-pyran (1.0 g, 5.7 mmol) was stirred at room temperature overnight, then heated for 2 h. The solution was diluted with water and adsorbed on to a column of SP-Sephadex C-25 resin. Elution with 0.2 M $NaClO_4$ gave one blue band which was acid stable and hence macrocyclic. On standing, this deposited blue crystals of the product (0.4 g, 10%). Found: C, 31.3; H, 5.6; N, 10.8. Calc. for $C_{17}H_{35}Cl_2CuN_5O_{12} \cdot H_2O$: C, 31.2; H, 5.7; N, 10.7%. Electronic spectrum (water): λ_{max} 568 nm (ε 116 M^{-1} cm^{-1}), 380 (sh, ε 120), 267 (ε 7900). IR spectrum (KBr disc): 1555, 1355 cm^{-1} (—NO_2).

(10-*Nitro*-10-(*hydroxymethyl*)-1,4,8,12-*tetraazacyclopentadecane*)*copper*(II) *perchlorate*, [Cu(**5**)]$(ClO_4)_2$

A solution of 4,7-diazadecane-1,10-diamine (1.0 g) and copper(II) nitrate trihydrate (1.3 g) in methanol (70 cm^3) was warmed and triethylamine (0.64 g), nitromethane (0.86 g) and aqueous formaldehyde (37%; 3 cm^3) were added. The mixture was warmed at *ca* 50°C for 1 h, and then allowed to cool to room temperature. Following dilution with water (500 cm^3) and acidification to pH 5, the mixture was sorbed onto a column of SP-Sephadex C-25 resin (20 × 3.5 cm) and eluted with aqueous $NaClO_4$ (0.2–0.4 M). Following removal of unreacted complexed tetraamine, the major band containing a macrocyclic species was removed, followed by two other minor bands whose identity was not elucidated fully. The major macrocyclic product was concentrated on a rotary evaporator and yielded fine purple crystals on standing. These were collected, washed with ethanol and air dried; they analysed with a molecule of $NaClO_4$ present. Found: C, 21.5; H, 4.1; N, 10.4. Calc. for $C_{12}H_{27}Cl_3CuN_5NaO_{15}$: C, 21.4; H, 4.05; N, 10.4%. Electronic spectrum (water): λ_{max} 572 nm (ε 96 M^{-1} cm^{-1}), 265 (ε 8000). IR Spectrum (KBr

disc): 3415 cm^{-1} (—OH), 1560, 1355 cm^{-1} ($—NO_2$).

1,4,8,12-*Tetraazacyclopentadecane*-10-*amine*-10-(11′-*undecanoic acid*) *pentahydrochloride hydrate ethanolate*, (**6**)·5HCl·H_2O·C_2H_5OH

To a solution of [Cu(**3**)]$(ClO_4)_2$ (1 g) in 1 : 1 ethanol–water (100 cm^3) was added Zn(Hg) prepared from 4 g of zinc shavings. The mixture was heated and stirred for 40 min, then filtered through Kieselguhr to give a clear, colourless solution. This was concentrated to a small volume on a rotary evaporator, diluted with ethanol (*ca* 200 cm^3) and treated with concentrated HCl (*ca* 10 cm^3) to produce a white precipitate which was collected, washed with ethanol and diethyl ether, and dried (0.4 g). Found: C, 43.4; H, 9.2; N, 10.5. Calc. for $C_{22}H_{47}N_5O_2$·5HCl·H_2O·C_2H_5OH: C, 43.7; H, 9.2; N, 10.6%. IR spectrum (KBr disc): 1724 cm^{-1} (—COOH), 1602 cm^{-1} (br, amine). ^{13}C NMR (D_2O): δ 25.0, 26.1, 27.1 (—N—C—*C*—C—N—, —*C*—C—COOH, —C(NH_2)—C—*C*—), 31.3–31.3 (overlapping peaks, side chain —C—*C*—C), 36.7, 38.9 (—*C*—COOH, —C(NH_2)—*C*—C—), 42.2, 45.6, 47.6 (—*C*—NH—), 177.6 (—COOH), (tert. C not observed); 17.0, 57.0 (EtOH). Addition of ether to the filtrate from the above isolation yielded a further precipitate (0.34 g), with microanalysis and spectroscopy consistent with formulation as a lipophilic macrocycle.

Further reactions

The strong nitro-carbon acid *p*-nitrobenzyl nitrite was prepared by reaction of silver nitrite with *p*-nitrobenzyl bromide;[6] separation of nitrito and nitro isomers from the reaction product was achieved via the carbanion.[7] Reaction with either copper(II) or nickel(II) tetraamines and formaldehyde in ethanol, in the presence or absence of base, produced coloured precipitates immediately, but these did not prove to contain macrocyclic species.

Physical methods

Electronic spectra were recorded with an Hitachi 150-20 spectrophotometer and IR spectra for complexes dispersed in KBr discs were recorded on Nicolet MX-1 FT–IR or Hitachi spectrometers. Nuclear magnetic resonance spectra were recorded using a Jeol FX-90Q spectrometer, with chemical shifts cited vs tetramethylsilane. Microanalyses were performed by the Australian National University microanalysis service.

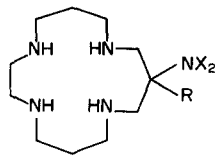

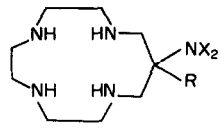

1	X=O	R=CH_2-COOH	1A
2	X=O	R=$(CH_2)_{10}$-CH_3	
3	X=O	R=$(CH_2)_{10}$-COOH	3A
4	X=O	R=CH_2-O-	
5	X=O	R=CH_2-OH	
6	X=H	R=$(CH_2)_{10}$-COOH	

RESULTS AND DISCUSSION

Of the range of nitro-substituted molecules investigated, each containing acidic hydrogens as a result of the electronic propoerties of the nitro substituent, all aliphatic molecules led to macrocyclization reactions. With the aromatic-substituted molecule *p*-nitrobenzyl nitrite, reaction to an isolable macrocyclic complex was not achieved; organic products and insoluble precipitates formed preferentially. At least with the aliphatic molecules, the chemistry which is well established with nitroethane earlier[1-4] persists, and would appear generally applicable.

A range of new pendant-arm macrocycles were identified in this study, employing copper(II) or nickel(II) as templating metal ion, and two different tetraamines as the precursor ligand. The macrocycles **1** and **1A** exhibit both a pendant nitro group and a pendant carboxylic acid group. The macrocycles **3** and **3A** also contain both pendant nitro and carboxylate groups, although in these cases the carboxylate is the terminal group of a long aliphatic, hydrophobic chain, —$(CH_2)_{10}$COOH. Both groups exhibit characteristic strong absorbances in the IR spectrum. These occur near 1545 and 1350 cm^{-1} for nitro groups. The acid side chains of the copper complex of **1** evidently exists in the carboxylate anion form, based on the strong absorbance at 1588 cm^{-1}. The complex of **3** has been isolated as both the acid (band at 1720 cm^{-1}) and carboxylate anion (band at 1550 cm^{-1}) species in different syntheses. The nickel analogues **1A** and **3A** have strong absorbances at 1730 and 1738 cm^{-1}, respectively, indicating that in these cases the free acid is present. The NMR spectrum of the diamagnetic nickel(II) complex of **1A** identifies the macrocycle clearly; resonances from the acid carbon (174 ppm), the tertiary carbon adjacent to the nitro group (93.0 ppm), the methylene adjacent to the acid group (38.0 ppm) and the ring methylenes all adjacent to secondary amines (46–52 ppm) were observed in

the ^{13}C NMR spectrum. Again, synthesis of the diamagnetic nickel(II) complex **3A** permitted characterization by NMR spectroscopy. The long-chain analogue **2**, with R = $(CH_2)_{10}CH_3$, was also prepared as the copper(II) complex. Macrocyclization (in all cases studied) is also indicated by stability in aqueous acid for extended periods. The presence of the long aliphatic chain in complexes of **2**, **3** and **3A** influences solubility properties, with complexes appreciably more soluble in polar organic solvents and less soluble in water, yet metal-based spectroscopic properties (such as electronic maxima) differ little from short-chain analogues. For example, the electronic maximum for the copper(II) complex with R = $(CH_2)_{10}CH_3$ (572 nm) is the same as that reported for the complex with R = CH_3.[2]

The complex with the protected alcohol, **4**, was isolated without hydrolysis of the protecting group to form a —CH_2—OH pendant, as indicated by microanalysis and IR spectroscopy. The —CH_2—OH pendant is present in the major macrocyclic product isolated from reaction with nitromethane, however. It was hoped that reaction with nitromethane would produce a complex with an R = H pendant, thus providing a macrocycle with an acidic hydrogen in the ring, available for further reaction. However, the acidity of this site initiated immediate reaction, since condensation with another molecule of formaldehyde has occurred, producing a —CH_2—OH pendant in **5**. The reaction between nitromethane and formaldehyde,

$$CH_3NO_2 + CH_2O \longleftrightarrow CH_2(CH_2OH)NO_2$$

is known to occur independently in solution,[8] so that the alcohol pendant may be introduced directly from this process. All three hydrogens in nitromethane are replaced by new C—C bonds in reaction with formaldehyde and $[M(H_2NCH_2CH_2NH_2)_3]^{n+}$ complexes, forming macrobicyclic species;[9] in the present case, macromonocycle formation requires only two of the three available acidic hydrogens, permitting other additional chemistry in this specific case.

The ligands **2**, **3** and **3A** represent new macrocycles with long hydrophobic "tails", somewhat related to ligand **7** reported previously.[10] Robustness is enhanced by reduction of the nitro group to a primary amine. Simple zinc/acid reduction in aqueous solution of both **2** and **3** has been performed; concomitant reduction of the copper ion occurs. In the former case, recomplexation to copper(II) has been performed as described in the Experimental. In the latter case, isolation of the free ligand **6** as a hydrochloride salt has been achieved. Characterization of the salt by microanalysis and NMR spectroscopy has indicated that reduction has been achieved without cleavage of the macrocycle. The properties of this new lipophilic polyamino acid will be pursued.

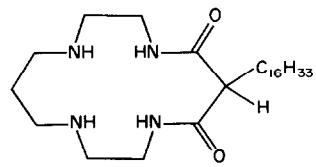

7

The general applicability of the formaldehyde/nitro-carbon acid condensation reaction with polyamines, where two primary amines are constrained in *cis*-disposed positions by a labile metal ion, has been demonstrated. A range of new macrocycles with various types of pendant groups have been prepared, and the facility of the chemistry suggests that this synthetic strategy offers a convenient route to a range of pendant-arm macrocycles.

Acknowledgement—Support of this research by the Australian Research Council is gratefully acknowledged.

REFERENCES

1. P. Comba, N. F. Curtis, G. A. Lawrance, A. M. Sargeson, B. W. Skelton and A. H. White, *Inorg. Chem.* 1986, **25**, 4260.
2. P. Comba, N. F. Curtis, G. A. Lawrance, M. A. O'Leary, B. W. Skelton and A. H. White, *J. Chem. Soc., Dalton Trans.* 1988, 2145.
3. G. A. Lawrance, T. M. Manning and M. A. O'Leary, *Polyhedron* 1988, **7**, 1263.
4. P. Comba, N. F. Curtis, G. A. Lawrance, M. A. O'Leary, B. W. Skelton and A. H. White, *J. Chem. Soc., Dalton Trans.* 1988, 497.
5. G. A. Lawrance and M. A. O'Leary, *Polyhedron* 1987, **6**, 1291.
6. N. Kornblum and D. C. Iffland, *J. Am. Chem. Soc.* 1955, **71**, 2137.
7. R. G. Cooke and A. K. McBeth, *J. Chem. Soc.* 1938, 1024.
8. H. O. House, *Modern Synthetic Reactions*. Benjamin/Cummings, California (1972).
9. A. M. Sargeson, *Chem. Br.* 1979, **15**, 23; R. J. Geue, T. W. Hambley, J. M. Harrowfield, A. M. Sargeson and M. R. Snow, *J. Am. Chem. Soc.* 1984, **106**, 5478.
10. M. Di Casa, L. Fabbrizzi, A. Perotti, A. Poggi and P. Tundo, *Inorg. Chem.* 1985, **24**, 1610.

Polyhedron Vol. 9, No. 18, pp. 2233–2237, 1990
Printed in Great Britain

0277–5387/90 $3.00+.00
© 1990 Pergamon Press plc

SYNTHESIS, SPECTROSCOPIC PROPERTIES AND BARRIERS TO BUT-2-YNE ROTATION OF THE NEW CATIONIC PHOSPHINE–BUT-2-YNE COMPLEXES, $[WI(CO)L\{Ph_2P(CH_2)PPh_2\}(\eta^2\text{-}MeC_2Me)][BF_4]$ {L = PMe_3, PMe_2Ph, $PMePh_2$, PPh_3, $PEtPh_2$, PEt_2Ph, PEt_3, P^nPr_3, P^nBu_3, $P(CH_2CH{=}CH_2)Ph_2$ AND $[Fe(\eta^5\text{-}C_5H_5)(\eta^5\text{-}C_5H_4PPh_2)]$}

PAUL K. BAKER* and KEVIN R. FLOWER

Department of Chemistry, University of Wales, Bangor, Gwynedd LL57 2UW, U.K.

(*Received* 20 *March* 1990; *accepted* 26 *April* 1990)

Abstract—The monobut-2-yne complex $[WI(CO)(NCMe)\{Ph_2P(CH_2)PPh_2\}(\eta^2\text{-}MeC_2Me)][BF_4]$ reacts with an equimolar quantity of phosphines, L {L = PMe_3, PMe_2Ph, $PMePh_2$, PPh_3, $PEtPh_2$, PEt_2Ph, PEt_3, P^nPr_3, P^nBu_3, $P(CH_2CH{=}CH_2)Ph_2$ and $[Fe(\eta^5\text{-}C_5H_5)(\eta^5\text{-}C_5H_4PPh_2)]$} in CH_2Cl_2 at room temperature to give the highly coloured acetonitrile displaced products $[WI(CO)L\{Ph_2P(CH_2)PPh_2\}(\eta^2\text{-}MeC_2Me)][BF_4]$ (**1–11**) in good yield. The barriers to but-2-yne rotation of a number of these complexes have been determined using variable temperature ^1H NMR spectroscopy. The but-2-yne ligands in **1–11** show ^{13}C NMR resonances above 200 ppm for the alkyne contact carbon chemical shifts, which suggests that the but-2-yne ligand is donating four electrons to the tungsten in these compounds.

The barrier to alkyne rotation of alkyne complexes of molybdenum(II) and tungsten(II) have received considerable attention in recent years. For example, the barriers to but-2-yne rotation of the monobut-2-yne complexes $[MoLL'(\eta^2\text{-}MeC_2Me)X][BF_4]$ (X = $\eta^5\text{-}C_5H_5$, L—L = $Me_2P(CH_2)_2PMe_2$, $Ph_2P(CH_2)_2PPh_2$ or $Ph_2P(CH{=}CH)PPh_2$; L = L′ = $PMePh_2$; L = CO, L′ = PEt_3, PPh_3 or PCy_3 for X = $\eta^5\text{-}C_9H_7$, L = CO, L′ = PEt_3 or PPh_3),[1,2] $[W(CO)(S_2CNEt_2)_2(\eta^2\text{-}MeC_2Me)]$,[3] $[Mo(\sigma\text{-}MeC{=}CMe_2)(CO)(\eta^2\text{-}MeC_2Me)(\eta^5\text{-}C_5H_5)]$,[4] $[Mo(SR)\{P(OMe)_3\}_2(\eta^2\text{-}MeC_2Me)(\eta^5\text{-}C_5H_5)][BF_4]$ (R = C_6H_5, $C_6H_4NO_2$, C_6H_4Me, C_6H_4OMe or $C_6H_4NH_2$),[5] $[Mo(SePh)\{P(OMe)_3\}_2(\eta^2\text{-}MeC_2Me)(\eta^5\text{-}C_5H_5)]$,[5] *cis*-$[WBr_2(CO)(CN^tBu)_2(\eta^2\text{-}MeC_2Me)]$,[6] *trans*-$[WBr_2(CO)(PPh_3)_2(\eta^2\text{-}MeC_2Me)]$,[6] $[WMe(CO)(\eta^2\text{-}MeC_2Me)(\eta^5\text{-}C_5H_4R)]$ (R = Me or Ph)[7] and $[MX_2(CO)L_2(\eta^2\text{-}MeC_2Me)]$ (for M = Mo, X = Cl, L = py, PEt_3 or PPh_3; X = Br, L = PEt_3; for M = W, X = Cl, L = PPh_3).[8] More recently we have reported the preparation and calculated the barriers to but-2-yne rotation of the tungsten diiodide complexes $[WI_2(CO)L_2(\eta^2\text{-}MeC_2Me)]$ {L = PMe_3, PMe_2Ph, $PMePh_2$, PPh_3, $PEtPh_2$, PEt_2Ph, PEt_3, P^nBu_3 or PPh_2Cy; L_2 = $Ph_2P(CH_2)PPh_2$}.[9] The complexes $[WI_2(CO)\{Ph_2P(CH_2)_nPPh_2\}(\eta^2\text{-}RC_2R)]$ (*n* = 1–6; R = Me or Ph) react with one equivalent of $Ag[BF_4]$ in acetonitrile at room temperature to give the cationic monoacetonitrile compounds $[WI(CO)(NCMe)\{Ph_2P(CH_2)_nPPh_2\}(\eta^2\text{-}RC_2R)][BF_4]$.[10]

In this paper we describe the preparation of the cationic monobut-2-yne complexes $[WI(CO)L\{Ph_2P(CH_2)PPh_2\}(\eta^2\text{-}MeC_2Me)][BF_4]$ {L = PMe_3, PMe_2Ph, $PMePh_2$, PPh_3, $PEtPh_2$, PEt_2Ph, PEt_3, P^nPr_3, P^nBu_3, $P(CH_2CH{=}CH_2)Ph_2$ and $[Fe(\eta^5\text{-}C_5H_5)(\eta^5\text{-}C_5H_4PPh_2)]$}, and the barrier to but-2-yne rotation of several of these complexes which have been determined using variable temperature ^1H NMR spectroscopy.

EXPERIMENTAL

Syntheses were carried out under an atmosphere of nitrogen using standard Schlenk-line techniques. CH_2Cl_2 was dried and distilled before use. The compound $[WI(CO)(NCMe)\{Ph_2P(CH_2)PPh_2\}(\eta^2\text{-}$

* Author to whom correspondence should be addressed.

$MeC_2Me)][BF_4]$ was prepared by the published method.[10] All chemicals were purchased from commercial sources, except $Ph_2P(CH_2)PPh_2$ which was synthesized by a literature method.[11]

Elemental analyses for carbon, hydrogen and nitrogen were determined on a Carlo Erba elemental analyser MOD 1106 (using helium as a carrier gas). IR spectra were recorded on a Perkin–Elmer 1430 ratio recording IR spectrophotometer. All ^1H and ^{13}C NMR spectra were recorded on a Bruker AC 250 CP/MAS NMR spectrometer (all spectra were calibrated against tetramethylsilane).

$[WI(CO)(PMe_3)\{Ph_2P(CH_2)PPh_2\}(\eta^2$ - $MeC_2Me)][BF_4]$ (1)

A solution of $[WI(CO)(NCMe)\{Ph_2P(CH_2)PPh_2\}(\eta^2$-$MeC_2Me)][BF_4]$ (0.5 g, 0.552 mmol) in CH_2Cl_2 (15 cm^3) in a Schlenk tube was frozen in liquid nitrogen. PMe_3 (0.0420 g, 0.552 mmol) was distilled into the Schlenk tube by direct pyrolysis of $[\{AgI(PMe_3)\}_4]$ (0.1680 g, 0.138 mmol) at 200°C *in vacuo*. After completion of pyrolysis the reaction Schlenk was opened to nitrogen and allowed to warm up to room temperature. After the reaction mixture had been stirring for 5 h, the solution was filtered and the solvent volume reduced to 1 cm^3 *in vacuo*. Dropwise addition of diethyl ether precipitated the red cationic complex $[WI(CO)(PMe_3)\{Ph_2P(CH_2)PPh_2\}(\eta^2$ - $MeC_2Me)][BF_4]$ (**1**), which on recrystallization from CH_2Cl_2/Et_2O yielded 0.28 g, 54% of pure product.

$[WI(CO)(PMe_2Ph)\{Ph_2P(CH_2)PPh_2\}(\eta^2$-$MeC_2Me)][BF_4]$ (2)

To $[WI(CO)(NCMe)\{Ph_2P(CH_2)PPh_2\}(\eta^2$-$MeC_2Me)][BF_4]$ (0.5 g, 0.552 mmol) dissolved in CH_2Cl_2 (15 cm^3), with continuous stirring under a stream of dry nitrogen, was added PMe_2Ph (0.079 cm^3, 0.552 mmol). After stirring the solution for 4 h, the solution was filtered and the solvent volume reduced to 2 cm^3 *in vacuo*. Dropwise addition of diethyl ether precipitated the red cationic complex $[WI(CO)(PMe_2Ph)\{Ph_2P(CH_2)PPh_2\}(\eta^2$-$MeC_2Me)][BF_4]$ (**2**), which on recrystallization from CH_2Cl_2/Et_2O yielded 0.29 g, 52% of pure product.

Similar reactions of $[WI(CO)(NCMe)\{Ph_2P(CH_2)PPh_2\}(\eta^2$-$MeC_2Me)][BF_4]$ with L {L = $PMePh_2$, PPh_3, $PEtPh_2$, PEt_2Ph, PEt_3, P^nPr_3, P^nBu_3, $P(CH_2CH{=}CH_2)Ph_2$ and $[Fe(\eta^5$-$C_5H_5)(\eta^5$-$C_5H_4PPh_2)]$} in CH_2Cl_2 at room temperature afforded the analogous cationic monodentate phosphine compounds $[WI(CO)L\{Ph_2P(CH_2)PPh_2\}(\eta^2$-$MeC_2Me)][BF_4]$ (**3–11**) (see Table 1 for colours and yields).

RESULTS AND DISCUSSION

Equimolar amounts of the cationic monoacetonitrile complex $[WI(CO)(NCMe)\{Ph_2P(CH_2)PPh_2\}(\eta^2$-$MeC_2Me)][BF_4]$ and L {L = PMe_3, PMe_2Ph, $PMePh_2$, PPh_3, $PEtPh_2$, PEt_2Ph, PEt_3, P^nPr_3, P^nBu_3, $P(CH_2CH{=}CH_2)Ph_2$ and $[Fe(\eta^5$-$C_5H_5)(\eta^5$-$C_5H_4PPh_2)]$} react in CH_2Cl_2 at room temperature to afford the substituted products **1–11** in good yield. The complexes **1–11** have been fully characterized by elemental analysis (C, H and N) (Table 1), IR (Table 2) and ^1H, and in selected cases ^{13}C, NMR spectroscopy (Tables 3 and 4). The complexes with L = PPh_3 (**4**) and $[Fe(\eta^5$-$C_5H_5)(\eta^5$-$C_5H_4PPh_2)]$ (**11**) were confirmed as CH_2Cl_2 solvates by repeated elemental analyses and ^1H and ^{13}C NMR spectroscopy (Tables 3 and 4). The compounds **1–11** are stable in the solid state when stored under nitrogen, however, they decompose in solution when exposed to air. Compounds **1–11** are soluble in polar solvents such as CH_2Cl_2, $CHCl_3$, acetone, etc., however, they are insoluble in hydrocarbon solvents and diethyl ether.

The structures of complexes **1–11** are highly likely to have the but-2-yne ligand *trans* to the iodide ligand, with the bidentate phosphine $Ph_2P(CH_2)PPh_2$, carbon monoxide and the monodentate phosphine, L, occupying the equatorial sites, since the X-ray crystal structures of the related cations $[WI(CO)L\{Ph_2P(CH_2)PPh_2\}(\eta^2$-$MeC_2Me)]^+$ [for L = $P(O^iPr)_3$[10] and $SC(NH_2)_2$[12]] have been determined and have this geometry. The spectroscopic properties of **1–11** are similar to these complexes and hence the proposed structure for **1–11** is shown in Fig. 1.

The IR spectra of **1–11** all show a single carbonyl resonance at $\sim$ 1955 cm^{-1}, and in selected cases very weak alkyne (C≡C) stretching bands at $\sim$ 1635 cm^{-1}, i.e. at a lower wavenumber compared to free but-2-yne due to donation of electron density from filled metal *d*-orbitals to empty π^*-orbitals on the coordinated but-2-yne ligand. Complexes **1–11** also show strong bands in the IR spectra at 1016 cm^{-1} and a strong sharp band at 529 cm^{-1} due to the ν(BF) of the tetrafluoroborate counter anion.[13]

The ^1H NMR spectra show the expected features for the structure shown in Fig. 1. The barrier to but-2-yne rotation of the complexes $[WI(CO)L\{Ph_2P(CH_2)PPh_2\}(\eta^2$-$MeC_2Me)][BF_4]$ (where L = PMe_3, PMe_2Ph, PPh_3, $PEtPh_2$, PEt_2Ph, PEt_3, P^nPr_3 and P^nBu_3) have been determined by variable temperature ^1H NMR spectroscopy. From a knowledge of the coalescence temperature, T_c, and the separation of the two methyl groups of the but-2-yne ligand ($\Delta\nu$), calculations using the equation $\Delta G^{\ddagger}_{T_c} = -RT_c \ln(\pi\Delta\nu h/\sqrt{2}K_BT_c)$[14,15] allows the

Table 1. Physical and analytical[a] data for the complexes $[WI(CO)L\{Ph_2P(CH_2)PPh_2\}(\eta^2\text{-}MeC_2Me)][BF_4]$

Complex	Colour	Yield	C	H
$[WI(CO)(PMe_3)\{Ph_2P(CH_2)PPh_2\}(\eta^2\text{-}MeC_2Me)][BF_4]$ (**1**)	Red	54	41.8 (42.2)	4.3 (4.0)
$[WI(CO)(PMe_2Ph)\{Ph_2P(CH_2)PPh_2\}(\eta^2\text{-}MeC_2Me)][BF_4]$ (**2**)	Red	52	45.2 (45.5)	3.7 (3.7)
$[WI(CO)(PMePh_2)\{Ph_2P(CH_2)PPh_2\}(\eta^2\text{-}MeC_2Me)][BF_4]$ (**3**)	Red–brown	57	48.0 (48.5)	3.9 (3.9)
$[WI(CO)(PPh_3)\{Ph_2P(CH_2)PPh_2\}(\eta^2\text{-}MeC_2Me)][BF_4]\cdot CH_2Cl_2$ (**4**)	Fawn	45	49.0 (48.6)	3.9 (3.7)
$[WI(CO)(PEtPh_2)\{Ph_2P(CH_2)PPh_2\}(\eta^2\text{-}MeC_2Me)][BF_4]$ (**5**)	Pink	58	49.3 (49.0)	3.9 (4.0)
$[WI(CO)(PEt_2Ph)\{Ph_2P(CH_2)PPh_2\}(\eta^2\text{-}MeC_2Me)][BF_4]$ (**6**)	Pink	53	45.9 (46.2)	3.8 (4.2)
$[WI(CO)(PEt_3)\{Ph_2P(CH_2)PPh_2\}(\eta^2\text{-}MeC_2Me)][BF_4]$ (**7**)	Pink	54	43.8 (44.0)	4.5 (4.4)
$[WI(CO)(P^nPr_3)\{Ph_2P(CH_2)PPh_2\}(\eta^2\text{-}MeC_2Me)][BF_4]$ (**8**)	Pink	50	46.6 (45.7)	5.2 (4.8)
$[WI(CO)(P^nBu_3)\{Ph_2P(CH_2)PPh_2\}(\eta^2\text{-}MeC_2Me)][BF_4]$ (**9**)	Pink	52	47.9 (47.3)	4.9 (5.2)
$[WI(CO)\{P(CH_2CH{=}CH_2)Ph_2\}\{Ph_2P(CH_2)PPh_2\}(\eta^2\text{-}MeC_2Me)][BF_4]$ (**10**)	Pink	49	49.8 (49.6)	4.2 (4.0)
$[WI(CO)\{[Fe(\eta^5\text{-}C_5H_5)(\eta^5\text{-}C_5H_4PPh_2)]\}\{Ph_2P(CH_2)PPh_2\}(\eta^2\text{-}MeC_2Me)][BF_4]\cdot CH_2Cl_2$ (**11**)	Fawn	48	48.4 (48.2)	3.7 (3.7)

[a] Calculated values in parentheses.

Table 2. IR data[a] for the complexes [WI(CO)L{$Ph_2P(CH_2)PPh_2$}(η^2-MeC_2Me)][BF_4]

Complex	ν(CO) (cm^{-1})	ν(C≡C) (cm^{-1})
1	1965 (s)	—[b]
2	1960 (s)	1635 (w)
3	1945 (s)	1635 (w)
4	1945 (s)	1625 (w)
5	1960 (s)	1620 (w)
6	1955 (s)	—[b]
7	1955 (s)	—[b]
8	1945 (s)	—[b]
9	1945 (s)	—[b]
10	1970 (s)	1635 (w)
11	1940 (s)	—[b]

[a] Spectra recorded as $CHCl_3$ films between NaCl plates; s, strong; w, weak.

[b] ν(C≡C) was not observed for these complexes.

barrier to but-2-yne rotation to be calculated. The barriers to but-2-yne rotation for complexes **1**, **2**, **4**, **5**, **6**, **7**, **8** and **9** are given in Table 5. The data in Table 5 show that from the highest barrier to but-2-yne rotation for L = PMe_3, $\Delta G^{\ddagger}_{T_c}$ = 55 kJ mol^{-1}, to the lowest barrier i.e. for L = PEt_2Ph, $\Delta G^{\ddagger}_{T_c}$ = 49 kJ mol^{-1}, there is only a difference of 6 kJ mol^{-1}. Since the accuracy of this method for calculating the barriers to but-2-yne rotation is ± 1 kJ mol^{-1} at best, it appears that the different steric and electronic effects of the phosphines in these complexes is having little effect on the barrier to but-2-yne rotation. These results are in contrast to the series of complexes [$WI_2(CO)L_2(\eta^2$-$MeC_2Me)$] where the electronic and steric effects of the phosphine ligands had a marked effect on the barrier to but-2-yne rotation.[9] For example, across the series L = PEt_3, PEt_2Ph, $PEtPh_2$ and PPh_3 for [WI_2(CO)$L_2(\eta^2$-$MeC_2Me)$] the values for $\Delta G^{\ddagger}_{T_c}$ are 58,

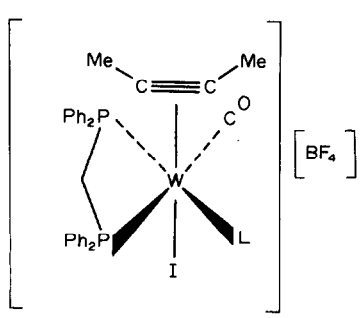

Fig. 1. Proposed structure of the complexes [WI(CO)L{$Ph_2P(CH_2)PPh_2$}(η^2-MeC_2Me)][BF_4] (**1**–**11**).

Table 3. ^{1}H NMR data[a] for the complexes [WI(CO)L{$Ph_2P(CH_2)PPh_2$}(η^2-MeC_2Me)][BF_4]

Complex	^{1}H (δ) (ppm)
1	7.29 (bm, 20H, Ph—*H*); 5.6 (bm, 2H, PCH_2P); 2.97 (s, 6H, ≡C*Me*); 1.49 (m, 9H, CH_3)
2	7.45 (bm, 25H, Ph—*H*); 5.43 (bm, 2H, PCH_2P); 2.97 (s, 6H, ≡C*Me*); 1.88 (t, 3H, CH_3, J_{P-H} = 4 Hz). 1.71 (t, 3H, C*H*, J_{P-H} = 4 Hz)
3	7.45 (bm, 30H, Ph—*H*); 5.63 (bm, 2H, PCH_2P); 2.97 (s, 6H, ≡C*Me*); 2.52 (d, 3H, CH_3, J_{P-H} = 4.2 Hz)
4	7.43 (bm, 35H, Ph—*H*); 5.62 (bm, 2H, PCH_2P); 5.27 (s, 2H, CH_2Cl_2); 2.94 (s, 6H, ≡C*Me*)
5	7.38 (bm, 30H, Ph—*H*); 5.43 (bm, 2H, PCH_2P); 2.38 (s, 6H, ≡C*Me*); 2.04 (bm, 2H, CH_2); 0.95 (m, 3H; CH_3)
6	7.35 (bm, 25H, Ph—*H*); 4.95 (m, 2H, PCH_2P); 2.92 (s, 6H, ≡C*Me*); 2.45 (bm, 4H, CH_2); 1.31 (t, 3H, CH_3, J_{P-H} = 5.2 Hz); 1.19 (t, 3H, CH_3, J_{P-H} = 5.1 Hz)
7	7.35 (bm, 20H, Ph—*H*); 5.15 (m, 2H, PCH_2P); 2.90 (s, 6H, ≡C*Me*); 2.35 (bm, 6H, CH_2); 1.35 (m, 9H, CH_3)
8	7.35 (bm, 20H, Ph—*H*); 5.15 (m, 2H, PCH_2P); 2.94 (s, 6H, ≡C*Me*); 2.35 (m, 6H, PCH_2); 1.75 (m, 6H, CH_2); 1.13 (t, 9H, CH_3, J_{H-H} = 7.5 Hz)
9	7.35 (bm, 20H, Ph—*H*); 5.13 (m, 2H, PCH_2P); 2.89 (s, 6H, ≡C*Me*); 2.25 (m, 6H, PCH_2); 1.65 (m, 6H, CH_2); 0.95 (t, 9H, CH_3, J_{H-H} = 7.5 Hz)
10	7.35 (bm, 30H, Ph—*H*); 5.66 (m, 2H, PCH_2P); 5.3 (m, 2H, PCH_2); 5.03 (m, 1H, =C*H*); 4.48 (m, 2H, =CH_2); 2.96 (s, 6H, ≡C*Me*)
11	7.38 (bm, 30H, Ph—*H*); 5.3 (s, 2H, CH_2); 4.8 (m, 2H, PCH_2P); 4.41–4.3 (bm, 9H, Cp—*H*); 2.93 (s, 6H, ≡C*Me*)

[a] Spectra run in $CDCl_3$ (+25°C) references to $SiMe_4$; s, singlet; bm, broad multiplet; m, multiplet; t, triplet.

56, 49 and 50, respectively. Whereas for the series of phosphines L = PEt_3, PEt_2Ph, $PEtPh_2$ and PPh_3 for the complexes [WI(CO)L{$Ph_2P(CH_2)PPh_2$}(η^2-MeC_2Me)][BF_4] the values for $\Delta G^{\ddagger}_{T_c}$ = 51, 49, 51 and 52, respectively, no significant trend is observed. This is likely to be due to the fact that the complexes [WI(CO)L{$Ph_2P(CH_2)PPh_2$}(η^2-MeC_2

Table 4. ^{13}C NMR data[a] for selected complexes [WI(CO)L{$Ph_2P(CH_2)PPh_2$}(η^2-MeC_2Me)][BF_4]

Complex	^{13}C (δ) (ppm)
1	221.98 (s, *C*≡*C*); 206.94 (s, *C*≡O); 133.07–127.92 (m, Ph—*C*); 36.4 (t, PCH_2P, J_{P-C} = 13.2 Hz); 24.2 (d, CH_2, J_{P-C} = 12 Hz); 19.74 (s, ≡C*Me*); 17.96 (t, CH_3, J_{P-C} = 5 Hz)
4	219.7 (s, *C*≡*C*); 207.2 (s, *C*≡O); 134.9–127.9 (m, Ph—*C*); 53.2 (s, CH_2Cl_2); 32.6 (t, PCH_2P, J_{P-C} = 13 Hz); 19.86 (s, ≡C*Me*)
6	224.29 (s, *C*≡*C*); 209.3 (s, *C*≡O); 137.2–127.8 (m, Ph—*C*); 33.2 (bs, PCH_2P); 27.3 (d, PCH_2, J_{P-C} = 15 Hz); 25.8 (d, PCH_2, J_{P-C} = 13.7 Hz); 19.7 (s, ≡C*Me*); 16.8 (s, CH_3)
9	221.81 (s, *C*≡*C*); 207.6 (s, *C*≡O); 134.2–126.9 (m, Ph—*C*); 35.3 (t, PCH_2P, J_{P-C} = 14.2 Hz); 26.8, 26.6, 24.73, 23.8 (cs, CH_2); 21.9 (s, ≡C*Me*); 10.7 (s, CH_3)

[a]Spectra recorded in $CDCl_3$ (+25°C) referenced to $SiMe_4$. s, singlet; d, doublet; t, triplet; b, broad; m, multiplet.

Table 5. Barriers of but-2-yne rotation for complexes of the type [WI(CO)L{$Ph_2P(CH_2)PPh_2$}(η^2-MeC_2Me)][BF_4]

Complex	T_c (K)	$\Delta\nu$ (Hz)	$\Delta G^{\ddagger}_{T_c}$ (kJ mol^{-1}) (±1)
1	268	57.25	55
2	252	61.29	51
4	260	90.26	52
5	253	79.66	51
6	257	223.42	49
7	258	101.8	51
8	265	97.9	53
9	259	87.5	52

Me)][BF_4] have only one monodentate phosphine different in the series, whereas for the previously reported complexes [$WI_2(CO)L_2(\eta^2$-$MeC_2Me)$][9] there are two monodentate or one bidentate phosphine which significantly affect the barrier to but-2-yne rotation in these neutral monobut-2-yne complexes. It is useful to note that the related triisopropylphosphite-containing complex [WI(CO){$P(O^iPr)_3$}{$Ph_2P(CH_2)PPh_2$}(η^2-MeC_2Me)]$^+$ [10] has a barrier to but-2-yne rotation, $\Delta G^{\ddagger}_{T_c}$ = 57 kJ mol^{-1}, i.e. similar to the compounds described in this paper.

The ^{13}C NMR spectra for selected complexes (Table 4) show alkyne contact carbon resonances above 200 ppm, which indicates[16] that the but-2-yne ligand is donating four electrons to the tungsten in these compounds. This is supported by the fact that the complexes [WI(CO)L{$Ph_2P(CH_2)PPh_2$}(η^2-MeC_2Me)][BF_4] obey the effective atomic number rule if the alkyne is donating four electrons to the metal in these compounds.

Acknowledgement—We thank the SERC for their support.

REFERENCES

1. M. L. H. Green, J. Knight and J. A. Segal, *J. Chem. Soc., Dalton Trans.* 1977, 2189.
2. S. R. Allen, P. K. Baker, S. G. Barnes, M. Green, L. Trollope, L. M. Muir and K. W. Muir, *J. Chem. Soc., Dalton Trans.* 1981, 873.
3. B. C. Ward and J. L. Templeton, *J. Am. Chem. Soc.* 1980, **102**, 1532.
4. S. R. Allen, M. Green, N. C. Norman, K. E. Paddick and A. G. Orpen, *J. Chem. Soc., Dalton Trans.* 1983, 1625.
5. S. R. Allen, T. H. Glauert, M. Green, K. A. Mead, N. C. Norman, A. G. Orpen, C. J. Schaverien and P. Woodward, *J. Chem. Soc., Dalton Trans.* 1984, 2747.
6. J. L. Davidson and G. Vasapollo, *J. Chem. Soc., Dalton Trans.* 1985, 2239.
7. H. G. Alt, *J. Organomet. Chem.* 1985, **288**, 149.
8. P. B. Winston, S. J. N. Burgmayer, T. L. Tonker and J. L. Templeton, *Organometallics* 1986, **5**, 1707.
9. E. M. Armstrong, P. K. Baker, M. E. Harman and M. B. Hursthouse, *J. Chem. Soc., Dalton Trans.* 1989, 295.
10. P. K. Baker, K. R. Flower, M. G. B. Drew and G. Forsyth, *J. Chem. Soc., Dalton Trans.* 1989, 1903.
11. K. Sommer, *Z. Anorg. Allg. Chem.* 1970, **376**, 37.
12. P. K. Baker, K. R. Flower, P. A. Bates and M. B. Hursthouse, *J. Organomet. Chem.* 1989, **372**, 263.
13. K. Nakamoto, *Infrared Spectra of Inorganic and Coordination Compounds*. John Wiley, New York (1963).
14. H. S. Gutowsky and C. H. Holm, *J. Chem. Phys.* 1956, **25**, 1228.
15. A. Allerhand, H. S. Gutowsky, J. Jones and R. A. Meinzer, *J. Am. Chem. Soc.* 1966, **88**, 3185.
16. J. L. Templeton and B. C. Ward, *J. Am. Chem. Soc.* 1980, **102**, 3288.

Polyhedron Vol. 9, No. 18, pp. 2239–2243, 1990
Printed in Great Britain

0277–5387/90 $3.00+.00
© 1990 Pergamon Press plc

THE SOLUTION STABILITY OF BINARY AND TERNARY COMPLEXES INVOLVING OXAAZAMACROCYCLIC LIGANDS

PABITRA K. BHATTACHARYA* and M. RAFIQUE ULLAH

Department of Chemistry, Faculty of Science, M.S. University of Baroda, Baroda 390002, India

and

RABAH A. KHALIL, SIMON J. KITCHEN and DAVID E. FENTON

Department of Chemistry, The University, Sheffield S3 7HF, U.K.

(*Received* 29 *March* 1990; *accepted* 26 *April* 1990)

Abstract—The formation constants of the binary complexes [CuL] and the ternary complexes [CuAL], where A refers to 2,2′-bipyridyl and L refers to oxaazamacrocyclic ligands, have been determined potentiometrically in 50% water–dioxan at 25°C (ionic strength 0.2 M $NaClO_4$). The constants have been correlated with the proposed structures of the binary and ternary complexes.

Tetraazamacrocyclic ligands are known to form very stable coordination complexes,[1–3] the stability of which is attributed to favourable enthalpy and entropy changes.[4–7] Interesting correlations between the metal ion size, the ligand hole size and the stability have been made;[8–10] the formation of such complexes is a slow process, however, and so study of the formation constants has mainly been confined to labile copper(II) species. The introduction of ethereal oxygen donor atoms into the macrocyclic rings results in faster reaction and the coordinating properties of the oxygen atoms may be assumed to be destabilizing.[11] Numerous transition, and non-transition, metal complexes with oxaazamacrocyclic ligands have now been synthesized[12–16] and the formation constants of a number of transition metal complexes have been determined.[17] For nickel(II) complexes of a series of O_2N_2 donor macrocycles it has been shown that the thermodynamic stability is dependent upon the macrocyclic ring size and is at a maximum for a 16-membered ring.[18,19] In contrast, for the copper(II) complexes no ring size dependence has been observed and this may be related to the ease with which copper(II) is able to accommodate different coordination geometries.[20]

In the present study the formation constants of the 1:1 copper(II) complexes of ligands (L^1–L^4) have been determined in 50% (v/v) water–dioxan together with those of the ternary complexes [Cu–bipy–L] (bipy = 2,2′-bipyridyl).

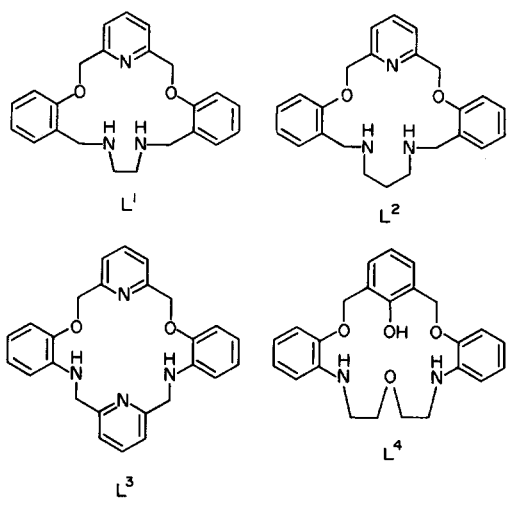

EXPERIMENTAL

Synthesis

The ligands L^1–L^4 were synthesized by the methods detailed in ref. 14. The complexes

* Author to whom correspondence should be addressed.

$Cu(L^1)(NO_3)_2$, $Cu(L^1)(ClO_4)_2$ and $Cu(L^2)(ClO_4)_2$ were prepared by reaction of the ligand and the appropriate hydrated metal salt in methanolic solutions.[15]

The ternary complexes were prepared by reaction of equimolar amounts of the macrocyclic complexes with stoichiometric amounts of either 1,10-phenanthroline (phen) or 2,2′-bipyridyl (bipy) in ethanol. The macrocyclic complex was first dissolved in warm ethanol and a solution of the ligand in ethanol added. The reactions proceeded as follows.

(i) $Cu(L^1)(ClO_4)_2$ *with* phen *or* bipy. The solution darkened slowly and a purple precipitate settled out. This was filtered off and dried. Found: C, 49.9; H, 4.0; N, 8.5. $Cu(L^1)(ClO_4)_2$, bipy ($C_{33}Cl_2CuH_{35}N_5O_{10}$) requires: C, 49.9; H, 4.2; N, 8.8%.

(ii) $Cu(L^1)(NO_3)_2$ *with* phen. A clear blue solution was obtained. This was reduced by rotary evaporation until a blue solid began to separate. The solid was filtered off and dried. Found: C, 54.3; H, 4.7; N, 12.3. $Cu(L^1)(NO_3)_2$,phen,$2H_2O$ ($C_{35}Cl_2CuH_{37}N_5O_{10}$) requires: C, 54.0; H, 4.7; N, 12.6%.

(iii) $Cu(L^2)(ClO_4)_2$ *with* phen. A green precipitate slowly settled out. This was filtered off and dried to give a green product of indeterminate composition.

Formation constants

All reagents used were of AR grade. Potentiometric titrations were carried out in 50% (v/v) water–dioxan using a GP electronics pH meter (No. 8021, accuracy ±0.01 pH units), at 25°C, using 0.2 M NaOH. For determination of ligand protonation constants the ligands (1.00×10^{-3}, 2.00×10^{-3} and 3.00×10^{-3} M) in 50 cm^3 of a 2.00×10^{-2} M $HClO_4$ solution ($I = 0.2$ M $NaClO_4$) were titrated with 0.2 M NaOH. The pH electrode was calibrated in aqueous solution using buffer solutions of pH 4, 7, and 9. Solvent corrections for pH were carried out as detailed earlier.[21]

The formation constants of the binary copper(II) complexes were determined under the same experimental conditions. For this the solution containing the metal ion and the ligands in the ratios 1:1, 1:2 and 1:3 (Cu^{2+}:L) in 50 cm^3 water–dioxan were titrated against standard alkali. The values were refined using SCOGS.[22] The species considered for the calculation of the protonation constants are L, $[LH]^+$ and $[LH_2]^+$, and for the binary constants are L, $[LH]^+$, $[LH_2]^+$, M and ML. These values were used as constants in calculating the formation constants of the ternary complexes. The formation constants of the ternary complexes were determined by titration of 50% (v/v) water–dioxan solutions (50 cm^3) of the reagents with concentrations of 2.00×10^{-3} and 1.00×10^{-3} M in the ratios M^{2+}:A:L = 1:1:1 and M^{2+}:A:L = 1:2:2 against carbonate-free standard NaOH. Titration of each set was carried out twice to check the reproducibility of the data. As macrocyclization is a slow process, sufficient time (2–3 min) was allowed between successive additions of NaOH solution to permit equilibrium to be reached, indicated by the system attaining constant pH. The experimental values of pH and volume of alkali used were fed into the computer and calculations were carried out using the computer program SCOGS.[22] The species considered were L, $[LH]^+$, $[LH_2]^+$, A, $[AH]^+$, M, [ML], [MA], $[MA_2]$ and MAL. The values of the protonation constants of the ligands and the formation constants of the binary complexes are presented in Table 1, and the values of the formation constants for the ternary complexes are presented in Table 2.

Mass spectra (FAB) of the ternary complexes

Fast atom bombardment mass spectra of the ternary complexes were recorded using a Kratos MS80RF mass spectrometer (accelerating voltage 4 kV, resolution 1500) coupled to a DS55 data system. The atom gun was an adapted saddle-field source (ION Tech Ltd) operated at *ca* 6 eV and a

Table 1. Proton–ligand formation constants ($\log K^H$ values) of the ligands and formation constants ($\log K$ values) of binary complexes of copper(II) with the ligands in 50% (v/v) water–dioxan and $\mu = 0.2$ M ($NaClO_4$) at 25°C (Standard deviation $\sigma\beta$ in parentheses)

Ligand	K_1^H	K_2^H	K_1	K_2
L^1	8.49(0.15)	5.04(0.19)	10.10(0.26)	—
L^2	9.26(0.40)	7.38(0.50)	9.17(0.15)	—
L^3	4.46(0.07)	2.50(0.07)	6.99(0.35)	—
L^4	3.72(0.10)	3.05(0.07)	5.75(0.00)	—
bipy	3.71(0.02)	—	7.00(0.04)	4.15(0.04)

Table 2. Stability constants of the mixed ligand complexes [Cu–bipy–L] in 50% (v/v) water–dioxan and $\mu = 0.2$ M ($NaClO_4$) at 25°C (Standard deviation $\sigma\beta$ in parentheses)

Ligand	Log K^{Cu}_{CuAL}	$\Delta \log K$
L^1	15.54(0.18)	−1.72
L^2	13.66(0.08)	−2.51
L^3	11.43(0.05)	−2.56
L^4	10.13(0.09)	−2.62

tube current of *ca* 2 mA. Xenon was used to provide the primary beam of atoms and the samples were mixed with a small amount of 3-nitrobenzyl alcohol matrix on a stainless steel probe. Spectra were recorded in the positive-ion mode at a scan speed of 30 s per decade.

RESULTS AND DISCUSSION

Only two protonation constants could be determined for each ligand; these correspond to those for the —NH protons. The protonation of the pyridinyl nitrogen is very much reduced because of the two protonated NH_3^+ sites in the ring.[23] The values for the protonation constants of the ligands L^1 and L^2 are higher than those for L^3 and L^4, and are comparable to those of 1,2-diaminoethane and 1,3-diaminopropane; this is because the nitrogen atoms are removed from the aromatic rings and so subjected to a reduced electron-withdrawing effect. The ligands L^3 and L^4, in which the nitrogen is linked directly to the aromatic ring, have lower protonation constants, which are comparable to those of the anilino-NH_2 group.

The complex formation can be shown by the following equilibrium.

$$M + L \rightleftharpoons ML$$

$$K^{M}_{ML} = \frac{[ML]}{[M][L]}.$$

It is observed that for complexes CuL^1 and CuL^2 the formation constants (10.10 and 9.17, respectively) are comparable to those for 1,2-diaminoethane and 1,3-diaminopropane complexes of copper(II).[24] For the CuL^3 and CuL^4 complexes the formation constants are lower in value because of coordination with the less basic nitrogen atoms.[14] The formation constant for CuL^1 is greater than that of CuL^2 and similarly that of CuL^3 is higher than that of CuL^4. This may be related to the increased ring sizes found in L^2 and L^4 as compared with L^1 and L^3 and also with the difference in the functional groups of L^3 and L^4.

The comparability of the formation complexes of CuL^1 and CuL^2 with those for complexes of aliphatic diamines suggests that coordination from the ethereal oxygens and the pyridinyl nitrogen might be weak. The crystal structure of $[Cu(L^1)H_2O](ClO_4)_2$ has been solved and shows that the copper is in a tetragonally elongated octahedral environment provided by the five ligand donor atoms and the water molecules.[25] The Cu—N distances are all within the standard range (2.02, 1.99 and 2.03 Å),[26] together with the Cu—O(water) at 2.02 Å. The axial Cu—O(ether) distances are long, 2.30 and 2.67 Å. In solution (dioxan–water) it is likely that the water is retained. The availability of 1(metal) : 2(ligand) complexes of L^1 both in solution and in the solid state[26] further suggests that it is also possible to release the pyridinyl-nitrogen in these complexes.

The formation of the ternary complexes takes place as follows:

$$Cu + A + L \rightleftharpoons CuAL$$

$$K^{Cu}_{CuAL} = \frac{[CuL]}{[Cu][A][L]}$$

$$CuA + L \rightleftharpoons CuAL$$

$$K^{CuA}_{CuAL} = \frac{[CuAL]}{[CuA][L]}$$

$$CuL + A \rightleftharpoons CuAL$$

$$K^{CuL}_{CuAL} = \frac{[CuAL]}{[CuL][A]}.$$

The difference in stability between the binary and ternary complexes is a way to characterize the tendency for ternary complex formation. Since more coordination positions are available for binding the first ligand than for binding the second ligand, the formation constant of the 1 : 1 complex is generally higher than that for the 1 : 2 complex.[27]

Table 3. Mass spectra of the ternary complexes

	X = ClO_4		X = NO_3
	L = phen	L = bipy	L = phen
$[Cu(L^1)(L)X]^+$	717	693	680
$[Cu(L^1)X]^+$	537	537	500
$[Cu(L_1)]^+$	438	438	438
$[(L^1)H]^+$	376	376	376
$[Cu(L)_2]^+$	423	—	423
$[Cu(L)]^+$	243	219	243

From a statistical consideration $K^{CuA}_{CuAL} < K^{Cu}_{CuL}$ or $K^{CuL}_{CuAL} < K^{Cu}_{CuA}$, therefore, $\Delta \log K$ ($= \log K^{CuA}_{CuAL} - \log K^{Cu}_{CuL}$ or $\log K^{CuL}_{CuAL} - \log K^{Cu}_{CuA}$) should be negative. In the ternary complexes studied here $\Delta \log K$ is small and negative and is comparable to the magnitude of $\Delta \log K$ in [Cu–bipy–neutral bidentate] ternary complexes.[28]

If the ternary complexes derived from bipy are octahedrally derived, the bipy can coordinate via two equatorial positions or by one equatorial and one axial position. The macrocycle would then have to become distorted in order to occupy the remaining coordination positions. The maximum expected coordination would then be seven (probably pentagonal bipyramidal) for L^1 and L^2 if all the donor atoms were involved. If the apparently weaker oxygen donors were not involved then five-coordination is likely. The $\Delta \log K$ values are comparable with those for [Cu–bipy–neutral bidentate] complexes and this suggests that the macrocycles are effectively coordinating via the two —NH donor sites only and so acting as bidentate ligands.

Studies on the speciation of L^1 have shown that binding through the diamino-nitrogen atoms of the macrocycle can occur and this is validated through the crystal structure of $[Ni(L^1)_2(NO_3)](NO_3)$, 2MeOH.[25] In this complex, which may be regarded as being similar to a ternary species due to the presence of the two ligand molecules, the nickel(II) is octahedrally coordinated by a bidentate nitrate anion and by two bidentate macrocycles in an exocyclic mode. The observation that the 1 : 2 species is retained in DMSO leads to the proposal that in the ternary complexes derived from L^1 or L^2 and bipy, a similar binding mode occurs for the macrocycle and so the macrocyclic nitrogen donors and the bipy provide a square-planar environment around the metal with accompanying axial molecules of solvation. The similarity of the $\Delta \log K$ values for these complexes and those derived from L^3 or L^4 and bipy suggests that the latter complexes also involve a bidentate binding mode for the macrocycle, probably through the nitrogen donors.

It was possible to isolate species from solution for complexes derived from the macrocycles L^1 and L^2 together with the ligands phen and bipy. The FAB mass spectra of the complexes isolated from solution indicated the presence of ternary complexes for $Cu(L^1)(L)(ClO_4)_2$, where L = phen or bipy, and for $Cu(L^1)(L)(NO_3)_2$, where L = phen, with the breakdown pattern for these species giving peaks corresponding to $[Cu(L^1)(L)X]^+$, $[Cu(L^1)X]^+$, $[Cu(L^1)]^+$, $[(L^1)H]^+$ and $[Cu(L)]^+$ (X = anion). The presence of the peaks such as $[Cu(L^1)]^+$ and $[Cu(L)]^+$ suggests that some reduction of either the metal or the ligand has occurred. No such spectrum was obtained for the product involving L^2 for which the breakdown pattern gave peaks corresponding to $[Cu(phen)_2ClO_4]^+$, $[Cu(phen)_2]^+$ and $[Cu(phen)]^+$, with very small peaks corresponding to $[Cu(L^2)]^+$ and $[(L^1)H]^+$. In the absence of crystals suitable for X-ray analysis it is only possible to speculate on the structures of the complexes, but it would seem likely that the complexes $Cu(L^1)(L)(ClO_4)_2$, where L = phen or bipy, would have a structure in which the macrocycle is bidentate as discussed above, with the second organic ligand and one perchlorate anion also coordinated to the metal. The presence of ligand bands in the same regions of the IR spectrum as the perchlorate band prevents an unambiguous assignment of the anion binding mode. The different colour of the $Cu(L^1)(L)(NO_3)_2,2H_2O$ complex would suggest a different arrangement, probably with the waters coordinated to the metal and with non-coordinated anions. The absence of a ternary complex in the reaction using L^2 may be related to the presence of a 1,3-trimethylene bridge in the macrocycle, leading to a less stronger bidentate chelating mode for L^2.

Acknowledgements—We thank the SERC for an award (to S.J.K.), the Iraqi Ministry of Higher Education and Scientific Research for an award (to R.A.K.) and the Government of India for a Research Fellowship (to M.R.U.) under the Indo–Bangladesh exchange programme.

REFERENCES

1. D. K. Cabbiness and D. W. Margerum, *J. Am. Chem. Soc.* 1969, **91**, 6540; 1970, **92**, 2151.
2. D. C. Olson and J. Vasilevskis, *Inorg. Chem.* 1969, **8**, 1611; 1971, **10**, 463 and 1228.
3. D. H. Busch, K. Farmery, V. Goedken, V. Katovic, A. C. Melnyk, C. R. Sperati and N. Tokel, *Am. Chem. Soc., Adv. Chem. Ser.* 1970, **100**, 44 and 52.
4. A, Anichini, L. Fabbrizzi, P. Paoletti and R. M. Clay, *J. Chem. Soc., Dalton Trans.* 1978, 578.
5. M. Kodama and E. Kimura, *J. Chem. Soc., Chem. Commun.* 1975, 326 and 891.
6. M. Kodama and E. Kimura, *J. Chem. Soc., Dalton Trans.* 1976, 116, 1720 and 2341.
7. F. P. Hinz and D. W. Margerum, *Inorg. Chem.* 1974, **13**, 2941.
8. L. Y. Martin, C. R. Sperati and D. H. Busch, *J. Am. Chem. Soc.* 1977, **99**, 2968.
9. Y. Hung, L. Y. Martin, S. C. Jaeckel, A. M. Tait and D. H. Busch, *J. Am. Chem. Soc.* 1977, **99**, 4029.
10. P. K. Bhattacharya, *J. Inorg. Nucl. Chem.* 1981, **43**, 41.
11. R. Barbucci and A. Vacca, *J. Chem. Soc., Dalton Trans.* 1977, 2363.
12. D. H. Cook, D. E. Fenton, M. G. B. Drew, S. G.

McFall and S. M. Nelson, *J. Chem. Soc., Dalton Trans.* 1977, 446.
13. L. F. Lindoy, H. C. Lip, J. H. Rea, R. J. Smith, K. Henrick, M. McPartlin and P. A. Tasker, *Inorg. Chem.* 1980, **19**, 3360.
14. D. E. Fenton, B. P. Murphy, A. J. Leong, L. F. Lindoy, A. Bashall and M. McPartlin, *J. Chem. Soc., Dalton Trans.* 1987, 2543.
15. S. J. Kitchen, PhD thesis, University of Sheffield (1989).
16. L. F. Lindoy, *The Chemistry of Macrocyclic Ligand Complexes*. Cambridge University Press, Cambridge (1989).
17. R. M. Izatt, J. S. Bradshaw, S. A. Nielsen, J. D. Lamb, J. J. Christensen and D. Sen, *Chem. Rev.* 1985, **85**, 271.
18. G. Anderegg, A. Ekstrom, L. F. Lindoy and R. J. Smith, *J. Am. Chem. Soc.* 1980, **102**, 2670.
19. K. Henrick, P. A. Tasker and L. F. Lindoy, *Prog. Inorg. Chem.* 1985, **33**, 1.
20. K. R. Adam, G. Anderegg, L. F. Lindoy, H. C. Lip, M. McPartlin, J. H. Rea, R. J. Smith and P. A. Tasker, *Inorg. Chem.* 1980, **19**, 2956.
21. N. D. Kulkarni and P. K. Bhattacharya, *Can. J. Chem.* 1987, **65**, 348.
22. I. G. Sayce, *Talanta* 1966, **15**, 1397; 1971, **18**, 653; I. G. Sayce and V. S. Sharma, *Talanta* 1972, **19**, 831.
23. J. J. Christensen, D. E. Smith, M. D. Slade and R. M. Izatt, *Thermochim. Acta* 1972, **5**, 35.
24. P. C. Parikh and P. K. Bhattacharya, *Ind. J. Chem.* 1975, **13**, 190.
25. N. A. Bailey, D. E. Fenton, S. J. Kitchen, P. A. Tasker and M. G. Williams, *J. Chem. Soc., Chem. Commun.* 1988, 1575.
26. B. Koren, M. Melnik, P. Sivy and F. Valach, *Struct. Bond.* 1983, **55**, 101.
27. H. Sigel and D. B. McCormick, *Accts Chem. Res.* 1970, **3**, 201.
28. P. J. Patel, V. K. Patel and P. K. Bhattacharya, *Inorg. Chem.* 1982, **21**, 3163.

Polyhedron Vol. 9, No. 18, pp. 2245–2249, 1990
Printed in Great Britain

0277–5387/90 $3.00+.00
© 1990 Pergamon Press plc

MIXED-LIGAND COMPLEXES—II.* (METHIONINATO)ETHYLENEDIBIGUANIDE COBALT(III) SALTS

R. K. RAY

Department of Chemistry, Rama Krishna Mission Vivekananda Centenary College, Rahara-743186, West Bengal, India

(*Received* 30 *January* 1989; *accepted after revision* 1 *May* 1990)

Abstract—A series of new cobalt(III) complexes of the formulation $[Co(meth\text{-}O^-)(EBG)]^{2+}$ (where meth-OH = DL-methionine, L-methionine; EBG = ethylenedibiguanide) has been prepared, and characterized using elemental analyses, conductivity measurements, visible and IR spectral data. The electronic absorption spectra reveal two ligand-field bands representing the transitions $^1A_{1g} \rightarrow {}^1T_{1g}$ and $^1A_{1g} \rightarrow {}^1T_{2g}$. The ligands obey their expected position in the spectrochemical series. The visible spectra of all the $[Co(meth\text{-}O^-)(EBG)]^{2+}$ salts are very similar, which reveals that coordination of methionine is through the amino and carboxylated groups. The mercaptide group of methionine remains uncoordinated in the mixed chelate $[Co(meth\text{-}O^-)(EBG)]^{2+}$.

The preparation and properties of the mixed chelate $[Co(meth\text{-}O^-)(EBG)]^{2+}$ (meth-OH = methionine; EBG = ethylenedibiguanide, **I**) were undertaken in order to examine the donor behaviour (SNO, SN or NO)[1–4] of methionine. Several other mixed chelates $[Co(AB)(EBG)]^{2+}$ containing one bidentate amino acid (ABH = glycine, DL-alanine, α-alanine, L-leucine, DL-valine, L-histidine) (donor set NO) and one ethylenedibiguanide (donor set NNNN) have been synthesized and characterized[5–7] in order to aid the elucidation of the structure of $[Co(meth\text{-}O^-)(EBG)]^{2+}$. The mode of chelation of methionine, a potentially flexidentate ligand, is discussed.

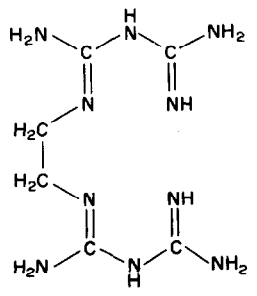

I

* For Part I, see ref. 6.

EXPERIMENTAL

Ethylenedibiguanide sulphate and diamine ethylenedibiguanide cobalt(III) hydroxide sulphate were prepared by published procedures.[8,9]

Analyses

Cobalt and nitrogen were determined as $CoSO_4$ and by the combustion method, respectively. Carbon and hydrogen were analysed by CDRI, Lucknow, India. Halides were determined as the silver salts and sulphate as barium sulphate. Electrical conductances were measured with a Philips PR 9500 conductivity bridge. IR spectra were recorded at CDRI, Lucknow. Solution spectra were obtained with a Hilger Uvispec spectrophotometer over the range 320–600 mm. Relevant data are given in Tables 1 and 2.

DL-(*Methioninato*)*ethylenedibiguanide cobalt*(III) *sulphate*

Diamine ethylenedibiguanide cobalt(III) hydroxide sulphate 4-hydrate (1 g) in water (20 cm^3) was allowed to react with heated DL-methionine (0.35 g in 20 cm^3 of water) on a steam bath for 1 h. After ammonia evolution had ceased, the solution was filtered, cooled and neutralized with cold, dilute H_2SO_4 (1:4) and filtered. After concentration and cooling, the filtrate deposited red–violet crystals,

Table 1. Characterization data for cobalt(III) mixed chelates

Complex	% Cobalt		% Carbon		% Hydrogen		% Nitrogen		% Anion	
	Calc.	Found	Calc.	Found	Calc.	Found	Calc.	Found	Calc.	Found
$[Co(DL\text{-meth-}O^-)(EBG)]SO_4 \cdot H_2O$	10.7	10.6	24.0	23.8	4.7	4.4	28.0	28.0	17.4	17.5
$[Co(DL\text{-meth-}O^-)(EBG)]Cl_2 \cdot 2H_2O$	10.8	10.8	24.3	24.0	5.1	4.8	28.4	28.5	13.1	13.1
$[Co(DL\text{-meth-}O^-)(EBG)]I_2 \cdot H_2O$	8.1	8.1	18.2	18.0	3.5	3.3	21.2	21.2	35.0	35.0
$[Co(L\text{-meth-}O^-)(EBG)]SO_4 \cdot H_2O$	10.7	10.5	24.0	23.6	4.7	4.5	28.0	28.3	17.4	17.6
$[Co(L\text{-meth-}O^-)(EBG)]Cl_2 \cdot 2H_2O$	10.8	10.6	24.3	24.5	5.1	4.7	28.4	28.2	13.1	12.9
$[Co(L\text{-meth-}O^-)(EBG)]I_2 \cdot H_2O$	8.1	7.9	18.2	18.5	3.5	3.3	21.2	21.1	35.0	34.8

EBG = Ethylenedibiguanide; DL-meth-OH = DL-methionine; L-meth-OH = L-methionine.

Table 2. Colour, conductance, chromophore and electronic spectra of cobalt(III) mixed chelates

Complex	Colour	Molar conductance (Ω^{-1} cm^2 mol^{-1}) in water at 25°C	Chromophore	Band I			Band II			Reference
				λ_{max} (nm)	Wave number (ν, cm^{-1})	Molar ε	λ_{max} (nm)	Wave number (ν, cm^{-1})	Molar ε	
$[Co(DL\text{-meth-}O^-)(EBG)]SO_4 \cdot H_2O$	Red–violet	218	CoN_5O	490	20,408	177	355	28,170	300	[a]
$[Co(DL\text{-meth-}O^-)(EBG)]Cl_2 \cdot 2H_2O$	Red–violet	207	CoN_5O	490	20,410	170	360	27,780	297	[a]
$[Co(DL\text{-meth-}O^-)(EBG)]I_2 \cdot H_2O$	Red–violet	211	CoN_5O	490	20,410	163	360	27,780	301	[a]
$[Co(L\text{-meth-}O^-)(EBG)]SO_4 \cdot H_2O$	Red–violet	209	CoN_5O	490	20,408	160	355	28,170	305	[a]
$[Co(L\text{-meth-}O^-)(EBG)]Cl_2 \cdot 2H_2O$	Red–violet	214	CoN_5O	490	20,410	169	360	27,780	309	[a]
$[Co(L\text{-meth-}O^-)(EBG)]I_2 \cdot H_2O$	Red–violet	201	CoN_5O	490	20,410	174	360	27,780	320	[a]
$[Co(gly\text{-}O^-)(EBG)]SO_4 \cdot 1.5H_2O$	Red–violet	328	CoN_5O	515	19,420	175	360	27,780	326	5
$[Co(gly\text{-}O^-)(bigH)_2]Cl_2 \cdot H_2O$	Red–violet	288	CoN_5O	490	20,410	150	365	27,400	175	7
$[Co(gly\text{-}O^-)(en)_2]Cl_2$	—	—	CoN_5O	487	20,530	98	346	28,900	107	3
$[Co(gly\text{-}O^-)(en)_2(Cl)]Cl$	—	—	CoN_5Cl	525	19,050	80	365	27,400	83	3
$[Co(DL\text{-}\alpha\text{-alan-}O^-)(bigH)_2]Cl_2$	Red–violet	246	CoN_5O	490	20,410	155	360	27,780	187	4
$[Co(\alpha\text{-alan-}O^-)(EBG)]Cl_2$	Red–violet	209	CoN_5O	490	20,410	175	360	27,780	325	6
$[Co(DL\text{-meth-}O^-)(bigH)_2]Cl_2$	Red–violet	—	CoN_5O	490	20,410	165	358	27,932	214	4
$[Co(SMCY\text{-}O^-)(en)_2]I_2 \cdot H_2O$	Brick red	227	CoN_5O	483	20,700	101	345	28,980	162	3
$[Co(CY^-\text{-}O^-)(en)_2]I \cdot H_2O$	Orange red	95	CoN_5S	490	20,410	128	600	16,670	43	3
$[Co(HCY\text{-}O^-)(en)_2]ICl \cdot H_2O$	Dark brown	553	CoN_5S	475	21,050	116	593	16,860	38	3

[a] This study.

α-alan-OH = α-alanine; bigH = biguanide; gly-OH = glycine; HCYOH = cysteine; SMCYOH = S-methyl-L-cysteine.

which were further purified from hot water and dried over $CaCl_2$ (yield, 0.8 g).

DL-(*Methioninato*)*ethylenedibiguanide cobalt*(III) *chloride*

This was obtained by metathesis of the complex sulphate (1 g) with barium chloride. After the removal of $BaSO_4$ the filtrate was concentrated to a small volume, cooled and filtered, when reddish-violet crystals separated. These were purified from hot water (yield, 0.8 g).

DL-(*Methioninanto*)*ethylenedibiguanide cobalt*(III) *idodide*

The reddish-violet iodide crystal salt was obtained by the addition of KI to a concentrated aqueous solution of the chloride (1 g). These were purified by two recrystallizations from hot water (yield, 0.8 g).

L-(*Methioninato*)*ethylenedibiguanide cobalt*(III) *sulphate*

L-Methionine (0.36 g in 20 cm^3 of water) and diamine ethylenedibiguanide cobalt(III) hydroxide base (1 g in 20 cm^3 of water) were reacted as described above and the solution was neutralized with dil. H_2SO_4. The red–violet crystalline salt was recrystallized from hot water (yield, 0.75 g).

L-(*Methioninato*)*ethylenedibiguanide cobalt*(III) *chloride*

This compound was obtained by metathesis of the complex sulphate (1 g) with $BaCl_2$. The filtrate after separation of $BaSO_4$ was concentrated to a small volume, cooled and filtered. The product was recrystallized from hot water (yield, 0.7 g).

L-(*Methioninato*)*ethylenedibiguanide cobalt*(III) *iodide*

The red–violet compound was obtained by a metathetic reaction using the above chloride salt (1 g) and KI, and was recrystallized from warm water (yield, 0.75 g).

RESULTS AND DISCUSSION

Busch, Dutta, Ray, Kauffman and others[3–7,10–13] have reported the isolation and detailed study of $[Co(AB)(bigH)_2]^{2+}$ (bigH = biguanide; ABH = amino acids), $[Co(AB)(EBG)]^{2+}$ (EBG = ethylenedibiguanide), $[Co(AB)(en)_2]^{2+}$ etc., in which the amino acids such as glycine (gly-OH) act as bidentate chelating ligands (NO donor) coordinating through the amino and carboxylate groups. Relatively little has been done with similar derivatives of tridentate ligands (histidine, cysteine, methionine, etc.) even though they offer the additional interesting question of which functional groups are utilized in chelation. Methionine is of particular interest in compounds of this composition because of the presence in its structure of three functional groups, only two of which can bind to the cobalt(III) in a given derivative.

Like other amino acids, methionine reacts with diamine ethylenedibiguanide cobalt(III) hydroxide sulphate liberating ammonia and a reddish solution resulted. On concentrating the solution to a small volume and neutralizing with acid the cations could be isolated. The salts are highly crystalline, appear homogeneous under the microscope and are very stable both in the solid state and in aqueous solution. The molar conductance measurements are indicative of the bi–univalent nature of the cations.[14,15] The high conductance value for $[Co(HCY\text{-}O^-)(en)_2]ICl$ ($pK_a = 3.7$)[16] indicates a highly dissociated form of the complex—the majority of the conductance value is due to ionization of the carboxyl group and release of the proton into solution (Table 2).[3]

Strong IR spectral bands around 3450–3100 cm^{-1} have been assigned to ν_{asy}(N—H) (3300–3380 cm^{-1}) and ν_{asy}(N—H) (3100–3150 cm^{-1}) modes of vibration of the guanyl group[6,17] and are observed almost in the same positions as those in the original ligand (EBG) but with a slight decrease in the intensities. This supports participation of EBG without deprotonation. The two bands at 3100–3200 cm^{-1} (NH_2 stretching region) indicate that the amino groups in these complexes are coordinated. Bands around 1650 cm^{-1} have been assigned to the ν(C=N) stretch, ν(N—H) deformation and ν(O—H) deformation vibrations. In ethylenedibiguanide sulphate ($EBG \cdot H_2SO_4$) the ν(C=N) stretch occurs at 1696 cm^{-1} and the ν(N—C—N) stretch at 1585 cm^{-1}.[18–20] A similar ν(N—C—N) stretching frequency for the other cobalt(III) biguanide complexes was noted at 1580 cm^{-1}.[19] Lowering of the ν(C=N) stretch (1655 cm^{-1}) and the ν(N—C—N) stretch (1545 cm^{-1}) in metal complexes is due to coordination with the nitrogen atoms of the =NH groups. The ν(C—N) stretch of the C—NH_2 group in both EBG and the corresponding cobalt(III) complexes is assigned at *ca* 1345–1375 cm^{-1}. Antisymmetrical COO^- stretching frequencies for other cobalt(III) complexes, viz. $[Co(CY^-\text{-}O^-)(en)_2]I$, $[Co(HCY\text{-}O^-)(en)_2]ICl$ and $[Co(SMCY\text{-}O^-)(en)_2]I_2$, are observed at 1616,

1721 and 1656 cm^{-1}, which represent $—CO_2^-$, —COOH and —OOCCo groups, respectively. No band at 1616 cm^{-1} has been observed, and therefore it can be concluded that the free carboxylate ion is not present.[3] An intense C=O stretching band for $[Co(CY^-\text{-}O^-)(en)_2]I$ occurs at 1616 cm^{-1}; the value being consistent with the presence of free carboxylate ion. For $[Co(SMCY\text{-}O^-)(en)_2]I_2$, the C=O stretching occurs at 1656 cm^{-1}, which is typical for coordinated carboxylate groups. The higher frequency noted for coordinated carboxylated groups is well established. The ν(C—N) stretch of the $C—NH_2$ group was located at *ca* 1345–1375 cm^{-1},[19] and chelate ring formation was confirmed when a new strong band appeared at 1200–1300 cm^{-1}.[20] This new band is not found in the studied ligand (EBG). In all metal chelates another new prominent band around 1200–1260 cm^{-1} appeared.[20,21] This is assigned to the following fragment of the molecular structure.

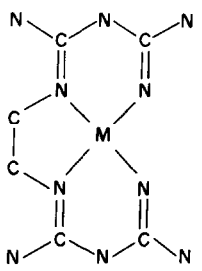

II

The electronic spectra of all the salts show two *d–d* absorption bands and their positions are consistent with assignments based on the C_{4v} symmetry approximated by the donor atoms (five nitrogens and one oxygen positioned octahedrally) rather than the true O_h symmetry.[22,23] The band at longer wavelength is assigned to the transition $^1A_{1g} \rightarrow {}^1T_{1g}$ and the one at shorter wavelength to $^1A_{1g} \rightarrow {}^1T_{2g}$. The visible spectra of all $[Co(meth\text{-}O^-)(EBG)]^{2+}$ salts are very similar to the spectra of $[Co(AB)(bigH)_2]^{2+}$ (ABH = amino acid), where the amino acids are chelated through the amino and carboxylated groups. In the visible spectra of $[Co(SMCY\text{-}O^-)(en)_2]I_2$ the two bands are observed at 483 and 345 nm. The bands are comparatively higher in frequency than the bands in the visible spectra of *cis*-$[Co(gly\text{-}O^-)(Cl)(en)_2]Cl$, $[Co(HCY\text{-}O^-)(en)_2]ICl$ and $[Co(CY^-\text{-}O^-)(en)_2]I_2$ (Table 2). This reflects the relative position of the groups in the spectrochemical series: $S^- < Cl^- < CO_2^-$.[24] From the nature of the spectral profile and their ε_{max} values, it appears that all of the studied complexes have CoN_5O chromophores instead of CoN_5S chromophores. This assumption is verified by comparing the spectra of several other cobalt(III) complexes containing CoN_5O and CoN_5S chromophores. Thus whereas the complexes containing the CoN_5O chromophore show a lower energy band at 490 nm and a higher energy band at 355–360 nm, the CoN_5S chromophore complexes exhibit these two bands at 590–600 nm and at 490 nm, respectively[3–7] (Table 2).

Acknowledgements—The Author is thankful to Professor R. L. Dutta, Department of Chemistry, Burdwan University and to Professor G. B. Kauffman, California State University, U.S.A., for laboratory and other research facilities. The Author is also indebted to the referee for stimulating discussion and valuable suggestions for the improvement of this article.

REFERENCES

1. R. L. Carlin and F. Caniziani, *J. Chem. Phys.* 1964, **40**, 371.
2. R. G. Neville and G. Gorin, *J. Am. Chem. Soc.* 1956, **78**, 4891, 4893.
3. V. M. Kothari and D. H. Busch, *Inorg. Chem.* 1969, **8**, 2276.
4. R. L. Dutta and A. Bhattacharya, *J. Ind. Chem. Soc.* 1980, **57**, 429; 1975 **52**, 1002.
5. R. L. Dutta and I. Malik, *J. Ind. Chem. Soc.* 1967, **44**, 866.
6. R. K. Ray and G. B. Kauffman, *Polyhedron* 1989, **8**, 1015.
7. R. L. Dutta, S. Sarkar and K. K. Bhattacharyya, *J. Ind. Chem. Soc.* 1973, **50**, 235.
8. P. Rây, *Chem. Rev.* 1961, **61**, 313.
9. K. Chakraborty and P. Rây, *J. Ind. Chem. Soc.* 1944, **81**, 41.
10. N. Matsuoka, J. Hidaka and Y. Shimura, *Bull. Chem. Soc. Jpn* 1966, **39**, 1257.
11. D. A. Buckingham and J. P. Collman, *Inorg. Chem.* 1967, **6**, 1803.
12. M. D. Alexander and D. H. Busch, *Inorg. Chem.* 1966, **5**, 602, 1590.
13. W. J. Stratton and D. H. Busch, *J. Am. Chem. Soc.* 1958, **80**, 3191.
14. W. J. Geary, *Coord. Chem. Rev.* 1971, **7**, 81.
15. M. M. Jones, *Elementary Coordination Chemistry*, p. 254. Prentice Hall, Englewood Cliffs, New Jersey (1964).
16. E. J. Cohn and J. T. Edsall, *Proteins, Amino Acids and Peptides*. Reinhold, New York (1943).
17. A. Albert and E. Spinner, *J. Chem. Soc.* 1960, 1221.
18. M. L. Simms, J. L. Atwood and D. A. Zatko, *J. Chem. Soc., Chem. Commun.* 1973, 46.

19. R. H. Skabo and P. W. Smith, *Aust. J. Chem.* 1969, **22**, 659.
20. P. V. Babykutty, C. P. Probhakaran, R. Anantanarayan and C. G. R. Nair, *J. Inorg. Nucl. Chem.* 1974, **36**, 3685.
21. A. Syamal and V. D. Ghakekar, *J. Inorg. Nucl. Chem.* 1978, **40**, 1606.
22. C. J. Ballhausen, *Introduction to Ligand Field Theory*, p. 259. McGraw Hill, New York (1962).
23. R. A. D. Wentworth and T. S. Piper, *Inorg. Chem.* 1965, **4**, 709.
24. J. Lewis and R. G. Wilkins, *Modern Coordination Chemistry*, p. 266. Interscience Publishers, New York (1960).

Polyhedron Vol. 9, No. 18, pp. 2251–2255, 1990
Printed in Great Britain

0277-5387/90 $3.00+.00
© 1990 Pergamon Press plc

NEW, STABLE, CHELATED, TETRACOORDINATED SILVER(I) COMPLEXES OF THE 2-(ARYLAZO)PYRIDINE LIGAND SYSTEM: SYNTHESIS, CHARACTERIZATION AND ASSESSMENT OF BONDING AND STRUCTURE

ALOK K. DEB, SUBRATA CHOUDHURY and SREEBRATA GOSWAMI*

Department of Chemistry, North-Eastern Hill University, Shillong 793 003, India

(*Received* 6 *December* 1989; *accepted* 1 *May* 1990)

Abstract—The 2-(arylazo)pyridines (L, **1**) in methanol gave bis-chelated silver complexes, $[AgL_2]^+$ (**2**), as the crystalline perchlorate salts which were characterized by elemental analyses. The complexes are 1:1 electrolytes in methanol. In contrast to the copper analogue, there is only a small shift of ν(N=N) to low energy in the IR spectrum of $[AgL_2]^+$ as compared to that of uncoordinated L, indicating a negligible $d\pi$–π^*(L) interaction. The high resolution ^{1}H NMR spectra of silver complexes with different substituted ligands (L^1–L^3) are reported. The complexes are quite stable and solutions in methanol and chloroform obey Beer's law.

This work stems from our continued interest in the transition metal chemistry of the azoimine ligand system (L, **1**) which is well-known as a versatile ligand capable of chelating[1–8] a wide range of metal ions. Recently, Datta and Chakravorty have reported[1] the 2-(phenylazo)pyridine chemistry of copper. The richness of this chemistry encouraged us to initiate research on the chemistry of the neighbouring element silver involving L.

Although silver(I) forms a great variety of complexes with N-donors, it is evident from a survey of the literature that the reports on stable, monomeric compounds of silver(I) with chelated ligands are scanty.[9,10] It is also well-documented that the metal ion has a pronounced tendency[11–13] to exhibit a linear two-coordination. The chemistry of monomeric silver(I) complexes of bidentate ligands with N,N-donors has grown primarily around 2,2′-bipyridine (bpy) and related ligands.[14,15] They are usually isolated in low yields and mostly used as intermediates for the preparation of the corresponding silver(II) complexes.[15] Many compounds of silver(I) are now known with soft donors like P, As, S, Se, etc., but they are mostly obtained as dimers or polymers.[16–19]

In this report we describe the high yield synthesis of stable, monomeric tetracoordinated silver(I) complexes of L. Assessment of structure and the stability of the complexes in solutions have been made on the basis of spectral data. Comparisons, where relevant, with the corresponding copper(I) complexes are also made. The four ligands used for the present work are abbreviated as L^1–L^4.

RESULTS AND DISCUSSION

(A) *Synthesis and formulation*

$AgNO_3$ reacts smoothly with L (**1**) in boiling methanol in the ratio of 1:2 to yield cationic $[AgL_2]^+$ (**2**), which have been isolated as perchlorate salts from the reaction mixture in high

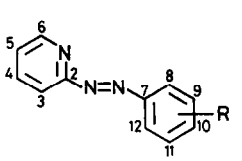

L

R=H : L^1
R=9-Me : L^2
R=10-Me : L^3
R=10-Cl : L^4

1

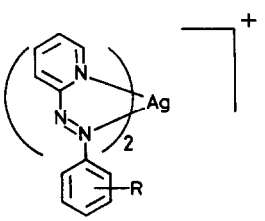

2

* Author to whom correspondence should be addressed.

yields (> 80%). The silver(I) complexes of L, obtained as dark brown needles, are stable and can be stored for a long time. They were characterized by elemental analyses which confirmed that the number of ligands (L) per silver is two. Magnetic susceptibility measurements showed that the compounds are diamagnetic (d^{10}) in nature, as expected. They are soluble in common polar organic solvents and are insoluble in non-polar benzene, hexane, etc. The molar conductance of $[AgL_2]ClO_4$ in methanol lies between 105 and 110 Ω^{-1} cm^2 mol^{-1} (Table 1), suggesting a 1 : 1 type of electrolytic nature of the compounds.[20] These results collectively conform to the formulation of the compounds as $[AgL_2]ClO_4$. We have also synthesized the corresponding $[CuL_2]ClO_4$ (L = L^1–L^4). These compounds have been synthesized by following the procedure described by Datta and Chakravorty.[1] Out of these four complexes, three with ligands L^2–L^4 are new. The IR data of the copper compounds have been compared with those of the silver complexes.

(B) *Bonding and assessment of structure*

(i) *IR spectra.* IR data were collected in the range 4000–300 cm^{-1} using KBr discs. Characteristic group frequencies are collected in Table 1. Some of these are found to be useful in identifying the geometry and bonding of the complexes and are considered here. The very broad structureless band, $\nu(ClO_4)$, at *ca* 1100 cm^{-1} suggests the lack of significant perchlorate coordination[21] in the solid state. Our main objective in studying the IR spectra of silver(arylazo)pyridines was to locate the ν(N=N) mode. The position of this band in our complexes was identified by comparison of the IR spectra of $[AgL_2]^+$ with those of $[CuL_2]^+$ and free L (Table 1). Since the N=N stretching frequency in free L appears[2] at *ca* 1425 cm^{-1}, we anticipated ν(N=N) in $[AgL_2]^+$ below this region. The IR spectra of $[AgL_2]^+$ systematically show a strong absorption at *ca* 1420 cm^{-1} (Table 1). Interestingly, the vibrational spectra of $[AgL_2]^+$ and the corresponding $[CuL_2]^+$ are nearly superimposable except for a single frequency shift from 1420 to 1380 cm^{-1} (Table 1). The band at 1380 cm^{-1} in $[CuL_2]^+$ has been assigned[1] to ν(N=N). Evidently, the band at *ca* 1420 cm^{-1} in $[AgL_2]^+$ is also due to ν(N=N). The ability of L to act as a strong π-acceptor towards electron-rich metal centres are well documented and the diagnostic test[1-7] for this interaction is the shift of ν(N=N) to lower frequencies in moving from free L to its complex. The small shift of ν(N=N) in $[AgL_2]^+$ suggests that the $d\pi$–π^*(L) interaction in the present silver(I) complexes is weak. This is similar to the bonding pattern in other silver(I) complexes with π-acid ligands having phosphorus and sulphur donors.[11] Near superimposability of the IR spectra of $[AgL_2]^+$ on those of $[CuL_2]^+$ suggests that like $[CuL_2]^+$, the gross stereochemistry of $[AgL_2]^+$ is tetrahedral.

(ii) *Electronic spectra.* The electronic spectra of the solutions of silver complexes were studied to assess their stabilities in solutions. 2-(Arylazo)-pyridines (**1**) and their silver complexes (**2**) show one absorption band of moderate intensity (ε, *ca* 1000 dm^3 mol^{-1} cm^{-1}) in the visible region, which has been assigned[22] to an n–π^* transition, centred primarily on the azo group. The small bathochromic shift of the absorption maximum in the silver complexes compared to that of free L indicates a weak interaction between N^2 and Ag^+. This observation is consistent with the IR data (*vide supra*). The silver complexes obey Beer's law in both $CHCl_3$ and MeOH. The intensity of the band at *ca* 460 nm does not change with dilution. Hence, the $[AgL_2]^+$ ion is stable in these solvents.

(iii) ^{1}H *NMR spectra.* The ^{1}H NMR data in $CDCl_3$ of the complexes are summarized in Table 2. Different protons are numbered as shown in Structure **1**. All the complexes display well-resolved spectra. The compounds with methyl substituted ligands, $[Ag(L^2)_2]^+$ and $[Ag(L^3)_2]^+$, systematically show a sharp and single methyl signal at δ_{Me} *ca* 2.3 ppm (Table 2).

The assignments of individual pyridyl ring proton signals were made[7,23-25] on the basis of their chemi-

Table 1. Some physical data of free L and complexes

Complex	IR (cm^{-1})[a] ν(C=N)	IR (cm^{-1})[a] ν(N=N)	Λ_M[c] (Ω^{-1} cm^2 mol^{-1})
L^1	1590[b]	1425[b]	
$[Cu(L^1)_2](ClO_4)$	1590	1375	110
$[Ag(L^1)_2](ClO_4)$	1590	1420	105
L^2	1590[b]	1425[b]	
$[Cu(L^2)_2](ClO_4)$	1585	1370	105
$[Ag(L^2)_2](ClO_4)$	1585	1420	110
L^3	1600	1425	
$[Cu(L^3)_2](ClO_4)$	1600	1375	107
$[Ag(L^3)_2](ClO_4)$	1595	1420	107
L^4	1600	1425	
$[Cu(L^4)_2](ClO_4)$	1595	1375	106
$[Ag(L^4)_2](ClO_4)$	1595	1420	108

[a] Unless otherwise stated, spectra were taken in KBr discs. All bands are of strong and medium intensity.

[b] The solvent used was methanol. Concentrations are *ca* 10^{-3} mol dm^{-3}.

Table 2. ^1H NMR[a] spectral data of $[Ag(L)_2](ClO_4)$[b]

Complex	δ (ppm) 6-H	5-H	4-H	3-H	12-H	11-H	10-H	9-H	8-H	9-Me	10-Me
$[Ag(L^1)_2](ClO_4)$	8.86	7.85	8.30	8.35	7.83	7.34–7.46	7.34–7.46	7.34–7.46	7.83		
$[Ag(L^2)_2](ClO_4)$	8.90	7.63–7.80	8.25	8.30	7.63–7.80	7.26	7.30		7.83–7.80	2.25	
$[Ag(L^3)_2](ClO_4)$	8.78	7.71–7.81	8.23	8.30	7.71–7.81	7.18		7.18	7.71–7.81		2.35

[a] In $CDCl_3$ using $SiMe_4$ as internal standard.
[b] Solubility of $[Ag(L^4)_2](ClO_4)$ in $CDCl_3$ is low, a well-resolved spectrum could not be obtained.

cal shifts and also by examining the spin–spin splitting patterns of the signals. Thus, the signal due to 6-H and 3-H appear as doublets, whereas 5-H and 4-H are triplets. The chemical shifts of the pyridyl protons of $[AgL_2]^+$ complexes are in the order: $\delta_{6\text{-H}} > \delta_{3\text{-H}} > \delta_{4\text{-H}} > \delta_{5\text{-H}}$. Large downfield shifts of the 5-H and 6-H protons in moving from free L to the coordinated L also have been observed. In fact, this is a common feature of the ^1H NMR spectra of the transition metal complexes of L.[25] The signals due to individual aryl protons were assigned mainly by the use of the relative intensities of the signals and also by examining the substitution induced effect on the splitting patterns. For example, 8-H and 12-H signals appear as coincident doublets in the complexes of L^1 and L^3, as expected. The 8-H signal of the corresponding L^2 complex should appear as a separate singlet. Unfortunately, the assignment of the 8-H proton in $[Ag(L^2)_2]^+$ has not been achieved so far because of serious overlap with other signals. It is also to be noted here that like the methyl protons, all of the aromatic protons exhibited only one signal for each proton. From this data it is very likely that both the chelate rings in $[AgL_2]^+$ are magnetically equivalent at least on the NMR time scale and the complexes contain an effective C_2-axis, which is also in agreement with the proposed tetrahedral structure of the complexes.

CONCLUSION

It is demonstrated that 2-(arylazo)pyridine ligands display high affinity towards silver(I). Stable, tetracoordinated, bis-chelated complexes of the type $[AgL_2]^+$ are isolated and throroughly characterized with the help of spectroscopic data. We wish to note here that the examples of stable, monomeric, tetra-coordinated silver(I) complexes are rare. The ease with which L reacts with silver(I) and the stability of the resultant bis complexes, even in solutions, are uncommon in silver(I) chemistry.

EXPERIMENTAL

Materials

The ligands were synthesized as previously.[26] The purification/preparation of solvents and supporting electrolytes was carried out as previously.[2] Reagents were used as received. The $AgNO_3$ salt was obtained from Glaxo Laboratories, Bombay. All other chemicals and solvents used for preparative work were of reagent grade and were used without further purification.

Physical measurements

Spectroscopic data were obtained with the use of the following instruments: Electronic spectra, Beckman 26 spectrophotometer; IR spectra (KBr disc, 4000–300 cm^{-1}), Perkin–Elmer IR-983 spectrophotometer; ^1H NMR spectra ($CDCl_3$), Varian EM 390. Solution electrical conductivity was measured using a Elico CM 82 T conductivity bridge with a solution concentration of *ca* 10^{-3} mol dm^{-3}. Magnetic susceptibilities were measured with a PAR vibrating sample magnetometer (Model 155) fitted with a Walker scientific magnet (Model L 75 FBAL).

Beer's Law verification of the solutions of $[Ag(L^1)_2](ClO_4)$ have been made spectrophotometrically using the following concentrations: (i) MeOH: 2.6678×10^{-4}, 4.0017×10^{-4}, 5.3357×10^{-4}, 6.2694×10^{-4}, 6.6696×10^{-4} M. (ii) $CHCl_3$: 2.7027×10^{-4}, 4.0541×10^{-4}, 4.8649×10^{-4}, 5.4054×10^{-4}, 6.7568×10^{-4} M.

Synthesis of bis[2-(phenylazo)pyridine]silver(I) perchlorate, $[Ag(L^1)_2](ClO_4)$

A sample of $AgNO_3$ (0.170 g, 1 mmol) in methanol (10 cm^3) was heated to reflux for 15 min, and to it a solution of L^1 (0.365 g, 2 mmol) in methanol (10 cm^3) was added. The mixture was further heated

to reflux for 3 h. The reddish-brown solution was then cooled and filtered through a G4 sintered glass funnel. To the cold filtrate a solution of aqueous $NaClO_4$ (*ca* 2 g in 10 cm^3 of water) was added with constant stirring. A dark coloured compound precipitated and was collected by filtration and washed thoroughly with water. Recrystallization of the compound from methanol–water (1 : 1) yielded a highly crystalline, dark brown product which was dried *in vacuo* over P_4O_{10}. Yield 0.46 g (80%). Found: C, 45.5; H, 3.0; Ag, 18.9; N, 14.2. Calc. for $C_{22}H_{18}ClN_6O_4Ag$: C, 46.0; H, 3.1; Ag, 18.8; N, 14.6%. λ_{max} ($CHCl_3$): 448 nm (ε, 935 dm^3 mol^{-1} cm^{-1} and λ_{max} (CH_3OH): 462 nm (ε, 990 dm^3 mol^{-1} cm^{-1}).

Syntheses of bis[2-(m-*tolylazo*)*pyridine*]*silver*(I) *perchlorate*, $[Ag(L^2)_2](ClO_4)$; *bis*[2-(p-*tolylazo*)*pyridine*]*silver*(I) *perchlorate*, $[Ag(L^3)_2](ClO_4)$; *and bis*[2-(p-*chlorophenylazo*)*pyridine*]*silver*(I) *perchlorate*, $[Ag(L^4)_2](ClO_4)$

These were prepared similarly using the appropriate ligand. $[Ag(L^2)_2](ClO_4)$: Yield, 95%. Found: C, 47.6; H, 3.5; Ag, 18.2; N, 13.8. Calc. for $C_{24}H_{22}ClN_6O_4Ag$: C, 47.9; H, 3.7; Ag, 17.9; N, 14.0%. λ_{max} ($CHCl_3$): 457 nm (ε, 720 dm^3 mol^{-1} cm^{-1}) and λ_{max} (CH_3OH): 462 nm (ε, 825 dm^3 mol^{-1} cm^{-1}). $[Ag(L^3)_2](ClO_4)$: Yield, 80%. Found: C, 47.7; H, 3.6; Ag, 18.0; N, 13.8. Calc. for $C_{24}H_{22}ClN_6O_4Ag$: C, 47.9; H, 3.7; Ag, 17.9; N, 14.0%. λ_{max} ($CHCl_3$): 450 nm (ε, 875 dm^3 mol^{-1} cm^{-1}) and λ_{max} (CH_3OH): 455 nm (ε, 1010 dm^3 mol^{-1} cm^{-1}). $[Ag(L^4)_2](ClO_4)$: Yield, 80%. Found: C, 40.9; H, 2.3; Ag, 16.6; N, 12.9. Calc. for $C_{22}H_{16}Cl_3N_6O_4Ag$: C, 41.1; H, 2.5; Ag, 16.8; N, 13.1%. λ_{max} ($CHCl_3$): 455 nm (ε, 765 dm^3 mol^{-1} cm^{-1}) and λ_{max} (CH_3OH): 458 nm (ε, 830 dm^3 mol^{-1} cm^{-1}).

Syntheses of bis[2-(*arylazo*)*pyridine*]*copper*(I) *perchlorate*, $[CuL_2](ClO_4)$ (L = L^2–L^4)

These were prepared from $Cu(ClO_4)_2 \cdot 6H_2O$ and appropriate L by following the method described by Datta and Chakravorty.[1] The analytical and spectral data are as follows: $[Cu(L^2)_2](ClO_4)$: Yield, 60%. Found: C, 51.5; H, 3.8; Cu, 11.2; N, 15.0. Calc. for $C_{24}H_{22}ClN_6O_4Cu$: C, 51.7; H, 3.9; Cu, 11.4; N, 15.1%. λ_{max} (CH_3OH): 700 and 560 nm (ε, 1570 and 5625 dm^3 mol^{-1} cm^{-1}). $[Cu(L^3)_2](ClO_4)$: Yield, 55%. Found: C, 51.6; H, 3.7; Cu, 11.2; N, 14.9. Calc. for $C_{24}H_{22}ClN_6O_4Cu$: C, 51.7; H, 3.9; Cu, 11.4; N, 15.1%. λ_{max} (CH_3OH): 700 and 560 nm (ε, 1480 and 5530 dm^3 mol^{-1} cm^{-1}). $[Cu(L^4)_2](ClO_4)$: Yield, 60%. Found: C, 44.0; H, 2.4; Cu, 10.3; N, 13.9. Calc. for $C_{22}H_{16}Cl_3N_6O_4Cu$: C, 44.1; H, 2.77; Cu, 10.6; N, 14.0%. λ_{max} (CH_3OH): 700 and 560 nm (ε, 1415 and 5262 dm^3 mol^{-1} cm^{-1}).

Acknowledgement—We thank RSIC, North-Eastern Hill University, Shillong, for the spectral data.

REFERENCES

1. D. Datta and A. Chakravorty, *Inorg. Chem.* 1983, **22**, 1085.
2. G. K. Lahiri, S. Bhattacharjee, S. Goswami and A. Chakravorty, *J. Chem. Soc., Dalton Trans.* 1990, 561; A. K. Deb, P. C. Paul and S. Goswami, *J. Chem. Soc., Dalton Trans.* 1988, 2051; S. Goswami, A. R. Chakravarty and A. Chakravorty, *Inorg. Chem.* 1983, **22**, 602; S. Goswami, A. R. Chakravarty and A. Chakravorty, *Inorg. Chem.* 1981, **20**, 2246; S. Goswami, A. R. Chakravarty and A. Chakravorty, *J. Chem. Soc., Chem. Commun.* 1982, 1288.
3. R. A. Krause and K. Krause, *Inorg. Chem.* 1980, **19**, 2600; T. Bao, K. Krause and R. A. Krause, *Inorg. Chem.* 1988, **27**, 759; R. A. Krause and K. Krause, *Inorg. Chem.* 1984, **23**, 2195.
4. B. K. Ghosh, S. Goswami and A. Chakravorty, *Inorg. Chem.* 1983, **22**, 3358; B. K. Ghosh, A. Mukhopadhyay, S. Goswami, S. Ray and A. Chakravorty, *Inorg. Chem.* 1984, **23**, 4633.
5. P. Bandyopadhyay, D. Bandyopadhyay, A. Chakravorty, F. A. Cotton, L. R. Falvello and S. Han, *J. Am. Chem. Soc.* 1983, **105**, 6327.
6. G. K. Lahiri, S. Goswami, L. R. Falvello and A. Chakravorty, *Inorg. Chem.* 1987, **26**, 3365.
7. M. N. Ackermann, C. R. Barton, C. J. Deodene, E. M. Specht, S. C. Keill, W. E. Schreiber and H. Kim, *Inorg. Chem.* 1989, **28**, 397.
8. A. K. Deb and S. Goswami, *J. Chem. Soc., Dalton Trans.* 1989, 1635.
9. G. Wilkinson, *Comprehensive Coordination Chemistry*, Vol. 5, p. 775. Pergamon Press, Oxford (1987).
10. S. Akabori, S. Sato, M. Sato and Y. Takanohashi, *Bull. Chem. Soc.* 1989, **62**, 1582.
11. F. A. Cotton and G. Wilkinson, *Advanced Inorganic Chemistry*, 5th edn, p. 942. John Wiley, New York (1988).
12. P. Gans and J. B. Gill, *J. Chem. Soc., Dalton Trans.* 1976, 779.
13. K. Nilson and A. Oskarsson, *Acta Chem. Scand., Ser. A*, 1982, **36**, 605.
14. J. M. Dale and C. V. Banks, *Inorg. Chem.* 1963, **2**, 591.
15. S. Swarnabala and M. V. Rajasekharan, *Inorg. Chem.* 1989, **28**, 662; D. P. Murtha and R. A. Walton, *Inorg. Chem.* 1973, **12**, 368.
16. Y. Inoguchi, B. Milewski-Mahrla, D. Neugebauer, P. G. Jones and H. H. Schmidbaur, *Chem. Ber.* 1983,

116, 1487; M. H. Douglas and R. Bau, *Inorg. Chem.* 1983, **22**, 4073.
17. H. Dietrich, W. Storck and G. Manecke, *J. Chem. Soc., Chem. Commun.* 1982, 1036; J. M. Paul, W. L. Birker and G. C. Verschoor, *J. Chem. Soc., Chem. Commun.* 1981, 322.
18. S. J. Berners Price, C. Brevard, A. Pagelot and P. J. Sadler, *Inorg. Chem.* 1985, **24**, 4278; 1986, **25**, 596; G. Salem, A. Schier and S. B. Wild, *Inorg. Chem.* 1988, **27**, 3029.
19. N. Barrow, H. Burgi, M. Camalli, F. Caruso, E. Fischer, L. M. Venanzi and L. Zambonelli, *Inorg. Chem.* 1983, **22**, 2356.
20. W. J. Greary, *Coord. Chem. Rev.* 1971, **7**, 81.
21. R. C. Elder, M. J. Heeg and E. Deutsch, *Inorg. Chem.* 1978, **17**, 427.
22. B. S. Raghavendra and A. Chakravorty, *Ind. J. Chem.* 1976, **14A**, 166.
23. W. Kaein and S. Kohlmann, *Inorg. Chem.* 1987, **26**, 68.
24. E. V. Brown and G. R. Granneman, *J. Am. Chem. Soc.* 1975, **97**, 621.
25. A. K. Mahapatra, B. K. Ghosh, S. Goswami and A. Chakravorty, *J. Ind. Chem. Soc.* 1986, **53**, 101.
26. N. Campbell, A. W. Henderson and D. Taylor, *J. Chem. Soc.* 1953, 1281; R. W. Faessinger and E. V. Brown, *J. Am. Chem. Soc.* 1951, **73**, 4606.

Polyhedron Vol. 9, No. 18, pp. 2257–2261, 1990
Printed in Great Britain

0277–5387/90 $3.00+.00
© 1990 Pergamon Press plc

VARIATION IN STABILITY OF MONOHALIDE COMPLEXES AND SOME PROPERTIES OF THE SOLVATED CATIONS WITHIN THE Mn^{2+}–Zn^{2+} SERIES

WACŁAW GRZYBKOWSKI

Department of Chemistry, Technical University of Gdańsk, 80-952 Gdańsk, Poland

(*Received* 18 *December* 1989; *accepted* 1 *May* 1990)

Abstract—The stability of the monohalide complexes of the divalent first-row transition metal cations in water as well as in other donor solvents follows the sequence: $MnX^+ > FeX^+ > CoX^+ > NiX^+ < CuX^+ > ZnX^+$. Moreover, some of the properties of the $M(solvent)_6^{2+}$ solvo-cations may be rationalized in terms of the same series. The observed sequence is opposite to that known as the Irving–Williams series.

The stability of the metal complexes in solution often is discussed in terms of hard and soft interactions of the metal cations and the respective ligands. This approach explains satisfactorily some of the observed variations and/or differences. More quantitative discussion is based upon the Gutmann's donor number (DN). Further and more profound analysis makes use of splitting the free-energy change into the enthalpy and entropy contributions.

However, these common and useful tools seem to be useless when the stability constants of similar but weak complexes are compared, and relatively small differences are discussed.

It seems to be well established that the stability constants of the monohalide complexes of the divalent first-row transition metal cations in water, as well as in most non-aqueous solvents, follow the sequence

$$MnX^+ > FeX^+ > CoX^+ > NiX^+ < CuX^+ > ZnX^+.$$

This series has been reported for both the MCl^+ and MBr^+ type complexes in water,[1,2] and for the MCl^+ complexes in dimethyl sulphoxide solutions.[3–5] The same trend was observed for the MF^+ complexes in water and methanol,[6] and for MCl^+ in methanolic solutions.[7] More recently, this series was reported for MCl^+ complexes in N,N-dimethylformamide (DMF) solution.[8] A similar sequence was obtained for MBr^+ type complexes in N,N-dimethylacetamide (DMA).[9,10]

The values of logarithms of the stability constants for most of the above mentioned systems are presented in Table 1. It was impossible to find data for the monohalide complexes of all the transition metal cations belonging to the Mn^{2+}–Zn^{2+} series, in the same solvent and obtained using the same method. This is due to the known sensitivity of iron(II) towards oxidation, and the high stability of di-, tri- and tetrahalide complexes of zinc(II), both responsible for most of the gaps existing in the table. Inspection of the collected data shows that the values for a given solvent vary within relatively narrow limits, while the copper(II) complexes are the most stable species within the series studied. Moreover, the lowest stabilities are displayed by the monohalide complexes in aqueous systems. Despite the gaps and experimental uncertainties, unavoidably present in the values of the similar data, the above sequence seems to be well established.

The same variation within the Mn^{2+}–Zn^{2+} series was observed for the first-step ionic association with the perchlorate anion in methanolic solution.[11]

The presented trend is distinctly opposite to the regularity

$$Mn^{2+} < Fe^{2+} < Co^{2+} < Ni^{2+} < Cu^{2+} > Zn^{2+}$$

well known as the Irving–Williams series[12] and obeyed by a large number of complexes in aqueous solution, especially when ligands have an N- or O-donor atom.

It has been shown by different authors that the stabilities of the monohalide complexes of the tran-

Table 1. The values of $\log \beta_1$ for monohalide complexes at 25°C

Solvent	H_2O			CH_3OH			DMSO	DMF	DMA
X^-	F^-	Cl^-	Br^-	ClO_4^-	F^-	Cl^-	Cl^-	Cl^-	Br^-
MnX^+	1.38	−0.30	−0.72	—	3.48	—	3.23	4.00	2.78
FeX^+	1.45	—	—	—	3.79	—	—	—	—
CoX^+	1.28	−0.66	−1.05	2.00	3.04	3.01	2.79	3.50	3.40
NiX^+	1.32	−0.80	−1.15	1.91	2.91	2.82	2.41	3.14	2.57
CuX^+	1.46	−0.05	−0.51	1.98	4.52	5.08	5.01	4.71	4.41
ZnX^+	1.30	−0.22	−0.72	1.81	3.36	3.89	—	—	—
Medium	[a]	[b]	[b]	[c]	[a]	[d]	[d]	[d]	[d]
Reference	6	1	2	11	6	7	5	8	10

[a] 0.5 M (TEAP).
[b] 3.0 M $M(ClO_4)_2$.
[c] From cond. data.
[d] Thermodynamic stability constants (variation of activity coefficients assumed to follow D–H equations).

sition metal cations are entropy controlled, i.e. the entropy term in free energy predominates over the enthalpy term, and although their enthalpies of formation are positive, the complexes have negative free energies of formation.[5,6] The results reported by Doe *et al.* clearly show that the ionic association of the transition metal perchlorates in methanol is also the consequence of unfavourable enthalpy and favourable entropy changes.[11]

The exceptions to the Irving–Williams series were considered as rather atypical behaviour. However, in the existing experimental data, the same trends and the same orders of magnitude, observed for non-aqueous systems, are an indication of the existence of a factor common for the complexes under consideration, and the sequence

$$Mn^{2+} > Fe^{2+} > Co^{2+} > Ni^{2+} < Cu^{2+} > Zn^{2+}$$

seems to be characteristic for the complexes whose stabilities are entropy controlled. The opposite situation, i.e. the enthalpy control of the complex formation, is related to reactions following the Irving–Williams series.

In Table 2 the available values of entropies of complex formation are listed along with the data for the ionic association of the perchlorates in methanol. Inspection of the collected data shows that for each of the solvents the entropy of formation of the CuX^+ complex is distinctly higher than that of the MnX^+, FeX^+, CoX^+, NiX^+ and ZnX^+ complexes or associates. Furthermore, the values for the latter species in DMSO and methanol may be considered as practically independent of the nature of the cation. The scatter of the data obtained for the aqueous systems seems to result from large experimental uncertainties in the very small stability constants of the monofluoride complexes.[6]

The divalent first-row transition metal ions are known to form well-defined coordination clusters in solution, and in the absence of coordinatively active anions exist as the $M(solvent)_6^{2+}$ type species in water as well as in most non-aqueous solvents.[13,14]

The equilibrium between the hexakis- and tetrakis-(solvent) species seems to be one of the factors controlling the solvation processes in DMA solution. The steric crowding caused by the acetyl groups stabilizes the $M(solvent)_4^{2+}$ solvates. However, at room temperature the tetrakis-(solvent) species exist as less than 5% of the total metal concentration, and $Co(DMA)_6^{2+}$ and $Ni(DMA)_6^{2+}$ are predominant species present in solutions of the respective perchlorates.[15,16] The

Table 2. Entropy of formation of MX^+ type complexes at 25°C

Solvent	CH_3OH		DMSO	H_2O
X^-	F^-	ClO_4^-	Cl^-	F^-
MnX^+	—	—	88.0	44
FeX^+	175	—	—	—
CoX^+	190	79.0	88.0	59
NiX^+	181	83.4	87.4	33
CuX^+	320	103.3	132.2	65
ZnX^+	180	86.8	—	48
Reference	6	11	5	6

Units: $J\,K^{-1}\,mol^{-1}$.

tetrakis-(solvent) species of the transition metal cations exist in N,N,N-hexamethylphosphortriamide (HMPA) solutions.[17]

Thermodynamical aspects of complex formation and the properties of the solvates cannot be discussed separately. It is obvious that the high entropy gain is related to the release of the solvent molecules during the inner-sphere complex formation, in accordance with

$$MS_6^{2+} + X^- \rightleftharpoons MXS_5^+ + S,$$

where S denotes a solvent molecule. The entropy gain on desolvation is increased on account of the loss of order in the bulk solvent. Substitution of the X^- anion for a solvent molecule in the first coordination sphere of a metal cation results in a substantial decrease in charge density. Thus, the total entropy change may be independent of the nature of the central metal ion with the same electrical charge. Distinctly higher entropy of formation of the $CuCl^+$ complex in DMSO was interpreted by Libuś and Pastewski in terms of formation of the pentacoordinated $CuCl(DMSO)_4^+$ complex, resulting in the liberation of two solvent molecules.[5] An analogous explanation was suggested by Doe *et al.* for the relatively high enthalpy and entropy values of the Cu^{2+}–ClO_4^- ion-pair in methanol.[11] The ClO_4^- anion which forms the ion-pair with the Cu^{2+} cation may be substituted for a methanol molecule in the primary solvation shell, while the ClO_4^- ions are outside this shell for other transition metal cations.

It is well known that the Jahn–Teller distorted octahedrons are observed for the structure of the primary solvation sphere of the Cu^{2+} cation. Two of the six solvent molecules are bound weakly to the Cu^{2+} ion with a long Cu^{2+}–donor atom of a solvent molecule distance, and they are more susceptible to ligand substitution as well as solvent exchange. Thus the reactivity of the Cu^{2+}–solvates and their position within the Mn^{2+}–Zn^{2+} series are a consequence of the $3d^9$ electronic structure.

The exchange of solvent molecules between the primary solvation shell of a cation and bulk solvent is a fundamental reaction for metal ions in solution. The kinetic parameters obtained from NMR studies of the first-row divalent transition metal cations indicate that the mechanism for solvent exchange varies from an associative activation mode for the early elements to a dissociative activation mode for the latter ones.[18] However, it has been reported by Merbach that the sequence of reactivity is independent of the exchange mechanism and the solvent following the series.

$$Cu^{2+} > Mn^{2+} > Fe^{2+} > Co^{2+} > Ni^{2+} > V^{2+},$$

which agrees well with the predictions based on the crystal-field theory.

The solvent-exchange rate constants for Mn^{2+}–Zn^{2+} are listed in Table 3 which includes data collected by Merbach,[19] Funahashi,[20] and Hewkin[21] plus that reported by other authors.[22-24]

Inspection of the data shows that Merbach's series can be presented by the sequence

$$Mn^{2+} > Fe^{2+} > Co^{2+} > Ni^{2+} < Cu^{2+} > Zn^{2+}$$

which reflects exactly the above variation of the respective stability constants within the Mn^{2+}–Zn^{2+} series.

The logarithms of the stability constants of the monohalide complexes in aqueous solution and the water-exchange rate constants are presented in Fig.

Table 3. Logarithms of first-order rate constants (s^{-1}, 25°C) for solvent exchange in the Mn^{2+}–Zn^{2+} cations

	Solvent					
	DMSO	DMF	H_2O	CH_3OH	CH_3CN	CH_3COOH
Mn^{2+}	6.8[a]	6.3	7.3	5.6	7.1	7.2[a]
Fe^{2+}	6.0[a]	6.0	6.6	4.7	5.8	6.6[a]
Co^{2+}	5.5[a]	5.6	6.5	4.3	5.5	6.1[a]
Ni^{2+}	3.5[a]	3.6	4.5	3.0	3.4	5.3[a]
Cu^{2+}	—	—	9.3[b]	7.5	7.2[c]	7.0[a]
Zn^{2+}	5.9[d]	—	7.5[b]	5.7[e]	—	—

[a] Reference 20.
[b] Reference 21.
[c] Reference 24.
[d] Reference 22.
[e] Reference 23.
Otherwise ref. 19.

1. In order to observe the dependence of the studied properties on the nature of the central metal ion, the data are plotted against the position of the metal cation within the Mn^{2+}–Zn^{2+} series, i.e. as a correlation with the number of 3*d* electrons. Moreover, the electrostriction partial molar volumes of the hydrated cations[25] are presented in this figure. The partial molar volume of the ion can be split into two major components. One of them, the intrinsic partial molar volume, is related to the size of an ion, while the second, the electrostriction partial molar volume, is determined by ion–solvent interactions. The correlation of the electrostriction volume with the rate constant of solvent exchange was reported earlier.[14]

It thus appears that the volume properties of the hydrates show a variation which may be interpreted in terms of ligand-field effects. According to the theory the highest LFSE is expected for the octahedral high-spin complexes of nickel(II). Thus, it is not surprising that the largest electrostriction is observed for $Ni(H_2O)_6^{2+}$. The position of $Cu(H_2O)_6^{2+}$ within the series is obviously due to the tetragonal elongation of two metal–ligand bonds arising from the Jahn–Teller effect. Otherwise, the evident parallel between the electrostriction volume of the cations and their lability appears to be easily understood. The faster the water-exchange mechanism the more distinct is the looseness of the structure of the nearest environment of the cation, irrespective of the mechanism for solvent exchange.

The striking parallel between the stability of the monohalide complexes and the rate of the water-exchange mechanism seems to be a distinct representation of the relationship between the thermodynamic and kinetic parameters. The greater the lability of the hydrates the higher the frequency of appearance and disappearance of the intermediate species. Their generation precedes entry of the X^- anion into the coordination sphere of the cation and MX^+ complex formation. The discussed analogy in the variation within the Mn^{2+}–Zn^{2+} series may be considered as a simple relationship between the probability of complex formation and its stability. Thus, it may be referred to the entropy change as a factor controlling stability of the monohalide complexes.

Analogous correlations for the methanol and DMF solutions are presented in Figs 2 and 3. Unfortunately, there are some gaps in the data and a full comparison cannot be completed. However, in accordance with the crystal-field theory, high lability of the $Cu(DMF)_6^{2+}$ may be expected, and the assumption that the Cu^{2+}–solvate is much more reactive than the Zn^{2+}–solvate does not need any additional support.

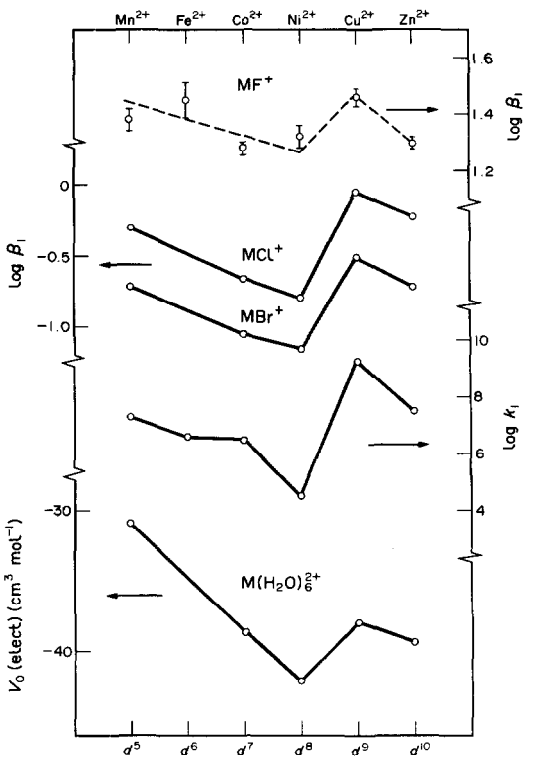

Fig. 1. Plots of logarithms of the stability constants of the monohalide complexes ($\log \beta_1$), logarithms of the rate constant for the water-exchange mechanism ($\log k_1$), and the electrostriction volumes $\bar{V}^0$(elect) against the position within the Mn^{2+}–Zn^{2+} series for the divalent cations in water.

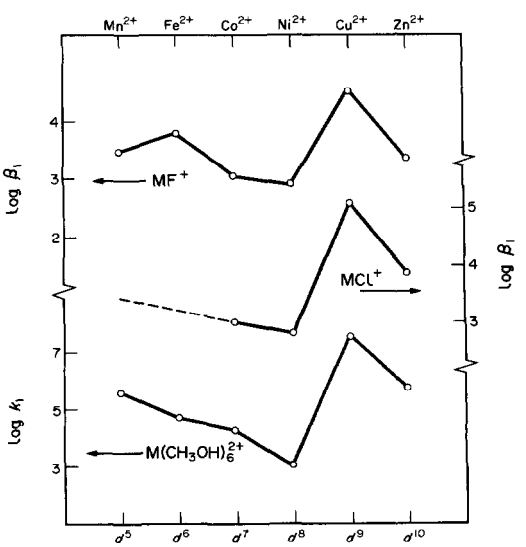

Fig. 2. Plots of logarithms of the stability constants ($\log \beta_1$) and logarithms of the rate constant ($\log k_1$) for the solvent exchange of the divalent cations in methanol.

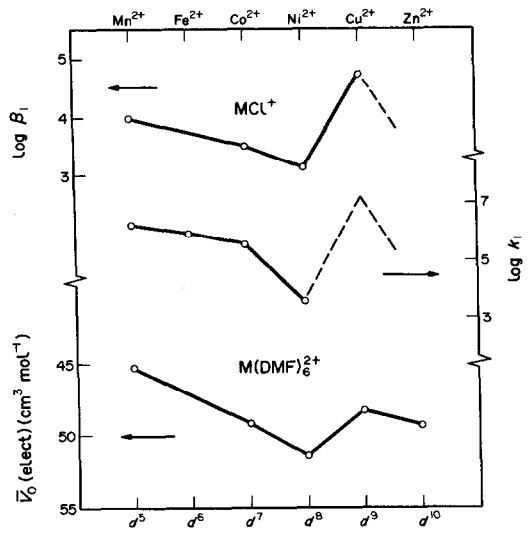

Fig. 3. Plots of logarithms of the stability constants of the MCl^+ type complexes, logarithms of the rate constant for solvent exchange, and the electrostriction volumes for the divalent cations in DMF.

Exceptional behaviour was observed for the monobromide complexes in DMA. The $MnBr^+$ complex exhibits significantly lower stability, its stability constant is lower than the value obtained for $CoBr^+$.[9,10] This difference exceeds the differences observed for MnF^+ and FeF^+ complexes in water and methanol, and is probably due to the sensitivity of iron(II) towards oxidation. The peculiarity of the DMA solutions may be related to the steric effects resulting in a lowering of the stability of the hexakis-(solvent) species.

Thus, the sequence

$$Mn^{2+} > Fe^{2+} > Co^{2+} > Ni^{2+} < Cu^{2+} > Zn^{2+}$$

seems to be valid for the cations forming the stable octahedral solvates. Moreover, it is independent of solvent and is related to the progressive filling of the 3*d* orbitals. The exchange of solvent molecules between the first coordination sphere of a metal cation and bulk solvent may be considered as the fundamental process for understanding the solvocation properties as well as complex formation and stability.

The relationships between the probability of complex formation and the stability constants were used in the mathematical models concerned with the formation of a stepwise series of mononuclear complexes. The pioneering and classical work was due to J. Bjerrum, while a more recent model was described by Mihailov.[26] However, the problem seems to be more complex and too difficult to be solved in terms of these oversimplified mathematical models.

Acknowledgement—This work was supported by Program CPBP-01.15 (870225).

REFERENCES

1. Z. Libuś and H. Tiałowska, *J. Sol. Chem.* 1975, **4**, 1011.
2. Z. Libuś and G. Kowalewska, *Polish J. Chem.* 1978, **52**, 709.
3. W. Libuś, R. Pastewski and T. Sadowska, *J. Chem. Soc., Faraday Trans. I* 1982, **78**, 377.
4. H. Strzelecki and W. Grzybkowski, *Polyhedron* 1988, **7**, 2473. 5. W. Libuś and R. Pastewski, *J. Sol. Chem.* 1988, **17**, 59.
6. L. R. Solomon, A. M. Bond, J. W. Bixler, D. R. Hallenbeck and K. M. Logsdon, *Inorg. Chem.* 1983, **22**, 1644.
7. H. Doe and T. Kitagawa, *Inorg. Chem.* 1982, **21**, 2272.
8. W. Grzybkowski and M. Pilarczyk, *J. Chem. Soc., Faraday Trans. I* 1986, **82**, 1745.
9. H. Strzelecki and R. Pastewski, *Bull. Pol. Acad. Chem.* 1987, **35**, 31.
10. R. Pastewski, *Bull. Pol. Acad. Chem.* 1988, **36**, 81.
11. H. Doe, T. Kitagawa and K. Sasabe, *J. Phys. Chem.* 1984, **88**, 3341.
12. H. Irving and R. Williams, *J. Chem. Soc.* 1953, 3192.
13. W. Libuś, B. Chachulski, W. Grzybkowski, M. Pilarczyk and D. Puchalska, *J. Sol. Chem.* 1981, **10**, 631.
14. W. Grzybkowski and M. Pilarczyk, *J. Chem. Soc., Faraday Trans. I* 1983, **79**, 2319.
15. S. F. Lincoln, A. M. Hounslow and A. N. Boffa, *Inorg. Chem.* 1986, **25**, 1038.
16. W. Grzybkowski and M. Pilarczyk, *Electrochim. Acta* 1987, **32**, 1601.
17. W. Grzybkowski and M. Pilarczyk, *J. Chem. Soc., Faraday Trans. I* 1988, **84**, 1551.
18. A. E. Merbach, *Pure Appl. Chem.* 1982, **54**, 1479.
19. C. Cossy, L. Helm and A. E. Merbach, *Helv. Chim. Acta* 1987, **70**, 1516.
20. A. Hioki, S. Funahashi, M. Ishi and M. Tanaka, *Inorg. Chem.* 1986, **25**, 1360.
21. D. J. Hewkin and R. H. Prince, *Coord. Chem. Rev.* 1970, **5**, 45.
22. D. M. W. Buck and P. Moore, *J. Chem. Soc., Dalton Trans.* 1976, 638.
23. S. A. Al-Baldawi and T. E. Gough, *Can. J. Chem.* 1969, **47**, 1417.
24. R. J. West and S. F. Lincoln, *J. Chem. Soc., Dalton Trans.* 1974, 281.
25. A. Lo Surdo and F. J. Millero, *J. Phys Chem.* 1980, **84**, 710.
26. M. H. Mihailov, *J. Inorg. Nucl. Chem.* 1974, **36**, 107.

Polyhedron Vol. 9, No. 18, pp. 2263–2266, 1990
Printed in Great Britain

0277–5387/90 $3.00+.00
© 1990 Pergamon Press plc

UV AND NMR STUDIES OF ALKYL-SUBSTITUTED GERMYL ANIONS

KUNIO MOCHIDA* and TSUYOSHI KUGITA

Department of Chemistry, Faculty of Science, Gakushuin University, 1-5-1 Mejiro, Tokyo 171, Japan

and

YASUHIRO NAKADAIRA

The University of Electro-Communications, 1-5-1 Chofugaoka, Chofu, Tokyo 182, Japan

(*Received* 23 *January* 1990; *accepted* 1 *May* 1990)

Abstract—Several (trialkylgermyl)alkali metals (M = Li, Na, K) were investigated by UV, ^{1}H and ^{13}C NMR spectroscopic methods to clarify the nature of a germanium–(alkali metal) bond. On conversion of a trialkylgermane to the corresponding germylalkali metals, the bathochromic shift of UV absorption maxima, upfield shift of the ^{1}H NMR signals and downfield shift of the ^{13}C NMR signal are observed.

Group 4B element-centred anions, homologues of carbanions, especially silyl and germyl anions have recently been recognized as useful synthetic reagents, and are effective for the introduction of the silyl and germyl groups into some types of organic compounds.[1] Although UV and NMR spectroscopic studies on properties of carbanions pertaining to their reactivities have been extensively carried out,[2] there have been relatively few reports on those of other group 4B element-centred anions.[3–15] Particularly on organogermyl anions, there have been no reports except one for phenyl-substituted germylalkali metals.[16] We describe herein the first information on UV and NMR spectroscopic characteristics of several (trialkylgermyl) alkali metal compounds and endeavour to clarify their spectroscopic properties.[1,17,18]

EXPERIMENTAL

^{1}H and ^{13}C NMR spectra were recorded on a JEOL FX 90Q instrument with HMPA–THF-d_8 solutions, and chemical shifts are referred to internal HMPA (δ 2.54 ppm for ^{1}H NMR) and THF-d_8 (δ 68.40 ppm for ^{13}C NMR). UV and visible spectra were recorded on a Shimazu UV-180 spectrometer.

Solvent

HMPA was distilled from CaH_2 under argon. THF-d_8 was distilled from sodium/benzophenone under argon.

Materials

Me_3GeCl, b.p. 115°C;[19] Me_3GeH, b.p. 26°C;[20] $(Me_3Ge)_2$, b.p. 137°C;[21] Et_3GeCl, b.p. 92°C/30 mmHg;[22] Et_3GeH, b.p. 123°C;[23] and $(Et_3Ge)_2$, b.p. 73°C/0.7 mmHg[24] were prepared by established methods.

Preparation of trialkylgermyl anions

(Trialkylgermyl)alkali metals were prepared from the reaction of the corresponding chlorides with alkali metals in HMPA–THF using the method described by Bulten and Noltes.[24]

UV absorption spectra of trialkylgermyl anions

The alkyl-substituted germyl anions are extremely sensitive to oxygen and moisture. A

* Author to whom correspondence should be addressed.

closed absorption cell was used to observe the UV absorption spectra of these anions.[26] The absorption cell apparatus used in this study consists of a 1 cm quartz absorption cell sealed to the side arm of a round-bottomed flask. The apparatus was connected to a high-vacuum system for alternate degassing and flushing with argon. Access to the flask was through a second side arm closed by a rubber syringe cap. The anions were prepared by contact of alkali metal with alkylgermyl chlorides in highly degassed HMPA–THF solvent in the round-bottomed flask.

NMR studies of trialkylgermyl anions

Alkyl-substituted germyl anions in HMPA–THF were prepared as described above. Approximately 1 cm^3 of the anion solution was transferred by means of a syringe into an argon-flushed NMR tube. The NMR tube containing the anion was degassed and sealed.

RESULTS AND DISCUSSION

Absorption spectra of trialkylgermyl anions

Electronic spectra of anions provide a good insight into the nature of their electronic structures. (Trialkylgermyl)alkali metal compounds have been generated from the corresponding chlorogermanes and alkali metals in HMPA–THF at room temperature quantitatively[24] and their formation can be rationalized by the dissociative electron-transfer attachment processes as shown below[16]

$$2\,R_3GeCl + 2\,M \longrightarrow (R_3Ge)_2 + 2\,MCl \quad (1)$$

$$(R_3Ge)_2 + 2\,M \longrightarrow 2\,R_3GeM \quad (2)$$

R = Me, Et, n-Pr, n-Bu; M = Li, Na, K.

All of the (trialkylgermyl)alkali metal compounds are yellow in HMPA–THF. As typical examples, the absorption spectra of Me_3GeM (M = Li, Na and K) are shown in Fig. 1. All show absorption maxima at 270–300 nm. The absorption maxima of starting trimethylchlorogermane and the intermediate, hexamethyldigermane, are known to be located below 220 nm.[25] Since measurements of these absorption spectra arising from germylalkali metals are possible only by the use of sealed UV cells in an inert gas atmosphere, the molar extinction coefficient could not be determined. The wavelength data for the absorption maxima (λ_{max}) of the (trialkylgermyl)alkali metal compounds in HMPA–THF are summarized in Table 1. Judging from the data in Table 1, the nature of the counterion has only a slight influence on λ_{max} which increases in the order Li ≃ Na < K. This implies that the germyl metal has highly ionic character, and hence in a qualitative way the absorption band observed may be stated to arise from the transition from the non-bonding orbital of the germyl anions (HOMO) to the lowest antibonding orbital of germanium–carbon bonds (LUMO). Similar small red shifts have been reported for the spectra of some organoalkali metals[26] and phenyl-substituted group 4B element-centred anions.[16]

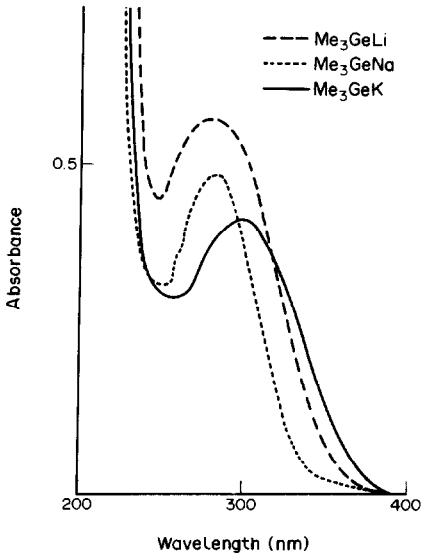

Fig. 1. UV spectra of (trimethylgermyl)alkali metals.

Table 1. Absorption data of UV spectra for alkyl-substituted germylalkali metals in HMPA–THF

Compound	λ_{max} (nm) for M = Li	Na	K
Me_3Ge	280	280	300
Et_3Ge	< 280	~ 280	290
n-Pr_3Ge	< 280	~ 280	290
n-Bu_3Ge	< 280	~ 280	290

A small but distinct substituent effect on absorption maxima is noted, namely, the (trimethylgermyl)alkali metal compounds exhibits it at longer wavelengths than the other (trialkylgermyl) alkali metal compounds (see Table 1).

^1H and ^{13}C NMR studies

The ^1H NMR chemical shifts of (trimethylgermyl)alkali metals and (triethylgermyl)alkali metals, and their related compounds are summarized in Table 2. As shown in Table 2, the

Table 2. ^{1}H chemical shifts of (trialkylgermyl)alkali metals and related species

Compound	δ (ppm) in HMPA–THF-d_8		
	C_2—H	C_2—H	Ge—H
Me_3GeLi	−0.35 (s)		
Me_3GeNa	−0.02 (s)		
Me_3GeK	−0.23 (s)		
Me_3GeCl	0.78 (2)		
Me_3GeH	0.21 (d)		3.83 (sept)
$(Me_3Ge)_2$	0.21 (s)		
Et_3GeLi	0.13 (q)	0.97 (t)	
Et_3GeNa	0.15 (q)	0.98 (t)	
Et_3GeK	0.17 (q)	0.98 (t)	
Et_3GeCl	0.97 (m)		
Et_3GeH	1.17 (m)		3.64 (m)
$(Et_3Ge)_2$	0.95 (m)		

Table 3. ^{13}C chemical shifts of (trialkylgermyl)alkali metals and related species

Compound	δ (ppm) in HMPA–THF-d_8	
	C_1	C_2
Me_3GeLi	12.59	
Me_3GeNa	6.72	
Me_3GeK	12.59	
Me_3GeCl	6.92	
Me_3GeH	−2.15	
$(Me_3Ge)_2$	−1.17	
Et_3GeLi	17.49	15.21
Et_3GeNa	17.36	15.21
Et_3GeK	17.56	15.27
Et_3GeCl	9.53	12.17
Et_3GeH	5.09	11.45
$(Et_3Ge)_2$	7.18	11.55

methyl proton signal of trimethylgermane is located at +0.21 ppm, whereas trimethylgermyllithium gives the corresponding signal slightly further upfield, −0.35 ppm. On the other hand, trimethylgermylsodium affords the signal at small but further upfield than those of trimethylgermyllithium and -potassium, this may be attributed to the difference in their degree of aggregation. The ethyl protons of triethylgermane appear as rather complex multiplets around +1.2 ppm. Metallation of the hydrogen atom of triethylgermane with lithium causes a considerable upfield shift of the signal due to the α-hydrogen (CH_2Ge) which appears as a quartet at +0.13 ppm. The influence of metallation on the chemical shift of the β-hydrogen (CH_3—C—Ge) is small, the signals appear at +0.97 ppm as a triplet. The ^{1}H NMR signals due to triethylgermylsodium and -potassium have very similar chemical shifts and patterns.

The ^{13}C NMR data of trimethyl- and triethylgermyl metals and their related compounds are summarized in Table 3. On metallation of trimethylgermane to trimethylgermyllithium, the ^{13}C NMR methyl signal moves to lower field, namely, from δ −2.15 to δ 12.59. Similarly, in the case of the ethyl derivatives, the ^{13}C NMR signal due to the α-carbon of the ethyl group shifts to lower field from δ 5.09 to δ 17.49. Similar trends in ^{13}C NMR data of triethylgermylsodium and -potassium are observed as shown in Table 3. The paramagnetic shift on metallation may be attributed to the decrease in transition energy which may cause a red shift of the UV absorption maxima described above. On metallation of a hydrocarbon with lithium, the ^{13}C NMR signal due to the α-carbon to lithium is reported to show an upfield shift in contrast to the germane mentioned above, whereas that of the β-carbon is shifted downfield from the corresponding hydrocarbons.[27]

Acknowledgements—The authors thank Professor Yoshito Takeuchi and Dr Toshie Hanazono of Tokyo University for recording the ^{13}C NMR spectra of some of the germyl anions.

REFERENCES

1. For example: D. D. Davies, *Organomet.Chem. Rev., Sect. A* 1970, **6**, 283; M. Fujita and T. Hiyama, *Yuki Gosei Kyokaishi* 1984, **42**, 293 and refs cited therein; M. Lesbre, P. Mazerolles and J. Satgé, *The Organic Compounds of Germanium*, pp. 646–655. John Wiley, New York (1971).
2. M. Szwarc, *Ions and Ion Pairs in Organic Reactions*. John Wiley, Vol. 1 (1972) and Vol. 2 (1974); E. Buncel and T. Durst, *Comprehensive Carbanion Chemistry*, Elsevier, Amsterdam, Vol. 1 (1980) and Vol. 2 (1984).
3. R. Waack and M. A. Doran, *Chem. Ind.* 1965, 564.
4. R. H. Cox, E. G. Janzen and W. B. Harrison, *J. Mag. Reson.* 1971, **4**, 274.
5. A. G. Evans, M. A. Hamid and N. H. Reese, *J. Chem. Soc.* 1971, 1110.
6. R. J. Hogan, P. A. Scherr, A. T. Weibel and J. P. Oliver, *J. Organomet. Chem.* 1975, **5**, 265.
7. J. B. Lambert and M. Uredameta-Perez, *J. Am. Chem. Soc.* 1978, **100**, 157.
8. G. A. Olah and R. J. Hunadi, *J. Am. Chem. Soc.* 1980, **102**, 6989.
9. R. J. Batchelor and R. Birchall, *J. Am. Chem. Soc.* 1983, **105**, 3848.

10. E. Bunsel, T. K. Venkatachalan, U. Edlund and B. Eliasson, *J. Chem. Soc., Chem. Commun.* 1984, 1476.
11. R. Sooriyakumaran and P. Boudjouk, *J. Organomet. Chem.* 1984, **271**, 289.
12. E. Buncel, T. K. Venkatachalan, B. Eliasson and U. Edlund, *J. Am. Chem. Soc.* 1985, **107**, 303.
13. U. Edlund, T. Lejon, T. K. Venkatachalan and E. Buncel, *J. Am. Chem. Soc.* 1985, **107**, 6408.
14. E. Buncel, T. K. Venkatachalan and U. Edlund, *Can. J. Chem.* 1986, **64**, 1674.
15. U. Edlund, T. Lejon, P. Pyyko, T. K. Venkatachalan and E. Buncel, *J. Am. Chem. Soc.* 1987, **109**, 5982.
16. K. Mochida, M. Wasaka, Y. Sakaguchi and H. Hayashi, *J. Am. Chem. Soc.* 1987, **109**, 7942.
17. K. Mochida and N. Matsushige, *J. Organomet. Chem.* 1982, **229**, 11.
18. W. Kitching, H. Olszowy and K. Harvey, *J. Org. Chem.* 1982, **47**, 1893.
19. A. E. Finholt, *Nucl. Sci. Abstr.* 1957, **6**, 617.
20. R. H. Fish and M. G. Kuivila, *J. Org. Chem.* 1966, **31**, 2445.
21. H. Gilman and V. Young, *J. Org. Chem.* 1936, **1**, 315.
22. H. H. Johnson, *J. Am. Chem. Soc.* 1953, **75**, 814.
23. H. H. Anderson, *J. Am. Chem. Soc.* 1957, **79**, 4913.
24. E. J. Bulten and J. G. Noltes, *Tetrahedron Lett.* 1966, **36**, 4389.
25. E. J. Bulten and J. G. Noltes, *J. Organomet. Chem.* 1969, **16**, P8.
26. R. Waack and M. A. Doran, *J. Am. Chem. Soc.* 1963, **85**, 1651.
27. R. D. Thomas, M. T. Clarke and T. C. Young, *J. Organomet. Chem.* 1987, **328**, 239.

Polyhedron Vol. 9, No. 18, pp. 2267–2272, 1990
Printed in Great Britain

0277–5387/90 $3.00+.00
© 1990 Pergamon Press plc

ELECTRON DISTRIBUTION WITHIN BIS(QUINONE)RUTHENIUM COMPLEXES. STRUCTURAL CHARACTERIZATION ON DELOCALIZED (BIPYRIDINE)BIS(QUINONE)RUTHENIUM AND ON THE LOCALIZED *TRANS*-BIS(3-CHLOROPYRIDINE)BIS(3,5-DI-TERT-BUTYL-1,2-SEMIQUINONE)RUTHENIUM(III) CATION

STEVEN R. BOONE and CORTLANDT G. PIERPONT*

Department of Chemistry and Biochemistry, University of Colorado, Boulder, CO 80309-0215, U.S.A.

(*Received* 19 *January* 1990; *accepted* 9 *May* 1990)

Abstract—Structural information obtained on complexes containing semiquinone and catecholate ligands has provided insights on charge distribution. Ligand C—O lengths found for *trans*-Ru(4-t-Bupy)$_2$(DBQ)$_2$ averaged 1.321(5) Å, midway between values of 1.34 and 1.29 Å expected for localized catecholate and semiquinone ligands. This value may arise from crystallographic disorder of a localized Ru^{III}(SQ)(Cat) species or it may result from charge delocalization over both quinone ligands. Crystallographic characterization of Ru(bpy)(Q)$_2$, where Q is the unsubstituted *o*-quinone ligand, has shown that the complex molecule crystallizes without imposed symmetry on the molecule, in a crystal structure that places both quinone ligands in different solid-state environments. The four independent C—O lengths average 1.321(5) Å, without significant variation, strongly suggesting charge delocalization over both quinone ligands. Characterization on the *trans*-Ru(3-Clpy)$_2$(DBQ)$_2^+$ cation, formed by one-electron oxidation of a neutral species that would be expected to show ligand charge delocalization, has shown ligand C—O lengths of 1.293(4) Å, exactly the value expected for semiquinone ligands. Oxidation of the neutral complex appears to occur at a ligand delocalized electronic level to give a ligand localized bis(semiquinone) product, Ru^{III}(SQ)$_2^+$.

Internal transfer of charge between electroactive transition metal ions and chelated *o*-quinone ligands sometimes complicates the assignment of formal charge within the chelate ring of complexes containing semiquinone and catecholate ligands.[1] Spectroscopic or magnetic properties may provide information on the oxidation state of the metal. Mössbauer spectra and variable-temperature magnetic susceptibility measurements have provided specific information on the charge distribution within the tris(semiquinone)iron(III) complexes, compounds that were among the first homoleptic semiquinone metal complexes.[2,3] Crystallographic molecular structure determinations have provided structural criteria for assigning charge distributions for complexes containing semiquinone and catecholate ligands.[1] Bond lengths to the metal are sometimes sensitive to both oxidation and spin state, but the structural features of the quinone ligand are nearly invariant. In particular, carbon–oxygen bond lengths of 1.34, 1.29 and 1.23 Å have been found from a large number of structure determinations to be characteristic of coordinated catecholate, semiquinone and *o*-benzoquinone electronic forms of the quinone ligands. Since localized charge assignments appear to be appropriate for the ligands of quinone complexes, charge delocalization between ligand and metal is thought to be less important for this class of compounds than for the oxidized 1,2-dithiolene or reduced 1,2-diimine complexes.[4]

Recent structural characterization on ruthenium quinone complexes seemed to show a break in this pattern of well-defined metal and quinone ligand

* Author to whom correspondence should be addressed.

charge assignments.[5] Spectroscopic characterization on the Ru(bpy)$(Q)_2$ and *trans*-Ru(py)$_2(Q)_2$ series failed to provide definitive information on charge distribution, and appeared to indicate electronic delocalization.[6] Structural characterization on *trans*-Ru(4-t-Bupy)$_2$(DBQ)$_2$, containing the 3,5-di-tert-butylquinone ligand, supported the idea of delocalization by showing that both quinone ligands were structurally equivalent with C—O lengths of 1.321(5) Å.[5] This value is midway between the semiquinone and catecholate values observed in other structures, and could potentially arise from disorder of semiquinone and catecholate ligands coordinated to ruthenium(III) in a complex molecule of localized charge distribution, Ru^{III}(4-t-Bupy)$_2$(DBSQ)(DBCat). Species with mixed-charge quinone ligands are known for the M^{III}(bpy)(DBSQ)(DBCat) (M = Cr, Fe, Co) series,[7–9] and the difference in charge between the two quinone ligands of Co(bpy)(DBSQ)(DBCat) appeared in the structural features of the molecule.[9] We now report the results of structural studies on two bis(quinone)ruthenium complexes with the hope that metrical features of the molecules will provide information on charge distribution and electronic structure. The first complex is Ru(bpy)$(Q)_2$, where the unsubstituted quinone ligands are not directly related by crystallographic symmetry and are contained in different solid-state environments in the crystal lattice. The second complex is the Ru(3-Clpy)$_2$(DBQ)$_2^+$ cation, which was obtained by oxidation of the neutral complex, and may provide information on the nature of the electronic level involved in the oxidation of the neutral parent complex.

RESULTS

Description of Ru(bpy)$(Q)_2$

The Ru(bpy)$(Q)_2$ molecule is isoelectronic with *trans*-Ru(4-t-Bupy)$_2$(DBQ)$_2$ and may be expected to have a similar charge distribution. Reasonable options for localized charge distribution for the Ru$(Q)_2$ regions of both complexes include $Ru^{II}(SQ)_2$, Ru^{III}(SQ)(Cat) and $Ru^{IV}(Cat)_2$. Ruthenium–nitrogen and ruthenium–oxygen bond lengths are more sensitive to the donor properties of the ligand than to electronic differences in the ruthenium ion, and are not reliable indicators of metal ion charge.[10] Carbon–oxygen lengths of the quinone ligands have been generally found to reflect ligand charge, and the formal charge of the quinone ligands can be used to determine the oxidation state of the metal. The two independent C—O lengths of *trans*-Ru(4-t-Bupy)$_2$(DBQ)$_2$ were 1.320(5) and 1.322(5) Å, indicating a charge for the ligand that was midway between SQ and Cat, with delocalization contributing to the similarity between the two ligands. A second possibility is that the charge distribution is localized as Ru^{III}(SQ)(Cat), but that the two different quinone ligands are disordered with the crystallographically-imposed inversion symmetry on the molecule.[5] The crystal structure of Ru(bpy)$(Q)_2$ consists of complex molecules with no imposed symmetry. A view of the molecule is shown in Fig. 1 and bond distances and angles are given in Table 1. Closest intermolecular contacts result from a weak stacking interaction between bipyridine ligands of adjacent molecules, shown in Fig. 2, through the inversion centre at [1/2,0,0]. Weaker pairing interactions occur between quinone ligands through inversion centres at [0,0,0] and [1/2,1/2,0], and the intermolecular interactions in the solid-state place the two quinone ligands in symmetrically different environments. If a localized Ru^{III}(SQ)(Cat) charge distribution is appropriate for the complex, the asymmetry in its solid-state environment may result in a structural difference between the two ligands. Effects of this type sometimes result in valence-trapped electronic structures for otherwise delocalized mixed-valence metal complexes,[11] and the structure of Co(bpy)(DBSQ)(DBCat) showed structurally dissimilar quinone ligands.[9] All four C—O lengths of the structure, given in Table 1, are within error of being identical, and the average value of 1.321(5) Å is identical to the average value found for *trans*-Ru(4-t-Bupy)$_2$(DBQ)$_2$.

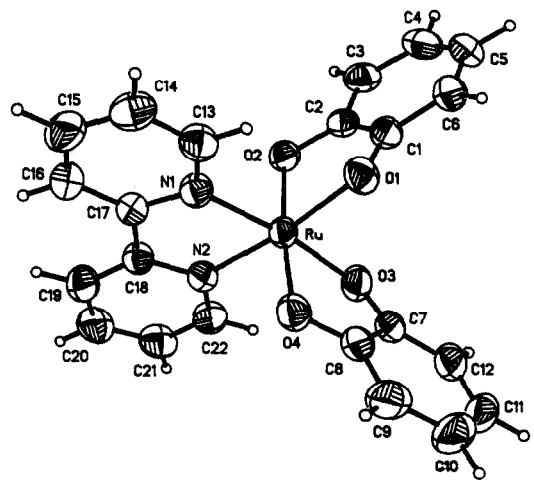

Fig. 1. View of the Ru(bpy)$(Q)_2$ molecule.

Bond lengths to the metal of Ru(bpy)$(Q)_2$ fail to provide information on metal charge but reveal features of ligand bonding. Ruthenium–oxygen bonds to the *trans*-oxygens, O(2) and O(4), are

Table 1. Selected bond distances and angles for Ru(bpy)$(Q)_2$

Bond distances (Å)			
Ru—O(1)	2.003(4)	O(3)—C(7)	1.322(4)
Ru—O(2)	1.977(3)	O(4)—C(8)	1.321(5)
Ru—O(3)	1.995(3)	C(1)—C(2)	1.424(6)
Ru—O(4)	1.981(3)	C(7)—C(8)	1.413(6)
Ru—N(1)	2.042(3)	N(1)—C(13)	1.346(7)
Ru—N(2)	2.055(4)	N(1)—C(17)	1.355(7)
O(1)—C(1)	1.316(5)	N(2)—C(18)	1.359(5)
O(2)—C(2)	1.326(6)	N(2)—C(22)	1.333(6)
Bond angles (°)			
O(1)—Ru—O(2)	81.8(1)	O(1)—Ru—O(3)	88.0(1)
O(2)—Ru—O(3)	94.9(1)	O(1)—Ru—O(4)	91.9(1)
O(2)—Ru—O(4)	173.1(1)	O(3)—Ru—O(4)	82.0(1)
O(1)—Ru—N(1)	98.1(2)	O(2)—Ru—N(1)	91.1(1)
O(3)—Ru—N(1)	172.0(2)	O(4)—Ru—N(1)	92.5(1)
O(1)—Ru—N(2)	173.2(1)	O(2)—Ru—N(2)	92.6(1)
O(3)—Ru—N(2)	96.2(1)	O(4)—Ru—N(2)	93.9(1)
N(1)—Ru—N(2)	78.2(2)		

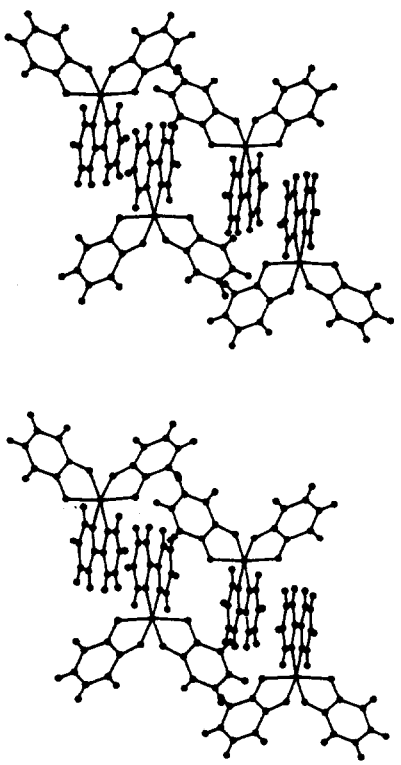

Fig. 2. Stereoview showing the bipyridine stacking interactions between adjacent Ru(bpy)$(Q)_2$ molecules.

shorter than Ru—O lengths to the oxygens *trans* to the bipyridine nitrogens. All four Ru—O lengths are relatively short due, presumably, to strong σ- and π-bonding interactions. Ruthenium–nitrogen lengths of 2.042(3) and 2.055(4) Å agree well with values of 2.045(5) and 2.054(5) Å found at sites *trans* to chloro ligands of *cis*-Ru(bpy)$_2Cl_2^+$.[10] Synergistic stabilization of *trans*-quinone Ru—O bonds also appears as a feature in Ru$(DBQ)_3$, where the average length is 1.972 Å and the bonds are among the shortest reported for all but lengths to oxo ligands.[12]

Bond angles about the ruthenium show that the complex has a regular octahedral structure with allowance for angular constraints of five-membered chelate rings. Bite angles of the quinone ligands are slightly larger [81.9(1)°] than the bipyridine bite angle of 78.2(2)°.

Description of trans-Ru(3-Clpy)$_2(DBSQ)_2^+$

The *trans*-Ru(3-Clpy)$_2(DBQ)_2^+$ cation is located about a crystallographic inversion centre which results in *trans* dispositions for the chloro substituents of the pyridine ligands and for the t-butyl substituents of the quinone ligands in the solid-state. A view of the cation is shown in Fig. 2, bond distances and angles are given in Table 2. Quinone C—O lengths of the cation are clearly indicative of charge distribution in this case. With values of 1.289(4) and 1.296(4) Å, they are both in the 1.29 Å range associated with semiquinone ligands.[1,3] Carbon–carbon bond lengths within the ring conform to the pattern noted for semiquinone ligands of other complexes[3] with a length for C(1)—C(2) which is slightly longer than the aromatic value, and shorter values for C(3)—C(4) and C(5)—C(6). Charge distribution for the cation is therefore $Ru^{III}(SQ)_2^+$, and a direct comparison can be made with

Table 2. Selected bond distances and angles for *trans*-Ru(3-Clpy)$_2$(DBSQ)$_2^+$

Bond distances (Å)			
Ru—O(1)	2.020(3)	O(1)—C(1)	1.289(4)
Ru—O(2)	2.000(2)	O(2)—C(2)	1.296(4)
Ru—N	2.085(2)	C(1)—C(2)	1.459(4)
C(2)—C(3)	1.427(5)	C(3)—C(4)	1.346(5)
C(4)—C(5)	1.452(5)	C(5)—C(6)	1.364(5)
C(1)—C(6)	1.415(5)		
Bond angles (°)			
O(1)—Ru—O(2)	79.8(1)	O(1)—Ru—N(1)	91.4(1)
O(2)—Ru—N(1)	88.9(1)		

neutral *trans*-Ru(4-t-Bupy)(DBQ)$_2$. Ruthenium–nitrogen lengths for the two structures are essentially the same with values of 2.085(3) Å for the cation and 2.079(3) Å for the neutral molecule. The average Ru—O length of the cation is 2.010(2) Å, slightly longer than the value of 1.994(3) Å for the neutral complex molecule. This may result from weaker donation to the metal by the partially reduced semiquinone ligands. The bite angle of the semiquinone ligand of *trans*-Ru(3-Clpy)$_2$(DBSQ)$_2^+$ is 79.8(1)°, slightly more contracted than the 80.5(1)° value of *trans*-Ru(4-t-Bupy)(DBQ$_2$).

DISCUSSION

Structural characterization on the neutral bis (quinone) complexes, *trans*-Ru(4-t-Bupy)$_2$(DBQ)$_2$ and Ru(bpy)(Q)$_2$, has provided results that indicate that the charge distributions for the two complexes are essentially the same. Carbon–oxygen lengths of the quinone ligands are intermediate between values expected for semiquinone and catecholate ligands. The localized charge form Ru^{III}(SQ)(Cat) with resonant delocalization over both ligands, eq. (1), is, perhaps, the most appropriate description for the electronic structure.

$$(SQ)Ru^{III}(Cat) \rightleftharpoons (Cat)Ru^{III}(SQ). \quad (1)$$

The electronic ground states of the oxidized 1,2-dithiolene and reduced 1,2-diimine complexes are ligand delocalized levels with little or no metal orbital contributions.[4] Electron pairing between the ruthenium(III) centre and the semiquinone radical ligand may occur by strong antiferromagnetic coupling or within the set of electronic levels that arise from strong molecular orbital interactions. The sharp NMR signals that the neutral complexes show seem to point most strongly to a delocalized MO electronic structure.

Reversible oxidation of the ligand delocalized level would result in an electronic form for the complex which is ostensibly a bis(semiquinone)species, eq. (2).

$$Ru^{III}(SQ)(Cat) \rightleftharpoons Ru^{III}(SQ)_2^+ + e^-. \quad (2)$$

This is in accord with the structural features of *trans*-Ru(3-Clpy)$_2$(DBSQ)$_2^+$. It also agrees with the EPR spectra recorded on the $S = 1/2$ cationic com-

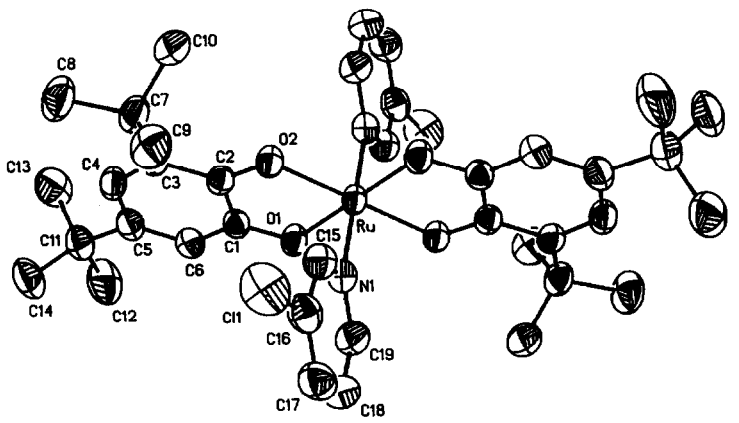

Fig. 3. View of the Ru(3-Clpy)$_2$(DBSQ)$_2^+$ cation.

plexes.[6] Resonances of the one-electron oxidation products are centred close to the free-electron g value, show no ligand proton hyperfine, and split to give weakly axial or rhombic signals at 77 K, with a difference between $g_{\parallel}$ and $g_{\perp}$ of 0.04. A slight metal orbital contribution to the ground state together with the large spin–orbit coupling constant of ruthenium(III) may be responsible for the anisotropy of the low-temperature glass spectrum.

Neutral quinone complexes have been prepared with metals on either side of ruthenium and osmium. With technetium and rhenium, charge-localized catecholate complexes, $M(Cat)_3$, are formed.[13] Palladium and platinum form bis(semiquinone) complexes, $M(SQ)_2$, with divalent metal ions.[14] Quinone complexes of rhodium and iridium await detailed characterization, but there is a marked tendency toward localized charge distributions for quinone complexes of metals other than ruthenium. Even the osmium analogues of the ruthenium complexes appear to show properties characteristic of charge-localized catecholate species.[12,15] Currently, the neutral bis and tris (quinone) complexes of ruthenium stand as the unique examples of delocalized quinone bonding with transition metals.

EXPERIMENTAL

Crystals used in this investigation were provided by Professor A. B. P. Lever of York University, Ontario, Canada.

Structure determination on $Ru(bpy)(C_6H_4O_2)_2$

A dark blue crystal of $Ru(bpy)(Q)_2$ suitable for crystallographic analysis was mounted and aligned on a Nicolet P3/F automated diffractometer. Crystal quality was examined by using rotational and axial photographs and was judged satisfactory for data collection. Information regarding data collection and structure determination is given in Table 3 and in the supplementary material. The location of the ruthenium atom was determined from a Patterson map; the locations of other atoms were determined from phases generated by using the ruthenium atom position. Fixed contributions for hydrogen atoms were included in final cycles of refinement. All non-hydrogen atoms of the molecule were refined with anisotropic thermal parameters. Final atomic coordinates for $Ru(bpy)(Q)_2$ and tables containing anisotropic thermal parameters and structure factors are available as supplementary material.

Structure determination on $[Ru(3\text{-}Clpy)_2(DBSQ)_2](PF_6)\cdot Et_2O$

A dark blue crystal of $[Ru(3\text{-}Clpy)_2(DBSQ)_2](PF_6)$, grown from a diethyl ether solution, was mounted and aligned on the diffractometer. Crystallographic information for the complex is given in Table 3 and in the supplementary material. The complex crystallizes in the centrosymmetric triclinic space group $P\bar{1}$ with one formula unit per unit cell.

Table 3. Crystallographic information for $Ru(bpy)(Q)_2$ and *trans*-$Ru(3\text{-}Clpy)_2(DBSQ)_2^+$

	$Ru(bpy)(Q)_2$	$[Ru(3\text{-}Clpy)_2(DBSQ)_2](PF_6)\cdot O(C_2H_5)_2$
Molecular weight	473.4	987.8
Colour	Dark blue	Dark blue
Crystal system	Triclinic	Triclinic
Space group	$P\bar{1}$	$P\bar{1}$
a (Å)	9.312(2)	8.513(3)
b (Å)	9.771(3)	11.907(5)
c (Å)	11.670(4)	12.762(5)
α (°)	91.90(3)	110.39(3)
β (°)	93.79(2)	106.48(3)
γ (°)	117.17(2)	94.48(3)
Volume (Å^3)	940.0(5)	1139.9(7)
Z	2	1
D_c (g cm^{-3})	1.67	1.44
μ (cm^{-1})	8.48	5.55
F(000)	476	511
Reflections [$F > 6\sigma(F)$]	2853	3682
R	0.042	0.040
R_w	0.053	0.056

Phases obtained from a structure factor calculation with the ruthenium atom at the origin [0,0,0] gave other non-hydrogen atoms of the complex cation and revealed the PF_6^- anion with the phosphorus atom located at the inversion centre [1/2,1/2,1/2]. Fluorine atoms of the anion were disordered about four sets of factional-atom locations. Final cycles of refinement revealed a cluster of peaks on the difference Fourier map located near the inversion centre at [0,0,1/2]. These peaks were judged to be a disordered diethyl ether solvate molecule, and were refined accordingly. Fixed contributions for the hydrogen atoms of the cation were included in the final cycles of refinement. Tables containing atomic coordinates, anisotropic thermal parameters and structure factors are available as supplementary material.

Acknowledgements—Our thanks to Professor A. B. P. Lever for providing crystalline samples of the complexes used in this investigation and to the National Science Foundation for providing support for this research under grant CHE 88–09923.

REFERENCES

1. C. G. Pierpont and R. M. Buchanan, *Coord. Chem. Rev.* 1981, **38**, 44.
2. R. M. Buchanan, S. L. Kessel, H. H. Downs, C. G. Pierpont and D. N. Hendrickson, *J. Am. Chem. Soc.* 1978, **100**, 7894.
3. S. R. Boone, G. H. Purser, H.-R. Chang, M. D. Lowery, D. N. Hendrickson and C. G. Pierpont, *J. Am. Chem. Soc.* 1989, **111**, 2292.
4. (a) J. A. McCleverty, *Prog. Inorg. Chem.* 1968, **10**, 49; (b) R. P. Burns and C. A. McAuliffe, *Adv. Inorg. Chem. Radiochem.* 1979, **22**, 303; (c) A. Vogler and H. Kunkely, *Comments Inorg. Chem.*, in press.
5. S. R. Boone and C. G. Pierpont, *Inorg. Chem.* 1987, **26**, 1769.
6. (a) A. B. P. Lever, P. R. Auburn, E. S. Dodsworth, M. Haga, W. Liu, M. Melnik and W. A. Nevin, *J. Am. Chem. Soc.* 1988, **110**, 8076; (b) A. B. P. Lever, P. R. Auburn, E. S. Dodsworth, M. Haga and W. A. Nevin, to be submitted for publication.
7. R. M. Buchanan, J. Claflin and C. G. Pierpont, *Inorg. Chem.* 1983, **22**, 2552.
8. M. W. Lynch, M. Valentine and D. N. Hendrickson, *J. Am. Chem. Soc.* 1982, **104**, 6982.
9. R. M. Buchanan and C. G. Pierpont, *J. Am. Chem. Soc.* 1980, **102**, 4951.
10. D. S. Eggleston, K. A. Goldsby, D. J. Hodgson and T. J. Meyer, *Inorg. Chem.* 1985, **24**, 4573.
11. U. Furholz, S. Joss, H. B. Burgi and A. Ludi, *Inorg. Chem.* 1985, **24**, 943.
12. S. Bhattacharya, S. R. Boone, G. A. Fox and C. G. Pierpont, *J. Am. Chem. Soc.* 1990, **112**, 1088.
13. (a) L. A. deLearie, R. C. Haltiwanger and C. G. Pierpont, *J. Am. Chem. Soc.* 1989, **111**, 4324; (b) L. A. deLeari, R. C. Haltiwanger and C. G. Pierpont, *Inorg. Chem.* 1987, **26**, 817.
14. (a) G. A. Fox and C. G. Pierpont, *J. Chem. Soc., Chem. Commun.* 1988, 806; (b) G. A. Fox and C. G. Pierpont, submitted for publication.
15. M. Haga, K. Isobe, S. R. Boone and C. G. Pierpont, in press.

Polyhedron Vol. 9, No. 18, pp. 2273–2283, 1990
Printed in Great Britain

0277–5387/90 $3.00+.00
© 1990 Pergamon Press plc

THE FORMATION OF COBALT AND NICKEL COMPLEXES ON CLAY SURFACES

NIGEL DAVISON and WILLIAM R. McWHINNIE*

Department of Chemical Engineering and Applied Chemistry, Aston University, Aston Triangle, Birmingham B4 7ET, U.K.

(*Received* 9 *November* 1989; *accepted* 9 *May* 1990)

Abstract—Treatment of hectorite exchanged with cobalt or nickel with various ligands is investigated. Basic ligands such as 2,2′-bipyridyl,1,2-diaminoethane (ethylenediamine, en) and ammonia readily afford complexes of nickel(II) and cobalt(III). In the case of ammonia, evidence is obtained for the isolation of an oxidation intermediate on the clay. More quantitative studies including some typical groundwater ligands such as pentanoic and butanoic acids reveal that the weak acid ligands are effective in displacing significant quantities of exchanged cobalt and nickel to solution; by contrast, some basic ligands can "stabilize" the more labile ion pair sorbed fractions of the metal on the clay surface. Although $[Ni(en)_3]^{2+}$ is much more strongly sorbed than Na^+ or Ca^{2+}, copper(II) ions release large quantities of nickel(II) to solution when aqueous $[Cu(H_2O)_6]^{2+}$ contacts $[Ni(en)_3]^{2+}$–hectorite. Tracer studies using ^{60}Co show that similar behaviour pertains at microscopic concentration levels to that observed with macroscopic concentrations.

The presence of organic material in groundwaters is well established,[1] but the possible influence of such materials on the sorption properties of metal ions on clay minerals is not well documented. Organic material, which has sites of Lewis basicity, may affect transition metal–sorbent interactions in three significant ways.

(1) Transport properties of the ion in the groundwater may be modified by complexation, indeed even precipitation could occur.
(2) Complex formation may promote desorption and hence alter the lability of the sorbed ion.
(3) The organic ligand may itself become sorbed onto the clay.

The direct sorption of ammonia from aqueous solution onto soils was first reported in 1852,[2] more recent work has covered such complex organic molecules as pesticides and other compounds of biological importance, e.g. amino acids and peptides.[3] The majority of transition metal sorption studies involving organic ligands have been concerned with the uptake of simple complexes onto the clay, e.g. tris(1,3-diaminopropane)cobalt(III) onto laponite,[4] and their characterization by a variety of spectroscopic methods.[5,6]

The fact that the presence of ligands could alter the lability of a metal ion sorbed onto a clay has obvious importance in the environmental context, particularly if the ions concerned were toxic or radioactive. We have recently been interested in factors affecting the lability of nickel(II) and cobalt(II) ions in clay environments and decided to explore the effect of ligands on this property. We have therefore carried out an initial qualitative study involving the addition of simple ligands to previously prepared Ni(Co) clay samples, and followed this with a more quantitative survey of the influence of typical groundwater organics. The work was carried out with hectorite which, due to the low iron content, is virtually colourless and thus facilitates the use of techniques such as visible adsorption spectroscopy.

EXPERIMENTAL AND RESULTS

Solution concentrations of cobalt and nickel were measured by atomic adsorption. It was established that the excess ligand in the solutions did not interfere with the metal analysis under the conditions used in this work.

* Author to whom correspondence should be addressed.

(A) *Qualitative study of the effect of ligands on cobalt- and nickel-saturated hectorite*

Samples of hectorite (sodium form; from Hector California) (15 g) were shaken with 0.1 M solutions of $NiCl_2$ or $CoCl_2$ (150 cm^3) for 3 days, filtered and left to air-dry. The clays were then resuspended in distilled water (150 cm^3) and shaken for a further 3 days, filtered and air-dried. The washing procedure was repeated and the air-dried clays were crushed to a fine powder prior to use in the following experiments.

Nickel(II) hectorite: 46 meq Ni^{2+} 100 g^{-1}; UV–vis: 395 nm, 660 nm; $d(001)$ = 15.1 Å (FWHM = 2.6 Å, where FWHM = full width at half maximum). Cobalt(II) hectorite: 50 meq Co^{2+} 100 g^{-1}; UV–vis; 459 nm, 512 nm; $d(001)$ = 15.3 Å (FWHM = 3.0 Å).

Treatment of Ni(Co) *clay with ligands.* Samples (2 g/0.5 mmol Ni^{2+}; 3 g/0.75 mmol Co^{2+}) of the above treated clays were contacted with a 0.03 M solution of NH_3 (50 cm^3, 1.5 mmol, i.e. Ni/NH_3 = 1:3, Co/NH_3 = 1:2). The mixture was stirred for 4 h, in the cobalt case ammonia-saturated air was passed through the solution during the period of the reaction. The solids were filtered, air-dried and subjected to XRD and diffuse reflectance analysis. In the nickel case no colour change was seen during the reaction, the clay retaining the green colour. By contrast the cobalt suspension turned brown within 3–4 min, the colour darkening after a further 20 min. In both cases the filtrates were colourless.

Similar experiments were then carried out with other ligands: ammonia (various ratios), 1,2-diaminoethane ("ethylenediamine", en), dimethylglyoxime (DMG) and 2,2′-bipyridyl (bipy). The reaction of the cobalt clay with en was carried out with the passage of en-saturated air. The ratios of reactants, XRD data and diffuse reflectance data for the ligand treated clays are given in Tables 1 and 2 (nickel), and Tables 3 and 4 (cobalt). Neither the 10:1 nor the 25:1 ammonia/cobalt clays gave a detectable ESR signal at room temperature.

Table 1. $d(001)$ Values obtained from Ni–hectorite treated with model organic ligands

Organic ligand added	Organic/Ni ratio	Colour of solid product	$d(001)$ (Å)	FWHM[a] (Å)
NH_3	3:1	Green	14.0	5.7
NH_3	10:1	Green[b]	12.8	3.6
NH_3	25:1	Green[b]	12.8	3.2
en	9:1	Violet–pink	14.7	3.6
DMG	6:1	Orange	14.3	2.8
bipy	5:1	Red–brown	18.2	3.0

[a] Full width of peak at half maximum peak height.

[b] The blue colour exhibited by both samples initially was lost on air-drying.

(B) *Typical groundwater ligands with nickel and cobalt hectorite*

A more quantitative approach was adopted for this section of the investigation, thus initially the following procedure was used to prepare clay samples: a sample of hectorite (15 g) was shaken with 0.1 M nickel chloride (cobalt chloride) solution (150 cm^3) for 3 days, filtered, then redispersed in a 1 M solution of $NiCl_2$ ($CoCl_2$) (150 cm^3) and shaken for a further 3 days prior to filtration. The clay was rinsed twice with distilled water, and a portion (5 g) was retained for further experiments [Ni(Co)–hectorite/rinse]. The remaining clay was dispersed in distilled water (100 cm^3), shaken for 2 h, then separated by ultracentrifugation. This procedure was repeated a further four times, after which the clay was left to air-dry [Ni(Co)–hectorite/wash].

Table 2. Peaks derived from diffuse reflectance spectra of Ni–hectorite treated with model organic ligands

Organic ligand added	Organic/Ni ratio	Absorption peaks (nm)			
NH_3	3:1	391(m-s)			669(w)
NH_3	10:1	392(m-s)			684(w)
NH_3	25:1	392(m-s)			686(w)
en	9:1	356(s)	456(w)	542(m-w)	
DMG	6:1	369(m-w)	422(m-w)	534(m-w)	
bipy	5:1	367(m-s)	422(w)	536(m-s)	

Peak intensities: s—strong, m—medium, w—weak, v—very.

Table 3. *d*(001) Values from Co–hectorite treated with model organic ligands

Weight of Co–hectorite used (g)	Organic ligand added	Organic/Co ratio	Colour of solid product	*d*(001) (Å)	FWHM (Å)
3.00	NH_3	2:1	Red–brown	13.1	3.2
2.00	NH_3	10:1	Yellow–brown	12.7	3.2
2.00	NH_3	25:1	Red–brown	13.5	3.0
1.75	en	1:1	Yellow–brown	14.9	4.0
1.75	en	9:1	Light brown	15.2	3.3

Table 4. Peaks derived from diffuse reflectance spectra of Co–hectorite treated with model organic ligands

Organic ligand added	Organic/Co ratio	Absorption peaks (nm)				
NH_3	2:1		385(m-w)		531(w)	
NH_3	10:1		384(m-w)		527(m-w)	
NH_3	25:1		399(m-w)	454(vw)		
en	1:1	348(w)		465(w)	518(m)	570(w)
en	9:1	349(s)		466(s)		573(w)

The metal contents of the clay were deduced from AA analysis of the contacting solutions, thus:

Ni–hectorite/rinse 64 meq 100 g^{-1}, *d*(001) 15.0 Å (FWHM 2.7 Å);
Ni–hectorite/wash 56 meq 100 g^{-1}, *d*(001) 15.1 Å (FWHM 2.5 Å);
Co–hectorite/rinse 69 meq 100 g^{-1}, *d*(001) 15.1 Å (FWHM 3.3 Å);
Co–hectorite/wash 64 meq 100 g^{-1}, *d*(001) 15.3 Å (FWHM 2.7 Å).

Reaction with ligands. Portions of the four clay types (0.2 g) were covered separately with solutions (10 cm^3) of ammonia (0.08 M), en (0.08 M), butanoic acid (BA, 0.08 M), pentanoic acid (PA, 0.08 M), and with distilled water. (n-Butanoic acid and n-pentanoic acid have been identified in "run off" from domestic waste disposal sites and may well be groundwater constituents. Also, they constitute useful, even if simplistic, models for humic and fulvic acids.) The mixtures were stirred for 3 days and the suspensions separated by ultracentrifugation. The solids were air-dried at room temperature and the supernatant liquids were retained for analysis. The appropriate ligand/metal reaction ratios were: Ni–hectorite/rinse, 12.5:1; Ni–hectorite/wash, 14.3:1; Co–hectorite/rinse, 11.6:1; Co–hectorite/wash, 12.5:1. Only in the cases of ammonia and en were rapid colour changes noted. Each clay specimen was examined by diffuse reflectance, XRD and IR. Results are given in Tables 5 and 6 (nickel), and in Tables 7 and 8 (cobalt).

The effect of differing metal/ligand ratios was then explored, thus Ni–clay specimens (0.2 g) were added separately to solutions of ammonia (12, 1.2 and 0.12 mM) and of butanoic acid (8.0, 0.8 and 0.08 mM) and treated as above. In parallel experiments, samples of the Co–hectorites (0.2 g) were treated with solutions of en (10 cm^3) (8.0, 0.8 and 0.08 mM) and butanoic acid (concentrations as for nickel). The visible absorption spectra and pH data for the supernatant solutions are shown in Tables 9 and 10, and data for the solids are in Tables 11 and 12.

Lability of complexed nickel(II) *on hectorite.* Ni–hectorite/wash (2.2 g) was added to an en solution (100 cm^3, 9.2 mmol) and stirred for 24 h. The suspension was then filtered and washed with three aliquots of distilled water (25 cm^3). The air-dried solid was a pale violet colour and gave *d*(001) 14.9 Å (FWHM 2.1 Å) and characteristic peaks at 550, 465 and 342 nm in the diffuse reflectance spectrum. The clay contained 56 meq Ni 100 g^{-1}.

Portions (0.2 g) of this $[Ni(en)_3]^{2+}$ clay were then added separately to solutions (10 cm^3) of NaCl (30, 6.0 and 1.2 mM); $CaCl_2$ (30, 6.0 and 1.2 mM); and

Table 5. Physical characteristics of Ni–hectorite clay samples after treatment with solutions of organic "ligands"

Clay	Organic added	Colour of solid product	d(001) (Å)	FWHM (Å)	Peaks resolved from diffuse reflectance spectrum (nm)			
Ni–hectorite/rinse	NH_3	Light green	12.5	3.1	394(m-w)			678(vw)
Ni–hectorite/rinse	en	Light mauve	14.9	2.5	342(m)	465(m-w)	555(vw)	
Ni–hectorite/rinse	BA	Very light green	16.3	3.6	394(w)			
Ni–hectorite/rinse	PA	Very light green	15.8	3.2	391(w)			
Ni–hectorite/rinse	Blank—dw	Light green	15.2	3.3	392(m-w)			665(vw)
Ni–hectorite/wash	NH_3	Light green	12.8	3.6	395(m-w)			676(vw)
Ni–hectorite/wash	en	Light mauve	14.9	2.2	345(m)	460(m-w)	556(vw)	
Ni–hectorite/wash	BA	Very light green	16.2	3.1	394(w)			
Ni–hectorite/wash	PA	Very light green	15.6	3.3	395(w)			
Ni–hectorite/wash	Blank—dw	Light green	15.0	2.8	396(m-w)			666(vw)

Abbreviations: NH_3—ammonia, en—ethylenediamine, BA—butanoic acid, PA—pentanoic acid, dw—distilled water.

Table 6. Physical characteristics of equilibrium solutions remaining from treatment of Ni–hectorite clays with organic "ligands"

Clay	Organic added	Initial solution pH	Final solution pH	Ni released from clay (meq/100 g)	Per cent Ni released	Peaks resolved from visible spectrum (nm)
Ni–hectorite/rinse	NH_3	10.36	10.23	0.048	0.08	ND
Ni–hectorite/rinse	en	10.82	10.78	0.19	0.30	ND
Ni–hectorite/rinse	BA	3.30	4.48	55	85	392(m)
Ni–hectorite/rinse	PA	3.31	4.46	52	82	392(m)
Ni–hectorite/rinse	Blank—dw	5.51	6.89	1.16	1.8	ND
Ni–hectorite/wash	NH_3	10.36	10.22	0.049	0.09	ND
Ni–hectorite/wash	en	10.82	10.62	0.21	0.37	ND
Ni–hectorite/wash	BA	3.30	4.37	48	85	392(m)
Ni–hectorite/wash	PA	3.31	4.40	50	89	392(m)
Ni–hectorite/wash	Blank—dw	5.51	6.58	0.82	1.4	ND

ND—no peaks detectable.

Table 7. Physical characteristics of Co–hectorite clay samples after treatment with solutions of organic "ligands"

Clay	Organic added	Colour of solid product	d(001) (Å)	FWHM (Å)	Peaks resolved from diffuse reflectance spectrum (nm)			
Co–hectorite/rinse	NH_3	Beige	13.1	4.0	381(m-w)	454(vw)	525(w)	593(vw)
Co–hectorite/rinse	en	Red–brown	15.4	3.7	342(m)	466(w)	562(vw)	
Co–hectorite/rinse	BA	Very light pink	16.4	4.1			522(w)	
Co–hectorite/rinse	PA	Very light pink	16.2	3.5		470(vw)	522(w)	
Co–hectorite/rinse	Blank—dw	Light pink	15.0	3.5		465(w)	521(m)	
Co–hectorite/wash	NH_3	Beige	13.0	3.6	386(m-w)	456(vw)	528(w)	585(vw)
Co–hectorite/wash	en	Red–brown	15.1	3.5	341(m-s)	464(w)	558(w)	
Co–hectorite/wash	BA	Very light pink	16.4	3.6		454(vw)	524(m-w)	
Co–hectorite/wash	PA	Very light pink	16.0	3.3		462(vw)	519(m)	
Co–hectorite/wash	Blank—dw	Light pink	15.1	3.0		459(w)	517(m)	

Table 8. Physical data from equilibrium solutions remaining after treatment of Co–hectorite clays with organic "ligands"

Clay	Organic added	Initial solution pH	Final solution pH	Co released from clay (meq/100 g)	Per cent Co released	Peaks resolved from visible spectrum (nm)
Co–hectorite/rinse	NH_3	10.36	10.27	0.058	0.08	ND
Co–hectorite/rinse	en	10.82	10.71	2.0	2.9	ND
Co–hectorite/rinse	BA	3.30	4.29	50	71	512(m)
Co–hectorite/rinse	PA	3.31	4.32	49	72	512(m)
Co–hectorite/rinse	Blank—dw	5.51	7.17	2.0	2.9	ND
Co–hectorite/wash	NH_3	10.36	10.02	0.048	0.08	ND
Co–hectorite/wash	en	10.82	10.71	2.1	3.3	ND
Co–hectorite/wash	BA	3.30	5.17	49	76	512(m)
Co–hectorite/wash	PA	3.31	3.84	49	77	512(m-w)
Co–hectorite/wash	Blank—dw	5.51	6.76	1.10	1.7	ND

Table 9. Physical data from equilibrium solutions remaining after treatment of Ni–hectorite clays with organic "ligand" solutions at various concentrations

Organic added	Organic/Ni ratio	Initial solution pH	Final solution pH	Ni released from clay (meq/100 g)	Per cent Ni released	Peaks resolved from visible spectrum (nm)
NH_3	3:1	9.98	9.44	0.014	0.02	ND
NH_3	1:5	9.20	7.08	0.18	0.32	ND
NH_3	1:50	6.68	6.75	0.43	0.76	ND
BA	1.4:1	3.66	4.68	14	25	394(m)
BA	1:7	4.02	6.56	3.8	6.6	393(vw)
BA	1:70	4.70	6.78	1.36	2.4	ND

Clay—Ni–hectorite/wash.

Table 10. Physical characteristics of Ni–hectorite clay samples after treatment with ammonia solutions at various concentrations

Organic added	Organic/Ni ratio	Colour of solid product	d(001) (Å)	FWHM (Å)	Peaks resolved from diffuse reflectance spectrum (nm)	
NH_3	3:1	Light green	13.8	5.6	392(m)	666(vw)
NH_3	1:5	Light green	16.0	3.3	393(m)	664(vw)
NH_3	1:50	Light green	15.8	3.1	392(m)	

Clay—Ni–hectorite/wash.

$CuCl_2$ (10 cm^3, 6.0 mM). Blank experiments with distilled water were also carried out. The suspensions were stirred for 3 days, and separated by ultracentrifugation as described above. Results from the physical investigation of the clay specimens and supernatant liquids are given in Table 13. In the case of copper(II)-treated clay a value of d(001) 13.0 Å (FWHM 1.5 Å) was obtained. The mauve–pink solid showed diffuse reflectance peaks at 558, 465 and 374 nm. The spectrum of the supernatant liquid gave maxima at 374 and 558 nm.

(C) *Microscopic effects*

If the environmental effects of cobalt(II) and nickel(II) were considered, it is likely that the con-

Table 11. Physical data from equilibrium solutions remaining after treatment of Co–hectorite clays with organic "ligand" solutions at various concentrations

Organic added	Organic/Co ratio	Initial solution pH	Final solution pH	Co released from clay (meq/100 g)	Per cent Co released	Peaks resolved from visible spectrum (nm)
en	1.25:1	10.47	7.23	0.36	0.56	ND
en	1:8	9.91	7.15	1.15	1.8	ND
en	1:80	9.17	7.07	0.93	1.5	ND
BA	1.25:1	3.51	4.81	18	28	466(w) 513(m)
BA	1:8	3.98	6.38	3.7	5.8	462(vw) 511(w)
BA	1:80	4.52	7.04	1.09	1.7	ND

Clay—Co–hectorite/wash.

Table 12. Physical characteristics of Co–hectorite clay samples after treatment with organic "ligand" solutions at various concentrations

Organic added	Organic/Co ratio	Colour of solid product	d(001) (Å)	FWHM (Å)	Peaks resolved from diffuse reflectance spectrum (nm)
en	1.25:1	Dark pink	15.1	4.0	348(m) 468(vw) 513(m-s) 557 (vw)
en	1:8	Light pink	15.1	3.3	347(vw) 511(m)
en	1:80	Light pink	15.0	3.4	462(w) 516(m)
BA	1.25:1	Very light pink	15.4	3.1	520(m-w)
BA	1:8	Light pink	15.1	3.0	462(vw) 517(m)
BA	1:80	Light pink	15.0	3.3	519(m)

Clay—Co–hectorite/wash.

Table 13. Nickel (copper) content and pH values of equilibrium solutions remaining after contacting $[Ni(en)_3]^{2+}$–hectorite with a number of inorganic salt solutions

Cation added	M^{n+}/Ni ratio	Ni in final solution (mmol dm^{-3})	Per cent Ni desorbed	Initial solution pH	Final solution pH
Na	5:1	0.052	0.94	5.76	8.92
Na	1:1	0.0121	0.22	5.69	8.75
Na	1:5	0.0058	0.10	5.65	8.84
Ca	5:1	0.37	6.7	5.72	8.88
Ca	1:1	0.18	3.2	5.65	8.85
Ca	1:5	0.047	0.85	5.57	8.58
dw	—	0.0039	0.07	5.51	8.92
Cu[a]	1:1	3.7	66	4.95	7.07

[a] Cu in final solution = 0.72 mmol dm^{-3}. Per cent Cu sorbed = 88.

dw—distilled water.

centrations of the ions in contact with a clay and the surrounding groundwaters would be very low, hence the conclusions that may be drawn from the macroscopic studies above may not extrapolate to the microscopic concentration levels that pertain in practice. We therefore decided to explore the microscopic regime by carrying out some experiments using ^{60}Co.

The work involved spiking a hectorite sample with a low concentration of ^{60}Co and treating the clay with various solutions of ligands. Analysis of the equilibrium solutions for cobalt content was then carried out.

Preparation of ^{60}Co*–hectorite.* Na–hectorite (2.92 g) was added to a 1.87 ppm solution of $^{60}CoCl_2$ (265.2 cm^3, 0.0084 mmol Co^{2+}) and shaken for 3 days. The suspension was then filtered and redispersed twice in distilled water prior to ultracentrifugation. The clay was air-dried for 3 days, and ground to a fine powder prior to use in subsequent experiments. γ-Spectrometric analysis of the contacting solutions indicated a cobalt content for the clay (i.e. ^{60}Co–hectorite) of 0.35 meq 100 g^{-1}.

Influence of ligands on ^{60}Co*–hectorite.* Portions of ^{60}Co–hectorite (0.204 g, 0.35 μmol Co^{2+}) were added separately to solutions (10.2 cm^3) of ammonia (0.44, 0.11 and 0.008 mM giving NH_3/Co ratios of 12.5 : 1, 3 : 1 and 1 : 5) and of butanoic acid (0.44, 0.044 and 0.0044 mM giving BA/Co ratios of 12.5 : 1, 1.25 : 1 and 1 : 8). Blank experiments in which the clay (0.204 g) was contacted with demineralized water were also carried out. All suspensions were stirred for 8 days and then ultracentrifuged, the solution phase being analysed for cobalt by γ-spectrometry. In the case of the 0.44 mM ammonia solution, ultacentrifugation did not remove all suspended material, hence the suspension was filtered through a 0.22 μ filter, all surfaces being subsequently washed with aqueous $CoCl_2$ to remove adhered ^{60}Co. The resulting clear solution was then analysed for radiocobalt. Relevant data are summarized in Table 14.

Physical measurements. X-ray diffraction (XRD) data were obtained with a Philips X-ray diffractometer using Co-K_α radiation with an iron filter. Traces were recorded at 1° 2θ min^{-1} in the range 1–4 $\times 10^3$ counts s^{-1} and could be observed from 3° 2θ upwards. UV–vis spectra were recorded, using a diffuse reflectance attachment for solids, on a Pye–Unicam SP 800 B spectrophotometer (300–800 nm). IR spectra were recorded with a Perkin–Elmer 599 B instrument; discs were pressed from 0.5 mg clay with 170 mg KBr. Some specimens were examined on a JEOL PE-IX type ESR spectrometer.

Table 14. Cobalt released from ^{60}Co–hectorite by solutions of organic compounds

Organic added	Organic/Co ratio	Co in final solution (μmol dm^{-3})	Per cent Co released
NH_3	12.5 : 1	0.28	0.80
NH_3[a]	12.5 : 1	0.025	0.07
NH_3	3 : 1	0.14	0.40
NH_3	1 : 5	0.82	2.4
BA	12.5 : 1	7.0	20
BA	1.25 : 1	3.3	9.4
BA	1 : 8	0.068	<0.18
dw	—	1.5	4.3

[a] After re-analysis.
BA—butanoic acid; dw—demineralized water.

Atomic absorption measurements were made with a Perkin–Elmer Model 460 AA spectrometer. Pre-analysed AnalaR samples of nickel and cobalt chloride hexahydrates were used as standards and 0.1% CsCl was added to all solutions prior to AA analysis to suppress ionization effects.

DISCUSSION

(A) *Preliminary survey*

It has previously been demonstrated that transition metal complex exchanged clays may be generated by contacting the clay with a solution of the chosen complex.[4,7,8] Little work has been carried out on the synthesis of complexes on clays *in situ* by allowing a transition metal ion exchanged clay to contact a solution of the appropriate ligand. The latter approach is of more interest if attempts are made to evaluate the influence of ligands on the lability of sorbed metal ions; the influence of groundwater organics on the lability of clay sorbed metal ions which may be toxic or radioactive, for example. We have been interested recently in gaining more information on the nature of exchange sites on hectorite and montmorillonite for iron exchanged clays (via Mössbauer spectroscopy[9]) and for cobalt and nickel exchanged clays (via XPS[10]). Since a major objective of this work was to obtain information on the environmental role of clays with respect to cobalt on nickel which might have been released to groundwaters, we restrict our attention in this paper to Co^{2+} and Ni^{2+} exchanged hectorite.

The clay samples used in the preliminary study were not totally saturated w.r.t. Ni^{2+} or Co^{2+}, they were, however, very rigorously washed and we

believe that the concentration of sorbed ion pairs on the clay surface is small,[11] i.e. the Co^{2+} and Ni^{2+} is mostly *exchanged* at interlayer and external sites. The samples gave values of $d(001)$ typical of a clay exchanged with dipositive ions (Tables 1 and 3);[12] further, diffuse reflectance spectra (Co^{2+}: 459 and 512 nm, Ni^{2+}: 395 and 660 nm) were consistent with $[M(H_2O)_6]^{2+}$ (M = Co, Ni) as the exchanged species.[13] We suggest at this juncture that a useful parameter in the following discussion may be the FWHM of the peak relating to the basal spacing [$d(001)$] of the clay, since the presence of different complex species in the interlayers will give rise to an inhomogeneity which will be reflected in a larger FWHM.

The addition of bipy to Ni–hectorite gave a clay with a diffuse reflectance spectrum characteristic of $[Ni(bipy)_3]^{2+}$, also the increase in $d(001)$ to 18.2 Å is indicative of the presence of a large complex ion.[14,15] The complex formed on addition of en to the Co–hectorite depends on the ratios, Co/en. A 1:1 ratio generated both $[Co^{III}(en)_3]^{3+}$ and $[Co^{II}(H_2O)_6]^{2+}$ (all experiments were carried out in air) as judged from the diffuse reflectance spectra and enhanced FWHM for $d(001)$ (4.0 Å); however a nine-fold excess of the ligand gave only $[Co^{III}(en)_3]^{3+}$ as evidenced from the diffuse reflectance spectrum[16] (note also FWHM for $d(001)$ is now 3.3 Å). We found no evidence for the presence of bis or tris complexes of cobalt(II) on the clay; we note that Schoonheydt *et al.*[5] have prepared a $[Co^{II}(en)_2]^{2+}$/hectorite. A 9:1 en/Ni ratio only was used, and this produced a clay containing both $[Ni(en)_2]^{2+}$ and $[Ni(en)_3]^{2+}$. Schoonheydt *et al.*[5] were able to generate $[Ni(en)_2]^{2+}$ on the surface of a montmorillonite clay and the band observed at 465 nm for this species agrees with the one noted here (456 nm, Table 2).

Although the dimethylglyoxime treated Ni–hectorite gave a spectrum typical of that expected for the square-planar bis(dimethylglyoximato) nickel(II)[17] complex, the value of $d(001)$ at 14.3 Å (Table 1) was larger than that normally expected for the presence of square-planar complexes (12.5–13.0 Å). It is suggested that the complex may in fact not be oriented parallel to the silicate sheets.

Treatment of the clays with ammonia produced some interesting results. In the case of Ni–hectorite all three ratios of Ni/NH_3 used (Table 1) gave a final clay that was green, however, whilst in contact with the ammonia solutions the 10:1 and 25:1 specimens exhibited a blue colour which we take to be evidence for the formation of $[Ni(NH_3)_6]^{2+}$. During the drying process ammonia is lost giving partially dehydrated clays. The 3:1 ratio clay (Tables 1 and 2) gives a spectrum suggesting that some $[Ni(H_2O)_6]^{2+}$ is present, however, both the value of $d(001)$ and more particularly the large FWHM indicate that the specimen is inhomogeneous. The 10:1 and 25:1 ratio treated clays are much more homogeneous and, whilst the diffuse reflectance spectra are consistent with a "NiO_6" environment, it appears that the ligand-field strength is lower than in $[Ni(H_2O)_6]^{2+}$. Also the value of $d(001)$ is inconsistent with the presence of the hexa-aquo-ion. We suggest therefore that, on loss of ammonia, at least two coordination sites are occupied by lattice silicate oxygen atoms giving $[Ni(O_{lat})_x(H_2O)_y]^{2+}$, where $x+y=6$ and $x \geqslant 2$; O_{lat} represents a silicate oxygen. We note that Tarasevich and Sivalov[18] observed bands at 403 and 694 nm for a partially dehydrated Co–montmorillonite and invoked a similar explanation.

Herman[19] also studied partially dehydrated Ni–montmorillonite, but no bands observed in that study correspond to those determined from the diffuse reflectance spectra of ammonia treated Co–hectorite (Table 4). Indeed it is clear from our results that coordinated ammonia is retained in the dry clay. Evidence for the presence of $[Co^{III}(NH_3)_6]^{3+}$ is obtained from the diffuse reflectance spectra of the 25:1 treated clay (454 nm) (Table 4). However, bands appear at 390 and 530 nm and we believe these arise from the formation of a species such as $[(NH_3)_5Co(O_2)(NH_3)_5]^{4+}$, which is an intermediate in the oxidation of cobalt(II) by molecular oxygen.[13] Such species are characteristically red or brown (as observed here). The $d(001)$ values (Table 3) are in the range 12.7–13.5 Å, rather low for the presence of species such as $[Co(NH_3)_6]^{3+}$ in any concentration. The cobalt/ammonia–hectorite specimens are ESR silent, a fact we take to eliminate the presence of superoxo-bridged species.

(B) *Groundwater ligands* (*Tables* 5–8)

Small quantities of longer chain carboxylic acids may be present in some groundwaters and pentanoic (PA) and butanoic acids (BA) were selected as being representative. The clay samples used in this work were prepared to achieve saturation of exchange sites with Ni^{2+} (Co^{2+}) but differed in the treatment given subsequently. Thus the samples labelled "rinse" were briefly rinsed with distilled water after exchange, whereas those labelled "wash" were rigorously washed with distilled water to remove, as far as possible, the "labile" ions sorbed as ion pairs.[11]

Treatment of the clays with PA and BA (see Experimental) resulted in an increase of initial solution pH and the release of > 70% of the exchanged nickel and cobalt to solution as the hexa-aquo-ions

(Tables 6 and 8); by contrast ammonia or en at the same concentration released less than 4% of the metal ion to solution—too little to give a detectable solution spectrum. Diffuse reflectance spectra of the acid treated clays [together with values of $d(001)$] (Tables 5–8) all indicate that the $[M(H_2O)_6]^{2+}$ ions are still present, but in much reduced concentration.

Although K_a for PA and BA is approximately 10^{-5} mol dm^{-3}, and the solution concentration of protons is low, in the presence of the clay we observed enhanced ionization of the acid and the displacement of M^{2+} (M = Ni, Co) by H^+. IR studies of the treated clays reveal that some acid was sorbed onto the clay. A band at 1690 cm^{-1} [ν(CO)] is significantly shifted from 1770 cm^{-1} of the hydrogen-bonded dimer[19] and that of the monomer, 1712 cm^{-1}. Yariv *et al.*[20] have investigated the sorption of benzoic acid into montmorillonite with differing exchanged ions (Ca^{2+}, Mg^{2+}, Cu^{2+}, Al^{3+}) but ν(CO) was invariant; however, when the montmorillonite was dehydrated, ν(CO) correlated with the Lewis acidity of the exchanged ion. It was proposed that the initial interaction was with a coordinated water molecule, but that direct metal–carboxylate interaction occurred on dehydration. We believe that the acid in our case interacts with coordinated water of the unreleased hexa-aquo-ions.

Treatment of the "rinse" and "wash" clays with distilled water induces, as anticipated, a greater loss of metal ion from the "rinse" specimen (but even the loss from the rigorously washed specimens is non-zero) (Tables 6 and 8). However, when the clays were treated with 0.08 M en or ammonia no differentiation between "wash" and "rinse" is seen and *less* metal is released to solution than with distilled water, with the exception of Co–hectorite/0.08 M en (Tables 6 and 8). This suggests that some metal complex ion pairs may be more tenaciously held on the clay surface than the corresponding $[M(H_2O)_6]^{n+}$–anion pairs and that they may be present even in rigorously washed clays. It is of interest to note that Pinnavaia and co-workers[21] believe that such species are responsible for the electroactivity of clay-modified electrodes.

Physical investigation of the ammonia and en treated clays (Tables 5 and 7) gave results which could be interpreted along the lines of section (A). Thus evidence for a degree of hydration was seen for the NH_3–Ni–hectorite on drying, and good evidence for the presence of both $[Ni(en)_2]^{2+}$ and $[Ni(en)_3]^{2+}$ was obtained from diffuse reflectance and IR data of the en–Ni–hectorites. The NH_3–Co–hectorite data seem to parallel those in Table 4, thus evidence for some $[Co^{III}(NH_3)_6]^{3+}$ is available ($\sim$ 460 and 590 nm); other peaks at $\sim$ 385 and $\sim$ 525 nm can be assigned, as previously, to a peroxocobalt(III) species. Careful examination of the IR spectrum reveals a significant peak at 1400 cm^{-1} attributed[22] to NH_4^+; indeed Mortland *et al.*[23] have shown that treatment of montmorillonite saturated by mono- or divalent ions was completely converted to NH_4^+. It is clear that conversion to NH_4^+ is less than complete in our case, but the observation of some NH_4^+ means that we must also consider the possibility of the presence of complementary mixed cobalt hydroxoammine species.

Addition of en to Co–hectorite generated $[Co^{III}(en)_3]^{3+}$ and, in this case, no evidence of redox intermediates was observed.

Tables 9–12 give data for the "wash" clay, which investigate the influence of varying ligand/metal ratios. Figure 1 presents a log–log plot of the per cent Ni(Co) desorbed as a function of initial ligand concentration. The per cent desorption by PA and BA is virtually a linear function of the ligand solution concentration. The significant dip in the en/NH_3 curves is attributed to the precipitation of metal hydroxide at ligand/metal ratios insufficient to involve complex formation, but where the hydroxide ion concentration is sufficient to exceed the solubility product of the metal hydroxide. Since we are dealing essentially with the lability of surface sorbed ion pairs from the "wash" clay, it seems likely that the hydroxide formation will be at the surface. As the ligand/metal ratio increases, complex formation proceeds, indeed if the third data point were ignored on the NH_3/Ni and en/Co plots (Fig. 1), the other data points also lie on a reasonable straight line. Not surprisingly, at very low ligand/metal ratios, the quantity of metal released tends to the value of distilled water alone. However, when, with basic ligands, the ratio is in the regime

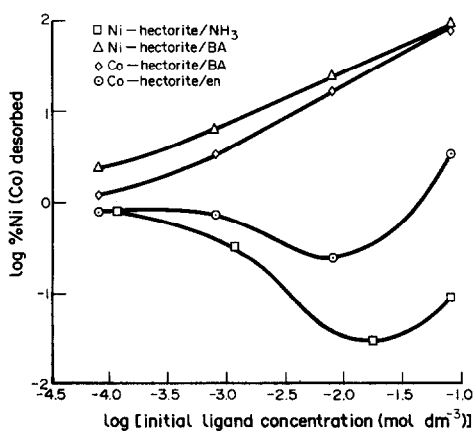

Fig. 1. Per cent Ni(Co) desorbed from Ni/Co–hectorite by various organic "ligands" at a number of initial solution concentrations.

of complex formation, in some cases *less* metal is released than from the distilled water treated as noted previously (e.g. see Co/en curve in Fig. 1). A variety of factors are involved, in the specific case of $[Co(en)_3]^{3+}$ a combination of a relatively low solvation energy for the large complex cation, together with a greater attraction of the tripositive ion, compared to $[Co(H_2O)_6]^{2+}$ for negative sites on the clay may be dominant. Others have noted the strong affinity of laponite, montmorillonite and bentonite for tripositive cobalt complexes $[Co(NH_3)_6]^{3+}$,[24] $[CoL_3]^{2+}$ (L = en, pn).[4,25,26] Indeed, even when the interlamellar ion is $[Ce(H_2O)_6]^{3+}$, Fripiat and Helsen[27] noted that $[Co(NH_3)_6]^{3+}$ was very strongly sorbed by montmorillonite.

Groundwaters will contain some inorganic cations, including possibly some transition metal ions, e.g. samples of pore water squeezed from Oxford clay contained 0.54–45 ppm amounts of iron, nickel and copper.[28] We undertook some experiments in which a $[Ni(en)_3]^{2+}$–hectorite was treated with various concentrations of NaCl, $CaCl_2$ and $CuCl_2$ (Table 13). The results are self explanatory. Not surprisingly Na^+ and Ca^{2+} have little success in mobilizing Ni^{2+} to the solution phase. By contrast Cu^{2+} is extremely effective at releasing nickel from the clay. Not only is the stability constant for the copper(II) complex greater, but the copper complex which in this instance is $[Cu(en)_2]^{2+}$ [$d(001)$ = 13.0 Å, a value typical for an intercalated square planar complex] has a greater affinity for the clay surface, an observation in agreement with the study of the thermodynamics of sorption of polyamine complexes on montmorillonite surfaces in which $[Cu(en)_2]^{2+}$ showed a greater affinity than $[Ni(en)_3]^{2+}$. Thus the relative affinities for the clay surface of two ions which form kinetically labile complexes may be strongly perturbed in the presence of some ligand species.

(C) *Microscopic effects*

The environmental concentrations of Co^{2+} and Ni^{2+} are likely to be low, hence it may not be appropriate to extrapolate from the data in sections (A) and (B) to situations in which the metal ion concentration may be in the ppb–ppm range. A sample of hectorite was spiked with ^{60}Co and treated as described in the Experimental (Table 14). The results are usefully summarized in Fig. 2. Again, as in the macroscopic studies, evidence for the stabilization of cobalt on the clay surface is seen for the basic ligand. With BA, at higher ligand/metal ratios cobalt is released to solution, but at this concentration level, a BA/Co ratio of 1 : 8 actually stabilized the cobalt relative to a simple distilled water treatment. At low absolute ligand/metal concentration ratios, a different mechanism seems operative, possibly explaining the non-linearity of this log–log plot in contrast to Fig. 1.

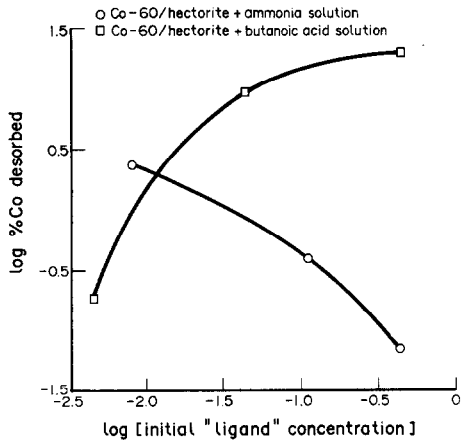

Fig. 2. Desorption of cobalt from a ^{60}Co–hectorite by organic "ligand" solutions.

The conclusion is then that groundwaters which are relatively rich in acidic ligands may labilize sorbed metal ions from clay minerals, but, by contrast, the presence of some basic ligands might actually increase the affinity of the ion for the clay surface.

Acknowledgement—N.D. thanks Aston University for a research studentship.

REFERENCES

1. L. H. Keith (Editor), *Identification and Analysis of Organic Pollutants in Water*. Ann Arbor Science Publishers Inc., Michigan (1976).
2. R. W. Grimshaw, *The Chemistry and Physics of Clays and Other Ceramic Materials*, 4th Edn. Benn, London (1971).
3. B. K. G. Theng, *The Chemistry of Clay–Organic Reactions*. Adam Hilger, London (1974).
4. G. N. Sarkar and J. L. Das Kanungo, *Ind. J. Trop. Agric.* 1983, **1**, 299.
5. R. A. Schoonheydt, F. Velghe and J. B. Utterhoeven, *Inorg. Chem.* 1979, **18**, 1842.
6. R. A. Schoonheydt and J. Pelgrims, *J. Chem. Soc., Faraday Trans.* 1983, **79**, 1169.
7. M. F. Traynor, M. M. Mortland and T. J. Pinnavia, *Clays, Clay Miner.* 1978, **26**, 318.
8. P. Peigneur, A. Maes and A. Cremers, 6th Int. Clay Conf. Proc. 1978: *Devs Sed.* 1978, **27**, 207.
9. N. Davison, W. R. McWhinnie and A. Hooper, *Inorg. Chim. Acta* 1989, **126**, 257.
10. N. Davison, W. R. McWhinnie and A. Hooper, submitted for publication.
11. P. Monsef-Mirzai and W. R. McWhinnie, *Inorg. Chim. Acta* 1983, **73**, 41.

12. A. Alietti, M. F. Brigatti, L. Poppi, V. Del Pennino, E. Mazzega and S. Valeri, *J. Coll. Int. Sci.* 1981, **84**, 301.
13. D. Nicholls, *Complexes and First Row Transition Elements*. Macmillan, London (1983).
14. R. A. Schoonheydt, *Devs Sed.* 1981, **34**, 163.
15. R. A. Palmer and T. S. Piper, *Inorg. Chem.* 1966, **5**, 864.
16. G. L. Roberts and F. H. Field, *J. Am. Chem. Soc.* 1950, **72**, 4232.
17. IUPAC (Commision on spectrochemical and other optical procedures for analysis): *Spectrophotometric Data for Colourimetric Analysis*, p. 397. Butterworths, London (1963).
18. Yu. I. Tarasevich and E. G. Sivalov, *Ukr. Khim. Zh.* 1975, **41**, 354.
19. R. C. Herman, *J. Chem. Phys.* 1940, **8**, 252.
20. S. Yariv, J. D. Russell and V. C. Farmer, *Isr. J. Chem.* 1966, **4**, 201.
21. R. D. King, D. C. Nocera and T. J. Pinnavaia, *J. Electroanal. Chem.* 1989, **239**, 43.
22. F. A. Miller and C. H. Wilkins, *Analyt. Chem.* 1952, **24**, 1253.
23. M. M. Mortland, J. J. Fripiat, J. Chaussidon and J. Utterhoeven, *J. Phys. Chem.* 1963, **67**, 248.
24. J. L. Das Kanungo, S. K. Chakravarti and S. K. Mukherjee, *J. Ind. Chem. Soc.* 1068, **45**, 685.
25. M. I. Knudson Jr and J. L. McAtee Jr, *Clays, Clay Miner.* 1973, **21**, 19.
26. J. L. Das Kanungo and G. N. Sarkar, *J. Ind. Chem. Soc.* 1984, **61**, 216.
27. J. J. Fripiat and J. Helsen, *Clays, Clay Miner.* 1966, **14**, 163.
28. N. Jeffries (A.E.A. Harwell), personal communication.

Polyhedron Vol. 9, No. 18, pp. 2285–2291, 1990
Printed in Great Britain

0277–5387/90 $3.00+.00
© 1990 Pergamon Press plc

SYNTHESIS OF NOVEL MIXED-LIGAND COMPLEXES OF LANTHANIDE IONS WITH 1,4-BIS-(1′-PHENYL-3′-METHYL-5′-PYRAZOLONE-4′)-1,4-BUTANEDIONE AND 1,10-PHENANTHROLINE AND THEIR UV, IR, ^{1}H NMR, FLUORESCENCE AND THERMAL ANALYSIS STUDIES

XIAOJING LI,* HUI WANYAN, WENJI DONG and RUDONG YANG

Department of Chemistry, Lanzhou University, Lanzhou 730000, China

(*Received* 19 *September* 1989; *accepted* 9 *May* 1990)

Abstract—The synthesis of 14 mixed-ligand solid complexes of lanthanide ions with 1,4-bis-(1′-phenyl-3′-methyl-5′-pyrazolone-4′)-1,4-butanedione (BPMPBD) and 1,10-phenanthroline (PHEN) in an alcohol–water solution is presented. The comosition of the complexes is determined as $Ln_2L_3P_2 \cdot nH_2O$ (Ln = Y, La, Pr, Sm–Lu; L = BPMPBD; P = PHEN; n = 4,5) by chemical and elemental analyses. The complexes are regarded as binuclear and characterized by IR, UV, ^{1}H NMR, fluorescence spectra, thermoanalysis and conductance methods.

1,4-Bis-(1′-phenyl-3′-methyl-5′-pyrazolone-4′)-1,4-butanedione (BPMPBD) is a 4-acyl-bis-pyrazolone in which two acylated pyrazolones are present as end groups of the diketone. The first 4-acyl-bis-pyrazolone was synthesized by Dong *et al.* in 1983[1] and later some derivatives and their complexes with lanthanide ions were reported.[2,3]

4-Acyl-bis-pyrazolones, in which there are four oxygen atoms available for complexation, are ideal chelating agents for lanthanides and actinides and are able to form mononuclear, polynuclear or heteronuclear complexes under differing conditions. These complexes are of interest because they provide the opportunity to study catalytic activity, energy transfer, electron transitions and the interaction between the metal ion and complexing agents. Some lanthanide ions when combined with 4-acyl-bis-pyrazolone exhibit excellent fluoresence[4] which provides an opportunity for studying their applications in analysis and optic materials.

In the present work the preparation and characterization of complex compounds formed by lanthanide elements (except for Ce, Sc and Pm) with BPMPBD (noted H_2L)—a tetradentate ligand and PHEN (noted P)—a bidentate ligand are reported first.

* Author to whom correspondence should be addressed.

EXPERIMENTAL

Reagents

BPMPBD (m.p. 222–222.5°C) was prepared by literature methods.[5] Found: C, 66.8; H, 5.0; N, 12.9. Calc. for BPMPBD ($C_{24}H_{21}N_4O_4$): C, 67.0; H, 5.1; N, 13.0%. Solutions of lanthanide nitrate were obtained by dissolving Ln_2O_3 (99.95%) in concentrated HNO_3 and evaporating the excess acid, followed by dilution to a certain concentration with distilled water. PHEN and other reagents were analysis grade.

Preparation of complex compounds

H_2L (0.220 g, 0.50 mmol) was dissolved in 30 cm^3 of alcohol solvent (95%) by adding an aqueous ammonia solution (2 N) and then the pH of this solution was adjusted to 5–6 with dilute HNO_3 solution. The PHEN (0.059 g, 0.33 mmol) ethanol solution and lanthanide nitrate (0.35 mmol) ethanol solution in the molar ratio $[H_2L]:[PHEN]:[Ln^{3+}] = 1.5:1:1.05$ were added successively to the H_2L ethanol solution and a precipitate appeared immediately. The precipitate was centrifugally separated after being stirred for 2 h and washed with dilute aqueous HNO_3 solution (pH = 3–4) until no Ln^{3+} and NH_4^+ could be detected in the washings.

Then the precipitate was washed with distilled water until the washings were neutral and did not contain NO_3^-. Finally the products were dried to constant weight at 40°C in a vacuum dryer after being washed 2 or 3 times with warm $CHCl_3$. The yields of the products were generally more than 75%.

Physical measurements and analyses

IR spectra, which were obtained as KBr discs and the dispersion media were free of water, were recorded with a Model FT-170SX IR spectrophotometer (U.S.A.). ^1H NMR spectra were obtained on a Model FA-80A spectrometer (U.S.A.). Fluorescence and UV spectra were recorded with a Model 850 fluorescence spectrophotometer (Japan) and a Model UV-730 spectrophotometer (China), respectively. A Model PCT-2 precision thermal analyser and Model DDS-11A conductometer were used, respectively, to determine the thermostability and conductivity of the complexes.

C, H and N analyses were performed with a Model 1106 elemental analyser (Italy). Water in the complexes was determined by thermoanalyses.

Lanthanide ions in the complexes were determined by the following method: A certain quantity of complex was decomposed by heating in a small amount of HNO_3–$HClO_4$ (1 : 1) solution and the excess acid was evaporated. This was diluted with distilled water and finally the Ln^{3+} was titrated with a standard solution of EDTA in a hexamethylenamine buffer solution.

RESULTS AND DISCUSSION

Composition and properties of the complexes

Table 1 contains the elemental analyses of the complexes. It is known from Table 1 that the composition of the complexes is $Ln_2L_3P_2 \cdot nH_2O$ ($n = 4$, 5) and the complexes are neutral, which also has been proved by their molar conductivity (3–8 Ω^{-1} cm^2 mol^{-1}) in DMSO solvent.[6]

All the complexes are insoluble in water, slightly soluble in ethanol, methanol, chloroform and benzene, and soluble in DMSO and DMF solvents. The complexes absorb moisture when they are exposed to the air.

IR spectra

All 14 complexes have similar IR spectra, which indicates that these complexes have similar structures.

The main changes found after complexing are:

(1) The C=O stretching frequency shifts from 1554 cm^{-1} in BPMPBD by about 22 cm^{-1} to a lower frequency (at 1532 cm^{-1}) in the complexes, and the strength of the vibration decreases, which is attributed to the interaction between the Ln^{3+} and carbonyl group in BPMPBD.
(2) The weak and broad band at 2600–3000 cm^{-1} in the IR spectrum of the free ligand BPMPBD, due to the intramolecular hydrogen bond formed between the carbonyl and hydroxyl group,

Table 1. Elemental analyses of the complexes

Compound	C% Calc.	C% Found	N% Calc.	N% Found	H% Calc.	H% Found	Ln% Calc.	Ln% Found
$Y_2L_3P_2 \cdot 4H_2O$	60.8	60.7	11.8	11.8	4.5	4.3	9.4	9.3
$La_2L_3P_2 \cdot 5H_2O$	57.3	57.2	11.1	10.9	4.3	4.3	13.8	13.9
$Pr_2L_3P_2 \cdot 4H_2O$	57.7	57.5	11.2	11.0	4.2	4.1	14.1	14.0
$Nd_2L_3P_2 \cdot 4H_2O$	57.5	57.4	11.2	11.3	4.2	4.0	14.4	14.3
$Sm_2L_3P_2 \cdot 4H_2O$	57.1	57.3	11.1	10.9	4.2	4.0	14.9	14.7
$Eu_2L_3P_2 \cdot 4H_2O$	57.0	56.9	11.1	11.0	4.2	4.1	15.0	15.0
$Gd_2L_3P_2 \cdot 4H_2O$	56.7	56.5	11.0	11.0	4.2	4.0	15.5	15.3
$Tb_2L_3P_2 \cdot 4H_2O$	56.6	56.7	11.0	11.1	4.2	4.1	15.6	15.6
$Dy_2L_3P_2 \cdot 4H_2O$	56.4	56.2	11.0	10.7	4.1	4.0	15.9	15.9
$Ho_2L_3P_2 \cdot 4H_2O$	56.3	56.2	10.9	10.9	4.1	4.1	16.1	16.0
$Er_2L_3P_2 \cdot 4H_2O$	56.2	56.0	10.9	10.9	4.1	4.0	16.3	16.1
$Tm_2L_3P_2 \cdot 4H_2O$	56.1	56.2	10.9	10.7	4.1	4.0	16.4	16.3
$Yb_2L_3P_2 \cdot 4H_2O$	55.9	55.9	10.9	10.7	4.1	4.0	16.8	16.6
$Lu_2L_3P_2 \cdot 4H_2O$	55.8	55.7	10.8	10.9	4.1	4.0	16.9	16.9

L = BPMPBD ($C_{24}H_{20}N_4O_4$-); P = PHEN ($C_{12}H_8N_2$).

disappears after chelation. The reason is that the intramolecular hydrogen bond is broken after chelation with lanthanide ions.

(3) The out-of-plane bending frequencies (δ_{C-H}) shift from 855 and 737 cm^{-1} in PHEN to 845 and 731 cm^{-1} in the complexes and the 1642 cm^{-1} band due to the stretching vibration of C=N of free PHEN is absent in these complexes, whereas a new band is observed around 1619 cm^{-1}, which is attributed to the fact that $\nu_{C=N}$ of chelated PHEN is overlapping with $\nu_{C=O}$ of BPMPBD at 1618 cm^{-1}, and increasing with the vibration strength. All these points can be taken as evidence of PHEN being bonded to lanthanide ions.

(4) The absorption peaks of ν_{Ln-O} and ν_{Ln-N} in the far-IR spectra appear, respectively, at about 415–436 cm^{-1} and 270–316 cm^{-1} which is similar to all other lanthanide complexes. This conforms to the result reported in the literature.[7]

(5) The presence of the broad absorption peak at 3450 cm^{-1} indicates the existence of water molecules in the complexes.

From the changes in the IR spectra, the analysis of the complex composition and the electroneutrality of the complexes above, it can be inferred that the complexes have a binuclear structure in which each of two Ln^{3+} ions combines with two complexing nitrogen atoms in each PHEN, and three BPMPBDs as tetradental ligands chelate two Ln^{3+} ions in two ways. One way is that the three BPMPBs bridge two Ln^{3+} ions side by side by means of the enolic form [see Fig. 1(a)]. The other method involves one of the three BPMPBDs bridging two Ln^{3+} ions and the other two chelating, respectively, one of the two Ln^{3+} ions [see Fig. 1(b)]. Which one of the two structures above is correct remains to be proved by studying the structure of the single crystal which is being grown in our laboratory.

UV spectra

The important UV absorption bands of the ligands and the complexes in CH_3OH solvent are listed in Table 2. No absorptions were observed in the visible for any of the compounds. It is clear that the spectra of the complexes are similar in character to that of ligands. The absorption maxima of the ligands remain either unchanged or suffer slight shifts in the complexes. This is because the spectra of the complexes are attributed mainly to that of the ligands and it appears reasonable to assign the absorption bands to π–π^* transitions.

Two weak absorption peaks of PHEN at 310 and 323 nm that are due to the n–π^* transition do not appear in the spectra of the complexes. The reason is that the solubility of the complexes in CH_3OH is so low that we cannot observe the n–π^* transition in the spectra.

^{1}H *NMR*

Table 3 contains the ^{1}H NMR spectral data for BPMPBD, PHEN and some complexes in DMSO.

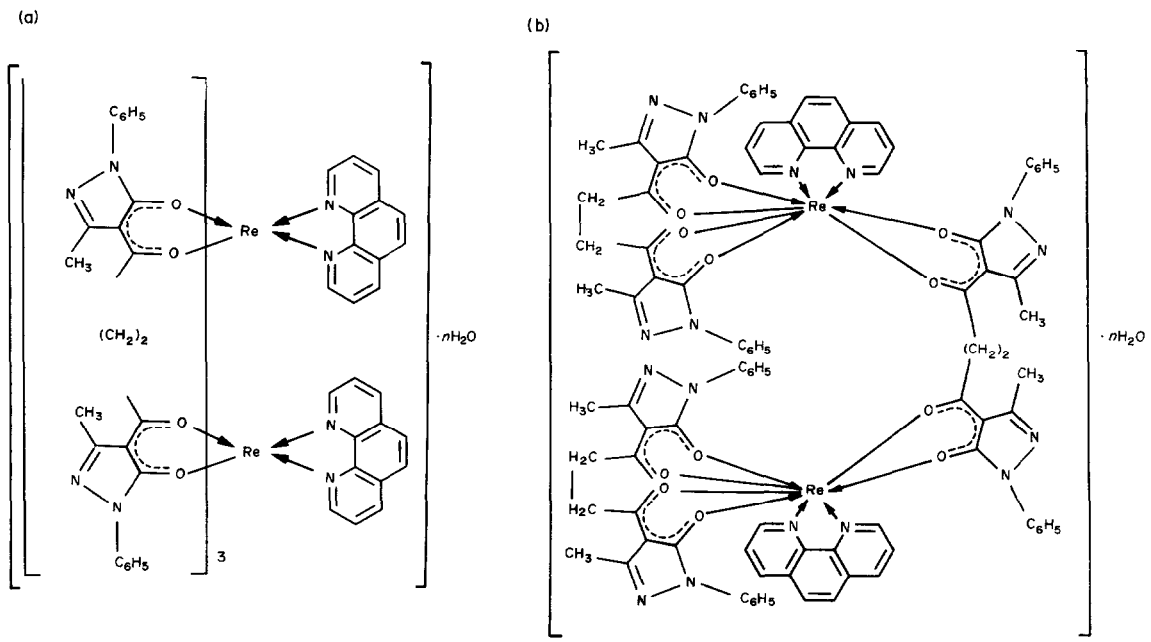

Fig. 1. The plausible structures of the complexes.

Table 2. UV spectral data for ligands and complexes

Compound	$\nu_{1(max)}$ (nm)	$\nu_{2(max)}$ (nm)	$\nu_{3(max)}$ (nm)
H_2L	218	231	262
PHEN	202	231	265
$Y_2L_3P_2$	220	231	266
$La_2L_3P_2$	222	230	266
$Pr_2L_3P_2$	223	231	265
$Nd_2L_3P_2$	221	233	265
$Sm_2L_3P_2$	221	232	264
$Eu_2L_3P_2$	220	231	266
$Gd_2L_3P_2$	222	228	265
$Tb_2L_3P_2$	221	229	264
$Dy_2L_3P_2$	221	230	264
$Ho_2L_3P_2$	222	231	265
$Er_2L_3P_2$	223	231	265
$Tm_2L_3P_2$	220	231	265
$Yb_2L_3P_2$	222	232	265
$Lu_2L_3P_2$	221	233	264

The methyl proton signal of the free ligand BPMPBD is observed as a singlet at 2.56 ppm and the methylidyne proton signal as a singlet at 3.23 ppm, while the benzene ring proton signals are observed as a multiplet at around 7.35–7.88 ppm. In our experiment, the hydroxyl proton signal of the enolic form of the BPMPBD ligand is not observed. Similar phenomena were observed in the literature.[5]

The proton signals of the free neutral ligand PHEN are found at 7.98, 8.12, 8.80 and 9.19 ppm.

In the complexes, the ^{1}H NMR spectra contain greater shifts and changes in comparison with the ^{1}H NMR of the free ligands. Meanwhile, the ^{1}H NMR spectra of the lanthanide ion complexes are obviously different due to the different number of unpaired $4f$ electrons and the different magnetism of lanthanide ions. The lanthanum ($4f^0$) complex exhibits a sharp ^{1}H NMR spectrum in which all protons suffer upfield shifts. The methyl and methylidyne signals have shifted from 2.56 to 2.05 ppm and from 3.23 to 2.75 ppm, respectively, while the phenyl multiplet has now shifted to 6.95–7.75 ppm. The proton signal of PHEN in the complex which has also shifted upfield appears at 7.82, 7.93, 8.45 and 9.10 ppm. This indicates that the deshielding effect of the electron atmosphere in the phenanthrene ring decreases after complexation of the nitrogen atoms in PHEN with the La^{3+} ion. The hydrogen proton signal of the waters in the complex is at 3.25 ppm, which should disappear when H_2O is exchanged by D_2O. In the samarium ($4f^5$) complex the proton signals become much weaker and broader than those in the lanthanum complex. The methyl and methylidyne signals have shifted to

Table 3. ^{1}H NMR spectral data[a] for the ligands and complexes (chemical shifts in ppm relative to TMS)

Compound	Methyl protons	Integrated intensity	Methylidyne protons	Integrated intensity	Benzene protons	Integrated intensity	PHEN protons	Integrated intensity	Hydroxyl protons	Integrated intensity
BPMPBD	2.56 (sh s)	6H	3.23 (sh m)	4H	7.35–7.88 (br m)	10H	—		—	
PHEN	—		—		—		7.98; 8.12; 8.80; 9.12 (m)	8H	—	
$La_2L_3P_2 \cdot 5H_2O$	2.05 (sh s) 2.18 (br s)	12H 6H	2.75 (sh m)	12H	6.95–7.75 (br m)	30H	7.82; 7.93; 8.45; 9.10 (m)	16H	3.25 (sh s)	10H
$Sm_2L_3P_2 \cdot 4H_2O$	2.32 (sh s)	18H	2.75 (sh m)	12H	7.20 (br m)	30H	8.70 (br m)	16H	3.28 (sh s)	8H
$Lu_2L_3P_2 \cdot 4H_2O$	2.13 (sh s) 2.30 (br s)	12H 6H	2.73 (br m)	12H	7.15–7.89 (br m)	30H	7.98; 8.07; 8.55; 9.11 (m)	16H	3.24 (sh s)	8H

sh, sharp; br, broad; s, singlet; m, multiplet.
[a] The ^{1}H NMR data were obtained at 80 MHz frequency.

2.32 and 2.75 ppm. The proton signals of phenyl and the phenanthrene ring become a broad multiplet appearing at 7.2–8.7 ppm. With the gadolinium ($4f^7$) complex no signal was observed at all. This may be due to a combination of large shifts and extensive broadening of the signals,[8] since the gadolinium ion has the maximum number of unpaired electrons and is therefore strongly paramagnetic. Hence this change from sharp and strong to broad and weak proton signals for the lanthanum, samarium and gadolinium ion complexes is obviously the result of an increase in paramagnetism in going from the lanthanum, samarium to gadolinium ions. In addition, the integrated intensity of the methyl protons is in the ratio 2 : 1; the ratio shows that the structure of complexes have non-equivalent ligands, with possibly structure type (b) (see Fig. 1).

Fluorescence

The terbium and samarium complexes exhibited excellent green and orange fluorescence, respectively, when the solid lanthanide complex samples were irradiated with UV light ($\lambda = 254$ nm). Fluorescence was not observed in the rest of the lanthanide complexes. The fluorescence spectral data of the ligands and complexes, measured in DMSO solvent, are displayed in Table 4. It can be seen from Table 4 that the terbium complex shows a high emission intensity when the samarium complex exhibits a weak emission intensity in DMSO, although it shows excellent fluorescence in the solid state. This may be due to the solvent effect. In addition to the terbium and samarium complexes, the dysprosium complex has a line emission that indicates the lowest triplet state energy level of the complexes lies above the resonance energy level of the lanthanide ions and efficient energy transfer from the triplet state. The neodymium and gadolinium complexes exhibit band emission attributable to L*–L luminescence. The praseodymium, europium, holmium, erbium and ytterbium complexes do not fluoresce or fluoresce very weakly due to internal quenching through strong coupling of the ions with the crystal forces.[9,10]

Thermal analysis

The thermal analysis for BPMPBD [see Fig. 2(a)] shows that the compound initially melts at 231°C and then begins to decompose from 260 to 565°C when it is heated in air. TG and DTA measurements of PHEN·H_2O indicate loss of water at 104°C, melting at 123°C and explosive decomposition from 217 to 318°C [see Fig. 2(b)].

Since all 14 complexes exhibit similar thermal analysis diagrams due to their similar structures, here we discuss thermostability of $Tb_2L_3P_2 \cdot 4H_2O$

Table 4. The fluorescence spectral data for the ligands and complexes in DMSO (1×10^{-3} M)

Compound	Ex	Em	Emission intensity	Transfer
H_2L	356	438	0.006	
PHEN	369	416	0.008	
$Pr_2L_3P_2$	359	601	0.007	$^3P_0$–$^3H_6$
$Nd_2L_3P_2$	371	427	0.002	Fluorescence of ligands
$Sm_2L_3P_2$	342	647	0.013	$^4G_{5/2}$–$^6H_{9/2}$
$Gd_2L_3P_2$	368	425	0.009	Fluorescence of ligands
$Tb_2L_3P_2$	346	490	0.316	$^5D_4$–$^7F_6$
	346	545	2.912	$^5D_4$–$^7F_5$
	346	584	0.347	$^5D_4$–$^7F_4$
	346	621	0.254	$^5D_4$–$^7F_3$
$Dy_2L_3P_2$	350	575	0.014	$^4F_{9/2}$–$^6H_{13/2}$
$Tm_2L_3P_2$	350	480	0.004	$^1D_2$–$^3H_4$
$Y_2L_3P_2$	—	—	—	Fluoresces very weakly or no fluorescence
$La_2L_3P_2$	—	—	—	
$Eu_2L_3P_2$	—	—	—	
$Ho_2L_3P_2$	—	—	—	
$Er_2L_3P_2$	—	—	—	
$Yb_2L_3P_2$	—	—	—	
$Lu_2L_3P_2$	—	—	—	

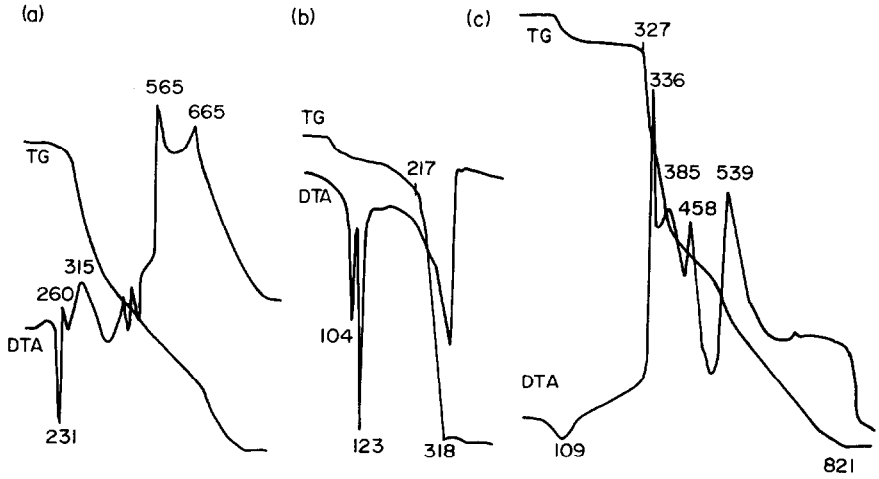

Fig. 2. The thermostability of the ligands and complexes: (a) H_2L(BPMPBD); (b) PHEN; (c) $Tb_2L_3P_2 \cdot 4H_2O$.

as an example [see Fig. 2(c)]. The compound loses water molecules at 109°C with a weight loss of about 3.41% (calc. 3.54%). These types of complexes have no melting point, so after losing water molecules the compound begins to decompose in the temperature range 327–821°C, in which four exothermic peaks appear successively on the DTA curve and obvious weight loss occurs on the TG curve. The total weight loss of the compound when heated was found to be 81.12%, which is nearly equal to the calculated 81.63% (considering the product of decomposition for $Tb_2L_3P_2 \cdot 4H_2O$ to be Tb_4O_7).

It is found from the discussion above that the complex is more thermostable than either BPMPBD and PHEN. In addition, the initial temperature of decomposition and the thermostability of the 14 complexes generally increase with decreasing ionic radii of the lanthanide ions (see Table 5). The "tetrad effect" phenomenon is found from the diagram of the relationship between the atomic numbers of lanthanide with the temperatures of the third

Table 5. The values of the thermal peaks of the complexes (°C)

Complexes	Y	La	Pr	Nd	Sm	Eu	Gd	Tb	Dy	Ho	Er	Tm	Yb	Lu
T_{abs}	102	104	126	113	108	104	106	109	110	108	107	105	107	120
$T_{exo(1)}$	343	312	317	320	329	332	336	336	345	342	346	343	345	349
$T_{exo(2)}$	382	374	378	386	380	383	384	385	396	401	392	364	399	400
$T_{exo(3)}$	461	449	462	454	459	452	447	458	463	457	455	455	465	462
$T_{exo(4)}$	546	524	540	536	540	541	535	539	550	555	546	529	551	536

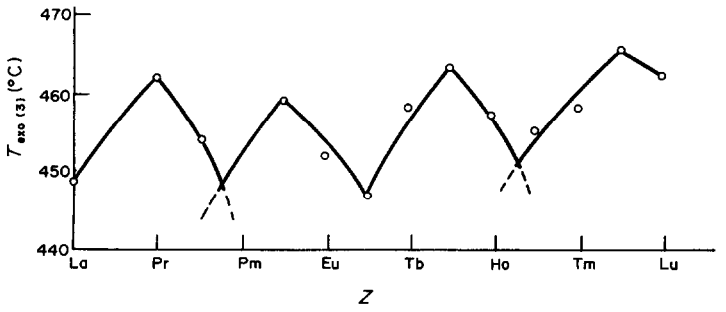

Fig. 3. The relationship of Z–$T_{exo(3)}$.

exothermal peak of each complex (see Fig. 3). This result is similar to that found in the literature.[11]

Acknowledgement—This research was sponsored by the fund of the Chinese Academy of Sciences.

REFERENCES

1. X. C. Dong, F. C. Liu and Y. L. Zhao, *Acta Chim Sinica* 1983, **41**, 848.
2. R. D. Yang, Y. H. Wan, Y. Yang and J. P. Wang, *Rare Earth* 1986, **5**, 1.
3. R. D. Yang, L. Q. Yang, J. M. Liu and W. J. Dong, *Book of Abstracts* XXV ICCC., Nanjing, China, July (1987), C3, p. 587.
4. Y. H. Wan, W. J. Dong, X. J. Li, C. Z. Feng and R. D. Yang, *Rare Earth* 1989, **2**, 1.
5. L. Q. Yang and R. D. Yang, *J. Lanzhou Univ.* 1988, **24**, 134.
6. W. J. Geary, *Coord. Chem. Rev.* 1971, **7**, 81.
7. K. Iftikhar, M. Sayeed and N. Ahmad, *Bull. Chem. Soc. Jpn* 1982, **55**, 2258.
8. E. C. Okafor, *J. Inorg. Nucl. Chem.* 1980, **42**, 1155.
9. T. Moeller, *The Chemistry of the Lanthanides*. Pergamon Press, Oxford (1973).
10. G. Blasse, *Handbook on the Physics and Chemistry of Rare Earths*, Vol. 4, p. 237. North-Holland, Amsterdam (1979).
11. X. J. Li, W. J. P. Dong, Y. H. Wan, W. G. Yang and R. D. Yang, *Inorg. Chem.*, in press.

Polyhedron Vol. 9, No. 18, pp. 2293–2298, 1990
Printed in Great Britain

0277–5387/90 $3.00+.00
© 1990 Pergamon Press plc

THE USE OF SILYLETHERS AND SILYLTHIOETHERS IN SYNTHESES OF OXOHALIDE AND THIOHALIDE COMPOUNDS OF MOLYBDENUM AND TUNGSTEN

VERNON C. GIBSON,* TERENCE P. KEE and ALAN SHAW

Department of Chemistry, University Science Laboratories, South Road, Durham DH1 3LE, U.K.

(*Received* 8 *January* 1990; *accepted* 11 *May* 1990)

Abstract—Convenient procedures for the preparation of molybdenum and tungsten oxo- and thiohalides are described which exploit reactions between transition metal halides and bis(silyl)ether and -thioether reagents, according to the general equation:

$$MCl_x + (Me_3Si)_2Y\ (Y = O,S) \longrightarrow M(Y)Cl_{x-2} + 2\,Me_3SiCl.$$

$W(O)Cl_4$ (**1**) and $Mo(O)Cl_3$ (**5**) are formed in high yield by room temperature treatment of WCl_6 and $MoCl_5$ with $(Me_3Si)_2O$ in CH_2Cl_2 solvent. $Mo(O)_2Cl_2$ (**6**) may be obtained from $Mo(O)Cl_4$ by an analogous room temperature procedure; efficient generation of $W(O)_2Cl_2$ (**2**) requires warming of $W(O)Cl_4$ with $(Me_3Si)_2O$ at 80°C in octane. In acetonitrile solvent, $W(O)Cl_4$ reacts with one equivalent of $(Me_3Si)_2O$ to give $W(O)_2Cl_2(CH_3CN)_2$ (**3**) in 70% yield. Treatment of $W(O)Cl_4$ with two equivalents of $(Me_3Si)_2O$ in CH_2Cl_2 leads to blue crystalline $W(O)_2Cl(OSiMe_3)$ (**4**), which is stable to elimination of Me_3SiCl to 100°C. $W(S)Cl_4$ (**7**), $W(S)_2Cl_2$ (**8**) and $Mo(S)Cl_3$ (**9**) are obtained by low temperature treatment of WCl_6, $W(S)Cl_4$ and $MoCl_5$, respectively, with one equivalent of $(Me_3Si)_2S$ in CH_2Cl_2 solvent. The mixed oxothiohalide compounds $W(O)(S)Cl_2$ (**10**) and $Mo(O)(S)Cl_2$ (**11**) may be isolated in good yield through the reaction of $W(O)Cl_4$ or $Mo(O)Cl_4$ with $(Me_3Si)_2S$ in CH_2Cl_2 at low temperature.

There is considerable interest in the chemistry of high oxidation state molybdenum and tungsten compounds containing oxo or sulphido ligands due to their importance in industrial and biological catalysis. The oxo- and thiohalides represent convenient starting materials for the study of these systems, and the oxo derivatives also allow access to analogous imido compounds by "NR" for "O" exchange. Although a variety of different routes to these materials has been developed over many years,[1] with few exceptions,[2] the vast majority of molybdenum and tungsten oxohalide syntheses require elevated temperatures, many involving hot tube/furnace procedures and further purification of the products (e.g. by sublimation) is often necessary. Thiohalide materials have generally proved more accessible under mild conditions.[1d,e,3]

In this paper, we describe straightforward procedures for the synthesis of oxo- and thiohalide compounds of molybdenum and tungsten which exploit reactions of transition metal halides with bis(silyl)ethers and bis(silyl)thioethers, respectively, according to the general equation (1):

$$MCl_x + (Me_3Si)_2Y\ (Y = O,S) \longrightarrow M(Y)Cl_{x-2} + 2Me_3SiCl. \quad (1)$$

The reactions are generally rapid, proceed at low temperature and give good yields of high purity materials. Base-free compounds may be obtained from either hydrocarbon or chlorocarbon solvents; the majority of these materials are insoluble in common solvents and therefore are not readily amenable to purification by solution procedures. However, since many metal halides and the $(Me_3Si)_2E$ (E = O,S) reagents may be readily purified by sublimation or distillation, materials of high purity may be obtained (provided moisture and oxygen are excluded during the preparations) and

* Author to whom correspondence should be addressed.

significantly, thiohalides free of oxide contaminants are accessible. Base adducts, which are formed in certain cases when the reaction is carried out in acetonitrile, can be readily purified by crystallization from the reaction solvent. This low temperature methodology is also suited to the synthesis of mixed oxythiohalide compounds such as $W(O)(S)Cl_2$ and $Mo(O)(S)Cl_2$ which have not proved conveniently accessible; indeed, to our knowledge, $Mo(O)(S)Cl_2$ has not been reported previously. Optimization of reaction conditions have led to some minor modifications of the procedures outlined in our earlier reports[4] of this synthetic approach.

RESULTS AND DISCUSSION

The treatment of WCl_6 with an equimolar amount of $(Me_3Si)_2O$ in CH_2Cl_2 at room temperature leads to deposition of $W(O)Cl_4$ (**1**) in the form of red crystals. If the reaction is carried out in hydrocarbon solvent, e.g. octane, the product is of similar purity but is obtained in the form of an amorphous orange powder. In contrast with other procedures, this method requires no further purification of the $W(O)Cl_4$ product once formed. $W(O)_2Cl_2$ (**2**) is best prepared by warming $W(O)Cl_4$ with an equimolar amount of $(Me_3Si)_2O$ in octane at 80°C for 4 h. The product is deposited as a finely-divided pale yellow amorphous powder. The solid gradually darkens if left to stand in the reaction mixture for a prolonged period, and its IR spectrum then shows contamination with siloxide groups, which suggests that a back reaction may occur with the liberated Me_3SiCl. Nevertheless, good quality $W(O)_2Cl_2$ may be obtained if the reaction is stopped as soon as the $W(O)Cl_4$ has been consumed (the end-point of the reaction can be judged when the orange colouration due to $W(O)Cl_4$ is discharged from the octane solution—typically *ca* 4 h). It did not prove possible to prepare **2** by treating **1** or WCl_6 with one or two equivalents, respectively, of $(Me_3Si)_2O$ in dichloromethane solvent at room temperature. Under these conditions, an amorphous off-white solid is obtained which gives strong bands at 1250 and 1000 cm^{-1} in the IR spectrum attributable to metal–siloxide species.[5] An additional broad absorption in the range 800–850 cm^{-1} is indicative of bridging oxo groups suggesting a heavily bridged oxo–siloxide lattice which we have found to be insoluble in all common solvents. The acetonitrile adduct $W(O)_2Cl_2(CH_3CN)_2$ (**3**), obtained previously by prolonged heating of **2** at 90°C in CH_3CN[6] (in a sealed tube), may be prepared in 70% yield by room temperature treatment of **1** with $(Me_3Si)_2O$ in acetonitrile solvent [eq. (2)]. Compound **1** is consumed to give a pale blue solution which upon concentration and cooling affords colourless crystals of **3**. It is not possible to replace all of the chloride groups on tungsten using $(Me_3Si)_2O$ since treatment of **1** with two equivalents of $(Me_3Si)_2O$ in CH_2Cl_2 gives $W(O)_2Cl(OSiMe_3)$ (**4**) [eq. (3)], which may be isolated as a pale blue microcrystalline solid in 70% yield.

$$\underset{(\mathbf{1})}{W(O)Cl_4} + (Me_3Si)_2O \xrightarrow{CH_3CN(S)} \underset{(\mathbf{3})}{W(O)_2Cl_2(CH_3CN)_2} + 2Me_3SiCl \quad (2)$$

$$\underset{(\mathbf{1})}{W(O)Cl_4} + 2(Me_3Si)_2O \xrightarrow{CH_2Cl_2} \underset{(\mathbf{4})}{W(O)_2Cl(OSiMe_3)} + 3Me_3SiCl. \quad (3)$$

Sharp absorptions at 1255 and 1000 cm^{-1}, and a broad absorption over the range 700–900 cm^{-1} in the IR spectrum are indicative of the siloxide ligand and bridging oxo groups, respectively. The methyls of the siloxide groups are also also seen as a singlet resonance at δ 0.42 ppm in the ^1H NMR spectrum ($CDCl_3$). Compound **4** does not eliminate Me_3SiCl to give WO_3 even upon prolonged warming at 100°C.

$MoCl_5$ reacts smoothly with an equimolar amount of $(Me_3Si)_2O$ to give a dark brown solid in high yield whose IR spectrum displays the terminal Mo=O stretch at 1007 cm^{-1}, characteristic of $Mo(O)Cl_3$ (**5**).[1c] $Mo(O)_2Cl_2$ (**6**) may be isolated in similar yield via the reaction of $Mo(O)Cl_4$ with $(Me_3Si)_2O$ under essentially analogous conditions; these are notably more mild than for the preparation of the tungsten analogue, **2**.

The reactions of metal halides with hexamethyldisilthiane, $(Me_3Si)_2S$, are generally exothermic and are therefore carried out at low temperature. Dropwise addition of a chilled (−30°C) dichloromethane solution of $(Me_3Si)_2S$ to a suspension of WCl_6 in CH_2Cl_2 at −78°C gives an immediate reaction which results in a red solution of $W(S)Cl_4$ (**7**). Two extractions with CH_2Cl_2 and a low temperature crystallization allows the thiohalide to be isolated in 80% yield. $W(S)_2Cl_2$ (**8**) may be isolated in similar yield as an insoluble blue–black amorphous solid upon treatment of $W(S)Cl_4$ with a molar equivalent of $(Me_3Si)_2S$. The synthesis of **8** has been reported on two previous occasions.[3b,7] However, in both cases full characterizing data were not given. An IR spectrum of **8** produced via the route described here reveals a strong terminal W=S

stretch at 538 cm^{-1} and bands at 365, 321 and 287 cm^{-1} due to ν(W—Cl). The mass spectrum also gives an envelope at m/z 318 due to the parent ion, with daughter fragments at m/z 286, 251 and 216 which correspond to $[M-S]^+$, $[M-S-Cl]^+$ and $[M-S-2Cl]^+$, respectively. $Mo(S)Cl_3$ (**9**) may be prepared by the reaction of $MoCl_5$ with $(Me_3Si)_2S$ in CH_2Cl_2 at −78°C. The data for **9** is found to be similar in all respects to those previously reported for $Mo(S)Cl_3$.[3b]

The relatively mild conditions under which $(Me_3Si)_2Y$ (Y = O,S) reagents react with molybdenum and tungsten halides suggested that it might prove possible to prepare mixed oxothiohalide materials such as $W(O)(S)Cl_2$ and $Mo(O)(S)Cl_2$. The molybdenum compound represents a potentially useful starting material for investigations of mixed oxo/thio molybdenum compounds of relevance to bio-inorganic systems. Although there have been reports of $W(O)(S)Cl_2$,[3b,8] routes to it are not entirely satisfactory and there is a paucity of characterizing data. To our knowledge, $Mo(O)(S)Cl_2$ is hitherto unknown. It was envisaged that $W(O)(S)Cl_2$ would prove more readily accessible by treatment of $W(S)Cl_4$ with $(Me_3Si)_2O$ rather than by the reaction of $W(O)Cl_4$ with $(Me_3Si)_2S$ (Scheme 1) since the thiane has been used on previous occasions to exchange an oxo ligand for a thio group.[9] However, these concerns were unfounded since $W(O)(S)Cl_2$ may be prepared by either permutation, presumably due to the very mild conditions and the swift reaction time (oxide for sulphide exchange often requires prolonged treatment of the oxide with the thiane reagent at ambient temperature[9]). Thus, CH_2Cl_2 solutions of either **1** or **7** react with equimolar amounts of $(Me_3Si)_2S$ or $(Me_3Si)_2O$, respectively, to give colourless supernatant solutions and in both cases an identical pale brown amorphous solid, which has been characterized as $W(O)(S)Cl_2$ (**10**) by elemental analysis, IR spectroscopy and mass spectrometry. The IR spectrum shows a characteristic terminal ν(W=S) stretch at 540 cm^{-1} and a strong broad absorption at 815 cm^{-1} is attributable to bridging oxo groups. The preference for terminal sulphide and bridging oxo ligands is also seen in the solid-state structures of **1** and **7**. The former is a linear oxo-bridged polymer[10] while **7** is a dimer with weak chlorine bridges

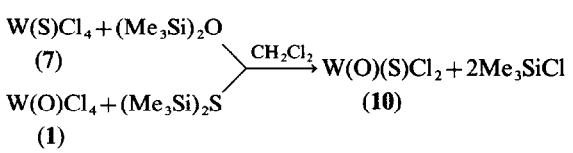

Scheme 1.

and a terminal sulphide ligand.[11] These features are also reproduced in the structure of $WCl_4 \cdot W(O)(S)Cl_2(dme)_2$ (dme = dimethoxyethane) reported by Rice and co-workers.[3b] The mass spectrum of **10** shows envelopes at m/z 604 and 302 attributable to dimeric and monomeric fragments, respectively.

$$Mo(O)Cl_4 + (Me_3Si)_2S \xrightarrow{CS_2} Mo(O)(S)Cl_2 + 2Me_3SiCl \quad (4)$$
$$(11)$$

$Mo(O)(S)Cl_2$ (**11**) is best prepared by treatment of $Mo(O)Cl_4$ with $(Me_3Si)_2S$ in CS_2 solvent [eq. (4)]. The pale brown solid formed in this reaction is found to be analytically pure. Its IR spectrum shows a terminal oxo stretch at 982 cm^{-1} and the absence of bands in the region 500–600 cm^{-1} suggests that the sulphide groups preferentially adopt bridging sites. The mass spectrum provides evidence for at least a dimeric structure; fragments are observed at m/z 361 and 342 corresponding to $[M_2-S-Cl]^+$ and $[M_2—O—2Cl]^+$, respectively, while an envelope at m/z 214 is due to $[M]^+$ with additional daughter fragments corresponding to further loss of oxygen, sulphur and chlorine groups.

In summary, reactions of molybdenum and tungsten halides with bis(silyl)ether and -thioether reagents provide straightforward syntheses of a range of molybdenum and tungsten oxo- and thiohalides which provide alternatives to the well-established hot tube/furnace methods.

EXPERIMENTAL

General

All manipulations of air- and/or moisture-sensitive materials were performed on a conventional vacuum/inert atmosphere (nitrogen or argon) line using standard Schlenk and cannula techniques, or in an inert atmosphere (nitrogen or argon) filled glove box.

The following solvents were dried by prolonged reflux over a suitable drying agent, being freshly distilled and deoxygenated prior to use (drying agent in parentheses): petroleum ether, b.p. 40–60°C (lithium aluminium hydride), b.p. 100–120°C (sodium), octane (sodium), acetonitrile (calcium hydride), dichloromethane (calcium hydride), carbon disulphide (4 Å molecular sieves) and diethyl ether (lithium aluminium hydride). NMR solvent: d-chloroform (phosphorus(V) oxide).

Elemental analyses were performed by the microanalytical services of this department. IR spectra were recorded on Perkin–Elmer 577 and 457 grating

spectrophotometers using either KBr or CsI windows. Absorptions abbreviated as: s (strong), m (medium), w (weak), br (broad), sp (sharp), sh (shoulder). Mass spectra were recorded on a VG 7070E mass spectrometer. ^{1}H NMR spectra were recorded on a Bruker AC 250 spectrometer at 250.13 MHz. $Mo(O)Cl_4$ was obtained by a literature procedure.[12] The following chemicals were obtained commercially and used as received unless stated otherwise: WCl_6 (Aldrich), $MoCl_5$ (Aldrich), hexamethyldisiloxane (Aldrich, distilled and stored over 4 Å molecular sieves), hexamethyldisilthiane (Fluka, distilled and stored over 4 Å molecular sieves).

Synthesis of $W(O)Cl_4$ **(1)**

A dichloromethane solution of $(Me_3Si)_2O$ (2.05 g, 12.6 mmol in 15 cm^3 of CH_2Cl_2) was added dropwise at room temperature to a stirred suspension of WCl_6 (5.0 g, 12.6 mmol) in dichloromethane (20 cm^3) over a period of 15 min. An immediate reaction ensued leading to deposition of $W(O)Cl_4$ in the form of red crystals. The mixture was stirred at room temperature for a further 60 min. The supernatant liquor was then decanted from the solid which was collected, washed with petroleum ether (2 × 10 cm^3, b.p. 40–60°C) and dried *in vacuo*. Yield, 4.28 g (99%). Elemental analysis for Cl_4OW: Found (Required): W, 53.9 (53.8); Cl, 41.2 (41.5)%; IR data (Nujol, CsI, cm^{-1}): 880–900(s,br), 387(s,br), 368(m,sh), 355(m,sh), 334(s,sp), 329(m,sh), 320(m,sh), 308(w,sh), 285(w).

Synthesis of $W(O)_2Cl_2$ **(2)**

An octane solution of $(Me_3Si)_2O$ (2.38 g, 14.7 mmol in 15 cm^3 of octane) was added to a stirred suspension of $W(O)Cl_4$ (5.0 g, 14.6 mmol) in octane (40 cm^3). The mixture was rapidly warmed to 80°C and stirred until the orange coloration of the octane solution was discharged to leave a yellow solid and a colourless solution. After cooling to room temperature, the supernatant solution was decanted from the solid, which was collected, washed with petroleum ether (2 × 20 cm^3; b.p. 40–60°C) and dried *in vacuo*. Yield, 3.99 g (95%). Elemental analysis for Cl_2O_2W: Found (Required): W, 63.7, (64.1); Cl, 24.4, (24.7)%; IR data (Nujol, CsI, cm^{-1}): 800–830(s,br).

Synthesis of $W(O)_2Cl_2(CH_3CN)_2$ **(3)**

An acetonitrile solution of $(Me_3Si)_2O$ (2.38 g, 14.7 mmol in 15 cm^3 of CH_3CN) was added dropwise at room temperature to a stirred suspension of $W(O)Cl_4$ (5 g, 14.6 mmol) in acetonitrile (40 cm^3) over a period of 15 min. The $W(O)Cl_4$ was consumed to give a pale blue solution which was stirred for a further 2 h. Filtration of this solution followed by concentration to half volume and cooling to −45°C gave white moisture-sensitive crystals of $W(O)_2Cl_2(CH_3CN)_2$. The remaining dark blue supernatant solution was decanted from the solid which was collected, washed with petroleum ether (2 × 10 cm^3, b.p. 40–60°C) and dried *in vacuo*. Yield, 3.77 g (70%). Elemental analysis for $C_4H_6Cl_2N_2O_2W$: Found (Required): W, 50.12, (49.84); Cl, 19.25, (19.22); H, 1.65, (1.64); C, 13.02, (13.03); N, 7.64, (7.59)%; IR data (Nujol, CsI, cm^{-1}): 2320(s,sp), 2300(s,sp), 1409(m), 1367(s,sp), 1040(m,sp), 1031(m,sh), 980(s,sp), 971(m,sh), 946(s,sh), 932(s,sh), 927(s,sp), 920(s,sh), 379(s,sp), 394(s,br), 380(m,sh).

Synthesis of $W(O)_2Cl(OSiMe_3)$ **(4)**

A dichloromethane solution of $(Me_3Si)_2O$ (0.96 g, 5.86 mmol in 15 cm^3 of CH_2Cl_2) was added dropwise to a stirred suspension of $W(O)Cl_4$ (1.0 g, 2.93 mmol) in dichloromethane (20 cm^3) at room temperature over a period of 15 min. The $W(O)Cl_4$ suspension reacted during stirring over 2 h to give a blue solution. Filtration, followed by concentration to half volume and cooling to −78°C, afforded blue crystals of $W(O)_2Cl(OSiMe_3)$. Yield, 0.7 g (70%). Elemental analysis for $C_3H_9ClO_3SiW$: Found (Required): W, 55.9 (56.7); Cl, 10.1 (10.9); C, 10.2 (11.1); H, 2.5 (2.8)%; IR data (Nujol, CsI, cm^{-1}): 1255(s,sp), 1002(s,br), 700–900(s,br), 280–360(s,br); ^{1}H NMR data (250 MHz, d-chloroform, 298 K): 0.42 (s, Si*Me*$_3$).

Synthesis of $Mo(O)Cl_3$ **(5)**

A dichloromethane solution of $(Me_3Si)_2O$ (2.97 g, 18.3 mmol in 15 cm^3 of CH_2Cl_2) was added dropwise at room temperature to a solution of $MoCl_5$ (5.0 g, 18.3 mmol) in dichloromethane (20 cm^3). The mixture was stirred at room temperature for 2 h to give a dark brown solid and a colourless solution. The supernatant solution was decanted from the solid, which was collected, washed with petroleum ether (2 × 20 cm^3, b.p. 40–60°C) and dried *in vacuo*. Yield 3.90 g (97.5%). Elemental analysis for Cl_3OMo: Found (Required): Cl, 48.69 (48.72)%; IR data (Nujol, CsI, cm^{-1}): 1007(s,sp), 398(s), 352(s), 309(m), 295(m,sh).

Synthesis of $Mo(O)_2Cl_2$ (**6**)

A dichloromethane solution of $(Me_3Si)_2O$ (3.2 g, 19.7 mmol in 15 cm^3 of CH_2Cl_2) was added dropwise at room temperature to a stirred suspension of freshly prepared $Mo(O)Cl_4$ (5.0 g, 19.7 mmol) in dichloromethane (20 cm^3). The mixture was stirred at room temperature for 4 h to give a pale brown solid suspended in a brown solution. The solid was isolated by cannula filtration, washed with light petroleum ether (2×20 cm^3, b.p. 40–60°C) and dried *in vacuo*. Yield 3.78 g (97%). Elemental analysis for Cl_2O_2Mo: Found (Required): Cl, 35.7 (35.7)%; IR data (Nujol, CsI, cm^{-1}): 800–830(s,br), 443(s,sp), 425(m,sh), 409(m,sh), 385(s,sp), 354(s,sp), 291(m,sp).

Synthesis of $W(S)Cl_4$ (**7**)

A suspension of WCl_6 (5.0 g, 12.6 mmol) in dichloromethane (20 cm^3) was cooled in a dry-ice/acetone slush bath and treated dropwise over a period of 15 min with a solution of $(Me_3Si)_2S$ (2.25 g, 12.6 mmol in 15 cm^3 of CH_2Cl_2) chilled to *ca* −30°C. An immediate reaction ensued leading to a red solution and precipitation of a brown, amorphous solid. The mixture was allowed to warm to room temperature and stirred for a further 30 min. Filtration of the supernatant solution followed by concentration and cooling to −78°C afforded red, moisture-sensitive crystals of $W(S)Cl_4$ (2.95 g, 65%). A second extraction of the residue with CH_2Cl_2 (20 cm^3) followed by crystallization resulted in a combined yield of 80% of analytically pure $W(S)Cl_4$. Elemental analysis for Cl_4SW: Found (Required): W, 51.5, (51.4); Cl, 39.5, (39.6); S, 9.0 (9.0)%; IR data (Nujol, CsI, cm^{-1}): 560(s,sp), 392(m,sh), 355(s), 306(m,sh), 285(w); mass spectral data, *m/z* (EI, 70 eV, W^{184}, S^{32}; Cl^{35}): 356 $[WSCl_4]^+$, 321 $[WSCl_3]^+$, 286 $[WSCl_2]^+$, 251 $[WSCl]^+$, 216 $[WS]^+$, 324 $[WCl_4]^+$, 289 $[WCl_3]^+$, 254 $[WCl_2]^+$, 219 $[WCl]^+$.

Synthesis of $W(S)_2Cl_2$ (**8**)

A solution of $WSCl_4$ (1.0 g, 2.8 mmol) in dichloromethane (20 cm^3) was cooled in a dry-ice/acetone slush bath and treated dropwise over a period of 15 min with a dichloromethane solution of $(Me_3Si)_2S$ (0.50 g, 2.8 mmol in 15 cm^3 of CH_2Cl_2) chilled to *ca* −30°C. An immediate reaction ensued, which after 30 min resulted in a colourless solution and a black, amorphous solid. The mixture was allowed to warm to room temperature and stirred for a further 2 h. The supernatant solution was decanted from the black solid, which was collected, washed with petroleum ether (2×10 cm^3, b.p. 40–60°C) and dried *in vacuo*. Yield, 0.72 g (81%). Elemental analysis for Cl_2S_2W: Found (Required): W, 57.64 (57.66); Cl, 21.69 (22.24); S, 19.90 (20.11)%; IR data (Nujol, CsI, cm^{-1}): 538(s,sp), 365(m,sh), 321(m,sh); mass spectral data, *m/z* (EI, 70 eV, W^{184}, S^{32}, Cl^{35}) 318 $[WS_2Cl_2]^+$, 286 $[WSCl_2]^+$, 251 $[WSCl]^+$, 216 $[WS]^+$.

Synthesis of $Mo(S)Cl_3$ (**9**)

A solution of $MoCl_5$ (1.0 g, 3.66 mmol) in dichloromethane (20 cm^3) was cooled in a dry-ice/acetone slush bath and treated dropwise over a period of 15 min with a dichloromethane solution of $(Me_3Si)_2S$ (0.65 g, 3.66 mmol in 15 cm^3 of CH_2Cl_2) chilled to *ca* −30°C. An immediate reaction ensued, which after 30 min had afforded a colourless solution and an olive green, amorphous solid. The mixture was allowed to warm to room temperature and stirred for 2 h. The supernatant solution was decanted from the solid which was collected, washed with petroleum ether (2×20 cm^3, b.p. 40–60°C) and dried *in vacuo*. Yield 0.75 g (87%). Elemental analysis for Cl_3SMo: Found (Required): S, 14.40 (13.68); Cl, 45.25 (45.38)%; IR data (Nujol, CsI, cm^{-1}): 398(s,br), 375(m,sh), 354(m), 346(w,sh), 290(m,br); mass spectral data *m/z* (EI, 70 eV, Mo^{96}; S^{32}, Cl^{35}, O^{16}): 326 $[Mo_2S_2Cl_2]^+$, 291 $[Mo_2S_2Cl]^+$, 259 $[Mo_2SCl]^+$, 233 $[MoSCl_3]^+$, 198 $[MoSCl_2]^+$, 163 $[MoSCl]^+$, 128 $[MoS]^+$.

Synthesis of $W(O)(S)Cl_2$ (**10**)

A chilled (*ca* −30°C) dichloromethane solution of $(Me_3Si)_2S$ (0.52 g, 2.93 mmol in 15 cm^3 of CH_2Cl_2) was added dropwise over a period of 15 min to a stirred suspension of $W(O)Cl_4$ (1.0 g, 2.93 mmol) in dichloromethane (20 cm^3) cooled in a dry-ice/acetone slush bath. An immediate reaction ensued, which after 30 min resulted in a colourless solution and a light brown, amorphous solid. The mixture was allowed to warm to room temperature and stirred for a further 2 h. The supernatant solution was decanted from the light brown solid, which was collected, washed with petroleum ether (2×10 cm^3, b.p. 40–60°C) and dried *in vacuo*. Yield, 0.73 g (82%). Elemental analysis for Cl_2SOW: Found (Required): W, 60.09, (60.71); S, 9.75, (10.59); Cl, 22.83, (23.42)%; IR data (Nujol, CsI, cm^{-1}): 815(s,br), 540(s,sp), 410(s), 372(m,br), 343(s,sp); mass spectral data *m/z* (EI, 70 eV, W^{184}, S^{32}, Cl^{35}) 604 $[W_2O_2S_2Cl_4]^+$, 585 $[W_2S_2O_3Cl_3]^+$, 566 $[W_2S_4Cl_2]^+$, 318 $[WS_2Cl_2]^+$, 302 $[WOSCl_2]^+$.

Synthesis of $Mo(O)(S)Cl_2$ (**11**)

A chilled (*ca* −30°C) carbon disulphide solution of $(Me_3Si)_2S$ (0.70 g, 3.92 mmol in 15 cm^3 of CS_2) was added dropwise over a period of 15 min to a stirred solution of $Mo(O)Cl_4$ (1.0 g, 3.92 mmol) in carbon disulphide (20 cm^3) cooled in a dry-ice/acetone slush bath. An immediate reaction ensued, which after 30 min resulted in a colourless solution and a light brown, amorphous solid. The mixture was allowed to warm to room temperature and stirred for 2 h. The supernatant solution was decanted from the solid, which was collected, washed with petroleum ether (2 × 20 cm^3, b.p. 40–60°C) and dried *in vacuo*. Yield 0.73 g (86%). Elemental analysis for Cl_2OSMo: Found (Required): S, 15.14 (14.92); Cl, 32.75 (32.99)%; IR data (Nujol, CsI, cm^{-1}): 982(s,sp), 851(w), 720(m), 473(s,sp), 378(s), 369(m,sh), 325(s,sp), 298(s,sh), 255(m); mass spectral data *m/z* (EI, 70 eV, Mo^{96}, S^{32}, Cl^{35}, O^{16}): 361 $[Mo_2O_2SCl_3]^+$, 342 $[Mo_2OS_2Cl_2]^+$, 326 $[Mo_2S_2Cl_2]^+$, 310 $[Mo_2OSCl_2]^+$, 214 $[MoOSCl_2]^+$, 198 $[MoSCl_2]^+$, 179 $[MoOSCl]^+$, 163 $[MoSCl]^+$, 147 $[MoOCl]^+$, 128 $[MoS]^+$, 112 $[MoO]^+$.

Acknowledgements—Research Corporation Trust and SERC are gratefully acknowledged for research grants (to V.C.G.) and SERC is thanked for studentships (to T.P.K. and A.S.).

REFERENCES

1. (a) K. Dehnicke, *Angew. Chem. Int. Edn. Engl.* 1965, **4**, 22; (b) R. A. Walton, *Prog. Inorg. Chem.* 1972, **16**, 135; (c) J. H. Canterford and R. Colton, *Halides of the Second and Third Row Transition Metals*. John Wiley, New York (1968); (d) M. J. Atherton and J. H. Holloway, *Adv. Inorg. Chem. Radiochem.* 1979, **22**, 171; (e) D. A. Rice, *Coord. Chem. Rev.* 1978, **25**, 199.
2. (a) S. F. Pedersen and R. R. Schrock, *J. Am. Chem. Soc.* 1982, **104**, 7483; (b) G. W. A. Fowles and J. L. Frost, *J. Chem. Soc. A* 1967, 671.
3. (a) D. A. Britnell, G. W. A. Fowles and D. A. Rice, *J. Chem. Soc., Dalton Trans.* 1974, 2191; (b) G. W. A. Fowles, R. J. Hobson, D. A. Rice and K. J. Shanton, *J. Chem. Soc., Chem. Commun.* 1976, 552.
4. (a) V. C. Gibson, T. P. Kee and A. Shaw, *Polyhedron* 1988, **7**, 579; (b) V. C. Gibson, A. Shaw and D. N. Williams, *Polyhedron* 1989, **8**, 549.
5. (a) R. M. Silverstein, G. C. Bassler and T. C. Morill, *Spectrometric Identification of Organic Compounds*, 4th Edn. John Wiley, New York (1981); (b) C. Eaborn, *Organosilicon Compounds*. Butterworth Scientific, London (1960).
6. B. J. Brisdon, *Inorg. Chem.* 1967, **6**, 1791.
7. K. M. Sharma, S. K. Anand, R. K. Multani and B. D. Jain, *Chem. Ind.* 1969, 1556.
8. D. Britnell, M. G. B. Drew, G. W. A. Fowles and D. A. Rice, *J. Chem. Soc., Chem. Commun.* 1972, 462.
9. Y. Do, E. D. Simhon and R. H. Holm, *Inorg. Chem.* 1983, **22**, 3809.
10. H. Hess and H. Hartung, *Z. Anorg. Allg. Chem.* 1966, **344**, 157.
11. M. G. B. Drew and R. Mandyczewsky, *J. Chem. Soc. A* 1970, 2815.
12. A. J. Nielson, *Inorg. Synth.* 1985, **23**, 195.

Polyhedron Vol. 9, No. 18, pp. 2299–2304, 1990
Printed in Great Britain

0277–5387/90 $3.00+.00
© 1990 Pergamon Press plc

SUBSTITUENT EFFECTS ON THE OXIDATION OF BENZOINS BY THE OCTACYANOMOLYBDATE(V) ION

H. A. HODALI* and R. A. EL-ZARU

Department of Chemistry, Faculty of Science, University of Jordan, Amman, Jordan

(*Received* 18 *December* 1989; *accepted* 11 *May* 1990)

Abstract—The kinetics of the oxidation of a series of benzoins (BH_2) by octacyanomolybdate(V) (OX^{3-}), in a buffered alkaline aqueous methanolic medium, have been studied spectrophotometrically. The experimental results are in agreement with the following rate law:

$$-1/2\,d[OX^{3-}]/dt = k[OX^{3-}][BH_2][OH^-],$$

and the following order of reactivity was observed: *o,o'*-dichloro- > *p,p'*-dichloro- > *m,m'*-dimethoxybenzoin > benzoin > *p,p'*-dimethoxy- > *o,o'*-dimethoxybenzoin. The rate measurements were used to calculate the thermodynamic activation parameters $\Delta G^{\ddagger}$, $\Delta H^{\ddagger}$ and $\Delta S^{\ddagger}$. The relative rates correlate very well with the Hammett substituent constants and support a negatively-charged intermediate. The effect of substituents correlated with a ρ-value of 1.36.

Octacyanomolybdate(V) has been employed in the oxidation of many classes of compounds, in both basic and acidic media. Examples are, the oxidation of hydrazine and substituted hydrazines,[1] iodide ions,[2] ascorbic acid[3,4] and benzenediols.[5] Acyloins (1,2-enediols), on the other hand, are readily oxidized by several oxidizing agents.[6,7] The kinetics of oxidation of benzoins (BH_2)[8] and aliphatic acyloins[9] by $[Fe(CN)_6]^{3-}$ in basic medium have been investigated. The oxidation reaction was found to be first-order with respect to each of the acyloin, the hexacyanoferrate(III) and the hydroxide ion. These findings prompted us to investigate the oxidation of benzoin and substituted benzoins by another oxidizing agent in order to compare its kinetic data with that obtained for $[Fe(CN)_6]^{3-}$, and also to study the effect of substituents on the rates of benzoin oxidation.

Herein, the kinetics of oxidation of a series of benzoins (**I–VI**) by $[Mo(CN)_8]^{3-}$ in alkaline medium are investigated. The results are used to calculate the reaction rates and thermodynamic parameters. The relative rate values were used along with the substituent constants (σ_m, σ_p) to find the value of the reaction constant (ρ).

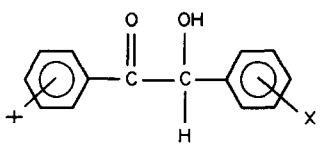

I , X = H
II , = *o*—OCH_3
III, = *p*—OCH_3
IV , = *m*—OCH_3
V , = *p*—Cl
VI , = *o*—Cl

EXPERIMENTAL

Materials

The benzoin used in this investigation was B.D.H. Analar grade, and was used without further purification. The substituted benzoins, *o,o'*-dichloro-,[10] *p,p'*-dichloro-,[10] *m,m'*-dimethoxy-,[11] *p,p'*-dimethoxy-,[11] *o,o'*-dimethoxybenzoin[11] and the cyano complexes, $K_4[Mo(CN)_8]\cdot 2H_2O$[12] and $Cs_3[Mo(CN)_8]\cdot 2H_2O$[13] were prepared by literature methods. The oxidizing agent, $Cs_3[Mo(CN)_8]\cdot 2H_2O$, was purified by recrystallization from water and was used as a primary standard. Analytical grade reagents and doubly-distilled water

* Author to whom correspondence should be addressed.

were used throughout the measurements. The desired buffer solutions for varying the pH of the reaction medium were prepared by mixing suitable volumes of 0.025 M borax and 0.10 M NaOH (pH = 9.0–10.0) or 0.05 M disodium hydrogen phosphate and 0.10 M NaOH (pH = 11.0–12.0). The pH was measured with a Metrohm 632 pH meter. The measured pHs were corrected for 50% v/v aqueous methanol using the relationship:[14] $pH_{corr} = pH_{meas} + 0.08$.

Kinetic measurements

The oxidation reactions were carried out in buffered alkaline aqueous methanol (50% v/v) using a thermostated bath to regulate the temperature to ±0.2°C. The ionic strength was adjusted to a constant value of 0.10 M by the addition of NaCl. Kinetic data were obtained by monitoring the decrease in the concentration of $[Mo(CN)_8]^{3-}$ at 390 nm with a thermostated Unicam SP8-500 spectrophotometer. Solutions of the benzoins and the octacyanomolybdate(V) were protected from light during the preparation and kinetic measurements.

Stoichiometry

The oxidation of benzoin was found to proceed by a 1:2 stoichiometry represented in eq. (1):[15]

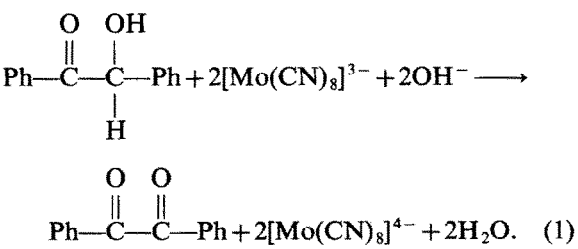

(1)

The formation of the 1,2-diketone (benzil), in high yield, was confirmed by a preparative scale reaction.[15]

RESULTS AND DISCUSSION

Effect of benzoin

Absorption measurements carried out at constant concentration of the oxidant, $[Mo(CN)_8]^{3-}$, the hydroxide ion and at constant ionic strength, but with varying concentrations of the benzoins (**I–VI**), showed a first-order dependence on the concentration of the benzoin (Table 1). The plot of $\ln(A_0/A_t)$ vs time for *m,m'*-dimethoxybenzoin (**IV**) is linear for about 75% of the reaction (Fig. 1). Similar plots were obtained for the other benzoins.

Table 1. Observed rate constants for the oxidation of benzoins (**I–VI**) by $[Mo(CN)_8]^{3-}$ [a]

	I[b]		**II**[b]		**III**[b]		**IV**[b]		**V**[b]		**VI**[b]	
10^3 BH_2	$10^4 k$ (s^{-1})	$10^2 k'$ ($M^{-1} s^{-1}$)	$10^4 k$ (s^{-1})	$10^2 k'$ ($M^{-1} s^{-1}$)	$10^4 k$ (s^{-1})	$10^2 k'$ ($M^{-1} s^{-1}$)	$10^4 k$ (s^{-1})	$10^2 k'$ ($M^{-1} s^{-1}$)	$10^4 k$ (s^{-1})	$10^2 k'$ ($M^{-1} s^{-1}$)	$10^4 k$ (s^{-1})	$10^2 k'$ ($M^{-1} s^{-1}$)
4.00	7.95	19.9	2.35	5.88	3.87	9.67	12.3	30.8	19.3	48.3	72.8	182
5.00	9.93	19.9	2.93	5.86	4.83	9.67	15.4	30.8	24.0	48.0	91.2	182
6.00	11.8	19.7	3.53	5.88	5.88	9.64	18.3	30.6	29.0	48.3	109	182
7.00	13.7	19.6	4.11	5.88	5.88	9.64	21.3	30.5	33.7	48.1	128	182
Average		19.8±0.2		5.87±0.01		9.65±0.02		30.6±0.2		48.2±0.2		182±1

[a] $[[Mo(CN)_8]^{3-}] = 1.0 \times 10^{-3}$ M, $T = 25.0$°C, pH = 11.0, $I = 0.10$ M.
[b] **I** = Benzoin, **II** = *o,o'*-dimethoxybenzoin, **III** = *p,p'*-dimethoxybenzoin, **IV** = *m,m'*-dimethoxybenzoin, **V** = *p,p'*-dichlorobenzoin, **VI** = *o,o'*-dichlorobenzoin, $k' = k/[BH_2]$.

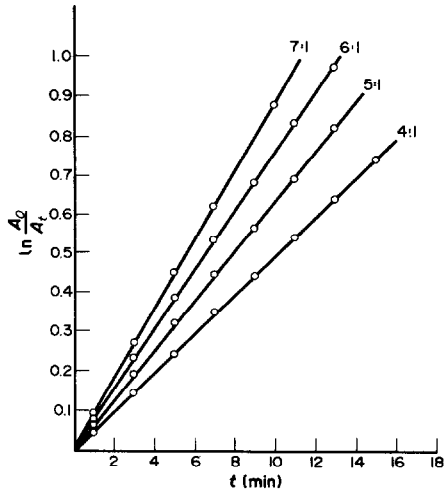

Fig. 1. Plots of $\ln(A_0/A_t)$ vs time for the oxidation of **IV** by $[Mo(CN)_8]^{3-}$ at different concentrations of **IV**.

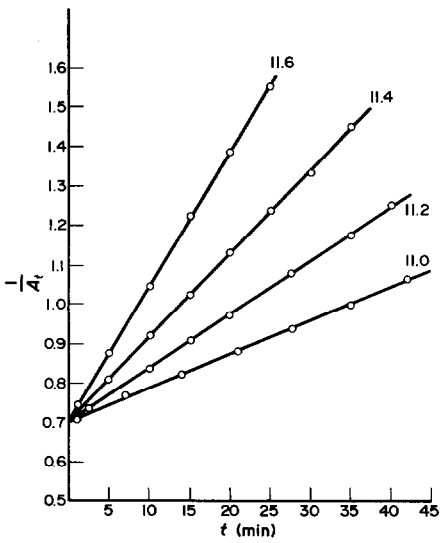

Fig. 2. Plots of $(1/A_t)$ vs time for the oxidation of **IV** by $[Mo(CN)_8]^{3-}$ at different pH values.

Effect of $[Mo(CN)_8]^{3-}$

Absorption measurements carried out at stoichiometric molar ratios of the reactants (benzoin (**I–IV**): oxidant ratio, 1:2) and at different pH values are shown in Table 2. The plots of $1/A_t$ vs t are linear, indicating a first-order dependence on both the benzoin and $[Mo(CN)_8]^{3-}$. The plot for *m,m'*-dimethoxybenzoin (**IV**) is shown in Fig. 2. Accordingly, the rate can be expressed as shown in eq. (2):

$$-d/dt[[Mo(CN)_8]^{3-}] = k[[Mo(CN)_8]^{3-}][\text{benzoin}]. \quad (2)$$

Effect of pH

The above kinetic measurements were used to obtain the plots of log k vs pH (Fig. 3). The slopes of these linear plots indicate first-order rate dependence on the hydroxide ion concentration. This is consistent with an overall rate defined by eq. (3). These kinetic measurements are also used to obtain the plots of k vs $1/[H^+]$ (Fig. 4). With the pH range available, the slopes of the straight lines obtained are used to evaluate approximate values of K_a for benzoins **I–IV** (Table 2).

$$-d/dt[[Mo(CN)_8]^{3-}] = k_{obs}[\text{benzoin}][Mo(CN)_8]^{3-}][OH^-]. \quad (3)$$

In view of the above data, the following simple

Table 2. Effect of pH on the rate of oxidation of benzoins (**I–IV**)[a]

		$10k$ ($M^{-1}s^{-1}$)			
pH	$10^{-11}/[H^+]$	**I**[b]	**II**[b]	**III**[b]	**IV**[b]
11.0	1.00	1.32	—	0.738	2.03
11.2	1.58	2.12	1.02	1.18	3.25
11.4	2.51	3.35	1.62	1.88	5.13
11.6	3.98	5.30	2.57	2.98	8.15
11.8	6.31	—	4.07	—	—

[a] $[BH_2] = 5.0\times10^{-4}$ M, $[[Mo(CN)_8]^{3-}] = 1.0\times10^{-3}$ M, $T = 25°C$, $I = 0.10$ M.

[b] Approximate values of K_a (where $K_a = KK_w$) are **I**: 1.8×10^{-12}; **II**: 6.4×10^{-13}; **III**: 7.1×10^{-13}; **IV**: 2.6×10^{-12}.

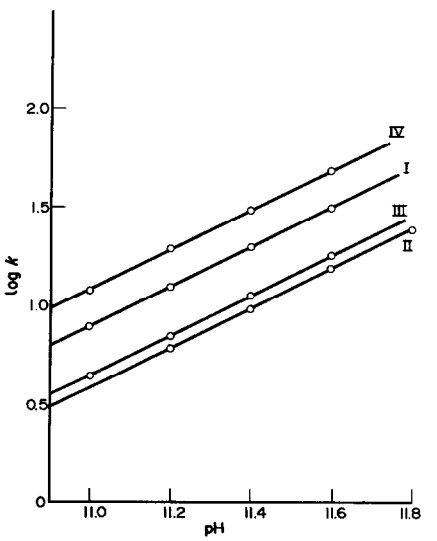

Fig. 3. Plots of log$k$ (in M^{-1} min^{-1}) vs pH for the oxidation of benzoins (**I–IV**) (See Table 2).

Table 3. Relative rate constants and the thermodynamic activation parameters for the oxidation of benzoins by $[Mo(CN)_8]^{3-}$ and $[Fe(CN)_6]^{3-}$ [a]

	$[Mo(CN)_8]^{3-}$					$[Fe(CN)_6]^{3-}$				
Compound	$10^4 k$ (s^{-1})	$\Delta H^{\ddagger}$ (kJ mol^{-1})	$\Delta S^{\ddagger}$ (J K^{-1} mol^{-1})	$\Delta G^{\ddagger}$ (kJ mol^{-1})	k_{rel}	$10^4 k$ [b] (s^{-1})	$\Delta H^{\ddagger}$ (kJ mol^{-1})	$\Delta S^{\ddagger}$ (J K^{-1} mol^{-1})	$\Delta G^{\ddagger}$ (kJ mol^{-1})	k_{rel}
I	7.95	62.0	−96.1	90.6	1.00	5.54	83.2	−27.5	91.4	1.00
II	2.35	62.3	−105	93.4	0.300	2.17	82.1	−39.1	93.8	0.392
III	3.87	82.0	−34.6	92.3	0.487	2.99	79.6	−45.0	93.0	0.540
IV	12.3	59.3	−102	89.7	1.54	8.27	76.8	−45.9	90.5	1.49
V	19.3	97.5	30.8	88.3	2.43	—	—	—	—	—
VI	72.8	103	62.0	84.5	9.17	48.9	94.5	28.4	86.0	8.83

[a] $[BH_2] = 4.0 \times 10^{-3}$ M, $[[Mo(CN)_8]^{3-}] = [[Fe(CN)_6]^{3-}] = 1.0 \times 10^{-3}$ M, $T = 25.0$°C, pH = 11.0, $I = 0.10$ M.
[b] Rate constants for the benzoins (I–IV) were obtained from ref. 8.

mechanism is proposed:[9]

$$BH_2 + OH^- \underset{}{\overset{K}{\rightleftharpoons}} BH^- + H_2O \quad (4)$$

$$BH^- + [Mo(CN)_8]^{3-} \xrightarrow{k_2} BH^{\cdot} + [Mo(CN)_8]^{4-} \quad (5)$$

$$BH^{\cdot} + [Mo(CN)_8]^{3-} + OH^- \xrightarrow{\text{Fast}} B + [Mo(CN)_8]^{4-} + H_2O. \quad (6)$$

On the assumption that step (6) proceeds by a fast one-electron oxidation, and step (5) is the rate-determining step, then the following third-order rate law can be easily derived [eq. (7)]:

$$-d[[Mo(CN)_8]^{3-}]/dt = k_2K[BH_2][[Mo(CN)_8]^{3-}][OH^-], \quad (7)$$

where $k_2K = k_{obs}$.

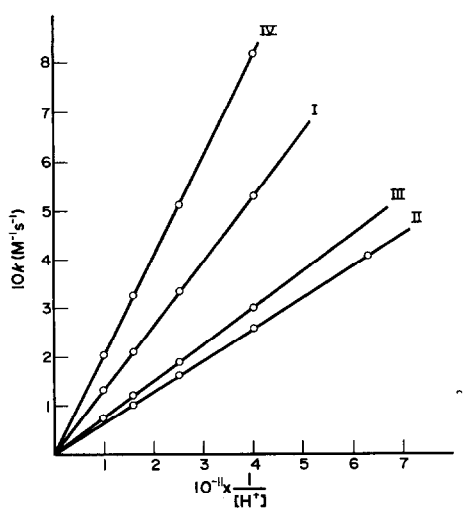

Fig. 4. Plots of k vs $1/[H^+]$ for the oxidation of benzoins (I–IV).

Relative reactivities

The relative reactivities of the benzoins studied are found in the following order (Table 3): **I** (1.00), **II** (0.300), **III** (0.487), **IV** (1.55), **V** (2.43), **VI** (9.17). The exceptionally high reactivity of *o,o'*-dichlorobenzoin (**VI**) and the relatively low reactivity of *o,o'*-dimethoxybenzoin (**II**) are attributed to the strong electron-withdrawing effect of the *o*-chloro substituents as compared with the electron-releasing effect of the *o*-methoxy groups. The electron-withdrawing groups are of importance in stabilizing the benzoin anion and thus enhancing its rate of oxidation. Similar trends were also observed for *p,p'*-dichlorobenzoin (**V**) and *p,p'*-dimethoxybenzoin (**III**). However, the higher reactivity of *m,m'*-dimethoxybenzoin (**IV**) compared with benzoin (**I**) is due to the stabilization of the intermediate benzoin anion through the mesomeric inductive effect of the *m*-methoxy group.

The values of $\log k_{rel}$ ($k_{rel} = k_{substituted}/k_{benzoin}$ under similar conditions) were plotted vs the substituent constants σ_m, σ_p. The substituent constants utilized here (Table 4) were derived from the ionization constant of the substituted benzoic acids[16,17] due

Table 4. Substituent effects on the oxidation of benzoins (III–V)[a]

Compound	$10^4 k$ (s^{-1})	k_{rel}	$\log k_{rel}$	σ
I	7.95	1.00	0.00	0.00
III	3.87	0.484	−0.315	−0.268
IV	12.3	1.54	0.187	0.115
V	19.3	2.43	0.385	0.240

[a] $[BH_2] = 4.0 \times 10^{-3}$ M, $[[Mo(CN)_8]^{3-}] = 1.0 \times 10^{-3}$ M, $T = 25$°C, pH = 11.0, $I = 0.10$ M.

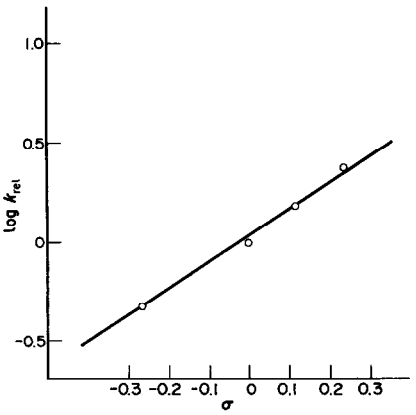

Fig. 5. Plots of $\log k_{rel}$ vs σ for the oxidation of benzoins **I, III, IV** and **V** (See Table 4).

to structural similarities. The slope of the linear plot obtained (Fig. 5) gives a Hammet ρ of +1.36. The sign and magnitude of ρ for this series of substituted benzoins are in good agreement with reported values for the cupric oxidation of acyloins[18] and *o*-hydroxyacetophenone.[19]

Thermodynamic parameters

The enthalpies of activation were evaluated by variation of the reaction temperature between 15 and 30°C under pseudo-first-order conditions ($[BH_2] = 4.0 \times 10^{-3}$ M, $[OX^{3-}] = 1.0 \times 10^{-3}$ M), at constant pH (11.0) and constant ionic strength (0.10 M). Plots of $-\log(k/T)$ vs $1/T$ gave straight lines for all the benzoins studied (**I–VI**). The values of $\Delta H^{\ddagger}$ were obtained from the slopes and the values of $\Delta S^{\ddagger}$, $\Delta G^{\ddagger}$ and k_{rel} were calculated at 25°C (Table 3, Fig. 6).

From the data accumulated in Table 3, a direct relationship between the benzoin reactivity and $\Delta S^{\ddagger}$ values could be easily formulated. The benzoin with the highest reactivity (**VI**) has the highest positive $\Delta S^{\ddagger}$ (+62.0) for the activated complex, while the least reactive (**II**) has the largest negative value of $\Delta S^{\ddagger}$ (−105). This can be explained in view of the closest approach through the formation of the activated complex, and thus, the value of $\Delta S^{\ddagger}$ is a function of the electron-transfer distance. For the high negative values of $\Delta S^{\ddagger}$, the electron transfer takes place at relatively short distances, which accordingly may be hindered by several factors such as, solvation, ion-pairing, hydrogen-bonding and substituent steric effects. The observed relationship between reactivity and electron-transfer distance was in full agreement with conclusions of other researchers[20] in this field.

For the purpose of comparison, the thermodynamic parameters, $\Delta H^{\ddagger}$, $\Delta S^{\ddagger}$ and $\Delta G^{\ddagger}$, for the oxidation of the benzoins (**I–IV**)[8] and **VI** with $[Fe(CN)_6]^{3-}$ were calculated under conditions similar to those employed for $[Mo(CN)_8]^{3-}$. The thermodyamic parameters for $[Fe(CN)_6]^{3-}$ are also found to be consistent and in perfect agreement with the above derived relationship between reactivity and electron-transfer distance (Table 3). However, the higher reactvity of $[Mo(CN)_8]^{3-}$ in comparison with $[Fe(CN)_6]^{3-}$ is mainly due to its higher reduction potential.[3]

REFERENCES

1. C. R. Dennis, A. J. Van Wyk, S. S. Basson and J. G. Leipoldt, *Inorg. Chem.* 1987, **26**, 270.
2. L. D. C. Bok, J. G. Leipoldt and S. S. Basson, *J. Inorg. Nucl. Chem.* 1975, **37**, 2151.

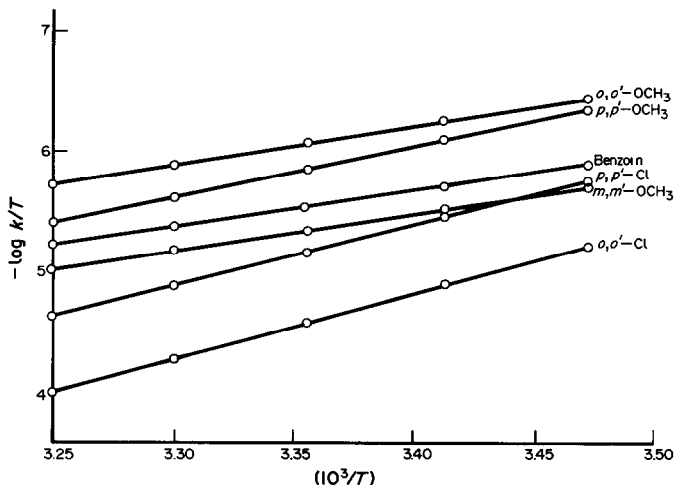

Fig. 6. Plots of $-\log(k/T)$ vs $1/T$ for the oxidation of benzoins (**I–VI**) by $[Mo(CN)_8]^{3-}$ at pH = 11.0 and $I = 0.10$.

3. E. Pelizzetti, E. Mentasti and E. Pramauro, *Inorg. Chem.* 1978, **17**, 1181.
4. R. A. El-Zaru and H. A. Hodali, *Polyhedron* 1990, **9**, 113.
5. E. Pelizzetti, E. Mentasti and E. Pramauro, *Inorg. Chem.* 1978, **17**, 1688.
6. R. A. El-Zaru and A. A. Jarrar, *Egypt. J. Chem.* 1977, **20**, 603.
7. R. A. El-Zaru, *Dirasat* 1978, **V**, 75.
8. A. A. Jarrar, R. A. El-Zaru and M. S. Mbarak, *Dirasat* 1979, **VI**, 7.
9. A. A. Jarrar, R. A. El-Zaru and A. S. Shahin, *Arab. J. Sci. Engng* 1988, **13**, 65.
10. R. E. Lutz and R. S. Murphey, *J. Am. Chem. Soc.* 1949, **71**, 480.
11. R. Adams and C. R. Marvel, *Org. Synth. Coll. Vol. 1*, 1941, 94.
12. J. C. Leipoldt, L. D. C. Bok and P. J. Cilliers, *Z. Anorg. Allg. Chem.* 1974, **409**, 343.
13. L. D. Bok, J. G. Leipoldt and S. S. Basson, *Z. Anorg. Allg. Chem.* 1975, **415**, 81.
14. R. G. Bates and R. A. Robinson, *Chemical Physics of Ionic Solutions* (Edited by B. C. Conway), Ch. 12. John Wiley, New York (1964); E. Kozakoova and B. Csefalvayova, *Chem. Zvesti* 1980, **34**, 610.
15. R. A. El-Zaru and A. Jarrar, *Chem. Ind.* 1977, 741.
16. P. Zuman and R. C. Patel, *Techniques in Organic Reaction Kinetics*, p. 230. John Wiley, New York (1984).
17. E. S. Amis and V. K. Lamer, *J. Am. Chem. Soc.* 1939, **61**, 905; E. S. Amis and J. F. Hinton, *Solvent Effects on Chemical Phenomena*, Vol. 1, Ch. 1. John Wiley, New York (1973).
18. H. A. Connon, B. G. Sheldon, K. E. Harding, L. E. Letterman, D. C. Fulton and W. G. Nigh, *J. Org. Chem.* 1973, **38**, 2020.
19. K. B. Wiberg and W. G. Nigh, *J. Am. Chem. Soc.* 1965, **87**, 3849.
20. H. Rau, R. Frank and G. Greiner, *J. Phys. Chem.* 1986, **90**, 2476.

Polyhedron Vol. 9, No. 18, pp. 2305–2308, 1990
Printed in Great Britain

0277–5387/90 $3.00+.00
© 1990 Pergamon Press plc

SUBSTITUTED METAL CARBONYLS—XIV. POLYNUCLEAR HETEROMETALLIC COMPLEXES OF Cr, Mo, W AND Mn SUPPORTED BY SINGLY-BRIDGING 1,1′-BIS(DIPHENYLPHOSPHINO)FERROCENE

T. S. A. HOR* and L.-T. PHANG

Department of Chemistry, Faculty of Science, National University of Singapore, Kent Ridge 0511, Singapore

(*Received* 7 *March* 1990; *accepted* 11 *May* 1990)

Abstract—A series of polynuclear heterometallic complexes $(OC)_5M(\mu\text{-dppf})M'(CO)_5$ (M, M′ = Cr, Mo, W; M ≠ M′) and $(OC)_5M(\mu\text{-dppf})Mn_2(CO)_9$ (dppf = 1,1′-bis(diphenylphosphino)ferrocene) has been synthesized at room temperature based on the metalloligand $M(CO)_5(\eta^1\text{-dppf})$. The use of amine oxide as a decarbonylant preserves the integrity of the Mn—Mn bond. The mixed metals are linked by a singly-bridging diphosphine group which does not perturb the two metal spheres.

Carbonyl complexes of the Group 6 metals which contain 1,1′-bis(diphenylphosphino)ferrocene (dppf) as a bridging, chelating and unidentate ligand are well represented in the literature.[1] Relatively rare are those in which dppf serves as a bridging ligand between atoms of two different metals. We recently reported the use of the unidentate-diphosphine complex $Fe(CO)_4(\eta^1\text{-dppf})$ as a metalloligand in the systematic synthesis of a series of novel mixed-metal carbonyls.[2] In view of the emerging importance of these functionalized metalloligands[3] and the chemistry of dinuclear complexes which are of relevance in solid-state and catalytic studies,[4] we herein report an extension of this avenue to the syntheses of the heterometallic Group 6 carbonyls and the hitherto unknown $(CO)_5M(\mu\text{-dppf})Mn_2(CO)_9$ (M = Cr, Mo, W) clusters.

RESULTS AND DISCUSSION

Trimethylamine *N*-oxide (TMNO)-induced decarbonylation of the binary carbonyls $M'(CO)_6$, followed by nucleophilic attack by $M(CO)_5(\eta^1\text{-dppf})$ (M, M′ = Cr, Mo, W; M ≠ M′) at ambient temperature (25°C), affords the desired heterometallics $(OC)_5M(\mu\text{-dppf})M'(CO)_5$ (Fig. 1). The basicity of the dangling phosphine and the generality of this route are exemplified by the ease of the conversion either with $M(CO)_5(dppf)$ or $M'(CO)_5(dppf)$ as the substrates, the only exception being the Mo—W complex which is best synthesized from $W(CO)_5(dppf)$. The carbonyl region

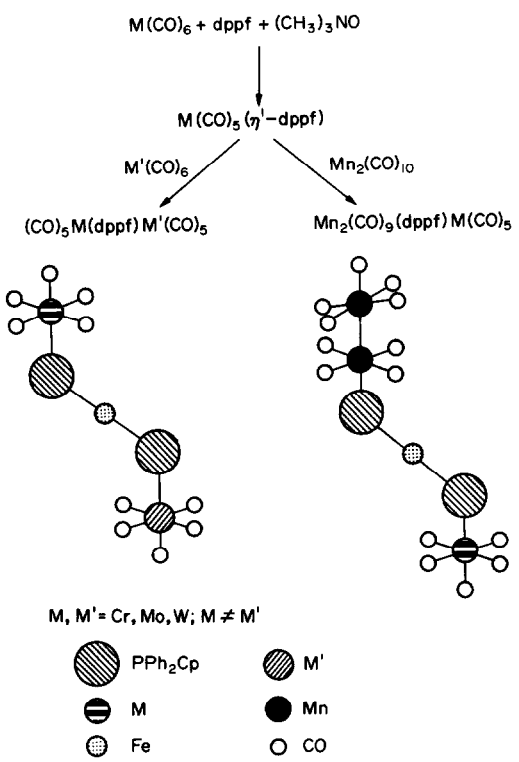

Fig. 1. Amine oxide-initiated synthesis of $(OC)_5M(dppf)M'(CO)_5$ and $(OC)_5M(dppf)Mn_2(CO)_9$, where dppf = $Fe(C_5H_4PPh_2)_2$.

* Author to whom correspondence should be addressed.

Table 1. Spectroscopic data of $(OC)_5M(dppf)M'(CO)_5$ and $(OC)_5M(dppf)Mn_2(CO)_9$, where dppf = $Fe(C_5H_4PPh_2)_2$

Complex	ν(CO) (cm^{-1})[a]	$\delta(^1H)$ (ppm)[b,c]	$\delta(^{31}P)$ (ppm)[b]
$(OC)_5Cr(dppf)Mo(CO)_5$	2073m, 2063m, 1988w, 1942s	7.25–7.42 (m, 20H), 4.27 (m, br, $2H_b^{Cr}+2H_b^{Mo}$), 4.04 (m, br, $2H_a^{Cr}+2H_a^{Mo}$)	47.52 (s, $-Ph_2PCr$), 28.54 (s, $-Ph_2PMo$)
$(OC)_5Cr(dppf)W(CO)_5$	2071m, 2063m, 1984w, 1940s	7.26–7.39 (m, 20H), 4.31 (m, br, $2H_b^{Cr}+2H_b^{W}$), 4.01 (m, br, $2H_a^{Cr}+2H_a^{W}$)	47.52 (s, $-Ph_2PCr$); 11.31 (t, $-Ph_2PW$), J(PW) 247 Hz
$(OC)_5Mo(dppf)W(CO)_5$	2072m, 1985w, 1948s	7.22–7.38 (m, 20H), 4.33 (m, br, $2H_b^{Mo}+2H_b^{W}$), 4.01 (m, br, $2H_a^{Mo}+2H_a^{W}$)	28.54 (s, $-Ph_2PMo$), 11.31 (t, $-Ph_2PW$), J(PW) 247 Hz
$(OC)_5Cr(dppf)Mn_2(CO)_9\cdot 1/3C_6H_{14}$	2091m, 2063m, 2009w, 1994s, 1936s	7.25–7.36 (m, 20H), 4.28 (m, br, $2H_b^{Cr}+2H_b^{Mn}$), 4.02 (m, br, $2H_a^{Cr}+2H_a^{Mn}$)	66.23 (s, br, $-Ph_2PMn$), 47.52 (s, $-Ph_2PCr$)
$(OC)_5Mo(dppf)Mn_2(CO)_9\cdot 1/4C_6H_{14}$	2091m, 2073m, 2009w, 1994s, 1947s	7.38 (m, 20H), 4.34 (m, br, $2H_b^{Mo}$), 4.24 (m, br, $2H_b^{Mn}$), 4.03 (m, br, $2H_a^{Mo}+2H_aMn$)	66.23 (s, br, $-Ph_2PMn$), 28.54 (s, $-Ph_2PMo$)
$(OC)_5W(dppf)Mn_2(CO)_9$	2091m, 2072m, 2009w, 1994s, 1935s	7.26–7.43 (m, 20H), 4.34 (m, br, $2H_b^{W}$), 4.27 (m, br, $2H_b^{Mn}$), 4.04 (m, br, $2H_a^{W}+2H_a^{Mn}$)	66.23 (s, br $-Ph_2PMn$), 11.31 (t, $-Ph_2PW$), J(PW) 244 Hz

[a] $CHCl_3$.
[b] $CDCl_3$.
[c] H_a and H_b refer to the external and internal cyclopentadienyl protons, respectively. H^M denotes the protons of the M- (M = Cr, Mn, Mo, W) coordinated phosphinocyclopentadienyl ring.

in the IR spectra of these complexes (Table 1) exhibit bands additive of their respective homonuclear analogues.[1e] This is best indicated by the resolutions of the high energy A_1 modes which have been discussed by Keiter *et al.*[5] Such an additive effect is also evident in the overlapping signals of the cyclopentadienyl ring protons in the ^1H spectrum, as well as the presence of two resonances with shift values comparable to those of the respective $M_2(CO)_{10}(\mu$-dppf) in the ^{31}P spectrum (Table 1). These spectral characteristics are consistent with two linked, yet essentially unperturbed coordination spheres. The present synthetic route requires the isolation of the pentacarbonyl metalloligand. This in many cases is found to be thermodynamically less stable compared to the chelate or bridged dimer,[6] as exemplified in the hitherto non-existence of complexes such as $M(CO)_5(\eta^1$-L—L) [L—L = $Ph_2P(CH_2)_nPPh_2$, $n > 3$; $Ph_2As(CH_2)_nAsPh_2$, $n > 1$; $Fe(C_5H_4AsPh_2)_2$]. Our earlier study on $M(CO)_5$(dppm)[7] also suggested that the nucleophilicity of the pendant phosphine can be significantly suppressed by the presumably steric crowding and hence is unsuitable as a precursor for mixed-metal syntheses. The good stability of $M(CO)_5$(dppf) and yet their ready conversion to the dimers are attributed to a delicate balance between the chelate bite, torsion angle and cone angle of dppf as a ligand. Though there are insufficient data to date to probe further into these parameters for different complexation modes of dppf, there is emerging evidence that dppf is not only a chelate ligand, as previously known, but a bridging ligand that can support metal–metal interaction should the situation dictate.[8]

With $Mn_2(CO)_{10}$, the metalloligand attaches itself axially,[9] as evident from IR data (Table 1), to one end of the molecule resulting in the novel $(OC)_5M(\mu$-dppf$)Mn_2(CO)_9$ complexes (Fig. 1) in reasonable yields. The negative mass susceptibility supports the diamagnetic nature of the complex, and together with molecular weight and microanalytical data preclude the possibility of a monomeric 17-electron manganese fragment. Heterometallic complexes of manganese with other metals are abundant and well-documented,[10] but, most of these reported are either dinuclear in nature or larger clusters but based on a single manganese sphere. It is thus envisaged that such an engagement of a $M(CO)_5$ unit onto the dimanganese framework,

as in the title complexes, without inducing metal–metal support between manganese and the metal, and without disrupting the Mn_2 entity, is partly owing to the characteristically low-energy requirement facilitated by the oxidative decarbonylation.[11] There is conflicting evidence in the literature on the stability of Mn—Mn bonds with respect to homolytic scission,[12] but the arguments tend to favour the bond being photosensitive but thermally resistant. Nucleophilic attack leading to the rupture of the metal–metal bond is, however, undisputed in many dinuclear species.[13] The absence of serious side-reactions arising from the fission of the Mn—Mn bond in the present complexes lends further support to the notion that nucleophilic attack of TMNO occurs on the carbonyl carbon instead of the metal centre.[14] This, together with our recent isolation of the other polynuclear Mn_2-based $(OC)_4Fe(\mu\text{-dppf})Mn_2(CO)_9$ and $(OC)_9Mn_2(\mu\text{-dppf})Mn_2(CO)_9$,[2b] affirms our prediction that there is a rich but largely unexplored low-energy substitution chemistry of dimanganese carbonyls.

Unlike many metal–metal bonded dimers, these singly ligand-bridged complexes are more open and flexible in their structures. The bridging dppf juxtaposes the two metals without significantly altering the reactivity pattern at each site. These characteristics, which contrast distinctly with the metal–metal bonded species and the dppm-bridged complexes[15] which emphasize the cooperative effect of the metals, provide the necessary impetus for our future directives.

EXPERIMENTAL

General procedures

All the preparations and reactions were carried out under a dry nitrogen atmosphere using standard Schlenk techniques. The general procedures and instruments used followed those described in our earlier reports.[1c,2] $M(CO)_5(\eta^1\text{-dppf})$ was prepared as previously described.[1e]

Preparations

$MM'(CO)_{10}(\mu\text{-dppf})$ (M,M′ = Cr, Mo, W; M ≠ M′). Solid $Mo(CO)_5(dppf)$ (0.201 g, 0.23 mmol) was added to a yellow mixture of $Cr(CO)_6$ (0.078 g, 0.35 mmol) and TMNO (0.037 g, 0.33 mmol) which had been stirring in THF (40 cm^3) for 15 min at 25°C. The resultant orange–yellow solution was further stirred for 3 h, after which the reaction mixture was filtered and the solvent removed *in vacuo*. Preparative TLC was used to separate the products, which were eluted with 15% CH_2Cl_2 in hexane solution. Further recrystallization from a CH_2Cl_2–hexane mixture yielded the required orange, heterometallic complex $(OC)_5Cr(dppf)Mo(CO)_5$ (0.082 g, 33%, Found: C, 53.7; H, 2.8. Calc. for $C_{44}H_{28}CrFeMoO_{10}P_2$: C, 53.8; H, 2.9%), together with an unidentified orange side product (0.033 g).

$(OC)_5Cr(dppf)W(CO)_5$ (0.054 g, 13%) was similarly prepared from $Cr(CO)_5(dppf)$ (0.313 g, 0.42 mmol), TMNO (0.060 g, 0.54 mmol) and $W(CO)_6$ (0.198 g, 0.56 mmol) with a reaction time of 4 h. (Found: C, 49.0; H, 2.5. Calc. for $C_{44}H_{28}CrFeO_{10}P_2W$: C, 49.4; H, 2.6%.)

$(OC)_5Mo(dppf)W(CO)_5$ was similarly obtained from $W(CO)_5(dppf)$ (0.201 g, 0.23 mmol), TMNO (0.032 g, 0.30 mmol) and $Mo(CO)_6$ (0.084 g, 0.32 mmol) with a reaction time of 2 h 15 min (Yield = 0.067 g (26%), Found: C, 47.7; H, 2.5. Calc. for $C_{44}H_{28}FeMoO_{10}P_2W$: C, 47.4; H, 2.5%.)

$MMn_2(CO)_{14}(\mu\text{-dppf})$ (M = Cr, Mo, W). A typical procedure of the synthesis involved the addition of solid $M(CO)_5(dppf)$ (0.3–0.4 g) to a stirred orange mixture of TMNO and $Mn_2(CO)_{10}$ in a stoichiometric ratio of 1:1.3:1.4 in THF for 3 h. Separation by preparative TLC (eluted with 15% CH_2Cl_2 in hexane), followed by recrystallization with hexane led to the isolation of the analytically pure orange–yellow complex.

$(OC)_5Cr(dppf)Mn_2(CO)_9 \cdot 1/3C_6H_{14}$: Yield = 56%; mass susceptibility, $\chi_g = -0.324 \times 10^{-6}$ c.g.s.; Found: C, 52.9; H, 3.0. Calc. for $C_{50}H_{33}CrFeMn_2O_{14}P_2$: C, 52.8; H, 2.9%. Mol. wt (benzene), Found: 1110. Calc.: 1108.

$(OC)_5Mo(dppf)Mn_2(CO)_9 \cdot 1/4C_6H_{14}$: Yield = 61%; mass susceptibility, $\chi_g = -0.312 \times 10^{-6}$ c.g.s.; Found: C, 50.6; H, 2.5. Calc. for $C_{50}H_{32}FeMn_2MoO_{14}P_2$: C, 50.6; H, 2.7%. Mol. wt (benzene), Found: 1150. Calc.: 1152.

$(OC)_5W(dppf)Mn_2(CO)_9$: Yield = 61%; mass susceptibility, $\chi_g = -0.223 \times 10^{-6}$ c.g.s.; Found: C, 46.3; H, 2.2. Calc. for $C_{48}H_{28}FeMn_2O_{14}P_2W$: C, 46.5; H, 2.3%.

Acknowledgements—The authors express their gratitude to Y. P. Leong for technical assistance and the National University of Singapore for financial support (Grant No. RP850030) and a scholarship to L.-T.P.

REFERENCES

1. (a) A. W. Rudie, D. W. Lichtenberg, M. L. Katcher and A. Davison, *Inorg. Chem.* 1978, **17**, 2859; (b) I. R. Butler, W. R. Cullen, T.-J. Kim, S. J. Rettig and J. Trotter, *Organometallics* 1985, **4**, 972; (c) P. K. Baker, S. G. Fraser and P. Harding, *Inorg. Chim. Acta* 1986, **116**, L5; (d) E. C. Alyea and S. Somogyvari, *Transition Met. Chem.* 1987, **12**, 310; (e)

T. S. A. Hor and L.-T. Phang, *J. Organomet. Chem.* 1989, **373**, 319.

2. (a) T. S. A. Hor and L.-T. Phang, *J. Organomet. Chem.* 1990, **381**, 121; (b) T. S. A. Hor and L.-T. Phang, *J. Organomet. Chem.*, in press.
3. (a) B. Demerseman, P. H. Dixneuf, J. Douglade and R. Mercier, *Inorg. Chem.* 1982, **21**, 3942; (b) S. R. Iyer, D. R. Tueting and N. E. Schore, *J. Organomet. Chem.* 1987, **320**, 339; (c) G. S. White and D. W. Stephan, *Inorg. Chem.* 1985, **24**, 1499; (d) W. Tikkanen, Y. Fujita and J. L. Petersen, *Organometallics* 1986, **5**, 888; (e) M. Sato, M. Sekino, M. Katada and S. Akabori, *J. Organomet. Chem.* 1989, **377**, 327.
4. (a) D. W. Stephan, *Coord. Chem. Rev.* 1989, **95**, 41 and refs therein; (b) W. L. Gladfelter and G. L. Geoffroy, *Adv. Organomet. Chem.* 1980, **18**, 207 and refs therein; (c) M. I. Bruce, *J. Organomet. Chem.* 1983, **242**, 147 and refs therein; (d) D. A. Roberts and G. L. Geoffroy, in *Comprehensive Organometallic Chemistry* (Edited by G. Wilkinson, F. G. A. Stone and E. W. Abel), Vol. 6, Ch. 40, p. 763. Pergamon Press, Oxford (1982); (e) J. F. Knifton, *J. Molec. Catal.* 1988, **47**, 99; (f) T. Hayashi, M. Konishi, K. Yokota and M. Kumada, *J. Organomet. Chem.* 1985, **285**, 359; (g) P. W. N. M. Van Leeuwen and C. F. Roobeek, *J. Molec. Catal.* 1985, **31**, 345.
5. R. L. Keiter, S. L. Kaiser, N. P. Hansen, J. W. Brodack and L. W. Cary, *Inorg. Chem.* 1981, **20**, 283.
6. (a) P. E. Garrou, *Chem. Rev.* 1981, **81**, 229 and refs therein; (b) S. O. Grim, J. D. Gaudio, R. P. Molenda, C. A. Tolman and J. P. Jesson, *J. Am. Chem. Soc.* 1974, **96**, 3416; (c) W. R. Cullen and J. D. Wollins, *Coord. Chem. Rev.* 1981, **39**, 1 and refs therein; (d) R. L. Keiter, K. M. Fasig and W. C. Lewis, *Inorg. Chem.* 1975, **14**, 201; (e) R. L. Keiter and D. P. Shah, *Inorg. Chem.* 1972, **11**, 191; (f) C. A. McAuliffe and W. Levason, *Studies of Inorganic Chemistry. 1. Phosphines, Arsines and Stilbines Complexes of the Transition Elements*, Ch. IV, p. 212. Elsevier, Amsterdam (1979).
7. T. S. A. Hor, *J. Organomet. Chem.* 1987, **319**, 213.
8. (a) D. T. Hill, G. R. Girard and F. L. McCabe, *Inorg. Chem.* 1989, **28**, 3529; (b) S. Onaka, A. Mizuno and S. Takagi, *Chem. Letts* 1989, **11**, 2037.
9. (a) M. L. Ziegler, H. Haas and R. K. Sheline, *Chem. Ber.* 1965, **98**, 2454; (b) C. U. Pittman Jr and G. O. Evans, *J. Organomet. Chem.* 1972, **43**, 361; (c) E. Singleton and R. H. Reimann, *J. Chem. Soc., Dalton Trans.* 1976, 2109.
10. (a) J. R. Johnson, D. M. Duggan and W. M. Risen Jr, *Inorg. Chem.* 1975, **14**, 1053; (b) R. A. Levenson and H. B. Gray, *J. Am. Chem. Soc.* 1975, **97**, 6042; (c) J. K. Ruff, *Inorg. Chem.* 1968, **7**, 1818; (d) N. Turp, *Coord. Chem. Rev.* 1986, **72**, 197 and refs therein.
11. (a) M. O. Albers and N. J. Coville, *Coord. Chem. Rev.* 1984, **53**, 227; (b) T.-Y. Luh, *Coord. Chem. Rev.* 1984, **60**, 255.
12. (a) A. E. Stiegman and D. R. Ryler, *Accts Chem. Res.* 1984, **17**, 61; (b) T. J. Meyer and J. V. Caspar, *Chem. Rev.* 1985, **85**, 187 and refs therein; (c) M. S. Wrighton and A. F. Hepp, *J. Am. Chem. Soc.* 1983, **105**, 5934; (d) J. P. Fawcett and A. J. Poë, *J. Chem. Soc., Dalton Trans.* 1977, 1302; (e) J. P. Fawcett, A. J. Poë and K. R. Sharma, *J. Am. Chem. Soc.* 1976, **98**, 1401; (f) R. A. Jackson and A. Poë, *Inorg. Chem.* 1978, **17**, 997; (g) L. F. Dahl and R. E. Rundle, *Acta Cryst.* 1963, **16**, 419; (h) D. Sonnenberger and J. D. Atwood, *J. Am. Chem. Soc.* 1980, **102**, 3484; (i) T. J. Oyer and M. S. Wrighton, *Inorg. Chem.* 1988, **27**, 3691; (j) D. R. Kidd, C. P. Cheng and T. L. Brown, *J. Am. Chem. Soc.* 1978, **100**, 4103; (k) P. M. Treichel, in *Comprehensive Organometallic Chemistry* (Edited by G. Wilkinson, F. G. A. Stone and E. W. Abel), Vol. 4, Ch. 29. Pergamon Press, Oxford (1982).
13. (a) H. Vahrenkamp, *Angew. Chem. Int. Edn Engl.* 1978, **17**, 379; (b) T. J. Meyers, *Prog. Inorg. Chem.* 1975, **19**, 1.
14. (a) Y.-L. Shi, Y.-C. Gao, Q.-Z. Shi, D. L. Kershner and F. Basolo, *Organometallics* 1987, **6**, 1528; (b) J.-K. Shen, Y.-C. Gao, Q.-Z. Shi and F. Basolo, *Organometallics* 1989, **8**, 2144; (c) J.-K. Shen, Y.-L. Shi, Y.-C. Gao, Q.-Z. Shi and F. Basolo, *J. Am. Chem. Soc.* 1988, **110**, 2414.
15. (a) X. L. R. Fontaine, G. B. Jacobsen, B. L. Shaw and M. Thornton-Pett, *J. Chem. Soc., Dalton Trans.* 1988, 741; (b) B. L. Shaw, M. J. Smith, G. N. Stretton and M. Thornton-Pett, *J. Chem. Soc., Dalton Trans.* 1988, 2099; (c) G. B. Jacobsen, B. L. Shaw and M. Thornton-Pett, *J. Chem. Soc., Dalton Trans.* 1987, 1509; (d) B. Chaudret, B. Delavaux and R. Poilblanc, *Coord. Chem. Rev.* 1988, **86**, 191 and refs therein; (e) R. J. Puddephatt, *Chem. Soc. Rev.* 1983, **12**, 99 and refs therein.

Polyhedron Vol. 9, No. 18, pp. 2309–2314, 1990
Printed in Great Britain

0277–5387/90 $3.00+.00
© 1990 Pergamon Press plc

COMPLEXES OF OSMIUM(III) DERIVED FROM O,O-DONOR LIGANDS

AHMED M. EL-HENDAWY

Chemistry Department, Faculty of Science, Damietta, Egypt

(*Received* 16 *March* 1990; *accepted* 11 *May* 1990)

Abstract—The complex $[Os^{III}Cl_3(PPh_3)_2MeOH]$ has been prepared and found to be a precursor for the synthesis of $[Os^{III}Cl_2(PPh_3)_2L]$ (L = monoanions of maltol, tropolone, acetylacetone, trifluoroacetylacetone, hexafluoroacetylacetone, benzoylacetone and dibenzoylmethane). These new complexes were characterized by spectroscopic measurements and exhibited a rich redox chemistry as demonstrated by cyclic voltammetry. The catalytic oxidation of alcohols in the presence of excess N-methylmorpholine-N-oxide by $[Os^{III}Cl_2(PPh_3)_2(acac)]$ has been studied and compared with that of the related ruthenium(III) complexes.

Mixed complexes of ruthenium(II) with triphenylphosphine and β-diketones, $[Ru(\beta\text{-diket})_2(PPh_3)_2]$, have been reported.[1] The low-spin ruthenium(III) complexes, $[RuX_2(\beta\text{-diket})(EPh_3)_2]$ (X = Cl, Br; E = P, As), have also been noted.[2,3] Recently,[4] we have prepared and characterized the complexes $[Ru^{III}Cl_2(PPh_3)_2L]$ (L = monoanions of maltol, kojic acid, tropolone and acetylacetone), but no work has so far been reported on similar complexes of osmium(III).

We now report the preparation of the new complexes $[Os^{III}Cl_2(PPh_3)_2L]$ [L = monoanions of maltol (malt), 3-hydroxy-2-methyl-4-pyrone; tropolone (trop), 2-hydroxy-2,4,6-cycloheptatrienone; acetylacetone (acac); trifluoroacetylacetone (tfacac); hexafluoroacetylacetone (hfacac); benzoylacetone (bac); and dibenzoylmethane (dbm)], starting with $[OsCl_3(PPh_3)_2MeOH]$. We also report their spectroscopic and electrochemical behaviour, together with the application of $[Os^{III}Cl_2(PPh_3)_2(acac)]$ to the catalytic oxidation of alcohols in the presence of N-methylmorpholine-N-oxide (NMO) as co-oxidant, since the analogous ruthenium(III) complex[4] and also the $Ru^{II}Cl_2(PPh_3)_3$/NMO system have been studied in this way.[5,6]

RESULTS AND DISCUSSION

On attempting to prepare *fac*-$[OsCl_3(PPh)_3]$ by the method of Taqui Khan *et al.*[7] using $Na_2[OsCl_6]$ instead of $(NH_4)_2[OsCl_6]$, a yellow solid was isolated and shown to be $[OsCl_3(PPh_3)_2MeOH]$ after recrystallization from methanol. Its IR spectrum has a strong broad band at 3473 cm^{-1} likely to have arisen from the ν(O—H) vibration, medium intensity bands at 2984 and 2911 cm^{-1} probably due to ν(C—H), and strong ones at 906 and 889 cm^{-1} which are attributed to the ν(C—O) of coordinated MeOH in the complex. These bands are absent both in $[RuCl_2(PPh_3)_3]$ and our present complexes $[OsCl_2(PPh_3)_2L]$ (L = O,O-donor ligand). We have also prepared $[RuCl_3(PPh_3)_2MeOH]$[8] and observed similar IR bands at 3505, 2941, 2836 and 1012 cm^{-1}, compared with those reported for $[RuCl_3(AsPh_3)_2MeOH]$[9] at 3480 and 1010 cm^{-1}.

Reaction of $[OsCl_3(PPh_3)_2MeOH]$ (**I**) with the O,O-donor ligands (HL) by refluxing for 0.5–2.5 h in methanol affords nice microcrystals with yields of 20–65%. Analytical data indicate that complexes have the formula $[OsCl_2(PPh_3)_2L]$ (L = malt, trop, acac, tfacac, hfacac, bac or dbm). These complexes are only soluble in CH_2Cl_2 and their molar conductivities are very low. Refluxing complex **I** alone in CH_3CN for a few hours gave a red solution from which red crystals were isolated. Analytical data were consistent with this being $[OsCl_3(PPh_3)_2CH_3CN]$, which was previously[10] prepared by long reflux of *trans*-$[OsCl_4(PPh_3)_2]$ in CH_3CN. Dissolution of **I** in CH_2Cl_2 and concentration of the solution by heating yields $[OsCl_3(PPh_3)_2CH_2Cl_2]$ as brown crystals.

The IR spectra of the complexes showed all the

bands due to triphenylphosphine and coordinated L. The general features are similar to those observed for analogous ruthenium complexes.[2-4] Characteristic bands of L are slightly shifted to lower wavenumbers; e.g. the band in the region 1555–1510 cm^{-1} for $[MCl_2(PPh_3)_2L]$ (M = Ru,[4] L = malt, trop, acac) was found at 1549–1510 cm^{-1} (M = Os). This band is tentatively assigned to ν(C═O), where a bathochromic shift (75–105 cm^{-1}) for the carbonyl groups upon coordination is expected.[11,12] A strong band attributed to ν(C—O) was found around 1350 cm^{-1} for $[OsCl_2(PPh_3)_2L]$ (L = trop, acac, bac, dbm), similar to those observed for analogous ruthenium complexes[4] and for $W_2O_5(trop)_2$.[13] The trifluoro- and hexafluoroacetylacetonato complexes show strong bands at 1296 and 1257 cm^{-1}, respectively, also arising from ν(C—O) vibrations. Only one band around 315 cm^{-1} has appeared in the $[OsCl_2(PPh_3)_2L]$ complexes, this is likely to be due to ν(Os—Cl).[14,15] This band is shifted to lower wavenumber in the osmium complexes compared with that observed near 335 cm^{-1} for ruthenium complexes.[4] The most important IR bands are listed in Table 1; the deep colours of the complexes make them unsuitable for Raman studies.

Magnetic susceptibility measurements for $[OsCl_3(PPh_3)_2MeOH]$ at room temperature showed a magnetic moment, μ_{eff}, of 1.48 BM corresponding to one unpaired electron. The other complexes $[OsCl_2(PPh_3)_2L]$, however, have μ_{eff} close to the spin-only value of one unpaired electron lying in the range 1.7–2.0 BM (Table 2), similar to those of *mer-* and *fac*-$[OsL'_3X_3]$ (L' = PBu^n_2Ph, PPr^n_2Ph, PPr^n_3; X = Cl, Br).[16] This suggests the low-spin d^5 $(t_2g)^5$ configuration for the osmium(III) ion in an octahedral environment, which is also the case for the analogous ruthenium(III) complexes.[4]

Electronic spectra and electron spin resonance

The UV–vis spectra of complexes in CH_2Cl_2 solution (Table 1) showed a broad band around 550 nm of low molar absorptivity (ε = 500 M^{-1} cm^{-1}) compared with those for analogous ruthenium(III) complexes[4,17,18] which have been observed at 600 nm. This band may owe its origin to a *d–d* transition. In $[OsCl_2(PPh_3)_2L]$ complexes (L = malt, trop), the band at 550 nm is replaced by high intensity bands in the region 700–500 nm which are tentatively assigned to the π(O,O donor) → $t_2(Os^{III})$ transition, while the weaker ligand-field bands may be obscured by such transitions. Similar bands also were found for $[Os(bipy)_2(acac)]^{2+}$ and $[RuCl_2(bipy)(acac)]$ at 530 nm (ε = 1500).[19] The strong bands in the 400 nm region or below could arise from Cl → t_2 transitions.[14,19]

The ESR spectra in CH_2Cl_2 frozen glasses of the complexes (concentration 5×10^{-3} M) were carried out at −170°C. Cooling was by means of cold nitrogen gas passed over the sample tube. The most significant spectra are those of $[OsCl_2(PPh_3)_2L]$ (L = acac, hfacac). The acetylacetone complex [Fig. 1(a)] shows only two peaks, $g_x = 2.96$ and $g_y = 1.59$, while the third component, g_z, is presumably very low (< 0.46) and lies beyond the maximum field obtainable (B_z > 1400 G). This is typically in accordance with the ESR spectrum of polycrystalline *mer*-$[OsCl_3(PBu^n_2Ph)_3]$ which has g values of 3.3, 1.65 and 0.36 in C_{2v} symmetry.[20] The hexafluoroacetylacetonate complex has another type of ESR spectrum [see Fig. 1(b)] with g_x = 3.00, $g_y = 1.63$ and $g_z = 1.53$, similar to that of $[RuCl_3(PBu^n_2Ph_3)_2]$[20] but with closer peaks (g_y and g_z). The X-ray crystal structure of $[OsCl_3(NH_3)(PPh_3)_2]$ (**A**)[21] has a distorted octahedral configuration with the movement of Cl atoms *cis* to N towards the nitrogen atom. A similar structure (**B**) for our compounds of C_2 symmetry is expected as shown below.

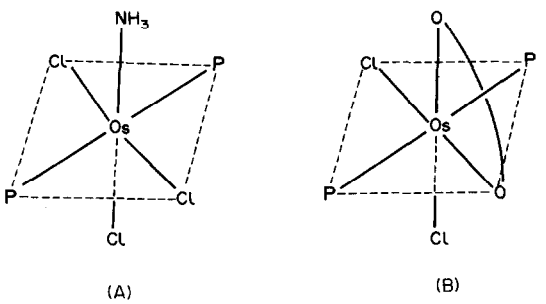

(A) (B)

(P = PPh_3, O–O = acac, hfacac)

Redox properties

The electrochemical properties of the complexes were investigated by cyclic voltammetric techniques. Voltammetric half-potential vs the Ag electrode for 0.1 M $Bu^n_4NPF_6$–CH_2Cl_2 solutions are presented in Table 2. The voltammogram reveals a pair of cathodic and anodic peaks in each case which correspond to Os^{III}/Os^{II} reduction and Os^{III}/Os^{IV} oxidation, respectively, and the peak separation (ΔE) for each complex is close to that anticipated for a Nernstian one-electron process (59 mV).[22] For $[OsCl_2(PPh_3)_2(acac)]$, a representative example (Fig. 2) compared with that of ferrocene [$E_{1/2}$ = 0.21 V, ΔE = 50 mV) under the same conditions, shows a quasi-reversible one-electron oxidation wave, $E_{1/2}$ = 0.78 V, ΔE = 70 mV, and of another wave reduction of $E_{1/2}$ = −0.56 V and ΔE = 80 mV.

Table 1. Analytical and spectroscopic data for complexes

Compound	Colour	Time of reflux, h (Yield)	Analysis, Found (Calc), % C	H	IR data, wavenumbers (cm^{-1}) ν(C=O)	ν(C—O)	ν(Os—Cl)	Other bands	UV–vis data, λ_{max}, nm (ε, $M^{-1}\,cm^{-1}$)
$[OsCl_3(PPh_3)_2MeOH]$	Yellow	4 (80)	52.9 (52.1)	4.0 (4.0)			306s	2984m, 2911w, 906s, 889s	692 (220), 490sh (541), 375 (3,050), 353 (2,800), 337 (2,700), 287sh (8,560), 260sh (18,000)
$[OsCl_2(PPh_3)_2(malt)]$	Green	0.6 (55)	54.7 (54.4)	3.9 (3.8)	1549s	—	310m		606 (1,080), 417 (3,380), 317 (8,060), 274 (12,200), 235 (52,420)
$[OsCl_2(PPh_3)_2(trop)]$	Deep brown	0.5 (50)	57.1 (56.9)	3.9 (3.9)	1510s	1347s	312m		713 (592), 654 (742), 558 (1,274), 486 (3,316), 423 (8,000), 332 (13,880), 315 (14,780), 235 (58,800)
$[OsCl_2(PPh_3)_2(acac)]$	Brown–red	0.5 (65)	55.6 (55.6) Cl: 7.9(8.0)	4.2 (4.2)	1519s	1367s	326m		558 (602), 449 (1,014), 363 (3,344), 354 (3,900), 294 (7,580), 277 (9,220), 268 (9,960), 234 (48,000)
$[OsCl_2(PPh_3)_2(tfacac)]$	Orange	2.5 (30)	52.2 (52.4)	3.6 (3.6)	1522s	1296s	321s		533 (426), 437 (1,914), 382 (4,140), 299 (7,620), 276 (8,760), 269 (9,400), 234 (46,840)
$[OsCl_2(PPh_3)_2(hfacac)]$	Brown	2.0 (35)	47.8 (47.2)	3.1 (3.1)	1447s	1257s	325m		533 (488), 461 (2,150), 421 (3,228), 417 (3,920), 309 (7,220), 276 (7,800), 268 (8,940), 234 (46,040)
$[OsCl_2(PPh_3)_2(bac)]$	Green	1.5 (15)	58.1 (58.3)	4.1 (4.1)	1550s 1520s	1359s	314m		580 (596), 313 (12,840), 233 (49,540)
$[OsCl_2(PPh_3)_2(dbm)]$	Green	1.5 (30)	60.7 (60.7)	4.1 (4.1)	1520s	1358s	318m		578 (532), 341 (18,100), 260 (29,860), 233 (55,240)
$[OsCl_3(PPh_3)_2CH_3CN]$	Red	2.0 (50)	52.7 (52.9) N: 1.65(1.6)	3.8 (3.8)			314m		
$[OsCl_3(PPh_3)_2CH_2Cl_2]$	Brown		49.6 (49.0)	3.5 (3.5)			323s		
$[RuCl_3(PPh_3)_2MeOH]$	Green							2941w, 2836w, 1012m	

Table 2. Magnetic moments and voltammetric half-wave potentials of the complexes

Complex	μ_{eff} (BM)	$E_{1/2}$ (reduction)	ΔE (V)	$E_{1/2}$ (oxidation)	ΔE	$E_{p,a}$[a]	Scan rate (mV s^{-1})
$[OsCl_3(PPh_3)_2MeOH]$	1.48	−0.76	0.070	+0.29	0.060		50, 100
$[OsCl_2(PPh_3)_2(malt)]$	1.74	−0.57	0.070	+0.59	0.240		10, 20, 50
$[OsCl_2(PPh_3)_2(trop)]$	1.66	−0.47	0.070	+0.63	0.250		20, 50, 100
$[OsCl_2(PPh_3)_2(acac)]$	1.89	−0.56	0.080	+0.78	0.070		20, 50, 100
$[OsCl_3(PPh_3)_2(tfacac)]$	2.01	−0.44	0.080	+0.94	0.080		10, 20, 50
$[OsCl_2(PPh_3)_2(hfacac)]$	1.92	−0.21	0.080	+1.21	0.060		10, 20, 50
$[OsCl_2(PPh_3)_2(bac)]$		−0.69	0.100	+0.64	0.080		10, 20, 50
$[OsCl_2(PPh_3)_2(dbm)]$	1.72	−0.66	0.080	+0.64	0.080		20, 50, 100
$[RuCl_2(PPh_3)_2(acac)]$		−0.41	0.070	—	—	+1.26	

[a] Corresponding anodic peak of oxidation.

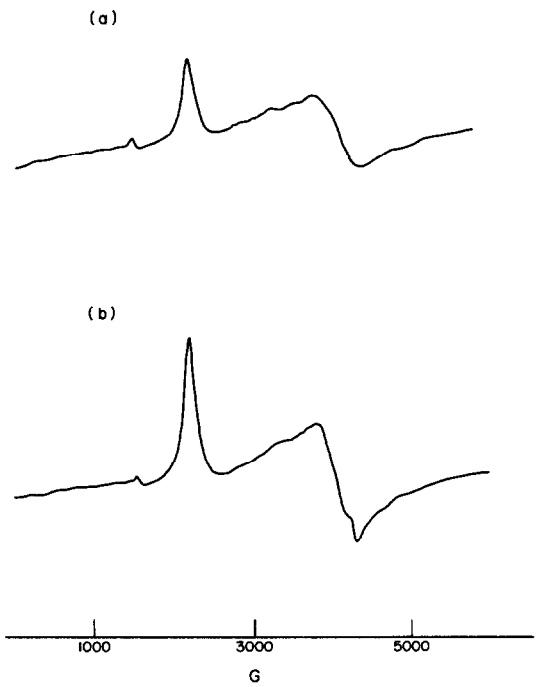

Fig. 1. (a) ESR spectra of *trans*-$[OsCl_2(PPh_3)_2(acac)]$; (b) ESR spectra of *trans*-$[OsCl_2(PPh_3)_2(hfacac)]$.

For scan rates (SR) between 10 and 100 mV s^{-1}, the ratio $i_p/(SR)^{1/2}$ (i_p = peak current) was constant and the ratio of the anodic to cathodic peak current is one, the peak separation being independent of the scan rate. This indicates that electron transfer is reversible or approaches reversibility and the mass transfer is limited. In tropolonato and maltolato complexes, the peak separation of the oxidation wave is 240–250 mV, indicating irreversible behaviour. The presence of such oxidation and reduction waves seems to be typical of osmium(III) halide complexes, e.g. $[OsCl_3(PPh_3)_2(CH_3CN)]$, $[OsCl_3(py)_2(PPh_3)]$[10] and $[Os^{III}X_2(PPh_3)_2L]$[23] (X = Cl, Br; HL = 2-hydroxypyridine, 2-hydroxy-6-methylpyridine and picolinic acid). From Table 2 which includes the cyclic voltammetric data, we conclude that $E_{1/2}$ of the reduction wave is shifted to lower or more negative values relative to $[OsCl_2(PPh_3)_2(acac)]$, reflecting an increase of basicity with more negative values of $E_{1/2}$ as the O,O-donor ligand changes in the order

hfacac < tfacac ≃ trop

< acac ≃ malt < dbm ≃ bac.

There is thus an anticipated increase in the ease of oxidization and decrease in the ease of reduction for the complexes containing benzoylacetone or dibenzoylmethane ligands. The stabilities of the Os^{IV}, Os^{III} and Os^{II} oxidation states in these complexes is reflected by the reversibility of these processes:

$$[OsCl_2(PPh_3)_2L]^+ \underset{-e^-}{\overset{+e^-}{\rightleftharpoons}} [OsCl_2(PPh_3)_2L]$$

$$\underset{-e^-}{\overset{+e^-}{\rightleftharpoons}} [OsCl_2(PPh_3)_2L]^-.$$

Catalytic oxidations

Since $[RuCl_2(PPh_3)_2(acac)]$[4] has been used in the presence of excess NMO for the catalytic oxidation of primary alcohols to aldehydes and secondary alcohols to ketones we tried to use $[OsCl_2(PPh_3)_2(acac)]$ (**II**) as an oxidation catalyst. Although it did catalytically oxidize *p*-methoxybenzyl alcohol to the aldehyde and α-tetralol to α-tetralone over 15 and 36 h, respectively, the yields were low (12 and 18%, respectively, with catalytic turnovers of 50) while piperonyl alcohol and benzohydrol were not oxidized at all. The low reactivity of the osmium

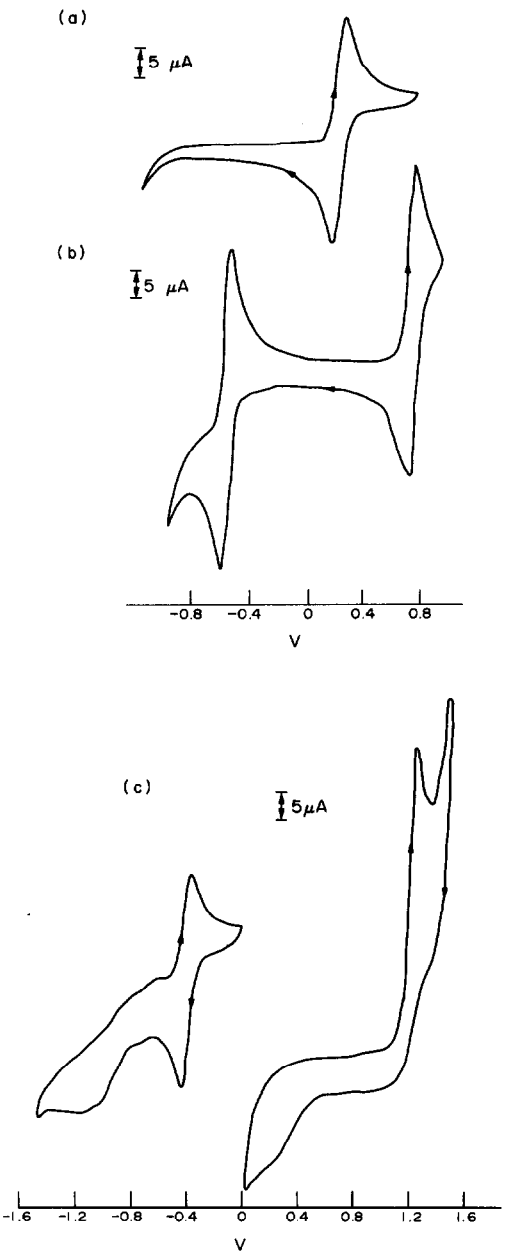

Fig. 2. Cyclic voltammogram, in CH_2Cl_2 with 0.1 M $(Bu^n{}_4N)PF_6$ as supporting electrolyte; volts vs Ag electrode, scan rate 100 mV s^{-1}: (a) Ferrocene; (b) *trans*-$[OsCl_2(PPh_3)_2(acac)]$ ($\sim 10^{-3}$ M), scan rate 50 mV s^{-1}; (c) *trans*-$[RuCl_2(PPh_3)_2(acac)]$ ($\sim 10^{-3}$ M).

complex in comparison with its ruthenium analogue is perhaps not surprising, thus $[RuO_4]^-$ is a much better oxidant than $[OsO_4]^-$.[24] In connection with the effectiveness of $[RuCl_2(PPh_3)(acac)]$ as an oxidant it is of interest to note that an extension of our earlier[4] cyclic voltammetric work on $[RuCl_2(PPh_3)_2(acac)]$ (**III**) to more positive potentials shows a further irreversible oxidation peak ($E = +1.26$ V) of height three times greater than the reduction wave at $E_{1/2} = -0.41$ V ($\Delta E = 70$ mV) vs Ag electrode. The latter wave is due to the Ru^{III}/Ru^{II} reduction,[4] so that the oxidation peak at 1.26 V probably arises from oxidation of Ru^{III} to Ru^{VI}; such an oxidation peak is not found for $[OsCl_2(PPh_3)_2(acac)]$, which gives only Os^{III}/Os^{IV} oxidation. This supports our earlier suggestion[4] that oxidations effected by **III** are likely to occur via higher oxidation states of ruthenium. It is also relevant that $[Ru(acac)_3]$, which has a similar cyclic voltammogram[4,25] to that of **II**, does not effect oxidations of alcohols in the presence of NMO.

EXPERIMENTAL

Preparation of complexes

All preparations use $[OsCl_3(PPh_3)_2MeOH]$ as starting material. This was prepared as follows; a solution of $Na_2[OsCl_6]\cdot 3H_2O$ (0.45 g, 0.9 mmol) in 2-methoxyethanol (60 cm^3) was degassed by passing N_2 through, then conc. HCl (30 cm^3) was added. The mixture was refluxed for 30 min. To the hot solution was added a solution of triphenylphosphine (1.0 g, 3.8 mmol) in 2-methoxyethanol (10 cm^3) and refluxing was continued for 3–4 h under nitrogen. The volume was reduced by 75% and the remaining solution was stored in a refrigerator overnight. After addition of methanol (50 cm^3) the solution was heated and cooled again, when a yellow solid appeared, which was washed thoroughly with water, methanol and ether. The product was recrystallized from methanol and dried *in vacuo*.

Preparation of $[OsCl_2(PPh_3)_2(acac)]$. The complex $[OsCl_3(PPh_3)_2MeOH]$ (0.42 g, 0.5 mmol) was dissolved in methanol (80 cm^3) and refluxed for 30 min on a steam bath until the solution became slightly dark yellow. Distilled acetylacetone (1 cm^3) was then added. A reddish-brown solution was obtained and after continuing reflux for another 30 min, nice brown crystals precipitated which were filtered off, washed with methanol and ether, and dried *in vacuo*.

Preparation of $[OsCl_2(PPh_3)_2L]$ (L = malt, trop, tfacac, hfacac, bac, dbm). A solution of $[OsCl_3(PPh_3)_2MeOH]$ (0.42 g, 0.5 mmol) in methanol (80 cm^3) was refluxed for 30 min, followed by the addition of the ligand (HL) (0.9 mmol). The mixture was refluxed for an appropriate time (as in Table 1). Nice microcrystals formed, which were filtered off, washed with a little methanol and ether and finally dried *in vacuo*. Analytical data are given in Table 1.

Catalytic oxidation by $[OsCl_2(PPh_3)_2(acac)]$ **(II)**

The oxidation of *p*-methoxybenzyl alcohol is typical. To a solution of *p*-methoxybenzyl alcohol (1 mmol) was added NMO (3 mmol) in CH_2Cl_2 (20 cm^3) and 2×10^{-2} mmol of compound **II**. The solution was stirred for 15 h in the presence of 4 Å molecular sieves (0.5 g). The mixture was evaporated to dryness and extracted with ether (2×25 cm^3). The combined ethereal extracts were filtered and evaporated to give *p*-methoxybenzaldehyde which was characterized and quantified as its 2,4-dinitrophenylhydrazone derivative.

The same experiment was carried out using $[Ru(acac)_3]$ (prepared by the literature method[26]) in place of **II** above. The red solution of the reaction mixture does not change and there was no oxidation.

IR spectra were measured on a Perkin–Elmer FT 1720 instrument as liquid paraffin mulls between CsI plates and as KBr discs. The electronic spectra were measured on a Philips PU 8740 UV–vis spectrophotometer or Varian 634 model. ESR spectra were recorded with a Varian E-12 spectrometer. Cyclic voltammetric studies were carried out on a potentiostat/generator (Oxford Electrodes) using a platinum working electrode and silver reference electrode in conjunction with a Philips PM 8043 X–Y recorder. Magnetic measurements were made on a Johnson Matthey magnetic susceptibility balance.

Acknowledgements—We thank the British Council for support, Dr W. P. Griffith for helpful advice, Dr J. F. Gibson for helpful discussion of ESR spectra and also Johnson Matthey Ltd for the loan of precious metals.

REFERENCES

1. J. D. Gilbert and G. Wilkinson, *J. Chem. Soc. A* 1969, 1749.
2. K. Natarajan and U. Agarwala, *Bull. Chem. Soc. Jpn* 1976, **49**, 2877.
3. O. K. Medhi and U. Agarwala, *Inorg. Chem.* 1980, **19**, 1381.
4. A. M. El-Hendawy and M. S. El-Shahawi, *Polyhedron* 1989, **8**, 2813.
5. K. B. Sharpless, K. Akashi and K. Oshima, *Tetrahedron Lett.* 1976, 2503.
6. K. Vijayasri, J. Rajaram and J. C. Kuriacose, *Proc. Ind. Acad. Sci.* 1986, **97**, 125.
7. M. M. Taqui Khan, S. Shareef Ahamed and R. A. Levenson, *J. Inorg. Nucl. Chem.* 1976, 1135.
8. T. A. Stephenson and G. Wilkinson, *J. Inorg. Nucl. Chem.* 1966, **28**, 945.
9. L. R. Ramirez, T. A. Stephenson and E. S. Switkes, *J. Chem. Soc., Dalton Trans.* 1973, 1770.
10. D. J. Salmon and R. A. Walton, *Inorg. Chem.* 1978, **17**, 2379.
11. K. Yamada, *Bull. Chem. Soc. Jpn* 1962, **35**, 1323.
12. M. M. Finnegan, T. G. Lutz, W. O. Nelson, A. Smith and C. Orvig, *Inorg. Chem.* 1987, **26**, 2171.
13. W. P. Griffith, C. A. Pumphrey and C. A. Shapski, *Polyhedron* 1987, **6**, 891.
14. S. M. Tetrick and R. A. Walton, *Inorg. Chem.* 1984, 379.
15. A. M. El-Hendawy, W. P. Griffith, M. N. Moussa and F. I. Taha, *J. Chem. Soc., Dalton Trans.* 1989, 901.
16. J. Chatt, G. J. Leigh, D. M. P. Mingos and R. Paske, *J. Chem. Soc. A* 1968, 2636.
17. O. K. Medhi and U. Agarwala, *J. Inorg. Nucl. Chem.* 1980, 1413.
18. K. Natarajan, R. K. Poddar and U. Agarwala, *J. Inorg. Nucl. Chem.* 1977, 431.
19. G. M. Bryant and J. E. Fergussion, *Aust. J. Chem.* 1971, **24**, 275.
20. A. Hudson and M. J. Kennedy, *J. Chem. Soc. A* 1969, 1116.
21. D. Bright and J. A. Ibers, *Inorg. Chem.* 1969, 1078.
22. R. S. Nicholson and I. Shain, *Analyt. Chem.* 1964, **36**, 706.
23. J. E. Armstrong and R. A. Walton, *Inorg. Chem.* 1983, 1545.
24. A. C. Dengel, A. M. El-Hendawy, W. P. Griffith and A. D. White, *Transition Met. Chem.* 1989, **14**, 230.
25. J. H. Tocher and J. D. Fackler, *Inorg. Chim. Acta* 1985, **102**, 211.
26. A. Endo, K. Shimiza, G. P. Sato and M. Mukaida, *Chem. Lett.* 1984, 437.

Polyhedron Vol. 9, No. 18, pp. 2315–2317, 1990
Printed in Great Britain

0277–5387/90 $3.00+.00
Pergamon Press plc

COMMUNICATION

THE CHAIN–POLYMERIC STRUCTURE OF THE COBALT CHLORIDE PYRIDINE-N-OXIDE COMPLEX $[CoCl_2(pyo)(H_2O)]_n$

MARK NIEUWENHUYZEN, WARD T. ROBINSON* and C. J. WILKINS*

Chemistry Department, University of Canterbury, Christchurch, New Zealand

(*Received* 4 *June* 1990; *accepted* 20 *July* 1990)

Abstract—An X-ray determination of the crystal structure of the cobalt chloride pyridine-N-oxide complex $CoCl_2(pyo)(H_2O)$ shows it to have a polymeric chain structure with mixed bridging by pyo and one chlorine atom. Octahedral coordination of cobalt is completed by the second chlorine atom and the water molecule. These latter two ligands show interchange of positions.

The cobalt chloride pyridine-N-oxide (pyo) complex of composition $CoCl_2(pyo)(H_2O)$ was identified in 1961.[1] Despite the low pyo:Co ratio, the pale red–violet colour of the compound is indicative of six-coordinate cobalt, presumably through ligand bridging. However, the nature of the bridging has remained unanswered.[2–4] The considerable structural information on copper halide–pyo complexes with low pyo:Cu ratios, including $CuCl_2(pyo)(H_2O)$,[5] affords no useful guide; copper develops five-coordination only, with the ligands in varying roles. Through crystal structure determination we have now established the chain polymeric nature of the compound. It represents a type quite apart from other cobalt halide–pyo complexes, which contain the $[Co(pyo)_6]^{2+}$ cation.[6]

EXPERIMENTAL

Preparation

Acicular crystals slowly separated from a violet methanol solution (4.0 cm^3) containing $CoCl_2 \cdot 6H_2O$ (0.30 g) and pyo (0.12 g). Conditions for formation of crystals suitable for diffraction (rather than microcrystalline material) were found rather critical and may depend upon water content. (Found: C, 24.9; H, 2.8; N, 5.8. Calc. for $C_5H_7Cl_2CoNO_2$: C, 24.7; H, 2.9; N, 5.8%.) The corresponding bromide obtained in the microcrystalline form gave: C, 18.6; H, 2.0; N, 4.2. Calc. for $C_5H_7Br_2CoNO_2$: C, 18.1; H, 2.1; N, 4.2%.

X-ray structure determination

Crystal size $0.06 \times 0.1 \times 0.4$ mm; monoclinic, space group $P2_1$, $Z = 2$; $a = 6.835(2)$, $b = 6.706(1)$, $c = 9.217(2)$ Å, $\beta = 102.96(0.02)°$, $U = 411.7(2)$ Å^3, $D_c = 1.96$, $D_m = 1.91$ (room temp.); $F(000) = 242$, $\mu = 26.82$ cm^{-1} (Mo-K_α). Data collection at 160 K, scan rate 2.44° min^{-1}, 2θ range 4–52° with $h = 0$–9, $k = 0$–9, $l = -12$ to 12; 974 unique reflections, 880 [$I > 2\sigma(I)$] used; transmission range 0.816–0.756, absorption correction applied.

Atoms were located from Patterson and difference Fourier syntheses. Refinement indicated the probability of disordering interchange of Cl(2) and O(2) to positions Cl(2′) and O(2′)—see Fig. 1. Partial occupancy was therefore introduced, but with tying between the Cl(2), Cl(2′) and O(2), O(2′) pairs. Excepting these pairs, all other non-hydrogen atoms were refined anisotropically with the weighting factor g fixed at 0.00025. Hydrogen atoms of pyo were located and their positions refined, giving convergence at $R = 0.0246$ and $R' = 0.0313$. Chirality was tested.

Bond lengths and bond angles are given in Table 1. Full data are deposited.

* Authors to whom correspondence should be addressed.

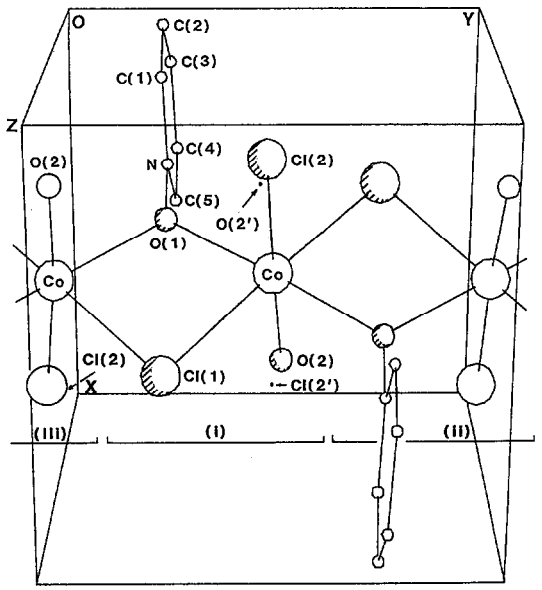

Fig. 1. The cell, containing its asymmetric units (i) x, y, z, (ii) $1-x$, $\frac{1}{2}+y$, $1-z$. The additional atoms Co, Cl(2) and O(2) to the left are from unit (iii) $1-x$, $y-\frac{1}{2}$, $1-z$. Inter-chain approaches to Cl(2) (i) are by O(2) (iv), C(1) (v), C(3) (vi) and C(4) (vi). Approaches to Cl(1) (i) are by C(2) (vii), C(3) (vii) and C(4) (vi). The symmetry codes are: (iv) $x-1$, y, z; (v) $-x$, $y+\frac{1}{2}$, $1-z$; (vi) x, y, $z+1$; (vii) $x+1$, y, $z+1$.

DISCUSSION OF STRUCTURE

The structure comprises a polymer chain developed through mixed bridging by Cl(1) and O(1) of pyo. The atoms Cl(2) and O(2) of the water molecule complete the octahedral coordination around cobalt (see Fig. 1). Refinement gave Cl(2) and O(2) as having 74.6(1.0)% site occupancy with Cl(2′) and O(2′) in the alternative interchanged directions (but at modified distances) contributing the balance. The polymer chains lie parallel to the Y axis, with the asymmetric units in a screw-axis relationship, but with the Co(i) coordinates 0.4915(2), 0.5000, 0.5008(1) there is a slight zigzag of the cobalt atoms. The mean plane through the chain ring atoms CoCl(1)CoO(1) is inclined 67.6° to the YZ face of the cell. The pyo ring is almost perpendicular (92.5°) to this mean plane, with all its carbon atoms involved in (inter- or intra-chain) C···Cl approaches of 3.5–3.8 Å. Atom deviations from ring planarity are small, with maximum 0.022 Å in the chain ring and 0.004 Å in the pyo ring. The atoms O(1) and C(1) lie, respectively, 0.020 and 0.086 Å from the pyo plane. The Co—Cl(1)—Co bridge shows definite asymmetry, with $l = 2.471(2)$, 2.494(2) Å, but asymmetry of Co—O(1)—Co is not certain [$l = 2.038(5)$, 2.047(5) Å]. The screw-axis, rather than mirror plane, relationship of successive units avoids compressed (3.35 Å) distances between pyo ring-planes and at the same time enables intra-chain Cl(1)···C(1)/C(5) approaches. Within the crystal as a whole, cohesion between the chains is provided by the inter-chain C/CH approaches to Cl(1) and Cl(2), and by inferred hydrogen-bonding between O(2) and Cl(2), or between O(2′) and Cl(2′). These O(2)···Cl(2) and O(2′)···Cl(2′) distances are 3.23 and 3.16 Å, respectively.

The structure, though of unusual type, can be considered in relation to that of $CoCl_2(H_2O)_2$ in which there is a chlorine-bridged chain of edge-sharing octahedra.[7] Interestingly, this chain structure also occurs, almost unmodified, as a component of the $[(CH_3)_3NH]CoCl_3 \cdot 2H_2O$ lattice.[8] In the present case, one of the two chlorine bridges between each successive cobalt pair is broken in favour of a pyo oxo-bridge; and in consequence only one water molecule is required to complete the cobalt octahedral coordination. From a comparison of bond lengths and angles (Table 2), it is

Table 1. Bond lengths (Å) and bond angles (°)

Co—Cl(1)	2.494(2), 2.471(2)	Co—Cl(2′)	2.572(9)
Co—O(1)	2.038(5), 2.047(5)	Co—O(2′)	2.007(26)
Co—Cl(2)	2.461(3)	N—O(1)	1.366(3)
Co—O(2)	2.106(8)	N—C(1)	1.334(4)
		N—C(5)	1.340(5)

Co—O(1)—Co	110.5(1)	Cl(2)—Co—O(2)	177.4(2)
Co—Cl(1)—Co	85.0	Cl(2′)—Co—O(2′)	174.5(8)
Cl(1)—Co—O(1)	82.0(1)	O(1)—N—C(1)	118.4(3)
N—O(1)—Co	124.7(4), 123.9(4)	O(1)—N—C(5)	118.4(3)
Cl(2)—Co—O(1)	91.0(1)	C(1)—N—C(5)	123.2(3)
Cl(2)—Co—Cl(1)	90.6(1)		

Table 2. Comparison of distances (Å) and angles (°) in related structures

	$CoCl_2(pyo)(H_2O)$	$CoCl_2(H_2O)_2$[7]	$[(CH_3)_3NH]CoCl_3 \cdot 2H_2O$[8]
Co—Cl[a]	2.471, 2.494	2.450, 2.478	2.456, 2.503
Cl—Co—Cl	91.0[b]	87.7	84.5
Co—Cl—Co	85.0	92.4	95.5
Co···Co	3.353	3.628	3.637
Co—OH_2	2.106, 2.007	2.040	2.078
O···Cl	3.23, 3.16[c]	3.219[c]	3.136[d]

[a] A persistent difference in these two bridging bond lengths is apparent.
[b] Cl—Co—O.
[c] Inter-chain hydrogen-bonded.
[d] Hydrogen-bonded to Cl^-.

Table 3. Powder diffraction data; *d* values and relative intensities

$CoCl_2(pyo)(H_2O)$	$NiCl_2(pyo)(H_2O)$	$CoBr_2(pyo)(H_2O)$
9.022(100)	8.992(100)	9.041(100)
6.754(67)	6.712(56)	7.164(31)
6.076(81)	6.050(73)	6.342(39)
4.894(18)	4.872(13)	
4.492(19)	4.479(20)	
3.150(37)	3.120(36)	3.199(25), 3.164(22)
3.030(21)	3.016(19)	3.091(12), 3.012(21)
2.527(14)	2.520(16)	2.724(16)
2.389(15)	2.372(7)	2.437(25)
2.019(15)	2.025(12), 2.010(12)	

Other reflections are: $CoCl_2(pyo)(H_2O)$, 1.602(10); $NiCl_2(pyo)(H_2O)$, 3.387(13); $CoBr_2(pyo)(H_2O)$, 4.077(12), 3.612(14), 2.837(16).

seen that the shorter Co—O—Co bridge provided by pyo causes reduction in the Co—Cl—Co bridge angle. Formation of a crystalline compound of this present structure can thus be seen as the outcome of several factors, including the ability of the chlorine bridging angle (normally in the range 85–95°) to vary, a favourable chain packing which accommodates the pyo rings within surrounding chlorine atoms, and the retention of inter-chain hydrogen-bonding of the kind in $CoCl_2(H_2O)_2$.[7]

The same structure evidently extends to $NiCl_2(pyo)(H_2O)$,[1] because its X-ray powder diffraction pattern is so closely similar to that of $CoCl_2(pyo)(H_2O)$, Table 3, as to indicate an isostructural relationship. The $CoBr_2(pyo)(H_2O)$ pattern is comparable, but differs in detail. We have found no evidence for the formation of cobalt complexes of composition $CoX_2(pyo)_2$, either monomeric—as known for $ZnCl_2(pyo)_2$[9]—or polymeric through halogen- or ligand-bridging. In the absence of water, cobalt chloride gives only $[Co(pyo)_6][CoCl_4]$.[10]

REFERENCES

1. J. V. Quagliano, J. Fujita, G. Franz, D. J. Phillips, J. A. Walmsley and S. Y. Tyree, *J. Am. Chem. Soc.* 1961, **83**, 3770.
2. N. M. Karayaniss, L. L. Pytlewski and C. M. Mikulski, *Coord. Chem. Rev.* 1973, **11**, 93.
3. J. A. Bertrand and D. L. Plymale, *Inorg. Chem.* 1964, **3**, 775.
4. D. H. Brown, D. Kenyon and D. W. A. Sharp, *J. Chem. Soc. A* 1969, 1474.
5. E. D. Estes and D. J. Hodgson, *Inorg. Chem.* 1976, **15**, 348 and refs therein.
6. J. S. Wood, R. K. Brown and N. S. Lehmann, *Acta Cryst.* 1986, **C42**, 410.
7. B. Morosin and E. J. Graeber, *Acta Cryst.* 1957, **16**, 1176.
8. D. B. Losee, J. N. McElearney, G. E. Shankle, R. L. Carlin, P. J. Cresswell and W. T. Robinson, *Phys. Rev.* 1973, **8**, 2185.
9. N. M. McConnell, R. O. Day and J. S. Wood, *Acta Cryst.* 1986, **C42**, 1094.
10. S. Jin, W. T. Robinson and C. J. Wilkins, to be published.

Polyhedron Vol. 9, No. 19, pp. 2319–2351, 1990
Printed in Great Britain

0277–5387/90 $3.00+.00
© 1990 Pergamon Press plc

POLYHEDRON REPORT NUMBER 33

SYNTHESIS, MOLECULAR STRUCTURES, PROPERTIES AND REACTIONS OF HALO- AND CARBONYL(AMINE)COPPER(I) COMPLEXES

KENNETH G. CAULTON

Department of Chemistry, Indiana University, Bloomington, IN 47405, U.S.A.

and

GEOFFREY DAVIES

Department of Chemistry, Northeastern University, Boston, MA 02115, U.S.A.

and

ELIZABETH M. HOLT

Department of Chemistry, Oklahoma State University, Stillwater, OK 74078, U.S.A.

CONTENTS

1. INTRODUCTION 2320

2. SYNTHESIS OF HALO(AMINE)COPPER(I) COMPLEXES 2321
   2.1. Aprotic conditions 2321
   2.2. Protic conditions 2321
   2.3. Amines employed 2321

3. MOLECULAR STRUCTURES AND PROPERTIES OF MONO- AND POLYMERIC HALO(AMINE)COPPER(I) COMPLEXES 2322
   3.1. General structural types 2322
      3.1.1. General considerations 2322
      3.1.2. Coordination number three 2322
      3.1.3. Crosslinked motifs 2323
   3.2. Bond lengths and angles 2323
   3.3. Caution 2324

4. CARBONYL COMPLEXES 2329
   4.1. Scope 2329
   4.2. General principles 2329
      4.2.1. Redox trends 2329
      4.2.2. Principles of CO binding 2329
      4.2.3. Characterization of solution behaviour 2329
   4.3. Bidentate amines 2330
   4.4. Tridentate amines 2331
   4.5. The influence of oxyacid anion co-ligands 2332
   4.6. General conclusions 2334

5. OXIDATION OF HALO(AMINE)COPPER(I) COMPLEXES BY DIOXYGEN . . . 2334
   5.1. General observations 2334
   5.2. Monodentate pyridine ligand systems 2336

5.3. Other amine ligand systems 2337
5.4. Stoichiometries, products and kinetics of oxidation of halo(amine)copper(I) complexes by dioxygen. General observations 2337
5.4.1. Solid or slurry oxidations 2337
5.4.2. Oxidation in protic solvents 2337
5.4.3. Biomimetic studies 2337
5.4.4. Aprotic halo(amine)copper(I) systems 2337
5.5. Stoichiometries of aprotic oxidation by dioxygen at ambient temperatures 2338
5.6. Oxidation kinetics 2339
5.7. Low temperature aprotic oxidation 2341

6. TRANSMETALLATION OF POLYNUCLEAR HALO(AMINE)COPPER(I) COMPLEXES WITH $M(NS)_n$ TRANSMETALLATORS AND OXIDATION OF THE PRODUCTS BY DIOXYGEN 2343
6.1. The discovery of transmetallation 2343
6.2. Transmetallation of halo(amine)copper(I) complexes with $M(NS)_n$ transmetallators . . 2344
6.3. Transmetallation kinetics and mechanisms 2345
6.4. Oxidation of the products of halo(amine)copper(I) transmetallation by dioxygen . . . 2346
6.5. Transmetallation of oxocopper(II) complexes 2346
6.6. Prospects for the development and use of transmetallation chemistry 2348

7. CONCLUDING REMARKS 2348

ACKNOWLEDGEMENTS 2348

1. INTRODUCTION

The element copper is very widely distributed as salts and complexes in plants, invertebrates, animals and common minerals. The known oxidation states are I, II, III and IV.[1]

Of these, the copper(II) or cupric form is by far the most common. Copper(II) displays a wide variety of coordination geometries in its many salts and complexes. Its most common coordination numbers are four, five and six.[2-6]

The next most common oxidation state is copper(I) or cuprous, which also forms a variety of complexes with common ligands. Aquocopper(I) readily disproportionates to elemental copper and aquocopper(II) but copper(I) may be stabilized against disproportionation under aprotic conditions in the presence of a variety of ligands, including amines. The most common coordination numbers for copper(I) are two, three and four.[7-12]

Most copper(I) salts and complexes are air-sensitive. Rates and products of oxidation by dioxygen very much depend on the coordinated ligands, the physical state (solid or in solution) and the presence of water. Copper(I) is stabilized by soft, π-acid ligands like iodides, phosphines,[7] arsines[7,8] and carbon monoxide,[9] while copper(II) has a strong preference for O-donors like water and hydroxide and hard N-donors like ammonia, pyridines and aliphatic polyamines.[2-6] This means that amine–copper(I) complexes are almost invariably air-sensitive, while at the same time implying that the rates and products of their oxidation can be modified or controlled with π-acids coordinated to copper(I).

Air-sensitivity and previous lack of success in growing single crystals of simple amine–copper(I) complexes were, until recently, the major reasons why the structural chemistry of copper(I) is much less well developed[10-12] than that of copper(II).[2-6] Availability of structural information is all the more important when we recall that copper(I), d^{10}, is transparent to common techniques like electronic and ESR spectroscopy and magnetic measurements that are so useful for copper(II) characterization.[2-6,13]

If we are to understand the mechanisms of oxidation of copper(I) complexes and of the many natural and synthetic oxidative reactions that are initiated and catalysed by the copper(I)/(II) couple,[11,14-17] then it is necessary to gather and classify as much information as possible on the underlying copper-based structures.

The aim of this Report is to update previous reviews[10-12] of the structural chemistry of simple halo(amine)copper(I) complexes. This information will be used to discuss recent progress in relating

structure to physical and chemical properties and to explain reactivity in stoichiometric and catalytic systems involving the copper(I)/copper(II) couple. Particular attention will be paid to reactions of halo(amine)copper(I) complexes with carbon monoxide and dioxygen that are so characteristic of copper(I). We also discuss aspects of copper(I)–dioxygen reactions that are the basis of many useful catalytic systems.[11,14-17]

2. SYNTHESIS OF HALO(AMINE)COPPER(I) COMPLEXES

Although copper(I) fluoride is unknown, the other copper(I) halides are common laboratory solids that are only slowly air-oxidized. Purified or freshly-made[18] copper(I) chloride, bromide and iodide thus serve as convenient starting materials for the synthesis of a wide variety of copper(I) complexes. Copper(I) complexes can be made under aprotic or protic conditions.

2.1. *Aprotic conditions*

Many halo(amine)copper(I) complexes may be made simply by adding the appropriate copper(I) halide to the liquid amine, either neat or dissolved in a solvent at a known concentration. However, stoichiometry is not necessarily always controllable by this method.

The preparation of halo(amine)copper(I) complexes in solution requires consideration of solubility as well as attention to maintenance of the copper(I) state. Copper(I) halides are soluble in acetonitrile and to some extent in acetone, methanol, ethanol, tetrahydrofuran, methylene chloride, nitrobenzene and di- and triglyme. The solubility of copper(I) halides in acetonitrile is due to solvent coordination. This and other solvents (and even excess free amine) may co-crystallize in the solid product. Copper(I) may be preserved by maintenance of an argon or dinitrogen atmosphere or by the addition of small amounts of ascorbic acid or hydrazine at any sign of green coloration.[19]

The slow extraction of CuX from a Soxhlet thimble by the distillate from a solvent–ligand[20] mixture has led to complex formation when CuX solubility in the solvent is low. Under these conditions, iodides normally form crystals of greater resistance to decomposition.

Crystallization may also be achieved by solvent diffusion techniques, evaporation of solvent at atmospheric conditions or under vacuum. The addition of a nitrobenzene solution of halo(amine)copper(I) complexes to deoxygenated hexane frequently leads to a solid product.[21] Crystallization from different solvents and at different temperatures has been shown to lead, on occasion, to complexes which differ in stoichiometry and/or structure.[22]

2.2. *Protic conditions*

CuI may be preserved in the cuprous state in saturated solutions of aqueous KI. Reactions under these conditions may lead to KCu_yI_z complexes without amine coordination.[23]

2.3. *Amines employed*

Copper(I) complexes of high stability are obtained with aromatic amines. Thus, many copper(I) halide–amine complexes are known with derivatives of pyridine. However, complexes with tertiary amines (N,N,N',N'-$Me_2NC_2H_4NMe_2$,[24] $Et_2NC_2H_4NEt_2$,[25] triethylamine[26]) and with secondary amines (morpholine,[27] piperidine,[28] N,N'-diisopropylethylenediamine[29] and aniline derivatives[30]) have also been isolated.

Complexes of formula CuXL, L = amine, have been the focus of research over a long period of time. Research groups such as that of Hardt *et al.*[31] focused on the wide variety of stoichiometries and emission properties evinced by these complexes in the solid state. Synthesis has frequently been carried out in neat liquid amine, resulting in an array of different materials. Characterization has too often been limited to an indication of the stoichiometry of reactants and the colour of the solid product. X-ray powder diffraction patterns are sometimes reported. Copper(I) iodide complexes are normally more stable with respect to air and moisture than the chlorides or bromides. Copper(I) fluoride–amine complexes are unreported. Complexes of stoichiometry Cu : X : L (L = ligand) of 1 : 1 : 0.5, 1 : 1 : 1, 1 : 1 : 1.5, 1 : 1 : 2, 1 : 1 : 2.5 and 1 : 1 : 3 have been noted. Many of these are aggregates and include bridging halides. Those of non-integral stoichiometry usually involve bidentate amines.

3. MOLECULAR STRUCTURES AND PROPERTIES OF MONO- AND POLYMERIC HALO(AMINE)COPPER(I) COMPLEXES

3.1. *General structural types*

In the drawings which follow, copper is cross (i.e. double) hatched, halogens are (singly) hatched, nitrogen and carbon are shaded, and oxygen is white.

3.1.1. *General considerations.* Single crystal X-ray diffraction reveals much of the structural chemistry of copper(I) halide complexes with amines to be based on the Cu_2X_2 rhombohedron which may be found in isolation, **I** ($Cu_2X_2L_4$), extended by the sharing of edges to form polymeric pleated sheets **II** [$(CuXL)_x$] or chairs **III** ($Cu_4I_4L_6$), and combined by face sharing to give cubes **IV** ($Cu_4X_4L_4$). Other motifs such as —Cu(L_2)—X—Cu(L_2)—X— chains **V**, $CuXL_3$ monomers **VI** and the $Cu_4X_4L_4$ distorted rectangle **VII** have also been observed. Copper normally achieves tetrahedral coordination by further binding to one or more amine molecules.

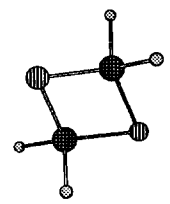

I

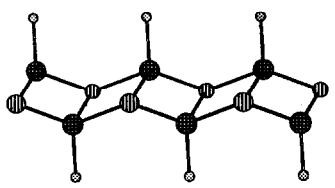

II

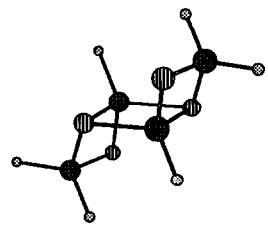

III

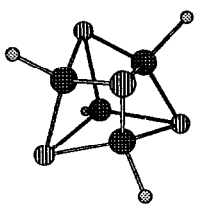

IV

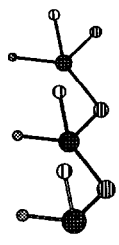

V

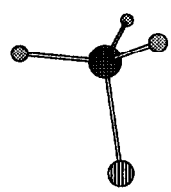

VI

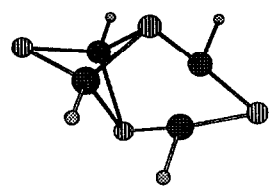

VII

3.1.2. *Coordination number three.* Bulky ligands such as *ortho*-disubstituted pyridine molecules may lead to three coordinate copper(I) atoms which are normally trigonal planar. The $Cu_2X_2L_2$ rhombohedron, $CuXL_2$ monomers, **VIII**,[32] $Cu_2X_2L_2$ rhombohedra (bent **IX**[33] or flat **X**[34]), Cu(L)—X—Cu(L)—X— chains [$(CuXL)_x$], **XI**,[33] and the $Cu_4I_4L_4$ distorted rectangle **VII**[22] are examples of complexes containing three-coordinate copper.

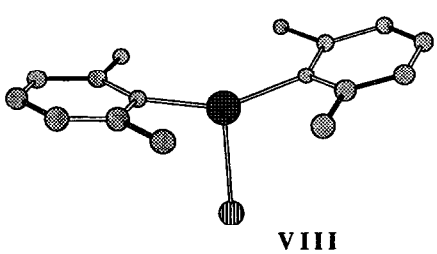

VIII

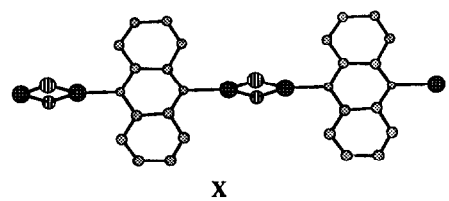

X

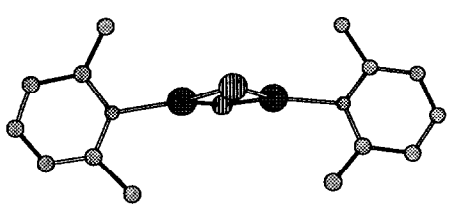

IX

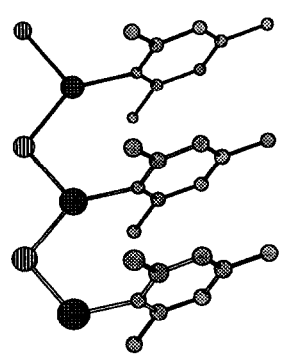

XI

3.1.3. *Crosslinked motifs.* There are examples of motifs (chairs and cubes) substituting intermotif Cu—X bonds for Cu—L binding. Thus, in addition to the Cu_4I_2(2-methylpyridine)$_6$ chair,[26] a Cu_4I_4(2-methylpyridine)$_2$ chair **XII**[35] has been isolated with Cu—I bonds linking adjacent chairs. Similarly, a linked (Cu—I), $Cu_4I_4(Et_3N)_3$ cube **XIII** has been observed.[26] Other types of crosslinking of motifs occur when ligands possess a second potentially coordinating group **XIV**. Thus, pyrazine, quinazoline, phenazine[34] and 3-cyanopyridine[19] lead to motifs of low ligand stoichiometry **XV** with full or partial utilization of additional donor sites on the organic ligand.

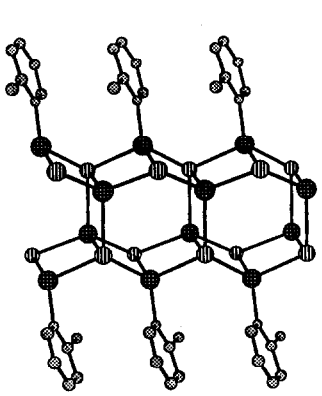

XII

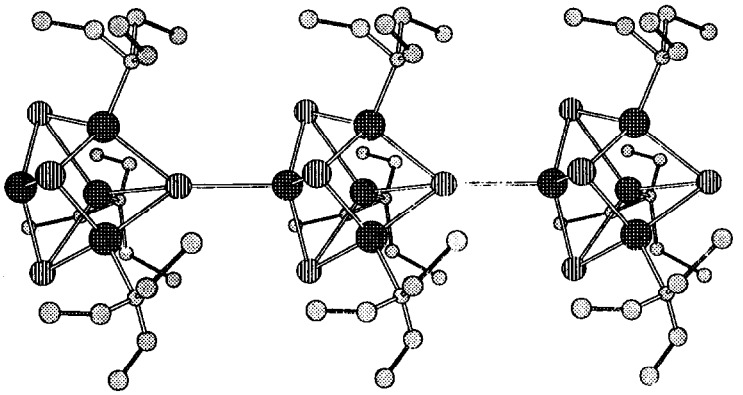

XIII

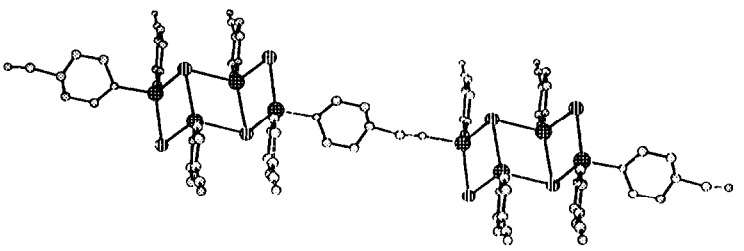

XIV

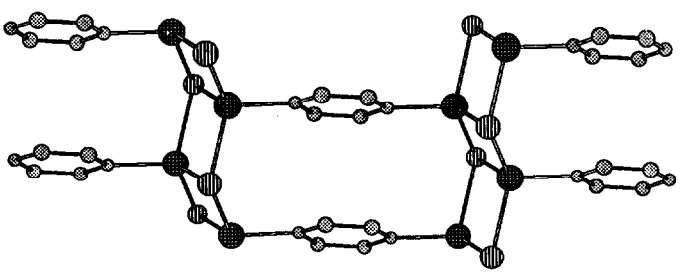

XV

It must be emphasized that there are authenticated cases where a single stoichiometry exists in more than one crystal and molecular structure: "CuI(pyridine)" is found as both a tetramer (cube)[47] and a pleated sheet polymer.[35]

3.2. *Bond lengths and angles*

The Cu_2X_2 rhombohedra, when not extended by edge or face sharing, display considerable variation in Cu—Cu separation (2.5–3.3 Å) which is achieved by distortion of angles within the rhomb. The Cu—Cu separation is normally shorter [2.535(9)–2.586(5) Å] in the ($Cu_2X_2L_2$) rhombohedron than in the corresponding $Cu_2X_2L_4$ complexes. The origins of this flexibility are unclear and may be due simply to crystal packing. In a series of rhombohedral Cu_2I_2 complexes with quinoline, the identity of the organic molecule co-crystallized in the unit cell appears to influence the rhomb

geometry without direct bonding to the metal. Thus, the Cu—Cu separation in Cu_2I_2(quinoline)$_4$ without a lattice guest is 3.364(5) Å,[22] with included CH_3CN is 3.137(2) Å[36] and with co-crystallized quinoline is 2.866(3) Å.[32] Cu_2X_2 rhombohedra are normally planar; however, there are examples of rhombohedra bent about the $X\cdots X$ axis, in one case by as much as 28°.[37]

While the length of the Cu—N bond appears to be a relatively constant, 2.01 Å, the length of the copper(I)–halide bond appears to be influenced by a number of factors: the coordination number of copper, the μ_2, μ_3 or terminal bonding nature of the halide, and the ratio of halide to amine bound to copper. Copper–halide distances also increase with an increase in the overall number of atoms bound to copper. Cu—I bond lengths average 2.55 Å in rhombohedra in which copper is three-coordinate, and elongate to 2.65–2.70 Å in rhombohedra in which copper is four-coordinate. There is less comparative data available for chloro and bromo complexes. Cu—I bonds lengthen as iodide is bound to successively more copper atoms; thus, Cu—X distances increase in the order: terminal $< \mu_2 < \mu_3$.[34] Cu—I distances at four-coordinate copper increase with decreasing numbers of Cu—I bonds (and a corresponding increase in the number of Cu—N bonds). For three complexes of CuI with 3-methylpyridine the distances vary as follows: ($NCuI_3$—cube) 2.649(2) Å,[38] (N_2CuI_2—rhombohedron) 2.655(3) Å,[39] (N_3CuI—monomer) 2.710(3) Å.[40]

Polymeric pleated sheet structures may show successive Cu—X bonds along the polymeric repeat direction to be equivalent or to alternate between long and short distances. For example, sheet polymer CuI(2-methylpyridine) crystallizes with alternating Cu—I bond lengths of 2.646(4) and 2.806(4) Å. This non-equivalence of Cu—X distance has also been observed in molecular species. Thus, in the Cu_2I_2 rhombohedron with N,N′-diisopropylethylenediamine, successive Cu—I distances are 2.661(1), 2.579(1), 2.666(1) and 2.581(1) Å,[29] while in the Cu_2Br_2 rhombohedron with 2,4-dimethyl-1,10-phenanthroline, alternating Cu—Br distances are 2.400(1) and 2.559(1) Å.[37]

3.3. *Caution*

Listed in Table 1 are the copper halo amine compounds which have been structurally characterized.

Table 1. Summary of structures determined by X-ray diffraction

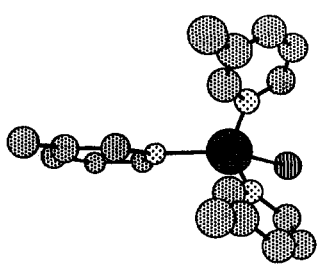

XVI

	Structure	Comments	Reference
(1) Monomer, $CuXL_3$	XVI		
X = I			
3-Methylpyridine			40
X = Br			
3-Methylpyridine			40
X = Cl			
3-Methylpyridine			40,42
(2) Monomer, $CuXL_2$	VIII		
X = I			
2,6-Dimethylpyridine			32
X = Br			
2,6-Dimethylpyridine			40
1-Benzyl-2-phenylbenzimidazole			43
N,N′-Diisopropylethylenediamine			29

Table 1—*continued*

X = Cl			
2,6-Dimethylpyridine			40
2,9-Dimethyl-1,10-phenanthrolene			37

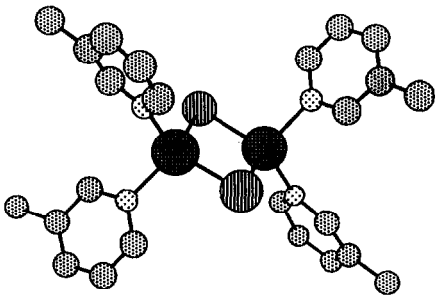

XVII

	Structure	Comments	Reference
(3) Rhombohedron, $Cu_2X_2L_4$			
X = I		Cu—Cu =	
Pyridine	XVII	2.699(5) flat	44
2-Methylpyridine		3.083(3) flat	32
2-Ethylpyridine		3.067(1) flat	32
3-Methylpyridine		2.782(3) flat	39
2,4-Dimethylpyridine		3.140(3) flat	41
3,5-Dimethylpyridine		2.683(1) flat	32
1,10-Phenanthroline (0.5 MeOH)		2.609(2) non-planar 28.6°	37
2,9-Dimethyl-1,10-phenanthrolene		3.024(2) flat	37
Quinoline		3.364(5) flat	22
CH_3CN in lattice		3.137(2) flat	36
Quinoline in lattice		2.866(3) flat	32
$AsMe_2(o\text{-}C_6H_4NMe_2)$		2.737 flat	45
N-N-Diisopropylethylenediamine		2.73	29
Isopropylquinaldate (O-coordination)		2.544(2) flat	46
n-Butylquinaldate (O-coordination)		2.53(1) flat	46
Methyl-2-pyridylacetate		3.427(7) flat	19
3-Cyanopyridine		2.660(2) flat	19
Benzimidazole		2.546(3) flat	43
N,N,N′,N′-Tetramethylenediamine		2.566(4) non-planar	24
X = Br			
2,4-Dimethylpyridine		3.091(3) flat	41
2-Methylpyridine		3.351(3) flat	41
Quinoline—quinoline included		3.140(4) flat	41
2,9-Dimethyl-1,10-phenanthroline		3.097(1) flat	37
N,N,N′,N′-Tetramethylethylenediamine		2.606(6)	25
X = Cl			
2,4-Dimethylpyridine		2.995(2) flat	41
2-Methylpyridine		3.145(3) flat	41
Quinoline—quinoline included		3.121(5) flat	41

	Structure	Comments	Reference
(4) Rhombohedron, $Cu_2I_2L_2$			
2,6-Dimethylpyridine	IX	2.586(5); 12.3° non-planar	33
2,2,6,6-Tetramethylpiperidine		2.535(9) flat	26
2-Phenylbenzimidazole		2.546(3) flat	43
Phenazine [$CuXL_{0.5}$]		cross-linked flat	34

Table 1—*continued*

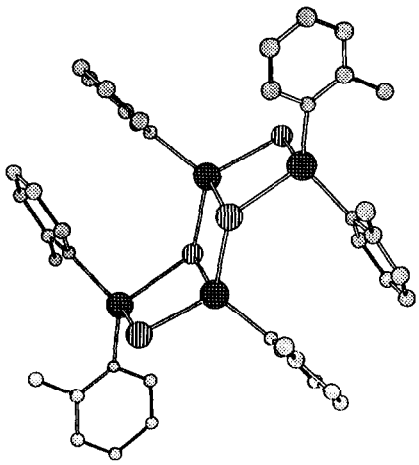

XVIII

	Structure	Comments	Reference
(5) Chair			
$Cu_4I_4L_6$			
2-Methylpyridine	**XVIII**		26
Cu_2I_2L			
2-Methylpyridine	**XII**	polymeric chair	35
$Cu_4I_4L_5$			
4-Cyanopyridine	**XIV**	(cross-linked chair)	19

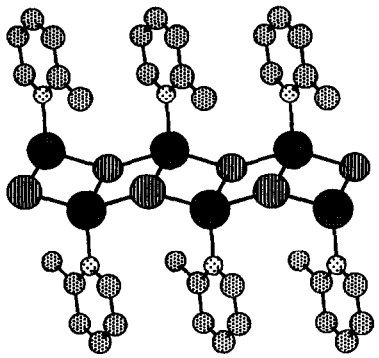

XIX

	Structure	Comments	Reference
(6) Polymeric pleated sheets, $(CuXL)_x$			
X = I			
Pyridine	**XIX**		38
2-Methylpyridine			39
2,4-Dimethylpyridine			39
3-Cyanopyridine			19
Benzylnicotinate			19
3-Pyridylacetonitrile			19
Methylnicotinate			19
Isopropylnicotinate			19
n-Butylnicotinate			19
n-Propylnicotinate			19
Nicotinamide			19
Isonicotinamide			19

Table 1—*continued*

Isonicotinic acid			19
Methylisonicotinate			1934
Pyrazine, $CuIL_{0.5}$		cross-linked	34
Quinoxaline, $CuIL_{0.5}$		cross-linked	43
Benzimidazole			
X = Br, Cl			33
Pyridine			

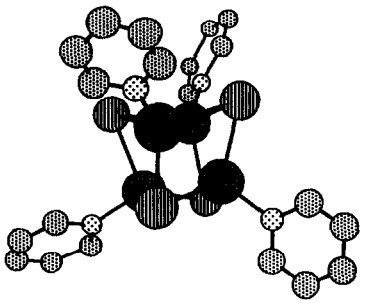

XX

	Structure	Comments	Reference
(7) Cube, $Cu_4X_4L_4$			
X = I			
Pyridine	XX		47
2-Methylpyridine			26
3-Methylpyridine			38
Morpholine			27
Piperidine			28
p-Chloroaniline$_2$(CH_3CN)$_2$			30
p-Toluidine$_2$(CH_3CN)$_2$			30
Phenylnicotinate			19
Isopropylnicotinate			19
Benzylnicotinamide			19
Benzimidazole · 3diglyme			43
N,N-Diethylnicotinamide			48
X = Br			
Et_3N			49
2-Methylpyridine			50
X = Cl			
Et_3N			49
[Bis(trimethylsilyl)methyl]pyridine			49
$Cu_4I_4L_3$			
Et_3N linked cube, Cu—I linkage	XIII		26

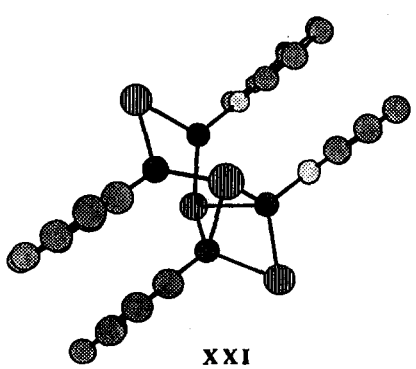

XXI

	Structure	Comments	Reference
(8) Distorted rectangle, $Cu_4X_4L_4$, X = I			
Quinoline	XXI		22

Table 1—*continued*

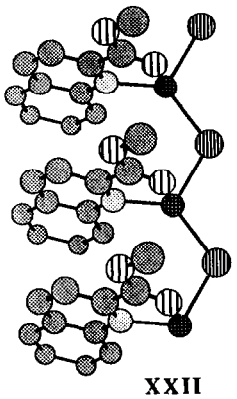

XXII

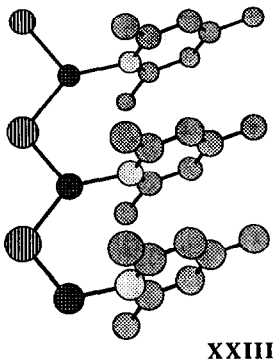

XXIII

	Structure	Comments	Reference
(9) Chain—$(CuXL)_x$, X = I			
X = I			
2,4,6-Trimethylpyridine (three-coordinate copper)	XI		33
Methylquinaldate (O-coordination)	XXII		46
Acridine (three-coordinate copper)	XXIII		26
X = Br, Cl			
Pyrazine, cross-linked	XV		34

It is evident that this field has advanced considerably based on intensive utilization of X-ray diffraction. It is equally evident from the multiplicity of complexes isolated with a single ligand under slightly different conditions of solvent, temperature and stoichiometry that a bulk sample may not duplicate the structure or composition of one single crystal. Similarly, these solid-state structures may correlate poorly (or even not at all!) with solution composition or structure. For example, a 2:1 mixture of CuI and quinoline refluxed in acetone/aqueous KI and crystallized at 55°C yielded $Cu_4I_4(quinoline)_4$ of stoichiometry 1:1.[22] $Cu_2I_2(quinoline)_4$ was crystallized at room temperature from a 1:2 mixture of CuI and quinoline refluxed in a similar manner in acetone and aqueous KI. $Cu_2I_2(quinoline)_4 \cdot quinoline$ was prepared from a solution of CuI in 2-methylpyridine to which quinoline was added (various complexes of CuI and 2-methylpyridine are known to arise from other synthetic procedures).[32] $Cu_2X_2(quinoline)_4 \cdot quinoline$ (X = Br or Cl) were prepared by crystallization of the parent halide from a solution of hot quinoline.[41] These $Cu_2I_2(quinoline)_4$ complexes display a rhombohedral motif with an additional quinoline molecule included in the unit cell. Thus, solvent and temperature of crystallization play a role in determining the structure of the product and the product does not necessarily display the stoichiometry of the reactants as combined. The crystalline materials on which our structural knowledge is based do not necessarily represent the stoichiometries or structures of the complexes formed in solution. Nor is it common practice to establish that the structure of the bulk solid material is the same as that of the single crystal selected for study. Routine comparison of an X-ray powder pattern calculated from the single crystal data with the pattern measured on the bulk solid is highly recommended.

A number of the polymeric pleated sheet and linear chain structures portrayed here exemplify the tendency of aromatic ligands to form planar ("graphitic") stacked arrays, both in molecules and especially in polymeric arrays. Since the coordination sphere of copper(I) appears to be easily deformable, it may be that such inter-ring stacking actually *controls* solid-state aggregation and geometry. Similarly, it is in this way that an included (lattice) aromatic molecule could be more than a passive bystander in the matter of solid-state structure. It has been reported that face-to-face

stacking of aromatic ligands influences luminescence behaviour,[22] when the interaromatic plane distance approaches 3.1 Å.

4. CARBONYL COMPLEXES

4.1. *Scope*

Although the scope of this review is nominally *halo amine* copper complexes, the full impact of the halide ligand upon bonding of the carbonyl only becomes clear by considering halide-free situations. As will be seen, it is the bridging ability of halide ligands which can cause these to competitively inhibit binding of carbon monoxide. We therefore temporarily expand the scope of the review in this section, in order to better understand the general phenomenon of CO binding by copper.

4.2. *General principles*

4.2.1. *Redox trends.* As mentioned in Section 1, a general characteristic of soluble copper(I) in an oxygen (e.g. acetylacetonate) or amine ligand environment is the occurrence of disproportionation [eq. (1)]:[10a]

$$2\,CuX \longrightarrow Cu^0 + CuX_2. \tag{1}$$

Such disproportionation of monovalent copper has been halted in several reports by stabilization via "soft" ligands (e.g. tertiary phosphines, CO, etc.). Binding of CO has been used to stabilize otherwise unstable copper(I)/ligand combinations.[51] Thus, while CuCl + NaOPh soon deposits Cu^0 in methanol or THF solvent, under one atm CO a carbonyl phenoxide complex is formed. Because of the ready reversibility of CO binding, addition of a second ligand (sometimes with replacement of CO gas by N_2) leads smoothly to complexes otherwise unobtainable.

A constructive application of the *reversible* redox reaction in eq. (1) occurs when CuX itself is not available. Then, the comproportionation of copper metal with CuX_2 (e.g. X = β-diketonate) in the presence of a soft ligand has furnished the corresponding monovalent copper complex, Cu(X)L.[52]

Floriani and co-workers have emphasized the tendency of copper(I) aryloxides to decompose to copper metal and have claimed that this represents disproportionation [eq. (2)]:[51]

$$2\,CuOAr \longrightarrow Cu^0 + Cu(OAr)_2. \tag{2}$$

While it is true that deposition of copper metal is accompanied by the appearance of a blue colour, we find[53] that this blue material (hydrocarbon soluble) when Ar = 2,4,6-^{t}Bu$_3$H$_2$C$_6$ is not a copper(II) complex. It can be sublimed at 30–50°C. Elemental analysis of the sublimed blue crystals show it to be the known[54] stable phenoxy radical. Thus, the blue colour of the stable radical can be mistaken as indicating copper(II), and the decomposition reaction is not disproportionation [eq. (2)], but rather homolysis [eq. (3)]:

$$CuOAr \longrightarrow Cu^0 + ArO^0. \tag{3}$$

4.2.2. *Principles of* CO *binding.* Another general observation is that copper(I) and CO are relatively poorly matched reaction partners. Carbon monoxide relies heavily on back-bonding for the strength of the M/C bond: witness the rarity of carbonyl compounds of oxidation number +3 and higher, as well as the rarity of carbonyl adducts of the non-transition metals. Copper(I), on the other hand, is reluctant to back-bond strongly: the high values of ν(CO) in copper carbonyls is the best indication of this. This is perhaps due to the increased metal nuclear charge of the late transition metals. In summary, CO binding to copper(I) is generally weak (yet there *are* exceptions!) and efforts are required (e.g. working under a CO atmosphere) to maintain them intact.

4.2.3. *Characterization of solution behaviour.* It remains true that progress in copper(I) carbonyl chemistry [and indeed much of the chemistry of copper(I)!] has been severely inhibited by excessive focus on that data which can be reliably gathered: solid-state structure by X-ray diffraction. While such work is both objective (i.e. unbiased by literature precedent and the chemists' preconceived thinking) and definitive, it provides no reliable guide to solution behaviour. Since most studies of chemical reactivity will take place in solution, and since copper(I) is kinetically labile, thus reaching

chemical equilibrium "immediately" (i.e. time of mixing) on change of phase (i.e. dissolving) we make a plea here for more systematic characterization of solution behaviour of newly isolated compounds. Such studies must employ spectral techniques which are diagnostic and definitive (e.g. the d^{10} configuration of copper(I) makes electronic spectra rather insensitive to the environment at the metal), and not obscured by time averaging (as is NMR at 25°C). The closed shell d^{10} configuration also makes NMR chemical shift changes small for ligands upon coordination. Finally, bridging the solid/solution phase change with measurements in both phases by the same spectral method promises to be exceptionally useful (e.g. solid-state NMR). It is unfortunate, in this regard, that copper NMR suffers from large quadrupolar signal broadening in all but close-to-T_d symmetry. Extending available methods for definitive characterization of species present in solution is an objective which warrants the attention of everyone who would subsequently explore the reactivity of copper(I) complexes in solution.

4.3. *Bidentate amines*

CuCl suspended in MeOH, THF or diglymes absorbs[55] CO, but only reversibly; attempts at isolation of the species giving CO absorption at 2070–2085 cm^{-1} result in partial loss of CO. CuBr and CuI absorb CO poorly, if at all. Addition of chelating diamines makes possible the isolation of copper(I) carbonyls, *when* $NaBPh_4$ *is added* (eq. (4), X = Cl, Br, I; TMEDA = N,N,N′,N′-tetramethylethylenediamine):

$$2\,CuX + 2\,TMEDA + 2\,CO + NaBPh_4 \longrightarrow NaX + [Cu_2(TMEDA)_2(CO)_2X]BPh_4. \qquad (4)$$

The structures, **XXIV**, for X = Cl, Br and I, all have two approximately tetrahedral coppers linked only by a bent and symmetrical halide bridge; each TMEDA is bidentate to a single metal. The identity of X has no influence on the Cu—C distances or on the Cu—X—Cu angle, but the TMEDA ligand bends further away from the halide as the halide becomes larger.[55]

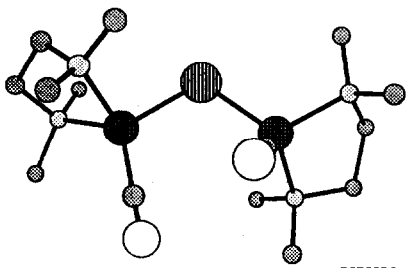

XXIV

Working in methanol, the situation is markedly different when $H_2NC_2H_4NH_2$ (en) is the amine. Then, depending on the en/Cu ratio, either (en)Cu(CO)(η^2-BPh_4) (**XXV**) or $[Cu_2(en)_3(CO)_2](BPh_4)_2$ (**XXVI**) is isolated.[56] The difference has been attributed to the fact that bulkier TMEDA cannot bridge, and does not permit approach of the bulky BPh_4^- unit for η^2-coordination. The interaction of copper with one *ortho* and one *meta* ring carbon is very weak (2.7–2.9 Å; cf. Cu—CO of 1.81

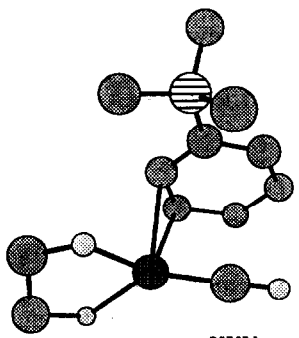

XXV

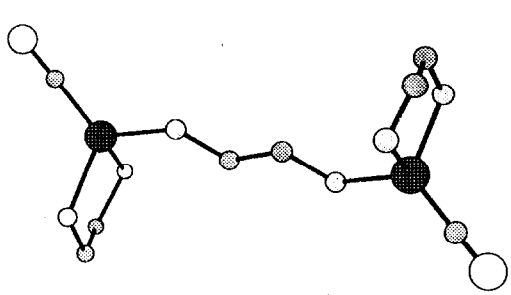

XXVI

Å), and it is suggested, based upon IR observations, that **XXV** transforms to $Cu(en)(CO)S^+$ on dissolving in methanol.

We suggest that there are additional possible factors at work. The presence or absence of halide as a reactive partner will depend in part on the solubility of NaX in the solvent employed. Moreover, the tertiary amine (TMEDA) is unique in precluding the hydrogen bonding available to secondary and primary (i.e. en) amines. Thus, $[Cu(^tBu)(H)NC_2H_4N(H)(^tBu)](OPh)]_2$ is a dimer by virtue of hydrogen bonding from one amine proton to the oxygen of the phenoxide on a second copper.[57] As an extension of this point, protic solvents can alter thermodynamics by hydrogen bonding to halide ligands. Ligands attached to late transition metals are expected to be particularly electron rich (i.e. good hydrogen bond participants) because π-donation from such ligands to the metal is minimal.[58]

Neither $[Cu_2(en)_3(CO)_2](BPh_4)_2$ nor $Cu(en)(CO)BPh_4$ loses CO in the solid state. Curiously, reaction of $Cu(en)(CO)BPh_4$ with $P(OEt)_3$, in methanol, displaces CO essentially quantitatively (rather than the η^2-BPh_4^-). In spite of this *displacement* of CO by added Lewis base, carbonylation of CuI in the presence of a large excess of en *does* give a carbonyl, $[Cu(en)_2(CO)]I$. Whether this contains five-coordinate CO or monodentate en is unknown. Another indication of the importance of competing nucleophiles is the observation that, with CuCl (rather than CuI), some of the above carbonylations are reversible. In summary, the authors note that the two crystallographically-characterized compounds may both arise from the common unit $Cu(en)(CO)^+$ or from $Cu(en)(CO)(MeOH)^+$, which can then bind BPh_4^- in the solid, or two of which can be linked by additional $H_2NC_2H_4NH_2$.

The reactivity of the labile coordination site in $Cu(bidentate)CO(solvent)^+$ is also evident in the composition and structure of $Cu_2(histamine)_3(CO)_2^+$ (**XXVII**) as its BPh_4^- salt.[59] Here, two of the

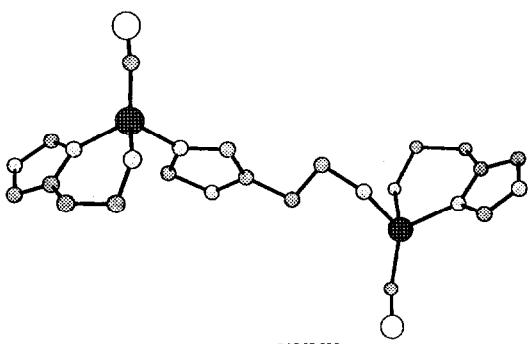

XXVII

histamines are each bidentate on a different metal, and the third links the two metals, thus making the two metal centres inequivalent. Two ν(CO) absorptions are evident in the solid state, at 2055 and 2066 cm^{-1}. The structure of the compound $Cu(histamine)(CO)BPh_4$, from a reaction with a lower histamine/Cu ratio, remains uncertain.

4.4. *Tridentate amines*

The "chelate effect" has been successfully utilized to enhance the stability of copper(I) amine/carbonyl complexes.[60] Thus, while ammonia/copper/carbonyls have eluded isolation,

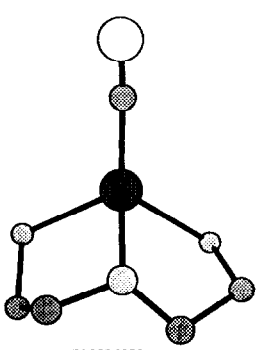

XXVIII

$Cu(NH_2C_2H_4NHC_2H_4NH_2)(CO)^+$ (**XXVIII**) is isolable and does not lose CO at 100°C in the solid state. The synthetic route, eq. (5):

$$CuI + dien + CO + NaBPh_4 \longrightarrow [Cu(dien)CO]BPh_4 + NaI \quad (5)$$

is noteworthy for its utilization of $NaBPh_4$ to not only provide a bulky counter ion for the cationic copper carbonyl, but also to remove I^- (in the form of poorly soluble NaI) as a potential nucleophile competing with CO. This compound exhibits a rather low ν(CO) value (2080 cm^{-1}).

Threefold-symmetric amines have also been employed[60–62] (e.g. $HBpz_3^-$, pz = pyrazolyl) to give a thermally stable molecular carbonyl, $Cu(CO)(HBpz_3)$, with ν(CO) = 2083 cm^{-1}. While resistant to decarbonylation in solution, it does lose CO during vacuum removal of solvent and thus provide access to an interesting composition, "$Cu(HBpz_3)$", which is in fact[63] a dimer containing *four*-coordinate copper (one-third of the pyrazole nitrogens bridge copper pairs). The more sterically "protecting" $HB(3,5\text{-}Me_2pz)_3^-$ ligand gives $CuCO[(HB(3,5\text{-}Me_2pz)_3]$ (ν(CO) = 2066 cm^{-1}). This requires pumping for 1 week at 65°C to effect decarbonylation, with formation of a dimer of structure wholly distinct from that of $[CuHBpz_3]_2$; each copper is in an approximately trigonal planar CuN_3 coordination environment.[63] This theme has been extended with $HB(3,5\text{-}R_2pz)_3^-$, where R = ^{i}Pr and Ph, to generate the corresponding monocarbonyls, as well as acetone and PMe_3 adducts.[64]

It thus appears clear that the tridentate ligands $HBpz_3^-$ and diethylenetriamine simplify the chemistry by closing off the additional equilibria which exist at the open coordination site of Cu(bidentate)CO^+. While this is advantageous for characterizing compounds involving a labile metal centre, it may be counterproductive in effecting catalysis of carbonylation reactions. Cu(en)(CO)(η^2-BPh_4) serves as an example of this point. Note also, in this regard, that copper(I) *di*carbonyl compounds are exceedingly rare.

4.5. *The influence of oxyacid anion co-ligands*

Tetrameric copper(I) benzoate reacts with CO in the presence of TMEDA to give a carbonyl complex (ν(CO) = 2080 cm^{-1}).[65] Upon addition of $NaBPh_4$ and work-up, some CO is lost to give the only example of a symmetrically *bridging* CO. The structures of the two cations $Cu_2(diamine)_2(\mu\text{-}O_2CPh)(\mu\text{-}CO)^+$ (**XXIX**), where diamine = $Me_2N(CH_2)_nNMe_2$ (n = 2, 3), are very similar. The

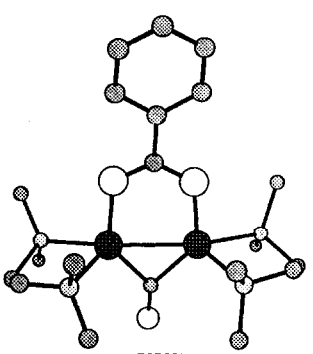

XXIX

bridging benzoate is thought to assist in stabilizing a *di*metal carbonyl (indeed it was selected for that purpose), and the Cu—C distances in the bridging carbonyl moiety (1.87 Å) are consistently short. The carbonyl carbon symmetrically bridges a short (2.41 Å) Cu—Cu distance, and the ν(CO) values ($\sim$ 1925 cm^{-1}) are the lowest reported for a copper carbonyl, yet the highest reported for a μ-CO. The μ-CO moiety becomes terminal in THF solution. This underscores the limited utility of solid-state structural information for solution behaviour.

Attempts to generalize this chemistry to acetate (replacing benzoate) reveals acetate loss in solution. In the presence of excess acetate, an acetato/terminal carbonyl complex could be isolated, which underwent *partial* conversion to a μ-carbonyl only at 60°C in the solid state.

The kinetic lability of copper(I) is thus seen to make impossible the observation and characterization of metastable (kinetically trapped) solution species. Only under unpredictable circumstances does low solubility (e.g. the benzoate complex above) permit isolation of unusual and

interesting species in the *solid* state. It bears mention that ethylenediamine[65] furnishes different steric and basicity properties, but also perhaps because of the considerable hydrogen bonding capability of the amine hydrogens. In the search for non-coordinating counterions which will not be competitive inhibitors of CO binding to copper(I), the group of Floriani has frequently employed BPh_4^-. While this is one of the best available "inert" counterions, we have already seen that a phenyl ring will sometimes function as a π-olefin donor.[56]

Doyle noted the dominance of (poly)amines as co-ligands among copper carbonyl complexes studied.[66] At the same time, it was known that $CuCl/AlCl_3$ (presumably $CuAlCl_4$) forms a benzene-soluble species which reversibly absorbs CO. Motivated by a desire to develop commercially-viable systems for the separation of CO as a component of gas mixtures, Doyle investigated[52,66] sulphonate (RSO_3^-) as a (weak) co-ligand for copper.

Doyle's synthesis is remarkably simple [eq. (6)]:

$$Cu_2O + 2\,CF_3SO_3H + 2\,CO \longrightarrow 2\,Cu(CO)O_3SCF_3 + H_2O \qquad (6)$$

with the evolved water being removed by added molecular seive. Under nitrogen, certain of the compounds (various R) lose CO. All lose CO in air due to oxidation to copper(II). Since the sulphonate vibrational bands were not diagnostic of structure, a single-crystal X-ray diffraction structure determination was carried out on $Cu(CO)O_3SEt$. As is often the case in species of stoichiometry LCuX, the solid is an infinite polymer with bridging X group. In $Cu(CO)O_3SEt$, all sulphonate oxygens are bound to copper, but each oxygen is terminal on a *different* copper, leading to a zigzag, one-dimensional chain of copper(I). These sulphonate carbonyl complexes react with diamines (e.g bipy, *o*-phen or TMEDA) to give $Cu(CO)(diamine)O_3SR$ compounds, but phosphines displace CO instead of sulphonate, to yield $CuL(O_3SR)$. The important conclusion is that there is some thermodynamic bias against a "soft/soft" $Cu(L)(CO)^+$ species. Significantly, mono-olefins, dienes and alkynes also displace CO rather than giving $CuL(CO)^+$ species.[66]

Floriani[67] has attempted to increase CO binding by offering it a particularly reactive metal/ligand fragment possessing an unstable (i.e. reactive) geometry: bent, two-coordinate copper(I) [eq. (7)]:

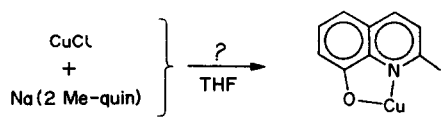

(7)

In fact, disproportionation takes place to give $Cu^{II}(2Me\text{-}quin)_2$. However, if eq. (7) is carried out under 1 atm CO, the thermodynamics of the disproportionation are reversed and $[Cu(2Me\text{-}quin)CO]_4$ may be isolated. This *air-stable* solid dissolves without decarbonylation in THF. An X-ray structure determination shows $[Cu(2Me\text{-}quin)CO]_4$ to have a non-planar eight-membered $(CuO)_4$ ring molecular structure, **XXX**, with the phenoxide oxygens functioning as μ_2-bridges. Four-

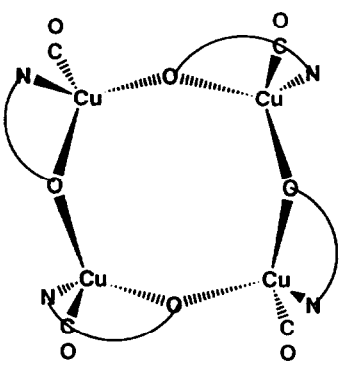

XXX

coordination at each copper is then achieved by terminal binding of CO and the pyridine nitrogen. There is no direct Cu—Cu interaction (they are 3.6 Å apart). *Para*-tolyl isocyanide does not rupture the phenoxide bridges, but instead displaces CO to give $[Cu(2Me\text{-}quin)(CNR)]_n$.

Under vigorous conditions (6–100 atm CO, 80–110°C) $[Cu(2Me\text{-}quin)CO]_4$ reacts to deoxygenate

a number of N/O functionalities [eqs (8)–(11)]:

$$PhNO \longrightarrow PhN(O){=}NPh \tag{8}$$

$$C_6H_5NO \longrightarrow C_6H_5N \tag{9}$$

$$RCH_2NO_2 \longrightarrow (RCN + H_2O) + RC(O)NH_2 + RCO_2H \quad (R = Et, {}^nPn, {}^nBu) \tag{10}$$

$$Me_2CHNO_2 \longrightarrow Me_2C{=}NOH \tag{11}$$

with evolution of CO_2. In certain cases the reaction was catalytic in copper, and, after eq. (8), 40% of the $[Cu(2Me\text{-}quin)CO]_4$ could be recovered.

4.6. *General conclusions*

Both thermodynamic and kinetic factors conspire to limit the number of copper carbonyls. The kinetics of both copper(I) and copper(II) are rapid enough that metastable species will only be detected with substantial effort and even then will only rarely be isolated. Copper in oxidation state II (and above) will probably strongly activate any coordinated CO to nucleophilic attack. Thus, in the presence of traces of water, rapid reduction [eq. (12)]:

$$Cu^{II}(CO)^{2+} + OH^- \longrightarrow Cu^{II}[C(O)OH]^+ \longrightarrow \begin{matrix} Cu^{II}{-}H^+ + CO_2 \\ \downarrow \\ Cu^I + \tfrac{1}{2}H_2 \end{matrix} \tag{12}$$

will occur. The thermodynamics of CO binding to copper(I) can be deduced from the observed high ν(CO) stretching frequencies; back-bonding is very weak, and thus the Cu—C bond is primarily a dative bond, with negligible multiple bond character. One might compare[68] the ν(CO) value of 2044 cm^{-1} in the d^0 complex $Cp^*_2Zr(H)_2CO$. Consider also that there are *no* known carbonyl compounds of the neighbouring metal zinc.

With the Cu^I—CO bond established as weak, it follows that other competitor ligands, even ones as weak as alcohol solvent or bridging halide, represent effective competitors, or even inhibitors of CO binding. While removal of halide from the system has been one effective strategy for halide binding, it is also possible to remove a maximum number of ligands (i.e. use simply unligated CuX), minimize the nucleophilicity of X^- (e.g. $AlCl_4^-$ or HSO_4^-) and choose the solvent to be nearly non-nucleophilic (e.g. benzene). In this way,[69] $CuAlCl_4/C_6H_6$, Cu supported on polystyrene, or CuCl in fuming sulphuric acid have been demonstrated to bind one CO (and even more!) per copper(I). Even here, however, the CO binding is reversible upon swings of pressure, and this property has been put to use for "scrubbing" CO impurities from industrial gases.

5. OXIDATION OF HALO(AMINE)COPPER(I) COMPLEXES BY DIOXYGEN

5.1. *General observations*

As pointed out in the Introduction and emphasized throughout this Report, one of the most characteristic reactions of halo(amine)copper(I) complexes is aerobic oxidation, often referred to as "autoxidation".[16,17] There has been continuous interest in copper(I) autoxidation since the catalytic properties of the products were first recognized.[70]

To work with the most air-sensitive halo(amine)copper(I) complexes is an object lesson in careful experimental technique. Very air-sensitive copper(I) systems are among the most effective known initiators and catalysts for metal-catalysed dioxygen reactions with protic substrates.[16,17,71]

The impetus for study of the reactions of copper(I) with air and dioxygen is the well known fact that pre-oxidation of copper(I) with dioxygen is required for initiation and catalysis of the most effective copper-catalysed oxidation systems.[16,17,71–73] In support of this principle, it is observed that halocopper(I) complexes made with 2,9-dimethyl-1,10-phenanthroline, N,N,N′,N′-tetrabenzylethylenediamine, 1,2-bis(diphenylphosphino)ethane and 2-(2-(dimethylamino)ethyl)pyridine

ligands are air-stable as solids; these solids are either insoluble or air-stable in solvents like methylene chloride and, as a consequence, are not the basis of useful catalytic systems.[74]

As might be expected from its π-acid character, iodide nearly always stabilizes copper(I) to oxidation and so most practical catalytic systems employ either copper(I) chloride or copper(I) bromide. Aprotic solvents are much preferred in such applications.[11,14,16,73]

We do not wish to disparage work on the autoxidation of copper(I) complexes in protic environments,[16,17,71] but would like to express the following opinion. The most straightforward method of studying the reactions of dioxygen with an air-sensitive metal complex is to work, if possible, in an inert, non-coordinating solvent like benzene,[75] toluene or methylene chloride.[21] The reason for this is that all aprotic reduced forms of dioxygen (that is, superoxide, peroxide, O^- and oxide) are protic bases and hence will be involved in acid–base reactions with any protic or aqueous environment. This acid–base behaviour makes study of the mechanisms of copper(I)-promoted reactions in alcohols or water extremely complicated and the results are not always easy to interpret.[16,17,71]

Most metal–dioxygen reactions are studied with the metal complex in excess, which calls for reasonable ($> ca$ 5 mM) ambient copper(I) solubility. Nitrobenzene and methylene chloride are effective, inert, aprotic solvents for most halo(amine)copper(I) complexes and offer a good range of dielectric properties (the dielectric constants are 34.8 and 8.9, respectively, at 25°C). This solvent dielectric difference is a useful probe of oxidation mechanisms (Section 5.5). Methylene chloride is a particularly convenient inert solvent for synthetic work because it is easily purified and evaporated (b.p. 40°C at 1 atm) and can also be used for gel permeation chromatographic product separations (Section 6.5).

Cryoscopic measurements in nitrobenzene (K_f 7.00°C m^{-1}) are appropriate for establishment of the molecularity of halo(amine)copper complexes in aprotic solution. The reason for this is that halides are good ligands for copper(I) and copper(II), especially in the presence of simple mono-, di- or triamines.[76] As a result, such halo(amine)copper complexes commonly exist either as neutral monomers or as polynuclear molecules in nitrobenzene and methylene chloride, depending on the experimental conditions.[11,14,21] This characteristic neutrality simplifies cryoscopy and at the same time eliminates uncertainty connected with the effects of ion-pairing[77,78] on the kinetics of copper(I) oxidation or copper(II) reduction. However, their neutrality often makes halo(amine)copper complexes difficult to crystallize from aprotic solvents (Section 2).

The driving force[11] for aprotic oxidation of a copper(I) complex by dioxygen is the formation of strong bonds between copper(II) and reduced dioxygen species.[14,16,21] The products might be superoxo-, peroxo- or oxocopper(II) complexes.[14,16,79–84] The stoichiometry of oxidation can be measured manometrically at ambient[21] or low[15,16,79] temperatures to determine the extent of dioxygen reduction.

Manometric measurements also establish whether or not the ligands attached to the copper(II) product(s) of oxidation are themselves oxidatively stable. If not, we often see two distinct stages of dioxygen consumption. The first stage is for copper(I) oxidation and the second is for ligand oxidation.[82] This behaviour is observed, for example, with N,N,N′,N′-tetraethylethylenediamine (TEED)[79–81] and 2-methylpyridine[82,83] ligands, both of which suffer alkyl substituent oxidation in the presence of excess dioxygen.

Quite a lot of effort has been expended on finding soluble halo(amine)copper(I) complexes whose ligands are oxidatively stable[82] and a list of desirable ligand characteristics has been drawn up.[14] The number of common, acceptable ligands is small because simple, dissolved halo(amine)copper(I) complexes have a great tendency to reduce dioxygen completely to oxide and the resulting oxocopper(II) products are strongly basic oxidants.[82,83] This means that oxocopper(II) complexes are very sensitive to water and will react with or oxidize most other protic substances.

Among the few common oxidatively stable ligands that form well-characterized, soluble, air-sensitive complexes with copper(I) halides in aprotic solvents are monodentate pyridine (py), ethylnicotinate (ENCA) and N,N-diethylnicotinamide (DENC). The ligand py has long been of interest because of its ability to promote a wide variety of copper-catalysed reactions of dioxygen (see below).[11,16,72,73]

Solubility of copper(I) halides is always greater with ENCA and DENC ligands than with py, which is an important synthetic consideration.[21,75,84] Bidentate ligands from the N,N,N′,N′-tetraalkyldiamine family also form useful dimeric halo(amine)copper(I) reductants for dioxygen[12,79–81]

but the dimeric oxocopper(II) products must be stabilized, for example by reaction with carbon dioxide (see below).[74,78,84]

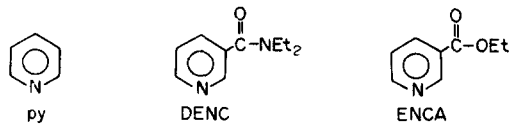

py DENC ENCA

We will now discuss the solution properties of halo(pyridine)– and halo(amine)–copper(I) complexes in more detail.

5.2. *Monodentate pyridine ligand systems*

The solubility of halo(pyridine)copper(I) complexes is usually greatest for the chloride but is also dependent on the pyridine ligand, molar ratio R = [pyridine]/[copper(I)], solvent and temperature. Solubility in ambient methylene chloride increases with DENC $\simeq$ ENCA $\gg$ py at $R = 1.0$. We will deal with the simplest molecular copper(I) systems first.

Cryoscopic determinations in nitrobenzene and measurements of the kinetics of copper(I) oxidation by dioxygen in an aprotic solvent can be used to establish the copper species present in a given aprotic system.[21,79–81] We find that N = DENC readily forms tetranuclear species $N_4Cu_4X_4$ that are "cubanes"[7,21,75] containing monodentate DENC, as indicated by an X-ray crystallographic study of the iodide,[75] PMR data and a characteristic, single sharp IR band at 1635 cm^{-1} for ν(C=O) in DENC.[7,21,75,85] These cubane tetramers have very little tendency to add DENC.[21] The common ligand DENC is therefore particularly attractive for generating simple tetrameric copper(I) reductant systems.[21,74]

Changing the amine ligand from N = DENC to N = ENCA has two very interesting effects. First, we now find that each copper(I) centre can coordinate up to *two* ENCA molecules in tetrameric molecules $N_4Cu_4X_4$ and $N_8Cu_4X_4$. Cryoscopic and kinetic measurements indicate that these species are both symmetrical, halo-bridged "cubanes"[7] with terminal N ligands.[21,75] This means that each copper(I) centre in $N_8Cu_4X_4$ is five-coodinate. Use of R between 1 and 2 presumably gives mixtures of $N_{8-x}Cu_4X_4$ species (x = 1–4). An ability to change the coordination number of copper(I) in a common tetrameric core structure is very important in establishing oxidation mechanisms (Section 5.6).[11,21]

Formation of $N_8Cu_4X_4$ is particularly favoured with N = ENCA and X = Br in nitrobenzene at $R = 2.0$. However, changing R from 1.0 to 2.0 in methylene chloride gives a system whose constituents very much depend on the total copper(I) concentration, especially when X = Cl. In fact, the predominant species in methylene chloride at low copper(I) concentrations is monomeric N_2CuCl, which dimerizes to $N_4Cu_2Cl_2$ with increasing [CuCl] but does not further dimerize to $N_4Cu_4Cl_4$ or $N_8Cu_4Cl_4$ species except at the highest practical copper(I) concentration in this solvent.[21]

As already noted, py gives less soluble complexes with copper(I) halides than do most *m*- or *p*-substituted monodentate pyridines. Although useful concentrations of $py_4Cu_4Cl_4$ can be obtained in nitrobenzene, this is not a practical proposition in methylene chloride.[11,21,86,87] The solubility is much higher at $R = 2.0$, but we now find a complicated mixture of soluble species py_2CuCl, $py_4Cu_2Cl_2$ and $py_8Cu_4Cl_4$, with the latter most favoured by high copper(I) concentrations (as found with ligand ENCA).[21] Marked sensitivity to the pyridine concentration [py] greatly complicates the kinetics of the well-known[73] oxidative coupling of phenols catalysed by oxo(pyridine)–copper(II) species in methylene chloride (Scheme 1).[14,16,79,81,82,86–88]

The most important recommendation of this Section is to establish the molecular forms of copper(I) halides in any particular amine/solvent system by cryoscopy or other suitable means before reactivity studies are made. This is, of course, absolutely essential in kinetic studies.[11,14,17,21,79–81,84,88] We note that the simplest known aprotic halocopper(I) systems with monodentate pyridine ligands in aprotic solvents are those made from DENC/CuX, which give tetrameric $(DENC)_4Cu_4X_4$ species over a wide range of copper(I) concentrations.[11,21,75,87]

5.3. *Other amine ligand systems*

Except for some examples of systems mentioned earlier,[74] most aliphatic mono- and polyamines L form very air-sensitive, soluble complexes with copper(I) halides.[14,16,17,73,79-81] These complexes characteristically exist as halo-bridged dimers both in the solid state (Section 2)[12,80] and in aprotic solvents.[79-81] They are excellent initiators for a wide variety of useful dioxygen reactions, most of which involve protic substrates.[12,14,16,73,79-81,88] The persistently short, 2.5–2.7 Å, Cu—Cu distances in LCu(X,X)CuL molecules (Section 2)[12,25] are important in determining the products and mechanisms of their oxidation by dioxygen[14,29-31] (Section 5.6). Dimeric halocopper(I) complexes with diamine ligands L show little tendency to add L or to break down to monomers in methylene chloride or nitrobenzene, but osmotic molecular weight measurements show that dimer breakdown is more likely to occur in acetonitrile (AN).[12] We note that $Cu(AN)_4Y$ salts, where Y is a variety of monoanions, are common starting materials for the synthesis of many amine–copper(I) complexes;[16] AN is a good ligand for copper(I) and for this reason greatly complicates measurements of the kinetics of copper(I) reactions with dioxygen in aqueous AN.[89] We should therefore avoid AN as an additive or solvent if the desired copper(I) products are polynuclear and contain only mono- or diamine ligands.

It has been accepted for some time that ligands containing N—H groups are not stable ligands for oxidized copper(I) halides.[11,16,73,82] The simplest solution to this problem is alkylation of all ligand N—H groups and the use of poly-N-(alkyl)polyamines as ligands in studies of copper(I) oxidation by dioxygen.[76,79-82]

5.4. *Stoichiometries, products and kinetics of oxidation of halo(amine)copper(I) complexes by dioxygen. General observations*

There have been many studies of copper(I) "autoxidation" reactions[16,17] which can be considered under four main headings.

5.4.1. *Solid or slurry oxidations.* Solid or slurry copper(I) oxidation systems are qualitative in the sense that the ultimate products often are unidentified solids, catalytic solutions or mixtures.[16,72,73,83] Studies of the stoichiometries and rates of such reactions by dioxygen uptake measurements may or may not give useful information, depending on whether the product is non-stoichiometric, the ligand is oxidatively unstable or the solvent is protic. Even in favourable circumstances, kinetic measurements of dioxygen uptake by solids or slurries often are irreproducible and are of questionable value in understanding oxidation and catalytic mechanisms.[90]

5.4.2. *Oxidation in protic solvents.*[16,17,71,89] Data obtained for oxidation of copper(I) complexes by dioxygen in protic solvents are a source of useful rate information. However, such systems often are not completely understandable in mechanistic terms because of the basic character of reduced forms of dioxygen and the inevitable presence of many different copper(I) reductant species and copper(II) oxidation products (see comments in Section 5.1).

5.4.3. *Biomimetic studies.* These are intended to duplicate the physical and chemical properties of the active sites of copper-containing proteins.[15,16] A careful choice of polyamine ligands has led to considerable success in this area, particularly with respect to the characterization of dimeric peroxocopper(II) cations at low temperatures and the discovery of stoichiometric oxygenase activity.[15,16,91-93] The use of aprotic solvents is appropriate because the active sites of copper-containing proteins probably are hydrophobic.[15,16,93] The stage is now set for kinetic and mechanistic studies of these interesting biomimetic systems. Success is likely because of the availability of X-ray structural information on the dimeric copper(I) reactants.[16,94] Information gained from studies of the kinetics of simple halo(amine)copper(I)–dioxygen systems should be useful in interpreting the data.[14]

5.4.4. *Aprotic halo(amine)copper(I) systems.* As already emphasized, halo(amine)copper(I) complexes are the basis of many practical catalytic systems that employ dioxygen as the formal oxidant.[11,14,16,73] Pre-oxidation of copper(I) with dioxygen is necessary for catalytic activity[11,14,72,73] and particular ligands survive the oxidation process in aprotic solvents.[11,14,74,82] For this reason we focus attention on the stoichiometries, products and kinetics of specific aprotic copper(I)–dioxygen systems in the following sections.

5.5. Stoichiometries of aprotic oxidation by dioxygen at ambient temperatures

The primary stoichiometries of ambient, aprotic oxidation of halo(amine)copper(I) complexes with coordinated ligands py, N and L by dioxygen are given in eqs (13)-(21):[11,14,21,79-84]

$$3py + 4CuX(s) + O_2 \longrightarrow py_3Cu_4X_4O_2 \textbf{(XXXIa)} \quad (13)$$

$$py_4Cu_4X_4 + O_2 \longrightarrow py_4Cu_4X_4O_2 \textbf{(XXXIb)} \quad (14)$$

$$4py_2CuX + O_2 \longrightarrow py_4Cu_4X_4O_2 + 4py \quad (15)$$

$$2py_4Cu_2X_2 + O_2 \longrightarrow py_4Cu_4X_4O_2 + 4py \quad (16)$$

$$py_8Cu_4X_4 + O_2 \longrightarrow py_4Cu_4X_4O_2 + 4py \quad (17)$$

$$N_4Cu_4X_4 + O_2 \longrightarrow N_4Cu_4X_4O_2 \textbf{(XXXII)} \quad (18)$$

$$N_8Cu_4X_4 + O_2 \longrightarrow N_4Cu_4X_4O_2 + 4N \quad (19)$$

$$2N_4Cu_2X_2 + O_2 \longrightarrow N_4Cu_4X_4O_2 + 4N \quad (20)$$

$$2L_2Cu_2X_2 + O_2 \longrightarrow 2L_2Cu_2X_2O \textbf{(XXXIII)} \quad (21)$$

$$2L_2Cu_2X_2O \rightleftharpoons L_4Cu_4X_4O_2. \quad (22)$$

These reactions invariably are studied in the presence of excess copper(I). It is understood here that the data refer to copper(I) oxidation in an inert, aprotic solvent, that py, N and X are oxidatively stable and that L are N,N,N′,N′-tetraalkyldiamines that only suffer slow oxidation in the presence of *excess* dioxygen.[11,14,21,79-82]

The most important features of these reactions are as follows.

(1) Every reaction results in complete dioxygen reduction to give oxocopper(II) products. The stoichiometries $\Delta[CuX]/\Delta[O_2] = 4.0$ distinguish these systems from those that give peroxocopper(II) products (Section 5.6).[14,16,92,93]

(2) Oxidation of monomeric, dimeric and tetrameric halo(pyridine)copper(I) complexes with dioxygen {eqs (13)–(17); the copper(I) halide actually is slurried in eq. (13)[21,87] and reactions (13)–(20) are written in order of increasing R and [CuX]} gives soluble tetrameric oxocopper(II) products that contain either three (in tetrameric product **XXXIa**) or four (in **XXXIb**) py ligands. Distinguishable[87] products **XXXIa** and **XXXIb** are catalytically active in a variety of useful dioxygen systems[16,73] but they cannot be isolated as intact solids.[11,21,83,87]

(3) The products **XXXII** of eqs (18)–(20) also are soluble tetrameric oxocopper(II) complexes that with monodentate N = DENC or ENCA are isolatable as intact solids.[21,75] These products are catalytically inactive in dioxygen reactions, which distinguishes them from products **XXXI**. However, they can be made catalytically active by addition of excesses of aliphatic alkylamines, which substitute for N.[11,21,87]

(4) By contrast, the products **XXXIII** of eqs (21) are oxocopper(II) dimers.[81] Reaction (22) evidently is prevented by (a) high affinity of copper(II) for bidentate L; (b) reluctance of copper(II) to be six-coordinate (it is five-coordinate in tetrameric pyridine-containing products $N_4Cu_4X_4O_2$);[21] and (c) the bulky alkyl substituents of the diamine ligands.[79-82]

(5) A variety of physical and chemical evidence indicates the following core structures for products **XXXI–XXXIII**.[11,14,21,81,87] One piece of chemical evidence comes from eqs (23) and (24):

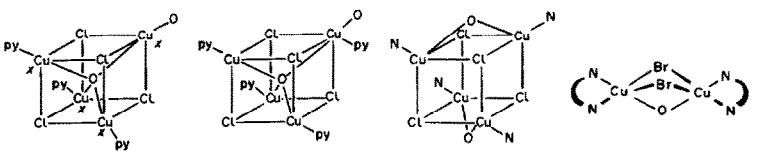

XXXIa **XXXIb** **XXXII** **XXXIII**

$$N_4Cu_4X_4O_2 + 2CO_2 \longrightarrow N_4Cu_4X_4(CO_3)_2 \textbf{(XXXIV)} \quad (23)$$

$$L_2Cu_2X_2O + CO_2 \longrightarrow L_2Cu_2X_2(CO_3) \textbf{(XXXV)} \quad (24)$$

Reaction (23) is not characteristic of products **XXXI**.[11,21,87] Reaction (24) is an important means of stabilizing products **XXXIII** against polymerization[80–82] and the monocarbonate products **XXXV** are useful "off-the-shelf" oxidative coupling initiators.[73,75]

(6) Most neutral oxo(halo)aminecopper(II) complexes disproportionate (with py and N ligands)[21,86,87] or polymerize (L ligands)[81] on attempted crystallization and only products **XXXV** have been crystallized intact. X-ray structural studies on examples of **XXXV** reveal symmetrical (with L = N,N,N′,N′-tetramethyl-1,3-propanediamine, TMPD) and asymmetrical (with L = TEED) μ-carbonato bridging systems that have *trans*- and *cis*-halide configurations in the respective dimers.[74,84] These different dimer configurations can also be *chemically* distinguished from the different products and kinetics of their reactions with 2,4,6-trichlorophenol.[78]

5.6. *Oxidation kinetics*

The kinetics of irreversible, aprotic oxidation of well-characterized excess monomeric, dimeric and tetrameric halo(amine)copper(I) complexes by dioxygen have been measured in benzene, methylene chloride and nitrobenzene.[11,21,75,79–81,88] Ambient oxidation of halo(amine)copper(I) complexes by dioxygen is driven by the formation of strong bonds between copper(II) and oxide. However, oxidation of copper(I) can be strongly inhibited by water and the oxocopper(II) products are very water sensitive.[82,88] For these reasons it is absolutely essential to use pure, anhydrous aprotic ligands and solvents in kinetic studies. The major results of this work are as follows.

(1) The characteristic rate laws for oxidation of monomeric, dimeric and tetrameric halo(amine) copper(I) complexes by dioxygen at ambient temperatures are given by eqs (25)–(27):

$$\text{Rate} = k_m[\text{monomer}]^3[O_2] \tag{25}$$

$$\text{Rate} = k_d[\text{dimer}]^2[O_2] \tag{26}$$

$$\text{Rate} = k_t[\text{tetramer}][O_2] \tag{27}$$

respectively. These rate laws apply to halocopper(I) complexes with py, N or L ligands because dioxygen is completely reduced by copper(I) under non-coordinating ambient aprotic solvent conditions to give oxocopper(II) products.[11,14,21,75,79–81] As a result, the rate laws directly reflect the copper(I) reductant molecularity.[21]

(2) Rate laws (13) demonstrate[21,90] that transfer of the third electron from copper(I) to the dioxygen molecule is required for irreversible dioxygen reduction.[11,14] The reason for this statement is that three monomeric copper(I) species are present in the activated complex associated with irreversible rate law (25). These three electrons are required to break the O—O bond in O_2. Two copper(I) dimers or one copper(I) tetramer contain the four electrons that reduce O_2 to two mols of oxide and so these are the stoichiometric constituents of the activated complexes for irreversible rate laws (26) and (27), respectively. Thus, a very important factor in reactions (13)–(19) is that the tetrameric halo(amine)copper(I) reductants contain the four electrons required to completely reduce a dioxygen molecule to two mols of oxide in a complementary reaction. This results in simple rate law (27)[21] (see also Section 6.4).

(3) Tetranuclear $py_8Cu_4Cl_4$ is oxidized about seven times more rapidly than $py_4Cu_4Cl_4$ by dioxygen in nitrobenzene at 25°C.[21,88] The corresponding second-order rate constant ratio for $(ENCA)_8Cu_4Cl_4$ and $(ENCA)_4Cu_4Cl_4$ is about four.[21] These observations indicate that dioxygen is not coordinated to copper(I) in the rate-determining oxidation step.[21,88]

(4) The oxidation rates are not very sensitive to the solvent dielectric constant and there is no spectral or kinetic evidence for reaction precursors or intermediates. This argues against a rate-determining step involving polar intermediates created by electron transfer from copper(I) to dioxygen.[11,21]

(5) Rate laws (27) with py and N ligands have very small experimental activation enthalpies (the range is 2.1–5.9 kcal mol^{-1}) and very negative activation entropies in the range $-(35–48)$ cal deg^{-1} mol^{-1} at 25°C. The activation enthalpies increase by about 2 kcal mol^{-1} on changing from X = Cl to X = Br in $(py,N)_4Cu_4X_4$ molecules. Very negative activation entropies indicate an associative rate-determining step. The activation parameters actually are quite well correlated by a plot of $\Delta H_t^{\ddagger}$ vs $\Delta S_t^{\ddagger}$, Fig. 1, which is further support for a common slow reaction step. The activation enthalpy for oxidation of $py_8Cu_4Cl_4$ is about 3 kcal mol^{-1}, lower than expected from the other activation

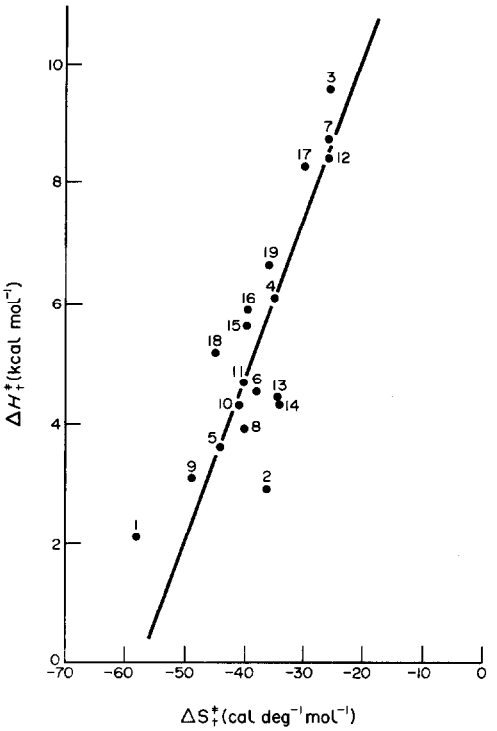

Fig. 1. Correlation of $\Delta H_t^{\ddagger}$ and $\Delta S_t^{\ddagger}$ (at 25°C) for oxidation of tetrameric copper(I)-containing molecules $N_mCu_{4-x}M_x(NS)_yX_4$[a] and L_4Cu_4[b] with dioxygen via rate laws (27) and (48) in nitrobenzene. Each point in the figure is identified in the following key. We conclude from this and other evidence (see text) that electron transfer from copper(I) to dioxygen is not rate-determining in any of the cited systems since correlation of the data is apparent for a wide range of redox driving forces and copper(I) reactants. The major factors that appear to influence $\Delta H_t^{\ddagger}$ and $\Delta S_t^{\ddagger}$ are the stiffness or electron density of the reductant molecular core, the effective nuclear charge of M and possible obstruction of O_2 insertion by NS ligands.[101,102]

KEY

Legend	N	m	M	x	y	Reference	Legend	N	m	M	x	y	Reference
1	py	4		0	0	88	11		3	Ni	1	1	101
2		8		0	0	21	12		3	Zn	1	1	101
3		3	Co	1	2	[c]	13	ENCA	4		0	0	21
4		3	Co	1	1	[c]	14		8		0	0	21
5		3	Ni	1	1	[c]	15	DENC	4		0	0	21[d]
6		3	Zn	1	1	[c]	16	ENCA	8		0	0	21[d]
7		3	Cu	1	1	[c]	17	DENC	3	Ni	1	1	101[d]
8	DENC	4		0	0	21,75	18		3	Co	1	2	102[d]
9		3	Co	1	2	102	19	L_4Cu_4					108a
10		3	Co	1	1	101							

[a] X = Cl unless noted otherwise; [b] L is 6-methyl-2-oxopyridinate (ref. 108); [c] M. A. El-Sayed, G. Davies, A. Abu-Raqabah and A. El-Toukhy, to be published; [d] X = Br.

parameters in Fig. 1 (see Section 7). This evidently is due to the presence of *five*-coordinate py_2CuCl_3 centres in this particular reductant.

The accumulated cryoscopic, spectral and kinetic evidence indicates that dioxygen *insertion* into the tetranuclear cores X_4[7,21,75] of $(py,N)_nCu_4X_4$ molecules is the rate-determining oxidation step. Insertion in this context means that the leading O atom of O_2 has to penetrate one of the six faces of $(py,N)_4Cu_4X_4$ before any electron transfer from copper(I) to dioxygen can take place. The X_4 core evidently is "stiffer" and dioxygen insertion is more obstructed with X = Br. However, the core evidently is "loosened" by an increase in the coordination number of copper(I) on addition of

py and ENCA ligands.[21,88] Dioxygen insertion seems to be obstructed in the same slow step of the corresponding oxidations of transmetallated halo(pyridine)copper(I) species $N_3Cu_3M(NS)_yX_4$ (Section 6.4).

Different product core structures **XXXI** and **XXXII** arise from different relative rates of (a) penetration of the X_4 core by the leading atom of O_2 and (b) concomitant dioxygen reduction by copper(I).[21,87,88] Electron transfer from copper(I) to O_2 is fastest in $py_8Cu_4Cl_4$ tetramers and partial insertion before complete electron transfer required to break the O—O bond results in asymmetrical core structures **XXXI** with ligand py.[21,87,88] Slower electron transfer in $N_mCu_4X_4$ systems results in symmetrical structures **XXXII**.[21]

The third-order rate constants, k_d, of eq. (26) and their activation parameters are very sensitive to the identity of py or N and to the alkyl substituents of ligands L in dimers $[(py,N)_4,L_2]Cu_2X_2$. Particular N-alkyl diamine substituents cause large differences of rate in methylene chloride and nitrobenzene.[81] It is very likely that activated complex assembly (not electron transfer) is the rate-determining step in halo(amine)copper(I) monomer and dimer oxidation by dioxygen.[21,79,81]

5.7. *Low temperature aprotic oxidation*

A great deal of effort has been expended on trying to limit the extent of dioxygen reduction by copper(I) and on characterization of the copper(II) products.[11,14,16,80,92,93] We have seen that there is a marked tendency for complete dioxygen reduction by low molecular weight halo(amine)copper(I) complexes. The physically isolated active sites of the high molecular weight copper-containing proteins called haemocyanins and tyrosinases contain only two copper centres.[16,93] It is known that the copper(I) forms of these metalloproteins reduce dioxygen under ambient conditions to give peroxocopper(II) species.[15,16,92,93] This information has stimulated great interest in making peroxocopper(II) models. Success has been achieved with carefully chosen binucleating tridentate amine ligands.[16,91–93] However, the peroxocopper(II) products are stable only at low temperatures ($< ca$ 240 K), which means that *temperature* is a very important means of controlling the extent of dioxygen reduction by copper(I).[14,16,79] This control could have kinetic or thermodynamic origins.[14,16]

Reducing the temperature simply reduces the rates of reactions (14) and (17)–(19) because each of these redox reactions is complementary. However, reactions (15), (16), (20) and (21) have the potential to generate superoxo- and peroxocopper(II) products because they involve monomeric and dimeric copper(I) complexes. In these cases the anticipated stoichiometries are given by eqs (28)–(30):[16,79]

$$M + O_2 \longrightarrow MO_2 \tag{28}$$

$$2M + O_2 \longrightarrow M_2O_2 \tag{29}$$

$$D + O_2 \longrightarrow DO_2, \tag{30}$$

where M and D represent copper(I) monomers and dimers, respectively. These stoichiometries can be determined manometrically.[15,16,79,91–93] We know of no evidence for the occurrence of reaction (28) in copper(I)–dioxygen systems.[14,79]

A recent study shows that the complete reduction of dioxygen by simple dimers $L_2Cu_2X_2$, eq. (18), can indeed be intercepted at low temperatures in methylene chloride to give peroxocopper products with L = TEED.[79] The products of eqs (18) and (31):

$$2L_2Cu_2Cl_2 + O_2 \longrightarrow (L_2Cu_2Cl_2)_2O_2\ (\mathbf{XXXVI}) \tag{31}$$

are green and blue, respectively. Low temperature blue products **XXXVI** actually are an equilibrium mixture of two, mixed-valence tetrameric peroxocopper species of stoichiometry $(L_2Cu_2X_2)_2O_2$ (Scheme 2).[79] This stoichiometry seems to be imposed by the 2.60 Å separation of the copper centres in $L_2Cu_2Cl_2$ (see refs 12, 25 and Section 2). Irreversible reaction (32) takes place over a very narrow temperature range (−40 to −30°C) because the activation enthalpy and entropy of reaction (32) are estimated to be 25 kcal mol^{-1} and 40 cal deg^{-1} mol^{-1} at 25°C, respectively, in methylene chloride.[79]

The chemistry summarized in Scheme 2 demonstrates that temperature is indeed a very important factor in controlling the extent of reduction of dioxygen by simple monomeric and dimeric copper(I)

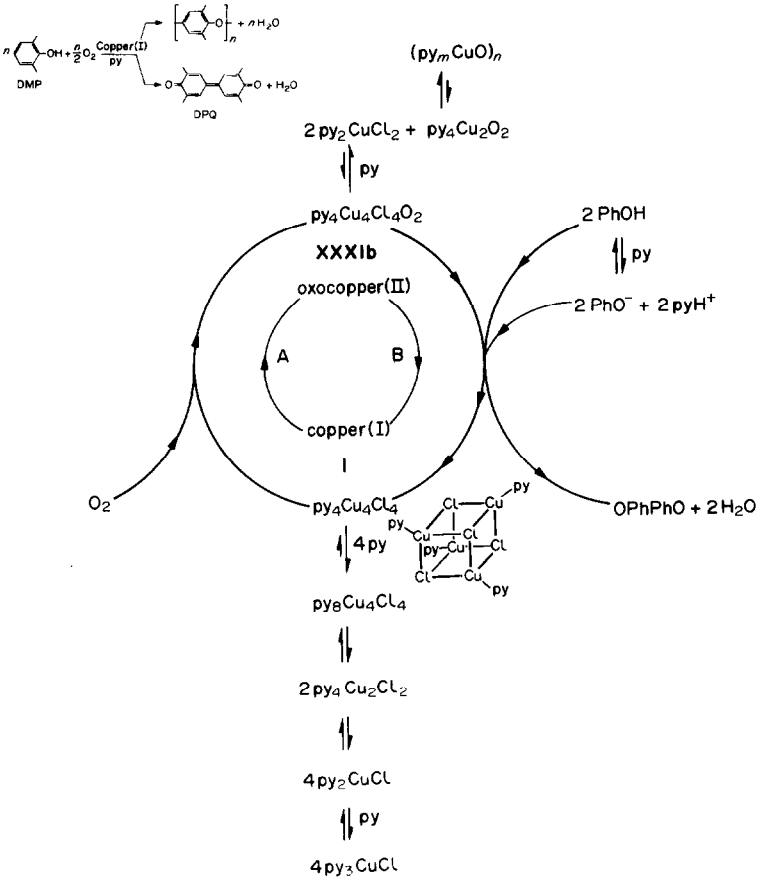

Scheme 1. Equilibria and the proposed[88] central catalytic components **A** and **B** of the py/CuCl/O_2/2,6-dimethylphenol (DMP) system that gives the oxidatively-coupled diphenoquinone product (inset) in methylene chloride and nitrobenzene.[11,73,86b] The catalytic intermediate in the cycle apparently has formal stoichiometry $py_3Cu_4Cl_4O(DMP)_2$.[88] The predominant product at higher pyridine concentrations is poly(2,6-dimethylphenylene oxide) (see inset).[73,88]

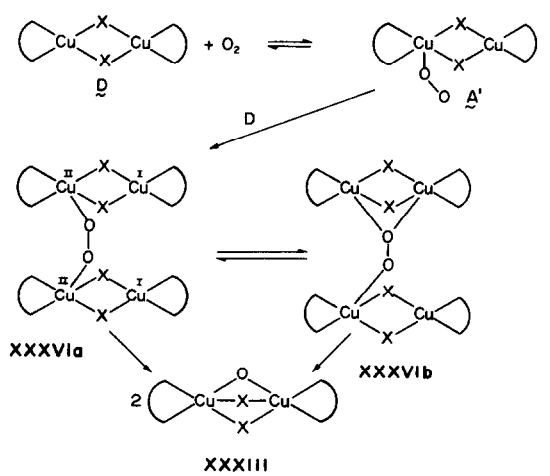

Scheme 2. Equilibria and irreversible reactions in the low temperature oxidation of $(TEED)_2Cu_2Cl_2$ (**D**) by O_2 in methylene chloride.[79] There is no firm evidence for the existence of significant concentrations of species **A′**. Peroxocopper complexes **XXXVIa** and **XXXVIb** [eq. (31)] are irreversibly converted to oxocopper(II) complex **III** in eq. (32) at $T \geq ca.\ -35°C$ (see text).[79]

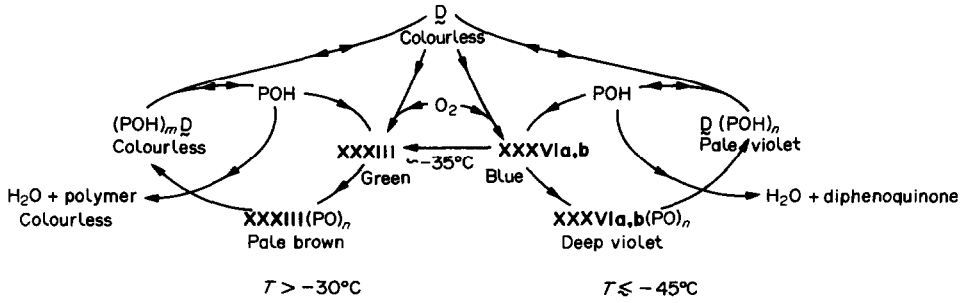

Scheme 3. Schematic catalytic cycles for the low and ambient temperature oxidative coupling of 2,6-dimethylphenol by the $L_2Cu_2Cl_2/O_2$ system of Scheme 2.[79]

complexes.[14,79] This control clearly is kinetic[14,79] because known reactions (29) and (30) have large equilibrium constants.[14–16]

After establishment of the underlying copper chemistry in Scheme 2 it was possible to show that the oxocopper(II) complex $(TEED)_2Cu_2Cl_2O$ from eq. (21) or (32):

$$(L_2Cu_2Cl_2)_2O_2 \longrightarrow 2L_2Cu_2Cl_2O \tag{32}$$

is the initiator and catalyst for the oxidative coupling of 2,6-dimethylphenol (DMP) to poly(2,6-dimethylphenylene oxide) by dioxygen (Scheme 3; also see inset of Scheme 1).[79] A similar approach shows that the catalytic intermediate in the corresponding system with $py_4Cu_4Cl_4$ as initiator in nitrobenzene is a formal oxocopper(II) complex of stoichiometry $py_3Cu_4Cl_4O(DMP)_2$.[88] The phenolic oxidation product in this case is the diphenoquinone (Scheme 1).[88]

The benefits of employing simple, well-characterized halo(amine)copper(I) complexes as reductants and non-coordinating, aprotic solvents as media in studies of copper(I) oxidation are obvious from the results of this Section. Neutrality of the copper(I) reactants considerably simplifies the interpretation of kinetic data for oxidation of copper(I).[14,21,79–81,88] We trust that the same systematic approach will be used in future studies of copper(I) "autoxidation" and copper-based catalysis.[16,73]

6. TRANSMETALLATION OF POLYNUCLEAR HALO(AMINE)COPPER(I) COMPLEXES WITH M(NS)$_n$ TRANSMETALLATORS AND OXIDATION OF THE PRODUCTS BY DIOXYGEN

Simple halo(amine)copper(I) complexes and the products of their aprotic reactions with dioxygen have a remarkable ability to serve as targets in aprotic reactions in which the copper centres are stoichiometrically replaced with other metals. These reactions are called transmetallation.[95]

6.1. *The discovery of transmetallation*[95]

Neutral oxocopper(II) complexes **XXXI–XXXIII** have not been crystallized intact.[11,21,87,88] Attempted crystallization of products **I** and **II** often gives crystalline products $(\mu_4\text{-O})(py,N)_4Cu_4X_6$ in a little understood series of disproportionation reactions.[21,86a,87] Products **XXXIII** must be freshly prepared because they polymerize in aprotic solvents, as indicated by cryoscopic measurements.[81]

The two important properties of products **XXXI–XXXIII** are that they are oxidants and strong protic bases. The need to distinguish as clearly as possible between the different basic oxo groups in their proposed core structures led us to examine their reactions with aprotic Lewis acids $M(NS)_2$, where NS is a monoanionic hydrazinecarbodithioate Schiff base ligand in structures **A–F** (Fig. 2).[95,96] We instead observed ambient, stoichiometric exchange of M for Cu, as exemplified by the reaction series summarized in eq. (33):[97]

$$(\mu_4\text{-O})(py,N)_4Cu_4X_6 + xC \longrightarrow (\mu_4\text{-O})(py,N)_4Cu_{4-x}Ni_xX_6 + xCu(NS)_2. \tag{33}$$

This new transmetallation chemistry has subsequently been shown to apply to a wide range of polynuclear copper targets.[98] However, we emphasize that it is *not* restricted to copper replacement.[98,99]

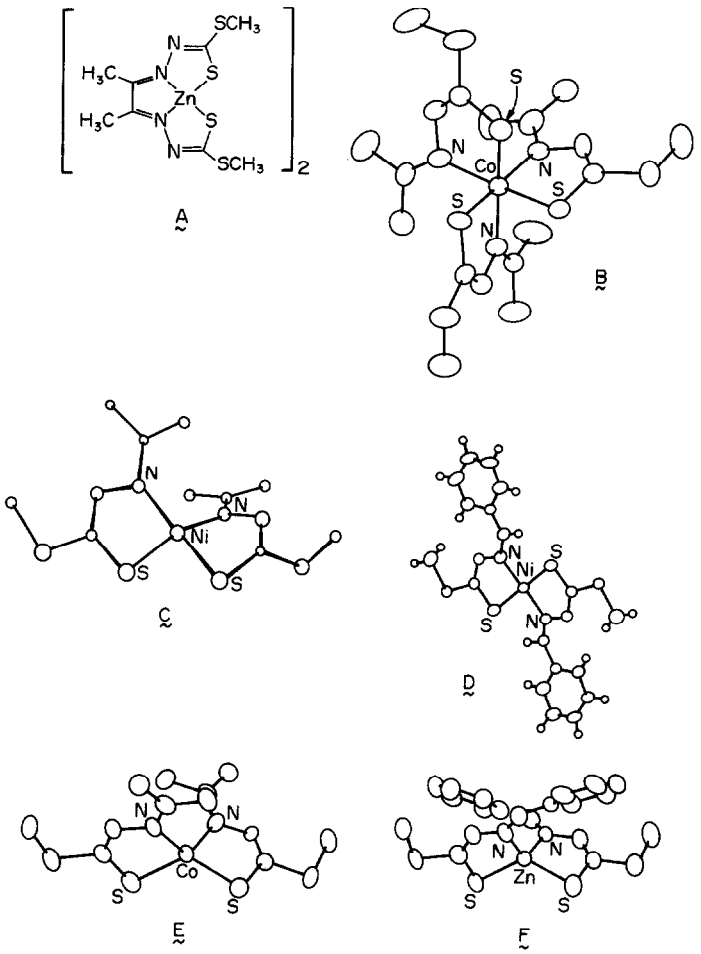

Fig. 2. Structures of S-methylhydrazinecarbodithioate transmetallators **A–F**.[96]

Transmetallation chemistry can be used to obtain literally hundreds of entirely new heteropolymetallic molecules that cannot be made by other means.[98]

The transmetallation phenomenon has been reviewed in detail[98] but the application of transmetallation still is in its infancy. Therefore, the remainder of this Report will highlight the most important aspects of halo(amine)copper(I) transmetallation with $M(NS)_n$ transmetallators and of oxidation of the transmetallated products with dioxygen.

6.2. *Transmetallation of halo(amine)copper(I) complexes with* $M(NS)_n$ *transmetallators*

Equations (34)–(40):

$$(py,N)_4Cu_4X_4 + M(NS)_2 \longrightarrow (py,N)_3Cu_3M(NS)X_4\,(\mathbf{XXXVII}) + (py,N) + Cu(NS)\,(s) \quad (34)$$

$$(py,N)_4Cu_4X_4 + 2M(NS)_2 \longrightarrow (py,N)_4M_2X_4 + 4Cu(NS)\,(s) \quad (35)$$

$$(py,N)_4Cu_4X_4 + Co(NS)_3 \longrightarrow (py,N)_3Cu_3Co(NS)_2X_4\,(\mathbf{XXXVIII}) + (py,N) + Cu(NS)\,(s) \quad (36)$$

$$(py,N)_4Cu_4X_4 + 2Co(NS)_3 \longrightarrow (py,N)_4Co_2X_4 + 2Cu(NS)_2 + 2Cu(NS)\,(s) \quad (37)$$

$$L_2Cu_2X_2 + M(NS)_2 \longrightarrow LCuM(NS)X_2 + L + Cu(NS)\,(s) \quad (38)$$

$$LCuM(NS)X_2 \longrightarrow LMX_2 + Cu(NS)\,(s) \quad (39)$$

$$LCuM(NS)X_2 + M(NS)_2 \longrightarrow (M(NS))_2X_2 + L + Cu(NS)\,(s) \quad (40)$$

summarize the stoichiometries of transmetallation of dimeric and tetrameric halo(amine)copper(I)

complexes with $M(NS)_n$ reagents **B**, **C** and **E** (Fig. 2) in methylene chloride and nitrobenzene under dinitrogen.

The advantage of using the S-methyl isopropylidenehydrazinecarbodithioate NS ligand system of these particular transmetallators is the precipitation of insoluble, pale yellow co-product Cu(NS) (s), which can be filtered, dried and weighed to establish transmetallation stoichiometries. The polymeric transmetallation products are identified by elemental analysis and by cryoscopic measurements in nitrobenzene.[98-104]

Reactions (34)–(40) have many interesting features, including the following.

(1) Reactions (34) and (36) are *direct* transmetallations.[86a] The word *direct* in this context means that the target and ultimate transmetallation product have the same molecularity. This is the most useful kind of transmetallation reaction because it allows the option of replacing all the copper in a given target with other metals and thus generates large transmetallation product families.[87,89,100]

(2) Reaction (34) proceeds even with M = copper(II) because Cu(NS) (s) is more stable than dissolved $Cu(NS)_2$. The product **XXXVII** in this case is a *mixed-valence* copper species.[101]

(3) Cryoscopic and spectroscopic measurements indicate that the first products of eqs (34) and (36) are tetrameric species containing only three ligands py or N.[88,99,101,102] This is evidently because each molecule contains three, four-coordinate (py,N)Cu centres, which means that M is five-coordinate in products **XXXVII** (that is, the NS ligand is bidentate, as indicated by a strong IR band at 1000 cm^{-1}).[96,101]

(4) Reactions (36) and (37) are preceded by rapid electron transfer from copper(I) to cobalt(III) in **B**.[99,102] This means that products **VIII** are mixed-valence species that formally contain two copper(I), one copper(II) and one cobalt(II) centres, as indicated by their electronic spectra.[99,102] Spectroscopic (electronic, IR) data also indicate that cobalt(II) in **XXXVIII** is five-coordinate and hence contains monodentate NS ligands (Scheme 4).[99,102]

(5) Reactions (35) and (37) are not direct because intramolecular NS ligand transfer (INLT) from M or cobalt to copper occurs on replacement of a second copper(I) centre of **XXXVII** or **XXXVIII** with **B**, **C** or **E**. INLT and intermolecular transmetallation thus are competitive processes in progressive copper(I) transmetallation.[99,102] This situation could be changed by altering the NS ligand or by employing M(NS) transmetallators.[98] However, systems based on reactions (35) and (37) are valuable new sources of heterometallic dimers because we can use equimolar $M(NS)_2$ and $M'(NS)_2$, where M and M′ are different metals, instead of two mols of $M(NS)_2$.[98-102]

(6) Reactions of species **XXXVIII** with mixtures of transmetallators $M(NS)_2$, $M'(NS)_2$ and **B** actually are quite selective.[99] This is partly because of decreasing thermodynamic transmetallator stability in the order $Cu(NS)_2 > Ni(NS)_2 > Co(NS)_2 > \mathbf{B} > Zn(NS)_2$[99] and partly because of differences in transmetallation rate laws for different M and NS.[98,105-107]

(7) Reactions (39) are a quantitative new source of LMX_2 complexes.[103] Faster reactions (40) give new dimers $[M(NS)]_2X_2$ whose stability depends on M.[103]

6.3. *Transmetallation kinetics and mechanisms*

The rate laws of transmetallation reactions that result in the replacement of a single metal centre in a polymetallic target can be determined by maintaining the target in large excess over the transmetallator.[97] The rate laws for these *mono*-transmetallation reactions, eqs (41)–(45):

$$\text{Rate} = k_{29}[\text{TM}][\text{T}]^2 \tag{41}$$

$$\text{Rate} = k_{30}[\text{TM}][\text{T}] \tag{42}$$

$$\text{Rate} = k_{31}[\text{TM}] \tag{43}$$

$$\text{Rate} = k_{32}[\text{TM}][\text{T}] + k_{-32} \tag{44}$$

$$\text{Rate} = k_{33}K_{33}[\text{TM}][\text{T}]/(1 + K_{33}[\text{T}]) \tag{45}$$

depend on the properties of the target R and transmetallator TM.[97,104-107]

Rate laws (41), (43) and (45) are indications of very weak, very strong and moderately strong transmetallation reaction precursors, respectively.[106,107] These precursors are proposed to be constructed via four-membered Cu—X—M—S rings between the reactants.[97,104-107] Excellent support

for this conclusion is that transmetallations of L_4Cu_4 (L is 6-methyl-2-oxopyridinate), which contains no halo ligands, are very much slower than those of halocopper targets under the same experimental conditions.[108] Reversible rate law (44) is only observed for the earliest events of transmetallation of particular copper(I) dimers $L_2Cu_2Cl_2$ in (polar) nitrobenzene. It does not actually refer to transmetallation, which is much slower in these cases than is discrete copper(II) replacement.[103,104]

The reader is referred to the original papers[97,104–107] for a detailed analysis of the information derived from different transmetallation rate laws. The most important factor for efficient known transmetallation systems involving halocopper targets and $M(NS)_n$ transmetallators seems to be the availability of nucleophilic X and S atoms in the respective labile reactants. These atoms are used to construct Cu—X—M—S precursor rings.[106,107] Other important attributes of halocopper species as transmetallation targets and $M(NS)_n$ reagents as transmetallators have been discussed in detail.[98,105–108]

6.4. *Oxidation of the products of halo(amine)copper*(I) *transmetallation by dioxygen*

Replacement of the redox-active metal centres of a catalyst with other metals is a powerful means of investigating catalytic mechanisms.[86a,109]

Products **XXXVII** and **XXXVIII** of eqs (34) and (36), respectively, react with dioxygen via eqs (46) and (47):

$$(py,N)_3Cu_3M(NS)X_4 + O_2 \longrightarrow \underset{\textbf{XXXIX}}{(\mu_4\text{-O},\mu\text{-O})N_3Cu_3M(H_2O)X_4} + 1/2N_2S_2 \qquad (46)$$

$$(py,N)_3Cu_3Co(NS)_2X_4 + O_2 \longrightarrow \underset{\textbf{XXXIXa}}{(\mu_4\text{-O},\mu\text{-O})N_3Cu_3Co(H_2O)X_4} + N_2S_2. \qquad (47)$$

The respective rate laws are eq. (48):[102,103]

$$d[\textbf{IX}]/dt = k_t[\textbf{XXXVII}, \textbf{XXXVIII}][O_2] \qquad (48)$$

Correlation of the activation parameters for common second-order rate laws (27) and (48) (Fig. 1)[21,88,101,102] indicates the same rate-determining dioxygen insertion mechanism (see Section 5.6). This very important observation shows that rapid oxidation of the coordinated NS ligands in **XXXVII** and **XXXVIII** to the disulphide N_2S_2 results from prior reduction of dioxygen by copper(I).[101,102] The impressive correlation of activation parameter data for oxidation of $(N,py)_mCu_{4-x}M_x(NS)_yX_4$[101,102] *and* L_4Cu_4[108a] complexes (L is 6-methyl-2-oxopyridinate) in Fig. 1 suggests contribution of some inherent property of the dioxygen molecule to $\Delta H_t^{\ddagger}$ and $\Delta S_t^{\ddagger}$ because L_4Cu_4 (point 19 in Fig. 1) has no halo core.

6.5. *Transmetallation of oxocopper*(II) *complexes*

Tetrameric oxocopper(II) products **XXXIX** and those from other copper(II) transmetallation systems[98] can easily be isolated by gel permeation chromatography with divinylbenzene/styrene copolymer resins under a positive dinitrogen pressure with methylene chloride as eluant.[86a]

Scheme 4 shows the proposed core structures of products **XXXIX**.[87,101,102] Evidence for these core structures comes from a variety of sources, including their behaviour on transmetallation with $M(NS)_n$ reagents, where characteristic CuO fragmentation is observed, eq. (49):[99,110]

$$\textbf{XXXIX} + xM'(NS)_2 \longrightarrow N_3M_{3-x}M'_xX_4O + CuO + 2Cu(NS)_2. \qquad (49)$$

The products $N_3M_{3-x}M'_xX_4O$ can be μ-oxo or μ_3-oxotrimers, Tr_1, because the CuO fragmentation patterns depend on the target and transmetallator.[110] The exception is with M = Cu in **XXXIX** and M′ = Ni in eq. (49), which gives no CuO fragmentation and leads to a complete, six-membered family of copper–nickel tetramers (μ_4-O, μ-O)$N_4Cu_{4-x}Ni_xCl_4$ (x = 0–4) through a sequence of site-selective transmetallation steps.[87] Scheme 4[110] illustrates the effects of reversing the oxidation/transmetallation sequence with halo(amine)copper(I) starting materials.

The patterns of transmetallation of copper(II) targets thus primarily depend on the target core structure and the transmetallator.[98] A very special kind of *trans*-effect operates specifically across the unrestrained[101] μ-oxo groups of species like **XXXII** in Scheme 4.[86a,108b,110] This means that one metal

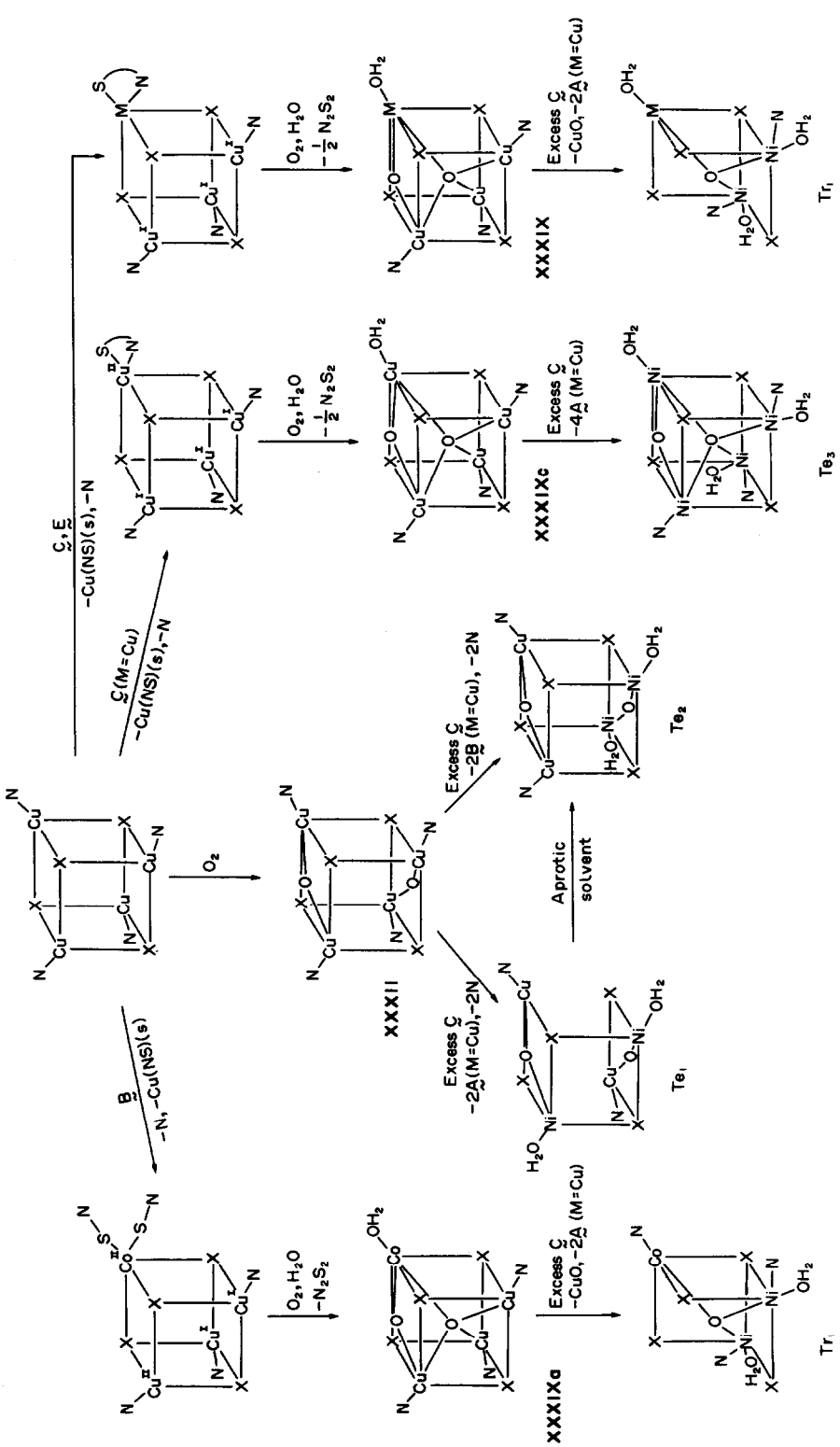

Scheme 4. Effects of changing the oxidation/transmetallation sequence in the reactions of copper(I) complexes $(DENC)_4Cu_4X_4$ with $M(NS)_n$ transmetallators **B**, **C** and **E** of Fig. 2.[102]

can either facilitate or retard the replacement by transmetallation of another metal that shares the same μ-oxo group. The *trans*-effect phenomenon results, for example, in selective replacement of metals *trans*- to cobalt(II) in $L_4Cu_{4-x}(Co,M)_xO_2$ molecules, where L is 6-methyl-2-oxopyridinate. The result is the generation of specific product isomers.[108b] The complete *trans*-effect order for Co, Ni, Cu and Zn centres has been worked out[108b] and appears to be general.[110] The *trans*-effect was only discovered because trimeric[110] and tetrameric[86a,108b,110] μ-oxocopper(II) targets were available for study.

6.6. *Prospects for the development and use of transmetallation chemistry*

All this remarkable transmetallation and oxidation chemistry was discovered as a result of a longstanding interest in copper-catalysed reactions of dioxygen.[11,82,83] It has already been demonstrated that transmetallation with redox-inactive metals like nickel(II) can be used to shut down active catalytic copper–dioxygen systems.[86a,88,109] Replacement of one metal in a polymeric catalyst with other redox-active or -inactive metals could have substantial effects on the efficiency and specificity of many metal-catalysed dioxygen reactions.[98]

There is substantial interest in the synthesis and use of heteropolymetallic molecules,[111,112] catalysts[112] and materials.[113] The objective is to modify the properties of existing materials in a beneficial manner. It is apparent that transmetallation chemistry has considerable potential in the synthesis of entirely new heteropolymetallic molecules, families of catalysts with closely similar structures but easily variable redox properties,[98] new alloys under very mild conditions[113] and large families of heterogeneous catalysts with systematically controllable properties.[98,113]

7. CONCLUDING REMARKS

Halo(amine)copper(I) complexes display a wide variety of molecular structures and physical properties. Carbonylcopper(I) complexes are relatively rare but there is sufficient structural information to illustrate their interesting structural variations. Chloro- and bromocopper(I) complexes with pyridine and alkylpolyamine ligands are very suitable for establishing the basic characteristics of aprotic copper(I) autoxidation and the mechanisms of catalysis by copper(I)–dioxygen systems. Polymeric halo(amine)copper(I) complexes and the products of their oxidation by dioxygen are excellent targets for the generation of many new heteropolymetallic molecules through transmetallation. Availability of these products should be of considerable value in the synthesis of new materials and in determining the mechanisms of metal-catalysed reactions.

Acknowledgements—This work was supported by Grant CHE-8717556 from the National Science Foundation and Grant 20022-AC3 from the Donors of the Petroleum Research Fund, administered by the American Chemical Society (to G.D.). G.D. particularly wishes to thank Professors Mohamed A. El-Sayed and Ahmed El-Toukhy for their many contributions to work on copper–dioxygen and transmetallation chemistry. All the drawings in this Report were prepared with the Chem 3D Molecular Modelling System supplied by Cambridge Scientific Computing, Inc.

REFERENCES

1. A. Butts, in *Copper, The Science and Technology of the Metal, its Alloys and Compounds*. Hafner Publishing Company, New York (1954).
2. A. F. Wells, in *Structural Inorganic Chemistry*, 5th edn, Ch. 25. Clarendon Press, Oxford (1984).
3. W. E. Hatfield and R. Whyman, *Transition Met. Chem.* 1969, **5**, 47.
4. (a) K. D. Karlin and J. Zubieta (Eds), *Copper Coordination Chemistry: Biochemical and Inorganic Perspectives*. Adenine Press, Guilderland, New York (1983); (b) K. D. Karlin and J. Zubieta (Eds), *Biological and Inorganic Copper Chemistry*, Vols I and II. Adenine Press, Guilderland, New York (1986).
5. D. W. Smith, *Coord. Chem. Rev.* 1976, **21**, 93.
6. R. Colton and J. H. Canterford, in *Halides of the First Row Transition Metals*. John Wiley, New York (1969).
7. M. R. Churchill and F. J. Rotella, *Inorg. Chem.* 1977, **16**, 3267 and refs therein.
8. P. G. Eller and P. W. R. Corfield, *Chem. Commun.* 1971, 105.

9. M. Pasquali and C. Floriani, in *Copper Coordination Chemistry: Biochemical and Inorganic Perspectives*, p. 311. Adenine Press, Guilderland, New York (1983).
10. (a) F. J. Jardine, *Adv. Inorg. Chem. Radiochem.* 1975, **17**, 115; (b) K. D. Karlin and J. A. Zubieta, *Inorg. Persp. Biol. Med.* 1979, **2**, 127.
11. G. Davies and M. A. El-Sayed, in Ref. 4(a), p. 281.
12. D. A. Haitko and M. F. Garbauskas, in Ref. 4(b), Vol. 2, p. 77.
13. B. J. Hathaway and D. E. Billing, *Coord. Chem. Rev.* 1970, **5**, 143.
14. G. Davies and M. A. El-Sayed, *Comm. Inorg. Chem.* 1985, **4**, 151.
15. K. D. Karlin and Y. Gultneh, *J. Chem. Educ.* 1985, **62**, 983.
16. K. D. Karlin and Y. Gultneh, *Prog. Inorg. Chem.* 1987, **35**, 219 and refs therein.
17. A. D. Zuberbuhler, in Ref. 4a, p. 238.
18. R. N. Keller and H. D. Wycoff, *Inorg. Synth.* 1946, **2**, 1.
19. J. A. Tompkins, PhD thesis, Oklahoma State University (1988).
20. N. P. Rath, PhD thesis, Oklahoma State University (1985).
21. G. Davies and M. A. El-Sayed, *Inorg. Chem.* 1983, **22**, 1257.
22. N. P. Rath, E. M. Holt and K. Tanimura, *J. Chem. Soc., Dalton Trans.* 1986, 2303.
23. N. P. Rath and E. M. Holt, *J. Chem. Soc., Chem. Commun.* 1985, 665.
24. L. M. Englehardt, R. I. Papasergio and A. H. White, *Aust. J. Chem.* 1984, **37**, 2207.
25. M. R. Churchill, G. Davies, M. A. El-Sayed, J. A. Fournier, J. P. Hutchinson and J. A. Zubieta, *Inorg. Chem.* 1984, **23**, 783.
26. P. C. Healy, C. Pakawatchai, C. Raston, B. W. Skelton and A. H. White, *J. Chem. Soc., Dalton Trans.* 1983, 1905.
27. V. Schramm and K. F. Fischer, *Naturwissenschaften* 1974, **61**, 500.
28. V. Schramm, *Inorg. Chem.* 1978, **3**, 714.
29. D. A. Haitko, *J. Coord. Chem.* 1984, **13**, 119.
30. N. P. Rath, E. M. Holt and K. Tanimura, *Inorg. Chem.* 1985, **24**, 3934.
31. Von H. D. Hardt and H. J. Stoll, *Z. Anorg. Allg. Chem.* 1978, **442**, 221; Von H. D. Hardt and H. J. Stoll, *Z. Anorg. Allg. Chem.* 1981, **480**, 199; Von H. D. Hardt and H. J. Stoll, *Z. Anorg. Allg. Chem.* 1981, **480**, 193; Von H. D. Hardt and P. Weber, *Z. Anorg. Allg. Chem.* 1978, **442**, 225.
32. P. C. Healy, C. Paikawatchai and A. H. White, *J. Chem. Soc., Dalton Trans.* 1983, 1917.
33. J. A. Campbell, C. L. Raston and A. H. White, *Aust. J. Chem.* 1984, **37**, 2201.
34. E. M. Holt, J. A. Tompkins, M. Draganjac, J. Armstrong and M. J. Bose, Abstract PC3, American Crystallographic Association, Austin, Texas, March 1987.
35. J. Strähle, W. Hiller, E. Eitel and D. Oehlkrug, *Z. Kristallogr.* 1980, **153**, 277; E. Eitel, D. Oehlkrug, W. Hiller and J. Strähle, *Z. Naturfor.* 1980, **B35**, 1247.
36. W. Hiller, *Z. Naturfor.* 1984, **B39**, 861.
37. P. C. Healy, C. Pakawatchai and A. H. White, *J. Chem. Soc., Dalton Trans.* 1985, 2531.
38. V. Schramm, *Cryst. Struct. Commun.* 1982, **11**, 1549.
39. N. P. Rath, J. L. Maxwell and E. M. Holt, *J. Chem. Soc., Dalton Trans.* 1986, 2449.
40. J. C. Dyason, P. C. Healy, C. Pakawatchai, V. A. Patrick and A. H. White, *Inorg. Chem.* 1985, **24**, 1957.
41. J. C. Dyason, L. M. Englehardt, P. C. Healy, C. Pakawatchai and A. H. White, *Inorg. Chem.* 1985, **24**, 1950.
42. E. W. Ainscough, A. G. Bingham, A. M. Brodie and K. L. Brown, *J. Chem. Soc., Dalton Trans.* 1984, 989.
43. A. Toth, C. Floriani, A. Chiesi-Villa and C. Guastini, *Inorg. Chem.* 1987, **26**, 3897.
44. J. C. Dyason, L. M. Englehardt, P. C. Healy and A. H. White, *Aust. J. Chem.* 1984, **37**, 2201.
45. R. Graziani, G. Bombieri and E. Forsellini, *J. Chem. Soc. A* 1971, 2331.
46. J. A. Tompkins, J. L. Maxwell and E. M. Holt, *Inorg. Chim. Acta* 1987, **127**, 1; G. W. Hunt and E. L. Amma, *J. Chem. Soc., Chem. Commun.* 1973, 869.
47. C. L. Raston and A. H. White, *J. Chem. Soc., Dalton Trans* 1976, 2153.
48. M. R. Churchill, G. Davies, M. A. El-Sayed, J. P. Hutchinson and M. W. Rupich, *Inorg. Chem.* 1982, **21**, 995.
49. J. C. Dyason, P. C. Healy, L. M. Englehardt, C. Pakawatchai, V. A. Patrick, C. L. Raston and A. H. White, *J. Chem. Soc., Dalton Trans* 1985, 831.
50. V. Schramm, *Cryst. Struct. Commun.* 1980, **9**, 1231.
51. P. Fiaschi, C. Floriani, M. Pasquali, A. Chiesi-Villa and C. Guastini, *Inorg. Chem.* 1986, **25**, 462.
52. G. Doyle, K. A. Eriksen and D. VanEngen, *Organometallics* 1985, **4**, 830.
53. P. Coan and K. G. Caulton, unpublished observations.
54. C. D. Cook and R. C. Woodworth, *J. Am. Chem. Soc.* 1953, **75**, 6242.
55. M. Pasquali, C. Floriani and A. Gaetani-Manfredotti, *Inorg. Chem.* 1981, **20**, 3382.
56. M. Pasquali, C. Floriani and A. Gaetani-Manfredotti, *Inorg. Chem.* 1980, **19**, 1191.
57. D. Haitko and M. F. Garbauskas, in Ref. 4b, p. 77.

58. J. M. Mayer, *Comm. Inorg. Chem.* 1988, **8**, 125.
59. M. Pasquali, G. Marini, C. Floriani, A. Gaetani-Manfredotti and C. Gaustini, *Inorg. Chem.* 1980, **19**, 2525.
60. M. Pasquali, F. Marchetti and C. Floriani, *Inorg. Chem.* 1978, **17**, 1684.
61. M. I. Bruce and A. P. P. Ostazewski, *J. Chem. Soc., Dalton Trans.* 1973, 2433.
62. M. R. Churchill, B. G. DeBoer, F. J. Rotella, O. M. Abusalah and M. I. Bruce, *Inorg. Chem.* 1975, **14**, 2051.
63. C. Mealli, C. S. Arcus, J. L. Wilkinson, T. J. Marks and J. A. Ibers, *J. Am. Chem. Soc.* 1976, **98**, 711.
64. N. Kitajima, K. Fujisawa, C. Fujimoto and Y. Moro-oka, *Chem. Lett.* 1989, 421.
65. M. Pasquali, C. Floriani, G. Venturi, A. Gaetani-Manfredotti and A. Chiesi-Villa, *J. Am. Chem. Soc.* 1982, **104**, 4092.
66. G. Doyle, K. A. Eriksen and D. VanEngen, *Inorg. Chem.* 1983, **22**, 2892.
67. C. Floriani, P. Fiaschi, A. Chiesi-Villa, C. Guastini and P. F. Zanazzi, *J. Chem. Soc., Dalton Trans.* 1988, 1607.
68. J. A. Marsella, C. J. Curtis, J. A. Bercaw and K. G. Caulton, *J. Am. Chem. Soc.* 1980, **102**, 7244.
69. H. Hirai, S. Hara and M. Komiyama, *Chem. Lett.* 1982, 1685.
70. C. Glaser, *Chem. Ber.* 1869, **2**, 422; *Ann. Chem. Pharm.* 1870, **154**, 159.
71. A. D. Zuberbuhler, *Met. Ions Biol. Syst.* 1974, **5**, 325; H. Gampp and A. D. Zuberbuhler, *Met. Ions Biol. Syst.* 1981, **12**, 133.
72. T. R. Demmin, M. D. Swerdloff and M. M. Rogic, *J. Am. Chem. Soc.* 1981, **103**, 5795 and refs therein.
73. A. S. Hay, H. S. Blanchard, G. E. Endres and J. W. Eustance, *J. Am. Chem. Soc.* 1959, **81**, 6335; G. F. Endres, A. S. Hay and J. W. Eustance, *J. Org. Chem.* 1963, **28**, 1300; A. S. Hay, *Adv. Polm. Sci.* 1967, **4**, 496; A. S. Hay, *Polm. Engng Sci.* 1976, **16**, 1; A. S. Hay, P. Shenian, A. C. Gowan, P. F. Erhardt, W. R. Haff and J. E. Therberg, in *Encyclopedia of Polymer Science and Tecnology*, p. 92. Interscience, New York (1969); H. L. Finkbeiner, A. S. Hay and D. M. White, Polymerization by oxidative coupling, in *Polymerization Processes* (Edited by C. E. Schildnecht and I. Skeist), p. 537 and refs therein. Wiley-Interscience, New York (1977).
74. M. R. Churchill, G. Davies, M. A. El-Sayed, M. F. El-Shazly, J. P. Hutchinson and M. W. Rupich, *Inorg. Chem.* 1980, **19**, 201.
75. M. R. Churchill, G. Davies, M. A. El-Sayed, J. P. Hutchinson and M. W. Rupich, *Inorg. Chem.* 1982, **21**, 995.
76. T. F. Brennan, G. Davies, M. A. El-Sayed, M. F. El-Shazly, M. W. Rupich and M. Veidis, *Inorg. Chim. Acta* 1981, **51**, 45.
77. R. W. Cruse, S. Kaderli, C. J. Meyer, A. D. Zuberbuhler and K. D. Karlin, *J. Am. Chem. Soc.* 1988, **110**, 5020.
78. G. Davies, M. F. El-Shazly and M. W. Rupich, *Inorg. Chem.* 1981, **20**, 3757.
79. G. Davies, M. A. El-Sayed and M. Henary, *Inorg. Chem.* 1987, **26**, 3266.
80. J. S. Thompson, in Ref. 4b, Vol. 2, p. 1.
81. M. A. Sayed, A. El-Toukhy and G. Davies, *Inorg. Chem.* 1985, **24**, 3387.
82. G. Davies, M. F. El-Shazly, D. R. Kozlowski, C. E. Kramer, M. W. Rupich and R. W. Slaven, *Adv. Chem. Ser.* 1979, **173**, 178.
83. I. Bodek and G. Davies, *Inorg. Chem.* 1978, **17**, 1814; *Inorg. Chim. Acta* 1978, **27**, 213.
84. M. R. Churchill, G. Davies, M. A. El-Sayed and J. P. Hutchinson, *Inorg. Chem.* 1982, **21**, 1002 and refs therein.
85. G. Davies, A. El-Toukhy, K. D. Onan and M. Veidis, *Inorg. Chim. Acta* 1985, **98**, 85.
86. (a) A. El-Toukhy, G.-Z. Cai, G. Davies, T. R. Gilbert, K. D. Onan and M. Veidis, *J. Am. Chem. Soc.* 1984, **106**, 4596; (b) G. Davies, M. A. El-Sayed and R. E. Fasano, *Inorg. Chim. Acta* 1983, **71**, 95.
87. G. Davies, M. A. El-Sayed, A. El-Toukhy, M. Henary and C. A. Martin, *Inorg. Chem.* 1986, **25**, 4479.
88. M. A. El-Sayed, A. Abu-Raqabah, G. Davies and A. El-Toukhy, *Inorg. Chem.* 1989, **28**, 1909.
89. R. D. Gray, *J. Am. Chem. Soc.* 1969, **91**, 56.
90. F. R. Hopf, M. M. Rogic and J. F. Wolf, *J. Phys. Chem.* 1983, **87**, 4681.
91. N. J. Blackburn, R. W. Strange, A. Farooq, M. S. Haka and K. D. Karlin, *J. Am. Chem. Soc.* 1988, **110**, 4263 and refs therein.
92. Z. Tyeklar, P. P. Paul, R. R. Jacobson, A. Farooq, K. D. Karlin and J. Zubieta, *J. Am. Chem. Soc.* 1989, **111**, 388.
93. Z. Tyeklar and K. D. Karlin, *Accts Chem. Res.* 1989, **22**, 241.
94. K. D. Karlin, R. W. Cruse, Y. Gultneh, J. C. Hayes, J. W. McKown and J. Zubieta, in Ref. 4b, Vol. 2, p. 101.
95. G. Davies, A. El-Toukhy, K. D. Onan and M. Veidis, *Inorg. Chim. Acta* 1984, **84**, 41.
96. K. D. Onan, G. Davies, M. A. El-Sayed and A. El-Toukhy, *Inorg. Chim. Acta* 1986, **113**, 109; 1986, **119**, 121 and refs therein.

97. G. Davies, M. A. El-Sayed and A. El-Toukhy, *Inorg. Chem.* 1986, **25**, 2269; *Inorg. Chem.* 1986, **25**, 3899.
98. G. Davies, M. A. El-Sayed and A. El-Touky, *Comm. Inorg. Chem.* 1989, **8**, 203.
99. G. Davies, M. A. El-Sayed, A. El-Toukhy, M. Henary, T. S. Kasem and C. A. Martin, *Inorg. Chem.* 1986, **25**, 3904.
100. A. Abu-Raqabah, G. Davies, M. A. Sayed, A. El Toukhy and M. Henary, *Inorg. Chem.* 1989, **28**, 1156.
101. G. Davies, M. A. El-Sayed, A. El-Toukhy, T. R. Gilbert and K. Nabih, *Inorg. Chem.* 1986, **25**, 1929.
102. G. Davies, M. A. El-Sayed, A. El-Toukhy, M. Henary and T. R. Gilbert, *Inorg. Chem.* 1986, **25**, 2373.
103. G. Davies, N. El-Kady, K. D. Onan, W. Shomaly, M. A. El-Sayed and A. El-Toukhy, *Inorg. Chim. Acta* 1988, **149**, 21.
104. G. Davies, N. El-Kady, M. A. El-Sayed, A. El-Toukhy and M. R. Shure, *Inorg. Chim. Acta* 1988, **149**, 31.
105. G. Davies, M. A. El-Sayed and A. El-Toukhy, *Inorg. Chem.* 1986, **25**, 1925.
106. G. Davies, N. El-Kady, M. A. El-Sayed, A. El-Toukhy and M. R. Shure, *Inorg. Chim. Acta* 1988, **149**, 42.
107. S. Al-Shehri, G. Davies, M. A. El-Sayed and A. El-Toukhy, *Inorg. Chem.* 1990, **29**, 1198, 1206.
108. (a) G.-Z. Cai, G. Davies, M. A. El-Sayed, A. El-Toukhy and T. R. Gilbert, in Ref. 4b, Vol. 2, p. 115; (b) G.-Z. Cai, G. Davies, M. A. El-Sayed and K. D. Onan, *Inorg. Chem.* 1986, **25**, 1935.
109. G. Davies, N. El-Kady, M. A. El-Sayed and A. El-Toukhy, *Inorg. Chim. Acta* 1985, **104**, 131.
110. M. Henary, G. Davies, A. Abu-Raqabah, M. A. El-Sayed and A. El-Toukhy, *Inorg. Chem.* 1988, **27**, 1872.
111. H. Vahrenkamp, *Comm. Inorg. Chem.* 1985, **4**, 253 and refs therein.
112. J. H. Sinfelt, *Bimetallic Catalysts.* John Wiley, New York (1983).
113. J. V. Marzik, L. G. Carreira and G. Davies, *J. Matl. Sci. Lett.* 1988, **7**, 833; G. Davies, B. C. Giessen and H.-L. Shao, *Matl. Lett.* 1990, **9**, 231.

Polyhedron Vol. 9, No. 19, pp. 2353–2357, 1990
Printed in Great Britain

0277–5387/90 $3.00+.00
© 1990 Pergamon Press plc

SYNTHESIS AND REDOX PROPERTIES OF A COPPER(II) COMPLEX OF N,N′,N″,N‴-TETRAKIS(2-QUINOLINEMETHYL-1-OXIDE)-1,4,8,11-TETRAAZACYCLOTETRADECANE

RENATA BILEWICZ*

Department of Chemistry, University of Warsaw, Pasteura 1, 02093 Warsaw, Poland

and

MAREK PIETRASZKIEWICZ

Institute of Physical Chemistry, Polish Academy of Sciences, Kasprzaka 44/52, 01224 Warsaw, Poland

(*Received* 22 *January* 1990; *accepted* 23 *March* 1990)

Abstract—1,4,8,11-Tetraazacyclotetradecane (cyclam) condensed with 2-chloro-methylquinoline-1-oxide yields the tetrasubstituted title compound, a ligand for copper(II). The redox properties of the copper(II) complex were characterized by voltammetric methods. Contrary to the complex with unsubstituted cyclam, the electroreduction proceeds stepwise with the generation of a copper(I) complex in the first step. The electron is transferred in a quasi-reversible process and the formal potential, $E^{\ominus}$, of the $Cu^{II}L/Cu^{I}L$ system was found to be −0.137 V in propylene carbonate and −0.113 V in N,N′-dimethylformamide.

Possible relationships to copper biochemistry have stimulated studies of the copper complexes with tetraaza macrocycles. Electroanalytical methods are used to determine the influence of structure on the reactivity of the copper complexes in the electron-transfer processes.[1] In biological systems copper compounds such as azurin or plastocyanin containing a single copper atom undergo rapid electron exchange which is assumed to be due to nearly identical geometries in the reduced and oxidized states.[2,3] The hydrophobic environment of the copper atom should minimize the solvent reorganization contributions. It is, therefore, believed that a properly tailored model ligand should provide a similar constrained environment for the copper atom and eliminate the large inner-coordination sphere changes observed for simple copper complexes during the electron-transfer reactions. In the case of the N_4-type ligands these attempts were, however, usually unsuccessful. The copper(I) complexes formed upon electroreduction of copper(II) were found to decompose or disproportionate to copper(II) and metallic copper. Stabilization of copper(I) was sometimes achieved with unsaturated N_4-type ligands or substituted cyclams.[4,5] Stable copper(I) complexes were observed for five-coordinate environments with a tetradentate ligand enforcing a nearly square-pyramidal geometry.[6–11] Direct electroreduction of $Cu^{II}N_4$ to the metal was reported by Fabrizzi and co-workers.[6,12] Air- and moisture-sensitive complexes of formally zero-valent copper were described by Bond and Khalifa.[11] On the other hand, electrochemical oxidation of the copper(II) complexes with some tetraazacyclotetradecane macrocycles was shown to yield copper(III) complexes[6,13] similarly to deprotonated peptide complexes.[14,15] In the present work, the cyclam substituted with heterocyclic N-oxide (Fig. 1) was used to complex the copper(II) ions. The complex was characterized by vol-

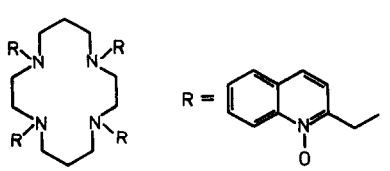

Fig. 1. The ligand studied.

*Author to whom correspondence should be addressed.

tammetry on glassy carbon and mercury electrodes with the aim of determining the accessibility of various oxidation states of copper.

EXPERIMENTAL

Chemicals

The solvents used: dichloromethane (CH_2Cl_2), acetonitrile (AN), N,N'-dimethyloformamide (DMF) and propylene carbonate (PC) were purified by distillation, dried and stored over 4 Å molecular sieves. Et_4NClO_4 (TEAP) was recrystallized from methanol and used in 0.1 mol dm^{-3} concentration as the supporting electrolyte. The ligand dissolved readily only in halogenated organic solvents, therefore CH_2Cl_2 was used to prepare the stock solution of the ligand.

Preparation of the complex

The title ligand was prepared as described previously.[16] The ligand (414 mg, 0.5 mmol) was stirred in ethanol (10 cm^3) with $Cu(NO_3)_2 \cdot 3H_2O$ (187.6 mg, 0.5 mmol) at 70°C for 1 h. Upon cooling the complex was crystallized slowly by vapour diffusion with ethyl ether to form deep green crystals. Yield: 386 mg, 76%. Found: C, 53.4; H, 4.6; N, 12.3. Calc. for $C_{50}H_{52}N_8O_4+Cu(NO_3)_2$: C, 53.5; H, 4.6; N, 12.5%.

Instrumentation

Voltammetry experiments were carried out in a three-electrode arrangement with a saturated calomel reference electrode and platinum foil counter electrode, both separated from the cell solution by a glass frit. The working electrode was either a static mercury drop electrode, SMDE 1 (Laboratorni Pristroje) of 0.014 cm^2 drop area, used in the dropping (sampled d.c. voltammetry) or hanging (cyclic voltammetry) mode, or a glassy carbon electrode, GCE (Bioanalytical Systems, Inc.) of 0.07 cm^2 area. The surface of the GCE was polished with a polishing microcloth using alumina powder (1 μm) and electrochemically treated by holding the potential at -1.5 V for 60 s and at $+0.3$ V for 60 s in the solution studied. All experiments including controlled-potential electrolysis with a mercury macrocathode were carried out using a BAS-100 Electrochemical Analyser (Bioanalytical Systems Inc.) with a KX-P1091 Printer (Panasonic) and HIPLOT DMP-40 Plotter (Houston Instrument).

The reference electrode potential was calibrated by using the ferrocene, $Fe(C_2H_5)_2$, oxidation process in the appropriate solvent so that the junction potential effects could be estimated. The cell resistance was externally compensated for by BAS-100.

RESULTS

Stoichiometry of the complex

In contrast to the behaviour of the ligand itself, the copper(II) complex dissolves readily in potentially coordinating solvents such as AN, DMF and PC. The stoichiometry of the complex was established by adding aliquots of the copper(II) solution to a sample containing a known amount of the macrocycle. On complexation the macrocycle dissolved and voltammograms were recorded 1 h after each aliquot addition. Two couples of peaks were formed, c_1/a_1 and c_2/a_2 (Fig. 2), increasing upon addition of copper(II). At concentration ratios, $C_{Cu^{II}}/C_L$, larger than one the peaks attained constant height and an additional peak corresponding to free copper(II) reduction to metallic copper was observed at potentials positive to that of peak c_1. This suggests that the macrocycle is able to accommodate a single copper ion. The same stoichiometry was found when aliquots of cyclam in CH_2Cl_2 were added to the copper(II) solution in DMF or PC. In AN the copper(II) complex is unstable and upon standing undergoes chemical reduction to the Cu^I–AN complex. The voltammogram exhibits a reduction peak at -0.36 V vs SCE on the GCE corresponding to the reduction of the Cu^I–AN complex to metallic copper. A similar potential for the Cu^I/Cu^0 couple in AN was reported by Farka and Iwamoto.[17] In AN solutions the anodic peak increases upon maintaining the electrode at -0.5 V prior to recording the anodic half-cycle. This confirms that copper(0) is formed during reduction and stripped off from the electrode surface during oxidation. Therefore, further experiments were carried out in DMF or PC. The low solubility of the complex in acetone or CH_2Cl_2 made it impossible to study the electrode processes in these non-coordinating solvents.

Voltammetry in PC

Voltammograms similar to those presented in Fig. 2 are obtained when the $Cu^{II}L$ complex is prepared externally and dissolved in 0.1 mol dm^{-3} TEAP solution in PC. For the c_1/a_1 couple of peaks the current ratio given by eq. (1):[18]

$$i_{pa}/i_{pc} = (i_{pa}/i_{pc})_0 + 0.485i/(i_{pc})_0 + 0.086, \quad (1)$$

where i is the current at the switching potential and the 0-index denotes that current is measured from

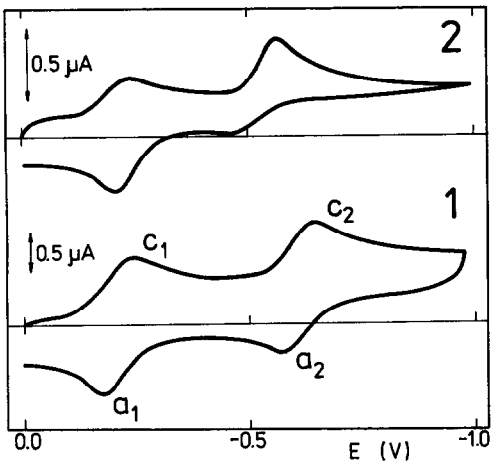

Fig. 2. Cyclic voltammograms for 2.32×10^{-4} mol dm^{-3} Cu^{II} after addition of 6.2 mg of the ligand recorded on (1) GCE and (2) SMDE in 0.1 mol dm^{-3} TEAP/PC solution. Scan rate: 20 mV s^{-1}.

the base line in the supporting electrolyte alone, was found to be unity (Table 1). The $E_{pc_1} - E_{pc_1/2}$ value close to 60 mV and the value of $E_{pa_1} - E_{pc_1}$ close to 60 mV at low scan rates and increasing with the increase of scan rate reveal quasi-reversibility of the system. The shifts of the cathodic and anodic peaks are symmetrical with respect to the midpoint potential, $(E_{pc} + E_{pa})/2$. The formal potential, $E^{\ominus}$, approximated by the midpoint potential value is given in Table 2. Figure 3 shows the c_1/a_1 couple of peaks recorded from 0 V towards negative potentials (curve 1) and a voltammogram recorded in the opposite direction—from −0.5 V, where the electrode is maintained for 1 min before initiating the anodic scan (curve 2). The curves appear identical which indicates the absence of complicating reactions and accumulation at the electrode. The heterogeneous rate constant, k^0, estimated from the anodic–cathodic peak separation by the method of Nicholson[19] was found to be $(8.3 \pm 0.2) \times 10^{-3}$ cm s^{-1} at the GCE.

Table 1. Cyclic voltammetry currents for 2×10^{-4} mol dm^{-3} $Cu^{II}L$ on GCE[a]

v (V s^{-1})	$(i_{c_1})_0$ (μA)	$(i_{a_1})_0$ (μA)	$(i)_0$ (μA)	(i_a/i_c)
0.01	0.94	0.53	0.60	0.95
0.02	1.37	0.81	0.89	0.99
0.05	2.16	1.33	1.54	1.05
0.10	3.10	1.88	2.13	1.02
0.15	3.79	2.29	2.79	1.05

[a] In DMF solution containing 0.1 mol dm^{-3} TEAP.

Table 2. Formal potentials[a] and diffusion coefficients of $Cu^{II}L$ in DMF and PC

Solvent	$E^{\ominus}$ (V)	$n\sqrt{D}$ (10^{-3} cm/$\sqrt{s}$)	D (10^{-6} cm^2/s)
PC	−0.137[b]	1.21	1.46
	−0.132[c]	1.23	1.51
DMF	−0.113[b]	2.26	5.11
	−0.116[c]	2.27	5.15

[a] Versus NHE, $E^{\ominus}$ is assumed to be $(E_{p_a} + E_{p_c})/2$ corrected for liquid junction potential.
[b] GCE.
[c] SMDE.

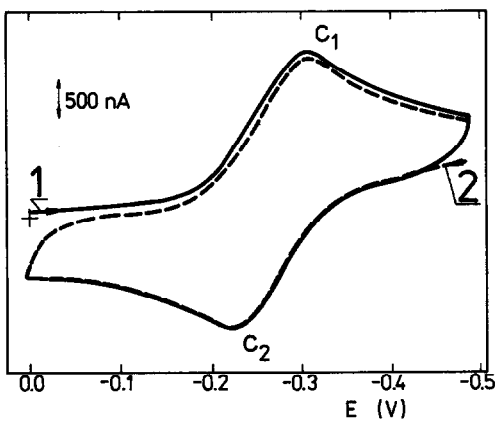

Fig. 3. Cyclic voltammograms of 4×10^{-4} mol dm^{-3} $Cu^{II}L$ on GCE in 0.1 mol dm^{-3} TEAP/PC solution. Scan rate: 50 mV s^{-1}. (——) Started from 0 V in the direction of negative potentials; (– – –) started from −0.5 V towards positive potentials.

Sampled d.c. voltammetry at the SMDE in the dropping mode gave a wave corresponding to peak c_1 with $E_{1/2}$ almost identical to the $E^{\ominus}$ value obtained from the cyclic voltammograms. The limiting currents increased linearly with the complex concentration and the $i_{lim}\sqrt{t_{drop}}$ was constant with increasing drop time, t_{drop}. The value $n\sqrt{D}$ was similar to that obtained from cyclic voltammetry, 2.3×10^{-3}. The slope of the wave $dE/d \log (i/i_d - i)$ was 59.16 mV.

The second reduction process was found to be chemically irreversible and largely dependent on the presence of traces of water, thus exhibiting that the product of this reduction step undergoes decomposition. Since no special effort was made to obtain solutions without traces of water this process was not studied more carefully.

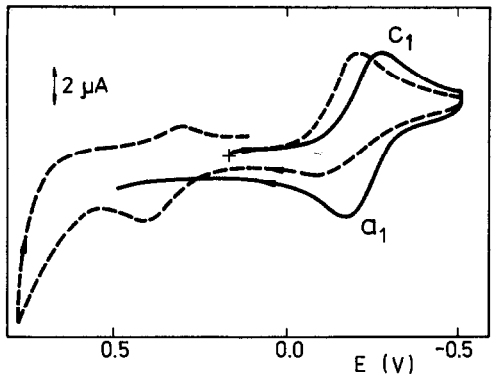

Fig. 4. The influence of (– – –) 5×10^{-3} mol dm^{-3} TEACl on the cyclic voltammograms of 5.6×10^{-4} mol dm^{-3} $Cu^{II}L$ in 0.1 mol dm^{-3} TEAP/DMF at the GCE. Scan rate: 50 mV s^{-1}.

Coulometry

To evaluate the number of electrons used in the first reduction step exhaustive electrolysis on a mercury pool electrode was carried out at −0.5 V, in solutions containing different concentrations of $Cu^{II}L$. The $i-q$ plots obtained were linear and extrapolation gave 0.98 F mol^{-1} at $i = 0$ as the mean value. The colour of the solution turned from green to yellow. The results confirmed consumption of 1e in the first step of reduction. The diffusion coefficients of $Cu^{II}L$ obtained in DMF and PC are depicted in Table 2.

Influence of chlorides

Addition of TEACl to the solution leads to a positive shift of the E_{pc_1} and a decrease of the a_1 peak. An additional anodic peak is formed at +0.460 V (Fig. 4). This points to chemical reaction following electron transfer, leading to the incorporation of Cl^- into the copper(I) complex. The new complex formed is more stable than Cu^IL.

Relative stabilities of the copper(II) and copper(I) complexes

Assuming that in the absence of chlorides the $E^{\ominus}$ value obtained from cyclic voltammetry approximates the thermodynamic formal potential of the $Cu^{II}L/Cu^IL$ pair, the ratio of stability constants of the complexes was calculated from eq. (2):[20]

$$(E^{\ominus}_{Cu^{II}/Cu^{I}})_{complex} = (E^{\ominus}_{Cu^{II}/Cu^{I}})_{uncomplexed} - 0.059 \log (K_{Cu^{II}L}/K_{Cu^{I}L}).$$

Using the value $(E^{\ominus}_{Cu^{II}/Cu^{I}})_{uncomplexed}$ equal to 0.0160 V vs NHE the ratio $K_{Cu^{II}L}/K_{Cu^{I}L}$ is 1×10^5, reflecting the higher stability of the copper(II) complex.

Conclusions

In most 14-membered saturated macrocycles the cavity is inappropriate for the larger copper(I) ion and the ability of these ligands to distort to tetrahedral geometry stabilizing copper(I) is reduced. Therefore, the copper(I) complex dissociates and disproportionates rapidly. The tetrasubstituted tetraazamacrocycle presented in this work was found to possess ligating properties both toward copper(II) and copper(I) ions. In contrast to the cyclam complex, substitution of the ligand with quinoline oxide groups renders the complexes insoluble in water and leads to enhancement of the stability of the copper(I) state. The reduction of the copper(II) complex is shifted 400 mV towards positive potentials, compared to the unsubstituted cyclam complex. Good ligands for copper(I), however, such as Cl^- or AN have to be avoided, since in their presence the Cu^IL complex undergoes fast chemical reactions leading to more stable copper(I) compounds.

Acknowledgements—This work was supported by Problems CPBP 01.15 and 3.20.

REFERENCES

1. P. Zanello, S. Tamburini, P. A. Vigato and G. A. Mazzocchini, *Coord. Chem. Rev.* 1987, **77**, 165.
2. K. D. Karlin and Y. Gultneh, *Prog. Inorg. Chem.* 1987, **35**, 219.
3. T. N. Sorrell, *Tetrahedron* 1989, **45**, 3.
4. J. M. Palmer, E. Papaconstantinou and J. F. Endicott, *Inorg. Chem.* 1969, **8**, 1516.
5. N. Jubran, H. Cohen, Y. Koresh and D. Meyerstein, *J. Chem. Soc., Chem. Commun.* 1984, 1683.
6. P. Zanello, R. Seeber, A. Cinquantini, G. Mazzochini and L. Fabrizzi, *J. Chem. Soc., Dalton Trans.* 1982, 893.
7. R. R. Gagne, J. L. Allison, R. S. Gall and C. A. Kowal, *J. Am. Chem. Soc.* 1977, **99**, 7170.
8. A. W. Addison, M. Carpenter, K. M. Lau and M. Wicholas, *Inorg. Chem.* 1978, **17**, 1545.
9. R. R. Gagne, J. L. Allison and D. M. Ingle, *Inorg. Chem.* 1979, **18**, 2767 and refs therein.
10. A. W. Addison, H. M. Hendricks, J. Reedijk and L. K. Thompson, *Inorg. Chem.* 1981, **20**, 103.
11. A. M. Bond and M. A. Khalifa, *Inorg. Chem.* 1987, **26**, 413.
12. L. Fabrizzi, A. Poggi and P. Zanello, *J. Chem. Soc., Dalton Trans.* 1983, 2191.
13. L. Fabrizzi and A. Poggi, *J. Chem. Soc., Chem. Commun.* 1980, 646.

14. C. A. Kowal and D. W. Margerum, *Inorg. Chem.* 1981, **20**, 2311.
15. J. M. Anast and D. W. Margerum, *Inorg. Chem.* 1981, **20**, 2319.
16. M. Pietraszkiewicz, J. Karpiuk, R. Bilewicz and S. P. Kasprzyk, *J. Coord. Chem.* 1990, **21**, 75.
17. F. Farka and R. T. Iwamoto, *J. Electroanal. Chem.* 1964, **8**, 55.
18. R. S. Nicholson, *Analyt. Chem.* 1966, **38**, 1406.
19. R. S. Nicholson, *Analyt. Chem.* 1965, **37**, 1351.
20. J. P. Gisselbrecht and M. Gross, *J. Electroanal. Chem.* 1981, **127**, 127.

Polyhedron Vol. 9, No. 19, pp. 2359–2370, 1990
Printed in Great Britain

0277–5387/90 $3.00+.00
© 1990 Pergamon Press plc

MOLECULAR ORBITAL STUDY OF THE STRUCTURE AND STABILITY OF TRANSITION METAL POLYHEDRAL BORANE COMPLEXES. POSITION OF BRIDGING HYDROGENS

ELUVATHINGAL D. JEMMIS,* P. N. V. PAVAN KUMAR* and G. NARAHARI SASTRY

School of Chemistry, University of Hyderabad, Central University, P.O. Hyderabad 500 134, India

(*Received* 4 *December* 1989; *accepted* 1 *May* 1990)

Abstract—The dependence of bridging hydrogen atoms on terminal hydrogen positions in *nido*-metalloboranes has been studied using the model compounds B_4H_8X (**6**, X = BH) and $B_4H_8Fe(CO)_3$ (**1d**). Calculations on B_5H_9 at both MNDO and extended Huckel levels have shown that the bridging hydrogen positions are controlled by the terminal hydrogen positions. Bridging hydrogen atoms might be observed above the B_n plane (towards the cap), if the caps have sufficiently diffuse orbitals. Model studies at both MNDO and extended Huckel levels of B_4H_8X [X = BeH^-, Li^- and $Fe(CO)_3$] supported these results. The effects of increasing ring size from B_4H_8 to B_5H_{10} are also studied. Suitable metal fragments for polyhedral borane ligands (rings) having five, six, seven, 11 and 13 vertex boron atoms can be selected using the ring–cap overlap match. Calculations have shown that $B_6H_6^{4-}$ (**13**) has more diffuse orbitals compared to $B_{11}H_{11}^{4-}$ (**14**) and $B_{13}H_{13}^{4-}$ (**15**). Compounds **14** and **15** preferred caps with less diffuse orbitals because of the rigidity of the ligands. The metal–ring boron distances in metalloboranes are controlled by this ring–cap compatibility. The concept of topological charge stabilization is also used in predicting the stabilities of various isomers of metalloboranes.

Boranes constitute one of the most studied polyhedral molecules with a variety of structural arrangements which are well understood using various electron-counting rules.[1] Two basically different types of hydrogen atoms, viz. terminal (H_t) and bridging (H_b) as in **1**, are present in many boranes. The bridging hydrogen atoms provide additional electrons required for a given structural type. B_5H_9 (**1a**) is a well-studied example of **1**, having both terminal and bridging hydrogen atoms.[2] The terminal hydrogen atoms here are bent towards the apical BH (X, cap)† and the bridging hydrogen atoms are bent away from it, lying below the B_4H_8 ring.[3] It is well documented in the literature that when there are only terminal hydrogens in the ring the diffuseness of the cap and the size of the ring control the position of terminal hydrogens.[4] In metal complexes of C_nH_n ring systems, the hydrogen atoms are bent away from the metal for smaller rings and towards the metal for larger rings to optimize the ring metal overlap match.[4a] Similarly, bending of ring substituents in pyramidal carbocyclic and polyhedral borane ring systems is also an attempt to optimize the ring–cap overlap.[4b,c,d] Based on this, a cap with more diffuse orbitals than appropriate for the ring orbitals should push the ring substituents away from it. When the cap orbitals are less diffuse than the ring orbitals, the ring substituents will be pushed towards the cap. The ideal situation involves optimum ring–cap overlap with no bending of ring-substituents, as excessive bending (in either way) weakens the ring-substituent σ bonds.

The situation is further complicated in polyhedral boranes because these contain bridging hydrogen atoms in addition to the terminal hydrogen atoms. Since the BH cap (X) orbitals are less diffuse than appropriate for the orbitals of the B_4H_8 ring, the terminal hydrogen atoms bend towards it as in **1a** and the bridging hydrogens are observed below the

* Authors to whom correspondence should be addressed.

† Throughout this paper apical or cap represents the unique vertex.

B_4 ring. Is it the only structure possible for bridged boranes? Can we think of a second minimum involving the bridging hydrogen atoms moved towards the cap (X)? Replacement of the BH cap by metal fragments with more diffuse orbitals should push the terminal hydrogen atoms below the B_4H_8 ring.[4] Does this affect the bridging hydrogen positions? If the terminal hydrogen positions can influence the bridging hydrogen positions, it should be possible to design compounds where the bridging hydrogen atoms attach themselves to the same side as that of the cap (X). This type of bonding has not been obtained for bridged boranes so far. In the first part of this paper the interdependence of bridging and terminal hydrogen positions is probed. The effects of ring size and differing capping groups on the positions of bridging hydrogen atoms are also analysed. Previous theoretical studies on these molecules did not address this problem.[5] We have selected B_4H_8X [X = BH, BeH^-, Li^- and $Fe(CO)_3$] (**1**, **2**) and $B_5H_{10}X$ [X = BH^+, BeH, Li and $Fe(CO)_3^+$] (**3**, **4**) for the theoretical study. Calculations are carried out using semi-empirical MNDO[6] [except for X = $Fe(CO)_3$] and the extended Huckel methods.[7] The MNDO calculations on **1a** and **3a** are already reported.[5e,c]

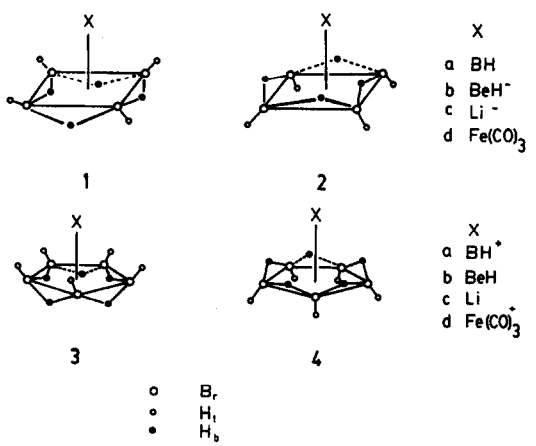

Apart from B_4H_8 and B_5H_{10}, many boranes and carbonates such as $C_2B_9H_{11}^{2-}$, $C_2B_3H_5^{4-}$ and $C_2B_4H_6^{2-}$ are available as ligands to the metal fragments. An extension of the ring–cap overlap analysis[4] helps us to find out suitable metal caps for given borane ligands. The above carborane anions are six-electron ligands similar to $C_5H_5^-$ but with a variety of orbital extensions. $C_2B_9H_{11}^{2-}$, the fragment of the icosahedral $C_2B_{10}H_{12}$ has a set of π-type MOs with totally different directional character in comparison to the pentagonal pyramidal $C_2B_4H_6^{2-}$ ligand. A survey of the available literature showed that 11 vertex boranes and carboranes are the most commonly found borane ligands to various metal fragments. To discover the stability order of a given borane ligand for different metal fragments as caps, we have selected ligands with five, six, seven, 11 and 13 vertex boron atoms for the theoretical study (second part of the paper). $Fe(CO)_3$ is taken as the model metal fragment. The metal–boron distances in the structurally-characterized complexes are examined to support the differences in the pentahapto and hexahapto borane ligands. A relationship is also sought between the topological charge stabilization rule[8] and the diffuse nature of the cap orbitals in metalloboranes. The qualitative arguments are supported by extended Huckel calculations with geometries and atomic parameters specified in the Appendix.[7]

RESULTS AND DISCUSSION

Initially a qualitative MO reasoning is presented to show why we expect two minima in bridged boranes. The electronic structure of **1** is similar to that of C_5H_5X (X = BH^+, CH^{2+}, etc.) molecules with three three-dimensionally delocalized MOs occupied by six electrons.[4] In **1** the square pyramidal B_4H_4X [X = BH, $Fe(CO)_3$, etc.] has two delocalized electrons. Four more are added by the four bridging hydrogen atoms. An alternative way of looking at **1** is to treat it as $B_4H_4X^{4-}$ with four protons attached at the sites of maximum electron density. With the terminal ring B_r—H_t (B_r corresponds to the ring boron atom as shown in **1**–**4**) bonds bent towards the cap (X) as in B_5H_9, the greater electron density should be found at the opposite side of the cap (X), i.e. below the ring (**5**). The same argument also leads to the expectation that the position of electron density should shift towards the cap, X (above the ring), if the terminal ring B_r—H_t bonds are bent away from the cap. From a localized picture of bonding we could anticipate the following. Both σ- and π-type MOs of the ring are involved in bonding with bridging hydrogen atoms. While the ring σ-bonding orbitals may prefer to interact with the "1*s*" orbitals of the bridging hydrogen atoms in the plane, the π-orbitals would have the node near the ring plane. The preferred positions for bridging hydrogen atoms to interact with them will be either below or above the ring. *This leads to the possibility of two minima for bridging hydrogens atoms.* The qualitative MO reasoning is supported by quantitative results on **1**–**4** using the semi-empirical MNDO method.

Various structures for B_4H_8X are optimized first by keeping the terminal hydrogen atoms towards the cap (X) and the bridging hydrogen atoms away from it (**1**) within C_{4v} symmetry. In **2** the positions

Table 1. Heats of formation and relative energies from MNDO for B_4H_8X (X = BH, BeH^- and Li^-) and $B_5H_{10}X$ (X = BH^+, BeH and Li). All values in kcal mol^{-1}

Molecule	ΔH_f	ΔH_f	$\Delta\Delta H_f$ (MNDO)[a]	$\Delta\Delta H_f$ (EHT)[b]
B_4H_8BH (**1a**)	31.3[c]	17.5[d]	124.0	199.9
B_4H_8BH (**2a**)	155.3			
$B_4H_8BeH^-$ (**1b**)	−13.6		39.2	79.2
$B_4H_8BeH^-$ (**2b**)	25.7			
$B_4H_8Li^-$ (**1c**)	38.8		17.3	38.0
$B_4H_8Li^-$ (**2c**)	56.1			
$B_5H_{10}BH^+$ (**3a**)	210.2[e]	194.0[f]	199.1	190.6
$B_5H_{10}BH^+$ (**3b**)	409.3			
$B_5H_{10}BeH$ (**3b**)	20.2		66.6	
$B_5H_{10}BeH$ (**4b**)	86.8			
$B_5H_{10}Li$ (**3c**)	37.2		34.7	
$B_5H_{10}Li$ (**4c**)	71.9			

[a] $\Delta\Delta H_f$ (MNDO) is obtained by subtracting the heats of formation of the two isomers.

[b] $\Delta\Delta H_f$ (EHT) is obtained by subtracting the sum of one-electron energies at the two minimum θ values (θ_2 and θ_2). See the text for θ description.

[c] Reference 5(e).

[d] D. D. Wagman, W. H. Evans, V. B. Parker, I. Halow, S. M. Bailey and R. H. Schumm, *Selected Values of Chemical Thermodynamic Properties*, National Bureau of Standards, Technical Note 270/3, Washington, D.C. (1968).

[e] Reference 5(c).

[f] Reference 10.

of both terminal and bridging hydrogen atoms are reversed and again all the geometric parameters are optimized within C_{4v} symmetry. A similar set of calculations was carried out on $B_5H_{10}X$ (**3** and **4**) keeping C_{5v} symmetry. The heats of formation and relative energy differences between the two sets of isomers **1** and **2**, and **3** and **4** are given in Table 1. MNDO-optimized bond lengths and bond angles are given in Table 2.

Table 1 shows that two minima are indeed poss-

Table 2. Optimum bond lengths and bond angles for B_4H_8X (**1**, **2**) and $B_5H_{10}X$ (**3**, **4**) from MNDO. Bond lengths in angstroms and bond angles in degrees

Molecule	B_r—B_r	B_r—H_t	B_r—H_b	B_r—X	X—H	X—H_t	X—H_b	DBH_t	XDH_b
B_4H_8BH (**1a**)	1.862	1.159	1.384	1.712	1.156	2.643	2.451	172.7	121.5
B_4H_8BH (**2a**)	1.703	1.164	1.711	2.181	1.169	2.979	1.339	180.5	41.9
$B_4H_8BeH^-$ (**1b**)	1.812	1.167	1.395	1.975	1.311	2.897	2.814	182.3	124.3
$B_4H_8BeH^-$ (**2b**)	1.712	1.170	1.584	2.284	1.312	3.118	1.617	176.0	50.2
$B_4H_8Li^-$ (**1c**)	1.775	1.175	1.404	2.188	—	3.060	3.087	183.5	125.2
$B_4H_8Li^-$ (**2c**)	1.716	1.175	1.547	2.473	—	3.293	1.821	174.2	53.3
$B_5H_{10}BH^+$ (**3a**)	1.814	1.170	1.371	1.801	1.171	2.674	2.534	158.1	116.8
$B_5H_{10}BH^+$ (**4a**)	1.716	1.170	1.495	2.166	1.177	3.121	1.622	175.8	53.3
$B_5H_{10}BeH$ (**3b**)	1.759	1.168	1.376	2.087	2.294	2.888	2.936	166.8	118.7
$B_5H_{10}BeH$ (**4b**)	1.710	1.166	1.461	2.324	1.288	3.321	1.872	166.8	58.3
$B_5H_{10}Li$ (**3c**)	1.718	1.172	1.383	2.391	—	3.067	3.313	166.8	119.3
$B_5H_{10}Li$ (**4c**)	1.706	1.167	1.443	2.614	—	3.586	2.106	163.9	60.1

ible. But in all the examples, structures with terminal hydrogen atoms towards the cap (X) and bridging hydrogen atoms away from it (X) are more stable. Our results on **1a** and **3a** in C_{4v} and C_{5v} symmetry are in agreement with the reported MNDO values.[5e,c] The relative energy differences ($\Delta\Delta H_f$) between the two isomers (**1** and **2**, and **3** and **4**) show that it is lowest for X = Li compared with BH or BeH (Table 1). The $\Delta\Delta H_f$ for a given cap is less for a four-membered ring compared to the corresponding five-membered ring. For example, with Li $\Delta\Delta H_f$ is 17.3 and 34.7 kcal mol^{-1} for the four- and five-membered rings, respectively (Table 1). This is because Li, being a very diffuse cap for a four-membered ring, pushes the terminal hydrogen atoms away from it in B_4H_8. This pushes the bridging hydrogen atoms towards the cap (X). Since the differences in the positions of the bridging and terminal hydrogen atoms are not very large, the energy difference between the two isomers **1** and **2** is lower for X = Li over B_5H_9. When the bridging hydrogen atoms are towards the cap (**2** or **4**), the B_r—B_r distance is found to be short compared to that in **1** or **3**, indicating that the electrons which bind the ring boron atoms are less delocalized to the bridging hydrogen atoms in this geometry. The B_r—H_b distance increases to large values as the H_b atoms are pushed towards the cap (X). At the same time the bridging hydrogen atoms developed some bonding interactions with the cap (Table 2). The variation in the terminal hydrogen positions (DBH_t in Table 2) in the two isomers is small for four-membered rings, with a maximum value of 8° for **1a** and **2a**. In the five-membered rings this increases to a maximum of 29° for **3c** and **4c**.

The above results using the MNDO method imply the possibility of two minima, one where the bridging hydrogen atoms are away from the cap (X) and the other where they are towards it. If the MNDO values are any indication for two minima in bridged boranes, caps with higher diffuse orbitals like metal fragments should show this trend more strongly. Our computational facilities do not permit quantitative studies with metalloboranes. We use the extended Huckel method to explain the possibility of two minima in bridged metalloboranes.

For the qualitative analysis we have selected B_5H_9 and $B_4H_8Fe(CO)_3$.[9] The possibility of a second minimum with bridging hydrogen atoms towards the cap on the B_4H_8X [X = BH and $Fe(CO)_3$] energy surface is studied in the following way. In the model B_5H_9 (**6**), ϕ is the angle made by d (middle of the ring), B_r and H_t. The angle made by d, e (middle of the B_r—Br bond) and H_b is θ. Energy curves are generated for the variation of bridging hydrogen atoms for fixed terminal hydrogen positions. In the calculations ϕ is kept at 120, 160° (terminal hydrogen atoms towards the cap, X), 180, 200 and 230° (terminal hydrogen atoms away from the cap, X) and θ is varied from 100 to 260° in 10° intervals for each value of ϕ. The total energy plots are given in Fig. 1. As anticipated above, for each value of ϕ the energy curve has two minima in θ (θ_1 and θ_2, as in Table 3). When ϕ is increased there is a lateral shift in the two minima. For example, when ϕ is 160°, the two minima are at 120 and 255° of θ and when it is changed to 200° they appear at 115 and 240°. The reasons for this are discussed below.

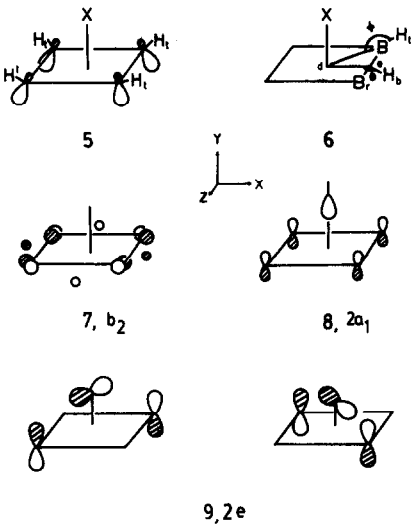

The Walsh diagram (Fig. 2, ϕ = 180°) shows the important MOs responsible for the change in total energy curves (**7**–**10**). The curve for MO b_2 (**7**), with no contribution from the terminal hydrogen atoms and the cap BH, is symmetric because the overlap between the bridging hydrogen atoms and the ring

Table 3. Comparison of the minimum in θ (θ_1 and θ_2) as a function of ϕ (**6**) for various caps of B_4H_8X (X = BH, BeH^-, Li^- and $Fe(CO)_3$). All values in degrees (obtained at the extended Huckel level)

Cap X	θ	ϕ 120	160	180	200	230
BH	θ_1	135	120	115	115	105
	θ_2	275	255	245	240	185
BeH^-	θ_1	135	120	120	110	100
	θ_2	265	250	245	240	230
Li^-	θ_1	135	120	110	110	100
	θ_2	270	255	250	245	235
$Fe(CO)_3$	θ_1	135	125	120	115	110
	θ_2	280	270	260	205	195

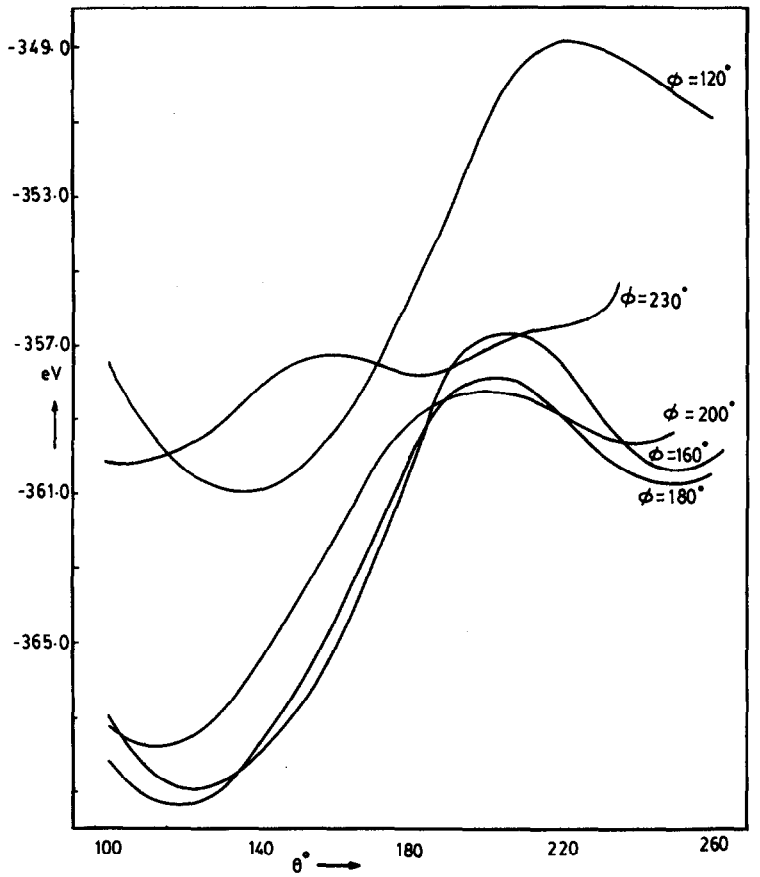

Fig. 1. Total energy plots for the variation of bridging hydrogen positions (θ) for a fixed terminal hydrogen position (ϕ) in B_5H_9 (**6**). ϕ is kept at 120, 160, 180, 200 and 230° and θ is varied from 100 to 260° in 10° intervals.

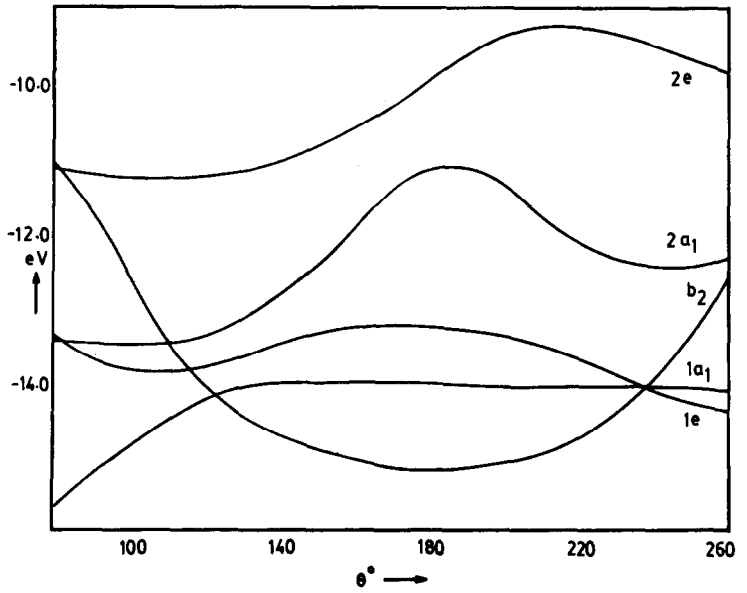

Fig. 2. Walsh diagram for the variation of the bridging hydrogen positions (θ) for a fixed terminal hydrogen position (ϕ) in B_5H_9 (**6**). ϕ is kept at 180°. Only the top five occupied MOs are shown.

boron atoms increases until θ becomes 180° and then starts decreasing with further increase of θ. Since there is no contribution from the terminal hydrogen atoms in b_2, similar curves are obtained with other values of ϕ. $2a_1$ reproduces the total energy plot closely (**8**). In **8** the bridging hydrogens can interact effectively with the ring p_y orbitals on either side of the node. A shift in the minimum value of θ is brought about by the change in the terminal hydrogen position. When the terminal hydrogen atoms are away from the cap (ϕ = 230°), the bridging hydrogen atoms are calculated to go towards it (X), as judged by the small barrier between the two minima in Fig. 1. This gives an indication that given a cap, which can push the terminal hydrogen atoms sufficiently below the B_4 ring, such as metal fragments, the bridging hydrogen atoms may be observed towards the cap. However, all the known metalloboranes had the terminal B_tH_t bonds bent towards the cap (X) so that the bridging hydrogens were away from the cap (X).[9c]

Calculations were carried out on the model metalloborane $B_4H_8Fe(CO)_3$ (**1d**) for the θ and ϕ values used in B_5H_9. Two minima in θ are found for each value of ϕ (Fig. 3). The minima shifted laterally with increasing values of ϕ (Table 3). An interesting point from the total energy plot is that when ϕ is at 230° [terminal hydrogen atoms away

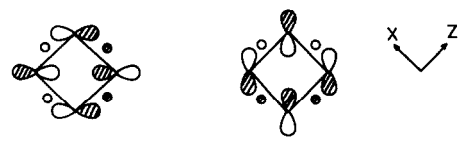

10, 1e

from the cap $Fe(CO)_3$] the energy minimum corresponded to a θ value (= 195°) where the bridging hydrogen atoms were bent towards the cap. Though such extreme values of ϕ may not be practical, these results along with the MNDO results discussed earlier indicate that the bridging hydrogen positions can be controlled by the terminal hydrogen positions.

Apart from $Fe(CO)_3$, caps from the main group

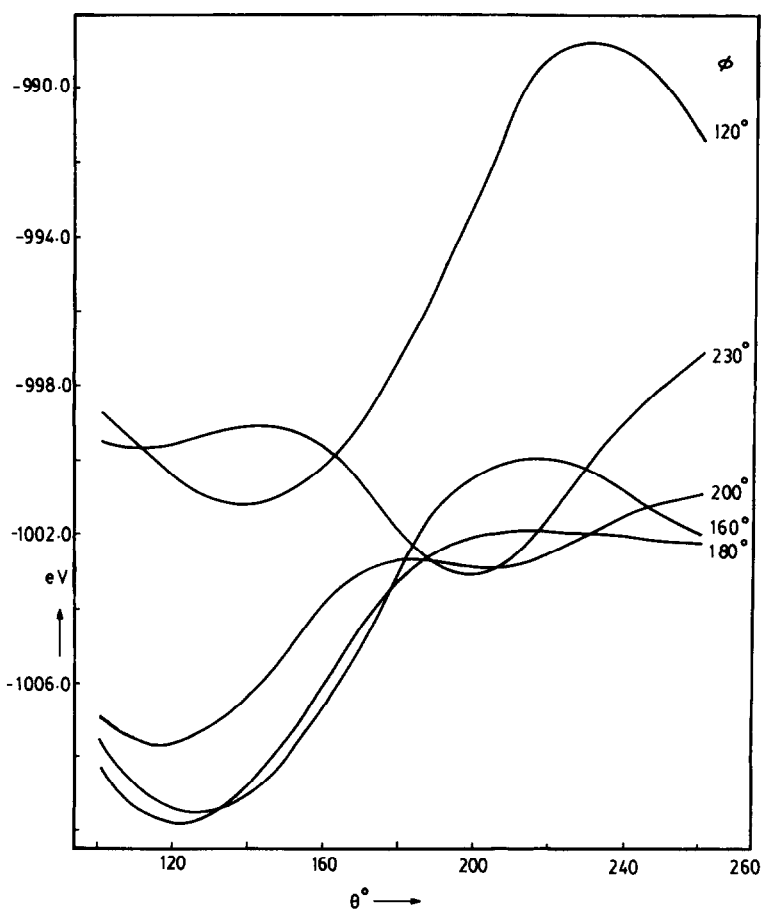

Fig. 3. Total energy plots for the variation of bridging hydrogen positions (θ) for a fixed terminal hydrogen position (ϕ) in $B_4H_8Fe(CO)_3$ (**1d**). ϕ is kept at 120, 160, 180, 200 and 230° and θ is varied from 100 to 260° in 10° intervals.

metals with diffuse orbitals are also tried to see the dependence of bridging hydrogen atoms on the terminal hydrogen positions. Table 3 indicates that two minima are obtained for both $B_4H_8BeH^-$ and $B_4H_8Li^-$. Therefore a smaller ring such as B_3H_6 should show the trend of bridging hydrogen atoms towards the cap (X) more strongly and caps like Li, BeH, $V(CO)_4$ and $Cr(CO)_4$ should also show this trend effectively.

Table 1 also gives the energy difference between the two θ minimum values (θ_1 and θ_2) for B_5H_9, $B_4H_8BeH^-$, $B_4H_8Li^-$ and $B_6H_{11}^+$ obtained from the extended Huckel method. A comparison of this to the $\Delta\Delta H_f$ of MNDO shows that even though the numbers from the extended Huckel method are always high, they follow the trends of MNDO results.

The role of ring size on the interdependence of terminal and bridging hydrogen positions is studied

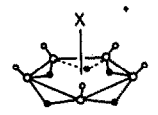

11

o B, • H_t • H_b

a b

X BH $Fe(CO)_3$

by changing the B_4 ring to a B_5 ring, $B_6H_{11}^+$ (**11a**), which is known to be a stable species with five bridging hydrogens.[10,5c] The variation of θ for each value of ϕ (160, 170, 180, 190 and 200°) in $B_6H_{11}^+$ (**11a**) gave again two minima. A comparison of the two θ minimum values (θ_1 and θ_2) for B_5H_9 and $B_6H_{11}^+$ showed that the bridging hydrogen atoms tend to occupy lower positions in $B_6H_{11}^+$ in relation to those of B_5H_9 (Table 4). The same trend is shown by the MNDO values (Table 2). This happens only when the terminal hydrogen atoms (H_t) are bent away from the cap. The difference in energy between the two θ minimum values for **11a** is 190.6 kcal mol^{-1} using the extended Huckel method. The corresponding value is found to be 199.1 kcal mol^{-1} with MNDO.

Similarly, calculations were carried out on $B_5H_{10}Fe(CO)_3^+$ (**11b**), obtained by replacing the BH cap in **11a** by $Fe(CO)_3$. Although **11b** is not known experimentally, the neutral derivative $B_5H_9Fe(CO)_3$ is known.[11] Related to this is $B_5H_{10}X$, where X = FeCp. Two isomers are known with this composition where FeCp occupies either the apical (cap) position or a site in the ring.[12] The bridging hydrogen atoms in **11b** are optimized for three values of ϕ (160, 180 and 200°). Again the energy curves show two minima (Table 4).

Table 4. Comparison of the minimum in θ (θ_1 and θ_2) as a function of ϕ (**6**) for the rings B_5H_9 (**6**) and $B_6H_{11}^+$ (**11a**) and $B_4H_8Fe(CO)_3$ (**1d**) and $B_5H_{10}Fe(CO)_3^+$ (**11b**). All values in degrees (obtained at the extended Huckel level)

Molecule	θ	ϕ 160	180	200
B_5H_9 (**6**)	θ_1	120	115	115
	θ_2	255	245	240
$B_6H_{11}^+$ (**11a**)	θ_1	120	110	100
	θ_2	250	240	235
$B_4H_8Fe(CO)_3$ (**1d**)	θ_1	125	120	115
	θ_2	270	260	205
$B_5H_{10}Fe(CO)_3^+$ (**11b**)	θ_1	120	115	105
	θ_2	275	250	240

We now use the above concept for compatibility of orbitals in overlap to find suitable caps for given borane ligands. Since most of the known metalloboranes and carboranes contain five, six, 11 and 13 BR and CR groups, borane ligands in planar (**12**, D_{5h}), pentagonal pyramidal (**13**, C_{5v}), icosahedral (**14**, C_{5v}), the hexagonal antiprismatic (**15**, C_{6v}) forms are chosen for the theoretical study. This involves the optimization of the ring terminal B—H bonds using the extended Huckel method. Since metal fragments (ML_ns) with varying cap orbitals are known, caps with a differing diffuse nature are simulated by changing the CFeC angle, α (**16**), in $Fe(CO)_3$.

The electronic structure of all these anionic ligands shows that the open face of the ligand has five (six in **15**) orbitals with varying hybridization. These are similar to the orbitals of the cyclo-

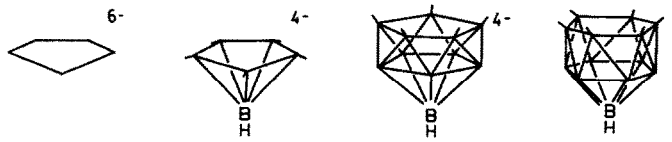

$B_5H_5^{6-}$ $B_6H_6^{4-}$ $B_{11}H_{11}^{4-}$ $B_{13}H_{13}^{4-}$

12 13 14 15

pentadienyl anion (Cp^-).[13] Their interaction with a metal fragment (ML_n) is also similar to that observed in the metallocenes. The strength of the interaction between the ring and ML_n depends on the extent to which the ring orbitals are hybridized and the size of the ring. For a given ring system, the out-of-plane bending value changes from positive (towards the cap) to negative (away from the cap) with decreasing diffuse nature of the cap. Thus the orbitals of $B_6H_6^{4-}$ (**13**) are splayed out, while those of the icosahedral fragments, $B_{11}H_{11}^{4-}$ (**14**) and $B_{13}H_{13}^{4-}$ (**15**), are bent in. The ring out-of-plane bendings in these ligands (**13–15**) are calculated to be 16.0, −22.6 and −25.0°, respectively, using the extended Huckel method. The value of 22.6° observed for $B_{11}H_{11}^{4-}$ (**14**), which is equal to that found in the icosahedral $B_{12}H_{12}^{2-}$, shows the rigidity of the ligand.

The interaction of these ligands (**12–15**) with the model transition metal fragment $Fe(CO)_3$ is studied while maintaining the CFeC angle α (**16**) at 90°. Combination of the planar $B_5H_5^{6-}$ and $Fe(Co)_3^{2+}$ gives $B_5H_5Fe(CO)_3^{4-}$ (**17**). The calculations gave a B—H bending angle of 13° towards the $Fe(CO)_3$ cap. When a BH^{2+} cap is attached from the second side of **17**, $B_6H_6Fe(CO)_3^{2-}$ (**18**) is obtained. This ion resembles $B_7H_7^{2-}$ (D_{5h}), where the ring hydrogen atoms are in the B_5 plane. In $B_6H_6Fe(CO)_3^{2-}$ (**18**), the ring hydrogen atoms are bent towards the metal cap by a small value, 3°. These two values are different to the optimum B—H bending angle (16°) found for $B_6H_6^{4-}$ (**13**).

$B_{11}H_{11}Fe(CO)_3^{2-}$ (**19**), obtained by the addition of $Fe(CO)_3^{2+}$ to $B_{11}H_{11}^{4-}$ (**14**), provides the opposite extreme to $B_6H_6Fe(CO)_3^{2-}$ (**18**). Calculations on **19** gave a B—H bending angle of 24° towards the $Fe(CO)_3$ cap. This is because with the B_5H_5 ring, $Fe(CO)_3$ preferred the B—H bonds to be bent towards the cap as in $B_5H_5Fe(CO)_3^{4-}$ (**17**). Since the ring hydrogen atoms in $B_{11}H_{11}^{4-}$ (**14**) are bent towards the vacant site by 22.6°, **14** provides it naturally for the incoming cap, $Fe(CO)_3$.

We consider three structures with a six-membered boron ring, $B_7H_7^{4-}$, $B_6H_6Fe(CO)_3^{4-}$ and $B_7H_7Fe(CO)_3^{2-}$, obtained from **13**, **17** and **18** by replacing the five-membered B_5H_5 ring with a B_6H_6 ring. The apical boron–ring boron distance in $B_6H_6^{4-}$ is 1.815 Å (MNDO). This is considerably longer (1.929 Å) in $B_7H_7^{4-}$ at the same level. The trends are similar to those reported using the PRDDO calculations, where the distances are 1.770 and 1.840 Å, respectively, for six- and seven-coordinate boron.[14a] The ring out-of-plane bending is calculated to be 25° (towards the BH cap) at the extended Huckel level. When the apical BH in $B_7H_7^{4-}$ is replaced by $Fe(CO)_3$, the ring out-of-plane angle is found to be 17°, towards the $Fe(CO)_3$ cap. Addition of another BH group from the oppposite side to $B_6H_6Fe(CO)_3^{4-}$ leads to $B_7H_7Fe(CO)_3^{2-}$. Here the ring out-of-plane value is 9° towards the $Fe(CO)_3$ cap at the extended Huckel level. $Fe(CO)_3$ orbitals find a natural match in the $B_{13}H_{13}$ ligand (**15**) as well, which has the BH bonds bent towards the missing apex by 26° as in $B_{13}H_{13}Fe(CO)_3^{2-}$ (**20**). The values indicate the more diffuse nature of the $Fe(CO)_3$ orbitals compared with those of BH. This is reflected in the energies of the following reactions (eqs (1)–(12), $ML_n = Fe(CO)_3$, numbers in parentheses correspond to values obtained with optimized CFeC angles). All the numbers being obtained at the extended Huckel level:

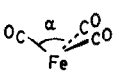

16

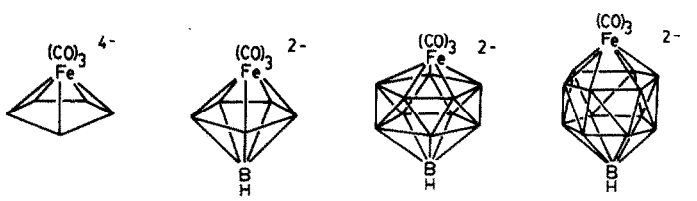

$B_5H_5Fe(CO)_3^{4-}$ (17) $B_6H_6Fe(CO)_3^{2-}$ (18) $B_{11}H_{11}Fe(CO)_3^{2-}$ (19) $B_{13}H_{13}Fe(CO)_3^{2-}$ (20)

$$B_4H_8ML_n + B_6H_6^{4-} \longrightarrow B_5H_9 + B_5H_5ML_n^{4-}$$
(**1d**) (**13**) (**1a**) (**17**)

$$\Delta E\ -39.5\ \text{kcal mol}^{-1} \quad (1)$$

$$B_4H_8ML_n + B_7H_7^{2-} \longrightarrow B_5H_9 + B_6H_6ML_n^{2-}$$
(1d) (23) (1a) (18)

ΔE −31.8 kcal mol^{-1} (2)

$$B_5H_{10}ML_n^{+} + B_6H_6^{4-} \longrightarrow B_6H_{11}^{+} + B_5H_5ML_n^{4-}$$
(3b) (13) (3a) (17)

ΔE −48.0 kcal mol^{-1} (3)

$$B_4H_8ML_n + B_5H_5^{4-} \longrightarrow B_5H_9 + B_4H_4ML_n^{4-}$$
(1d) (21) (1a) (22)

ΔE −32.4 kcal mol^{-1} (4)

$$B_{11}H_{11}ML_n^{2-} + B_5H_9 \longrightarrow B_{12}H_{12}^{2-} + B_4H_8ML_n$$
(19) (1a) (24) (1d)

ΔE −11.8 kcal mol^{-1} (5)

$$B_{13}H_{13}ML_n^{2-} + B_5H_9 \longrightarrow B_{14}H_{14}^{2-} + B_4H_8ML_n$$
(20) (1a) (25) (1d)

ΔE −19.7 kcal mol^{-1} (6)

$$B_{11}H_{11}ML_n^{2-} + B_7H_7^{2-} \longrightarrow B_{12}H_{12}^{2-} + B_6H_6ML_n^{2-}$$
(19) (23) (24) (18)

ΔE −43.7 (−48.9) kcal mol^{-1} (7)

$$B_{13}H_{13}ML_n^{2-} + B_7H_7^{2-} \longrightarrow B_{14}H_{14}^{2-} + B_6H_6ML_n^{2-}$$
(20) (23) (25) (18)

ΔE −51.5 (−54.0) kcal mol^{-1} (8)

$$B_{13}H_{13}ML_n^{2-} + B_6H_6^{4-} \longrightarrow B_{14}H_{14}^{2-} + B_5H_5ML_n^{4-}$$
(20) (13) (25) (17)

ΔE −59.2 (−60.2) kcal mol^{-1} (9)

$$B_{11}H_{11}ML_n^{2-} + B_6H_6^{4-} \longrightarrow B_{12}H_{12}^{2-} + B_5H_5ML_n^{4-}$$
(19) (13) (24) (17)

ΔE −51.3 (−55.1) kcal mol^{-1} (10)

$$B_6H_6ML_n^{2-} + B_{11}H_{11}^{4-} \longrightarrow B_{12}H_{12}^{2-} + B_5H_5ML_n^{4-}$$
(18) (14) (24) (17)

ΔE −61.0 (59.5) kcal mol^{-1} (11)

$$B_{13}H_{13}ML_n^{2-} + B_{12}H_{12}^{2-} \longrightarrow B_{14}H_{14}^{2-} + B_{11}H_{11}ML_n^{2-}$$
(20) (24) (25) (19)

ΔE −7.8 (−5.1) kcal mol^{-1}. (12)

Since $B_{11}H_{11}^{4-}$ and $B_{13}H_{13}^{4-}$ have less diffuse orbitals compared to the $B_6H_6^{4-}$ ligand, they prefer to interact with the group having less diffuse orbitals [BH rather than $Fe(CO)_3$] to form the more stable **24** and **25** [eqs (7)–(12)].[14] Obviously these numbers

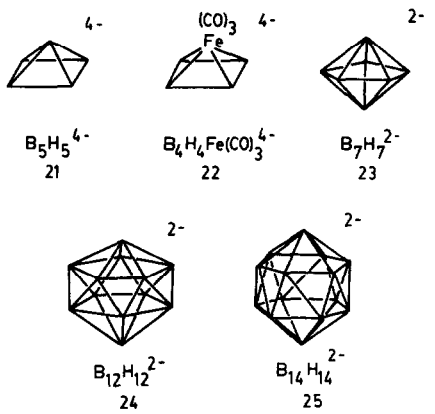

which are obtained from the sum of one-electron energies are only approximate. It is possible to change the metal and ligands in the transition metal fragment to give contracted or diffuse frontier orbitals so that the thermodynamics of the above reactions may be shifted in either direction. This is carried out as follows.

Initially the CFeC angle in $Fe(CO)_3$ is kept at 90°. To generate the required diffuse nature of the various metal fragments, the calculations are repeated on **12**–**15** by varying α in **16** but keeping the ring hydrogen atoms at the optimal positions found previously for $\alpha = 90°$. This shows that **12** prefers a metal cap with $\alpha = 99°$, whereas **13** prefers a cap with $\alpha = 103°$. This shows again that **13** prefers a cap with more diffuse orbitals. As anticipated, both **14** and **15** prefer caps with lower α, optimum values being 91 and 80°, respectively. The optimum α value for $B_7H_7Fe(CO)_3^{2-}$ is calculated to be 102° when the ring hydrogen atoms are kept in the boron plane. This indicates that $B_7H_7^{4-}$ in the C_{6v} geometry requires a diffuse metal cap if the ring hydrogen atoms are kept in the plane. The total energy corresponding to this structure is lower than that obtained when the ring hydrogen atoms are 9° towards the $Fe(CO)_3$ cap, even though all the interatomic distances between bonded atoms are kept constant. The numbers in parentheses refer to the values obtained for optimized CFeC angles.

Structural dependence

The differing diffuse nature of the above borane ligands (**13**–**15**) is also reflected in the experimentally observed M–B_r distances in the corresponding metalloboranes. Table 5 compares the

Table 5. M—B_r distances (Å) in metalloboranes and carboranes (**17–20**) available from X-ray data

Molecule	Fe—B	Reference
Five-atom ligand.		
$(CO)_3FeC_2B_3H_7$ (**17**)	2.125	15
Six-atom ligand,		
$(CO)_3FeC_2B_4H_4Me_2$ (**18**)	2.145	16
Eleven-atom ligand,		
$CpFeC_2B_9H_{11}$ (**19**)	2.090	17
Thirteen-atom ligand,		
$Cp_2Fe_2C_4B_8H_8Me_4$ (**20**)	2.106	18

M—B_r distances obtained from the X-ray diffraction data available in the literature for a given metal (Fe) with varying ligand sizes. The M—B_r distances are 2.125 Å in $(CO)_3FeC_2B_3H_7$,[15] 2.145 Å in $(CO)_3FeC_2B_4H_4Me_2$,[16] 2.090 Å in $CpFeC_2B_9H_{11}$[17] and 2.106 Å in $Cp_2Fe_2C_4B_8H_8Me_4$.[18] The longest distance (2.145 Å) is found with the $C_2B_4H_4Me_2$ ligand, which is the equivalent of **13**. The shorter values are found in $CpFeC_2B_9H_{11}$ (2.090 Å) and $Cp_2Fe_2C_4B_8H_8Me_4$ (2.106 Å), which are, respectively, equivalent to $B_{11}H_{11}^{4-}$ and $B_{13}H_{13}^{4-}$ ligands. The above analysis shows that ligand **13** prefers more diffuse caps, whereas both ligands **14** and **15** prefer caps with less diffuse orbitals. Since the ring *p*-orbitals are bent away from the vacant site in the B_5 ring of $B_6H_6^{4-}$, the distance between the ring and the cap will become longer in $(CO)_3FeC_2B_4H_4Me_2$. The reverse will be true with $B_{11}H_{11}^{4-}$ and $B_{13}H_{13}^{4-}$ ligands, which makes the ring to cap distance smaller in $CpFeC_2B_9H_{11}$ and $Cp_2Fe_2C_4B_8H_8Me_4$, which are in accordance with the predictions. Since structural data for all the borane ligands (**12–15**) with the same metal are not available, a comparison of the above mentioned could not be made for other metals. The basic idea that the bond distances between atoms would be short for optimal ring–cap interactions holds good in the examples known exprimentally.

Topological charge stabilization

According to the concept of topological charge stabilization,[8] when a more electronegative heteroatom is to be placed in a homoatomic ring system, it prefers the site of larger electron density. For example, $C_2B_5H_7$ can have four possible isomers in the pentagonal bipyramidal form, viz. 1,2-, 1,7-, 2,3- and 2,4-derivatives. Based on the charges in the isoelectronic reference C_6N^-, it is found that 2,4-positions carried more electron density. These two positions are occupied by the contracted CH groups in the most stable 2,4-isomer. BH groups with more diffuse orbitals than CH occupy the less negative 1,7-positions. This shows that diffuse nature and electropositive character go together. Since $Fe(CO)_3$ has more diffuse orbitals than BH, it would prefer to occupy more positive sites rather than BH.

To find out the relative positions of BH and $Fe(CO)_3$ caps in metalloboranes, the charges in various positions of the ligands $B_6H_6^{4-}$ (**13**), $B_6H_6Fe(CO)_3^{2-}$ (**18**), $B_{11}H_{11}Fe(CO)_3^{2-}$ (**19**) and $B_{13}H_{13}Fe(CO)_3^{2-}$ (**20**) are compared. In $B_6H_6^{4-}$ (**13**) the apical BH carries less negative charge (−0.14) than the remaining centres in the ring (−0.77). Therefore in pyramidal metalloboranes of the composition $B_5H_5ML_n$ the metal fragment (ML_n) would occupy the apical (cap) position, which is in agreement with experimental observations. In $B_6H_6Fe(CO)_3^{2-}$ (**18**) the apical BH position opposite to $Fe(CO)_3$ carries more positive charge (0.09) than the remaining centres in the ring (−0.24). A second metal fragment (ML_n) therefore may occupy that site. This explains the observation of 1,7-$Cp_2Co_2C_2B_3H_4Me$[19] and 1,7-$Cp_2Co_2C_2B_3H_3(\mu\text{-}C_3H_4)$.[20] Even though the apical BH position in $B_{11}H_{11}Fe(CO)_3^{2-}$ (**19**) carries less negative charge (−0.10) than the five BHs which are above it (−0.12, −0.13), it carries more charge than the top five BHs (−0.08, −0.11). However, the differences in the charges are much smaller than that discussed earlier with **13** and **18**. Therefore for the second metal fragment (ML_n) to occupy a site in **19**, we anticipate the various isomers not to differ in energy by large amounts. Again the apical BH position in $B_{13}H_{13}Fe(CO)_3^{2-}$ (**20**) carries less negative charge (−0.005) than the remaining centres (−0.14). Thus we can explain the formation of the complex $Cp_2Fe_2C_4B_8H_8Me_4$ with two CpFe caps in the apical positions.[18]

CONCLUSIONS

Metalloboranes with terminal (H_t) and bridging hydrogen atoms (H_b), as shown in **1–4**, are studied theoretically to understand the dependence of the positions of the bridging hydrogen atoms on those of the terminal hydrogen atoms. Model studies on B_5H_9 (**6**) showed that terminal hydrogen atoms do control the bridging hydrogen positions and predicted that bridging hydrogen atoms might be observed above the B_n plane (towards the cap) for caps with diffuse orbitals. Calculations on $B_4H_8Fe(CO)_3$ (**1d**), $B_4H_8BeH^-$ (**1b**) and $B_4H_8Li^-$ (**1c**) supported these ideas. The bridging hydrogen atoms in $B_4H_8Fe(CO)_3$ (**1d**) are found to be bent towards the cap atom when the terminal hydrogen atoms are below the B_4 ring.

Ring–cap overlap criterion is used to find suitable metal fragments for borane ligands with five, six, 11 and 13 vertex boron atoms. Hapto-five ligands such as $B_6H_6^{4-}$ (**13**) and $B_{11}H_{11}^{4-}$ (**14**) have very different orbitals arising from the varying terminal BH bond directions. This leads to the preference of $B_6H_6^{4-}$ (**13**) for metal caps with diffuse orbitals. Both $B_{11}H_{11}^{4-}$ (**14**) and $B_{13}H_{13}^{4-}$ (**15**) preferred caps with less diffuse orbitals because of the rigidity of the ligands. This results in longer M—B_r with $B_6H_6Fe(CO)_3^{2-}$ (**18**) and shorter M—B_r with $B_{11}H_{11}Fe(CO)_3^{2-}$ (**19**) and $B_{13}H_{13}Fe(CO)_3^{2-}$ (**20**). The experimentally known M—B_r distances varied accordingly. The variations of the metal–boron (M—B_r) distances in polyhedral metalloboranes can be understood from the directionality of the orbitals of the polyhedral ligand. Using the concept of topological charge stabilization we found that metal fragments (ML_n) occupy positions of less negative charge in metalloboranes. Accordingly a second ML_n should occupy the apical position (opposite to the first ML_n) in **18** and **20**, whereas in **19** the preference is not clear cut.

Acknowledgements—We thank the University of Hyderabad computer centre and the School of Chemistry Microcomputer for computations. P.N.V.P.K. and G.N.S. thank the CSIR for financial assistance.

REFERENCES

1. (a) W. N. Lipscomb, *Boron Hydrides*. Benjamin, New York (1963); (b) E. L. Muetterties, *Boron Hydride Chemistry*. Academic Press, New York (1975); (c) R. N. Grimes, in *Comprehensive Organometallic Chemistry* (Edited by G. Wilkinson, F. G. A. Stone and E. Abel), Vol. 1, Ch. 5.5, p. 459. Pergamon Press, Oxford (1982); (d) R. N. Grimes, *Metal Interactions with Boron Clusters*. Plenum Press, New York (1982); (e) M. E. O'Neill and K. Wade, in *Comprehensive Organometallic Chemistry* (Edited by G. Wilkinson, F. G. A. Stone and E. Abel), Vol. 1, p. 1. Pergamon Press, Oxford (1982); (f) N. N. Greenwood and A. Earnshaw, *Chemistry of Elements*, p. 204. Pergamon Press, Oxford (1984); (g) T. P. Fehlner and C. E. Housecroft, in *Molecular Structure and Energetics* (Edited by J. F. Liebman and A. Greenberg), Vol. 1, Ch. 6, p. 149. Florida (1986); (h) K. Wade, *Adv. Inorg. Chem. Radiochem.* 1976, **18**, 1; (i) R. W. Rudolph, *Accts Chem. Res.* 1976, **9**, 446; (j) R. E. Williams, *Adv. Inorg. Chem. Radiochem.* 1976, **18**, 67; (k) D. M. P. Mingos, *Accts Chem. Res.* 1984, **17**, 311; (l) B. K. Teo, *Inorg. Chem.* 1985, **24**, 115; (m) A. J. Stone, *Polyhedron* 1984, **3**, 1299; (n) R. J. Gillespie, W. W. Porterfield and K. Wade, *Polyhedron* 1987, **6**, 2129; (o) E. D. Jemmis, *J. Am. Chem. Soc.* 1982, **104**, 7017.
2. D. F. Gaines, *Accts Chem. Res.* 1973, **6**, 416.
3. (a) K. Hedberg, M. E. Jones and V. Schomaker, *Proc. Natl. Acad. Sci. U.S.* 1952, **38**, 679; (b) H. J. Hrostowski and R. J. Myers, *J. Chem. Phys.* 1954, **22**, 262; (c) W. J. Dulmage and W. N. Lipscomb, *Acta Cryst.* 1952, **5**, 260.
4. (a) M. Elian, M. M. L. Chen, D. M. P. Mingos and R. Hoffmann, *Inorg. Chem.* 1976, **15**, 1148; (b) K. Krogh-Jespersen, J. Chandrasekhar and P. v. R. Schleyer, *J. Org. Chem.* 1980, **45**, 1608; (c) E. D. Jemmis and P. v. R. Schleyer, *J. Am. Chem. Soc.* 1982, **104**, 4781; (d) E. D. Jemmis and P. N. V. Pavankumar, *Proc. Ind. Acad. Sci. (Chem. Sci).* 1984, **93**, 479.
5. (a) P. Brint and T. R. Spalding, *J. Chem. Soc., Dalton Trans.* 1980, 1236; (b) P. Brint, W. K. Pelin and T. R. Spalding, *J. Chem. Soc., Dalton Trans.* 1981, 546; (c) P. Brint, E. F. Healy, T. R. Spalding and T. Whelan, *J. Chem. Soc., Dalton Trans.* 1981, 2515; (d) D. R. Salahub, *J. Chem. Soc., Chem. Commun.* 1978, 385; (e) M. J. S. Dewar and M. L. Mckee, *J. Am. Chem. Soc.* 1977, **99**, 5231.
6. M. J. S. Dewar and W. Thiel, *J. Am. Chem. Soc.* 1977, **99**, 4799.
7. (a) R. Hoffmann, *J. Chem. Phys.* 1963, **39**, 1397; (b) R. Hoffmann and W. N. Lipscomb, *J. Chem. Phys.* 1962, **36**, 2179.
8. (a) B. M. Gimarc and J. J. Ott, *J. Am. Chem. Soc.* 1986, **108**, 4298; (b) J. J. Ott and B. M. Gimarc, *J. Am. Chem. Soc.* 1986, **108**, 4303.
9. (a) J. A. Ulman, E. K. Andersen and T. P. Fehlner, *J. Am. Chem. Soc.* 1978, **100**, 456; (b) N. N. Greenwood, C. G. Savory, R. N. Grimes, L. G. Sneddon, A. Davison and S. S. Wreford, *J. Chem. Soc., Chem. Commun.* 1974, 718; (c) Incidentally $B_4H_8Fe(CO)_3$ appears on the cover page of the book *Chemistry of Elements* by N. N. Greenwood and A. Earnshaw [ref. 1(f)] with bridging hydrogens below the B_4 ring.
10. H. D. Johnson II, V. T. Brice, G. L. Brubaker and S. G. Shore, *J. Am. Chem. Soc.* 1972, **94**, 6711.
11. T. P. Fehlner, J. Ragaini, M. Mangion and S. G. Shore, *J. Am. Chem. Soc.* 1976, **98**, 7085.
12. R. Weiss and R. N. Grimes, *Inorg. Chem.* 1979, **18**, 3291.
13. M. F. Hawthorne, *J. Organomet. Chem.* 1975, **100**, 97.
14. (a) L. D. Brown and W. N. Lipscomb, *Inorg. Chem.* 1977, **16**, 2989; (b) J. Bicerano, D. S. Marynick and W. N. Lipscomb, *Inorg. Chem.* 1978, **17**, 2041, 3443.
15. J. P. Brennan, R. N. Grimes, R. Schaeffer and L. G. Sneddon, *Inorg. Chem.* 1973, **12**, 2266.
16. R. D. Barreto, T. P. Fehlner and N. S. Hosmane, *Inorg. Chem.* 1988, **27**, 453 and refs therein.
17. A. Zalkin, D. H. Templeton and T. E. Hopkins, *J. Am. Chem. Soc.* 1965, **87**, 3988.
18. (a) J. R. Pipal and R. N. Grimes, *Inorg. Chem.* 1978, **17**, 6; (b) W. M. Maxwell, R. Weiss, E. Sinn and R. N. Grimes, *J. Am. Chem. Soc.* 1977, **99**, 4016.
19. W. T. Robinson and R. N. Grimes, *Inorg. Chem.* 1975, **14**, 3056.
20. J. R. Pipal and R. N. Grimes, *Inorg. Chem.* 1978, **17**, 10.

21. R. H. Summerville and R. Hoffmann, *J. Am. Chem. Soc.* 1976, **98**, 7240.

APPENDIX

The parameters for all the atoms used in the extended Huckel calculations are taken from previous studies: C, H, O, B, Be, Li[7] and Fe[21]. In B_5H_9 (**6**), B_r—B_r, B_r—X, B_r—H_t and B_r—H_b distances are kept at 1.800, 1.700, 1.230 and 1.360 Å, respectively. In $B_4H_8Fe(CO)_3$ (**1d**), the B_r—Fe distance is kept at 2.000 Å. Other distances involving the $Fe(CO)_3$ ligand are Fe—C = 2.000 Å and C—O = 1.150 Å. Fixed B_r—B_r and B_r—B_a (apical boron) of 1.770 Å and B—H = 1.150 Å are used in **12–15**. In **15**, B_r—B_a is kept at 1.86 Å. B_r—Fe is kept at 2.160 Å in **17–20**. The CFeC angle, α, in **16** is varied to simulate orbitals of different diffuse nature. The B_r—Li and B_r—Be distances are kept at 2.200 and 1.860 Å, respectively, in $B_4H_8Li^-$ and $B_4H_8BeH^-$.

Polyhedron Vol. 9, No. 19, pp. 2371–2374, 1990
Printed in Great Britain

0277–5387/90 $3.00+.00
Pergamon Press plc

STUDIES ON RARE EARTH COMPLEXES WITH CROWN ETHERS—XIX. SYNTHESIS AND CHARACTERIZATION OF THE COMPLEXES OF LANTHANIDE THIOCYANATES WITH DIBENZO-24-CROWN-8

LU TONGBU, GAN XINMIN, TANG NING and TAN MINYU*

Department of Chemistry, Lanzhou University, Lanzhou 730000, P.R.C.

(*Received* 20 *March* 1990; *accepted* 11 *May* 1990)

Abstract—The lanthanide thiocyanate complexes with DB24C8 have been prepared in acetonitrile medium. These new complexes with the general formula $[Ln(SCN)_3 \cdot DB24C8 \cdot 2H_2O \cdot CH_3CN]$ (Ln = La–Nd, Sm–Lu) have been characterized by elemental analysis, IR spectra, conductivity measurements and TG–DTA techniques. In the complexes, the ligand DB24C8, the thiocyanate groups and the water molecules are all coordinated to the metal ions.

Many rare earth–crown ether complexes have been investigated in recent years.[1–8] The previous research work was concentrated on some crown ethers with a relatively small cavity such as 12-crown-4, 15-crown-5 and 18-crown-6 as well as their derivatives,[2–7] while the rare earth complexes with larger cavity crown ethers were little reported.[8] In order to investigate the coordinating power of a large cavity crown ether with rare earth ions, we have recently synthesized the solid complexes of lanthanide thiocyanates with DB24C8, and investigated the composition and properties of these new complexes.

EXPERIMENTAL

Reagents

Hydrated lanthanide thiocyanates were prepared by the literature method.[9] DB24C8 was obtained from Shanghai Reagent Company and purified by recrystallization from ethanol before using, m.p. = 101.5–102.0°C.

Chemical and physical measurements

The metal ion was determined by EDTA titration using Xylenol-orange as an indicator. Carbon, nitrogen and hydrogen were determined using a Carlo Erba 1106 elemental analyser. The IR spectra were recorded in the 4000–200 cm^{-1} region using KBr pellets and a 170 SX FTIR spectrometer. Thermal analyses (TG and DTA) were performed on a Beijing PcT-2 thermobalance. The heating rate was 10°C min^{-1}. Conductivity measurements were carried out with a DDS-11A type conductivity bridge for freshly prepared solutions in acetone at 25°C.

Preparation of the complexes

A solution of 0.2 mmol $Ln(SCN)_3 \cdot xH_2O$ in 3 cm^3 of acetonitrile was added dropwise to a solution of 0.2 mmol DB24C8 in 4 cm^3 of acetonitrile. The mixture was stirred at room temperature for 24 h. The precipitated solid complex was filtered, washed with acetonitrile and diethyl ether, respectively, and dried in a desiccator (0.1 mmHg) over P_4O_{10} for 48 h. All the complexes are powdered solids with the characteristic colour of the corresponding lanthanide thiocyanates.

RESULTS AND DISCUSSION

The composition of the complexes

The analytical data for the newly synthesized complexes, listed in Table 1, indicate that all of the 14 complexes conform to a 1:1 stoichiometry of metal ion and crown ether.

* Author to whom correspondence should be addressed.

Table 1. Elemental analysis and molar conductance data

Compound[a]	%N Found (Calc.)	%C Found (Calc.)	%H Found (Calc.)	%M Found (Calc.)	Molar conductance (Ω^{-1} cm^2 mol^{-1})
$La(SCN)_3 \cdot L \cdot 2H_2O \cdot CH_3CN$	5.9 (6.7)	41.5 (41.5)	4.2 (4.6)	17.0 (16.6)	18.6
$Ce(SCN)_3 \cdot L \cdot 2H_2O \cdot CH_3CN$	7.2 (6.7)	41.5 (41.4)	4.5 (4.6)	16.3 (16.7)	17.9
$Pr(SCN)_3 \cdot L \cdot 2H_2O \cdot CH_3CN$	6.3 (6.7)	41.5 (41.4)	4.3 (4.6)	16.4 (16.8)	14.5
$Nd(SCN)_3 \cdot L \cdot 2H_2O \cdot CH_3CN$	7.2 (6.6)	41.2 (41.2)	4.4 (4.6)	17.3 (17.1)	14.7
$Sm(SCN)_3 \cdot L \cdot 2H_2O \cdot CH_3CN$	6.2 (6.6)	40.6 (40.9)	4.3 (4.6)	17.9 (17.7)	14.9
$Eu(SCN)_3 \cdot L \cdot 2H_2O \cdot CH_3CN$	6.1 (6.6)	41.0 (40.9)	4.3 (4.6)	18.0 (17.8)	15.3
$Gd(SCN)_3 \cdot L \cdot 2H_2O \cdot CH_3CN$	6.4 (6.5)	40.3 (40.6)	4.5 (4.5)	18.4 (18.3)	15.0
$Tb(SCN)_3 \cdot L \cdot 2H_2O \cdot CH_3CN$	6.2 (6.5)	40.2 (40.5)	4.3 (4.5)	18.7 (18.5)	16.2
$Dy(SCN)_3 \cdot L \cdot 2H_2O \cdot CH_3CN$	6.3 (6.5)	40.0 (40.4)	4.4 (4.5)	19.2 (18.8)	14.5
$Ho(SCN)_3 \cdot L \cdot 2H_2O \cdot CH_3CN$	6.6 (6.5)	40.0 (40.2)	4.3 (4.5)	19.3 (19.1)	10.4
$Er(SCN)_3 \cdot L \cdot 2H_2O \cdot CH_3CN$	6.4 (6.5)	40.3 (40.1)	4.5 (4.5)	19.4 (19.3)	12.3
$Tm(SCN)_3 \cdot L \cdot 2H_2O \cdot CH_3CN$	6.5 (6.4)	40.1 (40.1)	4.4 (4.5)	19.7 (19.4)	8.2
$Yb(SCN)_3 \cdot L \cdot 2H_2O \cdot CH_3CN$	6.5 (6.4)	40.1 (39.9)	4.4 (4.5)	20.1 (19.8)	9.0
$Lu(SCN)_3 \cdot L \cdot 2H_2O \cdot CH_3CN$	6.5 (6.4)	39.8 (39.8)	4.3 (4.5)	20.1 (20.0)	8.8

[a] L = DB24C8.

IR spectra

The most important IR peaks of the ligand and the complexes are reported in Table 2.

Compared with the free ligand, the absorptions of ν(Ar—O—R) and ν(R—O—R) of the complexes showed shifts towards lower wavenumbers. This provides evidence for the coordination of the crown ether with the metal ions. In addition, new bands, absent in the IR spectrum of the free ligand, are present in the 388–399 cm^{-1} region, which may be assigned to the ν(M—O_{crown}) stretching frequency.[8]

The IR absorptions of ν(CN), ν(CS) and δ(NCS) of the thiocyanate groups are present in the 2044–2058, 794–810 and 477–490 cm^{-1} regions, respectively, which suggests that the thiocyanate groups in the complexes are coordinated to the metal ions through the nitrogen atoms,[10] while the absence of absorptions near 2100, 700 and 420 cm^{-1} indicates that the sulphur atoms in the thiocyanate groups are not bonded to the metal ions.

In all the IR spectra of the complexes, strong bands which appear near 3400 and 1650 cm^{-1} are clearly due to ν(OH) and δ(HOH), respectively. Additionally, weak bands assigned to ρ_r(HOH) are found near 604 cm^{-1}, providing evidence that the water molecules in the complexes are also coordinated to the metal ions.[10] The presence of weak bands in the range 2250–2280 cm^{-1} due to ν[CN(CH_3CN)] suggests that the acetonitrile molecules in the complexes are not coordinated with the metal ions.[5]

Thermal analyses

The thermal analysis studies were performed by means of TG and DTA techniques. The thermal analytical data for some of the complexes are summarized in Table 3.

Table 2. The most important IR bands (cm^{-1})

Compound	ν(Ar—O—R)	ν(R—O—R)	ν(CN)[a]	ν(CS)	δ(NCS)	ν(CN)[b]	ν(Ln—O)	ν(OH)	δ(HOH)	ρr(H2O)
DB24C8	1224s	1102s								
La	1212s	1081s	2054s	794w	477m	2255m	396w	3463s	1648s	603m
Ce	1213s	1083m	2044s	796w	482m	2251m	396w	3399s	1676s	603m
Pr	1211s	1080m	2046s	809w	485m	2251m	394w	3402s	1652m	604m
Nd	1210s	1078m	2047s	802s	480m	2252m	390w	3485s	1660s	602m
Sm	1210s	1081m	2052s	809m	490m	2252m	392w	3467s	1649m	604m
Eu	1211s	1080m	2051s	808m	483m	2252m	388w	3461s	1649w	604m
Gd	1217s	1082s	2049s	809m	485m	2281m	396w	3454s	1660s	603m
Tb	1211s	1085m	2055s	809w	483m	2252m	391w	3402s	1650m	604m
Dy	1217s	1081s	2051s	809m	486m	2282m	391w	3452s	1661s	603m
Ho	1217s	1081s	2053s	809m	487m	2282m	396w	3452s	1662s	603m
Er	1217s	1081s	2055s	810m	487m	2283m	396w	3402s	1662s	603m
Tm	1218s	1081s	2057s	810m	488m	2283m	393w	3401s	1663s	603m
Yb	1218s	1081s	2058s	810m	487m	2283m	390w	3398s	1663s	603m
Lu	1218s	1081s	2058s	810m	488m	2284m	399w	3401s	1663s	603m

[a] The ν(CN) of the thiocyanate groups.
[b] The ν(CN) of the acetonitrile molecules.

Table 3. Thermal analytical data of some of the complexes

Compound	Endothermic peaks (°C)	Exothermic peaks (°C)	Total weight loss (%) Found	Calc.[a]
$La(SCN)_3 \cdot L \cdot 2H_2O \cdot CH_3CN$	126, 222	302, 494, 564	74.60	75.81
$Gd(SCN)_3 \cdot L \cdot 2H_2O \cdot CH_3CN$	121, 203	293, 478, 547	76.32	74.18
$Lu(SCN)_3 \cdot L \cdot 2H_2O \cdot CH_3CN$	104, 189	296, 466, 544	72.22	72.68

[a] Calculated weight loss for the change from the complexes to $Ln_2O_2SO_4$.
Ln = La, Gd, Lu.

The complexes of lanthanum, gadolinium and lutetium lose one acetonitrile molecule and two water molecules when heated to 126, 121 and 104°C, respectively. The weight losses found in this process are 8.82, 8.95 and 8.77%, respectively (Calc. 8.70, 8.82 and 8.34%, respectively).

After the loss of one acetonitrile molecule and two water molecules the three complexes melted when heated to 222, 203 and 189°C, respectively. In this process a small endothermic peak appeared in the DTA curve but no weight loss occurred in the TG curve of each complex. On raising the temperature further, the three complexes decomposed exothermically at 302, 293 and 296°C, respectively. After this other exothermic peaks and continuous weight loss were detected up to 850°C. At this temperature $Ln_2O_2SO_4$ (Ln = La, Gd and Lu) is formed.[11] The total weight loss found was approximately consistent with that calculated (Table 3). The DTA–TG curves of the other complexes are similar to those of the three complexes discussed above.

Solubility and molar conductance

All the complexes are sparingly soluble in benzene, chloroform and nitromethane, slightly soluble in water, methanol, ethanol and acetonitrile, and much more soluble in acetone, ethylacetate and tetrahydrofuran. The molar conductance values of the complexes measured in acetone at 25°C lie in the range 8.2–18.6 Ω^{-1} cm^2 mol^{-1} (Table 1), indicating that all the complexes are non-electrolytes.[12] This indicates that all the thiocyanate groups in the complexes are held in the coordination sphere.

From the data discussed above, it can be concluded that the large cavity crown ether DB24C8 can react with lanthanide thiocyanates in acetonitrile medium to form stable solid complexes, in which the ligand DB24C8, thiocyanate groups

and water molecules are coordinated to the metal ions, and therefore the correct molecular formula of the new prepared complexes should be $[Ln(DB24C8)(H_2O)_2(SCN)_3]\cdot CH_3CN$.

REFERENCES

1. J.-C. G. Bünzli and D. Wessner, *Coord. Chem. Rev.* 1984, **60**, 191.
2. R. D. Rogers and L. K. Kurihara, *Inorg. Chim. Acta* 1986, **116**, 171.
3. J.-C. G. Bünzli and A. Giorgetti, *Inorg. Chim. Acta* 1985, **110**, 215.
4. Zhou Jinping and Tan Minyu, *J. Chinese Rare Earth Soc.* 1983, **1**, 34.
5. Zhang Lianxiang, Lu Airu, Zhang Yuming and Chen Xiaoqing, *J. Chinese Rare Earth Soc.* 1988, **6**, 15.
6. Tan Minyu, Wang Xin, Gan Xinmin, Tang Ning, Guo Fang and Zhu Naijue, *Acta Chim. Sinica* 1989, **47**, 167.
7. Gan Xinmin, Tang Ning, Zhu Ying, Zhai Yingli and Tan Minyu, *J. Chinese Rare Earth Soc.* 1989, **7**, 13.
8. Qi Youxun, Tan Minyu and Zhai Yingli, *J. Inorg. Chem. Chin.* 1986, **2**, 87.
9. Zhang Yuehua and Yao Xinkan, *Hua Xue Shi Ji* 1982, **4**, 30.
10. K. Nakamoto, *Infrared and Raman Spectra of Inorganic and Coordination Compounds*, 3rd edn, pp. 227, 270–271. John Wiley, New York (1978).
11. L. Gmelin, *Gmelin Handbuch der Anorganischen Chemie*, 8th edn, System-Nummer 39 (C8), p. 326. Springer, Berlin (1981).
12. W. J. Geary, *Coord. Chem. Rev.* 1971, **7**, 81.

Polyhedron Vol. 9, No. 19, pp. 2375–2383, 1990
Printed in Great Britain

0277–5387/90 $3.00+.00
© 1990 Pergamon Press plc

NOVEL SQUARE PYRAMIDAL COPPER(II) COMPLEXES OF THE STEREOSPECIFIC LINEAR NSNN TETRADENTATE LIGAND, *N*-[(2-PYRIDYL)METHYL]-2-[(2-AMINOETHYL)THIO] ACETAMIDE (pygeH). THE CRYSTAL STRUCTURES OF [Cu(pyge)X] (X = Br, N_3)

PAUL J. TOSCANO,* KATHY J. FORDON, DEBORAH MACHERONE, SHUNCHENG LIU and JON ZUBIETA

Department of Chemistry, State University of New York at Albany, Albany, NY 12222, U.S.A.

(*Received* 29 *March* 1990; *accepted* 16 *May* 1990)

Abstract—The preparations of complexes of type [Cu(pyge)X] and [Cu(pyge)(OH_2)]BF_4, where pygeH is *N*-[(2-pyridyl)methyl]-2-[(2-aminoethyl)thio]acetamide and X is Br, N_3, NCO, NCS, $OC_6H_4NO_2$-*p*, and NO_2, are described. The new complexes have been characterized by elemental analysis, IR and electronic spectroscopy, magnetic moment, and in two cases (X = Br and $OC_6H_4NO_2$-*p*), EPR spectroscopy. The available data suggest that the complexes are of tetragonal, probably square pyramidal geometry in solution. X-ray structural analyses of [Cu(pyge)Br] (**1**) and [Cu(pyge)N_3] (**2**) were undertaken. Complex **1** crystallized in the monoclinic space group $P2_1/n$, $a = 9.676(2)$, $b = 9.147(2)$, $c = 15.171(3)$ Å, $\beta = 106.73(2)°$, $V = 1286.0(5)$ Å^3, $Z = 4$. Refinement was based on 1594 reflections and converged at $R = 0.059$, $R_w = 0.058$. Complex **2** crystallized in the monoclinic space group $P2_1/c$, $a = 9.925(2)$, $b = 9.354(3)$, $c = 15.141(4)$ Å, $\beta = 106.96(2)°$, $V = 1344.3(6)$ Å^3, $Z = 4$. Refinement was based on 1196 reflections and converged at $R = 0.065$, $R_w = 0.065$. The geometry of the complexes is best described as very slightly distorted square pyramidal, with the terminal amino group of the tetradentate ligand occupying the apical site. Origins of the observed stereospecificity and structural comparisons to octahedral [Co(pyge)$(NO_2)_2$] are discussed.

The study of the factors affecting the stereochemistry of copper(II) coordination compounds has been an area of intense research.[1–3] Part of this interest stems from attempts to model the copper-containing active sites in metalloproteins.[2–5] The copper(II) ion can accommodate a large range of coordination geometries.[1–3] This pliant ability of copper(II) has been likened to a kind of "plasticity" which is apparently overcome by the rigid tertiary structures of proteins to bind this ion in a specific geometry for a particular biological function.[1]

Recently, we have been investigating octahedral cobalt(III) coordination complexes containing stereospecific, linear NSNN tetradentate ligands, such as *N*-[(2-pyridyl)methyl]-2-[(2-aminoethyl) thio]acetamide (pygeH).[6–8] The ligand pygeH,

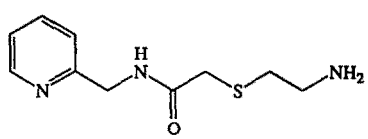

pygeH

after deprotonation, is designed to adopt the *cis*-β or unsymmetrical-*cis* geometry in octahedral compounds of type [Co(pyge)X_2].[6,8] The stereochemical control derives from the nature of the internal ligating atoms in the chelating ligand. The thioether atom shows a strong preference for pyramidal coordination when it is at the pivot point of two five-membered chelate rings in which the other donors are nitrogen or oxygen.[9] On the other hand, the deprotonated amide donor maintains planarity about that site.[10] In the course of our studies, it became of interest to apply this versatile ligand to a labile, stereochemically non-rigid situation as

* Author to whom correspondence should be addressed.

typified by the copper(II) ion. In this contribution, we wish to report upon the preparation and characterization of a series of novel five-coordinate complexes, [Cu(pyge)X], where X is a monodentate uninegative ligand, as well as $[Cu(pyge)(OH_2)]BF_4$. In addition, we have structurally characterized the complexes with X being either Br or N_3 in order to establish the solid-state stereochemistry and to make comparisons to the previously presented structure of octahedral $[Co(pyge)(NO_2)_2]$.[6]

EXPERIMENTAL

Materials and methods

Electronic spectra were determined on dilute *N,N*-dimethylformamide (DMF) or aqueous solutions using a Shimadzu UV-160 spectrophotometer at ambient temperature. Molar absorptivity coefficients are reported in $mol^{-1}\ dm^3\ cm^{-1}$. Room temperature magnetic susceptibilities were measured on a Johnson–Matthey susceptometer. Magnetic moments were calculated using literature diamagnetic corrections.[11] IR spectra were recorded from compressed KBr pellets using a Perkin–Elmer 1600 Series FT–IR spectrometer. Frozen EPR spectra were determined on glassy DMF/CH_2Cl_2 solutions at −196°C utilizing a Varian E-4 spectrometer calibrated with the diphenyl picryl hydrazyl radical. Room temperature EPR spectra in DMF solution were obtained in a special flat cell in order to minimize the dielectric effect of the solvent. Elemental analyses were determined by Atlantic Microlabs Inc. (Atlanta, Georgia).

Preparation of compounds

Unless otherwise noted, all starting materials and solvents were obtained from standard sources and used without further purification.

N-[(2-*Pyridyl*)*methyl*]-2-[(2-*aminoethyl*)*thio*]*acetamide dihydrobromide* (pygeH·2HBr)

The ligand was prepared via the literature method.[6] IR (KBr): 3226 (m), 3164 (m), 2865 (s), 1655 (s), 1612 (s), 1526 (s), 1484 (m), 1461 (s), 1421 (m), 1384 (w), 1372 (w), 1266 (m), 1249 (m), 1162 (w), 1102 (w), 1090 (w), 1078 (w), 1043 (w), 1027 (m), 958 (vw), 907 (vw), 893 (vw), 803 (w), 764 (m), 737 (w), 663 (vw), 558 (vw), 482 (vw).

[Cu(pyge)Br] (1)

Sodium metal (0.144 g, 6.3 mmol) was dissolved carefully in absolute ethanol (60 cm^3). Then pygeH·2HBr (1.20 g, 3.1 mmol) was added. After dissolution of the ligand, copper(II) acetate monohydrate (0.62 g, 3.1 mmol) was added. The suspension was stirred for 2 h and then the green precipitate was collected by filtration. The crude product was taken up in a minimum amount of water (*ca* 18 cm^3) and filtered. The filtrate was set aside for concentration and crystallization, giving 0.79 g (69.3%) of bright green product. Found: C, 32.6; H, 3.8; N, 11.4. Calc. for $C_{10}H_{14}BrCuN_3OS$: C, 32.7; H, 3.8; N, 11.4%. UV–vis (DMF): λ_{max} 673 (ε 170), 356 nm (ε 2300); $\mu_{eff} = 2.1$ BM; IR (KBr): 3324 (m), 3246 (m), 3150 (m), 2950 (m), 2894 (m), 2853 (m), 1605 (br s), 1583 (vs), 1566 (vs), 1484 (m), 1448 (m), 1423 (m), 1406 (m), 1390 (s), 1346 (w), 1285 (m), 1218 (m), 1159 (w), 1097 (w), 1052 (w), 1025 (m), 963 (m), 915 (s), 830 (m), 769 (s), 720 (w), 617 (w), 486 (m).

$[Cu(pyge)N_3]$ (2)

[Cu(pyge)Br] (0.20 g, 0.54 mmol) and sodium azide (0.175 g, 2.7 mmol) were added to water (7 cm^3). The solution was stirred for 2 h. Upon slow evaporation of the solvent, a pure dark green crystalline product was obtained (0.12 g, 67.4%). Found: C, 36.4; H, 4.3; N, 25.4. Calc. for $C_{10}H_{14}CuN_6OS$: C, 36.4; H, 4.3; N, 25.5%. UV–vis (DMF): λ_{max} 643 (ε 270), 389 nm (ε 4300), 360 (sh); $\mu_{eff} = 1.9$ BM; IR (KBr): 3322 (m), 3245 (m), 3155 (m), 2954 (w), 2900 (w), 2858 (w), 2057 (vs), 1609 (s), 1593 (vs), 1584 (vs), 1567 (vs), 1485 (m), 1404 (s), 1388 (s), 1346 (m), 1281 (m), 1217 (m), 1093 (vw), 1051 (w), 1026 (w), 972 (m), 919 (m), 827 (m), 765 (s), 720 (w), 620 (vw), 491 (w).

[Cu(pyge)NCO] (3)

[Cu(pyge)Br] (0.20 g, 0.54 mmol) and potassium cyanate (0.050 g, 0.62 mmol) were added to water (7 cm^3). After stirring the mixture for 2 h, the royal blue microcrystalline product that deposited was collected and dried (0.10 g, 73.9%). Found: C, 40.1; H, 4.3; N, 17.0. Calc. for $C_{11}H_{14}CuN_4O_2S$: C, 40.0; H, 4.3; N, 17.0%. UV–vis (DMF): λ_{max} 663 (ε 200), 354 nm (ε 2400); $\mu_{eff} = 1.9$ BM; IR (KBr): 3346 (m), 3247 (m), 3161 (m), 2950 (w), 2895 (w), 2859 (w), 2230 (vs), 1609 (vs), 1594 (vs), 1584 (vs), 1567 (vs), 1484 (m), 1443 (w), 1421 (m), 1406 (m), 1391 (s), 1346 (w), 1325 (m), 1280 (w), 1216 (w), 1154 (vw), 1093 (vw), 1050 (w), 1025 (w), 974 (w), 919 (m), 832 (m), 762 (s), 720 (w), 608 (w), 494 (w).

[Cu(pyge)NCS] (**4**)

[Cu(pyge)Br] (0.20 g, 0.54 mmol) and sodium thiocyanate (0.051 g, 0.63 mmol) were added to water (7 cm^3). After stirring the mixture for 2 h, the crude blue–green powder was collected. This material was recrystallized by dissolving it in boiling water (30 cm^3) and adding sodium thiocyanate (0.45 g) to the cooled solution. The blue–green microcrystalline product was collected, washed with cold water (5 cm^3), and dried (0.10 g, 70.5%). Found: C, 37.6; H, 4.0; N, 16.1. Calc. for $C_{11}H_{14}CuN_4OS_2$: C, 38.2; H, 4.1; N, 16.2%. UV–vis (DMF): λ_{max} 643 (ε 230), 362 nm (ε 2600); μ_{eff} = 1.9 BM; IR (KBr): 3300 (m), 3270 (m), 3167 (m), 2888 (vw), 2086 (vs), 1609 (vs), 1582 (vs), 1561 (vs), 1483 (m), 1405 (m), 1394 (s), 1342 (w), 1282 (w), 1227 (m), 1212 (w), 1145 (m), 1086 (vw), 1048 (w), 1028 (m), 970 (vw), 930 (vw), 894 (vw), 767 (s), 717 (vw), 637 (vw), 493 (w).

[Cu(pyge)($OC_6H_4NO_2$-*p*)] (**5**)

$AgNO_3$ (0.070 g, 0.41 mmol) was added to a solution of [Cu(pyge)Br] (0.15 g, 0.41 mmol) in H_2O (5 cm^3). The mixture was stirred for 15 min and filtered through Celite filtering aid to give a deep blue filtrate. Sodium *p*-nitrophenoxide (0.066 g, 0.41 mmol) was added to the filtrate. The resulting green solution was stirred for 2 h and allowed to go to dryness overnight. The sticky residue was triturated with methanol (3 cm^3) to give 0.11 g (60.4%) of dark green product which analysed as the monohydrate. Found: C, 43.4; H, 4.5; N, 12.6. Calc. for $C_{16}H_{20}CuN_4O_5S$: C, 43.3; H, 4.5; N, 12.6%. UV–vis (DMF): λ_{max} 673 (ε 220), 431 nm (ε 18,400); μ_{eff} = 1.9 BM; IR (KBr): 3359 (m), 3295 (m), 2870 (vw), 1607 (s), 1582 (vs), 1565 (vs), 1492 (s), 1462 (m), 1428 (w), 1404 (m), 1385 (m), 1351 (w), 1305 (vs), 1289 (vs), 1274 (vs), 1215 (w), 1171 (m), 1110 (s), 1050 (w), 1040 (w), 1023 (w), 1010 (w), 953 (w), 914 (m), 846 (m), 825 (w), 774 (m), 758 (m), 722 (w), 701 (w), 655 (m), 646 (m), 551 (w), 520 (w), 496 (vw), 466 (w).

[Cu(pyge)(NO_2)] (**6**)

A solution containing [Cu(pyge)(OH_2)]NO_3 (0.41 mmol in 5 cm^3 of water) was prepared as above in the synthesis of **5**. To this solution was added sodium nitrite (0.056 g, 0.82 mmol). The solvent was allowed to evaporate overnight and the residue was triturated with methanol (2 cm^3) to give 0.055 g (40%) of the dark green product. Found: C, 35.1; H, 4.1; N, 16.5. Calc. for $C_{10}H_{14}CuN_4O_3S$: C, 36.0; H, 4.2; N, 16.8%. UV–vis (DMF): λ_{max} 632 (ε 170), 354 nm (ε 2800); μ_{eff} = 1.9 BM; IR (KBr): 3298 (m), 3262 (w), 3163 (w), 2963 (vw), 2908 (vw), 2857 (w), 1609 (s), 1588 (vs), 1566 (vs), 1487 (m), 1450 (m), 1393 (s), 1354 (s), 1328 (s), 1290 (m), 1218 (w), 1163 (w), 1100 (vw), 1052 (vw), 1022 (w), 977 (w), 924 (w), 830 (w), 769 (m), 720 (w), 673 (vw), 645 (vw), 620 (vw), 491 (m), 472 (w).

[Cu(pyge)(OH_2)]BF_4 (**7**)

A solution containing [Cu(pyge)(OH_2)]NO_3 (0.41 mmol in 5 cm^3 of water) was prepared as above in the synthesis of **5**. To this solution was added sodium tetrafluoroborate (0.045 g, 0.41 mmol). After filtration, the solvent was allowed to concentrate to small volume to give 0.025 g (16%) of the very water-soluble blue product. Found: C, 30.8; H, 4.1. Calc. for $C_{10}H_{16}BCuF_4N_3O_2S$: C, 30.6; H, 4.1%. UV–vis (DMF): λ_{max} 607 (ε 200), 357 nm (ε 2300); IR (KBr): 3449 (br m), 3378 (m), 3307 (w), 1612 (vs), 1582 (vs), 1560 (vs), 1495 (w), 1415 (s), 1390 (s), 1346 (w), 1336 (w), 1251 (vw), 1213 (w), 1057 (s), 1026 (s), 961 (vw), 834 (vw), 771 (m), 718 (w), 552 (w), 477 (w).

Crystal structure analysis and refinement

Single crystals of compounds **1** and **2** suitable for X-ray diffraction studies were grown by concentration of saturated aqueous solutions at ambient temperature. A Nicolet R3m diffractometer in the θ–2θ mode with variable scan speed (3.0–20.0° min^{-1}) and graphite monochromated Mo-K_α (λ = 0.71073 Å) radiation was used to measure 2282 and 2332 unique reflections with $0 \leqslant 2\theta \leq 50°$, of which 1594 and 1196 reflections with $|F_o| > 6\sigma|F_o|$ were considered to be observed for **1** and **2**, respectively. Data were corrected for background, attenuators, Lorentz and polarization effects in the usual fashion, but not for absorption.[12] The structure of complex **1** was refined (with all non-hydrogen atoms anisotropic) to R = 0.059 and R_w = 0.058. In the case of complex **2**, difference Fourier maps indicated that the coordinated azide ligand was disordered. The disorder was successfully interpreted by assuming a model with two equally populated orientations of the azide group, approximately related by a 180° rotation around an axis passing through the copper atom and the central nitrogen atom of the azide ligand. Refinement of the structure of **2** (with all non-hydrogen atoms anisotropic, except the azide nitrogens) then proceeded to R = 0.065 and R_w = 0.065. Crystal data are summarized in Table 1. Atomic coordinates, full tables of bond lengths and angles, isotropic and aniso-

Table 1. Crystal/refinement data

	1	2
Compound	[Cu(pyge)Br]	[Cu(pyge)N_3]
Formula	$C_{10}H_{14}BrCuN_3OS$	$C_{10}H_{14}CuN_6OS$
M_r	367.8	329.9
Temperature (K)	298	298
Crystal system	Monoclinic	Monoclinic
Space group	$P2_1/n$	$P2_1/c$
a (Å)	9.676(2)	9.925(2)
b (Å)	9.147(2)	9.354(3)
c (Å)	15.171(3)	15.141(4)
β (°)	106.73(2)	106.96(2)
V (Å^3)	1286.0(5)	1344.3(6)
Z	4	4
D_c (g cm^{-3})	1.90	1.63
μ_{Mo} (cm^{-1})	49.2	17.8
Specimen (mm^3)	0.25 × 0.10 × 0.20	0.30 × 0.15 × 0.25
$2\theta_{max}$ (°)	50	50
N_{unique}	2282	2332
N_{obs}	1594	1196
R	0.059	0.065
R_w	0.058	0.065

tropic displacement factors, hydrogen atom parameters, and structure factors for complexes **1** and **2** have been deposited as supplementary data with the Editor or the Cambridge Crystallographic Data Centre.

RESULTS AND DISCUSSION

The reaction of pygeH·2HBr with $Cu(CH_3COO)_2 \cdot H_2O$ in basic ethanol solution, followed by recrystallization of the crude product from aqueous solution, led to the isolation of green air-stable [Cu(pyge)Br] (**1**) in good yield. Previously, it had been reported that pygeH·2HCl and $CuCl_2 \cdot 2H_2O$ in neutral ethanol solution gave square planar [Cu(pygeH)Cl]·2HCl, in which the terminal amino group is protonated and non-coordinating.[13] In the present instance, we have isolated only the neutral five-coordinate complex **1** (*vide infra*).

The bromide ligand of complex **1** can be substituted to give [Cu(pyge)X] either by direct metathesis with a suitable sodium or potassium salt [X = N_3 (**2**), NCO (**3**), NCS (**4**)] or via [Cu(pyge)(OH_2)]NO_3 prepared *in situ* from **1** and $AgNO_3$ [X = $OC_6H_4NO_2$-*p* (**5**) or NO_2 (**6**)]. The very water-soluble [Cu(pyge)(OH_2)]$^+$ cation could be isolated with some difficulty as the BF_4^- salt, **7**.

The IR vibrational spectra of the new series of complexes are essentially as expected. In all cases, moderately intense N—H stretches appear in the 3200–3350 cm^{-1} range. The C—H stretches diminish somewhat in intensity upon coordination and the deprotonated amide carbonyl stretch moves to lower energy. The pseudo-halide complexes **2–4** exhibit strong absorptions in the cumulated and triple bond region of their spectra.[14] The NCO group in **3** is likely N-bound with the symmetric and asymmetric stretches appearing at 2230 and 1325 cm^{-1}, respectively.[14,15] The determination of the coordination mode of the NCS group in **4** is more problematic; we have tentatively assigned the N-bound structure based upon electronic spectral data (*vide infra*). Complexes **5** (1275–1300 cm^{-1}), **6** (1354 and 1328 cm^{-1}) and **7** (3449 and 1025–1060 cm^{-1}) display absorptions in the expected regions for *p*-nitrophenolato, nitro, coordinated water and uncoordinated BF_4^- groups, respectively.[14]

The new copper(II) complexes are relatively soluble in DMF, giving solutions that are similar in colour to the original solid compound. The electronic spectra of [Cu(pyge)X] recorded in this solvent consist of one broad *d–d* band in the 630–675 nm range ($\varepsilon \sim$ 170–270 mol^{-1} dm^3 cm^{-1}) and a charge-transfer band at about 355–360 nm ($\varepsilon \sim$ 2500 mol^{-1} dm^3 cm^{-1}). The latter band, which is relatively invariant as a function of X ligand, can be assigned to $S(\sigma) \rightarrow Cu(d_{x^2-y^2})$ ligand-to-metal charge-transfer (LMCT).[16–18] The energy of the *d–d* band is consistent with a tetragonal,[19,20] probably five-coordinate structure with no apparent "intensity borrowing" from the LMCT band.[16] The energy of the *d–d* transition roughly follows the order expected from the spectrochemical series with $Br^- = p\text{-}NO_2C_6H_4O^- < NCO^- < N_3^- = NCS^- < NO_2^-$.[21] We have assigned the N-bound coordination mode to the NCS^- ligand in complex **4**, since its *d–d* transition occurs at the same energy as that for the azido complex, **2**. Complex **2** has an additional absorption at 389 nm ($\varepsilon \sim$ 4300 mol^{-1} dm^3 cm^{-1}) which is associated with azido-to-copper LMCT.[21] Although complex **5** is isolated as a monohydrate, we believe that the *p*-nitrophenolato group is bound to the copper ion, since the *d–d* transition for **5** in DMF occurs at considerably different energy than that for the aquo complex, **7**. Complex **5** also has a relatively intense absorption at 431 nm ($\varepsilon \sim$ 18,400 mol^{-1} dm^3 cm^{-1}) which can be assigned to phenolato-to-copper LMCT.[22,23]

On the other hand, in *dilute* aqueous solution, complexes **1–6** all form blue solutions that give virtually identical electronic absorptions at about 594 ± 3 nm ($\varepsilon \sim$ 200 mol^{-1} dm^3 cm^{-1}) and 330 nm ($\varepsilon \sim$ 3600 mol^{-1} dm^3 cm^{-1}) that are completely analogous to those of the independently prepared aquo complex **7** [594 nm (ε 160 mol^{-1} dm^3 cm^{-1}) and 329 nm (ε 3500 mol^{-1} dm^3 cm^{-1})]. These results suggest that the X ligand in [Cu(pyge)X] dissociates in aqueous solution to form the [Cu(pyge)(OH_2)]$^+$

cation. Further evidence for this assertion may be derived from the disappearance of the azido-to-copper charge-transfer band for **2** in water. Further, the spectrum of complex **5** in aqueous solution displays an absorption at ~ 400 nm that has essentially the same general shape and molar absorptivity ($\varepsilon \sim 28{,}000$ mol^{-1} dm^3 cm^{-1}) as sodium *p*-nitrophenoxide.

Complexes **2**–**6** were found to have $\mu_{eff} = 1.9 \pm 0.1$ BM at ambient temperature. For complex **1**, however, $\mu_{eff} = 2.1 \pm 0.1$ BM, which is slightly higher than the usual range of 1.80–1.90 BM for five-coordinate copper(II) complexes.[1] Interestingly, [CuLBr$_2$] (where L is MeNH(CH$_2$)$_3$S(CH$_2$)$_3$NHMe) was found to have $\mu_{eff} = 2.5 \pm 0.1$ BM;[24] it is not clear at this time whether the observed higher μ_{eff} for copper(II) bromo complexes of this type is a general phenomenon or an aberration in these two cases.

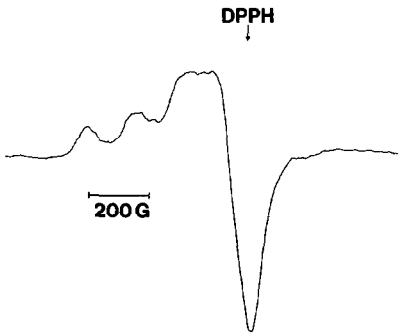

Fig. 1. The EPR spectrum of [Cu(pyge)Br] in frozen (−196°C) DMF–CH$_2$Cl$_2$ glass (*ca* 2.0×10^{-3} mol dm^{-3}). Microwave frequency was 9.25×10^9 Hz at 10 mW power, while the modulation was 0.82 G at 100 kHz.

The X-band EPR spectra of complexes **1** and **5** recorded in DMF–CH$_2$Cl$_2$ glass had similar g and A values. Though of relatively low resolution, they clearly gave the signature spectrum for an axially symmetric complex with a $d_{x^2-y^2}$ ground state ($g_\parallel > g_\perp > 2.0$).[1,25,26] An analysis of the frozen-state spectrum of **1** (see Fig. 1) gives $g_\perp = 2.041$, $g_\parallel = 2.189$, and $A_\parallel$ (Cu) $= 158 \times 10^{-4}$ cm^{-1}. The isotropic spectrum of **1** in DMF solution had $g_{iso} = 2.087$, which is very close to the value calculated from the frozen spectrum [$g_{iso} = 1/3(2g_\perp + g_\parallel) = 2.090$]. On the whole, these observations suggest that a tetragonal, probably square pyramidal, geometry obtains in DMF solution as well as in the solid phase (*vide infra*). In order to unambiguously assign the stereochemistry about the copper ion in the solid-state, the molecular structures of compounds **1** and **2** were determined by single crystal X-ray diffraction techniques.

Selected bond distances and angles for **1** are collected in Table 2. The structure (Fig. 2) is best described as a very slightly distorted square-based pyramid ($\tau = 0.83\%$).[1,27] The coordinating atoms in the basal plane [N(1), N(2), S(1) and Br(1)] are coplanar to within ±0.04 Å and the copper atom is 0.27 Å above this plane. The copper–ligand bond distances within the square plane[24,27–33] and bonding parameters within the ligand[6–8] are all within usual ranges found in related complexes. The Cu(1)—N(2) bond distance is short [1.930(8) Å], reflecting the deprotonation of this site.[34–36] The Cu(1)—N(3) apical bond length [2.218(7) Å] is

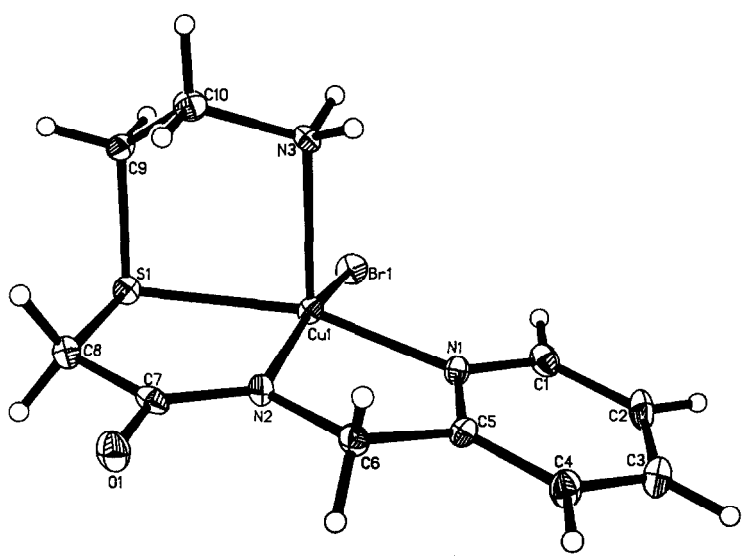

Fig. 2. Perspective view of the structure (20% probability ellipsoids) and atom labelling scheme for the non-hydrogen atoms of **1**; hydrogen atoms have arbitrary radii of 0.1 Å.

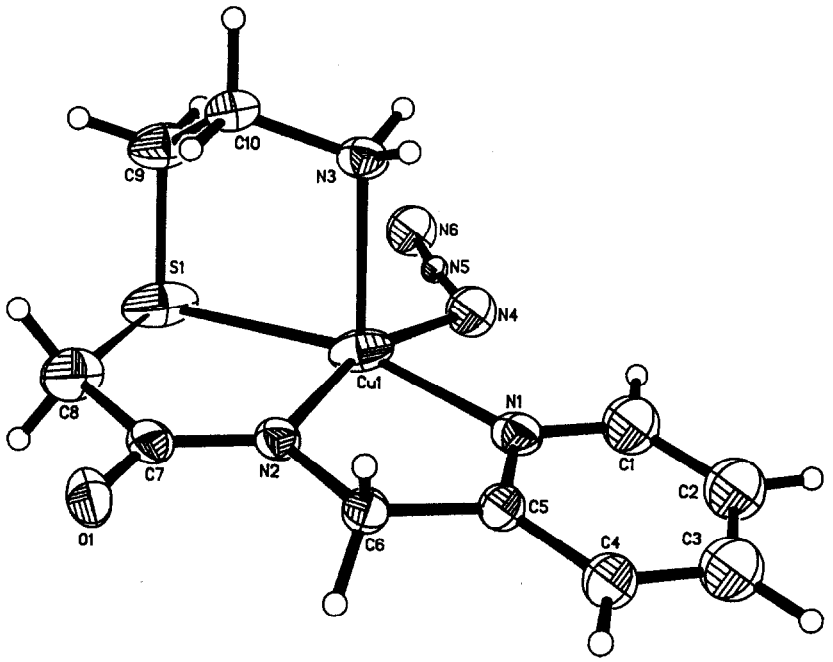

Fig. 3. Perspective view of the structure (20% probability ellipsoids) and atom labelling scheme for the non-hydrogen atoms of **2**; hydrogen atoms have arbitrary radii of 0.1 Å.

Table 2. Selected bond distances and angles for [Cu(pyge)Br] (**1**)

	r^a	N(2)^b	S(1)	N(3)	Br(1)
N(1)	2.017(7)	82.5(3)	163.1(2)	105.5(3)	97.2(2)
N(2)	1.930(8)		83.8(2)	98.9(3)	163.6(2)
S(1)	2.368(2)			86.6(2)	93.0(1)
N(3)	2.218(7)				97.0(2)
Br(1)	2.437(2)				

[a] Metal–ligand distance, Å.

[b] Other entries are the angles (°) subtended at the metal by the relevant atoms at the head of the row and column.

longer than typical copper(II)–amine distances[31] by ~ 0.20 Å and is slightly longer than predicted based upon correlations of apical bond lengths with copper out-of-plane distances.[1] This discrepancy likely arises from steric constraints imposed by the neighbouring sulphur ligating atom.

The structure of **2** is depicted in Fig. 3 and selected bond lengths and angles can be found in Table 3. Unfortunately, the azido ligand is disordered approximately about an axis containing the Cu(1)—N(5) vector (see Fig. 4), which necessarily limits discussion of the structure. The gross stereochemistry is best described as slightly distorted

Table 3. Selected bond distances and angles for [Cu(pyge)N_3] (**2**)

	r^a	N(2)^b	S(1)	N(3)	N(4); N(4′)^c
N(1)	2.024(10)	82.2(3)	164.3(3)	104.3(3)	83.6(7); 107.3(8)
N(2)	1.926(7)		84.1(3)	98.4(3)	162.9(7); 151.4(8)
S(1)	2.403(4)			85.5(3)	108.3(6); 81.4(8)
N(3)	2.189(8)				94.3(6); 104.9(8)
N(4)	2.091(19)				
N(4′)	2.009(20)				

[a] Metal–ligand distance, Å.

[b] Other entries are the angles (°) subtended at the metal by the relevant atoms at the head of the row and column.

[c] N(4) and N(4′) are the two equally populated positions of the coordinating atom of the disordered azide ligand (see text).

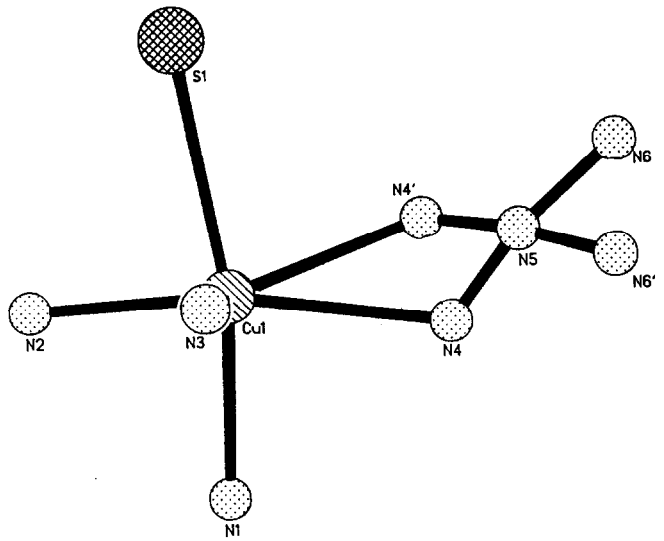

Fig. 4. The coordination sphere about the copper atom in **2** illustrating the disordered azide ligand.

square pyramidal (τ = 2.3% with the copper atom 0.18 Å above the basal plane or 21.5% and 0.32 Å, depending upon which azide orientation is chosen). Bonding parameters within the tetradentate ligand are about as expected and very similar to those found in the structure of **1**. Again, the Cu(1)—N(2) length is short [1.926(7) Å], while the apical Cu(1)—N(3) distance is long [2.189(8) Å]. The azido group is bound in a bent fashion[37-40] to the copper ion in both orientations [Cu(1)—N(4),N(4′)—N(5) = 118.5(17), 128.9(18)°] and is essentially linear [N(4),N(4′)—N(5)—N(6), N(6′) = 168.4(18), 171.4(34)°].

It is of interest to compare the structures of **1** and **2** to that previously determined for octahedral $[Co(pyge)(NO_2)_2]\cdot H_2O$ (**8**).[6] To a first approximation, the five-coordinate square pyramidal copper(II) complexes are derived from the six-coordinate cobalt(III) compound simply by the removal of the ligand *trans* to N(3). Thus, the stereospecific nature of the linear NSNN pyge ligand forces the copper complexes into a relatively undistorted tetragonal five-coordinate geometry.

Despite the structural similarities of **1** and **2** to the cobalt(III) complex (**8**), significant differences become apparent under closer examination. The Cu(1)—N(1) and Cu(1)—N(2) bond lengths are about 0.03–0.06 Å longer than their cobalt counterparts, as might be expected based upon the difference in ionic radii for copper(II) vs cobalt(III).[41] The Cu(1)—S(1) distance, however, is 0.14–0.16 Å longer than for the corresponding Co—S bond; the extra lengthening is likely due in part to the fact that the apical Cu(1)—N(3) distance is ~ 0.20–0.23 Å longer than for the analogous Co—N bond. Also, the copper ion is significantly out of the basal plane of the square pyramid (*ca* 0.25 Å), while the cobalt ion is essentially in the corresponding plane (0.03 Å below). In order to maintain the "bite" angle S(1)—M—N(3) (M = Cu for **1** and **2**; Co for **8**) for the out-of-plane chelate ring at about 87 ± 1°, the M—N(3) bond tilts back relative to the basal plane in the copper complexes. The angle made by the Cu(1)—N(3) bond to this plane is 80.9 and about 80° in **1** and **2**, respectively, as compared to the cobalt complex where this bond is essentially perpendicular to the equatorial plane (89.2°). Considerable strain is evident in this portion of the molecule as reflected in larger ligand torsion angles (Table 4) about S(1) in **1** and **2** as compared with **8**. Also, the S—C—C angles open up slightly but significantly to 115.4(6) and 113.5(6)° in **1** and 116.2(10) and 114.6(8)° in **2** as compared with 112.3(3) and 111.0(3)° in **8**.

Finally, several structures of various geometries for copper(II) complexes containing a flexible, linear NNNN or NSSN tetradentate ligand have been described. These include distorted square pyramidal with all four coordinating atoms of the tetradentate ligand in the basal plane,[30,31,42-45] distorted square pyramidal with an *internal* donating atom of the tetradentate ligand in the apical position,[27,46] trigonal bipyramidal,[30,47-51] distorted octahedral,[30,50-55] and square planar.[56] We note that the five-coordinate copper(II) complexes in the present report appear to constitute the first structurally characterized examples in which one of the *terminal* ligating atoms of the flexible, *linear* tetradentate ligand occupies the apical site in an essentially square pyramidal geometry. Thus in

Table 4. Ligand torsion angles (°)[a]

Atoms	1	2	8[b]
M—**1**—5—6	−4.6	−3.2	0.3
1—5—6—**2**	11.1	8.5	−7.0
5—6—**2**—M	12.8	10.1	10.9
5—6—**2**—7	−172.5	−175.3	−171.2
6—**2**—7—8	−178.5	−178.2	−175.6
M—**2**—7—8	7.3	7.9	2.1
2—7—8—S	−1.9	−3.3	8.9
7—8—S—M	2.4	1.0	−13.1
7—8—S—9	99.8	97.9	87.3
8—S—9—10	61.8	64.1	−72.6
M—S—9—10	−36.8	−33.3	28.4
S—9—10—**3**	58.7	56.2	−48.7
9—10—**3**—M	46.0	46.7	46.5

[a] Carbon atoms are denoted by number only; nitrogen atoms are in bold type; M refers to Cu for **1** and **2**, Co for **8**.

[b] Reference 7; the atom numbering scheme for **8** was different to that adopted in the present work.

conclusion, the present study reiterates the control of stereochemistry that can be achieved in even conformationally non-rigid systems such as copper(II) via the judicious choice of ligating atoms (NSNN) and chelate ring sizes.[9,32]

Acknowledgements—We gratefully acknowledge the generous support of the State University of New York Faculty Research Program and the U.S. Army Research Office under Grant DAAL 0338K0198. We also thank Professor C. Scholes for obtaining the room temperature EPR spectra.

REFERENCES

1. B. J. Hathaway, in *Comprehensive Coordination Chemistry* (Edited by G. Wilkinson, R. D. Gillard and J. A. McCleverty) Chap. 53. Pergamon Press, Oxford (1987).
2. K. D. Karlin and J. Zubieta (Eds), *Biological and Inorganic Copper Chemistry*, Vols 1 and 2. Adenine Press, Guilderland, New York (1986).
3. K. D. Karlin and J. Zubieta (Eds), *Copper Coordination Chemistry: Biochemical and Inorganic Perspectives*. Adenine Press, Guilderland, New York (1983).
4. H. Sigel (Ed.), *Metal Ions in Biological Systems*, Vol. 13. Marcel Dekker, New York (1981).
5. H. Sigel (Ed.), *Metal Ions in Biological Systems*, Vol. 12. Marcel Dekker, New York (1981).
6. P. J. Toscano, K. A. Belsky, L. M. Engelhardt, K. J. Fordon and A. H. White, *Inorg. Chem.* 1990, **29**, 1357.
7. P. J. Toscano, K. J. Fordon, L. M. Engelhardt, B. W. Skelton, A. H. White and P. A. Marzilli, *Polyhedron* 1990, **9**, 1079.
8. P. J. Toscano and L. G. Marzilli, *Inorg. Chem.* 1983, **22**, 3342.
9. B. Bosnich and A. T. Phillip, *J. Chem. Soc. A* 1970, 264.
10. H. C. Freeman, *Adv. Protein Chem.* 1967, **22**, 257. Several metal complexes with non-planar coordinated amides are now known: T. J. Collins and J. M. Workman, *Angew. Chem. Intl. Edn Engl.* 1989, **28**, 912 and refs therein.
11. L. N. Mulay, *Magnetic Susceptibility*. Interscience, New York (1966).
12. A. Bruce, J. L. Corbin, P. L. Dahlstrom, J. R. Hyde, M. Minelli, E. I. Stiefel, J. T. Spence and J. Zubieta, *Inorg. Chem.* 1982, **21**, 917.
13. M. Toprak, E. Gellert and O. Bekaroglu, *Transition Met. Chem. (Weinheim)* 1979, **4**, 372.
14. K. Nakamoto, *Infrared and Raman Spectra of Inorganic and Coordination Compounds*, 4th edn. John Wiley, New York (1986).
15. J. Kohout, M. Hvastijova and J. Gazo, *Coord. Chem. Rev.* 1978, **27**, 141.
16. D. E. Nikles, M. J. Powers and F. L. Urbach, *Inorg. Chem.* 1983, **22**, 3210.
17. A. R. Amundsen, J. Whelan and B. Bosnich, *J. Am. Chem. Soc.* 1977, **99**, 6730.
18. V. M. Miskowski, J. A. Thich, R. Solomon and H. J. Schugar, *J. Am. Chem. Soc.* 1976, **98**, 8344.
19. A. B. P. Lever, *Inorganic Electronic Spectroscopy*, 2nd edn. Elsevier, New York (1984).
20. F. A. Cotton and G. Wilkinson, *Advanced Inorganic Chemistry*, 4th edn, p. 814. John Wiley, New York (1980).
21. J. E. Huheey, *Inorganic Chemistry*, 3rd edn, p. 384. Harper & Row, New York (1983).
22. J. E. Pate, P. K. Ross, T. J. Thamann, C. A. Reed, K. D. Karlin, T. N. Sorrell and E. I. Solomon, *J. Am. Chem. Soc.* 1989, **111**, 5198.
23. K. D. Karlin and B. I. Cohen, *Inorg. Chim. Acta* 1985, **107**, L17.
24. E. C. Constable, P. J. Stotereau and M. G. B. Drew, *Polyhedron* 1989, **8**, 2749.
25. I. Bertini and A. Scozzafava, in *Metal Ions in Biological Systems* (Edited by H. Sigel), Vol. 12, Chap. 2. Marcel Dekker, New York (1981).
26. M. Symons, *Chemical and Biological Aspects of Electron-Spin Resonance Spectroscopy*. John Wiley, New York (1978).
27. A. W. Addison, T. N. Rao, J. Reedijk, J. van Rijn and G. C. Verschoor, *J. Chem. Soc., Dalton Trans.* 1984, 1349.
28. M. G. B. Drew, D. A. Rice and K. M. Richards, *J. Chem. Soc., Dalton Trans.* 1980, 2503.
29. Y. Nishida and K. Takahashi, *Inorg. Chem.* 1988, **27**, 1406.
30. A. Pajunen and S. Pajunen, *Acta Cryst.* 1986, **C42**, 53.
31. F.-J. Wu, S.-L. Wang, Y.-L. Liou and C.-S. Chung, *J. Chinese Chem. Soc.* 1989, **36**, 101 and refs therein.
32. P. J. M. W. L. Birker and J. Reedijk, in *Copper Coordination Chemistry: Biochemical and Inorganic Perspectives* (Edited by K. D. Karlin and J. Zubieta),

p. 409. Adenine Press, Guilderland, New York (1983).
33. M. I. Arriortua, J. L. Mesa, T. Rojo, T. Debaerdemaeker, D. Beltrán-Porter, H. Stratemeier and D. Reinen, *Inorg. Chem.* 1988, **27**, 2976.
34. H. Masuda, A. Odani and O. Yamauchi, *Inorg. Chem.* 1989, **28**, 624.
35. K. Matsumoto, S. Ooi, Y. Nakao, W. Mori and A. Nakahara, *J. Chem. Soc., Dalton Trans.* 1981, 2045.
36. P. de Meester and D. J. Hodgson, *Inorg. Chem.* 1978, **17**, 440.
37. D.-D. Klaehn, H. Paulus, R. Grewe and H. Elias, *Inorg. Chem.* 1984, **23**, 483.
38. M. A. S. Goher and T. C. W. Mak, *Inorg. Chim. Acta* 1984, **85**, 117.
39. R. F. Ziolo, M. Allen, D. D. Titus, H. B. Gray and Z. Dori, *Inorg. Chem.* 1972, **11**, 3044.
40. J. Via, M. I. Arriortua, T. Rojo, J. L. Mesa and A. Garcia, *Bull. Soc. Chem. Belg.* 1989, **98**, 179.
41. J. E. Huheey, *Inorganic Chemistry*, 3rd edn, p. 73. Harper & Row, New York (1983).
42. S. Juen, Z. Yishen, L. Baoshen and C. Liaorong, *Inorg. Chim. Acta* 1989, **162**, 29.
43. G. R. Brubaker, J. N. Brown, M. K. Yoo, R. A. Kinsey, T. M. Kutchan and E. A. Mottel, *Inorg. Chem.* 1979, **18**, 299.
44. G. Marongiu, E. C. Lingafelter and P. Paoletti, *Inorg. Chem.* 1969, **8**, 2763.
45. T.-Y. Lee, T.-J. Lee, C.-Y. Hong, M.-Y. Hsieh, D.-T. Wu and C.-S. Chung, *Acta Cryst.* 1986, **C42**, 1316.
46. J. F. Richardson and N. C. Payne, *Inorg. Chem.* 1978, **17**, 2111.
47. P. J. M. W. L. Birker, J. Helder, G. Henkel, B. Krebs and J. Reedijk, *Inorg. Chem.* 1982, **21**, 357.
48. F. J. Rietmiejer, P. J. M. W. L. Birker, S. Gorter and J. Reedijk, *J. Chem. Soc., Dalton Trans.* 1982, 1191.
49. P. J. M. W. L. Birker, E. F. Godefroi, J. Helder and J. Reedijk, *J. Am. Chem. Soc.* 1982, **104**, 7556.
50. E. Bouwman, A. Burik, J. C. Ten Hove, W. L. Driessen and J. Reedijk, *Inorg. Chim. Acta* 1988, **150**, 125.
51. E. Bouwman, R. Day, W. L. Driessen, W. Tremel, B. Krebs, J. S. Wood and J. Reedijk, *Inorg. Chem.* 1988, **27**, 4614.
52. E. Bouwman, J. C. Ten Hove, W. L. Driessen and J. Reedijk, *Polyhedron* 1988, **7**, 2591.
53. T. G. Fawcett, S. M. Rudich, B. H. Toby, R. A. Lalancette, J. A. Potenza and H. J. Schugar, *Inorg. Chem.* 1980, **19**, 940.
54. D. A. Wright and J. D. Quinn, *Acta Cryst.* 1974, **B30**, 2132.
55. J. van Rijn, W. L. Driessen, J. Reedijk and J.-M. Lehn, *Inorg. Chem.* 1984, **23**, 3584.
56. R. Boggs and J. Donohue, *Acta Cryst.* 1975, **B31**, 320.

Polyhedron Vol. 9, No. 19, pp. 2385–2391, 1990
Printed in Great Britain

0277–5387/90 $3.00+.00
© 1990 Pergamon Press plc

CLUSTER SYNTHESIS—XXVII. NEW SULPHIDO OSMIUM CARBONYL CLUSTER COMPLEXES FROM THE PYROLYSIS OF $Os_6(CO)_{16}(\mu_4\text{-}S)(\mu_3\text{-}S)$

RICHARD D. ADAMS,* GONG CHEN, MICHAEL P. POMPEO and SIXIU SUN

Department of Chemistry, University of South Carolina, Columbia, SC 29208, U.S.A.

(*Received* 9 *March* 1990; *accepted* 17 *May* 1990)

Abstract—When $Os_6(CO)_{16}(\mu_4\text{-}S)(\mu_3\text{-}S)$ (**1**) was heated to 125°C for 5 h in octane solvent, two new compounds $Os_6(CO)_{16}(\mu\text{-}S)_2$ (**2**), an isomer of **1**, and $Os_6(CO)_{15}(\mu_3\text{-}S)_3$ (**3**) were obtained in low yields, 10 and 7%, respectively. Both compounds were characterized by single-crystal X-ray diffraction analyses. The cluster of **2** can be described as two edge-fused butterfly tetrahedra that are further connected by an osmium–osmium bond between the wing-tip metal atoms. Compound **3** contains a raft-like cluster of six osmium atoms. Five of the metal atoms lie in an approximate plane. The sixth is folded out of the plane by 1.17 Å. Compound **3** also contains three triply-bridging sulphido ligands. Crystal data for **2**: $Os_6S_2O_{16}C_{16}$, $M = 1653.5$, monoclinic, $P2_1/c$ (No. 14), $a = 8.222(2)$, $b = 16.308(6)$, $c = 19.522(8)$ Å, $\beta = 92.46(3)°$, $V = 2615(3)$ Å^3, $D_c = 4.20$ g cm^{-3}, $Z = 4$, λ(Mo-K_α) = 0.71069 Å (graphite monochromator) $\mu = 293$ cm^{-1}. Methods: MITHRIL, difference Fourier, full-matrix least-squares. Refinement of 2246 reflections [$F^2 \geqslant 3\sigma(F^2)$] gave R and R_w values of 0.030 and 0.032, respectively. For **3**: $Os_6S_3O_{15}C_{15}$, $M = 1699.6$, triclinic, $P\bar{1}$ (No. 2), $a = 11.192(2)$, $b = 18.528(3)$, $c = 7.282(1)$ Å, $\alpha = 95.49(1)$, $\beta = 100.98(1)$, $\gamma = 98.20(2)°$, $V = 1455.5(5)$ Å^3, $D_c = 3.88$ g cm^{-1}, $Z = 2$, λ(Mo-K_α) = 0.71069 Å (graphite monochromator) $\mu = 263.9$ cm^{-1}. Methods: MITHRIL, difference Fourier, full-matrix least-squares. Refinement of 2789 reflections [$F^2 \geqslant 3\sigma(F^2)$] gave R and R_w values of 0.024 and 0.025, respectively.

The controlled pyrolysis of metal carbonyl complexes can be an effective, if not always an efficient, route to the preparation of metal carbonyl cluster complexes.[1] This method has been widely used in the preparation of higher nuclearity metal carbonyl clusters of the element osmium.[2] In the course of our studies of sulphur-containing cluster complexes of osmium,[3] we prepared and characterized the complex $Os_6(CO)_{16}(\mu_4\text{-}S)(\mu_3\text{-}S)$ (**1**).[4] We have now investigated the pyrolytic transformations of **1** and have obtained the two new sulphido osmium carbonyl cluster complexes, $Os_6(CO)_{16}(\mu_3\text{-}S)_2$ (**2**), an isomer of **1**, and $Os_6(CO)_{15}(\mu_3\text{-}S)_3$ (**3**). Both compounds have been characterized crystallographically. The results of this study are described herein.

EXPERIMENTAL

All reactions were carried out under an atmosphere of nitrogen. Octane was dried over sodium/benzophenoneketyl and distilled prior to use. Other reagent grade solvents were stored over 4 Å molecular sieves. All chromatographic separations were performed in air on TLC plates (Whatman 0.25 mm silica gel 60 Å F_{254}). IR spectra were recorded on a Nicolet 5DXB FT–IR spectrophotometer. Mass spectra were obtained on a VG Model 70SQ spectrometer by using electron impact ionization. $Os_6(CO)_{16}(\mu_4\text{-}S)(\mu_3\text{-}S)$ (**1**) was prepared by the previously reported procedure.[4]

Pyrolysis of $Os_6(CO)_{16}(\mu_4\text{-}S)(\mu_3\text{-}S)$ (**1**)

Compound **1** (50 mg) dissolved in 25 cm^3 of octane was heated to reflux for 5 h. The solvent was removed *in vacuo* and the residue was chromatographed by TLC. By using an 85:15, hexane–CH_2Cl_2 solvent mixture, the following compounds were separated in order of elution: grey–green $Os_6(CO)_{15}(\mu_3\text{-}S)_3$ (**3**) (2 mg, 7%), brown **1** (20 mg unreacted) and red–brown $Os_6(CO)_{16}(\mu_3\text{-}S)_2$ (**2**) (3 mg, 10%). Yields were calculated on the basis of the amount of **1** consumed in the reaction, and do not increase with increased reaction periods. For **2**: IR, ν(CO) (cm^{-1}) in hexane: 2080(w,sh), 2074(s),

* Author to whom correspondence should be addressed.

2070(s), 2053(w), 2030(vs). Mass spectral analysis (70 eV, 150°C): m/z for $^{192}Os = 1664-28x$, $x = 0$–16 $\{[M]^+ - x(CO)\}$. For **3**: IR, ν(CO) (cm^{-1}) in hexane: 2083(s), 2079(s), 2032(m), 2026(s), 2020(s), 2008(w). Mass spectral analysis (70 eV, 130°C): m/z for $^{192}Os = 1668-28x$, $x = 0$–15 $\{[M]^+ - x(CO)\}$.

Crystallographic analyses

Crystals of **2** and **3** suitable for diffraction analyses were grown from solutions in CH_2Cl_2–cyclohexane (1 : 1) solvent mixtures at 25°C. The data crystals were mounted in thin-walled glass capillaries. Diffraction measurements were made on a Rigaku AFC6S automatic diffractometer by using graphite-monochromatized Mo-K_α radiation. The unit cells were determined from 15 randomly selected reflections obtained by using the AFC6 automatic search, centre, index and least-squares routines. Crystal data, data collection parameters and results of the analyses are listed in Table 1. All intensity measurements were made by using the standard ω-scan (moving crystal–stationary counter) technique. Background measurements were made by 1/4 additional scan at each end of the scan. All data processing was performed on a Digital Equipment Corp. MICROVAX II computer by using the TEXSAN structure solving program library (Version 2.0) obtained from Molecular Structure Corp., The Woodlands, Texas. Neutral atom scattering factors were calculated by the standard procedures.[5a] Anomalous dispersion corrections were applied to all non-hydrogen atoms.[5b] Full-matrix least-squares refinements minimized the function: $\Sigma w(|F_{obs}| - |F_{calc}|)$, where $w = 1/\sigma(F)^2$, $\sigma(F) = \sigma(F_{obs}^2)/2F_{obs}$, and $\sigma(F_{obs}^2) = [\sigma(I_{raw})^2 + (0.02F_{obs}^2)^2]^{1/2}/Lp$.

Compound **2** crystallized in the monoclinic crystal system. The space group $P2_1/c$ was identified uniquely on the basis of the systematic absences observed during the collection of data. Compound **3** crystallized in the triclinic crystal system. The space group $P\bar{1}$ was assumed and confirmed by the successful solution and refinement of the structure. Both of the structures were solved by a combination of direct methods (MITHRIL) and difference Fourier techniques. For **2** only the osmium and oxygen atoms were refined with anisotropic ther-

Table 1. Crystal data for compounds **2** and **3**

	2	**3**
Empirical formula	$Os_6S_2O_{16}C_{16}$	$Os_6S_3O_{15}C_{15}\cdot 0.5C_6H_{12}$
Formula weight	1653.49	1699.2
Crystal system	Monoclinic	Triclinic
Lattice parameters		
a (Å)	8.222(2)	11.192(2)
b (Å)	16.308(6)	18.528(3)
c (Å)	19.522(8)	7.282(1)
α (°)		95.49(1)
β (°)	92.46(3)	100.98(1)
γ (°)		98.20(2)
V (Å^3)	2615(3)	1455.5(5)
Space group	$P2_1/c$ (No. 14)	$P\bar{1}$ (No. 2)
Z value	4	2
D_{calc} (g cm^{-3})	4.20	3.88
$F(000)$	2848	1476
μ(Mo-K_α) (cm^{-1})	292.97	263.90
Temperature (°C)	23	23
$2\theta_{max}$ (°)	43.0	44.0
Number of observations [$I > 3\sigma(I)$]	2246	2789
Number of variables	281	364
Residuals: R; R_w	0.030; 0.032	0.024; 0.025
Goodness-of-fit indicator	1.32	1.25
Maximum shift in final cycle	0.02	0.25
Largest peak in final difference map (e^-/Å^3)	1.12	1.11
Absorption correction:	Empirical	Analytical
Type		
Coeff. Max./Min.	1.00/0.43	0.41/0.05

mal parameters. All atoms of the molecule of **3** were refined anisotropically. In the final stages of refinement of **3** one half of a molecule of C_6H_{12} disordered about a centre of symmetry was identified. These atoms were refined with isotropic thermal parameters only.*

RESULTS AND DISCUSSION

The two new compounds $Os_6(CO)_{16}(\mu_3\text{-}S)_2$ (**2**) and $Os_6(CO)_{15}(\mu_3\text{-}S)_3$ (**3**) were obtained in low yields, 10 and 7%, respectively, from the thermal treatment of **1** at 125°C for 5 h. Both products were characterized by IR, mass spectrometry and single crystal X-ray diffraction analyses.

Compound **2** is an isomer of **1**. An ORTEP drawing of the molecular structure of **2** is shown in Fig. 1. Selected interatomic bond distances and angles are listed in Tables 2 and 3, respectively. The cluster has an unusual arrangement for the metal atoms. It could be described as a combination of two "butterfly" tetrahedra, Os(1)—Os(2)—Os(4)—Os(3) and Os(1)—Os(3)—Os(5)—Os(6) fused on one edge, Os(1)—Os(3), and joined at the wing-tips, Os(2)—Os(6). The Os—Os bonding distances span a wide range from 2.669(1) Å for the Os(1)—Os(3) bond to 3.033(1) Å for the Os(2)—Os(6) bond. The average Os—Os single bond value in $Os_3(CO)_{12}$ is 2.877(3) Å. A similarly short Os—Os value, 2.686(1) Å, was observed in **1**.[4] Long values, 3.00–3.12 Å, were observed in the 64-electron butterfly cluster complexes $Os_4(CO)_{11}L(\mu_3\text{-}S)_2$, L = CO,[7] PMe_2Ph[8] and $CNBu^t$,[8] but these bonds are believed to be substantially weakened due to the electron-rich character of the clusters.[7] Two contacts, Os(1)···Os(6) = 3.119(1) Å and Os(2)···Os(3) = 3.126(1) Å, are believed to be non-bonding interactions, but based purely on the bond lengths, there could be weak bonding interactions between these atom pairs. The molecule has an approximate two-fold rotation axis that passes through the midpoints of the Os(1)—Os(3) and Os(2)—Os(6) bonds. The triply-bridging sulphido ligands exhibit normal Os—S bond lengths.[9-10] The 16 carbonyl ligands do not deviate significantly from linearity. The mass spectrum of **2** shows the parent ion m/z = 1664 for ^{192}Os and ions corresponding to the loss of each of the 16 carbonyl ligands.

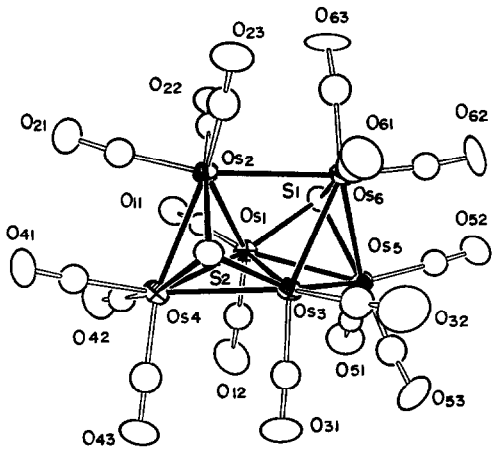

Fig. 1. An ORTEP drawing of $Os_6(CO)_{16}(\mu_3\text{-}S)_2$ (**2**) showing 50% probability thermal ellipsoids.

Table 2. Intramolecular distances for **2**

Os(1)—C(12)	1.83(3)	Os(3)—Os(6)	2.905(1)
Os(1)—C(11)	1.88(2)	Os(3)—Os(4)	2.912(2)
Os(1)—S(1)	2.330(6)	Os(3)—Os(5)	2.921(1)
Os(1)—Os(3)	2.669(1)	Os(4)—C(43)	1.88(3)
Os(1)—Os(5)	2.825(1)	Os(4)—C(41)	1.93(2)
Os(1)—Os(2)	2.863(1)	Os(4)—C(42)	1.94(3)
Os(1)—Os(4)	2.869(1)	Os(4)—S(2)	2.379(6)
Os(1)—Os(6)	3.119(1)	Os(5)—C(52)	1.89(2)
Os(2)—C(21)	1.89(2)	Os(5)—C(53)	1.93(3)
Os(2)—C(23)	1.89(3)	Os(5)—C(51)	1.95(3)
Os(2)—C(22)	1.92(2)	Os(5)—S(1)	2.380(6)
Os(2)—S(2)	2.407(5)	Os(5)—Os(6)	2.918(2)
Os(2)—Os(4)	2.850(2)	Os(6)—C(62)	1.90(2)
Os(2)—Os(6)	3.033(1)	Os(6)—C(61)	1.92(3)
Os(2)—Os(3)	3.126(1)	Os(6)—C(63)	1.95(3)
Os(3)—C(31)	1.85(2)	Os(6)—S(1)	2.402(6)
Os(3)—C(32)	1.93(3)	O—C(av)	1.14(3)
Os(3)—S(2)	2.322(6)		

Distances are in Å. Estimated standard deviations in the least significant figure are given in parentheses.

A process that shows the rearrangements of the bonds in the cluster of **1** to yield **2** is shown in Scheme 1. Atom labels in Scheme 1 correspond to those in Fig. 1. In addition, a carbonyl ligand must migrate from Os(1) to Os(6). It is not possible to predict the sequence of the bond rearrangements at this time.

Compound **2** contains a total of 88 cluster valence electrons. 90 electrons would be the count for two butterfly clusters (2 × 64) fused on an edge (minus 34).[11] The deficiency of two electrons accounts for the existence of the additional metal–metal bond between the atoms Os(2) and Os(6).

An ORTEP drawing of the molecular structure

* Complete tables of bond lengths, angles, atomic coordinates, thermal parameters and observed and calculated structure factors have been deposited as supplementary material with the Editor, from whom copies are available upon request. Atomic coordinates have also been deposited with the Cambridge Crystallographic Data Centre.

Table 3. Intramolecular bond angles for **2**

C(12)—Os(1)—S(1)	113.1(8)	C(43)—Os(4)—Os(1)	120.0(7)
C(12)—Os(1)—Os(3)	100.0(8)	C(43)—Os(4)—Os(3)	96.1(7)
C(12)—Os(1)—Os(5)	82.6(7)	C(41)—Os(4)—S(2)	89.5(7)
C(12)—Os(1)—Os(2)	147.7(7)	C(41)—Os(4)—Os(2)	97.5(7)
C(12)—Os(1)—Os(4)	88.1(7)	C(41)—Os(4)—Os(1)	148.1(7)
C(11)—Os(1)—S(1)	90.7(6)	C(41)—Os(4)—Os(3)	140.0(7)
C(11)—Os(1)—Os(3)	162.9(6)	C(42)—Os(4)—S(2)	164.1(7)
C(11)—Os(1)—Os(5)	132.9(6)	C(42)—Os(4)—Os(2)	110.2(7)
C(11)—Os(1)—Os(2)	98.1(6)	C(42)—Os(4)—Os(1)	77.4(7)
C(11)—Os(1)—Os(4)	101.0(6)	C(42)—Os(4)—Os(3)	127.9(7)
S(1)—Os(1)—Os(3)	101.8(1)	S(2)—Os(4)—Os(2)	53.9(1)
S(1)—Os(1)—Os(5)	54.0(1)	S(2)—Os(4)—Os(1)	93.4(1)
S(1)—Os(1)—Os(2)	99.0(2)	S(2)—Os(4)—Os(3)	50.8(1)
S(1)—Os(1)—Os(4)	156.7(2)	Os(2)—Os(4)—Os(1)	60.09(4)
Os(3)—Os(1)—Os(5)	64.17(3)	Os(2)—Os(4)—Os(3)	65.69(4)
Os(3)—Os(1)—Os(2)	68.69(4)	Os(1)—Os(4)—Os(3)	54.99(3)
Os(3)—Os(1)—Os(4)	63.33(4)	C(52)—Os(5)—S(1)	95.0(7)
Os(5)—Os(1)—Os(2)	115.67(5)	C(52)—Os(5)—Os(1)	147.3(7)
Os(5)—Os(1)—Os(4)	123.88(4)	C(52)—Os(5)—Os(6)	97.0(7)
Os(2)—Os(1)—Os(4)	59.63(4)	C(52)—Os(5)—Os(3)	140.7(7)
C(21)—Os(2)—S(2)	97.6(7)	C(53)—Os(5)—S(1)	168.1(7)
C(21)—Os(2)—Os(4)	81.2(7)	C(53)—Os(5)—Os(1)	120.0(7)
C(21)—Os(2)—Os(1)	120.8(7)	C(53)—Os(5)—Os(6)	117.1(7)
C(23)—Os(2)—S(2)	91.9(7)	C(53)—Os(5)—Os(3)	74.7(7)
C(23)—Os(2)—Os(4)	141.1(7)	C(51)—Os(5)—S(1)	96.9(6)
C(23)—Os(2)—Os(1)	149.2(7)	C(51)—Os(5)—Os(1)	93.8(6)
C(22)—Os(2)—S(2)	170.5(7)	C(51)—Os(5)—Os(6)	149.5(6)
C(22)—Os(2)—Os(4)	121.1(7)	C(51)—Os(5)—Os(3)	128.0(6)
C(22)—Os(2)—Os(1)	77.5(7)	S(1)—Os(5)—Os(1)	52.3(1)
S(2)—Os(2)—Os(4)	53.0(1)	S(1)—Os(5)—Os(6)	52.7(1)
S(2)—Os(2)—Os(1)	93.0(1)	S(1)—Os(5)—Os(3)	93.7(1)
Os(4)—Os(2)—Os(1)	60.29(3)	Os(1)—Os(5)—Os(6)	65.76(4)
C(31)—Os(3)—S(2)	106.0(7)	Os(1)—Os(5)—Os(3)	55.33(3)
C(31)—Os(3)—Os(1)	110.1(7)	Os(6)—Os(5)—Os(3)	59.67(3)
C(31)—Os(3)—Os(6)	154.1(7)	C(62)—Os(6)—S(1)	96.8(7)
C(31)—Os(3)—Os(4)	86.5(7)	C(62)—Os(6)—Os(3)	120.9(7)
C(31)—Os(3)—Os(5)	95.7(7)	C(62)—Os(6)—Os(5)	82.3(7)
C(32)—Os(3)—S(2)	95.4(7)	C(61)—Os(6)—S(1)	170.3(7)
C(32)—Os(3)—Os(1)	155.9(7)	C(61)—Os(6)—Os(3)	76.7(7)
C(32)—Os(3)—Os(6)	91.5(7)	C(61)—Os(6)—Os(5)	122.0(7)
C(32)—Os(3)—Os(4)	141.5(7)	C(63)—Os(6)—S(1)	93.6(8)
C(32)—Os(3)—Os(5)	98.9(7)	C(63)—Os(6)—Os(3)	150.3(7)
S(2)—Os(3)—Os(1)	100.2(1)	C(63)—Os(6)—Os(5)	141.8(8)
S(2)—Os(3)—Os(6)	99.6(1)	S(1)—Os(6)—Os(3)	93.7(1)
S(2)—Os(3)—Os(4)	52.6(1)	S(1)—Os(6)—Os(5)	52.0(1)
S(2)—Os(3)—Os(5)	155.3(1)	Os(3)—Os(6)—Os(5)	60.22(3)
Os(1)—Os(3)—Os(6)	67.89(4)	Os(1)—S(1)—Os(5)	73.7(2)
Os(1)—Os(3)—Os(4)	61.68(4)	Os(1)—S(1)—Os(6)	82.4(2)
Os(1)—Os(3)—Os(5)	60.51(4)	Os(5)—S(1)—Os(6)	75.2(2)
Os(6)—Os(3)—Os(4)	112.45(4)	Os(3)—S(2)—Os(4)	76.5(2)
Os(6)—Os(3)—Os(5)	60.11(3)	Os(3)—S(2)—Os(2)	82.7(2)
Os(4)—Os(3)—Os(5)	118.94(5)	Os(4)—S(2)—Os(2)	73.1(2)
C(43)—Os(4)—S(2)	106.0(8)	O—C(av)—Os	176(2)
C(43)—Os(4)—Os(1)	158.5(8)		

Angles are in degrees. Estimated standard deviations in the least significant figure are given in parentheses.

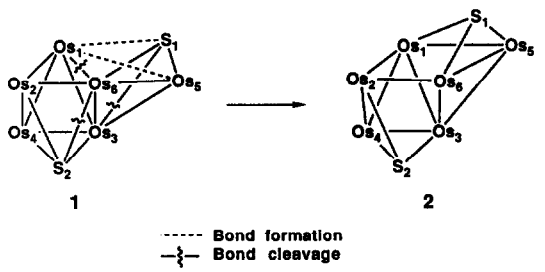

Scheme 1.

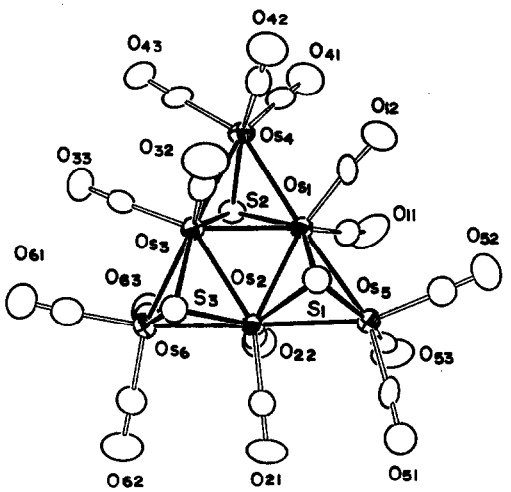

Fig. 2. An ORTEP drawing of $Os_6(CO)_{15}(\mu_3\text{-}S)_3$ (3) showing 50% probability thermal ellipsoids.

of 3 is shown in Fig. 2. Selected interatomic distances and angles are listed in Tables 4 and 5. The molecule exhibits a "raft-like" structure[12,13] for the six metal atoms. Five of the six metal atoms Os(1)–Os(5) lie within 0.16 Å of the least-squares plane that they define. Os(6) lies 1.17 Å from this plane.

Table 4. Intramolecular distances for 3

Os(1)—C(12)	1.91(2)	Os(3)—S(3)	2.364(3)
Os(1)—C(11)	1.93(2)	Os(3)—S(2)	2.364(3)
Os(1)—S(1)	2.384(3)	Os(3)—Os(4)	2.804(1)
Os(1)—S(2)	2.386(4)	Os(3)—Os(6)	2.813(1)
Os(1)—Os(2)	2.702(1)	Os(4)—C(41)	1.88(2)
Os(1)—Os(3)	2.7100(9)	Os(4)—C(43)	1.90(2)
Os(1)—Os(5)	2.8153(9)	Os(4)—C(42)	1.93(2)
Os(1)—Os(4)	2.8186(9)	Os(4)—S(2)	2.335(3)
Os(2)—C(22)	1.92(1)	Os(5)—C(51)	1.88(1)
Os(2)—C(21)	1.92(1)	Os(5)—C(52)	1.91(2)
Os(2)—S(3)	2.360(4)	Os(5)—C(53)	1.95(2)
Os(2)—S(1)	2.379(4)	Os(5)—S(1)	2.330(3)
Os(2)—Os(3)	2.7667(8)	Os(6)—C(62)	1.88(2)
Os(2)—Os(5)	2.786(1)	Os(6)—C(61)	1.92(2)
Os(2)—Os(6)	2.789(1)	Os(6)—C(63)	1.92(2)
Os(3)—C(32)	1.90(2)	Os(6)—S(3)	2.329(4)
Os(3)—C(33)	1.92(2)	O—C(av)	1.14(2)

Distances are in Å. Estimated standard deviations in the least significant figure are given in parentheses.

The cluster can be viewed as a central triangular cluster of three $Os(CO)_2$ groupings, Os(1), Os(2) and Os(3). The three edges of this triangle are bridged by $Os(CO)_3$ groupings which results in the formation of three triangular triosmium groups about the central triangle. Each of the outer three triangular groups contains a triply-bridging sulphido ligand. Two of these ligands, S(1) and S(3), lie on one side of the cluster while the other lies on the other side. All of the metal–metal bonds are shorter than those in the planar raft cluster complex $Os_6(CO)_{17}[P(OMe)_3]_4$ which has no bridging ligands.[12] However, they are very similar to the oxo-bridged Os—Os bonds in the raft cluster $Os_6(CO)_{18}(\mu_3\text{-}CO)(\mu_3\text{-}O)$,[13] and the sulphur-

Table 5. Intramolecular bond angles for 3

C(12)—Os(1)—S(1)	89.4(5)	S(2)—Os(1)—Os(2)	88.41(8)
C(12)—Os(1)—S(2)	121.4(4)	S(2)—Os(1)—Os(3)	54.85(9)
C(12)—Os(1)—Os(2)	144.6(5)	S(2)—Os(1)—Os(5)	131.89(7)
C(12)—Os(1)—Os(3)	118.2(4)	S(2)—Os(2)—Os(4)	52.51(7)
C(12)—Os(1)—Os(5)	102.7(4)	Os(2)—Os(1)—Os(3)	61.49(2)
C(12)—Os(1)—Os(4)	73.2(4)	Os(2)—Os(1)—Os(5)	60.62(2)
C(11)—Os(1)—S(1)	123.6(4)	Os(2)—Os(1)—Os(4)	121.97(3)
C(11)—Os(1)—S(2)	88.6(5)	Os(3)—Os(1)—Os(5)	121.05(3)
C(11)—Os(1)—Os(2)	112.4(4)	Os(3)—Os(1)—Os(4)	60.90(2)
C(11)—Os(1)—Os(3)	141.7(5)	Os(5)—Os(1)—Os(4)	175.60(3)
C(11)—Os(1)—Os(5)	73.1(4)	C(22)—Os(2)—S(3)	130.3(5)
C(11)—Os(1)—Os(4)	107.9(4)	C(22)—Os(2)—S(1)	135.3(5)
S(1)—Os(1)—S(2)	137.3(1)	C(22)—Os(2)—Os(1)	90.0(4)
S(1)—Os(1)—Os(2)	55.34(9)	C(22)—Os(2)—Os(3)	102.5(4)
S(1)—Os(1)—Os(3)	85.7(1)	C(22)—Os(2)—Os(5)	87.4(4)
S(1)—Os(1)—Os(5)	52.46(8)	C(22)—Os(2)—Os(6)	77.3(4)
S(1)—Os(1)—Os(4)	125.25(8)	C(21)—Os(2)—S(3)	96.4(4)

Continued overleaf

Table 5—*continued*

C(21)—Os(2)—S(1)	103.6(4)	C(41)—Os(4)—S(2)	99.5(4)
C(21)—Os(2)—Os(1)	148.0(4)	C(41)—Os(4)—Os(3)	152.8(4)
C(21)—Os(2)—Os(3)	149.9(4)	C(41)—Os(4)—Os(1)	104.6(4)
C(21)—Os(2)—Os(5)	86.5(4)	C(43)—Os(4)—S(2)	103.1(4)
C(21)—Os(2)—Os(6)	97.8(4)	C(43)—Os(4)—Os(3)	97.4(4)
S(3)—Os(2)—S(1)	89.8(1)	C(43)—Os(4)—Os(1)	152.5(4)
S(3)—Os(2)—Os(1)	106.55(8)	C(42)—Os(4)—S(2)	158.2(4)
S(3)—Os(2)—Os(3)	54.21(8)	C(42)—Os(4)—Os(3)	109.4(4)
S(3)—Os(2)—Os(5)	141.9(1)	C(42)—Os(4)—Os(1)	106.4(4)
S(3)—Os(2)—Os(6)	53.0(1)	S(2)—Os(4)—Os(3)	53.86(8)
S(1)—Os(2)—Os(1)	55.53(8)	S(2)—Os(4)—Os(1)	54.17(9)
S(1)—Os(2)—Os(3)	84.56(8)	Os(3)—Os(4)—Os(1)	57.64(2)
S(1)—Os(2)—Os(5)	52.93(8)	C(51)—Os(5)—S(1)	102.5(4)
S(1)—Os(2)—Os(6)	138.99(8)	C(51)—Os(5)—Os(2)	99.8(4)
Os(1)—Os(2)—Os(3)	59.40(2)	C(51)—Os(5)—Os(1)	153.5(4)
Os(1)—Os(2)—Os(5)	61.70(2)	C(52)—Os(5)—S(1)	99.9(4)
Os(1)—Os(2)—Os(6)	113.77(3)	C(52)—Os(5)—Os(2)	153.4(4)
Os(3)—Os(2)—Os(5)	120.06(3)	C(52)—Os(5)—Os(1)	103.2(4)
Os(3)—Os(2)—Os(6)	60.83(2)	C(53)—Os(5)—S(1)	158.7(4)
Os(5)—Os(2)—Os(6)	164.24(3)	C(53)—Os(5)—Os(2)	107.7(5)
C(32)—Os(3)—S(3)	85.9(4)	C(53)—Os(5)—Os(1)	107.9(4)
C(32)—Os(3)—S(2)	127.2(4)	S(1)—Os(5)—Os(2)	54.5(1)
C(32)—Os(3)—Os(1)	90.9(5)	S(1)—Os(5)—Os(1)	54.22(8)
C(32)—Os(3)—Os(2)	110.7(4)	Os(2)—Os(5)—Os(1)	57.68(2)
C(32)—Os(3)—Os(4)	76.1(4)	C(62)—Os(6)—S(3)	103.3(5)
C(32)—Os(3)—Os(6)	135.8(4)	C(62)—Os(6)—Os(2)	99.8(5)
C(33)—Os(3)—S(3)	103.3(4)	C(62)—Os(6)—Os(3)	154.6(5)
C(33)—Os(3)—S(2)	97.8(5)	C(61)—Os(6)—S(3)	103.1(5)
C(33)—Os(3)—Os(1)	150.0(4)	C(61)—Os(6)—Os(2)	156.3(5)
C(33)—Os(3)—Os(2)	141.1(4)	C(61)—Os(6)—Os(3)	103.8(4)
C(33)—Os(3)—Os(4)	92.3(4)	C(63)—Os(6)—S(3)	155.0(5)
C(33)—Os(3)—Os(6)	81.2(4)	C(63)—Os(6)—Os(2)	107.5(5)
S(3)—Os(3)—S(2)	138.1(1)	C(63)—Os(6)—Os(3)	103.6(4)
S(3)—Os(3)—Os(1)	106.2(1)	S(3)—Os(6)—Os(2)	54.0(1)
S(3)—Os(3)—Os(2)	54.08(8)	S(3)—Os(6)—Os(3)	53.75(8)
S(3)—Os(3)—Os(4)	157.5(1)	Os(2)—Os(6)—Os(3)	59.20(2)
S(3)—Os(3)—Os(6)	52.60(9)	Os(5)—S(1)—Os(2)	72.5(1)
S(2)—Os(3)—Os(1)	55.6(1)	Os(5)—S(1)—Os(1)	73.3(1)
S(2)—Os(3)—Os(2)	87.32(8)	Os(2)—S(1)—Os(1)	69.1(1)
S(2)—Os(3)—Os(4)	52.88(8)	Os(4)—S(2)—Os(3)	73.25(9)
S(2)—Os(3)—Os(6)	96.60(8)	Os(4)—S(2)—Os(1)	73.3(1)
Os(1)—Os(3)—Os(2)	59.12(2)	Os(3)—S(2)—Os(1)	69.6(1)
Os(1)—Os(3)—Os(4)	61.46(2)	Os(6)—S(3)—Os(2)	73.0(1)
Os(1)—Os(3)—Os(6)	112.76(3)	Os(6)—S(3)—Os(3)	73.7(1)
Os(2)—Os(3)—Os(4)	120.18(3)	Os(2)—S(3)—Os(3)	71.7(1)
Os(2)—Os(3)—Os(6)	59.97(2)	O—C(av)—Os	177(1)
Os(4)—Os(3)—Os(6)	147.84(3)		

Angles are in degrees. Estimated standard deviations in the least significant figure are given in parentheses.

bridged Os—Os bonds in $Os_3(CO)_9(\mu_3\text{-}CO)(\mu_3\text{-}S)$[10] and $Os_3(CO)_9(\mu_3\text{-}S)_2$.[9] Compound **3** contains 90 valence electrons which is the value expected for an electron-precise raft cluster of six metal atoms.[11,13] Stoichiometrically, the formation of **3** from **2** requires the addition of one sulphido ligand and the elimination of one carbonyl ligand. The mass spectrum of **3** showed the parent ion, $m/z = 1668$, for ^{192}Os and ions corresponding to the loss of each of the 15 carbonyl ligands. While the transformation seems to be simple, we have not yet been able to synthesize this interesting compound by a more direct route.

Acknowledgement—These studies were supported by the National Science Foundation under grant CHE-8919786.

REFERENCES

1. (a) M. D. Vargas and J. N. Nicholls, *Adv. Inorg. Radiochem.* 1986, **30**, 123; (b) P. Chini, *Inorg. Chim. Acta Rev.* 1968, 31.
2. (a) C. R. Eady, B. F. G. Johnson and J. Lewis, *J.*

Chem. Soc., Dalton Trans. 1975, 2606; (b) D. H. Farrar, B. F. G. Johnson, J. Lewis, P. R. Raithby and M. J. Rosales, *J. Chem. Soc., Dalton Trans.* 1982, 2051.
3. R. D. Adams, *Polyhedron* 1985, **4**, 2003.
4. R. D. Adams, I. T. Horváth and L. W. Yang, *J. Am. Chem. Soc.* 1983, **105**, 1533.
5. *International Tables for X-ray Crystallography*, Vol. IV. Kynoch Press, Birmingham, U.K. (1975): (a) Table 2.2B, pp. 99–101; (b) Table 2.3.1, pp. 149–150.
6. B. G. DeBoer and M. R. Churchill, *Inorg. Chem.* 1977, **16**, 878.
7. R. D. Adams and L. W. Yang, *J. Am. Chem. Soc.* 1983, **105**, 235.
8. R. D. Adams, I. T. Horváth and K. Natarajan, *Organometallics* 1984, **3**, 1540.
9. R. D. Adams, I. R. Horváth, B. E. Segmuller and L. Yang, *Organometallics* 1983, **2**, 144.
10. R. D. Adams, I. T. Horváth and H. S. Kim, *Organometallics* 1984, **3**, 548.
11. D. M. P. Mingos, *Accts Chem. Res.* 1984, **17**, 311.
12. R. J. Goudsmit, B. F. G. Johnson, J. Lewis, P. R. Raithby and K. H. Whitmire, *J. Chem. Soc., Chem. Commun.* 1982, 640.
13. R. J. Goudsmit, B. F. G. Johnson, J. Lewis, P. R. Raithby and K. H. Whitmire, *J. Chem. Soc., Chem. Commun.* 1983, 246.

Polyhedron Vol. 9, No. 19, pp. 2393–2397, 1990
Printed in Great Britain

0277–5387/90 $3.00+.00
© 1990 Pergamon Press plc

A ^{95}Mo NMR STUDY OF BIS[PENTACARBONYLMOLYBDENUM(0)] BRIDGING DITERTIARY PHOSPHINE COMPLEXES. THE CRYSTAL STRUCTURE OF $[Mo(CO)_5]_2(\mu\text{-}Ph_2PCH_2CH_2CH_2PPh_2)$

ELMER C. ALYEA,* GEORGE FERGUSON,* K. J. FISHER,†
ROBERT A. GOSSAGE and MICHAEL C. JENNINGS

Department of Chemistry and Biochemistry, University of Guelph, Guelph, Ontario N1G 2W1, Canada

(*Received* 27 *March* 1990; *accepted* 24 *May* 1990)

Abstract—Molybdenum-95 NMR data are presented for the series of ditertiary phosphine-bridged molybdenum dimers $[Mo(CO)_5]_2(\mu\text{-}Ph_2P(CH_2)_nPPh_2)$ (n = 2–6) (**II–VI**) and for the "dangling" phosphine complex $Mo(CO)_5(\eta^1\text{-}Ph_2PCH_2PPh_2)$ (**I**). Values of $\delta(^{95}Mo)$ in the range −1780 to −1788 ppm indicate that there is little effect on net molybdenum metal electron density as the number of bridging methylene groups increases from two to six. Steric effects are deemed as the cause for significantly lower molybdenum metal shielding in **I** [$\delta(^{95}Mo) = -1764$ ppm]. In $[Mo(CO)_5]_2(\mu\text{-}Ph_2PCH_2CH_2CH_2PPh_2)$ (**III**), the $PCH_2CH_2CH_2P$ moiety is maximally extended leading to a Mo---Mo separation of 8.2150(3) Å. The Mo—P distances are 2.545(1) and 2.519(1) Å. This structure, the first featuring a normal ditertiary phosphine bridging two Group 6 metal atoms, is compared with those known for other related molybdenum(0) pentacarbonyl phosphine complexes.

The vast majority of metal complexes incorporating potentially bidentate ditertiary phosphine ligands do so when the ligand acts in a chelating fashion. Ligands such as bis(diphenylphosphino)methane (dppm), 1,2-bis(diphenylphosphino)ethane (dppe) and 1,3-bis(diphenylphosphino)propane (dppp) are well known to form chelate complexes with many metal systems including the ones of Group 6. Carbonyl complexes of the type $M(CO)_4(\eta^2\text{-PP})$ (where M = Cr, Mo or W and PP = bidentate phosphine ligand) are well characterized and studied.[1–3] Considerably less well known are those carbonyl complexes in which the diphosphine acts as a bridging ligand between two metal carbonyl moieties. Studies of complexes of the type $[M(CO)_5]_2(\mu\text{-PP})$ (where M = Cr, Mo or W and PP = bidentate bridging phosphorus donor ligand) are few and most have dealt solely with synthetic techniques and simple characterization of these complexes.[4–9] Recently, however, Hor and his colleagues have begun some thermal stability and decomposition studies of these types of molecules.[8,10–12]

Crystallographically, no Group 6 metal carbonyl-bridged complex has been studied incorporating the ditertiary phosphine ligand type: $Ph_2P(CH_2)_nPPh_2$ (n = 1–6). A few diphosphane-bridged complexes have been characterized[13–15] as well as a dimolybdenum complex utilizing 1,1′-bis(diphenylphosphino)cobaltocene as a bridging ligand $\{[Mo(CO)_5]_2(\mu\text{-}Co(C_5H_4PPh_2)_2\}$.[16]

Since short and long chain ditertiary phosphine complexes of this type are currently of interest,[9–12] we felt that the recently studied $[Mo(CO)_5]_2(\mu\text{-}Ph_2P(CH_2)_nPPh_2)$ (n = 2–6) and $Mo(CO)_5(\eta^1\text{-dppm})$ complexes would be excellent choices to continue our investigation of the effects of various ligand systems on the molybdenum metal nucleus via ^{95}Mo NMR spectroscopy.[17] We also report the first crystal structure of a complex of this series; that of $[Mo(CO)_5]_2(\mu\text{-dppp})$.

* Authors to whom correspondence should be addressed.
† Present address: School of Chemistry, University of New South Wales, P.O. Box 1, Kensington, New South Wales 2033, Australia.

Table 1. Molybdenum-95 NMR data for $Mo(CO)_5(\eta^1$-PP) and $[Mo(CO)_5]_2(\mu$-PP) complexes

Complex	Solvent					
	CH_2Cl_2			CH_3CN		
	$\delta(^{95}Mo)^a$	$^1J_{MoP}{}^b$	$\Delta\nu_{1/2}{}^c$	$\delta(^{95}Mo)$	$^1J_{MoP}$	$\Delta\nu_{1/2}$
$Mo(CO)_5(\eta^1$-dppm) (I)	−1764	140	65	nm[d]	nm	nm
$[Mo(CO)_5]_2(\mu$-dppe) (II)	−1778	123	70	−1780	133	52
$[Mo(CO)_5]_2(\mu$-dppp) (III)	−1785	137	70	−1785	131	53
$[Mo(CO)_5]_2(\mu$-dppb)[e] (IV)	−1789	133	65	−1788	132	64
$[Mo(CO)_5]_2(\mu$-dpppent)[e] (V)	nm	nm	nm	−1785	122	52
$[Mo(CO)_5]_2(\mu$-dpph)[e] (VI)	nm	nm	nm	−1784	140	70

[a]Values in ppm relative to aqueous 2 M K_2MoO_4 at pH 11.

[b]Coupling in hertz.

[c]Peak-width at half-height values in hertz.

[d]nm = Not measured.

[e]dppb = 1,4-Bis(diphenylphosphino)butane, dpppent = 1,5-bis(diphenylphosphino)pentane, dpph = 1,6-bis(diphenylphosphino)hexane.

EXPERIMENTAL

The complexes studied were synthesized using the literature methods described by Hor.[8,9] Their purity was checked using IR and ^{31}P NMR spectroscopy and in the case of **III**, the thermal decomposition point. IR spectra were recorded using a Nicolet DXC-20 FTIR spectrometer from CH_2Cl_2 solutions in 0.5 cm^3 NaCl solution cells. Phosphorus-31 and molybdenum-95 NMR spectra were recorded from saturated CH_2Cl_2 or CH_3CN solutions at room temperature (22 ± 1°C) on a Bruker WH-400 NMR spectrometer operating at 161.92 and 26.08 MHz, respectively.

Crystals of **III** suitable for X-ray analysis were obtained by slow evaporation of an CH_3CN–MeOH (1:3 v/v) solution of **III** at ambient temperature. The crystal chosen was a colourless prism of approximate dimensions 0.44 × 0.70 × 0.98 mm.

Crystal data for $C_{37}H_{26}Mo_2P_2O_{10}$, $M_r = 884.44$, monoclinic, space group $P2_{1/a}$, $a = 12.555(3)$, $b = 17.652(4)$, $c = 17.381(3)$ Å, $\beta = 99.67(2)°$, $V = 3797(3)$ Å^3, $Z = 4$, $D_c = 1.55$ g cm^{-3}, $\mu = 7.8$ cm^{-1}, $F(000) = 1768$, Mo-K_α radiation ($\lambda = 0.71073$ Å), $T = 21°C$. 8645 reflections were measured on a CAD 4 diffractometer ($2\theta_{max} = 54°$), 8258 were unique and 6782 had $I > 3\sigma(I)$. Lorentz, polarization and empirical absorption corrections were applied. The structure was solved by direct methods (MULTAN). Refinement (with weights derived from counting statistics) by full-matrix least-squares calculations (with all hydrogen atoms allowed for but not refined) converged with $R = 0.030$ and $R_w = 0.046$ for the 6782 observed reflections. The final cycle of refinement had 460 variables and a maximum shift/error ratio of 0.03. A final difference map had no chemically significant features. Full details of the analysis are available from the Cambridge Crystallographic Data Centre or from the authors.

RESULTS AND DISCUSSION

^{95}Mo *NMR spectroscopy*

The ^{95}Mo NMR spectral data for the complexes studied appears in Table 1. Earlier studies by Hor[8,9] had shown similar IR and $\Delta(\delta^{31}P)$* NMR data for complexes **II–VI** indicating a similar overall strain on the bridging group regardless of the chain-length of the diphosphine bridge. We have demonstrated earlier that the net metal electron density, as indicated by $\delta(^{95}Mo)$, is not always related to the measured values of $\nu(C{\equiv}O)$ and $\Delta(\delta^{31}P)$.[17a] In this case, however, we find that $\delta(^{95}Mo)$ is virtually unchanged for complexes **III–VI**. Thus, it appears that $\delta(^{95}Mo)$ is also unaffected by the length of the chain of the bridging group. Steric crowding in complex **I** is likely the major contributing factor in producing the lower overall molybdenum shielding in that species. We observed previously that $\delta(^{95}Mo)$ values could vary over a 150 ppm range for $Mo(CO)_5PR_3$ complexes due to differing steric and electronic effects.[17d] This trend was also noticed in other studies on substituted molybdenum(0) carbonyl complexes.[17,18] In no case were two NMR

* $\Delta(\delta^{31}P) = \delta(^{31}P)$(complex) − $\delta(^{31}P)$(free ligand).

signals seen in the ^{95}Mo NMR spectra. Thus, at least in solution at ambient temperature, both of the metal centres have identical overall shielding; i.e. are magnetically equivalent. These relatively negative $\delta(^{95}Mo)$ values may relate to the great stability of these complexes[8,10–12] and indicate the ability of these ditertiary phosphine bridging ligands to shield the metal nucleus very efficiently. These complexes exhibit very similar metal shielding, in fact, to related monodentate phosphine complexes like $Mo(CO)_5PPh_2Et$ [$\delta(^{95}Mo) = -1789$ ppm].[17d] The one bond Mo—P coupling constants ($^1J_{MoP}$) and peak width at half-height values ($\Delta\nu_{1/2}$) (see Table 1) are also typical of a $Mo(CO)_5$ moiety bound to a triarylphosphine ligand.[17d] This indicates that the electronic field gradient around the metal atom is not greatly distorted and hence symmetry at the metal atom is high, as verified by the X-ray structural determination (*vide infra*).

Attempts to use ^{95}Mo NMR spectroscopy to characterize dimolybdenum species involving other bridging bidentate ligands are currently underway in our laboratory.

Crystal structure of **III**

Relevant bond lengths and bond angles for **III** appear in Table 2. The crystal structure determination of **III** (see Fig. 1) reveals that the two molybdenum centres occupy approximately octahedral geometry, as expected. However, the bulky pentacarbonyl molybdenum moieties have served to extend the bridging dppp ligand, in addition to widening the Mo—P—C angles [115.8(1)° av] from the expected tetrahedral angle of 109.5°. The $Mo(CO)_5$ units are staggered with respect to each other (Mo(1)—P(1)—P(2)—Mo(2) torsion angle 145.9°) and again steric considerations are invoked. Figure 1 clearly shows that one of the two phenyl rings on each phosphorus atom is oriented between two carbonyl ligands of its respective molybdenum. The Mo—P bond lengths [2.519(1) and 2.545(1) Å] are both shorter than those reported for $Mo(CO)_5PPh_3$ (2.560(1) Å)[19] $Mo(CO)_5P(p\text{-tolyl})_3$ (2.562(2) Å)[20] and in the dimer $[Mo(CO)_5]_2(\mu\text{-}Co(C_5H_4PPh_2)_2)$ (2.555(4) Å).[16] The Mo—P bond length in **III** is expectedly longer than in those cases where strong π-acceptor P ligands are incorporated, such as in $Mo(CO)_5P(CH_2CH_2CN)_3$ (2.506(1) Å).[19] In contrast to the "short" Mo—P bond distances in **III**, a longer Mo—P bond length might be expected in **I** due to steric effects. This would explain the failure by us and earlier workers[7,8] to synthesize $[M(CO)_5]_2(\mu\text{-dppm})$ (M = Mo, W). As noted above, the greater bulk of dppm as compared to the other ditertiary phosphine ligands was surmised as the main cause for the lesser shielding of the molybdenum nucleus in **I**. A structural study of **I** would therefore be of interest to address this hypothesis. Interestingly, dppe is even able to form dibridged bimetallic Group 6 $M^1M^2(CO)_{10}(\mu\text{-dppe})_2$ complexes.[21]

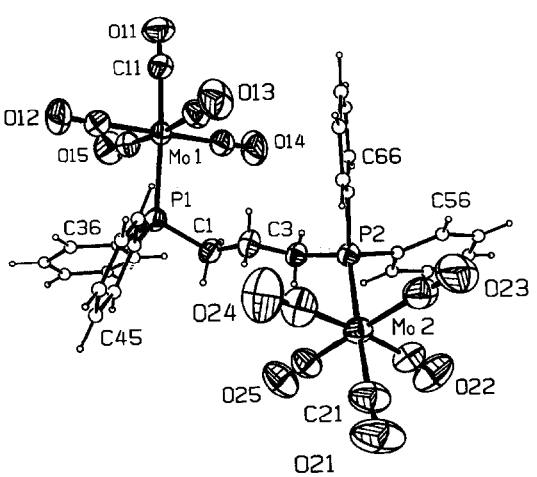

Fig. 1. A view of the $[Mo(CO)_5]_2(\mu\text{-}Ph_2PCH_2CH_2CH_2PPh_2)$ molecule with the crystallographic numbering scheme; ellipsoids are at the 50% level.

The Mo—C—O units are basically linear for Mo(1) and Mo(2) (see Table 2) and differ little from those of $Mo(CO)_5PPh_3$,[19] $Mo(CO)_5P(p\text{-tolyl})_3$[20] or $[Mo(CO)_5]_2(\mu\text{-}Co(C_5H_4PPh_2)_2)$.[16] Similarly, the OC—Mo—CO and OC_{trans}—Mo—P bond angles in **III** also reflect this similarity to the above species except that the OC_{trans}—Mo—P angles for Mo(1) and Mo(2) are significantly different (174.23(9) and 177.83(9)°, respectively).

The stability of the bridged-ligand series of complexes, as demonstrated by Hor and his colleagues,[8,10–12] can be attributed to a similar structural nature of the $Mo(CO)_5$ moieties to the fragment in $Mo(CO)_5PPh_3$[19] but with a considerably shorter, and likely therefore stronger, Mo—P bond. The ability of this series of dimers to withstand stressful thermal conditions[10–12] may make them very useful molecules in the design of larger clusters, metal dopants or in conductive metal polymeric systems.[22–24]

CONCLUSIONS

We have shown by ^{95}Mo NMR spectral studies that the molybdenum(0) nucleus is not greatly affected by the chain length when $n > 2$ in the series $[Mo(CO)_5]_2(\mu\text{-}Ph_2P(CH_2)_nPPh_2)$. Steric effects are likely the cause for deshielding the metal nucleus in $Mo(CO)_5(\eta^1\text{-dppm})$ and the inability to isolate

Table 2. Selected bond lengths (Å) and angles (°) for $[Mo(CO)_5]_2(\mu$-dppp)

Bond lengths (Å)			
Mo(1)—P(1)	2.545(1)	Mo(2)—P(2)	2.519(1)
Mo(1)—C(11)	2.006(3)	Mo(2)—C(21)	2.008(3)
Mo(1)—C(12)	2.012(3)	Mo(2)—C(22)	2.047(3)
Mo(1)—C(13)	2.033(3)	Mo(2)—C(23)	2.065(3)
Mo(1)—C(14)	2.046(3)	Mo(2)—C(24)	2.039(3)
Mo(1)—C(15)	2.035(3)	Mo(2)—C(25)	2.028(3)
C(1)—C(2)	1.519(3)	C(2)—C(3)	1.532(3)
P(1)—C(1)	1.834(3)	P(2)—C(3)	1.838(2)
O(11)—C(11)	1.127(4)	O(21)—C(21)	1.138(4)
O(12)—C(12)	1.144(3)	O(22)—C(22)	1.132(4)
O(13)—C(13)	1.141(4)	O(23)—C(23)	1.105(4)
O(14)—C(14)	1.137(4)	O(24)—C(24)	1.124(4)
O(15)—C(15)	1.123(3)	O(25)—C(25)	1.128(4)
P(1)—C(31)	1.834(2)	P(2)—C(51)	1.821(2)
P(1)—C(41)	1.816(3)	P(2)—C(61)	1.830(3)
Bond angles (°)			
P(1)—Mo(1)—C(11)	174.23(9)	P(2)—Mo(2)—C(21)	177.83(9)
P(1)—Mo(1)—C(12)	89.02(8)	P(2)—Mo(2)—C(22)	89.08(9)
P(1)—Mo(1)—C(13)	97.25(8)	P(2)—Mo(2)—C(23)	88.64(8)
P(1)—Mo(1)—C(14)	90.48(9)	P(2)—Mo(2)—C(24)	93.2(1)
P(1)—Mo(1)—C(15)	87.95(8)	P(2)—Mo(2)—C(25)	88.73(8)
C(11)—Mo(1)—C(12)	89.3(1)	C(21)—Mo(2)—C(22)	89.9(1)
C(11)—Mo(1)—C(13)	88.2(1)	C(21)—Mo(2)—C(23)	89.4(1)
C(11)—Mo(1)—C(14)	91.2(1)	C(21)—Mo(2)—C(24)	88.0(2)
C(11)—Mo(1)—C(15)	86.5(1)	C(21)—Mo(2)—C(25)	93.1(1)
C(12)—Mo(1)—C(13)	89.3(1)	C(22)—Mo(2)—C(23)	89.7(1)
C(12)—Mo(1)—C(14)	179.4(1)	C(22)—Mo(2)—C(24)	174.5(1)
C(12)—Mo(1)—C(15)	88.4(1)	C(22)—Mo(2)—C(25)	85.5(1)
C(13)—Mo(1)—C(14)	90.5(1)	C(23)—Mo(2)—C(24)	95.3(1)
C(13)—Mo(1)—C(15)	174.3(1)	C(23)—Mo(2)—C(25)	174.5(1)
C(14)—Mo(1)—C(15)	91.9(1)	C(24)—Mo(2)—C(25)	89.6(1)
Mo(1)—C(11)—O(11)	177.6(3)	Mo(2)—C(21)—O(21)	177.4(3)
Mo(1)—C(12)—O(12)	178.0(3)	Mo(2)—C(22)—O(22)	176.9(3)
Mo(1)—C(13)—O(13)	176.4(3)	Mo(2)—C(23)—O(23)	177.3(3)
Mo(1)—C(14)—O(14)	178.9(3)	Mo(2)—C(24)—O(24)	176.8(3)
Mo(1)—C(15)—O(15)	175.7(3)	Mo(2)—C(25)—O(25)	176.2(3)
Mo(1)—P(1)—C(1)	115.31(8)	Mo(2)—P(2)—C(3)	115.78(8)
Mo(1)—P(1)—C(31)	111.88(8)	Mo(2)—P(2)—C(51)	111.39(8)1
Mo(1)—P(1)—C(41)	119.40(9)	Mo(2)—P(2)—C(61)	120.91(4)1
C(1)—P(1)—C(31)	103.0(1)	C(3)—P(2)—C(51)	103.2(1)
C(1)—P(1)—C(41)	102.3(1)	C(3)—P(2)—C(61)	101.1(1)
C(31)—P(1)—C(41)	103.0(1)	C(51)—P(2)—C(61)	102.2(1)
P(1)—C(1)—C(2)	113.6(2)		
C(1)—C(2)—C(3)	111.0(2)		
P(2)—C(3)—C(2)	113.0(2)		

$[Mo(CO)_5]_2(\mu$-dppm). We have also reported the first crystal structure of any Group 6 metal complex with bridging ditertiary phosphine ligands. The structural differences and similarities of $[Mo(CO)_5]_2(\mu$-dppp) to related species have lent some insight into the stability of these molecules to stressful thermal conditions as noted by earlier work.

Acknowledgements—E.C.A. and G.F. thank N.S.E.R.C. for Infrastructure and Operating grants. R.A.G. acknowledges the Southwestern Ontario NMR Centre for assistance. E.C.A. dedicates this paper to the memory of his postdoctoral mentor, the late Professor Devon W. Meek, whose selfless devotion to his profession will continue to inspire.

REFERENCES

1. B. Chaudret, B. Delavaux and R. Poilblanc, *Coord. Chem. Rev.* 1988, **86**, 191.
2. R. J. Puddephatt, *Chem. Soc. Rev.* 1983, **12**, 99.
3. G. Wilkinson, F. G. A. Stone and E. W. Abel (Eds), *Comprehensive Organometallic Chemistry*, Vol. 3, Section 26.1.2.4.2. Pergamon Press, Oxford (1982).
4. H. Werner, R. Prinz, E. Bundschuh and K. Deckelmann, *Angew. Chem. Int. Edn Engl.* 1966, **5**, 606.
5. W. H. Dietsche, *Tetrahedron Lett.* 1966, **49**, 6187.
6. S. O. Grim, J. Del Gaudio, R. P. Molenda, C. A. Tolman and J. P. Jesson, *J. Am. Chem. Soc.* 1974, **96**, 3416.
7. (a) R. L. Keiter, S. L. Kaiser, N. P. Hansen, J. W. Brodack and L. W. Cary, *Inorg. Chem.* 1981, **20**, 283; (b) R. L. Keiter and D. P. Shah, *Inorg. Chem.* 1972, **11**, 191.
8. T. S. A. Hor, *J. Organomet. Chem.* 1987, **319**, 213.
9. T. S. A. Hor, *Inorg. Chim. Acta* 1989, **158**, 5.
10. H. S. O. Chan, T. S. A. Hor, C. S. M. Chiam and T. C. Chong, *J. Therm. Anal.* 1987, **32**, 1115.
11. T. S. A. Hor, *J. Organomet. Chem.* 1988, **340**, 51.
12. T. S. A. Hor and H. S. O. Chan, *Inorg. Chim. Acta* 1989, **160**, 53.
13. L. R. Nassimbeni, *Inorg. Nucl. Chem. Lett.* 1971, **7**, 187.
14. D. Sellman, *Angew. Chem. Int. Edn Engl.* 1973, **12**, 1020.
15. G. Huttner, P. Friedrich, H. Willenberg and H. D. Müller, *Angew. Chem. Int. Edn. Engl.* 1977, **16**, 260.
16. D. L. DuBois, C. W. Eigenbrot Jr., A. Miedaner and J. C. Smart, *Organometallics* 1986, **5**, 1405.
17. (a) E. C. Alyea, R. A. Gossage, J. Malito and Z. A. Munir, *Polyhedron* 1990, **9**, 1059; (b) E. C. Alyea, K. J. Fisher and R. A. Gossage, *Spectrochim. Acta* 1989, **45A**, 203; (c) E. C. Alyea and A. Somogyvari, *Can. J. Chem.* 1988, **66**, 397; (d) E. C. Alyea and A. Somogyvari, *Transition Met. Chem.* 1987, **12**, 310; (e) E. C. Alyea and A. Somogyvari, *Mag. Reson. Chem.* 1986, **24**, 357; (f) E. C. Alyea, A. Malek and J. Malito, *Inorg. Chim. Acta* 1985, **101**, 147.
18. (a) G. M. Gray, *Inorg. Chim. Acta* 1984, **81**, 157; (b) G. M. Gray, R. J. Gray and D. C. Berndt, *J. Mag. Reson.* 1984, **57**, 347; (c) A. M. Bond, S. W. Carr and R. Colton, *Organometallics* 1984, **3**, 541; (d) G. M. Gray and R. J. Gray, *Organometallics* 1983, **2**, 1026; (e) G. M. Gray and C. S. Kraihanzel, *Inorg. Chem.* 1983, **22**, 2959.
19. F. A. Cotton, D. J. Darensbourg and W. H. Ilsley, *Inorg. Chem.* 1981, **20**, 578.
20. E. C. Alyea, G. Ferguson and A. Somogyvari, *Organometallics* 1983, **2**, 668.
21. J. A. Iggo and B. L. Shaw, *J. Chem. Soc., Dalton Trans.* 1985, 1009.
22. E. Khor, H. S. O. Chan and T. S. A. Hor, *J. Mater. Sci.* 1989, **24**, 557.
23. T. S. A. Hor, H. S. O. Chan, L. Ying-Phooi and T. Mei-Mei, *J. Organomet. Chem.* 1989, **373**, 221.
24. E. Khor, H. S. O. Chan, T. S. A. Hor and J. R. Lusty, *J. Polym. Sci. Part C. Polymer Lett.* 1987, **25**, 471.

Polyhedron Vol. 9, No. 19, pp. 2399–2405, 1990
Printed in Great Britain

0277-5387/90 $3.00+.00
© 1990 Pergamon Press plc

FORMATION OF THE HEPTANITROSYLTRI-μ_3-THIOXOTETRAFERRATE(1−) ANION, $[Fe_4S_3(NO)_7]^-$ BY CAPTURE OF BIOLOGICAL SULPHUR IN REACTIONS WITH IRON(II) AND NITRITE

ANTHONY R. BUTLER, CHRISTOPHER GLIDEWELL*
and SHEILA M. GLIDEWELL

Chemistry Department, University of St Andrews, St Andrews, Fife KY16 9ST, U.K.

(*Received* 7 *February* 1990; *accepted* 7 *June* 1990)

Abstract—The reaction of cysteine with iron(II) sulphate heptahydrate and sodium nitrite, in aqueous solution at 118°C, yields $Na[Fe_4S_3(NO)_7]$; the yield is increased when the reducing agent sodium ascorbate is also present, and for certain reaction stoichiometries when nitrite is limiting the yield is quantitative. Sulphur is similarly captured, to form $Na[Fe_4S_3(NO)_7]$, from a range of other sources including several derivatives of cysteine, homocysteine, sodium thioglycolate, penicillamine and potassium benzylpenicillin, as well as from sodium thiosulphate. Glutathione and cystine both require the presence of sodium ascorbate for formation of $Na[Fe_4S_3(NO)_7]$, while methionine and 2-mercaptopyrimidine are among a number of sulphur compounds which do not provide $Na[Fe_4S_3(NO)_7]$ under these conditions. Both acid-hydrolysed casein and enzyme-hydrolysed casein, which contain low levels of both cystine and iron, react with sodium nitrite in the presence of sodium ascorbate to form $Na[Fe_4S_3(NO)_7]$, as does the synthetic Perigo medium. The $Na[Fe_4S_3(NO)_7]$ was identified by a combination of FTIR and ^{15}N NMR spectroscopy using 99% ^{15}N-labelled material and, in some cases, by isolation.

The mode of action by which nitrite inhibits the development of *Clostridium* species, and other food-spoilage organisms, in preserved foodstuffs has been the subject of investigation for a number of years.[1–6] In a laboratory medium (Perigo medium)[1] which supports the growth of *Clostridium* species, incubation with sodium nitrite not only caused a substantial reduction in the free nitrite concentration, but formed some new component in the medium, presumed[1] to be related to the consumption of nitrite, which was extremely inhibitory to the vegetative growth of a wide range of strains of a number of *Clostridium* species, including *Clostridium botulinum*.[1,2] The formation of an inhibitor associated with disappearance of nitrite has also been demonstrated using pig meat in place of the synthetic laboratory medium,[3] and similarly-formed inhibitors have been shown to be effective against a wide range of micro-organisms other than *Clostridium* species.[4] Earlier chemical studies[4,5] indicated that iron salts and a source of sulphur were required for the formation of the inhibitors.

Treatment[6] of vegetative cells of *C. botulinum* with nitrite in the presence of ascorbate resulted in loss of the ESR signal at $g = 1.94$, characteristic of the reduced form of a {4Fe–4S} iron–sulphur centre, and its replacement by an ESR signal at $g = 2.035$, characteristic of $[Fe(NO)_2X_2]$ complexes, most likely in this case of $[Fe(NO)_2(SR)_2]^-$. We have subsequently shown[7] that treatment with aqueous sodium nitrite of synthetic models for both {2Fe–2S} and {4Fe–4S} centres leads via $[Fe(NO)_2(SH)_2]^-$, identified[9] by ESR spectroscopy, to $[Fe_4S_3(NO)_7]^-$ isolable in yields around 40%.

In earlier work,[4] material with properties similar to those of $[Fe_4S_3(NO)_7]^-$ salts was extracted from a limited range of substrates treated with nitrite, with or without added iron salts, including casein hydrolysate, cysteine and thioglycolate. However, the evidence[4] for the identity of these extracts as a salt of $[Fe_4S_3(NO)_7]^-$ was suggestive only, not definitive. It relied on IR spectroscopy, Mössbauer

* Author to whom correspondence should be addressed.

spectroscopy and elemental analysis. Of these, the IR spectrum measured dispersively in Nujol is not adequately characteristic, while the interpretation of the Mössbauer isomer shifts and quadrupole splitting has proved to be controversial: it is not even clear how many quadrupole doublets characterize the spectra of $[Fe_4S_3(NO)_7]^-$ salts.[10-12] The reported analytical data[4] on the other hand were in excellent agreement with an atomic ratio Fe/S/N of 4:3:6 rather than 4:3:7 expected for the sodium or potassium salts of $[Fe_4S_3(NO)_7]^-$ or 4:3:8 expected for the ammonium salt. The presence of $[Fe_4S_3(NO)_7]^-$ in these extracts[4] is therefore not proven.

We have found that a combination of solution FTIR and ^{15}N NMR on isotopically labelled material provides definitive identification of the $[Fe_4S_3(NO)_7]^-$ anion: at high levels of ^{15}N labelling, the ^{15}N NMR spectrum comprises[13] a singlet of relative intensity one due to the unique apical nitrosyl ligand and a pair of doublets, forming an AX system, each of relative intensity three, due to the basal $Fe(NO)_2$ groups. While the chemical shifts are slightly solvent dependent, the overall spectrum is uniquely characteristic of $[Fe_4S_3(NO)_7]^-$: on the other hand, the ^{15}N NMR spectrum of the related dinuclear anion $[Fe_2S_2(NO)_4]^{2-}$ consists,[14] at any level of ^{15}N labelling, of a singlet, δ +37.8 in aqueous solution.

Here we report on the definitive identification of $[Fe_4S_3(NO)_7]^-$ as a reaction product from the interaction of nitrite and iron salts with a wide range of sulphur-containing substrates, including the capture of sulphur into $[Fe_4S_3(NO)_7]^-$ from a number of sulphur biochemicals including sulphur amino acids and their derivatives, peptides and penicillin derivatives, as well as other sulphur-containing systems.

EXPERIMENTAL

Samples of $[Fe_2(SR)_2(NO)_4]$ were prepared using previously published methods.[15,16] Samples of $Na[Fe_4S_3(NO)_7]$ were prepared by reaction of iron(II) sulphate heptahydrate with sodium sulphide and sodium nitrite in hot aqueous solution.[17] Acid-hydrolysed and enzyme-hydrolysed casein were obtained from Sigma: Perigo medium was prepared, and used, according to the literature.[1] 5,5-Diethylthiobarbituric acid was prepared by base-catalysed condensation of dimethyl diethylmalonate with thiourea.[18] Other organo-sulphur chemicals were the best available commercial grade and were used as received.

Preparation of $Na[Fe_4S_3(^{15}NO)_7]$

$Na^{15}NO_2$ (99% ^{15}N; MSD Isotopes) (0.10 g, 1.43 mmol), $Na_2S \cdot 9H_2O$ (0.35 g, 1.46 mmol) and $FeSO_4 \cdot 7H_2O$ (0.50 g, 1.80 mmol) were dissolved in water (500 cm^3). The solution was heated in an autoclave at 118°C for 20 min. After cooling, the solution was filtered through Hyflo-supercel, and the filtrate extracted with ether (6×50 cm^3). The organic extract was washed with water, dried and evaporated to provide $Na[Fe_4S_3(^{15}NO)_7]$ (80 mg, 70%), identified by IR and ^{15}N NMR spectroscopy.

IR spectra were recorded in tetrahydrofuran (THF) solution using 0.5 mm pathlength cells and a Perkin–Elmer Model 1710 FTIR spectrometer. ^{15}N NMR spectra were recorded in acetone solution, at ambient temperature, relative to 50% CH_3NO_2 in acetone, using a Brüker AM-300 spectrometer at 30.424 MHz. The IR spectra of authentic $Na[Fe_4S_3(NO)_7]$ (Fig. 1) were recorded using 0.002 mol dm^{-3} solutions in THF: $Na[Fe_4S_3(^{14}NO)_7]$, ν(NO) 1795(w), 1742(vs), 1707(m) cm^{-1}; $Na[Fe_4S_3(^{15}NO)_7]$, ν(NO) 1760(w), 1708(vs), 1673(m) cm^{-1}. The ^{15}N NMR spectrum of $Na[Fe_4S_3(^{15}NO)_7]$ was recorded using a saturated solution in acetone: δ_N, 11.8(s), (1N); 39.5 (d, J 3.8 Hz) and 80.6 (d, J 3.8 Hz) (AX, 6N). Electronic spectra were measured using a Pye–Unicam SP8-100 spectrophotometer, and ESR spectra were measured in 1 mm quartz capillaries using a Brüker ER200-D spectrometer.

Reactions of sodium nitrite and iron sulphate with characterized sulphur sources

(i) *Cysteine.* DL-Cysteine (2.0 g, 16.5 mmol), iron(II) sulphate heptahydrate (0.50 g, 1.80 mmol) and sodium nitrite (0.10 g, 1.45 mmol) were dissolved in water (1 dm^3) and the mixture was autoclaved at 118°C for 20 min. The mixture was cooled and filtered, and the filtrate exhaustively extracted with diethyl ether, until the extracts were colourless. The combined ether extracts were washed with water, dried and evaporated to provide $Na[Fe_4S_3(NO)_7]$ (21 mg, 18%) identified by FTIR and by analysis; Found Fe, 40.6; N, 17.5; S, 16.9. $Fe_4N_7NaO_7S_3$ requires Fe, 40.4; N, 17.7; S, 17.4%: derivatives by metathesis (a) $(Ph_4As)[Fe_4S_3(NO)_7]$; Found C, 31.2; H, 2.1; N, 10.6. $C_{24}H_{20}AsFe_4N_7O_7S_3$ requires C, 31.6; H, 2.2; 10.7%: (b) $(Ph_3PNPPh_3)[Fe_4S_3(NO)_7]$; Found C, 40.3; H, 2.7; N, 10.3. $C_{36}H_{30}Fe_4N_8O_7P_2S_3$ requires C, 40.5; H, 2.8; N, 10.5%. An entirely similar experiment using $Na^{15}NO_2$ (99% ^{15}N) provided $Na[Fe_4S_3(^{15}NO)_7]$ in like yield, identified by FTIR and ^{15}N NMR. No other iron–nitrosyl species were

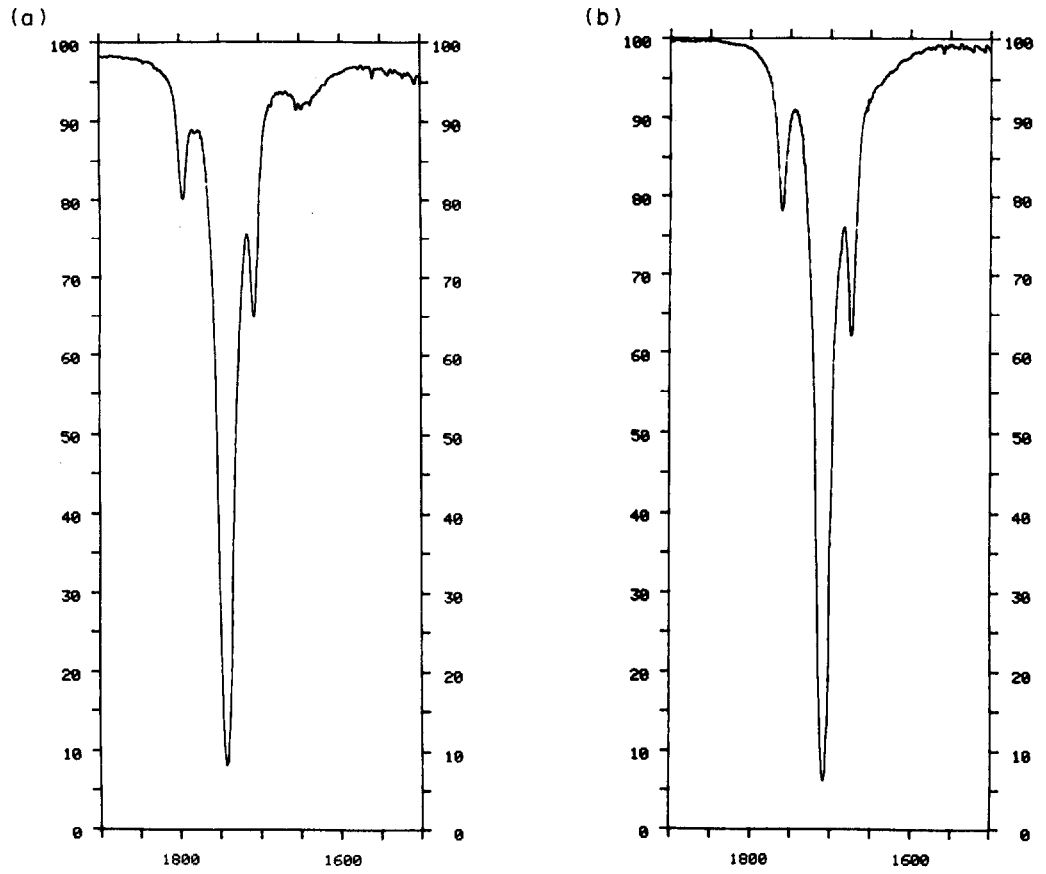

Fig. 1. FTIR spectra of the nitrosyl stretching region for (a) $Na[Fe_4S_3(^{14}NO)_7]$ and (b) $Na[Fe_4S_3(^{15}NO)_7]$: spectra recorded using 2×10^{-3} mol dm^{-3} solutions in THF.

isolated. When the reactions were repeated in the presence of sodium ascorbate (2.0 g, 10.1 mmol) under otherwise identical conditions the yield of $Na[Fe_4S_3(NO)_7]$ rose to 88 mg, 77%. The use of sodium ascorbate in the absence of cysteine or other sulphur sources provided nil $Na[Fe_4S_3(NO)_7]$. When the concentration of sodium nitrite was halved, the yields were little affected: by use of 0.05 g (0.72 mmol) of $NaNO_2$, 1.0 g (3.6 mmol) of $FeSO_4 \cdot 7H_2O$ and 8.0 g (66 mmol) of cysteine,[19] the yield of $Na[Fe_4S_3(NO)_7]$ rose to 39%, while in the presence of sodium ascorbate (13.1 g, 66 mmol) the yield of $Na[Fe_4S_3(NO)_7]$ was quantitative.

(ii) *Sodium thioglycolate.* In a reaction similar to the foregoing, but using sodium thioglycolate ($HSCH_2COO^-Na^+$; 2.0 g, 17.5 mmol) in place of cysteine, the isolated yield of $Na[Fe_4S_3(NO)_7]$, identified by FTIR, was 23.5 mg, 21%. Again proof of identity was reinforced by use of $Na^{15}NO_2$ and identification of $Na[Fe_4S_3(^{15}NO)_7]$ by both FTIR and ^{15}N NMR.

(iii) *Methyl thioglycolate, thioglycolic acid, thioethanol and 2-methyl-2-propanethiol.* The reaction mixture was in each case $NaNO_2$ (0.10 g, 1.45 mmol), $FeSO_4 \cdot 7H_2O$ (0.50 g, 1.80 mmol) and the sulphur source (16.5 mmol) in water (1 dm^3). Duplicate runs were made in the absence and in the presence of sodium ascorbate (3.3 g, 16.7 mmol). After autoclaving at 118°C for 20 min the mixtures were worked-up, as described above, to afford the known[16] complexes $[Fe_2(SR)_2(NO)_4]$, identified by FTIR. The results are summarized in Table 1.

(iv) *Other thiols, thiones and sulphides; elemental sulphur, sodium sulphite and sodium thiosulphate.* The reaction mixture was, in each case $NaNO_2$ (0.10 g, 1.45 mmol), $FeSO_4 \cdot 7H_2O$ (0.50 g, 1.80 mmol) and the sulphur source (16.5 mmol) in water (1 dm^3); where no $Na[Fe_4S_3(NO)_7]$ or $[Fe_2(SR)_2(NO)_4]$ was identifiable in the absence of sodium ascorbate, the run was repeated, as before, with the addition of sodium ascorbate (2.0 g, 10.1 mmol). The results are summarized in Table 1.

Reactions of sodium nitrite with casein hydrolysates

Sodium nitrite (0.10 g, 1.45 mmol) was dissolved in water (1 dm^3) and either acid-hydrolysed casein (150 g) or enzyme-hydrolysed casein (100 g) was

Table 1. Reactions of $FeSO_4 \cdot 7H_2O$ and $NaNO_2$ with sulphur sources

(i) Compounds providing $Na[Fe_4S_3(NO)_7]$ in the absence of sodium ascorbate:[a]

Cysteine;[b,c] *N*-acetylcysteine; cysteine methyl ester hydrochloride (52%); cysteine ethyl ester hydrochloride; homocysteine (6.5%); thioglycolic acid; sodium thioglycolate (21%);[b] penicillamine; potassium benzylpenicillin; 6-aminopenicillanic acid; sodium thiosulphate (20%); *N*-methylthiourea; *N,N'*-dimethylthiourea; *N,N'*-diphenylthiourea; thioacetanilide; thiocarbonyldiimidazole.

(ii) Compounds providing $Na[Fe_4S_3(NO)_7]$ only in the presence of sodium ascorbate:[a]

N-acetylpenicillamine; glutathione; cystine; *S*-methylcysteine; thiodiglycolic acid; thiazolidine-4-carboxylic acid; thiourea (8.9%); thiosemicarbazide; thioacetamide; 2-mercaptopyridine; 2-mercaptobenzothiazole.

(iii) Compounds providing no $Na[Fe_4S_3(NO)_7]$ even in the presence of sodium ascorbate:

Methionine; thiodiethanol; dithiothreitol;[d] 2-mercaptopyrimidine; 2-mercaptothiazoline; 2-mercapto-1-methylimidazole; 2-thiobarbituric acid; 2-thio-5,5-diethylthiobarbituric acid; 2-mercaptobenzimidazole; thiobenzanilide; *S*-(thiobenzyl)thioglycolic acid; thiamine hydrochloride; thioflavin-T; thioxanthen-9-one; 2-thiopheneacetic acid; 3-thiopheneacetic acid; sodium sulphite; octasulphur.

(iv) Compounds providing $Fe_2(SR)_2(NO)_4$:[e]

Methylthioglycolate (52, 72%); thioethanol; 2-methyl-2-propanethiol (0, 26%); thioglycolic acid.[c]

[a] Identification in every case by FTIR on THF solutions; when $Na[Fe_4S_3(NO)_7]$ was cleanly separable, without decomposition, from the reaction mixture, percentage yields are given.

[b] $Na[Fe_4S_3(NO)_7]$ confirmed also by use of $Na^{15}NO_2$ (99% ^{15}N) and ^{15}N NMR spectroscopy (see text).

[c] See text for discussion of yields.

[d] $Na[Fe_4S_3(NO)_7]$ formed in presence of $Na_2S_2O_4$.

[e] Identification and yields (without and with sodium ascorbate: see text) by FTIR on THF solutions.

added: these mixtures were autoclaved and worked-up as described above. Similar reactions were carried out using each of these sodium nitrite/casein hydrolysate mixtures with the following additives:[4]

(a) $FeSO_4 \cdot 7H_2O$ (0.50 g, 1.80 mmol);
(b) sodium ascorbate (2.0 g, 10.1 mmol);
(c) sodium thioglycolate (2.0 g, 17.5 mmol);
(d) $FeSO_4 \cdot 7H_2O$ (0.50 g, 1.80 mmol) and sodium ascorbate (2.0 g, 10.1 mmol);
(e) $FeSO_4 \cdot 7H_2O$ (0.50 g, 1.80 mmol) and sodium thioglycolate (2.0 g, 17.5 mmol).

The reactions under conditions (a) were also repeated using $Na_{15}NO_2$ in place of unlabelled sodium nitrite.

Reactions of sodium nitrite with Perigo medium

Sodium nitrite (0.10 g, 1.45 mmol) was added to 1 dm^3 of Perigo medium:[1] the mixture was autoclaved and worked-up as before. Similar runs were undertaken (a) using $Na^{15}NO_2$ instead of unlabelled sodium nitrite and (b) with the addition of $FeSO_4 \cdot 7H_2O$ (0.50 g, 1.80 mmol).

RESULTS AND DISCUSSION

When sodium nitrite and iron(II) sulphate heptahydrate were autoclaved at 118°C in dilute aqueous solution ($NaNO_2$, 100 ppm; $FeSO_4 \cdot 7H_2O$, 500 ppm) with DL-cysteine, the sodium salt of Roussin's black anion, $Na[Fe_4S_3(NO)_7]$, was isolated in 18% yield. This salt was identified unambiguously by a combination of FTIR, UV–vis, and, most characteristic, ^{15}N NMR spectroscopy: this latter technique, using 99% ^{15}N enrichment, showed that no other diamagnetic iron–nitrosyl complexes were formed. When excess of sodium ascorbate, as reducing agent, was present the isolated yield of $Na[Fe_4S_3(NO)_7]$ rose to 77%, based on sodium nitrite as the limiting component. Similar mixtures,

when held for 24 h at room temperature, gave no trace of $Na[Fe_4S_3(NO)_7]$.

An autoclaved mixture of $FeSO_4 \cdot 7H_2O$, $NaNO_2$ and cysteine in concentrations of 3.6×10^{-3}, 0.72×10^{-3} and 66×10^{-3} mol dm^{-3}, respectively, has been shown[19] to be extremely inhibitory when applied to growing cultures of *Clostridium sporogenes*. Using such mixtures, quantitative FTIR has shown that $Na[Fe_4S_3(NO)_7]$ is formed in 39% yield, based upon nitrite as the limiting component. When sodium ascorbate was also present at the same concentration as the cysteine, the conversion of nitrite to $Na[Fe_4S_3(NO)_7]$ was quantitative. Similar results were obtained using an iron(II) concentration of 1.8×10^{-3} mol dm^{-3}. This result is of interest as it has been found[19] that this autoclaved mixture exhibits the same level of inhibition, based on concentration of NO fragments, as pre-formed, unautoclaved $Na[Fe_4S_3(NO)_7]$, suggesting that this tetranuclear complex, or one of its dissociation products,[9] is the effective inhibitor. However, the observation[19] that the autoclaved mixture shows no ESR spectrum effectively rules out the presence of mononuclear iron–nitrosyl complexes of the types $[Fe(NO)_2(SR)_2]^-$, $[Fe(NO)(SR)_3]$ and $[Fe(NO)(SR)_3]^{3-}$, the common[9] products of $[Fe_4S_3(NO)_7]^-$ cleavage reactions in the presence of anionic sulphur nucleophiles.

The formation of $[Fe_4S_3(NO)_7]^-$ requires cleavage of the carbon–sulphur bonds in cysteine to liberate sulphide and reduction of iron(II) to a mean oxidation state of $-1/2$, followed by spontaneous self-assembly.[20] The role of sodium ascorbate, which causes a significant increase in the yields of $Na[Fe_4S_3(NO)_7]$ appears to be that of keeping the cysteine in the reduced, thiol form $HSCH_2CH(NH_2)COOH$: it is known[21] that the very slow oxidation by molecular oxygen of thiols, such as cysteine and glutathione, to the disulphide forms, cystine and diglutathione, is accelerated by iron salts. Consistent with this interpretation, when cystine was employed as the sulphur source, in the absence of sodium ascorbate, no $Na[Fe_4S_3(NO)_7]$ was formed: only upon addition of the reducing ascorbate was the cluster anion formed. This suggested that a thiol group might be essential for sulphur capture from organosulphur compounds into $[Fe_4S_3(NO)_7]^-$: subsequent investigation showed, however, that this was an over-simple hypothesis.

Although a number of other thiols including *N*-acetylcysteine, cysteine methyl ester hydrochloride, cysteine ethyl ester hydrochloride, homocysteine, sodium thioglycolate and penicillamine all gave $Na[Fe_4S_3(NO)_7]$ in the absence of sodium ascorbate, several thiols including glutathione, *N*-acetylpenicillamine, 2-mercaptopyridine and 2-mercaptobenzothiazole required the addition of sodium ascorbate before any $Na[Fe_4S_3(NO)_7]$ was formed, while the apparently related heterocyclic thiols (2-mercaptopyrimidine, 2-mercaptothiazoline, 2-mercapto-1-methylimidazole, and 2-mercaptobenzimidazole) gave no $Na[Fe_4S_3(NO)_7]$ even in the presence of sodium ascorbate. Dithiothreitol, which is oxidized with extreme ease,[22] provided no $Na[Fe_4S_3(NO)_7]$ even in the presence of sodium ascorbate. However in the presence of 1.50 g (8.6 mmol) of sodium dithionite, $Na[Fe_4S_3(NO)_7]$ was formed in 32% yield: control experiments in the absence of dithiothreitol showed no capture of sulphur from dithionite itself into $Na[Fe_4S_3(NO)_7]$.

In contrast, we have found that several thiones, including *N*-methylthiourea, *N*,*N*′-dimethylurea, *N*,*N*′-diphenylthiourea, thioacetanilide, and thiocarbonyldiimidazole, all provide $Na[Fe_4S_3(NO)_7]$ without added reductant, although sodium ascorbate is necessary for the formation of $Na[Fe_4S_3(NO)_7]$ from the related thiones, thiourea, thiosemicarbazide and thioacetamide, whereas thiobenzanilide and two thiobarbituric acids gave no $Na[Fe_4S_3(NO)_7]$ even in the presence of sodium ascorbate.

A similar spectrum of behaviour was observed with compounds containing sulphur bound in a C—S—C fragment (Table 1). In particular, methionine gave no $Na[Fe_4S_3(NO)_7]$ even in the presence of ascorbate. Hence of the three common sulphur-containing amino acids found in proteins, cysteine provides $Na[Fe_4S_3(NO)_7]$ even in the absence of sodium ascorbate as reductant, although more when the reductant is present; cystine provides $Na[Fe_4S_3(NO)_7]$ only in the presence of sodium ascorbate; and methionine does not yield $Na[Fe_4S_3(NO)_7]$.

In contrast to the reaction of sodium thioglycolate with iron(II) and nitrite which provides $Na[Fe_4S_3(NO)_7]$, in common with most thiols (Table 1), the neutral methyl thioglycolate provides instead the known[23] binuclear complex $[Fe_2(SCH_2COOCH_3)_2(NO)_4]$: the yield was 52%, rising to 72% in the presence of sodium ascorbate. Thioethanol likewise provided the known[23] $[Fe_2(SCH_2CH_2OH)_2(NO)_4]$ in the absence of sodium ascorbate, while 2-methyl-2-propanethiol, Me_3CSH, only gave $[Fe_2(SCMe_3)_2(NO)_4]$[24] (26%) when sodium ascorbate was present. When, in a control experiment, an authentic sample of $[Fe_2(SCH_2COOCH_3)_2(NO)_4]$ was autoclaved alone in aqueous medium at 118°C, it was recovered unchanged. The reaction of thioglycolic acid, $HSCH_2COOH$, with iron(II) and nitrite proved to be more complex: in unbuffered solution, the initial

iron-containing product was a rather labile oil whose IR spectrum, ν(NO) 1783 and 1756 cm^{-1}, ν(CO) 1732 cm^{-1}, was consistent with the presence of the neutral binuclear complex $[Fe_2(SCH_2COOH)_2(NO)_4]$, but attempts to purify this material by chromatography on silica led to its decomposition, to give $Na[Fe_4S_3(NO)_7]$ as the sole isolable iron nitrosyl complex. On the other hand, in buffered solution at pH 4, $Na[Fe_4S_3(NO)_7]$ was formed in 75% yield.

Of the three purely inorganic sulphur sources investigated, sodium thiosulphate, a well-established sulphur transfer agent, readily gave $Na[Fe_4S_3(NO)_7]$ in the absence of any reductant, while neither sodium sulphite nor elemental sulphur gave any evidence of sulphur transfer into the cluster anion. At room temperature, under a dinitrogen atmosphere, sodium thiosulphate reacts with sodium sulphide and iron(II) sulphate to yield[16] the μ-thiosulphato di-iron complex $[Fe_2(S_2O_3)_2(NO)_4]^{2-}$: this upon exposure to air, in solution, is readily transformed to $[Fe_4S_3(NO)_7]^-$, along with nitrate, nitrite and unidentified sulphur-containing, but nitrogen-free, by-products. It is probable that the reaction described here, forming $Na[Fe_4S_3(NO)_7]$ from $Na_2S_2O_3$ at 118°C, in air, proceeds via the di-iron thiosulphato complex, the mechanism of whose conversion to the tetra-iron complex still awaits elucidation.

Acid-hydrolysed casein typically contains *ca* 0.035% by weight of sulphur, incorporated as cystine, and *ca* 0.40% of sulphur, as methionine. Enzyme-hydrolysed casein, on the other hand, typically contains 0.045–0.08% sulphur as cystine and 0.30–0.40% sulphur as methionine. The experiments with single amino acids, described above, show that only cystine sulphur can be captured to form $Na[Fe_4S_3(NO)_7]$, while methionine sulphur remains bound. In our experiments the maximum available sulphur in runs using casein hydrolysates is therefore *ca* 1.6 mmol using acid-hydrolysed casein, and *ca* 1.4–2.5 mmol using enzyme-hydrolysed casein.

Each of the casein hydrolysates employed in this work was found, by AAS, to contain *ca* 20 ppm iron. Hence the maximum available iron in runs using acid-hydrolysed casein was 0.054 mmol, and with enzyme-hydrolysed casein, 0.036 mmol. Iron is thus clearly the limiting component in these experiments, and the maximum quantity of $Na[Fe_4S_3(NO)_7]$ which could be formed in the acid-hydrolysed casein runs was 5 mg.

When acid-hydrolysed casein was autoclaved with sodium nirite alone (see Experimental), no $Na[Fe_4S_3(NO)_7]$ was formed. This was expected since all the sulphur under these conditions is present as either cystine or methionine. However, in the presence of sodium ascorbate, which reduces cystine to cysteine, $Na[Fe_4S_3(NO)_7]$ was indeed detected by FTIR and confirmed by ^{15}N NMR spectroscopy in runs using $Na[^{15}NO_2]$. That the reduction of cystine was the limiting factor, rather than the state of the casein-bound iron, was shown by repeating the experiments in the presence of 500 ppm $FeSO_4 \cdot 7H_2O$. Again no $Na[Fe_4S_3(NO)_7]$ was produced unless sodium ascorbate was present. Use of the other additives suggested in previous work[4] led, as expected from the work on single sulphur sources, to an increase in the yield of $Na[Fe_4S_3(NO)_7]$. Results with enzyme-hydrolysed caseins were essentially identical, with the formation of $Na[Fe_4S_3(NO)_7]$ confirmed by the use of $Na[^{15}NO_2]$ and ^{15}N NMR spectroscopy, as before.

Since Perigo medium contains both sodium thioglycolate and enzyme-hydrolysed casein,[1] the observed formation of $Na[Fe_4S_3(NO)_7]$ was expected: in the absence of added iron, the level of $Na[Fe_4S_3(NO)_7]$ (which could not be satisfactorily separated from the rest of the mixture) was low, but its presence was confirmed by ^{15}N labelling. As expected, much higher yields were obtained in the presence of added iron. In none of the experiments using Perigo medium were any paramagnetic iron nitrosyl complexes detected by ESR spectroscopy, just as with the mixtures involving cysteine.[19]

The results with the casein hydrolysates show that even with very low levels of iron (20 ppm) and sulphur (0.035%) bound in proteins, a simple brief heat treatment with sodium nitrite under reducing conditions readily forms $Na[Fe_4S_3(NO)_7]$. Many canned foodstuffs, particularly meat products, undergo just such a heat treatment with sodium nitrite.

Acknowledgement—We thank AFRC for financial support.

REFERENCES

1. J. A Perigo, E. Whiting and T. E. Bashford, *J. Food Technol.* 1967, **2**, 377.
2. J. A. Perigo and T. A. Roberts, *J. Food Technol.* 1968, **3**, 91.
3. J. Ashworth and R. Spencer, *J. Food Technol.* 1972, **7**, 111.
4. J. Ashworth, A. Didcock, L. L. Hargreaves, B. Jarvis, C. L. Walters and L. F. Larkworthy, *J. Gen. Microbiol.* 1974, **84**, 403.
5. D. M. Moran, S. R. Tannenbaum and M. C. Archer, *Appl. Microbiol.* 1975, **30**, 838.
6. D. Reddy, J. R. Lancaster Jr and D. P. Cornforth, *Science* 1983, **221**, 769.
7. A. R. Butler, C. Glidewell, A. R. Hyde and J. C. Walton, *Inorg. Chim. Acta* 1985, **106**, L7.

8. R. H. Holm, *Chem. Soc. Revs* 1981, **10**, 455.
9. A. R. Butler, C. Glidewell and M.-H. Li, *Adv. Inorg. Chem.* 1988, **32**, 335.
10. W. Kerler, W. Neuwirth, E. Fluck, P. Kuhn and B. Zimmerman, *Z. Phys.* 1963, **173**, 321.
11. E. Kostiner, J. Steger and J. R. Rea, *Inorg. Chem.* 1970, **9**, 1939.
12. D. Sedney and W. M. Reiff, *Inorg. Chim. Acta* 1979, **34**, 231.
13. A. R. Butler, C. Glidewell, A. R. Hyde and J. McGinnis, *Inorg. Chem.* 1985, **24**, 2931.
14. C. Glidewell and I. L. Johnson, *Chem. Scripta.* 1987, **27**, 441.
15. A. R. Butler, C. Glidewell, A. R. Hyde, J. McGinnis and J. E. Seymour, *Polyhedron* 1983, **2**, 1045.
16. C. Glidewell, R. J. Lambert, M. B. Hursthouse and M. Motevalli, *J. Chem. Soc., Dalton Trans.* 1989, 2061.
17. G. Brauer (Ed.), *Handbuch der Präparativen Anorganischen Chemie*, 2nd edn, Vol. 2, p. 1526. Enke, Stuttgart (1960).
18. E. Fischer and A. Dilthey, *Lieb. Ann. Chem.* 1904, **335**, 334.
19. M. J. Payne, C. Glidewell and R. Cammack, *J. Gen Microbiol.*, submitted.
20. J. A. Ibers and R. H. Holm, *Science* 1980, **209**, 223.
21. M. Y. Hamed, J. Silver and M. T. Wilson, *Inorg. Chim. Acta* 1983,. **80**, 237 and refs therein.
22. W. W. Cleland, *Biochemistry* 1964, **3**, 480.
23. C. Glidewell, R. J. Lambert, M. E. Harman and M. B. Hursthouse, *J. Chem. Soc., Dalton Trans.*, in press.
24. C. Glidewell, M. E. Harman, M. B. Hursthouse, I. L. Johnson and M. Motevalli, *J. Chem. Res.* 1988, (S) 212, (M) 1676.

Polyhedron Vol. 9, No. 19, pp. 2407–2412, 1990
Printed in Great Britain

0277–5387/90 $3.00+.00
© 1990 Pergamon Press plc

SYNTHESIS AND MOLECULAR STRUCTURE OF [10-*endo*-(Ph_3PAu)-7,8-*nido*-$C_2B_9H_{11}$]$^-$: STRUCTURAL PATTERNS IN [$C_2B_9H_{11}X$]$^-$ ANIONS (X = H^+, $AuPPh_3^+$, $CuPPh_3^+$)

EWAN J. M. HAMILTON and ALAN J. WELCH*

Department of Chemistry, University of Edinburgh, Edinburgh EH9 3JJ, U.K.

(*Received* 20 *March* 1990; *accepted* 7 *June* 1990)

Abstract—Reaction of equimolar amounts of Tl[$TlC_2B_9H_{11}$], Ph_3PAuCl and [$PhCH_2NMe_3$]Cl affords the compound [$PhCH_2NMe_3$][$Ph_3PAuC_2B_9H_{11}$]. A single crystal X-ray diffraction study of this (as the CH_2Cl_2 solvate) reveals that the {Ph_3PAu} fragment is essentially *endo*-σ-bonded to B(10), in a similar manner to the *endo*-H atom in [7,8-*nido*-$C_2B_9H_{12}$]$^-$. In the title compound the gold atom is slipped towards B(10) by 0.87 Å from a position above the centre of the C_2B_3 carbaborane face. This parameter, together with ⟨B—B_{facial}⟩, ⟨B—C_{facial}⟩ and C—C, is discussed in relation to the corresponding parameters in [7,8-*nido*-$C_2B_9H_{12}$]$^-$ and [3-PPh_3-3,1,2-$CuC_2B_9H_{11}$]$^-$. The structural patterns thus revealed are traced to differing degrees of depopulation of the occupied π-molecular orbitals of [7,8-*nido*-$C_2B_9H_{11}$]$^{2-}$. Crystals of [$PhCH_2NMe_3$][10-*endo*-(Ph_3PAu)-7,8-*nido*-$C_2B_9H_{11}$]·CH_2Cl_2 are monoclinic, space group $P2_1/c$, with a = 9.5509(17), b = 19.232(3), c = 19.813(3) Å, β = 90.741(13)°. Using 4667 observed reflections the structure has been refined to R = 0.0487.

Since their initial syntheses and characterization more than 25 years ago,[1,2] carbametallaboranes have been the subject of intense research activity. The study of their chemistry has contributed significantly to such diverse areas as the development of current bonding theories[3] and homogeneous catalysis;[4] moreover, such compounds have the potential to be of future use, for example, in boron-neutron capture therapy of tumours.[5]

In the vast majority of carbametallaboranes the metal atom is more or less symmetrically disposed with respect to the ligating carbaborane face, although a sub-group, the "slipped" carbametallaboranes, are well known. In these, either the metal atom has access to > 18 valence electrons,[6] or the metal fragment is non-conical,[7] but in both cases (between which there is some degree of overlap) the reasons for the slipping are well understood.[8,9]

One class of slipped species that has received relatively little attention is that in which the metal atom is linearly coordinated, and thus essentially *endo*-σ-bonded to only one boron atom in the (now formally) open polyhedral face. This class is typified by the mercuracarbaborane [10-*endo*-(Ph_3PHg)-7,8-*nido*-$C_2B_9H_{11}$].[10] Recently, we established[11] that in [7,8-*nido*-$C_2B_9H_{12}$]$^-$ the 12th hydrogen atom also occupies an *endo*-terminal position [on B(10)]. Given that the structure of the anion [3-PPh_3-3,1,2-$CuC_2B_9H_{11}$]$^-$ has previously[12] been shown to involve the {Ph_3PCu} moiety reasonably symmetrically bonded to the five facial atoms (C_2B_3) of the carbaborane ligand, we considered it of interest to synthesize and structurally characterize the gold(I) analogue. In terms of the isolobal analogy[13] between H^+ and {Ph_3PAu^+} this species might be expected to show a greater structural similarity to [7,8-*nido*-$C_2B_9H_{12}$]$^-$ than to [3-PPh_3-3,1,2-$CuC_2B_9H_{11}$]$^-$, and thus might represent a further example of an essentially *endo*-σ-bonded $MC_2B_9H_{11}$ species.

EXPERIMENTAL

Synthesis and characterization

The reaction was carried out under dry N_2 using standard Schlenk-line techniques, with some sub-

* Author to whom correspondence should be addressed.

sequent manipulation in air. Solvents were dried and distilled under N_2 prior to use. The IR spectrum was recorded as KBr pellet on a Perkin–Elmer 598 spectrophotometer. NMR spectra were recorded on a Brucker WP200SY spectrometer as CD_2Cl_2 solution at 298 K. Microanalyses were performed by the departmental service. The starting materials, $Tl[TlC_2B_9H_{11}]$[14] and PPh_3AuCl,[15] were prepared by literature methods.

To a stirred mixture of solid $Tl[TlC_2B_9H_{11}]$ (0.2644 g, 0.489 mmol), PPh_3AuCl (0.2422 g, 0.490 mmol) and $[PhCH_2NMe_3]Cl$ {[BTMA]Cl} (0.0908 g, 0.489 mmol), was added CH_2Cl_2 (10 cm^3). The mixture was stirred overnight, filtered and the solvent removed from the pale orange filtrate *in vacuo*. Colourless needles of [BTMA]**1**·CH_2Cl_2 were obtained by diffusion of *n*-hexane into a CH_2Cl_2 solution at −30°C. Yield 0.1789 g, 45%. Found: C, 44.6; H, 5.3; N, 1.8. Calc. for $C_{30}H_{42}B_9NPAu \cdot CH_2Cl_2$: C, 45.0; H, 5.4; N, 1.7%. IR: ν_{max} at 2540 cm^{-1}. NMR: ^1H δ 7.40–7.75 (multiplet, 20H, C_6H_5), 4.41 (s, 2H, CH_2), 3.05 (s, 9H, CH_3) ppm, ^{11}B–{^1H} δ −16.19 (3B), −17.85 (2B), −21.94 (1B), −22.62 (2B), −35.94 (1B) ppm; ^{31}P δ 41.3 ppm.

Crystallographic study

A single crystal (0.1 × 0.1 × 0.5 mm) of [BTMA]**1**·CH_2Cl_2 was mounted on a glass fibre and set on an Enraf–Nonius CAD4 diffractometer equipped with graphite-monochromated Mo-K_α *X*-radiation (λ_{bar} = 0.71069 Å). Unit cell and orientation matrix from the least-squares refinement of the setting angles of 25 centred reflections ($12 < \theta < 13°$).

Crystal data. $C_{30}H_{42}B_9PAu \cdot CH_2Cl_2$, M = 812.83, monoclinic, space group $P2_1/c$, a = 9.5509(17), b = 19.232(3), c = 19.813(3) Å, β = 90.741(13)°, V = 3639.0 $Å^3$, Z = 4, D_{calc} = 1.483 g cm^{-3}, μ(Mo-K_α) = 42.5 cm^{-1}, $F(000)$ = 1612.

Data collected for $1 \leqslant \theta \leqslant 25°$ (h 0 → 11, k 0 → 22, l −23 → 23) by ω–2θ scans (ω scan width = 0.8 + 0.34 tan θ). Over the 194 h of data collection the intensities of two check reflections decayed to *ca* 89% of the original values, and the data were corrected appropriately (CADABS[16]). Of 5307 reflections measured, 4667 [$F \geqslant 2.0\sigma(F)$] were retained.

The structure was solved by Patterson synthesis (Au) and full-matrix least-squares refinement/ΔF syntheses (P, C, B, N, Cl, H_{cage}) using SHELX76.[17] Cage-carbon atoms were identified by internuclear distances and refined (as B) isotropic thermal parameters. Empirical absorption correction (DIFABS[18]) was applied after isotropic convergence. Data were weighted according to $w^{-1} = [\sigma^2(F) + 0.000513F^2]$. All non-hydrogen atoms were refined with anisotropic thermal parameters and phenyl rings were modelled as rigid, planar hexagons (C—C, 1.395 Å). Cage-hydrogen atoms were refined positionally, while all other hydrogen atoms were set in calculated positions (C—H, 1.08 Å). All hydrogen atoms were given a common isotropic thermal parameter, 0.108(5) $Å^2$ at convergence. R = 0.0487, R_w = 0.0482, S = 1.214, for 401 variables. Maximum and minimum residues in the ultimate ΔF synthesis were 0.94 (near Au) and −1.09 $eÅ^{-3}$, respectively. Atomic scattering factors for P, Cl, C, B, N and H inlaid in SHELX76; those for Au were obtained from *International Tables for X-Ray Crystallography*.[19]

Tables of final atomic positional and thermal parameters, a full list of bond angles, and tables of F_o/F_c values have been deposited as supplementary material with the Editor.

Theoretical study

An extended Huckel molecular orbital (EHMO) calculation was performed on [7,8-*nido*-$C_2B_9H_{11}]^{2-}$ with charge iteration [$H_{ii} = H_{ii}^\circ$ + (sense) × (charge)]. The model was derived from the crystallographic coordinates of [7,8-*nido*-$C_2B_9H_{12}]^-$[11] from which the *endo*-H(12) was removed. The calculation was made using the ICON8 program[20] and the weighted H_{ij} formula.[21] H_{ii}'s and Slater exponents for C, B and H were those inlaid in ICON8.

RESULTS AND DISCUSSION

Addition of CH_2Cl_2 to a solid equimolar mixture of $Tl[TlC_2B_9H_{11}]$, PPh_3AuCl and [BTMA]Cl afforded colourless [BTMA]**1** in reasonable yield. The compound was characterized by microanalysis (CH_2Cl_2 solvate) and multinuclear NMR spectroscopy. In particular, the ^{11}B NMR spectrum suggests that the anion has C_s molecular symmetry, subsequently confirmed by an X-ray diffraction study on [BTMA]**1**·CH_2Cl_2. Figure 1 shows a perspective view of the anion and demonstrates the atomic numbering. Table 1 lists internuclear distances and key interbond angles determined.

The anion **1** consists of a *nido*-{7,8-C_2B_9} framework with an *endo*-{PPh_3Au} unit bonded to B(10), Au—B(10) 2.222(9) Å (see Fig. 2 for a view of part of the molecule which emphasizes the orientation of the {AuP} unit relative to the carbaborane cage). Although in solution the molecule clearly displays C_s symmetry, in the solid the {AuP} unit is significantly displaced towards B(11), since Au···B(11) is 2.486(9) Å, cf. Au···B(9) 2.528(9)

Table 1. Interatomic distances (Å) and selected interbond angles (°) in [BTMA][10-*endo*-(PPh_3Au)-7,8-*nido*-$C_2B_9H_{11}$]

Au—P	2.2485(20)	B(4)—H(4)	1.02(10)
Au—B(9)	2.528(9)	B(5)—B(6)	1.813(13)
Au—B(10)	2.222(9)	B(5)—B(9)	1.785(13)
Au—B(11)	2.486(9)	B(5)—B(10)	1.751(13)
P—C(11)	1.816(9)	B(5)—H(5)	1.05(9)
P—C(21)	1.799(7)	B(6)—B(10)	1.790(13)
P—C(31)	1.815(6)	B(6)—B(11)	1.773(13)
B(1)—B(2)	1.752(13)	B(6)—H(6)	1.07(10)
B(1)—B(3)	1.744(14)	C(7)—C(8)	1.548(10)
B(1)—B(4)	1.729(14)	C(7)—B(11)	1.640(12)
B(1)—B(5)	1.808(14)	C(7)—H(7)	0.81(10)
B(1)—B(6)	1.792(13)	C(8)—B(9)	1.611(12)
B(1)—H(1)	1.12(9)	C(8)—H(8)	0.96(10)
B(2)—B(3)	1.774(14)	B(9)—B(10)	1.798(13)
B(2)—B(6)	1.759(13)	B(9)—H(9)	1.11(10)
B(2)—C(7)	1.707(12)	B(10)—B(11)	1.841(13)
B(2)—B(11)	1.798(13)	B(10)—H(10)	1.14(9)
B(2)—H(2)	1.08(9)	B(11)—H(11)	1.14(10)
B(3)—B(4)	1.725(14)	C(41)—C(47)	1.522(10)
B(3)—C(7)	1.708(13)	C(47)—N	1.536(11)
B(3)—C(8)	1,706(13)	C(48)—N	1.502(11)
B(3)—H(3)	1.14(9)	C(49)—N	1.505(11)
B(4)—B(5)	1.747(14)	C(50)—N	1.495(12)
B(4)—C(8)	1.670(12)	Cl(1)—C(99)	1.669(17)
B(4)—B(9)	1.805(14)	Cl(2)—C(99)	1.595(18)

P—Au—B(9)	143.53(21)	B(1)—B(5)—B(4)	58.2(5)
P—Au—B(10)	169.29(24)	B(1)—B(5)—B(6)	59.3(5)
P—Au—B(11)	138.08(21)	B(4)—B(5)—B(9)	61.5(5)
Au—P—C(11)	112.79(18)	B(6)—B(5)—B(10)	60.3(5)
Au—P—C(21)	112.62(23)	B(9)—B(5)—B(10)	61.1(5)
Au—P—C(31)	115.41(19)	B(1)—B(6)—B(2)	59.1(5)
C(11)—P—C(21)	105.2(3)	B(1)—B(6)—B(5)	60.2(5)
C(11)—P—C(31)	103.81(25)	B(2)—B(6)—B(11)	61.2(5)
C(21)—P—C(31)	106.1(3)	B(5)—B(6)—B(10)	58.2(5)
P—C(11)—C(12)	117.7(4)	B(10)—B(6)—B(11)	62.2(5)
P—C(11)—C(16)	122.3(4)	B(2)—C(7)—B(3)	62.6(5)
P—C(21)—C(22)	122.8(5)	B(2)—C(7)—B(11)	65.0(5)
P—C(21)—C(26)	117.2(5)	B(3)—C(7)—C(8)	63.0(5)
P—C(31)—C(32)	122.1(4)	B(3)—C(8)—B(4)	61.4(6)
P—C(31)—C(36)	117.8(4)	B(3)—C(8)—C(7)	63.1(5)
B(2)—B(1)—B(3)	61.0(6)	B(4)—C(8)—B(9)	66.7(6)
B(2)—B(1)—B(6)	59.5(5)	B(4)—B(9)—B(5)	58.2(5)
B(3)—B(1)—B(4)	59.6(6)	B(4)—B(9)—C(8)	58.2(5)
B(4)—B(1)—B(5)	59.1(5)	B(5)—B(9)—B(10)	58.5(5)
B(5)—B(1)—B(6)	60.5(5)	Au—B(10)—B(9)	77.1(4)
B(1)—B(2)—B(3)	59.3(5)	Au—B(10)—B(11)	74.8(4)
B(1)—B(2)—B(6)	61.4(5)	Au—B(10)—H(10)	98.7(48)
B(3)—B(2)—C(7)	58.7(5)	B(5)—B(10)—B(6)	61.6(5)
B(6)—B(2)—B(11)	59.8(5)	B(5)—B(10)—B(9)	60.4(5)
C(7)—B(2)—B(11)	55.7(5)	B(6)—B(10)—B(11)	58.4(5)
B(1)—B(3)—B(2)	59.8(5)	B(2)—B(11)—B(6)	59.0(5)
B(1)—B(3)—B(4)	59.8(6)	B(2)—B(11)—C(7)	59.3(5)
B(2)—B(3)—C(7)	58.7(2)	B(6)—B(11)—B(10)	59.3(5)
B(4)—B(3)—C(8)	58.2(5)	C(41)—C(47)—N	112.9(6)
C(7)—B(3)—C(8)	53.9(5)	C(47)—N—C(48)	111.8(6)
B(1)—B(4)—B(3)	60.6(6)	C(47)—N—C(49)	110.0(6)
B(1)—B(4)—B(5)	62.7(6)	C(47)—N—C(50)	106.8(6)
B(3)—B(4)—C(8)	60.3(5)	C(48)—N—C(49)	107.9(6)
B(5)—B(4)—B(9)	60.3(5)	C(48)—N—C(50)	110.3(7)
B(8)—B(4)—B(9)	55.1(5)	C(49)—N—C(50)	110.0(7)
		Cl(1)—C(99)—Cl(2)	115.4(10)

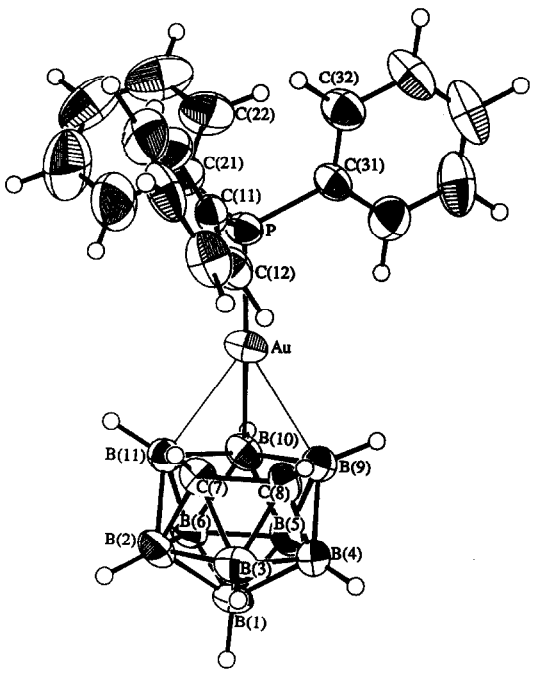

Fig. 1. Perspective view of [10-*endo*-(PPh_3Au)-7,8-*nido*-$C_2B_9H_{11}]^-$. Thermal ellipsoids drawn at the 50% probability level, but the hydrogen atoms are given an artificial radius of 0.1 Å for clarity. Phenyl rings numbered cyclically, C(*ij*) with $i = 1$–3, $j = 1$–6. Hydrogen atoms carry the same number as the boron or carbon to which they are attached.

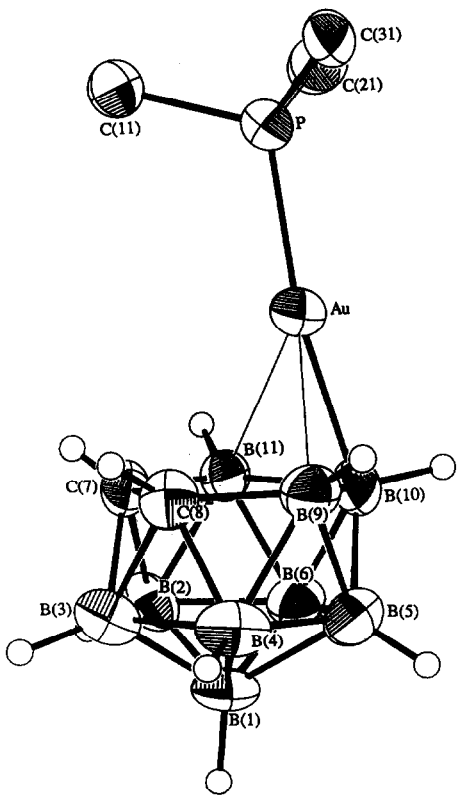

Fig. 2. Alternative view of the central portion of [10-*endo*-(PPh_3Au)-7,8-*nido*-$C_2B_9H_{11}]^-$.

Å, and P—Au···B(11) is 138.08(21)°, cf. P—Au···B(9) 143.53(21)°. The numbering scheme[22] for the carbaborane reflects its *nido* character. The upper C_2B_3 face is non-planar, being folded about the B(9)···B(11) vector with C(7), C(8) and B(10) below the best (least-squares) plane. Fold angles[23] are $\theta = 3.15°$ and $\phi = 3.28°$, and the gold atom, 2.062 Å above the least-squares plane, is slipped by 0.87 Å (= Δ) towards B(10). The lower pentagonal belt [B(2)B(3)B(4)B(5)B(6)] is effectively planar ($\sigma_{\text{lower belt}} = 0.006$ Å vs $\sigma_{\text{upper belt}} = 0.034$ Å).

Compound **1** was expressly synthesized and structurally analysed because of its potential relationship to [10-*endo*-H-7,8-*nido*-$C_2B_9H_{11}]^-$ (**2**)[11] and [3-PPh_3-3,1,2-$CuC_2B_9H_{11}]^-$ (**3**).[12] These three anions can notionally be partitioned into a common $[7,8\text{-}nido\text{-}C_2B_9H_{11}]^{2-}$ ligand and, respectively, $\{Ph_3PAu^+\}$, H^+ and $\{Ph_3PCu^+\}$ fragments, the last three being formally zero electron sources. Table 2 compares Δ, average B—B(facial), average B—C(facial) and C—C for anions **1**–**3** (note that the polyhedral numbering system[22] for *closo*-**3** differs from that for *nido*-**1** and *nido*-**2**). In all four parameters a constant trend is apparent, namely a small change in going from **2** to **1**, and a larger change (in the same direction in every case) in going from **1** to **3**.

To understand the origin of these structural patterns we have considered the form of the occupied π-frontier MO's of $[7,8\text{-}nido\text{-}C_2B_9H_{11}]^{2-}$, as given by a charge-iterated EHMO calculation. These orbitals are sketched in plan view in Fig. 3. The MO's of this species have been reported previously[9a] but the model used was idealized and the calculations were not charge-iterated. Our findings are in broad agreement with this earlier study, except that ψ_2 and ψ_3 are interchanged.

The unoccupied frontier MO's of $\{H_3PAu^+\}$ and $\{H_3PCu^+\}$ comprise[24] a valence (s–p_z) hybrid orbital and a degenerate pair of metal p_x, p_y atomic orbitals. For copper the latter are also valence orbitals, but for gold they are much higher-lying, their relative inaccessibility accounting for the tend-

Table 2. Comparison of key molecular parameters (Å) for compounds **1**–**3**

	2	**1**	**3**
Δ	0.91	0.87	0.27
⟨B—B_{facial}⟩	1.833(3)[a]	1.820(13)	1.768(10)
⟨B—C_{facial}⟩	1.610(3)	1.626(12)	1.666(10)
C—C	1.542(4)	1.548(10)	1.586(9)

[a] ESD of average is average ESD.

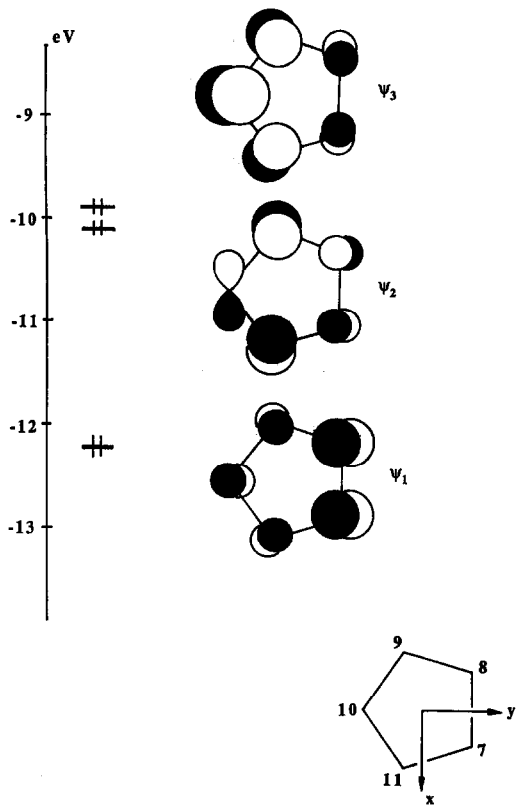

Fig. 3. The occupied π-frontier molecular orbitals of [7,8-*nido*-$C_2B_9H_{11}$]$^{2-}$.

ency of gold(I) to adopt linear coordination vs the tetrahedral coordination typical of copper(I).

The interaction of H^+ with [7,8-*nido*-$C_2B_9H_{11}$]$^{2-}$ to afford **2**, which has an *endo*-H atom bonded to B(10), has been discussed previously.[11] In essence, the key interaction is between H(1*s*) and ψ_3. In moving from H^+ to the formally isolobal {Ph_3PAu^+} some movement of the *endo*-fragment towards the centre of the C_2B_3 face is apparent (Δ from 0.91 to 0.87 Å), and is accompanied by a decrease in $\langle B—B_{facial}\rangle$, an increase in $\langle B—C_{facial}\rangle$ and an increase in C—C. When {Ph_3PAu^+} is replaced by {Ph_3PCu^+} all these structural changes are further magnified. Changing from **2** to **3** we go from a situation in which only ψ_3 is depopulated to one in which the equilibrium geometry results from an attempt to maximize the interaction of all three occupied carbaborane π-orbitals with the appropriate copper acceptor orbitals. The $\langle\psi_2/Cu(4p_x)\rangle$ interaction is maximized when the metal is essentially over the centre of the C_2B_3 face ($\Delta = 0$). Both the $\langle\psi_3/Cu(4p_y)\rangle$ and $\langle\psi_1/Cu(4s–4p_z)\rangle$ interactions would be optimized by a negative slip distortion, and thus the observation of a positive slip in **3** can only be the result of an attempt to maximize the overlap between ψ_3 (carbaborane HOMO) and Cu($4s–4p_z$) (metal LUMO).

Overall, the likely changes in depopulation of the ligand π-MO's as the series **2** → **1** → **3** is progressed are ψ_3 depopulated less, ψ_2 depopulated more and ψ_1 depopulated more. Consequent upon these are the following predicted changes in B—B, B—C and C—C facial distances:

(i) $\langle$B—B$\rangle$ will shorten, the reduced depopulation of ψ_3 outweighing the increased depopulation of ψ_1, since ψ_3 is heavily localized on B(9), B(10) and B(11), whereas ψ_1 lies predominantly on the facial carbon atoms.

(ii) $\langle$B—C$\rangle$ will lengthen, the changes in population of all three carbaborane π-MO's acting in concert.

(iii) C—C will lengthen, the increased depopulation of ψ_1 (localized on carbon) over-riding the effects of changes in the populations of ψ_2 and ψ_3 (both localized on boron).

The structural patterns detailed in Table 2 are fully consistent with these predictions, and indicate that whilst the bonding capabilities of {Ph_3PAu^+} and H^+ are broadly similar, in accord with the isolobal principle, there is firm evidence for some involvement of the high-lying Au($6p_x$,$6p_y$) atomic orbitals.

Finally we note the following:

(i) The mercuracarbaborane [10-*endo*-(Ph_3PHg)-7,8-*nido*-$C_2B_9H_{11}$][10] shows similar structural features to **2** and the isoelectronic **1** (Δ 0.92 Å, $\langle B—B_{facial}\rangle$ 1.86(2) Å, $\langle B—C_{facial}\rangle$ 1.61(2) Å, C—C 1.54(1) Å) consistent with its description as a σ-bonded [Hg—B(10)] species.

(ii) The above results may be contrasted with the effects on ring distances of {Ph_3PCu^+}[25] vs {Ph_3PAu^+}[26] complexation of $[C_5H_5]^-$ or its derivatives. Here, as one moves from {Ph_3PAu} *endo*-bonded to C(1) to {Ph_3PCu} bonded equally to all five carbon atoms, the C(1)—C(2), C(1)—C(5) bonds (≡B—B_{facial}) shorten, C(2)—C(3), C(4)—C(5) bonds (≡B—C_{facial}) lengthen, and the C(3)—C(4) bond (≡C—C) shortens. However, these structural differences are easily traced to the homocyclic nature of the $[C_5H_5]^-$ ligand vs the heterocyclic nature of the open face of [7,8-*nido*-$C_2B_9H_{11}$]$^{2-}$.

Acknowledgements—We thank the SERC for support (E.J.M.H.) and Johnson–Matthey for a generous loan of gold.

REFERENCES

1. M. F. Hawthorne, D. C. Young and P. A. Wegner, *J. Am. Chem. Soc.* 1965, **87**, 1818.

2. M. F. Hawthorne, D. C. Young, T. D. Andrews, D. V. Howe, R. L. Pilling, A. D. Pitts, M. Reintjes, L. F. Warren Jr and P. A. Wegner, *J. Am. Chem. Soc.* 1968, **90**, 879.
3. D. M. P. Mingos, *J. Chem. Soc., Dalton Trans.* 1977, 602.
4. C. W. Jung, R. T. Baker and M. F. Hawthorne, *J. Am. Chem. Soc.* 1981, **103**, 810.
5. Proceedings of Third International Symposium on Neutron Capture Therapy, *Strahlenther. Onkol.* 1989, **165**, 65.
6. M. F. Hawthorne, *J. Organomet. Chem.* 1975, **100**, 97.
7. A. J. Welch, *J. Chem. Soc., Dalton Trans.* 1975, 1473.
8. D. M. P. Mingos and M. I. Forsyth, *J. Organomet. Chem.* 1978, **146**, C37.
9. (a) D. M. P. Mingos, M. I. Forsyth and A. J. Welch, *J. Chem. Soc., Dalton Trans.* 1978, 1363; (b) M. J. Calhorda, D. M. P. Mingos and A. J. Welch, *J. Organomet. Chem.* 1982, **228**, 309.
10. H. M. Colquhoun, T. J. Greenhough and M. G. H. Wallbridge, *J. Chem. Soc., Dalton Trans.* 1979, 619.
11. J. Buchanan, E. J. M. Hamilton, D. Reed and A. J. Welch, *J. Chem. Soc., Dalton Trans.* 1990, 677.
12. Y. Do, H. C. Kang, C. B. Knobler and M. F. Hawthorne, *Inorg. Chem.* 1987, **26**, 2348.
13. R. Hoffmann, *Angew. Chem., Int. Ed. Engl.* 1982, **21**, 771.
14. M. P. Garcia, M. Green, F. G. A. Stone, R. G. Somerville, A. J. Welch, C. E. Briant, D. N. Cox and D. M. P. Mingos, *J. Chem. Soc., Dalton Trans.* 1985, 2343.
15. A. J. Carty and A. Efraty, *Inorg. Chem.* 1969, **8**, 543.
16. R. O. Gould and D. E. Smith, University of Edinburgh (1986).
17. G. M. Sheldrick, University of Cambridge (1976).
18. N. G. Walker and D. Stuart, *Acta Cryst.* 1983, **A39**, 158.
19. *International Tables for X-Ray Crystallography*, Vol. 4. Kynoch Press, Birmingham (1974).
20. J. Howell, A. Rossi, D. Wallace, K. Haraki and R. Hoffmann, *Quantum Chemistry Program Exchange*, No. 344. University of Indiana (1977).
21. J. H. Ammeter, H.-B. Burgi, J. C. Thibeault and R. Hoffmann, *J. Am. Chem. Soc.* 1982, **110**, 3686.
22. J. B. Casey, W. J. Evans and W. H. Powell, *Inorg. Chem.* 1983, **22**, 2228.
23. D. E. Smith and A. J. Welch, *Acta Cryst.* 1986, **C42**, 1717.
24. D. G. Evans and D. M. P. Mingos, *J. Organomet. Chem.* 1982, **232**, 171.
25. F. A. Cotton and J. Takats, *J. Am. Chem. Soc.* 1970, **92**, 2353.
26. T. V. Baukova, Yu. L. Slovokhotov and Yu. T. Struchkov, *J. Organomet. Chem.* 1981, **220**, 125.

Polyhedron Vol. 9, No. 19, pp. 2413–2418, 1990
Printed in Great Britain

0277–5387/90 $3.00+.00
© 1990 Pergamon Press plc

THE SYNTHESIS OF TRIDENTATE DIALKYLAMINO LIGANDS CONTAINING TERTIARY PHOSPHORUS OR ARSENIC DONORS

A. A. DANOPOULOS, A. R. WILLS and P. G. EDWARDS*

School of Chemistry and Applied Chemistry, University of Wales College of Cardiff, P.O. Box 912, Cardiff CF1 3TB, U.K.

(*Received* 3 *April* 1990; *accepted* 8 *June* 1990)

Abstract—Use of the trimethylsilyl protecting function on nitrogen enables the high yield preparation of the potentially tridentate ligands of the type $HN(CH_2CH_2ER_2)_2$ (E = P; R = Me, Et, ^{i}Pr and E = As; R = Me, Et) by nucleophillic substitution of halide in $Me_3SiN(CH_2CH_2Cl)_2$. The di-isopropylphosphino and diethylarsino derivatives have not previously been reported, the other derivatives described are now available in considerably improved yields via this new route. The failure of syntheses or poor yields obtained from unprotected amine precursors is explained by aziridine formation. Deprotonation of the amines provides series of chelating dialkylamido ligands enabling access to new classes of novel complexes.

During the course of a study of the coordination behaviour of the mixed tridentate ligands of the type $L(CH_2)_nX(CH_2)_nL$ (where L = σ-donor/π-acid and X = anionic σ/π base) with early transition metals and actinides, we found access to the compounds $(R_2ECH_2CH_2)_2NH$ (**A**) (R = alkyl, E = P, As) in good yield was not straightforward. These amines are of interest since they are readily deprotonated to give dialkylamides that are likely to form complexes with a range of metals stabilized by five-membered chelate rings, as well as being potentially capable of bridging. Previous studies with the similar diphosphinoamides $[(R_2PCH_2Si(Me)_2)_2N^-$ (R = alkyl or aryl)][1] and studies with $(R_2PCH_2CH_2)_2N^-$ (R = Me, Et)[2] and $(Et_2NCH_2CH_2)_2N^-$[3] demonstrate that new classes of interesting complexes may be obtained. Although the phenyl analogues of **A** are not new,[4] the extension of synthetic methods employed in the past to the preparation of the ligands **A** gives unsatisfactory results. In this paper we describe a general, high yield route to the desired amines, **A**, where R = Me, Et, ^{i}Pr (E = P) and Me, Et (E = As) using the trimethylsilyl protecting function on nitrogen.

* Author to whom correspondence should be addressed.

EXPERIMENTAL

(1) *Materials and methods*

All manipulations with phosphines, phosphides, arsines and arsenides were performed under nitrogen using standard techniques.[5] NMR spectra were obtained with a Bruker WM 360 spectrometer operating at 360 MHz (^{1}H) or 145 MHz $\{^{31}P[^1H]\}$ and referenced internally to the residual proton impurity in the solvent (C_6D_6, δ 7.27 ppm, ^{1}H) or externally to H_3PO_4 {85%, δ 0 ppm, $^{31}P[^1H]$}. IR spectra were obtained as neat films on a Perkin–Elmer 783 spectrometer and mass spectra were by the SERC Mass Spectroscopy Centre at Swansea on a VG Micromass 7070 by chemical ionization (NH_3), unless otherwise stated.

Solvents were dried by standard methods and distilled under nitrogen prior to use. Et_3N was distilled from sodium under nitrogen. Reagents prepared by literature routes were: Me_2PH,[6] Et_2PH,[7] $^iPr_2PH$,[8] R_2PLi[9] (R = Me, Et, ^{i}Pr), Me_2AsI[10] and Et_2AsI.[11] Other reagents were used as purchased.

(2) *Preparation of bis(2-chloroethyl)trimethylsilylamine* (**I**)

$(ClCH_2CH_2)_2NH \cdot HCl$ (10 g, 0.056 M) was suspended in a mixture of Et_3N (100 cm^3), Me_3SiCl

(40 cm^3) and $(CH_3)_2SO$ (0.25 cm^3) and the mixture was refluxed (16 h) under nitrogen with magnetic stirring. After cooling to room temperature, the off-white suspension was filtered and the excess volatile materials removed *in vacuo*. The yellow–orange oil remaining was $(ClCH_2CH_2)_2NSiMe_3$ (> 98% by NMR). Distillation of this oil was accompanied by decomposition, however, it may be applied directly to the preparations below with good results. Yield, 10.35 g (85% based on amine hydrochloride). Mass spectrum (values are for ions containing ^{35}Cl): 213 (M^+, 0.2%), 178 (M^+-Cl, 0.2%), 106 ($M^++1-SiMe_3-Cl$, 1.0%), 101 ($Me_3SiNCH_2^+$, 1.7%), 86 (Me_3SiN^+, 3.8%), 73 (Me_3Si^+, 93.8%), 56 ($CH_2NCH_2CH_2^+$, 100%).

(3) *Preparation of the bis(2-dialkylphosphinoethyl) amines (alkyl = methyl,* **II**; *ethyl,* **III**; *2-propyl,* **IV**)

The detailed procedure described here is for the ethyl derivative (**III**). To a solution of **I** (10.5 g, 0.049 M) in THF (50 cm^3) was added, at −40°C with stirring, a solution of Et_2PLi (12.5 g, 0.13 M) in THF (50 cm^3) over *ca* 0.5 h. After completion of the addition, the mixture was allowed to warm to room temperature and refluxed for 8 h. The cooled solution was then hydrolysed with water (200 cm^3), completion of hydrolysis of the protecting function being assured by further reflux (1 h) of the two-phase mixture. After cooling and separation of the phases, the aqueous phase was washed (Et_2O, 3 × 50 cm^3) and the combined organic phases dried ($MgSO_4$). This solution was filtered, the volatile solvents were distilled at atmospheric pressure, fractionation of the residue provided **III** as a colourless, viscous oil (b.p. 100–104°C/0.04 mm). Yield based on **I**, 80–92%. IR: 3250 (m, N—H), 1430 (s, CH_2), 1370 (s, CH_3), 1080 (s, CN). Mass spectrum (EI, 70 eV): 221 (M^++1-Et, 43%), 160 (M^+-PEt_2, 22.8%), 146 ($M^+-CH_2PEt_2$, 18.4%), 117 ($CH_2CH_2PEt_2$, 58.2%), 89 (PEt_2^+, 88.2%), 61 ($EtPH^+$, 100%).

Compounds **II** and **IV** are prepared in an analogous manner. Thus from **I** (27.96 g, 0.13 M) and Me_2PLi (18.36 g, 0.27 M) was obtained **II** by low pressure fractionation as a colourless oil (b.p. 78–80°C/0.05 mm). Yield based on **I**, 90–95%. IR: 3260 (m, NH), 1430 (s, CH_2), 1290 (m, CH_3), 1115 (s, CN). Mass spectrum: 194 (M^++1, 4.1%), 192 (M^+-1, 14.0%), 178 (M^+-Me, 89%), 164 ($M^+-1-2Me$, 5.6%), 150 (M^+-43, 8.5%), 132 (M^+-PMe_2, 58.7%), 118 ($M^+-CH_2PMe_2$, 79.9%), 89 ($CH_2CH_2PMe_2$, 95.4%), 61 (PMe_2^+, 100%). Alternatively **IV** may be prepared from **I** (6.5 g, 0.03 M) and $^iPr_2PLi$ (8.5 g, 0.07 M) and isolated as a colourless, viscous oil by vacuum distillation (b.p. 116°C/5 × 10^{-3} mm). Yield based on **I**, 55–60%. IR: 3270 (m), 1460 (s), 1367 (s), 1120 (m). Mass spectrum (CI, NH_3): 306 (M^++1, 0.1%), 263 ($M^+-{}^iPr$), 234 ($^iPr_2PP^iPr_2$, 0.6%), 220 ($M^+-2{}^iPr$, 1.8%), 188 ($M^+-P^iPr_2$), 174 ($M^+-CH_2P^iPr_2$, 29.7%), 160 ($M^+-CH_2CH_2P^iPr_2$, 1.0%), 145 ($M^+-HNCH_2CH_2P^iPr_2$, 90.2%), 117 ($P^iPr_2^+$, 100%).

(4) *Preparation of 2-bis(2-propylphosphino) ethylaziridine* (**V**)

To a cold (−40°C) solution of $^iPr_2PLi$ (5.00 g, 0.04 M) in THF (85 cm^3) was added bis(2-chloroethyl)aminehydrochloride (2.14 g, 0.012 M) in portions over 1 h. The yellow colour of the phosphide dissipated. The mixture was stirred (10 h), followed by hydrolysis with water (40 cm^3). After separation of phases, the aqueous layer was washed (Et_2O, 2 × 50 cm^3) and the combined organic fractions dried ($MgSO_4$). The solution was filtered and the solvents removed by ambient pressure distillation. Low pressure fractionation provided the product **V** (b.p. 50–52°C/0.05 mm). Yield based on aminehydrochloride, 1.68 g, 75%. IR: 3340 (m,br), 3050 (s), 2920 (s,br), 2830 (m), 2800 (m), 2740 (w), 2700 (w), 2660 (w), 1673 (w,br), 1460 (s), 1413 (w), 1385 (s), 1365 (s), 1302 (s), 1270 (m), 1237 (s), 1210 (m), 1185 (m), 1175 (w), 1155 (m), 1142 (m), 1103 (m), 1080 (m), 1055 (m), 1040 (m), 1020 (m), 944 (m), 960 (w), 925 (w), 907 (w), 879 (m), 860 (m), 824 (m), 779 (m), 750 (m), 725 (m), 679 (w), 654 (m), 618 (m), 537 (w), 489 (w), 478 (w), 434 (w), 420 (w). Mass spectrum: 187 (M^+, 1.1%), 186 (M^+-1, 1.2%), 145 ($M^+-NCH_2CH_2$, 10.4%), 144 ($M^+-{}^iPr$, 37.7%), 132 ($M^++1-CH_2NCH_2CH_2$, 8.9%), 118 ($^iPr_2P^++1$, 2.9%), 117 ($^iPr_2P^+$, 13.1%), 102 ($^iPr_2P^+-Me$, 94.1%), 73 ($PCH_2CH_2N^+$, 100%).

(5) *Preparation of the bis(2-dialkylarsinoethyl) amines (alkyl = methyl,* **VI**; *ethyl,* **VII**)

The following procedure is for the ethyl derivative **VII**. To a cooled (−40°C) solution of Et_2AsLi (5.38 g, 0.038 M) in THF (150 cm^3) was added dropwise with stirring a solution of **I** (3.42 g, 0.016 M). The resulting green solution was allowed to warm to room temperature and refluxed (0.5 h). The solution was then cooled (10°C) and hydrolysed with water (20 cm^3) causing the green colour to disappear. The mixture was again refluxed to ensure complete hydrolysis (0.5 h). The cooled mixture was then separated, the aqueous phase washed (Et_2O, 2 × 50 cm^3) and the combined organic phase dried ($MgSO_4$). After filtration and distillation of

the solvents at atmospheric pressure, the product was collected by fractionation at reduced pressure as a colourless liquid (b.p. 121°C/0.05 mm). Yield based on **I**, 4.4 g, 82%. IR: 3270 (w), 2930 (s,br), 2870 (s), 2818 (s), 2740 (m), 2685 (w), 2650 (w), 1455 (s), 1418 (m), 1375 (m), 1365 (w), 1332 (m), 1280 (m), 1265 (w), 1252 (w), 1220 (s), 1140 (m), 1115 (s), 1035 (m), 992 (w), 978 (w), 928 (w), 882 (w), 870 (w), 846 (m), 785 (m), 745 (s,br), 708 (m), 572 (s), 552 (w), 472 (w), 450 (w), 386 (w). Mass spectrum: 309 ($M^+ + 1 - Et$, 4.0%), 308 ($M^+ - Et$, 37.6%), 280 ($M^+ + 1 - 2Et$, 7.0%), 251 ($M^+ + 1 - 3Et$, 4.1%), 222 ($M^+ + 1 - 4Et$, 3.7%), 204 ($M^+ - AsEt_2$, 0.1%), 190 ($M^+ - CH_2AsEt_2$, 1.5%), 176 ($M^+ - CH_2CH_2AsEt_2$ or $M^+ + 1 - AsEt_2 - Et$, 4.8%), 174 ($M^+ - 1 - AsEt_2 - Et$, 6.8%), 133 ($AsEt_2^+$, 65.0%), 105 ($HAsEt^+$, 100%).

The methyl derivative **VI** may be prepared in a similar manner from Me_2AsNa. Thus from Me_2AsNa (19.74 g, 0.154 M) in THF (500 cm^3) and **I** (15.0 g, 0.070 M) was isolated **VI** by fractionation (17.0 g, 86% based on **I**, b.p. 124°C/3 mm). IR: 3250 (w,br), 2960 (m), 2920 (m), 2890 (m), 2790 (m), 2720 (w), 1810 (w,br), 1445 (m), 1410 (m), 1385 (vw), 1276 (w), 1253 (m), 1210 (vw), 1131 (m), 1105 (m), 1040 (w,br), 995 (w), 955 (w), 930 (w), 885 (m), 840 (m,br), 780 (w), 768 (w), 716 (w), 580 (s), 450 (vw), 360 (vw). Mass spectrum: 281 (M^+, 12.1%), 252 ($M^+ - 2Me$, 1.0%), 210 ($Me_2AsAsMe_2$, 0.6%), 176 ($M^+ - AsMe_2$, 25.6%), 162 ($M^+ - CH_2AsMe_2$, 50.5%), 148 ($M^+ - CH_2CH_2AsMe_2$, 7.5%), 122 ($NH_3 \cdot AsMe_2$, 20.5%), 119 ($CH_2AsMe_2^+$, 16.3%), 105 ($AsMe_2^+$, 5.4%), 71 ($M^+ - 2AsMe_2$, 100%).

For both **VI** and **VII**, the arsenide anion may be prepared directly from the dialkyliodoarsine in the reaction flask prior to addition of **I**.

RESULTS

The aminodiphosphines and -arsines (**II**, **III**, **IV**, **VI** and **VII**) have been synthesized according to the reaction sequence outlined in Scheme 1.

In addition, the aziridine (**VII**) has been prepared according to eq. (1). ^1H and $^{31}P[^1H]$ NMR data are presented in Table 1.

$$HCl \cdot N(CH_2CH_2Cl)_2 + 3LiP^iPr_2 \longrightarrow CH_2CH_2NCH_2CH_2P^iPr_2 + 3LiCl + 2HP^iPr_2. \quad (1)$$

DISCUSSION

(1) *Synthetic methods*

The reaction of $HCl \cdot HN(CH_2CH_2Cl)_2$ or the free amine, $HN(CH_2CH_2Cl)_2$, with dialkyl phosphido or arsenido nucleophiles ($^-ER_2$) in a ratio of 1 : 3 or 1 : 2, respectively, in THF or $NH_3(l)$, gives the desired aminodiphosphines or -arsines (**II**, **III**, **V**, **VI**) in low and variable yields. This procedure completely fails in attempted preparations of **IV**. Indeed, the reaction of the free amine [$HN(CH_2CH_2Cl)_2$] with $^-PPr_2$ leads to the dialkylphosphinoaziridine ($CH_2CH_2NCH_2CH_2PPr^i_2$, **VIII**) in reasonable yields (60%). Similar aziridines are obtained in the preparations of **II** and **III** also, although the proportion of aziridine to diphosphine is greatest for the di-isopropyl and decreases in the order $P^iPr_2 > PEt_2 > PMe_2 > AsEt_2 \approx AsMe_2$. This order parallels that of decreasing basicity and increasing nucleophilicity of the phosphido or arsenido anions. The mechanism we propose for aziridine formation is given in Scheme 2.

The proposed mechanism consists of a strong base-initiated intramolecular nucleophilic cyclization leading to the 2-chloroethylaziridine. Such base-initiated cyclizations of 2-haloalkylamines are well known and are the basis of the Gabriel synthesis of aziridines.[12] Further substitution of chloride results in the phosphinoaziridine. From this it is apparent that increasing the basicity and decreasing the nucleophilicity of the phosphide will decrease the yield of the diphosphinoamine in preference for the aziridine. The use of a protecting function on nitrogen should then suppress the first step and allow intermolecular substitution to predominate. Obviously such a protection must be stable to strong non-aqueous bases and nucleophiles and be readily removed after the substitution. We have

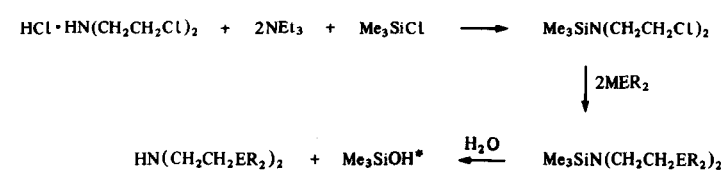

Scheme 1. (M = Li, Na; E = P, As.) *Note that other siloxanes may also be formed.

Table 1. NMR data for compounds I–VII[a]

Compound	δ $^{31}P[^1H]$	δ ^1H	Assignment
I		0.04 (s, 9H)	$Si(CH_3)_3$
		2.82 (t, 4H)	NCH_2CH_2Cl
		3.12 (t, 4H)	NCH_2CH_2Cl
II	−57.6	0.95 (d, 12H)	OCH_3
		1.49 (t, 4H)	PCH_2CH_2
		2.75 (q, 4H)	NCH_2CH_2
III	−28.2	1.09 (d of t, 12H)	PCH_2CH_3
		1.38 (q, 8H)	PCH_2CH_3
		1.58 (m, 4H)	PCH_2CH_2
		2.81 (m, 4H)	NCH_2CH_2
IV	−3.8	1.10 (m, 24H)	$PCHCH_3$
		1.61 (d of q, 4H)	PCH_2CH_2
		1.68 (d of sept., 4H)	$PCHCH_3$
		2.91 (q, 4H)	NCH_2CH_2
V	−2.0	0.90 (d, 2H)	NCH_2CH_2
		1.06 (m, 12H)	$PCHCH_3$
		1.70 (m, 6H)	PCH, PCH_2, NCH_2CH_2
		2.36 (m, 2H)	NCH_2CH_2
VI		0.92 (s, 12H)	$AsCH_3$
		1.33 (s, 1H)	NH
		1.58 (m, 4H)	$AsCH_2CH_2$
		2.73 (m, 4H)	NCH_2CH_2
VII		1.20 (t, 12H)	$AsCH_2CH_3$
		1.44 (q, 8H)	$AsCH_2CH_3$
		1.62 (t, 4H)	$AsCH_2CH_2$
		2.83 (t, 4H)	NCH_2CH_2

[a] Conditions are as described in the Experimental. All chemical shifts are in ppm.

previously reported[2] on the failure of benzyl since although the diphosphinobenzylamine is readily prepared in high yield, the benzyl function is not readily cleaved in this instance. Ideal for this purpose is the trimethylsilyl group since nitrogen–silicon bonds are readily cleaved by protic reagents (e.g. H_2O or MeOH). The use of trimethylsilyl in this context has been studied.[13] Our preferred method for the synthesis of **I** (Scheme 1) consists of the reaction of the aminehydrochloride with excess triethylamine in the presence of trimethylchlorosilane and a few drops of DMSO. DMSO increases the rate of silylation. This method has advantages over the prior liberation of free amine with either aqueous or non-aqueous bases followed by silylation, as low yields of mixures of unidentified silylamines are obtained from this procedure. Also, other silylating agents such as hexamethyldisilazane give unsatisfactory results. The substitution of chloride in **I** with phosphido or arsenido nucleophiles is suprisingly clean and has high yield; in the case of $^-PMe_2$ and $^-PEt_2$, almost quantitative yields of **II** and **III** are obtained if only a slight excess of phosphide is used. If the reaction is performed at −40 to −30°C, lithium–halogen exchange is minimized and hydrolysis of excess nucleophile and cleavage of the protecting function are conveniently simultaneous.

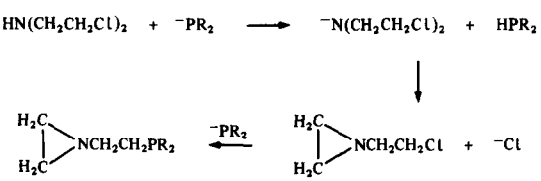

Scheme 2.

This route is also advantageous for the preparation of the diarsinoamines (**V**,**VI**), since contrary to a previous report,[14] the direct substitution of

chloride in $HCl \cdot N(CH_2CH_2Cl)_2$ or the free amine is not as successful as stated. We have not yet been able to reproduce the quoted yields, indeed total failure of this procedure is common, resulting in the isolation of considerable quantities of white solid after distillation of the more volatile liquid materials. From this white residue, we have isolated the ammonium salt, $HI \cdot HN(CH_2CH_2AsMe_2)_2$, by recrystallization from water. That the ammonium salt is isolated indicates that $^-AsMe_2$ is a better nucleophile than base for bis(2-chloroethyl) ammoniumhalide since substitution of the chlorides does not deprotonate the ammonium nitrogen. The source of iodide is no doubt NaI resulting from the preparation of $NaAsMe_2$ from $IAsMe_2$, presumably metathesis occurs with the hydrochloride due to the insolubility of NaCl under the conditions; we can not say whether this metathesis occurs before or after the substitution. The free ligand may then be reclaimed by treatment with base. We have also shown that on occasions, some mono-substituted amine, $Me_2AsCH_2CH_2N(H)CH_2CH_2Cl$, co-distills with the desired product (NMR) and slowly quaternizes (over several days) producing white crystalline solids.[15] This event seriously depletes the yield of the preparation, but can be minimized by more rigorous drying of the precursors [Me_2AsI and $HN(CH_2CH_2Cl)_2$] and by using a greater excess of arsenide.

(2) *Spectroscopic characterization*

The ^1H NMR spectra of the phosphorus-containing compounds consist of interpretable multiplets in the P–alkyl region (doublet for **II**, doublet of triplets and doublet of quartets for **III**). For **IV** there are two complicated resonances. The 2-propyl methyl protons give rise to an eight-line multiplet that appears as two overlapping doublets of doublets. We presume that this multiplicity of lines arises from the presence of rotamers due to restricted rotation of the adjacent 2-propyl P—C bonds. The unique proton gives rise to a straightforward doublet of septets. The methylene protons of the "backbone" also give rise to two multiplets in each case with the protons on carbons α to nitrogen being relatively deshielded with respect to those on carbons α to phosphorus. The resonance due to the protons on the carbon α to nitrogen appear as a binomial quartet as a result of two overlapping triplets, since homonuclear decoupling of this resonance from the protons on the carbons α to phosphorus gives rise to a doublet for **II**, **III** and **IV**. The magnitude of $^3J_{P-H}$ (*ca* 14 Hz for **II** and **IV**, 7.8 Hz for **II**) is greater than $^2J_{P-H}$ (*ca* 1.5–2 Hz for **II** and **IV**, 2.6 Hz for **II**) presumably due to alternation in the sign of the coupling constants between bonds, as has been reported previously[16] for ethyl phosphines. Resonances assignable to N—H protons were not observed, with the single exception of **VI** (δ 1.33 ppm, width at half height: 17 Hz).

The $^{31}P[^1H]$ NMR are single lines with the order of increasing deshielding $PMe_2 < PEt_2 < PPr^i_2$, a tendency already known for non-chelating analogues.[17] ^{31}P NMR spectra showed broadened lines for which P—H coupling could not be resolved under the conditions employed.

The compounds **II**–**VI** give rise to broad N—H stretches in the IR, in the region 3250–3280 cm^{-1}.

Mass spectroscopic data clearly support the characterizations of compounds **I**–**VII**. All the compounds presented here show a molecular ion with the exception of compounds **III** and **VI** where $M^+ - H - Et$ is observed. There are a number of common features in the fragmentation of **II**, **III**, **IV**, **VI** and **VII**. In each case, loss of one and/or two alkyl groups from the molecular ion is seen. Other fragments arising from E—C (E = P, As) and N—C and C—C cleavage are observed including R_2E, $R_2PCH_2CH_2$, $R_2ECH_2CH_2N$ and $R_2ECH_2CH_2NCH_2$. For the phosphines, the R_2P peaks are intense (100% for R = Me, ^{i}Pr; 88.2% for R = Et).

Acknowledgements—We would like to thank the University of Wales for a Studentship (A.R.W.) and the SERC for support (A.A.D.) and access to the Mass Spectrometry Centre at Swansea.

REFERENCES

1. M. D. Fryzuk and K. Bhangu, *J. Am. Chem. Soc.* 1988, **110**, 961; M. D. Fryzuk, A. Carter and A. Westerhaus, *Inorg. Chem.* 1985, **24**, 642.
2. A. A. Danopoulos and P. G. Edwards, *Polyhedron* 1989, **8**, 1339.
3. A. R. Wills and P. G. Edwards, *J. Chem. Soc., Dalton Trans.* 1989, 1253.
4. L. Sacconi and R. Morassi, *J. Chem. Soc. A* 1968, 2997; G. M. Whitesides, R. G. Nuzzo and M. E. Wilson, *J. Am. Chem. Soc.* 1978, **100**, 2269.
5. D. F. Shriver, *The Manipulation of Air Sensitive Compounds*. R. E. Krieger, Florida (1982).
6. A. Trenkle and H. Vahrenkamp, *Inorg. Synth.* 1982, **21**, 180.
7. K. Issleib and A. Tzchach, *Chem. Ber.* 1959, **92**, 704.
8. W. Voskuil and J. F. Arens, *Recl. Trav. Chim. Pays-Bas* 1963, **82**, 302.
9. K. Issleib and F. Krech, *J. Organomet. Chem.* 1968, **13**, 283.
10. I. T. Millar, H. Heaney, D. M. Heinekey and W. C. Fernelius, *Inorg. Synth.* 1960, **6**, 116.

11. N. I. Wigren, *Annalen* 1924, **437**, 285.
12. J. A. Deyrup, in *Chemistry of Heterocyclic Compounds* (Edited by A. Hassner), Wiley Interscience, New York (1983).
13. See for example T. Greene, *Protective Groups in Organic Synthesis*. Wiley Interscience, New York (1981).
14. R. Jaouhari, *Recl. Trav. Chim. Pays-Bas* 1988, **107**, 511.
15. P. G. Edwards and A. R. Wills, *Recl. Trav. Chim. Pays-Bas* 1989, **98**, 319.
16. S. L. Manatt, G. L. Juvinall and D. D. Ellerman, *J. Am. Chem. Soc.* 1963, **85**, 2664; G. Klose, *Annln Phys.* 1962, **9**, 262.
17. G. M. Kossolapoff and L. Maier, *Organo Phosphorus Chemistry*. Vol. 1. Wiley Interscience, New York (1972).

Polyhedron Vol. 9, No. 19, pp. 2419–2427, 1990
Printed in Great Britain

0277–5387/90 $3.00+.00
© 1990 Pergamon Press plc

SIMULATION OF PLASTICITY OF A COPPER(II) COORDINATION POLYHEDRON WITH A FORCE FIELD BASED ON COULOMBIC INTERACTIONS: CONFORMATIONAL ANALYSIS OF COPPER(II) CHELATES WITH α-AMINO ACIDS

J. SABOLOVIČ and N. RAOS*

Institute for Medical Research and Occupational Health, University of Zagreb, M. Pijade 158, 41001 Zagreb, Croatia, Yugoslavia

(*Received* 3 *April* 1990; *accepted* 8 *June* 1990)

Abstract—In order to simulate the plasticity of the copper(II) coordination sphere with the empirical force-field method (molecular mechanics), a square planar complex was defined as an octahedron consisting of four charges situated in the coordination plane, and two charges above and below the plane. Between these point charges only repulsive coulombic interactions take place besides harmonic bond-stretching interactions with the central atom. The model was parametrized on tetrahedrally distorted bis(L-N,N-dimethylvalinato) copper(II) (**1**). The obtained force field reproduced angles around copper in both planar and non-planar copper(II)-aminoacidates with r.m.s.-deviation from 0.15 to 3.4°. The enantioselectivity effect [energy difference between Cu(L-ligand)(L-ligand) and Cu(L-ligand)(D-ligand)] for compound **1** was reproduced within experimental error. The shape of the potential energy surface was analysed using the CuN_2O_2 "complex"; it yielded *cis* and *trans* conformations, but also many "false" minima. The model appears to be reliable for not too great deviations from planarity (15–30° for *trans* valence angles around copper).

There are two basic approaches in molecular-mechanics (or consistent force field) calculations[1,2] to simulate central atom coordination geometry. The first approach (based on "covalent" models) proposes an empirical potential dependent on bond lengths and valence angles around the metal atom, making consequently no basic difference between the "organic" and the "inorganic" parts of a molecule. The second approach assumes that between the central and ligated atoms only non-bonded, usually coulombic interactions take place ("ionic" models). The first approach has been thoroughly employed for conformational analysis of chelates with rigid coordination geometry, e.g. complexes of cobalt[3] and nickel.[4] A purely electrostatic model which treats atoms in the (first) coordination sphere as ionic species (only non-bonded, Lennard–Jones and Coulomb potentials were taken into account) has been applied to complexes of calcium with calcium-binding proteins,[5] e.g. calmodulin. Because calcium lacks any fixed shape of coordination polyhedron, this simple model proved successful.

The problem of simulating the plasticity of the copper(II) coordination sphere (the property of copper complexes that they usually do not form "regular", planar or tetrahedral coordination polyhedra[6,7]) with the molecular-mechanics method calls for modification of these simple models. In our previous papers dealing with tetracoordinated copper(II) bis-aminoacidates and their N-alkylated derivatives[8–15] we proposed two kinds of model. One treated the tetracoordinated (planar) copper(II) atom as being hexacoordinated, with two additional "dummy" atoms placed in the apical position.[10,15] The other was based on the new empirical potential dependent on the distortion coordinate β, defined as an angle between the bisectors of two O—Cu—N angles in opposite chelate rings.[11,12] In general, models with the distortion

* Author to whom correspondence should be addressed.

potential, V_β, proved to be better in reproducing the crystal geometry.

This paper deals with a new type of model, which is based on coulombic repulsion between ligated atoms. The model was inspired by the work of Kepert,[16] who tried to explain the variety of shapes of coordination polyhedra for many metallic and non-metallic elements proposing the repulsive potential between metal–ligand bonds. We adopted his general idea that the planarity of the copper(II) coordination sphere was due to the electron density situated above and below the plane of chelate rings.[16,17] Therefore, we proposed a model without any explicit angle-bending potential for the angles around copper, but with a bond-stretching potential for bonds with ligated and "dummy" atoms (i.e. apically placed charges). The model should, according to our classification, be regarded as "ionic", in contrast to our earlier models which can be described simply as "covalent".

METHODS

The conformational (strain) potential energy was calculated from the basic formula:

$$V = 1/2\sum_i k_{b,i}(b_i - b_{0,i})^2 + 1/2\sum_j k_{\theta,j}(\theta_j - \theta_{0,j})^2 + 1/2\sum_k V_n(1 \pm \cos n\varphi_k) + \sum_l (A_l \exp(-B_l r_l) - C_l r_l^{-6}) + \sum_{m \neq m'} \frac{q_m q_{m'}}{4\pi\varepsilon_0 r_{m'm}} + 1/2\sum_n k_{\chi,n}\chi_n^2, \quad (1)$$

in which b, θ, φ and χ stand for bond lengths, valence, torsional and out-of-plane angles, respectively; r is the non-bonded distance, k_b is an empirical parameter for bond stretching and k_θ for valence angle bending. Torsional interactions were determined with parameters V_n and n (height and multiplicity of the torsional barrier, respectively) and non-bonded interactions were computed from a Buckingham function with parameters A, B and C. The Coulomb potential, dependent on charge parameters ("elementary charges") q, was computed by taking into account only the atoms which define the shape of the coordination polyhedron (see Description of the model). In addition, the out-of-plane deformation potential for the carboxyl groups with a quadratic function dependent on parameter k_χ was also computed.

The parameters were the same as used in our previous research[12,15] with the exception of those developed in this paper (see Results and Discussion). Calculations were performed with Rasmussen's program for conformational analysis,[2] which was further modified to cope with the new model.

Description of the model

The coordination polyhedron is defined with five "real" atoms (M, N, N′, O and O′) situated in the plane of chelate rings, and two "dummy" ligand atoms (denoted as X and X′) placed above and below the plane. Between these atoms only bonding (with the central atom M) and coulombic interactions (between all non-bonded atoms, except between X and X′) were calculated.

The bond-stretching parameters (k_b and b_0) for M—O and M—N bonds [eq. (1)] were the same as used previously.[15] The parameter k_b for the M—X bond was defined so that at the distance b_{MX} from the central atom there was an equilibrium of attractive bonding (between M and X) and the repulsive coulombic forces (between X and ligated atoms). From that condition a simple equation for the calculation of the bond-stretching parameter can be derived ($b_{0,MX} = 0$):

$$k_{M-X} = q_Y q_X k'_b / 4\pi\varepsilon_0, \quad (2)$$

where q_Y is the charge parameter for atom O or N (it is taken to be equal), and q_X is the charge parameter for the "dummy" atom X or X′. K'_b is a sterical parameter dependent on appropriate bond lengths (b_{MX}, b_{MN}, b_{MO}), valence angles (θ_{XMN}, θ_{XMO}), and non-bonded distances between atoms in coordination polyhedron (r_{NX}, r_{OX}):

$$k'_b = \sum_Y r_{XY}^{\ 3} b_{MX}^{\ -1}(b_{MX} - b_{MY}\cos\theta_{XMY}), \quad (3)$$

where Y stands for N or O. The non-bonded distances r_{XY} can be easily calculated from bond lengths and valence angles:

$$r_{XY} = (b_{MX}^{\ 2} + b_{MY}^{\ 2} - 2b_{MX}b_{MY}\cos\theta_{XMY})^{1/2}. \quad (4)$$

Such a formulation [eqs. (2)–(4)] of the problem enabled us to express the M—X bond-stretching parameter as a function of three more basic parameters: (1) "elementary charges" centred on "real" atoms N and O, (2) charge of "electron cloud", i.e. "dummy" atoms X, and (3) distance of the apical charge from the nucleus of the central atom. Moreover, it is possible to choose such a sterical parameter k'_b to obtain a b_{MX} value in the realistic span of M—X distances (Fig. 1), having no reference to charge parameters q_Y and q_X.

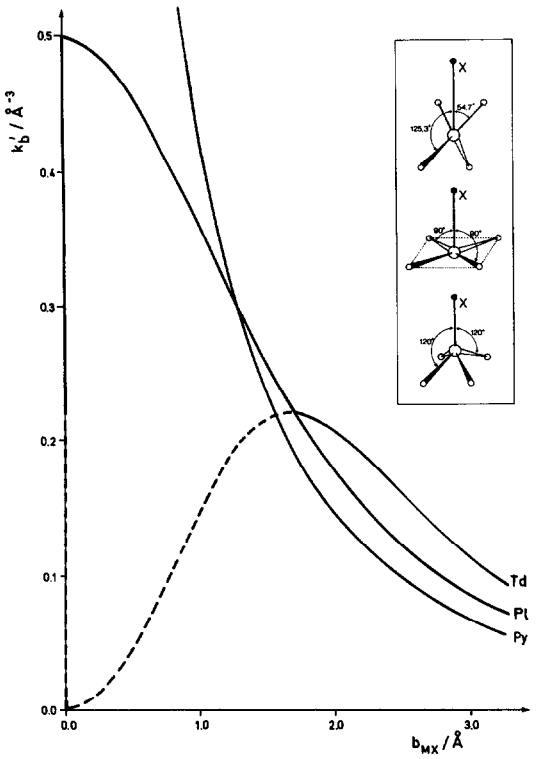

Fig. 1. Plot of the sterical parameter, k_b' [eq. (3)], vs bond length, b_{MX}, when $\partial V/\partial b_{MX} = 0$, "complex" $CuX_2O_2N_2$. Pl, planar (*trans*) configuration; Td, tetrahedral configuration; Py, pyramidal configuration. The points corresponding to the minima of the conformational energy are denoted by the heavy line, and points of maximum value of conformational energy are connected by the broken line. Lengths of the M—O and M—N bonds were taken to be equal (2.0 Å).

Comparison of structures, calculation of average Gibbs energy and construction of conformational energy diagrams

The root-mean-square deviation between crystal and theoretical structures was calculated from:

$$\varepsilon_{r.m.s.}(\Delta X) = \left(1/N \sum_{i=1}^{N} (\Delta X_i)^2\right)^{1/2}, \qquad (5)$$

where X stands for angles around copper (valence angles θ, distortion angle β and "torsional angle" φ_{ONNO}) when comparing the copper coordination geometry, or the interatomic distance, r, when checking the overall similarity. Symbol Δ denotes the difference between the values of the observable X in two structures. For checking of overall similarity, only distances between non-hydrogen atoms were taken into account.

The average Gibbs energy of the diastereomer (MLL or MDL) was calculated from the formula:

$$\langle G \rangle = \sum_i w_i G_i \Big/ \sum_i w_i, \qquad (6)$$

where G_i denotes the Gibbs energy of the ith conformer, and w_i stands for the statistical weight calculated from the Boltzmann formula. Details of calculations were given elsewhere.[13] The potential energy surface for distortion of the copper coordination polyhedron was constructed from the values of potential energy and appropriate values of two internal coordinates obtained after every iteration during the minimization of potential energy (procedure of Rasmussen and co-workers,[18] modified[12]). As the starting points for minimization, arbitrary conformations of the "complex" $CuX_2N_2O_2$ in the whole conformational space were constructed.

RESULTS AND DISCUSSION

The first step in checking the electrostatic model for simulation of the plasticity of the copper(II) coordination polyhedron was to prove how well it reproduced crystal geometry of copper(II) bis-complexes with α-amino acids and their N-alkylated derivatives (Table 1). Both bonding (k_b'), and charge (q_X, q_Y) parameters were systematically varied until the best agreement, in terms of $\varepsilon_{r.m.s.}(\Delta\theta)$ and $\varepsilon_{r.m.s.}(\Delta\theta,\Delta\beta,\Delta\varphi)$, between theoretical and crystal structures[10] of bis(L-N,N-dimethylvalinato) copper(II) has been achieved (Table 1). Although empirical parameters for molecular-mechanics calculation have no strict physical meaning, it has to be noted that obtained parameters (footnote to Table 1) are "realistic", in the sense that they reflect general charge distribution and molecular geometry. The sum of the q_Y charges equals -1.5 e, which is close to -2.0 e, the value to be expected if the complex is purely "ionic". The obtained k_{M-X} yielded M—X distances of about 2.2 Å, which corresponded approximately to the Cu—O (apical) bond length ($\approx$ 2.5 Å).

The obtained force field was checked on all tetracoordinated copper(II) bis-aminoacidates which showed no pronounced intermolecular interactions (Table 1). The new, electrostatic model gave better agreement with the X-ray structures of any model checked so far. The best model with a distortion coordinate potential (Model 5)[12] yielded better agreement with experimental data only in two cases (for the complexes with L-phenylalanine and rac.-N-benzylproline). The "abnormal" behaviour of the former molecule was also observed with other models[12] and was attributed to intramolecular

Table 1. Comparison of experimental and theoretical geometries of copper(II) bis-aminoacidates[a]

Angle	Crystal structure[b]	Model 6[c]	Model 5[d]	Angle	Crystal structure[b]	Model 6[c]	Model 5[d]
Bis-(L-N,N-dimethylvalinato)copper(II)[10]				Bis-(L-N-benzylprolinato)copper(II)[20]			
N—Cu—N′	161.45	160.06	161.41	N—Cu—N′	172.72	178.60	178.92
N—Cu—O	84.32	82.08	87.62	N—Cu—O	85.58	84.02	88.36
N—Cu—O′	97.07	98.58	93.34	N—Cu—O′	96.16	95.13	91.64
N′—Cu—O	95.30	98.57	93.34	N′—Cu—O	93.40	96.80	91.82
N′—Cu—O′	84.75	82.08	87.62	N′—Cu—O′	85.68	83.89	88.29
O—Cu—O′	175.51	176.27	174.04	O—Cu—O′	173.29	171.33	173.50
O′—N′—N—O	156.14	156.13	155.44	O′—N′—N—O	−165.54	172.41	172.39
β	170.49	169.30	171.29	β	−178.56	−173.43	−176.21
$\varepsilon_{r.m.s.}$ ($\Delta\theta$)		2.15	2.55	$\varepsilon_{r.m.s.}$ ($\Delta\theta$)		3.07	3.56
$\varepsilon_{r.m.s.}$ ($\Delta\theta$, $\Delta\beta$, $\Delta\varphi$)		1.91	2.21	$\varepsilon_{r.m.s.}$ ($\Delta\theta$, $\Delta\beta$, $\Delta\varphi$)		8.44	8.43
$\varepsilon_{r.m.s.}$ (Δr)		0.122	0.136	$\varepsilon_{r.m.s.}$ (Δr)		0.309	0.333
Bis-(L-leucinato)copper(II)[21]				Bis-(L-alaninato)copper(II)[22]			
N—Cu—N′	174.56	177.13	179.72	N—Cu—N′	175.47	179.25	180.00
N—Cu—O	84.19	82.69	88.13	N—Cu—O	83.83	83.12	88.30
N—Cu—O′	95.66	99.63	91.81	N—Cu—O′	95.51	96.75	95.51
N′—Cu—O	95.95	94.62	91.79	N′—Cu—O	96.18	97.33	91.77
N′—Cu—O′	84.17	83.04	88.27	N′—Cu—O′	84.44	82.80	88.16
O—Cu—O′	179.71	177.58	180.00	O—Cu—O′	179.25	179.55	180.00
O′—N′—N—O	174.71	−179.57	−179.98	O′—N′—N—O	175.79	−179.82	−179.95
β	176.16	−177.26	−179.64	β	176.66	−179.26	−179.69
$\varepsilon_{r.m.s.}$ ($\Delta\theta$)		2.32	3.90	$\varepsilon_{r.m.s.}$ ($\Delta\theta$)		1.85	3.84
$\varepsilon_{r.m.s.}$ ($\Delta\theta$, $\Delta\beta$, $\Delta\varphi$)		3.68	4.14	$\varepsilon_{r.m.s.}$ ($\Delta\theta$, $\Delta\beta$, $\Delta\varphi$)		2.65	3.87
$\varepsilon_{r.m.s.}$ (Δr)		0.242	0.293	$\varepsilon_{r.m.s.}$ (Δr)		0.161	0.207
Bis-(L-phenylalaninato)copper(II)[23]				(L-serinato)(glycinato)copper(II)[24]			
N—Cu—N′	175.86	171.70	179.69	N—Cu—N′	175.23	178.97	170.00
N—Cu—O	84.82	82.29	88.06	N—Cu—O	82.93	82.76	88.15
N—Cu—O′	96.43	88.77	91.76	N—Cu—O′	94.41	96.11	91.79
N′—Cu—O	94.62	105.89	91.86	N′—Cu—O	101.13	98.09	91.79
N′—Cu—O′	83.93	82.99	88.31	N′—Cu—O′	81.53	83.03	88.27
O—Cu—O′	176.85	170.69	179.28	O—Cu—O′	177.33	178.79	180.00
O′—N′—N—O	178.63	178.53	179.61	O′—N′—N—O	177.53	179.87	179.97
β	175.22	−171.05	−179.69	β	176.20	178.79	179.67
$\varepsilon_{r.m.s.}$ ($\Delta\theta$)		6.43	3.64	$\varepsilon_{r.m.s.}$ ($\Delta\theta$)		2.26	5.73
$\varepsilon_{r.m.s.}$ ($\Delta\theta$, $\Delta\beta$, $\Delta\varphi$)		7.39	3.72	$\varepsilon_{r.m.s.}$ ($\Delta\theta$, $\Delta\beta$, $\Delta\varphi$)		2.31	5.18
$\varepsilon_{r.m.s.}$ (Δr)		0.843	0.748	$\varepsilon_{r.m.s.}$ (Δr)		0.175	0.226
(L-N,N-diethylalaninato)(D-N,N-diethylalaninato)copper(II)[25]				Bis-(1-aminocyclopentane-1-carboxylato)copper(II)[22]			
N—Cu—N′	180.00	180.00	180.00	N—Cu—N′	180.00	180.00	180.00
N—Cu—O	84.07	83.51	87.99	N—Cu—O	83.84	83.66	88.44
N—Cu—O′	95.93	96.49	92.01	N—Cu—O′	96.16	96.34	91.56
N′—Cu—O	95.93	96.49	92.01	N′—Cu—O	96.16	96.34	91.56
N′—Cu—O′	84.07	83.51	87.99	N′—Cu—O′	83.84	83.60	88.44
O—Cu—O′	180.00	180.00	180.00	O—Cu—O′	180.00	180.00	180.00
O′—N′—N—O	180.00	180.00	180.00	O′—N′—N—O	180.00	180.00	180.00
β	180.00	180.00	180.00	β	180.00	180.00	180.00
$\varepsilon_{r.m.s.}$ ($\Delta\theta$)		0.46	3.20	$\varepsilon_{r.m.s.}$ ($\Delta\theta$)		0.15	3.76
$\varepsilon_{r.m.s.}$ ($\Delta\theta$, $\Delta\beta$, $\Delta\varphi$)		0.40	2.77	$\varepsilon_{r.m.s.}$ ($\Delta\theta$, $\Delta\beta$, $\Delta\varphi$)		0.13	3.25
$\varepsilon_{r.m.s.}$ (Δr)		0.061	0.089	$\varepsilon_{r.m.s.}$ (Δr)		0.171	0.238

Table 1 — *continued*

Angle	Crystal structure[b]	Model 6[c]	Model 5[d]	Angle	Crystal structure[b]	Model 6[c]	Model 5[d]
(L-N-benzylprolinato)(D-N-benzylprolinato)-copper(II)[26]				Bis-(α-aminoisobutyrato)copper(II)[27]			
N—Cu—N′	180.00	180.00	180.00	N—Cu—N′	180.00	180.00	180.00
N—Cu—O	87.89	83.68	88.20	N—Cu—O	83.92	82.83	88.19
N—Cu—O′	92.11	96.32	91.80	N—Cu—O′	96.08	97.17	91.81
N′—Cu—O	92.11	96.32	91.80	N′—Cu—O	96.08	97.17	91.81
N′—Cu—O′	87.89	83.68	88.20	N′—Cu—O′	83.92	82.83	88.19
O—Cu—O′	180.00	180.00	180.00	O—Cu—O′	180.00	180.00	180.00
O′—N′—N—O	180.00	180.00	180.00	O′—N′—N—O	180.00	180.00	180.00
β	180.00	180.00	180.00	β	180.00	180.00	180.00
$\varepsilon_{r.m.s.}$ ($\Delta\theta$)		3.44	0.25	$\varepsilon_{r.m.s.}$ ($\Delta\theta$)		0.89	3.49
$\varepsilon_{r.m.s.}$ ($\Delta\theta$, $\Delta\beta$, $\Delta\varphi$)		2.98	0.22	$\varepsilon_{r.m.s.}$ ($\Delta\theta$, $\Delta\beta$, $\Delta\varphi$)		0.77	3.02
$\varepsilon_{r.m.s.}$ (Δr)		0.313	0.333	$\varepsilon_{r.m.s.}$ (Δr)		0.055	0.099
(L-2-Aminobutyrato)(D-2-aminobutyrato)copper(II)[21]				(L-N-benzylvalinato)(D-N-benzylvalinato)copper(II)[28]			
N—Cu—N′	180.00	180.00	180.00	N—Cu—N′	180.00	180.00	180.00
N—Cu—O	84.55	82.64	88.13	N—Cu—O	85.02	83.54	88.35
N—Cu—O′	95.45	97.36	91.87	N—Cu—O′	94.98	96.30	91.65
N′—Cu—O	95.45	97.36	91.87	N′—Cu—O	94.98	96.61	91.65
N′—Cu—O′	84.55	82.64	88.13	N′—Cu—O′	85.02	83.54	88.35
O—Cu—O′	180.00	180.00	180.00	O—Cu—O′	180.00	180.00	180.00
O′—N′—N—O	180.00	180.00	180.00	O′—N′—N—O	180.00	−179.96	179.89
β	180.00	180.00	180.00	β	180.00	179.84	−179.99
$\varepsilon_{r.m.s.}$ ($\Delta\theta$)		1.56	2.92	$\varepsilon_{r.m.s.}$ ($\Delta\theta$)		1.21	2.72
$\varepsilon_{r.m.s.}$ ($\Delta\theta$, $\Delta\beta$, $\Delta\varphi$)		1.35	2.53	$\varepsilon_{r.m.s.}$ ($\Delta\theta$, $\Delta\beta$, $\Delta\varphi$)		1.05	2.35
$\varepsilon_{r.m.s.}$ (Δr)		0.278	0.321	$\varepsilon_{r.m.s.}$ (Δr)		0.228	0.216

[a] All angles are expressed in degrees and $\varepsilon_{r.m.s.}$ (Δr) values in Å (only non-hydrogen atoms were taken into account).
[b] References correspond to crystal structures.
[c] Model with coulombic interactions (see Methods). Force-field parameters: $q_X = -0.750$ e, $q_Y = -0.375$ e, $k_{M-X} = 14.0101$ kcal mol^{-1} Å^{-2}, $b_{0,M-X} = 0$.
[d] The best model with distortion coordinate potential; taken from ref. 12.

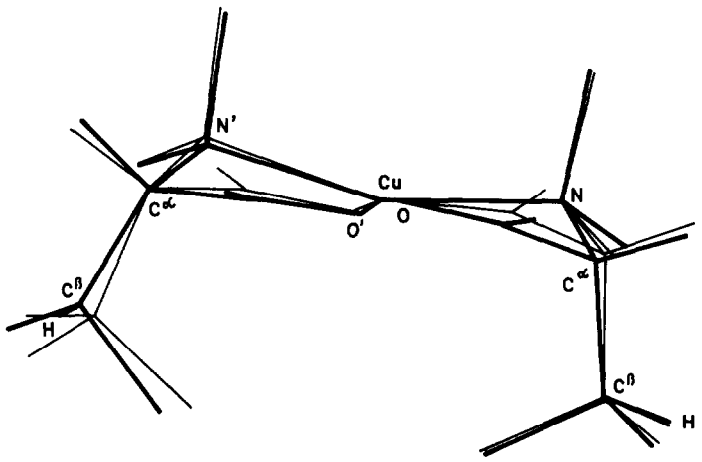

Fig. 2. Comparison of the X-ray structure[10] (heavy line) and theoretical structure (thin line) of bis(L-N,N-dimethylvalinato)copper(II).

Table 2. The statistical analysis (mean and standard deviation) of angles around copper in chelates with amino acids. Data from Table 1[a]

Angle	Crystal structure	Model 6	Model 5
Distorted molecules ($n = 6$)			
N—Cu—N′	172.55(5.07)	174.29(6.86)	176.62(6.81)
N—Cu—O	84.28(0.82)	82.83(0.63)	88.10(0.24)
N—Cu—O′	95.87(0.83)	95.83(3.49)	92.02(0.59)
N′—Cu—O	96.10(2.43)	98.55(3.51)	92.06(0.57)
N′—Cu—O′	84.08(1.27)	82.97(0.53)	88.15(0.24)
O—Cu—O′	176.99(2.18)	175.70(3.47)	177.80(2.87)
O′—N′—N—O	176.21(11.15)	174.59(8.70)	174.58(8.99)
β	176.03(3.19)	181.18(6.31)	179.35(3.84)
Square-planar molecules ($n = 6$)			
N—Cu—N′	180.00(0.00)	180.00(0.00)	180.00(0.00)
N—Cu—O	84.88(1.41)	83.31(0.41)	88.22(0.15)
N—Cu—O′	95.12(1.41)	96.66(0.43)	91.78(0.15)
N′—Cu—O	95.12(1.41)	96.72(0.40)	91.78(0.15)
N′—Cu—O′	84.88(1.41)	83.30(0.41)	88.22(0.15)
O—Cu—O′	180.00(0.00)	180.00(0.00)	180.00(0.00)
O′—N′—N—O	180.00(0.00)	180.01(0.02)	180.02(0.04)
β	180.00(0.00)	180.01(0.02)	180.02(0.04)

[a] All values are given in degrees. Standard deviations are given in parentheses.

interactions in the crystal lattice (stacking of phenyl rings, apical ligation of carboxylic oxygens and hydrogen bondings).[23] Both molecules gave higher distortion from ideal planar geometry (N—Cu—O = 90°) with Model 6 than with Model 5, indicating —at least in that case—that the force field was "too loose".

The valence angles around copper were substantially better reproduced with the new model. The linear correlation of measured vs calculated *trans*-angles yielded both the correlation coefficient and slope ($r = 0.68$, $B = 1.08$ for O—Cu—O; $r = 0.88$, $B = 1.19$ for N—Cu—N) acceptable, but the distortion angle ($r = 0.73$, $B = 1.44$) and torsion angle, O′—N′—N—O ($r = 0.58$, $B = 0.44$) were less successfully reproduced. The numbers are close to those achieved with other empirical force-field models.[12] Some improvement was achieved for *cis*-angles (N—Cu—O) which gave upon linear regression a correlation coefficient in the range 0.2–0.4 (< 0.1 for other force fields). Also, the electrostatic model did not yield "too stick" a force field (the force field which gave theoretical values of valence angles too close to their "standard" values, e.g. 90 and 180°) like models with distortion coordinate potential.[12] The mean of the angles in the theoretical structures is in the range of mean angles in the crystal structures (Table 2). Such good agreement was not obtained for the models with a distortion coordinate potential, e.g. Model 5.

The second test for validity of the model is to check its ability to reproduce the diastereoselectivity (or more specifically: enantioselectivity)* effect (Table 3). Contrary to the models with a distortion coordinate potential,[11,12] which gave too high values for the difference between MLL and MDL isomers ($\Delta G = 5.42$–7.43 kJ mol^{-1}), the electrostatic model revealed the value of the enantioselectivity effect in the very limits of experimental error. Comparably good results were obtained only with the "dummy" atom model[9] ($\Delta G = 2.95$ kJ mol^{-1}) but, unfortunately, that model did not give a correct geometry of copper coordination.

The model was further checked on the $CuX_2N_2O_2$ "molecule" in order to study the shape of the potential energy surface in the absence of "additional" sterical influences. Systematically

*The enantioselectivity effect is defined as Gibbs energy difference between MLL and MDL (L and D denote configuration of the ligand) isomers: $\Delta G = -RT \ln (\beta_{MLD}/\beta_{MDL})$; β is the cumulative stability constant of the appropriate complex.

Table 3. Estimation of conformational potential, Gibbs energy and statistical weights of the two isomers of bis-(N,N-dimethylvalinato)copper(II)[a]

Number	Conformational potential MLL	MDL	ΔV	Gibbs energy MLL	MDL	ΔG
1–3	32.750 (0.0000)	34.508 (0.0000)	−1.758	27.502 (0.0000)	28.604 (0.0000)	−1.102
1–6	13.827 (0.0036)	13.292 (0.0006)	0.535	18.148 (0.0006)	12.434 (0.0020)	5.714
3–3	32.769 (0.0000)	35.324 (0.0000)	−2.555	25.790 (0.0000)	27.316 (0.0000)	−1.526
3–4	28.152 (0.0000)	26.241 (0.0000)	1.911	22.623 (0.0001)	20.198 (0.0001)	2.425
3–6	14.410 (0.0029)	13.129 (0.0006)	1.281	13.151 (0.0046)	13.306 (0.0014)	−0.155
4–6	8.201 (0.0349)	8.287 (0.0045)	−0.086	6.932 (0.0570)	7.490 (0.0144)	−0.558
5–5	28.352 (0.0000)	24.569 (0.0000)	3.783	31.136 (0.0000)	26.893 (0.0000)	4.243
6–6	0.0000 (0.9549)	−5.101 (0.9917)	5.101	0.000 (0.9332)	−2.972 (0.9794)	2.972
Estimated enantioselectivity	5.41				3.26	
Experimental value[9]		2.9...4.0				

[a] All energy values are expressed in kJ mol^{-1}. Statistical weights are given in parentheses. The minima of the conformational energy are denoted as in ref. 8. Zero points: $V = 878.031$ kJ mol^{-1}, $G = 2380.583$ kJ mol^{-1}. The enantioselectivity was calculated from the energy of all 21 conformers; for conformers with high energy (not referred to here) energies were not computed after minimization, but approximative values for both strain and Gibbs energy were taken (approximation $E(n-m) = 1/2[E(n-n)+E(m-m)]$, where n and m were code numbers of the conformers).

minimizing the energy of a great number of starting configurations, only two "real" (*trans*, 1 and *cis* 2; Table 4) minima were obtained. These two minima have virtually the same energy. The slight deviation from planarity ($|\beta| = 180°$) of the *cis* minimum can be explained by the small asymmetry of the system (Cu—O and Cu—N bond lengths are not equal). The tetrahedral minimum has not been possible to achieve, but the tetrahedral configuration appeared only as a transition state at a considerably high energy ($V \approx 930$ kJ mol^{-1}).

Because of the lack of a repulsive potential

Table 4. Some characteristic minima of conformational energy for the "complex" $CuX_2N_2O_2$[a]

Number	NMN′	NMO	NMO′	N′MO	N′MO′	OMO	XMX	ONNO	β	MX	V
1	180.0	90.0	90.0	90.0	90.0	180.0	180.0	180.0	180.0	2.1985	854.78
2	89.96	89.99	180.00	180.00	89.99	90.06	179.52	0.0	−179.9	2.1985	854.79
3	119.09	74.74	74.74	74.74	74.74	117.44	0.0	179.83	99.59	1.9376	784.17
4	74.53	74.73	118.27	118.27	74.73	74.97	0.0	0.0	99.59	1.9376	784.18
5	74.53	118.27	74.73	74.73	118.27	74.97	0.0	0.0	−0.35	1.9376	784.18
6	69.03	69.70	69.70	108.86	108.86	107.46	0.0	88.20	−87.56	1.9499	790.30
7	110.17	107.71	69.71	107.71	69.26	70.32	0.0	−55.14	88.76	1.9472	790.33
8	167.91	56.31	111.60	111.60	56.31	55.29	0.0	0.0	111.60	1.9623	820.53
9	0.0	0.0	0.0	0.0	0.0	0.0	0.0	—	0.0	1.8682	1988.71
10	0.0	180.0	0.0	180.0	0.0	180.0	0.0	—	180.0	0.5324	1565.82

[a] All angles are expressed in degrees, M—X bond lengths in Å and conformational potential (V) in kJ mol^{-1}.

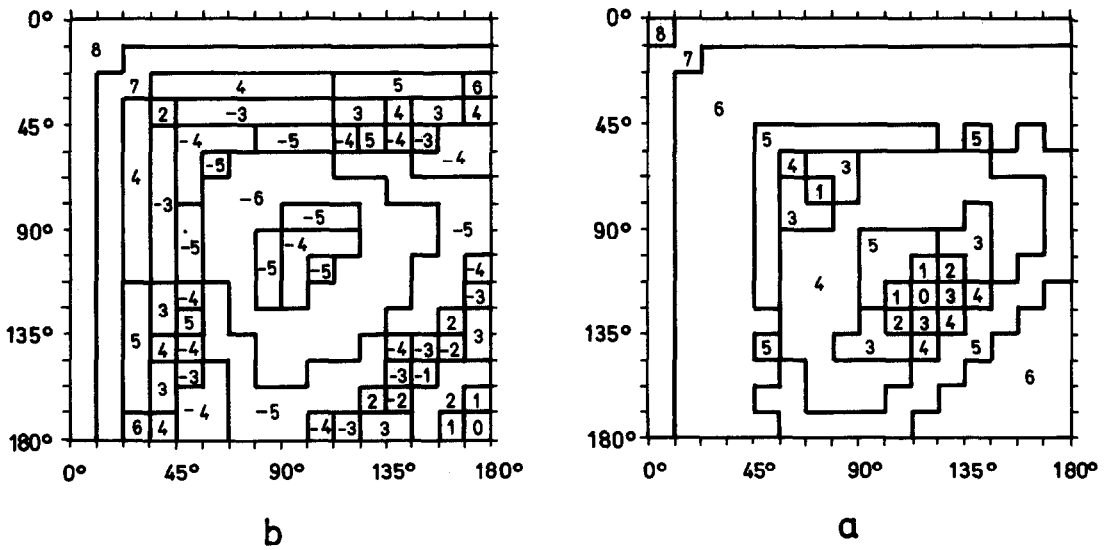

Fig. 3. A diagram of the potential (conformational) energy of the *trans*-$CuX_2N_2O_2$ "complex" in the frame of coordinates N—M—N and O—M—O. The energy ranges (in kcal mol^{-1}) in the appropriate region of the diagram are expressed by the numbers: (a) 0 (< 0.001), 1 (0.001–0.01), 2 (0.01–0.1), 3 (0.1–1), 4 (1–5), 5 (5–10), 6 (10–50), 7 (50–100), 8 (100–1000); (b, absolute values) 0 (< 0.001), 1 (0.001–0.1), 2 (0.1–1), 3 (1–5), 4 (5–10), 5 (10–15), 6 (15–20), 7 (20–50), 8 (50–100). Zero values correspond to $V = 187.420$ kcal mol^{-1} (Min. 3, Table 4) (a) and $V = 204.298$ kcal mol^{-1} (Min. 1, Table 4) (b).

between apically placed charges, the system easily degenerates to the "pentacoordinated complex" $CuXN_2O_2$, i.e. two X "atoms" come atop each other (X—Cu—X′ = 0). As a consequence, a large series of "false" minima was obtained (Table 4), which should be described as (distorted) pyramids (Nos 3, 4), trigonal bipyramids (Nos 6, 7) and even "linear molecules" (Nos 9, 10). Unfortunately, some of these minima (e.g. Nos 3–8) even have a lower conformational energy than the "real" ones.

General properties of the model can be studied by analysing the shape of the potential energy surface (Figs 3 and 4). There is obviously a very flat region around the *trans* minimum (a nearly analogous plot can be drawn for the *cis* minimum, but in the frame of different valence angles). Upon larger distortion

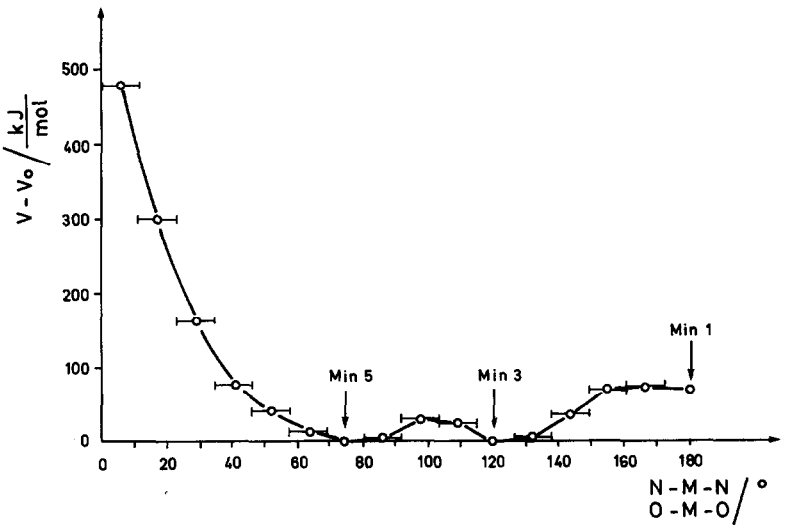

Fig. 4. Plot of the conformational energy of the "complex" $CuX_2N_2O_2$ in the frame of the N—M—N coordinate for the points (obtained from Fig. 3 and Table 4) where N—M—N ≈ O—M—O. The zero point is taken to be equal to 784.165 kJ mol^{-1} (Min. 3, Table 4).

(> 15–30° for N—M—N′ and O—M—O′ angles), the $CuX_2N_2O_2$ "complex" is placed in the lower regions of potential energy surface yielding the "false" minima. In the vicinity of *trans* and *cis* minima the $CuX_2N_2O_2$ "complex" is very flexible, changing its conformational energy by less than 5 kJ mol^{-1} upon distortion.

In conclusion, we can state that the electrostatic model reproduced the geometry of the tetracoordinated copper(II) bis-aminoacidates better than the models checked previously.[10,12] The plasticity of the copper(II) coordination sphere is also evident, because the model generated a very flat potential energy surface for small deviations from planarity (Fig. 3). Unfortunately, for higher deviations it gave a large number of "false" minima (Table 4), and was also incapable of yielding the tetrahedral minimum, which was obtained with the models based on the distortion potential.[12] We tried to solve the problems of false minima by suppressing the "degeneration" of the hexacoordinated to pentacoordinated copper atom through introduction of an additional angle-bending potential for the X—Cu—X′ angle. This attempt did not prove successful, because starting conformations generally did not converge to the minimum even after a very strong potential was applied ($k_{X—M—X} = 1000$ kcal mol^{-1}, $\theta_{X—M—X,0} = 180°$). Fortunately, in our class of compounds the deviation from planarity was not so high as to induce transition of coordination octahedron to any five-top solid. However, the use of the model for conformation analysis of highly distorted structures would call for further development.

REFERENCES

1. G. R. Brubaker and D. W. Johnson, *Coord. Chem. Rev.* 1984, **53**, 1.
2. S. R. Niketić and Kj. Rasmussen, *The Consistent Force Field: A Documentation.* Springer, Berlin (1977); Kj. Rasmussen, *Potential Energy Functions in Conformational Analysis.* Springer, Berlin (1985).
3. S. R. Niketić and Kj. Rasmussen, *Acta Chem. Scand.* 1981, **A35**, 623.
4. G. J. McDougall, R. D. Hancock and J. C. A. Boeyens, *J. Chem. Soc., Dalton Trans.* 1978, 1438.
5. K. Hori, J. N. Kushick and H. Weinstein, *Biopolymers* 1988, **27**, 1865.
6. J. Gažo, I. B. Bersuker, J. Garaj, M. Kobašova, J. Kohout, H. Langefelderova, M. Melnik, M. Serator and F. Valach, *Coord. Chem. Rev.* 1976, **19**, 253.
7. B. J. Hathaway, *Coord. Chem. Rev.* 1982, **41**, 423.
8. N. Raos and Vl. Simeon, *Croat. Chem. Acta* 1983, **56**, 79.
9. N. Raos and Vl. Simeon, *Croat. Chem. Acta* 1985, **58**, 127.
10. B. Kaitner, B. Kamenar, N. Paulić, N. Raos and Vl. Simeon, *J. Coord. Chem.* 1987, **15**, 373.
11. J. Sabolović, N. Raos and Kj. Rasmussen, *Croat. Chem. Acta* 1989, **62**, 495.
12. J. Sabolović and N. Raos, *Polyhedron* 1990, **9**, 1277.
13. N. Raos and Vl. Simeon, *Croat. Chem. Acta* 1984, **57**, 1217.
14. B. Kamenar, M. Penavić, A. Škorić, N. Paulić, N. Raos and Vl. Simeon, *J. Coord. Chem.* 1988, **17**, 85.
15. N. Raos, S. R. Niketić and Vl. Simeon, *J. Inorg. Biochem.* 1982, **16**, 1.
16. D. L. Kepert, *Inorganic Stereochemistry.* Springer, Berlin (1982).
17. M. C. Favas and D. L. Kepert, *Prog. Inorg. Chem.* 1980, **27**, 325.
18. S. Melberg and Kj. Rasmussen, *Carbohydrate Res.* 1979, **69**, 27; S. R. Niketić and Kj. Rasmussen, *Acta Chem. Scand.* 1981, **A35**, 213.
19. V. A. Davankov, S. V. Rogozhin, A. A. Kurganov and Ya. Zhuchkova, *J. Inorg. Nucl. Chem.* 1975, **37**, 369.
20. G. G. Aleksandrov, Yu. T. Struchkov and A. A. Kurganov, *Zh. Strukt. Khim.* 1973, **14**, 492.
21. T. G. Fawcett, M. Ushay, J. P. Rose, R. A. Lalancette, J. A. Potenza and H. J. Schugar, *Inorg. Chem.* 1979, **18**, 327.
22. M. A. Hitchman, L. Kwan, L. M. Engelhardt and A. H. White, *J. Chem. Soc., Dalton Trans.* 1987, 457.
23. D. van der Helm, M. B. Lawson and E. L. Enwall, *Acta Cryst.* 1971, **B27**, 2411.
24. I. A. Dyakon, S. V. Donu, L. F. Chapurina and A. S. Avilov, *Kristallografia* 1984, **29**, 384.
25. C. P. Nash and W. P. Schaefer, *J. Am. Chem. Soc.* 1969, **91**, 1319.
26. G. G. Aleksandrov, Yu. T. Struchkov, A. A. Kurganov, S. V. Rogozhin and V. A. Davankov, *Zh. Strukt. Khim.* 1972, **13**, 671.
27. R. Calvo, M. A. Mesa, G. Oliva, J. Zukerman-Schpector, O. R. Nascimento, M. Tovar and R. Arce, *J. Chem. Phys.* 1984, **81**, 4584.
28. G. G. Aleksandrov and Yu. T. Struchkov, *Zh. Strukt. Khim.* 1975, **16**, 228.

Polyhedron Vol. 9, No. 19, pp. 2429–2432, 1990
Printed in Great Britain

0277–5387/90 $3.00+.00
© 1990 Pergamon Press plc

STABILITY CONSTANTS FOR THE LEAD(II)–HALIDE SYSTEMS

G. T. HEFTER

School of Mathematical and Physical Sciences, Murdoch University, Murdoch, WA 6150, Australia

(*Received* 12 *December* 1989; *accepted* 15 *June* 1990)

Abstract—The stability constants of the complexes of lead(II) with fluoride, chloride, bromide and iodide in aqueous solution have been measured by potentiometric titrations with a lead amalgam at 25°C and an ionic strength of 1.00 M ($NaClO_4$). The overall stability constants show an interesting "mixed" order with $\log \beta_n$ for $F^- > (Cl^- < Br^- < I^-)$ for $n = 1, 2$, although the fluoride system shows no tendency to form higher order complexes. The stepwise stability constants for each system show variations which may reflect a change in the coordination number of lead(II) from six to four.

Lead(II) is usually considered to be a "borderline" metal ion in Lewis acid terms.[1-3] As such, its stability constants (β_n) with related ligands often show unusual patterns compared with archetypal class A (hard) or class B (soft) metal ions.[1-3] In terms of its halide complexes, lead(II) was thought[1] to exhibit class A behaviour with β_n values having the order $F^- < Cl^- < Br^- < I^-$. However, it was later shown[3,4] that this apparent order was based on an erroneous indirect estimation[5] of $\beta_n[PbF_n^{2-n}(aq)]$. Instead, a mixed order: $F^- > (Cl^- < Br^- < I^-)$ prevails.[3]

Whilst this mixed order was derived[3] from existing literature data, many of the published studies[6-8] disagree markedly as to the relative importance of individual complexes. Thus, it was thought worthwhile to undertake a re-investigation of these systems under comparable conditions. The present paper reports stability constants for the complexes of lead(II) with fluoride, chloride, bromide and iodide in aqueous solution at 25°C and $I = 1$ M ($NaClO_4$) obtained by potentiometric titrations using a lead amalgam electrode.

EXPERIMENTAL

Reagents and apparatus

All chemicals were of analytical reagent grade. A stock solution of lead(II)–perchlorate was prepared by neutralizing (pH 5.0) freshly prepared lead(II)–carbonate[9] with perchloric acid. The concentration was determined polarographically using 5 N purity lead metal as a standard. Ligand solutions were made up by weight from the sodium salts. Sodium fluoride was purified by the method of Lingane.[10] The chloride, bromide, and iodide salts were recrystallized from "conductivity" water then dried at 150°C under vacuum for 24 h. Iodide solutions were prepared and stored under argon to prevent aerial oxidation.

Lead amalgam was prepared by electrolysis of an acidified lead(II)–nitrate solution continually deaerated with argon. The liquid amalgam (about 1% Pb) was transferred to argon-filled storage flasks with a glass syringe. Ionic strength (I) was maintained at 1.00 M with sodium perchlorate and temperature at 25.0 ± 0.1°C. The pH of all the solutions was adjusted to 5.0 ± 0.1 where the presence of HF, HF_2^- and lead(II)–hydroxy species may be ignored.[11,12] All solutions were stored in polyethylene containers.

Measurements were performed under argon on cells which may be represented by:

$$Ag|AgCl, 5\ M\ NaCl \| 5\ M\ NaClO_4 \| x\ M\ Pb^{2+},\ y\ M\ X^-,\ I = 1\ M\ (NaClO_4)|Pb(Hg).$$

No corrections were made for liquid junction potentials but separate measurements[13] and cal-

culations[14] indicated that such corrections were negligible.

The lead amalgam was calibrated using the *in situ* techniques described previously.[11,13] Providing freshly prepared amalgam was used and oxygen was rigorously excluded, calibration slopes were always close to Nernstian (29.6 mV) down to $\sim 10^{-5}$ M Pb^{2+}. In Pb^{2+}-buffered solutions (i.e. in the presence of excess halide) satisfactory response could be obtained down as low as 10^{-7} M in free Pb^{2+}. Care had to be taken to avoid precipitation of PbX_2, a problem which severely limited the range of concentrations which could be studied. All other experimental details are as described previously.[13]

Calculations

Using the usual mass balance relationships, it is readily shown that providing $[Pb^{2+}] \ll [X^-]$ then

$$\frac{1}{[X^-]_T}\left\{\frac{[Pb^{2+}]_T}{[Pb^{2+}]} - 1\right\} = F_0(X) = \sum_1^n \beta_n [X^-]_T^n \quad (1)$$

where $F_0(X)$ represents the experimentally determined left-hand side of the equation, the subscript T refers to the total or analytical concentration and β_n are the overall stability constants (expressed in terms of concentrations) for the reactions

$$Pb^{2+}(aq) + n X^-(aq) \overset{\beta_n}{\rightleftharpoons} PbX_n^{2-n}(aq).$$

The β_n values may be obtained numerically by a least-squares fit of $F_0(X)$ vs $[X^-]_T$ data or graphically, following De Ford and Hume.[15] Both techniques were used and gave identical results within the limits of experimental error.

RESULTS AND DISCUSSION

Typical experimental data for the Pb^{II}/Cl^- system are presented in Table 1; similar data were obtained for the other halide systems. The stability constants obtained are summarized in Table 2. These values are, in general, in good agreement with literature data obtained under comparable conditions,[6,7] although the present data have the advantage of greater self-consistency.

Higher order complexes

The lead(II)–halide systems show interesting variations in their extent of formation of higher order complexes. Thus, even though β_1 and β_2 are greatest for fluoride complexes (Table 2) no higher order complexes ($n > 2$) are formed, consistent with the insolubility of PbF_2 (s) in excess fluoride.[4,8] No evidence was found in the present study for

Table 1. Typical potentiometric titration data for the Pb^{2+}/Cl^- system, 25°C, I = 1.0 M ($NaClO_4$)

E (V)	$[Pb^{2+}]_T$ (10^4 M)	$[Pb^{2+}]^a$ (10^5 M)	$[Cl^-]_T$ (10M)	$F_0(X)^b$ (M^{-1})	$F_1(X)^c$ (M^{-2})	$F_2(X)^c$ (M^{-3})
0.4809	1.27	9.33	0.378	9.5	13	—[d]
0.4841	1.22	7.00	0.727	10.2	17	65
0.4856	1.20	6.18	0.894	10.5	17	56
0.4869	1.18	5.54	1.05	10.8	17	49
0.4882	1.16	4.92	1.21	11.2	18	51
0.4896	1.14	4.40	1.36	11.7	20	58
0.4920	1.10	3.62	1.64	12.4	21	53
0.4942	1.07	3.00	1.91	13.4	23	58
0.4960	1.04	2.55	2.15	14.3	25	59
0.4979	1.00	2.19	2.39	14.9	25	53
0.5037	0.898	1.34	3.20	17.8	28	48
0.5059	0.853	1.07	3.55	20.2	32	55
0.5080	0.813	0.850	3.86	22.1	34	57
0.5100	0.775	0.680	4.14	25.1	39	65
0.5115	0.742	0.572	4.40	27.0	41	66

Overall result: $\beta_1 = 9.0 \pm 0.5\ M^{-1}$, $\beta_2 = 12 \pm 1\ M^{-2}$, $\beta_3 = 57 \pm 6\ M^{-3}$

[a] Obtained graphically from an *in situ* calibration curve[13] (data not shown).

[b] As defined in eq. (1)

[c] As defined in ref. 15.

[d] Data not used for calculation of β_3.

Table 2. Summary of overall stability constants for the lead(II)–halide systems, 25°C, $I = 1.0$ M ($NaClO_4$)[a]

Ligand	$\log\beta_1$	$\log\beta_2$	$\log\beta_3$	$\log\beta_4$
F^-	1.46±0.01	2.52±0.05	—	—
Cl^-	0.93±0.02	1.08±0.04	1.72±0.05	—
Br^-	1.10±0.04	1.38±0.04	2.38±0.10	—
I^-	1.18±0.07	2.30±0.05	3.16±0.07	4.8±0.3

[a] β_n in units of M^{-n}, with estimated overall errors.

complexes higher than $n = 3$ for Cl^- or Br^- or $n = 4$ for I^- even at $[X^-]/[Pb^{2+}]$ ratios of up to 70,000.

Relative stabilities

The present results (Table 2) confirm the "mixed" stability order $F^- > (Cl^- < Br^- < I^-)$ previously inferred for the lead(II)–halide complexes, at least for $PbX^+(aq)$ and $PbX_2^0(aq)$. The absence of higher order complexes for Pb^{2+}/F^- implies *complexed* lead(II) shows a classical class B (soft) stability order: $F^- < Cl^- < Br^- < I^-$. Interestingly, in non-aqueous solvents such as DMF[16] and DMSO[17] the lead(II)–halides generally show clear class A (hard) behaviour with stability constants $Cl^- > Br^- > I^-$ (no F^- data are available) although there is some evidence for mixed orderings.

Figure 1 plots the *stepwise* stability constants K_n ($= \beta_n/\beta_{n-1}$) for the lead(II)–halide systems. On statistical grounds, $\log K_n$ is expected to decrease with increasing n since there are fewer available coordination sites for an incoming ligand.[18] Substantial departures are usually due to changes in coordination number.[19] Such changes generally occur abruptly, i.e. in a single step, producing an anomaly in the stability constant order.[19] Figure 1 suggests such anomalies exist for the lead(II)–halide systems with $K_3 > K_2$ for Cl^- and Br^- and $K_4 > K_3$ for I^-. By analogy with zinc(II), cadmium(II) and mercury (II)[19] the coordination change may be envisaged as:

$$PbX_n(H_2O)_{6-n}^{2-n} + X^- \rightleftharpoons PbX_{n+1}(H_2O)_{3-n}^{1-n} + 3H_2O,$$

where the geometry of lead(II) changes from (pseudo) octahedral to (pseudo) tetrahedral.

Such changes are usually more readily apparent in the corresponding enthalpy and entropy changes than in $\log K_n$.[19] Unfortunately, no calorimetric study of these systems has been made[6–8] and the data which can be calculated from the published temperature dependence of the stability constants are dubious. For example, the value of ΔH_1 [$PbF^+(aq)$] which can be calculated from the data of Bond[4,20] is nearly 20 kJ mol^{-1} more negative than any other monofluoride complex.[3] Similarly, independent determinations[21] of ΔH_1 [$PbX^+(aq)$] differ by *ca* 14, 3 and 48 kJ mol^{-1} for X = Cl^-, Br^- and I^-, respectively. Not surprisingly therefore, the available data cannot be used to confirm or refute a possible change in coordination number. A thorough calorimetric investigation of the lead(II)–halide systems would be clearly of considerable interest in understanding the behaviour of these complexes.

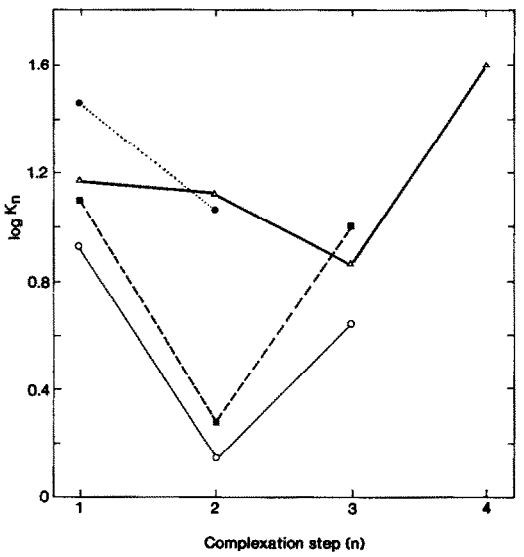

Fig. 1. Plot of stepwise stability constants ($\log K_n$) calculated from Table 2 against the complexation step (n) at 25°C, $I = 1.0$ M ($NaClO_4$): F^- (●); Cl^- (○); Br^- (■); I^- (△).

REFERENCES

1. S. Ahrland, J. Chatt and N. R. Davies, *Quart. Rev. Chem. Soc.* 1958, **12**, 265.
2. R. G. Pearson, *J. Am. Chem. Soc.* 1963, **85**, 3533.
3. G. T. Hefter, *Coord. Chem. Rev.* 1974, **12**, 221.
4. A. M. Bond and G. T. Hefter, *Inorg. Chem.* 1970, **9**, 1021.
5. R. E. Connick and A. D. Paul, *J. Am. Chem. Soc.* 1958, **80**, 2069.
6. L. G. Sillen and A. E. Martell, *Stability Constants of Metal-Ion Complexes*, Special Publications 17 (1964) and 25 (1971), Chem. Soc., London.
7. E. Hoegfeldt, *Stability Constants of Metal-Ion Complexes, Part A: Inorganic Ligands*. IUPAC Chemical Data Series No. 21, Pergamon Press, Oxford (1982).
8. A. M. Bond and G. T. Hefter, *Critical Survey of*

Stability Constants and Related Thermodynamic Data of Fluoride Complexes in Aqueous Solution. IUPAC Chemical Data Series No. 27, Pergamon Press, Oxford (1980).
9. P. Pascal (Ed.), *Nouveau Traité de Chimie Minerale*, 3rd edn, Vol. 8, p. 753. Masson, Paris (1963).
10. J. J. Lingane, *Analyt. Chem.* 1967, **39**, 881.
11. G. T. Hefter, *J. Solution Chem.* 1984, **13**, 457.
12. C. F. Baes and R. E. Mesmer, *The Hydrolysis of Cations*. Wiley-Interscience, New York (1976).
13. G. T. Hefter, *J. Electroanal. Chem.* 1972, **39**, 345.
14. G. T. Hefter, *Analyt. Chem.* 1982, **54**, 2518.
15. D. D. DeFord and D. N. Hume, *J. Am. Chem. Soc.* 1951, **73**, 5321.
16. V. M. Samoilenko and M. P. Zhukov, *Ukr. Khim. Zh.* 1970, **36**, 765.
17. V. M. Samoilenko and M. P. Lyashenko, *Zh. Neorg. Khim.* 1973, **18**, 2402.
18. F. J. C. Rossotti, in *Modern Coordination Chemistry* (Edited by J. Lewis and R. G. Wilkins). Wiley-Interscience, New York (1960).
19. S. Ahrland, in *The Chemistry of Nonaqueous Solvents* (Edited by J. J. Lagowski), Vol. 5A. Academic Press, New York (1978).
20. A. M. Bond, *Anal. Chim. Acta* 1971, **53**, 159.
21. J. J. Christensen and R. M. Izatt, *Handbook of Metal–Ligand Heats*, 3rd edn. Marcel Dekker, New York (1980).

Polyhedron Vol. 9, No. 19, pp. 2433–2435, 1990
Printed in Great Britain

0277-5387/90 $3.00+.00
© 1990 Pergamon Press plc

COMMUNICATION

CYCLIC VOLTAMMETRIC STUDIES OF PENTACYANO(PHOSPHINE)FERRATE(II) COMPLEXES

M. M. MONZYK and R. A. HOLWERDA*

Department of Chemistry and Biochemistry, Texas Tech University, Lubbock, TX 79409, U.S.A.

(*Received* 3 *June* 1990; *accepted* 4 *July* 1990)

Abstract—Half-wave potentials for nine $[Fe(CN)_5L]^{2-/3-}$ couples are reported, where L = P(cyclohexyl)$_3$ (0.321 V), $AsPh_3$ (0.564 V), $SbPh_3$ (0.560 V) and P(Ph-*p*-X)$_3$; X = H (0.522 V), F (0.557 V), Cl (0.585 V), OCH_3 (0.492 V), CH_3 (0.505 V) and CF_3 (0.632 V); $E_{1/2}$ referenced to SHE at 25.0°C, pH 5.0, I = 0.2 M ($NaOAc/NaNO_3$). Linear Hammett plots of $E_{1/2}$ and $\log(K_X/K_H)$ ($\rho = -3.06$) vs σ_p demonstrate that the thermodynamic oxidizability of $[Fe(CN)_5P(Ph\text{-}p\text{-}X)_3]^{3-}$ complexes is moderately sensitive to inductive characteristics of *p*-X groups. The electrochemical reversibility and aqueous solution stability characteristics of $[Fe(CN)_5P(Ph\text{-}p\text{-}X)_3]^{2-/3-}$ couples meet the requirements for biochemical redox mediators in the 0.49–0.63 V vs SHE interval.

Recently completed studies of palladium(II) linkage isomerization processes showed that the rate of carbon-bonded to π-bonded chloranilate (CA^{2-}; 2,5-dioxo-3,6-dichloro-1,4-benzoquinone) rearrangement, induced by incoming PR_3 ligands, depends strongly on triphenylphosphine *para*-substituents.[1,2] Indeed, ^{31}P NMR coordination chemical shifts, phosphine precursor complexation binding constants and intramolecular isomerization rate constants all vary linearly with the Hammett σ_p parameter, suggesting that the polarization of phosphorus 3*p* electron density toward the electrophilic palladium(II) centre strongly destabilizes *trans* Pd–carbanion C bonds.[1] In this way, chloranilate is constrained to function as a weaker σ-donor in the π-CA^{2-} linkage isomer.

Pentacyanoferrate(II) complexes of the form $[Fe(CN)_5L]$ (L = NCS^-, N_3^-, H_2O, NH_3, PPh_3) are useful in probing the dependence of outer-sphere electron transfer rates on thermodynamic driving force.[3–5] Although the IR, electronic, ^{57}Fe Mössbauer and ^{31}P NMR spectral characteristics of $[Fe(CN)_5PR_3]^{3-}$ complexes have been described,[6,7] the dependence of iron(III,II) reduction potentials on phosphine substituents has not been reported. In order to further examine the inductive contributions of phosphine ligands towards bivalent metal centres, we have determined the half-wave potentials of $[Fe(CN)_5P(Ph\text{-}p\text{-}X)_3]^{2-/3-}$ couples (X = H, F, Cl, OCH_3, CH_3, CF_3) by cyclic voltammetry in aqueous solution. For comparison, the $E_{1/2}$ values derived from pentacyanoferrate(II) adducts with P(cyclohexyl)$_3$, $AsPh_3$ and $SbPh_3$ are also reported. In light of these results, the feasibility of $[Fe(CN)_5(Ph\text{-}p\text{-}X)_3]^{3-}$ species as redox mediators will be assessed.

EXPERIMENTAL

Reagent grade chemicals and triply-distilled water were used throughout. Tricyclohexylphosphine, triphenylarsine, triphenylantimony and triphenylphosphines with *p*-H, *p*-F, *p*-Cl, *p*-OCH_3, *p*-CH_3 and *p*-CF_3 substituents were obtained from Strem. Pentacyanoferrate(II) adducts with these ligands were prepared from $Na_3[Fe(CN)_5(NH_3)]\cdot 3H_2O$ by literature procedures,[6,8] vacuum-dried at room temperature and shown to be pure by elemental analyses for C, H and N (Desert Analytics, Tucson, Arizona). All Na_3[Fe

* Author to whom correspondence should be addressed.

$(CN)_5L]$ complexes subjected to electrochemical study were reported previously,[6,8] except for those where L = $P(C_6H_{11})_3(\cdot 5H_2O)$ and $P(C_6H_4\text{-}p\text{-}CF_3)_3$ $(\cdot 4H_2O)$.

Cyclic voltammograms of nitrogen-purged, 1 mM electroactive solute solutions thermostated to 25.0°C were carried out at a sweep rate of 50 mV s^{-1} with a Bioanalytical Systems CV–1B triangular wave generator and a Hewlett–Packard 7004B *X–Y* recorder. Carbon paste working, gold auxiliary and saturated calomel reference electrodes were employed in $I = 0.2$ M, buffered (HOAc/NaOAc) solutions containing 0.1 M each of sodium acetate and sodium nitrate supporting electrolytes. The carbon paste working electrode was renewed and polished prior to each series of scans on a $Na_3[Fe(CN)_5L]$ complex. Measured potentials were converted to the SHE scale by using hydroxyethylferrocene ($E_{1/2} = 402$ mV vs SHE) as an internal calibrant.[9,10] Reported half-wave potentials were calculated as the average of anodic and cathodic peak potentials ($i_{pa}/i_{pc} = 1.0$) and are the mean of at least three independent trials.

RESULTS AND DISCUSSION

Cyclic voltammograms of $K_4Fe(CN)_6$ and $Na_3[Fe(CN)_5L]$ (L = $P(C_6H_{11})_3$, $AsPh_3$, $SbPh_3$, $P(C_6H_4\text{-}p\text{-}X)_3$; X = H, F, Cl, OCH_3, CH_3, CF_3) in aqueous solution generally exhibit quasi-reversible, one-electron oxidation waves with peak-to-peak separations of 80–120 mV at a sweep rate of 50 mV s^{-1}; substantially larger ΔE_p values were found for $[Fe(CN)_5AsPh_3]^{3-}$ (180 mV) and $Fe(CN)_6^{4-}$ (260 mV), however. In all cases, half-wave potentials calculated as $(E_{pa} + E_{pc})/2$ are independent of sweep rate in the interval 50–300 mV s^{-1}. Table 1 summarizes the $E_{1/2}$ {iron(III,II)} data and represents a comparison with other pentacyanoferrate(III,II) couples of interest. Half-wave potentials of the $[Fe(CN)_5PPh_3]^{2-/3-}$ and $Fe(CN)_6^{3-/4-}$ couples are in reasonable agreement with potentiometrically-measured E^0 values of 0.54 and 0.40 V vs SHE, respectively ($I = 0.05$ M).[3]

As anticipated, $E_{1/2}$ increases substantially with electron-withdrawing capability of the X substituent in $[Fe(CN)_5P(Ph\text{-}p\text{-}X)_3]^{3-}$ complexes. Hammett plots of $E_{1/2}$ or $\log(K_X/K_H)$ ($= \{E_{1/2}(H) - E_{1/2}(X)\}/0.0591$) vs σ_p (Fig. 1) are reasonably linear, with least-squares slopes of 0.181 ± 0.015 and -3.06 ± 0.25, respectively (correlation coefficient = 0.987). In contrast, there is little change or consistent trend in thermodynamic oxidizability when the donor atom is varied from P to As to Sb while holding the phenyl substituent constant. Finally, it should be noted that the entire range in $E_{1/2}$ for triphenylphosphine complexes (0.140

Table 1. Half-wave potentials derived from the oxidation of $[(CN)_5Fe^{II}L]$ complexes[a]

L	$E_{1/2}\{Fe^{III,II}\}$ (V vs SHE)	$\log(K_X/K_H)$[b]	$\sigma_p(X)$[c]
CN^-	0.404		
	0.40[d]		
NH_3	0.33[d]		
H_2O	0.54[d]		
N_3^-	0.24[d]		
PPh_3	0.522	0.000	0.000
	0.54[d]		
P(cyclohexyl)$_3$	0.321		
P(Ph-*p*-OCH_3)$_3$	0.492	0.508	−0.268
P(Ph-*p*-CH_3)$_3$	0.505	0.288	−0.170
P(Ph-*p*-F)$_3$	0.557	−0.592	0.062
P(Ph-*p*-Cl)$_3$	0.585	−1.07	0.227
P(Ph-*p*-CF_3)$_3$	0.632	−1.86	0.54
$AsPh_3$	0.564		
$SbPh_3$	0.560		

[a] 25.0°C, pH 5.0, $I = 0.2$ M. Uncertainty in $E_{1/2}$ estimated at ±0.005 V.

[b] $\log(K_X/K_H) = [E_{1/2}(L = PPh_3) - E_{1/2}(L = P(Ph\text{-}p\text{-}X)_3)]/0.0591$.

[c] Hammett constant of *p*-X phenyl substituent.

[d] Reduction potentials reported in ref. 3 (25°C, $I = 0.05$ M).

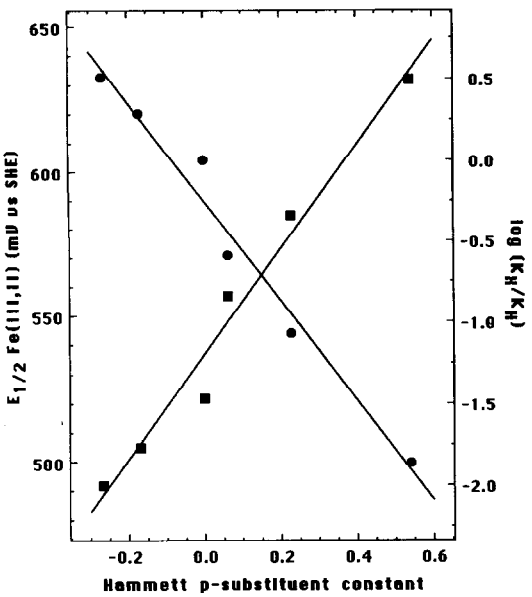

Fig. 1. Linear least-squares correlations of $[Fe(CN)_5P(Ph\text{-}p\text{-}X)_3]^{2-/3-}$ half-wave potentials (■) and $\log(K_X/K_H)$ values (●) with Hammett *p*-substituent constants; 25.0°C, $I = 0.2$ M, pH 5.0.

V) is modest when compared with the difference (0.201 V) between half-wave potentials for the $[Fe(CN)_5PPh_3]^{2-/3-}$ couple and its analogue with a saturated phosphine substituent, $[Fe(CN)_5P(cyclohexyl)_3]^{2-/3-}$. Looked at in perspective, the π-accepting capabilities of triphenylphosphines always exceed those of trialkylphosphines, even when the former contain effective electron-donating functions such as a methoxy group. All of the $Na_3[Fe(CN)_5P(Ph\text{-}p\text{-}X)_3]$ compounds considered here exhibit the electrochemical reversibility and aqueous solution stability characteristics required of biochemical redox mediators. Although the potential range spanned by these reductants is modest, few other suitable mediators are available in the 0.49–0.63 V vs SHE interval.[10]

Triphenylphosphine *p*-substituent effects on the oxidizability of $[Fe(CN)_5P(Ph\text{-}p\text{-}X)_3]^{3-}$ complexes are comparable to those of *p*-substituents on the phenylferricenium/phenylferrocene couple, for which the slope of a $\log(K_X/K_H)$ vs σ_p plot is -2.41.[11] In contrast, a much more negative ρ value of -8.43 pertains in the case of mono- and disubstituted ferrocenes in which substituents are directly bonded to the cyclopentadienyl rings.[12] With regard to phosphine-induced C-bonded to π-bonded chloranilate linkage isomerization with $[Pd(CA)(P\{Ph\text{-}p\text{-}X\}_3)_2]$, the ρ value of -3.12, characteristic of second phosphine ligand pre-equilibrium binding,[1] is surprisingly similar to that of -3.06 which governs $[Fe(CN)_5P(Ph\text{-}p\text{-}X)_3]^{2-}$ reduction, verifying that extensive polarization of the P donor atom accompanies ligation of palladium(II). The sensitivity of the linkage isomerization rate constant to phosphine basicity is considerably smaller ($\rho = -1.32$).[1]

Acknowledgement—We thank the Robert A. Welch Foundation (Grant D-735) for support of this research.

REFERENCES

1. W.-Y. Jeong and R. A. Holwerda, *Inorg. Chem.* 1989, **28**, 2674.
2. W.-Y. Jeong and R. A. Holwerda, *Inorg. Chem.* 1988, **27**, 2571.
3. R. Stasiw and R. G. Wilkins, *Inorg. Chem.* 1969, **8**, 156.
4. J. C. Cassatt and C. P. Marini, *Biochemistry* 1974, **13**, 5323.
5. P. Leupin, N. Al-Shatti and A. G. Sykes, *J. Chem. Soc., Dalton Trans.* 1982, 927.
6. H. Inoue, M. Sasagawa, E. Fluck and T. Shirai, *Bull. Chem. Soc., Jpn* 1983, **56**, 3434.
7. H. Inoue, M. Sasagawa and E. Fluck, *Z. Naturfor.* 1985, **40b**, 22.
8. R. Nast and K. W. Krüger, *Z. Anorg. Allg. Chem.* 1965, **341**, 189.
9. M. C. Garcia and R. A. Holwerda, *J. Inorg. Biochem.* 1987, **30**, 167.
10. R. Szentrimay, P. Yeh and T. Kuwana, in *Electrochemical Studies of Biological Systems* (Edited by D. T. Sawyer), ACS Symp. Ser. No. 38, p. 143. American Chemical Society, Washington, DC (1977).
11. J. G. Mason and M. Rosenblum, *J. Am. Chem. Soc.* 1960, **82**, 4206.
12. E. G. Perevalova, S. P. Gubin, S. A. Smirnova and A. N. Nesmeyanov, *Dokl. Ak. Nauk SSSR* 1964, **155**, 857.

Polyhedron Vol. 9, No. 20, pp. 2437–2442, 1990
Printed in Great Britain

0277–5387/90 $3.00+.00
© 1990 Pergamon Press plc

POTENTIOMETRIC INVESTIGATIONS ON THE CADMIUM(II)–AMINO ACID–IMIDAZOLE SYSTEMS (AMINO ACID = GLYCINE, DL-α-ALANINE OR DL-VALINE)

ZUBAIDA KHATOON and KABIR-UD-DIN*

Department of Chemistry, Aligarh Muslim University, Aligarh-202 002, India

(*Received* 6 *June* 1989; *accepted* 15 *January* 1990)

Abstract—The formation constants of mixed-ligand complexes of Cd^{II} with glycine, DL-α-alanine or DL-valine as primary ligands and imidazole as secondary ligand have been determined potentiometrically under physiological like conditions [temp. = 37°C, $\mu = 0.15$ (KNO_3)]. The formation constants for binary systems involving the amino acids and imidazole were also determined under identical conditions. The experimental pH-titration data were analysed using computer program SUPERQUAD. The relative stability of each ternary complex was compared with that of the corresponding binary complexes in terms of $\Delta \log K$ and $\log X$ values.

The ligand imidazole (IM) plays an important role in biochemistry because of its presence in histamine and histidine residues in proteins. The work reported on the interaction of serum albumin with zinc, cadmium and lead ions has demonstrated that the principal sites on the protein molecules responsible for metal binding are the IM group of histidine.[1,2] The effectiveness of the IM group for acting as a metal binding site was attributed to its great flexibility, its availability at physiological pH and its capacity to form both σ and π bonds with metal ions. The neutral IM coordinates via the tertiary nitrogen atom rather than the imino nitrogen of the heterocyclic ring.[4,5]

In the present work we are reporting results of potentiometric investigations on mixed-ligand complexes of Cd^{II} with glycine (GL), DL-α-alanine (AL) or DL-valine (VL) as primary ligands and IM as secondary ligand. Protonation constants of the free ligands, stoichiometry of binary and ternary complexes and their formation constants were computed by analysing the pH-titration data with SUPERQUAD computer program[6] which is an improved version of widely used MINIQUAD program.[7] The values of formation constants for ternary systems containing Cd^{II}–GL–IM were compared with literature values.[8] As no formation constant data on mixed-ligand systems of Cd^{II} with AL, VL and IM are available, the values are being reported for the first time in the present work.

EXPERIMENTAL

The ligands GL (BDH, India), AL, IM (BDH, England) and VL (SDS', India) were used as obtained. Ligand stock solutions were prepared by dissolving calculated amounts in doubly-distilled water. The IM stock solution was standardized by pH-titration with standard nitric acid. Stock solution of nitrate salt of Cd^{II} (S. Merck, India) was prepared in 0.05 M HNO_3. The metal content was determined by complexometric EDTA titration.[9]

Carbonate-free NaOH (the titrant) was prepared and standardized against standard potassium hydrogen phthalate solution.

All the titrations were performed at 37°C (±0.1) in a double-walled glass cell through the outer jacket of which water circulated from a constant temperature bath. Ionic-strength (μ) of all the solutions to be titrated was adjusted to 0.15 by adding requisite amounts of KNO_3. The initial volume of the titration solution in each case was 50 cm^3. Oxygen-free nitrogen gas was passed into the solutions before titrations and then over the solutions during titrations. The titrant was added to the cell

* Author to whom correspondence should be addressed. Present address: Department of Chemistry, Faculty of Science, Garyounis University, Benghazi, Libya.

and changes in pH were monitored with a digital pH-meter (ELICO, model LI-120, accuracy: ±0.01 pH unit) using ELICO type EK-62 glass and ELICO type ER-70 calomel electrodes. The pH standard was taken as 4.02 for 0.05 M potassium hydrogen phthalate solution. The electrode system was calibrated by the method of Irving *et al.*[10]

The pK_w of H_2O was taken to be 13.38 at 37°C and $\mu = 0.15$.[11]

Methods

The protonation constants of the free ligands were evaluated as described.[12]

In studying the binary systems, Cd^{II}–AA ratios were 1 : 3 and 1 : 6 while Cd^{II}–IM ratios were 1 : 13.5 and 1 : 22. In the ternary systems, Cd^{II}–AA–IM ratios were 1 : 2 : 4.5 and 1 : 2 : 8.7. The metal ion concentration was *ca.* 2×10^{-3} M. Nitric acid was used to lower the pH of initial solution mixtures in both the binary and ternary systems. The titrations were terminated when either the pH-meter readings became unstable showing a continuous downward drift or visual precipitations occurred.

Titration data analyses, using the SUPERQUAD program, were performed on a VAX-11/780 computer. The procedure used to select the correct equilibrium model was similar to those reported previously.[12,13] The model which gave the best statistical fit to the titration data, as suggested by Gans *et al.*,[6] was assumed to be the true model taking into account the systematic errors in the

Table 1. Protonation constants of free ligands and formation constants of binary and ternary complexes of Cd^{2+}

System	p	q	r	s	log β (S.D.)[a]	pH range	No. of titrations	No. of data points	σ	χ^2	Literature values
H^+–GL	0	1	0	1	9.29(0.02)	7.50–11.00	3	51	2.7	7	
	0	1	0	2	11.62(0.02)	2.00–4.20	3	42	2.6	14	
H^+–AL	0	1	0	1	9.41(0.05)	7.75–11.00	3	60	2.4	10	
	0	1	0	2	11.75(0.02)	2.00–4.50	3	41	1.6	7	
H^+–VL	0	1	0	1	9.31(0.03)	7.50–10.95	3	70	2.9	6	
	0	1	0	2	11.55(0.04)	2.05–4.50	3	51	1.3	9	
H^+–IM	0	0	1	1	6.91(0.00)	4.50–7.50	3	45	2.8	4	
Cd^{2+}–GL	1	1	0	0	4.26(0.01)	6.50–9.55	2	44	1.1	7	4.62,[b] 4.30[c]
	1	2	0	0	7.78(0.01)						6.59,[b] 7.70[c]
	1	3	0	0	10.11(0.04)						9.80[c]
	1	1	0	−2	−14.41(0.08)						
Cd^{2+}–AL	1	1	0	0	4.05(0.02)	6.60–9.60	2	42	1.5	3	4.24[c]
	1	2	0	0	7.25(0.04)						7.54[c]
	1	3	0	0	9.77(0.05)						9.54[c]
	1	1	0	−1	−4.89(0.08)						
	1	1	0	−2	−14.74(0.14)						
Cd^{2+}–VL	1	1	0	0	3.70(0.02)	6.40–9.35	2	44	2.6	11	3.95[c]
	1	2	0	0	6.62(0.06)						6.81[c]
	1	1	0	−1	−5.07(0.05)						
Cd^{2+}–IM	1	0	1	0	2.70(0.06)	4.70–8.20	2	67	3.5	5	2.74,[b] 2.62[d]
	1	0	2	0	4.98(0.06)						4.65[d]
Cd^{2+}–GL–IM	1	1	1	0	7.03(0.16)	6.00–9.50	2	53	1.2	8	8.03[b]
	1	1	2	0	9.37(0.06)						
	1	1	1	−1	−1.28(0.12)						
Cd^{2+}–AL–IM	1	1	1	0	6.72(0.15)	6.15-9.06	2	55	4.2	10	
Cd^{2+}–VL–IM	1	1	1	0	6.35(0.10)	6.20–9.10	2	68	2.4	7	

Temp. = 37°C; $\mu = 0.15$ (KNO_3).

[a] Standard deviation in log β.

[b] Ref. 8.

[c] C. P. S. Chandel and C. M. Gupta, *Bull. Chem. Soc. Jpn.* 1984, **57**, 2303; temp. = 30°C, $\mu = 1.0$.

[d] C. Tanford and M. L. Wagner, *J. Am. Chem. Soc.* 1953, **75**, 434; temp. = 35°C, $\mu = 0.15$.

experimental data. Finally, the results were assessed on the basis of σ and χ^2 values (for details of χ^2 statistics based on weighted residuals, see Ref. 14). Plots of residuals were also examined to assess the results.[6]

RESULTS AND DISCUSSION

Protonation constants of the free ligands

The protonation constants of ligands GL, AL, VL and IM, evaluated with the aid of the SUPERQUAD program,[12] are given in Table 1.

Binary systems

The formation constants of Cd^{II}–AA and Cd^{II}–IM binary complexes were determined under conditions identical with those of ternary systems, i.e. at 37°C and ionic-strength 0.15 (KNO_3). The values, given in Table 1, show good agreement with the literature values after allowing for changes in experimental conditions as well as in methods of calculation.

With the AAs, Cd^{II} formed $Cd(GL)^+$, $Cd(GL)_2$, $Cd(GL)_3^-$, $Cd(AL)^+$, $Cd(AL)_2$, $Cd(AL)_3^-$, $Cd(VL)^+$ and $Cd(VL)_2$ complexes. In each case, at least one hydroxy species was also detected. El-Ezaby *et al.*[8] have reported formation of a protonated species of Cd^{II} with GL at Cd^{II}–GL ratios of 1 : 1, 1 : 2 and 1 : 3. The stability order in terms of ligands has been found to be GL > AL > VL. The higher stability of GL complexes can be explained due to absence of alkyl chain in GL. Substitution of the methyl group on the α-carbon atom produces a small decrease in $\log\beta$ values but further lengthening of the GL skeleton shows a marked influence on stability.

Under our experimental conditions, formation of only two complexes, *viz.* $Cd(IM)^{2+}$ and $Cd(IM)_2^{2+}$, was observed with IM. Higher species were taken into consideration but were rejected during the refinement.

Distribution curves for various species of Cd^{II} formed in the binary systems with GL, AL, VL or IM as a function of pH at AA = 0.012 M and IM = 0.044 M are shown in Fig. 1.

Ternary systems

The general four-component equilibrium can be written as:

$$pM + q(AA) + r(IM) + sH \rightleftharpoons M_p(AA)_q(IM)_rH_s \quad (1)$$

(p, q, r, s are the stoichiometric coefficients corresponding to Cd^{2+}, AA^-, IM and H^+, respectively; charges are omitted for brevity).

The overall formation constants are defined as:

$$\beta_{pqrs} = \frac{[M_p(AA)_q(IM)_rH_s]}{[M]^p[AA]^q[IM]^r[H]^s}. \quad (2)$$

In the present work results of three mixed-ligand systems, *viz.* Cd^{II}–GL–IM, Cd^{II}–AL–IM and Cd^{II}–VL–IM, are reported. The studies were performed in the pH range 6.0–9.5.

A number of models in sequence were examined with the SUPERQUAD program. Those models were rejected for which value(s) of σ and/or χ^2 were large. Formation constants for the best models examined for the ternary complexes are reported in Table 1. Slight variations in the values of the protonation constants and the formation constants of the binary complexes had no effect on the chosen ternary model; however, the changes observed in the formation constants for the latter were within the experimental error.

For Cd^{II}–GL–IM system, formation of 1 : 1 : 1 : 0, 1 : 2 : 2 : 0 and 1 : 1 : 1 : −1, while for the other systems only 1 : 1 : 1 : 0 complex species have been detected.

The parameters $\Delta\log K_1$, $\Delta\log K_2$, $\log X$ and $\Delta\log\beta$ are generally used to indicate the relative stability of ternary complexes as compared with the binary ones; these are given in Table 2. $\Delta\log K_1$, $\Delta\log K_2$ and $\log X$ represent the formation constants for equilibria (3), (5) and (7) and are calculated from relations (4), (6) and (8), respectively. $\Delta\log\beta$ is the difference between the experimental and the calculated values of β (calculated on the basis of statistical grounds).

$$Cd(AA) + Cd(IM) \rightleftharpoons Cd(AA)(IM) + Cd \quad (3)$$

$$\Delta\log K_1 = \log\beta_{Cd(AA)(IM)} - [\log\beta_{Cd(AA)} + \log\beta_{Cd(IM)}] \quad (4)$$

$$Cd(AA) + Cd(IM)_2 \rightleftharpoons Cd(AA)(IM)_2 + Cd \quad (5)$$

Table 2. The values of $\Delta\log K_1$, $\Delta\log K_2$, $\log X$ and $\Delta\log\beta_{1110}$ for Cd^{II}–AA–IM ternary systems

	AA		
Parameter	GL	AL	VL
$\Delta\log K_1$	0.07	−0.03	−0.05
$\Delta\log K_2$	0.13		
$\log X$	1.29	1.21	1.10
$\Delta\log\beta_{1110}$	0.34	0.30	0.25

Temp. = 37°C; μ = 0.15 (KNO_3).

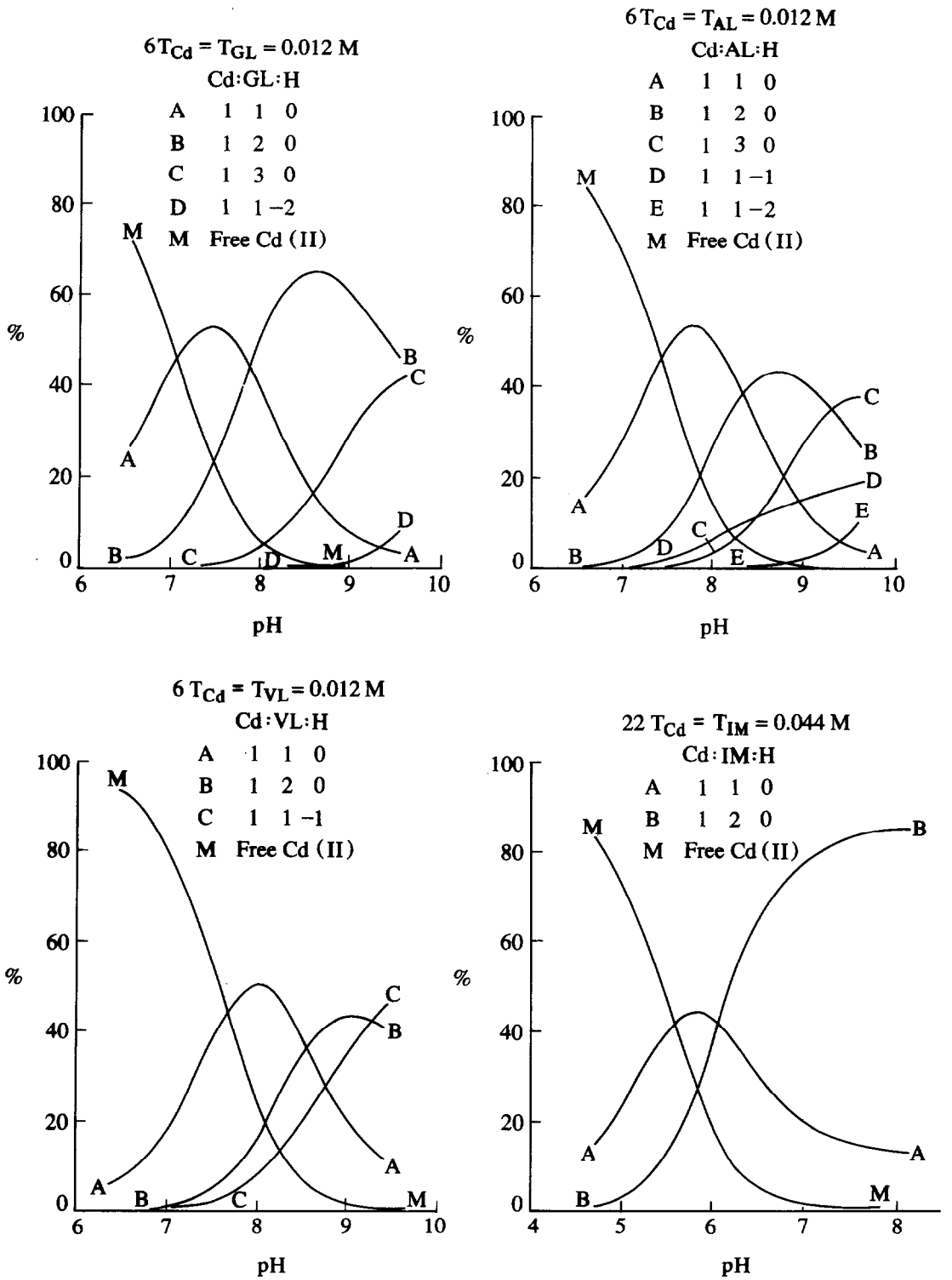

Fig. 1. SUPERQUAD computed species distributions with pH for binary systems of Cd^{II}.

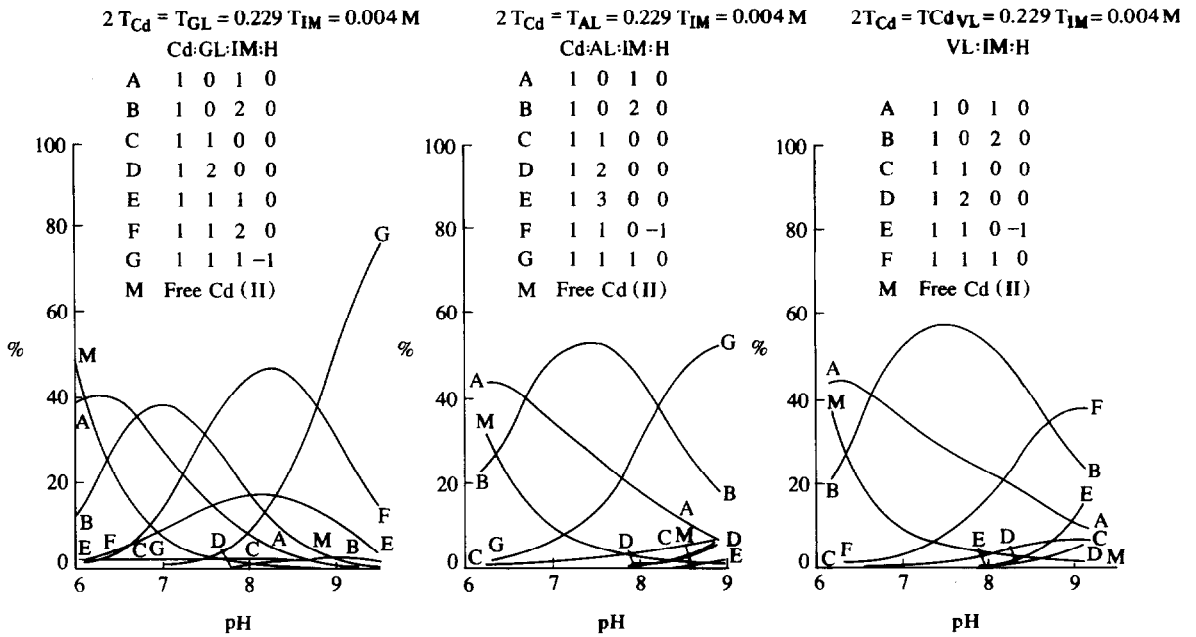

Fig. 2. SUPERQUAD computed species distributions with pH for ternary systems of Cd^{II}.

$$\Delta \log K_2 = \log \beta_{Cd(AA)(IM)_2} - [\log \beta_{Cd(AA)} + \log \beta_{Cd(IM)_2}] \quad (6)$$

$$Cd(AA)_2 + Cd(IM)_2 \rightleftharpoons 2Cd(AA)(IM) \quad (7)$$

$$\log X = 2 \log \beta_{Cd(AA)(IM)} - [\log \beta_{Cd(AA)_2} + \log \beta_{Cd(IM)_2}] \quad (8)$$

$$\Delta \log \beta = \log \beta(\text{exptl}) - \log \beta(\text{calcd}). \quad (9)$$

$\Delta \log K_1$ values which are very close to zero indicate no marked stabilization of the 1:1:1:0 ternary complexes of Cd^{II} formed by equilibrium (3). In other words, imidazole binds better to Cd^{II} than to the binary $Cd(AA)^+$ complexes. This is due to the fact that more coordination positions are available on Cd^{II} than on $Cd(AA)^+$ complexes. However, positive values of $\log X \simeq 1$ (which are greater than the statistical value of 0.6) show that the formation of 1:1:1:0 ternary complexes is favoured by equilibrium (7) or, in other words, 1:2 binary species are less stable than the 1:1:1:0 ternary species. Positive values of $\Delta \log \beta_{1110}$ also show higher stability for the 1:1:1:0 mixed-ligand species compared to binary ones. For the $Cd(GL)(IM)_2^+$ ternary complex, the value of $\Delta \log K_2$ is near to zero showing no marked stabilization over the present binary ones or, in other words, equilibrium (5) is not much favoured in the right direction. Addition of two IM molecules to Cd^{II} and to $Cd(GL)^+$ were equally favoured.

The speciation plots (Fig. 2) of Cd^{II}–AA–IM ternary systems at 1:2:8.7 ratio show that the respective values of maximum concentrations for 1:1:1:0 species were 17.5, 52.5 and 36% respectively with GL, AL and VL while maximum concentration of $Cd(GL)(IM)_2^+$ was 47%. In the case of the Cd^{II}–GL–IM system, formation of the hydroxy species started at *ca.* pH 7 and was *ca.* 76% at pH 9.5.

Acknowledgements—We thank the Chairman, Department of Chemistry, for providing necessary facilities. One of us (Z.K.) is grateful to the CSIR (India) for awarding a SRF.

REFERENCES

1. C. Tanford, *J. Am. Chem. Soc.* 1952, **74**, 211.
2. F. R. N. Gurd and D. S. Goodman, *J. Am. Chem. Soc.* 1952, **74**, 670.
3. H. C. Freeman, *Inorganic Biochemistry*. Elsevier, Amsterdam/New York (1973).
4. L. Hunter and J. A. Marriot, *J. Chem. Soc.* 1941, 777.
5. T. J. Lane and K. P. Quinalan, *J. Am. Chem. Soc.* 1960, **82**, 2994.
6. P. Gans, A. Sabatini and A. Vacca, *J. Chem. Soc., Dalton Trans.* 1985, 1195.
7. (a) A. Sabatini, A. Vacca and P. Gans, *Talanta* 1974,

21, 53; (b) P. Gans, A. Sabatini and A. Vacca, *Inorg. Chim. Acta* 1976, **18**, 237; (c) M. Micheloni, A. Sabatini and A. Vacca, *Inorg. Chim. Acta* 1977, **25**, 41.
8. M. S. El-Ezaby, M. Rashad and N. M. Moussa, *Polyhedron* 1983, **2**, 245.
9. C. N. Reilley, R. W. Schmid and F. Sadek, *J. Chem. Edu.* 1959, **36**, 555, 619.
10. H. M. Irving, M. G. Miles and L. D. Pettit, *Anal. Chim. Acta* 1967, **38**, 475.
11. G. Berthon, P. M. May and D. R. Williams, *J. Chem. Soc., Dalton Trans.* 1978, 1433.
12. Zubaida Khatoon and Kabir-ud-Din, *Transition Met. Chem.* 1989, **14**, 34.
13. Zubaida Khatoon and Kabir-ud-Din, *Transition Met. Chem.* 1990, **15**, 217.
14. A. Vacca and A. Sabatini, *Computational Methods for the Determination of Formation Constants* (Edited by D. J. Legget). Plenum Press, New York (1985).

Polyhedron Vol. 9, No. 20, pp. 2443–2447, 1990
Printed in Great Britain

0277–5387/90 $3.00+.00
© 1990 Pergamon Press plc

COMPLEXING ABILITY OF BIS(PHENYL-2-PICOLYLKETONATO)COPPER(II) TOWARDS DIFFERENT METAL(II) AND METAL(III) SALTS

ALI EL-DISSOUKY* and ADEL Z. EL-SONBATI

Chemistry Departments, Faculties of Science, Alexandria and Mansoura Universities, Egypt

(*Received* 4 *October* 1989; *accepted* 3 *April* 1990)

Abstract—A series of binuclear and trinuclear adducts of the bis(phenyl-2-picolylketonato)copper(II), $[Cu(PPK)_2]$, were prepared with Mg^{2+}, Ca^{2+}, Co^{2+}, Ni^{2+}, Cu^{2+}, La^{3+}, Nd^{3+} and UO_2^{2+} salts. The metal halides gave the binuclear adducts, while the nitrates gave trinuclear adducts. The spectral data show that the planarity of the copper(II) environment in the binuclear adducts is higher, while that in the trinuclear adducts is lower compared to that in the mononuclear complex. Furthermore, the planarity of the adducts was found to be inversely proportional to the ionic radius of the M^{2+} ion in the binuclear adducts. The magnetic susceptibilities of $[Cu(PPK)_2CuX_2]$ and $[\{Cu(PPK)_2\}_2Cu(NO_3)_2]$ complexes were studied over the temperature range of 766–300 K. The magnetic parameters were found to be related to the stereochemistry around the bridging ligand.

In earlier studies,[1–6] the formation and characterization of the complexes of some heterocyclic nitrogen-containing keto-enolates were reported. However, no work has been traced concerning the complexing ability of these complexes. In this paper we report the synthesis and characterization of some binuclear and trinuclear adducts of the bis(phenyl-2-picolylketonato)copper(II) with some metal(II), metal(III) and UO_2^{2+} salts. This work is of interest because of the interesting magnetic and electronic properties of the adducts which are formed. Furthermore, the binuclear and trinuclear copper(II) adducts provide models for metalloenzymes.

EXPERIMENTAL

Physical measurements

Electronic and IR spectra were measured on Pye Unicam SP8-400 and SP3-300 spectrophotometers, respectively. Magnetic susceptibilities were measured on a Faraday magnetic balance and using $HgCo(SCN)_4$ as magnetic susceptibility standard. Molar conductivities were measured on 10^{-3} M solutions of the complexes in nitrobenzene at 20°C using a systronics (303 model) with direct reading conductivity meter. The elemental analyses given in Table 1, were carried out at the Microanalysis Unit at the University of Manchester, U.K. The metal analyses were made using a Chimatzu absorption-flame photometer, Model AA-610S.

Synthesis of the complexes

All chemicals were analar reagent grade and used as supplied. Bis(phenyl-2-picolylketonato) copper(II) was prepared as reported earlier.[1] The binuclear adducts with the general formula $[Cu(PPK)_2MX_2]$ ($M = Mg^{2+}$, Ca^{2+}, Co^{2+}, Ni^{2+} or Cu^{2+} and $X = Cl^-$ or Br^-) were prepared by the general method, *viz.* a suspension of $[Cu(PPK)_2]$ (0.01 mol) in absolute ethanol (30 cm^3) containing MX_2 (0.012 mol). This mixture was stirred at room temperature for 6–8 h and filtered. The filtrate was allowed to stand for 24–36 h at room temperature. The fine crystalline product which was formed in each case was collected by filtration and recrystallized from ethanol. Yield: 82–94%.

* Author to whom correspondence should be addressed. Present address: Chemistry Department, Faculty of Science, Alexandria University, Alexandria, Egypt.

The trinuclear complexes $[\{Cu(PPK)_2\}_2M(NO_3)_n]$ (M = Ca^{2+}, Co^{2+}, Ni^{2+}, Cu^{2+}, Mg^{2+}, La^{3+}, Nd^{3+} or UO_2^{2+} and $n = 2$ or 3) were prepared as follows. Hydrated metal nitrate (0.015 mol) was added to 50 cm^3 of the appropriate solvent (THF, Me_2CO or EtOH) containing $[Cu(PPK)_2]$ (0.03 mol). The reaction mixture was refluxed for 15–20 min, cooled to room temperature and the solid product was collected in each case by filtration and recrystallized from the suitable solvent(s). Yield: 66–79%.

RESULTS AND DISCUSSION

Bis(phenyl-2-picolylketonato)copper(II) reacts with metal(II) and metal(III) halides giving only the binuclear adducts, $[Cu(PPK)_2MX_2]$, while with the metal(II) and metal(III) nitrates, the trinuclear adducts, $[\{Cu(PPK)_2\}_2M(NO_3)_n]$, are formed, Table 1. The adducts are air-stable and decompose above 300°C. They are also soluble in most common organic solvents but can be recovered unchanged from their solution when using non-coordinating solvents. In the solvents such as Py, DMF or DMSO, a drastic change in the colour was observed. This could be due to the dissociation of the adducts and/or formation of new compounds. However, further studies will be performed in the future on the effects of the counter ions and the coordinating solvents on the formation and the behaviour of such adducts.

The molar conductivity of the adducts, Table 1, indicate their non-electrolytic nature.

The IR spectra of PPK and $[Cu(PPK)_2]$ were discussed in previous communications.[1-4] The spectra of the binuclear and trinuclear adducts under investigation exhibit a medium band at 1400–1410 cm^{-1}, due to ν(C—O), compared to that at 1440 cm^{-1} in the complex,[2,3] $[Cu(PPK)_2]$, consistent with the withdrawal of electron density from the oxygen

Table 1. Analytical data and some physical properties of the adducts

Compound	Colour	Decomposition[a] temperature	Λ_M[b]	% Found (% Calc.) C	H	N	Cu	M
$[Cu(PPK)_2CuCl_2]$	Olive green	228	2.08	52.3 (52.9)	3.3 (3.4)	4.6 (4.8)	21.3 (21.5)	
$[Cu(PPK)_2CuBr_2]$	Green	256	1.96	45.7 (45.9)	3.0 (2.9)	3.9 (4.1)	18.6 (18.7)	
$[Cu(PPK)_2CoCl_2]$	Dark green	235	2.00	52.9 (53.3)	3.4 (3.4)	4.9 (4.8)	11.0 (10.9)	10.0 (10.1)
$[Cu(PPK)_2NiCl_2]$	Dark green	220	3.23	53.0 (53.3)	3.3 (3.4)	4.9 (4.8)	11.0 (10.8)	10.2 (10.0)
$[Cu(PPK)_2NiBr_2]$	Olive green	247	2.18	49.9 (46.3)	2.9 (3.0)	4.3 (4.2)	9.4 (9.4)	8.8 (8.7)
$[Cu(PPK)_2MgCl_2]$	Light green	219	3.00	56.1 (56.6)	3.6 (3.6)	5.2 (5.1)	11.3 (11.5)	4.4 (4.4)
$[Cu(PPK)_2CaCl_2]$	Light green	222	3.18	54.8 (55.1)	3.4 (3.5)	5.0 (4.9)	11.3 (11.2)	7.0 (7.1)
$[\{Cu(PPK)_2\}_2Cu(NO_3)_2]$	Violet	289	4.10	56.3 (56.8)	3.7 (3.6)	7.5 (7.7)	17.5 (17.4)	
$[\{Cu(PPK)_2\}_2Ni(NO_3)_2]$	Purple	301	2.08	56.7 (57.1)	3.6 (3.7)	7.7 (7.6)	11.5 (11.6)	5.5 (5.4)
$[\{Cu(PPK)_2\}_2Ca(NO_3)_2]$	Reddish-brown	278	2.80	57.6 (58.0)	3.8 (3.7)	7.5 (7.8)	11.6 (11.8)	3.8 (3.7)
$[\{Cu(PPK)_2\}_2Mg(NO_3)_2]$	Reddish-brown	291	2.92	58.7 (58.9)	3.9 (3.8)	8.1 (7.9)	12.0 (12.0)	2.3 (2.3)
$[\{Cu(PPK)_2\}_2La(NO_3)_3]$	Brown	342	2.00	50.2 (50.5)	3.1 (3.2)	8.0 (7.9)	10.3 (10.3)	
$[\{Cu(PPK)_2\}_2Nd(NO_3)_3]$	Brown	336	3.40	50.0 (50.3)	3.2 (3.2)	8.1 (7.9)	10.1 (10.2)	
$[\{Cu(PPK)_2\}_2UO_2(NO_3)_2]$	Yellow–brown	346	2.96	46.1 (46.7)	2.9 (3.0)	7.5 (7.3)	9.5 (9.5)	

[a] Decomposition temperature (°C).

[b] Molar conductivity of 10^{-3} M solution in nitrobenzene at 25 ± 1°C.

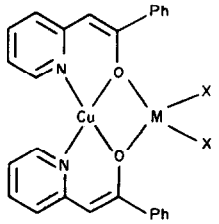

M = Ca^{2+}, Mg^{2+}, Co^{2+}, Ni^{2+} or Cu^{2+} and X = Cl^- or Br^-

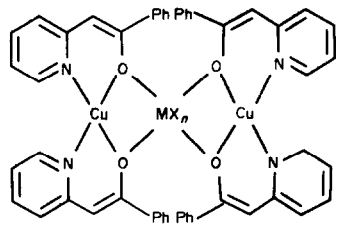

M = Mg^{2+}, Ca^{2+}, Ni^{2+} or Cu^{2+}; $n = 2$
M = La^{3+} or Nd^{3+}; $n = 3$
X = NO_3^-

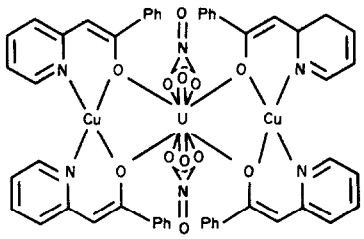

(I)

atom due to polymerization. In addition, the spectra of all the complexes display bands in the region 1580–1586 cm^{-1} compared to those at 1605 cm^{-1} in the spectrum of $[Cu(PPK)_2]$. This band could be assigned to the ν(C=N) of the pyridine moiety. The spectra of all the binuclear adducts contain bonds at 288–296 and 222–218 cm^{-1}, characteristic of coordinated, terminal ν(M—Cl) and ν(M—Br), respectively. The IR spectra of the nitrato complexes (except of uranyl) display absorption bands at 1440–1460 (ν_1), 1026–1030 (ν_2), 742–738 (ν_3), 1340–1378 (ν_4), 712–718 (ν_5) and 810–815 cm^{-1} (ν_6). Such bands are not observed in PPK or $[Cu(PPK)_2]$, and are consistent with the coordinated nitrato group.[7] Moreover, two weak bands are also observed due to the nitrato combination mode at 1700–1800 cm^{-1}. The magnitudes of separation of ν_1 and ν_4 of *ca* 82–100 cm^{-1} indicate the exclusive presence of the monodentate coordinating nitrato group and clearly eliminate the presence of ionic NO_3^-. In the case of the uranyl trinuclear adduct, the spectrum shows a series of bands at 1150 (ν_1), 1285 (ν_4), 1302 (ν_2), 740 (ν_3), 712 (ν_5) and 816 (ν_6), in addition to two weak bands at 1780 and 1736 cm^{-1}. The separation of ν_1 and ν_4 of 265 cm^{-1} and the separation of the combination modes of 44 cm^{-1} indicate the bidentate nature of NO_3^- in the uranyl complex. According to the elemental analyses, conductivity measurements and IR data, structures **Ia**, **Ib** and **Ic** could be assumed for the binuclear and trinuclear adducts. The possibility of the presence of both mono- and bidentate nitrato groups together is ruled out as these would require four bands (two sets corresponding to each type of coordination)[8] in the range 1700–1800 cm^{-1}.

The absorption electronic spectral bands and the extinction coefficients of the *d–d* bands are given in Table 2. The complex, $[Cu(PPK)_2]$, showed a *d–d* band centred at 18,000 cm^{-1}. On the other hand, the binuclear adducts $[Cu(PPK)_2CuX_2]$ (X = Cl^- or Br^-) presented two bands around 18,600–18,700 and 10,600–10,700 cm^{-1}. These are assigned to the *d–d* bands of CuN_2O_2 and CuO_2X_2, respectively. Furthermore, the spectrum of $[\{Cu(PPK)_2\}_2 Cu(NO_3)_2]$ exhibits two asymmetric ligand-field bands at 18,900 and 15,700 cm^{-1}. It is reasonable to assign the high-frequency band to the *d–d* transition for CuN_2O_2 and the low-frequency band to the CuO_6 chromophore. In addition to the *d–d* transition band characteristic of CuN_2O_2 in the binuclear complexes, $[Cu(PPK)_2MX_2]$ (M = Co^{2+} or Ni^{2+} and X = Cl^- or Br^-), the spectra exhibit bands at 15,400 and 14,800 cm^{-1} characteristic of tetrahedral cobalt(II) and at 20,700–20,800 cm^{-1} due to a square-planar nickel(II), as proved by the magnetic data. From the data given in Table 2, one could conclude that the planarity of the CuN_2O_2 chromophore in the binuclear complexes increases

Table 2. Room temperature magnetic moments and the electronic absorption spectra[a] of the adducts

Compound	μ_{eff} (BM)	$\bar{\nu}$ (cm^{-1}) (log ε)
$[Cu(PPK)_2CuCl_2]$	1.56	18,600 (2.62), 10,700 (2.18)
$[Cu(PPK)_2CuBr_2]$	1.48	18.600 (2.71), 10,600 (2.18)
$[Cu(PPK)_2CoCl_2]$	4.03	18.000 (2.54), 15,400, 14,800 (2.50)
$[Cu(PPK)_2NiCl_2]$	1.74	18,800 (2.49), 20,700 (2.30)
$[Cu(PPK)_2NiBr_2]$	1.76	18,800 (2.56), 20,700 (2.30)
$[Cu(PPK)_2MgCl_2]$	1.73	18,000 (2.50)
$[Cu(PPK)_2CaCl_2]$	1.74	18,000 (2.56)
$[\{Cu(PPK)_2\}_2Cu(NO_3)_2]$	1.52	17,700 (2.36), 10,000 (1.30)
$[\{Cu(PPK)_2\}_2Ni(NO_3)_2]$	1.49	17,700 (2.43), 10,000 (1.08)
$[\{Cu(PPK)_2\}_2Ca(NO_3)_2]$	1.56	17,700 (2.32), 10,000 (1.04)
$[\{Cu(PPK)_2\}_2Mg(NO_3)_2]$	1.62	17,700 (2.48), 10,000 (1.06)
$[\{Cu(PPK)_2\}_2La(NO_3)_3]$		17,500 (2.51), 10,000 (1.06)
$[\{Cu(PPK)_2\}_2Nd(NO_3)_3]$		17,500 (2.49), 10,100 (1.06)
$[\{Cu(PPK)_2\}_2UO_2(NO_3)_2]$	1.76	17,500 (2.48), 10,000 (1.03)

[a] Ethanolic solution.

in the order, $Ni^{2+} > Co^{2+} > Mg^{2+} > Ca^{2+} > La^{3+}$. Thus it is assumed that this effect becomes greater as the size of the second metal ion decreases.

The electronic spectra of the lanthanide(III) and uranyl adducts display one broad band around 17,500–17,600 cm^{-1} and a much weaker one appears in some cases around 10,000 cm^{-1}. The shift of the band characteristic of CuN_2O_2 towards lower energy could be described in terms of the distortion increase of the nearly planar copper(II) environments towards the tetrahedral geometry in these trinuclear adducts. Furthermore, for the alkaline earth and *d*-metal ions, in the trinuclear adducts, this band appears around 17,500–17,700 cm^{-1} indicating a higher distortion decrease towards the tetrahedral geometry relative to the lanthanides. However, in several cases, the appearance of one broad band of relatively low intensity is consistent with rather symmetrical structues. By combining both the well-known tendency of the copper(II) ion to expand its coordination sphere and the existing ambiguity in the assignments of a certain geometry based upon electronic spectra,[9] the spectra of the present adducts may also represent apical expansion through cation–solvent or anion-bridged interactions towards a distorted octahedron.

The magnetic susceptibilities of the formed adducts were measured in the temperature range 76–300 K. The room temperature magnetic moments are given in Table 2. The variable temperature magnetic susceptibilities for trinuclear and binuclear copper(II) adducts are shown in Fig. 1. The room temperature magnetic moments for the

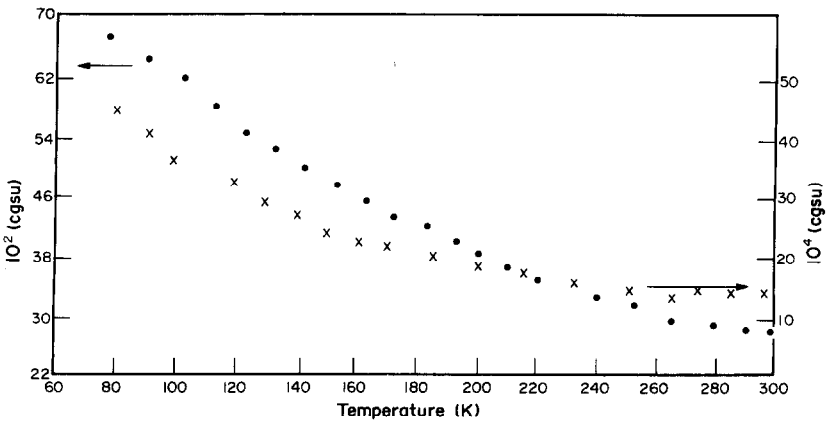

Fig. 1. Magnetic susceptibilities/mol vs temperature curves for: $[Cu(PPK)_2CuCl_2]$ (●) and $[\{Cu(PPK)_2\}_2Cu(NO_3)_2]$ (×).

copper adducts were found to be lower than the expected spin-only value for an unpaired electron on each copper(II). Using the Bleaney–Bowers equation [eq. (1)] for binuclear adducts and eq. (2) for trinuclear adducts,[10] the magnetic parameters were determined by best fit techniques; $g = 2.068$ and $J = -42$ cm^{-1} for $[Cu(PPK)_2CuCl_2]$; $g = 2.066$ and $J = -39$ cm^{-1} for $[Cu(PPK)_2CuBr_2]$; and $g = 2.052$ and $J = -36$ cm^{-1} for $[\{Cu(PPK)_2\}_2Cu(NO_3)_2]$. In all cases N_α was found to be 60×10^{-6} cgs/Cu^{2+}.

$$\chi_A = \left[\frac{N\beta^2 g^2}{3kT}\right][1 + 1/3 \exp^{-2J/kT}]^{-1} + N_\alpha \quad (1)$$

$$\chi_A = \left[\frac{N\beta^2 g^2}{12kT}\right]\left[\frac{e^{2x} + 10e^{3x} + 1}{e^{2x} + 2e^{3x} + 1}\right] + N_\alpha, \quad (2)$$

where $x = -J/kT$ and the other symbols have their usual meanings. The values of J indicate that the spin of the adjacent copper ions are antiferromagnetically coupled. It should be indicated here that the analytical, spectral and the magnetic data support the polynuclear nature of these complexes, with the overall symmetry being low and the g values not being appreciably different from 2.0. The low values of J obtained for the binuclear complexes could be attributed to the distortion and the low symmetry around the bridging oxygen. This distortion (towards planarity) leads to a decrease of the super-exchange integral through the oxygen bridge, resulting in a lower absolute value of J.

REFERENCES

1. M. F. El-Shazly, T. M. Salem, A. M. Hindawey and A. El-Dissouky, *Inorg. Chim. Acta* 1977, **25**, 55.
2. A. El-Dissouky, S. A. El-Shazly and M. Gaafar, *Transition Met. Chem.* 1983, **8**, 175.
3. A. El-Dissouky, G. B. Mohamad and A. Z. El-Sonbati, *Inorg. Chim. Acta* 1983, **74**, 279.
4. A. El-Dissouky and L. S. Refaat, *Inorg. Chim. Acta* 1984, **87**, 213.
5. A. El-Dissouky, A. M. Hindawey and A. Abdel-Salam, *Inorg. Chim. Acta* 1986, **119**, 207.
6. A. El-Dissouky, A. Fahmy and A. Amer, *Inorg. Chim. Acta* 1987, **133**, 311.
7. K. Nakamoto, *Infrared Spectra of Inorganic and Coordination Compounds*. John Wiley, New York (1970).
8. I. S. Ahuja, R. Singh and C. P. Rai, *J. Molec. Struct.* 1978, **49**, 201.
9. E. D. McKenzie, *J. Chem. Soc. A* 1970, 3095.
10. B. Bleany and K. D. Bowers, *Proc. R. Soc., Lond. Ser. A.* 1952, **214**, 451.

Polyhedron Vol. 9, No. 20, pp. 2449–2453, 1990
Printed in Great Britain

0277–5387/90 $3.00+.00
© 1990 Pergamon Press plc

CHARACTERIZATION AND ELECTRICAL PROPERTIES OF MoO_2Cl_2 COMPLEXES WITH N-ARYL-N′-(SUBSTITUTED THIAZOLYL) THIOUREAS AND UREAS

K. L. MADHOK* and CHITRA GUPTA

School of Studies in Chemistry, Jiwaji University, Gwalior-474011 (M.P.) India

(*Received* 29 *January* 1990; *accepted* 1 *May* 1990)

Abstract—MoO_2Cl_2 formed six-coordinate complexes with N-(substituted)-N′-(substituted thiazolyl) thioureas and ureas of the general formula $[MoO_2(RNHC{=}SNHR')_2]Cl_2$ and $[MoO_2(RNHC{=}ONHR')_2]Cl_2$, where R = thiazolyl, 4-phenyl and 5-nitrothiazolyl groups and R′ = $-C_2H_5$, $-C_6H_5$, *o*-$C_6H_4(CH_3)$, *p*-$C_6H_4(CH_3)$ and $-C_6H_5CO$. The complexes have been characterized by elemental analysis, molar conductance, magnetic susceptibility, IR, UV–vis and ^1H NMR spectral data. Electrical measurements show that the room temperature conductivities range from 2.3×10^{-8} to 4×10^{-4} Ω^{-1} cm^{-1}. The activation energies (E_a) for conduction have been determined.

The chemistry of oxomolybdenum(VI) complexes involving NS-, SS- and SO-donor ligands has interested coordination chemists in recent years, as evidenced by the flurry of papers published in this area.[1–7] Most simple molybdenum(VI) coordination compounds contain the *cis*-dioxo MoO_2^{2+} cation. Complexes of the type MoO_2L_2 are known,[8–10] where L is a molecule of bidentate Schiff base. Electrical properties of several metal—copper(II), cobalt(II), nickel(II) and platinum(II)—complexes have been investigated.[11–13] Applications of metal complexes as semiconductors[14] and for gas detection[15] have been reported. Earlier communications[16–24] have described the metal chelates of C=S, C=O and C=NH donor ligands, but nothing is reported on the synthesis and physicochemical properties of dioxodichloro-Mo^{VI}-N-aryl-N′-(substituted thioazolyl) thioureas and ureas which was the subject of the present work.

EXPERIMENTAL

All the chemicals used were either BDH "AnalaR" quality or E. Merck "GR" quality. The ligands N-aryl-N′-(substituted thiazolyl) thioureas and N-aryl-N′-(substituted thiazolyl) ureas were prepared[25] by refluxing substituted-2-aminothiazole with respective isothiocyanates, RNCS, and isocyanates, RNCO, where R is alkyl, aryl or substituted aryl groups. The purity of these ligands was checked by melting point, elemental analysis and IR spectral studies.

General method for the preparation of MoO_2Cl_2 *complexes*

All the preparative work of metal complexes was carried out in a dry box. MoO_2Cl_2 was prepared by Zado's method[26] and characterized on the basis of elemental analyses and IR peaks. Molybdenum(VI) dioxydichloride complexes were prepared by the following general method. An ethereal solution of the ligand (50 cm^3, 0.2 M) was added dropwise, with constant stirring, to an ethereal solution of an equal volume (0.1 M) of anhydrous MoO_2Cl_2. During the course of the reaction the temperature was maintained below 10°C. After addition of the ligand was complete, the reaction mixture was allowed to stand for 2 h to attain equilibrium. A coloured complex separated out in most of the cases. In the cases of *o*-T4PTTU, *p*-T4PTTU, *o*-T5TTU and *p*-T5NTTU, the coloured complexes were separated out by distilling off the excess solvent. Complex compounds thus obtained were washed several times with dry ether until free of excess ligand and then dried *in vacuo*. The complexes were characterized on the basis of their melting points and elemental analyses (Table 1). Molyb-

* Author to whom correspondence should be addressed.

Table 1. Analytical data of MoO_2Cl_2 complexes with N-Aryl-N′-(substituted thiazolyl) thioureas and ureas

Compound	Formula (Empirical)	Melting point (°C)	Analysis of the complexes % Found Mo	S	Cl	% Calculated Mo	S	Cl
Molybdenum dioxydichloride (M)	MoO_2Cl_2 Yellow–Orange	—	48.5	—	35.5	48.7	—	35.0
M·2PTTU	$MoO_2Cl_2 \cdot 2C_{10}H_9N_3S_2$	135	14.1	19.3	10.7	14.4	19.1	10.6
M·2*o*-TTTU	$MoO_2Cl_2 \cdot 2C_{11}H_{11}N_3S_2$	132	13.8	18.4	10.2	13.8	18.4	10.2
M·2*p*-TTTU	$MoO_2Cl_2 \cdot 2C_{11}H_{11}N_3S_2$	134	13.7	18.4	10.0	13.8	18.4	10.2
M·2BzTTU	$MoO_2Cl_2 \cdot 2C_{11}H_9N_3S_2O$	145	13.3	17.6	9.8	13.2	17.7	9.8
M·2EtTTU	$MoO_2Cl_2 \cdot 2C_6H_9N_3S_2$	127	16.6	22.4	12.3	16.8	22.3	12.4
M·2PTU	$MoO_2Cl_2 \cdot 2C_{10}H_9N_3SO$	145	15.0	20.0	11.0	15.1	20.1	11.2
M·2P5NTTU	$MoO_2Cl_2 \cdot 2C_{10}H_8N_4S_2O_2$	140	12.8	17.0	9.3	12.7	16.9	9.4
M·2OT5NTTU	$MoO_2Cl_2 \cdot 2C_{11}H_{10}N_4S_2O_2$	142	12.4	16.4	9.0	12.2	16.3	9.0
M·2*p*-T5NTTU	$MoO_2Cl_2 \cdot 2C_{11}H_{10}N_4S_2O_2$	139	12.0	16.4	9.0	12.2	16.3	9.0
M·2Bz5NTTU	$MoO_2Cl_2 \cdot 2C_{11}H_8N_4S_2O_3$	138	11.8	15.8	8.8	11.8	15.7	8.7
M·2Et5NTTU	$MoO_2Cl_2 \cdot 2C_6H_8N_4S_2O_2$	144	14.6	19.0	10.2	14.5	19.3	10.7
M·2P5NTU	$MoO_2Cl_29 \cdot 2C_{10}H_8N_4SO_3$	139	13.0	8.9	9.8	13.2	8.8	9.8
M·2P4PTTU	$MoO_2Cl_2 \cdot 2C_{16}H_{13}N_3S_2$	140	11.7	15.6	8.5	11.7	15.6	8.6
M·2*o*-T4PTTU	$MoO_2Cl_2 \cdot 2C_{17}H_{15}N_3S_2$	138	11.3	15.2	8.8	11.4	15.2	8.5
M·2*p*-T4PTTU	$MoO_2Cl_2 \cdot 2C_{17}H_{15}N_3S_2$	138	11.3	15.0	8.5	11.4	15.2	8.5
M·2Bz4PTTU	$MoO_2Cl_2 \cdot 2C_{17}H_{13}N_3S_2O$	130	11.0	14.6	8.0	11.0	14.6	8.1
M·2Et4PTTU	$MoO_2Cl_2 \cdot 2C_{12}H_{13}N_3S_2$	128	13.4	17.4	9.9	13.2	17.7	9.8
M·2P4PTU	$MoO_2Cl_2 \cdot 2C_{16}H_{13}N_3SO$	129	12.3	8.2	9.1	12.2	8.1	9.0

denum was estimated as lead molybdate; sulphur as barium sulphate by fusing the complexes with a 1 : 1 mixture of sodium peroxide and sodium carbonate, extracting the melt with water and then neutralizing with dilute HCl, when $BaSO_4$ precipitated; and chlorine as silver chloride by the method of Piria and Schiff.[27] The analytical data are in good agreement with those calculated for MoO_2Cl_2–ligand (1 : 2) complexes. Melting points were determined in open capillary tubes on a Unimelt temperature instrument and are uncorrected.

Magnetic measurements were carried out on a Gouy balance using a field strength of 5×10^3 gauss and mercury tetrathiocyanatocobaltate(II), Hg[Co(SCN)$_4$], as the standard. Molar conductances were determined in N,N-dimethylformamide using a Digital Conductivity meter CC601, with a cell constant of 1.11 (Century Instruments Pvt. Ltd, Chandigarh, India). The IR spectra of the ligands and their metal complexes were determined using KBr pellets on a Perkin–Elmer Grating IR spectrophotometer, Model 577, in the range 400–300 cm^{-1}. Absorption spectra of MoO_2Cl_2 complexes were measured in CH_2Cl_2 by standard methods using a UV–vis spectrophotometer (Model Shimadzu-UV–vis spectrophotometer-260, Japan).

For electrical measurements the compounds were made into discs of diameter 12 mm and thickness 0.4–0.8 mm. Concentrically, on the flat faces of each disc, electrodes were provided by applying a silver-based conductive paint. The electrical conductivities (σ) of the complexes were measured in the temperature range 30–115°C by employing a conductivity cell and a digital picoammeter (ESA 813 Electronic Corporation of India Ltd).

RESULTS AND DISCUSSION

All the MoO_2Cl_2 complexes are dark yellow–brown, and sparingly soluble in common organic solvents, except N,N-dimethylformamide in which they are more soluble. On heating, all of the complexes decompose or melt with decomposition above 145°C, but are easily decomposed by mineral acids. The analytical results (Table 1) indicate a 1 : 2 ratio of MoO_2Cl_2–ligand which corresponds to the general empirical formula $[MoO_2 \cdot L_2]Cl_2$. The very low solubility of these complexes in suitable solvents precluded molecular weight determinations. The molar conductances of the complexes in DMF and nitrobenzene were in the ranges 144.0–164.2 and 38.0–48.2 Ω^{-1} cm^2 mol^{-1}, respectively. The molar conductance results indicate that the complexes are 1 : 2 electrolytes.[28] The magnetic susceptibilities of the complexes were found to be in the

Table 2. IR spectral data of the ligands and their MoO_2Cl_2 complexes (in cm^{-1})

Compound	ν(Mo—S)	ν(C—S) stretch	ν(C=O)	ν(N—H)	ν(C—N)	Mo=O stretch
PTTU	—	740 s	—	3210	1535 s	—
$[MoO_2(PTTU)_2]Cl_2$	348 m	732 w	—	3208	1542 m	870 m, 904 m
o-TTTU	—	745 m	—	3220 m	1545 m	—
$[MoO_2(o\text{-}TTTU)_2]Cl_2$	358 m	735 m	—	3220 m	1550 m	875 m, 912
p-TTTU	—	740 s	—	3212 m	1535 m	—
$[MoO_2(p\text{-}TTTU)_2]Cl_2$	360 m	735 w	—	3214 b	1542 m	872 s, 910 m
BzTTU	—	755 s	—	3225 m	1540 s	—
$[MoO_2(BzTTU)_2]Cl_2$	370	742 m	—	3228	1550 m	870 m, 915 b
EtTTU	—	742 m	—	3225	1540 s	—
$[MoO_2(EtTTU)_2Cl_2$	362	730 m	—	3225	1560 m	872 s, 908 m
PTU	—	—	1730 s	3200	1538 s	—
$[MoO_2(PTU)_2]Cl_2$	—	—	1720 m	3200	1546 m	870 m, 914 m
P5NTTU	—	760 s	—	3215	1542 w	—
$[MoO_2(P5NTTU)_2]Cl_2$	380	745 m	—	3215	1555 w	875 m, 920 m
o-T5NTTU	—	765 s	—	3220	1540 m	—
$[MoO_2(o\text{-}T5NTTU)_2]Cl_2$	375	750 m	—	3220	1550 m	880 s, 918 m
p-T5NTTU	—	758 m	—	3208	1535m	—
$[MoO_2(p\text{-}T5NTTU)_2]Cl_2$	372	742 m	—	3210	1545 m	878 m, 910 m
Bz5NTTU	—	762 s	—	3223	1532 s	—
$[MoO_2(Bz5NTTU)_2]Cl_2$	370	750 m	—	3222	1545 m	875 m, 915 m
Et5NTTU	—	755 m	—	3225	1530 s	—
$[MoO_2(Et5NTTU)_2]Cl_2$	382	745 m	—	3225	1538 m	880 s, 916 m
P5NTU	—	—	1715 m	3220	1532 m	—
$[MoO_2(P5NTU)_2]Cl_2$	—	—	1700 m	3218	1548 m	885 m, 920 s
P4PTTU	—	748 s	—	3210	1540 s	—
$[MoO_2(P4PTTU)_2]Cl_2$	390	740 w	—	3212	1556 s	874 m, 918 m
o-T4PTTU	—	756 s	—	3210	1550 m	—
$[MoO_2(o\text{-}T4PTTU)_2]Cl_2$	376	740 m	—	3210	1555 m	870 m, 910 m

range -0.48 to -0.90×10^{-6} G, indicating their diamagnetic nature.

The UV spectra of the ligands display bands around 240–265 nm in methylene chloride which are shifted to 275–320 nm in MoO_2Cl_2 complexes. This shift is attributed to the fact that during complex formation, the energy level is lowered due to stabilization of the excited state. All the electronic spectral bands are due to M ← S charge-transfer absorption. Moore and Larsen[29] have observed that S → M charge-transfer in xanthate complexes appears at 6000 cm^{-1} below that of the corresponding dithiocarbamate complexes, and have suggested that xanthates are much greater reducing agents than dithiocarbamates. In our case, it is observed from the spectral data that the present ligands are not reducing agents.

In the IR spectra of thioazolyl-substituted thiocarbamides in KBr, bands appearing at 740–760 cm^{-1} have been assigned to ν(C=S) modes.[30] In MoO_2Cl_2 complexes these bands are reduced in intensity (Table 2). The lowering of C=O frequencies (1715–1730 cm^{-1} in PTU and P5NTU) on complexation (1720 and 1700 cm^{-1}) seems to be a more reliable indication of formation of the M—O bond. Furthermore, a slight increase in the C—N stretching frequency on coordination also supports the view that bonding is through sulphur and oxygen in these complexes. The band appearing at 348–390 cm^{-1} in MoO_2Cl_2 complexes of thiocarbamides is assignable to an Mo—S band. A lowering of the Mo=O stretching vibrations (from 960 cm^{-1} in MoO_2Cl_2 to 904–920 cm^{-1} in complexes) occurs in all the complexes and may be ascribed to chelation. The thiazole nucleus is observed to show the bands in the region 1588, 1480, 1340 and 1025 cm^{-1}, respectively. These bands are observed at lower frequencies and at reduced intensities in the complexes. The bands appearing at 3000–3225 cm^{-1} have been assigned to ν_s(NH) and ν_{as}(NH), the latter being the higher frequency bands. There is a little change in this band on complexation.

The ^1H NMR spectra of PTTU, *o*-TTTU, BzTTU, P4TTU and *p*-T4PTTU indicate four distinct resonances: (i) a sharp singlet (δ 7.4–7.8 ppm) due to the $-C_6H_5$ ring proton; (ii) a broad mul-

tiplet (δ 3.2–3.4 ppm) due to the *o,p*-$CH_3C_5H_4$ ring protons; (iii) a sharp signal (δ 2.2–2.5 ppm) due to the protons of the CH_3 groups; (iv) a doublet at δ 4.38–4.6 ppm due to the NH protons of the —CSNH group. Finally, a singlet at δ 8.4–8.7 ppm is possibly due to the protons of the thiazolyl ring. On account of poor solubility, the NMR spectra of MoO_2Cl_2 complexes with the above ligands were taken in deuterated DMSO. The spectra of molybdenum(VI) complexes show the signal due to the —CNH group does not undergo any shift. The positions of the —C_6H_5 and *o,p*-$CH_3C_5H_4$ ring protons remain unperturbed, ruling out the possibility of coordination of the —NH group of —NHC_6H_5. The lone pair of electrons on the sulphur and nitrogen of the thiazole ring causes paramagnetic shielding of the 4- and 5-protons. Formation of the dative bond using this electron pair of sulphur greatly reduces the paramagnetic shielding, causing a significant upfield shift for the adjacent protons. In other words, we can state that there is a decrease in the electron density of the thiozolyl ring upon adduct formation. This decrease causes a reduction of the paramagnetic anisotropic effect. This will result in an almost uniform upfield shift for all the ring protons. In the molybdenum complexes of PTTU, *o*-TTTU, BzTTU, P4PTTU and *p*-T4PTTU, an upfield sift of heterocyclic ring protons by 2–3.8 ppm is observed, confirming coordination through the thiazolyl sulphur.

In Fig. 1 the logarithm of electrical conductivity (σ) of $MoO_2Cl_2 \cdot 2PTTU$ against the reciprocal of temperature (T) in K is shown. The band gaps E_g for the condution process were calculated using the equation:

$$\sigma = \sigma_0 e^{-E_g/2kT},$$

where σ is the conductivity at T (K), σ_0 is a constant and k is Boltzmann's constant. The slopes of the straight lines of $\log\sigma$ vs $1/T$ were accurately determined by using the least-squares method. The electrical conductivities of the complexes are in the ranges 2.3×10^{-8}–10^{-6} and 4×10^{-7}–10^{-4} Ω^{-1} cm^{-1}. On comparison of these ranges with the electrical conductivity range of the semiconductors (given by Kittel[31]), it is observed that PTTU, *o*-TTTU and *p*-T4PTTU complexes are good semiconductors with band gaps ranging from 1.09 to 1.40 eV. It is also observed that complexes having a substituent in the *para* position in the ligands have greater conductivities than if the substituents are in the *ortho* positions. The Seebeck coefficient (α) measurements in these complexes showed that complexes of PTTU, Et4PTTU and P4PTU are n-type semicondutctors (negative α values) and all other MoO_2Cl_2 complexes are p-type semiconductors (positive α values).

MoO_2Cl_2 has been found to have a tetrahedral structure by Skinner.[32] It seems probable that on complexation with N-aryl-N′-(substituted thiazolyl) thioureas and ureas, the coordination number of molybdenum increases to six and a complex compound with distorted octahedral structure is formed having d^2sp^3 hybridization. Chelation with these bidentate ligands and the displacement of

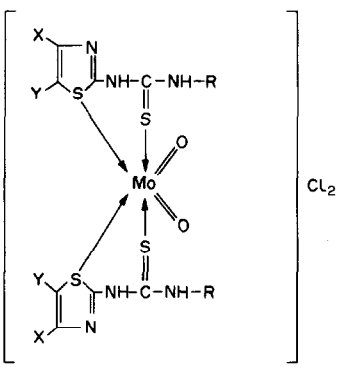

I

For L			
PTTU	; R=$-C_6H_5$	; X=H	; Y=H
o-TTTU	; R=$-C_6H_4(CH_3)$	; X=H	; Y=H
p-TTTU	; R=$-C_6H_4(CH_3)$	; X=H	; Y=H
BzTTU	; R=$-C_6H_5CO$	; X=H	; Y=H
EtTTU	; R=$-C_2H_5$	; X=H	; Y=H
P5NTTU	; R=$-C_6H_5$	; X=H	; Y=$-NO_2$
o-T5NTTU	; R=$-C_6H_4(CH_3)$	; X=H	; Y=$-NO_2$
p-T5NTTU	; R=$-C_6H_4(CH_3)$	; X=H	; Y=$-NO_2$
Bz5NTTU	; R=$-C_6H_5CO$	; X=H	; Y=$-NO_2$
Et5NTTU	; R=$-C_2H_5$	; X=H	; Y=$-NO_2$
p-4PPTU	; R=$-C_6H_5$	; X=C_6H_5	; Y=H
o-T4PTTU	; R=$-C_6H_4(CH_3)$	; X=C_6H_5	; Y=H
p-T4PTTU	; R=$-C_6H_4(CH_3)$	; X=C_6H_5	; Y=H
Bz4PTTU	; R=$-C_6H_5CO$	; X=C_6H_5	; Y=H
Et4PTTU	; R=$-C_2H_5$	; X=C_6H_5	; Y=H

Complex of MoO_2Cl_2 with N-(substituted)-N′-(substituted thiazolyl) thiourea.

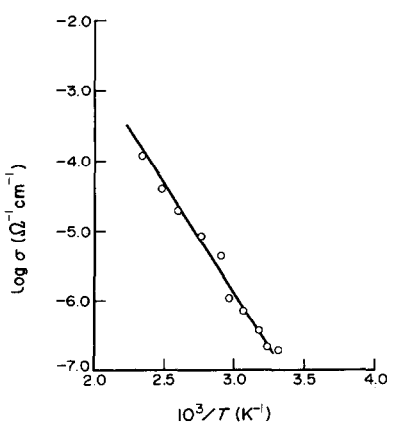

Fig. 1. Plot of $\log\sigma$ vs $1/T$ for $[MoO_2(PTTU)_2]Cl_2$.

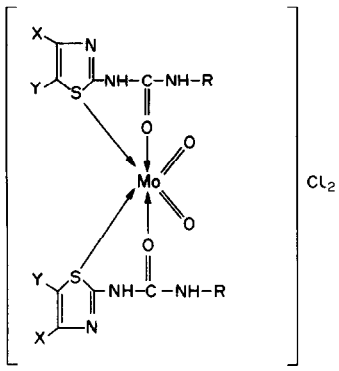

II

For L

PTU ; R = $-C_6H_5$; X = H ; Y = H

P5NTU ; R = $-C_6H_5$; X = H ; Y = NO_2

P4PTU ; R = $-C_6H_5$; X = C_6H_5 ; Y = H

Complex of MoO_2Cl_2 with N-(substituted)-N′-(substituted thiazolyl) urea.

chlorine atoms to the outside of the coordination sphere further confirms the observations of Griffith and Wickins[31] that in MoO_2Cl_2 chlorine atoms are present in the *cis* position. On the basis of the above data the complex compounds may be represented by structures **I** and **II**.

Acknowledgements—The authors are thankful to Professor R. P. Bhatnagar, Head, Chemistry Department, Professor K. P. Srivastava of B.I.T.S., Pilani, and Director R. R. L. Jammu, for providing the necessary laboratory facilities.

REFERENCES

1. W. E. Newton, J. L. Corbin and J. W. McDonald, *J. Chem. Soc., Dalton Trans.* 1974, 104.
2. K. Yamanouchi and J. H. Enemark, *Inorg. Chem.* 1979, **18**, 1626.
3. J. T. Spence, M. Minelli and P. Kroneck, *J. Am. Chem. Soc.* 1980, **102**, 4538.
4. S. Purohit, A. P. Koley, L. S. Prasad, P. T. Manoharan and S. Ghosh, *Inorg. Chem.* 1989, **28**, 3735.
5. B. V. Merinov, A. B. Kuzharov and N. G. Furmanova, *Kristallografia* 1986, **31**, 93.
6. B. D. Gupta and W. U. Malik, *J. Less-Common Met.* 1969, **17**, 277.
7. J. Singh, K. Lal and S. P. Gupta, *S. Afr. J. Sci.* 1979, **75**, 62.
8. S. O. Oh and B. K. Koo, *Taehan Hwa Hakhoe Chi.* 1985, **29**, 226.
9. S. O. Oh and B. K. Koo, *Taehan Hwa Hakhoe Chi.* 1985, **29**, 257.
10. S. O. Oh and B. K. Koo, *Taehan Hwa Hakhoe Chi.* 1986, **30**, 441.
11. J. R. Allan, H. J. Bowley, D. L. Gerrard, A. D. Paton and K. Turvey, *Inorg. Chim. Acta* 1987, **132**, 41.
12. J. R. Allan, H. J. Bowley, D. L. Gerrard, A. D. Paton and K. Turvey, *Thermochim. Acta* 1987, **122**, 403.
13. J. R. Allan, H. J. Bowley, D. L. Gerrard, A. D. Paton and K. Turvey, *J. Coord. Chem.* 1988, **17**, 255.
14. W. Zygfryd and D. Brown, *Wiad. Chem.* 1973, **27**, 38.
15. N. R. Byrd and M. B. Sheratte, *Sci. Tech. Aerosp. Rep.* 1976, **4**, 14.
16. K. L. Madhok and K. P. Srivastava, *Ind. J. Chem.* 1980, **A19**, 808.
17. K. L. Madhok, *Inorg. Chim. Acta* 1982, **61**, 103.
18. K. P. Srivastava and K. L. Madhok, *Ind. J. Chem.* 1978, **16A**, 359.
19. K. P. Srivastava and K. L. Madhok, *J. Inorg. Nucl. Chem.* 1978, **40**, 1821.
20. K. P. Srivastava and K. L. Madhok, *J. Chem. Engng Data (ACS)* 1978, **23**, 256.
21. K. P. Srivastava, G. P. Srivastava, S. K. Arya and K. L. Madhok, *J. Chem. Engng Data (ACS)* 1980, **25**, 173.
22. K. L. Madhok, *Polyhedron* 1987, **6**, 1807.
23. K. L. Madhok, *Polyhedron* 1984, **3**, 39.
24. K. L. Madhok, *Ind. J. Chem.* 1985, **24A**, 122.
25. K. P. Srivastava, I. K. Jain and K. L. Madhok, *Proc. Ind. Acad. Sci. (Chem. Sci.)* 1981, **90**, 309.
26. F. Zado, *J. Inorg. Nucl. Chem.* 1963, **25**, 1115.
27. H. T. Clarke, *A Handbook of Organic Analysis*, p. 308. Edward Arnold, London (1960).
28. G. J. Sutton, *Aust. J. Chem.* 1971, **24**, 919.
29. F. W. Moore and M. L. Larson, *Inorg. Chem.* 1967, **6**, 998.
30. A. Yamaguchi, R. B. Penland, S. Lowe, C. Curran and J. V. Quagliano, *J. Am. Chem. Soc.* 1958, **80**, 527.
31. C. Kittel, *Introduction to Solid State Physics*, 5th edn, p. 207. Wiley Eastern Limited, New Delhi (1984).
32. A. F. Wells, *Structural Inorganic Chemistry*, p. 387. Clarendon Press, London (1962).

Polyhedron Vol. 9, No. 20, pp. 2455–2461, 1990
Printed in Great Britain

0277–5387/90 $3.00+.00
© 1990 Pergamon Press plc

COMPLEXATION OF EUROPIUM(III) AND AMERICIUM(III) WITH IONIZABLE MACROCYCLIC LIGANDS

V. K. MANCHANDA* and P. K. MOHAPATRA

Radiochemistry Division, B.A.R.C., Bombay-400085, India

(*Received* 14 *March* 1990; *accepted* 11 *May* 1990)

Abstract—The complexation of europium(III) and americium(III) with ionizable macrocyclic ligands, i.e. 1,7-diaza-4,10,13-trioxacyclopentadecane-N,N′-diacetic acid (K21DA) and 1,10-diaza-4,7,13,16-tetraoxacyclooctadecane-N,N′-diacetic acid (K22DA), has been investigated using the solvent extraction technique. Both trivalent cations formed marginally stronger complexes with K22DA than that with K21DA. Apart from the size effect, steric constraints associated with the metal coordination of carboxylate groups attached to the macrocyclic ring appeared to play an important role in complex formation. An attempt was made, wherever possible, to compare the results of macrocyclic ligands with those of ethylene diamine diacetic acid (analogous non-cyclic ligand). The studies carried out on americium(III) up to pH 6.0 in the presence of macrocyclic ligands in the aqueous phase did not reveal any precipitation or adsorption of metal ion. Speciation diagrams in the pH range 3.0–6.0 for the systems Am^{III}–K21DA and Am^{III}–K22DA have been deduced.

During the past two decades, size-selective complexation behaviour of macrocyclic ligands with ions of alkali metals and alkaline earths has been investigated in depth.[1–4] Ion–dipole interaction has been found to be the principal binding force of these metal ions with the macrocyclic ligands.[5] In view of their low-lying partly filled *f*-orbitals, a large number of lanthanide and actinide ions have the electronic configuration (ns^2np^6, where $n = 5$ or 6) analogous to that of monovalent alkali metal ions and divalent alkaline earth ions. In spite of their configurational similarities, the literature on lanthanide macrocyclic complexes and particularly actinide macrocyclic complexes is very scarce.[6,7] Amongst the actinide ions, evaluation of thermodynamic stability data has been carried out only for uranium(VI) complexes.[8,9] Other actinide ions, e.g. Pu^{IV}, Am^{III} and Cm^{III}, were studied for their extraction behaviour using macrocyclic reagents as auxiliary ligands where they acted as neutral oxo-donors.[10–12] No systematic size correlation of the ionic radii of these cations with cavity size of the ligands has been reported so far.

Chang and co-workers[13–15] have investigated the coordination behaviour of ionizable macrocyclic ligands with lanthanide ions and found 1,7-diaza-4,10,13-trioxacyclopentadecane-N,N′-diacetic acid (K21DA) and 1,10-diaza-4,7,13,16-tetraoxacyclooctadecane-N,N′-diacetic acid (K22DA) to possess some selectivity features. Loncin *et al.*[16] found 1,4,7,10-tetraazacyclododecane-N,N′,N″,N‴-tetracetic acid (DOTA) to form the strongest complexes with lanthanides known to date. On the other hand, due to the large increase in the cation solvation energy, interactions of lanthanide and actinide ions (in their high oxidation states) with neutral cyclic polyethers in aqueous solution were found to be too weak to be measured experimentally.[17,18] Ionizable macrocyclic ligands are likely to have strong electrostatic interactions with actinide ions, along with guest–host interactions which are predominantly size selective in nature. These ligands have also gained importance due to their ability to transfer metal ions towards non-aqueous media even in the absence of any other organophilic counter anion.[19]

A typical trivalent actinide ion americium(III) and the analogous lanthanide ion europium(III), along with the 15-membered macrocyclic ligand K21DA and 18-membered macrocyclic ligand K22DA, were chosen for the present investigations. These ligands are reported to offer cavities of a size compatible with the ionic radii of the trivalent ions considered here.[20,21] Due to the presence of oxygen

* Author to whom correspondence should be addressed.

and nitrogen as donor atoms, similar to their behaviour with lanthanides,[22,23] these ligands are expected to interact better with the americium(III) ion compared to the ligands which have only oxygen donor atoms.[24,25] Potentiometric titration techniques were used as previously[13,14] for the determination of complex formation constants of K21DA and K22DA with several lanthanide ions including europium(III). The solvent extraction technique involving tracer concentrations of the metal and milligram amounts of macrocyclic ligand at a constant pH was used in the present work. Apart from overcoming the difficulties encountered in treating the complex equilibria involving polynuclear species as required for potentiometric data, the use of the solvent extraction tracer technique was also helpful in dispensing with the use of elaborate glove-box facilities which is a pre-requisite for handling milligram amounts of americium.

Equilibrium constants obtained in the present work for 1 : 1 complexes revealed that with both macrocyclic ligands americium(III) forms stronger complexes than europium(III). Some observations regarding the prominent equilibria involved and the speciation diagrams have also been included in this paper.

EXPERIMENTAL

Reagents

Proanalysi grade thenoyltrifluoroacetone (TTA) of E. Merck and G.R. grade xylene supplied by Lobo-chemie Indo Austranal. Co. were used. Tetramethylammonium chloride (Fluka Chemie A.G.) and tetramethylammonium hydroxide (Aldrich Chemical Co. Inc.) were used for ionic strength adjustments and for the preparation of buffer solutions, respectively. The ^{241}Am used was obtained by beta decay of ^{241}Pu and was purified by an ion-exchange technique. The ^{152,154}Eu obtained by irradiating spec. pure Eu_2O_3 was used without further purification. Purity of the tracers was confirmed by gamma spectrometry. The syntheses of K21DA and K22DA were carried out by the method reported earlier.[26]

Solvent extraction studies

An aliquot of the radioactive tracer was heated to dryness and then dissolved in a buffer solution of the desired pH and ionic strength (0.1 M). Buffer solutions were prepared using tetramethylammonium hydroxide to avoid possible complexation of the macrocyclic ligand with alkali metal ions. For the same reason the ionic strength adjustment was carried out with tetramethylammonium chloride.

The stock solution of TTA (0.4 M) in xylene was equilibrated with 0.1 M $HClO_4$ overnight to convert it into the ketohydrate form. Subsequently the organic phase was equilibrated with an aqueous solution of desired pH (without radiotracer) to remove traces of $HClO_4$ present.

The concentrated organic extract required for back extraction experiments was prepared by equilibrating 0.4 M TTA in xylene as the organic phase, and radiotracers in the concentration range 10^{-5}–10^{-6} M at pH 3.0 (chloroacetate buffer) as the aqueous phase. The organic phase in the subsequent experiments was obtained by approximately 20 times dilution of this organic concentrate. To study the effect of variation of TTA concentration on distribution coefficient, a varying volume of the radiotracer-loaded organic phase diluted with a suitable volume of xylene was equilibrated with the aqueous phase containing a fixed concentration of K21DA/K22DA at pH 4.6 and i.s. = 0.1 M. To study the effect of the variation of ligand concentration, a varying volume of the freshly prepared K21DA/K22DA solution at pH 4.6 along with a suitable volume of an inert 0.1 M (tetramethylammonium chloride) solution was used as the aqueous phase.

To study the effect of variation of pH, the aqueous phase was pipetted in steps from a ligand solution ($\sim$ 100 cm^3) after adjustment of the pH to the required value by dropwise addition of conc. HCl solution. The equilibrium pH was measured after completion of the experiment.

After equilibration, the two phases were allowed to settle in a waterbath for about 20 min and then were centrifuged for 2 min before assaying. Suitable aliquots of the two phases (20×10^{-3} to 200×10^{-3} cm^3) were pipetted carefully avoiding any cross-contamination. Americium and europium were assayed using a NaI well-type gamma scintillation detector with the appropriate base line voltage and window widths. Distribution coefficients were calculated by dividing the counts per minute per unit volume of the organic phase by the counts per minute per unit volume of the aqueous phase. All experiments were carried out at 25 ± 0.1°C.

Calculations

In the absence and presence of the macrocyclic ligand (H_4L) in the aqueous phase, distribution coefficients D_0 and D are given as

$$D_0 = \frac{[Am(TTA)_3]_0}{[Am^{3+}]_a\left(1+\sum_i \beta_i^{OH}[OH^-]^i+\sum_j \beta_j^{Ac}[Ac^-]^j+\sum_k \beta_k^{Cl}[Cl^-]^k+\sum_l \beta_l^{TTA}[TTA^-]^l\right)} \quad (1)$$

$$D = \frac{[Am(TTA)_3]_0}{[Am^{3+}]_a\left(1+\sum_i \beta_i^{OH}[OH^-]^i+\sum_j \beta_j^{Ac}[Ac^-]^j+\sum_k \beta_k^{Cl}[Cl^-]^k+\sum_l \beta_l^{TTA}[TTA^-]^l+\sum_m \beta_m^{L}[L^{2-}]^m\right)} \quad (2)$$

In the above expression, the concentration of the $AmHL^{2+}$ type species has been neglected in view of the much larger complexation of the L^{2-} ion.[27] By substituting the terms corresponding to hydroxy, acetate, chloride and TTA complexes with I, J, K, and L, respectively, eqs (1) and (2) can be arranged as

$$\frac{1}{D} = \frac{1}{D_0} + \sum_m \beta_m^{L}[L^{2-}]^m \frac{1}{D_0}\cdot\frac{1}{1+C},$$

where $C = I+J+K+L$, or

$$\left(\frac{D_0}{D}-1\right)(1+C) = \beta_1^{L}[L^{2-}]+\beta_2^{L}[L^{2-}]^2+\cdots \quad (3)$$

Depending upon whether the AmL^+ species or a combination of AmL^+ and AmL_2^- species co-exist at equilibrium, we can graphically obtain β_1^{L} alone or both β_1^{L} and β_2^{L} by plotting either

$$\left(\frac{D_0}{D}-1\right)(1+C) \text{ or } \left(\frac{D_0}{D}-1\right)(1+C)/[L^{2-}] \text{ vs } [L^{2-}].$$

The concentration of $[L^{2-}]$ at equilibrium is computed from the total ligand concentration by the following equation:

$$[H_4L^{2+}]_t = [H_4L^{2+}]+[H_3L^+]+[H_2L]+[HL^-]+[L^{2-}]+[AmL^+]+2[AmL_2^-].$$

Since $[Am]_t \ll [H_4L^{2+}]_t$; the last two terms can be neglected.

$$[H_4L^{2+}]_t = [L^{2-}]_e\left(1+\frac{[H^+]}{k_4}+\frac{[H^+]^2}{k_3k_4}+\frac{[H^+]^3}{k_2k_3k_4}+\frac{[H^+]^4}{k_1k_2k_3k_4}\right),$$

where k_1, k_2, k_3 and k_4 denote proton ligand dissociation constants.[13,14] The value of C is obtained from the literature.[28] $[H^+]$ was obtained from the pH using the relation:[29]

$$[H^+] = 10^{-(pH-0.11)} \quad (i.s. = 0.1).$$

RESULTS

Equilibration time

We reported earlier, the variation of the extraction rate constants with variation of lanthanide(III) ion, ligand and pH in the system Ln^{III}–(K21DA/K22DA)–TTA–$CHCl_3$.[30,31] It was observed that the rate of attainment of equilibrium in the forward direction was inversely related to the pH. It was necessary to shake the extraction tube for several hours (> 8) at pH 4.6 to reach equilibrium. On the other hand, the equilibrium was attained in about 20 min at this pH if approached from the reverse direction. This can be explained on the basis of slow dissociation kinetics of the Am–macrocyclic complex in the aqueous phase which governs the forward extraction rate. The reverse extraction rate appeared to be governed by either the rate of transfer of the $Am(TTA)_3$ species from the organic phase to the aqueous phase, or the dissociation rate of this species in the aqueous phase. No attempt was made in the present work to investigate the mechanism of extraction in the forward direction. Results of the studies carried out to investigate the influence of [TTA], $[H_4L^{2+}]$ and $[H^+]$ on equilibrium states (when approached from the reverse direction) for the systems Am^{III}–(K21DA/K22DA)–TTA are given in Table 1.

Effect of variation of TTA *concentration*

Variation of $\log D$ with $\log[TTA]_0$ was investigated at pH 4.6 for Am^{III}–(K21DA/K22DA) systems. Dependency of ~ 3 suggested the presence of the $Am(TTA)_3$ species in the organic phase.

Effect of variation of ligand concentration

Figure 1 shows the variation of $\log D$ vs $\log[H_4L^{2+}]$ at pH 4.6 for americium(III) and europium(III) with both ligands. A linear relationship of $\log D$ vs $\log[H_4L^{2+}]$ with a slope of -1 for the system Am^{III}–K22DA–TTA at pH 4.6 suggested that at this pH and in the ligand concentration range chosen, americium(III) was present predominantly as AmL^+ in the aqueous phase. A slope of ~ 1 was also seen in the straight line plots of $\log(D_0/D-1)(1+C)$ vs $\log[L^{2-}]$. According to eq. (3) given in the section on calculations, this could

Table 1. Dependencies on log D of log[TTA], log[K21DA]/[K22DA] and pH

System	Variable parameter	Range of variation	Dependency of log D[a]	Experimental conditions[b]
Am^{III}–K21DA–TTA	[K21DA]	1.76×10^{-4}–2.64×10^{-3} M	−0.74	[TTA] = 2.35×10^{-2} M; pH = 4.6
	pH	3.20–4.70	2.7–1.0	[TTA] = 1.1×10^{-1} M
				[K21DA] = 3.16×10^{-4} M
Am^{III}–K22DA–TTA	[TTA]	3.16×10^{-2}–3.16×10^{-1} M	3.02	[K22DA] = 5.0×10^{-4} M; pH = 4.6
	[K22DA]	4.25×10^{-5}–4.25×10^{-4} M	−1.04	[TTA] = 2.35×10^{-2} M; pH = 4.6
	pH	2.9–5.0	1.9–0.4	[TTA] = 1.1×10^{-1} M
				[K22DA] = 2.2×10^{-4} M

[a] Dependency of log D as the pH varies continuously.
[b] Temperature, 25°C; i.s. = 0.1.

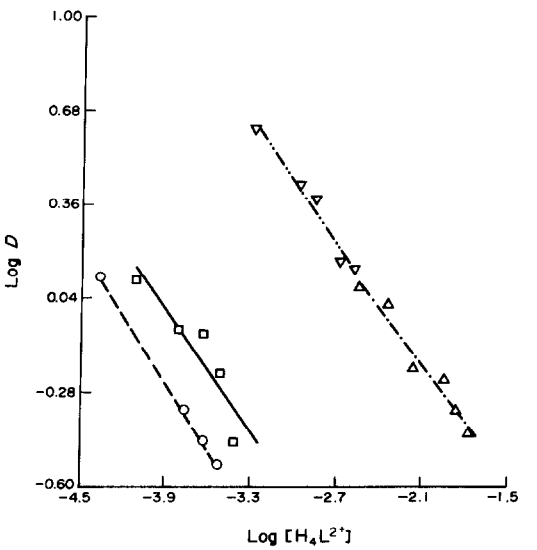

Fig. 1. Variation of log D vs log[H_4L^{2+}]; [TTA] = 2.35×10^{-2} M: i.s. = 0.1. (◇) Am^{III}–K21DA; (△) Eu^{III}–K21DA; (○) Am^{III}–K22DA; (□) Eu^{III}–K22DA.

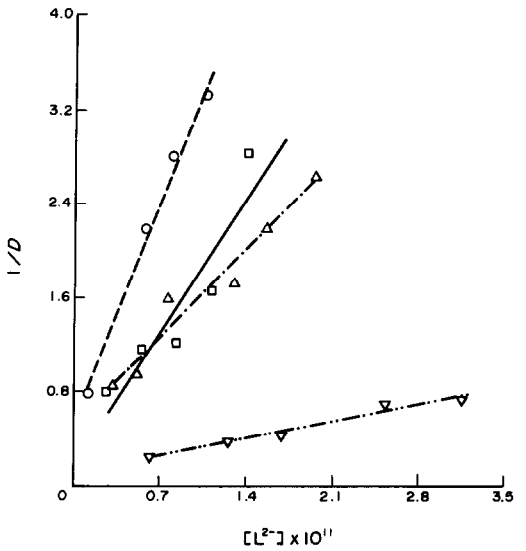

Fig. 2. Variation of $1/D$ vs [L^{2-}]; pH = 4.6; [TTA] = 2.35×10^{-2} M; i.s. = 0.1. (◇) Am^{III}–K21DA; (△) Eu^{III}–K21DA; (○) Am^{III}–K22DA; (□) Eu^{III}–K22DA.

be taken as evidence for the presence of 1 : 1 species in the aqueous phase. An attempt was made to compute complex formation constants by assuming that the small variation in slope from unity was experimental error. The D_0 value used was obtained by extrapolation of the plot of $1/D$ vs [L^{2-}] (Fig. 2). This was particularly important since the experimentally observed D_0 referred to the extraction of a different species.[32] Values of log K obtained for the systems studied in the present work are given in Table 2. In a few cases, whenever the graphical method was followed (Fig. 2) for the determination of log K values, an excellent agreement with the values obtained by the simple algebraic method was found.

Complex formation constants were specifically obtained for the systems Eu–K21DA and Eu–K22DA to ascertain the acceptability of the present approach. Agreement of the values obtained by potentiometric methods as well as by the present method, as shown in Table 2, is fairly good. It should be borne in mind that apart from the errors involved in the measurement of pH and distribution data, the values obtained using the present method were also influenced by the literature data on acetate complexation of these ions. On the other hand,

Table 2. Complex formation constants and ionic radii of metal ions with K21DA, K22DA and EDDA

Metal ion	i.r. (Å)	Method	$\log\beta_1$ K21DA	K22DA	EDDA
Am^{III}	1.09	Solvent extraction	12.86±0.03	13.33±0.11	—
Eu^{III}	1.07	Solvent extraction	12.23±0.08	12.33±0.12	—
		Potentiometric[a]	11.85±0.11	12.02±0.11	8.38
Pu^{IV}[b]	0.96	Solvent extraction	21.52±0.31	19.11±0.05	18.90±0.06

[a] Reference 14.
[b] Reference 34.

uncertainty in the potentiometric data was only related to the errors of pH measurements.

Variation of pH

Figure 3(a) shows the variation of $\log D$ as a function of pH for the system Am^{III}–K21DA–TTA. The concentration of K21DA was maintained constant at 3.16×10^{-4} M. The slope of the plot was found to change from ~ 2.7 (at pH 3.2) to ~ 1.0 (at pH 4.6). Table 1 shows the $\log D$ dependencies on [TTA], $[H_4L^{2+}]$ and pH in the systems Am^{III}–(K21DA/K22DA)–TTA. On the basis of this data it is possible to write the two-phase equilibria under different pH conditions as follows:

$$Am(TTA)_3(o)+3H^+(a)\rightleftharpoons Am^{3+}(a)+3HTTA(o) \quad \text{(i)}$$
(dominating at pH < 3.0)

$$Am(TTA)_3(o)+H_3L^+(a)\rightleftharpoons AmL^+(a)+3HTTA(o) \quad \text{(ii)}$$

$$Am(TTA)_3(o)+H_2L(a)+H^+(a)\rightleftharpoons AmL^+(a)+3HTTA(o). \quad \text{(iii)}$$
(dominating at pH ~ 4.6).

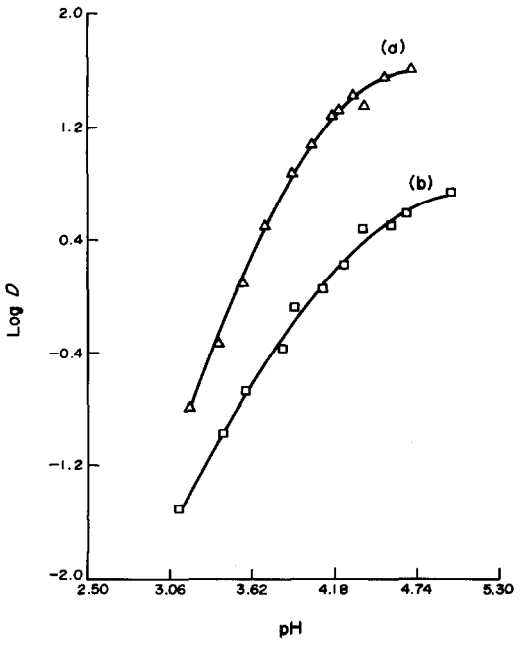

Fig. 3. Variation of $\log D$ vs pH; [TTA] = 1.1×10^{-1} M; i.s. = 0.1 M. (△) Am^{III}–K21DA–TTA; [K21DA] = 3.16×10^{-4} M; (□) Am^{III}–K22DA–TTA, [K22DA] = 2.2×10^{-4} M.

Curve (a) in Fig. 3 also reveals that the dependency of $\log D$ on pH increases with decreasing pH. At pH < 3.0 it appears that there is not much aqueous complexation of americium(III) and the two-phase equilibrium is represented as in (i). The slope of 2.6 in the pH range 3.2–3.8 and 1.6 in the pH range 3.8–4.2 suggests decreasing contribution of equilibrium (i) and increasing contributions of equilibriums (ii) and (iii) with increasing pH.

Experiments carried out substituting K21DA with K22DA under identical conditions resulted in distribution ratios which were too low to be measured reliably. Curve (b) in Fig. 3 refers to [K22DA] = 2.2×10^{-4} M. Throughout the pH range studied (3.1–5.0), in spite of the lower concentration, the K22DA curve was found to be below that of K21DA. This is explained in view of the stronger complexation of americium(III) with K22DA. As expected, even the slope values in a given pH range were lower than those observed for K21DA curve. The slope of ~ 1.0 suggesting predominance of eq. (iii) was observed in the pH range 3.9–4.4 rather than > 4.6 [as seen for curve (a)]. The decrease of the slope below 1.0 in both cases at pH > 4.7 could possibly be attributed to the presence of hydrolysed species of the type Am(K21DA/K22DA)OH in the aqueous phase at equilibrium.

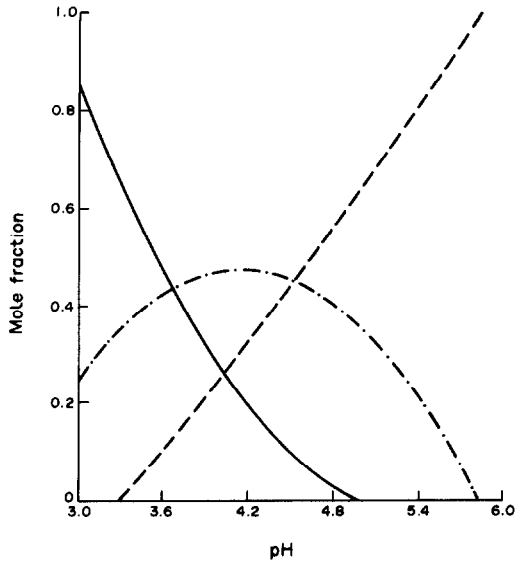

Fig. 4. Speciation diagram of americium(III); [K21DA] = 1.0×10^{-3} M. Am^{3+} (——); $Am(OH)^{2+}$ (—·—·—); $Am(K21DA)^{+}$ (– – –).

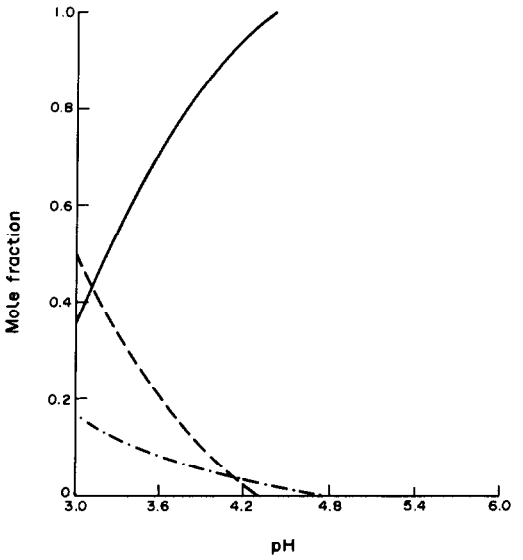

Fig. 5. Speciation diagram of americium(III): [K22DA] = 1.0×10^{-3} M. Am^{3+} (– – –); $Am(OH)^{2+}$ (—·—·—); $Am(K22DA)^{+}$ (——).

Speciation

Figure 4 shows the variation of $[Am^{3+}]$, $[Am(OH)^{2+}]$ and $[AmL^{+}]$ (L = K21DA) as a function of pH. This diagram was constructed using the pK_a data of K21DA,[14] the hydrolysis constant of Am^{3+},[32] the stability constant data obtained in the present work and ligand concentration. At pH 3.0; the major species is Am^{3+} which does not complex K21DA at all. With increasing pH, the Am^{3+} concentration decreases and that of AmL^{+} increases. Am^{3+} is quantitatively converted to AmL^{+} at pH 5.8. The concentration of $Am(OH)^{2+}$ species passes through a maximum at pH 4.0. The speciation diagram for K22DA, constructed similarly, is shown in Fig. 5. In contrast to Fig. 4, there is a significant concentration of the AmL^{+} species even at pH 3.0. This is in agreement with the difference in the nature of the potentiometric titration curves obtained for K21DA and K22DA in the presence of a lanthanide ion like Eu^{3+}.[13,14] Quantitative complexation of Am^{3+} with K22DA occurs even at pH 4.2. Concentration of Am^{3+} as well as $Am(OH)^{2+}$ decreases continuously with increasing pH.

DISCUSSION

The coordination number of lanthanide(III) ions in macrocyclic lanthanide complexes has been reported[6] to vary in the range 8–12 as revealed by their X-ray crystal structure analysis. It is reasonable to assume that the ionic radius of americium(III) in the present case is $\geqslant 1.09$ Å.[21] On the other hand, the cavity size of K21DA appears to be 0.97 ± 0.13 Å (typical of 15-membered ligands) and that of K22DA is 1.45 ± 0.15 Å (typical of 18-membered ligands).[20] In view of the empirical guest–host size correlation arrived at by Christensen *et al.*,[33] it is probable that whereas americium(III) and europium(III) may be loosely held in the K22DA cavity, no such encapsulation is possible in the K21DA cavity. Larger $\log K$ values for americium(III) over europium(III) (Table 2) may be explained on the basis of better availability of f orbitals for participation in the bonding of the actinide ion. Similar results have been reported by several workers on the basis of their studies with macrocyclic[10,24] as well as non-cyclic ligands.[23]

Table 2 also shows the $\log K$ values of the complexes of plutonium(IV) with K21DA, K22DA and EDDA.[34] It may be noted that the larger complex formation constants of plutonium(IV) with K21DA compared to that with K22DA is in sharp contrast to the observed behaviour of americium(III) and trivalent lanthanides. This is explained on the basis of better size compatability of the plutonium(IV) ion (i.r. = 0.96 Å) with K21DA (cavity size = 0.97 ± 0.13 Å). The observed trend in $\log K$ values for trivalent lanthanides[13,14] and of americium(III) for different ligands is EDDA < K21DA < K22DA. This could be rationalized if one considers that steric constraints increase with decrease of the metal ion radius as well as with the increase of ring size.

There has been an attempt to use thorium(IV) and europium(III) as model tetravalent and

trivalent ions for investigating the preferential stabilization of the former using the heteropolytungstate ion.[35] This work has gained in importance due to the increasing interest in the stabilization of the unusual tetravalent state of some *trans*-plutonium elements.[36] In view of the data available in the present work, 15-membered macrocyclic ligands with ionizable pendent groups appear to be promising for the stabilization of americium(IV) [analogous to plutonium(IV)] over americium(III).

Acknowledgements—The authors are thankful to Dr P. R. Natarajan, Head, Radiochemistry Division, B.A.R.C., for his keen interest and encouragement in this work. They are also thankful to Dr C. A. Chang, Squibb Institute for Medical Reseach, New Brunswick, New Jersey, U.S.A., for his valuable suggestions.

REFERENCES

1. I. M. Kolthoff, *Analyt. Chem.* 1979, **51**, 1R.
2. E. Weber and F. Vogtle, *Top. Curr. Chem.* 1981, **98**, 1.
3. J. M. Lehn, *Accts Chem. Res.* 1978, **11**, 5.
4. C. J. Pedersen, in *Synthetic Multidentate Macrocyclic Compounds* (Edited by R. M. Izatt and J. J. Christensen). Academic Press, New York (1978).
5. J. M. Lehn, *Struct. Bonding* 1973, **16**, 1.
6. J. C. G. Bunzli, *Handbook on the Physics and Chemistry of Rare Earths* (Edited by K. A. Gschneidner Jr and L. Eyring). Elsevier Science Publishers, (1985).
7. R. M. Izatt, J. S. Bradshaw, S. A. Nielsen, J. D. Lamb, J. J. Christensen and D. Sen, *Chem. Rev.* 1985, **85**, 271.
8. M. Brighli, P. Fux, J. Lagrange and P. Lagrange, *Inorg. Chem.* 1985, **24**, 80.
9. J. Lagrange, J. P. Metabanzoulou, P. Fux and P. Lagrange, *Polyhedron* 1989, **8**, 2251.
10. D. D. Ensor and D. J. Pruett, *Sep. Sci. Tech.* 1988, **23**, 1345.
11. H. F. Ally, S. M. Khalifa, J. D. Navratil and M. T. Saba, *Solv. Ext. Ion Exch.* 1985, **3**, 623.
12. J. N. Mathur and P. K. Khopkar, *Solv. Ext. Ion Exch.* 1988, **6**, 111.
13. C. A. Chang and M. E. Rowland, *Inorg. Chem.* 1983, **22**, 3866.
14. C. A. Chang and V. O. Ochaya, *Inorg. Chem.* 1986, **25**, 355.
15. C. A. Chang, P. H. Chang, V. K. Manchanda and S. P. Kasprzyk, *Inorg. Chem.* 1988, **27**, 3786.
16. M. F. Loncin, J. F. Desreux and E. Merciny, *Inorg. Chem.* 1986, **25**, 2646.
17. R. M. Izatt, D. J. Eatough and J. J. Christensen, *Struct. Bonding* 1973, **16**, 61.
18. P. K. Mohapatra and V. K. Manchanda, *Radiochemistry and Radiation Chemistry Symposium*, Nagpur, India, AL 05 (1990).
19. S. I. Kang, A. Czech, B. P. Czech, L. E. Stewart and R. A. Bartsch, *Anal. Chem.* 1985, **57**, 1713.
20. N. K. Dalley, in *Synthetic Multidentate Macrocyclic Compounds* (Edited by R. M. Izatt and J. J. Christensen). Academic Press, New York (1978).
21. R. D. Shannon, *Acta Cryst.* 1976, **A32**, 751.
22. G. Anderegg, *Helv. Chim. Acta* 1981, **64**, 1790.
23. M. C. Almasio, F. Arnaud-Neu and M. J. Schwing-Weill, *Helv. Chim. Acta* 1983, **66**, 1296.
24. D. D. Ensor and A. H. Shah, *Solv. Ext. Ion Exch.* 1983, **1**, 241.
25. D. D. Ensor and N. Nicks, *Solv. Ext. Ion Exch.* 1988, **6**, 621.
26. V. K. Manchanda, *Radiochim. Acta* 1989, **48**, 213.
27. R. Delgado and J. J. R. Frausto da Silva, *Talanta* 1982, **29**, 815.
28. G. R. Choppin and A. C. Muscatello, *Inorg. Chim. Acta* 1985, **109**, 67.
29. P. Glentworth, B. Wiseall, C. L. Wright and A. J. Mahmood, *J. Inorg. Nucl. Chem.* 1968, **30**, 967.
30. C. A. Chang, V. K. Manchanda and J. Peng, *Inorg. Chim. Acta* 1987, **130**, 117.
31. C. A. Chang, V. K. Manchanda and J. Peng, *Solv. Ext. Ion Exch.* 1989, **7**, 413.
32. P. K. Mohapatra and P. K. Khopkar, *Polyhedron* 1989, **8**, 2071.
33. J. J. Christensen, J. O. Hill and R. M. Izatt, *Science* 1971, **174**, 459.
34. V. K. Manchanda and P. K. Mohapatra, *Inorg. Chim. Acta* 1990, **170**, 141.
35. A. Saito and J. J. Shibikawa, *Radio Nucl. Chem. Letts* 1988, **126**, 189.
36. P. G. Eller and R. A. Penneman, *J. Less-Common Metals* 1987, **127**, 19.

Polyhedron Vol. 9, No. 20, pp. 2463–2467, 1990
Printed in Great Britain

0277–5387/90 $3.00+.00
© 1990 Pergamon Press plc

SOME COPPER(I) AND COPPER(II) COMPLEXES OF TWO NEW POTENTIALLY HEPTADENTATE TRIPODAL SCHIFF BASE LIGANDS

ELMER C. ALYEA,* GEORGE FERGUSON and MICHAEL JENNINGS

Department of Chemistry and Biochemistry, University of Guelph, Guelph, Ontario N1G 2W1 Canada

and

BAOLONG LI, ZHENG XU and XIAOZENG YOU

Coordination Chemistry Institute, Nanjing University, Nanjing, P.R.C.

and

SHIXIONG LIU

Institute of Structural Chemistry, Fuzhou University, Fuzhou, P.R.C.

(*Received* 27 *September* 1989; *accepted* 21 *May* 1990)

Abstract—Two potentially heptadentate tripodal Schiff base ligands, tris[4-(2-thienyl)-3-aza-3-butenyl]amine (S_3tren) and tris[4-(2-furyl)-3-aza-3-butenyl]amine (O_3tren) have been prepared and characterized by ^1H and ^{13}C NMR spectral data. For the complexes [Cu(E_3tren)]BPh_4 (E = S, O), NMR spectral shifts clearly indicate coordination of all four nitrogen donor atoms. X-ray analysis for [Cu(S_3tren)]BPh_4 shows trigonal pyramidal geometry for the copper(I) cation, with all Co---S distances [average of 3.344(4) Å] being too great for any bonding interaction. IR, ESR and electronic spectral data for the green copper(II) complexes, $CuX_2 \cdot S_3$tren (X = Cl, Br), indicate six-coordination in the solid state and square pyramidal geometry (with halide dissociation) in freshly prepared dimethylformamide solutions.

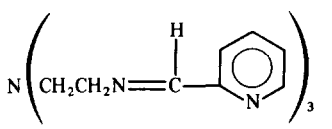

(1) py_3tren

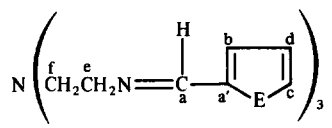

(2) E = S, S_3tren; (3) E = O, O_3tren

Although seven-coordination is readily achieved by many metal ions,[1,2] the ability of a single ligand to supply all seven donor atoms is rare.[3] The best studied potentially heptadentate ligand, tris[4-(2-pyridyl)-3-aza-3-butenyl]amine, known as py_3tren (**1**), was designed to give transition metal complexes having mono-capped trigonal antiprismatic coordination polyhedra.[4,5] A recent detailed assessment of the bonding properties of py_3tren in a series of $[M(py_3tren)]^{2+}$ (M = Mn, Fe, Co, Ni, Cu and Zn) complexes shows, however, that the seventh bond to the apical or bridgehead nitrogen atom may only be considered as "weakly bonding" in the case of manganese [2.794(2) Å] and cobalt [2.870(2) Å].[5] In order to overcome the domineering influence of the three pendant α-diimine chelating arms on the resultant metal geometry, we have prepared two new analogous ligands that contain thiophene and furan moieties in the pendant arms. These potentially heptadentate tripodal Schiff base ligands, called S_3tren (**2**) amd O_3tren (**3**) are expected to

* Author to whom correspondence should be addressed.

enhance metal interaction with the bridgehead nitrogen atom as compared to py_3tren.[5] The importance of multidentate nitrogen–sulphur ligands in copper model systems for the "blue" copper oxidases and electron transfer proteins[6] led us to explore the coordinating ability of **2** and **3** with both copper(I) and copper(II) ions, which we report in this paper.

The syntheses of the new potentially heptadentate ligands **2** and **3** were readily effected by the Schiff base condensation of tris(2-aminoethyl)amine (tren) with the appropriate aldehyde. S_3tren precipitated from the absolute ethanol solution as a white solid in 93% yield (m.p. 135–137°C) and gave satisfactory elemental analysis; O_3tren was isolated as an easily hydrolysed oil and thus was characterized by spectral methods. ^1H and ^{13}C NMR spectral data (coupled and decoupled) acquired on a Bruker WH-400 spectrometer provided confirmatory evidence for the formation of the expected three azomethine linkages. The assignment of ^1H and ^{13}C resonances according to the above structural formula for **2** and **3** (Table 1) was based on those observed for the precursors. Characteristic mass spectral molecular ion and IR ν(C=N) stretching frequencies occurred at 428 m/z, 1637 cm^{-1} (**2**) and at 380 m/z, 1647 cm^{-1} (**3**). An X-ray crystallographic analysis of S_3tren has confirmed the tripodal geometry of the ligand and revealed the conjugation of the thiophene moieties with the azomethine linkages.[7]

The reactions of **2** with CuX_2 salts gave [CuL]Y and $CuX_2 \cdot L$, where Y = I_3, BPh_4 and X = Cl, Br, N_3, SCN, ClO_4, NO_3. The copper(I) complexes were obtained by the addition of excess NaY to solutions containing $Cu(OAc)_2$ and L; $[Cu(O_3tren)]BPh_4$ was isolated in a similar fashion. Copper(II) is well known to be easily converted to copper(I) by various mild reducing agents or ligands,[8a] for example, the tripodal ligand tris(2-methylthioethyl)amine (NS_3-Me) forms $[Cu(NS_3\text{-Me})]I_3$ due to the instability of the initial copper(II) com-

Table 1. ^1H and ^{13}C NMR spectral data

Compound	^1H data[a] δ(ppm) and J(Hz)	^{13}C data[a] δ(ppm) and J(Hz)
S_3tren[b]	8.10 (H_a), 7.36 (H_c, d, J_{cd} = 5.2), 6.99 (H_d, dd, J_{cd} = 5.1, J_{bd} = 3.7), 6.69 (H_b, d, J_{bd} = 3.7), 3.58 (H_e, t, J_{ef} = 5.7), 2.82 (H_f, t, J_{ef} = 5.7)	155.29 (C_a, d, J = 161.6), 142.73 ($C_{a'}$), 130.28 (C_c, d, J = 176.7), 128.35 (C_d, d, J = 194.8), 127.28 (C_b, d, J = 168.8), 59.58 (C_e, t, J = 134.4), 55.67 (C_f, t, J = 132.7)
O_3tren[b]	7.91 (H_a), 6.45–6.42 (H_b, H_c, H_d, m), 3.63 (H_e, t, J_{ef} = 5.9), 2.88 (H_f, t, J_{ef} = 6.1)	151.44 ($C_{a'}$), 150.63 (C_a, d, J = 161.6), 144.48 (C_c, d, J = 202.6),[c] 113.76 (C_d, d, J = 175.9),[c] 111.51 (C_b, d, J = 176.7),[c] 59.71 (C_e, t, J = 134.3), 55.35 (C_f, t, J = 133.1)
$[Cu(S_3tren)]BPh_4$[d]	8.78 (H_a), 7.76 (H_b, dd, J_{bd} = 3.7, J_{ab} = 1.2), 7.63 (H_c, d, J_{cd} = 5.2), 7.34 (H, phenyl, m), 7.18 (H_d, dd, J_{cd} = 5.2, J_{bd} = 3.7), 6.92 (H, phenyl, t, J = 7.4), 6.77 (H, phenyl, t, J = 7.3), 3.80 (H_e, t, J = 5.3), 3.13 (H_f, t, J = 5.4)	[e]
$[Cu(O_3tren)]BPh_4$[d]	8.33 (H_a), 7.47 (H_b, d, J_{bd} = 1.4), 7.44 (H_c, d, J_{cd} = 3.5), 7.34 (H, phenyl, t, J = 3.1), 6.92 (H, phenyl, t, J = 7.3), 6.77 (H, phenyl, t, J = 7.2), 6.65 (H_d, dd, J_{cd} = 3.5, J_{bd} = 1.6), 3.81 (H_e, dd, J = 5.9, J = 4.8), 3.16 (H_f, dd, J = 6.3, J = 5.0)	[e]

[a] d = doublet, dd = doublet of doublets, m = multiplet, t = triplet.
[b] $CDCl_3$ solution.
[c] Tentative assignment.
[d] $(CD_3)_2CO$ solution.
[e] Insufficiently soluble.

plex, $[Cu(NS_3\text{-}Me)I]ClO_4$.[8b] The isolation of $[ML](OAc)(BPh_4)$ complexes, where M = Mn, Fe, Co, Ni and L = **2** and **3**, has also been accomplished and spectral and structural characterization is underway.[9] Preliminary ^1H NMR spectral data for $[CuL]BPh_4$, where L = **2** and **3**, and ESR and visible spectra data for $CuX_2 \cdot S_3tren$, where X = Cl and Br, are presented here.

Downfield shifts of proton resonances in the ^1H NMR spectra of $[CuL]BPh_4$ (L = **2** and **3**), compared to those observed for the free ligands, clearly indicate coordination of all four nitrogen donor atoms. The shifts are the most dramatic for the azomethine protons [(H_a) 0.68 (**2**) vs 0.42 (**3**) ppm] and ethylene protons [0.22, 0.31 (**2**) vs 0.18, 0.29 ppm (**3**) for H_e and H_f, respectively]. Resonances due to ring protons are also shifted downfield in the complexes (Table 1), but it is less clear whether this occurs due to E atom complexation. The large shift for H_b (1.07 and 1.03 ppm for **2** and **3**, respectively) could occur simply as a result of increased conjugation with the C=N linkage; the shift of only *ca* 0.2 ppm, which occurs for H_d in both complexes, supports this idea rather than coordination of the E atoms. However, the shift for H_c is much larger for **3** (1.01 vs 0.27 ppm for **2**), implying that the Cu—O interaction is significantly greater than the Cu—S interaction. X-ray investigations are underway to resolve this ambiguity; results for $[CuL]BPh_4$ (L = **2**) confirm the adoption of trigonal pyramidal geometry for the copper(I) ion,* with all Cu---S distances (average of 3.344(4) Å) being too great for any bonding interaction (Fig. 1).* The cation has non-crystallographic three-fold symmetry, with the sulphur atoms being twisted

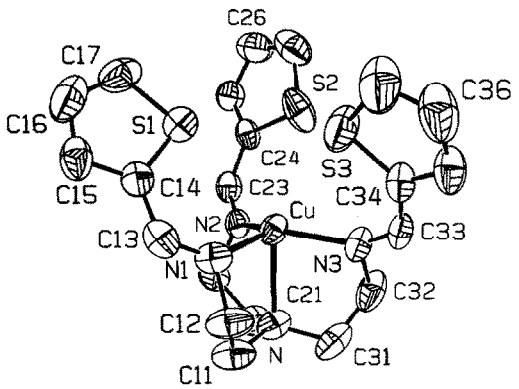

Fig. 1. A view of the $[CuN(CH_2CH_2N{=}CH\text{-}C_4H_3S)_3]^+$ cation with the crystallographic numbering scheme; ellipsoids are at the 50% level.

an average of 40.2° from being eclipsed with the equatorial nitrogen atoms; an angle of 60° corresponds to a trigonal antiprism. The Cu—N distances to the equatorial nitrogens [N(1), N(2), N(3)] are 2.028(5), 2.006(4) and 1.999(4) Å, respectively, while the N(ap)—Cu—N(eq) and N(eq)—Cu—N(eq) angles are 82.1(2) and 118.2(2)° (av.), respectively. The Cu—N(ap) distance is 2.310(5) Å, with the copper atom being 0.275(1) Å above the plane of the equatorial azomethine nitrogen atoms and the apical tertiary amine atom (N) lying 2.035(1) Å below that plane. Other relevant interatomic distances and angles are given in Table 2. Not surprisingly, the coordination geometry is remarkedly similar to that recently described for the cationic copper(I) complex of the related tripodal Schiff base ligand $N[CH_2CH_2N{=}CH(C_6H_5)]_3$ (Ph_3tren).[10] Principal dimensions in that case were Cu—N(ap) 2.232(2) Å, Cu—N(eq) 2.010(2) Å (av) and N(ap)—Cu—N(eq) 84.2(1)° (av), N(eq)—Cu—N(eq) 118.9° (av).

The green complexes of formulation $CuX_2 \cdot S_3tren$ (X = Cl, Br) have similar structures to each other, with spectral evidence indicating six-coordination in the solid state and five-coordination in solution. IR spectra of the solids show coordination of the azomethine nitrogen atoms [ν(C=N) shifts from 1637 to 1616 cm^{-1}], the presence of lattice water in the chloride [ν(O—H) at 3396 cm^{-1}], and ν(Cu—X) bands typical of octahedral geometry (240 and 209 cm^{-1} for Cl and Br, respectively). Three g values are observed in the ESR spectra of powder samples (Table 3) with the minimum g value being less than 2.03, as is typical of distorted *cis*-octahedral geometry.[11] Freshly prepared frozen dimethylformamide solutions gave axial ESR spectra with $g_\parallel > g_\perp$ (Table 2), suggesting a $d_{x^2-y^2}$ electronic ground state of square pyramidal

* Crystal data for $C_{45}H_{44}CuN_4S_3B$, M_r = 811.4, monoclinic, space group $P2_1/c$, a = 11.774(1), b = 17.738(2), c = 22.917(4) Å, β = 121.08(1)°, V = 4099(3) Å^3, Z = 4, Mo-K_α radiation (λ = 0.71069 Å, T = 298 K. A Gaussian absorption was applied (μ = 7.39 cm^{-1}). The structure was solved by a combination of direct methods and difference Fourier synthesis. Successful refinement was by full-matrix least-squares with R = 0.046 and R_w = 0.060 for 3996 reflections with $I > 3\sigma(I)$. Pertinent bond distances and angles can be found in the text and in Table 2. A transformation of the coordinates from $P2_1/c$ using the matrix

$$\begin{bmatrix} -1 & 0 & 0 \\ 0 & 1 & 0 \\ -1 & 0 & -1 \end{bmatrix}$$

will give a $P2_1/n$ monoclinic cell [a = 11.774(1), b = 17.738(2), c = 19.627(4) Å, β = 90.17(1)°] which is isomorphous with $[CuN(CH_2CH_2N{=}CH\text{-}C_6H_5)_3]^+[BPh_4]^-$.[10]

Table 2. Molecular dimensions

(a) Interatomic distances (Å)

Cu—N	2.310(5)	N—C(11)	1.461(7)
Cu—N(1)	2.027(5)	N—C(21)	1.456(7)
Cu—N(2)	2.006(4)	N—C(31)	1.459(7)
Cu—N(3)	1.999(4)	N(1)—C(12)	1.482(7)
Cu—S(1)	3.276(3)	N(1)—C(13)	1.268(7)
Cu—S(2)	3.361(4)	N(2)—C(22)	1.475(6)
Cu—S(3)	3.396(5)	N(2)—C(23)	1.268(6)
S(1)—C(14)	1.711(7)	N(3)—C(32)	1.472(7)
S(1)—C(17)	1.699(7)	N(3)—C(33)	1.270(6)
S(2)—C(24)	1.705(7)	C(11)—C(12)	1.515(8)
S(2)—C(27)	1.714(7)	C(13)—C(14)	1.430(10)
S(3)—C(34)	1.706(6)	C(21)—C(22)	1.516(8)
S(3)—C(37)	1.704(7)	C(23)—C(24)	1.435(9)
		C(31)—C(32)	1.496(9)
		C(33)—C(34)	1.431(7)

(b) Bond angles (°)

N—Cu—N(1)	81.2(2)	N—C(11)—C(12)	110.8(5)
N—Cu—N(2)	82.8(2)	N(1)—C(12)—C(11)	109.2(5)
N—Cu—N(3)	82.3(2)	N(1)—C(13)—C(14)	126.0(5)
N(1)—Cu—N(2)	110.9(2)	S(1)—C(14)—C(13)	123.2(6)
N(1)—Cu—N(3)	117.9(2)	S(1)—C(14)—C(15)	110.3(6)
N(2)—Cu—N(3)	125.5(2)	C(13)—C(14)—C(15)	126.6(6)
Cu—N—C(11)	104.7(4)	N—C(21)—C(22)	110.4(5)
Cu—N—C(21)	102.8(4)	N(2)—C(22)—C(21)	110.3(5)
Cu—N—C(31)	103.2(4)	N(2)—C(23)—C(24)	126.6(5)
C(11)—N—C(21)	114.6(5)	S(2)—C(24)—C(23)	123.9(6)
C(11)—N—C(31)	115.0(5)	C(23)—C(24)—C(25)	125.5(6)
C(21)—N—C(31)	114.5(5)	N—C(31)—C(32)	111.1(5)
Cu—N(1)—C(12)	107.0(4)	N(3)—C(32)—C(31)	110.7(5)
Cu—N(1)—C(13)	134.8(4)	N(3)—C(33)—C(34)	126.2(5)
C(12)—N(1)—C(13)	117.1(5)	S(3)—C(34)—C(33)	124.3(6)
Cu—N(2)—C(22)	107.9(4)	C(33)—C(34)—C(35)	124.4(6)
Cu—N(2)—C(23)	135.7(4)		
C(22)—N(2)—C(23)	116.0(5)		
Cu—N(3)—C(32)	105.9(4)		
Cu—N(3)—C(33)	136.9(4)		
C(32)—N(3)—C(33)	115.6(5)		

Table 3. Electronic and ESR spectral data[a]

Compound	*d–d* Transitions (cm^{-1})[b]	g_1[c]	g_2[c]	g_3[c]	$g_\parallel$[d]	$g_\perp$[d]
$CuCl_2 \cdot S_3$tren	14,300(180), 10,000(sh)	2.21	2.16	2.02	2.22(154)	1.96
$CuBr_2 \cdot S_3$tren	14,500(220), 10,000(sh)	2.20	2.15	2.02	2.24(159)	2.05

[a] Dimethylformamide solutions.

[b] Molar extinction coefficient (ε) is in parentheses, sh is shoulder.

[c] Spin-Hamiltonian parameters for powders at room temperature.

[d] Spin-Hamiltonian parameters for frozen solutions at 77 K. Hyperfine coupling constants ($A_\parallel$) in units of 10^{-4} cm^{-1} are in parentheses.

geometry.[12] Conductance data for 10^{-3} M DMF solutions (Λ_M = 62.5 and 68.2 Ω^{-1} mol^{-1} cm^2 for the chloride and bromide, respectively) are in agreement with the complexes being 1 : 1 electrolytes.[13] These fresh DMF solutions showed electronic spectral bands at 14,300 cm^{-1} (ε = 180, Cl) and 14,500 cm^{-1} (ε = 220, Br), with low energy shoulders near 10,000 cm^{-1}; such visible absorption bands are expected for square pyramidal copper(II) complexes.[10,14] Preliminary electronic and ESR spectral data for these and other $CuX_2 \cdot S_3$tren complexes currently under study indicate that octahedral to square pyramidal to trigonal bipyramidal structural changes can occur; these results will be reported elsewhere.

Acknowledgements—The authors thank NSERC Canada for operating grants and an infrastructure grant (E.C.A. and G.F.) and a CIDA Research Associateship (Z.X.).

REFERENCES

1. M. G. B. Drew, *Prog. Inorg. Chem.* 1977, **23**, 67.
2. D. L. Kepert, *Prog. Inorg. Chem.* 1979, **25**, 41.
3. M. Calligaris and L. Randaccio, in *Comprehensive Coordination Chemistry* (Edited by G. Wilkinson, R. D. Gillard and J. A. McCleverty), Vol. 2, Ch. 20, p. 735. Pergamon Press, Oxford (1987).
4. L. J. Wilson and N. J. Rose, *J. Am. Chem. Soc.* 1968, **90**, 6041.
5. R. M. Kirchner, C. Mealli, M. Bailey, N. Howe, L. P. Torre, L. J. Wilson, L. C. Andrews, N. J. Rose and E. C. Lingafelter, *Coord. Chem. Rev.* 1987, **77**, 89.
6. K. D. Karlin and J. Zubieta (Eds), *Copper Coordination Chemistry: Biochemical & Inorganic Perspectives*. Adenine Press, Guilderland, N.Y. (1983).
7. E. C. Alyea, S. Liu, B. Li, Z. Xu and X. Z. You, *Acta Cryst.* 1989, **C45**, 1566.
8. (a) F. A. Cotton and G. Wilkinson, *Advanced Inorganic Chemistry*, 4th edn, p. 800. John Wiley, New York (1980); (b) M. Suzuki, H. Kanatomi, H. Koyama and I. Murase, *Bull. Chem. Soc. Jpn* 1980, **53**, 1961.
9. E. C. Alyea, G. Ferguson, M. Jennings, B. Li, Z. Xu and X. Z. You, unpublished results (1989).
10. E. C. Alyea, G. Ferguson, M. Jennings and Z. Xu, *Polyhedron* 1990, **9**, 739.
11. B. J Hathaway and D. E. Billing, *Coord. Chem. Rev.* 1970, **5**, 143.
12. T. N. Sorrell and D. L. Jameson, *Inorg. Chem.* 1982, **21**, 1014.
13. W. J. Geary, *Coord. Chem. Rev.* 1971, **7**, 81.
14. A. B. P. Lever, *Inorganic Electronic Spectroscopy*, 2nd edn. Elsevier, Amsterdam (1984).

Polyhedron Vol. 9, No. 20, pp. 2469–2476, 1990
Printed in Great Britain

0277–5387/90 $3.00+.00
© 1990 Pergamon Press plc

PREPARATION AND REACTIVITY OF *CIS*-BIS(CYCLOPENTADIENYLDIPHENYLPHOSPHINE)(TETRACARBONYL)MOLYBDENUM AND *CIS*-[1,3-BIS(DIPHENYLPHOSPHINO)DICYCLOPENTADIENE](TETRACARBONYL)MOLYBDENUM. X-RAY CRYSTAL STRUCTURE OF $2[(C_5H_5)Mo]_2(\mu\text{-}PPh_2)_2(CO)(O)\cdot C_6H_{14}$

WAI-KWOK WONG*

Department of Chemistry, Hong Kong Baptist College, Kowloon, Hong Kong

and

FONG LUNG CHOW and HUA CHEN

Department of Applied Biology and Chemical Technology, Hong Kong Polytechnic, Hung Hom, Kowloon, Hong Kong

and

RU-JI WANG and THOMAS C. W. MAK*

Department of Chemistry, The Chinese University of Hong Kong, Shatin, N.T., Hong Kong

(*Received* 7 *March* 1990; *accepted* 7 *June* 1990)

Abstract—The interaction of $C_7H_8Mo(CO)_4$ with 2 equivalents of $Ph_2P(C_5H_5)$ in hexane at −2°C gives two isomers of *cis*-$[Ph_2P(C_5H_5)]_2Mo(CO)_4$ (**II** and **III**) in high yield. In toluene, the coordinated $Ph_2P(C_5H_5)$ ligands of **II** and **III** undergo intramolecular Diels–Alder dimerization at room temperature producing *cis*-[1,3-bis(diphenylphosphino)dicyclopentadiene](tetracarbonyl)molybdenum (**IV**) in quantitative yield. Compound **IV** can also be prepared in high yield by the interaction of *cis*-$Mo(CO)_4(Ph_2PCl)_2$ with 2 equivalents of $(C_5H_5)Tl$ in refluxing toluene. Pyrolysis of **IV** gives a hexane solvate $2[(C_5H_5)Mo]_2(\mu\text{-}PPh_2)_2(CO)(O)\cdot C_6H_{14}$ (**VI**) in low yield, the structure of which was determined by X-ray crystallography.

We recently reported[1] the synthesis of *cis*-[1,3-bis(diphenylphosphino)dicyclopentadiene](tetracarbonyl)molybdenum (**IV**), via the interaction of *cis*-$Mo(CO)_4(Ph_2PCl)_2$ with 2 equivalents of $(C_5H_5)Tl$ and postulated that **IV** was produced via intramolecular Diels–Alder dimerization of the $Ph_2P(C_5H_5)$ ligands of the proposed intermediate *cis*-$[Ph_2P(C_5H_5)]_2Mo(CO)_4$ (**II**). Metal-promoted intramolecular Diels–Alder cycloaddition between coordinated phospholes and coordinated vinylphosphines has also been described recently.[2] Here we report the isolation of **II** and demonstrate that **IV** is indeed formed via intramolecular Diels–Alder dimerization of the coordinated cyclopentadienyldiphenylphosphine of **II**.

* Authors to whom correspondence should be addressed.

RESULTS AND DISCUSSION

Interaction of $C_7H_8Mo(CO)_4$ *with* $Ph_2P(C_5H_5)$

(i) *At room temperature.* When $C_7H_8Mo(CO)_4$ was treated with 2 equivalents of $Ph_2P(C_5H_5)$ in hexane, light yellow crystals of stoichiometry $(C_{34}H_{30}P_2)Mo(CO)_4$ (**IV**) were obtained in high

yield (85%). The IR spectrum (KBr) of **IV** exhibits three absorptions at 2017s, 1916s and 1880 vs(br) cm^{-1}. The absorption pattern is indicative of a *cis*-configuration for the four terminal carbonyl groups. The mass spectrum shows the highest peak at *m/z* 596, corresponding to the $(M-4CO)^+$ fragment ($C_{34}H_{30}P_2Mo$). The $^{31}P\{^1H\}$ NMR spectrum exhibits two doublets of relative intensity 1 : 1 centred at δ 23.4 (J = 24.4 Hz) and 37.2 ppm (J = 24.4 Hz), respectively. The ^1H NMR spectrum is very complicated. In addition to the phenyl resonances, it exhibits three multiplets of relative intensity 1 : 1 : 1 centred at δ 6.67, 6.19 and 5.19 ppm, respectively, in the olefinic proton region and four multiplets of relative intensity 2 : 1 : 3 : 1 centred at δ 2.94, 2.74, 2.02 and 0.74 ppm, respectively, in the aliphatic proton region. The spectroscopic data suggest that the phosphine ligand is 1,3-bis(diphenylphosphino)dicyclopentadiene (**I**) formed via intramolecular Diels–Alder dimerization of (diphenylphosphino)cyclopentadiene as shown in Eq. (1):

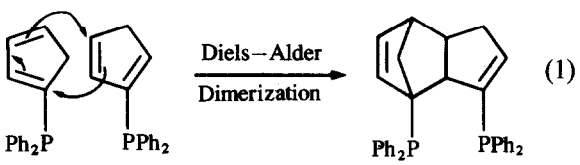

(1)

I

The X-ray diffraction study of **IV** has established a *cis*-configuration for the four terminal carbonyl groups and confirmed that the two $Ph_2P(C_5H_5)$ ligands indeed did undergo dimerization to produce the 1,3-bis(diphenylphosphino)dicyclopentadiene ligands.[1]

(ii) *At* −2°C. When $C_7H_8Mo(CO)_4$ was treated with 2 equivalents of $Ph_2P(C_5H_5)$ at −2°C in hexane, compounds **II** and **III** were obtained. The major product, **II**, recrystallized from hexane, has a stoichiometry $[Ph_2P(C_5H_5)]_2Mo(CO)_4$. The IR spectrum in KBr exhibits three absorption at 2014s, 1899 vs(br), 1877 vs(br) cm^{-1}, indicative of a *cis*-configuration for the four terminal carbonyls. The $^{31}P\{^1H\}$ NMR spectrum exhibits a singlet at δ 23.2 ppm indicating that the two phosphorus ligands are equivalent. Other than the broad complex multiplets centred at δ 7.18 ppm for the phenyl resonances, the ^1H NMR spectrum shows a broad complex multiplet and a broad singlet of relative intensity 3 : 2 centred at δ 6.50 and 2.81 ppm for the olefinic protons and the aliphatic protons of the C_5H_5 ring, respectively. Based on the above spectroscopic data, two structures are possible for **II**. These are **IIa** and **IIb** as shown below.

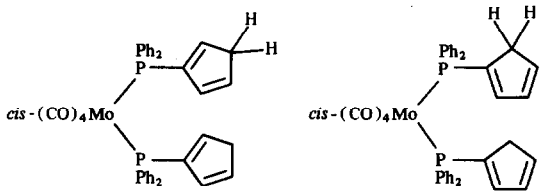

IIa **IIb**

If **II** adopts structure **IIb**, one would then expect that the aliphatic protons of the carbon β to the phosphorus would couple with the phosphorus to give a doublet. The fact that the aliphatic protons resonance shows a singlet suggests that the protons are attached to the carbon γ to the phosphorus atom. In terms of steric hindrance the C_5H_5 ring of **IIa** probably has less steric interaction with the other substituents on the phosphorus than that of **IIb**. Thus, based on the splitting pattern and steric argument, structure **IIa** is assigned to **II**. ^1H and $^{31}P\{^1H\}$ NMR studies show that **II** in C_6D_6 at ambient temperature isomerizes to **IV** quantitatively.

The minor product, **III**, is always contaminated with **II**. However, ^1H and $^{31}P\{^1H\}$ NMR studies show that a mixture of **II** and **III** in C_6D_6 at ambient temperature isomerizes to **IV** quantitatively, and no other products are observed. This suggests that the stoichiometry of **III** is the same as **II** and is $[Ph_2P(C_5H_5)]_2Mo(CO)_4$. The IR spectrum of **III** in KBr exhibits three absorptions at 2014s, 1988 vs(br), 1877 vs(br) cm^{-1}, indicative of a *cis*-configuration for the four terminal carbonyls. The $^{31}P\{^1H\}$ NMR spectrum exhibits two doublets of relative intensity 1 : 1 centred at δ 21.1 (J_{P-P} = 24.4 Hz) and δ 30.8 (J_{P-P} = 24.4 Hz) ppm, suggesting the presence of two non-equivalent phosphorus ligands. Other than the phenyl and olefinic resonances, ^1H NMR shows a doublet (J_{P-H} = 15.0 Hz) and a singlet of relatively intensity 1 : 2 at δ 4.07 and 2.89 ppm, respectively. The chemical shift and coupling constant of the doublet at δ 4.07 ppm is similar to that of the unique proton of the (Me_4C_5H) ring (δ 4.23 ppm; J_{P-H} = 15.3 Hz) of the complex $[(Me_4C_5H)PPh_2]Mo(CO)_5$ (**V**) whose structure has been established by an X-ray diffraction study[3] and is shown below.

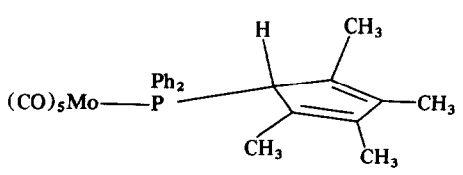

V

The chemical shift of the singlet at δ 2.89 ppm is similar to the aliphatic protons of **II**. Based on the above spectroscopic data, the following structure is assigned to **III**.

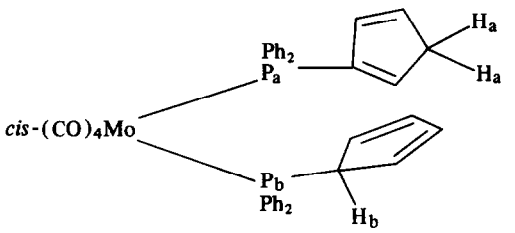

III

Based on the assigned structures, assignment of ^{31}P NMR data can be made and is shown in Table 1.

Interaction of cis-$Mo(CO)_4(Ph_2PCl)_2$ *with* $(C_5H_5)Tl$

When *cis*-$Mo(CO)_4(Ph_2PCl)_2$ was treated with 2 equivalents of $(C_5H_5)Tl$ in toluene at room temperature, no reaction was observed after 48 h. However, if the reaction was carried out overnight in refluxed toluene, compound **IV** was obtained in high yield (80%). The formation of **IV** probably involves the mechanism shown in Scheme 1. *Cis*-$Mo(CO)_4(Ph_2PCl)_2$ reacts with $(C_5H_5)Tl$ to produce intermediate **II** which then undergoes a series of rearrangements and finally intramolecular Diels–Alder cycloaddition to produce the final product **IV**. The mechanism is further supported by the fact that **II** and **III** isomerize to **IV** quantitatively at room temperature.

Thermolysis of **IV**

Pyrolysis of **IV** in the solid state produces a red crystalline compound **VI** of stoichiometry $C_{35}H_{30}O_2P_2Mo_2$ in low yield. The IR spectrum (KBr) of **VI** exhibits a strong absorption at 1807 cm^{-1} in the terminal carbonyl region. The $^{31}P\{^1H\}$ NMR spectrum exhibits a singlet at δ 167.2 ppm.

Table 1. ^1H and $^{31}P\{^1H\}$ NMR data

Compound	$^1H^a$	Assignment	$^{31}P^b$	Assignment
II	7.18m(20)	$Ph_2P(C_5H_5)$	23.2s	$Ph_2P(C_5H_5)$
	6.50m(6)	Olefinic protons of C_5H_5		
	2.81br,s(4)	Aliphatic protons of C_5H_5		
III	7.26m(20)	$Ph_2P(C_5H_5)$	21.2d(1)	$Ph_2P_a(C_5H_5)$; J_{P-P} = 24.2 Hz
	6.48m(7)	Olefinic protons of C_5H_5	30.8d(1)	$Ph_2P_b(C_5H_5)$; J_{P-P} = 24.2 Hz
	4.07d(1)	H_b; J_{P-H} = 15.0 Hz		
	2.89s(2)	H_a		
IV	7.33m(20)	Ph_2P	23.4d(1)	P_a; J_{P-P} = 24.4 Hz
	6.67m(1)	Olefinic protons of the dicyclopentadiene ligand	37.2d(1)	P_b; J_{P-P} = 24.4 Hz
	6.19m(1)			
	5.19m(1)			
	2.94m(2)	Aliphatic protons of the dicyclopentadiene ligand		
	2.74m(1)			
	2.02m(3)			
	0.74m(1)			
V	7.80m(4)	$Ph_2P(C_5Me_4H)$	37.0s	$Ph_2P(C_5Me_4H)$
	7.55m(6)			
	4.23d(1)	$P(C_5Me_4H)$; J_{P-H} = 15.3 Hz		
	1.74br,s(6)	$P(C_5Me_4H)$		
	1.42s(6)			
VI	8.14m(4)	μ-PPh_2	167.2s	μ-PPh_2
	7.46m(4)			
	7.19m(12)			
	4.97s(5)	C_5H_5		
	4.78m(5)	C_5H_5		

[a] In $CDCl_3$ at 30°C, referenced to Me_4Si (δ 0.00).
[b] In $CDCl_3$ at 30°C, referenced to external 85% H_3PO_4 (δ 0.0), negative for upfield shift.
Abbreviations: s, singlet; d, doublet; m, multiplet; br, broad.

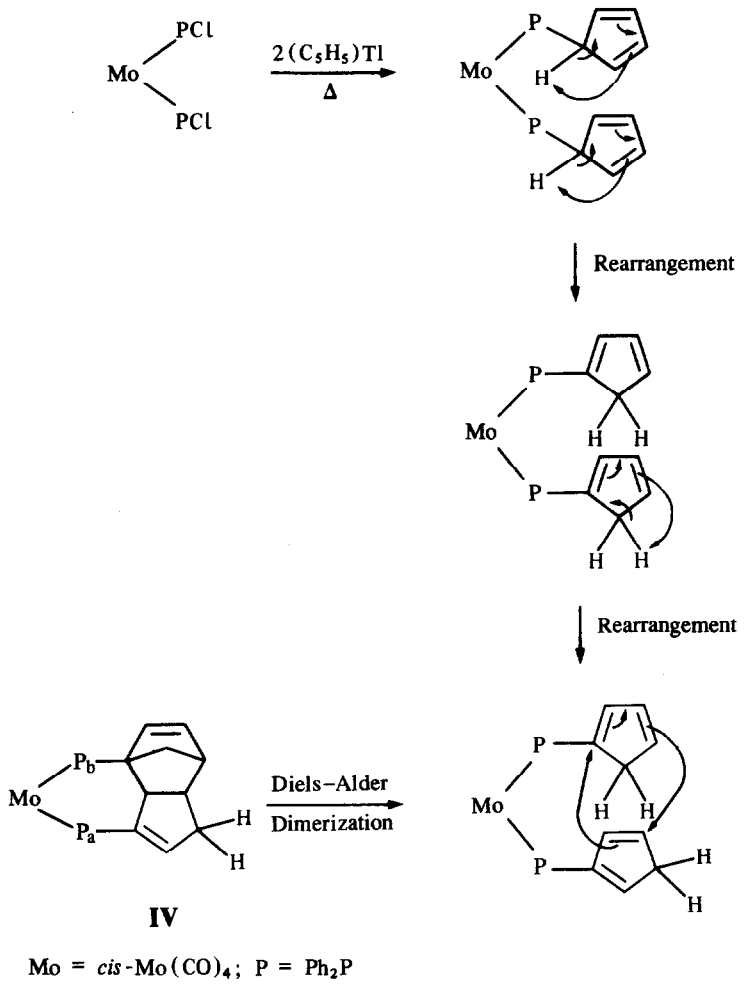

IV

Mo = *cis*-Mo(CO)$_4$; P = Ph_2P

Scheme 1.

The low-field chemical shift suggests the presence of phosphido-bridged ligands.[4] The ^{1}H NMR spectrum exhibits a set of three multiplets of total relative intensity 20, centred at δ 8.14, 7.46 and 7.19 ppm for the phenyl protons, a singlet of intensity 5 at δ 4.97 ppm, and a multiplet of relative intensity 5 at δ 4.78 ppm for the C_5H_5 rings.

The structure of **VI** was determined by an X-ray diffraction study of its hexane solvate, 2 **VI** · C_6H_{14}. The crystal data and other parameters for the X-ray structural analysis are listed in Table 2. The hexane molecules centred about a crystallographic inversion centre, exhibits two-fold disorder.

A perspective drawing of **VI** is shown in Fig. 1. Selected bond lengths and bond angles are given in Table 3. The structure is consistent with its spectroscopic data and **VI** can be formulated as $[(C_5H_5)Mo]_2(\mu\text{-}PPh_2)_2(CO)(O)$. The dimer can be considered as a $Mo^{(II)}$—$Mo^{(IV)}$ mixed-valent compound. Mo(1) to which the oxo group is attached is formally in a +4 oxidation state and Mo(2) where the carbonyl is attached is formally in a +2 oxidation state. For the two molybdenum atoms to obey the 18-electron rule, a double bond should exist between them.

This is reflected by the shorter Mo—Mo distance of 2.941(1) Å in comparison with those in the analogous complexes $M_2(CO)_8(\mu\text{-}PEt_2)_2$ (M = Mo, 3.06 Å and M = W, 3.05 Å).[5] The coordination polyhedron around each molybdenum atom can be described as a distorted tetrahedron if the metal–metal bond is neglected, with the cyclopentadienyl group occupying one coordination site, and two bridging phosphorus atoms and the oxo atom [for Mo(1)] or the carbonyl group [for Mo(2)] occupying the other three sites (Fig. 1). The oxo and carbonyl ligands are *trans* to each other as reflected by the torsion angle O(1)—Mo(1)—Mo(2)—C(2) of 178.6°. The planar Mo_2P_2 core (within ±0.036 Å) is similar to that found in $M_2(CO)_8(\mu\text{-}PEt_2)_2$ (M = Mo, W)[5] and $W_2(CO)_8(\mu\text{-}PPh_2)_2$,[6] but different from the butterfly Fe_2P_2 core in $Fe_2(CO)_6(\mu\text{-}PPh_2)_2$.[7] The Mo=O bond distance of 1.687(6) Å falls in the range reported for the other

Table 2. Data collection and processing parameters

Molecular formula	$2[(C_5H_5)Mo]_2(\mu\text{-}PPh_2)_2(CO)(O)\cdot C_6H_{14}$
Molecular weight	1559.14
Colour and habit	Dark red plate
Unit cell parameters	$a = 9.554(a)$ Å $\alpha = 76.58(1)°$ $b = 13.418(2)$ Å $\beta = 71.63(1)°$ $c = 14.363(2)$ Å $\gamma = 88.00(1)°$ $V = 1698.3(5)$ Å^3 $Z = 1$ $F(000) = 790$
Density (calcd)	1.524 g cm^{-3}
Space group	$P\bar{1}$ (No. 2)
Radiation	Graphite-monochromatized MoK_α, $\lambda = 0.71073$ Å
Standard reflections	$(11\bar{2})$, (204)
Intensity variation	±8%
R_{int} (from merging of equivalent reflections)	0.053
Absorption coefficient	8.45 cm^{-1}
Crystal size	$0.10 \times 0.32 \times 0.35$ mm^3
Mean μr	0.108
Transmission factors	0.773–0.884
Scan type and rate	ω; 3.01–15.63° min^{-1}
Scan range	0.60° below $K\alpha_1$ to 0.70° above $K\alpha_2$
Background counting	Stationary counts for one-fifth of scan time at each end of scan range
Collection range	h, $\pm k$, ± 1; $2\theta_{max} = 50°$
Unique data measured	5947
Observed data with $\|F_o\| \geqslant 6\sigma(\|F_o\|)$, n	3839
Number of variables, p	391
$R_F = \Sigma\|\|F_o\|-\|F_c\|\|/\Sigma\|F_o\|$	0.053
Weighting scheme	$w = [\sigma^2(F_o)+0.0015\|F_o\|^2]\underline{1}$
$R_G = [\Sigma w(\|F_o\|-\|F_c\|)^2/\Sigma w\|F_o\|^2]^{1/2}$	0.082
$S = [\Sigma w(\|F_o\|-\|F_c\|)^2/(n-p)]^{1/2}$	1.606
Residual extrema in final difference map	+1.78 to −0.93 eÅ^{-3}

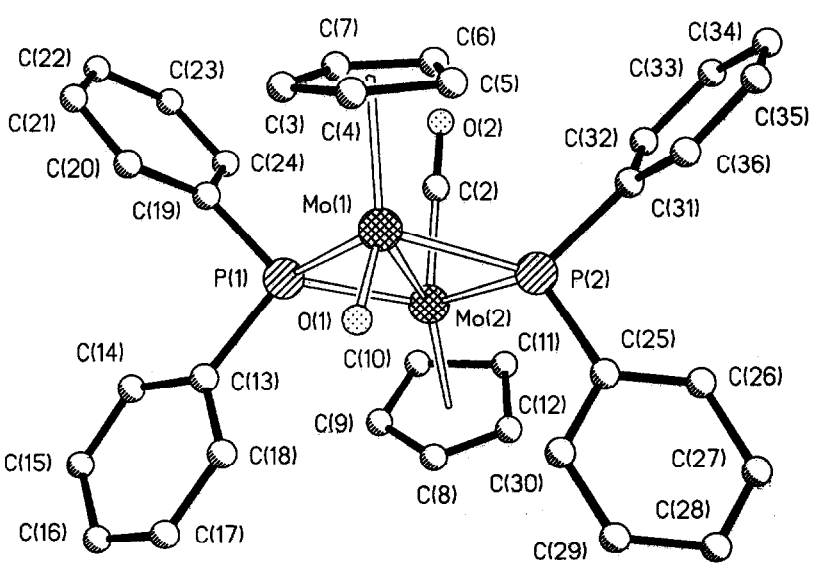

Fig. 1. A perspective drawing of **VI** with thermal ellipsoids at 30% probability.

Table 3. Selected bond lengths (Å) and bond angles (°) in the Mo_2P_2 core of the $[(C_5H_5)Mo]_2(\mu\text{-}PPh_2)_2(CO)(O)$ molecule

Mo(1)—Mo(2)	2.941(1)	C(2)—O(2)	1.15(1)
Mo(1)—P(1)	2.459(2)	Mo(2)—P(1)	2.324(2)
Mo(1)—P(2)	2.463(2)	Mo(2)—P(2)	2.324(2)
Mo(1)—O(1)	1.687(6)	Mo(2)—C(2)	1.95(1)
Mo(1)—Cp(1)	2.085(8)[a]	Mo(2)—Cp(2)	2.008(8)[a]
Mo(2)—Mo(1)—P(1)	50.0(1)	Mo(1)—Mo(2)—P(1)	54.2(1)
Mo(2)—Mo(1)—P(2)	50.0(1)	Mo(1)—Mo(2)—P(2)	54.3(1)
P(1)—Mo(1)—P(2)	99.9(1)	P(1)—Mo(2)—P(2)	108.3(1)
Mo(2)—Mo(1)—O(1)	111.9(2)	Mo(1)—Mo(2)—C(2)	89.0(2)
P(1)—Mo(1)—O(1)	102.0(2)	P(1)—Mo(2)—C(2)	90.4(2)
P(2)—Mo(1)—O(1)	102.7(2)	P(2)—Mo(2)—C(2)	91.8(3)
Mo(2)—Mo(1)—Cp(1)	124.4(2)	Mo(1)—Mo(2)—Cp(2)	148.5(2)
P(1)—Mo(1)—Cp(1)	113.2(3)	P(1)—Mo(2)—Cp(2)	118.8(3)
P(2)—Mo(1)—Cp(1)	112.2(3)	P(2)—Mo(2)—Cp(2)	119.0(3)
O(1)—Mo(1)—Cp(1)	123.7(4)	C(2)—Mo(2)—Cp(2)	122.4(4)
Mo(1)—P(1)—Mo(2)	75.8(1)	Mo(1)—P(2)—Mo(2)	75.8(1)
Mo(1)—P(1)—C(13)	116.6(3)	Mo(1)—P(2)—C(25)	117.1(2)
Mo(2)—P(1)—C(13)	118.5(2)	Mo(2)—P(2)—C(25)	118.3(3)
Mo(1)—P(1)—C(19)	116.2(2)	Mo(1)—P(2)—C(31)	117.0(2)
Mo(2)—P(1)—C(19)	128.0(3)	Mo(2)—P(2)—C(31)	128.2(3)
C(13)—P(1)—C(19)	101.2(4)	C(25)—P(2)—C(31)	100.4(4)
Mo(2)—C(2)—O(2)	176.1(7)		

[a]Cp(1) is the centre of the ring composed of carbon atoms C(3)—C(7), and Cp(2) is the centre of the C(8)—C(12) ring.

molybdenum oxo complexes.[8,9] In accordance with the different oxidation states of the metal atoms, the Mo(1)—P [av. 2.461(2) Å] and Mo(1)—Cp(1) [2.085(8) Å] bonds are significantly longer than Mo(2)—P [av. 2.324(2) Å] and Mo(2)—Cp(2) [2.008(8) Å], respectively. The bond lengths and angles involving the carbon atoms are all normal and there are no unusual intermolecular contacts in the crystal packing.

EXPERIMENTAL

Microanalyses were performed by Butterworth (U.K.). IR spectra were recorded on a Perkin–Elmer 983 spectrometer; data given in cm^{-1} in KBr pellets. NMR spectra were recorded on a JEOL FX90Q spectrometer. Chemical shifts of ^1H NMR spectra were referenced to internal deuterated solvents and then recalculated to TMS = 0.0 ppm. ^{31}P NMR spectra were referenced to external 85% H_3PO_4.

All operations were carried out under nitrogen or *in vacuo*. All chemicals used were of reagent grade. Solvents were dried by standard procedures, distilled and deaerated prior to use. Melting points were taken in sealed capillaries and are uncorrected.

$Ph_2P(C_5H_5)$,[10] $(C_5H_5)Tl$,[10] $C_7H_8Mo(CO)_4$[11] and *cis*-$Mo(CO)_4(Ph_2PCl)_2$[12] were prepared according to literature methods.

Preparation of cis-$[Ph_2P(C_5H_5)]_2Mo(CO)_4$

A solution of $C_7H_8Mo(CO)_4$ (0.5 g, 1.7 mmol) in hexane (50 cm^3) was added dropwise to a freshly prepared solution of $Ph_2P(C_5H_5)$ (0.9 g, 3.6 mmol) in hexane (50 cm^3) at −2°C. After stirring at −2°C for 2 h, the solution was filtered. The filtrate was concentrated to *ca* 60 cm^3 and cooled to −20°C to give white crystalline products which were a mixture of **II** and **III**.

The white crystalline products were then extracted with cold hexane (2 × 20 cm^3) at 0°C. The hexane solution was then concentrated to *ca* 20 cm^3 at 0°C and cooled to −20°C to give pure **II** as a white crystalline solid, which was filtered and dried *in vacuo*. Yield: 0.9 g, 75%; m.p. 202–204°C (decomposed). Found (required): C, 64.5 (64.4); H, 4.0 (4.2); P, 9.0 (8.8)%. IR (KBr), ν(CO): 2014s, 1899 vs(br), 1877 vs(br) cm^{-1}.

Further recrystallization of the filtrate only produced a mixture of **II** and **III**.

Preparation of **IV**

(i) A solution of $C_7H_8Mo(CO)_4$ (0.5 g, 1.7 mmol) in hexane (50 cm^3) was added dropwise to a freshly

prepared solution of $Ph_2P(C_5H_5)$ (0.9 g, 3.6 mmol) in hexane at ambient temperature. After stirring for 3 h at ambient temperature, white precipitates were obtained. The precipitates were filtered and recrystallized from a 1:1 toluene–hexane mixture (20 cm^3) to give light yellow crystals which were dried *in vacuo*. Yield: 1.1 g, 88%; m.p. 198–200°C (decomposed). Found (required): C, 64.4 (64.4); H, 4.1 (4.2); P, 8.9 (8.8)%. IR (KBr), ν(CO): 2017s, 1916s, 1880 vs(br) cm^{-1}.

(ii) A solution of *cis*-$Mo(CO)_4(Ph_2PCl)_2$ (0.9 g, 1.5 mmol) in toluene (50 cm^3) was added dropwise to a suspension of $(C_5H_5)Tl$ (0.9 g, 3.3 mmol) in toluene (50 cm^3) at ambient temperature. The solution was stirred at ambient temperature for 48 h, but no reaction was observed. The solution was then refluxed overnight and allowed to cool to room temperature and filtered. The filtrate was then concentrated under reduced pressure to *ca* 20 cm^3. n-Hexane was then added until the solution turned cloudy. Upon standing at room temperature overnight, light yellow crystals of **IV** were obtained. Yield: 0.9 g, 85%.

Pyrolysis of **IV**

Compound **IV** (0.9 g, 1.2 mmol) was heated at 200°C *in vacuo*. The complex gradually turned black with evolution of gas as the temperature was raised. After heating for 4 h at 200°C, gas evolution ceased. The black residue was cooled down to room temperature, dissolved in a minimum amount of $CHCl_3$, and chromatographed on silica gel using toluene as eluent. A brown band was collected and the solvent was evaporated *in vacuo*. The residue was redissolved in a minimum amount of $CHCl_3$ and chromatographed again on silica gel using a hexane–toluene mixture as eluent. Three bands were obtained. Band A was obtained by eluting with hexane–toluene (2:3), and bands B and C were obtained with hexane–toluene (1:2). Solvents were removed *in vacuo*. Bands A and B yielded only a small amount of solid material and were discarded. Band C gave considerably better yield and recrystallization of the residue, with toluene–hexane, gave dark red prisms which were dried *in vacuo*. Yield: 0.2 g, 22%; m.p. >280°C. Found (required): C, 57.4 (57.1); H, 4.2 (4.1); P, 8.1 (8.4)%. IR (KBr), ν(CO): 1807s cm^{-1}.

$^{31}P\{^1H\}$ *NMR studies*

(i) *Isomerization of* **II**. **II** (20 mg) was dissolved in 0.5 cm^3 of $CDCl_3$ at 10°C. The isomerization process was monitored by $^{31}P\{^1H\}$ NMR spectroscopy at 4-h intervals for 12 h. Within the period,

Table 4. Atomic coordinates ($\times 10^5$ for Mo; $\times 10^4$ for other atoms) and equivalent isotropic temperature factors[a] ($Å^2 \times 10^4$ for Mo and P; $\times 10^3$ for other atoms)

Atom	*x*	*y*	*z*	U_{eq}
Mo(1)	14224(8)	17883(5)	82515(5)	479(3)
Mo(2)	37807(8)	18294(5)	63410(5)	475(3)
P(1)	2432(2)	380(2)	7440(2)	473(6)
P(2)	3050(2)	3225(2)	7058(2)	478(6)
O(1)	2076(6)	1559(5)	9240(4)	65(1)
C(2)	2306(9)	2067(6)	5644(6)	66(1)
O(2)	1501(8)	2204(5)	5185(5)	94(1)
C(3)	−1056(8)	1145(7)	8809(7)	73(1)
C(4)	−1020(8)	1961(7)	9268(7)	69(1)
C(5)	−592(8)	2872(7)	8500(7)	72(1)
C(6)	−511(8)	2586(7)	7550(6)	65(1)
C(7)	−786(8)	1529(7)	7765(7)	68(1)
C(8)	6196(9)	1517(9)	6371(9)	128(1)
C(9)	5867(9)	873(8)	5941(7)	84(1)
C(10)	5586(9)	1324(7)	5031(7)	85(1)
C(11)	5788(10)	2404(9)	4898(9)	142(1)
C(12)	6213(9)	2423(9)	5849(9)	130(1)
C(13)	3394(8)	−598(6)	8112(6)	59(1)
C(14)	3550(9)	−1572(6)	7914(7)	76(1)
C(15)	4408(9)	−2283(7)	8289(8)	97(1)
C(16)	5092(10)	−1993(8)	8969(8)	121(1)
C(17)	4936(10)	−1075(8)	9167(8)	102(1)
C(18)	4108(9)	−351(7)	8727(7)	81(1)
C(19)	1104(8)	−413(6)	7234(6)	56(1)
C(20)	37(8)	−1025(6)	8027(7)	66(1)
C(21)	−1014(9)	−1585(7)	7867(8)	85(1)
C(22)	−1036(9)	−1577(7)	6909(8)	92(1)
C(23)	45(10)	−998(7)	6120(7)	85(1)
C(24)	1116(8)	−396(6)	6266(6)	61(1)
C(25)	4354(8)	3797(6)	7509(6)	53(1)
C(26)	4980(8)	4776(6)	6991(7)	67(1)
C(27)	6100(9)	5169(7)	7281(7)	78(1)
C(28)	6572(9)	4636(7)	7974(7)	78(1)
C(29)	5940(9)	3656(8)	8489(7)	84(1)
C(30)	4858(8)	3250(7)	8274(6)	67(1)
C(31)	2149(8)	4383(6)	6580(5)	49(1)
C(32)	2077(9)	4591(6)	5619(6)	64(1)
C(33)	1375(9)	5452(6)	5263(7)	72(1)
C(34)	746(9)	6087(7)	5899(8)	82(1)
C(35)	792(9)	5881(7)	6835(7)	75(1)
C(36)	1504(9)	5024(6)	7172(7)	68(1)
C(37)	3856(8)	4661(11)	−345(13)	171(1)
C(38)	2367(8)	4058(9)	193(12)	150(1)
C(39)	1092(6)	4746(5)	47(12)	134(1)
C(40)	−311	4058	361	54(1)
C(41)	−1713(8)	4644(8)	727(8)	158(1)
C(42)	−2277(12)	5144(11)	−158(10)	154(1)

[a] U_{eq} defined as one third of the trace of the orthogonalized *U* tensor. Atoms C(37)—C(42) belong to the disordered hexane molecule and have site occupancy factors of $\frac{1}{2}$.

II isomerized to **IV** quantitatively. Throughout the course of the reaction, no other resonance signals, other than those of **II** and **IV**, were observed.

(ii) *Isomerization of a mixture of* **II** *and* **III**. **II** and **III** (20 mg) were dissolved in 0.5 cm^3 of $CDCl_3$ at 10°C. The isomerization process was monitored by $^{31}P\{^1H\}$ NMR spectroscopy every 4 h for 12 h. Within the period, both **II** and **III** isomerized to **IV** quantitatively. Throughout the course of the reaction, no other resonances, other than those of **II**, **III** and **IV** were observed.

X-ray diffraction studies

Crystals of **VI** suitable for X-ray diffraction study were grown from toluene–n-hexane as a solvate of stoichiometry 2 **VI** · C_6H_{14}.

Raw intensities collected at 21°C on a Nicolet R3m/V diffractometer were processed with the profile fitting procedure of Diamond[13] and corrected for absorption using ψ-scan data[14] (details in Table 4). Two molybdenum atoms was located by direct phase determination and the coordinates of the other non-hydrogen atoms were derived from successive difference Fourier syntheses. The carbon atoms of the disordered solvent (n-hexane) were found on a subsequent difference Fourier map and interatomic distance constraints of 1.540(2) and 2.52(1) Å were applied to adjacent carbons and alternate carbons. The non-hydrogen atoms were refined anisotropically and the carbon atoms of the solvent molecule isotropically. Hydrogen atoms of the phenyl and cyclopentadienyl groups were generated geometrically (C—H bond fixed at 0.96 Å) and allowed to ride on their respective parent carbon atoms. These hydrogen atoms were assigned appropriate isotropic thermal parameters and included in the structure factor calculation. The hydrogen atoms of the disordered hexane molecule were ignored. Computations were performed using the SHELTXL-PLUS program package[15] on a DEC MicroVAX-II computer. Analytic expressions of atomic scattering factors were employed, and anomalous dispersion corrections were incorporated.[16] The maxima in the last difference map all lie in the neighbourhood of the solvent molecule.

REFERENCES

1. W. K. Wong, F. L. Chow, H. Chen and T. C. W. Mak, *J. Organomet. Chem.* 1989, **377**, C65.
2. R. Vac, J. H. Nelson, E. B. Milosavljevic, L. Solujic and J. Fischer, *Inorg. Chem.* 1989, **28**, 4132.
3. W. K. Wong, F. L. Chow, H. Chen, R.-J. Wang and T. C. W. Mak, *Polyhedron*, in press.
4. A. J. Carty, C. A. Fyfe, M. Lettinga, S. Johnson and L. H. Randall, *Inorg. Chem.* 1989, **28**, 4120 and refs therein.
5. M. H. Linck and L. R. Nassimbeni, *Inorg. Nucl. Chem. Lett.* 1973, **9**, 1105.
6. S.-G. Shyu, M. Calligaris, G. Nardin and A. Wojcicki, *J. Am. Chem. Soc.* 1987, **109**, 3617.
7. A. Wojcicki, *Inorg. Chem. Acta* 1985, **100**, 125.
8. C. D. Garner and J. M. Charnock, *Comprehensive Coordination Chemistry* (Edited by G. Wilkinson, R. D. Gillard and J. A. McCleverty), Vol. 3, p. 1329. Pergamon Press, Oxford (1987).
9. D. Coucouvanis and S.-M. Koo, *Inorg. Chem.* 1989, **28**, 2.
10. G. K. Anderson and M. Lin, *Organometallic* 1988, **7**, 2285.
11. J. J. Eisch and R. B. King, *Organometallic Synthesis*, Vol. 1, pp. 124–125. Academic Press, New York (1965).
12. D. T. Thompson, *British Patent*, 1,156,336 (Cl.C07f), 25 June 1969, Appl. 2 August 1966–2 March 1967; 4 pp.
13. R. Diamond, *Acta Cryst.* 1969, **A25**, 43.
14. G. Kopfmann and R. Huber, *Acta Cryst.* 1968, **A24**, 348.
15. G. M. Sheldrick, *Crystallographic Computing 3*: Data Collection, Structure Determination, Proteins, and Databases (Edited by G. M. Sheldrick, C. Kruger and R. Goddard), p. 175. Oxford University Press, New York (1985).
16. *International Tables for X-ray Crystallography*, Vol. IV, pp. 55, 99 and 149. Kynoch Press, Birmingham (1974). (Now distributed by Kluwer Academic Publishers, Dordrecht.)

Polyhedron Vol. 9, No. 20, pp. 2477–2481, 1990
Printed in Great Britain

0277–5387/90 $3.00+.00
© 1990 Pergamon Press plc

ADDITION OF RHg^+ FRAGMENTS TO P—P BONDS OF HETEROATOMIC CLUSTERS

MASSIMO DI VAIRA, DONELLA ROVAI and PIERO STOPPIONI*

Dipartimento di Chimica, Università di Firenze, Via Maragliano 77, 50144 Firenze, Italy

(*Received* 19 *March* 1990; *accepted* 7 *June* 1990)

Abstract—Treatment of a dichloromethane solution of [(triphos)MP_3] [triphos = 1,1,1-tris(diphenylphosphinomethyl)ethane; M = Co, Rh] with RHgCl (R = CH_3, C_6H_5) in the presence of $TlPF_6$ affords the compounds [(triphos)MP_3HgR]PF_6·solvent (M = Co, Rh; R = CH_3, C_6H_5). An X-ray crystallographic analysis on the [(triphos)CoP_3HgCH_3]PF_6 derivative has shown that the mercury atom of the $HgCH_3$ fragment is bound to two phosphorus atoms of the P_3 unit of [(triphos)CoP_3].

The neutral compounds [(triphos)MP_3] [triphos = 1,1,1-tris(diphenylphosphinomethyl)ethane; M = Co, Rh, Ir] which have a pseudo-tetrahedral core formed by three unsubstituted phosphorus atoms and one cobalt group metal, stabilized by the tripod tridentate ligand triphos, exhibit distinct reactivity. The heteroatomic polarized MP_3 core interacts with electrophilic organic reagents[1] and transition metal–ligand fragments[2] through one P atom or the P_3 triangular face.

We have recently found[3] that the interaction of the $[Au(PR_3)]^+$ (R = CH_3, C_6H_5) cations with the MP_3 core is accompanied by an unusual labilization of the phosphane ligand bound to gold and formation of compounds in which the gold atom bridges two [(triphos)MP_3] units, being linked to a P—P edge of the P_3 group of each unit. It was therefore of interest to examine the reactions of [(triphos)MP_3] with sources of HgY^+ (Y = halide or hydrocarbyl), which are isoelectronic with $[AuPR_3]^+$ and present different bonding abilities according to the nature of Y. Mercury(II) compounds have been found to be capable of binding to transition metals yielding different compounds. The most familiar interactions consist of the linear M—HgY or M—Hg—M arrangements;[4] the HgY fragments in the presence of metal clusters may end over a metal–metal edge[5] or a triangular face of the metal polyhedron.[6] The complexes in which the HgY^+ moiety bridges a metal–metal bond or caps a triangular face of an organometallic cluster, are endowed with good stability and redistribution reactions, analogous to those extensively investigated for organomercurial compounds,[7] have been observed.[8]

EXPERIMENTAL

All reactions and manipulations were performed under an atmosphere of dry oxygen-free nitrogen. Solvents were freshly distilled under nitrogen from the appropriate drying agents immediately before use. The $^{31}P\{^1H\}$ and ^1H NMR spectra were obtained in CD_2Cl_2 using a VARIAN VXR 300 spectrometer operating at 121.4 and 300.1 MHz and are referred to external 85% H_3PO_4 and internal TMS, respectively. Analytical data for carbon, hydrogen and cobalt were obtained in the Microanalytical Laboratory of the Chemistry Department; phosphorus, mercury and rhodium elemental analyses were performed by Mykroanalytisches Labor Pascher, Remagen, F.R.G. [(triphos)MP_3] (M = Co,[9] Rh[10]) were prepared as previously described. CH_3HgCl (Merck), C_6H_5HgCl (Ega Chemie) and $TlPF_6$ (Strem Chemicals) were used as supplied. All the compounds were collected on a sintered-glass frit, in a closed system, and washed with benzene and light petroleum (b.p. 40–70°C) in turn before being dried under a stream of nitrogen.

Synthetic procedures

Synthesis of the compounds. [(triphos)CoP_3HgCH_3]PF_6. CH_3HgCl (0.13 g, 0.5 mmol) dissolved

* Author to whom correspondence should be addressed.

in tetrahydrofuran (30 cm^3) was added to a dichloromethane solution (40 cm^3) of [(triphos)CoP_3] (0.39 g, 0.5 mmol) and solid $TlPF_6$ (0.17 g, 0.5 mmol) was added to the resulting solution. The mixture was stirred at room temperature for 4 h and filtered. Orange crystals of [(triphos)CoP_3HgCH_3]PF_6 were obtained by addition of benzene and slow concentration. The compound crystallizes, as also found from the X-ray work, with dichloromethane solvate molecules whose amount was assigned mainly in accordance with the results of the structural investigation (see below) (yield 85%). Found: C, 43.1; H, 3.9; Co, 4.8; Hg, 16.7; P, 18.1. [(triphos)CoP_3HgCH_3]$PF_6 \cdot 0.7CH_2Cl_2$, $C_{42.7}H_{43.4}Cl_{1.4}CoF_6HgP_7$, requires: C, 42.9; H, 3.7; Co, 4.9; Hg, 16.8; P, 18.1%. NMR ^1H: δ 1.13 (3H, s, $HgCH_3$, ^2J 180 Hz), 1.69 (3H, s, CCH_3), 2.53 (6H, s, PCH_2), 7.04 (30H, m, arom. H). The same procedure was used to obtain [(triphos)$CoP_3HgC_6H_5$]$PF_6 \cdot 0.7CH_2Cl_2$ (yield 80%). Found: C, 45.7; H, 3.7; Co, 4.5; Hg, 15.7; P, 17.1. [(triphos)$CoP_3HgC_6H_5$]$PF_6 \cdot 0.7CH_2Cl_2$, $C_{47.7}H_{45.4}Cl_{1.4}CoF_6HgP_7$, requires: C, 45.5; H, 3.6; Co, 4.7; Hg, 15.9; P, 17.2%. NMR ^1H: δ 1.71 (3H, s, CCH_3), 2.52 (6H, s, PCH_2), 7.05 (30H, m, arom. H). The rhodium derivatives, which also crystallize with dichloromethane, were obtained through the same procedure by reacting [(triphos)RhP_3], RHgCl (R = CH_3, C_6H_5) and $TlPF_6$ in 1 : 3 : 3 stoichiometric ratios. Found: C, 41.9; H, 3.7; Hg, 16.2; P, 17.5; Rh, 8.3. [(triphos)RhP_3HgCH_3]$PF_6 \cdot 0.5CH_2Cl_2$ (yield 75%), $C_{42.5}H_{43}ClF_6HgP_7Rh$, requires: C, 41.7; H, 3.5; Hg, 16.4; P, 17.7; Rh, 8.4%. Found: C, 44.2; H, 3.7; Hg, 15.4; P, 16.6; Rh, 8.0. [(triphos)$RhP_3HgC_6H_5$]$PF_6 \cdot 0.5CH_2Cl_2$ (yield 75%), $C_{47.5}H_{45}ClF_6HgP_7Rh$, requires: C, 44.4; H, 3.5; Hg, 15.6; P, 16.9; Rh, 8.0%.

X-ray crystal structure

Diffraction data for [(triphos)CoP_3HgCH_3]$PF_6 \cdot 0.7CH_2Cl_2$. Crystals of the compound did not provide good material for X-ray diffraction, giving broad reflections. An Enraf–Nonius CAD4 diffractometer and Mo-K_α radiation (λ = 0.71069 Å) were used for all operations, which were performed at room temperature. The crystal used for intensity data collection and determination of lattice constants was an elongated prism with dimensions 0.15 × 0.15 × 0.50 mm. Lattice constants were determined by least-squares refinement of the angular settings of 20 reflections with $18 \leqslant 2\theta \leqslant 28°$.

Crystal data. $C_{42.7}H_{43.4}Cl_{1.4}CoF_6HgP_7$, M_r = 1196.59, triclinic, a = 12.988(3), b = 13.654(3), c = 14.954(5) Å, α = 66.99(5), β = 85.28(8), γ = 70.91(9)°, U = 2304(1) Å, Z = 2, D_c = 1.724 g cm^{-3}, $F(000)$ = 1178.8, μ(Mo-K_α) = 41.5 cm^{-1}, space group $P\bar{1}$.

The intensities of all reflections with $l \geqslant 0$ were measured in the range $5 \leqslant 2\theta \leqslant 44°$ in the ω–2θ scan mode with a scan width of $(1.30 + 0.35 \tan\theta)°$ and variable 4–8° min^{-1} scan speed. No crystal decay was observed. Of the total 5656 reflections recorded, 3211 having $I > 3\sigma(I)$ were used for structure determination. Intensity data were corrected for Lorentz and polarization effects and, at isotropic convergence after the structure was solved, they were also corrected for absorption by an empirical procedure.[11] The principal computer programs used in the crystallographic calculations are listed in refs 11–14.

Crystal structure determination. The structure was solved by a combination of direct methods and heavy-atom procedures. In the least-squares refinement the function $\Sigma w(|F_o| - |F_c|)^2$ was minimized with weights $w = [\sigma^2(F_o) + 0.0015|F_o|^2]^{-1}$. The scattering factors for the neutral atoms and the anomalous dispersion corrections for cobalt and mercury were taken from ref. 15. Atoms heavier than carbon were assigned anisotropic thermal parameters, whereas the other atoms were refined isotropically. The U_c value in the solvate CH_2Cl_2 molecule was assumed to be approximately equal to the mean of the U_{eq} values for the chlorine atoms and not refined. Hydrogen atoms were introduced in calculated positions (C—H = 0.95 Å) with fixed thermal parameters, each *ca* 20% larger than that of the corresponding carbon atom. Phenyl groups of the triphos ligand were refined as rigid bodies with idealized geometry. The triphos and $HgCH_3$ methyl groups were also refined as rigid bodies. The C—Cl distances in the CH_2Cl_2 molecule were constrained to a unique value, which was refined. The 0.7 occupancy factor assigned to the solvent molecule resulted from a compromise choice which was made in view of the results of sets of refinement cycles performed with different, fixed values for the CH_2Cl_2 population parameter. The value finally considered to be satisfactory ensured: (1) a low R value; (2) reasonable chlorine thermal parameters (U_{eq} values close to those of the fluorine atoms in the anion); and (3) acceptable values for the (unique) C—Cl bond length and the Cl—C—Cl angle in the solvate molecule. The highest peaks in the final ΔF map, with heights < 2 $eÅ^{-3}$, were in the region of the mercury atom. The largest shift/error ratios in the final cycles were < 0.06 and the final R values were R = 0.083 and R_w = 0.086. Final atomic positional and thermal parameters, bond lengths and angles and F_o/F_c values have been deposited as supplementary material with the Editor, from whom

copies are available on request. Atomic coordinates have also been submitted to the Cambridge Crystallographic Data Centre.

RESULTS AND DISCUSSION

Treatment of a dichloromethane solution of [(triphos)MP_3] with RHgCl (R = CH_3, C_6H_5), in a 1:1 stoichiometric ratio for M = Co and two-fold excess for M = Rh, in the presence of $TlPF_6$, affords compounds of formula [(triphos)$MP_3HgR]PF_6$·solvent (M = Co, Rh; R = CH_3, C_6H_5). The compounds are obtained as analytically pure orange crystals in good yield. They are mildly air-sensitive and are soluble in dichloromethane and acetone. The rhodium derivatives decompose quickly in solution yielding the parent [(triphos)RhP_3]; such behaviour prevented any characterization of the rhodium compounds in solution. On the other hand, the reaction of the [(triphos)MP_3] compounds (M = Co, Rh) with HgX_2 (X = Cl, Br) in the presence of $TlPF_6$, the stoichiometric ratios of the reagents being 1:1:1, affords decomposition of the MP_3 core. The cobalt derivative yields the (triphos)Co^{II} species, whose presence was confirmed by the precipitation and characterization of [(triphos)CoI][16] after addition of NaI dissolved in ethanol.

The structure of the [(triphos)CoP_3HgCH_3] PF_6·$0.7CH_2Cl_2$ compound consists of [(triphos)$CoP_3HgCH_3]^+$ dimetal cations, PF_6^- anions and interposed CH_2Cl_2 solvent molecules. Figure 1 shows a perspective view of the cation. Selected values of bond distances and angles in the structure are listed in Table 1. The cobalt atom in the dimetal core is coordinated by the three phosphorus atoms of the triphos ligand and by those of the P_3 unit, as in the parent [(triphos)CoP_3] compound.[9] The mercury atom is linked in a slightly asymmetrical fashion to two phosphorus atoms of the P_3 unit and to the methyl carbon. The Hg—P distances are definitely larger (by 0.18 Å, in the mean) than the Au—P distances found for the $[Au\{(triphos)MP_3\}_2]PF_6$ (M = Co, Rh, Ir) compounds, where the gold atom bridges between two [(triphos)MP_3] units, being linked to one pair of P_{P3} atoms of each unit.[3] They are also larger than the Hg—P distances generally found for mercury phosphine derivatives.[17] The P—P bond into which insertion of the $HgCH_3$ unit occurs lengthens from 2.141(2) Å in the parent compound, where the three P—P bonds are symmetry equivalent, to 2.293(8) Å. The other two P—P bonds of the P_3 unit are substantially unaffected by the insertion. Of the three Co—P_{P3} bonds, which measure 2.301(1) Å in the compound [(triphos)CoP_3], the one lying opposite the $HgCH_3$ group lengthens to 2.349(6) Å whereas the other two shorten to 2.25(1) Å in the mean. The Co—$P_{triphos}$ distances are essentially unchanged. The overall pattern of such deformations is similar to that already found for the gold derivatives mentioned above.[3] The distortions in

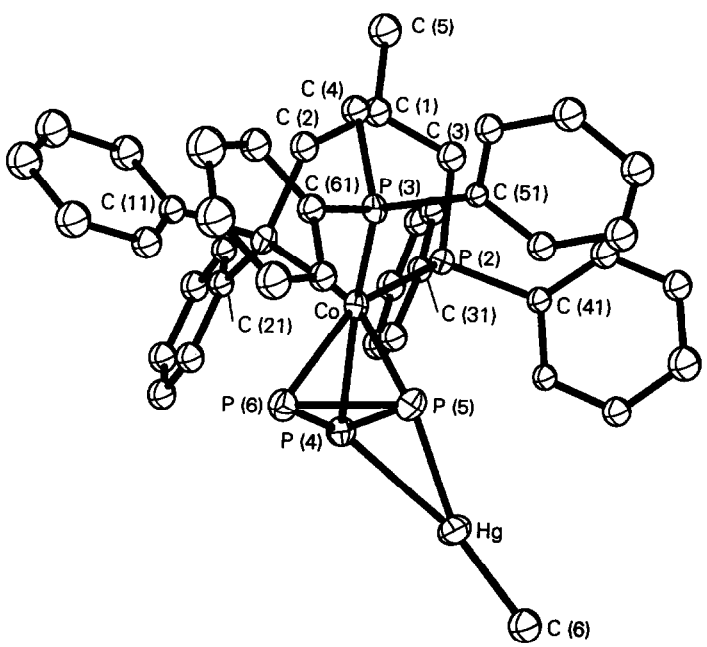

Fig. 1. Perspective view of the cation in the structure of [(triphos)$CoP_3HgCH_3]PF_6$·$0.7CH_2Cl_2$ with 20% probability ellipsoids. Only the first carbon atom of each phenyl group is labelled.

Table 1. Selected bond distances (Å) and angles (°) for the compound [(triphos)CoP_3HgCH_3]$PF_6 \cdot 0.7CH_2Cl_2$

Co—P(1)	2.197(5)	P(4)—P(5)	2.293(8)
Co—P(2)	2.198(6)	P(4)—P(6)	2.119(8)
Co—P(3)	2.183(6)	P(5)—P(6)	2.145(8)
Co—P(4)	2.255(6)	Hg—P(4)	2.679(6)
Co—P(5)	2.245(6)	Hg—P(5)	2.579(6)
Co—P(6)	2.349(6)	Hg—C(6)	2.08(2)
P(1)—Co—P(2)	89.8(2)	P(5)—P(4)—P(6)	58.0(3)
P(1)—Co—P(3)	92.5(2)	P(4)—P(5)—P(6)	56.9(3)
P(2)—Co—P(3)	95.8(2)	P(4)—P(6)—P(5)	65.1(3)
P(4)—Co—P(5)	61.3(2)	P(4)—Hg—P(5)	51.7(3)
P(4)—Co—P(6)	54.8(2)	P(4)—Hg—C(6)	153.9(3)
P(5)—Co—P(6)	55.6(2)	P(5)—Hg—C(6)	154.4(3)

the triangular P_3 group, due to insertion of the present mercury, or of the above gold systems,[3] are notably smaller than those undergone upon insertion of the PtL_2[18] or CPh_2[19] groups. This has to be ascribed to the different electronic requirements of the systems involved. On the other hand, the angle, of 130.4(2)°, between the plane of the P_3 unit and that defined by the atoms Hg, P(4) and P(5) is in the range of values found for the analogous hinge angles in the gold[3] as well as the PtL_2[18] or CPh_2[19] derivatives. The methyl carbon of the $HgCH_3$ group lies strictly in the plane defined by the P(4), P(5) and Hg atoms.

The cobalt compounds exhibit in their ^1H NMR spectra (see the Experimental) the triphos signals with the expected shifts; the methyl mercury derivative presents in addition the CH_3 signal whose chemical shift and coupling constant to mercury are comparable to those reported for other CH_3Hg compounds.[20] The $^{31}P\{^1H\}$ NMR spectra at room temperature exhibit the PF_6^- multiplet with the expected shift (δ −145.4) and two broad, well separated resonances having a 1 : 1 intensity ratio (Table 2). The lower field signal is assigned to the phosphorus atoms of the triphos ligand and the higher field one to the unsubstituted phosphorus atoms, as the corresponding chemical shifts are not significantly different from those found for the parent [(triphos)CoP_3] compound (Table 2).[21] As the equivalence on the NMR time-scale both of the $P_{triphos}$ signals and of the P_{P3} signals is inconsistent with the structure in the solid state, variable temperature $^{31}P\{^1H\}$ spectra were recorded. The two resonances, strongly affected by the cobalt quadrupole moment, become sharper on cooling and their shifts remain substantially unchanged down to −80°C (Table 2). On lowering the temperature further each of the above signals begins to coalesce,

Table 2. $^{31}P\{^1H\}$ NMR data for the complexes

Compound	T (K)	δ (ppm)[a] P(triphos)	δ (ppm)[a] $P(P_3)$
[(triphos)CoP_3HgCH_3]PF_6	Ambient	39.98(br)	−267.34(br)
	180	39.04(br)	−268.17(br)
[(triphos)$CoP_3HgC_6H_5$]PF_6	Ambient	37.88(br)	−250.51(br)
	185	39.05(br)	−255.30(br)
		37.20(br)	−260.55(br)
[(triphos)CoP_3][b,c]	Ambient	38.16(br)	−276.21(br)

[a] Chemical shifts are relative to 85% H_3PO_4. Positive chemical shifts are downfield: br = broad. The complexes were dissolved in CD_2Cl_2.

[b] ^{31}P NMR data at room temperature for this molecule are reported for comparison purposes.

[c] Reference 20.

but it was not possible to freeze the fluxional process even at the lowest temperature reached (−94°C). The [(triphos)CoP_3] compound and the isoelectronic [(triphos)CoP_2X]BF_4 (X = S, Se) species[22] undergo dynamic processes in solution, even at low temperatures, which cause the equivalence of the three phosphorus atoms of the triphos ligand as well as of those in the cyclic units (P_3 or P_2X). This is probably due to rotation of the cyclic unit with respect to the triphos–metal fragment. Although such processes are expected to occur also in the present compounds, they are not sufficient to account for the equivalence of the P_3 phosphorus atoms which is only consistent with the HgR fragment undergoing rapid motion over sets of positions in the P_3 rings. The HgR fragment, which in the solid state is bound to a P—P edge, may accomplish such motion in solution through an intermediate state in which the mercury unit is either capping the P_3 face or σ-bonded to one phosphorus atom of the P_3 group. Both arrangements are consistent with the geometrical preferences exhibited by HgR units toward metal polyhedra.[4,6] The difference between the two Hg—P bond lengths in the structure of [(triphos)CoP_3HgCH_3]PF_6 (see above) and the preference of mercury for low coordination numbers, suggest that a possible intermediate may have mercury σ-bound to one phosphorus atom of the P_3 ring.

The above results show that the chemical behaviour of the HgY^+ fragments toward the MP_3 core depends on the nature of Y: when a covalent Hg—Y bond is present (Y = CH_3, C_6H_5) addition of the metal fragment to a P—P edge results, whereas in presence of a predominantly ionic Hg—Y bond (Y = Cl, Br) demolition of the MP_3 core is attained. Such demolition is likely to occur with involvement of the solvent, as found for the bimolecular oxymercuriation reactions of olefin compounds.[23] It has to be observed, in this connection, that the mixed MP_3 core behaves differently from metal clusters, which form stable adducts with HgY moieties irrespectively of the nature of Y.[8]

REFERENCES

1. G. Capozzi, L. Chiti, M. Di Vaira, M. Peruzzini and P. Stoppioni, *J. Chem. Soc., Chem. Commun.* 1986, 1799.
2. M. Di Vaira and L. Sacconi, *Angew. Chem. Int. Ed. Engl.* 1982, **21**, 330.
3. M. Di Vaira, M. Peruzzini and P. Stoppioni, *J. Chem. Soc., Dalton Trans.* 1990, 109.
4. C. A. Ghilardi, S. Midollini, S. Moneti, A. Orlandini, G. Scapacci and D. Dakternieks, *J. Chem. Soc., Chem. Commun.* 1989, 1686, and refs cited therein.
5. R. Fahmy, K. King, E. Rosenberg, A. Tiripicchio and M. Tiripicchio Camellini, *J. Am. Chem. Soc.* 1980, **102**, 3626.
6. E. G. Mednikov, V. V. Bashilov, V. I. Sokolov, Yu. L. Slovokhotov and Yu. T. Struchkov, *Polyhedron* 1983, **2**, 141.
7. J. L. Wardell, *Comprehensive Organometallic Chemistry* (Edited by G. Wilkinson, F. G. A. Stone and E. W. Abel), Vol. 2, p. 892. Pergamon Press, Oxford (1982).
8. T. J. Henly and J. R. Shapley, *Organometallics* 1989, **8**, 2729.
9. C. A. Ghilardi, S. Midollini, A. Orlandini and L. Sacconi, *Inorg. Chem.* 1980, **19**, 301.
10. C. Bianchini, C. Mealli, A. Meli and L. Sacconi, *Inorg. Chim. Acta* 1979, **37**, L543.
11. N. Walker and D. Stuart, *Acta Cryst.* 1983, **A39**, 158.
12. G. M. Sheldrick, SHELX 76, System of Computing Programs. University of Cambridge (1976).
13. M. C. Burla, M. Camalli, G. Cascarano, C. Giacovazzo, G. Polidori, R. Spagna and D. Viterbo, *J. Appl. Cryst.* 1989, **22**, 389.
14. C. K. Johnson, ORTEP-II, Report ORNL-5138. Oak Ridge National Laboratory, Tennessee (1976).
15. *International Tables for X-ray Crystallography*, Vol. 4. Kynoch Press, Birmingham (1974).
16. L. Sacconi and S. Midollini, *J. Chem. Soc., Dalton Trans.* 1972, 1213.
17. K. Brodersen and H.-U. Hummel, *Comprehensive Coordination Chemistry.* (Edited by G. Wilkinson, R. D. Gillard and J. A. McCleverty), Vol. 5, p. 1082. Pergamon Press, Oxford (1987).
18. M. Di Vaira, S. Moneti, M. Peruzzini and P. Stoppioni, *J. Organomet. Chem.* 1984, **266**, C8; M. Di Vaira, P. Stoppioni and M. Peruzzini, *Acta Cryst.* 1987, **C43**, 1284.
19. M. Di Vaira, L. Niccolai, M. Peruzzini and P. Stoppioni, *Organometallics* 1985, **4**, 1888.
20. R. D. Bach and A. T. Weibel, *J. Am. Chem. Soc.* 1976, **98**, 6241.
21. M. Di Vaira, L. Sacconi and P. Stoppioni, *J. Organomet. Chem.* 1983, **250**, 183.
22. M. Di Vaira, M. Peruzzini and P. Stoppioni, *J. Chem. Soc., Dalton Trans.* 1984, 359.
23. F. Freeman, *Chem. Rev.* 1975, **75**, 439.

Polyhedron Vol. 9, No. 20, pp. 2483–2489, 1990
Printed in Great Britain

0277–5387/90 $3.00+.00
© 1990 Pergamon Press plc

SYNTHESIS AND CHARACTERIZATION OF SOME β-DIKETONATE DERIVATIVES OF HYDROTRIS(3,5-DIMETHYLPYRAZOLYL)BORATOOXOVANADIUM(IV). THE CRYSTAL AND MOLECULAR STRUCTURE OF HYDROTRIS(3,5-DIMETHYLPYRAZOLYL)BORATO PENTANE-2,4-DIONATO OXOVANADIUM(IV)

ROY L. BEDDOES, DAVID COLLISON, FRANK E. MABBS* and MOHAMMAD A. PASSAND

Chemistry Department, University of Manchester, Manchester M13 9PL, U.K.

(*Received* 30 *March* 1990; *accepted* 8 *June* 1990)

Abstract—A series of compounds of formulation LVOB, where B = pentane-2,4-dionato, 3-chloropentane-2,4-dionato, 1-phenylbutane-1,3-dionato, 1,3-diphenyl-1,3-propanedionato, 4,4,4-trifluoro-1-(2-thenyl)-butane-1,3-dionato and 1,1,1-trifluoro-pentane-2,4-dionato, have been prepared and characterized by elemental analyses, EPR, electronic absorption, IR and mass spectrometry and by cyclic voltammetry. The single crystal X-ray structure of LVO(acac) is also reported. The compound crystallizes in the monoclinic space group $P2_1/c$, $a = 14.943(1)$, $b = 8.127(3)$, $c = 20.894(4)$ Å, $\beta = 113.26(1)°$, $Z = 4$. The unit cell comprises discrete six-coordinate molecules, which have approximate mirror symmetry and exhibit the expected lengthening of the V—N bond *trans* to the terminal oxo group. (V—N(31) = 2.328(2) Å compared with V—N(11) = 2.111(2) and V—N(21) = 2.120(2) Å.) The terminal V=O length is 1.596(2) Å. The atoms within the six-membered ring, comprising vanadium and the pentane-2,4-dionato ligand, are not co-planar with significant tilting (21.5°) about the oxygen–oxygen vector of the ligand.

We have a continuing interest in establishing the relationship between the geometric structures, the reactivity, and the electronic structures of *d*-transition metal compounds. Of particular interest to us are compounds of oxovanadium(IV)[1] and oxomolybdenum(V).[2,3] Not only are these species amenable to study by a wide range of spectroscopic techniques they are also being found in an increasing number of metalloproteins. As part of a substantial continuing programme of study we have already been involved[3] in the synthesis and characterization of a range of LMoO(X)(Y) compounds, where L = the sterically demanding hydrotris(3,5-dimethylpyrazolyl)borato ligand. X and Y are mononegative, unidentate ligands or the mononegative donor atoms of a bidentate ligand, which give electrically neutral complexes. We are currently extending the use of the ligand L to oxovanadium chemistry. The use of mononegative, bidentate ligands, B, to give compounds of formulation LVOB preserves six-coordination and electrical neutrality. These properties enhance the solubilities of the compounds in non-aqueous solvents and also their resistance to hydrolysis. We have already made a preliminary report[4] of the synthesis of LVOB, where B = β-diketonato or N,N-diethyldithiocarbamato, and since then Carrano and co-workers[5] have reported the synthesis of LVO(acac), where acac = pentane-2,4-dionato, as well as the synthesis and X-ray structures of $LVCl_2$dmf, LVOCldmf, where dmf = N,N-dimethylformamide, and $K[LVCl_2(Me_2pz)]$, where Me_2pz = 3,5-dimethylpyrazolide. This present communication extends our preliminary report[4] to include more detailed spectroscopic characterization of the β-diketonato complexes and the X-ray crystal structure of LVO(acac). The detailed single crystal EPR spectroscopy of some of these β-diketonato complexes will be reported elsewhere.

* Author to whom correspondence should be addressed.

EXPERIMENTAL AND RESULTS

Preparation of the compounds

This is most conveniently accomplished under non-aqueous conditions according to eq. (1):

$$VOB_2 + KL \xrightarrow[\text{Solvent}]{50\text{–}60^\circ C} LVOB + KB. \quad (1)$$

VOB_2

VOB_2, where B = pentane-2,4-dionato (acac), 3-chloro-pentane-2,4-dionato (Clacac), 1-phenyl-butane-1,3-dionato (bzac), 1,3-diphenyl-1,3-propanedionato (dbzac), 4,4,4-trifluoro-1-(2-thenyl)-butane-1,3-dionato (thtf), and 1,1,1-trifluoro-pentane-2,4-dionato (tfa), were each prepared by adding a stoichiometric quantity of the β-diketone in ethanol to a concentrated aqueous solution of oxovanadium(IV) sulphate. The pH of the solution was adjusted with dilute aqueous sodium bicarbonate until the required complex precipitated. The precipitate was filtered off, washed with water, dried in air and used without further purification.

KL

This was prepared according to the literature method.[6]

LVOB

These were all prepared by heating KL (5 mmol) and VOB_2 (5 mmol) in sodium dried toluene (100 cm^3) at 50°C for 15–20 h. The methods of isolation of the desired compounds varied slightly in each case as follows.

LVO(acac). The solution was filtered and the volume was reduced *in vacuo* to 30 cm^3. On cooling this solution a pale blue precipitate was obtained. The precipitate was washed with ice-cold sodium-dried toluene, followed by diethyl ether. Found: C, 51.9; H, 6.4; N, 18.1; B, 2.5; V, 11.0. Calc.: C, 51.8; H, 6.3; N, 18.1; B, 2.3; V, 11.0%.

LVO(Clacac). A dark brown solid was filtered off, washed with toluene followed by diethyl ether. The solid was dissolved in dichloromethane and crystallized by the addition of methanol. Found: C, 48.0; H, 5.6; N, 16.6; V, 10.1. Calc.: C, 48.3; H, 5.7; N, 16.9; V, 10.2%.

LVO(dbzac). The solution was filtered and the filtrate evaporated to dryness *in vacuo*. The resulting olive-green solid was dissolved in dichloromethane and crystallized by the addition of methanol. Found; C, 60.5; H, 5.7; N, 15.2; V, 8.6. Calc.: C, 61.3; H, 5.7; N, 14.3; V, 8.7%.

LVO(bzac)·0.5CH_3CN. The solution was filtered and the filtrate evaporated to dryness *in vacuo*. The resulting green solid was dissolved in dichloromethane and reprecipitated by the addition of methanol. The compound was finally crystallized from methylcyanide. Found: C, 57.5; H, 6.1; N, 16.7; V, 9.3. Calc.: C, 57.2; H, 6.0; N, 16.7; V, 9.3%.

LVO(thtf). The grey precipitate was filtered off and washed with toluene and then with diethyl ether. The compound was crystallized from methylcyanide. Found: C, 46.5; H, 4.4; N, 14.4; V, 8.4. Calc.: C, 47.2; H, 4.5; N, 14.3; V, 8.7%.

LVO(tfa). The green precipitate was filtered off and then crystallized from methylcyanide. Found: C, 46.3; H, 5.1; N, 16.0; V, 9.9. Calc.: C, 46.4; H, 5.1; N, 16.2; V, 9.8%.

The yields in each of these preparations were in the range of 30–40%.

Physical methods

IR spectra. IR spectra of the compounds in KBr discs were recorded using a Perkin–Elmer 1710 IR Fourier transform spectrometer. The B—H and V=O stretching frequencies are summarized in Table 1.

Cyclic voltammograms. Cyclic voltammograms of the compounds in dried methylcyanide were obtained with a Princeton Applied Research Model 173 potentiostat/galvanostat and a Model 175 universal programmer using a glassy carbon working electrode and a saturated calomel reference electrode. The supporting electrolyte was 0.2 M $[Bu^n_4N][BF_4]$ with ferrocene as an internal standard. The results are summarized in Table 1.

Electron paramagnetic resonance (EPR) spectra. EPR spectra of fluid and frozen toluene solutions of LVOB were obtained at both *X*- and *Q*-band frequencies using a Varian E112 spectrometer. Temperature control was achieved as previously described.[7] The spin-Hamiltonian parameters were obtained via spectrum simulation at both frequencies using our previously described simulation methods.[8] The principal g and A values are given in Table 1.

Electronic absorption spectra. Electronic absorption spectra of the compounds in toluene were obtained using a Varian 2390 spectrophotometer over the wavelength range 3000–250 mm. The band maxima of the compounds along with those of other relevant oxovanadium(IV) compounds are given in Table 2.

Mass spectra. Mass spectra of the compounds were obtained using *a Kratos MS25 spectrometer*

Table 1. IR, electrochemical and EPR data for LVOB

Compound	ν(B—H) (cm⁻¹)	ν(V=O) (cm⁻¹)	$E(V^{V}/V^{IV})$ vs SCE[a] E (V)	ΔE (mV)	I_{pa}/I_{pc}	g_{iso}	A_{iso}/G	g_1	g_2	g_3	A_1/G	A_2/G	A_3/G
LVO(acac)	2510	963	1.145	80	1.04	1.972±0.002	98.9±0.1	1.950±0.001	1.980±0.001	1.983±0.001	177.8±0.6	63.8±0.1	59.0±0.1
LVO(Clacac)	2519	961	1.232	82	1.04	1.970±0.001	99.2±0.2	1.949±0.001	1.979±0.001	1.982±0.001	177.0±0.1	63.8±0.1	59.0±0.1
LVO(dbcac)	2522	959	1.175	82	1.02	1.971±0.001	100.5±1.3	1.948±0.001	1.979±0.001	1.982±0.001	178.0±0.1	64.0±0.1	59.0±0.1
LVO(bzac)	2520	965	1.164	79	1.05	1.972±0.002	99.3±0.2	1.949±0.001	1.979±0.001	1.982±0.001	177.0±0.1	63.8±0.1	59.0±0.1
LVO(thtf)	2526	967	1.395	95	0.95	1.971±0.001	101.0±0.1	1.948±0.001	1.979±0.001	1.982±0.001	178.5±0.1	63.8±0.1	59.0±0.1
LVO(tfa)	2539	963	1.399	82	1.01	1.969±0.001	101.0±0.2	1.948±0.002	1.979±0.001	1.982±0.001	178.5±0.5	64.3±0.3	59.3±0.3

[a] The results quoted are for a scan rate of 100 mV s⁻¹. For ferrocene under the same conditions $E = 0.428$ V, $\Delta E = 75$ mV, $I_{pa}/I_{pc} = 1.05$. Errors on g and A values cover the range of values required to fit the spectra at both X- and Q-band frequencies.

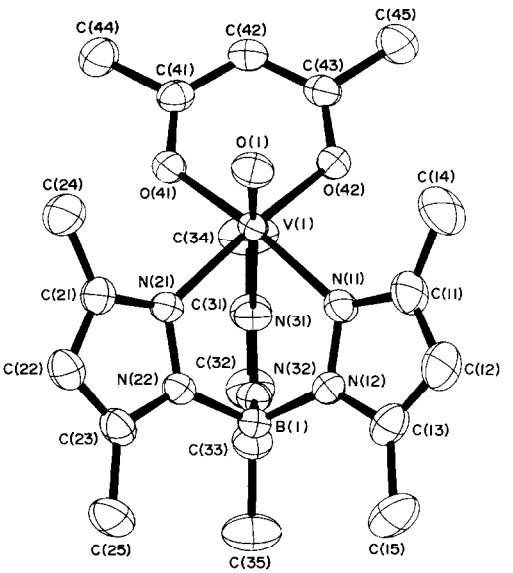

Fig. 1. Atomic numbering, and a view down the edge of the approximate mirror plane, in LVO(acac).

with electron impact to effect ionization. The results are summarized in Table 3.

Single crystal X-ray structure determination of LVO(acac). The determination at ambient temperatures was achieved using an Enraf–Nonius CAD4 diffractometer. The crystals were grown from methylcyanide solution by slow evaporation. The data collection parameters are given in Table 4. The solution of the structure was achieved by a combination of Patterson and difference Fourier methods. The least-square refinement minimized $\Sigma w^2(|F_o|-|F_c|)^2$ with the weighting $w^{-1} = (1.307-0.105F+0.00343F^2)^{1/2}$. The positions of all atoms were refined. The atomic numbering scheme is shown in Fig. 1, whilst selected bond lengths and angles are given in Table 5. The non-hydrogen atoms were refined with anisotropic thermal parameters, but for the hydrogen atoms only isotropic temperature factors were refined. Lists of atomic coordinates, bond lengths and angles, thermal parameters, plus the observed and calculated structure factors are deposited as supplementary material.

DISCUSSION

The X-ray crystal structure of LVO(acac) shows it to consist of discrete six-coordinate molecules. The molecular geometry is that of a distorted octahedron (see Fig. 1). There is no crystallographically imposed symmetry in the molecules, but there is an approximate mirror plane containing the atoms O(1)—V(1)— and those of the pyrazolyl ring N(31),

Table 2. Electronic absorption spectra of LVOB and some related VOB_2 compounds

Compound	Band maxima, cm^{-1} (Absorption coefficient, $dm^3\ mol^{-1}\ cm^{-1}$)				
LVO(acac)[a]	13,110 (54)	17,620 (11)	24,220 (50)	25,110 (50)	31,950 (8680)
LVO(Clacac)[a]	13,120 (55)	17,250 (10)	23,100 (35)	24,200 (~ 30)	30,030 (7410)
LVO(tfa)[1]	13,140 (49)	17,000 (9)	22,570 (31)	24,130 (27)	31,890 (7620)
LVO(thtf)[a]	13,140 (52)	16,900 (12)	21,200 (~ 50)	27,980 (23,400)	—
LVO(bzac)[a]	13,150 (50)	17,370 (10)	21,960 (63)	23,300 (63)	29,290 (15,270)
LVO(dbzac)[a]	13,050 (52)	16,970 (12)	20,830 (87)	27,190 (20,550)	35,260 (11,200)
$VO(acac)_2$[b]	15,440 (60)	16,880 (67)	25,810 (128)	—	—
$VO(bzac)_2$[b]	15,380 (85)	16,670 (85)	21,740 (140)	—	—

[a] Toluene solution.
[b] Benzene solution (H. J. Stoklosa and J. R. Wasson, *J. Inorg. Nucl. Chem.* 1967, **38**, 677).

etc. This is illustrated in Fig. 1, which shows a view of the molecule down the edge of this approximate mirror plane. As expected there is a significant lengthening of the V—N bond *trans* to the terminal oxo group (V(1)—N(31) = 2.328(2) Å) compared with those *cis* to this group (V(1)—N(11) = 2.111(2) and V(1)—N(21) = 2.120(2) Å). The V—N bond lengths in LVO(acac) compare favourably with those of equivalent bonds in other five- and six-coordinate $[LVO]^+$ compounds.[5,9] However, the terminal V(1)—O(1) bond length (1.596(2) Å) is significantly shorter than that reported in six-coordinate LVOCl(dmf) (1.649(5) Å), but is similar to those in $LVO(R_2dtc)$,[9] where R = ethyl or n-propyl (1.587(8) and 1.602(6) Å, respectively). No unusual features were observed in the dimensions of the pyrazolyl rings.

The carbon–oxygen and carbon–carbon bond lengths within the pentane-2,4-dionato ligand are comparable to those observed in other oxovanadium(IV) pentane-2,4-dionato compounds.[10] However, the atoms within the six-membered ring comprising the vanadium and the pentane-2,4-dionato ligand are not co-planar. There is a significant tilting about the O(41)–O(42) direction (see Fig. 2). The dihedral angle between the plane formed by V(1), O(41), O(42) and the best plane of the pentane-2,4-dionato ligand is 21.5°. We attribute this distortion to interaction with the methyl group [C(34)] on the pyrazolyl ring which is *trans* to the terminal oxo group. There are some relatively short contacts between the hydrogen atoms of this methyl group and the oxygen and carbon atoms of the

Table 3. Mass spectral data for LVOB compounds

Compound	Relative molecular mass	Peak maxima of multiplets
LVO(acac)	463	463,[a] 447,[d] 368,[c] 364[b]
LVO(Clacac)	497	497,[a] 383,[c] 364[b]
LVO(dbzac)	587	587,[a] 492,[c] 364,[b] 235[e]
LVO(bzac)	525	525,[a] 430,[c] 364[b]
LVO(thtf)	585	585,[a] 569,[d] 490,[c] 364[b]
LVO(tfa)	517	517,[a] 422,[c] 364[b]

[a] Parent ion peak.
[b] LVO.
[c] Parent minus 3,5-dimethylpyrazolyl.
[d] Parent minus oxygen atom.
[e] Unassigned.

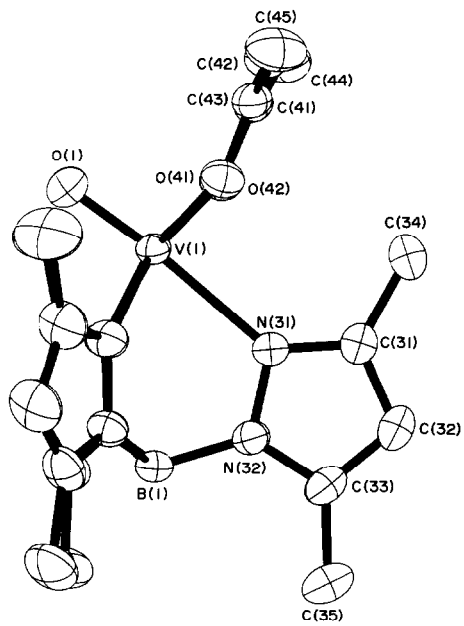

Fig. 2. A view of LVO(acac), illustrating the tilt of the {V(acac)} fragment about the O(41)–O(42) direction.

Table 4. Crystallographic data

Molecular formula	$C_{20}H_{29}N_6O_3BV$
Formula weight	463.2
Crystal dimensions (mm)	$0.35 \times 0.23 \times 0.52$
Space group	$P2_1/C$ (No. 14)
Unit cell (from 25 reflections)	
a (Å)	14.943(1)
b (Å)	8.127(3)
c (Å)	20.894(4)
β (°)	113.26(1)
D_{calc} (g cm^{-3})	1.32
Z	4
$F(000)$	972
(Mo-K_α) (Å)	0.71069
μ (cm^{-1})	4.8
θ_{range} (°)	1–25
Scanwidth, type	ω–θ $(0.7+0.35\tan\theta)$
Range of indices	h: 0 to 17; k: 0 to 9; l: −24 to 22
Absorption corrections	None
Number of reflections measured	4430
Number of unique reflections	3346
Number of parameters	397
R (%)	3.37
R_w (%)	3.63
Max. shifted/ESD	0.35
Largest peaks in difference Fourier (e/Å^3)	+0.3 and −0.2

$R_w = \sqrt{\Sigma w\Delta^2}/\Sigma wF_o^2$, $\Delta = |F_o| - |F_c|$.

Table 5. Selected bond lengths (Å) and bond angles (°) for LVO(acac)

Bond lengths

V(1)—O(1)	1.596(2)	N(11)—C(11)	1.345(3)	N(31)—C(31)	1.330(3)
V(1)—O(41)	2.004(1)	C(11)—C(12)	1.390(4)	C(31)—C(32)	1.395(3)
V(1)—O(42)	2.013(1)	C(12)—C(13)	1.368(4)	C(32)—C(33)	1.368(4)
V(1)—N(11)	2.111(2)	C(13)—N(12)	1.345(3)	C(33)—N(32)	1.347(3)
V(1)—N(21)	2.120(2)	N(12)—N(11)	1.374(2)	N(32)—N(31)	1.374(2)
V(1)—N(31)	2.328(2)				
O(41)—C(41)	1.269(3)	N(21)—C(21)	1.332(2)	B(1)—N(12)	1.546(3)
C(41)—C(42)	1.401(3)	C(21)—C(22)	1.392(3)	B(1)—N(22)	1.547(3)
C(42)—C(43)	1.391(3)	C(22)—C(23)	1.367(3)	B(1)—N(32)	1.532(3)
O(42)—C(43)	1.274(3)	C(23)—N(22)	1.346(3)		
		N(22)—N(21)	1.373(2)		

Bond angles

O(1)—V(1)—N(31)	175.4(1)	O(41)—V(1)—O(42)	86.8(1)
O(1)—V(1)—O(41)	97.2(1)	O(41)—V(1)—N(21)	91.0(1)
O(1)—V(1)—O(42)	96.9(1)	O(42)—V(1)—N(11)	92.2(1)
O(1)—V(1)—N(11)	96.0(1)	N(11)—V(2)—N(21)	87.4(1)
O(1)—V(1)—N(21)	94.9(1)	N(11)—V(1)—N(31)	81.0(1)
V(1)—O(41)—C(41)	126.2(1)	N(21)—V(1)—N(31)	81.5(1)
V(1)—O(42)—C(43)	124.9(1)	O(41)—V(1)—N(31)	85.9(1)
O(41)—C(41)—C(42)	124.6(1.2)	O(42)—V(1)—N(31)	86.7(1)
O(42)—C(43)—C(42)	125.0(1.6)		
C(41)—C(42)—C(43)	123.6(1)		

Table 6. Interatomic distances between the C(34)-methyl group and the pentane-2,4-dionato ligand

	C(34)	H(341)	H(342)	H(343)
O(41)	3.309(3)	4.19	2.64(5)	3.54(3)
O(42)	3.353(3)	4.36	3.22(5)	2.89(5)
C(41)	3.475(4)	4.25	2.67(5)	3.55(5)
C(42)	3.649(4)	4.44	3.01(5)	3.37(5)
C(43)	3.555(4)	4.45	3.22(5)	3.02(5)
C(44)	4.264	4.79	3.36	4.50
C(45)	4.462	> 5	4.29	3.71

pentane-2,4-dionato ligand (see Table 6). The relatively large tilting of the pentane-2,4-dionate ligand in the present compound is in contrast to a tilt of only 3.6° in six-coordinate VO(acac)$_2$ γ-picoline.[10b]

In view of the similarity of the β-diketonate ligands used in this work, and the small variations in ν(V═O) and ν(B—H) (see Table 1), we assume that all of the compounds have essentially the same distorted octahedral geometry as that formed in LVO(acac). This distorted geometry is reflected in the EPR and electronic absorption spectra of the compounds. The appearance of the frozen solution spectra, at both *X*- and *Q*-band frequencies was indicative of, at most, rhombic EPR symmetry (i.e. $g_1 \neq g_2 \neq g_3$ and $A_1 \neq A_2 \neq A_3$, but with the principal axes of g and A tensors coincident). All of the spectra were satisfactorily simulated on this basis and the mean values of the relevant parameter from both frequencies are shown in Table 1. Although the anisotropies, particularly between g_2 and g_3, and A_2 and A_3, are small they are necessary for satisfactory simulation. The averages of the principal g and A values are in good agreement with the isotropic values obtained from fluid solutions. Not surprisingly, in view of the similarity of the ligand donor atoms, the individual spin-Hamiltonian parameters show little variation over the series of compounds with no effects of the substituents on the β-diketonate being detected.

The electronic absorption spectra also reflect the low symmetry of the compounds in that, for four out of the six compounds studied, we observe four bands which can be attributed to *d–d* transitions based on their absorption coefficients (see Table 2). In the other two compounds the equivalent fourth band would be masked by the intense charge-transfer band from the UV region of the spectrum. Four *d–d* bands have also previously been reported for some low symmetry Schiff-base oxovanadium(IV) compounds.[11] This observation implies the complete removal of degeneracy within the *d*-orbitals of the vanadium. In our initial interpretation of the dilute single crystal EPR data for LVO(Et$_2$dtc), where Et$_2$dtc = N,N-diethyldithiocarbamato, we assumed an electronic structure based on a distortion from D_{3d} point symmetry.[4] However, both the electronic absorption and EPR spectra of the present compounds are also compatible with approximate mirror symmetry (ideally C_s) in the molecules. Further single crystal EPR studies on LVOB and LVO(R$_2$dtc) are in progress to resolve this ambiguity.

The LVOB complexes in methylcyanide solutions all exhibited quasi-reversible one-electron oxidation as assessed by cyclic voltammetry, and by comparison with the simultaneous measurements on ferrocene (see Table 1). The quasi-reversibility was demonstrated by the linear plots of peak current vs the square root of the scan rate, by $\Delta E > 59$ mV which tended towards 59 mV as the scan rate decreased, and by I_{pa}/I_{pc} close to unity. The potentials fall in the narrow range 1.145–1.399 V, suggesting a metal-based process. Those compounds which have electron-withdrawing substituents on the β-diketonate ligand are slightly more difficult to oxidize. Two of the compounds, LVO(bzac) ($E = -1.409$ V, $\Delta E = 83$ mV, $I_{pa}/I_{pc} = 1.00$) and LVO(thtf) ($E = -1.139$ V, $\Delta E = 82$ mV, $I_{pc}/I_{pc} = 1.03$), also, gave quasi-reversible one-electron reductions. The other compounds exhibited ill-defined irreversible reductions. These results, demonstrating the instability of the $[LVOB]^+$ species, are in accordance with our previous observations that the $\{LMoE\}^{2+}$ moiety, where E = O or S, only afford isolable species by achieving six-coordination and overall electrical neutrality.

The LVOB compounds were also examined by mass spectroscopy (see Table 3). The relative molecular masses of each compound are based upon a rounded sum of the relative atomic masses. The mass numbers in Table 3 refer to the peak of maximum intensity within a multiplet. The multiplets arise from the isotopic distribution within the light atoms. For all of the compounds studied we observed the parent ion and the $[LVO]^+$ ion. In addition, all of the compounds except LVO(Clacac) gave a multiplet assignable to the loss of one 3,5-dimethylpyrazolyl ring. These observations are directly comparable with the mass spectroscopy of LMoO(X)(Y) compounds.[3]

Acknowledgements—We gratefully acknowledge financial support from the Royal Society (to D.C.) and from the SERC. We thank Mr O. S. Mills for the design and provision of the software required for the solution of the crystal structure.

REFERENCES

1. D. Collison, B. Gahan, C. D. Garner and F. E. Mabbs, *J. Chem. Soc., Dalton Trans.* 1980, 667; B. Gahan and F. E. Mabbs, *J. Chem. Soc., Dalton Trans.* 1983, 1695, 1713; D. Collison, B. Gahan and F. E. Mabbs, *J. Chem. Soc., Dalton Trans.* 1983, 1705; J. K. Money, K. Folting, J. C. Huffman, D. Collison, J. Temperley, F. E. Mabbs and G. Christou, *Inorg. Chem.* 1986, **25**, 4583; D. Collison, B. Gahan and F. E. Mabbs, *J. Chem. Soc., Dalton Trans.* 1987, 111; D. Collison, F. E. Mabbs, J. Temperley, G. Christou and J. C. Huffman, *J. Chem. Soc., Dalton Trans.* 1988, 309; F. E. Mabbs and J. Temperley, *Spectrochim. Acta* 1989, **45A**, 285.
2. C. D. Garner, L. H. Hill, F. E. Mabbs, D. L. McFadden and A. T. McPhail, *J. Chem. Soc., Dalton Trans.* 1977, 853, 1202; C. D. Garner, P. Lambert, F. E. Mabbs and T. J. King, *J. Chem. Soc., Dalton Trans.* 1979, 1191; C. D. Garner, N. C. Howlader, F. E. Mabbs, P. M. Boorman and T. J. King, *J. Chem. Soc., Dalton Trans.* 1978, 1350; C. D. Garner, N. C. Howlader, F. E. Mabbs, A. T. McPhail and K. D. Onan, *J. Chem. Soc., Dalton Trans.* 1978, 1848; B. Gahan, N. C. Howlader and F. E. Mabbs, *J. Chem. Soc., Dalton Trans.* 1981, 142.
3. D. Collison, F. E. Mabbs, J. H. Enemark and W. E. Cleland Jr, *Polyhedron* 1986, **5**, 423; C. G. Young, D. Collison, F. E. Mabbs and J. H. Enemark, *Inorg. Chem.* 1987, **26**, 2925; W. E. Cleland Jr, K. M. Barnhart, K. Yamonouchi, D. Collison, F. E. Mabbs, R. B. Ortega and J. H. Enemark, *Inorg. Chem.* 1987, **26**, 1017; C. S. J. Chang, D. Collison, F. E. Mabbs and J. H. Enemark, *Inorg. Chem.* 1990, **29**, 2261.
4. D. Collison, F. E. Mabbs, M. A. Passand, K. Rigby and W. E. Cleland Jr, *Polyhedron* 1989, **8**, 1827.
5. E. Kime-Hunt, K. Spartalian, M. DeRusha, C. M. Nunn and C. J. Carrano, *Inorg. Chem.* 1989, **28**, 4392.
6. S. J. Trofimenko, *J. Am. Chem. Soc.* 1967, **89**, 6288.
7. D. Collison, B. Gahan and F. E. Mabbs, *J. Chem. Soc., Dalton Trans.* 1987, 111.
8. D. Collison and F. E. Mabbs, *J. Chem. Soc., Dalton Trans.* 1982, 1565; B. Gahan and F. E. Mabbs, *J. Chem. Soc., Dalton Trans.* 1983, 1713.
9. W. E. Cleland Jr, private communication of unpublished results.
10. (a) R. P. Dodge, D. H. Templeton and A. Zalkin, *J. Chem. Phys.* 1961, **35**, 55: P. Hon, R. L. Belford and C. E. Pfluger, *J. Chem. Phys.* 1965, **43**, 3111; (b) Shao Meicheng, Wang Lifeng and Zhang Zeying, *Acta Chim. Sinica* 1983, **41**, 985.
11. K. S. Patel, G. A. Kolawole and A. Earnshaw, *J. Inorg. Nucl. Chem.* 1981, **43**, 3107.

Polyhedron Vol. 9, No. 20, pp. 2491–2495, 1990
Printed in Great Britain

0277–5387/90 $3.00+.00
© 1990 Pergamon Press plc

PREPARATION OF TEREPHTHALOYL DERIVATIVES OF CYCLIC TRIAMINES AND THEIR SELECTIVITIES TOWARD COPPER(II), NICKEL(II) AND ZINC(II) IONS

MANABU FUJIWARA,* JUN MATSUDA and HISANOBU WAKITA

Department of Chemistry, Faculty of Science, Fukuoka University, Nanakuma, Jonan-ku, Fukuoka 814-01, Japan

(*Received* 3 *January* 1990; *accepted* 8 *June* 1990)

Abstract—Three polymeric ligands containing 9-, 10- and 12-membered cyclic triamines have been prepared by the reaction of cyclic triamine with terephthaloyl chloride. They are insoluble in water and ordinary organic solvents, but under heterogeneous conditions they can adsorb some transition metal ions [copper(II), nickel(II), and zinc(II)] very rapidly. The complexing abilities of the 9- and 10-membered polymeric ligands are stronger in the order zinc(II) < nickel(II) < copper(II), but that of the 12-membered polymeric ligand is nickel(II) < zinc(II) < copper(II).

Selective separation of heavy metal ions is an important subject in the fields of industrial and analytical chemistries. For this purpose, many extractants and chelating resins have been synthesized and some of them have been applied in practice. Tabushi and co-workers[1] reported that the lipophilic cyclams (saturated tetraaza macrocycles) with long alkyl side-chains are able to extract heavy metal ions from aqueous solution to an organic phase. However, the selectivity of these ligands is not very satisfactory. They also reported that the cyclam bound chemically on polystyrene is a good adsorbent for heavy metal ions.[2] Nevertheless, its adsorption rate is very slow and it takes about 3 h for the half-adsorption of the copper(II) ion. Zolotov *et al.*[3] reported that the macrocyclic Schiff base ligand (6,8,15,17 - tetramethyldibenzo - 5,9,14,18 - tetraazacyclotetradecene) exhibits a high selectivity for copper(II) in solvent extraction. Its extraction rate was found to be very slow on account of its rigid structure. In our previous paper,[4] we reported the preparation of polymeric ligands containing the tetraaza macrocycle as an integral part of the polymer backbone, and the complexing ability for copper(II) and nickel(II) under heterogeneous conditions. These polymeric ligands possess a high selectivity for copper(II). In addition, their complexation rates are faster than that of the corresponding monomer ligand, but are not yet satisfactory for practical use. Though many studies on the tetraaza macrocycles and their metal complexes have been reported, a few studies on cyclic triamines and their metal complexes have been carried out.[5] For the complexes with cyclic triamines, the transition metal ion does not incorporate well into the hole of the cyclic triamine, but just sits on the cyclic triamine plane. This means their stability constants may be small but their complexation rates are very high. In this paper, we report the preparation and characterization of the polymeric compounds containing the cyclic triamines and the application to the selective adsorbent for the copper(II) ion.

EXPERIMENTAL

Preparation of the terephthaloyl derivative

To a chloroform solution (300 cm^3) of the free cyclic triamine[6] (1,4,7-triazacyclononane, 1,4,7-triazacyclodecane, or 1,5,9-triazacyclododecane) (0.005 mol) containing pyridine (0.015 mol) as a base, was added dropwise a chloroform solution (200 cm^3) of terephthaloyl chloride (0.006 mol). The mixed solution was refluxed for 24 h. The pale-yellow precipitate formed after the reaction was filtered on a glass filter, washed with dilute sodium hydroxide solution, deionized water and

* Author to whom correspondence should be addressed.

ethanol, and dried *in vacuo*. Three types of polymeric ligands* containing 9-, 10- and 12-membered triamines in the polymer backbone were prepared in about 60% yields.

Preparation of the copper(II) complex with the terephthaloyl derivative

To an aqueous solution (50 cm^3) of copper(II) acetate tetrahydrate (0.030 mol) was added the polymeric ligand (0.003 unit mol). The mixed solution was stirred for 3 h at room temperature, then, the precipitate changed to pale-blue. The bluish precipitate was filtered on a glass filter, washed with water and ethanol, and dried *in vacuo*.

Procedure for the binding of metal(II) ions by the polymeric ligand

The binding of metal(II) ions by the terephthaloyl derivative was carried out using a 10-cm^3 test tube with stopper, in which an aqueous solution (10 cm^3) of metal(II) acetate [copper(II), nickel(II) or zinc(II)] and the uniformly powdered terephthaloyl derivative (10.0 mg) were contained. The test tube was shaken for an appropriate time from 10 to 180 min at room temperature. After shaking, the terephthaloyl derivative was filtered off. The concentration of the metal(II) ion remaining in the filtrate was determined by atomic absorption spectrometry.

RESULTS AND DISCUSSION

The terephthaloyl derivatives are insoluble in water, dilute sodium hydroxide solution and common organic solvents, suggesting that they have rather high molecular weights. The first amine moiety of one cyclic triamine in the terephthaloyl derivative may remain unsubstituted, while its second and third amine moieties react with terephthaloyl chloride to form two amide bonds per one cyclic triamine. The end groups of the polymeric compound are probably carboxyl groups, which are formed by the reaction of one carbonyl chloride in the terephthaloyl chloride by washing with water. The chemical structure of the polymeric compounds estimated from IR spectral data and the results of elemental analyses is shown in Fig. 1. Wieghardt

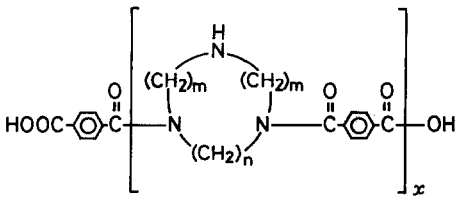

Fig. 1. Structural model of the terephthaloyl derivatives. $m = n = 2$: 9-membered triamine–terephthaloyl derivative; $m = 2, n = 3$: 10-membered triamine–terephthaloyl derivative; $m = n = 3$: 12-membered triamine–terephthaloyl derivative.

et al.[7] reported a similar example where only two nitrogen atoms in a cyclic triamine react with tolylsulphonyl chloride to produce the disubstituted triamine.

Elemental analysis of the terephthaloyl derivative

The elemental analyses of terephthaloyl derivatives are summarized in Table 1. The appropriate x values in Fig. 1, the degree of the polymerization, were estimated from the results of elemental analyses. For the 9-membered triamine–terephthaloyl derivative, the ratio of C:H:N is 16.4:18.7:3.0, where the value of N is fixed at 3.0 because the nitrogen atoms in the polymeric compound belong to only the triamine ring moiety. When the x value is 3.4, the calibrated values of C:H:N are 16.4:18.8:3.0, in good agreement with the found values. In other chemical structures where the end group is one of the cyclic amine moieties, bis(cyclic triamine) connected with terephthaloyl bridge, tris(*p*-carbonylbenzoyl)-cyclic triamine and cross-linked polymer, no x values can be calculated in good agreement with the found values of both C and H.

For the 10-membered triamine–terephthaloyl derivative, the ratio of C:H:N is 15.8:19.6:3.0, and the x value is 10.0. For the 12-membered triamine–terephthaloyl derivative, the ratio of C:H:N is 18.3:24.1:3.0, and the x value is 6.2. These results indicate that the terephthaloyl deriva-

Table 1. Elemental analyses of 9-, 10- and 12-membered triamine–terephthaloyl derivatives

Terephthaloyl derivative	C (%)	H (%)	N (%)
9-Membered	63.92	6.13	13.58
10-Membered	65.46	6.83	14.50
12-Membered	66.90	7.42	12.81

* The IR spectra of the terephthaloyl derivatives have characteristic absorption bands at 3300, 2980, 1730, 1650, 1555, 1480, 1445, 1375, 1290, 1140, 1025, 865, 745 and 730 cm^{-1}. These results indicate that these terephthaloyl derivatives have some unsubstituted amine moieties, amide bonds and disubstituted benzene rings.

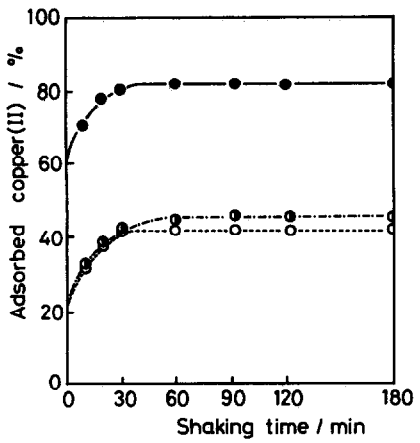

Fig. 2. Effect of shaking time on the adsorption of the copper(II) ion. Adsorbent: (——●——) 9-membered triamine–terephthaloyl derivative (10.0 mg); (-·-◑-·-) 10-membered triamine–terephthaloyl derivative (10.0 mg); (---○---) 12-membered triamine–terephthaloyl derivative (10.0 mg).

tives are polymeric and their molecular weights are probably in the range 1050–2900 depending upon their members of the cyclic triamines.

Binding of metal(II) *ions by the polymeric ligand*

Effect of shaking time. Figure 2 shows the effect of shaking time on the percentage of copper(II) ions bound by the 9-, 10- and 12-membered triamine–terephthaloyl derivatives. For the 9-membered polymeric ligand, the percentage of bound copper(II) ions reached 70% after shaking for only 10 min. This percentage increased with additional shaking for 10 and 20 min. With 30 min shaking, 82% of copper(II) ions were bound by the polymeric ligand. This value implies that 25% of the cyclic triamine moieties in the polymeric ligand were operative for capture of a copper(II) ion and 75% were not. The percentages of other metal(II) ions, nickel(II) and zinc(II), bound by the polymeric ligand were 64 and 55% after shaking for 30 min, respectively. These values are small in comparison with that of copper(II). Within 30 min the reaction between the polymeric ligand and metal(II) ions attained the adsorption equilibria.

For the 10-membered polymeric ligand, the percentage of bound copper(II) ions was 33% after shaking for 10 min. This percentage increased with additional shaking. After 30 min shaking, 45% of copper(II) ions were bound by the polymeric ligand. This value is much smaller than that for the 9-membered polymeric ligand. The percentages of bound nickel(II) and zinc(II) ions were 36 and 28%, respectively, and also much smaller than those of the 9-membered polymeric ligand. However, the complexing ability of the 10-membered polymeric ligand for the metal(II) ions is stronger in the order of zinc(II) < nickel(II) < copper(II), similar to that of the 9-membered polymeric ligand, and the adsorption equilibria between the 10-membered polymeric ligand and metal(II) ions were attained after about 30 min, which is also similar to that of the 9-membered polymeric ligand.

For the 12-membered polymeric ligand, the percentages of bound copper(II), nickel(II) and zinc(II) ions were 42, 15 and 26% after 30 min, respectively. The values for copper(II) and zinc(II) ions are slightly smaller, but that for nickel(II) is much smaller than for the 10-membered polymeric ligand. This leads to the result that the complexing ability of the 12-membered polymeric ligand for metal(II) ions is stronger in the order of nickel(II) < zinc(II) < copper(II), which is different to the order for the 9- and 10-membered polymeric ligands. These results indicate that the structure of the metal(II) complex with the 12-membered polymeric ligand is distinct from those of metal(II) complexes with other polymeric ligands. This may be caused by the differences in the ring size of the cyclic triamines contained within the polymeric ligands. In fact, the ring size of the 12-membered triamine is too large to bind the metal(II) ion at three positions by facial coordination. However, the equilibria between the 12-membered polymeric ligand and metal(II) ions are attained within 30 min, which is similar to the values found for the 9- and 10-membered polymeric ligands. The adsorption rates of metal(II) ions by these polymeric ligands were found to be very fast under such heterogeneous conditions. For other systems containing chelating agents in the solid phase and metal ions in aqueous solutions, the adsorption equilibria were not attained until after more than 48 h.[8]

Effect of pH *on binding capacity.* Figures 3–5 show the effects of the pH of the sample solution on the binding capacity of the polymeric ligands for copper(II), nickel(II) and zinc(II) ions. The pH values were adjusted from 4.0 to 5.5 by using acetate buffer solutions (0.200 mol dm^{-3}) and to above 5.5 by the addition of appropriate amounts of 1.0 mol dm^{-3} sodium hydroxide solution. The shaking time was 1 h.

For the 9-membered polymeric ligand, below pH 4.0 the binding capacity for copper(II) was very small (0.03 mmol g^{-1}) and for nickel(II) and zinc(II) was complete zero. The capacity for copper(II) increased with increasing pH of the sample solution to 6.8. The capacity increased to 0.82 mmol g^{-1}. These behaviours agree well with the result obtained from the pH titration of the corresponding mono-

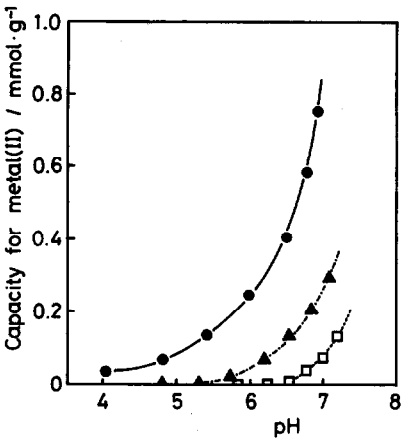

Fig. 3. Effect of pH on the capacity of the 9-membered polymeric ligand for the metal(II) ions. (——●——): copper(II); (-·-▲-·-): nickel(II); (---□---): zinc(II).

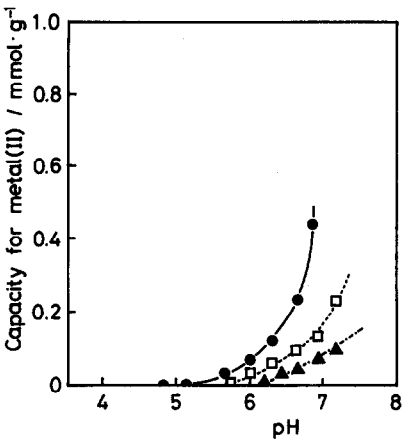

Fig. 4. Effect of pH on the capacity of the 10-membered polymeric ligand for the metal(II) ions. (——●——): copper(II); (-·-▲-·-): nickel(II); (---□---): zinc(II).

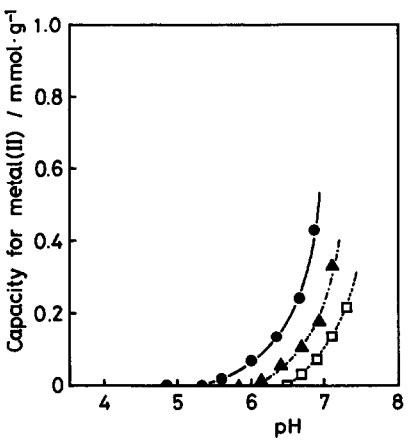

Fig. 5. Effect of pH on the capacity of the 12-membered polymeric ligand for the metal(II) ions. (——●——): copper(II); (-·-▲-·-): nickel(II); (---□---): zinc(II).

meric triamine. In acidic solution, the metal(II) ion and a proton combine with cyclic triamine competitively. In solution around neutral pH, metal(II) ions are coordinated by the cyclic triamine. In alkaline solution, the hydroxyl ion and triamine coordinate to the metal(II) ion competitively. Therefore, the capacity of the triamine–terephthaloyl derivative for the metal(II) ion is probably the highest around neutral acidity of the sample solution. On the other hand, no nickel(II) or zinc(II) was bound by the polymeric ligand below pH 5.3 and 6.5, respectively. The capacity for nickel(II) and zinc(II) ions increased with increasing pH of the sample solution. The values for nickel(II) and zinc(II) increased to 0.21 and 0.04 mmol g^{-1} at pH 6.8, respectively. These are much smaller than the value for copper(II). These results indicate that the 9-membered polymeric ligand binds more strongly in the order of zinc(II) < nickel(II) ≪ copper(II), suggesting that the nature of the triaza ring in the polymeric ligand influences the binding properties of the polymeric ligand towards metal(II) ions.

For the 10-membered polymeric ligand, below pH 5.3 copper(II), nickel(II) and zinc(II) ions were not bound. The binding capacities of this polymeric ligand for copper(II), nickel(II) and zinc(II) increased remarkably with increasing pH of the sample solutions from pH 5.3, 6.1 and 6.6, respectively. At pH 6.8, the binding capacities for copper(II), nickel(II) and zinc(II) were 0.44, 0.19 and 0.07, respectively. The value for copper(II) is much smaller than that of the 9-membered polymeric ligand, but these values for nickel(II) and zinc(II) are slightly smaller and slightly larger than those for the 9-membered polymeric ligand, respectively. These results indicate that the polymeric ligands exert different effects of ionic strength to each other. For the 12-membered polymeric ligand, below pH 5.2 copper(II), nickel(II) and zinc(II) ions were not bound. The binding capacities of this polymeric ligand for copper(II), nickel(II) and zinc(II) increased remarkably with increasing pH of the sample solutions from pH 5.2, 6.2 and 5.7, respectively. The increasing slope for nickel(II) is rather small. At pH 6.8, the capacities for copper(II), nickel(II) and zinc(II) were 0.44, 0.07 and 0.14 mmol g^{-1}, respectively. The capacity for nickel(II) is smaller than that for zinc(II). The complexing ability of the 12-membered polymeric ligand for metal(II) ions is stronger in the order nickel(II) < zinc(II) < copper(II), which is different from those of the 9- and 10-membered polymeric ligands. These results indicate that the structure of the metal(II) complex with the 12-membered polymeric ligand is distinct from those of metal(II) complexes with other polymeric ligands, as mentioned above.

Reflectance spectra of polymeric ligands and their copper(II) complexes

The diffused reflectance spectra of polymeric ligands and their copper(II) complexes were measured. The 9- and 12-membered polymeric ligands have weak absorption bands at 442 and 418 nm, respectively. These bands can be assigned to π–π^* transitions.

The copper(II) complex with the 9-membered polymeric ligand exhibits two absorption bands at 670 and 428 nm. The former can be assigned to ligand-field transitions and the latter may be assigned to charge-transfer transitions. The absorption spectrum of the copper(II) complex with the parent monomeric ligand, CuL^{2+} (L = 1,4,7-triazacyclononane), in H_2O shows an absorption band at 637 nm.[9] This result indicates that the ligand-field strength of the terephthaloyl derivative (9-membered polymeric ligand) is weakened considerably in comparison with that of the parent cyclic triamine. This was caused by the introduction of the terephthaloyl groups, the electron-withdrawing substituents.

The copper(II) complex with the 12-membered triamine–terephthaloyl derivative exhibits absorption bands at 666 and 424 nm. These may be also assigned to ligand-field transitions and charge-transfer transitions, respectively. The absorption spectrum of the copper(II) complex with 1,5,9-triazacyclododecane in H_2O shows an absorption band at 689 nm.[9] The absorption band of the copper(II) complex with the terephthaloyl derivative was shifted not to longer wavelengths, but to shorter wavelengths by about 20 nm in comparison with that of the unsubstituted 12-membered triamine. As mentioned above, the structure of the copper(II) complex with the 12-membered polymeric ligand may be different from that of the corresponding parent triamine. This difference influences the adsorption character of the 12-membered polymeric ligand, where the polymeric ligand binds to the zinc(II) ion more strongly than to the nickel(II) ion.

REFERENCES

1. I. Tabushi and M. Fujiyoshi, *Hetereocycles* 1977, **7**, 851; I. Tabushi, Y. Taniguchi and H. Kato, *Tetrahedron Lett.* 1977, 1049.
2. I. Tabushi, Y. Kuroda, H. Kato, T. Hirai, H. Okino, M. Fujiyoshi and Y. Taniguchi, *Japan Kokai Patent* 77,110,290 (1977).
3. Yu. A. Zolotov, V. F. Ionov, V. A. Bodnja, G. A. Larikova, N. V. Niz'eva, G. E. Vlasova and E. V. Rybakova, *Zh. Anal. Khim.* 1982, **37**, 1543.
4. N. Kubota, M. Fujiwara, T. Matsushita and T. Shono, *Polyhedron* 1985, **4**, 1051.
5. L. T. Taylor and D. H. Busch, *Inorg. Chem.* 1969, **8**, 1366; R. Yang and L. J. Zompa, *Inorg. Chem.* 1976, **15**, 1499; L. J. Zompa, *Inorg. Chem.* 1978, **17**, 2531; L. J. Murphy, Jr and L. J. Zompa, *Inorg. Chem.* 1979, **18**, 3278.
6. H. Koyama and T. Yoshino, *Bull. Chem. Soc. Jpn* 1972, **45**, 481.
7. K. Wieghardt, I. Tolksdorf and W. Herrmann, *Inorg. Chem.* 1985, **24**, 1230.
8. M. Fujiwara, Y. Nakajima, T. Matsushita and T. Shono, *Polyhedron* 1985, **4**, 1859.
9. T. J. Riedo and T. A. Kaden, *Helv. Chim. Acta* 1979, **62**, 1089.

Polyhedron Vol. 9, No. 20, pp. 2497–2506, 1990
Printed in Great Britain

0277–5387/90 $3.00+.00
© 1990 Pergamon Press plc

EFFECT OF UREA ON THE SPECIATION OF 1,10-PHENANTHROLINE COMPLEXES OF TOXIC METAL IONS—COMPUTER AUGMENTED MODELLING STUDIES

N. PADMAJA, M. SARATCHANDRA BABU, G. NAGESWARA RAO, R. SAMBASIVA RAO and KARRI V. RAMANA*

Bioinorganic Chemistry Laboratories, School of Chemistry, Andhra University, Visakhapatnam-530 003, India

(*Received* 3 *April* 1990 ; *accepted* 8 *June* 1990)

Abstract—The speciation of Pb^{II} and Cd^{II} complexes of 1,10-phenanthroline has been studied in varying concentrations (0–29.64% w/w) of urea solutions maintaining an ionic strength of 0.16 mol dm^{-3} (NaCl) at 30°C. The strength of the acid and the base was checked using the Gran plot method. Titrations were performed with a wide range of metal to ligand ratios (1 : 2–1 : 6). The primary alkalimetric data are pruned either with SCPHD (2.0) or by a new graphical procedure. The approximate equilibrium constants thus obtained were refined with MINIQUAD 75. The selection of best chemical models was based on statistical parameters and residual analysis. Since the active form of the ligand is LH^+, the species detected are ML, ML_2 and ML_3 only. Global stability constants were evaluated using ANOVA. The solvent effects have been analysed in terms of macroscopic properties of the solvent mixture with ESOCE. The trend in β values of the proton–ligand and the metal–ligand complexes with the dielectric constant is explained on the basis of electrostatic and non-electrostatic forces.

The role of urea is significant in the metabolism, though it acts as denaturant of DNA,[1] proteins,[2] insulin[3] and other macromolecules.[4] Acinus (micro-circulatory unit of the liver) contains periportal and perivenous cells which convert the ammonia in the blood into non-toxic urea.[5] The synthesis of urea is maximal[6] at physiological pH (7.4) and markedly decreased at pH 7.05. The release of the urea thus produced is regulated[7] by sympathetic and para-sympathetic nerves. The patients with urea toxicity (ureamia) exhibit the symptoms as pneumonitis, pericardiatis, gastrointestinal disorders and peripheral neuropathy. The lethal dose of urea to fish[8] (*Channa punctatus*) is 27 000 ppm. This is significant with respect to water pollution by fertilizers containing urea; feeding experimental animals resulted[9] in reduced venous concentrations of plasma amino acids. Urea from urea-based fertilizer is degraded to ammonia in soil by urease (Ni-containing enzyme), the activity of which is essential for plant growth. In addition urea can be used as a drug in the treatment of syndrome of inappropriate antidiuretic hormone secretion (SIADH).[10]

The globular structure of protein in aqueous solution may be due to the hydrophobic interactions. The contact between non-polar side chains of proteins and water requires an unfavourable arrangement of water molecules. There are many such contacts in an unfolded conformation but relatively few in a globular one, which is stabilized in spite of its own low conformational entropy.[11] Two alternative mechanisms are proposed for the denaturing effect of urea on proteins: (1) Direct interaction of urea molecules with amide and peptide groups which destroys intermolecular hydrogen bond and hydrophobic interactions[12] that are involved in the maintenance of ternary structure of DNA, macromolecules, etc. (2) Urea exerts its influence through changes in the water structure.[13] The negative heat capacities of transfer of certain amino acids[14] from water to aqueous urea solution and the increments in the critical micelle concentration[15] of certain micelles, suggest that urea may reduce the co-operative structure of water. Hence it is proposed to

* Author to whom correspondence should be addressed.

study the urea–water interactions in order to understand the denaturing property of urea.

Toxicity of metals occurs when an organism is unable to cope with the additional metal concentration by direct usage, storage or excretion. The toxicity effects of heavy metal ions may also be the result of their strong bonding with reactive groups of enzymes. Hence studies of the interaction of toxic metal ions with bioligands in the presence of urea throw light on: (1) the understanding of the mechanism of the adverse effect of these cations on metabolic processes, (2) in suggesting antidotes and (3) on the effect of denaturant on the speciation.

In the present study the complexation of Pb^{II} and Cd^{II} with 1,10-phenanthroline (phen) is studied electrometrically in urea–water mixtures.

Table 1. Total initial concentration of ingredients (mmol)

% w/w Urea	Metal ion	TMO	TLO	TLO : TMO
0.00, 5.80, 11.52, 20.31, 29.64	Pb^{II}	0.1997	0.400	1 : 2
			0.500	1 : 2.5
			0.600	1 : 3
		0.0998	0.400	1 : 4
			0.500	1 : 5
			0.600	1 : 6
	Cd^{II}	0.1958	0.400	1 : 2
			0.500	1 : 2.5
			0.600	1 : 3
		0.0979	0.400	1 : 4
			0.500	1 : 5
			0.600	1 : 6

EXPERIMENTAL

Solutions of phen (E. Merck), Pb^{II} and Cd^{II} were prepared in doubly distilled water. All other solutions were of A.R. grade and were prepared in doubly distilled water. Urea was recrystallized twice from ethanol[16] and was dried at 60°C for 2 h. Stock urea solutions were prepared and stored frozen. The solution was never allowed to stand at room temperature for more than 24 h before its usage. The strength of the alkali was determined using the Gran plot method.[17] The errors in the concentrations of ligand, metal ions and alkali were subjected to analysis of variance (ANOVA) by the computer program COSWT (concentration of solution by weight method).[18]

The titrations were carried out in the medium containing varying amounts of urea maintaining an ionic strength of 0.16 mol dm^{-3} with NaCl at 30 ± 0.05°C. The measurements were recorded with a Systronic (model 335) pH meter of 0.01 readability in conjunction with a glass and calomel electrode. The glass electrode was equilibrated in a well-stirred urea–water mixture containing inert electrolyte. Titration of strong acid with alkali was carried out at regular intervals to check whether complete equilibration was achieved or not. The calomel electrode was refilled with urea–water mixture of equivalent composition as that of the titrand. In each of the titrations, the titrand consists of mineral acid of approximately 1 mmol in a total volume of 50 cm^3. Titrations with different ratios (1 : 2–1 : 6) of metal–ligand are carried out with 0.3 mol dm^{-3} NaOH (Table 1). The details of experimental procedure and titration assembly are given elsewhere.[19]

Modelling strategy

The approximate stability constants of protonation or complexation of phen were calculated either with the computer program SCPHD (2.0)[20] or by a graphical method developed[21] in our laboratory (Fig. 1). The best fit chemical model for each system investigated was arrived at using non-linear least squares analysis using MINIQUAD 75,[22] which exploits the advantage of constrained least squares method in the initial refinement and reliable convergence of undamped, unconstrained Marquardt algorithm. The variation of stepwise equilibrium constants of proton–ligand as well as metal–ligand species was analysed on electrostatic grounds using ESOCE and on the basis of solute–solute and solute–solvent interactions.

RESULTS AND DISCUSSION

Mathematical models for proton–ligand equilibria

Although phen is a bifunctional base, its behaviour in aqueous solutions involves the addition of

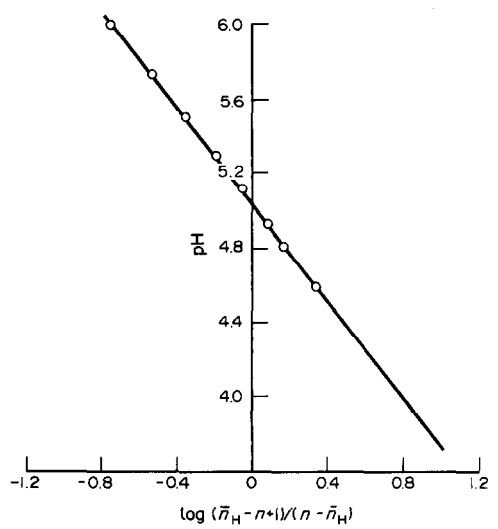

Fig. 1. Evaluation of stepwise stability constants by graphical method.

a single proton. There is evidence, based on shifts in the UV spectra, that it accepts a second proton in more concentrated acid ($pk_a = -1.6$); this proton cannot be detected by pH metry. Hence in the pH range of 2–10, phen exists as monoprotonated form and its equilibrium can be represented as

$$L + H^+ \rightleftharpoons LH^+ ; K_1^H = [LH^+]/[L][H^+]. \quad (1)$$

Secondary formation function $\bar{n}_H$ is the average number of protons bound per mole of ligand, and the equilibrium constants are related by eq. (2):

$$\bar{n}_H = K_1^H \times FHi/(1 + K_1H \times FHi), \quad (2)$$

where FHi is the free hydrogen ion concentration. $\bar{n}_H$ in terms of ligand concentration can be represented as

$$\bar{n}_H = (Ei + OHi - ALKi - FHi)/TLEi, \quad (3)$$

where TLEi, Ei and OHi are the total ligand, total acid and hydroxyl ion concentrations due to autoionization of water, respectively. ALKi is the concentration of alkali. The formation curves along with alkalimetric titration curves for a typical system are given in Fig. 2. The overlapping of formation curves indicates the precision of the titrations and the existence of a single equilibrium.

Binary complexes

The complexation of phen with Pb^{II} or Cd^{II} can be represented as

$$pM^{2+} + qLH^+ \rightleftharpoons MpL_q^{2+} + qH^+. \quad (4)$$

The formation function $\bar{n}$ (average number of ligands bound per mole of metal ion) is given by eq. (5):

$$\bar{n}_i = \frac{TLEi \times nHi - (Ei + OHi - ALKi - FHi)}{nHi \times TMEi}. \quad (5)$$

Since phen is a neutral base and in the experimental conditions only one proton is attached to the nitrogen atom, there is no possibility for the existence of protonated species, which is corroborated by the overlapping of formation curves

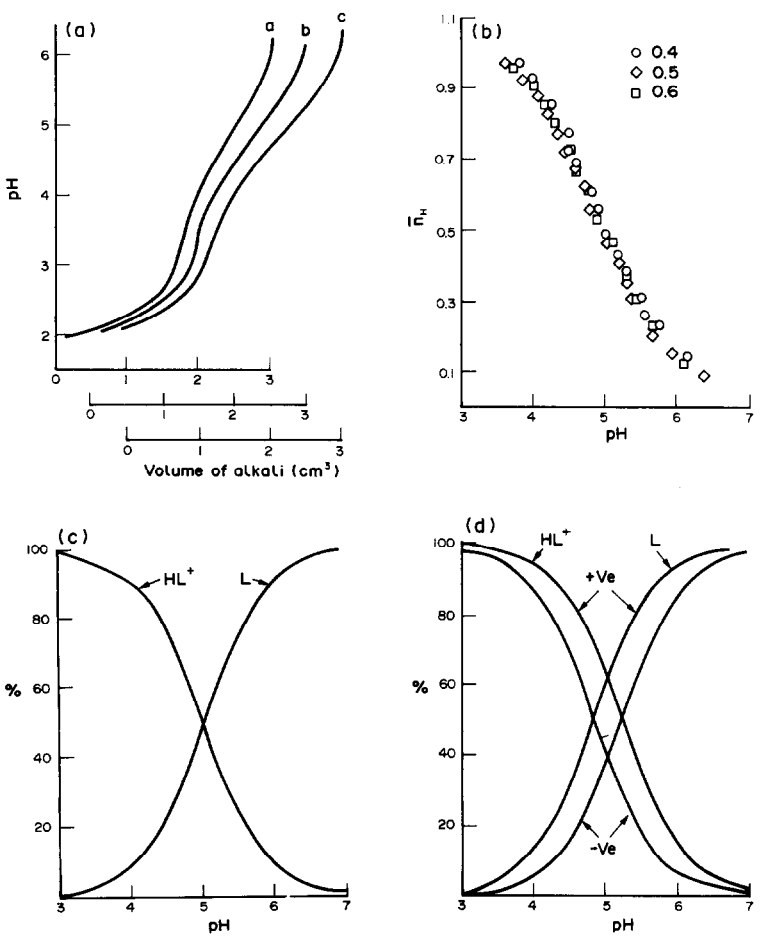

Fig. 2. Alkalimetric titration curves: (a) formation curves; (b) species distribution diagrams; and (c) effect of errors in $\log \beta$ on the concentration of species (d) of phen in aqueous solution.

for different ratios of the metal and ligand concentrations. Since the ratio of TLO and TMO is greater than unity in all those experiments the formation of polynuclear complexes is not considered. The chemical models for proton–ligand and metal–ligand equilibria from MINIQUAD 75 are given in Tables 2 and 3, respectively. 1,10-Phenanthroline contains two imine nitrogen atoms which are potential sites for coordination of metal ligands. Since each ligand molecule satisfies two coordination positions of a metal ion, the highest complex expected will be ML_3. Hence three species [ML, ML_2 and ML_3) are tried for modelling purposes. Very low standard deviations in $\log\beta$ and small values of U—the sum of squares of deviations in concentrations of ligand and hydrogen atom at all experimental points—indicate precision in $\log\beta$ and the best fit model for the experimental data, respectively. Since each of the χ^2 values in this study is less than $\chi^2_{\nu 0.5}$ it can be inferred that residuals form a part of normal distribution. Very small values of the mean (-9.324×10^{-7}), the standard deviation (2.244×10^{-4}) and the mean deviation (1.936×10^{-4}) for a typical system (phen in a 20.31% urea–water mixture) corroborate that the residuals are around a zero mean with little dispersion. For an ideal distribution, the values of kurtosis and skewness should be 3.0 and 0.0, respectively. Small deviation of kurtosis from the ideal value indicates that the residual forms a leptokurtic or platikurtic pattern which are similar to those found by Cassasas *et al.*[23] These statistics thus show that the best fit mathematical models given in Tables 2 and 3 are adequate for the representation of present equilibria.

Global stability constants

Since many titrations were performed with different initial ligand concentrations, there is a

Table 2. Chemical models of acido–basic equilibria of phen in urea–water mixtures along with population stability constants

% w/w	Expt. No.	$\log K_1$ (SD)	pH Range	NP	U/(NP-m) $\times10^8$	Skewness	Kurtosis	χ^2	R
0.00	1	5.080(2)	3.5–7.0	12	0.7337	−1.54	4.69	4.00	0.0286
	2	5.040(2)	3.5–7.0	15	0.8233	−1.06	3.10	3.60	0.0246
	3	4.997(2)	3.5–7.0	18	0.1487	−1.00	2.82	6.22	0.0278
	Average[a]	5.040(2)							
	Pooled data	5.025(1)	3.5–7.0	45	0.1138	−0.91	3.29	13.64	0.0285
5.80	1	4.972(2)	3.5–7.0	14	0.3498	−1.68	4.71	8.00	0.0176
	2	4.884(3)	3.5–7.0	19	0.3281	−1.11	3.28	6.00	0.0124
	3	4.927(2)	3.5–7.0	23	0.8599	−1.70	4.55	7.88	0.0203
	4	4.936(2)	3.5–7.0	26	0.1679	−1.77	5.08	8.32	0.0221
	Average[a]	4.941(10)							
	Pooled data	4.913(3)	3.5–7.0	82	0.1732	−1.71	6.25	20.15	0.0216
11.52	1	4.867(4)	3.7–7.0	12	0.1550	−2.02	6.26	7.33	0.0417
	2	4.788(1)	3.7–7.0	14	0.6366	−1.49	6.22	10.86	0.0214
	3	4.826(2)	3.7–7.0	14	0.0790	−1.10	4.77	8.00	0.0238
	4	4.642(1)	3.7–7.0	17	0.1256	−1.76	8.99	13.06	0.0258
	Average[a]	4.773(32)							
	Pooled data	4.746(1)	3.7–7.0	57	0.0220	−0.29	4.26	16.11	0.0402
20.31	1	4.781(4)	3.8–7.0	8	0.9885	−0.29	4.26	16.11	0.0402
	2	4.634(2)	3.8–7.0	7	0.7207	−0.23	3.10	1.00	0.0301
	3	4.639(2)	3.8–7.0	7	0.5883	−2.0	2.52	5.43	0.0185
	4	4.660(3)	3.8–7.0	6	0.6981	−0.06	1.85	2.67	0.0165
	Average[a]	4.678(14)							
	Pooled data	4.677(11)	3.8–7.0	28	0.1044	−0.11	2.43	14.29	0.0268
29.64	1	4.480(12)	3.0–7.0	6	1.2403	−0.03	1.81	1.33	0.0295
	2	4.340(7)	3.0–7.0	6	0.7717	−0.05	2.10	4.00	0.0188
	3	4.362(7)	3.0–7.0	6	0.8442	−0.03	1.82	2.67	0.0196
	4	4.308(6)	3.0–7.0	6	0.8522	−0.03	1.59	4.00	0.0165
	Average[a]	4.373(15)							
	Pooled data	4.363(3)	3.0–7.0	24	0.8979	−0.03	2.03	4.00	0.0125

$U=\sum_{i=i}^{NP}(TLC_i-TLE_i)^2+(THC_i-THE_i)^2$; NP = number of points; SD = standard deviation in log K; Na(Cl) = 0.16 mol dm^{-3}; T = 303°K.

[a] Population stability constants; pH meter readability = 0.01.

Table 3. Best fit chemical models of M^{II}–phen complexes in urea–water mixtures along with statistical parameters

% w/w Urea	log β (SD) 110	120	130	pH Range	NP	U/(NP-m) ×10⁶	χ^2	R	Skewness	Kurtosis
				Pb^{II}–phen						
0.00	2.872(3)	6.498(4)		2.0–6.0	77	0.3074	173.40	0.1042	−0.02	3.09
5.80	3.017(4)	6.443(9)		2.4–6.0	80	0.5410	14.73	0.0530	−0.03	3.87
11.52	3.373(2)	6.452(5)		2.0–6.0	136	0.2697	251.61	0.0821	−0.02	4.01
20.31	3.615(3)	6.509(4)		2.0–6.0	179	0.4983	149.91	0.1041	−0.29	4.00
29.64	3.891(5)	6.672(8)		2.3–6.0	119	0.1217	47.01	0.0233	−0.46	3.65
				Cd^{II}–phen						
0.00	4.912(6)	9.007(8)	11.213(4)	2.6–6.0	56	1.0045	30.00	0.0372	−0.72	4.04
5.80	3.695(7)	8.572(6)	11.599(8)	2.4–6.0	134	5.0252	65.50	0.0465	−0.71	4.54
11.52	3.983(2)	8.545(9)	11.497(5)	2.4–6.0	165	1.3591	46.76	0.0697	−0.21	3.81
20.31	4.446(1)	8.890(5)	11.360(5)	2.0–6.0	184	7.5154	31.04	0.0422	−0.44	4.17
29.64	5.288(8)	9.732(11)	—	2.0–6.0	77	6.0893	67.15	0.0198	−2.03	12.16

possibility that the difference in log β values of the separate experiments was due to the inter and intra titration variability. Braibanti *et al.*[24] subjected the stability constants obtained from different experiments to ANOVA and named the resulting constants as population stability constants or global stability constants; these are of practical utility for either inter comparison or for critical compilation in spite of their higher SD's. Population stability constants are given in Table 2 for protonation equilibria and in Table 4 for a typical system of metal–ligand equilibria.

Effect of systematic errors in the best fit model

MINIQUAD 75 does not have provision to study the effect of systematic errors in the concentrations of ingredients and electrode calibration on the magnitude of equilibrium constant. In order to rely upon the best chemical model for critical evaluation and application under varied experimental conditions with different accuracies of data acquisition, an investigation was made by introducing pessimistic errors in the concentration of alkali, mineral acid, ligand and in the correction factor, log F. The results of a typical sample in Table 5 emphasise that the errors in alkali and mineral acid affect the stability constants more than those in ligand and correction factor.

Effect of urea on the equilibria

(a) *Acido–basic equilibria.* The results show that log formation constant decreases with an increase in dielectric constant. Since 1/D is a linear function of (D−1)/(2D+1) [see Fig. 3(b)] the analysis of variation of $\log K^H$ with dielectric constant is confined to only 1/D using ESOCE[25] and Forsethe[26] computer programs. As the shape of the curves [Fig. 3(d)] do not suggest a higher polynomial trend,

Table 4. Stability constants obtained from separate and pooled data and population stability constants for Cd^{II}–phen in 20.31% w/w urea–water mixture

% w/w	log β (SD) 110	120	130	pH Range	NP	U/(NP-m) ×10⁷	χ^2	R	Skewness	Kurtosis
20.31										
1	4.747(14)	9.043(5)	11.273(3)	2.0–6.0	26	1.7704	8.77	0.0200	−1.36	5.69
2		9.041(3)	11.427(5)	2.0–6.0	31	2.6474	12.89	0.0192	−2.14	12.48
3		8.998(2)	11.194(9)	2.0–6.0	32	1.2895	13.67	0.0123	−0.42	4.46
4	4.232(3)	8.247(12)		2.0–6.0	31	1.3247	30.78	0.0352	−0.19	6.06
5	4.424(8)	7.989(13)								
6	4.568(5)	8.013(8)		2.0–6.0	32	7.4504	34.83	0.0313	−0.32	6.77
Average	4.485(4)	8.555(4)	11.295(2)	2.0–6.0	32	2.0188	17.33	0.0155	−1.65	8.35
pooled	4.446(1)	8.890(5)	11.360(4)	2.0–6.0	184	7.5154	31.04	0.0422	−0.44	4.17

Table 5. Effect of systematic errors on the protonation (11.52% w/w) and complex (20.31% w/w) equilibria of phen with Cd^{II}

Ingredient	% Error	log β (SD) 011	110	120	130
log F	−5	4.716(6)	Rej.	8.563(5)	10.231(4)
	−2	4.725(6)	3.998(3)	8.747(6)	10.933(6)
	0	4.746(1)	4.446(1)	8.890(5)	11.360(4)
	+2	4.766(5)	4.777(2)	9.073(6)	11.751(3)
	+5	4.776(6)	5.208(3)	9.414(7)	12.287(5)
Alkali	−5	4.900(4)	4.520(1)	8.589(7)	Rej.
	−2	4.809(9)	4.453(3)	8.794(6)	Rej.
	0	4.746(1)	4.446(1)	8.890(5)	11.360(4)
	+2	4.687(3)	4.491(8)	8.957(6)	12.03(27)
	+5	4.603(1)	4.656(2)	8.996(11)	12.721(24)
Acid	−5	4.544(9)	5.199(8)	9.313(12)	13.407(20)
	−2	4.664(3)	4.684(5)	9.078(6)	12.301(23)
	0	4.746(1)	4.446(1)	8.890(5)	11.360(4)
	+2	4.825(9)	4.283(6)	8.673(6)	Rej.
	+5	4.945(6)	4.077(8)	8.312(9)	Rej.
Ligand	−5	4.798(7)	4.393(6)	8.809(6)	10.885(5)
	−2	4.765(5)	4.318(5)	8.676(7)	Rej.
	0	4.756(1)	4.446(1)	8.890(5)	11.360(4)
	+2	4.725(5)	4.499(6)	8.966(5)	11.769(3)
	+5	4.693(5)	4.582(6)	9.073(5)	12.144(2)
Metal	−5		4.447(8)	8.959(6)	11.759(3)
	−2		4.445(7)	8.917(6)	11.525(3)
	0		4.446(1)	8.890(5)	11.360(4)
	+2		4.448(5)	8.862(6)	11.181(4)
	+5		4.454(3)	8.819(6)	10.869(6)

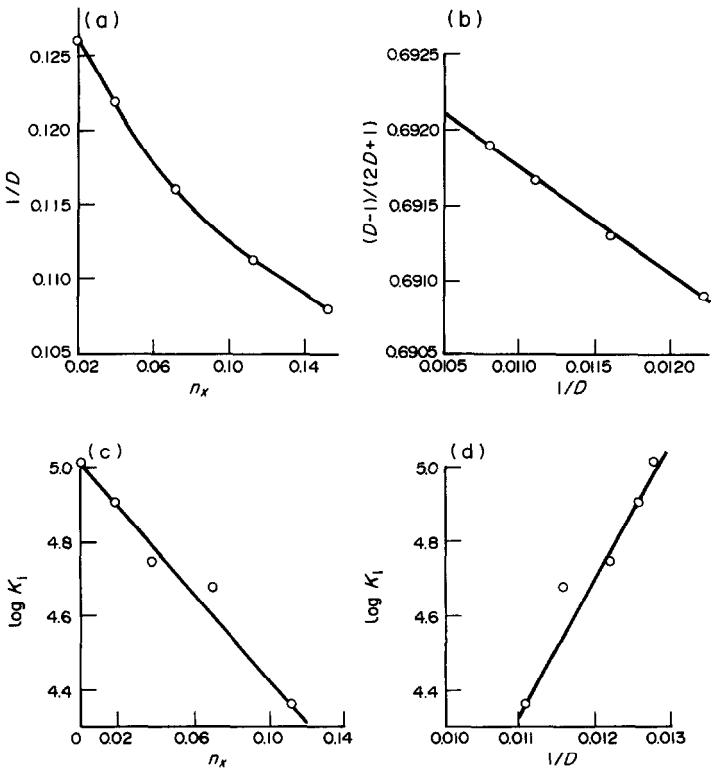

Fig. 3. Correlation of log K with mole fraction and reciprocal of dielectric constant in urea–water mixtures.

we arrived at a linear model based on the standard deviation. The changes in $\log K^H$ for the protonation equilibria of phen with mole fraction (n_x) of urea are also linear with monotonic decrease [Fig. 3(c)].

Cationic weak acids (HL^+) formed from a neutral base and protons are isoelectric processes and, as such, electrostatic charging effects should have minimal influence on the equilibrium. Thus electrostatic considerations alone reveal that $\log K^H$, in binary mixed solvents, should either remain constant or increase by a small amount. As such they are good model compounds to study specific solute–solvent interactions as a function of cosolvent content. An increase in cosolvent content increases the ion–dipole forces between the proton and nitrogen atom of the solute to a lesser extent than ion–dipole forces between a proton and the more electronegative donor oxygen atom of the solvent. Thus a decrease in $\log K^H$ with cosolvent content is expected and for systems in which it passes through a minimum, it has been assumed that the interaction between proton and nitrogen would be greater than that between proton and oxygen atom of water.

The heat capacity studies indicate that urea neither decreases nor increases the water structure[16] and it is well known[27] that structure breaking solutes shift the water PMR signal up field and structure making solutes shift it down field. It was observed that the addition of urea does not alter the chemical shift of water protons until the solute concentration is 7 M.[16,28] This supports the view that urea mixes freely with water so as to leave the solution as much structured as water. Even beyond 7 M the change in the chemical shift is very meagre which is probably due to the aggregation of urea molecules. The flickering cluster model was proposed[29] for water, wherein each water molecule is considered to be an integral part of flickering clusters instead of belonging solely to monomeric or cluster species. Introduction of urea molecules into the heart of flickering clusters can be achieved without prejudice to the geometry of urea molecules. Due to this interposition of urea in the cluster the life time of the clusters may be extended and the dimensions of the voids may be changed, which accounts for the increased solubility of hydrocarbons in aqueous urea over that in water.

Dielectric relaxation studies show that the number of water molecules around urea with a relaxation time different from that of pure water is usually small.[30] The calculations of molecular dynamics suggest that there is only a slight difference in aqueous solution of urea and pure water and hence urea can enter into water without appreciable distortion of the solvent structure.[31] The only difference is in urea–water mixtures, the water molecule is firmly fixed to urea. That means the hydration structure around the urea molecule is more rigid than that of pure water. It is observed[32] that five water molecules are attached to one molecule of urea in the first hydration shell whose positions are in the direction of *trans* H, *cis* H and carbonyl lone pair. Water molecules in the second hydration shell are also fixed rather firmly. From these observations it appears that the urea molecule can enter into the water structure without breaking it noticeably as a whole. So the water structure may be certainly changed in the vicinity of urea within the first or second hydration shell, though the potential energy of the whole system is almost the same as that of pure water. Urea molecules do not affect the water structure beyond the secondary hydration shell.

(b) *Metal–ligand equilibria.* The change in stepwise formation constants ($\log K^M$) of complexes of phen with Pb^{II} and Cd^{II} with variation of concentration of urea are depicted in Figs 4 and 5. In the case of Pb^{II}, $\log K_1^M$ and $\log K_2^M$ monotonically increased and decreased, respectively, with the mole fraction of the solute, whereas for Cd^{II}, a minimum for ML and maxima for ML_2 and ML_3 are observed. A similar trend is observed in the case of $\log K_n^M$ vs 1/D. These results show the predominance of non-electrostatic forces.

Distribution of species

The distribution diagrams obtained from DISPLOT[33] [Fig. 2(c)] show that the dissociation of the proton which is associated with nitrogen takes place in the pH range 3.0–5.0. The ionization begins at 2.5 and ends at 7.0. As the concentration of the protonated ligand (HL^+) decreases, the concentration of free ligand (L) increases. As such, 50% of each of these species exist at that pH where it is equal to $\log K$. Since the second protonation constant is -1.9 the species LH_2^{2+} does not exist in the pH range of investigation (2.5–7.0).

The effect of systematic errors on the concentrations of the species is given in [Fig. 2(d)]. It is evident from this figure that even the small changes in determination of stability constants may lead to large variations in the concentration of the species. This type of study is significant in determining total parenteral nutrition.

Since HL is the predominant form of the ligand in the pH range 2.0–7.0, there is no scope for the formation of protonated metal complexes in these systems. The best fit model contains mononuclear, unprotonated, unhydroxylated species, viz. ML and ML_2 in the case of Pb^{II}, and ML, ML_2 and

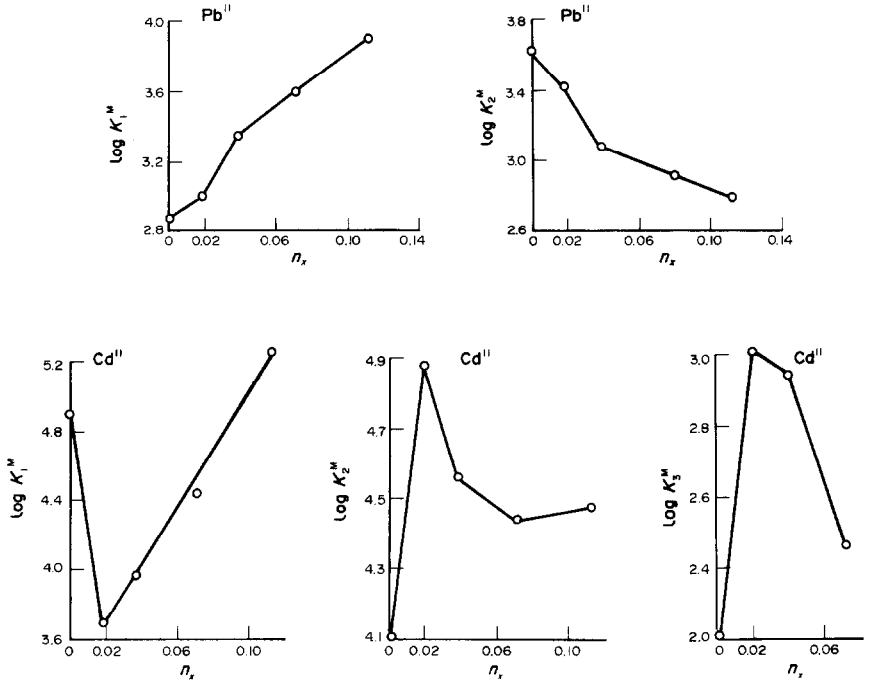

Fig. 4. Variation of log K^M of M^{II}–phen complexes with mole fraction of urea.

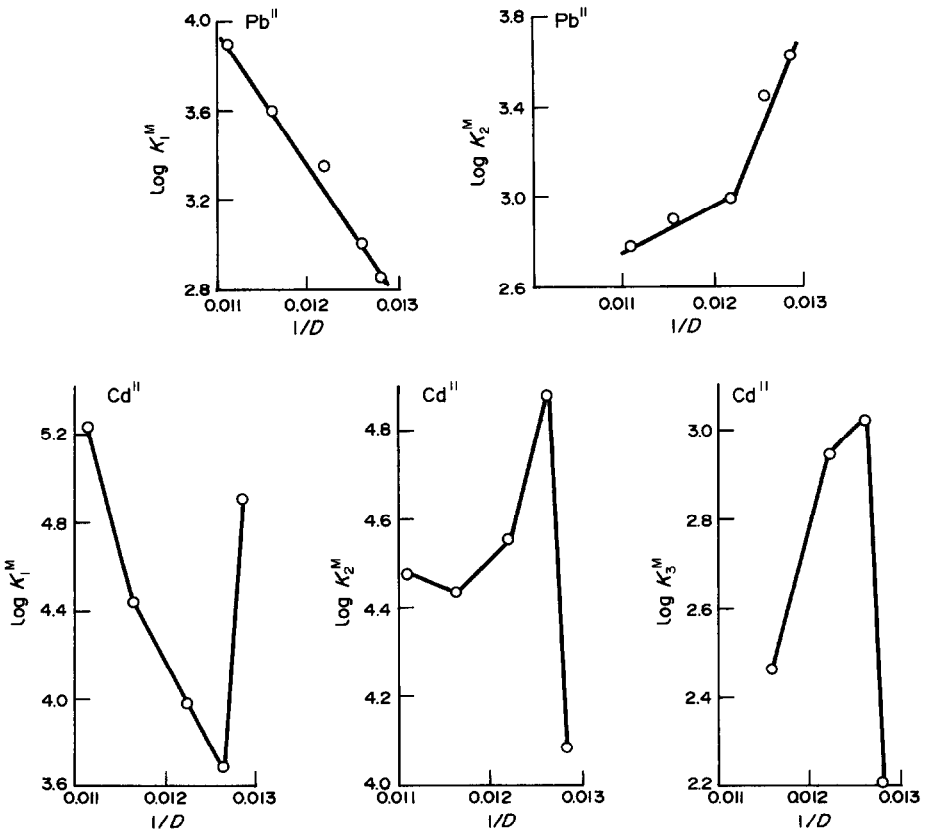

Fig. 5. Correlation of log K^M of M^{II}–phen complexes with the reciprocal of the dielectric constant of urea–water mixtures.

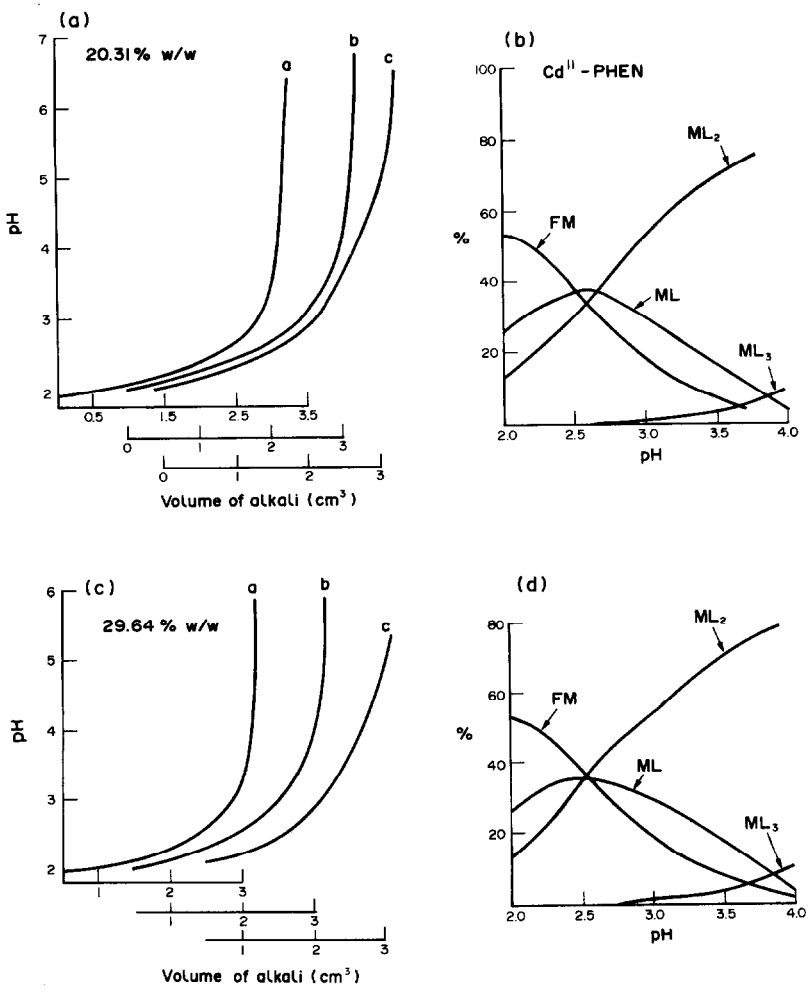

Fig. 6. Alkalimetric titration curves and species distribution diagrams of urea–water mixtures.

ML_3 for Cd^{II} (Table 3). The hydroxylated complexes such as ML(OH) and $ML_2(OH)$ were rejected by MINIQUAD 75 in the pH range studied.

It is clear from the typical distribution diagrams (Fig. 6) that the equilibria correspond to the simultaneous formation of ML, ML_2 and ML_3. As the concentration of urea is increased, the stability of the metal–ligand complex is decreased which is concluded from the distribution diagrams. Although the same species are formed in the entire range of the concentration of urea, the difference in the pH region and the extent of formation of the species are due to the effect of the metal ion, characteristic intermediate complexes and solute on the different processes existing in the solution.

ML_3 species could not be detected for the Pb^{II} ion, may be because of the following reasons: (1) the small size of the lead ion cannot accommodate three molecules of phen around itself due to steric hindrance of the ligand molecules, (2) as there are no *d* electrons, the overlap of metal–ligand orbitals are very small which leads to the formation of no complexes at all or of very weak complexes which in no time may become dissociated, the dissociation being much faster than formation. On the other hand the Cd^{II} ion has filled *d* orbitals which have $d\pi$–$p\pi$ interaction with the ligand and so the formation of ML_3 species is observed though not with considerable stability. However, at higher concentrations of urea (29.64%) there is no formation of ML_3 species even in the case of Cd^{II}. This may be due to the competition between the ligand (phen) and the solute (urea) molecules towards the metal ion.

REFERENCES

1. P. H. Vonhippel and T. Schleich, *Structure and Stability of Biological Macromolecules* (Edited by S. N. Timasheff and C. J. Forman), p. 69. Dekker, New York (1968).

2. A. E. Russel and D. R. Cooker, *Biochem. J.* 1969, **113**, 221.
3. H. Thurow, *Proc. Int. Insulin Symp.* 1979, 215.
4. R. J. Siezen and J. G. Bendels, *Exp. Eye Res.* 1982, **34**, 969.
5. A. R. Poso, K. E. Penttila, E. M. Soulinna and K. O. Lindros, *Biochem. J.* 1986, **239**, 263.
6. C. Remesy, C. Demigne and P. Fafournoux, *Eur. J. Biochem.* 1986, **158**, 283.
7. C. Balle and K. Jungermann, *Eur. J. Biochem.* 1986, **158**, 13.
8. G. J. Sri Vastava and O. Srivastava, *Ind. J. Phys. Nat. Sci.* 1981, **1**, 71.
9. D. A. Danilson, K. E. Webb Jr and J. H. Herbein, *J. Anim. Sci.* 1987, **64**, 842.
10. C. I. Miyagawa, *Drug Intell. Clin. Pharm.* 1986, **20**, 527.
11. P. L. Whilney and C. Tanford, *J. Biol. Chem.* 1962, **237**, 1375.
12. J. A. Gordon and W. P. Jencks, *Biochemistry* 1963, **2**, 47.
13. G. G. Hammes and J. C. Swann, *Biochemistry* 1967, **6**, 1591.
14. G. C. Ureshek and L. Bengamin, *J. Phys. Chem.* 1964, **68**, 2476.
15. M. J. Schick, *J. Phys. Chem.* 1964, **68**, 2476.
16. S. Subramanian, D. Balasubramanian and J. C. Ahluwalia, *J. Phys. Chem.* 1969, **73**, 266.
17. G. Gran, *Analyst* 1952, **77**, 661; *Anal. Chim. Acta* 1988, **206**, 111.
18. R. Sambasiva Rao, K. M. M. Krishna Prasad, A. Satyanarayana and C. Kamala Sastry, unpublished work.
19. C. Rambabu, R. Sambasiva Rao, A. Satyanaryana and P. V. Krishna Rao, *Chim. Acta Turc.* 1986, **14**, 75.
20. R. Sambasiva Rao, A. Satyanarayana and G. Nageswara Rao, unpublished work.
21. G. Nageswara Rao, K. V. Ramana and R. Sambasiva Rao, *Ind. J. Chem.* 1987, **26**, 849.
22. P. Gans, A. Sabatini and A. Vacca, *Inorg. Chim. Acta* 1976, **18**, 237.
23. E. Cassasas, N. Filekla and R. Tauler, *Anal. Chim. Acta* 1980, **191**, 399, 1413.
24. A. Braibanti, G. Mori, F. Dallavalle and B. Veroni, *Talanta* 1982, **29**, 725.
25. R. Sambasiva Rao, A. Satyanarayana, C. Rambabu and P. V. Krishna Rao, *9th Int. CODATA Conf.*, Jerusalem (1984).
26. (a) G. E. Forsethe, *J. Soc. Ind. Appl. Maths* 1957, **5**, 74; (b) B. Carnahan, H. A. Luther and J. L. Wilkes, *Applied Numerical Methods.* John Wiley, New York (1969).
27. K. A. Hartman, *J. Phys. Chem.* 1966, **70**, 270.
28. E. G. Finar, F. Franks and M. I. Tait, *J. Am. Chem. Soc.* 1972, **94**, 4424.
29. H. S. Frank and W. Y. Wen, *Disc. Faraday. Soc.* 1957, **24**, 133.
30. (a) E. S. Grant, S. E. K Fe and R. Shack, *Adv. Molec. Relax. Processes* 1972, **4**, 217; (b) U. Kattae, H. Geike and R. Potlel, *J. Phys. Chem.* 1986, **90**, 5464.
31. J. C. Owicki and H. A. Scheraga, *J. Am. Chem. Soc.* 1977, **99**, 7403.
32. P. Cristinziano, F. Lelg, P. Amodeo, G. Barona and V. Barone, *J. Chem. Soc. Faraday I* 1989, **85**, 621.
33. G. Nageswara Rao, A. Ravindrababu, S. V. V. Satyanarayana Rao, R. Sambasiva Rao, A. Satyanarayana and K. V. Ramana, *Acta Cien. Indica* 1989, **15**, 321.

Polyhedron Vol. 9, No. 20, pp. 2507–2510, 1990
Printed in Great Britain

0277–5387/90 $3.00+.00
© 1990 Pergamon Press plc

SYNTHESIS AND SPECTRAL PROPERTIES OF THE NOVEL DICATIONIC BIMETALLIC PHOSPHINE-BRIDGED COMPOUNDS $[W_2I_2(\mu\text{-L—L})(CO)_2(dppm)_2(\eta^2\text{-}MeC_2Me)_2][BF_4]_2$ {dppm = $Ph_2P(CH_2)PPh_2$; L—L = $Ph_2P(CH_2)_nPPh_2$, n = 1–6 OR $[Fe(\eta^5\text{-}C_5H_4PPh_2)_2]$}

PAUL K. BAKER* and KEVIN R. FLOWER

Department of Chemistry, University of Wales, Bangor, Gwynedd LL57 2UW, U.K.

(*Received* 5 *April* 1990; *accepted* 15 *June* 1990)

Abstract—Two equivalents of the cationic monobut-2-yne complex $[WI(CO)(NCMe)(dppm)(\eta^2\text{-}MeC_2Me)][BF_4]$ react with one equivalent of the bidentate phosphine ligands L—L {L—L = $Ph_2P(CH_2)_nPPh_2$, n = 1–6 or $[Fe(\eta^5\text{-}C_5H_4PPh_2)_2]$} in CH_2Cl_2 at room temperature, to rapidly afford the bimetallic phosphine-bridged compounds $[W_2I_2(\mu\text{-L—L})(CO)_2(dppm)_2(\eta^2\text{-}MeC_2Me)_2][BF_4]_2$ (**1–7**) in high yield. Equimolar quantities of $[WI(CO)(NCMe)(dppm)(\eta^2\text{-}MeC_2Me)][BF_4]$ and dppm react in CH_2Cl_2 at room temperature to afford a mixture of $[W_2I_2(\mu\text{-dppm})(CO)_2(dppm)_2(\eta^2\text{-}MeC_2Me)_2][BF_4]_2$, $[WI(CO)(\eta^1\text{-dppm})(dppm)(\eta^2\text{-}MeC_2Me)][BF_4]$ and unreacted dppm. ^{13}C NMR spectroscopy shows that each but-2-yne ligand in these bimetallic complexes are utilizing both their filled $p\pi$-orbitals and donating four electrons to the tungsten in these compounds.

Although the preparation and reactions of cationic alkyne complexes of molybdenum(II) and tungsten(II) have been much studied in recent years,[1–14] hitherto no examples of complexes of this type containing bimetallically bridged-phosphine ligands have been reported. Bimetallic complexes containing bridging bidentate phosphines such as $Ph_2P(CH_2)PPh_2$ (dppm) have received considerable attention in recent years; in particular by Shaw and co-workers.[15] In this paper we describe the synthesis and spectral properties of some new dicationic bimetallic phosphine-bridged alkyne compounds of the type $[W_2I_2(\mu\text{-L—L})(CO)_2(dppm)_2(\eta^2\text{-}MeC_2Me)_2][BF_4]_2$ {L—L = $Ph_2P(CH_2)_nPPh_2$, n = 1–6 and $[Fe(\eta^2\text{-}C_5H_4PPh_2)_2]$}.

EXPERIMENTAL

All reactions were carried out using standard Schlenk-line techniques. The cationic but-2-yne complex, $[WI(CO)(NCMe)(dppm)(\eta^2\text{-}MeC_2Me)][BF_4]$, was prepared by the published method.[16] All chemicals were purchased from commercial sources except dppm which was prepared by the literature method.[17] The solvent CH_2Cl_2 was dried and distilled over P_4O_{10}. Elemental analyses for carbon, hydrogen and nitrogen were determined using a Carlo Erba Elemental Analyser MOD 1106 (using helium as a carrier gas). IR spectra were recorded on a Perkin–Elmer 1430 ratio recording IR spectrophotometer. ^1H and ^{13}C NMR spectra were recorded on a Bruker AC250 CP/MAS NMR spectrometer (all spectra were calibrated against tetramethylsilane). ^{31}P NMR spectra were recorded on a Bruker WH 400 NMR spectrometer at the University of Warwick (spectra calibrated against 85% H_3PO_4).

$[W_2I_2(\mu\text{-dppm})(CO)_2(dppm)_2(\eta^2\text{-}MeC_2Me)_2][BF_4]_2$ (1)

To $[WI(CO)(NCMe)(dppm)(\eta^2\text{-}MeC_2Me)][BF_4]$ (0.5 g, 0.552 mmol) dissolved in CH_2Cl_2 (15 cm^3), with continuous stirring under a stream of dry nitrogen, was added $Ph_2P(CH_2)PPh_2$ (0.106 g, 0.276 mmol). After stirring for 5 h the solution was filtered and the solvent volume reduced to 2 cm^2 *in vacuo*. Dropwise addition of dry Et_2O precipitated the orange–brown cationic complex $[W_2I_2(\mu\text{-dppm})$

* Author to whom correspondence should be addressed.

Table 1. Physical and analytical[a] data for the complexes $[W_2I_2\{\mu\text{-L—L}\}(CO)_2(dppm)_2(\eta^2\text{-MeC}_2\text{Me})_2][BF_4]_2$

Complex	Colour	Yield (%)	Analytical data C	H
$[W_2I_2\{\mu\text{-Ph}_2\text{P(CH}_2\text{)PPh}_2\}(CO)_2(dppm)_2(\eta^2\text{-MeC}_2\text{Me})_2][BF_4]_2$ (**1**)	Orange–brown	43	48.0 (48.3)	3.6 (3.7)
$[W_2I_2\{\mu\text{-Ph}_2\text{P(CH}_2\text{)}_2\text{PPh}_2\}(CO)_2(dppm)_2(\eta^2\text{-MeC}_2\text{Me})_2][BF_4]_2$ (**2**)	Orange–brown	44	48.8 (48.6)	4.1 (3.8)
$[W_2I_2\{\mu\text{-Ph}_2\text{P(CH}_2\text{)}_3\text{PPh}_2\}(CO)_2(dppm)_2(\eta^2\text{-MeC}_2\text{Me})_2][BF_4]_2$ (**3**)	Orange–brown	42	49.2 (48.8)	4.0 (3.9)
$[W_2I_2\{\mu\text{-Ph}_2\text{P(CH}_2\text{)}_4\text{PPh}_2\}(CO)_2(dppm)_2(\eta^2\text{-MeC}_2\text{Me})_2][BF_4]_2$ (**4**)	Orange–brown	39	49.0 (49.0)	4.1 (3.9)
$[W_2I_2\{\mu\text{-Ph}_2\text{P(CH}_2\text{)}_5\text{PPh}_2\}(CO)_2(dppm)_2(\eta^2\text{-MeC}_2\text{Me})_2][BF_4]_2$ (**5**)	Orange–brown	48	49.0 (49.3)	4.1 (4.0)
$[W_2I_2\{\mu\text{-Ph}_2\text{P(CH}_2\text{)}_6\text{PPh}_2\}(CO)_2(dppm)_2(\eta^2\text{-MeC}_2\text{Me})_2][BF_4]_2$ (**6**)	Orange–brown	44	49.2 (49.5)	4.3 (4.1)
$[W_2I_2\{\mu\text{-[Fe}(\eta^5\text{-C}_5\text{H}_4\text{PPh}_2)_2]\}(CO)_2(dppm)_2(\eta^2\text{-MeC}_2\text{Me})_2][BF_4]_2$ (**7**)	Orange–brown	35	49.8 (49.4)	4.0 (3.7)

[a] Calculated values in parentheses.

$(CO)_2(dppm)_2(\eta^2\text{-MeC}_2\text{Me})_2][BF_4]_2$ (**1**), which upon recrystallization from CH_2Cl_2–Et_2O yielded 0.25 g (43%) of pure product.

Similar reactions of $[WI(CO)(NCMe)(dppm)(\eta^2\text{-MeC}_2\text{Me})][BF_4]$ with $Ph_2P(CH_2)_nPPh_2$ (n = 2–6) and $[Fe(\eta^5\text{-C}_5\text{H}_4\text{PPh}_2)_2]$ (2:1 molar ratio), in CH_2Cl_2 at room temperature, afforded the analogous cationic complexes $[W_2I_2\{\mu\text{-Ph}_2\text{P(CH}_2\text{)}_n\text{PPh}_2\}(CO)_2(dppm)_2(\eta^2\text{-MeC}_2\text{Me})_2][BF_4]_2$ and $[W_2I_2\{\mu\text{-[Fe}(\eta^5\text{-C}_5\text{H}_4\text{PPh}_2)_2]\}(CO)_2(dppm)_2(\eta^2\text{-MeC}_2\text{Me})_2][BF_4]_2$ (**2–7**) (see Table 1 for physical and analytical data).

RESULTS AND DISCUSSION

The starting material for this research is $[WI(CO)(NCMe)(dppm)(\eta^2\text{-MeC}_2\text{Me})][BF_4]$, which is prepared by reacting the neutral di-iodide compound $[WI_2(CO)(dppm)(\eta^2\text{-MeC}_2\text{Me})]$ with an equimolar amount of $Ag[BF_4]$ in acetonitrile at room temperature to afford the iodide displaced product $[WI(CO)(NCMe)(dppm)(\eta^2\text{-MeC}_2\text{Me})][BF_4]$.[16] The complex $[WI(CO)(NCMe)(dppm)(\eta^2\text{-MeC}_2\text{Me})][BF_4]$ reacts with L—L {L—L = $Ph_2P(CH_2)_nPPh_2$, n = 1–6 and $[Fe(\eta^5\text{-C}_5\text{H}_4\text{PPh}_2)_2]$} in a 2:1 molar ratio in CH_2Cl_2 at room temperature to give the novel bimetallic compounds $[W_2I_2(\mu\text{-L—L})(CO)_2(dppm)_2(\eta^2\text{-MeC}_2\text{Me})_2][BF_4]_2$ (**1–7**) in high yield. Complexes **1–7** have been fully characterized by elemental analysis (C, H and N) (Table 1), IR (Table 2), ^1H and, in selected cases, ^{13}C NMR spectroscopy (Tables 3 and 4). Complexes **1–7** are stable in the solid state when stored under nitrogen, however, they slowly decompose when exposed to air in solution. Complexes **1–7** are all moderately soluble in CH_2Cl_2 or $CHCl_3$, but they are insoluble in hydrocarbon solvents and Et_2O. The bidentate ferrocenylphosphine complex is less soluble than its $Ph_2P(CH_2)_nPPh_2$ counterparts.

The IR spectra of **1–7** showed broad, single carbonyl bands between 1955 and 1960 cm^{-1}, which would be expected since the two tungsten atoms in **1–7** are well separated by phosphine and carbon linkages. The IR spectra also show weak $\nu(C{\equiv}C)$ alkyne stretching bands at a considerably lower wavenumber compared with free but-2-yne, which

Table 2. IR data[a] for the compounds $[W_2I_2(\mu\text{-L—L})(CO)_2(dppm)_2(\eta^2\text{-MeC}_2\text{Me})_2][BF_4]_2$

Complex	$\nu(C{\equiv}O)$ cm^{-1}	$\nu(C{\equiv}C)$ cm^{-1}
1	1955 (s)	—
2	1960 (s)	—
3	1960 (s)	1630 (vw)
4	1955 (s)	1635 (vw)
5	1960 (s)	1635 (vw)
6	1955 (s)	1630 (vw)
7	1956 (s)	1620 (vw)

[a] Spectra recorded in $CHCl_3$ as thin films between NaCl plates. s, strong; vw, very weak.

Table 3. ^{1}H NMR data for the compounds $[W_2I_2(\mu\text{-L—L})(CO)_2(dppm)_2(\eta^2\text{-MeC}_2\text{Me})_2][BF_4]_2$

Complex	^{1}H (δ) ppm
1	8.09–6.5 (m, 60H, Ph); 5.55 (bm, 4H, PCH_2P); 4.73 (bm, 2H, PCH_2P); 2.58, 2.4, 2.35, 2.25 (4 × s, 12H, ≡C*Me*)
2	8.22–6.85 (m, 60H, Ph), 4.85 (bm, 4H, PCH_2P); 3.01, 2.76, 2.57, 2.46, (4 × s, 12H, ≡C*Me*); 2.15 (bm, 4H, PCH_2)
3	8.08–6.51 (m, 60H, Ph); 4.85 (bm, 4H, PCH_2P); 3.0, 2.61, 2.46, 2.2 (4 × s, 12H, ≡C*Me*); 2.0 (bm, 6H, CH_2)
4	7.84–6.79 (m, 60H, Ph), 4.8 (bm, 4H, PCH_2P); 3.0 2.61, 2.46, (3 × s, 12H, ≡C*Me*); 1.69 (bm, 8H, CH_2)
5	7.84–6.8 (m, 60H, Ph); 4.85 (bm, 4H, PCH_2P); 3.0, 2.58, 2.49, (3 × s, 12H, ≡C*Me*); 1.60 (bm, 10H, CH_2)
6	8.2–6.73 (m, 60H, Ph); 4.83 (bm, 4H, PCH_2P); 3.0, 2.6, 2.46, 2.38 (4 × s, 12H, ≡C*Me*); 1.68–1.30 (bm, 12H, CH_2)
7	8.2–6.73 (m, 60H, Ph); 4.88 (bm, 4H, PCH_2P); 4.6, 4.32, 4.29 (3 × s, 8H, Cp-*H*); 3.0, 2.76, 2.52 (3 × s, 12H, ≡C*Me*)

[a] Spectra recorded in $CDCl_3$ (+25°C) referenced to $SiMe_4$. s, singlet; m, multiplet; bm, broad multiplet.

is due to back donation of electron density from filled metal *d*-type orbitals into empty π^*-orbitals of the but-2-yne. Strong, broad bands at ~ 1020 cm^{-1}, ν(BF), are also observed in the IR spectra of **1–7** due to the tetrafluoroborate anion.[18]

The ^{1}H and ^{13}C NMR spectra of **1–7** show there to be a number of isomers in solution. Unsuccessful attempts were made to grow suitable single crystals of **1–7** for X-ray crystallography. One likely structure of **1–7** is shown in Fig. 1, which has iodide *trans*- to a but-2-yne ligand on each tungsten atom. The X-ray crystal structures of [WI(CO)L(dppm)(η^2-MeC_2Me)]$^+$ [L = P(O^{i}Pr)$_3$[16] and $SC(NH_2)_2$[19]] have been determined and have the geometry displayed in Fig. 1, where each of the phosphine atoms of the bidentate bridging phosphine have replaced the tri-isopropylphosphite and thiourea ligands in [WI(CO)L(dppm)(η^2-MeC_2Me)]$^+$ to give the bridging complexes $[W_2I_2(\mu\text{-L—L})(CO)_2(dppm)_2(\eta^2\text{-MeC}_2\text{Me})_2][BF_4]_2$.

The reactions of two equivalents of [WI(CO)(NCMe)(dppm)(η^2-MeC_2Me)][BF_4] with one equivalent of L—L {L—L = $Ph_2P(CH_2)_nPPh_2$, n = 1–6 and [Fe(η^5-$C_5H_4PPh_2)_2$]} must initially afford a monodentate phosphine complex of the type [WI(CO)(η^1-L—L)(dppm)(η^2-MeC_2Me)][BF_4] which rather than displacing an iodide to give the dicationic complexes of the type [W(CO)(dppm){$PPh_2(CH_2)_nPPh_2$}(η^2-MeC_2Me)][BF_4]I, the free end of the phosphine reacts with another equivalent of [WI(CO)(NCMe)(dppm)(η^2-MeC_2Me)][BF_4] to give the bimetallic phosphine-bridged compounds **1–7**. It is interesting to note that reaction of the more electron rich and sterically constrained bidentate nitrogen donor ligands N—N (N—N = 2,2′-bipyridine, 1,10-phenanthroline, etc.) with an equimolar amount of [WI(CO)(NCMe)(dppm)(η^2-MeC_2Me)][BF_4] gave the dicationic complexes [W(CO)(N—N)(dppm)(η^2-MeC_2Me)][BF_4]I.[20]

Equimolar quantities of [WI(CO)(NCMe)(dppm)(η^2-MeC_2Me)][BF_4] and dppm shows the series of resonances due to **1**, a single resonance at δ = −21.53 ppm due to uncoordinated dppm. There is also an additional set of low intensity resonances which is likely to be due to the monodentate coordinated complex [WI(CO)(η^1-dppm)(dppm)(η^2-MeC_2Me)][BF_4]. There is com-

Table 4. ^{13}C NMR data for the complex $[W_2I_2(\mu\text{-L—L})(CO)_2(dppm)_2(\eta^2\text{-MeC}_2\text{Me})_2][BF_4]_2$

Complex	^{13}C (δ) ppm
2	229.86, 224.76, 219.98, 219.5, 216.96 (5 × s, *C*≡*C*); 205.85, 202.0, 201.9 (3 × s, C≡O); 137.6–126.29 (m, Ph); 32.3 (bm, PCH_2P); 28.7 (bm, PCH_2); 22.6, 22.4, 21.9, 20.96 (4 × s, ≡C*Me*)
3	222.94, 221.0 (2 × s, *C*≡*C*); 191.64 (s, C≡O); 138.49–126.3 (m, Ph); 31.7–22.04 (m, PCH_2, CH_2); 18.95, 17.23, 16.26 (3 × s, ≡C*Me*)
5	222.88, 222.4, 221.75, 219.22 (4 × s, *C*≡*C*); 212.35, 208.7, (2 × s, C≡O); 135.4, 126.6 (m, Ph); 33.02–23.03 (m, PCH_2P, PCH_2, CH_2); 19.41, 18.26, 17.88, 16.94, (4 × s, ≡C*Me*)

[a] Spectra recorded in $CDCl_3$ (+25°C) referenced to $SiMe_4$. s, singlet; t, triplet; m, multiplet; b, broad.

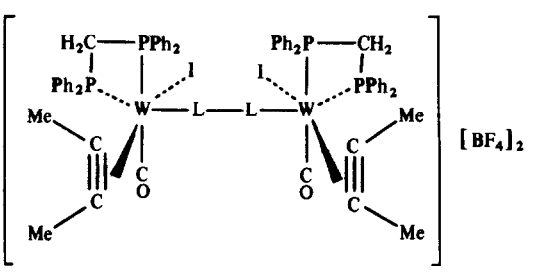

Fig. 1. One possible structure of the bimetallic complexes $[W_2I_2(\mu\text{-L—L})(CO)_2(dppm)_2(\eta^2\text{-MeC}_2\text{Me})_2][BF_4]_2$.

petition from [WI(CO)(NCMe)(dppm)(η^2-MeC_2Me)][BF_4] for both dppm and [WI(CO)(η^1-dppm)(dppm)(η^2-MeC_2Me)][BF_4]. Whereas when a pure sample of **1** is reacted with one equivalent of dppm the ^{31}P NMR spectrum of this mixture displayed only resonances for **1** and free dppm at $\delta = -21.53$ ppm.

The ^{13}C NMR spectra of **2**, **3** and **5** showed a number of resonances above 200 ppm due to both carbonyl ligands and alkyne contact carbon atoms, which again suggests the existence of several isomers in solution. Alkyne contact carbon resonances above 200 ppm indicate[21] that the but-2-yne ligands are utilizing both their filled $p\pi$-orbitals and are formally donating four-electrons each to the tungsten atoms in these compounds.

Acknowledgements—We thank Dr O. W. Howarth for measuring several ^{31}P NMR spectra at the University of Warwick and we thank the SERC for support.

REFERENCES

1. M. Bottrill and M. Green, *J. Chem. Soc., Dalton Trans.* 1977, 2365.
2. C. T. Lam, P. W. R. Corfield and S. J. Lippard, *J. Am. Chem. Soc.* 1977, **99**, 617.
3. W. Beck and K. Schloter, *Z. Naturfor.* 1978, **33B**, 1214.
4. P. L. Watson and R. G. Bergman, *J. Am. Chem. Soc.* 1980, **102**, 2698.
5. K. Sünkel, U. Nagel and W. Beck, *J. Organomet. Chem.* 1981, **222**, 251.
6. S. R. Allen, P. K. Baker, S. G. Barnes, M. Green, L. Trollope, L. M. Muir and K. W. Muir, *J. Chem. Soc., Dalton Trans.* 1981, 873.
7. C. Caravana, C. M. Giandomenico and S. J. Lippard, *Inorg. Chem.* 1982, **21**, 1860.
8. J. C. Jeffery, J. C. V. Laurie, I. Moore and F. G. A. Stone, *J. Organomet. Chem.* 1983, **258**, C37.
9. F. R. Kreissl, W. Sieber and W. Wolfgruber, *Angew. Chem. Int. Edn Engl.* 1983, **22**, 493.
10. K. R. Birdwhistell, T. L. Tonker and J. L. Templeton, *J. Am. Chem. Soc.* 1985, **107**, 4474.
11. M. Green, *Polyhedron* 1986, **5**, 427.
12. M. Green, *J. Organomet. Chem.* 1986, **300**, 93.
13. H. P. Kim, S. Kim, R. A. Jacobson and R. J. Angelici, *Organometallics* 1986, **5**, 2481.
14. P. K. Baker, E. M. Armstrong and M. G. B. Drew, *Inorg. Chem.* 1988, **27**, 2287.
15. (a) A. Blagg, A. T. Hutton, P. G. Pringle and B. L. Shaw, *J. Chem. Soc., Dalton Trans.* 1984, 1815; (b) F. S. M. Hassan, D. P. Markham, P. G. Pringle and B. L. Shaw, *J. Chem. Soc., Dalton Trans.* 1985, 279; (c) J. A. Iggo and B. L. Shaw, *J. Chem. Soc., Dalton Trans.* 1985, 1009; (d) A. Blagg and B. L. Shaw, *J. Chem. Soc., Dalton Trans.* 1987, 221; (e) A. Blagg, B. L. Shaw and M. Thornton-Pett, *J. Chem. Soc., Dalton Trans.* 1987, 769; (f) G. B. Jacobsen, B. L. Shaw and M. Thornton-Pett, *J. Chem. Soc., Dalton Trans.* 1987, 1489; (g) A. Blagg, P. G. Pringle and B. L. Shaw, *J. Chem. Soc., Dalton Trans.* 1987, 1489; (h) G. B. Jacobsen, B. L. Shaw and M. Thornton-Pett, *J. Chem. Soc., Dalton Trans.* 1987, 1509; (i) A. Blagg, R. Robson, B. L. Shaw and M. Thornton-Pett, *J. Chem. Soc., Dalton Trans.* 1987, 2171.
16. P. K. Baker, K. R. Flower, M. G. B. Drew and G. Forsyth, *J. Chem. Soc., Dalton Trans.* 1989, 1903.
17. V. K. Sommer, *Z. Anorg. Allg. Chem.* 1970, **376**, 37.
18. K. Nakamoto, *Infrared Spectra of Inorganic and Coordination Compounds*. John Wiley, New York (1963).
19. P. K. Baker, K. R. Flower, P. A. Bates and M. B. Hursthouse, *J. Organomet. Chem.* 1989, **372**, 263.
20. P. K. Baker and K. R. Flower, unpublished results.
21. J. L. Templeton and B. C. Ward, *J. Am. Chem. Soc.* 1980, **102**, 3288.

Polyhedron Vol. 9, No. 20, pp. 2511–2516, 1990
Printed in Great Britain

0277–5387/90 $3.00+.00
© 1990 Pergamon Press plc

OCTAHEDRAL METAL CARBONYLS—LXXIII.† DISPLACEMENT OF AROMATIC SOLVENTS (SOLV) FROM (SOLV)$Cr(CO)_5$ COMPLEXES GENERATED AFTER FLASH PHOTOLYSIS: MODES OF BONDING AND MECHANISM

SHULIN ZHANG and GERARD R. DOBSON‡

Department of Chemistry and Center for Organometallic Research,
University of North Texas, Denton, TX 76203-5068, U.S.A.

(*Received* 23 *March* 1990; *accepted* 15 *June* 1990)

Abstract—Rates of solvent displacement by 1-hexane (hex) from 17 (solv)$Cr(CO)_5$ transients generated after pulsed laser flash photolysis (solv = aromatic solvent, $C_6H_{6-n}X_n$; X = alkyl, perfluoroalkyl (R, R_f); F, Cl, Br; n = 0–4),

$$(\text{solv})Cr(CO)_5 + \text{hex} \longrightarrow (\eta^2\text{-hex})Cr(CO)_5 + \text{solv},$$

have been determined. Analyses of the rate constants in terms of the steric and electronic properties of solv indicate that the rections take place via initial slow fission of a solv—Cr bond. The data also indicate that for R, R_f and F substituents, solv is coordinated to Cr "edge on" via an isolated C=C bond, while for solv which contain Cl and Br substituents, coordination to Cr takes place through halogenic lone pairs. Aside from influences of the mode of coordination of solv to Cr, rates increase with increasing electron-withdrawing properties and increasing steric bulk of the substituents.

Recent studies have begun to provide an understanding of solvation–desolvation reactions taking place after flash photolyisis of metal carbonyls; in these studies, $Cr(CO)_6$ has been the exemplar. Thus, several groups have investigated the very rapid solvation reactions which take place after coordinatively-unsaturated [$Cr(CO)_5$] is produced,[1] and others have studied the strengths of Cr—alkane bonds by time-resolved photoacoustic calor imetry.[2,3] Still other studies have focused attention on the rates and mechanisms of displacement of solvent molecules such as alkanes,[2,4,5] benzene[6] and chlorobenzene[7] from (solvent)$Cr(CO)_5$ molecules by Lewis bases [L; eq. (1)]:

$$(\text{solvent})Cr(CO)_5 + L \longrightarrow LCr(CO)_5 + \text{solvent}. \quad (1)$$

In this last regard it is interesting to note that evidence suggests two solvent displacement mechanisms [eq. (2)] to be operative. For (*n*-heptane)$Cr(CO)_5$, in which *n*-heptane is coordinated to Cr via an "agostic"[8] C—H—Cr interaction, both the interchange pathway (2a) and the dissociative pathway (2b) have been found to be assessible,[2,4] while for benzene[6] and chlorobenzene[7] as solvents the dissociative pathway is much more pronounced. Moreover, for these last two solvents, modes of bonding also may differ. Thus, strong evidence has been presented which supports coordination of benzene via an "edge-on", isolated double bond.[6] On the other hand, the mode of bonding of chlorobenzene to Group VI-B metals, whether "edge-on" or via coordination through a lone pair of electrons on Cl, has been the subject of some discussion;[9] X-ray structural studies have shown both modes of bonding of substituted benzenes, "edge-on",[10] and coordinate, through a halogenic lone pair,[11] to take place.

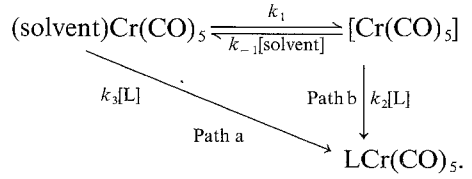

(2)

† Part LXXII: S. Zhang and G. R. Dobson, *J. Organomet. Chem.*, in press.

‡ Author to whom correspondence should be addressed.

All these observations have prompted a broader investigation of solvent displacement reactions of (solv)$Cr(CO)_5$ complexes according to eq. (1), where solv are aromatic hydrocarbons containing zero or more alkyl, perfluoromethyl, F, Cl or Br substituents and L = 1-hexene. It was of particular interest to study changes in rates of solv displacement from (solv)$Cr(CO)_5$ as a function of the steric and electronic nature of the aromatic solvents since, where linear free energy relationships are observed to exist, it may be concluded that reactions are mechanistically similar.

EXPERIMENTAL

Materials

Chromium hexacarbonyl (Pressure Chemical Co.) was vacuum sublimed before use. Benzene and toluene (Mallinckrodt), *t*-butylbenzene (Eastman), cyclohexylbenzene, cumene, ethylbenzene, 1,2,3,4-tetramethylbenzene, *o*-xylene and *m*-xylene (Aldrich), and mesitylene (Fisher) were all fractionally distilled from sodium under nitrogen. α,α,α-Trifluorotoluene, *o*-bromofluorobenzene and *p*-xylene (Lancaster Synthesis), bromobenzene (Matheson), and chlorobenzene, *o*-dichlorobenzene and fluorobenzene (Aldrich) were fractionally distilled from P_4O_{10} under nitrogen. 1-Hexene (Aldrich) was fractionally distilled from anhydrous $MgSO_4$.

Flash photolysis studies

Flash photolysis studies were carried out employing equipment previously described,[12] except that either a Lumonics TE-430 ($Xe/F_2/He$ gas fill, 351 nm, 10 ns FWHI, 25 mJ/pulse maximum energy) or Tachisto 800 ($Xe/F_2/He$ gas fill, 20 ns FWHI, 200 mJ/pulse maximum energy) excimer laser was employed as the photolysis source. Typically, solutions *ca* 3.5×10^{-3} M in $Cr(CO)_6$, containing at least a 100-fold excess of the 1-hexene "trap" in the aromatic solvent, were employed so that pseudo-first-order reaction conditions were obtained. The observation wavelength was 490 nm, which monitored the disappearance of (solv)$Cr(CO)_5$; the temperature was maintained at 25.00(5)°C through the use of a jacketed cell and an external circulating bath. Depending upon the signal-to-noise ratio observed for a given solvent, pseudo-first-order rate constants obtained from plots of $\ln(A_t-A_\infty)$ vs time were determined from the averages of from one to 10 traces. No significant differences were observed for individual traces obtained after the first or after subsequent flashes, an observation which indicates that flash photolysis of (1-hexene)$Cr(CO)_5$ affords the same photolysis product as does $Cr(CO)_6$, i.e. $[Cr(CO)_5]$. Rate constants were determined employing at least four sets of data taken at different concentrations of 1-hexene. The data were analysed employing in-house, Asyst©-based computer programs designed for the laboratory's 286-based microcomputer. Limits of error are given in parentheses as the uncertainty of the last digit(s) of the cited value to one standard deviation.

RESULTS AND DISCUSSION

Evidence has strongly indicated that the reactions taking place after pulsed laser flash photolysis of $Cr(CO)_6$/bz/hex solutions (bz = benzene; hex = 1-hexene) proceed according to eq. (3):[6]

$$Cr(CO)_6 \xrightarrow[+bz]{h\nu} (bz)Cr(CO)_5 \xrightarrow{+hex} (\eta^2\text{-hex})Cr(CO)_5. \tag{3}$$

Rate data for this reaction obtained over very wide concentration ranges of bz (the solvent) and hex (the "trapping agent"), to [hex] = *ca* 6 M, obey the rate law

$$-d[(bz)Cr(CO)_5]/dt = \frac{k[(bz)Cr(CO)_5][hex]}{[bz]+k'[hex]}. \tag{4}$$

Since [bz], [hex] ≫ $[(bz)Cr(CO)_5]$ (Experimental),

$$k_{obs} = k[hex]/([bz]+k'[hex]). \tag{5}$$

This rate law was interpreted in terms of a dissociative mechanism for benzene displacement, eq. (6):

$$\begin{array}{l} (bz)Cr(CO)_5 \underset{k_{-1}[bz]}{\overset{k_1}{\rightleftharpoons}} [Cr(CO)_5] \\ \qquad\qquad\qquad\qquad \Big\downarrow k_2[hex] \\ \qquad\qquad\qquad\qquad (\eta^2\text{-hex})Cr(CO)_5. \end{array} \tag{6}$$

For this mechanism, assuming a steady-state concentration of $[Cr(CO)_5]$, k [eq. (5)] = k_1k_2/k_{-1} and $k' = k_2/k_{-1}$.

It is reasonable to assume (for the present) that the mechanism given in eq. (6) also applies to other aromatic solvents, such as those investigated here. Under the reaction conditions employed in the present study, [hex] ≪ [solv], and since it has been observed for benzene that $k' < 1$ (*vide infra*), [solv] ≫ k'[hex]. It is also to be noted, since [solv] ≫ [hex], that [solv] will be approximately constant as [hex] is varied, and thus that [solv] ≃ $[solv]_0$, the concentration of the pure solvent. Under these

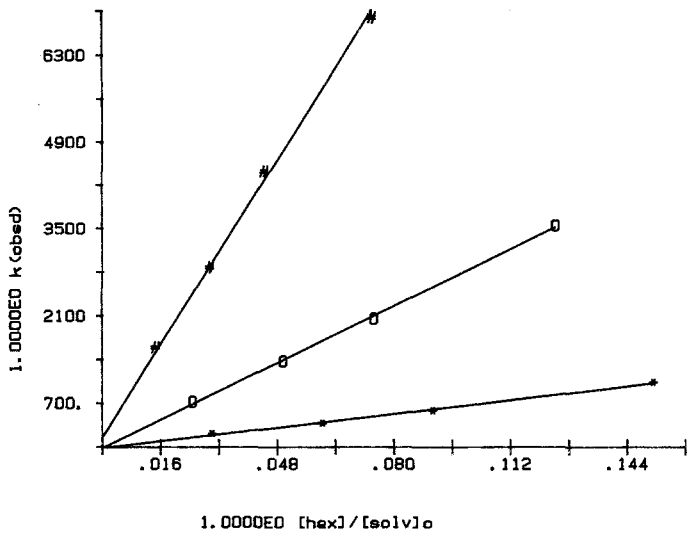

Fig. 1. Plots of k_{obs} vs [hex]/[solv]$_0$ for reactions of (solv)Cr(CO)$_5$ complexes with hex at 25°C (solv = aromatic solvent; hex = 1-hexene). #: solv = cumene; ○: solv = *o*-xylene; *: solv = 1,2,3,4-tetramethylbenzene.

conditions, eq. (5) becomes,

$$k_{obs} \simeq k([hex]/[solv]_0), \quad (7)$$

and plots of the pseudo-first-order rate constants, k_{obs}, vs [hex]/[solv]$_0$ will afford the rate constants, k ($= k_1k_2/k_{-1}$).

Figure 1 exhibits plots of k_{obs} vs [hex]/[solv]$_0$ for three representative solv (cumene, *o*-xylene and 1,2,3,4-tetramethylbenzene) which demonstrate the adherence of these reactions to the rate law given in eq. (7); the other solvents studied also obey this rate law. The rate constants, k, determined at 25.0°C for 17 solv, are presented in Table 1.

For the mechanism shown in eq. (6), of the rate constants which comprise k ($= k_1k_2/k_{-1}$), k_2, the rate constant for interaction of [Cr(CO)$_5$] with hex, is the same for all solvents. Thus, observed changes in rate are attributable to changes in k_1/k_{-1}, the equilibrium constant for desolvation; however, both these rate constants, k_1 and k_{-1}, should be

Table 1. Rate constants for displacement of aromatic solvents from photogenerated (solv)Cr(CO)$_5$ complexes

Number	Solvent	$10^{-4}k$ (s^{-1})
1	α,α,α-Trifluorotoluene, $C_6H_5CF_3$	550(57)
2	Fluorobenzene, C_6H_5F	106(4)
3	Benzene, C_6H_6	12.2(11)
4	Cumene, $C_6H_5CH(CH_3)_2$	8.84(29)
5	Mesitylene, 1,3,5-$C_6H_3(CH_3)_3$	7.69(22)
6	Ethylbenzene, $C_6H_5CH_2CH_3$	7.27(16)
7	*t*-Butylbenzene, $C_6H_5C(CH_3)_3$	6.85(26)
8	*o*-Dichlorobenzene, *o*-$C_6H_4Cl_2$	6.57(18)
9	Cyclohexylbenzene, C_6H_5(*c*-C_6H_{11})	6.05(47)
10	Toluene, $C_6H_5CH_3$	4.32(40)
11	Chlorobenzene, C_6H_5Cl	3.75(7)
12	*m*-Xylene, *m*-$C_6H_4(CH_3)_2$	2.85(6)
13	*p*-Xylene, *p*-$C_6H_4(CH_3)_2$	2.45(8)
14	*o*-Xylene, *o*-$C_6H_4(CH_3)_2$	2.16(1)
15	*o*-Bromofluorobenzene, *o*-C_6H_4BrF	0.915(18)
16	1,2,3,4-Tetramethylbenzene, 1,2,3,4-$C_6H_2(CH_3)_4$	0.684(27)
17	Bromobenzene, C_6H_5Br	0.30(3)

influenced by the steric and electronic properties of solv.

The value of k_{-1}, the rate constant for interaction of solv with $[Cr(CO)_5]$, is expected to be very large since available data indicate that solvation of photogenerated $[Cr(CO)_5]$ takes place on the ps–fs time-scale.[2] Thus there should be little solv—Cr bond-making in attaining the transition state, and consequently there is expected to be relatively little influence of k_{-1} on k among various solv. Thus, differences in the values for k, which vary by some 1750-fold, will be determined largely by differences in k_1, the rate constants for solv dissociation.

Turning first to consideration of the data for benzene and nine monosubstituted aromatic solvents (1–4, 6, 7, 9–11, 17; Table 1), rates have been correlated with the "aromatic" substituent constants, σ_m, σ_p and MR, presented by Hansch and co-workers.[13] Bearing in mind that evidence strongly suggests that in $(bz)Cr(CO)_5$, bz is bonded to Cr "edge-on" through a C=C bond[6] and that σ_m and σ_p are electronic substituent constants for adjacent carbons, the sums of these $(\sigma_m+\sigma_p)$ are taken as the electronic substituent constants, E, used for this study. The MR values, taken from molar refractivity data,[14] have been used to represent steric influences. The electronic and steric substituent constants, E and MR respectively, are presented in Table 2. The observed second-order rate constants, k (eq. 7), were correlated with E and MR for the aromatic solvents 1–4, 6, 7, 9–11, 17, through use of the equation:

$$\log k = aE+b(MR)+c, \qquad (8)$$

employing a multilinear regression. This fit afforded a correlation coefficient, R, of 0.072. With the exclusion of the rate constants for arenes 11 and 17 (chlorobenzene and bromobenzene), this fit improves to $R = 0.979$ and obeys eq. (9):

$$\log k = 1.70E+0.069(MR)+5.14. \qquad (9)$$

Equation (9) indicates that rate constants for displacement of monosubstituted aromatic solvents from their $(solv)Cr(CO)_5$ complexes increase with the increasing charge-withdrawing properties of the substituent and also with increasing substituent bulk. On this basis, the rates of dissociation of chlorobenzene and bromobenzene are abnormally slow. Figure 2 exhibits a plot of $\log(k_{calc}-k_{exp})$ vs E, MR. The "spikes" (both positive and negative) thus represent differences between the experimentally-determined rate constants, k_{exp}, and the rate constants calculated by employing eq. (9), k_{calc}. The figure clearly demonstrates the good fit for the rate constants for solv 1–4, 6, 7, 9 and 10, and the poor fit of k for solv 11 and 17, chlorobenzene (CB) and bromobenzene, to eq. (9).

Table 2. Aromatic substituent constants[13]

Substituent (—X)	σ_m	σ_p	E $(=\sigma_m+\sigma_p)$	MR
$-CF_3$	0.42	0.54	0.97	5.02
—F	0.34	0.06	0.40	0.92
$-CH(CH_3)_2$	−0.07	−0.15	−0.22	14.98
—H	0.00	0.00	0.00	1.03
$-C(CH_3)_3$	−0.10	−0.20	−0.30	19.62
$-C_6H_{11}$	−0.07[a]	−0.22	−0.29	26.69
$-CH_2CH_3$	−0.07	−0.15	−0.22	10.3
$-CH_3$	−0.07	−0.17	−0.24	5.65
—Cl	0.37	0.23	0.60	6.03
—Br	0.39	0.23	0.62	8.88

[a] This value is not available in ref. 13; it is assumed to be the same as that for $-CH(CH_3)_2$.

The good correlation of the data for the aromatic solvents 1–4, 6, 7, 9 and 10 indicates that the displacement of each solv in this group from its $(solv)Cr(CO)_5$ complex is mechanistically similar and that coordination of each solv to Cr also is similar in nature. This group of solv includes bz, which is displaced from $(bz)Cr(CO)_5$ via the mechanism shown in eq. (6), and which is coordinated "edge-on" to Cr.[6]

Chlorobenzene also is displaced from its $(CB)Cr(CO)_5$ complex via a dissociative mechanism;[7] the much slower rates of displacement of chlorobenzene and bromobenzene thus are not related to mechanistic differences; they instead are most reasonably attributable to a different mode of bonding to Cr of these solvents, via lone pairs on the halogen atoms rather than through "edge-on" olefinic bonding. This mode of bonding has been widely observed in a number of related systems (*vide supra*).[11]

This supposition was further probed through determination of the rate of displacement of *n*-butyl chloride (BC) by hex from photogenerated $(BC)Cr(CO)_5$. This rate (k, [eq. (7)] $= 2.27(8)\times10^3$ s^{-1}), is slower than is the rate of displacement of CB, as is expected on the basis of the electron-withdrawing nature of $-C_6H_5$ relative to that of $-C_4H_9$, a trend consistent with a similar mode of bonding of both CB and BC to Cr. *n*-Butyl chloride, being aliphatic, *must* bond to Cr via a lone pair of electrons on Cl, since solvents coordinating via a C—H—Cr "agostic" interaction are much more susceptible to solvent displacement.[2,4,5]

On the other hand, fluorobenzene (FB) is a member of the group of eight aromatic solvents which

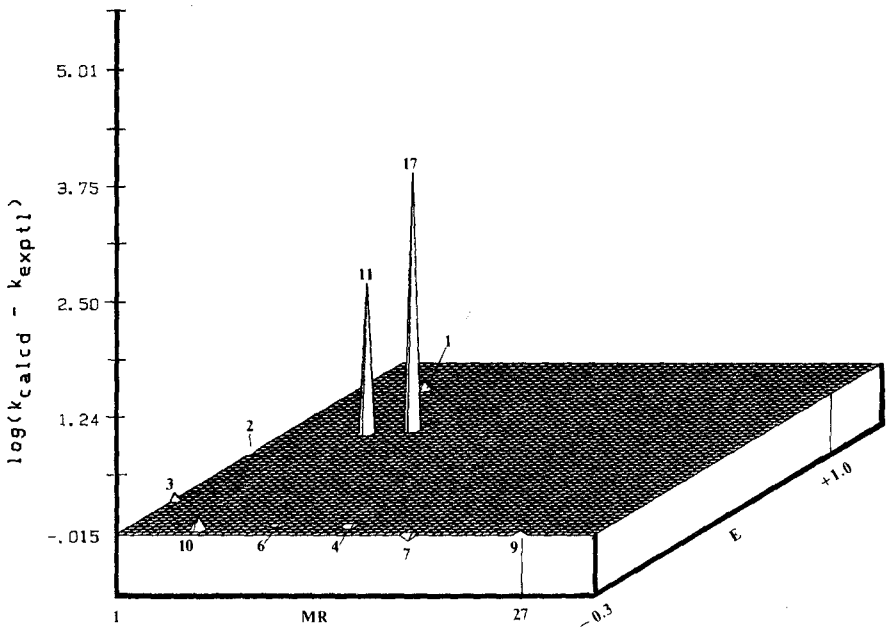

Fig. 2. Plot of $\log(k_{calc}-k_{exp})$ vs E, MR, the electronic and steric parameters (Table 2) for 10 aromatic solvents: 1—α,α,α-trifluorotoluene; 2—fluorobenzene; 3—benzene; 4—cumene; 6—ethylbenzene; 7—*t*-butylbenzene; 9—cyclohexylbenzene; 10—toluene; 11—chlorobenzene; 17—bromobenzene. The numbers refer to Table 1.

the evidence presented above indicates are bonded to Cr via an isolated C=C bond. Oishi has presented evidence which he interprets as indicative of a similar mode of bonding of FB to Cr in (η^6-anisole)(η^2-FB)$Cr(CO)_2$ produced upon photolysis of (η^6-anisole)$Cr(CO)_3$ in FB solution.[15] The "change-over" in the mode of bonding from F to Cl is reasonably attributable to the decrease in electronegativity of X along the series F, Cl, Br; a decrease which would be expected to produce an increase in the coordinating ability of X. Note in this regard (Table 1) that a 12-fold increase in the rate of displacement of solv is observed for chlorobenzene vs bromobenzene.

Relative rates observed for the displacement of aromatic solvents from their (solv)$Cr(CO)_5$ complexes containing the series of five halogenated benzenes (2, 8, 11, 15, 17; Table 1) also are consistent with coordination of Cl and Br to the metal in disubstituted solv containing these substituents (8, 15). As would be expected, these rates increase with the increasing electron-withdrawing abilities of the halogens, i.e. as the coordinating abilities of X decrease.

From Table 1 it can be seen that the solv studied also includes a series of six methyl-substituted benzenes (5, 10, 12–14, 16). It is noted, with the exception of mesitylene, that the rates decrease from that observed for benzene with increasing methyl-substitution, as expected based upon the electron-releasing nature of methyl substituents relative to H and "edge-on" C=C bonding to Cr. The faster rate observed for mesitylene suggests that coordination of arenes to the metal takes place preferentially at an " unsubstituted" double bond in which there is less steric crowding, a bond which mesitylene, alone of these six solv, does not possess. Employing 2 E and 2 MR for the two methyl groups in xylene molecules and eq. (9), the best agreement between the calculated and experimentally-determined rate constants, k_{calc} and k_{exp}, is for *p*-xylene (2.6×10^4 s^{-1} in each case) which suggests Cr–arene bond formation involving the unsubstituted *o*- and *m*-carbons.

Acknowledgements—The financial support of this research by the National Science Foundation (CHE-8800127) is gratefully acknowledged. We thank Texas Instruments, Inc. for the generous gift of the Tachisto excimer laser.

REFERENCES

1. (a) J. A. Welch, K. S. Peters and V. Vaida, *J. Phys. Chem.* 1982, **68**, 1941; (b) J. D. Simon and K. S. Peters, *Chem. Phys. Lett.* 1983, **68**, 53; (c) J. D. Simon and X. Xie, *J. Phys. Chem.* 1986, **90**, 6751; (d) J. D. Simon and X. Xie, *J. Phys. Chem.* 1987, **91**, 5538; (e) L. Wang, X. Zhu and K. G. Spears, *J. Am. Chem. Soc.* 1988, **110**, 8695; (f) L. Wang, X. Zhu and K. G. Spears, *J. Phys. Chem.* 1989, **93**, 2; (g)

J. D. Simon and X. Xie, *J. Phys. Chem.* 1989, **93**, 291; (h) A. G. Joly and K. A. Nelson, *J. Phys. Chem.* 1989, **93**, 2876.
2. G. K. Yang, V. Vaida and K. S. Peters, *Polyhedron* 1988, **7**, 1619.
3. J. Morse, G. Parker and T. J. Burkey, *Organometallics* 1989, **7**, 2471.
4. S. Zhang and G. R. Dobson, *Inorg. Chim. Acta* 1989, **165**, L11.
5. (a) J. M. Kelly, D. V. Bent, H. Herrmann, D. Schulte-Frohlinde and E. A. Koerner von Gustorf, *J. Organomet. Chem.* 1974, **69**, 259; (b) R. Bonneau and J. M. Kelly, *J. Am. Chem. Soc.* 1980, **102**, 1220; (c) J. M. Kelly, C. Long and R. Bonneau, *J. Phys. Chem.* 1983, **87**, 3344.
6. S. Zhang, V. Zang, H. C. Bajaj, G. R. Dobson and R. van Eldik, *Inorg. Chem.*, in press.
7. G. R. Dobson and S. Zhang, *J. Coord. Chem.* 1990, **21**, 155.
8. M. Brookhart and M. L. H. Green, *J. Organomet. Chem.* 1983, **250**, 395.
9. S. Zhang and G. R. Dobson, *Inorg. Chem.* 1990, **29**, 598.
10. (a) J. Browning, M. Green, B. R. Penfold, J. Spencer and F. G. A. Stone, *J. Chem. Soc., Chem. Commun.* 1973, 31; (b) J. Browning and J. R. Penfold, *J. Cryst. Molec. Struct.* 1974, **4**, 335; (c) R. E. Cobbledick and F. W. B. Einstein, *Acta Cryst.* 1978, **B34**, 1849; (d) J. R. Sweet and W. A. G. Graham, *J. Am. Chem. Soc.* 1983, **105**, 305; (e) H. van der Heijden, A. G. Orpen and P. Pasman, *J. Chem. Soc., Chem. Commun.* 1985, 1576; (f) S. T. Belt, S. B. Duckett and R. N. Perutz, *J. Chem. Soc., Chem. Commun.* 1989, 928; (g) W. D. Jones and L. Dong, *J. Am. Chem. Soc.* 1989, **111**, 8722.
11. (a) D. N. Lawson, J. A. Osborn and G. Wilkinson, *J. Chem. Soc. A* 1966, 1733; (b) R. H. Crabtree, J. W. Faller, M. F. Mellea and J. M. Quirk, *Organometallics* 1982, **1**, 1361; (c) R. Uson, J. Fornies, M. Tomas, F. A. Cotton and L. R. Falvello, *J. Am. Chem. Soc.* 1984, **106**, 2482; (d) R. H. Crabtree, M. F. Mellea and J. M. Quirk, *J. Am. Chem. Soc.* 1984, **106**, 3913; (e) M. J. Burk, R. H. Crabtree and E. M. Holt, *Organometallics* 1984, **3**, 638; (f) F. L. Barcelo, P. Lahuerta, M. A. Ubeda, C. Foces-Foces, F. H. Cano and M. Martinez-Ripoll, *J. Chem. Soc., Chem. Commun.* 1985, 43; (g) X. Solans, M. Font-Altaba, M. Aguilo, C. Miratvilles, J. Besteiro and P. Lahuerta, *Cryst. Struct. Commun.* 1985, **C41**, 841; (h) F. A. Cotton, P. Lahuerta, M. Sanau, W. Schwotzer and I. Solana, *Inorg. Chem.* 1986, **25**, 3526; (i) F. L. Barcelo, F. A. Cotton, P. Lahuerta, R. Llusar, M. Sanau, W. Schwotzer and M. Ubeda, *Organometallics* 1986, **5**, 808; (j) M. J. Burk, B. Seegmuller and R. H. Crabtree, *Organometallics* 1986, **6**, 2241; (k) F. J. Liotta, Jr, G. Van Duyne and B. K. Carpenter, *Organometallics* 1987, **6**, 1010; (l) F. L. Barcelo, F. A. Cotton, P. Lahuerta, M. Sanau, W. Schwotzer and M. A. Ubeda, *Organometallics* 1987, **6**, 1105; (m) R. J. Kulawiec, E. M. Holt, M. Lavin and R. H. Crabtree, *Inorg. Chem.* 1987, **26**, 2559; (n) R. M. Catala, D. Cruz-Garritz, A. Hills, D. L. Hughes, R. L. Richards, P. Soss and H. Torrens, *J. Chem. Soc., Chem. Commun.* 1987, 261; (o) C. H. Winter, A. Arif and J. A. Gladysz, *J. Am. Chem. Soc.* 1987, **109**, 7560; (p) F. L. Barcelo, P. Lahuerta, M. A. Ubeda, C. Foces-Foces, F. H. Cano and M. Martinez-Ripoll, *Organometallics* 1988, **7**, 584; (q) R. J. Kulawiec and R. H. Crabtree, *Organometallics* 1988, **7**, 1891.
12. S. Zhang and G. R. Dobson, *Inorg. Chem.* 1989, **28**, 324.
13. C. Hansch, A. Leo, S. H. Unger, K. H. Kim, O. Nikaitani and E. J. Lien, *J. Med. Chem.* 1973, **16**, 1207.
14. A. I. Vogel, *J. Chem. Soc.* 1948, 1833.
15. S. Oishi, *J. Organomet. Chem.* 1987, **335**, 207.

Polyhedron Vol. 9, No. 20, pp. 2517–2526, 1990
Printed in Great Britain

0277–5387/90 $3.00+.00
© 1990 Pergamon Press plc

CONVERSION OF LONG-CHAIN TERMINAL ALCOHOLS AND SECONDARY AMINES INTO TERTIARY AMINES USING RUTHENIUM(II) TERTIARY PHOSPHINE COMPLEXES AS HOMOGENEOUS CATALYSTS*

SANJOY GANGULY and D. MAX ROUNDHILL†

Department of Chemistry, Tulane University, New Orleans, LA 70118, U.S.A.

(*Received* 9 *April* 1990; *accepted* 15 *June* 1990)

Abstract—$RuCl_2(PPh_3)_3$ acts as a homogeneous catalyst for the condensation reaction between long-chain terminal alcohols and secondary amines to give tertiary amines. Supporting evidence is presented for a pathway involving an intermediate aldehyde which undergoes Schiff base formation with the secondary amine. Small amounts of amine side product are formed from catalysed alkyl group transfer reactions between the amines in the solution. A secondary pathway involving decarbonylation of the aldehyde leads to the formation of alkane and $RuHCl(CO)(PPh_3)_3$. Mechanistic probes are presented and discussed, and the scope of the reaction with secondary alcohols and ketones is presented.

The catalysed synthesis of amines having long-chain alkyl groups is of potential commercial value because of the use of these compounds in the production of detergents. A plausible synthetic approach to these compounds involves the condensation reaction between long-chain terminal alcohols and secondary amines [eq. (1)]:

$$Me(CH_2)_nOH + R_2NH \longrightarrow Me(CH_2)_nNR_2 + H_2O. \quad (1)$$

This reaction has been the focus of considerable study for an extended period of time, and numerous heterogeneous catalysts have been developed for accelerating this reaction.[2] The reaction has received less study as a transformation which can be catalysed under homogeneous conditions, but complexes of ruthenium and other transition metals have been used for similar dehydration reactions.[3] An example of such a process is the use of ruthenium triphenylphosphine complexes as homogeneous catalysts for the conversion of ethylene glycol into both monoamines and diamines.[4] This paper reports our use of ruthenium(II) complexes as homogeneous catalysts for the conversion of long-chain terminal alcohols into tertiary amines by the general condensation reaction shown in eq. (1). Alcohols ranging in carbon chain length from 10 to 18 have been used [$n = 9, 13, 15, 17$ in eq. (1)], and secondary amines have been employed which have methyl, ethyl, 1-propyl and phenyl substituents as the R group in R_2NH.

EXPERIMENTAL

Alcohols and secondary amines were commercial samples and used as supplied. The complexes $RuCl_2(PPh_3)_3$, $RuCl_2(PN)_2$, $RuCl_2(dppe)_2$, $RuCl_2(bipy)_2$ and $RuCl_2(CO)_2(PPh_3)_2$ were synthesized using literature procedures.[5] Triphenylphosphine (Aldrich) and stannous chloride were commercial samples. The catalytic reactions were carried out in a Parr pressure vessel fitted with a 45 cm^3 reaction cup. The reaction cup was heated in an aluminium block, and the reaction mixture stirred by a magnetic stir bar. The cooled reaction mixture was filtered through alumina to remove the ruthenium complexes, and the eluant analysed on a Hewlett–Packard Model 5830 gas chromatograph–mass spectrometer. Prior to the GC–MS analysis, dodecane (0.75 g, 4.4 mmol) was added to a mixture of the alcohol (10 mmol) and secondary amine (10 mmol). The yield of product tertiary amine was obtained by comparing the peak areas of the reac-

* For a preliminary communication, see ref. 1.
† Author to whom correspondence should be addressed.

tant alcohol and product amine with that of the standard dodecane. The relative detector sensitivity for equimolar amounts of terminal alcohol, product amine and dodecane was 1.7:1.3:1 with an accuracy of better than 5%. Our product yields are accurate to approximately 5%, and the selectivity in the majority of cases is greater than 90%. The lowered selectivity in some reactions was reduced because of a catalysed amine scrambling reaction. The yields of other amine products were obtained by GC–MS comparison with dodecane. The complex which was recovered from the reaction at the end of each catalytic run was $RuHCl(CO)L(PPh_3)_2$, where L is a secondary amine. The complex $RuHCl(CO)(PPh_3)_3$ was prepared by the literature procedure and characterized by a combination of IR, ^1H and $^{31}P\{^1H\}$ NMR spectroscopy: $\nu(CO)$ 2020, 1922, 1903 cm^{-1}; ^1H NMR: δ −7.2 [$^2J(PH_{cis}) = 23.7$ Hz, $^2J(PH_{trans}) = 104.9$ Hz]; $^{31}P\{^1H\}$ NMR: δ 13.5s, 39.6s [$^2J(PP)$ 0 Hz].[6] Addition of excess diethylamine to a solution of $RuHCl(CO)(PPh_3)_3$ gave $RuHCl(CO)(HNEt_2)(PPh_3)_2$, which was characterized by ^1H and $^{31}P\{^1H\}$ NMR spectroscopy: ^1H NMR: δ −14.5t [$^2J(PH) = 19.6$ Hz]; $^{31}P\{^1H\}$ NMR: δ 47.6s.

RESULTS

When a terminal alcohol, $Me(CH_2)_nOH$ (n = 9, 13, 15, 17), is reacted with a secondary amine, R_2NH (R = Me, Et, 1-Pr, Ph), at 120°C for 2.5 h in the absence of any catalyst, no observable quantity of tertiary amine $Me(CH_2)_nNR_2$ is formed. When the complex $RuCl_2(PPh_3)_3$ (50 μmol) is added to such a reaction mixture containing an alcohol (10 mmol) and a secondary amine (10 mmol) at 120°C, tertiary amine is formed as the product after 2.5 h reaction time (Table 1). After the reaction is complete the only ruthenium complex which can be detected in the solution is $RuHCl(CO)L(PPh_3)_2$, where L is the secondary amine used as the reactant. When the amine L is removed from this solution by evaporation, the complex $RuHCl(CO)(PPh_3)_3$ is formed.[6] This reaction is readily reversible since we find that the addition of excess secondary amine (L) to $RuHCl(CO)(PPh_3)_3$ gives $RuHCl(CO)L(PPh_3)_2$ [eq. (2)]:

$$RuHCl(CO)L(PPh_3)_2 \underset{L}{\overset{PPh_3}{\rightleftharpoons}} RuHCl(CO)(PPh_3)_3 \quad (L = R_2NH). \tag{2}$$

Table 1. Conversion of terminal alcohols and secondary amines into tertiary amines[a]

Terminal alcohol	Secondary amine[b]	Tertiary amine	Yield (%)[c]	Turnover number[d]
$C_{10}H_{21}OH$	$NHMe_2$	$C_{10}H_{21}NMe_2$	52	104
$C_{10}H_{21}OH$	$NHEt_2$	$C_{10}H_{21}NEt_2$	24	48
$C_{10}H_{21}OH$	$NHPr_2$	$C_{10}H_{21}NPr_2$	26	52
$C_{10}H_{21}OH$	$NHPh_2$	$C_{10}H_{21}NPh_2$	52	104
$C_{14}H_{29}OH$	$NHMe_2$	$C_{14}H_{29}NMe_2$	75	150
$C_{14}H_{29}OH$	$NHEt_2$	$C_{14}H_{29}NEt_2$	28	56
$C_{14}H_{29}OH$	$NHPr_2$	$C_{14}H_{29}NPr_2$	23	46
$C_{14}H_{29}OH$	$NHPh_2$	$C_{14}H_{29}NPh_2$	50	100
$C_{16}H_{33}OH$	$NHMe_2$	$C_{16}H_{33}NMe_2$	45	90
$C_{16}H_{33}OH$	$NHEt_2$	$C_{16}H_{33}NEt_2$	21	42
$C_{16}H_{33}OH$	$NHPr_2$	$C_{16}H_{33}NPr_2$	24	47
$C_{16}H_{33}OH$	$NHPh_2$	$C_{16}H_{33}NPh_2$	49	98
$C_{18}H_{37}OH$	$NHMe_2$	$C_{18}H_{37}NMe_2$	82	164
$C_{18}H_{37}OH$	$NHEt_2$	$C_{18}H_{37}NEt_2$	14	28
$C_{18}H_{37}OH$	$NHPr_2$	$C_{18}H_{37}NPr_2$	21	42

[a] Reaction conditions: 2.5 h at 120°C with $RuCl_2(PPh_3)_3$ (0.5%) added.

[b] The propyl group is the 1-propyl.

[c] Yield of tertiary amine for a reaction containing equal moles of terminal alcohol and secondary amine.

[d] Turnover number based on moles tertiary amine obtained per mole of $RuCl_2(PPh_3)_3$ catalyst.

Table 2. Comparative yield of $C_{16}H_{33}NPr_2$ for different catalytic conditions[a]

Catalyst	Temperature (°C)	Yield of $C_{16}H_{33}NPr_2$ (%)
$RuCl_2(PPh_3)_3$	25	0[b]
$RuCl_2(PPh_3)_3$	70	4[b]
$RuCl_2(PPh_3)_3$	120	24
$RuCl_2(PPh_3)_3 + PPh_3$ (4 moles)	120	51
$RuCl_2(PPh_3)_3 + SnCl_2 \cdot 2H_2O$	120	13
$RuCl_2(PN)_2$	120	0
$RuCl_2(PN)_2 + PPh_3$ (4 moles)	120	0
$RuHCl(CO)(PPh_3)_3$	120	0
$RuCl_2(dppe)_2$	120	0
$RuCl_2(bipy)_2$	120	0
$RuCl_2(CO)_2(PPh_3)_2$	120	5
$RuCl_2(PPh_3)_3$	160	47
$RuCl_2(PPh_3)_3 + PPh_3$ (4 moles)	160	56
$RuCl_2(PN)_2$	160	15
$RuCl_2(PN)_2 + PPh_3$ (4 moles)	160	72

[a] Reaction time 2.5 h; catalyst concentration 0.5%.
[b] Reaction time 30 h.

The complexes $RuHCl(CO)L(PPh_3)_2$ and $RuHCl(CO)(PPh_3)_3$ are inactive as catalysts for reaction (1), and $RuCl_2(PPh_3)_3$ does not catalyse the reverse reaction. At 120°C, the chelate complexes $RuCl_2(PN)_2$ (PN = *o*-diphenylphosphino-N,N-dimethylaniline), $RuCl_2(dppe)_2$, $RuCl_2(bipy)_2$ and the dicarbonyl complex $RuCl_2(CO)_2(PPh_3)_2$ are also inactive as homogeneous catalysts for reaction (1). At the higher temperature of 160°C, $RuCl_2(PN)_2$ will catalyse the formation of $C_6H_{33}NPr_2$ from $C_{16}H_{33}OH$ and $NHPr_2$. When the reaction temperature is lowered to 25°C, $RuCl_2(PPh_3)_3$ is inactive as a catalyst for the formation of $C_{16}H_{33}NPr_2$ over a time period of 30 h, and comparable reaction conditions at 70°C give only a 4% yield of $C_{16}H_{33}NPr_2$ after 30 h (Table 2). Although triphenylphosphine itself is not a catalyst for reaction (1), the addition of 4 moles of triphenylphosphine per mole of $RuCl_2(PPh_3)_3$ to solutions which contain $RuCl_2(PPh_3)_3$ or $RuCl_2(PN)_2$ results in increased yields of amine (Table 2). The complex $RuCl_2(PN)_2$ is not recovered at the end of the catalytic reaction at 160°C under conditions where 4 moles of triphenylphosphine are added. Instead in the $^{31}P\{^1H\}$ NMR spectrum we observe a single resonance at δ 25 due to an unidentified complex. The yield of tertiary amine is dependent on both the alcohol and secondary amine. The highest yields are obtained with $NHMe_2$ and $C_{14}H_{29}OH$ or $C_{18}H_{37}OH$, and the lowest yield with $NHEt_2$ and $C_{18}H_{37}OH$ (Table 1). Secondary and tertiary alcohols do not react; thus in the presence of $RuCl_2(PPh_3)_3$ at 170°C for 2.5 h with dipropylamine, the secondary alcohols 2-propanol, 2-octanol, 4-methylcyclohexanol, *t*-butanol and phenol give no tertiary amine products.

The catalytic reaction with primary alcohols and secondary amines exhibits an induction period of approximately 30 min before significant amounts of tertiary amine product are formed. This induction period is reduced when 4 moles of PPh_3 per mole of $RuCl_2(PPh_3)_3$ are added to the solution. Data collected in Table 3 show that the catalysed reaction between $C_{10}H_{21}OH$ and $NHPr_2$ gives increased yields of $C_{10}H_{21}NPr_2$ with added triphenylphosphine at all times after this 15 min induction period. At the early stages of the reaction the $^{31}P\{^1H\}$ NMR spectrum shows the presence of $RuCl_2(PPh_3)_3$ (δ 45, 60) as the only phosphorus containing ruthenium complex, whereas at the late stages of the catalysis complete conversion to $RuHCl(CO)(NHPr)(PPh_3)_2$ (δ 47.8) has occurred. No other complexes are observed in significant amounts. In the presence of added triphenylphosphine we observe the formation of $RuHCl(CO)(NHPr)(PPh_3)_2$ after 90 min, whereas in the absence of added triphenylphosphine we only observe this compound after 180 min.

At the higher temperature of 180°C and the longer reaction time of 10 h we observe the

$RuCl_2(PPh_3)_3$ catalysed conversion of secondary alcohols into tertiary amines by condensation with primary amines, but not with secondary amines. Thus after the 10 h reaction time we obtain a 43% yield of 4-methylcyclohexylphenylamine from 4-methylcyclohexanol and aniline, and a 22% yield of 4-methylcyclohexyl hexylamine from 4-methylcyclohexanol and 1-hexylamine [eq. (3)].

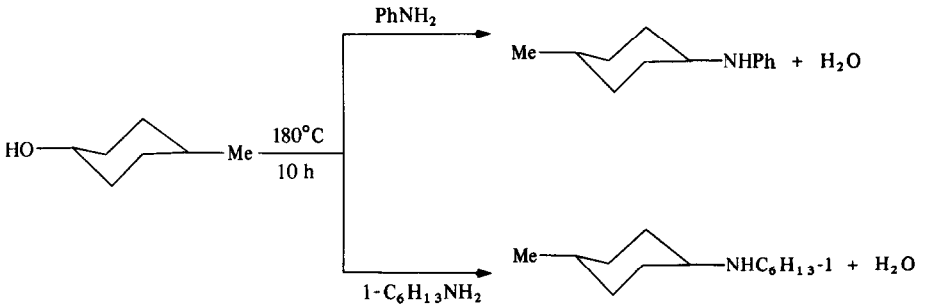

(3)

With 4-methycyclohexanol and dipropylamine we observe no product amine after 10 h, but after 16 h reaction time the compound 4-methylcyclohexyldipropylamine is formed in 13% yield. Under catalytic conditions at 120°C we observe no tertiary amine formation from dipropylamine and secondary alcohols or ketones. Previous workers have, however, reported that $RuCl_2(PPh_3)_3$ acts as a homogeneous catalyst for the condensation of aniline with *both* secondary and primary alcohols, therefore we have investigated further the scope of this reaction.[7] Under catalysed conditions at 180°C for 10 h we find that aniline and 1-hexylamine undergo condensation reactions with both cyclic and acyclic alcohols and ketones [eq. (4)].

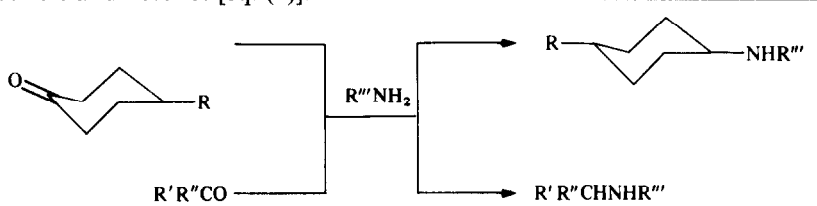

(4)

(R = H,Me; R' = R'' = C_2H_5; R' = CH_3, R'' = Ph; R' = 1-C_6H_{13}, R'' = CH_3; R''' = Ph, 1-C_6H_{13})

The yields of product amine are generally low (Table 4), especially for the case where a secondary amine reactant is employed.

In the catalysed condensation reactions of aniline with both 3-pentanone and acetophenone, the respective yields of 3-pentylphenylamine and acetophenyl phenylamine are increased by approximately four-fold when the reaction is carried out under a pressure of hydrogen.[8] For the case of secondary amines and ketones the yield of tertiary amine is very low even when the catalyst is composed of $RuCl_2(PPh_3)_3$ with 4 moles of triphenylphosphine under a hydrogen pressure of 1300 psig (Table 5).

In some cases the selectivity of the condensation reaction (1) is lowered by a redistribution reaction, whereby the initially formed amine undergoes alkyl group interchange to give a series of different tertiary and secondary amines. This reaction is observed in the reaction between terminal alcohols and secondary amines (Table 6), secondary alcohols and both primary and secondary amines (Table 7), and ketones and primary amines (Table 8). The data in Tables 6–8 show no particular pattern. For the terminal alcohols we only observe significant redistribution products when dipropylamine is used. In addition to the product $RNPr_2$, the amines R_2NPr, NPr_3 and RNHPr (R = $C_{10}H_{21}$, $C_{14}H_{29}$, $C_{16}H_{33}$, $C_{18}H_{37}$) are formed in varying amounts depending on the alcohol ROH (Table 6). Similar results are found when secondary alcohols are used (Table 7). For the case of ketones we observe no amine redistribution products when the reaction is carried out in the absence of hydrogen, when the amine yield is very low. Under a pressure of hydrogen the yield of amine is increased, and redistribution products are observed (Table 8).

DISCUSSION

The complex $RuCl_2(PPh_3)_3$ acts as a homogeneous catalyst for the condensation of terminal alcohols with secondary amines to give tertiary amines. At the end of the 2.5 h reaction time the complex has been converted completely into

Table 3. Conversion of 1-decyl alcohol and dipropylamine into decyldipropylamine both in the absence and presence of triphenylphosphine[a]

Time (m)	Yield of $C_{10}H_{21}NPr_2$ (%) No PPh_3	PPh_3
0	0	0
15	0	0
30	0.1	0.86
45	0.25	5.53
60	0.60	7.78
75	1.65	20.80
90	16.82	21.60
105	18.30	35.10
120	19.70	39.00
135	20.80	47.70
150	24.50	50.60
180	27.00	56.20

[a] Reaction conditions: 3 h at 120°C; 1.00×10^{-2} moles of 1-decyl alcohol and 1.00×10^{-2} moles of dipropylamine; 5.22×10^{-5} moles of $RuCl_2(PPh_3)_3$ and 2.08×10^{-4} moles of PPh_3.

$RuHCl(CO)(amine)(PPh_3)_2$. Separate experiments with $RuHCl(CO)(PPh_3)_3$ and secondary amine verify that this complex is not itself a catalyst for the condensation reaction. The initial step of the reaction apparently results in the formation of an intermediate alkoxide complex which can undergo β-hydrogen transfer to give an aldehydic intermediate. In the presence of excess secondary amine we do not detect any aldehydic intermediates because of their rapid condensation with amine. Two pieces of evidence support the postulate that intermediate aldehydes are formed. The first supportive evidence is the formation of both $RuHCl(CO)L(PPh_3)_2$ (L = amine) and small quantities of alkane in the catalytic reaction. Well-documented examples exist which show that aldehydes are decarbonylated by platinum metal group complexes to give alkanes and carbonyl metal complexes.[9] The second support comes from a series of separate catalysed and uncatalysed reactions between butyraldehyde and diethylamine at 120°C for 2.5 h reaction time (Table 9). In the absence of catalyst the products of the reaction are the eneal, $CH_3(CH_2)_2CH{=}C(C_2H_5)CHO$, and the eneamine, $CH_3CH_2CH{=}CHN(C_2H_5)_2$, in a 44:1 ratio. In the presence of $RuCl_2(PPh_3)_3$ the products are the eneal and tertiary amine, $(C_4H_9)N(C_2H_5)_2$, in a 8.9:1 ratio. In the presence of hydrogen under a pressure of 1300 psig the catalytic reaction is selective for $(C_4H_9)N(C_2H_5)_2$. These results can be explained by eq. (5)

$$\begin{array}{l} RCH_2CHO \underset{H_2O}{\overset{Et_2NH}{\rightleftharpoons}} RCH{=}CHNEt_2 \xrightarrow{H_2} RCH_2CH_2NEt_2 \\ \quad \Updownarrow \\ RCH_2CH{=}CH(R)CHO \end{array} \qquad (5)$$

$(R = C_2H_5)$,

Table 4. Conversion of ketones and primary or secondary amines into secondary or tertiary amines both in the absence and presence of hydrogen

Ketone	Primary amine	Secondary amine	Yield (%)[a]	Yield (%)[b]
$(C_2H_5)_2CO$	$PhNH_2$	$(C_2H_5)_2CHNHPh$	5	21
CH_3COPh	$PhNH_2$	$CH_3(Ph)CHNHPh$	5	23
$1\text{-}C_6H_{13}COCH_3$	$1\text{-}C_6H_{13}NH_2$	$CH_3(1\text{-}C_6H_{13})CHNHC_6H_{13}$	5	50
$1\text{-}C_6H_{13}COCH_3$	$PhNH_2$	$CH_3(1\text{-}C_6H_{13})CHNHPh$	9	35
	$1\text{-}C_6H_{13}NH_2$	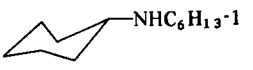	7	31
	$PhNH_2$		8	25
	$PhNH_2$		6	25
$(C_2H_5)_2CO$	$NHPr_2$	$((C_2H_5)_2CH)Pr_2N$	0	5[c]
CH_3COPh	$NHPr_2$	$(CH_3CHPh)Pr_2N$	0	4[c]

[a] Reaction conditions are 180°C for 10 h with $RuCl_2(PPh_3)_3$.

[b] Reaction conditions are 180°C for 10 h with $RuCl_2(PPh_3)_3$ and 1300 psig hydrogen.

[c] Conditions as for 2 but with 4 moles of triphenylphosphine added.

Table 5. Conversion of ketones and secondary amines into tertiary amines

Ketone	Secondary amine	Tertiary amine	Yield (%)
$(C_2H_5)_2CO$	$NHPr_2$	$(C_2H_5)_2CHNPr_2$	5
CH_3COPh	$NHPr_2$	$CH_3(Ph)CHNPr_2$	4
$(CH_3)_2CO$	$NH(CH_2)_4$	$(CH_3)_2CHN(CH_2)_4$	5
	$NHPr_2$		5
$1\text{-}C_6H_{13}COCH_3$	$NHPr_2$	$CH_3(1\text{-}C_6H_{13})CHNPr_2$	6
$(C_2H_5)_2CO$	$NH(CH_2)_4$	$(C_2H_5)_2CHN(CH_2)_4$	6

Reaction conditions: 10 h at 180°C with $RuCl_2(PPh_3)_3$ and 4 moles of PPh_3 under a hydrogen pressure of 1300 psig.

Table 6. Redistribution amine products from the catalytic reaction between terminal alcohols and secondary amines[a]

Alcohol	Amine	Product (%)[b] $RNPr_2$	R_2NPr	NPr_3	RNHPr
$C_{10}H_{21}OH$	$NHPr_2$	63	3	6	—
$C_{14}H_{29}OH$	$NHPr_2$	23	2	3	6
$C_{16}H_{33}OH$	$NHPr_2$	24	—	8	11
$C_{18}H_{37}OH$	$NHPr_2$	21	—	1	—

[a] Reaction conditions: 2.5 h at 120°C with $RuCl_2(PPh_3)_3$.
[b] R = $C_{10}H_{21}$, $C_{14}H_{29}$, $C_{16}H_{33}$, $C_{18}H_{37}$.

Table 7. Reaction of secondary alcohols with primary and secondary amines[a]

Alcohol (ROH)	Amine ($R'NH_2$)	Product (%) RNHR′	R_2NR'	RNR'_2	R'_2NH	R_2NH	R'_3N
	$PhNH_2$	43	7	—	—	—	—
	$1\text{-}C_6H_{13}NH_2$	22	13	25	7	5	12
$2\text{-}C_8H_{17}OH$	$1\text{-}C_6H_{13}NH_2$	33	—	—	—	—	6
$2\text{-}C_8H_{17}OH$	$PhNH_2$	18	—	—	—	—	—
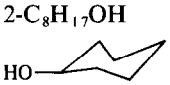	$1\text{-}C_6H_{13}NH_2$	21	3	—	—	—	—
$2\text{-}C_5H_{11}OH$	$1\text{-}C_6H_{13}NH_2$	—	—	5	—	—	—
Alcohol (ROH)	Amine (R'_2NH)		RNR'_2	RNHR′	R'_3N	RNH_2	
$(CH_3)_2CHOH$	$NHPr_2$	—	—	—	30	—	—
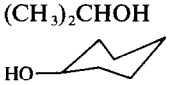	$NHPr_2$	—	13	14	35	—	—
$2\text{-}C_8H_{17}OH$	$NHPr_2$	—	—	—	4	—	—
	$NHPr_2$	—	14	—	6	—	—

[a] Reaction conditions: 10 h at 180°C with $RuCl_2(PPh_3)_3$.

Table 8. Redistribution products from the reaction of ketones with primary amines,[a] $RuCl_2(PPh_3)_3$, with 4 moles of PPh_3 and 1300 psig hydrogen

Ketone (RR'CO)	Amine ($R''NH_2$)	Product amines (%)[b] A	B	C	D	E	F
$(CH_3CH_2)_2CO$	$1\text{-}C_6H_{13}NH_2$	13	—	—	—	12	8
$(CH_3CH_2)_2CO$	$PhNH_2$	21	—	—	—	—	—
CH_3COPh	$1\text{-}C_6H_{13}NH_2$	26	21	13	—	—	5
CH_3COPh	$PhNH_2$	23	—	—	—	0.5	—
$1\text{-}C_6H_{13}COCH_3$	$1\text{-}C_6H_{13}NH_2$	50	—	—	5	—	—
$1\text{-}C_6H_{13}COCH_3$	$PhNH_2$	35	—	—	—	—	—
	$1\text{-}C_6H_{13}NH_2$	31	—	—	2	1	—
	$PhNH_2$	25	—	—	4	—	—
	$PhNH_2$	25	—	—	4	—	—

[a] Reaction conditions: 10 h at 180°C with 4 moles of PPh_3 and 1300 psig hydrogen added.

[b] A = $(RR'CH)NHR''$, B = $(RR'CH)_2NH$, C = $(RR'CH)_2NR''$, D = $(RR'CH)NR''_2$, E = R''_2NH, F = R''_3N.

whereby the condensation reaction to eneamine is in competition with the self-condensation of the aldehyde to give the aldol eneal product. The formation of saturated amine results from the function of $RuCl_2(PPh_3)_3$ as a hydrogenation catalyst for the intermediate eneamine, and the hydrogenation step is accelerated under hydrogen pressure.

At 120°C for 2.5 h we do not observe any catalysed condensation reaction between dipropylamine and secondary or tertiary alcohols. This

Table 9. Reaction products from butyraldehyde and diethylamine

Conditions[a]	Product ratio	Yield (%)
No catalyst	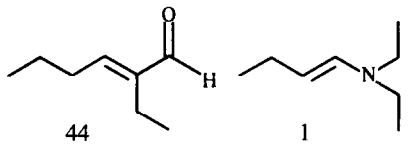 44 : 1	77
No catalyst (1300 psi H_2)	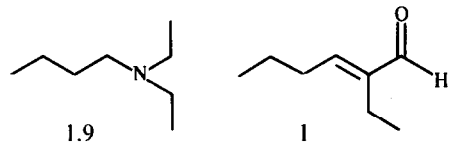 1.9 : 1	66
$RuCl_2(PPh_3)_3$	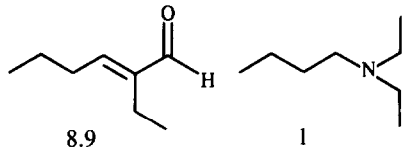 8.9 : 1	77
$RuCl_2(PPh_3)_3$ (1300 psi H_2)	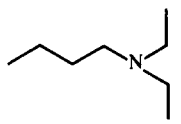	32

[a] Conditions are 120°C for 2.5 h.

observation may be due to the failure of $RuCl_2(PPh_3)_3$ to catalyse either the dehydrogenation of secondary alcohols to ketones or the hydrogenative condensation of ketones with the secondary amine. Under conditions with $RuCl_2(PPh_3)_3$ for 10 h at 180°C we detect *no* tertiary amine formation with 3-pentanone and dipropylamine, diethylamine or pyrrolidine, or with acetophenone and dipropylamine. Furthermore when the alcohol is 2-octanol, 3-pentanol or cyclohexanol we detect no ketone formation.

The data in Table 2 show that $RuCl_2(PPh_3)_3$, but not $RuCl_2(dppe)_2$, $RuCl_2(PN)_2$ (PN = 2-diphenylphosphino-N,N-dimethylaniline) or $RuCl_2(bipy)_2$, is a homogeneous catalyst for the condensation reaction between terminal alcohols and secondary amines. The difference between $RuCl_2(PPh_3)_3$ and the other complexes is that $RuCl_2(PPh_3)_3$ is a 16-electron complex, whereas the other complexes have 18-electron configurations. The failure of $RuCl_2(PN)_2$ to catalyse the formation of tertiary amines implies that under our experimental conditions the ligand is not hemilabile, whereby the dimethylamino moiety hinges away from the metal centre to create a vacant coordination site.[5] Adding tin(II) chloride to $RuCl_2(PPh_3)_3$ does not increase its catalytic activity by introducing $SnCl_3^-$ as a good leaving ligand. Adding triphenylphosphine causes an increase in catalytic activity of $RuCl_2(PPh_3)_3$ Triphenylphosphine itself is inactive as a homogeneous catalyst for reaction (1). From the data in Table 3 it is unclear as to the precise function of triphenylphosphine in accelerating the formation of tertiary amines. Since we observe the formation of $RuHCl(CO)(NHPr_2)(PPh_3)_2$ at an earlier stage of the reaction than we do in the absence of triphenylphosphine, it appears that the complete catalytic cycle has been accelerated. Several possibilities can be excluded or considered unlikely. One of these is that chloride ion is replaced by triphenylphosphine to give a catalytically more reactive cationic ruthenium(II) complex. We have eliminated this possibility because solutions of $RuCl_2(PPh_3)_3$ show no increased conductivity upon addition of excess triphenylphosphine. A second possibility is that triphenylphosphine acts to extend the catalyst lifetime of $RuCl_2(PPh_3)_3$; this postulate is disfavoured by the observation that the catalytically inactive complex $RuHCl(CO)NHPr_2(PPh_3)_2$ is formed at shorter reaction times in the presence of added triphenylphospine than is found in comparable catalytic runs in its absence.

The proposed catalytic pathway for the condensation reaction between terminal alcohols and secondary amines is shown in Scheme 1. In this scheme a key step is the Schiff base condensation reaction between secondary amine and the inter-

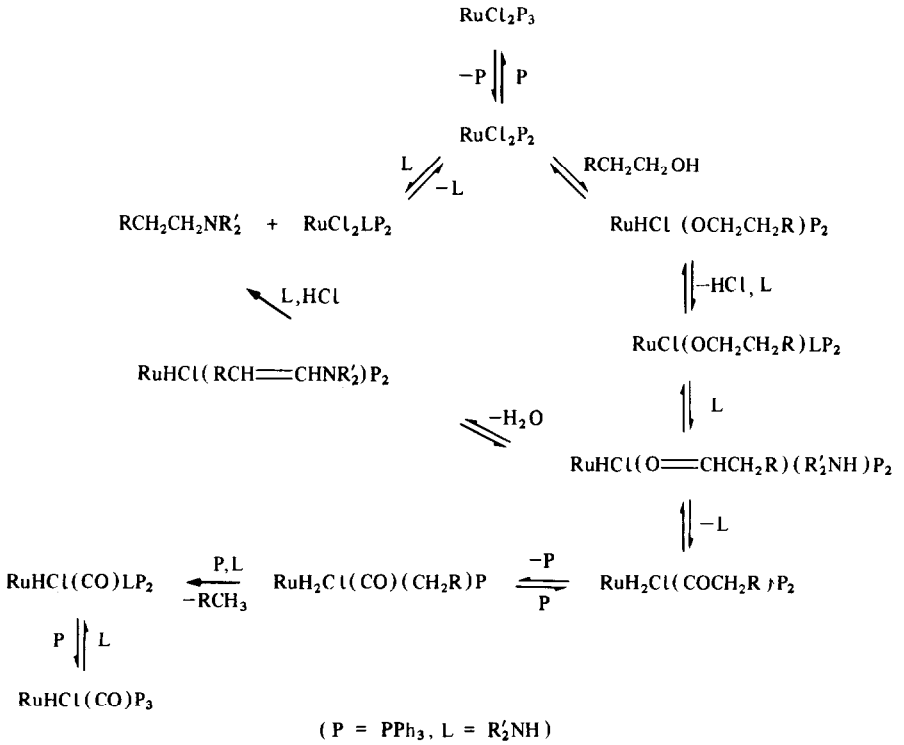

(P = PPh_3, L = R'_2NH)

Scheme 1.

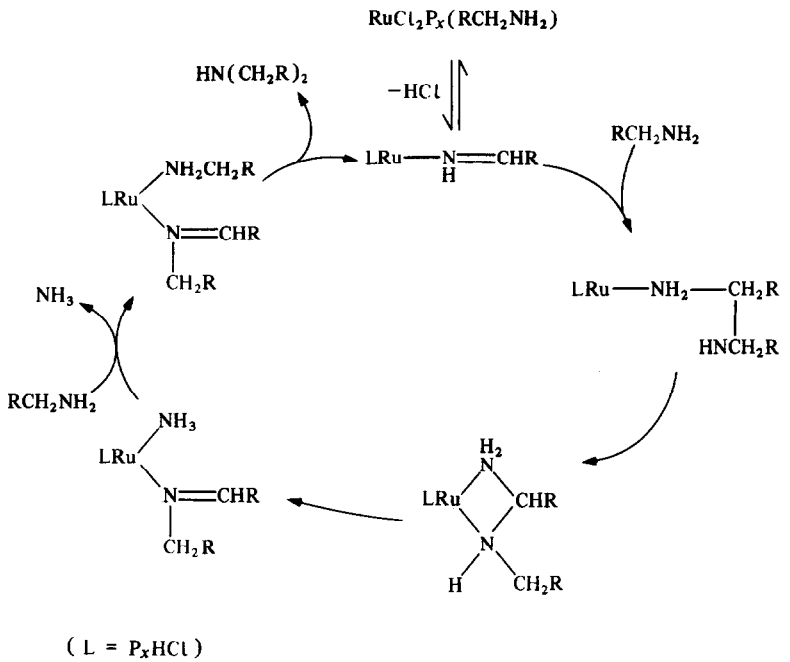

Scheme 2.

mediate aldehyde formed by β-hydrogen transfer. The tertiary amine product is then obtained by the catalysed hydrogenation of the imine formed in this Schiff base condensation. Two plausible explanations for the accelerating effect of triphenylphosphine are that it displaces the complexed aldehyde ligand to facilitate its reaction in the free state with secondary amine, or that it functions to accelerate the catalytic hydrogenation of imine to tertiary amine.

The condensation reaction between ketones and amines under catalytic conditions with $RuCl_2(PPh_3)_3$ requires a higher temperature than does the condensation reaction between primary alcohols and amines. The primary product is the secondary amine, and the yield is increased under a pressure of hydrogen [eq. (6)].

$$R_2CO + R'NH_2 + H_2 \longrightarrow R_2CHNHR' + H_2O \quad (6)$$

For secondary amines as reactants, tertiary amines are not formed in the absence of hydrogen, and even under 1300 psig hydrogen pressure the yields are very low [eq. (7)].

$$R_2CO + R'_2NH + H_2 \longrightarrow R_2CHNR'_2 + H_2O \quad (7)$$

These results support a pathway whereby the final amine is produced by catalytic hydrogenation of an intermediate imine formed in an equilibrium condensation reaction between the ketone and reactant amine [eq. (8)].

$$R_2CO + R'NH_2 \underset{H_2O}{\overset{-H_2O}{\rightleftharpoons}} R_2C{=}NR' \xrightarrow{H_2} R_2CHNHR' \quad (8)$$

We propose that the catalytic activity of $RuCl_2(PPh_3)_3$ results from its functioning as a hydrogenation catalyst for the intermediate imine. This imine is formed in equilibrium with the ketone and amine, and its catalysed hydrogenation to the product amine drives the equilibrium away from the reactant.

The amine redistribution reaction results in decreased selectivity of the catalysed condensation reactions between amines and either alcohols or ketones. These side products cannot be eliminated from the product because this redistribution reaction occurs subsequent to the formation of the initial amine product. Previous researchers have found that these redistribution reactions are catalysed by a series of different ruthenium complexes.[10] The pathway used to explain these reactions is shown in Scheme 2.

Acknowledgements—We thank the Louisiana Board of Regents for support of this research through the Louisiana Educational Quality Support Fund. We thank Johnson Matthey Inc. for a loan of ruthenium trichloride.

REFERENCES

1. S. Ganguly, F. L. Joslin and D. M. Roundhill, *Inorg. Chem.* 1989, **28**, 4562.
2. H. J. Hubert and K. D. Tillmetz, *Ger. Offen. Patent* 3432015 (1986), *Chem. Abstr.* 1986, **105**, 42326c; L. H. Slaugh and G. W. Schoenthal, *Ger. Offen. Patent* 2844984 (1979), *Chem. Abstr.* 1979, **91**, 19882q; S. Murahashi, T. Shimamura and I. Moritani, *J. Chem. Soc., Chem. Commun.* 1974, 931; A. Baiker and J. Kijenski, *Catal. Rev.-Sci. Engng* 1985, **27**, 653; A. Baiker and W. Richarz, *Tetrahedron Lett.* 1977, 1937; P. Y. Fong, K. R. Smith and J. D. Sauer, *Eur. Patent* (1988), *Chem. Abstr.* 1988, **110**, 40803k; Z. Feng and X. Tang, *Riyong Huaxue Gongye* 1988, 1, *Chem. Abstr.* 1988, **109**, 75656w; I. D. Dobson, P. S. Williams and A. W. Lidy, *Eur. Patent* (1988), *Chem. Abstr.* 1988, **110**, 57112g; C. E. Haberman, *U.S. Patent* 4772750 (1988), *Chem. Abstr.* 1988, **111**, 57046j.
3. J. A. Marsella, *AU Patent* 564225 (1987), *Chem. Abstr.* 1987, **108**, 169619t; C. F. Hobbs and D. E. McMackins, *U.S. Patent* 4120901 (1978), *Chem. Abstr.* 1978, **90**, 54459h; Y. Tsuji, R. Takeuchi, H. Ogawa and Y. Watanabe, *Chem. Lett.* 1986, 293; R. Grigg, T. R. B. Mitchell, S. Sutthivaiyakit and N. Tongpenyai, *J. Chem. Soc., Chem. Commun.* 1981, 611; D. M. Fenton, *U.S. Patent* 3708539 (1973), *Chem. Abstr.* 1973, **78**, 124001f; S. Murahashi, K. Kando and T. Hakata, *Tetrahedron Lett.* 1982, **23**, 229.
4. J. A. Marsella, *J. Org. Chem.* 1987, **52**, 467.
5. P. S. Hallman, T. A. Stephenson and G. Wilkinson, *Inorg. Synth.* 1970, **12**, 237; T. B. Rauchfuss and D. M. Roundhill, *J. Am. Chem. Soc.* 1974, **96**, 3098; J. Chatt and R. G. Hayter, *J. Chem. Soc.* 1961, 896; J. T. Mague and J. P. Mitchener, *Inorg. Chem.* 1972, **11**, 2714; R. Mason, D. W. Meek and G. R. Scollary, *Inorg. Chim. Acta* 1976, **16**, L11; G. L. Gaines, P. E. Behnken and S. J. Valenty, *J. Am. Chem. Soc.* 1978, **100**, 6549; T. A. Stephenson and G. Wilkinson, *J. Inorg. Nucl. Chem.* 1966, **28**, 945.
6. N. Ahmad, J. J. Levison, S. D. Robinson and M. F. Uttley, *Inorg. Synth.* 1974, **15**, 45.
7. Y. Watanabe, Y. Tsuji, H. Ige, Y. Ohsugi and T. Ohta, *J. Org. Chem.* 1984, **49**, 3359.
8. The role of hydrogen is discussed in a review: A. Baiker, *Stud. Surf. Sci. Catal.* 1988, **41**, 283.
9. M. C. Baird, C. J. Nyman and G. Wilkinson, *J. Chem. Soc. A.* 1968, 348.
10. A. Arcelli, B. T. Khai and G. Porzi, *J. Organomet. Chem.* 1982, **231**, C31; C. W. Jung, J. D. Fellmann and P. E. Garrou, *Organometallics* 1983, **2**, 1042; L. Shvo and R. M. Laine, *J. Chem. Soc., Chem. Commun.* 1980, 753; R. D. Adams and J. E. Babin, *Organometallics* 1988, **7**, 963; R. M. Laine, D. W. Thomas and L. W. Cary, *J. Am. Chem. Soc.* 1982, **104**, 1763.

Polyhedron Vol. 9, No. 20, pp. 2527–2531, 1990
Printed in Great Britain

0277–5387/90 $3.00+.00
© 1990 Pergamon Press plc

SYNTHESIS OF NEW SYMMETRICAL *MESO*-SUBSTITUTED PORPHYRINS: TETRA-6-QUINOLINE PORPHYRIN, TETRA-6-[N-METHYL(^{13}C) QUINOLINE] PORPHYRIN TETRAIODIDE SALT AND THEIR COPPER(II) COMPLEXES

JAMES D. McCURRY* and JAMES E. ROBERTS†

Lehigh University, Department of Chemistry, Bethlehem, PA 18015, U.S.A.

(*Received* 26 *February* 1990; *accepted* 15 *June* 1990)

Abstract—The synthesis and spectroscopic characterization of a series of *meso*-substituted porphyrins based on a new parent compound, tetra-6-quinoline porphyrin, is described. Successful preparation of the parent compound was accomplished by the synthesis of 6-quinoline carboxaldehyde followed by reaction with pyrrole via the Rothemund condensation. The quinoline nitrogens were then methylated with ^{13}C-methyl iodide to form the uniformly labelled tetra-6-[N-methyl(^{13}C) quinoline] porphyrin tetraiodide salt. Copper(II) complexes of the parent compound and the ^{13}C labelled porphyrin were also successfully prepared and characterized.

Porphyrin compounds have been extensively studied due to their important metabolic role in oxygen transport, electron transport and photosynthesis.[1] Synthetic porphyrins are often used as models to understand the chemistry of naturally occurring porphyrins and have recently found application as structural probes for nucleotides and as tumour imaging agents.[2,3] For our work porphyrins were chosen as model compounds for the investigation of paramagnetic relaxation in solid-state nuclear magnetic resonance. The ability of porphyrins to complex paramagnetic metals and their simple rigid geometry allow simplification of the structural terms in the paramagnetic relaxation equation. In our laboratory, a number of symmetric free base and copper(II) *meso*-tetra-[N-methyl(^{13}C) pyridyl] porphyrin tetraiodide salts have been synthesized. The ^{13}C labelling improved sensitivity and selectivity for the NMR relaxation experiments. These syntheses were performed by the Adler-modified Rothemund condensation of equimolar amounts of pyrrole with pyridylaldehydes.[4,5]

A logical extension of the N-methylated pyridyl porphyrins was the preparation of an N-methylated quinoline porphyrin series, specifically tetra-6-[N-methyl(^{13}C) quinoline] porphyrin (see Fig. 1). Since a number of *meso*-tetra-aryl porphyrins have been prepared via the Rothemund condensation,[6–9] the challenge was finding a method for the synthesis of 6-quinoline carboxaldehyde since it is not commercially available or reported in the literature. The aldehyde synthesis was accomplished by the partial oxidation of 6-methyl quinoline, which is commercially available. Teague and Roe reported a simple preparation of 3-quinoline carboxaldehyde from 3-methyl quinoline using selenium oxide.[10] Once the 6-quiniline carboxaldehyde was prepared, the porphyrin synthesis proceeded analogous to the pyridyl series. The ^{13}C label was introduced to the quinoline nitrogen using ^{13}C-methyl iodide.

EXPERIMENTAL

All synthetic methods were first attempted with non-labelled materials. Products were characterized for structure and purity before proceeding to isotropically enriched syntheses. The following descriptions and results are only reported for the isotropically enriched products when applicable. All solvents and reagents used were reagent grade. Elemental analyses were performed in duplicate and the averages reported. UV–vis spectroscopy was accomplished with a Perkin–Elmer Lambda V spectrometer using 1 cm matched quartz cells, a 0.2 nm slit width and a scan speed of 60 nm min^{-1} from

* Current address: Hewlett Packard, Valley Forge, PA 19482, U.S.A.

† Author to whom correspondence should be addressed.

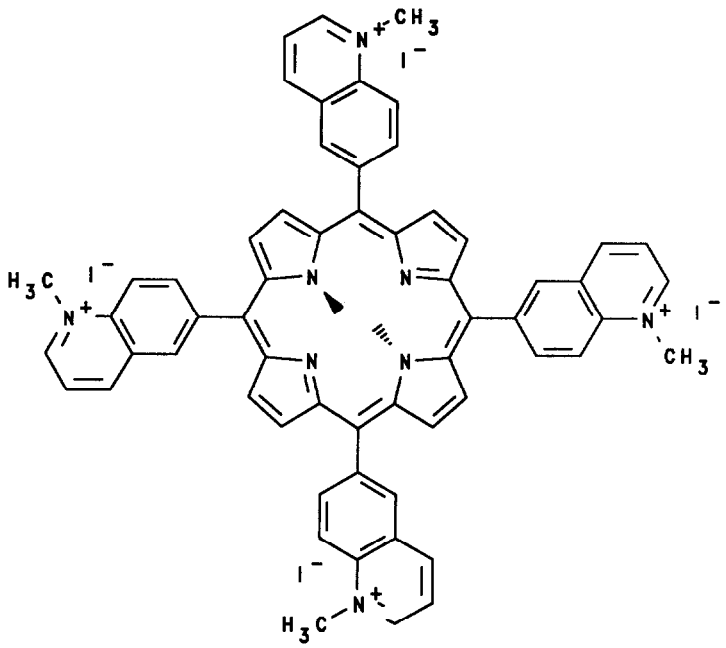

Fig. 1. Structure of tetra-6-[N-methyl(^{13}C) quinoline] porphyrin tetraiodide salt.

700 to 350 nm. ^{1}H NMR spectroscopy was performed with a Bruker AM 500 with resonances referenced to TMS (0.0 ppm). A Matson Sirus 100 FT–IR was used for IR spectroscopy with the sample cast as a film between potassium bromide windows. Gas chromatography–mass spectrometry (GC–MS) analysis was accomplished with a Hewlett–Packard 5970A equipped with a 25 m × 0.25 mm i.d. thin film SP-1 capillary column.

(1) *6-Quinoline carboxaldehyde*

A 500 cm^3 three-necked flask containing 25.0 g (0.18 mol) of 6-methyl quinoline (Aldrich Chemical Co.) was equipped with an immersion thermometer, a powder addition funnel and a magnetic stirring bar. Into the powder addition funnel was placed 20.0 g (0.18 mol) of selenium(IV) oxide. The 6-methyl quinoline was heated to 180°C and the selenium oxide was slowly added to the stirring quinoline.[11] The complete addition of the SeO_2 took approximately 1 h and was controlled so that the temperature never exceeded 210°C. After cooling to room temperature 100 cm^3 of ethyl ether was placed in the flask and a reflux condenser replaced the addition funnel. The ether was refluxed for 20 min, cooled and decanted from the flask, leaving the dark brown tar behind. This procedure was repeated twice more. The combined ether extracts were dried over magnesium sulphate, filtered and the ether removed with a rotary evaporator. A damp yellow solid was recovered and an IR spectrum was taken to confirm the presence of an aldehyde functionality (ν = 1700 cm^{-1}). Further analysis by GC–MS was performed to determine the presence and purity of quinoline aldehyde. The product was further purified by fractional distillation under vacuum to obtain 9.1 g (33% yield) of 6-quinoline carboxaldehyde as a pale yellow solid. The aldehyde was immediately used for porphyrin synthesis before any significant oxidation occurred.

(2) *Tetra-6-quinoline porphyrin* (T6QP)

The quinoline aldehyde (9.1 g, 58.0 mmol) prepared above was placed in a flask and dissolved in 150 cm^3 of propionic acid. After dissolution, freshly distilled pyrrole (4.0 g, 58.0 mmol) was added and the mixture was refluxed for 2 h. After cooling to room temperature, the propionic acid was removed by rotary evaporation leaving a shiny black tar. The tar was dissolved in 100 cm^3 of chloroform. A flash chromatography column (45 cm × 5 cm) was packed with neutral activated alumina (Brockman activity 1, 80–200 mesh) and the chloroform solution containing the tar was placed on the column. The porphyrin was chromatographed on the column with 10% (v/v) pyridine–dichloromethane. Long wavelength UV light was used to follow the porphyrin elution band through the column. Fractions containing the porphyrin were combined and the solvent removed by rotary evaporation. A total of 500 mg of tetra-6-quinoline porphyrin was recovered as dark purple crystals (1% yield). A UV–vis and a ^{1}H NMR spectra were recorded for this novel

compound. A Beer's law analysis was also performed in order to calculate the Soret band extinction coefficient. Found: C, 82.0; H, 4.3; N, 13.4. Calc.: C, 82.1; H, 4.2; N, 13.7%.

(3) *Tetra*-6-[N-*methyl*(^{13}C) *quinoline*] *porphyrin tetraiodide salt* (T6NMQP)

Methylation of the quinoline nitrogens was accomplished by refluxing tetra-6-quinoline porphyrin (0.3 g, 0.37 mmol) and ^{13}C-methyl iodide (5.0 g, 34.3 mmol) in 50% (v/v) chloroform–dimethylformamide for 24 h. After cooling to room temperature, the reaction mixture was mixed with 250 cm^3 of dichloromethane to precipitate the product. The methylated porphyrin salt was recovered by filtration and was washed with 15 cm^3 portions of hot dichloromethane until the filtrate was clear. The result was recovery of 0.51 g of product as a brown solid (99% yield). A UV–vis spectrum and ^{1}H proton NMR spectrum were recorded for this porphyrin. A Soret band extinction coefficient was also calculated from a Beer's law plot. Found: C, 48.5; H, 3.4; N, 7.8. Calc.: C, 48.4; H, 3.3; N, 8.1%.

(4) *Copper–tetra*-6-[N-*methyl*(^{13}C) *quinoline*] *porphyrin tetraiodide salt* (Cu–T6NMQP)

The porphyrin was metallated by mixing methylated quinoline porphyrin (75 mg, 0.05 mmol) and $CuCl_2(H_2O)_2$ (75 mg, 0.44 mmol) in 25 cm^3 of dimethylformamide and refluxing for 1 h. The resulting solution was chilled to 0°C and stored at that temperature overnight to precipitate the product. A total of 62 mg of copper–tetra-6-[N-methyl(^{13}C) quinoline] porphyrin tetraiodide salt was recovered from the solvent by filtration followed by cold (0°C) acetone washings (85% yield). A UV–vis spectrum was taken for this porphyrin with the determination of a Soret band extinction coefficient from the Beer's law plot.

(5) *Copper–tetra*-6-*quinoline porphyrin* (Cu–T6QP)

The tetra-6-quinoline porphyrins are novel compounds so the non-methylated free base porphyrin was metallated with copper in order to complete UV–vis spectral characterization for the series. Starting with tetra-6-quinoline porphyrin (75 mg, 0.09 mmol) and $CuCl_2(H_2O)_2$ (75 mg, 0.44 mmol), 80 mg of copper–tetra-6-quinoline porphyrin was obtained using the metallation procedure described above (100% yield). A UV–vis spectrum was obtained and a Soret band extinction coefficient was determined from the Beer's law analysis.

RESULTS AND DISCUSSION

The successful oxidation of the 6-methyl quinoline to form 6-quinoline carboxaldehyde was initially confirmed by the presence of a carbonyl IR band at 1700 cm^{-1} in the crude reaction product. Further characterization was accomplished by GC–MS. The gas chromatogram shows the presence of two major components in the product. The mass spectra were compared with reference spectra of 6-methyl quinoline and 3-quinoline carboxaldehyde.[12] Analysis of the mass spectra revealed the two components to be methyl quinoline and quinoline carboxaldehyde. Higher oxidation products such as quinoline alcohols and carboxylic acids were not detected. Attempts to rigorously purify the aldehyde were not attempted since the next reaction step, porphyrin condensation, would not be adversely affected by the presence of methyl quinoline while further handling of the reaction product would result in aldehyde losses.

The 6-quinoline porphyrin series represents a new *meso*-substitution. Spectroscopic analyses for these compounds were carried out with UV–vis and NMR. The UV–vis spectrum for the tetra-6-quinoline porphyrin is shown in Fig. 2(A). The features show a strong Soret band at 424 nm with *Q*-bands at 518, 553, 592 and 640 nm. The relative intensities for these features are typical for symmetric *meso*-substituted porphyrins.[1] The copper–tetra-6-quinoline UV–vis spectrum is shown in Fig. 2(B). This spectrum shows the hypso characteristics typical for copper porphyrins where the intensity sequence is Soret $\gg \alpha > \beta$ and the energies are slightly blue shifted.[1] The spectral features and Soret band extinction coefficients for the four quinoline porphyrins are summarized in Table 1.

^{1}H NMR spectroscopy was used to further characterize both free-base porphyrin structures. The tetra-6-quinoline porphyrin ^{1}H NMR in $CDCl_3$ showed resonances in the aromatic region (7.5–9.5 ppm) whose chemical shifts are similar to those reported for 6-quinoline.[13] A large singlet resonance at 8.8 ppm is due to the eight chemically equivalent β-pyrrole protons on the parent porphyrin ring. The only other peak of interest occurred at -2.6 ppm which represented the two protons on the porphyrin core nitrogens. Integration of the quinoline protons and the β-pyrrole protons gave an intensity ratio of 3:1, thus indicating a symmetrically substituted product.

The ^{1}H NMR spectra of the tetra-6-[N-methyl (^{13}C) quinoline] porphyrin in perdeuterated dimethyl sulphoxide was taken in order to determine the extent of methylation and is shown in Fig. 3. A ^{1}H resonance from the N-methyl(^{13}C) protons

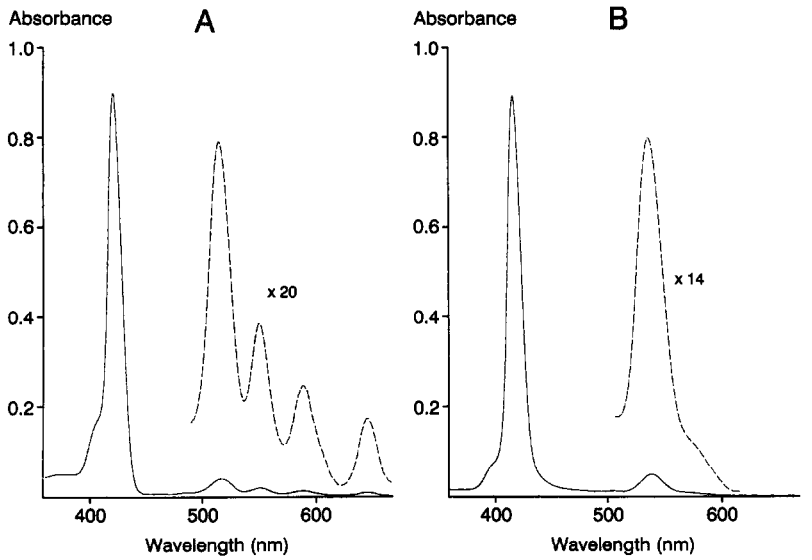

Fig. 2. (A) UV–vis spectrum of tetra-6-quinoline porphyrin in chloroform. *Q*-band expansion: × 20. (B) UV–vis spectrum of copper tetra-6-quinoline porphyrin in chloroform. *Q*-band expansion: × 14. The methylated porphyrins exhibit similar UV–vis spectra, with the observed spectral features summarized in Table 1.

was observed at 5.0 ppm with a ^{1}H–^{13}C *J*-coupling of 145.1 Hz. The doublet appearance of this resonance confirmed all methyl groups originated from the 99% ^{13}C labelled methyl iodide. Integration of the aromatic resonances (8.0–10.0 ppm) and the N-methyl(^{13}C) resonance gave an intensity ratio of 2:1. This indicated complete methylation of the porphyrin. Resonances due to residual water and protonated DMSO were observed at 3.4 and 2.5 ppm, respectively.

Although no rigorous solubility work was performed with these porphyrins, it was observed that the N-methylated iodide salts exhibited distilled water solubilities comparable to the tetra-4-(N-

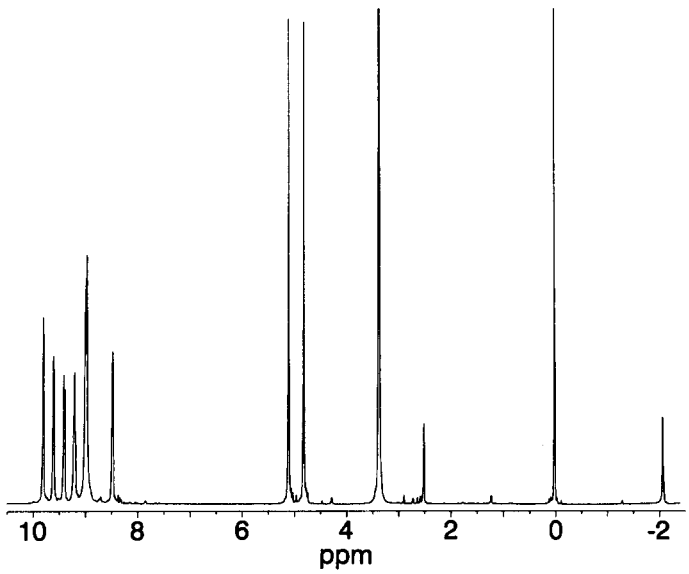

Fig. 3. ^{1}H NMR spectrum of tetra-6-[N-methyl(^{13}C) quinoline] porphyrin tetraiodide salt in perdeuterated dimethylsulphoxide. The resonances resulting from the porphyrins' protons are described in the text. The resonance at 4.4 ppm is due to residual water and the resonance at 2.5 ppm is due to protonated DMSO.

Table 1. Absorption spectral features and Soret band extinction coefficients for tetra-6-quinoline porphyrin series

Porphyrin	Spectral features (nm)[a] B	Q_y (1,0]	Q_y [0,0]	Q_x [1,0]	Q_x [0,0]	Extinction coefficients (ε) ($M^{-1}\,cm^{-1} \times 10^5$)
T6QP	424	518	553	592	650	
	(22.7)	(1.0)	(0.6)	(0.3)	(0.2)	
T6NMQP	419	516	554	580	637	2.39
	(14.5)	(1.0)	(0.4)	(0.4)	(0.2)	
Cu–T6QP	420	541	580	—	—	
	(18.3)	(1.0)	(0.2)			
Cu–T6NMQP	418	543	580	—	—	2.36
	(9.0)	(1.0)	(0.3)			

[a]Peak intensities relative to the first Q-band $\{Q_y$ [1,0]$\}$ are shown below the wavelengths in parentheses.

methyl pyridyl) porphyrins. The non-methylated porphyrins were soluble in methylene chloride and chloroform.

CONCLUSIONS

Selenium oxide was shown to be a good reagent for the mild oxidation of 6-methyl quinoline without the formation of higher oxidation products. The yields for this reaction were sufficient to provide enough aldehyde for the porphyrin synthesis. The Adler modified Rothemund condensation of the quinoline aldehyde with pyrrole was successful for the formation of the desired *meso*-substituted porphyrin, however, yields were very low. The four quinoline porphyrins prepared in this work had UV–vis spectra whose features were consistent with symmetric aryl-*meso* substitution on the porphyrin ring. These UV–vis spectra were sufficient for the quantitation and confirmation of product formation.

Acknowledgements—We would like to acknowledge the assistance of Dr Natalie Foster, Dr Douglas Brown and William Anderson. This work was supported by grant No. DMR-8553275 from the Solid State Chemistry Program of the Division of Materials Research at the National Science Foundation (J.E.R.). Additional support was obtained through the Presidential Young Investigator Program (J.E.R.) from: Air Products and Chemicals, American Cyanamid, Cambridge Isotopes Laboratories, Hercules and Monsanto Company.

REFERENCES

1. D. Dolphin, *The Porphyrins*. Academic Press, New York (1978).
2. R. F. Pasternak, E. H. Gibbs and J. J. Villafranca, *Biochemistry* 1983, **22**, 2406.
3. D. R. Doirion and C. J. Gomer (Eds), *Porphyrin Localization and Treatment of Tumors*. A. R. Liss, New York (1984).
4. A. D. Adler, F. R. Longo and W. Shergalis, *J. Am. Chem. Soc.* 1964, **86**, 3145.
5. A. D. Adler, F. R. Longo, J. D. Finarelli, J. Goldmacher, J. Assour and L. Korsakoff, *J. Org. chem.* 1968, **32**, 476.
6. S. Sugata, S. Yamanouchi and Y. Matsushima, *Chem. Pharm. Bull.* 1977, **25**, 884.
7. E. B. Fleischer, *Inorg. Chem.* 1962, **1**, 493.
8. P. Hambright and E. B. Fleischer, *Inorg. Chem.* 1970, **9**, 1757.
9. P. Hambright, T. Gore and M. Burton, *Inorg. Chem.* 1976, **15**, 2314.
10. C. E. Teague and A. Roe, *J. Am. Chem. Soc.* 1951, **73**, 688.
11. Selenium oxide is described in the Merck Index (ref No. 8386) as an intense local irritant of the skin and eyes. *The Merck Index, 11th edn.* Merck and Co., Inc., Rahway, New Jersey (1989).
12. EPA/NIH Mass Spectra Data Base, Vol. 1; U.S. Government Printing Office, Washington, D.C. (1978).
13. G. Jones, *The Chemistry of Heterocyclic Compounds, A Series of Monographs, Quinolines, Part 1* (Edited by A. Weissberger and E. C. Taylor). John Wiley, New York (1977).

Polyhedron Vol. 9, No. 20, pp. 2533–2547, 1990
Printed in Great Britain

0277–5387/90 $3.00+.00
© 1990 Pergamon Press plc

SYNTHETIC AND STRUCTURAL STUDIES ON COBALT CARBONYL COMPLEXES CONTAINING INDIUM

L. M. CLARKSON, K. McCRUDDEN and N. C. NORMAN*

Department of Chemistry, The University, Newcastle upon Tyne NE1 7RU, U.K.

and

L. J. FARRUGIA

Department of Chemistry, The University, Glasgow G12 8QQ, U.K.

(*Received* 11 *April* 1990; *accepted* 20 *June* 1990)

Abstract—The reaction between $InCl_3$ and one equivalent of $K[Co(CO)_3(PPh_3)]$ affords the complex $[InCl_2(PPh_3)\{Co(CO)_4\}]$ (**8**), which was characterized by X-ray diffraction. Compound **8** crystallizes in the triclinic space group $P\bar{1}$ with $a = 15.044(4)$, $b = 10.292(3)$, $c = 16.937(6)$ Å, $\alpha = 89.61(3)$, $\beta = 110.14(3)$, $\gamma = 91.04(2)°$ and $Z = 4$. The structure contains two essentially identical molecules per asymmetric unit and comprises an indium centre bonded to two chlorine atoms, a PPh_3 ligand and a $Co(CO)_4$ fragment in a tetrahedral coordination geometry. The solution state rearrangement of **8** to a complex, **9**, containing $Co(CO)_3(PPh_3)$ fragments is described and discussed. The reaction between $InCl_3$ and two equivalents of $K[Co(CO)_3(PPh_3)]$ affords two complexes. The first was characterized as $[Co(CO)_3(PPh_3)_2][InCl_2\{Co(CO)_4\}_2]$ (**10**) by X-ray crystallography. Compound **10** crystallizes in the triclinic space group $P\bar{1}$ with $a = 13.466(5)$, $b = 14.176(6)$, $c = 16.162(4)$ Å, $\alpha = 75.47(3)$, $\beta = 115.19(2)$, $\gamma = 114.17(3)°$ and $Z = 2$. The structure is a salt containing the $[Co(CO)_3(PPh_3)_2]^+$ cation and the indium-centred anion $[InCl_2\{Co(CO)_4\}_2]^-$. The latter contains an indium centre bonded to two chlorine atoms and two $Co(CO)_4$ fragments in a tetrahedral geometry. Spectroscopic data on the second complex obtained from this reaction indicates the formula $[InCl\{Co(CO)_3(PPh_3)\}_2]$ (**12**). We have also characterized the anion of **10** as its PPN salt (PPN = $Ph_3PNPPh_3^+$), $[PPN][InCl_2\{Co(CO)_4\}_2]$ (**11**). Compound **11** crystallizes in the triclinic space group $P\bar{1}$ with $a = 9.957(2)$, $b = 20.262(3)$, $c = 23.058(5)$ Å, $\alpha = 82.16(2)$, $\beta = 86.13(2)$, $\gamma = 84.00(2)°$ and $Z = 4$. The two crystallographically independent anions are similar in all respects to the anion in **10**. The reaction between $InCl_3$ and three equivalents of $K[Co(CO)_3(PPh_3)]$ affords $[In\{Co(CO)_3(PPh_3)\}_3]$ (**14**), spectroscopic data for which are described and discussed. We have also examined the reaction between InCl and $[Co_2(CO)_6(PPh_3)_2]$ which affords the dicobalt–indium chloride complex $[InCl(PPh_3)\{Co(CO)_3(PPh_3)\}_2]$ (**13**). Spectroscopic and analytical data are presented for all new complexes together with a discussion of their solution state properties which involve partial dissociation and rearrangement reactions.

Many examples exist of compounds containing transition metal–indium bonds.[1,2] In this introduction, however, we shall restrict ourselves primarily to those compounds which contain cobalt and are therefore of most relevance to this work.

One of the earliest such compounds to be described was $[In\{Co(CO)_4\}_3]$ (**1**), prepared by Hieber and Teller[3] from the metallic elements and

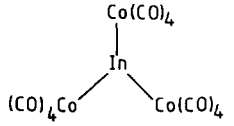

1

* Author to whom correspondence should be addressed.

CO under high pressure. This compound was later prepared by Schrauzer *et al.*[4] from indium metal, $[Co_2(CO)_8]$ and CO in toluene at high pressure and reported to be a catalyst for the dimerization of norbornadiene, and a subsequent report by Robinson and Schussler[5] presented details of a crystal structure determination which revealed a trigonal planar indium centre bonded to three $Co(CO)_4$ fragments. The reaction between **1** and $[Co(CO)_4]^-$ has been described by Robinson and co-workers[6] and affords the anionic complex $[In\{Co(CO)_4\}_4]^-$ (**2**). The solution state properties of **2** were also reported[6] with regard to dissociation; in CH_2Cl_2 it is essentially undissociated whereas in THF it dissociates to give **1** and $[Co(CO)_4]^-$, whilst in DMSO complete dissociation to $[In]^{3+}$ and $[Co(CO)_4]^-$ is observed. Two further Lewis base adducts with **1** were also mentioned, viz. $[In(OPPh_3)\{Co(CO)_4\}_3]$ and $[Cl(In\{Co(CO)_4\}_3)_2]^-$.

Indium halide fragments coordinated to cobalt have also been known for many years. Graham has described the insertion of InBr into $[Co_2(CO)_8]$ in THF which affords $[InBr(THF)\{Co(CO)_4\}_2]$ (**3**),[7] although the THF is readily lost to give $[InBr\{Co(CO)_4\}_2]$ (**4**), which is presumed to be dimeric. The same reaction, however, if carried out in benzene yields the polynuclear complex $[In_3\{Co(CO)_4\}_3(\mu\text{-}Br)_3\{\mu_3\text{-}Co(CO)_3\}]$ (**5**),[7,8] the structure of which was determined by X-ray crystallography.[8,9] Compound **3** is also produced from the reaction between $InBr_3$ and $2Na[Co(CO)_4]$ in THF and Graham has also described[7b] the synthesis of $[In(acac)\{Co(CO)_4\}_2]$ from **3** and the synthesis of **1** from $InBr_3$ and $3Na[Co(CO)_4]$.

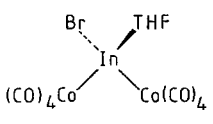

3

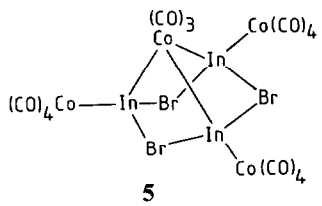

5

The anionic complex $[InBr_2\{Co(CO)_4\}_2]^-$ (**6**) has been prepared as the $[NEt_4]$ salt, from the reaction between InBr and $[Co_2(CO)_8]$ in the presence of $[NEt_4]Br$ and structurally characterized,[10] and Hsieh and Mays[11] have described the synthesis of

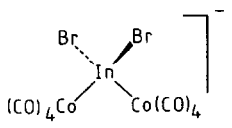

6

$[InCl\{Co(CO)_4\}_2]$ (**7**) by three methods: (i) $InCl_3 + 2Na[Co(CO)_4]$, (ii) insertion of InCl into $[Co_2(CO)_8]$ and (iii) reaction of InCl with $[Hg\{Co(CO)_4\}_2]$.

Finally, we note that Ruff[12] has reported the reaction between $InBr_3$ and one equivalent of $[PPN][Co(CO)_4]$ which gives the adduct $[PPN][InBr_3\{Co(CO)_4\}]$ and Burlitch *et al.*[13] have described the synthesis of the adduct $[PPN][InPh_3\{Co(CO)_4\}]$ from $[PPN][Co(CO)_4]$ and $InPh_3$ ($PPN = Ph_3PNPPh_3^+$].

Herein we report details of our own work involving the reactions between $InCl_3$ and $K[Co(CO)_3(PPh_3)]$.

RESULTS AND DISCUSSION

The reaction between $InCl_3$ and one equivalent of $K[Co(CO)_3(PPh_3)]$ in THF gave a pale yellow solution from which very pale yellow crystals were obtained after work-up and crystallization from CH_2Cl_2–hexane mixtures. An IR spectrum obtained on a solution of these crystals in THF is shown in Fig. 1(a) with numerical data in Table 1. In order to determine the structure of this complex, an X-ray diffraction study was undertaken, the results of which are presented in Fig. 2 and Table 2. The structure comprises an indium centre in a tetrahedral coordination environment bonded to two chlorine atoms, a $Co(CO)_4$ fragment and a PPh_3 ligand, $[InCl_2(PPh_3)\{Co(CO)_4\}]$ (**8**) and can

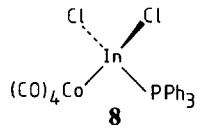

8

be described as a phosphine adduct of the neutral, trivalent indium complex, $[InCl_2\{Co(CO)_4\}]$. Two

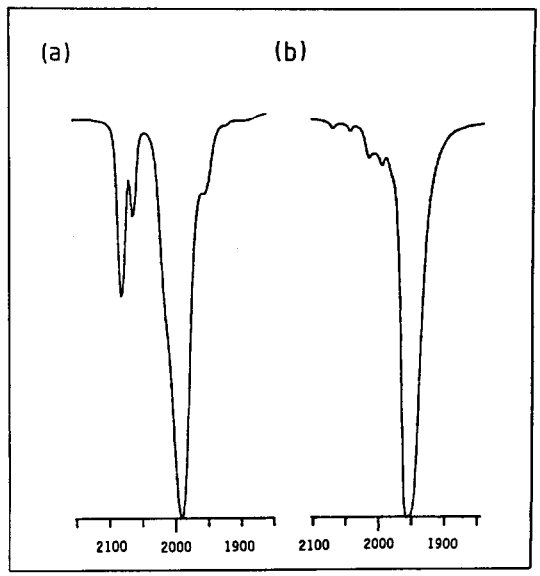

Fig. 1. IR spectra in the carbonyl stretching region, (a) **8** and (b) **9**, recorded in THF solution.

Table 1. Spectroscopic and analytical data for the complexes

Compound	ν(CO) (cm^{-1})[a]	Analysis[b] C	H
$[InCl_2(PPh_3)\{Co(CO)_4\}]$ (**8**)	2080m, 2063w, 1991s, 1955sh[c]	42.4 (42.7)	2.3 (2.5)
$[Co(CO)_3(PPh_3)_2][InCl_2\{Co(CO)_4\}_2]$ (**10**)	2077w, 2060m, 1995s, 1886m	46.1 (47.2)	2.3 (2.5)
$[Ph_3PNPPh_3][InCl_2\{Co(CO)_4\}_2]$ (**11**)	2077w, 2060m, 1993s, 1886m	—	
$[InCl(PPh_3)\{Co(CO)_3(PPh_3)\}_2]$ (**13**)	2021w, 2000w, 1952s	57.4 (56.3)	3.6 (3.5)
$[In\{Co(CO)_3(PPh_3)\}_3]$ (**14**)	1988w, 1943s	57.8 (56.9)	3.6 (3.4)
	1994w, 1947s[d]		
	1994w, 1946s[e]		
	1980w, 1936s, 1838w[f]		

[a] Measured in THF solution.
[b] Values shown are percentages; calculated values in parentheses.
[c] w = weak, m = medium, s = strong, sh = shoulder with respect to intensities.
[d] Measured in CH_2Cl_2 solution.
[e] Measured in toluene solution.
[f] Measured in MeCN solution.

molecules of **8** are present in the asymmetric unit of the unit cell which are similar in their gross structural form except in the conformations about the In—Co bond. Thus the torsion angle defined by P(1)—In(1)—Co(1)—C(2) differs by about 25° in the two molecules, whereas the orientation of the PPh_3 ligand relative to the $InCl_2$ fragment differs by only 5°. The In—Co bond lengths [In(1a)—Co(1a) 2.540(3), In(1b)—Co(1b) 2.543(3) Å] are in the usual range for such bonds, which we will discuss later, and are axial with respect to the trigonal bipyramidal geometry about cobalt. The In—P lengths are 2.607(5) and 2.611(5) Å which can be compared with a standard single bond value of 2.60 Å derived from the sum of the covalent radii of indium and phosphorus.[14] While phosphine complexes of indium halides are quite common[15] the only published structural data of which we are aware are for the complex $[InCl_3(PPh_3)_2]$[16] for which the In—P bond lengths are 2.701(5) and 2.723(5) Å, slightly longer than those in **8** possibly as a result of increased steric crowding around the indium centre.

Analytical data for **8** are given in Table 1 and are in accord with the formula derived from the X-ray analysis. However, when a sample of **8** was

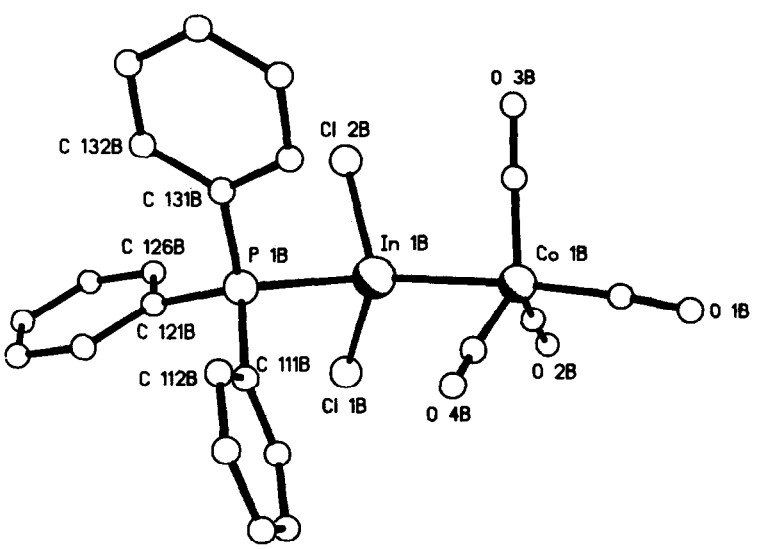

Fig. 2. Molecular structure of one molecule of **8** showing the atom numbering scheme adopted. Hydrogen atoms omitted for clarity.

Table 2. Selected bond lengths (Å) and angles (°) for $[InCl_2(PPh_3)\{Co(CO)_4\}]$ (**8**)[a]

In(1a)—Co(1a)	2.540(3)	In(1a)—P(1a)	2.607(5)
In(1a)—Cl(1a)	2.385(5)	In(1a)—Cl(2a)	2.359(6)
In(1b)—Co(1b)	2.543(3)	In(1b)—P(1b)	2.611(5)
In(1b)—Cl(1b)	2.380(5)	In(1b)—Cl(2b)	2.370(6)
Co(1a)—In(1a)—P(1a)	121.1(2)	Co(1a)—In(1a)—Cl(1a)	113.5(3)
Co(1a)—In(1a)—Cl(2a)	113.6(2)	P(1a)—In(1a)—Cl(1a)	99.1(2)
P(1a)—In(1a)—Cl(2a)	100.0(2)	Cl(1a)—In(1a)—Cl(2a)	107.6(2)
Co(1b)—In(1b)—P(1b)	120.6(2)	Co(1b)—In(1b)—Cl(1b)	116.3(2)
Co(1b)—In(1b)—Cl(2b)	114.3(2)	P(1b)—In(1b)—Cl(1b)	99.5(2)
P(1b)—In(1b)—Cl(2b)	98.9(2)	Cl(1b)—In(1b)—Cl(2b)	104.6(2)

[a] Numbers in parentheses are the estimated standard deviation in the least significant digit in this and all subsequent tables.

dissolved in CD_2Cl_2 in order to obtain a ^{31}P NMR spectrum, the initially colourless solution became yellow after a few minutes and a small amount of white solid was precipitated, some of which slowly redissolved. The ^{31}P NMR spectrum obtained on this sample showed signals at 63.4 and 6.4 ppm, the former consistent with PPh_3 bonded to cobalt[17] and the latter with free phosphine or possibly phosphine bonded to indium. Moreover, on removal of the CO_2Cl_2 and after dissolving the resultant yellow oil in THF, the IR spectrum obtained revealed that a rearrangement had certainly taken place [Fig. 1(b)], whilst the peak values ($\nu C{\equiv}O$ 2076w, 2050w, 2021w, 2002w, 1957s cm^{-1}), especially the major, intense absorption at 1957 cm^{-1}, were also suggestive of a $Co(CO)_3(PPh_3)$ fragment.[17] Thus **8** would appear to rearrange in CD_2Cl_2 solution affording a complex in which PPh_3 is bonded to cobalt, presumably of the form $[InCl_2\{Co(CO)_3(PPh_3)\}]$ (**9**). However, crystals of **8** were originally obtained from CH_2Cl_2 solution after work-up of the reaction. It would therefore appear that whilst **9** is the major compound present in solution, and, of course, the anticipated product from this reaction, a small amount of **8** is also present which crystallizes more readily under the conditions employed. The subsequent rearrangement of **8** into **9** after redissolution in CH_2Cl_2 suggests that an equilibrium shown in eq. (1) is present which in CH_2Cl_2 solution lies predominantly to the right. However, as **8** is apparently less soluble than **9**, crystallization affords **8** which progressively shifts the equilibrium in solution to the left-hand side [as represented in eq. (1)]. This cannot be the whole story since the rearrangement of **9** to **8** requires more CO, relative to cobalt and indium, than is originally present in the reaction. We suggest that this accounts for the low isolated yields of **8** (typically 48%) but we have not observed or isolated any carbonyl-deficient compounds from this reaction.

$$[InCl_2(PPh_3)\{Co(CO)_4\}] \quad (\mathbf{8}) \rightleftharpoons [InCl_2\{Co(CO)_3(PPh_3)\}] + CO \quad (\mathbf{9}) \quad (1)$$

As a partial explanation for these results, we note that the observed lability of the PPh_3 ligand on cobalt is in accord with the generally observed substitution lability of ligands in CoL_4 fragments.[18] However, we did not encounter such problems in the chemistry of $K[Co(CO)_3(PPh_3)]$ with antimony or bismuth halides[17] and suggest that the reason for these observations in the system described above is that the Lewis acidic indium centre effectively competes with the cobalt for the phosphine ligand.

In an effort to obtain **8** by another, potentially higher yield route we carried out the following reaction. $InCl_3$ was dissolved in THF together with one equivalent of PPh_3. After stirring for 15 min, one equivalent of $K[Co(CO)_4]$ was added and work-up followed by crystallization from CH_2Cl_2–hexane mixtures afforded a pale yellow crystalline material which analysed correctly for **8**.* When these crystals were dissolved in CD_2Cl_2 a colour change from colourless to yellow was observed and the ^{31}P NMR spectrum was similar to that observed previously for **8** and showed signals at 63.4 and 6.2 ppm. Removal of the CD_2Cl_2 and redissolution in THF gave a yellow solution, the IR spectrum of which was identical to that shown in Fig. 1(b), i.e. that of **9**. The THF solution IR spectrum of the original pale yellow crystals showed a pattern almost ident-

* Found: C, 42.5; H, 2.3. Compound **8** requires: C, 42.7; H, 2.5 (Table 1).

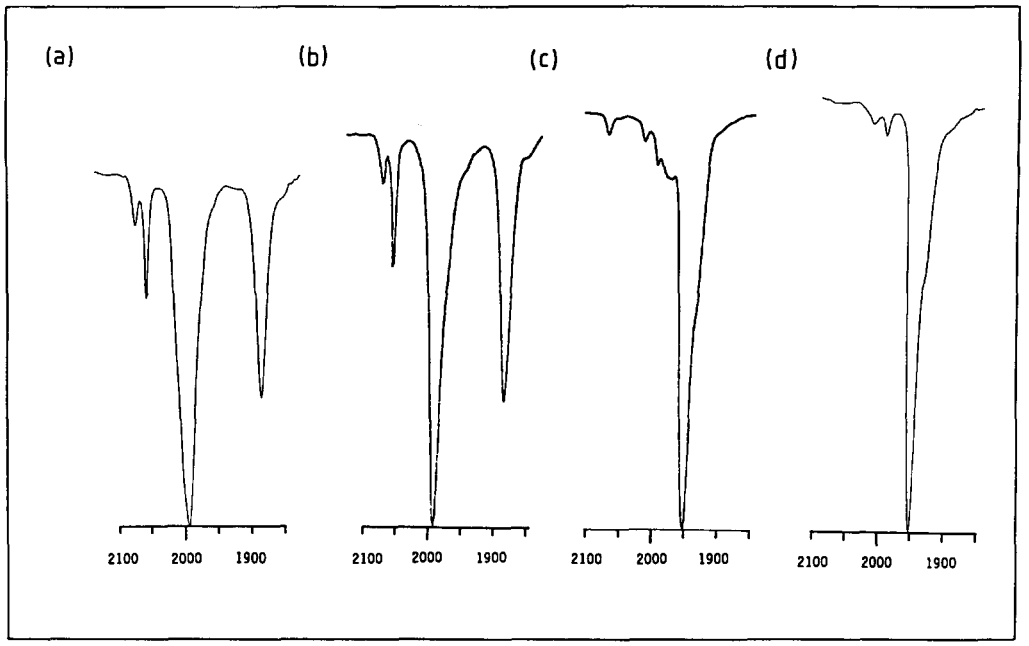

Fig. 3. IR spectra in the carbonyl stretching region, (a) **10**, (b) **11**, (c) **12** and (d) **13**.

ical to that found for **8** [Fig. 1(a)] but with values 2090m, 2075w, 2004s cm^{-1}, i.e. approximately 10–12 cm^{-1} higher in frequency. We have no explanation for this particular observation except to say that we cannot be sure as to whether the solid-state structure found for **8** is also present in THF solution (it is certainly not present in CH_2Cl_2 solution). The pattern of absorptions in the IR spectrum is consistent with a $Co(CO)_4$ group, but the extent to which the phosphine remains coordinated to indium is unclear. It may well be concentration dependent and thereby affect the frequencies observed in the IR spectra but not the number and intensity of the peaks.*

The reaction between $InCl_3$ and two equivalents of $K[Co(CO)_3(PPh_3)]$ is more complex and gives rise to at least two products. Work-up followed by recrystallization from THF–hexane mixtures afforded a heterogeneous sample consisting of yellow plate-like crystals and an orange crystalline powder. An IR spectrum was obtained on a THF solution of the yellow crystals [Fig. 3(a), Table 1] together with a ^{31}P NMR spectrum which showed a singlet at 55.9 ppm (CD_2Cl_2), but in order to ascertain the structure, an X-ray diffraction study was carried out. The results are presented in Figs 4 and 5 and Table 3 and establish the structure as a salt with the formula $[Co(CO)_3(PPh_3)_2][InCl_2\{Co(CO)_4\}_2]$ (**10**). The cation $[Co(CO)_3(PPh_3)_2]^+$ has not been previously characterized by X-ray methods and comprises a trigonal bipyramidal cobalt centre with axial PPh_3 ligands and equatorial carbonyls.[19] The anion $[InCl_2\{Co(CO)_4\}_2]^-$ consists of a tetrahedral indium centre bonded to two chlorine atoms and two $Co(CO)_4$ fragments, the latter adopting a configuration such that the indium occupies an axial site in the trigonal bipyramidal coordination geometry around the cobalt, as was also observed for **8**. The Co—In bond lengths [In(1)—Co(1) 2.617(2) and In(1)—Co(2) 2.608(2) Å] are slightly longer than those observed in **8** but comparable to those observed in the dibromo analogue $[InBr_2\{Co(CO)_4\}_2]^-$ (**6**),[10] [In—Co 2.638(12), 2.644(14) molecule A and 2.637(12), 2.596(14) Å molecule B]. Other In—Co bond lengths of interest are those in **5**[8,9] [terminal $(CO)_4Co$—In 2.532(5), 2.585(5), 2.582(6) Å; μ-$(CO)_3Co$—In 2.573(5), 2.637(6), 2.591(5) Å] and in **1**[5] [In—Co 2.590(3), 2.595(3), 2.597(3) Å]. Clearly, a value of 2.50–2.65 Å is typical for a In—Co single bond though little else of any significance can be gathered from these values. We note, however, that in all cases where indium is bonded to a $Co(CO)_4$ fragment, it resides in an axial position with respect to the cobalt centre.

We will return to the formation of **10** and the nature of the second product shortly but at this stage it is useful to include the results of another

* We have no evidence for the rearrangement of **8** to **9** in THF solution.

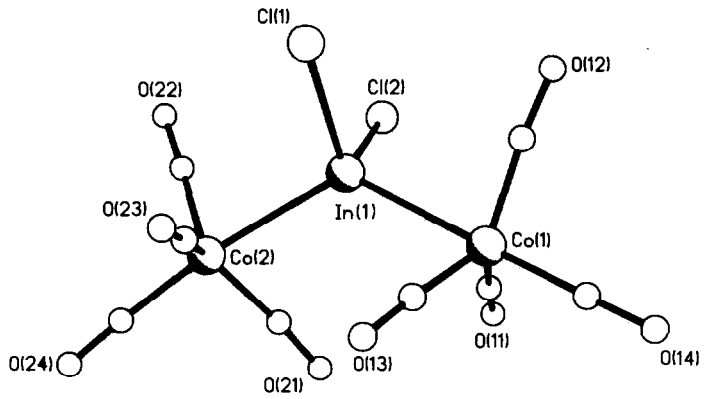

Fig. 4. Molecular structure of the anion $[InCl_2\{Co(CO)_4\}_2]^-$ of **10** showing the atom numbering scheme adopted.

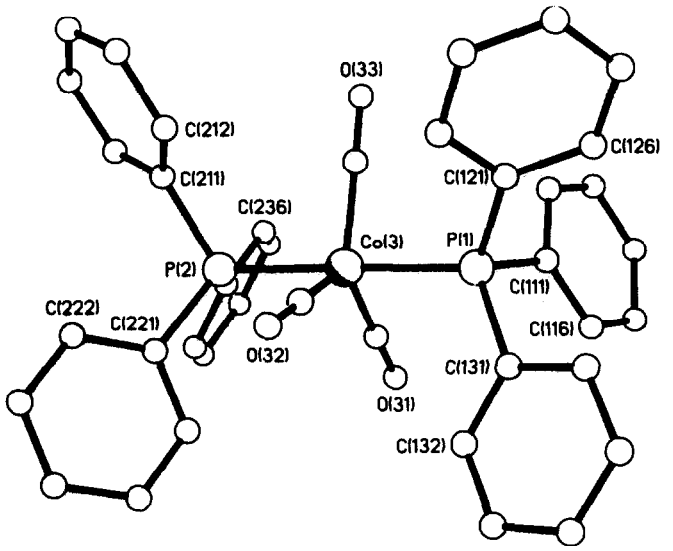

Fig. 5. Molecular structure of the cation $[Co(CO)_3(PPh_3)_2]^+$ of **10** showing the atom numbering scheme adopted. Hydrogen atoms omitted for clarity.

Table 3. Selected bond lengths (Å) and angles (°) for $[Co(CO)_3(PPh_3)_2][InCl_2\{Co(CO)_4\}_2]$ (**10**)

In(1)—Co(1)	2.617(2)	In(1)—Co(2)	2.608(2)
In(1)—Cl(1)	2.420(3)	In(1)—Cl(2)	2.407(2)
Co(1)—In(1)—Co(2)	121.5(1)	Co(1)—In(1)—Cl(1)	110.1(1)
Co(1)—In(1)—Cl(2)	106.3(1)	Co(2)—In(1)—Cl(1)	104.7(1)
Co(2)—In(1)—Cl(2)	110.2(1)	Cl(1)—In(1)—Cl(2)	102.5(1)

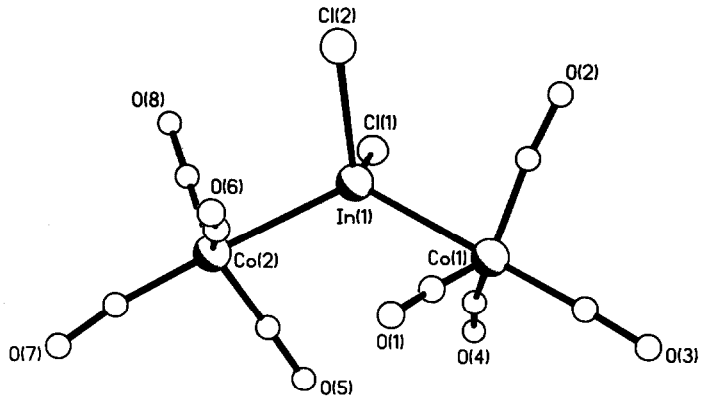

Fig. 6. Molecular structure of one of the anions $[InCl_2\{Co(CO)_4\}_2]^-$ of **11** showing the atom numbering scheme adopted.

Table 4. Selected bond lengths (Å) and angles (°) for $[PPN][InCl_2\{Co(CO)_4\}_2]$ (**11**)

In(1)—Co(1)	2.600(4)	In(1)—Co(2)	2.621(4)
In(1)—Cl(1)	2.417(7)	In(1)—Cl(2)	2.420(6)
In(2)—Co(3)	2.625(4)	In(2)—Co(4)	2.609(4)
In(2)—Cl(3)	2.409(6)	In(2)—Cl(4)	2.398(7)
Co(1)—In(1)—Co(2)	120.2(2)	Co(1)—In(1)—Cl(1)	107.0(2)
Co(1)—In(1)—Cl(2)	111.7(2)	Co(2)—In(1)—Cl(1)	109.1(2)
Co(2)—In(1)—Cl(2)	104.7(2)	Cl(1)—In(1)—Cl(2)	102.7(3)
Co(3)—In(2)—Co(4)	123.5(2)	Co(3)—In(2)—Cl(3)	108.1(2)
Co(3)—In(2)—Cl(4)	104.9(2)	Co(4)—In(2)—Cl(3)	106.8(2)
Co(4)—In(2)—Cl(4)	109.4(3)	Cl(3)—In(2)—Cl(4)	102.1(3)

crystal structure determination carried out on the complex $[PPN][InCl_2\{Co(CO)_4\}_2]$ (**11**), obtained from the reaction between $InCl_3$ and two equivalents of $[PPN][Co(CO)_4]$.[20] The results for **11** are presented in Fig. 6 and Table 4 and show that both the crystallographically-independent anions, $[InCl_2\{Co(CO)_4\}_2]^-$, are similar in all respects to **10**. The In—Co bond lengths are *ca* 2.6 Å [In(1)—Co(1) 2.600(4), In(1)—Co(2) 2.621(4); In(2)—Co(3) 2.625(4), In(2)—Co(4) 2.609(4) Å] whilst the Co—In—Co and Cl—In—Cl angles differ by no more than 3.3 and 0.6°, respectively. Moreover, the relative orientations of the $Co(CO)_4$ fragments are also similar as judged by the torsion angles Cl(2)—In(1)—Co(1)—C(11) [−49.2(3)°] and Cl(2)—In(1)—Co(2)—C(23) [−155.3(4)°] in **10** compared with the corresponding angles in **11** of −44.6(10) and −160.6(9)° for molecule A and −50.1(10) and −154.3(12)° for molecule B.

The solution IR spectrum of **11** [Fig. 3(b), Table 1] is very similar to that observed for **10**. Both were obtained in THF but the absorption at 1886 cm^{-1} is characteristic of $[Co(CO)_4]^-$ [20] and therefore indicates that partial In—Co bond heterolysis occurs in this solvent.* Dissociation in polar coordinating solvents is commonly observed in the chemistry of transition metal indium compounds, as cited in the Introduction for **1** and **2**[6] and as reported for related complexes containing $Mo(CO)_3(\eta\text{-}C_5H_5)$[2] and $Mn(CO)_5$[21] fragments (see later).

Turning now to the mechanistic origin of **10**, the lability of the PPh_3 ligands on cobalt is again evident since the cobalt centres bonded to indium have clearly lost the phosphine present in the starting anionic complex, $[Co(CO)_3(PPh_3)]^-$, whereas the cobalt in the counter cation, $[Co(CO)_3(PPh_3)_2]^+$, has an additional phosphine ligand. The formation of **10** under the reaction conditions employed is fully repeatable and this reaction, together with that

* In the spectrum of **10** [Fig. 3(a)], we assume that the signals arising from $[Co(CO)_3(PPh_3)_2]^+$ are masked by the strong absorption at 1995 cm^{-1}.

which afforded **8**, were indicative of a situation in which $Co(CO)_3(PPh_3)$ fragments bonded to indium were very prone to phosphine loss. However, the second complex formed in the reaction between $InCl_3$ and two equivalents of $K[Co(CO)_3(PPh_3)]$ does appear, on the basis of spectroscopic data, to contain the $In–Co(CO)_3(PPh_3)$ moiety. This complex, **12**, was isolated as an orange powder and has an IR spectrum in THF solution with an intense absorption at 1952 cm^{-1} and much weaker peaks at 2075, 2021 and 2000 cm^{-1} [Fig. 3(c)] which is characteristic of a $Co(CO)_3(PPh_3)$ fragment. We were unable to obtain enough sample for either microanalysis or a ^{31}P NMR spectrum, however, the similarity between the spectra for **12** [Fig. 3(c)] and **9** [Fig. 1(b)] is readily apparent and provides further evidence for the presence of one, or more, $Co(CO)_3(PPh_3)$ groups. Moreover, we were able to obtain further insight into the nature of **12** due to some results obtained from a different project concerned with the insertion of indium monochloride into metal–metal bonds.[22] Thus the reaction between InCl and $[Co_2(CO)_6(PPh_3)_2]$[23] afforded a yellow crystalline complex, **13**, the THF solution IR spectrum of which is shown in Fig. 3(d), which again comprises a single strong absorption at 1952 cm^{-1} (Table 1). The ^{31}P NMR spectrum of **13** exhibited two broad singlets at 63.4 and 37.5 ppm in an approximate ratio of 2:1, the former attributable to a PPh_3 ligand bonded to cobalt (cf. the signal observed at 63.4 ppm for **9**). The latter signal is not due to free PPh_3 but may well be associated with an additional phosphine bonded to indium. We propose, therefore, the following formula for **13**, $[InCl(PPh_3)\{Co(CO)_3(PPh_3)\}_2]$, and support for this is also provided by the microanalytical data (Table 1). Mass spectra are often difficult to obtain for phosphine complexes due to facile loss of phosphine but an FAB mass spectrum obtained for **13** showed a signal at *m/z* 925 due to the ion $[In\{Co(CO)_3(PPh_3)\}_2]^+$; further details are given in the Experimental.

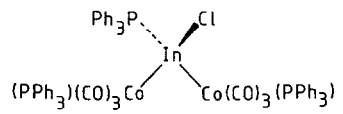

13

Thus, in summary, we feel that the nature of **13** is fairly well established by the spectroscopic and analytical data and suggest on the basis of the similarity of the IR spectra, that **12** is either the same complex or very closely related; perhaps $[InCl\{Co(CO)_3(PPh_3)\}_2]$.

The reaction between $InCl_3$ and three equivalents of $K[Co(CO)_3(PPh_3)]$ in THF afforded an orange solution from which well-formed orange crystals were obtained after work-up and recrystallization from CH_2Cl_2. Unfortunately these crystals lost solvent very rapidly when removed from the mother liquor and were unsuitable for X-ray diffraction studies. Similar problems were encountered with crystals obtained from other solvents [see Experimental] and as a result it was not possible to obtain an X-ray crystal structure. Nevertheless, an IR spectrum obtained on this material (Fig. 7, Table 1) and microanalytical data (Table 1) were consistent with the anticipated formula, $[In\{Co(CO)_3(PPh_3)\}_3]$ (**14**), a complex analogous to $[In\{Co(CO)_4\}_3]$ (**1**),[5] the probable structure of which is indicated in the diagram below.

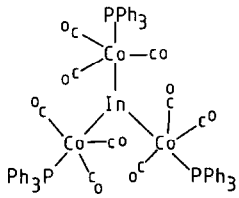

14

As we have discussed previously with regard to **9**, **12** and **13**, the appearance of a single strong absorption at *ca* 1940–1960 cm^{-1} is characteristic of a $Co(CO)_3(PPh_3)$ fragment, but the absence of absorptions at or around 1926 and particularly at 1830 cm^{-1}, due to the anion $[Co(CO)_3(PPh_3)]^-$,[20] indicate that **14** does not dissociate in THF, in contrast to the situation observed for $[In\{M(CO)_3(\eta\text{-}C_5H_5)\}_3]$ (M = Mo, W).[2] Spectra obtained for **14** in toluene, CH_2Cl_2 and MeCN are very similar

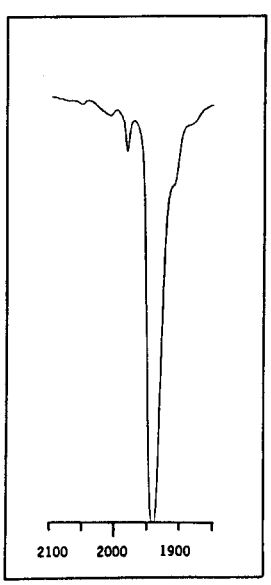

Fig. 7. IR spectrum in the carbonyl stretching region for **14** in THF solution.

to that observed in THF (Table 1), although a small peak observed at 1838 cm^{-1} MeCN is suggestive of a small degree of dissociation in this solvent. The extent to which complexes of the general form $In(ML_n)_3$ dissociate in various solvents is clearly very dependent on the nature of the metal fragment, ML_n, and the solvent system, but we will defer a detailed discussion of this phenomenon to a future publication.

A FAB mass spectrum recorded on a sample of **14** showed a signal at *m/z* 925 corresponding to the fragment ion $[In\{Co(CO)_3(PPh_3)\}_2]^+$ but of greater interest were the ^{31}P NMR spectra which were obtained in CD_2Cl_2 solution. The spectrum observed, at 298 K, on a solution with a concentration of about 3×10^{-2} mol dm^{-3} is shown in Fig. 8(a) with chemical shift data given in Table 5. This spectrum was obtained on a solution derived from a completely homogeneous crop of well-formed crystals of **14** and yet it was evident that a number of phosphine-containing complexes were present in solution. All signals in the range 55–65 ppm are consistent with the presence of cobalt bonded PPh_3 groups with the strong intense signal at 62.2 ppm most likely due to **14**. However, the signals at 37.4 and −4.2 ppm probably arise from indium-bound phosphine and free phosphine, respectively, and thus clearly indicate some form of equilibrium/rearrangement process is present in this solvent. This behaviour was observed and has been discussed for **8**/**9** and is not unexpected, but of further interest is the fact that the spectra obtained are clearly temperature dependent. ^{31}P NMR spectra obtained at 253, 233 and 213 K are shown in Figs 8(b)–(d), respectively, and indicate a number of trends. Firstly it is apparent that the signals at 62.2 and −4.2 ppm (298 K) decrease in intensity relative to those at 56.0 and 35.9 ppm (213 K), and also that the signal at −4.2 (298 K) shifts up field to −10.5 ppm on cooling to 213 K. These changes are reversible on warming the sample to room temperature and clearly indicate the presence of an equilibrium between various species although with the data available, any speculation as to the nature of this equilibrium and the species present would be idle. A concentration dependence is also evident when the spectrum shown in Fig. 8(a) is compared with that obtained at a concentration of *ca* 1.5×10^{-3} mol dm^{-3} at 298 K shown in Fig. 8(e). However, as before, the nature of any equilibria which give rise to these differences is unclear.

In concluding this section of the paper we will merely state that a number of reactions have been carried out within the reaction system defined by $InCl_3 + nK[Co(CO)_3(PPh_3)]$ which give rise to a number of compounds some of which we have been able to characterize fully whilst on the nature of others, we are forced to speculate. An important point to be made, however, is that the structures observed in the solid state are not always those present in solution and also that the anticipated products are often either unobserved or unstable with respect to subsequent rearrangement. An important factor in this latter observation is the lability of PPh_3 on the cobalt centre and the apparent affinity of the indium centre for phosphine.

As will be evident from the foregoing discussion, much of the chemistry described herein at times seemed rather intractable and we were not well disposed towards the idea of an extensive study of the reactivity of any of these complexes. Two reactions were carried out, however, and are worth mentioning at this point. Treatment of a solution of **14** with 0.5 equivalents of $InCl_3$ in THF led to a lightening of the orange colour of the solution, an IR spectrum of which showed a single strong absorption at 1952 cm^{-1}. This observed frequency is the same as that found for **12** and **13** and is there-

Table 5. ^{31}P NMR chemical shift data for **14** at different temperatures and concentrations[a]

Temperature (K)	Chemical shifts (ppm)						
298[b]		63.4	62.2	58.6	55.9	37.4	−4.2
253[b]	63.0	63.7	62.2		55.9	35.5	−7.0
233[b]	62.9	63.5	62.5		55.9	35.7	−9.2
213[b]	63.1	63.4	62.7		56.0	35.9	−10.5
298[c]	64.1	63.4	62.1	58.5	55.9		−4.1

[a]All spectra are ^1H decoupled and referenced to 85% H_3PO_4 (external), positive values to high frequency. Plots of all spectra are displayed in Fig. 8(a)–(e).

[b]Concentration $\approx 3 \times 10^{-2}$ mol dm^{-3}.

[c]Concentration $\approx 1.5 \times 10^{-2}$ mol dm^{-3}.

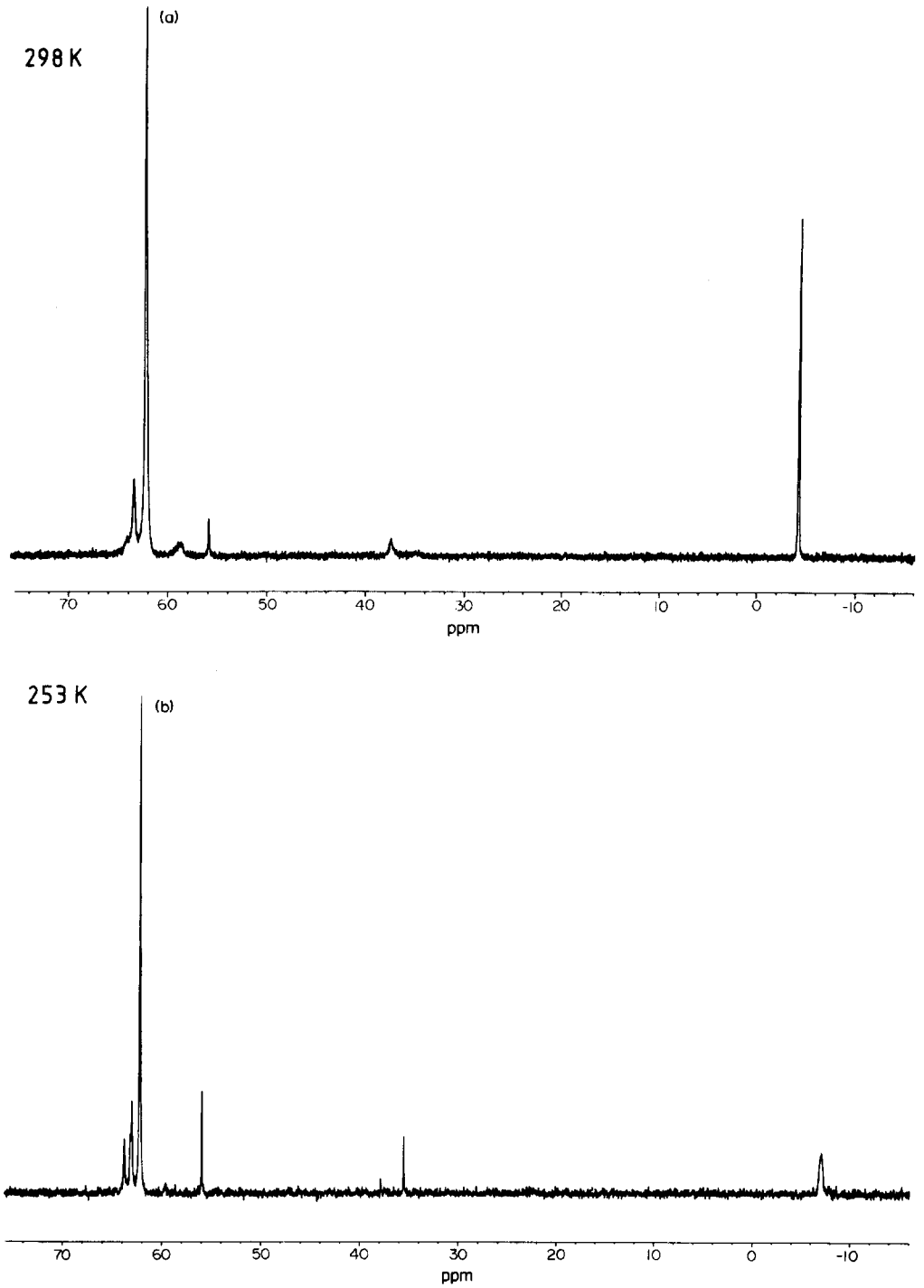

Fig. 8. ^{31}P NMR spectra for **14** measured in CD_2Cl_2 solution. Spectra (a)–(d) were recorded for a solution of approximate concentration 3×10^{-2} mol dm^{-3} at 298, 253, 233 and 213 K, respectively. Spectrum (e) was recorded for a solution of approximate concentration 1.5×10^{-2} mol dm^{-3} at 298 K. Chemical shifts are listed for all spectra in Table 5.

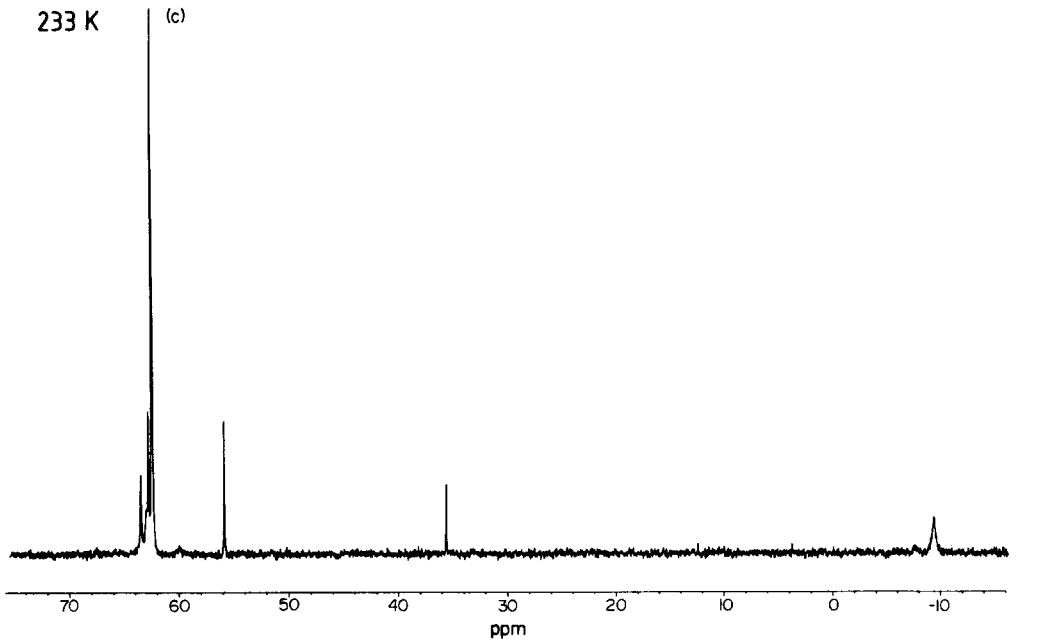
233 K
(c)
70
60
50
40
30
20
10
0
-10
ppm

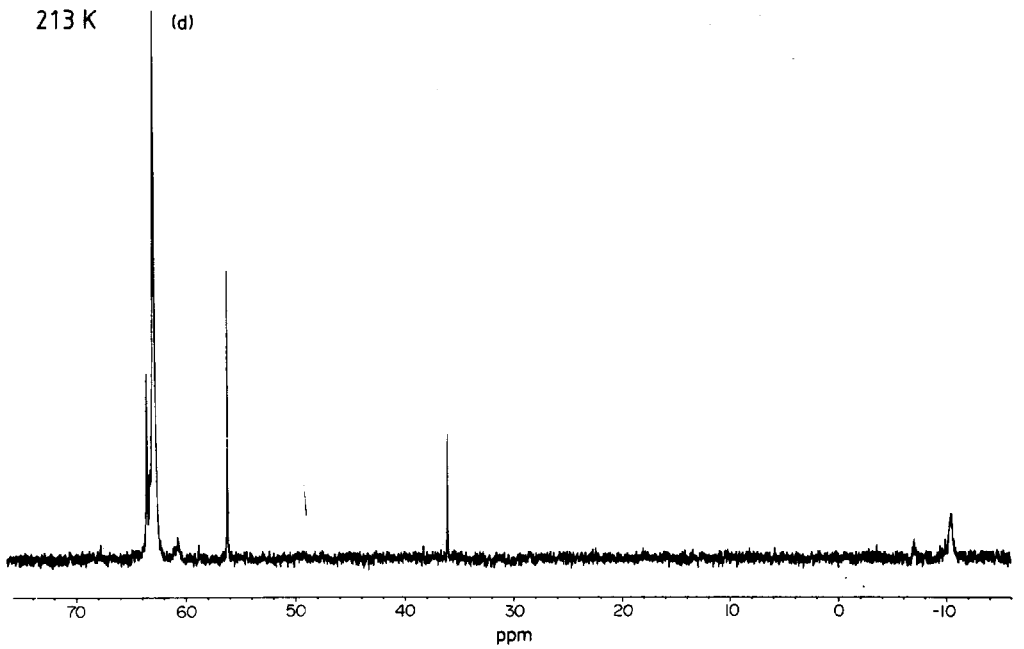
213 K
(d)
70
60
50
40
30
20
10
0
-10
ppm

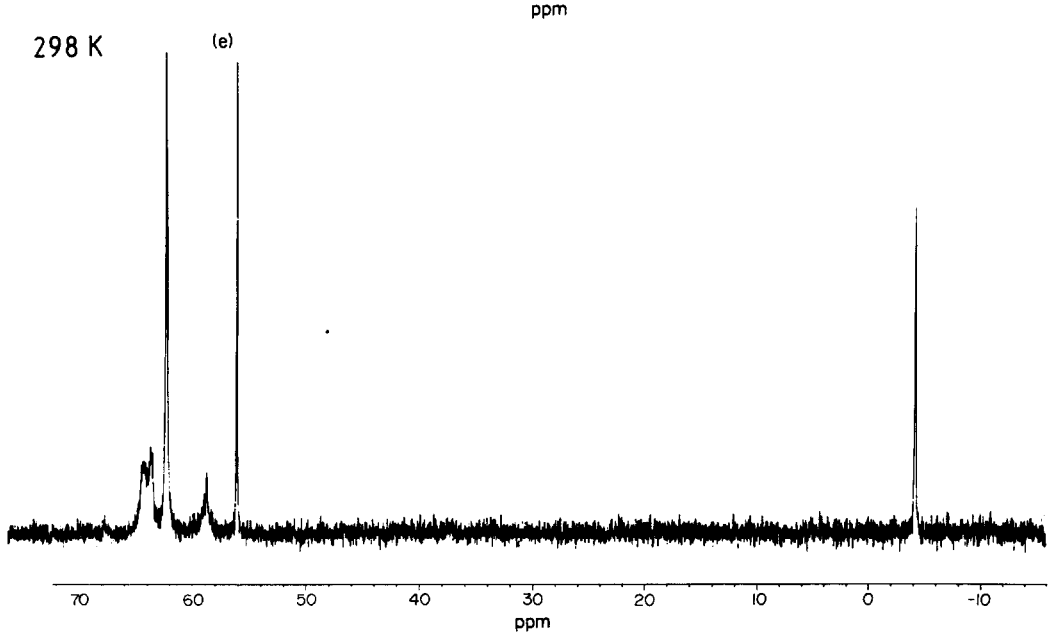
298 K
(e)
70
60
50
40
30
20
10
0
-10
ppm

fore consistent with the formation of a dicobalt indium compound as shown in eq. (2):

$$2[In\{Co(CO)_3(PPh_3)\}_3] + InCl_3 \rightleftharpoons 3[InCl\{Co(CO)_3(PPh_3)\}_2]. \quad (2)$$

We have observed similar chemistry in the related system with $[In\{Mo(CO)_3(\eta\text{-}C_5H_5)\}_3]$[24] and also for analogous antimony[25] and bismuth[17,26] complexes.

The second reaction which we carried out was between $[In\{Co(CO)_4\}_3]$ (**1**)[7b] and three equivalents of PPh_3. On work-up, an orange, crystalline material was obtained, the IR spectrum of which was identical to that obtained previously for **14**.

In closing we note that the thallium analogue of **14**, $[Tl\{Co(CO)_3(PPh_3)\}_3]$ (**15**), has been reported, originally by Hieber[27] and more recently by Robinson[28] and Burlitch.[29] The latter report gives IR data for **15** in THF solution (viz. 1987m, 1954s, 1922w sh) which is similar to that observed for **14**. A more detailed discussion of the similarities and differences between indium and thallium in these types of complexes is both interesting and illuminating and we shall have more to say on this matter in a future paper.

EXPERIMENTAL

General procedures

All experiments were performed using standard Schlenk techniques under an atmosphere of dry oxygen-free dinitrogen. All solvents were freshly distilled over appropriate drying agents immediately prior to use. ^1H and ^{13}C NMR spectra were recorded on a Bruker WP200 spectrometer operating at 200.13 and 50.324 MHz, respectively, and are referenced to Me_4Si, positive values to high frequency. ^{31}P NMR spectra were obtained on a Bruker WM300 instrument operating at 121.49 MHz. FAB mass spectra were recorded on a Kratos MS80 spectrometer using a *m*-nitrobenzyl alcohol matrix. IR spectra were recorded on a Nicolet 20 SXB FTIR spectrophotometer, and microanalytical data were obtained at the University of Newcastle.

$InCl_3$, $[Co_2(CO)_8]$, PPh_3 and $[Co_2(CO)_6(PPh_3)_2]$ were procured commercially and used without further purification.

IR and analytical data for the new compounds are presented in Table 1 whilst ^{31}P NMR data are given in the text and Table 5.

Preparations

Preparation of $K[Co(CO)_3(PPh_3)]$. This was prepared in a two stage reaction. $K[Co(CO)_4]$ was prepared according to the procedure given by Edgell[30] and more recently by Ellis[31] from $[Co_2(CO)_8]$ and KOH, whilst $K[Co(CO)_3(PPh_3)]$ was prepared from $K[Co(CO)_4]$ and PPh_3 according to Wojcicki.[18]

Reaction between $InCl_3$ *and* 1 $K[Co(CO)_3(PPh_3)]$. A solution of $K[Co(CO)_3(PPh_3)]$, prepared from $[Co_2(CO)_8]$ (0.105 g, 0.307 mmol) and PPh_3 (0.161 g, 0.614 mmol), in THF (30 cm^3) was added to a stirred solution of $InCl_3$ (0.136 g, 0.614 mmol) in THF (10 cm^3), and cooled to $-78°C$ by means of a dry ice–ethanol bath. During the addition a slight deepening of the yellow colour was observed together with the formation of a very finely dispersed white precipitate. After complete addition, the reaction mixture was warmed to room temperature and stirred for a further 3 h. Removal of all volatiles followed by extraction in CH_2Cl_2 and filtration through Celite afforded a yellow solution from which, after reduction of the solvent volume and slow diffusion of hexane at $-30°C$ over a period of 2–3 days, very pale yellow plate-like crystals of **8** were obtained which were suitable for X-ray diffraction studies (48% yield).

Reaction between $InCl_3$ *and* 2 $K[Co(CO)_3(PPh_3)]$. A solution of $K[Co(CO)_3(PPh_3)]$, prepared from $[Co_2(CO)_8]$ (0.354 g, 1.034 mmol) and PPh_3 (0.542 g, 2.068 mmol), in THF (30 cm^3) was added to a stirred solution of $InCl_3$ (0.229 g, 1.034 mmol) in THF (10 cm^3), pre-cooled to 0°C. During the addition, a marked deepening of the yellow colour was observed ($K[Co(CO)_3(PPh_3)]$ in THF is usually a very pale yellow) together with the formation of a fine white precipitate. After warming to room temperature, the reaction mixture was stirred for a further 1.5 hours. Filtration through Celite, followed by reduction of the solvent volume to 5 cm^3, followed by slow diffusion of hexane (30 cm^3) at $-30°C$ over a period of 5 days afforded small yellow crystals and a white solid (KCl). Repeated recrystallizations from CH_2Cl_2–hexane mixtures afforded X-ray quality crystals of **10**, and an orange powder, **12**.

NMR data for **10**: ^1H (CD_2Cl_2) δ 7.60 and 7.44 (m, phenyls); $^{13}C\text{-}\{^1H\}$ (CD_2Cl_2) δ 134.7 and 131.8 (m, *o*-, *m*-, *p*-phenyls).

Reaction between InCl *and* $[Co_2(CO)_6(PPh_3)_2]$. InCl (0.070 g, 0.466 mmol) and $[Co_2(CO)_6(PPh_3)_2]$ (0.378 g, 0.466 mmol) were stirred in toluene (10 cm^3) at 80°C for 7 h. After this time the toluene was removed *in vacuo* and the resulting yellow powder redissolved in CH_2Cl_2 and filtered through Celite. The solvent from the yellow filtrate was removed *in vacuo* and the resulting yellow solid recrystallized from THF–hexane at $-30°C$, which afforded yellow crystals of **13**.

NMR data for **13**: ^{1}H (CD_2Cl_2) δ 7.75, 7.60, 7.39 (m, phenyls); ^{13}C-{^{1}H} δ 133.8 (m, *o*-C_6H_5), 131.1 (s, *p*-C_6H_5), 129.3 (m, *m*-C_6H_5). Mass spectra (FAB): *m/z* 925, P′ [P′ = In{Co(CO)$_3$(PPh$_3$)}$_2$]; 841, P′ − 3CO; 785, P′ − 5CO; 642, [Co_2(PPh$_3$)$_2$]; 321, [Co(PPh$_3$)]; 114, [In].

Reaction between $InCl_3$ *and* 2 [PPN][Co(CO)$_4$] A solution of $InCl_3$ (0.035 g, 0.160 mmol) in THF (10 cm^3) was added to a stirred solution of [PPN][Co(CO)$_4$][20] (0.302 g, 0.320 mmol) in THF (10 cm^3) at room temperature. The pale yellow solution was stirred for 18 h affording a slightly turbid pale green solution. Purification by column chromatography on Florisil with Et_2O–THF (3:1) as eluant afforded a yellow oil after removal of all voltatiles *in vacuo*. Redissolution in CH_2Cl_2 followed by filtration through Celite gave a clear yellow solution from which, after concentration of the solvent volume and slow diffusion of hexane at −30°C, pale yellow needles of **11** suitable for X-ray diffraction were obtained.

Reaction between $InCl_3$ *and* 3 K[Co(CO)$_3$(PPh$_3$)]. A stirred solution of K[Co(CO)$_3$(PPh$_3$)], prepared from [Co_2(CO)$_8$] (0.748 g, 2.187 mmol) and PPh_3 (1.147 g, 4.374 mmol), in THF (20 cm^3) was cooled to 0°C and maintained at this temperature. To this was added a solution of $InCl_3$ (0.325 g, 1.458 mmol) dropwise over a period of a few minutes, resulting in a turbid yellow solution. After complete addition, the reaction mixture was allowed to warm to room temperature and was stirred for a further 24 h, during which time a colour change from yellow to orange was observed. Filtration through Celite, followed by removal of all volatiles *in vacuo* afforded an orange oil. Extraction in CH_2Cl_2, followed by filtration through Celite gave a clear orange solution from which, after reduction of the solvent volume and slow diffusion of hexane at −30°C, a crude crystalline solid was obtained. Recrystallization from a concentrated solution in CH_2Cl_2 afforded well-formed crystals of **14**. The crystals rapidly lost solvent on removal of the mother liquor and were thus unsuitable for X-ray studies.

Crystallization from 1,2-dichloroethane, chlorobenzene, 1,2-dichlorobenzene, $CHCl_3$, THF–hexane and acetone–hexane gave crystals of varying degrees of visual quality but none proved suitable for X-ray diffraction.

NMR data for **14**: ^{1}H (CD_2Cl_2) δ 7.67-7.27 (m, phenyls); ^{13}C-{^{1}H} (CD_2Cl_2) δ 134.1 (m, *o*-C_6H_5), 131.1 (s, *p*-C_6H_5), 129.3 (m, *m*-C_6H_5). Mass spectra (FAB): *m/z* 925, P′ [P′ = In{Co(CO)$_3$(PPh$_3$)}$_2$]; 896, P′ − 1CO; 841, P′ − 3CO; 785, P′ − 5CO; 757, P′ − 6CO; 667, [Co(CO)$_3$(PPh$_3$)]; 583, [Co(PPh$_3$)$_2$]; 321, [Co(PPh$_3$)]; 262, [PPh$_3$]; 114, [In]; 77, [Ph].

X-ray crystallographic studies

Structure determination of [$InCl_2$(PPh$_3$){Co(CO)$_4$}] (**8**). A pale yellow crystal of approximate dimensions 0.5 × 0.4 × 0.3 mm was mounted in a general position on a glass fibre and coated with acrylic resin. Data were collected at ambient temperatures, using the θ–2θ scan mode, on a CAD4F automated diffractometer with graphite-monochromated X-radiation. Unit cell parameters were determined by refinement of the setting angles ($\theta \geqslant 12°$) of 25 reflections. The standard reflections $\bar{8}06$ and $3\bar{4}5$ were measured every 2 h and after *ca* 5100 data, these showed a catastrophic decrease in intensities. As a result only data to $h = 7$ were obtained (theoretical maximum value for h is 17 where $\theta \leqslant 22.5°$). A decay correction in two linear sections was applied, as were Lorentz–polarization and absorption/extinction (DIFABS)[32] corrections. A total of 5371 measured reflections (θ range 2–22.5°, h 0 → 7, k −12 → +12, l −20 → +20) yielded 5011 independent data, of which 2856 having an intensity $> 2.5\sigma(I)$ were considered observed and used for structure solution and refinement. The distribution of normalized structure factors indicated the centrosymmetric space group $P\bar{1}$, and this was confirmed by successful structure solution and refinement. The structure was solved by direct methods (MITHRIL)[33] and subsequent electron density difference syntheses. The structure consists of two molecules in the asymmetric unit, which are approximately related by the symmetry operation (1/2−x, 1/2+y, 1/2−z), and the structure can be refined in the monoclinic space group $P2_1/n$. The true space group, however, is undoubtedly $P\bar{1}$, for several reasons.

(i) The α and (particularly) the γ unit cell angles differ significantly from 90°.

(ii) Although the zones $h0l$; $h+l = 2n+1$ and $0k0$; $k = 2n+1$ are systematically weak, the Laue symmetry is clearly not monoclinic. A substantial number of reflection pairs hkl and $h\bar{k}l$ differ significantly in intensities, as observed in values for R(merge) [2.7% for $P\bar{1}$ and 17.9% for $P2_1/n$].

The structure was refined using full-matrix least-squares, minimizing the function $\Sigma\omega(|F_o| - |F_c|)^2$. The weighting scheme $\omega = [\sigma^2(F_o)]^{-1}$ was used and judged satisfactory. $\sigma(F_o)$ was estimated from counting statistics. The In, Co, Cl and P atoms were allowed anisotropic thermal motion, the other atoms refined with isotropic thermal parameters. The phenyl groups were refined as rigid groups with idealized geometry (C—C = 1.395, C—H = 1.0 Å) with individually refined isotropic thermal parameters for the carbon atoms, and fixed parameters

(0.05 Å^2) for the hydrogen atoms. Refinement using a total of 227 parameters converged to give the residuals presented in Table 6 with mean and maximum Δ/σ values of 0.004 and 0.064, respectively, in the final cycle. A final electron density difference synthesis showed no chemically significant features (max $\Delta\rho = +1.03$, min $\Delta\rho = -0.55$ eÅ^{-3}). The ESD of an observation of unit weight (S) was 2.12. Neutral atom scattering factors were taken from ref. 34 with corrections applied for anomalous scattering. All calculations were carried out on a MicroVAX 3600 computer using the Glasgow GX suite of programs.[35] The two molecules are similar in general, but differ in some small details (see text). The Co—C bond lengths (*mean* 1.71 Å for molecule A, 1.77 Å for molecule B, ESDs 0.02–0.03 Å) differ somewhat, and the Co(2a)—C(4a)—0(4a) angle of 136(3)° is decidedly non-linear. This is probably an artefact of the poor quality truncated data set, and has no chemical significance.

Structure determination of $[Co(CO)_3(PPh_3)_2][InCl_2\{Co(CO)_4\}_2]$ (**10**). In general, this was performed as described above for **8**. The points of difference are as follows:

(i) Standard reflections 22$\bar{8}$, 7$\bar{4}\bar{7}$ and 351 showed a slight decrease in intensity of *ca* 1.5% in 10,000 reflections.

(ii) A total of 7040 measured reflections (θ range 2–22.5°, h 0 → 14, k −15 → 15, l −17 → 17) yielded 6941 independent data, of which 4763 having an intensity $>3\sigma(I)$ were considered observed.

(iii) All non-hydrogen atoms apart from the aryl carbons were allowed anisotropic thermal motion. The phenyl groups were refined as rigid groups as for **8**.

(iv) Refinement using 343 parameters converged to give the residuals shown in Table 6 with mean and maximum Δ/σ values of 0.0002 and 0.002, respectively, in the final cycle. A final electron density difference synthesis showed no significant features (max $\Delta\rho = +0.66$, min $\Delta\rho = -0.5$ eÅ^{-3}). S was 2.09.

Structure determination of $[Ph_3PNPPh_3][InCl_2\{Co(CO)_4\}_2]$ (**11**). As for **8** except:

(i) Standard reflections 381 and 40$\bar{7}$ showed no significant variations in intensity.

(ii) A total of 12,770 measured reflections (θ range 2–22.5°, h 0 → 10, k −22 → 22, l −24 → 24) yielded 11,945 independent data. Due to the small crystal size and poor diffraction, only 4044 reflections having an intensity $>2\sigma(I)$ were considered observed and used for structure solution and refinement.

(iii) Due to matrix size limitations, the parameter list was divided into two blocks of 272 and 335 parameters, and each refined in separate cycles. The Co, In, Cl and P atoms were allowed anisotropic thermal motion, all other atoms were refined using isotropic thermal parameters. The phenyl rings were refined as rigid groups as for **8**.

(iv) Refinement converged to give the residuals shown in Table 6 with mean and maximum Δ/σ

Table 6. Crystallographic data

Compound	**8**	**10**	**11**
Chemical formula	$C_{22}H_{15}Cl_2CoInO_4P$	$C_{47}H_{30}Cl_2Co_3InO_{11}P_2$	$C_{44}H_{30}Cl_2Co_2InNO_8P_2$
fw	619.0	1195.2	1066.3
Crystal system	Triclinic	Triclinic	Triclinic
Space group	$P\bar{1}$	$P\bar{1}$	$P\bar{1}$
a (Å)	15.044(4)	13.466(5)	9.957(2)
b (Å)	10.292(3)	14.176(6)	20.262(3)
c (Å)	16.937(6)	16.162(4)	23.058(5)
α (°)	89.61(3)	75.47(3)	82.16(2)
β (°)	110.14(3)	115.19(2)	86.13(2)
γ (°)	91.04(2)	114.17(3)	84.00(2)
V (Å^3)	2461.6(14)	2536(2)	4576(2)
Z	4	2	4
d_{calc} (g cm^{-3})	1.67	1.56	1.55
$F(000)$	1216	1188	2128
μ(Mo-K_α) (cm^{-1})	19.03	16.27	14.43
λ (Å)	0.71069	0.71069	0.71069
Temperature (K)	298	298	298
R	0.054	0.047	0.071
R_w	0.060	0.052	0.065

values of 0.0002 and 0.002, respectively, in the final cycle. A final electron density difference synthesis showed no significant features (max $\Delta\rho = +0.66$, min $\Delta\rho = -0.5$ eÅ^3). S was 2.09.

Relevant crystallographic data for all complexes is presented in Table 6.*

Acknowledgement—We thank the SERC for a studentship (L.M.C.).

REFERENCES

1. N. A. Compton, R. J. Errington and N. C. Norman, *Adv. Organomet. Chem.*, in press.
2. L. M. Clarkson, W. Clegg, N. C. Norman, A. J. Tucker and P. M. Webster, *Inorg. Chem.* 1988, **27**, 2653 and refs therein.
3. W. Hieber and U. Teller, *Z. Anorg. Allg. Chem.* 1942, **249**, 43.
4. G. N. Schrauzer, B. N. Bastian and G. A. Fosselius, *J. Am. Chem. Soc.* 1966, **88**, 4890.
5. W. R. Robinson and D. P. Schussler, *Inorg. Chem.* 1973, **12**, 848.
6. W. R. Robinson and D. P. Schussler, *J. Organomet. Chem.* 1971, **30**, C5. See also, J. M. Burlitch, R. B. Peterson, H. L. Conder and W. R. Robinson, *J. Am. Chem. Soc.* 1970, **92**, 1783, for a brief mention of **2**.
7. (a) D. J. Patmore and W. A. G. Graham, *Chem. Commun.* 1965, 591; (b) D. J. Patmore and W. A. G. Graham, *Inorg. Chem.* 1966, **5**, 1586.
8. P. D. Cradwick, W. A. G. Graham, D. Hall and D. J. Patmore, *Chem. Commun.* 1968, 872.
9. P. D. Cradwick and D. Hall, *J. Organomet. Chem.* 1970, **22**, 203.
10. P. D. Cradwick, *J. Organomet. Chem.* 1971, **27**, 251.
11. A. T. T. Hsieh and M. J. Mays, *J. Organomet. Chem.* 1972, **37**, 9.
12. J. K. Ruff, *Inorg. Chem.* 1968, **7**, 1499.
13. J. M. Burlitch, M. E. Leonowicz, R. B. Peterson and R. E. Hughes, *Inorg. Chem.* 1979, **18**, 1097.
14. Values taken from J. Emsley, *The Elements*. Clarendon Press, Oxford (1989).
15. A. J. Carty and D. G. Tuck, *Prog. Inorg. Chem.* 1975, **19**, 243.
16. M. V. Veidis and G. J. Palenik, *Chem. Commun.* 1969, 586.
17. W. Clegg, N. A. Compton, R. J. Errington, D. C. R. Hockless, N. C. Norman, M. Ramshaw and P. M. Webster, *J. Chem. Soc., Dalton Trans.* 1990, 2375.
18. F. Ungváry and A. Wojcicki, *J. Am. Chem. Soc.* 1987, **109**, 6848.
19. Bond lengths and angles for $[Co(CO)_3(PPh_3)_2]^+$; Co(3)—P(1) 2.233(3), Co(3)—P(2) 2.234(3), Co(3)—CO av 1.781 Å; P(1)—Co(3)—P(2) 178.8(1), P(1)—Co(3)—CO av 90.4, P(2)—Co(3)—CO av 89.7, CO—Co(3)—CO av 120.0°.
20. J. K. Ruff and W. J. Schlientz, *Inorg. Synth.* 1976, **15**, 85. Infrared values for [PPN][$Co(CO)_4$] (MeCN, 1890s) and [PPN][$Co(CO)_3(PPh_3)$] (MeCN, 1926m, 1830vs, br) are taken from Y. Zhen, W. G. Feighery, C.-K. Lai and J. D. Atwood, *J. Am. Chem. Soc.* 1989, **111**, 7832. Our own data for $[Co(CO)_4]^-$ in THF give a value of 1886 cm^{-1}.
21. A. T. T. Hsieh and M. J. Mays, *Chem. Commun.* 1971, 1234; A. T. T. Hsieh and M. J. Mays, *J. Chem. Soc., Dalton Trans* 1972, 516.
22. L. M. Clarkson, N. C. Norman and L. J. Farrugia, *J. Organomet. Chem.* 1990, **390**, C10.
23. This is similar to the reaction between InBr and $[Co_2(CO)_8]$ which, in THF, affords $[InBr(THF)\{Co(CO)_4\}_2]$, ref. 7, and to the reaction between InCl and $[Co_2(CO)_8]$ which affords $[InCl\{Co(CO)_4\}_2]$, ref. 11.
24. L. M. Clarkson and N. C. Norman, unpublished observations.
25. A. M. Barr, M. D. Kerlogue, N. C. Norman, P. M. Webster and L. J. Farrugia, *Polyhedron* 1989, **8**, 2495.
26. W. Clegg, N. A. Compton, R. J. Errington, N. C. Norman, A. J. Tucker and M. J. Winter, *J. Chem. Soc., Dalton Trans.* 1988, 2941.
27. W. Hieber and R. Breu, *Chem. Ber.* 1957, **90**, 1259.
28. S. E. Pederson and W. R. Robinson, *Inorg. Chem.* 1975, **14**, 2360.
29. J. M. Burlitch and T. W. Theyson, *J. Chem. Soc., Dalton Trans.* 1974, 828.
30. W. F. Edgell and J. Lyford, *Inorg. Chem.* 1970, **9**, 1932.
31. J. E. Ellis, P. T. Barger, M. L. Winzenburg and G. F. Warnock, *J. Organomet. Chem.* 1990, **383**, 521.
32. N. Walker and D. Stuart, *Acta Cryst.* 1983, **A39**, 158.
33. C. J. Gilmore, *J. Appl. Cryst.* 1984, **17**, 42.
34. *International Tables for X-ray Crystallography*, Vol. 4, Kynoch Press, Birmingham (1974).
35. P. R. Mallinson and K. W. Muir, *J. Appl. Cryst.* 1985, **18**, 51.

*Supplementary material available: Tables of fractional coordinates for **8**, **10** and **11** have been deposited with the Cambridge Crystallographic Data Centre. Tables listing complete bond lengths and angles, anisotropic thermal parameters, hydrogen atom parameters and observed and calculated structure factors are available from the Editor.

Polyhedron Vol. 9, No. 20, pp. 2549–2551, 1990
Printed in Great Britain

0277–5387/90 $3.00+.00
© 1990 Pergamon Press plc

COMMUNICATION

THE SYNTHESES OF HIGH OXIDATION STATE METAL COMPLEXES CONTAINING THE TRIPODAL LIGAND $[(\eta^5\text{-}C_5H_5)Co\{P(OMe)_2(=O)\}_3]^-$ AND THE X-RAY CRYSTAL STRUCTURE OF $[(\eta^5\text{-}C_5H_5)Co\{P(OMe)_2(=O)\}_3ReO_3]$

HILARY J. BANBERY, WASIF HUSSAIN, IONA G. EVANS, THOMAS A. HAMOR,* CHRISTOPHER J. JONES* and JON A. McCLEVERTY*

School of Chemistry, University of Birmingham, Edgbaston, Birmingham, B15 2TT, U.K.

and

HEINZ-JOSEF SCHULTE, BIRGIT ENGLES and WOLFGANG KLÄUI*

Institut für Anorganische Chemie der Technischen Hochschule, Templergraben 55, D-5100 Aachen, F.R.G.

(*Received* 3 *May* 1990; *accepted* 10 *August* 1990)

Abstract—The new complexes $[(\eta^5\text{-}C_5H_5)Co\{P(OR)_2(=O)\}_3MO_3]$ (M = Re, R = Me or Et; M = Tc, R = Me) have been synthesized from the reaction between $[(\eta^5\text{-}C_5H_5)Co\{P(OR)_2(=O)\}_3]^-$ and MO_4^-. The rhenium complexes may also be prepared by oxidation of $[(\eta^5\text{-}C_5H_5)Co\{P(OR)_2(=O)\}_3Re(CO)_3]$. The oxidation of $[(\eta^5\text{-}C_5H_5)Co\{P(OR)_2(=O)\}_3Mo(CO)_3H]$ affords the dimer, $[(\eta^5\text{-}C_5H_5)Co\{P(OR)_2(=O)\}_3MoO_2]O$, which is also obtained from MoO_4^{2-} and the tripodal ligand. The reaction between WO_4^{2-} and $[(\eta^5\text{-}C_5H_5)Co\{P(OR)_2(=O)\}_3]^-$ affords either the dimer, $[(\eta^5\text{-}C_5H_5)Co\{P(OR)_2(=O)\}_3WO_2]O$ (R = Me, Et), or the monomer, $[(\eta^5\text{-}C_5H_5)Co\{P(OR)_2(=O)\}_3WO_3]^-$ (R = Et). An X-ray diffraction study of $[(\eta^5\text{-}C_5H_5)Co\{P(OMe)_2(=O)\}_3ReO_3]$ confirms that the rhenium has a distorted octahedral coordination geometry consisting of three facial oxygen atoms from the tripodal ligand and three rhenyl oxo-groups [mean Re=O, 1.703(7) Å; mean O=Re=O, 102.5(7)°].

Complexes of rhenium(VII) with polydentate ligands are rare.[1] The compounds [ReO_3Cl(2,2′-bipyridyl)] and [ReO_3Cl(*o*-phenanthroline)] provide well characterized examples of complexes containing bidentate ligands coordinated to the $\{Re(=O)_3\}^+$ moiety,[2] and more recently the complex $[ReO_2(OSiMe_3)_2\{N{=}P(Ph)_2CH_2PPh_2\}]$, which contains the $\{Re(=O)_2\}^{3+}$ moiety, has been reported.[3] However, there has been little work on rhenium(VII) complexes with ligands containing three or more donor atoms. Wieghardt *et al.* have recently described the synthesis and structure of [(1,4,7-triazacyclononane)ReO_3]$^+$.[4] Organometallic derivatives of rhenium(VII) are also known, two examples being methyltrioxorhenium[5] and $[(\eta^5\text{-}C_5Me_5)ReO_3]$.[6] We were interested in establishing whether a high-valent rhenium(VII) chemistry might be developed using tridentate oxygen ligands to bind to an MO_3 (M is an early *d*-block metal) fragment. To this end we have examined the oxidation reactions of $[(\eta^5\text{-}C_5H_5)Co\{P(OR)_2(=O)\}_3M(CO)_3]^z$ (M = Re, $z = 0$; M = Mo, $z = 1-$)[7,8] and the reactions between the uninegative tripodal ligand[9,10] $[(\eta^5\text{-}C_5H_5)Co\{P(OR)_2(=O)\}_3]^-$ (R = Me or Et) and MO_4^x (M = Tc or Re and $x = 1-$; M = Mo or W and $x = 2-$).

* Authors to whom correspondence should be addressed.

The oxidation of $[(\eta^5\text{-}C_5H_5)Co\{P(OR)_2(=O)\}_3Re(CO)_3]$ with peracetic acid affords the rhenium(VII) complex $[(\eta^5\text{-}C_5H_5)Co\{P(OR)_2(=O)\}_3ReO_3]$, which can also be prepared by acidification of a solution containing $[(\eta^5\text{-}C_5H_5)Co\{P(OR)_2(=O)\}_3]^-$ and ReO_4^- [ν(Re=O) 940 and 910 cm^{-1}, R = Me]. The ^1H NMR spectra of these compounds are consistent with the presence of three-fold symmetry in the molecule, and the presence of a distorted octahedral structure about rhenium has been confirmed by the X-ray diffraction study described below. A similar reaction was found to occur with TcO_4^- [ν(Tc=O) 906 and 892 cm^{-1}, R = Me]. The oxidation of $[(\eta^5\text{-}C_5H_5)Co\{P(OEt)_2(=O)\}_3W(CO)_3H]$ ($L_{OEt}W(CO)_3H$) affords the tungsten(VI) dimer $[\{L_{OEt}WO_2\}_2O]$.[11] We have prepared in a similar way the analogous molybdenum(VI) complex and confirmed its oxo-bridged structure by an X-ray crystal structure determination.[12] This compound and its counterpart with R = Me may also be prepared directly by acidification of a solution containing $[(\eta^5\text{-}C_5H_5)Co\{P(OR)_2(=O)\}_3]^-$ (R = Me, Et) and MoO_4^{2-} or, for R = Me, $Mo_2O_7^{2-}$ [ν(Mo=O) 935 and 902 cm^{-1}, R = Me, Et]. The ^1H NMR spectra of these complexes are consistent with the absence of either a three-fold symmetry axis or a plane of symmetry, in accord with the crystallographic results. The compounds are non-conducting in MeOH solution. The reactions of $[(\eta^5\text{-}C_5H_5)Co\{P(OR)_2(=O)\}_3]^-$ (R = Me or Et) with WO_4^{2-} give differing results depending upon the nature of R. In the case where R = Me the compound obtained is non-conducting in MeOH solution and exhibits a ^1H NMR spectrum, which is consistent with the absence of symmetry in the complex [ν(W=O) 950 and 905 cm^{-1}]. Using a shorter reaction time in the case where R = Et affords a product which forms a conducting solution in MeOH and exhibits a ^1H NMR spectrum which shows only one environment for the methyl groups of the ethyl substituents [ν(W=O) 950–broad and 905 cm^{-1}], consistent with the formulation $Na[L_{OEt}WO_3]$. However, crystals grown from this solution have been found, by an X-ray diffraction study, to contain the dimer $[\{L_{OEt}WO_2\}_2O]$.

The crystals of $[(\eta^5\text{-}C_5H_5)Co\{P(OMe)_2(=O)\}_3ReO_3]$ are monoclinic, space group $P2_1/c$ with $a = 8.524(4)$, $b = 15.395(6)$, $c = 47.138(13)$ Å, $\beta = 94.66(4)°$ and $Z = 12$; $D_c = 2.215$ g cm^{-3}, μ(Mo-K_α) = 70.9 cm^{-1}. 5218 reflections measured on an Enraf–Nonius CAD-4 diffractometer in the range $2 < \theta < 23°$ and having $I > 3.5\sigma(I)$ were used in the analysis. The structure was solved by Patterson and Fourier methods and refined[13] by least-squares with anisotropic temperature factors for the heavier atoms and isotropic temperature factors for the oxygen and carbon atoms. Hydrogen atoms were included in calculated positions. The refinement converged (all calculated shift/ESD ratios $< 0.2\sigma$) to R, R_w 0.071, 0.106 with weights $w = 1/[\sigma^2(F)+0.00001F^2]$ and residual electron density within ± 1.95 e Å^{-3}. An empirical absorption correction was applied using DIFABS.[14]

The compound crystallizes with three independent molecules in the unit cell; one of these is illustrated[15]* in Fig. 1. The other two molecules have virtually identical structures. Apart from the cyclopentadienyl ring the molecules approximate

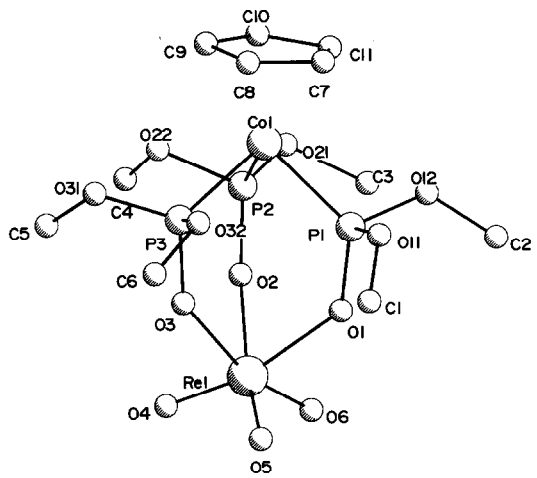

Fig. 1. A view of molecule A showing the atom labelling. Hydrogen atoms have been omitted for clarity. Selected bond distances (Å) and angles (°) for molecule A:

Re(1)—O(1)	2.13(2)	Re(1)—O(4)	1.73(2)
Re(1)—O(2)	2.10(2)	Re(1)—O(5)	1.68(3)
Re(1)—O(3)	2.16(2)	Re(1)—O(6)	1.72(2)
Co(1)—P(1)	2.118(10)	P(1)—O(1)	1.57(2)
Co(1)—P(2)	2.151(10)	P(2)—O(2)	1.52(2)
Co(1)—P(3)	2.146(9)	P(3)—O(3)	1.51(2)

O(1)—Re(1)—O(2)	79.1(8)
O(1)—Re(1)—O(3)	81.8(7)
O(2)—Re(1)—O(3)	79.3(8)
O(4)—Re(1)—O(5)	106.2(12)
O(4)—Re(1)—O(6)	100.1(11)
O(5)—Re(1)—O(6)	100.1(11)
Co(1)—P(1)—O(1)	121.1(8)
Co(1)—O(2)—O(2)	117.7(10)
Co(1)—P(3)—O(3)	117.2(9)
P(1)—O(1)—Re(1)	134.0(11)
P(2)—O(2)—Re(1)	140.4(14)
P(3)—O(3)—Re(1)	139.9(13)

* The atomic coordinates have been deposited with the Cambridge Crystallographic Data Centre.

to three-fold symmetry. Mean bond lengths are: Re=O, 1.703(7); Re—O, 2.131(10); P=O(Re), 1.537(11); P—O(Me), 1.593(9); P—Co, 2.143(5) Å. The coordination geometry at rhenium is essentially octahedral with maximum angular deviation from ideal values, 18.2°, in an O=Re—O *trans* angle (*trans* angle range 161.8–165.2°, mean 163.5°). The angles between the rhenyl oxo-groups are large [mean 102.5(7)°], presumably due to repulsion between the short electron-rich double bonds. Concomitantly the other *cis* angles are generally less than 90°.

The Co—P bond length is somewhat shorter than the mean lengths of 2.183, 2.175, 2.173 and 2.165 Å found in the crystal structures of $[(\eta^5\text{-}C_5H_5)Co\{P(OMe)_2(=O)\}_2\{P(OMe)_3\}]$,[16] $[(L_{OEt})_2M]$ (M = Sn, Pb)[17] and $[L_{OEt}Rh(CO)_3RhL_{OEt}]$,[18] respectively. The angles subtended at the cobalt atom by the three phosphorus atoms are close to 90° [mean 89.6(4)°]. The cyclopentadienyl rings are all planar to within the limits of experimental error [maximum displacements 0.03(6), 0.01(6) and 0.10(7) Å for the three independent molecules]. The cobalt atom is essentially equidistant from the ring carbon atoms, the relevant distances being in the ranges 2.02(4)–2.07(4), 1.99(4)–2.11(5) and 2.05(4)–2.15(4) Å in $[(\eta^5\text{-}C_5H_5)Co\{P(O)(OMe)_2\}_2\{P(OMe)_3\}]$[16] and $[(L_{OEt})_2M]$ (M = Sn, Pb).[17] The overall average Co—C distance in $[(\eta^5\text{-}C_5H_5)Co\{P(OMe)_2(=O)\}_3ReO_3]$ is 2.07(2) Å, which may be compared with the mean values of 2.096, 2.082 and 2.079 Å in these three molecules.[16,17]

Acknowledgements—We are grateful to Ms C. A. Fletcher for experimental assistance and to the SERC, Amersham International plc and Johnson Matthey plc for support (to H.J.B., W.H. and I.G.E., respectively).

REFERENCES

1. K. A. Conner and R. A. Walton, *Comprehensive Coordination Chemistry* (Edited by G. Wilkinson, R. D. Gillard and J. A. McCleverty), Ch. 43. Pergamon Press, Oxford (1987).
2. V. S. Sergeinko, T. S. Khodashova, M. A. Porai-Koshits and L. A. Butman, *Sov. J. Coord. Chem. (Engl. Transl.)* 1977, **3**, 822.
3. K. V. Katti and R. G. Cavell, *Inorg. Chem.* 1989, **28**, 3033.
4. K. Wieghardt, C. Pomp, B. Nuber and J. Weiss, *Inorg. Chem.* 1986, **25**, 1659.
5. I. R. Beattie and P. J. Jones, *Inorg. Chem.* 1979, **18**, 2318.
6. W. A. Herrmann, *Angew. Chem. Int. Ed.* 1988, **27**, 1297.
7. W. Kläui, J. Okuda, M. Scotti and M. Valderrama, *J. Organomet. Chem.* 1985, **280**, C26.
8. W. Kläui, A. Müller and M. Scotti, *J. Organomet. Chem.* 1983, **253**, 45.
9. W. Kläui, *Z. Naturfor.* 1979, **B34**, 1403.
10. S. S. Salam, C. J. Jones and J. A. McCleverty, *J. Chem. Soc., Dalton Trans.* 1988, 2769.
11. W. Kläui, A. Müller, W. Eberspach, R. Boese and I. Goldberg, *J. Am. Chem. Soc.* 1987, **109**, 164.
12. H. Hamers, A. Müller and W. Kläui, unpublished results.
13. G. M. Sheldrick, SHELX76, Program for Crystal Structure Determination. University of Cambridge (1976).
14. N. Walker and D. Stuart, *Acta Cryst.* 1983, **39A**, 158.
15. W. D. S. Motherwell and W. Clegg, PLUTO, Program for Drawing Crystal and Molecular Structures. University of Cambridge (1978).
16. D. K. Towle, S. J. Landon, T. B. Brill and T. H. Tulip, *Organometallics* 1982, **1**, 295.
17. E. M. Holt, W. Kläui and J. J. Zuckerman, *J. Organomet. Chem.* 1987, **335**, 29.
18. W. Kläui, M. Scotti, M. Valderrama, S. Rojas, G. M. Sheldrick, P. G. Jones and T. Schroeder, *Angew. Chem., Int. Ed.* 1985, **24**, 683.

Polyhedron Vol. 9, No. 21, pp. 2553–2566, 1990
Printed in Great Britain.

0277–5387/90 $3.00+.00
Pergamon Press plc

POLYHEDRON REPORT NUMBER 34

RECENT DEVELOPMENTS IN THE CHEMISTRY OF MONO- AND DINUCLEAR COMPLEXES OF THE MACROCYCLIC DIANION, 5,7,12,14-TETRAMETHYLDIBENZO[b,i][1,4,8,11] TETRAAZACYCLOTETRADECINE

F. A. COTTON* and JOANNA CZUCHAJOWSKA

Laboratory for Molecular Structure and Bonding and Department of Chemistry, Texas A&M University, College Station, TX 77843, U.S.A.

CONTENTS

1. INTRODUCTION 2553

2. MONONUCLEAR COMPLEXES 2554
   2.1. Early transition metals (Groups IV, V, VI) 2554
   2.2. Middle transition metals (Groups VII, VIII, IX) 2559
   2.3. The metals nickel, copper and zinc 2562

3. DINUCLEAR COMPLEXES 2562
   3.1. The diruthenium compounds 2563
   3.2. The dirhodium compound 2563
   3.3. The dichromium and dimolybdenum compounds 2563

4. CONCLUSIONS 2565

1. INTRODUCTION

A high level of activity in the synthesis and structural characterization of transition metal complexes containing macrocyclic ligands continues unabated. One reason that such systems have aroused interest is their ability to model biological phenomena, such as the binding of small molecules, e.g. O_2 or CO, to iron in various haem systems. Full understanding of this process has been an elusive one for biologists and chemists alike. It is understandable then, why special attention has been paid to synthetic macrocycles which resemble but also differ from the naturally occurring porphyrins. However, the chemistry of metal–macrocycle complexes is also of fundamental interest.

The title macrocyclic ligand, a dianion which is usually abbreviated tmtaa, shares many common characteristics with porphyrins, but it features some important differences. Thus, while it is of bio-inorganic interest, it also has many other characteristics that make it of fundamental interest in its own right. The similarities to porphyrins are as follows: (1) the four nitrogen atoms of H_2tmtaa are confined to a plane, as in the porphyrins (see I); (2) upon metal complexation, the ligand usually

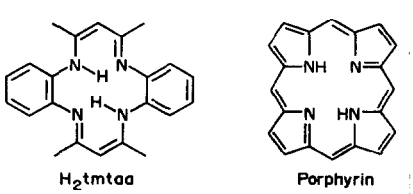

H_2tmtaa Porphyrin

I

* Author to whom correspondence should be addressed.

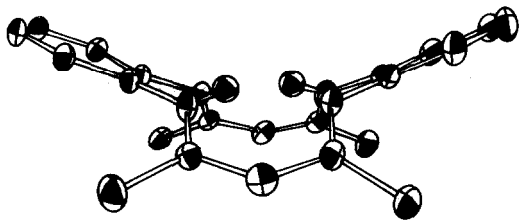

Fig. 1. Side view of H_2tmtaa showing its saddle shape even in the free state.

deprotonates to give a dianion; and (3) tmtaa has a completely conjugated system of double bonds. The differences between tmtaa and the naturally occurring systems, however, account for the non-bio-inorganic interest and hence for the proliferation of new and interesting compounds. The 14-membered ring size of tmtaa, as compared to a 16-membered one in porphyrins, favours shorter metal–nitrogen distances. Secondly, in contrast to the completely delocalized framework of porphyrins, each of tmtaa's two negative charges tends to be localized only over the 2,4-pentanediiminato chelate rings. Lastly, even though tmtaa can be described as conjugated, it is an anti-aromatic ($4n$) system, whereas porphyrins exhibit a $4n+2$ π-electron aromaticity.

Tmtaa was first synthesized by Jäger[1] via a template condensation reaction of *o*-phenylenediamine with 2,4-pentanedione. Its modified synthesis[2] and a crystal structure[3] were reported much later by Goedken and co-workers. It has three special steric features which dictate its reactivity and coordination geometry: (1) Its "core size" is about 1.902 Å, which is about 0.1 Å smaller than that of porphyrins. (2) A saddle shape conformation is produced by the internal steric constraints (e.g. methyl–phenyl repulsions) and this causes displacement of the coordinated metal from the N_4 plane. (3) Because the saddle shape has the *o*-phenylene rings and the diiminate framework displaced in opposite directions, the two remaining coordination sites on the metal centre become chemically inequivalent. Figure 1 shows the saddle shape as it exists even in the free ligand, H_2tmtaa.[3]

The present article provides a concise summary of most of what is known about transition metal–tmtaa complexes. However, we do not attempt to discuss all of them. Rather the most important trends in our judgement will be noted and a few compounds with special features will be emphasized. Tables 1 and 2 list the known tmtaa complexes with information on their properties, including structures in the relatively few cases where these are known. It should be mentioned again that H_2tmtaa itself is structurally characterized.[3]

2. MONONUCLEAR COMPLEXES

2.1. *Early transition metals* (*Groups* IV, V, VI)

General trends. The organometallic chemistry of the early transition metals, although a broad and active field today, mainly depends on such stabilizing ligands as cyclopentadiene and substituted cyclopentadienes.[4] It was not until the early 1980s that the title ligand was introduced to this field as an ancillary ligand for stabilizing M—C functionalities.

In 1982, Goedken and co-workers synthesized Ti(tmtaa)Cl_2[5] and other Ti(tmtaa)$(R)_n$ type compounds (where R = O, S, alkyl groups and n = 1, 2) which were the first examples of a wide group of compounds subsequently synthesized. Since then, the macrocyclic stabilization effect of tmtaa has allowed for a more diverse chemistry of the group IV, V and VI transition metals, to be discussed presently.

There are two efficient synthetic routes employed in the preparation of the M(tmtaa)$(Cl)_n$ (n = 1, 2) type compounds listed in Table 1 for Group IV, V and VI metals. They are as follows: (1) reaction of an early transition metal halide with H_2tmtaa under basic reaction conditions (e.g. in the presence of NEt_3); and (2) reaction of a metal halide with an activated form of H_2tmtaa, Li_2(tmtaa), in tetrahydrofuran (THF). The lithium compound is formed upon reacting n-Bu–Li with H_2tmtaa in a 2:1 ratio at -10°C in THF.

Metal	Complex	Average M—N distance (Å)	Distance of M from N_4 plane (Å)	Other measurements	References
Group IV					
Ti	$Ti(L)Cl_2$	2.042(4)	0.91		5
	Ti(L)Cl	Unpublished results			6
	Ti(L)(cp)	2.114(6)	0.889(1)	Mag. suscept. (μ_{eff} = 1.81 BM, 292 K)	6, 7
	Ti(L)O	No structure		Mass spec., IR	5
	$Ti(L)O_2$	No structure		Mass spec., IR	5
	$[Ti(L)]_2O^+$	No structure		IR	5
	Ti(L)S	No structure		Mass spec., IR	5
	$Ti(L)(C_2O_4)$	No structure		Mass spec., IR, CV	5
	$Ti(L)(C_7H_8S_2)$	No structure		Mass spec., IR, CV	5
	$Ti(L)(S)_2$	No structure		Mass spec., IR	5
	$Ti(L)(C_6H_6O_2)$	No structure		Mass spec., CV	5
Zr	$Zr(L)Cl_2$		1.070(2)	NMR	8
	$Zr(L)(CH_2Ph)_2$	2.189(8)	1.019(2)	NMR	8
	Zr(L—Me)(Me)(THF)	2.185(5)	1.049(1)	NMR	8
Group V					
V	V(L)O	2.017(2)–2.026(2)	0.678(1)	CV, ESR, IR	9, 10
	$V(L)Cl_2$	No structure		CV, ESR, IR	10
	V(L)S	No structure		CV, ESR, IR	10
	$[V(L)—N—V(L)]^+$	No structure		CV, ESR, IR	10
	$[V(L)(O)]_2^{2+}$	No structure		CV, ESR, IR	10
	$[V(L)(O)]_2$	No structure		Mass spec., IR, UV–vis	10
	V(L)Cl	Unpublished results			6
	V(L)(mes)	2.002(8)	0.626	Mag. suscept. (μ_{eff} = 2.90 BM, 293 K)	6
	V(L)(cp)	2.104(4)	0.875(1)	Mag. suscept. (μ_{eff} = 2.76 BM, 292 K)	6,9
Nb	$Nb(L)Cl_2$	2.122(2)–2.127(3)	0.970(2)	Chem. anal., mag. suscept. (μ_{eff} = 1.9 BM, 293 K)	11
Group VI					
Cr	Cr(L)Cl	1.971(6)	0.435(1)	UV–vis	12
Mo	$Mo(L)(CO)_4$	No structure		NMR, UV–vis, IR	13
	$[Mo(L)O]^{+\cdot}$	2.034(4)–2.041(4)	0.737(1)	CV, ESR, IR	15
	Mo(L)O	No structure		CV, NMR, IR	15
W	$W(L)(CO)_4$	2.240(7)	1.526	NMR, UV–vis, IR	13, 14
Group VII					
Mn	$Mn(L)NEt_3$	2.110(3)–2.117(3)	0.730	UV–vis, IR, ESR, chem. anal.	16, 17
	$Mn(L)N(n\text{-}Pr)_3$	No structure		UV–vis, IR, ESR, chem. anal.	16
	Mn(L)Cl	No structure		UV–vis, IR, ESR, chem. anal., mag. suscept. (μ = 4.96–5.05 BM, RT)	16
	Mn(L)Br	No structure		UV–vis, IR, ESR, chem. anal., mag. suscept. (μ = 4.96–5.05 BM, RT)	16
	Mn(L)SCN	No structure		UV–vis, IR, ESR, chem. anal., mag. suscept. (μ = 4.96–5.05 BM, RT)	16
	$Mn(L)N_3$	No structure		UV–vis, IR, ESR, chem. anal., mag. suscept. (μ = 4.78 BM, RT)	16

Table 1—*continued*

Metal	Complex	Average M—N distance (Å)	Distance of M from N_4 plane (Å)	Other measurements	References
Group VIII					
Fe	Fe(L)	1.918(3)	0.114	Mass spec., UV–vis, mag. suscept. (μ_{eff} = 3.69 BM, RT)	18, 3
	Fe(L)Cl	2.002	0.600	IR, mass spec., chem. anal., mag. suscept. (μ_{eff} = 5.95 BM, RT)	17, 18
	Fe(L)(CO)	1.927(4)	0.290	IR, chem. anal.	18, 19
	Fe(L)(NO)	1.716(11)		IR, chem. anal. ESR, mag. suscept. (μ_{eff} = 1.91 BM, 292 K)	20
	[Fe(L)Na(thf)$_3$]	1.093(9)	0.086(2)	Mag. suscept. (μ_{eff} = 2.92 BM, 292 K)	21
	Fe(L)(CO)C_5H_5N	1.941(2)	0.050	IR, chem. anal.	18, 19
	Fe(L)(CO)NH_2NH_2	1.944(9)	0.110	IR, chem. anal.	19, 22
	Fe(L)(py)$_2$	No structure			18
	Fe(L)(C_6H_5)	1.904–1.915	0.230	IR	23
	(Fe(L))$_2$O	2.054	0.698	IR, chem. anal., mag. suscept. (μ_{eff} = 1.96 BM, RT)	18, 24
Ru	Ru(L)(CO)	No structure		IR, NMR, mass spec., CV	25
	Ru(L)(py)$_2$	No structure		IR, NMR, mass spec., CV	25
	Ru(L)(MeCN)$_2^+$	No structure		IR, mass spec., CV	25
	Ru_2(L—L)$Cl_2(CO)_2$	No structure		IR, mass spec.	25
	Ru(L)(PMePh$_2$)$_2$	2.031(1)	0.000	NMR, UV–vis	26
Group IX					
Co	Co(L)	No structure		Mag. suscept. (μ_{eff} = 2.85 BM, RT)	27
	Co(L)Cl	No structure		Mag. suscept. (μ_{eff} = 2.67 BM, RT)	27
	Co(L)Br	No structure		Mag. suscept. (μ_{eff} = 3.15 BM, RT)	27
	Co(L)I	1.901	0.234	Mag. suscept. (μ_{eff} = 2.80 BM, RT)	27, 28
	[Co(L)Na(thf)$_3$]	Unreported		Diamagnetic	21
	[Co(L)(py)]$^+$	No structure		NMR	27
	[Co(L—(CH_2CH_2))]py$^+$	1.892	0.000	IR	29
	[Co(L=O)$(NH_3)_2$]$^+$	No structure		IR, NMR, chem. anal.	27
Rh	Rh_2(L)$(CO)_4$	2.071(1)		UV–vis, IR, NMR, mass spec.	30
	Rh_2(L)$(CO)_4^+$	2.11(1)		IR, NMR, UV–vis	30
Ni, Cu and Zn					
Ni	Ni(L)	No structure		NMR	1
	[Ni(L)Na(thf)$_3$]		0.006(4)	Mag. suscept. (μ_{eff} = 1.89 BM, 292 K)	21
	[Ni(L)—(L)Ni]$^{2+}$	No structure		ESR, CV, IR, NMR	31
	Ni(L)—(L)Ni	No structure		CV, IR, NMR	31
Cu	Cu(L)	No structure		UV–vis, mass spec. Raman, mag. suscept. (μ_{eff} = 1.85 BM, RT)	32, 33
Zn	Zn(L)NEt_3	No structure		IR, NMR, UV–vis	16
	Zn(L)N(n-Pr)$_3$	No structure		IR, NMR, UV–vis	16

Table 2. Listing of the dimeric $[M(tmtaa)]_2$ type complexes

Metal	Complex	Average M—N distance (Å)	Distance of M from N_4 plane (Å)	Other measurements	References
Cr	$[Cr(L)]_2$	1.993(3)–2.009(3)	0.50(2)	IR, NMR, chem. anal.	34, 35
Mo	$[Mo(L)]_2$	2.084(6)–2.096(6)	0.50(2)	CV, UV–vis	36
	$[Mo(L)]_2^{+\cdot}$		0.57	CV, ESR	36
	$[Mo(L)]_2^{-\cdot}$	No structure		CV, ESR	36
Ru	$[Ru(L)]_2^+$	No structure		CV, mag. suscept. (μ_{eff} = 1.55 BM, RT)	25
	$[Ru(L)]_2$	No structure		CV, mass spec., mag. suscept. (μ_{eff} = 2.88 BM, RT)	25
	$[Ru(L)]_2^{2+}$	No structure		CV	25
Rh	$[Rh(L)]_2$	1.982(6)–1.998(6)	0.222(1)	NMR, UV–vis	37

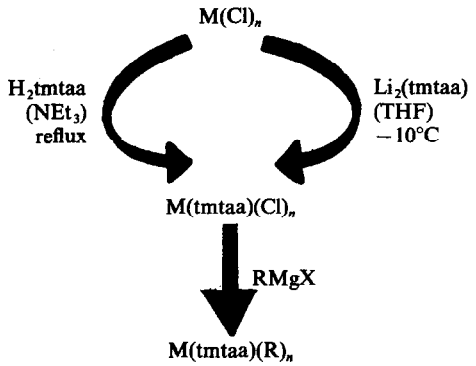

Despite the seemingly disparate character of the compounds listed in Table 1, a number of features tie them all together. First, there is the inherent predisposition of tmtaa to push the metal out of the N_4 plane (see Introduction). Indeed, all the monomeric compounds discussed in this section have the metal located well out of the N_4 plane. The displacements range from 0.435 Å for Cr(tmtaa)Cl[12] to 1.070 Å for $Zr(tmtaa)Cl_2$.[8] The degree of metal displacement is a function of the size of the metal ion: $Zr(tmtaa)Cl_2$, mentioned above, shows the maximum distortion; its first row analogue, $Ti(tmtaa)Cl_2$,[5] on the other hand, shows the smaller distortion of 0.91 Å, consistent with the smaller radius of titanium.[38] The second feature is that most $M(tmtaa)(Cl)_n$ type complexes are easily alkylated with Grignard reagents, often leading to novel M—C functionalities. These alkyl groups are found *cis* to each other,[8] as shown in Fig. 2; this is somewhat unusual in light of the many six-coordinate complexes of the middle transition metals which possess a *trans* ligand arrangement [e.g. Fe(tmtaa)(CO)(py)].[18,19] The axial halides in these early transition metal compounds are themselves found in the *cis* arrangement.

The extent to which the metal atoms are displaced from the N_4 plane is greater for these early transition metals than for any of the later ones. One way to rationalize this is to regard the coordination sphere as a distorted trigonal prism, as shown schematically in **II**. This point of view

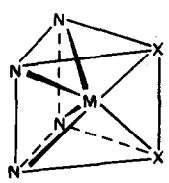

II

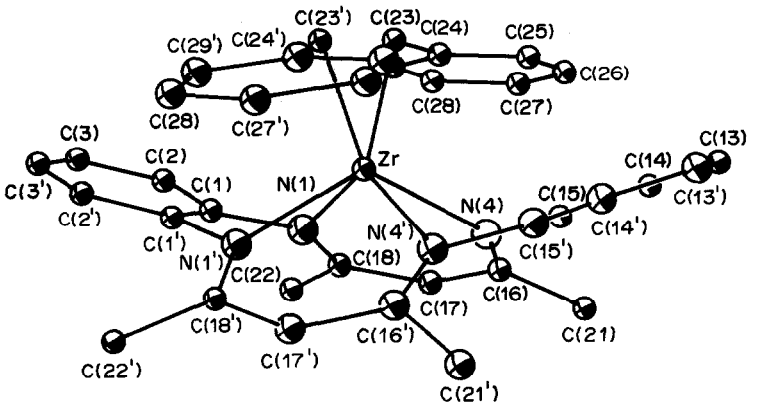

Fig. 2. An ORTEP diagram of the six-coordinate zirconium complex, illustrating the *cis* arrangement of the axial ligands.

is consistent with the large displacement and with the presence of two X ligands, both on the same side (i.e. *cis*) and is in harmony with Girolami's recent work[4] showing that the trigonal prism is a "natural" geometry for six-coordinate d^0 metal ions.

Peculiarities. A zirconium complex, Zr(tmtaa-Me)(Me)(THF),[8] demonstrates that during a substitution reaction occurring at the metal centre, the ligand itself can undergo some transformation, as shown in **III**. Floriani and co-workers report that although the familiar saddle shape

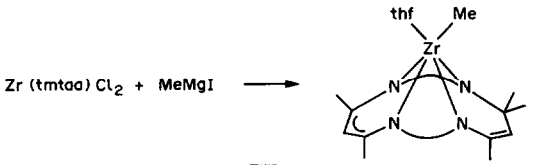

III

of tmtaa is retained in this complex, the ligand no longer behaves as a dianion, but instead acts as a trianion. Although, the exact route to the formation of this compound is obscure, it is clear that the ligand undergoes methylation at the carbon atom of one C=N group. The zirconium(IV) is 1.049 Å out of the N_4 plane, the largest displacement seen to date.

Yet another anomaly worth mentioning is provided by the $M(H_2tmtaa)(CO)_4$ compounds, where M = Mo,[13] W,[13,14] shown in Fig. 3. The metal is bonded to only two of the four nitrogen atoms of tmtaa and the ligand remains neutral upon coordinating to the $M(CO)_4$ moiety. These complexes are obtained by reaction of $M(CO)_6$ with H_2tmtaa at high temperatures. In these reactions, one of the two nitrogen protons migrates to a methine carbon atom so that the ligand can now be represented by **IV**. The saddle shape conformation of this isomeric H_2tmtaa becomes even more pronounced than that of the normal form.

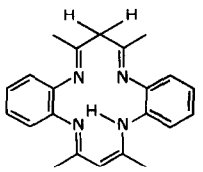

IV

In a very recent report[36a] it has been shown that $(tmtaa)(M)(CO)_4$, where M = Mo and W, can be converted to the cation, $[(tmtaa)M(CO)_3NO]^+$, which may then react with CH_3CN to give the "scorpion" like product shown in Fig. 4. This seven-coordinate cationic complex is quite remarkable, because it contains a tridentate tmtaa moiety. The latter was transformed from a bidentate unit by formation of an imine appendage which in turn resulted from the insertion of an acetonitrile molecule into a C—H bond of the coordinated —N=C—CH_2—C=N— fragment.

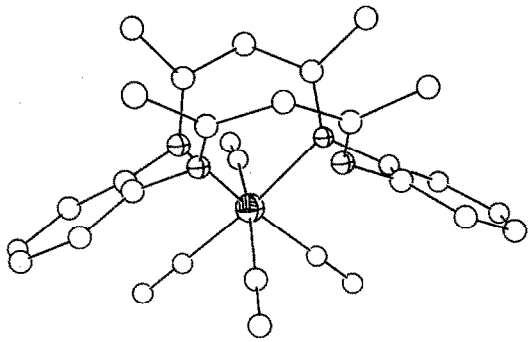

Fig. 3. Side view of the $W(H_2tmtaa)(CO)_4$ complex, illustrating the metal's coordination to only two nitrogen atoms of the ligand.

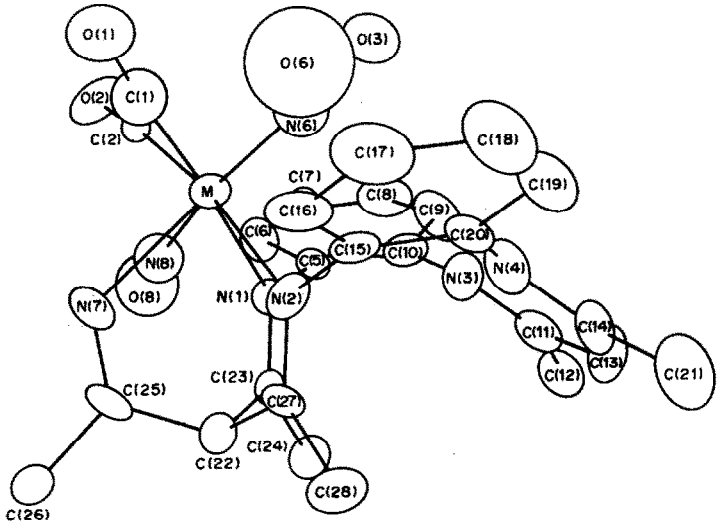

Fig. 4. An ORTEP diagram of the "scorpion"-like $[W(CO)_3NO(C_{24}H_{27}N_5)]BF_4 \cdot CH_3CN$ complex.

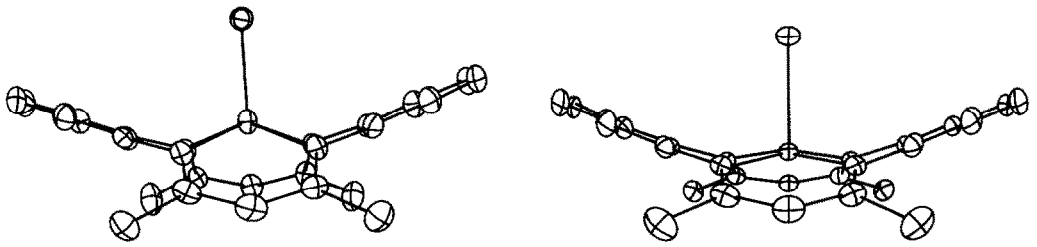

Fig. 5. Side view of Fe(tmtaa)Cl (left) and Co(tmtaa)Cl (right).

The compound (tmtaa)CrCl[12] is of unusual interest as the only known square pyramidal complex of chromium(III). It can be easily prepared in essentially quantitative yield. It has three unpaired electrons, which is in accord with a molecular orbital treatment of the electronic structure. The structure closely resembles that of the analogous iron(III) complex shown in Fig. 5.

2.2. *Middle transition metals* (*Groups* VII, VIII, IX)

General trends. Unlike the early transition metals discussed above, these metals have been found in various macrocyclic systems for over two decades. Study of these systems is especially important because of their potential practical uses. For example, metals such as manganese, iron and cobalt

have long been known to take active parts in many biological functions, i.e. binding of small molecules in haems. The same metals in synthetic macrocycles can provide us, then, with significant clues to the understanding of the natural systems. Such was the motivation behind the extensive study of the middle transition metals with tmtaa, done concurrently by Goedken and Dabrawiak, beginning in the early 1970s.

The first row metals, manganese, iron and cobalt, clearly dominate the list in this section. Their chemistry upon complexation to the macrocyclic ligand is quite similar for all of them despite their differences in ionic radii, oxidation numbers and spin states. First, iron and cobalt form the four-coordinate complexes of the type M^{II}(tmtaa). Fe(tmtaa)[3,18] and Co(tmtaa)[27] are both low spin M^{II} systems with $\mu_{eff} = 3.69$ and 2.86 BM, respectively. Only Fe(tmtaa) has been structurally characterized; there are, however, many features common to the two compounds in terms of their chemical behaviour. These two four-coordinate complexes readily coordinate axial ligands to satisfy their coordinatively unsaturated geometry. Reaction of Fe(tmtaa) with $CHCl_3$ or CCl_4 leads to the five-coordinate, high-spin complex, Fe(tmtaa)Cl.[17,18] Similarly, Co(tmtaa) reacts with X_2 or CHX_3 (X = Cl, Br, I) to give Co(tmtaa)X[27] ($S = 1$ spin configuration). Both structures are shown in Fig. 5.

The displacements out of the N_4 plane for iron(III) and cobalt(III) centres are 0.600 and 0.234 Å, respectively. The redirecting of the N_4 lone pairs towards the metal is much greater in the case of the bigger ion, Fe^{3+}.[38] Manganese forms similar five-coordinate complexes but via a different synthetic route.[16] Mn(tmtaa)X, where X = Cl, Br, I, are high-spin d^4 systems. Although nothing is known about their structures, the compounds are well characterized by IR, ESR and magnetic susceptibility measurements.

There are a number of six-coordinate complexes (mostly of iron and cobalt), all of them containing the axial ligands *trans* to each other. The few crystal structures available establish with certainty the configuration of tmtaa as it accommodates the additional ligands. A good example of such a complex is Fe(tmtaa)(CO)(NH_2NH_2),[19,22] shown in Fig. 6. This octahedral iron(II) complex has the carbon monoxide molecule strongly bound to the iron (C—Fe = 1.75 Å), producing a *trans* effect at the hydrazine site. This, together with the steric interactions between tmtaa and hydrazine, results in an abnormally long iron–nitrogen$_{(base)}$ bond of 2.12 Å. The low-spin Fe^{2+} centre is displaced from the N_4 plane towards the carbon monoxide by 0.11 Å; this displacement is similar to that in the other low-spin Fe^{2+} complex, four-coordinate Fe(tmtaa), discussed earlier.

Although there are other six-coordinate compounds known of metals such as cobalt and ruthenium, useful comparisons cannot be made because of the lack of crystallographic studies. Compounds such as $[Co(L)(py)_2]^+$,[27] Ru(L)$(py)_2$[25] or $[Ru(L)(MeCN)_2]^+$[25] are all well-defined, but by NMR and IR only.

Finally, it ought to be pointed out that the chemistry of the second and third row middle transition metals is quite unexplored. Rhenium, osmium and iridium have yet to play a role in tmtaa chemistry.

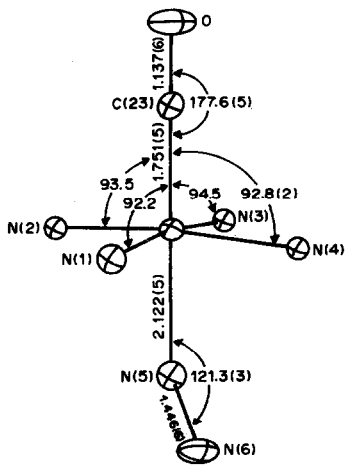

Fig. 6. Bond distances and angles in the six-coordinate Fe(tmtaa)(CO)(NH_2NH_2) complex.

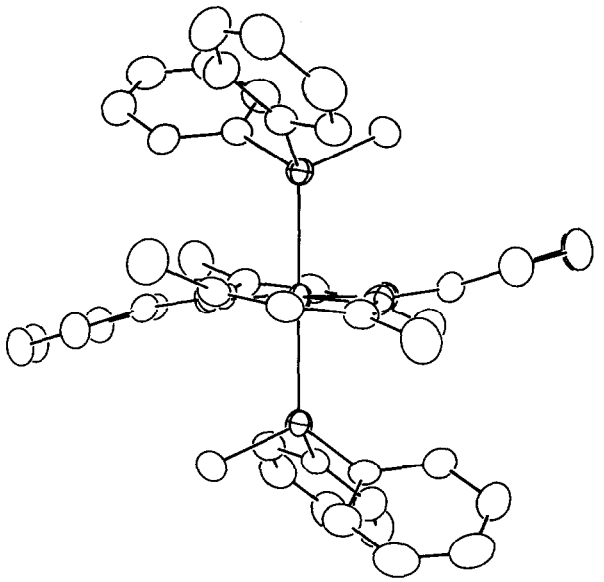

Fig. 7. Side view of the molecule illustrating the step-like shape of the ligand.

Peculiarities. $Ru(tmtaa)(PMePh_2)_2$[26] is a novel complex in which the conventional geometry of the ligand is altered. The octahedral environment of the ruthenium atom consists of four equatorially bound nitrogen atoms of tmtaa and two axially bound phosphorus atoms of $PMePh_2$. The axial, bulky phosphines force the ligand out of the saddle shape and into a "step-like" geometry, with the two benzenoid rings *trans* to each other, relative to the N_4 plane (Fig. 7). This centrosymmetric complex is the only example of a complex in which the saddle shape of tmtaa is destroyed in this fashion. The low-spin t_{2g}^6 electron configuration gives the ruthenium(II) a small enough effective radius to allow it to fit into four nitrogen atoms.

Another complex with unusually interesting features is obtained from a reaction of $Co(tmtaa)(py)_2^+$[24] with acetylene under basic conditions. The final product, Fig. 8, contains the dianionic yet pentadentate tmtaa macrocycle with a vinylide carbon σ-donor occupying one of the two axial sites of the metal. This structure may be compared with that shown in Fig. 4.

The formation of this remarkable product is favoured by a strained coordination environment of the metal ion and the activated character of the methine carbon of tmtaa.

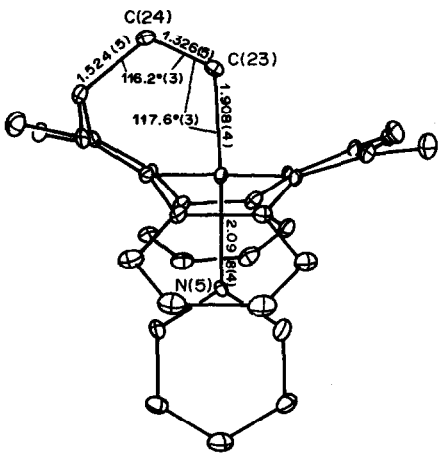

Fig. 8. Side view of $[Co(C_{24}H_{24}N_4)(C_5H_5N)]^+$ illustrating the pentadentate coordination of tmtaa.

2.3. *The metals nickel, copper and zinc*

The last class of mononuclear complexes to be discussed is that formed by the late transition metals and zinc. The first report of tmtaa coordination in 1969 mentioned the four-coordinate nickel complex, Ni(tmtaa).[1] Since then, there has been but a handful of other examples, with nickel and copper as the only two late transition metals. Dabrawiak and co-workers[31] found that Ni(tmtaa) undergoes elecrochemical oxidation which leads to the formation of a dimer, **Va**. The two macrocyclic fragments are joined through a carbon–carbon single bond. Under basic conditions this dimeric cation easily loses two protons to give the complex **Vb**. Presumably, a radical mechanism

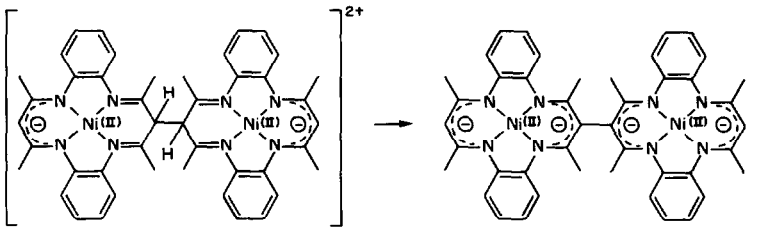

Va **Vb**

leads to the joining of the two macrocycles, in the end giving the neutral dimer. Its postulated structure is supported by IR and ^{1}H NMR data. (Similar chemistry has been seen with an oxovanadium complex of tmtaa, reported by Goedken and co-workers.)[10]

The element zinc exhibits somewhat different chemical behaviour when coordinated to tmtaa. The complexation of zinc(II) with the macrocycle takes place only in the presence of a base,[16] such as NEt_3 or $N(n\text{-}Pr)_3$, and the resulting product contains a tertiary amine strongly coordinated to the metal centre. The $Zn(tmtaa)(NR_3)$ type complexes are most probably square pyramidal in geometry, as shown by molecular models, with the metal displaced from the N_4 plane thus facilitating the binding of the amine, as shown in **VI**. (Potentially severe steric interactions between the alkyl

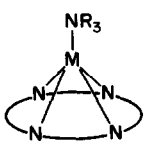

VI

groups of the amine and the macrocyclic fragment are diminished when the metal is pushed out of the N_4 plane.)

One can speculate that the displacement of zinc(II) is similar to that for manganese(II) since the ionic radii of the two cations[38] are relatively large and both exceed the hole size of tmtaa. There have been no reports of $M(tmtaa)NR_3$ type complexes with nickel or copper despite some preliminary attempts by Dabrawiak to synthesize the nickel ones.

The only copper complex reported is Cu(tmtaa).[32,33] It has one unpaired electron and spectroscopic data are also reported but the structure is unknown. In view of the well-known strong preference of copper(II) for square coordination, this might have a stepped conformation like that in $Ru(tmtaa)(PPh_2Me)_2$.

3. DINUCLEAR COMPLEXES

The chemistry of unbridged $[M(tmtaa)]_2$ type dimers is small in comparison to the large field of monomeric species. These metal–metal bonded complexes with non-bridging macrocycles warrant more study in view of their stability despite the potential steric repulsions of the macrocyclic ligand. Furthermore, these porphyrin-like systems have potential as catalysts in redox processes. Since there is but a handful of $[M(tmtaa)]_2$ complexes known to date, it is worthwhile to consider each of them explicitly.

3.1. *The diruthenium compounds*

The first compounds of the type $[M(tmtaa)]_2$ to be reported were those of ruthenium. In 1978, Warren and Goedken[25] reported the chemistry summarized in the scheme below, **VII**. Unfortunately, no structural data have yet been presented.

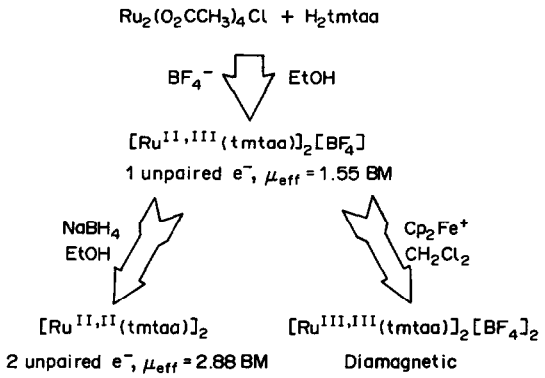

VII

From the magnetic data it can be inferred that the electron configurations for the neutral molecule, the +1 and the +2 ions are, respectively, $\sigma^2\pi^4\delta^2\delta^{*2}\pi^{*2}$, $\sigma^2\pi^4\delta^2\delta^{*2}\pi^*$ and $\sigma^2\pi^4\delta^2\delta^{*2}$. These are analogous to those believed to occur in the analogous porphyrin systems.

3.2. *The dirhodium compound*

The compound $Rh_2(tmtaa)_2$ has been prepared and structurally characterized.[37] It has the tmtaa rings in the usual saddle conformation and a Rh—Rh distance of 2.619(6) Å, consistent with a $\sigma^2\pi^4\delta^2\delta^{*2}\pi^{*4}$ configuration and a net single bond. A side view of this molecule showing how the two tmtaa rings are rotated 90° to each other to allow a snug fit is presented in Fig. 9.

3.3. *The dichromium and dimolybdenum compounds*

Several publications[35,36] have appeared dealing with the molybdenum compound and its derivatives. $Mo_2(tmtaa)_2$ is easily prepared by reaction of $Mo_2(O_2CCH_3)_4$ with Li_2tmtaa and it has been shown that it can be both oxidized and reduced, as shown below in **VIII**. The structures of both the

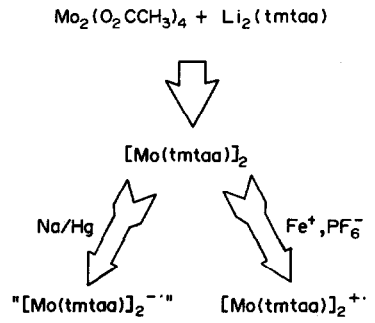

VIII

neutral molecule and the cation have been reported and they are essentially identical except for a change in the Mo—Mo bond distance from 2.175(1) Å for the molecule to 2.221(1) Å for the cation. This change of 0.046 Å upon removal of one δ electron is similar to that found in other cases. Figure 10 shows the structures of both of these species (and the Cr_2 and Rh_2 molecules as well) projected down the M—M axis. Conversely, the side view of the $Rh_2(tmtaa)_2$ structure shown in Fig. 9 is essentially the same for the other three species.

An especially interesting example of a M—M multiply bonded species of tmtaa appeared recently with the synthesis of $[Cr(tmtaa)]_2$.[34,35] Chromium(II) is well-known for forming unusually short Cr—Cr quadruple bonds under certain conditions. Only a few of them, however, exist in unbridged

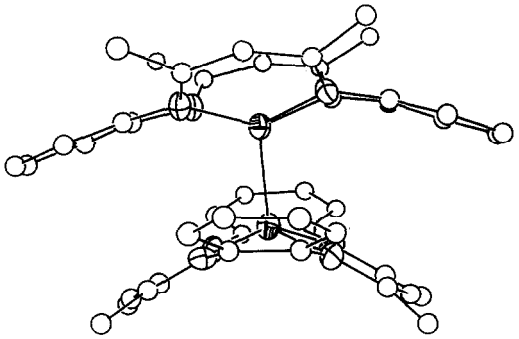

Fig. 9. An ORTEP diagram of the $[Rh(tmtaa)]_2$ molecule showing how the saddle-shaped ligands fit together snugly.

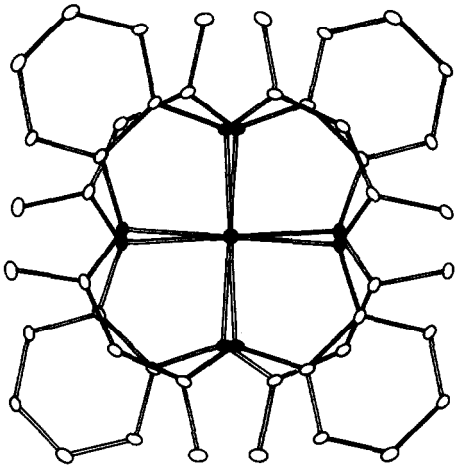

Fig. 10. An ORTEP view of the $[Mo(tmtaa)]_2$ molecule down the M—M axis.

systems. There are all together five efficient ways of synthesizing the $[Cr(tmtaa)]_2$ compound, three reported by one group[34] and two by another.[35]

$$Me_8Cr_2(LiTHF)_4 + 2tmtaaH_2 \xrightarrow{-4CH_4}$$

$$2Mes_2Cr(THF)_3 + 2tmtaaH_2 \xrightarrow{-4MesH}$$

$$2CrCl_2(THF)_2 + 2(tmtaa)Li_2 \xrightarrow{-4LiCl} [(tmtaa)Cr]_2.$$

$$Cr_2(O_2CCH_3)_4 + 2(tmtaa)Li_2 \xrightarrow{-2Li(O_2CCH_3)}$$

$$2Cp_2Cr + 2tmtaaH_2 \xrightarrow{-4CpH}$$

As before, X-ray crystallographic studies show that the two tmtaa fragments possess the saddle-shape geometry and are rotated by nearly 90° relative to one another, as indicated in Figs 9 and 10.

The Cr—Cr distance is 2.101(1) Å in the crystal form that is isomorphous with $Mo_2(tmtaa)_2$. This is short enough to show that a multiple bond exists in the dimer. Calculations[35] show that

there is only a triple bond between the two chromium atoms because metal–ligand interactions lead to a diminished overlap between the δ-bonding $d_{x^2-y^2}$ orbitals. In the molybdenum compound, on the other hand, significant δ-bonding exists.

In summary, unbridged $[M(tmtaa)]_2$ type complexes are stable, despite the steric repulsions of the macrocyclic moieties. There are two main features of the ligand which serve to reduce the potentially severe steric interactions which might have been expected when the macrocyclic fragments are brought together within a bonding distance of the metals. They are, as mentioned in the discussion of monomeric compounds: (1) the ability of the ligand to displace the metal out of the N_4 plane; and (2) its flexibility to adjust the saddle shape according to the size of a metal and axial ligands (another M(tmtaa) fragment, in this case). The limited number of reactions that have been so far investigated in the case of the dimers $[Mo(tmtaa)]_2$, $[Ru(tmtaa)]_2$ and $[Ru(tmtaa)]_2^+$ point to a facile cleavage of Mo—Mo and Ru—Ru bonds. The molybdenum dimer reacts first with tetracyanoethylene (TCNE) and then presumably with some traces of water to produce monomeric $[MoO(tmtaa)][C_3(CN)_5]$.[36b] The ruthenium(II) dimer, on the other hand, dissociates in the presence of CO or pyridine to give monomers of Ru(tmtaa)(CO) and $Ru(tmtaa)(py)_2$. Furthermore, $[Ru(tmtaa)]_2^+$ disproportionates in the presence of carbon monoxide and acetonitrile forming Ru(tmtaa)(CO) and $[Ru(tmtaa)(CH_3CN)_2]^+$.

There is still a lot to be accomplished in the field of unbridged tmtaa dimers. Metals such as vanadium, tungsten, osmium, manganese and iron to mention a few, have the potential for forming these compounds; their synthesis may be simply a matter of time.

4. CONCLUSIONS

The syntheses of unbridged $[M(tmtaa)]_2$ type compounds highlight the fascinating chemistry of the dibenzo[b,i][1,4,8,11]tetraazacyclotetradecine macrocyclic ligand. The latter bears many similarities to porphyrinato systems, but its chemical behaviour seems to be even more diverse. The unique features of tmtaa with regard to electronic delocalization, core size and framework flexibility are responsible for the variety of complexes reported to date. In turn, these complexes give us an insight into the effects of metal electronic configuration, charge and size upon the structure and properties of the macrocyclic framework. These and other matters are of continuing interest to us and other research groups as we discover new "M(tmtaa)" type systems.

Acknowledgement—We thank the National Science Foundation for support.

REFERENCES

1. E. G. Jäger, *Z. Anorg. Chem.* 1969, **364**, 177.
2. V. L. Goedken, J. Molin-Case and Y.-A. Whang, *Chem. Commun.* 1973, 337.
3. V. L. Goedken, J. J. Pluth, S. M. Peng and B. Bursten, *J. Am. Chem. Soc.* 1976, **98**, 8014.
4. P. M. Morse and G. S. Girolami, *J. Am. Chem. Soc.* 1989, **111**, 4114.
5. V. L. Goedken and J. A. Ladd, *Chem. Commun.* 1982, 142.
6. S. Ciurli, C. Floriani, A. Chiesi-Villa and C. Guastini, *Chem. Commun.* 1986, 1401.
7. C.-H. Yang and V. L. Goedken, *Chem. Commun.* 1986, 1101.
8. C. Floriani, S. Ciurli, A. Chiesi-Villa and C. Guastini, *Angew. Chem. Int. Ed. Engl.* 1987, **26**, 70.
9. F. A. Cotton, J. Czuchajowska and X. Feng, *Inorg. Chem.*, in press.
10. V. L. Goedken and J. A. Ladd, *Chem. Commun.* 1981, 910.
11. C. Floriani, M. Mazzanti, S. Ciurli, A. Chiesi-Villa and C. Guastini, *J. Chem. Soc., Dalton Trans.* 1988, 1361.
12. F. A. Cotton, J. Czuchajowska, L. R. Falvello and X. Feng, *Inorg. Chim. Acta* 1990, **172**, 135.
13. L. G. Bell and J. C. Dabrawiak, *Chem. Commun.* 1975, 512.
14. F. A. Cotton and J. Czuchajowska, *Polyhedron* 1990, **9**, 1217.
15. J. M. Giraudon, J. E. Guerchais, J. Sala-Pala and L. Toupet, *Chem. Commun.* 1988, 921.
16. D. R. Neves and J. C. Dabrawiak, *Inorg. Chem.* 1976, **15**, 129.
17. M. C. Weiss, B. Bursten, S. M. Peng and V. L. Goedken, *J. Am. Chem. Soc.* 1976, **98**, 8021.
18. V. L. Goedken and Y. Park, *Chem. Commun.* 1975, 214.
19. V. L. Goedken, S. M. Peng, J. Molin-Norris and Y. Park, *J. Am. Chem. Soc.* 1976, **98**, 8391.
20. P. Berno, C. Floriani, A. Chiesi-Villa and C. Guastini, *J. Chem. Soc., Dalton Trans.* 1988, 1409.

21. S. Ciurli, E. M. Meyer, C. Floriani, A. Chiesi-Villa and C. Guastini, *Chem. Commun.* 1987, 281.
22. V. L. Goedken, J. Molin-Case and Y. Whang, *Chem. Commun.* 1973, 337.
23. V. L. Goedken, S. M. Peng and Y. Park, *J. Am. Chem. Soc.* 1974, **96**, 284.
24. M. C. Weiss and V. L. Goedken, *Inorg. Chem.* 1979, **18**, 819.
25. L. F. Warren and V. L. Goedken, *Chem. Commun.* 1978, 909.
26. F. A. Cotton and J. Czuchajowska, *Polyhedron* 1990, **9**, 1221.
27. M. C. Weiss and V. L. Goedken, *J. Am. Chem. Soc.* 1976, **98**, 3389.
28. M. C. Weiss and V. L. Goedken, *Chem. Commun.* 1976, 531.
29. M. C. Weiss, G. C. Gordon and V. L. Goedken, *J. Am. Chem. Soc.* 1979, **101**, 857.
30. G. C. Gordon, P. W. Dehaven, M. C. Weiss and V. L. Goedken, *J. Am. Chem. Soc.* 1978, **100**, 1003.
31. F. C. McElroy and J. C. Dabrawiak, *J. Am. Chem. Soc.* 1976, **98**, 7112.
32. W. H. Woodruff, R. W. Pastor and J. C. Dabrawiak, *J. Am. Chem. Soc.* 1976, **98**, 7999.
33. L. A. Nafie, R. W. Pastor, J. C. Dabrawiak and W. H. Woodruff, *J. Am. Chem. Soc.* 1976, **98**, 8007.
34. J. J. H. Edema, S. Gambarotta, P. van der Sluis, W. J. J. Smeets and A. L. Spek, *Inorg. Chem.* 1989, **28**, 3782.
35. F. A. Cotton, J. Czuchajowska and X. Feng, *Inorg. Chem.*, in press.
36. (a) D. Mandon, J. M. Giraudon, L. Toupet, J. Sala-Pala and J. E. Guerchais, *J. Am. Chem. Soc.* 1987, **109**, 3490; (b) J. M. Giraudon, J. E. Guerchais, J. Sala-Pala and L. Toupet, *Chem. Commun.* 1988, 921; (c) J. M. Giraudon, D. Mandon, J. Sala-Pala, J. E. Guerchais, J. M. Kerbaol, Y. LeMest and P. L'Haridon, *Inorg. Chem.* 1990, **29**, 707.
37. (a) S. L. Van Voorhees and B. B. Wayland, *Organometallics* 1987, **6**, 204; (b) F. A. Cotton and J. Czuchajowska, unpublished.
38. R. D. Shannon, *Acta Cryst.* 1976, **A32**, 751.

ADDENDUM

Since the submission of this manuscript for publication, we have been informed of an interesting compound relevant to this review. J. Guerchais and co-workers synthesized a metal–metal bonded dimolybdenum compound (see below) that is the first of its kind. The $[Mo_2]^{4+}$ core is bonded to only one tmtaa ligand which acts as a bridging ligand for the two metal centres. Two acetate groups are *cis* to each other, also bridging the molybdenum atoms. This dimer has the molybdenum–molybdenum distance of 2.105(1) Å, suggesting a quadruple bond. It will be interesting to see if other compounds with the ligand in this posture can be made.

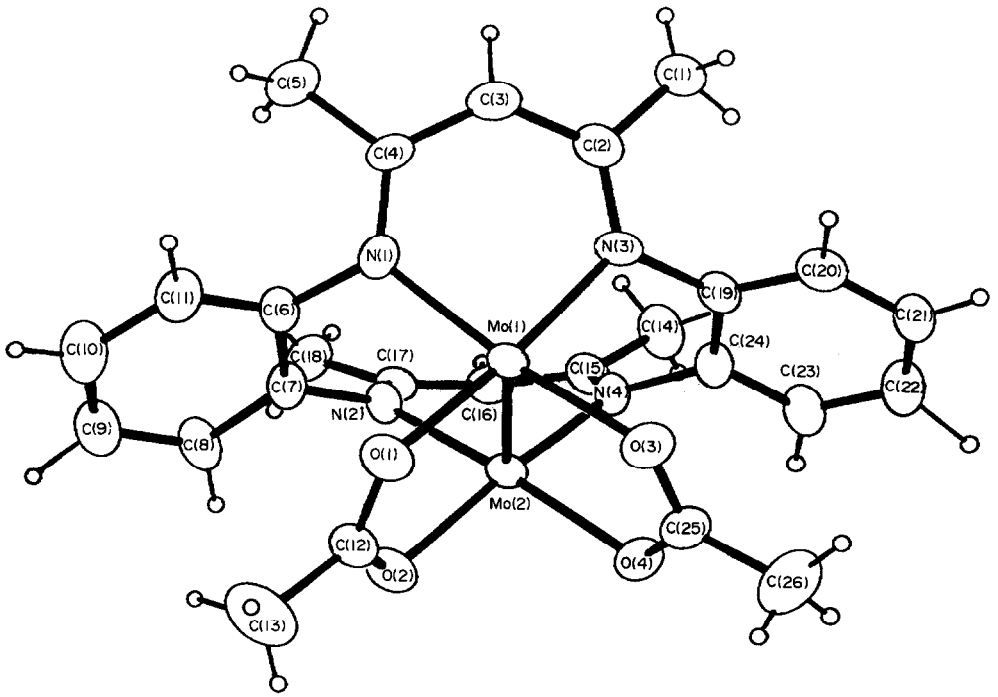

21. S. Ciurli, E. M. Meyer, C. Floriani, A. Chiesi-Villa and C. Guastini, *Chem. Commun.* 1987, 281.
22. V. L. Goedken, J. Molin-Case and Y. Whang, *Chem. Commun.* 1973, 337.
23. V. L. Goedken, S. M. Peng and Y. Park, *J. Am. Chem. Soc.* 1974, **96**, 284.
24. M. C. Weiss and V. L. Goedken, *Inorg. Chem.* 1979, **18**, 819.
25. L. F. Warren and V. L. Goedken, *Chem. Commun.* 1978, 909.
26. F. A. Cotton and J. Czuchajowska, *Polyhedron* 1990, **9**, 1221.
27. M. C. Weiss and V. L. Goedken, *J. Am. Chem. Soc.* 1976, **98**, 3389.
28. M. C. Weiss and V. L. Goedken, *Chem. Commun.* 1976, 531.
29. M. C. Weiss, G. C. Gordon and V. L. Goedken, *J. Am. Chem. Soc.* 1979, **101**, 857.
30. G. C. Gordon, P. W. Dehaven, M. C. Weiss and V. L. Goedken, *J. Am. Chem. Soc.* 1978, **100**, 1003.
31. F. C. McElroy and J. C. Dabrawiak, *J. Am. Chem. Soc.* 1976, **98**, 7112.
32. W. H. Woodruff, R. W. Pastor and J. C. Dabrawiak, *J. Am. Chem. Soc.* 1976, **98**, 7999.
33. L. A. Nafie, R. W. Pastor, J. C. Dabrawiak and W. H. Woodruff, *J. Am. Chem. Soc.* 1976, **98**, 8007.
34. J. J. H. Edema, S. Gambarotta, P. van der Sluis, W. J. J. Smeets and A. L. Spek, *Inorg. Chem.* 1989, **28**, 3782.
35. F. A. Cotton, J. Czuchajowska and X. Feng, *Inorg. Chem.*, in press.
36. (a) D. Mandon, J. M. Giraudon, L. Toupet, J. Sala-Pala and J. E. Guerchais, *J. Am. Chem. Soc.* 1987, **109**, 3490; (b) J. M. Giraudon, J. E. Guerchais, J. Sala-Pala and L. Toupet, *Chem. Commun.* 1988, 921; (c) J. M. Giraudon, D. Mandon, J. Sala-Pala, J. E. Guerchais, J. M. Kerbaol, Y. LeMest and P. L'Haridon, *Inorg. Chem.* 1990, **29**, 707.
37. (a) S. L. Van Voorhees and B. B. Wayland, *Organometallics* 1987, **6**, 204; (b) F. A. Cotton and J. Czuchajowska, unpublished.
38. R. D. Shannon, *Acta Cryst.* 1976, **A32**, 751.

ADDENDUM

Since the submission of this manuscript for publication, we have been informed of an interesting compound relevant to this review. J. Guerchais and co-workers synthesized a metal–metal bonded dimolybdenum compound (see below) that is the first of its kind. The $[Mo_2]^{4+}$ core is bonded to only one tmtaa ligand which acts as a bridging ligand for the two metal centres. Two acetate groups are *cis* to each other, also bridging the molybdenum atoms. This dimer has the molybdenum–molybdenum distance of 2.105(1) Å, suggesting a quadruple bond. It will be interesting to see if other compounds with the ligand in this posture can be made.

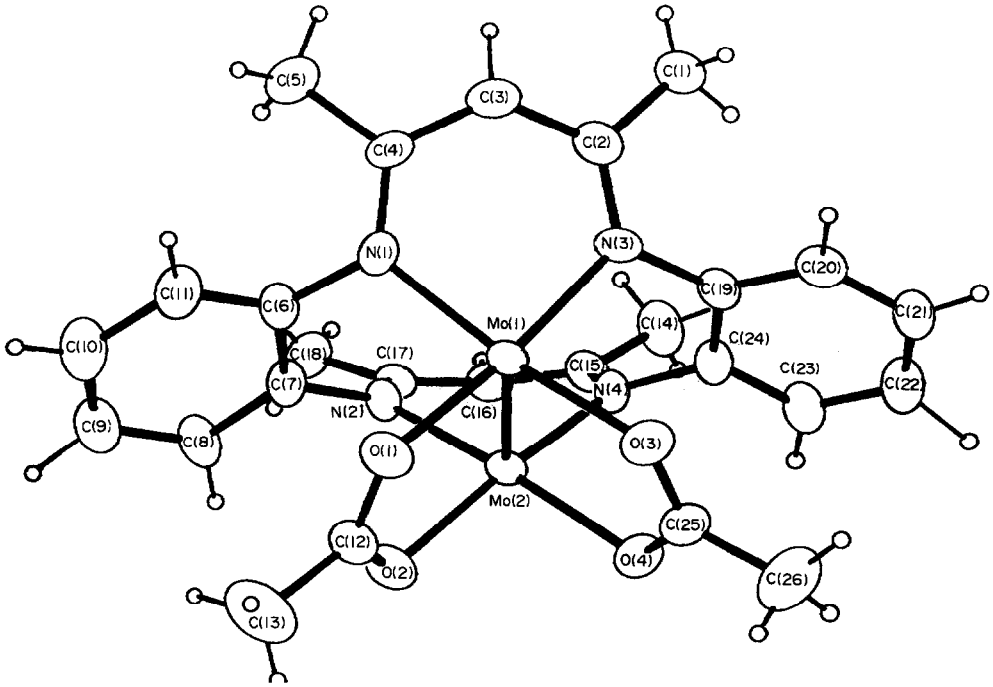

Polyhedron Vol. 9, No. 21, pp. 2567–2574, 1990
Printed in Great Britain

0277–5387/90 $3.00+.00
© 1990 Pergamon Press plc

STUDIES ON THE COBALT(II)–DIPEPTIDE–IMIDAZOLE SYSTEM; A NEW DIOXYGEN CARRIER

ANDRZEJ VOGT*

Institute of Chemistry, University of Wrocław, 14 Joliot-Curie Str., 50-383 Wrocław, Poland

and

ALEKSANDER KUFELNICKI

Institute of Chemistry, Medical Academy of Łódź, 1 Muszyński Str., 90-151 Łódź, Poland

and

BOGUSŁAWA JEŻOWSKA-TRZEBIATOWSKA*

Institute of Low Temperatures and Structure Research, Polish Academy of Sciences, Wrocław, Poland

(*Received* 21 *November* 1989; *accepted* 3 *April* 1990)

Abstract—A series of new mixed cobalt(II) complexes with dipeptide and imidazole, which are dioxygen carriers, was synthesized. The oxygen-free, high-spin octahedral form of the active complex, the reversible dimeric complex with a μ-peroxo bridge as the oxygenated form and the irreversible complex with a μ-superoxo bridge have been examined by spectrophotometric (UV, vis, near-IR), ESR, potentiometric and gas-volumetric methods. Both the electron and the molecular structures have been proposed for each species.

Searching for synthetic models which are close to biological systems capable of reversible oxygen uptake,[1–3] we have investigated a group of mixed-ligand complexes imitating the proximal histidine environment in haemoglobin. The complexes were formed from cobalt(II) ions with dipeptides (dipept) and imidazole (Himid). Related mixed-ligand systems with amino acids (amac) and imidazole[4–7] have proved to be excellent inorganic oxygen and nitric oxide carriers—the considerable influence of the imidazole axial ligand on the thermodynamic stability as well as on inhibition of intramolecular oxidation (auto-oxidation) has been revealed.

The use of peptides instead of amino acids causes some complications due to additional coordination through the deprotonated amide groups. This mode of coordination, very important in metal–peptide complexes in general,[8] is also of essential importance in the oxygen uptake reactions.[9–11] Taking into account the interesting properties of the imidazole-containing systems, we have extended our studies to mixed-ligand complexes with peptides (starting with dipeptides), as a further step towards biological systems.

EXPERIMENTAL

Reagents

All the dipeptides used (glycylglycine, glycyl-L-alanine, L-alanyl–glycine and L-alanyl–L-alanine) were p.a., Fluka AG. Imidazole, p.a., was obtained from Merck. The blue–violet $Co(imid)_2$ polymeric complex was obtained according to the procedure described in ref. 4. For the preparation of the μ-superoxo complex, ceric ammonium nitrate, Merck, p.a., was used. The other reagents (nitric acid, sulphuric acid, sodium hydroxide, potassium nitrate, acetone) were obtained from POCh Gliwice.

* Authors to whom correspondence should be addressed.

Physical measurements

Electronic absorption spectra in the UV–vis and near-IR regions were recorded on a Cary 14 spectrophotometer in a thermostatted cell compartment at 0–1°C, using cuvettes of diameter 0.05, 0.1 and 1 cm. The ESR spectra were recorded on a SE/X 2543 (X band) spectrometer at room-temperature. An external manganese standard was applied. Volumetric measurements were made at ~0°C in an isobaric measurement system described in ref. 11, additionaly provided with a modified double-walled reaction vessel, making possible the introduction of solid $Co(imid)_2$ samples. The pH values were recorded simultaneously by means of a N517 digital pH meter with a combined SAgP-201W electrode. The same pH-meter set-up was used in all other potentiometric measurements.

Preparation of complexes

The solution samples of the active form were synthesized and stored under an oxygen-free atmosphere in order to avoid the formation of oxygenated forms. For spectroscopic investigations we used 0.3 mmol of $Co(imid)_2$ and 0.9 mmol of dipeptide in 1 cm^3 of water—the solution was bubbled with pure N_2 in a gas washer. In the potentiometric and gasometric measurements the total volume of solution amounted to 40 cm^3. For the spectrophotometric measurements the samples of the solution of the active form were prepared directly in a cuvette with a soft silicone stopper according to the procedure mentioned above. Prior to the measurements the reagents were weighed in the cuvette. The water used in the preparation was initially de-aerated in a syringe connected to the cuvette through a needle and then injected into the cell.

The O_2-containing form (μ-peroxo-bridged) was synthesized and stored under a pure oxygen atmosphere at 0°C. The cooled oxygen was bubbled through the sample over *ca* 10 min. For absorption spectra the cuvettes were filled and transported to the spectrophotometer at the same low temperature. The μ-superoxo type complex was prepared in a cool chamber by the addition of 1 cm^3 of the oxygenated form to 1 cm^3 of 0.2 M $(NH_4)_2[Co(NO_3)]_6$ in strongly acidic medium (2 M HNO_3). For ESR measurements a small sample of the solution was collected, maintaining the low temperature, using a syringe with a polypropylene tube into a silica tube. The cuvettes used in the spectrophotometric measurements were filled and transported in a cooled Dewar vessel.

RESULTS AND DISCUSSION

The active form

Most of the systems taking up molecular oxygen reversibly in aqueous solutions are simple metal–ligand systems.[1,3] The studies on O_2 transporters forming a ternary arrangement (Co–chelating ligand–N-base) appear to be much more interesting as closer models of the prosthetic groups. Nevertheless, investigation of the structure of these complexes, as well as of the equilibria involved, is a more complicated problem. The ternary system under study belongs to the most effective dioxygen carriers, since many cycles of the displacement of equilibrium (1) may be accomplished without noticeable loss in efficiency of the system

$$\text{Active form} \underset{N_2}{\overset{O_2}{\rightleftharpoons}} \text{Oxygenated form.} \qquad (1)$$

For all the dipeptides used, very similar spectral curves of the active form have been obtained (Fig. 1), characteristic of high-spin cobalt(II) six-coordinated complexes.[12] The main bands at *ca* 500 nm ($\varepsilon \sim 10$) and *ca* 1100 nm ($\varepsilon \sim 1$) correspond to the quartet spin-allowed transitions $^4T_{1g} \rightarrow {}^4T_{1g}(P)$ and $^4T_{1g} \rightarrow {}^4T_{2g}$, both the bands being strongly asymmetric owing to admixture of the spin-forbidden transitions to doublet states.

The observed rise in pH during dissolution of $Co(imid)_2$ in isoelectric dipeptide medium is due to reaction (2) in which the imidazole molecule—a relatively strong N-base— is released:

$$Co(imid)_2 + \text{dipept}^{\pm} \rightleftharpoons Co(imid)\text{dipept} + \text{Himid}, \qquad (2)$$

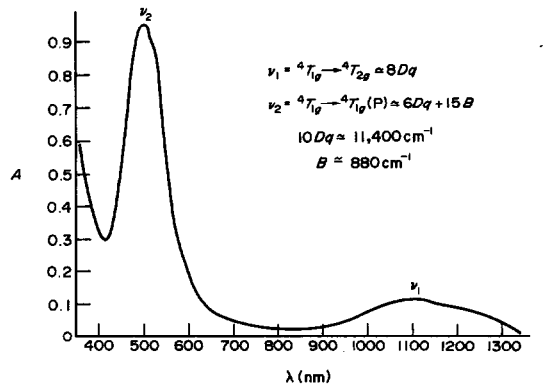

Fig. 1. Visible, near-IR spectrum of the "active" form of the O_2 carrier cobalt(II)–alanylalanine–Himid under N_2: solvent, H_2O; temperature, 0–1°C; *C*, 0.1 M.

where

imid =

$$\text{imid} + \text{H} \rightleftharpoons \text{Himid} \quad (\log K_{1\text{H}} = 14.29 \pm 0.04)^{13}$$

Himid =

$$\text{Himid} + \text{H} \rightleftharpoons \text{H}_2\text{imid} \quad (\log K_{2\text{H}} = 7.03 \pm 0.03)^{13}$$

dipept$^{\pm}$, dipept = dipept^{-}, dipeptH$_{-1}$ denote the neutral, anionic (—NH_3^+ deprotonated) and amide deprotonated forms, respectively.

The appearance of free imidazole was proved by isolation, involving precipitation with acetone of all acetone-insoluble components (complexes and unreacted dipeptide) and then qualitative identification—IR spectra. Reaction (2) is followed by metal-promoted amide deprotonation

$$\text{Co(imid)dipept} \rightleftharpoons \text{Co(Himid)dipeptH}_{-1}. \qquad (3)$$

The correctness of eqs (2) and (3) was confirmed by the results of acid–base titrations (Fig. 2, Table 1); almost 4 mmol of acid per mmol of cobalt were needed to neutralize the solution, which may be explained by the set of equations:

$$\text{Co(Himid)dipeptH}_{-1} + \text{H} \rightleftharpoons \text{Co(dipeptH}_{-1}) + \text{H}_2\text{imid} \qquad (4)$$

$$\text{Co(dipeptH}_{-1}) + 2\text{H} \rightleftharpoons \text{Co} + \text{dipept}^{\pm} \qquad (5)$$

$$\text{Himid} + \text{H} \rightleftharpoons \text{H}_2\text{imid}. \qquad (6)$$

It should be underlined that the proton balance indicates unequivocally a 1 : 1 dipeptide-to-metal ratio.

The oxygenated form

Oxygenation of the active form after stabilization of pH caused a decrease in pH for all the systems (however to a variable extent), Fig. 3. The latter fact may be easily explained by examining the data of quantitative determination of released imidazole during the formation of the oxygenated complex (Table 2). This determination was made after precipitation of the O_2-containing form, in a similar manner as was described earlier for the active form and then by potentiometric titration of the imidazole in the filtrate. Thus we can say that the drop in pH during dioxygen complex formaion (Fig. 3) is due to displacement of equilibria—the greater the shift of equilibrium towards oxygen uptake (i.e. the higher the quantity of imidazole released, Table 2) the lower the decrease in pH.

Hence, the reversible dioxygen fixation consists of replacement of the H_2O molecule by O_2 but this substitution does not influence the pH.

The volumetric measurements indicated the stoichiometry characteristic of μ-peroxo dimers; O_2 : Co = 1 : 2 (Table 3). From the data in Table 3, the maximum of dioxygen fixation occurs at a 1 : 1 dipeptide-to-metal ratio (Fig. 4). This is additional proof for the proposed structure of the active complex.

The increase in concentration ratio above 1 : 1 gives rise to a distinct decrease in dioxygen fixation yield. This should be interpreted as the shift of the complexing equilibria towards the inactive Co(dipept)$_2$ species.

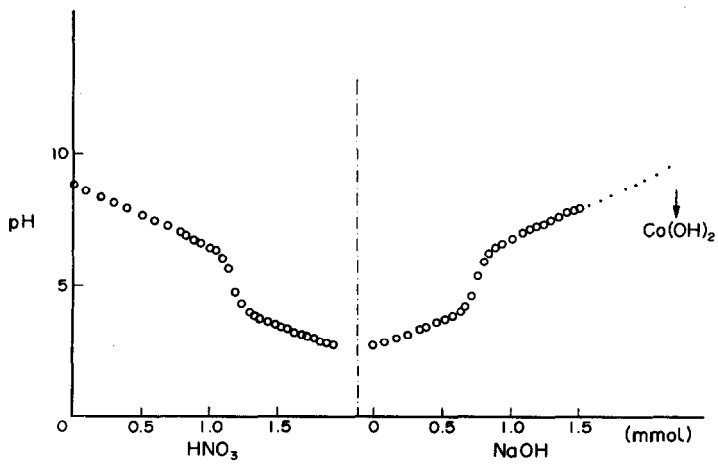

Fig. 2. Acid–base titration of the cobalt(II)–dipeptide–imidazole system under oxygen-free conditions. Gly–ala, 0.9 mmol; Co(imid)$_2$, 0.3 mmol.

Table 1. Titration data for the cobalt(II)–dipeptide–imidazole system [Temperature = 0–1°C, $\mu = 0.1$ (KNO_3)]

Dipeptide	mmol of $Co(imid)_2$	mmol of dipeptide	mmol of HNO_3	mmol HNO_3 / mmol CO
Gly–gly	0.3000	0.9022	1.199	3.997
	0.3009	0.6002	1.200	3.902
	0.2994	1.2000	1.162	3.881
	0.2010	0.8031	0.780	3.881
Gly–L-ala	0.2983	0.9004	1.156	3.875
L-Ala–gly	0.2983	0.9018	1.143	3.832
L-Ala–L-ala	0.3000	0.9015	1.162	3.873

Dioxygen uptake by the active complex is accompanied by rapid increase in optical density within the near-UV (Fig. 5), the visible region being overlapped by the forming bands up to the near-IR. At the same time the *d–d* transitions characteristic of the active form disappear. These changes in optical density are reflected in the change of colour of the solution from pale pink for the active form to dark red–brown for the oxygenated form.

The position (300–400 nm) and intensity of both LMCT bands in the UV are highly typical of singly-bridged complexes of the μ-peroxo type. The presence of two charge-transfer bands is due to the splitting of π^* antibonding orbitals of the dioxygen molecule into two components (π^*_h and π^*_v) owing to the lack of co-planarity of the Co—O—O—Co moiety.[14] On the lower energetic slope of this band pair we may observe a shoulder at *ca* 500 nm characteristic of the $^1A_{1g} \rightarrow {}^1T_{1g}$ transition in cobalt(III) low-spin complexes.[12] The intensity of the

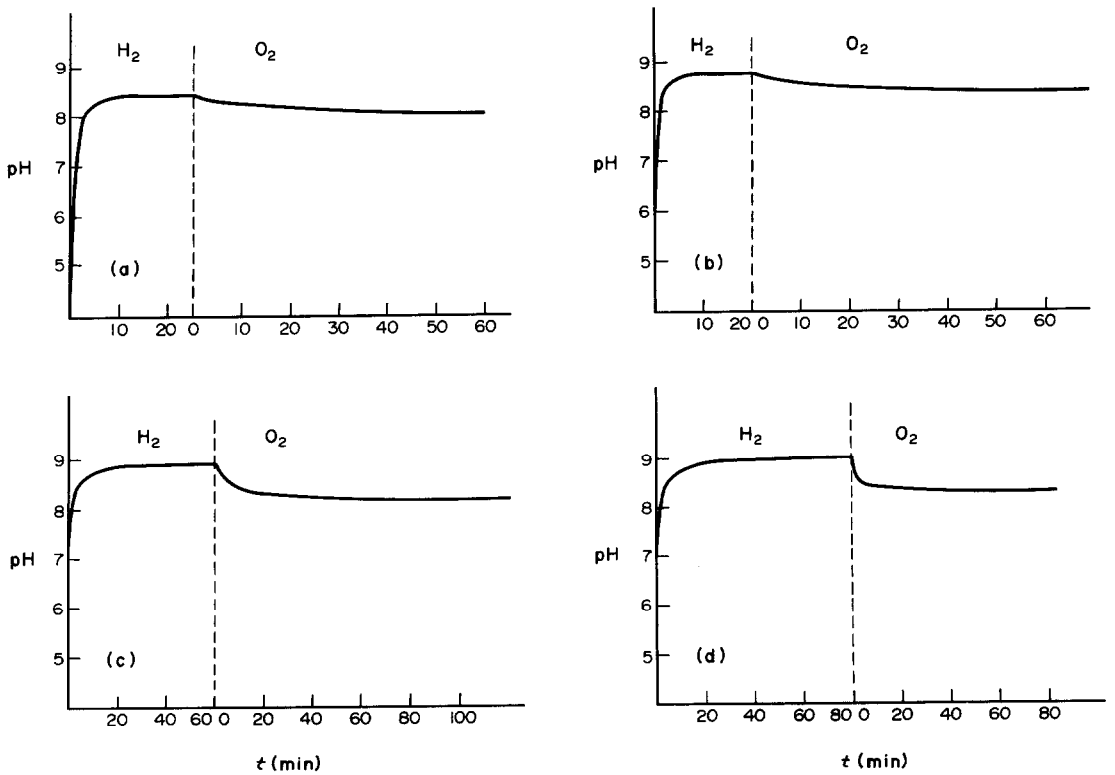

Fig. 3. pH changes during formation and oxygenation of the "active" complex at ~0°C. Dipeptide, 0.9 mmol; $Co(imid)_2$, 0.3 mmol. (a) Gly–gly, (b) gly–ala, (c) ala–gly and (d) ala–ala.

Table 2. The releasing data of imidazole during μ-peroxo complex formation (mmol of imidazole per mmol of cobalt)

Dipeptide	0.3 mmol $Co(imid)_2$+ 0.9 mmol dipeptide	0.6 mmol $Co(imid)_2$+ 1.8 mmol dipeptide
Gly–gly	0.953	0.979
Gly–L-ala	0.695	0.827
L-Ala–gly	0.574	0.523
L-Ala–L-ala	0.364	0.489

charge-transfer bands decreases in time, simultaneously with the formation of much weaker *d–d* bands which could be assigned to monomeric, low-spin aquodipeptide cobalt(III) complexes.

The reaction of molecular oxygen uptake by the active form of the complexes under study is very fast. The reverse process, i.e. detachment of the molecule by lowering the O_2 pressure over the solution, is much slower, the rate being highly dependent on temperature. The temperature, however, is an unfavourable factor as it remarkably accelerates the auto-oxidation reactions of the oxygenated form leading to inactive cobalt(III) complexes. Therefore all experiments with the oxygenated form have been carried out at the lowest possible temperature (0–1°C). As was evidenced spectrophotometrically, the auto-oxidation is just moderated enough at this temperature to be neglected during the investigations.

Table 3. Stoichiometry and thermodynamic data for O_2 uptake in the cobalt(II)–dipeptide–imidazole system [Temperature = 0–1°C, μ = 0.1 (KNO_3)]

Dipeptide	$C_L : C_{Co}$	$\frac{\text{mmol } O_2}{\text{mmol Co}}$	$\log K_{O_2}$[a]
Gly–gly	0.5 : 1	0.1951	2.166
	0.75 : 1	0.2539	2.373
	1.0 : 1	0.4128	3.035
	2.0 : 1	0.3052	2.555
L-Ala–gly	0.5 : 1	0.2372	2.315
	1.0 : 1	0.4297	3.139
	2.0. 1	0.4128	3.035
Gly–L-ala	0.5 : 1	0.2372	2.315
	1.0 : 1	0.3748	2.836
	2.0 : 1	0.3722	2.827
L-Ala–L-ala	0.5. 1	0.2485	2.355
	1.0 : 1	0.4003	2.964
	2.0. 1	0.4270	3.127

[a] $K_{O_2} = C_{O_2}/(C_{Co} - 2C_{O_2}) \cdot [O_2]$, where C_{O_2} = [Adduct], $[O_2] = 2.183 \times 10^{-3}$.

The μ-superoxo form

The μ-peroxo complexes are readily irreversibly oxidated in acidic medium by strong oxidizing agents (Ce^{4+}, Cl_2, MnO_4^-, $HClO_4$) to green–violet products. The electronic spectra of the latter complexes displayed a characteristic charge-transfer band, $d\pi \rightarrow \pi^*_v$, in the near-IR (Fig. 6), typical of cobalt complexes containing a μ-superoxo bridge. The position of this band (*ca* 700 nm), $\varepsilon \sim 10^2$, was almost independent of the type of dipeptide, unlike the related complexes without imidazole (Table 4). The mixed-ligand species were also much more kinetically stable.

By using the mentioned MLCT band we carried out a spectrophotometric titration of the system with Ce^{4+} ions in 1 M HNO_3 medium; the results [0.5 mmol of Ce^{4+} per mmol of Co (Fig. 7)] suggest consumption of one electron per two cobalt ions which confirms the one-electron oxidation of the μ-peroxo bridge to the μ-superoxo bridge.

The presence of the μ-superoxo bridge in the green–violet complexes is indicated by the ESR spectra. For all the investigated systems, isotropic ESR signals were observed (Fig. 8) consisting of a 15-line hyperfine structure arising from symmetric coupling of the unpaired electron with two equi-

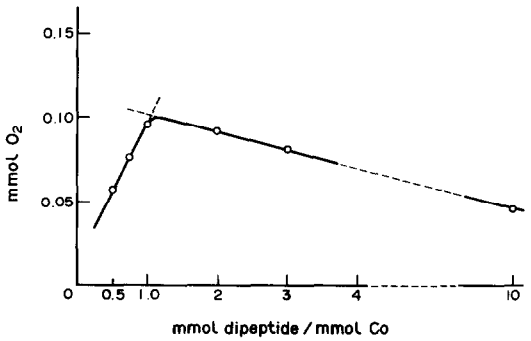

Fig. 4. Dependence of the quantity of oxygen bound on the dipeptide-to-metal ratio for the cobalt(II)–glygly–Himid system, $Co(imid)_2$.

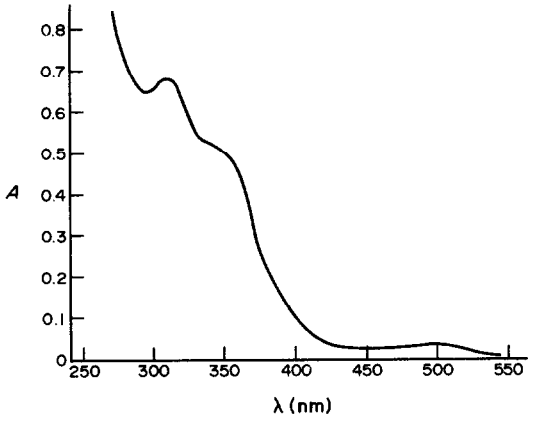

Fig. 5. Absorption spectrum of the cobalt(Gly–ala)Himid oxygenated form. Solvent, H_2O; temperature, 0–1°C; C^0_{Co}, 0.040 M; path length, l, 0.1 cm.

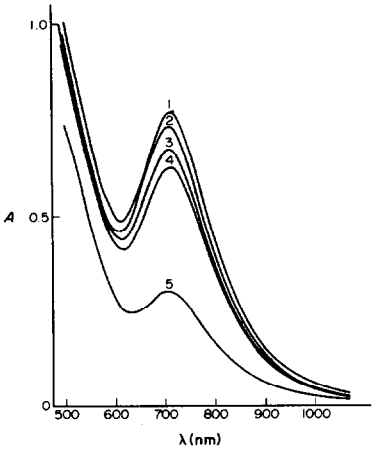

Fig. 6. Absorption spectrum of the cobalt(Gly–ala)Himid μ-superoxo complex. Curves: 1—after 5 min, 2—30 min, 3—90 min, 4—180 min, 5—48 h. Solvent, H_2O, 1 M HNO_3; temperature, 0–1°C; C^0_{Co}, 0.15 M; path length, l, 0.1 cm.

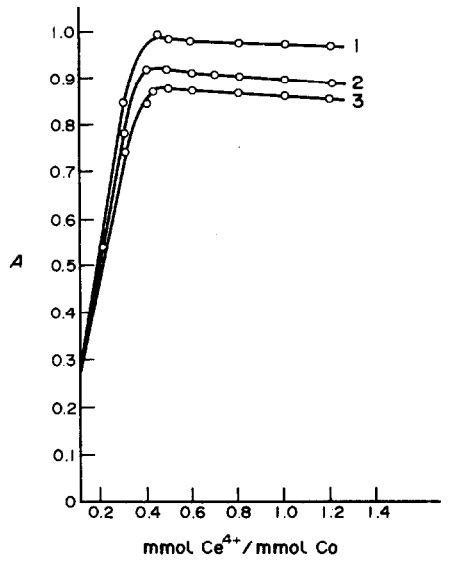

Fig. 7. Spectrophotometric titration of the cobalt(II)–dipeptide (amac)–O_2 system with Ce^{4+} ions in 1 M HNO_3 medium. Temperature, 0–1°C, 1—L-ala, 2—gly–L-ala, 3—gly–gly.

valent cobalt ion nuclei of spin 7/2. Both the parameters of the spin Hamiltonian were similar, contrary to the complexes without imidazole (Table 5), thus indicating a considerable unification of structure.

As is the case for numerous dioxygen complexes the small value of the A_{iso} hyperfine splitting constant of order 1 mT, in comparison with 10 mT for simple cobalt(II) complexes,[15] indicates strong delocalization of electron density from the metal to the dioxygen bridge (up to 90%).

CONCLUSIONS

The results presented above suggest that the active (oxygen-free) form is a mixed-ligand complex

Table 4. Position of the $d\pi \rightarrow \pi^*_v$ band and half-lives of the μ-superoxo type complexes without and with imidazole

	Without Himid		With Himid	
Dipeptide	Max. (nm)	$t_{0.5}$ (min)	Max. (nm)	$t_{0.5}$ (min)
Gly–gly	735	105.2	700	98.07
Gly–L-ala	~740	—[a]	710	350.2
L-Ala–gly	780	22.95	710	199.7
L-Ala–L-ala	800	75.55	710	280.4

[a] Very weak band.

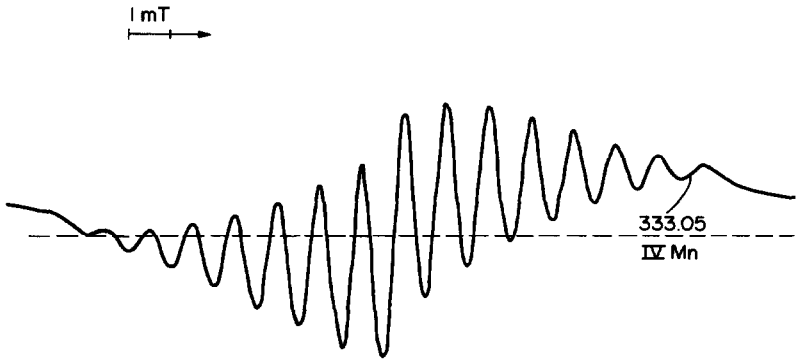

Fig. 8. ESR spectrum of the cobalt(Ala-gly)Himid μ-superoxo complex.

of distorted octahedral structure. In the proposed structure the dipeptide molecule chelated through the amine nitrogen, carbonyl oxygen and deprotonated amide group defines the equatorial plane—water and imidazole as the axial ligands (Fig. 9).

In the presence of O_2 the water is reversibly replaced by dioxygen and then the diamagnetic, low-spin complexes of cobalt(III) character are formed, with a μ-peroxo (—O_2^{2-}—) bridge. The studied system is a relatively effective dioxygen carrier, capable of oxygen transport in many cycles. As we have observed, this system is less resistant to auto-oxidation than the relative Co–amac–imidazole one, but is more resistant than the Co–dipeptide–OH^- system (without imidazole). The oxygenated form undergoes, in acidic medium, rapid oxygenation to an irreversible cobalt(III) complex with a monoelectron reduced O_2^- bridge of the μ-superoxo type (Fig. 10).

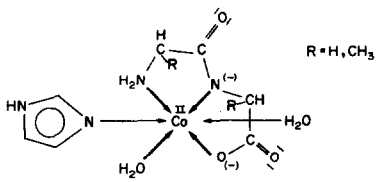

Fig. 9. Proposed structure of the "active" form of the cobalt(II)–dipeptide–imidazole system.

The irreversible μ-superoxo complexes are much more resistant to intramolecular oxidation than the complexes containing the μ-peroxo bridge.

It should be emphasized that for our complexes we have observed a distinct unification of structures, unlike in the complexes without imidazole where a great influence of the primary dipeptide

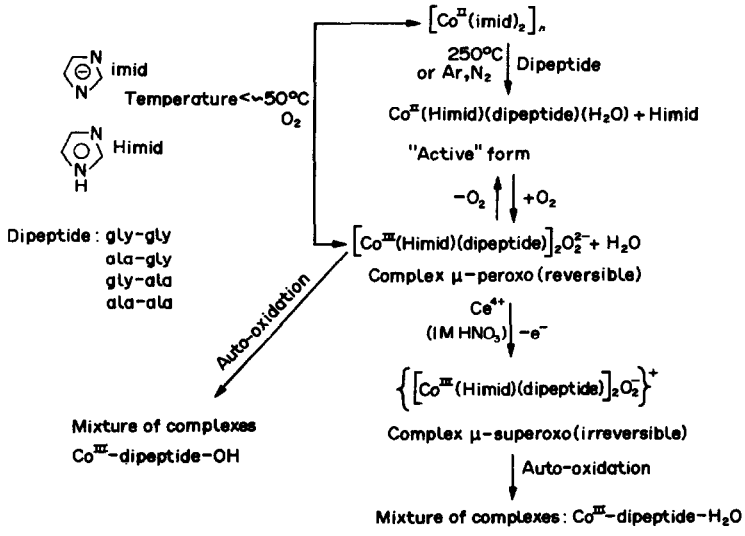

Fig. 10. Scheme of reactions for the formation of the active and O_2-containing complexes.

Table 5. ESR parameters of the μ-superoxo type complexes without and with imidazole

Dipeptide	Without Himid		With Himid	
	A_{iso} (mT)	g	A_{iso} (mT)	g
Gly–gly	10.3	2.030	10.7	2.026
Gly–L-ala	10.3	—[a]	10.6	2.026
L-Ala–gly	10.6	2.050	10.3	2.026
L-Ala–L-ala	13.3	2.034	10.3	2.027

[a] Lack of distinct line centre.

structure on electron density distribution in the metal–ligand moiety was established.[11]

REFERENCES

1. R. D. Jones, D. A. Summerville and F. Basolo, *Chem. Rev.* 1979, **79**, 139.
2. A. E. Martell, *Accts Chem. Res.* 1982, **15**, 155.
3. E. C. Niederhoffer, J. H. Timmons and A. E. Martell, *Chem. Rev.* 1984, **84**, 137.
4. B. Jeżowska-Trzebiatowska, A. Vogt, H. Kozłowski and A. Jezierski, *Bull. Acad. Polon. Sci., Ser. Sci. Chim.* 1972, **20**, 187.
5. S. Bagger and K. Gibson, *Acta Chem. Scand.* 1972, **26**, 2972.
6. B. Jeżowska-Trzebiatowska, *Pure and Appl. Chem.* 1974, **38**, 367.
7. B. Jeżowska-Trzebiatowska, K. Gerega and A. Vogt, *Inorg. Chim. Acta* 1978, **31**, 183.
8. H. Sigel and R. B. Martin, *Chem. Rev.* 1982, **82**, 385.
9. W. R. Harris, G. McLendon and A. E. Martell, *J. Am. Chem. Soc.* 1976, **98**, 8378.
10. W. R. Harris and A. E. Martell, *J. Am. Chem. Soc.* 1977, **99**, 6746.
11. A. Kufelnicki, *Polish J. Chem.* 1988, **62**, 19; 1988, **62**, 641; A. Kufelnicki, *Polish J. Chem.*, in press.
12. A. B. P. Lever, *Inorganic Electronic Spectroscopy*, pp. 318–321. Elsevier, Amsterdam (1968).
13. R. M. Smith and A. E. Martell, *Critical Stability Constants*, Vol. 2, p. 144. Plenum Press, New York (1975).
14. A. B. P. Lever and H. B. Gray, *Accts Chem. Res.* 1978, **11**, 348.
15. M. C. R. Symons, *Chemical and Biochemical Apsects of Electron-spin Resonance Spectroscopy*. Van Nostrand, New York (1978).

Polyhedron Vol. 9, No. 21, pp. 2575–2578, 1990
Printed in Great Britain

0277–5387/90 $3.00+.00
© 1990 Pergamon Press plc

THE SYNTHESIS AND CHARACTERIZATION OF DI-μ-(METHOXY)-BIS-SQUARATOCOPPER(II)

LINCOLN A. P. M. HALL

Department of Chemistry, The University of the West Indies,
St. Augustine, Trinidad, West Indies

(*Received* 13 *February* 1990; *accepted* 7 *June* 1990)

Abstract—The complex di-μ-(methoxy)-bis-squaratocopper(II), prepared by reacting methanolic solutions of $CuSO_4 \cdot 5H_2O$ and squaric acid in an atmosphere of dry nitrogen, appears to be square planar based on the results of elemental and EXAFS spectroscopic analysis.

Although metal halides have been successfully used in the synthesis of squarates from alcoholic solutions, attempts to prepare a copper(II) squarate from a primary alcohol using copper(II) halides have failed.[1–5] However, if copper(II) sulphate is used, a red–brown complex is formed from methanol. The EXAFS spectroscopic analysis suggests that the complex is square planar. As far as is known, this complex is the first directly synthesized square-planar squarate.

EXPERIMENTAL

Two hundred cm^3 volumes of hot, deaerated 6.5×10^{-3} M squaric acid (obtained from Sigma Chemical Company) and 7.6×10^{-3} M $CuSO_4 \cdot 5H_2O$ methanolic solutions were mixed and allowed to stand in an inert atmosphere. The red–brown complex which formed was collected and dried as described elsewhere.[2] The $CuSO_4 \cdot 5H_2O$ and methanol were of AnalaR grade and obtained from BDH, Poole, U.K. Yield: 0.13 g (40%). Found: C, 28.7; H, 1.7; Cu, 31.1. Calc. for $C_{10}H_8O_{10}Cu_2$: C, 28.9; H, 1.9; Cu, 30.6%.

A sample of the red–brown complex was left exposed to the atmosphere for a few days until it became completely converted to a yellow–green complex. Found: C, 25.1; H, 3.2; Cu, 26.0. Calc. for $C_{10}H_{16}O_{14}Cu_2$: C, 24.6; H, 3.3; Cu, 26.1%.

The IR spectra between 4000 and 600 cm^{-1} were recorded using both Nujol and hexachlorobutadiene as mulling agents. The spectra between 600 and 400 cm^{-1} were recorded using a Nujol mull and AgBr as window material. A reflectance spectrum was taken between 40,000 and 10,000 cm^{-1}. The magnetic susceptibility was determined using $Hg[Co(SCN)_4]$ as calibrant, and the copper content was determined by atomic absorption spectrophotometry.

The EXAFS spectra were measured at 77 K using finely powdered samples of the complex, diluted with boron nitride, and placed in an aluminium sample holder. The synchrotron was operated at 2 GeV energy and an average current of 180 mA. Data collection was carried out at station 9.2 at the SRS, Daresbury Laboratory, using a Si(220) double crystal order-sorting monochromator, with harmonic rejection at 50%. The transmission method of data collection was used. Analysis of the data was carried out using the program "EXCURV88".

RESULTS AND DISCUSSION

The IR spectrum of the complex obtained with the Nujol mull shows the O—H stretch at 3450 cm^{-1}. The very weak absorption at 1780 cm^{-1} is attributed to C=O stretching while the band around 1600 cm^{-1} is assumed to be due to C—C and C—O stretching vibrations.[6] The peaks at 1010 and 1090 cm^{-1} are assigned to the C—O stretching vibrations of the bridging methoxy groups, since similar peaks appear in the spectrum of neat methanol.[7] The absorption at 710 cm^{-1} is a typical squarate band.[8] The absorptions that occur at 520, 440, 430 and 420 cm^{-1}, respectively, have been assigned to Cu—O stretching which is responsible for absorptions at 520 and 435 cm^{-1} in the IR spectrum of $Cu(OMe)_2$.[9] The IR spectrum obtained from the HCB mull showed absorptions at about

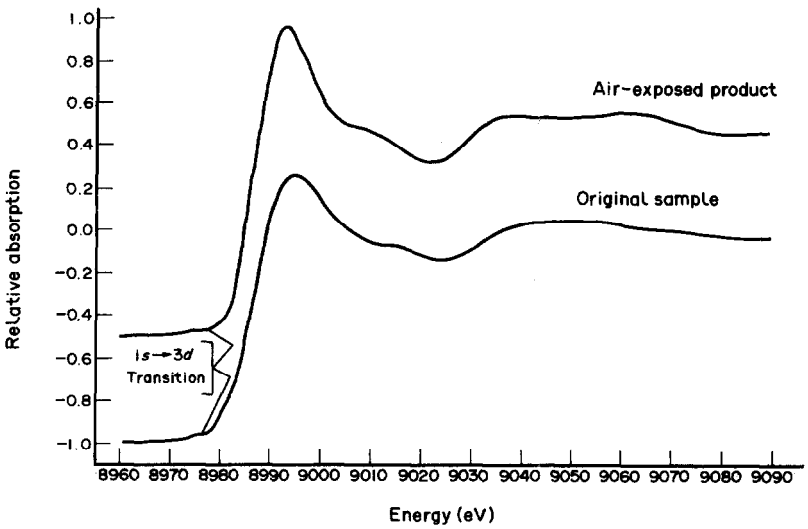

Fig. 1. Comparison of the X-ray absorption spectra of I and II.

1450 and 2930 cm^{-1} which have been identified as CH_3 bands from the bridging methoxy groups.[7]

The UV–vis spectrum shows three absorptions at 10,500–16,000, 19,100 and 20,500 cm^{-1} and is similar to the spectra of the square-planar copper(II) complexes $Cu(DPM)_2$, (DPM represents the anion of 2,2,6,6-tetramethylheptane-3,5-dione) and $Cu(3\text{-}Meacac)_2$ (Meacac represents 3-methylpentane-2,4-dionato).[10,11] $Cu(DPM)_2$, $Cu(3\text{-}Meacac)_2$ and di-μ-(methoxy)-bis-squaratocopper(II) all contain the CuO_4 chromophore. The red–brown squarate (the title compound) is much darker in colour than the yellow–brown copper(II) squarate chloride which apparently has a distorted tetrahedral structure;[3] square-planar copper(II) complexes are frequently red.[12] In addition, the electronic spectrum of copper(II) squarate chloride does not have an absorption at *ca* 19,000 cm^{-1} which is generally present in the spectra of square-planar copper(II) complexes.[10,11]

The EXAFS spectrum (Fig. 1) shows the $1s \rightarrow 3d$ quadrupole transition at 8979 eV which is indicative of the copper(II) oxidation state. The first coordination shell can be fit with four oxygen atoms at 1.93 Å. The EXAFS also shows the presence of a second coordination shell which can be reproduced with either one copper atom at ~ 2.75 Å or two carbon atoms at 2.77 Å (Figs 2, 3 and 4). The copper fit (Debye–Waller factor 0.016) is preferable since the Debye–Waller factor for the two carbon atoms–four oxygen atoms fit (0.002) is rather small.

The edge-width (calculated as the interval between half edge-height and the maximum) of the *K*-edge is 8.6 eV while the edge-width for the air-exposed product is 6.6 eV (Fig. 1). The yellow–

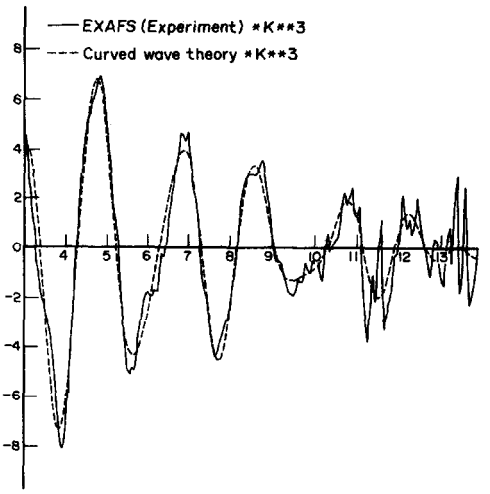

Fig. 2. EXAFS simulation with four oxygen, two carbon and one copper atoms.

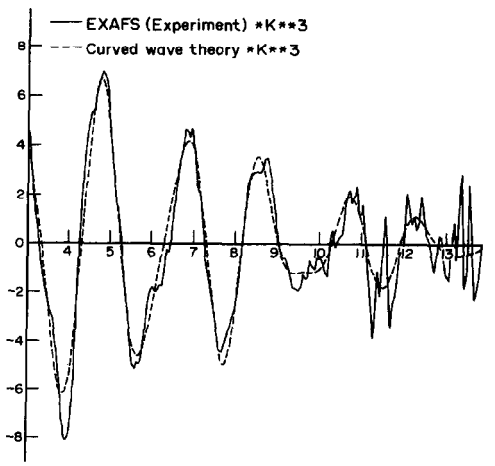

Fig. 3. EXAFS simulation with four oxygen and one copper atoms.

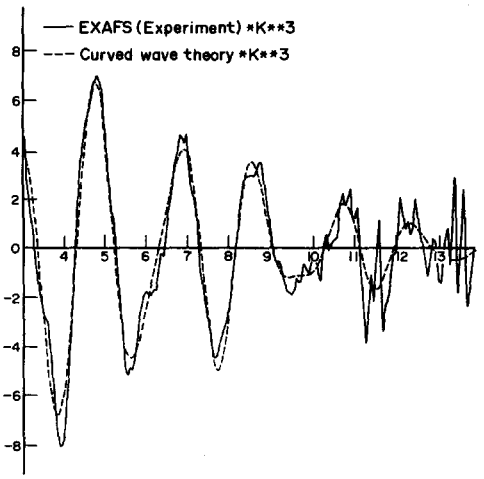

Fig. 4. EXAFS simulation with four oxygen and two copper atoms.

green, air-exposed complex is found to be octahedral from the evidence given later (*vide infra*). The following structures are proposed.

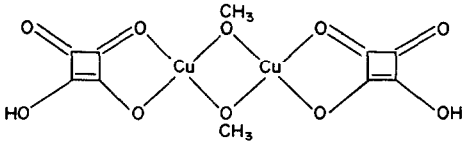

I

Di-μ-(methoxy)-bis-squaratocopper(II).

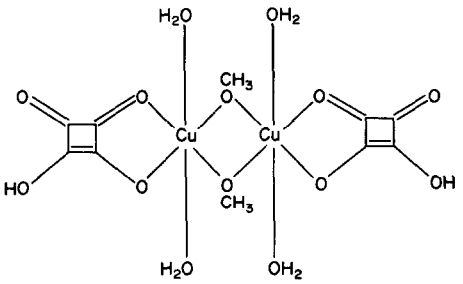

II

Air-exposed product.

The IR spectrum of the air-exposed product shows a number of changes. The O—H stretch at 3450 cm^{-1} in the spectrum of the unexposed complex is replaced by a broad band that extends from 2700 to 3700 cm^{-1}. This is assumed to be due to the O—H stretch in the coordinated water molecules in **II**.[13] The peak at 1010 cm^{-1} observed in the IR spectrum of **I** does not appear in the IR spectrum of **II**, while the peak at 1090 cm^{-1} appears as a multiplet with peaks at 1090, 1110 and 1122 cm^{-1} in the spectrum of **II**. Thus, one of the C—O stretching vibrations of the bridging methoxy groups is lost in **II**. The number of Cu—O absorptions is also reduced. The peak at 520 cm^{-1} does not appear in the spectrum of **II**, while there are only two peaks at 435 and 450 cm^{-1} instead of the three peaks observed in this region in the spectrum of **I**. The reduction in the number of C—O and Cu—O absorptions has been attributed to the higher symmetry of **II**.

The 2 eV change in edge-width in the EXAFS spectra of **I** and **II** suggests that **I** is square planar and **II** octahedral. Bhaskare and Kulkarni[14] illustrated a similar, although greater, difference in edge-width between octahedral copper glutamate (edge-width, 7.58) and square-planar copper oxide (edge-width, 9.98). The Cu—O bond lengths of 1.93 Å in **I** are also consistent with square-planar CuO_4.[15–18] The absence of any pre-edge feature suggests that if there is any axial ligation in **I** the ligands are either > 3 Å or < 2.3 Å from the copper atoms.[18] However, the EXAFS simulation shows no evidence of any ligand at short distance. In addition, any contribution at 2.75 Å should result in a pre-edge feature if there is axial ligation. The evidence, therefore, indicates that **I** is square planar with Cu—O and Cu—Cu distances of 1.93 and 2.74 Å, respectively, and a Cu—O—Cu angle of ~ 90° as shown in the following diagram. The Cu—Cu bond length of 2.74 Å is longer than 2.61–2.65 Å required for direct Cu—Cu bonding.[19]

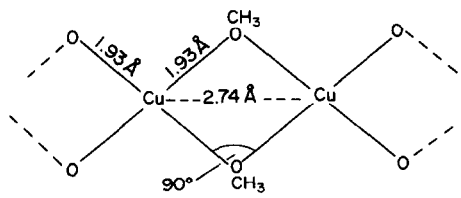

Analysis of the EXAFS spectrum of the air-exposed product (Fig. 5) suggests that it is most

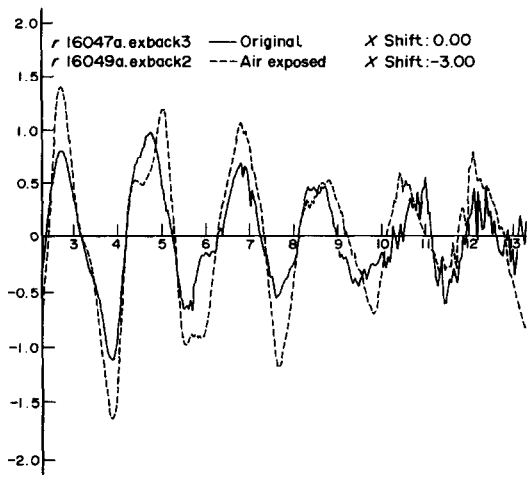

Fig. 5. Comparison of the EXAFS simulations of **I** and **II**.

likely six-coordinate with the fit to the first shell giving six oxygen atoms at 1.93 Å. It is quite likely that the restricted space between layers in the complex forces the copper to adopt an octahedral geometry without the expected Jahn–Teller distortion.

The room temperature magnetic moment of the title complex is 1.84 BM which is consistent with copper(II).

Tetrahedral, five-coordinate and octahedral squarates have been prepared before under anaerobic conditions.[1–5] The square-planar geometry present in this complex completes the list of common geometries shown by first-row transition metal complexes and illustrates the fact that the nature of the solvents and salts used in the preparation of squarates under anaerobic conditions affects the coordination and shape of the complex synthesized.

Acknowledgements—The author wishes to thank Dr S. S. Hasnain and Dr R. W. Strange from the Daresbury Laboratory in Warrington, U.K., for their help in obtaining the EXAFS spectra and the latter for his help in interpreting the EXAFS spectra.

REFERENCES

1. O. St. C. Headley and L. A. Hall, *Polyhedron* 1985, **4**, 1697.
2. O. St. C. Headley and L. A. Hall, *Polyhedron* 1986, **5**, 1829.
3. D. I. Maharaj and L. A. Hall, *Inorg. Chim. Acta* 1988, **145**, 235.
4. D. I. Maharaj and L. A. Hall, *Polyhedron* 1988, **7**, 2155.
5. L. A. Hall, *Polyhedron* 1989, **8**, 1335.
6. N. R. West and Y. Niu, *J. Am. Chem. Soc.* 1963, **85**, 2589.
7. M. H. Randall, *Infrared Determination of Organic Structures*, p. 191. Van Nostrand, Canada (1952).
8. F. G. Baglin and C. B. Rose, *Spectrochim. Acta* 1970, **26A**, 2298.
9. R. W. Adams, R. L. Martin and G. Winter, *Aust. J. Chem.* 1967, **20**, 773.
10. F. A. Cotton and J. J. Wise, *Inorg. Chem.* 1967, **6**, 917.
11. B. Hathaway, D. Billing and R. Dudley, *J. Chem. Soc. A* 1970, 1420.
12. A. B. P. Lever, *Inorganic Electronic Spectroscopy*, p. 376. Elsevier, Amsterdam (1984).
13. S. M. Condren and H. O. McDonald, *Inorg. Chem.* 1973, **12**, 57.
14. C. K. Bhaskare and S. Y. Kulkarni, *Proc. Ind. Acad. Sci. (Chem. Sci.)* 1986, **97**, 25.
15. H. Koyama, H. Saitoy and H. Kuroya, *J. Inst. Polytech. Osaka City Univ. Serec.* 1953, **4**, 43.
16. S. Asbrink and L. J. Norrby, *Acta Cryst.* 1970, **B26**, 8.
17. P. C. Healey and A. H. White, *J. Chem. Soc., Dalton Trans.* 1972, 1913.
18. R. Cini, P. Colamarino, P. L. Orioli, L. S. Smith, P. R. Newman, H. D. Gillman and P. Nannelli, *Inorg. Chem.* 1977, **16**, 3233.
19. J. N. van Niekerk and F. R. L. Schoening, *Acta Cryst.* 1953, **6**, 227.

Polyhedron Vol. 9, No. 21, pp. 2579–2584, 1990
Printed in Great Britain

0277–5387/90 $3.00+.00
© 1990 Pergamon Press plc

TRIPODAL LIGANDS WITH MIXED DONORS. SYNTHESIS OF 2-DIPHENYLPHOSPHINOMETHYL-2-PHENYLTHIOMETHYL-1-METHOXYPROPANE (PSO) AND ITS TRANSITION METAL COMPLEXES

SHIUH-TZUNG LIU,* CHONG-LUNG TSAO, MING-CHU CHENG and SHIE-MING PENG

Department of Chemistry, National Taiwan University, Taipei, Taiwan 10764, R.O.C.

(*Received* 20 *March* 1990; *accepted* 7 *June* 1990)

Abstract—A tripodal ligand containing phosphorus, sulphur and oxygen donors has been synthesized and its coordination in chromium(0), molybdenum(0), tungsten(0), manganese(I) and palladium(II) complexes has been investigated. X-ray crystal structures of the chromium, tungsten and palladium compounds have been determined, and the conformations of the six-membered chelate rings of these complexes are discussed.

The design of new polydentate ligands for coordination studies has been interesting and challenging work. As part of our interest in tripodal terdentate ligands, we wished to synthesize such species which contain both "soft" and "hard" donor sites. Such ligands could be used to study the selectivity studies toward transition metals. In our early work,[1] we described several tripodal ligands that contain only two different donor sites, **1** and **2**. However, tripodal terdentates containing three different donor atoms would be more attractive for coordination chemists. Only a few such species have been reported,[2,3] and none containing phosphorus. Here, we report the synthesis of a tripodal phosphine ligand with three different donors, 2-diphenylphosphinomethyl-2-phenylthiomethyl-1-methoxypropane (abbreviated as PSO) **3**, and its complexation toward various transition metals.

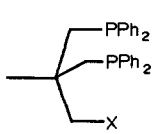

1 X = OMe (P_2O)
2 X = SPh (P_2S)

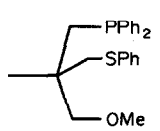

3

* Author to whom correspondence should be addressed.

RESULTS AND DISCUSSION

Synthesis of ligand

The synthetic approach to **3** is shown in Scheme 1. From **4**, compound **5** was prepared according to a modification of the reported method.[4] The oxetane ring was opened by the benzenethiolate anion to generate the sulphide–alcohol **6**. Mesylation of the hydroxy function of **6**, followed by treatment with diphenylphosphide anion, produced the desired phosphine compound (±)-**3**, after anaerobic chromatography of the crude product on a column of degassed silica gel. This terdentate was characterized by a spectroscopic method and elemental analysis. The ^{31}P NMR spectrum shows a single peak at −24.78 ppm, upfield from the reference of 85% H_3PO_4, which is the characteristic absorption of a tertiary phosphine.

Group VI *complexes*

The group VI carbonyl complexes, (PSO)M$(CO)_4$, in which M = Cr (**8a**), Mo (**8b**) and W (**8c**), were readily prepared by means of the direct ligand substitution reaction. The complexes **8a**–**8c** were made by the thermal reaction of **3** with the corresponding $M(CO)_6$ in boiling, degassed xylene. Attempts to prepare (PSO)Mo$(CO)_3$ failed. The substitution reaction of Mo(η^6-cyclohepatriene)$(CO)_3$ by PSO led to the isolation of **8b** instead

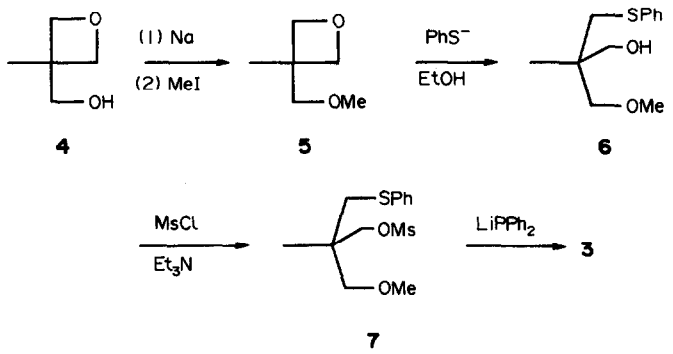

Scheme 1.

of $(PSO)Mo(CO)_3$. Other thermal substitution reactions or photochemical activation of **8b** were unable to force the oxygen donor to become co-ordinated. All purified tetracarbonyl metal complexes have been identified by both spectroscopic and elemental analyses; their data are summarized in Table 1.

Crystals of **8a** and **8c** were grown from hexane and dichloromethane solvents and are isomorphous. The structure of **8a** shows the chromium centre to have an octahedral stereochemistry with four carbonyls, and the phosphorus and the sulphur donors of PSO bound to the metal (Figs 1 and 2). All bond distances and bond angles are within normal ranges; some selected bond distances and bond angles are given in Table 2. The M—C distances for both **8a** and **8c** *trans* to phosphorus are longer than those *trans* to sulphur; this effect is believed to be a consequence of the presence of metal-to-sulphur π-back-donation.[2,4]

Manganese(I) *complexes*

From the reaction of equimolar **3** and $Mn(CO)_5Br$ in boiling chloroform, a yellow crystalline solid of complex **9** was isolated. The IR spectrum

Table 1. Spectroscopic and analytical data of complexes **8a–8c**

Complex	^{1}H NMR	^{31}P NMR ($\Delta_{\delta P}$)[a]	IR [ν(CO)] (cm^{-1})	Analysis
8a	7.56–7.34 (m, 15 H), 3.05 (s, 3 H) 2.82–3.09 (m, 4 H) 2.63 (dd, J = 24.6, J_{P-C-H} = 8 Hz, 1 H) 2.35 (dd, J = 24.6, J_{P-C-H} = 8 Hz, 1 H) 0.86 (s, 3 H)	37.36 (62.1)	2008 1960 1912 1885	$C_{28}H_{27}OPSCr$ Calc. C, 60.2; H, 4.9 Found C, 60.1; H, 5.1
8b	7.62–7.35 (m, 15 H), 3.12 (s, 3 H) 3.18 (d, J = 10.8 Hz, 1 H) 3.02 (d, J = 10.8 Hz, 1 H) 3.02 (d, J = 9.4 Hz, 1 H) 2.94 (d, J = 9.4 Hz, 1 H) 2.67 (dd, J = 15, J_{P-C-H} = 7 Hz, 1 H) 2.47 (dd, J = 15, J_{P-C-H} = 7 Hz, 1 H) 0.95 (s, 3 H)	18.51 (43.3)	2019 1976 1916 1891	$C_{28}H_{27}OPSMo$ Calc. C, 55.8; H, 4.5 Found C, 56.2; H, 4.5
8c	7.70–7.32 (m, 15 H), 3.13 (s, 3 H) 3.30 (d, J = 11.4 Hz, 1 H) 3.16 (d, J = 11.4 Hz, 1 H) 3.01 (d, J = 5.8 Hz, 1 H) 2.94 (d, J = 5.8 Hz, 1 H) 2.80 (dd, J = 14.6, J_{P-C-H} = 8 Hz, 1 H) 2.60 (dd, J = 14.6, J_{P-C-H} = 8 Hz, 1 H) 0.97 (s, 3 H)	3.36 (28.1)	2014 1929 1910 1883	$C_{28}H_{27}OPSW$ Calc. C, 48.7; H, 3.9 Found C, 49.5; H, 4.0

[a] Coordination chemical shifts ($\Delta_{\delta P}$) = δ_p(complex) − δ_p(free ligand), in ppm.

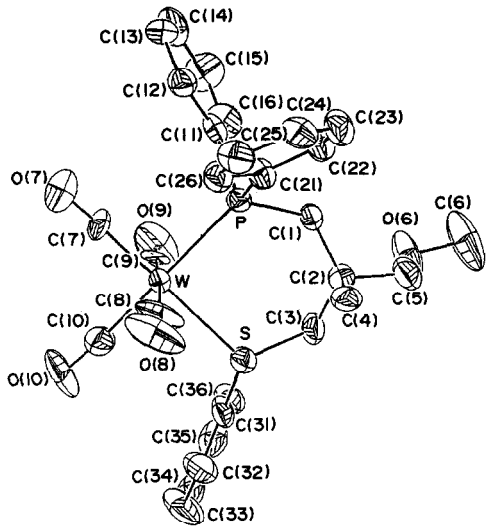

Fig. 1. The ORTEP drawing of **8c**.

(ν(CO) = 2034, 1961, 1907 cm^{-1}) of **9** shows three terminal CO stretches in *fac*-geometry.[5] Both ^{31}P and ^{1}H NMR spectra indicate that phosphorus and sulphur donors bind to the metal centre with the oxygen site uncoordinated. This evidence indicates the structure of **9** to be an octahedral complex with phosphorus, sulphur and bromide in a *fac*-arrangement.

Another way to achieve complex **9** is by the reaction of **3** and $Mn_2(CO)_{10}$ to generate [(PSO)Mn $(CO)_3]_2$ (**10**), followed by treatment with bromine (Scheme 2). It is interesting to note that both IR and ^{1}H NMR spectra of **10** are similar to those of **9**; only the ^{31}P chemical shifts for both complexes have a slight difference (δ 25.66 of **9** vs δ 27.63 of **10**). However, we have not determined the exact structure of **10**.

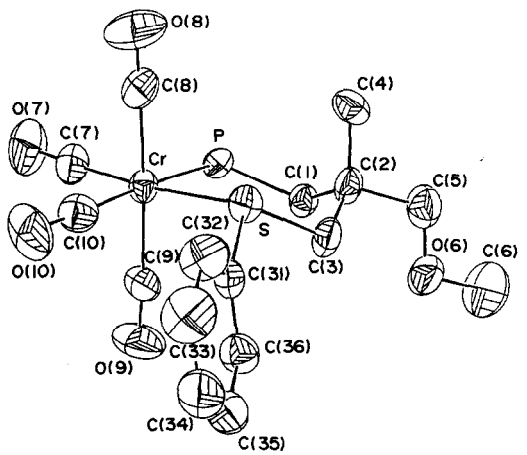

Fig. 2. The ORTEP drawing of **8a** (phenyl groups omitted for clear view).

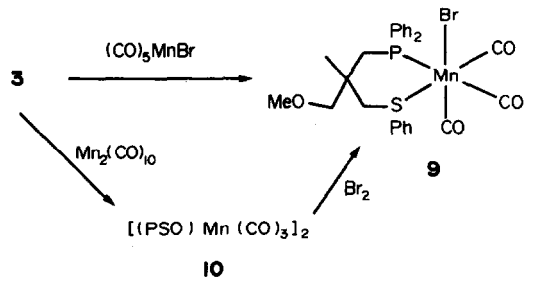

Scheme 2.

Palladium(II) *complex*

The reaction of equimolar amounts of **3** and $PdCl_2$ in acetonitrile afforded the desired complex (PSO)$PdCl_2$ (**11**) as a yellow, crystalline solid upon recrystallization. Both ^{1}H and ^{31}P NMR spectroscopic data of the compound indicate that the potentially terdentate PSO ligand acts in a bidentate mode with phosphorus and sulphur atoms binding to palladium metal in a *cis*-fashion. This structure has been further determined by the single-crystal X-ray diffraction method. Figure 3 shows an ORTEP view of the complex with all non-hydrogen atoms labelled. The coordination geometry around palladium is a square-planar arrangement with the palladium atom slightly [0.197(4) Å] out of the plane defined by S,P,Cl(1),Cl(2). Selected bond dis-

Table 2. Selected bond distances (Å) and bond angles (°) of complexes **8a**, **8c** and **11**

	8a M = Cr	**8c** M = W	**11** M = Pd
M—P	2.385(2)	2.510(3)	2.235(2)
M—S	2.420(2)	2.546(4)	2.285(2)
M—C(7)	1.806(6)	1.88(1)	
M—C(8)	1.911(7)	2.07(1)	
M—C(9)	1.879(6)	1.82(2)	
M—C(10)	1.820(6)	1.94(1)	
M—C(11)			2.289(2)
M—C(12)			2.381(2)
P—C(1)	1.820(5)	1.82(1)	1.830(6)
S—C(3)	1.822(6)	1.81(1)	1.824(7)
C(1)—C(2)	1.549(9)	1.54(2)	1.524(7)
C(2)—C(3)	1.538(8)	1.56(2)	1.518(9)
S—M—P	91.85(7)	89.7(1)	97.81(6)
P—M—C(7)	88.8(2)	89.8(4)	
S—M—C(10)	92.0(2)	91.2(4)	
C(7)—M—C(10)	87.8(3)	89.8(6)	
C(8)—M—C(9)	174.7(3)	175.6(5)	
P—M—C(11)			86.26(7)
S—M—C(2)			84.77(7)
C(11)—M—C(12)			91.15(7)

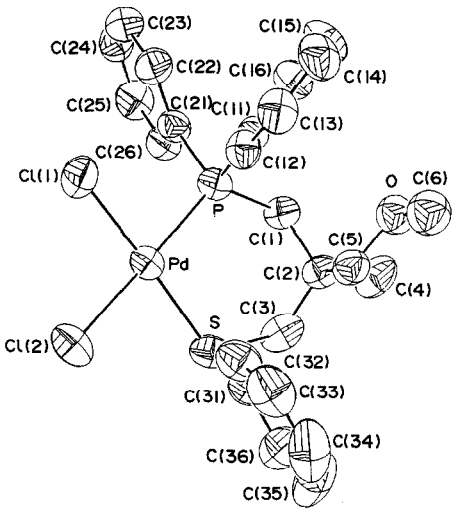

Fig. 3. ORTEP drawing of complex **11**.

tances and angles are listed in Table 2. The Pd—Cl bond *trans* to the phosphorus atom is longer, as expected, than that *trans* to the sulphur atom, probably due to the "*trans* effect".

Conformational analysis

Table 3 presents all torsional angles around the six-membered chelate rings of the complexes, which also facilitates their comparison. The characteristic $+g$, $-g$ alternations indicate the conformations of the six-membered chelate rings of **8a**, **8c** and **11** to be in chair forms, which are considered the most stable.[6,7] However, these chair conformations are all slightly distorted, especially in the palladium complex (Fig. 3).

In the previous investigation,[1a,1b] we found that the conformations of $(P_2S)Mo(CO)_4$ and $(P_2O)Cr(CO)_4$ were in twist-boat forms mainly due to the steric interactions of substituents along the chelate rings, as shown in Fig. 4(a). Apparently, the trivalent thioether (coordination to the metal) helps to relieve some 1,3-diaxial interactions in the chelate rings of complexes **8a** and **8c**, so that the chelate rings are able to adopt chair forms [Fig. 4(b)].

Table 3. Torsional angles (°) around the six-membered chelate rings of complexes **8a**, **8c** and **11**

	8a M = Cr	**8c** M = W	**11** M = Pd
M—P—C(1)—C(2)	−52.5(3)	−54.1(7)	43.5(3)
P—C(1)—C(2)—C(3)	80.3(4)	81.8(10)	−71.9(4)
C(1)—C(2)—C(3)—S	−81.1(4)	−82.4(10)	67.0(4)
C(2)—C(3)—S—M	57.7(3)	57.6(6)	−34.9(3)
C(3)—S—M—P	−28.8(2)	−28.9(4)	6.4(2)
S—M—P—C(1)	25.4(2)	26.0(4)	−9.9(2)

In contrast to an equatorial position, the phenyl group attached to the sulphur atom is situated in an axial position in the palladium complex **11**. This difference obviously suggests the "eclipsed" interaction of the equatorial phenyl group and the chloride ligand to be larger than the 1,3-diaxial interaction. Of course, another factor contributing to this outcome is that the larger angle of S—Pd—P [97.81(6)°] increases the distance between phosphorus and sulphur, which leads to the decrease of the 1,3-diaxial interaction between the phenyl groups.

The resolution of the chiral ligand PSO and its applications are currently in progress.

EXPERIMENTAL

The general information has been described in detail previously.[1] Compound **4** was prepared according to the reported method.[8]

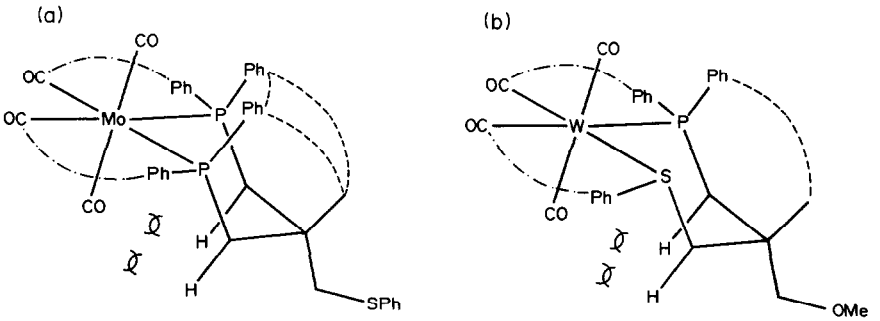

Fig. 4. (a) Three types of major steric interactions of $(P_2S)Mo(CO)_4$ in the chair conformation: (i) 1,3-diaxial interactions (---); (ii) "eclipsed" interactions between apical ligands (CO) and phenyl groups (—·—·—); (iii) interactions between apical ligands and axial hydrogen atoms (𝔍). (b) The steric interaction of $(PSO)W(CO)_4$ in the chair form.

3-Methoxymethyl-3-methyloxetane (**5**)

Freshly-cut sodium metal (3.7 g) was added to a solution of **4** (16.27 g, 0.16 mol) in toluene (40 cm^3). The mixture was heated to reflux overnight. Iodomethane (12 cm^3, 0.16 mol) was added to the above solution, which was then stirred at room temperature for 36 h. The reaction mixture was quenched with water (50 cm^3) and the organic layer was separated. The organic portion was extracted with ether (20 $cm^3 \times 3$). All organic extracts were combined, dried and concentrated. The residue was distilled to give compound **5** (10.0 g, 54%) as a clear liquid: b.p. 138–142°C/760 mm (similar to literature[9]).

2-Hydroxymethyl-2-phenylthiomethyl-1-methoxypropane (**6**)

Freshly-cut sodium metal (4.15 g, 180.4 mmol) was added to ethanol (70 cm^3) under a nitrogen atmosphere. After all the sodium had reacted, thiophenol (18 cm^3, 175.3 mmol) was added to the ethoxide solution slowly, this was then stirred for 30 min. Compound **5** (6.63 g, 57.2 mmol) was transferred into the above solution and the resulting mixture was heated to reflux overnight. Water (20 cm^3) followed by ether (40 cm^3) was added to the reaction mixture. The organic layer was separated, and the aqueous layer was extracted with ether (30 $cm^3 \times 2$). The combined organic extracts were dried and concentrated. The residue was chromatographed on silica (100 g) with elution by 5% ethyl acetate in hexane. The desired compound **6** was obtained as a viscous, yellow liquid (8.08 g, 62%). ^{1}H NMR: δ 7.40–7.00 (m, 5 H), 3.48 (d, $J = 9$ Hz, 1 H), 3.42 (d, $J = 9$ Hz, 1 H), 3.20 (d, $J = 3$ Hz, 2H), 3.15 (s, 3 H), 3.08 (d, $J = 9$ Hz, 1 H), 2.92 (d, $J = 9$ Hz, 1 H), 2.70 (br, 1 H), 0.80 (s, 3 H). Found: C, 63.1; H, 8.1. Calc. for $C_{12}H_{18}O_2S$: C, 63.7; H, 8.1%.

2-Diphenylphosphinomethyl-2-phenylthio-1-methoxypropane (**3**)

The hydroxy compound **6** was transformed into mesylate **7** according to a standard procedure described previously.[1b] To a solution of diphenylphosphine (3.23 g, 17.2 mmol) in THF (100 cm^3) was added a 2.50 M hexane solution of *n*-butyllithium (17.0 cm^3) at ice-cooled temperature. After stirring for 30 min, compound **7** (4.24 g, 13.9 mmol), in a small portion of THF, was added to the phosphide anion solution. The resulting mixture was heated to reflux for 4 h; degassed water (10 cm^3) was then added. The organic layer was separated, dried and concentrated. The crude product was chromatographed on silica (100 g) with elution by 40% ethyl acetate in hexane. The desired tripodal ligand, PSO, was obtained as a viscous, colourless

Table 4. Summary of crystal data of complexes **8a**, **8c** and **11**

	8a	**8c**	**11**
Formula	$CrPSC_{28}H_{27}O_5$	$WPSC_{28}H_{27}O_5$	$PdPSC_{24}H_{23}Cl_2O$
Crystal size (mm)	$0.7 \times 0.7 \times 0.5$	$0.6 \times 0.6 \times 0.5$	$0.5 \times 0.5 \times 0.5$
Lattice	Orthorhombic	Orthorhombic	Orthorhombic
Space group	$Pna2_1$	$Pna2_1$	$Pbca$
a (Å)	16.786(8)	16.896(8)	16.223(3)
b (Å)	12.728(9)	12.768(4)	15.447(3)
c (Å)	12.754(4)	12.837(5)	19.737(3)
V (Å^3)	2725.1	2769.3	4945.7
Z	4	4	8
$F(000)$	1088	1240	2064
Temperature (K)	300	300	300
μ (mm^{-1})	0.57	4.42	1.11
Transmission	0.94–1.0	0.65–1.0	0.85–1.0
$2\theta_{max}$	54	55	50
h, k, l	21, 16, 16	21, 16, 16	19, 18, 23
λ (Å)	0.7093	0.7093	0.7093
Number of reflections	3097	3318	4350
Number of observed reflections	2208 ($> 2.5\sigma$)	2477 ($> 2.0\sigma$)	2682 ($> 2.5\sigma$)
Number of variables	325	325	270
$R(F)$	0.045	0.040	0.037
$R_w(F)$	0.034	0.037	0.037
S	2.42	3.81	2.87

liquid. ^{1}H NMR: δ 7.60–7.00 (m, 15 H), 3.10 (s, 2 H), 3.00 (s, 3 H), 2.90 (s, 2 H), 2.20 (d, J_{P-C-H} = 3 Hz, 2 H), 0.90 (s, 3 H). Found: C, 73.1; H, 7.0. Calc. for $C_{24}H_{27}OPS$: C, 73.1; H, 6.9%.

Preparation of **8a–8c**

The ligand PSO and an equimolar amount of group VI metal carbonyl ($M(CO)_6$, M = Cr, Mo and W) were dissolved in an aromatic solvent (toluene or xylene) and heated to reflux for 8–10 h. The desired complexes were isolated by chromatography on silica. All spectroscopic and analytic data are given in Table 1.

Preparation of (PSO)$Mn(CO)_3Br$ (**9**)

A solution of $BrMn(CO)_5$ (45.7 mg, 0.17 mmol) and PSO (65.5 mg, 0.17 mmol) in chloroform was refluxed for 30 min. After addition of hexane, the solution was allowed to stand for several days. The complex *fac*-(PSO)$Mn(CO)_3Br$ was crystallized as yellowish needles (65.3 mg, 64%). IR: ν(C≡O) 2034, 1961, 1907 cm^{-1}. ^{1}H NMR: δ 7.90–7.30 (m, 15 H), 3.25 (s, 3 H), 3.09 (d, J = 8.84 Hz, 1 H), 3.03 (d, J = 8.84 Hz, 1 H), 2.71 (d, J = 11 Hz, 1 H), 2.64 (d, J = 11 Hz, 1 H), 2.44 (dd, J = 10, 15.3 Hz, 1 H), 2.15 (dd, J = 10, 15.3 Hz, 1 H), 0.61 (s, 3H). ^{31}P NMR: δ 25.66. Found: C, 48.7; H, 4.0. Calc. for $C_{27}H_{27}O_4PSMnBr$: C, 49.1; H, 4.1%.

Preparation of (PSO)$PdCl_2$ (**11**)

This complex was obtained as a yellow, crystalline solid by stirring a mixture of PSO and $PdCl_2$ in acetonitrile, followed by recrystallization from dichloromethane and ethyl acetate, m.p. (dec.) 190°C. ^{1}H NMR: δ 7.94–7.30 (m, 15 H), 3.03 (s, 3 H), 2.97 (d, J = 5 Hz, 1 H), 2.95 (d, J = 5 Hz, 1 H), 2.89 (d, J = 2.7 Hz, 1 H), 2.87 (d, J = 2.7 Hz, 1 H), 2.49 (dd, J = 22.5, 12 Hz, 1 H), 2.09 (dd, J = 22.5, 12 Hz, 1 H), 0.93 (s, 3 H). ^{31}P NMR: δ 17.81. Found: C, 50.1; H, 4.7. Calc. for $C_{24}H_{27}OPSPdCl_2$: C, 50.4; H, 4.8%.

Crystallographic analysis of complexes **8a**, **8c** *and* **11**

Cell parameters were determined on a CAD-4 diffractometer by a least-squares treatment. Atomic scattering factors wee taken from the *International Tables for X-ray Crystallography*.[10] Computation was carried out by using the NRCC SDP VAX package.[11] Relevant data are summarized in Table 4.

Acknowledgement—Financial support from the National Science Council (R.O.C.) is acknowledged.

REFERENCES

1. (a) S.-T. Liu, H.-E. Wang, M.-C. Cheng and S.-M. Peng, *J. Organomet. Chem.* 1989, **376**, 333; (b) S.-T. Liu, G.-J. Liu, C.-H. Yieh, M.-C. Cheng and S.-M. Peng, *J. Organomet. Chem.* 1990, **387**, 83; (c) S.-T. Liu, C.-H. Yieh and H.-J. Lu, *Phosphorus, Sulfur and Silicon* 1989, **44**, 261.
2. S. G. Murray and F. R. Hartley, *Chem. Rev.* 1981, **81**, 365 and refs therein.
3. For recent review in tripodal polyphosphines see: L. Sacconi and F. Mani, in *Transition Metal Chemistry* (Edited by G. A. Melson and B. N. Figgis), Vol. 8, p. 179. Marcel Dekker, New York (1982).
4. M. F. Lappert, D. B. Shaw and G. M. McLaughlin, *J. Chem. Soc., Dalton Trans.* 1979, 427.
5. C. S. Kraihanzel, J. M. Ressner and G. M. Gray, *Inorg. Chem.* 1982, **21**, 879.
6. J. R. Gollogly and C. J. Hawkins, *Inorg. Chem.* 1972, **11**, 156.
7. M. R. Churchill, A. L. Rheingold and R. L. Keiter, *Inorg. Chem.* 1981, **20**, 2730.
8. D. B. Pattison, *J. Am. Chem. Soc.* 1957, **79**, 3455.
9. A. J. McAlees, R. McCrindle and A. R. Woon-Fat, *Inorg. Chem.* 1976, **15**, 1065.
10. *International Tables for X-ray Crystallography*, Vol. IV. Kynoch Press, Birmingham (1974).
11. E. J. Gabe and F. L. Lee, *Acta Cryst.* 1981, **A37**, S339.

Polyhedron Vol. 9, No. 21, pp. 2585–2589, 1990
Printed in Great Britain

0277–5387/90 $3.00+.00
© 1990 Pergamon Press plc

ELECTRONIC STRUCTURE OF THIOCHLOROANIONS OF MOLYBDENUM

LUDMIŁA SZTERENBERG

Institute of Chemistry, University of Wrocław, 50-383 Wrocław, F. Joliot-Curie 14, Poland

(*Received* 5 *April* 1990; *accepted* 8 *June* 1990)

Abstract—The electronic structure and bonding properties of the $[Mo_3(\mu_3\text{-}S)(\mu\text{-}S_2)_3Cl_6]^{2-}$, $[Mo_2(\mu\text{-}S_2)(\mu\text{-}Cl)_2Cl_6]^{2-}$ and $[Mo_2(\mu\text{-}S_2)_2Cl_8]^{2-}$ ions have been studied using the Fenske–Hall method. On the basis of the two-centre overlap populations, the roles and the strengths of the metal–metal and metal–ligand bonds have been determined.

Metal compounds in which two transition metal elements are joined via the sulphur or halogen atoms and which contain the metal–metal bonds are well known. This class of complexes is of biological and catalytic interest. There is as yet no definitive evidence for the presence of disulphur complexes in biological systems. However, it was suggested that the reaction of xanthine oxidase with cyanide yielding thiocyanate and the inactive disulpho-form of the enzyme involves abstraction of a sulphur atom from a disulphur complex or from a persulphido group.[1–3]

In continuation of our theoretical investigations of the Mo—S clusters model,[4–6] this paper reports the results of the determination of the electronic structure of polynuclear molybdenum thioanions with a structural unit in which both sulphur atoms of the disulphur ligand are bonded to each of the two metal atoms. The electronic structures of the $[Mo_3(\mu_3\text{-}S)(\mu\text{-}S_2)_3Cl_6]^{2-}$, $[Mo_2(\mu\text{-}S_2)(\mu\text{-}Cl)_2Cl_6]^{2-}$ and $[Mo_2(\mu\text{-}S_2)_2Cl_8]^{2-}$ ions, as well as of the S_2^{n-} ligand (where $n = 0$–2), were calculated by the parameter-free Fenske–Hall method.

COMPUTATIONAL DETAILS

The semi-quantitative Fenske–Hall LCAO molecular orbital method[7] was applied in our study. The method is an approximate Hartree–Fock–Roothaan SCF LCAO MO molecular orbital approach which involves neither arbitrary nor adjustable parameters, depending only upon the choice of wave functions and atomic coordinates as input data. The operation is self-consistent.

The interatomic distances and angles used for the examined complexes were based upon their structural determinations for $[Mo_3(\mu\text{-}S)(\mu\text{-}S_2)_3Cl_6]^{2-}$, $[Mo_2(\mu\text{-}S_2)(\mu\text{-}Cl)_2Cl_6]^{2-}$[8] and $[Mo_2(\mu\text{-}S_2)_2Cl_8]^{2-}$[9] (Fig. 1).

RESULTS AND DISCUSSION

The calculated distribution of charges in the studied complex ions is shown in Tables 1 and 2. The results obtained for some energy eigenvalues are given in Table 3 and Fig. 2. As a result of these, four groups of the occupied orbitals were observed. The *s* orbitals of sulphur and chlorine ligands that do not form effective M—L bonds are the lowest occupied ones. The next group of orbitals displays mainly the *p* character of the ligand atoms and the 4*d* character of molybdenum. This group is followed by the π non-bonding ligand orbitals. The highest occupied molecular orbitals are the strongly delocalized, multicentre orbitals having pre-

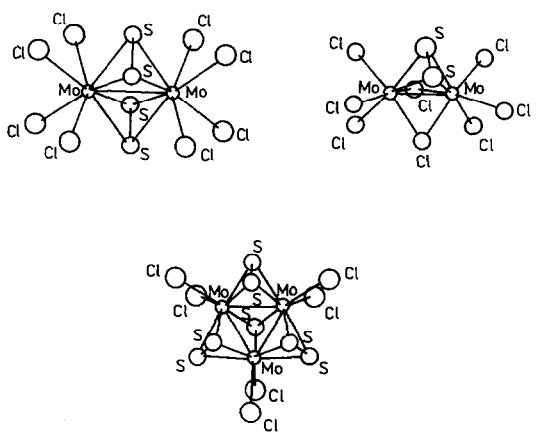

Fig. 1. The geometry of the studied complexes.

Table 1. Calculated atomic charges

	I[a]	II[b]	III[c]
Mo	+1.087	+1.029	+0.844
$S_{(\mu\text{-}S_2)}$	−0.025	−0.082	−0.103
$S_{(\mu\text{-}S)}$			−0.489
Cl_b		−0.360	
Cl_t	−0.510	−0.530	−0.571

[a] $[Mo_2(\mu\text{-}S_2)_2Cl_8]^{2-}$.
[b] $[Mo_2(\mu\text{-}S_2)(\mu\text{-}Cl)_2Cl_6]^{2-}$.
[c] $[Mo_3(\mu\text{-}S)(\mu\text{-}S_2)_3Cl_6]^{2-}$.

Table 2. Charge distributions for the molybdenum atoms

	I[a]	II[b]	III[c]
d	4.467	4.484	4.707
s	0.215	0.249	0.218
p	0.230	0.236	0.230

[a] $[Mo_2(\mu\text{-}S_2)_2Cl_8]^{2-}$.
[b] $[Mo_2(\mu\text{-}S_2)(\mu\text{-}Cl)_2Cl_6]^{2-}$.
[c] $[Mo_3(\mu\text{-}S)(\mu\text{-}S_2)_3Cl_6]^{2-}$.

dominantly the character of the 4*d* orbitals of molybdenum and of the *p* orbitals of the ligands. The lowest unoccupied molecular orbitals have predominantly the character of the 4*d* orbitals of molybdenum. The description of bonding in the studied system is based on the following sequence of metal–metal orbitals (Fig. 2, Table 3): $\sigma^2(d_{z^2})\sigma^*(d_{z^2})$ for $[Mo_2(\mu\text{-}S_2)_2Cl_8]^{2-}$, $\sigma^2(d_{z^2})^2\delta^1(d_{x^2-y^2})\delta^{*1}(d_{x^2-y^2})\sigma^*(d_{z^2})$ for $[Mo_2(\mu\text{-}S_2)(\mu\text{-}Cl_2)Cl_6]^{2-}$ and $\sigma^2(d_{z^2})\pi^4(d_{xz})\pi^*(d_{xz})$ for $[Mo_3(\mu_3\text{-}S)(\mu\text{-}S_2)_3Cl_6]^{2-}$ (where the σ, π and δ orbitals denote the bonding combinations of the valence *d* orbitals of molybdenum, while σ^*, π^* and δ^* are their corresponding antibonding counterparts). For the $[Mo_2(\mu\text{-}S_2)_2Cl_8]^{2-}$

Table 3. *d–d* Interactions of investigated anions

Molecular orbital	$[Mo_2(\mu\text{-}S_2)_2Cl_8]^{2-}$	Energy levels (eV) and occupations	
47		↓↑	−2.26
	$[Mo_2(\mu\text{-}S_2)(\mu\text{-}Cl_2)Cl_6]^{2-}$		
40		↓↑	−1.77
41		↑	0.54
42	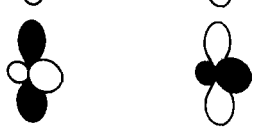	↑	0.89
	$[Mo_3(\mu\text{-}S)(\mu\text{-}S_2)_3Cl_6]^{2-}$		
50	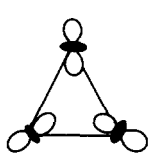	↓↑	−3.17
51	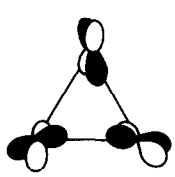	↑↑ ↓↑	−2.33

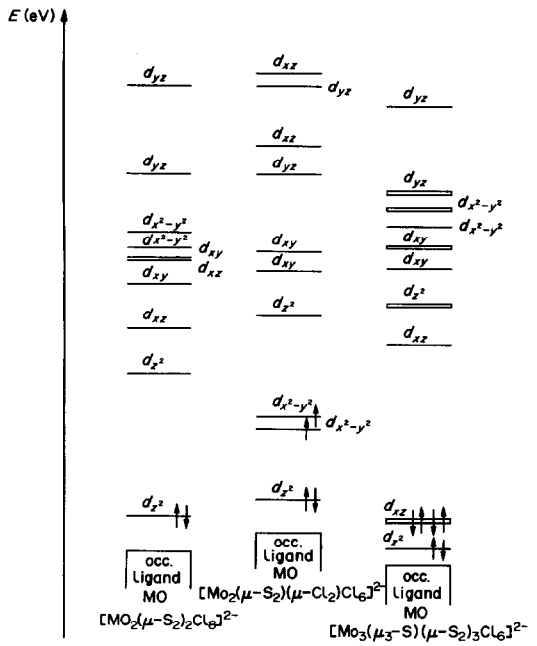

Fig. 2. Molecular orbital diagrams showing the highest filled and lowest unfilled orbitals for the anions investigated.

complex anion the HOMO orbital is occupied by two electrons. The results of calculations for the high- and low-spin systems suggested the presence of the low-spin configuration. The high-spin system proved to be energetically unstable. In such a case the $\sigma^1\sigma^{*1}$ configuration does not form effective Mo—Mo bonding, either. No experimental data on the magnetic properties of the examined system are available, and no temperature-dependent paramagnetism should be expected here, which was also indicated by the $\Delta E_{\text{HOMO-LUMO}}$ splitting value of about 5 eV. Instead, the scheme obtained for the $[Mo_2(\mu\text{-}S_2)(\mu\text{-}Cl_2)Cl_6]^{2-}$ ion is in good agreement with the magnetic and spectroscopic experimental data, but without contradiction of the existence of σ character in the Mo—Mo bonding. The presence of the chloride bridge atoms is responsible for the appearance of the δ bonding and antibonding orbitals (because of the Mo—Mo interaction) between the σ and σ^* orbitals. Since in all of the three examined cases the σ–σ^* splitting remained of the same order, we could dispel the doubts of Müller and co-workers[8] about the unchanged spectroscopic and magnetic properties of the $[Mo_2(\mu\text{-}S_2)(\mu\text{-}Cl_2)Cl_6]^{2-}$ ion as compared with those of the monomeric molybdenum(V) complex ions. The magnetically undetectable electrons of the $[Mo_2(\mu\text{-}S_2)(\mu\text{-}Cl_2)Cl_6]^{2-}$ ion are localized on the Mo—Mo axis in the molecular σ orbital, while the two other electrons occupy the δ and δ^* orbitals. The moderately intensive band at about 12.5×10^3 cm^{-1} in the electronic absorption spectrum of the $[Mo_2(\mu\text{-}S_2)(\mu\text{-}Cl_2)Cl_6]^{2-}$ complex ion was attributed to the $\sigma(d_{z^2}) \rightarrow \delta(d_{x^2-y^2})$ transition, while the shoulder on the intensive band at about 23×10^3 cm^{-1} should be attributed to the $\delta(d_{x^2-y^2}) \rightarrow \sigma^*(d_{z^2})$ one-electron excitation.

More detailed characteristics of bonding are given by Mülliken's overlap populations. Nevertheless, although they are not significant in the absolute scale, comparison of the values for similar systems led to reasonable trends. Taking into account the above-mentioned limitations, the conclusions can be applied to the molybdenum–molybdenum and molybdenum–ligand bonding. The most important overlap populations of the examined complexes are presented in Table 4. The data in Table 4 also confirm a predominant contribution of the $d\sigma$ orbitals to the metal–metal bonding. The contribution of the $d\pi$ and $d\delta$ orbitals is several times lower than those of the $d\sigma$ orbitals. In all of the complexes the Mo—Mo overlap population value is of the same order. Although the Mo—Mo bond plays an important role in electron delocalization, the main contribution to the formation of a stable MoS_2Mo cluster is found to arise from the bonding interaction between the sulphur and the metal atoms, since the former is an electron donor, possessing the capability of strong electron delocalization. In all the studied cases, the two-centre overlap population revealed some consistencies about the metal–ligand bond strengths. The bonding interaction between the d orbitals of

Table 4. Two-centre overlap populations

	I[a]	II[b]	III[c]
$d_{z^2}-d_{z^2}$	0.0712	0.0893	
d–d	0.0735	0.0900	0.0803
Total Mo—Mo	0.1004	0.1086	0.1306
d-$S_{(\mu\text{-}S_2)}$	0.1140	0.1125	0.0956
Total Mo—$S_{(\mu\text{-}S_2)}$	0.1498	0.1425	0.1510
d-$S_{(\mu\text{-}S)}$			0.1221
Total Mo—$S_{(\mu\text{-}S)}$			0.2035
d-Cl_b		0.0775	
Total Mo—Cl_b		0.1453	
d-Cl_t	0.1005	0.0980	0.0907
Total Mo—Cl_t	0.1630	0.1853	0.1731
S—S (in μ-S_2)	0.3661	0.3799	0.3847

[a] $[Mo_2(\mu\text{-}S_2)_2Cl_8]^{2-}$.
[b] $[Mo_2(\mu\text{-}S_2)(\mu\text{-}Cl)_2Cl_6]^{2-}$.
[c] $[Mo_3(\mu\text{-}S)(\mu\text{-}S_2)_3Cl_6]^{2-}$.

Table 5. Selected results of MO calculations on the disulphur ligand and the examined complexes

		S_2	S_2^-	S_2^{2-}	μ-S_2 in I[a]	μ-S_2 in II[b]	μ-S_2 in III[c]
Mülliken gross atomic charges		0.0	−0.5	−1.0	−0.03	−0.08	−0.1
Mülliken gross population	s	1.78	1.79	1.81	1.79	1.78	1.76
	p_x	1.50	1.50	2.00	1.49	1.54	1.53
	p_y	1.50	2.00	2.00	1.50	1.52	1.53
	p_z	1.22	1.20	1.19	1.24	1.25	1.26
One-centre densities	s	1.72	1.75	1.77	1.75	1.73	1.70
	p_x	1.46	1.46	2.00	1.37	1.42	1.42
	p_y	1.46	2.00	2.00	1.36	1.39	1.40
	p_z	0.96	0.95	0.93	1.04	1.03	1.05
Two-centre overlap population		0.39	0.34	0.29	0.36	0.37	0.38

[a] $[Mo_2(\mu\text{-}S_2)_2Cl_8]^{2-}$.
[b] $[Mo_2(\mu\text{-}S_2)(\mu\text{-}Cl_2)Cl_6]^{2-}$.
[c] $[Mo_3(\mu_3\text{-}S)(\mu\text{-}S_2)_3Cl_6]^{2-}$.

Table 6. Selected orbital energies (in eV) and per cent composition of the respective molecular orbitals in $[Mo_2(\mu\text{-}S_2)_2Cl_8]^{2-}$

Molecular orbital	Orbital energies	Per cent character
19	−9.00	40.0 p_x S; 35.0 d_{xy} Mo
20	−8.80	48.6 p_y S; 34.4 d_{xz} Mo
21	−7.67	50.7 p_z Cl; 28.0 $d_{x^2-y^2}$ Mo
22	−7.38	69.5 p_z Cl; 11.4 d_{yz} Mo
23	−7.13	34.0 p_y S; 32.7 d_{xy} Mo
24	−7.13	32.0 p_z Cl; 18.3 d_{z^2} Mo
25	−6.90	35.6 p_x Cl; 18.9 d_{yz} Mo
47[a]	−2.26	48.0 d_{z^2} Mo; 9.8 p_x Cl
48	+2.77	62.2 d_{z^2} Mo; 21.4 $d_{x^2-y^2}$ Mo; 26.8 p_x S
49	+3.61	56.2 d_{xz} Mo; 26.8 p_x S

[a] HOMO.

the metal and ligand falls in the oder:

$$P(d\text{Mo–}\mu S_2) > P(d\text{Mo–Cl}_t) > P(d\text{Mo–}\mu\text{Cl}).$$

The strong metal–bridge (μS_2) bonding is evidence for the stability of such systems. The stability is due to the extensive electron delocalization in the Mo—μS_2—Mo arrangement. The negative charge on the sulphur of the free S_2^{2-} ligand decreases drastically in the complexes (Table 5). When S_2^{2-} is a bidentate bridge ligand, the flow of charge π_g,π_u from the disulphur unit to the metal is more effective. Calculations show that the extensive electron delocalization is a general feature of the cluster compounds investigated. It usually appeared as the larger contribution of the π electrons on the μ-S_2 atoms to the free orbitals of the metal. The major contribution of the π bonds, Mo—S_2, is shown in Table 6 by the quantitative molecular orbital scheme for the $[Mo_2(\mu\text{-}S_2)_2Cl_8]^{2-}$ ion.

REFERENCES

1. R. J. P. Williams, *The Biological Role of Molybdenum*. Climax Molybdenum Company, London (1978).
2. V. Massey and D. Edmondson, *J. Biol. Chem.* 1970, **245**, 6595.
3. A. Müller, W. A. Jaegermann and J. H. Enemark, *Coord. Chem. Rev.* 1982, **46**, 245.

4. L. Szterenberg and B. Jeżowska-Trzebiatowska, *Bull. Acad. Polon. Sci.* 1981, **XXIX**, 219.
5. L. Szterenberg and B. Jeżowska-Trzebiatowska, *Inorg. Chim. Acta* 1982, **59**, 363.
6. L. Szterenberg and B. Jeżowska-Trzebiatowska, *Bull. Acad. Polon. Sci.* 1988, **36**, 363.
7. M. B. Hall and R. F. Fenske, *Inorg. Chem.* 1972, **11**, 768.
8. P. Klingelhöfer, U. Müller, C. Friebel and J. Pebler, *Z. Anorg. Allg. Chem.* 1986, **543**, 22.
9. D. Fenske, *Z. Anorg. Allg. Chem.* 1985, **520**, 7.

Polyhedron Vol. 9, No. 21, pp. 2591–2595, 1990
Printed in Great Britain.

0277–5387/90 $3.00+.00
© 1990 Pergamon Press plc

PROPERTIES IN SOLID AND SOLUTION OF $[Pd(PPr_3^n)(NO_2)_3][As(C_6H_5)_4]$

GIUSEPPE BRUNO,* SEBASTIANO CAMPAGNA, MATTEO CUSUMANO,* ANTONINO GIANNETTO and VITTORIO RICEVUTO

Dipartimento di Chimica Inorganica e Struttura Molecolare, Salita Sperone 31, Vill. S. Agata, 98010 Messina, Italy

(*Received* 5 *January* 1989; *accepted after revision* 15 *June* 1990)

Abstract—The crystal structure of $[Pd(PPr_3^n)(NO_2)_3][As(C_6H_5)_4]$ has been determined by single X-ray diffraction: $[Pd(PPr_3^n)(NO_2)_3][As(C_6H_5)_4]$, $Mr = 788.0$, orthorhombic, $P2_12_12_1$, $a = 17.781(2)$, $b = 15.050(2)$, $c = 13.397(1)$ Å, $V = 3585.1(5)$ Å^3, $Z = 4$, $Dx = 1.46$ Mg m^{-3}, λ(Mo-K_α) = 0.71073 Å, $\mu = 14.5$ cm^{-1}, $F(000) = 1608$, $T = 294$ K, $R = 0.056$ for 2620 independent reflections with $I > 3\sigma(I)$. The complex $[Pd(PPr_3^n)(NO_2)_3][As(C_6H_5)_4]$ is essentially square-planar. The bond distance palladium-to-nitrogen *trans* to phosphine of 2.25 Å is the longest observed so far in palladium(II) complexes. The rate of replacement of the nitro-group *trans* to phosphine by piperidine has been studied in the title complex and in *trans*-$[Pd(PPr_3^n)(NO_2)_2Cl][As(C_6H_5)_4]$ at 25°C in dichloromethane. The second order rate constants k_2 (dm^3 mol^{-1} s^{-1}) are, respectively, $(72.8 \pm 1.1) \times 10^3$ and $(36.8 \pm 2.0) \times 10^3$. The enhancement of the relative lability of NO_2 with respect to Cl suggests that the nitro group is either weakly bound to palladium in solution, as in the solid, or is coordinated through oxygen.

We have recently[1] reported that by reaction of the tetrameric complex $[Pd_4(PPr_3^n)_4(NO_2)_8]$ with nucleophiles, anionic complexes of *n*-propylphosphine of the type $[Pd(PPr_3^n)X_3][As(C_6H_5)_4]$ (X = Cl, Br, NO_2, etc.) are obtained. In this paper we report the properties in solid and solution of one of these substances, i.e. $[Pd(PPr_3^n)(NO_2)_3][As(C_6H_5)_4]$. In particular, we describe the structure in the solid compound, as determined by a single-crystal X-ray study, and in order to search for a possible relation between structure and reactivity, we report the kinetics of substitution, by piperidine, of the group X *trans* to PPr_3^n in $[Pd(PPr_3^n)(NO_2)_2X][As(C_6H_5)_4]$ (X = NO_2 or Cl) in dichloromethane at 25°C.

EXPERIMENTAL

The preparation of the complexes $[Pd(PPr_3^n)(NO_2)_3][As(C_6H_5)_4]$ and *trans* $[Pd(PPr_3^n)(NO_2)_2Cl][As(C_6H_5)_4]$ has already been reported.[1] Piperidine was distilled over KOH pellets. All the solvents were of the highest quality commercially available and used as received.

The conductivity measurements were performed with a Radiometer CDM3 conductivity bridge. Ultraviolet–vis. spectra were recorded by using a Perkin–Elmer Lambda 5 spectrophotometer. Infrared spectra in the range 250–4000 cm^{-1} were recorded as Nujol mulls on a Perkin–Elmer 783 spectrometer.

The kinetics were followed with a standard Durrum–Gibson stopped-flow spectrophotometer equipped with a photometric log amplifier model D-131. Absorbance changes, at selected wavelengths, were displayed on a Gould 054100 storage oscilloscope and traces were recorded on a Radiometer REC 61 potentiometric recorder.

In all cases a large excess of reagent was used to provide pseudo-first-order conditions and to force the reactions to completion. Pseudo-first-order rate constants $k_{obs.}$ (s^{-1}) were obtained either from the gradients of the plots $\log(A_t - A_\infty)$ vs time or from non-linear least-squares fit of experimental data to $A_t = A_0 + (A_0 - A_\infty) \exp(-k_{obs.}t)$, where A_0, A_∞ and $k_{obs.}$ were the parameters to be optimized (A_0 = absorbance after mixing of the reagents, A_∞ = absorbance at completion of reaction). The $k_{obs.}$ values were reproducible to better than ±5%.

* Author to whom correspondence should be addressed.

X-ray data collection and structure refinement

Diffraction data were collected on a Nicolet R3/m diffractometer using graphite-monochromated Mo-K_α($\lambda = 0.71073$ Å) radiation. During the course of the intensity data collection the crystal showed no loss in intensity.

Accurate unit-cell dimensions and crystal orientation matrices were obtained from least-squares refinement of 2θ, ω, χ and ψ values of 25 strong reflections in the range $15° < 2\theta < 30°$. Lorentz and polarization corrections were applied to the intensity data. The structure was solved by using standard Patterson methods, successive least-squares refinements, and difference Fourier maps. Non-hydrogen atoms were refined anisotropically; the carbon atoms of the triphenylarsine cation were refined isotropically. Hydrogen atoms were added at calculated positions and included in the structure factor calculations with a common thermal parameter ($U = 0.08$ Å^2). As usual a general high thermal motion is present in the propyl chains. For this reason some of the C—C bond distances were refined with fixed geometry [d(C—C) = 1.52(2) Å].

Of 5030 independent reflections, measured with a 2θ–ω scan technique in the range $4 < 2\theta < 55$, 2620 having $I > 3\sigma(I)$ were used to refine 237 parameters to final residuals of $R = 0.056$ and $Rw = 0.063$.

The weighting scheme used in the last refinement cycles was: $w = 1.000/(\sigma^2(F_o) + 0.002826F_o^2)$. Reversing the sign of the imaginary anomalous-scattering component of the title compound, which has the non-centrosymmetric space group $P2_12_12_1$, increased R from 0.056 to 0.072. This difference is highly significant, and therefore the model has the correct absolute configuration.

Scattering factors for non-hydrogen atoms were taken from Ref. 2 and for hydrogen atoms from Ref. 3. Anomalous dispersion corrections were taken from Ref. 4. All calculations were performed with SHELX76[5] and PARST[6] set of programs on the IBM 4341 computer at the "Centro di Calcolo dell' Università di Messina". The refined structure was plotted with use of the PLUTO and ORTEP programs (Figs 1 and 2). Atom coordinates, full lists of bond distances and bond angles, anisotropic temperature factors, calculated and observed structure factors are available as supplementary material (Table SI–SIV).

RESULTS AND DISCUSSION

The title compound, obtained by reaction in methanol of the tetrameric complex $[Pd_4(PPr_3^n)_4(NO_2)_8]$, in the presence of $[As(C_6H_5)_4](NO_3)$ 1:10, with excess $NaNO_2$, is a yellow crystalline solid. On the basis of elemental analysis and the IR spectrum the substance can be formulated as $[Pd(PPr_3^n)(NO_2)_3][As(C_6H_5)_4]$. In fact the IR spectrum, besides two bands at 800 and 750 cm^{-1} characteristic of $[As(C_6H_5)]^+$, shows two bands at 1330 and 1398 cm^{-1} assignable to NO stretching.[7] The single crystal X-ray determination of this study confirms that the complex has a square-planar structure with the nitro groups coordinated through nitrogen.

Molecular structure of $[Pd(PPr_3^n)(NO_2)_3][As(C_6H_5)_4]$

The crystal structure of the title compound, depicted in Fig. 1, where the atomic labelling is shown, consists of discrete anion in which the palladium atom is four-coordinated and the $[As(C_6H_5)_4]^+$ cation is separated by normal Van der Waals' interactions. In Fig. 2 a stereoview of the anion is reported. Selected bond distances and angles are given in Table 1.

The local anion geometry is, as expected, square-planar slightly distorted with N3—Pd—P and N1—Pd—N2 bonds angles of 178.3(3) and 178.3(5)°. The weighted mean plane through the four basal donor atoms and the metal atom shows slight distortion from planarity with N1 and N2 deviating by −0.028(10) and 0.034(15) Å, respectively. P and N3 are 0.002(4) and 0.013(9) Å; the palladium atom is −0.015(1) out of this plane. The Pd—P bond distance of 2.263(4) Å is comparable with the value of 2.252(3)Å found in $[Pd_2(PPr_3^n)(NCS)(SCN)_2(\mu\text{-}CN)]$[8] and is not significantly longer than the value of 2.243(5) Å found in $[Pd(PPr_3^n)(NO_2)_2Cl][As(C_6H_5)_4]$,[1] where *n*-propylphosphine is *trans* to the chlorine atom. The two nitro groups *trans* to each other are both bonded to palladium through their nitrogen atoms. The Pd—N1 and Pd—N2 bond distances, are 2.01(1) and 2.01(1) Å, respectively, and are comparable with the corresponding values reported for *trans*-$[Pd(PPr_3^n)(NO_2)_2Cl][As(C_6H_5)_4]$,[1] *trans*-$[Pd(PPhMe)_2(NO_2)_2]$,[9] *trans*-$[Pd(PEt_3)_2(NO_2)_2]$,[9] $[Pd_4(PPr_3^n)_4(NO_2)_8]$[10] and $[Pd(dien)(NO_2)]$.[11] The geometry of these two nitro groups is characterized by an N—O bond length which ranges from 1.16(2) to 1.26(2) Å and by the O—N—O bond angles which are 118(1)° for O22—N2—O21 and 122(1)° for O12—N1—O11. The two nitro group planes are rotated with respect to the palladium coordination plane by 86.9(8) and 92.3(9)° while the rotation of the third nitro group (O31—N3—O32), *trans* to PPr_3^n, significantly deviates from the orthogonality to the metal coordination plane [118.5(12)°]. In addition the bond distance Pd—N3 of 2.25(1) Å

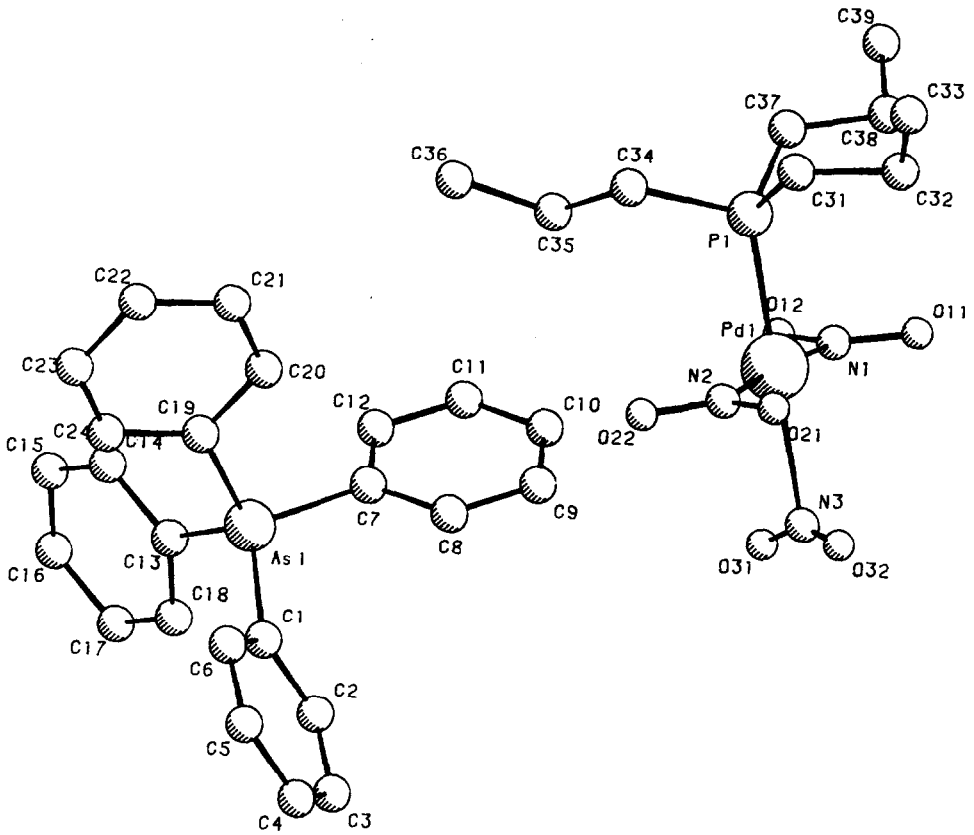

Fig. 1. Perspective view of the $[Pd(PPr_3^n)(NO_2)_3][As(C_6H_5)_4]$ structure.

is, to our knowledge, the longest so far observed for the palladium-to-nitrogen bond. Such an arrangement suggests that some interaction between the oxygen atoms of the nitro group and palladium occurs as in an incipient nitro–nitrito isomerization. It is difficult to explain the Pd—N bond lengthening on the basis of PPr_3^n *trans* influence only and the presence of the adjacent nitro groups has probably to be taken into account.

In the tetraphenylarsonium cation, which has a nearly perfect tetrahedral geometry, the As—C bond distances are as usual and require no special comment.

Conductivity measurements show that $[Pd(PPr_3^n)(NO_2)_3][As(C_6H_5)_4]$ is a 1:1 electrolyte in the common organic solvents. In addition, in solution of coordinating media, the complex undergoes partial solvation. In fact, the shape of the

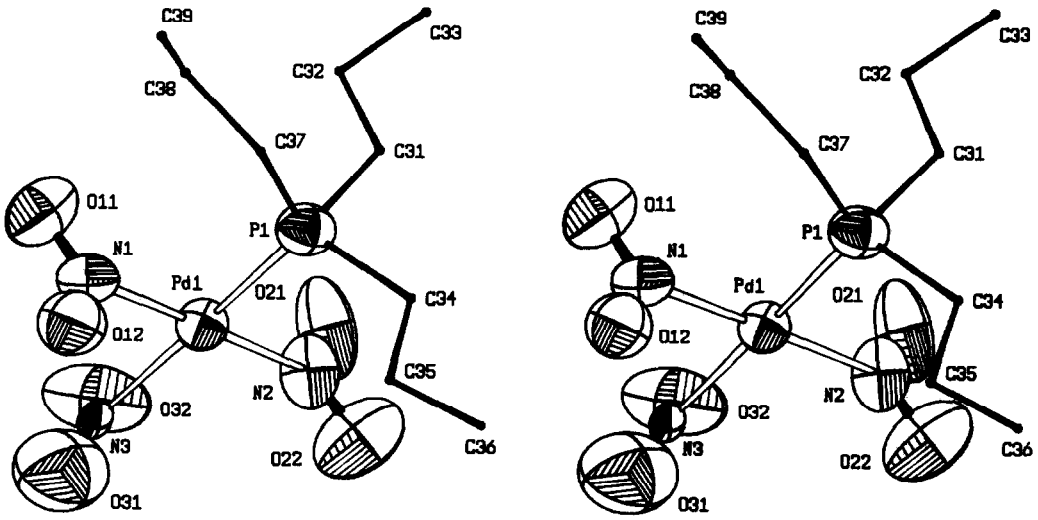

Fig. 2. Stereoview of the anion $[Pd(PPr_3^n)(NO_2)_3]^-$.

Table 1. Selected bond lengths (Å) and bond angles (°)

	Bond distances (Å)		
Pd—P	2.263(4)	Pd—N2	2.01(1)
Pd—N1	2.01(1)	P—C31	1.82(2)
Pd—N3	2.25(1)	P—C37	1.71(2)
P—C34	1.88(2)	N1—O12	1.21(2)
N1—O11	1.24(2)	N2—O22	1.16(2)
N2—O21	1.26(2)	N3—O32	1.06(2)
N3—O31	1.00(2)	As—C13	1.89(1)
As—C7	1.87(1)	As—C19	1.88(1)
	Angles (°)		
N2—Pd—N3	89.5(4)	N1—Pd—N2	178.3(5)
N1—Pd—N3	89.1(4)	P—Pd—N2	89.2(4)
P—Pd—N3	178.3(3)	Pd—P—C37	119.2(8)
P—Pd—N1	92.2(4)	Pd—P—C31	122.5(6)
Pd—P—C34	112.6(6)	C31—P—C37	110(1)
C34—P—C37	103.3(9)	Pd—N1—O12	119(1)
C31—P—C34	81.6(8)	O11—N1—O12	122(1)
Pd—N1—O11	119(1)	Pd—N2—O21	118(1)
Pd—N2—O22	124(1)	Pd—N3—O32	115(1)
O21—N2—O22	118(1)	O31—N3—O32	126(1)
Pd—N3—O31	117(1)	N3—O32—O31	26(1)
N3—O31—O32	27.7(9)	C31—C32—C33	109(1)
P—C31—C32	109(1)	C34—C35—C36	109(1)
P—C34—C35	110(1)	C37—C38—C39	109(1)
P—C37—C38	109(1)	C7—As—C19	109.3(6)
C13—As—C19	109.0(6)	C7—As—C13	109.8(6)

electronic spectrum of the complex changes on changing concentration. In the presence of free NO_2^-, which should suppress solvolysis, the spectrum of the complex in CH_3CN, MeOH, DMF, etc. overlaps with that recorded, under the same experimental conditions, in poorly coordinating media such as CH_2Cl_2 or $CHCl_3$.

The three nitro groups coordinated to palladium are easily replaced by the common nucleophiles. The process, which is rapid at room temperature, occurs in three observable steps. We have followed, by stopped-flow technique, the kinetics of substitution, by piperidine, of the first nitro group in the title compound and in *trans*-$[Pd(PPr_3^n)(NO_2)_2Cl][As(C_6H_5)_4]$ in dichloromethane at 25°C. As expected on the basis of the large *trans* effect of phosphine,[12] the first leaving group is that coordinated in the *trans* position with respect to PPr_3^n; this can be easily shown by the identity of the electronic spectra after reaction with piperidine, in a ratio 1 : 1, under the same experimental conditions (1) and (2):

$$[Pd(PPr_3^n)(NO_2)_3]^- + pip \rightarrow trans-[Pd(PPr_3^n)(NO_2)_2(pip)] + NO_2^-, \quad (1)$$

$$trans-[Pd(PPr_3^n)(NO_2)_2Cl]^- + pip \rightarrow trans-[Pd(PPr_3^n)(NO_2)_2(pip)] + Cl^-. \quad (2)$$

The kinetics of these reactions, under pseudo-first-order conditions with respect to the complex, obey the simple rate law

$$k_{obs.} = k_2[\text{piperidine}]. \quad (3)$$

The k_2 values (Fig. 3) are $(72.8 \pm 1.1) \times 10^3$ dm^3 mol^{-1} s^{-1} and $(36.8 \pm 2.0) \times 10^3$ dm^3 mol^{-1} s^{-1}, respectively. The lability of NO_2^-, larger than that of Cl^-, is abnormal; usually, in fact, chloride is a much better leaving group than nitrite.[13] These findings could be directly related to the structure

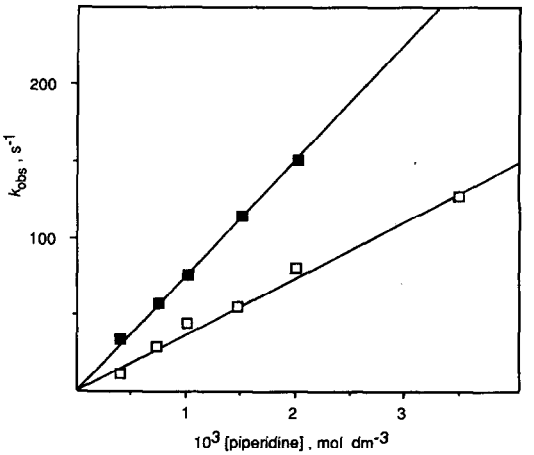

Fig. 3. Plot of $k_{obs.}$ (s^{-1}) vs [piperidine] (mol dm^{-3}) for reaction (1) ■ and reaction (2) □.

Table 2. Values of observed rate constants, $k_{obs.}$ (s^{-1}), for reaction of $[Pd(PPr_3'')(NO_2)_2X][As(C_6H_5)_4]$ (X = NO_2 or Cl) with piperidine in CH_2Cl_2 at 25°C

[Piperidine] (mol dm^{-3})	$k_{obs.}$ (NO_2) (s^{-1})	$k_{obs.}$ (Cl) (s^{-1})
4×10^{-4}	35.1	11.3
7.5×10^{-4}	57.5	30.2
10×10^{-4}	77.8	45.5
15×10^{-4}	115.0	56.7
20×10^{-4}	150.1	80.9
35×10^{-4}		127.5

of $[Pd(PPr_3'')(NO_2)_3][As(C_6H_5)_4]$ if we assume that also in solution the nitro group *trans* to phosphine is very weakly bound to palladium. Alternatively, the enhanced lability of NO_2 with respect to Cl could be accounted for assuming that in solution, NO_2 is bonded through oxygen. Nitro–nitrito isomerization is in fact conceivable taking into account that one of the oxygen atoms of the nitro group *trans* to phosphine interact to some extent with palladium already in the solid state. It is unfortunate that spectra in solution were of bad quality so that the bonding mode of NO_2 could not be established. Synthetic work is in progress in order to study to what extent the bond lengthening and the lability enhancement of NO_2 *trans* to palladium may be related to the presence of the adjacent nitro groups.

REFERENCES

1. G. Bruno, S. Campagna, M. Cusumano, A. Giannetto and V. Ricevuto, *Polyhedron* 1989, **8**, 161.
2. D. T. Cromer and J. B. Mann, *Acta Cryst.* 1968, **A24**, 321.
3. R. F. Stewart, *J. Chem. Phys.* 1970, **53**, 3175.
4. *International Tables for X-ray Crystallography*, Vol. IV. Kynoch Press, Birmingham (1974).
5. G. M. Sheldrick, *System of Computing Programs*, University of Cambridge (1976).
6. M. Nardelli, *Comput. Chem.* 1983, **7**, 95.
7. M. Hitchman and G. L. Rowbottom, *Coord. Chem. Rev.* 1982, **42**, 55.
8. G. Bombieri, G. Bruno, M. Cusumano, G. Guglielmo and V. Ricevuto, *Polyhedron* 1985, **4**, 1365.
9. L. M. Tack, J. L. Hubbard, G. R. Kriek, J. Dubrawski and J. H. Enemark, *Cryst. Struct. Commun.* 1981, **10**, 385.
10. G. Bombieri, G. Bruno, M. Cusumano and G. Guglielmo, *Acta Cryst.* 1984, **C40**, 409.
11. N. Bresciani Pahor, M. Calligaris and L. Randaccio, *J. Chem. Soc., Dalton Trans.* 1976, 725.
12. T. P. Cheesman, A. L. Odell and H. A. Raethel, *Chem. Commun.* 1968, 1496.
13. L. Cattalini, in *Reaction Mechanism in Inorganic Chemistry* M. T. P. Internat. Rev. Sci., Ser. 1, Vol. 9 (Edited by M. L. Tobe). Butterworths, London (1972); L. Cattalini, M. Cusumano, V. Ricevuto and M. Trozzi, *J. Chem. Soc., Dalton Trans.* 1975, 771.

Polyhedron Vol. 9, No. 21, pp. 2597–2602, 1990
Printed in Great Britain

0277–5387/90 $3.00+.00
© 1990 Pergamon Press plc

EPR INVESTIGATIONS ON BIS(DITHIOPHOSPHINATO)COPPER(II) COMPLEXES MAGNETICALLY DILUTED IN THE CORRESPONDING NICKEL(II) SINGLE CRYSTALS AND X-RAY CRYSTAL STRUCTURE OF BIS(DI-n-PROPYLDITHIOPHOSPHINATO)NICKEL(II)

N. D. YORDANOV*

Institute of Kinetics and Catalysis, Bulgarian Academy of Sciences, 1113 Sofia, Bulgaria

and

G. GOCHEV **and** O. ANGELOVA

Chemistry Department, University of Sofia, 1126 Sofia, Bulgaria

and

J. MACICEK

Institute of Applied Mineralogy, Bulgarian Academy of Sciences, 1000 Sofia, Bulgaria

(*Received* 15 *December* 1989; *accepted* 21 *June* 1990)

Abstract—Bis(diethyldithiophosphinato)nickel(II), $[(C_2H_5)_2PS_2]_2Ni$ and bis(di-n-propyl dithiophosphinato)nickel(II), $[(n\text{-}C_3H_7)_2PS_2]_2Ni$, single crystals doped with the corresponding copper(II) complexes have been prepared and studied by EPR spectroscopy. The components of the **g**-tensor, ^{63}Cu hyperfine coupling tensor and ^{63}Cu nuclear quadrupole coupling tensor have been determined. An X-ray crystal structure determination of bis(di-n-propyldithiophosphinato)nickel(II) shows the nickel atom to lie at a centre of symmetry, coordinated by four sulphur atoms at 2.220(4) and 2.230(3) Å.

In the analysis of EPR data for single-crystal systems special attention is paid to the cases where the various tensor axes do not coincide. For transition metal ions in low symmetry sites the anisotropy of the various tensors, in general, is large and any non-coincidence of the tensor axes can lead to large off-diagonal matrix elements. For this reason the first-order treatment gives only qualitative agreement with experiment. Moreover, in the first-order treatment the nuclear quadrupole coupling has no contribution to the allowed transitions. Independently of this, however, some authors use powdered spectra to calculate the quadrupole interaction.[1]

In this paper the results obtained from single-crystal EPR spectra of $^{63}Cu^{II}$ dithiophosphinato complexes, $[Cu(dtph)_2]$ (**I**), magnetically diluted in the corresponding $Ni(R_2\text{-}dtph)_2$ host lattices, are presented and the structural data are compared with those available from X-ray crystal analysis.

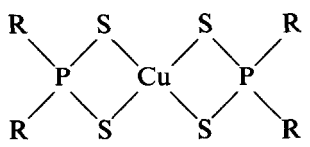

R = Et, Pr^n

(I)

The molecular and crystal structure of $Ni(Me_2\text{-}dtph)_2$[2a] and $Ni(Et_2\text{-}dtph)_2$[2b] are known, while the structure of $Ni(Pr^n{}_2\text{-}dtph)_2$, obtained by X-ray analysis, is reported in the present paper.

* Author to whom correspondence should be addressed.

EXPERIMENTAL

Preparation of the complexes

$(Et_2$-dtph)Na and $(Pr^n{}_2$-dtph)Na have been synthesized according to the methods described.[3] $Ni(R_2$-dtph$)_2$ complexes (R = Et or n-Pr) have been obtained by precipitation of an aqueous solution of the corresponding $Na(R_2$-dtph) and $NiCl_2$. The complexes thus obtained have been recrystallized twice from $CHCl_3$. ^{63}CuO (AERE, Harwell) has been transformed to $^{63}CuCl_2$ through dissolution in HCl followed by evaporation to dryness.

$^{63}Cu/Ni(dtph)_2$ complexes have been prepared by exchange of about 1% of Ni^{II} with $^{63}Cu^{II}$ in $CHCl_3$–water solution, followed by evaporation of the organic phase. The single crystals have been obtained from a chloroform–n-heptane (1 : 1 v/v) solution of $^{63}Cu/Ni(dtph)_2$ by slow evaporation in an open beaker.

EPR measurement and refinement

The single-crystal EPR spectra have been recorded on a Bruker ER 420 X-band spectrometer at room temperature. The microwave frequency has been measured by a Systron–Donner Model 6016 frequency counter with an accuracy of about 50 kHz. The magnetic field has been determined with an accuracy of about 0.5 G by means of a NMR gaussmeter B-H 12. For the orientation of the single crystals in the magnetic field a two-circle goniometer GO-2 has been employed.

The EPR spectra have been recorded by rotation of the single crystals about three mutually perpendicular axes (defining an arbitrary Cartesian reference frame) every 5 or 10°.

The set of experimentally obtained EPR spectra can be described by the spin hamiltonian

$$\mathcal{H} = \beta\vec{H}\cdot\mathbf{g}\cdot\vec{S}+\vec{S}\cdot\mathbf{A}\cdot\vec{I}+\vec{I}\cdot\mathbf{P}\cdot\vec{I}-g_n\beta_n\vec{H}\cdot\vec{I},$$

the various terms in which have their usual meaning. The choice of this spin hamiltonian is based on the facts that the four hyperfine lines are not equally spaced (this inequality varies in a complex way from one spectrum to another) and that in some directions so-called "forbidden" lines appear. To find the components of the various tensors in the chosen reference frame, the method described[4] has been used where perturbation corrections to the energy levels up to second-order are taken into account. In the present study, however, the quantity

$$S = \left\{\frac{1}{(2I+1)n}\sum_{i=1}^{n}\sum_{m+-I}^{I}[h\nu_i - f(i,m,p_1,p_2,\ldots)]^2\right\}^{1/2},$$

where $I = 3/2$ and i runs over all the spectra, was minimized, the parameters p_α (the components of the tensors) being varied simultaneously by means of a modified, simplex procedure.[5] Since this procedure is relatively slow, starting values for the components of the **g** and **A** tensors were taken as those obtained from the first-order treamtent. A value for $S = 0.5\times10^{-4}$ cm^{-1} (which is comparable with the experimental error) has been chosen for goodness of fit. After satisfactory convergence, the **g**, **A** and **P** tensors have been diagonalized and the principal values, as well as the principal directions of them, have been obtained.

Crystallographic study

A prismatically-shaped crystal of $Ni(Pr^n{}_2$-dtph$)_2$ with approximate dimensions, $0.12\times0.08\times0.10$ mm, has been analysed on a computer-controlled Enraf–Nonius CAD4 diffractometer with graphite-monochromatized Mo-K_α radiation. The diffraction data have been collected at a temperature of 292 K, using the ω–2θ scan technique.

The crystals of bis(di-n-propyldithiophosphinato) nickel(II) have been found to be monoclinic, space group $P2_1/n$, $a = 8.165(2)$, $b = 8.706(1)$, $c = 14.935(3)$ Å, $\beta = 103.76(2)°$, $V = 1031.1(7)$ Å^3, $Z = 2$, $D_c = 2.714$ g cm^{-3}, μ(Mo-K_α) = 29.5 cm^{-1}, $F(000) = 888$, $R = 0.053$ for 649 observed reflections with $I > 3\sigma(I)$.

Accurate cell constants have been obtained from a least-squares refinement of the setting angles of 22 reflections in the range $14.05 < \theta < 15.53°$.

A total of 2972 reflections have been collected in the range $\sin\theta/\lambda < 0.527$ (h: −8 to 8, k: −9 to 9, l: −15 to 15) with a zigzag scanning mode. The intensities of equivalent reflections have been averaged. From 1374 unique reflections, only $N_o = 649$ reflections with $I > 3\sigma(I)$ have been used in further calculations.

The structure has been solved by the heavy-atom method. The nickel atom has been located from the three-dimensional Patterson map. The positions of the remaining non-hydrogen atoms have been obtained from subsequent Fourier and difference-Fourier syntheses. The structure has been refined by a geometrically restrained (on P—C and C—C bonds) least-squares fitting, where the function $\Sigma w(|F_o|-|F_c|)^2$ has been minimized with weights w defined as $w = 4F_o^2/[\sigma^2(F_o)]^2$. The highest positive peak in the final difference Fourier map was 2.19 e Å^{-3}. An empirical extinction correction of the form $F_{(corr)} = F/(1+gI)$ with $g = 0.253\times10^{-6}$ has been applied. Atomic scattering factors and anomalous dispersion coefficients for neutral atoms have been taken from *International Tables* (1974). Positional

and thermal parameters have been deposited along with tables of F_o/F_c values.

All calculations have been carried out on a PDP 11/44M computer with a locally modified SDP/PDP V3.0 crystallographic package.

RESULTS AND DISCUSSION

EPR study

Typical EPR spectra of ^{63}Cu/Ni(Pr^n$_2$-dtph)$_2$ and ^{63}Cu/Ni(Et$_2$-dtph)$_2$ single crystals for two different, arbitrarily chosen orientations with respect to the magnetic field are shown in Fig. 1(a) and (b). The EPR spectrum of ^{63}Cu/Ni(Pr^n$_2$-dtph)$_2$ [Fig. 1(a)] is based upon two quartets which shows that the copper(II) occupies two different sites in the crystal, whereas the EPR spectrum of ^{63}Cu/Ni(Et$_2$-dtph)$_2$ [Fig. 1(b)] corresponds only to one site. Each line of a given quartet is further split into three lines (with relative intensities 1:2:1) due to the interaction of the copper(II) unpaired electron with two equivalent ^{31}P nuclei ($I = 1/2$). This superhyperfine splitting is isotropic within experimental error and is of the order of 5.5 G.

The experimentally obtained EPR spectra are in agreement with the crystallographic data for the crystals of Ni(Et$_2$-dtph)$_2$[2b] and Ni(Pr^n$_2$-dtph)$_2$ (reported in the present paper). The number of molecules per unit cell is equal for both compounds ($Z = 2$), but their mutual orientation is different. In accordance with the space group symmetry and atomic coordinates of these compounds, the two molecules in the case of Ni(Et$_2$-dtph)$_2$ are magnetically equivalent, whereas in the case of Ni(Pr^n$_2$-dtph)$_2$ they differ.

The results obtained after digital processing of the EPR data are shown in Tables 1 and 2. In Table 1 the principal values of the **g**, **A** and **P** tensors are presented, and in Table 2 the angles that determine the mutual orientations of the **g** and **A** tensors.

It is seen from Table 2 that the principal directions of the **g** and **A** tensors for ^{63}Cu/Ni(Et$_2$-dtph)$_2$ nearly coincide to within the angle setting error ($\approx 1°$).

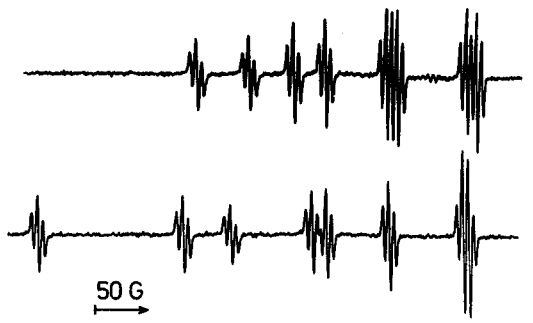

Fig. 1(a). Single crystal EPR spectra of ^{63}Cu/Ni(Pr^n$_2$-dtph)$_2$ for two different arbitrarily chosen orientations of the magnetic field.

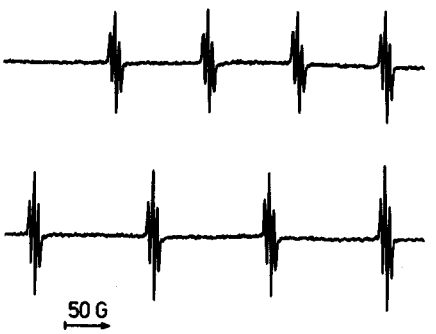

Fig. 1(b). Single crystal EPR spectra of ^{63}Cu/Ni(Et$_2$-dtph)$_2$ for two different arbitrarily chosen orientations of the magnetic field.

For the ^{63}Cu/Ni(Pr^n$_2$-dtph)$_2$ complex, the principal values of the **g**, **A** and **P** tensors (Table 1) for the two different sites are equal (if we keep in mind that $|\Delta g_i| \approx 5 \times 10^{-4}$; $|\Delta A_i|$, $|\Delta P_i| \approx 0.5 \times 10^{-4}$ cm^{-1}). It is seen from Table 2, however, that only the directions of g_3 and A_3 coincide, whereas the directions of A_1 and A_2 are rotated in the plane (g_1, g_2) to an angle of about 10° but in a different direction for each site. One possible reason for this is the fact that the **g** and **A** tensors are close to axial symmetry and consequently the error in the determination of the principal directions in a plane

Table 1. Principal values of the **g**, **A** and **P** tensors for ^{63}Cu/Ni(Pr^n$_2$-dtph)$_2$ and ^{63}Cu/Ni(Et$_2$-dtph)$_2$ (A_i and P_i are in units of 10^{-4} cm^{-1})

	Complex	g_1	g_2	g_3	A_1	A_2	A_3	P_1	P_2	P_3
Pr^n	Site 1	2.0230	2.0259	2.1082	27.7	29.9	145.0	1.8	−1.9	0.1
	Site 2	2.0223	2.0255	2.1080	28.5	30.5	145.6	2.1	−2.4	0.3
Et		2.0226	2.0246	2.1066	26.6	28.4	150.0	1.2	2.4	−3.6

Table 2. Angles between the principal directions of the g and A tensors for ^{63}Cu/Ni(Pr^n$_2$-dtph)$_2$ and ^{63}Cu/Ni(Et$_2$-dtph)$_2$

Complex		A_1	A_2	A_3	Site 2 g_1	Site 2 g_2	Site 2 g_3
Pr^n Site 1	g_1	11	101	89	79	85	168
	g_2	79	11	90	85	8	84
	g_3	91	90	1	12	96	79
Site 2	g_1	13	77	90			
	g_2	103	13	90			
	g_3	90	90	0			
Et	g_1	2	88	90			
	g_2	92	2	90			
	g_3	90	90	0			

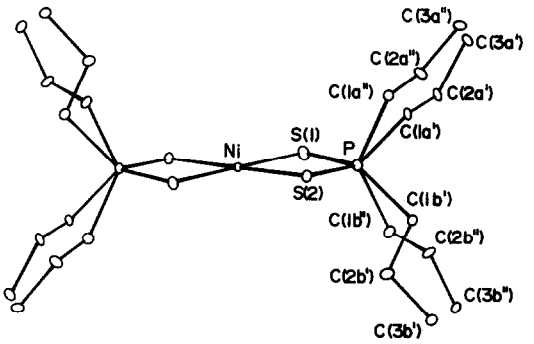

Fig. 2. The molecule of Ni(Pr^n$_2$-dtph)$_2$ along with the atom labelling scheme.

perpendicular to the principal direction, corresponding to $g_3(A_3)$, is relatively large.

It is assumed that the directions of g_3 and A_3 are perpendicular to the molecular plane (CuS_4 plane). It is seen from Table 2 that the directions of g_3 for the two sites of ^{63}Cu/Ni(Pr^n$_2$-dtph)$_2$ make an angle of 79°. The angle between the molecular-plane normals calculated from the crystallographic data is about 77°, which is very close to the calculated value from the EPR data. This result suggests that the copper(II) complex takes the structure of the host lattice without distorting it. In Table 1 the principal values of the nuclear quadrupole coupling tensor, **P**, are also presented. In magnitude they correspond to the values obtained by other authors for analogous complexes of ^{63}Cu^{II}. It is well known, however, that the determination of the nuclear quadrupole coupling tensor from EPR spectra is not very accurate. As a confirmation of this, Table 3 presents the results obtained by various research groups for the complexes ^{63}Cu(acac)$_2$ as well as ^{63}Cu(dtc)$_2$ (which are analogous to the complexes studied here). The differences in the results for one and the same complex are most probably due to the large relative error in deriving the components of the nuclear quadrupole coupling tensor. Nevertheless, the second-order terms due to the nuclear quadrupole coupling and nuclear hyperfine interaction (the latter vary from 0 to about 5×10^{-4} cm^{-1} depending on the direction of the magnetic field) give a satisfactory explanation of the behaviour of the distances between the hyperfine resonance lines. The magnitude of the difference between the calculated and experimentally obtained values of the magnetic field, at which the hyperfine resonance lines appear, is seldom greater than 1 G and in most cases is less than 0.8 G, i.e. within the experimental error.

Crystallographic study

The molecule of Ni(Pr^n$_2$-dtph)$_2$ along with the atom labelling scheme is shown in Fig. 2. The packing of the molecules within the unit cell is shown in Fig. 3, and selected bond lengths and angles are listed in Table 4.

The nickel atom lies at a centre of symmetry and

Table 3. Principal values of the nuclear quadrupole coupling tensor for ^{63}Cu(dtc)$_2$ and ^{63}Cu(acac)$_2$ obtained by various research groups (in units of 10^{-4} cm^{-1})

Complex	P_1	P_2	P_3	Method	Reference
Cu(dtc)$_2$ in py	−2.4	−2.6	5.0	Frozen solution–EPR	1
Cu/Zn(Et$_2$-dtc)$_2$	−1.6	−0.5	2.1	Single crystal–EPR	4
Cu/Pd(acac)$_2$	1.45	3.39	−5.11	Single crystal–EPR	6
	−0.68	−1.54	2.45	Single crystal–ENDOR	7
	−2.3	−2.3	4.6	Single crystal–EPR	8

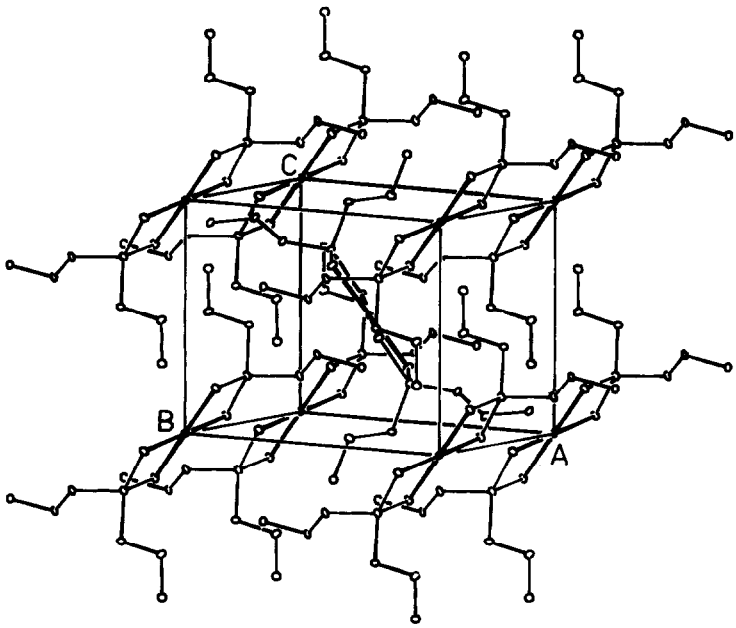

Fig. 3. The packing of the $Ni(Pr^n_2\text{-dtph})_2$ molecules within the unit cell.

is coordinated by four sulphur atoms at 2.220(4) and 2.230(3) Å. The intramolecular Ni···P distance is 2.838(4) Å. The shortest Ni···Ni distances are well "spatially balanced": 8.165(*a*-axis), 8.706(*b*-axis) and 8.768 Å (a half of the unit-cell body diagonal). In a radius of 4.0 Å the nickel atom has intermolecular contacts only with the disordered methyl-carbon atoms C(3a″) (3.59(2) Å) and C(3a′) (4.00(2) Å). The phosphorus atom deviates from the NiS_4 plane by 0.35 Å and has a highly distorted tetrahedral configuration with angle variations from 90(2) to 132(1)°. The average P—S distance of 1.989(5) Å is comparable with the same distances found in bis(dimethyldithiophosphinato) nickel(II) (2.01(1) Å)[2a] and bis(diethyldithiophosphinato)nickel(II) (2.00(1) Å).[2b] A perceptible variation of P—C bond lengths (1.74–1.92 Å) from their average value of 1.85 Å is observed. The disordered propyl groups (Fig. 2) take up predominantly two sets of positions, both with 50% occupancy. The discrete $Ni(Pr^n_2\text{-dtph})_2$ molecules are packed in a zigzag motif and are joined by a van der

Table 4. Selected bond distances (Å) and angles (°) for $Ni(Pr^n_2\text{-dtph})_2$ (standard deviations are given in parentheses)

Ni—S(1)	2.220(4)	P—C(1a′)	1.74(2)	P—C(1a″)	1.90(2)
Ni—S(2)	2.230(3)	P—C(1b′)	1.86(2)	P—C(1b″)	1.92(2)
S(1)—P	1.978(5)	C(1a′)—C(2a′)	1.40(2)	C(1a″)—C(2a″)	1.39(4)
S(2)—P	1.999(6)	C(2a′)—C(3a′)	1.56(3)	C(2a″)—C(3a″)	1.52(3)
		C(1b′)—C(2b′)	1.46(3)	C(1b″)—C(2b″)	1.50(3)
		C(2b′)—C(3b′)	1.57(3)	C(2b″)—C(3b″)	1.56(3)
S(1)—Ni—S(2)	88.4(1)	Ni—S(2)—P	84.1(2)	P—C(1a′)—C(2a′)	120(2)
S(1)—Ni—S(2′)	91.6(1)	S(1)—P—S(2)	102.5(2)	C(1a′)—C(2a′)—C(3a′)	114(2)
Ni—S(1)—P	84.8(2)	S(1)—P—C(1a′)	115.0(7)	P—C(1b′)—C(2b′)	110(2)
		S(1)—P—C(1b′)	125.5(9)	C(1b′)—C(2b′)—C(3b′)	113(3)
		S(2)—P—C(1a′)	114.5(9)	C(1a″)—P—C(1b″)	139(1)
		S(2)—P—C(1b′)	109.4(9)	C(1a″)—C(2a″)—C(3a″)	121(3)
		C(1a′)—P—C(1b′)	90(2)	C(1b″)—C(2b″)—C(3b″)	110(2)

Waals' interaction. The only intermolecular distance shorter than 3.5 Å is C(2a′)···C(2a′) (3.33(2) Å).

Acknowledgements—The financial support of the Committee of Sciences and High Education (Project 538) and the Bulgarian Academy of Sciences are gratefully acknowledged.

REFERENCES

1. D. L. Liczwek, R. L. Belford, J. R. Pilbrow and J. S. Hyde, *J. Phys. Chem.* 1983, **87**, 2509.
2. (a) P. E. Jones, G. B. Ansell and L. Katz, *J. Chem. Soc., Chem. Commun.* 1968, 78 ; *Acta Cryst.* 1969, **B25**, 1939 ; (b) P. S. Shelty and Q. Fernando, *Acta Cryst.* 1969, **B25**, 1294.
3. W. A. Higgins, P. W. Vogel and W. G. Craig, *J. Am. Chem. Soc.* 1955, **77**, 1864 ; W. Kuchen, K. Stvolenberg and J. Metter, *Chem. Ber.* 1963, **96**, 1733.
4. C. P. Keijzers, Thesis, Nijmegen (1974).
5. S. N. Deming and S. L. Morgan, *Analyt. Chem.* 1973, **45**, 278A ; J. W. Copper, *Introduction to Pascal for Scientists.* Wiley Interscience, New York (1981).
6. G. J. Baker and J. B. Raynor, *J. Chem. Soc., Dalton Trans.* 1986, 2663.
7. S. Kita, M. Hashimoto and M. Iwaizumi, *J. Magn. Res.* 1982, **46**, 361.
8. A. H. Maki and B. R. McGarvey, *J. Chem. Phys.* 1958, **29**, 31.

Polyhedron Vol. 9, No. 21, pp. 2603–2608, 1990
Printed in Great Britain

0277–5387/90 $3.00+.00
© 1990 Pergamon Press plc

SYNTHESIS AND CHARACTERIZATION OF NOVEL TRIPLY-BRIDGED BINUCLEAR COPPER(I) COMPLEXES CONTAINING [3,6-BIS(3,5-DIMETHYLPYRAZOL-1-YL)PYRIDAZINE] (PPDMe) AS A TETRADENTATE BRIDGING LIGAND: X-RAY CRYSTAL STRUCTURE OF $[Cu_2(\mu\text{-DPPM})_2(\mu\text{-PPDMe})][BF_4]_2$ [DPPM = BIS(DIPHENYLPHOSPHINO)METHANE]

M. PILAR GAMASA, JOSE GIMENO,* ELENA LASTRA and JUAN M. RUBIO GONZALEZ

Departamento de Química Organometálica, Facultad de Química, Universidad de Oviedo, 33071 Oviedo, Spain

and

SANTIAGO GARCIA-GRANDA

Departamento de Química Física y Analítica, Facultad de Química, Universidad de Oviedo, 33071 Oviedo, Spain

(*Received* 29 *March* 1990; *accepted* 21 *June* 1990)

Abstract—Triply-bridged cationic binuclear copper(I) complexes $[Cu_2(\mu\text{-L—L})_2(\mu\text{-PPDMe})]^{2+}$, PPDMe = [3,6-bis(3,5-dimethylpyrazol-1-yl)pyridazine], have been prepared. Treatment in dichloromethane at room temperature of $[Cu_2(\mu\text{-L—L})_2(CH_3CN)_2][BF_4]_2$ with PPDMe in a 1:1 molar ratio gives $[Cu_2(\mu\text{-L—L})_2(\mu\text{-PPDMe})][BF_4]_2$, L—L = bis(diphenylphosphino)methane (dppm) (**1**), 1,1-bis(diphenylphosphino)ethane(mdppm) (**2**) and 2-(diphenylphosphino)pyridine (dppy) (**3**). The crystal structure of **1** has been determined by X-ray diffraction methods. Crystals of **1**, containing dichloromethane molecules of crystallization, are monoclinic, space group $C2/c$, with $Z = 8$ in a unit cell of dimensions $a = 38.100(2)$, $b = 12.7888(7)$, $c = 28.55(1)$ Å, $\beta = 91.79(4)°$. The structure was refined to $R = 0.115$ for 2129 observed reflections, with the tetrafluoroborate anions and the dichloromethane molecules highly disordered. In the binuclear complex **1** the two copper atoms in a distorted tetrahedral arrangement are at a distance of 3.452(7) Å, bridged by two dppm ligands through P atoms and with one PPDMe acting as a dichelate tetradentate ligand through two N pyrazolyl atoms and the two pyridazine N atoms. ^1H and $^{31}P\{^1H\}$ NMR data are discussed.

Binuclear copper(I) and copper(II) complexes form a significant group of derivatives in the coordination chemistry of copper which are currently receiving special attention mainly due to the studies related to the reactivity of dioxygen in biological systems.[1,2] Since it is known[3] that the crystal structure of the active site in deoxyhaemocyanin contains a binuclear copper(I) moiety, particular interest has been focussed on the synthesis of these type of complexes to use as reactivity models for this and other binuclear copper proteins.[4]

We have recently reported[5] a systematic method for the preparation of the scarcely known triple-bridged binuclear copper(I) complexes containing the moieties $Cu_2(\mu\text{-dppm})$ (**A**) and $Cu_2(\mu\text{-dppm})_2$ (**B**), with dppm = bis(diphenylphosphino)methane

* Author to whom correspondence should be addressed.

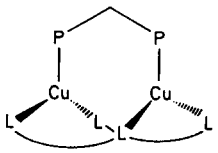

(A)

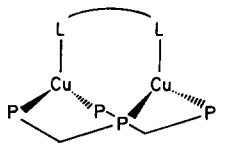

(B)

as bridging ligands. These systems have shown to be excellent precursors for the incorporation of one or two L—L anionic bidentate ligands to give binuclear copper(I) complexes with three mixed eight-membered bimetallic rings (L—L = 6-methylpyridin-2-olate, 3,5-dimethylpyrazolate, 1,3-di-*p*-tolyltriazenide or acetate). We have also prepared cationic binuclear copper(I) triply-bridged complexes containing the $Cu_2(\mu\text{-dppy})_3$ moiety [dppy = 2-(diphenylphosphino)pyridine] (**C**).[6]

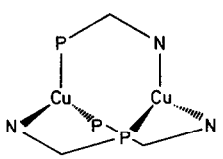

(C)

The present paper reports the preparation of novel triply-bridged cationic binuclear copper(I) complexes $[Cu_2(\mu\text{-L—L})_2(\mu\text{-PPDMe})][BF_4]_2$, L—L = bis(diphenylphosphino)methane (dppm) (**1**), 1,1-bis(diphenylphosphino)ethane (mdppm) (**2**), 2-(diphenylphosphino)pyridine (dppy) (**3**), containing

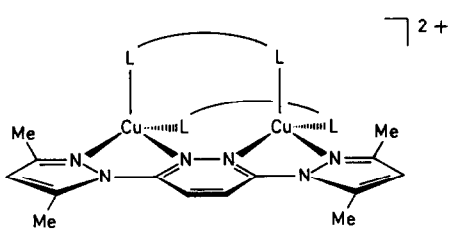

L-L = dppm (1), mdppm (2), dppy (3)

3,6-bis(3,5-dimethylpyrazol-1-yl)pyridazine (PPD Me) as a tetradentate bridging group. The X-ray single crystal structure determination of **1** shows the two copper atoms in a distorted tetrahedral arrangement held at a distance of 3.452(7) Å by three bridging ligands, two dppm ligands and one PPDMe acting as a dichelating tetradentate ligand. These complexes can be related to a series of binuclear copper(II) complexes prepared by Thomson *et al.* with PPDMe[7] and similar polydentate bridging nitrogen heterocycles[8] of importance as structural/magnetic probes for the binuclear copper active sites in oxyhaemocyanin and enzymes involved in oxidase and oxygenase activity and reversible oxygen uptake.

RESULTS AND DISCUSSION

Synthesis and spectroscopic characterization

Treatment of a solution of $[Cu_2(\mu\text{-L—L})_2(MeCN)_2][BF_4]_2$ in dichloromethane, at room temperature, with an equimolar amount of PPDMe gives a solution from which the binuclear cationic complexes **1–3** can be isolated as tetrafluoroborate salts

$$[Cu_2(\mu\text{-L—L})_2(MeCN)_2]^{2+} + PPDMe \longrightarrow [Cu_2(\mu\text{-L—L})_2(PPDMe)]^{2+} + 2MeCN. \quad (1\text{–}3)$$

All the complexes are air-stable in the solid state and have been characterized by elemental analyses, conductance measurements in solution and ^1H and $^{31}P\{^1H\}$ NMR spectroscopy. Selected data are given in Table 1. In addition, the structure of complex **1** has been determined by X-ray diffraction. Conductance values of the complexes in acetone show that they are 1 : 2 electrolytes and IR spectra (Nujol) exhibit the expected ν(B—F) absorptions (1000–1100 cm^{-1}) in addition to those characteristic of the bridging phosphine ligands and PPDMe (see Experimental).

^1H NMR spectra in CD_2Cl_2 at room temperature (Table 1) exhibit aromatic, methylene (CH_2P_2 and $HCMeP_2$) and methyl signals of the ligands (PPDMe and mdppm), in accord with the proposed binuclear nature of the complexes and the dichelating coordination of PPDMe. The spectrum of complex **1** shows methylene resonances (CH_2P_2) at δ 3.19 ppm as one unresolved triplet or multiplet showing the (ABXX′) or (AA′BB′X_2) spin system with accidental degeneracy of chemical shifts expected for the two sets of chemically inequivalent protons $CH_aH_bP_2$. This is typical of the binuclear complexes containing the $Cu_2(\mu\text{-dppm})_2$ moiety with boat–boat or boat–chair conformations.[5,9] The corresponding proton and methyl resonances of the pyridazine (pydz) and pyrazolyl (pz) groups appear as singlets [δ 8.7 (pydz), 6.01 (pz), 1.61 and 2.77 (Me) ppm], showing that they are chemically equivalent. This is consistent with the proposed symmetrical dichelate bridging system of PPDMe and in agreement with the X-ray structure deter-

Table 1. Analytical,[a] molar conductance[b] and ^{1}H NMR[c] data

Compound	C	N	H	^{1}H NMR	Λ_M
$[Cu_2(\mu\text{-dppm})_2(\mu\text{-PPDMe})][BF_4]_2$ (1)	56.1 (56.1)	5.9 (6.1)	4.4 (4.5)	8.70 (s, 2H, pydz), 7.4–6.6 (m, 40H, PC_6H_5), 6.01 (s, 2H, pz), 3.19 (t, 4H, P_2CH_2) ^2J(P—H) 4 Hz, 2.77 (s, 6H, CH_3), 1.61 (s, 6H, CH_3)	212
$[Cu_2(\mu\text{-mdppm})_2(\mu\text{-PPDMe})][BF_4]_2$ (2)	58.0 (58.0)	5.9 (6.2)	4.9 (4.7)	8.6 (s, 1H, pydz), 8.5 (s, 1H, pydz), 8.0–6.5 (m, 40H, C_6H_5), 5.85 (s, 1H, pz), 5.60 (s, 1H, pz), 3.60 (m, 1H, PCH), 2.71 (s, 6H, CH_3), 2.62 (s, 3H, CH_3), 1.28 (s, 3H, CH_3), 1.07 (m, 3H, $PCCH_3$)	193
$[Cu_2(\mu\text{-dppy})_2(\mu\text{-PPDMe})][BF_4]_2$ (3)	52.8 (52.6)	10.3 (10.2)	4.1 (4.0)	8.78 (m, 1H, pydz), 8.32 (m, 1H, pydz), 8.0–6.8 (m, 28H, C_6H_4N, C_6H_5), 6.27 (s, 2H, pz), 2.70 (s, 6H, CH_3), 2.29 (s, 3H, CH_3), 2.17 (s, 3H, CH_3)	200

[a] Calculated values are given in parentheses.
[b] In acetone solution (5×10^{-4} M) at 20°C (Ω^{-1} cm^2 mol^{-1}).
[c] ^{1}H (32.20 MHz) chemical shifts (δ) in ppm, measured in $CDCl_3$ at ambient temperature; pydz = pyridazine, pz = pyrazol, s = singlet, d = doublet, t = triplet.

mination (see below), although a small deviation of the two pyrazole rings from planarity is observed.

This unsymmetrical arrangement of the pyrazole rings seems to be more effective in complexes **2** and **3** even in solution, since the proton NMR spectra show two different signals for the pyridazine protons and for the 3-methyl pyrazolyl groups (see Table 1), clearly indicating the chemical inequivalence of these groups, probably due to a larger distortion from the planarity of the heterocycle ligand. This apparently does not affect the 5-methyl groups, located at the opposite position with respect to the copper coordination environment, for which the spectra only show one singlet signal.

$^{31}P\{^1H\}$ NMR spectra at room temperature exhibit a single resonance [δ −7.37 (**1**) and 2.09 (**3**) ppm] showing that all phosphorus atoms in each molecule are chemically equivalent. For complex **3** this appears to indicate a "head to tail" configuration of the dppy ligand, which is consistent also with the aforementioned chemical equivalence of the 5-methyl groups.

Description of the crystal structure of $[Cu_2(\mu\text{-dppm})_2(\mu\text{-PPDMe})][BF_4]_2$ (**1**)

The crystal structure of complex **1** consists of binuclear $[Cu_2(\mu\text{-dppm})_2(\mu\text{-PPDMe})]^{2+}$ cations, BF_4^- anions and dichloromethane molecules of crystallization. The structure of the cation together with the atomic numbering scheme is depicted in Fig. 1 and selected bond distances and angles are collected in Table 2. Although the poor quality of the crystals due to their small size, along with the

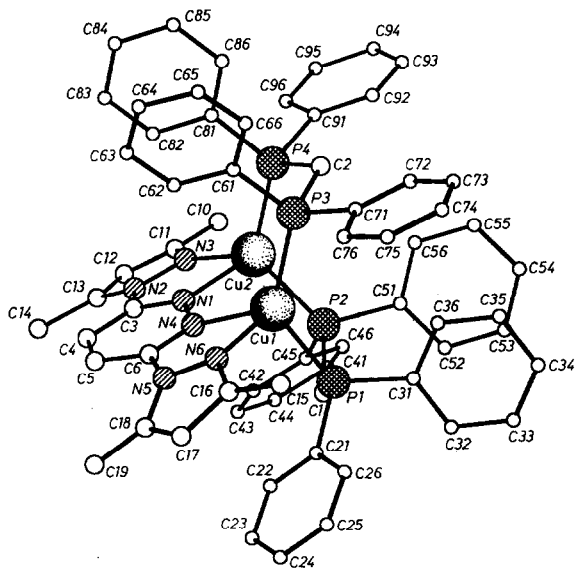

Fig. 1. View of the structure of $[Cu_2(\mu\text{-dppm})_2(\mu\text{-PPDMe})]^{2+}$ (**1**) with the hydrogen atoms omitted for clarity.

Table 2. Selected values of bond lengths (Å) and bond angles (°) (with ESDs)

Cu(1)—Cu(2)	3.452(7)	Cu(1)—P(1)	2.29(1)
Cu(1)—P(3)	2.23(1)	Cu(1)—N(4)	2.08(3)
Cu(1)—N(6)	2.16(3)	Cu(2)—P(2)	2.26(1)
Cu(2)—P(4)	2.26(2)	Cu(2)—N(1)	2.08(3)
Cu(2)—N(3)	2.09(3)	P(1)—C(1)	1.85(4)
P(1)—C(21)	1.78(3)	P(1)—C(31)	1.81(3)
P(2)—C(1)	1.82(4)	P(2)—C(41)	1.86(3)
P(2)—C(51)	1.79(3)	P(3)—C(2)	1.86(4)
P(3)—C(61)	1.81(3)	P(3)—C(71)	1.84(3)
P(4)—C(2)	1.81(4)	P(4)—C(81)	1.81(3)
P(4)—C(91)	1.83(3)	N(1)—N(2)	1.38(4)
N(3)—N(4)	1.35(4)	N(3)—C(3)	1.29(6)
N(4)—C(6)	1.31(5)	N(5)—N(6)	1.39(5)
P(1)—Cu(1)—P(3)	129.5(5)	P(1)—Cu(1)—N(4)	100.9(9)
P(1)—Cu(1)—N(6)	103.(1)	P(3)—Cu(1)—N(4)	117.7(9)
P(3)—Cu(1)—N(6)	117.(1)	N(4)—Cu(1)—N(6)	75.(1)
P(2)—Cu(2)—P(4)	124.8(5)	P(2)—Cu(2)—N(1)	108.(1)
P(2)—Cu(2)—N(3)	106.(1)	P(4)—Cu(2)—N(1)	117.(1)
P(4)—Cu(2)—N(3)	114.(1)	N(1)—Cu(2)—N(3)	75.(1)
Cu(1)—P(1)—C(1)	114.(1)	Cu(1)—P(1)—C(21)	110.(1)
Cu(1)—P(1)—C(31)	122.(1)	C(1)—P(1)—C(21)	104.(2)
C(1)—P(1)—C(31)	102.(2)	C(21)—P(1)—C(31)	102.(1)
Cu(2)—P(2)—C(1)	116.(1)	Cu(2)—P(2)—C(41)	109.(1)
Cu(2)—P(2)—C(51)	121.(1)	C(1)—P(2)—C(41)	99.(2)
C(1)—P(2)—C(51)	106.(2)	C(41)—P(2)—C(51)	103.(1)
Cu(1)—P(3)—C(2)	115.(1)	Cu(1)—P(3)—C(61)	116.(1)
Cu(1)—P(3)—C(71)	111.(1)	C(2)—P(3)—C(61)	105.(2)
C(2)—P(3)—C(71)	102.(2)	C(61)—P(3)—C(71)	105.(1)
Cu(2)—P(4)—C(2)	113.(1)	Cu(2)—P(4)—C(81)	120.(1)
Cu(2)—P(4)—C(91)	113.(1)	C(2)—P(4)—C(81)	104.(2)
C(2)—P(4)—C(91)	102.(2)	C(81)—P(4)—C(91)	102.(1)
P(1)—C(1)—P(2)	116.(2)	P(3)—C(2)—P(4)	115.(2)
Cu(2)—N(1)—N(2)	114.(2)	Cu(2)—N(1)—C(11)	141.(3)
N(2)—N(1)—C(11)	105.(3)	Cu(2)—N(3)—N(4)	120.(2)
Cu(2)—N(3)—C(3)	119.(3)	N(4)—N(3)—C(3)	121.(3)
Cu(1)—N(4)—N(3)	120.(2)	Cu(1)—N(4)—C(6)	119.(2)
N(3)—N(4)—C(6)	120.(3)	Cu(1)—N(6)—N(5)	111.(2)
Cu(1)—N(6)—C(16)	133.(3)	N(5)—N(6)—C(16)	111.(3)

high disorder of the tetrafluoroborate anions and the dichloromethane molecules of crystallization, led to a rather high value of R (0.115), structural information of chemical significance can be obtained. In the binuclear cation the two copper atoms are held at a distance of 3.452(7) Å by three bridging ligands, two dppm ligands bonded through the P atoms and one PPDMe molecule acting as a bridge tetradentate ligand via the nitrogen atoms, N(3) and N(4), of the pyridazine group and the N(1) and N(6) atoms of the pyrazolyl groups. Both copper atoms are in a distorted tetrahedral arrangement determined by two P and two N atoms, with N—Cu—N angles of 75(1)° showing the small bite chelating angle of the PPDMe ligand similar to that found[7] in the binuclear square-planar copper(II) complexes $[Cu_2(\mu\text{-PPDMe})(\mu\text{-OH})Cl_2]^+$ and $[Cu_2(\mu\text{-PPDMe})(\mu\text{-OH})(NO_3)_2(H_2O)_2]^+$ [av. 78.1(2)°]. The coordinated heterocycle is not planar, as is shown by the dihedral angle of the two pyrazolyl groups of 28(2)° and the two different angles of each pyrazolyl group with the pyridazine ring [14(1) and 22(1)°]. This contrasts with the essential planarity shown by the PPDMe ligand in the above mentioned binuclear copper(II) complexes.

The conformations of the two PCuCuP bridges are approximately "eclipsed", which is also shown by $[Cu_2(\mu\text{-dppm})_2(\mu\text{-Mepy-O})]^+$ (Mepy-O = 6-

methylpyridin-2-olate)[5] in which the eight-membered Cu(μ-dppm)$_2$Cu ring adopts a boat–boat conformation. Unexpectedly, the structure of complex **1** shows the corresponding dimetallic ring in an approximately boat–chair conformation. The Cu—P and Cu—N distances [av. 2.26(2) and 2.10(3) Å, respectively] are in the range typical of four-coordinated copper(I) complexes.[6,9]

EXPERIMENTAL

Measurements

C, H and N analyses were carried out with a Perkin–Elmer 240 microanalyser. The IR spectra were recorded over the 4000–600 cm^{-1} range on a Perkin–Elmer 1720X FT spectrometer using Nujol mulls between NaCl plates. Conductivities were measured at room temperature with a Jenway PCM 3 conductimeter. NMR spectra were recorded on a Bruker AC300 at 300 MHz (^{1}H) or 121.5 MHz (^{31}P) using $SiMe_4$ or 85% H_3PO_4 as standard references.

Synthesis

All reactions were performed under dry nitrogen and the solvents were dried by standard methods and distilled under nitrogen before use. PPDMe[10] was synthesized according to the reported improved method.[7] The compounds [Cu$_2$(μ-*L*—L)$_2$(MeCN)$_2$][BF$_4$]$_2$ were prepared as described earlier.[6,9]

Preparation of [Cu$_2$(μ-L—L)$_2$(μ-PPDMe)][BF$_4$]$_2$; L—L = dppm (**1**), mdppm (**2**), dppy (**3**)

To a solution of [Cu$_2$(μ-L—L)$_2$(MeCN)$_2$][BF$_4$]$_2$ (0.5 mmol) in CH_2Cl_2 (40 cm^3), PPDMe (0.134 g, 0.5 mmol) was added and the mixture stirred at room temperature for 12 h. After filtration, a solid was obtained by addition of diethyl ether (10 cm^3) to the partially evaporated solution. Yields (%) and colours: **1**, 80, yellow; **2**, 70, orange; **3**, 50, yellow. IR (Nujol mulls, cm^{-1}): **1**, 1450sh, 1430s, 1372w, 1355w, 1100vs,br, 760w, 735m, 710w, 685m; **2**, 1570m, 1300w, 1055s,br, 760m, 735m, 730w, 700m. ^{31}P{^{1}H} NMR (CD_2Cl_2): **1**, −7.37 ppm; **2**, 2.09 ppm.

Crystallographic data collection and refinement of the structure of [Cu$_2$(μ-dppm)$_2$(μ-PPDMe)][BF$_4$]$_2$·4/3CH_2Cl_2 (**1**)

Crystals of **1** (obtained from a mixture of dichloromethane–di-isopropylether by slow diffusion) were small and due to loss of the solvent of crystallization, especially when they are dried *in vacuo*, they gradually become a powder. A yellow crystal of approximate dimensions 0.03 × 0.1 × 0.4 mm was used for the X-ray analyses and was apparently unchanged during the measurements (no decay of intensities was observed). Crystal data are collected in Table 3. Geometric and intensity data were taken on an Enraf–Nonius CAD-4 automated diffract-

Table 3. Crystal data for [Cu$_2$(μ-dppm)$_2$(μ-PPDMe)][BF$_4$]$_2$·4/3CH_2Cl_2

Formula	$C_{64}H_{60}B_2F_8N_6P_4 \cdot 4/3CH_2Cl_2$
Molecular weight	1451.1
Crystal system	Monoclinic
Space group	*C*2/*c*
Cell dimensions	
a (Å)	38.100(2)
b (Å)	12.7888(7)
c (Å)	28.55(1)
β (°)	91.79(4)
Cell volume (Å^3)	13,905(5)
Z	8
ρ(calc.) (g cm^{-3})	1386
μ (cm^{-1})	8.70
F(000)	5935
Temperature for data collection (°C)	22
h, *k*, *l* range	−45 to 45; 0 to 15; 0 to 33
Total number of reflections	13,459
Number of unique reflections	12,250
Number of reflections used, $I > 2\sigma(I)$	2129
Number of parameters	276
Final *R*	0.115

ometer equipped with graphite-monochromated Mo-K_α ($\lambda = 0.71073$ Å) radiation. All reflections measured are in the range $0 \leqslant \theta \leqslant 25°$. The structure was solved by the heavy atom method localizing the rest of the atoms by cycles of DIRDIF[11] and difference Fourier syntheses. Full-matrix least-squares with anisotropic thermal parameters in the last cycles for the Cu and P atoms and unit weights were used for refinement (SHELX76 program).[12] The hydrogen atoms were included in idealized positions (C—H 1.08 Å) with an overall isotropic temperature factor [final value of $U = 0.11(2)$ Å^2]. The phenyl rings, tetrafluoroborate anions and the dichloromethane molecules were refined as rigid bodies. Initially, the structure was solved in the space group *Cc* and changed to *C*2/*c* after a centre of symmetry was found. The tetrafluoroborate anions and the two dichloromethane molecules of crystallization were highly disordered, each molecule of the solvent having an occupancy factor of approximately 2/3. Atomic scattering factors were taken from *International Tables for X-ray Crystallography*.[13]

Acknowledgements—We thank the Dirección General de Investigación Científica y Técnica (DGICYT) for financial support (Proyecto PB87-912) and the Ministerio de Educación y Ciencia for a fellowship grant (to E.L.).

REFERENCES

1. (a) *Copper Coordination Chemistry: Biochemical Inorganic Perspectives* (Edited by K. D. Karlin and J. Zubieta). Adenine Press, Guiderland, New York (1983); (b) *Biological and Inorganic Copper Chemistry* (Edited by K. D. Karlin and J. Zubieta). Adenine Press, Guiderland, New York (1986); (c) K. D. Karlin and Y. Gultneh, *J. Chem. Educ.* 1985, **62**, 983.
2. K. D. Karlin and Y. Gultneh, *Prog. Inorg. Chem.* 1987, **35**, 219.
3. W. P. J. Gaykema, A. Volbeda and W. G. J. Hol, *J. Molec. Biol.* 1986, **187**, 255.
4. T. N. Sorrell, *Tetrahedron* 1989, **45**, 3.
5. J. Diez, M. P. Gamasa, J. Gimeno, M. Lanfranchi and A. Tiripicchio, *J. Chem. Soc., Dalton Trans.* 1990, 1027.
6. M. P. Gamasa, J. Gimeno, E. Lastra, A. Tiripicchio and M. Tiripicchio Camellini, *J. Chem. Soc., Dalton Trans.* 1989, 1499.
7. L. K. Thomson, T. C. Won, D. B. Murphy, E. J. Gabe, F. L. Lee and Y. Le Page, *Inorg. Chem.* 1985, **24**, 4719.
8. L. K. Thomson, A. W. Hanson and B. S. Ramaswamy, *Inorg. Chem.* 1984, **23**, 2459; S. K. Mandal, T. C. Woon, L. K. Thomson, M. J. Newlands and E. J. Gabe, *Aust. J. Chem.* 1986, **39**, 1007; L. K. Thomson, S. K. Mandal, E. J. Gabe, F. L. Lee and A. W. Addison, *Inorg. Chem.* 1987, **26**, 657; L. K. Thomson, F. L. Lee and E. J. Gabe, *Inorg. Chem.* 1988, **27**, 39.
9. J. Diez, M. P. Gamasa, J. Gimeno, A. Tiripicchio and M. Tiripicchio Camellini, *J. Chem. Soc., Dalton Trans.* 1987, 1275.
10. J. Elguero, R. Jacquier and S. Mondon, *Bull. Soc. Fr.* 1970, 1346.
11. P. T. Beurskens, W. P. Bosman, H. M. Doesburg, T. H. E. M. Van den Hark, P. A. J. Prick, J. H. Noordik, G. Beurskens, R. O. Gould and V. Parthasarathi, in *Conformation in Biology* (Edited by R. Srinivasan and R. H. Sarma), pp. 389–406. Adenine Press, New York (1982).
12. G. M. Sheldrick, SHELX, a Program for Crystal Structure Determination. University of Cambridge, U.K. (1976).
13. *International Tables for X-ray Crystallography*, Vol. IV. Kynoch Press, Birmingham (Present distributor: D. Reidel, Dordrecht) (1974).

Polyhedron Vol. 9, No. 21, pp. 2609–2612, 1990
Printed in Great Britain

0277-5387/90 $3.00+.00
© 1990 Pergamon Press plc

STABILITY CONSTANTS OF DODECAOXOHEXAPHOSPHATE(III) COMPLEXES WITH DIVALENT METAL CATIONS IN POTASSIUM CHLORIDE SOLUTION

TOSHIO NAKASHIMA,* HIDEMI TANAKA and GOHSUKE SUGIHARA

Department of Chemistry, Faculty of Science, Fukuoka University, Nanakuma, Jonan-ku, Fukuoka 814-01, Japan

and

HIROHIKO WAKI

Department of Chemistry, Faculty of Science, Kyushu University, Hakozaki, Higashi-ku, Fukuoka 812, Japan

(*Received* 23 *April* 1990; *accepted* 22 *June* 1990)

Abstract—The stability constants of the dodecaoxohexaphosphate(III) ligand anion with magnesium(II), iron(II), nickel(II) and copper(II) ions were spectrophotometrically determined in aqueous solutions of different ionic strengths (potassium chloride) at room temperature. An optical method based on the measurement of the absorbance ratio at two wavelengths was employed in combination with an equimolar dilution procedure. The logarithmic stability constants of the magnesium, iron(II), nickel and copper complexes with dodecaoxohexaphosphate(III) were, for example at $I = 1$, found to be 5.16, 5.11, 5.39 and 4.76, respectively. Unusual behaviour of the iron(II) complex on the ionic strength dependence of the constant were observed and discussed.

Since the dodecaoxohexaphosphate(III) salt (DOHP) was first synthesized by Blaser and Worms,[1] the structure has been determined by X-ray analysis,[2] and the hydrolytic behaviour[3,4] and the characteristic absorption spectrum[3] have been investigated. For the metal complex formation only the stability constant of the silver complex has been reported.[5] Our preliminary experiments showed that the ring structure characteristic absorption peak at 355 nm shifts to longer wavelengths on complexation with a divalent metal ion. This tendency may be utilized in determining the stability constant. The stability constants of metal–DOHP complexes are in general very large,[6] therefore it may be convenient to use an equimolar metal–ligand dilution method[7] in the analyses. We found that the absorbance measurements at two wavelengths give more accurate results in spite of a considerable overlapping of the spectra of the free ligand and its metal complex.

EXPERIMENTAL

Materials

Potassium, magnesium(II), iron(II), nickel(II) and copper(II) chlorides of commercially available analytical grade were supplied by Kishida Chemicals. DOHP was prepared by the procedure of Blaser and Worms. Double-distilled water was used in all experiments.

Determination of the molar absorption coefficient of DOHP

The molecular weight of prepared DOHP is unknown because of its indefinite hydration

* Author to whom correspondence should be addressed.

number, thus the molar absorption coefficient was determined from the absorbance and the elemental phosphorus analysis of a solution of DOHP sodium salt. The latter was made by decomposition of DOHP with acid into phosphate monomers, followed by absorption measurements using an ordinary molybdenum(VI)–molybdenum(V)[8] method. The molar absorption coefficient of DOHP was evaluated to be 269 ± 0.5 at 355 nm, at room temperature.

Spectral measurements

The pH of a 10–15 cm^3 solution containing potassium chloride and equimolar 5×10^{-3} mmol metal ion and DOHP was adjusted to 7–8.5 in order to minimize hydrolysis of the metal[9] and protonation of DOHP.[10] Then the spectrum of the solution was measured in a 5-cm path quartz cell, using a Spectrophotometer Model U-best 30 (Japan Spectroscopic Co. Ltd). Under these conditions all of DOHP is considered to form the complex with each metal ion due to the high stability of the complex. From the measurements, therefore, the molar absorption coefficients of each metal complex can be determined. This solution was successively diluted with potassium chloride solution of the same concentration to dissociate the complex further. After each dilution a spectral analysis was made. If necessary, the pH was controlled within the pH region by using hydrochloric acid or potassium hydroxide solution. All the calculations were carried out on a personal computer.

RESULTS AND DISCUSSION

When the free ligand DOHP and its one-to-one metal complex are in co-existence, the absorption of the solution is represented by

$$A = \varepsilon^{P}[P]d + \varepsilon^{MP}[MP]d, \tag{1}$$

where ε^{P} and ε^{MP} represent the molar absorption coefficients of free DOHP and its complex, and d represents the cell length. Since the signals from the free ligand and its complex are, in general, not separated, two wavelengths, one of 355 nm for the free ligand peak and the other being an apparent peak wavelength for a ligand–metal complex composite spectrum, were employed. Taking the ratio of absorbances at these two wavelengths,

$$R = \frac{A_{max}}{A_{355}} = \frac{\varepsilon^{P}_{max}[P] + \varepsilon^{MP}_{max}[MP]}{\varepsilon^{P}{}_{355}[P] + \varepsilon^{MP}_{355}[MP]} = \frac{\varepsilon^{P}_{max} + \varepsilon^{MP}_{max}\beta_1[M]}{\varepsilon^{P}_{355} + \varepsilon^{MP}_{355}\beta_1[M]}, \tag{2}$$

where β_1 represents a stability constant

$$\beta_1 = [MP]/[M][P] \tag{3}$$

and P represents the DOHP ligand. When the metal and DOHP are equimolar in the solution, the free metal concentration can be solved as

$$[M] = (-1 + \sqrt{1 + 4\beta_1 C_P})/2\beta_1 \tag{4}$$

where C_P is the total concentration of DOHP,

$$C_P = [P] + [MP]. \tag{5}$$

From eqs (2) and (4) the following equation for analysis of β_1 is derived:

$$\beta_1 = \frac{\left\{1 + \dfrac{2(R\varepsilon^{P}_{355} - \varepsilon^{P}_{max})}{\varepsilon^{MP}_{max} - R\varepsilon^{MP}_{355}}\right\}^2 - 1}{4C_P}. \tag{6}$$

By substituting the molar absorption coefficients and all known quantities into eq. (6), the stability constants can be evaluated.

Since the stability constants of DOHP complexes with divalent metal ions are very high,[6] and an equimolar solution mixture of DOHP and a divalent metal of the appropriate concentrations can give quantitative formation of the one-to-one complexes, the molar absorption coefficient of the complex can be calculated. Figure 1 shows the absorption spectra with molar absorption coefficients for various one-to-one metal complexes of DOHP. As can be seen from the figure, the peak at 355 nm for DOHP shifted by about 10 nm to longer wavelengths on forming the one-to-one complex with a divalent metal ion, while other peaks in the UV region did not shift appreciably. Furthermore, the molar absorption coefficient of the complex at maximum wavelength in general decreased from that of free DOHP. This pronounced change did not occur for iron(II) and alkali metal cations. In the case of calcium, precipitation gradually took place on mixing with DOHP, thus the stability constant of the Ca–DOHP complex could not be determined.

Table 1 provides molar absorption coefficients for DOHP and its complexes at 355 nm, and the individual peak wavelengths. The stability constants calculated from eq. (6), using R values determined after each dilution of equimolar DOHP/metal solution with potassium chloride solution of the same ionic strength, are plotted against the total concentration of DOHP (Fig. 2). The values initially decreased and then became constant at individual ionic strengths. These vlaues in the low concentration range were thus taken as the stability constants of the 1 : 1 metal–DOHP complex, and are tabulated in Table 2.

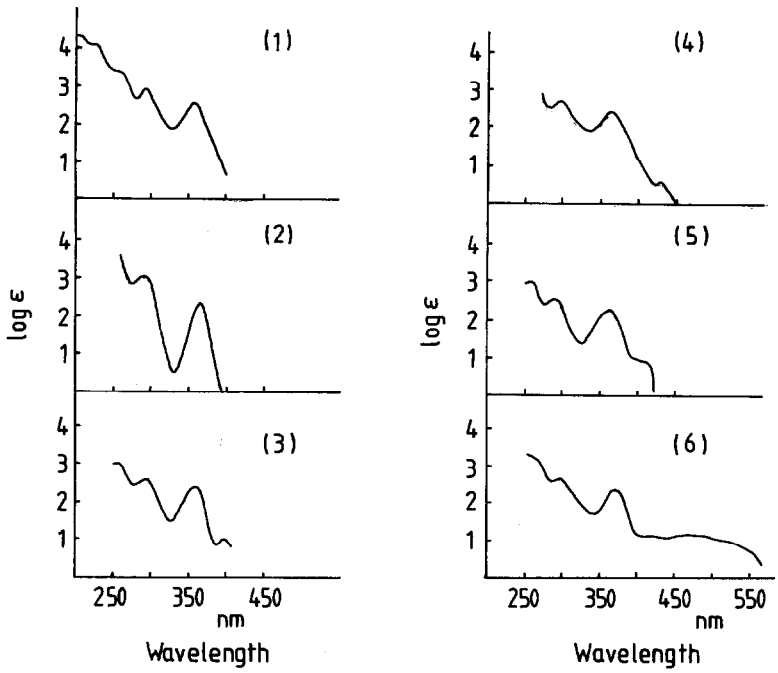

Fig. 1. Absorption spectra of DOHP and equimolar complexes of DOHP with different cations. (1) DOHP only (pH 8.5); (2) Mg–DOHP (pH 8.2); (3) Ca–DOHP (pH 8.3); (4) Fe–DOHP (pH 7.5); (5) Ni–DOHP (pH 8.2); (6) Cu–DOHP (pH 7.0).

To obtain the true stability constants, inert supporting electrolytes such as tetramethylammonium salts may be preferable for the measurements. However, the stability of DOHP complexes is usually too high, therefore dissociation did not appreciably take place even after large dilution. Therefore in our measurements, potassium chloride solution was used to obtain appreciable dissociation by which analyses could be made. Accordingly the values tabulated in Table 2 may be considered to be conditional constants from this point of view. The constants in all cases decreased with increasing ionic strength as expected, although this was not appreciable in the case of the iron(II) complex. Although the plot of $\log \beta_1 \sim \sqrt{I}$ was fairly linear, extrapolation to zero ionic strength may not give a thermodynamic stability constant, because the system may involve ion-pair formation of DOHP with potassium ions.[11] In any case, the order of the stability constant, β_1, was $Fe^{II} < Cu^{II} < Ni \approx Mg$ at lower ionic strengths.

Table 1. Molar absorption coefficients of the complex peak and free DOHP at the longest wavelength

	Wavelength of peak (nm)	ε^{MP}_{max}	ε^{MP}_{355}	ε^{P}_{max}
Mg	365	199	139	97.0
Fe	364	265	219	110
Ni	367	188	112	74.0
Cu	367	205	113	73.5
Ca	361	220	182	150
DOHP	355	—	—	269[a]

[a] Molar absorption coefficient of DOHP only, i.e. (ε^{P}_{355}).

The tendency of decreasing stability constants was almost similar in magnesium, nickel and copper complexes, which may be due to the variation of activity coefficients of each species concerned. Unique behaviour was found for the iron(II) complex, where the stability constants only slightly change in the range studied. The reason may be because the iron(II) complex has a different structure from that of other metal complexes. A free DOHP anion has the possibility to adopt two forms, the chair form or the boat form, although the chair form may be more stable in solution. The complexes with copper, magnesium and nickel probably adopt a boat form so that the four oxygen atoms can bind together to the metal cations. On the other hand, the iron(II) complex probably exists in the chair

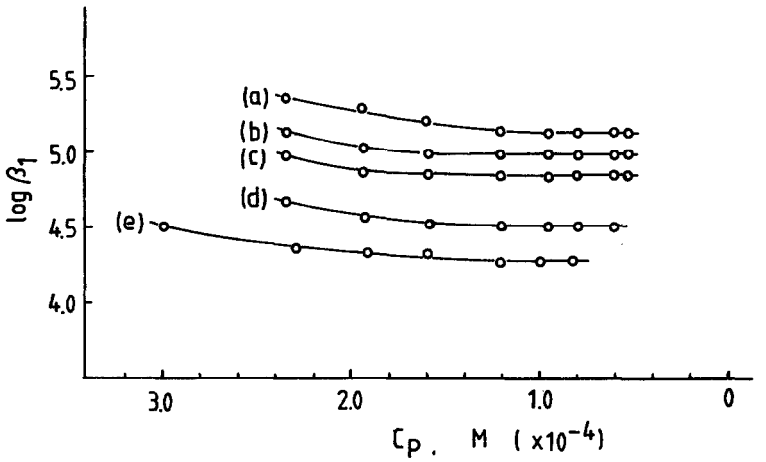

Fig. 2. Stability constants of the Mg–DOHP complex at different dilution stages. (a) $I = 1.0$; (b) $I = 1.5$; (c) $I = 2.0$; (d) $I = 2.5$; (e) $I = 3.0$.

form, therefore the iron(II) ion of coordination number six can retain its ability to accept a chloride ligand. The additional binding of the chloride ligands to the metal in the complex may undoubtedly promote the increase of the conditional stability constant through the enlarged numerator of [MP]/[M][P]. This assumption on the structure may be supported by the fact that the molar absorption coefficient of the iron(II)–DOHP complex, $\varepsilon = 265$ mol^{-1} dm^3 cm, is very close to that of free DOHP ligand, $\varepsilon = 269$ mol^{-1} dm^3 cm.

In addition to the present dual-wavelength method, a conventional single-wavelength method[12] was also applied to the stability constant analyses. However, the latter was more erroneous compared with the former, where two measurable quantities are involved at a given point of the complex system.

Table 2. Dependence of logarithmic stability constants on ionic strength

	Ionic strength					
	0.5	1.0	1.5	2.0	2.5	3.0
Mg	5.77	5.16	4.95	4.82	4.49	4.26
Fe^{II}	5.13	5.11	5.06	5.07	5.09	4.97
Ni	—	5.39	5.21	4.95	4.72	4.60
Cu	5.16	4.76	4.50	—	—	—

REFERENCES

1. B. Blaser and K. H. Worms, *Z. Anorg. Allg. Chem.* 1959, **300**, 237.
2. J. Weiss, *Z. Anorg. Allg. Chem.* 1960, **306**, 30.
3. T. Nakashima, H. Waki and S. Ohashi, *J. Inorg. Nucl. Chem.* 1977, **39**, 1751.
4. T. Nakashima, S. Nakamura, H. Sutoh and S. Ohashi, *J. Inorg. Nucl. Chem.* 1981, **43**, 612.
5. H. Waki and T. Nakashima, *J. Inorg. Nucl. Chem.* 1979, **41**, 113.
6. H. Waki, T. Kubo, T. Nakashima and S. Ohashi, Preprint of the 32nd Autumn Meeting of the *Chem. Soc. Jpn* (1975) at Kyushu University, Fukuoka.
7. G. Cilento and D. L. Sanioto, *Z. phys. Chem., Leipzig* 1963, **333**, 223.
8. I. Hosokawa and F. Ohshima, *Water Res.* 1973, **7**, 283.
9. R. M. Smith and A. E. Martell (Eds), *Critical Stability Constants.* Plenum Press, New York (1976).
10. T. Nakashima, Y. Uchimura, H. Waki and S. Ohashi, Preprint of the 43rd Spring Meeting of the *Chem. Soc. Jpn* (1981) at Nippon University, Tokyo.
11. T. Nakashima, *Bull. Cent. Res. Inst. Fukuoka Univ.* 1989, **19**, 149.
12. F. T. C. Rossotti and H. Rossotti, *The Determination of Stability Constants.* McGraw-Hill, New York (1961).

Polyhedron Vol. 9, No. 21, pp. 2613–2617, 1990
Printed in Great Britain

0277-5387/90 $3.00+.00
© 1990 Pergamon Press plc

THEORETICAL ASPECTS OF AN EQUILIBRIUM STUDY IN THE NON-DISSOCIATING MOLECULAR SOLVENT ACETIC ACID

M. A. KHAN, J. MEULLEMEESTRE, M. J. SCHWING and F. VIERLING*

Laboratoire de Chimie-Physique, URA n° 405, EHICS, Université Louis Pasteur, 1 rue Blaise Pascal, F-67008 Strasbourg Cedex, France

(*Received* 23 *April* 1990; *accepted* 22 *June* 1990)

Abstract—The bromide complexes of copper(II) were studied spectrophotometrically in acetic acid. This non-dissociating solvent presents secondary equilibria such as perchlorate ⇄ acetate and in the case of copper acetate in acetic acid, monomer ⇄ dimer. A matrix rank treatment of the optical densities identified four mononuclear bromo complexes which are formulated as Cu(OAc)Br, $CuBr_2$, $LiCuBr_3$ and Li_2CuBr_4. The overall stability constants of these species are $\log\beta_1 = 3.2$, $\log\beta_2 = 6.5$, $\log\beta_3 = 7.7$ and $\log\beta_4 = 7.7$. The electronic spectra of the individual species, in this solvent, are reported for the first time. The *d–d* transition band of the tetrabromocuprate is calculated to be at 1120 nm and confirms the structure of a flattened tetrahedron.

According to the classification of the solvents based on the dielectric constant, ε_r, solvents with values of $\varepsilon_r < 15$ are classified as non-dissociating molecular solvents. Acetic acid, $\varepsilon_r = 6.2$, falls under this category and is therefore non-ionic in character and species present in this solvent exist as ion-pairs or ionic aggregates.[1] However, an equilibrium study in this solvent poses a host of theoretical problems which we shall indicate with a concrete example. Having already reported studies of halogenocuprates in different protic and aprotic solvents[2–5] we shall illustrate these problems with the help of results of copper(II) bromides in acetic acid, at 25°C and at a constant molecular environment maintained at 1 mol dm^{-3}.

1. PROBLEM OF THE NATURE OF SALT

In all our previous studies the metal coordinator was introduced into the solution by using a solution of copper(II) perchlorate. However, at low concentration of copper perchlorate in acetic acid, the formation of copper acetate is remarked. Copper perchlorate has a characteristic absorption band at 790 nm, whereas copper acetate absorbs at 680 nm. Eswein *et al.*[6] and Sawada *et al.*[7] have reported the absorption of copper acetate at 670 and 685 nm, respectively. In acetic solutions and at higher concentrations of copper perchlorate, its characteristic maximum is clearly observed at 790 nm. With dilution of the solution this maximum undergoes a hypsochromic effect and shifts to 680 nm, thus indicating the presence of copper acetate. Figure 1(a) and (b) shows the effect of dilution of copper perchlorate solution in acetic acid, respectively, in the presence, as well as in the absence, of lithium perchlorate (1 mol dm^{-3}). There is therefore an equilibrium between perchlorate and acetate:

$$Cu(ClO_4)_2 \rightleftarrows Cu(ClO_4)(OAc) \rightleftarrows Cu(OAc)_2.$$

Copper perchlorate absorbs at 790 nm, copper acetate at 680 nm and, in between, a mixed salt of the two has an absorption maximum at about 720 nm.[10]

Under these conditions a study of the halogeno complexes of copper in acetic acid with copper perchlorate is nearly impossible because the form of the non-complexed copper in the solution is unknown: whether it is in the form of perchlorate or acetate, or in the form of the mixed salt especially when the concentration of copper is low. Furthermore, Fig. 1(a) indicates that even the addition of lithium perchlorate as indifferent electrolyte fails to stabilize copper in the form of copper perchlorate.

* Author to whom correspondence should be addressed.

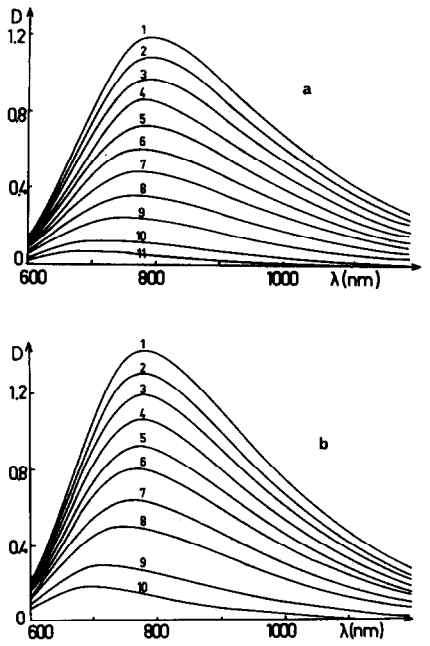

Fig. 1. Dilution of copper(II) perchlorate solution in acetic acid: (a) in the absence of $LiClO_4$; (b) in the presence of $LiClO_4$.

Consequently in a study of the halogeno complexes of copper(II) in acetic acid, copper must be added in the form of copper acetate.

2. MONOMER–DIMER EQUILIBRIUM

The use of copper acetate in acetic acid engenders a different type of problem, that of the existence of a monomer–dimer equilibrium: $2Cu(OAc)_2 \rightleftarrows Cu_2(OAc)_4$. Yamada *et al.*[8] and Martin and Whitley[9] have shown that the absorption band of copper acetate in acetic acid at 365 nm is due to metal–metal bonding in copper acetate which exists as a dimer in solution. Sawada *et al.*[10] have reported this absorption maximum at 370 nm. This band is not observed in our work because of low copper concentration, but it is observed at 372 nm in concentrated solutions of copper acetate $[Cu^{II}] > 4 \times 10^{-3}$ mol dm^{-3}.

The equilibrium constant of the monomer–dimer equilibrium has been determined by Kochi and Bubramanian[11] and is equal to 5×10^{-4}. These authors have also reported the feeble absorption intensity of the dimer band ($\varepsilon < 60$ dm^3 mol^{-1} cm^{-1}). The existence of the monomer and dimer species has been confirmed with the help of magnetic susceptibility measurements by Sawada *et al.*,[7] who have shown that the copper acetate in acetic acid has a dimeric structure, whereas the chloro complexes of copper are monomeric in nature.

Taking into consideration all these factors: (1) the low value of the equilibrium constant of monomer $\rightleftarrows$ dimer, (2) the very low absorption intensity of the dimer, (3) the disappearance of copper acetate in favour of the formation of bromo complexes, in our study, as well as the low concentrations of copper solutions, it can be assumed that copper acetate is in the monomeric form as far as this work is concerned. This hypothesis is further sustained by the fact that addition of small quantities of perchloric acid, which is the case in our study, favours the monomeric species.[11]

3. EQUILIBRIUM OF BROMO COMPLEXES OF COPPER(II) IN ACETIC ACID

In dissociating protic or aprotic solvents, the complexes involved in the equilibrium reaction are either charged or neutral species, generally cations more solvated than anions and sometimes completely unsolvated anions such as CuX_4^{2-}, the electronic spectrum of which was demonstrated as solvent independent.[3]

On the contrary, in the non-dissociating aprotic solvents such as THF[4] or protic solvents such as acetic acid, the species are present as ion-pairs or ion-aggregates and the successive equilibria in solution can be written as:

$$Cu(OAc)_2 + LiBr \rightleftarrows Cu(OAc)Br, LiOAc$$

$$Cu(OAc)_2 + 2LiBr \rightleftarrows CuBr_2, 2LiOAc$$

$$Cu(OAc)_2 + 3LiBr \rightleftarrows LiCuBr_3, 2LiOAc$$

$$Cu(OAc)_2 + 4LiBr \rightleftarrows Li_2CuBr_4, 2LiOAc. \quad (a)$$

However, the so-called non-dissociating solvents are only so by definition in the case of relative permittivity values, ε_r, lower than 15. For acetic acid which has an ε_r of 6.2 there is nevertheless the feeble ionization present. The presence of such voluminous ion-aggregates as $LiCuBr_3$, 2LiOAc or Li_2CuBr_4, 2LiOAc is quite improbable. Consequently, the sequence of the equilibria should be written in the following way:

$$Cu(OAc)_2 + LiBr \rightleftarrows Cu(OAc)Br + LiOAc$$

$$Cu(OAc)_2 + 2LiBr \rightleftarrows CuBr_2 + 2LiOAc$$

$$Cu(OAc)_2 + 3LiBr \rightleftarrows LiCuBr_3 + 2LiOAc$$

$$Cu(OAc)_2 + 4LiBr \rightleftarrows Li_2CuBr_4 + 2LiOAc. \quad (b)$$

As a matter of fact, the equilibrium constants corresponding to formulation (b) are different from those used in ionic media or aprotic dissociating

solvents. This difference is essentially due to the presence of the LiOAc concentration in the numerator. Amuli *et al.*[4] maintained the molecular environment constant in THF by the addition of $LiClO_4$, which enabled its exact analytical concentration to be known. By analogy, LiOAc should be used in these solutions. Unfortunately, copper(II) possesses good coordination ability with lithium acetate, unlike with perchlorate, and would consequently lead to another set of equilibria which overlap with the copper(II) bromides under study. Without addition of LiOAc, calculation of its concentration, taking into account equilibria (b), is quite impossible.

Therefore, the determination of the equilibrium constants of the copper(II) bromo complexes is performed using formulation (a) generalized by:

$$Cu(OAc)_2 + jLiBr \rightleftarrows \text{complex j},$$

with an equilibrium constant $\beta_j = [\text{complex j}]/[Cu(OAc)_2][LiBr]^j$.

4. COPPER(II) BROMIDES IN ACETIC ACID

Keeping in view all the above aspects we report below the results of copper(II) bromo complexes in acetic acid. Eswein *et al.*[6] have already reported the existence of the tri- and tetrabromocuprates in acetic acid absorbing at 625 and 510 nm, respectively. Yatsimirskii and Mal'Kova have calculated the stability constants of the mono- and dibromo complexes ($\log\beta_1 = 2.60$ and $\log\beta_2 = 6.42$) in acetic acid.[12] In another publication, these authors postulated the presence of tetra- and hexabromo complexes in concentrated solutions.[13]

Figure 2 shows the experimental spectra of the copper(II) bromides in the UV–vis and the near-IR regions. As soon as the ligand is added to the copper solutions, the copper absorption band at 260 nm diminishes with the appearance of several maxima:

an absorption band at 285 nm which increases in intensity with concentration and at the same time undergoes a hypsochromic shift until 267 nm for $C = 1.0$ mol dm^{-3};

another maximum at 350 nm, increasing with concentration until $C = 0.01$ mol dm^{-3}, with a bathochromic shift until 370 nm. For $\geqslant 0.03$ mol dm^{-3} this maximum diminishes in intensity and shifts back to 350 nm;

the appearance in the visible range of two absorption bands at 435 and 640 nm following the same evolution pattern as the 350 nm band. In addition to these bands in the visible spectrum, another band appears at 520 nm for ligand concentrations superior to 0.1 mol dm^{-3};

in the near-IR, the maximum at 860 nm increases in intensity until $C = 0.05$ mol dm^{-3} and then diminishes in favour of a large band centred at 1170 nm.

A matrix rank treatment of optical densities was executed to determine the minimum number of species present in the solution,[14] which indicated the presence of at least three complexes. The theoretical expressions and the mathematical treatment have

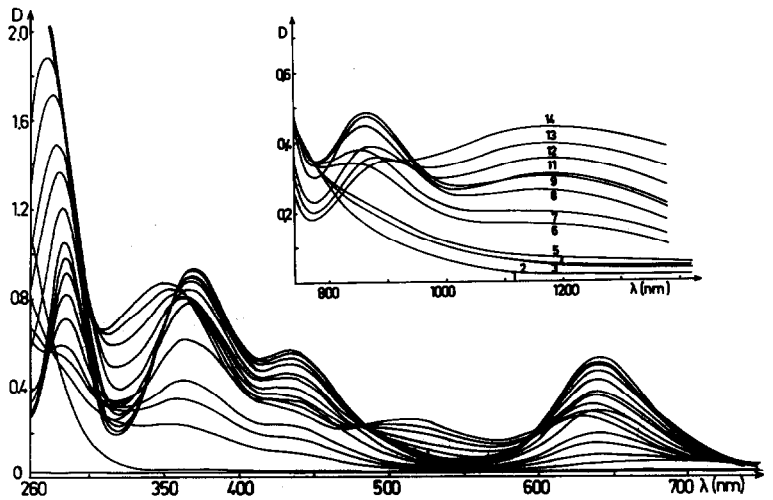

Fig. 2. Copper(II) bromide absorption spectra in acetic acid. (a) UV–vis, $B = 5 \times 10^{-4}$ M, $l = 0.5$ cm, spectra/$10^3 \times C$ (M): 1/0.5; 2/0.8; 3/1; 4/1.5; 5/2; 6/3; 7/5; 8/10; 9/30; 10/60; 11/100; 12/200; 13/400; 14/600; 15/800; 16/1000. (b) Proche IR, $B = 1.5 \times 10^{-3}$ M, $l = 2$ cm, spectra/$10^3 \times C$ (M): 1/0; 2/0.5; 3/1; 4/1.5; 5/2; 6/4; 7/5; 8/7; 9/10; 10/40; 11/100; 12/400; 13/700; 14/1000.

Table 1. Results of the numerical analysis of the theoretical models [1,2,3] and [1,2,3,4]

Overall stability constant	Model [1,2,3]	Model [1,2,3,4]
β_1	$(8.9\pm6.0)\times10^2$	$(1.7\pm0.7)\times10^3$
β_2	$(2.0\pm1.0)\times10^6$	$(3.0\pm1.1)\times10^6$
β_3	$(8.9\pm6.0)\times10^6$	$(5.5\pm3.0)\times10^7$
β_4	—	$(5.5\pm3.5)\times10^7$
σ_t	0.069	0.052

Table 2. The characteristic charge-transfer and the *d–d* transition bands of the copper(II) bromo complexes in acetic acid

CuOAcBr	$CuBr_2$	$LiCuBr_3$	$LiCuBr_4$
314(3080)	284(3650)	275(7160)	260(11,000)
	370(4000)	370(3080)	336(4600)
	440(2440)	440(1840)	410 sh
			520(1570)
			590 sh
	640(2200)	640(1800)	
752(126)	860(157)	880(152)	780 sh
960 sh	1130(86)	1220(112)	1120(166)

been explained in one of our earlier publications.[3] The computation was performed on the [1,2,3] and [1,2,3,4] theoretical models, i.e. the mono-, di- and tribromo complexes and the mono-, di-, tri- and tetrabromo complexes, respectively. The results are summarized in Table 1.

The quadratic mean $\langle\sigma_t\rangle$ has a significantly lower value for the model with four complexes. Consequently the presence of four mononuclear bromo complexes is concluded and, in acetic acid, they are formulated as Cu(OAc)Br, $CuBr_2$, $LiCuBr_3$ and Li_2CuBr_4. The values of the stability constants are used to determine the specific molar extinction coefficients, ε_j, to calculate the electronic spectra of the individual species represented in Fig. 3. The characteristic charge-transfer bands, as well as the *d–d* transitions for the individual complexes, are reported in the Table 2.

The formation curves of the four complexes are represented in Fig. 4, and it is seen that $CuBr_2$ covers a large range of ligand concentration. Even with a maximum experimental concentration of 1.0 mol dm^{-3}, where 49% of the third and 49% of the fourth complex are formed, small quantities of the dibromo complex are still present.

Our earlier works concerning the structure in solution of the tetrachlorocuprates have demonstrated both the square-planar and flattened tetrahedron configurations depending upon the solvents. As regards the tetrabromo complex, all studies converge to attribute the flattened tetrahedron structure for it. In the solid state, this configuration has a very specific *d–d* transition band at 1111 nm and above. Our calculations show its maximum at 1120 nm and therefore, by comparison with solids, the structure of the tetrabromocuprate, in acetic acid solution, is that of a flattened tetrahedron.

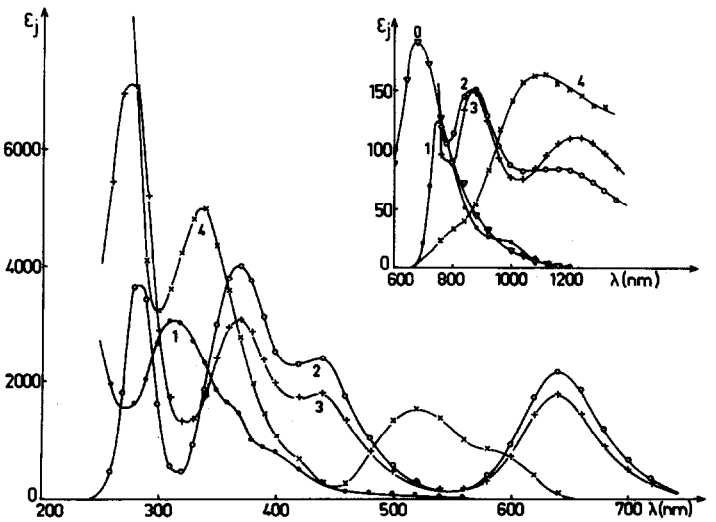

Fig. 3. Calculated electronic spectra of the copper(II) bromo complexes in acetic acid: (0) $Cu(OAc)_2$, (1) Cu(OAc)Br, (2) $CuBr_2$, (3) $LiCuBr_3$, (4) Li_2CuBr_4.

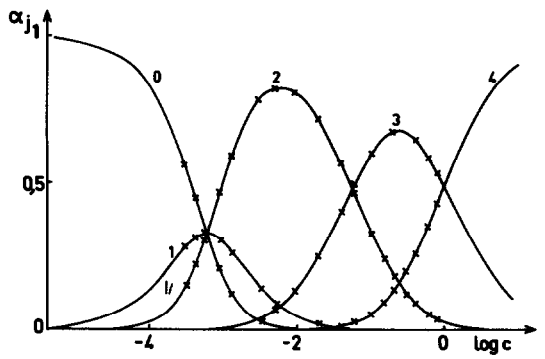

Fig. 4. Degree of formation of the copper(II) bromo complexes in acetic acid, (c is the effective concentration of LiBr); ($\times$) experimental points.

EXPERIMENTAL

Anhydrous acetic acid, pro-analysis (Merck), was used after the addition of a calculated amount of acetic anhydride, p.a. Merck, along with three drops of 0.001 M perchloric acid, 70% p.a. Merck, and then allowing the solution to stand overnight.[1] Copper solutions were prepared from stock solutions of copper(II) acetate, p.a. Merck, and $Cu(ClO_4)_2 \cdot 6H_2O$, p.a. Merck. Lithium bromide, p.a. Merck, and lithium perchlorate, p.a. Fluka, were used without any purification.

The final analytical concentration of copper was 5×10^{-4} mol dm^{-3} for measurements in the UV–vis and 3.75×10^{-3} mol dm^{-3} in the IR region. In these spectral ranges ligand concentrations were varied from 10^{-3} to 1.0 mol dm^{-3} with spectrophotometric cells of 0.5 and 2.0 cm, respectively.

Acetic acid was used as the spectrophotometric reference solution. The final solutions of copper and bromide were prepared just before measurements to avoid any possibility of errors due to instability. The absorption of the solutions was measured with the help of CARY 17D with digital interfacing and a Periferic Zip 30 rapid printer. The numerical analysis was performed on an IBM 3081 D computer.

REFERENCES

1. A. I. Popov, *The Chemistry of Non-aqueous Solvents* (Edited by J. J. Lagowski), Part III. Academic Press, New York (1970).
2. M. A. Khan and M. J. Schwing, *Inorg. Chem.* 1976, **15**, 2202; *Bull. Soc. Chim. Fr.* 1977, **3–4**, 399.
3. M. Elleb, J. Meullemeestre, M. J. Schwing and F. Vierling, *Inorg. Chem.* 1980, **19**, 2699; 1982, **21**, 1477.
4. C. Amuli, J. Meullemeestre, M. J. Schwing and F. Vierling, *Inorg. Chem.* 1983, **22**, 3567; 1986, **25**, 856; *Nouv. J. Chim.* 1987, **11**, 27.
5. M. A. Khan, J. Meullemeestre, M. J. Schwing and F. Vierling, *Polyhedron* 1983, **2**, 459; *Inorg. Chem.* 1989, **28**, 3306.
6. R. P. Eswein, E. S. Howald, R. A. Howald and D. P. Keeton, *J. Inorg. Nucl. Chem.* 1967, **29**, 437.
7. K. Sawada, H. Ohtaki and M. Tanaka, *J. Inorg. Nucl. Chem.* 1972, **34**, 3455.
8. S. Yamada, H. Nakamura and R. Tuchida, *Bull. Chem. Soc. Jpn* 1957, **30**, 953.
9. R. L. Martin and A. Whitley, *J. Chem. Soc.* 1958, 1394.
10. K. Sawada, H. Ohtaki and M. Tanaka, *J. Inorg. Nucl. Chem.* 1972, **34**, 625.
11. J. K. Kochi and R. V. Bubramanian, *Inorg. Chem.* 1965, **4**, 1527.
12. K. B. Yatsimirskii and T. V. Mal'Kova, *Russ. J. Inorg. Chem.* 1961, **6**, 426.
13. T. V. Mal'Kova and K. B. Yatsimirskii, *Russ. J. Inorg. Chem.* 1963, **8**, 169.
14. Z. Z. Hugus and A. A. El Awady, *J. Phys. Chem.* 1971, **75**, 2594.

Polyhedron Vol. 9, No. 21, pp. 2619–2623, 1990
Printed in Great Britain

0277–5387/90 $3.00+.00
© 1990 Pergamon Press plc

ROTATIONAL BARRIERS IN DIALKYLAMINOCHLOROSPHINES: STERIC EFFECTS ON THE PREPARATION OF CAGE COMPLEXES

DAVID S. BADER and MARK M. TURNBULL*

Department of Chemistry, Clark University, 950 Main Street, Worcester, MA 01610, U.S.A.

(*Received* 2 *April* 1990; *accepted* 4 *July* 1990)

Abstract—The barrier to rotation about the P—N bond in a series of N,N-dialkylphenylphosphonamidous chlorides has been measured. The barriers fall into two groups based on the alkyl substituents being primary (barrier = 11.6 ± 0.1 kcal mol^{-1}) or secondary (barrier = 13.4 ± 0.2 kcal mol^{-1}). The difference in barrier height is interpreted in terms of the steric requirements of the alkyl substituents. This steric argument is used to explain the observed difference in reactivity of $(R_2N)_2P(O)H$ compounds with $Mo(CO)_6$.

In 1983, Wong *et al.*[1] discovered the thermal condensation reaction between $(^iPr_2N)_2P(O)H$ and $Mo(CO)_6$ to give the cage complex **1** (R = ^{i}Pr), containing the unusual tetraoxatetraphosphorinane ring which binds the two metals centres together [see eq. (1)]:

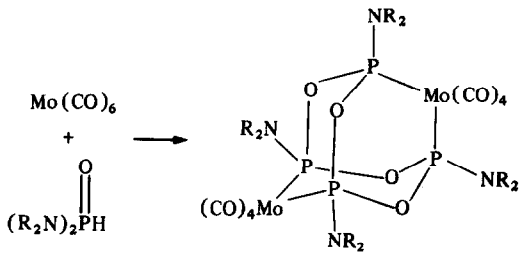

(1)

(1)

Further work using other phosphine oxides, $(R_2N)_2P(O)H$ (R = cyclohexyl, ethyl, benzyl)[2a] and (R = methyl),[2b] indicated that the yield of cage-like product depended upon the alkyl groups on the amino-substituents; larger groups such as isopropyl and cyclohexyl (= c-hex) gave high yields of the corresponding **1**, while the smaller substituents, methyl, ethyl and benzyl, gave virtually no **1** (detectable spectroscopically, but not isolated).

We interpreted this marked reactivity difference as a steric dependence, where increased steric bulk was somehow responsible for the cage-forming process. This idea was in agreement with the proposed pathway,[3] wherein initial formation of the coordinated phosphinous acid, **2**, is followed by elimination of dialkylamine to generate the coordinated phosphinidene oxide, **3**, which then goes on to form **1** [see eq. (2)]. The existence of the chromium analogue of **3** has been shown by Niecke *et al.*[4] and provides support for this pathway. Relief of steric strain in the conversion of **2** to **3** might provide the driving force for the loss of dialkylamine. It is reasonable that more crowded molecules would undergo this reaction more easily since coordinated phosphinous acids (similar to **2**, but where there are alkyl, aryl or alkoxy substituents in place of the amino groups) are generally isolable, stable species.[5]

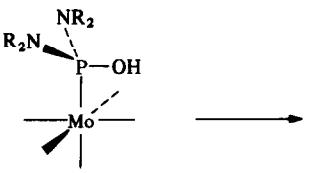

(2)

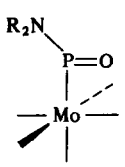

(3)

1 (2)

* Author to whom correspondence should be addressed.

We believed that one way to quantify this steric effect would be to examine the barrier to rotation about the P—N bond for the various dialkylamino substituents. Such a relationship would have a useful predictive value for attempting the synthesis of **1** with other amino substituents.

RESULTS AND DISCUSSION

Measurement of the rotational barriers in compounds of the general structure $(R_2N)_2P(O)H$, the actual starting materials for the synthesis of **1**, would provide a direct measure of the steric requirements for the dialkylamino groups involved. However, we were unable to detect any change in the ^{13}C NMR spectrum of $(^iPr_2N)_2P(O)H$ from 330 to 185 K. This was not suprising since the spectrum of $Ph(Me_2N)P(O)Cl$ remains unchanged down to 193 K.[6] Jennings and co-workers, however, had detected the barrier for $Ph(^iPr_2N)P(S)Cl$, which showed coalescence at 208 K,[7] and thus we had hoped that we would be able to detect the barrier for at least the bulky (^{i}Pr and c-hex) oxy-analogues. Because of our inability to study the actual compounds used in the preparation of **1**, we turned to the phenylphosphonamidous chlorides $[Ph(R_2N)PCl]$.

The magnitude of this barrier was first determined by dynamic ^1H NMR spectroscopy of $Ph(Me_2N)PCl$ in 1968.[8] Since that time many workers have studied the phenomenon and the effects of varying the substituents at phosphorus and nitrogen.[9] More recently, Martin and co-workers have examined the P—N bond character of aminophosphines through ^{15}N and ^{31}P NMR chemical shifts and coupling constants.[10] The barrier is attributed to the combined effects of lone pair–lone pair repulsions, N—P double-bond character and steric effects. We felt that in a series of dialkylaminophosphines such as $Ph(R_2N)PCl$ (**4**), where the only variant was the alkyl group, the electronic contributions (lone pair effects and double bond character) would remain reasonably constant. Therefore the difference in the rotational barriers would provide us with a direct measure of the changing steric contribution from the dialkylamino substituents. Dakternieks and Di Giacomo[11] have used similar arguments to explain the effect of varying the P substituents in similar diethylaminophosphines. The barriers to rotation for some of these compounds (R = Me, Et, ^{i}Pr) have been previously reported,[9] but at widely different temperatures, making a direct comparison difficult.

We determined the thermodynamic activation parameters for P—N rotation in the series $Ph(R_2N)PCl$ [R = Me (**4a**), Et (**4b**), Bz (**4c**), ^{i}Pr (**4d**) and c-hex (**4e**)] to see if the steric effects derived therefrom would provide a useful measure of the success of the related $(R_2N)_2P(O)H$ compounds to produce **1**. Compounds **4a–e** were prepared by standard techniques (see Experimental). Treatment of $PhPCl_2$ with two equivalents of the appropriate amine gave the corresponding $Ph(R_2N)PCl$, compound **4**, in 70–90% yield.

$$PhPCl_2 + R_2NH \longrightarrow Ph(R_2N)PCl \quad (3)$$

(4)

^{13}C NMR {H} spectra were obtained for the dialkylaminophosphines (**4a–e**). Spectra were obtained within the liquid range of the solvent, d_6-acetone (200–330 K). Chemical shifts and coupling constants for the low and high temperature limiting spectra are given in Table 1. Rotational frequencies at each temperature were determined by the Complete Bandshape Analysis[12] method for the coalescing doublets of the carbons adjacent to the nitrogen atom for all compounds.

The observed $^2J_{PNC}$ coupling constants for the low and high temperature limiting spectra indicate that the signs of the low temperature couplings must be opposite. For example, $(Me_2N)PhPCl$ shows two doublets with observed couplings of 13 and 35 Hz at 200 K and a doublet with an observed coupling of 11 Hz at 330 K. These values are clearly consistent with couplings of opposite sign as has been observed previously.[9b] Wehrli and co-workers showed the $^2J_{PNC}$ coupling to be dependent upon the dihedral angle between the C—N bond and the phosphorus lone pair; for angles near 0° the value is large and positive and for angles near 180° the value is small and negative. We have assigned our spectra accordingly.

For **4d** and **4e**, the high temperature spectra could not be obtained below the boiling point of the

Table 1. ^{13}C NMR chemical shifts and coupling constants for the α-carbon of aminophosphines **4a–e**[a]

Compound, R	Low temperature	High temperature
4a, Me	37.2(−13), 42.7(35)	40.4(11)
4b, Et	41.1(−13), 45.9(37)	44.7(13)
4c, Bz	50.1(−12), 55.3(36)	53.6(12)
4d, ^{i}Pr	45.1(26), 52.6(−13)	[b]
4e, Cyx	54.9(23), 60.9(−12)	[b]

[a] In d_6-acetone. Chemical shifts in ppm referenced to solvent (*J* in Hz).

[b] High temperature limit above solvent boiling point.

solvent. Hence, the opposite signs of the observed low temperature coupling constants could not be confirmed, but have been assigned that way by analogy assuming the molecules have similar conformations. However, both **4d** and **4e** show a substantial reduction of the large coupling constant (by about 10 Hz) compared to the primary-alkyl substituted **4a–c**. In addition, the chemical shifts of the large and small coupled doublets in **4d** and **4e** are reversed with respect to **4a–c**, the lower field resonances of **4d** and **4e** having the smaller coupling constants. These effects suggest significant differences in the ground state conformations of **4** as a function of R and thus our assignment of opposite signs to the coupling constants may be inappropriate. Clearly, however, the similarity of spectra within an alkyl type and the differences of the spectra between the alkyl types supports our hypothesis that these compounds constitute two distinct groups.

Standard Eyring plots of $1/T$ vs $\ln k/T$ for each series of spectra yielded $\Delta H^{\ddagger}$ and $\Delta S^{\ddagger}$. These values and the calculated values for $\Delta G^{\ddagger}$ at 298 K are given in Table 2 along with the correlation coefficient for the Eyring plots from which they were derived. Only those spectra not near the high or low temperature limits were used. As has been previously noted,[13] non-linearity was observed at very low and very high rotational rates. Errors introduced by spin–spin coupling and scalar coupling of nuclei are systematic and lead to low values of $\Delta H^{\ddagger}$ and consequently more negative values of $\Delta S^{\ddagger}$, but these are mutually compensating errors, with respect to the calculation of $\Delta G^{\ddagger}$, at the moderate temperatures used in these experiments. In addition, at very low and high rotational rates the errors in comparing the simulated and experimental spectra become significant. At very low rates (< 20–30 Hz), changes of 20% or more produce no visible change in the spectrum. The same is true at high rotational rates (above ≈ 20,000 Hz) and thus these data were not used. A comparison of our results with the literature values is given in Table 3.

Examination of the rotational barriers of **4a–e** shows distinct similarities among compounds with the same type of alkyl group (primary or secondary) and an abrupt break between these groups. Those aminophosphines with primary alkyl groups, **4a–c**, exhibit a barrier of 11.6 ± 0.1 kcal mol^{-1} while those with secondary alkyl groups, **4d** and **4e**, show a barrier of 13.4 ± 0.2 kcal mol^{-1}. We contend that because these are all alkyl-substituted amines, the electronic contribution of the different groups should be relatively constant. Thus the difference in rotational barriers must result from the different steric constraints of the alkyl groups. The absolute difference between the rotational barriers of the two groups is small, 1.8 kcal mol^{-1}, and thus raises the question of how valid conclusions based upon that difference can be. We believe that the even smaller spread of values within each group (0.2 and 0.3 kcal, about 15% of the separation between the groups) supports our hypothesis that the primary or secondary nature of the alkyl group plays the major role in distinguishing the rotational barriers for these compounds.

We are gratified that the two sets of dialkylamino substituents resulting from examination of the rotational barriers correspond to the two sets defined by the reaction of $(R_2N)_2P(O)H$ with $Mo(CO)_6$. We conclude that when R is primary, intermediate **2** in the cage synthesis is too low in energy to undergo the critical elimination reaction to form **3**. Steric crowding in the case of secondary alkyl groups raises the energy of **2**, thus lowering the activation barrier to the production of **3** and thence on to **1**.

The one remaining question is whether the barriers to rotation in **4** and the steric differences derived therefrom, are reasonable models for the interactions occurring in the proposed intermediate **2**. The question is not whether the actual values for

Table 2. Calculated enthalpies, entropies[a] and free energies of activation[b] for rotation about the P—N bond of N,N-dialkylaminophenylchlorophosphines

Compound, R	$\Delta H^{\ddagger}$	$\Delta S^{\ddagger}$	$\Delta G^{\ddagger}$	r^c
4a, Me	8.30	−10.9	11.5	(0.977)
4b, Et	8.32	−10.6	11.5	(0.996)
4c, Bz	7.20	−15.0	11.7	(0.992)
4d, ^{i}Pr	9.10	−14.2	13.3	(0.993)
4e, Cyx	10.7	−9.8	13.6	(0.999)

[a] $\Delta H^{\ddagger}$ and $\Delta G^{\ddagger}$ in kcal mol^{-1}, $\Delta S^{\ddagger}$ in cal mol^{-1} K.
[b] $\Delta G^{\ddagger}$ reported at 298 K.
[c] Correlation coefficients of corresponding Eyring plot.

Table 3. Comparison of rotational barriers[a] with literature values[b]

Compound	Literature value (T K)	This work
4a	10.9 (223)	10.8
4b	10.8 (216)	10.6
4d	12.8 (258)	12.8

[a] All in kcal mol^{-1}.
[b] Taken from ref. 9(a).

the rotational barriers are comparable, but rather whether the *relative* values are comparable. In the case of **4**, one dialkylamino group is varied with the rest of the structure held constant (phenyl and chloro substituents). In intermediate **2**, the phosphorus atom is tetracoordinate with another dialkylamino group replacing the phenyl substituent, a hydroxyl group in place of chlorine and a $Mo(CO)_5$ fragment coordinated to the phosphorus lone pair. The tetracoordinate nature of the phosphorus atom will clearly change the electronic and lone pair repulsion contributions to the barrier, but the steric requirements will be exaggerated relative to the model compounds, leading to even greater energy differences between the two sets of dialkylamino substituents in **2**.

Further work is in progress to test the predictive power of these results. We intend to vary the steric congestion about the amino group in a regular fashion using the series piperidine, (+)- and (−)-2-methylpiperidine, and 2,6-dimethylpiperidine. The measured rotational barriers for these $Ph(R_2N)PCl$ compounds should allow us to predict the subsequent success of using the diaminophosphine oxides to produce **1**.

EXPERIMENTAL

All procedures were carried out using standard Schlenk techniques under an argon atmosphere. Dichloromethane was distilled from CaH_2. Ether was distilled from Na/benzophenone ketyl. All amines were purchased from Aldrich Chemicals and distilled from KOH. $PhPCl_2$ was purchased from Alfa Products and used without further purification. IR spectra were recorded on a Perkin–Elmer 1330 spectrophotometer and were calibrated against polystyrene. NMR spectra were recorded on a Bruker AC-200 spectrometer (courtesy of the Worcester NMR Consortium) and calibrated against TMS (^1H), solvent (^{13}C) or external Ph_3P (^{31}P). ^{13}C and ^{31}P NMR spectra were broadband proton-decoupled unless otherwise noted. Elemental analyses were performed by MultiChem Laboratories, Inc. Lowell, MA.

$Ph(c\text{-}hex_2N)PCl$ (**4e**)

$PhPCl_2$ (4.07 cm^3, 5.37 g, 30.0 mmol) was dissolved in 50 cm^3 of CH_2Cl_2 and cooled to −78°C. Dicyclohexylamine (11.9 cm^3, 10.9 g, 60.0 mmol) was added dropwise over the course of 10 min with vigorous stirring. The reaction mixture was allowed to warm to room temperature and stirred for 12 h. 50 cm^3 of Et_2O was added, the resulting mixture was filtered and the precipitate washed with 4 × 15 cm^3 of Et_2O. The solvent was removed *in vacuo* from the combined filtrate and washings to give a viscous pale yellow oil, 8.48 g (88%). Found: C, 64.6; H, 7.9; N, 3.6. Calc. for $C_{18}H_{27}ClNP$: C, 66.7; H, 8.4; N, 4.3% (We believe the discrepancy in analysis is due to the compound's susceptibility to hydrolysis. No impurities were detected by NMR spectroscopy and a repeat analysis was not attempted.) IR (neat): 3045m, 2910vs, 2840s, 1060s, 745s, 695s. ^1H NMR: δ 7.74 (br m, 2H, *o*-Ph), 7.43 (br m, 3H, *m*- and *p*-Ph), 3.0 (br, 2H, NCH), 1–2 (br m, 20H, CH_2's). ^{13}C NMR: δ 140.6 (d, $J = 28$ Hz), 131.4 (d, $J = 22$ Hz), 130.2 (s), 129.0 (s), 58.5 (br), 34.8 (br), 26.8 (s), 26.2 (s). ^{31}P NMR: δ 134.

Compounds **4a–d**

These were prepared by procedures analogous to that for **4e**. Isolated material was characterized by comparison of physical properties and ^1H NMR spectra with the literature data.[9] The broadband proton-decoupled ^{31}P NMR spectra at room temperature and high temperature limiting ^{13}C NMR are reported here for reference:

$Ph(Me_2N)PCl$ (**4a**): ^{31}P NMR (d_6-acetone): δ 145. ^{13}C NMR (d_6-acetone): δ 140.2 (d, $J = 27$ Hz), 131.1 (d, $J = 20$ Hz), 130.6 (s), 129.3 (s), 40.4 (d, $J = 11$ Hz). $Ph(Et_2N)PCl$ (**4b**): ^{31}P NMR (d_6-acetone): δ 141. ^{13}C NMR (d_6-acetone) −δ 140.0 (d, $J = 30$ Hz), 131.1 (d, $J = 20$ Hz), 130.5 (s), 129.2 (s), 44.7 (d, $J = 13$ Hz), 14.2 (d, $J = 5$ Hz). $Ph(Bz_2N)PCl$ (**4c**): ^{31}P NMR (d_6-acetone): δ 139. ^{13}C NMR (d_6-acetone): δ 139.6 (d, $J = 30$ Hz), 137.2 (s), 131.3 (d, $J = 22$ Hz), 130.8 (s), 129.2 (s), 129.9 (s), 128.0 (s), 53.5 (d, $J = 12$ Hz). $Ph(^iPr_2N)PCl$ (**4d**): ^{31}P NMR (d_6-acetone): −δ 132. ^{13}C NMR (d_6-acetone): δ 140.3 (d, $J = 19$ Hz), 131.3 (d, $J = 21$ Hz), 130.5 (s), 129.4 (s), 49.4 (br), 24.4 (s), 23.5 (d, $J = 13$ Hz).

Data analysis methods

Fourier transform ^{13}C NMR {H} spectra were obtained for each compound from 200 to 330 K. Samples were prepared at a concentration of 5%. Probe temperatures were determined by calibration against the temperature-dependent chemical shifts of ethylene glycol (above room temperature) or methanol (below room temperature).

Magnetic resonance spectra were simulated by the "Complete Bandshape Method".[12b] The lineshape equation, implemented on an IBM–XT personal computer, was designed to simultaneously simulate two pairs of coalescing resonances and thus accommodated simulation of the exchanging

doublets. In brief, calculated NMR spectra were obtained as follows: experimental frequencies and linewidths, as well as a projected rate constant, were input into the program to yield a set of contracted Lorentzian line-shape functions. The line-shape functions were then multiplied over the experimental frequency range to yield a calculated spectrum whose rate constant and transverse relaxation times could be adjusted to obtain the best fit with the experimental spectrum as determined by eye. We estimate the error in the rotational frequencies to be 5% or less.

Acknowledgement—We wish to thank Clark University for a University College Summer Undergraduate Research Fellowship (D.S.B.).

REFERENCES

1. E. H. Wong, M. M. Turnbull, E. J. Gabe, F. L. Lee and Y. Le Page, *J. Chem. Soc., Chem. Commun.* 1983, 776.
2. (a) E. H. Wong, M. M. Turnbull, K. D. Hutchinson, C. Valdez, E. J. Gabe, F. L. Lee and Y. Le Page, *J. Am. Chem. Soc.* 1988, **110**, 8422; (b) M. M. Turnbull and C. M. Banse, unpublished results.
3. E. H. Wong, E. J. Gabe and J.-P. Charland, *J. Chem. Soc., Chem. Commun.* 1988, 1632.
4. E. Niecke, M. Englemann, H. Zorn, B. Krebs and G. Henkel, *Angew. Chem. Int. Edn Eng.* 1980, **19**, 710.
5. For example see (a) C. S. Kraihanzel and C. M. Bartish, *J. Am. Chem. Soc.* 1972, **94**, 3572; (b) E. H. Wong, F. C. Bradley, L. Prasad and E. J. Gabe, *J. Organomet. Chem.* 1984, **263**, 167.
6. M. P. Simonnin, J. J. Basselier and C. Charrier, *Bull. Soc. Chim. France* 1967, 3544.
7. J. Burdon, J. C. Hotchkiss and W. B. Jennings, *J. Chem. Soc., Perkin Trans. 2* 1976, 1052.
8. A. H. Cowley, M. J. S. Dewar and W. R. Jackson, *J. Am. Chem. Soc.* 1968, **90**, 4185.
9. (a) A. H. Cowley, M. J. S. Dewar, W. R. Jackson and W. B. Jennings, *J. Am. Chem. Soc.* 1970, **92**, 5206; (b) M. Simonnin, R. Lequan and F. W. Wehrli, *J. Chem. Soc., Chem. Commun.* 1972, 1204; (c) J. Burdon, J. C. Hotchkiss and W. B. Jennings, *J. Chem. Soc., Perkin Trans. 2* 1976, 1052.
10. J.-P. Gouesnard, J. Dorie and G. J. Martin, *Can. J. Chem.* 1980, **58**, 1295.
11. D. Dakternieks and R. Di Giacomo, *Phosphorus and Sulfur* 1985, **24**, 217.
12. (a) H. S. Gutowsky and C. H. Holm, *J. Chem. Phys.* 1956, **25**, 1228; (c) J. Sandstrom, *Dynamic NMR Spectroscopy*. Academic Press, London (1982).
13. (a) W. E. Stewart and T. H. Siddall, *Chem. Rev.* 1970, **70**, 517; (b) M. B. Robin, F. A. Bovey and H. Basch, *The Chemistry of Amides* (Edited by J. Zabicky). John Wiley, London (1970).

Polyhedron Vol. 9, No. 21, pp. 2625–2634, 1990
Printed in Great Britain

0277–5387/90 $3.00+.00
© 1990 Pergamon Press plc

t-BUTYLIMIDO COMPLEXES OF CHROMIUM. X-RAY CRYSTAL STRUCTURES OF $Cr(NBu^t)_2(PMe_2Ph)Cl_2$ AND $[Cr(NBu^t)_2(C_5H_4N)_2(\eta^1\text{-}O_3SCF_3)]O_3SCF_3$

ANDREAS A. DANOPOULOS, WA-HUNG LEUNG and GEOFFREY WILKINSON†

Johnson Matthey Laboratory, Chemistry Department, Imperial College, London SW7 2AY, U.K.

and

BILQUIS HUSSAIN-BATES and MICHAEL B. HURSTHOUSE†

Chemistry Department, Queen Mary and Westfield College, Mile End Road, London E1 4NS, U.K.

(*Received* 22 *June* 1990; *accepted* 5 *July* 1990)

Abstract—The compound $Cr(NBu^t)_2Cl_2$ has been synthesized and converted to $Cr(NBu^t)_2(NHBu^t)Cl$, $Cr(NBu^t)_2(NHBu^t)_2$ and $Li_2Cr(NBu^t)_4$, the latter completing the series of Group 6 compounds, $Li_2M(NBu^t)_4$, M = Cr, Mo, W. The five-coordinate adducts, $Cr(NBu^t)_2Cl_2L$, L = PMe_3, PMe_2Ph and Bu^tNC, have been characterized as well as $[Cr(NBu^t)_2Cl_2]_2(\mu\text{-}Ph_2PCH_2CH_2PPh_2)$ and the six-coordinate $Cr(NBu^t)_2Cl_2$(2,2′-bipyridyl). Chloride substitution reactions of $Cr(NBu^t)_2Cl_2$ lead to the compounds, $Cr(NBu^t)_2(\eta^1\text{-}O_2CMe)_2$, $[Cr(NBu^t)_2(PMe_3)_2](O_3SCF_3)_2 \cdot 0.5MeCN$, $[Cr(NBu^t)_2py_2(\eta^1\text{-}O_3SCF_3)]SO_3CF_3$ and $[Cr(NBu^t)_2(bpy)_2](PF_6)_2$. The isocyanide, $[Cr(NBu^t)_2Cl_2(Bu^tNC)]$, with MeLi gives the η^2-iminoacyl $Cr(NBu^t)_2[\eta^2\text{-}(Bu^tN{=}CMe)]Cl$. Interaction of $Cr(NBu^t)_2Cl_2$ with alkylating agents at low temperatures gives the chromium(V) dimer $[Cl(Bu^tN)Cr(\mu\text{-}NBu^t)]_2$ in a one-electron per chromium reduction and the same product is obtained by reduction of the dihalide with $(\eta^5\text{-}C_5H_5)_2Co$. X-ray structures of compounds listed in the title have been determined.

In previous papers we have described the synthesis, X-ray structures and some reactions of the lithium derivatives of the species $[M(NBu^t)_4]^{2-}$, M = Mo and W,[1] and $[Re(NBu^t)_4]^-$.[1a,2] A preliminary note on the chromium(VI) analogue[3] is now expanded and this paper also includes a number of reactions of $Cr(NBu^t)_2Cl_2$.[3]

We have also previously described the chromium(VI) diaryls, $Cr(NBu^t)_2Ar_2$, Ar = $C_6H_2Me_3$-2,4,6(mesityl, mes), $C_6H_3Me_2$-2,6, the X-ray structures of the mesityl and of the reaction product with Bu^tNC, i.e. $Cr(NBu^t)_2[\eta^2\text{-}mesC{=}NBu^t]mes$; an unstable acyl from the reaction with CO, $Cr(NBu^t)_2(COmes)_2$ was characterized spectroscopically.[4]

After completion of the present study, a recent paper has described $Cr(NBu^t)_2X_2(py)$, X = Cl, Br, some bulky dialkyls, e.g. $Cr(NBu^t)_2(CH_2SiMe_3)_2$, similar to the aryls, and η^5-cyclopentadienyl compounds of the type $Cr(\eta^5\text{-}C_5H_5)(NBu^t)_2R$, R = alkyl or bromide.[5]

Analytical and physical data for new compounds are collected in Table 1. Reactions of $Cr(NBu^t)_2Cl_2$ are summarized in Scheme 1.

RESULTS AND DISCUSSION

(1) *Bis(t-butylimido)dichlorochromium*(VI)

As in previous work,[4,5] the starting material is $Cr(NBu^t)_2(OSiMe_3)_2$[6] from which, by interaction

† Authors to whom correspondence should be addressed.

Table 1. Analytical and physical data for chromium compounds

Compound	Colour	Melting point (°C)	Analysis (%)[a] C	H	N	Cl
$Cr(NBu^t)_2Cl_2$ (**1**)	Red	68–70	36.4 (36.2)	6.8 (6.8)	10.5 (10.5)	
$Cr(NBu^t)_2(NHBu^t)Cl$ (**2**)	Orange	148–150	47.6 (47.8)	9.4 (9.3)	13.8 (13.9)	12.1 (11.7)
$Cr(NBu^t)_2(NHBu^t)_2$ (**3**)	Red–purple	57–60	55.9 (56.8)	11.0 (11.2)	16.0 (16.5)	
$Cr(NBu^t)_2[N(SiMe_3)Bu^t)]Cl$ (**4**)	Red	165–170	48.0 (48.2)	9.5 (9.6)	11.0 (11.3)	
$Li_2Cr(NBu^t)_4$ (**5**)	Red	> 250[b]	53.8 (54.9)	10.5 (10.3)	16.0 (15.9)	
$Cr(NBu^t)_2Cl_2(PMe_2Ph)$ (**6**)	Dark yellow	164[b]	47.6 (47.6)	7.3 (7.2)	6.9 (6.9)	
$Cr(NBu^t)_2Cl_2(PMe_3)$ (**7**)	Yellow	142[b]	29.6 (29.8)	5.2 (5.0)	7.8 (7.7)	
$Cr(NBu^t)_2Cl_2(CNBu^t)$ (**8**)	Orange	130[b]	44.8 (44.8)	7.8 (7.8)	11.9 (12.0)	
$Cr_2(NBu^t)_4Cl_4(\mu\text{-dppe})$ (**9**)	Yellow	192[b]	54.1 (54.2)	6.5 (6.5)	6.0 (6.0)	
$Cr(NBu^t)_2Cl_2(bpy)$ (**10**)	Orange–yellow	141[b]	51.4 (51.3)	6.1 (6.2)	13.0 (13.3)	
$Cr(NBu^t)_2(O_2CMe)_2$ (**11**)	Dark orange	63–64	46.0 (46.2)	7.5 (7.7)	8.7 (9.0)	
$[Cr(NBu^t)_2py_2(OTf)]OTf$ (**12**)[c]	Orange	161[b]	37.1 (37.8)	4.3 (4.4)	8.7 (8.8)	
$Cr(NBu^t)(PMe_3)_2(OTf)_2(MeCN)_{0.5}$ (**13**)	Pale green	131[b]	30.7 (30.7)	5.8 (5.6)	5.4 (5.3)	
$[Cr(NBu^t)_2(bpy)_2](PF_6)_2$ (**14**)	Purple	175–176[b]	42.2 (42.2)	4.1 (4.2)	10.2 (10.5)	
$Cr(NBu^t)_2(Bu^tNCMe)Cl$ (**15**)	Dark yellow	90–92	51.1 (51.3)	9.0 (9.2)	12.9 (12.8)	
$Cr(NBu^t)_2(NPPh_3)_2$ (**16**)	Red–purple	190–193	71.4 (70.8)	6.5 (6.4)	7.4 (7.5)	
$[(Bu^tN)ClCr(\mu\text{-}NBu^t)]_2$ (**17**)	Yellow–green	225–227	45.0 (45.4)	8.1 (8.5)	12.9 (13.2)	16.0 (16.7)
$[Cr(NBu^t)(NHBu^t)(\mu\text{-}NBu^t)]_2$ (**18**)	Green	175–176	53.8 (54.1)	10.5 (10.5)	15.7 (15.7)	

[a] Calculated values given in parentheses.
[b] Decomposes.
[c] OTf = CF_3SO_3.

with boron trichloride in dichloromethane, the chloride, $Cr(NBu^t)_2Cl_2$ (**1**), can be prepared in multigram quantities. The reaction is very sensitive to conditions; longer reaction times or higher temperatures than those specified in the Experimental lead to reduced yields, possibly due to polymer formation and/or reduction by chloride ion (cf. reduction of CrO_2Cl_2 by BCl_3[7]). Other main group or transition metal halides ($AlCl_3$, PCl_5, $TiCl_4$, $ZrCl_4$) react similarly but the products are difficult to separate and BCl_3 is the preferred reagent because of the ease of removal of excess chlorinating agent and side products. The chloride (**1**) has been claimed previously,[5,8] but the materials reported were evidently impure oils; our product is a red crystalline solid that can be conveniently purified by sublimation. It is extremely sensitive to moisture; it is less oxidizing than CrO_2Cl_2 as is evident from its reactivity and this is doubtless due to increased π-donation to the metal by the imido group.[6b] The ^1H NMR spectrum is strongly dependent on the nature of the solvent; aromatic solvents induce upfield shifts, possibly due to weak complex formation (cf. the adduct with pyridine[5]). In the $^{13}C\text{-}\{^1H\}$ NMR

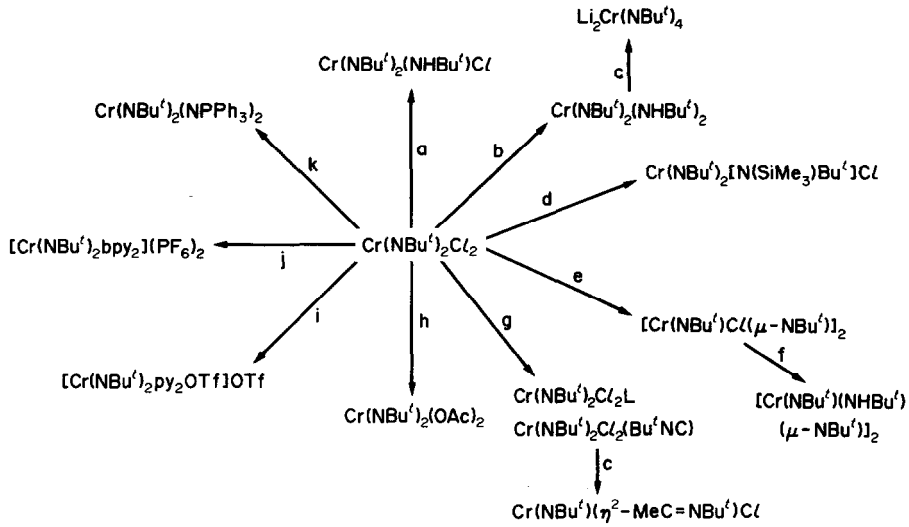

Scheme 1. Reactions of $Cr(NBu^t)_2Cl_2$. (a) Bu^tNH_2 or $Bu^tNH(SiMe_3)$; (b) Bu^tNHLi (2 eq); (c) MeLi, Et_2O; (d) $LiN(SiMe_3)(Bu^t)\cdot Et_2O$; (e) $Zn(CH_2CMe_3)_2$, *CpLi or Cp_2Co; (f) Bu^tNHLi; (g) L = PMe_2Ph, PMe_3, Bu^tNC, bpy; (h) AgOAc; (i) $AgSO_3CF_3$+py; (j) bpy, $AgCF_3SO_3$, PF_6^-; (k) $LiNPPh_3$.

spectrum the Δ parameter[6b,9] (Δ = 53 ppm) indicates the presence of electrophilic, probably linear, $MNBu^t$ groups and the high order of the Cr—N bond is supported by the IR stretching frequency.

(2) *Bis(t-butylimido)(t-butylamido)chlorochromium* (VI) (**2**), *bis(t-butylimido)bis(t-butylamido)chromium*(VI) (**3**), *bis(butylimido)[t-butyl(trimethylsilyl)amido]chlorochromium*(VI) (**4**) *and dilithium tetrakis (t-butylimido)chromate*(VI) (**5**)

The interaction of the dichloride with excess Bu^tNH_2 proceeds according to eq. (1):

$$Cr(NBu^t)_2Cl_2 + 2Bu^tNH_2 = Cr(NBu^t)_2(Bu^tNH)Cl + Bu^tNH_3Cl. \quad (1)$$

Further substitution does not occur even under forcing conditions, while the use of less bulky amines gives intractable products.

t-Butylsilylamine reacts similarly only to give the monoamido species (**2**), eq. (2):

$$Cr(NBu^t)_2Cl_2 + Bu^tNH(SiMe_3) = Cr(NBu^t)_2(Bu^tNH)Cl + SiMe_3Cl. \quad (2)$$

Compound **2** is monomeric (mass spectrum) and remarkably inert towards substitution of the chloride by a variety of nucleophiles. Methyllithium gives intractable products and there is no reaction with more bulky alkyl lithium or Grignard reagents. The compound can be recovered after treatment with Na/Hg or Mg in tetrahydrofuran.

The bis-amido compound, $Cr(NBu^t)_2(NHBu^t)_2$ (**3**) is obtained from $Cr(NBu^t)_2Cl_2$ with two equivalents of $LiNHBu^t$ in toluene but in rather low yield evidently because of competing reduction reactions. The bis-amido compound could not be obtained either at elevated temperature or by use of more polar solvents.

Attempts to obtain $Cr(NBu^t)_3$ (the isoelectronic analogue of CrO_3) from **2** via α-elimination of HCl by thermal or photochemical treatment or by interaction with strong neutral (Et_3N, proton sponge) or anionic (Bu^tLi) bases were unsuccessful and the starting material is recovered. A possible alternative route involved synthesis of $Cr(NBu^t)_2[N(SiMe_3)Bu^t]Cl$ (**4**) by interaction of $Cr(NBu^t)_2Cl_2$ with $LiNBu^t(SiMe_3)\cdot Et_2O$ but thermolysis in THF or toluene gives a green material from which, on work-up, only orange crystals of $Cr(NBu^t)_2(NHBu^t)Cl$ can be isolated; the solvent evidently acts as a source of hydride. There was no reaction in hexane.

Deprotonation of **3** with lithium alkyls under conditions similar to those used for synthesis of the molybdenum and tungsten analogues[1c] gives $Li_2Cr(NBu^t)_4$ (**5**).

Although crystals of **5** suitable for X-ray study could not be obtained, the compound is evidently isostructural with the molybdenum and tungsten analogues[1] and can be formulated as $(Bu^tN)_2Cr(\mu\text{-}NBu^tLi)_4Cr(NBu^t)_2$, as the spectroscopic properties of the three compounds are very similar. Thus the ^1H NMR spectrum of **5** has two singlets (ratio 1 : 3)

at 1.60 and 1.30 ppm corresponding to linear and bent metal–imido groups, respectively (cf. W, 1.67, 1.48; Mo, 1.66, 1.47 ppm). The IR bands for linear and bent groups are at 1230 and 1190 cm^{-1}, respectively.

(3) *Adducts and chloride-substituted compounds from* $Cr(NBu^t)_2Cl_2$

(a) *Adducts.* The pyridine compound, $Cr(NBu^t)_2Cl_2(py)$, was obtained from $Cr(NBu^t)_2(OSiMe_3)_2$ by action of HCl in Et_2O followed by pyridine.[5] Interaction of $Cr(NBu^t)_2Cl_2$ with PMe_2Ph, PMe_3 and Bu^tNC readily gives rise to the corresponding mono-adducts (**6**, **7** and **8**), as expected for addition to the 16-electron Lewis acid (**1**). These adducts are insoluble in toluene but are fairly soluble in THF or in CH_2Cl_2 in which they are non-conductors. There is no evidence even in refluxing THF for transfer of an imido group to the phosphine as occurs for the monoimido tetraphenylporphyrin complex of chromium(IV),[10] where the phosphineimide and chromium(II) porphyrin are obtained. Interaction of **1** with $Ph_2P(CH_2)_2PPh_2$ (dppe) formed a dppe bridged dimer (**9**) which again has five-coordinate chromium(VI). The reluctance to give an octahedral species may be attributed to the strong *trans* influence of the imido ligand[6b] which precludes having a phosphorus atom *trans* to it (cf. similar observations for tungsten imido complexes[11]). However, interaction with 2,2′-bipyridyl (bpy) does give a six-coordinate adduct $Cr(NBu^t)_2Cl_2(bpy)$ (**10**) which can be converted to the cation, $[Cr(NBu^t)_2(bpy)_2]^{2+}$, as discussed below.

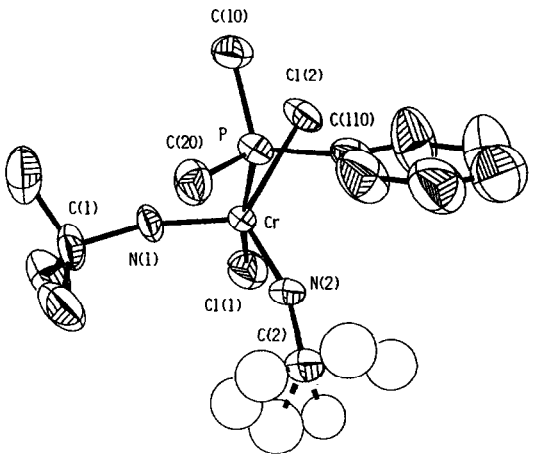

Fig. 1. The structure of $Cr(NBu^t)_2Cl_2(PMe_2Ph)$.

The structure of $Cr(NBu^t)_2Cl_2(PMe_2Ph)$ has been determined by X-ray crystallography.

A diagram of the molecule is shown in Fig. 1 and selected bond lengths and angles are given in Table 2. The geometry is quite clearly best described as trigonal bipyramidal, with the phosphine and one chlorine occupying the axial sites. The Cr—Cl_{ax} and Cr—Cl_{eq} distances are very similar, reflecting the lack of any *d* electrons and Cr—P π-bonding. One surprising feature is that in the equator, the N—Cr—N angle is the smallest, whereas repulsions between the electron density in the imido bonds might be expected to require enlargement of this. A similar feature has been found in the trigonal

Table 2. Selected bond lengths (Å) and bond angles (°) for $Cr(NBu^t)_2Cl_2(PMe_2Ph)$

Bond lengths			
P(1)—Cr(1)	2.392(5)	Cl(1)—Cr(1)	2.351(5)
Cl(2)—Cr(1)	2.342(5)	N(1)—Cr(1)	1.638(11)
N(2)—Cr(1)	1.641(12)	C(10)—P(1)	1.799(15)
C(20)—P(1)	1.812(15)	C(110)—P(1)	1.816(12)
C(1)—N(1)	1.453(17)	C(2)—N(2)	1.446(17)
C(12)—C(1)	1.529(24)	C(13)—C(1)	1.572(25)
C(11)—C(1)	1.480(22)		
Bond angles			
Cl(1)—Cr(1)—P(1)	167.1(1)	Cl(2)—Cr(1)—P(1)	81.5(2)
Cl(2)—Cr(1)—Cl(1)	86.4(2)	N(1)—Cr(1)—P(1)	93.2(4)
N(1)—Cr(1)—Cl(1)	95.3(4)	N(1)—Cr(1)—Cl(2)	122.3(5)
N(2)—Cr(1)—P(1)	91.6(5)	N(2)—Cr(1)—Cl(1)	93.1(5)
N(2)—Cr(1)—Cl(2)	124.1(5)	N(2)—Cr(1)—N(1)	113.4(6)
C(10)—P(1)—Cr(1)	115.2(6)	C(20)—P(1)—Cr(1)	111.6(6)
C(20)—P(1)—C(10)	103.8(8)	C(110)—P(1)—Cr(1)	112.5(5)
C(1)—N(1)—Cr(1)	166.4(10)	C(2)—N(2)—Cr(1)	163.6(10)

bipyramidal $Re(NBu^t)_2Cl_3$.[2] The Cr–imido functions have normal geometries with short Cr—N bonds (1.635 Å) and slight bends of *ca* 14° in the Cr—N—C group. Both imido groups are required to act as 4e donors to provide an 18e configuration at chromium.

(b) *Chloride substitution reactions.* Some of these have been noted above. Interaction of **1** with silver acetate gives $Cr(NBu^t)_2(\eta^1\text{-}O_2CMe)_2$ (**11**) as a low melting solid, readily soluble in organic solvents. The η^1-coordination is in accord with both IR and NMR data.

Interaction of **1** with silver trifluoromethanesulphonate (AgOTf) in acetonitrile removes Cl^- as AgCl and the adduct $Cr(NBu^t)_2(MeCN)_n(OTf)_2$ is obtained, but only as an orange oil that has not crystallized; addition of pyridine or PMe_3 allows isolation of the respective crystalline products, **12**, **13**. In the latter case the analysis corresponds to $[Cr(NBu^t)_2(PMe_3)_2](OTf)_2 \cdot 0.5MeCN$ (**13**) and the presence of MeCN was also confirmed by IR and ^1H NMR spectra. From spectroscopic data the pyridine complex (**12**) is clearly $[Cr(NBu^t)_2py_2(\eta^1\text{-}OTf)](OTf)$, with one η^1-triflate bound to five-coordinate chromium(VI); in MeCN at 25°C the molar conductivity (183 Ω^{-1} cm^2 mol^{-1}) is somewhat higher than usual for a 1 : 1 electrolyte which suggests some dissociation of coordinated triflate in dilute solution. The X-ray structure of the salt is shown in Fig. 2 and bond lengths and angles are given in Table 3.

The geometry of the cation is again suitably described as trigonal bipyramidal, this time with the axial sites occupied by the pyridine donors. The distribution of ligands in the equator reflects that found in the dichloro complex described above,

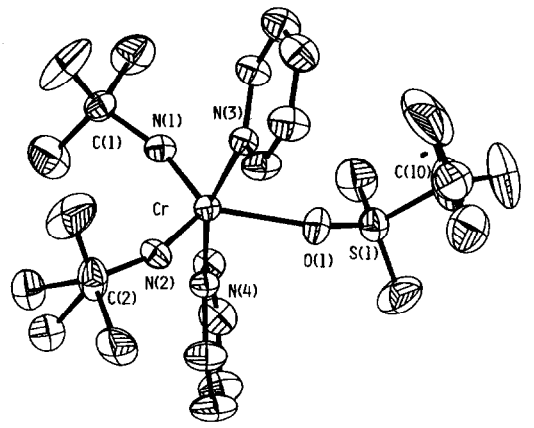

Fig. 2. The structure of the cation in $[Cr(NBu^t)_2(C_5H_4N)_2(\eta^1\text{-}O_3SCF_3)]CF_3SO_3$.

with the smallest angle between the two imido bonds. The Cr—N—C groups are again slightly bent, with angles of *ca* 163°, although normal Cr≡NR interactions are again required to provide an 18e configuration for chromium. It may be noted that a similar tungsten compound $W(NBu^t)_2(NH_2Bu^t)_2(\eta^1\text{-}OTf)_2$ is octahedral with *cis*-η^1-O_3SCF_3 groups.[1b,c]

Interaction of $Cr(NBu^t)_2Cl_2(bpy)$ (**10**) with AgOTf and additional bpy in MeCN leads to the cation $[Cr(NBu^t)_2(bpy)_2]^{2+}$ that can be precipitated as its PF_6^- salt (**14**), which is sparingly soluble in THF and CH_2Cl_2 but very soluble in MeCN in which Λ_M = 250 Ω^{-1} cm^2 mol^{-1} (1 : 2 electrolyte). The solid salt is unaffected by water, methanol or dilute normal acids. The *cis* geometry for the two NBu^t ligands in the octahedral complex is suggested

Table 3. Selected bond lengths (Å) and bond angles (°) for $[Cr(NBu^t)_2py_2(\eta^1\text{-}OTf)]^+$

Bond lengths			
O(1)—Cr(1)	2.028(7)	N(1)—Cr(1)	1.629(7)
N(2)—Cr(1)	1.615(7)	N(3)—Cr(1)	2.062(7)
N(4)—Cr(1)	2.067(7)	O(1)—S(1)	1.466(6)
Bond angles			
N(1)—Cr(1)—O(1)	127.1(3)	N(2)—Cr(1)—O(1)	121.0(3)
N(2)—Cr(1)—N(1)	111.8(4)	N(3)—Cr(1)—O(1)	79.6(3)
N(3)—Cr(1)—N(1)	96.4(3)	N(3)—Cr(1)—N(2)	93.9(3)
N(4)—Cr(1)—O(1)	82.8(3)	N(4)—Cr(1)—N(1)	94.8(3)
N(4)—Cr(1)—N(2)	94.5(3)	N(4)—Cr(1)—N(3)	162.4(2)
S(1)—O(1)—Cr(1)	137.3(3)	C(1)—N(1)—Cr(1)	163.2(5)
C(2)—N(2)—Cr(1)	161.9(5)	C(31)—N(3)—Cr(1)	121.4(5)
C(35)—N(3)—Cr(1)	120.9(5)	C(41)—N(4)—Cr(1)	121.8(5)
C(45)—N(4)—Cr(1)	120.1(5)		

by two types of C_5H_4N rings of the bpy ligands (two N atoms *trans* to NBu^t) according to the NMR data.

The isocyanide complex, $Cr(NBu^t)_2Cl_2(CNBu^t)$ (**8**), was treated with MeLi in diethyl ether in the expectation that nucleophilic attack might lead to a carbene complex. However, the product was the η^2-iminoacyl complex, $[Cr(NBu^t)_2(\eta^2\text{-}Bu^tN{=}CMe)Cl]$ (**15**), that was characterized spectroscopically. A related iminoacyl,[4] characterized crystallographically, was obtained by transfer of a mesityl group in $Cr(NBu^t)_2(mes)_2$ to the carbon atom of Bu^tNC in an "insertion" reaction. The present complex is presumably formed by methyl transfer to the isocyanide carbon atom in an intermediate $Cr(NBu^t)_2Cl(Me)(CNBu^t)$. The IR spectrum has a characteristic $\nu(C{=}N)$ stretch at 1760 cm^{-1} (cf. refs 2 and 4).

The interaction of $Cr(NBu^t)_2Cl_2$ with two equivalents of $LiN{=}PPh_3$ in toluene gives the bisphosphineiminato compound, $Cr(NBu^t)_2(NPPh_3)_2$ (**16**). Although phosphineiminato complexes are well established,[12] the use of $LiNPPh_3$ as a phosphineiminato transfer agent is not common. From the three resonance forms possible for the metal–ligand system, viz.

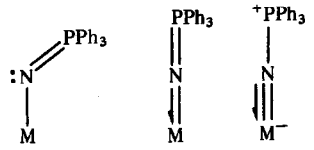

(I) **(II)** **(III)**

We consider that form **I** contributes more in the present case in view of the IR absorption (1075 cm^{-1}) at the lower limit of the ν(P—N) region, 1050–1200 cm^{-1}.[12]

Complex **16**, although it reacts with high oxidation state oxo compounds like CrO_2Cl_2, $CrO_2(OSiMe_3)_2$, OsO_4 or $MoO_2(S_2CNEt_2)_2$, does not form a nitrido-bridged dimer with elimination of Ph_3PO; such a reaction occurs with free phosphine imines and the oxo species, OsO_4 and OsO_3NBu^t.[13]

(4) *Reduction reactions of* $Cr(NBu^t)_2Cl_2$

The dialkyls[5] such as the neopentyl were obtained by alkylation of $Cr(NBu^t)_2(py)Br_2$ and the authors state that "The choice of alkylating agent is clearly critical in order to prevent reduction". We had independently shown that $Cr(NBu^t)_2Cl_2$ at 0–5°C in diethyl ether with $LiCH_2CMe_3$ and $LiCH_2SiMe_3$ gives the dialkyls identical to those described.[5] However, we find additionally that at low temperatures the diamagnetic chromium(V) dimer, $[(Bu^tN)ClCr(\mu\text{-}NBu^t)]_2$ (**17**), only is obtained; the same product is obtained by reaction of **1** with LiC_5Me_5. An oxo analogue of this imido species is not known. It seems reasonable to assume that reduction (with Li or Mg alkyls acting as one-electron reductants) and alkylation, are competing reactions, with substitution being kinetically favoured, while the thermodynamically preferred product is **17**. (cf. The similar rhenium(VI) compound[2].)

The confirmation of a one-electron reduction process is shown by the reaction of **1** with $(\eta^5\text{-}C_5H_5)_2Co$ [eq. (3)]:

$$2Cr(NBu^t)_2Cl_2 + 2Cp_2Co = 2Cp_2Co^+Cl^- + [Cl(NBu^t)Cr(\mu\text{-}NBu^t)]_2. \quad (3)$$

So far, attempts to reduce $Cr(NBu^t)_2Cl_2$ in the presence of various O, N and P donors, alkenes, etc., by use of Na/Hg or Mg, have given only brown intractable products.

The dimer **17** reacts with $LiNHBu^t$ in diethyl ether to give the first imido amido complex of chromium(V), namely $[Cr(NBu^t)(NHBu^t)(\mu\text{-}NBu^t)]_2$ (**18**); the high solubility of the compound in hexane, even at −78°C, makes isolation in high yields difficult. The ^1H NMR spectrum of the diamagnetic compound consists of six singlets, which on close examination are found to comprise two sets of three singlets. A similar spectrum has been observed for the isoelectronic vanadium analogue,[14] $[V(NBu^t)(NHBu^t)(\mu\text{-}NBu^t)]_2$, which is also highly petroleum soluble. The spectra probably result from the double bond character of the $Cr{=}NHBu^t$ bond which restricts rotation about the Cr—N bond,[15] giving two sets of isomers.

We have been unable to obtain X-ray quality crystals of compounds **17** and **18** due to twinning. However, the structures with bridged NBu^t groups are well established by IR and NMR spectra. The chromium(V) atom is thus four-coordinate in both cases and there could be a metal–metal interaction, although this seems unlikely. The diamagnetism of the compounds is presumably due to superexchange interaction of unpaired electron density on each metal atom via the imido bridge. The situation is thus similar to that found for the rhenium(VI) compound, $[(Bu^tN)_2(\mu\text{-}Bu^tN)Re]_2$, which has been characterized by X-ray diffraction.[2]

EXPERIMENTAL

Experimental procedures and instrumentation have been described.[2,16] The following starting materials were prepared by literature methods:

$Cr(NBu^t)_2(OSiMe_3)_2$,[6a] $Zn(CH_2CMe_3)_2$[17] and $(C_6H_5)_3P{=}NH$,[18] $LiNHBu^t$ was prepared by interaction of Bu^tNH_2 with Bu^nLi in hexane at −78°C and $LiNBu^t(SiMe_3)\cdot Et_2O$ by deprotonation of $Bu^tNHSiMe_3$ with LiMe in Et_2O. In mass spectra (EI at 70 eV) all *m/e* values show appropriate isotopic envelopes due to chromium isotopes. NMR data are in ppm relative to Me_4Si in C_6D_6 unless otherwise stated; ^{31}P spectra are referenced to external H_3PO_4. IR data are in cm^{-1} in Nujol mulls unless otherwise stated.

(1) *Bis(t-butylimido)dichlorochromium*(VI) (**1**)

To a solution of $Cr(NBu^t)_2(OSiMe_3)_2$ (6.0 g, 0.016 mol) in CH_2Cl_2 (60 cm^3) at 0°C was added dropwise with stirring over 5 min a solution of BCl_3 in hexane (32 cm^3 of 1M solution; 0.032 mol). The solution becomes slightly darker in colour and after addition of BCl_3 was allowed to warm to room temperature and stirred for 2 h. Longer reaction times depress the yield. Volatiles were recovered in vacuum leaving an oily residue which after *ca* 1 h in vacuum solidifies. The solid was extracted with hot hexane until the extracts were colourless (*ca* 4×50 cm^3); removal of solvent left a red residue which was sublimed (80–100°C/0.01 mm Hg) to a cold probe. Yield 55–65%.

MS: 264(M^+); 249(M^+-Me); 233(M^+-MeNH_2). NMR ^1H: 1.14s; ($CDCl_3$) 1.60 s; $^{13}C\{^1H\}$ ($CDCl_3$): 30.4, $C(CH_3)_3$; 82.5 $C(Me_3)$. IR: 1258 (NBu^t); 358 (CrCl).

(2) *Bis(t-butylimido)(t-butylamido)chlorochromium* (VI) (**2**)

Method A. A solution of **1** (1.0 g, 3.8 mmol) and $Bu^tNH(SiMe_3)$ (1.45 g, 10 mmol) in hexane (30 cm^3) was refluxed (*ca* 12 h) when the colour changed from dark red to orange–red. After removal of volatiles in vacuum the orange solid was crystallized from hot hexane. Yield: 0.75 g (66%).

Method B. To **1** (0.5 g, 1.9 mmol) in hexane (10 cm^3) was added Bu^tNH_2 (2 cm^3) and the solution refluxed for 8 h. Work-up as above gave 0.2 g (35%) of product, spectroscopically identical with that prepared as above. MS: 301 (M^+); 286 (M^+-Me); 271 (M^+-2Me); 230 (M^+-NBu^t). NMR ^1H: 1.30 [s, 18H, $NC(CH_3)_3$]; 1.21 [s, 9H, $NHC(CH_3)_3$]. IR: 3250 (NH), 1202 (NBu^t), 358 (CrCl).

(3) *Bis(t-butylimido)bis(t-butylamido)chromium*(VI) (**3**)

A toluene (20 cm^3) solution of **1** (0.5 g, 1.89 mmol) at −78°C was added via a cannula to a cold (−78°C) solution of $LiNHBu^t$ (0.3 g, 3.77 mmol) in toluene (20 cm^3) over *ca* 10 min and the mixture allowed to warm over 12 h, during which time the colour changed from orange–red to dark purple. The volatiles were removed and the residue extracted with hexane (3×20 cm^3); the filtered extracts were evaporated and the residue sublimed (80°C/0.05 mm Hg) to give a red–purple crystalline solid. Yield: 0.25 g (40%).

MS: 338 (M^+); 323 (M^+-Me); 308 (M^+-2Me). NMR ^1H: 1.39 [s, 18H, $NHBu^t$]; 1.35 [s, 18H, (NBu^t)].

(4) *Bis(t-butylimido)[t-butyl(trimethylsilyl)amido] chlorochromium* (**4**)

To **1** (0.3 g, 1.13 mmol) in toluene (30 cm^3) at −78°C was added dropwise via a cannula, a solution of $LiNBu^t(SiMe_3)\cdot Et_2O$ (0.26 g, 1.13 mmol) in toluene (20 cm^3) and the mixture allowed to warm to room temperature with stirring (12 h). Removal of volatiles and extraction of the residue with hexane (2×20 cm^3), filtration and evaporation of the solution left a red–purple solid which was sublimed (100°C/0.05 mm Hg). Yield: 0.18 g (*ca* 45%).

NMR ^1H ($CDCl_3$): 1.60 {s, 9H, $N(SiMe_3)[C(CH_3)_3]$}; 1.54 [s, 18H, $NC(CH_3)_3$]; 0.51 [s, 9H, $SiMe_3$].

(5) *Dilithium tetrakis(t-butylimido)chromate*(VI) (**5**)

To a solution of $Cr(NBu^t)_2(NHBu^t)_2$ (0.3 g, 0.9 mmol) in hexane–ether (3 : 1, 20 cm^3) at −78°C was added dropwise a solution of Bu^nLi (0.65 cm^3 of a 2.68 M solution). After stirring for 10 min at −78°C the mixture was allowed to warm (1 h) and then was heated (30°C, 0.5 h), after which volatiles were removed and the residue extracted with hexane (3×10 cm^3); concentration (5 cm^3) and cooling (−20°C, 2 days) gave red crystals which could be recrystallized from Et_2O. Yield: 0.03 g (*ca* 10%).

IR: 1224 (linear $CrNBu^t$); 1184 (bent $CrNBu^t$). NMR ^1H: 1.30 [s, 27H, (bent imido)]; 1.60 [s, 9H (linear imido)]. In $CDCl_3$ values are 1.40 and 1.56.

(6) *Bis(t-butylimido)(dimethylphenylphosphine)dichlorochromium*(VI) (**6**)

To a solution of **1** (0.2 g, 0.75 mmol) in toluene (10 cm^3) was added PMe_2Ph (0.1 cm^3, 1.5 mmol). The resulting mixture was stirred at room temperature for 3 h. The yellow precipitate was collected, washed with hexane and recrystallized from THF at −20°C. Yield: 0.13 g (52%).

NMR ^1H ($CDCl_3$): 1.52 (s, 18H, NBu^t); 2.08 (6H,

d, PMe_2, $^3J_{P-H}$ = 11.95 Hz) and aromatic protons; $^{31}P-\{^1H\}$ ($CDCl_3$): 30.67.

(7) *Bis(t-butylimido)(trimethylphosphine)dichlorochromium*(VI) (**7**)

This was prepared as for **6** from **1** (0.2 g, 0.75 mmol) and PMe_3 (0.075 cm^3) in toluene. Recrystallization from THF at −20°C afforded a yellow microcrystalline solid. Yield: 0.14 g (60%).

NMR ^1H ($CDCl_3$): 1.54 (s, 18H, NBu^t); 1.83 (d, 9H, P*Me*$_3$); $^{31}P-\{^1H\}$ ($CDCl_3$): 28.72.

(8) *Bis(t-butylimido)(t-butylisocyanide)dichlorochromium*(VI) (**8**)

This was prepared as for **6** from **1** (0.2 g, 0.75 mmol) and Bu^tNC (0.1 cm^3) in toluene. Recrystallization from THF–hexane at −20°C gave an orange microcrystalline solid. Yield: 0.12 g (45%).

IR (Nujol and KBr disk): 2237 (NC).

(9) *Bis(t-butylimido)[μ-bis(diphenylphosphino)ethane]tetrachlorodichromium*(VI) (**9**)

This was prepared as for **6** from **1** (0.2 g, 0.75 mmol) and dppe (0.3 g, 0.75 mmol) in toluene. Recrystallization from CH_2Cl_2–hexane gave a yellow microcrystalline solid. Yield: 0.2 g (40%).

NMR ^1H (CD_2Cl_2): 1.32 (s, 36H, NBu^t); 3.38 (m, 4H, *CH*$_2$PPh$_2$); $^{31}P-\{^1H\}$ (CD_2Cl_2): 50.53.

(10) *Bis(t-butylimido)(2,2′-bipyridyl)dichlorochromium*(VI) (**10**)

As for **6** but from **1** (0.29, 0.75 mmol) and 2,2′-bipyridine (0.12 g, 0.75 mmol) in toluene (20 cm^3). Yield: 0.23 g, (75%).

NMR ^1H ($CDCl_3$): 1.62 (s, 18H, NBu^t) and aromatic protons.

(11) *Bis(t-butylimido)di-η^1-acetatochromium*(VI) (**11**)

To a well-stirred suspension of Ag(OAc) (0.25 g, 1.5 mmol) in toluene (10 cm^3) was added $Cr(NBu^t)_2Cl_2$ (0.29, 0.75 mmol) in toluene (10 cm^3). The resulting mixture was stirred at room temperature overnight and filtered. The orange filtrate was evaporated to dryness and the residue extracted with hexane (10 cm^3) which was concentrated (to *ca* 5 cm^3) and cooled at −78°C to give bright orange crystals. Yield: 0.15 g (64%).

MS: 253 ($M^+ - CH_3CO_2$). IR: 1666, 1525, (CO_2). NMR ^1H ($CDCl_3$): 1.55 (s, 18H, Bu^t); 2.15 (s, 6H, C*H*$_3$CO$_2$).

(12) *Bis(t-butylimido)bis(pyridine)-η^1-O-trifluoromethylsulphonatochromium*(VI) (*trifluoromethylsulphonate*) (**12**)

To a solution of **1** (0.2 g, 0.75 mmol) in MeCN (10 cm^3) was added AgOTf (0.4 g, 1.5 mmol) in MeCN (10 cm^3). The mixture was stirred at room temperature for 1 h, filtered, and the orange filtrate evaporated. The residue was extracted with CH_2Cl_2 (20 cm^3), then pyridine (0.13 cm^3, 1.5 mmol) was added and the solution stirred for 3 h at room temperature. On reduction of volume (to *ca* 5 cm^3), excess of Et_2O (25 cm^3) was added; the orange precipitate was collected, washed with Et_2O (2 × 5 cm), and recrystallized from CH_2Cl_2–Et_2O. Yield: 0.34 g (73%).

NMR ^1H (CD_3CN): 1.66 (s, 18H, NBu^t) and aromatic protons.

(13) *Bis(t-butylimido)bis(trimethylphosphine)chromium*(VI) *bis(trifluoromethylsulphonate)*(0.5 *acetonitrile*) (**13**)

This was prepared as for **12** from **1** (0.2 g, 0.75 mmol), Ag(OTf) (0.4 g, 1.5 mmol) and PMe_3 (0.15 cm, 1.5 mmol). Yield: 0.2 g (40%). Λ_M (MeCN 25°C): 200 Ω^{-1} cm^2 mol^{-1}.

NMR ^1H (CD_2Cl_2): 1.61 (s, 18H, NBu^t); 1.92 (d, 18H, $^3J_{P-H}$ = 12 Hz; PMe_3). $^{31}P-\{^1H\}$ (CD_2Cl_2): 31.80.

(14) *Bis(t-butylimido)bis(2,2′-bipyridine)chromium*(VI)*bis(hexafluorophosphate)* (**14**)

To a solution of $Cr(NBu^t)_2Cl_2$(bpy) (0.55 g, 1.3 mmol) in MeCN (10 cm^3) was added 2 equivalents of Ag(OTf) (0.66 g, 2.6 mmol) in MeCN (10 cm^3). The solution was stirred at room temperature for 1 h, filtered and to the filtrate was added another equivalent of bpy (0.2 g). After stirring for an additional 6 h the solution was reduced in volume (5 cm^3) and a saturated methanolic solution of $[Bu^n{}_4N]PF_6$ added. The dark purple precipitate was collected, washed with THF and Et_2O, and recrystallized from MeCN–Et_2O. Yield: 0.4 g (39%).

NMR ^1H (CD_3CN): 1.45 (s, 19H, NBu^t) and aromatic protons.

(15) *Bis(t-butylimido)[η^2-methyl(t-butylimino)methyl]chromium*(VI) (**15**)

To a suspension of the isocyanide adduct (**8**) (0.3 g, 1 mmol) in Et_2O (20 cm^3) at −78°C was added MeLi (3 cm^3, 0.33 M in Et_2O) and the mixture slowly warmed to room temperature. After stirring

overnight the solution was filtered, evaporated to dryness and the residue extracted with hexane ($2 \times 10\ cm^3$). This extract was concentrated (to *ca* 10 cm^3) and cooled at $-20°C$ to give yellow crystals. Yield: 0.15 g (49%).

IR: 1760 (CN). NMR ^1H (C_6D_6): 1.30 (s, 18H, NBu^t); 1.35 (s, 9H, $C{=}NBu^t$); 2.30 (s, 3H, $Me{-}C{=}N$).

(16) *Bis(t-butylimido)bis(triphenylphosphineimino) chromium*(VI) (**16**)

A solution of **1** (0.25 g, 9.5 mmol) in toluene (10 cm^3) was added to a suspension of $LiNPPh_3$ (0.54 g, 1.9 mmol) in toluene (20 cm^3) at $-78°C$. The solution was stirred and allowed to warm overnight; filtration and evaporation of the filtrate gave a residue that was crystallized from Et_2O as dark red needles. Yield: 0.3 g (42%).

IR: 1194 (Bu^tN); 1075 (N=P); 712, 694, aromatic CH bands. NMR ^1H ($CDCl_3$): 1.28 (s, 18H, $NCMe_3$); 7.1, 8.05 (m, 30H, aromatic). $^{31}P\{^1H\}$: 8.93.

(17) *Bis[t-butylimido(chloro)(μ-t-butylimido)]dichromium*(V) (**17**)

Method A. To $Cr(NBu^t)_2Cl_2$ (0.2 g, 0.75 mmol) in toluene (20 cm^3) at $-78°C$ was added dineopentylzinc (0.5 g, 2.5 mmol), when the colour changed from red to orange–yellow. After warming with stirring (2 h), volatiles were removed and the residue extracted with hexane ($3 \times 5\ cm^3$); filtration, concentration and cooling ($-20°C$) gave green–yellow crystals. Yield: 0.06 g (*ca* 35%) based on Cr.

Method B. To a solution of $Cr(NBu^t)_2Cl_2$ (0.2 g, 0.75 mmol) in toluene (10 cm^3) was added $(C_5H_5)_2Co$ (0.15 g, 0.75 mmol) in toluene (10 cm^3). After stirring for *ca* 12 h, the solution was filtered from $(C_5H_5)_2CoCl$ and worked-up as above. Yield: 0.05 g (30%).

MS: 458 (M^+); 443 ($M^+ - Me$); 402 ($M^+ - iso$-

Table 4. Crystal data, details of intensity measurements and structure refinement

Compound	$Cr(NBu^t)_2(PMe_2Ph)Cl_2$	$[Cr(NBu^t)_2py_2(\eta^1\text{-}OTf)]OTf$
Molecular weight	403.295	662.595
Crystal system	Monoclinic	Triclinic
a (Å)	10.227(3)	14.069(2)
b (Å)	18.465(10)	10.879(1)
c (Å)	11.809(2)	9.768(3)
α (°)	90	92.74(3)
β (°)	108.46(2)	89.11(1)
γ (°)	90	93.61(3)
Volume (Å^3)	2115.93	1491.83
Space group	*Cc*	$P\bar{1}$
Z	4	2
D_c (g cm^{-3})	1.266	1.475
μ (cm^{-1})	8.558	5.830
$F(000)$	848	680
h, k, l range	$0 \rightarrow 11$	$-15 \rightarrow 15$
	$0 \rightarrow 20$	$0 \rightarrow 11$
	$-13 \rightarrow 13$	$-10 \rightarrow 10$
Total number of reflections	1680	4389
Number of unique reflections	1560	4131
Number of reflections used [$F > 3\sigma(F)$]	1331	2887
Number of parameters	203[a]	442[b]
Weighting scheme paramater g in $w = 1/[\sigma^2(F)+gF_o^2]$	0.002	0.002
Final R	0.0511	0.0734
Final R_w	0.0566	0.0813

[a] Methyl carbons of the Bu^t group at C(2) are disordered over orientations.

[b] Methyl carbons of the Bu^t group at C(2) and the fluorines at C(10) in the cation, and the sulphonyl oxygens and the fluorines in the anion are all disordered and represented in each case by four sites with suitable occupancies.

butene); 387 ($M^+ - NBu^t$). NMR ^1H: 1.74 (s, 18H, terminal imido); 1.12 (s, 18H, bridging imido).

(18) *Bis[(t-butylamido)(t-butylimido)(μ-t-butylimido)] dichromium*(V) (**18**)

To the chloro compound (**17**) (0.15 g, 0.33 mmol) in Et_2O (10 cm^3) at −78°C was added $LiNHBu^t$ (0.052 g, 0.66 mmol) in Et_2O (10 cm^3). The mixture was slowly warmed to room temperature, stirred overnight and filtered. The bluish-green filtrate was evaporated and the residue was extracted with hexane (10 cm^3). Concentration of the hexane extract (to 5 cm^3) and cooling at −78°C afforded highly-soluble dark green crystals. Yield: 0.08 g (35%).

MS: 532 (M^+); 517 ($M^+ - CH_3$); 502 (M^+ − isobutene); 460 ($M^+ - Bu^tNH$); 388 ($M^+ - 2Bu^tNH$).

X-ray crystallography

Crystals of both compounds were sealed under argon in glass capillaries. Unit cell and intensity data were obtained using standard procedures on a CAD4 diffractometer. Experimental details are given in Table 4. The structures were solved and developed via the heavy atom method and refined by full-matrix least-squares. Both crystals showed large and variable mosaic spread, indicating lower than preferred crystal quality, and structure refinement was hampered by disorder. Details are given in Table 4. Lists of final coordinates, displacement factor coefficients, bond lengths and angles, together with F_o/F_c values have been deposited as supplementary data with the Editor. Coordinates have also been deposited with the Cambridge Crystallographic Data Centre.

Acknowledgements—We thank the SERC (A.A.D.) and the Croucher Foundation, Hong Kong (W.-H.L.) for support.

REFERENCES

1. A. A. Danopoulos, G. Wilkinson, B. Hussain-Bates and M. B. Hursthouse: (a) *J. Chem. Soc., Chem. Commun.* 1989, 896; (b) *Polyhedron* 1989, **8**, 2947; (c) *J. Chem. Soc., Dalton Trans.* 1990, 2753.
2. A. A. Danopoulos, C. J. Longley, G. Wilkinson, B. Hussain-Bates and M. B. Hursthouse, *Polyhedron* 1989, **8**, 2657.
3. A. A. Danopoulos, G. Wilkinson, B. Hussain-Bates and M. B. Hursthouse, *Polyhedron* 1990, **9**, 1009.
4. A. C. Sullivan, G. Wilkinson, M. Motevalli and M. B. Hursthouse, *J. Chem. Soc., Dalton Trans.* 1988, 53.
5. N. Meijboom, C. J. Schaverien and A. G. Orpen, *Organometallics* 1990, **9**, 774.
6. (a) W. A. Nugent and R. L. Harlow, *Inorg. Chem.* 1980, **19**, 777; (b) W. A. Nugent and J. M. Mayer, *Metal–Ligand Multiple Bonds*. John Wiley, New York (1988).
7. R. B. Johannesen and H-L. Krauss, *Chem. Ber.* 1964, **97**, 2094.
8. W. A. Nugent, *Inorg. Chem.* 1983, **22**, 965.
9. W. A. Nugent and B. L. Haymore, *Coord. Chem. Rev.* 1980, **31**, 123.
10. R. L. Elliot, P. J. Nichols and B. O. West, *Polyhedron* 1987, **6**, 2191.
11. A. J. Nielsen, *Polyhedron* 1987, **6**, 1657.
12. (a) K. Dehnicke and J. Strahle, *Polyhedron* 1989, **8**, 707; (b) B. F. G. Johnson, B. L. Haymore and J. L. Dilworth, in *Comprehensive Coordination Chemistry* (Edited by G. Wilkinson, R. D. Gillard and J. A. McCleverty), Vol. 2, p. 124. Pergamon Press, Oxford (1987).
13. A. O. Chong, K. Oshima and K. B. Sharpless, *J. Am. Chem. Soc.* 1977, **99**, 3420.
14. A. A. Danopoulos and G. Wilkinson, to be published.
15. M. H. Chisholm and I. P. Rothwell, in *Comprehensive Coordination Chemistry* (Edited by G. Wilkinson, R. D. Gillard and J. A. McCleverty), Vol. 2, p. 177. Pergamon Press, Oxford (1987); M. F. Lappert, P. P. Power, A. R. Sanger and R. C. Srivastava, *Metal and Metalloid Amides*, p. 483. Ellis Harwood, Chichester (1980); L. M. Jackman and F. A. Cotton, *Dynamic Nuclear Magnetic Resonance Spectroscopy*. John Wiley, New York (1975).
16. A. A. Danopoulos, A. C. C. Wong, G. Wilkinson, B. Hussain and M. B. Hursthouse, *J. Chem. Soc., Dalton Trans.* 1990, 315.
17. R. R. Schrock and J. D. Fellman, *J. Chem. Soc.* 1978, **100**, 3359.
18. L. Birkofer, A. R. Her and P. Richter, *Chem. Ber.* 1963, **96**, 2750.

Polyhedron Vol. 9, No. 21, pp. 2635–2640, 1990
Printed in Great Britain

0277–5387/90 $3.00+.00
© 1990 Pergamon Press plc

BINUCLEAR COMPLEXES CONTAINING A DIMETALLATED OLEFIN. THE CRYSTAL AND MOLECULAR STRUCTURES OF $[Ir_2(CO)_2(C_6H_5)(CNC(CH_3)_3)(\mu\text{-}RC{=}CR)((C_6H_5)_2PCH_2P(C_6H_5)_2)_2]B(C_6H_5)_4 \cdot 0.4(CH_3)_2CO$ AND $[Rh_2Cl_2(CO)_2(\mu\text{-}RC{=}CR)((C_6H_5)_2PC_5H_4N)_2] \cdot 2C_2H_4Cl_2$ ($R = CO_2CH_3$)

J. T. MAGUE

Department of Chemistry, Tulane University, New Orleans, LA 70118, U.S.A.

(*Received* 30 *March* 1990; *accepted* 11 *July* 1990)

Abstract—X-ray structure analysis of the complexes $[Ir_2(CO)_2(C_6H_5)(CNC(CH_3)_3)(RC_2R)((C_6H_5)_2PCH_2P(C_6H_5)_2)_2]B(C_6H_5)_4$ (**1**) and $[Rh_2Cl_2(CO)_2(RC_2R)((C_6H_5)_2PC_5H_4N)_2]$ (**2**) ($R = CO_2CH_3$) shows that both contain the RC_2R moiety bound as a dimetallated olefin. The metal–metal separations [**1**: 2.8987(4) Å, **2**: 2.6528(5) Å] indicate that significant metal–metal interaction is present. The results provide confirmation of the presence of a σ-bonded (to iridium) phenyl group in **1**. In both complexes the carbonyl ligands are *trans* to the dimetallated olefin. Complex **1** is monoclinic, $P2_1/n$, $a = 19.901(5)$, $b = 19.416(4)$, $c = 24.138(8)$ Å, $\beta = 100.82(2)°$, $Z = 4$, 6812 reflections [$I \geqslant 3\sigma(I)$], $R = 0.048$, $R_w = 0.066$. Complex **2** is monoclinic, Cc, $a = 20.808(2)$, $b = 12.368(2)$, $c = 20.514(2)$ Å, $\beta = 111.446(8)°$, $Z = 4$, 3361 reflections [$I \geqslant 3\sigma(I)$], $R = 0.038$, $R_w = 0.053$.

In a recent publication[1] we reported that the attempted thermal decarbonylation of $[Ir_2(CO)_3Cl(\mu\text{-}RC_2R)(DPPM)_2]BPh_4$ ($R = CO_2Me$, DPPM = $Ph_2PCH_2PPh_2$) in refluxing THF formed $[Ir_2Cl_2(CO)_2(RC_2R)(DPPM)_2]$ and what was suggested to be $[Ir_2(CO)_2(Ph)(RC_2R)(DPPM)_2]BPh_4$ (**3**) in approximately equal amounts. The latter was proposed to derive from attack of an iridium species on the tetraphenylborate ion. In related work, $[Rh_2Cl_2(\mu\text{-}RC_2R)(Ph_2PC_5H_4N)_2]$ (**4**) ($R = CO_2Me$) has been reported[2] to reversibly add carbon monoxide to form a dicarbonyl adduct. We now report determination of the structures of the more stable *tert*-butylisocyanide adduct of **3** (**1**) and of the carbonyl adduct of **4** (**2**) which confirm the previously proposed compositions.

EXPERIMENTAL

The complex $[Ir_2(CO)_2(Ph)(CNC(CH_3)_3)(RC_2R)(DPPM)_2]BPh_4$ (**1**) ($R = CO_2Me$), prepared as previously described,[1] was crystallized by the slow diffusion of hexane and diethyl ether into an acetone solution. A pale yellow needle was wedged into a thin-walled glass capillary containing the mother liquor to retard loss of solvent of crystallization and the capillary was sealed with epoxy cement. Bright orange crystals of **2** were obtained from the slow diffusion of toluene into a CO-saturated 1,2-dichloroethane solution of the complex, prepared *in situ* from $[Rh_2Cl_2(\mu\text{-}RC_2R)(Ph_2PC_5H_4N)_2]$ ($R = CO_2CH_3$)[2] and carbon monoxide. An irregular crystal was secured with epoxy cement in the end of a thin-walled glass capillary containing the mother liquor to retard solvent loss. Intensity data were collected at room temperature on an Enraf–Nonius CAD-4 diffractometer. General procedures for the data collection and refinement have been published,[3] while details specific to the present study appear in Table 1.

Least-squares refinement of 25 reflections ($16.03 \leqslant \theta \leqslant 20.95$ for **1**; $19.94 \leqslant \theta \leqslant 24.65$ for **2**) accurately centred on the diffractometer provided final unit cell parameters. Systematic absences observed in the data collection uniquely determined the space group for **1**, while for **2** either Cc or $C2/c$ was indicated. The choice of Cc was suggested by a density measurement and confirmed

Table 1. Crystallographic data for **1** and **2**

Formula	$C_{93}H_{84}P_4O_6NBIr_2 \cdot 0.4C_3H_6O$	$C_{46}H_{42}P_2N_2O_6Cl_6Rh_2$
Formula weight	1853.98	1199.29
Crystal system	Monoclinic	Monoclinic
Space group	$P2_1/n$	Cc
a (Å)	19.901(5)	20.808(2)
b (Å)	19.496(4)	12.368(2)
c (Å)	24.138(8)	20.514(2)
β (°)	100.82(2)	111.446(8)
V (Å^3)	8871	4914
Z	4	4
ρ(calc.) (g cm^{-3})	1.39	1.62
Radiation	Mo-K_{α_1} graphite monochromated, $\lambda = 0.71073$ Å	
Linear absorbance coefficient (cm^{-1})	31.1	10.9
Range of transmission factors	0.845–1.000	—
θ range (°)	1.4–21.0	0.5–25.0
Scan type	ω–2θ	ω–2θ
Scan width (°)	$0.80+0.20 \tan\theta$	$0.80+0.20 \tan\theta$
Scan rate (° min^{-1})	1.2–16.5	1.5–16.5
Attn factor	11.87	11.87
p Factor in weight[a]	0.04	0.04
Unique data	9457	4430
Data, $I \geqslant 3\sigma(I)$	6812	3361
Number of variables	565	287
Largest shift/ESD, final cycle	0.31	0.18
R[b]	0.048	0.038
R_w[c]	0.066	0.053
GOF[d]	2.223	1.841

[a] The weighting scheme for the final refinement was $w = 1/(\sigma_F)^2$, where $\sigma_F = \sigma_{F^2}/2F$ and $\sigma_{F^2} = [(\sigma_I)^2 + (pF^2)^2]^{1/2}$.
[b] $R = \Sigma ||F_o| - |F_c|| / \Sigma F_o$.
[c] $R_w = [w(F_o - |F_c|)^2 / \Sigma w(F_o)^2]^{1/2}$.
[d] $GOF = [\Sigma w(F_o - |F_c|)^2 / (N_o - N_v)]^{1/2}$ (N_o, N_v are number of observations and variables, respectively).

by the successful refinement. Both data sets were corrected for an approximately linear decay (**1**: 12.3%; **2**: 0.8%) in the intensity monitors. An empirical absorption correction (ψ scans for six reflections, $83 \leqslant \chi \leqslant 89°$) was also applied for **1**, but not for **2** because of the inaccessibility of suitable reflections. Solution was by direct methods and refinement by full-matrix least-squares (Enraf–Nonius, SDP software package) with hydrogen atoms included as fixed contributions (C—H = 0.95 Å, isotropic thermal parameters 1.3 times that of attached carbon) riding on attached carbon atoms. Solvent of crystallization was found in both crystals. The acetone in **1** was given an occupancy of 0.4 based on a trial refinement of the occupancy factors of the constituent atoms. For **2**, two molecules of 1,2-dichloroethane were found. In the ensuing refinement of **2** the solvent molecules were not well-behaved and the phenyl groups showed very irregular geometries. A degree of disorder was indicated for the solvent by difference maps but could not be resolved. Therefore the refinement was completed employing a restrained refinement[4,5] of the solvent molecules and phenyl groups alternating with normal refinement of the remaining non-hydrogen atoms. The solvent molecules and phenyl rings were closely restrained (±0.02 Å), respectively, to the observed geometry[6] and to planar hexagons (C—C = 1.390 Å). The final difference maps for both structures were essentially featureless. Final crystallographic data have been deposited with the Editor as supplementary material.

DISCUSSION

The crystal structure of **1** consists of well-separated $[Ir_2(CO)_2(C_6H_5)(CNC(CH_3)_3)(\mu\text{-DMAD})(DPPM)_2]^+$ (DMAD = $C_2(CO_2Me)_2$) cations, tetraphenylborate anions and solvent acetone

molecules. A perspective view of the inner coordination sphere of the cation is shown in Fig. 1. The salient feature of the cation is the presence of a phenyl group bonded to iridium, confirming the composition proposed from analytical and spectroscopic data.[1] Pertinent bond distances and interbond angles appear in Table 2, from which it is evident that the coordination about each metal is roughly octahedral with the major distortion resulting from the bonding constraints of the acetylenic ligand. This moiety is clearly bound as a dimetallated olefin, as evidenced by the C(3)—C(4) distance of 1.32(1) Å and the approximately trigonal planar environment about these atoms. The Ir(1)—C(3) and Ir(2)—C(4) distances are slightly different but this is probably not significant. They are significantly longer than those in the precursor $[Ir_2(CO)_3Cl(\mu\text{-DMAD})(DPPM)_2]^+$ (**5**) [2.055(5), 2.077(5) Å][1] but compare favorably with the longer Ir—C distance [2.133(6) Å] found in $[Ir_2Cl_2(CO)_2(\mu\text{-DMAD})(DPPM)_2]$ (**6**)[7] and therefore, are not considered to be unusually long. The Ir(1)—Ir(2) distance of 2.8987(4) Å is somewhat longer than that in **5** [2.8933(2) Å], which likely reflects a greater *trans* influence of the axial phenyl group in **1** as compared to the carbonyl group in **5**. Nevertheless, it is significantly shorter than the intraligand P---P distances [P(1)---P(4) = 3.030(3), P(2)---P(3) = 3.005(3) Å], indicating an attractive interaction between the metal atoms. Although the metal–metal distances in **1** and **5** are rather long for an Ir—Ir bond [c.f. Ir—Ir = 2.7793(3) Å in **6**], significant metal–metal interaction is required to accomodate the observed diamagnetism and the longer distances observed for the former two compared with that in **6** are probably the result of their cationic nature.

Many of the other structural features of **1** can be attributed to steric factors. Thus the plane of the phenyl group on Ir(I) is twisted by only *ca* 7° from the mean equatorial plane. This phenyl ring is substantially sandwiched between those built on C(111) and C(211) and makes close contacts with two *ortho*-hydrogens [C(12)---H(112) = 2.90, C(16)---H(212) = 2.89 Å], which effectively prevent it from assuming another orientation. While all the Ir—P distances are within the range previously found in **5** and **6**, the more typical value for DPPM-bridged di-iridium complexes is 2.32–2.33 Å.[8-10] The longer values seen for Ir(1)—P(2) and Ir(2)—P(4) are probably the result of the contacts H(226)---C(12) (2.67 Å) and H(426)---C(17) (2.82 Å) which involve a phenyl group on each of these phosphorus atoms. These contacts also account for the departure of the axial ligands (phenyl and isocyanide) from collinearity with the metal–metal bond. Both bend towards the DMAD moiety. Finally, as has been noted in **5** and **6**, there is a twist of the two sides of the cation about the Ir—Ir axis of 6.4°.

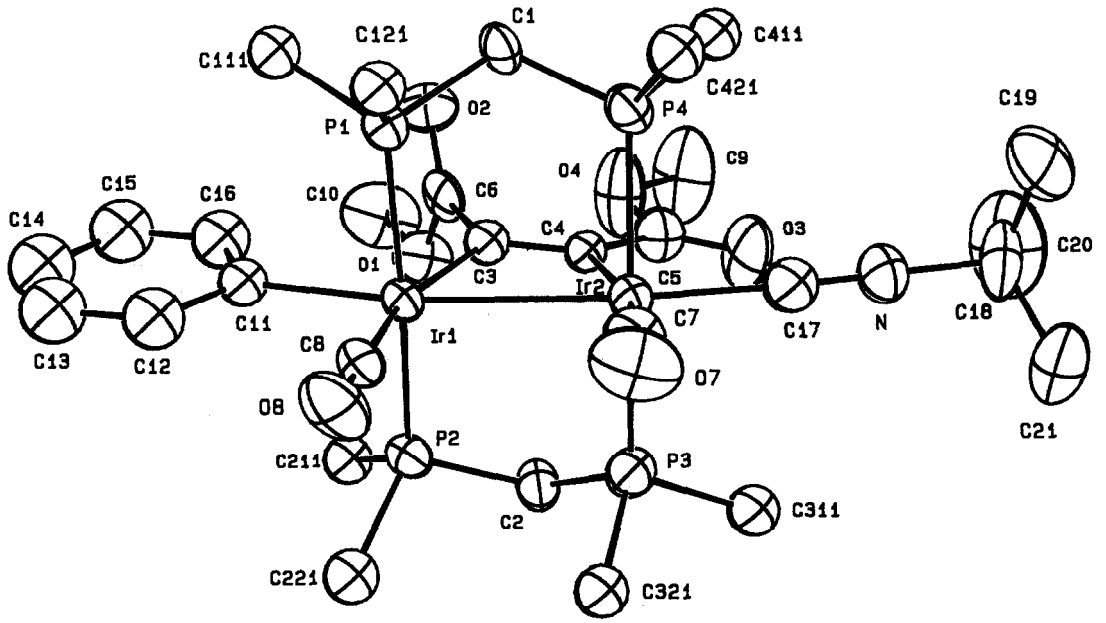

Fig. 1. A perspective view of the inner coordination sphere of the $[Ir_2(CO)_2(C_6H_5)(CNC(CH_3)_3)(\mu\text{-}H_3CO_2CC{=}CCO_2CH_3)((C_6H_5)_2PCH_2P(C_6H_5)_2)_2]^+$ cation (**1**). Thermal ellipsoids are shown at the 50% level and only the *ipso*-carbon atoms of the ligand phenyl rings are shown.

Table 2. Bond distances (Å) and interbond angles (°) for $[Ir_2(CO)_2(C_6H_5)(CNC(CH_3)_3)(\mu\text{-}H_3CO_2CC{=}CCO_2CH_3)((C_6H_5)_2PCH_2P(C_6H_5)_2)_2]B(C_6H_5)_4$ (**1**)

Bond distances			
Ir(1)—Ir(2)	2.8987(4)	Ir(2)—C(17)	2.02(1)
Ir(1)—P(1)	2.346(2)	P(1)—C(1)	1.830(8)
Ir(1)—P(2)	2.376(2)	P(4)—C(1)	1.827(8)
Ir(1)—C(3)	2.149(8)	P(2)—C(2)	1.808(8)
Ir(1)—C(8)	1.86(1)	P(3)—C(2)	1.835(8)
Ir(1)—C(11)	2.171(8)	C(3)—C(4)	1.32(1)
Ir(2)—P(3)	2.341(2)	C(7)—O(7)	1.16(1)
Ir(2)—P(4)	2.373(2)	C(8)—O(8)	1.17(1)
Ir(2)—C(4)	2.118(7)	C(17)—N	1.16(1)
Ir(2)—C(7)	1.89(1)	N—C(18)	1.51(1)

Interbond angles			
Ir(2)—Ir(1)—P(1)	90.88(5)	P(3)—Ir(2)—P(4)	170.10(8)
Ir(2)—Ir(1)—P(2)	93.76(5)	P(3)—Ir(2)—C(4)	89.4(2)
Ir(2)—Ir(1)—C(3)	67.8(2)	P(3)—Ir(2)—C(7)	93.3(3)
Ir(2)—Ir(1)—C(8)	96.9(2)	P(3)—Ir(2)—C(17)	92.0(3)
Ir(2)—Ir(1)—C(11)	169.7(2)	P(4)—Ir(2)—C(4)	81.0(2)
P(1)—Ir(1)—P(2)	170.12(8)	P(4)—Ir(2)—C(7)	96.6(3)
P(1)—Ir(1)—C(3)	90.1(2)	P(4)—Ir(2)—C(17)	87.1(3)
P(1)—Ir(1)—C(8)	91.8(3)	C(4)—Ir(2)—C(7)	164.6(3)
P(1)—Ir(1)—C(11)	85.9(2)	C(4)—Ir(2)—C(17)	97.7(3)
P(2)—Ir(1)—C(3)	83.6(2)	C(7)—Ir(2)—C(17)	97.3(4)
P(2)—Ir(1)—C(8)	96.3(3)	Ir(1)—C(3)—C(4)	111.0(6)
P(2)—Ir(1)—C(11)	88.1(2)	Ir(1)—C(3)—C(6)	126.6(6)
C(3)—Ir(1)—C(8)	164.6(3)	C(4)—C(3)—C(6)	122.4(7)
C(3)—Ir(1)—C(11)	102.4(3)	Ir(2)—C(4)—C(3)	112.0(6)
C(8)—Ir(1)—C(11)	92.9(3)	Ir(2)—C(4)—C(5)	122.6(6)
Ir(1)—Ir(2)—P(3)	87.60(6)	C(3)—C(4)—C(5)	125.4(7)
Ir(1)—Ir(2)—P(4)	90.96(5)	Ir(1)—C(8)—O(8)	178.6(7)
Ir(1)—Ir(2)—C(4)	68.5(2)	Ir(2)—C(7)—O(7)	179.2(9)
Ir(1)—Ir(2)—C(7)	96.5(3)	Ir(2)—C(17)—N	173.4(8)
Ir(1)—Ir(2)—C(17)	166.2(2)	C(17)—N—C(18)	175(1)

The crystal structure of **2** consists of well-separated $[Rh_2Cl_2(CO)_2(\mu\text{-DMAD})(Ph_2PC_5H_4N)_2]$ molecules and two independent, partially disordered solvent 1,2-dichloroethane molecules. A perspective view of the inner coordination sphere is shown in Fig. 2, while pertinent bond distances and interbond angles appear in Table 3. Again, it is clear from these data that the DMAD moiety is bound as a dimetallated olefin. The Rh(1)—C(17) and Rh(2)—C(11) distances are significantly different but there does not appear to be any obvious reason for this. The former, however, compares well with those found previously in $[(\eta^5\text{-}C_5H_5)Rh(\mu\text{-DMAD})(\mu\text{-}Ph_2PC_5H_4N)Rh(CO)(\mu\text{-Cl})]_2$ (**7**).[11] The Rh(1)—Rh(2) distance of 2.6528(1) Å is midway between the corresponding distances found in **7** [2.661(1) Å] and $[Rh_2Cl_2(CO)_2(NC_5H_4{=}C(CH_3)C_6H_4)_2]$ (**8**) [2.639(2) Å],[12] but is considerably longer than that in $[Rh_2Cl_2(\mu\text{-CO})(Ph_2PC_5H_4N)_2]$ (**9**) [2.612(1) Å].[13] This is not surprising since **2**, **7** and **8** are formally rhodium(II) complexes, while **9** contains rhodium(I). As the metal–metal distance in **2** is significantly less than the intraligand P—N distances [P(1)---N(1) = 2.761(8), P(2)---N(2) = 2.679(8) Å], an attractive interaction is clearly present. The coordination about each metal is approximately octahedral with the primary distortion again being the result of the bonding constraints of the DMAD moiety. The Rh—Cl distances differ only slightly but are significantly longer than the mean value found for **8** [2.464(4) Å]. There does not appear to be an obvious reason for this difference although we note that each chlorine makes a rather close contact with the *ortho*-hydrogen of the adjacent pyridyl group [Cl(1)---H(10) = 2.675, Cl(2)---

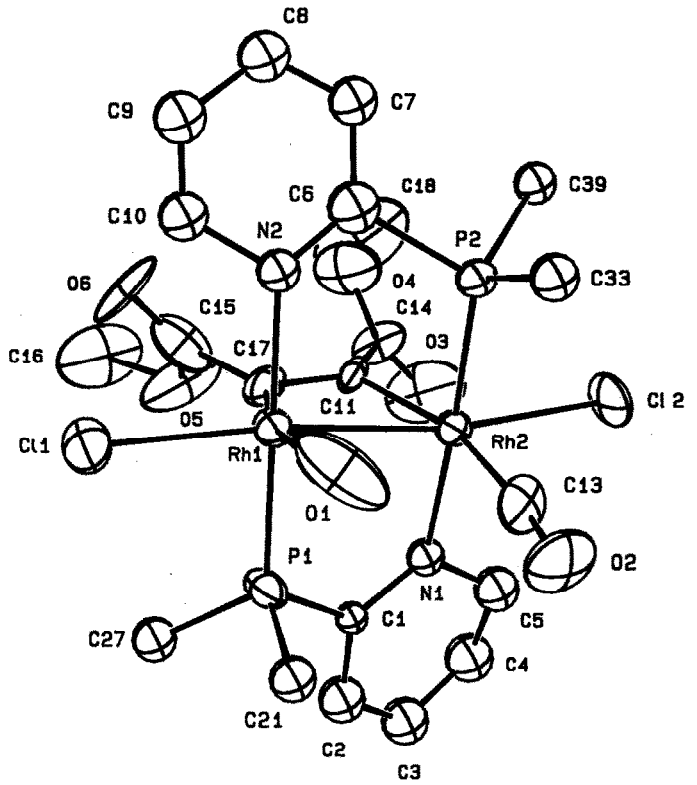

Fig. 2. A perspective view of the inner coordination sphere of $[Rh_2Cl_2(CO)_2(\mu\text{-}H_3CO_2CC{=}CCO_2CH_3)((C_6H_5)_2PC_5H_4N)_2]$ (**2**). Thermal ellipsoids are drawn at the 50% level and only the *ipso*-carbons of the phenyl rings are shown.

Table 3. Bond distances (Å) and interbond angles (°) for $[Rh_2Cl_2(CO)_2(\mu\text{-}H_3CO_2CC{=}CCO_2CH_3)((C_6H_5)_2PC_5H_4N)_2]$ (**2**)

Bond distances

Rh(1)—Rh(2)	2.6528(5)	Rh(2)—C(13)	1.96(2)
Rh(1)—Cl(1)	2.519(4)	Rh(2)—C(11)	2.09(1)
Rh(1)—P(1)	2.259(4)	P(1)—C(1)	1.82(1)
Rh(1)—N(2)	2.148(8)	P(2)—C(6)	1.86(1)
Rh(1)—C(12)	1.98(1)	N(1)—C(1)	1.40(1)
Rh(1)—C(17)	2.01(1)	N(2)—C(6)	1.29(2)
Rh(2)—Cl(2)	2.490(4)	C(12)—O(1)	1.08(2)
Rh(2)—P(2)	2.244(4)	C(13)—O(2)	1.16(2)
Rh(2)—N(1)	2.171(7)	C(11)—C(17)	1.338(8)

Interbond angles

Rh(2)—Rh(1)—Cl(1)	170.3(1)	Rh(1)—Rh(2)—C(13)	97.4(4)
Rh(2)—Rh(1)—P(1)	86.3(1)	Cl(2)—Rh(1)—P(2)	86.3(2)
Rh(2)—Rh(1)—N(2)	93.8(2)	Cl(2)—Rh(1)—N(1)	92.5(2)
Rh(2)—Rh(1)—C(12)	96.1(4)	Cl(2)—Rh(1)—C(11)	103.4(4)
Rh(2)—Rh(1)—C(17)	71.6(4)	Cl(2)—Rh(1)—C(13)	89.6(5)
Cl(1)—Rh(1)—P(1)	86.3(1)	P(2)—Rh(1)—N(1)	172.1(2)
Cl(1)—Rh(1)—N(2)	93.5(2)	P(2)—Rh(2)—C(11)	91.6(3)
Cl(1)—Rh(1)—C(12)	90.5(5)	P(2)—Rh(2)—C(13)	96.7(4)
Cl(1)—Rh(1)—C(11)	102.4(4)	N(1)—Rh(2)—C(11)	81.0(4)
P(1)—Rh(1)—N(2)	180(0)	N(1)—Rh(2)—C(13)	91.1(4)
P(1)—Rh(1)—C(12)	93.2(4)	C(11)—Rh(2)—C(13)	165.0(5)
P(1)—Rh(1)—C(17)	91.8(4)	Rh(1)—C(17)—C(11)	111(1)
N(2)—Rh(1)—C(12)	86.8(5)	Rh(1)—C(17)—C(15)	127(1)
N(2)—Rh(1)—C(17)	88.2(4)	C(11)—C(17)—C(15)	119(2)
C(12)—Rh(1)—C(17)	166.4(5)	Rh(2)—C(11)—C(17)	106(1)
Rh(1)—Rh(2)—Cl(2)	170.3(1)	Rh(2)—C(11)—C(14)	124(1)
Rh(1)—Rh(2)—P(2)	86.1(1)	C(14)—C(11)—C(17)	130(2)
Rh(1)—Rh(2)—N(1)	94.1(2)	Rh(1)—C(12)—O(1)	174(1)
Rh(1)—Rh(2)—C(11)	70.7(4)	Rh(2)—C(13)—O(2)	174(1)

H(5) = 2.537 Å]. It may, therefore, be that the lengthening is due to steric factors and this may also account for the fact that the Rh—Cl bonds are not collinear with the metal–metal axis. The Rh—N distances are significantly shorter than those found in **8** [2.25(1), 2.26(1) Å], consistent with a lower *trans* influence of phosphorus as compared with the σ-bonded phenyl group in **8**. The two sides of the molecule are twisted, with respect to one another, by 14.7°. This is probably largely steric in origin so as to minimize contacts between the phenyl group built on C(39) and the adjacent carbomethoxy group.

The ^{31}P and ^{13}C NMR spectra of **2** were reported to indicate the complex readily exchanges carbon monoxide in solution.[2] The low temperature limiting spectra of freshly prepared **2** indicated the presence of two species, the minor component having a symmetrical ^{31}P spectrum and the major component a spectrum interpreted as the AB portion of an ABXY spin system (X = Y = Rh). The latter was proposed to indicate a structure in which one rhodium had chlorine equatorial and the carbonyl axial, while on the other metal the ligand positions were reversed. The symmetrical spectrum was attributed to a species having the structure found here. The observation that the material isolated by slow crystallization at room temperature in the presence of carbon monoxide is the symmetrical isomer, together with the observed lability of **2** indicates that the latter is presumably the thermodynamically more stable isomer while the unsymmetrical species is formed under kinetic control.

Acknowledgements—The support of the Tulane University Chemistry Department and the Pennzoil Corporation are gratefully acknowledged.

REFERENCES

1. J. T. Mague, C. L. Klein, R. J. Majeste and E. D. Stevens, *Organometallics* 1984, **3**, 1860.
2. J. T. Mague, *Organometallics* 1986, **5**, 918.
3. J. T. Mague and C. L. Lloyd, *Organometallics* 1988, **7**, 983.
4. J. Konnert, *Acta Cryst.* 1976, **32A**, 614.
5. J. Konnert and W. A. Hendrickson, *Acta Cryst.* 1980, **36A**, 344.
6. T. B. Reed and W. N. Lipscomb, *Acta Cryst.* 1953, **6**, 45.
7. B. R. Sutherland and M. Cowie, *Organometallics* 1984, **3**, 1869.
8. M. Cowie, G. Vasopollo, B. R. Sutherland and J. P. Ennett, *Inorg. Chem.* 1986, **25**, 2648.
9. B. R. Sutherland and M. Cowie, *Inorg. Chem.* 1984, **23**, 2324.
10. R. Eisenberg, C. P. Kubiak and C. Woodcock, *Inorg. Chem.* 1980, **19**, 2733.
11. E. Rotondo, S. LoSchavio, G. Bruno, C. G. Arena, R. Gobetto and F. Faraone, *Inorg. Chem.* 1989, **28**, 2944.
12. D. Dowerah, L. J. Radonovich, N. F. Woolsey and M. J. Heeg, *Organometallics* 1990, **9**, 614.
13. J. P. Farr, M. M. Olmstead, C. T. Hunt and A. L. Balch, *Inorg. Chem.* 1981, **20**, 1182.

Polyhedron Vol. 9, No. 21, pp. 2641–2645, 1990
Printed in Great Britain

0277–5387/90 $3.00+.00
© 1990 Pergamon Press plc

IRON MACROCYCLIC COMPLEXES: THE SYNTHESIS AND SINGLE CRYSTAL X-RAY STRUCTURE OF $[Fe([18]aneN_2S_4)](BPh_4)_2 \cdot 2MeCN \cdot 1/2MeOH$ {$[18]aneN_2S_4$ = 1,4,10,13-TETRATHIA-7,16-DIAZACYCLOOCTADECANE}

NIGEL ATKINSON and AIDAN J. LAVERY

Department of Physical Sciences, The Polytechnic, Queensgate, Huddersfield HD1 3DH, U.K.

and

ALEXANDER J. BLAKE, GILLIAN REID and MARTIN SCHRÖDER*

Department of Chemistry, University of Edinburgh, West Mains Road, Edinburgh EH9 3JJ, U.K.

(*Received* 17 *May* 1990; *accepted* 20 *July* 1990)

Abstract—Reaction of $FeCl_2$ with one molar equivalent of $[18]aneN_2S_4$ in refluxing MeOH–H_2O for 15 min affords a deep blue solution containing the complex cation $[Fe([18]aneN_2S_4)]^{2+}$. Addition of excess BF_4^- or BPh_4^- counterions gives the complex as a blue solid. A single crystal X-ray structure determination of $[Fe([18]aneN_2S_4)](BPh_4)_2 \cdot 2MeCN \cdot 1/2MeOH$ shows iron(II) bound to all six macrocyclic donor atoms in a distorted octahedral geometry, Fe—N = 2.022(4), 2.037(5), Fe—S = 2.2578(17), 2.2588(16), 2.2673(16), 2.2674(15) Å. The macrocycle binds to give a *rac* configuration with each $SCH_2CH_2NCH_2CH_2S$ linkage bound meridionally to the metal centre. Solutions of $[Fe([18]aneN_2S_4)](BF_4)_2$ show two irreversible, overlapping oxidations at E_{pa} = +0.78 and +0.88 V vs Fc/Fc^+.

We have recently been investigating the coordination chemistry of the potentially hexadentate macrocycles $[18]aneN_2S_4$ (1,4,10,13-tetrathia-7,16-diazacyclooctadecane) and $Me_2[18]aneN_2S_4$ (7,16-dimethyl-1,4,10,13-tetrathia-7,16-diazacyclooctadecane).[1] In the course of this work we have observed that these macrocycles bind readily to transition metal centres, leading to unusual stereochemical and electrochemical properties. Importantly, we have found that $[18]aneN_2S_4$ binds octahedrally to metal centres to give exclusively the *rac* isomer, as originally proposed by Black and McLean.[1,2] As a continuation of these studies we report herein the synthesis and single crystal structure of $[Fe([18]aneN_2S_4)](BPh_4)_2 \cdot 2MeCN \cdot 1/2MeOH$.

* Author to whom correspondence should be addressed.

RESULTS AND DISCUSSION

Treatment of $FeCl_2 \cdot 4H_2O$ with one molar equivalent of $[18]aneN_2S_4$ in refluxing MeOH–H_2O (1 : 1 v/v) under N_2 for 15 min affords a deep blue solution. Addition of excess $NaBF_4$ or $NaBPh_4$ yields a blue precipitate, which can be recrystallized

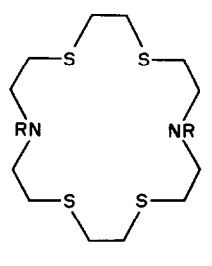

$[18]aneN_2S_4$: R = H
$Me_2[18]aneN_2S_4$: R = Me

Scheme 1.

from MeCN. Prolonged refluxing results in decomposition giving an insoluble orange precipitate.

The IR spectrum of the tetrafluoroborate salt shows peaks at 3240 and 3080 cm^{-1} corresponding to N—H stretching vibrations, ν(N—H), as well as other peaks indicative of the presence of coordinated [18]aneN_2S_4. Peaks at 1050, 535 and 520 cm^{-1} are characteristic of the BF_4^- counterion. The FAB mass spectrum of this product shows molecular ion peaks at $m/z = 469$, 401 and 381, assigned to $[^{56}Fe([18]aneN_2S_4)BF_4]^+$, $[^{56}Fe([18]aneN_2S_4)\cdot H_2O+H]^+$ and $[^{56}Fe([18]aneN_2S_4-H)]^+$, respectively. The ^1H NMR spectrum measured in CD_3NO_2 shows a complex second-order multiplet in the range $\delta = 2.15$–3.85 ppm assigned to the methylene protons of the coordinated macrocycle. The ^{13}C NMR spectrum of the complex, measured in CD_3NO_2 at 298 K, exhibits 12 distinct resonances, indicating the presence of two different isomers in solution in a ratio of roughly 3:2, (δ = 52.26, 51.90, 39.82, 39.46, 33.56 and 32.96 ppm for one isomer; 52.41, 51.80, 38.90, 38.08, 35.46 and 34.94 ppm for the other isomer). These results are consistent with the presence of two alternative forms of the *rac* configuration. These diastereoisomers, **I** and **II**, differ in the relative orientations of the N—H functions (Fig. 1) and each gives rise to six methylene carbon resonances.[3] The UV–vis spectrum of the product shows absorption bands at $\lambda_{max} = 572$ nm ($\varepsilon_{max} = 171$ M^{-1} cm^{-1}), 424 (152) and 344 (103) which are assigned as *d–d* transitions on the basis of the magnitudes of their extinction coefficients and their solvent independence. In addition, there is a much more intense band at 238 nm (19,570) which is assigned tentatively as a S → Fe charge-transfer transition. This evidence, together with microanalytical data, indicates the product to be the low-spin iron(II) species [Fe([18]aneN_2S_4)]$(BF_4)_2$. The corresponding BPh_4^- salt, [Fe([18]aneN_2S_4)]$(BPh_4)_2$, can be prepared by using $NaBPh_4$ in place of $NaBF_4$ in the above synthesis.

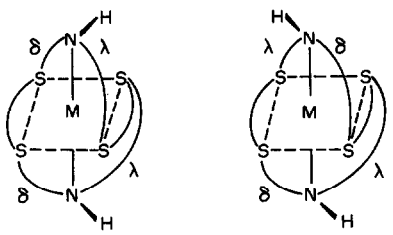

Fig. 1. Isomers **I** and **II** for *rac*-[M([18]aneN_2S_4)]$^{x+}$.

Deep blue, columnar crystals of suitable quality for a single crystal X-ray structure determination were obtained by slow evaporation from a solution of [Fe([18]aneN_2S_4)]$(BPh_4)_2$ in MeCN–EtOH. The structure confirms a *rac* configuration for [Fe([18]aneN_2S_4)]$^{2+}$ (Fig. 2), with all six macrocyclic donor atoms bound to the Fe^{II} centre, Fe—S(1) = 2.2674(15), Fe—S(4) = 2.2673(16), Fe—S(10) = 2.2578(17), Fe—S(13) = 2.2588(16), Fe—N(7) = 2.037(5), Fe—N(16) = 2.022(4) Å. Thus, the two Fe—S bond lengths in one SCH_2CH_2S chain are essentially equal, but different from those in the other SCH_2CH_2S linkage. This is consistent with predictions based on the influence of the N—H functions which give rise to approximate non-crystallographic C_2 symmetry [Fig. 2(b)] and six distinct methylene carbon resonances. Furthermore, the orientations of the two N—H groups confirm that the complex exists as isomer **I** in the crystal selected.[3] The *rac* configuration observed probably reflects the preference for *gauche* torsions at C—S linkages and *anti* torsions at C—N (secondary amine) linkages.[4] There is a small, but significant, tetrahedral distortion of the sulphur-donor atoms out of the least-squares S_4 coordination plane, with S(1) and S(13) lying 0.137 and 0.139 Å, respectively, above the plane, while S(4) and S(10) lie 0.137 and 0.139 Å, respectively, below. The structure also shows that the N—H groups in [Fe([18]aneN_2S_4)]$^{2+}$ participate in strong hydrogen-bonding interactions with the two MeCN molecules: H(7)···N(6S) = 2.079(9) Å, angle N(7)—H(7)···N(6S) = 137.4(5)°, H(7)···N(6S)—C(5S) = 171.1(7)°; H(16)···N(3S) = 2.078(9) Å, angle N(16)—H(16)···N(3S) = 139.4(4)°, H(16)···N(3S)—C(2S) = 166.5(7)°.

Cyclic voltammetry of [Fe([18]aneN_2S_4)]$(BF_4)_2$, measured in MeCN (0.1 M $^nBu_4NBF_4$ supporting electrolyte) at platinum electrodes, shows two overlapping, irreversible oxidations at $E_{pa} = +0.78$ and +0.88 V vs Fc/Fc^+, assigned tentatively to Fe^{II}/Fe^{III} couples for the two *rac* isomers. The irreversibility may be due to deprotonation of the oxidation product. The Fe^{II}/Fe^{III} couple for the related low-spin, bis-trithia and bis-triaza macrocyclic species, [Fe([9]aneS_3)$_2$]$^{2+}$ and [Fe([9]aneN_3)$_2$]$^{2+}$, occur at $E_{1/2} = +0.98$[5] and −0.59 V vs Fc/Fc^+, respectively.[6]

EXPERIMENTAL

IR spectra were recorded as KBr and CsI discs using a Perkin–Elmer 598 spectrometer over the range 200–4000 cm^{-1}. UV–vis spectra were measured in quartz cells using Perkin–Elmer Lambda 9 and Pye Unicam SP8-400 spectrophotometers. Microanalyses were performed by the Edinburgh

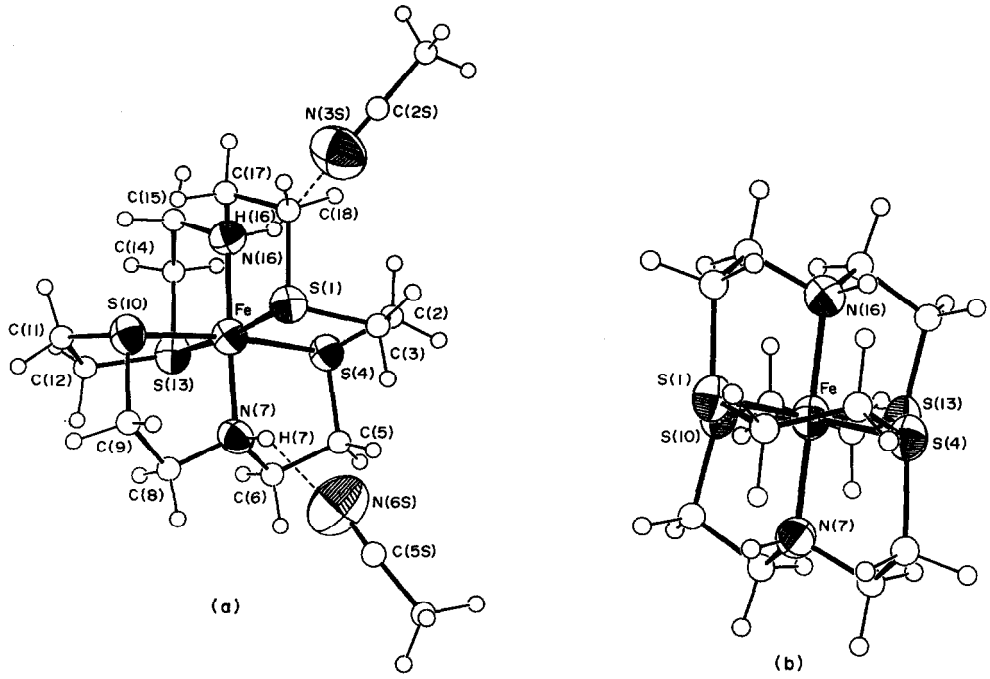

Fig. 2. Two views of the single crystal structure of $[Fe([18]aneN_2S_4)]^{2+}$: (a) showing hydrogen-bonded MeCN solvent molecules, with numbering scheme adopted; (b) view along the approximate, non-crystallographic C_2-axis.

University Chemistry Department Microanalytical service. Electrochemical measurements were performed on a Bruker E310 Universal Modular Polarograph. All readings were taken using a three-electrode potentiostatic system in acetonitrile containing 0.1 M $^nBu_4NPF_6$ or $^nBu_4NBF_4$ as supporting electrolyte. Cyclic voltammetric measurements were carried out using a double platinum electrode and an Ag/AgCl reference electrode. All potentials are quoted vs ferrocene/ferrocenium, Fc/Fc^+. Mass spectra were measured by electron impact on a Kratos MS 902 and by fast atom bombardment on a Kratos MS 50TC spectrometer. ^1H and ^{13}C NMR spectra were obtained on Bruker WP80 and WP200 instruments.

(a) *Synthesis of* $[Fe([18]aneN_2S_4)](BF_4)_2$

Reaction of $FeCl_2 \cdot 4H_2O$ (22 mg, 0.107 mmol) and $[18]aneN_2S_4$ (35 mg, 0.107 mmol) in refluxing, degassed MeOH–H_2O (35 cm^3, 1 : 1 v/v), for 15 min under N_2, afforded a deep blue solution. Cooling, reducing the volume to 10 cm^3 and filtering the reaction mixture into a solution of excess $NaBF_4$ in MeOH gave a blue precipitate which was recrystallized from MeCN and diethyl ether (Yield: 40 mg, 83%). Found: C, 26.0; H, 4.8; N, 5.0. Calc. for $[C_{12}H_{26}N_2S_4Fe](BF_4)_2$: C, 25.9; H, 4.7; N, 5.0%. FAB mass spectrum (3-NOBA matrix): Found m/z = 469, 401 and 381. Calc. for $[^{56}Fe([18]aneN_2S_4)BF_4]^+$, M^+ = 469; $[^{56}Fe([18]aneN_2S_4)\cdot H_2O]^+$, M^+ = 400; $[^{56}Fe([18]aneN_2S_4)]^+$, M^+ = 382. UV–vis spectrum (MeCN): λ_{max} = 572 nm (ε_{max} = 171 M^{-1} cm^{-1}), 424 (152), 344sh (103), 238 (19,570). ^1H NMR spectrum (80.13 MHz, CD_3NO_2, 298 K): δ = 2.15–3.85 ppm (m, CH_2, 24H). ^{13}C DEPT NMR spectrum (50.32 MHz, CD_3NO_2, 298 K): δ = 52.26, 51.90 ($2\times NCH_2$); 39.82, 39.46 ($2\times NCH_2CH_2S$); 33.56, 32.96 ppm ($2\times SCH_2CH_2S$) major isomer; δ = 52.40, 51.80 ($2\times NCH_2$); 38.90, 38.08 ($2\times NCH_2CH_2S$); 35.46, 34.94 ppm ($2\times SCH_2CH_2S$) minor isomer. IR spectrum (KBr disc): 3240m, 3080m, 2920m, 1460m, 1420m, 1380w, 1320w, 1295w, 1050vs b, 930w, 790m, 535m, 520m cm^{-1}.

(b) *Synthesis of* $[Fe([18]aneN_2S_4)](BPh_4)_2$

Method as for (a), using $NaBPh_4$ in place of $NaBF_4$. Recrystallization from MeCN–EtOH gave the product as blue crystals. FAB mass spectrum (3-NOBA matrix): Found m/z = 381. Calc. for $[^{56}Fe([18]aneN_2S_4)]^+$, M^+ = 382. IR spectrum (KBr disc): 3180m, 3040m, 2980w, 2920w, 1575m, 1475m, 1460m, 1420m, 1405m, 1380w, 1305w, 1260w, 1170w, 1120w, 1080w, 1060w, 1030w, 990w, 970w, 920w, 840w, 820w, 785w, 755m, 735vs, 710vs, 610vs, 470w cm^{-1}.

Single crystal X-ray structure determination of $[Fe([18]aneN_2S_4)](BPh_4)_2 \cdot 2MeCN \cdot 1/2MeOH$

Slow evaporation from a solution of the complex in a 1:1 v/v mixture of MeCN–EtOH gave deep blue, columnar crystals. The selected crystal ($0.69 \times 0.27 \times 0.27$ mm) was sealed in a glass capillary to prevent solvent loss. Crystal data: $[C_{12}H_{26}N_2S_4Fe]^{2+} \cdot 2(C_{24}H_{20}B^-) \cdot 2MeCN \cdot 1/2MeOH$, $M = 1119.0$, triclinic, space group $P\bar{1}$, $a = 11.8615(8)$, $b = 15.4285(12)$, $c = 17.9412(13)$ Å, $\alpha = 67.301(3)$, $\beta = 78.542(4)$, $\gamma = 76.696(3)°$,

Table 1. Bond lengths, angles and torsion angles for $[Fe([18]aneN_2S_4)]^{2+}$

Bond lengths (Å) with standard deviations

Fe—S(1)	2.2674(15)	C(6)—N(7)	1.485(7)
Fe—S(4)	2.2673(16)	N(7)—C(8)	1.498(8)
Fe—N(7)	2.037(5)	C(8)—C(9)	1.524(9)
Fe—S(10)	2.2578(17)	C(9)—S(10)	1.819(7)
Fe—S(13)	2.2588(16)	S(10)—C(11)	1.822(6)
Fe—N(16)	2.022(4)	C(11)—C(12)	1.526(9)
S(1)—C(2)	1.826(6)	C(12)—S(13)	1.817(6)
S(1)—C(18)	1.826(6)	S(13)—C(14)	1.804(6)
C(2)—C(3)	1.503(8)	C(14)—C(15)	1.532(9)
C(3)—S(4)	1.823(6)	C(15)—N(16)	1.477(8)
S(4)—C(5)	1.843(6)	N(16)—C(17)	1.503(7)
C(5)—C(6)	1.528(8)	C(17)—C(18)	1.518(8)

Angles (°) with standard deviations

S(1)—Fe—S(4)	90.66(5)	S(4)—C(5)—C(6)	108.6(4)
S(1)—Fe—N(7)	92.50(13)	C(5)—C(6)—N(7)	108.2(5)
S(1)—Fe—S(10)	90.16(6)	Fe—N(7)—C(6)	112.1(3)
S(1)—Fe—S(13)	172.77(6)	Fe—N(7)—C(8)	114.0(4)
S(1)—Fe—N(16)	86.02(13)	C(6)—N(7)—C(8)	111.2(4)
S(4)—Fe—N(7)	85.61(13)	N(7)—C(8)—C(9)	108.0(5)
S(4)—Fe—S(10)	173.20(6)	C(8)—C(9)—S(10)	112.1(4)
S(4)—Fe—S(13)	90.46(6)	Fe—S(10)—C(9)	98.06(21)
S(4)—Fe—N(16)	91.94(13)	Fe—S(10)—C(11)	106.55(20)
N(7)—Fe—S(10)	87.62(13)	C(9)—S(10)—C(11)	104.0(3)
N(7)—Fe—S(13)	94.71(13)	S(10)—C(11)—C(12)	114.5(4)
N(7)—Fe—N(16)	177.13(18)	C(11)—C(12)—S(13)	114.7(4)
S(10)—Fe—S(13)	89.56(6)	Fe—S(13)—C(12)	106.68(20)
S(10)—Fe—N(16)	94.85(13)	Fe—S(13)—C(14)	98.99(21)
S(13)—Fe—N(16)	86.80(13)	C(12)—S(13)—C(14)	103.3(3)
Fe—S(1)—C(2)	103.46(20)	S(13)—C(14)—C(15)	110.5(4)
Fe—S(1)—C(18)	100.00(19)	C(14)—C(15)—N(16)	108.7(5)
C(2)—S(1)—C(18)	101.4(3)	Fe—N(16)—C(15)	114.4(4)
S(1)—C(2)—C(3)	112.8(4)	Fe—N(16)—C(17)	112.1(3)
C(2)—C(3)—S(4)	113.5(4)	C(15)—N(16)—C(17)	111.4(4)
Fe—S(4)—C(3)	103.29(20)	N(16)—C(17)—C(18)	108.7(4)
Fe—S(4)—C(5)	99.95(19)	S(1)—C(18)—C(17)	109.3(4)
C(3)—S(4)—C(5)	101.3(3)		

Torsion angles (°) with standard deviations

C(18)—S(1)—C(2)—C(3)	−68.8(5)	C(8)—C(9)—S(10)—C(11)	79.1(5)
C(2)—S(1)—C(18)—C(17)	130.8(4)	C(9)—S(10)—C(11)—C(12)	−78.3(5)
S(1)—C(2)—C(3)—S(4)	−46.8(5)	S(10)—C(11)—C(12)—S(13)	−32.6(6)
C(2)—C(3)—S(4)—C(5)	−69.1(5)	C(11)—C(12)—S(13)—C(14)	−79.6(5)
C(3)—S(4)—C(5)—C(6)	130.7(4)	C(12)—S(13)—C(14)—C(15)	79.8(5)
S(4)—C(5)—C(6)—N(7)	−50.8(5)	S(13)—C(14)—C(15)—N(16)	49.2(6)
C(5)—C(6)—N(7)—C(8)	−175.9(5)	C(14)—C(15)—N(16)—C(17)	−174.2(5)
C(6)—N(7)—C(8)—C(9)	−172.7(5)	C(15)—N(16)—C(17)—C(18)	−177.0(5)
N(7)—C(8)—C(9)—S(10)	49.2(6)	N(16)—C(17)—C(18)—S(1)	−49.6(5)

$V = 2925.6$ Å^3 [from 2θ values for 27 reflections measured at $\pm\omega(32 < 2\theta < 35°$, $\lambda = 1.54184$ Å, $T = 298$ K)], $Z = 2$, $D_c = 1.270$ g cm^{-3}, μ(Cu-K_α) = 3.712 cm^{-1}, $F(000) = 1186$.

Data collection and processing. Stoë STADI-4 four-circle diffractometer, graphite-monochromated Cu-K_α radiation, ω–2θ scans using the learnt-profile method.[7] 8245 reflections measured ($2\theta_{max} = 120°$, h $-13 \rightarrow 12$, k $-15 \rightarrow 17$, l $-18 \rightarrow 20$) giving 6110 with $F > 6\sigma(F)$. No significant crystal decay.

Structure analysis and refinement. The iron position was deduced from a Patterson synthesis. Iterative cycles of least-squares refinement and difference Fourier syntheses[8] located the positions of all other non-hydrogen atoms. Corrections for absorption (max. 0.356, min. 0.171) were applied using ψ scans. Two fully-occupied MeCN molecules and one half-occupied MeOH molecule from the solvent were found to be associated with each $[Fe([18]aneN_2S_4)]^{2+}$ cation. Strong hydrogen-bonding interactions between the macrocyclic N—H functions and the two MeCN molecules may account for the well-ordered nature of these solvent molecules, whereas the MeOH molecule is disordered and does not participate in significant hydrogen-bonding interactions. Hydrogen atoms were included in fixed, calculated positions, and the phenyl rings of the BPh_4^- counteranion were refined as rigid groups.[8] Anisotropic thermal parameters were refined for Fe, S, N, B and C atoms. The weighting scheme $w^{-1} = \sigma^2(F) + 0.000509F^2$ gave satisfactory agreement analyses. At final convergence, $R = 0.0668$, $R_w = 0.0947$, $S = 1.232$ for 591 independent parameters, and the final difference Fourier synthesis showed no feature above 0.60 or below -0.61 e Å^{-3}. Illustrations were prepared using ORTEPII,[9] molecular geometry calculations utilized CALC,[10] and scattering factor data were inlaid[8] or taken from ref. 11. Bond lengths, angles and torsion angles are given in Table 1. Fractional atomic coordinates and thermal parameters, together with observed and calculated structure factors have been deposited with the Editor, from whom copies are available on request. Atomic coordinates have also been deposited with the Cambridge Crystallographic Data Centre.

Acknowledgement—We thank the SERC for support.

REFERENCES

1. G. Reid and M. Schröder, *Chem. Soc. Rev.* 1990, **19**, 43; G. Reid, A. J. Blake, T. I. Hyde and M. Schröder, *J. Chem. Soc., Chem. Commun.* 1988, 1397; N. Atkinson, A. J. Blake, M. G. B. Drew, G. Forsyth, A. J. Lavery, G. Reid and M. Schröder, *J. Chem. Soc., Chem. Commun.* 1989, 984.
2. D. St. C. Black and I. A. McLean, *J. Chem. Soc., Chem. Commun.* 1968, 1004; *Tetrahedron Lett.* 1969, 3961; *Aust. J. Chem.* 1971, **24**, 1401.
3. R. W. Hay, B. Jeragh, S. F. Lincoln and G. H. Searle, *Inorg. Nucl. Chem. Lett.* 1978, **14**, 435.
4. S. R. Cooper, *Accts Chem. Res.* 1988, **21**, 141; R. E. Wolf, J. R. Hartman, J. M. E. Storey, B. M. Foxman and S. R. Cooper, *J. Am. Chem. Soc.* 1987, **109**, 4328.
5. K. Wieghardt, H. J. Küppers and J. Weiss, *Inorg. Chem.* 1985, **24**, 3067; H. J. Küppers, K. Wieghardt, B. Nuber, J. Weiss, E. Bill and A. X. Trautwein, *Inorg. Chem.* 1987, **26**, 3762; A. J. Blake, A. J. Holder, T. I. Hyde and M. Schröder, *J. Chem. Soc., Chem. Commun.* 1989, 1433.
6. P. Chaudhuri and K. Wieghardt, *Prog. Inorg. Chem.* 1987, **35**, 329; K. Wieghardt, W. Schmidt, W. Herrmann and H. J. Küppers, *Inorg. Chem.* 1983, **22**, 2953.
7. W. Clegg, *Acta Cryst.* 1981, **A37**, 22.
8. G. M. Sheldrick, SHELX76, Program for Crystal Structure Refinement. University of Cambridge, U.K. (1976).
9. P. D. Mallinson and K. W. Muir, ORTEPII, Interactive Version. *J. Appl. Cryst.* 1985, **18**, 51.
10. R. O. Gould and P. Taylor, CALC, Fortran77 version. University of Edinburgh, Scotland (1985).
11. D. T. Cromer and J. L. Mann, *Acta Cryst.* 1968, **A24**, 321.

Polyhedron Vol. 9, No. 21, pp. 2647–2649, 1990
Printed in Great Britain.

0277–5387/90 $3.00+.00
© 1990 Pergamon Press plc

COMMUNICATION

DETERMINATION OF *CIS–TRANS* ISOMERS OF AMINE AND PYRIDINE PLATINUM(II) COMPLEXES BY *J*(Pt—H) COUPLING CONSTANTS

T. B. T. HA,* J.-P. SOUCHARD, F. L. WIMMER and N. P. JOHNSON

Laboratoire de Pharmacologie et de Toxicologie Fondamentales du CNRS, 205, route de Narbonne, 31077 Toulouse Cedex, France

(*Received* 14 *March* 1990; *accepted* 4 *July* 1990)

Abstract—The coupling constants ^3J(Pt—H) of $[Pt(Xpy)_2L_2]$ and $[Pt(Xpy)(dmso)I_2]$ complexes (Xpy = pyridine, 4-Me-py, 3,5-diMe-py, 4-Cl-py, 4-CN-py, 4-$HOCH_2$-py, 4-CH_3COO-py; L = Cl, I, Br, ONO_2) have been recorded. The ^3J(Pt—H) values of the *cis* complexes are 42 ± 2 Hz, while those of the *trans* derivatives are 31.5 ± 2.5 Hz. ^2J(Pt—H) of $[Pt(XNH_2)_2L_2]$ complexes (X = CH_3, cyclopropyl, cyclobutyl, cyclopentyl, cyclohexyl, cycloheptyl; L = Cl, I, ONO_2) also have been recorded. The ^2J(Pt—H) values of the *cis* complexes are 66.5 ± 1.5 Hz, those of the *trans* derivatives are 58 ± 2 Hz. These results show that measurement of Pt—H coupling constants is a rapid method of identifying the *cis* and the *trans* isomers of platinum(II) complexes.

Different methods have been used to distinguish *cis* and *trans* isomers of platinum(II) complexes. For identifying *cis*- and *trans*-$[Pt(Xpy)_2Cl_2]$, several chemical tests are available:[1]

—Oxyphenylenetelluronium hydrogen sulphate which gives a red coloration with the *cis* isomer.
—Hydrobromic acid gives a bright yellow precipitate with the *cis* isomer while the *trans* isomer gives a whitish precipitate.
—Silver oxide reacts with the *cis* isomer to give a yellow glassy mass; with the *trans* isomer white needles are formed.
—Kurnakov's test[2–4] which involves addition of thiourea and precipitation of the thiourea complexes.

In addition, several methods are available for analysing mixtures of *cis*- and *trans*-$[Pt(NH_3)_2Cl_2]$. Paper chromatography,[5] TLC and HPLC are employed mainly for detecting one isomer in the presence of the other. Solutions containing *cis*- and *trans*-$[Pt(NH_3)_2Cl_2]$ can also be analysed by measuring optical absorbances before and after controlled reaction with allyl alcohol.[6] However, ^{195}Pt NMR spectroscopy has proved to be insufficiently sensitive at low concentrations, and laser Raman spectroscopy did not yield useful signals.[5]

In this paper, we report the ^3J(Pt—H) coupling constants (Table 1) of 28 complexes of general formulae $[Pt(Xpy)_2Cl_2]$, $[Pt(Xpy)_2I_2]$, $[Pt(Xpy)_2(ONO_2)_2]$ and $[Pt(Xpy)(dmso)I_2]$; (Xpy = pyridine or substituted pyridines). The ^{1}H NMR spectra have been recorded in deuterated acetone, chloroform or dmso. The coupling constants, ^3J(Pt—H), between Pt and H(α) of the pyridines are 42 ± 2 Hz for the *cis* complexes and 31.5 ± 2.5 Hz for the *trans* isomers. In addition the ^2J(Pt—H) values of 21 complexes of general formulae $[Pt(XNH_2)_2I_2]$, $[Pt(XNH_2)_2Cl_2]$ and $[Pt(XNH_2)_2(ONO_2)_2]$ (X = CH_3, cyclopropyl, cyclobutyl, cyclopentyl, cyclohexyl, cycloheptyl) were recorded (Table 2). The difference between the values for the *cis* and *trans* isomers is smaller: 66.5 ± 1.5 Hz for the *cis* and 58 ± 2 Hz for the *trans* complexes.

Thus, the *J*(Pt—H) coupling constants are characteristic of the geometry of the complex. These results may reflect a general *trans* effect on coupling constants in platinum complexes,[7] and their

* Author to whom correspondence should be addressed.

Table 1. Pt—H coupling constants, ^3J(Pt—H) (Hz), of *cis*- and *trans*-[Pt(A_1A_2)L_2]

A_1	A_2	L	*Cis*	*Trans*	Reference
py	py	Cl	42[b]	34[b]	10
		I	41[a]	33[b]	This work
		ONO_2	43[a]	30[b]	This work
4-Me-py	4-Me-py	Cl	42[b]	33[b]	10
		I	41[a]	31[b]	This work
		ONO_2	43[a]	29[a]	This work
3,5-diMe-py	3,5-diMe-py	I	41[a,b]	32.5[b]	This work
		ONO_2	43[a]		This work
4-Cl-py	4-Cl-py	ONO_2	40[a]		This work
4-CN-py	4-CN-py	Cl	40[a,b]	33.5[b]	This work
		I	40[a]	33[a]	This work
4-$HOCH_2$-py	4-$HOCH_2$-py	ONO_2	42[a]		This work
dmso	py	I		33[b]	12
dmso	4-Me-py	I		33[b]	12
dmso	3,5-diMe-py	I		33.5[b]	12
dmso	4-Cl-py	I		32.5[b]	12
dmso	4-CN-py	I		34[b]	12
CO	py	Cl		30[a]	13
		Br		29[a]	13

[a] CD_3COCD_3 solvent.
[b] $CDCl_3$ solvent.
py = pyridine; 4-Me-py = 4-methylpyridine; 3,5-diMe-py = 3,5-dimethylpyridine; 4-Cl-py = 4-chloropyridine; 4-CN-py = 4-cyanopyridine; 4-$HOCH_2$-py = 4-hydroxymethylpyridine; dmso = dimethylsulphoxide.

Table 2. Pt—H coupling constants, ^2J(Pt—H) (Hz), of *cis*- and *trans*-[Pt(XNH_2)$_2L_2$]

X	L	*Cis*	*Trans*
CH_3	I	68[a]	60[a]
	ONO_2	68[a]	
	Cl	67[b]	58[b]
Cyclopropyl	I	66[a]	
Cyclobutyl	I	66[a]	
	ONO_2	67[a]	
Cyclopentyl	I	66[a]	
	ONO_2	67[a]	
	Cl	66[b]	58[a]
Cyclohexyl	I	66[a]	58[a]
	ONO_2	66[a]	58[a]
Cycloheptyl	I	67[a]	60[a]
	ONO_2	68[a]	
	Cl	65[b]	56[a], 57[c]

[a] CD_3COCD_3 solvent.
[b] CD_3SOCD_3 solvent.
[c] $CDCl_3$ solvent.

measurement is an easy and rapid method of distinguishing *cis* and *trans* isomers.

EXPERIMENTAL

Preparation of the complexes

The complexes *cis*- and *trans*-$[Pt(Xpy)_2Cl_2]$ and $[Pt(XNH_2)_2Cl_2]$ were prepared from K_2PtCl_4 by well established methods.[1,8–10]

Cis- and *trans*-$[Pt(Xpy)_2I_2]$ and $[Pt(XNH_2)_2I_2]$ and their nitrato derivatives were prepared according to Souchard *et al.*[11]

Trans-[Pt(dmso)(Xpy)I_2] complexes were prepared according to Ha *et al.*[12]

Spectral measurements

^{1}H NMR spectra were recorded on a Bruker 250 MHz Fourier transform spectrometer at ambient temperature. dmso solutions were prepared immediately prior to measurement. Coupling in pyridine complexes gave distinct satellite peaks, while some broadening due to chemical shift anisotropy was observed for the amine complexes.

REFERENCES

1. G. B. Kauffman, *Inorg. Synth.* 1963, **7**, 249.
2. N. S. Kurnakov, *J. Russ. Phys. Chem. Soc.* 1893, **25**, 565.
3. A. A. Grinberg, M.I. Gelfman and S. I. Pechenyuk, *Russ. J. Inorg. Chem.* (Engl. Transl.) 1970, **15**, 252.
4. N. S. Kurnakov, *J. Prakt. Chem.* 1894, **50**, 481.
5. F. Basolo, M. Lederer, L. Ossicini and K. H. Stephen, *J. Chromatogr.* 1963, **10**, 262.
6. C. P. Hicks and M. Spiro, *J. Chem. Soc., Chem. Commun.* 1981, 131.
7. W. McFarlane, *J. Chem. Soc., Dalton Trans.* 1974, 324.
8. P. D. Braddock, T. A. Connors, M. Jones, A. R. Khokhar, D. H. Melzack and M. L. Tobe, *Chem. Biol. Interac.* 1975, **11**, 145.
9. L. K. Thompson, *Inorg. Chim. Acta* 1980, **38**, 117.
10. N. Farrell, T. B. T. Ha, J.-P. Souchard, F. L. Wimmer, S. Cros and N. P. Johnson, *J. Med. Chem.* 1989, **32**, 2240.
11. J.-P. Souchard, F. L. Wimmer, T. B. T. Ha and N. P. Johnson, *J. Chem. Soc., Dalton Trans.* 1990, 307.
12. T. B. T. Ha, F. L. Wimmer, J. Jaud, J.-P. Souchard and N. P. Johnson, *J. Chem. Soc., Dalton Trans.* 1990, 1251.
13. P. S. Hall and D. A. Thornton, *Polyhedron* 1987, **6**, 85.

Polyhedron Vol. 9, No. 21, pp. 2651–2653, 1990
Printed in Great Britain

0277-5387/90 $3.00+.00
© 1990 Pergamon Press plc

COMMUNICATION

TRANSMETALLATION OF A BINUCLEAR COMPLEX OF NICKEL(0): SYNTHESIS AND MOLECULAR STRUCTURE OF [NiPt(μ-CNMe)(CNMe)($Ph_2PCH_2PPh_2$)$_2$Cl][Cl]

KEVIN S. RATLIFF, PHILLIP E. FANWICK and CLIFFORD P. KUBIAK*

Department of Chemistry, Purdue University, West Lafayette, IN 47907, U.S.A.

(*Received* 21 *May* 1990; *accepted* 16 *July* 1990)

Abstract—The transmetallation of the dinickel complex $Ni_2(CNMe)_3(dppm)_2$ (**1**) with $Pt(dppm)Cl_2$ (dppm = $PPh_2CH_2PPh_2$) yields the heterobimetallic complex [NiPt$(CNMe)_2$ $(dppm)_2$Cl][Cl] (**2**). The structure of **2** was determined by X-ray crystallography. The Ni—Pt bond distance of 2.5892(9) Å indicates a strongly interacting mixed-metal core. In the presence of one equivalent of methyl isocyanide, the chloride bound to platinum can be removed with $TlPF_6$ to form the tris-isocyanide complex [NiPt$(CNMe)_3$ $(dppm)_2$][PF_6]$_2$ (**3**).

The formation of heterobimetallic complexes which alloy different metal atoms is of interest for their potential to exhibit cooperative reactivities and unusual chemical and physical properties. Structurally characterized heterobimetallic complexes having a discrete metal–metal bond between nickel and platinum have not been known previously. Recently, several examples of heterobimetallic complexes have been prepared using metallation and transmetallation techniques. Shaw and co-workers have used a synthetic strategy based on the transmetallation of relatively labile d^{10} metal ions, Cu^I, Ag^I, Au^I or Hg^{II}, by d^8 ions such as Rh^I or Ir^I.[1] We recently reported the metallation and transmetallation of the homobinuclear Ni^0 complex $Ni_2(\mu$-CNMe)(CNMe)$_2$(dppm)$_2$ (dppm = $Ph_2PCH_2PPh_2$), (**1**) with Pd^{II},[2] Au^I,[3] Ni^{II}[4] and Hg^{II}[5] salts. Here we report the transmetallation of **1** with $Pt(dppm)Cl_2$,[6] to form the strongly bonded Ni—Pt heterobimetallic complex [NiPt(μ-CNMe)(CNMe)$(dppm)_2$Cl][Cl] (**2**).

* Author to whom correspondence should be addressed. Research Fellow of the Alfred P. Sloan Foundation, 1987–1991.

EXPERIMENTAL

Complex **2** was prepared from $Ni_2(CNMe)_3$ $(dppm)_2$ (0.2803 g, 0.27 mmol) and $(dppm)PtCl_2$[7] (0.1807 g, 0.27 mmol) in THF. The solution turned red and a bright red solid precipitated from solution. The solid was collected by filtration and washed with a small amount of THF and then pentane. The solid was dried; yield = 0.2065 g, 0.17 mmol, 65%. ^{1}H NMR (CD_2Cl_2): δ 8.1–7.1 (m, 40H), δ 3.12 (m, 4H), δ 2.83 (s, 6H). $^{31}P\{^1H\}$ NMR (CD_2Cl_2): AA′BB′, $\delta(P_A)$ = 31.0, $\delta(P_B)$ = 23.3; $J(PtP_A)$ = 2716 Hz; $J(PtP_B)$ = 528 Hz. IR(KBr) ν(CN): 2187(s), 1715(s) cm^{-1}.

Crystal data for **2**·2CH_3CN. The complex crystallized with two molecules of acetonitrile in the crystal lattice. $PtNiCl_2P_4N_4C_{58}H_{56}$, FW = 1257.72, monoclinic space group $P2_1/n$, a = 15.324(1), b = 18.354(2), c = 20.190(2) Å, V = 5639(2) Å^3, Z = 4, d_{calc} = 1.481 g cm^{-3}. Crystal dimensions: 0.50 × 0.35 × 0.28 mm. The structure was solved by MULTAN least-squares Fourier methods and was refined to R and R_w values of 0.032 and 0.039, respectively, for 601 variables and 5235 observations with $I \geq 3.0\sigma(I)$ with Mo-K_α radiation. Data were corrected for absorption

empirically, $\mu = 30.85$ cm^{-1}. Further details can be found in the supplementary material.

Complex **3** was prepared from complex **2** (0.250 g, 0.213 mmol) and $Tl(PF_6)$ (0.153 g, 0.44 mmol), in CH_3CN, in the presence of one equivalent of methylisocyanide. The solution turned orange and TlCl precipitated out of solution. The solution was filtered and the solvent removed. The solid was then recrystallized from THF–pentane. Yield = 0.275 g, 0.19 mmol, 90%. ^{1}H NMR (CD_2Cl_2): δ 7.6–7.1 (m, 40H), δ 4.63 (m, 4H), δ 2.67 (s, 6H), δ 2.32 (s, 3H). ^{31}P{^{1}H} NMR (CD_2Cl_2): AA′BB′, $\delta(P_A) = 10.31$, $\delta(P_B) = 6.76$, $J(PtP_A) = 2444$ Hz. IR(KBr) ν(CN): 2230(m), 2194(s), 2143(m) cm^{-1}.[7]

RESULTS AND DISCUSSION

Treatment of a THF solution of **1** with one equivalent of $Pt(dppm)Cl_2$ leads directly to the transmetallated product, **2**, in 65% yield:

$$Ni_2(\mu\text{-CNMe})(CNMe)_2(dppm)_2 + Pt(dppm)Cl_2 \longrightarrow [NiPt(\mu\text{-CNMe})(CNMe)(dppm)_2Cl][Cl] \quad (1)$$

The IR spectrum of **2** exhibits one terminal and one bridging isocyanide ν(CN) band at typical values of 2187 and 1715 cm^{-1}, respectively. The isocyanides, however, are equivalent on the ^{1}H NMR time scale and appear as a singlet at 2.83 ppm. The ^{31}P {^{1}H} NMR spectrum of **2** is an AA′BB′ spin system [$\delta(P_A) = 30.60$ ppm, $\delta(P_B) = 23.36$ ppm] with ^{195}Pt coupling constants of $^1J(PtP_A) = 2781$ Hz and $^2J(PtP_B) = 528$ Hz, thus indicating a Ni—Pt heterobinuclear complex. Crystals of **2** suitable for X-ray diffraction were obtained from slow diffusion of Et_2O into a concentrated acetonitrile solution of **2**. An ORTEP drawing of **2** is presented in Fig. 1. The molecule consists of a strongly bonding Ni—Pt core with d(Ni—Pt) = 2.5892(9) Å. Holah *et al.* have synthesized the heterobimetallic complex $NiPtCl_2(\mu\text{-CO})(dppm)_2$ which possesses a significantly longer Ni—Pt separation of 2.689(2) Å.[8] Compound **2** adopts a distorted "A-frame" geometry with the platinum atom remaining essentially square planar and the nickel atom adopting a distorted tetrahedral geometry. A skeletal view of **2** with selected bond distances and bond angles is shown in Fig. 2. The formation of **2** from $Ni_2(\mu\text{-CNMe})(CNMe)_2(dppm)_2$ and $Pt(dppm)Cl_2$ presumably follows an initial metallation of the dinickel complex with $Pt(dppm)Cl_2$ followed by the expulsion of a Ni^0 fragment.[2]

In the presence of one equivalent of methyl isocyanide, the chloride bound to the platinum atom

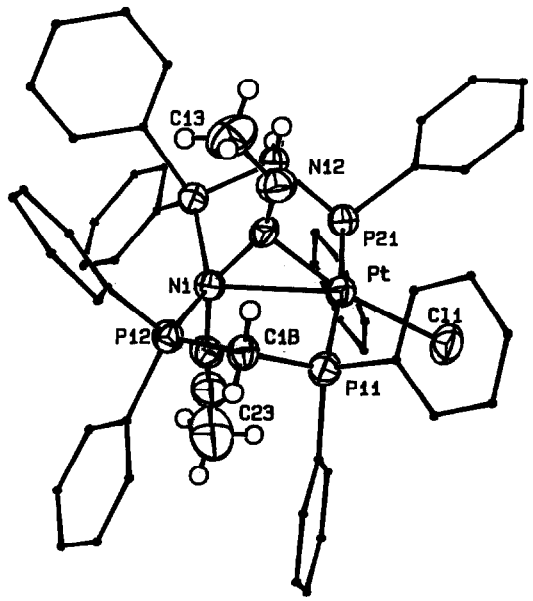

Fig. 1. ORTEP drawing of $[NiPt(\mu\text{-CNMe})(CNMe)(dppm)_2Cl]^+$ (**2**).

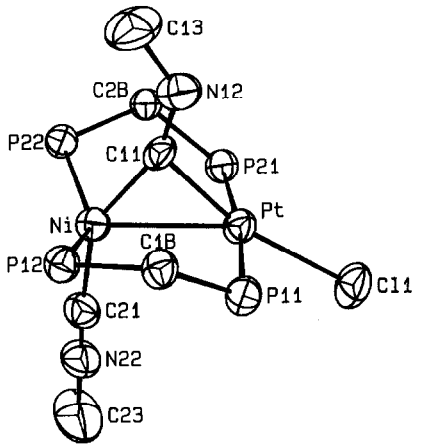

Fig. 2. Skeletal view of **2** with selected bond distances (Å) and bond angles (°): Ni—Pt, 2.5892(9); P(11)—Pt—P(21), 173.47(6); Cl(1)—Pt—C(11), 163.2(2); P(12)—Ni—P(22), 140.65(7); P(12)—Ni—C(21), 103.6(2); P(22)—Ni—C(11), 88.2(2); C(11)—Ni—C(21), 146.7(3).

can be removed using thallium(I) salts to form the tris-isocyanide complex, $[NiPt(CNMe)_3(dppm)_2]^{2+}$ (**3**).[7]

$$[NiPt(CNMe)_2(dppm)_2Cl][Cl] + 2Tl(PF_6) + CNMe \longrightarrow [NiPt(CNMe)_3(dppm)_2][PF_6]_2 \quad (2)$$

The latter complex is analogous to the homobinuclear complex $[Ni_2(CNMe)_3(dppm)_2]^{2+}$[9] and the heterobinuclear complex $[NiPd(CNMe)_3$

$(dppm)_2]^{2+}$ [2] which were recently prepared in our laboratories.

The IR spectrum of **3** reveals only terminal isocyanide bands at $\nu(CN) = 2230$, 2194 and 2143 cm^{-1}. The $^{31}P\{^1H\}$ NMR spectrum of **3** is also an AA'BB' spin system with $\delta(P_A) = 10.18$ ppm and $\delta(P_B) = 6.76$ ppm. The spectrum, however, only shows ^{195}Pt coupling to one set of phosphorus atoms, with a coupling constant of $^1J(PtP_A) = 2444$ Hz. The absence of ^{195}Pt coupling to the phosphorus atoms bound to the nickel atom indicates that there is a significant weakening of the metal–metal interaction between the nickel and platinum atoms compared with **2**. The ^1H NMR spectrum reveals two types of methyl isocyanides at δ 2.68 and 2.32 ppm in a ratio of 2 : 1. Attempts at forming X-ray quality crystals have been unsuccessful, however, spectroscopic data as well as previous X-ray structural studies of $[Ni_2(CNMe)_3dppm_2]^{2+}$ and $[NiPd(CNMe)_3dppm_2]^{2+}$ suggest the following weakly metal–metal′ interacting structure.

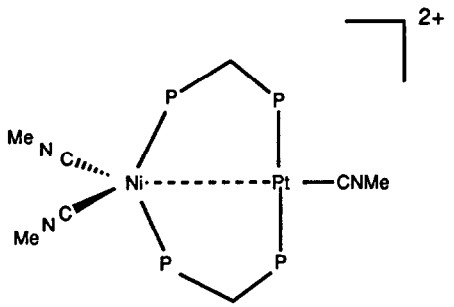

3

The synthesis of this Ni—Pt complex completes the series of $[Ni—M(CNMe)_3(dppm)_2]^{2+}$ (M = Ni, Pd, Pt) complexes. Further studies on the metallation and transmetallation of $Ni_2(\mu\text{-}CNMe)(CNMe)_2(dppm)_2$ are continuing.

Supplementary material available: atomic coordinates have been deposited with the Director, Cambridge Crystallographic Data Centre.

Acknowledgements—This work was supported by NSF (CHE-8707963). We are also grateful to NSF for support of the Chemical X-ray diffraction facility at Purdue. K.S.R. gratefully acknowledges a David Ross graduate Fellowship.

REFERENCES

1. (a) A. Blaff, A. T. Hutton, P. G. Pringle and B. L. Shaw, *Inorg. Chim. Acta* 1983, **76**, L265; (b) G. R. Copper, A. T. Hutton, D. M. McEwan, P. G. Pringle and B. L. Shaw, *Inorg. Chim. Acta* 1983, **76**, L267; (c) C. R. Langrick, P. G. Pringle and B. L. Shaw, *J. Chem. Soc., Dalton Trans.* 1984, 1233; (d) S. W. Carr and B. L. Shaw, *J. Chem. Soc., Dalton Trans.* 1986, 1815.
2. J. Ni, P. E. Fanwick and C. P. Kubiak, *Inorg. Chem.* 1988, **27**, 2017.
3. H. P. Kim, P. E. Fanwick and C. P. Kubiak, *J. Organomet. Chem.* 1988, **346**, C39.
4. K. S. Ratliff, G. K. Broeker, P. E. Fanwick and C. P. Kubiak, *Angew. Chem. Int. Edn Engl.* 1990, **29**, 395.
5. J. K. Gong, J. Huang, P. E. Fanwick and C. P. Kubiak, *Angew. Chem. Int. Edn Engl.* 1990, **29**, 396.
6. $Pt(dppm)Cl_2$ was prepared by the 1 : 1 reaction of $(COD)PtCl_2$ with dppm in CH_2Cl_2: J. X. McDermott, J. F. White and G. M. Whitesides, *J. Am. Chem. Soc.* 1976, **98**, 6521.
7. The complex has also been prepared by the decomposition of the heterotrinuclear complex $[Ni_2Pt(CNMe)_5(dppm)_2][PF_6]_2$: J. Ni, PhD thesis, Purdue University (1990).
8. D. G. Holah, A. N. Hughes, V. R. Magnuson, H. A. Mirza and K. O. Parker, *Organometallics* 1988, **7**, 1233.
9. D. L. DeLaet, R. DelRosario, P. E. Fanwick and C. P. Kubiak, *J. Am. Chem. Soc.* 1987, **109**, 754.

Polyhedron Vol. 9, No. 21, pp. 2655–2657, 1990
Printed in Great Britain

0277–5387/90 $3.00+.00
© 1990 Pergamon Press plc

COMMUNICATION

REACTION OF O_2 WITH $\{\eta^3$-HB(3-Bu^{t}pz)$_3\}$MgCH$_2$Si(CH$_3$)$_3$: FACILE Si—C BOND CLEAVAGE AND FORMATION OF $\{\eta^3$-HB(3-Bu^{t}pz)$_3\}$MgOSi(CH$_3$)$_3$

RUNYU HAN and GERARD PARKIN*

Department of Chemistry, Columbia University, New York, NY 10027, U.S.A.

(*Received* 25 *June* 1990; *accepted* 31 *July* 1990)

Abstract—The reaction of the magnesium trimethylsilylmethyl complex $\{\eta^3$-HB(3-Bu^{t}pz)$_3\}$MgCH$_2$Si(CH$_3$)$_3$ with O_2 gives the trimethylsiloxide derivative $\{\eta^3$-HB(3-Bu^{t}pz)$_3\}$MgOSi(CH$_3$)$_3$ as a result of facile cleavage of the Si—C bond.

The reaction of molecular oxygen with metal alkyl derivatives is of fundamental importance in view of the role that metal-based oxidations play in systems as diverse as industrial and biological processes.[1] We have recently reported the insertion of O_2 into the Mg—C bond of a series of alkyl complexes $\{\eta^3$-HB(3-Bu^{t}pz)$_3\}$MgR [3-Bu^{t}pz = 3-C_3N_2Bu^{t}H$_2$; R = CH$_3$, CH$_2$CH$_3$, CH(CH$_3$)$_2$, C(CH$_3$)$_3$] to give alkylperoxo derivatives $\{\eta^3$-HB(3-Bu^{t}pz)$_3\}$MgOOR [eq. (1)]:[2]

$$\{\eta^3\text{-HB(3-Bu}^t\text{pz)}_3\}\text{MgR} + O_2 \longrightarrow \{\eta^3\text{-HB(3-Bu}^t\text{pz)}_3\}\text{MgOOR}. \quad (1)$$

Here we report that the analogous reaction of the trimethylsilylmethyl derivative $\{\eta^3$-HB(3-Bu^{t}pz)$_3\}$MgCH$_2$SiMe$_3$ with O_2 is accompanied by facile Si—C bond cleavage and the formation of the trimethylsiloxide derivative, $\{\eta^3$-HB(3-Bu^{t}pz)$_3\}$MgOSiMe$_3$.

The trimethylsilylmethyl derivatives $\{\eta^3$-HB(3-Bu^{t}pz)$_3\}$MgCH$_2$SiMe$_3$† and $\{\eta^3$-HB(3,5-Me$_2$pz)$_3\}$MgCH$_2$SiMe$_3$† [3,5-Me$_2$pz = 3,5-C_3N_2(CH$_3$)$_2$H] are obtained by metathesis of (Me$_3$SiCH$_2$)$_2$Mg with either Tl$\{\eta^3$-HB(3-Bu^{t}pz)$_3\}$ or K{HB(3,5-Me$_2$pz)$_3$}, respectively [eqs (2) and (3)]:

$$(\text{Me}_3\text{SiCH}_2)_2\text{Mg} \xrightarrow{\text{Tl}\{\eta^3\text{-HB(3-Bu}^t\text{pz)}_3\}} \{\eta^3\text{-HB(3-Bu}^t\text{pz)}_3\}\text{MgCH}_2\text{SiMe}_3 \quad (2)$$

$$(\text{Me}_3\text{SiCH}_2)_2\text{Mg} \xrightarrow{\text{K\{HB(3,5-Me}_2\text{pz)}_3\}} \{\eta^3\text{-HB(3,5-Me}_2\text{pz)}_3\}\text{MgCH}_2\text{SiMe}_3. \quad (3)$$

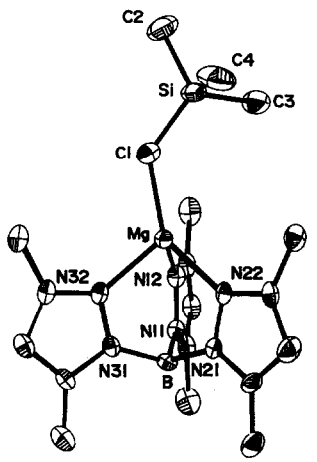

Fig. 1. ORTEP drawing for $\{\eta^3$-HB(3,5-Me$_2$pz)$_3\}$MgCH$_2$SiMe$_3$.

* Author to whom correspondence should be addressed.

† Selected ^{1}H NMR data (C_6D_6, RT, 200 MHz). $\{\eta^3$-HB(3-Bu^{t}pz)$_3\}$MgCH$_2$SiMe$_3$: δ 1.40 [9H, s, HB{C$_3$N$_2$H$_2$C(CH$_3$)$_3\}_3$], 5.80 [d, 1H, HB{C$_3$N$_2$H$_2$C(CH$_3$)$_3\}_3$], 7.33 [d, 1H, HB{C$_3$N$_2$H$_2$C(CH$_3$)$_3\}_3$], −0.49 [2H, s, MgCH$_2$SiMe$_3$], 0.54 [9H, s, Si(CH$_3$)$_3$]. $\{\eta^3$-HB(3,5-Me$_2$pz)$_3\}$MgCH$_2$SiMe$_3$: δ 2.10 and 2.23 [s, HB{C$_3$N$_2$H(CH$_3$)$_2\}_3$], 5.44 [s, HB{C$_3$N$_2$H(CH$_3$)$_2\}_3$], −0.64 [2H, s, MgCH$_2$SiMe$_3$], 0.51 [9H, s, Si(CH$_3$)$_3$]. $\{\eta^3$-HB(3-Bu^{t}pz)$_3\}$MgOSiMe$_3$: δ 1.44 [9H, s, HB{C$_3$N$_2$H$_2$C(CH$_3$)$_3\}_3$], 5.77 [d, 1H, HB{C$_3$N$_2$H$_2$C(CH$_3$)$_3\}_3$], 7.28 [d, 1H, HB{C$_3$N$_2$H$_2$C(CH$_3$)$_3\}_3$], 0.53 [9H, s, Si(CH$_3$)$_3$].

The molecular structure of $\{\eta^3$-HB(3,5-$Me_2pz)_3\}MgCH_2SiMe_3$ has been determined by single crystal X-ray diffraction, as shown in Fig. 1.*

The reaction of $\{\eta^3$-HB(3,5-$Me_2pz)_3\}MgCH_2SiMe_3$ with O_2 has been examined using ^1H NMR spectroscopy which demonstrates the formation of a complex mixture of products, of which the bis {tris(3,5-dimethylpyrazolyl)hydroborato} derivative $\{\eta^3$-HB(3,5-$Me_2pz)_3\}_2Mg$[3] is a major constituent [eq. (4)]:

$$\{\eta^3\text{-HB(3,5-Me}_2\text{pz)}_3\}\text{MgCH}_2\text{SiMe}_3 \xrightarrow{O_2} \{\eta^3\text{-HB(3,5-Me}_2\text{pz)}_3\}_2\text{Mg} + \cdots \quad (4)$$

In view of the greater stability that may be provided by the more sterically demanding tris(3-t-butylpyrazolyl)hydroborato ligand system, and in particular the inability to form the corresponding bis{tris(3 - t - butylpyrazolyl)hydroborato}magnesium derivative,[3] we examined the reaction of $\{\eta^3$-HB(3-Bu^{t}pz)$_3\}MgCH_2SiMe_3$ with O_2. The reaction was indeed observed to be much cleaner than the reaction of $\{\eta^3$-HB(3,5-$Me_2pz)_3\}MgCH_2SiMe_3$ with O_2 and the major product (after 1 h at room temperature) was identified as the trimethylsiloxide derivative, $\{\eta^3$-HB(3-Bu^{t}pz)$_3\}MgOSiMe_3$ [eq. (5)].† Formaldehyde was also observed as a product of this reaction.

$$\{\eta^3\text{-HB(3-Bu}^t\text{pz)}_3\}\text{MgCH}_2\text{SiMe}_3 \xrightarrow{O_2} \{\eta^3\text{-HB(3-Bu}^t\text{pz)}_3\}\text{MgOSiMe}_3 + (\text{CH}_2\text{O})_n. \quad (5)$$

* Crystal data for $\{\eta^3$-HB(3,5-$Me_2pz)_3MgCH_2SiMe_3$: $C_{19}H_{33}N_6BSiMg$, $M = 408.8$, monoclinic, space group $C2/c$ (No. 15), $a = 23.897(8)$, $b = 8.010(2)$, $c = 30.072(8)$ Å, $\beta = 119.71(2)°$, $U = 5000(2)$ Å^3, $Z = 8$, $D_c = 1.09$ g cm^{-3}, $F(000) = 1760$ electrons, μ(Mo-K_α) = 1.4 cm^{-1}, $T = 295$ K, crystal dimensions 0.18 mm × 0.54 mm × 0.60 mm. Intensity data were collected on a Nicolet R3m diffractometer using monochromated Mo-K_α X-radiation ($\lambda = 0.71073$ Å) and were corrected for Lorentz and polarization effects. A total of 1863 unique reflections were collected in the range $3° < 2\theta < 45°$, of which 1489 with $F_o > 5\sigma(F_o)$ were used in the structure determination. The structure was solved using direct methods and standard difference map techniques. Most of the hydrogen atoms were located in the difference map after all the non-hydrogen atoms were located and refined anisotropically, but hydrogens on carbon were allowed to refine in calculated positions [$d_{C-H} = 0.96$ Å; U_{iso} (H) = $1.2U_{iso}$(C)]. Block-diagonal least-squares refinement converged to $R = 0.0599$ ($R_w = 0.0602$), with the maximum shift-to-σ ratio of 0.023 for the last cycle. The final difference map showed no significant features, with the highest final peak 1.0 e Å^{-3}. Atomic coordinates, bond lengths and angles, and thermal parameters have been deposited at the Cambridge Crystallographic Data Centre.

Characterization of the trimethylsiloxide derivative $\{\eta^3$-HB(3-Bu^{t}pz)$_3\}MgOSiMe_3$ is also provided by the independent synthesis from $\{\eta^3$-HB(3-Bu^{t}pz)$_3\}MgCl$ and $KOSiMe_3$ [eq. (6)]:

$$\{\eta^3\text{-HB(3-Bu}^t\text{pz)}_3\}\text{MgCl} + \text{KOSiMe}_3 \longrightarrow \{\eta^3\text{-HB(3-Bu}^t\text{pz)}_3\}\text{MgOSiMe}_3 + \text{KCl}. \quad (6)$$

The reaction of $\{\eta^3$-HB(3-Bu^{t}pz)$_3\}MgCH_2SiMe_3$ with O_2 most likely involves a radical chain process, as proposed for the reactions of $\{\eta^3$-HB(3-Bu^{t}pz)$_3\}MgR$[2] and other metal alkyl derivatives with O_2.[5] Thus, a potential mechanism for the formation of $\{\eta^3$-HB(3-Bu^{t}pyz)$_3\}MgOSiMe_3$ involves the generation of $Me_3SiO^\bullet$ as a result of the rearrangement of the radical intermediate $Me_3SiCH_2O_2^\bullet$ [eq. (7)]. The formation of a strong Si—O bond would be expected to provide an effective driving force for such a transformation.

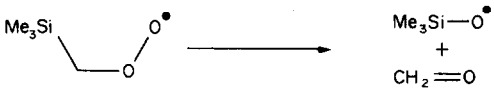

(7)

Support for a radical-chain mechanism is provided by the observation of (i) mild inhibition of the reaction of $\{\eta^3$-HB(3-Bu^{t}pz)$_3\}MgCH_2SiMe_3$ with O_2 in the presence of galvinoxyl, a radical trap, and (ii) crossover products in the reactions of O_2 with mixtures of (a) $\{\eta^3$-HB(3-Bu^{t}pz)$_3\}MgCH_2SiMe_3$ and $\{\eta^3$-HB(3,5-$Me_2pz)_3\}MgC(CH_3)_3$ [eq. (8)], and of (b) $\{\eta^3$-HB(3,5-$Me_2pz)_3\}MgCH_2SiMe_3$ and $\{\eta^3$-HB(3-Bu^{t}pz)$_3\}MgC(CH_3)_3$ [eq. (9)]:[6]

$$\{\eta^3\text{-HB(3-Bu}^t\text{pz)}_3\}\text{MgCH}_2\text{SiMe}_3 + \{\eta^3\text{-HB(3,5-Me}_2\text{pz)}_3\}\text{MgC(CH}_3)_3 \longrightarrow \{\eta^3\text{-HB(3-Bu}^t\text{pz)}_3\}\text{MgOOC(CH}_3)_3 + \{\eta^3\text{-HB(3-Bu}^t\text{pz)}_3\}\text{MgOSiMe}_3 + \cdots \quad (8)$$

$$\{\eta^3\text{-HB(3-Bu}^t\text{pz)}_3\}\text{MgC(CH}_3)_3 + \{\eta^3\text{-HB(3,5-Me}_2\text{pz)}_3\}\text{MgCH}_2\text{SiMe}_3 \longrightarrow \{\eta^3\text{-HB(3-Bu}^t\text{pz)}_3\}\text{MgOSiMe}_3 + \{\eta^3\text{-HB(3-Bu}^t\text{pz)}_3\}\text{MgOOC(CH}_3)_3 + \cdots \quad (9)$$

Organic products arising from facile cleavage of Si—C bonds of other trialkylsilyl metal derivatives upon autoxidation have been previously observed, and thus provide a precedent for the reactions described here. For example, treatment of the Grignard reagent Me_3SiCH_2MgCl with O_2, followed by hydrolysis, gave significant quantities of Me_3SiOH, $(Me_3Si)_2O$ and CH_2O.[7] Thus, these observations provide further evidence that such cleavage reactions may be a general feature of trimethylsilylmethyl derivatives upon autoxidation.

Acknowledgement—We thank the donors of the Petroleum Research Fund, administered by the ACS, for partial support of this research.

REFERENCES

1. (a) H. Mimoun, *Comprehensive Coordination Chemistry* (Edited by G. Wilkinson, R. D. Gillard and J. A. McCleverty), Vol. 6, pp. 317–410. Pergamon Press, Oxford (1987); (b) R. A. Sheldon and J. K. Kochi, *Metal Catalyzed Oxidations of Organic Compounds.* Academic Press, New York (1981); (c) R. K. Grasselli and J. D. Burrington, *Adv. Catal.* 1981, **30**, 133; (d) R. K. Grasselli, J. D. Burrington and J. F. Brazdil, *Faraday Discuss. Chem. Soc.* 1981, **72**, 203; (e) R. A. Sheldon, *J. Molec. Catal.* 1983, **20**, 1; (f) A. E. Martell, *Pure Appl. Chem.* 1983, **55**, 125; (g) B. G. Malmstrom, *Ann. Rev. Biochem.* 1982, **51**, 21; (h) M. F. Perutz, *Ann. Rev. Biochem.* 1979, **48**, 327; (i) R. D. Jones, D. A. Summerville and F. Basolo, *Chem. Rev.* 1979, **79**, 139; (j) R. E. White, *Ann. Rev. Biochem.* 1980, **49**, 315; (k) F. P. Guengerich and T. L. Macdonald, *Accts Chem. Res.* 1984, **17**, 9; (l) J. P. Collman, *Accts Chem. Res.* 1977, **10**, 265.
2. R. Han and G. Parkin, *J. Am. Chem. Soc.* 1990, **112**, 3662.
3. R. Han and G. Parkin, *J. Organomet. Chem.*, in press.
4. Over a period of days at room temperature, the minor product, which may be tentatively assigned as the trimethylsilylperoxo derivative $\{\eta^3\text{-HB(3-Bu}^t\text{pz)}_3\}\text{MgOOCH}_2\text{SiMe}_3$, is slowly converted to $\{\eta^3\text{-HB(3-Bu}^t\text{pz)}_3\}\text{MgOSiMe}_3$.
5. (a) A. G. Davies and B. P. Roberts, *Accts Chem. Res.* 1972, **5**, 387; (b) A. G. Davies and B. P. Roberts, *J. Chem. Soc. B* 1968, 1074; (c) R. C. Lamb, P. W. Ayers, M. K. Toney and J. F. Garst, *J. Am. Chem. Soc.* 1966, **88**, 4261; (d) C. Walling and A. Cioffari, *J. Am. Chem. Soc.* 1970, **92**, 6609; (e) E. J. Panek and G. M. Whitesides, *J. Am. Chem. Soc.* 1972, **94**, 8768; (f) F. R. Jensen and R. C. Kiskis, *J. Organomet. Chem.* 1973, **49**, C46; (g) A. G. Davies and B. P. Roberts, *J. Chem. Soc. B* 1968, 1074; (h) P. B. Brindley and M. J. Scotton, *J. Chem. Soc., Perkin Trans. II* 1981, 419.
6. In view of the decomposition that arises as a result of the reaction of $\{\eta^3\text{-HB(3,5-Me}_2\text{pz)}_3\}\text{MgR}$ derivatives with O_2, only the $\{\eta^3\text{-HB(3-Bu}^t\text{pz)}_3\}\text{MgX}$ derivatives can be definitively identified as crossover products.
7. J. J. Eisch and G. R. Husk, *J. Org. Chem.* 1964, **29**, 254.

Polyhedron Vol. 9, No. 21, pp. 2659–2662, 1990
Printed in Great Britain

0277–5387/90 $3.00+.00
© 1990 Pergamon Press plc

COMMUNICATION

THE FIRST METAL COMPLEXES CONTAINING TELLURIUM–SULPHUR–NITROGEN ANIONS; X-RAY STRUCTURE OF $[Pt(TeSN_2H)(PMe_2Ph)_2][BF_4]$

PAUL F. KELLY, ALEXANDRA M. Z. SLAWIN, DAVID J. WILLIAMS and J. DEREK WOOLLINS*

Department of Chemistry, Imperial College of Science, Technology and Medicine, South Kensington, London SW7 2AY, U.K.

(*Received* 21 *May* 1990; *accepted* 10 *August* 1990)

Abstract—Reaction of $Te_3N_2SCl_2$ with *cis*-$PtCl_2(PMe_2Ph)_2$ and 1,8-diazabicylo[5.4.0] undec-7-ene provides the first route to a metal–tellurium–sulphur–nitrogen complex, $Pt(TeSN_2)(PMe_2Ph)_2$ (**1**), the only example of a complex containing the $TeSN_2^{2-}$ ligand. Complex **1** reacts with a dilute solution of $HBF_4 \cdot Et_2O$ to give $[Pt(TeSN_2H)(PMe_2Ph)_2][BF_4]$ (**2**), the X-ray structure of which reveals the first example of a M–Te–S–N ring. Complexes **1** and **2** are air-stable.

Recently we reported the preparation of $Pt(ESN_2)(PR_3)_2$ and $[Pt(ESN_2H)(PR_3)_2][BF_4]$ (E = S or Se).[1,2]† Since these compounds have interesting structural properties we have now developed a synthetic route to the tellurium analogue. This has been achieved by utilizing the only known (though poorly characterized) Te—S—N heterocycle, $Te_3N_2SCl_2$, prepared by reaction of $[(Me_3Si)_2N]_2S$ with $TeCl_4$ in THF.[3] Here we report details of the synthesis of $Pt(TeSN_2)(PMe_2Ph)_2$ (**1**) and $[Pt(TeSN_2H)(PMe_2Ph)_2][BF_4]$ (**2**) and the X-ray crystal structure of **2**.

Reaction of a CH_2Cl_2 solution of *cis*-$PtCl_2(PMe_2Ph)_2$ with $Te_3N_2SCl_2$, in the presence of dbu (dbu = 1,8-diazabicyclo[5.4.0]undec-7-ene), gives, after work-up, a yellow solid which analyses as **1**, the first example of a M—Te—S—N species. We have been unable to resolve the X-ray crystal structure‡ of **1** due to

$$PtCl_2(PPMe_2Ph)_2 + Te_3N_2SCl_2 \xrightarrow[4\,dbu]{CH_2Cl_2} \underset{(1)}{Pt(TeSN_2)(PMe_2Ph)_2} + 4[dbuH]Cl + 2Te \quad (1)$$

$$Pt(TeSN_2)(PMe_2Ph)_2 + HBF_4 \longrightarrow \underset{(2)}{[Pt(TeSN_2H)(PMe_2Ph)_2][BF_4]} \quad (2)$$

disorder problems [as was the case for $Pt(SeSN_2)(PMe_2Ph)_2$]; however **1** is readily protonated [eq. (2)] by HBF_4 to give **2**. The X-ray crystal structure of **2** reveals (Fig. 1) square-planar coordination of the platinum with the metal bonded to the tellurium of the $TeSN_2H^-$ anion. The Pt—P(1) and Pt—P(2) distances [2.313(3) and 2.257(3) Å] are significantly different from each other and reflect the *trans* geometry of the phosphorus atoms with respect to tellurium and nitrogen. However, these distances are the same as those observed in the sulphur and selenium analogues, **3** and **4**.

* Author to whom correspondence should be addressed.

† $Pt(S_2N_2)(PR_3)_2$ complexes are best prepared by reaction of *cis*-$PtCl_2(PR_3)_2$ with $S_4N_4H_4$ and the base dbu, whilst $Pt(SeSN_2)(PR_3)_2$ complexes are made by reaction of the dichloro species with $[Se_2N_2SCl]_2$ in liquid ammonia. The complexes can be readily protonated on the metal-bound nitrogen by the action of acids such as HBF_4.

‡ Crystal data: Complex **1**, monoclinic, $a = 19.810(8)$, $b = 9.677(5)$, $c = 10.972(5)$ Å, $\beta = 107.10(3)°$, space group *Cc* or *C*2/*c*. Due to severe disorder problems the detailed structure could not be resolved.

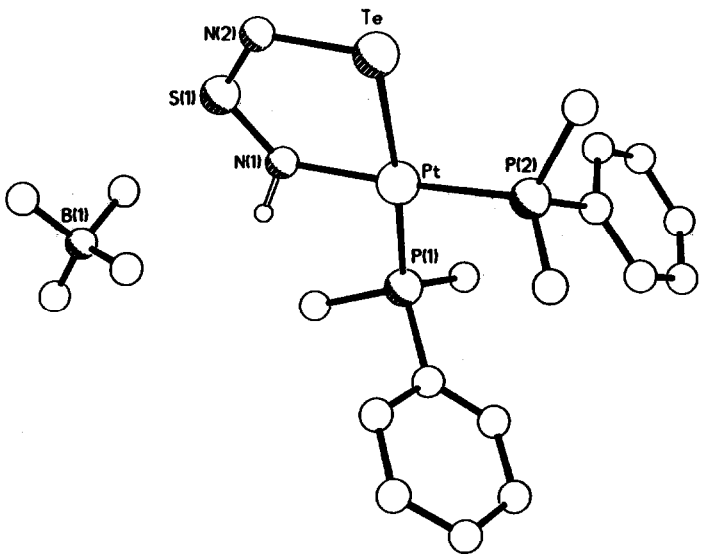

Fig. 1. The X-ray structure of $[Pt(TeSN_2H)(PMe_2Ph)_2][BF_4]$ (**2**) in the crystal. Important bond lengths (Å) and angles (°):

Pt—P(1)	2.313(3)	N(2)—S(1)	1.532(14)
Pt—P(2)	2.257(3)	S(1)—N(1)	1.569(11)
Pt—Te	2.553(1)	Pt—N(1)	2.046(11)
Te—N(2)	1.993(13)		

P(1)—Pt—P(2)	94.5(1)	Te—N(2)—S(1)	120.3(6)
N(1)—Pt—Te	84.9(3)	N(2)—S(1)—N(1)	111.6(6)
Pt—Te—N(2)	95.6(3)	S(1)—N(1)—Pt	127.6(6)

This is consistent with the ^{31}P NMR wherein the $^1J\{^1P-^{195}Pt\}$ coupling constants for the two phosphorus atoms are quite different from each other, but are not greatly changed upon varying E (E = Te, Se, S).* Despite the significantly increased covalent radius of tellurium versus selenium and sulphur and the consequent increase in the Pt—E and E—N(2) bond lengths (E = Te, Se, S) in **2** relative to **3** and **4**, the gross structure of the molecule remains virtually unchanged throughout the series; complexes **2**–**4** being crystallographically isostructural.† The only significant change in the ring geometry other than at E is at N(1) where there is a significant increase in the Pt—N(1)—S(1) angle [127.6(6) in **2**, cf. 122.8(4) and 121.4(4)° in **3** and **4**, respectively]. There are no Te—S—N structures available for comparison. As in **3** and **4**, the cations form infinite stacks in the crystal. Within the stacks of dimer pairs the intradimer $PtTeSN_2$ ring separation is 3.55 Å and the interdimer separation is 4.35 Å.‡ The ^{31}P NMR spectra of $Pt(ESN_2)(PR_3)_2$ (E = S, Se) have characteristic $^{31}P-^{195}Pt$ coupling constants. In **1** there are additional $^2J\{^{31}P-^{195}Te\}$ couplings for P(1) (Fig. 2) and P(2) of 146 and 103 Hz, respectively. To the best of our knowledge there have been no previous reports of a $^2J\{^{31}P-^{125}Te\}$ coupling directed through a metal.

The chemistry of S–N anions such as $S_2N_2^{2-}$ and S_3N^- is well known[4] and, as we have recently demonstrated,[5,6] selenium analogues can also be prepared. The development of Te—N and Te—S—N chemistry has, until now, been limited because of the lack of suitable starting materials (Te_4N_4 is poorly characterized and extremely hazardous). The work reported here demonstrates that Te—S—N species can be stabilized. The ease of synthesis of **1** and **2**, coupled with their ease of handling and stability, should greatly facilitate the development of this hitherto unexplored area of chemistry. We are currently investigating the incorporation of **2**–**4** in molecular metals.

* The $^1J\{^{31}P-^{195}Pt\}$ coupling constants for P(1) and P(2) are 2559, 2687, 2642 and 3240, 3227, 3171 Hz for E = S, Se and Te, respectively.

† The Pt—E, E—N(2) bond lengths (Å) and the Pt—E—N(2) angles (°) are 2.283(2), 2.401(1), 2.553(1); 1.649(8), 1.833(9), 1.993(13); and 104.4(3), 100.2(2), 95.6(3) for the S, Se and Te compounds, respectively.

‡ There are short non-bonded anion–cation contacts between F(1) and S(1) (3.17 Å) and F(1) and N(1) (3.26 Å).

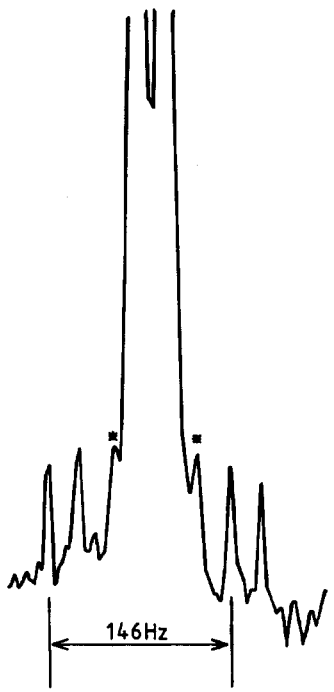

Fig. 2. The ^{31}P NMR spectrum of the phosphorus *trans* to tellurium in complex **1**. Peaks marked with an asterisk (*) are spinning sidebands.

EXPERIMENTAL

$Pt(TeSN_2)(PMe_2Ph)_2$ (1)

A vigorously stirred suspension of $Te_3N_2SCl_2$[3] (0.21 g, 0.41 mmol) and *cis*-$PtCl_2(PMe_2Ph)_2$ (0.22 g, 0.41 mmol) in CH_2Cl_2 (60 cm^3) was treated with excess dbu (*ca* 0.5 cm^3), and the resulting mixture stirred for 4 h. This yielded an orange solution together with large amounts of a finely-divided black precipitate of tellurium which was removed by twice filtering through celite, in air. Removal of the CH_2Cl_2 *in vacuo* gave an orange–brown oil which was triturated with degassed water, yielding a yellowish solid which was filtered, washed with more water, then dried *in vacuo*. Addition of hexane to a CH_2Cl_2 solution of this product yielded pure $Pt(TeSN_2)(PMe_2Ph)_2$ (**1**) (0.21 g, 78%) as a yellow solid. Found: C, 29.7; H, 3.3; N, 4.1. Calc.: C, 29.2; H, 3.4; N, 4.3%. ^{31}P NMR: AX spectrum, δ_a 0.8 ppm [$^1J(^{195}Pt–^{31}P)$ 2786 Hz], δ_x −30.2 ppm (^1J 2839 Hz). IR: 1080 (s), 619 (s), 374 (m) and 349 (m) cm^{-1}.

$[Pt(TeSN_2H)(PMe_2Ph)_2][BF_4]$ (2)

Protonation was achieved by treating a solution of **1** (0.1 g, 0.15 mmol) in CH_2Cl_2 (30 cm^3) with a solution of excess $HBF_4 \cdot Et_2O$ (3 drops) in CH_2Cl_2 (60 cm^3) over a period of 1 min. After stirring for 5 min the volume of the solution was reduced to $\approx$ 5 cm^3 and a reddish solid precipitated with Et_2O (100 cm^3). After drying, the solid was extracted into CH_2Cl_2 (20 cm^3), filtered to remove some residual red solid and tellurium, then slowly treated with hexane, with stirring, to give $[Pt(TeSN_2H)(PMe_2Ph)_2][BF_4]$ (**2**) (95 mg, 84%) as well-formed microcrystals. Crystals suitable for X-ray crystallography were grown by slow hexane diffusion into a dilute CH_2Cl_2 solution of **4**. Found: C, 25.7; H, 3.0; N, 4.2. Calc.: C, 25.7; H, 3.1; N, 3.8%. ^{31}P NMR: AX spectrum, δ_a −1.5 ppm [$^1J(^{195}Pt–^{31}P)$ 2642 Hz], δ_x −35.6 ppm (^1J 3171 Hz). IR: (bands between 100 and 1200 cm^{-1} obscured by vibrations due to BF_4^-), 619 (w) and 315 (w) cm^{-1}.

Crystal data. Complex **2**, $C_{16}H_{23}BF_4N_2P_2PtSTe$, $M = 746.9$, monoclinic, $a = 8.479(2)$, $b = 17.365(5)$, $c = 16.061(7)$ Å, $\beta = 103.79(3)°$, $U = 2297$ Å^3, space group $P2_1/n$, $Z = 4$, $D_c = 2.16$ g cm^{-3}, μ(Cu-K_α) = 242 cm^{-1}. Refined unit cell parameters were obtained by centring 16 reflections on a Nicolet R3m diffractometer. 3100 independent reflections were measured ($2\theta \leqslant 116°$) with Cu-K_α radiation (graphite monochromator) using ω-scans. 2747 had $|F_o| > 3\sigma(|F_o|)$ and were considered to be observed. Data were corrected for Lorentz and polarization factors and an empirical absorption correction based on 372 azimuthal measurements was applied; maximum and minimum transmission factors: 0.182 and 0.058, respectively. The structure was solved by direct methods. The positions of hydrogen atoms were idealized, C—H = 0.96 Å, assigned isotropic thermal parameters, $U(H) = 1.2\ U_{eq}(C)$ and allowed to ride on their parent carbon atoms. Refinement was by block-cascade full-matrix least-squares to $R = 0.054$, $R_w = 0.056$ [$w^{-1} = \sigma^2(F) + 0.00128F^2$]. The maximum and minimum residual electron density in the final ΔF map were 2.52 and −2.01 e Å^{-3}. Computations were carried out on an Eclipse S140 computer using the SHELXTL program system. Further details of the crystal structure can be obtained from the Director of the Cambridge Crystallographic Data Centre, University Chemical Laboratory, Lensfield Road, Cambridge CB2 1EW, U.K. Any request should be accompanied by the full literature citation for this communication.

Acknowledgements—We are grateful to Johnson Matthey for loans of precious metals. J.D.W. is currently the Sir Edward Frankland Fellow of the Royal Society of Chemistry.

REFERENCES

1. R. Jones, P. F. Kelly, C. P. Warrens, D. J. Williams and J. D. Woollins, *J. Chem. Soc., Chem. Commun.* 1986, 711.
2. C. A. O'Mahoney, I. P. Parkin, D. J. Williams and J. D. Woollins, *Polyhedron* 1989, **8**, 2215.
3. A. V. Zibarev, G. G. Furin and G. G. Yakobson, *Izv. Akad NSSR Ser. Khim.* 1985, **12**, 2774.
4. P. F. Kelly and J. D. Woollins, *Polyhedron* 1986, **5**, 607.
5. P. F. Kelly, A. M. Z. Slawin, D. J. Williams and J. D. Woollins, *J. Chem. Soc., Chem. Commun.* 1989, 408.
6. P. F. Kelly, I. P. Parkin, A. M. Z. Slawin, D. J. Williams and J. D. Woollins, *Angew. Chem.* 1989, **101**, 1052.

Polyhedron Vol. 9, No. 22, pp. 2663–2673, 1990
Printed in Great Britain

0277-5387/90 $3.00+.00
© 1990 Pergamon Press plc

SYNTHESIS, SPECTROSCOPIC AND MAGNETIC PROPERTIES OF COPPER(II) COMPLEXES OF NOVEL POLYAZA CHAIN MOLECULES

R. BARIZ and C. BRÉMARD*

Laboratoire de Spectrochimie Infrarouge et Raman, (LASIR) UPR A 2631 L CNRS
Bât. C.5, Université de Lille I, 59655 Villeneuve d'Ascq Cedex, France

and

G. NOWOGROCKI and S. SUEUR✝

Laboratoire de Cristallochimie et Physicochimie du Solide, URA 0452 CNRS, E.N.S.C. de Lille, Université de Lille I, BP. 108, 59655 Villeneuve d'Ascq Cedex, France

(*Received* 18 *January* 1990; *accepted* 1 *May* 1990)

Abstract—The coordination of copper(II) chloride to the large linear polyazadioxime molecules 4,4-diaza-3,6-dimethyl-3,5-octadiene-2,7-dione-2,7-dioxime and -4,5,8,9-tetraaza-3,6,7,10-tetramethyl-3,5,7,9-dodecatetraene-2,11-dione-2,11-dioxime (abbreviated, respectively, H_2doxN_2 and H_2doxN_4) has been studied. These polymetallic complexes are an unusual route for bridging paramagnetic ions through a direct polyatomic pathway to give an antiferromagnetic linear chain of the ribbon type. Without available X-ray data the molecular geometries of the polymetallic compounds are characterized by vibrational, electronic and EPR spectroscopy, as well as by magnetic susceptibility measurements between 300 and 4.2 K. The binuclear $Cu_2(H_2doxN_2)Cl_4$ complex shows antiferromagnetic intradimer super exchange, $2J = -38$ cm^{-1}, and the trinuclear $Cu_3(H_2doxN_4)Cl_6$ complex shows antiferromagnetic intratrimer superexchange between neighbouring centres, $2J = -25$ cm^{-1}, propagated through the diaza bonds.

The polymetallic complexes of macromolecules are ubiquitous in conductive materials and biology. They are involved in a large number of processes; electron transport, metal storage or intermediates in redox reactions. In this respect, the interaction of metallic ions with large molecules is currently receiving much attention. Among the large chain molecules of interest, the linear conjugated macromolecules such as polyacetylenes and carotenoids are by far the most studied.[1] Unfortunately, the interactions of these polyene molecules occur only with the low oxidation state of metallic species such as carbonyl complexes. Ligands containing the —N=C—C=N— grouping are among the best known chelating agents, e.g. dimethylglyoxime, biacetyldihydrazone, 2,2′-bipyridine, etc. Larger polyaza chain molecules containing this grouping can be synthesized by condensation reactions between 1,2-diketones and hydrazines. Some polyaza ligands containing two —N=C—C=N— groupings and related metallic complexes have been previously synthesized.[2–14]

Recently, the syntheses and vibrational analysis of larger polyazadioxime oligomers have been reported.

The coordinating properties of the polyaza ligands are expected to differ from the coordinating properties of the corresponding monomeric systems, because of the several possible stereoisomers arising from the conformational changes of the backbone of the ligands.[13,14] The coordination of polyazadioxime molecules to copper(II) chloride was undertaken because the complexes exhibit a bridging route that consists of a polyatomic direct bonding pathway and conjugated bonding throughout the ligand.[13] The nature of

* Author to whom correspondence should be addressed.

magnetic and electronic interactions in magnetically coupled systems is the subject of much speculation,[15-19] but with the rapid growth in the number of reference complexes more information is being obtained. The spectroscopic and magnetic study of the copper(II) complexes of a series of polyazadioxime chain molecules promises to be a useful addition to the study of magnetic coupling propagated via a large polyatomic pathway.

EXPERIMENTAL

Synthesis of the polyazadioxime chain molecules

All chemicals were of reagent grade and were utilized without further purification except dehydration.

Dimethylglyoxime or 2,3-butanedione-2,3-dioxime (abbreviated hereafter H_2dox) was recrystallized from ethanol.

4,4 - *Diaza* - 3,6 - *dimethyl* - 3,5 - *octadiene* - 2,7-*dione*-2,7-*dioxime*, H_2doxN_2 (**2**). This was obtained by a method previously described.[7] Found: C, 49.0; H, 7.2; N, 28.2; O, 16.1. Calc. for $C_8H_{14}N_4O_2$: C, 48.5; H, 7.0; N, 28.3; O, 16.2%. Mass spectrum, *m/z* (%): 198(5); 182(10.8); 181(100); 165(5); 122(13.6); 98(29.4); 68(15.1); 58(32.2); 45(4.3).

4,4-*Diaza*[15]-3,6-*dimethyl*-3,5-*octadiene*-2,7-*dione*-2,7-*dioxime*, $H_2dox^{15}N_2$ (**2**). A solution of $^{15}N_2H_4 \cdot H_2O$ in dry ethanol was obtained from $^{15}N_2H_4 \cdot H_2SO_4$ (95%) (10^{-3} mol) and NaOH (2×10^{-3} mol). The solution of hydrazine hydrate was added dropwise to 0.222 g (2×10^{-3} mol) of 2,3-butanedione dissolved in 50 cm^3 of dry ethanol under vigorous stirring. The mixture was refluxed for 24 h and the volume reduced to 10 cm^3. Then the solution was kept at 0°C. After 24 h the pale yellow solid obtained was filtered and washed with cold methanol and diethyl ether. The product was dried *in vacuo*, yield 80%. Mass spectrum, *m/z* (%): 200(6); 184(150); 183(100); 182(4).

4,5,8,9 - *Tetraaza* - 3,6,7,10 - *tetramethyl* - 3,5,7,9-*dodecatetraene*-2,11-*dione*-2,11-*dioxime*, H_2doxN_4 (**3**). Biacetyldihydrazone or 2,3-butanedione-2,3-dihydrazone was obtained as previously described.[20,21]

0.114 g (10^{-3} mol) of biacetyldihydrazone was dissolved in 50 cm^3 of warm dry ethanol. This solution was added dropwise to 30 cm^3 of a stirred solution of dry ethanol containing 0.222 g (2×10^{-3} mol) of biacetyl monoxime. The mixture was refluxed for 24 h and then cooled to room temperature. After 24 h the yellow–orange microcrystals were filtered off and washed with cold ethanol and diethyl ether. The crystals were dried *in vacuo*, yield 80%. Found: C, 51.9; H, 7.54; N, 30.2; O, 9.9. Calc. for $C_{12}H_{20}N_6O_2$: C, 51.4; H, 7.1; N, 30.0; O, 11.4%. Mass spectrum, *m/z* (%): 280(9); 263(10.2); 204(4.7); 198(8); 182(10.5); 181(100); 163(8.1); 136(5.3); 123(9.4); 98(43); 68(20.1); 58(48).

4,5,8,9,12,13 - *Hexaaza* - 3,6,7,10,11,14 - *hexamethyl*-3,5,7,9,11,13 - *hexadecahexene* - 2,15 - *dione*-2,15-*dioxime*, H_2doxN_6 (**4**).[22] Bis(biacetyl)azine dihydrazone or 4,4-diaza-3,6-dimethyl-3,5-octadiene-2,7-dione-2,7-dihydrazone was obtained as previously described.[2] 0.196 g (10^{-3} mol) of bis(biacetyl)azine dihydrazone was dissolved in 50 cm^3 of warm dry ethanol. This solution was added dropwise to a stirred solution of 0.222 g (2×10^{-3} mol) of biacetyl monoxime in 30 cm^3 of dry ethanol. The mixture was refluxed for 24 h and then cooled to room temperature. After 24 h the yellow–orange microcrystals were filtered off and washed with cold ethanol and diethyl ether. The crystals were dried *in vacuo*, yield 80%. Found: C, 52.7; H, 7.13; N, 30.7; O, 7.1. Calc. for $C_{16}H_{26}N_8O_2$: C, 53.0; H, 7.2; N, 30.9; O, 8.8%. Mass spectrum, *m/z* (%): 362(4.1); 280(12.2); 263(25.4); 198(6.5); 181(43); 164(13.1); 98(100); 81(24.6); 51(11.4).

Poly(1,4-*diaza*-2,3-*dimethyl*-*butadiene*) (**5**). A solution of biacetyl (2×10^{-3} mol) in dry ethanol was added dropwise to N_2H_4 (2×10^{-3} mol) dissolved in 100 cm^3 of dry ethanol under vigorous stirring. The mixture was refluxed for 72 h and then cooled to room temperature. The pasty product obtained was washed with ethanol and diethyl ether. The product was dried *in vacuo*. Found: C, 60.1; H, 9.2; N, 31.2. Calc. for $(C_4H_6N_2)_n$: C, 58.5; H, 7.3; N, 34.1%.

Synthesis of the copper(II) *and zinc*(II) *complexes*

$Cu(H_2dox)Cl_2$ (**6**) *and* $Cu(H_2dox)Br_2$ (**7**). These were obtained as described in the literature.[23] Found: C, 19.3; H, 3.2; N, 11.1; Cu, 26.1; Cl, 28.2. Calc. for $CuC_4H_8N_2O_2Cl_2$: C, 19.2; H, 3.2; N, 11.2; Cu, 25.4; Cl, 28.3%. Found: C, 14.2; H, 2.4; N, 8.3; Cu, 18.7; Br, 46.8. Calc. for $CuC_4H_8N_2O_2Br_2$: C, 14.1; H, 2.4; N, 8.2; Cu, 18.7; Br, 47.1%.

$Cu_2(H_2doxN_2)Cl_4$ (**8**). To 50 cm^3 of a dry solution of hot ethanol containing 0.198 g (10^{-3} mol) of H_2doxN_2 were added dropwise and under vigorous stirring 20 cm^3 of a solution of dry ethanol containing 0.541 g (3×10^{-3} mol) of $CuCl_2$. After 12 h, green crystals separated.

They were collected by filtration, washed with cold ethanol and diethyl ether and dried *in vacuo*, yield 90%. Found: C, 21.9; H, 3.3; N, 11.8; Cu, 26.9; Cl, 29.3. Calc. for $Cu_2C_8H_{14}N_4O_2Cl_4$: C, 21.0; H, 3.0; N, 12.0; Cu, 27.2; Cl, 30.0%.

$Cu_2(H_2doxN_2)Br_4$ (**9**). This was obtained in a similar manner except $CuBr_2$ was used in place of $CuCl_2$, yield 90%. Found: C, 15.0; H, 2.4; N, 8.4; Cu, 19.4; Br, 49.1. Calc. for $Cu_2C_8H_{14}N_4O_2Br_4$: C, 14.9; H, 2.1; N, 8.7; Cu, 19.7; Br, 49.6%.

$Zn_2(H_2doxN_2)Cl_4$ (**10**). 0.198 g (10^{-3} mol) of H_2doxN_2 was dissolved into 50 cm^3 of hot dry ethanol. This solution was added dropwise under vigorous stirring to 20 cm^3 of dry diethyl ether containing 0.410 g (3×10^{-3} mol) of $ZnCl_2$. After 6 h, pale yellow crystals were collected by filtration under dry argon, washed rapidly with dry diethyl ether and dried *in vacuo*, yield 80%. Found: C, 20.8; H, 3.2; N, 11.5; Zn, 26.9; Cl, 30.5. Calc. for $Zn_2C_8H_{14}N_4O_2Cl_4$: C, 20.4; H, 3.0; N, 11.9; Zn, 27.8; Cl, 30.2%.

$Cu_3(H_2doxN_4)Cl_6$ (**11**). 0.280 g (10^{-3} mol) of H_2doxN_4 was dissolved into 60 cm^3 of hot dry ethanol. This solution was added dropwise under vigorous stirring to 20 cm^3 of dry ethanol containing 0.853 g (5×10^{-3} mol) of $CuCl_2$. After 24 h, dark green crystals were filtered off, washed with ethanol and diethyl ether and dried *in vacuo*, yield 90%. Found: C, 21.0; H, 3.1; N, 12.2; Cu, 26.8; Cl, 30.7. Calc. for $Cu_3C_{12}H_{20}N_6O_2Cl_6$: C, 21.1; H, 2.9; N, 12.3; Cu, 27.2; Cl, 31.1%.

Attempt to obtain $Cu_4(H_2doxN_6)Cl_8$ (**12**). The method used is similar to that used for $Cu_3(H_2doxN_4)Cl_6$ (**11**). Unfortunately, even in the presence of an excess of $CuCl_2$, the resulting compound does not correspond to a definite product but to a mixture of $Cu_3(H_2doxN_6)Cl_6$ and $Cu_4(H_2doxN_6)Cl_8$.

Physical measurements

The IR spectra were recorded on a FT–IR Bruker IFS 113V instrument using the KBr disc method of Nujol mulls (4000–500 cm^{-1}) and polyethylene disc method (500–20 cm^{-1}).

The Raman spectra were recorded using a triple monochromator Dilor RTI 30 instrument. The exciting lines used were the radiations of a krypton (647.1 nm) or argon (514.5, 488.0, 457.9 nm) ion laser. Sample spinning cell techniques were used and the absorbing samples were diluted in solid K_2SO_4 and pressed to form pellets.

The electronic spectra were run on a "Jobin et Yvon" DUOSPAC 203 instrument, using Nujol mulls.

EPR spectra were recorded at X-band on a Varian E.109 spectrometer at room and liquid nitrogen temperatures using powder samples. The magnetic field was calibrated with a DPPH marker.

Magnetic measurements were performed on a Faraday type magnetometer equipped with a helium continuous-flow cryostat in the 4–300 K temperature range. $HgCo(NCS)_4$ was used as a susceptibility standard. Diamagnetic corrections for **7** and **10** were taken as -236 and -342×10^{-6} cm^3 mol^{-1}, respectively. The data were also corrected for the temperature independent paramagnetism (TIP) of the copper(II) ions, 60×10^{-6} cm^3 mol^{-1}.

RESULTS

Synthesis of the copper(II) *and zinc*(II) *polyaza complexes*

The polyazadioxime chain molecules are capable of chelating metallic ions through the nitrogen-donor atoms. The coordination capabilities of the polyaza chain molecules depend on the nature of the metallic ion and the counterion.

In the presence of $CuCl_2$, H_2dox forms a well-known complex $Cu(H_2dox)Cl_2$ (**6**)[6] which has been structurally well characterized[24,25] (Fig. 1). The conformational changes in the backbone of the H_2dox ligand result in a torsion of 180° around the N=C—C=N single bond. Upon coordination, the backbone of the ligand changes from the C_{2h} to C_{2v} point symmetry group.

In the presence of MX_2 (M = Cu, Zn; X = Cl, Br), H_2doxN_2 forms binuclear complexes $M_2(H_2doxN_2)X_4$. All the complexes are poorly soluble in dry ethanol. They crystallize immediately without dramatic rearrangement of the backbone of the chain molecule except for torsional motions. Among the possible stereoisomers of the H_2doxN_2 molecule (Fig. 2) the (*E,E,E,E*) s all *trans* conformation is the most probable.[21] When the ligand is dissolved in the presence of an excess of MX_2, the conformational changes of the H_2doxN_2 molecule result in a torsion of 180° around the N=C—C=N single bonds and the coordination constrains the

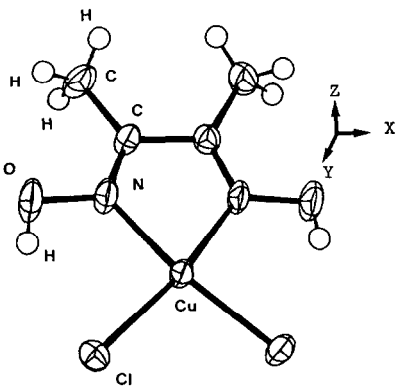

Fig. 1. Molecular structure of $Cu(H_2dox)Cl_2$ (from refs 24 and 25).

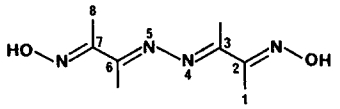

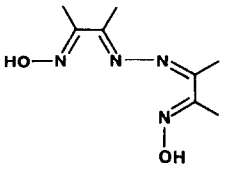

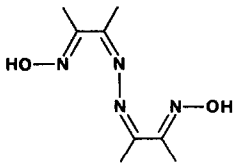

Fig. 2. Possible stereoisomers of the H_2doxN_2 molecule.

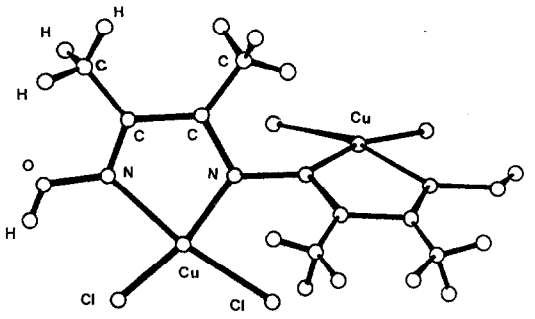

Fig. 3. Idealized molecular geometry of $Cu_2(H_2doxN_2)Cl_4$ (**8**).

(*E,E,E,E*) s *cis*, s *gauche*, s *cis* conformation (Fig. 3). Upon coordination, the backbone of the planar subunits N=C—C=N change from C_{2h} to C_{2v} symmetry. The resulting symmetry of the complex is at the very most C_2.

Unfortunately attempts to obtain suitable crystals for X-ray analysis failed and no definitive structural assignment could be made. Nevertheless the structure of a parent ketazine complex has been reported earlier[13] and supports the reasonable structural assumptions concerning all the complexes under study (Fig. 3). The bridge connecting the two metal centres consists of an azine linkage. The complex is not planar, there is a rotation about the N—N bond to minimize the intra- and intermolecular contacts. To prevent the precipitation of fortuitous compounds such as $M(H_2doxN_2)X_2$, the ligand is introduced dropwise to a vigorously stirred solution containing a large excess of metallic salts. Elemental analyses were undertaken after numerous attempts with different metal–ligand ratios, and are in good agreement with the proposed formulation $M_2(H_2doxN_2)X_4$ with the range [2.5–5] for the metal–ligand ratio.

The geometry of the backbone of the coordinated H_2doxN_2 molecule depends on the counterion X of the metallic compounds MX_2. As previously reported,[14] coordination of H_2doxN_2 with $Cu(ClO_4)_2$ leads to a template rearrangement of the H_2doxN_2 molecule. In the $[Cu(HdoxN_2)]_2[ClO_4]_2$ complex, the $HdoxN_2^-$ anion acts as a planar tridentate ligand with an (*E,E,Z,E*) s *cis*, s *trans*, s *cis* conformation, Fig. 4.

Among the possible stereoisomers of the H_2doxN_4 molecule, the (*E,E,E,E,E,E*) all *trans* conformation is the most probable,[21] Fig. 5. When the H_2doxN_4 ligand is dissolved in the presence of an excess of MX_2 (M = Cu, X = Cl, Br) the conformational modifications of the H_2doxN_4 molecule, upon coordination, arise from a torsion of 180° around the C—C single bonds (Fig. 5) and

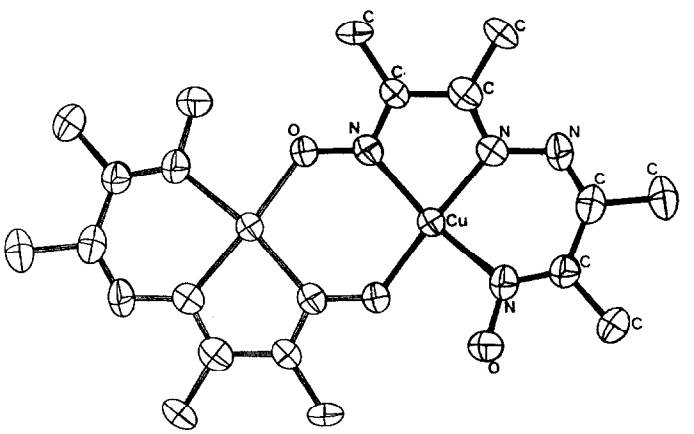

Fig. 4. View of the "basal plane" of the dication $[Cu(HdoxN_2)]_2^{2+}$ (from ref. 14).

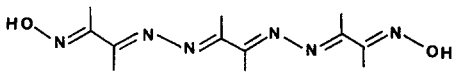

(E,E,E,E,E,E ; S trans, S trans, S trans, S trans, S trans)

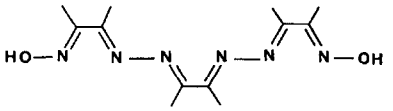

(E,E,E,E,E,E ; S Cis, Strans, S Cis, S trans, S Cis)

Fig. 5. Conformational changes of the (*E,E,E,E,E,E*) stereoisomer of the H_2doxN_4 molecule.

the preferred conformation in $Cu_3(H_2doxN_4)Cl_6$ becomes (*E,E,E,E,E,E*) s *cis*, s *gauche*, s *cis*, s *gauche*, s *cis*.

The bridges connecting the three metal centres consist of two azine linkages. The symmetry of the planar N=C—C=N subunits evolves from C_{2h} to C_{2v}. The resulting symmetry of the complex is at the very most C_2 because of the rotation around the N—N bonds to minimize the intra- and intermolecular contacts. The resulting structure of the tricopper complex may be expected to be a non-planar spiral structure rather than a planar zigzag structure.

It should be noted that the elemental analyses concerning the $Cu_3(H_2doxN_4)Cl_6$ compound are in good agreement with the proposed formulation if the metal–ligand ratio is in the [4–7] range.

Attempts to obtain pure tetrametallic complexes, $M_4(H_2doxN_6)Cl_8$, have failed to date, and the numerous elemental analyses are not in good agreement with the proposed formulation in the range [4–8] for the metal–ligand ratio. The elemental analyses likely correspond to a mixture of $Cu_3(H_2doxN_6)Cl_6$ and $Cu_4(H_2doxN_6)Cl_8$ complexes. The conformational changes in the backbone of the $doxN_6$ molecule do not occur for all four subunits before precipitation of the compound. In the same way, if the polycondensation between biacetyl and hydrazine is undertaken under template synthesis conditions, no significant metal content is detected. It is probable that the all s *trans* conformation of the polymer remains, even in the presence of a large excess of $CuCl_2$.

Vibrational spectroscopy

IR and Raman spectroscopies have been used to establish the conformational changes of the ligand backbones during the complexation and the mode of bonding in the coordination sphere of the metallic ions copper(II) and zinc(II). Therefore, the assignments of the most characteristic Raman and IR bands of both polyaza chain molecules and related metallic complexes have been undertaken by comparison between ^{14}N and ^{15}N labelled compounds' spectra, Cl and Br, Cu and Zn derivatives, respectively. The effects of site and crystal in the solid state are probably weak and not resolved with the resolution used to run the spectra at room temperature. So, the spectra are interpreted using the molecular structure hypothesis in the solid state.

The vibrational spectra of all the compounds H_2dox, H_2doxN_2, H_2doxN_4 and H_2doxN_6 are in good agreement with a C_{2h} symmetry group.[21,22,26] Indeed with C_{2h} symmetry, the normal vibrations are either Raman active (A_g+B_g) or IR active (A_u+B_u). It should be noted that the spectra of the polyaza chain molecules are particularly characteristic of the N=C(CH$_3$)C(CH$_3$)=N subunits with planar C_{2h} local symmetry.

The coordination of metallic moieties such as MX_2 (M = Cu, Zn; X = Cl, Br) to subunits, through the two nitrogen atoms, imposes a 180° rotation around the C—C bond to give subunits with C_{2v} symmetry group. The A_1, B_1 and B_2 modes are IR active, whereas all the vibration modes A_1, A_2, B_1 and B_2 are Raman active. The polymetallic complexes of the large polyazadioxime molecules arise from the linkage of two, three or four subunits with C_{2v} local symmetry, the resulting symmetry group is at the most C_2 for all of the compounds.

The band pattern of the spectra of the polymetallic complexes resemble that of the MH_2doxX_2 spectra, therefore assignments can be made in correspondence with the results from the vibrational analysis of the monomeric species. The main Raman and IR peaks of the copper(II) complexes $Cu(H_2dox)Cl_2$, $Cu_2(H_2doxN_2)Cl_4$ and $Cu_3(H_2doxN_4)Cl_6$ are collected in Table 1. The lines observed in the ν(C=N) region are indicative of the skeletal change upon coordination. Indeed, the ν(C=N—OH) and ν(C=N—N) modes are both IR and Raman active for all the metallic compounds under study. These results are in good agreement with local C_{2v} symmetry of the subunits for all the ligands with the all *E* configuration in $[Cu(HdoxN_2)_2][ClO_4]_2$, inducing four bands in the ν(C=N) region which are IR and Raman active. This result is in good agreement with a C_s symmetry of the ligand.[14]

The lines observed in the spectral range 1400–600 cm^{-1}, attributed to deformation, rocking and wagging motions of the methyl groups, indicate poorly the skeletal change of the polyaza molecules upon coordination. The more sensitive indications of the conformational changes are the skeletal deformation and torsion motions which are active

Table 1. Characteristic vibrational modes (cm^{-1}) of copper(II) complexes with polyaza chain molecules

$Cu(H_2dox)Cl_2$		$Cu_2(H_2doxN_2)Cl_4$		$Cu_3(H_2doxN_4)Cl_6$		Tentative assignment
IR	Raman	IR	Raman	IR	Raman	
1660w		1650w	1650w	1660w	1660w	ν(C=N—O)
1600w	1600m	1580s	1580s	1580s	1580m	ν(C=N—N)
1195s		1190		1190s		ν(C—CH_3)
1090s						ν(C—C)
1070s		1060s		1047s		ν(N—O)
813s		810m		860m		ν(C—CH_3)
708s		757s				
650s		617s		614m		
580s		575s	570w			
524s		510m		520w		
485sh	485w	485w				
						ν(Cu—N)
476s		470w				
340w		380m				
						ν(Cu—Cl)
315sh		314s	315w	310s		
297s		268m	268w		262w	
						$\delta(CuN_2)$
230m	230m		230w			
200m	200m	189m				
170m	170w	186w		186w		$\delta(CuCl_2)$
142w	142w	166w		168w		
130w	130w	127w				
117w	117w	120w				

s, strong; m, medium; w, weak: sh, shoulder.

in the far wavenumber range, Table 1, however, the interpretation is not straightforward.

The assignments of the most characteristic vibrational modes of the coordination sphere MN_2X_2 are achieved by comparison with those of $Cu(H_2dox)X_2$ (X = Cl, Br) and the zinc analogue complexes. Among the $4A_1+A_2+B_1+3B_2$ expected vibration modes for the MN_2X_2 moieties, only the intense IR modes ν_{as},ν_s(M—X) and δ(XMX) are unequivocally assigned. Indeed, the weak ν_s and ν_{as}(M—N) stretching modes are masked by the intense bands arising from the MCl_2 vibrations and are only clearly observed with X = Br. Nevertheless, when the complexes contain more than one MN_2X_2 subunit, the Raman and IR bands are broad.

Electronic transitions

The electronic spectra of the copper(II) complexes exhibit several bands at: 270 (s), 310 (s), 350 (sh), 460 (sh), 690 (w) nm for $Cu(H_2dox)Cl_2$; 280 (s), 330 (s), 350 (sh), 470 (sh), 690 (w), 760 (w) nm for $Cu_2(H_2doxN_2)Cl_4$; 320 (s), 370 (s), 350 (sh), 490 (sh), 690 (w), 740 (w), 770 (w) nm for $Cu_3(doxN_4)Cl_6$, with the respective intensities s (strong), sh (shoulder) and w (weak). The assignments of these electronic transitions may be facilitated by comparing the spectra with those of the corresponding free ligand and zinc(II) complex. Indeed the two strong absorptions near 300 nm are observed both in the free ligand and metallic complex spectra. They are attributed readily to internal ligand $\pi \rightarrow \pi^*$ transition. In addition, the weak and broad absorptions around 700 nm are not observed for the zinc(II) analogues and are assigned to $d \rightarrow d$ transitions in copper(II) complexes. The medium absorptions, observed as shoulders near 350 and 470 nm in all the spectra of metallic complexes, probably arise from $d \rightarrow \pi^*$ metal–ligand charge-transfers. The charge-transfer character of the latter transitions can be verified if the Raman spectra of the metallic complexes are carried out at different exciting lines within the contour of the charge-transfer bands. A pre-resonance Raman effect was detected particularly for the Raman bands in the ν(C=N) region, Table 1. The Raman band intensities of the ν_s(C=N) modes are enhanced more and

more if the exciting line wavelength decreases from 647.1, 514.5, 488.0 to 457.9 nm. These features indicate that the orbitals of the C=N group participate in the π^* molecular orbital involved in the charge-transfer transition. It should be noted that the intense Raman band corresponding to the ν(N—N) bond in the free polyaza ligands is not enhanced by resonance effects and may be clearly detected only in the $Zn_2(doxN_2)Cl_4$ complex at 1055 cm^{-1} with off-resonance conditions. The *d–d* bands are too broad to be used as a "criterion of stereochemistry".[27,28] Indeed, four *d–d* transitions are expected for one CuN_2Cl_2 chromophore with C_{2v} local symmetry from $d_{z^2}(a_1)$; $d_{x^2-y^2}(a_1)$; $d_{xz}(b_2)$; $d_{yz}(a_2)$ to the ground state $d_{xy}(b_1)$. $Cu(H_2dox)Cl_2$ exhibits ill-defined absorptions around 700 nm as generally reported for copper(II) complexes with square-planar stereochemistry. For di- and tri-copper(II) complexes, there are two and three CuN_2Cl_2 chromophores and the respective electronic absorption spectra exhibit untractable absorptions near 700 nm for the elucidation of the stereochemistry.

Magnetic susceptibility and EPR spectra

The theory of exchange interactions in copper(II) dimers and trimers has been treated in detail previously.[16,18,19,29]

The crystal structure[24] and magnetic susceptibility[23] of $Cu(H_2doxCl_2)Cl_2$ have previously been reported. The complex consists of dimeric $[Cu(H_2dox)Cl_2]_2$ units that are essentially isolated from each other, although the dimeric moieties are linked together through hydrogen bonds to form an infinite linear chain.[25] The bridging Cu_2Cl_2 unit is constrained to be planar by the presence of the crystallographic inversion centre in the middle of the dimer. The geometry of each copper can be described as a distorted tetragonal-pyramidal arrangement, the bridging chloride occupying the apical site.

Magnetic suspectibility measurements[21] show that the exchange coupling constant was found to be small, $2J = +0.30$ cm^{-1}, where J is defined by the well-known spin-Hamiltonian:

$$H = -2JS_1 \cdot S_2, \qquad (1)$$

for a pair of $S = 1/2$ ions; $-2J$ represents the energy gap between the two low-lying states resulting from the spin coupling. As previously reported,[23] the EPR spectrum of $Cu(H_2dox)Cl_2$, run at room temperature, exhibits a clear resolution of the **g** tensor principal components into a parallel $g_\parallel = 2.21$ and a perpendicular $g_\perp = 2.03$ component. On lowering the temperature to 77 K the spectrum shows a complete **g** tensor anisotropy with $g_x = 2.02$, $g_y = 2.04$ and $g_z = 2.21$. The corresponding bromide derivative $Cu(H_2dox)Br_2$, exhibits a broad quasi-isotropic feature centred at $\langle g \rangle = 2.03$ at room temperature.[23] On lowering the temperature to 77 K, only a weak change is observed in the EPR spectrum. It should be noted that the signals observed for non-dilute powdered samples are only a good estimation of the crystal **g** tensor components rather than the molecular **g** tensor components.

The magnetic susceptibility of the dicopper(II) complex $Cu_2(H_2dox)N_2)Cl_4$ is plotted in Fig. 6 as a function of temperature. The magnetic susceptibility per copper exhibits a broad maximum around 30 K, which rapidly drops as the temperature is lowered. This type of temperature-dependent behaviour is expected for an antiferromagnetically coupled copper(II) binuclear molecule. The magnetic susceptibility per copper may be calculated using the Bleaney–Bowers expression.[30]

$$\chi_{Cu} = N\beta^2 g^2/kT[3+\exp(-2J/kT)]^{-1}[1-\rho] + \rho N\beta^2 g^2/4kT + \chi_{TIP}. \qquad (2)$$

In eq. (2) the symbols have their usual meaning. The formula gives the magnetic susceptibility per mole of copper atom in the coupled system, corrected for TIP and paramagnetic impurities. The curve through the data points in Fig. 6 was obtained from the best fit of the data to eq. (2) with the parameters $g = 2.08 \pm 0.03$, $\rho = 0.08 \pm 0.01$ and $2J = -38.5 \pm 2$ cm^{-1}. The magnetic data of the dicopper(II) complex $Cu_2(H_2doxN_2)Cl_4$ are analogous to those reported previously[13] for the parent complex $Cu_2(pmk)Cl_4$. The magnitude of $-2J$ suggests that the dominant pathway for exchange is superexchange through the Cu—N—N—Cu azine bridge. Earlier magnetic susceptibility measurements show that the exchange couplings through the Cu–Cl–Cu exchange pathway are weak for $[Cu(H_2dox)Cl_2]_2$ and $Cu_2(pmk)Cl_4$[13] compounds. The g value obtained from the magnetic measurements for the $Cu_2(H_2doxN_2)Cl_4$ compound, $g = 2.08 \pm 0.03$, is in good agreement, within the experimental error range, to the isotropic $\langle g \rangle$ value deduced from the EPR data, $\langle g \rangle = 1/3(g_\parallel + 2g_\perp) = 2.1$. At 77 K two components can be observed, $g_\perp = 2.06$ and $g_\parallel = 2.18$, in the EPR spectrum of $Cu_2(H_2doxN_2)Cl_4$. The spectrum appears to be in agreement with a triplet spin state, $S = 1$, by the temperature dependence although any half-field signal is observed. The molecular **g** tensors of the two magnetic sites were found to be identical and analogous to that of the monomeric species $Cu(H_2dox)Cl_2$. It should be noted that the signals remain broad even at low temperature and the zero-

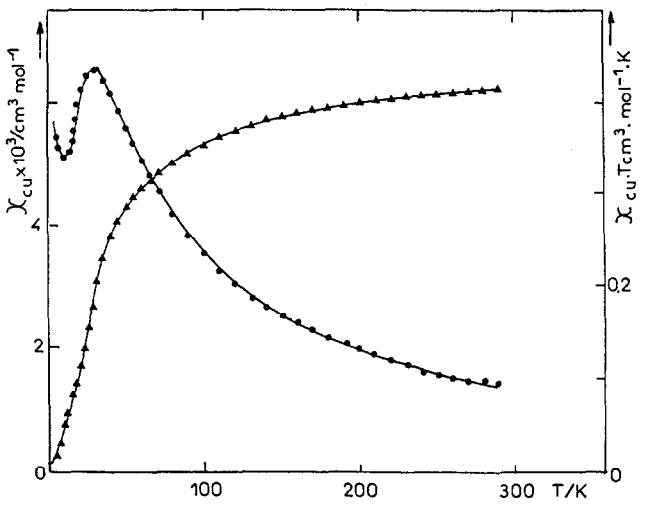

Fig. 6. Magnetic susceptibility per copper (●) and the product $\chi_{Cu}T$ (▲) plotted as a function of temperature for $Cu_2(H_2doxN_2)Cl_4$. The curve through the data is the best fit of the data to eq. (2), as described in the text.

field splitting parameters cannot be drawn out as previously reported for dicopper(II) analogues.[31]

The temperature dependence of χ_{Cu} vs T for $Cu_3(H_2doxN_4)Cl_6$, represented in the form of the product $\chi_{Cu}T$, the magnetic susceptibility per mole of copper multiplied by the temperature, is shown in Fig. 7. The general form of the magnetic data for $Cu_3(doxN_4)Cl_6$ is appropriate for a trimer with dominant exchange interactions between adjacent copper atoms.[32,36] To characterize the exchange interaction in symmetric trimers, the spin-Hamiltonian may be written:

$$H = -2J_{12}(S_1 \cdot S_2 + S_2 \cdot S_3) - 2J_{13}S_1 \cdot S_3. \quad (3)$$

The exchange integral J_{12} refers to two adjacent copper atoms and J_{13} to the interaction between the terminal copper atoms by coupling S_1 and S_3 to give an intermediate spin state S^*, and then coupling S^* to S_2 to give a total spin state S. The low-lying states are a ground doublet state 1/2(0), an excited doublet state 1/2(1) and an excited quartet state 3/2(1) using the notation $S(S^*)$.[32] Different **g** tensor values correspond to the different $S(S^*)$ states according to the relation previously reported.[36] As long as the trinuclear complex has two equivalent ions, the two spin doublets are not mixed and the g values for the various multiplets can be easily expressed as a linear combination of the **g** tensors of the individual ions. Therefore the most general expression for the magnetic susceptibility of a sym-

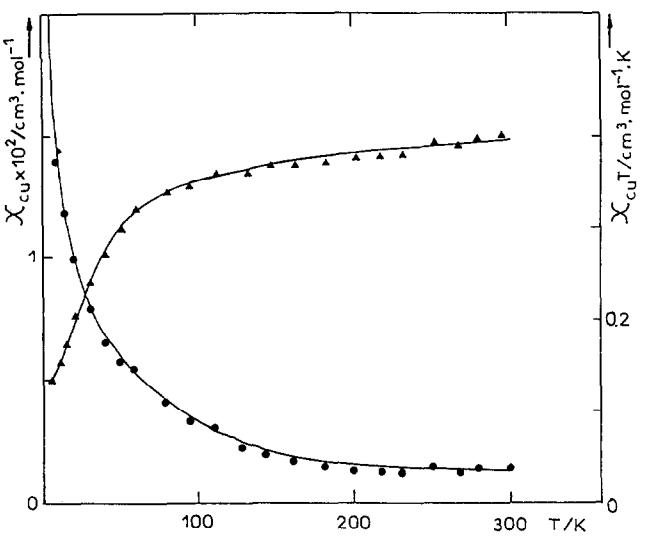

Fig. 7. Magnetic susceptibility per mole of copper (●) and the product $\chi_{Cu}T$ (▲) as a function of temperature for $Cu_3(H_2doxN_4)Cl_4$. The curve through the data is the best fit of the data to eq. (4) as described in the text.

metric trimer is reduced to the following equation[32] if $\mathbf{g}_1 = \mathbf{g}_2 = \mathbf{g}_3 = \mathbf{g}$ and if J_{13} is assumed to be negligible as expected for nearly linear tricopper complexes. It should be noted that neither the nonplanar spiral structure nor the planar zigzag structure exhibits a strictly linear alignment of the Cu_3 system.

$$\chi_{Cu} = N\beta^2 g^2/12kT[X/Y]+\chi_{TIP}$$
$$X = 10\exp[J_{12}/kT]+\exp[-2J_{12}/kT]+1$$
$$Y = 2\exp[J_{12}/kT]+\exp[-2J_{12}/kT]+1. \quad (4)$$

The experimental values of $\chi_{Cu}T$ have been fit to eq. (4) by treating g and J_{12} as adjustable parameters. The resulting best fit is shown as the solid line in Fig. 7. The best fit is achieved with $g = 2.13\pm0.05$ and $2J_{12} = -25\pm3$ cm^{-1}. The reasonable agreement between calculated and experimental $\chi_{Cu}T$ values supports the hypothesis effected and discussed earlier in detail.[32,36] The magnetic data show that the coupling between the internal and the two external copper ions of the trimer is antiferromagnetic, therefore, the **g** tensor of the ground spin doublet is given by[36] $\mathbf{g} = 4/3\mathbf{g}_1 - 1/3\mathbf{g}_2$, where $\mathbf{g}_1 = \mathbf{g}_3$ and $\mathbf{g}_2$ are local **g** tensors for external and internal copper nuclei, respectively. The temperature dependence of the apparent **g** values obtained from powder EPR spectra can be compared to these reported previously for tricopper(II) analogues.[36] Above 77 K the two spin doublets and the spin quartet are populated and the observed spectrum at a given temperature above 77 K would be a thermal average of the spectra of the three multiplets. If the individual local **g** tensors are analogous, as assumed the **g** components obtained at 77 K in the EPR spectrum, $g_x = 2.06$, $g_y = 2.19$, $g_z = 2.23$, are relevant to the doublet ground state with an average value $\langle g \rangle = 2.16$ in accordance with the magnetic data.

DISCUSSION

Without X-ray data for the polymetallic complexes under study, it is not possible to analyse the relationship between the structural and magnetic properties of complexes of the types $Cu(H_2dox)Cl_2$, $Cu_2(H_2doxN_2)Cl_4$ and $Cu_3(H_2doxN_4)Cl_6$. Indeed, even if the gross molecular structures can be reasonably assumed from the experimental data of the present work, they cannot predict the magnetic behaviour since a small modification of the structural parameters may drastically modify the magnetic properties of the polymetallic complexes. However, it is possible from a small number of basic concepts to explain qualitatively the magnetic properties and to deduce some structural evidence.[18,37] The spin–spin coupling in the polycopper(II) complexes under study may be propagated through the Cu—N—N—Cu azine exchange pathway or either of the Cu—Cl—Cu exchange pathways.

If the intermolecular chlorine–copper contacts form a coordination polyhedron close to a tetragonal pyramidal geometry, the exchange interaction between the two copper ions would be weak, as observed previously for $[Cu(H_2dox)Cl_2]_2$ and $Cu_2(pmk)Cl_4$.[13,38,39]

The magnetic orbital lies in the plane determined by the four closest atoms N_2Cl_2. If these atoms lie in a plane, the magnetic orbital would have little density out of the plane and the amount of overlap onto the bridging chlorine would be small. It is important to note that the fitted curves shown in Figs 6 and 7 did not require significant corrections for interdimer magnetic coupling arising from the possible intermolecular chlorine bridging contacts. It is clear from magnetic susceptibility data that chain behaviour is not obtained. By analogy with the $Cu(H_2dox)Cl_2$ complex, the $Cu_2(H_2doxN_2)Cl_4$ and $Cu_3(H_2doxN_4)Cl_6$ complexes would be expected to exhibit negligible exchange interactions via the chloride bridges, and the propagation of magnetic coupling occurs via the direct azine pathway resulting in intramolecular antiferromagnetic superexchange.

The coordination polyhedron of each copper(II) ion in $Cu_2(H_2doxN_2)Cl_4$ and $Cu_3(H_2doxN_4)Cl_6$ is deduced to be nearly planar as reported previously for the $[Cu(H_2dox)Cl_2]_2$ complex.[24,25] In the square-planar environment the most destabilized orbital occupied by the unpaired electron of copper (II) ion is of the d_{xy} type.[18] This points from the metal towards the four nearest neighbours N_2Cl_2 in an antibonding fashion. It can be expected that the main factor governing the magnitude of the antiferromagnetic interaction via the extended azine bridge will be the overlap of magnetic orbitals. Both the orientation and delocalization of the magnetic orbitals favour their overlapping and thus the antiferromagnetic interaction. The possibility of the former method is governed by the torsional angle of the ketazine bond C=N—N=C, which is indicative of the relative orientation of the d_{xy} magnetic orbitals. However, the delocalization depends on the energy gap between the copper(II) orbitals and the ligand orbitals, which depends on the torsional angles of the azine functions. The delocalization in the monomeric subunits is transmitted through the azine bond via the σ molecular orbital system only, according to the assumed dihedral angle between the planar monomeric fragments, the π molecular

orbital system is not delocalized over the entire molecules.

It is tempting to compare the present $2J$ values with those obtained for parent dimeric complexes. The antiferromagnetic coupling constants reported for $Cu_2(pmk)Cl_4$[13] and for $Cu_2(H_2doxN_2)Cl_4$ in the present study are in the same order, -52 and -38 cm^{-1}, respectively. They suggest a dihedral angle between the two planar monomeric fragments of more than 30° in $Cu_2(H_2doxN_2)Cl_4$. Indeed if a coplanar conformation of the two monomeric fragments is constrained through a rigid ligand such as pyridazine-3,6-diformyldioxime, H_2piox, to form the $Cu_2(Hpiox)_2(ClO_4)_2(H_2O)_2$ complex,[40] the magnitude of the antiferromagnetic coupling is very large and close to 500 cm^{-1}. This strong interaction is due to the strict co-planarity of the two magnetic orbitals and to their delocalization through the σ and π systems of the ligands. Analogous conclusions[41,43] can be drawn from earlier reports concerning parent complexes with pyridazine, imidazolato and triazolato bridging ligands.

The knowledge of the magnetic exchange pathway for $Cu_2(H_2doxN_2)Cl_4$ indicates that for the non-planar tricopper complex, $Cu_3(H_2doxN_4)Cl_6$, the magnitude of the superexchange between the two external copper(II) ions is expected to be negligible as is assumed in strictly linear tricopper complexes.[34] The antiferromagnetic coupling constant value between the two adjacent copper(II) ions is of the same order as that observed for the dimer analogue $Cu_2(H_2doxN_2)Cl_4$, -25 and -38 cm^{-1}, respectively. From the results obtained in the present work, it should be reasonable to speculate that the magnitude of the antiferromagnetic coupling between two adjacent copper(II) ions in the linear tetracopper(II) complex, $Cu_4(H_2doxN_6)Cl_8$, or in the copper(II) linear chains of the twisted ribbon type, is in the same range as that measured in $Cu_3(H_2doxN_4)Cl_6$, although these compounds have not been successfully synthesized as yet.

Acknowledgement—We thank J. M. Leblanc from the Université du Mans (France) for the magnetic measurements and helpful discussions.

REFERENCES

1. D. N. Batchelder and D. Bloor, *Advances in Infrared and Raman Spectroscopy* (Edited by R. J. H. Clark and R. E. Hester), Vol. 11, p. 133. Wiley, Heyden (1984).
2. W. J. Stratton and D. H. Busch, *J. Am. Chem. Soc.* 1960, **82**, 4834.
3. W. J. Stratton and D. H. Busch, *J. Am. Chem. Soc.* 1958, **80**, 1286.
4. W. J. Stratton and D. H. Busch, *J. Am. Chem. Soc.* 1958, **80**, 3191.
5. W. J. Stratton, M. F. Rettig and R. F. Drury, *Inorg. Chim. Acta* 1969, **3**, 97.
6. W. J. Stratton, *Inorg. Chem.* 1970, **9**, 517.
7. W. J. Stratton and P. J. Ogren, *Inorg. Chem.* 1970, **9**, 2588.
8. J. E. Andrew and A. B. Blake, *J. Chem. Soc. A* 1969 1413.
9. P. W. Ball and A. B. Blake, *J. Chem. Soc. A* 1969, 1415.
10. A. Dei, D. Gatteschi and E. Piergentile, *Inorg. Chem.* 1979, **18**, 89.
11. C. Benelli, A. Dei and D. Gatteschi, *Inorg. Chem.* 1982, **21**, 1284.
12. M. Ghedini, G. Demunno, G. Denti, A. M. Monotti Lanfredi and A. Tiripicchio, *Inorg. Chim. Acta* 1982, **57**, 87.
13. C. J. O'Connor, R. J. Romananch, D. M. Robertson, E. E. Eduok and F. R. Fronczek, *Inorg. Chem.* 1983, **22**, 449.
14. A. Abraham, J. M. Capon, G. Nowogrocki, S. Sueur and C. Brémard, *Polyhedron* 1985, **4**, 1761.
15. R. E. Coffman and G. R. Buettner, *J. Phys. Chem.* 1979, **83**, 2387.
16. E. A. Boudreaux and L. N. Mulay, *Theory and Applications of Molecular Paramagnetism.* John Wiley, New York (1976).
17. C. G. Pierpont, L. C. Francesconi and D. N. Hendrickson, *Inorg. Chem.* 1978, **17**, 3470.
18. O. Kahn, *Angew. Chem. Int. Edn Engl.* 1985, **24**, 834 and refs cited therein.
19. R. L. Carlin, *Magnetochemistry.* Springer, Heidelberg (1986).
20. D. H. Busch and J. C. Baileur, *J. Am. Chem. Soc.* 1956, **78**, 1137.
21. R. Bariz, C. Brémard, J. Laureyns and J. C. Merlin, *J. Molec. Struct.* 1986, **142**, 439.
22. F. Abraham, R. Bariz and C. Brémard, unpublished works.
23. M. Mégnamisi Bélombé and M. A. Novotny, *Inorg. Chem.* 1980, **19**, 2470 and refs cited therein.
24. D. H. Svedung, *Acta Chim. Scand.* 1969, **23**, 2865.
25. J. M. Capon, Thesis Lille, France (1984).
26. V. Tabacik and V. Pellegrin, *Spectrochim. Acta* 1979, **35**, 961.
27. B. J. Hathaway and D. E. Billing, *Coord. Chem. Rev.* 1970, **5**, 143.
28. B. J. Hathaway, *Coord. Chem. Rev.* 1983, **52**, 87.
29. C. J. O'Connor, *Prog. Inorg. Chem.* 1982, **29**, 203.
30. B. Bleaney and K. D. Bowers, *Proc. R. Soc. London, Ser. A* 1952, **214**, 451.
31. A. Bencini, D. Gatteschi, C. Zanchini, J. G. Haasnoot, R. Prins and Reedijk, *J. Inorg. Chem.* 1985, **24**, 2812.
32. D. B. Brown, J. R. Wasson, J. W. Hall and W. E. Hatfield, *Inorg. Chem.* 1977, **16**, 2526.
33. C. Benelli, R. K. Bunting, D. Gatteschi and C. Zanchini, *Inorg. Chem.* 1984, **23**, 3074.
34. Y. Journaux, J. Sletten and O. Kahn, *Inorg. Chem.* 1986, **25**, 439.

35. W. Haase and S. Gehring, *J. Chem. Soc., Dalton Trans.* 1985, 2609.
36. L. Banci, A. Bencini and D. Gatteschi, *Inorg. Chem.* 1983, **22**, 2681.
37. D. Çatteschi, O. Kahn and R. D. Willett (Eds), *Magneto Structural Correlations in Exchange Coupled Systems*, NATO ASI Ser. C. Vol. 140. D. Reidel, Dordrecht (1984).
38. W. E. Marsh, K. C. Patel, W. E. Hatfield and D. J. Hodgson, *Inorg. Chem.* 1983, **22**, 511.
39. C. P. Landee and R. E. Greeney, *Inorg. Chem.* 1986, **25**, 3771.
40. B. Mernari, Thesis Lille, France (1987).
41. L. K. Thompson, F. W. Hartstock, P. Robichand and A. W. Hanson, *Can. J. Chem.* 1984, **62**, 2755.
42. L. K. Thompson, A. W. Hanson and B. S. Ramaswamy, *Inorg. Chem.* 1984, **23**, 2459.
43. G. Kolks, S. L. Lippard, J. V. Waszczak and H. R. Lilienthal, *J. Am. Chem. Soc.* 1982, **104**, 717.

Polyhedron Vol. 9, No. 22, pp. 2675–2679, 1990
Printed in Great Britain

0277–5387/90 $3.00+.00
© 1990 Pergamon Press plc

THE CHEMISTRY OF IRON IN BIOSYSTEMS—IV. COMPLEX FORMATION BETWEEN IRON(III) AND 5-SULPHOSALICYLIC ACID, IN AQUEOUS SOLUTION

V. SALVADÓ and X. RIBAS

Departament de Química, Col.legi Universitari de Girona (U.A.B.), Pça. Hospital 6, 17071 Girona, Spain

and

M. VALIENTE*

Química Analítica, Universitat Autònoma de Barcelona, 08193 Bellaterra, Barcelona, Spain

(*Received* 26 *April* 1989; *accepted after revision* 7 *June* 1990)

Abstract—The study of soluble complexes formed in aqueous solution between iron(III) and 5-sulphosalicylic acid (H_3L) has been carried out by means of potentiometric techniques, at 25°C, employing 0.5 mol dm^{-3} $NaNO_3$ as inert ionic media. The results, obtained by a proper numerical analysis of the experimental data, show the formation of the following metal complexes in solution (charges omitted; the values between parentheses correspond to the respective stability constants): FeHL ($\log \beta_{111} = 19.12$), FeL ($\log \beta_{011} = 17.05$), Fe_2L_3 ($\log \beta_{023} = 48.41$), FeL_2 ($\log \beta_{012} = 26.42$) and FeL_3 ($\log \beta_{013} = 32.76$). As seen, in the presence of 5-sulphosalicylic acid, iron(III) forms a polynuclear complex of stoichiometry Fe_2L_3, which has not been reported before.

As a continuation of our interest to study naturally occurring ligands bearing carboxylic groups as complexing agents for iron(III) ions,[1–3] 5-sulphosalicylic acid has been chosen. The ligand has a structural similarity with salicylic acid and higher solubility. Also, the use of 5-sulphosalicylic acid avoids precipitation of ferric hydroxide in aqueous solution.

In the molecule of 5-sulphosalicylic acid, the carboxylic and hydroxylic groups are attached to a benzene ring. This fact brings some different characteristics to 5-sulphosalicylic acid with respect to the previously studied ligands, i.e. increasing the rigidity of the chelating ring as well as the acidic character of the hydroxylic group.

5-Sulphosalicylic acid is used in laboratories as a colorimetric reagent for iron(III) ions.[4] Data for the iron(III)–5-sulphosalicylic acid system reported in the literature and summarized in Table 1, show a general agreement of the proposed models,[5–10] regarding M : L stoichiometries of 1:1, 1:2 and 1:3. Despite this, some important differences are observed between the values of stability constants proposed in ref. 10 with respect to other authors.[7–9] This fact encouraged us to carry out a detailed and systematic study of the complexing equilibria in the iron(III)–5-sulphosalicylic acid system, using 0.5 M NO_3^- as ionic medium. The present work has been thus undertaken in order to obtain precise information on the system iron(III)–5-sulphosalicylic acid by a proper characterization of the chemical reactions involved.

EXPERIMENTAL

The study is based on experimental data including measurements of the free hydrogen ion concentration, h, in a number of aqueous solutions containing iron(III) and 5-sulphosalicylic acid. The method, based on potentiometric titrations, has been described in detail before.[1–3]

For the different experiments, the analytical concentrations of iron(III), B, and 5-sulphosalicylate C, in the test solutions, were varied in the range

* Author to whom correspondence should be addressed.

Table 1. Summary of literature data on iron(III)–5-sulphosalicylate complexes, in aqueous solutions

Model (H : M : L)	Method	Ionic medium	Reference
1 : 1 : 1, 2 : 1 : 2	Potentiometric and spectrophotometric	1.0 M (H, Na)ClO_4	5
1 : 1 : 1, 2 : 1 : 2, 3 : 1 : 3	Spectrophotometric	0.1 M KNO_3	6
0 : 1 : 1, 0 : 1 : 2, 0 : 1 : 3	Potentiometric	3.0 M $NaClO_4$	7
0 : 1 : 1, 0 : 1 : 2, 0 : 1 : 3	Spectrophotometric	0.5 M KNO_3	8
0 : 1 : 1, 0 : 1 : 2, 0 : 1 : 3	Spectrophotometric	0.05 M —	9
0 : 1 : 1, 0 : 1 : 2, 0 : 1 : 3	Potentiometric and spectrophotometric	0.5 M $NaNO_3$	10
1 : 1 : 1, 0 : 1 : 1, 0 : 2 : 3, 0 : 1 : 2, 0 : 1 : 3	Potentiometric	0.5 M $NaNO_3$	This work

Table 2. Results obtained on the protolytic equilibria of 5-sulphosalicylic acid in aqueous 0.5 M $NaNO_3$, by graphical and numerical methods

Method	U	σ (mV)	$\log \beta_1$	$\log \beta_2$
Graphical[12]	—	—	11.34	13.72
Numerical[13,14]	10.5	0.39	11.39±0.01	13.72±0.01

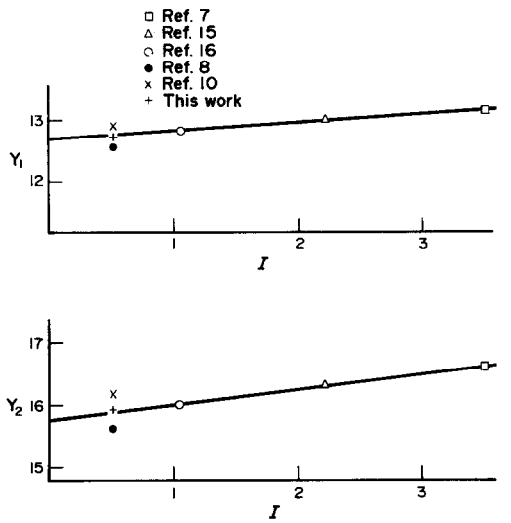

Fig. 1. Correlation of the protolytic constants of 5-sulphosalicylic acid by means of the Specific Interaction Theory (SIT).

0.8–1.0 mmol dm^{-3} and 9.0–25.0 mmol dm^{-3}, respectively. The pH was varied in the range 1.5–7.5.

The experiments were carried out in a thermostatic bath at 25±0.1°C.

RESULTS

Protolytic equilibria of 5-sulphosalicylic acid

By using the potentiometric technique, with test solutions of $B = 0$ the protonation constants of the 5-sulphosalicylic ion were determined at the above mentioned conditions. The results obtained include only mononuclear species (no aggregates were detected in the analysis of data). The constants were evaluated by using a graphical method[12] and later refined with the least-square fitting programs LETAGROP[13] and SUPERQUAD.[14] The final values are given in Table 2. A comparison of these results with those determined by other authors[7,8,10,15,16] has been carried out by a correlation procedure using the specific ionic interaction theory[17] and related coefficients obtained from refs 17 and 18; Fig. 1 gives the results of this correlation. As seen by this treatment, our values give a good correlation with those obtained with diverse ionic media and also fit better than the protonation constants proposed in refs 8 and 10.

Iron(III)–5-sulphosalicylate complexes

The formation of soluble complexes between iron(III) and 5-sulphosalicylate can be expressed by the general equation:

$$pH + qFe + rL \rightleftharpoons H_pFe_qL_r; \quad \beta_{pqr}, \qquad (1)$$

where β_{pqr} represents the formation constant of corresponding p, q, r complex species. Figure 2 shows the experimental data obtained, plotted in the form Z vs $-\log h$ at different B and C levels.

Z represents the number of H^+ bound to the total 5-sulphosalicylate, defined by:

$$Z = (A - h + K_w \cdot h^{-1})/C, \qquad (2)$$

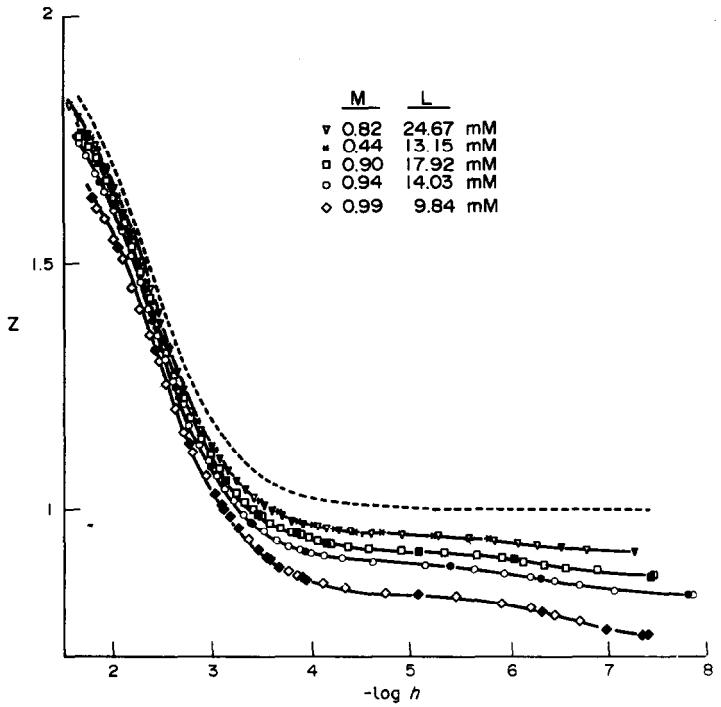

Fig. 2. Z plotted vs $-\log h$ for the different sets of experiments. Full points represent back titrations. Solid lines have been calculated by the model proposed in the present work.

where A represents the analytical concentration of hydrogen ion.

In order to verify our equilibrium data, back titrations were performed using the same analytical composition of the system. These data also are plotted. The good agreement between the forward and back titration data also shows that no irreversible processes take part in the complexation reactions.

The stoichiometry of the complexes as well as the constant β_{pqr} have been determined by means of numerical analysis of the obtained data. For this purpose, the computer programs LETAGROP[13] and SUPERQUAD[14] were used. The results obtained from this treatment are collected in Table 3. As seen, the introduction of a polynuclear species of stoichiometry Fe_2L_3 contributes definitively to the best fit of the model to the experimental data. This species has not been reported before.

Thus, the best fit of the experimental data is obtained when the species FeHL, FeL, Fe_2L_3, FeL_2 and FeL_3 are formed. These results are expressed

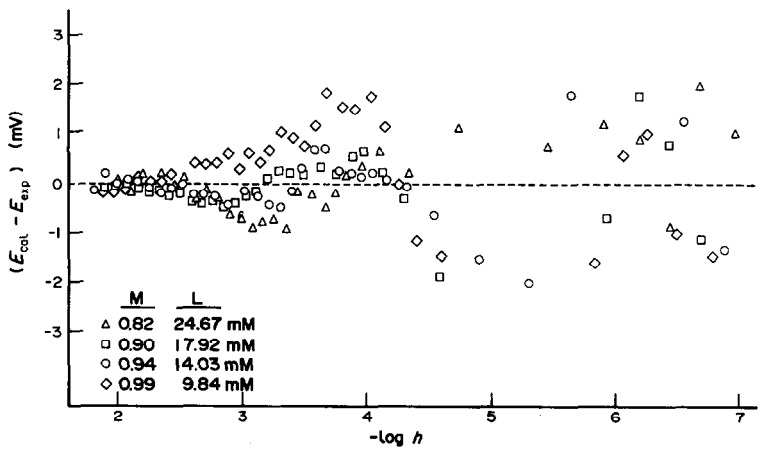

Fig. 3. Residuals $(E_{calc}-E_{exp})$ (mV) values plotted vs $-\log h$ for the different experimental data on the basis of the model proposed by eqs (3)–(7).

Table 3. Results obtained on the numerical treatment of the experimental data for the system iron(III)–5-sulphosalicylate

Model	(p,q,r)	U	σ (mV)	$\log \beta_{pqr}$
I	0,1,1	0.16×10^5	10.45	18.0±0.15
	0,1,2			26.8±0.05
	0,1,3			32.9±0.06
II	1,1,1	0.19×10^5	11.52	19.6±0.11
	0,1,1			17.2±0.08
	−1,1,1			12.6±0.05
	−2,1,1			5.4±0.12
III	2,1,2	0.17×10^5	10.76	rejected
	1,1,2			31.3±0.04
	0,1,2			26.7±0.06
	−1,1,2			19.6±0.06
IV	3,1,3	0.17×10^5	11.71	rejected
	2,1,3			44.7±0.07
	1,1,3			40.1±0.06
	0,1,3			32.9±0.05
V	1,1,1	0.14×10^5	9.79	19.5±0.10
	0,1,1			17.2±0.07
	−1,1,1			rejected
	1,1,2			31.3±0.06
	0,1,2			26.7±0.05
	2,1,3			rejected
	1,1,3			rejected
	0,1,3			32.9±0.06
VI	1,1,1	0.14×10^5	9.71	19.5±0.09
	0,1,1			17.2±0.05
	−2,1,1			rejected
	1,1,2			31.3±0.08
	0,1,2			26.5±0.06
	−1,1,2			rejected
	1,1,3			rejected
	0,1,3			32.9±0.06
VII	1,1,1	0.58×10^3	1.89	19.1±0.06
	0,1,1			17.1±0.04
	0,2,3			48.4±0.04
	1,1,2			rejected
	0,1,2			26.4±0.03
	0,1,3			32.8±0.05

The standard deviation σ (mV) is defined as $(U/[N_{p-Nk}\beta])^{1/2}$. N_k is the number of constants to adjust. The error in the constant values is given as $\pm3\sigma$ (log β). When $\sigma(k) > 0.2\beta$, the "best" value of log β and the maximum value, Max, log $[\beta+3\sigma(\beta)]$ are given.

by the following reaction equations; corresponding β_{pqr} values are given:

$$Fe+L+H \rightleftharpoons FeHL;\ \log\beta_{111} = 19.12\pm0.02 \quad (3)$$

$$Fe+L \rightleftharpoons FeL;\ \log\beta_{011} = 17.05\pm0.02 \quad (4)$$

$$2Fe+3L \rightleftharpoons Fe_2L_3;\ \log\beta_{023} = 48.41\pm0.01 \quad (5)$$

$$Fe+2L \rightleftharpoons FeL_2;\ \log\beta_{012} = 26.42\pm0.01 \quad (6)$$

$$Fe+3L \rightleftharpoons FeL_3;\ \log\beta_{013} = 32.76\pm0.02. \quad (7)$$

Using this set of complexes, we systematically considered new complexes by using a statistical process of LETAGROP called "Species Selector".[19] In this sense, taking into account the acidic properties of Fe^{3+}, the new complexes included species of the type $Fe_p(OH)_qL_r$. Altogether, 43 new complexes were tried, but the model expressed by eqs (3)–(7) still gives the best fit of the experimental data.

Figure 3 shows the residual values of $(E_{calc}-E_{exp})$ in mV. As seen, there is no evidence of systematic deviations on the proposed model.

DISCUSSION

The results obtained in the present work correspond to the complex formation between iron(III) and 5-sulphosalicylic acid, in an aqueous solution of 0.5 M $NaNO_3$ ionic medium.

The experimental data have been shown to correspond to the equilibrium state of the system and no irreversible processes have been found to take part in the reactions studied.

The complex species formed are represented by eqs (3)–(7), and Fig. 4 shows the distribution diagrams of the species, calculated by the program HALTAFALL,[20] in the pH range 1.5–8.0. This model is in partial agreement with the results previously reported.[5–10] The mononuclear species FeL, FeL_2 and FeL_3 are reported in most of these studies[7–10] and their stability constants appear to be well-defined in the present work. In the case of the protonated species reported in refs 5 and 6, FeHL, FeH_2L_2 and FeH_3L_3, only one species, FeHL, has been found in our analysis. On the other hand, the numerical treatment of the obtained data has shown that a deprotonated binuclear iron(III)–5-sulphosalicylate complex, Fe_2L_3, is formed and, as seen in Fig. 4, is present in a wide pH interval. This species has not been reported before. This type of result follows the tendency of carboxylic ligands bearing hydroxyl groups to form polynuclear complex species with iron(III).[1]

On the other hand, the model proposed in the present work may be interpreted mechanistically by stepwise addition of deprotonated ligand to the metal ion. The formation of the polynuclear species may also be a consequence of such an addition by following the suggested reaction:

$$2FeL+L \rightleftharpoons Fe_2L_3. \quad (8)$$

The high stability of Fe_2L_3 species could explain

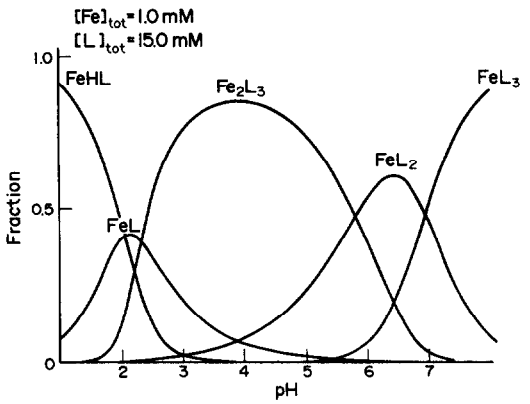

Fig. 4. Fraction diagram of the iron(III)–5-sulphosalicylic acid complexes as a function of $-\log h$.

the possibility of the proposed reaction (8) by compensating for the low acidity of the hydroxyl group.

In Fig. 2, the full lines represent calculated values of Z vs $-\log h$ using the proposed model [eqs (3)–(7)]. The close fit to the experimental values determines a high confidence level of this model.

REFERENCES

1. V. Salvadó, X. Ribas, M. Blanco and M. Valiente, *Inorg. Chim. Acta* 1987, **137**, 155.
2. V. Salvadó, X. Ribas, V. Zelano, G. Ostacoli and M. Valiente, *Polyhedron* 1989, **8**, 813.
3. V. Salvadó, X. Ribas and M. Valiente, *J. Chem. Res. (M)* 1989, 2533.
4. F. D. Snell and C. T. Snell, *Colorimetric Methods of Analysis*, Vol. 4. Van Nostrand, New York (1979).
5. B. P. Nikolskii, V. V. Palchevskii, A. D. Chegodaeva and N. K. Barkova, *Dokl. Akad. Nauk SSSR* 1970, **194**, 1100.
6. G. Popa and E. Dascalescu, *An. Univ. Bucuresti Chim.* 1972, **21**, 113.
7. A. Agren, *Acta Chem. Scand.* 1954, **8**, 266.
8. W. A. E. McBryde, J. L. Rohn, J. S. Penciner and J. A. Page, *Canad. J. Chem.* 1970, **48**, 2574.
9. K. Ogawa and N. Tobe, *Bull. Chem. Soc. Jpn* 1966, **39**, 223.
10. M. Morin, M. R. Pâris and J. P. Scharpf, *Anal. Chim. Acta* 1971, **57**, 123.
11. X. Ribas, V. Salvadó, V. Zelano, G. Ostacoli and M. Valiente, unpublished data.
12. L. G. Sillén, *Acta Chem. Scand.* 1956, **10**, 186.
13. P. Brauner, L. G. Sillén and R. Whiteker, *Arkiv. Kemi* 1969, **31**, 365.
14. A. Vacca and A. Sabattini, *J. Chem. Soc., Dalton Trans.* 1985, 1195.
15. R. Nasanen and P. Merilain, *Suomen Kem.* 1961, **34**, 75.
16. R. P. Martin and R. A. Paris, *Bull. Soc. Chim. Fr.* 1964, **80**, 1195.
17. L. Ciavatta, *Ann. Chim. (Rome)* 1980, **70**, 551.
18. C. F. Bages and R. E. Mesmer, *The Hydrolysis of Cations*. John Wiley, New York (1976).
19. L. G. Sillén and B. Warnqvist, *Arkiv. Kemi* 1968, **31**, 341.
20. N. Ingri, W. Kakolowicz, L. G. Sillén and B. Warnqvist, *Talanta* 1967, **14**, 1261.

Polyhedron Vol. 9, No. 22, pp. 2681–2687, 1990
Printed in Great Britain

0277–5387/90 $3.00+.00
© 1990 Pergamon Press plc

KINETICS AND MECHANISM OF THE LIGAND SUBSTITUTION REACTION OF AQUO-ETHYLENEDIAMINETETRAACETATO COMPLEX OF RUTHENIUM(III) WITH 4,6-DIMETHYL-2-MERCAPTOPYRIMIDINE LIGAND IN AQUEOUS MEDIUM

M. M. TAQUI KHAN,* DEBABRATA CHATTERJEE, AMJAD HUSSAIN and M. A. MOIZ

Discipline of Coordination Chemistry and Homogeneous Catalysis, Central Salt and Marine Chemicals Research Institute, Bhavnagar-364 002, India

(*Received* 3 *July* 1989; *accepted after revision* 15 *June* 1990)

Abstract—The kinetics of the ligand substitution reaction of aquo-ethylenediaminetetraacetato ruthenate(III) with 4,6-dimethyl-2-mercaptopyrimidine were studied as a function of ligand concentration, temperature (30–45°C) and pH (1.4–9.0). The reaction proceeds with the formation of a red complex (λ'_{max} = 510 nm) which undergoes a pH dependence change (pK_a = 4.5) to form a violet product (λ_{max} = 560 nm). Activation parameters for both the reactions were calculated and compared with other experimental results under identical experimental conditions. The mechanism of the substitution process was explained in terms of the labilization effect of the coordinated ethylenediaminetetraacetate ligand. An associative interchange (Ia) mechanism was suggested for the substitution reaction of H_2O by the ligand 4,6-dimethyl-2-mercaptopyrimidine followed by the displacement of coordinated carboxylate group in which deprotonation of coordinated ligand and reorganization of the coordination sphere of the metal ion takes place. The sum of acid dissociation and chelation constants for red to violet complex formation computed potentiometrically at 30°C and μ = 0.1 M KCl is 3.58.

Ligand substitution reactions on pentacoordinated chelated ruthenium(III) complexes have long been a subject of much interest.[1–2] Recently, the kinetic behaviour of ethylenediaminetetraacetate and the N-(hydroxyethyl)-ethylenediaminetetraacetate complex of ruthenium(III) with a series of anionic and neutral ligands was reported.[3–4] The remarkable lability of the water molecule in the complexes was explained due to the formation of a hydrogen bond between the free carboxylate oxygen and the coordinated water molecule. The transient coordination of a pendant group also plays an important role which causes the rapid replacement of a coordinated water molecule.[5–6] It was reported recently[7] that 2-mercaptopyridine can behave as a monodentate as well as a bidentate ligand, leading to a mixture of red and green products, respectively. The 2-mercaptopyrimidine ligand can exist in its tautomeric form in aqueous solution with a protonated N-atom.[8] The available thione group, however, is capable of forming a bond with the transition metal ions.[9] The ligand 4,6-dimethyl-2-mercaptopyrimidine[6] is an ambidentate ligand that can coordinate through the sulphur and the ring nitrogen atom. We have, therefore, undertaken the study of the substitution reaction of H_2O in [Ru(Hedta)(H_2O)] with the ligand L in aqueous solution. The reaction proceeds at low pH by the coordination of the 2-mercapto group in the metal ion to give a red complex in the first instant. At higher pH > (4.5) the red complex changes to a violet complex where both S and N of the ligand are combined to the metal ion in a bidentate manner. The equilibrium and rate constants for the formation of the mixed ligand Ru^{III}–EDTA–L

* Author to whom correspondence should be addressed.

complex have been computed by potentiometric and spectrophotometric studies.

EXPERIMENTAL

$K[Ru(H\text{-}edta)(Cl)]\cdot 2H_2O$ was prepared and characterized by following the published procedure.[10,11] It rapidly hydrolyses in aqueous solution to $Ru(H\text{-}edta)(H_2O)$[2,11] (with a $\lambda_{max} = 283$ nm and $\varepsilon_{283}^{max} = 2800$). The composition of the red product complex [ethylenediaminetetraacetato-4,6-dimethyl-2-mercaptopyrimidineruthenium(III)] in solution was determined by recording the spectra of four different solutions in which concentration of metal and ligand was maintained at 1 : 1, 1 : 2, 1 : 3 and 1 : 10, respectively. The pH of each solution was kept fixed at 1. The spectra of the 1 : 1 solution ($\lambda_{max} = 510$ nm and $\varepsilon_{510}^{max} = 2280$) nicely matched with the other solutions containing higher ligand concentrations. The violet compound ethylenediaminetetraacetato - 4,6 - dimethyl - 2 - mercaptopyrimidineruthenium(III) was produced in the solution by treating the red product with a slight excess of NH_4OH ($\lambda_{max} = 560$ nm and $\varepsilon_{560}^{max} = 1750$). The 1 : 1 metal–ligand composition was determined by a similar manner at pH 9.0.

All other chemicals used were A.R. grade. Doubly distilled water was used throughout this study. Acetate, phosphate and borate buffers were used to control the pH and $NaClO_4$ for adjusting ionic strength.

Potentiometric titrations were performed under an argon atmosphere as described elsewhere[12] using a Metrohm 682 titrator in manual mode. Formation constants were computed at 30°C ($\mu = 0.1$ M KCl) by a curve fitting method using the program PKAS.[13]

For recording spectra and other spectrophotometric measurements a Shimadzu UV-160 spectrophotometer equipped with temperature controller TCC-240A was used. The substitution reaction was followed by using a Hi-Tech SF-140 stopped-flow spectrophotometer. The absorbance time plots for the biphasic reaction (formation of red complex and its conversion to violet product) were analysed with the aid of ADS-1 data acquisition and analysis system equipped with the stopped-flow unit. pH measurements were carried out with a Digisun pH meter with an accuracy of ± 0.001 unit. The rate constant data are reproducible within $\pm 4\%$.

RESULTS AND DISCUSSION

Preliminary kinetic experiments demonstrated that the employed buffer component, viz. acetate, phosphate and borate, as well as the medium selected to control the ionic strength of solutions did not react with the Ru^{III} complex. The nucleophilicity of 4,6-dimethyl-2-mercaptopyrimidine is so high that the other potential nucleophiles, used either as buffer or to control the ionic strength of the medium, had no significant effect on the behaviour of the system when these were added to the solution containing entering ligand prior to the mixing with the aquo complex within the stopped-flow mixing chamber.[14]

The substitution reaction of $Ru(H\text{-}edta)(H_2O)$ with 4,6-dimethyl-2-mercaptopyrimidine ligand was studied under pseudo first-order conditions and in contrast with the preceding work performed by Matsubara and Creutz,[2] two successive reactions were detected in this work. The first reaction leading to the red complex was due to the substitution of the water molecule in $Ru(H\text{-}edta)(H_2O)$ by the 4,6-dimethyl-2-mercaptopyrimidine in which the sulphur atom of the ligand is coordinated to the metal ion. The characteristic red colour is due to sulphur to metal charge-transfer.[15] The second reaction was associated with the partial or total conversion of the red complex to a violet complex where the ligand 4,6-dimethyl-2-mercaptopyrimidine acts as a chelate by the coordination of the sulphur atom of 2-mercapto and the ring nitrogen atom.

The observed rate constant for the first reaction in the formation of red complex depends on the ligand concentration of the entering ligand and it increases linearly with the increase of ligand concentration at constant pH, ionic strength and temperature (Fig. 1). As there is no intercept in the plot, it can be assumed that the reverse aquation is not appreciable under experimental conditions. The observed rate constant for the conversion of red complex to violet complex in the second reaction is independent of the entering ligand concentration at a fixed pH and temperature (Table 1). This shows

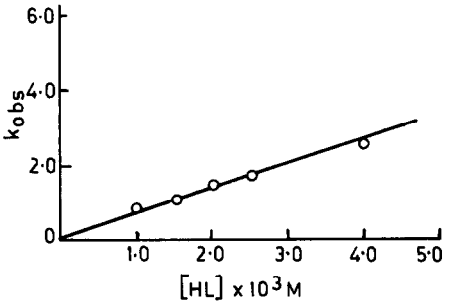

Fig. 1. Effect of [HL] on k_{obs} for the reaction of Ru(edta)$(H_2O)^-$ with 4,6-dimethyl-2-mercaptopyrimidine at pH = 5 (acetate buffer), $\mu = 0.2$ M ($NaClO_4$), [Ru(edta)$(H_2O)^-$] = 1×10^{-4} M, $T = 30$°C.

Table 1. Values of k_{obs} and k'_{obs} as a function of ligand concentration [Complex 1] = 1.1×10^{-4} M, pH = 5, $T = 30°C$, $\mu = 0.2$ M ($NaClO_4$)

[Ligand] (M)	$10^{-1} k_{obs}$ s^{-1}	k'_{obs} s^{-1}
1×10^{-3}	0.78	0.98
1.5×10^{-3}	1.01	1.01
2.0×10^{-3}	1.39	1.00
2.5×10^{-3}	1.68	1.01
4×10^{-3}	2.54	1.03

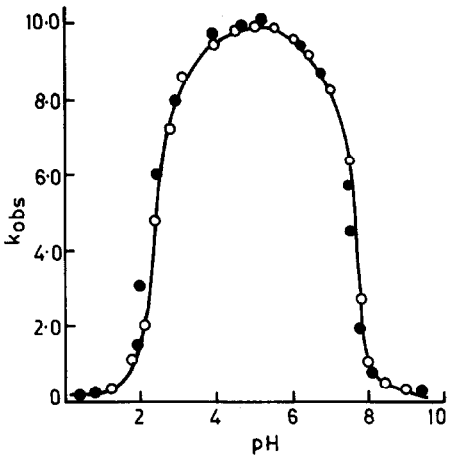

Fig. 2. Variation of k_{obs} with pH at 30°C. [Complex 1] = 1×10^{-4} M, [HL] = 1.5×10^{-3} M, $\mu = 0.2$ M ($NaClO_4$); (○) observed rate constant; (●) calculated by using resolved rate constant.

that the second step involves a deprotonation of the coordinated ligand. The relatively lower values of the observed rate constant for the conversion of red to violet complex reflects that the proton transfer reaction in this step is diffusion controlled[14] and the measured rate cannot be ascribed to a simple acid–base reaction. The deprotonated form of 4,6-dimethyl-2-mercaptopyrimidine is a potentially bidentate ligand. In the formation of the violet complex ethylenediaminetetraacetato-4,6-dimethyl-2-mercaptopyrimidineruthenium(III), the ligand binds through the ring nitrogen by the displacement of a coordinated carboxylate group which would lead to the change in the absorption spectrum from red to violet with an appreciable reorganization of the coordination sphere of the metal ion.[9,15] It is worthwhile to note here that no change in red colour was found when Ru(H-edta)(H_2O) was reacted with 4-mercaptopyridine even at high pH.[7]

The pH dependence of the formation of red complex is associated with the substitution lability of the various Ru^{III}–edta species, viz Ru(H-edta)(H_2O), Ru(edta)(H_2O)$^-$ and Ru(edta)$(OH)^{2-}$. The characteristic pH dependence (Fig. 2) for this substitution reaction can be explained in terms of the following equilibria:

$$\text{Ru(H-edta)}(H_2O) \overset{K_1}{\rightleftharpoons} \text{Ru(edta)}(H_2O)^- + H^+ \quad pK_1 = 2.4,$$

$$\text{Ru(edta)}(H_2O)^- \overset{K_2}{\rightleftharpoons} \text{Ru(edta)}(OH)^{2-} + H^+ \quad pK_2 = 7.6,$$

and the reaction pathways:

$$\text{Ru(H-edta)}(H_2O) + HL \xrightarrow{k_1} \text{Ru(H-edta)(HL)} + H_2O, \quad (1)$$

$$\text{Ru(edta)}(H_2O)^- + HL \xrightarrow{k_2} \text{Ru(edta)(HL)} + H_2O, \quad (2)$$

$$\text{Ru(edta)}(OH)^{2-} + HL \xrightarrow{k_3} \text{Ru(edta)(HL)} + OH^-, \quad (3)$$

where HL represents neutral 4,6-dimethyl-2-mercaptopyrimidine ligand with one protonated N atom.

Now considering the above acid dissociation equilibria among the reactants, the following rate expression was derived:

$$k_{obs} = \frac{k_1[H^+]^2 + k_2K_1[H^+] + k_3K_1K_2}{[H^+]^2 + K_1[H^+] + K_1K_2}[HL]. \quad (4)$$

It is seen from Fig. 2 that the two inflections in the bell-shaped curve occur exactly at pH = pK_1 and pH = pK_2. A similar result was reported by Matsubara and Creutz.[2] At very low pH (< 1) only the Ru(H-edta)(H_2O) species which is less labile than Ru(edta)(H_2O)$^-$ is predominant in the solution and the significant contribution to the rate is due to reaction (1) only. Hence eq. (4) at very low pH reduces to $k_{obs} = k_1[HL]$. At very high pH (>9), only reaction (3) in which Ru(edta)$(OH)^{2-}$ is predominant can be considered. So at high pH, eq. (4) is reduced to $k_{obs} = k_3[HL]$. It can be clearly seen from Fig. 2 that in the pH range $4 < pH < 6$, k_{obs} reaches a maximum limit. In this pH range, almost complete deprotonation of Ru(H-edta)(H_2O) occurs to form the most labile deprotonated Ru(edta)(H_2O)$^-$. Hence, in this pH range k_{obs} can be equated to $k_2[HL]$. The values of k_2 do not change appreciably in the pH range $4 < pH < 6$ as substantiated by plotting the limiting form of eq. (4) as a function of $[H^+]$ at pH < 5 and pH > 5. The

limiting form of eq. (4) can be written as follows:

$$k_{obs} = \left(k_1 + \frac{K_2K_1}{[H^+]}\right)\left(1 + \frac{K_1}{[H^+]}\right)^{-1}, \quad \text{at pH} < 5 \tag{5}$$

and

$$k_{obs} = \left(k_3 + \frac{k_2[H^+]}{K_2}\right)\left(1 + \frac{[H^+]}{K_2}\right), \quad \text{at pH} > 5. \tag{6}$$

The values of k_2 thus obtained, 7.74×10^3 and 7.8×10^3 M^{-1} s^{-1}, at 30°C are significantly larger than $k_1 = 63$ M^{-1} s^{-1} and $k_3 = 50.6$ M^{-1} s^{-1}. An identical rate–pH profile was obtained when k_{obs} (calculated by resolving rate constant values) is plotted against pH. The calculated (theoretical) curve superimposes which substantiates the various assumptions in rate expressions (1)–(3).

In the second reaction it was found that the k'_{obs} (observed rate constant for the conversion of red to violet complex) value increases with the decrease of hydrogen ion concentration in the solution.

The pH dependence (Fig. 3) of the conversion of red complex to violet in the second reaction can be interpreted in terms of the following reversible proton transfer to and from the monodentate red complex and subsequent chelation of the deprotonated red complex to produce chelated violet complex in solution.

$$RH^+ + H_2O \overset{K_a}{\rightleftharpoons} R + H_3O^+, \tag{7}$$

$$R \underset{k_{-4}}{\overset{k_4}{\rightleftharpoons}} V, \tag{8}$$

where RH^+ and R represent the protonated and deprotonated forms of the red complex, respectively, and V represents the chelated violet complex. Now considering the above acid dissociation equilibrium (7) and chelation step (8), the following rate expression was derived:

$$k'_{obs} = \frac{\{k_{-4}K_a + [H_3O^+]\} + k_4K_a}{K_a + [H_3O^+]}. \tag{9}$$

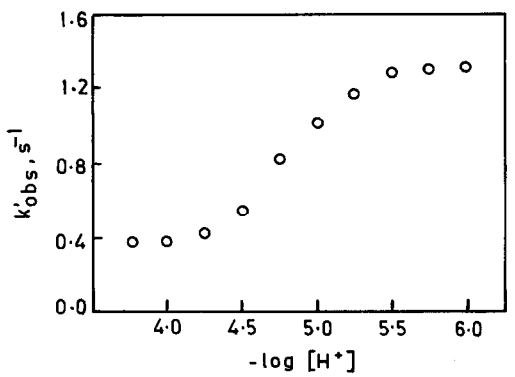

Fig. 3. Variation of k'_{obs} with pH at 30°C. [Complex 1] = 1×10^{-4} M, [HL] = 1.5×10^{-3} M, $\mu = 0.2$ M ($NaClO_4$).

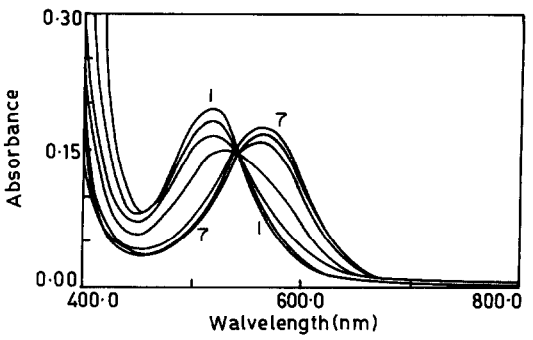

Fig. 4. Electronic spectra of Ru(edta)$(H_2O)^-$ with 4,6-dimethyl-2-mercaptopyrimidine at different pH. [Complex 1] = 1×10^{-4} M = [HL], $T = 30$°C, $\mu = 0.2$ M ($NaClO_4$), pH of (1) 1.42, (2) 2.89, (3) 3.78, (4) 4.45, (5) 5.00, (6) 6.80, (7) 7.89.

It is seen in Fig. 3, the k'_{obs} values are independent of pH in the low acid ($K_a \gg [H_3O^+]$) and high acid ($[H_3O^+] \gg K_a$) regions and go from $k_{obs} = k_{-4}$ at high acid concentration to $k'_{obs} = k_4 + k_{-4}$ at low acid concentration. The values of k_4 and k_{-4} thus obtained are 0.91 and 0.41 s^{-1}, respectively. The pK_a (negative logarithm of the apparent equilibrium constant) value is determined (pK_a = 4.79) by using the values of k_4 and k_{-4} in eq. (9). In this case, the negative logarithm of the equilibrium constant is not strictly speaking a pK_a but rather the sum of the pK_a of RH^+ and log of the chelation equilibrium.

The red and violet complexes co-exist in solution with an isobestic point at 542 nm (Fig. 4). The pK_a value for the conversion of red to violet complex determined spectrophotometrically by plotting absorbance vs pH (Fig. 5) is 4.5.

To determine the acid dissociation constant and the chelation constant for the formation of 1 : 1 Ru(edta)-4,6-dimethyl-2-mercaptopyrimidine complex the potentiometric titrations were carried out at 30°C, $\mu = 0.10$ M KCl.

The free ligand titration of 4,6-dimethyl-2-mercaptopyrimidine [Fig. 6(a)] shows no inflection but only a buffer region between $a = 0$–1. The proton dissociation constant calculated from the program PKAS[14] was $10^{-8.79}$.

The titration curve for 1 : 1 Ru(H-edta)(H_2O) and 4,6-dimethyl-2-mercaptopyrimidine under Ar [Fig. 6(b)] gave two inflections at $a = 1.0$ and 2.0. The plausible reactions in the buffer region between

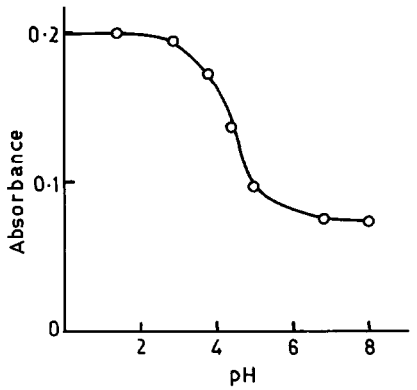

Fig. 5. Change in absorbance at 510 nm with hydrogen ion concentration at 30°C, $\mu = 0.2$ M ($NaClO_4$), [Complex 1] = [HL] = 1×10^{-4} M.

$a = 0$–1 are as follows:

$$MLH \rightleftharpoons ML + H^+,$$

$$K_a = [ML][H^+]/[MLH], \quad (10)$$

$$ML + HA \overset{K_{MLAH}}{\rightleftharpoons} MLAH, \quad (11)$$

where MLH = [Ru(H-edta)(H_2O)] and HA = 4,6-dimethyl-2-mercaptopyrimidine.

The dissociation constant for equilibrium (10) as reported earlier[13] is $10^{-2.36}$. In equilibrium (11), since there is no liberation of proton, the formation constant of MLAH cannot be determined by potentiometry. The formation constant of MLAH obtained by spectrophotometry is $10^{4.75}$. The buffer region between $a = 1$–2 indicates the dissociation of proton from the MLAH species and the following equilibrium is assumed:

$$MLAH \overset{K_{MLA}}{\rightleftharpoons} MLA + H^+, \quad (12)$$

$$K_{MLA} = [MLA][H^+]/[MLAH].$$

The proton dissociation constant for equilibrium (12) calculated by program PKAS is $10^{-6.19}$, dissociation of proton is followed by chelation:

$$MLA \overset{K_{Ch}}{\rightleftharpoons} MLA\,(chelate). \quad (13)$$

From the equilibria (10)–(12) the chelation constant was calculated as $10^{2.61}$.

The sum of the chelation constant [eq. (13)] and dissociation constant [eq. (12)] determined spectrophotometrically, $10^{-4.5}$, agrees with that determined potentiometrically, i.e. $10^{-3.58}$. The difference of 1.0 log K unit may be accounted for by the use of different techniques in elucidating the constants.

The effect of temperature on the substitution reaction was studied under limiting condition, i.e. where a minor change in pH due to change in temperature would not affect the observed rate constants. Rate constant data for both the reactions at different temperatures are shown in Table 2. Activation parameters for both the reactions are shown in Table 3 along with some related data obtained from literature for comparison purposes. It is seen from Table 3 that the low value of $\Delta H^{\ddagger}$ and negative value of $\Delta S^{\ddagger}$ for this substitution reaction clearly support the associative character of the substitution process and are in close agreement with those reported for other substitution reactions. Labilization of water molecules in this reaction may be explained on the basis of hydrogen bonding between the uncoordinated acetic acid moiety [in the case of Ru(H-edta)(H_2O)] and H_2O. Matsubara and Creutz[2] reported the possibility of a dissociative mode of activation resulting from the eventual labil-

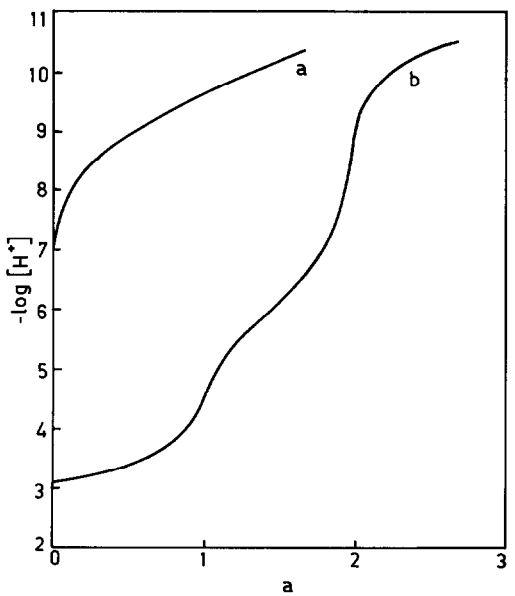

Fig. 6. Potentiometric titration curve of (a) 4,6-dimethyl-2-mercaptopyrimidine free ligand, (b) 1 : 1 4,6-dimethyl-2-mercaptopyrimidine and Ru(H-edta)(H_2O) complex.

Table 2. Values of specific rate constants as a function of temperature at pH = 5.0, $\mu = 0.2$ M ($NaClO_4$), [Complex 1] = 1.1×10^{-4} M

Temperature (°C)	$k \times 10^{-3}$ M^{-1} s^{-1}	k_{r-v} s^{-1}
30	7.8	1.01
35	9.55	1.55
40	11.34	2.32
45	14.08	3.45

Table 3. Comparison of the activation parameters of some model reactions with these substitution reactions and conversion of red to violet complex

System	$\Delta H^{\ddagger}$ (KJ mol^{-1})	$\Delta S^{\ddagger}$ (J mol^{-1}·deg)	$\Delta H^{\ddagger}_{r\to v}$ (KJ mol^{-1})	$\Delta S^{\ddagger}_{r\to v}$ (J mol^{-1}·deg)	Reference
Ru(edta)(H_2O)–Pyrazine	24.10	−84.0			2
Ru(edta)(H_2O)–Acetonitrile	34.86	−100.8			2
Ru(edta)(H_2O)–Thiourea	22.3±1.4	−105±5			3
Ru(edta)(H_2O)-2-mercaptopyridine	24.4	−84.0			7
Ru(edta)(H_2O)-4,6-dimethyl-2-mercaptopyrimidine	29±1	−76±3	62±2	33±3	This work

ization of the Ru^{III}—OH_2 bond through hydrogen bonding between the pendant carboxylate group and water molecule, but this possibility was recently ruled out by Eldik,[3,4] where a significantly negative volume of activation ($\Delta V^{\ddagger}$) was required for the substitution of Ru(H-edta)(H_2O) by a series of neutral and anionic ligands which is a characteristic of an associative process. The slightly higher value of $\Delta H^{\ddagger}$ as compared to 2-mercaptopyridine[7] may be due to the presence of two methyl groups which cause some steric hindrance in forming activated species, which is also indicated by a larger value of $\Delta S^{\ddagger}$ (Table 3).

A comparatively larger activation energy for the second reaction as compared to the first indicates the displacement of coordinated carboxylate group in the formation of the tetracoordinated EDTA in the complex ethylenediaminetetraacetato-4,6-dimethyl-2-mercaptopyrimidineruthenium(III). It is assumed that the deprotonation of the coordinated mercaptopyrimidine ligand leads to a chelated product ethylenediaminetetraacetate-4,6-dimethyl-2-

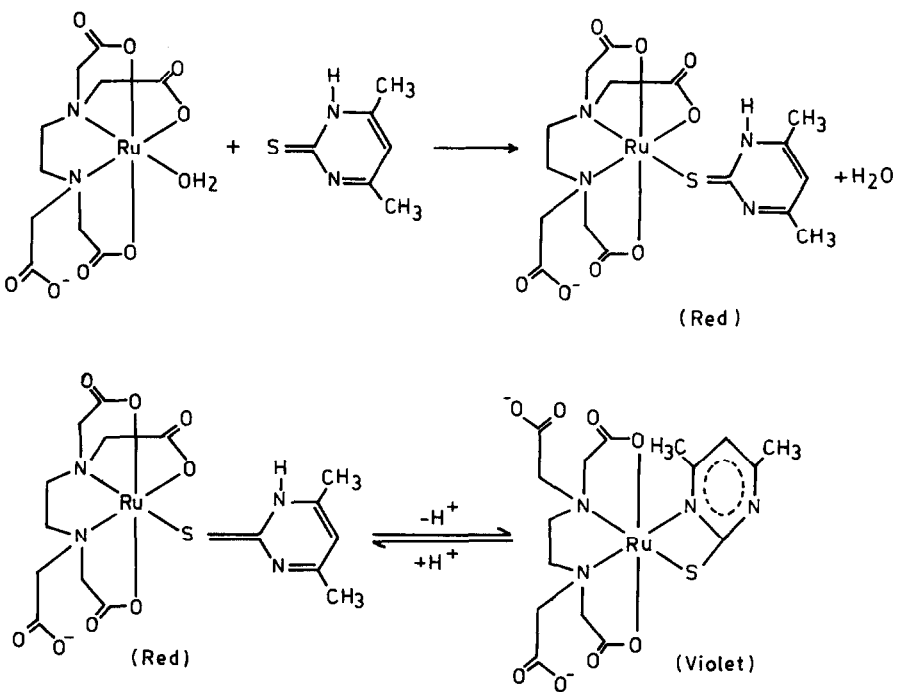

Fig. 7. Mechanism of the substitution of $Ru(edta)(H_2O)^- + HL \rightarrow Ru(edta)(L)^- + H_2O$ (where HL = 4,6-dimethyl-2-mercaptopyrimidine).

mercaptopyrimidineruthenium(III), obtained by the opening of the coordinated carboxylate group by a pH dependent process.

Based on the above mentioned experimental facts, it is suggested that the substitution of water molecules from the ethylenediaminetetraacetate complex of ruthenium(III) proceeds through an associative interchange (Ia) mechanism followed by the conversion of pentacoordinated-EDTA–Ru^{III}–L to tetracoordinated-EDTA–Ru^{III}–L chelated product (Fig. 7).

REFERENCES

1. K. Shimizu, *Bull. Chem. Soc. Jpn* 1977, **50**, 2921.
2. T. Matsubara and C. Creutz, *Inorg. Chem.* 1979, **18**, 1956.
3. H. C. Bajaj and R. Van Eldik, *Inorg. Chem.* 1988, **27**, 4052.
4. H. C. Bajaj and R. Van Eldik, *Inorg. Chem.*, in press.
5. H. Ogino, T. Watanabe and N. Tanaka, *Inorg. Chem.* 1975, **14**, 2093.
6. H. Ogino, M. Shimaru and N. Tanaka, *Inorg. Chem.* 1979, **18**, 2497.
7. H. E. Toma, P. S. Santos, M. P. D. Mattioli and L. A. A. Oliveira, *Polyhedron* 1987, **6**, 603.
8. R. A. Jones and A. R. Katritzky, *J. Chem. Soc.* 1958, 3610.
9. B. P. Kennedy and A. B. P. Lever, *Can. J. Chem.* 1972, **50**, 3488.
10. E. E. Mercer and R. R. Buckley, *Inorg. Chem.* 1965, **4**, 1692.
11. A. A. Diamantis and J. V. Dubrawsky, *Inorg. Chem.* 1981, **20**, 1142.
12. M. M. Taqui Khan, Amjad Hussain, G. Ramachandriah and M. A. Moiz, *Inorg. Chem.* 1986, **25**, 3023.
13. R. J. Molekaitis and A. E. Martell, *Can. J. Chem.* 1982, **60**, 168.
14. F. Caldin, *Fast Reactions in Solution*, p. 262. Wiley Eastern, New York (1964).
15. S. R. Fletcher and A. C. Skapski, *J. Chem. Soc.* 1964, **30**, 706.

Polyhedron Vol. 9, No. 22, pp. 2689–2691, 1990
Printed in Great Britain

0277–5387/90 $3.00+.00
© 1990 Pergamon Press plc

THE SYNTHESES OF MONO-AROMATIC CARBOXYLIC DERIVATIVES OF BIS(η^5-CYCLOPENTADIENYL)ZIRCONIUM(IV)

YAO-KUN ZHOU* and HONG-MING CHEN

Department of Chemistry, Lanzhou University, Lanzhou, Gansu Province, P.R.C.

(*Received* 16 *January* 1990; *accepted* 21 *June* 1990)

Abstract—Fifteen mono-aromatic carboxylic derivatives of the type Cp_2ZrCl 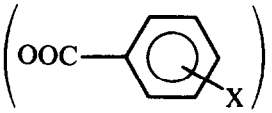 (where Cp = cyclopentadienyl; X = *o*-Br, *m*-Br, *p*-Br, *o*-Cl, *p*-Cl, *o*-I, *p*-I, *o*-F, *m*-F, *m*-NO_2, *p*-NO_2, *p*-Me, *p*-CN, *o*-NH_2 and H) have been prepared by the reaction of Cp_2ZrCl_2 with the sodium salts of aromatic acids in a 1 : 1 molar ratio in benzene at 30°C. The compositions, structures and coordinative modes of the carboxylate ligands in these derivatives have been characterized by elemental analysis, IR and ^{1}H NMR spectra.

The preparation of bis-aromatic derivatives of bis(η^5-cyclopentadienyl)titanium(IV) was reported as a patent,[1] and it was claimed that they could be used as catalysts in alkene polymerization. Subsequent work[2–4] has shown that some derivatives have physiological activities. A perusal of the literature reveals that most of the work has been restricted to titanium(III and IV), with less work on derivatives of zirconium(IV).[5] We have synthesized and characterized 15 mono-aromatic carboxylic derivatives of bis(η^5-cyclopentadienyl)zirconium (IV) dichloride.

EXPERIMENTAL

All the reaction systems were protected with nitrogen. Benzene was dried by distilling it over the sodium ketyl of benzophenone, petroleum ether (60–90°C) by distilling it over CaH_2 for about 24 h, and bis(η^5-cyclopentadienyl)zirconium(IV) dichloride was prepared by the literature procedures.[6]

Measurement

The carbon, hydrogen and nitrogen analyses were carried out on a 1106 type elemental analytical instrument. Zirconium was determined gravimetrically as ZrO_2.

IR spectra were obtained with a FT-5DX (4000–400 cm^{-1}, KBr) instrument, while ^{1}H NMR spectra were obtained on an FT-80A spectrometer (solvents, $DCCl_3$ or D_3CCCD_3; internal standard, TMS). The melting points were determined using a Kofler melting point apparatus.

Preparation of the sodium salts of aromatic carboxylic acids

All of them were prepared by the reaction of aromatic carboxylic acids with alcoholic sodium in the same molar ratio. The products were dried at constant temperature *in vacuo*.

Syntheses of the derivatives

Anhydrous sodium salts of aromatic carboxylic acid (1 mmol), Cp_2ZrCl_2 (1 mmol) and benzene (50 cm^3) were stirred for 10 h at 30°C and the precipitated sodium chloride was filtered off. The filtrate was concentrated to 5 cm^3 under reduced pressure, then the appropriate amount of anhydrous petroleum ether (60–90°C) was added. The white solid obtained was recrystallized from benzene–petroleum ether (60–90°C).

* Author to whom correspondence should be addressed.

RESULTS AND DISCUSSION

The substitution reactions of Cp_2ZrCl_2 with the anhydrous sodium salts of aromatic carboxylic acids were carried out in the same ratio:

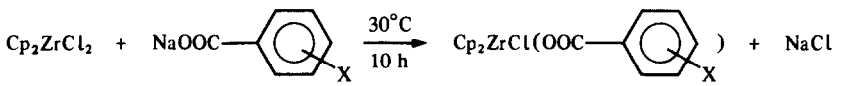

(here, Cp = cyclopentadienyl; X = *o*-Br, *m*-Br, *p*-Br, *o*-Cl, *p*-Cl, *o*-I, *p*-I, *o*-F, *m*-F, *m*-NO_2, *p*-NO_2, *p*-Me, *p*-CN, *o*-NH_2 and H).

This reaction occurred readily under these conditions. All the products were obtained in high yields. They are white crystals and are sensitive to moisture. They can be dissolved easily in polar organic solvents like CH_2Cl_2, $CHCl_3$, acetone, etc. However, they are insoluble in n-hexane or petroleum ether. All of them have sharp melting points. The elemental analytical and physical data of the products are given in Table 1.

IR spectra

In the carboxylato complexes, the symmetrical O—C—O stretching frequency (ν_1) and asymmetrical O—C—O stretching frequency (ν_2) are of importance since their position and separation ($\nu_2 - \nu_1$) can help in determining the type of bonding in the metal carboxylate.[7] We referred to the stan-

Table 1. Yields, melting points and elemental analytical data of the compounds

S. No.	X	Yield (%)	Melting point (°C)	Analysis (%) Found (Calc.) C	H	N	Zr
I	*o*-Br	67.8	91–92	44.4 (44.7)	3.1 (3.1)		20.2 (20.0)
II	*m*-Br	73.6	138–139	44.6 (44.7)	3.1 (3.1)		
III	*p*-Br	83.7	160–162	45.1 (44.7)	3.1 (3.1)		
IV	*o*-Cl	73.2	95–97	49.4 (49.5)	3.4 (3.4)		
V	*p*-Cl	68.3	173–174	49.5 (49.5)	3.4 (3.4)		22.3 (22.1)
VI	*o*-I	70.6	120–122	40.6 (40.5)	2.8 (2.8)		18.4 (18.1)
VII	*p*-I	80.5	127–129	40.6 (40.5)	2.8 (2.8)		
VIII	*o*-F	87.2	121–122	51.5 (51.6)	3.5 (3.6)		23.4 (23.0)
IX	*m*-F	82.0	129–130	51.5 (51.6)	3.6 (3.6)		
X	*m*-NO_2	75.2	174–176	48.3 (48.3)	3.4 (3.3)	3.3 (3.3)	
XI	*p*-NO_2	75.6	191–192	48.3 (48.3)	3.3 (3.3)	3.3 (3.3)	21.7 (21.6)
XII	*p*-Me	71.8	159–161	54.9 (55.1)	4.4 (4.4)		23.5 (23.3)
XIII	*p*-CN	91.2	189–190	54.0 (53.6)	3.5 (3.5)		22.9 (22.6)
XIV	*o*-NH_2	84.6	138–140	52.5 (52.0)	4.1 (4.1)	3.6 (3.6)	23.5 (23.2)
XV	H	86.2	155–157	53.9 (54.0)	4.0 (4.0)		24.4 (24.1)

dard spectra of the sodium salts of aromatic carboxylic acids and found that the separation values ($\nu_2-\nu_1$) are about 190 cm^{-1}. Our experimental results indicated that the separation values ($\nu_2-\nu_1$) for these derivatives are also about 190 cm^{-1} and therefore deduce that the coordinative mode of the carboxylates is the bidentate bridging structure.

Absorption bands indicating the presence of the cyclopentadienyl group appear at ≈ 3100 [ν(C—H)], ~ 1440 [ν(C—C)], ~ 1020 [δ(CH) in-plane] and ~ 810 cm^{-1} [δ(CH) out-of-plane]. All these bands correspond to those of bis(η^5-cyclopentadienyl)zirconium(IV) dichloride. The data indicate that the cyclopentadienyl rings remain delocalized and π-bonded to the metal, and maintain their aromatic nature.

^{1}H *NMR spectra*

In these derivatives, the chemical shifts of the cyclopentadienyl protons are at 6.21–6.43 ppm, which is upfield compared to Cp_2ZrCl_2.[8] The results correspond with the aroxyl bis(η^5-cyclopentadienyl)zirconium(IV).

Comparing with $Cp_2ZrCl(OOC-C_6H_5)$, the higher the electronegativities of the substituting groups in the aromatic rings, the more downfield are the chemical shifts of the cyclopentadienyl protons. However, as the substituting groups (X) are F, Cl, Br and I; *o*-X and *p*-X have different influences on the chemical shifts of the cyclopentadienyl. For *o*-X (X = F, Cl, Br and I), the chemical shifts of the cyclopentadienyl protons are almost the same except for F (F: 6.43, Cl: 6.32, Br: 6.30, I: 6.31). Whereas for *p*-X (X = Cl, Br and I), the chemical shifts are different (Cl: 6.43, Br: 6.24, I: 6.21). The results correspond to those reported by Beachell and Butter in the aromatic carboxylato bis(η^5-cyclopentadienyl)titanium(IV).[9]

REFERENCES

1. National Lead Company, *Brit. Pat.* 1961, 858.
2. A. Z. Rubezhov and S. P. Gubin, *Adv. Organomet. Chem.* 1972, **10**, 347.
3. O. P. Pandy, *Acta Chim. Hung.* 1984, **116**, 29.
4. Yao-hua Xu, *You Ji Hua Xue* 1984, **5**, 336.
5. S. K. Sengupta and B. P. Barnanwal, *Rev. Roum. Chim.* 1983, **28**, 287.
6. L. T. Reynolds and G. Wilkinson, *J. Inorg. Nucl. Chem.* 1959, **9**, 86.
7. K. Chandra, *J. Inorg. Nucl. Chem.* 1980, **42**, 187.
8. A. F. Reid and P. C. Wailes, *J. Organomet. Chem.* 1964, **2**, 329.
9. H. C. Beachell and S. A. Butter, *Inorg. Chem.* 1965, **4**, 1133.

Polyhedron Vol. 9, No. 22, pp. 2693–2697, 1990
Printed in Great Britain

0277–5387/90 $3.00+.00
© 1990 Pergamon Press plc

STRUCTURE AND SPECTROSCOPIC STUDY OF AN AZIDE–COPPER(II) DINUCLEAR COMPLEX: $[Cu(pymep)(N_3)_2]_2 \cdot 2H_2O$

T. ROJO,* J. I. R. LARRAMENDI, I. DURAN, J. L. MESA, J. VIA† and M. I. ARRIORTUA†

Departamentos de Química Inorgánica y Mineralogía-Petrología,† Facultad de Ciencias, Universidad del País Vasco, Apdo. 644, E-48080 Bilbao, Spain

(*Received* 29 *March* 1990; *accepted* 21 *June* 1990)

Abstract—The compound of formula $[Cu(C_{14}H_{15}N_3)(N_3)_2]_2 \cdot 2H_2O$ [where $C_{14}H_{15}N_3$ is N-(2′-(6-methyl)pyridyl)methylene-2-(2′-pyridyl)ethylamine (pymep)] has been synthesized and its crystal structure determined by X-ray diffraction methods. The structure consists of centrosymmetric dimeric molecules, $[Cu(pymep)(N_3)_2]_2 \cdot 2H_2O$, in which the water molecules form hydrogen bonds with the azide groups. The geometry of the coordination polyhedron around the copper(II) ion is near to trigonal bipyramid. The X-band ESR powder spectrum shows a weak-intensity signal corresponding to the $\Delta M_s = \pm 2$ forbidden transition, which indicates a magnetic interaction between the copper(II) ions of the dimeric compound.

Many bivalent transition metal ions form complexes of the type $[ML_{III}X_2]$,[1–4] where L_{III} is a tridentate ligand and X is a negatively charged unidentate ion (halide or pseudo-halide). Structural data are available for several $[CuL_{III}X_2] \cdot nH_2O$ compounds [L_{III} is 2,2′:6′,2″-terpyridine (terpy), pyridine-2-aldehyde 2′-pyridylhydrazone (paphy) or N-(2′-(6-methyl)pyridyl)methylene-2-(2′-pyridyl) ethylamine (pymep)] showing the copper(II) ion to be five-coordinate[5–10] or exceptionally, hexacoordinate.[11]

Monomeric $[CuL_{III}X_2] \cdot nH_2O$ complexes can be considered as precursors of the condensed systems. Recently, we have established a synthetic strategy of new one-dimensional systems of copper(II) with tridentate ligands of general formula $[CuL_{III}XY]$ (X = coordinating anion, Y = coordinating or non-coordinating anion) which include bi- and polynuclear species.[12] In this way, the ability and adaptability of the azide ion (N_3^-) as a bridging ligand is well established,[13,14] and two bridge modes, end-on and end-to-end, have been observed in the polynuclear complexes.[14] In this work, we present the crystal structure and a spectroscopic study of the $[Cu(pymep)(N_3)_2] \cdot H_2O$ dimeric complex.

* Author to whom correspondence should be addressed.

EXPERIMENTAL

Preparation of the $[Cu(pymep)(N_3)_2] \cdot H_2O$

This compound was synthesized by a different method from the one described in the literature.[15] Diluted solutions of $CuCl_2 \cdot 2H_2O$ in water and the N-(2′-(6-methyl)pyridyl)methylene-2-(2′-pyridyl) ethylamine compound in ethanol were mixed in a 1 : 1 molar ratio. The resulting solution was treated with a slight excess of NaN_3 pseudo-halide to give a microcrystalline, dark green precipitate. It was filtered, washed with water and diethyl ether and stored in a desiccator over P_4O_{10} for 48 h. Prismatic crystals were obtained by slow evaporation of an ethanolic solution containing the resulting compound. Found: C, 43.1; H, 4.3; N, 32.6. $[Cu(C_{14}H_{15}N_3)(N_3)_2] \cdot H_2O$ requires: C, 43.0; H, 4.4; N, 32.3%. The thermogravimetric analysis indicates the presence of one water molecule per copper(II) ion. The dehydration of the compound starts at $\approx 80°C$.

X-ray crystallography

A specimen with dimensions $0.17 \times 0.08 \times 0.02$ mm was selected. Preliminary cell dimensions and

space group symmetry were obtained from Weissenberg and oscillation photographs. The crystal was mounted on a Enraf–Nonius CAD-4 diffractometer equipped with graphite-monochromatized Cu-K_α radiation. Accurate cell parameters were obtained by a least-squares refinement of the setting angles of 25 reflections with $16 \leqslant 2\theta \leqslant 30°$.

Crystal data. $[Cu(C_{14}H_{15}N_3)(N_3)_2]\cdot H_2O$, $M = 390.5$, $P2_1/n$, $a = 10.543(2)$, $b = 9.653(1)$, $c = 16.638(3)$ Å, $\beta = 97.90(2)°$, $U = 1677(4)$ Å^3, $Z = 4$, $D_m = 1.57(3)$, $D_x = 1.55$ g cm^{-3}, $\lambda(Cu\text{-}K_{\alpha 1}) = 1.54059$ Å, $\mu(Cu\text{-}K_\alpha) = 21.14$ cm^{-1}, $F(000) = 796$, $T = 294$ K. The density was measured by flotation in a chloroform 1,1,2,2-tetrabromoethene mixture.

A total of 2277 reflections were recorded in the range $2 \leqslant 2\theta \leqslant 80°$ with h: $-8 \rightarrow 8$; k: $0 \rightarrow 8$; l: $-13 \rightarrow 13$, using the ω–2θ scan technique. Three orientation and two intensity control reflections were checked every 50 reflections and every hour, respectively, and showed no significant variation. Data were corrected for Lorentz-polarization effects. No absorption corrections have been made. After averaging of the symmetry-related reflections 1011 unique reflections were obtained, of which 947 had $I \geqslant 2\sigma(I)$. The structure was solved by direct methods, using the MULTAN 84 system,[16] and refined by full-matrix least-squares, using the SHELX 76 program.[17] The function minimized was $\Sigma\omega[|F_o|-|F_c|]^2$, where $\omega = [\sigma^2(F_o)+0.001797(F_o)^2]^{-1}$. Positions of the hydrogen atoms were computed and refined with overall isotropic thermal parameters and the remaining atoms anisotropically. The final R was 0.039 ($R_\omega = 0.043$) for all observed reflections. At the end of the refinement the maximum peak in the final ΔF map was 0.24 e Å^{-3}. Scattering factors were taken from the *International Tables for X-ray Crystallography*.[18] All calculations were carried out on a Microvax Computer at the computer centre of the Basque University. The geometric calculations were made with XANADU[19] and molecular illustrations were drawn with SCHAKAL 88.[20] Further details are presented as supplemenary data, together with thermal parameters, bond lengths and angles, mean average planes and structure factors.

Physical measurements

Water was determined thermogravimetrically using a Perkin–Elmer TGS-1 thermobalance. The IR spectrum was obtained on a Perkin–Elmer 1430 spectrophotometer using KBr pellets. The electronic reflectance spectrum at 298 K was measured with a Perkin–Elmer Lambda-9 UV–vis/NIR spectrophotometer on a powder sample. A Bruker ER 200 tt spectrometer, equipped with a standard low-temperature device, operating at X-band calibrated by an NMR probe for the magnetic field and a HP 5342A frequency counter for the microwave frequency, was used to record the ESR powder spectra of the complex at different temperatures.

RESULTS AND DISCUSSION

Selected bond lengths and angles are given in Table 1. The structure of the compound is shown in Fig. 1, together with the atomic numbering system.

The structure consists of $[Cu(pymep)(N_3)_2]_2\cdot 2H_2O$ centrosymmetric dimeric molecules. The coordination polyhedron around the copper(II) ion is better described as a distorted trigonal bipyramid. The axial sites are occupied by the two outer nitrogen atoms [N(1), N(3)] of the tridentate ligand [Cu—N(1),N(3), 2.039(7), 2.038(6) Å, respectively], while the equatorial sites are occupied by the central nitrogen atom [N(2)] of this ligand [Cu—N(2), 2.080(6) Å] and by two nitrogen atoms [N(4), N(7)] belonging to the azide groups [Cu—N(4), N(7), 2.039(8), 1.986(7) Å, respectively]. In the coordination polyhedron, the average value of the angles N_{axial}—Cu—$N_{equatorial}$ is 90(5)°, while the equatorial angles N(2)—Cu—N(4), N(2)—Cu—N(7) and N(4)—Cu—N(7) are 107.9(3), 122.6(3) and 129.5(3)°, respectively, and the axial angle N(1)—Cu—N(3) is 169.8(4)°. The separation of the copper(II) ion from the plane defined by the N(2), N(4), N(7) atoms is 0.02 Å. Likewise, the distortion of the coordination polyhedron, from trigonal bipyramid ($\Delta = 0$) towards a regular square pyramid ($\Delta = 1$), has been calculated according to the Muetterties and Guggenberger description.[21,22] The value obtained, $\Delta = 0.11$ (Table 2), is in good agreement with a topology near to trigonal bipyramid.

In the dimeric molecule, each water molecule forms intramolecular hydrogen bonds with both the N(4) of one azide group [Ow···N(4), 2.882(9) Å] and the $N(9)^i$ atom of the azide group belonging to the other half of the dimer [Ow···$N(9)^i$, 3.02(1) Å; $i = 1-x, -y, -z$]. The intradimer copper–copper distance is 6.970(2) Å.

The azide groups are found to be linear within experimental error [angles N(4)—N(5)—N(6) and N(7)—N(8)—N(9) are 177.8(7) and 176.5(8)°, respectively]. The values for the angles Cu—N(4)—N(5) and Cu—N(7)—N(8) [119.0(5) and 130.9(5)°, respectively] lie within the expected range for the angle of a trigonally hybridized nitrogen.[13] The different N—N distances in both azide groups support the asymmetry of these groups. In the N(4)—N(5)—N(6)

Table 1. Selected bond distances (Å) and angles (°) in the [Cu(pymep)(N$_3$)$_2$]·H$_2$O complex, with ESDs in parentheses

Coordination polyhedron and azide groups			
Cu—N(1)	2.039(7)	Cu—N(2)	2.080(6)
Cu—N(3)	2.038(6)	Cu—N(4)	2.039(8)
Cu—N(7)	1.986(7)	Cu—Cu^i	6.970(2)
N(4)—N(5)	1.191(14)	N(5)—N(6)	1.153(15)
N(7)—N(8)	1.179(12)	N(8)—N(9)	1.143(13)
Ow···N(4)	2.882(9)	Ow···N(9)^i	3.02(1)
N(1)—Cu—N(2)	91.3(3)	N(1)—Cu—N(4)	91.1(3)
N(1)—Cu—N(7)	89.6(3)	N(3)—Cu—N(2)	78.8(3)
N(3)—Cu—N(4)	94.1(3)	N(3)—Cu—N(7)	93.8(3)
N(1)—Cu—N(3)	169.8(4)	N(2)—Cu—N(4)	107.9(3)
N(2)—Cu—N(7)	122.6(3)	N(4)—Cu—N(7)	129.5(3)
Cu—N(4)—N(5)	119.0(5)	Cu—N(7)—N(8)	130.9(5)
N(4)—N(5)—N(6)	177.8(7)	N(7)—N(8)—N(9)	176.5(8)
Mean values of the pymep ligand			
C—C	1.40(7)	C—N	1.33(6)
C—C—C	119(3)	C—N—C	119(3)

Symmetry code: $i = 1-x, -y, -z$.

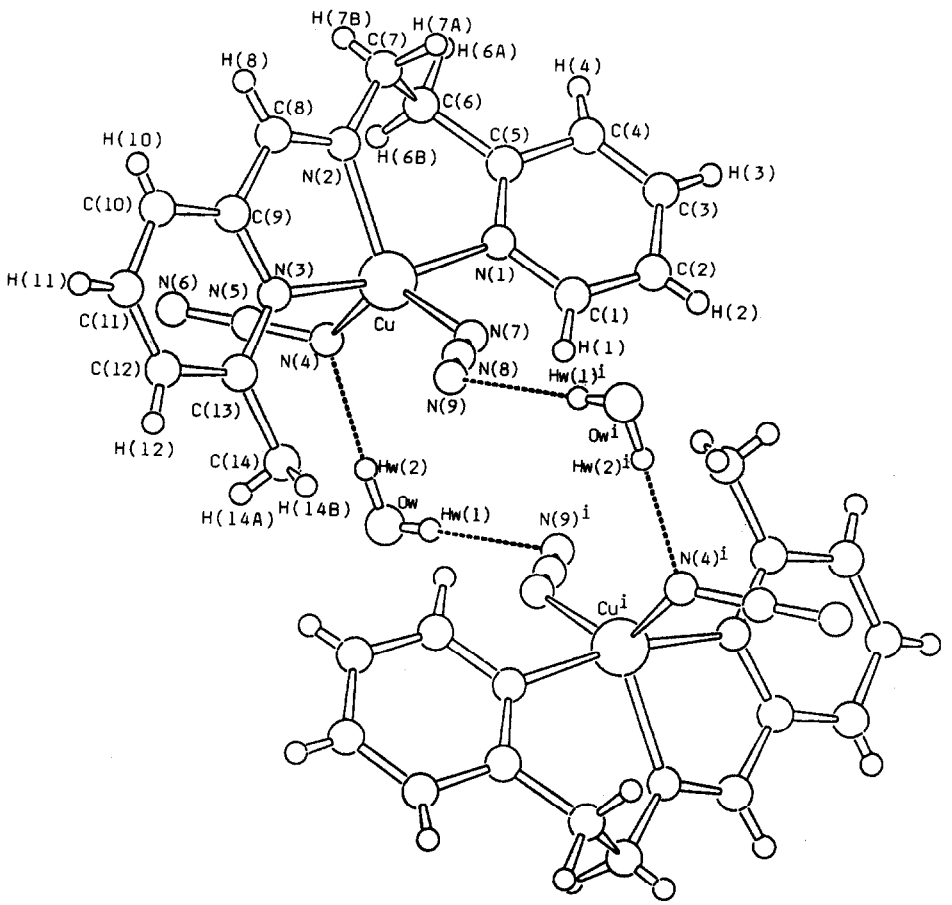

Fig. 1. Stereoscopic view and atomic numbering of the [Cu(pymep)(N$_3$)$_2$]·H$_2$O complex.

Table 2. Dihedral angles (°) and distortion (Δ) of the coordination polyhedron for the $[Cu(pymep)(N_3)_2]\cdot H_2O$ compound compared with the ideal geometries trigonal bipyramid (TBP) and regular square pyramid (SPr)

Dihedral angle	TBP	$[Cu(pymep)(N_3)_2]\cdot H_2O$	SPr
δa_1	101.5	97.1	121.8
δa_3	101.5	108.8	121.8
δa_4	101.5	101.6	121.8
δa_6	101.5	105.5	121.8
δa_2	101.5	100.7	73.9
δa_5	101.5	96.6	73.9
δe_1	53.1	58.9	73.9
δe_2	53.1	54.1	73.9
δe_3	53.1	45.9	0
Δ	0	0.11	1

$\Delta = |[(\delta a_1 + \delta a_3 + \delta a_4 + \delta a_6) - 406.0]/182.7| + |[(\delta a_2 + \delta a_5) - 203.0]/248.41| + |[(\delta e_1 + \delta e_2) - 106.2]/187.2| + |(53.1 - \delta e_3)/477.9|$.

azide group, the N—N distances are 1.191(14) and 1.153(15) Å for N(4)—N(5) and N(5)—N(6), respectively. In the other azide group, N(7)—N(8)—N(9), the N(7)—N(8) and N(8)—N(9) distances are 1.179(12) and 1.143(13) Å, respectively. In both cases, the longest N—N distance is closest to the Cu—N bond.

The interest in the IR spectrum of the complex lies mainly on the bands due to the water molecule and azide groups. For the water molecule, only the stretching vibration has been observed at 3340 cm^{-1}. For the azide groups, the crystal structure shows that both groups are crystallographically independent. Thus, two bands are expected to appear in the IR spectrum due to the antisymmetric stretching mode, $\nu_{as}(N_3)$, of the azide groups, and similarly, two further bands are expected to occur corresponding to the symmetric stretching mode, $\nu_s(N_3)$.[23] According to these considerations, four bands can be observed in the IR spectrum. The strong bands at 2055 and 2035 cm^{-1} may be accounted for by the antisymmetric stretching frequency of the azide groups. The symmetric stretching vibrations, much weaker than the antisymmetric stretching vibration, are at 1350 and 1315 cm^{-1}. Two peaks at frequencies 680 and 675 cm^{-1}, corresponding to the bending mode, can also be observed in the IR spectrum.

In the visible region, the reflectance electronic spectrum, at room temperature, exhibits one broad and unresolved band centred around 13,000 cm^{-1}. The position of the intensity maximum in the absorption envelope agrees with the observations of Hathaway and co-workers[24,25] on $[CuN_5]$ chromophores with geometries near to trigonal bipyramid.

The X-band ESR powder spectrum (Fig. 2) shows an orthorhombic signal, which corresponds to the $\Delta M_s = \pm 1$ allowed transition [$g_1 = 2.220$ (2.214), $g_2 = 2.167$ (2.174) and $g_3 = 2.039$ (2.034) at 298 and (110) K]. In addition to this signal, a weak intensity absorption at ≈ 1600 gauss can be observed, which corresponds to the $\Delta M_s = \pm 2$ forbidden transition and indicates a magnetic interaction between the copper(II) ions of the dimeric molecule.

In the title compound, magnetic interactions can be propagated by a superexchange pathway through an extended bridging network formed by two azide groups and one water molecule connected by hydrogen bonds (see Fig. 1). The Cu—Cu^i distance (through the extended bridging network) is 12.3 Å, and for such distance the expected $|J|$ value ranges between 10^{-2} and 10^{-3} cm^{-1}, according to the experimentally determined function for long-range antiferromagnetic superexchange proposed by Coffman and Buettner.[26] However, a direct dipolar interaction, which is known to vary as r^{-3} (r being the interspin distance) can not be assumed negligible in this compound ($D_d = 10^{-2}$ cm^{-1}). It must be pointed out that, for the detection of the magnetic interactions with exchange coupling constants of $|J| < 0.1$ cm^{-1}, the magnetic measurements should be performed at temperatures lower than 2 K.

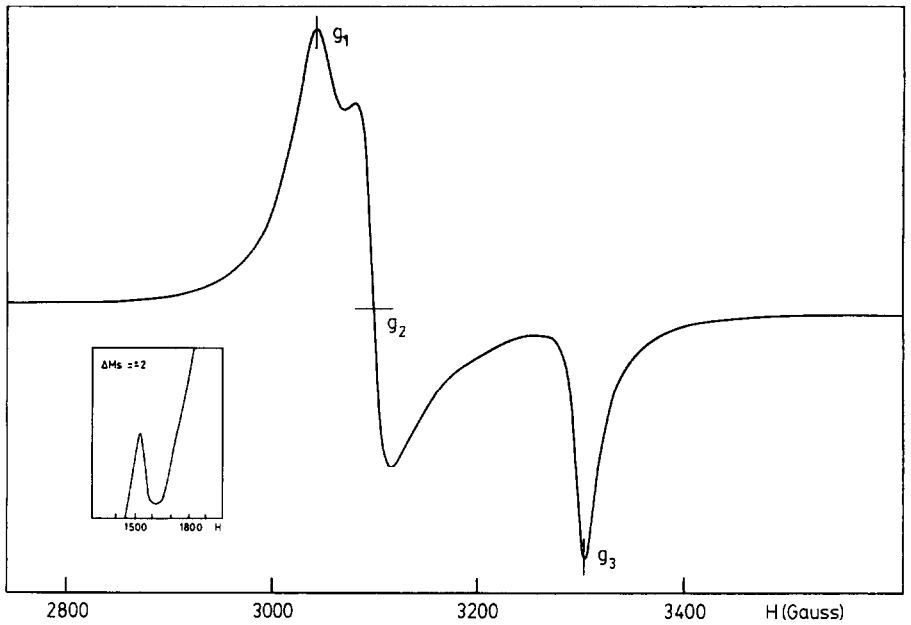

Fig. 2. X-band ESR spectrum of a powdered sample of the [Cu(pymep)(N$_3$)$_2$]·H$_2$O complex at room temperature.

Acknowledgements—This work was supported in part by a grant (UPV 130.310.0014/88) from the University of the Basque Country, which we gratefully acknowledge.

REFERENCES

1. D. L. Kepert, E. S. Kucharski and A. H. White, *J. Chem. Soc., Dalton Trans.* 1980, 1932.
2. J. V. Folgado, E. Escrivá, A. Beltrán and D. Beltrán, *Transition Met. Chem.* 1986, **11**, 485.
3. J. V. Folgado, E. Escrivá, A. Beltrán and D. Beltrán, *Transition Met. Chem.* 1987, **12**, 306.
4. M. I. Arriortua, R. Cortés, L. Lezama, T. Rojo, X. Soláns and M. Font-Bardía, *Inorg. Chim. Acta* 1990, **174**, 263.
5. T. Rojo, M. Vlasse and D. Beltrán, *Acta Cryst.* 1983, **C39**, 194.
6. W. Henke, S. Kramer and D. Reinen, *Inorg. Chem.* 1983, **22**, 2858.
7. M. I. Arriortua, J. L. Mesa, T. Rojo, T. Debaerdemaeker, D. Beltrán, H. Stratemeier and D. Reinen, *Inorg. Chem.* 1988, **27**, 2976.
8. T. Rojo, A. García, J. L. Mesa, J. Vía and M. I. Arriortua, *Inorg. Chim. Acta* 1988, **149**, 159.
9. J. L. Mesa, M. I. Arriortua, L. Lezama, J. L. Pizarro, T. Rojo and D. Beltrán, *Polyhedron* 1988, **7**, 1383.
10. J. I. R. Larramendi, B. Díaz, J. L. Mesa, T. Rojo, J. Vía and M. I. Arriortua, *Transition Met. Chem.*, submitted.
11. J. L. Mesa, T. Rojo, M. I. Arriortua, G. Villeneuve, J. V. Folgado, A. Beltrán and D. Beltrán, *J. Chem. Soc., Dalton Trans.* 1989, 53.
12. T. Rojo, J. L. Mesa, M. I. Arriortua, J. M. Savariault, J. Galy, G. Villeneuve and D. Beltrán, *Inorg. Chem.* 1988, **27**, 3904.
13. Z. Dori and R. F. Ziolo, *Chem. Rev.* 1973, **73**, 247.
14. R. D. Willett, D. Gatteschi and O. Khan (Eds), *Magneto-structural Correlations in Exchange Coupled Systems*, p. 57. NATO ASI Series, Reidel, Dordrecht, Holland (1985).
15. Y. Nakao, *Inorg. Chim. Acta* 1983, **74**, 159.
16. P. Main, G. Germain and M. M. Woolfson, MULTAN 84. A System of Computer Programs for the Automatic Solution of Crystal Structures from X-ray Diffraction Data. University of York, U.K. and Louvain, Belgium (1984).
17. G. M. Sheldrick, SHELX 76. Program for Crystal Structure Determination. University of Cambridge, U.K. (1976).
18. *International Tables for X-ray Crystallography*, Vol. 4, pp. 72–79. Kynoch Press, Birmingham (1974).
19. P. Roberts and G. M. Sheldrick, XANADU. Program for Torsion Angle, Mean Plane and Libration Correction Calculations. University of Cambridge, U.K. (1975).
20. E. Ketler, SCHAKAL 88. A Fortran Program for the Graphic Representation of Molecular and Crystallographic Models. University of Freiburg (1988).
21. E. L. Muetterties and L. J. Guggenberger, *J. Am. Chem. Soc.* 1974, 1748.
22. J. L. Mesa, M. I. Arriortua, L. Lezama, J. L. Pizarro, T. Rojo and D. Beltrán, *Polyhedron* 1988, **7**, 1383.
23. I. Agrell, *Acta Chem. Scand.* 1971, **25**, 2965.
24. B. J. Hathaway and D. E. Billing, *Coord. Chem. Rev.* 1970, **5**, 143.
25. B. J. Hathaway, *Struct. Bond.* 1984, **57**, 55 and refs therein.
26. R. Coffman and G. R. Buettner, *J. Chem. Phys.* 1979, **83**, 2387.

Polyhedron Vol. 9, No. 22, pp. 2699–2704, 1990
Printed in Great Britain

0277–5387/90 $3.00+.00
© 1990 Pergamon Press plc

SPECTROSCOPIC STUDIES AND CRYSTAL STRUCTURE OF BIS(N-2-PYRIDINYLCARBONYL-2-PYRIDINECARBOXIMIDATO) MANGANESE(II) MONOHYDRATE: ZERO-FIELD SPLITTING PARAMETERS

DOLORES MARCOS, JOSÉ-VICENTE FOLGADO and DANIEL BELTRÁN-PORTER*

UIBCM, Departament de Química Inorgànica, Universitat de València, Dr Moliner 50, 46100 Burjassot, València, Spain

and

MARIA T. DO PRADO-GAMBARDELLA, SANDRA H. PULCINELLI and REGINA H. DE ALMEIDA-SANTOS

Instituto de Física e Química de São Carlos, Universidade de São Paulo, C. Postal 369, CEP 13560, São Carlos, Brazil

(*Received* 30 *March* 1990; *accepted* 21 *June* 1990)

Abstract—The X-ray crystal structure of bis(N-2-pyridinylcarbonyl-2-pyridinecarboximidato)manganese(II) monohydrate, $Mn(BPCA)_2 \cdot H_2O$, has been determined. It consists of discrete neutral $Mn(BPCA)_2$ entities linked two by two through water molecules hydrogen bonded to ligand carbonyl groups. The coordination geometry around the manganese ions can be described approximately as very distorted compressed octahedral. ESR spectra at X- and Q-band are reported for the title compound as well as for manganese(II) doped into $Zn(BPCA)_2 \cdot H_2O$ powder samples. Zero-field splitting parameters, D and E, are calculated at 298 and 130 K. The D values are 0.073 and 0.078 cm^{-1}, respectively, whereas λ ($= E/D$) is far away from zero (0.23 and 0.24 cm^{-1}, respectively) in good agreement with the actual low symmetry of the MnN_6 chromophores.

A part of our research is focused on the study of the interaction between N-donor tridentate rigid ligands (L_{III}) and transition metal ions, and we have recently reported the structural and spectroscopic properties of a series of compounds containing the $Cu(L_{III})_2^{n+}$ entities [L_{III} = BPCA (N-2-pyridinylcarbonyl-2-pyridinecarboximidate anion), $n = 0$; L_{III} = tpt (2,4,6-tris(2-pyridyl)-1,3,5-triazine) or terpy (2,2′:6′,2″-terpyridine), $n = 2$].[1,2] In these complexes the CuN_6 polyhedra can be considered as tetragonally elongated octahedra with a slight orthorhombic component superimposed as a consequence of the rigidity of the tridentate ligands together with the Jahn–Teller effect. Both cases, dynamic and static structures have been observed.[1,2]

We are now studying the behaviour of the BPCA ligand with metallic ions other than copper(II). We report here the crystal structure and spectroscopic studies of the compound $Mn(BPCA)_2 \cdot H_2O$. Since the $Zn(BPCA)_2 \cdot H_2O$ compound is isostructural with the manganese(II) complex, accurate zero-field parameters have been estimated from the ESR spectra on manganese(II)-doped zinc samples.

EXPERIMENTAL

Preparation of $Mn(BPCA)_2 \cdot H_2O$

The HBPCA ligand was isolated as described in ref. 3. Solutions of HBPCA (0.22 mmol) in acetone

* Author to whom correspondence should be addressed.

(2 cm^3) and $Mn(NO_3)_2 \cdot 4H_2O$ (0.11 mmol) in water (15 cm^3) were mixed with stirring. The pH of the resulting orange solution was slowly changed to *ca* 8 (with aqueous NaOH). Red–brown crystals appeared after several hours, these were isolated by filtration, washed with cold acetone and stored in a desiccator over silica gel. Found: C, 54.8; H, 3.4; Mn, 10.4; N, 15.9. Calc. for $C_{24}H_{18}MnN_6O_5$: C, 54.9; H, 3.4; Mn, 10.5; N, 16.0%.

Samples of $Zn(BPCA)_2 \cdot H_2O$ were prepared in the same way but using $Zn(NO_3)_2 \cdot 6H_2O$ instead of manganese(II) nitrate. Doped samples, with a nominal per cent of manganese(II) between 1 and 5, were obtained starting from an adequate mixture of the metallic nitrates.

Physical measurements

IR spectra (KBr pellets) were recorded in the 4000–250 cm^{-1} region using a Pye Unicam SP 2000 spectrophotometer. Diffuse reflectance and solution (chloroform) electronic spectra were recorded on a Perkin–Elmer Lambda 9 UV–vis/NIR spectrophotometer. ESR spectra were recorded on Bruker ER 200D (X-Band) and on Varian E15 (Q-band) spectrometers equipped with a variable temperature device. Water was determined thermogravimetrically by means of a Setaram B70 simultaneous TGA–DTA thermobalance and X-ray powder diffraction patterns ($2° < 2\theta < 50°$) were obtained by means of a Kristalloflex 810 Siemens diffractometer using Cu-K_α radiation and silicon powder as internal reference.

Crystallographic study

Crystal data. Red–brown prismatic crystals of $C_{24}H_{18}MnN_6O_5$, $M = 524.9$, monoclinic, space group $P2_1/c$, $a = 9.192(1)$, $b = 8.821(1)$, $c = 28.920(4)$ Å, $\beta = 97.01(1)°$, $V = 2327(1)$ $Å^3$, $Z = 4$, $D_c = 1.498$ g cm^{-3}, μ(Mo-K_α) = 5.62 cm^{-1}, λ(Mo-K_α) = 0.70926 Å. Manganese and zinc compounds are isostructural and data for the zinc complex have been reported previously.[1]

Data collection. A well-formed crystal of dimensions $0.33 \times 0.20 \times 0.10$ mm was mounted on an Enraf–Nonius CAD-4 diffractometer equipped with a graphite monochromator. The cell dimensions were obtained by least-squares refinement of 25 well-centred reflections. From systematic absences the space group $P2_1/c$ was assumed. Examination of four standard reflections monitored after each 50 reflections showed no substantial intensity decay. A total of 5631 reflections were measured ($2° < 2\theta < 46°$; $-10 < h < 10$, $0 < k < 9$, $0 < l < 31$) with the variable-speed ω–2θ technique; of which 3222 were unique and 1518 with $I > 3\sigma(I)$ were used in the determination of the structure. Lorentz, polarization and absorption corrections (transmission factor range, 0.887–0.951) were applied.

Structure solution and refinement. The structure was solved using direct methods locating the manganese, nitrogen and oxygen atoms. The remaining non-hydrogen atoms were located from successive Fourier syntheses. Refinement of the structure was carried out with the SHELX76 system[4] by weighted anisotropic full-matrix least-squares methods. All hydrogen atoms were calculated assuming C—H = 1.08 Å and were included in the refinement with a fixed isotropic thermal parameter ($B_{iso} = 6$ $Å^2$). The final R_w value was $R_w = 0.056$ (364 parameters refined). $\Sigma w(|F_o| - |F_c|)^2$ was minimized with $w = 1/[\sigma^2(F_o)]$ with $\sigma^2(F_o)$ from counting statistics. In the final difference map the residual maxima were less than 1 e $Å^{-3}$. Atomic scattering factors and corrections for anomalous dispersion for the manganese atom were taken from *International Tables for X-ray Crystallography*.[5] The geometrical calculations were performed with XANADU[6] and DISTAN,[7] and molecular illustrations were drawn with ORTEP.[8] Final atomic coordinates, thermal parameters and F_o/F_c values have been deposited with the Editor as supplementary data.

RESULTS AND DISCUSSION

Crystal structure

Figure 1 shows a perspective view of the $Mn(BPCA)_2$ units with the atomic numbering scheme, and Fig. 2 shows a stereoscopic view of the unit cell. Selected bond distances and angles are listed in Table 1. The structure consists of neutral $Mn(BPCA)_2$ entities linked two by two through hydrogen bonding involving water molecules and carbonyl groups from BPCA ligands, as shown by contact distances listed in Table 1.

Obviating the angular distortions owing to the rigidity of BPCA ligand (see Table 1), the geometry of the MnN_6 polyhedra can be regarded as very distorted compressed octahedral. This compression along the N(2)—Mn—N(5) axis is the result of the rigid structure of the BPCA ligands, which enforce shorter metal–N(central) bond distances.

The N(1), N(2), N(3) and N(5) atoms define a plane (within ±0.10 Å) from which the manganese atom lies 0.07 Å away. The N(2), N(4), N(5) and N(6) atoms, however, deviate more (±0.15 Å) from their least-squares plane, the manganese atom being

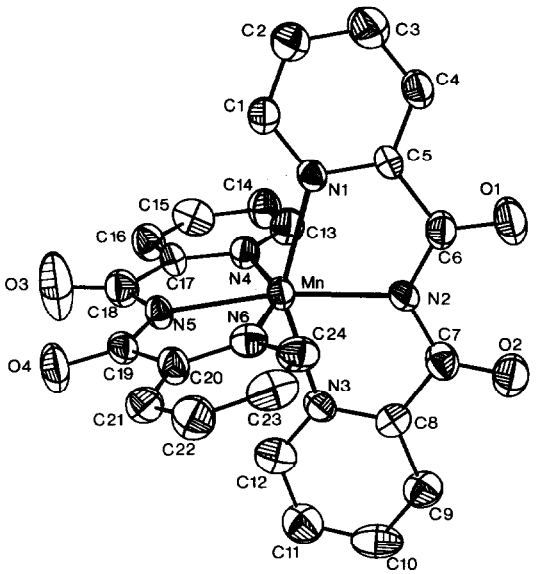

Fig. 1. Perspective view and atomic numbering of the $Mn(BPCA)_2$ units.

only 0.002 Å from this plane. Both mean planes make an angle of 87.0°.

The adaptation of the BPCA ligands to the pseudo-octahedral geometry of the MnN_6 polyhedra requires deformations of the ligand framework. Both ligands are unequivalent and neither of them can be considered planar. In fact, deviations of non-hydrogen atoms from the calculated mean planes are 0.30 Å in one of the ligands and 0.32 Å in the other. Furthermore, it should be noted that the values of the angles around the carbon atoms involved in the carbonyl groups significantly differ from the idealized value of 120°.

Infrared and electronic spectra

The IR spectrum of the title compound shows two noteworthy features, namely the presence of bands at 3550(m) and 3480(m) cm^{-1}, assignable to the O—H stretching vibrations of the water molecule, and that of two intense bands at 1700(vs) and 1685(vs) cm^{-1}, which are due to the C=O stretching vibrations of BPCA carbonyl groups. The shape and position of the ν(OH) bands, in addition to the thermoanalytical data (water is evolved endothermically at low temperature; peak temperature, 80°C), are consistent with water molecules involved in hydrogen bonds of moderate strength.[9] The splitting of the C=O band, which appears as an unique band at 1750(vs) cm^{-1} in the spectrum of the HBPCA ligand,[1,3] might be due to the presence of two different BPCA in the complex, since only one of them is involved in the hydrogen

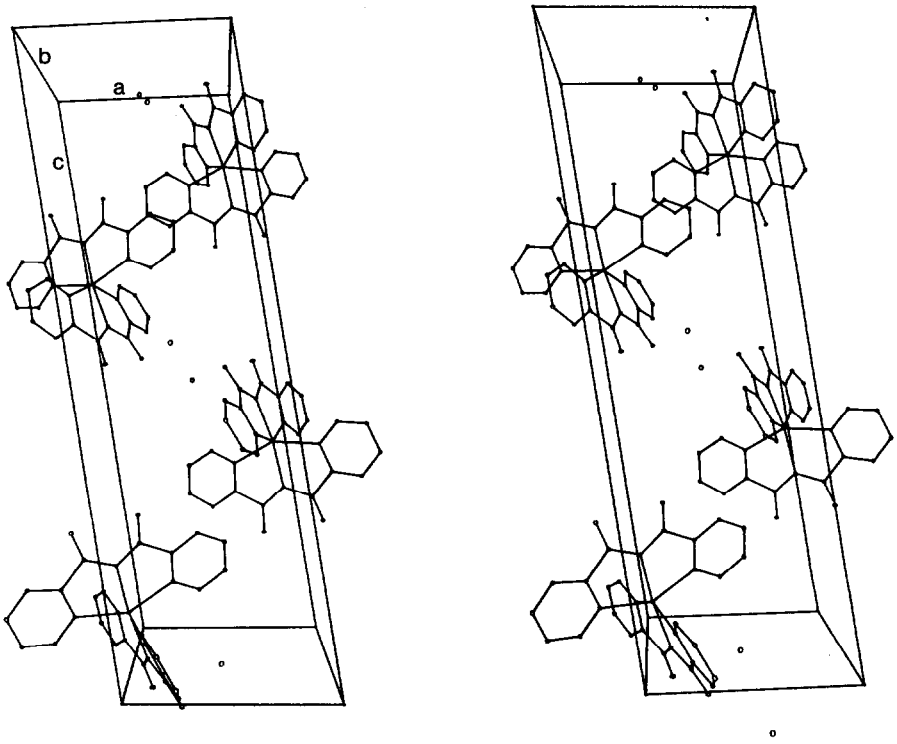

Fig. 2. Stereoscopic view of the unit cell for $Mn(BPCA)_2 \cdot H_2O$.

Table 1. Selected bond distances (Å) and angles (°) for $Mn(BPCA)_2 \cdot H_2O$ with ESDs in parentheses

Distances			
Mn—N(1)	2.216(7)	Mn—N(2)	2.179(7)
Mn—N(3)	2.255(7)	Mn—N(4)	2.285(8)
Mn—N(5)	2.169(7)	Mn—N(6)	2.236(8)
Angles			
N(1)—Mn—N(2)	74.8(3)	N(1)—Mn—N(3)	149.0(3)
N(1)—Mn—N(4)	94.2(3)	N(1)—Mn—N(5)	111.2(3)
N(1)—Mn—N(6)	89.8(3)	N(2)—Mn—N(3)	74.4(3)
N(2)—Mn—N(4)	98.0(3)	N(2)—Mn—N(5)	169.5(3)
N(2)—Mn—N(6)	114.1(3)	N(3)—Mn—N(4)	93.8(3)
N(3)—Mn—N(5)	99.8(3)	N(3)—Mn—N(6)	99.3(3)
N(4)—Mn—N(5)	73.4(3)	N(4)—Mn—N(6)	147.5(3)
N(5)—Mn—N(6)	75.1(3)		
Hydrogen bonding			
O(w)···O(3)′	2.89(1)	O(3)—O(w)—O(3)′	91.5(3)
O(w)···O(3)	3.15(1)	O(4)—O(w)—O(3)′	130.4(3)
O(w)···O(4)	3.19(1)	O(3)—O(w)—O(4)	51.3(3)

O(3)′ from O(3) after $1-x$, $1-y$, $1-z$.

bonds. This is supported by the observation of an unsplit carbonyl band centred at 1700 cm^{-1} in the IR spectra of the thermally dehydrated $Mn(BPCA)_2$ samples. Similarly, this carbonyl band appears unsplit and centred at 1700 cm^{-1} in the IR spectra of the anhydrous $Ni(BPCA)_2$ complex.[3] Hence the carbonyl groups involved in the hydrogen bonds must be those which produce the absorption at lower wavenumbers, in correspondence to weaker C=O bonds.[1]

Both the reflectance and solution (chloroform) electronic spectra of the compound show only a very strong broad band above 16,000 cm^{-1}, probably due to charge-transfer transitions, which produces the red–brown colour of the samples.

ESR spectroscopy

ESR spectra have been obtained at both X- and Q-band for manganese(II) ions doped into $Zn(BPCA)_2 \cdot H_2O$ at 298 and 130 K. The pure manganese(II) samples give, at room temperature, a strong, broad, symmetrical signal centred at $g_{eff} = 2.00$ and other less intense features at lower and higher magnetic field. This fact suggests a low value for D,[10,11] where D is the axial zero-field splitting parameter in the spin Hamiltonian

$$\mathcal{H} = g\beta HS + D(S_z^2 - 1/3S^2) + E(S_x^2 - S_y^2). \quad (1)$$

The spectra recorded at 130 K [Fig. 3(top)] showed only small changes in the position of the outer signals. An accurate estimation of D and E was not possible at this stage because of the width of the overlapping signals. However, a first evaluation of $0.07\ cm^{-1} < |D| < 0.08\ cm^{-1}$ was made from these spectra. On the contrary, the doped into zinc(II) samples showed a large number of transitions with well-resolved hyperfine structure [Fig. 3(bottom)]. Obviously, the resolution decreases with increasing concentration of manganese(II) in the samples.

The program POWDER[12] was used to calculate the resonance fields by exact diagonalization of the matrix derived from eq. (1) and good agreement with the experimental resonance fields was found with $g = 2.00$ and the data in Table 2. The calculated positions of the signals deviated from the experimental values by less than 25 gauss.

Owing to the small D value and the good resolution of the hyperfine splitting, the sign of D could be determined from the mean spacing of the hyperfine components in the $\pm 3/2 \leftrightarrow \pm 5/2$ transitions, with the magnetic field parallel to z.[13] This

Table 2. Zero-field splitting parameters for $Mn(BPCA)_2 \cdot H_2O$

Temperature (K)	$\lvert D\rvert$ (cm^{-1})	$\lvert E\rvert$ (cm^{-1})	$\lambda\ (= E/D)$
298	0.073	0.017	0.23
130	0.078	0.019	0.24

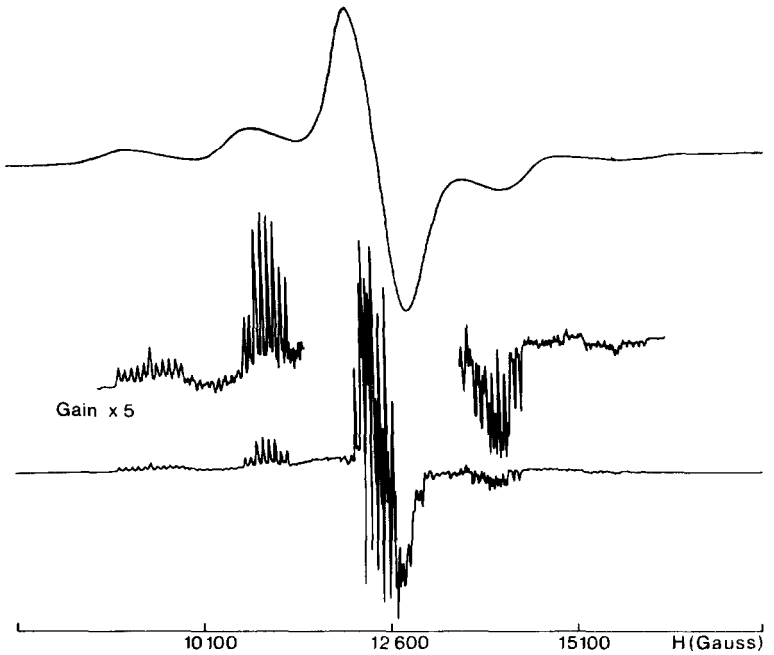

Fig. 3. Q-Band ESR powder spectra, at 130 K, of $Mn(BPCA)_2 \cdot H_2O$ (top) and $Zn(BPCA)_2 \cdot H_2O$ doped with 1% Mn (bottom).

spacing was greater for the lowest (84 gauss) than for the highest (74 gauss) field observed transition. Assuming that A is negative, as is usually the case for manganese(II), D must be also negative.

The estimated D values indicate that the axial distortion in the MnN_6 chromophores is not very large. This is in full accord with the molecular structure discussed before, since the tetragonality of the chromophore (defined as the ratio between the mean equatorial Mn—N distance and the mean axial Mn—N distance) is only 1.038, if we take the shortest Mn—N distances as the direction of the axial axis. Besides this, the negative D found corresponds to the observed compression of the "octahedra" along an approximate four-fold axis.[10] On the other hand, the λ ($= E/D$) values, near the limiting value of 1/3, fit extremely well with the actual low symmetry of the MnN_6 chromophores.

Finally, it can be noted that the hyperfine parameter A is somewhat lower than found in other manganese(II) complexes.[10,11,14,15] This must be due to the very low symmetry of the MnN_6 chromophores, together with a considerable density of unpaired electrons on the ligands.[1]

Acknowledgements—This work was supported partially by a grant from CAICYT which we acknowledge. D.M. and J.V.F. thank the MEC and Generalitat Valenciana, respectively, for research fellowships. We are grateful to Professor Dr D. Reinen (Marburg, F.R.G.) for making available the Varian E15 spectrometer and for his hospitality to one of us (J.V.F.).

REFERENCES

1. D. Marcos, R. Martínez-Mañez, J. V. Folgado, A. Beltrán-Porter, D. Beltrán-Porter and A. Fuertes, *Inorg. Chim. Acta* 1989, **159**, 11.
2. J. V. Folgado, W. Henke, R. Allmann, H. Stratemeier, D. Beltrán-Porter, T. Rojo and D. Reinen, *Inorg. Chem.* 1990, **29**, 2035.
3. J. V. Folgado, D. Marcos and D. Beltrán-Porter, unpublished work.
4. G. M. Sheldrick, SHELX76, Program for Crystal Structure Determination. Cambridge University, U.K. (1976).
5. *International Tables for X-ray Crystallography*, Vol. 4, pp. 72–99. Kynoch Press, Birmingham (1974).
6. P. Roberts and G. M. Sheldrick, XANADU, Program for Crystallographic Calculations. Cambridge University, U.K. (1975).
7. J. Burzlaff, V. Bohme and M. Gomm, DISTAN. University of Erlangen, F.R.G. (1977).
8. C. K. Johnson, ORTEP, Report ORNL-3794. Oak Ridge National Laboratory, Oak Ridge, Tennessee (1965).
9. J. R. Ferraro, *Low-frequency Vibrations of Inorganic and Coordination Compounds*, p. 65. Plenum Press, New York (1971).

10. M. Goodgame and J. N. Okey, *J. Chem. Soc., Dalton Trans.* 1985, 75 and refs therein.
11. M. Goodgame and J. N. Okey, *Inorg. Chim. Acta* 1985, **103**, 67 and refs therein.
12. POWDER, Program to Simulate an ESR Spectrum of Polycrystalline or Glassy Materials, IBM PC version (1986).
13. R. B. Birdy and M. Goodgame, *Inorg. Chem.* 1979, **18**, 472.
14. G. M. Woltermann and J. R. Wasson, *Inorg. Chem.* 1973, **12**, 2366.
15. A. Ozarowsky, B. R. McGarvey, A. B. Sarkar and J. E. Drake, *Inorg. Chem.* 1988, **27**, 628.

Polyhedron Vol. 9, No. 22, pp. 2705–2708, 1990
Printed in Great Britain

0277–5387/90 $3.00+.00
© 1990 Pergamon Press plc

PERTURBED ANGULAR CORRELATION STUDIES OF THE Hf–EDTA COMPLEX

S. K. DAS, B. S. TOMAR and SATYA PRAKASH*

Radiochemistry Division, Bhabha Atomic Research Centre, Trombay, Bombay 400 085, India

(*Received* 23 *April* 1990; *accepted* 22 *June* 1990)

Abstract—The integral perturbed angular correlation (IPAC) technique has been used to determine the stability constant of the Hf–EDTA complex in 4.6 M $HClO_4$. The stability constant ($\log K$) was found to be: 30.1 ± 0.44. The time differential perturbed angular correlation (TDPAC) study of polycrystalline Hf–EDTA was carried out to estimate the quadrupole interaction frequency (w_Q) and the asymmetry of the EFG for the complex, before and after heating at 160°C. These parameters are very similar in these two cases and indicate the possibility of partial polymerization through OH bridging, whereby the immediate chemical surrounding of the hafnium nucleus is expected to remain unchanged.

The perturbed angular correlation (PAC) technique has been effectively used to study hyperfine interactions. Use of this technique in condensed matter physics has been reviewed by Heer and Novey.[1] However, use of this technique in chemistry is relatively recent. Adloff[2] has reviewed several aspects of structural chemistry and solution chemistry, namely, polymerization, complexation, hot atom chemistry, etc., which are amenable to PAC studies. Another review by Rinneberg[3] covers the application of this technique in various fields of research. A report by Lerf and Butz[4] provides data on nuclear quadrupole interactions in several compounds studied by this technique.

Attempts have been made to determine the stability constants of the zirconium complex with EDTA using conventional chemical techniques such as spectrophotometry[5] and ion exchange chromatography.[6] In all these cases the solutions used were made up with low acidity in which zirconium or hafnium is known to polymerize.[7] This restricts these techniques for the direct determination of stability constants, since one has to correct for hydrolysis of the metal ion. While the stability constant of Zr–EDTA at higher acidity (> 3 M), at which zirconium is not polymerized, has been determined,[8] this value for Hf–EDTA has not been determined at higher acidity. Adloff[2] has discussed the potential of IPAC in the determination of stability constants. However, no such attempt has been made so far. In the present work, the sensitivity of the IPAC technique has been exploited in the study of complexation of hafnium(IV) with EDTA and the determination of its stability constant in 4.6 M $HClO_4$.

It is well known from IR data[9] that the Hf–EDTA complex contains four water molecules, of which, two are in the inner sphere and the remaining two are in the outer sphere. The thermal analysis of this complex revealed that at 160°C, 3.6 moles of water are lost. However, there are uncertainties regarding the structure of the complex after removal of the water molecules by heating. In the event of removing the water molecules from the inner sphere, the electronic distribution around the hafnium nucleus would change, resulting in a different EFG. Consequently, the angular correlation pattern would also be altered. To investigate these aspects a TDPAC study has been carried out with polycrystalline Hf–EDTA, before and after heating the sample at 160°C.

EXPERIMENTAL

Sample preparation

Neutron irradiated $HfOCl_2 \cdot 8H_2O$ was dissolved in 5 cm^3 of 6 M HCl to make the stock solution. 0.2 cm^3 aliquots of this solution were transferred to several glass ampoules of 3-mm diameter and dried

* Author to whom correspondence should be addressed.

under an IR lamp. Samples of different Hf : EDTA ratios were made by adding EDTA solutions of determined concentrations prepared in 4.6 M $HClO_4$ in these ampoules. The resultant clear solutions were kept overnight to ensure uniform mixing. These samples were checked for the coincidence of the 133–482 keV cascade at various angles, namely 90, 135 and 180°, using a set-up consisting of two $3'' \times 3''$ NaI(Tl) detectors coupled to a fast–slow coincidence circuit.

For TDPAC measurements Hf–EDTA crystals were prepared following the method described in ref. 9. Nearly 10 mg of inactive hafnium oxychloride was added to an irradiated sample and dissolved in 2 cm^3 of water. This solution was diluted with water to nearly 10 cm^3 and an equimolar quantity of Na_2EDTA was added to this solution with heating. A white precipitate appeared which vanished on further heating. The solution was then evaporated to nearly 1 cm^3 and cooled. The Hf–EDTA complex was crystallized by adding nearly 25 cm^3 of acetone and leaving the solution for 24 h. TDPAC counts were taken for this sample, before and after heating at 160°C, for 4 h at 90 and 180° angles using a set-up consisting of two $1\frac{1}{2}'' \times 1\frac{1}{2}''$ NaI(Tl) detectors coupled to a fast–slow coincidence circuit with a resolving time of 1.4 ns for the above cascade. Nearly 10,000 counts were collected in the peak position of the time spectrum. The detectors were kept at a distance of 14 cm away from the sample so that the solid angle correction was negligible.

RESULTS AND DISCUSSION

Integral measurements

The integral attenuation coefficients A_2G_2 were obtained from the coincidence counts using the formula

$$W(\theta) = 1 + A_2G_2P_2(\cos\theta) + A_4G_4P_4(\cos\theta), \quad (1)$$

where A_k values are the radiation parameters, G_k values are the attenuation factors and P_k values are the Legendre polynomials. The A_2G_2 values as a function of the Hf : EDTA ratio are plotted in Fig. 1. The figure shows that A_2G_2 decreases initially and saturates at a Hf : EDTA ratio close to unity, indicating the formation of a 1 : 1 complex. The stability constant of this complex was then obtained in the following way.

The stability constant of the complex MY in

$$M + Y \rightleftharpoons MY$$

is given by

$$K = [MY]/[M][Y]. \quad (2)$$

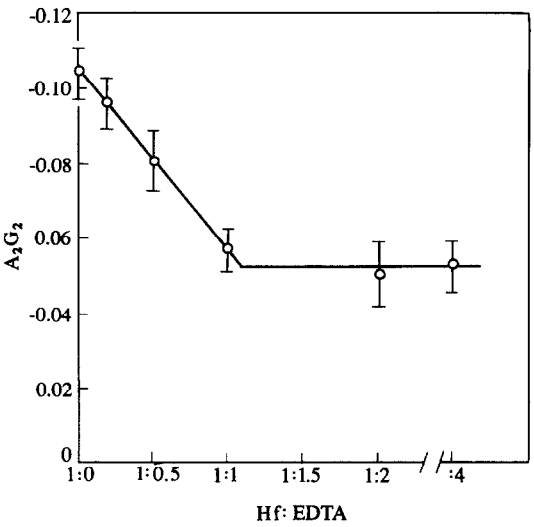

Fig. 1. A_2G_2 vs Hf : EDTA at 4.6 M $HClO_4$.

Alternatively,

$$K = f_A/f_F[Y], \quad (3)$$

where f_A and f_F are the fractions of the complex and the free metal ion, respectively, that is

$$f_A + f_F = 1. \quad (4)$$

For any intermediate value of Hf : Y, the observed attenuation factor can be written as

$$G_2 = f_AG_{2A} + f_FG_{2F}, \quad (5)$$

where G_{2A} and G_{2F} are the integral attentuation factors for the complex and the free metal ion, respectively. G_{2F} is the value of G_2 (Fig. 1) which corresponds to the case when no EDTA is present, and G_{2A} is the saturation value of G_2. f_A and f_F were obtained from eqs (4) and (5).

The free EDTA concentration, [Y], in the medium is obtained from the stepwise dissociation constants of EDTA and is given by

$$[Y] = ([H_4Y]_0 - f_A[M]_0) \Big/ \left(1 + \frac{[H^+]^6}{K_1K_2K_3K_4K_5K_6} + \frac{[H^+]^5}{K_1K_2K_3K_4K_5} + \frac{[H^+]^4}{K_1K_2K_3K_4} + \frac{[H^+]^3}{K_2K_3K_4} + \frac{[H^+]^2}{K_3K_4} + \frac{[H^+]}{K_4}\right), \quad (6)$$

where $[\ ]_0$ represents the initial concentration, and K_5 and K_6 are the dissociation constants for the protonated EDTA species. The dissociation constants for EDTA at the ionic strength (4.6) used in this experiment have been calculated from the extended Debye–Huckel theory using the parameters obtained by fitting the data from ref. 10.

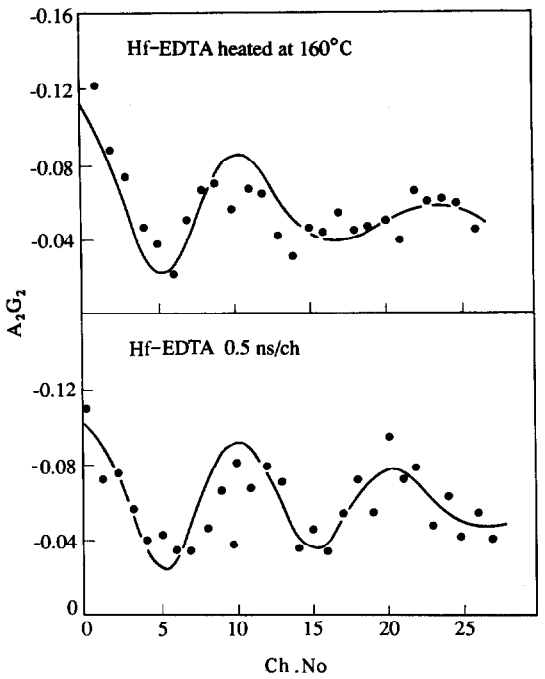

Fig. 2. Time differential perturbed angular correlation spectra for polycrystalline Hf–EDTA.

Substituting [Y] from eq. (6) and the values of f_A and f_F, we obtain the stability constant from eq. (3). The value of the stability constant thus obtained is: $\log K = 30.1 \pm 0.44$.

The present data is in good agreement with the literature data obtained by Caletka *et al.*[8] for Zr–EDTA. The data obtained by Intorre and Martell,[5] Tikhonova,[6] and Morgan and Justus[11] are lower than the present data. This may be attributed to hydrolysis of the metal ion at low acidity.

TDPAC measurements

The A_2G_2 values were obtained from the time spectra at 90 and 180° using expression (1), by neglecting the A_4G_4 term as its magnitude is insignificant compared to A_2G_2. TDPAC patterns for the Hf–EDTA complex, before and after heating at 160°C, are shown in Fig. 2. The continuous curve represents the least-square fit, from which the quadrupole interaction frequency (w_Q), the asymmetry parameter (η) and the width of the frequency distribution (δ) were obtained by using the following equation,[12]

$$G_2(t) = \sum_{n=0}^{3} S_{2n} \cos w_n t \, e^{-(1/2)\delta^2 w_n^2 t^2} \, e^{-(1/2)w_n^2 \tau^2}, \quad (7)$$

where w_ns are the frequencies of the transitions among the m states of the intermediate level. For $\eta = 0$, $w_1 = 6w_Q$, where

$$w_Q = eQV_{zz}/4I(2I-1)\hbar,$$

Q being the quadrupole moment of the intermediate state of spin, I, and V_{zz} is the electric field gradient (EFG). S_{2n} are the amplitudes of the corresponding transitions and are dependent on the asymmetry (η) of the EFG, and τ is the resolving time of the set-up.

Table 1. Time differential angular correlation data for the Hf–EDTA complex

Sample	w_Q (MHz)	η	δ (%)
Unheated	22.9 ± 0.6	0.80	5 ± 1
	21.7 ± 0.5[a]	0.86[a]	—
Heated	20.1 ± 0.6	0.70	9 ± 2

[a] From ref. 13.

Our data are presented in Table 1, along with the literature data for the unheated sample.[13] The quadrupole interaction frequencies for the two cases are almost the same. It is known from the thermal analysis[9] that on the average 3.6 molecules of water are lost at 160°C after prolonged heating. If this evaporation takes place from a single molecule of Hf–EDTA, then firstly, the eight-coordination of hafnium(IV) would have been disturbed and secondly, this would have changed the electron distribution around the hafnium nucleus drastically, resulting in a very different value of w_Q

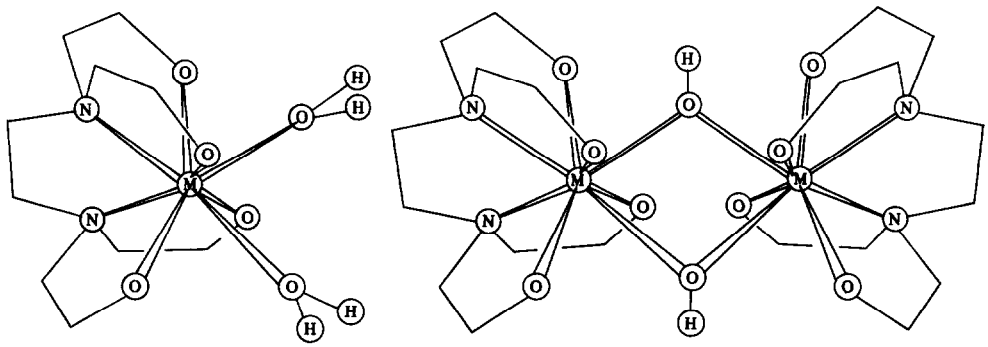

Fig. 3. Structures of monomeric and polymeric Hf–EDTA complexes.[14]

in the two cases. The close values of w_Q observed can be attributed to the probable partial polymerization through OH bridging, as suggested for the Th–EDTA complex[14] (see Fig. 3). This figure shows that the nature of the bonds and the coordination number of the metal ion in the complex, as well as in the polymeric species, remain practically unchanged. Thus the electron distribution around the hafnium nucleus remains almost unchanged, leading to a nearly constant w_Q.

Acknowledgements—The authors thank Shri J. K. Samuel for his help in setting up the PAC equipment. Thanks are also due to Dr P. R. Natarajan, Head, Radiochemistry Division, for his keen interest in this work.

REFERENCES

1. E. Heer and T. B. Novey, in *Solid State Physics* (Edited by F. Seitz and D. Turnbull), Vol. 9, p. 199. Academic Press, New York (1959).
2. J. P. Adloff, *Radiochim. Acta* 1978, **25**, 57.
3. H. H. Rinneberg, *Atom. Energy Rev.* 1978, **172**, 477.
4. A. Lerf and T. Butz, *Hyp. Int.* 1987, **36**, 275.
5. B. J. Intorre and A. E. Martell, *Inorg. Chem.* 1964, **3**, 81.
6. L. I. Tikhonova, *Russ. J. Inorg. Chem.* 1967, **12**, 494.
7. S. K. Das, B. S. Tomar and S. Prakash, *Radiochim. Acta* 1986, **40**, 213.
8. R. Caletka, M. Kyrs and J. Rais, *J. Inorg. Nucl. Chem.* 1964, **26**, 1443.
9. H. G. Langer, *J. Inorg. Nucl. Chem.* 1964, **26**, 59.
10. F. F. Carini and A. E. Martell, *J. Am. Chem. Soc.* 1952, **74**, 5745.
11. L. O. Morgan and N. L. Justus, *J. Am. Chem. Soc.* 1956, **78**, 38.
12. R. Beraud, I. Berkes, J. Daniere, G. Marest and R. Rougny, *Nucl. Inst. Meth.* 1969, **69**, 41.
13. J. Ch. Abbe and A. Marques Netto, *J. Inorg. Nucl. Chem.* 1975, **37**, 2239.
14. R. F. Bogucki and A. E. Martell, *J. Am. Chem. Soc.* 1958, **80**, 4170.

Polyhedron Vol. 9, No. 22, pp. 2709–2716, 1990
Printed in Great Britain

0277–5387/90 $3.00+.00
© 1990 Pergamon Press plc

PREPARATION AND PROPERTIES OF AMIDO HALIDE COMPLEXES OF NIOBIUM AND TANTALUM AND THEIR REACTIONS WITH ALKYNES

YUAN-WEI CHAO, SUZETTE POLSON* and DAVID E. WIGLEY†

Carl S. Marvel Laboratories of Chemistry, Department of Chemistry, University of Arizona, Tucson, AZ 85721, U.S.A.

(*Received* 16 *April* 1990; *accepted* 4 *July* 1990)

Abstract—A one-step procedure for the preparation of new mixed-amido halides of niobium and tantalum from their pentahalides and the trimethylsilylamine reagents, Me_3SiNR_2, is described. Thus, high yields of the monokis(amides), $M(NEt_2)Cl_4(OEt_2)$ (**1**, M = Ta; **2**, M = Nb), and the bis(amides), $Ta(NR_2)_2Cl_3(L)$ (**3**, R = Et, L = Et_2O; **4**, R = Et, L = THF; **5**, R = Me, L = THF), can be obtained by this procedure and crystallized as Et_2O or THF adducts. The dimeric niobium amide, $[Nb(NEt_2)_2Cl_3]_2$ (**6**), and the monomeric tris(amide), $Nb(NEt_2)_3Cl_2$ (**7**), are also prepared from Me_3SiNEt_2 and $NbCl_5$ in a single step, under the appropriate conditions. The use of Me_3SiNR_2 compounds as amidation reagents can be extended to prepare the alkoxide amides, $Ta(NEt_2)(DMP)Cl_3(OEt_2)$ (**8**), $Ta(NEt_2)(DIPP)Cl_3(OEt_2)$ (**9**) and $Ta(NEt_2)(DIPP)_2Cl_2(OEt_2)$ (**10**), from the addition of Me_3SiNEt_2 to solutions of the phenoxide compounds, $Ta(DMP)Cl_4(OEt_2)$, $Ta(DIPP)Cl_4(OEt_2)$ and $Ta(DIPP)_2Cl_3(OEt_2)$, respectively (DIPP = 2,6-diisopropylphenoxide, DMP = 2,6-dimethylphenoxide). Complex **10** can be further alkoxylated using $LiDIPP \cdot OEt_2$ to provide base-free $Ta(NEt_2)(DIPP)_3Cl$ (**11**). When **10** is reduced using two equivalents of NaHg in the presence of the appropriate alkyne, the adducts $(PhC{\equiv}CPh)Ta(NEt_2)(DIPP)_2$ (**12**), $(Me_3CC{\equiv}CH)Ta(NEt_2)(DIPP)_2$ (**13**) and $(Me_3SiC{\equiv}CMe)Ta(NEt_2)(DIPP)_2$ (**14**) are formed.

The *selective* preparation of simple amido halides, $M(NR_2)_xCl_y$, of the early transition metals has been difficult to achieve with amidolithium or -sodium reagents unless the ligand is extremely bulky.[1,2] Various strategies to prepare mixed-ligand compounds of smaller amides have been developed, including: (i) the exhaustive amidation of the metal halide, followed by the reaction of the resulting homoleptic complex with a halide source like Me_3SiCl;[3–5] (ii) redistribution reactions of homoleptic or partially substituted complexes;[6,7] and (iii) reactions of the halides with the secondary amine itself, which typically provide adducts $M(NR_2)_xCl_{5-x}(HNR_2)$.[8,9] The disadvantages of these approaches are that they require multiple steps from the pentachlorides or provide adducts in which the coordinated amine may not be labile.

The reaction of early metal halides with silylethers constitutes a convenient method to selectively *alkoxylate* the metal and provide mixed-alkoxy halides.[10–12] For example, Gibson has reported[10] the preparation of $[Nb(OR)Cl_4]_2$ (where R = Me, Et, $SiMe_3$) and we have prepared[11] $[Ta(OR)Cl_4]_2$ and $Ta(OR)Cl_4(OEt_2)$ (where OR = 2,6-dialkylphenoxides) in high yields from the reactions of the pentachlorides with the appropriate trimethylsilyl ethers, Me_3SiOR. Since these and related tantalum alkoxide derivatives are useful precursors to reactive tantalum(III) arene complexes,[11,13] and since π-donor ligands may be singularly important in defining the course of reaction of these compounds,[14,15] we have sought to prepare new amido halides of niobium and tantalum which may exhibit a similar reactivity.

* Participant, National Science Foundation—Research Experiences for Undergraduates, Department of Chemistry, University of Arizona (1989).

† Author to whom correspondence should be addressed.

Preparations of dialkylamido complexes of the groups 4–6 metals from silylamine reagents and metal halides are known,[16] but typically require the metal fluorides to exploit the formation of a strong Si—F bond (in byproduct Me_3SiF) as a driving force. In this paper, we report the preparation of new niobium and tantalum compounds of the form $M(NR_2)_xCl_{5-x}$, and extend these amidation reactions to include the preparation of alkoxide amides of the type $Ta(NR_2)(OR)_xCl_{4-x}$. The reductions of one of these derivatives, viz. $Ta(NEt_2)(DIPP)_2Cl_2(OEt_2)$ (DIPP = 2,6-diisopropylphenoxide), in the presence of alkynes is also reported.

RESULTS AND DISCUSSION

The transformations observed in this study are summarized in eqs (1)–(6) and in Scheme 1. Spectroscopic data for the compounds are given in the Experimental.

Monokis- and bis(amido) halide complexes

The need to develop routes to a number of *mixed* π-donor ligand complexes[14] has prompted us to explore the use of trimethylsilylamines as selective $-NR_2$ transfer reagents in group 5 chemistry. When one equivalent of Me_3SiNEt_2 reacts with $TaCl_5$ in diethyl ether, an immediate reaction ensues to provide solutions from which $Ta(NEt_2)Cl_4(OEt_2)$ (**1**) can be isolated in high yields, eq. (1). Based upon the single ν(Ta—Cl) mode in its

$$MCl_5 + 1\ Me_3SiNEt_2 \xrightarrow{Et_2O} \underset{\substack{1,\ M=Ta\\ 2,\ M=Nb}}{\text{N, Cl, Cl, M, Cl, Cl, O}} \quad (1)$$

far-IR spectrum and the *trans* isomers observed in the monokis-alkoxides, $Ta(OR)Cl_4(OEt_2)$,[11] $Ta(OSi[2\text{-}MeC_6H_4]_3)Cl_4(OEt_2)$[17] and $Ta(OPh)Cl_4L$ (L = pyridine or α-picoline),[18] **1** is formulated as a monomeric, *trans* structure. The analogous niobium complex can be isolated in high yield as purple crystals by the same route, eq. (1).

We have reported previously that excess Me_3SiNEt_2 reacts with $TaCl_5$ (in toluene–Et_2O) to provide dimeric $[Ta(NEt_2)_2Cl_3]_2$ in high yields.[14] This complex was observed to react with pyridine, which disrupted the dimeric structure and provided *cis,mer*-$Ta(NEt_2)_2Cl_3$(pyridine).[14] Oxygen donor solvents, viz. Et_2O or THF, also disrupt the dimeric structure to afford the six-coordinate, monomeric complexes, $Ta(NEt_2)_2Cl_3(OEt_2)$ (**3**) and $Ta(NEt_2)_2Cl_3(THF)$ (**4**) in good yields, eq. (2). Although $[Ta(NEt_2)_2Cl_3]_2$ is itself prepared in a toluene–Et_2O solution, simply removing all of the reaction vola-

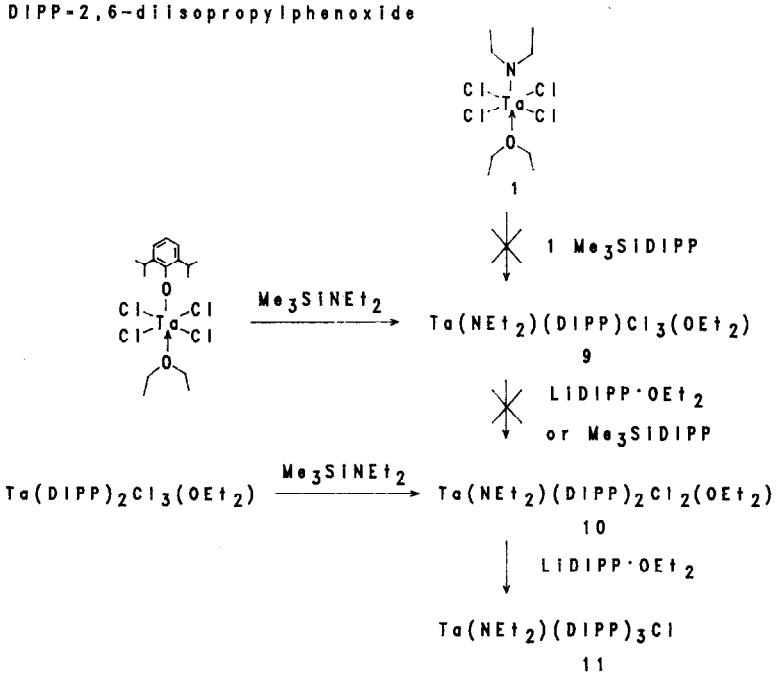

Scheme 1.

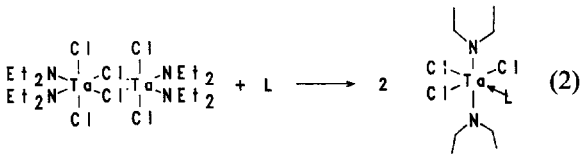

(2)

3, L-Et_2O
4, L-THF

tiles from this solution does not afford the etherate **3**.[14] However, by preparing solutions of this dimer in *neat* Et_2O and cooling them to −30°C, high yields of the monoetherate $Ta(NEt_2)_2Cl_3(OEt_2)$ (**3**) are obtainable. The dimethylamido analogue of **4**, viz. $Ta(NMe_2)_2Cl_3(THF)$ (**5**), is readily prepared in a single step from $TaCl_5$, Me_3SiNMe_2 and THF.

The structures of these complexes of the formula $Ta(NR_2)_2Cl_3$(O-donor) appear to differ from the analogous $Ta(NR_2)_2Cl_3$(N-donor) compounds such as $Ta(NEt_2)_2Cl_3$(pyridine)[14] or $Ta(NMe_2)_2Cl_3(HNMe_2)$.[3] The pyridine and dimethylamine adducts possess a *cis,mer* geometry, as manifested by inequivalent amide ligands in their ^1H and ^{13}C NMR spectra and by a structural determination of the latter complex.[3] The solution *equivalency* of the amide ligands in complexes **3** and **4** requires either the *fac* isomer, or the *trans,mer* geometry, as depicted in eq. (2). Single crystals of the etherate **3** were examined by X-ray crystallography.[19] Although the difference between N and O atoms in the ligands could not be unambiguously distinguished by crystallography, the *mer* arrangement of the NEt_2 and OEt_2 ligands was clearly established.[19] This crystallographic result, in concert with the NMR data, requires the *trans,mer* geometry for **3** as shown in reaction (2). Accordingly, the THF adducts **4** and **5** are also assigned as *trans,mer* structures.

Niobium amido halide complexes

We have extended the utility of this method to the preparation of the dialkyl amides of niobium. Reactions (3) and (4) summarize the syntheses of niobium bis(amide) (**6**) and tris(amide) (**7**) chlorides. Based upon the equivalent amide ligands of **6** in solution, and the presumed relation of this compound to its tantalum analogues, $[Ta(NEt_2)_2Cl_3]_2$[14] and $[Ta(NMe_2)_2Cl_3]_2$,[3] we assign the structure of **6** as shown in eq. (3). However,

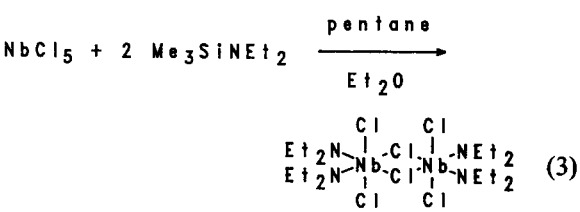

(3)

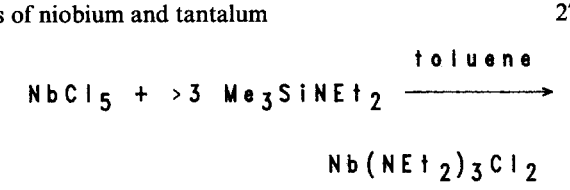

(4)

solution molecular weight measurements of **7** reveal a *monomeric* structure (calc. for monomer: 380. Found: 415 ± 40), unlike its dimeric tantalum analogue $[Ta(NMe_2)_3Cl_2]_2$ reported by Chisholm *et al.*[3] Thus, the equivalency of the diethylamido ligands (by ^1H and ^{13}C NMR spectroscopy) requires that either all three NEt_2 ligands occupy the equatorial positions of a trigonal bipyramid, or more likely, **7** exists as a fluxional five-coordinate structure in solution. Thus, by using the trimethylsilyl-based reagents, controlled amidation of $NbCl_5$ can be effected to afford $Nb(NEt_2)_nCl_{5-n}$ complexes for $n = 1$, 2 or 3.

Our earlier preparation of "base-free" monokis(alkoxides) $[Ta(DIPP)Cl_4]_2$ (DIPP = 2,6-di-isopropylphenoxide) and $[Ta(DMP)Cl_4]_2$ (DMP = 2,6-dimethylphenoxide)[11] prompted attempts to prepare their dialkylamido analogues $[Ta(NR_2)Cl_4]_2$. However, the reaction of $TaCl_5$ in CH_2Cl_2 or $CHCl_3$ solution resulted in the formation of brown solutions from which no tractable products could be isolated.

Amido alkoxides of tantalum

Mixed π-donor ligation may be useful for fine-tuning the reactivity of group 5 intermediates in reduction reactions,[14] therefore we have sought to extend these amidation reactions in order to prepare amido alkoxides. Thus, the monokis(alkoxide) $Ta(DMP)Cl_4(OEt_2)$[11] (DMP = 2,6-dimethylphenoxide) reacts with equimolar Me_3SiNEt_2 to afford $Ta(NEt_2)(DMP)Cl_3(OEt_2)$ (**8**) in *ca* 70% isolated yield, reaction (5). The structure of **8** is most

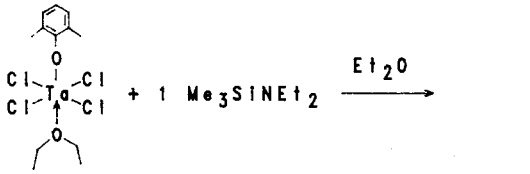

(5)

8

DMP-2,6-dimethylphenoxide

likely characterized by *mer*-chlorides, but whether the π-donor ligands are *trans* as in **3** and **4** or *cis* as in $Ta(NEt_2)_2Cl_3$(pyridine)[14] is not known.

We selected the DIPP compounds to extend this synthetic procedure to higher substituted phenoxide analogues as summarized in Scheme 1. Thus, both

$Ta(NEt_2)(DIPP)Cl_3(OEt_2)$ (**9**) and $Ta(NEt_2)(DIPP)_2Cl_2(OEt_2)$ (**10**) are readily prepared through the reactions of Me_3SiNEt_2 with $Ta(DIPP)Cl_4(OEt_2)$[11] and $Ta(DIPP)_2Cl_3(OEt_2)$,[11] respectively. However, compound **9** has not, in our hands, been prepared from the reaction of **1** with one equivalent of $Me_3SiDIPP$ or $LiDIPP \cdot OEt_2$ in Et_2O, although this preparative route would seem viable, Scheme 1. Likewise, $Ta(NEt_2)(DIPP)_3Cl$ (**11**) is not accessible through the reaction of the tantalum tris(phenoxide), $Ta(DIPP)_3Cl_2(OEt_2)$,[20] with Me_3SiNEt_2, however, **11** can be synthesized from the addition of $LiDIPP \cdot OEt_2$ to **10**, Scheme 1. Finally, compound **10** is not readily available from the reaction of **9** with either $LiDIPP \cdot OEt_2$ or $Me_3SiDIPP$ for reasons which are not readily apparent.

Reactions of amide complexes with alkynes

The reduction of $Ta(OR)_nCl_{5-n}$ complexes in the presence of alkynes may provide alkyne adducts,[14,21] metallacyclopentadienes[14,21] or arene complexes,[11,13] depending upon the nature of the π-donor ligands, including the steric constraints they may place upon the metal. The reactivity of these mixed-ligand compounds with alkynes was initiated with compound **10**, eq. (6). Thus, when **10** is

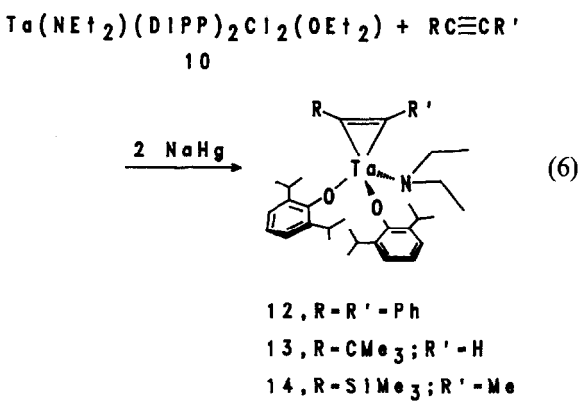

(6)

reduced using two equivalents of NaHg in the presence of the appropriate alkyne, the adducts $(PhC{\equiv}CPh)Ta(NEt_2)(DIPP)_2$ (**12**), $(Me_3CC{\equiv}CH)Ta(NEt_2)(DIPP)_2$ (**13**) and $(Me_3SiC{\equiv}CMe)Ta(NEt_2)(DIPP)_2$ (**14**) are formed. The $PhC{\equiv}CPh$ and $Me_3SiC{\equiv}CMe$ adducts, **12** and **14**, are readily isolated as crystalline solids, but $(Me_3CC{\equiv}CH)Ta(NEt_2)(DIPP)_2$ (**13**) has not been induced to crystallize, although remarkably clean NMR spectra have been obtained for this compound. In reactions of **10** with smaller alkynes such as $EtC{\equiv}CEt$, only intractable oils were obtained and no evidence for metallacyclopentadienes or higher cyclo-oligomers was obtained.

DISCUSSION

There are few *general* routes to mixed-ligand $M(\pi\text{-donor})_nCl_{5-n}$ complexes which will permit control over the extent of the π-donor substitution based upon anything other than the size of the ligand.[22] This trend has resulted in few early metal compounds $M(L)_x(L')_yCl_z$, where L and L′ are different π-donors. The need for a variety of d^2 "$Ta(\pi\text{-donor})_x$" moieties for use in carbon—carbon bond-forming reactions[23] has prompted the search to control the extent of substitution by *reagent selection* such that reactions with small ligands might be halted at the partially substituted stage. Our need for mixed-alkoxy halides has led to the completion of the series for the compounds $Ta(DIPP)_nCl_{5-n}$ (where $n = 1$–4) in yields of 50–85% which demonstrate this methodology, reactions (7)–(10). Additionally, the trimethylsilyl reagents provide more smooth, clean and controlled reactivity than is usually available from using the protic reagents (viz. HDIPP) which release HCl upon reaction. Therefore, with the precedent provided by the work of Gibson and co-workers,[10,12a] as well as these reactions, we have developed analogous routes to the preparation of new amido halides and amido alkoxides of the group 5 metals, using sterically innocuous amido ligands.

$$TaCl_5 + 1\,Me_3SiDIPP + Et_2O \longrightarrow Ta(DIPP)Cl_4(OEt_2)^{11} \quad (7)$$

$$TaCl_5 + 2\,Me_3SiDIPP \text{ or } 2\,LiDIPP \cdot OEt_2 \longrightarrow Ta(DIPP)_2Cl_3(OEt_2)^{11} \quad (8)$$

$$Ta(DIPP)_2Cl_3(OEt_2) + 1\,LiDIPP \cdot OEt_2 \longrightarrow Ta(DIPP)_3Cl_2(OEt_2)^{20a} \quad (9)$$

$$Ta(DIPP)_2Cl_3(OEt_2) + \text{excess } K^+DIPP^- \longrightarrow Ta(DIPP)_4Cl^{24} \quad (10)$$

We note that the mixed-ligand *fluorides* of niobium and tantalum, $M(NEt_2)_nF_{5-n}$ (for $n = 1$ or 2), have been prepared by Winfield and co-workers in a metathetical reaction between the pentafluorides and the trimethylsilylamine, Me_3SiNEt_2.[16d] However, the tris(amido) fluorides are not available by this route, as $M(NEt_2)_2F_3$ (M = Nb or Ta) are the highest substituted products arising from the reaction between $[MF_5]_4$ and neat Me_3SiNEt_2. Both $M(NEt_2)F_4$ and $M(NEt_2)_2F_3$ have been formulated as polymeric, fluoro-bridged structures based primarily upon their IR spectra.[16d]

EXPERIMENTAL

All experiments were performed under a nitrogen atmosphere either by standard Schlenk techniques[25] or in a Vacuum Atmospheres HE-493 drybox at room temperature (unless otherwise indicated). Solvents were purified under nitrogen by standard techniques[26] and transferred to the drybox without exposure to air. The "cold" solvents used to wash isolated solid products were cooled to *ca* −20°C before use. In all preparations, the Me_3SiNR_2 reagent was weighed (although both the weights and the volumes are recorded for convenience) and the reagent additions were carried out over a period of *ca* 1 min. In all complexes, DIPP = 2,6-diisopropylphenoxide and DMP = 2,6-dimethylphenoxide.

Tantalum(V) chloride and niobium(V) chloride (both resublimed) were purchased from Alfa and used as received. Me_3SiNMe_2 and Me_3SiNEt_2 were obtained from Petrarch and used as received. $Me_3SiDIPP$,[11] Me_3SiDMP,[11] $LiDIPP \cdot OEt_2$,[14] $Ta(DIPP)Cl_4(OEt_2)$,[11] $Ta(DMP)Cl_4(OEt_2)$,[11] $Ta(DIPP)_2Cl_3(OEt_2)$[11] and $[Ta(NEt_2)_2Cl_3]_2$[14] were prepared by our previously reported methods.

^1H (250 MHz) and ^{13}C (62.9 MHz) NMR spectra were recorded at probe temperature (unless otherwise specified) on a Bruker WM-250 spectrometer in C_6D_6 solvent. Chemical shifts (reported downfield of Me_4Si) are referenced internally to C_6D_6 *protio* solvent impurities (δ 7.15) or solvent ^{13}C resonances (δ 128.0). Routine coupling constants are not listed. IR spectra in the region of 600–180 cm^{-1} were recorded as CsI pellets on a Perkin–Elmer PE-983 spectrometer. Molecular weight measurements were determined by vapour pressure osmometry using a device similar to the one previously described.[27] All microanalytical samples were handled under nitrogen and were combusted with WO_3 (Desert Analytics, Tucson, Arizona).

$Ta(NEt_2)Cl_4(OEt_2)$ (1)

Neat Me_3SiNEt_2 (0.17 g, 0.23 cm^3, 1.19 mmol) was added dropwise to a solution of $TaCl_5$ (0.42 g, 1.19 mmol) in 20 cm^3 of diethyl ether. The solution immediately took on a yellow colour, which slowly changed to bright orange over 20 min. The best yields were obtained by allowing the reaction to stir at room temp. for 2 days. The solvent was then removed *in vacuo* to provide the product as an orange solid (0.49 g, 1.04 mmol, 87%) which was sufficiently pure for further reactions. This compound was recrystallized from a minimum volume of diethyl ether at −30°C to provide 0.39 g of analytically pure, orange, crystalline product (0.82 mmol, 79%). ^1H NMR (C_6D_6): δ 4.74 (q, 4 H, OCH_2CH_3), 4.08 (br, 4 H, NCH_2CH_3), 0.96. 0.87 (t, 6 H each, OCH_2CH_3 and NCH_2CH_3). ^{13}C NMR (C_6D_6): δ 67.3 (OCH_2CH_3), 51.1 (NCH_2CH_3), 12.4, 11.7 (OCH_2CH_3 and NCH_2CH_3). IR (CsI): ν(Ta—Cl) = 324 cm^{-1}. Found: C, 20.7; H, 4.4. Calc. for $C_8H_{20}Cl_4NOTa$: C, 20.5; H, 4.3%.

$Nb(NEt_2)Cl_4(OEt_2)$ (2)

To a sample of $NbCl_5$ (0.45 g, 1.70 mmol) dissolved in 15 cm^3 of diethyl ether was added, dropwise, Me_3SiNEt_2 (0.24 g, 0.31 cm^3, 1.70 mmol). Multiple colour changes occurred over 5 min, resulting finally in a purple solution. After stirring this solution for 10 h, the solvent was removed *in vacuo* to afford the product as a purple solid which was washed with pentane and dried *in vacuo*; yield 0.52 g (1.37 mmol, 80%). $Nb(NEt_2)Cl_4(OEt_2)$ obtained in this manner is sufficiently pure for further reactions, but can be recrystallized from diethyl ether at −30°C to yield 0.49 g (1.28 mmol or 76%) of purple crystals. ^1H NMR (C_6D_6): δ 4.50 and 4.10 (q, 4 H each, NCH_2CH_3 and OCH_2CH_3), 1.01 and 0.82 (t, 6 each, NCH_2CH_3 and OCH_2CH_3). ^{13}C NMR (C_6D_6): δ 67.2 (OCH_2CH_3), 55.8 (NCH_2CH_3), 12.4 and 10.3 (NCH_2CH_3 and OCH_2CH_3). IR (CsI): ν(Nb—Cl) = 342 cm^{-1}. Found: C, 25.1; H, 5.4. Calc. for $C_8H_{20}Cl_4NNbO$: C, 25.2; H, 5.3%.

$Ta(NEt_2)_2Cl_3(OEt_2)$ (3)

$[Ta(NEt_2)_2Cl_3]_2$ (0.60 g, 0.69 mmol) was dissolved in 10 cm^3 of diethyl ether and stored at −30°C for 24 h, over which time the etherate crystallized out in 74% yield (0.52 g). ^1H NMR (C_6D_6): δ 3.91 (q, 8 H, NCH_2CH_3), 3.38 (q, 4 H, OCH_2CH_3), 1.08 (t, 6 H, OCH_2CH_3), 0.88 (t, 12 H, NCH_2CH_3). ^{13}C NMR (C_6D_6): δ 65.8 (OCH_2CH_3), 46.5 (NCH_2CH_3), 14.4 (OCH_2CH_3), 12.0 (NCH_2CH_3). Found: C, 28.0; H, 6.2. Calc. for $C_{12}H_{30}Cl_3N_2OTa$: C, 28.5; H, 6.0%.

$Ta(NEt_2)_2Cl_3(THF)$ (4)

Excess THF (1.5 cm^3) was added to a slurry of $[Ta(NEt_2)_2Cl_3]_2$ (0.60 g, 0.69 mmol) in 10 cm^3 of pentane. An immediate reaction ensued to afford a clear, yellow–orange solution. After stirring this solution for 1 h, the reaction volatiles were removed *in vacuo* to yield the product as an orange solid. The product could be washed with cold Et_2O to provide 0.65 g (1.29 mmol, 94%) of $Ta(NEt_2)_2Cl_3(THF)$. The compound was recrystallized from diethyl ether at −30°C in 79% yield (0.54

g, 1.07 mmol). ^{1}H NMR (C_6D_6): δ 4.17 (q, 8 H, NCH_2CH_3), 3.99 (m, 4 H, $O(CH_2CH_2)_2$), 1.21 (m, 4 H, $O(CH_2CH_2)_2$), 1.00 (t, 12 H, NCH_2CH_3). ^{13}C NMR (C_6D_6): δ 73.6 (C_α, THF), 47.0 (NCH_2CH_3), 25.4 (C_β, THF), 11.7 (NCH_2CH_3). Found: C, 28.8; H, 5.6; Cl, 20.2. Calc. for $C_{12}H_{28}Cl_3N_2OTa$: C, 28.6; H, 5.6; Cl, 21.1%.

$Ta(NMe_2)_2Cl_3(THF)$ (**5**)

Neat Me_3SiNMe_2 (1.17 g, 1.53 cm^3, 10 mmol) was added to a solution of $TaCl_5$ (0.90 g, 2.51 mmol) in 20 cm^3 of toluene–diethyl ether (3 : 1), which formed an immediate red–orange colour. After stirring this mixture for 8 h, 2 cm^3 of THF were added, and the reaction volatiles were removed *in vacuo* to afford 0.94 g of the product as an orange powder (2.09 mmol, 84%). Analytically pure samples of $Ta(NMe_2)_2Cl_3(THF)$ were obtained as red crystals in 52% yield by crystallization from THF–pentane solution at −30°C. ^{1}H NMR (C_6D_6): δ 3.92 (m, 4 H, $O(CH_2CH_2)_2$), 3.81 (br s, 12 H, NCH_3), 1.16 (m, 4 H, $O(CH_2CH_2)_2$). ^{13}C NMR (C_6D_6): δ 74.0 (C_α, THF), 48.3 (NCH_3), 25.4 (C_β, THF). Found: C, 21.7; H, 4.6. Calc. for $C_8H_{20}Cl_3N_2OTa$: C, 21.5; H, 4.5%.

$[Nb(NEt_2)_2Cl_3]_2$ (**6**)

To a solution of $NbCl_5$ (0.40 g, 1.48 mmol) in 20 cm^3 of pentane–diethyl ether (1 : 1) was added neat Me_3SiNEt_2 (0.43 g, 0.56 cm^3, 2.96 mmol), which immediately produced a dark brown colour. After 70 min, the solution was filtered and the volatiles were removed from the filtrate *in vacuo* to afford 0.83 g of product as a red–brown solid (1.19 mmol, 80%). This compound was obtained analytically pure in 68% yield (0.69 g, 1.00 mmol of dimer) by recrystallizing from toluene–pentane solution at −30°C. ^{1}H NMR (C_6D_6): δ 3.72 (q, 8 H, NCH_2CH_3), 0.84 (t, 12 H, NCH_2CH_3). ^{13}C NMR (C_6D_6): δ 47.7 (NCH_2CH_3), 11.3 (NCH_2CH_3). Found: C, 28.0; H, 6.0; N, 8.0. Calc. for $C_8H_{20}Cl_3N_2Nb$: C, 28.0; H, 5.8; N, 8.1%.

$Nb(NEt_2)_3Cl_2$ (**7**)

To a stirred suspension of $NbCl_5$ (0.51 g, 1.89 mmol) in 15 cm^3 of toluene was added Me_3SiNEt_2 (1.09 g, 1.40 cm^3, 7.55 mmol), which resulted in a rapid reaction and the formation of a brown solution. After 2 h, the reaction volatiles were removed *in vacuo* to afford a brown solid which was extracted with a minimum of diethyl ether (*ca* 3 cm^3), filtered and the filtrate was cooled to −30°C. The yellow crystals of $Nb(NEt_2)_3Cl_2$ which formed (0.69 g, 0.91 mmol, 48%) were collected and dried *in vacuo*. ^{1}H NMR (C_6D_6): δ 3.83 (q, 12 H, NCH_2CH_3), 1.00 (t, 18 H, NCH_2CH_3). ^{13}C NMR (C_6D_6): δ 47.2 (NCH_2CH_3), 12.1 (NCH_2CH_3). Molecular weight (CH_2Cl_2 soln): Calc. for monomeric $Nb(NEt_2)_3Cl_2$: 380. Found: 415±40. Found: C, 38.1; H, 8.11; N, 11.0. Calc. for $C_{12}H_{30}Cl_2N_3Nb$: C, 38.1; H, 7.9; N, 11.1%.

$Ta(NEt_2)(DMP)Cl_3(OEt_2)$ (**8**)

To a stirred solution of $Ta(DMP)Cl_4(OEt_2)$ (0.77 g, 1.49 mmol) in 15 cm^3 of diethyl ether was added Me_3SiNEt_2 (0.22 g, 0.29 cm^3, 1.51 mmol). After 48 h, the solution was pumped to dryness to yield a yellow solid. This solid was dissolved in a minimum volume (*ca* 3 cm^3) of diethyl ether and the solution was cooled to −30°C to provide 0.59 g of the product as yellow crystals (1.07 mmol, 71%). ^{1}H NMR (C_6D_6): δ 6.87–6.69 (A_2B mult, 3 H, H_{aryl}), 4.44, 3.94 (q, 4 H each, NCH_2CH_3 and OCH_2CH_3), 2.61 (s, 6 H, $OC_6H_3Me_2$), 0.94, 0.86 (t, 6 H each, NCH_2CH_3 and OCH_2CH_3). ^{13}C NMR (C_6D_6): δ 158.3 (C_{ipso}), 130.8 (C_o), 129.3 (C_m), 124.7 (C_p), 66.3 (OCH_2CH_3), 51.8 (NCH_2CH_3), 18.6 ($OC_6H_3Me_2$), 12.4, 12.3 (OCH_2CH_3 and NCH_2CH_3). Found: C, 34.2; H, 5.3. Calc. for $C_{16}H_{29}Cl_3NO_2Ta$: C, 34.6; H, 5.3%.

$Ta(NEt_2)(DIPP)Cl_3(OEt_2)$ (**9**)

To a stirred solution of $Ta(DIPP)Cl_4(OEt_2)$ (0.76 g, 1.32 mmol) in 10 cm^3 of diethyl ether was added Me_3SiNEt_2 (neat) (0.21 g, 0.28 cm^3, 1.44 mmol). After 6 h, the solution was pumped to dryness, the resulting solid was extracted with 1 cm^3 of diethyl ether–pentane (1 : 1) and the solution cooled to −30°C. The yellow crystals of **9** which formed were collected and dried *in vacuo*; yield 0.41 g (0.67 mmol, 51%). ^{1}H NMR (C_6D_6): δ 7.10–6.89 (A_2B mult, 3 H, H_{aryl}), 4.47 (q, 4 H, NCH_2CH_3), 4.00 (spt, 2 H, $CHMe_2$), 3.93 (q, 4 H, OCH_2CH_3), 1.28 (d, 12 H, $CHMe_2$), 0.98, 0.90 (t, 6 H each, NCH_2CH_3 and OCH_2CH_3). ^{13}C NMR (C_6D_6): δ 155.0 (C_{ipso}), 141.3 (C_o), 125.5 (C_p), 124.7 (C_m), 66.2 (OCH_2CH_3), 51.3 (NCH_2CH_3), 26.4 ($CHMe_2$), 25.1 ($CHMe_2$), 12.5, 11.8 (NCH_2CH_3 and OCH_2CH_3). Found: C, 39.0; H, 6.2. Calc. for $C_{20}H_{37}Cl_3NO_2Ta$: C, 39.3; H, 6.1%.

$Ta(NEt_2)(DIPP)_2Cl_2(OEt_2)$ (**10**)

To a solution of $Ta(DIPP)_2Cl_3(OEt_2)$ (1.35 g, 0.46 cm^3, 1.88 mmol) in 15 cm^3 of diethyl ether was added Me_3SiNEt_2 (0.35 g, 0.47 cm^3, 2.41 mmol). After the solution was stirred for 2 h, it was filtered

and the volatiles removed from the filtrate *in vacuo*. Dissolving the resulting yellow solid in Et_2O and cooling the solution to $-30°C$ afforded 1.34 g (1.78 mmol, 94%) of yellow crystals of the product. ^1H NMR (C_6D_6): δ 7.19–6.94 (A_2B mult, 6 H, H_{aryl}), 4.26, 3.60 (q, 4 H each, NCH_2CH_3 and OCH_2CH_3), 4.07 (spt, 4 H, $CHMe_2$), 1.38 (d, 24 H, $CHMe_2$), 1.03 and 0.96 (t, 6 H each, NCH_2CH_3 and OCH_2CH_3). ^{13}C NMR (C_6D_6): δ 155.3 (C_{ipso}), 140.7 (C_o), 124.3 (C_m), 123.9 (C_p), 65.2 (OCH_2CH_3), 49.8 (NCH_2CH_3), 26.3 ($CHMe_2$), 25.4 ($CHMe_2$), 14.1, 10.6 (OCH_2CH_3 and NCH_2CH_3). Found: C, 52.5; H, 7.9. Calc. for $C_{36}H_{64}Cl_2NO_3Ta$: C, 52.3; H, 7.8%.

$Ta(NEt_2)(DIPP)_3Cl$ (**11**)

To a vigorously stirred solution of $Ta(NEt_2)(DIPP)_2Cl_2(OEt_2)$ (0.61 g, 0.81 mmol) in 15 cm^3 of diethyl ether was added solid $LiDIPP \cdot OEt_2$ (0.21 g, 0.81 mmol). After 8 h, the cloudy, pale yellow solution was filtered and the filtrate was pumped to dryness to afford a solid. Extraction of this solid with 3 cm^3 of Et_2O and cooling the solution to $-30°C$ afforded 0.41 g (0.50 mmol, 62%) of product as pale yellow crystals. ^1H NMR (C_6D_6): δ 7.09–6.89 (A_2B mult, 9 H, H_{aryl}), 4.07 (q, 4 H, NCH_2CH_3), 3.63 (spt, 6 H, $CHMe_2$), 1.20 (d, 36 H, $CHMe_2$), 1.01 (t, 6 H, NCH_2CH_3). ^{13}C NMR (C_6D_6): δ 156.7 (C_{ipso}), 138.9 (C_o), 123.9 (C_m), 123.8 (C_p), 50.6 (NCH_2CH_3), 27.2 ($CHMe_2$), 24.5 ($CHMe_2$), 14.9 (NCH_2CH_3). Found: C, 58.6; H, 7.6. Calc. for $C_{48}H_{61}ClNO_3Ta$: C, 58.6; H, 7.5%.

$(PhC{\equiv}CPh)Ta(NEt_2)(DIPP)_2$ (**12**)

To a solution of $Ta(NEt_2)(DIPP)_2Cl_2(OEt_2)$ (**10**) (0.44 g, 0.58 mmol) in 10 cm^3 of diethyl ether was added $PhC{\equiv}CPh$ (0.11 g, 0.60 mmol) and 0.5% NaHg amalgam (0.19 cm^3, 1.16 mmol). After this mixture was stirred for 10 h, the resulting pale yellow solution was filtered through Celite and the filtrate was pumped to dryness. Extracting the resulting solid with 1 cm^3 of pentane and cooling the extract to $-30°C$ afforded white crystals of **12** in 40% yield (0.17 g, 0.23 mmol). ^1H NMR (C_6D_6): δ 7.41 [pseudo d, 4 H, H_o (C_6H_5)], 7.12–6.94 [m, 12 H, H_{aryl} (DIPP) and H_m, H_p (C_6H_5)], 3.99 (q, 4 H, NCH_2CH_3), 3.56 (spt, 4 H, $CHMe_2$), 1.22 and 1.21 (overlapping d, 12 H each, $CHMe_2$), 0.98 (t, 6 H, NCH_2CH_3). ^{13}C NMR (C_6D_6): δ 214.6 (C_{alkyne}), 158.2 (C_{ipso}, DIPP), 142.6 (C_{ipso}, C_6H_5), 137.3 (C_o, DIPP), 128.7, 128.6 (C_o and C_m, C_6H_5), 127.7 (C_p, C_6H_5), 123.6 (C_m, DIPP), 122.5 (C_p, DIPP), 46.4 (NCH_2CH_3), 27.3 ($CHMe_2$), 23.9, 23.8 ($CHMe_2$), 15.0 (NCH_2CH_3). Found: C, 63.8; H, 7.1. Calc. for $C_{42}H_{54}NO_2Ta$: C, 64.2; H, 6.9%.

$(Me_3CC{\equiv}CH)Ta(NEt_2)(DIPP)_2$ (**13**)

To a solution of $Ta(NEt_2)(DIPP)_2Cl_2(OEt_2)$ (**10**) (0.44 g, 0.58 mmol) in 10 cm^3 of diethyl ether was added $Me_3CC{\equiv}CH$ (0.14 cm^3, 1.10 mmol) and 0.5% NaHg amalgam (0.19 cm^3, 1.16 mmol). After stirring this mixture for 8 h, the resulting yellow solution was filtered through Celite and the solvent removed *in vacuo* to afford the product as a yellow oil. The yield of **13** obtained in this reaction was 0.12 g (0.20 mmol, 34%). This compound has not been induced to crystallize, therefore no analyses were attempted. ^1H NMR (C_6D_6): δ 10.95 (s, 1 H; $HC{\equiv}CCMe_3$), 7.08–6.90 (A_2B mult, 6 H, H_{aryl}), 4.00 (q, 4 H, NCH_2CH_3), 3.40 (spt, 4 H, $CHMe_2$), 1.28 and 1.19 (d, 12 H each, $CHMe_2$), 1.09 (s, 9 H, $HC{\equiv}CCMe_3$), 1.06 (t, 6 H, NCH_2CH_3). ^{13}C NMR (C_6D_6): δ 232.4, 196.8 (C_{alkyne}), 157.9 (C_{ipso}), 136.9 (C_o), 123.4 (C_m), 122.2 (C_p), 48.1 (NCH_2CH_3), 30.9 (CMe_3), 27.0 ($CHMe_2$), 24.2, 23.6 ($CHMe_2$), 16.3 (NCH_2CH_3). The resonance for CMe_3 was not observed or is obscured by another signal.

$(Me_3SiC{\equiv}CMe)Ta(NEt_2)(DIPP)_2$ (**14**)

To a solution of $Ta(NEt_2)(DIPP)_2Cl_2(OEt_2)$ (**10**) (0.51 g, 0.62 mmol) in 10 cm^3 of diethyl ether was added $Me_3SiC{\equiv}CMe$ (0.13 g, 1.24 mmol) and 0.5% NaHg amalgam (0.42 cm^3, 1.24 mmol). After this solution was stirred for 8 h, the resulting pale yellow mixture was filtered through Celite and the filtrate was pumped to dryness. Extracting the resulting solid with *ca* 2 cm^3 of pentane and cooling the extract to $-30°C$ afforded the product as pale yellow crystals; yield 0.22 g (0.31 mmol, 45%). ^1H NMR (C_6D_6): δ 7.09–6.90 (A_2B mult, 6 H, H_{aryl}), 3.91 (q, 4 H, NCH_2CH_3), 3.33 (spt, 4 H, $CHMe_2$), 3.01 (s, 3 H, $Me_3SiC{\equiv}CMe$), 1.29, 1.19 (d, 12 H each, $CHMe_2$), 1.03 (t, 6 H, NCH_2CH_3), 0.05 (s, 9 H, $Me_3SiC{\equiv}CMe$). ^{13}C NMR (C_6D_6): δ 230.7, 220.3 (C_{alkyne}), 158.2 (C_{ipso}), 136.8 (C_o), 123.4 (C_m), 122.0 (C_p), 48.4 (NCH_2CH_3), 27.2 ($CHMe_2$), 24.6 ($Me_3SiC{\equiv}CMe$), 23.9, 23.6 ($CHMe_2$), 15.6 (NCH_2CH_3), 0.3 ($Me_3SiC{\equiv}CMe$). Found: C, 55.9; H, 7.8. Calc. for $C_{34}H_{56}NO_2SiTa$: C, 56.7; H, 7.8%.

Acknowledgements—We wish to acknowledge the National Science Foundation for support of this research (CHE-8919367), the Department of Chemistry of the University of Arizona for partial support of this work, and Mr Scott T. Haubrich for the initial preparation of $Nb(NEt_2)Cl_4(OEt_2)$.

REFERENCES

1. (a) D. C. Bradley, M. B. Hursthouse, K. M. A. Malik and G. B. C. Vuru, *Inorg. Chim. Acta* 1980, **44**, L5; (b) D. C. Bradley, M. B. Hursthouse, K. M. Abdul Malik, A. J. Nielson and G. B. Chota Vuru, *J. Chem. Soc., Dalton Trans.* 1984, 1069; (c) C. Airoldi, D. C. Bradley, H. Chudzynska, M. B. Hursthouse, K. M. A. Malik and P. R. Raithby, *J. Chem. Soc., Dalton Trans.* 1980, 2010; (d) R. A. Andersen, *Inorg. Chem.* 1979, **18**, 3622; (c) R. A. Andersen, *Inorg. Chem.* 1979, **18**, 1724; (f) R. A. Andersen, *Inorg. Chem.* 1979, **18**, 2928.
2. For the preparation and structures of homoleptic amides of niobium and tantalum, see: (a) D. C. Bradley and I. M. Thomas, *Can. J. Chem.* 1962, **40**, 1355; (b) D. C. Bradley and I. M. Thomas, *Can. J. Chem.* 1962, **40**, 449; (c) D. C. Bradley and M. H. Gitlitz, *J. Chem. Soc. A* 1969, 980; (d) C. Heath and M. B. Hursthouse, *J. Chem. Soc., Chem. Commun.* 1971, 143.
3. M. H. Chisholm, J. C. Huffman and L.-S. Tan, *Inorg. Chem.* 1981, **20**, 1859.
4. (a) M. Akiyama, M. H. Chisholm, F. A. Cotton, M. W. Extine and C. A. Murillo, *Inorg. Chem.* 1977, **16**, 2407; (b) H. Bürger and K. Wiegel, *J. Organomet. Chem.* 1977, **124**, 279.
5. This method is often used in the preparation of mixed-alkoxy halides of the early metals. See: D. C. Bradley, R. C. Mehrotra and D. P. Gaur, *Metal Alkoxides*. Academic Press, London (1978).
6. See, for example: (a) E. C. Alyea, D. C. Bradley, M. F. Lappert and A. R. Sanger, *J. Chem. Soc., Chem. Commun.* 1969, 1064; (b) M. F. Lappert and A. R. Sanger, *J. Chem. Soc. A* 1971, 874; (c) H. Bürger and C. Kluess, *J. Organomet. Chem.* 1976, **108**, 69; (d) J. S. Basi, D. C. Bradley and M. H. Chisholm, *J. Chem. Soc. A* 1971, 1433.
7. M. H. Chisholm, L.-S. Tan and J. C. Huffman, *J. Am. Chem. Soc.* 1982, **104**, 4879.
8. (a) G. W. A. Fowles and C. M. Pleass, *J. Chem. Soc.* 1957, 1674; (b) G. W. A. Fowles and C. M. Pleass, *J. Chem. Soc.* 1957, 2078; (c) P. J. H. Carnell and G. W. A. Fowles, *J. Less-Common Met.* 1962, **4**, 40; (d) P. J. H. Carnell and G. W. A. Fowles, *J. Chem. Soc.* 1959, 4113; (e) P. A. Bates, A. J. Nielson and J. M. Waters, *Polyhedron* 1985, **4**, 1391.
9. Acetamide and thioacetamide compounds of the group 5 metals can arise from the insertion of isocyanates and isothiocyanates into metal–carbon bonds. See, for example: (a) M. G. B. Drew and J. D. Wilkins, *J. Chem. Soc., Dalton Trans.* 1974, 198; (b) J. D. Wilkins, *J. Organomet. Chem.* 1974, **65**, 383; (c) J. D. Wilkins, *J. Organomet. Chem.* 1974, **67**, 269.
10. V. C. Gibson, T. P. Kee and A. Shaw, *Polyhedron* 1988, **7**, 2217.
11. D. J. Arney, P. A. Wexler and D. E. Wigley, *Organometallics* 1990, **9**, 1282.
12. (a) V. C. Gibson and T. P. Lee, *J. Chem. Soc., Chem. Commun.* 1989, 656; (b) L. B. Handy, K. G. Sharp and F. F. Brinckman, *Inorg. Chem.* 1972, **11**, 523.
13. P. A. Wexler and D. E. Wigley, *J. Chem. Soc., Chem. Commun.* 1989, 664.
14. Y.-W. Chao, P. A. Wexler and D. E. Wigley, *Inorg. Chem.* 1989, **28**, 3860.
15. (a) M. A. Bruck, A. S. Copenhaver and D. E. Wigley, *J. Am. Chem. Soc.* 1987, **109**, 6525; (b) K. R. Ballard, I. M. Gardiner and D. E. Wigley, *J. Am. Chem. Soc.* 1989, **111**, 2159.
16. (a) A. Majid, R. R. McLean, D. W. A. Sharp and J. M. Winfield, *Z. Anorg. Chem.* 1971, **385**, 85; (b) H. Bürger and H.-J. Neese, *Z. Anorg. Chem.* 1969, **365**, 243; (c) H. Bürger and H.-J. Neese, *Z. Anorg. Chem.* 1969, **370**, 275; (d) J. C. Fuggle, D. W. A. Sharp and J. M. Winfield, *J. Chem. Soc., Dalton Trans.* 1972, 1766.
17. S. G. Bott and A. C. Sullivan, *J. Chem. Soc., Chem. Commun.* 1988, 1577.
18. K. C. Malhotra, U. K. Banerjee and S. C. Chaudhry, *J. Ind. Chem. Soc.* 1980, **57**, 868.
19. M. A. Bruck, unpublished results.
20. (a) J. R. Strickler, M. A. Bruck, P. A. Wexler and D. E. Wigley, *Organometallics* 1990, **9**, 266; (b) G. R. Clark, A. J. Nielson and C. E. F. Rickard, *Polyhedron* 1987, **6**, 1765.
21. J. R. Strickler, P. A. Wexler and D. E. Wigley, *Organometallics* 1988, **7**, 2067.
22. L. R. Chamberlain, I. P. Rothwell and J. C. Huffman, *Inorg. Chem.* 1984, **23**, 2575.
23. See, for example: (a) L. R. Chamberlain, I. P. Rothwell and J. C. Huffman, *J. Chem. Soc., Chem. Commun.* 1986, 1203; (b) L. R. Chamberlain, L. D. Durfee, P. E. Fanwick, L. M. Kobriger, S. L. Latesky, A. K. McMullen, B. D. Steffey, I. P. Rothwell, K. Folting and J. C. Huffman, *J. Am. Chem. Soc.* 1987, **109**, 6068; (c) B. D. Steffey, R. W. Chesnut, J. L. Kerschner, P. J. Pellechia, P. E. Fanwick and I. P. Rothwell, *J. Am. Chem. Soc.* 1989, **111**, 378; (d) K. C. Wallace, J. C. Dewan and R. R. Schrock, *Organometallics* 1986, **5**, 2162; (e) K. C. Wallace and R. R. Schrock, *Macromolecules* 1987, **20**, 448.
24. Y.-W. Chao, D. P. Smith and D. E. Wigley, manuscript in preparation. [We note that $Ta(DIPP)_4Cl$ can also be prepared from the slow reaction of $TaCl_5$ and excess $LiDIPP \cdot OEt_2$ in benzene–Et_2O solution (cf. ref. 22).]
25. D. F. Shriver and M. A. Drezdzon, *The Manipulation of Air-sensitive Compounds*, 2nd edn. John Wiley, New York (1986).
26. D. D. Perrin and W. L. F. Armarego, *Purification of Laboratory Chemicals*, 3rd edn. Pergamon Press, Oxford (1988).
27. B. J. Burger and J. E. Bercaw, in *Experimental Organometallic Chemistry* (Edited by A. L. Wayda and M. Y. Darensbourg). ACS Symp. Ser. 357, Washington, D. C. (1987).

Polyhedron Vol. 9, No. 22, pp. 2717–2720, 1990
Printed in Great Britain

0277-5387/90 $3.00+.00
©1990 Pergamon Press plc

PREPARATION AND ^{199}Hg NMR STUDY OF SOME MERCURY(II) THIOLATE COMPLEXES

LAURENCE CARLTON* and DAVID WHITE

Department of Chemistry, University of the Witwatersrand, Johannesburg, Republic of South Africa

(*Received* 14 *March* 1990; *accepted* 5 *July* 1990)

Abstract—Mercury-199 NMR parameters are reported for the complexes $Hg(SPr^i)_2$, $Hg(SPh)_2$, $Hg(SCH_2CH_2OH)_2$, $Hg(SCH_2CO_2H)_2$, $Hg(SCH_2CH_2CO_2H)_2$ and $Hg(Sbt)_2$ (Sbt = benzthiazole-2-thiolate) which are readily prepared in moderate to good yield by the reaction of HgO with the free thiol. The ^{199}Hg chemical shift of $Hg(SPr^i)_2$ in a variety of solvents falls in a range −723 to −884 ppm; possible modes of interaction of the solvent with the metal are discussed.

The properties of mercury thiolate complexes are relevant to the study of biochemical systems that interact with the metal[1–3] and the development of antidotes to mercury poisoning.[4–6] Mercury-199 NMR spectroscopy has a potentially useful contribution to make in these areas but, as yet, few studies have reported ^{199}Hg NMR data.[7]

The isotope ^{199}Hg, spin 1/2, occurs in 16.84% natural abundance; relaxation processes (principally chemical shift anisotropy[8] at high magnetic field strengths) are effective and NMR data acquisition can be fairly rapid. The sensitivity of the ^{199}Hg nucleus to changes in its chemical environment is reflected in the observed chemical shift range of over 3000 ppm.[9] This makes ^{199}Hg NMR well suited to the detection of changes in the bonding and conformation of mercury complexes.

EXPERIMENTAL

Reagents were obtained from various sources and used without further purification. THF, pyrrolidine, benzene and toluene were distilled from sodium, dichloromethane was distilled from phosphorus pentoxide, acetone was distilled from potassium carbonate, pyridine, pyrrole, DMF, acetonitile and ether were distilled from calcium hydride and DMSO, n-hexane, isopropylamine, diisopropylamine and triethylamine were dried over calcium hydride. Other solvents were of the highest available purity and used without further treatment. Complexes were prepared under nitrogen.

NMR spectra were recorded at 22°C on a Bruker AC 200 FT spectrometer operating at 200.13 MHz (^{1}H), 50.32 MHz (^{13}C) and 35.84 MHz (^{199}Hg). ^{199}Hg spectra were obtained using a spectral width of 50,000 Hz and acquisition time of 0.33 s.

Preparation of $Hg(SPr^i)_2$[10]

A mixture of mercuric oxide (3.22 g, 14.9 mmol) and isopropyl thiol (2.26 g, 30 mmol) in dichloromethane (80 cm^3) at room temperature was stirred for 2 days. The solution was concentrated and an excess of hexane was added. On standing at −20°C for 12 h bis(isopropylthiolato)mercury was obtained as colourless needles (3.81 g, 10.9 mmol, 73%) Found: C, 20.0; H, 4.0. $C_6H_{14}HgS_2$ requires: C, 20.5; H, 4.0%. ^{1}H NMR (DMSO) δ 3.57 (sept, 1H, J 6.6 Hz), 1.31 (d, 6H, J 6.6 Hz). ^{13}C NMR (DMSO) δ 33.9, 31.0 ppm.

Preparation of $Hg(SPh)_2$[5]

A mixture of mercuric oxide (6.44 g, 29.8 mmol) and thiophenol (6.55 g, 60 mmol) in ethanol (80 cm^3) at room temperature was stirred for 12 h. The product was collected in a sinter, washed with ethanol and dried *in vacuo* to give bis(phenylthiolato)mercury as a white powder (10.51 g, 25.1 mmol, 84%) Found: C, 33.7; H, 2.3. $C_{12}H_{10}HgS_2$ requires: C, 34.4; H, 2.4%. ^{1}H NMR (DMSO) δ

* Author to whom correspondence should be addressed.

7.36 (mult, 2H), 7.11 (mult, 3H). ^{13}C NMR (DMSO) δ 136.9, 131.5, 128.4, 124.5 ppm.

Preparation of $Hg(SCH_2CH_2OH)_2$

A mixture of mercuric oxide (3.22 g, 14.9 mmol) and 2-mercaptoethanol (2.33 g, 30 mmol) in ethanol (80 cm^3) at room temperature was stirred for 12 h. The product was collected in a sinter, washed with ethanol and dried *in vacuo* to give bis(2-hydroxyethanethiolato)mercury as a white powder (1.61 g, 4.5 mmol, 31%) Found: C, 13.0; H, 2.8. $C_4H_{10}HgO_2S_2$ requires: C, 13.5; H, 2.8%. ^{1}H NMR (DMSO) δ 5.24 (s, 1H) 3.33 (t, 3H, *J* 5.9 Hz), 2.87 (t, 3H, *J* 5.9 Hz). ^{13}C NMR (DMSO) 63.3, 30.2 ppm.

Preparation of $Hg(SCH_2CO_2H)_2$[11]

A mixture of mercuric oxide (3.22 g, 14.9 mmol) and thioglycolic acid (2.78 g, 30 mmol) in ethanol (80 cm^3) at room temperature was stirred for 12 h. The product was collected in a sinter, washed with ethanol and dried *in vacuo* to give bis(acetic acid thiolato)mercury as a white powder (5.40 g, 14.1 mmol, 95%) Found: C, 12.7; H, 1.7. $C_4H_6HgO_4S_2$ requires: C, 12.6; H, 1.6%. ^{1}H NMR (DMSO) δ 11.75 (s, 1H) 3.67 (s, 2H). ^{13}C NMR (DMSO) δ 175.5, 29.4 ppm.

Preparation of $Hg(SCH_2CH_2CO_2H)_2$

A mixture of mercuric oxide (3.22 g, 14.9 mmol) and 3-mercaptopropionic acid (3.20 g, 30 mmol) in dichloromethane (80 cm^3) at room temperature was stirred for 12 h. The product was collected in a sinter, washed with dichloromethane and dried *in vacuo* to give bis(propionic acid-3-thiolato)mercury as a white powder (1.71 g, 4.2 mmol, 28%). Found: C, 16.9; H, 2.4. $C_6H_{10}HgO_4S_2$ requires: C, 17.5; H, 2.5%. ^{1}H NMR (DMSO) δ 12 (broad, 1H), 3.05 (t, 2H, *J* 6.8 Hz), 2.56 (t, 2H, *J* 6.8 Hz). ^{13}C NMR (DMSO) δ 174.1, 39.4, 22.1 ppm.

Preparation of $Hg(Sbt)_2$

A mixture of mercuric oxide (3.22 g, 14.9 mmol) and benzthiazole-2-thiol (4.98 g, 30 mmol) in dichloromethane at room temperature was stirred for 3 days. The product was collected in a sinter, washed with dichloromethane and dried *in vacuo* to give bis(benzthiazole-2-thiolato)mercury as a white powder (6.4 g, 12.0 mmol, 81%). Found: C, 29.8; H, 1.5; N, 4.9. $C_{14}H_8HgN_2S_4$ requires: C, 31.5; H, 1.5; N, 5.3%. ^{1}H NMR (DMSO) 7.88 (mult, 1H), 7.61 (mult, 1H), 7.30 (mult, 2H). ^{13}C NMR (DMSO) δ 167.5, 152.7, 137.0, 125.9, 123.8, 121.1, 120.0 ppm.

RESULTS AND DISCUSSION

The complexes $Hg(SR)_2$ are readily prepared in moderate to good yield by the reaction of HgO with the free thiol in dichloromethane or ethanol at room temperature. $Hg(SPr^i)_2$ is soluble in all common solvents except water while $Hg(SPh)_2$, $Hg(SCH_2CH_2OH)_2$, $Hg(SCH_2CO_2H)_2$, $Hg(SCH_2CH_2CO_2H)_2$ and $Hg(Sbt)_2$ are soluble only in DMSO and DMF.

Mercury-199 chemical shifts (Table 1) for the complexes in DMSO solution are found in the range -882 to -1206 ppm relative to $HgMe_2$. This upfield shift may result from the involvement of sulphur lone pair electrons in bonding to the metal. No spin–spin coupling is observed between ^{199}Hg and either hydrogen or ^{13}C, and all ^{199}Hg resonance lines appear as singlets.

From the similarity in the chemical shifts of $Hg(SPr^i)_2$ and $Hg(SCH_2CH_2OH)_2$ it is clear that in the latter the influence of the OH group over four bonds is negligible. For $Hg(SCH_2CH_2CO_2H)_2$, with carboxyl groups positioned a similar distance from the metal, the upfield shift of over 70 ppm relative to $Hg(SPr^i)_2$ must arise from diamagnetic through space shielding by the carbonyls. The closer proximity of the carbonyls to the metal in $Hg(SCH_2CO_2H)_2$ causes a further upfield shift. With aromatic rings positioned at a distance of two bonds from the metal in $Hg(SPh)_2$ and $Hg(Sbt)_2$, the effects of diamagnetic shielding are more pronounced, amounting in the case of Hg(Sbt) to an upfield shift of 324 ppm relative to $Hg(SPr^i)_2$.

Table 1. Mercury-199 spectral data for the complexes $Hg(SR)_2$[a]

	δ Hg[b]	$\nu_{1/2}$[c]	T_1 (Hg)[d]
$Hg(SCH_2CH_2OH)_2$	-882	15	0.10
$Hg(SPr^i)_2$	-884	5	0.15
$Hg(SCH_2CH_2CO_2H)_2$	-959	20	0.06
$Hg(SCH_2CO_2H)_2$	-985	65	0.07
$Hg(SPh)_2$	-1112	7.5	0.11
$Hg(Sbt)_2$	-1206	95	0.06

[a] Solvent DMSO: DMSO-d_6 ($\sim$ 20:1), concentration 0.1 M, temperature 22°C, 400–2400 transients recorded from each.

[b] Chemical shifts in ppm from neat $HgMe_2$ (external standard), negative values to high field.

[c] Line widths at half height in hertz.

[d] Spin–lattice relaxation times in seconds.

Table 2. The ^{199}Hg chemical shift of $Hg(SPr^i)_2$ in various solvents[a]

Solvent	δ Hg	Solvent	δ Hg	Solvent	δ Hg
Dimethylsulphoxide	−884	Pyrrole	−828	Diethyl ether	−789
Dimethylformamide	−871	Acetic acid	−822	Toluene	−783
Tetrahydrofuran	−845	Isopropanol[b]	−804	Benzene	−783
Acetonitrile	−836	Dichloromethane	−800	n-Hexane	−779
Methanol[b]	−834	Chloroform	−797	Diisopropylamine	−749
Nitromethane[b]	−834	Furan	−795	Pyrrolidine	−745
Acetone	−832	Thiophene	−794	Triethylamine	−733
Pyridine	−832	Isopropyl thiol	−791	Isopropylamine	−723

[a] Chemical shifts in ppm from neat $HgMe_2$ (external standard), negative values to high field; concentration 0.1 M; temperature 22°C.

[b] ~ 0.05 M (saturated).

Spin–lattice relaxation times, measured by the inversion-recovery method, are short and fall in a narrow range of 0.06–0.15 s. The dominant relaxation effects are likely to be spin-rotation and chemical shift anisotropy.[12] The broadening of the resonance lines of $Hg(SCH_2CO_2H)_2$ and $Hg(Sbt)_2$ suggests that in these compounds spin–spin relaxation processes are also operating; these might be expected to arise from conformational changes involving restricted rotation about the Hg—S or S—C bonds.

The ^{199}Hg chemical shift of $Hg(SPr^i)_2$ in a variety of solvents is shown in Table 2 and appears (with the exception of measurements in THF and methanol) to fall into four groups according to the nature of the solvent: (i) O- and N-donors in which the donor atom is involved in π-bonding (δ −822 to −884); (ii) O- and S-donors in which the donor atom is not π-bonded, Cl-donors (δ −789 to −804); (iii) aliphatic and aromatic hydrocarbons (δ −779 to −783); (iv) aliphatic amines (δ −723 to −749). Groups (i)–(iii) follow an order of decreasing dipole moment but the position of group (iv) on this scale is clearly anomalous. If the coordinating properties of hexane and its contribution to the ^{199}Hg chemical shift can be regarded as minimal (as found for $HgMe_2$[12]) it is possible to draw a number of conclusions.

The interaction between the solvents of group (i) and mercury favours an overall diamagnetic shielding by π-bonded groups of the solvent, i.e. the chemical shifts (relative to that measured in hexane) can be attributed to effects of solvent magnetic anisotropy. The fact that the increasing upfield shift roughly parallels the increase in dipole moment of the solvent suggests that electrostatic forces are involved in the ordering of the solvent in the region close to the metal.

Solvents of group (ii) provide a small diamagnetic shielding while for those of group (iii) there is no significant shielding. The data provide no evidence for an interaction of the π systems of benzene and toluene with the metal; the chemical shift in these solvents is only marginally different from that observed in hexane. This contrasts with the finding of Sens *et al.*[12] for dimethyl mercury, where a shift to high field of 56 ppm was observed on changing from hexane to benzene. The presence of sulphur would seem to discourage the interaction of the metal with the aromatic π system of a non-polar hydrocarbon.

Solvents of group (iv) contribute an overall paramagnetic shielding which is likely to arise from the mixing of atomic orbitals (i.e. nitrogen lone pair and mercury 6*p*) induced by a Lewis acid–base interaction.

Acknowledgement—We thank the University of the Witwatersrand for financial support.

REFERENCES

1. G. A. Neville and T. Drakenberg, *Can. J. Chem.* 1974, **52**, 616.
2. P. G. Schultz, K. G. Au and C. T. Walsh, *Biochemistry* 1985, **24**, 6840.
3. S. M. Miller, D. P. Ballou, V. Massey, C. H. Williams and C. T. Walsh, *J. Biol. Chem.* 1986, **261**, 8081.
4. G. Pouskouleli, P. Kourounakis and T. Theophanides, *Inorg. Chim. Acta* 1977, **24**, 45.
5. A. J. Canty and R. Kishimoto, *Inorg. Chim. Acta* 1977, **24**, 109.
6. D. L. Rabenstein, A. P. Arnold and R. D. Guy, *J. Inorg. Biochem.* 1986, **28**, 279.
7. G. K. Carson and P. A. W. Dean, *Inorg. Chim. Acta* 1982, **66**, 157.

8. J. D. Kennedy and W. McFarlane, *J. Chem. Soc. Faraday II* 1976, **72**, 1653.
9. R. Garth Kidd and R. J. Goodfellow, in *NMR and the Periodic Table* (Edited by R. K. Harris and B. Mann), p. 266. Academic Press, London (1978).
10. E. Wertheim, *J. Am. Chem. Soc.* 1929, **51**, 3661.
11. W. Stricks, I. M. Kolthoff and A. Heyndrickx, *J. Org. Chem.* 1954, **76**, 1515.
12. M. A. Sens, N. K. Wilson, P. D. Ellis and J. D. Odom, *J. Magn. Reson.* 1975, **19**, 323.

Polyhedron Vol. 9, No. 22, pp. 2721–2726, 1990
Printed in Great Britain

0277–5387/90 $3.00+.00
© 1990 Pergamon Press plc

THE PREPARATION OF THE NEW COMPARTMENTAL LIGAND 1-(2-HYDROXYPHENYL)-3-(2-THIOMETHOXYPHENYL)-1,3-PROPANEDIONE AND ITS INTERACTIONS WITH METAL IONS

U. RUSSO, M. VIDALI and B. ZARLI*

Dipartimento di Chimica Inorganica, Metallorganica e Analitica, Via Loredan, 4-35131, Padova, Italy

(*Received* 21 *May* 1990; *accepted* 5 *July* 1990)

Abstract—The preparation of the ligand 1-(2-hydroxyphenyl)-3-(2-thiomethoxyphenyl)-1,3-propanedione (H_2htmp) is reported along with its physicochemical characterization. The compound is present in the solid state as an unique enol tautomer, while in solution both the enol and the keto tautomers are present. By reaction with metal salts, mononuclear complexes of the type $M(H_2htmp)_2Cl_2$ (M = Pt, Pd) and $M(Hhtmp)_2 \cdot 2H_2O$ (M = Cu, Ni and Co) were isolated and characterized by physicochemical measurements. In addition homo- and heterobinuclear complexes have been prepared.

The design and synthesis of coordination compounds containing two or more different metal ions in adjacent sites are interesting because they provide the path to study multi-electron redox reactions, magnetic exchange interactions and the possible activation of small substrate molecules. Moreover, these complexes can be used to mimic enzymatic metal sites.[1–4]

To obtain heterobinuclear complexes we have prepared and studied the trinucleating ligand 1-(2-hydroxyphenyl)-3-(2-thiomethoxyphenyl)-1,3-propanedione (H_2htmp) which presents three types of reacting sites, one in the centre of the molecule (the β-diketone moiety) and two in the outer sites (the β-ketophenyl and the thioether moiety).

This ligand gives mononuclear and homo- and heterobinuclear complexes allowing, consequently, the synthesis of MM′M″ linear trinuclear compounds that are otherwise difficult to obtain.[5–7]

The present paper reports the preparation of several mono- and binuclear complexes with this ligand. All the compounds described herein are air-stable, both in the solid state and in solution.

EXPERIMENTAL

All the solvents used in the preparation were freshly distilled. Melting points were recorded on a Fisher stage melting point apparatus and are not corrected. IR spectra were recorded on a Nicolet FTIR 5DX spectrometer as KBr pellets or in Nujol mulls. The electronic spectra were recorded on a Cary 17 UV spectrophotometer in DMSO solution and Nujol dispersion. The ^{1}H NMR spectra (200 MHz) were obtained on a Brucker spectrometer in $CDCl_3$ solution.

Preparation of 1-(2-*hydroxyphenyl*)-3-(2-*thiomethoxyphenyl*)-1,3-*propanedione* (H_2htmp)

o-Hydroxyacetophenone (50 mmol) was dissolved in toluene (15 cm^3); two drops of methanol were added and the solution was slowly added to a 60% NaH suspension in toluene (170 cm^3). The resulting yellow suspension was gently refluxed for 15 min. After which, a toluene solution (100 cm^3) of methyl *o*-methylthiosalicylate (55 mmol) was added dropwise. The suspension was refluxed for 6 h, and then allowed to cool down to room temperature. The precipitate was filtered, washed with diethyl ether and dried *in vacuo*. It was added to ice-cooled water, stirred for 10 min, and then acidified to pH = 1 with conc. HCl and the solid extracted with diethyl ether. The organic phase was separated, washed with a 5% $NaHCO_3$ solution and water. After decantation of the aqueous phase, the ethereal phase was dried over Na_2SO_4. Evaporation of the organic solution gave a yellow solid, which upon

* Author to whom correspondence should be addressed.

recrystallization from methanol gave 7.4 g of pure ligand, m.p. 69–70°C (yield, 52%).

Preparation of $M(H_2htmp)Cl_2$ (M = Pd, Pt)

The ligand (2 mmol) was dissolved in benzene (100 cm^3) and the appropriate metal chloride (1 mmol) was added with stirring. The resulting solution was stirred for 48 h. The product was filtered, washed with benzene, ethanol and diethyl ether, and dried *in vacuo*. The same products were obtained when ethanol was used as solvent.

Preparation of $M(Htmp)_2 \cdot nH_2O$ (M = Cu, $n = 0$; M = Ni *or* Co, $n = 2$)

The ligand (2 mmol) was dissolved in ethanol and the appropriate metal acetate or chloride hydrate (1 mmol) was added with stirring. The resulting solution was stirred for 6 h. The obtained precipitate was filtered, washed with ethanol and diethyl ether, and dried *in vacuo*. The same products were obtained when benzene was used as solvent.

Preparation of homobinuclear $M_2(htmp)_2 \cdot H_2O$ *complexes* (M = Ni *or* Co, $n = 4$; M = Cu, $n = 0$)

An ethanolic solution of the ligand (2 mmol) and of lithium hydroxide (4 mmol) was added to a warm ethanol solution of the appropriate metal acetate (1 mmol). The resulting mixture was allowed to reflux for 8 h and then cooled to room temperature. The precipitate was filtered and washed several times with ethanol and diethyl ether, and then dried *in vacuo*.

Preparation of $CuNi(htmp)_2 \cdot 2H_2O$

Lithium hydroxide (2 mmol) was added to an ethanolic suspension of the mononuclear compound (1 mmol) and the solution was stirred at room temperature for 30 min. Then a solution of the metal acetate (1 mmol) in ethanol was added and the mixture refluxed for 8 h. The solid was filtered, washed with ethanol and diethyl ether, and dried *in vacuo*.

Preparation of $PdCu(Hhtmp)_2Cl_2$

The complex can be prepared by reaction of the mononuclear $Cu(Hhtmp)_2$ and $PdCl_2$, or of $Pd(H_2htmp)_2Cl_2$ and copper(II) acetate in an ethanolic solution.

RESULTS AND DISCUSSION

The ligand has been synthesized in three steps (see Scheme 1) starting from thiosalycylic acid. In the first step the thiolo group is methylated by methyl iodide. After conversion into the methyl ester it reacted with *o*-hydroxyacetophenone in the presence of sodium hydride.

The compound gives microanalytical and mass spectral data consistent with the structure; the fragmentation pattern of the compound is reported in Fig. 1. The X-ray structure of the ligand[8] showed that the compound is present, at least in the solid state, only as its enol tautomer (see Fig. 2).

The hydroxyl IR stretching band of the ligand consists of a broad signal (400 cm^{-1} wide) centred at approx. 3050 cm^{-1}; this band may result from two broad, overlapping OH absorptions. Both the position and the extreme width are compatible with strong intramolecular association. In the carbonyl region only one band at 1609 cm^{-1} is present, due to chelating C=O—H, while no band due to free C=O is observed.

The enol tautomer is the major form in $CDCl_3$ solution. A freshly prepared chloroform solution showed the presence of the enol form, together with

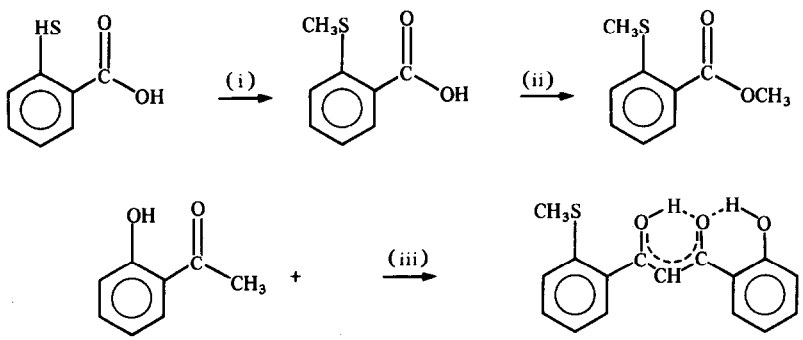

Scheme 1. Reaction steps in the preparation of H_2htmp: (i) dimethylsulphate; (ii) thionyl chloride, methanol; and (iii) 60% NaH, toluene.

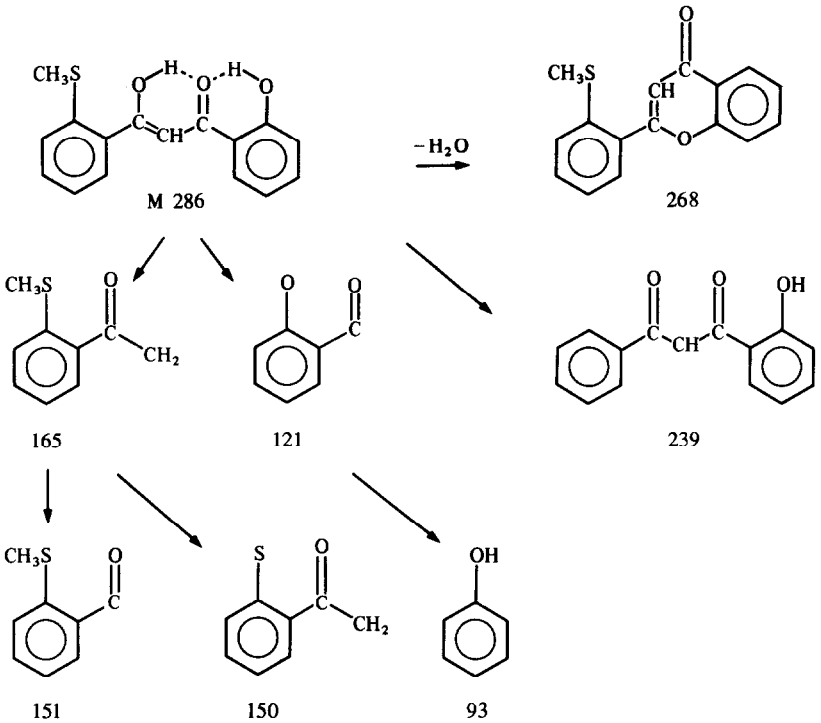

Fig. 1. Fragmentation pattern of 1-(2-hydroxyphenyl)-3-(2-thiomethoxyphenyl)-1,3-propanedione.

extraneous material, amounting to about 18%. The pre-eminent ^{1}H NMR resonances occur at 2.5, 6.75, 12 and 15.45 ppm and have been assigned to the C*H*$_3$S, C*H*, phenolic O*H* and enolic O*H* of the enol form, respectively. Other weak signals are at 2.4, 4.65 and 11.9 ppm and may be assigned to the SC*H*$_3$, methylene and phenolic O*H* of the ketonic tautomer. The integration peak areas are in agreement with these assignments. The other multiple bands in the range 6.9–8.0 ppm are due to aromatic hydrogens.

Interaction with metal salts

Reactions of $PdCl_2$ or $PtCl_2$ with the ligand, in benzene or ethanol solution, gave compounds of the type $M(H_2htmp)_2Cl_2$. Both the cream-coloured platinum(II) and palladium(II) complexes present similar IR spectra; in the 1700–1400 cm^{-1} region there are peaks at 1609, 1578 and 1562 cm^{-1}, present also in the free ligand, which are attributed to the C=O, benzene ring and C=C stretching modes, respectively. The complexes display a band at 385–375 cm^{-1} assigned to the ν(M—S) stretching vibration, since this band is not present in the spectra of the free ligand or of other metal complexes. The two bands at 318 and 301 cm^{-1}, and 328 and 310 cm^{-1}, are assigned to the Pd—Cl and Pt—Cl stretches, respectively. We suggest a coordination geometry of the type shown in Fig. 3(A) for these complexes.

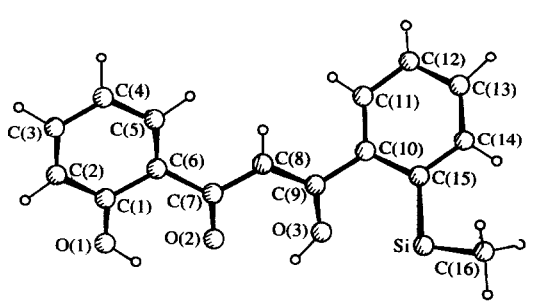

Fig. 2. Molecular structure of $C_{16}H_{14}O_3S$ and the atom labelling scheme.

The ^{1}H NMR spectrum of $Pd(H_2htmp)_2Cl_2$, in d_6-DMSO solution, is virtually identical to that of the free ligand; it shows that the organic moiety is uncoordinated to the palladium, at least in DMSO solution, and involved in a keto–enol equilibrium, where the enol tautomer is predominant. The pre-eminent peaks occur at 2.47 (SC*H*$_3$), 7.13 (C*H*), 11.6 (phenolic O*H*) and 15.75 (enolic O*H*). The 2.40 (SC*H*$_3$), 4.82 (C*H*$_2$) and 11.2 (phenolic O*H*) peaks can be assigned to the keto form. The integrated peak areas are in agreement with these assignments. From this solution a crystalline compound was obtained, and its elemental analysis agrees with the formula $Pd(DMSO)_2Cl_2$.

Table 1. Analytical data

Compound	C (%) Calc.	C (%) Found	H (%) Calc.	H (%) Found	S (%) Calc.	S (%) Found	Metal (%) Calc.	Metal (%) Found
H_2htmp	67.1	67.6	4.9	4.9	11.2	11.3		
$Cu(Hhtmp)_2$	60.6	60.7	4.1	4.2	10.1	9.8	14.2	14.0
$Ni(Hhtmp)_2 \cdot 2H_2O$	57.7	57.5	3.9	4.1	9.6	9.8	8.8	8.3
$Co(Hhtmp)_2 \cdot 2H_2O$	57.7	57.6	3.9	4.0	9.6	9.8	8.8	8.5
$Pt(H_2htmp)_2Cl_2$[a]	41.2	41.5	3.0	2.9	6.9	7.1	20.3	20.4
$Pd(H_2htmp)_2Cl_2$[b]	51.2	51.6	3.8	3.7	8.5	8.3	14.2	13.8
$Cu_2(htmp)_2$	55.2	55.8	3.5	3.2	9.2	9.0	18.3	18.7
$Ni_2(htmp)_2 \cdot 4H_2O$	50.7	50.3	3.7	3.3	8.4	8.1	15.5	15.8
$Co_2(htmp)_2 \cdot 4H_2O$	50.7	50.3	3.7	3.4	8.4	8.2	15.5	15.9
$CuNi(htmp)_2 \cdot 2H_2O$	52.9	52.6	3.9	3.4	8.8	8.5	8.7(Cu)	8.3
							8.1(Ni)	7.8
$PdCu(Hhtmp)_2Cl_2$[c]	47.4	47.7	3.2	3.0	7.9	7.6	7.8(Cu)	8.0
							13.2(Pd)	12.8

[a] Calc.: Cl, 7.6. Found: Cl, 8.0.
[b] Calc.: Cl, 9.4. Found: Cl, 9.7.
[c] Calc.: Cl, 8.7. Found: Cl, 8.9.

By reacting the ligand H_2htmp with copper(II), nickel(II) and cobalt(II) metal salts, in benzene or ethanol solution, complexes of the type $M(Hhtmp)_2 \cdot nH_2O$ have been obtained. Their almost identical IR spectra suggest that the same type of coordination is present in all the compounds. Characteristic absorption bands are found in the 1600–1500 cm^{-1} region; on the basis of literature data,[9] we assign the band occurring near 1610 cm^{-1} in both the spectra to the C=O and the band at about 1510 cm^{-1} to the C=C stretching modes of the coordinated acetylacetonate moiety. The absorption band at 3400 cm^{-1} in the complexes containing water molecules is consistent with the analytical data. From these IR data either of the structures shown in Fig. 3(B) or (C) can be proposed for the 1 : 2 chelate.

The room temperature magnetic moments are in the range typical for planar copper(II) and octahedral nickel(II) and cobalt(II) complexes.

The electronic spectrum of the copper(II) shows a band at 670 nm, as expected for a square-planar copper(II) β-diketonate complex. Moreover, this band, which is attributed to the ligand field *d–d* transition, is more similar to that of bis(dibenzoylacetonato)copper(II) than to that of bis(*o*-hydroxyacetophenonato)copper(II) which has two peaks in this region. The nickel complex shows absorption bands between 500 and 1300 nm as expected for octahedral ones. The cobalt(II) com-

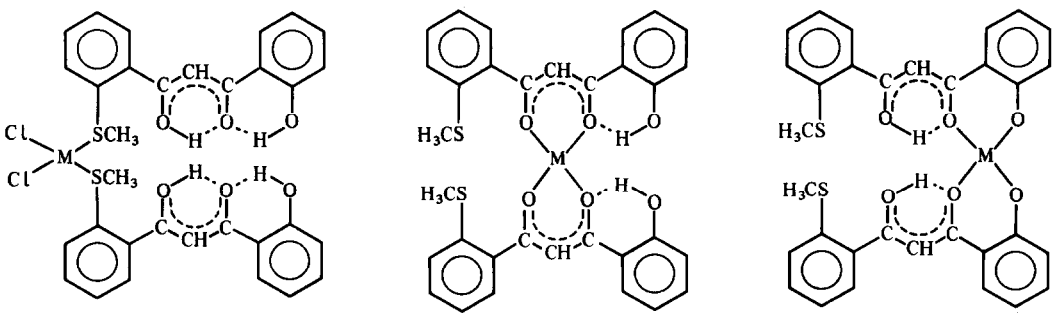

Fig. 3. (A) Proposed structure for $M(H_2htmp)_2Cl_2$, M = Pd or Pt; (B) and (C) possible structures of $M(Hhtmp)_2 \cdot nH_2O$, M = Cu, Ni or Co.

Table 2. Spectroscopic data and magnetic moments

Compound	IR (cm^{-1}) frequency in the 1650–1500 cm^{-1} range			UV (nm)			μ (BM)
H_2htmp	1610	1580	1560				
$Cu(Hhtmp)_2$	1614	1586	1538	670			1.78
$Ni(Hhtmp)_2 \cdot 2H_2O$	1612	1580	1527	680	1110		2.92
$Co(Hhtmp)_2 \cdot 2H_2O$	1600	1571	1516	530	600	1150	4.60
$Pd(H_2htmp)_2Cl_2$	1609	1578	1562	—	—		Diamagnetic
$Pt(H_2htmp)_2Cl_2$	1608	1580	1562	—	—		Diamagnetic
$Cu_2(htmp)_2$	1615	1590	1560	670 broad			1.39
$Ni_2(htmp)_2 \cdot 4H_2O$	1610	1535	1510	650	1115		3.80
$Co_2(htmp)_2 \cdot 4H_2O$	1590	1543	1510	600			6.38
$CuNi(htmp)_2 \cdot 2H_2O$	1612	1585	1500	690	1100		2.59
$PdCu(Hhtmp)_2Cl_2$	1615	1593	1560	670	—		1.82

plex has a low intensity band at *ca* 1150 and two bands at 600 and 530 nm; these features are typical of a weak octahedral field, and the magnetic moment (4.60 BM) is of the same order as those found in other high-spin octahedral cobalt(II) complexes. We suggest that nickel, cobalt and copper are coordinated to the acetylacetone group as shown in Fig. 3(B).

Homobinuclear complexes

These complexes can be obtained by reaction of the ligand with the appropriate metal salts, or by reaction of the mononuclear compound with metal acetate. Their electronic and IR spectra suggest that these complexes are of the type shown in Fig. 4. The IR spectra show bands in the region 1650–1500 cm^{-1}, which are typical of coordinated carbonyl groups and ethylenic C=C bonds. The presence of water is confirmed by a broad band at 3450–3000 cm^{-1}, due to the stretching mode of coordinated water. The electronic spectrum of the copper chelate in DMSO solution or in a Nujol mull, shows a broad band at 670 nm due to the *d–d* transition, as expected for copper(II) acetylacetonate or hydroxyacetophenonate complexes. The nickel(II) compound has very broad bands at 1100 cm^{-1} and at 645 nm, similar to those found for some nickel(II) diketonate complexes.[10] The electronic spectrum of the cobalt complex is very similar to that of $Co(acac)_2 \cdot 2py$[11] and is consistent with octahedral coordination. The magnetic moments, at room temperature, of the dinuclear compounds are lower than the spin-only values, similar to those obtained for analogous adducts in which antiferromagnetic coupling is operative.[12]

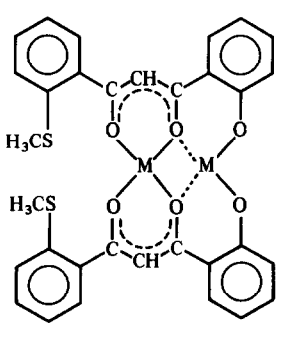

M = Cu^{2+}; Ni^{2+}; Co^{2+}

Fig. 4. Probable structure for the linear homobinuclear complexes.

Heterobinuclear complexes

The complexes can be prepared by reaction of the mononuclear complexes with the appropriate metal salts; however, it is necessary to pay attention to the temperature reaction since the copper and nickel mononuclear complexes can be converted into the 2/2 chelate by heating above 60°C. Their IR data are essentially the same as that of the corresponding homobinuclear complexes. The strong band in the 1585–1630 cm^{-1} region is attributable to the coordinated C=O group, and the band in the 1500–1570 cm^{-1} region corresponds to the C=C vibration. Moreover, the $PdCu(Hhtmp)_2Cl_2$ complex shows bands due to the Pd—S and Pd—Cl stretching modes. The magnetic property is explained by assuming that the entire paramagnetism arises from the copper(II) centre; on this basis the magnetic moment is as expected for the isolated d^9 copper(II) ion.

The room temperature magnetic moment of $NiCu(htmp)_2 \cdot 2H_2O$ (2.59 BM) is lower than the

spin-only values, and is similar to those found for analogous complexes in which a magnetic exchange coupling takes place.[13] Work is in progress to prepare the trinuclear chelates.

Acknowledgements—We thank Mrs Sandra Boesso and Mr Letterio Turiaco for technical assistance. This work has been supported by the Italian MPI.

REFERENCES

1. U. Casellato, P. A. Vigato and M. Vidali, *Coord. Chem. Rev.* 1977, **23**, 31.
2. S. E. Groh, *Isr. J. Chem.* 1976–1977, **15**, 277.
3. U. Casellato, P. A. Vigato, D. E. Fenton and M. Vidali, *Chem. Soc. Rev.* 1979, **8**, 199.
4. K. D. Karlin and Y. Gultneh, *J. Chem. Educ.* 1985, **62**, 983.
5. R. L. Lintvedt, B. A. Schoenfelner, C. Ceccarelli and M. D. Glick, *Inorg. Chem.* 1984, **23**, 2867.
6. F. J. Rietmeijer, G. A. Van Albada, R. A. G. DeGraaff, J. G. Haasnoot and J. Reedijk, *Inorg. Chem.* 1985, **24**, 3597.
7. L. L. Borer, R. Horsma, O. A. Rajan and E. Sinn, *Inorg. Chem.* 1986, **25**, 3652.
8. U. Casellato, R. Graziani, M. Vidali, R. Purrello and G. Maccarrone, *J. Cryst. Spectr. Res.* 1987, **17**, 323.
9. H. Musso and H. Junge, *Tetrahedron Lett.* 1966, **33**, 4003.
10. S. Pinchas, B. L. Silver and I. Laulicht, *J. Chem. Phys.* 1967, **46**, 1506.
11. R. H. Holm, G. W. Everett and A. Chakravorty, *Prog. Inorg. Chem.* 1966, **7**, 183.
12. J. T. Hashagen and J. P. Fawcett Jr, *J. Am. Chem. Soc.* 1965, **87**, 2821.
13. M. Vidali, G. Rizzardi, P. A. Vigato, U. Casellato, S. Kida and J. Okawa, *Inorg. Chim. Acta* 1979, **34**, 19.

Polyhedron Vol. 9, No. 22, pp. 2727–2732, 1990
Printed in Great Britain

0277–5387/90 $3.00 + .00
© 1990 Pergamon Press plc

IRON SANDWICHES AS MOLECULAR RESERVOIR MATERIALS: DESIGN, ELECTRONIC PROPERTIES AND PROSPECTS*

D. ASTRUC,† M.-H. DESBOIS, M. LACOSTE and F. MOULINES

Laboratoire de Chimie Organique et Organométallique, URA CNRS N° 35, 351 cours de la Libération, 33405 Talence Cedex, France

and

J.-R. HAMON

Laboratoire de Chimie des Organométalliques, URA CNRS N° 347, Campus de Beaulieu, Université de Rennes I, 35042 Rennes Cedex, France

and

F. VARRET

Département Recherches Physiques, URA CNRS N° 71, Université de Paris VI, 75252 Paris Cedex 05, France

(*Received* 6 *July* 1990; *accepted* 17 *July* 1990)

Abstract—Two aspects of the properties of iron sandwich complexes as molecular reservoir materials are reviewed in a prospective way: (i) electronic properties in the solid state in mononuclear, Jahn–Teller active 19-electron iron(I) complexes and binuclear, 37-electron mixed-valence complexes, showing the coupling between the electronic structure and the lattice; and (ii) solution properties of iron sandwiches as molecular reservoirs of electrons, protons, hydrogen atoms and hydrides.

Iron sandwich complexes have potential as molecular reservoir materials insofar as several oxidation states can be isolated and handled without breakdown. Thermal stability can be obtained in the [FeCp(arene)] series (Cp = C_5H_5) if the arene is permethylated or bulky enough so that the iron(I) radical centre is sterically protected. Binuclear complexes of this series can be linked either via the Cp ligand (fulvalene bridge) or via the arene ligand (bis- or polyarene bridge).

In this short prospective review, we wish to emphasize two aspects of the reservoir properties of these compounds: (i) the solid-state electronic features of the paramagnetic sandwiches in the context of a discoid, monodimensional stacking; and (ii) their function as molecular reservoirs of electrons, protons, hydrogen atoms and hydrides.

The ferromagnetic properties of decamethylferricinium salts disclosed by Miller's group have encouraged organometallic chemists to design the synthesis of complexes with the aim of obtaining new solid-state properties.[1]

Several years ago, it was found that large differences of steric bulk of the two ligands on the iron(I) sandwich complex [FeCp(C_6Me_6)] induce a specific packing arrangement with alternating positions of the arene ligand along the chains[2] (Fig. 1). The

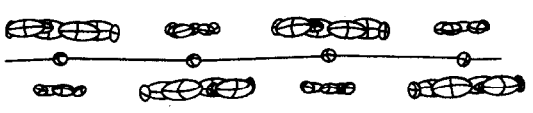

Fig. 1. Alternating sandwich positions in the lattice observed in the X-ray crystal structure of [Fe^{I}Cp(C_6Me_6)].[2]

* Paper presented at the Symposium on Applied Organometallic Chemistry, Pokolbin, N.S.W., Australia, 10–12 July, 1989.

† Author to whom correspondence should be addressed.

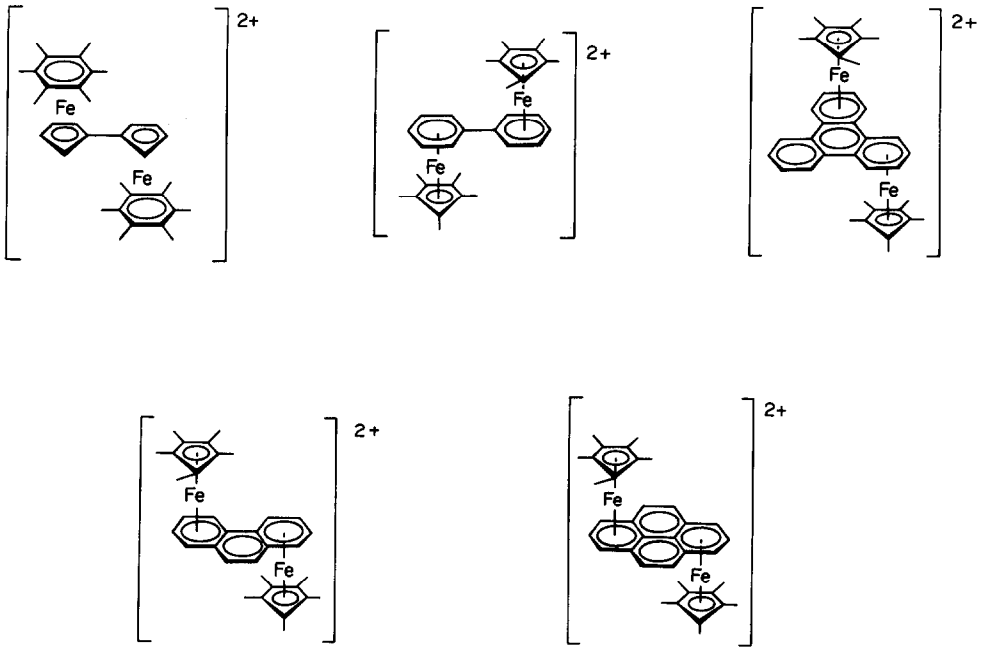

variation of the quadrupole splitting (QS) of the Mössbauer doublet as a function of temperature was assigned to the (Boltzmann) law of thermal population of the upper Kramers' level (Fig. 2). The latter originates from the Jahn–Teller distortion caused by single occupancy of the doubly degenerate e^*_1 orbital.[3] Although this law is valid for dilute iron(I) samples or for sandwiches having comparable steric bulks of the two ligands (disorder in the solid state) such as $[Fe(C_5R_5)(C_6R_6)]$, R = H or Me (Fig. 3), it is no longer true in the solid state. The lattice arrangement induces a specific dynamic cooperative Jahn–Teller distortion responsible for the splitting of the low-temperature Mössbauer

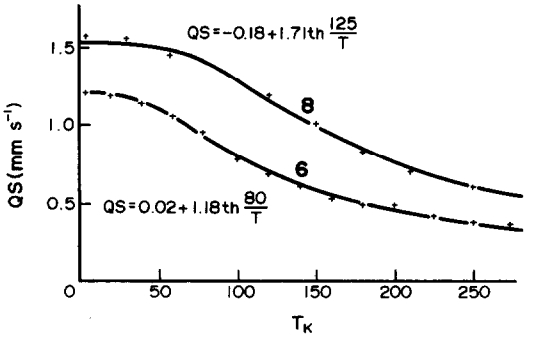

Fig. 2. Variation of QS as a function of temperature in the 19-electron complexes $[Fe(C_5Me_5)(C_6Me_6)]$ (top curve) and $[Fe(Cp)(C_6H_6)]$ (bottom curve). The thermal population of the upper Kramers' level was fitted by the indicated laws (rhombic distortion of the Jahn–Teller-active iron(I) sandwiches). In other iron(I) sandwiches with different ring sizes, phase transitions are observable along these curves [see refs 2 and 7(a)].

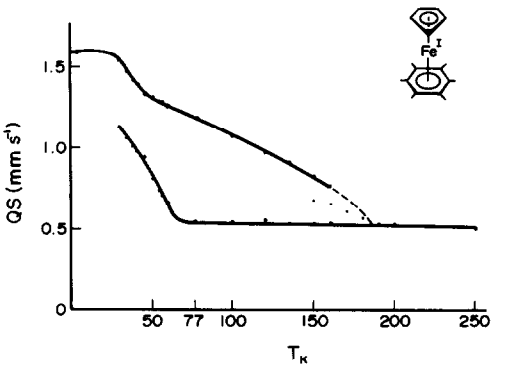

Fig. 3. Splitting of the Mössbauer quadrupole doublet of $[Fe^ICp(C_6Me_6)]$.

doublet of $[FeCp(C_6Me_6)]$ into two doublets (Fig. 4). This phenomenon is accompanied by second-order phase transitions as indicated by the differential thermal analysis and by the breaks in the

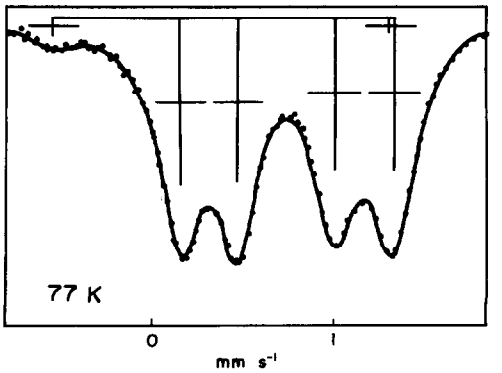

Fig. 4. Mössbauer spectrum of $[FeCp(C_6Me_6)]$ at 77 K. Note the splitting into two equal contributions.

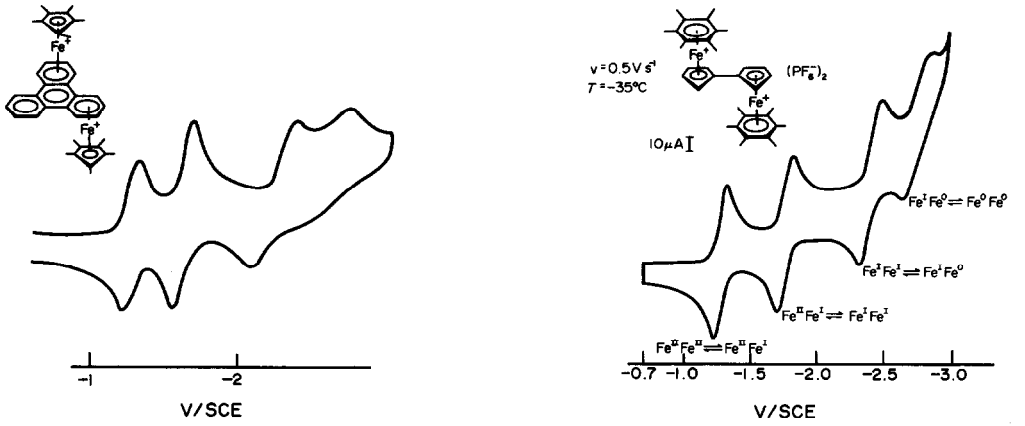

Fig. 5. Cyclic voltammograms of dinuclear iron sandwiches at −30°C (Hg cathode, DMF, $^nBu_4N^+BF_4^-$ 0.1 M; scan rate: 0.1 V s^{-1}).

curve of the variation of the quadrupole splitting as a function of temperature.

These data established the cooperativity between the electronic structure of iron(I) sandwiches and the solid-state lattice.

Cyclic voltammograms of the dinuclear complexes bridged either by the fulvalene or by a polyaromatic ligand show four well separated waves, three of which are chemically and electrochemically reversible (Fig. 5). Only the fourth reduction wave, at very negative potential (around $E_p = -2.5$ V vs SCE), corresponds to a slow electron-transfer in every case (possibly due to a structural change). But three of the five oxidation states are thermally stable and can be isolated: the 36-electron, 37-electron and 38-electron complexes (in the polyaromatic series, the 38-electron species are stable only up to 0°C). The two unpaired electrons in the 38-electron complexes are antiferromagnetically coupled (fulvalene, phenanthrene or pyrene bridges). Systems with biphenyl or dihydrophenanthrene as the bridge are 36-electron complexes with a bicylohexadienylidene bridge. Indeed the voltammograms of the binuclear complexes with a bridge of the biphenyl type show only a two-electron wave (C_5H_5 series) or two close one-electron waves (C_5Me_5 series). In the fulvalene and C_5Me_5 series, 37-electron mixed-valence complexes have been synthesized. Their Mössbauer spectra show the absence of Jahn–Teller activity and delocalization of the electron over the two iron centres, on the Mössbauer time scale (10^7 s^{-1}) down to 4 K.[4] Thus, these compounds can be viewed as models for organometallic conductors with stacked sandwiches, e.g. electron reservoirs in the solid state. The analogy could be extended to vertical stacks with cyclophane bridges (Fig. 6). Stacks with 37-elecron complexes and organic acceptors such

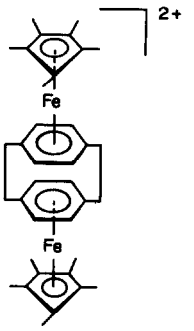

Fig. 6.

as TCNE or TCNQ would be of interest with respect to their magnetic properties. A diruthenium analogue has recently been made with $TCNQ^-$ by the Dupont group but with a diamagnetic organoruthenium cation.[5]

Remarkably, sandwich complexes, the structures of which are very different from those of redox metalloproteins (except that they have iron in common), are shown to achieve comparable functions of relays to convey electrons, protons and hydrogen atoms in chemical systems.

The stable redox couple $[Fe^{II/I}Cp(C_6Me_6)]^{+/0}$ and its water-soluble derivative $[Fe^{II/I}(CpCO_2)(C_6Me_6)]^{0/-}$ are redox catalysts for the cathodic reduction of NO_3^- to NH_3 in basic media, whereas NO_3^- is not electro-active in such media otherwise[6,7] (Scheme 1).

The ability of the iron(I) sandwich complexes to store electrons has also been recognized in a variety of stoichiometric processes with organic and inorganic acceptors (TCNQ, $TCNQ^-$, phenazine, O_2, H_2O, CO_2, organometallic cations, aldehydes, ketones, alkynes), and the presence of a salt has

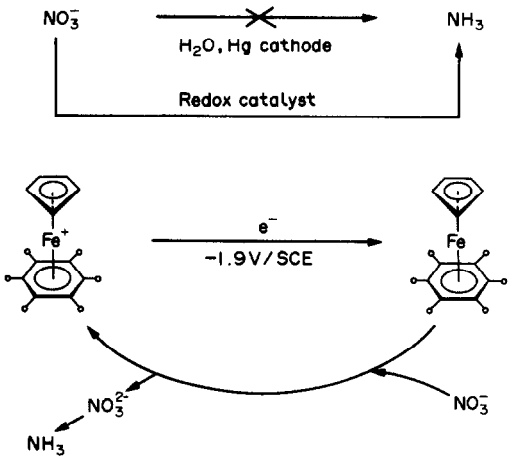

Scheme 1. Redox catalysis of the cathodic reduction of NO_3^- to NH_3 mediated by iron sandwiches.

been shown to have a dramatic role on the course of these reductions.[7] Dinuclear complexes such as $[Fe_2Cp_2diphenyl]^{2+/0}$, which can transfer two electrons in one step, are sought after redox catalysts for the reduction of H^+ to H_2 in energy conversion devices. The iron(I) sandwiches are also excellent initiators for electron-transfer chain-catalysed reactions which must be initiated by reducing agents (for instance, ligand exchange reactions,[7b] Scheme 2).

The complexes $[Fe^{II}Cp(arene)]^+$ in which the arene ligand bears one or several methyl substituent(s) are excellent reservoirs of protons. A series of deprotonation–alkylation sequences leads to multiple hexa-alkylation, finishing with the formation of tentacled iron-sandwich complexes with a variety of structures.[8] New discoid molecules are expected using this strategy (Scheme 3).

Extensive proton transfers are responsible for the deuteration of the benzylic hydrogens using $D_2O + NaOD$ (1 N).[9]

Hydrogen atom transfers are also possible to and from the 19-electron complex $[Fe^ICp(C_6Me_6)]$. A hydrogen atom is removed by O_2 according to an electron-transfer mechanism followed by proton transfer.[7a] The 18-electron complex formed bears an exocyclic methylene which can trap a hydrogen atom from Pd/H_2 and reforms the 19-electron complex.[10] The latter reacts also with Pd/H_2 at 20°C or with $NaBH_4$ or $LiAlH_4$ to give further hydrogen atom transfer (Scheme 4).

Similarly, the bimetallic phenanthrene and dihydrophenanthrene complexes can transfer several electrons and hydrogen atoms,[11] a function achieved by vitamin K.

The function of iron–arene sandwiches as reservoirs of hydride is useful (for purpose of protection by H^-) in arene activation mediated by temporary complexation to iron. Bis-arene iron dications do not react properly with carbon nucleophiles to form C—C bonds but give electron transfer. However, protection by hydride allows further formation of C—C bonds leading to mono- or heterofunctional cyclohexadienes (Scheme 5). The hydride removal (deprotection) follows an electron pathway as shown by Mandon.[12c,d]

Several transition metal hydrides are able to catalyse the reduction of alkyl halides by $NaBH_4$.[12b]

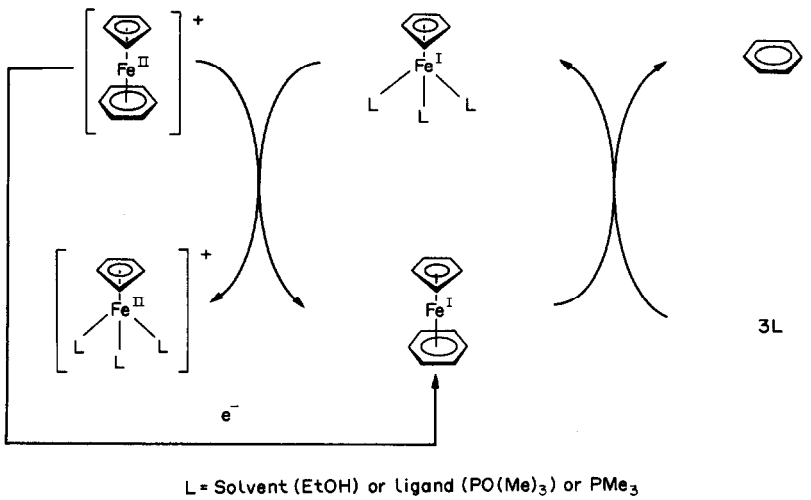

Scheme 2. Mechanism of the electrocatalytic ligand exchange of an arene by three two-electron ligands induced by electrons.

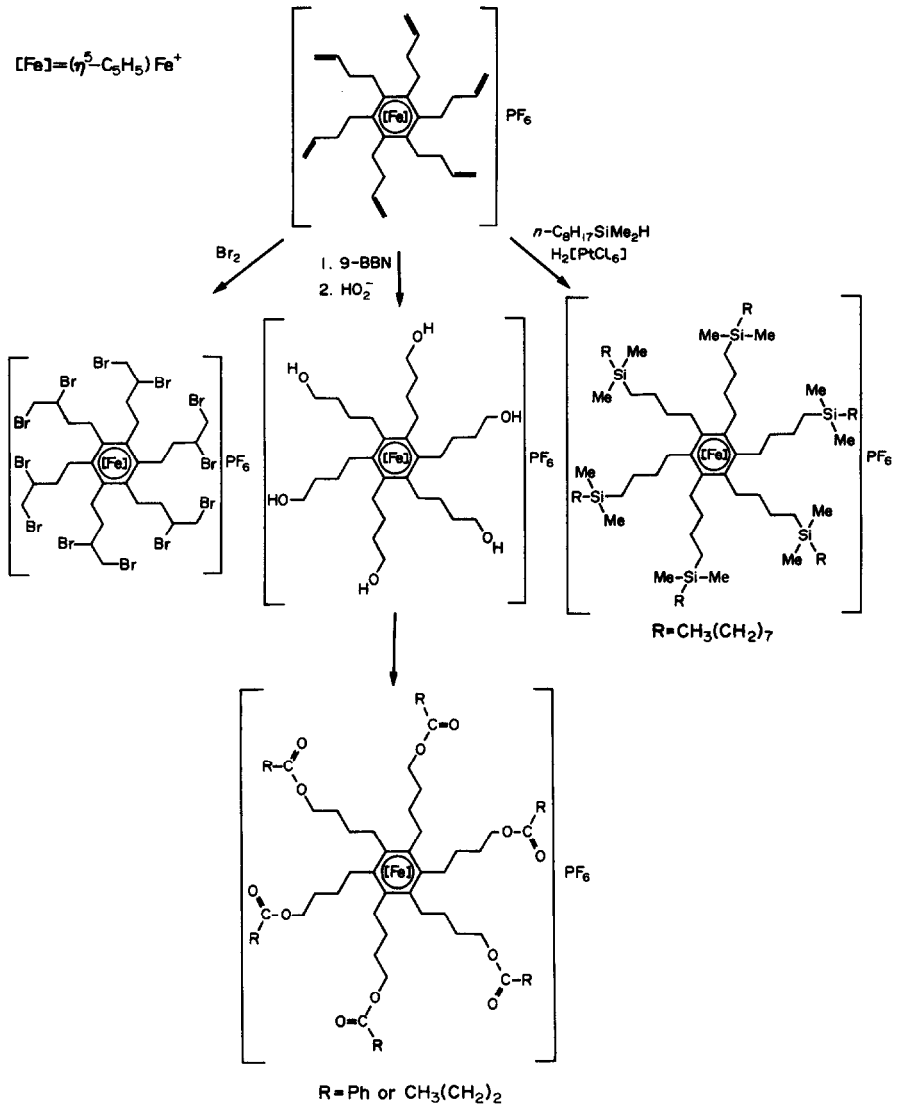

Scheme 3. Syntheses of tentacled iron sandwiches.

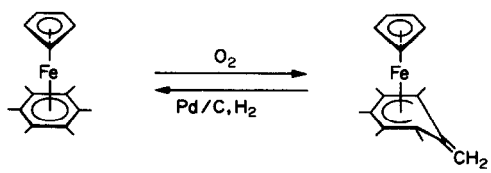

Scheme 4. Reversible hydrogen atom transfer in iron sandwiches.

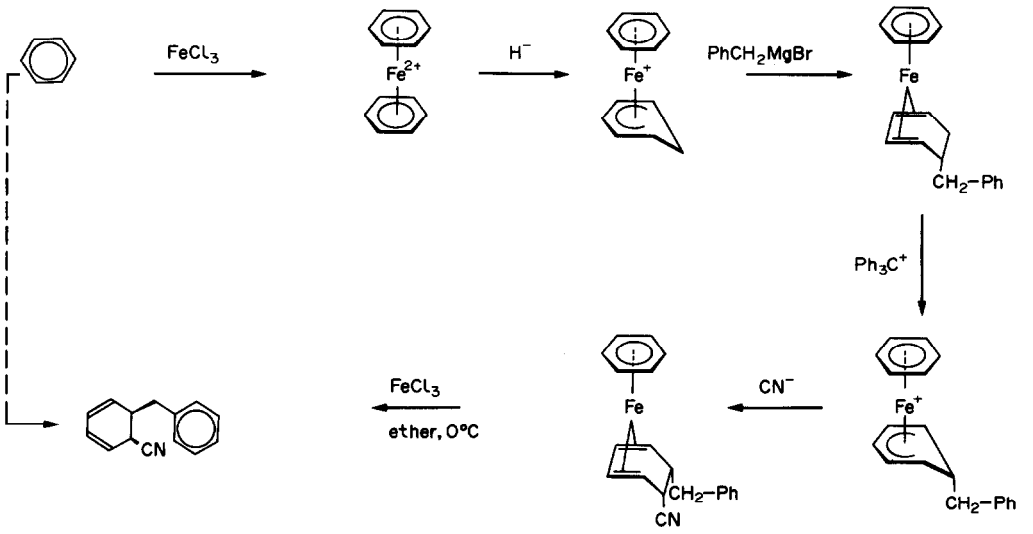

Scheme 5. Hydride reservoir: protection by hydride for the transformation of benzene into heterobifunctional cyclohexadienes.

This is also the case for $[Fe(C_5R_5)(CO)_2H]$ (R = H, Me). These metal–hydride complexes behave as hydride reservoirs rather than as true transition metal catalysts in the sense that the role of the metal is quite ancillary. This is perhaps the limiting case between the two concepts of reservoir (relay) which trans*port* (trans*locate*) small particles with minimal structural change and transition metal catalysts which involve a deep change at the metal centre during the catalytic cycle. Both are needed for artificial as well as for natural processes.

REFERENCES

1. J. S. Miller, *Chem. Rev.* 1988, **88**, 201.
2. D. Astruc, J.-R. Hamon, G. Althoff, E. Román, P. Batail, P. Michaud, J.-P. Mariot, F. Varret and D. Cozak, *J. Am. Chem. Soc.* 1979, **101**, 5445.
3. J. H. Ammeter, *J. Magn. Reson.* 1987, **30**, 299.
4. (a) M.-H. Desbois, D. Astruc, J. Guillin, J.-P. Mariot and F. Varret, *J. Am. Chem. Soc.* 1985, **107**, 52; (b) M. Lacoste, F. Varret, L. Toupet and D. Astruc, *J. Am. Chem. Soc.* 1987, **109**, 6504.
5. M. D. Ward, P. J. Fagan, F. C. Calabrese and D. C. Johnson, *J. Am. Chem. Soc.* 1989, **11**, 1719.
6. (a) E. Román, R. Dabard, C. Moinet and D. Astruc, *Tetrahedron Lett.* 1979, **16**, 1433; (b) A. Buet, A. Darchen and C. Moinet, *J. Chem. Soc., Chem. Commun.* 1979, 447.
7. (a) D. Astruc, *Accts Chem. Res.* 1986, **19**, 377; (b) D. Astruc, *Angew. Chem. Int. Edn Engl.* 1988, **27**, 643; (c) C. Moinet, E. Román and D. Astruc, *J. Electroanal. Interfac. Chem.* 1981, **121**, 241; (d) A. Darchen, *J. Chem. Soc., Chem. Commun.* 1983, 768.
8. F. Moulines and D. Astruc, *Angew. Chem. Int. Edn Engl.* 1988, **27**, 1347.
9. J.-R. Hamon and D. Astruc, *J. Organomet. Chem.*, submitted.
10. P. Michaud and D. Astruc, *Angew. Chem. Int. Edn Engl.* 1982, **21**, 918.
11. M. Lacoste, B. Gloaguen and D. Astruc, manuscript in preparation.
12. (a) D. Astruc, in *The Chemistry of the Metal–Carbon Bond* (Edited by F. R. Hartley and S. Patay), Vol. 4, pp. 625–731. John Wiley, New York (1987); (b) P. Michaud, C. Lapinte and D. Astruc, *Ann. N.Y. Acad. Sci.* 1983, **415**, 97; (c) D. Mandon, L. Toupet and D. Astruc, *J. Am. Chem. Soc.* 1986, **108**, 1320; (d) D. Mandon and D. Astruc, *Organometallics* 1989, **8**, 2372.

Polyhedron Vol. 9, No. 22, pp. 2733–2739, 1990
Printed in Great Britain

0277–5387/90 $3.00+.00
© 1990 Pergamon Press plc

PLATINUM GROUP METAL–KETOXIME COMPLEXES: CRYSTAL STRUCTURE OF HYDROGEN *FAC*-TRIS(DIMETHYLVIOLURATO)RUTHENATE(II) HEPTAHYDRATE

M. ANGUSTIAS ROMERO and JUAN MANUEL SALAS*

Departamento de Química Inorgánica, Facultad de Ciencias, Universidad de Granada, 18071 Granada, Spain

and

MICHEL SIMARD, MIGUEL QUIRÓS and ANDRÉ L. BEAUCHAMP*

Département de Chimie, Université de Montréal, C.P. 6128, Succ. A, Montréal, Québec H3C 3J7, Canada

(*Received* 5 *February* 1990; *accepted* 20 *July* 1990)

Abstract—Eight complexes of the anions of monomethyl- and dimethylvioluric acids with the metals ruthenium, rhodium, palladium and platinum have been isolated and characterized by elemental analysis, IR spectroscopy, NMR and thermogravimetry. IR spectra suggest bidentate coordination through the nitroso group and the carbonyl oxygen in position six. Analysis of dehydration processes of rhodium complexes allows us to distinguish between crystallization water, coordinated water and H_3O^+ cations. The crystal structure of hydrogen *fac*-tris(dimethylviolurato)ruthenate(II) heptahydrate has been solved by X-ray diffraction. The existence of ruthenium(II) in this compound instead of ruthenium(III) has been checked by recording its NMR spectra. The metal atom lies on a crystallographic three-fold axis, with three symmetry-related bidentate dimethylviolurato anions in its coordination sphere, defining the *fac* isomer. Water molecules build a very intricate hydrogen-bonding network.

Violuric acids are the 5-isonitroso derivatives of barbituric acid. These compounds show a great ability to form complexes with a large number of metal ions under different conditions of temperature and acidity. They have found immense analytical applications for the identification and determination of several metal ions.[1–6] Acidity constants and metal complexation constants of violuric acids have been studied by several authors.[7–18]

Some complexes of these ligands with transition metal ions have been isolated and characterized by spectroscopic techniques.[19–26] Violurato derivatives show, in these compounds, π-acceptor properties acting as strong-field ligands.[27]

X-ray studies carried out on this type of complex indicate that violurato ligands generally behave as bidentate groups through the nitrogen atom of the oxime group and an oxygen atom from a vicinal carbonyl group.[28–38]

As part of our work on the coordination behaviour of pyrimidine derivatives,[39–41] we report here the synthesis, spectroscopic characterization and thermal behaviour of eight new ruthenium(II), palladium(II), rhodium(III) and platinum(II) complexes of monomethyl- (HMV) and dimethyl- (HDMV) violuric acids, and the crystal structure of the complex hydrogen *fac*-tris(dimethylviolurato) ruthenate(II) heptahydrate.

EXPERIMENTAL

Reagents

Monomethyl- and dimethylvioluric acids were obtained in our laboratory by well-known pro-

* Authors to whom correspondence should be addressed.

cedures.[42,43] Elemental analyses were undertaken by the Technical Services of Granada University using a Perkin–Elmer 240C microanalyser.

Preparation of the ketoximato complexes

$(H_3O)[Ru(DMV)_3]\cdot 6H_2O$ *and* ML_2 *complexes.* The title ruthenium(II) complex and the ML_2 complexes (where M = Pd^{II} or Pt^{II} and L = MV or DMV anions) were prepared by adding 1 mmol of $RuCl_3$, $Na_2[PdCl_4]$ or $(NH_4)_2[PtCl_4]$ to a stirred solution of 2 mmol of HMV or HDMV in 50 cm^3 of distilled water. Yellow palladium complexes or green platinum complexes immediately precipitated. In the case of the ruthenium compound, the dark red solution was held at room temperature for a few days, and small black crystals appeared.

The isolated products were collected and quickly washed with small amounts of water and ethanol and dried in air. Elemental analysis (Calc. in parentheses): $(H_3O)[Ru(DMV)_3]\cdot 6H_2O$: C, 27.7 (27.7); H, 4.1 (4.2); N, 16.8 (16.1)%. $Pd(MV)_2$: C, 25.9 (26.9); H, 1.6 (1.8); N, 18.0 (18.8)%. $Pd(DMV)_2$: C, 30.0 (30.3); H, 2.5 (2.5); N, 18.0 (17.7)%. $Pt(MV)_2$: C, 22.6 (22.4); H, 1.6 (1.5); N, 15.5 (15.7)%. $Pt(DMV)_2$: C, 25.4 (25.6); H, 2.1 (2.1); N, 15.4 (14.9)%.

$Ru(NO)_2(DMV)_2Cl$. The procedure is the same as for the synthesis of $(H_3O)[Ru(DMV)_3]\cdot 6H_2O$, but involves a large excess of $NaNO_2$ adding to the reaction mixture. C, 24.6 (25.5); H, 2.0 (2.1); N, 19.5 (19.8)%.

$(H_3O)[Rh(DMV)_2Cl_2]\cdot 2H_2O$. Commercial $RhCl_3\cdot xH_2O$ (0.2 g) was added to a solution of dimethyl violuric acid (0.4 g) in hot methanol (50 cm^3). The reaction mixture was stirred at 50°C for 15 min. After cooling, the yellow solution was held at room temperature for a few days, when small yellow crystals appeared. The product was washed with methanol and air dried. C, 23.4 (24.1); H, 3.2 (3.2); N, 14.2 (14.1)%.

$[Rh(DMV)_2Cl(H_2O)]\cdot 2H_2O$. The synthesis is analogous to the previous one, but using DMSO as solvent instead of methanol. C, 25.5 (25.7); H, 3.2 (2.9); N, 15.4 (15.0)%.

Physical measurements

Infrared spectra were obtained on a Perkin–Elmer 983G spectrophotometer using KBr (4000–250 cm^{-1}) or polyethylene (600–180 cm^{-1}) pellets.

^1H and ^{13}C NMR spectra were recorded on a Brucker AM300 spectrometer using hexadeuterated dimethylsulphoxide as solvent.

Thermogravimetric measurements were carried out on a Mettler TG-50 thermobalance, using a heating rate of 20°C min^{-1} and a dynamic atmosphere of pure air (100 cm^3 min^{-1}). The nature of the final pyrolysis products was checked by IR spectroscopy.

Data collection and structure determination

A shiny, black, hexagonal, prismatic crystal mounted in open air was used for X-ray work. The unit cell, obtained by usual methods on an Enraf–Nonius CAD-4 diffractometer, shows trigonal or hexagonal symmetry, the first indicated by non-equivalence of hkl and $hk\bar{l}$ reflections. Systematic absences were consistent with space groups $P\bar{3}c1$ and $P3c1$. The structure solved and refined well in $P\bar{3}c1$.

The intensity data were obtained with a Syntex $P\bar{1}$ diffractometer as described earlier,[44] by using graphite-monochromatized Mo-K_α radiation. All hkl and $hk\bar{l}$ reflections within a sphere limited by $2\theta < 50°$ ($0 \leqslant h \leqslant 17$, $0 \leqslant k \leqslant 17$, $-22 \leqslant l \leqslant 22$) were collected. Three standard reflections checked every 47 measurements showed random fluctuation within $\pm 2.6\%$.

A total of 3672 reflections were measured. After averaging, the number of independent reflections reduced to 1840, of which 1279 with $I > 3\sigma(I)$ were used for structure determination. These data were corrected for Lorentz and polarization, but not for absorption ($\mu = 5.82$ cm^{-1}).

The ruthenium atom was located at equipoint 4*d* by means of the Patterson synthesis. All other atoms, including 28 water molecules, were readily located from a ΔF map calculated by the SHELX package.[45] The structure was refined anisotropically by full-matrix least-squares. Individual weights based on counting statistics were applied.

Water oxygen OW(3), initially placed on the two-fold axis (equipoint 4*f*), showed abnormally large thermal motion. It was displaced from the axis, and its three coordinates were allowed to refine (occupancy factor = 1/2). After convergence, more reasonable temperature factors were obtained, indicating that this water molecule was statistically distributed over two symmetry-related sites near the axis.

The methyl hydrogens were also found to be disordered over two equally populated sets of sites. Each set of hydrogen atoms was treated as a semi-rigid body, and a common isotropic temperature factor was refined for the six half-hydrogens of each group. Water hydrogens were not detected. Final agreement factors were $R = 0.036$ and $R_w = 0.045$.

The scattering curves and anomalous dispersion terms for ruthenium were obtained from standard sources.[46,47] The final atomic coordinates and equi-

valent temperature factors are part of the supplementary material, which also includes tables of anisotropic temperature factors, least-squares plane calculations, distances and angles in hydrogen bonds, and structure factor amplitudes.

Crystal data

$(H_3O)[Ru(C_6N_3O_4H_6)_3]\cdot 6H_2O$, FW = 780.6, trigonal, space group $P\bar{3}c1$, $a = 14.007(8)$, $c = 18.333(8)$ Å, $V = 3115.0$ Å^3, $D_c = 1.664$ g cm^{-3}, $Z = 4$, $F(000) = 399$, $\lambda(\text{Mo-}K_\alpha) = 0.71069$ Å (graphite monochromator), $\mu(\text{Mo-}K_\alpha) = 5.82$ cm^{-1}, $T = 293$ K, crystal dimensions (faces): 0.33 mm (001–00$\bar{1}$), 0.28 mm (100–$\bar{1}$00), 0.28 mm (010–0$\bar{1}$0) and 0.28 mm (1$\bar{1}$0–$\bar{1}$10).

RESULTS AND DISCUSSION

Spectroscopic studies

In Table 1, the most important absorption bands of the IR spectra are collected. These values agree well with the literature values for bidentate N(5)—O(6) violurate anions,[48] in which a π-electron delocalization takes place in the five member chelate ring [M—N(5)—C(5)—C(6)—O(6)].

An additional intense, broad band appears in the spectrum of $Ru(NO)_2(DMV)_2Cl$ at 1912 cm^{-1}, clearly assignable to ν(N≡O) of the coordinated nitrosyl groups.[37] This spectrum does not show bands assignable to the existence of nitro groups.

Chlorine-containing compounds show, in the low frequency area, bands due to ν(M—Cl), which suggest that chlorine atoms are in the inner coordination sphere of these complexes.

^{1}H and ^{13}C NMR spectra of $(H_3O)[Ru(DMV)_3]\cdot 6H_2O$ are well solved showing sharp signals, which clearly indicates that the initial ruthenium(III) has been reduced to ruthenium(II). The positions of these signals are the same as reported by Brémard *et al.*[27] for the sodium salt of this complex anion. A complete interpretation of the ^{13}C spectrum has been carried out by these authors.

Thermal behaviour

Thermal decomposition of hydrated compounds begins with the loss of water molecules. This process appears as two or three weight loss effects in the DTG diagram of rhodium complexes, showing the non-equivalence of the present water molecules. A third of them (which is directly coordinated to metal atom or supporting the extra proton) are completely eliminated at about 180°C. In the case of $(H_3O)[Ru(DMV)_3]\cdot 6H_2O$, a single broad weight loss effect is observed for dehydration involving the seven molecules.

The two TG diagrams corresponding to rhodium complexes show, in the 200–360°C temperature range, a new weight loss effect. The corresponding values are in good agreement with the expected values for the elimination of chlorine atoms. After this, pyrolytic decomposition of the organic moiety takes place, finishing around 430°C. This process occurs for the ruthenium complexes in the range 220–380°C, whereas for the palladium and platinum complexes, it occurs between 330 and 420°C (see Table 2).

The final residues were identified by IR spectroscopy. They are PdO or Pt, respectively, for palladium(II) and platinum(II) compounds, with good agreement between experimental and calculated values. For ruthenium and rhodium complexes, the residue is mainly the corresponding metal, but the presence of non-stoichiometric oxides, unburned carbon and even metastable carbonate (in the case of $[Rh(DMV)_2Cl(H_2O)]\cdot 2H_2O$) is observed.

Table 1. Infrared data (cm^{-1})

	ν(C=O)	ν[C(6)—C(5)—N(5)]	ν(N=O)	ν(M—Cl)
$(H_3O)[Ru(DMV)_3]\cdot 6H_2O$	1708, 1647	1555, 1511	1428	—
$Ru(NO)_2(DMV)_2Cl$[a]	1731, 1678	1549, 1525	1416	304
$[Rh(DMV)_2Cl(H_2O)]\cdot 2H_2O$	1725, 1677	1565, 1518	1405	294
$(H_3O)[Rh(DMV)_2Cl_2]\cdot 2H_2O$	1721, 1668	1544	1408	360, 304
$Pd(MV)_2$	1742, 1648	1613, 1504	1414	—
$Pd(DMV)_2$	1719, 1675	1560, 1515	1411	—
$Pt(MV)_2$	1737, 1656	1600, 1513	1413	—
$Pt(DMV)_2$	1726, 1676	1548, 1518	1416	—

[a] ν(N≡O) = 1912 cm^{-1}.

Table 2. Thermal decomposition

Compound	Process	Temperature range (°C)	% Acc. weight loss Experimental	Calculated
$(H_3O)[Ru(DMV)_3]\cdot 6H_2O$	Dehydration	45–130	15.2	16.15
	Pyrolysis	200–380	85.2	—
$Ru(NO)_2(DMV)_2Cl$	Pyrolysis	220–380	82.1	—
$[Rh(DMV)_2Cl(H_2O)]\cdot 2H_2O$	Dehydration[a]	45–190	10.3	9.64
	Dehalogenation	200–350	≈16	15.97
	Pyrolysis	350–430	72.0	—
$(H_3O)[Rh(DMV)_2Cl_2]\cdot 2H_2O$	$-2H_2O$	45–120	6.9	6.03
	$-H_2O$	120–170	10.9	9.05
	Dehalogenation	200–370	≈19	20.44
	Pyrolysis	370–430	81.2	—
$Pd(MV)_2$	Pyrolysis	325–425	71.1	72.58
$Pd(DMV)_2$	Pyrolysis	325–425	74.6	74.20
$Pt(MV)_2$	Pyrolysis	325–425	64.3	63.54
$Pt(DMV)_2$	Pyrolysis	350–425	66.1	65.35

[a] Three steps.

Description of the structure

An ORTEP view of the complex is shown in Fig. 1. The complex consists of discrete anions in which ruthenium is octahedrally coordinated by three dimethylviolurate anions acting as bidentate ligands. The ligand forms a five-membered chelate ring via the oxygen, O(6), and the N(5) atom of the nitroso group. The metal sits on a crystallographic three-fold axis, and the three ligands define the *fac* stereoisomer. The molecules are individually chiral, but the compound is racemic, the Δ and Λ enantiomers being related by the cell inversion centre.

Interatomic distances and bond angles are listed in Table 3. The distances, angles and other features of the coordination sphere are very similar to those of the analogous $[(violurate)_3Ru]^-$ complex,[34] with the difference that the present molecule is closer to idealized symmetry because it lies on a crystallographic three-fold axis. The present Ru—O and Ru—N distances are not significantly different from those found in the above ruthenium(II) viol-

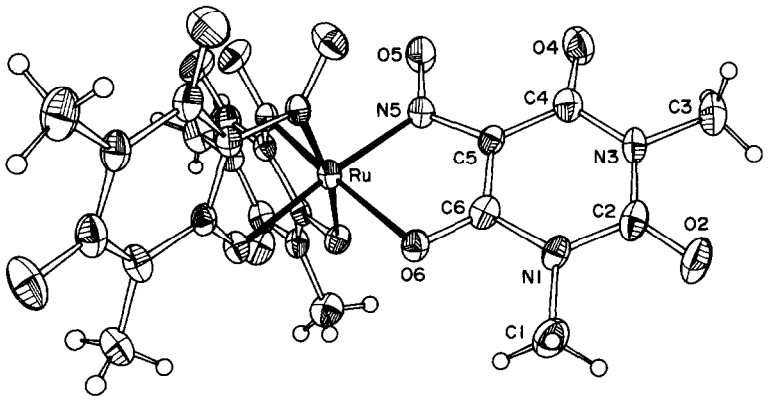

Fig. 1. ORTEP drawing of the *fac*-Ru(dimethylviolurate)$_3$ anion. Ellipsoids are drawn at the 50% probability level. Hydrogen atoms are shown as spheres of arbitrary size. The ligands are related by a crystallographic three-fold axis running through the ruthenium atom.

Table 3. Distances and angles in hydrogen *fac*-Ru(dimethylviolurate)$_3$ · 7H$_2$O

Distances (Å)			
Ru—O(6)	2.099(4)	N(3)—C(4)	1.383(7)
Ru—N(5)	1.960(4)	C(4)—O(4)	1.231(6)
N(1)—C(1)	1.467(7)	C(4)—C(5)	1.434(8)
N(1)—C(2)	1.389(8)	C(5)—N(5)	1.382(7)
N(1)—C(6)	1.367(7)	C(5)—C(6)	1.407(6)
C(2)—O(2)	1.210(8)	N(5)—O(5)	1.258(5)
C(2)—N(3)	1.379(7)	C(6)—O(6)	1.266(6)
N(3)—C(3)	1.461(8)		
Angles (°)			
O(6)—Ru—N(5)	80.8(1)	N(3)—C(2)—O(2)	122.6(5)
O(6)—Ru—O(6)	90.6(1)	C(2)—N(3)—C(4)	125.2(4)
N(5)—Ru—N(5)	93.8(2)	C(2)—N(3)—C(3)	116.4(4)
O(6)—Ru—N(5) (*cis*)	95.6(1)	C(4)—N(3)—C(3)	118.0(4)
O(6)—Ru—N(5) (*trans*)	169.4(1)	N(3)—C(4)—C(5)	114.6(5)
Ru—O(6)—C(6)	109.5(3)	N(3)—C(4)—O(4)	119.0(5)
Ru—N(5)—O(5)	125.6(3)	C(5)—C(4)—O(4)	126.4(5)
Ru—N(5)—C(5)	114.3(3)	C(4)—C(5)—C(6)	121.7(4)
C(5)—N(5)—O(5)	120.0(4)	C(4)—C(5)—N(5)	124.9(4)
C(2)—N(1)—C(6)	112.2(4)	C(6)—C(5)—N(5)	113.1(4)
C(2)—N(1)—C(1)	118.0(4)	N(1)—C(6)—C(5)	118.7(4)
C(6)—N(1)—C(1)	119.3(4)	N(1)—C(6)—O(6)	119.2(4)
N(1)—C(2)—N(3)	117.2(5)	C(5)—C(6)—O(6)	122.1(4)
N(1)—C(2)—O(2)	120.2(5)		

urate compound. The angles around the metal correspond to an octahedron with a trigonal distortion, originating mainly from the small N(5)—Ru—O(6) angle of 80.8(1)° imposed in the chelate ring by the "bite" of the ligand.

Since the crystal structure of dimethylvioluric acid has not been determined, the ligand will be compared with violuric acid,[28,49] assuming that methylation has no dramatic effect. As a logical consequence of deprotonation and greater delocalization in the chelate ring, the C(5)—C(6) and N(5)—O(5) bonds of violuric acid [1.505(8) and

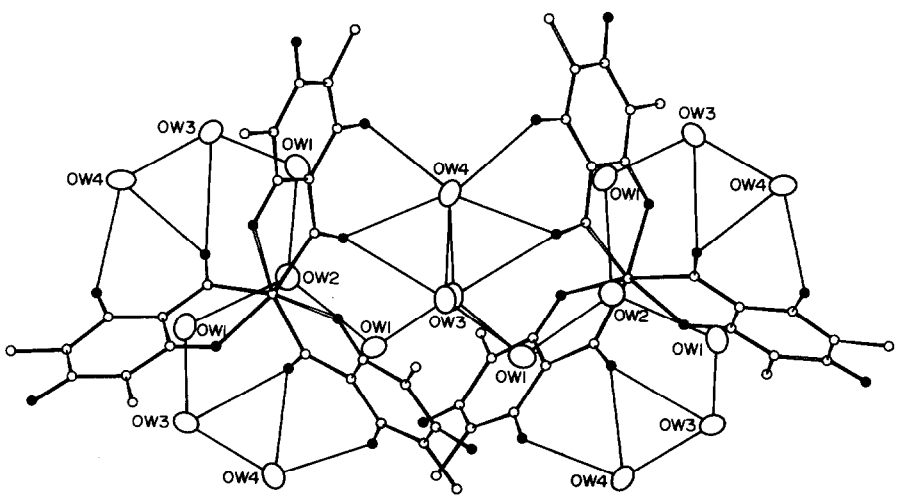

Fig. 2. Hydrogen bonding network in the unit cell. The lines represent hydrogen bonds, but the hydrogen positions could not be determined. The two sites on which OW(3) is disordered are shown in the centre of the drawing. Oxygen atoms are shown as dark spheres and can be identified by comparison with Fig. 1.

Table 4. Distances (Å) between atoms possibly involved in hydrogen bonding

OW(2)—OW(1)	$(x, y, z; 1-y, 1+x-y, z$ and $-x+y, 1-x, z)$	2.800(7)
OW(1)—OW(3)	$(-y, x-y, z)$	2.73(2)
OW(1)—OW(3)	$(y, x, 1/2-z)$	2.47(2)
OW(1)—O(5)	$(x-y, 1-y, 1/2-z)$	2.967(6)
OW(1)—O(4)	$(x-y, 1-y, 1/2-z)$	3.056(7)
OW(3)—OW(4)	(x, y, z)	2.49(2)
OW(3)—O(5)	$(x-y, -y, 1/2-z)$	2.90(2)
OW(4)—O(5)	$(x, y, z$ and $x-y, -y, 1/2-z)$	2.868(5)
OW(4)—O(4)	$(x, y, z$ and $x-y, -y, 1/2-z)$	2.778(6)

1.327(8) Å, respectively][28,49] are shortened in the complex [1.407(6) and 1.258(5) Å, respectively], whereas the C(5)—N(5) and C(6)—O(6) bonds are lengthened [1.274(7) and 1.175(8) Å vs 1.382(7) and 1.266(6) Å, respectively]. Also, the angles around C(5) are severely distorted. The C(6)—C(5)—N(5) and C(4)—C(5)—N(5) angles are 115.1(6) and 125.7(6)°, respectively, in violuric acid. They occur in the opposite order [121.7(4) and 113.1(4)°] for the chelate. No such distortion is detected around C(6). These features are similar to those found in other violurate[32–34,37,50] and dimethylviolurate[35,36] complexes with various metals. The remaining distances and angles are fairly similar to those of violuric acid.

The pyrimidine ring shows significant, but small, deviations from planarity: the largest distances are found for C(2) [0.039(5) Å], N(3) [−0.023(4) Å] and C(4) [0.018(5) Å]. Exocyclic atoms are more displaced, most of them are situated on the same side as the metal atom, which lies at 0.0883(3) Å away from the plane. The largest deviations are found for the nitroso group [N(5), 0.116(4) and O(5), 0.170(3) Å], but O(2) [0.101(4) Å] and the C(1) methyl group [0.103(6) Å] are also appreciably displaced.

The water molecules participate in an intricate network of hydrogen bonds (Fig. 2); details on their geometry are provided in the supplementary material. The distances are collected in Table 4. The unit cell contains, altogether, 28 water molecules: 12 of them [OW(1)] are in general positions, four OW(2) molecules lie on a three-fold axis, whereas the six OW(4) molecules occupy a two-fold axis. Six extra water molecules [OW(3)] are each disordered over two sites slightly off the two-fold axis. Each ligand is connected to this network via the oxygen atoms of the 5-nitroso and 4-carbonyl groups.

The extra proton that balances the charge of the complex anion has not been detected. However, the position of OW(2) on the three-fold axis, its relationship via hydrogen bonding [in which OW(2) must be the donor] with the three nearby OW(1) molecules and the fact that there is one OW(2) per ruthenium atom, lead us to believe that OW(2) actually represents an H_3O^+ cation.

Acknowledgements—We are grateful to Professor F. D. Rochon (Université de Québec à Montréal) for helping in the determination of the cell dimensions and collecting the X-ray diffraction data. We wish to thank the Natural Sciences and Engineering Research Council of Canada and CICYT (research project 402/86) for financial support of this research, and the Spanish Ministry of Education and Science for a scholarship to M.Q.

REFERENCES

1. P. A. Leermakers and W. A. Hoffman, *J. Am. Chem. Soc.* 1958, **80**, 5663.
2. M. E. Taylor and R. J. Robinson, *Analyt. Chem.* 1962, **34**, 533.
3. L. V. Ershova and V. V. Noskov, *Zh. Anal. Khim.* 1971, **26**, 2406.
4. J. Beltrán and J. Faus, *J. Chromatogr.* 1975, **103**, 392.
5. R. S. Chawla and R. P. Singh, *J. Ind. Chem. Soc.* 1975, **52**, 169.
6. R. S. Chawla, Y. Dutt and R. P. Singh, *Talanta* 1969, **16**, 119.
7. C. Bremard, *Bull. Soc. Chim. Fr.* 1975, 953.
8. Y. Vandewalle and J. Nicole, *C.R. Hebd. Séanc. Acad. Sci., Paris* 1976, **282**, 1073.
9. J. M. Degorre, J. Hennion and J. Nicole, *C.R. Hebd. Séanc. Acad. Sci., Paris* 1977, **284**, 671.
10. C. Bremard, G. Nowogrocki and S. Sueur, *Inorg. Chem.* 1978, **17**, 3220.
11. Y. Vandewalle and J. Nicole, *Bull. Soc. Chim. Fr.* 1978, 363.
12. J. M. Degorre, A. Delannoy, J. Hennion and J. Nicole, *Bull. Soc. Chim. Fr.* 1979, 477.
13. J. D. López, J. M. Salas, M. Melgarejo and C. Valenzuela, *An. Quím.* 1981. **77B**, 40.
14. E. Garcia-España, J. Moratal and J. Faus, *J. Coord. Chem.* 1982, **12**, 41.

15. B. R. Singh and R. Ghosh, *Thermochim. Acta* 1982, **53**, 257.
16. B. P. Singh, V.K. Bhardwaj, B. R. Singh and R. Ghosh, *Thermochim. Acta* 1983, **64**, 139.
17. J. M. Moratal, A. Prades, M. Julve and J. Faus, *Thermochim. Acta* 1985, **89**, 343.
18. E. García-España, M. Julve, J. Moratal and J. Faus, *New J. Chem.* 1988, **12**, 59.
19. S. Sueur, C. Bremard and G. Nowogrocki, *J. Inorg. Nucl. Chem.* 1976, **38**, 2037.
20. J. Faus and J. Moratal, *An. Quím.* 1980, **76B**, 169.
21. C. Bremard, G. Nowogrocki and S. Sueur, *J. Chem. Soc., Dalton Trans.* 1981, 1856.
22. H. T. Kuek, B. O. West and J. K. Yandell, *Inorg. Chim. Acta* 1981, **52**, 1.
23. J. D. López, J. M. Salas, M. P. Sánchez and C. Valenzuela, *An. Quím.* 1982, **78B**, 368.
24. M. A. Romero, J. M. Salas, J. D. López and C. Valenzuela, *An. Quím.* 1983, **79B**, 383.
25. J. D. López, M. A. Romero, J. M. Salas and C. Valenzuela, *An. Quím.* 1983, **79B**, 477.
26. M. A. Romero, J. M. Salas, A. García and C. Valenzuela, *An. Quím.* 1983, **79B**, 507.
27. C. Brémard, B. Mouchel and S. Sueur, *Inorg. Chem.* 1983, **22**, 3562.
28. B. M. Craven and Y. Mascarenhas, *Acta Cryst.* 1964, **17**, 407.
29. M. H. Guillier, *C. R. Hebd. Séanc Acad. Sci., Paris* 1963, 427.
30. C. Riche, *C. R. Hebd. Séanc Acad. Sci., Paris* 1965, **260**, 2516.
31. M. Hamelin, *C. R. Hebd. Séanc Acad. Sci., Paris* 1967, **264**, 2034.
32. M. Hamelin, *Acta Cryst.* 1972, **B28**, 228.
33. C. L. Raston and A. H. White, *J. Chem. Soc., Dalton Trans.* 1976, 1915.
34. F. Abraham, G. Nowogrocki, S. Sueur and C. Bremard, *Acta Cryst.* 1978, **B34**, 1466; 1980, **B36**, 799.
35. M. A. Romero, D. Martin, J. D. López and C. Valenzuela, *An. Quím.* 1983, **79B**, 200.
36. C. Ruiz-Valero, A. Monge, E. Gutiérrez and E. Gutiérrez, *Acta Cryst.* 1983, **C39**, 1214; 1984, **C40**, 811.
37. F. Abraham, G. Nowogrocki, S. Sueur and C. Bremard, *Acta Cryst.* 1983, **C39**, 838.
38. J. M. Salas, M. A. Romero, K. Aoki and K. K. Chacko, *Inorg. Chim. Acta*, submitted for publication.
39. M. N. Moreno, J. M. Salas, E. Colacio, M. P. Sánchez and F. Nieto, *Acta Cryst.* 1986, **C42**, 407.
40. M. A. Romero, J. M. Salas, R. López and M. D. Gutiérrez, *Polyhedron* 1988, **7**, 659.
41. M. D. Gutiérrez, R. López, M. A. Romero and J. M. Salas, *Can. J. Chem.* 1988, **66**, 249.
42. C. Valenzuela, J. M. Salas and J. D. López, *An. Quím.* 1980, **76B**, 251.
43. C. Valenzuela, R. Galisteo and J. D. López, *An. Quím.* 1978, **74B**, 402.
44. E. Colacio Rodríguez, J. Ruiz Sánchez, J. D. López González, J. M. Salas Peregrín, M. J. Olivier, M. Quirós and A. L. Beauchamp, *Inorg. Chim. Acta* 1990, **171**, 151.
45. G. M. Sheldrick, SHELX-76, Crystallographic Program System. University of Cambridge, U.K. (1976).
46. D. T. Cromer and J. T. Waber, *Acta Cryst.* 1965, **18**, 104.
47. D. T. Cromer, *Acta Cryst.* 1965, **18**, 17.
48. J. M. Enemark and R. D. Feltham, *Coord. Chem. Rev.* 1974, **13**, 339.
49. B. M. Craven and W. J. Takei, *Acta Cryst.* 1964, **17**, 415.
50. M. Hamelin, *Acta Cryst.* 1976, **B32**, 364.

Polyhedron Vol. 9, No. 22, pp. 2741–2745, 1990
Printed in Great Britain

0277–5387/90 $3.00+.00
© 1990 Pergamon Press plc

REACTIVITY OF CYCLOMETALLATED PALLADIUM(II) DIMER COMPLEXES WITH DIPHOSPHINES

JOSE M. VILA,* MIGUEL GAYOSO, JESUS J. FERNANDEZ, JUAN M. ORTIGUEIRA and ANTONIO SUAREZ

Department of Inorganic Chemistry, University of Santiago, 15706 Santiago de Compostela, Spain

(*Received* 13 *June* 1990; *accepted* 25 *July* 1990)

Abstract—The new complexes $[\{Pd(2,3,4\text{-}(MeO)_3C_6HC(H)=NR)\}_2(\mu\text{-}L\text{—}L)(\mu\text{-}O_2CMe)](O_2CMe)$ [where L—L = $Ph_2PCH_2PPh_2$ (dppm), $Ph_2PC(=CH_2)PPh_2$ (vdpp); R = Cy, 2′,4′,6′-$(Me)_3C_6H_2$] were synthesized as 1 : 1 electrolytes by treating the cyclometallated Schiff base palladium(II) acetato-bridged dimers with the appropriate diphosphine in a 1 : 1 molar ratio. These were converted into the analogous halide-bridged complexes by treatment with NaX. Reaction of the palladium(II) cyclometallated halide-bridged dimers with dppm or vdpp in 1 : 1 and 1 : 2 molar ratios gave the dinuclear and mononuclear species, $[\{Pd(2,3,4\text{-}(MeO)_3C_6HC(H)=NR)\}_2(\mu\text{-}L\text{—}L)(\mu\text{-}X)](X)$ and $[Pd\{2,3,4\text{-}(MeO)_3C_6HC(H)=NR\}(L\text{—}L\text{-}P,P)](PF_6)$, respectively, as 1 : 1 electrolytes. The stereochemistry of the complexes is discussed on the basis of spectroscopic data. The compounds were characterized by microanalysis (C, H, N), IR and ^1H and $^{31}P\{^1H\}$ NMR spectroscopy.

Cyclometallation reactions have drawn much attention in the past years and reviews covering them have appeared.[1–4] These reactions have been used as pathways to new products in organic synthesis.[5] We have extensively studied the cyclometallation of differently substituted Schiff bases[6,7] (where the question of regioselectivity has arisen),[8] imidazole ligands[9] and diimines[10] by palladium(II) and manganese (I), which produces dimer and monomer species. The latter were obtained from the dimer complexes by bridge splitting reactions with neutral ligands, such as tertiary phosphines, and anionic ligands, such as acetylacetonate. When we attempted similar reactions with diphosphines of the type $Ph_2PCH_2PPh_2$ (dppm) or $Ph_2PC(=CH_2)PPh_2$ (vdpp), we obtained new dinuclear species with both diphosphine, and halide-bridging ligands and mononuclear species with a chelating diphosphine, depending on the molar ratio used.[11] In the present paper we report a further new type of cyclometallated complex of palladium(II) with Schiff bases, in which the two metal centres are bridged by a diphosphine ligand and an acetato group to give dinuclear 1 : 1 electrolytes. Halide-bridged analogues and mononuclear complexes are also described.

EXPERIMENTAL

Solvents were purified by the standard methods.[12] Chemicals were reagent grade. Palladium(II) acetate and dppm were purchased from Aldrich Chemie and Ventron, respectively; vdpp was made as in the literature.[13] Elemental analyses were carried out on a Perkin–Elmer elemental analyser 240-B. IR spectra were recorded as Nujol mulls or polythene discs on a Perkin–Elmer 180 spectrophotometer. NMR spectra were obtained on $CDCl_3$ solutions and referred to the high frequency of $SiMe_4$ (^1H) or 85% H_3PO_4($^{31}P\{^1H\}$) and were recorded on a Bruker WM-250 spectrometer.

The synthesis of the Schiff base ligands (**a**, **b**), of the acetato-bridged (**1a**, **1b**) and of the halide-bridged (**2a**, **3a**, **2b**, **3b**) dimer complexes has been described by us in an earlier paper.[8]

Synthesis of the complexes

$[\{Pd(2,3,4\text{-}(MeO)_3C_6HC(H)=NCy)\}_2(\mu\text{-}Ph_2PCH_2PPh_2)(\mu\text{-}O_2CMe)](O_2CMe)$ (**4a**). To a solu-

* Author to whom correspondence should be addressed.

tion of the acetato-bridged dimer **1a** (0.05 g, 0.06 mmol) in acetone (*ca* 10 cm^3), dppm (0.02 g, 0.06 mmol) was added. After stirring for 3 h at room temperature, a precipitate formed which was filtered off and dried *in vacuo*. Recrystallization from dichloromethane–n-hexane afforded the desired complex as a yellow solid. Complexes **5a**, **4b** and **5b** were made similarly.

[{Pd(2,3,4 - $(MeO)_3C_6HC(H)$=NCy)}$_2$(μ - $Ph_2PCH_2PPh_2$)(μ-Cl)](Cl) (**6a**). To a suspension of the chloro-bridged dimer **2a** (0.05 g, 0.06 mmol) in acetone (*ca* 10 cm^3), dppm (0.02 g, 0.06 mmol) was added. The mixture was stirred for 3 h at room temperature and the resulting precipitate was filtered off and dried *in vacuo*. Recrystallization from dichloromethane–n-hexane gave the desired complex as a white solid. Complexes **7–9a** and **6–9b** were made similarly.

[Pd{2,3,4 - $(MeO)_3C_6HC(H)$=NCy}($Ph_2PCH_2PPh_2$-*PP*)](${PF_6}$) (**10a**). To a suspension of the chloro-bridged dimer **2a** (0.05 g, 0.06 mmol) in acetone (*ca* 10 cm^3), dppm (0.05 g, 0.12 mmol) and NH_4PF_6 (0.02 g, 0.12 mmol) were added. The mixture was stirred for 2 h at room temperature, aqueous acetone was added and the resulting solid was filtered off and dried *in vacuo*. Recrystallization from dichloromethane–n-hexane gave the final compound as an orange solid. Complexes **11a**, **10b** and **11b** were made similarly.

RESULTS AND DISCUSSION

In a previous paper[8] we described the preparation and characterization of the acetato-, chloro- and bromo-bridged dimer complexes [(**1–3**)**a**, (**1–3**)**b**] which were the necessary precursors for the synthesis of the compounds in the present paper. The cyclopalladated moiety in the compounds now described bears the same characteristics as the parent dimer compounds. The ν(C=N) stretching band (Table 1) appears at lower frequency than that corresponding to the free imines, in agreement with expected nitrogen coordination.[14] The HC=N ^{1}H NMR resonance in each compound appears shifted to lower frequency by *ca* 0.3–0.4 ppm relative to the free ligand[15] (Table 2). The H(5) proton (see numbering scheme in Fig. 1) appears as a doublet in the phosphine-bridged complexes, and as a doublet of doublets in the phosphine-chelated complexes, by coupling to one or two ^{31}P. The remaining pro-

Table 1. Microanalytical, colour, yield and IR data[a]

	Colour	Yield (%)	Analytical data, found (calc.) (%) C	H	N	IR data (cm^{-1}) ν(C=N)[b]	ν(COO)[c]	ν(Pd—X)
4a	Yellow	51	57.8 (57.5)	5.7 (5.4)	2.4 (2.6)	1610s	1565m 1407m	
5a	Yellow	56	55.2 (55.6)	5.7 (5.6)	2.2 (2.0)	1605m	1575m 1405m	
6a	White	81	56.1 (55.8)	5.5 (5.5)	2.3 (2.2)	1609m		288m
7a	Yellow	81	55.4 (55.0)	5.4 (5.5)	2.3 (2.0)	1608s		285m
8a	Yellow	52	52.3 (51.9)	5.1 (5.1)	2.1 (2.0)	1604m		170m
9a	Yellow	63	52.7 (52.4)	5.0 (5.2)	2.0 (1.9)	1611s		175m
10a	Orange	68	54.0 (53.6)	4.9 (4.8)	1.5 (1.5)	1600s		
11a	Orange	68	54.6 (54.7)	4.8 (4.6)	1.5 (1.5)	1600m		
4b	White	88	60.0 (60.0)	5.4 (5.2)	2.1 (2.1)	1608m	1576m 1400m	
5b	White	73	60.4 (60.1)	5.4 (5.4)	2.1 (1.9)	1607m	1572m 1405m	
6b	White	70	59.6 (60.0)	5.1 (5.3)	2.2 (2.0)	1610s		278m
7b	Yellow	77	58.9 (58.5)	5.1 (5.1)	2.2 (2.2)	1612m		283m
8b	Yellow	55	54.8 (55.2)	4.9 (5.3)	2.0 (1.9)	1611m		172m
9b	White	54	55.8 (56.0)	4.8 (4.9)	2.1 (2.2)	1612m		174m
10b	White	64	52.7 (52.8)	4.9 (5.1)	1.5 (1.4)	1608m		
11b	Yellow	82	52.5 (52.9)	4.6 (4.7)	1.5 (1.4)	1611m		

[a] Molecular weight values, found (calc.): **4a**, 1220 (1268); **6a**, 1199 (1221); **4b**, 1362 (1340); **5b**, 1315 (1293); **7b**, 1267 (1305).

[b] ν(C=N) values for **a**: 1625s; **b**: 1631m (cm^{-1}).

[c] The higher value corresponds to ν_{as}(COO) and the lower one to ν_s(COO).

Table 2. $^{1}H^{a}$ and $^{31}P\{^{1}H\}^{b}$ NMR data[c,d]

	δ(HC=N)	δ[H(5)]	δ(MeO)	δ(O_2CMe)	δ(P)	δ(CH_2)
a[e]	8.56s	6.70d	3.92s			
		^{3}J[H(5)H(6)] = 8.8	3.88s			
			3.87s			
4a	8.25d	5.63d	3.80s	2.17s	31.9s	4.85t
	^{4}J(PH) = 7.9	^{4}J(PH) = 7.0	3.59s			^{2}J(PH) = 11
			2.88s			
5a	8.30d	6.36d	3.87s	2.17s	46.8s	5.15m
	^{4}J(PH) = 7.6	^{4}J(PH) = 10.2	3.60s			
			2.56s			
6a	8.18d	5.51d	3.90s		29.0s	4.77t
	^{4}J(PH) = 8.4	^{4}J(PH) = 6.7	3.67s			^{2}J(PH) = 12
			2.96s			
7a	8.31d	6.29d	3.91s		45.6s	5.10m
	^{4}J(PH) = 8.3	^{4}J(PH) = 6.8	3.63s			
			2.94s			
8a	8.20d	5.49d	3.91s		29.6s	4.96t
	^{4}J(PH) = 8.9	^{4}J(PH) = 7.0	3.68s			^{2}J(PH) = 12.4
			2.90s			
9a	8.34d	6.01d	3.93s		47.3s	5.17m
	^{4}J(PH) = 7.7	^{4}J(PH) = 6.9	3.64s			
			2.89s			
10a	8.38d	5.39dd	3.98s		−27.7d (P_B)	4.28dd
	^{4}J(PH) = 7.8	^{4}J(P_BH) = 11.4	3.74s		−3.3d (P_A)	^{2}J(P_AH) = 11.5
		^{4}J(P_AH) = 8.0	3.07s		^{2}J(PP) = 63.9	^{2}J(P_BH) = 8.1
11a	8.39d	6.06dd	3.99s		−4.4d (P_B)	5.12m
	^{4}J(PH) = 7.8	^{4}J(P_BH) = 11.0	3.76s		12.5d (P_A)	
		^{4}J(P_AH) = 8.1	3.09s		^{2}J(PP) = 17.1	
b[e,f]	8.46s	6.80d	3.93s			
		^{3}J[H(5)H(6)] = 8.9	3.90s			
			3.85s			
4b[f]	8.08d	5.56d	3.81s	0.56s	30.9s	4.81t
	^{4}J(PH) = 7.6	^{4}J(PH) = 6.3	3.62s			^{2}J(PH) = 10.5
			2.97s			
5b[f]	8.07d	5.58d	3.86s	0.67s	45.9s	5.21m
	^{4}J(PH) = 7.6	^{4}J(PH) = 6.2	3.62s			
			2.62s			
6b[f]	8.01d	5.51d	3.84s		31.2s	4.90t
	^{4}J(PH) = 7.7	^{4}J(PH) = 6.1	3.65s			^{2}J(PH) = 13
			2.89s			
7b[f]	8.20d	6.40d	3.87s		52.5s	5.20m
	^{4}J(PH) = 8.0	^{4}J(PH) = 6.5	3.63s			
			2.45s			
8b[f]	8.10d	5.47d	3.84s		29.8s	5.14t
	^{4}J(PH) = 7.9	^{4}J(PH) = 6.5	3.66s			^{2}J(PH) = 12
			2.91s			
9b[f]	8.14d	6.06d	3.78s		47.9s	5.25m
	^{4}J(PH) = 7.6	^{4}J(PH) = 7.0	3.64s			
			2.66s			
10b[f]	8.18d	6.01dd	3.95s		−32.7d (P_B)	4.25dd
	^{4}J(PH) = 7.6	^{4}J(P_BH) = 10.5	3.76s		−8.5d (P_A)	^{2}J(P_AH) = 11.8
		^{4}J(P_AH) = 7.6	3.15s		^{2}J(PP) = 65.6	^{2}J(P_BH) = 8.0
11b[f]	8.14d	5.95dd	3.97s		−4.2d (P_B)	5.05m
	^{4}J(PH) = 7.6	^{4}J(P_BH) = 10.4	3.78s		12.1d (P_A)	
		^{4}J(P_AH) = 7.7	3.15s		^{2}J(PP) = 18.2	

[a] Spectra measured at 250 MHz (*ca* +20°C); chemical shifts (δ) in ppm (±0.01) to high frequency of $SiMe_4$.
[b] Spectra measured at 100.6 MHz (*ca* +20°C); chemical shifts (δ) in ppm (±0.1) to high frequency of 85% H_3PO_4.
[c] Coupling constants in hertz.
[d] s, singlet; d, doublet; dd, doublet of doublets; t, triplet; m, multiplet.
[e] δ[*H*(6)]: **a**, 7.68d [^{3}J[H(6)H(5)] = 8.8 Hz]; **b**, 7.95d [^{3}J[H(6)H(5)] = 8.9 Hz].
[f] Other protons: **4b**, 6.90s, 2.42s, 2.28s; **5b**, 6.94s, 2.31s, 2.17s; **6b**, 6.94s, 2.38s, 2.32s; **7b**, 6.98s, 2.36s, 2.17s; **8b**, 6.94s, 2.38s, 2.33s; **9b**, 6.92s, 2.27s, 2.10s; **10b**, 6.67s, 2.23, 2.17s; **11b**, 6.67s, 2.28s, 2.21s.

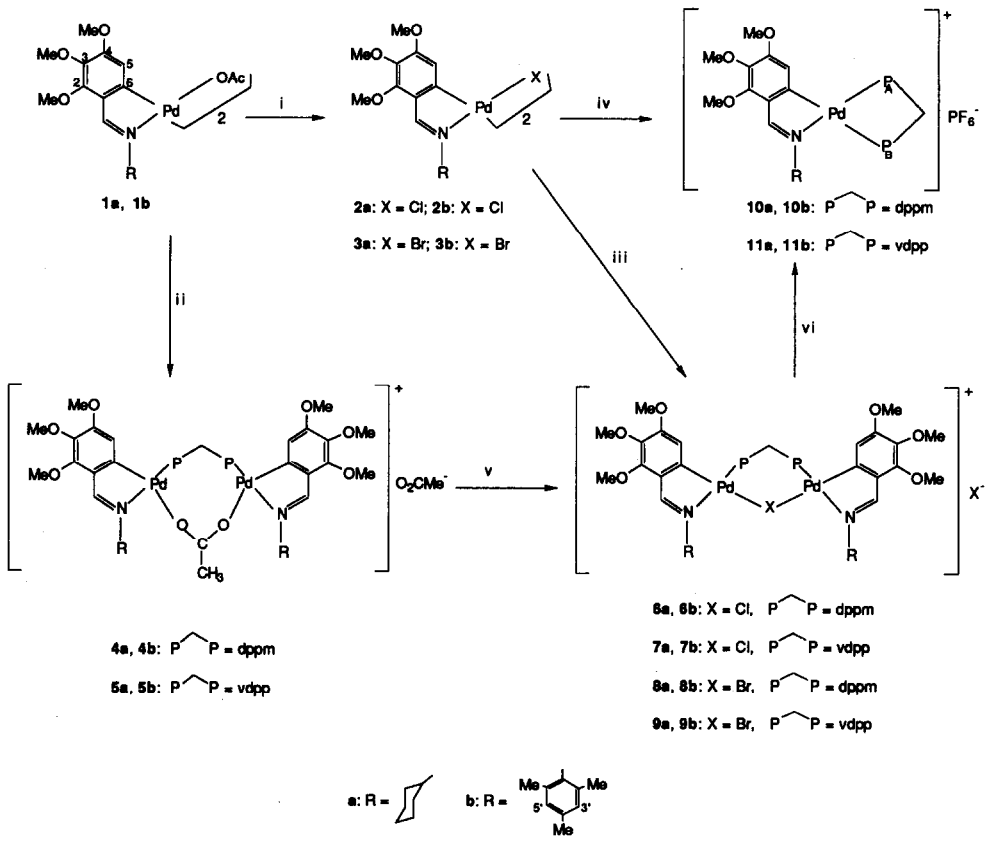

Fig. 1. (i) NaX in aqueous acetone; (ii) 1 equiv. dppm or vdpp in acetone; (iii) 1 equiv. dppm or vdpp in acetone; (iv) 2 equiv. dppm or vdpp + NH_4PF_6 in acetone; (v) NaX in aqueous acetone; (vi) 1 equiv. dppm or vdpp + NH_4PF_6 in acetone.

tons [H(3)′, H(5)′, CH_3, CH_3O] have been assigned unequivocally from chemical shift data and relative intensities (Table 2). The values of the conductivity data (130–155 Ω^{-1} cm^2 mol^{-1} in 10^{-3} mol dm^{-3} solutions in dry acetonitrile) indicate the compounds to be 1 : 1 electrolytes.[16]

Treatment of the acetato-bridged dimer complexes, **1a** and **1b**, with the diphosphines dppm or vdpp in a 1 : 1 dimer–diphosphine molar ratio gave the hitherto unknown complexes **4a**, **5a**, **4b** and **5b**, where one acetato ligand has been replaced by a diphosphine ligand to yield a dinuclear complex with two different bridging ligands. The complexes have been fully characterized by their microanalysis (C, H, N), IR and $^{31}P\{^1H\}$ and ^1H NMR spectroscopy (see Experimental, Tables 1 and 2 and Fig. 1). The IR spectra show the characteristic ν(COO) bands at 1565, 1407 (**4a**), 1575, 1405 (**5a**), 1576, 1400 (**4b**) and 1572, 1405 (**5b**) cm^{-1}; their separation, in each compound, is characteristic of a bridging acetato group.[17] These bands remain when the acetato anion was exchanged for the hexafluorophosphate ion by treatment with NH_4PF_6, showing that they are due to the bridging acetato group. The ^1H NMR spectra show singlets at δ 2.17 (**4a**), 2.13 (**4b**), 0.56 (**5a**) and 0.67 (**5b**) ppm for the O_2CMe(bridging) protons; the lower frequency shift of the latter two resonances is due to the shielding influence of the nitrogen-bonded aromatic ring. The $^{31}P\{^1H\}$ NMR spectra show a singlet, suggesting the two ^{31}P nuclei to be equivalent.

Treatment of the halide-bridged dimer complexes (**2a**, **3a**, **2b**, **3b**) with dppm or vdpp in a 1 : 1 dimer–diphosphine molar ratio gave the complexes (**6–9**)**a** and (**6–9**)**b** where the two metal centres are bridged by a diphosphine ligand and a halogen atom (see Experimental, Tables 1 and 2). These compounds could also be prepared in good yield by treatment of the parent acetato complexes (**4a**, **5a**, **4b**, **5b**) with aqueous sodium chloride or bromide (see Fig. 1). They are 1 : 1 electrolytes (*vide supra*), in contrast to similar compounds reported with bis(diphenylphosphino)ethane (dppe),[18] in which there are two terminal Pd—X bonds and the molecule is not ionic, in accordance with the larger "bite" of dppe as opposed to dppm or vdpp. The IR spectra show only one ν(Pd—X) band for each compound; its rather low frequency suggesting the halogen is *trans* to carbon rather than nitrogen.[19,20] These IR results are in agreement with a parallel disposition

of the Schiff base ligands; in an antiparallel arrangement the halogen atom would be *trans* to the phenyl carbon of one ligand and *trans* to the imine nitrogen of the other, resulting in two different IR ν(Pd—X) bands. The CH_3O[C(4)] NMR resonance is shifted to lower frequency due to the shielding effect of the phosphine phenyl ring.[7] In an antiparallel arrangement one would observe two different resonances for the two inequivalent CH_3O[C(4)] groups, as one of them would not be influenced by the phenyl ring of the phosphine. In a similar complex, the X-ray single crystal determination shows this geometry to be correct.[11]

Reaction of the halide-bridged dimer complexes (**2a**, **3a**, **2b**, **3b**) with dppm or vdpp, and NH_4PF_6, in a dimer–diphosphine 1 : 2 molar ratio affords the mononuclear species **10a**, **11a**, **10b** and **11b**. These can also be made by treatment of (**6–9**)**a** and (**6–9**)**b** with dppm or vdpp, and NH_4PF_6. The final products are identical, whether the chloro or bromo species is used, as the halogen is exchanged by the hexafluorophosphate ion. The $^{31}P\{^1H\}$ NMR shows two doublets for the two inequivalent phosphorus nuclei. The lower frequency doublet is assigned to the phosphorus nucleus *trans* to the phenyl carbon, C(6), and the higher frequency doublet to the phosphorus nucleus *trans* to the imine nitrogen. This is based on the assumption that a ligand of greater *trans* influence shifts the ^{31}P resonance of the phosphorus nucleus *trans* to it to lower frequency.[21] Selective decoupling experiments on compounds **10a**, **11a**, **10b** and **11b** confirm this. *H*(5) gives rise to a doublet of doublets because of coupling to both phosphorus nuclei [^4J(PH) *ca* 11 and 8 Hz]. The HC=N proton resonance (doublet) is coupled only to one phosphorus nucleus [^4J(PH) *ca* 7.5 Hz], presumably that *trans* to it. Selective irradiation of the P_B resonance (assuming this to be the ^{31}P nucleus *trans* to the phenyl carbon atom) reduces the *H*(5) resonance to a doublet [^4J(PH) *ca* 8 Hz], whilst the *H*C=N resonance remains a doublet [^4J(PH) *ca* 7.5 Hz]. Selective irradiation of the P_A resonance reduces the *H*(5) resonance to a doublet [^4J(PH) *ca* 11 Hz] and the *H*C=N resonance to a singlet. Selective irradiation also allows the correct assignment of the $^2J(PCH_2)$ couplings (Table 2).

Acknowledgements—We wish to thank Dr X. L. R. Fontaine (University of Leeds) for some helpful discussions and the Spanish Ministerio de Educacion y Ciencia (DGICYT) for funding.

REFERENCES

1. M. I. Bruce, *Angew. Chem. Int. Edn Engl.* 1977, **16**, 73.
2. I. Omae, *Chem. Rev.* 1979, **79**, 289.
3. I. Omae, *Coord. Chem. Rev.* 1984, **53**, 261.
4. V. V. Dunina, O. A. Zalevskaya and V. M. Potapov, *Russ. Chem. Rev.* 1988, **57**, 250.
5. A. D. Ryabov, *Synthesis* 1985, **3**, 233.
6. J. M. Vila, A. Suarez, M. T. Pereira, E. Gayoso and M. Gayoso, *Synth. React. Inorg. Met.-Org. Chem.* 1988, **18**, 47.
7. J. M. Vila, A. Suarez, M. T. Pereira, E. Gayoso and M. Gayoso, *Polyhedron* 1987, **6**, 1003.
8. J. M. Vila, M. T. Pereira, E. Gayoso and M. Gayoso, *Transition Met. Chem.* 1986, **11**, 342.
9. A. Suarez, J. M. Vila, M. T. Pereira, E. Gayoso and M. Gayoso, *J. Organomet. Chem.* 1987, **335**, 359.
10. J. M. Vila, J. M. Ortigueira, M. C. Rodriguez, M. T. Pereira and M. Gayoso, unpublished results.
11. J. M. Vila, J. M. Ortigueira, E. Gayoso, M. Gayoso, A. Castineiras, W. Hiller and J. Strahle, *Inorg. Chim. Acta*, accepted.
12. D. D. Perrin, W. L. F. Armarego and D. R. Perrin, *Purification of Laboratory Chemicals*, 2nd edn. Pergamon Press, Oxford (1983).
13. I. J. Colquhoun and W. McFarlane, *J. Chem. Soc., Dalton Trans.* 1982, 1915.
14. H. Onoue and I. Moritani, *J. Organomet. Chem.* 1972, **43**, 431.
15. Y. A. Ustinyuk, V. A. Chertov and J. V. Barinov, *J. Organomet. Chem.* 1971, **29**, C53.
16. W. J. Geary, *Coord. Chem. Rev.* 1971, **7**, 81.
17. K. Nakamoto, *IR and Raman Spectra of Inorganic and Coordination Compounds*, 4th edn. Wiley-Interscience, New York (1986).
18. J. Dehand, M. Pfeffer and M. Zinsius, *Inorg. Chim. Acta* 1975, **13**, 229.
19. R. C. Elder, R. D. P. Cruea and R. F. Morrison, *Inorg. Chem.* 1976, **15**, 1623.
20. B. Crociani, R. Boschi, R. Pietropaolo and U. Belluco, *J. Chem. Soc. A* 1970, 531.
21. P. S. Pregosin and R. W. Kunz, ^{31}P and ^{13}C NMR of Transition Metal Phosphine Complexes, in *NMR* 16 (Edited by P. Diehl, E. Fluck and R. Kosfeld). Springer, Berlin (1979).

Polyhedron Vol. 9, No. 22, pp. 2747–2750, 1990
Printed in Great Britain

0277–5387/90 $3.00+.00
© 1990 Pergamon Press plc

COPPER COMPLEXES OF 2-THIOURACIL

YANG WEI-DA* and HU YIN-PING

Department of Chemistry, East China Normal University, Shanghai 200062, P.R.C.

(*Received* 7 *November* 1989; *accepted* 1 *August* 1990)

Abstract—The preparation of five copper complexes of 2-thiouracil (turH) is described. Their stoichiometric formulae, confirmed by elemental analysis and molecular weight determination in DMSO, are as follows: $Cu(turH)_2Cl$ (**II**), Cu(turH)Br (**III**), $Cu_2(turH)_3Cl_2$ (**IV**), $Cu_4(tur)_4$ (**V**) and Cu(tur)Cl (**VI**). Their tentative structures have been assigned on the basis of IR and electronic spectra, molar conductance and magnetic susceptibility data. The turH acts as a monodentate ligand via its exocyclic sulphur in **II** and **IV**, but is bidentate in **III** and **VI** by using SN(3) and ON(3) donor sets, respectively. However, in tetramer **V** it seems more likely that the deprotonated ligand behaves as a tridentate bridge. In addition, the only copper(II) complex which has been isolated might take the dimeric structure through the oxygen bridges in its crystal lattice.

2-Thiouracil (turH) (**I**) is known as a basic constituent of some t-RNAs[1] and exhibits anti-tumour and anti-thyroid activity because it readily incorporates into nucleic acids.[2] The interactions of various transition metal ions with nucleo-bases have attracted much attention in the past decade. However, little work has been carried out regarding the nature of turH complexes formed with the monovalent copper.[3] In this paper we will report the synthesis and the binding sites which occur in five novel copper complexes based on their various physicochemical properties.

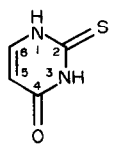

(I)

EXPERIMENTAL

Materials

2-Thiouracil was purchased from the Shanghai Chemical Reagent Factory No. 2, and used after recrystallization from acetone. All the remaining chemicals were reagent grade.

Preparation of the complexes

A warm solution of turH (150 mg, 1.18 mmol) in acetone (150 cm^3) was added dropwise to a methanolic solution (30 cm^3) of $CuCl_2 \cdot H_2O$ (285 mg, 1.68 mmol). After refluxing and stirring for 2 h, light yellow crystals (complex **II**) gradually separated. These were hot filtered off, thoroughly washed with methanol and acetone and finally dried *in vacuo*. The yield obtained was approx. 20%.

Complex **III** was readily prepared by the same procedure except that $CuBr_2$ was used as the appropriate halide. The pale yellow coloured product was isolated in *ca* 35% yield.

Complex **IV** was prepared by dropping a suspension of ligand (320 mg, 2.50 mmol) in warm 6% HCl (10 cm^3) into an aqueous solution (5 cm^3) of cupric acetate (250 mg, 1.25 mmol), with constant stirring. An additional portion of 6% HCl (3–4 cm^3) was subsequently added, until a yellow–green powder resulted from the turbid black coloured solution. After further stirring for 3 h the solution turned light green and the colour of the suspended solid changed to pale yellow. The crude product was filtered and purified in a 4 : 1 (v/v) mixed solvent of acetone and ethanol. The final product was obtained in a 24% yield.

* Author to whom correspondence should be addressed.

The preparation of complex **V** was essentially the same as presented above for the initial reaction, except that rapid filtration followed as soon as the yellow–green solid appeared in the reaction mixture. The precipitate was then purified by the same procedure as described earlier. The resulting solid was ivory coloured, with a yield of *ca* 17%.

The cupric complex **VI** was obtained by the same method as for complex **II** but with a molar ratio of 1:1 (the actual quantity of both reactants used was 0.8 mmol) and simply using methanol as the reaction medium. The resulting compound was a yellow–green microcrystalline product in a yield of *ca* 50%. In this case, the reason why the ligand does not exhibit its reducing power is still obscure.

Physicochemical measurements

IR spectra were recorded on a Perkin–Elmer 580B spectrometer using KBr discs. Electronic spectra were obtained on a Beckman DU-7 spectrometer using DMSO as the solvent. Conductivity measurements were made in 10^{-3} mol dm^{-3} dimethylformamide at 20°C with a DDS-11A conductivity meter. Magnetic susceptibility data were determined by a Faraday's balance, employing Mohr's salt as the calibrant. The molecular weight of each complex was obtained using the Rast method and extrapolating the freezing-point depression data for various concentrations in DMSO as its molality approached infinite dilution. EPR spectra were obtained with a JES-FE2XG spectrometer and g values were calculated using the double calibrant method.[4]

RESULTS AND DISCUSSION

The analytical and some relevant physicochemical data of the title complexes are shown in Table 1. The results from the molecular weight determination show that all the complexes are monomeric in DMSO, except complex **V** which is a tetramer. The magnetic and visible spectral data show that all the copper in **II**–**V** is cuprous, but bivalent in **VI**. The low molar conductivities of the title complexes in DMF indicate non-electrolytic behaviour.[5] The considerable magnitude of Λ_M (34–39 S cm^2 mol^{-1}) obtained may be due to some ligand exchange between the strong polar solvent molecule and the halide group. The small value (*ca* 18 S cm^2 mol^{-1}) for complex **V** probably arises from the partial degradation of the tetramer (which is less soluble in DMF) caused by heating during the preparation of the tested solution.

The characteristic IR data for the free ligand and the complexes are presented in Table 2. It is clear

Table 1. Analytical and other physicochemical data for copper complexes

Complex		C (%)	H (%)	N (%)	Cu (%)	Molecular weight	Λ_m [a]	λ_{max} [b]	Effective magnetic moment (BM)
$Cu(turH)_2Cl$	(II)	26.7(27.0)[c]	2.2(2.3)	15.5(15.8)	17.6(17.9)	335(355)[d]	38.0	Nil	Diamagnetic
Cu(turH)Br	(III)	18.0(17.7)	1.3(1.5)	10.2(10.3)	22.8(23.4)	252(272)	33.8	Nil	Diamagnetic
$Cu_2(turH)_3Cl_2$	(IV)	25.9(24.7)	1.6(2.0)	14.6(14.4)	21.1(21.8)	563(582)	39.0	Nil	Diamagnetic
Cu(tur)	(V)	25.6(25.2)	1.8(1.6)	13.9(14.7)	32.7(33.3)	697(763)[e]	17.6	Nil	Diamagnetic
Cu(tur)Cl	(VI)	21.2(21.2)	1.7(1.3)	12.3(12.4)	28.4(28.1)	235(226)	37.0	825	1.98 (295 K), 1.34 (77 K)

[a] Millimolar conductivity in DMF.
[b] Maximum absorption (nm) in visible region in DMSO.
[c,d] Calculated data given in parentheses.
[e] Data for tetramer.

Table 2. Selected IR bands of the ligand and complexes (cm^{-1})

Compound		O—H	N—H	C=O	Thioamide band I	Thioamide band II	Thioamide band IV
turH	(I)	—	3090s,br	1685s	1570s	1217s	838m
$Cu(turH)_2Cl$	(II)	—	3090s,br	1685s	1558s	1208s	835m
Cu(turH)Br	(III)	3480w,br	3100s	1672s	1553s	1210s	832m
$Cu_2(turH)_3Cl_2$	(IV)	—	3100s,br	1685s	1560s	1210s	833m
$Cu_4(tur)_4$	(V)	3400m,br	3100s,br	1675s	1530s, 1510s	1213m	822m
Cu(tur)Cl	(VI)	—	3085s	—	1566s	1224s	838m

that thioamide bands I, II and IV for all the complexes shift towards lower frequencies, as compared to the free turH and among these the largest band-shift is noted for thioamide band I. It is reasonable to expect that the thiocarbonyl sulphur of turH (or tur^-) is used in bonding in **II**–**V**, since copper(I) is a soft acid in nature, but their bonding modes seem to be different. If copper(I) is given the common coordination number of three, possible structures for **II** and **IV** may be depicted as shown in Fig. 1(a) and (b). The bathochromic shift of the C=O group, along with the concomitant appearance of the absorption of ν(O—H) (*ca* 3500 cm^{-1}) in the IR spectra for **III** and **V**, implies that N(3) of the pyrimidine ring also coordinates to the metal.[6] Thus the structure for **III** may be illustrated as in Fig. 1(c). Moreover, in the case of **V** a new spectral feature was observed, i.e. splitting of the thioamide band I into a doublet, which shifts to lower wavenumbers (1510 and 1530 cm^{-1}). If compared to the other cuprous complexes, this is presumably a sign that tur^- serves as a tridentate bridge involving a N(1)SN(3) donor set, hence, Fig. 1(d) would be expected for the tentative structure of $Cu_4(tur)_4$. The most informative compound among those reported is the cupric complex, in which the binding sites of the ligand are more likely to be the ON(3) bite rather than the SN(3) ligand coordination sphere, as evidenced by the disappearance of the vibration of the C=O group, and the thioamide band IV remaining constant, which is considered to be mainly due to the contribution from ν(C=S).[7]

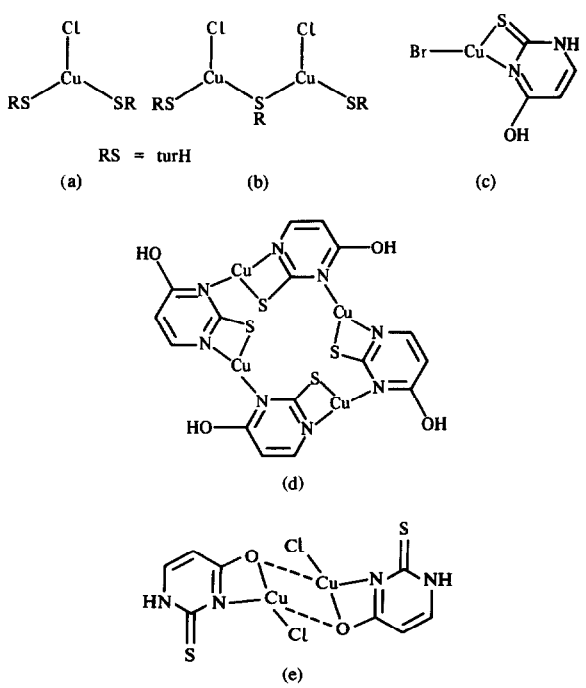

Fig. 1. Postulated structures for the copper complexes: (a) $Cu(turH)_2Cl$, (b) $Cu_2(turH)_3Cl_2$, (c) Cu(turH)Br, (d) $Cu_4(tur)_4$ and (e) dimer of Cu(tur)Cl.

Although complex **VI** is shown to be a monomer by the molecular weight determination, its effective magnetic moment at 77 K (1.34 BM) is considerably lower than in the literature (1.70–2.20 BM),[8] which indicates moderate antiferromagnetic coupling between the adjacent copper(II) centres. The polycrystalline *X*-band EPR data for **VI** are consistent with the magnetic susceptibility measurements mentioned above. In addition to the strong full-field transitions observed (g value of 2.2 at 3100 G), a weak half-field transition signal (corresponding to $\Delta M_s = \pm 2$) with a g value of *ca* 4.3 at 1170 G was also examined. The appearance of the latter signal provides further support to the postulated spin-coupled species in the solid complex.[9,10] Consequently, a dimeric form would be taken in the lattice for the copper(II) complex [Fig. 1(e)]. On account of the magnetic data, an O-bridged structure seems to be preferred to a Cl-bridged structure because of the greater antiferromagnetism normally given by the former in binuclear copper(II) species. Nevertheless, with such stereochemical conditions both the copper(II) and μ-oxygen atoms are forced to form less stable, fused four-membered rings. Con-

sidering the same circumstances as in the molecular weight determination previously discussed, the possibility of complex **III** accepting a dimer form is also not excluded. Attempts to grow single crystals of complex **V** suitable for X-ray study have proved unsuccessful.

Acknowledgement—The authors wish to thank the National Natural Science Foundation of China for financial support, under the Grant 2860358.

REFERENCES

1. M. Y. W. Yu, J. Sediak and R. H. Lindsay, *Arch. Biochem. Biophys.* 1973, **155**, 111.
2. J. F. Holland, R. Guthrie, P. Sheeke and H. Tieckelmann, *Cancer Res.* 1958, **18**, 776.
3. G. W. Hunt and E. L. Amma, *J. Chem. Soc., Chem. Commun.* 1973, 869.
4. H.-Q. Xue, *Physics* (Chinese) 1982, **12**, 170.
5. R. J. Angelici, *Synthesis and Technique in Inorganic Chemistry*, 2nd edn, p. 213. Saunders, Philadelphia (1977).
6. J. F. Villa and H. C. Nelson, *J. Indian Chem. Soc.* 1978, **55**, 631.
7. I. P. Khullar and U. Agarwala, *Aust. J. Chem.* 1974, **27**, 1877.
8. B. N. Figgis and J. Lewis, in *Modern Coordination Chemistry* (Edited by J. Lewis and R. G. Wilkins), Ch. 6. Interscience Publishers, New York (1960).
9. J. F. Villa, R. Doyle, H. C. Nelson and J. L. Richards, *Inorg. Chim. Acta* 1977, **25**, 49.
10. H. C. Nelson and J. F. Villa, *Inorg. Chim. Acta* 1979, **34**, L235.

Polyhedron Vol. 9, No. 22, pp. 2751–2757, 1990
Printed in Great Britain

0277–5387/90 $3.00+.00
Pergamon Press plc

FERROCENYL LIGANDS—II. IN SEARCH OF REDOX-ACTIVE FERROCENYL LIGANDS. THE PREPARATION AND CHARACTERIZATION OF TWO SCHIFF'S BASE DERIVATIVES OF 1,1′-DIACETYLFERROCENE. THE CRYSTAL AND MOLECULAR STRUCTURE OF THE 2-PYRIDYLHYDRAZONE OF 1,1′-DIACETYLFERROCENE

A. HOULTON, J. R. DILWORTH, R. M. G. ROBERTS* and J. SILVER*

Department of Chemistry and Biological Chemistry, University of Essex, Wivenhoe Park, Colchester CO4 3SQ, U.K.

and

M. G. B. DREW*

Department of Chemistry, University of Reading, Reading RG6 2AD, U.K.

(*Received* 14 *May* 1990; *accepted* 6 *August* 1990)

Abstract—With the aim of producing redox-active ferrocenyl ligands, the synthesis and characterization of two arylhydrazones, phenyl (**1**) and pyridyl (**2**), of 1,1′-diacetylferrocene (DAF) are reported. The X-ray crystal and molecular structure of **2**, as its acetate salt, has been determined and refined to $R = 0.072$ for 3449 independent reflections; $[FeC_{24}N_6H_{26}]^{2+} \cdot 2[CH_3CO_2]^-$ crystallizes in the triclinic, space group $P\bar{1}$, $a = 15.273(15)$, $b = 17.493(18)$, $c = 11.722(13)$ Å, $\alpha = 97.4(1)$, $\beta = 75.8(1)$, $\gamma = 70.4(1)°$, $U = 2781.5$ Å^3, $Z = 4$. The delocalization of the bonding observed in the substituents on the Cp rings is discussed in comparison with other relevant structures. Similar reactions of DAF with ethylamine, aniline or n-butylamine failed to yield new products.

Attempts to synthesize metal complexes from **1** and **2** failed to yield well characterized materials. In fact, the stability of both complexes in the presence of metal ions was low, with iron(III) species being produced. While not isolated in the pure form, this iron(III) species did not appear to be a ferrocinium derivative.

There is considerable current interest in the production of metal–metal interactions, particularly when these are between two different metals.[1] Of interest to us is the use of organometallic, particularly ferrocenyl, ligands to achieve this goal.[2,3] In addition to the wide variety of substitution patterns available for the ferrocenyl moiety, such molecules have the feature that the ferrocenyl group can, in principle, act as a redox centre.[4] This would permit the electronic "tuning" of a coordinated metal by oxidizing the ferrocenyl group to its ferricinium derivative.[5,6]

A further reason for interest in oxidizable ferrocenyl ligands is the fact that ferricinium ions have anti-tumour activity while the parent ferrocene has not.[7] Also, very recently, reports of the activity of platinum and gold complexes[8,9] of 1,1′-bis(diphenylphosphino)ferrocene (Fdpp) against experimental tumours have appeared. However, complexes of Fdpp do not readily undergo oxidation[10] and we have recently discussed why this should be the case.[11] The synthesis of oxidizable ferrocenyl ligands would allow the design of multifunctional drugs.

It is thus of considerable interest to synthesize ferrocenyl ligands with low oxidation potentials. Due to the acknowledged coordination chemistry of

* Authors to whom correspondence should be addressed.

Schiff's bases[12] we undertook a study of ferrocenyl derivatives with the above aim. We here report the reaction of some primary amines and arylhydrazines with 1,1′-diacetylferrocene (DAF). The stability and suitability of these complexes as ligands is discussed. The crystal and molecular structure of the 2-pyridylhydrazone of DAF is also presented and compared with relevant structures.

EXPERIMENTAL

The melting points are uncorrected. The ^{13}C NMR spectra were obtained on a Bruker WP80 FT spectrometer. The ferrocenyl carbons were numbered conventionally, C(1) being the *ipso*-carbon. The phenyl carbon resonances were numbered similarly and distinguished by primes. For the pyridyl derivatives the pyridine ring is numbered conventionally starting from the N atom. Analysis was performed at the University of Manchester, U.K. Mössbauer data were recorded at 80 K and isomer shifts (δ) are referred to natural iron at room temperature on a spectrometer previously described.[13] All solvents and reagents were used as purchased unless otherwise specified.

Reaction of DAF *and phenylhydrazine* (1)

DAF (1 g, 3.7 mmol) (Aldrich) was dissolved in dried ethanol (using 3 Å molecular sieve) (100 cm^3) and phenylhydrazine (2 cm^3, 20 mmol) (BDH) was added. The solution was refluxed for 1 h and the volume reduced to 25 cm^3. Cooling in ice overnight afforded dark red crystals which were filtered off, dried and stored in a desiccator. Compound **1** was obtained in 59.5% yield (m.p. 115–116°C). IR (cm^{-1}): 1600 ν(C=N). Found: C, 68.8; H, 5.8; N, 11.8. Calc. for $C_{26}H_{26}N_4Fe$: C, 69.3; H, 5.8; N, 12.4%.

1,1′-*Bis(pyridylhydrazone)* (2)

DAF (1 g, 3.7 mmol) (Aldrich) and 2-hydrazinopyridine (1 g, 9.2 mmol) (Aldrich) were dissolved in dried ethanol (100 cm^3) and 1 cm^3 of glacial acetic acid was added. The mixture was refluxed for 1 h and the volume then reduced to 25 cm^3. Cooling in ice overnight afforded dark red crystals which were filtered off, dried and stored in a desiccator. The compound was isolated as the acetate salt. Compound **2** was obtained in 82% yield (3 mmol) (m.p. 128–130°C). IR (cm^{-1}): 1610 ν(C=N). Found: C, 58.0; H, 5.4; N, 13.9. Calc. for $C_{28}H_{32}N_6O_4Fe$: C, 58.7; H, 5.6; N, 14.6%.

Primary amines with DAF

Reactions were tried with ethylamine, aniline and n-butylamine in place of the hydrazines. Changes of solvent to propan-1-ol and toluene and carrying the reaction out under nitrogen were also tried. In all cases no reaction was observed, DAF being recovered quantitatively.

X-ray data collection and structure determination of 2

The crystal structure determination was performed at the University of Reading.

The crystal data for $[FeC_{24}N_6H_{26}]^{2+} \cdot 2[CH_3CO_2]^-$, $M = 578.1$, triclinic, $a = 15.273(15)$, $b = 17.493(18)$, $c = 11.722(13)$ Å, $\alpha = 97.4(1)$, $\beta = 75.8(1)$, $\gamma = 70.4(1)°$, $U = 2781.5$ Å^3, $F(000) = 1200$, $D_m = 1.36$ g cm^{-3}, $Z = 4$, Mo-K_α radiation ($\lambda = 0.7107$ Å), μ(Mo-K_α) = 6.0 cm^{-1}, space group $P\bar{1}$, $R = 0.072$.

A crystal of approximate size 0.25 × 0.3 × 0.3 mm was set up to rotate about the a axis on a Stoe Stadi2 diffractometer and data were collected via variable width w scan. Background counts were 20 s and a scan rate of 0.0333 ° s^{-1} was applied to a width of $(1.5+\sin\mu/\tan\theta)$. 7122 independent reflections were measured, of which 3449 with $I > 3\sigma(I)$ were used in subsequent refinement.

The structure was determined by the heavy-atom method. All non-hydrogen atoms were refined anisotropically. Hydrogen atoms bonded to carbon were in fixed positions. The methyl hydrogen atoms were refined as rigid groups. Hydrogen atoms bonded to the nitrogen atoms were identified in a difference Fourier map and also included in fixed positions.

The structure was given a weighting scheme in the form $w = 1/[\sigma^2(F)+0.003F^2]$. The final R value was 0.072 ($R_w = 0.077$). In the final cycle of refinement all shift/error ratios were $< 0.3\sigma$. The final difference Fourier map showed no peaks greater than 0.8 e Å^{-3}. Calculations were carried out using SHELX76 and some of our own programs on the Amdahl V7 at the University of Reading.

RESULTS AND DISCUSSION

All attempts to prepare Schiff's base type complexes from DAF and primary amines such as ethylamine, aniline and n-butylamine failed to yield new products. In all cases DAF was recovered from the reaction mixtures. However, reactions did occur on replacement of the amines with substituted hydrazines (the phenyl and 2-pyridyl). In the latter case, glacial acetic acid was required for reaction to occur.

The Mössbauer data for the compounds prepared and DAF are presented in Table 1. The quadrupole splitting (QS) of 2.15(1) mm s^{-1} for DAF is in perfect agreement with the previously reported value[14] and indicates that the acetyl groups are electron-withdrawing. The QS increases however when the =O is replaced by either =NNHPh or =NNhPyH$^+$, but the values are still lower than ferrocene itself (QS = 2.37 mm s^{-1}) indicating that electron-withdrawal is still occurring, although to a lesser extent. We have previously shown there to be a linear correlation between QS and oxidation potential.[15] The increase in QS indicates a decrease in the oxidation potential for **1** and **2** compared to DAF.

However, electrochemical investigations revealed these complexes to be unsuitable as redox ligands. Preliminary cyclic voltammetry studies showed that chemical reactions were taking place in solution. In order to identify the reaction products, a controlled potential electrolysis (CPE) experiment was undertaken. CPE of **1** in MeCN at +0.8 V resulted in a dark brown solid which was analysed by Mössbauer spectroscopy. The resulting spectra showed two sites; a ferrocenyl site (86%) and a high-spin iron(II) site ($\delta \sim 1.24$ mm s^{-1}, $\Delta \sim 3.46$ mm s^{-1}) (14%). There was no evidence of a ferrocinium type site. In order to establish if this was an electrochemical reaction, a control experiment was carried out in which a sample of **1** was dissolved in MeCN under N_2 and stirred. Isolation of the resulting solid gave a Mössbauer spectrum very similar to that of the CPE study, indicating that **1** is not stable in solution even under N_2. This was a disappointing result with regard to our initial objectives.

Furthermore, all attempts to prepare metal complexes of **1** and **2** failed to yield well characterized materials. Reaction of **1** with zinc acetate, $ZnCl_2$, $Tl(ac)_2$, $CuCl_2$, $HgCl_2$, $NiCl_2 \cdot 6H_2O$ and $AgNO_3$ were tried. Analysis via ^{57}Fe Mössbauer spectroscopy (for selected data see Table 1) revealed at least two species in the isolated materials; commonly a ferrocenyl site (which sometimes matched those of the starting material although in one case (with $CuCl_2$) the parameters clearly matched those of DAF indicating hydrolysis had occurred), and one or more new sites with parameters around $\delta = 0.49$ mm s^{-1} and $\Delta = 0.82$ mm s^{-1}. These parameters are characteristic of an iron(III) species,[16] but unlike ferrocinium,[17] the most obvious oxidation product. Also the colour, brown, and the fact that under conditions where the only possible oxidant was oxygen, the site was still present would suggest that the species is not a ferrocinium type complex and is a decomposition product of the ferrocenyl moiety. Both **1** and **2** were sensitive to moisture and turned orange–brown (and **1** turned black on one occasion) on standing in air. Mössbauer spectroscopy of these latter materials revealed these samples to contain sites similar to those found with metal salts.

These results would indicate that oxygen is necessary for the formation of the iron(III) materials seen and tentatively suggest them to be μ-oxo iron(III) species,[18] especially as the spectra of these iron(III) species nearly always exhibited symmetric doublets.

Table 1. Mössbauer data (at 80 K)

	δ (mm s^{-1})	Δ (mm s^{-1})
DAF	0.51(1)	2.15(1)
1	0.53(1)	2.29(1)
2	0.53(1)	2.27(1)
1+$Zn(Ac)_2$	0.53(1)	2.29(1)
	0.49(1)	0.82(1)
1+$HgCl_2$	0.53(1)	2.29(1)
	0.49(1)	0.94(3)
1 CPE+0.8 V	1.24(3)	3.46(1)
	0.52(1)	2.09(2)
1+$AgNO_3$	0.46(1)	0.73(1)
1+$CuCl_2$	0.53	2.29[a]
	0.49	0.70
2+Tl acetate	0.53	2.27[a]
	0.32	0.61

[a] Site held.

The crystal and molecular structure of **2**

Table 2 contains selected bond distances and angles for **2**. The asymmetric unit consists of two independent $[FeC_{24}N_6H_{26}]^{2+}$ cations (A and B) and four independent $[CH_3CO_2^-]_2$ anions. Figure 1 shows the set of the three ions for the salt (A set shown) and includes the numbering sequence. Figure 2 shows a view of a $[C_{12}H_{13}N_3]$ fragment, hydrogen bonded to one acid molecule. Table 3 lists the O···N distances for this pairing. The O···N

Table 2. Selected bond lengths for **2**

Fe—$C_{(av)}$	2.070
C—$C(Cp)_{(av)}$	1.440
C(1)—$C(6)_{(av)}$	1.460
C=$N_{(av)}$	1.289
N—$N_{(av)}$	1.384
N—$C(Py)_{(av)}$	1.381

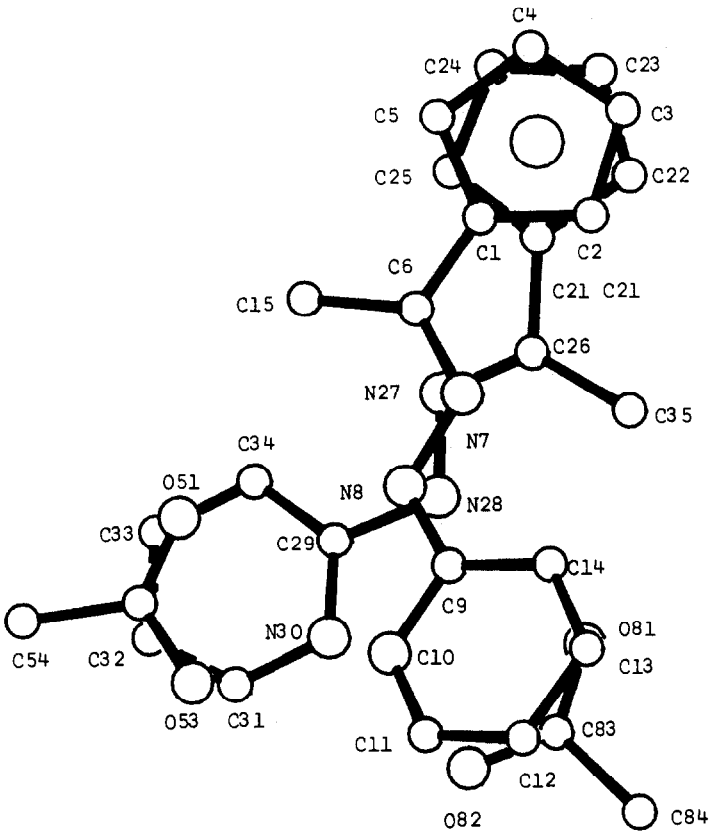

Fig. 1. Molecular structure of $[FeC_{24}N_6H_{26}]^{2+}$ $[CH_3CO_2^-]_2$ showing the atomic numbering scheme.

distances to the pyridine nitrogen are the shorter, within the range 2.58(2)–2.66(2) Å, with the corresponding distances to the aliphatic NH being in the range 2.94(2)–2.98(2) Å. The hydrogen bond scheme was compatible with the electron density observed in a difference Fourier map. For six of the eight linkages, the hydrogen atom was clearly identified bonded to the nitrogen atom; for the other two [N(30) and N(8B)], a peak was located closer to the nitrogen atom than to the oxygen atom but slightly further than the correct bonding distance. Figure 3 shows a profile view of the ferrocenyl cation alone to demonstrate the relative orientations of the Cp and pyridinium planes (see Table 4). In the acetate group all bond lengths are typical.[19–21]

Table 3. O···N distances for the anion–cation pair

	Molecule A (Å)	Molecule B (Å)
$N_{Ali}\cdots O$		
N(8)—O(*n*1)	2.98(2)	2.94(2)
N(28)—O(*m*1)	2.95(2)	2.95(2)
N(Py)···O		
N(10)—O(*n*2)	2.61(2)	2.58(2)
N(30)—O(*m*2)	2.66(2)	2.66(2)

n = 5 in A, 7 in B; m = 8 in A, 6 in B.

Table 4. Angles between the pyridyl and Cp planes[a]

	Molecule A (°)	Molecule B (°)
P(1)—P(2)	30.6	15.4
P(1)—P(3)	1.6	2.4
P(1)—P(4)	21.0	14.7
P(2)—P(3)	29.3	14.1
P(2)—P(4)	10.3	2.2
P(3)—P(4)	19.5	13.1

[a] Least-squares results for molecules A and B. All atoms included within planes are within 0.02 Å.
P(1), atoms C(1), C(2), C(3), C(4), C(5):
In A C(6) −0.04, N(7) 0.35; In B C(6) 0.06, N(7) 0.42
P(2), atoms C(9), N(10), C(11), C(12), C(13), C(14):
In A N(8) 0.06, N(7) 0.19; In B N(8) −0.00, N(7) 0.06
P(3) atoms C(21), C(22), C(23), C(24), C(25):
In A C(26)0.10,N(27) −0.07; InBC(26)0.15,N(27) −0.02
P(4), atoms C(29), N(30), C(31), C(32), C(33), C(34)
In A N(28) −0.05,N(27)0.08; InBN(28)0.05,N(27) −0.01.
Molecule B similarly labelled.

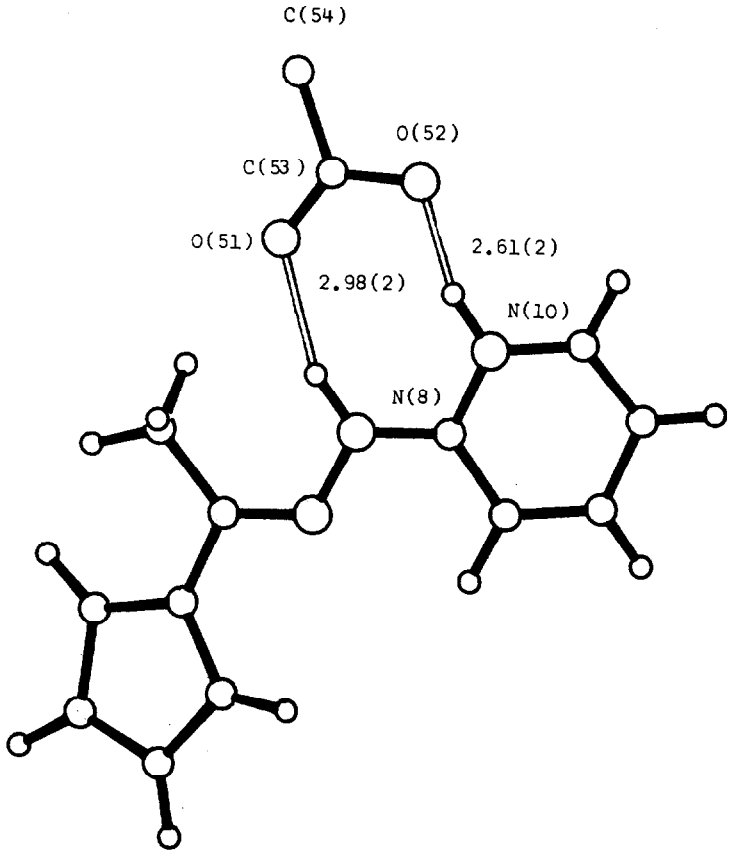

Fig. 2. View of the $[C_{12}H_{13}N_3]$ fragment hydrogen bonded to one acid anion. Hydrogen bonds are shown as unshaded lines.

As is apparent from Fig. 2, the $[FeC_{24}N_6H_{26}]^{2+}$ $[CH_3CO_2^-]_2$ grouping has approximately C_2 symmetry. The Fe—C distances are as expected for a ferrocene derivative,[22] ranging from 2.026(15) to 2.135(17) Å. The two Cp rings are staggered (all *trans* C—Fe—C angles are within 4° of 180°). This is quite unusual for a ferrocene derivative. We have surveyed a large number of substituted ferrocenes and have found the most common configuration to be eclipsed.[22] Previous studies of 1,1′-disubstituted ferrocenes, such as diacetylferrocene[23] and ferrocenedicarboxylic acid,[24] have

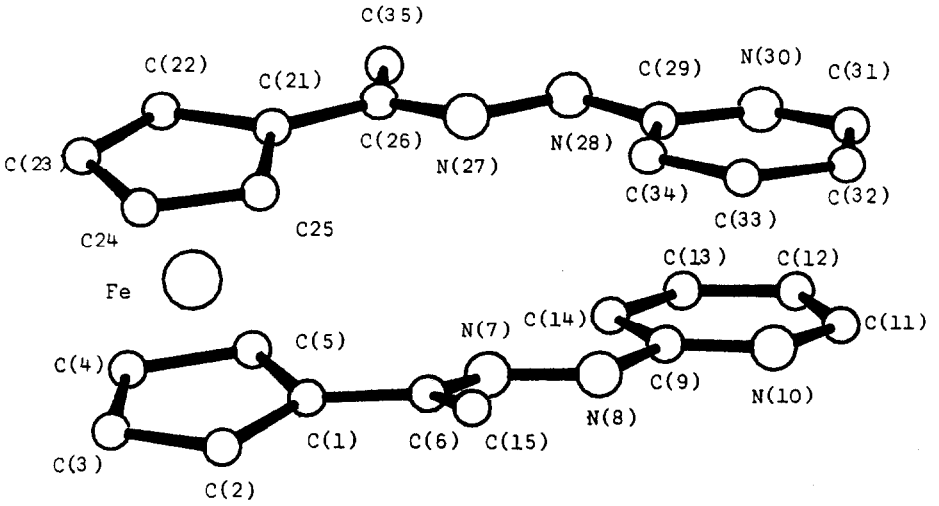

Fig. 3. Profile view of $[FeC_{24}N_6H_{26}]^{2+}$ showing the atomic numbering scheme.

eclipsed conformations with twist angles of 4.7° for the former and 1.6° for the latter.

The cyclopentadienyl rings in both molecules A and B are planar, as are the pyridine rings (see Table 3). The ring-tilt between the two Cp rings is small at 1.6 and 2.4° in A and B, respectively, giving a mean of 2.0°. The two pyridine rings are inclined at 10.3 and 2.2° with respect to each other for A and B. The angle α between the plane defined by the Cp and pyridine rings of each side chain exhibits a wide range, from 13.1 to 30.6°. The largest pair of angles are present in molecule A, with angles of 19.5 and 30.6°. There appears to be little chemical non-equivalence between the two substituent arms and hence these differences are probably due to packing forces.

Palenik *et al.*[25] have reported the structures of 5-hydroxy-2-formylpyridine thiosemicarbazone (5OH2FPTSC) and acetone thiosemicarbazone (ATSC). It is interesting to note that the former compound exhibits an *E* configuration as does the hydrazone prepared here. These authors also compared these structures with other semicarbazones and semicarbazides.[25] They showed that ATSC and various semicarbazides had a significantly longer average N(1)—N(2) bond length at 1.404(8) Å than did the semicarbazones (excluding ATSC) at 1.372(3) Å. They attributed the shortening as being due to the interaction of the N—N bond with the group attached to the sp^2 carbon of the C=N bond, concluding that aryl thiosemicarbazones could be treated as extensively delocalized systems.

Table 5 lists the structural parameters found by Palenik *et al.*,[25] with the corresponding distances for **2**. All the bond lengths and angles in **2** are typical, although the N—C bond at 1.377 Å is clearly the longest in the series and may reflect the fact that sulphur and not carbon is present as the terminal atom in the side chain of the thiosemicarbazones.

The average N—N distances of 1.384 Å in **2** indicates some interaction with the Cp ring, which is in accordance with the view of Palenik *et al.*[25] However, this is at the upper limit for such distances and suggests that the interaction is small.

Table 5. Comparison of the C=N—N—C fragments of **2** with some relevant structures

	C=N (Å)	N—N (Å)	N—C (Å)	Reference
$\mathbf{2}_{(av)}$	1.289	1.384	1.377	This work
5OHFPTSC	1.270	1.379	1.336	25
ATSC	1.286	1.398	1.342	25

^{13}C *NMR data*

The ^{13}C NMR data for the hydrazones and parent hydrazines appear in Table 6. The assignments of the phenyl resonances in the phenylhydrazones were made using the known additivity factors.[26] A similar approach was used for the 2-pyridyl carbons.[27] For the latter, good agreement was found between the observed and calculated shifts for the neutral pyridinyl substituent. This finding is at variance with the X-ray structure which shows an acetate molecule bound to hydrogens of the pyridinium and secondary amine nitrogen atoms. Such binding, however, must be weak and is disrupted in polar solvents such as acetone.

The cyclopentadienyl carbons C(3),C(4) (β) are deshielded relative to the C(2),C(5) (α) carbons, indicating electron-withdrawal by the hydrazone substituent. The β position in ferrocene shows similar effects to the *para* position in benzene,[28] the chemical shifts of which appear to be largely controlled by charge density. The C(3),C(4) resonances are about 2 ppm upfield from those of diacetylferrocene,[29] which supports the conclusion from the Mössbauer data that electron-withdrawal by the hydrazino group is less than that for the acetyl group. For the ferrocenylphenylhydrazone, the shift of the *para* [C(4)′] carbon is almost identical to that of phenylhydrazine itself, which suggests

Table 6. ^{13}C chemical shifts of hydrazones[a]

Hydrazone	C(1)	C(2)	C(3)	C(4)	C(1)′[b]	C(2)′	C(3)′	C(4)′	C(5)′	C(6)′	C=N	Me
$Fc(CMe{=}NNHPh)_2$	87.9[c]	67.8[c]	70.4[c]	—	142.3	113.6	129.7	119.5	129.7	113.6	147.4	13.7
$Fc[CMe{=}NNH(2\text{-}py)]_2$	87.1[c]	68.2[c]	70.8[c]	—	—	158.5	108.4	139.2	115.5	147.1	145.5	14.1
PhCMe=NNHPh	—	125.3[d]	128.1[d]	127.4[d]	—	113.0	128.8	119.2	128.8	113.0	146.1	11.4
PhCMe=NNH(2-Py)	—	126.2[d]	128.7[d]	128.7[d]	—	158.3	107.8	138.4	115.9	147.9	143.9	12.4

[a] In ppm from TMS.
[b] Primes refer to nitrogen-bound phenyl-carbon atoms.
[c] Ferrocenyl carbon signals.
[d] Carbon atoms of carbon-bound phenyl groups.

that the lone pair on the nitrogen atom of the secondary amine is not appreciably delocalized around the imine grouping. One point of particular interest is the geometry of the imine group. The above X-ray analysis clearly shows an *E* configuration. It has been demonstrated[30] that the stereochemistry of the imino group can be unambiguously determined in solution by the ^{13}C shifts of the carbon atoms in the α-position to the imine (in our case the methyl group). Thus hydrazones of *E* geometry have the α-carbon shifted upfield by 12–15 ppm relative to the parent ketone, whereas a *Z* geometry causes only a 3–6 ppm upfield shift. For both ferrocenylhydrazones in this study upfield shifts of about 14 ppm are found, showing that the *E* geometry is preserved in solution.

CONCLUSIONS

The instability of the hydrazones of DAF, reported here, precludes their use as organometallic ligands. This instability was not due to hydrolysis, resulting in DAF, as might have been expected, but the formation of an iron(III) product, which was not a ferrocinium type complex. We tentatively suggest, from Mössbauer data, that these species are μ-oxo iron(III) complexes. More importantly, however, these hydrazones did not show promise as ligands. Also, they did not appear to undergo the typically reversible ferrocene–ferrocinium oxidation, the second feature we were trying to achieve for the complexes. We note that while this manuscript was in preparation, reports of lanthanide complexes of the condensation products of formylferrocene and ferrocenylformyl acetone with benzoylhydrazine[31] and ethylenediamine,[32] respectively, were made. However, neither study investigated the possible redox behaviour of the complexes. In the latter case[32] Mössbauer data were reported and the QS for the series ranged from 2.24 to 2.27 mm s^{-1}. These values are relatively low and would indicate a high potential for the ferrocenyl oxidation in these complexes. We are continuing to investigate suitable redox-active ligands.

REFERENCES

1. O. Kahn, *Struct. Bond. (Berlin)* 1987, **69**, 89.
2. A. Houlton, P. T. Bishop, R. M. G. Roberts, J. Silver and M. Herberhold, *J. Organomet. Chem.* 1989, **364**, 381.
3. A. Houlton, R. M. G. Roberts, M. G. Drew and J. Silver, *J. Chem. Soc., Dalton Trans.* 1990, 1543.
4. N. G. Connelly and N. E. Geiger, *Adv. Organomet. Chem.* 1984, **23**, 1.
5. J. C. Kotz and C. L. Nivert, *J. Organomet. Chem.* 1973, **52**, 387.
6. J. C. Kotz, C. L. Nivert, J. M. Lieber and R. C. Reed, *J. Organomet. Chem.* 1975, **91**, 87.
7. P. Köpf-Maier, H. Köpf and E. W. Neuse, *J. Cancer Res. Clin. Oncol.* 1984, **108**, 336.
8. B. Longato, G. Pilloni, G. Valle and B. Corain, *Inorg. Chem.* 1988, **27**, 956.
9. D. T. Hill, G. R. Girard, F. L. McCabe, R. K. Johnson, P. D. Stupik, J. H. Zhang, W. M. Reiff and D. S. Eggleston, *Inorg. Chem.* 1989, **28**, 3529.
10. B. Corain, B. Longato, G. Fauero, D. Ajò, G. Pilloni, U. Russo and F. R. Kreissl, *Inorg. Chim. Acta* 1989, **157**, 259.
11. A. Houlton, J. R. Miller, R. M. G. Roberts and J. Silver, *J. Chem. Soc., Dalton Trans.* 1990, 2181.
12. F. A. Cotton and G. Wilkinson, *Advances in Inorganic Chemistry*, 5th edn. Interscience, New York (1988).
13. M. Y. Hamed, R. C. Hider and J. Silver, *Inorg. Chim. Acta* 1982, **66**, 13.
14. N. L. Good, J. Buttone and D. Foyt, *Ann. N.Y. Acad. Sci.* 1974, **239**, 193.
15. J. Silver and R. M. G. Roberts, *J. Organomet. Chem.* 1984, **263**, 235.
16. T. C. Gibb, *Principles of Mössbauer Spectroscopy*. Chapman and Hall, London (1980).
17. G. K. Wertheim and R. H. Herber, *J. Chem. Phys.* 1963, **38**, 2106.
18. P. G. Debrunner, in *Iron Porphyrins* (Edited by A. B. P. Lever and H. B. Grey), Part 3, p. 208. VCH, Deerfield, Florida (1989).
19. R. E. Jones and D. H. Templeton, *Acta Cryst.* 1958, **11**, 484.
20. V. Amirthalingam and V. M. Padnanabhan, *Acta Cryst.* 1958, **11**, 896.
21. J. N. Niekirk, F. R. L. Schoening and J. H. Talbot, *Acta Cryst.* 1953, **6**, 501.
22. R. M. G. Roberts, J. Silver, B. M. Yamin, M. G. B. Drew and U. Eberhardt, *J. Chem. Soc., Dalton Trans.* 1988, 1549.
23. G. J. Palenik, *Inorg. Chem.* 1970, **9**, 2424.
24. G. J. Palenik, *Inorg. Chem.* 1969, **8**, 2744.
25. G. J. Palenik, D. F. Rendle and W. S. Carter, *Acta Cryst.* 1974, **B30**, 2390.
26. D. F. Ewing, *Org. Magn. Reson.* 1979, **12**, 499.
27. E. Pretsch, T. Clerc, J. Seibl and W. Simon, in *Strukturaufklärung organischer Verbindungen*. Springer, Berlin (1976).
28. A. A. Koridze, P. V. Petrovskii, A. I. Mokhov and A. I. Lutsenko, *J. Organomet. Chem.* 1977, **136**, 57.
29. B. E. Mann and B. F. Taylor, *^{13}C NMR Data for Organometallic Compounds*. Academic Press, London (1981).
30. C. A. Bunnell and P. L. Fuchs, *J. Org. Chem.* 1977, **42**, 2614.
31. M. Yongxiang, M. Zhongqian, Z. Gang, M. Yun and Y. Min, *Polyhedron* 1989, **8**, 2105.
32. P. Hu, L. Zhang, X. Zhu, X. Liu, L. Ji and Y. Chen, *Polyhedron* 1989, **8**, 2459.

Polyhedron Vol. 9, No. 22, pp. 2759–2761, 1990
Printed in Great Britain

0277–5387/90 $3.00+.00
© 1990 Pergamon Press plc

COMMUNICATION

INELASTIC NEUTRON SCATTERING STUDY OF HYDRIDE LIGANDS IN $[(\mu_2\text{-H})_2Os_3(CO)_{10}]$: EVIDENCE FOR A DIRECT H—H INTERACTION

WILSON C-K. POON*

Department of Applied Physics and Physical Electronics, Portsmouth Polytechnic, Park Building, King Henry I Street, Portsmouth PO1 2DZ, U.K.

PAUL DALLIN

School of Chemical Sciences, University of East Anglia, Norwich NR4 7TJ, U.K.

BRIAN F. G. JOHNSON

University Chemical Laboratory, Lensfield Road, Cambridge CB2 1EW, U.K.

ELISABETH A. MARSEGLIA

Cavendish Laboratory, Madingley Road, Cambridge CB3 0HE, U.K.

and

JOHN TOMKINSON

Neutron Division, Rutherford Appleton Laboratory, Chilton, Didcot, Oxon OX11 0QX, U.K.

(*Received* 30 *January* 1990; *accepted* 29 *August* 1990)

Abstract—The inelastic neutron scattering (INS) spectrum of $[(\mu_2\text{-H})_2Os_3(CO)_{10}]$ has been recorded; bands due to M—H vibrations are clearly seen and evidence has been found for a direct interaction between the two hydrogen ligands.

Inelastic neutron scattering (INS) has long been used as a tool in the study of metal–hydrogen interactions in bulk metal hydrides[1] but, apart from an early communication by White and Wright,[2] the technique has not been exploited in the investigation of hydrido-ligands in transition metal cluster complexes. This is somewhat surprising, given the difficulties encountered in investigating M—H modes using IR and Raman spectroscopy due to their inherently weak intensities and large band widths. Conventionally, the detection and assignment of such bands relies on their preferential sharpening at lower temperature.[3] Even with such sharpening, however, overlap with other bands is still considerable, making band assignment and detailed modelling formidable tasks.

The triosmium cluster, $[(\mu_2\text{-H})_2Os_3(CO)_{10}]$, is unusual in that it contains 46 valence electrons and, consequently, is one of the relatively few examples of an unsaturated, low nuclearity cluster. Both single crystal X-ray and neutron diffraction studies have been carried out[5] and show that the central triangular osmium core contains one Os—Os distance which is considerably shorter (264 pm) than the other two (288 pm). This short edge is spanned

* Author to whom correspondence should be addressed. Now at Department of Physics, University of Edinburgh, Mayfield Road, Edinburgh EH9 3JZ, U.K.

by the two bridging hydrogen ligands and as such provides a rare example of a μ_2-H bridging system of the type observed in the molecular structure of diborane. We now wish to provide information which we believe provides evidence for a substantial H—H interaction of the type recently found for a number of mononuclear dihydrogen complexes.

In Fig. 1 is shown the INS spectrum of $[(\mu_2\text{-}H)_2Os_3(CO)_{10}]$ which has been obtained on the TFXA spectrometer at the ISIS pulsed neutron facilities of the Rutherford Appleton Laboratory. The physics of the neutron scattering process in general, and the "intensity optimized" nature of TFXA in particular, means that the only motion expected to be represented strongly in this spectrum is that due to the hydrogen atoms.[4] From previous work on hydrido-clusters,[6,7] we expect to and indeed do find modes in the 600–1600 cm^{-1} region; these are due mainly to M—H vibrations. In addition, there are two strong INS bands below *ca* 650 cm^{-1}. These bands are found at frequencies normally associated with M—C stretching and carbonyl bending vibrations (650–300 cm^{-1}); and M—M stretches and metal–carbon deformations (< 250 cm^{-1}), respectively. However, they are expected to couple with the M—H vibrations, thereby gaining intensity and consequently appearing in these regions of the INS spectrum. Lastly, the weak features found near 1400 cm^{-1} and above 1600 cm^{-1} may be assigned to overtones and combinations arising from the main M—H vibrations.

Quantitative calculations are in progress using the data analysis package CLIMAX, specially developed for INS spectra,[8] and the results have indicated the following noteworthy points.

(i) In the analysis of the M—H vibrations, interactions between the hydrogen ligands are found to be very important. For example, if such interactions are ignored then the two strongest peaks seen in the INS spectrum at *ca* 650 cm^{-1} would be expected to collapse into one. These interactions have been quantitatively modelled to provide an excellent fit with the INS data. Significantly, it is this observation which provides the first, clear example of H—H interactions of the type recently found in mononuclear dihydrogen complexes. These interactions are also of interest in the modelling of the behaviour of hydrogen on metal surfaces.

(ii) The bands below *ca* 650 cm^{-1} should allow a detailed investigation of hydrogen dynamics in response to carbonyl motion. This could have important implications for those interested in hydrogen migration in hydrido-clusters and in modelling the bulk–metal hydride bond[9] using hydridocarbonyl cluster compounds.

(iii) The availability of data on combinations and overtones will enable us to build up a detailed model of the anharmonic hydrogen local potential, which will eventually allow comparison with work along a similar direction on hydrogen potentials in bulk metals.[10]

We have also measured the INS spectrum of $[(\mu_2\text{-}H)_4Os_4(CO)_{12}]$ (Fig. 2). Although the structure of this material is known and μ_2-bridging hydrido-ligands suggested from a consideration of the Os—Os bond lengths,[11] the positions of the hydrogen atoms have not been resolved with certainty. Bearing in mind that INS is primarily a probe of local hydrogen dynamics, the striking similarity of the spectra of $[(\mu_2\text{-}H)_2Os_3(CO)_{10}]$ and $[(\mu_2\text{-}H)_4Os_4(CO)_{12}]$ immediately supports the assignment of μ_2-bridging hydrido-ligands to this structure. Detailed analysis of this spectrum using CLIMAX is also in progress.

In summary, we have shown that the technique

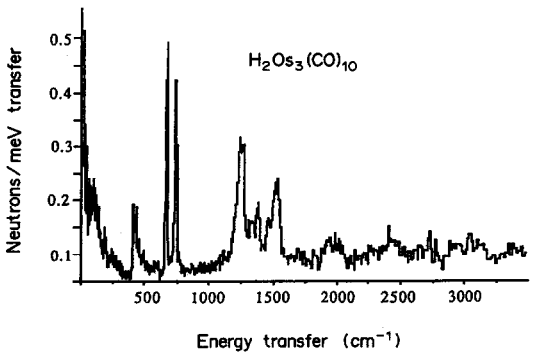

Fig. 1. The inelastic neutron scattering spectrum of $[(\mu_2\text{-}H)_2Os_3(CO)_{10}]$. The strongest bands in the 600–1600 cm^{-1} region are due to Os—H vibrations. Other bands are assigned in the text.

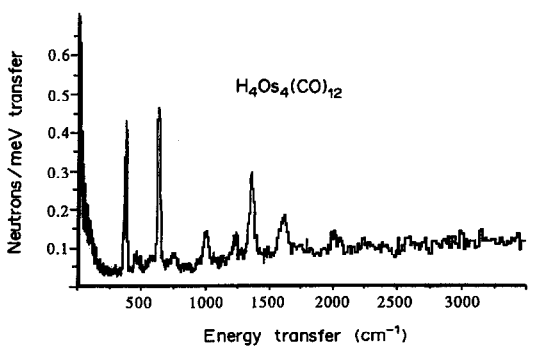

Fig. 2. The inelastic neutron scattering spectrum of $[(\mu_2\text{-}H)_4Os_4(CO)_{12}]$. The similarity with the spectrum in Fig. 1 strongly suggests the presence of μ_2-bridging hydrido-ligands in this material.

of INS spectroscopy is extremely useful in the detection and assignment of vibrational modes in hydridocarbonyl metal clusters. In particular we have indicated that, in $[(\mu_2\text{-H})_2Os_3(CO)_{10}]$, the interactions between the two hydrogen ligands are important and can be modelled quantitatively.

REFERENCES

1. For a recent review see, T. Springer, Hydrogen in metals I, Vol 28 of *Topics in Applied Physics* (Edited by G. Alefeld and J. Völkl). Springer, New York (1978).
2. J. W. White and C. J. Wright, *J. Chem. Soc., Chem. Commun.* 1970, 971.
3. See recent work by C. E. Anson, G. D'Alfonso, U. A. Jayasooriya and P. L. Stanghellini, *J. Organomet. Chem.* 1989, **372**, 85.
4. See J. Tomkinson, *Neutron Scattering at a Pulsed Source* (Edited by R. J. Newport, B. D. Rainford and R. Cywinski). Adam Hilger, London (1988).
5. A. G. Orpen, A. V. Rivera, E. G. Bryan, D. Pippard, G. M. Sheldrick and K. D. Rouse, *J. Chem. Soc., Chem. Commun.* 1978, 723.
6. I. A. Oxton, *Rev. Inorg. Chem.* 1982, **4**, 1.
7. H. Knözinger, *Metal Clusters in Catalysis* (Edited by B. C. Gates, L. Guozi and H. Knözinger). Elsevier, Amsterdam (1986).
8. Details on CLIMAX can be obtained through either John Tomkinson at the RAL or Don Kearley at the ILL (Grenoble).
9. See, for example, A. Dedieu and S. Nakamura, *Quantum Chemistry: The Challenge of Transition Metals and Coordination Chemistry* (Edited by A. Veillard), NATO ASI Series C, Vol. 176.
10. See, for example, J. Eckert, J. A. Goldstone, D. Tonks and D. Richter, *Phys. Rev. B* 1983, **27**, 1980, on the anharmonic potential of H in Nb and Ta.
11. B. F. G. Johnson, J. Lewis, P. R. Raithby and C. Zuccaro, *Acta Cryst.* 1981, **B37**, 1728.

Polyhedron Vol. 9, No. 22, pp. 2763–2765, 1990
Printed in Great Britain

0277–5387/90 $3.00+.00
Pergamon Press plc

COMMUNICATION

NEW SYNTHETIC PATHWAYS INTO THE ORGANOMETALLIC CHEMISTRY OF GALLIUM

MALCOLM L. H. GREEN,* PHILIP MOUNTFORD, GEOFFREY J. SMOUT and S. ROBERT SPEEL

Inorganic Chemistry Laboratory, South Parks Road, Oxford OX1 3AQ, U.K.

(*Received* 23 *July* 1990; *accepted* 4 *September* 1990)

Abstract—Ultrasonic irradiation of gallium metal with di-iodine and alkyl iodides, RI, rapidly gives high yields of $[RGaI_2]$ via a reactive intermediate material "GaI". "GaI" also inserts into the metal–iodine bonds of $[Fe(\eta\text{-}C_5H_5)(CO)_2I]$ and $[Mo(\eta\text{-}C_5H_4Me)(CO)_3I]$ as witnessed by the synthesis of $[Fe(\eta\text{-}C_5H_5)(CO)_2Ga(\eta^1\text{-}C_5H_4Me)_2\cdot$pyridine] and $[Mo(\eta\text{-}C_5H_4Me)(CO)_3GaI_2\cdot Et_2O]$, whose crystal structures have been determined.

We report an improved and very convenient synthesis for monoalkylgallium di-iodide compounds $[RGaI_2]$. Previous routes to these compounds have involved the exchange reaction between the reactive and costly Me_3Ga and GaI_3,[1] or prolonged thermal reaction (1–2 weeks) between Ga and I_2 or thermally prepared "GaI" with RI.[2] A metal vapour synthesis route gave mixtures of the mono- and di-alkylated derivatives.[3]

We have found that sonication of liquid gallium metal with di-iodine and alkyl iodides (RI) rapidly gives high yields of the monoalkylgallium di-iodides $[RGaI_2]$. Typically, gallium metal (0.70 g, 10 mmol), di-iodine (1.27 g, 5 mmol) and the alkyl halide (*ca* 2 cm^3) in toluene (10 cm^3) were sonicated under N_2 using a Heat-Systems Ultrasonics cell disruptor direct immersion horn sonicator, supplying *ca* 375 W, 20 kHz.[4]

The mixture was warmed to melt the gallium (m.p. 30°C) before sonication. Upon sonication the gallium metal dispersed, the initially purple mix becoming first grey and then, after 2–8 min, turning into a colourless solution. Recrystallization of the products from toluene gave high yields of white crystalline $[RGaI_2]$ [**1(a)**; R = Me (70%) (**b**); R = Et (82%) (**c**); R = ^{n}Pr (80%) (**d**); R = ^{i}Pr (55%) (**e**); R = ^{n}Bu (90%) (**f**); R = n-pentyl (76%); **1e**, **1f** liquid at room temperature]. Cryoscopic molecular weight determinations in *p*-xylene for **1a–c** indicate a degree of association of 1.6–1.9 (for *ca* 0.06–0.3 M in monomer equivalents).

Many Lewis adducts are known for alkylgallium dichlorides,[5] but adducts of $[RGaI_2]$ are confined largely to those of $MeGaI_2$ with R′SH (R′ = Me, Et, ^{n}Pr and ^{t}Bu).[6] Therefore, we have explored further reactions of $[RGaI_2]$.

Treatment of **1a–f** with Lewis bases [Et_2O, THF, pyridine, acridine, PMe_3, PPh_3, $P(OPh)_3$ and $AsPh_3$] gave 1:1 adducts, characterized by ^{1}H NMR and IR spectroscopy and mass spectrometry, all adducts showing a band near 540 cm^{-1} in the IR spectrum associated with ν(Ga—C). The adducts of **1b** with PPh_3 and $AsPh_3$ dissociate on subjection to EI mass spectrometry, but cryoscopic molecular weight determinations in *p*-xylene showed them to be essentially monomeric in this solvent.

Sonication of gallium metal and di-iodine in toluene in the absence of alkyl iodide gave a pale green powder "GaI" (**2**). This material is surprisingly reactive and behaves as a monovalent gallium system. Thus treatment of **2** with excess RI and stirring at room temperature overnight or sonicating for a few minutes gave the monoalkylgallium di-iodides (**1**). Treatment of **2** with toluene solutions of tetrahydrofuran or PPh_3 gave apparent disproportionation to products that analysed as $GaI_2\cdot$THF and $GaI_3\cdot PPh_3$, respectively,

* Author to whom correspondence should be addressed.

together with the corresponding quantity of gallium metal.*

The "GaI" prepared by sonication has a powder diffraction pattern that does not correspond either to that reported previously by Corbett or Chadwick and their co-workers,[7,8] or to those for low-valent gallium iodides reported by Gerlach *et al.*[9] It may, however, be similar to the thermally-prepared "GaI" of Wilkinson and Worral, which they showed to contain at least Ga, Ga_2I_3 and Ga_2I_4 by Raman spectroscopy.[2] Their "GaI" reacted much more slowly than our sonicated "GaI" with RI, possibly due to particle size effects. We were interested to see whether "GaI" (**2**) would undergo oxidative addition reactions with metal–iodine bonds. Room temperature reaction with [Fe(η-C_5H_5)$(CO)_2$I] and recrystallization of the product from ether gave [Fe(η-C_5H_5)$(CO)_2GaI_2\cdot(Et_2O)_n$] (**3a**). A similar but heated reaction of **2** with [Mo(η-C_5H_4Me)$(CO)_3$I] gave large amber crystals of [Mo(η-C_5H_4Me)$(CO)_3GaI_2\cdot Et_2O$] (**4a**). [Mo(η-C_7H_7)$(CO)_2$I] and [Mo(η-C_5H_4Me)$(CO)_3]_2$ gave [Mo(η-C_7H_7)$(CO)_2GaI_2\cdot$THF] (**5**) and [(Mo(η-C_5H_4Me)$(CO)_3)_2$GaI] (**6**) by essentially analogous reactions. The adducts **3a** and **4a** readily lose some ether, although the last traces are retained tenaciously. As with the simple alkylgallium di-iodides, both **3a** and **4a** readily undergo displacement of Et_2O to form 1 : 1 adducts with pyridine (**3b**, **4b**).

Treatment of **3a** with 2 equivalents of NaC_5H_4Me followed by reaction with pyridine

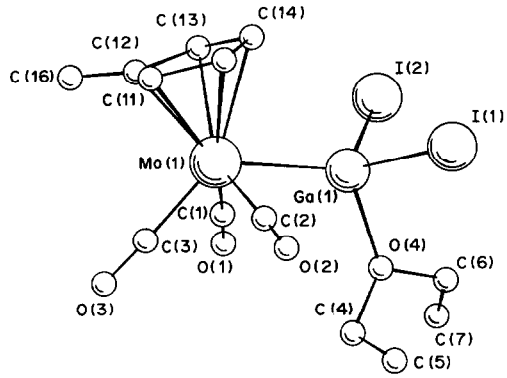

Fig. 1. Molecular structure of [Mo(η-C_5H_4Me)$(CO)_3$ $GaI_2\cdot Et_2O$] (**4a**). Hydrogen atoms omitted for clarity. Selected bond lengths (Å) and angles (°) as follows:

Mo(1)—Ga(1)	2.582(2)	Mo(1)—$Cp_{cent.}$	1.99
Mo(1)—C(1)	1.99(2)	Ga(1)—I(1)	2.593(2)
Mo(1)—C(2)	1.98(2)	Ga(1)—I(2)	2.582(2)
Mo(1)—C(3)	1.99(2)	Ga(1)—O(1)	2.04(1)

Mo(1)—Ga(1)—O(1)	115.8(3)
Mo(1)—Ga(1)—I(1)	122.06(9)
Mo(1)—Ga(1)—I(2)	113.88(9)
I(1)—Ga(1)—I(2)	106.20(9)
I(1)—Ga(1)—O(1)	96.9(3)
I(2)—Ga(1)—O(1)	98.4(3)
$Cp_{cent.}$—Mo(1)—Ga(1)	108.9

where $Cp_{cent.}$ refers to the computed centroid of the η-C_5H_4Me ring.

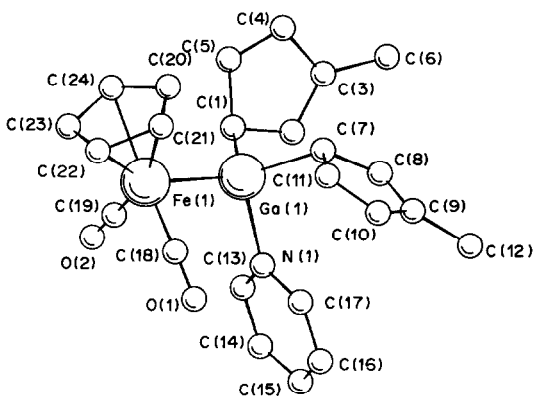

Fig. 2. Molecular structure of [Fe(η-C_5H_5)$(CO)_2$Ga(η^1-$C_5H_4Me)_2\cdot$pyridine] (**7**). Hydrogen atoms omitted for clarity. Selected bond lengths (Å) and angles (°) as follows:

Fe(1)—Ga(1)	2.4272(9)	Ga(1)—N(1)	2.101(4)
Fe(1)—C(18)	1.734(8)	Ga(1)—C(1)	2.076(5)
Fe(1)—C(19)	1.744(7)	Ga(1)—C(7)	2.058(5)
Fe(1)—$Cp_{cent.}$	1.73		

Fe(1)—Ga(1)—N(1)	108.9(1)
Fe(1)—Ga(1)—C(1)	113.6(2)
Fe(1)—Ga(1)—C(7)	119.1(2)
$Cp_{cent.}$—Fe(1)—G(1)	119.5

where $Cp_{cent.}$ refers to the computed centroid of the η-C_5H_5 ring.

* Satisfactory analyses have been obtained for all compounds except the Et_2O adducts, where all ether was removed before analysis. Compounds **1** and their adducts with Lewis bases were characterized by ^{1}H NMR, mass spectrometry and IR, all compounds showing bands in the Ga—C stretching region. ^{1}H NMR data for selected compounds {benzene[$^2H_6$]} at 300 MHz; chemical shifts (δ) in ppm.

3b: 9.12 (d, 2H, pyridine), 6.46 (t, 1H, pyridine), 6.23 (t, 2H, pyridine), 4.30 (s, 5H, η-C_5H_5). (**3c**; ether-free **3a**): 3.99 (s).

4a: 4.72 (d, 4H, η-C_5H_4Me), 3.80 (q, 4H, $(MeCH_2)_2O$), 1.59 (s, 3H, η-C_5H_4Me), 0.92 (t, 6H, $(MeCH_2)_2O$). **4b**: 9.03 (d, 2H, pyridine), 6.42 (t, 1H, pyridine), 6.16 (t, 2H, pyridine), 4.91, 4.84 (AA′, BB′, 4H, η-C_5H_4Me), 1.69 (s, 3H, η-C_5H_4Me).

5: 4.69 (s, 7H, η-C_7H_7), 3.95 (t, 2H, THF), 1.21 (m, 2H, THF).

6: 4.88, 4.77 (AA′, BB′, 4H, η-C_5H_4Me), 1.47 (s, 3H, η-C_5H_4Me).

7: 8.28 (d, 2H, pyridine), 6.71 (t, 1H, pyridine), 6.43 (br. s, 4H, η^1-C_5H_4Me), 6.41 (br., 2H, pyridine), 5.74 (br. s, 4H, η^1-C_5H_4Me), 4.35 (s, 5H, η-C_5H_5), 2.25 (s, 6H, η^1-C_5H_4Me).

gives pale diamond-shaped crystals of [Fe(η-C_5H_5)$(CO)_2$Ga(η^1-$C_5H_4Me)_2$·pyridine] (**7**) in modest yield.

The crystal structures of **4a** (Fig. 1) and **7** (Fig. 2) have been determined* and they confirm the presence of a transition metal–gallium bond in each compound. The Ga—Fe bond length of 2.4272(9) Å in **7** is comparable to those in [$(CH_2{=}CH)$Ga(THF)$Fe(CO)_4]_2$ of 2.510(1) and 2.521(2) Å.[10]

In conclusion, we have shown that sonication is a most convenient way of making alkylgallium diiodides. Sonochemically-produced "GaI" behaves as a highly-reactive monovalent gallium system and can provide a new route to compounds containing transition metal–gallium bonds.

*Crystal data for **4a**: $C_{13}H_{17}GaI_2MoO_4$, crystal dimensions *ca* $0.3\times0.4\times0.5$ mm, triclinic, space group $P\bar{1}$, $a = 12.570(5)$, $b = 10.049(14)$, $c = 11.919(18)$ Å, $\alpha = 138.47(7)$, $\beta = 91.12(7)$, $\gamma = 94.31(7)°$, $3 \leqslant 2\theta \leqslant 46°$, $V = 988.9$ Å^3, $D_c = 2.209$ g cm^{-3}, $Z = 2$, $\mu = 50.84$ cm^{-1}, $F(000) = 612$, $R = 0.068$, $R_w = 0.061$ for 2071 observed reflections [$I > 3\sigma(I)$].

Crystal data for **7**: $C_{24}H_{24}FeGaNO_2$, crystal dimensions *ca* $0.2\times0.2\times0.4$ mm, triclinic, space group $P\bar{1}$, $a = 9.828(2)$, $b = 10.134(3)$, $c = 12.955(7)$ Å, $\alpha = 121.29(3)$, $\beta = 96.34(3)$, $\gamma = 90.13(2)°$, $3 \leqslant 2\theta \leqslant 48°$, $V = 1093.1$ Å^3, $D_c = 1.474$ g cm^{-3}, $Z = 2$, $\mu = 19.15$ cm^{-1}, $F(000) = 496$, $R = 0.045$, $R_w = 0.057$ for 2303 observed reflections [$I > 3\sigma(I)$].

Data were collected using an Enraf–Nonius CAD4-F diffractometer employing graphite-monochromated Mo-K_α radiation ($\lambda = 0.71069$ Å). The heavy-atom positions were located using direct methods and the other non-hydrogen atoms located from subsequent difference syntheses. The structures were refined using full-matrix least-squares procedures with anisotropic thermal parameters for all non-hydrogen atoms. Hydrogen atoms were placed in calculated positions (C—H = 0.96 Å) with an isotropic thermal parameter of 1.3 times that of their supporting carbon atom, and refined riding on that carbon atom. Crystallographic calculations were carried out using the Oxford CRYSTALS package.[11] Atomic coordinates, bond lengths and angles, observed and calculated structure factors, and thermal parameters have been deposited at the Cambridge Crystallographic Centre.

REFERENCES

1. G. G. Hoffmann, *Z. Naturf.* 1985, **40B**, 335.
2. M. Wilkinson and I. J. Worral, *J. Organomet. Chem.* 1979, **166**, 293.
3. K. B. Starowieski and K. S. Klabunde, *Appl. Organomet. Chem.* 1989, **3**, 219.
4. K. S. Suslick (Ed.), *Ultrasound: Its Chemical, Physical and Biological Effects.* VCH Publishers, New York (1987).
5. U. Kruerke (Ed.), *Gmelin Handbook of Inorganic Chemistry: Organogallium Compounds, Part* 1. Springer, Berlin (1987).
6. G. G. Hoffmann, *Z. Anorg. Allg. Chem.* 1984, **514**, 196.
7. J. D. Corbett and R. K. McMullan, *J. Chem. Soc.* 1955, **77**, 4217.
8. J. R. Chadwick, A. W. Atkinson and B. G. Huckstepp, *J. Inorg. Nucl. Chem.* 1966, **28**, 1021.
9. C. Gerlach, W. Hönle and A. Simon, *Z. Anorg. Allg. Chem.* 1982, **486**, 7.
10. J. C. Vanderhooft, R. D. Ernst, F. W. Cagle Jr, R. J. Neustadt and T. H. Cymbaluk, *Inorg. Chem.* 1982, **21**, 1876.
11. D. J. Watkin, J. R. Carruthers and P. W. Betteridge, CRYSTALS User Guide. Chemical Crystallography Laboratory, University of Oxford (1985).

Polyhedron Vol. 9, No. 23, pp. 2767–2802, 1990
Printed in Great Britain

0277–5387/90 $3.00 + .00
© 1990 Pergamon Press plc

POLYHEDRON REPORT NUMBER 35

COORDINATIVELY UNSATURATED TRIPALLADIUM AND TRIPLATINUM CLUSTERS: MODELS FOR REACTIONS ON METAL SURFACES

RICHARD J. PUDDEPHATT†

Department of Chemistry, University of Western Ontario, London, Canada N6A 5B7

and

LJUBICA MANOJLOVIC-MUIR and KENNETH W. MUIR

Department of Chemistry, University of Glasgow, Glasgow G12 8QQ, U.K.

CONTENTS

1. INTRODUCTION 2768
   1.1. Historical perspective 2768
   1.2. The chemical problems and strategy 2768
      1.2.1. Coordinatively unsaturated clusters 2768
      1.2.2. Preventing cluster fragmentation 2769
2. THE SYNTHESIS OF COMPLEXES $[M_3(\mu_3\text{-CO})(\mu\text{-DPPM})_3]^{2+}$ 2771
3. STRUCTURE AND BONDING IN THE CLUSTER CATIONS 2773
4. COORDINATION CHEMISTRY OF THE CLUSTERS 2774
   4.1. Reactions with carbon monoxide 2774
   4.2. Reactions with phosphine and phosphite ligands 2775
   4.3. Reactions with isocyanide ligands 2776
   4.4. Reactions with SnX_3^- ligands 2777
   4.5. Reaction with hydride 2778
   4.6. Reactions with halide and related ligands 2779
   4.7. Reactions with diphosphine ligands 2780
   4.8. Reactions with other bidentate ligands 2781
   4.9. Summary of coordination chemistry 2782
5. REACTIONS WITH ELECTROPHILES 2784
6. REACTION WITH PLATINUM(0) COMPLEXES AND WITH MERCURY(0) . . . 2785
7. OXIDATIVE ADDITION REACTIONS 2787
   7.1. Reactions with H—S and H—Se bonds 2787
   7.2. Reactions with C=S bonds 2788
   7.3. Reactions with P—H bonds 2790
8. REACTIONS WITH ALKYNES 2791
   8.1. Reactions of $[Pt_3(\mu_3\text{-CO})(\mu\text{-dppm})_3]^{2+}$ 2791
   8.2. Reactions with $[Pt_3(\mu_3\text{-H})(\mu\text{-dppm})_3]^{+}$ 2793
   8.3. Comparison to the surface chemistry of HCCH 2795
9. CATALYSIS OF THE WATER GAS SHIFT REACTION 2795
10. CONFORMATIONS OF dppm LIGANDS 2796
11. CONCLUSIONS 2799

† Author to whom correspondence should be addressed.

1. INTRODUCTION

This review is mostly concerned with the chemistry of a class of coordinatively unsaturated cluster complexes of platinum and, to a lesser extent, palladium, and with a study of the relationship of this chemistry to that which is known or thought to occur on a platinum surface during chemisorption and catalysis. The relationship of the chemistry of coordinatively unsaturated clusters† with the chemistry of a metal surface was not fully appreciated until about 15 years ago.[1,2] Prior to this, the development of organometallic chemistry and heterogeneous catalysis had proceeded much more independently of one another, but it is remarkable how platinum has played a dominant role in both fields. A brief historical outline to illustrate this point is given below.

1.1. *Historical perspective*

The phenomenon now known as catalysis was first reported by H. Davy who observed the flameless combustion of coal gas in the presence of a platinum wire in 1817. The first commercial application of catalysis was in Dobereiner's lighters, which were based on his observation of the spontaneous combustion of hydrogen in the presence of a finely divided platinum catalyst in 1823. From such modest beginnings, heterogeneous platinum metal catalysis is now of major significance. Some applications still involve combustion catalysis and related effects, with applications in catalytic converters, afterburners and heaters for example, but there are also major uses in the oxidation of ammonia and in the reforming (platforming) of petroleum for fuels and petrochemicals.[3]

Just as platinum was the first heterogeneous catalyst discovered, so it was also a constituent of the first organometallic compound to be reported. The compound was Zeise's salt $K[PtCl_3(C_2H_4)]$ which was discovered in 1827, just 10 years after Davy's discovery and 9 years before Berzelius in 1836 coined the term catalysis to describe this new phenomenon.[3,4] The first metal carbonyl was also a platinum complex, $[\{PtCl_2(CO)\}_n]$, prepared by Schutzenberger in 1868. Alkylplatinum and hydridoplatinum complexes were prepared by Chatt in the 1950s, and it was in this period also that the bonding in Zeise's salt and related compounds was described in the general terms which are now used. The mechanisms of many reactions of organoplatinum complexes have been determined and have contributed to our understanding of the mechanisms of homogeneously catalysed reactions.

It is now recognized that chemisorption and the reactions occurring in heterogeneous catalysis are forms of coordination chemistry and organometallic chemistry of the metal surface. There are analogies with transition metal chemistry both in terms of the reactions involved and the structures of the surface species. For example, in terms of reactions of metal surfaces and complexes, respectively, non-dissociative chemisorption is like coordination, and dissociative chemisorption is like oxidative addition.[1,2,5] When carbon monoxide binds to a platinum(111) surface, it can bind at on-top (terminal) or two-fold (doubly bridging) sites and perhaps also at three-fold (triply bridging) sites; the surface mobility of carbon monoxide is due to easy migration between these sites (Fig. 1).[6,7] Such metal–carbonyl bonding modes are also common in metal cluster complexes, and the mobility of carbon monoxide on metal surfaces is analogous to carbonyl fluxionality.[1,2,5] Similarly, the dissociative chemisorption of dihydrogen on a metal surface is analogous to the oxidative addition of dihydrogen to a metal cluster complex. In each case, the H—H bond is cleaved and the resulting hydrogen atoms usually bind in bridging positions between two or three metal atoms.[1,2] Many other examples will be considered below.

1.2. *The chemical problems and strategy*

1.2.1. *Coordinatively unsaturated clusters.* In designing coordinatively unsaturated clusters to mimic surface reactions, the late transition elements and particularly rhodium, iridium, palladium and platinum are most attractive since, in the lower oxidation states, these elements often form

† For the purpose of modelling surface reactions it is advantageous to have all metal atoms in the cluster complex coordinatively unsaturated but, in more general terms, a single site of coordinative unsaturation is all that is required.

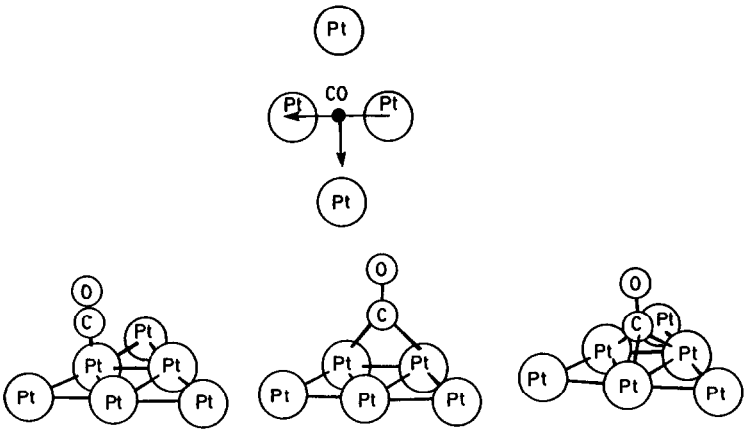

Fig. 1. The binding modes of carbon monoxide on a platinum(111) surface and, above, a top view indicating how a small motion can transform a doubly bridging CO to a terminal or triply bridging CO.

complexes in which the metal has the 16-electron configuration.[4] For example, the square planar mononuclear d^8 complexes have a vacant p_z orbital, and this feature is often carried over to the binuclear and cluster complexes of these elements. In contrast, the transition elements in the centre of the periodic table usually adopt the 18-electron configuration and their cluster complexes are usually coordinatively saturated [e.g. $Os_3(CO)_{12}$] or have a single site of unsaturation [e.g. $Os_3H_2(CO)_{10}$].[8–10] Cobalt and nickel also tend to form coordinatively saturated clusters.[11] The coordinatively unsaturated binuclear and cluster complexes of rhodium and iridium have played an important rôle in the mimicry of surface reactions,[1,2,12–17] but this review will treat only such complexes of palladium and platinum.

1.2.2. *Preventing cluster fragmentation.* The major problem in developing the cluster–surface analogy with the late transition elements is that the metal–metal bonds in their binuclear or cluster complexes are not sufficiently robust to resist cluster fragmentation during many chemical reactions.[18–23] The first studies of platinum clusters were made by Chatt and Chini, who found that the clusters $[Pt_3(\mu\text{-}CO)_3L_4]$ reacted with excess phosphine ligand (L) to give the mononuclear complexes $[Pt(CO)L_3]$ or $[PtL_4]$.[18] Nevertheless, despite this problem, an impressive chemistry of the clusters $[M_3(\mu\text{-}L)_3L'_3]$ and $[M_3(\mu\text{-}L)_3L'_4]$, where L = CO or SO_2 and L′ = tertiary phosphine, has been developed in which the cluster nuclearity is maintained or increased,[18–23] and much of this chemistry has been reviewed.[19,20,24] For example, Farrar and coworkers showed that, with bulky phosphine ligands, the complexes $[Pt_3(\mu\text{-}CO)_3L_3]$ undergo phosphine ligand exchange at a rate much greater than the rate of cluster fragmentation, and that the reactions proceed by reversible formation of $[Pt_3(\mu\text{-}CO)_3L_4]$.[21] Mingos and coworkers showed that carbonyl groups of these cluster complexes could be replaced by sulphur dioxide to give $[Pt_3(\mu\text{-}SO_2)_3L_3]$, while isocyanides could displace both the carbonyl and the phosphine ligands.[19,22,25] The electron-rich clusters $[Pt_3(\mu\text{-}CO)_3L_3]$ can also act as Lewis bases, forming complexes to Lewis acids such as M^+, LM^+ (M = Cu, Ag, Au, L = phosphine ligand), Hg or Hg^{2+};[26–31] examples of the product clusters are $[Au\{Pt_3(\mu\text{-}CO)_3(PPh_3)_3\}_2]^+$ and $[Pt_3(\mu_3\text{-}AuPCy_3)(\mu\text{-}CO)_3(PCy_3)_3]^+$. This combination of electrophilic and nucleophilic character of the platinum(0) clusters is promising in terms of catalytic behaviour. There are excellent accounts of structure and bonding in these complexes, which rationalize their dual character.[32–35]

In order to stabilize cluster complexes with respect to fragmentation, it is desirable to use bridging ligands which bind more strongly than the μ-CO, μ-RNC, μ-SO_2 or μ-H ligands which are typically present in palladium and platinum cluster complexes.[19,20] The ligand $Ph_2PCH_2PPh_2$, dppm, has proved to be one of the most useful bridging groups and its use in stabilizing binuclear complexes has been reviewed.[36–38] It is important to note here that much of the chemistry of the binuclear complexes $[M_2Cl_2(\mu\text{-dppm})_2]$, M = Pd or Pt, can be considered to mimic the chemistry occurring at a two-fold site on a metal surface. Many small unsaturated molecules insert into the metal–

metal bond, and the metal centres are susceptible to attack by both nucleophilic and electrophilic reagents.[36–38] Where the nucleophile or electrophile is metal-centred, these reactions can lead to formation of heteronuclear cluster complexes (eq. 1).[39–45]

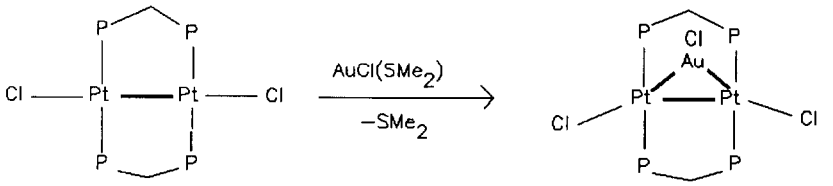

(1)

More robust Pt_3 and Pt_2M clusters could be prepared by reaction of $[Pt_2(\mu\text{-S})(\mu\text{-dppm})(\eta^1\text{-dppm})_2]$ with suitable Lewis acids, as shown in Scheme 1. The product complexes contain a μ_3-S or μ_4-S bridge as well as three μ-dppm ligands, and are therefore inert towards fragmentation. A typical structure is shown in Fig. 2.[46] However, these complexes were inert towards reaction with most organic ligands and attempts to form additional metal–metal bonds in the clusters were unsuccessful.[47]

Fortunately, the strategy of locking three metal atoms together in a triangle by μ-dppm ligands to give reactive, coordinatively unsaturated clusters was ultimately successful and this review describes the chemistry which has been developed so far.

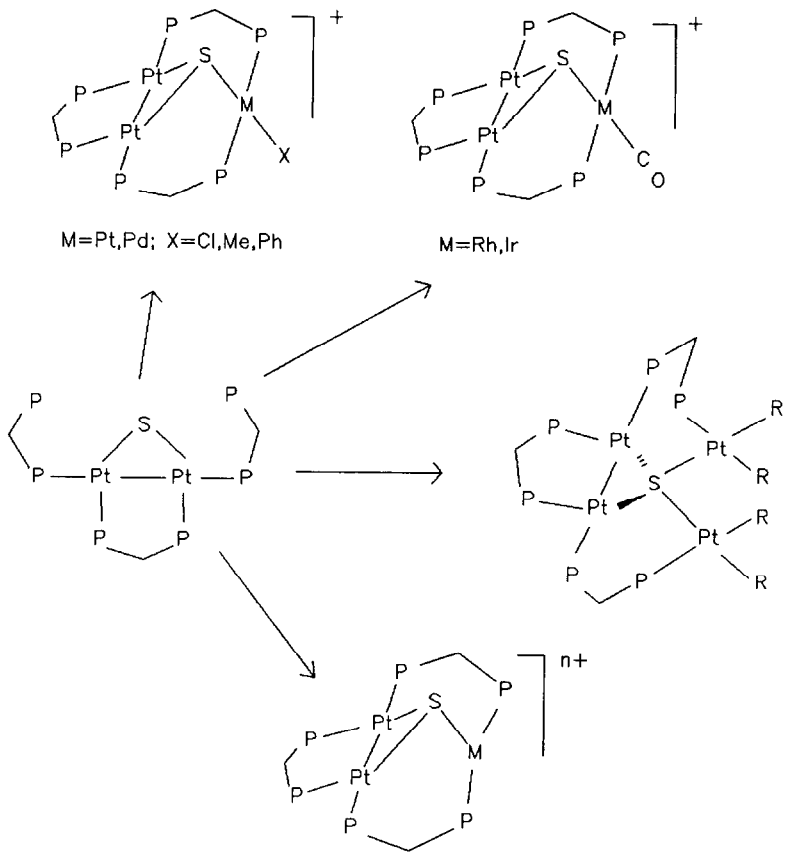

Scheme 1. R = Me or Ph.

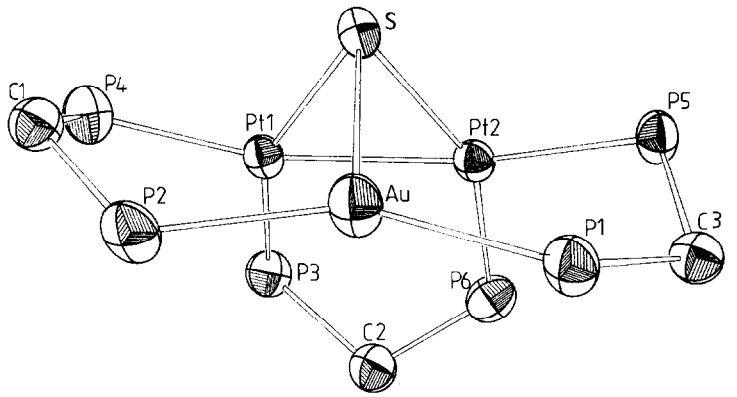

Fig. 2. A view of the $[Pt_2Au(\mu_3\text{-}S)(\mu\text{-}dppm)_3]^+$ cation. Distances are Pt—Pt = 2.61(1) Å, and Pt—Au = 3.25(1) and 3.11(1) Å. The Pt—Au distances are non-bonding.

2. THE SYNTHESIS OF COMPLEXES $[M_3(\mu_3\text{-}CO)(\mu\text{-}DPPM)_3]^{2+}$

The cluster complex cations were prepared by reaction of $[M(O_2CCF_3)_2(dppm)]$ with carbon monoxide in aqueous acetone, according to eq. (2), M = Pd or Pt, X = CF_3CO_2:

$$3[MX_2(dppm)] + 3CO + 2H_2O \longrightarrow [M_3(\mu_3\text{-}CO)(\mu\text{-}dppm)_3]X_2 + 4HX + 2CO_2. \quad (2)$$

For M = Pd, the reaction occurs at room temperature[48,49] but, for M = Pt, a temperature of 100°C is needed.[50] When M = Pd, the reaction was shown to proceed by way of dipalladium(I) intermediates $[Pd_2(O_2CCF_3)_2(\mu\text{-}dppm)_2]$ and $[Pd_2(\mu\text{-}CO)(O_2CCF_3)_2(\mu\text{-}dppm)_2]$.[49] For M = Pt, the major intermediate species was the diplatinum(I) hydride $[Pt_2H(CO)(\mu\text{-}dppm)_2]^+$. This reaction mixture gave efficient catalysis of the water gas shift reaction and, when much H_2 was produced, the complex hydride $[Pt_2H_3(\mu_3\text{-}dppm)_2]^+$ was also identified in the reaction mixture.[51] For M = Pt, the reduction was studied for a wider variety of ligands $R_2PCH_2PR_2$. The clusters $[Pt_3(\mu_3\text{-}CO)(\mu\text{-}R_2PCH_2PR_2)_3]^{2+}$ were formed when R = Ph, 4-MeC_6H_4 or 3,5-$Me_2C_6H_3$, but reduction led only to $[Pt_2H(CO)(\mu\text{-}R_2PCH_2PR_2)_2]^+$ when R = 2-MeC_6H_4, probably due to steric hindrance by the 2-MeC_6H_4 substituents.[51]

The mechanism of reaction is believed to involve formation of shortlived M^0(dppm) species according to Scheme 3, followed by sequential reaction to give the binuclear and trinuclear complexes according to Scheme 2 (M = Pt) and Scheme 3 (M = Pd).[49,51]

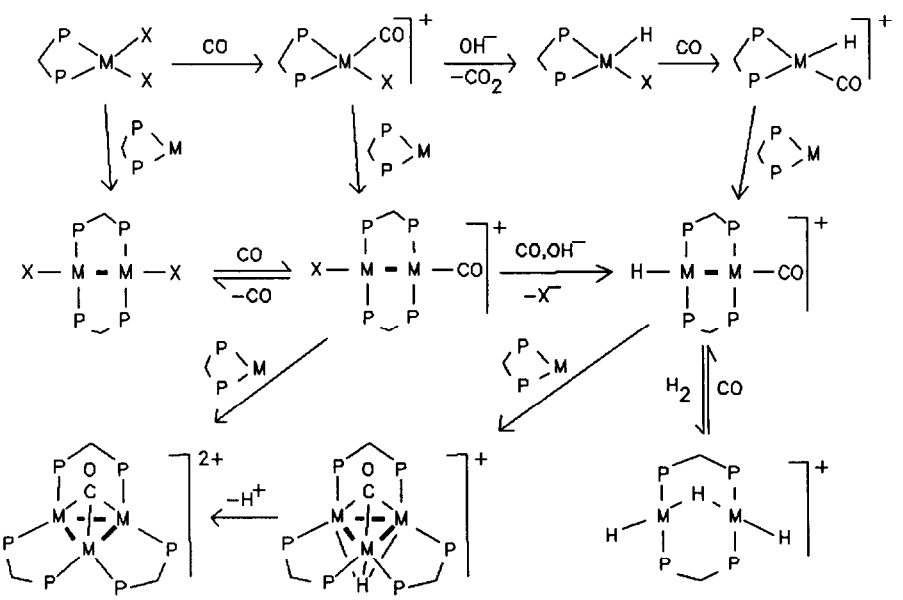

Scheme 2.

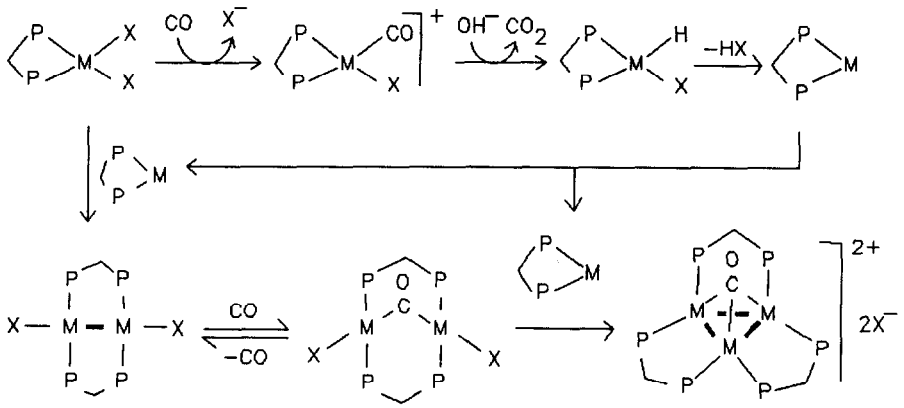

Scheme 3.

Finally, reduction does not always stop at the M_3 stage. When M = Pt, further reduction can occur to give $[Pt_4(\mu\text{-H})(\mu\text{-CO})_2(\mu\text{-dppm})_3(\eta^1\text{-dppm})]^+$ which can be oxidized to give $[Pt_4(\mu\text{-H})(\mu\text{-CO})_2(\mu\text{-dppm})_3\{Ph_2PCH_2P(O)Ph_2\}]^+$ or $[Pt_4(\mu\text{-CO})_2(\mu\text{-dppm})_3\{Ph_2PCH_2P(O)Ph_2\}]$.[51–53] This step does not occur if the reduction of $[Pt(O_2CCF_3)_2(dppm)]$ is carried out in the presence of some free acid CF_3CO_2H.[54] Indeed, the Pt_4 clusters are decomposed by acid or by Ag^+ to give back the parent cation $[Pt_3(\mu_3\text{-CO})(\mu\text{-dppm})_3]^{2+}$.

The structure of a trinuclear complex, $[Pt_3(\mu_3\text{-CO})(\mu\text{-dppm})_3]^{2+}$ (**1**), is shown in Fig. 3.[50] It contains a triangular Pt_3 cluster, with Pt—Pt distances [2.613(1), 2.638(1) and 2.650(1) Å] indicative of platinum–platinum single bonds (2.58–2.80 Å).[55–57] The edges of the Pt_3 triangle are spanned by three dppm ligands to form an approximately latitudinal (planar) Pt_3P_6 skeleton. One face of the Pt_3 triangle is capped by a carbonyl group coordinating the metal centres in a symmetrical triply bridging mode [Pt—C 2.080(9), 2.089(8) and 2.095(9) Å]. This is the first example of a cluster complex containing a $Pt_3(\mu_3\text{-CO})$ group. Even the largest platinum clusters studied previously contain only terminal and μ_2-CO ligands.[19,20] In **1**, the bulky phenyl and methylene groups of the dppm ligands form a fence around each face of the latitudinal Pt_3P_6 skeleton, so that the metal centres are easily accessible only from above and below the Pt_3 plane. This structural feature, illustrated in Fig. 4,[58] is retained in many crystallographically characterized adducts of **1** with small molecules and ions.

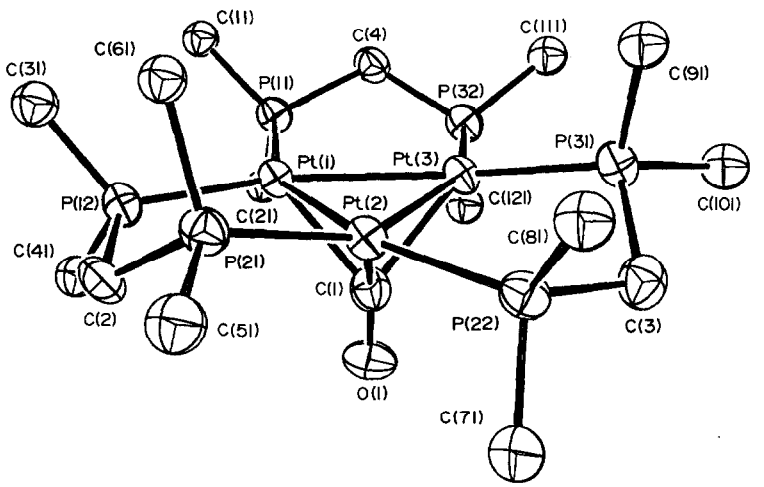

Fig. 3. A view of the $[Pt_3(\mu_3\text{-CO})(\mu\text{-dppm})_3]^{2+}$ cation. In each phenyl ring only the carbon atom attached to phosphorus is shown. Reproduced by permission from *Organometallics* 1986, **5**, 345.

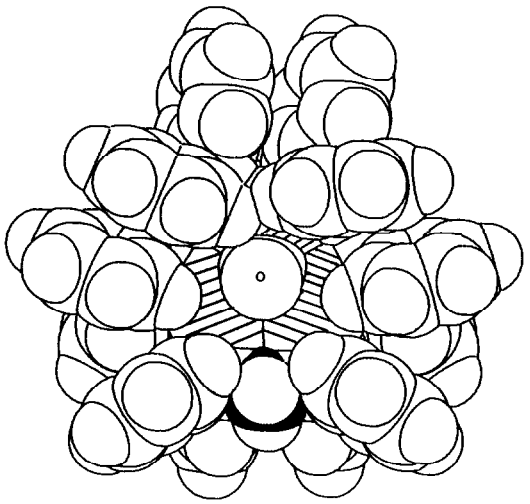

Fig. 4. A space-filling model of the $[Pt_3(SCN)(\mu_3\text{-}CO)(\mu\text{-}dppm)_3]^+$ cation showing the steric environment of the μ_3-CO group which lies in a cavity bounded by six phenyl groups. Platinum atoms are cross-hatched and methylene carbon atoms are shaded. Reproduced by permission from *Inorg. Chem.* 1986, **25**, 4192.

3. STRUCTURE AND BONDING IN THE CLUSTER CATIONS

The bonding in $[Pt_3(\mu_3\text{-}CO)(\mu\text{-}dppm)_3]^{2+}$ has been modelled, using EHMO analysis, by considering it to be formed from a planar (latitudinal) Pt_3L_6 unit and CO^{2+}. Calculations have been based on $Pt_3(CO)_6$ and $Pt_3(\mu\text{-}H_2PCH_2PH_2)_3$ units as models for the $Pt_3(\mu\text{-}dppm)_3$ unit,[33,35] and a typical MO correlation diagram is given in Fig. 5.[35] The highest energy filled orbitals a_1 and e are

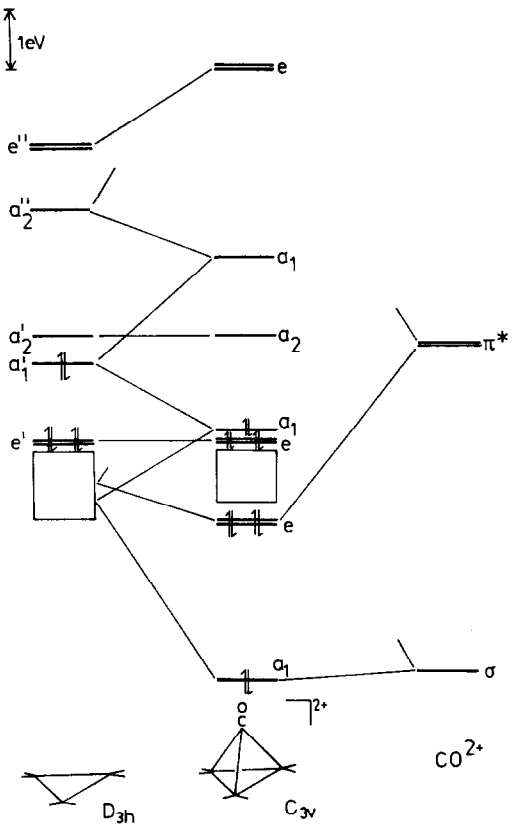

Fig. 5. An interaction diagram for the $[Pt_3(\mu_3\text{-}CO)(\mu\text{-}dppm)_3]^{2+}$ cation, considering it to be formed from $[Pt_3(\mu\text{-}dppm)_3]$ and CO^{2+}.

metal–metal bonding and are analogous to the Walsh orbitals in cyclopropane. These are the orbitals which will be used when the cluster interacts with Lewis acids. Of the lowest energy unoccupied orbitals, a_2 is metal–metal antibonding while a_1 and e are combinations derived mostly from the empty $6p_z$ orbital on each platinum atom and therefore have mostly metal–metal non-bonding character. Since Lewis bases will normally approach from below the Pt_3L_6 plane, the initial interaction will be with the a_1 or e levels of the cluster and this should not affect the metal–metal bonding to a great extent. However, if a ligand can migrate to an edge of the cluster and hence interact with the metal–metal antibonding orbital a_2, cleavage or weakening of a metal–metal bond is expected to occur.[32–35]

It is, of course, the presence of the empty $6p_z$ orbitals (a_1 and e) on platinum which gives the clusters their coordinatively unsaturated character. In terms of electron counting, the $[Pt_3(\mu_3\text{-CO})(\mu\text{-dppm})_3]^{2+}$ cluster has 42 electrons in the valence shell and, in principle at least, it could reach coordinative saturation by adding three extra 2-electron donor ligands to give the 48-electron count. In practice, one or two ligands can be added to give 44e, 46e and perhaps even 48e clusters, as discussed in the next section.

4. COORDINATION CHEMISTRY OF THE CLUSTERS

In this section, the chemistry of the cluster complexes $[M_3(\mu_3\text{-CO})(\mu\text{-dppm})_3]^{2+}$, M = Pd or Pt, with 2-electron and 4-electron donor ligands will be described. It will be seen that added ligands can bind at terminal or bridging sites on the M_3 triangle and that they can influence the mode of coordination of the carbonyl ligand. There are some unique forms of fluxionality of these complexes, and the mechanism of ligand substitution in the clusters is made clear by the direct study of the adducts.

4.1. *Reactions with carbon monoxide*[59]

This chemistry is illustrated in Scheme 4.

The clusters **1**, M = Pd or Pt, add carbon monoxide rapidly and reversibly to give **2** or **3** and, when M = Pt, a second carbonyl can be added to give **4**. Exchange between all these species was rapid on the NMR time scale at room temperature, but the equilibria involving addition or loss of carbon monoxide could be frozen out at −80°C. However, for the 1 : 1 adduct, the NMR spectra indicated that the molecule had D_{3h} symmetry even at −90°C, and hence suggested structure **3**, whereas the IR spectra indicated that both terminal and bridging carbonyls were present and hence suggested structure **2**. It was therefore proposed that fluxionality involving **2** ⇌ **3** is rapid even at −90°C. EHMO calculations suggest very similar energies for **2** and **3**, consistent with the experimental observations.[35]

This work is significant for two reasons. Firstly, it shows how terminal, μ_2 and μ_3 carbonyl groups can be close in energy when coordinated to a Pt_3 triangle, and that the resulting fluxionality can mimic the easy migration of CO on a platinum surface.[6,7] Secondly, the sequence of reactions **1** ⇌ **2** ⇌ **3** ⇌ **2′** ⇌ **1** of Scheme 4 illustrates very clearly how carbonyl substitution can occur very easily by reversible addition of carbon monoxide. Indeed exchange of carbon monoxide in **1** by ^{13}CO occurs very rapidly at room temperature.[59]

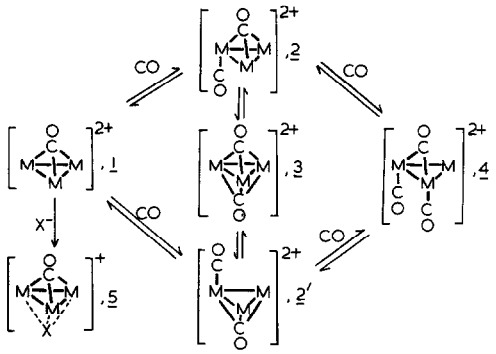

Scheme 4.

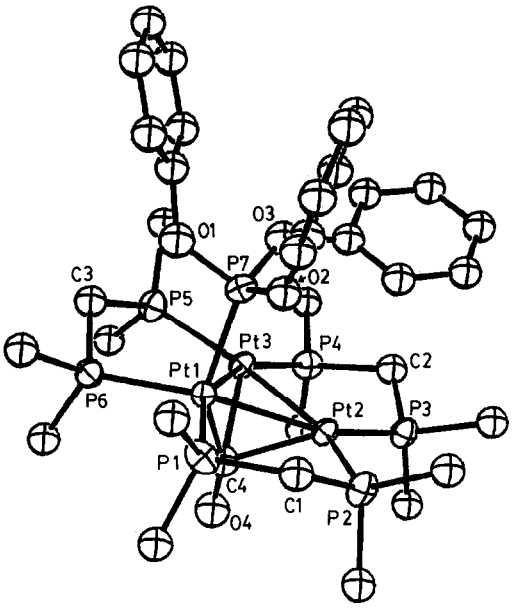

Fig. 6. The structure of the $[Pt_3(\mu_3\text{-CO})\{P(OPh)_3\}(\mu\text{-dppm})_3]^{2+}$ cation.

4.2. *Reactions with phosphine and phosphite ligands*[60,61]

The cluster $[Pt_3(\mu_3\text{-CO})(\mu\text{-dppm})_3]^{2+}$ adds monodentate phosphine or phosphite ligands (L) to give $[Pt_3(\mu_3\text{-CO})L(\mu\text{-dppm})_3]^{2+}$ (**5**), and the structure of the adduct with $L = P(OPh)_3$ is shown in Fig. 6. This structure reveals that the phosphite ligand adds to a single platinum centre, Pt(1). It is also interesting to note that the carbonyl ligand is no longer in a symmetrical μ_3-bridging mode, but is bound more strongly to Pt(1) than to the other two platinum atoms. Pertinent bond lengths are shown in Table 1. They can be rationalized by considering that CO^{2+} acts as an acceptor ligand for the Pt_3L_7 fragment so that it binds preferentially to the most electron-rich platinum centre, i.e. to the PtL_3 centre. As can be seen in Fig. 6, the adducts are sterically crowded and their formation

Table 1. Selected bond lengths (Å) in Pd_3 cluster complexes $[Pd_3(\mu_3\text{-X})(\mu_3\text{-CO})(\mu\text{-dppm})_3]^{+\,a\text{-}c}$

X^-	$CF_3CO_2^-$	Cl^-	I^-
Pd(1)—Pd(2)	2.576(1)[c]	2.604(1)	2.599(1)
Pd(2)—Pd(3)	2.610(1)	2.586(1)	2.591(1)
Pd(3)—Pd(1)	2.607(2)	2.583(1)	2.599(1)
⟨Pd—Pd⟩	2.598(19)	2.591(11)	2.596(5)
Pd—P	2.30–2.34	2.30–2.32	2.30–2.33
Pd(1)—C	2.175(11)	2.14(2) 2.14(2)[b]	2.137(8)
Pd(2)—C	2.141(12)	2.25(2) 2.21(3)	2.192(8)
Pd(3)—C	2.080(10)	2.17(2) 2.14(2)	2.160(8)
⟨PdC⟩	2.132		2.163
ref.	48,73	72	73

[a] As discussed in the text, these complexes may be considered to have 48 electrons counts if the halide acts as a 6-electron ligand.

[b] There is Cl—CO disorder, and the two sets of Pd—C distances correspond to two positions of the disordered CO ligand.

[c] One $CF_3CO_2^-$ oxygen weakly binds to Pd(1) [Pd(1)—O(1) 2.83 Å], and the other bridges Pd(2)—Pd(3) [Pd(2)—O(2) 2.77 Å, Pd(3)—O(2) 2.92 Å].

becomes less favourable for more sterically demanding phosphines. The limit appears to be reached with PPh_3 which forms a complex in solution at −90°C. At room temperature, however, this complex is essentially fully dissociated.

A remarkable property of these complexes is that the added ligand L can migrate around the Pt_3 ring, according to eq. (3), at a rate fast enough to cause NMR fluxionality. The transition state is thought to be the triply bridged species **6**. For the adduct with $L = PF_3$, the NMR spectrum, even at −90°C, is that expected for a complex with three-fold symmetry and it is possible that bridging PF_3 groups could be present in the ground state.[61] These are the first observations of phosphine fluxionality in transition metal cluster complexes.[62] The ligands PH_3 and PF_3 are also thought to bind as terminal ligands when adsorbed onto platinum(111) or nickel(111) surfaces.[63]

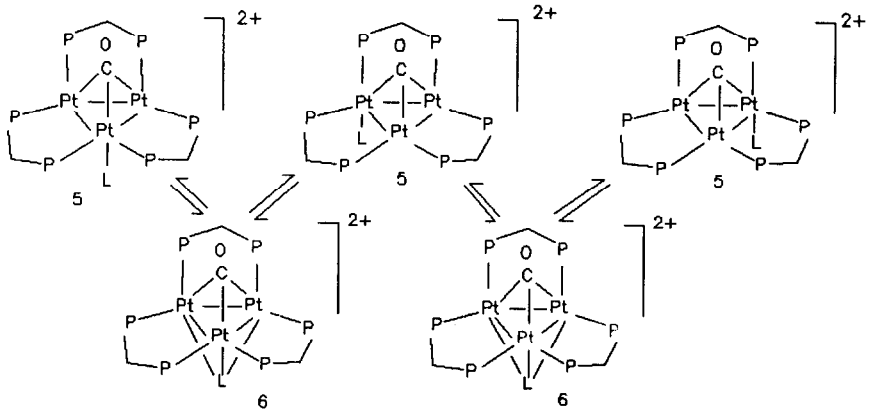

(3)

4.3. *Reactions with isocyanide ligands*[64]

The chemistry of the bulky isocyanide ligands RNC, R = t-Bu, Cy or 2,6-$Me_2C_6H_3$, with the platinum cluster **1** is shown in eq. (4). Again, the first equivalent of RNC adds as a terminal ligand, but a second equivalent may then displace the carbonyl ligand.

Remarkably, the product contains two terminal isocyanide ligands bound to the same platinum atom, as shown in Fig. 7. These molecules may also exhibit fluxional behaviour, of the type described for the phosphine adducts. In terms of the surface analogy, MeNC is adsorbed onto platinum(111) in a mixture of terminal (linear MeNC) and μ_2 (bent MeNC) bonding modes.[64] In neither the surface nor the cluster reactions is there evidence for the presence of $Pt_3(\mu_3\text{-CNR})$ groups, except possibly as intermediates in the fluxional process.

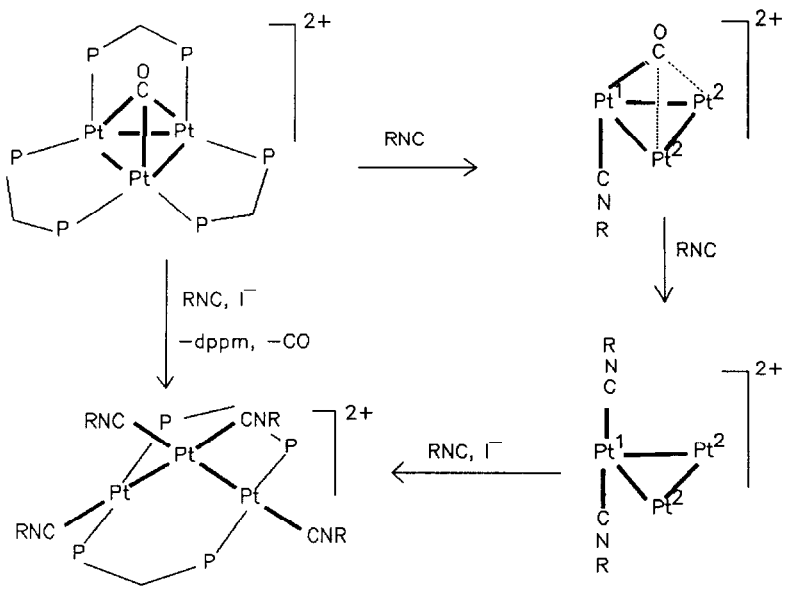

(4)

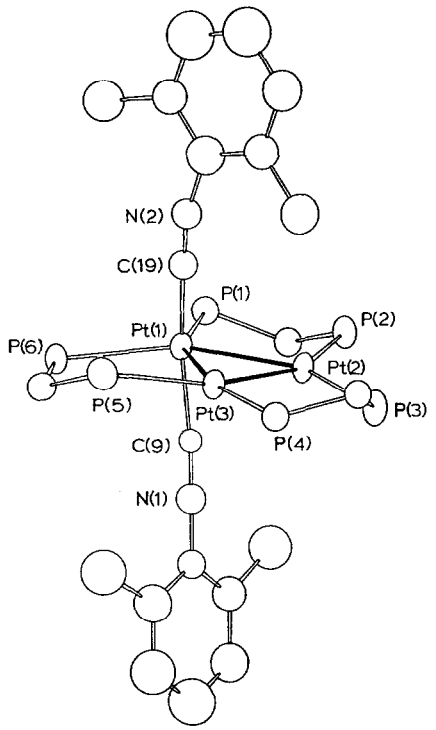

Fig. 7. The structure of the $[Pt_3(XyNC)_2(\mu\text{-dppm})_3]^{2+}$ cation.

4.4. *Reactions with* SnX_3^- *ligands*

Like the isocyanides, the anions SnX_3^-, X = F^- or Cl^-, can form 1 : 1 adducts with $[Pt_3(\mu_3\text{-}CO)(\mu\text{-dppm})_3]^{2+}$ and can also add a second equivalent with replacement of carbonyl.[65,66] However, unlike the phosphines or isocyanides, the SnX_3^- ligands bind to the Pt_3 cluster in a triply bridging

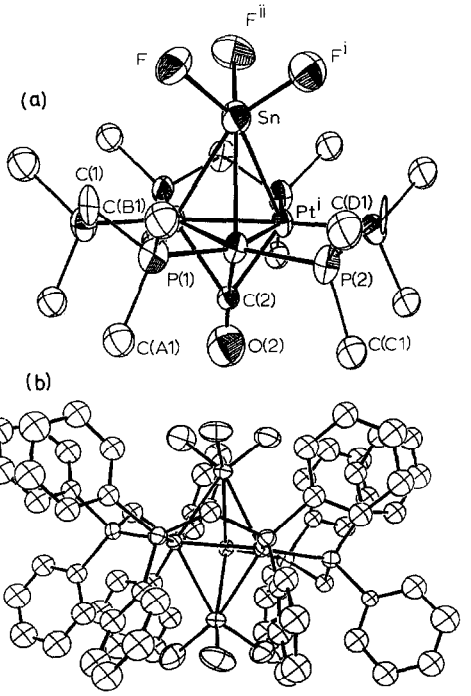

Fig. 8. The structures of μ_3-SnF_3 complexes. (a) $[Pt_3(\mu_3\text{-}CO)(\mu_3\text{-}SnF_3)(\mu\text{-dppm})_3]^+$. Reproduced by permission from *J. Chem. Soc., Chem. Commun.* 1989, 161. (b) $[Pt_3(\mu_3\text{-}SnF_3)_2(\mu\text{-dppm})_3]$.

mode to form trigonal bipyramidal $Pt_3(\mu_3\text{-}CO)(\mu_3\text{-}SnX_3)$ and $Pt_3(\mu_3\text{-}SnX_3)_2$ linkages in $[Pt_3(\mu_3\text{-}CO)(\mu_3\text{-}SnF_3)(\mu\text{-}dppm)_3]^+$ and $[Pt_3(\mu_3\text{-}SnF_3)_2(\mu\text{-}dppm)_3]$ (Fig. 8). The $Pt_3(\mu_3\text{-}Sn)$ linkages in $[Pt_3(\mu_3\text{-}CO)(\mu_3\text{-}SnF_3)^-(\mu\text{-}dppm)_3]^+$ and $[Pt_3(\mu_3\text{-}SnF_3)_2(\mu\text{-}dppm)_3]$ are essentially covalent, the Pt—Sn bond lengths [2.699(2)–2.830(2) Å] lying within the accepted range for platinum–tin single bonds (2.6–2.8 Å).[67,68]

A complex in which SnX_3^- is the only triply bridging ligand $[Pt_3\{\mu_3\text{-}SnMe_2(O_2PF_2)\}(\mu\text{-}dppm)_3]^+$ was prepared in a different way, by reaction of Me_2SnH_2 with $[Pt_3(\mu_3\text{-}CO)(\mu\text{-}dppm)_3][PF_6]_2$.[65] The structure of this complex [Pt—Sn 2.702(3)–2.766(2) Å] is closely similar to that of the parent cation (Fig. 3), from which it can be considered derived by replacement of the carbon monoxide ligand by a $SnMe_2(O_2PF_2)^-$ ion.

It is noteworthy that the ligands PR_3 and SnX_3^- are isolobal and yet they give quite different ground state structures on addition to $[Pt_3(\mu_3\text{-}CO)(\mu\text{-}dppm)_3]^{2+}$. The ground state structure of the tin complexes, containing a $Pt_3(\mu_3\text{-}CO)(\mu_3\text{-}SnX_3)$ unit, probably corresponds to the transition state (**6**) for fluxionality of the phosphine and phosphite complexes [eq. (3)].

It is possible to use the above results to predict that SnX_3^- ligands will bind at triply bridging sites on a platinum surface, and that such groups may be present in some important heterogeneous bimetallic platinum, tin catalysts.[65]

4.5. *Reaction with hydride*[69]

This reaction occurs according to eq. (5), the source of H^- being $Na[BH_4]$. Whilst there is little doubt that complex **8** has the structure shown, with an unusual $Pt_3(\mu_3\text{-}H)$ group, the structure of **7** is less certain. The NMR spectra at low temperature indicate three-fold symmetry and hence structure **7**, but the IR spectrum has $\nu(CO) = 1982\ cm^{-1}$ which suggests a terminal carbonyl group. Given the easy fluxionality of several related complexes, as discussed previously, it is obviously possible that **7** has a structure of lower symmetry in the ground state, such as $[Pt_3(\mu_3\text{-}H)(CO)(\mu\text{-}dppm)_3]^+$, where the carbonyl ligand is terminal.

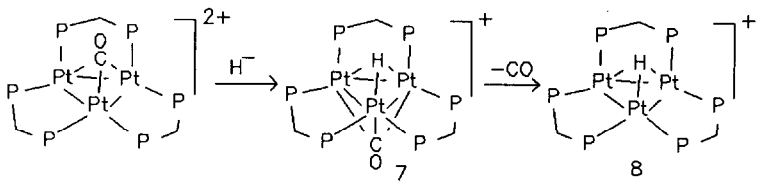

(5)

The complex **8** readily undergoes inversion of the $Pt_3(\mu_3\text{-}H)$ group and it has been suggested that this occurs by way of a planar $Pt_3(\mu_3\text{-}H)$ transition state. This is then related to the mechanism by which hydrogen atoms are thought to migrate from the surface to the bulk phase in metallic platinum or palladium. Hydrogen atoms on the platinum(111) surface may be present as PtH, $Pt_2(\mu_2\text{-}H)$ or $Pt_3(\mu_3\text{-}H)$ groups, but $Pt_3(\mu_3\text{-}H)$ groups are most stable.[70]

The hydride complex **8** can also add phosphite ligands to give the complexes $[Pt_3(\mu_3\text{-}H)L(\mu\text{-}dppm)_3]^+$ with $L = P(OR)_3$; R = Me, Et or Ph. Evidence from NMR spectroscopy indicates the structure **9**, with an asymmetric $Pt_3(\mu_3\text{-}H)$ bridge. Again, the stronger bond of hydrogen to the platinum atom with the highest coordination number can be rationalized by considering the complex to be formed from Pt_3L_7 and H^+, with the proton binding most strongly to the most electron-rich metal centre.[71]

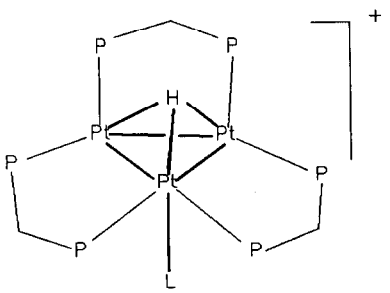

9

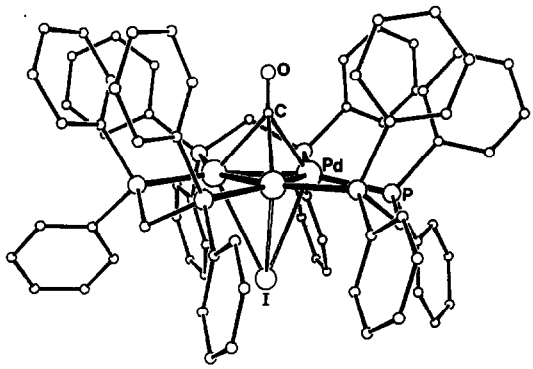

Fig. 9. The structure of the cation $[Pd_3(\mu_3\text{-}I)(\mu_3\text{-}CO)(\mu\text{-}dppm)_3]^+$.

4.6. *Reactions with halide and related ligands*[72,73]

The complexes $[M_3(\mu_3\text{-}CO)(\mu\text{-}dppm)_3]^{2+}$ with M = Pd or Pt add halide ligands to give $[M_3(\mu_3\text{-}CO)X(\mu\text{-}dppm)_3]^+$ and, for M = Pd, the halide is triply bridging, as illustrated by the structure of Fig. 9.[72] The complexes readily undergo halide for halide substitution reactions. The structures of the palladium adducts with X = Cl or I, characterized crystallographically, show that the halide occupies the second capping site of the Pd_3 triangle and thus completes a trigonal bipyramidal $Pd_3(\mu_3\text{-}X)(\mu_3\text{-}CO)$ unit (Fig. 9).[72,73] The finer structural details of this unit are obscured in the chloride adduct by μ_3-CO/Cl disorder. However, in the iodide adduct, which is not disordered, the iodide ligand is roughly equidistant from the metal atoms, with Pd—I distances of 2.951(1), 3.031(1) and 3.083(1) Å. These distances are substantially longer than those considered typical of normal Pd—I σ-bonds (about 2.6 Å).[74,75] It is then possible that the $Pd_3(\mu_3\text{-}I)$ interaction is largely electrostatic in origin, although weak covalent character is indicated by the UV–vis spectra. A $\mu_3\text{-}X^-$ ligand could be considered as a 6-electron donor and, on that assumption, the complexes $[M_3(\mu_3\text{-}X)(\mu_3\text{-}CO)(\mu\text{-}dppm)_3]^+$ would have a coordinatively saturated 48-electron configuration. Ligand addition does not much affect the Pd—Pd distances as shown by the data in Table 1.

The pseudohalide SCN^- also forms 1 : 1 adducts with the complexes $[M_3(\mu_3\text{-}CO)(\mu\text{-}dppm)_3]^{2+}$.[58] However, in $[Pt_3(SCN)(\mu_3\text{-}CO)(\mu\text{-}dppm)_3]^+$ the thiocyanate acts as a terminal ligand (Figs 10 and 4), as is obvious from the Pt—S [2.656(4) Å] and Pt···S [3.243(4) and 3.380(4) Å] distances, which can be compared with those normally found for covalent Pt—SCN bonds (2.3–2.4 Å).[76] Addition of the terminal SCN^- ligand, which occupies a longitudinal position with respect to the Pt_3 triangle,

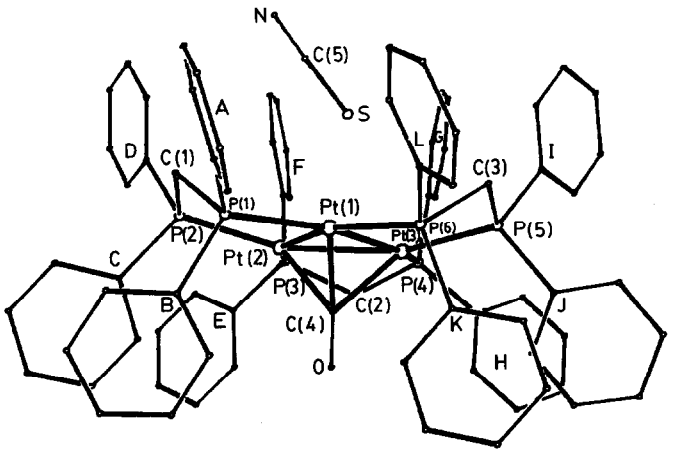

Fig. 10. The structure of the cation $[Pt_3(SCN)(\mu_3\text{-}CO)(\mu\text{-}dppm)_3]^+$. Reproduced by permission from *Inorg. Chem.* 1986, **25**, 4191.

Table 2. Selected interatomic distances (Å) and angles (°) in 1:1 adducts of $[Pt_3(\mu_3\text{-CO})(\mu\text{-dppm})_3]^{2+}$ and ligands, L

L	—	μ_3-SnF_3^-	SCN^-	$P(OPh)_3$	μ-$S_2CNMe_2^-$	μ-$Me_2PCH_2PMe_2$f
Electron count	42e	44e	44e	44e	46e	46e
Pt(1)—Pt(2)	2.638(1)	2.638(3)[a]	2.620(1)	2.656(2)	2.612(1)	2.628(1)
Pt(2)—Pt(3)	2.613(1)	2.638(3)	2.625(1)	2.626(2)	2.622(1)	2.648(1)
Pt(3)—Pt(1)	2.650(1)	2.638(3)	2.623(1)	2.636(2)	2.605(1)	2.620(1)
⟨Pt—Pt⟩[b]	2.634(19)	2.638(3)	2.623(3)	2.639(15)	2.613(9)	2.632(14)
Pt—P[c]	2.27–2.30	2.28–2.30	2.27–2.31	2.29–2.34	2.24–2.36	2.25–2.34
Pt(1)—C	2.095(9)	2.16(5)	2.042(13)	1.93(3)	2.01(1)	2.049(8)
Pt(2)—C	2.089(8)	2.16(5)	2.165(13)	2.16(3)	2.67(1)	2.425(8)
Pt(3)—C	2.080(9)	2.16(5)	2.175(13)	2.27(3)	2.02(1)	2.061(9)
⟨Pt—C⟩[d]	2.088	2.16(5)	2.127	2.12	2.235	2.178
Δ(Pt—C)[d]	0.006	—	0.060	0.14	0.308	0.174
C—O	1.154(9)	1.14(4)	1.165(14)	1.21(4)	1.22(1)	1.19(1)
Pt(1)—C—O	132(1)	135(2)	144(1)	155(2)	137(1)	140(1)
Pt(2)—C—O	133(1)	135(2)	130(1)	121(2)	—	121(1)
Pt(3)—C—O	135(1)	135(2)	129(1)	120(2)	141(1)	139(1)
ref.	50	65	58	61	80	77

[a] This complex has crystallographically imposed three-fold symmetry.

[b] Mean and range ESD of Pt—Pt distances.

[c] For latitudinal Pt—P bonds only.

[d] ⟨Pt—C⟩ is the mean of the three Pt—C distances; Δ(Pt—C) is the RMS deviation of the three M—C distances from their mean and is a rough measure of the asymmetry of the $M_3(CO)$ binding.

causes a slight slippage of the μ_3-CO ligand towards the SCN^- substituted platinum atom, as is evident from the Pt—C bond lengths shown in Table 2. The rapid fluxionality of this complex, observed even at −80°C, indicates that the terminal $\rightleftharpoons$ μ_3-thiocyanate transformation occurs very easily.

4.7. *Reactions with diphosphine ligands*[77,78]

The complexes $[M_3(\mu\text{-CO})(\mu\text{-dmpm})_4]^{2+}$, M = Pt or Ni, dmpm = $Me_2PCH_2PMe_2$, are prepared by reaction of $[Pt_2(\mu\text{-dmpm})_3(PPh_3)]$ with carbon dioxide and water, or by reduction of nickel(II) salts with $NaBH_4$ in the presence of carbon dioxide and dmpm, respectively.[77,78] They can be considered as adducts of the unknown clusters $[M_3(\mu_3\text{-CO})(\mu\text{-dmpm})_3]^{2+}$ with the bidentate ligand dmpm. The arrangement of the fourth dmpm ligand and the carbonyl group, with respect to the latitudinal $M_3(\mu\text{-dmpm})_3$ fragment in the two adducts, is shown in Fig. 11. In both complexes the fourth dmpm ligand is bonded to the M_3 cluster in an edge-bridging longitudinal mode. The carbonyl ligand forms a distorted μ_3-CO bridge in the nickel complex,[78] but in the platinum complex it acts primarily as a μ_2-ligand bridging the same platinum atoms to which the fourth longitudinal dmpm ligand is also attached (a semi-bridging interaction with the third platinum centre is possible).[77] In both cases the carbonyl binds most strongly to the metal centres with highest coordination number. This is consistent with the explanation given for distortions in monodentate phosphine adducts in section 4.2. The complex $[Ni_3(\mu_3\text{-CO})(\mu\text{-dmpm})_4]^{2+}$ is the first example of a 46-electron Ni_3 cluster; nickel clusters are usually coordinatively saturated.

Whilst $[Pt_3(\mu\text{-CO})(\mu\text{-dmpm})_4]^{2+}$ adopts a rigid structure,[77] the nickel analogue is fluxional in the sense that the fourth dmpm ligand can migrate around the Ni_3 triangle as shown in eq. (6).[78] More remarkable is the observation that $[Pt_3(\mu_3\text{-CO})(\mu\text{-dppm})_3]^{2+}$ can reversibly add a fourth dppm ligand to give $[Pt_3(\mu_3\text{-CO})(\mu\text{-dppm})_4]^{2+}$. This complex, which must be subject to very severe steric effects, is fluxional even at −90°C, as shown by eq. (6).[79]

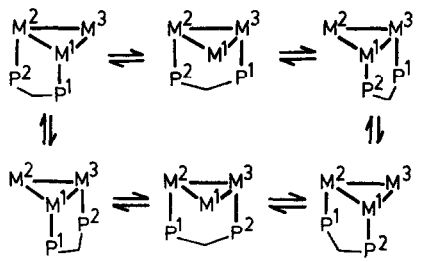

(6)

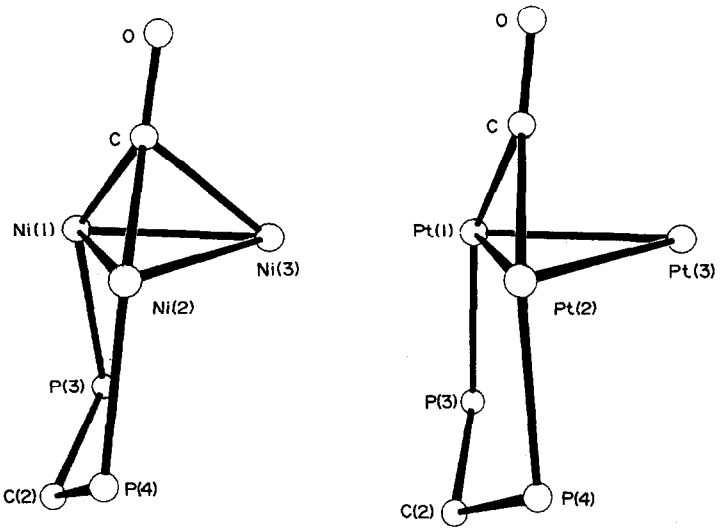

Fig. 11. The structures of the cations $[Ni_3(\mu\text{-CO})(\mu\text{-dmpm})_4]^{2+}$ and $[Pt_3(\mu\text{-CO})(\mu\text{-dmpm})_4]^{2+}$.

4.8. *Reactions with other bidentate ligands*[80]

The dithio ligands, $R_2NCS_2^-$ and R_3PCS_2, form similar complexes of formula $[Pt_3(\mu\text{-CO})(\mu\text{-}S_2CNR_2)(\mu\text{-dppm})_3]^+$ or $[Pt_3(\mu\text{-CO})(\mu\text{-}S_2CPR_3)(\mu\text{-dppm})_3]^{2+}$. From the structure of the adduct shown in Fig. 12, it is obvious that, on addition of N,N-dimethyldithiocarbamate to $[Pt_3(\mu_3\text{-CO})(\mu\text{-}$

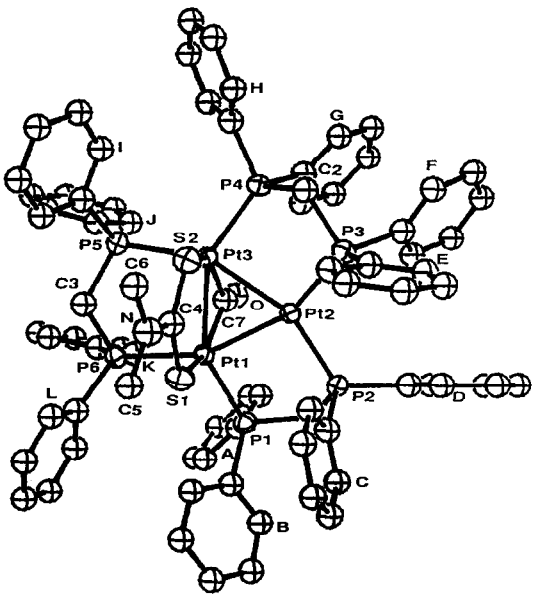

Fig. 12. The structure of the cation $[Pt_3(\mu\text{-CO})(\mu\text{-}S_2CNMe_2)(\mu\text{-dppm})_3]^+$.

dppm)$_3$]$^{2+}$, the carbonyl ligand has slipped from the symmetrical μ_3-bonding mode to bridge two platinum atoms only, and they are the same atoms to which the μ-$S_2CNMe_2^-$ ligand is also bonded. Even at low temperature, the ^{31}P NMR spectra indicate three-fold symmetry and so fluxionality analogous to that of eq. (6) is obviously very easy in these complexes.

4.9. *Summary of coordination chemistry*

Molecular structures of many cluster complexes discussed above have been determined by X-ray crystallography. Selected structural data are presented in Tables 1 and 2. The coordination chemistry of the complexes with M = Pt is summarized in Scheme 5. It is now obvious that the complexes [$M_3(\mu_3$-CO)(μ-dppm)$_3$]$^{2+}$, M = Pd or Pt, can add one or two 2-electron donor ligands or a bidentate 4-electron donor ligand to give 44-electron and 46-electron clusters. When the additional ligand is a weakly bound halide or trifluoroacetate it can be argued that the cluster valence electron count may even reach 48-electron.

The complexes discussed so far contain a triangular M_3 cluster and a $M_3(\mu$-dppm)$_3$ fragment in which the M_3P_6 unit adopts a planar, latitudinal conformation. In most complexes the M_3 triangle is close to equilateral and, where small differences in the individual M—M bond lengths are observed, no correlation with the electronic properties of the cluster is usually obvious. Thus, in [$Pt_3(\mu_3$-CO)(μ-dppm)$_3$]$^{2+}$, where all three metal centres are electronically identical, the Pt—Pt distances vary from 2.613(1) to 2.650(1) Å, whereas in [Pt_3(SCN)(μ_3-CO)(μ-dppm)$_3$]$^+$, where the thiocyanate ligand interacts with one metal atom only, the Pt—Pt distances are virtually constant, at 2.620(1)–2.625(1) Å. However, the latitudinal M—P bonds tend to lengthen with increase in the coordination number of the metal atom. In [$Pt_3(\mu$-S_2CNMe_2)(μ-CO)(μ-dppm)$_3$]$^+$, for example, the Pt—P bonds range from 2.244(3) to 2.357(3) Å, the shorter bonds involving the four-coordinate platinum atom and the longer ones involving the two six-coordinate platinum atoms which are bridged by $S_2CNMe_2^-$ and carbon monoxide ligands. In the complexes [$M_3(\mu_3$-CO)(μ-dppm)$_3$]$^{2+}$ and their adducts with anionic ligands the mean Pt—P distances [2.28–2.29 Å] are slightly shorter than the mean Pd—P distances [2.31–2.32 Å], and this may reflect the harder acid character of palladium compared with that of platinum.[81]

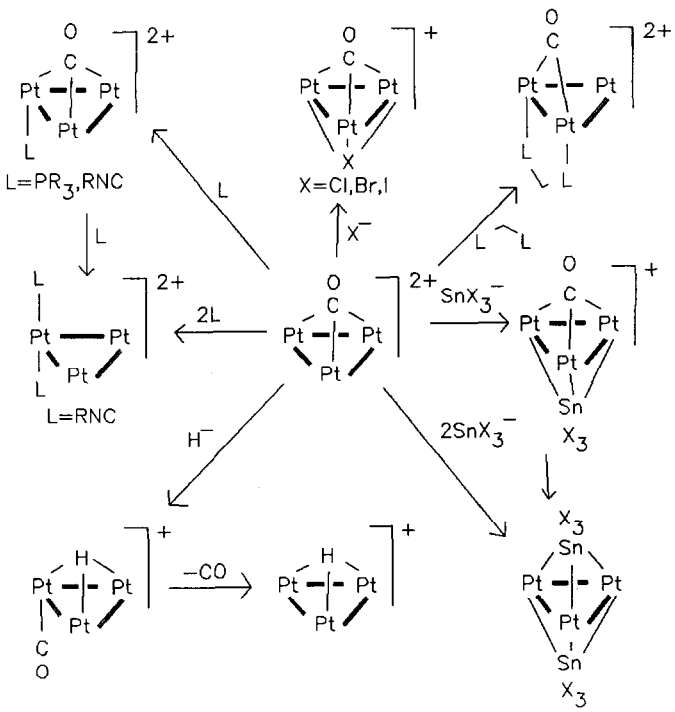

Scheme 5.

Of particular interest is the observation that the mean M—M bond lengths show little variation in these complexes. Thus, mean Pt—Pt distances vary only from 2.61 to 2.64 Å; mean Pd—Pd distances are slightly shorter, 2.59–2.60 Å, reflecting the difference in the Pauling metallic radii (Pt 1.295, Pd 1.283 Å).[82] It is therefore clear that the additional ligands bind to $[M_3(\mu_3\text{-CO})(\mu\text{-dppm})_3]^{2+}$ using the empty $6p_z$ orbitals of the metal atoms rather than empty metal–metal σ^* orbitals of the cluster, and this conclusion is supported by theoretical considerations.[33,35]

The additional ligands can interact with one, two or all three metal centres in the $[M_3(\mu_3\text{-CO})(\mu\text{-dppm})_3]^{2+}$ complexes (Scheme 5). Most monodentate ligands add as terminal groups, but the halides and SnX_3^- ligands form $M_3(\mu_3\text{-X})$ and $M_3(\mu_3\text{-SnX}_3)$ linkages. Isocyanide and SnX_3^- are also capable of replacing the carbonyl group.

The added ligands can affect the geometry of the $M_3(\mu_3\text{-CO})$ unit, and symmetrical μ_3-, asymmetrical μ_3- and symmetrical μ_2-bonding modes are all represented (Tables 1 and 2). The two extreme bonding modes are found in $[Pt_3(\mu_3\text{-CO})(\mu\text{-dppm})_3]^{2+}$ and $[Pt_3(\mu_2\text{-S}_2\text{CNMe}_2)(\mu\text{-CO})(\mu\text{-dppm})_3]^+$, for example. In complexes where the additional ligands interact with one metal centre only, one short and two long M—C bonds are observed, the short bond involving the metal atom with higher coordination number. Similar slippage is apparent in the $[Pt_3(\mu_3\text{-H})(L)(\mu\text{-dppm})_3]^+$ complexes, where the hydride ligand binds more strongly to the platinum atom with higher coordination number.

The degree of slippage of the carbonyl group from the symmetrical μ_3-bridging mode, judged by the r.m.s. deviations of the M—C distances from their mean value (Tables 1 and 2), reflects the donor ability of the added ligand, increasing along the series $\mu_3\text{-I} < \mu_3\text{-}\eta^2\text{-}CF_3CO_2^- < SCN^- < P(OPh)_3$. The C—O bond lengths also appear to increase with donor ability of the added ligand, suggesting an increase in carbon monoxide π^* orbital occupancy, but this observation must be considered tentative in view of the high standard deviations for some of the observed C—O distances. We and Evans considered the carbonyl derivatives and suggested that π-backbonding to carbon monoxide was stronger from the platinum atom with higher coordination number as shown in **A** below, and that this effect led to the shorter Pt—CO distance involving the same platinum atom (Fig. 6).[35,58,77]

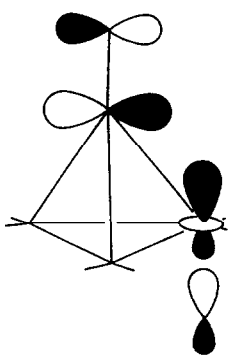

A

However, this rationalization obviously cannot be applied to the hydride derivatives. A more general, simple way to understand the observations is to consider that the complexes are formed by interaction of the $[Pt_3(L)(\mu\text{-dppm})_3]$ fragment with CO^{2+} or H^+, each of which has a vacant σ-acceptor orbital. Therefore the CO^{2+} or H^+ will bind preferentially to the platinum atom with highest electron density, i.e. the platinum atom with highest coordination number. The π-backbonding component in the Pt—CO bonding would then be a secondary effect, rather than the primary effect responsible for the observed distortions of the $Pt_3(\mu_3\text{-CO})$ group. The μ-CO bonding mode in the complexes $[Pt_3(\mu\text{-CO})(\mu\text{-LL})(\mu\text{-dppm})_3]^{2+}$ can be rationalized in an analogous fashion, i.e. by considering the CO^{2+} electrophile interacting with the hypothetical $Pt_3(\mu\text{-dppm})_3(\mu\text{-LL})$ unit.

Finally, the ligand binding modes and fluxionality involving ligand migration between platinum centres are similar in many ways to the processes thought to occur on a platinum surface and, when known, the activation energies are also similar. In both the cluster and surface chemistry, the key

property in this respect is the similarity in the energies of the PtL, $Pt_2(\mu\text{-L})$ and $Pt_3(\mu_3\text{-L})$ groups. As an example, the activation energy for carbon monoxide migration on platinum(111) is estimated as 7 kcal mol^{-1}, while the activation energy for fluxionality can be estimated as < 10 kcal mol^{-1}.[7,59]

5. REACTIONS WITH ELECTROPHILES[83]

The cluster $[Pt_3(\mu_3\text{-H})(\mu\text{-dppm})_3]^+$ (**8**) can act as a base in reactions with electrophilic reagents, as illustrated in Schemes 6 and 7. It can add one proton to give $[Pt_3(\mu_3\text{-H})_2(\mu\text{-dppm})_3]^{2+}$ (**10**) and then another proton to give $[Pt_3(\mu_2\text{-H})_3(\mu\text{-dppm})_3]^{3+}$ (**11**). These reactions are reversible, so that addition of base gives back the parent cluster (Scheme 6).

Complex **10** reacts with carbon monoxide with loss of H_2 to give back the cluster $[Pt_3(\mu_3\text{-CO})(\mu\text{-dppm})_3]^{2+}$ but phosphine and phosphite ligands add to give $[Pt_3H_2(L)(\mu\text{-dppm})_3]^{2+}$, which are thought, on the basis of NMR studies, to have structure **12**.

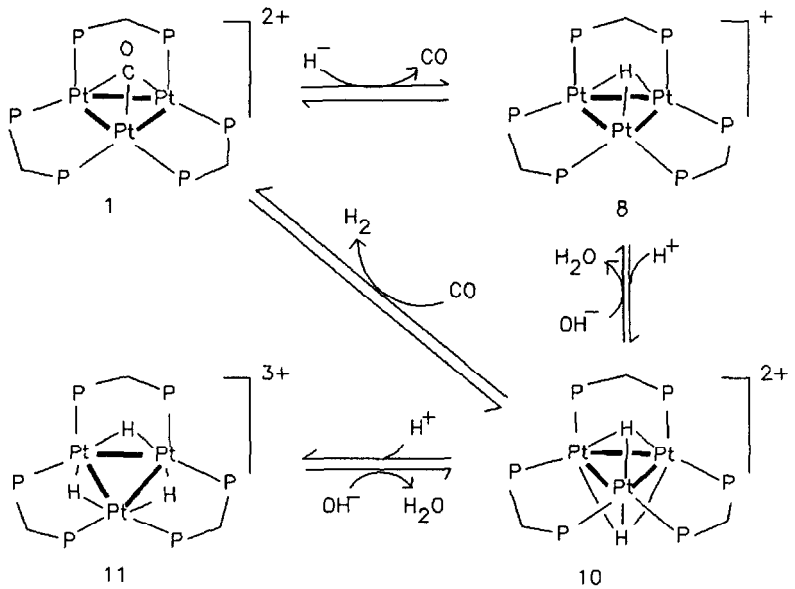

Scheme 6.

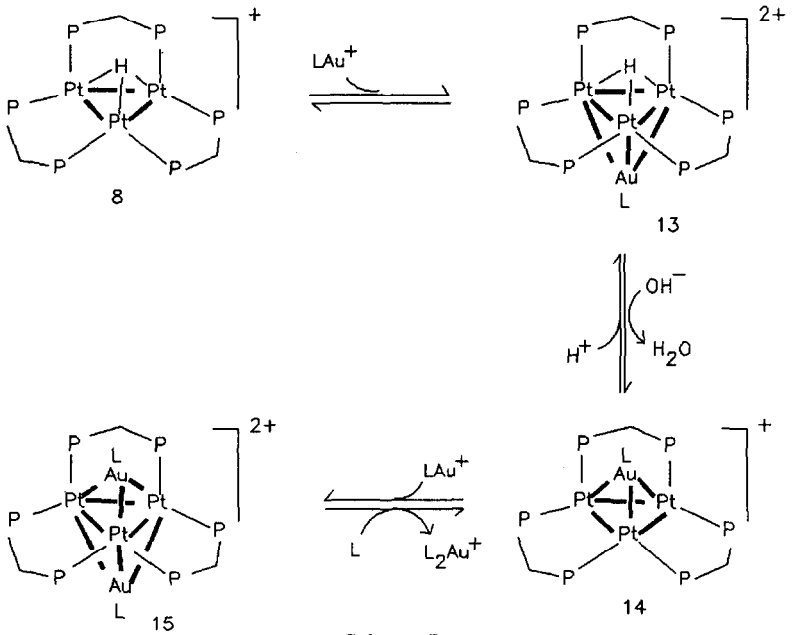

Scheme 7.

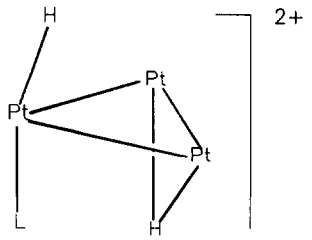

12

The fragment LAu^+ is isolobal with H^+, and similar chemistry results from its reaction with $[Pt_3(\mu_3\text{-}H)(\mu\text{-}dppm)_3]^+$, as shown in Scheme 7. These reactions also give a clear picture of how electrophilic substitution reactions can occur at the Pt_3 face of the cluster, i.e. by addition of an electrophile at one face followed by loss of an electrophile from the other face.

In terms of electron-counting, addition or loss of H^+ or LAu^+ does not affect the formal coordinative unsaturation at the Pt_3 centre but, in complexes such as **10**, **13** or **15** in which both faces of the Pt_3 triangle are capped, both electrophiles are competing for the electron density of the same a_1 bonding orbital of the Pt_3 fragment, and so the ligands are more weakly bound than in complexes such as **8** or **14** in which only one face of the Pt_3 triangle is capped. This is shown by dramatic reductions in the coupling constants ^1J(PtH) or ^2J(PtAuP) for the bis(capped) clusters.[83]

6. REACTION WITH PLATINUM(0) COMPLEXES AND WITH MERCURY(0)[52,53,71]

The addition of electrophilic d^{10} gold fragments to the Pt_3 clusters leads to cluster expansion as shown in section 5, and it was of interest to compare the corresponding chemistry of nucleophilic d^{10} species such as platinum(0) complexes. The complex $[Pt(CO)_2L_2]$, L = PPh_3, reacts with $[Pt_3(\mu_3\text{-}H)(\mu\text{-}dppm)_3]^+$ to give $[Pt_4(\mu\text{-}H)(\mu\text{-}CO)_2(L)(\mu\text{-}dppm)_3]^+$. A similar complex with L = η^1-dppm is often a by-product during the synthesis of $[Pt_3(\mu_3\text{-}CO)(\mu\text{-}dppm)_3]^{2+}$ (see section 2), and its formation probably occurs by addition of a platinum(0) fragment to a Pt_3 cluster. In both complexes the Pt_4 clusters have the butterfly structure, as shown in Fig. 13, which is expected for 58-electron clusters of platinum. The cluster can be considered to be formed from the $Pt(CO)_2L$ fragment acting as a 2-electron donor to the Pt_3 triangle of **1**, and in this sense it is an example of ligand addition (section 4). In this case, the extra platinum bridges an edge of the Pt_3 triangle and, consistent with the trend discussed in section 4, the hydride ligand moves to bridge the same edge. The Pt_4 complexes are fluxional and the mechanism shown in eq. (7) has been established. This fluxionality leads to effective

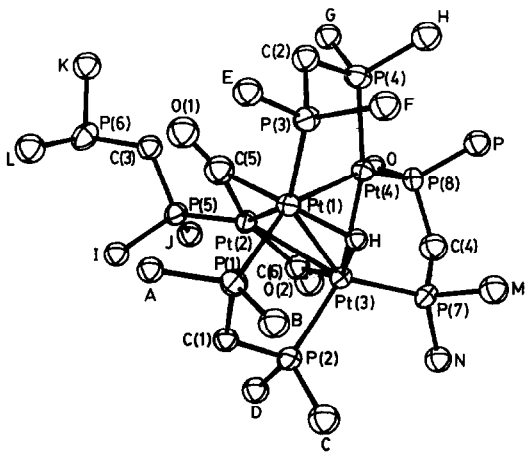

Fig. 13. The structure of the cation $[Pt_4(\mu\text{-}H)(\mu\text{-}CO)_2(\mu\text{-}dppm)_3(\eta^1\text{-}dppm)]^+$. For each phenyl ring only the carbon atom attached to phosphorus is shown. Reproduced by permission from *J. Chem. Soc., Chem. Commun.* 1988, 150.

three-fold symmetry of the clusters, since the hydride and the $LPt(CO)_2$ fragments can move rapidly from edge to edge of the $Pt_3(\mu\text{-dppm})_3$ triangle.[53]

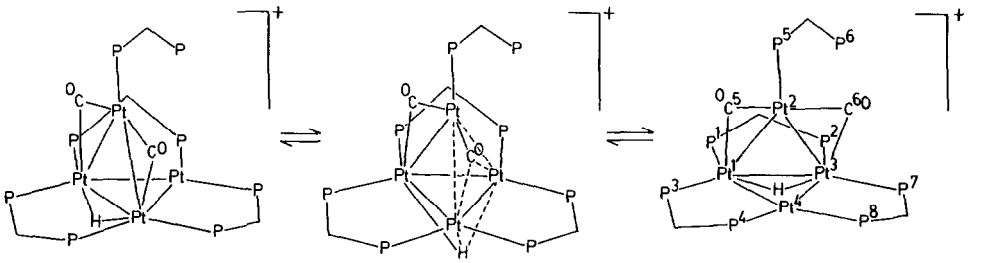

(7)

Elemental mercury reacts easily with $[Pt_3(\mu_3\text{-CO})(\mu\text{-dppm})_3]^{2+}$ to give $[Pt_3(\mu_3\text{-CO})(\mu_3\text{-Hg})(\mu\text{-dppm})_3]^{2+}$ and, in the presence of Me_3NO whose rôle is to abstract carbon monoxide from platinum, to give $[Pt_3(\mu_3\text{-Hg})_2(\mu\text{-dppm})_3]^{2+}$ (Scheme 8). In these complexes, EHMO calculations indicate that the mercury atom acts as a weak donor using its $6s^2$ electron pair and a weak π-acceptor using its vacant $6p_\pi$ orbitals and so remains essentially neutral. There is an analogy with the tin(II) complexes discussed in section 4.4, since tin(II) also has the s^2 configuration, and the mercury adducts can also be considered as coordination complexes. Similar complexes with Hg or Hg_2 bridging two Pt_3 units are known, but no other simple Pt_3Hg clusters are known. A structure is shown in Fig. 14, and the

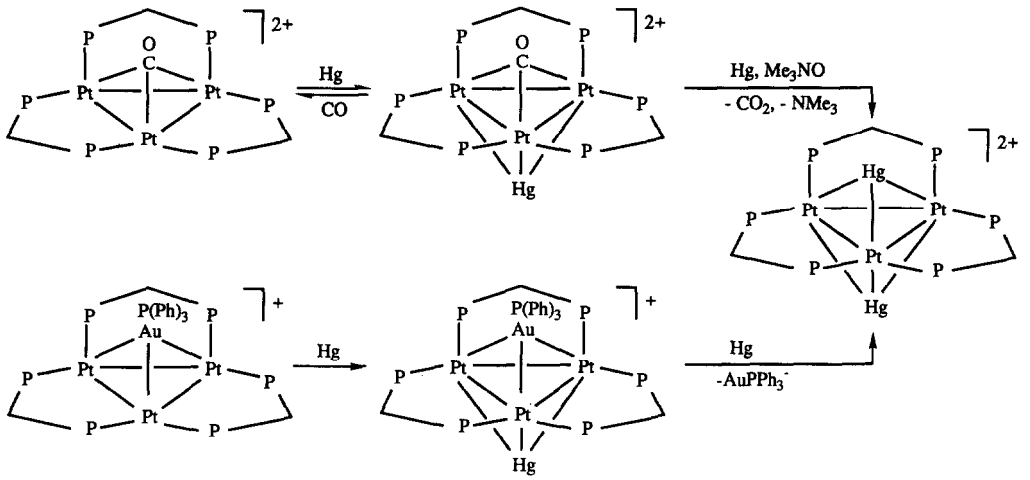

Scheme 8.

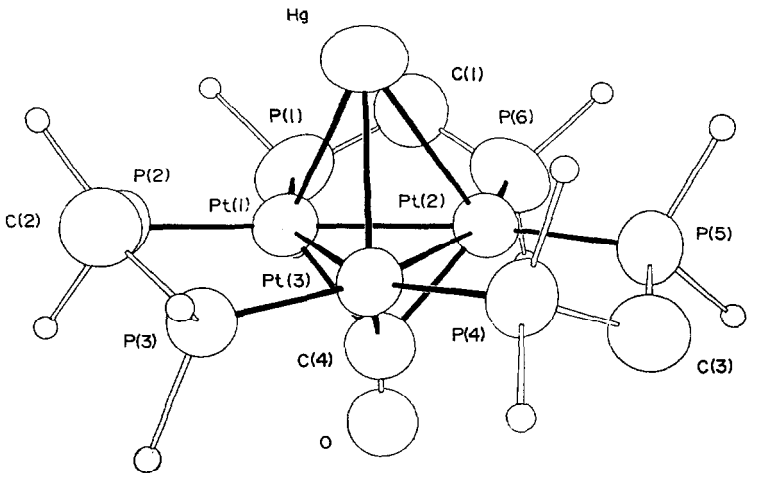

Fig. 14. The structure of $[Pt_3(\mu_3\text{-CO})(\mu_3\text{-Hg})(\mu\text{-dppm})_3]^{2+}$.

Pt_3Hg unit can be considered as a likely model for mercury on a platinum(111) surface. The adsorption of mercury atoms on metal surfaces is difficult to study because of the extreme ease of amalgamation.

7. OXIDATIVE ADDITION REACTIONS

In the clusters $[Pt_3(\mu_3\text{-}CO)(\mu\text{-}dppm)_3]^{2+}$ or $[Pt_3(\mu_3\text{-}H)(\mu\text{-}dppm)_3]^{+}$, the oxidation state of each platinum is formally +2/3 and oxidation by two units leads to a mean oxidation state of +4/3 for each platinum. In these products the three-fold symmetry is lost and they are easily identified as $Pt^{I}_2Pt^{II}$ complexes, in which the Pt^{II} centre is bound to the Pt^{I}_2 unit only by the two μ-dppm ligands and by an extra bridging group introduced during the reaction. In some cases, the Pt^{II} centre breaks away completely. For example, the reaction of $[Pt_3(\mu_3\text{-}CO)(\mu\text{-}dppm)_3]^{2+}$ with HCl gave $[Pt_2Cl_2(\mu\text{-}dppm)_2]$ and $[PtCl_2(dppm)]$, whilst reaction with hydrogen gave $[Pt_2H_2(\mu\text{-}H)(\mu\text{-}dppm)_2]^{+}$ as the only detectable product. This section will describe in detail only those reactions which occurred without cluster fragmentation.

7.1. *Reactions with* H—S *and* H—Se *bonds*[84–86]

The chemistry of $[Pt_3(\mu_3\text{-}CO)(\mu\text{-}dppm)_3]^{2+}$ with reagents H_2E or REH (E = S or Se) is illustrated in Scheme 9. It is likely that in all cases a coordination complex $[Pt_3(\mu_3\text{-}CO)(EHR)(\mu\text{-}dppm)_3]^{2+}$ is formed, and this step has been monitored for R = Et or Ph, E = S and R = Ph, E = Se. Next, oxidative addition of the E—H bond occurs with loss of carbon monoxide and cleavage of two metal–metal bonds to give $[Pt_3H(\mu_3\text{-}ER)(\mu\text{-}dppm)_3]^{2+}$. When R = H or t-Bu, loss of R^+ then occurs to give $[Pt_3H(\mu_3\text{-}E)(\mu\text{-}dppm)_3]^{+}$ or, when R = Ph, reaction with more REH can give hydrogen and $[Pt_3(EPh)(\mu_3\text{-}EPh)(\mu\text{-}dppm)_3]^{2+}$. The palladium cluster reacts in a similar way, but the Pd—H bond formed is more reactive. The structure of $[Pt_3H(\mu_3\text{-}S)(\mu\text{-}dppm)_3]^{+}$ (Fig. 15) shows clearly the $Pt^{I}_2Pt^{II}$ formulation with just one metal–metal bond [Pt^{I}—Pt^{I} 2.597(4) and $Pt^{I}\cdots Pt^{II}$ 3.574(2), 3.678(7) Å].[84,85] Another approach is to consider these as 46-electron clusters in which the extra four electrons resulting from the oxidative addition reaction occupy metal–metal anti-bonding molecular orbitals, thus leading to cleavage of two metal–metal bonds.

These reactions are of interest as models for poisoning of platinum or palladium catalysts, and much work has been carried out to understand the heterogeneous reaction between platinum and hydrogen sulphide. On a platinum(111) surface, hydrogen sulphide first forms a coordination complex, then undergoes dissociation to give H and HS groups on the surface, and finally loses hydrogen to give adsorbed sulphide present as $Pt_3(\mu_3\text{-}S)$ groups.[86] This chemistry is then very similar to that observed with the model complex $[Pt_3(\mu_3\text{-}CO)(\mu\text{-}dppm)_3]^{2+}$.

An unusual reaction of $[Pt_3H(\mu_3\text{-}S)(\mu\text{-}dppm)_3]^{+}$ occurs with $[AuCl(PPh_3)]$ and $AgNO_3$ to give

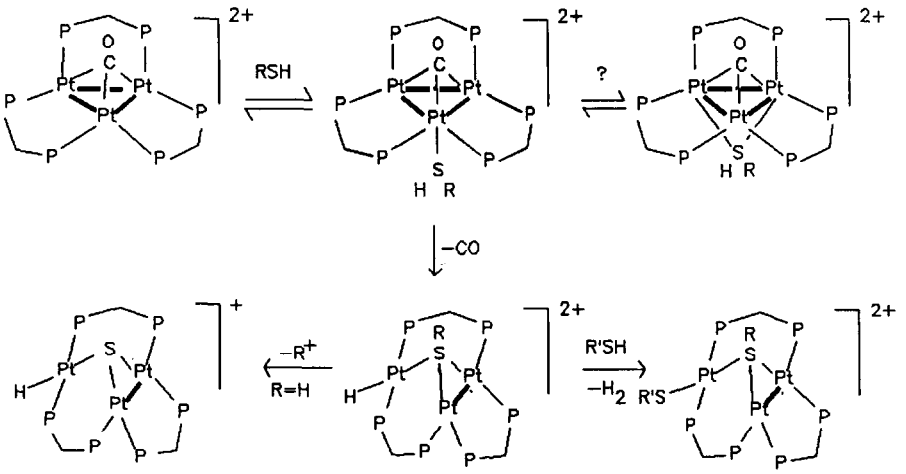

Scheme 9.

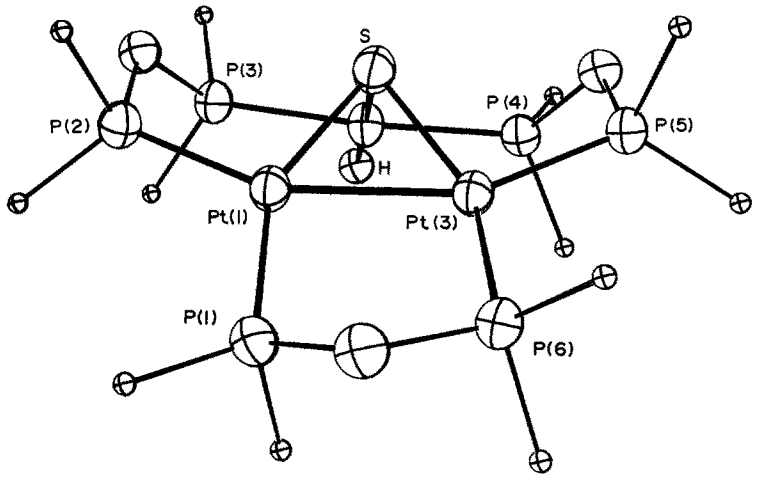

Fig. 15. The structure of the cation $[Pt_3H(\mu_3\text{-}S)(\mu\text{-dppm})_3]^+$. Reproduced by permission from *J. Chem. Soc., Chem. Commun.* 1986, 1809.

$[Pt_3(AuPPh_3)(\mu_3\text{-}S)(\mu_3\text{-}AgCl)(\mu\text{-dppm})_3]^+$ and HNO_3.[87] The structure of the heterometallic product (**16**) is shown in Fig. 16. It can be considered derived from that of the parent complex by replacement of H^+ with isolobal $AuPPh_3^+$, and addition of an AgCl unit to the vacant capping site of the Pt_3 triangle, to form a $Pt_3(\mu_3\text{-}Ag)$ unit [Pt—Pt 2.615(3), 2.619(3), Pt···Pt 3.631(2)–3.726(2), Pt—Ag 2.768(4)–2.861(4) Å].† A notable feature of this complex is the presence of a short Pt—Au bond not supported by bridging groups [2.577(3) and 2.575(3) Å].[45,88–90]

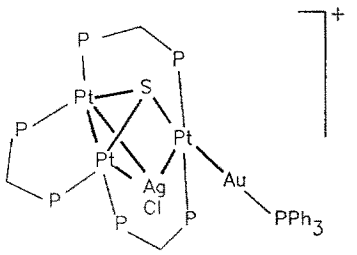

16

7.2. *Reactions with* C=S *bonds*

As discussed in section 4.5, the thiocyanate ligand forms complexes $[M_3(\mu_3\text{-}CO)(SCN)(\mu\text{-dppm})_3]^+$, M = Pd or Pt, but these rearrange either thermally or photochemically with cleavage of the sulphur–carbon bond to give $[M_3(CN)(\mu_3\text{-}S)(\mu\text{-dppm})_3]^+$, eq. (8).[58]

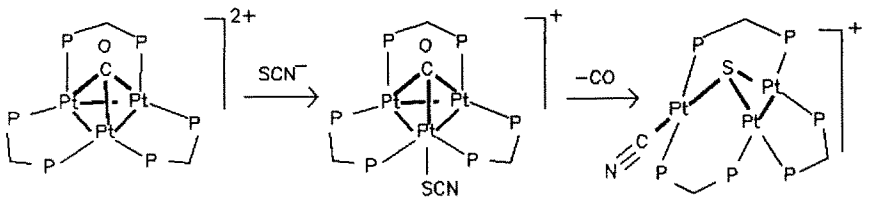

(8)

† In the crystal structure of $[Pt_3(AuPPh_3)(\mu_3\text{-}AgCl)(\mu_3\text{-}S)(\mu\text{-dppm})_3][PF_6]$ the asymmetric unit comprises two cations and two anions.

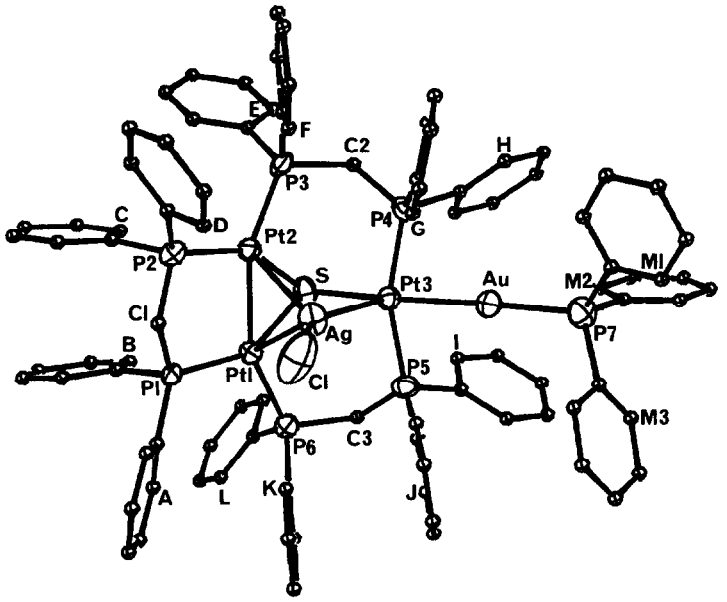

Fig. 16. The structure of one of the two crystallographically independent $[Pt_3(\mu_3\text{-}S)(AuPPh_3)(\mu_3\text{-}AgCl)(\mu\text{-}dppm)_3]^+$ cations. The structure of the second cation differs from that shown above only slightly. Reproduced by permission from *Inorg. Chem.* 1988, **27**, 4516.

When M = Pt, similar reactions occur with the neutral reagents COS, CS_2 and RNCS to give $[Pt_3(\mu_3\text{-}CO)(SCE)(\mu\text{-}dppm)_3]^{2+}$ and then $[Pt_3(CE)(\mu_3\text{-}S)(\mu\text{-}dppm)_3]^{2+}$, E = O, S or RN [eq. (9)].[91]

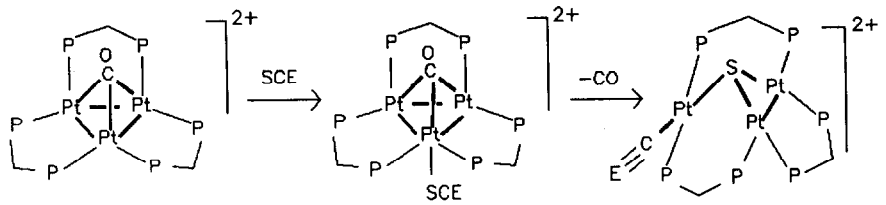

(9)

Mechanistic studies on these reactions have been carried out. The reactions with SCN^- and CS_2 are retarded by free carbon monoxide, but no long-lived intermediates could be detected. However, the reactions of $[Pt_3(\mu_3\text{-}C^*O)(\mu\text{-}dppm)_3]^{2+}$ with both COS and RNCS gave $[Pt_3(C^*O)(\mu_3\text{-}S)(\mu\text{-}dppm)_3]^{2+}$ as kinetic product, with loss of carbon monoxide and RNC, respectively, and in the isothiocyanate reactions, subsequent displacement of C*O by RNC gave the thermodynamic product $[Pt_3(CNR)(\mu_3\text{-}S)(\mu\text{-}dppm)_3]^{2+}$. Thus there appear to be two mechanistic pathways possible for these reactions, as illustrated in Scheme 10.

An interesting property of the μ_3-S complexes described in sections 1.2, 7.1 and 7.2 is the fluxionality, involving inversion about the sulphur atom, which leads to an effective plane of symmetry containing the $Pt_3(\mu_3\text{-}S)(\mu\text{-}dppm)_3$ unit [eq. (10)].[46,47,85,97]

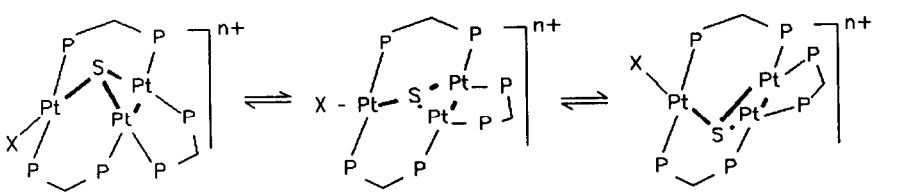

(10)

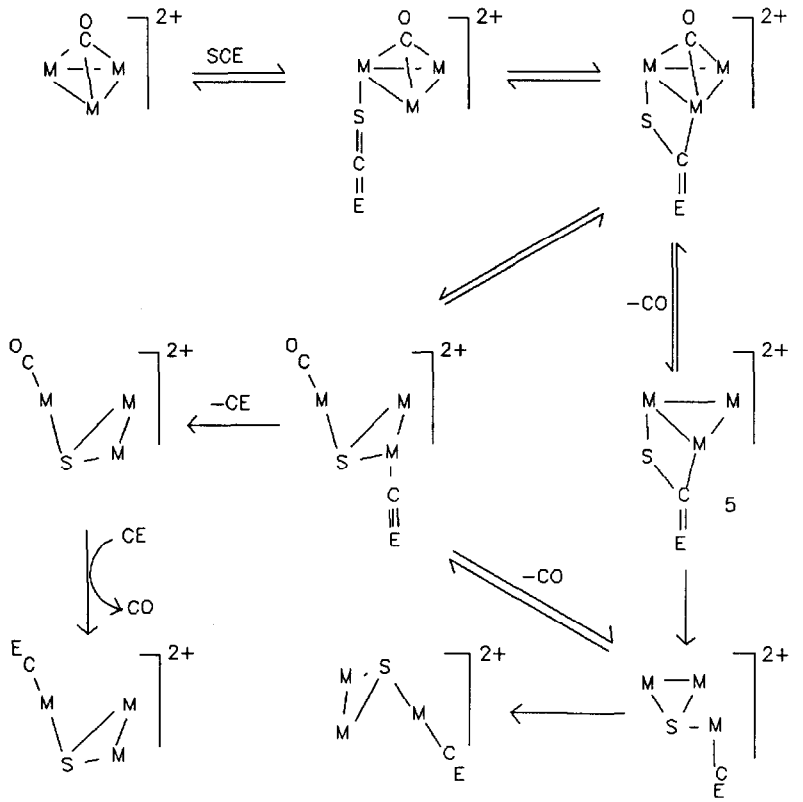

Scheme 10.

7.3. *Reactions with* P—H *bonds*[92]

The complex $[Pt_3(\mu_3\text{-}CO)(\mu\text{-}dppm)_3]^{2+}$ reacts with $PhPH_2$ to give $[Pt_3(CO)(\mu_3\text{-}PPh)(\mu\text{-}dppm)_3]^{2+}$ and hydrogen. The carbonyl ligand in this phosphinidene bridged cluster is labile and is easily displaced by many other ligands, as shown in Scheme 11. It is not known why hydridoplatinum

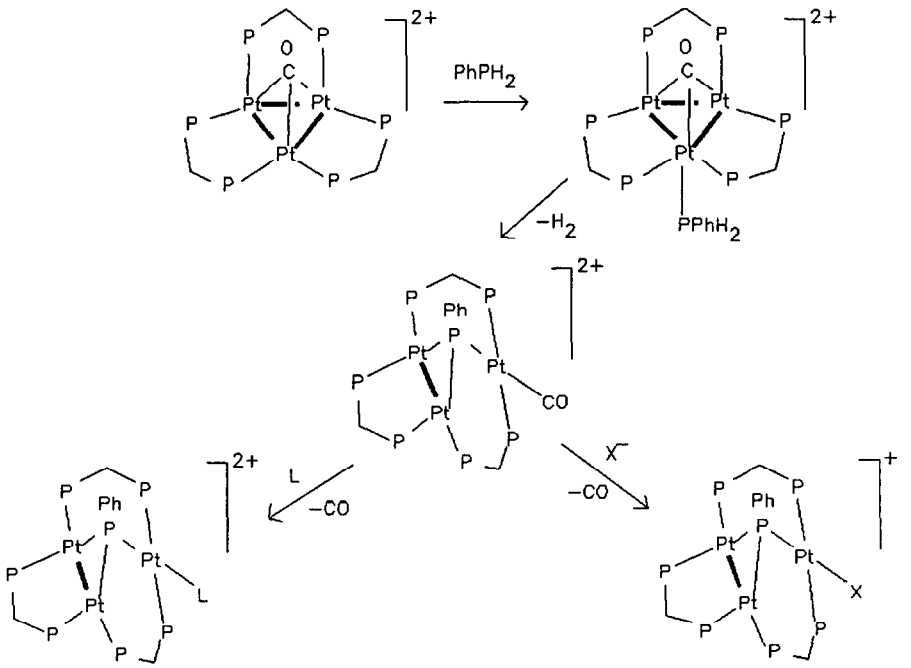

Scheme 11.

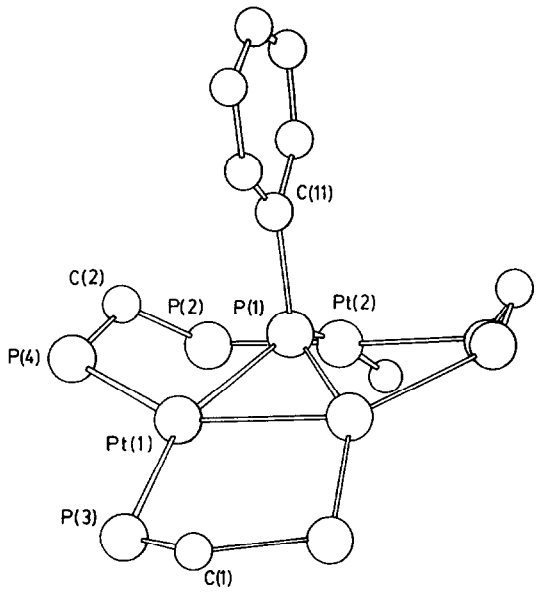

Fig. 17. The structure of the $[Pt_3(\mu_3\text{-PPh})(OH)(\mu\text{-dppm})_3]^+$ cation.

complexes are not formed in these reactions (compare with Scheme 9). However, the reasons are kinetic in origin since the complex $[Pt_3H(\mu_3\text{-PPh})(\mu\text{-dppm})_3]^+$ (Scheme 11) can be prepared though it is reactive. A typical structure is shown in Fig. 17.

In a similar reaction, excess PH_3 gives $[Pt_3(PH_3)(\mu_3\text{-PH})(\mu\text{-dppm})_3]^{2+}$, an unusual example of a μ_3-PH group. On a platinum(111) surface PH_3 adsorbs as a terminal ligand at low temperature and then loses all hydrogen to give adsorbed phosphide, $Pt_3(\mu_3\text{-P})$, while the surface chemistry of $PhPH_2$ has not been studied.[63] There are obvious similarities and differences when compared to the cluster chemistry. Certainly, the cluster complex reactions proceed by way of an intermediate coordination complex $[Pt_3(\mu_3\text{-CO})(L)(\mu\text{-dppm})_3]^{2+}$, L = PH_2Ph or PH_3, which then loses hydrogen by a stepwise reaction sequence. This is similar to the surface science.

8. REACTIONS WITH ALKYNES

8.1. *Reactions of* $[Pt_3(\mu_3\text{-CO})(\mu\text{-dppm})_3]^{2+}$

The reactions of acetylene and some derivatives of acetylene with $[Pt_3(\mu_3\text{-CO})(\mu\text{-dppm})_3]^{2+}$ are shown in Scheme 12. The reactions give initially the carbonyl(alkyne) complexes **17** or **20**, but these easily lose carbon monoxide to give **18** or **21**, or undergo displacement of carbon monoxide by other ligands to give complexes such as **19**. The structure of the complex **19** is shown in Fig. 18, which shows that the acetylene adopts the μ_3-(η^2-||) bonding mode and that there is just one metal–metal bond. The acetylene is a 4-electron ligand, and so **19** is a 46-electron cluster. The structure is similar to those found for the oxidative addition products with $Pt_3(\mu_3\text{-S})$ or $Pt_3(\mu_3\text{-PPh})$ groups (section 7), rather than to the complexes with simple donor ligands (sections 4.7 and 4.8), and so it is perhaps most reasonable to consider the acetylene addition as a form of oxidative addition. Thus the acetylene forms σ-bonds to Pt(2) and Pt(3) and the resulting dimetallated ethylene acts as a 2-electron donor to Pt(1).[93]

The complexes **18** and **21** are characterized spectroscopically as containing acetylene in the less common μ_3-(η^2-⊥) bonding mode. The complex **18** is fluxional, as shown in Scheme 12, such that the acetylene can migrate around the Pt_3 triangle. Both complexes are coordinatively unsaturated, with the 44-electron configuration, and ligand addition and alkyne-for-alkyne exchange occur readily. The presence of two metal–metal bonds in **18** and **21** is predicted on the basis of the NMR data, and is consistent with the theoretical prediction for a 44-electron cluster of platinum. Thus Wade's

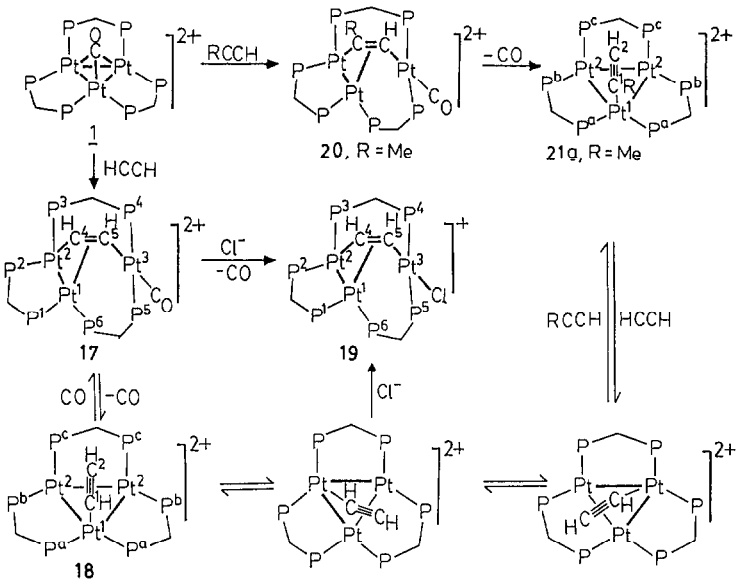

Scheme 12.

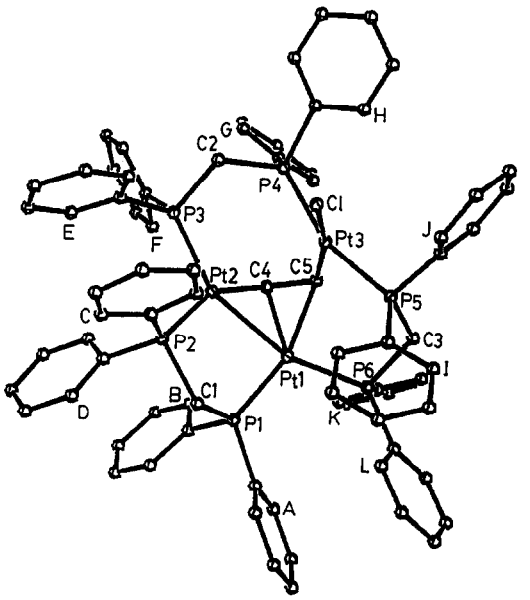

Fig. 18. The structure of the cation $[Pt_3Cl(HC{\equiv}CH)(\mu\text{-dppm})_3]^+$, illustrating the μ_3-(η^2-||) coordination of the acetylene [C(4) and C(5)] to the Pt_3 unit.

rules (modified for the platinum atoms preferring a 16-electron count) predict an *arachno* or *hypho* structure (Fig. 19) for the Pt_3C_2 core in **18** or **19**, respectively.

Reaction of sodium acetylide with $[Pt_3(\mu_3\text{-CO})(\mu\text{-dppm})_3]^+$ or, better, with complex **17** or **19** gave the complex **22**. This complex contains an acetylene ligand in the μ_3-(η^2-||) bonding mode and an unusual bis(diphenylphosphino)propenyl ligand, formed by formal insertion of acetylide into a C—H bond of a μ-dppm ligand. The structure of **22** is shown in Fig. 20.[94]

In all of the reactions described above, the acetylene does not rearrange to vinylidene or other possible structures.

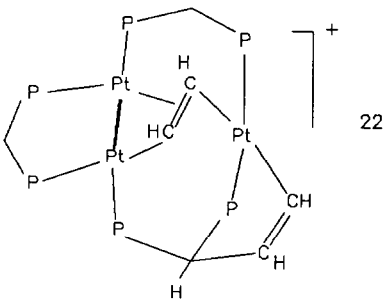

22

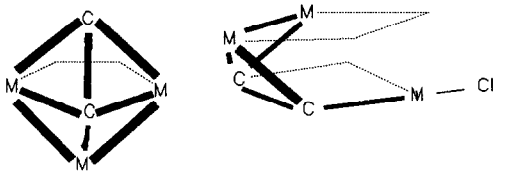

Fig. 19. A depiction of the M_3C_2 cores of the cations $[Pt_3(HCCH)(\mu\text{-dppm})_3]^{2+}$, **18**, and $[Pt_3Cl(HCCH)(\mu\text{-dppm})_3]^{+}$, **19**, showing the proposed relation to a pentagonal bipyramid and a square antiprism, respectively.

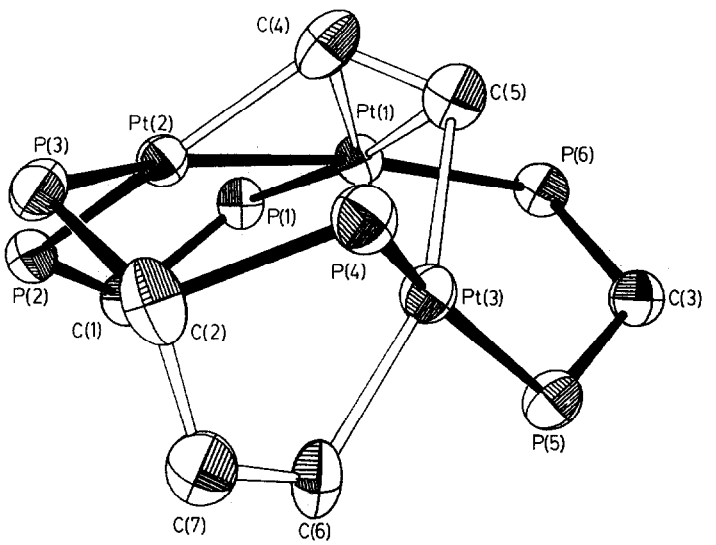

Fig. 20. The structure of the cation $[Pt_3(HCCH)(\mu\text{-dppm})_2\{\mu_2\text{-}\eta^3\text{-}(Ph_2P)_2CHCH{=}CH\}]^{+}$ with all phenyl groups omitted for clarity. The acetylene ligand [C(4), C(5)] bridges the M_3 unit in the $\mu_3\text{-}(\eta^2\text{-}\|)$ fashion also shown in Fig. 18. In this structure a CCH^{-} ion has inserted into a C(2)—H bond to give a $(Ph_2P)_2CHCH{=}CH$ ligand which is bonded to Pt(3) through C(6). Reproduced by permission from *J. Am. Chem. Soc.* 1989, **111**, 745.

8.2. *Reactions with* $[Pt_3(\mu_3\text{-H})(\mu\text{-dppm})_3]^{+}$

These reactions are shown in Scheme 13. The reaction of HCCH with $[Pt_3(\mu_3\text{-H})(\mu\text{-dppm})_3]^{+}$ at $-80°C$ gave a weak acetylene complex, which reacted further, in the absence of excess acetylene, to give the vinylidene complex, **23**, or, in the presence of excess acetylene, to give the vinyl(acetylene) complex, **24**.[95,96] Complex **23** did not react with excess acetylene to give **24**.

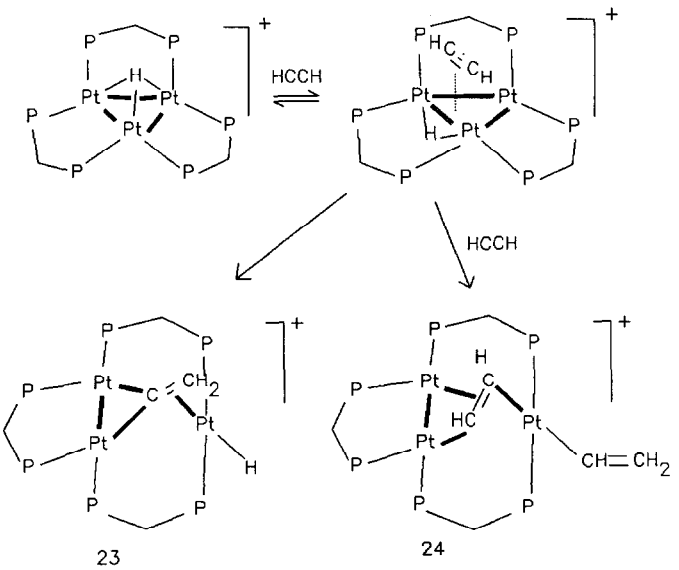

Scheme 13.

Some light was shed on the mechanism of these reactions by labelling studies, using combinations $Pt_3D + HCCH$ or $Pt_3H + DCCD$. It was found that H,D scrambling occurred between the hydride and vinylidene sites of **23** and that H,D scrambling occurred between the hydride and all vinyl sites of **24**, but that no H,D scrambling occurred in the acetylene ligand of **24**. These results, and the observation that **23** could not be converted to **24**, were interpreted in terms of the mechanism of Scheme 14. It is assumed that the acetylene adduct $[Pt_3(\mu\text{-H})(\mu\text{-dppm})_3(HCCH)]^+$ first rearranges to the intermediate 44-electron vinyl cluster **A**, and that there is then a very rapid scrambling between vinyl complex **A**, vinylidene(hydride) complex **B** and ethylidyne complex **C**, all of which are 44-electron clusters. This process naturally leads to H,D scrambling. Finally, the stable 46-electron clusters **23** and **24** are formed by isomerization of **B** or by reaction of **A** with excess acetylene, respectively.[96]

The acetylene complex **24** is analogous to complexes such as **19**, except that the acetylene is *trans* to vinyl instead of chloride. This difference is sufficient to lead to fluxionality of the HCCH ligand in **24** but not in **19**. The vinyl group probably labilizes the *trans* bond, and the resulting mechanism of fluxionality is shown in eq. (11).

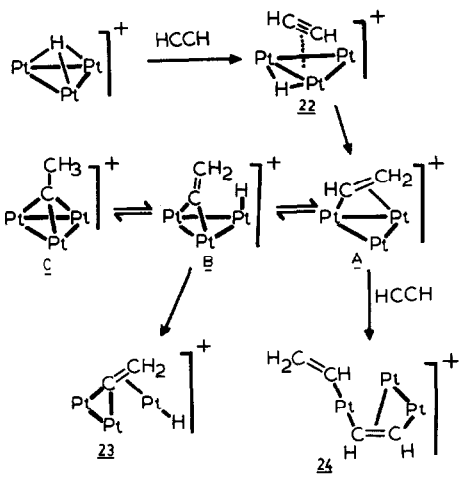

Scheme 14.

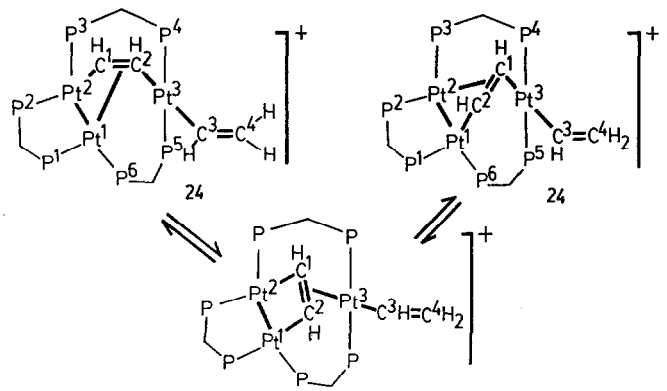

(11)

8.3. *Comparison to the surface chemistry of* HCCH[97,98]

Acetylene adsorbs to the platinum(111) surface at low temperature in the μ_3-(η^2-||) bonding mode, but then rearranges on warming. On the platinum(111) surface, the stable species is thought to be the ethylidyne, $Pt_3(\mu_3\text{-}CCH_3)$, but on lower symmetry surfaces the vinylidene, μ_3-η^2-C=CH_2, is thought to be present. The extra hydrogen atom needed to form ethylidyne is presumably provided by dissociation of acetylene, initially to CCH and H, on the surface. Species such as CCH, CH, or C are thought to be present on other metal surfaces as major products, and there is some evidence also for vinyl groups on the surfaces, at least as intermediates. On the platinum(111) surface, it has been suggested that the sequence of reactions for formation of ethylidyne is $Pt_3(\mu_3\text{-}\eta^2\text{-HCCH}) \rightarrow Pt_3(\mu_3\text{-}\eta^2\text{-C=}CH_2)H \rightarrow Pt_3(\mu_3\text{-}CCH_3)$, and that H,D exchange between adsorbed hydrogen and ethylidyne involves reversible isomerization $Pt_3(\mu_3\text{-}CCH_3) \rightleftharpoons Pt_3(CH\text{=}CH_2)$, with the H,D exchange step occurring in the vinyl group.[97-99]

In the model cluster systems, no rearrangement of acetylene groups, $Pt_3(HCCH)$, to vinylidene, $Pt_3(C\text{=}CH_2)$, or other groups occurred unless a hydride ligand was present on the cluster (sections 8.1 and 8.2), and this suggests that acetylene rearrangement on a metal surface may require at least catalytic amounts of surface hydrogen. In the model systems, the first step involves combination of hydride and acetylene ligands to give vinyl. At this stage there is good evidence for H,D exchange processes and these may well involve reversible formation of vinylidene and ethylidyne groups analogous to steps proposed to occur on a platinum(111) surface.[99] The vinylidene group may be stable in the clusters as may a terminal vinyl group. However, ethylidyne, which appears to be the most stable species on the platinum(111) surface,[97-99] is at best a reaction intermediate in the model cluster complexes.

9. CATALYSIS OF THE WATER GAS SHIFT REACTION[51,52]

While the major efforts described above have been to mimic chemisorption and related phenomena on metal surfaces, it would obviously also be useful to mimic the catalytic activity of metal surfaces. The latter aim has not been realized, but the cluster $[Pt_3(\mu_3\text{-}CO)(\mu\text{-dppm})_3]^{2+}$ is a useful catalyst for the water gas shift (WGS) reaction, $CO + H_2O \rightarrow CO_2 + H_2$.

From a kinetic point of view, the catalysis is first order in cluster complex and inverse first order in pressure of carbon monoxide (Fig. 21). The reaction occurs more rapidly in aqueous methanol containing higher H_2O–MeOH ratios provided that solubility is sufficient. The mechanism of Scheme 15 is thought probable. All of the individual steps in the proposed catalytic cycle have been shown to occur readily, with the exception of the step involving attack of hyroxide on $[Pt_3(\mu_3\text{-}CO)(\mu\text{-dppm})_3]^{2+}$ to give carbon dioxide and $[Pt_3(\mu_3\text{-}H)(\mu\text{-dppm})_3]^{+}$, which is suggested to be rate determining. There are good precedents for attack of hydroxide on cationic carbonyls of platinum, but a terminal carbonyl may be necessary. The inhibition of catalysis by excess carbon monoxide may be due to the parallel formation of $[Pt_3(CO)_2(\mu\text{-dppm})_3]^{2+}$ or $[Pt_3(CO)_3(\mu\text{-dppm})_3]^{2+}$ (section 4.1), which may be less reactive to attack by hydroxide.

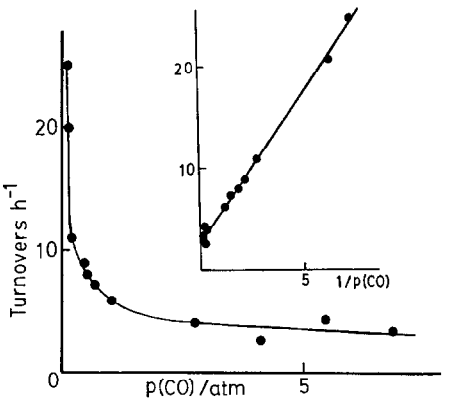

Fig. 21. Dependence of turnover rate for the WGS reaction catalysed by $[Pt_3(\mu_3\text{-}CO)(\mu\text{-}dppm)_3]^+$ in aqueous methanol at 100°C on the pressure of carbon monoxide. The inset shows the corresponding plot of turnover rate versus $1/p(CO)$.

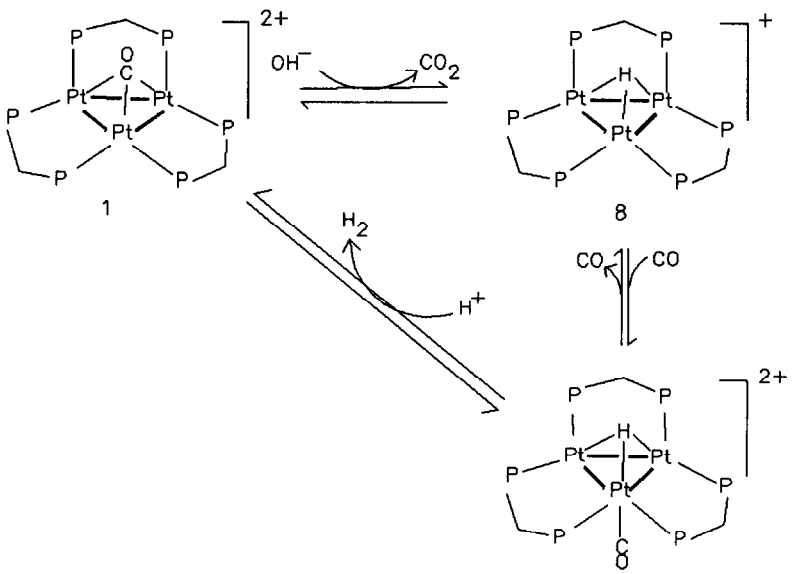

Scheme 15.

10. CONFORMATIONS OF dppm LIGANDS

Molecular structures of nearly all complexes discussed here contain a $M_3(\mu_3\text{-dppm})_3$ fragment in which the metal atoms form a triangular arrangement edge-bridged by three dppm ligands. In most complexes the metal atoms form three M—M bonds, and such complexes contain an approximately latitudinal M_3P_6 unit. In the complexes where only one M—M bond is observed, the M—P bonds are substantially bent out of the M_3 plane.

When a dppm ligand bridges a M—M bond a five-membered M_2P_2C ring is formed. Crystallographic studies have shown that, in the cluster complexes discussed here, such rings usually adopt an envelope shape with the CH_2 group at the flap. This conformation of the M_2P_2C rings permits a near-zero P—M—M—P torsion angle, required by the latitudinal M_3P_6 core, and M—P—C—P torsion angles, w_1 and w_2, corresponding to nearly staggered conformations of the dppm ligands around the P—CH_2 bonds. A correlation plot[100] of w_1 and w_2 angles observed in

different complexes (Fig. 22) thus shows a cluster of points centred on $w_1 = -w_2 = 50°$, characterizing a symmetrical envelope conformation of the M_2P_2C rings. The plot also shows combinations of w_1 and w_2 values consistent with M—M separation of 2.60 Å in rings of average dimensions (M—P = 2.30 Å, P—C = 1.83 Å, M—P—C = 109° and P—C—P = 111°). In such rings $w_1 = -w_2 = 50°$ represents the dppm conformation of lowest energy, corresponding to the smallest distortions from staggering ($w_1 = -w_2 = 60°$) about the P—CH bonds, allowed by the constraint M—M = 2.60 Å. For dppm ligands bridging two metal atoms which are not directly bonded to each other, the observed M—P—C—P torsion angles are typically $w_1 = 65°$ and $w_2 = -40°$ (Fig. 22). Thus the rupture of the M—M bonds and the increase in M···M separations to 3.1–3.6 Å causes a relatively small change in conformation of the dppm ligands, the w_1 and w_2 torsion angles changing typically by about 10–15°. This analysis therefore shows that dppm ligands can bridge a pair of metal atoms at M—M separations of 2.58–3.60 Å without adopting energetically unfavourable conformations, irrespective of whether or not the metal atoms are bonded to each other. It is then not surprising that the dppm ligands are capable of preventing fragmentation of these trinuclear complexes into binuclear and/or mononuclear species.

In the complexes which contain three M—M bonds, and therefore three envelope shaped M_2P_2C rings, two conformations of the *triangulo*-$M_3(\mu\text{-dppm})_3$ fragment are observed: (A) all three CH_2 flaps lie above the same face of the M_3 triangle, and (b) two CH_2 flaps lie above and one below the M_3 triangle. In type (A) complexes six equatorial phenyl groups project above the M_3 triangle and six axial phenyl groups project below it (Fig. 23). In type (B) complexes four equatorial plus two axial, and two equatorial plus four axial, phenyl groups lie above the opposite faces of the M_3 triangle. Therefore, in both types of complexes the two faces of the M_3 cluster are exposed to sterically different environments, the steric hindrance increasing with the number of axial phenyl groups (Fig. 24). The observed molecular structures of these complexes illustrate clearly that ligands adding to the $M_3(\mu\text{-dppm})$ fragment show a preference for the M_3 face with the greater number of equatorial phenyl groups.

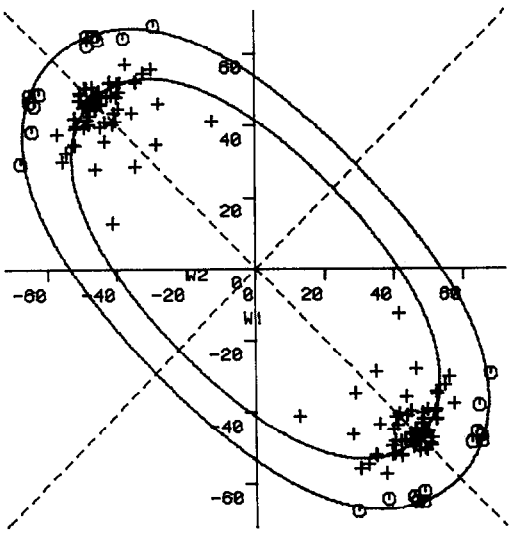

Fig. 22. Conformational map for dppm ligands in complexes with $M_3(\mu\text{-dppm})_3$ skeletons. The M—P—C—P torsion angles, w_1 and w_2, for each ligand are plotted against each other. Crosses correspond to ligands bridging M—M bonds and open circles to ligands bridging two metal atoms which are not bonded to each other (M···M 3.1–3.6 Å). Also shown are the combinations of w_1 and w_2 corresponding to M—M = 2.60 Å (inner curve) and 3.00 Å (outer curve) for a M_2P_2C ring with M—P = 2.30 Å, P—C = 1.83 Å, M—P—C = 109° and P—C—P = 111°. The diagonal broken lines $w_1 = w_2$, and $w_1 = -w_2$ are lines of mirror symmetry in the map, and relate isometric ligand conformations. The clustering about $w_1 = -w_2 = 50°$ (or $w_2 = -w_1 = 50°$) for rings with M—M bonds is especially obvious.

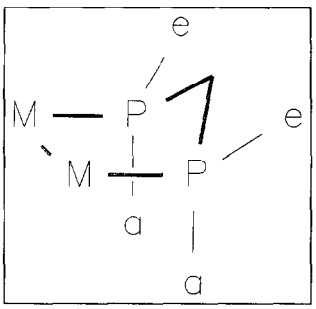

Fig. 23. The symmetrical envelope conformation of an M_2P_2C ring. Axial (a) and equatorial (e) substituent positions are also shown.

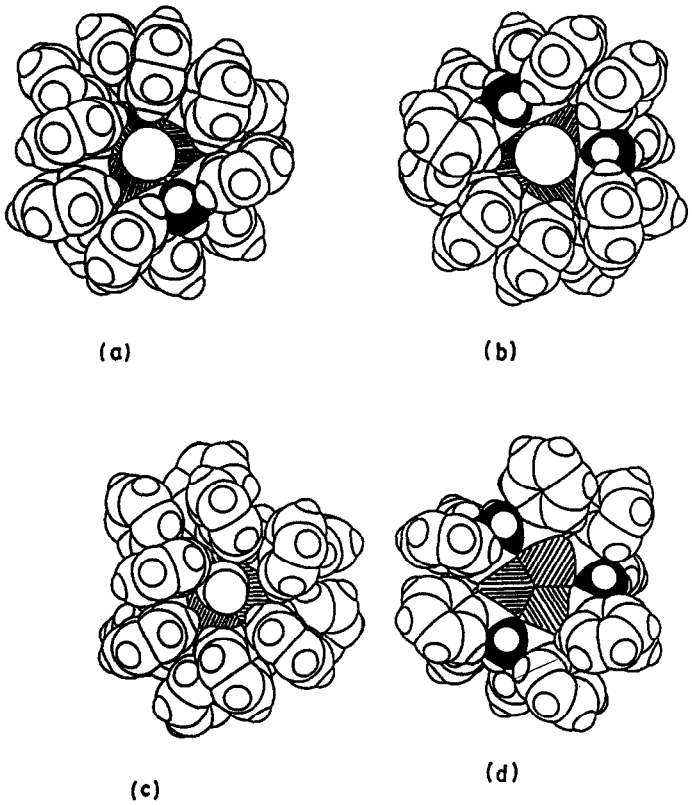

Fig. 24. The steric environments of M_3 faces in *triangulo*-$M_3(\mu\text{-dppm})_3$ complexes illustrated by space-filling models. Metal atoms are hatched and dppm methylene carbon atoms are shown in black. In all cases the complex is viewed along normal to the M_3 plane. (a) $[Pd_3(\mu_3\text{-I})(\mu_3\text{-CO})(\mu\text{-dppm})_3]^+$ viewed from the μ_3-CO side. The carbonyl is surrounded by two equatorial phenyl groups (adjacent to methylene carbon) and four axial phenyl groups. (b) The same cation viewed from the μ_3-I side. The iodo ligand is surrounded by four equatorial and two axial phenyl groups. Rotation of (a) by 180° about the vertical axis gives (b). (c) $[Pt_3(\mu_3\text{-CO})\{P(OPh)_3\}(\mu\text{-dppm})_3]^{2+}$ viewed from the μ_3-CO side. The carbonyl ligand is surrounded by six axial phenyl groups but the asymmetry in the $(\mu_3\text{-CO})Pt_3$ bonding does not appear to be caused by steric effects. (d) The same cation rotated 180° about the vertical axis to show the face to which the phosphite ligand is attached. The phosphite ligand is not shown. All phenyl groups are equatorial. Comparison of (a)–(d) suggests that steric hindrance above the M_3-face increases along the series (d) < (b) < (a) < (c).

11. CONCLUSIONS

The results described above show that coordinatively unsaturated cluster complexes, which are stabilized with respect to cluster fragmentation, can mimic some of the properties of a metal surface. Perhaps the most important property of the clusters is the ability to coordinate small molecules under very mild conditions in ways that mimic adsorption on a metal surface at low temperature. Such coordination compounds can typically be formed at $-80°C$ in solution and can be characterized by multinuclear NMR techniques. Where the molecules are stable at room temperature, they can be crystallized and characterized crystallographically. The best mimics for the structures of surface bound molecules have been based on derivatives of the iron group clusters, such as $[M_3(CO)]_{12}$, M = Fe, Ru or Os.[1,2,8–11] However, these are coordinatively saturated and must undergo carbonyl dissociation in order to bind small molecules. Since carbonyl dissociation is not usually easy, the coordination of small molecules often requires forcing conditions. In this sense, the coordinatively unsaturated clusters of the late transition metals are better mimics of a coordinatively unsaturated metal surface, particularly in terms of reactivity and reaction mechanism.

The ligands bound to the Pt_3 clusters may adopt terminal, μ_2 or μ_3 bonding modes and the energy differences between these different forms is evidently small in many cases. This frequently leads to very easy fluxionality. For example, the unique fluxionality of phosphine and diphosphine ligands is clearly a result of this phenomenon and is directly related to the coordinative unsaturation of the clusters. The fluxionality then gives useful mimicry of the mobility of coordinated molecules on a metal surface.

The oxidative addition of small molecules to the clusters mimics dissociative chemisorption on a metal surface and typically involves the preliminary step of simple coordination, mimicking low temperature non-dissociative chemisorption, as described above. It is in these cases of oxidative addition that metal–metal bonds are usually broken, and hence when the rôle of the μ-dppm ligands in preventing cluster fragmentation is particularly useful. The coordination and rearrangement of acetylene on the Pt_3 clusters, and the use of the clusters as catalysts for the WGS reaction, are further examples of processes where the dppm ligands prevent cluster fragmentation.

In summary, these clusters are very crude models for a metal surface but they are able to mimic many of the chemical properties of a platinum(111) surface. Clearly, the design, synthesis and study of coordinatively unsaturated clusters can also be a productive and worthwhile area of research in its own right.

Acknowledgements—We thank NATO for a travel grant in aid of collaborative research. R. J. Puddephatt thanks the NSERC (Canada) for financial support and Drs G. Ferguson and N. C. Payne for stimulating collaborations. Special thanks are due to the talented graduate students and postdoctoral fellows who did all the work; their names are given in the references.

REFERENCES

1. E. L. Muetterties, *Bull. Soc. Chim. Belg.* 1975, **84**, 959; 1976, **85**, 451.
2. E. L. Muetterties, *J. Organomet. Chem.* 1980, **200**, 177.
3. D. McDonald and L. B. Hunt, *A History of Platinum and its Allied Metals*. Johnson Matthey, Europa Publications, London (1982).
4. J. P. Collman, L. S. Hegedus, J. R. Norton and R. G. Finke, *Principles and Applications of Organotransition Metal Chemistry*. University Science Books, Mill Valley, California (1987).
5. M. R. Albert and Y. T. Yates Jr, *The Surface Scientist's Guide to Organometallic Chemistry*. ACS, Washington (1987).
6. A. B. Anderson and M. K. Awad, *J. Am. Chem. Soc.* 1985, **107**, 7854.
7. B. E. Hayden and A. M. Bradshaw, *Surf. Sci.* 1983, **125**, 787; B. Poelsma, L. K. Verheij and G. Comsa, *Phys. Rev. Lett.* 1982, **49**, 1731.
8. H. Vahrenkamp, *Adv. Organomet. Chem.* 1983, **22**, 169.
9. M. I. Bruce, *Coord. Chem. Rev.* 1987, **76**, 1.
10. A. J. Deeming, *Adv. Organomet. Chem.* 1986, **26**, 1.

11. F. A. Cotton and G. Wilkinson, *Advanced Inorganic Chemistry*, 5th edn. Wiley, New York (1988).
12. R. R. Burch, A. J. Shusterman, E. L. Muetterties, R. G. Teller and J. M. Williams, *J. Am. Chem. Soc.* 1983, **105**, 3546.
13. M. D. Fryzuk, T. Jones and F. W. B. Einstein, *Organometallics* 1984, **3**, 185; M. D. Fryzuk, *Organometallics* 1982, **1**, 408.
14. R. D. Brost and S. R. Stobart, *J. Chem. Soc., Chem. Commun.* 1989, 498.
15. C. Woodcock and R. Eisenberg, *Inorg. Chem.* 1985, **24**, 1287; D. H. Berry and R. Eisenberg, *Organometallics* 1987, **6**, 1796.
16. B. R. Sutherland and M. Cowie, *Organometallics* 1984, **3**, 1869; R. McDonald, B. R. Sutherland and M. Cowie, *Inorg. Chem.* 1987, **26**, 3333.
17. J. Wu, P. E. Fanwick and C. P. Kubiak, *Organometallics* 1987, **6**, 1805.
18. J. Chatt and P. Chini, *J. Chem. Soc. A* 1970, 1538.
19. D. M. P. Mingos and R. W. M. Wardle, *Transition Met. Chem.* 1985, **10**, 441.
20. N. K. Eremenko, E. G. Mednikov and S. S. Kurasov, *Russ. Chem. Rev.* 1985, **54**, 394.
21. C. S. Browning, D. H. Farrar, R. Gukathasan and S. A. Morris, *Organometallics* 1985, **4**, 1750; D. H. Farrar, R. R. Gukathesan and S. A. Morris, *Inorg. Chem.* 1984, **23**, 3258.
22. D. G. Evans, M. F. Hallam, D. M. P. Mingos and R. W. M. Wardle, *J. Chem. Soc., Dalton Trans.* 1987, 1889; S. G. Bott, M. F. Hallan, O. J. Ezomo, D. M. P. Mingos and I. D. Williams, *J. Chem. Soc., Dalton Trans.* 1988, 1461; D. M. P. Mingos, I. D. Williams and M. J. Watson, *J. Chem. Soc., Dalton Trans.* 1988, 1509.
23. C. Couture, D. H. Farrar, D. S. Fisher and R. R. Gukathasan, *Organometallics* 1987, **6**, 532.
24. H. C. Clark and V. K. Jain, *Coord. Chem. Rev.* 1984, **55**, 151.
25. C. E. Briant, D. I. Gilmour, D. M. P. Mingos and R. W. M. Wardle, *J. Chem. Soc., Dalton Trans.* 1985, 1693.
26. M. F. Hallam, D. M. P. Mingos, T. Adatia and M. McPartlin, *J. Chem. Soc., Dalton Trans.* 1988, 335.
27. A. Albinati, A. Moor, P. S. Pregosin and L. M. Venanzi, *J. Am. Chem. Soc.* 1982, **104**, 7672.
28. A. Albinati, K.-H. Dahmen, A. Togni and L. M. Venanzi, *Angew. Chem. Int. Ed. Engl.* 1985, **24**, 766.
29. D. M. P. Mingos and R. W. M. Wardle, *J. Chem. Soc., Dalton Trans.* 1986, 73.
30. D. M. P. Mingos, P. Oster and D. J. Sherman, *J. Organomet. Chem.* 1987, **320**, 257.
31. Y. Yamamoto, H. Yamazaki and T. Sakurai, *J. Am. Chem. Soc.* 1982, **104**, 2329.
32. D. G. Evans and D. M. P. Mingos, *J. Organomet. Chem.* 1982, **240**, 321.
33. C. Mealli, *J. Am. Chem. Soc.* 1985, **107**, 2245.
34. D. J. Underwood, R. Hoffmann, K. Tatsumi, A. Nakamura and Y. Yamamoto, *J. Am. Chem. Soc.* 1985, **107**, 5968.
35. D. G. Evans, *J. Organomet. Chem.* 1988, **352**, 397.
36. R. J. Puddephatt, *Chem. Soc. Rev.* 1983, 99.
37. A. L. Balch, *Homogeneous Catalysis with Metal Phosphine Complexes* (Edited by L. Pignolet). Plenum Press, New York (1983).
38. B. Chaudret, B. Delavaux and R. Poilblanc, *Coord. Chem. Rev.* 1988, **86**, 191.
39. P. Braunstein, J.-M. Jud, Y. Dusausoy and J. Fischer, *Organometallics* 1983, **2**, 180.
40. J. Ni and C. P. Kubiak, *Inorg. Chim. Acta* 1987, **127**, L37.
41. M. C. Grossel, R. P. Moulding and K. R. Seddon, *J. Organomet. Chem.* 1983, **253**, C50.
42. P. Braunstein, C. de M. de Bellefon and M. Ries, *J. Organomet. Chem.* 1984, **262**, C14; P. Braunstein, C. de M. de Bellefon, M. Ries and J. Fischer, *Organometallics* 1988, **7**, 332; P. Braunstein, C. de M. de Bellefon, M. Ries, J. Fischer, S.-E. Bouaoud and D. Grandijean, *Inorg. Chem.* 1988, **27**, 1327.
43. D. M. Hoffman and R. Hoffmann, *Inorg. Chem.* 1981, **20**, 3543.
44. P. R. Sharp, *Inorg. Chem.* 1986, **25**, 4185.
45. G. J. Arsenault, Lj. Manojlovic-Muir, K. W. Muir, R. J. Puddephatt and I. Treurnicht, *Angew. Chem. Int. Ed. Engl.* 1987, **26**, 86; Lj. Manojlovic-Muir, K. W. Muir, I. Treurnicht and R. J. Puddephatt, *Inorg. Chem.* 1987, **26**, 2418; G. J. Arsenault and R. J. Puddephatt, *Can. J. Chem.* 1989, **67**, 1800.
46. N. Hadj-Bagheri and R. J. Puddephatt, *J. Chem. Soc., Chem. Commun.* 1987, 1269; N. Hadj-Bagheri, Ph.D. thesis, University of Western Ontario, 1988.
47. N. Hadj-Bagheri and R. J. Puddephatt, *Inorg. Chem.* 1989, **28**, 2384.
48. Lj. Manojlovic-Muir, K. W. Muir, B. R. Lloyd and R. J. Puddephatt, *J. Chem. Soc., Chem. Commun.* 1983, 1336.
49. B. R. Lloyd and R. J. Puddephatt, *Inorg. Chim. Acta* 1984, **90**, L77.
50. G. Ferguson, B. R. Lloyd and R. J. Puddephatt, *Organometallics* 1986, **5**, 344.
51. B. R. Lloyd, Ph.D. thesis, University of Western Ontario, 1985; I. R. Jobe, Ph.D. thesis, University of Western Ontario, 1988.
52. A. A. Frew, R. H. Hill, Lj. Manojlovic-Muir, K. W. Muir and R. J. Puddephatt, *J. Chem. Soc., Chem. Commun.* 1982, 198.

53. G. Douglas, Lj. Manojlovic-Muir, K. W. Muir, M. C. Jennings, B. R. Lloyd, M. Rashidi and R. J. Puddephatt, *J. Chem. Soc., Chem. Commun.* 1988, 149.
54. G. Schoettel and R. J. Puddephatt, unpublished work.
55. Lj. Manojlovic-Muir, K. W. Muir and T. Solomon, *J. Organomet. Chem.* 1979, **179**, 479.
56. Lj. Manojlovic-Muir and K. W. Muir, *J. Organomet. Chem.* 1981, **219**, 129.
57. Lj. Manojlovic-Muir, K. W. Muir, M. C. Grossel, M. P. Brown, C. D. Nelson, A. Yavazi, E. Kallas, R. P. Moulding and K. R. Seddon, *J. Chem. Soc., Dalton Trans.* 1986, 1955.
58. G. Ferguson, B. R. Lloyd, Lj. Manojlovic-Muir, K. W. Muir and R. J. Puddephatt, *Inorg. Chem.* 1986, **25**, 4190.
59. B. R. Lloyd, A. Bradford and R. J. Puddephatt, *Organometallics* 1987, **6**, 424.
60. A. Bradford, M. C. Jennings and R. J. Puddephatt, *Organometallics* 1988, **7**, 792.
61. A. M. Bradford, G. Douglas, Lj. Manojlovic-Muir, K. W. Muir and R. J. Puddephatt, *Organometallics* 1990, **9**, 409.
62. R. F. Alex and R. K. Pomeroy, *Organometallics* 1987, **6**, 2437; D. H. Farrar and J. A. Lunniss, *J. Chem. Soc., Dalton Trans.* 1987, 1249; M. R. Shaffer and J. B. Keister, *Organometallics* 1986, **5**, 561.
63. G. E. Mitchell, M. A. Henderson and J. M. White, *Surf. Sci.* 1987, **191**, 425; M. D. Alvey and J. T. Yates Jr, *J. Am. Chem. Soc.* 1988, **110**, 1782.
64. A. M. Bradford, Lj. Manojlovic-Muir, K. W. Muir and R. J. Puddephatt, unpublished work; A. M. Bradford, N. C. Payne, R. J. Puddephatt, D. S. Yang and T. B. Marder, *J. Chem. Soc., Chem. Commun.*, in press; T. Szilagyi, *Appl. Surf. Sci.* 1988, **35**, 19; N. R. Avery and T. W. Matheson, *Surf. Sci.* 1984, **143**, 11a.
65. G. Douglas, M. C. Jennings, Lj. Manojlovic-Muir, K. W. Muir and R. J. Puddephatt, *J. Chem. Soc., Chem. Commun.* 1989, 159.
66. M. C. Jennings, G. Schoettel, S. Roy, R. J. Puddephatt, G. Douglas, Lj. Manojlovic-Muir and K. W. Muir, *Inorg. Chem.*, in press.
67. L. J. Guggenberger, *J. Chem. Soc., Chem. Commun.* 1968, 512.
68. G. K. Campbell, P. B. Hitchcock, M. F. Lappert and M. C. Mirza, *J. Organomet. Chem.* 1985, **289**, C1.
69. B. R. Lloyd and R. J. Puddephatt, *J. Am. Chem. Soc.* 1985, **107**, 7785.
70. A. M. Baro and H. Ibach, *Surf. Sci.* 1980, **92**, 237; J. Lee, J. P. Cowin and L. Wharton, *Surf. Sci.* 1983, **130**, 1; K. Mortensen, F. Besenbacher, I. Stensgaard and C. Klink, *Surf. Sci.* 1989, **211/212**, 813.
71. R. Ravindranath, N. C. Payne and R. J. Puddephatt, unpublished work.
72. Lj. Manojlovic-Muir, K. W. Muir, B. R. Lloyd and R. J. Puddephatt, *J. Chem. Soc., Chem. Commun.* 1985, 536.
73. Lj. Manojlovic-Muir and K. W. Muir, unpublished work.
74. L. Y. Ukhin, N. A. Dolgopolova, L. G. Kuzmina and Y. T. Struchkov, *J. Organomet. Chem.* 1981, **210**, 263.
75. A. S. Hirschin, W. K. Musker, M. M. Olmstead and J. L. Dallas, *Inorg. Chem.* 1981, **20**, 1702.
76. The CSSR programs were used to scan the Cambridge Structural Database. See: *CSSR Manual*, 3rd edn; Daresbury, England (1985).
77. S. S. M. Ling, N. Hadj-Bagheri, Lj. Manojlovic-Muir, K. W. Muir and R. J. Puddephatt, *Inorg. Chem.* 1987, **26**, 231.
78. G. Ferguson, M. C. Jennings, H. A. Mirza and R. J. Puddephatt, *Organometallics* 1990, **9**, 1576.
79. A. M. Bradford and R. J. Puddephatt, *New J. Chem.* 1988, **12**, 427.
80. A. M. Bradford, R. J. Puddephatt, G. Douglas, Lj. Manojlovic-Muir and K. W. Muir, *Organometallics* 1990, **9**, 1579.
81. J. M. Wisner, T. J. Bartczak and J. A. Ibers, *Organometallics* 1986, **5**, 2044.
82. L. Pauling, in *The Nature of the Chemical Bond*, 3rd edn, p. 256. Cornell University Press, Ithaca (1960).
83. R. Ramachandran, N. C. Payne and R. J. Puddephatt, *J. Chem. Soc., Chem. Commun.* 1989, 128.
84. M. C. Jennings, N. C. Payne and R. J. Puddephatt, *J. Chem. Soc., Chem. Commun.* 1986, 1809.
85. M. C. Jennings, N. C. Payne and R. J. Puddephatt, *Inorg. Chem.* 1987, **26**, 3776.
86. R. J. Koestner, M. Salmeron, E. B. Kollin and J. L. Gland, *Surf. Sci.* 1986, **172**, 68.
87. M. C. Jennings and R. J. Puddephatt, *Inorg. Chem.* 1988, **27**, 4280; G. Douglas, M. C. Jennings, Lj. Manojlovic-Muir and R. J. Puddephatt, *Inorg. Chem.* 1988, **27**, 4516.
88. P. Braunstein, H. Lehner, D. Matt, A. Tiripicchio and M. Tiripicchio-Camellini, *Angew-Chem. Int. Ed. Engl.* 1984, **23**, 90, 304.
89. H. H. Murray, D. A. Briggs, G. Garzon, R. G. Raptis, C. L. Porter and J. P. Fackler Jr, *Organometallics* 1987, **6**, 1992.
90. P. G. Jones, *Gold Bull.* 1986, **19**, 46.
91. A. M. Bradford, M. C. Jennings and R. J. Puddephatt, *Organometallics* 1989, **8**, 2367.
92. M. C. Jennings and R. J. Puddephatt, unpublished work.

93. G. Douglas, Lj. Manojlovic-Muir, K. W. Muir, M. Rashidi, C. M. Anderson and R. J. Puddephatt, *J. Am. Chem. Soc.* 1987, **109**, 6527.
94. M. C. Jennings, Lj. Manojlovic-Muir and R. J. Puddephatt, *J. Am. Chem. Soc.* 1989, **111**, 745.
95. M. Rashidi and R. J. Puddephatt, *J. Am. Chem. Soc.* 1986, **108**, 7111.
96. M. Rashidi and R. J. Puddephatt, *Organometallics* 1988, **7**, 1636.
97. C. M. Mate, C.-T. Kao, B. E. Bent and G. A. Somorjai, *Surf. Sci.* 1988, **197**, 183, and references therein.
98. P. K. Wang, C. P. Slichter and J. H. Sinfelt, *Phys. Rev. Lett.* 1984, **53**, 82.
99. K. M. Ogle and J. M. White, *Surf. Sci.* 1986, **165**, 234.
100. J. D. Dunitz, in *X-Ray Analysis and the Structure of Organic Molecules*, p. 447. Cornell University Press, Ithaca (1979).

Polyhedron Vol. 9, No. 23, pp. 2803–2808, 1990
Printed in Great Britain

0277–5387/90 $3.00+.00
© 1990 Pergamon Press plc

A ^{59}Co NMR STUDY OF STEREOISOMERISM OF COBALT(III) COMPLEXES WITH POLYDENTATE AMINOCHELATE LIGANDS

T. SH. KAPANADZE, YU. V. KOKUNOV and YU. A. BUSLAEV*

N. S. Kurnakov Institute of General and Inorganic Chemistry,
U.S.S.R. Academy of Sciences, Moscow, U.S.S.R.

(*Received* 4 *April* 1989; *accepted after revision* 15 *June* 1990)

Abstract—The stereoisomerization of complexes with polydentate aminochelate ligands dien (diethylenetriamine), trien (triethylenetetramine), tetraen (tetraethylenepentamine) and cyclam (1,4,8,11-tetraazacyclotetradecane) were investigated by ^{59}Co NMR in aqueous solutions. Their structure and preference of certain isomeric formations were studied. It was found that for the $[Co(dien)(NO_2)_2NH_3]Cl$ complex, out of four geometric isomers observed, those with *mer*-configuration dominate. *Trans*-complexes with tetradentate ligand (trien), configurationally are more labile than *cis*-complexes and the stability of geometric isomers increases in the order *trans* $< \alpha < \beta$. While when the cyclic tetradentate ligand (cyclam) coordinates to cobalt, mainly complexes with *trans*-configuration are formed. Formation of all four alternative geometric isomers for Co^{III} complexes containing pentadentate ligand (tetraen) is found.

Different stereoisomeric forms are possible for octahedral Co^{III} complexes with polydentate amine ligands. These forms will differ in the nitrogen atom binding with the central atom of cobalt.

In Co^{III} complexes with polydentate amines there are several sources of asymmetry (complex configuration, conformation of chelate cycles, asymmetric character of donor nitrogen atoms) resulting in the appearance of complicated diastereoisomeric forms. Therefore, to determine the absolute configuration of these isomers is rather difficult, although, undoubtedly, attractive. High sensitivity of the Co^{III} nucleus to structural changes allows (using ^{59}Co NMR) the existence of different types of isomerism to be determined in the solutions of Co^{III} complexes with chelate ligands.

This work was aimed at investigating, by ^{59}Co NMR, the stereoisomerization reaction of Co^{III} complexes containing polydentate amine ligands: dien, trien, tetraen and cyclam.

EXPERIMENTAL

The cobalt(III) complex compounds were synthesized according to known procedures: $[Co(dien)(NO_2)_2NH_3]Cl$,[1] $[Co(NH_3)_3(NO_2)_2Py]Cl$,[2] $[Co(trien)X_2]Y_{1;3}$,[3,4] $[Co(cyclam)X_2]Y_{1;3}$,[5,6] ($X = NO_2^-$, NH_3, Cl^-; $Y = Cl^-$, ClO_4^-). Solutions, containing *trans*-$[Co(trien)(OH)_2]^+$ and $[Co(cyclam)(OH)_2]^+$ were obtained by passing *trans*-$[Co(trien)Cl_2]Cl$ and *trans*-$[Co(cyclam)Cl_2]Cl$; $[Co(tetraen)X]Y_{1;3}$[7] ($X = NH_3$; OH^-, Cl^-, H_2O; $Y = Cl^-$, ClO_4^- and $ZnCl_4^{2-}$) through an ion-exchange column (form-OH). ^{59}Co NMR spectra of the fresh aqueous solutions with a concentration of 0.05–0.1 mol dm^{-3} were recorded on a Bruker AM-400 (resonance frequency 94.45 MHz) at room temperature. Chemical shifts are given relative to $[Co(NH_3)_6]Cl_3$.

RESULTS AND DISCUSSION

Octahedral Co^{III} complexes containing one molecule of tridentate ligand (dien) can exist in two isomeric forms (*mer*- and *fac*-).[8–12]

The presence of different monodentate ligands in the coordination sphere leads to an increase in the number of geometric isomers. Four resonance signals corresponding to isomers (Table 1) were found in the ^{59}Co NMR spectrum of an aqueous solution of $[Co(dien)(NO_2)_2NH_3]Cl$.

Intensity ratios of signals show that for Co^{III} complexes (with one molecule dien) the formation

* Author to whom correspondence should be addressed.

Table 1. ^{59}Co NMR spectra of $[Co(dien)(NO_2)_2NH_3]Cl$ aqueous solutions after 10 min

Isomers' assignment		δ ^{59}Co (ppm)	Line widths ($\Delta\nu 1/2$ Hz)	Relative intensity
fac-	aed,bf,c	−1430	280	6.12
	aed,cf,b	−1480	310	3.22
mer-	edc,ab,f	−1530	420	33.05
	edc,af,b	−1550	650	56.78

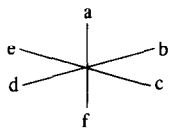

of the *mer*-configuration is preferable compared with the formation of *fac*-isomers.

It should be noted that for the bis-complex of diethylenetriamine $[Co(dien)_2]^{3+}$, which is realized in the form of three topological isomers: S-*fac*, u-*fac* and *mer*,[13–16] meridional coordination of dien over facial coordination is also preferable. However, as was shown by Keene and Searle,[17] when PO_4^{3-} or SeO_3^{2-} oxyanions are present in the solution, the equilibrium shifts to the preferred formation of *fac*-isomers (S-*fac* > u-*fac* > *mer*). They assume that an enhanced proportion of the *fac*-isomers is responsible for the differential specific associations between the oxyanions and the three isomeric cations.

When triethylenetetramine is coordinated to cobalt the formation of three geometric isomers α-*cis* (S-*cis*), β-*cis* (u-*cis*) and *trans*- is possible.[18] We found the formation of the above geometric isomers for complexes $[Co(trien)X_2]^{n+}$ (where $X = NO_2^-$, NH_3, OH^-) (Table 2).

Presence of two asymmetric nitrogen atoms—NH-group—in the ligand trien increases the number of possible isomers.[3,18] Analysing the stereomodels of the geometric isomers mentioned, Buckingham *et al.*[19] showed that two enantiomers, Δ (SS) and Λ (RR), are possible in the case of the α-*cis* configuration of the complex. For the complexes of β-*cis* configuration the possibility of four stereoisomers, Λ (SS), Λ (SR), Δ (RR) and Δ (RS), was considered, but for the *trans*-complex the presence of two optical isomers (SS), (RR) and *meso*-form (SR) was considered. However, wide lines in the ^{59}Co NMR spectrum for the dinitro-complex $[Co(trien)(NO_2)_2]Cl$ [Fig. 1(a)] evidently do not allow the observation of diastereoisomers in the solution caused by insignificant structural effects. Substitution of the nitro-group by an ammonia molecule or hydroxo-group in tetramine Co^{III} complexes makes the resonance signals in the ^{59}Co NMR spectrum noticeably narrow. Thus, a low intensity signal (−665 ppm) is present in the spectrum of the freshly prepared *trans*-$[Co(trien)(NH_3)_2]Cl_3$ as a result of *trans*-(R,S)-*meso*-form formation [Fig. 1(b)] besides an intense signal corresponding to the sum of optical isomers R,R (S,S) of *trans*-configuration. Intensity ratios of signals show that for *trans*-complexes with triethylenetetramine, SS- and RR-configurations are much preferable because in the case of R,S-species formation all three five-member cycles reveal different conformations (λ, ε, δ), as was assumed by Shibata,[4] which, evidently, requires a higher strain of the chelate rings. It should be noted that in solutions of *trans*-$[Co(trien)X_2]^{n+}$ in all cases α- and β-*cis* isomers were present as a result of *trans* → *cis* isomerization. Isomerization of *trans* $\rightleftharpoons$ α-*cis* $\rightleftharpoons$ β-*cis* at pH = 7 at 25°C proceeds spontaneously and in time equilibrium shifts to the formation of α- and β-*cis* isomers. Timed ^{59}Co NMR spectra analyses for $[Co(trien)X_2]^{n+}$ complexes leads to the conclusion that the stability of geometric isomers increases in the order *trans* < α < β-*cis*. The presence of two broad signals (Fig. 2) in the $[Co(trien)(NH_3)OH]^{2+}$ spectrum is a result of the dimer complexes existence in the solution bonded to each other through a bridging OH-group. In the formation of

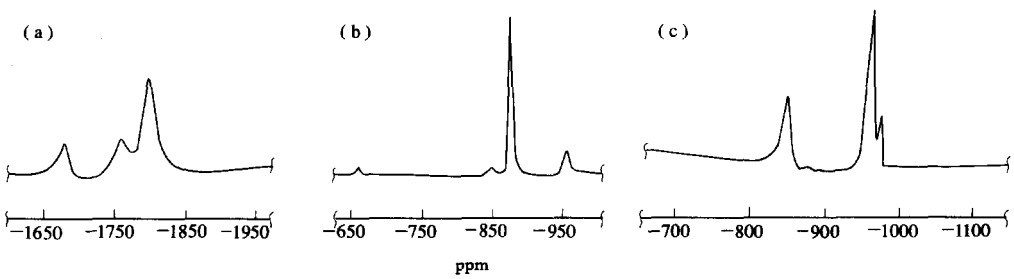

Fig. 1. ^{59}Co NMR spectra of (a) $[Co(trien)(NO_2)_2]Cl$, (b) *trans*-$[Co(trien)(NH_3)_2]Cl_3$, and (c) *cis*-$[Co(trien)(NH_3)_2](ClO_4)_3$ in aqueous solution after 15 min. The assignments of the lines are given in Table 2.

Table 2. ^{59}Co NMR data of isomers' assignments for $Co(trien)X_2^{n+}$ complexes ($X = NO_2^-$, NH_3, $n = 1,3$)

Complex	Absolute configuration	δ ^{59}Co (ppm)	$\Delta\nu 1/2$ (Hz)
$[Co(trien)(NO_2)_2]^+$	*trans*	−1800	685
	α-cis	−1680	510
	β-cis	−1760	560
trans-$[Co(trien)(NH_3)_2]^{3+}$	*trans*-RR(SS)	−880	250
	trans-RS	−665	260
	α-cis	−850	350
	β-cis	−955	325
β-cis-$[Co(trien)(NH_3)_2]^{3+}$	*β-cis* Λ-SS(-RR)	−955	325
	β-cis Λ-SR(-RS)	−973	310
	β-cis *α-cis*	−850	350

dimer complexes all four geometric isomers can participate (Table 3).

It is known[5] when the cyclic tetramine ligand—cyclam—is coordinated to cobalt, complexes with *trans*-configuration are mainly formed. Whereupon, all four nitrogen atoms can be asymmetric centre. That is why the possibility of five diastereoisomers RRRR, RSRR, SSRR, RSSR and RSRS was considered with regard to the orientation of hydrogen atoms.[6]

The possible existence of such isomers was discussed in the literature,[5,6,20–22] but the formation of more than two isomers for *trans*-complexes was never mentioned.

$[Co(cyclam)(NH_3)_2]Cl_3$ obtained as a result of reaction of *trans*-$[Co(cyclam)Cl_2]Cl$ with liquid ammonia gives one resonance signal (−620 ppm) in aqueous solutions, so out of five possible isomers only one *trans*-form is stable (Table 4). No other isomers appeared when the pH or temperature of the solution were changed. In the solution of *cis*-$[Co(cyclam)(NH_3)_2]^{3+}$ spontaneous *cis* → *trans* isomerization was observed. Increase of the basicity (pH > 10) favoured *cis* → *trans* isomerization and the complex with the *trans*-configuration dominated in the solution.

Evidently, this is the result of the amine ligands deprotonation in basic solutions which makes the chelate rings inversion easier in turn. Formation of all five configuration isomers was observed in the solution of *cis*-$[Co(cyclam)(OH)_2]^+$ (Table 4). The presence of a dihydroxo-complex of *cis*-configuration was proved. In the spectrum of this solution in the presence of optically active anions of *d*-tartaric acid, the signal (993 ppm) assigned to *cis*-$[Co(cyclam)(OH)_2]^+$ shifted to higher field and split into two (987 and 981 ppm) as a result of diastereoisomers $\Lambda d \rightleftharpoons \Delta d$ formation. Since the *cis*-complex has no symmetry plane, only this complex can exist in two enantiomeric Λ- and Δ-forms.

Earlier authors[23] succeeded in separating optically the active isomer *cis*-Λ-$[Co(cyclam)en]Cl_3$. So, for Co^{III} complexes with cyclam only, complexes with the *trans*-configuration are more stable in solution. While only one form out of five possible diastereoisomers is mainly formed as follows from the intensity ratios of signals for *trans*-complexes, but not three, as was assumed on the basis of the model compound calculations.[20]

One could assume as well, the existence of all five types of diastereoisomers for *cis*-complexes. However, *cis*-complexes are formed as a racemic compound of two enantiomers Λ-SSSS (Δ-RRRR) in which five- and six-member chelate cycles have more stable gauche- and chair-conformations, therefore steric hindrance must be minimal.

Dissolving *β*-$[Co(tetraen)Cl](ClO_4)_2$ in 10% aqueous solution of ammonia led to the formation of a

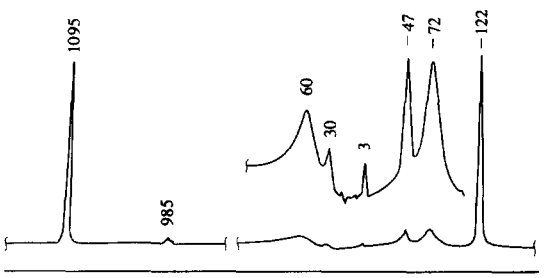

Fig. 2. ^{59}Co NMR (9.395 T) spectra of the reaction products of 0.1 M *α-cis*-$[Co(trien)Cl_2]Cl$ in 2% aqueous solution of ammonium after 2 days.

Table 3. ^{59}Co NMR data of Co^{III} complexes assigned from the reaction of α-*cis*-$[Co(trien)Cl_2]^+$ and NH_4OH

Complexes	Absolute configuration	δ ^{59}Co (ppm)	$\Delta\nu 1/2$ (Hz)
$[Co(trien)(NH_3)OH]^{2+}$	*trans*	−122	165
	α-*cis*	30	205
	β-*cis* { aedc,f,b	−47	280
	β-*cis* { aedc,b,f	3	185
$[Co_2(trien)_2(NH_3)_2OH]^{5+}$		−72	850
		60	1030
$[Co(trien)(OH)_2]^+$	{ *trans*-RR(SS)	1095	130
	{ *trans*-RS	985	150

mixture of hydroxo- and ammonium complexes:

$$[Co(tetraen)Cl]^{2+} \xrightarrow[H_2O]{NH_3} [Co(tetraen)OH]^{2+} + [Co(tetraen)NH_3]^{3+},$$

both complexes being formed in all four possible isomeric forms (Table 5).[24–27]

A wide signal in the region −380 to −460 ppm consisting of several overlapping lines [Fig. 3(a)] indicated the hydroxo- complexes' dimerization through the bridging OH-group. As all four types of hydroxo-complex could participate in the dimer formation, various combinations of isomeric forms are possible (for example, α- and β- and so on).

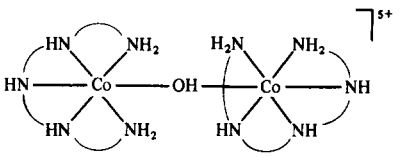

α β

Each combination of the complex must produce two separate resonance signals in the ^{59}Co NMR spectrum. Evidently, the complicated shape of the signal from binuclear hydroxo-complexes is thus explained. ^{59}Co NMR data for similar binuclear μ-peroxo-O_2 complexes $[Co(tetraen)_2]O_2^{4+}$ are given in Refs 30 and 31. On making the solution acid, the bridging bond in [(tetraen)Co-OH-Co(tetraen)]$^{5+}$

Table 4. ^{59}Co NMR spectra of (a) an aqueous solution of *cis*-$[Co(cyclam)(NH_3)_2]Cl_3$ after 2 days and (b) species observed after 2 h for the reaction *cis*-$[Co(cyclam)Cl_2]Cl + NH_4OH \rightarrow$ product

Complexes	^{59}Co (ppm)	$\Delta\nu 1/2$ (Hz)	Relative intensity
(a)			
trans-$[Co(cyclam)(NH_3)_2]^{3+}$	−620	1800	80
cis-$[Co(cyclam)(NH_3)_2]^{3+}$	−590	1005	20
(b)			
$[Co(cyclam)(OH)NH_3]^{2+}$			
trans {	140	290	88
trans {	100	310	5
cis	−3	250	6.5
$[Co(cyclam)(OH)_2]^+$			
	1092	140	93.15
	1185	—	1.05
trans[a]	1153	—	1.55
	1086	—	0.75
	1045	—	0.85
cis Λ, Δ	993	—	1.78

[a]Conformation isomers.

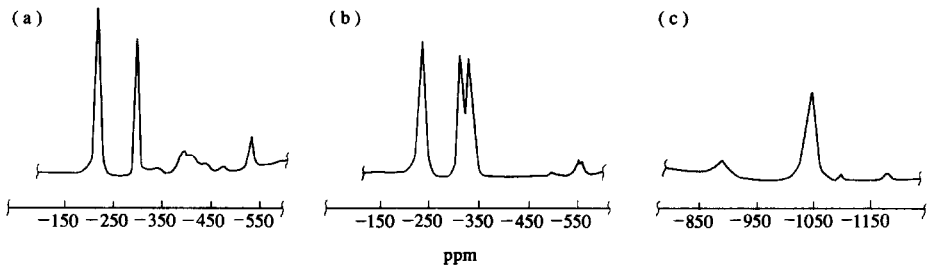

Fig. 3. ^{59}Co NMR spectra (a, c) of the products observed after 1 h for the reaction β-[Co(tetraen)Cl]$(ClO_4)_2$ in 10% aqueous solution of ammonium and (b) of 0.1 M [Co(tetraen)OH]$(ClO_4)_2$ with 0.6 M H_2 *d*-tart.

is easily broken resulting in the formation of mononuclear water complexes.

In the literature discussing the symmetry of all the four considered geometric isomers, opinions differ. In some reports[28,29] it was assumed that all four isomers must be asymmetric. However, later it was proved[25,32] that out of the four isomers, the α-isomer has the plane of symmetry and cannot exist in optically active form. Other authors[25] succeeded in separating Λ- and Δ-enantiomers and proved the existence of optically active forms for the β-isomer. In the type of complexes discussed, besides the chiral configuration of the chelate rings there is one more source of optical activity—three asymmetric atoms of the secondary nitrogen.

It was found by X-ray analysis[26] that the β-isomer is realized in two stable diastereoisomeric forms differing by the orientation of the hydrogen atoms bonded to the nitrogen atom (NH-group) on *trans*-coordination with the NH_2-group (—NH—Co—NH_2—). Moreover, for bedcf, the existence of four diastereoisomers is assumed on the basis of stereo-models of these complexes, but for aedfc,b and aedcf,b the formation of only one form was discussed.[26] It is necessary to note that in all the considered amine ligands, the nitrogen atoms participating in complex formation are four coordinated, i.e. they have tetrahedral surrounding and are configurationally stable. So, different orientations of hydrogen atoms predetermine the conformation of chelate cycles—the curve of the ligand chain where carbon atoms not participating in complex formation are placed.

The presence of optical isomers dependent on the different Λ- and Δ-configurations of the complexes was found for two geometric isomers. In the spec-

Table 5. ^{59}Co NMR spectra from the reaction of β-[Co(tetraen)Cl]$^{2+}$ and aqueous solution of ammonium

Complexes	^{59}Co (ppm)	Δν1/2 (Hz)	Relative intensity
[Co(tetraen)OH]$^{2+}$			
α-(aedfc,b)	225	950	55.20
β-(bedfc,a)	310	470	35.85
(aedcf,b)	490	210	1.45
(bedcf,a)	545	290	7.35
[Co(tetraen)]$_2$OH^{5+}			
	380[a]	—	—
	400[a]	—	—
	415[a]	—	—
	435[a]	—	—
[Co(tetraen)NH_3]$^{3+}$			
-(aedfc,b)	−885	1350	15.60
-(bedfc,a)	−1040	1220	79.15
(aedcf,b)	−1100	420	2.95
(bedcf,a)	−1170	485	3.15

[a]Remarks are in the text.

trum of the aqueous solution [Co(tetraen)OH] $(ClO_4)_2$ in the presence of *d*-tart^{2-} [Co : (*d*-tart)$^{2-}$ = 1 : 6] all four signals were slightly shifted to a higher field and two signals corresponding to β-(bedfc,a) and (bedcf,a) isomers, having neither a plane nor a symmetry centre, were split because of the binding of optically active anions in the second coordination sphere with the formation of Λ-*d* and Δ-*d* diastereoisomers [Fig. 3(b)]. No formation of diastereoisomers was found due to the different orientation of hydrogen atoms at the secondary nitrogen atoms, which in the case of tetradentate ligands (trien and cyclam) contribute to the shielding of the cobalt(III) central atom. It is known[33,34] that for Co^{III} complexes with anions of ethylenediaminetetraacetic acid where asymmetric nitrogen atom with different substituents is also present. However, consideration of the chelate cycles' geometry showed that nitrogen can have only S-configuration. Evidently, formation of geometric isomers with pentadentate ligand (tetraen) also requires such a curve of the chelate cycles when only a definite orientation of the hydrogen atom is stabilized.

REFERENCES

1. S. P. H. Grayton, C. F. Zitomer and J. Lambert, *Inorg. Synth.* 1963, 7, 211.
2. B. Adell, *Z. Anorg. Allg. Chem.* 1957, **B289**, 313.
3. A. M. Sargeson and G. H. Searle, *Inorg. Chem.* 1967, **6**, 787.
4. M. Shibata, *Modern Syntheses of Cobalt (III) Complexes*, p. 7. Akademie Verlag, Berlin (1983).
5. B. Bosnich, C. K. Poon and M. L. Tobe, *Inorg. Chem.* 1965, **4**, 1102.
6. C. K. Poon and M. L. Tobe, *Inorg. Chem.* 1968, **7**, 2398.
7. D. A. House and C. S. Garner, *Inorg. Chem.* 1967, **6**, 272.
8. P. H. Crayton and J. A. Mattern, *J. Inorg. Nucl. Chem.* 1960, **13**, 248.
9. Y. Tanito, Y. Saito and H. Kuroya, *Bull. Chem. Soc. Jpn* 1953, **26**, 420.
10. E. V. Popa, M. D. Mazus and V. N. Biyushkin, in *Investigtion of Coordination Compounds Chemistry and Physico-Chemical Methods of Analysis*, p. 43. Kishinev: Izd-vo AN MSSR (1969).
11. V. P. Tarasov, T. Sh. Kapanadze, I. B. Baranovski, G. V. Tsintsadze, S. G. Drobyshev and Yu. A. Buslaev, *Koord. Khim.* 1984, **10**, 368.
12. T. Sh. Kapanadze, V. P. Tarasov, G. V. Tsintsanze and Yu. A. Buslaev, *Koord. Khim.* 1987, **13**, 1261.
13. Y. Yoshilawa and K. Yamasaki, *Bull. Chem. Soc. Jpn* 1972, **45**, 179.
14. F. R. Keene and G. H. Searle, *Inorg. Chem.* 1972, **11**, 148.
15. S. C. F. Au-Yeung and D. R. Eaton, *J. Magn. Reson.* 1983, **52**, 351.
16. T. Sh. Kapanadze, Yu. V. Kokunov, G. V. Tsintsadze and Yu. A. Buslaev, *Dokl. AN SSSR.* 1989, **304**, 1139.
17. F. R. Keene and G. H. Searle, *Inorg. Chem.* 1974, **13**, 2173.
18. A. M. Sargeson and G. H. Searle, *Inorg. Chem.* 1965, **4**, 45.
19. D. A. Buckingham, P. A. Marzilli and A. M. Sargeson, *Inorg. Chem.* 1967, **6**, 1032.
20. R. H. Boyd, *J. Chem. Phys.* 1968, **49**, 2574.
21. T. F. Lai and C. K. Poon, *Inorg. Chem.* 1976, **15**, 1562.
22. L. Prasad and S. C. Nyburg, *Acta Cryst.* 1987, **C43**, 1038.
23. M. Nonoyama and O. Nirai, *Inorg. Chim. Acta* 1981, **54**, L.283.
24. M. Nogradi, *Stereochemistry*. Akademiai Kiado, Budapest (1981).
25. D. A. House and C. S. Garner, *Inorg. Chem.* 1966, **5**, 2097.
26. M. R. Snow, D. A. Buckingham, P. A. Marzilli and A. M. Sargeson, *Chem. Comm.* 1969, 891.
27. T. Sh. Kapanadze, V. P. Tarasov, G. V. Tsintsadze and Yu. A. Buslaev, *Koord. Khim.* 1987, **13**, 1261.
28. W. C. Fernelius and B. E. Bryant, *J. Am. Chem. Soc.* 1953, **75**, 1735.
29. J. Selbin, *J. Inorg. Nucl. Chem.* 1961, **17**, 84.
30. S. C. F. Au-Yeung and D. R. Eaton, *Can. J. Chem.* 1983, **61**, 2431.
31. S. C. F. Au-Yeung and D. R. Eaton, *Inorg. Chim. Acta.* 1983, **76**, L.141.
32. R. T. M. Fraser, *Proc. Chem. Soc.* 1963, **7**, 262.
33. C. W. Maricondi and B. E. Douglas, *Inorg. Chem.* 1972, **11**, 688.
34. P. A. Cheltsov, O. N. Andrianova and N. A. Ezerskaya, *Koord. Khim.* 1977, **3**, 1220.

Polyhedron Vol. 9, No. 23, pp. 2809–2814, 1990
Printed in Great Britain

0277–5387/90 $3.00+.00
© 1990 Pergamon Press plc

THE OLIGOMERIZATION OF LOWER OLEFINS BY CATALYSTS DERIVED FROM Ni(sacsac)(PBu_3)Cl*

STEPHEN J. BROWN, ANTHONY F. MASTERS† and MILAN VENDER

Department of Inorganic Chemistry, University of Sydney, NSW 2006, Australia

and

JOHN I. SACHINIDIS and PETER A. TREGLOAN†

Department of Inorganic Chemistry, University of Melbourne, Parkville, Victoria 3052, Australia

(*Received* 6 *July* 1990; *accepted* 17 *July* 1990)

Abstract—The dimerization of butenes by a catalyst system derived from (pentane-2,4-dithionato)chlorotri-n-butylphosphinenickel(II) and diethylaluminium chloride in chlorobenzene has been investigated. The data are consistent with the presence of two catalytic species in solution. The concentrations of the catalysts appear to decrease with time, at a rate which is first-order in catalyst concentration, and the initial oligomerization rate appears to be second-order in olefin concentration.

The catalytic oligomerization of low molecular weight olefins has been practised commercially for about 50 years.[1] It remains a reaction of considerable industrial significance, and is utilized today in the production of fuels and specialty chemicals. A number of catalyst types have been used, and new catalysts are still being developed. The interest in new catalysts derives from the requirements of higher selectivity accompanying high activity. Although complexes of many transition metals are active as oligomerization catalysts,[2,3] nickel-based systems have received perhaps the greatest attention.[4–7] Both Shell's higher olefin process and IFP's Dimersol™ process utilize nickel-based catalyst precursors.[8,9]

The air-stable, 16-electron compounds Ni(R^2–R^1sacR^3sac)($PL^1L^2L^3$)Cl (R^j, L^j = alkyl or aryl, sacsac$^-$ = $C_5H_7S_2^-$ = dithioacetylacetonate anion = pentane-2,5-dithionate anion) form extremely active olefin oligomerization catalysts when activated by a suitable co-catalyst.[10–15]

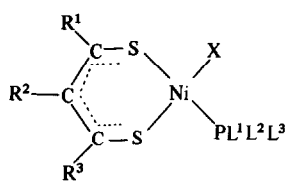

I

These systems are extremely active, oligomerizing ethylene at turnover numbers greater than 1000 mol of ethylene per mole of nickel per second at atmospheric pressure and room temperature. Catalysts derived from compounds **I** are also extremely active olefin double bond shift isomerization catalysts. The high rates of reactions observed in these systems make the study of the catalytic reaction extremely difficult. However, manageable reaction rates can be obtained using butenes as substrates. This may be a consequence of the low thermodynamic equilibrium concentration of 1-butene at ambient temperatures. Internal olefins appear to be oligomerized less rapidly than terminal olefins by catalysts derived from **1**. 1-Butene or *cis*- or *trans*-butene substrates are rapidly isomerized to close to the thermodynamic equilibrium mixture.

We have previously reported on the kinetics of,

* Paper presented at the Symposium on Applied Organometallic Chemistry, Pokolbin, NSW, Australia, 10–12 July 1989.

† Authors to whom correspondence should be addressed.

and product distributions from, a series of reactions between butenes and catalysts derived from **I** ($R^1 = R^3 = CH_3$, $R^2 = H$) with different phosphine ligands.[13] An empirical mathematical model was developed for the latter stages of the reaction ($t > ca$ 3/4 h). This model was able to describe the catalyst performance with a high degree of accuracy. For all of the catalysts tested, the butene concentration varied non-linearly with time, and was found empirically to obey the relationship

$$\ln(m_b) = A\exp(Bt) + C, \quad (1)$$

where m_b is the mass of residual butene, and A, B and C are empirical constants specific to individual catalysts. This equation was shown to be of the same form as equations developed by Dumas and Hsu to describe the kinetics of butadiene polymerization catalysed by homogeneous nickel-based species.[16] Dumas and Hsu showed that the behaviour described by eq. (1) is consistent with the "instantaneous" activation of a single catalytic species such that the polymerization reaction is first-order in both substrate and catalyst concentrations [eq. (2)], and that the disappearance of the active form of the catalyst is first-order in catalyst concentration [eq. (3)].

$$\delta m_b/\delta t = -k_b m_b m_c \quad (2)$$

$$\delta m_c/\delta t = -k_c m_c \quad (3)$$

In these expressions m_b and m_c are the masses of residual butene and catalyst, respectively, and k_b and k_c are the oligomerization and catalyst disappearance rate constants, respectively. Our analysis was limited to the latter stages of the reaction, and the fit of our model to the data over that period was excellent. However, a systematic deviation of our data from the model was observed during the initial period of the reaction. The precision of the data during the initial period did not allow a more complete analysis of the reaction during this phase of the reaction.

We have now refined the experiment by the addition of automated data acquisition. This has enabled us to collect a significant data population during the initial reaction period. An analysis of the catalyst behaviour during the initial reaction period is presented herein.

RESULTS AND DISCUSSION

In this study, we have concentrated on the catalysts derived from Ni(sacsac)(PBu_3)Cl and Et_2AlCl in chlorobenzene. The similarity of the behaviour of all of the catalysts reported in our previous study suggests that the behaviour observed for this catalyst system is probably obeyed by all catalysts **I**. We have shown previously, that the initial rate of propylene oligomerization in reactions at constant propylene pressure is proportional to the concentration of nickel precursor, provided that the nickel : Et_2AlCl ratio is high.[14] Within the concentration limits available, a similar first-order

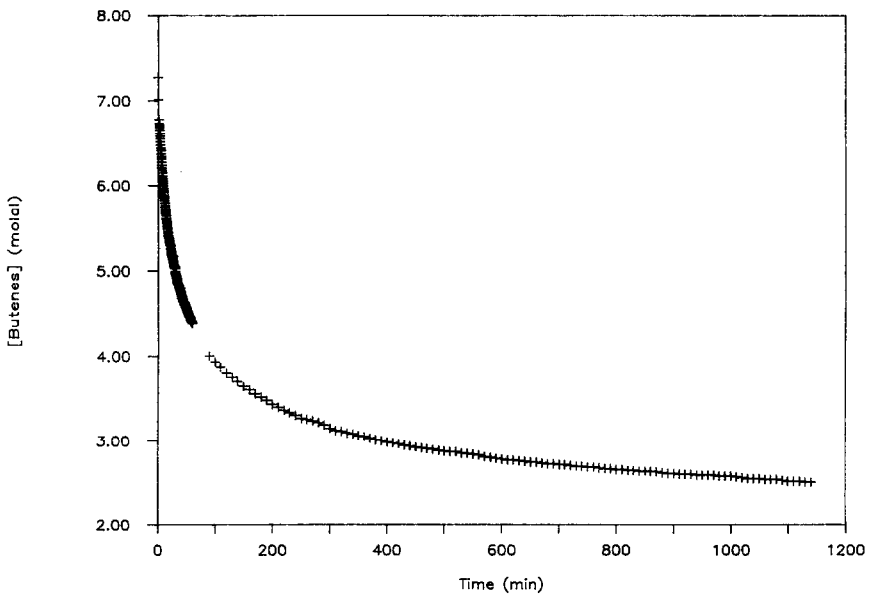

Fig. 1. Time dependence of butene concentration. Initial concentrations (molal): Ni, 0.005626; Al, 0.1824; C_4H_8, 7.19.

dependence of the initial rate on the Ni(sacsac) (PBu_3)Cl concentration is suggested in the present system.

Figure 1 illustrates the concentration of residual butene as a function of time for a typical reaction. There is an initial rapid decrease in the butene concentration, followed by a slower consumption of the remaining butene. The data can be divided into an initial ($0 \leqslant t \leqslant 1$ h) and an advanced ($4.5 \leqslant t \leqslant 19$ h) stage of the reaction.

Figure 2 shows that the data obtained during the latter period of the reaction can be modelled extremely well by eqs (1)–(3), as we have shown previously[13] (we note, however, that reasonable fits at these slow reaction rates can also be obtained from alternative models). The regression is characterized by an index of determination of 0.999, and is statistically significant at a probability level greater than 99.99%. This behaviour is consistent with a model in which the oligomerization reaction is first-order in the concentrations of both butene substrate and the catalyst, and in which the amount of active catalyst decreases at a rate which is first-order in catalyst concentration.

It is clear, however, from Fig. 2, that the reaction cannot be described by this model at short reaction times.

The data obtained during the initial reaction period is best accommodated by an empirical regression function of the form

$$1/m_b = D\exp(Et)+F, \qquad (4)$$

where, again, m_b is the mass of residual butene, and D, E and F are empirical constants specific to the catalyst. The fit of this function to the decrease in butene concentration, as a function of time, during the initial period is illustrated in Fig. 3. The regression of Fig. 3 also has an index of determination larger than 0.999 (statistical significance higher than 99.99%). No simple regression has been found for the transition period between 1 and 4.5 h of the reaction time. This is indicated by the systematic deviations of the experimental points from the linear regressions in both Figs 2 and 3.

It can be demonstrated that the form of eq. (4) is consistent with a kinetic model which is first-order with respect to catalyst concentration and second-order with respect to butene concentration [eq. (5)], with the disappearance of catalyst described by eq. (6)

$$\delta m_b/\delta t = -k'_b m_b^2 m_{c'} \qquad (5)$$

$$\delta m_{c'}/\delta t = -k'_c m_{c'}, \qquad (6)$$

where $m_{c'}$ is the mass of residual catalyst, and k'_b and k'_c are the oligomerization and catalyst disappearance rate constants, respectively, for this reaction stage. The values of the constants of eq. (4) are then

$$D = -(k'_b/k'_c)(m_c)_0 \qquad (7)$$

$$E = -k'_c \qquad (8)$$

$$F = 1/(m_b)_0 - D. \qquad (9)$$

Here, $(m_c)_0$ and $(m_b)_0$ are the initial amounts of catalyst and butene, respectively.

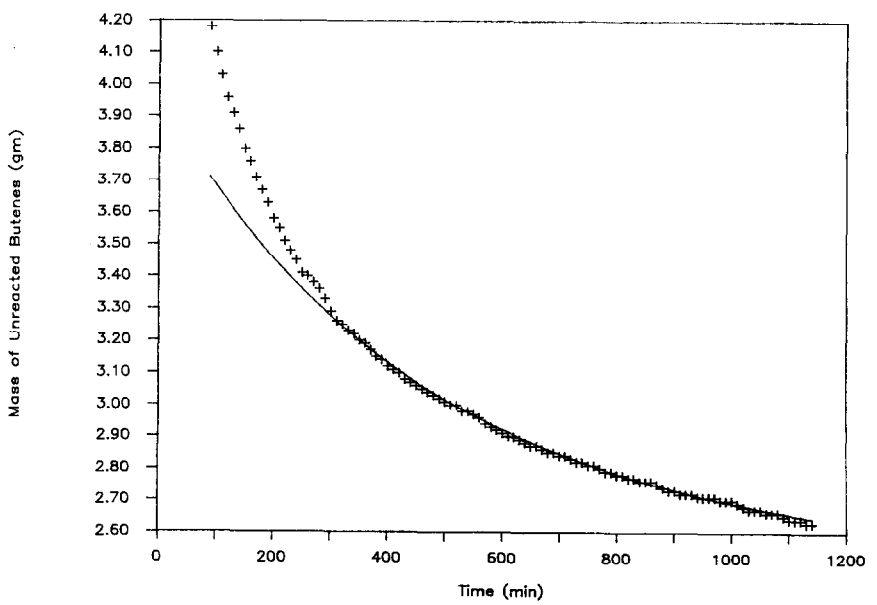

Fig. 2. Fit (solid line) to experimental data (points) during the latter period of butene oligomerization.

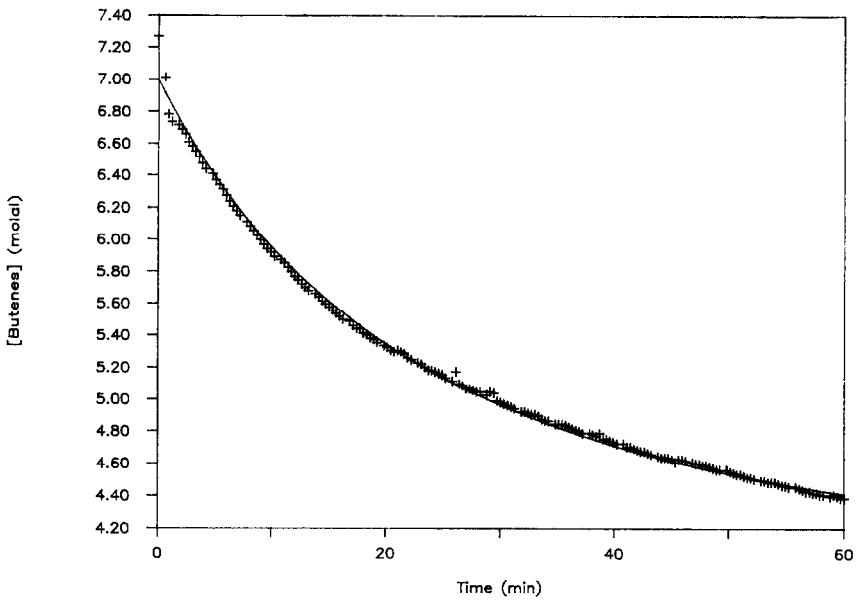

Fig. 3. Fit (solid line) to experimental data (points) during the initial period of butene oligomerization.

The data then suggest a system in which there are two catalytic species, **A** and **B**, in solution, both oligomerizing butene and both being consumed at rates which are first-order in catalyst concentration. However, the reaction order with respect to butene concentration during the initial reaction period during which catalyst **A** dominates, may differ from that during the advanced reaction period, during which catalyst **B** dominates. The detailed natures of catalysts **A** and **B** are at present unknown. Our analysis does not discriminate between models in which (a) one catalyst is generated more rapidly than the other, (b) the first catalyst "decomposes" into the second, or (c) both catalysts are generated "instantaneously". With the assumption of option (c), a comparison of reaction rates for the initial and advanced reaction stages indicates that initially the two reaction rates differ by about a factor of three, with catalyst **A** predominating. After about 1 h, the two reaction rates are about equal, and after about 4 h the two reaction rates differ by about a factor of 20, with catalyst **B** predominating. This change in the ratio of reaction rates agrees very well with the observed transformation from one reaction phase into the other.

Propylene oligomerization, catalysed by other nickel complex/aluminium haloalkyl systems, has been reported to be first-order in nickel, and second-order in olefin concentrations.[17,18] However, relatively short reaction times were used in these studies. Both first- and second-order kinetics with respect to olefin concentration can be accommodated by the conventional mechanism involving a nickel–hydride intermediate and a sequence of olefin coordination, olefin insertion and β-hydride elimination steps.[5,19] If the insertion of the second olefin molecule into the nickel–alkyl bond is rate-determining, the reaction order with respect to olefin will depend on the reversibility of the insertion of the first olefin molecule into the nickel–hydride bond.

We have conducted numerous experiments varying the concentrations of the reagents and the reaction times and have found the behaviour described above to be quite general. A mechanism involving two parallel, coupled catalytic cycles involving two different catalysts has been postulated previously to describe the oligomerization of 1-butene by the catalyst derived from (C_8H_{13})Ni(acac) ($acac^-$ = 2,4-pentanedionato anion.)[20]

Some care is required in interpreting the experimental data in terms of rate constants derived from the relationships above. Although the initial concentrations of the Ni(sacsac)(PBu_3)Cl and Et_2AlCl precursors are known, the true concentrations of actual catalysts in the reaction are not. There is no guarantee that the precursor and catalyst concentrations are related by a simple direct proportionality, nor that the proportionality factor approaches unity. Moreover, we, and others, have demonstrated that the role(s) of the alkylaluminium and other co-reactants can be non-trivial.[13,14,17,18] Accordingly, we prefer to use the present data to provide a qualitative, rather than quantitative, description of the system.

The nature of the catalyst consumption process

is also unknown at present. However, we have observed that the addition of an extra aliquot of Ni(sacsac)(PBu_3)Cl to the reactor after the reaction had practically ceased resulted in additional butene consumption. The revival of the reaction was observed regardless of whether both Ni(sacsac)(PBu_3)Cl and Et_2AlCl were injected simultaneously, or whether only Ni(sacsac)(PBu_3)Cl was added. The addition of Et_2AlCl alone had no apparent effect.

These reactions are highly selective ($\geq 95\%$) for dimerization. A small fraction of higher oligomer products is formed. We have observed that the C_{16} fraction of the reaction products is almost always significantly larger than the C_{12} fraction. Thus, it seems that the dimerization of octenes is favoured over the addition of butene to the octenes.

The amounts of hexenes produced increase with the concentration of Et_2AlCl. This behaviour is consistent with the suggestion that the active catalyst may be in equilibrium with excess Et_2AlCl.[14]

EXPERIMENTAL

All manipulations were carried out in an inert atmosphere of argon or butenes using standard vacuum manifold techniques. Solvents were AR grade and were dried and distilled under argon before use. Diethylaluminium chloride (Merck and Aldrich) was used as received. The compound Ni(sacsac)(PBu_3)Cl was prepared from Ni(sacsac)$_2$ and $NiCl_2(PBu_3)_2$ by the method reported previously,[21,22] and its identity confirmed by NMR spectroscopy. *trans*-2-Butene (Matheson technical grade) was used as received. The presence of small amounts of 1-butene, and *cis*-2-butene in the *trans*-2-butene was established by gas chromatographic analysis. No other impurities were detected by this technique. Gas chromatographic analyses were performed on an SGE 25m QC2/BP1 0.25 mm capillary column using a Hewlett Packard 5890A gas chromatograph equipped with an FID and a Hewlett Packard 3393A integrator.

Butenes were oligomerized in batch experiments in a magnetically stirred stainless steel tubular reactor system. The temperature inside the reactor was monitored and maintained constant by immersion of the reactor in a stirred, controlled temperature bath at 25.0 ± 0.2°C. The oligomerization experiments were conducted as described previously,[13] except that the temperature and pressure were monitored via a thermocouple and a calibrated pressure transducer (Sensym, Inc. (U.S.A.) SSX100A) respectively, connected to a data logger (Data Electronics (Australia) DATATAKER DT100). The pressure transducer was calibrated over the range 0–600 kPa using both the known pressure–temperature dependence for butenes, and direct pressure measurements by a mercury manometer. The logging program enabled the collection of data in regular preselected intervals. Typically, data were logged every 20 s for about 1 h, and every 10 min thereafter. The logged values were averages of readings over the logging interval. Data analysis was as described previously,[13] but used a reduced population of the experimental data, particularly for the latter period of the reaction. The reliability of the final results could be shown to be unaltered by this data reduction. The yield predicted from the time–pressure–temperature analysis was checked by a careful mass balance and gas chromatographic analyses of the reaction products. The useful range of catalyst concentrations available with this method is limited by two factors. Firstly, the relatively slow rate of butene oligomerization limits the lower range of catalyst concentrations effective in producing manageable reaction rates. Secondly, the potential contribution to the partial pressure of any ethane produced by decomposition of Et_2AlCl limits the higher range of catalyst concentrations. In general, the useful range of concentrations is between $5–60 \times 10^{-4}$ molal for Ni(sacsac)(PBu_3)Cl, and up to 9×10^{-2} molal for Et_2AlCl.

Acknowledgements—We thank the National Energy Research Development and Demonstration Council, the Australian Research Council and the Potter Foundation for generous financial support.

REFERENCES

1. G. D. Hobson and W. Pohl, *Modern Petroleum Technology*, 4th edn. Applied Science, Barking, Essex (1973).
2. G. Le Febvre and Y. Chauvin, *Aspects of Homogeneous Catalysis* (Edited by R. Ugo), Vol. 1, Ch. 3, p. 107. D. Reidel, Dordrecht (1970).
3. G. W. Parshall, *Homogeneous Catalysis. The Applications and Chemistry of Catalysis by Soluble Transition Metal Complexes*. Wiley Interscience, Brisbane (1980).
4. P. W. Jolly and G. Wilke, *The Organic Chemistry of Nickel*, Vol. 2. Academic Press, New York (1975).
5. B. Bogdanović, *Adv. Organomet. Chem.* 1979, **17**, 105.
6. P. W. Jolly, in *Comprehensive Organometallic Chemistry* (Edited by G. Wilkinson, F. G. A. Stone and E. W. Abel), Vol. 8, p. 615. Pergamon Press, Oxford (1982).
7. W. Keim, A. Behr and M. Roper, *Comprehensive Organometallic Chemistry* (Edited by G. Wilkinson, F. G. A. Stone and E. W. Abel), Vol. 8, p. 371. Pergamon Press, Oxford (1982).

8. E. R. Freitas and C. R. Gum, *Chem. Engng Prog.* 1979, **75**, 73.
9. Y. Chauvin, J. F. Gaillard, D. V. Quang and J. W. Andrews, *Chem. Ind.* (*Lond.*) 1974, 375.
10. K. J. Cavell and A. F. Masters, *J. Chem. Res.* 1983, 72.
11. A. F. Masters and K. J. Cavell, *U.S. Pat.* 4533651. CSIRO (1985).
12. V. W. L. Chin, A. F. Masters, M. Vender and R. J. Tyler, *Studies in Surface Science and Catalysis* (Edited by D. M. Bibby, C. D. Chang, R. F. Howe and S. Yurchak), Vol. 36, p. 421. Elsevier, Amsterdam (1988).
13. S. J. Brown, A. F. Masters and M. Vender, *Polyhedron* 1988, **7**, 2009.
14. S. J. Brown, L. M. Clutterbuck, A. F. Masters, J. I. Sachinidis and P. A. Tregloan, *App. Catal.* 1989, **48**, 1.
15. S. J. Brown and A. F. Masters, *J. Organomet. Chem.* 1989, **367**, 371.
16. C. Dumas and C. C. Hsu, *Chem. Engng Commun.* 1983, **24**, 37.
17. O. T. Onsager, H. Wang and U. Blindheim, *Helv. Chim. Acta* 1969, **52**, 196.
18. E. Balbolov, M. Mitkova and K. Kurtev, *J. Organomet. Chem.* 1988, **352**, 247.
19. O. T. Onsager and J. E. Johansen, *The Chemistry of the Metal–Carbon Bond* (Edited by F. R. Hartley and S. Patai), Vol. 3, p. 205. John Wiley, Brisbane (1985).
20. M. Peuckert, PhD thesis. Rheinisch-Westfälischen Technischen Hochschule Aachen (1980).
21. K. J. Cavell, D. G. Hay, A. F. Masters and G. A. Williams, *Aust. J. Chem.* 1985, **38**, 369.
22. J. P. Fackler Jr and A. F. Masters, *Inorg. Chim. Acta* 1980, **39**, 111.

Polyhedron Vol. 9, No. 23, pp. 2815–2822, 1990
Printed in Great Britain

0277–5387/90 $3.00+.00
© 1990 Pergamon Press plc

FISCHER–TROPSCH CATALYSTS DERIVED FROM SURFACE CONFINED $[H_nFeCo_3(CO)_{12}]^{n-1}$ ($n = 0, 1$)*

R. S. ARMSTRONG, T. BELL, A. F. MASTERS† and M. A. WILLIAMS‡

Department of Inorganic Chemistry, University of Sydney, NSW 2006 Australia

and

A. L. CHAFFEE§

CSIRO Division of Fuel Technology, Private Mail Bag 7, Menai, NSW 2234 Australia

(*Received* 6 *July* 1990; *accepted* 17 *July* 1990)

Abstract—The preparation and characterization of species in which $[H_nFeCo_3(CO)_{12}]^{n-1}$ ($n = 0, 1$) are supported on partially dehydroxylated silica and on aminated silica are reported. $[HFeCo_3(CO)_{12}]$, deposited onto aminated silica, yields the cluster anion, $[FeCo_3(CO)_{12}]^-$, bound to the surface. However, when $[HFeCo_3(CO)_{12}]$ is loaded onto partially dehydroxylated silica, deprotonation does not occur and the surface species is the cluster hydride. The cluster anion, as $K^+[FeCo_3(CO)_{12}]^-$, can be deposited onto both supports. The cluster anion, as $PrNH_3^+[FeCo_3(CO)_{12}]^-$, can also be loaded onto partially dehydroxylated silica. All depositions occur without the formation of other IR detectable carbonyl-containing species and with the metal framework remaining intact. The supported clusters are precursors of active catalysts for the Fischer–Tropsch reaction at 1 atm. The catalysts, derived from the precursors by thermal activation under hydrogen, are active for at least 120 h. The order of activity is as follows: $[HFeCo_3(CO)_{12}]$/partially dehydroxylated silica $< K^+[FeCo_3(CO)_{12}]^-$/partially dehydroxylated silica $\approx K^+[FeCo_3(CO)_{12}]^-$/aminated silica $\ll PrNH_3^+[FeCo_3(CO)_{12}]^-$/partially dehydroxylated silica $\approx [HFeCo_3(CO)_{12}]^-$/aminated silica. Only the catalysts derived from the last two precursors contain significant amounts of nitrogen. This is consistent with the formation of metal nitride phases in these catalysts and may correlate with their higher activity. Moreover, this formation of nitride phases occurs only when the nitrogen is in close association with the metal cluster. During the thermal activation of all the catalysts there was no loss of metal and the iron to cobalt ratio remained at 1 : 3. The effects of operational parameters on product distribution and CO conversion rates obtained with the catalyst produced from $[HFeCo_3(CO)_{12}]$ deposited onto aminated silica are also reported.

Transition metal carbonyl cluster compounds have attracted increasingly greater interest as possible models of metal surfaces[1,2] and as precursors of supported metal catalysts.[3,4] These clusters often have been absorbed onto partially dehydroxylated metal oxide supports,[5] and confined to the surface either by tight ion pairing with ionic support moieties,[5] or by bond formation via reaction between the cluster and surface hydroxyl groups.[6,7] Alternatively, metal carbonyl compounds have been immobilized on functionalized metal oxide surfaces by appropriate ligating or ionic groups bound to the surface as chemical anchors.[8]

Immobilized catalysts derived from mixed-metal carbonyl clusters have been claimed to exhibit more desirable behaviour than catalysts prepared from

*Paper presented at the Symposium on Applied Organometallic Chemistry, Pokolbin, NSW, Australia, 10–12 July 1989.

† Author to whom correspondence should be addressed.

‡ Present address: School of Science and Technology, University of Western Sydney, Nepean, P.O. Box 10, Kingswood, NSW 2750, Australia.

§ Present address: BHP Melbourne Research Laboratories, P.O. Box 264, Clayton, Victoria 3168, Australia.

either a mixture of metal salts, or a mixture of carbonyl clusters of the same metal stoichiometry.[9] Choplin *et al.*[10] showed that thermal decomposition of supported heterometallic carbonyl clusters yields very small heterometallic particles which have the same bulk composition as that of the starting cluster. In contrast, mixtures of homometallic carbonyl clusters supported on metal oxides appear to decompose into separate metallic phases.[11]

Hemmerich *et al.*[12,13] reported the deposition of $[HFeCo_3(CO)_{12}]$ onto an amine-modified silica support. This is a rare example of the utilization of the acid–base chemistry of an amine group in cluster anchoring. Thermal activation of this supported cluster was reported to produce a catalyst which contained dimetallic particles of the same stoichiometry as $[HFeCo_3(CO)_{12}]$. This catalyst was active in the Fischer–Tropsch reaction, showing reasonable reaction rates and a remarkable selectivity to gasoline-range products. Recently, we reported our initial comparisons[14] of this catalyst system to the work of Hemmerich.[12,13] The structure of the metal carbonyl cluster bonded to the silica surface after loading is easily characterized for this system. However, the surface species, which is produced by thermal activation of the carbonyl cluster and is the active Fischer–Tropsch catalyst, has not been identified. We present, here, further work investigating the nature of the species produced on the surface when $[H_nFeCo_3(CO)_{12}]^{n-1}$ ($n = 0, 1$) are deposited onto modified silica. Results of the Fischer–Tropsch reaction with these species as catalyst precursors are also reported.

EXPERIMENTAL

All synthetic manipulations were carried out in an air-free dry argon atmosphere using Schlenk techniques. Dichloromethane and acetone were dried by distillation from calcium hydride and potassium carbonate, respectively. Silica gel 40 (surface area 675 $m^2\ g^{-1}$, 35–70 mesh) was obtained from Merck. The 3-aminopropyltriethoxysilane (Dynamit Nobel Chemie, Dynasylan AMEO™) was obtained from Plastral Trading and distilled before use under argon. Dicobaltoctacarbonyl (Strem) and iron pentacarbonyl (Aldrich) were used as received. $[HFeCo_3(CO)_{12}]$, $K^+[FeCo_3(CO)_{12}]^-$ and $PrNH_3^+[FeCo_3(CO)_{12}]^-$ were prepared by the methods of Chini *et al.*[15]

Supports

Partially dehydroxylated silica. Silica gel 40 (15 g) was heated *in vacuo* at 300°C for 3 h to produce approx. 13 g of partially dehydroxylated silica.

Aminated silica. Partially dehydroxylated silica (10 g) was refluxed with AMEO (13 g) in toluene (100 cm^3) for 6 h. The solution was filtered and the solid was washed with toluene for 24 h in a Soxhlet extractor. The aminated silica was finally dried *in vacuo*. Yield: approx. 16 g.

Catalyst precursors

$[HFeCo_3(CO)_{12}]$/*aminated silica* (*catalyst precursor* **A**). $[HFeCo_3(CO)_{12}]$ (1.0 g, 1.8 mmol) was dissolved in acetone (50 cm^3) and stirred at room temperature for 2 h with aminated silica (4 g). The solvent was removed *in vacuo*, and the resultant solid was washed with pentane (50 cm^3). The solid was then dried overnight *in vacuo*. Analyses: wt% of element before (after) catalysis—Fe 1.7(2.3), Co 5.2(6.3), N 1.89(0.80), Co/Fe 2.9(2.6).

$[HFeCo_3(CO)_{12}]$/*partially dehydroxylated silica* (*catalyst precursor* **B**). $[HFeCo_3(CO)_{12}]$ (1.0 g, 1.8 mmol) was dissolved in dichloromethane (50 cm^3) and stirred at room temperature for 2 h with partially dehydroxylated silica (4 g). The solvent was removed *in vacuo* and the resultant solid was dried overnight *in vacuo*. Analyses: wt% of element before (after) catalysis—Fe 1.8(2.0), Co 5.5(6.3), Co/Fe 2.9(3.0).

$K^+[FeCo_3(CO)_{12}]^-$/*partially dehydroxylated silica* (*catalyst precursor* **C**). $K^+[FeCo_3(CO)_{12}]^-$ (1.0 g, 1.6 mmol) was dissolved in acetone (50 cm^3) and stirred at room temperature for 2 h with partially dehydroxylated silica (4 g). The solvent was removed *in vacuo*, and the resultant solid was washed with pentane (50 cm^3). The solid was then dried overnight *in vacuo*. Analyses: wt% of element before (after) catalysis—Fe 1.6(1.8), Co 4.9(5.5), Co/Fe 2.9(2.9).

$K^+[FeCo_3(CO)_{12}]^-$/*aminated silica* (*catalyst precursor* **D**). $K^+[FeCo_3(CO)_{12}]^-$ (1.0 g, 1.6 mmol) was dissolved in acetone (50 cm^3) and stirred at room temperature for 2 h with aminated silica (4 g). The solvent was removed *in vacuo*, and the resultant solid was washed with pentane (50 cm^3). The solid was then dried overnight *in vacuo*. Analyses: wt% of element before (after) catalysis—Fe 1.6(2.1), Co 4.8(6.8), N 1.80(0.11), Co/Fe 2.8(3.1).

$PrNH_3^+[FeCo_3(CO)_{12}]^-$/*partially dehydroxylated silica* (*catalyst precursor* **E**). $PrNH_3^+[FeCo_3(CO)_{12}]^-$ (1.0 g, 1.6 mmol) was dissolved in acetone (50 cm^3) and stirred at room temperature for 2 h with partially dehydroxylated silica (4 g). The solvent was removed *in vacuo*, and the resultant solid was washed with pentane (50 cm^3). The solid was then dried overnight *in vacuo*. Analyses: wt% of element before (after) catalysis—Fe 1.6(2.0), Co 5.0(6.3), N 0.40(0.39), Co/Fe 3.0(3.0).

Testing of catalysts

Catalysts were tested for Fischer–Tropsch activity at atmospheric pressure in a fixed-bed reactor as previously described.[16] The catalyst precursors were activated in a stream of hydrogen (space velocity 500 h^{-1}) at 200°C for 2 h. A hydrogen–carbon monoxide–water vapour mixture (total space velocity 500 h^{-1}) was used as the feed gas, and was preheated to 200°C prior to entering the stainless steel reaction vessel (10 cm × 1 cm i.d.) which was maintained at constant temperature. The products of the reaction were monitored for a minimum of 12 h.

Carbon monoxide conversion rates, carbon dioxide selectivity, and C_1 and C_2 hydrocarbon selectivity were monitored at approx. 20 min intervals with a Shimadzu 8AIT gas chromatograph fitted with a thermal conductivity detector and a packed column (10 ft × ⅛ in i.d., Chromosorb 102, S.G.E., Australia) and were continuously data-logged.

Variable temperature and gas feed composition experiments were performed sequentially on the same sample. Time was allowed for these systems to come to "steady state" before data-logging recommenced.

Full product distributions (C_1–C_{29} hydrocarbons and oxygenates) were obtained at least once during the reaction period using a Hewlett–Packard 5890A gas chromatograph equipped with a flame ionization detector and a fused silica capillary column (50 m × 0.02 mm i.d., EP-5, S.G.E., Australia). The error in the percentage of diesel and wax obtained from a catalyst test is greater than for the lower hydrocarbons due to retention of these products on the catalyst support. The long reaction times used in these experiments, however, should minimize these errors. Comparison of the results obtained from the continuous monitoring system (Shimadzu gas chromatograph) and the full product distribution (Hewlett–Packard gas chromatograph) for the selectivity to C_1 and C_2 hydrocarbons indicated that the magnitude of this error was low in all cases.

Metal analyses were obtained by atomic absorption spectroscopy. C, H and N analyses were determined by combustion using a Leco CHN600 analyser. Fourier transform IR spectra of catalyst precursors were obtained using a Digilab FTIR FTS20/80 spectrophotometer. Diffuse reflectance IR spectra of $[HFeCo_3(CO)_{12}]$/aminated silica (catalyst precursor **A**) under activation conditions were obtained using a Mattson Cygnus 100 spectrophotometer. The sample was contained in a Harrick environmental cell.

RESULTS AND DISCUSSION

The supports used in this study were partially dehydroxylated silica and aminated silica. The former was prepared from silica gel 40 (35–70 mesh) by heating *in vacuo* for 3 h. Aminated silica was synthesized by the condensation of AMEO onto silica with the elimination of ethanol.[17] The same cluster loadings and catalytic results were obtained irrespective of whether or not ethanol was removed via a Dean Stark apparatus.

$[HFeCo_3(CO)_{12}]$ was loaded onto aminated silica by evaporation of an acetone solution of the cluster to form catalyst precursor **A**. The IR spectrum of the resultant catalyst precursor (Table 1) showed

Table 1. Carbonyl stretching frequencies of $[H_nFeCo_3(CO)_{12}]^{n-1}$ (n = 0, 1) deposited on various supports[a]

Cluster species	Support	Catalyst precursor	CO stretching frequency (cm^{-1})
$[HFeCo_3(CO)_{12}]$	Aminated silica	**A**[e]	2064w 2004s 1966m 1928m 1818m
$[HFeCo_3(CO)_{12}]$	Partially dehydroxylated silica	**B**	2102w 2062vs,br 2023s,sh 1984w 1884m
$K^+[FeCo_3(CO)_{12}]^-$	Partially dehydroxylated silica	**C**	2064w 2003s 1967m 1928m 1820m
$K^+[FeCo_3(CO)_{12}]^-$	Aminated silica	**D**	2063w 2003s 1967m 1927m 1820m
$PrNH_3^+[FeCo_3(CO)_{12}]^-$	Partially dehydroxylated silica	**E**	2064w 2004s 1967m 1928m 1819m
$Et_4N^+[FeCo_3(CO)_{12}]^-$[b,d]			2063w 2006s 1971w 1933m 1828m
$[HFeCo_3(CO)_{12}]$[c,d]			2098w 2058s 2051s 2030m 1988m 1889s

[a] KBr disc spectrum unless otherwise stated.
[b] Acetone solution spectrum.
[c] CCl_4 solution spectrum.
[d] Reference 15.
[e] Surface species is $[SIL—(CH_2)_3NH_3]^+[FeCo_3(CO)_{12}]^-$ (SIL = Surface≡Si).

five bands in the region 2200–1600 cm^{-1}. These data are consistent with the deprotonation of $[HFeCo_3(CO)_{12}]$ to form the carbonyl anion, $[FeCo_3(CO)_{12}]^-$,[15] deposited onto the surface. The anion is formed by the acid–base reaction of the hydride cluster, $[HFeCo_3(CO)_{12}]$, with ultimate transfer of the hydride to the amine anchor [eq. (1)]. The deposition of the cluster onto the support is quite easily followed by IR spectroscopy, the clusters $[HFeCo_3(CO)_{12}]$ and $[FeCo_3(CO)_{12}]^-$ exhibiting distinct and different spectra[15] in the region of the carbonyl stretching frequencies.

$$SIL{-}(CH_2)_3NH_2 + [HFeCo_3(CO)_{12}] \longrightarrow SIL{-}(CH_2)_3NH_3^+[FeCo_3(CO)_{12}]^- \quad (1)$$

SIL = Surface≡Si

There appears to be a small shift in the bridging carbonyl stretching frequency to lower frequencies. The shift is monotonic with increasing cluster loading. For small cluster loadings, this difference is at the limit of experimental significance, but is consistently observed. Tight ion pairing interactions between bridging carbonyls of supported anionic clusters and cationic surface species are detectable by a shift of the bridging carbonyl IR absorption to lower frequencies.[5,18] However in the present case, this shift is also observed for the anion on supports without this amine anchor (Table 1). Thus, this shift in the bridging carbonyl IR absorption cannot be attributed necessarily to an interaction of the anion with the alkylammonium anchor or the support, analogous to that postulated for supported $[Fe_3(CO)_{11}]^-$.[5]

The IR spectrum of $[HFeCo_3(CO)_{12}]$ deposited onto aminated silica (catalyst precursor **A**) indicated that no new carbonyl species, other than supported $[FeCo_3(CO)_{12}]^-$, were formed during the deposition process. In particular, Choplin *et al.*[19] reported the deposition of $[HFeCo_3(CO)_{12}]$ onto partially dehydroxylated magnesia. The hydride cluster was deprotonated by the magnesia surface and bound as $[FeCo_3(CO)_{12}]^-$. These authors postulated that $[Co(CO)_4]^-$ was a possible decomposition product accompanying the formation of the anionic cluster on the surface.[19] We have no IR evidence of any surface confined $[Co(CO)_4]^-$ in our product (no absorption at $\simeq$ 1890 cm^{-1}).[20]

Elemental analysis of catalyst precursor **A** showed $\simeq$ 7% metal by weight and an iron to cobalt ratio of 1 : 3, the same ratio as for the original cluster. Temperature-programmed reduction (TPR) experiments of this supported cluster under hydrogen showed no peaks due to reduction of metal species. The IR, TPR and elemental data are consistent with deposition of the metal cluster onto the silica surface without any detectable metal oxidation and with the preservation of the cluster metal framework.

IR spectra were obtained from the $[HFeCo_3(CO)_{12}]$/aminated silica system (catalyst precursor **A**) at a variety of temperatures and under conditions which mimic the thermal catalyst activation process. Upon heating to 110°C in a stream of 1 : 1 carbon monoxide–hydrogen, complete loss of carbonyl ligands from the cluster was observed. Cooling the sample in a carbon monoxide stream does not regenerate the starting supported cluster, nor any other carbonyl-containing species detectable by IR spectroscopy. For this catalyst precursor the elemental analysis of the solid obtained after catalyst activation (and use) shows the same total metal content and the same iron to cobalt ratio as before activation. This contrasts with the work of Czekaj and Geoffroy[21] who have recently shown that bulk $[HFeCo_3(CO)_{12}]$ is volatilized at about 80°C in a carbon monoxide stream. Furthermore, these authors suggest that under these conditions, $[HFeCo_3(CO)_{12}]$ decomposes to $Fe(CO)_5$, $Co_4(CO)_{12}$ and H_2.[21] Thus, cluster decomposition to yield volatile $Fe(CO)_5$ does not occur in our system, in which thermal degradation of the precursor apparently yields metal domains with the same overall stoichiometry as those of the starting supported cluster. This is consistent with the results of Choplin *et al.*[10,19] who established that $[FeCo_3(CO)_{12}]^-$, deposited onto partially dehydroxylated magnesia, starts to decompose at 50°C, and when thermally degraded at 400°C in a stream of hydrogen gives very small bimetallic particles. The individual particles were shown to have the same bulk composition as that of the starting $[HFeCo_3(CO)_{12}]$.

Results of the Fischer–Tropsch testing of the catalyst system derived from precursor **A** are collected in Tables 2 and 3. This catalyst shows activity in the Fischer–Tropsch reaction and remains active for long periods (at least 120 h). Methane production, whilst not excessive, is undesirably high and under all conditions the products follow a typical Shultz–Flory distribution with α-values (propagation probabilities)[22] of around 0.7. The olefin content of the product is high, especially in the range C_3–C_5, and the oxygenate content is low. The overall product distribution does not change appreciably with time. Aminated silica with no loaded metal cluster showed no carbon monoxide conversion under the same activation and testing processes.

Table 2 contains the variance with temperature of the product parameters over the range 220–280°C. Carbon monoxide conversion rates increase with

Table 2. Differences in Fischer–Tropsch reaction as a function of temperature for catalyst **A**, derived from $[HFeCo_3(CO)_{12}]$ deposited onto aminated silica

Temperature (°C)	220	240	260	280
CO conversion (mmol CO/g met/h)	34.4	82.6	144.9	320.3
Fuel product (%)	96.4	92.8	87.3	81.3
CO_2 (%)	3.6	7.2	12.7	18.7
Fuel product distribution (%)				
CH_4	11.1	15.9	20.0	26.7
LPG[a]	35.0	32.9	29.8	40.8
Petrol[b]	53.9	50.9	38.6	30.0
Diesel[c]	0.0	0.3	6.3	2.5
Wax[d]	0.0	0.0	5.4	0.0
Olefin component (%)				
Fuel product	67.8	53.5	29.9	49.8
LPG[a]	86.4	72.6	48.2	77.4
Petrol[b]	69.7	58.1	37.2	58.5
Diesel[c]		32.5	18.5	27.0
Wax[d]			1.0	
Oxygenate component (%)				
Fuel product	3.8	2.4	0.7	3.0

[a] LPG—C_2–C_4 hydrocarbons.
[b] Petrol—C_5–C_{12} hydrocarbons and C_1–C_5 oxygenates.
[c] Diesel—C_{13}–C_{19} hydrocarbons.
[d] Wax—C_{20}–C_{29} hydrocarbons.
Conditions : gas feed—1 : 1 H_2 : CO.

Table 3. Differences in Fischer–Tropsch reaction as a function of feed compositions for catalyst **A**, derived from $[HFeCo_3(CO)_{12}]$ deposited onto aminated silica

Feed conditions H_2 : CO : H_2O	2 : 1 : 0	1 : 1 : 0	2 : 4 : 1
CO conversion (mmol CO/g met/h)	95.7	82.6	75.1
Fuel products (%)	94.8	92.8	84.8
CO_2 (%)	5.2	7.2	15.2
Fuel product distribution (%)			
CH_4	19.6	15.9	11.2
LPG[a]	30.9	32.9	32.2
Petrol[b]	46.7	50.9	55.2
Diesel[c]	2.8	0.3	1.4
Olefin component (%)			
Fuel product	43.3	53.5	68.6
LPG[a]	65.0	72.6	87.3
Petrol[b]	48.8	58.1	72.0
Diesel[c]	14.6	32.5	52.5
Oxygenate component (%)			
Fuel product	2.1	2.4	3.2

[a] LPG—C_2–C_4 hydrocarbons.
[b] Petrol—C_5–C_{12} hydrocarbons and C_1–C_5 oxygenates.
[c] Diesel—C_{13}–C_{19} hydrocarbons.
Conditions: temperature—240°C.

increasing temperature and the catalyst is inactive below 210°C. A calculation of the energy of activation of the Fischer–Tropsch reaction for this catalyst, using the Arrhenius equation, gives a result of 82(±9) kJ mol^{-1}. This compares with values of 108 kJ mol^{-1} for iron and 112 kJ mol^{-1} for cobalt, both deposited onto alumina.[23] The product distribution also changed with temperature over the temperature range studied. Carbon dioxide production increased with temperature from 3 to 19%, as did the amount of methane which rose from 11 to 27%. The petrol fraction was reduced with increasing temperature. Changes in the selectivity to olefins were not systematic with the temperature rise. Thus the desirable increase in carbon monoxide conversion rate at higher temperatures is offset by an undesirable increase in methane and carbon dioxide production.

Table 3 summarizes the changes in the carbon monoxide conversion rate and product selectivity in the Fischer–Tropsch reaction with changes in the gas feed composition. The carbon monoxide conversion rate increases with increasing hydrogen content of the feed gas. The production of carbon dioxide decreases with an increase in the hydrogen content. This decrease is due, in principle, to the shift in the equilibrium position in the water–gas shift reaction. An increase in the hydrogenation of surface species (i.e. increase in methane produced and decrease in olefin fraction) is also observed with rising hydrogen content.

Amine modification of the silica surface appears to be necessary to anchor $[FeCo_3(CO)_{12}]^-$ to silica by solution processes using $[HFeCo_3(CO)_{12}]$. If unmodified silica is used as a support, the silica remains almost colourless after contact with a solution of $[HFeCo_3(CO)_{12}]$, and only a weak IR absorption is observed at 2004 cm^{-1}.[24] We have deposited $[HFeCo_3(CO)_{12}]$ on partially dehydroxylated silica by evaporation from its dichloromethane solution to yield catalyst precursor **B**. The IR spectrum (Table 1) clearly indicates the

Table 4. Fischer–Tropsch reaction for $[H_nFeCo_3(CO)_{12}]^{n-1}$ ($n = 0, 1$) deposited on various supports

Cluster species	$[HFeCo_3(CO)_{12}]$	$[HFeCo_3(CO)_{12}]$	$K^+[FeCo_3(CO)_{12}]^-$	$K^+[FeCo_3(CO)_{12}]^-$	$PrNH_3^+[FeCo_3(CO)_{12}]^-$
Support	Aminated silica	Silica	Silica	Aminated silica	Silica
Catalyst	**A**	**B**	**C**	**D**	**E**
CO conversion (mmol CO/g met/h)	82.6	7.5	24.4	34.4	73.2
Fuel product (%)	92.8	95.1	82.2	86.5	78.6
CO_2 (%)	7.2	4.9	17.8	13.5	21.4
Fuel product distribution (%)					
CH_4	15.9	17.3	10.3	11.3	11.3
LPG[a]	32.9	35.8	33.8	32.4	28.3
Petrol[b]	50.9	46.3	54.6	51.4	49.4
Diesel[c]	0.3	0.6	1.4	4.9	11.0
Olefin component (%)					
Fuel product	53.5	42.3	71.4	65.3	49.0
LPG[a]	72.6	65.8	91.9	80.3	72.5
Petrol[b]	58.1	40.3	72.8	71.9	52.9
Diesel[c]	32.5	0.0	44.4	47.4	21.1
Oxygenate component (%)					
Fuel product	2.4	2.2	3.9	3.8	2.3

[a] LPG—C_2–C_4 hydrocarbons.
[b] Petrol—C_5–C_{12} hydrocarbons and C_1–C_5 oxygenates.
[c] Diesel—C_{13}–C_{19} hydrocarbons.
Conditions: gas feed—1 : 1 H_2 : CO; temperature—240°C.

presence of the hydrido cluster rather than the anionic cluster, $[FeCo_3(CO)_{12}]^-$, on the support. By contrast, $[HFeCo_3(CO)_{12}]$ is readily bound to alumina or magnesia as the anion.[10,19,24] Elemental analysis of the silica supported catalyst precursor **B** showed that the iron to cobalt ratio of 1:3 was maintained.

The $[HFeCo_3(CO)_{12}]$/partially dehydroxylated silica system (catalyst **B**) is also active in the Fischer–Tropsch reaction (Table 4), but the rate of carbon monoxide conversion is more than an order of magnitude lower than that of the $[HFeCo_3(CO)_{12}]$/aminated silica system (catalyst **A**). The product distribution was found to be similar in both cases. Partially dehydroxylated silica with no loaded metal cluster showed no carbon monoxide conversion under the same activation and testing processes. Elemental analysis of the used catalyst showed no loss of metal and the same iron to cobalt ratio as for the catalyst precursor. The reasons for this dramatic loss of activity are unclear at present. However, it appears that for good carbon monoxide conversion rates, the surface bound catalyst precursor must be the cluster anion.

The anionic metal cluster, $[FeCo_3(CO)_{12}]^-$, was loaded onto partially dehydroxylated silica by evaporation of an acetone solution of $K^+[FeCo_3(CO)_{12}]^-$ to produce catalyst precursor **C**. The IR spectrum (Table 1) and elemental analysis of this supported species indicate that the cluster was deposited as the anion with its metal framework intact. The catalyst derived from this precursor (catalyst **C**) also showed a carbon monoxide conversion rate substantially lower than that observed for the catalyst prepared from $[HFeCo_3(CO)_{12}]$ loaded onto aminated silica (catalyst **A**). However, the reaction rate for catalyst **C** was higher than that of the material derived from hydride cluster deposited onto partially dehydroxylated silica (catalyst **B**). Elemental analyses of catalyst **C** showed no loss of iron or cobalt. Hemmerich *et al.*[12] have suggested that the amine anchors react with the clusters under Fischer–Tropsch conditions to form metal nitride phases. The nitrogen content for the $[HFeCo_3(CO)_{12}]$/aminated silica species after catalysis (catalyst **A**) was still significant at 1.5 nitrogen atoms per $FeCo_3$ unit. However, the nitrogen content for aminated silica (with no loaded metal cluster), after it was tested as a catalyst, indicated that the amine anchors were lost in the absence of loaded metal cluster. This is consistent with the formation of metal nitride phases during activation. Schultz *et al.*[25] showed that iron nitrides have a greater activity in the Fischer–Tropsch reaction than do simple iron phases. This work of Schultz *et al.*[25] supports the view that the increased activity of catalyst **A** is due to the presence of metal nitrides.

$K^+[FeCo_3(CO)_{12}]^-$ was also deposited onto aminated silica by this "incipient wetness" technique with acetone as the solvent, to prepare catalyst precursor **D**. This system showed a low carbon monoxide conversion rate compared with that obtained for $[HFeCo_3(CO)_{12}]$ on aminated silica (catalyst **A**). The carbon monoxide conversion rate and product distribution for catalyst **D** (Table 4) are similar to those observed for this anion loaded onto partially dehydroxylated silica (catalyst **C**). Elemental analysis showed the iron to cobalt ratio before and after catalysis to be 1:3 as expected. The nitrogen content for catalyst **D** was 0.2 nitrogen atoms per $FeCo_3$ unit, compared with the result for $[HFeCo_3(CO)_{12}]$ on aminated silica (catalyst **A**) of 1.5 nitrogen atoms per $FeCo_3$ unit. Thus, despite the presence of surface nitrogen in the catalyst precursor, metal nitrides were not formed during activation of catalyst **D**. This fact is consistent with its activity being low. Therefore, even though the amine anchor may be present, as in catalyst precursor **D**, the available nitrogen must form a close association with the metal cluster anion for the production of metal nitride phases.

The cluster anion was therefore loaded onto partially dehydroxylated silica as $PrNH_3^+[FeCo_3(CO)_{12}]^-$ to yield catalyst precursor **E**. The propylammonium countercation was chosen to mimic the charged amine anchor. The carbon monoxide conversion rate for the catalyst produced from this precursor (catalyst **E**) was high and is similar to the value obtained using the catalyst derived from $[HFeCo_3(CO)_{12}]$ deposited onto aminated silica (catalyst **A**). The nitrogen content for catalyst **E** is high (0.8 nitrogen atoms per $FeCo_3$ unit), indicating the presence of metal nitride phases and is consistent with the observation of higher carbon monoxide conversion rates. The product distributions of catalysts **A** and **E** show a large difference only in the carbon dioxide and diesel selectivity. The other fuel product selectivities and the selectivity to olefin and to oxygenate are quite similar for these two catalysts.

Acknowledgements—We thank the CSIRO/University of Sydney Collaborative Research Scheme for financial support. M.A.W. thanks the Australian Institute for Nuclear Science and Engineering for a Postdoctoral Fellowship. We thank Plastral Trading for generous gifts of AMEO.

REFERENCES

1. J. Evans, *Chem. Soc. Rev.* 1981, **10**, 159.
2. E. L. Muetterties, T. N. Rhodin, E. Band, C. F. Brucker and W. R. Pretzer, *Chem. Rev.* 1979, **79**, 91.

3. A. K. Smith and J. M. Basset, *J. Molec. Catal.* 1977, **2**, 229.
4. B. C. Gates, L. Guczi and H. Knozinger (Eds), *Metal Clusters in Catalysis*. Elsevier, Amsterdam (1986).
5. F. Hughes, J. M. Basset, Y. Ben Taarit, A. Choplin, M. Primet, D. Rojas and A. K. Smith, *J. Am. Chem. Soc.* 1982, **104**, 7020.
6. A. K. Smith, F. Hughues, A. Theolier, J. M. Basset, R. Ugo, G. M. Zanderighi, J. L. Bilhou, V. Bilhou-Bougnol and W. F. Graydon, *Inorg. Chem.* 1979, **18**, 3104.
7. C. C. Santini, J. M. Basset, B. Fontal, J. Krause, S. Shore and C. Charrier, *J. Chem. Soc., Chem. Commun.* 1987, 512.
8. J. Evans and B. P. Gracey, *J. Chem. Soc., Chem. Commun.* 1980, 852.
9. Y. Iwasawa and M. Yamada, *J. Chem. Soc., Chem. Commun.* 1985, 675.
10. A. Choplin, L. Huang, A. Theolier, P. Gallezot, J. M. Basset, U. Siriwardane, S. G. Shore and R. Mathieu, *J. Am. Chem. Soc.* 1986, **108**, 4224.
11. J. M. Basset and A. Choplin, *J. Molec. Catal.* 1983, **21**, 95.
12. R. Hemmerich, W. Kiem and M. Roper, *J. Chem. Soc., Chem. Commun.* 1983, 428.
13. M. Roper, R. Hemmerich and W. Kiem, *Chem. Ingen. Tech.* 1984, **56**, 152.
14. R. S. Armstrong, T. Bell, A. L. Chaffee, V. W. L. Chin, H. J. Loeh, A. B. J. Lucchese, A. F. Masters and M. A. Williams, *Appl. Catal.* 1989, **47**, 243.
15. P. Chini, L. Colli and M. Peraldo, *Gazz. Chim. Ital.* 1960, **90**, 1005.
16. A. L. Chaffee and H. J. Loeh, *Appl. Catal.* 1986, **26**, 123.
17. K. G. Allum, D. R. Hancock, I. V. Howell, S. McKenzie, R. C. Pitkethly and P. J. Robinson, *J. Organomet. Chem.* 1975, **87**, 203.
18. J. R. Wilkinson and L. J. Todd, *J. Organomet. Chem.* 1976, **118**, 199.
19. A. Choplin, L. Huang, J. M. Basset, R. Mathieu, U. Siriwardane and S. G. Shore, *Organometallics* 1986, **5**, 1547.
20. J. K. Ruff and W. J. Schlientz, *Inorg. Synth.* 1974, **15**, 84.
21. C. L. Czekaj and G. L. Geoffroy, *Inorg. Chem.* 1988, **27**, 8.
22. G. Henrici-Olivé and S. Olivé, *Catalyzed Hydrogenation of Carbon Monoxide*, p. 143. Springer, Berlin (1984).
23. M. A. Vannice, *J. Catal.* 1975, **37**, 449.
24. F. Guglielminotti, D. Osella and P. L. Stanghellini, *J. Organomet. Chem.* 1985, **281**, 291.
25. J. F. Schultz, M. Abelson, L. Shaw and R. B. Anderson, *Ind. Engng Chem.* 1957, **49**, 2055.

Polyhedron Vol. 9, No. 23, pp. 2823–2831, 1990
Printed in Great Britain

0277–5387/90 $3.00+.00
© 1990 Pergamon Press plc

SYNTHESIS OF HETEROGENEOUS OLEFIN-OLIGOMERIZATION CATALYSTS USING HOMOGENEOUS NICKEL-CHELATE COMPLEXES AS A BASIS*

ALISON M. A. BENNETT, GARY A. FOULDS† and DAVID A. THORNTON

Departments of Chemistry and Chemical Engineering, University of Cape Town, Rondebosch 7700, South Africa

(*Received* 6 *July* 1990; *accepted* 17 *July* 1990)

Abstract—The synthesis and characterization of two nickel(II) catalyst precursors are described. The first is derived from cross-linking of the bis(glycidyl ether) of bis(1-*p*-hydroxyphenyl-1,3-butanedionato)nickel(II) with 1,2-diaminoethane and the second is obtained from polystyrene-supported chloro-2,4-pentanedithionatotriphenylphosphine-nickel(II). The compounds and their homogeneous precursors have been examined for their activity in catalysing the oligomerization of 1-hexene using triethylaluminium and ethylaluminiumdichloride as co-catalysts. Results obtained indicate that the polymeric complexes are active when $AlEtCl_2$ is used as a co-catalyst, but not when $AlEt_3$ is used. Furthermore, oligomerization is accompanied by isomerization, while a high selectivity for dimers is observed. Analysis of the complexes after catalytic runs reveals that some leaching of the nickel ions from the polymers has taken place.

Olefin oligomerization is a fundamental reaction in the upgrading of low molecular weight olefins to high value chemicals and synthetic fuels. Oligomerization may be effected using homogeneous or heterogeneous catalysts and industrial processes have been based on both systems. Examples of these are SHOP[1] and DIMERSOL,[2] which are homogeneous, and MOGD,[3] which is heterogeneous. Both systems have their advantages and disadvantages. Homogeneously-catalysed reactions are generally more efficient, specific and reproducible than those catalysed heterogeneously. However, heterogeneous catalysts are chemically and thermally more stable and also obviate the separation problems encountered in homogeneously-catalysed processes.

In combination with a suitable Lewis acid, almost any soluble nickel compound will show activity for olefin oligomerization. Compounds with oxidation states ranging from zero to two have been used and several comprehensive reviews cover the subject.[5–7] The oligomerization activity of β-ketoenolate and related complexes, **I**, has been extensively studied.[8–13] In particular, bis(2,4-pentanedionato)nickel(II) exhibits high activity in the presence of various Lewis acids and shows remarkable selectivity to linear oligomers if AlR_3 (R = alkyl) is used as co-catalyst.[10]

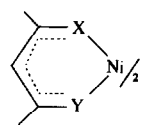

X = Y = O[8]
X = O, Y = NH[13]

(I)

Closely related to the β-ketoenolate complex catalysts are the systems reported by Cavell and Masters,[14–17] in which the β-ketoenolate ligand has been replaced by its dithio analogue, **II**. In addition, the introduction of the phosphine moiety has a pronounced effect, both on reactivity and selectivity.[16,18] Some of these complexes are among the most active oligomerization catalysts known.

* Paper presented at the Symposium on Applied Organometallic Chemistry, Pokolbin, NSW, Australia, 10–12 July 1989.

† Author to whom correspondence should be addressed. Present address: CSIRO, Division of Coal and Energy Technology, Lucas Heights Research Laboratories, NSW, Australia.

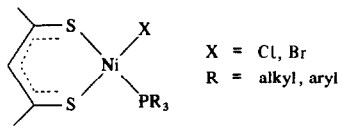

(II)

The aim of the present work is to exploit the advantages of both systems by heterogenizing the most promising of the soluble nickel-complex catalysts. We have chosen $[Ni(acac)_2]_3$ (Hacac = 2,4-pentanedione) and [Ni(sacsac)(PPh_3)Cl] (Hsac sac = pentane-2,4-dithione) as a basis for preparing polymeric analogues, the former for its selectivity in forming linear isomers when used with AlR_3 (R = alkyl) and the latter for its high activity. We have investigated the reactions of 1-hexene with the polymeric complexes, **IV** and **V**, and their monomeric homogeneous precursors, **III** and **II** (X = Cl, R = Ph), respectively, in a series of batch experiments, using $AlEt_3$ and $AlEtCl_2$ as co-catalysts. 1-Hexene was chosen as the reactant olefin for its manageable reactivity and ease of handling. In addition, since the lower olefins are more reactive,[4] complexes that oligomerize 1-hexene should certainly be active for the oligomerization of lower olefins.

EXPERIMENTAL

All reactions were performed using standard Schlenk tube techniques under dry argon. 1-Hexene and toluene were dried over sodium wire and freshly distilled under dry nitrogen before use. The starting materials $[Ni(PPh_3)_2Cl_2]$[19] and $[Ni(sacsac)_2]$[20] were prepared using methods described in the literature. Polystyrene polymer, 2% cross-linked with divinyl benzene and functionalized with PPh_3 at a concentration of 0.00306 mol PPh_3/g polymer, was purchased from Aldrich. Triethylaluminium (25% w/w in toluene) and ethylaluminium dichloride (25% w/w in toluene) were purchased from Aldrich and used as supplied.

Preparation of bis(p-*hydroxyphenyl*-1,3-*butanedionato*)*nickel*(II) (**III**) *and the polymeric nickel complex* **IV**

Bis(*p*-hydroxyphenyl-1,3-butanedionato)nickel(II) (**III**) and the polymeric nickel compound, **IV**, which is derived from complex **III**, were prepared according to the reaction scheme depicted in Fig. 1.[21] The detailed experimental procedure relating to each reaction sequence and the charac-

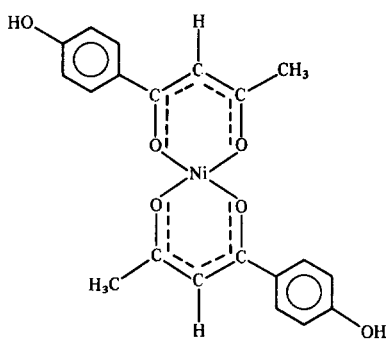

(III)

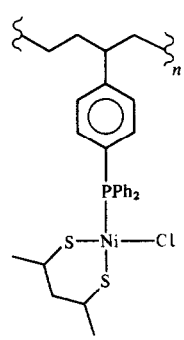

(V)

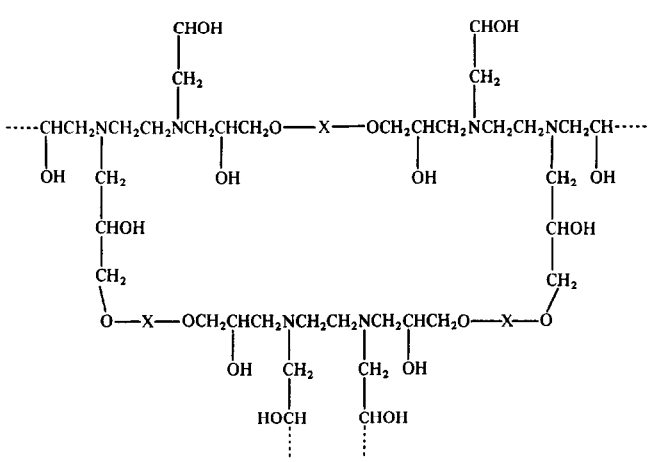

(IV)

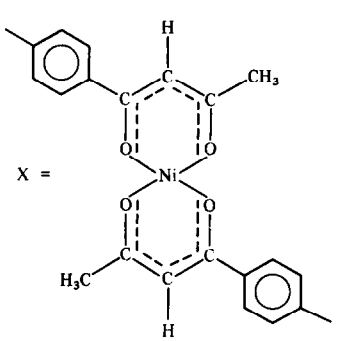

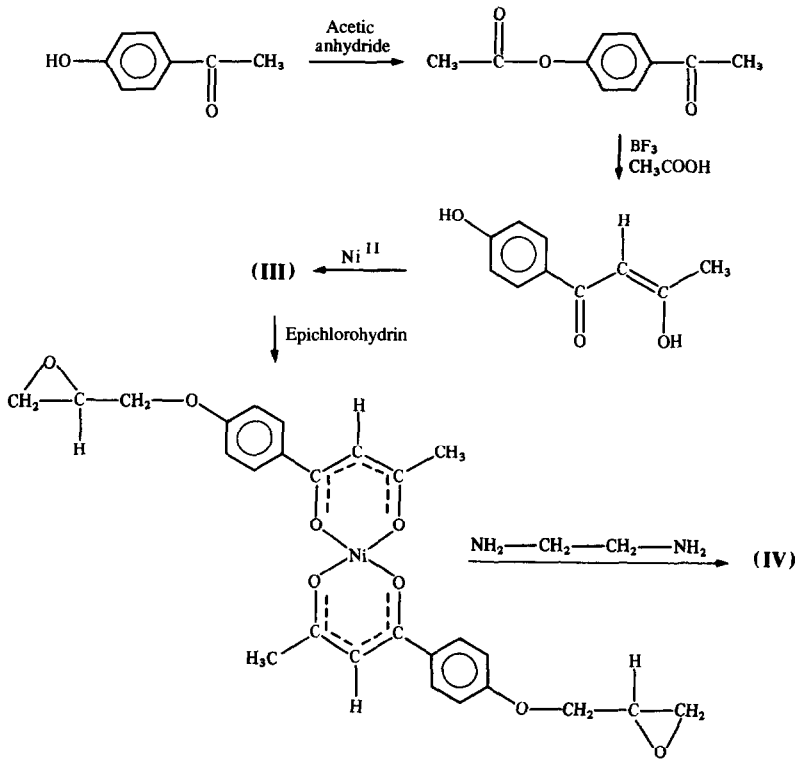

Fig. 1. Reaction scheme for the preparation of polymer **IV**.

terization of each intermediate are reported elsewhere.[22]

Preparation of [Ni(sacsac)(PPh_3)Cl]

[Ni(sacsac)(PPh_3)Cl] was prepared in a similar manner to that described previously.[23] [Ni(sacsac)$_2$] (0.48 g, 1.5 mmol) and [$NiCl_2(PPh_3)_2$] (0.98 g, 1.5 mmol) were dissolved in deoxygenated benzene (40 cm^3) and refluxed for 3 h under nitrogen. The resultant solution was filtered while hot. Removal of the solvent from the filtrate yielded a black oily residue. This residue was taken up in the minimum of acetone. Slow addition of n-heptane, with scratching, yielded black crystals. Recrystallization in this manner was repeated until microanalytical purity was established.

Preparation of the polymeric nickel complex **V**

[Ni(sacsac)(PPh_3)Cl] (2.181 g, 4.47 mmol) was dissolved in deoxygenated benzene (50 cm^3). Sufficient PPh_3-functionalized polystyrene polymer (2.0 g) was added to the solution, which was then refluxed for 48 h. The dark brown, polymeric, supported nickel complex, **V**, was filtered and washed with benzene until the washings were colourless.

Analyses of complexes

The purity and composition of the compounds were determined by microanalysis (C, H and N) and Energy Dispersive X-ray analysis (EDX) (Ni) (Table 1). Further characterization was achieved using ^1H and ^{13}C NMR spectroscopy, IR spectroscopy and thermogravimetry. NMR spectra were run at ambient temperature on a Varian ZX 200 spectrometer using CH_3OD or $CDCl_3$ as solvent and TMS as reference. IR spectra were determined as Nujol mulls (4000–1500 and 1300–300 cm^{-1}) or hexachlorobutadiene mulls (4000–1700 and 1500–1300 cm^{-1}) between CsI plates on a Perkin–Elmer 983 spectrophotometer, and as Nujol mulls between polyethylene plates (500–80 cm^{-1}) on a Digilab FTS-16 B/D interferometer. Thermogravimetric analysis was performed on a Stanton Redcroft thermal analyser.

1-*Hexene oligomerization*

Oligomerization was carried out in batch mode using a magnetically-stirred glass reactor. To exclude the presence of any water associated with the nickel catalyst, each was dissolved or slurried in toluene, transferred to the reactor and azeotroped

Table 1. Analytical data

Compound	Calculated C (%)	H (%)	N (%)	Ni (%)	Found C (%)	H (%)	N (%)	Ni (%)
III	58.2	4.4	—	13.6	57.7	4.1	—	13.6
IV	[a]	[a]	[a]	—	50.6	4.3	8.7	14.3
[Ni(sacsac)(PPh_3)Cl]	56.6	4.5	—	—	57.1	4.2	—	—
V					67.3	4.0	—	6.2
IV[b]					20.8	4.8	2.0	3.5
V[b]					70.2	5.6	—	0.8

[a] Theoretical values are dependent on the degree of cross-linking which is not known.
[b] Percentage nickel determined after catalytic run.

for several hours under argon (concentration of nickel in toluene = 10^{-3} mol nickel/60 cm^3 toluene). The reactor, heated by a thermostatted oil bath, was allowed to stabilize at 40°C, before injecting the co-catalyst (25% w/w in toluene) into the reactor via a septum (Ni : Al ratio 1 : 1 for $AlEt_3$ and 1 : 10 for $AlEtCl_2$). The reaction temperature, which was monitored throughout, rose intitially (45°C) before slowly returning to 40°C. The reactor was maintained under a positive pressure of argon and samples (1 cm^3) were taken with a syringe at regular time intervals. The samples were immediately mixed with methanol to quench the reaction by catalyst deactivation.

Product analysis

The liquid products were filtered (to remove deactivated nickel complex precipitate) and analysed by gas–liquid chromatography, using methanol as an internal standard. Product analysis was determined using a Varian 3600 GC with a 0.531 mm i.d., 30 m long, fused silica megabore column, coated with a 1.5 μm film of DB 101 (100% methylpolysiloxane). Products have been reported as mass % :

$$\text{mass \% (olefin } i) = \frac{(\text{Peak area olefin } i)R_{fi}}{\sum_{i=1}^{n} [(\text{Peak area olefin } i)R_{fi}]}$$

where n = number of olefins present
R_{fi} = response factor of olefin i*.

* The response factor of an olefin with a carbon number greater than five is taken as unity.

RESULTS AND DISCUSSION

IR spectra

Selected bands from the IR spectra of compounds **II**, **III**, **IV** and **V** are listed in Table 2. The carbonyl stretch, ν(C═O), occurs at 1610 cm^{-1} for *p*-hydroxybenzoylacetone and a shift of 10 cm^{-1} to lower wavenumber is an indication that complexation with nickel(II) to yield the monomeric complex **III** has occurred. This vibration is also present in the polymeric complex **IV** and occurs at 1590 cm^{-1}. Of particular interest are the metal–ligand vibrations, ν(Ni—O), which occur at 435 and 271 cm^{-1} for the monomer, **III**, and at 429 and 276 cm^{-1} for the cured epoxy polymer, **IV**. These bands have been assigned by comparison with the spectrum of *trans*-$[Ni(acac)_2(H_2O)_2]$[24] and by metal-ion substitution studies.[24] The bands at 3281 and 3164 cm^{-1} are assigned to the asymmetric and symmetric N—H stretches in the cured polymer **IV** which do not, of course, occur in the spectrum of the monomer **III**. In addition, the presence of ν(N—H) indicates that

Table 2. Characteristic bands (cm^{-1}) in the IR spectra of the polymeric complexes and their homogeneous precursors

	III	**IV**	[Ni(sacsac)(PPh_3)Cl]	**V**
ν(C═O)	1600	1590		
ν(Ni—O)	435	429		
	271	276		
$\nu(N—H)_{as}$		3281		
$\nu(N—H)_s$		3164		
ν(C═S)			715	710
ν(Ni—S)			382	393
			290	
ν(Ni—Cl)			332	338

only a degree of cross-linking has been achieved, while the absence of any bands which may reasonably be assigned to ν(Ni—N) eliminates the possibility of coordination of ethylenediamine.

In considering the spectra of [Ni(sacsac)(PPh_3)Cl] (**II**; R = Ph, X = Cl) and the polymer **V**, the bands which impart important structural information are ν(C=S), ν(Ni—S), ν(Ni—P) and ν(Ni—Cl). The ν(C=S) band occurs at 715 cm^{-1} in the complex [Ni(sacsac)(PPh_3)Cl] and is shifted to 710 cm^{-1} in the spectrum of the polymer **V**. Assignment of ν(Ni—S) has been made with reference to a recent study[24] in which the IR spectrum of [Ni$(sacsac)_2$] was analysed. The ν(Ni—Cl) band was assigned on the basis of halide substitution.[24] The assignment of ν(Ni—P) is as yet unclear. However, a detailed IR study of the complexes **II** is presently being undertaken with a view to assigning ν(Ni—P).

Finally, the fact that the metal–ligand bands are not significantly shifted when the monomeric complexes are converted into their polymeric derivatives strongly suggests that the square-planar environment of the nickel(II) ion is unchanged.

^{1}H *and* ^{13}C *NMR spectra*

Due to their limited solubility, the NMR spectra of the complexes **III**, and the polymers **IV** and **V** could not be determined. ^{1}H and ^{13}C NMR spectra confirmed the identity of [Ni(sacsac)(PPh_3)Cl] (Table 3).

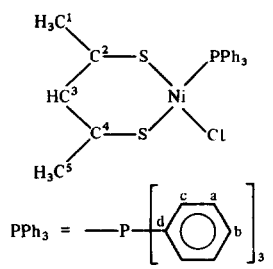

Table 3. ^{1}H and ^{13}C NMR spectra of [Ni(sacsac)(PPh_3)Cl][a]

^{1}H(ppm)		^{13}C(ppm)	
C^1H_3, C^5H_3	2.28	C^1, C^5	31.56
		C^2, C^4	Not observed
C^3H	Obscured	C^3	130.84
		C^a	128.13 (doublet)
Ph	7.4–7.9	C^b	130.53
	(multiplet)	C^c	135.04 (doublet)
		C^d	Not observed

[a] Spectra were run at ambient temperature using $CDCl_3$ as solvent and TMS as reference.
J_{CCP} = 9.8, J_{CCCP} = 10.2.

The chemical shifts are similar to those reported for [Ni(sacsac)(PEt_3)Cl].[23] At ambient temperature the methyl resonances are magnetically equivalent. This equilibration has been attributed to phosphine or halide exchange.[23] As also found for the complex [Ni(sacsac)(PEt_3)Cl], the relaxation time of the quaternary carbon atoms is insufficiently short for these resonances to be observed.

TGA/DTA studies

The TGA/DTA curves for the polymeric complexes **IV** and **V** are shown in Figs 2 and 3, respectively. It is clear that the polymer **V** is stable to over 200°C, whereas the epoxy polymer **IV** exhibits a mass loss at much lower temperatures. A total mass loss of 80% is observed for polymer **V**, with the final residue being NiO. Consequently, 14.5% of the polymer mass is nickel, which is consistent with the EDX analysis which yielded 14.3% by mass of nickel. A total mass loss of 76% is observed for the epoxy polymer **IV**. However, the residue is not NiO, but a more complex acid-insoluble material.

1-*Hexene oligomerization*

In the oligomerization studies, it was decided not only to investigate the effect of catalyst, but also the

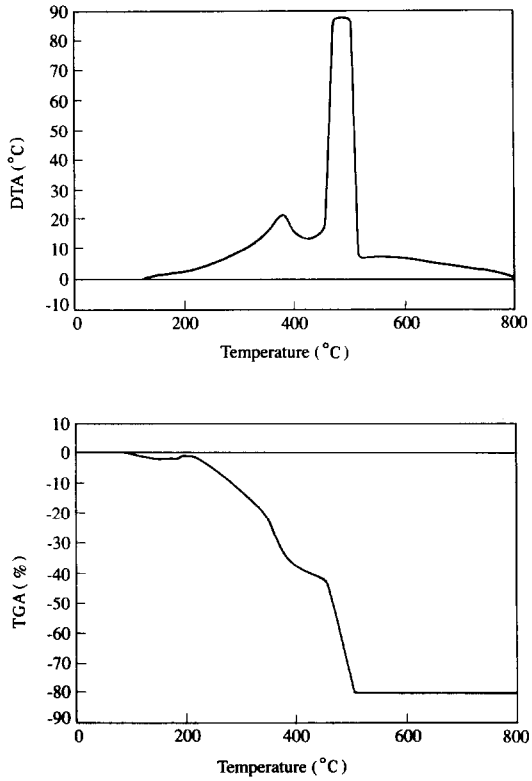

Fig. 2. TGA/DTA curves for polymer **IV**.

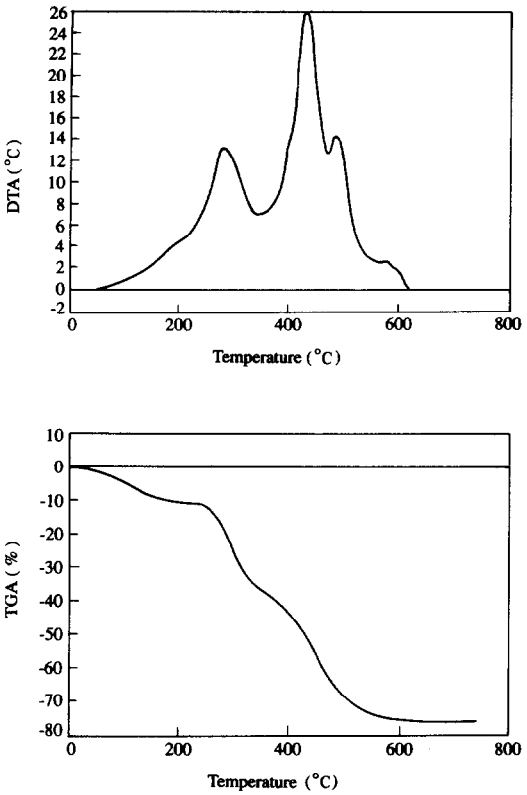

Fig. 3. TGA/DTA curves for polymer **V**.

effect of co-catalyst on the activity and selectivity of the reaction. We have utilized $AlEt_3$ and $AlEtCl_2$ co-catalysts, because firstly, the order of reactivity for the chloride-containing Lewis acids is $AlEt_2Cl < Al_2Et_3Cl_3 < AlEtCl_2$[22] and secondly, because a unique selectivity for linear product formation is obtained when $AlEt_3$ is used in a 1:1 ratio with bis(β-ketoenolato)nickel(II) complexes in "chloride-free" solvents.[10,25] The latter phenomenon is illustrated in Figs 4 and 5 where 1-hexene

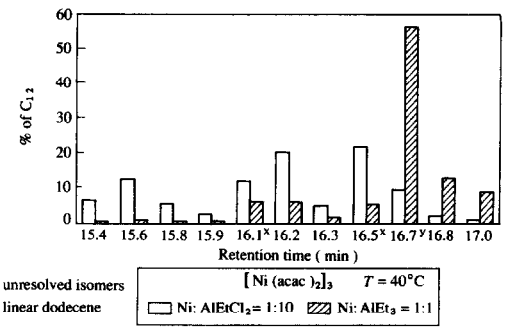

Fig. 5. C_{12} isomer distributions using $[Ni(acac)_2]_3$ with $AlEt_3$ and $AlEtCl_2$ as co-catalysts.

has been oligomerized by $[Ni(acac)_2]_3$ in the presence of an equimolar amount of $AlEt_3$ and a 10-fold excess of $AlEtCl_2$. Clearly, $AlEtCl_2$ has the higher activity, but Fig. 5 reveals the striking difference in C_{12} selectivity.

Compounds **III**, **IV** and **V** were not active when tested with an equimolar amount of $AlEt_3$. These complexes are insoluble and it is possible that the stability of the complexes, coupled with their insolubility, may preclude the formation of the active species in the presence of the weak Lewis acid.

The polymeric nickel complex, **IV**, and its monomeric precursor, **III**, are both active as oligomerization catalysts when a 10-fold excess of $AlEtCl_2$ is utilized as co-catalyst. As is commonly found in these systems, oligomerization is accompanied by isomerization to internal olefins.[26]

Figure 6 shows the conversion of 1-hexene using the monomeric complex, **III**, as catalyst. This complex, which is suspended in toluene, dissolves on the addition of $AlEtCl_2$ and the reaction thus proceeds in a homogeneous manner. As for other homogeneous catalysts of this type, the monomeric complex, **III**, exhibits high initial activity and is, in fact,

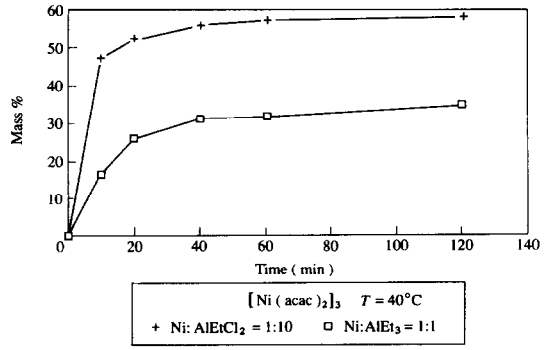

Fig. 4. Dimerization of 1-hexene using $[Ni(acac)_2]_3$ with $AlEt_3$ and $AlEtCl_2$ as co-catalysts.

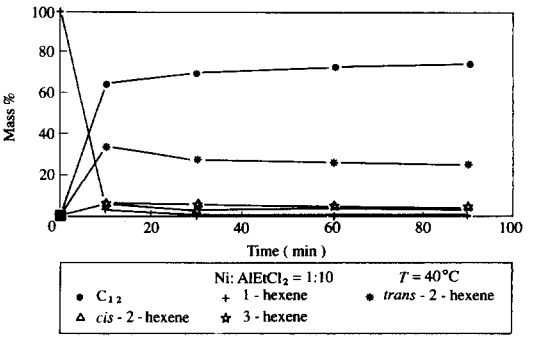

Fig. 6. Conversion of 1-hexene using complex **III** with $AlEtCl_2$ as co-catalyst.

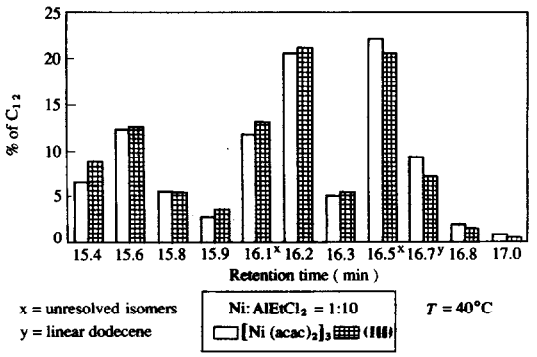

Fig. 7. C_{12} isomer distributions using $[Ni(acac)_2]_3$ and complex **III** with $AlEtCl_2$ as co-catalyst.

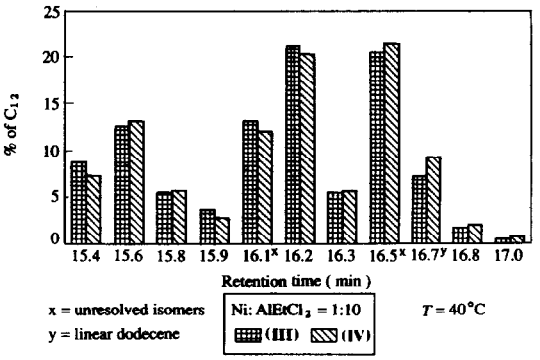

Fig. 9. C_{12} isomer distributions using complex **III** and polymer **IV** with $AlEtCl_2$ as co-catalyst.

more active than $[Ni(acac)_2]_3$ (Fig. 4). This may be due to the electronic effect of the ligand which now has a *p*-hydroxyphenyl substituent replacing a methyl group. The C_{12} isomers produced by the monomeric complex, **III**, and $[Ni(acac)_2]_3$ are shown in Fig. 7. It is clear that they are very similar and it is likely that a similar reaction mechanism is involved.

The nickel polymer, **IV**, exhibits a different trend from that observed for its monomeric homogeneous precursor, **III** (Fig. 8). Although conversion is still rapid, the isomerization reaction predominates in the early stages producing a large percentage of *cis*- and *trans*-2-hexene and 3-hexene. That oligomerization proceeds at a slower pace is probably due to the fact that the internal C_6 olefins have to be converted to the α-olefin. This is evident from a concomitant decrease in the internal C_6 olefins as C_{12} dimers are produced. No active species have been presented in the literature to describe the activity of supported catalysts. However, the similarity in C_{12} isomer distribution for both the polymeric complex and its homogeneous precursor is clearly illustrated in Fig. 9, implying that both systems comprise a similar active species. In addition, both monomer **III** and polymer **IV** produce dimers only, with no higher oligomers being formed.

Turning to [Ni(sacsac)(PPh_3)Cl] and the phosphine supported polymer, **V**, the situation is similar to the system described above in that the supported catalyst is initially less active than its homogeneous precursor (Figs 10 and 11). Similarly, C_6 isomerization is dominant in the early stages but is followed by increasing oligomerization. As observed by Cavell and Masters,[14] who studied the oligomerization of propylene using [Ni(sacsac)(PPh_3)Cl] and a polymer-supported analogue, the oligomer (C_{12}) isomer distribution is similar when the homogeneous catalyst is heterogenized onto an organic support (Fig. 12). This is indicative of the operation of a similar active species in both systems. Comparison of the C_{12} isomer distribution formed by the polymeric complexes, **IV** and **V**, respectively, reveals substantial differences between the two systems (Fig. 13). These differences can probably be ascribed to the influence of the phos-

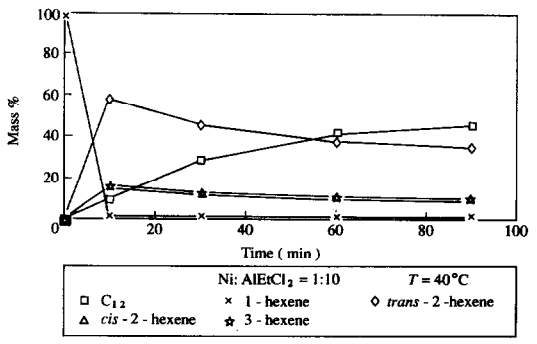

Fig. 8. Conversion of 1-hexene using polymer **IV** with $AlEtCl_2$ as co-catalyst.

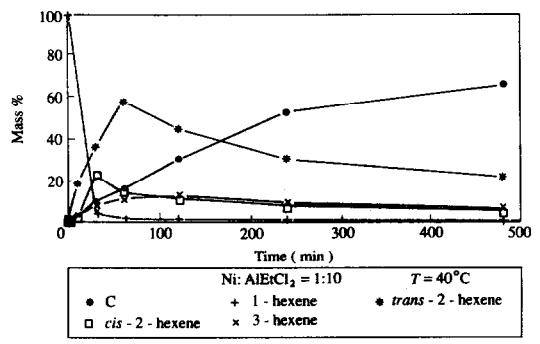

Fig. 10. Conversion of 1-hexene using polymer **V** with $AlEtCl_2$ as co-catalyst.

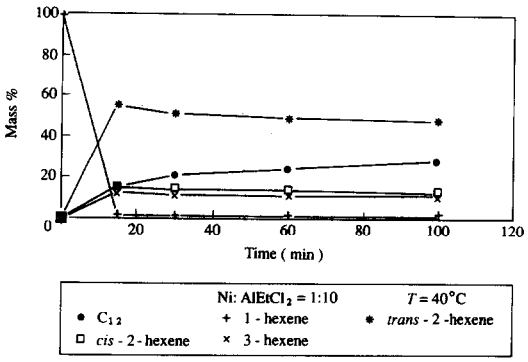

Fig. 11. Conversion of 1-hexene using [Ni(sacsac)(PPh$_3$)Cl] with AlEtCl$_2$ as co-catalyst.

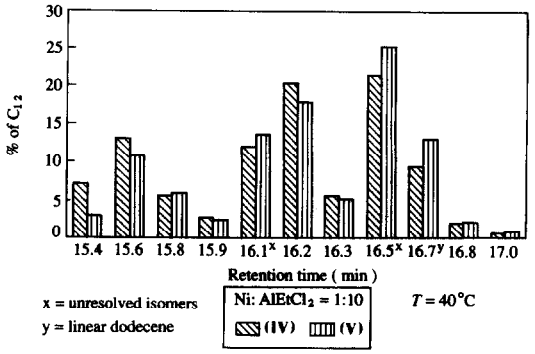

Fig. 13. C$_{12}$ isomer distributions using polymers **IV** and **V** with AlEtCl$_2$ as co-catalyst.

phine ligand on the reaction.[18] Analysis of the polymer **V**, after reaction, revealed that the percentage nickel had decreased from 6.2% to less than 1%. This suggests excessive weeping and some doubt exists as to whether only polymer-bound nickel was responsible for oligomerization. As a result of the excessive weeping, the polymer **V** could not be used for successive runs, a major drawback of this system.

In conclusion, the epoxy polymer, **IV**, shows promise as an olefin oligomerization catalyst, particularly in view of its thermal and chemical stability.[21] However, the non-selectivity towards yielding a linear product and the fact that only dimers are formed, are two factors that require further investigation. We are presently examining the synthesis of nickel(I) complexes and methods for their polymerization, since a number of these complexes have been shown to be active for the homogeneous oligomerization of olefins to linear products.[12] In addition, it also obviates the use of a co-catalyst.

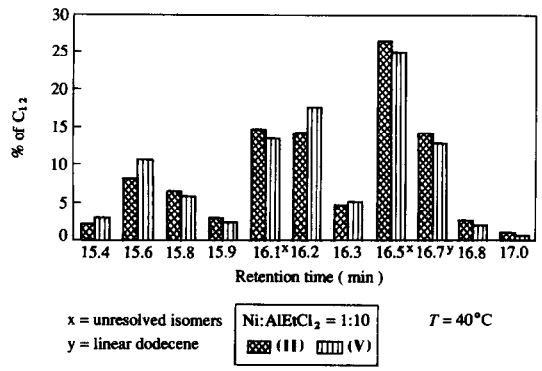

Fig. 12. C$_{12}$ isomer distributions using [Ni(sacsac)(PPh$_3$)Cl] and polymer **V** with AlEtCl$_2$ as co-catalyst.

Acknowledgements—We wish to thank the National Energy Council and the CSIR for financial support (to A.M.A.B.).

REFERENCES

1. R. S. Bauer, H. Ching, P. W. Glockner, W. Keim and H. van Zwet, *US Pat.* 3635937 (1972).
2. Y. Chauvin, J. F. Gaillard, D. V. Quang and J. W. Andrews, *Chem. Ind. (Lond.)* 1974, 375.
3. R. J. Quann, L. A. Green, S. A. Tabak and F. J. Krambeck, *Ind. Engng Chem. Res.* 1988, **27**, 565.
4. G. Lefebvre and Y. Chauvin, in *Aspects of Homogeneous Catalysis* (Edited R. Ugo), Vol. 1, p. 107. Carlo Manfredi, Milan (1970).
5. V. S. Feldblyum and N. V. Obeschalova, *Russ. Chem. Rev.* 1968, **37**, 789.
6. P. W. Jolly and G. Wilke, in *The Organic Chemistry of Nickel*, Vol. 2. Academic Press, New York (1975).
7. P. W. Jolly, in *Comprehensive Organometallic Chemistry*, p. 615. Pergamon Press, New York (1982).
8. J. Ewers, *Angew. Chem. Int. Edn* 1966, **5**, 584.
9. J. R. Jones, *J. Chem. Soc. C* 1971, 117.
10. J. R. Jones and T. J. Symes, *J. Chem. Soc. C* 1971, 1124.
11. W. Keim, B. Hoffmann, R. Lodewick, M. Peuckert and G. Schmitt, *J. Molec. Catal.* 1979, **6**, 79.
12. W. Keim, A. Behr and G. Kraus, *J. Organomet. Chem.* 1983, **251**, 377.
13. G. Henrici-Olive and S. Olive, *Transition Met. Chem.* 1976, **1**, 109.
14. K. J. Cavell and A. F. Masters, *J. Chem. Res. Symp.* 1983, 72.
15. K. J. Cavell and A. F. Masters, *Aust. J. Chem.* 1986, **39**, 1129.
16. S. J. Brown, A. F. Masters and M. Vender, *Polyhedron* 1988, **7**, 2009.
17. S. J. Brown, L. M. Clutterbuck, A. F. Masters, J. I. Sachinidis and P. A. Tregloan, *Appl. Catal.* 1989, **48**, 1.
18. B. Bogdanovic, *Adv. Organomet. Chem.* 1979, **17**, 105.

19. L. M. Venanzi, *J. Chem. Soc.* 1958, 719.
20. C. G. Barraclough, R. L. Martin and I. M. Stewart, *Aust. J. Chem.* 1962, **22**, 891.
21. M. E. B. Jones, M. F. Lynch, D. A. Thornton and R. F. Webb, *Makromolec. Chem.* 1961, **50**, 232.
22. A. M. A. Bennett, G. A. Foulds and D. A. Thornton, to be submitted for publication.
23. J. P. Fackler and A. F. Masters, *Inorg. Chim. Acta* 1980, **39**, 111.
24. A. M. A. Bennett, G. A. Foulds and D. A. Thornton, *Polyhedron* 1989, **8**, 2305 and refs cited therein.
25. K. Zhou, Z. Gao and W. Keim, *Proceedings, 8th Int. Congr. on Catalysis*, Vol. V, p. 429. Berlin (1984).
26. Y. Chauvin, N. H. Phung, N. Guichard and G. Lefebvre, *Bull. Soc. Chim. Fr.* 1966, 3223.

Polyhedron Vol. 9, No. 23, pp. 2833–2837, 1990
Printed in Great Britain

0277–5387/90 $3.00+.00
© 1990 Pergamon Press plc

COPPER(I) COMPLEXES FROM $[Cu(PPh_3)_4]ClO_4$ AND SOME HETEROCYCLIC THIONES AS LIGANDS. THE CRYSTAL STRUCTURE OF $[Cu(py2SH)_2(PPh_3)_2]ClO_4 \cdot 2CHCl_3$

P. KARAGIANNIDIS,* P. ASLANIDIS and S. PAPASTEFANOU

Department of General and Inorganic Chemistry, Aristotelian University of Thessaloniki, Thessaloniki 54006, Greece

and

D. MENTZAFOS, A. HOUNTAS and A. TERZIS

X-ray Laboratory, NCR "Democritos", 153 10 Ag. Paraskevi, Athens, Greece

(*Received* 16 *February* 1990; *accepted* 20 *July* 1990)

Abstract—Reactions of $[Cu(PPh_3)_4]ClO_4$ with heterocyclic thiones (L) [L = pyridine-2-thione (py2SH), pyrimidine-2-thione (pymtH), 1,3-thiazolidine-2-thione (tzdtH), 1-methyl-1,3-imidazoline-2-thione (meimtH), benz-1,3-imidazoline-2-thione ($bzimtH_2$), benz-1,3-thiazoline-2-thione (bztzH), 5-nitro-2-benz-1,3-imidazoline-2-thione ($nbzimtH_2$) 5-methyl-2-benz-1,3-imidazoline-2-thione ($mebzimtH_2$) and quinazolinone-2-thione ($qnotH_2$)] yield mononuclear complexes of the general formula $[Cu(L)_2(PPh_3)_2]ClO_4 \cdot 2CHCl_3$. The complexes have been characterized by elemental analysis, IR, UV–vis and NMR spectroscopy. The crystal structure of $[Cu(py2SH)_2(PPh_3)_2]ClO_4 \cdot 2CHCl_3$ has been determined by single-crystal X-ray diffraction methods. The copper atom has S_2P_2 tetrahedral coordination with Cu—S 2.363, 2.377(1) Å and Cu—P 2.301, 2.315(1) Å.

There has been considerable interest during the past few years in complexes of heterocyclic thiones and transition metals, stemming from the similarity of these ligands with thiolated nucleosides.[1] Notably, major interest has grown in copper complexes due to the biological importance of copper–sulphur interactions in Cu^I/Cu^{II} redox systems.[2]

Recently the structures of a number of simple complexes of copper(I) with heterocyclic thiones, and also of mixed complexes with heterocyclic thiones and triphenylphosphine ligands, have been reported.[3–5] As part of our continuing investigation into the synthesis and chemical structural properties of copper(I) complexes, we report here the preparation and characterization of a new series of complexes of the general formula $[Cu(L)_2(PPh_3)_2]ClO_4$.

* Author to whom correspondence should be addressed.

EXPERIMENTAL

Physical measurements

Elemental analyses of carbon, nitrogen, hydrogen and copper, IR, electronic and NMR spectra, conductivities and magnetic susceptibility measurements were performed as described previously.[5]

Starting materials

$[Cu(PPh_3)_4]ClO_4$ was prepared from $CuClO_4$ and PPh_3 as described in the literature.[6] All thione ligands, supplied by EGA or Aldrich, were used after recrystallization from ethanol. Triphenylphosphine, copper(II) perchlorate and all solvents were of reagent grade and were used without further purification in the synthetic work.

Preparation of the complexes

$[Cu(PPh_3)_4]ClO_4$ (1 mmol) was dissolved in 30 cm^3 of chloroform and treated with 20 cm^3 of a 1 mmol solution of the appropriate ligand in the same solvent. The reaction mixture was refluxed for 2 h, filtered and cooled to room temperature. Slow evaporation of the solvent at room temperature gave the microcrystalline solid, which was filtered off, washed with ether and dried *in vacuo*.

Collection and reduction of intensity data

Complete crystal and intensity collection data are reported in Table 1. Unit cell dimensions were derived from least-squares refinement of the setting angles of 15 automatically centred reflections in the range $13 < 2\theta < 24°$ on a SYNTEX $P2_1$ diffractometer. The intensities of three standards monitored after every 67 reflections were stable, with a scatter of less than 3% from their respective means. Lorentz and polarization corrections were applied.

Solution and refinement of the structure

The positional coordinates of copper, chlorine, sulphur and phosphorus atoms were deduced by direct methods using the SHELX 76 program.[7] The rest of the non-hydrogen atoms were revealed by subsequent ΔF calculations. The difference map showed the existence of two solvent molecules (chloroform) in the asymmetric unit, one of them being disordered. The difference map shows two positions, A and B, for the disordered $CHCl_3$. The

Table 1. Summary of crystal and intensity collection data

Formula	$Cu(SNC_5H_5)_2(PC_{18}H_{15})_2ClO_4(CHCl_3)_2$
FW	1148.6
a (Å)	11.054(2)
b (Å)	12.455(3)
c (Å)	19.733(5)
α (°)	100.38(2)
β (°)	99.83(2)
γ (°)	96.11(2)
V (Å^3)	2607(1)
Z	2
D_{calc} (Mg m^{-3})	1.463
D_{meas} (Mg m^{-3})	1.45
Space group	$P\bar{1}$
Radiation	Mo-K_α (λ = 0.71069 Å)
μ (cm^{-1})	9.19
Scan speed (° min^{-1})	2.0–15.0
Scan range (°)	1.6 plus $\alpha_1-\alpha_2$
Background counting (s)	0.5 of scan time
2θ limit (°)	45.0
Data collected	7048
Data unique	6266
Data used	5104
$F_o >$	$4.0\sigma(F_o)$
R_{int}	0.0122
Range of $h\ k\ l$	$0 \rightarrow 9, -13 \rightarrow 13, -21 \rightarrow 20$
Weighting scheme	$1/w = \sigma^2(F_o)+0.0008\ \|F_o\|^2$
$F(000)$	1168
Number of refined parameters	642
$\|\Delta/\sigma\|_{max}$	0.510
$(\Delta p)_{max}$ (eÅ^{-3})	0.561
$(\Delta p)_{min}$ (eÅ^{-3})	−0.626
R (obs)[a]	0.0494
R (all data)[a]	0.0621
R_w (obs)[b]	0.0632
R_w (all data)[b]	0.0666

[a] $R = \Sigma|\Delta F|/\Sigma|F_o|$.

[b] $R_w = [\Sigma w(\Delta F)^2/\Sigma w|F_o|^2]^{1/2}$.

site occupancies of the positions A and B were refined, keeping the sum of the two constant at 1.0, and the Cl—Cl and C—Cl distances constrained to 2.84(1) and 1.73 Å. The occupancy refined to 0.809(3) Å for the A position. Refinement was carried out by blocked full-matrix least-squares, in which $\Sigma w\Delta^2$ was minimized. The hydrogen atoms were calculated as riding on carbon atoms at 1.02 Å. Non-hydrogen atoms were refined using anisotropic temperature factors and hydrogen atoms isotropic temperature factors. Atomic scattering factors were taken from the *International Tables for X-ray Crystallography*.[8]

RESULTS AND DISCUSSION

It is well known that copper(I) complexes with heterocyclic thiones have a wide variety of stoichiometries and structure types depending on both the thione ligand and the counter ion. Generally, the number of ligands bound to the univalent metal seems to be influenced by both the chemical nature of the ligands and the geometry they impose. In fact, in the absence of triphenylphosphine, three or four ligand molecules are present in pyridine-2-thione complexes for nitrate[9] and perchlorate[10] derivatives. However, in the presence of triphenylphosphine it seems that the counter ion does not change the core geometry and a distorted tetrahedral coordination about the copper atom is obtained.

The crystal structure of mononuclear or binuclear halide complexes, e.g. [Cu(py2SH)$(PPh_3)_2$Br] and $[Cu(py2SH)(PPh_3)Br]_2$[3] shows that coordination about copper involves the halogen atom. Interestingly, the reaction of $[Cu(PPh_3)_2NO_3]$ with heterocyclic thiones results in the formation of the complexes $[Cu(L)_2(PPh_3)_2]NO_3$ in which the anion is not coordinated to copper.[5]

The reaction of $[Cu(PPh_3)_4]ClO_4$ with these heterocyclic thiones (L) yields a variety of crystalline products. These products fall into two general groups corresponding to either a 1:1 or to a 2:1 ligand-to-metal ratio; no species containing more than two heterocyclic thione ligands per copper ion have been observed. On changing the solvent, products of different composition have been isolated, but their analytical results were poor and irreproducible.

All the complexes described herein are air- and moisture-stable solids, but their solutions are oxidized within a few days. They are diamagnetic, as would be expected for d^{10} species, and behave as 1:1 electrolytes in acetonitrile solutions. Table 2 lists the compounds we have isolated with their colours, melting points and analytical data. The

Table 2. Some physical properties and analytical data of the complexes

Compound	Yield (%)	Colour	Melting point (°C)	Analysis, found (calc.) (%)			
				C	H	N	Cu
$[Cu(py2SH)_2(PPh_3)_2]ClO_4 \cdot 2CHCl_3$	88	Yellow	147	50.4 (50.2)	3.6 (3.7)	2.5 (2.4)	5.6 (5.5)
$[Cu(pymtH)_2(PPh_3)_2]ClO_4 \cdot 2CHCl_3$	90	Yellow	107	48.9 (48.0)	3.5 (3.5)	5.0 (4.9)	5.6 (5.5)
$[Cu(tzdtH)_2(PPh_3)_2]ClO_4 \cdot 2CHCl_3$	82	White	171	46.0 (45.4)	3.8 (3.6)	2.6 (2.4)	5.3 (5.4)
$[Cu(meimtH)_2(PPh_3)_2]ClO_4 \cdot 2CHCl_3$	79	Pale yellow	135	47.7 (47.8)	3.7 (3.8)	4.9 (4.8)	5.6 (5.5)
$[Cu(bztzH)_2(PPh_3)_2]ClO_4 \cdot 2CHCl_3$	66	Yellow	176	50.9 (50.8)	3.8 (3.4)	2.4 (2.3)	5.3 (5.2)
$[Cu(bzimtH_2)_2(PPh_3)_2]ClO_4 \cdot 2CHCl_3$	68	White	191	50.3 (50.9)	3.6 (3.6)	4.8 (4.6)	5.4 (5.2)
$[Cu(qnotH_2)_2(PPh_3)_2]ClO_4 \cdot 2CHCl_3$	79	Red	114	51.2 (50.7)	3.7 (3.5)	4.1 (4.4)	5.1 (4.9)
$[Cu(mebzimtH_2)_2(PPh_3)_2]ClO_4 \cdot 2CHCl_3$	65	White	175	50.8 (51.6)	3.8 (3.8)	4.5 (4.5)	5.1 (5.1)
$[Cu(nbzimtH_2)_2(PPh_3)_2]ClO_4 \cdot 2CHCl_3$	86	Yellow	92	46.9 (47.4)	3.7 (3.2)	6.2 (6.4)	4.7 (4.8)

Table 3. Main bond distances (Å) and angles (°)

Distances (Å)			
Cu—P(1)	2.301(1)	C(71)—N(1)	1.347(7)
Cu—P(2)	2.315(1)	C(81)—C(82)	1.395(7)
Cu—S(1)	2.377(1)	C(82)—C(83)	1.368(9)
Cu—S(2)	2.363(1)	C(83)—C(84)	1.375(9)
P(1)—C(11)	1.825(5)	C(84)—C(85)	1.364(9)
P(1)—C(21)	1.837(5)	C(85)—N(2)	1.340(8)
P(1)—C(31)	1.820(4)	C(81)—N(2)	1.357(6)
P(2)—C(41)	1.822(5)	Cl—O(1)	1.415(5)
P(2)—C(51)	1.824(4)	Cl—O(2)	1.370(6)
P(2)—C(61)	1.821(5)	Cl—O(3)	1.412(6)
S(1)—C(71)	1.706(5)	Cl—O(4)	1.413(4)
S(2)—C(81)	1.707(5)	C(A)—Cl(1)	1.737(6)
C(71)—C(72)	1.407(8)	C(A)—Cl(2)	1.746(7)
C(72)—C(73)	1.361(8)	C(A)—Cl(3)	1.738(7)
C(73)—C(74)	1.380(10)	C(B1)—Cl(4)	1.734(6)
C(74)—C(75)	1.342(9)	C(B1)—Cl(5)	1.735(5)
C(75)—N(1)	1.358(8)	C(B1)—Cl(6)	1.733(4)
Angles (°)			
P(1)—Cu—P(2)	121.5(0)	Cu—P(1)—C(31)	114.2(1)
P(1)—Cu—S(1)	105.3(0)	Cu—P(2)—C(41)	111.3(2)
P(2)—Cu—S(1)	106.0(1)	Cu—P(2)—C(51)	116.8(2)
P(1)—Cu—S(2)	112.9(0)	Cu—P(2)—C(61)	118.2(2)
P(2)—Cu—S(2)	107.6(0)	Cu—S(1)—C(71)	116.9(2)
S(1)—Cu—S(2)	101.3(0)	Cu—S(2)—C(81)	115.9(1)
Cu—P(1)—C(11)	118.1(1)	S(1)—C(71)—N(1)	121.7(4)
Cu—P(1)—C(21)	111.6(1)	S(2)—C(81)—N(2)	119.4(4)

results of the elemental analyses show good agreement with the suggested formulae.

Description of the structure

Relevant distances and angles are listed in Table 3. Figure 1 contains a labelled diagram of the cation with an adjacent perchlorate group.

The pyridine-2-thione acts as a monodentate ligand coordinating through the sulphur atom. The $Cu_2X_2L_2$ core geometry is very similar to that of the complex $[Cu(py2SH)_2(PPh_3)_2]NO_3$. The coordination of copper(I) is distorted tetrahedral, with a mean distance of 2.370 Å for Cu—S and 2.308 Å for Cu—P. The Cu—S distances are somewhat shorter than the sum of the covalent tetrahedral radii for copper and sulphur (2.39 Å); they are not sufficiently short to suggest appreciable metal–sulphur multiple bonding.

The Cu—P(1) and Cu—P(2) bond lengths [2.301(1) and 2.315(1) Å, respectively] are in good agreement with the distances in $[Cu(PPh_3)_2(BF_4)]$[11] and $[Cu(PPh_3)_2(pymtH)Br]$.[3]

The angles at the copper atoms are nearly tetrahedral. This result is a consequence of the approximately equal steric factors near the copper coordination sphere. However, the P—Cu—P angle of 121.5° deviates considerably from the tetrahedral value of 109.47°, but falls in the range of values

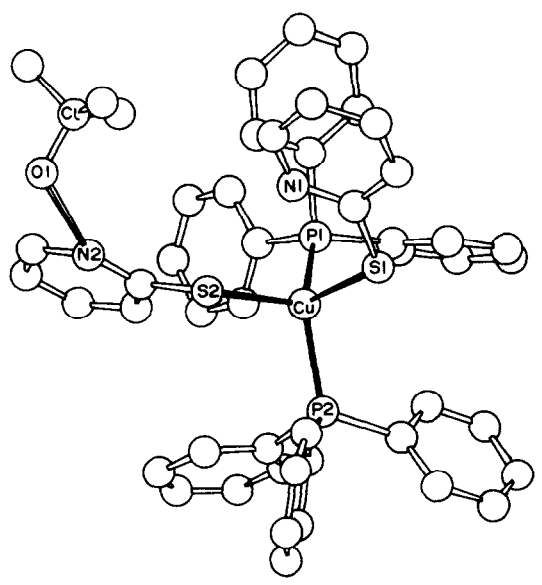

Fig. 1.

reported for other bis(triphenylphosphine)copper(I) compounds.[12]

It is suitable to present the results as a comparison between the compounds $[Cu(tzdtH)_2(PPh_3)_2]NO_3$ (**I**)[5] and $[Cu(py2SH)_2(PPh_3)_2]ClO_4$ (**II**). The interatomic parameters associated with each of the molecules **I** and **II** are similar, which indicates that the molecules are very nearly identical. A difference between the two molecules is found in the interaction of S(1) with copper atoms, namely, Cu—S [2.377(1) and 2.363(1) Å for molecule **I**, and 2.373(1) and 2.382(1) Å for molecule **II**] and associated S(1)—Cu—S(2) angles of 101.3(0) and 115.4(0)°, respectively.

A slightly greater difference is observed in the Cu—P distances [2.301(1) and 2.315(1) Å for molecule **I**, and 2.292(1) and 2.310(1) Å for molecule **II**], which is associated with a small increase in the angle P—Cu—P [121.5(0)° for molecule **I** and 123.2(0)° for molecule **II**].

Electronic spectra

The UV–vis spectra of the complexes in $CHCl_3$ at ambient temperature, as expected, show no *d–d* transitions but consist of two strong absorption bands with maxima at ~360 and ~280 nm, which can be assigned as intraligand transitions.

IR spectra

IR spectra of the studied complexes are in agreement with the X-ray diffraction data with respect to the monodentate sulphur donating character of the ligands investigated. In fact, only small changes upon coordination can be observed in the 3400–3100 cm^{-1} region for bands assigned to N—H stretching vibrations, suggesting that the nitrogen atoms are not involved in bonding.[11]

The pattern of vibrations and the directions of the shifts in the position of the four "thioamide" bands[12,13] are very similar to those observed for the analogous nitrate complexes[4] in which the coordination also takes place through the thione sulphur atom.

The monodentate nature of the ligands is further confirmed by the presence of new bands around 350 cm^{-1}, which can be assigned to the ν(Cu—S) vibration,[12] and the absence of the corresponding ν(Cu—N).

Ionic perchlorate is indicated by the presence of an intense broad band at 1090 cm^{-1}, as well as a band of medium intensity at 620 cm^{-1}, in the solid state IR spectra of all the complexes.[14,15]

Supplementary material

Lists of observed and calculated structure factors, of positional and anisotropic thermal parameters of the non-hydrogen atoms, of positional and isotropic thermal parameters of the hydrogen atoms are available from the authors on request. Atomic coordinates have been deported with the Cambridge Crystallographic Data Centre.

REFERENCES

1. (a) I. P. Evans and G. Wilkinson, *J. Chem. Soc., Dalton Trans*, 1974, 946; (b) B. P. Kennedy and A. B. P. Lever, *Can. J. Chem.* 1972, **50**, 3488.
2. E. S. Raper, *Coord. Chem. Rev.* 1985, **61**, 115.
3. P. Karagiannidis, P. Aslanidis, D. P. Kessissoglou, B. Krebs and M. Dartman, *Inorg. Chim. Acta* 1989, **156**, 47.
4. P. Karagiannidis, P. Aslanidis, S. Papastefanou, D. Mentzafos, A. Hountas and A. Terzis, *Inorg. Chim. Acta* 1989, **156**, 277.
5. C. Lecomte, S. Skoulika, P. Aslanidis, P. Karagiannidis and S. Papastefanou, *Polyhedron* 1989, **8**, 1103.
6. F. A. Cotton and D. M. L. Goodgame, *J. Chem. Soc.* 1960, 5267.
7. G. H. Sheldrick, SHELX 76, A program for crystal structure determination. University of Cambridge, U.K. (1976).
8. *International Tables for X-ray Crystallography*, Vol. IV. Kynoch Press, Birmingham (1974).
9. S. C. Kokkou, S. Fortier, P. J. Rentzeperis and P. Karagiannidis, *Acta Cryst.* 1983, **C39**, 178.
10. S. C. Kokkou, V. Schramm and P. Karagiannidis, *Acta Cryst.* 1985, **C41**, 1040.
11. E. S. Raper and J. L. Brooks, *J. Inorg. Nucl. Chem.* 1977, **39**, 2163.
12. L. J. Bellamy, *The Infrared Spectra of Complex Molecules*. John Wiley, New York (1966).
13. E. Lieber, C. N. R. Rao, C. N. Pillai and R. D. Hites, *Can. J. Chem.* 1958, **36**, 801.
14. S. D. Ross, *Spectrochim. Acta* 1962, **18**, 225.
15. E. S. Raper, J. R. Creighton, J. D. Wilson, W. Clegg and A. Milne, *Inorg. Chim. Acta* 1988, **149**, 265.

Polyhedron Vol. 9, No. 23, pp. 2839–2845, 1990
Printed in Great Britain

0277–5387/90 $3.00+.00
© 1990 Pergamon Press plc

DINUCLEAR μ-PYRAZOLE NICKEL(II), COBALT(II), CADMIUM(II) AND ZINC(II) COMPLEXES WITH DINUCLEATING PYRAZOLE-DERIVED LIGANDS

J. PONS,* X. LÓPEZ, E. BENET and J. CASABÓ*

Departament de Química, Universitat Autónoma de Barcelona, 08193 Bellaterra, Barcelona, Spain

and

F. TEIXIDOR* and F. J. SÁNCHEZ

Institut de Ciència dels Materials (C.S.I.C.), 08193 Bellaterra, Barcelona, Spain

(*Received* 20 *March* 1990; *accepted* 25 *July* 1990)

Abstract—New pyrazole-derived ligands, 3,5-bis(2-pyridyl)pyrazole (HL), 2-(6-methyl) pyridyl-2-pyridyl-3,5-pyrazole (HL^1) and 3,5-bis-2-(6-methyl)pyridyl-3,5-pyrazole (HL^2), are reported. Complexes of formulae $[ML(NO_3)]\cdot xH_2O$ (M = Co^{II}, Ni^{II}, Zn^{II} and Cd^{II}), $[ML(NCS)]\cdot H_2O$ (M = Co^{II}, Ni^{II}, Zn^{II} and Cd^{II}), $[ML^1(NO_3)]\cdot H_2O$ (M = Ni^{II} and Co^{II}), $[M_2L^2(NO_3)_2(OH)]\cdot H_2O$ (M = Ni^{II} and Co^{II}), $[M_2L^1Cl_2(OH)]$ (M = Co^{II} and Ni^{II}) were synthesized and characterized by IR and UV–vis spectroscopies and magnetic susceptibility measurements. Dinuclear compounds containing a di-μ-pyrazole bridge are found in nitrate and thiocyanate complexes with the first two ligands, while mixed μ-hydroxo, μ-pyrazole-bridged structures are found in chloride complexes with the second ligand and nitrate complexes with the last ligand.

Research on the coordination chemistry of pyrazole-derived ligands has progressed very rapidly in the last years. The synthesis of metallocycles of the type $M(pz)_nM'$, where pz is the pyrazole or pyrazole-derived ligand, is one of the major areas of interest.[1] Very recently, the interest in this $M(pz)_nM'$ metallocycle type of compounds has increased due to the possibility of the synthesis of mixed μ-OH, μ-pz-bridged compounds of rhodium(III), nickel(II), palladium(II) or platinum(II). These compounds are very interesting due to the enhanced nucleophilicity of the OH group. The high-field ^1H NMR[2,3] observed for the —OH proton supports this assumption.

Trofimenko in his extensive and well documented review[1] inspires further studies on these $M(pz)_nM'$ metallocycles. Both metal ions are close enough to undergo synchronous or stepwise reactions with small molecules, possibly of a catalytic nature. Numerous double pz-bridged bimetallic complexes, $M(pz)_2M'$, are known, commonly with monodentate or bidentate ligand groups completing the coordination of the metal ions. With few exceptions, the $(AA)M(pz)_2M'(AA)$ complexes have a boat configuration, in which the $M(pz)_2M'$ core is not planar. In the unusual $(C_5H_5)_2Ti(pz)_2Ti(C_5H_5)_2$ complex, the two pz rings are coplanar, but the Ti atoms lie 0.4 Å above and below the central ring plane, resulting in an overall chair conformation.[4] This non-planarity sometimes causes difficulty in synthesizing compounds with interesting catalytic and physical properties. The puckered nature of the $M(pz)_2M'$ core and the non-planarity of the whole complex is generally due to the non-rigid complex skeleton and the exo-nature (pyrazole independent) of the ligands used to complete the coordination of the metal ions.

In a recent paper[5] we reported an interesting pz-derived ligand affording strictly planar, dinuclear di-μ-pz-bridged complexes. The 3,5-bis(2-pyridyl)pyrazole (HL) has proved to be an excellent tetradentate, dinucleating ligand giving dinuclear

* Authors to whom correspondence should be addressed.

complexes with first row transition metal ions. The nickel complex of this ligand, $[Ni_2L_2(MeOH)_4]Cl_2 \cdot 2H_2O$, has a molecular structure in which both ligand molecules and both metal ions are coplanar.[5] Furthermore, four solvent molecules complete the hexacoordination of the nickel(II) ion. On the other hand, the copper(II) complex shows an interesting tetrahedral tetramer structure, cubane-like, involving $\pi(h^5)$ Cu^{II}–pz dimer–dimer interactions.[6] In this paper we report on two new, closely related 3,5-bis(2-pyridyl)pyrazole-derived ligands (Fig. 1) and their comparative coordination chemistry toward the first transition metal series and group 12 metal ions.

EXPERIMENTAL

General

All reagents were commercial grade materials and were used without further purification. All solvents (methanol, ethanol) were previously deoxygenated in a vacuum line and all reactions were routinely carried out under nitrogen atmosphere.

Analyses (C, N, H) were performed in our microanalytical laboratory on a Perkin–Elmer 240-B instrument. IR spectra were run on a Perkin–Elmer FT spectrophotometer as KBr pellets or Nujol films. Electronic spectra were run on a Kontron UV–vis spectrophotometer in the solid state (KBr pellets). ^1H and ^{13}C NMR were recorded on a Brucker AM 400WB spectrometer.

Magnetic susceptibility measurements were made using a Faraday type balance equipped with a liquid nitrogen cryostat. Diamagnetic corrections were calculated from Pascal Tables and direct diamagnetic susceptibility measurements of the ligands. No TIP (temperature independent paramagnetism) corrections were used in the calculations. From the Curie–Weiss plot of the magnetic measurements, the Curie constant, C, was calculated and the g value was derived by the equation $C = 0.125 \times g^2 \times S(S+1)$, where S is the spin value of the corresponding metal ion.

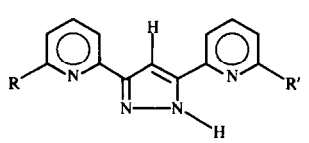

Fig. 1. Pyrazole-derived ligands: R = R′ = H: HL; R = CH_3, R′ = H: HL^1; R = R′ = CH_3: HL^2.

Materials

The compound 6-methyl-2-picolinic acid[7] was prepared by previously reported procedures. The ligand molecule, 3,5-bis(2-pyridyl)pyrazole (HL), was synthesized as previously described.[5]

Synthesis of the ligands

Preparation of methyl-6-methyl-2-picolinate. A 500-cm^3 round-bottom flask, equipped with a reflux condenser and addition funnel, was charged with 6-methyl-2-picolinic acid (11.4 g, 83.1 mmol) and methanol (25 cm^3). H_2SO_4 (12.5 cm^3) was slowly added (1 h) through the funnel. The resulting solution was then gently refluxed for 2 h, allowed to cool to room temperature and then poured into a mixture of 10 g of ice in 90 cm^3 of water. The solution was neutralized (Na_2CO_3), and then filtered and extracted with several portions of ethyl ether (50 cm^3 each). The extract was dried overnight (anhydrous Na_2SO_4) and filtered. The solvent was eliminated by rotary evaporation and the residue placed on the vacuum line at 80°C to eliminate the last traces of water. Yield: 10.3 g; 82%. IR spectrum (KBr): ν(C=O) 1723 cm^{-1}; ν(C=C) 1593 cm^{-1}. ^1H NMR (d_6-dmso, ppm): 2.6 (s, 3, CH_3—py); 4.0 (s, 3, CH_3—CO); 7.53 (t, 1, *H*—py); 7.9 (d, 2, *H*—py). ^{13}C NMR (d_6-dmso, ppm): 23.6, CH_3—py; 52.0, CH_3—CO; 121.8, 126.5, 137.24, 146.79, 158.26 (C_5H_5N); 165.28 (*C*O). Found: C, 63.2; H, 5.6; N, 8.7. Calc. for $C_8H_9NO_2$: C, 63.6; H, 6.0; N, 9.3%.

Preparation of 2-pyridyl-2-(6-methyl)pyridyl-1,3-propanedione. Under a dinitrogen atmosphere, a 250-cm^3 Schlenk flask was charged with sodium (0.67 g, 28.0 mmol). Ethanol (20 cm^3) was added and the mixture was stirred until all the sodium was consumed. The ethanol was eliminated *in vacuo*. Dry toluene (25–30 cm^3), methyl-6-methyl-2-picolinate (4.39 g, 29.0 mmol) and pyridyl-methyl-ketone (4.95 g, 40.9 mmol) were added in this order, always slowly, to the white residue of sodium ethanolate. The mixture was stirred until a yellowish precipitate separated (0.5 h), then it was gently warmed until the sodium salt of the β-diketone was formed (6 h). The salt was filtered and dried. The resulting solid was slowly added to a vigorously stirred solution of acetic acid (30 cm^3), water (30 cm^3) and ice (100 g), yielding a solid which was filtered and dried *in vacuo*. Yield: 4.5 g; 64.6%. IR spectrum (KBr): ν(C=O) 1615 cm^{-1}; ν(C=C) 1564 cm^{-1}. ^1H NMR ($CDCl_3$, ppm): 2.58 (s, 3 CH_3—py); 4.8 [$H_2C(C{=}O)_2$]; 7.1–8.1 [m, 7, *H*—py, *H*C=C(O)]; 8.6 (s, 1, *H*—py): Found: C,

69.4; H, 4.9; N, 11.1. Calc. for $C_{14}H_{12}N_2O_2$: C, 69.0; H, 5.0; N, 11.7%.

Preparation of 2-(6-*methyl*)*pyridyl*-2-*pyridyl*-3,5-*pyrazole* (HL^1). A 100-cm^3 Schlenk flask connected to a Dean–Stark apparatus was charged with 2-pyridyl-2-(6-methyl)-pyridyl-1,3-propanedione (1 g, 4.2 mmol) and hydrazine (0.24 g, 7.5 mmol). Benzene (70 cm^3) was added, and the mixture was then refluxed for 18 h, allowed to cool to room temperature and then filtered. Yield: 0.9 g; 91.5%. IR spectrum (KBr): ν(N—H) 3283 cm^{-1}; ν(C=C), ν(C=N) 1581–1562 cm^{-1}. ^1H NMR ($CDCl_3$, ppm): 2.50 (s, 3, CH_3—py); 7.0 (d, 1, *H*—py); 7.1 (d, 1, *H*—py); 7.35 (s, 1, *H*—pyrazole); 7.5–7.8 (m, 3, *H*—py); 7.90 (d, 1, *H*—py); 8.6 (s, 1, *H*—py); 10.4 [b, 1, *H*—N(pyrazole)]. ^{13}C-NMR ($CDCl_3$, ppm): 158, 149, 136, 122.7, 122.4, 120, 112 (C_5H_3N); 149, 101 (C_3HN_2); 24.4 (CH_3). Found: C, 71.2; H, 5.1; N, 23.4. Calc, for $C_{14}H_{12}N_4$: C, 71.2; H, 5.1; N, 23.7%.

Preparation of 1,3-*bis*[2-(6-*methyl*)*pyridyl*]-1,3-*propanedione*. Under a dinitrogen atmosphere, a 250-cm^3 Schlenk flask was charged with sodium (0.63 g, 27.4 mmol). Deoxygenated absolute ethanol (20 cm^3) was added and the mixture was stirred until all the sodium was consumed. The ethanol was eliminated *in vacuo* to yield a white solid. Dry toluene (25–30 cm^3), methyl-6-methyl-2-picolinate (4 g, 26.5 mmol) and 6-methylpyridyl-2-methyl-ketone[8] (3.61 g, 26.7 mmol) were added in this order, always slowly, to the white residue of sodium ethanolate. Upon stirring the mixture overnight, a pale orange precipitate separated, which was filtered and dried. The resulting solid was slowly added to a vigorously stirred solution of acetic acid (20 cm^3), water (20 cm^3) and ice (70 g), yielding a white solid which was filtered and dried *in vacuo*. Yield: 3.1 g; 46.0%. IR spectrum (KBr): ν(C=O) 1614 cm^{-1}; ν(C=C), ν(C=N) 1581 cm^{-1}. ^1H NMR ($CDCl_3$ ppm): 2.54 (s, 6, CH_3—py); 4.67 [s, $H_2C(C{=}O)_2$]; 7.1 [s, *H*C=C(O)]; 7.13 (d, 2, *H*—py); 7.57 (t, 2, *H*—py); 7.8 (d, 2, *H*—py). ^{13}C NMR ($CDCl_3$, ppm): 184.7 (*C*=O); 158.5, 152, 136, 126, 118 (C_5H_3N); 94.5 [H*C*=C(py)]; 24.5 (CH_3). Found: C, 70.0; H, 5.5; N, 10.7. Calc for $C_{15}H_{14}N_2O_2$: C, 70.8; H, 5.6; N, 11.0%.

Preparation of 3,5-*bis*-2-(6-*methylpyridyl*)-3,5-*pyrazole* (HL^2). A 100-cm^3 Schlenk flask connected to a Dean–Stark apparatus was charged with 1,3-bis-[2-(6-methyl)pyridyl]-1,3-propanedione (1 g, 3.9 mmol) and hydrazine (0.20 g, 6.1 mmol). Benzene (60 cm^3) was added and the mixture was then refluxed for 18 h. Upon cooling, a solid separated which was filtered and vacuum dried. Yield: 0.7 g; 69.2%. IR spectrum (KBr): ν(N—H) 3293 cm^{-1}; ν(C=C), ν(C=N) 1579–1562 cm^{-1}. ^1H NMR ($CDCl_3$, ppm): 2.58 (s, 6, CH_3—py); 7.1 (d, 2, *H*—py); 7.35 (s, 1, *H*—pyrazole); 7.61 (t, 2, *H*—py); 7.67 (d, 2, *H*—py); 11 [b, 1, *H*—N(pyrazole)]. ^{13}C NMR ($CDCl_3$, ppm): 158, 148, 136, 122, 117 (C_5H_3N); 147, 101 (C_3HN_2); 24.4 (CH_3). Found: C, 69.1; H, 5.5; N, 21.1. Calc for $C_{15}H_{14}N_4 \cdot 0.5H_2O$: C, 69.5; H, 5.8; N, 21.6%.

Synthesis of the metal complexes

Synthesis of the nitrate complexes $[ML(NO_3)] \cdot xH_2O$ (M = Co^{II}, Ni^{II}, Zn^{II} *and* Cd^{II}). These complexes were synthesized as previously described.[5]

Synthesis of the thiocyanate complexes $[ML(NCS)] \cdot H_2O$ (M = Co^{II}, Ni^{II}, Zn^{II} *and* Cd^{II}). The appropriate thiocyanate salt (9×10^{-4} mol: $Ni(NCS)_2$, 0.16 g; $Co(NCS)_2 \cdot 3H_2O$, 0.21 g; $Zn(NCS)_2$, 0.16 g; $Cd(NCS)_2$, 0.216 g) in solid was added to a solution of the ligand (0.1 g; 4.5×10^{-4} mol) in ethanol (99%, 20 cm^3). The resulting mixture was stirred for 6 h and the clear solution obtained left to stand at room temperature for 24 h. All operations were carried out at room temperature, but in the case of the cadmium complex, the reaction was carried out under refluxing conditions. A crystalline precipitate appeared in all cases, which was filtered, washed with ethanol and vacuum dried.

Synthesis of the nitrate complexes $[ML^1(NO_3)] \cdot H_2O$ (M = Ni^{II} *and* Co^{II}). The appropriate metal salt (8.4×10^{-4} M: $Ni(NO_3)_2 \cdot 6H_2O$, 0.24 g; $Co(NO_3)_2 \cdot 6H_2O$, 0.24 g) was added to a solution of the ligand (0.1 g, 4.2×10^{-4} mol) in EtOH (99%, 40 cm^3). The mixture was concentrated and a crystalline precipitate appeared, which was filtered, washed with ethanol and vacuum dried.

Synthesis of the nitrate complexes $[M_2L^2(NO_3)_2(OH)] \cdot H_2O$ (M = Ni^{II} *and* Co^{II}). The appropriate metal salt (4×10^{-4} mol: $Ni(NO_3)_2 \cdot 6H_2O$, 0.12 g; $Co(NO_3)_2 \cdot 6H_2O$, 0.12 g) was added to a solution of the ligand (0.05 g, 2×10^{-4} mol) in ethanol (99%, 40 cm^3). The mixture was heated and carried to dryness. The resulting solid was treated with tetrahydrofurane and ethyl ether. Finally, a crystalline solid precipitate was obtained, which was filtered, washed with THF and ether and vacuum dried.

Synthesis of the chloride complexes $[M_2L^1Cl_2(OH)]$ (M = Co^{II} *and* Ni^{II}). The appropriate metal salt (8.4×10^{-4} mol: $CoCl_2 \cdot 6H_2O$, 0.20 g; $NiCl_2 \cdot 6H_2O$, 0.20 g) was added to a solution of the ligand (0.1 g, 4.2×10^{-4} mol) in ethanol (99%, 40 cm^3). The mixture was heated at 60°C for 2 h and then left to stand at room temperature. A crystalline solid precipitate was obtained, which was filtered, washed with ethanol and ether and vacuum dried.

Table 1. Analytical and physical data

Compound	Colour	Yield (%)	Analysis[a] C (%)	N (%)	H (%)
$[CoL(NO_3)]\cdot 2H_2O$	Orange	58	(41.3)	(18.5)	(3.5)
			41.2	18.5	3.4
$[NiL(NO_3)]\cdot H_2O$	Purple	63	(43.4)	(19.5)	(3.1)
			43.1	19.0	3.1
$[ZnL(NO_3)]\cdot 2H_2O$	Colourless	45	(40.6)	(18.2)	(3.4)
			40.4	18.2	3.3
$[CdL(NO_3)]\cdot H_2O$	Colourless	42	(37.7)	(16.9)	(2.7)
			37.4	17.3	2.8
$[CoL(NCS)]\cdot H_2O$	Dark red	42	(47.2)	(19.7)	(3.1)
			47.1	19.8	3.1
$[NiL(NCS)]\cdot H_2O$	Grey–green	38	(47.2)	(19.7)	(3.1)
			47.3	19.4	3.1
$[ZnL(NCS)]\cdot H_2O$	Colourless	51	(46.4)	(19.3)	(3.1)
			45.9	19.3	3.0
$[CdL(NCS)]\cdot H_2O$	Colourless	48	(41.0)	(17.1)	(2.7)
			40.9	16.9	2.6
$[Ni_2L^1Cl_2(OH)]$	Dark green	53	(38.2)	(12.7)	(2.7)
			38.0	12.6	2.7
$[Co_2L^1Cl_2(OH)]$	Dark green	47	(38.1)	(12.7)	(2.7)
			38.1	12.5	2.7
$[NiL^1(NO_3)]\cdot H_2O$	Dark green	53	(45.0)	(18.7)	(3.5)
			44.9	18.6	3.2
$[CoL^1(NO_3)]\cdot H_2O$	Dark red	49	(44.9)	(18.7)	(3.5)
			44.3	18.6	3.4
$[Ni_2L^2(NO_3)_2(OH)]\cdot H_2O$	Green	48	(34.3)	(15.9)	(3.1)
			34.1	15.6	3.0
$[Co_2L^2(NO_3)_2(OH)]\cdot H_2O$	Bright red	50	(34.2)	(16.0)	(3.1)
			34.1	15.9	3.2

[a] Calculated analytical values are given in parentheses.

Table 1 reports the analytical and physical data for all the reported compounds.

RESULTS AND DISCUSSION

The β-diketone compounds, 1,3-bis[2-(6-methyl) pyridyl]-1,3-propanedione and 2-pyridyl-2-(6-methyl)pyridyl-1,3-propanedione, have been synthesized following a Claisen condensation of the appropriate ketones and esters. Equation (1) schematically represents this reaction.

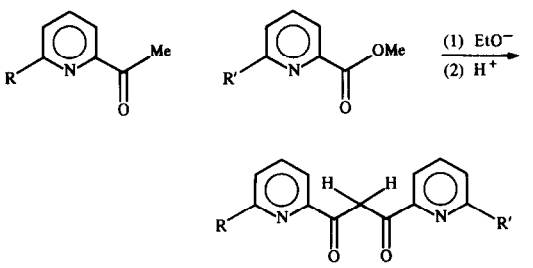

(1)

Further treatment of these β-diketone compounds with hydrazine in benzene yielded the expected pz-derived ligands, 3,5-bis-2-(6-methyl) pyridyl-3,5-pyrazole and 2-(6-methyl)pyridyl-2-pyridyl-3,5-pyrazole.

In chloroform solution the β-diketones described here are in equilibrium with the corresponding keto-enols. These last species are dominant, in an approximate ratio of 20% β-diketone: 80% keto-enol.

IR spectra of the nitrate complexes

The IR spectra of the nitrate-containing complexes are a valuable tool to elucidate their stereochemistry. Frequently, such studies are based on the behaviour of the $\nu_3(E', D_{3h})$ band, which is very sensitive to the coordination mode of the nitrate group. In general there are several bands which are due to the organic ligands in the N—O stretching mode region, which makes the analysis of the ν_3 band difficult. Lever and Mantovani[9] have dem-

Table 2. Selected IR absorption bands (cm^{-1})

$[CoL(NO_3)]\cdot 2H_2O$	1768	
$[NiL(NO_3)]\cdot H_2O$	1766, 1753	
$[ZnL(NO_3)]\cdot 2H_2O$	1767	
$[CdL(NO_3)]\cdot H_2O$	1767	1743, 1733
$[NiL^1(NO_3)]\cdot H_2O$		1743, 1739, 1733
$[CoL^1(NO_3)]\cdot H_2O$		1742, 1738, 1733
$[Ni_2L^2(NO_3)_2(OH)]\cdot H_2O$	1711	1743
$[Co_2L^2(NO_3)_2(OH)]\cdot H_2O$	1764	1728
$[CoL(NCS)]\cdot H_2O$	2078	
$[NiL(NCS)]\cdot H_2O$	2093	
$[ZnL(NCS)]\cdot H_2O$	2076	
$[CdL(NCS)]\cdot H_2O$	2070, 2130	

onstrated the utility of the $\nu_1+\nu_4(E', D_{3h})$ combination band for structural purposes. This band appears near 1750 cm^{-1} and is not generally overlapped by other ligand bands. Table 2 shows the IR absorptions in the $(\nu_1+\nu_4)$ combination band region for the complexes synthesized.

The cobalt and zinc complexes of the ligand HL show one single band in this region, indicating ionic behaviour of the nitrate group. The nickel(II) complex exhibits two bands, shifted only 13 cm^{-1}, in the same region. This splitting is not typical for a real unidentate nitrate group,[9] but could be explained by considering that either the two ionic nitrate groups are placed in different lattice sites or is induced by non-symmetric intermolecular hydrogen bond interactions with the water molecules in the crystal. Moreover, all these compounds exhibit one single, strong band in the ν_3 mode region at 1385 cm^{-1}, as is expected for an ionic nitrate group.[10]

The complex compounds of the ligand HL^1 exhibit three bands in the combination band region, shifted by only 9–10 cm^{-1} between them. This behaviour could also be explained by assuming ionic character of the nitrate group. The splitting and the difference in position of these bands with respect to the complexes of the ligand, HL, could be explained by assuming that relatively strong but rather symmetric intermolecular lattice or hydrogen bond interactions exist in the crystal. Consequently, with this hypothesis all these compounds exhibit only one strong band in the ν_3 mode region, as is expected for an ionic nitrate anion.

The complexes of the ligand HL^2 present two clear and well defined bands separated by 28–36 cm^{-1}. This behaviour is typical for a monodentate nitrate group.[9] In addition, these compounds exhibit two bands in the N—O stretching mode region at 1456, 1299 (Ni) and 1456, 1289 (Co) cm^{-1}, as is expected for a monodentate nitrate group.[10] The cadmium compound of the ligand HL also exhibits two well defined bands at 1767 and 1743–1733 cm^{-1}, similar to the aforementioned complexes of the ligand HL^2, indicating a similar monodentate coordination mode of the nitrate group in this complex. The second band is split into two components separated by only 10 cm^{-1}, but this splitting is probably due to non-symmetrical intermolecular lattice forces in the crystal.

IR spectra of the thiocyanate complexes

We have synthesized four thiocyanate complexes of the ligand HL of general formula $[MLNCS\cdot H_2O]$. The cobalt, nickel and zinc thiocyanate complexes exhibit only one band in the ν(CN) mode region at 2078, 2093 and 2076 cm^{-1}, respectively. On the contrary, the cadmium(II) complexes exhibit two bands in the same region at 2070 and 2130 cm^{-1} (Table 2). N-thiocyanate complexes have been reported in the literature where the ν(CN) band appears at similar frequencies: $[Co(NCS)_4]^{2-}$ (2065 cm^{-1}), $[Ni(NCS)_4]^{2-}$ (2112, 2103 cm^{-1}), $[Zn(NCS)_4]^{2-}$ (2072 cm^{-1}).[10] Even though our compounds are not tetrahedral, we could tentatively assign a nitrogen coordinated mode for all of them except the cadmium(II) compound, which is probably sulphur coordinated.[11]

Electronic spectra

Good electronic spectra for the complexes with the ligand HL [Ni^{II} and Co^{II}] were obtained by diffuse reflectance methods. Both nickel(II) compounds show two bands in the visible region, one at 560 nm $[NiL(NO_3)]\cdot H_2O$ or 550 nm $[NiL(NCS)]\cdot H_2O$, $[\nu_3{}^3A_{2g} \rightarrow {}^3T_{1g}(P), O_h]$ and a second band split into two components at 794 and 750 nm $[NiL(NO_3)]\cdot H_2O$ or 790 and 756 nm $[NiL(NCS)]\cdot H_2O$ $[\nu_2{}^3A_{2g} \rightarrow {}^3T_{1g}(F), O_h]$. These

spectra are characteristic of an octahedral nickel(II) complex[12] with a tetragonal distortion splitting the ν_2 band. Both cobalt(II) compounds show two bands as a shoulder of an intense charge-transfer band, at 693 and 500 nm $[CoL(NO_3)]\cdot 2H_2O$ or 650 and 500 nm $[CoL(NCS)]\cdot H_2O$, typical for an octahedral cobalt(II) complex.[13] The similarity of the electronic spectra of the thiocyanate and nitrate complexes of nickel(II) and cobalt(II) confirms the coordination mode of the thiocyanate group through the nitrogen in all of the complexes.

Magnetic susceptibility data

Magnetic susceptibility data for the compounds studied have been run from room temperature down to 77 K. Table 3 displays only relevant data at two temperatures. The nickel nitrate and nickel thiocyanate complexes of ligand HL and HL^1 display Curie–Weiss behaviour in the temperature interval studied and show values for the magnetic moment at room temperature typical of octahedral nickel(II) complexes.[14] The slight variation with temperature could be explained by assuming an antiferromagnetic interaction between both nickel(II) ions in the dinuclear molecule. The higher values observed in the hydroxo compounds of ligands HL^1 and HL^2 suggest distorted tetrahedral coordination of the nickel(II) ions in the compound.[14] Also, in this case, antiferromagnetic interactions between the metal ions could be assumed.

The cobalt nitrate compounds of ligands HL and HL^1 also show Curie–Weiss behaviour down to 77 K. The magnetic moment values and their variation are typical for an octahedral coordinated cobalt(II) ion.[14] The smaller values of the magnetic moment for the μ-OH compounds suggest a distorted tetrahedral coordination for the cobalt(II) ion.[14] In all cases, a slight antiferromagnetic interaction between the cobalt(II) ions could be assumed, being smaller in the case of the hydroxo compounds. The practically Curie behaviour of the μ-OH compounds suggests a small effective spin–orbit coupling constant. This small value explains the spin-only value of the magnetic moment (3.89 BM) found in these compounds.[15] The cobalt thiocyanate compound exhibits an anomalous low magnetic moment.

Table 3. Magnetic susceptibility measurements

	MB (77 K)	MB (293 K)	g
$[CoL(NO_3)]\cdot 2H_2O$	4.07	4.74	2.61
$[CoL^1(NO_3)]\cdot H_2O$	4.67	4.85	2.52
$[CoL(NCS)]\cdot H_2O$	3.43	3.81	2.04
$[Co_2L^1Cl_2(OH)]$	3.75	3.89	2.03
$[Co_2L^2(NO_3)_2(OH)]\cdot H_2O$	3.97	4.09	2.11
$[NiL(NO_3)]\cdot H_2O$	2.36	2.94	2.31
$[NiL^1(NO_3)]\cdot H_2O$	2.84	2.92	1.72
$[NiL(NCS)]\cdot H_2O$	2.32	2.73	2.07
$[Ni_2L^1Cl_2(OH)]$	2.75	3.66	3.05
$[Ni_2L^2(NO_3)_2(OH)]\cdot H_2O$	2.72	3.57	1.77

CONCLUSIONS

Di-μ-pyrazole-bridged complexes

Nitrate and thiocyanate complexes of ligands HL and HL^1 exhibit a metal–ligand stoichiometry of 1:1. The IR spectra of the nitrate complexes show ionic behaviour of the nitrate group for all the complexes, except for the cadmium(II) compound. IR spectra of the thiocyanate complexes show a nitrogen coordination mode for the thiocyanate group. We could assign a dinuclear, di-μ-pz-bridged structure (Fig. 2) to these compounds, similar to that found in the nickel(II) compound $[Ni_2L_2(MeOH)_4]Cl_2\cdot 2H_2O$.[5] Solvent molecules or nitrate groups complete the coordination of the metal ions in the nitrate complexes, and solvent molecules and —NCS groups in the thiocyanate complexes, in agreement with the magnetic measurements.

Mixed μ-hydroxo,μ-pyrazole-bridged complexes

The nitrate complexes of the ligand HL^2 and the chloride complexes of the ligand HL^1 show a metal–ligand stoichiometry of 2:1. IR spectra of the nitrate complexes display monodentate coordinated nitrate groups. We could assign a mixed μ-OH, μ-pz-bridged structure (Fig. 3) to these compounds, with nitrate ions coordinated to the metal ions $[(NO_3)M(\mu\text{-}OH)(\mu\text{-}L^2)M(NO_3)]\cdot H_2O$. A similar mixed bridged structure is assigned to the chloride complexes of ligand HL^1. Distorted tetrahedral coordination could be assigned to the metal ions in

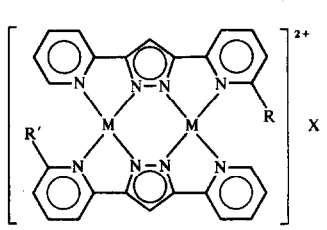

Fig. 2. Diagrammatic drawing of the proposed structure of the di-μ-pyrazole complexes. R = R′ = H: HL; R = CH_3, R′ = H: HL^1; R = R′ = CH_3: HL^2.

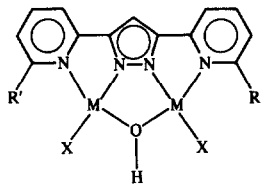

Fig. 3. Diagrammatic drawing of the proposed structure of the mixed μ-hydroxo, μ-pyrazole complexes. R = R′ = H: HL; R = CH_3, R′ = H: HL^1; R = R′ = CH_3: HL^2.

these latter compounds, due to the voluminous OH group, according to the magnetic measurements.

Steric problems due to the methyl groups probably do not allow coordination of the two ligand molecules in the dimethylated HL^2 compound. In the case of the monomethylated ligand HL^1, the *trans* disposition of the methyl groups from each ligand allows the metal–ligand stoichiometry of 1:1. The non-methylated ligand, HL, seems to favour di-μ-pz-bridged complexes, but with the dimethylated ligand, HL^2, only stoichiometric relations, metal–ligand 2:1, are found. The monomethylated ligand, HL^1, forms di-μ-pz complexes with poor coordinating anions like NO_3^-, but with strong coordinating ones, like Cl^-, mixed bridged structures are formed.

Acknowledgements—This work was supported by grant No. MAT88-0179-C02-01 from the Spanish Government (C.I.C.Y.T., Comisión Interministerial de Ciencia y Tecnología) and by "Fundación Ramon Areces", Spain.

REFERENCES

1. S. Trofimenko, *Prog. Inorg. Chem.* 1985, **34**, 115.
2. L. A. Oro, D. Carmona, M. P. Lamata, M. C. Apreda, C. Foces-Foces, F. H. Cano and P. M. Maitlis, *J. Chem. Soc., Dalton Trans.* 1984, 1823.
3. G. López, G. García, J. Ruíz, G. Sánchez, J. García and C. Vicente, *J. Chem. Soc., Chem. Commun.* 1989, 1045.
4. B. F. Fieselman and G. D. Stucky, *Inorg. Chem.* 1978, **17**, 2074.
5. J. Casabó, J. Pons, K. S. Siddiqi, F. Teixidor, E. Molins and C. Miravitlles, *J. Chem. Soc., Dalton Trans.* 1989, 1401.
6. J. Casabó, J. Pons and F. Teixidor, *Inorg. Chem.*, submitted.
7. G. Black, E. Depp and B. B. Corson, *J. Org. Chem.* 1949, **14**, 14.
8. H. B. Amin and R. J. Taylor, *J. Chem. Soc., Perkin Trans* 1979, **2**, 624.
9. A. B. P. Lever and E. Mantovani, *Inorg. Chem.* 1971, **10**, 817.
10. K. Nakamoto, *Infrared Spectra of Inorganic and Coordination Compounds*, 2nd edn. John Wiley, New York (1970).
11. R. A. Bailey, S. L. Kozak, T. W. Michelsen and W. N. Mills, *Coord. Chem. Rev.* 1971, **6**, 407.
12. E. Whiling, *Coord. Chem. Rev.* 1973, **10**, 227.
13. R. L. Carlin, *Transition Met. Chem.* 1965, **1**, 1.
14. R. L. Carlin, *Magnetochemistry*. Springer, Berlin (1986).
15. F. A. Cotton and G. Wilkinson, *Advanced Inorganic Chemistry*, 3rd edn. John Wiley, New York (1972).

Polyhedron Vol. 9, No. 23, pp. 2847–2857, 1990
Printed in Great Britain

0277–5387/90 $3.00+.00
© 1990 Pergamon Press plc

PROTONATION AND METAL COMPLEXATION STUDIES ON SOME OXA-DIAZA MACROCYCLIC LIGANDS

M. FÁTIMA CABRAL, JUDITE COSTA, RITA DELGADO, J. J. R. FRAÚSTO DA SILVA† and M. FERNANDA VILHENA

Centro de Química Estrutural, Instituto Superior Técnico, Lisbon, Portugal

(*Received* 18 *June* 1990; *accepted* 25 *July* 1990)

Abstract—Some 9- and 10-membered oxa-diaza macrocyclic ligands and their N-acetate derivatives have been synthesized and their protonation patterns studied by ^{1}H NMR and potentiometric techniques. The stability constants of the complexes formed by these ligands with several alkaline–earth and first-series transition metal ions, zinc, cadmium and lead, were determined by potentiometry and the values were compared with those formed with the analogous 9-membered tri-aza macrocyclic ligands and with 12-membered oxa-triaza ligands. The substitution of one nitrogen by an oxygen atom in the backbone of the macrocyclic ring has pronounced effects both on the kinetics of the complexation reactions (faster equilibration) and on the stability of the metal complexes formed (decreased stability). The differences in this last case are analysed for two pairs of cyclic amines ([9]aneN$_3$/[9]aneN$_2$O and [12]aneN$_4$/[12]aneN$_3$O) with the first transition metal ions and for the corresponding N-acetate derivatives with the first transition and alkaline–earth metal ions.

A large number of macrocyclic compounds have been synthesized and their metal complexes studied in the past three decades. However, less attention has been paid to the tridentate macrocyclic compounds, recently reviewed,[1,2] with the exception of compound **I**, 1,4,7-triazacyclononane, and some of its N-functionalized derivatives, namely the triacetate (**II**).

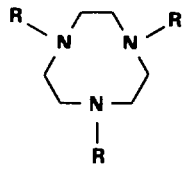

I: R ≡ H—1,4,7-triazacyclononane
II: R ≡ CH_2COOH—1,4,7-triazacyclononane-N,N′,N″-triacetic acid (NOTA)

With the aim of investigating the effect of substitution of a nitrogen atom by an oxygen donor atom in the ring of macrocyclic ligands on the behaviour and selectivity of their metal complexes with some divalent metal ions, we decided to study the compounds listed below (**III–VI**).

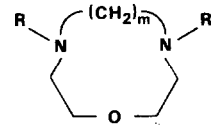

III: $m = 2$, R ≡ H—1-oxa-4,7-diazacyclononane ([9]aneN$_2$O)
IV: $m = 2$, R ≡ CH_3—4,7-dimethyl-1-oxa-4,7-diazacyclononane (N-Me$_2$[9]aneN$_2$O)
V: $m = 2$, R ≡ CH_2COOH—1-oxa-4,7-diazacyclononane-4,7-diacetic acid (N-ac$_2$[9]aneN$_2$O)
VI: $m = 3$, R ≡ H—1-oxa-4,8-diazacyclodecane ([10]aneN$_2$O).

In view of the propensity of most divalent transition metal ions for the coordination number 6 in their complexes, most tridentate macrocycles coordinate to metal ions so that they occupy three facial sites on the coordination sphere of the metal. Furthermore, 2:1 ligand to metal complexes are possible with ligands **III**, **IV** and **VI**, whilst ligand **V** seems ideally suited to wrap around the metal ions.

† Author to whom correspondence should be addressed.

EXPERIMENTAL

Reagents

All the ligands were synthesized and purified in our laboratories. The chemicals used were of reagent grade and organic solvents were purified by standard methods.

Synthesis and characterization of the ligands

The cyclic amine **III** was synthesized by Richman–Atkins procedure,[3] involving the condensation of 0.05 mol (18.40 g) of the disodium salt of ethylenediamine ditosylate and 0.05 mol (20.72 g) of ditosylated diethyleneglycol at 110°C in dry dimethylformamide. The ditosylated cyclic amine obtained, after recrystallization from benzene–*n*-hexane (yield: 75%), was refluxed with a mixture of glacial acetic acid, 48% hydrobromic acid and phenol for 28 h. The required product (**III**) was precipitated with ether, filtered, and washed with acetone. Recrystallization was carried out with methanol–acetone, and the pure product was obtained in 71% yield; m.p. 167–169°C.

The methylated amine (**IV**) was obtained by refluxing the dihydrobromide [9]aneN_2O with formic acid and formaldehyde for 24 h.[4] The pure product was obtained, as an oil, by vacuum distillation and was characterized by ^{1}H NMR spectroscopy and potentiometric titration.

The N-acetate derivative (**V**) was prepared by reaction of 4.6 mmol (1.33 g) of **III** (in the dihydrobromide form) with 9.2 mmol (1.28 g) of bromoacetic acid and 4.9 mmol (1.13 g) of $BaCl_2 \cdot 2H_2O$ in aqueous alkaline solution. The temperature was kept between 25–30°C and the pH below 8.6, for 10 days. After the reaction the pH was adjusted to 1.4 with 5 M H_2SO_4, the mixture concentrated and the precipitated inorganic salts filtered off. The product was recrystallized from methanol–acetone and purified by anion-exchange chromatography using a Dowex 1-X8 (20–50 mesh) resin in the OH^- form, by elution with formic acid, 0.1 M. Yield: 62%; m.p. 200–202°C. ^{1}H NMR (D_2O–DSS and pD*† 0.20): δ 4.033 ppm (4H, triplet), δ 3.764 ppm (4H, singlet), δ 3.549 ppm (4H, triplet). Elemental analysis for the molecular formula $C_{10}N_2O_5H_{19}Cl$ (Mol. wt = 282.73): Found: N, 9.9; H, 6.8; C, 42.5. Calc.: N, 10.2; H, 6.6; C, 42.7%.

† Operational pD, i.e. value measured with a pH meter standardized with conventional aqueous pH 4 and 7 buffer solutions.

Compound **VI** was prepared by a procedure similar to that used for the synthesis of [9]aneN_2O, using 0.05 mol (19.12 g) of the disodium salt of trimethylenediamine ditosylate and 0.05 mol (20.72 g) of ditosylated diethyleneglycol. The resulting product was recrystallized from methylene chloride–methanol (yield: 59%) and characterized by ^{1}H NMR spectroscopy ($CDCl_3$–TMS): δ 7.7–7.3 ppm (8H, multiplet); δ 3.76 ppm (4H, triplet): δ 3.24 ppm (8H, multiplet), δ 2.43 ppm (6H, singlet) and δ 2.42 ppm (2H, multiplet).

The detosylation was achieved by the method described above and the recrystallization was carried out with methanol–acetone. Yield: 74%, m.p. = 237–239°C, ^{1}H NMR (D_2O–DSS): δ 3.97 ppm (4H, multiplet), δ 3.37 ppm (8H, multiplet) and δ 2.17 ppm (2H, multiplet).

Equipment

For the potentiometric titrations a Crison Digilab 517 measuring instrument was used together with an Ingold U1330 glass electrode and a Radiometer K401 saturated calomel reference electrode described previously.[5] Titrations were carried out in a thermostatted cell at 25.0 ± 0.1°C and the ionic strength of the solutions kept at 0.01 M with KNO_3.

The pH measurements for the NMR titrations were made using a pH M64 Digilab Radiometer (or a Crison micropH 2002) instrument fitted with a combined Ingold 405 M3 microelectrode.

^{1}H NMR spectra were recorded at 100 MHz and probe temperature in a JEOL JNM 100 PTF spectrometer coupled to a JEOL 980A computer.

Solutions

Analytical grade metal nitrates were used and the metal content of the solutions checked by titration with EDTA. The CO_2-free potassium hydroxide solution was prepared as described before.[5] Solutions of the ligands for NMR measurements ($\approx$ 0.01 M) were made up in D_2O (99.8 atom % deuterium from Merck) and the pD* was adjusted by adding DCl or CO_2-free KOD. In all cases sodium 3-(trimethylsilyl)-1-propane sulphonate (DSS) was used as internal reference.

Calculations

The protonation and the stability constants were determined from the potentiometric titrations using the Superquad program.[6] The results were obtained from a minimum of two titrations for which the C_M–C_L ratios were 1 : 1, 1 : 2 and, in some cases, 2 : 1. The errors quoted were calculated by propagation

rules from the standard deviations of the overall constants obtained for about 50 readings in each set of titrations, given by the program, and do not represent the total experimental errors.

It was found that copper(II) and zinc(II) solutions equilibrate with the cyclic amines (**III, IV** and **VI**) during the course of titrations within 5 min of each addition of titrant; cobalt(II) needed 15 min to equilibrate with ligand **III**, and 10 min with ligands **IV** and **VI**, but nickel(II) reacted very slowly, requiring up to 15 min with ligand **VI**, 30 min with ligand **III** and far more with ligand **IV**. With this last ligand it was not possible to perform automated titrations; an out-of-cell technique would be required for the purpose, but it was not undertaken in the present work. Ligand **V** equilibrates more rapidly in the reactions with metal ions, requiring only 90 s for Mn^{2+}, Zn^{2+}, Pb^{2+} and Fe^{2+}, but 5 min with Co^{2+} and 15 min with Ni^{2+}.

The fractions of protonation were obtained from the experimental NMR titration curves using a multiple linear regression program.[7]

RESULTS AND DISCUSSION

Protonation constants and sequence of protonation

The protonation constants of the ligands studied in the present work or obtained from the literature for the same set of ligands are summarized in Table 1. Other ligands are included in this table for comparison.

The first protonation constant for [9]aneN_2O is similar to that of [9]aneN_2S, and also to those of linear amines, a situation not usually found with other macrocyclic compounds,[1] for which $\log K_1$ is generally higher than for the linear amines (this tendency can be seen in Table 1, comparing compounds [9]aneN_3 and diethylenetriamine). The values of the table agree with the interpretation of the higher values of $\log K_1$ being due to the formation of internal hydrogen bonds within the ring cavity, the magnitude of which decreases in the series N ≫ O > S.[1,13]

The values of the second protonation constants

Table 1. Protonation constants ($\log K_i$)[a] for some oxa-diaza, thia-diaza and triaza cyclononane derivatives and some similar linear derivatives ($T = 25°C$)

Ligand	$\log K_1$	$\log K_2$	$\log K_3$	$\log K_4$
[9]aneN_2O	9.677±0.006[b] 9.59[c]	5.45±0.01[b] 5.32[c]		
N-Me_2[9]aneN_2O	8.80±0.03[b]	4.82±0.08[b]		
N-ac_2[9]aneN_2O	10.57±0.01[b] 10.8[d]	4.02±0.03[b]	1.8±0.3[b]	< 1[b]
[10]aneN_2O	10.09±0.07[b]	6.31±0.09[b]		
[9]aneN_3	10.42[e]	6.82[e]	< 1	
N-Me_3[9]aneN_3	11.7[f]	5.1[f]	≈ 0.4[f]	
N-ac_3[9]aneN_3	11.41[g]	5.74[g]	3.16[g]	1.71[g]
(NOTA)	11.73[j]	5.742[j]	3.160[j]	1.955[j]
[9]aneN_2S	9.67[h]	3.98[h]		
$H_2N(CH_2)_2NH(CH_2)_2OH$ (HEEN)	9.59[i]	6.60[i]		
$H_2N(CH_2)_2O(CH_2)_2NH_2$ (ODEN)	9.75[i]	8.90[i]		
$H_2N(CH_2)_2NH(CH_2)_2NH_2$ (DIEN)	9.70[i]	8.98[i]	4.25[i]	

[a] Protonation constants $K_i = [H_iL]/[H_{i-1}L][H^+]$.
[b] Present work, $T = 25.0 \pm 0.1°C$; $I = 0.10$ M KNO_3.
[c] From ref. 8, $I = 0.1$ M $NaNO_3$.
[d] From ref. 9, $I = 0.1$ M $NaClO_4$.
[e] From ref. 10, $I = 0.1$ M $NaNO_3$.
[f] From ref. 11, $I = 0.1$ M $NaClO_4$.
[g] From ref. 12, $I = 0.1$ M $NaNO_3$.
[h] From ref. 13, $I = 0.1$ M $NaNO_3$.
[i] From ref. 14, $I = 0.1$ M.
[j] From ref. 15, $I = 0.1$ M $NaNO_3$.

($\log K_2$) for the cyclic amines are lower than those of the linear amines. This decrease of basicity can be explained in terms of the electrostatic repulsions between two closely neighbouring ammonium nitrogens, i.e. between the incoming protons and those already bound to the neighbouring nitrogen atoms. This effect decreases with the distance between the two nitrogen atoms, as shown by the value of $\log K_2$ for [10]aneN_2O, where the two nitrogen atoms are separated by a propane chain. Hancock *et al.*[13] suggested that the decreasing values of $\log K_2$ in the series [9]aneN_3 (6.82), [9]aneN_2O (5.45) and [9]aneN_2S (3.98) is probably due to the involvement of the donor atoms in a cooperative stabilization of the attached proton by hydrogen bonding. In fact, with similar linear ligands the $\log K_2$ values do not vary much with the change of the central donor atom from nitrogen, to oxygen or to sulphur, indicating that the inductive effects are not important.[13] Lower than expected values and in the same order also result if the addition of the second proton involves breaking of the hydrogen bonds previously formed since this represents an unfavourable contribution to the heat of the reaction.[16]

More difficult to explain is the value for the first protonation constant of the dimethylated amine (**IV**). In fact, the inductive effect of the methyl groups should make this value higher than that of the parent amine (**III**), as it happens for N-Me_3[9]aneN_3 compared with [9]aneN_3, but this is not the case.

Similar arguments explain the higher value of $\log K_1$ of compound **V**. In this case, the possible formation of hydrogen bonds between the protonated nitrogen and the carboxylate groups help to stabilize the protonated species and contribute to higher $\log K_1$ values.

The explanation of the values of protonation constants of the N-acetate derivative is not straightforward (exception made for $\log K_1$); likewise, it is not immediately evident which are the following basic centres to be protonated, the carboxylate groups or the other nitrogen atom, as it happens with the diaza[16] and triaza[11] macrocycles. However, following the titration by NMR spectrometry measurements, it is possible to understand the sequence of the protonation.

For a quantitative treatment of the sequence of protonation, it is helpful to have a model compound which adopts configurational structures similar to the compound to be studied and whose titration curves are easy to interpret.[7,11,16–19] Compound **IV**, the methylated amine, seems to have the required conditions.

Indeed, the titration curves obtained by NMR measurements of this compound are very simple. The spectrum at pD* 4.92 can be seen in Fig. 1. For

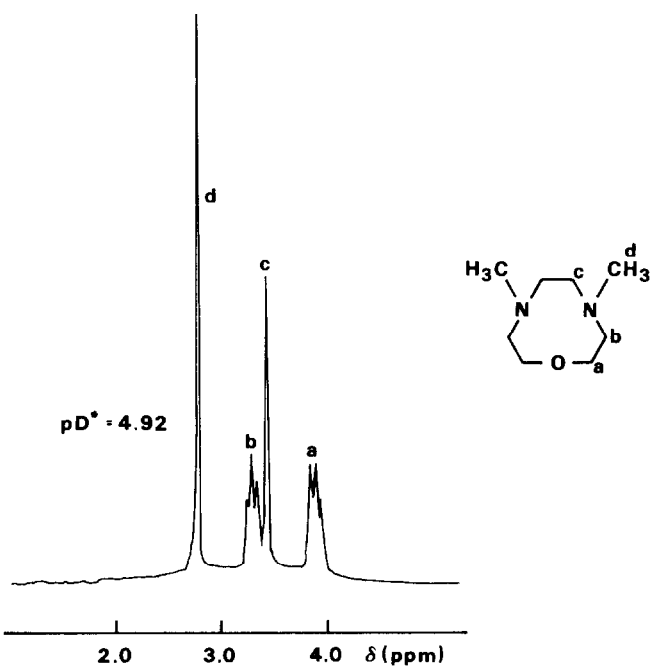

Fig. 1. ^{1}H NMR spectrum of N-Me_2[9]aneN_2O (**IV**) at pD* 4.92.

values of pD* < 8 the spectra present four resonances, although the resonances of the methylenic protons *b* and *c* are indistinguishable for higher pD* values. The assignment of the resonances is straightforward: methylenic protons *a* and the methyl protons *d* are singlets, which can be distinguished by the area ratio 2:3; methylenic protons *a*, deshielded by the electronegative oxygen atom nearby, appear at lower field. The assignment of methylenic protons *b* is made by double-resonance experiments, irradiating the methylenic protons *a*.

The titration curves present two net inflexions, with all the resonances shifting to lower field. One of them, in the pD* range 10.5–7.5, corresponds to the protonation of 50% of the nitrogen atoms, and the second one, in the pD* range 7.0–3.0 corresponds to the protonation of the remaining nitrogen groups.

For $n = 1$ and $n = 2$ (n being the number of equivalents of acid added to the ligand completely deprotonated), it is possible to use Sudmeier and Reilley's quantitative approach[17] to determine the values of the shielding constants (C_{ij}):

$$\Delta\delta_i = \sum_{j=1}^{N} C_{ij} f_j \qquad (1)$$

$$\sum_{j=1}^{N} \alpha_j f_j = n, \qquad (2)$$

where $\Delta\delta_i = \delta_i^{obs} - \delta_i^{o}$, δ_i^{obs} is the observed shift of the i non-labile proton of a methylenic group and δ_i^{o} the intrinsic shift of the fully deprotonated form of the ligand; f_j is the protonation fraction of the various neighbouring basic groups, usually expressed as percentage of protonation (the contributions of the different basic sites being additive); α_j is the number of equivalent sites of protonation and N is the number of basic sites.

C_{ij} represents the $\Delta\delta_i$ value of the methylenic proton i caused by full protonation of a given basic site j. In the present work we refer by C_N the shielding constant relative to the α methylenic protons caused by the protonation of a nitrogen atom and by $C_{N'}$ the corresponding value for the β methylenic protons; C_{COO^-} is the shielding constant relative to the methylenic protons caused by the protonation of a carboxylate group.

The values of C_{ij} determined for the model compound, N-Me_2[9]aneN_2O, are summarized in Table 2.

From this table it can be seen that the values of C_N and $C_{N'}$ are different for the various methylenic protons and increase with the value of pD* (except $C_{N'}$). The variation of the shielding constants with pD*, also found for all other macrocyclic compounds studied before[7,11,16,18,19] has been ascribed to different conformations of the macrocyclic ring.

With these shielding constants it is possible to calculate the fractions of protonation f_j for the N-acetate derivative (**V**), from the experimental δ_i^{obs} obtained by the titration curves, by the combination of equation (2) and four equations of type (1) (one equation for each methylenic proton of the molecule). The set of simultaneous linear equations can be solved using a multiple linear regression program.[7] Naturally, it is necessary to assign previously the various resonances of compound **V**.

In Fig. 2 is shown the spectrum of N-ac_2[9]ane N_2O at pD* 0.2 and the titration curves for the entire pD* range. The spectra exhibit four different resonances at low pD* (< 7) and only three resonances for pD* values higher than 7 (resonances *b* and *c* being superimposed), that can be assigned by the methods already described for the methylated amine. The methylene protons *c* and *d* are singlets, whilst *a* and *b* are triplets; the two triplets can be easily assigned by double-resonance experiments, the protons *a* appearing at lower field due to the deshielding effect of the adjacent oxygen atom. The methylene protons *c* are also easily assigned since they are affected by the same basic centre as *b* and have a similar titration profile. The methylene protons *d* appear at a lower field and have a completely different titration profile, being sensitive to the titration of the two centres (1 and 2).

The titration curves exhibit a pronounced inflexion in the pD* range 12–9, when all the resonances shift downfield; this probably corresponds to the protonation of 50% of the nitrogen atoms (by potentiometric studies it can be seen that in this

Table 2. Shielding constants (C_N and $C_{N'}$) determined from N-Me_2[9]aneN_2O (in ppm)

pD* = 7.46 (n = 1)				pD* = 2.55 (n = 2)			
$C_{N'}$[a]	C_N[b]	$(C_N - C_{N'})$[c]	C_N[d]	$C_{N'}$[a]	C_N[b]	$(C_N + C_{N'})$[c]	C_N[d]
0.35	0.82	0.92	0.67	0.32	0.93	1.17	0.72

pD* range there is only one protonation step). For lower pD* values, between 5–1.5, resonances *b* and *c* move slightly to low field, but methylenic protons *d* have a more pronounced shift, whilst methylenic protons *a* practically do not shift. It seems that, in this pD* range, the carboxylate groups are being protonated, as the potentiometric measurements indicate two protonation steps at this pD* region (cf. Table 1), but the shift of protons *b* and *c* can only be understood if hydrogen bonds between carboxylated groups and protonated nitrogen are formed. For very low pD* values (below 2) there is a continuous shift of all the resonances indicating that full protonation of the last centre is not achieved.

The application of Sudmeier and Reilley's quantitative approach to this compound, assuming that the shielding constants listed in Table 2 are appropriate for this ligand and considering $C_{COO^-} = 0.20$ ppm (the value generally adopted[19]), leads to the protonation fractions shown in Table 3.

All the values in Table 3 seem coherent with our comments above. The value of f_{COO^-} for $n = 4$ is too high, because it was assumed that for the last pD* value of the titration (pD* = 0.19) the fourth equivalent of acid was completely added, which is not true. Indeed, it appears that only about 80% of protonation of the nitrogen atoms is achieved, the carboxylate groups being protonated before the last nitrogen.

So it is possible to conclude that the first proton added to the completely deprotonated compound **V** will protonate one of the indistinguishable nitrogen atoms, the second and third protonate the carboxylate groups, and the last equivalent of acid added protonates the last nitrogen up to about 80% for pD* ≈ 0. N-ac$_2$[9]aneN$_2$O is therefore one

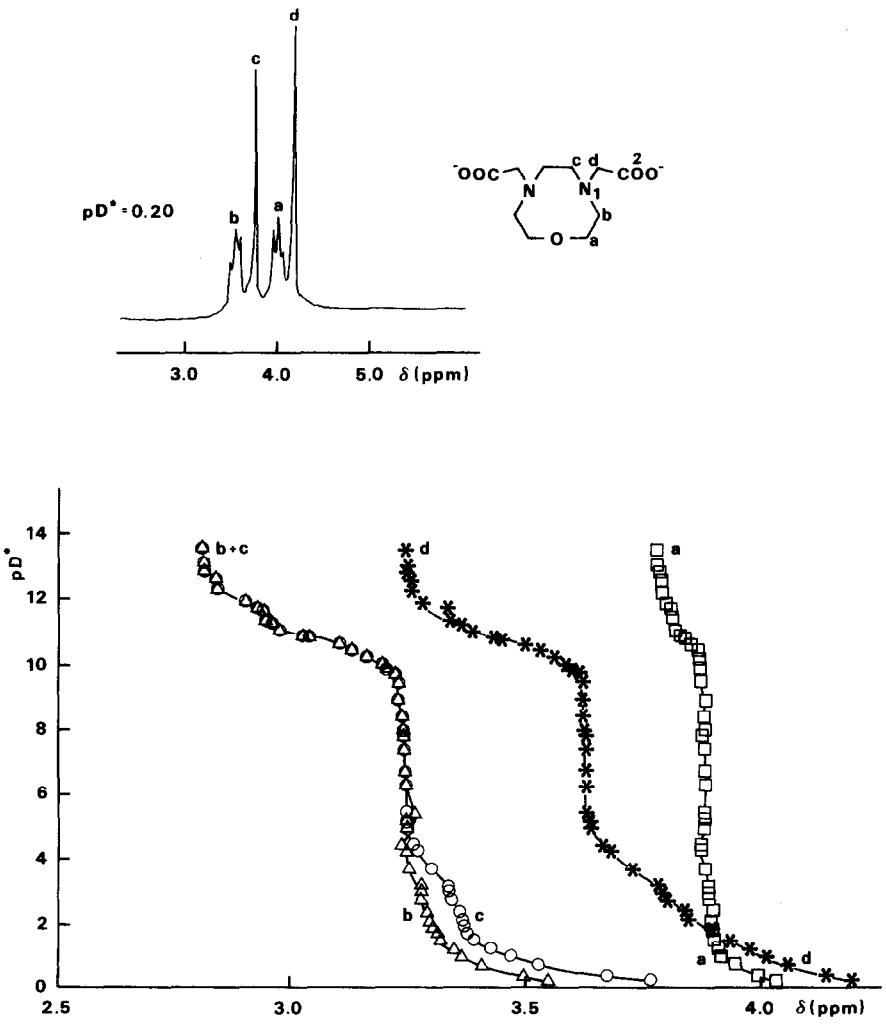

Fig. 2. ^{1}H NMR spectrum of N-ac$_2$[9]aneN$_2$O (**V**) at pD* 0.20 and titration curves pD* versus δ (ppm).

Table 3. Protonation fractions (%) for N-ac$_2$[9]aneN$_2$O

pD*	n	f_N	f_{COO^-}
7.42	1	50±4	0±4
3.17	2	48±2	52±2
1.48	3	54±4	96±4
0.19	4[a]	83±4	117±4

[a] At the end of the titration.

more macrocycle whose nitrogen atoms are less basic than the carboxylates, contrary to what happens with the linear complexones.[7,11,18,19]

It is now easy to explain the protonation constants of this compound, listed in Table 1. Log K_2 is a normal value for the protonation of a carboxylate group linked to a non-protonated nitrogen atom. The protonation of the second carboxylate is counteracted by the positive charge of the nitrogen atom and the possible breaking of the hydrogen bond $^+HN\cdots{}^-OOC—$, hence the protonation constant is lower (1.8). The last protonation constant is a very low value ($\log K < 1$) because it corresponds to the protonation of a nitrogen atom at short distance from the other protonated nitrogen, the electrostatic repulsion being even stronger given the relatively rigid structure of the ring.

It is curious to note that subsequent to the protonation of the first nitrogen, formation of hydrogen bonds between carboxylate groups and protonated nitrogen possibly occurs; for $n = 2$ the protonated carboxylate can also form hydrogen bonds with the non-protonated nitrogen. It might be thought that the model compound, the corresponding methylated amine, would not be a good model since it cannot form this type of hydrogen bond, as in the case of the similar 12-membered compounds.[19] The difference derives from the simpler NMR spectrum of the compound studied in the present work due to its symmetry, hence a smaller number of equations result for the system of equations (1) and (2) and the problem did not arise.

The comparison of the protonation constants of N-ac$_2$[9]aneN$_2$O and NOTA (I) is interesting. In fact, the second acid equivalent added to NOTA still protonates a nitrogen atom but the total posi-

Table 4. Stability constants ($\log K_i$)[a] of some 9- and 10-membered oxa-diaza macrocyclic ligands ($T = 25°C$)

Metal ion	Species	Ligand				
		[9]aneN$_2$O[b]		[10]aneN$_2$O[b]	N-ac$_2$[9]aneN$_2$O[b]	
Li^+	ML	—		—	1.42±0.05	
Mg^{2+}	ML	—		—	3.68±0.01	5.2[c]
Ca^{2+}	ML	—		—	5.36±0.02	5.0[c]
Sr^{2+}	ML	—		—	3.95±0.01	3.3[c]
Ba^{2+}	ML	—		—	3.13±0.02	3.3[c]
Mn^{2+}	ML	3.0±0.1		—	7.73±0.01	
	ML_2	(3.8±0.1)			—	
Fe^{2+}	ML	(5.00±0.06)		—	9.70±0.01	
Co^{2+}	ML	6.33±0.05		5.4±0.1	11.48±0.02	
	ML_2	5.30±0.08		5.6±0.1	—	
Ni^{2+}	ML	8.05±0.05	8.59[d]	6.48±0.04	11.89±0.02	
	ML_2	7.85±0.01	7.27[d]	4.6±0.1	—	
Cu^{2+}	ML	10.80±0.01	10.85[d]	9.30±0.03	13.37±0.09	
	ML_2	8.80±0.04	8.64[d]	6.50±0.07	—	
Zn^{2+}	ML	6.40±0.04	6.32[d]	5.1±0.1	12.53±0.01	
	ML_2	5.7±0.1	5.07[d]	5.00±0.07	—	
Pb^{2+}	ML	—	5.17[e]	—	12.00±0.03	
Cd^{2+}	ML	—	4.48[e]	—	10.56±0.01	
	ML_2	—	3.40[e]	—	—	

[a] Stability constants $K_{ML} = [ML]/([M][L])$; $K_{ML_2} = [ML_2]/[ML][L]$.
[b] Present work, $I = 0.10$ M KNO_3.
[c] From ref. 9, $I = 0.1$ M $NaClO_4$.
[d] From ref. 8, $I = 0.1$ M $NaNO_3$.
[e] From ref. 20, $I = 0.1$ M $NaNO_3$.

tive charge spreads over the three nitrogens of the ring[11] and a higher $\log K_2$[12] than that found for V is obtained. The third proton added goes to a carboxylate but $\log K_3$ is smaller than expected for the protonation of such a group, due to the repulsion of the partially charged nitrogen to which it is bonded.

Stability constants with some metal ions

The values of the stability constants of some metal complexes studied in this work together with some values found in the literature for the same complexes are summarized in Table 4.

The 1:1 complexes of [9]aneN_2O and [10]aneN_2O have coordinated water molecules which ionize for pH > 6 giving hydroxo species. The constants (pK) corresponding to the equilibrium: $ML \rightleftarrows MLOH + H^+$ are listed below:

Metal ions	[9]aneN_2O	[10]aneN_2O
Mn^{2+}	9.59	—
Co^{2+}	8.93	7.68
Cu^{2+}	7.22	7.20
Zn^{2+}	8.40	7.64

As expected, the values of pK for the complexes of [10]aneN_2O are lower since the complexes of this ligand are less stable and hydrolyse at lower pH.

Some stability constants of the complexes of the ligand N-Me_2[9]aneN_2O were also determined, and the constants obtained for the ML species were: 5.76 ± 0.07 for Co^{2+}, 7.76 ± 0.02 for Cu^{2+} and 6.58 ± 0.06 for Zn^{2+}. With Cu^{2+} and Zn^{2+} hydroxo complexes are also formed. The values for this ligand are smaller than those obtained for [9]aneN_2O, and only ML species are formed, which means that the steric hindrance of the methyl substituents prevents the formation of ML_2 species.

In Table 4 the values obtained by Hancock *et al.* for [9]aneN_2O, and by Ewin and Hill for N-ac_2[9]aneN_2O are also indicated. Our values are in good agreement with those of Hancock *et al.* for Cu^{2+} and Zn^{2+}, but not with those for Ni^{2+}. The equilibrium of formation of Ni^{2+} complexes with [9]aneN_2O is slow to attain (cf. Experimental section) and discrepancies can easily arise. It is worth noting that the substitution of a nitrogen atom for an oxygen in the ring of the macrocycle increases the rate of formation of the complex. Indeed, Zompa found that 3–4 months were necessary to reach the equilibrium of metal–ligand solutions of triaza cyclic amines.[10,21] A similar situation was found with the 12-membered macrocycles,[5] making the mixed oxygen–nitrogen macrocyclic compounds more attractive for applications, as already referred by Hancock *et al.*[8]

However, the values for N-ac_2[9]aneN_2O obtained by Ewin and Hill for the alkaline–earth metal ions are significantly different from ours, especially in the case of Mg^{2+}. These authors performed their measurements in a different medium, $NaNO_3$, but no complex formation with Na^+ appears to occur with this ligand. The discrepancy may therefore result from the different method used by these authors, i.e. calorimetric measurements.

It is interesting to note that in all systems studied in the present work the analysis of the titration data indicate the absence of protonated complex species, even for low pH values. This is an indication of the particularly favourable conformations of these compounds as tridentate chelating ligands.

The Irving–William's order of stability is obeyed for all the ligands, but some Cu^{2+} complexes are less stable than expected, namely the Cu^{2+}–N-ac_2[9]aneN_2O complex which has a stability constant lower than that of EDDA and even than that of DACODA, a N-acetate diazamacrocycle with propane chains separating the nitrogen atoms (see Table 5).

The increase of the size of the ring of the amines, from 9- to 10-membered, leads to a decrease in the stability of the complexes with the transition metal ions studied. This does not happen with the analogous triazamacrocycles, for which the Co^{2+} complex of [10]aneN_3 is more stable than that of [9]aneN_3, and the Cu^{2+} and Zn^{2+} complexes of the two ligands have similar stabilities (although the values published present some dispersion[1,2]).

We can see from Table 4 that the values for log K_{ML_2} for the cyclic amines are only slightly lower than those of log K_{ML}, evidence of the easy addition of the second ligand in facial arrangement to form a hexacoordinated complex. This does not occur with the analogous linear ligands, e.g. ODEN, listed in Table 5.

Comparing the values of stability constants of metal complexes for N-ac_2[9]aneN_2O (Table 4) with those of ethylenediaminediacetic acid (EDDA; Table 5), a linear ligand with the same four donor atoms, it can be seen that the values for the macrocyclic ligand are slightly higher than those for the linear ligand, except for Ni^{2+} and especially Cu^{2+}, whose complexes are considerably less stable than those of EDDA.

More interesting is the comparison of the 9- and 12-membered ligands as to the replacement of one nitrogen for an oxygen atom in the macrocyclic ring. Table 6 summarizes the results of stability constants for the amines and Table 7 the results for the N-acetate derivatives.

Table 5. Stability constants ($\log K_i$) for some metal complexes, collected from the literature ($T = 25°C$)

Metal ion	Species	$H_2N(CH_2)_2O(CH_2)_2NH_2$ (ODEN)[a]	[9]aneN$_3$[b]	N-ac$_3$[9]aneN$_3$ (NOTA)	EDDA[a]	DACODA[f]
Mg^{2+}	ML	—	—	9.69[c]; 8.93[d]	3.95	3.38
Ca^{2+}	ML	—	—	8.92[c]; 8.81[d]	—	4.10
Sr^{2+}	ML	—	—	6.83[c]	—	3.14
Ba^{2+}	ML	—	—	5.10[c]	—	2.70
Mn^{2+}	ML	—	5.8	14.3[e]	7.05	6.90
	ML_2		3.6			
Co^{2+}	ML	8.70	13.4; 11.2	17.5[e]	11.23	9.35
	ML_2	4.40	10.5; 7.8		4.20	
Ni^{2+}	ML	5.90	12.4; 13.6	—	13.65	10.70
	ML_2	3.62	6.8; 11.8	—	—	—
Cu^{2+}	ML	8.97	15.4; 15.1	19.8[e]; 21.63[c]	16.2	16.44
	ML_2	3.72	12.01; 12.01		—	—
Zn^{2+}	ML	5.74	11.3; 11.7	18.3[e]	11.11	11.90
	ML_2	4.12	9.2; 10.0		—	
Cd^{2+}	ML	5.27	9.5; 9.5	16.0[e]	9.1	10.25
	ML_2	4.06	8.4; 8.4		—	
Pb^{2+}	ML	6.10	10.3	16.6[e]	10.7	9.29
	ML_2	—	5.1			

[a] From ref. 14, $I = 0.1$ M.
[b] From ref. 1, the values were selected from two different authors of the list given in ref. 1.
[c] From ref. 15, $I = 0.10$ M $NaNO_3$.
[d] From ref. 12, $I = 0.1$ M $NaNO_3$.
[e] From ref. 22, $I = 0.1$ M KNO_3.
[f] From ref. 27, $I = 0.1$ M KNO_3.

Table 6. Comparison of stability constants ($\log K_{ML}$) for 9- and 12-membered amines, when a nitrogen atom of the ring is replaced by an oxygen atom

Metal ions	Species	[9]aneN$_3$[a]	[9]aneN$_2$O[b]	Δ^h	[12]aneN$_4$	[12]aneN$_3$O[f]	Δ^i
Co^{2+}	ML	11.2	6.33	4.87	—	10.52	—
	ML_2	7.8	5.30	2.50			
Ni^{2+}	ML	13.6	8.05	5.55	16.4[c]	12.19	4.2
	ML_2	11.8	7.85	3.95	—		
Cu^{2+}	ML	15.1	10.80	4.3	24.8[d]	15.74	9.1
	ML_2	12.01	8.80	3.21			
Zn^{2+}	ML	11.7	6.40	5.3	16.2[e]	10.43	5.8
	ML_2	10.0	5.70	4.3			
Cd^{2+}	ML	9.5	5.17[g]	4.33	—	—	—
	ML_2	8.4		—			
Pb^{2+}	ML	10.3	4.48[g]	5.82	—	—	—
	ML_2	5.1	3.40[g]	1.7			
H^+	HL	10.42	9.68	0.74	10.7	10.11	0.59
	H_2	6.82	5.45	1.37	9.7	8.53	1.17

[a] Selected from Table 5.
[b] Our values, present work.
[c] From ref. 23, $I = 0.1$ M $NaNO_3$.
[d] From ref. 24, $I = 0.2$ M $NaCl_4$.
[e] From ref. 14, $I = 0.1$ M.
[f] Our results, not published.
[g] From ref. 20, $I = 0.1$ M $NaNO_3$.
[h] Difference in log units between stability constants of [9]aneN$_3$ and [9]aneN$_2$O.
[i] Difference in log units between stability constants of [12]aneN$_4$ and [12]aneN$_2$O.

Table 7. Comparison of stability constants (log K_{ML}) for 9- and 12-membered complexones, when one nitrogen atom of the macrocyclic ring is replaced by an oxygen atom

Metal ions	N-ac$_3$[9]aneN$_3$O (NOTA)[a]	N-ac$_2$[9]aneN$_2$O	Δ[g]	DOTA[c]	N-ac$_3$[12]aneN$_3$O[e]	Δ[h]
Mg^{2+}	9.69; 8.93	3.68	6.01; 5.25	11.915	10.253	1.66
Ca^{2+}	8.92; 8.81	5.36	3.56; 3.45	17.226	12.984	4.24
Sr^{2+}	6.83	3.95	2.88	15.22	11.370	3.85
Ba^{2+}	5.10	3.13	1.97	12.873	9.915	2.96
Mn^{2+}	14.3	7.73	6.57	20.202[d]	16.09	4.11
Fe^{2+}	—	9.70	—	20.22[d]	16.55	3.67
Co^{2+}	17.5	11.48	6.02	20.27	19.54	0.73
Ni^{2+}	—	11.89	—	20.03	18.04	1.99
Cu^{2+}	19.8; 21.63	13.37	6.43; 8.26	22.25	20.17	2.08
Zn^{2+}	18.3	12.53	5.77	21.099	18.66	2.44
Cd^{2+}	16.0	10.56	5.44	21.31[d]	19.25[f]	2.06
Pb^{2+}	16.6	12.00	4.6	22.69[d]	19.18[f]	3.51
H^+	11.73	10.57	1.16	12.09	11.61	0.48
	5.74	4.08	1.66	9.680	7.70	1.98
	3.16	1.8	1.4	4.548	4.05	0.50
				4.130	2.77	1.36

[a] Values from Table 5.
[b] Values from Table 4.
[c] Values from ref. 25, DOTA = N-ac$_4$[12]aneN$_4$.
[d] Our values, submitted for publication.
[e] Our values, ref. 5.
[f] Our values, not published.
[g] Difference in log units between stability constants of NOTA and N-ac$_2$[9]aneN$_2$O.
[h] Difference in log units between stability constants of DOTA and N-ac$_3$[12]aneN$_3$O.

There are few values in the literature for [12]aneN$_4$ due to the slow kinetics of formation of the complexes, but the values summarized in Table 6 seem to indicate that for the ML complexes there is a decrease of 4–5 log units in the values of stability constants when a nitrogen atom of the macrocyclic ring is replaced by an oxygen atom. This difference is verified for the 9- and 12-membered macrocycles. The Cu^{2+} complex of the 12-membered macrocycles is an exception, the difference being of about 9 log units. For the ML_2 complexes of the 9-membered ligands the same difference is about 2–4 log units. Note that the basicities of the two ligand pairs are very similar.

However, when we compare the corresponding complexones (N-acetate derivatives of the two families of ligands—Table 7) the differences are more pronounced. For the alkaline–earth metal ions, except Mg^{2+} that seems to prefer the NOTA ligand, the value of Δ is larger for the 12-membered system but decreases with the ionic potential of the metal ion for the two systems. For the 9-membered ligands the difference for the first transition series metal ions is of about 5–6 log units, whilst for the 12-membered ligands the difference is only about 2 log units (equal to the difference in basicities of the two ligands) except for Mn^{2+}, Fe^{2+} and Pb^{2+} complexes for which the difference is about 4 log units (as it is for Ca^{2+}).

The smaller difference of Δ for the transition metal ions of the complexes for the 12-membered ligands that have 8 and 7 potential donor atoms, was explained before[5] by the fact that some of the donor atoms may not be involved in the coordination to the metal ion due to the strict stereochemical requirements for covalent bonding. When all the donor atoms are involved in the coordination, as is the case of the alkaline–earth metal ions and Pb^{2+}, the differences between the two families of ligands are 3–4 log units and cannot be explained in terms of differences of basicity. The electronic structure of these cations allows an optimal adjustment to all donor atoms of DOTA to maximize the electrostatic interactions.[5] The same seems to happen with the complexes of NOTA with Ca^{2+} and, particularly, with Mg^{2+}, due to the smaller size of this latter ion. These effects are reflected in the enthalpy and entropy changes of formation o the alkaline–earth metal complexes with these ligands collected in Table 8.

Table 8. Enthalpy and entropy changes for the formation of 1 : 1 metal-to-ligand complexes of alkaline–earth ions and cyclic complexes (values from the literature). Units: ΔH, kcal mol^{-1}; ΔS, cal mol^{-1} K^{-1}

Metal ion	N-ac$_2$[9]aneN$_2$O[a]			N-ac$_3$[9]aneN$_3$ (NOTA)[b]			N-ac$_3$[12]aneN$_3$O[c]			DOTA[d]		
	log K[e]	ΔH	ΔS	log K	ΔH	ΔS	log K	ΔH	ΔS	log K	ΔH	ΔS
Mg^{2+}	5.2	5.70	42.8	9.69	+0.4	45	10.254	+2.4	55	11.92	+1.9	61
Ca^{2+}	5.0	−2.70	14.1	8.92	−5.9	21	12.985	−10.1	25	17.23	−11.7	40
Sr^{2+}	3.3	−0.93	12.0	6.83	−2.1	24	11.370	−9.6	20	15.22	−10.5	35
Ba^{2+}	3.3	−0.78	12.7	5.10	−1.38	19	9.915	−8.1	18	12.87	−8.5	30

[a] From ref. 9.
[b] From ref. 15.
[c] From ref. 19, our values.
[d] From ref. 26, our values.
[e] From ref. 9, not our values, for coherence of the results in this Table.

From the values of this Table it can be seen that the increase in stability of the NOTA complexes when compared with N-ac$_2$[9]aneN$_2$O seems to be due to both more favourable heats and entropies of reaction. The same happens when we compare N-ac$_3$[12]aneN$_3$O and DOTA, but the higher stability of the alkaline–earth metal complexes of the latter ligand is now clearly due to more favourable entropies of reaction, which shows the involvement of its four acetate groups and argues again in favour of a "cage" coordinating structure.

Acknowledgements—The authors thank the Instituto Nacional de Investigação Científica and the Junta Nacional de Investigação Científica e Tecnológica for financial assistance.

REFERENCES

1. P. Chaudhuri and K. Wieghardt, *Prog. Inorg. Chem.* 1987, **35**, 329.
2. R. Bhula, P. Osvath and D. C. Weatherburn, *Coord. Chem. Rev.* 1988, **91**, 89.
3. J. E. Richman and T. J. Atkins, *J. Am. Chem. Soc.* 1974, **96**, 2268; T. J. Atkins, J. E. Richman and W. F. Oettle, *Org. Synth.* 1973, **58**, 2435.
4. E. K. Barefield and F. Wagner, *Inorg. Chem.* 1973, **12**, 2435.
5. M. T. S. Amorim, R. Delgado, J. J. R. Fraústo de Silva, M. C. T. A. Vaz and M. F. Vilhena, *Talanta* 1988, **35**, 741.
6. P. Gans, A. Sabatini and A. Vacca, *J. Chem. Soc., Dalton Trans.* 1985, 1195.
7. J. R. Ascenso, R. Delgado and J. J. R. Fraústo da Silva, *J. Chem. Soc., Perkin Trans. II*, 1985, 781.
8. R. D. Hancock and V. J. Thom, *J. Am. Chem. Soc.* 1982, **104**, 291.
9. G. Ewin and J. O. Hill, *J. Chem. Res. (S)*, 1985, 334; (M), 1985, 3501.
10. R. Yang and L. J. Zompa, *Inorg. Chem.* 1976, **15**, 1499.
11. C. F. G. C. Geraldes, M. C. Alpoim, M. P. M. Marques, A. D. Sherry and M. Singh, *Inorg. Chem.* 1985, **24**, 3876.
12. M. J. Van der Merve, J. C. A. Boeyens and R. D. Hancock, *Inorg. Chem.* 1985, **24**, 1208.
13. S. M. Hart, J. C. A. Boeyens, J. P. Michael and R. D. Hancock, *J. Chem. Soc., Dalton Trans.* 1983, 1601.
14. R. Smith and A. E. Martell, *Critical Stability Constants*, Vol. 2. Plenum Press, New York (1975); and Vol. 5. Plenum Press, New York (1982).
15. A. Bevilacqua, R. I. Gelb, W. B. Hebard and L. J. Zompa, *Inorg. Chem.* 1987, **26**, 2699.
16. J. R. Ascenso, M. A. Santos, J. J. R. Fraústo da Silva, M. C. T. A. Vaz and M. G. B. Drew, *J. Chem. Soc., Dalton Trans.*, accepted.
17. J. L. Sudmeier and C. N. Reilley, *Anal. Chem.* 1964, **36**, 1698, 1707.
18. J. F. Desreux, E. Merciny and M. F. Loncin, *Inorg. Chem.* 1981, **20**, 987.
19. M. T. S. Amorim, J. R. Ascenso, R. Delgado, J. J. R. Fraústo da Silva, *J. Chem. Soc., Dalton Trans.*, accepted.
20. V. J. Thom, S. Shaikjee and R. D. Hancock, *Inorg. Chem.* 1986, **25**, 2992.
21. L. J. Zompa, *Inorg. Chem.* 1978, **17**, 2531.
22. H. Hama and T. S. Takamoto, *Nippon Kagaku Kaishi* 1975, **7**, 1182.
23. A. Evers and R. D. Hancock, *Inorg. Chim. Acta* 1989, **160**, 245.
24. M. Kodama and E. Kimura, *J. Chem. Soc., Chem. Commun.* 1975, 326.
25. R. Delgado and J. J. R. Fraústo da Silva, *Talanta* 1982, **29**, 815.
26. R. Delgado, J. J. R. Fraústo da Silva and M. C. T. A. Vaz, *Inorg. Chim. Acta* 1984, **90**, 185.
27. J. Ascenso, J. J. R. Fraústo da Silva, M. A. Santos and M. C. T. A. Vaz, XXVI Int. Conf. on Coordination Chemistry, Porto (1988).

Polyhedron Vol. 9, No. 23, pp. 2859–2861, 1990
Printed in Great Britain

0277–5387/90 $3.00+.00
© 1990 Pergamon Press plc

COMMUNICATION

SYNTHESIS AND X-RAY STRUCTURAL CHARACTERIZATION OF A (η^3-PHOSPHAALLYL)TUNGSTEN P-OXIDE

FRANÇOIS MERCIER, LOUIS RICARD and FRANÇOIS MATHEY*

Laboratoire de Chimie du Phosphore et des Métaux de Transition, DCPH,
Ecole Polytechnique, 91128 Palaiseau Cedex, France

(*Received* 9 *July* 1990; *accepted* 4 *September* 1990)

Abstract—The oxidation of (η^3-1-aryl-1-phosphaallyl)(η^5-cyclopentadienyl)dicarbonyltungsten (Ar = 2,4,6-^{t}Bu$_3$C$_6$H$_2$) by hydrogen peroxide affords the corresponding P-oxide which retains the phosphaallyl η^3-coordination according to X-ray crystal structure analysis.

Today numerous phosphorus analogues of unsaturated hydrocarbon π-complexes are known.[1] These products have been described either with a free lone pair or with an additional η^1-complexation at phosphorus. All the attempts at obtaining the corresponding P-oxides have been unsuccessful until now. Some theoretical studies have been performed on various η^5-phosphacyclopentadienyl complexes.[2] They show that the energetic gap between the HOMO and the lone pair orbital is sufficiently large to explain why it is difficult to oxidize these products at phosphorus while retaining the η^5-complexation of the ring. The situation is similar with the η^3-1-phosphaallyl complexes. They exist either with a free lone pair (**A**)[3] or with additional complexation at phosphorus (**B**).[4] The corresponding P-oxides (**C**) are unknown. We wish to describe the first product of type **C** which is also the first representative of the phosphoryl analogues of unsaturated hydrocarbon π-complexes.

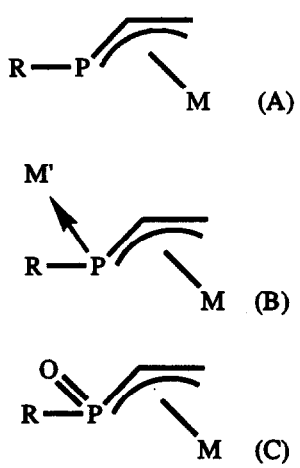

Complex **1**,[3a] as a mixture of two isomers, was oxidized by aqueous hydrogen peroxide in benzene to afford the corresponding isomers of P-oxide (**2**) [eq. (1)].

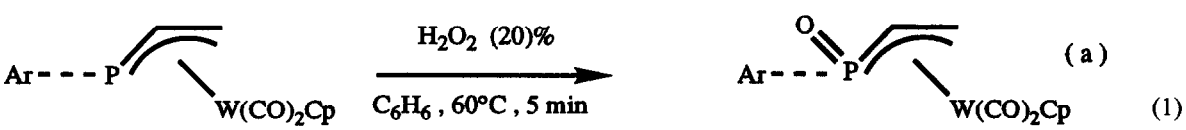

(1)

1 a, b

2 a, b (40)%

Ar = 2,4,6 ^{t}Bu$_3$C$_6$H$_2$

* Author to whom correspondence should be addressed.

The two isomers of **2*** separately crystallized in hexane–dichloromethane (90 : 10). The X-ray crystal structure analysis of the major isomer, **2a**, was carried out (Fig. 1).† The structural features of the phosphaallyl unit [PC(1)C(2)] are absolutely normal. The P=O bond length is also in the normal range. The overall structure of **2a** is similar to the *anti* structure of the previously described molybdenum[4c] and cobalt complexes,[3b] with the *ipso*-carbon of the P-substituent [C(3)] lying in the PC(1)C(2) plane and outside of the PC(1)C(2) angle. The C(2)—C(1)—P—O(1) dihedral angle (47.4°) is close to the corresponding C(2)—C(1)—P—M′ angle in the molybdenum complex (55.2°).[4c] If the structural parameters of **2a** are surprisingly normal, on the contrary, the strong electron-withdrawing effect of the phosphoryl group drastically alters the spectroscopic parameters. The CO stretching frequencies are shifted to higher values (1962 and 1888 cm^{-1} in **2a** vs 1935 and 1850 cm^{-1} in **1**[3a]). Similarly, the C(1) carbon is substantially shielded [δ C(1) 25.5 in **2a** vs 69.7 in **1a**[3a]] suggesting a strong polarization of the C(1)—C(2) bond. We ascribe the stability of **2** to the use of the very bulky supermesityl substituent at phosphorus.[5] In addition, the gap between the HOMO and the lone pair orbital in complexes such as **A** is probably smaller than in η^5-phosphacyclopentadienyl complexes.

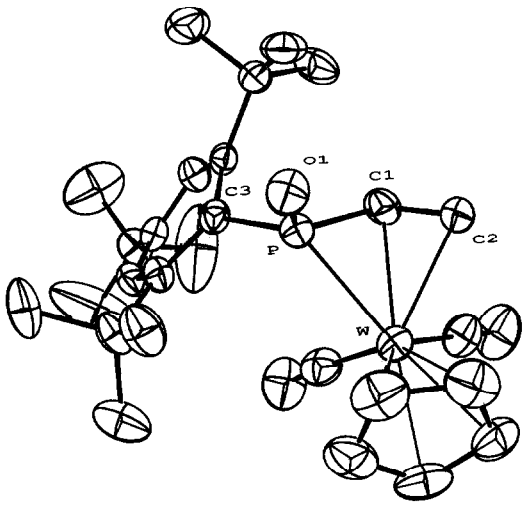

Fig. 1. Structure of **2a** in the crystal.[6] Ellipsoids are scaled to enclose 50% of the electronic density. Hydrogen atoms are omitted for clarity. Important bond distances (Å) and angles (°):

W—P	2.488(1)	P—C(1)	1.762(4)
W—C(1)	2.335(4)	P—C(3)	1.839(4)
W—C(2)	2.344(5)	C(1)—C(2)	1.414(6)
P—O(1)	1.487(3)		

P—W—C(1)	42.7(1)	W—P—C(3)	119.7(1)
P—W—C(2)	66.0(1)	O(1)—P—C(1)	117.7(2)
C(1)—W—C(2)	35.2(1)	O(1)—P—C(2)	117.8(2)
W—P—O(1)	118.9(1)	C(1)—P—C(3)	105.1(2)
W—P—C(1)	64.0(1)	P—C(1)—C(2)	111.5(4)

EXPERIMENTAL

Complex **1** (0.61 g, 1 mmol), as a mixture of two isomers, was heated at 60°C for 5 min with aqueous hydrogen peroxide (20%, 0.5 cm^3, 4 mmol) in benzene (3 cm^3). After evaporation, extraction of the residue with dichloromethane, drying with Na_2SO_4 and evaporation of CH_2Cl_2, the resulting crude product was chromatographed on silica gel 70–230 mesh. Some impurities were removed with dichloromethane, then complex **2** was eluted with ethyl acetate–methanol (90 : 10) as a mixture of isomers. Yield 0.24 g (*ca* 40%). The two isomers separately crystallized in hexane–dichloromethane (90 : 10).

REFERENCES

1. Two complementary reviews are available: F. Mathey, *New J. Chem.* 1987, **11**, 585; J. F. Nixon, *Chem. Rev.* 1988, **88**, 1327.

* Major isomer, **2a**: ^{31}P NMR (CD_2Cl_2): δ +34.6, $^1J(^{31}P-^{183}W)$ = 73.2 Hz; ^{13}C NMR (CD_2Cl_2): δ 25.53 (d, ^1J(C—P) = 42.7 Hz, CH—P), 31.02 (s, Me *para*), 33.92 (s, Me *ortho*), 92.99 (s, Cp); IR (CH_2Cl_2): ν (CO) 1962, 1888 cm^{-1}; MS (EI, 70 eV, ^{184}W): m/z 624 (M^+, 8%), 568 ($M^+ - 2CO$, 27%), 378 ($M^+ - ArH$, 23%), 350 ($M^+ - ArH - CO$, 100%), 322 ($M^+ - ArH - 2CO$, 55%). Calc. for $C_{27}H_{37}O_3PW$: C, 51.93; H, 5.97. Found: C, 51.91; H, 5.91. Minor isomer **2b**: ^{31}P NMR (CD_2Cl_2): δ +44.0, $^1J(^{31}P—^{183}W)$ = 148.9 Hz.

† X-ray structure determination for **2a**: crystals of **2a**, $C_{27}H_{37}O_3PW$, were grown at room temperature from a hexane–dichloromethane (90 : 10) solution of the compound. Data were collected at 18 ± 1° on an Enraf–Nonius CAD4 diffractometer. The crystal structure was solved and refined using the Enraf–Nonius supplied SDP package. The compound crystallizes in space group $P2_1/n$, a = 10.057(1), b = 14.030(1), c = 18.942(2) Å, β = 93.04(1)°; V = 2669.08(76) $Å^3$; Z = 4; d_{calc} = 1.562 g cm^{-3}; Mo-K_α radiation (λ = 0.71073 Å), graphite monochromator; μ = 45.3 cm^{-1}; $F(000)$ = 1248. A total of 7762 unique reflections was recorded in the range $2 \leqslant 2\theta \leqslant 60.0°$, of which 2914 were considered as unobserved [$F^2 < 3.0\sigma(F^2)$], leaving 4848 for solution and refinement. The structure was solved by Patterson methods, yielding a solution for the tungsten and phosphorus atoms. The hydrogen atoms were included as fixed contributions in the final stages of least-squares refinement, while using anisotropic temperature factors for all other atoms. A non-Poisson weighting scheme was applied with a p factor equal to 0.05. The final R factors were R = 0.029, R_w = 0.037; G.O.F. = 1.03.

2. C. Guimon, G. Pfister-Guillouzo and F. Mathey. *New J. Chem.* 1979, **3**, 725; N. M. Kostic and R. F. Fenske, *Organometallics* 1983, **2**, 1008; C. Guimon, D. Gonbeau, G. Pfister-Guillouzo, G. de Lauzon and F. Mathey, *Chem. Phys. Lett.* 1984, **104**, 560.
3. (a) F. Mercier and F. Mathey, *Organometallics* 1990, **9**, 863; (b) F. Mercier, C. Hugel-Le Goff, L. Ricard and F. Mathey, *J. Organomet. Chem.* 1990, **389**, 389.
4. (a) F. Mercier, J. Fischer and F. Mathey, *Angew. Chem., Int. Edn Engl.* 1986, **25**, 357; (b) F. Mercier, C. Hugel-Le Goff and F. Mathey, *Organometallics* 1988, **7**, 955; (c) C. Hugel-Le Goff, F. Mercier, L. Ricard and F. Mathey, *J. Organomet. Chem.* 1989, **363**, 325.
5. The use of the supermesityl substituent also allowed the stabilization of the elusive phosphaalkene P-oxides: R. Appel, F. Knoch and H. Kunze, *Angew. Chem., Int. Edn Engl.* 1984, **23**, 157.

Polyhedron Vol. 9, No. 23, pp. 2863–2865, 1990
Printed in Great Britain

0277-5387/90 $3.00+.00
© 1990 Pergamon Press plc

COMMUNICATION

FORMATION OF MOLYBDENUM–TIN HETEROBIMETALLIC COMPLEXES. REACTIONS OF NEW [(phen){P(4-XC_6H_4)$_3$}Mo(CO)$_3$] (X = Cl, F, CH_3, OCH_3) COMPOUNDS WITH TIN(IV) HALIDES AND ORGANOHALIDES

M. CANO*

Departamento de Química Inorgánica, Facultad CC Químicas, Universidad Complutense 28040 Madrid, Spain

and

M. PANIZO

Departamento de Química, Facultad Ciencias, Universidad Autónoma, 28049 Madrid, Spain

(*Received* 24 *August* 1990; *accepted* 17 *September* 1990)

Abstract—The preparation of [(phen){P(4-XC_6H_4)$_3$}Mo(CO)$_3$] (X = Cl, F, CH_3, OCH_3) complexes and their characterization by IR and ^{31}P NMR spectroscopies have been studied. The reactions of the above compounds with R_nSnCl_{4-n} (R = C_6H_5, CH_3; n = 0, 1) are also described.

Tin tetrahalides and organohalides have been found to react readily with several substituted carbonyl group VIB compounds to yield heterobimetallic M—Sn complexes.[1–4]

In a previous paper from this laboratory,[5] we have shown that the reactions of [(bipy){P(4-XC_6H_4)$_3$}Mo(CO)$_3$] with tin derivatives, $SnCl_4$ and R_nSnCl_{4-n} (R = C_6H_5, CH_3; n = 0, 1), give the seven-coordinate complexes [(bipy){P(4-XC_6H_4)$_3$}Mo(CO)$_2$(Cl)(R_nSnCl_{3-n})] or [(bipy)Mo(CO)$_3$(Cl)(R_nSnCl_{3-n})] depending on the tin derivative and phosphine employed. These complexes contain a Mo—Sn bond.

On the other hand, it has recently been reported that the reaction of M(CO)$_3$(NN) fragments [M = Mo, W; NN = 2,2′-bipyridine (bipy), 1,10-phenanthroline (phen)] with mercury halides can be interpreted as the insertion of the former between the atoms of the Hg—X bonds, and this was demonstrated by the isolation of trimetallic complexes X—M—Hg—M′—X (M′ = Mo, W).[6] The same type of reaction has been reported using [Fe(SnX_3)(CO)$_2$(η^5-C_5H_5)] or [(bipy)M(Cl)($SnCl_3$)(CO)$_3$] (X = Cl, Br, I; M = Mo, W) as probes to react with the [M(CO)$_3$(bipy)(NCMe)] complexes (M = Mo, W) giving trimetallic arrays through the insertion of the M(CO)$_3$(bipy) fragments into Sn—X bonds.[7]

Our bimetallic compounds described above could be considered as containing the Mo(CO)$_3$(bipy) unit acting as a bridge between the chloride and tin atoms. However, this behaviour can only be considered as proof of the formation of the dicarbonyl phosphine complexes [(bipy){P(4-XC_6H_4)$_3$}Mo(CO)$_2$(Cl)(R_nSnCl_{3-n})] if the unit [{P(4-XC_6H_4)$_3$}Mo(CO)$_2$(bipy)] is inserted into the Sn—X bonds.

As an extension of the above results and to clarify this behaviour, we are studying the related reactions between [(phen){P(4-XC_6H_4)$_3$}Mo(CO)$_3$] and $SnCl_4$, $C_6H_5SnCl_3$ and CH_3SnCl_3. In this paper we

* Author to whom correspondence should be addressed.

Table 1. IR and ^{31}P NMR data for [(phen){P(4-XC_6H_4)$_3$}Mo(CO)$_3$] complexes and ^{31}P NMR and reference data for P(4-XC_6H_4)$_3$ phosphines

X	IR data (cm^{-1}) ν(CO)[a]			$\delta(^{31}P)$ (ppm)[b]	$\delta(^{31}P)$ (ppm)[c]	pka[c]	$\Delta(\delta^{31}P)$[d]
Cl	1920vs,	1825s,	1792s	38.3, 24.35	−8.7	1.03	47, 33.05
F	1919vs,	1824s,	1791s	37.17	−9.3	1.97	46.47
CH_3	1914vs,	1816s,	1788s	36.33	−8.3	3.84	44.63
OCH_3	1913vs,	1815s,	1787s	34.13	−10.6	4.59	44.73

[a] Spectra recorded in CH_2Cl_2 solution; s, strong; vs, very strong.
[b] Complex values, in $CHCl_3$ solution.
[c] Free ligand values, ref. 15.
[d] $\Delta(\delta^{31}P) = \delta(^{31}P)_{complex} - \delta(^{31}P)_{free\ ligand}$.

describe the new [(phen){P(4-XC_6H_4)$_3$}Mo(CO)$_3$] compounds and some of their reactions with tin derivatives.

Refluxing mixtures of (phen)Mo(CO)$_4$ and P(4-XC_6H_4)$_3$ in acetone in the molar ratio 1 : 1 gave, in all cases, the tricarbonyl complexes [(phen){P(4-XC_6H_4)$_3$}Mo(CO)$_3$] which have been characterized by analytical data [Found: C, 54.8; H, 2.7; N, 3.9. Calc. for $C_{33}H_{20}N_2O_3PClMo$: C, 54.7; H, 2.8; N, 3.9% (X = Cl). Found: C, 58.7; H, 3.01; N, 4.2. Calc. for $C_{33}H_{20}N_2O_3PFMo$: C; 58.6; H, 3.0; N, 4.1% (X = F). Found: C, 65.1; H, 4.4; N, 4.2. Calc. for $C_{36}H_{29}N_2O_3PMo$: C, 65.1; H, 4.4; N, 4.2% (X = CH_3). Found: C, 60.4; H, 4.0; N, 3.9. Calc. for $C_{36}H_{29}N_2O_6PMo$: C, 60.7; H, 4.1; N, 3.9% (X = OCH_3)], IR and ^{31}P NMR spectroscopies (Table 1).

The new complexes are microcrystalline, air-stable solids, soluble in organic solvents. Their IR spectra in CH_2Cl_2 solution show, in all cases, three strong carbonyl stretching bands. This has been attributed to the formation of a *fac*-isomer,[8] but there are slight ambiguities in the literature and the IR data may not always conclusively distinguish between the *fac*- and *mer*-isomers.[9–13] The ^{31}P NMR data (when X = F, CH_3, OCH_3) are consistent (Table 1) with the above suggestion; however, when X = Cl an additional signal at 24.35 ppm could be attributed to the presence of a new isomer.

Recently we reported the formation of a mixture of *fac*- and *mer*-isomers for [Mo(CO)$_3$(η^2-NN)(η^1-dppm)] [NN = phen, 2,9-dimethyl-1,10-phenanthroline (dmp); dppm = bis(diphenylphosphino) methane].[14] The ^{31}P NMR data for the phen derivative, δ 20.3 (*mer*-isomer) and 28.7 ppm (*fac*-isomer), are very similar to those displayed by [(phen){P(4-ClC_6H_4)$_3$}Mo(CO)$_3$], δ 38.3 and 24.35 ppm, and, therefore, a similar *fac–mer* mixture could be suggested in this case.

The ν(CO) frequencies and $\Delta(\delta^{31}P)$ chemical shift values show a general increase with decreasing phosphine ligand basicity[15] (Table 1). This has previously been found for other molybdenum(0) carbonyl complexes.[16]

We have also started to study the reactivity of the above complexes with tin derivatives and we describe the results of the reactions of one of these compounds.

The tricarbonyl complex [(phen){P(4-ClC_6H_4)$_3$}Mo(CO)$_3$] reacts with $SnCl_4$, $C_6H_5SnCl_3$ and CH_3SnCl_3 in a refluxing acetone–dichloromethane mix-

Table 2. Analytical and IR data for [(phen){P(4-ClC_6H_4)$_3$}Mo(CO)$_2$(Cl)(R_nSnCl_{3-n})] (R = C_6H_5, CH_3; n = 0, 1)

R	Analysis (%)[a] C	H	N	IR data (cm^{-1}) ν(CO)[b]	
Cl	40.9(41.0)	2.1(2.1)	3.1(3.0)	1912vs,	1841vs
C_6H_5	44.7(45.7)	2.5(2.5)	2.9(2.8)	1909vs,	1831vs
CH_3	41.9(42.3)	2.4(2.5)	3.0(3.0)	1907vs,	1839vs

[a] Required values are given in parentheses.
[b] Nujol mulls; vs, very strong.

ture in a 1:1 mol ratio. Evolution of CO was observed and new Mo—Sn complexes [(phen){P(4-$ClC_6H_4)_3$}$Mo(CO)_2(Cl)(R_nSnCl_{3-n})$] were formed in all cases. Therefore, insertion of the [(phen){P(4-$ClC_6H_4)_3$}$Mo(CO)_2$] units into the Sn—Cl bonds could be suggested to explain this behaviour.

The complexes isolated are microcrystalline, air-stable solids, and have been characterized by their analytical data and IR spectroscopy (Table 2). The IR spectra confirm the existence of Cl—Mo—Sn arrays,[7] but the low solubility of the compounds precluded good NMR spectral data. Mössbauer spectroscopy is probably the best method for knowing the nature of coordination around the tin atom in these types of compound and we are trying to obtain additional information. We are also preparing a new series of Mo—Sn compounds with the rest of the tricarbonylphosphine complexes.

REFERENCES

1. R. Kummer and W. A. G. Graham, *Inorg. Chem.* 1968, **7**, 310.
2. T. E. Reed and D. G. Hendricker, *Chubu Kogyo Baigaku Kiyo A* 1978, 175.
3. W. R. Cullen and R. K. Pomeroy, *Inorg. Chem.* 1975, **14**, 939.
4. P. K. Baker and A. Bury, *J. Organomet. Chem.* 1989, **359**, 189.
5. M. Panizo and M. Cano, *J. Organomet. Chem.* 1985, **287**, 221.
6. P. Correa, M. E. Vargas and J. Granifo, *Polyhedron* 1987, **6**, 1781.
7. J. Granifo, *Polyhedron* 1990, **9**, 1187.
8. F. A. Cotton and C. S. Kraihanzel, *J. Am. Chem. Soc.* 1962, **84**, 4432.
9. E. E. Isaacs and W. A. G. Graham, *Inorg. Chem.* 1975, **14**, 2560.
10. T. S. A. Hor and S. M. Chee, *J. Organomet. Chem.* 1987, **331**, 23.
11. T. S. A. Hor, *Inorg. Chim. Acta* 1987, **128**, L3.
12. J. Dalton, I. Paul, J. G. Smith and F. G. A. Stone, *J. Chem. Soc. A* 1968, 1208.
13. A. Blagg, S. W. Carr, G. R. Cooper, I. D. Dobson, J. B. Gill, D. C. Goodall, B. L. Shaw, N. Taylor and T. Boddington, *J. Chem. Soc., Dalton Trans.* 1985, 1213.
14. M. Cano, J. A. Campo, V. Pèrez-García, E. Gutierrez Puebla and C. Alvarez-Ibarra, *J. Organomet. Chem.* 1990, **382**, 397.
15. T. Allman and R. Goel, *Can. J. Chem.* 1982, **60**, 716.
16. G. M. Gray and R. J. Gray, *Organometallics* 1983, **2**, 1026.

Polyhedron Vol. 9, No. 23, pp. 2867–2871, 1990
Printed in Great Britain

0277–5387/90 $3.00+.00
Pergamon Press plc

COMMUNICATION

NEW BINUCLEATING AMIDO LIGANDS, SYNTHESIS AND STRUCTURES OF COPPER(II) AND MANGANESE(III) COMPLEXES

KAREN BERTONCELLO, GARY D. FALLON and KEITH S. MURRAY*

Department of Chemistry, Monash University, Clayton, Victoria 3168, Australia

(*Received* 28 *August* 1990; *accepted* 27 *September* 1990)

Abstract—New binucleating ligands containing μ-alkoxo backbones and amido-pyridyl or amido-phenol "end" groups have been synthesized. The syntheses and structures of mononuclear Cu^{II} and binuclear (Cu^{II}—Cu^{II} and Mn^{III}—Mn^{III}) complexes are described. The crystal structure of a novel doubly-bridged Mn^{III}—Mn^{III} complex shows that each six-coordinate manganese is bridged by endogenous μ-alkoxo and exogenous μ-acetato groups. Chemical or electrochemical oxidations will be required to obtain higher oxidation state metallo species.

We are in the process of developing new binucleating ligand systems of the types shown, LH_3 and $L'H_5$, which differ from the well studied Schiff-base[1] or tripodal amino-pyridyl[2] analogues in so far as the salicylideneimine or amino-pyridyl end groups of the latter are replaced by amido-pyridyl or amido-phenol groups. The endogenous μ-alkoxo backbone remains common to all classes. These types of ligands are being used to prepare binuclear (or higher nuclearity) Cu—Cu, Ni—Ni, Fe—Fe and Mn—Mn complexes primarily to use as models for polymetallic bio-sites of these metal ions, for example in Type 3 copper-containing proteins,[3] iron oxo-proteins[4] or the manganese–water oxidation centre (W.O.C.) of Photosystem II.[5] It was felt that incorporation of chelating amido fragments of the type shown, especially in deprotonated forms could potentially stabilize high oxidation state metal ion combinations such as Cu^{II}—Cu^{III}, Cu^{III}—Cu^{III}, Mn^{III}—Mn^{III}, Mn^{III}—Mn^{IV}, etc., some of which have been postulated to be important in the biological systems mentioned above. Studies by other groups[6–8] and our own[9] on related mononuclear amido-chelate species have shown that these oxidation states can be obtained. It was also felt that the planar-deprotonated —CON^-— groups might impose geometric features at the metal ions and the endogenous bridging moiety different to those observed in the Schiff-base and tripodal-pyridyl analogues.

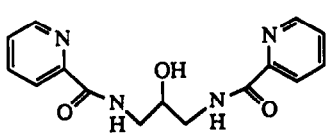

LH_3

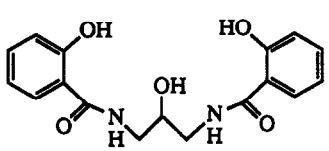

$L'H_5$

The ligands LH_3 and $L'H_5$ were synthesized by reaction of 1,3-diaminopropan-2-ol with the corresponding ester of the 2-carboxypyridine or 2-carboxyphenol precursor, and were fully characterized by analytical and spectroscopic methods. Variations have been made, for instance, in the length and symmetry of the diamine backbone. Macro-

* Author to whom correspondence should be addressed.

Table 1. Mononuclear and binuclear complexes of amido-pyridyl (LH_3) and amido-phenol ($L'H_5$) ligands

Complex	Colour	μ_{eff} (BM) at 295 K (per M ion)
Ligand LH_3		
$Mn(LH_3)Cl_2$	Colourless	5.81
$Cu(LH_3)(ClO_4)_2$	Pale blue	1.63
$Cu(LH)\cdot 2H_2O$	Violet	1.92
$Ni(LH)\cdot H_2O$	Orange	0
$Cu_2L(OAc)\cdot 2.5H_2O$	Blue	1.61[a]
$Cu_2L(CF_3CO_2)\cdot 4H_2O\cdot MeOH$	Blue	1.61
Ligand $L'H_5$		
$[Mn_2L'(OAc)py_4]py\cdot H_2O$	Dark green	4.82
$Mn_2L'(OAc)(MeOH)_4$	Dark green	4.63

[a] A value of 1.70 BM was obtained on a sample obtained by heating, *in vacuo*, the sample used for crystallography, *viz.* $Cu_2L(H_2O)(OAc)\cdot 0.5DMF$. The DMF is easily lost at 295 K.

cyclic analogues of these open-chain amido ligands are also currently being explored. There is an early report of a related macrocyclic system based on the 4-methylphenol-2,6-dicarboxy backbone.[10]

Transition metal ions can readily be incorporated into these ligands and some results were noted which did not always accord with preconceived notions of the relative pK_a values of the various donor groups on the ligand, and probably relate to a subtle interplay of acidity, stability, solubility, hydrogen bonding and nature of solvent. Thus, reaction of LH_3 with metal salts in methanol in the ratio 1 : 2, in the absence of base, yielded crystalline 1 : 1 "adducts" such as $Cu^{II}(LH_3)(ClO_4)_2$ and $Mn^{II}(LH_3)Cl_2$ (Table 1). Similar adducts were obtained by Vagg and co-workers[11] using related non-binucleating pyridyl-amide ligands and polymeric structures were postulated for such species in the solid state. Addition of a base such as NaOH, to a 1 : 1 or 1 : 2 mixture of LH_3 and $Cu(CF_3CO_2)_2$, yielded the violet-coloured complex $Cu(LH)\cdot 2H_2O$, in which the ligand acted as a tetradentate chelate and still retained the protonated, non-bonded alcohol moiety but had undergone deprotonation of the amido NH groups. A crystal structure determination* confirmed the planar CuN_4 coordination imposed by LH^{2-} on copper [Fig. 1(a)] and showed hydrogen-bonded lattice interactions involving water molecules and amide-oxygen or alcohol-oxygen atoms. The Cu—N(amido) and Cu—N (pyridyl) distances are normal.[12] The analogous square-planar $Ni(LH)\cdot H_2O$ complex was likewise obtained and displayed IR, ^1H NMR and mass spectral data compatible with the copper(II) structure.

Binuclear μ-carboxylate copper(II) complexes of LH_3 were obtained using a 2 : 1 copper carboxylate-to-ligand ratio with DMF or MeCN as preferred solvents. FAB mass spectral measurements clearly show the $Cu_2L(RCO_2)$ parent ion. A low temperature crystal structure determination† of Cu_2L

*Crystal data on $Cu(LH)\cdot 2H_2O$: $C_{15}H_{18}CuN_4O_5$, fw = 397.9, monoclinic, $a = 7.998(2)$, $b = 22.696(6)$, $c = 9.463(3)$ Å, $\beta = 109.94(2)°$. Space group: $P2_1/a$, $Z = 4$, $D_c = 1.64$ g cm^{-3}, $D_M = 1.64(1)$ g cm^{-3}, $F(000) = 820$, μ(Mo-K_α) = 1.39 mm^{-1}, λ(Mo-K_α) = 0.71073 Å, $T = 20(1)°C$. Structure solved by Patterson and Fourier methods and refined by full-matrix least-squares (positional and anisotropic thermal parameters for Cu, O, N and isotropic thermal parameters for all other atoms). $R = 0.061$, $R_w = 0.072$ for 152 parameters and 1905 observed [$F > 6\sigma(F)$] data from 3716 measured. The limits of data collection were $3.5 \leqslant 2\theta \leqslant 55°$.

†Crystal data on $Cu_2L(H_2O)(OAc)\cdot 0.5DMF$: $C_{18.5}H_{21.5}Cu_2N_{4.5}O_{6.5}$, fw = 538.0, triclinic, $a = 8.662(1)$, $b = 10.010(1)$, $c = 12.833(2)$ Å, $\alpha = 83.27(1)$, $\beta = 73.61(1)$, $\gamma = 79.35(1)°$. Space group: $P\bar{1}$, $Z = 2$, $D_c = 1.71$ g cm^{-3}, $F(000) = 548$, μ(Mo-K_α) = 2.08 mm^{-1}, λ(Mo-K_α) = 0.7107 Å, $T = -100(1)°C$. Structure solved by Patterson and Fourier methods and refined by full-matrix least-squares (positional and anisotropic thermal parameters for Cu and isotropic thermal parameters for all other atoms). $R = 0.045$, $R_w = 0.052$ for 147 parameters and 2716 observed [$F > 6\sigma(F)$] data from 3680 measured. The limits of data collection were $3.5 \leqslant 2\theta \leqslant 50°$. DMF is disordered about the origin. C(8) is also disordered above and below the C(7), C(9), O(2) plane.

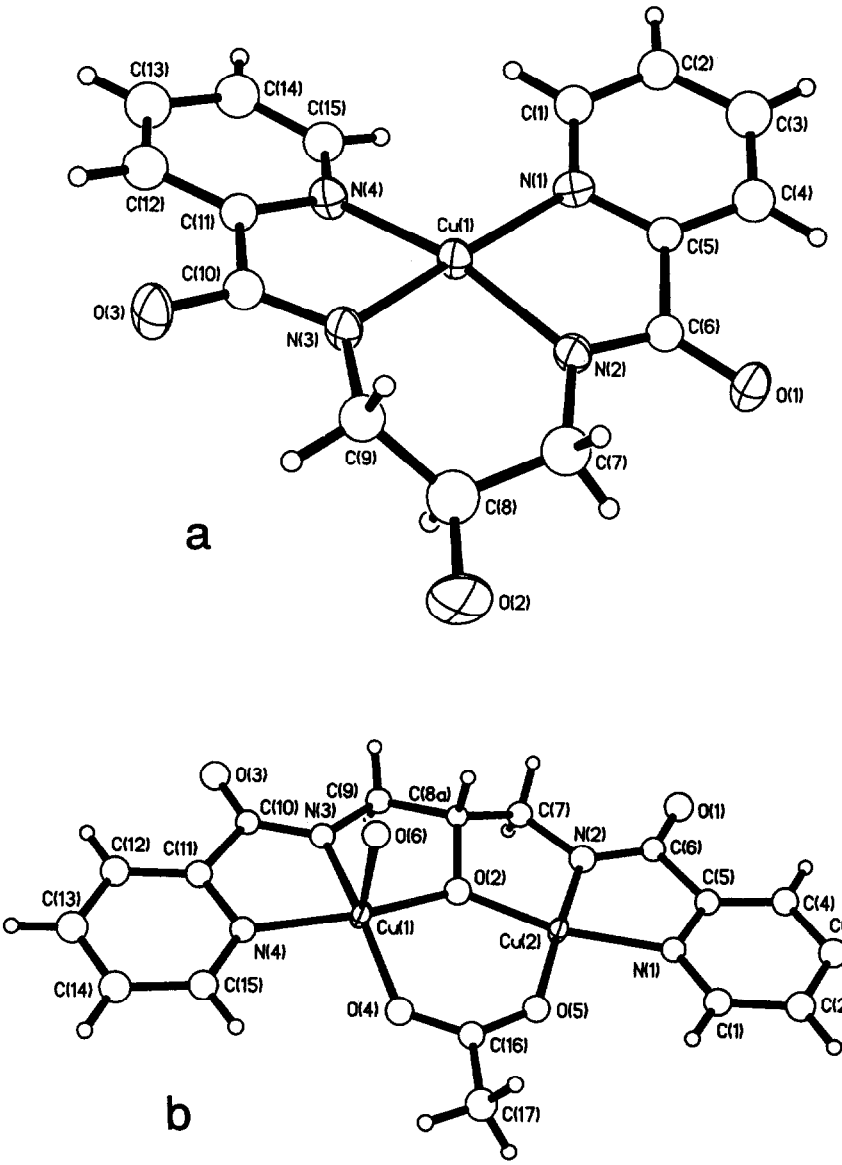

Fig. 1. (a) ORTEP drawing of $Cu(LH)\cdot 2H_2O$. The solvated H_2O molecules are not shown. Selected bond lengths (Å): Cu(1)—N(1) = 2.064(5); Cu(1)—N(2) = 1.956(5); Cu(1)—N(3) = 1.949(5); Cu(1)—N(4) = 2.026(6); Cu(1)—O(1) = 2.533; C(6)—O(1) = 1.257(8); C(6)—N(2) = 1.291(9); C(10)—O(3) = 1.259(9); C(10)—N(3) = 1.309(9). Hydrogen-bonded contacts: O(1)···O(5) = 2.78; O(2)···O(5) = 2.69; O(3)···O(4) = 2.80; O(3)···O(4′) = 2.82; O(4)···(5) = 2.72 [where O(4) and O(5) are water oxygens]. (b) ORTEP drawing of $Cu_2L(H_2O)(OAc)0.5DMF$. The solvated DMF molecules not shown. C(8) is disordered, only the site above the C(7), C(9), O(2) plane is shown. Selected bond lengths (Å): Cu(1)—N(3) = 1.913(4); Cu(1)—N(4) = 2.003(4); Cu(1)—O(2) = 1.907(4); Cu(1)—O(4) = 1.963(3); Cu(1)—O(6) = 2.344(4); Cu(2)—N(1) = 1.992(4); Cu(2)—N(2) = 1.899(5); Cu(2)—O(2) = 1.874(3); Cu(2)—O(5) = 1.923(4); C(6)—O(1) = 1.250(6); C(6)—N(2) = 1.317(6); C(10)—O(3) = 1.258(6); C(10)—N(3) = 1.312(6). Cu(1)···Cu(2) = 3.416. Selected bond angle (°): Cu(1)—O(2)—Cu(2) = 129.2(2).

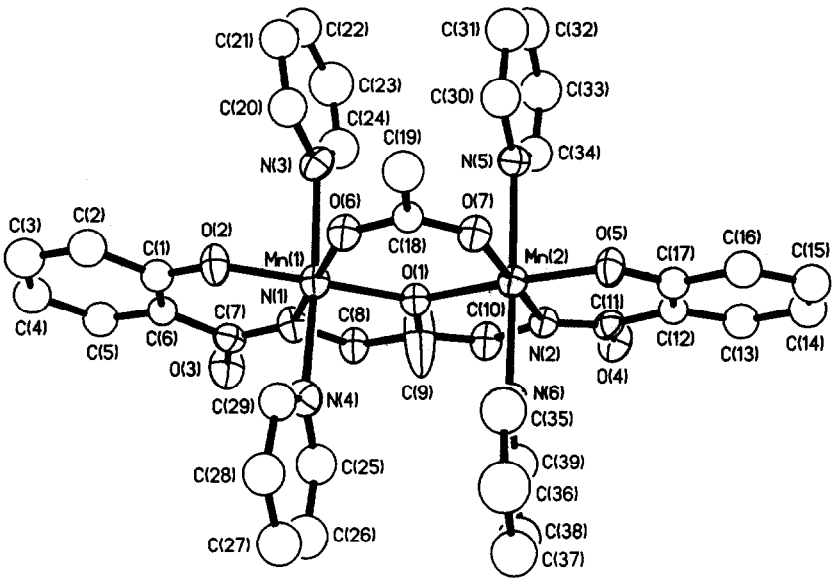

Fig. 2. ORTEP drawing of $[Mn_2L'(OAc)py_4]py \cdot H_2O$. The solvated py and H_2O molecules are not shown. Selected bond lengths (Å) and angles (°): Mn(1)—O(1) = 1.938(5); Mn(1)—O(6) = 1.995(5); Mn(1)—O(2) = 1.848(5); Mn(1)—N(1) = 1.919(6); Mn(1)—N(3) = 2.362(6); Mn(1)—N(4) = 2.389(7); Mn(2)—O(1) = 1.942(4); Mn(2)—O(7) = 1.977(5); Mn(2)—O(5) = 1.851(5); Mn(2)—N(2) = 1.927(6); Mn(2)—N(5) = 2.410(6); Mn(2)—N(6) = 2.389(7). Mn···Mn = 3.552(2); Mn(1)—O(1)—Mn(2) = 132.5(2).

$(H_2O)(OAc) \cdot 0.5DMF$ confirmed that the binucleating ligand had been fully deprotonated and that the two CuN_2O_2 planar moieties were coplanar and were bridged, as desired, by the endogenous μ-alkoxo-oxygen atom and the exogenous $\eta^1:\eta^1:\mu_2$-bridging acetate group. One of the copper atoms has an axially-bonded water molecule [Fig. 1(b)]. A Cu—Cu distance of 3.416 Å and Cu—O(R)—Cu angle of 129.2(2)° were generally in accord with the observed magnetic moment of 1.70 BM (at 295 K), which in turn is indicative of weak antiferromagnetic coupling. Interestingly, Okawa and co-workers[13] have recently observed weak ferromagnetic coupling in a μ-acetato-bridged Cu^{II}—Cu^{II} complex of another binucleating amido ligand system which contains a μ-pyrazolato endogenous bridging group. Unfortunately, no structural data were obtainable which could be compared with those for $Cu_2L(H_2O)(OAc) \cdot 0.5DMF$.

Crystalline μ-pyrazolate-bridged complexes such as $[Cu_2L(3,5\text{-}Me_2\text{-}pyz)]$ were obtained using $Cu(ClO_4)_2$ in the presence of NaOH and ligand. Na^+ and ClO_4^- ions were incorporated into the lattice of some of these derivatives. This is a feature sometimes observed in metal–amido chelate compounds[6,9] and is related to the ability of amide oxygen atoms to bind to Na^+ as well as to the chelated metal.

One of the most interesting groups of binuclear complexes is that formed from manganese(III) and the ligand $L'H_5$. These complexes are of general formula $Mn_2L'(OAc)(B)_4$, where B = pyridine, γ-picoline and methanol, and are formed by reacting $[Mn_3O(OAc)_6py_3](ClO_4)$[14] or $Mn(OAc)_3$, in air, with $L'H_5$ using the neat pyridine base or methanol as solvent. Such conditions are basic enough to cause removal of five protons from $L'H_5$. The molecular structure* of the pyridine derivative, shown in Fig. 2, consists of two octahedrally-coordinated manganese(III) ions bridged by both

*Crystal data on $[Mn_2L'(OAc)py_4]py \cdot H_2O$: $C_{44}H_{43}Mn_2N_7O_8$, fw = 907.7, triclinic, $a = 9.218(3)$, $b = 13.637(4)$, $c = 17.291(5)$ Å, $\alpha = 99.50(2)$, $\beta = 91.44(2)$, $\gamma = 100.14(3)°$. Space group: $P\bar{1}$, $Z = 2$, $D_c = 1.43$ g cm^{-3}, $F(000) = 940$, μ(Mo-K_α) = 0.63 mm^{-1}, λ(Mo-K_α) = 0.71073 Å, $T = 20(1)°C$. Structure solved by Patterson and Fourier methods and refined by full-matrix least-squares [positional and anisotropic thermal parameters for Mn, O, N and C(7) through C(11) and isotropic thermal parameters for all other atoms]. $R = 0.062$, $R_w = 0.079$ for 355 parameters and 3456 observed [$F > 6\sigma(F)$] data from 5489 measured. The limits of data collection were $4.0 \leqslant 2\theta \leqslant 45°$. The stereochemistry around C(9) is trigonal but should be tetrahedral and is, therefore, disordered. An attempt to refine C(9) as occupying two sites, above and below the C(8), C(10), O(1) plane, was unsuccessful.

the μ-alkoxo-oxygen atom of $(L')^{5-}$, with a Mn—O—Mn angle of 132.5(2)°, and by a $\eta^1:\eta^1:\mu_2$-bridging acetate group. The Mn—Mn distance is 3.552(2) Å. A doubly-bridged Mn^{III}_2 structure of this, or any other type, is quite rare in the general context of models for the polynuclear manganese site in the W.O.C. or in manganese catalase enzymes.[5] The whole of the binucleating $(L')^{5-}$ ligand moiety is remarkably planar, presumably through a combination of favourable geometry around the manganese atoms and incorporation of deprotonated amide fragments along the backbone. It is interesting to note that the Mn—O and Mn—N distances provided by $(L')^{5-}$ are similar to those recently deduced from EXAFS for the W.O.C. of Photosystem II, whereas the Mn—N(pyridine) and Mn···Mn distances are longer than those obtained from fits of the first and second shell EXAFS peaks.[15]

The room temperature magnetic moment, per manganese, of $[Mn_2L'(OAc)py_4]py \cdot H_2O$ is 4.82 BM, which is close to the uncoupled $S = 2$ value. Similar weak coupling has been observed recently in other doubly- and triply-bridged Mn^{III}—Mn^{III} systems.[5] An irreversible oxidation wave, observed in the cyclic voltammogram of DMF solutions of this complex at +1.1V (reference to SCE), is assigned to $Mn^{III} \rightarrow Mn^{IV}$. Thus, in contrast to other recently reported mononuclear amido-manganese chelates,[7,8] a stronger oxidant than air is required to obtain Mn^{IV} or Mn^{V} species.

Studies of reactivity, electrochemistry and variable temperature susceptibility are in progress on the various compounds described here.

Supplementary data. Tables of atomic coordinates, thermal parameters, bond lengths and angles have been deposited at the Cambridge Crystallographic Data Centre.

REFERENCES

1. (a) D. E. Fenton, in *Advances in Inorganic Bioinorganic Mechanisms* (Edited by A. G. Sykes), Vol. 2, p. 187. Academic Press, New York (1983); (b) F. L. Urbach, in *Metal Ions in Biological Systems* (Edited by H. Sigel), Vol. 13, Ch. 3. Marcel Dekker, New York (1982); (c) K. S. Murray, in *Biological and Inorganic Copper Chemistry* (Edited by K. D. Karlin and J. Zubieta), Vol. 2, p. 161. Adenine Press, New York (1986).
2. (a) K. D. Karlin and Y. Gultneh, *Prog. Inorg. Chem.* 1987, **35**, 219; (b) T. N. Sorrell, *Tetrahedron* 1989, **45**, 3.
3. E. I. Solomon, in *Metal Clusters in Proteins* (Edited by L. Que Jr), ACS Symposium Series No. 372, p. 116 (1988).
4. (a) S. J. Lippard, *Angew. Chem. Int. Edn* 1988, **27**, 344; (b) L. Que Jr and R. S. Scarrow, in *Metal Clusters in Proteins* (Edited by L. Que Jr), ACS Symposium Series No. 372, p. 152 (1988).
5. (a) G. Christou, *Accts Chem. Res.* 1989, **22**, 328; (b) K. Wieghardt, *Angew. Chem. Int. Edn* 1989, **28**, 1153; (c) G. Brudvig and R. H. Crabtree, *Prog. Inorg. Chem.* 1989, **37**, 99; (d) V. L. Pecoraro, *Photochem. Photobiol.* 1988, **49**, 249.
6. T. J. Collins and S. W. Gordon-Wyllie, *J. Am. Chem. Soc.* 1989, **111**, 4511, and refs therein.
7. M. Koikawa, H. Okawa and S. Kida, *J. Chem. Soc., Dalton Trans.* 1988, 641.
8. S. K. Chandra, S. B. Choudhury, D. Ray and A. Chakravorty, *J. Chem. Soc., Chem. Commun.* 1990, 474.
9. K. Bertoncello, G. D. Fallon and K. S. Murray, *Inorg. Chim. Acta* 1990, **174**, 57.
10. H. Okawa, M. Honda and S. Kida, *Chem. Lett.* 1972, 1027.
11. D. J. Barnes, R. L. Chapman, F. S. Stephens and R. S. Vagg, *Inorg. Chim. Acta* 1981, **51**, 155.
12. (a) R. L. Chapman, F. S. Stephens and R. S. Vagg, *Inorg. Chim. Acta* 1980, **43**, 29; (b) M. Antolovich, D. J. Phillips and A. D. Rae, *Inorg. Chim. Acta* 1989, **156**, 189.
13. T. Kamiusuki, H. Okawa, E. Kitaura, M. Koikawa, N. Matsumoto, S. Kida and H. Oshio, *J. Chem. Soc., Dalton Trans.* 1989, 2077.
14. J. B. Vincent, H. R. Chang, K. Folting, J. C. Huffmann, G. Christou and D. N. Hendrickson, *J. Am. Chem. Soc.* 1987, **109**, 5703.
15. J. E. Penner-Hahn, R. M. Fronko, V. L. Pecoraro, C. F. Yocum, S. D. Betts and N. R. Bowlby, *J. Am. Chem. Soc.* 1990, **112**, 2549.

Polyhedron Vol. 9, No. 24, pp. 2873–2878, 1990
Printed in Great Britain

0277–5387/90 $3.00+.00
© 1990 Pergamon Press plc

SYNTHESIS, CHARACTERIZATION AND STRUCTURE OF COMPLEXES OF *o*-AMINOPHENOL-N,N,O-TRIACETIC ACID WITH COBALT(II), NICKEL(II), MANGANESE(II) AND ZINC(II)

ZHANG HUALIN* and LI PEIYI

Department of Chemistry, Fudan University, Shanghai, P.R.C.

and

WANG BOYI, WU JIANHUA and ZHENG PEIJU

Center of Analysis and Measurement, Fudan University, Shanghai, P.R.C.

(*Received* 11 *December* 1989; *accepted* 20 *July* 1990)

Abstract—The potassium salt of *o*-aminophenol-N,N,O-triacetic acid (APTA) and $KMnL \cdot H_2O$, $KCoL \cdot 3H_2O$, $KNiL \cdot 3H_2O$, $KZnL \cdot 3ZH_2O$, $Co(CoL)_2 \cdot 7H_2O$ and $Ni(NiL)_2 \cdot 8H_2O$ (L^{3-} : anion of APTA) have been synthesized and characterized by elementary analysis, thermogravimetric analysis, molar conductance, IR spectra, magnetic measurements and electronic spectra. The coordination environments of these metal ions have been discussed on the basis of these studies. The single crystal structure of cobalt(II)–APTA has been determined as $CoL \cdot 0.5Co(H_2O)_6 \cdot 4H_2O$, which contains two types of cobalt(II). One type of cobalt(II) is coordinated with six water molecules to form $Co(H_2O)_6^{2+}$, the other is chelated by APTA to form a distorted octahedron and linked into an infinite chain anion $[CoC_6H_4(OCH_2COO)N(CH_2COO)_2^-]_n$, in which each cobalt(II) atom is linked with neighbouring cobalt(II) atoms through two carboxylate oxygen atoms of the phenoxyacetate group. Water molecules occupy interstices in the structure.

Amino carboxylates, as one type of organic ligand, have found wide uses in many important fields as a result of their excellent coordination abilities. *o*-Aminophenol-N,N,O-triacetic acid (APTA) is a new kind of ligand in which iminodiacetic acid is incorporated into the *ortho* position on the ring of phenoxyacetic acid. It is interesting to study the derivatives of phenoxyacetic acid, not only for their special physiological action[1,2] but also for their potential coordination ability,[3,4] especially the coordination behaviour of ethereal oxygen.[5,6] Generally, isolated ethereal oxygen is weakly linked to metal ions or not bonded at all. However, when a strong coordination group is introduced adjacent to an ethereal oxygen, the coordination ability of the ethereal oxygen is greatly increased due to the chelate effect. Therefore the title ligand and its complexes with manganese(II), cobalt(II), nickel(II) and zinc (II) were synthesized and characterized by thermal analysis, IR spectra, electronic spectra and magnetic moments, and the single crystal structure of the cobalt(II) complex determined. On the basis of the physicochemical measurements, the coordination stereochemistry of complexes has been discussed in view of the nature of APTA and the central metal ions.

EXPERIMENTAL

Preparation of compounds

Monopotassium salt of APTA (KH_2L)[7]

o-Aminophenol (0.25 mol) was added to an aqueous solution of $ClCH_2COOK$ (1 mol). The mixture was heated under N_2 with continuous stirring and the pH was maintained above 10 using 5 mol dm^{-3}

* Author to whom correspondence should be addressed.

KOH. After $1\frac{1}{2}$ h, $ClCH_2COOK$ (0.25 mol) was added to ensure the reaction was complete and the mixture was allowed to continue refluxing until the pH of the solution remained constant. The solution was then acidified to pH 3.3 with 6 mol dm^{-3} HCl after cooling and the mixture was allowed to stand overnight. The product was recrystallized twice from deionized water to give the white microcrystalline monopotassium salt of APTA (KH_2L, L^{3-} = anion of APTA). Melting point: 208°C (dec.). Found: C, 44.8; H, 3.8; N, 4.3. Calc. for $C_{12}H_{12}NO_7K$: C, 44.9; H, 3.8; N, 4.4%.

$KM^{II}L \cdot xH_2O$

(a) $KMnL \cdot H_2O$. $MnCO_3$ (1 mmol) was added to KH_2L (1 mmol) in 10 cm^3 of H_2O and the mixture was stirred under N_2 until the pH of the mixture reached 6. 15 cm^3 of ethanol was added to the filtrate and the product was recrystallized with water–ethanol (1 : 1).

(b) $KCoL \cdot 3H_2O$, $KNiL \cdot 3H_2O$ *and* $KZnL \cdot 3H_2O$. $M^{II}CO_3$ (1 mmol) was added to KH_2L (1 mmol) in 20 cm^3 of H_2O and the mixture was mildly heated with stirring until the pH of the mixture reached 6. The filtrate was evaporated on a 70°C water bath until the microcrystalline product appeared on the surface of the solution, then an equal volume of ethanol was added. The complex salt precipitated from solution after a few hours and was recrystallized from water–ethanol (1 : 1).

$M^{II}(M^{II}L)_2 \cdot xH_2O$ (M = Co, Ni)

KH_2L (1 mmol) was added to 40 cm^3 of an aqueous solution containing $M^{II}(NO_3)_2$ (1.5 mmol). The pH of the solution was adjusted to 3.5 with dilute NaOH. The solution was then evaporated until the microcrystals precipitated from solution. The product was recrystallized from water and dried at 60–70°C.

$CoL \cdot 0.5Co(H_2O)_6 \cdot 4H_2O$

The microcrystals of $Co(CoL)_2 \cdot 7H_2O$ were dissolved in water and this was allowed to evaporate at room temperature. The single crystal obtained from solution was used for X-ray analysis without being dried at temperatures higher than room temperature.

The results of elementary analysis, molar conductivity and thermogravimetric analysis of these complex salts are listed in Tables 1, 2 and 3, respectively.

Apparatus

Microanalyses for C, H and N were performed with a Perkin–Elmer 2400C elementary analyser. Metal analyses were carried out by EDTA complexation titration. Molar conductance measurements were obtained in deionized water using a DDS-11A conductivity apparatus. The thermogravity measurements were performed using a LCT-2 differential thermal analyser in an air atmosphere and at a heating rate of 5°C min^{-1}. IR spectra were recorded using a IFS113V IR Fourier spectrometer and KBr discs. The electronic spectra of aqueous solution in the UV–vis region were recorded on a Shimadzu 240 UV–vis spectrophotometer, and in the near-IR region on a Hitachi 330 IR spectrophotometer. The absorption spectra of solid compounds in the UV–vis region were monitored with a Hitachi 557 UV–vis spectrophotometer. Magnetic susceptibilities were determined at room temperature by the Gouy method using $(NH_4)_2Fe(SO_4)_2 \cdot 5H_2O$ as a calibrant, and the diamagnetic corrections for ligand and H_2O were applied. The X-ray intensity data from a single crystal were collected on a CAD4 diffractometer with Mo-K_α radiation using the ω–2θ scan mode. A total of 3565 independent reflections in the range $\theta \leqslant 25$ were measured, of which 2363

Table 1. The elementary analysis data of M^{II}–APTA complexes[a]

Complex	C (%)	H (%)	N (%)	M (%)
$KMnL \cdot H_2O$	36.4(36.7)	3.3(3.5)	3.5(3.5)	13.9(14.0)
$KCoL \cdot 3H_2O$	33.5(33.3)	3.6(3.7)	3.3(3.2)	13.8(13.6)
$KNiL \cdot 3H_2O$	33.4(33.4)	3.5(3.7)	3.1(3.2)	13.5(13.6)
$KZnL \cdot 3H_2O$	32.5(32.8)	3.6(3.7)	3.3(3.2)	14.7(14.9)
$Co(CoL)_2 \cdot 7H_2O$	33.5(33.4)	4.2(4.0)	3.3(3.3)	20.3(20.5)
$Ni(NiL)_2 \cdot 8H_2O$	32.7(32.7)	4.2(4.1)	3.3(3.2)	19.9(20.0)

[a] Values in parentheses are calculated according to the formula listed in the above table.

Table 2. Molar conductivities of M^{II}–APTA complexes at 20°C ($\sim 10^{-3}$ mol dm^{-3} aqueous solution)

Complex	S (cm^2 mol^{-1})
KMnL·H_2O	94.9
KCoL·$3H_2O$	83.9
KNiL·$3H_2O$	84.5
KZnL·$3H_2O$	77.6
$Co(CoL)_2 \cdot 7H_2O$	130.3
$Ni(NiL)_2 \cdot 8H_2O$	135.3

reflections with $I \geqslant 3\sigma(I)$ were considered to be observable. An Lp correction was applied. The structure was solved by direct methods and difference Fourier syntheses. The positions of hydrogen atoms were calculated. The refinements were carried out by full-matrix least-squares procedures with anisotropic temperature factors for non-hydrogen atoms and isotropic temperature factors for hydrogen atoms. The final R is 0.063. The calculations were performed on a PDP 11/44 using the SDP program. Atomic scattering factors were taken from the *International Tables for X-ray Crystallography* (1974).

RESULTS AND DISCUSSION

Structure of $[CoC_6H_4(OCH_2COO)N(CH_2COO)_2] \cdot 0.5[Co(H_2O)_6] \cdot 4H_2O$

$[CoC_6H_4(OCH_2COO)N(CH_2COO)_2] \cdot 0.5[Co(H_2O)_6] \cdot 4H_2O$, $Mr = 989.45$, orthorhombic, *Pbnm*, $a = 9.343(2)$, $b = 18.447(3)$, $c = 24.100(5)$ Å, $Z = 4$, $V = 4153.5$ Å^3, $D_c = 1.582$ g cm^{-3}, $\mu = 6.591$ cm^{-1}, $R = 0.063$ for 2363 observed reflections. The bond lengths and angles are listed in Tables 4 and 5. A view of $[CoC_6H_4(OCH_2COO)N(CH_2COO)_2]^-$ is shown in Fig. 1. There are two different coordination environments of cobalt(II) in the complex. One kind of cobalt(II) is chelated by APTA and linked into an infinite chain anion $\{[CoC_6H_4(OCH_2COO)N(CH_2COO)_2]^-\}_n$, and the other kind of cobalt(II) is coordinated by six water molecules to form $[Co(H_2O)_6]^{2+}$.

In the anion group, the central cobalt atom is bonded to N, O(1), O(3), O(5), O(6) and O(7) to form a severely distorted octahedron, in which O(6) is another carboxylate oxygen atom of the phenoxyacetate group in an adjacent Co^{II}–APTA unit, and

Table 3. The results of thermogravimetric analysis of M^{II}–APTA complexes

Complex	Calc. H_2O (%)	Found H_2O (%)	H_2O Loss temperature range
KMnL·H_2O	4.6	4.6	190–240°C
KCoL·$3H_2O$	12.5	12.5	65–135°C
KNiL·$3H_2O$	12.5	12.4	50–190°C
KZnL·$3H_2O$	12.3	12.0	45–190°C
$Co(CoL)_2 \cdot 7H_2O$	14.6	14.6	120–185°C
$Ni(NiL)_2 \cdot 8H_2O$	16.4	16.0	120–255°C

Table 4. Bond distances in angstroms

Co—O(1)	2.065(3)	O(1)—C(8)	1.267(5)
Co—O(3)	2.056(3)	O(2)—C(8)	1.254(5)
Co—O(5)	2.104(3)	O(3)—C(10)	1.261(5)
Co—O(6)	2.077(3)	O(4)—C(10)	1.245(5)
Co—O(7)	2.053(3)	O(5)—C(6)	1.375(4)
Co—N	2.234(3)	O(5)—C(11)	1.429(4)
Co(1)—O(8)	2.115(5)	O(6)—C(12)	1.242(4)
Co(1)—O(9)	2.063(3)	O(7)—C(12)	1.263(4)
Co(1)—O(10)	2.011(4)	N—C(1)	1.454(5)
Co(1)—O(11)	2.143(5)	N—C(7)	1.469(5)
Co(1)—O(12)	2.181(4)	N—C(9)	1.484(5)
C(1)—C(2)	1.392(5)	C(1)—C(6)	1.396(5)
C(2)—C(3)	1.369(6)	C(3)—C(4)	1.385(7)
C(4)—C(5)	1.379(6)	C(5)—C(6)	1.369(6)
C(7)—C(8)	1.516(6)	C(9)—C(10)	1.515(6)
C(11)—C(12)	1.510(5)		

Numbers in parentheses are ESDs in the least significant digits.

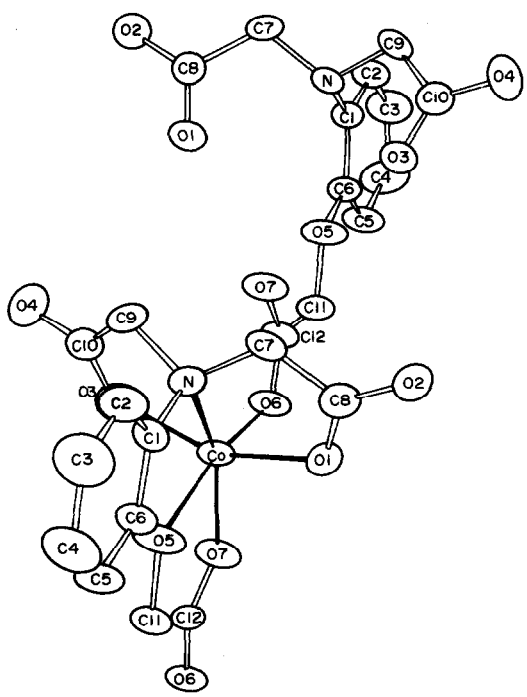

Fig. 1. Structure of CoL^-.

Table 5. Bond angles in degrees

O(1)—Co—O(3)	152.9(1)	O(10)—Co(1)—O(11)	83.8(1)
O(1)—Co—O(5)	94.1(1)	O(10)—Co(1)—O(12)	175.4(2)
O(1)—Co—O(6)	89.8(1)	O(11)—Co(1)—O(12)	91.5(1)
O(1)—Co—O(7)	103.8(1)	C(6)—O(5)—C(11)	122.0(3)
O(1)—Co—N	77.7(1)	C(1)—N—C(9)	111.5(3)
O(3)—Co—O(5)	95.1(1)	C(1)—N—C(7)	112.1(3)
O(3)—Co—O(6)	88.8(1)	C(7)—N—C(9)	113.4(3)
O(3)—Co—O(7)	103.2(1)	N—C(1)—C(2)	121.6(3)
O(3)—Co—N	79.7(1)	N—C(1)—C(6)	120.3(3)
O(5)—Co—O(6)	162.8(1)	C(2)—C(1)—C(6)	118.2(4)
O(5)—Co—O(7)	75.4(1)	C(1)—C(2)—C(3)	120.5(4)
O(5)—Co—N	77.1(1)	C(2)—C(3)—C(4)	120.4(4)
O(6)—Co—O(7)	87.4(1)	C(3)—C(4)—C(5)	120.0(4)
O(6)—Co—N	120.1(1)	C(4)—C(5)—C(6)	119.5(4)
O(7)—Co—N	152.5(1)	O(5)—C(6)—C(1)	114.8(3)
O(8)—Co(1)—O(9)	88.9(1)	O(5)—C(6)—C(5)	123.7(3)
O(8)—Co(1)—O(10)	96.2(1)	C(1)—C(6)—C(5)	121.4(4)
O(8)—Co(1)—O(11)	180.00(0)	N—C(7)—C(8)	112.3(3)
O(8)—Co(1)—O(12)	88.5(1)	O(1)—C(8)—O(2)	124.3(4)
O(9)—Co(1)—O(9)	177.3(2)	O(1)—C(8)—C(7)	118.6(4)
O(9)—Co(1)—O(10)	89.32(9)	O(2)—C(8)—C(7)	117.0(4)
O(9)—Co(1)—O(11)	91.1(1)	N—C(9)—C(10)	113.5(3)
O(9)—Co(1)—O(12)	90.77(9)	O(3)—C(10)—O(4)	124.9(4)
O(3)—C(10)—C(9)	118.9(4)	O(4)—C(10)—C(9)	116.1(3)
O(5)—C(11)—C(12)	106.4(3)	O(6)—C(12)—O(7)	124.9(3)
O(6)—C(12)—C(11)	116.1(3)	O(7)—C(12)—C(11)	119.1(3)

Numbers in parentheses are estimated standard deviations in the least significant digits.

the discrete units of Co^{II}–APTA are linked through two carboxylate oxygen atoms of phenoxyacetate to form an infinite chain polynuclear complexing-anion, in which the cobalt atoms are arranged in a zigzag mode. Here, APTA acts as a hexadentate ligand and the phenyl group—C(1), C(2), C(3), C(4), C(5) and C(6), amine nitrogen N, ethereal oxygen O(5), phenoxyacetate group–C(11), C(12), O(6), O(7) and cobalt atom are roughly co-planar within 0.08 Å. The Co^{II}—N bond length in Co^{II}–APTA is longer than that in Co^{II}—HBATA (HBATA : *o*-hydroxybenzylamine-N,N,O-triacetic acid, one of the analogues of APTA), but the Co^{II}—O(ether) bond length is shorter than that in Co^{II}—HBATA[8] [Co—N, 2.120 Å; Co—O(ether), 2.233 Å]. Obviously, the longer bond length of Co^{II}—N in Co^{II}—APTA can be ascribed to the weaker basicity of the aromatic amine nitrogen of APTA due to the p–π conjugation system. The comparatively shorter bond length of Co^{II}—O(ether) in Co^{II}—APTA may be rationalized as being due to the higher electron density on the ethereal oxygen of APTA as a result of more extensive electronic delocalization on the conjugated system (in APTA the delocalized π bond is π_8^{10}, while in HBATA is π_7^8). Since the weak coordinating ability of ethereal oxygen is generally accepted, it is quite natural that the Co^{II}—N bond length (2.120 Å) is shorter than that of Co^{II}—O(ether) (2.233 Å) in Co^{II}—HBATA. However, the sequence of bond lengths in Co^{II}—APTA is reversed, but if referred to the structural parameters of the protonated complex of cobalt(II) with APDA (*o*-aminophenol-N,N-diacetic acid),[9] in which the Co^{II}—N bond length (2.156 Å) is quite close to that of Co^{II}—O(phenol) (2.154 Å), the above structural character is not abnormal. Firstly, the formation of the phenoxyacetate chelate ring reinforces the interaction between cobalt(II) and oxygen(ether) and secondly, unlike HBATA in which the C—N bond can revolve freely to reach the most stable steric arrangement, the co-plane of the benzene ring with the nitrogen atom makes APTA more rigid in the steric adjustment. So the least tension framework is attained only by adjusting the bond lengths of Co^{II}—N and Co^{II}—O (ether). Consequently, while the Co^{II}—O(ether) bond is strengthened, the Co^{II}—N bond is weakened. For the same reason, in Co^{II}—APTA

there is more space left for the sixth coordination atom, which makes it possible for Co^{II}—APTA to adopt a chain polynuclear structure.

From the crystal structures of Co^{II}—APTA and Co^{II}—HBATA, it can be predicted that although the coordination ability of ethereal oxygen is relatively weak, it would greatly increase when a strong coordination group adjoins to the ethereal oxygen and forms a chelate ring with it; it would be so, especially when the adjacent group would affect the electronic effects on ethereal oxygen.

Infrared spectra

The most characteristic bands in the IR spectra of KH_2L and its complexes are given in Table 6.[10] The characteristic absorptions of coordinated APTA in complexes shift toward lower or higher frequency as compared with uncoordinated APTA, which indicates that APTA is coordinated to the metal ion through the carboxylate oxygen, ethereal oxygen and aromatic amine nitrogen. Generally, when a carboxylate group is coordinated to a metal in the form of (a), the stronger the interaction, the larger the $\Delta\nu_{(a)}$ [$\Delta\nu = \nu_{as}(-COO^-) - \nu_s(-COO^-)$], while in the form of (b), $\Delta\nu_{(b)}$ is smaller than $\Delta\nu_{(a)}$.[11]

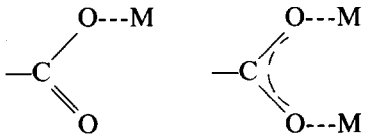

(a) (b)

The results reveal a different order ($\Delta\nu$: $KZnL \cdot 3H_2O < KNiL \cdot 3H_2O < KCoL \cdot 3H_2O < KMnL \cdot H_2O$) to the Erving and Williams M^{II} stability order ($Zn^{II} < Ni^{II} < Co^{II} > Mn^{II}$) which may probably be attributed to the existence of the (b) coordination pattern in the cobalt(II) complex.

Table 7. Magnetic moments of complexes of APTA with Co^{II}, Ni^{II} and Mn^{II} at room temperature

Complex	μ_{eff} (BM)
$KCoL \cdot 3H_2O$	4.71
$KNiL \cdot 3H_2O$	3.16
$KMnL \cdot H_2O$	5.88
$Co(CoL)_2 \cdot 7H_2O$	4.79[a]
$Ni(NiL)_2 \cdot 8H_2O$	3.26[a]

[a] Values are corrected for the paramagnetism of $Co(H_2O)_6^{2+}$ and $Ni(H_2O)_6^{2+}$.

Magnetism

The magnetic moments of complexes are collected in Table 7. All compounds except $KZnL \cdot 3H_2O$ are high spin. Usually, μ_{eff} values for high-spin octahedral cobalt(II) complexes range from 4.8 to 5.2 BM.[12] The μ_{eff} value for Co^{II}—APTA is slightly lower than 4.8 BM, which implicates that the coordination geometry around each cobalt atom is a distorted octahedron,[13] as illustrated in Fig. 1. The μ_{eff} value for Ni^{II}—APTA falls within the normal range (2.9–3.4 BM[12]), which indicates the octahedral arrangement around nickel(II) in its high-spin APTA complexes. The μ_{eff} value for Mn^{II}—APTA is close to the $\mu_{s.o.}$ value, which provides no more information than that APTA is a weak-field ligand. The thermogravimetric analysis, however, shows that there is one water molecule coordinated to manganese(II),

Table 6. The infrared spectra of KH_2L and M^{II}–APTA complexes (cm^{-1})

Species	ν(—C(=O)—)	ν(—C(=O)—O$^-$)	$\nu(\phi$—N)	$\nu(\phi$—O—C)	ν(O—H)
KH_2L	1730(vs)	1657(s) 1430(m)	1337(m)	1250(s) 1058(m)	
$KMnL \cdot H_2O$		1619(vs) 1421(s) 1595(sh) 1401(s)	1323(m)	1259(s) 1065(m)	3133
$KCoL \cdot 3H_2O$		1606(vs) 1405(s)	1307(m)	1253(s) 1035(m)	3421
$KNiL \cdot 3H_2O$		1611(vs) 1397(s)	1297(m)	1249(s) 1034(m)	3442
$KZnL \cdot 3H_2O$		1605(vs) 1409(s)	1308(m)	1257(s) 1039(m)	3442
$Co(CoL)_2 \cdot 7H_2O$		1607(vs) 1408(s) 1597(vs) 1395(s)	1329(m)	1246(s) 1039(m)	3355
$Ni(NiL)_2 \cdot 8H_2O$		1606(vs) 1592(vs) 1399(s)	1328(m)	1245(s) 1038(m)	3359

Table 8. The electronic spectra of M^{II}–APTA complexes

Complex	State	ν_1 (nm)	ν_2 (nm)	ν_3 (nm)	Dq (cm^{-1})	B (cm^{-1})	β
$KCoL \cdot 3H_2O$	aq.	1215		520	934	802	0.83
$Co(CoL)_2 \cdot 7H_2O$	aq.[a]	1215		520			
$KCoL \cdot 3H_2O$	solid			518			
$Co(CoL)_2 \cdot 7H_2O$	solid			520			
$KNiL \cdot 3H_2O$	aq.	1075	650	392	930	852	0.83
$Ni(NiL)_2 \cdot 8H_2O$	aq.[a]	1075	650	392			
$KNiL \cdot 3H_2O$	solid		650	390			
$Ni(NiL)_2 \cdot 8H_2O$	solid		656	395			

For Co^{II}–APTA: $\nu_1\ {}^4T_{1g}(F)\text{---}{}^4T_{2g}(P)$; $\nu_2\ {}^4T_{1g}\text{---}{}^4A_{2g}$; $\nu_3\ {}^4T_{1g}\text{---}{}^4T_{1g}(P)$

For Ni^{II}–APTA: $\nu_1\ {}^3A_{2g}\text{---}{}^3T_{2g}$; $\nu_2\ {}^3A_{2g}\text{---}{}^3T_{1g}(F)$; $\nu_3\ {}^3A_{2g}\text{---}{}^3T_{1g}(P)$

[a] A $M(H_2O)_6(NO_3)_2$ solution of the same concentration as reference.

therefore manganese(II) is probably located in the central area of a distorted octahedron.

Electronic spectra

The electronic spectra of complexes are given in Table 8. The similarity of the absorption spectra of $KCoL \cdot 3H_2O$ or $KNiL \cdot 3H_2O$ and $Co(CoL)_2 \cdot 7H_2O$ or $Ni(NiL)_2 \cdot 8H_2O$ in solution or in the solid state suggests that the structure of the complex anion in both states is independent of the counter-ion. The main features of these spectra are consistent with the octahedral geometry around cobalt (II) and nickel(II). The absorption bands were assigned and approximate *Dq*, *B* and β were evaluated for an ideal octahedron (see Table 8). Both β values are less than one, which suggests the existence of some electron delocalization in cobalt (II) and nickel(II) complexes. Since the zinc(II) complex is colourless and antimagnetic, the absorption spectrum of the cobalt(II)-dopped zinc(II) complex was recorded in order to gain some insight into the coordination geometry around zinc(II). It gives an absorption peak around 535 nm, which is similar to Co(II)—APTA in its appearance and red shifts about 15 nm in its location. So the zinc(II) atom is probably octahedrally coordinated to APTA.

Acknowledgement—This work was supported by the National Natural Science Foundation of China as an item of major project.

REFERENCES

1. A. Chiriac, V. Chiriac, D. Ciubotariu, S. Holban and Z. Simon, *Eur. J. Med. Chem.-Chim. Ther.* 1983, **18**, 507.
2. D. D. Perrin, *Nature* 1961, **191**, 253.
3. R. Sahai and A. K. Chaudhary, *Monatsh. Chem.* 1982, **113**, 681.
4. G. Smith, E. J. O'Reilly, C. H. L. Kennard, K. Stadnicka and B. Oleksyn, *Inorg. Chim. Acta* 1981, **47**, 111.
5. Y. Hasegawa and G. R. Choppin, *Inorg. Chem.* 1977, **16**, 2931.
6. Zhang Hualin and Xu Kangcheng, *Huaxue Xuebao* 1985, **43**, 562.
7. Zhang Hualin and Zhou Meisheng, private communication.
8. Wu Guang, Wang Boyi, Zheng Peiju, Cheng Longchun, Xu Junxing, Zhang Peiyue, Zhang Huinong and Zhang Hualin, *Wuji Huaxue*, 1988, **4**(1), 97.
9. A. E. Obodovskaya and L. M. Shkol'nikova, *Koord. Khim.* 1979, **5**, 762.
10. K. Nakanishi and P. H. Solomon, *Infrared Absorption Spectroscopy*, 2nd ed., Holden-Day, San Francisco (1977).
11. G. B. Deacon and R. J. Phillips, *Coord. Chem. Rev.* 1980, **33**, 227.
12. F. A. Cotton and G. Wilkinson, *Advanced Inorganic Chemistry*, 4th ed., John Wiley, New York (1980).
13. M. Cartwright, D. A. Edwards and J. M. Potts, *Inorg. Chim. Acta* 1979, **34**, 211.
14. A. B. P. Lever, *Inorganic Electronic Spectroscopy*, 2nd ed., Elsevier, Amsterdam (1984).

Polyhedron Vol. 9, No. 24, pp. 2879–2885, 1990
Printed in Great Britain

0277–5387/90 $3.00+.00
© 1990 Pergamon Press plc

INTERACTION OF HETEROCYCLIC THIOAMIDES WITH TELLURIUM(II) AND TELLURIUM(IV). SYNTHESES AND CRYSTAL STRUCTURES OF BIS[2-(2-THIOXO-1,3-THIAZOLIDIN-3-YL)-4,5-DIHYDRO-1,3-THIAZOLIUM]HEXABROMOTELLURATE(IV) AND TRIS(1-METHYLIMIDAZOLE-2-(3H)-THIONE)TELLURIUM(II) BROMIDE

V. KUMAR and G. ARAVAMUDAN*

Department of Chemistry, Indian Institute of Technology, Madras 600 036, India

and

M. SESHASAYEE

Department of Physics, Indian Institute of Technology, Madras 600 036, India

(*Received* 15 *December* 1989; *accepted after revision* 20 *July* 1990)

Abstract—Reaction of 1,3-thiazolidine-2-thione with tellurium(IV) in hydrobromic acid medium gave the hexabromotellurate, $[C_6H_9N_2S_3]_2^{2+}[Te^{IV}Br_6]^{2-}$ (**3**). Reaction of 1-methylimidazoline-2-(3H)-thione (L″) with tellurium(IV), in hydrobromic acid medium, gave the mixed-ligand tellurium(II) complex $[Te^{II}L''_3Br]^+Br^-$ (**4**). The structures of $[C_6H_9N_2S_3]_2^{2+}$ $[Te^{IV}Br_6]^{2-}$ (**3**) and $[Te^{II}L''_3Br]^+Br^-$ were determined by single crystal X-ray diffraction methods. In **3** the unit cell contains $[TeBr_6]^{2-}$ anions and two $[C_6H_9N_2S_3]^+$ cations. There is no direct bonding between the metal atom and the cations. In the anion only slight angular deviations from the perfect octahedral geometry are observed. The lone pair of electrons on tellurium(IV) is found to be stereochemically inert. In the cation the two five-membered heterocyclic rings adopt different conformations. In complex **4**, in the solid state, the planar $[Te^{II}L''_3Br]^+$ cation and Br^- anion are held together by ionic interactions. In the cation, L″ is bonded to the central tellurium atom through the sulphur atom.

The heterocyclic thioamides, 1,3-thiazolidine-2-thione (L) and 1-methylimidazoline-2(3H)-thione (L″), are ambidentate ligands in that they can coordinate through the heterocyclic nitrogen or the exocyclic sulphur atom.[1–5] Thiols are capable of undergoing reductive complexation reactions with tellurium(IV) and selenium(IV).[6–9] The interaction of thiols, like 3-mercaptopropionic acid, cysteine, etc., has led to the isolation of the bis(thiolato) complex of tellurium(II) and selenium(II). Interaction of L with transition metals like palladium, cadmium, etc., have resulted in the formation of complexes in which the ligand L remains intact.[10,11] Kubiak and Glowiak[12] on trying to prepare the zinc complex of L, noticed the formation of a new compound of overall composition, $[L'H]^+[ZnCl_3(H_2O)]^-$;

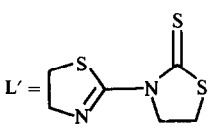

Ainscough *et al.*[13] noticed the formation of $Cu^IL'Cl_2$ during the interaction of L with copper(II) in nitromethane as solvent. Earlier, with selenium(IV), we observed the formation of the hydrobromide of L′.[14] The disulphide, 2,2′-dithiobis[4,5-dihydrothiazole], formed by the oxidation of L is known to rearrange on acid catalysis giving the

* Author to whom correspondence should be addressed.

thiocarbonyl derivative, L′.[15] Complexes of L″ with the metal ions Cr^{III},[16] Co^{II},[17] Ni^{II},[18] Cu^{I},[19,20] Zn^{II},[21] Pd^{II},[22] Pt^{II},[23] Cd^{II},[24] Pb^{II}[25] have been reported. Reaction between copper(II) salts and L″ produced a wide variety of compounds whose composition was dependent on the nature of the solvent, the coodinating properties of the counter ion as well as the molar ratios of the reactants. Agnus *et al.*[26] have reported a Cu^{I}–Cu^{II} cluster featuring the mercaptide anion of L″. Two structures have also been reported which involve an oxidized form of L″, namely 1,1′-dimethyl-2,2′-dimidazolylmonosulphide.[27,28] During the interaction of copper(II) salts with L″, copper(II) is reduced by L″ to copper(I), while L″ is oxidized to the corresponding disulphide. L″ is also known to form 1 : 1 charge-transfer complexes with di-iodine.[29] During the interactions of the thioamides, L and L″, with tellurium(IV) in acid media, attempts to isolate bis(thiolato) complexes of tellurium(II) were made.

The interaction of L with tellurium(IV) in acid media, such as HCl, H_2SO_4, etc., did not yield any isolable crystalline products. However, on employing HBr medium, the formation of the hexabromotellurate (**3**) was observed. The mixed-ligand tellurium(II) complex, $[Te^{II}L''_3Br]^+[Br]^-$ (**4**) was obtained during the interaction of L″ with tellurium(IV) in HBr medium. In this paper, we report the syntheses and crystal structure determinations of **3** and **4**.

EXPERIMENTAL

Preparation of bis[2-(2-*thioxo*-1,3-*thiazolidin*-3-*yl*)-4,5-*dihydro*-1,3-*thiazolium*]*hexabromotellurate*(IV) (**3**)

Ligand L (0.48 g, 4 mmol) was dissolved in 15 cm^3 of methyl alcohol. To this was slowly added tellurium dioxide (0.159 g, 1 mmol) in 5 cm^3 of 4 N hydrobromic acid. The solution gradually turned yellow. After about 24 h, a mixture of orange–red coloured solid and yellow needles of L′ (the thione derivative) were formed. To this, 20 cm^3 of acetonitrile were added, stirred for 15 min and filtered. The filtrate was deep red in colour. The filtrate on slow evaporation at room temperature yielded small, red, transparent crystals of **3**. Found: C, 13.6; H, 1.7; N, 5.7; S, 17.9; Br, 46.4; Te, 11.9. $TeC_{12}H_{18}N_4S_6Br_6$ requires: C, 14.2; H, 1.8; N, 5.5; S, 18.9; Br, 47.1; Te, 12.5%. IR (cm^{-1}): 1575 (s, C=N); 1360 (m, C⋯N); 1040 (m, C=S). ^1H NMR (DMSO-d_6): δ 3.25–3.45 (d, —CH_2—S—C=S); 3.50–3.70 (d, —CH_2S); 3.80–4.10 (d, —CH_2—N—C=S); 4.60–4.80 (d, —CH_2—N—).

Preparation of bromotris(1-*methylimidazoline*-2-(3H)-*thione*)*tellurium*(II) *bromide* (**4**)

Ligand L″ (0.33 g, 3 mmol) was dissolved in 10 cm^3 of methyl alcohol. To this was slowly added tellurium dioxide (0.08 g, 0.5 mmol) in 5 cm^3 of 4 N hydrobromic acid. A deep red colour was produced. The solution on slow evaporation at room temperature yielded small, red, transparent crystals of **4**. The yield was nearly quantitative. Found: C, 21.8; H, 2.5; N, 12.8; Br, 24.8; Te, 19.8. $TeC_{12}H_{18}N_6S_3Br_2$ requires: C, 22.9; H, 2.9; N, 13.1; Br, 25.4; Te, 20.3%. IR (cm^{-1}): 3270–3110 (b, —NH); 1560 (s, C=N); 1395 (s, C⋯N); 960 (m, C⋯S). ^1H NMR (DMSO-d_6): 3.5 (s, —CH_3); 6.7 (d, —CH); 7.1 (d, —CH); 12.2 (b, —NH).

X-ray structure determination of **3** *and* **4**

Crystal data and data collection parameters for **3** and **4** are given in Tables 1 and 2, respectively. The intensity data were corrected for Lorentz and polarization effects. The structures were solved by the heavy-atom method. The positions of tellurium and bromine were obtained from the respective Patterson map. Successive difference Fourier maps revealed the positions of all the remaining non-hydrogen atoms. Non-hydrogen atoms were refined anisotropically by the full-matrix least-squares method using SHELX 76.[30] The scattering factors for tellurium were obtained from Cromer and Mann.[31] Refinement was continued using a weighting scheme of $w = 1/[\sigma^2(F_o)+g|F_o|^2]$ (g being 0.0075 for **3** and 0.0267 for **4**) until the $(\text{shift/ESD})_{max}$ in non-hydrogen parameters was less than 0.01. For both **3** and **4**, the hydrogen atoms did not appear in the final difference Fourier map and their positions were geometrically fixed and not refined. Maximum electron densities in the final difference Fourier map were 2.76 for **3** and 4.35 $eÅ^{-3}$ for **4**, but were rejected due to their proximities to tellurium.

DISCUSSION

Formation aspects of complex **3**

The hexabromotellurate, $[C_6H_9N_2S_3]_2^{2+}[Te^{IV}Br_6]^{2-}$, presents an interesting example of some subtle aspects of coordination. Tellurium(IV) exhibits borderline behaviour from the concept of HSAB[31] theory. Therefore the thione sulphur of L′ would have been expected to coordinate to tellurium(IV). However, bromide, which is a relatively harder base, is coordinated to

Table 1. Crystallographic data for $[C_6H_9N_2S_3]_2^{2+}[TeBr_6]^{2-}$

(a) *Physical and crystal data*

Formula: $TeC_{12}H_{18}N_4S_6Br_6$	Molecular weight: 1017.66
Crystal system: monoclinic	V: 1404. 68 Å^3
Space group: $P2_1/c$	Z: 2
a: 8.618(5) Å	ρ_{exp}: 2.35 g cm^{-3}
b: 11.401(7) Å	ρ_x: 2.36 g cm^{-3}
c: 14.327(5) Å	μ(Mo-K_α): 9.78 mm^{-1}

Morphology: Parallelopiped (0.175 × 0.24 × 0.16) mm

(b) *Data collection*

Temperature 293 K	Horizontal APT: [2.75 + 1.25 tan θ] mm
Crystal detector: 173 mm	Vertical APT: 4.0 mm
Take-off angle: 6.0°	Scan mode: ω–2θ
Maximum Bragg angle: θ = 25°	Scan angle: [0.80 + 0.35 tan θ]°

Standard intensity reflections: 5 2 6, $\bar{5}$ 2 $\bar{6}$, 4 3 7

Standard orientation reflections: 4 $\bar{3}$ 5, 5 2 6, 1 $\bar{1}$ 10

Scan speed parameters: SIGPRE[a] = 0.6, SIGMA[a] = 0.032, VPRE[a] = 6.66 mm^{-1}, TMAX[a] = 30 s

Independent recorded reflections: 3873

[a] These parameters are as described in A. Mossett, J. J. Bonnett and J. Galy, *Acta Cryst.* 1977, **B33**, 2633.

tellurium. This can be explained on the basis of the effect of the cation in stabilizing the huge anion, $[TeBr_6]^{2-}$. The formation of the title compound can be explained by the oxidation of L, **1**, in air to the corresponding disulphide, **2**, which in hydrobromic acid medium undergoes rapid intramolecular rearrangement with the extrusion of one sulphur to give the corresponding thione derivative $[L'H]^+$, which brings out the anion from the solution to give **3** as given in Scheme 1.

Table 2. Crystallographic data for $[TeL_3Br]^+Br^-$

(a) *Physical and crystal data*

Formula: $TeC_{12}H_{18}N_6S_3Br_2$	Molecular weight: 629.92
Crystal system: triclinic	V: 1061.69(4) Å^3
Space group: $P\bar{1}$	Z: 2
a: 10.058(8) Å	ρ_{exp}: 1.95 g cm^{-3}
b: 10.700(9) Å	ρ_x: 1.96 g cm^{-3}
c: 10.886(11) Å	μ(Mo-K_α) = 5.27 mm^{-1}
α: 108.15(8)°	Radiation: (Mo-K_α) = 0.71069 Å
β: 95.92(7)°	
γ: 103.68(7)°	

Morphology: Parallelipiped (0.125 × 0.16 × 0.24) mm

(b) *Data collection*

Temprature: 293 K	Horizontal APT: [2.75 + 1.25 tan θ] mm
Crystal detector: 173 mm	Vertical APT: 4.0 mm
Take-off angle: 6.0°	Scan mode: ω–2θ
Maximum Bragg angle: θ = 25°	Scan angle: [0.80 + 0.35 tan θ]°

Standard intensity reflections: 2 7 0, 5 4 $\bar{1}$, $\bar{1}$ 2 4

Standard orientation reflections: 2 7 0, $\bar{4}$ 6 1, $\bar{1}$ 3 4

Scan speed parameters: SIGPRE[a] = 0.6; SIGMA[a] = 0.032; VPRE[a] = 6.66° mm^{-1}; TMAX[a] = 60 s

Independent recorded reflections: 3999

[a] These parameters are as described in A. Mossett, J. J. Bonnett and J. Galy, *Acta Cryst.* 1977, **B23**, 2633.

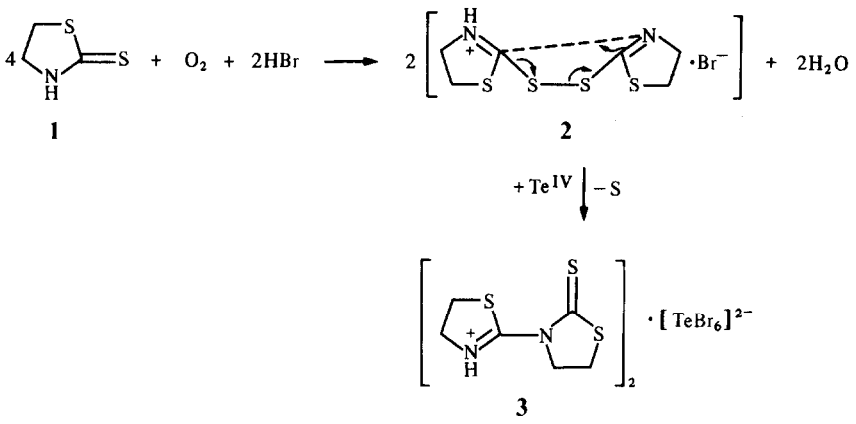

Scheme 1.

Structure of complex **3**

Selected bond lengths and angles are given in Table 3. Figure 1 shows the PLUTO[32] plot of the molecule, while Fig. 2 shows the packing of the molecules in the unit cell.

According to VSEPR[33] theory, a distorted octahedral configuration is expected for systems of the type TeX_6^{2-} (X = Cl, Br, I) which contain six bonding electron pairs and one non-bonding electron pair in the valence shell of tellurium(IV). However, structural investigations on many TeX_6^{2-} anions show a regular octahedral structure. It is observed that the location of tellurium on an inversion centre always produces an undistorted or very slightly distorted octahedron. Highly distorted octahedrons are found with the tellurium atom in a non-centrosymmetric point symmetry group (Table 4). According to Pearson,[34] only small deviations from ideal $m\bar{3}m$ symmetry will be allowed when the point group is of lower symmetry than $m\bar{3}m$.

The hexabromotellurate (**3**) crystallizes in the centrosymmetric space group $P2_1/c$. Only half the molecule is unique, the other half being related by an inversion centre. The tellurium atom of the $[TeBr_6]^{2-}$ anion is at the inversion centre and the $TeBr_6$ octahedron shows slight deviations from the perfect octahedral requirements, with the Br(1)—Te—Br(2) angle being 87.2(2)°. The geometry of the anion is similar to that observed in other centrosymmetric systems. In the cation, the bond parameters are similar to those observed in the hydrobromide of L′. One of the five-membered rings, i.e. the dihydrothiazole ring, adopts the half chair conformation, while the other five-membered ring, namely the thiazolidine thione ring, adopts the envelope conformation.

Table 3. Main bond lengths (Å) and bond angles (°) in **3**, with ESDs in parentheses

Te—Br(1)	2.700(1)	Br(1)—Te—Br(2)	87.2(2)
Te—Br(2)	2.708(1)	Br(1)—Te—Br(3)	89.8(3)
Te—Br(3)	2.691(1)	Br(2)—Te—Br(3)	89.9(3)

The nature of interaction of L″ *with tellurium*(IV)

Tellurites are good oxidizing agents for thiols as indicated by the E_0 values for the two redox systems:

$$RSH + 2H^+ + 2e^- \rightleftharpoons 2RSH; \quad E_0 = 0.07 - 0.03\,V$$

and

$$TeO_3^{2-} + 6H^+ + 4e^- \rightleftharpoons Te^0 + 3H_2O;$$

$$E_0 = 0.53\,V.$$

But the observed reaction is not the reduction of tellurium(IV) to tellurium(0), but the stabilization

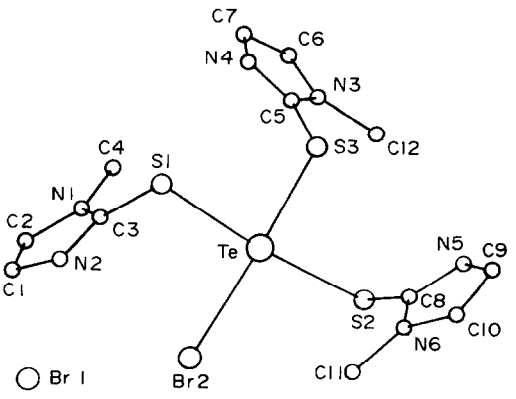

Fig. 1. PLUTO plot of the molecule.

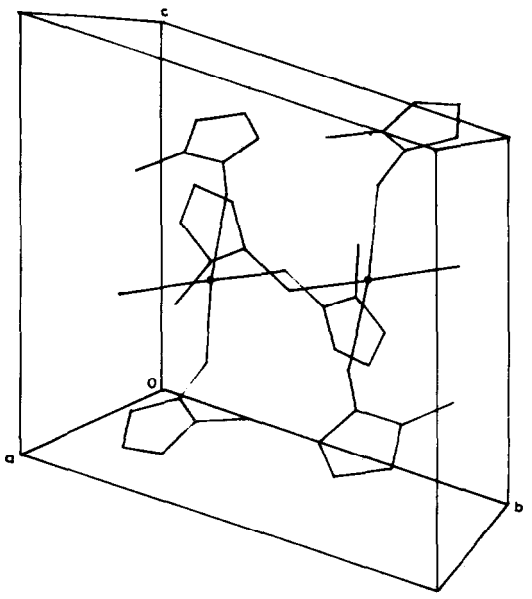

Fig. 2. Packing of the molecules in the unit cell.

of the intermediate and the uncommon oxidation state of +2 of tellurium by thione and bromide complexation. There are two interesting aspects which have to be highlighted. Firstly, this is the first instance in planar tellurium(II) chemistry wherein a three sulphur–one halogen coordination of ligands is reported. Secondly, $[TeL''_3Br]^+Br^-$ forms even in presence of excess ligand, L'', under these conditions formation of $[TeL''_4]^{2+}$ is to be expected. The competitive ligating abilities of thione and bromide have resulted in the formation of a complex which involves both ionic and coordinated bromide. During the reductive complexation reaction with tellurium(IV), L'' becomes oxidized. The first oxidation product should be the disulphide, as is well known in the reactions of excess thioureas and enolizable thiones with tellurium(IV) in acid medium.[40] The fate of the oxidation products of L'' in the solution phase is being investigated.

Table 5. Main bond lengths (Å) and bond angles (°) in **4**, with ESDs in parentheses

Te—S(1)	2.712(3)	Te—S(3)	2.575(3)
Te—S(2)	2.690(3)	Te—Br(2)	2.836(1)
S(1)—Te—S(2)	173.4(1)	S(2)—Te—S(3)	92.7(1)
S(3)—Te—Br(2)	169.4(1)	S(2)—Te—Br(2)	94.0(1)
S(1)—Te—S(3)	81.5(1)	S(1)—Te—Br(2)	92.2(1)

Structure of complex **4**

Selected bond lengths and angles are given in Table 5. Figure 3 shows the PLUTO plot of the molecules, while Fig. 4 shows the packing of the molecules in the unit cell.

The ligands L'' are monodentate and bonded through the sulphur atom to tellurium, with an average Te—S bond length of 2.659 Å. The tellurium atom in the +2 oxidation state, surrounded by three sulphur atoms and a bromide atom, exhibits a characteristically planar geometry.[41] The three sulphur atoms of the ligands, S(1), S(2) and S(3), and the bromine, Br(2), define an approximate plane with deviations of 0.119(5), 0.103(5), −0.149(4) and −0.124(2) Å out of this plane, respectively. The tellurium atom lies 0.05(1) Å out of this plane. The angles subtended at the central tellurium range from 81.5(4) to 94.0(1)° and their sum is 360.4(3)°. The bonding can be explained on the basis of two linear three-centre systems involving p_x and p_y orbitals of tellurium(II) with two ligand σ-orbitals.[42] The angles S(2)—Te—S(1) = 173.4(1) and Br(2)—Te—S(3) = 169.1(4)° show that the two three-centre systems are approximately linear. One of the Te—S distances, Te—S(3) = 2.575(3) Å, is shorter than the other two Te—S distances of 2.712(3) and 2.690(3) Å, probably reflecting the *trans* influence of the bromide atom on S(3). All the L'' ligands are planar and their dimensions are essentially the

Table 4. Comparison of TeX_6^{2-} octahedra

Compound	Space group	Point symmetry for Te	Geometry	Reference
$(H_3N—C_2H_4—NH_3)^{2+}TeCl_6^{2-}$	$P\bar{1}$	$\bar{1}$	Undistorted	35
$(H_3N—C_3H_6—NH_3)^{2+}TeCl_6^{2-}$	*Pnma*	*m*	Distorted	36
$[(MeNH)_2CS_2]^{2+}TeCl_6^{2-}$	$Pna2_1$	1	Distorted	37
$(C_2H_5—CHNH_3—COOH)_2^{2+}TeBr_6^{2-}$	$P2_1/c$	$\bar{1}$	Undistorted	38
$[(CONH_2)_2(CH_2)_2]_2H_2TeBr_6$	$C2/c$	2	Distorted	39
$(C_6H_9N_2S_3)_2^{2+}TeBr_6^{2-}$	$P2_1/c$	$\bar{1}$	Slightly distorted	Present work

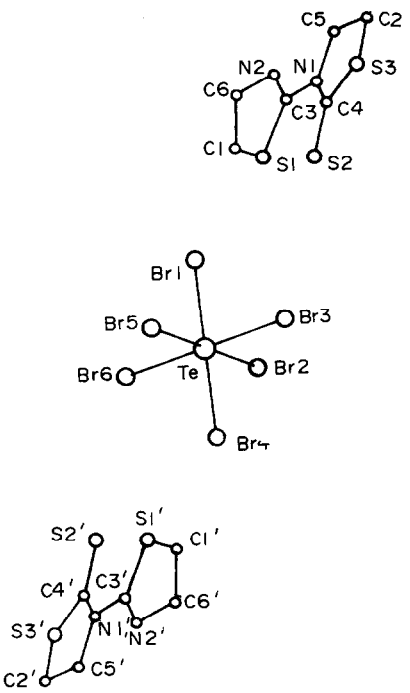

Fig. 3. PLUTO plot of the molecule.

same amongst themselves and are as found in the complexes of L″ with zinc(II), nickel(II), cobalt(II) and lead(II). In the ligands the C—S and C—N bond distances show extensive delocalization in the thioamide moiety. The C—N distances involving the ethylenic carbon atoms are longer than those within the thioamide portion of the ligands. The Te—S—C angles of 99.5(3), 101.8(3) and 102.7(3)° show that the sulphur atoms are essentially sp^3 in character with the $\rangle C^+—S^-$ canonical structure dominating in the coordinated ligand. Two adjacent L″ groups are above the plane defined by tellurium, three sulphur atoms and one bromine atom, while the other L″ group is situated below this plane.

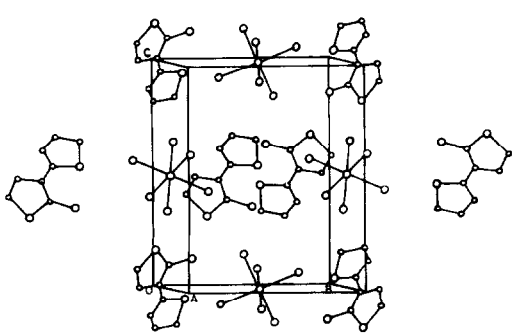

Fig. 4. Packing of the molecules in the unit cell.

Atomic coordinates, thermal parameters, full lists of bond lengths and angles and lists of F_o/F_c values have been deposited as supplementary data with the Editor, from whom copies are available on request. Atomic coordinates have also been deposited with the Cambridge Crystallographic Data Centre.

Acknowledgement—One of the authors (V.K.) thanks the Council of Scientific and Industrial Research, CSIR, New Delhi, India, for the award of a fellowship.

REFERENCES

1. J. Dehand and J. Jordanov, *Inorg. Chim. Acta* 1976, **17**, 37.
2. E. S. Raper and J. L. Brookes, *J. Inorg. Nucl. Chem.* 1977, **39**, 2163.
3. E. Buncel, A. R. Norris, S. E. Taylor and W. J. Racz, *Can. J. Chem.* 1982, **60**, 3033.
4. P. P. Singh, O. P. Agarwala and A. K. Gupta, *Inorg. Chim. Acta* 1976, **18**, 19.
5. E. R. Clarke and M. A. Al-Turaihi, *J. Inorg. Nucl. Chem.* 1976, **38**, 1441.
6. G. C. Rout, M. Seshasayee, G. Aravamudan and S. Sowrirajan, *Acta Cryst.* 1984, **C40**, 963.
7. S. Sowrirajan, G. Aravamudan, M. Seshasayee and G. C. Rout, *Acta Cryst.* 1985, **C41**, 576.
8. G. C. Rout, M. Seshasayee, G. Aravamudan and S. Sowrirajan, *Polyhedron* 1984, **3**, 921.
9. G. C. Rout, M. Seshasayee, G. Aravamudan and S. Sowrirajan, *J. Cryst. Spec. Res.* 1985, **15**, 377.
10. M. Kubiak and T. Glowiak, *Acta Cryst.* 1982, **B38**, 2031.
11. M. Kubiak and T. Glowiak, *Acta Cryst.* 1985, **C41**, 1580.
12. M. Kubiak and T. Glowiak, *Acta Cryst.* 1986, **C42**, 419.
13. E. W. Ainscough, B. F. Anderson, E. N. Baker, A. G. Bingham, M. L. Brader and A. M. Brodie, *Inorg. Chim. Acta* 1985, **105**, L5.
14. V. Kumar, G. Aravamudan, V. Ganesh, M. Seshasayee, D. Heijdenrijk and H. Schenk, *Phosphorus, Sulfur and Silicon* 1989, **45**, 15.
15. A. G. M. Barrett, D. H. R. Barton and R. Colle, *J. Chem. Soc., Perkin Trans.* 1980, **1**, 665.
16. E. S. Raper, S. Redshaw and J. R. Creighton, *Inorg. Chim. Acta* 1984, **87**, L1.
17. E. M. Holt, S. L. Holt and K. H. Watson, *J. Am. Chem. Soc.* 1970, **92**, 2721.
18. E. S. Raper, M. E. O'Neill and J. A. Daniels, *Inorg. Chim. Acta* 1980, **41**, 201.
19. L. P. Battaglia, A. B. Corradi, M. Nardelli and M. E. V. Tani, *J. Chem. Soc., Dalton Trans.* 1976, 143.
20. E. R. Atkison, D. J. Gardiner, A. R. W. Jackson and E. S. Raper, *Inorg. Chim. Acta* 1985, **98**, 35.
21. I. W. Nowell, A. G. Cox and E. S. Raper, *Acta Cryst.* 1979, **35B**, 1947.
22. L. M. Butler, J. R. Creighton, R. E. Outghred, E. S.

Raper and I. W. Nowell, *Inorg. Chim. Acta* 1983, **75**, 149.
23. M. E. O'Neill, E. S. Raper, J. A. Daniels and I. W. Nowell, *Inorg. Chim. Acta* 1982, **66**, 79.
24. E. S. Raper and I. W. Nowell, *Inorg. Chim. Acta* 1980, **43**, 165.
25. S. Bristow, J. A. Harrison and L. J. Farrugia, *Polyhedron* 1987, **6**, 2177.
26. Y. Agnus, R. Louis and R. Weiss, *J. Chem. Soc., Chem. Commun.* 1980, 87.
27. D. A. Baldwin, J. C. A. Boeyens, R. G. Copperthwaite, J. H. N. Loubser and A. J. Markwell, *J. Cryst. Spec. Res.* 1984, **14**, 157.
28. D. A. Baldwin, J. C. A. Boeyens, L. Denner and A. J. Markwell, *J. Cryst. Spec. Res.* 1986, **16**, 763.
29. F. Freeman, J. W. Ziller, H. N. Po and M. C. Kiendl, *J. Am. Chem. Soc.* 1988, **110**, 2586.
30. G. M. Sheldrick, SHELX 76—A Program for Crystal Structure Determination. University of Cambridge, U.K. (1976).
31. D. T. Cromer and J. B. Mann, *Acta Cryst.* 1968, **24**, 321.
32. S. Motherwell, PLUTO—A Plotting Program for Molecular Crystal Packing Diagrams. University of Cambridge, U.K. (1978).
33. R. J. Gillespie and R. S. Nyholm, *Quart. Rev. Chem. Soc.* 1957, **11**, 339.
34. R. G. Pearson, *Symmetry Rules for Chemical Reactions*. John Wiley, New York (1976).
35. W. Abriel, *Acta Cryst.* 1986, **B42**, 449.
36. W. Abriel and C. Friedrich, *Z. Naturfor.* 1985, **40b**, 1691.
37. U. Rosso, G. Valle and S. Calogero, *J. Chem. Soc., Dalton Trans.* 1980, 2303.
38. F. Dahan and O. Lefebvre-Soubeyran, *Acta Cryst.* 1976, **B32**, 2859.
39. F. Dahan and O. Lefebvre-Soubeyran, *Acta Cryst.* 1976, **B32**, 2863.
40. P. R. Sethuraman, M. R. Udupa and G. Aravamudan, *J. Inorg. Nucl. Chem.* 1973, **35**, 3291.
41. O. Foss and S. Hauge, *Acta. Chem. Scand.* 1959, **13**, 1252.
42. O. Foss, *Selected Topics in Structural Chemistry*, p. 145. Universitetsforlaget, Oslo (1967).

Polyhedron Vol. 9, No. 24, pp. 2887–2893, 1990
Printed in Great Britain

0277–5387/90 $3.00+.00
© 1990 Pergamon Press plc

COORDINATION CHEMISTRY OF CHELATING NITROGEN LIGANDS WITH TUNGSTEN CARBONYL NITRILES

BRIAN P. BUFFIN* and THOMAS G. RICHMOND†

Department of Chemistry, University of Utah, Salt Lake City, UT 84112, U.S.A.

(*Received* 3 *June* 1990; *accepted* 2 *August* 1990)

Abstract—The reactions of a series of Schiff base ligands (**1–4**) prepared by condensation of pyridine-2-carboxaldehyde and 2-X-anilines (X = F, Cl, Br, OMe) with $W(CO)_3(RCN)_3$ results in the formation of deeply coloured complexes $W(CO)_3$(**1–4**)(NCR) which readily react with carbon monoxide to afford $W(CO)_4$(**1–4**). The ligand **5**, prepared from pyridine-2-carboxaldehyde and N,N-dimethylethylenediamine, coordinates to $W(CO)_3$ through the conjugated pyridine–imine chelate to afford complexes with a pendant dimethylamino group which reacts with electrophiles. Of the ligands studied, only the *bis*-amine, pyridine ligand **8**, coordinates to $W(CO)_3$ in a tridentate manner. These reactions provide insight into the geometric and electronic factors which influence coordination of nitrogen containing ligands at a *fac*-tricarbonyl metal centre.

Recent work from our laboratory involves the investigation of the metal carbonyl coordination chemistry of multidentate nitrogen donor ligands with pendant aryl halide groups. This research led to the discovery of chelate assisted carbon–halogen bond activation at a tungsten carbonyl metal centre, including the observation of the first well defined oxidative addition of carbon–fluorine bonds under mild conditions at a transition metal centre.[1]

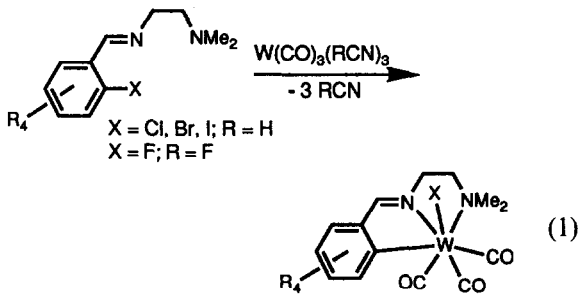

(1)

Suitably designed ligands also control the regiochemistry of this process.[2]

In order more fully to understand the coordination chemistry of "hard" nitrogen based chelating ligands with tungsten carbonyl nitrile starting materials, we chose to explore the chemistry of a number of related Schiff base ligands. Since we were interested in the possibility of aryl halide coordination[3] as a possible intermediate in the aforementioned oxidative addition reactions, we have investigated the chemistry of several Schiff base ligands derived from pyridine-2-carboxaldehyde and *ortho*-substituted anilines (X = F, Cl, Br, OMe). A number of chelate stabilized complexes of aryl halides have been noted in the literature.[3,4] At very electrophilic metal centres, monodentate aryl and alkyl halides function as ligands.[5] Examples of aryl ether coordination in chelate structures have also been reported.[6] Although ligands **1–4** readily coordinate to tungsten as bidentate N-bound donors, no interactions of the pendant group X with the metal centre could be detected. Accordingly, we examined the coordinating properties of the ligand **5** derived from pyridine-2-carboxaldehyde and N,N-dimethylethylenediamine, which contains a very basic dimethylamino group and is known to coordinate in a tridentate manner to several transition metals.[7] Surprisingly, this ligand functions only as a bidentate donor. Only the reduced ligand **8** behaves as a tridentate donor in a tungsten tricarbonyl compound.

This work provides insight into the coordination chemistry of hard, nitrogen based donor ligands at

* Abstracted in part from the MS thesis of B.P.B., University of Utah (1990).

† Author to whom correspondence should be addressed.

octahedral metal centres containing a *fac*-tricarbonyl moiety. This research is also relevant to the growing interest in the behaviour of classical nitrogen[8] and oxygen[9] donor ligands at low valent metal centres.

EXPERIMENTAL

All manipulations were carried out under a nitrogen atmosphere by employing standard Schlenk or glove box techniques unless stated otherwise.[10] Solvents were dried in the indicated manner and distilled prior to use: dichloromethane (P_2O_5), toluene (Na), hexanes (Na/Ph_2CO), acetonitrile (3 Å molecular sieves), $CDCl_3$ (3 Å molecular sieves), DMSO-d_6 (Na). All other reagents were obtained from commercial suppliers and used as received. A literature recipe was used to prepare $W(CO)_3(RCN)_3$ and $W(CO)_4(RCN)_2$ (R = Et, Pr).[11] Schiff base ligands were prepared by condensation of aldehyde and amine in ethanol followed by vacuum distillation, and the expected signals were observed in IR and NMR spectra. Crude **5** was reduced by treatment with excess $NaBH_4$ (4 eqn.) in refluxing methanol, followed by aqueous workup and vacuum distillation to afford **8** in 69% yield.

NMR spectra were obtained on a Varian XL-300 spectrometer. All chemical shifts are reported in δ (ppm) units with the following abbreviations: d = doublet, m = multiplet, s = singlet, and t = triplet. Proton and carbon spectra were referenced to tetramethylsilane by using solvent peaks as internal standards. Fluorine NMR chemical shifts were referenced to internal CCl_3F. Phosphorus chemical shifts were referenced to external 85% H_3PO_4. IR spectra were recorded on a BioRad model FTS-40 FTIR spectrometer operating with a resolution of either 1.0 or 2.0 cm^{-1}. Solution spectra were obtained in 0.1 mm CaF_2 cells. Thin films of liquid ligands and mineral oil mulls of solids were placed between KBr plates for spectral acquisition. Visible spectra were recorded on a Varian CARY 2200 UV–vis spectrophotometer in 1.00 cm quartz cuvettes and a 450 W low pressure mercury lamp filtered through Pyrex was employed for irradiations. Microanalyses were performed by Desert Analytics (Tucson, AZ).

$W(CO)_4$(1)

A 100 cm^3 Schlenk flask equipped with a magnetic stir bar was charged with 4.0 g (9.2 mmol) of $W(CO)_4(PrCN)_2$ and 1.8 g (9.2 mmol) of **1** and then flushed with nitrogen. Methylene chloride (30 cm^3) was added by syringe producing a deep blue–green solution almost immediately. Carbon monoxide gas was then bubbled through the solution for 15 min to afford an intense purple solution reminiscent of the aqueous permanganate ion. The solution was then filtered through a Celite plug, and hexane (30 cm^3) was layered on top of the CH_2Cl_2 solution. After allowing the solvents to diffuse for about 12 h, the methylene chloride was partially removed under reduced pressure. Isolation of the precipitated solid by filtration and washing with pentane gave 3.5 g (7.1 mmol, 77% yield) of a dark purple, air-stable, solid after vacuum drying. IR(CH_2Cl_2): ν_{CO} = 2010s, 1904vs, 1890sh, 1842s cm^{-1}. ^1H NMR ($CDCl_3$, 20°C): δ 9.143 (1H, d, 5.4 Hz), 8.684 (1H, d, 2.5 Hz, J_{W-H} = 7 Hz), 7.778 (1H, app. t, 1.5 Hz), 7.764 (1H, d, 1.1 Hz), 7.354 (1H, m), 7.263 (1H, m), 7.118 (3H, m). $^{13}C\{^1H\}$ NMR($CDCl_3$, 20°C): δ 218.49, 214.10, 197.46, 165.73, 155.19, 152.89 (d, J_{CF} = 249 Hz), 136.43, 129.28 (d, J_{C-F} = 8 Hz), 128.89, 127.21, 125.85, 124.65 (d, J_{C-F} = 4 Hz), 116.81, 116.68 (d, J_{CF} = 20 Hz). ^{19}F NMR($CDCl_3$, 20°C): δ −127.91 (m, br). λ_{max} (toluene) = 581 nm. Found: C, 38.8; H, 1.7; N, 5.5. Calc. for $C_{16}H_9FN_2O_4W$: C, 38.7; H, 1.8; N, 5.6%.

$W(CO)_3(CH_3CN)$(2)

A 100 cm^3 Schlenk flask was charged with 1.9 g (4.4 mmol) of $W(CO)_3(EtCN)_3$ and flushed with nitrogen. Acetonitrile (40 cm^3) was added by syringe to produce a brown–yellow solution which precipitated $W(CO)_3(CH_3CN)_3$ within 10 min. Addition of 0.95 g of **2b** in CH_3CN resulted in an immediate colour change to deep turquoise blue. Removal of solvent under reduced pressure followed by recrystallization from CH_2Cl_2–hexanes gave 1.4 g (2.7 mmol, 61% yield) of purple crystals. IR(CH_3CN): ν_{CO} = 1909vs, 1799s, br cm^{-1}. Found: C, 38.2; H, 2.3; N, 7.9. Calc. for $C_{17}H_{12}ClN_3O_3W$: C, 38.8; H, 2.3; N, 8.0%.

$W(CO)_4$(2)

Carbon mononoxide gas was bubbled through the blue methylene chloride solution left from the recrystallization of $W(CO)_3(CH_3CN)$(**2**). A colour change from blue to deep purple was observed. Crystallization from hexanes afforded 0.32 g (0.62 mmol) of air-stable lavender solid. Including the above product, this accounts for 75% of the W starting material. IR(CH_2Cl_2): ν_{CO} = 2010s, 1904vs, 1890sh, 1844s cm^{-1}. ^1H NMR($CDCl_3$, 20°C): δ 9.199 (1H, d, 5.4 Hz), 8.693 (1H, s, J_{W-H} = 4 Hz), 7.822 (2H, d, 4.7 Hz), 7.338 (3H, m), 7.143 (2H, m). $^{13}C\{^1H\}$ NMR($CDCl_3$, 20°C): δ 218.87, 213.99, 197.52, 165.64, 155.07, 152.97,

136.32, 133.84, 130.50, 128.86, 128.48, 127.57, 127.20, 124.63, 119.00. λ_{max} (toluene) = 580 nm. Found: C, 37.4; H, 2.0; N, 5.7. Calc. for $C_{16}H_9ClN_2O_4W$: C, 37.5; H, 1.8; N, 5.5%.

$W(CO)_4$(3)

$W(CO)_4$(**3**) was prepared in an analogous manner to the complex derived from **1** to afford a 65% yield of a dark purple air-stable solid. IR(CH_2Cl_2): ν_{CO} = 2010s, 1905vs, 1891sh, 1844s cm^{-1}. ^1H NMR($CDCl_3$, 20°C): δ 9.912 (1H, d, 5.4 Hz), 8.682 (1H, s, J_{W-H} = 6 Hz), 7.829 (2H, m), 7.556 (1H, d, 7.9 Hz), 7.311 (3H, m), 7.086 (1H, m). $^{13}C\{^1H\}$ NMR($CDCl_3$, 20°C): δ 218.85 (J_{W-C} = 18.8 Hz), 214.01, 197.64 (J_{W-C} = 11.5 Hz), 165.69, 155.03, 152.98, 150.49, 136.35, 133.63, 128.89, 128.69, 128.25, 127.23, 124.53, 114.04. λ_{max} (toluene) = 581 nm.

$W(CO)_4$(4)

$W(CO)_4$(**4**) was prepared in a similar manner to the complex derived from **1** in 73% yield as an air-stable dark purple solid. IR(CH_2Cl_2): ν_{CO} = 2008s, 1900vs, 1882sh, 1836s cm^{-1}. ^1H NMR($CDCl_3$, 20°C): δ 9.300 (1H, d, 5.9 Hz), 8.792 (1H, s, J_{W-H} = 5 Hz), 7.903 (2H, m), 7.319 (3H, m), 7.046 (2H, m), 3.870 (3H, s). $^{13}C\{^1H\}$ NMR($CDCl_3$, 20°C): δ 218.96, 214.88, 198.30, 164.90, 155.43, 152.86, 150.37, 141.20, 136.27, 128.83, 128.32, 126.75, 123.70, 120.68, 112.22, 55.76. λ_{max} (toluene) = 568 nm. Found: C, 39.9; H, 2.3; N, 5.5. Calc. for $C_{17}H_{12}N_2O_5W$: C, 40.2; H, 2.4; N, 5.5%.

$W(CO)_4$(5)

A 100 cm^3 Schlenk flask equipped with a magnetic stir bar was charged with 4.00 g (8.42 mmol) of $W(CO)_3(PrCN)_3$ and then flushed with nitrogen. Methylene chloride (30 cm^3) was added by syringe, and the resulting brown solution was degassed and flushed with nitrogen. Addition of 1.49 g (8.42 mmol) of **5** by pipette under a positive flow of nitrogen immediately produces a bright royal blue solution. Carbon monoxide was then bubbled through the solution for 15 min during which time the solution colour changed to a deep red–purple. The flask was then charged with carbon monoxide gas, sealed, and the solution stirred for 12 h to complete conversion to the tetracarbonyl compound. The solution was then filtered through a Celite plug, and hexanes (20 cm^3) were layered on top of the methylene chloride solution. After letting the solvents diffuse for 3 h, methylene chloride was partially removed under reduced pressure on a rotary evaporation apparatus. The solid formed was isolated by filtration and washed with pentane. After vacuum drying, 3.18 g (6.74 mmol, 80% yield) of an air-stable brown solid was isolated. IR (CH_2Cl_2): ν_{CO} = 2008s, 1897s, 1883sh, 1834s cm^{-1}. ^1H NMR($CDCl_3$, 20°C): δ 9.200 (1H, d, 5.9 Hz), 8.678 (1H, s), 7.890 (1H, m), 7.786 (1H, m), 7.350 (1H, m), 4.193 (2H, app. t, 5.9 Hz), 2.946 (2H, app. t, 5.9 Hz), 2.294 (6H, s). $^{13}C\{^1H\}$ NMR($CDCl_3$, 20°C): δ 216.85, 215.01, 198.33, 163.62, 155.39, 152.77, 136.49, 127.39, 126.43, 63.82, 60.18, 45.57. λ_{max} (toluene) = 538 nm. Found: C, 35.5; H, 3.1; N, 8.8. Calc. for $C_{14}H_{15}N_3O_4W$: C, 35.5; H, 3.2; N, 8.9%.

[9][BF_4]

A nitrogen atmosphere drybox was utilized to transfer 0.34 g (2.3 mmol) of trimethyloxonium tetrafluoroborate into a 100 cm^3 Schlenk flask. After removing the flask from the drybox, methylene chloride (25 cm^3) was added under a positive nitrogen flow, and the flask was cooled to −78°C. A solution of 1.0 g (2.1 mmol) of $W(CO)_4$(**5**) in 25 cm^3 CH_2Cl_2 was slowly added by syringe to the solution. Allowing the mixture to warm to room temperature and stirring for 24 h resulted in formation of a red–orange precipitate. Filtration and vacuum drying afforded 1.06 g (1.84 mmol, 88% yield) of crude solid. Crystallization with CH_3CN–Et_2O gave analytically pure red–brown crystals. IR(CH_3CN): ν_{CO} = 2013s, 1901vs, 1883sh, 1835s cm^{-1}. ^1H NMR(CD_3CN, 20°C): δ 9.122 (1H, m), 9.038 (1H, s), 8.071 (2H, m), 7.543 (1H, m), 4.543 (2H, app. t, 8.0 Hz), 3.807 (2H, app. t, 8.0 Hz), 3.214 (9H, s). $^{13}C\{^1H\}$ NMR(CD_3CN, 20°C): δ 215.93, 215.02, 199.07, 170.96, 155.54, 153.57, 139.02, 129.86, 128.78, 66.60, 59.09, 54.76. λ_{max} (CH_3CN) = 502 nm. Found: C, 31.3; H, 3.1; N, 7.3. Calc. for $C_{15}H_{18}BF_4N_3O_4W$: C, 31.3; H, 3.2; N, 7.3%.

[9][I]

No precautions were taken to exclude atmospheric oxygen or moisture in this synthesis. $W(CO)_4$(**5**) (0.20 g, 0.42 mmol) was dissolved in 5 cm^3 CH_2Cl_2, and methyl iodide (0.35 g, 2.47 mmol) was added to the solution. After 5 min an IR spectrum indicated that a reaction had occurred. Allowing the solution to stand for 15 h resulted in the formation of 0.10 g (0.16 mmol, 38% yield) of air-stable metallic grey crystals. IR(CH_3CN): ν_{CO} = 2012s, 1900vs, 1881sh, 1835s cm^{-1}. ^1H NMR(CD_3CN, 20°C): δ 9.215 (1H, s), 9.134 (1H, m), 8.076 (2H, m), 7.549 (1H, m), 4.580 (2H, app.

t, 8.0 Hz), 3.879 (2H, app. t, 8.0 Hz), 3.241 (9H, s). $^{13}C\{^1H\}$ NMR(CD_3CN, 20°C): δ 215.89, 215.00, 199.07, 170.90, 155.51, 153.61, 138.97, 129.86, 128.77, 66.44, 58.98, 54.86. λ_{max} (CH_3CN) = 502 nm. Found: C, 29.1; H, 2.9; N, 6.7. Calc. for $C_{15}H_{18}IN_3O_4W$: C, 29.3; H, 2.9; N, 6.8%.

$W(CO)_3$(**8**)

A 100 cm^3 Schlenk flask equipped with a magnetic stir bar was charged with 2.0 g (4.6 mmol) of $W(CO)_3(EtCN)_3$ and flushed with nitrogen. Acetonitrile (20 cm^3) was added by syringe to produce a yellow–brown solution which precipitated $W(CO)_3(CH_3CN)_3$ within 5 min. Slow addition of **8** (0.83 g, 4.6 mmol) in 20 cm^3 CH_2Cl_2 under a positive flow of nitrogen resulted in the immediate precipitation of a bright orange solid. The mixture was stirred for 12 h, at which time the precipitate was removed by filtration. Washing with methylene chloride and vacuum drying afforded 1.7 g (3.8 mmol, 82% yield) of a bright orange solid. IR (CH_3CN): ν_{CO} = 1892s, 1760s, br cm^{-1}. ^1H NMR(DMSO-d_6, 20°C): δ 8.840 (1H, m), 7.916 (1H, m), 7.530 (1H, m), 7.359 (1H, m), 6.125 (1H, br), 4.252 (2H, s), 3.105 (1H, m), 2.821 (3H, s), 2.604 (1H, m), 2.254 (1H, m), 2.147 (3H, s), 1.828 (1H, m). $^{13}C\{^1H\}$ NMR(DMSO-d_6, 20°C): δ 225.78, 225.57, 224.57, 161.58, 151.13, 137.89, 123.84, 122.06, 59.57, 59.29, 55.24, 51.21, 49.43. Found: C, 34.5; H, 3.7; N, 9.4. Calc. for $C_{13}H_{17}N_3O_3W$: C, 34.9; H, 3.8; N, 9.4%.

RESULTS

Schiff base ligands were prepared by condensation of aldehyde and amine components in ethanol and purified as oils by vacuum distillation. A deep blue solution was formed upon addition of the ligands **1**–**4** to a CH_2Cl_2 solution of $W(CO)_3(RCN)_3$ indicative[12] of coordination of the ligands as at least bidentate nitrogen donors (see Scheme 1). Of particular interest was the possibility of X-group interaction with the metal. In the case of **2**, $W(CO)_3$(MeCN)(**2**) was prepared in acetonitrile solution and characterized by elemental analysis after recrystallization from CH_2Cl_2–hexanes. That this material maintains its integrity upon recrystallization in the absence of acetonitrile is consistent with nitrile coordination to the metal centre, rather than a solvate. In addition a weak C≡N stretch assigned to coordinated acetonitrile is observed in a mineral oil mull at 2272 cm^{-1} (free CH_3CN in mineral oil absorbs at 2256 cm^{-1}). This increase in frequency is as observed for $W(CO)_{5-x}(CH_3CN)_x$ complexes.[13] A combination band,[14] arising from the symmetrical C—H deformation and the C—C stretch, at 2306 cm^{-1} (CH_3CN at 2293 cm^{-1}) is also detected. The expected two band pattern in the carbonyl region for the pseudo C_{3v}

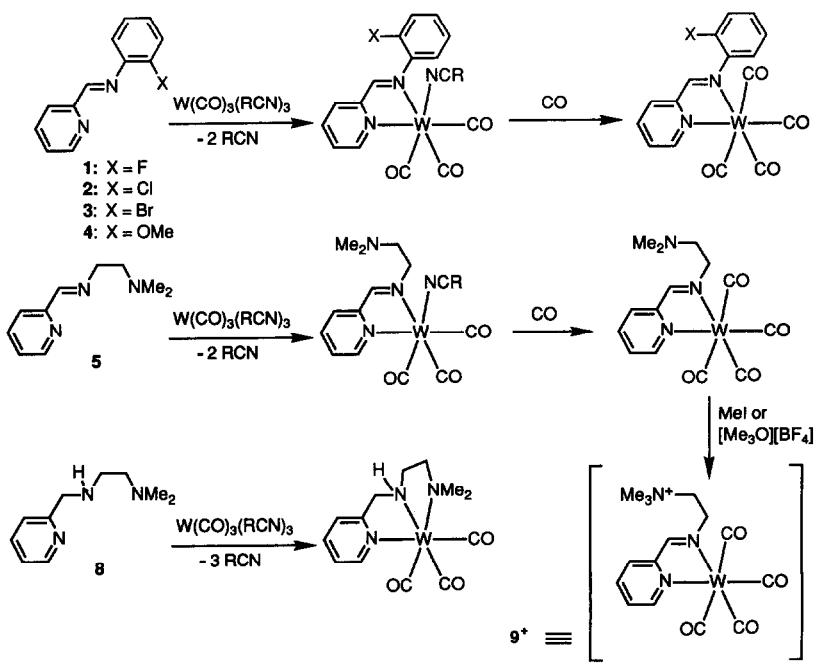

Scheme 1.

tricarbonyl arrangement (ν_{CO} = 1909s, 1799s, br cm^{-1}) is observed.

Numerous other attempts to promote X-group coordination to the metal centre utilizing ligands **1–4** in the absence of carbon monoxide or excess RCN invariably resulted in some decomposition and eventual scavenging of carbon monoxide and formation of the tetracarbonyl products $W(CO)_4$(**1–4**). A more convenient synthesis of the tetracarbonyl complexes was effected by addition of carbon monoxide to solutions of the tricarbonyl complexes or utilizing $W(CO)_4(RCN)_2$ as a starting material. These were fully characterized by IR and NMR spectroscopic methods and elemental analysis. The deep purple colours [λ_{max} (toluene) = 568–581 nm] are consistent with literature precedent for coordination of conjugated pyridine–imine ligands.[12] Diagnostic of ligand coordination is the down field shift of the *ortho*-proton on the pyridine ring by 0.4–0.6 ppm upon coordination to the $W(CO)_4$ centre. Tungsten-183 satellites of 4–8 Hz were detected on the imine protons of the coordinated ligands.

Attempts to remove a carbonyl ligand photochemically were unsuccessful, resulting in decomposition of the complexes to colourless solutions at long irradiation times under vacuum or nitrogen purge in toluene solution. As expected,[15] carbon monoxide substitution was observed in the presence of 1 eqiv. PPh_3 to afford the green (λ_{max} = 656 nm) complex $W(CO)_3(PPh_3)$(**1**) which is characterized by its isosbestic formation from $W(CO)_4$(**1**) and its ^{31}P NMR spectra showed δ = 32.64 with $^1J_{WP}$ = 27 Hz.

Addition of ligand **5** to a CH_2Cl_2 solution of $W(CO)_3(RCN)_3$ resulted in a royal blue solution (ν_{CO} = 1904s, 1790vs, br) assigned to $W(CO)_3(RCN)_3$(**5**) as illustrated in Scheme 1. High solubility and rapid scavenging of carbon monoxide to afford the deep red–purple $W(CO)_4$(**5**) precluded isolation of $W(CO)_3(RCN)$(**5**). The structure of $W(CO)_4$(**5**) is assigned on the basis of its spectroscopic properties and elemental analysis. The down field shift of the *ortho*-proton on the pyridine of 0.58 ppm and the deep colour of the complex are indicative of bidentate ligand coordination, but tungsten satellites could not be resolved on the slightly broad imine proton.

Decomposition resulted upon attempted photochemical dissociation of carbon monoxide to generate $W(CO)_3$(**5**). Treatment of **5** with (cycloheptatriene)$W(CO)_3$ in hexanes results in an ill-defined solid which is poorly soluble in CH_2Cl_2 or CH_3CN with ν_{CO} = 1964s, 1896s, br, 1832s cm^{-1}. These bands are compatible with a dimeric or oligomeric structure or perhaps a *mer*-$W(CO)_3$(**5**) complex but are inconsistent with a *fac*-$W(CO)_3$(**5**) structure.

The chemical reactivity of the non-coordinated dimethylamino group is as expected for a free amine. Alkylating agents $[Me_3O][BF_4]$ or MeI react rapidly to afford the cationic complexes $[\mathbf{9}]^+$ in excellent and fair yields, respectively. The CO stretching frequencies increase by 4–6 cm^{-1} upon alkylation. Appropriate integration and a *ca* 1 ppm downfield shift are observed for the transformation from NMe_2 to $[NMe_3]^+$ groups. Protonation of **5** in CH_3CN with CH_3COOH, CF_3COOH, HPF_6(aq) or HCl(aq) afforded $[H(\mathbf{5})]^+$ characterized by ν_{CO} = 2012s, 1900vs, 1882sh and 1837s, and λ_{max} (CH_3CN) = 502 nm red shifted by 13 nm from **5** in CH_3CN. No attempts were made to isolate salts of $[H(\mathbf{5})]^+$.

Tridentate coordination was finally achieved utilizing the ligand **8** prepared by reduction of **5** with $NaBH_4$. Addition of **8** to a MeCN solution of $W(CO)_3(RCN)_3$ resulted in immediate precipitation of the bright orange solid $W(CO)_3$(**8**) characterized by ν_{CO} = 1892s and 1760s, br cm^{-1}, ^1H and ^{13}C NMR spectroscopic methods and elemental analysis.

DISCUSSION

Attempts to promote coordination of weakly basic X-groups to the $W(CO)_3$ using the pyridine–imine ligand systems **1–4** proved unsuccessful although, as expected from literature precedent,[12] the ligand systems readily bind to yield $W(CO)_3$(**1–4**)(NCR) complexes. Although the remaining nitrile is quite labile with a half-life for exchange in related systems of the order of seconds at room temperature,[16] no interaction of the X-group was detected. The lability of the nitrile ligand, which is in contrast to the somewhat related phosphine based complex $W(CO)_3(NCMe)(\eta^2\text{-}Ph_2PCH_2PPh_2)$,[17] is also apparent in the facile scavenging of carbon monoxide to afford $W(CO)_4$(**1–4**). Photolysis of these complexes in toluene solution also failed to provide any evidence for X-group coordination. The expected entropic advantage for coordination of the X-group in the chelate complex does not appear to be sufficient to compete with acetonitrile as a ligand. Molecular models suggest that the ligand system is not flexible enough to enable the X-group to coordinate readily to afford a facial tridentate donor. The conjugation of the imine with the aryl ring would tend to favour planarity for the ligand system.

Perhaps the most surprising result of this research is the failure of the ligand **5**, which contains the flexible pendant N,N-dimethylaminoethyl group in addition to the pyridine–imine functionality, to fully chelate upon reaction with $W(CO)_3(RCN)_3$.

The deep purple colour is consistent with coordination through the pyridine–imine chelate, rather than through an amine–imine chelate. Alkylation of the free dimethylamino group provides conclusive evidence for this mode of coordination. Apparently the π-acceptor ability[12,18] of the observed chelate is dominant in determining the regiochemistry of coordination rather than the higher base strength of the potential amine–imine regioisomer. Tridentate binding is observed only in the saturated ligand system **8** which has sufficient flexibility to fully coordinate to the *fac*-$W(CO)_3$ moiety. Comparison of the ligands **5** and **8** shows that the coordinating ability of the pendant dimethylamino group relative to acetonitrile depends markedly on the geometry of the ligand system. In spite of its much higher protonic basicity, the dimethylamino group cannot compete effectively with acetonitrile as a ligand in the geometry imposed by pyridine–imine chelate. Photochemical removal of carbon monoxide from $W(CO)_4$(**5**) also did not induce the NMe_2 group to coordinate.

It is clear that in order to observe chelation of weakly basic X-groups, ligand geometry is crucial, particularly in octahedral complexes enforced by the *fac*-$W(CO)_3$ group. As illustrated by the contrasting behaviour of **5** and **8**, this is true even for quite basic ligands. Two recently reported examples[6] of chelate stabilized aryl ether coordination at $Mo(CO)_3$ provide rather diverse models for the desired interaction, as does the structure of a complex containing a bicyclic triene ligand with a pendant bromocarbon coordinated to $Mo(CO)_3$.[19]

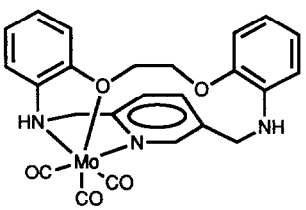

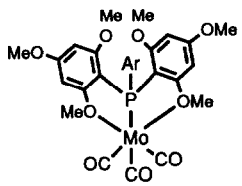

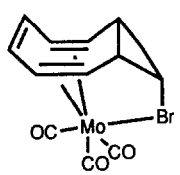

(2)

The contrasting behaviour of these ligands emphasizes the predominance of steric over electronic factors in these systems. Only flexible ligands capable of assuming a facial arrangement are able to coordinate in a tridentate manner. The choice of starting material may also influence the success of attaining coordination of weak X-groups. Our choice of $W(CO)_3(RCN)_3$ allows for direct comparison with our previous studies, but at the expense of introducing competitive nitrile ligands which may hinder observation of halide,[20] perhaps alkoxide,[6] but probably not dimethylamino group interactions with a metal centre. Interestingly, we note that our C—X activating systems[1] are characterized by relatively rigid ligand backbones which may actually disfavour non-productive halocarbon coordination and thus promote metal insertion into C—X bonds.

Acknowledgements—This work was supported in part by the National Science Foundation through a PYI grant to T.G.R. and by the Donors of the Petroleum Research Fund administered by the American Chemical Society.

REFERENCES

1. T. G. Richmond, M. A. King, E. P. Kelson and A. M. Arif, *Organometallics* 1987, **6**, 1995. T. G. Richmond, C. E. Osterberg and A. M. Arif, *J. Am. Chem. Soc.* 1987, **109**, 8091. C. E. Osterberg, M. A. King, A. M. Arif and T. G. Richmond, *Angew. Chem. Int. Ed. Engl.* 1990, **29**, 888. For related chemistry at Pt^{II} see: C. M. Anderson, R. J. Puddephatt, G. Ferguson and A. J. Lough, *J. Chem. Soc., Chem. Commun.* 1989, 1297.
2. M. J. Poss, A. M. Arif and T. G. Richmond, *Organometallics* 1988, **7**, 1669.
3. R. J. Kulawiec and R. H. Crabtree, *Coord. Chem. Rev.* 1990, **99**, 89.
4. R. H. Crabtree, J. W. Faller, M. F. Mella and J. M. Quirk, *Organometallics* 1982, **1**, 1361. M. R. Colsman, M. D. Noirot, M. M. Miller, O. P. Anderson and S. H. Strauss, *J. Am. Chem. Soc.* 1988, **110**, 6886. R. M. Catala, D. M. Cruz-Garritz, A. Hills, D. L. Hughes, R. L. Richards, P. Sosa and H. Torrens, *J. Chem. Soc., Chem. Commun.* 1987, 261.
5. C. H. Winter, A. M. Arif and J. A. Gladysz, *J. Am. Chem. Soc.* 1987, **109**, 7560. C. H. Winter and J. A. Gladysz, *J. Organomet. Chem.* 1988, **354**, C33. R. J. Kulawiec and R. H. Crabtree, *Organometallics* 1988, **7**, 1891.
6. H. Adams, N. A. Bailey, D. E. Fenton, P. D. Hempstead, B. A. Hewes, S. J. Kitchen and M. J. Winter, *Polyhedron* 1989, **8**, 1857. K. R. Dunbar, S. C. Haefner and D. J. Burzynski, *Organometallics* 1990, **9**, 1347.
7. G. Zakrzewshi and L. Sacconi, *Inorg. Chem.* 1968, **7**, 1034. P. Bamfield, R. Price and R. G. J. Miller, *J. Chem. Soc. (A)* 1969, 1447.
8. P. Chauduri and K. Wieghardt, *Prog. Inorg. Chem.* 1987, **35**, 329.
9. X.-L. Luo, G. K. Schulte and R. H. Crabtree, *Inorg. Chem.* 1990, **29**, 682.
10. D. F. Shriver and M. A. Drezdon, *Manipulation of Air Sensitive Compounds*, 2nd edn. Wiley, New York (1986).
11. G. J. Kubas, *Inorg. Chem.* 1983, **22**, 692.
12. G. van Kotcn and K. Vricze, *Adv. Organomet. Chem.* 1982, **21**, 151. H. Brunner and W. A. Herrman, *J. Organomet. Chem.* 1973, **57**, 183.

13. B. L. Ross, J. G. Grasselli, W. M. Ritchey and H. D. Kasez, *Inorg. Chem.* 1963, **2**, 1023.
14. B. N. Storhoff and H. C. Lewis Jr, *Coord. Chem. Rev.* 1977, **23**, 1.
15. R. W. Balk, T. Snoeck, D. J. Stufkens and A. Oskam, *Inorg. Chem.* 1980, **19**, 3015. D. P. Drolet, L. Chan and A. J. Lees, *Organometallics* 1988, **7**, 2502. C. E. Johnson and W. C. Trogler, *J. Am. Chem. Soc.* 1981, **103**, 6352.
16. T. G. Richmond, *Coord. Chem. Rev.* 1990, in press.
17. D. J. Darensbourg, D. J. Zalewski, C. Plepys and C. Campana, *Inorg. Chem.* 1987, **26**, 3727.
18. Q.-Z. Shi, T. G. Richmond, W. C. Trogler and F. Basolo, *Organometallics* 1982, **1**, 1033.
19. F. J. Liotta Jr, G. Van Duyne and B. K. Carpenter, *Organometallics* 1987, **6**, 1010.
20. M. J. Burk, R. H. Crabtree and E. M. Holt, *Organometallics* 1984, **3**, 638.

Polyhedron Vol. 9, No. 24, pp. 2895–2899, 1990
Printed in Great Britain

0277–5387/90 $3.00+.00
© 1990 Pergamon Press plc

THE COMPLEXES OF IRON(III) WITH D-GLUCOPYRANOSYL ESTERS OF GLYCINE

M. TONKOVIĆ, Š. HORVAT, J. HORVAT, S. MUSIĆ and O. HADŽIJA*

Ruđer Bošković Institute, 41000 Zagreb, Yugoslavia

(*Received* 5 *April* 1990; *accepted* 6 *August* 1990)

Abstract—The complexes of iron(III) with unprotected, partially protected and fully protected glycine glycosides were prepared and characterized. The dependence between the protection level of the ligands and the composition of the complexes was observed, i.e. molecular weight of the complexes decreases with increasing level of ligand protection.

In recent years, research concerning synthesis of glycopeptides has been directed towards the development of highly receptor selective and specific derivatives for clinical use. The promising results obtained by incorporation of sugar moieties into biologically active peptides[1,2] and the increasing evidence that the carbohydrate moieties in glycoproteins are involved in recognitive and other biological regulative mechanisms[3] led us to examine the chelating properties of some simple model compounds in which N-acylated or free amino acids are linked by the glycosidic ester bond to a protected or unprotected carbohydrate molecule.

Previous studies[4–6] have shown that glucopyranosyl esters of amino acids, although readily hydrolysed, may also undergo transesterification and transamination reactions through nucleophilic attack at the 1-ester carbonyl group. Since the reactions mentioned point out the enhanced electrophilic properties of the 1-ester carbonyl carbon, it seemed of interest to study the complex formation of iron with this type of ligand.

Many papers concerning formation, preparation and characterization of the complexes of iron(III) with amino acids, sugars and polysaccharides appear in the literature,[7–19] but to our knowledge, complexes with amino acid glycosides have not been described so far. Therefore, in this paper we report the preparation and physicochemical properties of such complexes and on the basis of the analytical data, the probable structures are proposed.

EXPERIMENTAL

Materials

Abbreviations of ligands (Fig. 1): GGT, 1-*O*-glycyl-β-D-glucopyranose trifluoroacetate; AcGGT, 2,3,4,6-tetra-*O*-acetyl-1-*O*-glycyl-β-D-glucopyranose trifluoroacetate; AcGGTBoc, 2,3,4,6-tetra-*O*-acetyl-1-*O*-(*N*-t-butoxycarbonyl-glycyl)-β-D-glucopyranose. All chemicals used were of analytical grade.

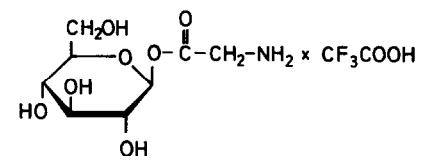

GGT

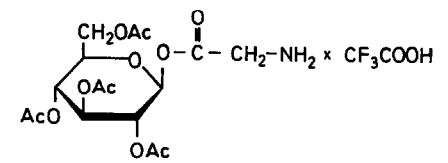

AcGGT

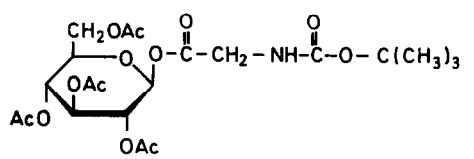

AcGGTBoc

Fig. 1. Structures of amino acid glycosides.

* Author to whom correspondence should be addressed.

Methods of preparation

D-Glucopyranosyl esters of glycine (GGT, AcGGT, AcGGTBoc) have been synthesized by the procedure reported earlier.[20]

Iron(III) complexes of GGT, AcGGT and AcGGTBoc were prepared by mixing 0.1 M aqueous iron(III) nitrate with solid ligands in 1 Fe^{III}: 2 dm^3 molar ratio. The solid complexes were obtained by evaporation of these solutions *in vacuo* and dried in a desiccator over silica gel. Redissolution of the complexes in water yielded brown solutions, except the iron(III)–AcGGTBoc complex where a white precipitate was formed. The precipitate was removed by filtration and the clear solution was lyophylized.

Methods of analyses

Carbon, hydrogen, nitrogen and iron were estimated by standard microanalytical methods. IR spectra were recorded on a Perkin–Elmer spectrophotometer, model 580B. ^{57}Fe Mössbauer spectroscopy was performed using a commercial spectrophotometer (Wissenschaftliche Elektronik GmbH, F.R.G.) with a $^{57}Co/Rh$ source, and the chemical shift is given with respect to metallic iron. Thermogravimetric analyses were performed using Cahn RG electrobalance (U.S.A.). Molecular weights were determined by gel filtration on a Sephadex G-25 column (0.9 × 20 cm) in 0.01 M acetic acid by comparing the elution volumes of the complexes with those of standards: bacitracin (mol. wt 1450) and phenylazobenzyloxycarbonyl-Pro-Leu-Gly-Pro-D-Arg (mol. wt 777). Blue Dextran 2000 was used for the void volume determination. Homogeneity of the complexes was established by thin layer chromatograhy on silica gel, using visualization of spots with: 10% sulphuric acid, ninhydrin–HBr and by inspection under UV light. Paper electrophoresis was performed on Whatman No. 1 paper, at room temperature, with a voltage gradient of 30 V cm^{-1} in Tris–HCl buffer (pH 7.2). Visualization of the complex was performed by peptide reagent and a 2% solution of potassium hexacyanoferrate(II).

RESULTS AND DISCUSSION

In Table 1 the results of chemical analyses and physicochemical measurements of the complexes are presented. The complexes are amorphous and

Table 1. Analytical data of the iron(III)–amino acid glycoside complexes

Methods of analysis	Results					
	Iron(III)–GGT		Iron(III)–AcGGT		Iron(III)–AcGGTBoc	
Elemental microanalysis	Calc. (%)	Found (%)	Calc. (%)	Found (%)	Calc. (%)	Found (%)
C	25.6	25.6	31.9	31.8	28.9	28.7
H	3.7	4.8	5.0	4.9	5.1	5.4
N	6.5	6.8	3.1	3.0	6.4	6.6
Fe	6.0	5.5	4.1	4.6	6.4	6.9
NO_3	15.4	—	4.6	4.8	21.3	—
Thermogravimetric analysis (TGA)	Weight loss at: RT–347°C 81.86% RT–727°C 85.98%		Weight loss at: RT–128°C 25.27% RT–342°C 83.44% RT–741°C 93.46%		Weight loss at: RT–128°C 26.14% RT–342°C 82.53% RT–811°C 93.69%	
Thin layer chromatography (TLC)	Solvent: *n*-Butanol–acetone–HCl–acetylacetone–water (60:40:1:0.5:20) $R_{f(GGT)} = 0.24$ $R_{firon(III)} = 0.05$ $R_{firon(III)\text{-}GGT} = 0.11$		Solvent: Methanol–benzene–acetic acid (20:10:15) $R_{f(AcGGT)} = 0.81$ $R_{firon(III)} = 0.92$ $R_{firon(III)\text{-}AcGGT} = 0.52$		Solvent: Methanol–benzene–acetic acid (20:10:15) $R_{f(AcGGTBoc)} = 0.98$ $R_{firon(III)} = 0.92$ $R_{firon(III)\text{-}AcGGTBoc} = 0.70$	
Approximate molecular weight determination	—		Calc. 2703.7	Found > 1450 < 5000	Calc. 872.8	Found > 777 < 1450

soluble in water giving a pale brown solution. Thin layer chromatography showed the spots migrating differently from the ligands and iron(III) ion. The molecule of the complex consists of a carbohydrate moiety and the inorganic part consists of iron, nitrate and water. It is known[21] that when heated carbohydrates lose the first molecule of water at 120–190°C, the second and third ones at 165–250°C. Thermal decomposition of iron nitrate starts at 127°C. All three complexes showed by TGA a significant decomposition in the temperature range from room temperature to 342–347°C. In that range all water molecules were evaporated, including those in the carbohydrate moiety, while the decomposition of nitrate began; decarboxylation of the molecule takes place in that temperature range also. The complexes are decomposed completely at 727–811°C. From the IR spectra characteristic bands of the ligands and the complexes are summarized in Table 2. The bands at 830–840 and 390–400 cm^{-1}, which appeared only in the IR spectra of the complexes, corresponding to Fe—O, Fe—OH stretching vibrations, confirmed the existence of such complexes. The bands at about 830 cm^{-1} may be due to inorganic nitrate also.[22,23] The bands at 590–610 cm^{-1} present in the spectra of ligands and complexes, but being much stronger and of different shape in the latter, also can be attributed to the Fe—O stretching vibration. Medium intensity bands in the range 1465–1200 cm^{-1} assigned to —CCH, $—CH_2$ and —COH bending vibrations exhibit shifts to higher frequencies which can be attributed to complexation. The opposite phenomenon is observed in the range 1770–1735 cm^{-1} which is probably due to the coordination with iron. The bands at 1680–1640 and 1465–1420 cm^{-1} assigned, respectively, to the asymm (COO—) and sym (COO—) modes of carboxylate group with differences of about 200 cm^{-1}, indicate bidentate coordination via carboxylate oxygen.[12,19] All spectra of ligands and complexes exhibit bands with maxima at 3380–3480 cm^{-1} originating from O—H stretching vibration which can be ascribed to hydroxy groups of ligands and/or to adsorbed and coordinated water molecules. In the electrophoresis all three complexes moved toward the cathode indicating positive charge. Approximate molecular weight determination showed that iron(III)–AcGGT has a molecular weight >1450, and iron(III)–AcGGTBoc molecular weight between 1450–777.

On the basis of the results of elemental analyses the following formulae of the complexes can be proposed: $Fe_3OL_6(NO_3)_7(H_2O)_5$ for iron(III)–GGT; $Fe_2O_2L_4(NO_3)_2(H_2O)_{20}$ for iron(III)–AcGGT; and $FeL(NO_3)_3(H_2O)_7$ for iron(III)–AcGGTBoc.

It appears that the coordination of the carboxyl group to a trimeric iron unit (Fe_3O) is a general feature for the coordination of amino acids, namely, the coordination to an oxygen is more strongly favoured where iron(III) is involved, than the coordination to the nitrogen of the amino group.[12] The overall structure of these molecules is that of a central oxygen atom bonded to three iron atoms, which are bonded to oxygens of the carboxyl groups

Table 2. Principal bands (cm^{-1}) of IR spectral data of amino acid glycosides and their iron(III) complexes

GGT	Iron(III)–GGT	AcGGT	Iron(III)–AcGGT	AcGGTBoc	Iron(III)–AcGGTBoc	Assignment[a]
3450s	3380s,b	3480m	3380s,b	3395s	3400s,b	ν(O—H) assoc.
1770m	1755m	1750vs	1730s	1745vs 1720m	1725s	ν(C=O)
1680m 1630sh	1650s	1680s	1680w 1645m		1640s	$\delta(NH_3)^+$; $\delta(H_2O)$; $\nu(COO^-)$ asymm.
1435m	1465w	1440s	1455sh	1420w	1420w	δ(COH); $\delta(CH_2)$; δ(CCH)
1200s	1210w	1415w				
1325w	1355w 1385w	1390s 1315sh	1375s 1350sh	1390w 1370s	1350b,m	$\nu(COO^-)$ sym; $\nu(NO_3)^-$ $\delta(C—CH_3)$
1200s	1210w	1230s	1250m	1230vs	1260w	ν(C—O); δ(COH); $\delta(CH_2)$; δ(CCH)
	830m		835s		840m	$\nu(NO_3^-)$; ν(Fe—O—H)
610m	590m,b 400s	600m	610m,b 390m,b	610m	610bm 400m	ν(Fe—O)

[a] Assignments were performed according to refs 9, 22–26.

of the amino acid residues. The structures of the complexes formed are consistent with a basic iron(III)–acetate structure.[27] On the basis of analytical data it seems very likely that iron(III)–GGT complex, where the ligand, having non-protected glucose, is linked glycosidically with glycine trifluoroacetate, has a structure essentially the same as described above. The trifluoroacetate of the amino acid glycoside is present as a zwitter-ion and the amino nitrogen is not involved in iron ligand bonding.

Experimental data indicate some differences in the structures of iron(III)–AcGGT and iron(III)–AcGGTBoc complexes.

Even though AcGGT has the structure very similar to GGT, i.e. zwitter-ion capable for complexation with iron(III) by the same manner, elemental analysis and molecular weight indicate the formula $Fe_2O_2L_4(NO_3)_2(H_2O)_{20}$ which presumes an oxo bridging of two irons. This presumption is supported by the IR spectrum where bands of: 835s, 610mb and 390mb cm^{-1} can be attributed to oxo bridges between two iron atoms.[28] Resembling structures are found by crystallographic studies of natural iron–protein complexes.[29–31]

The molecular weight of the iron(III)–AcGGTBoc complex indicates a monomeric structure. This structure, supported by elemental analysis, may be realized by bidentate coordination via two carbonyl oxygens forming a seven-membered ring. Four coordination sites of iron are completed with water molecules. The results of Mössbauer spectroscopy support the above presumption. The values of isomer shift, δ (0.370 mm s^{-1}), quadrupole splitting, ΔE (0.732 mm s^{-1}), and line width Γ (0.403 mm s^{-1}), show that iron is present only in the form of iron(III) and is in the octahedral position. However, a relatively high value of quadrupole splitting indicates that the octahedral structure of the Fe^{III} ion is distorted, which can be ascribed to the asymmetric position of the ligands. These results point out the enhanced electrophilic properties of the 1-ester carbonyl carbon in the fully protected ligand, and may be related to the observed susceptibility of protected β-D-glucopyranosyl esters of amino acids toward nucleophilic attack.[6] The likely structures of the complexes resulting from the above data are presented in Fig. 2, indicating that the structure differences are determined by the protection level of the ligands.

Acknowledgements—Thanks are due to the Self-Managed Community of Interest for Scientific Research of SR Croatia for financial support. The authors are grateful to Miss B. Špoljar and Mrs R. Herman for elemental analyses, and Dr B. Ladešić for electrophoresis.

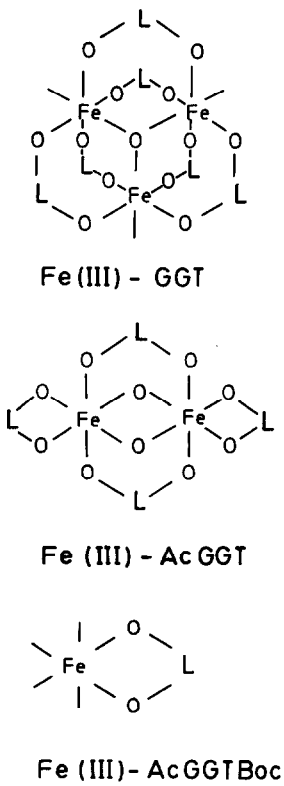

Fig. 2. Presumed structures of the complexes of iron(III) with D-glucopyranosyl esters of glycine.

REFERENCES

1. R. E. Rodriguez, F. D. Rodriguez, M. P. Sacristan, J. L. Torres, G. Valencia and J. M. Garcia Anton, *Neurosci. Lett.* 1989, **101**, 89.
2. J. Horvat, Š. Horvat, C. Lemieux and P. W. Schiller, *Int. J. Peptide Protein Res.* 1988, **31**, 499.
3. H. Kunz, *Angew. Chem. Int. Ed.* 1987, **26**, 294.
4. Š. Horvat and D. Keglević, *Carbohydr. Res.* 1976, **47**, 35.
5. D. Keglević, M. Pongračić and J. Horvat, *Carbohydr. Res.* 1980, **80**, 63.
6. Š. Horvat and D. Keglević, *Carbohydr. Res.* 1982, **108**, 89.
7. E. M. Holt, S. L. Holt, W. F. Tucker, R. O. Asplund and K. J. Watson, *J. Am. Chem. Soc.* 1974, **96**, 2621.
8. G. Micera, S. Deiana, C. Gessa and M. Petrera, *Inorg. Chim. Acta* 1981, **56**, 109.
9. R. N. Puri and R. O. Asplund, *Inorg. Chim. Acta* 1981, **54**, 187.
10. R. N. Puri and R. O. Asplund, *Inorg. Chim. Acta* 1982, **66**, 49.
11. M. Tonković, S. Musić, I. Nagy-Czako, A. Vertes and O. Hadžija, *Acta Chim. Acad. Sci. Hung.* 1982, **110**, 197.
12. W. F. Tucker, R. O. Asplund and S. L. Holt, *Arch. Biochem. Biophys.* 1975, **166**, 433.
13. S. Balt, M. W. G. DeBolster and G. Visser-Luirink, *Inorg. Chim. Acta* 1983, **78**, 121.

14. M. Tonković, O. Hadžija and I. Nagy-Czako, *Inorg. Chim. Acta* 1983, **80**, 251.
15. B. W. Fitzsimmons, A. Hume, L. F. Larkworthy, M. H. Turnbull and A. Yavari, *Inorg. Chim. Acta* 1985, **106**, 109.
16. S. H. Laurie, *Inorg. Chim. Acta* 1986, **123**, 15.
17. L. Nagy, K. Burger, J. Kurti, M. A. Mostafa, L. Korecz and I. Kiricsi, *Inorg. Chim. Acta* 1986, **124**, 55.
18. M. Tonković, O. Hadžija, B. Ladešić, B. Klaić and S. Musić, *Inorg. Chim. Acta* 1989, **161**, 81.
19. S. Deiana, L. Erre, G. Micera, P. Piu and C. Gessa, *Inorg. Chim. Acta* 1980, **46**, 249.
20. D. Keglević, Đ. Ljevaković and Š. Valenteković, *Croat. Chem. Acta* 1974, **46**, 115.
21. R. C. MacKenzie (Ed.), *Differential Thermal Analysis*, Vol. 2. Academic Press, London (1972).
22. D. H. Williams and I. Fleming, *Spectroscopic Methods in Organic Chemistry*. McGraw Hill, London (1973).
23. K. Nakamoto, *Infrared and Raman Spectra of Inorganic and Coordination Compounds*. Wiley, New York (1978).
24. H. A. Tajmir-Riahi, *Inorg. Chim. Acta* 1988, **153**, 155.
25. V. Moreno, K. Dittmer and J. V. Quagliano, *Spectrochim. Acta* 1960, **16**, 1368.
26. M. L. Dhar and O. Singh, *Z. Naturforsch.* 1986, **41b**, 82.
27. B. N. Figgis and G. B. Robertson, *Nature* 1965, **205**, 694.
28. Th. G. Spiro and P. Saltman, *Structure and Bonding* 1969, **6**, 124.
29. R. E. Stenkamp, L. C. Siecker, L. H. Jensen and J. Sanders-Loehr, *Nature* 1981, **291**, 263.
30. W. T. Elam, E. A. Stern, J. D. McCallum and J. Sanders-Loehr, *J. Am. Chem. Soc.* 1982, **104**, 6369.
31. R. E. Stenkamp, L. C. Siecker and L. H. Jensen, *J. Am. Chem. Soc.* 1984, **106**, 618.

Polyhedron Vol. 9, No. 24, pp. 2901–2909, 1990
Printed in Great Britain

0277–5387/90 $3.00+.00
Pergamon Press plc

PREPARATION AND REACTIVITY OF $PhP(C_5Me_4H)_2$ AND $Ph_2P(C_5Me_4H)$. X-RAY CRYSTAL STRUCTURES OF $Mo(CO)_5[Ph_2P(C_5Me_4H)]$ AND $(\eta^5\text{-}C_5Me_4H)Mo(CO)(\mu\text{-}PPh_2)_2Mo[(\eta^5\text{-}C_5Me_4)P(O)Ph_2](CO)\cdot 1/4C_6H_{14}$

WAI-KWOK WONG*

Department of Chemistry, Hong Kong Baptist College, Kowloon, Hong Kong

and

FONG LUNG CHOW, HUA CHEN and BOON WAI AU-YEUNG

Department of Applied Biology and Chemical Technology, Hong Kong Polytechnic, Hung Hom, Kowloon, Hong Kong

and

RU-JI WANG and THOMAS C. W. MAK*

Department of Chemistry, The Chinese University of Hong Kong, Shatin, New Territories, Hong Kong

(*Received* 4 *May* 1990; *accepted* 6 *August* 1990)

Abstract—The phosphine ligands $PhP(C_5Me_4H)_2$, **I**, and $Ph_2P(C_5Me_4H)$, **II**, can be prepared via the interaction of $PhPCl_2$ and Ph_2PCl with two and one equivalent(s) of $(C_5Me_4H)Li$, respectively. At ambient temperature, $C_7H_8Mo(CO)_4$ reacts with **I**–**II** to give the corresponding $Mo(CO)_5L$ complex, **III**–**IV** [**III**, $L = PhP(C_5Me_4H)_2$; **IV**, $L = Ph_2P(C_5Me_4H)$], in moderate yield (60–65%). In refluxing hexane, $C_7H_8Mo(CO)_4$ reacts with **II** to give $(\eta^5\text{-}C_5Me_4H)Mo(CO)(\mu\text{-}PPh_2)_2Mo[(\eta^5\text{-}C_5Me_4)P(O)Ph_2](CO)\cdot 1/4C_6H_{14}$, **V**, in low yield (10%). Structures of **IV** and **V** have been determined by X-ray crystallography.

The (diphenylphosphino)cyclopentadienyl anion, $Ph_2P(C_5H_4)^-$, has been shown to be a very versatile reagent in organometallic synthesis. Its use as a difunctional reagent to bring two hetero metal centres in close proximity has received considerable attention.[1] Although the chemistry of the anion has been investigated extensively, relatively few studies have been done on its parent compound, $Ph_2P(C_5H_5)$. Recently, we have demonstrated that coordinated $Ph_2P(C_5H_5)$ ligands in *cis*-$Mo(CO)_4[Ph_2P(C_5H_5)]_2$ underwent Diels–Alder dimerization to produce the 1,3-bis(diphenylphosphino) dicyclopentadiene ligand.[2] In this paper, we wish to report the preparation and reactivity of the tetramethylcyclopentadienyl analogues $PhP(C_5Me_4H)_2$, **I**, and $Ph_2P(C_5Me_4H)$, **II**.

* Authors to whom correspondence should be addressed.

RESULTS AND DISCUSSION

Preparation of phosphine ligands

(i) $PhP(C_5Me_4H)_2$, **I**. The interaction of $PhPCl_2$ with two equivalents of $(C_5Me_4H)Li$ in hexane produced a pale orange viscous oil from which white crystalline needles, **I**, were obtained upon cooling to −20°C. The mass spectrum of the white needles shows the highest peak at *m/z* 350, corresponding to the molecular ion $M^+[PhP(C_5Me_4H)_2]^+$, and a peak at *m/z* 229 corresponding to the $[M-(C_5Me_4H)]^+$ fragment. The $^{31}P\{^1H\}$ NMR spec-

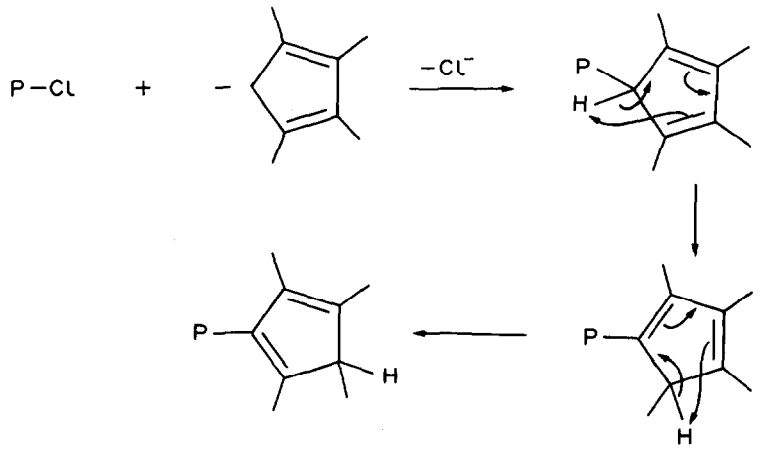

Scheme 1.

trum of **I** shows a singlet at δ 12.5 ppm. The ^{1}H NMR spectrum exhibits a multiplet of relative intensity 5, centred at δ 7.24 ppm for the phenyl protons; a broad singlet of relative intensity 2 at δ 3.92 ppm for the unique protons of the two C_5Me_4H rings; and three broad singlets of relative intensities 6:6:12 at δ 2.08, 1.75 and 1.61 ppm, respectively, for the methyl protons of the two C_5Me_4H rings. The resonance of the unique protons at δ 3.92 ppm corresponds to aliphatic rather than olefinic protons. The above spectroscopic evidence indicates that **I** is bis(2,3,4,5-tetramethylcyclopenta-1,4-dienyl)phenylphosphine which is formed via a series of proton migrations as shown in Scheme 1.

Two structures are possible for **I**. These are **Ia** and **Ib** as shown below:

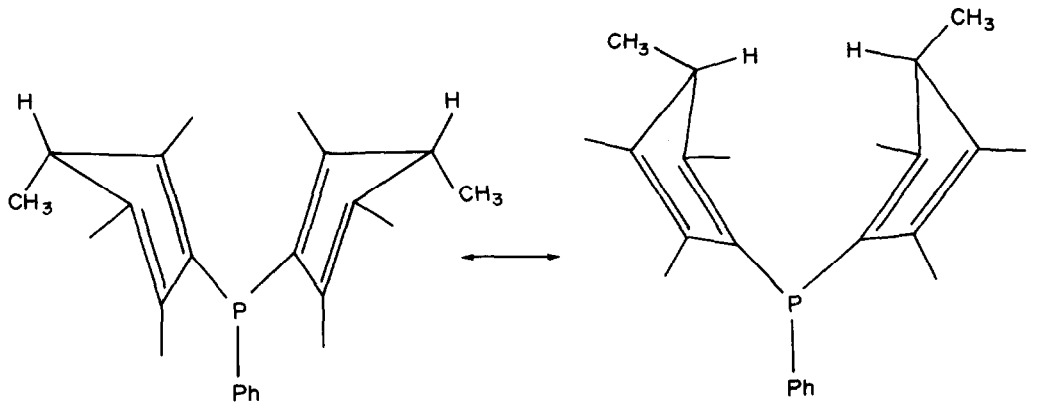

Ia

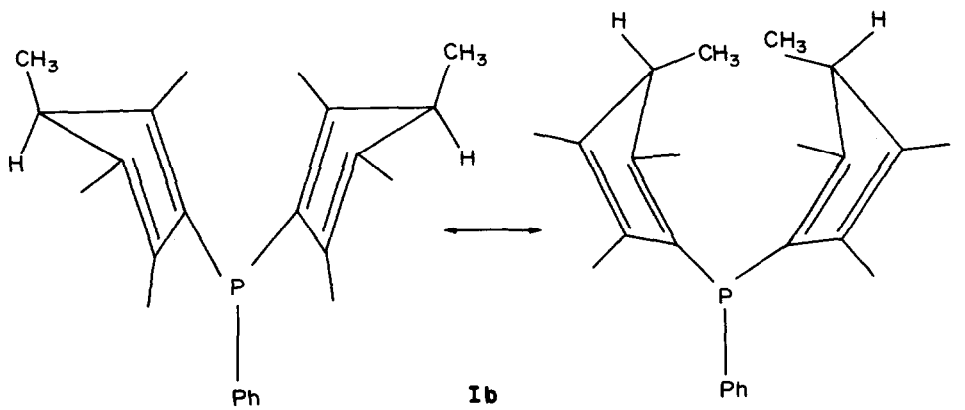

Ib

As shown in the resonance structures, steric interaction between the two C_5Me_4H rings is less in **Ia** than in **Ib**. Thus, structure **Ia** is assigned to **I**.

(ii) $Ph_2P(C_5Me_4H)$, **II**. The interaction of Ph_2PCl with one equivalent of $(C_5Me_4H)Li$ in hexane produced a thick yellow oil, **II**. The mass spectrum of **II** shows the highest peak at *m/z* 306, corresponding to the molecular ion, M^+ $[Ph_2P(C_5Me_4H)^+]$, and an intense peak at *m/z* 122, corresponding to the fragment $(C_5Me_4H_2)^+$. The $^{31}P\{^1H\}$ NMR spectrum of **II** exhibits two singlets of equal intensity at δ −24.6 and 0.8 ppm, indicating the presence of equal amounts of the two isomers of **II**. The ^1H NMR spectrum exhibits a complex multiplet of total intensity 10 centred at δ 7.27 ppm for the phenyl protons, two broad singlets of equal intensity of total intensity 1 at δ 3.69 and 2.64 ppm for the unique proton of the C_5Me_4H ring, and a set of broad singlets of total intensity 12 range δ 1.54–1.91 ppm for the methyl protons of the C_5Me_4H ring. The appearance of two resonances at δ 3.69 and 2.64 ppm for the unique proton further demonstrates the presence of two isomers of **II**. The chemical shifts of the unique protons correspond to aliphatic protons. The above spectroscopic evidence indicates that **II** is (2,3,4,5-tetramethylcyclopenta-1,4-dienyl)phosphine. Structures **IIa** and **IIb** can be assigned to the two isomers of **II** as shown below:

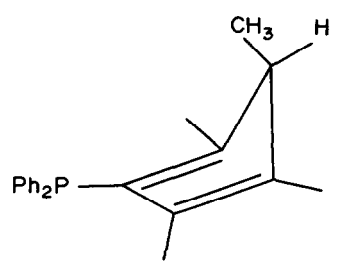

IIa

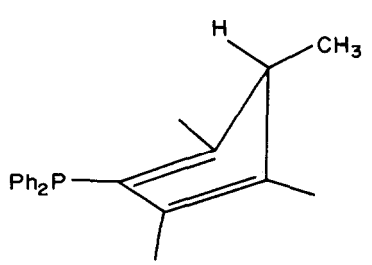

IIb

Interaction of $C_7H_8Mo(CO)_4$ *with the phosphine ligands*

(i) When $C_7H_8Mo(CO)_4$ was treated with two equivalents of $PhP(C_5Me_4H)_2$ at room temperature in hexane, white crystals of stoichiometry $Mo(CO)_5[PhP(C_5Me_4H)_2]$, **III**, were obtained in moderate yield (60%). The infrared spectrum (KBr) of **III** exhibits three absorptions at 2067s, 1979s, and 1927vs (br) cm^{-1} at the terminal carbonyl region. The $^{31}P\{^1H\}$ NMR spectrum shows a singlet at δ 40.8 ppm. The ^1H NMR spectrum exhibits two multiplets of relative 2 : 3 intensity centred at δ 7.56 and 7.28 ppm, respectively, for the phenyl protons; a doublet of relative intensity 2 centred at δ 4.18 ppm (J_{P-H} = 10.5 Hz) for the unique protons of the C_5Me_4H rings; and three broad singlets of relative intensity 6 : 12 : 6 at δ 2.17, 1.69 and 1.50 ppm, respectively, for the methyl protons of the C_5Me_4H rings. The ^1H NMR chemical shift and the splitting pattern of the unique proton of the C_5Me_4H rings of **III** is similar to that of **IV** which has been confirmed by X-ray crystallography (vide infra) to be at the carbon α to the phosphorus. Based on the above data, the following structure can be assigned to **III**.

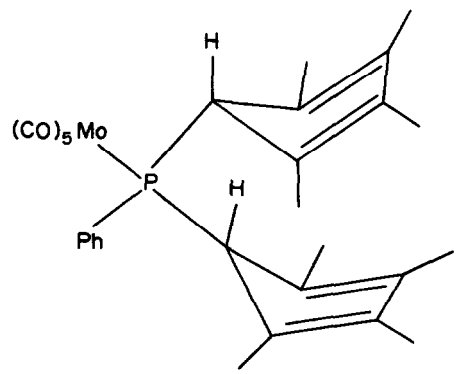

III

Compound **III** is probably formed via a series of proton migrations as shown in Scheme 1 but in the reversed direction. The formation of coordinated bis(2,3,4,5 - tetramethylcyclopenta - 2,4 - dienyl) phenylphosphine reflects that in the complexed form, the 2,3,4,5-tetramethylcyclopenta-2,4-dienyl derivative is probably less sterically hindered than the 2,3,4,5 - tetramethyl - cyclopenta - 1,4 - dienyl analogue.

(ii) When $C_7H_8Mo(CO)_4$ was treated with two equivalents of $Ph_2P(C_5Me_4H)$ at room temperature in hexane, white crystals of stoichiometry $Mo(CO)_5[Ph_2P(C_5Me_4H)]$, **IV**, were obtained in moderate yield (65%). The IR spectrum (KBr) of **IV** exhibits three absorptions at 2070s, 1983s, and 1927vs (br) cm^{-1} at the terminal carbonyl region. The $^{31}P\{^1H\}$ NMR spectrum of **IV** shows a singlet at δ 37.0 ppm. The ^1H NMR spectrum exhibits two multiplets of relative intensity 4 : 6 centred at δ 7.68 and 7.24 ppm, respectively for the phenyl protons; a doublet

of relatively intensity 1 centred at δ 4.23 ppm (J_{P-H} = 15.3 Hz) for the unique proton of the C_5Me_4H ring; and three broad singlets of relative intensity 3:3:6 at δ 1.76, 1.73 and 1.42 ppm, respectively, for the methyl protons of the C_5Me_4H ring. The ^1H NMR chemical shift and splitting pattern of the unique proton suggests that the proton is an aliphatic proton and is attached to the carbon α to the phosphorus. The above spectroscopic evidence indicates that the phosphine ligand is a (2,3,4,5-tetramethylcyclopenta - 2,4 - dienyl)diphenylphosphine ligand. Thus, the following structure can be assigned to **IV**:

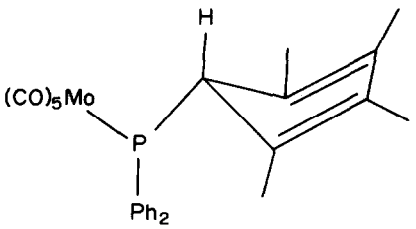

IV

The structure of **IV** was confirmed by X-ray crystallography. Crystals suitable for the diffraction study were grown from hexane. The crystal data and other parameters for the X-ray structural analysis are listed in Table 1. A perspective drawing of **IV** is shown in Fig. 1. Selected bond lengths and bond angles are given in Table 2. The cyclopentadienyl group is a planar five-membered ring (within $\pm$0.006 Å). The P(1)—C(31)—C(32) angle of 111.8(4)°, together with the C—C distances of 1.52(1) Å for C(31)—C(32) and C(31)—C(35) as well as 1.35(1), 1.46(1) and 1.36(1) Å for C(32)—C(33), C(33)—C(34) and C(34)—C(35), respectively, indicate that the phosphine is indeed a (2,3,4,5-tetramethylcyclo-2,4-pentadienyl)diphenylphosphine ligand. The molybdenum atom in complex **IV** retains the octahedral coordination of its parent $Mo(CO)_6$.[3] The X-ray structural analysis showed that there are two distinctly different Mo—C distances in complex **IV**. The carbonyl is *trans* to the $Ph_2P(C_5Me_4H)$ ligand and has a Mo—$C_{ax.}$ bond of 1.989(8) Å which is significantly shorter than the Mo—C bonds involving the equatorial carbonyl groups [av. Mo—$C_{eq.}$ = 2.050(9) Å]. This structural feature has been observed in analogous complexes such as $Mo(CO)_5P(CH_2CH_2CN)_3$ and $Mo(CO)_5PPh_3$.[4] The Mo—P bond of 2.555(2) Å is comparable to that found in $Mo(CO)_5PPh_3$[4] [2.560(1) Å] but is significantly longer than those in $Mo(CO)_5P(CH_2CH_2CN)_3$[4] [2.506(1) Å] and $Mo(CO)_5[P(CH_2)_6N_3]$[5] [2.479(5) Å]. As expected, one of the

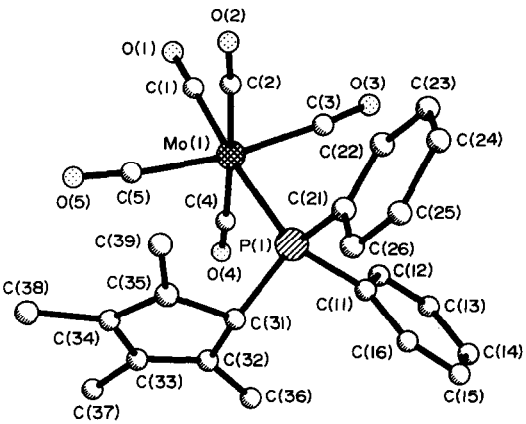

Fig. 1. A perspective view of the molecular structure of **IV**.

phenyl groups of $Ph_2P(C_5Me_4H)$ is oriented so that the P(1)—C(11) bond lies approximately over the bisector of an equatorial C—Mo—C angle to minimize the steric interactions, which can be quantitatively expressed by the torsion angles C(3)—Mo(1)—P(1)—C(11) = −43.8(4)° and C(4)—Mo(1)—P(1)—C(11) = 49.3(4)°.

(iii) When $C_7H_8Mo(CO)_4$ was treated with two equivalents of **I** in refluxed hexane for 3 days, dark red crystals of **V** were obtained in low yield (10%). The IR spectrum of **V** in KBr exhibits two absorptions at 1891s and 1820s cm^{-1} at the terminal carbonyl region. The $^{31}P\{^1H\}$ NMR spectrum of **V** exhibits two singlets of relative intensity 2:1 at δ 83.6 and 20.6 ppm, respectively. The ^1H NMR spectrum exhibits two multiplets and a broad singlet of relative intensity 4:8:18, centred at δ 7.72, 7.42 and 7.25 ppm, respectively, for the phenyl protons; a broad singlet of relative intensity 1 at δ 5.63 ppm in the olefinic region for the unique proton of the C_5Me_4H ring; and a broad singlet, two singlets, a multiplet and a singlet of relative intensity 3:3:12:3:3, centred at δ 1.91, 1.63, 1.53, 1.25 and 1.08 ppm, respectively, for the methyl protons of the C_5Me_4H rings.

The structure of **V** was determined by an X-ray diffraction study of its hexane solvate, $\mathbf{V} \cdot 1/4C_6H_{14}$. The crystal data and other parameters for the X-ray structural analysis are listed in Table 1. A perspective drawing of **V** is shown in Fig. 2. Selected bond lengths and bond angles are given in Table 3. The structure can be formulated as (η^5-C_5Me_4H)Mo(CO)(μ - PPh_2)$_2$Mo[(η^5 - C_5Me_4)P(O)Ph_2](CO) and is consistent with the spectroscopic data. Thus, the ^{31}P chemical shifts at δ 83.4 and 20.6 ppm of relative intensity 2:1 can be assigned to the two phosphido-bridged ligands and

Table 1. Data collection and processing parameters

	IV	V
Molecular formula	$(CO)_5Mo[(C_6H_5)_2P(C_5H(CH_3)_4)]$	$[C_5H(CH_3)_4][C_5(CH_3)_4POPh_2]$ $\cdot(Ph_2P)_2Mo_2(CO)_2\cdot xC_6H_{14}$ ($x \simeq 0.25$)
Molecular weight	542.38	1082.45 (for $x = 0.25$)
Colour and habit	colourless plane	dark red prism
Unit cell parameters		
a (Å)	11.339(3)	13.450(3)
b (Å)	13.219(4)	13.457(5)
c (Å)	9.578(6)	15.676(3)
α (°)	117.69(2)	78.27(2)
β (°)	85.99(3)	76.82(2)
γ (°)	82.54(2)	70.94(2)
V (Å^3)	1247(1)	2585(1)
Z	2	2
$F(000)$	552	1113
Calculated density (g cm^{-3})	1.444	1.390 (for $x = 0.25$)
Space group	$P\bar{1}$ (No. 2)	$P\bar{1}$ (No. 2)
Radiation	graphite-monochromatized Mo-K_α, $\lambda = 0.71073$ Å	
Standard reflections	(222), (411)	(2$\bar{3}$7), (317)
Intensity variation	±3%	±2%
R_{int} (from merging of equiv. reflections)	0.020	0.015
Absorption coefficient (cm^{-1})	6.07	6.06
Crystal size (mm^3)	0.10 × 0.34 × 0.42	0.24 × 0.44 × 0.80
Mean μr	0.087	0.149
Transmission factors	0.801 to 0.836	0.682 to 0.799
Scan type and rate (° min^{-1})	ω–2θ; 3.01 to 15.63	ω–2θ; 3.01 to 15.63
Scan range	0.60 ° below K_{α_1} to 0.70° above K_{α_2}	
Background counting	stationary counts for one-fifth of scan time at each end of scan range	
Collection range	h, ±k, ±l; $2\theta_{max} = 50°$	h, ±k, ±l; $2\theta_{max} = 50°$
Unique data measured	4410	9096
Obs. data with $\lvert F_o\rvert \geq 6\sigma(\lvert F_o\rvert)$, n	3687	7550
Number of variables, p	299	606
$R_F = \Sigma \lvert\lvert F_o\rvert - \lvert F_c\rvert\rvert / \Sigma \lvert F_o\rvert$	0.062	0.039
Weighting scheme, w	$\frac{1-\exp(-4\sin^2\theta/\lambda^2)}{\sigma^2(F_o)+0.0006\lvert F_o\rvert^2}$	$\frac{1}{\sigma^2(F_o)+0.00005\lvert F_o\rvert^2}$
$R_G = [\Sigma w(\lvert F_o\rvert - \lvert F_c\rvert)^2 / \Sigma w\lvert F_o\rvert^2]^{1/2}$	0.087	0.069
$S = [\Sigma w(\lvert F_o\rvert - \lvert F_c\rvert)^2/(n-p)]^{1/2}$	1.723	4.512
Residual extreme in final difference map (eÅ^{-3})	+1.11 to −1.25	+1.14 to −0.42

the phosphine oxide, respectively. The dimer can be considered as a Mo^{II}—Mo^{II} compound. For the two molybdenum atoms to obey the 18-electron rule, a double bond should exist between them. This is reflected by the shorter Mo—Mo distance of 2.744(1) Å in comparison with those in the analogous P-bridged complexes $M_2(CO)_8(\mu\text{-}PEt_2)_2$[6] (M=Mo, 3.06 and M=W, 3.05) and the unbridged complex $Mo_2(CO)_6(\eta^5\text{-}C_5H_5)_2$[7] [3.235(1) Å]. The coordination polyhedron around each Mo atom can be described as a distorted tetrahedron if the metal–metal bond is neglected, which is similar to that in $Mo_2(\eta^5\text{-}C_5H_5)_2(\mu\text{-}PPh_2)_2(CO)(O)$.[8] The coordination geometries of the Mo atoms in these two complexes differ markedly in that the Cp(1)—Mo(1)—Mo(2)—Cp(2) moiety in complex **V** is approximately linear with angles of 165.8(2)° and 179.3(2)° for Cp(1)—Mo(1)—Mo(2) and Cp(2)—Mo(2)—Mo(1), respectively, but the corresponding angles in $Mo_2(\eta^5\text{-}C_5H_5)_2(\mu\text{-}PPh_2)_2(CO)(O)$ are 124.4(2)° and 148.5(2)°, respectively. The Mo_2P_2 core in **V** has the same planar

Table 2. Selected bond lengths (Å) and bond angles (°) for **IV**

Mo(1)—P(1)	2.555(2)	Mo(1)—C(1)	1.989(8)
Mo(1)—C(2)	2.061(8)	Mo(1)—C(3)	2.043(8)
Mo(1)—C(4)	2.043(9)	Mo(1)—C(5)	2.05(1)
O(1)—C(1)	1.13(1)	O(2)—C(2)	1.13(1)
O(3)—C(3)	1.13(1)	O(4)—C(4)	1.13(1)
O(5)—C(5)	1.12(1)	P(1)—C(11)	1.843(8)
P(1)—C(21)	1.846(6)	P(1)—C(31)	1.867(6)
P(1)—Mo(1)—C(1)	176.2(3)	P(1)—Mo(1)—C(2)	89.1(2)
C(1)—Mo(1)—C(2)	90.3(3)	P(1)—Mo(1)—C(3)	88.4(3)
C(1)—Mo(1)—C(3)	87.8(4)	C(2)—Mo(1)—C(3)	90.8(4)
P(1)—Mo(1)—C(4)	90.8(2)	C(1)—Mo(1)—C(4)	90.0(4)
C(2)—Mo(1)—C(4)	176.0(3)	C(3)—Mo(1)—C(4)	93.2(4)
P(1)—Mo(1)—C(5)	100.4(2)	C(1)—Mo(1)—C(5)	83.3(3)
C(2)—Mo(1)—C(5)	86.9(3)	C(3)—Mo(1)—C(5)	170.8(4)
C(4)—Mo(1)—C(5)	89.2(4)	Mo(1)—C(1)—O(1)	179.0(9)
Mo(1)—C(2)—O(2)	177.2(6)	Mo(1)—C(3)—O(3)	176(1)
Mo(1)—C(4)—O(4)	177.6(8)	Mo(1)—C(5)—O(5)	174(1)
Mo(1)—P(1)—C(11)	117.8(2)	Mo(1)—P(1)—C(21)	114.3(2)
C(11)—P(1)—C(21)	98.1(3)	Mo(1)—P(1)—C(31)	116.1(2)
C(11)—P(1)—C(31)	102.7(3)	C(21)—P(1)—C(31)	105.8(3)

(within ± 0.082 Å from the least-squares plane) configuration as found in other analogous phosphido-bridged complexes.[6,8] The two carbonyl groups are *trans* to each other and approximately perpendicular to the Mo_2P_2 plane. Both cyclopentadienyl rings are planar conjugated groups with sp^2 hybridized C atoms and normal C—C bond lengths [av. 1.428(8) Å], which is in accord with the ^1H NMR results.

EXPERIMENTAL

Microanalyses were performed by Butterworth (U.K.). IR spectra were recorded on a Perkin–

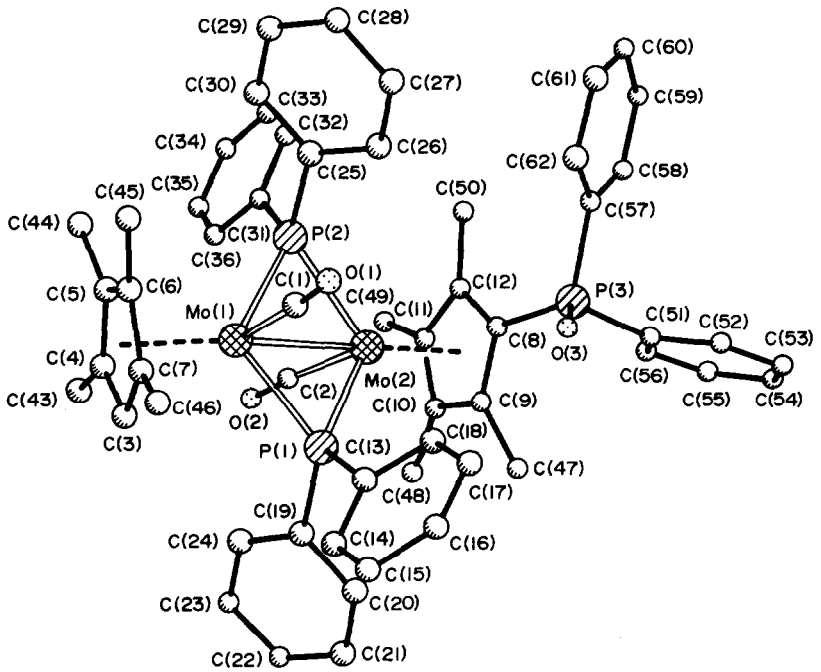

Fig. 2. A perspective view of the molecular structure of **V**.

Table 3. Selected bond lengths (Å) and bond angles (°) for **V**

Mo(1)—Mo(2)	2.744(1)		
Mo(1)—P(1)	2.400(2)	Mo(2)—P(1)	2.417(2)
Mo(1)—P(2)	2.418(2)	Mo(2)—P(2)	2.425(2)
Mo(1)—C(1)	1.928(5)	Mo(2)—C(2)	1.909(5)
Mo(1)—Cp(1)	2.011(5)[a]	Mo(2)—Cp(2)	2.026(5)
C(1)—O(1)	1.157(7)	C(2)—O(2)	1.173(6)
P(1)—C(13)	1.821(5)	P(2)—C(25)	1.834(6)
P(1)—C(19)	1.817(6)	P(2)—C(31)	1.830(6)
P(3)—O(3)	1.485(5)	P(3)—C(8)	1.799(5)
P(3)—C(51)	1.821(6)	P(3)—C(57)	1.804(8)
Mo(2)—Mo(1)—P(1)	55.6(1)	Mo(1)—Mo(2)—P(1)	55.0(1)
Mo(2)—Mo(1)—P(2)	55.6(1)	Mo(1)—Mo(2)—P(2)	55.4(1)
P(1)—Mo(1)—P(2)	110.6(1)	P(1)—Mo(2)—P(2)	109.8(1)
Mo(2)—Mo(1)—C(1)	84.9(2)	Mo(1)—Mo(2)—C(2)	70.6(2)
P(1)—Mo(1)—C(1)	82.6(2)	P(1)—Mo(2)—C(2)	82.0(2)
P(2)—Mo(1)—C(1)	84.0(2)	P(2)—Mo(2)—C(2)	83.5(2)
Mo(2)—Mo(1)—Cp(1)	165.8(1)	Mo(1)—Mo(2)—Cp(2)	179.3(1)
P(1)—Mo(1)—Cp(1)	123.8(2)	P(1)—Mo(2)—Cp(2)	124.3(2)
P(2)—Mo(1)—Cp(1)	124.9(2)	P(2)—Mo(2)—Cp(2)	125.4(2)
C(1)—Mo(1)—Cp(1)	109.3(2)	C(2)—Mo(2)—Cp(2)	109.2(2)
Mo(1)—C(1)—O(1)	172.7(6)	Mo(2)—C(2)—O(2)	169.2(5)
Mo(1)—P(1)—Mo(2)	69.4(1)	Mo(1)—P(2)—Mo(2)	69.0(1)
Mo(1)—P(1)—C(13)	118.3(2)	Mo(1)—P(2)—C(25)	114.9(2)
Mo(2)—P(1)—C(13)	125.3(2)	Mo(2)—P(2)—C(25)	125.8(2)
Mo(1)—P(1)—C(19)	124.4(2)	Mo(1)—P(2)—C(31)	128.0(2)
Mo(2)—P(1)—C(19)	116.87(2)	Mo(2)—P(2)—C(31)	117.2(2)
C(13)—P(1)—C(19)	102.1(3)	C(25)—P(2)—C(31)	101.7(3)
O(3)—P(3)—C(8)	114.5(3)	O(3)—P(3)—C(51)	112.8(3)
C(8)—P(3)—C(51)	103.1(3)	O(3)—P(3)—C(57)	111.7(3)
C(8)—P(3)—C(57)	112.3(3)	C(51)—P(3)—C(57)	101.4(3)

[a] Cp(1) is the centre of the ring composed of carbon atoms C(3)—C(7), and Cp(2) is the centre of C(8)—C(12) ring.

Elmer 983 spectrometer; data given in cm^{-1} in KBr pellets. NMR spectra were recorded on a JEOL FX90Q spectrometer. Chemical shifts of ^1H NMR spectra were referenced to internal deuterated solvents and then recalculated to TMS = 0.0 ppm. ^{31}P NMR spectra were referenced to external 85% H_3PO_4. Mass spectra were obtained on a VG7070F spectrometer.

All operations were carried out under nitrogen or *in vacuo*. All chemicals used were of reagent grade. Solvents were dried by standard procedures, distilled, and deaerated prior to use. Melting points were taken in sealed capillaries and are uncorrected.

$C_5Me_4H_2$[9] and $C_7H_8Mo(CO)_4$[10] were prepared according to literature methods.

Preparation of $PhP(C_5Me_4H)_2$, **I**

A three-necked round-bottom flask (250 cm^3) fitted with a gas inlet, magnetic stirring bar and pressure-equalizing addition funnel was charged with 1,2,3,4-tetramethylcyclopentadiene (5.4 g, 44.3 mmol). Anhydrous tetrahydrofuran (100 cm^3) was syringed into the flask. The solution was then cooled to about −5°C, and *n*-BuLi (26 cm^3, 1.6 M, 41.6 mmol) was added dropwise to the solution over a period of 1 h. During the period, a white precipitate was formed. The reaction mixture was then warmed to room temperature slowly and allowed to stir overnight. The mixture was cooled to −78°C. Dichlorophenylphosphine (2.8 cm^3, 20 mmol) was then added dropwise to the solution. The white precipitate gradually disappeared and the solution changed to clear yellow. The solution was then warmed to room temperature and stirring was continued for another 2 h. The solvent was removed *in vacuo*. The residue was extracted with hexane (2 × 50 cm^3). The combined hexane filtrate was evaporated *in vacuo* to give a pale orange viscous oil from which white needles were obtained upon

cooling to −20°C. Yield (pale orange oil): 5.6 g, 80%.

^{1}H NMR ($CDCl_3$): δ 7.24 (m, 5H), 3.92 (br s, 2H), 2.08 (br s, 6H), 1.75 (br s, 6H), 1.61 (br s, 12H); $^{31}P\{^1H\}$ NMR ($CDCl_3$): δ 12.5(s) IR(neat, cm^{-1}): 3053m, 2963s, 2912s, 2855s, 2738w, 1955w, 1813w, 1584w, 1544w, 1479w, 1433s, 1378s, 1326w, 1302w, 1253w, 1215m, 1183m, 1140m, 1109m, 1088m, 1068m, 1025m, 976s, 897w, 844m, 794w, 744s, 710m, 696s, 633w, 566m, 539m, 514m, 486m. MS: *m/z* 350. The purity of the pale orange oil was judged to be 95% by $^{31}P\{^1H\}$ NMR.

Preparation of $Ph_2P(C_5Me_4H)$, **II**

The procedure was the same as the preparation of **I**. $C_5Me_4H_2$ (4.1 g, 33.6 mmol), *n*-BuLi (1.6 M, 20 cm^3, 32 mmol) and Ph_2PCl (7.0 g, 31.7 mmol) were used. A pale orange oil was obtained. Yield: 8.0 g, 72%. ^{1}H NMR ($CDCl_3$): δ 7.27 (m, 1.0 H), 3.69 and 2.64 (two br s of total 1H), 1.54–1.91 (sets of s, 12H); $^{31}P\{^1H\}$ NMR ($CDCl_3$): δ −24.6 and 0.8 (two s of equal intensity). IR (neat, cm^{-1}): 3068m, 3052m, 2963s, 2916s, 2872s, 1948w, 1883w, 1808w, 1750w, 1583m, 1478m, 1431s, 1327m, 1304m, 1274w, 1216m, 1181m, 1156m, 1130m, 1093s, 1068m, 1026m, 999s, 980s, 895m, 846m, 791w, 740s, 696s. MS: *m/z* 305. The purity of the pale orange oil was judged to be 90% by $^{31}P\{^1H\}$ NMR.

Preparation of $Mo(CO)_5[PhP(C_5Me_4H)_2]$, **III**

A solution of $C_7H_8Mo(CO)_4$ (1.15 g, 3.8 mmol) in hexane (50 cm^3) was added dropwise to a solution of **I** (2.8 g, 7.9 mmol) in hexane (20 cm^3). The solution was allowed to stir at room temperature for 18 h. The solution was filtered. The filtrate was concentrated to *ca* 20 cm^3 and chromatographed on silica gel under nitrogen atmosphere using hexane as eluent. A pale yellow band was separated. The solution was concentrated to *ca* 20 cm^3 and cooled to −20°C to give white needles which were filtered and dried *in vacuo*. Yield: 1.3 g, 60%; m.p. 113–115°C [Found (required): C, 59.6(59.4); H, 5.4(5.3); P, 5.2(5.3)]. ^{1}H NMR ($CDCl_3$): δ 7.56 (m, 2H), 7.28 (m, 3H), 4.18 (d, J_{P-H} = 10.5 Hz, 2H), 2.17 (br s, 6H), 1.69 (br s, 12H), 1.50 (br s, 6H); $^{31}P\{^1H\}$ NMR ($CDCl_3$): δ 40.8(s). IR in KBr, ν_{CO}: 2067s, 1979s and 1927vs (br) cm^{-1}.

Preparation of $Mo(CO)_5[Ph_2P(C_5Me_4H)]$, **IV**

A solution of $C_7H_8Mo(CO)_4$ (1.7 g, 5.7 mmol) in hexane (50 cm^3) was added dropwise to a solution of **II** (3.6 g, 11.6 mmol) in hexane (20 cm^3). The solution was allowed to stir overnight at room temperature, upon which a brown solution was obtained. The solution was filtered and the filtrate was evaporated to dryness *in vacuo*. The residue was then dissolved in a minimum amount of toluene and then chromatographed on silica gel using toluene as eluent. A brown band was collected. The solution was evaporated to dryness *in vacuo*. The residue was re-dissolved in a minimum amount of toluene and chromatographed on silica gel using hexane–toluene (10:1) mixture as eluent. A light yellow band and a crimson band were obtained. The solvent of the light yellow band was removed *in vacuo*. The residue was dissolved in a minimum amount of toluene, and hexane was added until it started to turn cloudy. At this point, a small amount of toluene was added to make the solution clear again. The resultant solution was then cooled to −20°C to give white crystals which were filtered and dried *in vacuo*. Yield: 2.0 g, 65%; m.p. 152–154°C (decomp.) [Found (required): C, 57.6(57.6); H, 4.3(4.2); P, 5.2(5.7)]. ^{1}H NMR ($CDCl_3$): δ 7.68 (m, 4H), 7.24 (m, 6H), 4.23 (d, J_{P-H} = 15.3 Hz, 1H), 1.76 (br s, 3H), 7.24 (m, 6H), 4.23 (d, J_{P-H} = 15.3 Hz, 1H), 1.76 (br s, 3H), 1.73 (br s, 3H), 1.42 (br s, 6H); $^{31}P\{^1H\}$ NMR ($CDCl_3$): δ 37.0 (s). IR in KBr, ν_{CO}: 2070s, 1983s, 1927vs (br) cm^{-1}.

Attempts to isolate products from the crimson band were unsuccessful.

Preparation of **V**

A solution of $C_7H_8Mo(CO)_4$ (0.9 g, 3.0 mmol) in hexane (50 cm^3) was added dropwise to a solution of **II** (2.0 g, 6.5 mmol) in hexane (20 cm^3). The solution was refluxed for 3 days. A dark solution with dark precipitate was obtained. The solution was filtered. Attempts to isolate crystalline product from the filtrate were unsuccessful. The dark precipitate was dissolved in a minimum amount of toluene, and chromatographed on silica gel using toluene as eluent. An orange–red band was obtained. The solvent of the orange–red band was evaporated to dryness *in vacuo* to give a dark red residue. The residue was then re-dissolved in a minimum amount of methylene chloride, and hexane was added until it started to turn cloudy. At this point, a small amount of methylene chloride was added to make the solution clear again. The resultant solution was allowed to evaporate slowly in air. After two days, dark red prisms of stoichiometry $C_{56}H_{55}O_3P_3Mo_2 \cdot 1/4(C_6H_{14})$ were formed. They were filtered and dried *in vacuo*. Yield: 0.2 g, 12%; m.p. > 300°C [Found (required): C, 64.0(63.8); H, 5.7(5.4); P, 8.2(8.6)]. ^{1}H NMR ($CDCl_3$): δ 7.72 (m, 4H), 7.42 (m, 8H), 7.25 (br s, 18H), 5.63 (br s, 1H),

1.91 (br s, 3H), 1.63 (s, 3H), 1.53 (s, 12H), 1.25 (m, 3H), 1.08 (s, 3H); $^{31}P\{^1H\}$ NMR ($CDCl_3$): δ 83.6 (s, 2P), 20.6 (s, 1P). IR in KBr, ν_{CO}: 1891s and 1820s cm^{-1}.

X-ray crystallography

Raw intensities collected on a Nicolet R3m/V four-circle diffractometer at room temperature (294 K) were processed with the profile-fitting procedure of Diamond[11] and corrected for absorption using ψ-scan data.[12] Details of data collection and processing for complexes **IV** and **V** are listed in Table 1.

(i) *Complex* **IV**. Patterson superposition yielded the positions of all non-hydrogen atoms which were subjected to anisotropic refinement. The hydrogen atoms were generated geometrically (C—H bonds fixed at 0.96 Å) and allowed to ride on their respective parent C atoms; all hydrogen atoms were assigned appropriate isotropic temperature factors and included in the structure-factor calculations.

(ii) *Complex* **V**. The Mo_2P_2 core was located by direct phase determination and the coordinates of the other non-hydrogen atoms were derived from successive difference Fourier syntheses. A disordered *n*-hexane solvent molecule located about a crystallographic inversion centre was found on a subsequent difference Fourier map, and interatomic distance constraints of 1.500(2) and 2.490(2) Å were applied to pairs of adjacent and alternate carbon atoms, respectively. The occupancies of these carbon atoms were fixed at 1/2 in the refinement to be compatible with reasonable values of their temperature factors. All non-hydrogen atoms were subjected to anisotropic refinement. Hydrogen atoms except those of the solvent molecule were generated geometrically (C—H bonds fixed at 0.96 Å) and allowed to ride on their respective C atoms; they were assigned appropriate isotropic temperature factors and included in the structure-factor calculations.

Computations were performed using the SHELXL-PLUS program package[13] on a DEC MicroVAX-II computer. Analytic expressions of atomic scattering factors were employed, and anomalous dispersion corrections were incorporated.[14]

Acknowledgement—We thank the Hong Kong Polytechnic and UPGC for financial support.

REFERENCES

1. G. K. Anderson and M. Lin, *Organometallics* 1988, **7**, 2285, and refs therein.
2. W. K. Wong, F. L. Chow, H. Chen and T. C. W. Mak, *J. Organomet. Chem.* 1989, **377**, C65.
3. W. Rüdorff and U. Hoffmann, *Z. Phys. Chem.* (*B*) 1935, **28**, 351; T. C. W. Mak, *Z. Kristallogr.* 1984, **166**, 277.
4. F. A. Cotton, D. J. Darensbourg and W. H. Ilsley, *Inorg. Chem.* 1981, **20**, 578.
5. J. R. DeLerno, L. M. Trefonas, M. Y. Darensbourg and R. J. Majeste, *Inorg. Chem.* 1976, **15**, 816.
6. M. H. Linck and L. R. Nassimbeni, *Inorg. Nucl. Chem. Lett.* 1973, **9**, 1105.
7. R. D. Adams, D. M. Collins and F. A. Cotton, *Inorg. Chem.* 1974, **13**, 1086.
8. W. K. Wong, F. L. Chow, H. Chen, R.-J. Wang and T. C. W. Mak, *Polyhedron* 1990, **9**, 2469.
9. C. M. Fendrick, L. D. Schertz, V. W. Day and T. J. Marks, *Organometallics* 1988, **7**, 1828.
10. J. J. Eisch and R. B. King, *Organometallic Synthesis*, Vol. 1, pp. 124–125. Academic Press, New York (1965).
11. R. Diamond, *Acta Cryst. A* 1969, **25**, 43.
12. G. Kopfmann and R. Hubber, *Acta Cryst. A* 1968, **24**, 348.
13. G. M. Sheldrick, in *Crystallographic Computing 3: Data Collection, Structure Determination, Proteins and Databases* (Edited by G. M. Sheldrick, C. Krüger and R. Goddard), p. 175. O.U.P., New York (1985).
14. *International Tables for X-ray Crystallography*, Vol. IV, pp. 55, 99 and 149. Kynoch Press, Birmingham (1974). (Now distributed by Kluwer Academic Publishers, Dordrecht.)

Polyhedron Vol. 9, No. 24, pp. 2911–2918, 1990
Printed in Great Britain

0277–5387/90 $3.00+.00
© 1990 Pergamon Press plc

COPPER THIOETHER CHEMISTRY: SYNTHESIS AND X-RAY CRYSTAL STRUCTURES OF BINUCLEAR COPPER(I) COMPLEXES $[Cu_2(L)]^{2+}$ {L = [24]aneS$_8$, [28]aneS$_8$}* INCORPORATING OCTATHIA MACROCYCLES

ALEXANDER J. BLAKE, ANNE TAYLOR and MARTIN SCHRÖDER†

Department of Chemistry, University of Edinburgh, West Mains Road, Edinburgh EH9 3JJ, Scotland, U.K.

(*Received* 10 *May* 1990; *accepted* 6 *August* 1990)

Abstract—Reaction of L {L = [24]aneS$_8$, [28]aneS$_8$} with two molar equivalents of $[Cu(NCMe)_4]X$ ($X^- = ClO_4^-$, BF_4^-, PF_6^-) in MeCN affords the white binuclear copper(I) complexes $[Cu_2(L)]^{2+}$. A single crystal X-ray structure determination of $[Cu_2([24]aneS_8)](BF_4)_2$ shows two tetrahedral copper(I) centres, each of which is coordinated to four thioether sulphur-donors, Cu—S(1) = 2.263(3), Cu—S(4) = 2.363(3), Cu—S(7) = 2.349(3), Cu—S(10) = 2.261(3) Å. The Cu···Cu distance is 5.172(3) Å. A single crystal X-ray structure determination of $[Cu_2([28]aneS_8)](ClO_4)_2$ shows that this complex also contains two tetrahedral copper(I) centres, each coordinated to four thioether sulphur-donors, Cu—S(1) = 2.278(5), Cu—S(4) = 2.333(5), Cu—S(8) = 2.328(5), Cu—S(11) = 2.268(5) Å. The Cu···Cu distance of 6.454(3) Å is greater than in $[Cu_2([24]aneS_8)]^{2+}$, reflecting the greater cavity size in $[Cu_2([28]aneS_8)]^{2+}$. Cyclic voltammetry of $[Cu_2([24]aneS_8)]^{2+}$ and $[Cu_2([28]aneS_8)]^{2+}$ at platinum electrodes in MeCN (0.1 M $^nBu_4NPF_6$) shows irreversible oxidations at E_{pa} = +0.88 V, +0.92 V vs Fc/Fc^+, respectively, at a scan rate of 200 mV s^{-1}. Coulometric measurements in MeCN confirm these oxidations to be two-electron (one electron per copper) processes to give binuclear copper(II) species. Oxidation of the binuclear copper(I) precursors with H_2SO_4 or HNO_3 affords ESR-active copper(II) species which presumably incorporate SO_4^{2-} and NO_3^- bridges.

The study of mono- and binuclear $Cu^{II/I}$ complexes as models for copper-containing metallo-enzymes is well established.[1] Several biological systems involve copper coordinated to sulphur,[2] and this has led several groups to investigate the incorporation of $Cu^{II/I}$ centres into thioether crowns.[3–8] Rorabacher and co-workers have reported a series of studies on the complexation of copper(II) and copper(I) by polythia macrocyclic ligands.[3,5,6] The single crystal X-ray structure of $[Cu([15]aneS_5)]^{2+}$ shows a square-based pyramidal stereochemistry, Cu—S_{eq} = 2.289(2), 2.315(2), 2.331(2), 2.338(2), Cu—S_{ap} = 2.398(2) Å with the copper atom 0.41 Å out of the basal plane.[5] Reduction of $[Cu([15]aneS_5)]^{2+}$ affords $[Cu([15]aneS_5)]^+$, in which the copper(I) centre has a distorted tetrahedral geometry in the solid state, Cu—S = 2.243(5), 2.245(5), 2.317(5), 2.338(5) Å; the fifth sulphur-donor is non-bonding and is disordered over two sites, Cu···S = 3.442(12) and 3.560(11) Å. The self-exchange electron-transfer rate constant for $[Cu([15]aneS_5)]^{2+/+}$ is very rapid ($k = 3 \times 10^4$ M^{-1} s^{-1}).[5] Cooper and co-workers have reported[7] a similar, rapid Cu—S bond cleavage on reduction of $[Cu([18]aneS_6)]^{2+}$. $[Cu([18]aneS_6)]^{2+}$ shows a tetragonally elongated octahedral stereochemistry, Cu—S = 2.323(1), 2.402(1), 2.635(1) Å. Reduction of this complex affords $[Cu([18]aneS_6)]^+$ which, like $[Cu([15]aneS_5)]^+$, shows a tetrahedral stereochemistry at the metal centre, Cu—S = 2.245(2), 2.253(2), 2.358(2), 2.360(2) Å.[7] The interconversion of $Cu^{II/I}$ centres with [15]aneS$_5$ and [18]aneS$_6$ com-

*[24]aneS$_8$: 1,4,7,10,13,16,19,22-octathiacyclotetracosane; [28]aneS$_8$: 1,4,8,11,15,18,22,25-octathiacyclooctacosane.

† Author to whom correspondence should be addressed.

plexes therefore leads to the formation and breaking of one and two Cu—S bonds, respectively.

These results suggested that tetrahedral coordination of copper(I) to thioether crowns was preferred, as would be expected for a d^{10} metal centre. We have been interested in the synthesis of binuclear copper complexes of thioether macrocycles and have reported previously the synthesis of the binuclear copper(I) species $[Cu_2(L)(NCMe)_2]^{2+}$ {L = [18]aneS$_6$,[4] Me$_2$[18]aneN$_2$S$_4$[9]}. In these systems, however, the 18-membered rings are too small and lack sufficient sulphur-donors to encapsulate two copper(I) centres tetrahedrally. As a result, a solvent MeCN molecule completes the tetrahedral coordination sphere at each copper(I) centre. We argued that larger ring S$_8$-donor crowns would be capable of encapsulating two copper(I) ions tetrahedrally to give a binuclear, homoleptic thioether product. We report herein the synthesis and single crystal X-ray structure determination of two such complexes, $[Cu_2(L)]^{2+}\cdot 2X^-$ {L = [24]aneS$_8$, $X^- = BF_4^-$; L = [28]aneS$_8$, $X^- = ClO_4^-$}.

RESULTS AND DISCUSSION

Reaction of L {L = [24]aneS$_8$, [28]aneS$_8$} with two molar equivalents of $[Cu(NCMe)_4]X$ (X^- = ClO_4^-, BF_4^-, PF_6^-), in MeCN under reflux, affords the white, binuclear copper(I) complexes $[Cu_2(L)]^{2+}\cdot 2X^-$. This assignment of the products is based on IR, NMR and FAB mass spectroscopy and elemental analysis. In order to confirm the connectivity and stereochemistry at the copper(I) centres, and also the conformation of these coordinated large-ring thia macrocycles, single crystal X-ray structure determinations were carried out. Although examples of coordination compounds with these octathia ligands have been described previously,[10,11] none has been characterized crystallographically.

A single crystal X-ray structure determination on $[Cu_2([24]aneS_8)](BF_4)_2$ confirms [Fig. 1(a) and (b)] the complex to be a genuine binuclear copper(I) complex. The two copper(I) centres are related by a crystallographic inversion centre and are each coordinated to four thioether sulphur-donors, Cu—S(1) = 2.263(3), Cu—S(4) = 2.363(3), Cu—S(7) = 2.349(3), Cu—S(10) = 2.261(3) Å. These bond lengths are comparable with Cu—S distances in related copper(I)–thioether complexes.[4-8] The Cu···Cu distance of 5.172(3) Å indicates that the two copper(I) centres are non-interacting. The angles at the copper(I) centres are distorted from those values expected for a tetrahedron, ∠S(1)CuS(4) = 94.54(10), ∠S(1)CuS(7) = 120.20(11),

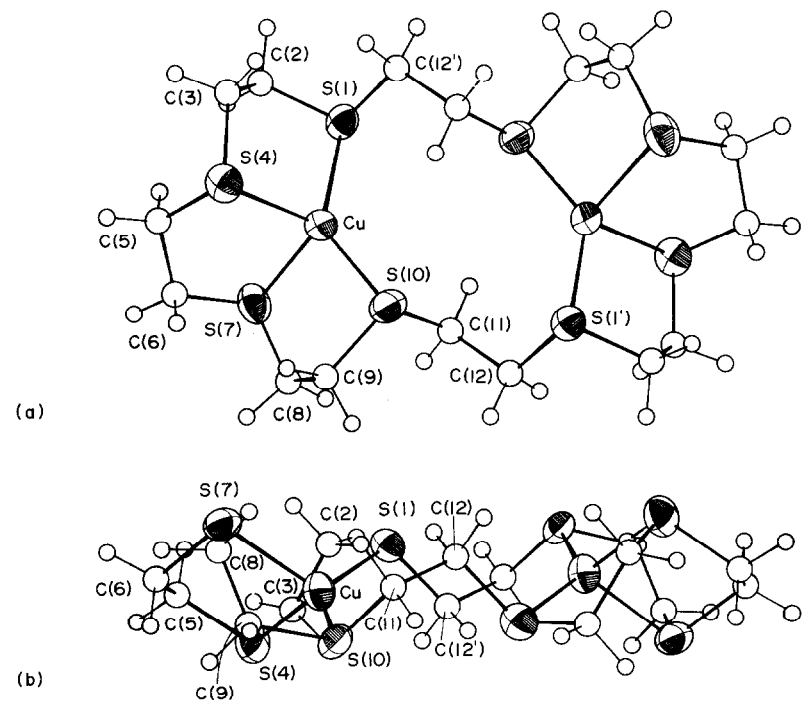

Fig. 1. (a) View of the $[Cu_2([24]aneS_8)]^{2+}$ cation with atom numbering scheme adopted; (b) Orthogonal view showing the conformation of the macrocycle.

∠S(1)CuS(10) = 133.86(11), ∠S(4)CuS(7) = 91.81(10), ∠S(4)CuS(10) = 116.39(10), ∠S(7)CuS(10) = 93.57(10)°. The structure of $[Cu_2([28]aneS_8)](ClO_4)_2$, the analogous complex with the larger, 28-membered ring macrocycle, shows similar features: a single crystal X-ray structure determination of this species [Fig. 2(a) and (b)] also shows two tetrahedral copper(I) centres each coordinated to four thioether sulphur-donors, Cu—S(1) = 2.278(5), Cu—S(4) = 2.333(5), Cu—S(8) = 2.328(5), Cu—S(11) = 2.268(5) Å, ∠S(1)CuS(4) = 93.69(19), ∠S(1)CuS(8) = 108.78(19), ∠S(1)CuS(11) = 133.39(20), ∠S(4)CuS(8) = 105.66(18), ∠S(4)CuS(11) = 119.79(19), ∠S(8)CuS(11) = 93.25(18)°. The Cu···Cu distance of 6.454(3) Å is greater than in $[Cu_2([24]aneS_8)]^{2+}$, reflecting the greater cavity size of $[28]aneS_8$.

These results confirm that the 24- and 28-membered ring ligands are large enough to encapsulate two isolated tetrahedral metal centres. Interestingly, we have found that $[24]aneS_8$ and $[28]aneS_8$ can also complex two palladium(II) ions to give the $[Pd_2(L)]^{4+}$ species.[12,13] The coordination geometry at palladium(II) in these complexes is likely to be square-planar. Thus, the binucleating octathia ligands, $[24]aneS_8$ and $[28]aneS_8$, are capable of complexing both tetrahedral *and* square-planar metal centres. This opens up the possibility of unusual redox capabilities; for example, reduction of the square-planar, binuclear platinum(II) complexes $[Pt_2(L)]^{4+}$ should afford the platinum(0) species $[Pt_2(L)]$ in which the metal centres are tetrahedral. Control of this four-electron reduction couple should lead to interesting substrate activation reactions such as O_2 reduction, although ligand oxidation reactions may be a problem in this case.

Cyclic voltammetry of $[Cu_2(L)]^{2+}$ at platinum electrodes in MeCN (0.1 M $^nBu_4NPF_6$) shows irreversible oxidations at $E_{pa} = +0.88$ V {L = $[24]aneS_8$} and $E_{pa} = +0.92$ V vs Fc/Fc^+ {L = $[28]aneS_8$}, at a scan rate of 200 mV s^{-1}. Coulometric measurements confirm these oxidations to be two-electron processes (one electron per copper) to afford green $Cu^{II/I}$ products, $\lambda_{max} = 428$ {L = $[24]aneS_8$}; 560, 406 nm {L = $[28]aneS_8$}. The fact that these oxidations are electrochemically irreversible is not surprising since the resultant copper(II) centres would be expected to tend towards octahedral or at least five coordination, and would therefore require extra ligation. We have, therefore, undertaken a preliminary study of the chemical oxidation of $[Cu_2(L)]^{2+}$ with, for example, $NOBF_4$, HNO_3 and H_2SO_4. Oxidation of the complexes affords stable, coloured paramagnetic species, the ESR spectra of which suggest that the two copper(II) centres are non-interacting.

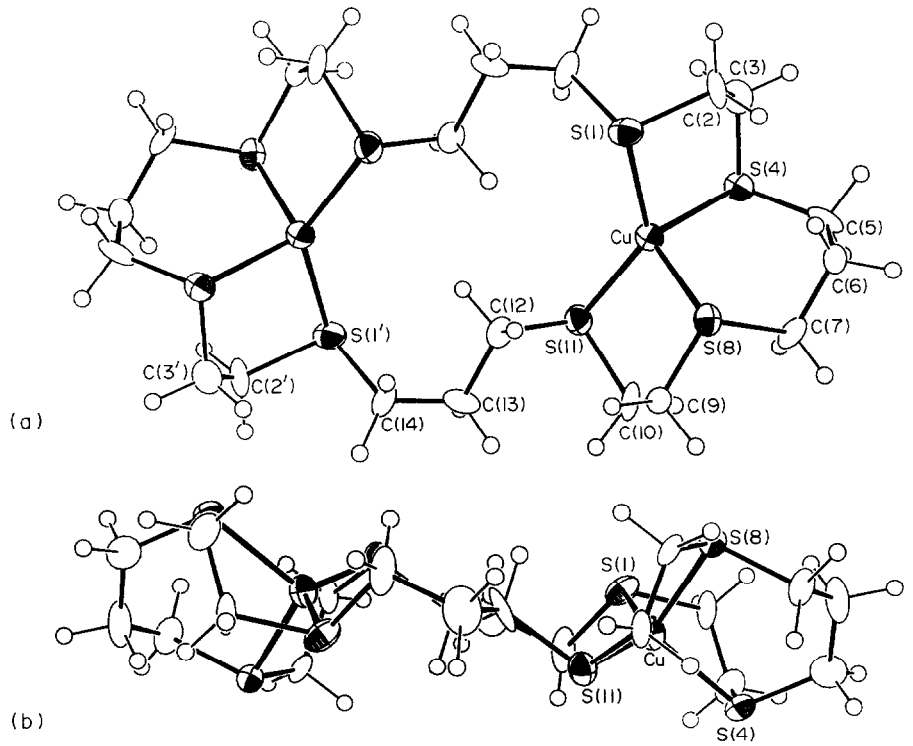

Fig. 2. (a) View of the $[Cu_2([28]aneS_8)]^{2+}$ cation with atom numbering scheme adopted; (b) Orthogonal view showing the conformation of the macrocycle.

Current work is aimed at elucidating the structures and chemistry of these binuclear copper(II) complexes, and to study the redox chemistry of the binuclear copper(I) precursors with small molecule substrates.

EXPERIMENTAL

IR spectra were measured as Nujol mulls, KBr and CsI discs using a Perkin–Elmer 598 spectrometer over the range 200–4000 cm^{-1}. UV–vis spectra were measured in quartz cells using Perkin–Elmer Lambda 9 and Pye Unicam SP8-400 spectrophotometers. Microanalyses were performed by the Edinburgh University Chemistry Department microanalytical service. ESR spectra were recorded as solids or as frozen glasses down to 77 K using a Bruker ER200D X-band spectrometer. ^1H and ^{13}C NMR spectra were recorded at 200.13 and 50.32 MHz, respectively, on a Bruker WP200 spectrometer. Electrochemical measurements were performed on a Bruker E310 Universal Modular Polarograph. All readings were taken using a three-electrode potentiostatic system in acetonitrile containing 0.1 M $^nBu_4NPF_6$ or $^nBu_4NBF_4$ as supporting electrolyte. Cyclic voltammetric measurements were carried out using a double platinum electrode and a Ag/AgCl reference electrode. All potentials are quoted versus ferrocene/ferrocinium, Fc/Fc^+. Mass spectra were run by electron impact on a Kratos MS 902 and by fast atom bombardment on a Kratos MS 50TC spectrometer.

Synthesis of $[Cu_2([24]aneS_8)](PF_6)_2$

To a solution of [24]aneS$_8$ (0.192 g, 0.4 mmol), dissolved in refluxing MeCN (20 cm^3), was added $[Cu(NCMe)_4]PF_6$ (0.298 g, 0.8 mmol). The solution was refluxed for 2 h, filtered and the volume reduced to 5 cm^3. Addition of Et_2O and cooling to −20°C afforded a white precipitate which was recrystallized from acetone–Et_2O to give the desired complex in 78% yield. Found: C, 21.2; H, 3.6. Calc. for $C_{16}H_{32}Cu_2S_8P_2F_{12}$: C, 21.4; H, 3.6%. IR spectrum (KBr disc): 2980, 2920, 1420, 1395, 1320, 1290, 1255, 1210, 1170, 1150, 1130, 1120, 1080, 1050, 920, 840, 740w, 680, 660w, 630w, 610w, 560 and 455 cm^{-1}. FAB mass spectrum (3-NOBA matrix): Found: $M^+ = 753$, 607. Calc. for $[^{63}Cu_2([24]aneS_8)PF_6]^+$: $M^+ = 753$; $[^{63}Cu_2([24]aneS_8)-H]^+$: $M^+ = 607$, with correct isotopic distributions. ^1H NMR spectrum (CD_3CN, 298 K, 200.13 MHz): $\delta = 2.93$–2.97 ppm (32H). ^{13}C NMR spectrum (CD_3CN, 298 K, 50.32 MHz): $\delta = 32.54$ ppm (CH_2).

The complex $[Cu_2([24]aneS_8)](BF_4)_2$ can be prepared in 72% yield by the same method by using $[Cu(NCMe)_4]BF_4$ as a starting material. Found: C, 24.7; H, 4.1. Calc. for $C_{16}H_{32}Cu_2S_8B_2F_8$: C, 24.6; H, 4.1%. IR spectrum (KBr disc): 2980, 2920, 1425, 1410, 1285, 1255, 1200w, 1170w, 1050br, 920w, 910w, 890w, 850, 820, 770, 680, 620w, 520, 455 and 415 cm^{-1}. FAB mass spectrum (3-NOBA matrix): Found $M^+ = 694$, 606. Calc. for $[^{63}Cu_2([24]aneS_8-H)BF_4]^+$: $M^+ = 694$; $[^{63}Cu_2([24]aneS_8)-2H]^+$: $M^+ = 606$, with correct isotopic distributions. ^1H NMR spectrum (CD_3CN, 298 K, 80.13 MHz): $\delta = 2.93$–2.13 ppm (32H).

Crystal structure determination of $[Cu_2([24]aneS_8)](BF_4)_2$

[1,4,7,10,13,16,19,22 - octathiacyclotetracosane - (S^1, S^4, S^7, S^{10})(S^{13}, S^{16}, S^{19}, S^{22})dicopper(I)]$^{2+}$ · $2BF_4^-$. A colourless plate, 0.85 × 0.36 × 0.035 mm, grown by diffusion of Et_2O vapour into a solution of the complex in MeCN, was mounted on a Stoë STADI-4 four-circle diffractometer.

Crystal data. $C_{16}H_{32}Cu_2S_8^{2+} \cdot 2BF_4^-$, $M = 781.5$, monoclinic, space group $P2_1/n$ (alt. $P2_1/c$, No. 14), $a = 6.480(6)$, $b = 20.040(11)$, $c = 11.327(6)$ Å, $\beta = 91.84(5)°$, $U = 1470$ Å^3 [from 2θ values of 22 reflections measured at $\pm\omega(2\theta = 24$–$26°$, $\bar{\lambda} = 0.71073$ Å), $T = 298$ K], $Z = 2$, $D_{calc} = 1.765$ g cm^{-3}, $\mu = 2.014$ mm^{-1}, $F(000) = 792$.

Data collection and processing. STADI-4 diffractometer, graphite-monochromated Mo-K_α X-radiation, $T = 298$ K, ω–2θ scans using the learnt-profile method,[14] 2231 unique data collected ($2\theta_{max}$ 45°, h $-6 \rightarrow 6$, k $0 \rightarrow 21$, l $0 \rightarrow 12$), giving 1468 with $F \geqslant 4\sigma(F)$ for use in all calculations. No significant crystal decay was observed.

Structure solution and refinement. A Patterson synthesis located the copper atom and iterative cycles of least-squares refinement and difference

Table 1. Bond lengths for $[Cu_2([24]aneS_8)]^{2+}$ (with standard deviations)

Cu—S(1)	2.263(3)	C(5)—C(6)	1.503(16)
Cu—S(4)	2.363(3)	C(6)—S(7)	1.817(12)
Cu—S(7)	2.349(3)	S(7)—C(8)	1.808(12)
Cu—S(10)	2.261(3)	C(8)—C(9)	1.561(16)
S(1)—C(2)	1.800(10)	C(9)—S(10)	1.814(12)
C(2)—C(3)	1.520(14)	S(10)—C(11)	1.811(10)
C(3)—S(4)	1.816(10)	C(11)—C(12)	1.524(14)
S(4)—C(5)	1.837(12)	C(12)—S(1′)[a]	1.807(11)

[a] Primed atoms are related to their unprimed equivalents by inversion through ($\frac{1}{2}$, 0, 0).

Table 2. Bond angles for $[Cu_2([24]aneS_8)]^{2+}$ (with standard deviations)

S(1)—Cu—S(4)	94.54(10)	C(3)—S(4)—C(5)	101.8(5)
S(1)—Cu—S(7)	120.20(11)	S(4)—C(5)—C(6)	110.3(8)
S(1)—Cu—S(10)	133.86(11)	C(5)—C(6)—S(7)	113.1(8)
S(4)—Cu—S(7)	91.81(10)	Cu—S(7)—C(6)	98.0(4)
S(4)—Cu—S(10)	116.39(10)	Cu—S(7)—C(8)	98.8(4)
S(7)—Cu—S(10)	93.57(10)	C(6)—S(7)—C(8)	102.3(5)
Cu—S(1)—C(2)	97.8(3)	S(7)—C(8)—C(9)	116.2(8)
Cu—S(1)—C(12′)	110.8(4)	C(8)—C(9)—S(10)	112.7(8)
C(2)—S(1)—C(12′)	100.9(5)	Cu—S(10)—C(9)	97.7(4)
S(1)—C(2)—C(3)	115.4(7)	Cu—S(10)—C(11)	107.9(3)
C(2)—C(3)—S(4)	116.3(7)	C(9)—S(10)—C(11)	103.6(5)
Cu—S(4)—C(3)	97.3(3)	S(10)—C(11)—C(12)	113.1(7)
Cu—S(4)—C(5)	96.4(4)	C(11)—C(12)—S(1′)	112.7(7)

Fourier synthesis located the remaining non-hydrogen atoms. At isotropic convergence, corrections (min. 0.750, max. 1.615) for absorption were applied using DIFABS.[15] Disorder in the BF_4^- counter-anion was modelled by two fully-occupied and four half-occupied fluorine atoms. Refinement (by least-squares on F[16]) with anisotropic thermal for all ordered non-hydrogen atoms and with hydrogen atoms in fixed, calculated positions converged at R, $R_w = 0.0652$, 0.0827, respectively, $S = 1.141$ for 157 refined parameters, and the final ΔF synthesis showed no feature above 0.79 e $Å^{-3}$. The weighting scheme, $w^{-1} = \sigma^2(F) + 0.000264F^2$, gave satisfactory agreement analyses and in the final cycle $(\Delta/\sigma)_{max}$ was 0.072. Bond lengths, angles and torsion angles are listed in Tables 1–3.

Synthesis of $[Cu_2([28]aneS_8)](PF_6)_2$

To a solution of [28]aneS$_8$ (0.215 g, 0.4 mmol) dissolved in refluxing MeCN (25 cm^3) was added $[Cu(NCMe)_4]PF_6$ (0.298 g, 0.8 mmol). The solution was refluxed for 2 h, filtered and the volume reduced to 5 cm^3. Addition of Et_2O and cooling to −20°C afforded a white precipitate which was recrystallized from acetone–Et_2O to give the desired complex in 82% yield. Found: C, 25.2; H, 4.2. Calc. for $C_{20}H_{40}Cu_2S_8P_2F_{12}$: C, 25.2; H, 4.3%. IR spectrum (KBr disc): 2980, 2920, 1440, 1430, 1420, 1410, 1340w, 1300, 1290, 1255, 1245, 1210w, 1140, 1130, 1020, 935, 840, 740, 660 and 555 cm^{-1}. FAB mass spectrum (3-NOBA matrix): Found: $M^+ = 809$, 663. Calc. for $[^{63}Cu_2([28]aneS_8)PF_6]^+$: $M^+ = 809$; $[^{63}Cu_2([28]aneS_8)-H]^+$: $M^+ = 663$, with correct isotopic distributions. ^{1}H NMR spectrum (CD_3CN, 298 K, 200.13 MHz): $\delta = 2.75$–3.10 ppm (28H). ^{13}C NMR spectrum (CD_3CN, 298 K, 50.32 MHz): $\delta = 33.60$, 31.50, 25.56 ppm (CH_2).

The complex $[Cu_2([28]aneS_8)](ClO_4)_2$ can be prepared in 80% yield by the same method by using $[Cu(NCMe)_4]ClO_4$ as a starting material. Found: C, 27.5; H, 4.6. Calc. for $C_{20}H_{40}Cu_2S_8Cl_2O_8$: C, 27.4; H, 4.7%. IR spectrum (KBr disc): 2960, 2920, 2850, 1440, 1405, 1340w, 1300w, 1255, 1240, 1140, 1090, 940w, 920, 910, 850, 840, 805w, 635 and 625 cm^{-1}. FAB mass spectrum (3-NOBA matrix): Found: $M^+ = 763$, 663. Calc. for $[^{63}Cu_2([28]aneS_8)^{35}ClO_4]^+$: $M^+ = 763$; $[^{63}Cu_2([28]aneS_8)-H]^+$: $M^+ = 663$, with correct isotopic distributions. ^{1}H NMR spectrum (CD_3CN, 298 K, 200.13 MHz): $\delta = 2.72$–2.97 ppm (28H). ^{13}C NMR spectrum (CD_3CN, 298 K, 50.32 MHz): $\delta = 33.14$, 31.23, 26.10 ppm (CH_2).

Table 3. Torsion angles for $[Cu_2([24]aneS_8)]^{2+}$ (with standard deviations)

C(12′)—S(1)—C(2)—C(3)	70.7(8)	C(6)—S(7)—C(8)—C(9)	77.6(9)
S(1)—C(2)—C(3)—C(4)	51.1(9)	S(7)—C(8)—C(9)—S(10)	49.9(11)
C(2)—C(3)—S(4)—C(5)	70.6(8)	C(8)—C(9)—S(10)—C(11)	63.7(9)
C(3)—S(4)—C(5)—C(6)	−147.6(8)	C(9)—S(10)—C(11)—C(12)	91.2(8)
S(4)—C(5)—C(6)—S(7)	64.9(9)	S(10)—C(11)—C(12)—S(1′)	68.2(8)
C(5)—C(6)—S(7)—C(8)	−141.7(8)		

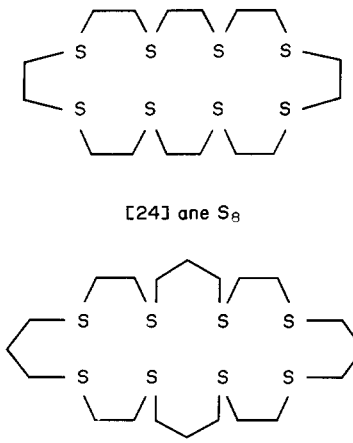

Scheme 1.

Crystal structure determination of $[Cu_2([28]aneS_8)](ClO_4)_2$

[1,4,8,11,15,18,22,25 - octathiacyclooctacosane - (S^1,S^4,S^8,S^{11})(S^{15},S^{18},S^{22},S^{25}) dicopper(I)]$^{2+}\cdot 2ClO_4^-$. A pale yellow needle, $0.47\times0.05\times0.05$ mm, grown by diffusion of Et_2O vapour into a solution of the complex in MeCN, was cooled to 173 ± 0.1 K on a Stoë STADI-4 four-circle diffractometer equipped with an Oxford Cryosystems low-temperature device.[18]

Crystal data. $C_{20}H_{40}Cu_2S_8^{2+}\cdot 2ClO_4^-$, M = 863.0, monoclinic, space group $P2_1/n$ (alt. $P2_1/c$, No. 14), a = 6.999(7), b = 20.000(21), c = 11.780(7) Å, β = 102.37(7)°, U = 1611 Å^3 [from setting angles of 10 reflections with 2θ = 20–22°, $\bar{\lambda}$ = 0.71073 Å, T = 173 K], Z = 2, D_{calc} = 1.779 g cm^{-3}, μ = 2.032 mm^{-1}, $F(000)$ = 888.

Table 4. Bond lengths for $[Cu_2([28]aneS_8)]^{2+}$ (with standard deviations)

Cu—S(1)	2.278(5)	C(6)—C(7)	1.56(3)
Cu—S(4)	2.333(5)	C(7)—S(8)	1.794(20)
Cu—S(8)	2.328(5)	S(8)—C(9)	1.804(17)
Cu—S(11)	2.268(5)	C(9)—C(10)	1.493(25)
S(1)—C(2)	1.835(20)	C(10)—S(11)	1.850(19)
C(2)—C(3)	1.55(3)	S(11)—C(12)	1.761(20)
C(3)—S(4)	1.802(19)	C(12)—C(13)	1.56(3)
S(4)—C(5)	1.795(19)	C(13)—C(14)	1.50(3)
C(5)—C(6)	1.50(3)	C(14)—S(1′)[a]	1.849(21)

[a] Primed atoms are related to their unprimed equivalents by inversion through $(2-x, 1-y, 1-z)$.

Data collection and processing. STADI-4 diffractometer, graphite-monochromated Mo-K_α X-radiation, T = 173 K, ω–2θ scans using the learnt-profile method,[14] 2727 data collected ($2\theta_{max}$ 45°, h $-7\rightarrow7$, k $0\rightarrow21$, l $0\rightarrow12$), 1799 unique (R_{int} 0.071), giving 1039 reflections with $F\geqslant4\sigma(F)$ for use in all calculations. Linear isotropic crystal decay (*ca* 21%) corrected for during data reduction, no absorption correction.

Structure solution and refinement. A Patterson synthesis located the metal atom and iterative cycles of least-squares refinement and different Fourier synthesis located the remaining non-hydrogen atoms: these were then refined (by least-squares on F[16]) with anisotropic thermal parameters for all non-hydrogen atoms and with hydrogen atoms in fixed, calculated positions. At final convergence R, R_w = 0.0656, 0.0784, respectively, S = 0.947 for 182 refined parameters, and the final ΔF synthesis showed no feature above 0.74 e Å^{-3}. An isotropic extinction parameter refined to $6(4)\times10^{-8}$. The

Table 5. Bond angles for $[Cu_2([28]aneS_8)]^{2+}$ (with standard deviations)

S(1)—Cu—S(4)	93.69(19)	C(6)—C(7)—S(8)	107.5(13)
S(1)—Cu—S(8)	108.78(19)	Cu—S(8)—C(7)	100.5(6)
S(1)—Cu—S(11)	133.39(20)	Cu—S(8)—C(9)	99.6(6)
S(4)—Cu—S(8)	105.66(18)	C(7)—S(8)—C(9)	100.8(8)
S(4)—Cu—S(11)	119.79(19)	S(8)—C(9)—C(10)	117.4(12)
S(8)—Cu—S(11)	93.25(18)	C(9)—C(10)—S(11)	113.3(12)
Cu—S(1)—C(2)	97.2(6)	Cu—S(11)—C(10)	99.3(6)
S(1)—C(2)—C(3)	111.1(13)	Cu—S(11)—C(12)	108.4(7)
C(2)—C(3)—S(4)	115.1(13)	C(10)—S(11)—C(12)	99.8(9)
Cu—S(4)—C(3)	98.6(6)	S(11)—C(12)—C(13)	115.3(14)
Cu—S(4)—C(5)	108.5(6)	C(12)—C(13)—C(14)	113.7(17)
C(3)—S(4)—C(5)	102.4(9)	C(13)—C(14)—S(1′)	108.0(14)
S(4)—C(5)—C(6)	121.8(14)	C(14)—S(1′)—C(2′)	100.1(9)
C(5)—C(6)—C(7)	111.1(16)		

Table 6. Torsion angles for $[Cu_2([28]aneS_8)]^{2+}$ (with standard deviations)

S(1)—C(2)—C(3)—S(4)	−56.2(16)	S(8)—C(9)—C(10)—S(11)	−48.3(16)
C(2)—C(3)—S(4)—C(5)	−80.6(15)	C(9)—C(10)—S(11)—C(12)	−70.6(14)
C(3)—S(4)—C(5)—C(6)	91.5(16)	C(10)—S(11)—C(12)—C(13)	−59.1(15)
S(4)—C(5)—C(6)—C(7)	63.8(20)	S(11)—C(12)—C(13)—C(14)	−167.6(14)
C(5)—C(6)—C(7)—S(8)	−101.4(16)	C(12)—C(13)—C(14)—S(1′)	69.7(19)
C(6)—C(7)—S(8)—C(9)	169.3(13)	C(13)—C(14)—S(1′)—C(2′)	149.6(14)
C(7)—S(8)—C(9)—C(10)	−75.0(14)	C(14)—S(1′)—C(2′)—C(3′)	68.6(14)

weighting scheme $w^{-1} = \sigma^2(F) + 0.0007F^2$ gave satisfactory agreement analyses and in the final cycle $(\Delta/\sigma)_{max}$ was 0.11. Bond lengths, angles and torsion angles are listed in Tables 4–6.

Atomic scattering factors were inlaid[17] except for copper,[18] molecular geometry calculations utilized CALC[19] and figures were produced by ORTEPII.[20] Atomic coordinates, displacement factor coefficients and F_o/F_c tables have been deposited.

Acknowledgement—We thank the SERC for support.

REFERENCES

1. S. G. Murray and F. R. Hartley, *Chem. Rev.* 1981, **81**, 365; K. D. Karlin and J. Zubieta (Eds), *Copper Coordination Chemistry: Biochemical and Inorganic Perspectives*. Adenine Press, New York (1983); D. E. Fenton, *Advances in Inorganic and Bioinorganic Mechanisms* (Edited by A. G. Sykes), p. 187. Academic Press, London (1983); D. E. Fenton, *Pure Appl. Chem.* 1989, **61**, 903 and refs therein.
2. L. Rydel and J. O. Lundgren, *Nature (Lond.)* 1976, **261**, 344; P. M. Collman, H. C. Freeman, J. M. Guss, M. Murata, V. A. Norris, J. A. M. Ramshaw and M. P. Venkatappa, *Nature (Lond.)* 1978, **272**, 319; H. C. Freeman, *Coordination Chemistry* (Edited by J. P. Laurent), Vol. 21, p. 29. Pergamon Press, Oxford (1981); E. T. Adman and L. H. Jensen, *Isr. J. Chem.* 1981, **21**, 8.
3. D. B. Rorabacher, M. J. Martin, M. J. Koenigbauer, M. Malik, R. R. Schroeder, J. F. Endicott and L. A. Ochrymowycz, in *Copper Coordination Chemistry: Biochemical and Inorganic Perspectives* (Edited by K. D. Karlin and J. Zubieta), p. 167. Adenine Press, New York (1983); D. B. Rorabacher, M. M. Bernado, A. M. Q. Vande Linde, G. H. Leggett, B. C. Westerby, M. J. Martin and L. A. Ochrymowycz, *Pure Appl. Chem.* 1988, **60**, 501 and refs therein.
4. R. O. Gould, A. J. Lavery and M. Schröder, *J. Chem. Soc., Chem. Commun.* 1985, 1492.
5. P. W. R. Corfield, C. Ceccarelli, M. D. Glick, I. W.-Y. Moy, L. A. Ochrymowycz and D. B. Rorabacher, *J. Am. Chem. Soc.* 1985, **107**, 2399.
6. T. E. Jones, D. B. Rorabacher and L. A. Ochrymowycz, *J. Am. Chem. Soc.* 1975, **97**, 7485; T. E. Jones, L. L. Zimmer, L. L. Diaddario, D. B. Rorabacher and L. A. Ochrymowycz, *Inorg. Chem.* 1975, **14**, 7163; N. S. Ferris, W. H. Woodruff, D. B. Rorabacher, T. E. Jones and L. A. Ochrymowycz, *J. Am. Chem. Soc.* 1978, **100**, 5939; L. L. Diaddario, L. L. Zimmer, T. E. Jones, L. S. W. L. Sokol, R. B. Cruz, E. L. Yee, L. A. Ochrymowycz and D. B. Rorabacher, *J. Am. Chem. Soc.* 1979, **101**, 3511; L. L. Diaddario Jr, E. R. Dockal, M. D. Glick, L. A. Ochrymowycz and D. B. Rorabacher, *Inorg. Chem.* 1985, **24**, 356; I. R. Young, L. A. Ochrymowycz and D. B. Rorabacher, *Inorg. Chem.* 1986, **25**, 2576; V. B. Pett, G. H. Leggett, T. H. Cooper, P. R. Reed, D. Situmeang, L. A. Ochrymowycz and D. B. Rorabacher, *Inorg. Chem.* 1988, **27**, 2164.
7. J. R. Hartman and S. R. Cooper, *J. Am. Chem. Soc.* 1986, **108**, 1202.
8. M. D. Glick, D. P. Gavel, L. L. Diaddario and D. B. Rorabacher, *Inorg. Chem.* 1976, **15**, 1190; B. V. Gorewit and W. K. Murker, *J. Coord. Chem.* 1976, **5**, 67; W. N. Setzer, C. A. Ogle, G. S. Wilson and R. S. Glass, *Inorg. Chem.* 1983, **22**, 266; H-J. Küppers, K. Wieghardt, Y.-H. Tsay, C. Krüger, B. Nuber and J. Weiss, *Angew Chem.* 1987, **99**, 583; *Angew. Chem. Int. Edn. Engl.* 1987, **26**, 575; S. C. Rawle, G. A. Admans and S. R. Cooper, *J. Chem. Soc., Dalton Trans.* 1988, 93; C. M. Lucas, L. Shuang, M. J. Newlands, J.-P. Charland and E. J. Gabe, *Can. J. Chem.* 1988, **66**, 1506; C. M. Lucas, L. Shuang, M. J. Newlands, J.-P. Charland and E. J. Gabe, *Can. J. Chem.* 1989, **67**, 639.
9. N. Atkinson, A. J. Blake, M. G. B. Drew, G. Forsyth, A. J. Lavery, G. Reid and M. Schröder, *J. Chem. Soc., Chem. Commun.* 1989, 984.
10. A. J. Blake and M. Schröder, *Adv. Inorg. Chem.* 1990, **35**, 1.
11. R. E. DeSimone and T. M. Tighe, *J. Inorg. Nucl. Chem.* 1976, **38**, 1623; D. Sevdić and H. Meider, *J. Inorg. Nucl. Chem.* 1977, **39**, 1403; A. C. Braithwaite, C. E. F. Rickard and T. N. Waters, *Aust. J. Chem.* 1981, **34**, 2665; K. Saito, Y. Masudo and E. Sekido, *Anal. Chim. Acta* 1983, **151**, 447.
12. K. Travis and D. H. Busch, *J. Chem. Soc., Chem. Commun.* 1970, 1041.
13. G. Reid, PhD thesis. University of Edinburgh, U.K. (1989).
14. W. Clegg, *Acta Cryst.* 1981, **A37**, 22.
15. N. Walker and D. Stuart, DIFABS, Program for

Empirical Absorption Correction, *Acta Cryst.* 1983, **A39**, 158.
16. G. M. Sheldrick, SHELX76, Program for Crystal Structure Refinement. University of Cambridge, U.K. (1976).
17. J. Cosier and A. M. Glazer, *J. Appl. Cryst.* 1986, **19**, 105.
18. D. T. Cromer and J. L. Mann, *Acta Cryst.* 1968, **A24**, 321.
19. R. O. Gould and P. Taylor, CALC, Program for Molecular Geometry Calculations. University of Edinburgh, U.K. (1985).
20. P. D. Mallinson and K. W. Muir, ORTEPII, Interactive Version, *J. Appl. Cryst.* 1985, **18**, 51.

Polyhedron Vol. 9, No. 24, pp. 2919–2924, 1990
Printed in Great Britain

0277–5387/90 $3.00+.00
© 1990 Pergamon Press plc

COPPER THIOETHER CHEMISTRY: THE SYNTHESIS AND SINGLE CRYSTAL X-RAY STRUCTURES OF $[Cu_2([18]aneS_6)(NCMe)_2](ClO_4)_2$ AND $[Cu([9]aneS_3)(AsPPh_3)](ClO_4)$

ALEXANDER J. BLAKE, ROBERT O. GOULD, ALAN J. HOLDER, AIDAN J. LAVERY and MARTIN SCHRÖDER*

Department of Chemistry, University of Edinburgh, West Mains Road, Edinburgh EH9 3JJ, Scotland, U.K.

(*Received* 5 *June* 1990; *accepted* 10 *August* 1990)

Abstract—Reaction of $[18]aneS_6$ with two molar equivalents of $[Cu(NCMe)_4](ClO_4)$ in CH_2Cl_2–MeCN affords the binuclear copper(I) complex $[Cu_2([18]aneS_6)(NCMe)_2](ClO_4)_2$. The single crystal X-ray structure of the complex shows a centrosymmetric cation with two tetrahedral copper(I) centres each coordinated to three thioether S-donors of $[18]aneS_6$, Cu—S(1) = 2.3200(15), Cu—S(4) = 2.3415(16), Cu—S(7) = 2.3250(15) Å, and to one MeCN molecule, Cu—N(1) = 1.939(5) Å, to give an overall NS_3-donation at the metal centres. Additionally, S(7′) shows a long-range interaction, Cu···S(7′) = 3.318(2) Å thus distorting the coordination geometry of the metal ion towards trigonal bipyramidal. The metal–metal separation of 4.428(2) Å suggests that there is no significant interaction between the copper centres of the dimer. Reaction of $[9]aneS_3$ with one molar equivalent of $[Cu(NCMe)_4](ClO_4)$ in refluxing MeCN in the presence of ligands, L, affords the adducts $[Cu([9]aneS_3)L]^+$ (L = PPh_3, $AsPh_3$). The single crystal X-ray structure of the complex $[Cu([9]aneS_3)(AsPh_3)](ClO_4)$ shows tetrahedral AsS_3 coordination at copper(I) with $[9]aneS_3$ bound facially to the metal centre, Cu—S = 2.303(6), Cu—As = 2.322(4) Å.

The bioinorganic chemistry of copper is dominated by mono- and binuclear $Cu^{II/I}$ complexes which may model the stereochemical, electronic and redox properties of certain metalloproteins.[1] Several biological systems incorporate copper coordinated to sulphur,[2] and this has led to the study of $Cu^{II/I}$ complexes of thioether crowns, and a series of mononuclear species have now been synthesized including $[Cu([9]aneS_3)_2]^{2+}$,[3] $[Cu([9]aneS_3)I]$,[4] $[CuCl_2([12]aneS_3)_2]$,[5] $[Cu([14]aneS_4)]^+$,[6] $[Cu(OClO_3)_2([14]aneS_4)]$,[7] $[Cu([15]aneS_5)]^{2+/+}$[8] and $[Cu([18]aneS_6)]^{2+/+}$.[9] More recently, $Cu^{II/I}$ complexes of thiophene-containing crowns have also been reported.[10] However, few examples of binuclear copper complexes of thioether macrocycles have been described. The minicycle $[9]aneS_3$ has been shown by Cooper and co-workers to form the binuclear copper(I) species $[Cu_2([9]aneS_3)_3]^{2+}$ which incorporates one bridging and two facially bound trithia ligands.[11] Similarly, $[16]aneS_4$ has been found to bridge $CuCl_2$ fragments in $[Cu_2Cl_4([16]aneS_4)]$,[12] and more recently we have established that the larger ring octathia crowns $[24]aneS_8$ and $[28]aneS_8$ can fully encapsulate two copper(I) centres in a tetrahedral manner.[13] However, the intermediate ring $[18]aneS_6$, the sulphur analogue of 18-crown-6 ($[18]aneO_6$), is too small and lacks sufficient S-donors to fully encapsulate two copper(I) centres in the same way. Although a series of mononuclear transition metal complexes of $[18]aneS_6$ have been reported,[16] we thought it possible that $[18]aneS_6$ could still act as a binucleating ligand to copper(I) centres if external ligation were available. We report herein the synthesis and structure of the binuclear copper(I) complex $[Cu_2([18]aneS_6)(NCMe)_2]^{2+}$[14] and the related monomeric fragments $[Cu([9]aneS_3)(L)]^+$ (L = NCMe, PPh_3, $AsPh_3$).[15]

* Author to whom correspondence should be addressed.

RESULTS AND DISCUSSION

Addition of two molar equivalents of $[Cu(NCMe)_4](ClO_4)$ to a solution of $[18]aneS_6$ in CH_2Cl_2–MeCN, followed by warming the solution to 35°C for 0.5 h under N_2 affords a pale yellow solution. Addition of $NaClO_4$ to the cooled solution gives the binuclear copper(I) complex $[Cu_2([18]aneS_6)(NCMe)_2](ClO_4)_2$. If the metal insertion is carried out under more vigorous conditions, the mononuclear species $[Cu([18]aneS_6)]^+$ is isolated.[9] $[Cu_2([18]aneS_6)(NCMe)_2](ClO_4)_2$ can be recrystallized from MeCN to afford pale brown crystals of the complex. $[Cu_2([18]aneS_6)(NCMe)_2](ClO_4)_2$ crystallizes with imposed $C_i(\bar{1})$ symmetry. A single crystal X-ray structure determination of the complex shows (Fig. 1) a centrosymmetric cation with two identically bound copper(I) centres. Each copper(I) is coordinated to three thioether S-donors of $[18]aneS_6$, Cu—S(1) = 2.3200(15), Cu—S(4) = 2.3415(16), Cu—S(7) = 2.3250(15) Å, and to one MeCN molecule, Cu—N(1) = 1.939(5) Å, to give overall NS_3-donation at the tetrahedral metal centres, ∠S(1)CuS(4) = 92.05(5), ∠S(1)CuS(7) = 114.69(5), ∠S(1)CuN(1) = 120.55(14), ∠S(4)CuS(7) = 91.59(5), ∠S(4)CuN(1) = 122.85(14), ∠S(7)CuN(1) = 110.89(14)°. S(7′) shows a long-range interaction to the copper centre, Cu···S(7′) = 3.318(2) Å, thus distorting the coordination geometry of the metal ion towards trigonal bipyramidal. The Cu···Cu separation of 4.428(2) Å suggests that there is no significant interaction between these centres, although S(7) and S(7′), which are separated by nine bonds within the coordinated macrocycle, approach one another to a distance of 3.635(3) Å. The S-atoms of the hexathia ring adopt a chair-like conformation with the S-donors coordinated to copper forming a plane 0.98 Å from the plane of the S-donors coordinated to copper; each copper(I) centre lies 1.08 Å above its coordinated S_3-plane.

$[Cu_2([18]aneS_6)(NCMe)_2](ClO_4)_2$ is the first example of a binuclear copper complex with $[18]aneS_6$, although several binuclear organometallic species such as $[Rh_2(C_5Me_5)_2Cl_2([18]aneS_6)]^{2+}$ and $[M_2(arene)_2Cl_2([18]aneS_6)]^{2+}$ (M = Ru, Os) in which the hexathia ligand is bound in an *exo*, bidentate manner to each metal fragment have been reported.[16,17] Similar *exo* coordination has been proposed in a series of binuclear molybdenum carbonyl complexes.[18] Solutions of $[Cu_2([18]aneS_6)(NCMe)_2]^{2+}$ in MeCN and $MeNO_2$ are stable to the atmosphere, reflecting the stabilization of copper(I) afforded by the NS_3-donor set. However, in dmf or on addition of N-donor ligands such as py, oxidation of the complex occurs to afford intractable copper(II) materials.

The above results confirm the preferred tetrahedral coordination for copper(I) thioether complexes and suggested that related tetrahedral species $[Cu([9]aneS_3)(L)]^+$ (L = PR_3, AsR_3) should be isolable.[14,19] Reaction of $[9]aneS_3$ with one molar equivalent of $[Cu(NCMe)_4](ClO_4)$ in refluxing MeCN affords a colourless solution of $[Cu([9]aneS_3)(NCMe)]^+$. $[Cu([9]aneS_3)(NCMe)]^+$ does not appear to react with CO in MeCN, while reaction with py and PEt_3 affords ill-defined air-sensitive products.[4] However, reaction with ligands, L, in warm MeCN affords the adducts $[Cu([9]aneS_3)L]^+$ (L = PPh_3, $AsPh_3$). The single crystal X-ray structure of $[Cu([9]aneS_3)(AsPh_3)](ClO_4)$ shows (Fig. 2) the cation located on a crystallographic three-fold axis with imposed C_3 symmetry. Distorted tetrahedral AsS_3 coordination is observed at the copper(I) with $[9]aneS_3$ bound facially to the metal centre, Cu—S = 2.303(6), Cu—As = 2.322(4) Å. Coordination of $[9]aneS_3$ to tetrahedral metal centres is rare,[4,11,20] with the ∠SCuS angle of 94.5(2)° being substantially reduced from the values

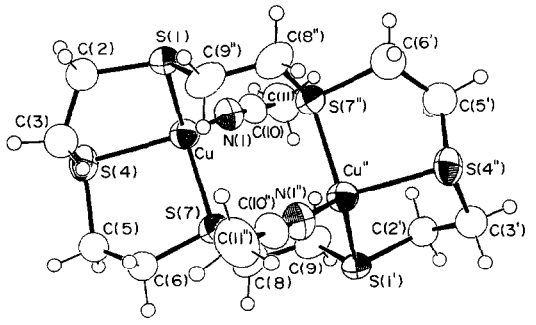

Fig. 1. Structure of $[Cu_2([18]aneS_6)(NCMe)_2]^{2+}$ with numbering scheme adopted. Left side shows major conformation, right side minor conformation.

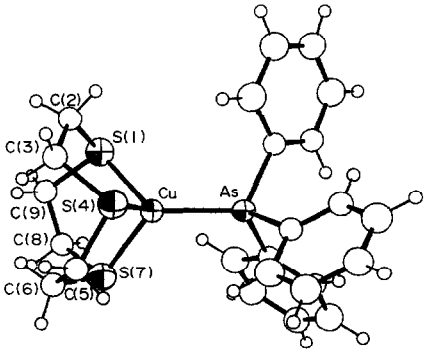

Fig. 2. Structure of $[Cu([9]aneS_3)(AsPh_3)]^+$ with numbering scheme adopted.

expected for a tetrahedral metal centre; this reflects the small bite of facially coordinated [9]aneS$_3$, $\angle$SCuAs = 122.0(2)°. During the course of this work,[15] Wieghardt and co-workers reported the synthesis of [Cu([9]aneS$_3$)I] directly from CuI and [9]aneS$_3$.[4] The structure of [Cu([9]aneS$_3$)I] shows tetrahedral copper(I), Cu—S = 2.329(1), 2.331(1), 2.343(1) Å, Cu—I = 2.490(1) Å, $\angle$S(1)CuS(2) = 92.6(1), $\angle$S(1)CuS(3) = 93.1(1), $\angle$S(2)CuS(3) = 93.9(1), $\angle$S(1)CuI = 128.6(1), $\angle$S(2)CuI = 121.3(1), $\angle$S(3)CuI = 118.7(1).[4] These structural features are therefore quite similar to those of [Cu([9]aneS$_3$)(AsPh$_3$)]$^+$.

We are currently investigating the oxidative chemistry of [Cu$_2$([18]aneS$_6$)(NCMe)$_2$]$^{2+}$ and related binuclear copper(I) thioether complexes such as [Cu$_2$(L)]$^{2+}$ (L = [24]aneS$_8$, [28]aneS$_8$), and of the mononuclear species of type [Cu([9]aneS$_3$)L]$^+$ in the presence of small molecule substrates.

EXPERIMENTAL

IR spectra were measured as Nujol mulls, KBr and CsI discs using a Perkin–Elmer 598 spectrometer over the range 200–400 cm^{-1}. UV–vis spectra were measured in quartz cells using Perkin–Elmer Lambda 9 and Pye Unicam SP8-400 spectrophotometers. Microanalyses were performed by the Edinburgh University Chemistry Department microanalytical service. Mass spectra were run by electron impact on a Kratos MS 902 and by fast atom bombardment on a Kratos MS 50TC spectrometer. ^{1}H NMR spectra were recorded at 80 MHz on a Bruker WP80 spectrometer.

Synthesis of [Cu([18]aneS$_6$)(NCMe)$_2$](ClO$_4$)$_2$

[Cu(NCMe)$_4$](ClO$_4$) (0.09 g, 2.78×10^{-4} mol) was added to a solution of [18]aneS$_6$ (0.05 g, 1.38×10^{-4} mol) in CH$_2$Cl$_2$–MeCN (20 cm^3, 1:1 v/v) under N$_2$. The reaction mixture was warmed gently for 0.5 h to afford a pale yellow solution. Addition of NaClO$_4$ to the cooled solution gave a pale yellow product which was recrystallized from MeCN to give [Cu$_2$([18]aneS$_6$)(NCMe)$_2$](ClO$_4$)$_2$ in up to 50% yield. Found: C, 24.9; H, 3.8; N, 3.8. Calc. for [Cu$_2$([18]aneS$_6$)(NCMe)$_2$](ClO$_4$)$_2$: C, 25.0; H, 3.9; N, 3.6%.

X-ray structure determination of [Cu$_2$([18]aneS$_6$)(NCMe)$_2$](ClO$_4$)$_2$

A colourless crystal (0.75 × 0.5 × 0.2 mm) suitable for X-ray analysis was obtained from MeCN solution.

Crystal data. $C_{16}H_{30}Cu_2N_2S_6^{2+}2ClO_4^-$, M = 768.7, triclinic, space group $P\bar{1}$, a = 9.184(6), b = 9.317(3), c = 9.598(7) Å, α = 81.18(4), β = 73.07(6), γ = 67.93(3)°, V = 727.2 Å^3, D_c = 1.76 g cm^{-3} [from setting angles of 12 reflections (2θ = 16–22°, $\bar{\lambda}$ = 0.71073 Å)], Z = 1; F(000) = 392, $\bar{\lambda}$(Mo-K_α) = 0.71073 Å, μ = 2.11 cm^{-1}.

Data collection and processing. Enraf–Nonius CAD4 four-circle diffractometer, ω–2θ scans, 2539 reflections measured to 2θ = 50°, giving 1926 with $F \geqslant 6\sigma(F)$. No significant crystal decay.

Strucure analysis and refinement. The copper atoms were located using a Patterson synthesis, and application of DIRDIF[21] gave positions for all other non-hydrogen atoms, showing the cation to contain two copper atoms bonded to one macrocycle arranged about a centre of symmetry. On refinement,[22] unrealistic bond lengths, angles and high thermal parameters indicated significant disorder at C(2), C(3), C(5) and C(6). This was resolved into two alternative conformations which refined eventually to site occupancies of 0.55 and 0.45. Hydrogen atoms bonded to all carbon atoms were included in calculated positions and not refined. The ClO$_4^-$ ion is disordered mainly about a molecular three-fold axis. After absorption corrections using DIFABS[23] (maximum correction 20%), anisotropic thermal parameters were refined for all non-hydrogen atoms except the disordered methylene region. In the final cycles, the extensively correlated positional and thermal parameters for the ClO$_4^-$ ion were held constant. At convergence, R and R_w = 0.044 and 0.056, respectively, for 128 parameters, giving a maximum Δ/σ of 0.2. A final difference synthesis showed no peaks or troughs greater than ±0.8 eÅ^{-3}. Bond lengths, angles and torsion angles are given in Table 1.

Synthesis of [Cu([9]aneS$_3$)(PPh$_3$)](ClO$_4$)

Reaction of [Cu(NCMe)$_4$](ClO$_4$) (0.23 g, 7.03×10^{-4} mol) with [9]aneS$_3$ (0.13 g, 7.22×10^{-4} mol), in refluxing MeCN (30 cm^3) under N$_2$, affords a yellow solution which after 1 h turns colourless. PPh$_3$ (0.21 g, 8.1×10^{-4} mol) in MeCN (5 cm^3) was added and the reaction mixture warmed to 40°C for 0.5 h. On cooling a white product crystallized from solution. The complex was recrystallized from MeNO$_2$ (5 cm^3) to give [Cu([9]aneS$_3$)(PPh$_3$)](ClO$_4$) in 70% yield. Found: C, 46.9; H, 4.4. Calc. for [Cu([9]aneS$_3$)(PPh$_3$)](ClO$_4$): C, 47.6; H, 4.5%. IR spectrum (KBr disc): 3040, 1478, 1437, 1404, 1328, 1303, 1279, 815, 748, 709, 695, 620, 529, 502 and 440 cm^{-1}. ^{1}H NMR spectrum (80 MHz, CD$_3$NO$_2$, 298 K): δ = 7.5 (m, 15H, PPh$_3$), 3.06 pm (m, CH_2, 12H).

Table 1. Bond lengths (Å), bond angles and in-ring torsion angles (°) for $[Cu_2([18]aneS_6)(NCMe)_2](ClO_4)_2$[a]

Cu—S(1)	2.3200(15)	S(4)—C(5)	1.921(11)
Cu—S(4)	2.3415(16)	S(4)—C(5′)	1.655(15)
Cu—S(7)	2.3250(15)	C(5)—C(6)	1.491(15)
Cu—N(1)	1.939(5)	C(5′)—C(6′)	1.476(22)
S(1)—C(2)	1.800(11)	C(6)—S(7)	1.785(10)
S(1)—C(9″)	1.818(6)	C(6′)—S(7)	1.882(16)
S(1′)—C(2′)	1.865(13)	S(7)—C(8)	1.816(6)
C(2)—C(3)	1.518(16)	C(8)—C(9)	1.498(9)
C(2′)—C(3′)	1.514(19)	N(1)—C(10)	1.129(7)
C(3)—S(4)	1.837(11)	C(10)—C(11)	1.443(9)
C(3′)—S(4)	1.883(13)		

S(1)—Cu—S(4)	92.05(5)	C(3)—S(4)—C(5)	98.4(5)
S(1)—Cu—S(7)	114.69(5)	Cu—S(4)—C(3′)	97.8(4)
S(1)—Cu—N(1)	120.55(14)	Cu—S(4)—C(5′)	100.1(5)
S(4)—Cu—S(7)	91.59(5)	C(3′)—S(4)—C(5′)	105.7(7)
S(4)—Cu—N(1)	122.85(14)	S(4)—C(5)—C(6)	115.7(7)
S(7)—Cu—N(1)	110.89(14)	S(4)—C(5′)—C(6′)	113.1(11)
Cu—S(1)—C(2)	98.1(4)	C(5)—C(6)—S(7)	113.7(7)
Cu—S(1)—C(9″)	109.43(20)	C(5′)—C(6′)—S(7)	112.6(11)
C(2)—S(1)—C(9″)	109.9(4)	Cu—S(7)—C(6)	103.8(3)
Cu—S(1)—C(2′)	98.8(4)	Cu—S(7)—C(8)	105.05(21)
C(2′)—S(1)—C(9″)	89.2(4)	C(6)—S(7)—C(8)	110.9(4)
S(1)—C(2)—C(3)	116.2(8)	Cu—S(7)—C(6′)	93.6(5)
S(1)—C(2′)—C(3′)	106.8(9)	C(6′)—S(7)—C(8′)	91.3(5)
C(2)—C(3)—S(4)	107.7(7)	S(7)—C(8)—C(9)	110.9(4)
C(2′)—C(3′)—S(4)	114.3(9)	S(1″)—C(9)—C(8)	111.1(4)
Cu—S(4)—C(3)	96.0(3)	Cu—N(1)—C(10)	173.3(5)
Cu—S(4)—C(5)	98.3(3)	N(1)—C(10)—C(11)	179.0(6)

C(9″)—S(1)—C(2)—C(3)	−80.4(8)	C(3′)—S(4)—C(5′)—C(6′)	−143.3(11)
C(2)—S(1)—C(9″)—C(8″)	−172.0(5)	S(4)—C(5)—C(6)—S(7)	−49.0(10)
C(9″)—S(1)—C(2′)—C(3′)	−160.5(8)	S(4)—C(5′)—C(6′)—S(7)	64.8(13)
C(2′)—S(1)—C(9″)—C(8″)	−179.6(6)	C(5)—C(6)—S(7)—C(8)	−78.5(8)
S(1)—C(2)—C(3)—S(4)	−61.9(9)	C(5′)—C(6′)—S(7)—C(8)	−151.0(11)
S(1)—C(2′)—C(3′)—S(4)	62.1(10)	C(6)—S(7)—C(8)—C(9)	−164.2(5)
C(2)—C(3)—S(4)—C(5)	151.0(7)	C(6′)—S(7)—C(8)—C(9)	178.4(6)
C(2′)—C(3′)—S(4)—C(5′)	65.4(11)	S(7)—C(8)—C(9)—S(1″)	60.2(5)
C(3)—S(4)—C(5)—C(6)	−61.4(9)		

[a] Atoms marked ″ related to unmarked atoms by operation $-x, -y, -z$.

Synthesis of $[Cu([9]aneS_3)(AsPh_3)](ClO_4)$

This complex was prepared in a similar manner using $AsPh_3$ in place of PPh_3. Found: C, 44.1; H, 4.2. Calc. for $[Cu([9]aneS_3)(AsPh_3)](ClO_4)$: C, 44.4; H, 4.19%. IR spectrum (KBr disc): 3044, 1480, 1437, 1404, 1333, 1302, 1278, 813, 740, 694, 620, 473, 346 and 322 cm^{-1}. ^1H NMR spectrum (80 MHz, CD_3CN, 298 K): $\delta = 7.40$ (br s, 15H, $AsPh_3$), 2.87 ppm (br s, CH_2, 12H).

Structure determination of $[Cu([9]aneS_3)(AsPh_3)](ClO_4)$

A colourless plate, $0.4 \times 0.2 \times 0.08$ mm, was mounted on a Stoë STADI-4 four-circle diffractometer.

Crystal data. $C_{24}H_{27}AsCuS_3^{2+}\ 2ClO_4^-$, $M = 749.0$, trigonal, space group $R\bar{3}$, $a = 11.126(6)$, $c = 37.255(12)$ Å, $U = 3994.6$ Å^3 (from setting angles for 21 reflections with $2\theta = 20$–$21°$,

Table 2. Bond lengths (Å), bond angles and in-ring torsion angles (°) with standard deviations for $[Cu([9]aneS_3)(AsPh_3)](ClO_4)$

Cu—As	2.322(4)	C(10)—C(15)	1.402(20)
Cu—S(1)	2.303(6)	C(11)—C(12)	1.39(3)
S(1)—C(2)	1.86(3)	C(12)—C(13)	1.38(3)
C(2)—C(3)	1.40(4)	C(13)—C(14)	1.34(3)
C(3)—S(4)	1.806(22)	C(14)—C(15)	1.411(23)
As—C(10)	1.935(13)	Cl(1)—O(1)	1.47(3)
C(10)—C(11)	1.355(21)	Cl(2)—O(2)	1.30(6)

As—Cu—S(1)	122.02(19)	As—C(10)—C(11)	123.6(11)
S(1)—Cu—S(4)	94.49(20)	As—C(10)—C(15)	116.6(10)
Cu—As—C(10)	115.7(4)	C(11)—C(10)—C(15)	119.7(13)
C(10)—As—C(10′)	102.6(6)	C(10)—C(11)—C(12)	120.7(17)
Cu—S(1)—C(9)	99.1(7)	C(11)—C(12)—C(13)	120.2(21)
Cu—S(1)—C(2)	96.1(9)	C(12)—C(13)—C(14)	119.8(19)
C(9)—S(1)—C(2)	103.4(11)	C(13)—C(14)—C(15)	121.2(16)
S(1)—C(2)—C(3)	119.3(20)	C(10)—C(15)—C(14)	118.2(14)
C(2)—C(3)—S(4)	118.1(18)		

C(9)—S(1)—C(2)—C(3)	66.4(23)	S(1)—C(2)—C(3)—S(4)	44.3(27)
C(2)—C(3)—S(4)—C(5)	−124.6(20)		

$\bar{\lambda} = 0.71073$ Å, $T = 295$ K), $Z = 12$, $D_c = 1.870$ g cm^{-3}, $\mu = 2.53$ mm^{-1}, $F(000) = 2274$.

Data collection and processing. Stoë STADI-4 diffractometer, graphite-monochromated Mo-K_α X-radiation, $T = 295$ K, ω–2θ scans using the learnt profile method,[24] 3424 unique reflections ($2\theta_{max}$ 45°, h −9 to 10, k 0 to 11, l 0 to 40) collected, assuming space group $P\bar{3}$, giving 1137 with $F \geqslant 6\sigma(F)$. No significant crystal decay or movement was apparent. All significant data had $(-h + k + l) = 3n$ or $(h - k + l) = 3n$ and the data were analysed as those for a rhombohedral twin. The 1721 data meeting one of these conditions included 673 from the obverse twin, 655 from the reverse twin, 33 common to both with the same indices ($l = 0$ or $h = k = 0$) and 360 ($l = 3n$) containing symmetry-independent contributions from the two twins. Scaling difficulties made it impossible to use the third and fourth classes of data. The first two classes were scaled together after altering the indices for the reverse twin to those for the corresponding obverse axes (hkl to $-h-kl$), and gave a total of 716 data with a merging R of 0.054: of these, 416 with $F \geqslant 6\sigma(F)$ were used to solve and refine the structure.

Structure solution and refinement. The copper and arsenic atoms were located from a Patterson function and subsequent difference maps located all other non-hydrogen atoms of the cation, which is essentially ordered with imposed 3 (C_3) symmetry. The two independent perchlorate ions have imposed $\bar{3}$ (S_6) symmetry. The oxygen atoms are extensively disordered, but refined reasonably well with a single atom for each group in a general position with a site occupancy of 2/3. The non-hydrogen atoms of the cation were then refined anisotropically; hydrogen atoms were refined in fixed, idealized positions with C—H = 1.08 Å, tetrahedral or trigonal geometry as appropriate, and fixed temperature factors of $U_{iso} = 0.05$ Å^2 in the phenyl ring and 0.10 Å^2 in the macrocycle.[22] At final convergence R and $R_w = 0.052$ and 0.064, respectively, $S = 1.06$ for 116 refined parameters: in the final ΔF synthesis the maximum residuals were ± 0.80 eÅ^{-3} near the heavy atoms or perchlorate ions and ± 0.25 eÅ^{-3} elsewhere. No extinction or absorption corrections were made. The weighting scheme $w^{-1} = \sigma^2(F) + 0.0017F^2$ gave satisfactory agreement analyses and in the final cycle $(\Delta/\sigma)_{max}$ was 0.05. Bond lengths, angles and torsion angles are given in Table 2.

Atomic scattering factors were inlaid[22] or taken from ref. 25, molecular geometry calculations utilized CALC[26] and the figures were produced by ORTEPII.[27]

Acknowledgement—We thank the SERC for support.

REFERENCES

1. S. G. Murray and F. R. Hartley, *Chem. Rev.* 1981, **81**, 365; *Copper Coordination Chemistry: Biochemical and Inorganic Perspectives* (Edited by K.

D. Karlin and J. Zubieta). Adenine Press, New York (1983); D. E. Fenton, *Advances in Inorganic and Bioinorganic Mechanisms* (Edited by A. G. Sykes), p. 187. Academic Press, London (1983); D. B. Rorabacher, M. J. Martin, M. J. Koenigbauer, M. Malik, R. R. Schroeder, J. F. Endicott and L. A. Ochrymowycz, in *Copper Coordination Chemistry: Biochemical and Inorganic Perspectives* (Edited by K. D. Karlin and J. Zubieta), p. 167. Adenine Press, New York (1983); D. B. Rorabacher, M. M. Bernado, A. M. Q. Vande Linde, G. H. Leggett, B. C. Westerby, M. J. Martin and L. A. Ochrymowycz, *Pure Appl. Chem.* 1988, **60**, 501 and refs therein; D. E. Fenton, *Pure Appl. Chem.* 1989, **61**, 903.

2. L. Rydel and J. O. Lundgren, *Nature* 1976, **261**, 344; P. M. Collman, H. C. Freeman, J. M. Guss, M. Murata, V. A. Norris, J. A. M. Ramshaw and M. P. Venkatappa, *Nature* 1978, **272**, 319; H. C. Freeman, *Coordination Chemistry* (Edited by J. P. Laurent), Vol. 21, p. 29. Pergamon Press, Oxford (1981); E. T. Adman and L. H. Jensen, *Isr. J. Chem.* 1981, **21**, 8.
3. W. N. Setzer, C. A. Ogle, G. S. Wilson and R. S. Glass, *Inorg. Chem.* 1983, **22**, 266.
4. H-J. Küppers, K. Wieghardt, Y-H. Tsay, C. Krüger, B. Nuber and J. Weiss, *Angew. Chem.* 1987, **99**, 583; *Angew. Chem. Int. Ed. Engl.* 1987, **26**, 575.
5. S. C. Rawle, G. A. Admans and S. R. Cooper, *J. Chem. Soc., Dalton Trans.* 1988, 93.
6. E. R. Dockal, L. L. Diaddario, M. D. Glick and D. B. Rorabacher, *J. Am. Chem. Soc.* 1977, **99**, 4530; L. L. Diaddario Jr, E. R. Dockal, M. D. Glick, L. A. Ochrymowycz and D. B. Rorabacher, *Inorg. Chem.* 1985, **24**, 356.
7. M. D. Glick, D. P. Gavel, L. L. Diaddario and D. B. Rorabacher, *Inorg. Chem.* 1976, **15**, 1190.
8. P. W. R. Corfield, C. Ceccarelli, M. D. Glick, I. W-Y. Moy, L. A. Ochrymowycz and D. B. Rorabacher, *J. Am. Chem. Soc.* 1985, **107**, 2399.
9. J. R. Hartman and S. R. Cooper, *J. Am. Chem. Soc.* 1986, **108**, 1202.
10. C. M. Lucas, L. Shuang, M. J. Newlands, J-P. Charland and E. J. Gabe, *Can. J. Chem.* 1988, **66**, 1506; C. M. Lucas, L. Shuang, M. J. Newlands, J-P. Charland and E. J. Gabe, *Can. J. Chem.* 1989, **67**, 639.
11. J. A. Clarkson, R. Yagbasan, P. J. Blower and S. R. Cooper, *J. Chem. Soc., Chem. Commun.* 1989, 1244.
12. B. V. Gorewit and W. K. Murker, *J. Coord. Chem.* 1976, **5**, 67.
13. A. J. Blake, A. Taylor and M. Schröder, *Polyhedron* 1990, **9**, 2911. For other complexes of S_8-donor macrocycles see: K. Travis and D. H. Busch, *J. Chem. Soc., Chem. Commun.* 1970, 1041; R. E. DeSimone and T. M. Tighe, *J. Inorg. Nucl. Chem.* 1976, **38**, 1623; D. Sevdić and H. Meider, *J. Inorg. Nucl. Chem.* 1977, **39**, 1403; A. C. Braithwaite, C. E. F. Rickard and T. N. Waters, *Aust. J. Chem.* 1981, **34**, 2665; K. Saito, Y. Masudo and E. Sekido, *Analyt. Chim. Acta* 1983, **151**, 447.
14. R. O. Gould, A. J. Lavery and M. Schröder, *J. Chem. Soc., Chem. Commun.* 1985, 1492.
15. A. J. Holder, PhD thesis. University of Edinburgh (1987).
16. A. J. Blake and M. Schröder, *Adv. Inorg. Chem.* 1990, **35**, 1.
17. M. Schröder, *Pure Appl. Chem.* 1988, **60**, 517.
18. D. Sevdić and L. Fekete, *Inorg. Chim. Acta* 1982, **57**, 111; D. Sevdić and L. Fekete, *Polyhedron* 1985, **4**, 1371; D. Sevdić, M. Curić and L. J. Tušek-Božić, *Polyhedron* 1989, **8**, 505.
19. N. Atkinson, A. J. Blake, M. G. B. Drew, G. Forsyth, A. J. Lavery, G. Reid and M. Schröder, *J. Chem. Soc., Chem. Commun.* 1989, 984.
20. A. J. Blake, R. O. Gould, J. A. Greig, A. J. Holder, T. I. Hyde and M. Schröder, *J. Chem. Soc., Chem. Commun.* 1989, 876.
21. P. T. Beurskens, W. P. Bosman, H. M. Doesbury, Th. E. M. van den Hark, P. A. J. Prick, J. H. Noordik, G. Beurskens, R. O. Gould and V. Parthasarathia, DIRDIF, Applications of Direct Methods to Difference Structure Factors. University of Nijmegen, Netherlands (1983).
22. G. M. Sheldrick, SHELX76, Program for Crystal Structure Refinement. University of Cambridge, England (1976).
23. N. Walker and D. Stuart, DIFABS, Program for Empirical Absorption Corrections, *Acta Cryst.* 1983, **A39**, 158.
24. W. Clegg, *Acta Cryst.* 1981, **A37**, 22.
25. D. T. Cromer and J. L. Mann, *Acta Cryst.* 1968, **A24**, 321.
26. R. O. Gould and P. Taylor, CALC, Program for Molecular Geometry Calculations. University of Edinburgh, Scotland (1985).
27. P. D. Mallinson and K. W. Muir, ORTEPII, Interactive Version, *J. Appl. Cryst.* 1985, **18**, 51.

Polyhedron Vol. 9, No. 24, pp. 2925–2929, 1990
Printed in Great Britain

0277–5387/90 $3.00+.00
© 1990 Pergamon Press plc

RHODIUM MACROCYCLIC COMPLEXES: THE SYNTHESIS AND SINGLE CRYSTAL X-RAY STRUCTURE OF $[Rh([18]aneN_2S_4)](PF_6)_3 \cdot 3H_2O$ ([18]aneN$_2$S$_4$ = 1,4,10,13-TETRATHIA-7,16-DIAZACYCLOOCTADECANE)

ALEXANDER J. BLAKE, GILLIAN REID and MARTIN SCHRÖDER*

Department of Chemistry, University of Edinburgh, West Mains Road, Edinburgh EH9 3JJ, Scotland, U.K.

(*Received* 27 *April* 1990; *accepted* 29 *August* 1990)

Abstract—Reaction of $[Rh(H_2O)_6]^{3+}$ with one molar equivalent of [18]aneN$_2$S$_4$ in refluxing MeOH–H_2O (1:1 v/v) for 12 h affords an orange solution from which the complex $[Rh([18]aneN_2S_4)](PF_6)_3$ can be isolated upon addition of NH_4PF_6. A single crystal X-ray structure determination shows a distorted octahedral geometry at rhodium(III) involving the four thioether and two aza-donors of the macrocycle. The complex cation adopts a *rac*-configuration via meridional coordination of the two $SCH_2CH_2NCH_2CH_2S$ linkages.

We have been investigating the synthesis, structures and redox properties of transition metal complexes incorporating polythia and polyaza macrocyclic ligands.[1] Recently, we have extended our interests to the coordination chemistry of the potentially hexadentate macrocycles [18]aneN$_2$S$_4$ and Me$_2$[18]aneN$_2$S$_4$.[2] In their original report on the synthesis of [18]aneN$_2$S$_4$, Black and McLean proposed that this macrocycle would coordinate to first row transition metal ions to give octahedral complexes with the *rac*-configuration (Fig. 1):[3] our studies have confirmed this suggestion.[2,4] These results contrast with those obtained for the hexathia analogue, [18]aneS$_6$, which coordinates octahedrally to a range of transition metal ions to give the *meso*-configuration exclusively.[5] Importantly, we have also shown that substitution of N—H for N—Me in these macrocycles results in dramatic changes to the stereochemical and electrochemical properties of their copper(II) and palladium(II) complexes: [18]aneN$_2$S$_4$ facilitates generation of a mononuclear palladium(III)—N$_2$S$_4$ ionophore, while Me$_2$[18]aneN$_2$S$_4$ stabilizes palladium(I).[2] We wished to extend this study to the binding of [18]aneN$_2$S$_4$ to rhodium(III) centres, and we report herein the synthesis and single crystal X-ray structure of $[Rh([18]aneN_2S_4)](PF_6)_3 \cdot 3H_2O$. The related octahedral macrocyclic rhodium(III) complex $[Rh([9]aneS_3)_2]^{3+}$ and its reduction to unusual mononuclear rhodium(II) and rhodium(I) species has been described.[6]

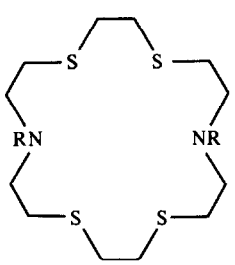

[18]aneN$_2$S$_4$: R = H

Me$_2$[18]aneN$_2$S$_4$: R = Me

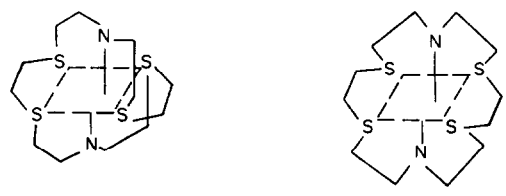

rac *meso*

Fig. 1. *Meso*- and *rac*-configurations for [M([18]aneN$_2$S$_4$)]$^{x+}$.

* Author to whom correspondence should be addressed.

RESULTS AND DISCUSSION

Treatment of $[Rh(H_2O)_6]^{3+}$ with one molar equivalent of [18]aneN$_2$S$_4$ in refluxing MeOH–H_2O for *ca* 12 h affords a bright orange solution containing the complex cation $[Rh([18]aneN_2S_4)]^{3+}$. Addition of excess NH_4PF_6 yields the complex as an orange precipitate which can be recrystallized from H_2O. The IR spectrum of the complex shows N—H stretching vibrations, ν(N—H), at 3240 and 3080 cm^{-1}, as well as other bands characteristic of coordinated [18]aneN$_2$S$_4$ and PF_6^- counterions. The FAB mass spectrum exhibits molecular ion peaks at $M^+ = 719$, 573 and 427: these are assigned to $[^{103}Rh([18]aneN_2S_4)(PF_6)_2]^+$, $[^{103}Rh([18]aneN_2S_4\text{-}H)PF_6]^+$ and $[^{103}Rh([18]aneN_2S_4\text{-}2H)]^+$, respectively. This evidence, together with microanalytical data, confirms the formulation $[Rh([18]aneN_2S_4)](PF_6)_3$ for the product. The complex can also be isolated as the BPh_4^- salt by using $NaBPh_4$ in place of NH_4PF_6 in the above preparation. The ^{1}H NMR spectrum of $[Rh([18]aneN_2S_4)](BPh_4)_3$ confirms a ratio of three BPh_4^- counterions to one [18]aneN$_2$S$_4$ macrocycle.

Single crystals of $[Rh([18]aneN_2S_4)](PF_6)_3 \cdot 3H_2O$ suitable for X-ray analysis were obtained by slow concentration of an aqueous solution of the complex. The structure of $[Rh([18]aneN_2S_4)]^{3+}$ shows (Fig. 2) the d^6 rhodium(III) ion coordinated by all six donor atoms of the macrocycle, with the N-donors occupying mutually *trans* positions. The observed bond lengths [Rh—S(1) = 2.3289(14), Rh—S(4) = 2.3416(14), Rh—S(10) = 2.3353(14), Rh—S(13) = 2.3349(14), Rh—N(7) = 2.083(4), Rh—N(16) = 2.101(5) Å] are similar to those in the related macrocyclic complexes $[Rh([9]aneS_3)_2]^{3+}$ [Rh—S = 2.3316(14), 2.3335(12), 2.3335(12) Å][6] and $[Rh([9]aneN_3)_2]^{3+}$ [Rh—N = 2.065(19), 2.073(21), 2.058(18) Å].[7] Consistent with other structurally characterized octahedral transition metal complexes $[M([18]aneN_2S_4)]^{x+}$ ($M = Ag^I$, $x = 1$; $M = Ni^{II}$, Fe^{II}, Hg^{II}, $x = 2$; $M = Co^{III}$, $x = 3$),[4] $[Rh([18]aneN_2S_4)]^{3+}$ adopts a *rac*-configuration involving meridional coordination of the two $SCH_2CH_2NCH_2CH_2S$ linkages to the central rhodium(III) ion. Angles around the rhodium(III) ion deviate considerably from ideal octahedral values and there is a significant tetrahedral distortion of the thioether-donor atoms out of the least-squares S_4 coordination plane, with S(4) and S(10) both lying 0.175 Å above this plane, and S(1) and S(13) lying 0.174 and 0.176 Å below. This tetrahedral distortion is likely to originate from the restricted bite angle of the $SCH_2CH_2NCH_2CH_2S$ chains of the macrocycle. The magnitude of this distortion in $[Rh([18]aneN_2S_4)]^{3+}$ is less than in $[Ag([18]aneN_2S_4)]^+$, consistent with the smaller ionic radius of rhodium(III) (66.5 pm) compared with silver(I) (115 pm).[8] To our knowledge, $[Rh([18]aneN_2S_4)]^{3+}$ represents the first characterized complex involving encapsulation of rhodium(III) by an 18-membered ring macrocyclic ligand.

The $[Rh([18]aneN_2S_4)]^{3+}$ cation participates in significant hydrogen-bonding through the N—H functions of the macrocycle, H_2O solvent molecules and fluorine atoms of the PF_6^- counterions: H(7)···O(1S) = 1.888(7) Å, angle N(7)—(H7)···O(1S) = 166.9(5)°; H(16)···O(2S) = 1.726(8)

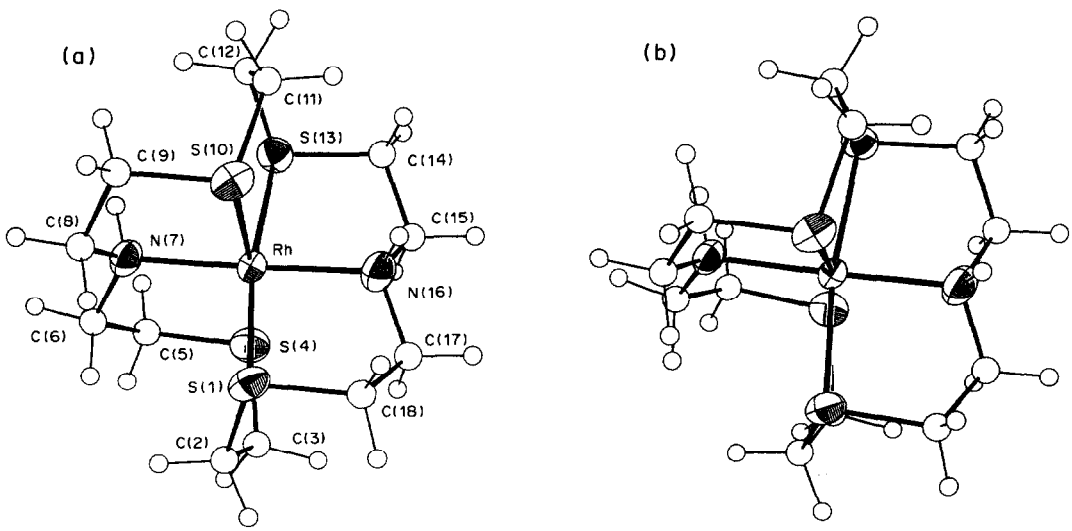

Fig. 2. Two views of the $[Rh([18]aneN_2S_4)]^{3+}$ cation: (a) with numbering scheme adopted and (b) orthogonal view showing the configuration adopted.

Å, angle N(16)—H(16)···O(2S) = 170.9(5)°; F(28)···O(3S) = 2.822(15) Å and O(2S)···O(3S) = 2.655(11) Å.

Since $[Rh([18]aneN_2S_4)](PF_6)_3$ dissolves only very sparingly in organic solvents such as MeCN, $MeNO_2$ and Me_2CO, all electrochemical measurements were performed using the much more soluble BPh_4^- salt. Cyclic voltammetry of $[Rh([18]aneN_2S_4)](BPh_4)_3$ in MeCN (0.1 M $^nBu_4NBPh_4$ supporting electrolyte) at platinum electrodes shows an irreversible reduction. At 298 K, this occurs at $E_{pc} = -1.34$ V vs Fc/Fc^+ (scan-rate = 180 mV s^{-1}). Upon lowering the temperature to 238 K and increasing the scan-rate to 400 mV s^{-1}, the reduction shifts cathodically to −2.02 V vs Fc/Fc^+ but remains irreversible. Coulometric measurements show that this process, which generates a yellow solution, corresponds to a two-electron reduction. These data suggest that the reduction corresponds to the formation of a d^8 rhodium(II) $[Rh([9]aneS_3)_2]^{2+}$ ($E_{1/2}$ for rhodium(III)/thia macrocyclic complex, $[Rh([14]aneS_4)]^{4+}$, has been reported previously.[9] Importantly, the trithia macrocycle $[9]aneS_3$ stabilizes both the d^7 rhodium(II) $[Rh([9]aneS_3)_2]^{2+}$ ($E_{1/2}$ for rhodium(III)/(II) = −0.71 V vs Fc/Fc^+) and the d^8 rhodium(I) complex $[Rh([9]aneS_3)_2]^+$ ($E_{1/2}$ for rhodium(II)/(I) = −1.08 V vs Fc/Fc^+).[6] Such stabilization is not achieved in the analogous tri-aza complex $[Rh([9]aneN_3)_2]^{3+}$ which shows two irreversible reductions at much more cathodic potentials, $E_{pc} = -1.93$ and −2.32 V vs Fc/Fc^+.[7]

EXPERIMENTAL

IR spectra were recorded as KBr and CsI discs using a Perkin–Elmer 598 spectrometer over the range 200–4000 cm^{-1}. UV–vis spectra were measured in quartz cells using Perkin–Elmer Lambda 9 and Pye Unicam SP8-400 spectrophotometers. Microanalyses were performed by the Edinburgh University Chemistry Department Microanalytical Service. Electrochemical measurements were performed on a Bruker E310 Universal Modular Polarograph. All readings were taken using a three-electrode potentiostatic system in acetonitrile containing 0.1 M $^nBu_4NPF_6$ or $^nBu_4NBPh_4$ as supporting electrolyte. Cyclic voltammetric measurements were carried out using a double platinum electrode and an Ag–AgCl reference electrode. All potentials are quoted vs ferrocene/ferrocenium, Fc/Fc^+. Mass spectra were run by electron impact on a Kratos MS 902 and by fast atom bombardment on a Kratos MS 50TC spectrometer. ^1H and ^{13}C NMR spectra were obtained on Bruker WP80 and WP200 instruments.

(a) *Synthesis of* $[Rh([18]aneN_2S_4)](PF_6)_3$

A fresh solution of $[Rh(H_2O)_6]^{3+}$ was prepared by treatment of $RhCl_3$ with three molar equivalents of $AgNO_3$ in refluxing H_2O. Reaction of $[Rh(H_2O)_6]^{3+}$ (0.140 mmol) with $[18]aneN_2S_4$ (45 mg, 0.138 mmol) in refluxing MeOH–H_2O (30 cm^3, 1:1 v/v) for 12 h afforded an orange solution. Addition of excess NH_4PF_6 gave an orange solid which was filtered, recrystallized from H_2O and dried *in vacuo* (yield: 71 mg, 54%). Found: C, 16.4; H, 2.9; N, 3.4. Calc. for $[C_{12}H_{26}N_2S_4Rh](PF_6)_3$: C, 16.7; H, 3.0; N 3.2%. FAB mass spectrum (3-NOBA matrix): Found: m/z = 719, 573 and 427. Calc. for $[^{103}Rh([18]aneN_2S_4)(PF_6)_2]^+$: m/z = 719, $[^{103}Rh([18]aneN_2S_4)PF_6]^+$: m/z = 574, $[^{103}Rh([18]aneN_2S_4)]^+$: m/z = 429: IR spectrum (KBr disc): 3240m, 3080w, 2980w, 2880w, 1465m, 1420m, 1380w, 1290w, 1230w, 1210w, 1175w, 1140m, 1065w, 1020w, 1000w, 970w, 840vs, 740m, 555vs, 495w cm^{-1}.

Single crystal structure determination of $[Rh([18]aneN_2S_4)](PF_6)_3 \cdot 3H_2O$. Recrystallization of the complex from aqueous solution yielded orange plates (0.62 × 0.62 × 0.15 mm) suitable for a single crystal X-ray crystallographic study.

Crystal data. $[C_{12}H_{26}N_2S_4Rh](PF_6)_3 \cdot 3H_2O$, M = 918.2, monoclinic, space group $P2_1/n$, a = 11.7097(12), b = 13.9470(11), c = 19.1954(17) Å, β = 107.048(6)°, V = 2997.2 $Å^3$ [from 2θ values of 35 reflections measured at $\pm\omega$ ($34 < 2\theta < 35°$, λ = 0.71073 Å, T = 298 K)], D_c = 2.035 g cm^{-3}, Z = 4, μ(Mo-K_α) = 1.118 mm^{-1}, F(000) = 1832.

Data collection and processing. A Stoë STADI-4 four-circle diffractometer, graphite-monochromated Mo-K_α radiation and ω–2θ scans using the learnt-profile method[10] were used. Of 4424 unique reflections measured ($2\theta_{max} = 45°$, h −12 → 12, k 0 → 14, l 0 → 20) 4125 with $F > 6\sigma(F)$ were used in all calculations. There was no significant crystal decay and no absorption correction was applied.

Structure analysis and refinement. The rhodium atom was located from a Patterson synthesis and the structure was developed by iterative cycles of least-squares refinement and difference Fourier synthesis.[11] During refinement some disorder of one of the PF_6^- counterions was observed. This was modelled successfully using partial F atoms, which integrated to six F atoms per P atom. Three fully occupied H_2O solvent molecules were found to be associated with each cation, although the H atoms on these could not be located. Anisotropic thermal parameters were refined for Rh, S, P, O, N and all fully occupied F atoms. Macrocyclic H atoms were included in fixed, calculated positions. The weighting scheme $w^{-1} = \sigma^2(F) + 0.007342F^2$ gave satis-

Table 1. Bond lengths, angles and torsion angles for $[Rh([18]aneN_2S_4)]^{3+}$, with standard deviations in parentheses

Bond lengths (Å)

Rh—S(1)	2.3289(14)	C(6)—N(7)	1.488(7)
Rh—S(4)	2.3416(14)	N(7)—C(8)	1.498(8)
Rh—N(7)	2.083(4)	C(8)—C(9)	1.497(8)
Rh—S(10)	2.3353(14)	C(9)—S(10)	1.834(6)
Rh—S(13)	2.3349(14)	S(10)—C(11)	1.833(6)
Rh—N(16)	2.101(5)	C(11)—C(12)	1.482(8)
S(1)—C(2)	1.811(6)	C(12)—S(13)	1.821(6)
S(1)—C(18)	1.826(7)	S(13)—C(14)	1.833(6)
C(2)—C(3)	1.500(8)	C(14)—C(15)	1.514(9)
C(3)—S(4)	1.826(6)	C(15)—N(16)	1.507(8)
S(4)—C(5)	1.821(6)	N(16)—C(17)	1.486(8)
C(5)—C(6)	1.507(8)	C(17)—C(18)	1.505(10)

Angles (°)

S(1)— Rh—S(4)	88.83(5)	S(4)—C(5)—C(6)	111.2(4)
S(1)— Rh—N(7)	92.59(12)	C(5)—C(6)—N(7)	109.2(5)
S(1)— Rh—S(10)	92.49(5)	Rh—N(7)—C(6)	110.7(3)
S(1)— Rh—S(13)	171.43(5)	Rh—N(7)—C(8)	113.2(3)
S(1)— Rh—N(16)	85.29(13)	C(6)—N(7)—C(8)	114.1(4)
S(4)— Rh—N(7)	85.25(12)	N(7)—C(8)—C(9)	109.9(5)
S(4)— Rh—S(10)	171.33(5)	C(8)—C(9)—S(10)	111.6(4)
S(4)— Rh—S(13)	91.44(5)	Rh—S(10)—C(9)	97.31(19)
S(4)— Rh—N(16)	94.70(13)	Rh—S(10)—C(11)	104.56(20)
N(7)— Rh—S(10)	86.13(12)	C(9)—S(10)—C(11)	104.9(3)
N(7)— Rh—S(13)	95.97(12)	S(10)—C(11)—C(12)	115.1(4)
N(7)— Rh—N(16)	177.88(17)	C(11)—C(12)—S(13)	115.5(4)
S(10)— Rh—S(13)	88.52(5)	Rh—S(13)—C(12)	103.96(19)
S(10)— Rh—N(16)	93.95(13)	Rh—S(13)—C(14)	98.20(19)
S(13)— Rh—N(16)	86.15(13)	C(12)—S(13)—C(14)	104.7(3)
Rh—S(1)—C(2)	103.65(19)	S(13)—C(14)—C(15)	111.9(4)
Rh—S(1)—C(18)	98.11(21)	C(14)—C(15)—N(16)	109.8(5)
C(2)—S(1)—C(18)	103.3(3)	Rh—N(16)—C(15)	111.8(4)
S(1)—C(2)—C(3)	114.1(4)	Rh—N(16)—C(17)	109.1(4)
C(2)—C(3)—S(4)	113.8(4)	C(15)—N(16)—C(17)	112.8(5)
Rh—S(4)—C(3)	103.04(21)	N(16)—C(17)—C(18)	108.8(5)
Rh—S(4)—C(5)	98.07(19)	S(1)—C(18)—C(17)	109.9(5)
C(3)—S(4)—C(5)	102.0(3)		

Torsion angles (°)

C(18)—S(1)—C(2)—C(3)	−67.1(5)	C(8)—C(9)—S(10)—C(11)	75.0(5)
C(2)—S(1)—C(18)—C(17)	134.2(5)	C(9)—S(10)—C(11)—C(12)	−74.6(5)
S(1)—C(2)—C(3)—S(4)	−47.8(5)	S(10)—C(11)—C(12)—S(13)	−41.3(6)
C(2)—C(3)—S(4)—C(5)	−66.9(5)	C(11)—C(12)—S(13)—C(14)	−69.6(5)
C(3)—S(4)—C(5)—C(6)	131.1(4)	C(12)—S(13)—C(14)—C(15)	79.1(5)
S(4)—C(5)—C(6)—N(7)	−52.8(5)	S(13)—C(14)—C(15)—N(16)	50.9(6)
C(5)—C(6)—N(7)—C(8)	−176.4(5)	C(14)—C(15)—N(16)—C(17)	−172.6(5)
C(6)—N(7)—C(8)—C(9)	−173.9(5)	C(15)—N(16)—C(17)—C(18)	−178.1(5)
N(7)—C(8)—C(9)—S(10)	52.2(6)	N(16)—C(17)—C(18)—S(1)	−56.4(6)

factory agreement analyses. At final convergence, $R = 0.0618$, $R_w = 0.0978$ and $S = 1.460$ for 384 independent parameters, and the final difference Fourier synthesis showed no feature above 1.39 or below -1.14 eÅ^{-3}. Illustrations were prepared using ORTEPII,[12] molecular geometry calculations utilized CALC,[13] and scattering factor data were inlaid[11] or taken from ref. 14. Bond lengths, angles and torsion angles are given in Table 1. Atomic coordinates, thermal parameters and lists of observed and calculated structure factors have been deposited with the Editor, from whom copies are

available on request. Atomic coordinates have also been deposited with the Cambridge Crystallographic Data Centre.

(b) *Synthesis of* $[Rh([18]aneN_2S_4)](BPh_4)_3$

Method as for (a) but using $NaBPh_4$ in place of NH_4PF_6 and recrystallizing from MeCN (yield: 116 mg, 68%). FAB mass spectrum (3-NOBA matrix): Found: $m/z = 427$. Calc. for $[^{103}Rh([18]aneN_2S_4)]^+$: $m/z = 429$. ^1H NMR spectrum (80.13 MHz, CD_3NO_2, 298 K): $\delta = 2.0$–3.9 (br, m, CH_2, 24H), 6.8–8.0 ppm (m, BPh_4^-, 60H). IR spectrum (KBr disc): 3200vs, 3020m, 3010w, 2990m, 2970w, 2960w, 2910w, 1950w, 1900w, 1820w, 1570m, 1470m, 1420m, 1385m, 1300w, 1260w, 1180m, 1145m, 1120w, 1060w, 1020m, 990w, 910m, 860w, 840m, 740vs, 710vs, 705vs, 620m, 590m, 485m, 460m cm^{-1}.

Acknowledgements—We thank the SERC for support and Johnson Matthey plc for generous loans of platinum metal salts.

REFERENCES

1. A. J. Blake and M. Schröder, *Adv. Inorg. Chem.* 1990, **35**, 1; M. Schröder, *Pure Appl. Chem.* 1988, **60**, 517; M. N. Bell, A. J. Blake, R. O. Gould, A. J. Holder, T. I. Hyde, A. J. Lavery, G. Reid and M. Schröder, *J. Inclusion Phenom.* 1987, **5**, 169.
2. G. Reid, A. J. Blake, T. I. Hyde and M. Schröder, *J. Chem. Soc., Chem. Commun.* 1988, 1397; A. J. Blake, G. Reid and M. Schröder, *J. Chem. Soc., Dalton Trans.* 1990, in press; N. Atkinson, A. J. Blake, M. G. B. Drew, G. Forsyth, A. J. Lavery, G. Reid and M. Schröder, *J. Chem. Soc., Chem. Commun.* 1989, 984.
3. D. St. C. Black and I. A. McLean, *J. Chem. Soc., Chem. Commun.* 1968, 1004; *Tetrahedron Lett.* 1969, 3961; *Aust. J. Chem.* 1971, **24**, 1401.
4. G. Reid and M. Schröder, *Chem. Soc. Revs* 1990, **19**, 239.
5. A. J. Blake, R. O. Gould, A. J. Holder, T. I. Hyde and M. Schröder, *Polyhedron* 1989, **8**, 513; J. R. Hartman, E. J. Hintsa and S. R. Copper, *J. Am. Chem. Soc.* 1986, **108**, 1208; S. R. Cooper, S. C. Rawle, J. R. Hartman, E. J. Hintsa and G. A. Adams, *Inorg. Chem.* 1988, **27**, 1209; J. R. Hartman and S. R. Cooper, *J. Am. Chem. Soc.* 1986, **108**, 1202; R. E. Wolf, J. R. Hartman, J. M. Storey, B. M. Foxman and S. R. Cooper, *J. Am. Chem. Soc.* 1987, **109**, 4328.
6. A. J. Blake, R. O. Gould, A. J. Holder, T. I. Hyde and M. Schröder, *J. Chem. Soc., Dalton Trans.* 1988, 1861; A. J. Blake, A. J. Holder, T. I. Hyde and M. Schröder, *J. Chem. Soc., Chem. Commun.* 1987, 987; S. C. Rawle, R. Yagbasan and S. R. Cooper, *J. Am. Chem. Soc.* 1987, **109**, 6181.
7. A. J. Blake, T. I. Hyde and M. Schröder, unpublished results.
8. R. D. Shannon, *Acta Cryst.* 1976, **A32**, 751.
9. T. Yoshida and T. Ueda, *J. Chem. Soc., Chem. Commun.* 1985, 1137; W. D. Lemke, K. E. Travis, N. E. Takvoryan and D. H. Busch, *Adv. Chem. Ser.* 1977, 358.
10. W. Clegg, *Acta Cryst.* 1981, **A37**, 22.
11. G. M. Sheldrick, SHELX76, Program for Crystal Structure Refinement. University of Cambridge, England (1976).
12. P. D. Mallinson and K. W. Muir, ORTEPII, interactive version, *J. Appl. Cryst.* 1985, **18**, 51.
13. R. O. Gould and P. Taylor, CALC, Fortran77 version. University of Edinburgh, Scotland (1985).
14. D. T. Cromer and J. L. Mann, *Acta Cryst.* 1968, **A24**, 321.

Polyhedron Vol. 9, No. 24, pp. 2931–2935, 1990
Printed in Great Britain

0277–5387/90 $3.00+.00.
© 1990 Pergamon Press plc

MERCURY MACROCYCLIC COMPLEXES: THE SYNTHESIS OF $[Hg([18]aneN_2S_4)]^{2+}$ AND $[Hg(Me_2[18]aneN_2S_4)]^{2+}$. THE SINGLE CRYSTAL X-RAY STRUCTURE OF $[Hg([18]aneN_2S_4)](PF_6)_2 \cdot 4/3H_2O$

ALEXANDER J. BLAKE, GILLIAN REID and MARTIN SCHRÖDER*

Department of Chemistry, University of Edinburgh, West Mains Road, Edinburgh EH9 3JJ, Scotland, U.K.

(*Received* 18 *June* 1990; *accepted* 13 *August* 1990)

Abstract—Reaction of $HgSO_4$ with one molar equivalent of L{L = [18]aneN$_2$S$_4$ (1,4,10,13-tetrathia-7,16-diazacyclooctadecane) or Me$_2$[18]aneN$_2$S$_4$ (7,16-dimethyl-1,4,10,13-tetrathia-7,16-diazacyclooctadecane)} in refluxing MeOH–H_2O for 15 min affords a colourless solution containing the complex cation $[Hg(L)]^{2+}$. Addition of excess PF_6^- counterion gives the complex $[Hg([18]aneN_2S_4)](PF_6)_2 \cdot 4/3H_2O$ as a cream coloured solid. A single crystal X-ray structure determination shows mercury(II) bound to a severely distorted octahedral arrangement of the six macrocyclic donor atoms, Hg—S = 2.655(5), 2.735(4), 2.751(4), 2.639(5) Å, Hg—N = 2.473(11), 2.472(17) Å. The cation is in a *rac* configuration with the two $SCH_2CH_2NCH_2CH_2S$ linkages bound meridionally to the metal centre.

In the course of our continuing study of the coordination chemistry of the potentially hexadentate macrocycles [18]aneN$_2$S$_4$ and Me$_2$[18]aneN$_2$S$_4$, we have observed that these large ring systems readily bind to a range of transition metal ions, and that the resultant complexes can often exhibit unusual stereochemical and electrochemical properties.[1] Importantly, we have found that [18]aneN$_2$S$_4$ binds octahedrally to first and second row transition metal centres to give the *rac* isomer exclusively, thus confirming the original proposals by Black and McLean.[2] We were interested to determine whether coordination of [18]aneN$_2$S$_4$ to a large third row metal ion would result in a different configuration for the macrocycle or in distortion from a regular octahedral *rac* configuration. We therefore extended this study to the complexation of mercury(II) with these macrocyclic ligands and report herein the synthesis of $[Hg([18]aneN_2S_4)]^{2+}$ and $[Hg(Me_2[18]aneN_2S_4)]^{2+}$. The single crystal structure of $[Hg([18]aneN_2S_4)](PF_6)_2 \cdot 4/3H_2O$ is also described. Few examples of macrocyclic mercury thioether complexes have been reported. The dimeric species $[Hg_2([14]aneS_4)Cl_4]$ involves exodentate coordination of two thia-donors, with two Cl^- ligands completing the tetrahedral environment at each mercury(II) ion,[3] while we have previously reported the synthesis and structure of $[Hg([9]aneS_3)_2]^{2+}$. This complex cation involves facial coordination of each trithia macrocycle to give a centrosymmetric, tetragonally compressed stereochemistry, Hg—S_{ap} = 2.638(3), Hg—S_{eq} = 2.728(3), 2.712(3) Å.[4]

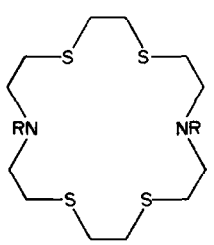

[18] aneN$_2$S$_4$: R=H
Me$_2$ [18] aneN$_2$S$_4$: R=Me

Scheme 1.

RESULTS AND DISCUSSION

Treatment of $HgSO_4$ with one molar equivalent of [18]aneN$_2$S$_4$ in refluxing MeOH–H_2O (1 : 1 v/v)

* Author to whom correspondence should be addressed.

for 30 min affords a colourless solution. Addition of excess NH_4PF_6 yields a cream coloured precipitate which was recrystallized from MeCN. The IR spectrum of this product shows a peak at 3295 cm^{-1} corresponding to an N—H stretching vibration, ν(N—H), as well as other peaks indicative of the presence of coordinated [18]aneN$_2$S$_4$ and PF_6^- counterion. The FAB mass spectrum exhibits molecular ion peaks at $m/z = 672$ and 527 assigned to $[^{202}Hg([18]aneN_2S_4)PF_6-H]^+$ and $[^{202}Hg([18]aneN_2S_4)-H]^+$, respectively. The ^1H NMR spectrum measured in CD_3NO_2 at 298 K shows a broad multiplet in the range $\delta = 2.25-3.90$ ppm assigned to the methylene protons of the coordinated macrocycle, as well as a broad resonance at 7.05 ppm due to the N—H functions. These data, together with microanalytical data, indicate the formulation $[Hg([18]aneN_2S_4)](PF_6)_2$ for the product.

Colourless crystals were obtained by vapour diffusion of diethyl ether into a solution of $[Hg([18]aneN_2S_4)](PF_6)_2$ in MeCN. The structure shows (Fig. 1) mercury(II) bound via all six macrocyclic donor atoms, Hg—S(1) = 2.655(5), Hg—S(4) = 2.735(4), Hg—S(10) = 2.751(4), Hg—S(13) = 2.639(5), Hg—N(7) = 2.473(11), Hg—N(16) = 2.472(17) Å, and confirms a *rac* configuration for $[Hg([18]aneN_2S_4)]^{2+}$. This result is consistent with all other structurally characterized octahedral complexes of [18]aneN$_2$S$_4$.[1] The Hg—S bond lengths observed are similar to those in $[Hg([9]aneS_3)_2]^{2+}$.[4] Two alternative diastereoisomers of *rac*-$[M([18]aneN_2S_4)]^{x+}$ are possible: these differ in the relative orientations of their N—H groups (Fig. 2).[5] Each isomer has C_2 symmetry and therefore should give rise to six different ^{13}C NMR resonances. Our single crystal X-ray study shows that $[Hg([18]aneN_2S_4)]^{2+}$ exists as a distorted form isomer **II** in the crystal selected.

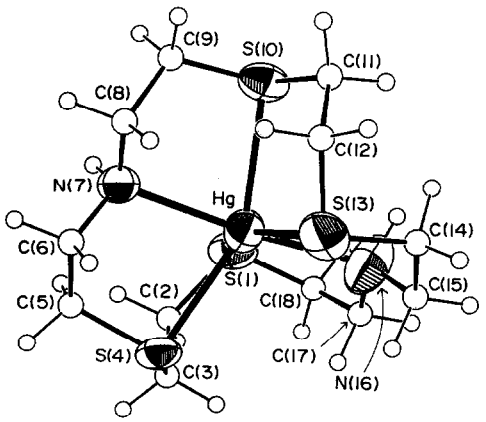

Fig. 1. Single crystal structure of $[Hg([18]aneN_2S_4)]^{2+}$ with numbering scheme adopted.

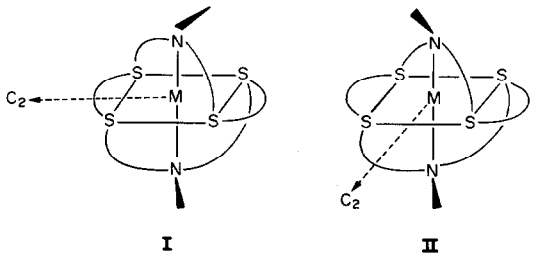

Fig. 2. Isomers I and II for *rac*-$[M([18]aneN_2S_4)]^{x+}$.

Interestingly, our single crystal structure determinations on a range of first row metal complexes *rac*-$[M([18]aneN_2S_4)]^{x+}$ have usually shown these to exist as isomer **I**, although ^{13}C NMR studies on the complexes where M = iron(II) or rhodium(III) have clearly shown that both isomers are present in solution.[1] The ligand conformation and M–donor bond lengths observed in the crystal structure of $[Hg([18]aneN_2S_4)]^{2+}$ lead to approximate, non-crystallographic C_2 symmetry. The structure of $[Hg([18]aneN_2S_4)]^{2+}$ also reveals a severe tetrahedral distortion of the S-donor atoms out of the best S_4 coordination plane, with S(1) and S(13) lying 0.658 and 0.664 Å, respectively, above the plane, while S(4) and S(10) lie 0.670 and 0.652 Å, respectively, below. It is likely that this distortion is a consequence of the fact that the radius of the mercury(II) ion (102 pm)[6] is too large for the macrocyclic cavity, especially with the limited bite angle of the $SCH_2CH_2NCH_2CH_2S$ chains.

The di-N-methylated complex $[Hg(Me_2[18]aneN_2S_4)](PF_6)_2$ has been prepared by a route analogous to that employed for $[Hg([18]aneN_2S_4)](PF_6)_2$, and characterized by microanalyses, IR, ^1H NMR spectroscopy and FAB mass spectrometry. By analogy with our earlier studies on $[Pd(L)]^{2+}$, $[Cu(L)]^{2+}$ and $[Ag(L)]^+$ [1] we propose that $[Hg(Me_2[18]aneN_2S_4)]^{2+}$ is in a *meso* configuration involving facial binding of the $SCH_2CH_2NCH_2CH_2S$ chains, due to the steric effect of replacing NH by the bulkier NMe groups. Studies are currently underway to confirm these proposals.

Cyclic voltammetry of $[Hg([18]aneN_2S_4)](PF_6)_2$ measured in MeCN (0.1 M $^nBu_4NPF_6$ supporting electrolyte) at platinum electrodes shows an irreversible reduction at $E_{pc} = -1.16$ V vs Fc/Fc^+. Subsequent scans lead to the generation of new waves, suggesting the formation of daughter products. Cyclic voltammetry of $[Hg(Me_2[18]aneN_2S_4)](PF_6)_2$ under the same conditions shows an irreversible reduction at $E_{pc} = -0.60$ V vs Fc/Fc^+. Subsequent scans lead to the appearance of a chemically-reversible reduction at

$E_{1/2} = -0.46$ V vs Fc/Fc^+. These results indicate that reduction of the mercury(II) complexes is followed by some chemical reaction, possibly involving formation of solvated species which exhibit a different electrochemistry. In both cases, reduction to mercury metal occurs over a period of a few seconds. $[Hg([9]aneS_3)_2]^{2+}$ shows a chemically-reversible reduction at $E_{1/2} = -0.15$ V vs Fc/Fc^+.[4]

EXPERIMENTAL

IR spectra were recorded as KBr and CsI discs using a Perkin–Elmer 598 spectrometer over the range 200–4000 cm^{-1}. UV–vis spectra were measured in quartz cells using Perkin–Elmer Lambda 9 and Pye Unicam SP8-400 spectrophotometers. Microanalyses were performed by the Edinburgh University Chemistry Department Microanalytical service. Electrochemical measurements were performed on a Bruker E310 Universal Modular Polarograph. All readings were taken using a three-electrode potentiostatic system in acetonitrile containing 0.1 M $^nBu_4NPF_6$ or $^nBu_4NBF_4$ as supporting electrolyte. Cyclic voltammetric measurements were carried out using a double platinum electrode and an Ag/AgCl reference electrode. All potentials are quoted vs ferrocene/ferrocenium, Fc/Fc^+. Mass spectra were run by electron impact on a Kratos MS 902 and by fast atom bombardment on a Kratos MS 50TC spectrometer. ^1H and ^{13}C NMR spectra were obtained on Bruker WP80 and WP200 instruments.

(a) *Synthesis of* $[Hg([18]aneN_2S_4)](PF_6)_2$

Reaction of $HgSO_4$ (30 mg, 0.101 mmol) and $[18]aneN_2S_4$ (35 mg, 0.107 mmol) in refluxing $MeOH–H_2O$ (35 cm^3, 1 : 1 v/v) for 15 min under N_2 afforded a colourless solution. Cooling, reducing the volume to 10 cm^3 and filtering the reaction mixture into a solution of excess NH_4PF_6 in MeOH gave a cream precipitate which was recrystallized from MeCN and diethyl ether (Yield : 60 mg, 73%). Found: C, 17.7; H, 3.4; N, 3.5; S, 16.3. Calc. for $[C_{12}H_{26}N_2S_4Hg](PF_6)_2$: C, 17.6; H, 3.2; N, 3.4; S, 15.7%. FAB mass spectrum (3-NOBA matrix): Found $m/z = 672$ and 527. Calc. for $[^{202}Hg([18]aneN_2S_4)PF_6]^+$ $m/z = 673$; $[^{202}Hg([18]aneN_2S_4)]^+$ $m/z = 528$. ^1H NMR spectrum (80.13 MHz, CD_3NO_2, 298 K): $\delta = 2.25$–3.90 (m, b, CH_2, 24H), 7.05 ppm (b, NH, 2H). ^{13}C DEPT NMR (50.32 MHz, CD_3NO_2, 298 K) suggests fluxional behaviour in solution: two sets of resonances in a ratio of approximately 3 : 1; major component $\delta = 45.41$ (NCH_2), 30.57, 27.52 ppm ($2\times SCH_2$); minor component $\delta = 43.57$ (NCH_2), 29.05, 28.94ppm ($2\times SCH_2$). IR spectrum (KBr disc): 3295m, 2920m, 2860m, 1465m, 1420m, 1320w, 1280w, 1100m, 1040w, 1000w, 940w, 840vs, br, 740w, 555vs cm^{-1}.

Single crystal X-ray structure determination on $[Hg([18]aneN_2S_4)](PF_6)_2 \cdot 4/3H_2O$. Colourless tablets suitable for single crystal X-ray analysis were obtained by vapour diffusion of diethyl ether into a solution of the complex in MeCN. The selected crystal ($0.39 \times 0.21 \times 0.12$ mm) was sealed in a glass capillary tube to prevent solvent loss.

Crystal data. $[C_{12}H_{26}N_2S_4Hg]^{2+} \cdot 2PF_6^- \cdot 4/3H_2O$, $M = 841.1$. Monoclinic, space group $C2/c$, $a = 22.904(8)$, $b = 10.141(4)$, $c = 26.516(9)$ Å, $\beta = 121.544(24)°$, $V = 5249$ Å^3 [from 2θ values for 48 reflections measured at $\pm\omega$ ($23.9 < 2\theta < 25.8°$, $\lambda = 0.71073$ Å, $T = 298$ K)], $Z = 8$, $D_c = 2.129$ g cm^{-3}, μ(Mo-K_α) = 6.334 cm^{-1}, $F(000) = 3232$.

Data collection and processing. Stoë STADI-4 four-circle diffractometer, graphite-monochromated Mo-K_α radiation and ω–2θ scans using the learnt-profile method[7] were used. 4496 reflections measured ($2\theta_{max} = 45°$, h $-24 \rightarrow 15$, k $0 \rightarrow 10$, l $0 \rightarrow 28$) giving 2500 with $F > 6\sigma(F)$. Initial corrections for absorption (min. 0.1833, max. 0.3412) were made by means of ψ-scans. Crystal decay (30%) was approximately linear and isotropic.

Structure analysis and refinement. The mercury position was deduced from a Patterson synthesis. Iterative cycles of least-squares refinement and difference Fourier syntheses[8] located the positions of all other non-hydrogen atoms. Final corrections for absorption (max. 1.624, min. 0.921) were made using DIFABS.[9] During refinement the bond linking C(17) to C(18) was observed to be unusually short. Thus, the bond lengths, C(17)–C(18) and C(17)—N(16) were constrained to be 1.50 Å. Two mutually incompatible 2/3-occupied H_2O solvent molecules were found per $[Hg([18]aneN_2S_4)]^{2+}$ cation. Hydrogen atoms were included in fixed, calculated positions. Anisotropic thermal parameters were refined for Hg, S, N, P, F and C atoms. The weighting scheme $w^{-1} = \sigma^2(F) + 0.000277F^2$ gave satisfactory agreement analyses. At final convergence $R = 0.0490$, $R_w = 0.0615$, $S = 1.104$ for 302 independent parameters, and the final difference Fourier synthesis showed no feature above 0.86 or below -1.71 eÅ^{-3}: this trough lies close to the mercury ion. Illustrations were prepared using ORTEPII,[10] molecular geometry calculations utilized CALC,[11] and scattering factor data were inlaid[5] or taken from ref. 12. Bond lengths, angles and torsion angles are given in Table 1. Fractional atomic coordinates, thermal parameters, together

with observed and calculated structure factors, have been deposited with the Editor, from whom copies are available on request. Atomic coordinates have also been deposited with the Cambridge Crystallographic Data Centre.

(b) *Synthesis of* $[Hg(Me_2[18]aneN_2S_4)](PF_6)_2$

Method as for (a) above, using $HgSO_4$ (30 mg, 0.101 mmol) and $Me_2[18]aneN_2S_4$ (35 mg, 0.099 mmol). Product isolated as a pale green solid (yield: 56 mg, 67%). Found: C, 19.7; H, 3.6; N, 3.2. Calc. for $[C_{14}H_{30}N_2S_4Hg](PF_6)_2$: C, 19.9; H, 3.6; N, 3.3%. FAB mass spectrum (3-NOBA matrix): Found $m/z = 574$. Calc. for $[^{202}Hg([18]aneN_2S_4)H_2O]^+$ $m/z = 574$. ^1H NMR spectrum (80.13 MHz, CD_3NO_2, 298 K): $\delta = 2.60$–3.65 (m, b, CH_2, 24H), 2.43 ppm (s, CH_3, 6H). IR spectrum

Table 1. Bond lengths, angles and torsion angles for $[Hg([18]aneN_2S_4)]^{2+}$, with standard deviations in parentheses

		Bond lengths (Å)	
Hg—S(1)	2.655(5)	C(5)—C(6)	1.510(22)
Hg—S(4)	2.735(4)	C(6)—N(7)	1.409(19)
Hg—N(7)	2.473(11)	N(7)—C(8)	1.460(20)
Hg—S(10)	2.751(4)	C(8)—C(9)	1.501(23)
Hg—S(13)	2.639(5)	C(9)—S(10)	1.832(17)
Hg—N(16)	2.472(17)	S(10)—C(11)	1.817(16)
S(1)—C(2)	1.797(17)	C(11)—C(12)	1.550(23)
S(1)—C(18)	1.747(18)	C(12)—S(13)	1.805(16)
C(2)—C(3)	1.502(23)	S(13)—C(14)	1.808(20)
C(3)—S(4)	1.807(17)	C(14)—C(15)	1.51(3)
S(4)—C(5)	1.834(16)	C(15)—N(16)	1.47(3)
		Angles (°)	
S(1)—Hg—S(4)	81.59(13)	S(4)—C(5)—C(6)	111.8(11)
S(1)—Hg—N(7)	103.1(3)	C(5)—C(6)—N(7)	112.1(13)
S(1)—Hg—S(10)	105.74(13)	Hg—N(7)—C(6)	111.6(9)
S(1)—Hg—S(13)	151.12(14)	Hg—N(7)—C(8)	109.2(9)
S(1)—Hg—N(16)	75.8(4)	C(6)—N(7)—C(8)	113.9(12)
S(4)—Hg—N(7)	76.5(3)	N(7)—C(8)—C(9)	114.9(13)
S(4)—Hg—S(10)	152.03(12)	C(8)—C(9)—S(10)	116.3(12)
S(4)—Hg—S(13)	104.47(13)	Hg—S(10)—C(9)	98.5(5)
S(4)—Hg—N(16)	108.3(4)	Hg—S(10)—C(11)	100.7(5)
N(7)—Hg—S(10)	75.5(3)	C(9)—S(10)—C(11)	104.6(7)
N(7)—Hg—S(13)	105.7(3)	S(10)—C(11)—C(12)	117.1(11)
N(7)—Hg—N(16)	174.8(5)	C(11)—C(12)—S(13)	117.4(11)
S(10)—Hg—S(13)	82.29(13)	Hg—S(13)—C(12)	102.2(5)
S(10)—Hg—N(16)	99.7(4)	Hg—S(13)—C(14)	98.1(7)
S(13)—Hg—N(16)	75.5(4)	C(12)—S(13)—C(14)	103.0(8)
Hg(1)—S(1)—C(2)	103.0(6)	S(13)—C(14)—C(15)	111.4(14)
Hg(1)—S(1)—C(18)	102.1(6)	C(14)—C(15)—N(16)	106.5(16)
C(2)—S(1)—C(18)	105.8(8)	Hg—N(16)—C(15)	112.6(12)
S(1)—C(2)—C(3)	117.9(12)	Hg—N(16)—C(17)	108.1(12)
C(2)—C(3)—S(4)	118.4(12)	C(15)—N(16)—C(17)	111.2(16)
Hg—S(4)—C(3)	100.2(6)	N(16)—C(17)—C(18)	115.8(16)
Hg—S(4)—C(5)	94.7(5)	S(1)—C(18)—C(17)	117.1(13)
C(3)—S(4)—C(5)	103.7(7)		
		Torsion angles (°)	
C(18)—S(1)—C(2)—C(3)	70.8(14)	C(8)—C(9)—S(10)—C(11)	−87.5(13)
C(2)—S(1)—C(18)—C(17)	−95.7(15)	C(9)—S(10)—C(11)—C(12)	67.6(13)
S(1)—C(2)—C(3)—S(4)	55.0(17)	S(10)—C(11)—C(12)—S(13)	56.1(15)
C(2)—C(3)—S(4)—C(5)	59.3(14)	C(11)—C(12)—S(13)—C(14)	59.7(14)
C(3)—S(4)—C(5)—C(6)	−144.6(11)	C(12)—S(13)—C(14)—C(15)	−149.6(13)
S(4)—C(5)—C(6)—N(7)	69.2(15)	S(13)—C(14)—C(15)—N(16)	68.9(17)
C(5)—C(6)—N(7)—C(8)	−176.8(13)	C(14)—C(15)—N(16)—C(17)	−176.0(15)
C(6)—N(7)—C(8)—C(9)	−176.0(13)	C(15)—N(16)—C(17)—C(18)	177.0(16)
N(7)—C(8)—C(9)—S(10)	−51.0(17)	N(16)—C(17)—C(18)—S(1)	−44.6(21)

(KBr disc): 2950m, 2840m, 1465m, 1450m, 1430m, 1320m, 1280w, 1260w, 1230m, 1210w, 1170w, 1130w, 1090m, 1050m, 1030w, 1010w, 990w, 950w, 930m, 840vs, br, 740m, 725m, 690w, 640w, 620w, 555vs cm^{-1}.

Acknowledgement—We thank the SERC for support.

REFERENCES

1. G. Reid and M. Schröder, *Chem. Soc. Revs* 1990, **19**, 239; G. Reid, A. J. Blake, T. I. Hyde and M. Schröder, *J. Chem. Soc., Chem. Commun.* 1988, 1397; N. Atkinson, A. J. Blake, M. G. B. Drew, G. Forsyth, A. J. Lavery, G. Reid and M. Schröder, *J. Chem. Soc., Chem. Commun.* 1989, 984.
2. D. St. C. Black and I. A. McLean, *J. Chem. Soc., Chem. Commun.* 1968, 1004; *Tetrahedron Lett.* 1969, **1**, 3961; *Aust. J. Chem.* 1971, **24**, 1401.
3. N. W. Alcock, N. Herron and P. Moore, *J. Chem. Soc., Chem. Commun.* 1976, 886.
4. A. J. Blake, A. J. Holder, T. I. Hyde, G. Reid and M. Schröder, *Polyhedron* 1989, **8**, 2041.
5. R. W. Hay, B. Jeragh, S. F. Lincoln and G. H. Searle, *Inorg. Nucl. Chem. Lett.* 1978, **14**, 435.
6. R. D. Shannon, *Acta Cryst.* 1976, **A32**, 751.
7. W. Clegg, *Acta Cryst.* 1981, **A37**, 22.
8. G. M. Sheldrick, SHELX76, Program for Crystal Structure Refinement. University of Cambridge, England (1976).
9. N. Walker and D. Stuart, DIFABS, Program for Empirical Absorption Corrections, *Acta Cryst.* 1983, **A39**, 158.
10. P. D. Mallinson and K. W. Muir, ORTEPII, interactive version, *J. Appl. Cryst.* 1985, **18**, 51.
11. R. O. Gould and P. Taylor, CALC, Fortran77 version. University of Edinburgh, Scotland (1985).
12. D. T. Cromer and J. L. Mann, *Acta Crystallogr.* 1968, **A24**, 321.

Polyhedron Vol. 9, No. 24, pp. 2937–2939, 1990
Printed in Great Britain

0277–5387/90 $3.00 + .00
© 1990 Pergamon Press plc

SYNTHESIS AND X-RAY STUDIES OF DI-μ-CYANATO-BIS[{CYANATO(N,N-DIMETHYLETHYLENEDIAMINE)}COPPER(II)]

A. E. MAURO,* S. I. KLEIN and J. S. SALDAÑA

Instituto de Química de Araraquara, UNESP, C.P. 174, 14800, Araraquara, Brazil

and

C. A. De SIMONE, J. ZUKERMAN-SCHPECTOR and E. E. CASTELLANO

Instituto de Física e Química de São Carlos, USP, 13560, São Carlos, Brazil

(*Received* 3 *May* 1990; *accepted* 8 *August* 1990)

Abstract—The compound di-μ-cyanato-bis[{cyanato(N,N-dimethylethylenediamine)}copper(II)] was synthesized, and studied by IR spectroscopy and X-ray diffraction. It is dimeric with bridging and terminal cyanate groups, and the copper atoms show a square-based pyramid coordination geometry.

One of our research lines relates to the synthesis, reactivity and solid-state structural characterization of copper compounds with nitrogen-based ligands.[1–3] Recently, we synthesized an azido complex with a bidentate amine,[4] whose structural features prompted us to extend the investigation to copper(II) cyanato complexes. The structural parameters that emerge from the copper–pseudohalogen amine complexes merit attention, since they may be related to those of biological interest, such as copper-containing proteins.[5] In addition, it must be pointed out that the pseudohalogens bonded to copper may be made to react with organic nitrogen-based ligands present at the metal's coordination sphere, in analogy to other metal-induced organic synthesis. It is also a fact that lesser attention has been given to cyanate than to other pseudohalogen copper complexes, and we consider it desirable to fill in this gap. We therefore prepared $[Cu(NCO)_2(diMeen)]_2$ (diMeen = N,N-dimethylethylenediamine) and subjected this complex to a full IR and X-ray crystallographic characterization.

* Author to whom correspondence should be addressed.

EXPERIMENTAL

Synthesis of $[Cu(NCO)_2(diMeen)]_2$

To a solution of 0.681 g (2.82 mmol) of $Cu(NO_3)_2 \cdot 3H_2O$ in 25 cm^3 of methanol was added 0.30 cm^3 (2.82 mmol) of diMeen, followed by a dropwise addition of 0.49 g (6.05 mmol) of KNCO in 3.5 cm^3 of water. The mixture was stirred for 30 min and the solid obtained was filtered, washed with ether and dried *in vacuo*. Recrystallization from methanol gave blue crystals suitable for X-ray analysis. The elemental analysis results were in agreement with the proposed formula.

IR spectrum

The IR spectrum of the title complex was recorded as CsI pellets on a Carl Zeiss Specord 75 IR spectrophotometer.

Crystal structure determination of $[Cu(NCO)_2(diMeen)]_2$

Crystal data: $C_{12}H_{24}Cu_2N_8O_4$, $M = 471.08$, monoclinic, space group $P2_1/c$, $a = 12.216(2)$,

$b = 10.662(1)$, $c = 14.997(4)$ Å, $\beta = 96.09(3)°$, $V = 1942.29(9)$ Å^3, $Z = 4$, $D_c = 1.61$ g cm^{-3}, λ(Mo-K_α) = 0.71073 Å, $\mu = 21.44$ cm^{-1}, $F(000) = 968$.

A dark-blue single crystal of approximate dimensions 0.125 × 0.3 × 0.3 mm was used in data collection on an Enraf-Nonius CAD-4 diffractometer, using graphite monochromated Mo-K_α radiation. Twenty-five reflections ($12 < \theta < 19°$) were used for least-squares determination of the cell constants, and 2286 reflections with $I > 3\sigma(I)$ were used in the structure determination and refinement. The structure was solved by direct methods[6] and difference Fourier synthesis,[7] using atomic scattering factors from reference 8. Refinement by least-squares minimized $\Sigma_w(|F_o| - |F_c|)^2$; atomic coordinates, anisotropic thermal parameters and scale factor refined; isotropic thermal parameters for H atoms located geometrically.[7] Final $R = 0.0429$. Lists of atomic parameters, observed and calculated structure factors, and anisotropic thermal coefficients for all atoms have been deposited with the Editor as supplementary material.

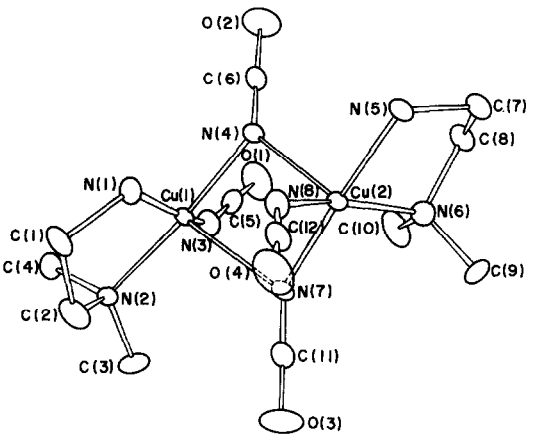

Fig. 1. Molecular structure of $[Cu(NCO)_2(diMeen)]_2$.

RESULTS AND DISCUSSION

The IR spectrum of $[Cu(NCO)_2(diMeen)]_2$ showed absorption bands for coordinated cyanate groups[9–11] at 2210w, 2170s, νCN; 1185m, νCO; 645m and 615w, δNCO, cm^{-1}. In the spectrum, the occurrence of two bands assignable to the νCN vibrational mode suggested the presence of cyanate groups with differing modes of coordination. In particular the large splitting of 30 cm^{-1} observed for δNCO indicated the presence of at least one bridging cyanate group.

The X-ray diffraction study confirmed that the title compound is in fact dimeric. The structure of the complex molecule with the atom-numbering scheme is shown in Fig. 1. Selected bond lengths and bond angles are given in Table 1. Each copper atom is surrounded by five nitrogen atoms belonging to two bridging cyanates, one terminal cyanate and two diMeen nitrogens. The coordination geometry for each metal is that of a square-based pyramid, with the bridging cyanato nitrogens occupying the apical positions in both cases. The copper atoms are displaced from the basal planes made up of N(1), N(2), N(3), N(4); and N(5), N(6), N(7), N(8) by only 0.161(1) and 0.194(1) Å, respectively, and although the basal planes are crystallographically parallel, the two halves of the dimer are not related by a centre of symmetry. The angles between the apical and the basal nitrogens of the pyramids vary from 82.2° to 102°, about the theoretical value of 90°. These angles and those within the metal and the nitrogens of the basal plane relate closely to those found in the complex $[Cu(N_3)_2(tMeen)]_2$, where the geometry around the copper atoms is similar.[12]

It is instructive at this point to compare the different polyhedra formed by the metal and the nitrogen atoms of the title compound and those of the related $[Cu(N_3)_2(tMeen)]_2$ and $[Cu(N_3)_2(diEten)]_2$. In the tMeen complex two azido groups bridge the metals in an "end-to-end" fashion resulting in a very long Cu...Cu distance of 5.004 Å, whereas for the diEten compound[4] two N_3 groups are "end-on" bridging with a short Cu...Cu distance of 3.37 Å. Unlike the present complex, $[Cu(N_3)_2(diEten)]_2$ displays a centre of symmetry, and its overall structure is better understood if the copper atoms are placed in the centre of trigonal bipyramids, with the nitrogen of the bridging azide and that of the NH_2 end of diEten at the axial sites. In this complex the Cu...NH_2 distance is smaller than the Cu...NEt_2 distance, which is the opposite of that expected if purely inductive effects were taken into account, and it is interesting that the same trend is again observed for $[Cu(NCO)_2(diMeen)]_2$. In this latter complex, the presence of cyanate rather than azido groups forced such a distortion that the compound entirely lost its centre of symmetry by allowing the NH_2 ends of the diMeen ligands to be on the same side of the dimer. This effect may be of electronic origin, caused by the replacement of the azide by cyanate as the pseudohalogen, rather than by the change from diEten to diMeen as the chelating ligand. Curiously, the net effect is a further shortening of the Cu...Cu distance in $[Cu(NCO)_2(diMeen)]_2$ to 3.2464(9) Å; this fine interplay of electronic effects caused by pseudohalide substitution might be further enlightened by the structural details of a mixed

Table 1. Relevant distances (Å) and angles (°) for $[Cu(NCO)_2(diMeen)]_2$

Cu(1)—Cu(2)	3.2464(9)	Cu(2)—N(8)	1.976(5)
Cu(1)—N(1)	2.004(4)	C(5)—O(1)	1.186(8)
Cu(1)—N(2)	2.057(4)	C(6)—O(2)	1.183(9)
Cu(1)—N(3)	1.936(5)	C(11)—O(3)	1.191(9)
Cu(1)—N(4)	2.028(5)	C(12)—O(4)	1.201(9)
Cu(1)—N(7)	2.466(5)	N(3)—C(5)	1.140(8)
Cu(2)—N(4)	2.346(5)	N(4)—C(6)	1.133(8)
Cu(2)—N(5)	2.003(4)	N(7)—C(11)	1.157(8)
Cu(2)—N(6)	2.085(5)	N(8)—C(12)	1.143(8)
Cu(2)—N(7)	1.982(5)		
N(1)—Cu(1)—N(2)	84.5(2)	N(4)—Cu(2)—N(8)	100.5(2)
N(1)—Cu(1)—N(3)	162.7(2)	N(5)—Cu(2)—N(6)	83.5(2)
N(1)—Cu(1)—N(4)	87.6(2)	N(5)—Cu(2)—N(7)	175.7(2)
N(1)—Cu(1)—N(7)	95.1(2)	N(5)—Cu(2)—N(8)	90.0(2)
N(2)—Cu(1)—N(3)	92.4(2)	N(6)—Cu(2)—N(7)	93.1(2)
N(2)—Cu(1)—N(4)	172.1(2)	N(6)—Cu(2)—N(8)	160.2(2)
N(2)—Cu(1)—N(7)	99.0(2)	N(7)—Cu(2)—N(8)	92.4(2)
N(3)—Cu(1)—N(4)	95.0(2)	N(3)—C(5)—O(1)	178.0(7)
N(3)—Cu(1)—N(7)	102.2(2)	N(4)—C(6)—O(2)	178.3(7)
N(4)—Cu(1)—N(7)	82.2(2)	N(7)—C(11)—O(3)	178.1(7)
N(4)—Cu(2)—N(5)	96.8(2)	N(8)—C(12)—O(4)	177.8(7)
N(4)—Cu(2)—N(6)	98.9(2)	Cu(1)—N(4)—Cu(2)	95.5(2)
N(4)—Cu(2)—N(7)	86.3(2)	Cu(1)—N(7)—Cu(2)	93.1(2)

azido–cyanato copper dimer which is presently under investigation.[13]

As to other cyanato complexes, $[Cu(NCO)_2(diMeen)]_2$ shows longer Cu...N distances for the nitrogens of the bridging groups, but the distances compare well with those of another copper complex which contains 2,2-lut[14] and to those of the interesting $[Cu_2(C_{17}H_{22}N_4O)(C_2H_3O_2)(NCO)][PF_6]$.[15]

Acknowledgements—We thank CNPq, FAPESP and FINEP for financial support.

REFERENCES

1. J. Z. Schpector, E. E. Castellano, G. Oliva, A. E. Mauro and M. R. Roveri, *Acta Cryst.* 1985, **C41**, 204.
2. J. Z. Schpector, E. E. Castellano, A. E. Mauro and M. R. Roveri, *Acta Cryst.* 1986, **C42**, 302.
3. S. I. Klein, A. E. Mauro, M. A. Momesso, C. C. Porta, R. H. A. Santos and M. T. P. Gambardella, *Química Nova* 1987, **10**, 314.
4. O. L. Casagrande, S. I. Klein, A. E. Mauro and K. Tomita, *Trans. Met. Chem.* 1989, **14**, 45.
5. P. Chaudhuri, K. Oder, K. Wirghardt, B. Nuber and J. Weiss, *Inorg. Chem.* 1986, **25**, 2818.
6. G. M. Sheldrick, SHELX 86. Program for Crystal Solution, University of Göttingen, F.R.G. (1986).
7. G. M. Sheldrick, SHELX 76. A Program for Crystal Structure Determination, University of Cambridge, U.K. (1976).
8. *International Tables for X-ray Crystallography*, Vol. 4. Kynoch Press, Birmingham (1974).
9. K. Nakamoto, *Infrared Spectra of Inorganic and Coordination Compounds*. Wiley Interscience, New York (1970).
10. J. Nelson and S. M. Nelson, *J. Chem. Soc.* 1969, 1597.
11. J. L. Burmeister and T. P. O'Sullivan, *Inorg. Chim. Acta* 1969, **3**, 479.
12. I. B. Waksman, S. Sikorav and O. Kahn, *J. Cryst. Spectrosc. Res.* 1983, **13**, 303.
13. A. E. Mauro (Manuscript in preparation).
14. F. Valach, M. Dunaj-Jurco, J. Garaj and M. Hvastijová, *Coll. Czech. Chem. Commun.* 1974, **39**, 380.
15. M. L. Boillot, O. Kahn, C. J. O'Connor, J. Gouteron, S. Jeannin and Y. Jeannin, *J. Chem. Soc., Chem. Commun.* 1985, 178.

Polyhedron Vol. 9, No. 24, pp. 2941–2952, 1990
Printed in Great Britain

0277–5387/90 $3.00+.00
© 1990 Pergamon Press plc

PREPARATION AND CHARACTERIZATION OF $M_2(SeAr')_6$ AND MIXED LIGAND $M_2(OR)_2(SeAr')_4$ SPECIES (M = Mo, W)

MALCOLM H. CHISHOLM,* JOHN C. HUFFMAN, IVAN P. PARKIN and WILLIAM E. STREIB

Department of Chemistry and Molecular Structure Center, Indiana University, Bloomington, IN 47405, U.S.A.

(*Received* 22 *June* 1990; *accepted* 10 *August* 1990)

Abstract—Toluene solutions of $M_2(NMe_2)_6$ (M = Mo, W) react with mesitylene selenol (Ar'SeH) to give $M_2(SeAr')_6$ complexes. $Mo_2(OR)_6$ (R = ^{t}Bu, $CH_2{}^t$Bu) react with excess (> 6 fold) Ar'SeH to give $Mo_2(SeAr')_6$, whilst $W_2(OR)_6(py)_2$ (R = ^{i}Pr, $CH_2{}^t$Bu) react with excess (> 6 fold) Ar'SeH to give $W_2(OR)_2(SeAr')_4$. Reaction of $Mo_2(OPr^i)_6$ with Ar'SeH produces $Mo_2(OPr^i)_2(SeAr')_4$ which crystallizes in two different space groups. These arene–selenato complexes are air-stable and insoluble in common organic solvents. X-ray crystallographic studies revealed that the $Mo_2(SeAr')_6$ and $W_2(SeAr')_6$ compounds are isostructural in the solid state and adopt ethane-like staggered configurations with the following important structural parameters, M—M (W—W/Mo—Mo) 2.3000(11)/2.2175(13) Å, M—Se 2.430 (av.)/2.440 (av.) Å, M—M—Se 97.0° (av.)°. In the solid state $W_2(O^iPr)_2(SeAr')_4$ adopts the anti-configuration with crystallographically imposed C_i symmetry and W—W 2.3077(7) Å, W—Se 2.435 (av.) Å, W—O 1.858(6) Å; W—W—Se 100.27(3)°, 93.8(3)° and W—W—O 108.41(17)°. $Mo_2(OPr^i)_2(SeAr')_4$ crystallizes in both $P\bar{1}$ and $A2/a$ space groups in which the molecules are isostructural with each other and the tungsten analogue. Important bond lengths and angles are Mo—Mo 2.180(24) Å, Mo—Se 2.432(av.) Å, Mo—O 1.872(9) Å, Mo—Mo—Se 99.39(9)°, 94.71(8)°, Mo—Mo—O 107.55(28)°.

The synthesis of metal–metal multiply bonded compounds has been extensively explored, especially for molybdenum and tungsten.[1] Indeed M_2R_6 (M = Mo, W) compounds are formed for a range of ligands R = alkoxy, amido, thiolate and various mixed species of general formula $M_2R'_2R_4$, e.g. $M_2Cl_2(NMe_2)_4$.[2–4]

Previously, there have been a few reports of Cr, Mo and W aryl selenolate complexes.[5] Two examples which contain μ_2 bridging SePh ligands have been structurally determined by X-ray crystallography,[6,7] namely, $(C_7H_7)Mo(\mu\text{-SePh})_3Mo(CO)_3$ and $(\eta^5\text{-}C_5H_5)(NO)Cr(\mu\text{-SePh})_2Cr(NO)(\eta^5\text{-}C_5H_5)$. Aryl selenium and tellurium complexes of general formula $[M(C_5H_5)_2(EPh)_2]$ (M = Ti, V, Nb, Mo, W; E = S, Se, Te) have been characterized by elemental analysis and IR spectroscopy and are thought to have terminal aryl-chalcogen ligands.[8] One tungsten compound containing an aryl-selenolate ligand has been studied by X-ray crystallography, $(\eta^7\text{-}C_7H_7)W(CO)_2(SePh)$, and contains a terminal aryl-selenide ligand.[7]

Homoleptic complexes supported by selenolate ligands are known[9–14] for mercury $[Ph_4P][Hg(SePh)_3]$, lead $[Ph_4As][Pb(SePh)_3]$, tin $[Sn(SePh)_4]$ and silicon $[(Si(SePh)_3)_2]$. These species are suggested to have only terminal selenolate ligands. Molybdenum and tungsten compounds of formulation $[OM(SePh)_4]$ and $[M_2O_2(ER)_6OMe]^-$ (R = S, Se; R = aryl) have been made and characterized by UV–vis, EPR and elemental analysis.[14,15] An X-ray crystal structure of the thiolate derivative indicates that the dinuclear species has one bridging μ_2 thiolate group and two μ_2 oxo species, with the remainder of the ligands being terminal.[16,17] The selenide derivatives of these complexes have inferred structures based upon the thiolato chemistry.

Here we report the synthesis and characteriz-

* Author to whom correspondence should be addressed.

ation of homoleptic molybdenum and tungsten multiply bonded compounds supported by mesitylene selenol ligands. The choice of the mesityl group was influenced by considerations of steric bulk and C—S bond cleavage.[3,4] The preparations of $M_2(OR)_2(SeAr')_4$ (M = Mo, W) are also presented. To our knowledge these are the first examples of homoleptic transition metal selenolate complexes.[5,18]

RESULTS AND DISCUSSION

Syntheses and characterization

$M_2(SeAr')_6$ and $M_2(SeAr')_4(OR)_2$ compounds. All the reactions were performed at room temperature in toluene or toluene–hexane mixtures. Reaction of $M_2(NMe_2)_6$ (M = Mo, W) with excess (> 6 fold) Ar'SeH produced the completely substituted $M_2(SeAr')_6$ complex, eq. (2) (N.B. Ar', here and after is used for the mesitylene ligand; 2,4,6-trimethyl benzene):

$$M_2(NMe_2)_6 + 6Ar'SeH = M_2(SeAr')_6 + 6HNMe_2. \quad (1)$$

$Mo_2(OR)_6$ (R = ^{t}Bu, $CH_2{}^t$Bu) also reacts with Ar'SeH to give complete substitution, eq. (2). The alcohol generated can be detected in the ^{1}H NMR spectra of the filtrate:

$$Mo_2(OR)_6 + 6Ar'SeH = Mo_2(SeAr')_6 + 6HOR. \quad (2)$$

Surprisingly, reaction of $W_2(OR)_6 \cdot py_2$ (R = $CH_2{}^t$Bu, ^{i}Pr), $W_2(O^t Bu)_6$ or $Mo_2(OR)_6$ (R = ^{i}Pr, ^{c}Hex) with excess (> 6 fold) of mesitylene selenol does not produce the fully substituted species, but rather the tetrasubstituted species $M_2(OR)_2(SeAr')_4$, eq. (3):

$$W_2(OR)_6py_2 + 4Ar'SeH = W_2(OR)_2(SeAr')_4 + 4HOR + 2py \quad (3a)$$

$$Mo_2(OR)_6 + 4Ar'SeH = Mo_2(OR)_2(SeAr')_4 + 4HOR. \quad (3b)$$

The reason for the complete substitution in the amide case for both Mo and W [eq. (1)], when compared to the analogous sulphur chemistry is not obvious.[3] One explanation could be the complete insolubility of the products in eq. (3) in common organic solvents, thus providing a driving force for the reaction.

The reaction of $M_2(OR)_6$ with a six-fold excess of mesitylene selenol leads to complete substitution at room temperature in the case of some molybdenum compounds (OR = ^{t}Bu, $CH_2{}^t$Bu) but stops at the tetrasubstituted tungsten species. The complete substitution at room temperature in the molybdenum case (OR = ^{t}Bu, $CH_2{}^t$Bu) is surprising in the light of the corresponding thiolate chemistry where forcing conditions (80°C) are required. Possibly the larger covalent radius of selenium compared with sulphur (0.09 Å) is sufficient to alter the relative reactivity of the intermediate $M_2(EAr')_x(OR)_{6-x}$ (x = 1–5) compounds (E = S, Se). The increased acidity of a selenol compared with a thiol would also facilitate the generation of the selenolate.

In general, the reaction to form the $Mo_2(SeAr')_6$ species occurs faster for amide [eq. (1)] than alkoxide replacement [eq. (2)]. The rate of reaction (as judged by the rate of product precipitation) is dependent on the bulk of the alkoxide with the ^{t}OBu derivative requiring less time for reaction than the $OCH_2{}^t$Bu derivative [eq. (2)]. This indicates a degree of steric control in the reaction. The tungsten reaction to form $W_2(OR)_2(SeAr')_4$ is much slower than the reaction to form the fully substituted molybdenum species. At room temperature little reaction occurs between $W_2(OBu^t)_6$ and mesitylene selenol after 6 days in hydrocarbon solvents. However a reaction time of 2 weeks in THF followed by cooling to −20°C for 30 days allowed isolation of $W_2(O^tBu)_2(SeAr')_4$.

Reaction of $Mo_2(OR)_6$ (R = ^{t}Bu, $CH_2{}^t$Bu) with Ar'SeH goes to complete substitution and formation of $Mo_2(SeAr')_6$ [eq. (2)], whilst for R = Pr^i and cyclohexyl (^{c}Hex), the tetrasubstituted species $Mo_2(SeAr')_4(OR)_2$ are formed. This is probably due to the solubility of the tetrasubstituted derivative. For R = ^{i}Pr and ^{c}Hex the tetrasubstituted species are very insoluble, whilst a purported $Mo_2(SeAr')_4(OR)_2$ (R = ^{t}Bu, $CH_2{}^t$Bu) species would be expected to be more soluble (based on the relative solubilities of $Mo_2(OBu^t)_6$, $Mo_2(OCH_2{}^tBu)_6$ and $Mo_2(O^cHex)_6$ in hydrocarbon solvents).

Treatment of a solution of $Mo_2Cl_2(NMe_2)_4$ in toluene with excess mesitylene selenol also leads to $Mo_2(SeAr)_6$ formation, eq. (4). The yields of the product are comparable to those obtained by the other routes, although the microanalysis is slightly inferior.

$$Mo_2Cl_2(NMe_2)_4 + 6HSeAr' = Mo_2(SeAr')_6 + 2HCl + 4HNMe_2. \quad (4)$$

The $M_2(SeAr')_6$ and $M_2(OR)_2(SeAr')_4$ (M = Mo, W) compounds were characterized by IR spectroscopy, melting points and X-ray crystallography. Unfortunately, the insolubility precluded an NMR study of the $M_2(SeAr')_6$ product. However,

the mixed alkoxide/selenolate species $M_2(OR)_2(SeAr')_4$ are slightly soluble in THF, chloroform or toluene to about 15 mg in 100 cm^3 of solvent.

The homoleptic compounds $M_2(SeAr')_6$ are relatively air-stable and show little detectable physical changes (IR/m.p./colour) even when stored in the light over 5 months. They are insoluble in and show no decomposition by water. Addition of 6 M HNO_3 to the hexaselenolates causes slow decomposition but requires a long time for reaction due to the high crystallinity of the sample. These physical properties are probably attributable to the hydrophobic exterior presented by the mesitylene ligands.

The IR spectra of the hexaselenolates exhibit the expected ligand vibrations due to coordinated mesitylene selenol and a stretch at low frequency at *ca* 285 or 260 cm^{-1} (in the molybdenum and tungsten cases, respectively), which can be assigned to M—Se vibrations. The mixed $M_2(SeAr')_4(OR)_2$ species exhibit vibrations due to both the selenolate and alkoxide ligands.

The ^1H NMR spectra of $M_2(SeAr')_4(OR)_2$ (M = Mo, R = Pr^i, cyclohexyl; M = W, R = Pr^i, Bu^t, neopentyl) measured at room temperature show the expected resonances for both the selenolate and alkoxide ligands in the correct integral ratios and are consistent with the anti-rotamer. The spectra required a long accumulation time because of the low solubility of the materials.

$M_2(SeAr')_2(NMe_2)_4$. The reaction between $M_2Cl_2(NMe_2)_4$ and mesitylene selenium Grinard Ar'SeMgBr in THF leads to the precipitation of yellow crystals, $M_2(SeAr')_2(NMe_2)_4$ in a 40% yield based on eq. (5). These compounds are slightly soluble in THF–toluene and chloroform, and are air and light sensitive, especially in solution. The ^1H NMR spectrum of $M_2(ScAr')_2(NMe_2)_4$ in benzene reveals only the anti-rotamer. The corresponding thiolate $Mo_2(SAr')_2(NMe_2)_4$ adopts an ethane staggered geometry about the metal–metal triple bond with the aryl thiolato ligands in an anti-configuration in the solid state. Attempts to obtain an X-ray determination of the selenolate derivative were hampered by problems of twinning. The IR spectra of $M_2(SeAr')_2(NMe_2)_4$ have bands directly assignable to the amide and coordinated selenolate ligands.

$$M_2Cl_2(NMe_2)_4 + 2Ar'SeMgBr = M_2(SeAr')_2(NMe_2)_4 + 2MgBrCl. \quad (5)$$

Attempted preparations of phenylselenolates. The reactions between $M_2(NMe_2)_6$ or $M_2(OR)_6 \cdot L_2$ (M = Mo, W, L = py, $HNMe_2$) and selenophenol (HSePh) at room temperature in hydrocarbon solvents produce a purple precipitate for molybdenum and a black solid for tungsten. The reactions with $M_2(NMe_2)_6$ produce ammonium salts as evidenced by the IR spectra of both the molybdenum and tungsten products. In the molybdenum case the reaction is extremely rapid and the product formulated as having an empirical formula $[Mo_4(SePh)_{10}Se_2]H_2NMe_2$ on the basis of microanalysis and IR spectroscopy. The latter showed vibrations associated with the selenophenol ligand as well as the $Me_2NH_2^+$ ion at 2700 and 2400 cm^{-1} ($\bar{\nu}$ NH) for the complex.[18] The product is also air-stable (no change in IR spectrum over 1 month at room temperature in air) and insoluble in organic solvents. The reaction between $Mo_2(O^tBu)_6$ and phenylselenol also produces a purple solid which has a very similar IR to $[Mo_4(SePh)_{10}Se_2]H_2NMe_2$, but missing the vibrations associated with the $Me_2NH_2^+$ ion. However, new bands at 3200 and 1630 cm^{-1}, as well as OBu^t vibrations suggest hydrogen bonding involving $[H_2O^tBu]^+$.

The reaction between $W_2(NMe_2)_6$ and selenophenol proceeded in an analogous manner to the molybdenum compounds and produced a black solid, the microanalysis and IR of which are consistent with the empirical formula $[W_4Se_4(SePh)_{10}]H_2NMe_2$. This material is insoluble in common solvents once isolated. If the reaction to form this material is performed in THF the tungsten species is not precipitated until after 2 days, compared with 3 h for reactions in hydrocarbon solvents.

The solubility of the compounds produced in the reaction of non-sterically protected selenophenols with tungsten and molybdenum amides and alkoxides was not improved by the use of *para*-substituted selenophenols such as *p*-$EtOC_6H_6$—SeH.

Solid state structures of $M_2(SeAr')_6$ (M = Mo, W)

Crystal data for the $M_2(SeAr')_6$ compounds are given in Table 1; selected bond lengths and angles in Table 2. An ORTEP view of the molecule showing the atom numbering scheme used in the tables is shown in Fig. 1 for $W_2(SeC_6H_2Me_3)_6$, and a view down the Mo—Mo axis in $Mo_2(SeC_6H_2Me_3)_6$ is given in Fig. 2.

The sample of $W_2(SeAr')_6$ that was examined crystallographically, crystallized from the reaction involving $W_2(NMe_2)_6$ and Ar'SeH on standing at room temperature for 4 days. No included solvent was present and the compound formed with a crystallographically imposed centre of symmetry in the space group $P\bar{1}$.

The sample of $Mo_2(SeC_6H_2Me_3)_6$ used for X-ray analysis, crystallized from the reaction solution involving $Mo_2(O^tBu)_6$ with excess mesitylene

Table 1. Summary of crystal data

	I	II	III	IV	V
Empirical formula	$W_2C_{54}H_{66}Se_6$	$Mo_2C_{54}H_{66}Se_6$	$W_2C_{42}H_{58}O_2Se_4$	$Mo_2C_{42}H_{58}Se_4O_2$	$Mo_2C_{42}H_{58}Se_4O_2$
Colour of crystal	Brown	Red	Red	Yellow	Red–Orange
Crystal dimensions (mm)	$0.14\times0.16\times0.28$	$0.25\times0.25\times0.25$	$0.30\times0.30\times0.16$	$0.25\times0.25\times0.25$	$0.08\times0.10\times0.52$
Space group	$P\bar{1}$	$P\bar{1}$	$P\bar{1}$	$P\bar{1}$	$A2/a$
Cell dimensions					
Temperature (°C)	−155	−155	−155	−155	−155
a (Å)	11.727(4)	11.747(2)	10.805(1)	10.846(2)	23.971(7)
b (Å)	11.765(3)	11.725(2)	11.434(1)	11.355(2)	8.692(2)
c (Å)	11.158(3)	11.139(2)	9.428(1)	9.396(1)	22.001(7)
α (°)	95.66(1)	95.49(1)	98.28(1)	98.68(1)	
β (°)	95.93(2)	96.11(1)	110.62(1)	110.57(1)	110.10(1)
γ (°)	118.27(2)	118.20(1)	88.75(1)	88.51(1)	
Z (molecules/cell)	1	1	1	1	4
Volume (Å^3)	1329.32	1325.59	1078.26	1070.63	4489.73
Calculated density (g cm^{-3})	1.944	1.730	1.969	1.710	1.613
Wavelength (Å)	0.71069	0.71069	0.71069	0.71069	0.71069
Molecular weight	1556.58	1380.76	1278.46	1102.64	1102.64
Linear absorption coefficient (cm^{-1})	85.178	45.741	88.206	39.710	37.920
Detector to sample distance (cm)	22.5	22.5	22.5	22.5	22.5
Sample to source distance (cm)	23.5	23.5	23.5	23.5	23.5
Average Ω scan width at half-height	0.25	0.25	0.25	0.25	0.25
Scan speed (° min^{-1})	8.0	8.0	8.0	4.0	4.0
Scan width (+dispersion)	2.0	2.0	2.0	2.0	2.0
Individual background (s)	3	3	4	6	8
Aperture size (mm)	3.0×4.0	3.0×4.0	3.0×4.0	3.0×4.0	3.0×4.0
2θ Range (°)	6–45	6–45	6–45	6–45	6–45
Total number of reflections collected	3552	4398	3023	3369	6447
Number of unique intensities	3480	3467	2834	2797	2938
Number with $F > 0.0$	3306	3256	2758	2603	2582
Number with $F > 2.33\sigma(F)$	3142	2936		2415	2302
Number with $F > 3^*\sigma(F)$			2417		
$R(F)$	0.0443	0.0417	0.0330	0.056	0.0703
$R_w(F)$	0.0436	0.0415	0.0357	0.0559	0.0634
Goodness of fit for the last cycle	1.424	1.037	1.910	1.415	1.515
Maximum δ/σ for the last cycle	0.18	0.12	0.049	0.05	0.35

Table 2. Selected bond distances (Å) and angles (°) for the $M_2(SeC_6H_2Me_3)_6$ molecules

		Distance	
A	B	W	Mo
M(1)	M(1)′	2.3000(11)	2.2175(13)
M(1)	Se(2)	2.4214(15)	2.4324(11)
M(1)	Se(3)	2.4278(14)	2.4385(11)
M(1)	Se(4)	2.4457(16)	2.4568(12)
Se(2)	C(5)	1.951(11)	1.938(7)
Se(3)	C(14)	1.956(11)	1.956(7)
Se(4)	C(23)	1.957(11)	1.956(7)

			Angle	
A	B	C	W	Mo
M(1)	M(1)′	Se(2)	96.46(5)	96.56(5)
M(1)	M(1)′	Se(3)	96.92(4)	97.18(5)
M(1)	M(1)′	Se(4)	97.68(5)	98.17(5)
Se(2)	M(1)	Se(3)	116.91(5)	116.70(4)
Se(2)	M(1)	Se(4)	120.13(5)	120.04(4)
Se(3)	M(1)	Se(4)	118.54(5)	118.48(4)
M(1)	Se(2)	C(5)	104.3(3)	104.64(22)
M(1)	Se(3)	C(14)	106.1(3)	106.57(22)
M(1)	Se(4)	C(23)	105.6(3)	105.82(21)

selenol in toluene at room temperature overnight. The molybdenum compound was isostructural with the tungsten analogue.

A comparison of the parameters associated with the central $X_3M{\equiv}MX_3$ core in structurally characterized homoleptic alkyls, amides, alkoxides and thiolates has been made previously.[4] For related molecules the W—W distance is longer by *ca* 0.08 Å than the Mo—Mo distances.[3,4] This difference is found in the $M_2(SeAr')_6$ compounds.

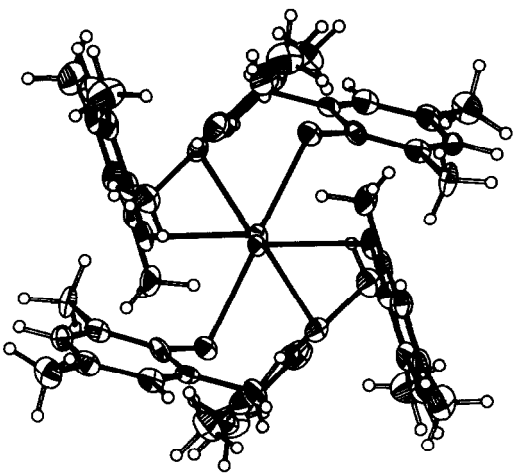

Fig. 2. ORTEP view down the Mo—Mo axis in $Mo_2(SeAr')_6$.

The M—Se distance in $M_2(SeAr')_6$ is (within the 3 σ criteria) the same for Mo and W, 2.43(av.) Å. This M—Se distance is significantly shorter than that observed in the mononuclear $(\eta^7\text{-}C_7H_7)W(CO)_2SePh$ complex, 2.588(2) Å, and the dimeric $(C_6H_7)Mo(\mu\text{-}SePh)_3Mo(CO)_3$ complex, *ca* 2.56 (av.) Å.[6,7] The metal–selenium bond lengths are also shorter than that in the "diselenide complex" $[W_2(CO)_{10}Se_4][SbF_4]_2$, 2.626(2) and 2.631(2) Å,

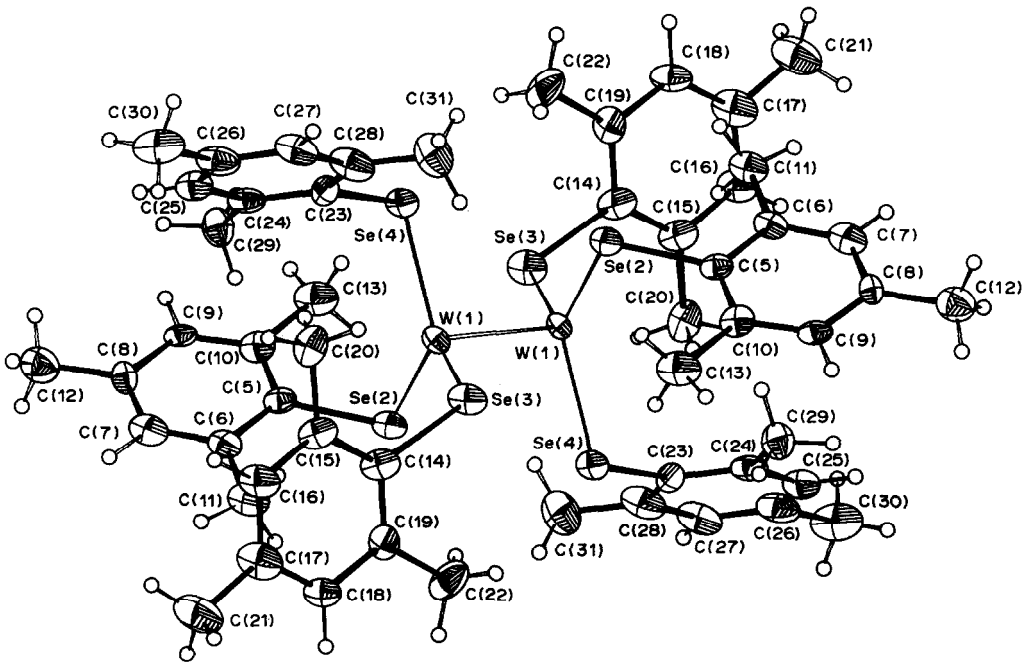

Fig. 1. ORTEP view of $W_2(SeAr')_6$.

respectively.[16] Although these distances are not directly comparable due to differing electronic and steric effects produced by different sets of ligands, the relative shortness of the M—Se bonds in the $M_2(SeAr)_6$ complexes is suggestive of metal–selenium π-bonding. The presence of the methyl groups on the mesitylene ligand probably help to stop bridge formation in the $M_2(SeAr)_6$ complexes.

The M—M—X angles in $M_2(SeAr')_6$ span a small range 96.4–98.2°, and are essentially the same for both the tungsten and molybdenum complexes. These angles are more acute than those in the homoleptic alkyl, amide or alkoxide M_2R_6 complexes, where 100–103° is the normal.[1] The thiolate $M_2(SAr')_6$ complexes[4] have M—M—X angles of comparable magnitude to the selenolate complexes; Mo—Mo—S = 96.6(2)°, W—W—S = 97.4(av.)°. The smaller angles for the selenates and thiolates can be explained in terms of the arrangement of all six mesityl groups, which are distal with respect to the central M—M core. In a typical alkoxide case, e.g. $Mo_2(OCH_2Bu^t)_6$,[1] four groups are distal and two are proximal generating larger and smaller M—M—X angles, with the average angle being larger than the thiolate or selenolate case.

The Mo—Mo distance in $Mo_2(SeAr')_6$ of 2.2176(13) Å is typical of those found in $(Mo{\equiv}Mo)^{6+}$ containing compounds (d = 2.15–2.23 Å) and slightly shorter than the corresponding $Mo_2(SAr')_6$ complex at 2.228(1) Å. The W—W bond in $W_2(SeAr')_6$ is also typical of a $(W{\equiv}W)^{6+}$ moiety at 2.300 Å, and is further significantly shorter (0.012 Å) than the corresponding thiolate analogue.[4]

The M—Se distances are longer (by 0.11 Å) in $M_2(SeAr')_6$ than the M—S bond lengths in $M_2(SAr')_6$ complexes. This is not surprising as selenium has a larger covalent radius than sulphur (1.11 Å compared with 1.02 Å). For the $M_2(SAr')_6$ molecules a case of substantial M—S π-bonding has been forwarded on the basis of the short Mo—S distances observed when compared with the relevant covalent radii.[3] The case for selenium to metal π-bonding can be similarly made, especially since sulphur and selenium have the same electronegativities on the Pauling scale.[20] In general, the covalent radius of selenium is 0.09 Å greater than for sulphur in analogous compounds. The M—S distances in the thiolate analogues $M_2(SAr')_6$ are 0.15 Å shorter than those expected on the basis of covalent radii. This has led to the suggestion of substantial π character in the metal to sulphur bond.[3,4] In the $M_2(SeAr')_6$ species, the M—Se bond lengths are 0.11 Å longer than the sulphur analogue. This indicates that there is a contraction of 0.13 Å in the M—Se bond lengths [0.15+0.09−0.11] in the homoleptic species that may be attributable to the existence of Se-to-M π-bonding. Other reported M—Se bond lengths include 2.512(3) Å in $Sn(SePh)_4$ and 2.727(1) Å in $[Ph_4As][Pb(SePh)_3]$.[11,12]

$M_2(SeAr')_4(O^iPr)_2$

Crystal data for the $M_2(SeAr')_4(O^iPr)_2$ molecules are given in Table 1; selected bond lengths and angles in Table 3. An ORTEP view of the tungsten derivative showing the atom numbering scheme used in the tables is given in Fig. 3, and a stereo-

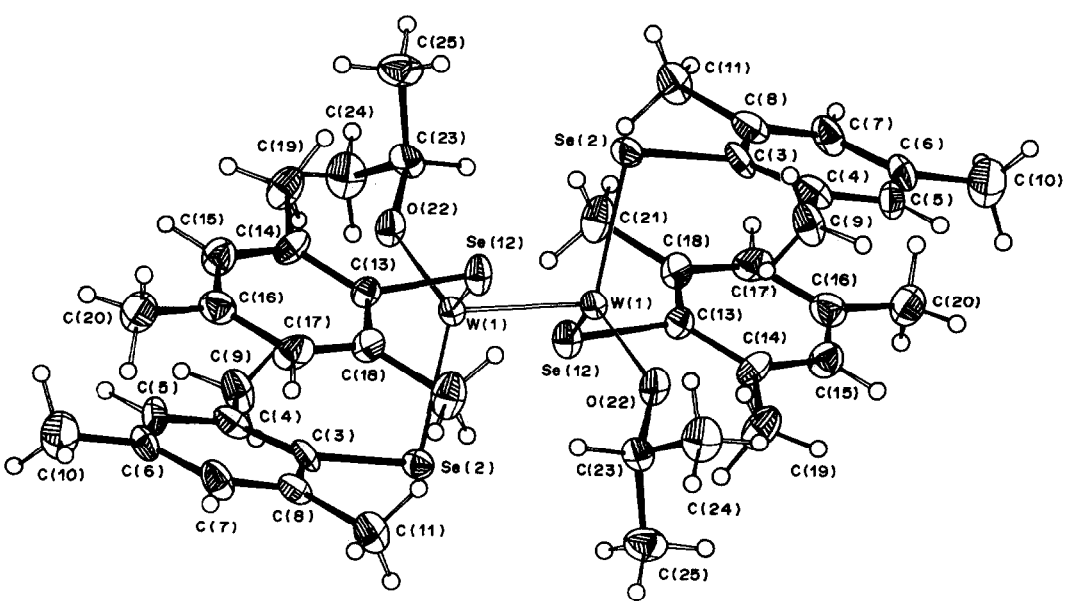

Fig. 3. ORTEP view of $W_2(SeAr')_4(OPr^i)_2$.

Table 3. Selected bond distances (Å) and bond angles (°) for $M_2(SeC_6H_2Me_3)_4(O^iPr)_2$ molecules

		Distance		
A	B	W	Mo[a]	Mo'[b]
M(1)	M(1)'	2.3077(7)	2.2192(17)	2.2180(24)
M(1)	Se(2)	2.4303(10)	2.4353(14)	2.4281(21)
M(1)	Se(12)	2.4410(10)	2.4476(14)	2.4427(19)
M(1)	O(22)	1.858(6)	1.873(6)	1.872(9)
Se(2)	C(3)	1.955(9)	1.938(10)	1.954(13)
Se(12)	C(13)	1.959(9)	1.955(9)	1.947(13)
O(22)	C(23)	1.449(10)	1.435(11)	1.441(16)

			Angle		
A	B	C	W	Mo[a]	Mo'[b]
M(1)'	M(1)	Se(2)	100.27(3)	100.17(6)	99.39(9)
M(1)'	M(1)	Se(12)	93.85(3)	94.04(5)	94.71(8)
M(1)'	M(1)	O(22)	108.41(17)	108.55(20)	107.55(28)
Se(2)	M(1)	Se(12)	120.14(3)	119.73(5)	118.59(7)
Se(2)	M(1)	O(22)	111.32(18)	112.68(21)	113.8(3)
Se(12)	M(1)	O(22)	118.43(18)	117.28(2)	117.9(3)
W(1)	Se(2)	C(3)	90.07(25)	89.9(3)	94.6(4)
W(1)	Se(12)	C(13)	107.72(25)	106.7(3)	106.0(4)
W(1)	O(22)	C(23)	140.5(5)	139.8(6)	140.2(8)
Se(2)	C(3)	C(4)	121.2(6)	120.8(7)	119.0(10)
Se(2)	C(3)	C(8)	118.5(6)	120.1(7)	119.0(10)

[a] Yellow plates.
[b] Orange–red needles.

view of the molecule looking down the Mo—Mo bond axis is given in Fig. 4.

The crystal used for X-ray analysis crystallized from the reaction solution of $W_2(OPr^i)_6(py)_2$ with excess ArScH on standing at room temperature. The molecule has a crystallographically imposed centre of inversion in the space group $P\bar{1}$. The mesityl and isopropyl groups are with respect to the W—W bond distal and proximal, respectively, and the structure is very similar to that adopted by $Mo_2(OPr^i)_2(SAr)_4$.

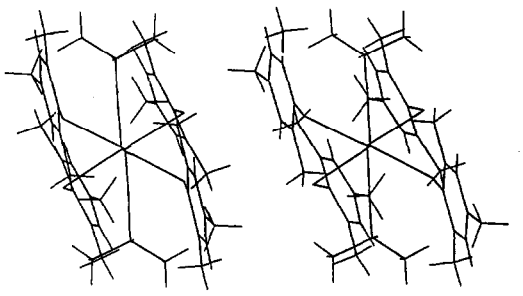

Fig. 4. Stereo-view of $Mo_2(SeAr')_4(OPr^i)_2$ down the Mo—Mo axis.

The crystals of $Mo_2(SeAr')_4(O^iPr)_2$ used for the analysis are crystallized out of the reaction solution of $Mo_2(O^iPr)_6$ with excess (> 6-fold) mesitylene selenol, on cooling the reaction to −20°C after 10 days at room temperature. Two types of crystals were observed from the reaction mixture, yellow plates (10%) and red–orange needles (90%). Both samples were examined crystallographically and found to be $Mo_2(SeAr')_4(O^iPr)_2$. The molecules have a centre of symmetry and were found to be isostructural with each other and the tungsten species $W_2(SeAr')_4(O^iPr)_2$.

The W—W distance of 2.3077(7) Å in $W_2(SeAr')_4(O^iPr)_2$ is typical of a W—W triple bond although slightly longer than the bond length observed in $W_2(SeAr')_6$. The W—Se bond lengths are comparable within the 3σ criteria to those observed in the homoleptic compound. The W—O bond lengths at 1.858(6) Å are slightly shorter than those normally observed in multiple bonded tungsten compounds supported by alkoxide ligands (*ca* 1.94–1.89(av.) Å).[1] This difference is not considered significant as it is comparable to the difference between the bond lengths in $Mo_2(OCH_2{}^tBu)_6$.[1,21]

Thus, the substitution of four alkoxy groups by four areneselenolate ligands has little overall effect on the RO-to-M bonding. As was observed for the homoleptic compounds the W—Se and Mo—Se bond lengths are shorter than expected on the basis of covalent radii, suggestive of Se-to-M π-bonding.

The W—W—O angle at 108.41(17) is close to those observed for other alkoxides. The two W—W—Se angles are significantly different at 93.85(3) and 100.27(3)°, respectively. This pattern was observed for the similar compound $Mo_2(O^iPr)_2(SAr')_4$ which had angles of 95.4(0) and 99.8(0)°.[4]

The Mo—Mo bond distances 2.2192(17) and 2.2180(24) Å in $Mo_2(SeAr')_4(O^iPr)_2$ are normal for triple bonds between molybdenum atoms and equivalent to that in $Mo_2(SeAr')_6$. The other bond lengths and bond angles are essentially the same as those in the tungsten analogue $W_2(SeAr')_4(O^iPr)_2$.

EXPERIMENTAL

All reactions were performed under a nitrogen atmosphere in degassed and distilled solvents. The preparation of $M_2(NMe_2)_6$ (M = Mo, W), $M_2(OR)_6$ (M = Mo, W ; R = $CH_2{}^tBu$)$_3$, ^tBu, ^iPr, ^cHex and $W_2(OR)_6(py)_2$ (R = ^iPr, $CH_2{}^tBu$; L = py, $HNMe_2$) were as previously described.[21-24] Phenyllithium, mesitylene magnesium bromide and selenium metal were purchased from Aldrich Chemical Co. Mesitylene selenol was prepared from the reaction of mesityl Grinard and elemental selenium as described below. ^{1}H NMR spectra were obtained in d^8-THF, $CDCl_3$ or C_6D_6 on a Nicolet 360 spectrometer operating at 360.12 MHz and referenced to internal residual protio THF, chloroform and benzene at 1.73, 7.24 and 7.15 ppm, respectively. Mass spectra were obtained on a Kratos MS450. IR spectra were recorded either as KBr discs or Nujol mulls using a Perkin–Elmer 283 spectrophotometer. Elemental analyses were obtained from Oneida Research Services (Whiteborough, New York).

Mesitylene Selenol

To a solution of mesitylene magnesium bromide (50 cm^3 of 1 M solution in THF) was added over 1 h with stirring grey selenium powder (4.0 g, 50 mmol). The solution was stirred overnight at room temperature with all the selenium dissolving to produce a light-green solution. The solution was hydrolysed by the cautious dropwise addition of water (20 cm^3) followed by 20 cm^3 of 6 N HCl. The upper orange THF layer was collected and dried over anhydrous $MgSO_4$ for 24 h. After filtration from the $MgSO_4$ the THF was removed *in vacuo* to leave a yellow oil (6.8 g, 34.4 mmol, 69%) which was purified by distillation (*ca* 55°C, 1.10^{-4} torr). MS: M^+ = 199; ^{1}H NMR (C_6H_6): δ = 6.67 (s, 2H), 2.18 (s, 6H), 2.04 (s, 3H). IR (KBr plates): 3000br, 2930s, 2900s, 2850sh, 2300w, 1540m, 1435s, 1370m, 1350w, 1270w, 1025s, 870w, 840s, 680s, 540s, 340m cm^{-1}. (Introduction of air helps to provide formation of mesitylene diselenide which crystallizes from the oil on standing.) $(C_6H_2Me_3Se)_2$; MS: M^+ = 396, ^{1}H NMR: δ = 6.69 (s, 4H), 2.31 (s, 12H), 2.03 (s, 6H).

Phenyl Selenol

To a solution of phenyllithium (25 cm^3, 1.8 M solution in cyclohexane–diethyl-ether 80:20) was added THF (5 cm^3) and powdered grey selenium (3.55 g, 0.045 mol). The reaction was stirred for 18 h at room temperature with all the selenium dissolving to give a light-green solution. The solution was hydrolysed by the cautious dropwise addition of water (15 cm^3) (very exothermic reaction), followed by 6 N HCl (15 cm^3). The upper orange layer was decanted and dried over anhydrous $MgSO_4$. Removal of the solvent under vacuum gave selenophenol (4.42 g, 0.27 mmol, 60%), which was purified by distillation at 57°C/8 torr.

[*Caution*: Phenyl and mesitylene selenol are very malodorous and all operations should be performed in a well ventilated hood. The glassware is best cleaned after the reaction by soaking in sodium hypochlorite (4% solution) for 1 day, decanting off the liquid then adding to a KOH–EtOH bath.]

$W_2(SeAr')_6$

$W_2(NMe_2)_6$ (0.100 g, 0.158 mmol) was dissolved in toluene (20 cm^3) at room temperature. Mesitylene selenol (0.250 g, 1.25 mmol) was added dropwise to the stirred solution causing an immediate darkening in colour from yellow to red. The stirring was continued for 5 min then the solution allowed to stand at ambient temperature for 3 days, during which time dark-red–brown crystals of $W_2(SeAr')_6$ (0.154 g, 0.0985 mmol, 62.3%) formed. These were collected by filtration, washed with hexane (20 cm^3) and THF (20 cm$_3$) and air dried. Found: C, 41.7; H, 4.3; N, 0.0. Calc.: C, 42.2; H, 4.2%. IR (KBr disc): 3000m, 2945m, 2895m, 1585w, 1552w, 1520w, 1442vs, 1420vs, 1360m, 1290s, 1161w, 1080w, 1015sh, 1002vs, 940w, 866w, 835vs, 716w, 690w, 554w, 535m, 455w, 400w, 325sh, 315m, 245s cm^{-1}. M.p. = 162–164°C, decomp. These crystals were suitable for X-ray analysis as described below.

$Mo_2(SeAr')_6$

Mesitylene selenol (0.40 g, 2.01 mmol) was dissolved in toluene–hexane (10 : 10 cm^3) and stirred for 0.5 h at room temperature. Solid $Mo_2(NMe_2)_6$ (0.100 g, 0.122 mmol) was added to produce an immediate colour change in the solution to dark-red and after 10 min with stirring, to dark-brown with a red precipitate. The mixture was stirred overnight and the solid collected by filtration and washed with hexane (20 cm^3), THF (30 cm^3), toluene (20 cm^3) and diethyl-ether (20 cm^3); $Mo_2(SeAr')_6$ (0.186 g, 0.134 mmol, 61%). IR (KBr disc): 3000m, 2960m, 2900m, 2840m, 1708w, 1588w, 1552w, 1535w, 1520w, 1442vs, 1430vs, 1390sh, 1368s, 1290s, 1162m, 1080w, 1016s, 1002vs, 940m, 865m, 838vs, 716m, 690s, 556m, 540s, 460w, 410w, 331m, 320sh, 285vs cm^{-1}. M.p. 168–172°C, decomp. Found: C, 46.9; H, 4.7; N, 0.0. Calc. for $Mo_2(SeAr')_6$: C, 47.0; H, 4.8%.

Alternative procedure 1. To a solution of $Mo_2(OBu^t)_6$ (0.100 g, 0.159 mmol) in toluene (20 cm^3) at room temperature was added excess mesitylene selenol (0.25 g, 1.26 mmol). The solution was stirred for 5 min, causing an intense dark-red colour. This was allowed to stand at room temperature for 5 days to produce dark-red crystals of $Mo_2(SeC_6H_2(CH_3)_3)_6$ (0.148 g, 0.107 mmol, 67%). Found: C, 47.7; H, 4.8; N, 0.0. Calc.: C, 47.0; H, 4.8%. IR and melting points were identical to the compounds made above. The crystals were of X-ray quality and the structure was determined as outlined above.

The reaction can also be repeated with the same procedure, reaction scale and conditions, but using $Mo_2(OCH_2{}^tBu)_6$ instead of $Mo_2(OBu^t)_6$ to give $Mo_2(SeAr')_6$ (0.095 g, 0.068 mmol, 43%).

Alternative procedure 2. To a solution of $Mo_2Cl_2(NMe_2)_4$ (0.035 g, 0.08 mmol) in toluene (35 cm^3) at room temperature was added mesitylene selenol (0.20 g, 1.00 mmol) to generate a dark-red coloured solution. The solution was stirred for 5 min and then left to stand overnight (10 h) to produce brown–red crystals. The crystals were filtered and washed with THF (10 cm^3), ethanol (15 cm^3), toluene (15 cm^3) and diethyl-ether (10 cm^3); $Mo_2(SeAr')_6$ (0.035 g, 0.025 mmol, 33%). Found: C, 47.5; H, 4.7; N, 0.10. Calc.: C, 47.0; H, 4.8%.

$W_2(SeAr')_4(O^iPr)_2$

Solid $W_2(OPr^i)_6(py)_2$ (0.100 g, 0.114 mmol) was added to a stirred solution of mesitylene selenol (0.40 g, 2.0 mmol) in toluene (20 cm^3) at room temperature generating a dark-red solution. The solution was stirred by a magnetic follower for 10 min and then allowed to stand for 3 days at room temperature. This produced red crystals of $W_2(SeAr')_4(O^iPr)_2$ (0.068 g, 0.077 mmol, 67%) which were collected by filtration and washed with pentane (20 cm^3) and THF (20 cm^3). Found: C, 39.5; H, 4.5; N, 0.0. Calc.: C, 39.4; H, 4.5%. IR (KBr disc): 3000w, 2945m, 2895m, 2845sh, 1580w, 1560w, 1430vs, 1410s, 1380sh, 1362m, 1350m, 1310m, 1380m, 1150m, 1090s, 1005s, 960vs, 845m, 832s, 710m, 695w, 600m, 550w, 530w, 460m, 440m cm^{-1}. M.p. 135°C darkens, does not melt below 360°C. ^1H NMR at 22°C in $CDCl_3$: $\delta = 6.85$ (s, 8H), 4.03 (br, 2H), 2.35 (s, 24H), 2.24 (s, 12H), 1.28 (s, 12H).

$W_2(SeAr')_4(OCH_2{}^tBu)_2$

Solid $W_2(OCH_2{}^tBu)_6(py)_2$ (0.091 mg, 0.087 mmol) was added to a stirred solution of mesitylene selenol (0.20 g, 1.00 mmol) in toluene (20 cm^3) at room temperature to form a dark-red solution. The solution was allowed to stand at room temperature for 8 days and then cooled to −20°C for 3 days to produce red crystals of $W_2(SeAr')_4(OCH_2{}^tBu)_2$ (0.040 g, 0.29 mmol, 33%). IR (KBr disc): 3000w, 2940s, 2900m, 2840s, 1455s, 1435m, 1385m, 1365m, 1355m, 1285m, 1170w, 1030vs, 940w, 930w, 860w, 840s, 745w, 725m, 685vs, 605w, 605w, 550w, 535w, 460w, 445w, 410w, 390w, 310w, 270w cm^{-1}. ^1H NMR at 22°C ($CDCl_3$): $\delta = 6.85$ (s, 8H), 3.33 (s, 4H), 2.31 (s, 24H), 2.24 (s, 12H), 0.84 (s, 18H).

$W(O^tBu)_2(SeAr')_4$

Mesitylene selenol (0.20 g, 1.0 mmol) was added dropwise to a stirred solution of $W_2(O^tBu)_6$ (0.050 g, 0.062 mmol) in THF (10 cm^3) at room temperature. This caused an immediate darkening of the solution to dark red. The mixture was allowed to stand at room temperature for 2 weeks and then cooled to −20°C for 30 days. This produced lustrous red crystals of $W_2(O^tBu)_2(SeAr')_4$ which were obtained by decanting the solution and washing with hexane (5 cm^3), toluene (5 cm^3) and THF (5 cm^3) (0.021 g, 0.016 mmol, 26%). ^1H NMR at 26°C (C_6D_6): $\delta = 6.68$ (s, 8H), 2.182 (s, 24H), 2.042 (s, 12H), 1.036 (s, 18H). IR (KBr disc): 2958s, 2900sh, 1450s, 1365m, 1351m, 1288w, 1225m, 1150s, 1010s, 960vs, 900w, 835s, 690w, 600w, 540s, 460s, 410s, 390s, 315w, 270s cm^{-1}. Found: C, 40.6; H, 4.4; N, 0.0. Calc.: C, 40.5; H, 4.7%.

$Mo_2(SeAr')_4(O^cHex)_2$

Mesitylene selenol (0.20 g, 1.00 mmol) was added dropwise with stirring to a slurry of $Mo_2(O^cHex)_6$ (0.05 g, 0.064 mmol) in toluene (20 cm^3). The solu-

tion turned dark red, and after 10 min with stirring all the $Mo_2(O^cHex)_6$ has reacted and dissolved. The solution was allowed to stand at room temperature for 24 h, during which time red crystals were precipitated. The crystals were collected by filtration and washed with hexane (10 cm^3) and toluene (10 cm^3) to give $Mo_2(SeAr')_4(O^cHex)_2$ (0.026 g, 0.21 mmol, 33%). IR (KBr disc): 3000m, 2920s, 1595w, 1560w, 1440s, 1400w, 1370m, 1350m, 1335w, 1290m, 1245w, 1230w, 1160w, 1140w, 1080w, 1035vs, 1005vs, 965s, 945m, 880w, 860w, 840vs, 790s, 720w, 700vs, 630sh, 600w, 555w, 540w, 500w, 460w, 450w, 410w, 375w, 345w, 330w, 315w, 295m, 274w, cm^{-1}. ^1H NMR at 25°C (C_6D_6): $\delta = 6.54$ (s, 8H), 2.24 (s, 24H), 2.15 (s, 12H), 1.6 (br, 10H), 0.85 (br, 12H).

$Mo_2(SeAr')_4(O^iPr)_2$

$Mo_2(O^iPr)_6$ (0.050 g, 0.092 mmol) was dissolved in toluene (20 cm^3) at room temperature to generate an orange solution. Mesitylene selenol (0.30 g, 1.5 mmol) was added dropwise with stirring generating a dark-red colour in solution. The mixture was allowed to stand at room temperature for 3 days and then cooled to −20°C for 2 days to produce a mixture of red needles (90%) and yellow plates (10%), both of which were $Mo_2(O^iPr)_2(SeAr')_4$ (0.035 g, 0.032 mmol, 35%). The crystals were collected by decanting the solution and washing with 10 cm^3 of both pentane and diethyl-ether. The filtrate was combined with pentane (10 cm^3) and cooled to −20°C to produce a fine orange–red precipitate of $Mo_2(O^iPr)_2(SeAr')_4$ (0.015 g, combined yield 45%). Found: C, 46.2; H, 4.7; N, 0.0. Calc.: C, 45.7; H, 5.3%. ^1H NMR (C_6D_6): $\delta = 6.93$ (s, 2H), 6.89 (s, 4H), 6.86 (s, 2H), 4.07 (scpt, 2H), 2.41 (s, 6H), 2.32 (s, 6H), 2.29 (s, 12H), 1.29 (d, 12H). IR (KBr disc): 2995m, 2942s, 2895s, 2835m, 1580w, 1445s, 1425s, 1360m, 1350m, 1310m, 1275m, 1160w, 1150m, 1115m, 1090s, 1020m, 1004m, 960vs, 835s, 720w, 690w, 600m, 550w, 535w, 460m, 440m, 330w, 290s cm^{-1}.

$M_2(NMe_2)_4(SeAr')_2$ (M = Mo, W)

Mesitylene magnesium bromide (0.46 cm^3, 1 M soln in THF) was added to THF (10 cm^3) at room temperature. Solid elemental grey selenium (0.36 g, 0.46 mmol) was added and the mixture stirred for 0.5 h until all the selenium had dissolved leaving a clear colourless solution. Solid $Mo_2Cl_2(NMe_2)_4$ (0.100 g, 0.27 mmol) was added and the solution rapidly stirred for 1 min, generating a clear yellow solution. The solution was allowed to stand overnight producing yellow needle-like crystals. The solution was filtered and the crystals washed with *n*-pentane (10 cm^3) and diethyl-ether (10 cm^3) to give $Mo_2(SeAr')_2(NMe_2)_4$, (0.060 g, 0.086 mmol), 32%). The filtrate was cooled to −20°C to produce a second crop (0.012 g, 0.0156 mmol overall yield 38%). The crystals were air sensitive and insoluble in hexane, acetone, THF and water. IR (Nujol mull) 1440sh, 1380w, 1233m, 1125m, 1028m, 1010m, 940vs, 937vs, 837m, 710w, 695w, 650w, 550m, 540m, 460w, 440w, 335m. ^1H NMR (C_6D_6): $\delta = 6.79$ (s, 4H), 4.38 (br, 12H), 2.54 (s, 12H), 2.09 (br, 18H). Analogous reaction conditions and reaction scale gave for tungsten; $W_2(SeAr')_2(NMe_2)_4$ (yield 0.061 g, 0.065 mmol). IR (Nujol mull): 1440sh, 1380w, 1335m, 1160w, 1130m, 1110m, 1060m, 1030m, 1010m, 945vs, 840m, 710m, 695m, 550m, 540m, 380w, 340 cm^{-1}. ^1H NMR (C_6D_6): $\delta = 6.82$ (s, 4H), 4.38 (br, 12H), 2.54 (s, 12H), 2.13 (br, 18H). Found: C, 33.2; H, 4.4; N, 4.9. Calc.: C, 33.2; H, 4.9; N, 5.9%.

Reactions involving selenophenol with $M_2(NMe_2)_6$ *and* $M_2(OR)_6$ *compounds* (M = Mo, W)

Molybdenum

To $Mo_2(NMe_2)_6$ (0.05 g, 0.11 mmol) dissolved in toluene (10 cm^3) was added selenophenol (0.25 g, 0.15 mmol), generating a purple colour in solution and a purple precipitate. The reaction was allowed to stand at room temperature for 3 days, and the purple precipitate isolated by filtration, washed with THF (5 cm^3), hexane (5 cm^3) and toluene (5 cm^3). The solid (0.076 g) was insoluble in common solvents, air-stable and seemingly inert to hydrolysis. Found: C, 35.2; H, 2.6; N, 0.7. Calc. for $[Mo_4(SePh)_{10}Se_2]H_2NMe_2$: C, 34.7; H, 2.9; N, 0.6%. IR (KBr disc): 3020br, 2920m, 2700m br, 2400m br, 1550m, 1530m, 1460m, 1450m, 1425m, 1370m, 1310w, 1285w, 1240w, 1165w, 1140w, 1090w, 1055m, 1005m, 1005s, 990m, 930w, 875m, 835m, 800w, 725s, 680s, 655m, 600sh, 550sh, 510sh, 455m, 410w, 395w, 340w, 310w, 295w cm^{-1}. [Reaction of $Mo_2(O^tBu)_6$ with selenophenol under the same conditions produces a purple solid which has similar IR bands to the above save no stretch at 2700, 2400 and 1450 cm^{-1}, but stretches at 1630 and 3200 cm^{-1}.]

Tungsten

To $W_2(NMe_2)_6$ (0.050 g, 0.08 mmol) dissolved in toluene (10 cm^3) at room temperature was added selenophenol (0.25 g, 1.59 mmol). This produced an intermediate darkening of the solution to red.

After 1 day at room temperature a black precipitate is produced, which was collected by filtration (after 3 days), washed with hexane (10 cm^3), toluene (10 cm^3) and diethyl-ether (15 cm^3). The precipitate is slightly soluble in THF, air-stable and seemingly inert to hydrolysis. Found: C, 27.7; H, 1.7; N, 0.6. Calc. for $[W_4(SePh)_{10}Se_4]H_2NMe_2$: C, 28.0; H, 2.1; N, 0.5%. IR (KBr disc): 3020br, 2920m, 2650m br, 2310m br, 1550m, 1530m, 1460m, 1450m, 1425m, 1370m, 1310w, 1285w, 1240w, 1165w, 1140w, 1090w, 1055m, 1005m, 1005s, 990m, 930w, 875m, 835m, 8002, 725s, 680s, 655m, 600sh, 550sh, 510sh, 455m, 410w, 395w, 340w, 310w, 295w cm^{-1}. Reaction involving $W_2(O^iPr)_6 \cdot (HNMe_2)_2$ with selenophenol under the same conditions gave the same product.

X-Ray Structure Determinations

General operating facilities, procedures and programmes have been previously described.[25] A summary of the crystal data is given in Table 1.

$W_2(SeAr')_6$

A suitable crystal was located and transferred to the goniostat using standard inert atmosphere handling techniques employed by the IUMSC and cooled to -155°C for characterization and data collection.

A systematic search of a limited hemisphere of reciprocal space located no symmetry or systematic absences, indicating a triclinic space group. Subsequent solution and refinement of the structure confirmed the centrosymmetric choice, $P\bar{1}$.

Data were collected in the usual manner using a continuous θ–2θ scan with a fixed background. Data were reduced to a unique set of intensities and associated σ in the usual manner. The structure was solved by a combination of direct methods (MULTAN 78) and Fourier techniques. A different Fourier synthesis revealed some but not all, hydrogen atoms. All hydrogen atoms positions were therefore calculated using idealized geometries and d(C—H) = 0.95 Å. These calculated positions were fixed for the final cycles of refinement.

Data were corrected for absorption. A final difference Fourier was featureless, with the largest peak being 1.19 e/Å^3 at the metal site.

As shown in the figures and tables, the molecule lies at a crystallographic centre of inversion.

$Mo_2(SeAr')_6$

Mounting and cooling were performed identically to the tungsten analogue.

A systematic search of a limited hemisphere of reciprocal space located a set of diffraction maxima with no symmetry or systematic absences, indicating a triclinic space group. The morphology was essentially the same as the tungsten analogue, and examination of the reciprocal space revealed that the structures are indeed isomorphous.

Data were collected in the usual manner using a continuous θ–2θ scan with a fixed background. Data were reduced to a unique set of intensities and associated σ in the usual manner. The heavy atom coordinates from the tungsten analogue were used as a starting point for the refinement. All hydrogen atoms were clearly visible in a difference Fourier synthesis phased on the non-hydrogen parameters. All hydrogen atoms were refined isotropically and non-hydrogen atoms anisotropically in the final cycles.

A final difference Fourier was featureless, with the largest peak being 0.45 e/Å^3. No absorption correction was performed.

$W_2(O^iPr)_2(SeAr')_4$

A crystal of suitable size was mounted using silicon grease and was transferred to a goniostat where it was cooled to -155°C for characterization and data collection. A search of limited hemisphere of reciprocal space revealed no symmetry or systematic absences. An initial choice of space group $P\bar{1}$ was confirmed by the successful solution of the structure. Following intensity data collection and correction for absorption, data processing gave a residual of 0.010 for 145 unique intensities which had been measured more than once. Four standards measured every 300 data showed no significant trends.

The structure was solved by a combination of direct methods (MULTAN 78) and Fourier techniques. The tungsten and selenium positions were obtained from an E-map. Subsequent iterations of least-squares refinement and different Fourier revealed all of the remaining non-hydrogen atoms. Hydrogen atoms were placed in fixed calculated positions to improve the refinement of the non-hydrogen atoms. Hydrogen thermal parameters were fixed at one plus the isotropic thermal parameter of the atom to which they were bonded.

In the final cycles of refinement all non-hydrogen atoms were refined with anisotropic thermal parameters to a final $R(F) = 0.033$. The final difference map was reasonably clean. There were heavy atom residuals of 0.81–1.67 e/Å^3. All other residual peaks were 0.76 e/Å^3 or less. The centre of the molecule is at a crystallographic centre of symmetry.

$Mo_2(O^iPr)_2(SeAr')_4$

The sample consisted of reddish-orange needles and a minor component (estimated 10%) of yellow plate-like crystals. Both components were examined and transferred to the gonistat where they were cooled to $-155°C$ for characterization and data collection. For the major component a systematic search of limited hemispherical reciprocal space located a set of diffraction maxima with symmetry and systematic absences corresponding to a monoclinic space group. It was later discovered that an *A*-centring was present, the system was not reindexed, leading to the choice of $A2/a$ (standard setting $C2/c$).

Data were collected using a continuous θ–2θ scan with fixed background. Data were reduced to a unique set of intensities and associated σ in the usual manner. The structure was solved by a combination of direct methods (MULTAN 78) and Fourier techniques. A different Fourier synthesis revealed the location of some but not all hydrogen atoms. All hydrogen atoms were assigned idealized geometries d(C—H) = 0.95 Å. These calculated positions were fixed for the final cycles of refinement. The structure is essentially the same as the tungsten complex above.

The minor component (yellow plates) was also isostructural with the major component (orange–yellow needles). A structure analysis using the same procedure as above was based on a triclinic unit cell with $P\bar{1}$ symmetry.

Acknowledgements—We thank the National Science Foundation for financial support. I.P.P. acknowledges SERC for a NATO postdoctoral fellowship. Atomic Positional Parameters have been deposited with the Director, Cambridge Crystallographic Centre.

REFERENCES

1. M. H. Chisholm, *Polyhedron* 1983, **2**, 681.
2. Alkyls: F. Huq, W. Mowat, A. Shortland, A. C. Skapski and G. Wilkinson, *J. Chem. Soc., Chem. Commun.* 1971, 1079; M. H. Chisholm, F. A. Cotton, M. W. Extine and B. R. Stults, *Inorg. Chem.* 1976, **15**, 2252.
   Amides: M. H. Chisholm, F. A. Cotton, B. A. Frenz, W. W. Reichert, L. W. Shive and B. R. Stults, *J. Am. Chem. Soc.* 1976, **98**, 4469; M. H. Chisholm, F. A. Cotton, M. W. Extine and B. R. Stults, *J. Am. Chem. Soc.* 1976, **98**, 4477.
3. M. H. Chisholm, J. F. Corning and J. C. Huffman, *Inorg. Chem.* 1984, **23**, 754.
4. M. H. Chisholm, J. F. Corning, K. Folting and J. C. Huffman, *Polyhedron* 1985, **4**, 383.
5. G. Wilkinson, B. Gillard and J. McCleverty (Eds), *Comprehensive Coordination Chemistry*, Vol. 2, p. 661. Pergamon Press, Oxford (1987).
6. A. Rettenmeier, K. Weidenhammer and M. L. Ziegler, *Z. Anorg. Chem.* 1981, **473**, 91.
7. J. Rott, E. Guggotz, A. Rettenmeier and M. L. Ziegler, *Z. Naturforsch* 1982, **37B**, 13.
8. M. Sato and T. Yoshida, *J. Organomet. Chem.* 1974, **67**, 395.
9. H. J. Gysling, *Coord. Chem. Rev.* 1982, **42**, 133.
10. I. G. Dance, *Polyhedron* 1986, **5**, 1037.
11. D. H. Barton and H. Dadoun, *Nouv. J. Chem.* 1982, **6**, 53.
12. P. A. W. Dean, J. J. Vittal and N. C. Payne, *Inorg. Chem.* 1984, **23**, 4232.
13. P. Krebs, *Angew. Chem. Intl. Ed. Engl.* 1983, **22**, 113.
14. G. R. Hanson, A. A. Brunette, A. C. McDonell, K. S. Murray and A. G. Wedd, *J. Am. Chem. Soc.* 1981, **103**, 1953.
15. J. R. Bradbury, A. F. Masters, A. C. McDonell, A. A. Brunette, A. M. Bond and A. G. Wedd, *J. Am. Chem. Soc.* 1981, **103**, 1959.
16. C. Belin, T. Makani and J. Roziere, *J. Chem. Soc., Chem. Commun.* 1985, 118.
17. I. G. Dance, A. G. Wedd and I. W. Boyd, *Aust. J. Chem.* 1978, **31**, 519; J. R. Bradbury, M. F. Mackay and A. G. Wedd, *Aust. J. Chem.* 1978, **31**, 2423.
18. M. H. Chisholm, I. P. Parkin, J. C. Huffman and W. E. Streib, *J. Chem. Soc., Chem. Commun.* 1990, 920.
19. A. J. Gorden and R. A. Ford (Eds), *The Chemists Companion. A Handbook of Practical Data Techniques and References*, p. 83. Wiley, New York (1972).
20. A. L. Allred and E. G. Rochow, *J. Inorg. Nucl. Chem. Lett.* 1958, **5**, 264.
21. M. H. Chisholm, F. A. Cotton, C. A. Murillo and W. W. Reichert, *Inorg. Chem.* 1977, **16**, 1801.
22. M. H. Chisholm, F. A. Cotton, B. A. Frenz, W. W. Reichert and B. R. Stults, *J. Am. Chem. Soc.* 1976, **98**, 4477.
23. M. Akiyama, M. H. Chisholm, F. A. Cotton, M. W. Extine, D. A. Haitko, D. Little and P. E. Fanwick, *Inorg. Chem.* 1979, **18**, 2266.
24. M. H. Chisholm, *Polyhedron* 1983, **2**, 681.
25. M. H. Chisholm, K. Folting, J. C. Huffman and C. C. Kirkpatrick, *Inorg. Chem.* 1984, **24**, 1021.

Polyhedron Vol. 9, No. 24. pp. 2953–2958, 1990
Printed in Great Britain

0277–5387/90 $3.00+.00
© 1990 Pergamon Press plc

SYNTHESIS AND CRYSTAL STRUCTURE OF THE COMPLEX $[MoW(OEt)(\mu\text{-}CH_2)\{\mu\text{-}C(C_6H_4Me\text{-}4)C(Me)O\}(\eta^7\text{-}C_7H_7)(\eta^5\text{-}C_2B_9H_{10}Me)]$

STEPHEN J. DOSSETT, MASSIMINO U. PILOTTI and F. GORDON A. STONE*

Department of Inorganic Chemistry, The University of Bristol, Bristol BS8 1TS, U.K.

(*Received* 21 *June* 1990; *accepted* 10 *August* 1990)

Abstract—The complex $[MoW(\mu\text{-}CC_6H_4Me\text{-}4)(CO)_2(\eta^7\text{-}C_7H_7)(\eta^5\text{-}C_2B_9H_{10}Me)]$ reacts with diazomethane in Et_2O containing EtOH to afford the dimetal compound $[MoW(OEt)(\mu\text{-}CH_2)\{\mu\text{-}C(C_6H_4Me\text{-}4)C(Me)O\}(\eta^7\text{-}C_7H_7)(\eta^5\text{-}C_2B_9H_{10}Me)]$. The structure of this product was established by X-ray diffraction. The Mo—W bond [2.778(4) Å] is bridged by a CH_2 group [μ-C—Mo 2.14(3), μ-C—W 2.02(3) Å] and by a $C(C_6H_4Me\text{-}4)C(Me)O$ fragment [Mo—O 2.11(3), W—O 2.18(2), Mo—$C(C_6H_4Me\text{-}4)$ 2.41(3), W—$C(C_6H_4Me\text{-}4)$ 2.09(3), Mo—C(Me) 2.26(3) Å]. The molybdenum atom is η^7-coordinated by the C_7H_7 ring and the tungsten atom is η^5-coordinated by the open pentagonal face of the *nido*-icosahedral $C_2B_9H_{10}Me$ cage. The tungsten atom also carries a terminally bound OEt group [W—O 1.88(3) Å]. The ^1H and $^{13}C\text{-}\{^1H\}$ NMR data for the dimetal compound are reported and discussed.

As part of a continuing study[1] of the ligating properties of the C≡W bonds in the salts $[X][W(\equiv CR)(CO)_2(\eta^5\text{-}C_2B_9H_9R'_2)]$ [X = $N(PPh_3)_2$, NEt_4 or PPh_4; R = alkyl, aryl or alkynyl; R′ = H or Me] we have recently prepared the electronically unsaturated 32 valence electron dimetal complex $[MoW(\mu\text{-}CC_6H_4Me\text{-}4)(CO)_2(\eta^7\text{-}C_7H_7)(\eta^5\text{-}C_2B_9H_{10}Me)]$ (**1**) by treating $[NEt_4][W(\equiv CC_6H_4Me\text{-}4)(CO)_2(\eta^5\text{-}C_2B_9H_{10}Me)]$ with $[Mo(CO)_2(NCMe)(\eta^7\text{-}C_7H_7)][BF_4]$ in CH_2Cl_2.[2] Compound **1** reacts with $PHPh_2$ to afford $[MoW(\mu\text{-}PPh_2)\{\mu\text{-}C(OH)C(C_6H_4Me\text{-}4)\}(CO)(\eta^7\text{-}C_7H_7)(\eta^5\text{-}C_2B_9H_{10}Me)]$ (**2**), a complex having a very unusual structure.[3] In further studies on the reactivity of species of type **1** with nucleophilic reagents, we report herein a novel dimetal compound resulting from the reaction between **1** and diazomethane. We have previously shown that the latter reagent readily adds CH_2 groups to heteronuclear dimetal compounds with bridging alkylidyne groups, but having cyclopentadienyl $\eta^5\text{-}C_5R_5$ (R = H or Me) ligands attached to the Mo or W centres instead of an $\eta^5\text{-}C_2B_9$ cage, as in **1**.

* Author to whom correspondence should be addressed, at the Department of Chemistry, Baylor University, Waco, TX 76798-7348, U.S.A.

RESULTS AND DISCUSSION

Treatment of a Et_2O solution of **1** with an excess of CH_2N_2 resulted in an immediate colour change of the solution from red to orange–brown. Column chromatography of the mixture on alumina removed several products formed in such trace amounts that they could not be identified. However, continued elution of the column led to the recovery of significant amounts of an orange crystalline solid **3**. Although the IR and NMR data for this species did not allow structural characterization, nevertheless it was apparent that an unusual compound had formed. Thus the IR spectrum revealed the absence of any CO groups. Moreover, the ^1H and $^{11}B\text{-}\{^1H\}$ NMR spectra showed that no B—H→Mo bridge-bond was present, as occurs in the precursor **1**. The $^{13}C\text{-}\{^1H\}$ NMR spectrum displayed no resonances attributable to CO ligands nor to a μ-C alkylidyne carbon-nucleus, although peaks were observed indicating that the C_7H_7 ring and the $C_2B_9H_{10}Me$ cage were present. An X-ray diffraction study on the complex **3** was evidently necessary. Although the crystals were twinned, it was possible to establish the structure, and in this manner **3** was identified as the dimetal compound $[MoW(OEt)(\mu\text{-}CH_2)\{\mu\text{-}C(C_6H_4Me\text{-}4)C(Me)O\}(\eta^7\text{-}C_7H_7)(\eta^5\text{-}C_2B_9H_{10}Me)]$.

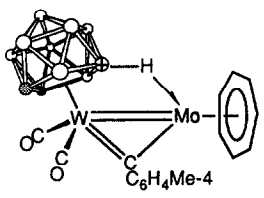

(1)

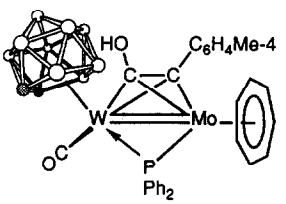

(2)

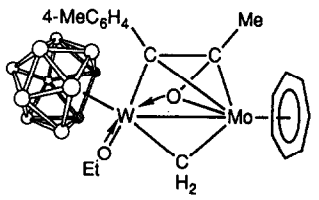

(3)

○BH ◉CH ●CMe ⊕B

Selected bond distances and angles are listed in Table 1, and the molecule is shown in Fig. 1. The Mo—W bond [2.778(4) Å] is bridged by a CH_2 group [Mo—C(40) 2.14(3), W—C(40) 2.02(3) Å], and also by a $C(C_6H_4Me\text{-}4)C(Me)O$ fragment. The oxygen atom of the latter is bonded to both metal centres [Mo—O(2) 2.11(3), W—O(2) 2.18(2) Å], as is the carbon atom C(30) of the $C(C_6H_4Me\text{-}4)$ group [Mo—C(30) 2.41(3), W—C(30) 2.09(3) Å]. However, the carbon atom C(20) of the CMe moiety is linked only to the molybdenum [Mo—C(20) 2.26(3) Å]. As expected, the latter carries the C_7H_7 ring, while the carbaborane cage is η^5-coordinated via its open pentagonal face to the tungsten atom. Unexpectedly, the tungsten is bonded to an OEt group. The W—O(1) distance [1.88(3) Å] is appreciably shorter than the W—O(2) separation, implying a degree of multiple bonding in the former linkage, as depicted in the structural formula for **3** displayed, with the ligand functioning formally as a three-electron donor. The electron contributions from the various ligands, as well as the presence of the metal–metal bond, allow both metal centres to acquire filled 18 electron shells, so that the compound is electronically saturated with 34 valence electrons.

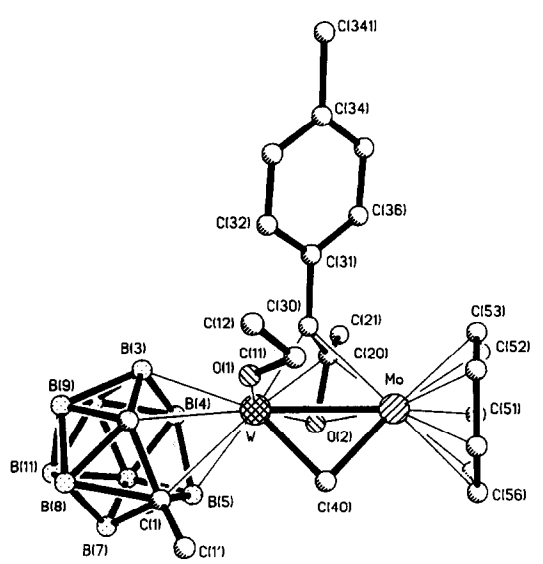

Fig. 1. The molecular structure of $[MoW(OEt)(\mu\text{-}CH_2)\{\mu\text{-}C(C_6H_4Me\text{-}4)C(Me)O\}(\eta^7\text{-}C_7H_7)(\eta^5\text{-}C_2B_9H_{10}Me)]$ (**3**) showing the atom-numbering scheme.

The origin of the ethoxy group in compound **3** derives from ethanol used in the generation of diazomethane (see Experimental section). In an attempt to increase the yield of **3**, typically *ca* 15%, ethanol was added to the reaction mixture, but this produced no advantageous result. Having established the molecular structure of complex **3**, it was possible to interpret satisfactorily all the NMR data.

The $^{11}B\text{-}\{^1H\}$ NMR spectrum showed seven peaks at δ 4.2, 1.1, −6.7, −7.9, −8.8, −10.1 and −14.2 ppm. The signals at −8.8 and −10.1 ppm each corresponded in intensity to two boron nuclei, while each of the remaining resonances was of an intensity expected for one boron nucleus. The peaks at δ 4.2 and 1.1 ppm became doublets [J(BH) 130 Hz] in a fully-coupled ^{11}B NMR spectrum, confirming that they are attributable to BH groups with two-centre two-electron bonds. The fully-coupled ^{11}B spectrum was measured because the observed chemical shifts at 4.2 and 1.1 ppm fall into the region where signals due to exo-polyhedral three-centre two-electron B—H→Mo groups are often seen. However, in a fully-coupled ^{11}B NMR spectrum these groups, if present, have resonances with $^1H—^{11}B$ couplings of *ca* 80 Hz, e.g. for compound **1** the B—H→Mo signal is at δ 11.7 ppm, with J(BH) 77 Hz.[2]

The ^1H and $^{13}C\text{-}\{^1H\}$ NMR spectra of complex **3** are also in agreement with the structure revealed by X-ray diffraction. In the ^1H spectrum the signal for the $\mu\text{-}CH_2$ group occurs as an AB pattern at δ 5.64 and 5.77 with J(AB) 10 Hz, while in the $^{13}C\text{-}\{^1H\}$ spectrum the resonance for the $\mu\text{-}CH_2$ ligand is at δ 147.9 ppm, and shows $^{183}W—^{13}C$ satellite peaks [J(WC) 40 Hz]. Compounds with metal–metal bonds bridged by methylene groups commonly have ^{13}C resonances in the range δ 100–200 ppm,[5] and thus complex **3** is no exception.

The $^{13}C\text{-}\{^1H\}$ NMR spectrum of compound **3** shows the expected signals for all the other groups

Table 1. Selected bond distances (Å) and angles (°) for the complex [MoW(OEt)(μ-CH$_2$){μ-C(C$_6$H$_4$Me-4)C(Me)O}(η^7-C$_7$H$_7$)(η^5-C$_2$B$_9$H$_{10}$Me)] (**3**)

W—Mo	2.778(4)	W—O(1)	1.88(3)	W—O(2)	2.18(2)	W—C(30)	2.09(3)
W—C(40)	2.02(3)	W—C(1)	2.57(4)	W—C(2)	2.59(5)	W—B(3)	2.47(4)
W—B(4)	2.48(4)	W—B(5)	2.43(4)	Mo—O(2)	2.11(3)	Mo—C(20)	2.26(3)
Mo—C(30)	2.41(3)	Mo—C(40)	2.14(3)	Mo—C(50)	2.24(4)	Mo—C(51)	2.27(4)
Mo—C(52)	2.34(4)	Mo—C(53)	2.25(5)	Mo—C(54)	2.23(5)	Mo—C(55)	2.26(6)
Mo—C(56)	2.32(5)	O(1)—C(11)	1.46(5)	C(11)—C(12)	1.35(6)	O(2)—C(20)	1.44(4)
C(20)—C(21)	1.51(5)	C(20)—C(30)	1.45(5)	C(30)—C(31)	1.47(3)	C(1)—C(2)	1.72(5)
C(1)—B(5)	1.69(6)	C(1)—B(7)	1.77(7)	C(1)—B(8)	1.87(6)	C(2)—B(3)	1.78(6)
C(2)—B(8)	1.74(7)	C(2)—B(9)	1.76(7)	B(3)—B(4)	1.68(6)	B(3)—B(9)	1.76(7)
B(3)—B(10)	1.71(6)	B(4)—B(5)	1.80(5)	B(4)—B(6)	1.68(6)	B(4)—B(10)	1.70(6)
B(5)—B(6)	1.74(7)	B(5)—B(7)	1.86(7)	B(6)—B(7)	1.70(7)	B(6)—B(10)	1.80(6)
B(6)—B(11)	1.75(8)	B(7)—B(8)	1.78(7)	B(7)—B(11)	1.61(7)	B(8)—B(9)	1.68(6)
B(8)—B(11)	1.82(8)	B(9)—B(10)	1.68(7)	B(9)—B(11)	1.73(7)	B(10)—B(11)	1.77(6)
Mo—W—O(1)	99.3(8)	Mo—W—O(2)	48.7(6)	O(1)—W—O(2)	147(1)	Mo—W—C(30)	57.3(9)
O(1)—W—C(30)	91(1)	O(2)—W—C(30)	66(1)	Mo—W—C(40)	50(1)	O(1)—W—C(40)	92(1)
O(2)—W—C(40)	74(1)	C(30)—W—C(40)	107(1)	W—Mo—O(2)	50.7(7)	W—Mo—C(20)	62.2(9)
O(2)—Mo—C(20)	38.1(9)	W—Mo—C(30)	46.9(8)	O(2)—Mo—C(30)	61(1)	C(20)—Mo—C(30)	36(1)
W—Mo—C(40)	46.2(9)	O(2)—Mo—C(40)	73(1)	C(20)—Mo—C(40)	103(1)	C(30)—Mo—C(40)	93(1)
W—O(1)—C(11)	142(2)	O(1)—C(11)—C(12)	110(1)	W—O(2)—Mo	80.7(9)	W—O(2)—C(20)	92(2)
Mo—O(2)—C(20)	77(1)	Mo—C(20)—O(2)	65(1)	Mo—C(20)—C(21)	133(3)	O(2)—C(20)—C(21)	115(3)
Mo—C(20)—C(30)	78(2)	O(2)—C(20)—C(30)	106(3)	C(21)—C(20)—C(30)	136(3)	W—C(30)—Mo	75.8(9)
W—C(30)—C(20)	95(2)	Mo—C(30)—C(20)	66(2)	W—C(30)—C(131)	138(2)	Mo—C(30)—C(31)	129(2)
C(20)—C(30)—C(31)	125(3)	W—C(40)—Mo	84(1)				

present. Thus diagnostic resonances for the cage-carbon nuclei of the carbaborane ligand occur at δ 77.1 (CH) and 62.9 ppm (*C*Me), both peaks being broad due to unresolved ^{11}B—^{13}C coupling. Signals for the ethoxide ligand occur at δ 78.7 (OCH_2) and 17.1 ppm (OCH_2*Me*). A specific assignment of peaks for the CMe moiety of the C(C_6H_4Me-4)*C*(*Me*)O fragment is not possible since they occur with the resonances for the C_6H_4Me-4 group. Thus signals at 138.2 and 138.0 ppm are ascribed to one or other of the C^4(C_6H_4) and *C*(Me)O nuclei, and a pair of resonances at δ 21.6 and 21.2 ppm can be assigned to the C(*Me*)O and Me-4 groups. The resonance for the C*Me* group of the carbaborane ligand is seen at δ 32.1 ppm, a characteristic chemical shift for such a group. Remaining resonances in the ^{13}C-{^1H} NMR spectrum of **3** are observed at 164.5 [C^1(C_6H_4)], 129.7, 129.2 (C_6H_4), 128.5 (*C*C_6H_4Me-4) and 90.8 ppm (C_7H_7). These assignments correlate with those observed for these groups in earlier work.

The μ-C(C_6H_4Me-4)C(Me)O fragment present in compound **3** has been found previously in the complexes [WMn{μ-C(C_6H_4Me-4)C(Me)O}(CO)$_5$(η-C_5H_5)] (**4**) and [MoW{μ-C(C_6H_4Me-4)C(Me)O}(CO)$_4$(η-C_5H_5)$_2$] (**5**).[6] The bridge bonding in **3**, with the oxygen atom linked to both metal centres, is similar to that present in **4**. In contrast, in complex **5** the C(Me)O moiety is η^2-coordinated to the tungsten atom, and there is no Mo—O bond.

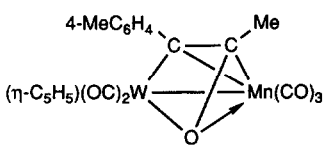

(4)

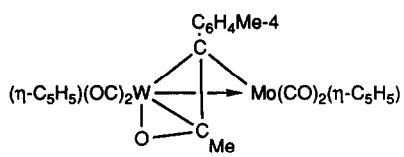

(5)

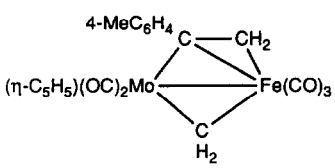

(6)

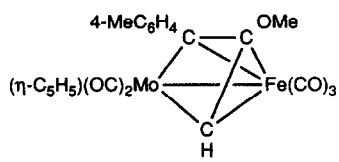

(7)

Compounds **4** and **5** are obtained from reactions between [W(≡CC_6H_4Me-4)(CO)$_2$(η-C_5H_5)] and [MnMe(CO)$_5$] and [MoMe(CO)$_3$(η-C_5H_5)], respectively. Both species result from a coupling of the *p*-tolylmethylidyne group in the tungsten reagent with an acyl group, very probably generated at the manganese or molybdenum centres. The formation of the μ-C(C_6H_4Me-4)C(Me)O ligand in **3** is clearly complex and must involve several steps; thereby accounting both for the relatively low yield and the observation of trace amounts of unidentified products. The synthesis of **3** from **1** requires reaction of the latter with two CH_2 fragments in a stepwise fashion. A double addition of methylene groups is unusual, but there is precedent in the formation of the compounds [MoFe(μ-CH_2){μ-σ:η-C(C_6H_4Me-4)=CH_2}(CO)$_5$(η-C_5H_5)] (**6**) and [MoFe{μ-C(C_6H_4Me-4)C(OMe)CH}(CO)$_5$(η-C_5H_5)] (**7**) from [MoFe(μ-CC_6H_4Me-4)(CO)$_6$(η-C_5H_5)] and CH_2N_2.[4c] Some possible intermediates in the synthesis of **3**, modelled on earlier work, are shown in Scheme 1.

As mentioned earlier, compound **1** is electronically unsaturated, and intermediate **A** is therefore reasonable based on the known facile addition of CH_2 groups across the metal–metal bonds of many such species.[4,5,7–11] The transformation from **A** into **B** involves a lifting of the B—H→Mo bond, concomitant with coordination of an ethanol molecule at the tungsten centre. The ability of η^5-C_2B_9 cage-systems to adopt either a spectator rôle as in **B** or a non-spectator rôle as in **A**, thereby filling a dual rôle as either a four- or a six-electron donor at a dimetal centre, is well established.[1–3] The oxidative addition of ethanol at a dimetal centre, step **B** to **C**, so as to generate a molecule with the elements (EtO)W—Mo(H) has ample precedent in the work of Chisholm *et al.*[12] on the reactions of the compounds [1,2-M_2R_2(NMe_2)$_4$] (M = Mo or W, R = alkyl) with alcohols. Intermediate **C** would

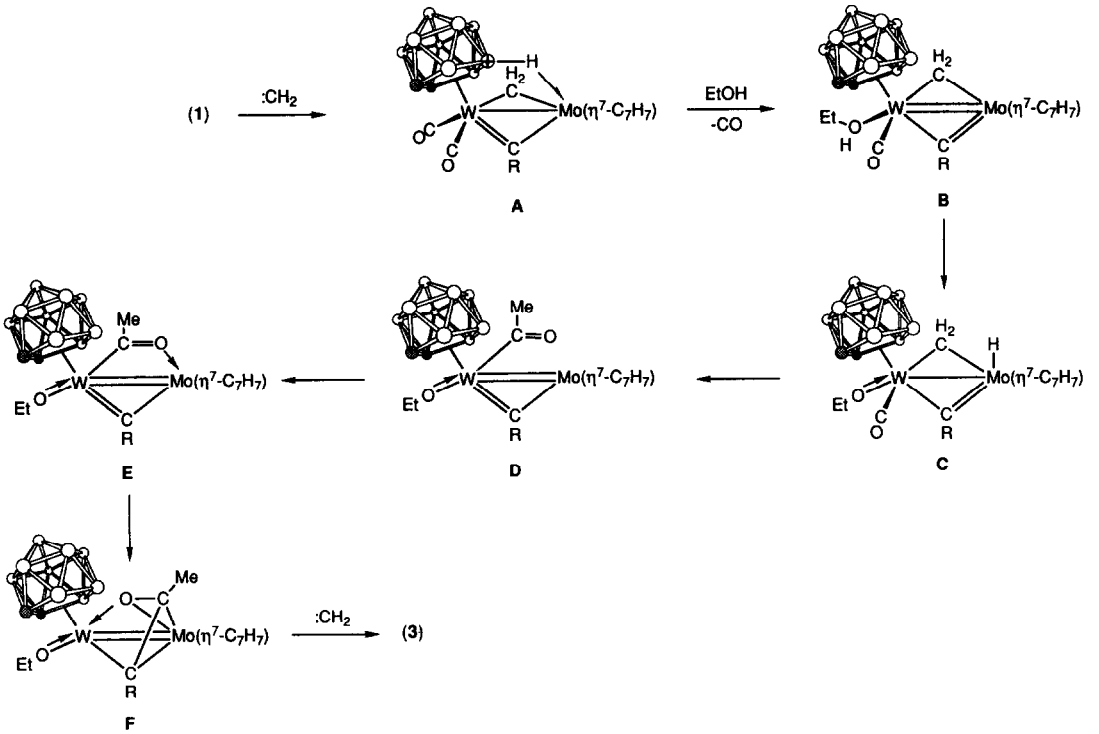

Scheme 1. R = C$_6$H$_4$Me-4; ○BH, ◎CH, ●CMe, ⊕ B.

readily generate a Me group,[8] and the latter by migrating to a molecule of CO could afford the acyl species **D**. The final steps **D** → **E** → **F** involve the acyl ligand adopting a μ-η^2 bonding mode,[13] followed by coupling with the *p*-tolylmethylidyne fragment, as observed previously.[6] Several of the postulated steps in the reaction scheme require transformations between structures with multiple or single metal–metal bonds. We have encountered this process in the reactions of alkynes at dimolybdenum centres,[14] and it probably results from a need for the metal atoms to attain where possible a filled 18-electron valence shell, as implied by some of the intermediates depicted in Scheme 1.

EXPERIMENTAL

Solvents were rigorously dried before use, and all reactions were carried out in Schlenk tubes under oxygen-free nitrogen. Alumina used for chromatography was BDH aluminium oxide (Brockman activity II). The compound [MoW(μ-CC$_6$H$_4$Me-4)(CO)$_2$(η^7-C$_7$H$_7$)(η^5-C$_2$B$_9$H$_{10}$Me)] (**1**) was prepared as previously described.[2] The NMR measurements were made with JEOL JNM GX270 and GX400 spectrometers. The ^{11}B-{^{1}H} NMR chemical shifts are positive to high frequency of BF$_3$·Et$_2$O (external).

Synthesis of the complex [MoW(OEt)(μ-CH$_2$){μ-C(C$_6$H$_4$Me-4)C(Me)O}(η^7-C$_7$H$_7$)(η^5-C$_2$B$_9$H$_{10}$Me)]

A solution of compound **1** (0.20 g, 0.30 mmol) in Et$_2$O (10 cm^3) was treated with an excess of CH$_2$N$_2$ [*ca* 10 mmol in Et$_2$O (10 cm^3), generated using an Aldrich Chemical Co. Diazald kit which employs an EtOH–H$_2$O–Et$_2$O mixture as solvent]. Following addition of CH$_2$N$_2$, the red solution immediately became orange–brown in colour. Solvent was removed *in vacuo*, and the residue was dissolved in a mixture of CH$_2$Cl$_2$–hexane (*ca* 5 cm^3, 2 : 1) and chromatographed (column 2 × 25 cm). Elution with CH$_2$Cl$_2$–hexane (1 : 4) removed traces of inseparable fractions. Continued elution and increasing the concentration of CH$_2$Cl$_2$ removed an orange band. Evaporation of solvent *in vacuo* followed by crystallization of the residue from CH$_2$Cl$_2$–hexane (1:4) afforded orange microcrystals of [MoW(OEt)(μ-CH$_2$){μ-C(C$_6$H$_4$Me-4)C(Me)O}(η^7-C$_7$H$_7$)(η^5-C$_2$B$_9$H$_{10}$Me)] (**3**) (0.032 g, 15%) (Found: C, 38.7; H, 6.0%. C$_{23}$H$_{37}$B$_9$MoO$_2$W requires C, 38.2; H, 5.2%). NMR (in CD$_2$Cl$_2$): ^{1}H, δ 1.11 [apparent triplet, 3 H, OCH$_2$*Me*, *J*(HH) 7], 2.31, 2.46, 2.54 (s × 3, 9 H, CMe and Me-4), 3.60 [s br, 1 H, CH(C$_2$B$_9$H$_{10}$Me)], 3.81–4.00 (m, 2 H, OC*H*$_2$Me), 5.29 (s, 7 H, C$_7$H$_7$), 5.64, 5.77 [(AB), 2 H, μ-CH$_2$, *J*(AB) 10], 6.99, 7.12 [(AB)$_2$, 4 H, C$_6$H$_4$,

J(AB) 7 Hz]; ^{13}C-{^{1}H}, δ 164.5 [C^{1}(C_6H_4)], 147.9 [μ-CH_2, J(WC) 40 Hz], 138.2, 138.0 [C^{4}(C_6H_4) and O*C*Me], 129.7, 129.2 (C_6H_4), 128.5 (*C*C_6H_4Me-4), 90.8 (C_7H_7), 78.7 (O*C*H_2Me), 77.1 [br, *C*H($C_2B_9H_{10}$Me)], 62.9 [br, *C*Me($C_2B_9H_{10}$Me)], 32.1 [C*Me*($C_2B_9H_{10}$Me)], 21.6, 21.1 (Me-4 and C*Me*), 17.1 ppm (OCH$_2$*Me*); ^{11}B-{^{1}H}, δ 4.2 (1 B), 1.1 (1 B), −6.7 (1 B), −7.9 (1 B), −8.8 (2 B), −10.1 (2B), −14.2 ppm (1 B).

Crystal structure determination for **3**

Diffracted intensities were collected at 298 K from a crystal of dimensions *ca* 0.45 × 0.30 × 0.20 mm on a Siemens R3m/V four-circle diffractometer. Of the 5182 unique reflections collected (θ–2θ scans, $3° \leqslant 2\theta \leqslant 50°$), 2506 had $F \geqslant 10\sigma(F)$, and only these were used for structure solution and refinement. The data were corrected for Lorentz and polarization effects, and for X-ray absorption, the latter by an empirical method based on azimuthal scan data.[15]

Crystal data. $C_{23}H_{37}B_9MoO_2W$, $M = 722.6$, monoclinic space group $P2_1/n$, $a = 11.724(6)$, $b = 17.12(1)$, $c = 14.87(1)$ Å, $\beta = 100.07(5)°$, $U = 2939(2)$ Å^3, $Z = 4$, $D_c = 1.64$ g cm^{-3}, $F(000) = 1408$ electrons, Mo-K_α X-radiation (graphite monochromator), $\bar{\lambda} = 0.71073$ Å, μ(Mo-K_α) = 44.3 cm^{-1}.

The structure was solved by first locating the metal atoms by direct methods, and then using successive difference Fourier syntheses to locate the remaining atoms except hydrogens. The latter were included in calculated positions (C—H 0.96 and B—H 1.10 Å),[16] with fixed isotropic thermal parameters. Only the metal atoms, and O(2), C(20), and C(21) were refined anisotropically. Poor quality data resulted from crystal twinning, as revealed by the peak profiles. Refinement by full matrix least squares led to $R = 0.10$ ($R' = 0.10$). A weighting scheme of the form $w^{-1} = [\sigma^2(F) + 0.005|F|^2]$ gave a satisfactory analysis of variance. The final electron-density difference synthesis showed one peak of 5.7 eÅ^{-3} near the W atom; this high value being due to the poor quality of the data. Calculations were performed on a DEC micro-Vax II computer with the SHELXTL PLUS system of programs,[15] scattering factors with corrections for anomalous dispersion were taken from ref. 17.

Additional material available from the Cambridge Crystallographic Data Centre comprise the atom coordinates, thermal parameters, and remaining bond distances and angles.

REFERENCES

1. F. G. A. Stone, *Adv. Organomet. Chem.* 1990, **31**, 53.
2. S. J. Dossett, I. J. Hart and F. G. A. Stone, *J. Chem. Soc., Dalton Trans.* 1990, 3481.
3. S. A. Brew, S. J. Dossett, J. C. Jeffery and F. G. A. Stone, *J. Chem. Soc., Dalton Trans.* 1990, 3709.
4. (a) M. R. Awang, R. D. Barr, M. Green, J. A. K. Howard, T. B. Marder and F. G. A. Stone, *J. Chem. Soc., Dalton Trans.* 1985, 2009; (b) E. Delgado, J. Hein, J. C. Jeffery, A. L. Ratermann, F. G. A. Stone and L. J. Farrugia, *J. Chem. Soc., Dalton Trans.* 1987, 1191; (c) M. E. Garcia, N. H. Tran-Huy, J. C. Jeffery, P. Sherwood and F. G. A. Stone, *J. Chem. Soc., Dalton Trans.* 1987, 2201.
5. W. A. Herrmann, *Adv. Organomet. Chem.* 1982, **20**, 159.
6. I. J. Hart, J. C. Jeffery, R. M. Lowry and F. G. A. Stone, *Angew. Chem. Int. Ed. Engl.* 1988, **27**, 1703.
7. M. J. Winter, *Adv. Organomet. Chem.* 1989, **29**, 101.
8. R. B. Calvert and J. R. Shapley, *J. Am. Chem. Soc.* 1977, **99**, 5225; A. J. Shultz, J. M. Williams, R. B. Calvert, J. R. Shapley and G. D. Stucky, *Inorg. Chem.* 1979, **18**, 319.
9. L. J. Farrugia, M. Green, D. R. Hankey, M. Murray, A. G. Orpen and F. G. A. Stone, *J. Chem. Soc., Dalton Trans.* 1985, 177.
10. M. Green, R. M. Mills, G. N. Pain, F. G. A. Stone and P. Woodward, *J. Chem. Soc., Dalton Trans.* 1982, 1309.
11. W. A. Herrmann, J. Plank, C. Bauer, M. L. Ziegler, E. Guggolz and R. Alt, *Z. Anorg. Allg. Chem.* 1982, **85**, 487; W. A. Herrmann, C. Bauer, G. Kriechbaum, H. Kunkely, M. L. Ziegler, D. Speth and E. Guggolz, *Chem. Ber.* 1982, **115**, 878.
12. M. H. Chisholm and R. J. Tatz, *Organometallics* 1986, **5**, 1590; M. H. Chisholm, B. W. Eichorn, K. Folting, J. C. Huffman and R. J. Tatz, *Organometallics* 1986, **5**, 1599.
13. J. C. Jeffery, A. G. Orpen, F. G. A. Stone and M. J. Went, *J. Chem. Soc., Dalton Trans.* 1986, 173; and references therein.
14. S. A. R. Knox, R. F. D. Stansfield, F. G. A. Stone, M. J. Winter and P. Woodward, *J. Chem. Soc., Dalton Trans.* 1982, 173.
15. G. M. Sheldrick, SHELXTL PLUS programs for use with the Siemens R3m/V X-ray system.
16. P. Sherwood, BHGEN, a program for the calculation of idealised H-atom positions for a *nido*-icosahedral carbaborane fragment, Bristol (1986).
17. *International Tables for X-Ray Crystallography*, Vol. 4. Kynoch Press, Birmingham (1974).

Polyhedron Vol. 9, No. 24, pp. 2959–2964, 1990
Printed in Great Britain

0277–5387/90 $3.00+.00
© 1990 Pergamon Press plc

SYNTHESIS AND CHEMISTRY OF THE BIS(TRIMETHYLSILYL)AMIDO BIS-TETRAHYDROFURANATES OF THE GROUP 2 METALS MAGNESIUM, CALCIUM, STRONTIUM AND BARIUM. X-RAY CRYSTAL STRUCTURES OF $Mg[N(SiMe_3)_2]_2 \cdot 2THF$ AND RELATED $Mn[N(SiMe_3)_2]_2 \cdot 2THF$

DONALD C. BRADLEY,* MICHAEL B. HURSTHOUSE,* ALI A. IBRAHIM, K. M. ABDUL MALIK, MAJID MOTEVALLI, REINHOLD MÖSELER, HAROLD POWELL, JOHN D. RUNNACLES and ALICE C. SULLIVAN*

Department of Chemistry, Queen Mary and Westfield College, Mile End Road, London E1 4NS, U.K.

(*Received* 29 *June* 1990; *accepted* 12 *August* 1990)

Abstract—Transamination reactions utilizing the compound mercuric bis(trimethylsilyl)amide, $Hg\{N(SiMe_3)_2\}_2$, in tetrahydrofuran (THF), and the metals Na, Mg, Ca, Sr, Ba and Al have been investigated. Thus the THF solvated compounds $Na[N(SiMe_3)_2] \cdot THF$ and $M[N(SiMe_3)_2]_2 \cdot 2THF$, M = Mg, Ca, Sr and Ba (**1–4**), have been prepared. The X-ray crystal structures of **1** and the related manganese compound $Mn[N(SiMe_3)_2]_2 \cdot 2THF$ (**5**) are reported. Interaction of the silylamides, **2–4**, with a range of crown ethers apparently proceeded with elimination of silylamine, $(Me_3Si)_2NH$, and novel ring opening of the crown ethers, generating species containing a donor alkoxide ligand with a vinyl ether function, presumably, $—O(CH_2CH_2O)_nCH{=}CH_2$ (n = 3–5). The silylamides **2–4** were also cleanly converted to the corresponding alkoxides (from ^1H NMR data) in reactions with stoichiometric quantities of 3-ethyl-3-pentanol.

The utility of σ-organomercury(II) compounds in redox transorganylation reactions is well established.[1] We have observed that mercury bis(trimethylsilyl)amide may be employed similarly for the amination of metals from groups 1 and 2 but not 3. In this paper we present details of these transamination reactions including the crystal and molecular structure of one of the products and of the analogous manganese compound. We also include a preliminary account of the reactions of the new silylamides with a range of crown-ethers and the alcohol, 3-ethyl-3-pentanol.

RESULTS AND DISCUSSION

Mercuric silylamide, $Hg[N(SiMe_3)_2]_2$, was prepared in the manner described by Burger,[2] and transamination reactions [eq. (1)]

$$n/2\,Hg[N(SiMe_3)_2]_2 + M \xrightarrow{THF} M[N(SiMe_3)_2]_n \cdot xTHF + n/2\,Hg \quad (1)$$

$$M = Na \quad n = 1, x = 1$$

$$M = Mg, Ca, Sr \text{ and } Ba \quad n = 2, x = 2$$

were explored for metals from groups 1–3 with decreasing electropositive character. Thus while the reaction with sodium proceeded smoothly at room temperature and the alkaline earth metals Mg, Ca, Sr and Ba reacted slowly in refluxing THF, there was no reaction with aluminium turnings even when surface cleaning agents like mercuric chloride were employed. It is noteworthy that attempted direct reactions between the alkaline earth metals Ca, Sr and Ba and the silylamine, $(Me_3Si)NH$, were unsuccessful despite the presence of catalytic quantities of mercuric chloride.

The new compounds **1–4** were isolated as colourless or pale cream crystalline solids. They showed

* Authors to whom correspondence should be addressed.

good thermal stability, with melting points decreasing down the group, but were extremely sensitive to air. The presence of two coordinated THF molecules was indicated by ^{1}H NMR spectroscopy. Surprisingly, the chemical shift of the single resonance observed for the trimethylsilyl protons was insensitive to the nature of the central metal atom for compounds **2**–**4**. The variable temperature NMR spectra recorded for the strontium compound, **3**, in the temperature range 293–203 K showed that the single resonance persisted although it was somewhat broadened at lower temperatures. A monomeric tetrahedral structure was confirmed by X-ray crystallography for the magnesium and related manganese compounds $M[N(SiMe_3)_2]_2 \cdot 2THF$. Mass spectra could only be obtained for $M[N(SiMe_3)_2]_2 \cdot 2THF$ (M = Mg, Mn). For the magnesium compound the highest mass peak observed (*m/z* 488) corresponded to the three-coordinated species, $\{Mg[N(SiMe_2)_2]_2 \cdot THF\}^+$, whereas for the manganese compound a species corresponding to the four-coordinated complex, $\{Mn[N(SiMe_3)_2]_2 \cdot 2THF\}^+$, was observed together with some fragment ions. Wannagat and co-workers had previously isolated the unsolvated species and the monomeric monoetherate, $Mg[N(SiMe_3)_2]_2 \cdot OEt_2$, from the reaction between diethylmagnesium and the silylamine, $(Me_3Si)_2NH$.[3,4] The crystal structures of the unsolvated manganese dimer, $\{Mn[N(SiMe_3)_2]_2\}_2$, the solvated three-coordinate manganese monomer, $Mn[N(SiMe_3)_2]_2 \cdot THF$, and the solvated samarium species, $Sm[N(SiMe_3)_2] \cdot 2THF$, have been mentioned in the literature.[5,6] It is noteworthy that the THF in compounds **2** and **5** could be replaced by pyridine giving stable bis-pyridine complexes, $M[N(SiMe_3)_2]_2 \cdot 2py$ (M = Ca, Mn). The manganese complex has been shown by single crystal X-ray diffraction to have a distorted tetrahedral structure.*

Crystal structures

The structure of the compounds $M[N(SiMe_3)_2]_2 \cdot 2THF$ (M = Mg, Mn) is given in Fig. 1 and substantial deviation from ideal tetrahedral geometry is apparent. The crystal data are given in Table 1 and selected bond lengths and angles are collected in Table 2. While the difference in the M—O bond lengths closely parallel the difference in the ionic radii (with Mg^{2+} 0.66 Å and Mn^{2+} 0.80 Å), the M—N distances are remarkably

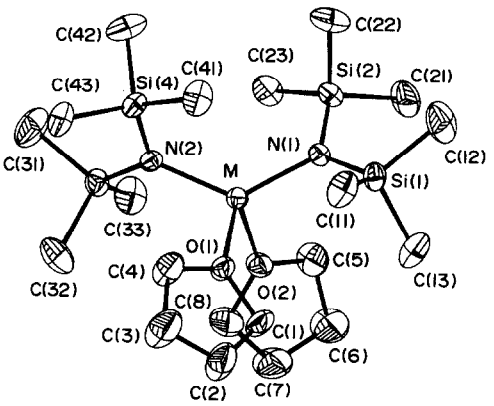

Fig. 1.

similar and apparently long—cf. Al—N 1.78 Å in $Al[N(SiMe_3)_2]_3$.[7] At the same time the N—Si distances in the Mg^{2+} and Mn^{2+} structures are short, a feature previously correlated with the ionic character of the $—N(SiMe_3)_2$ ligand,[8,9] although here the Si—N—Si angles are not particularly wide. This, together with the long M—N bonds, probably reflects severe interligand repulsions. Both complexes exhibited some tetrahedral flattening, with the dihedral angle between the planes described by O,M,O and N,M,N atoms wider than that expected for tetrahedral geometry.

Reactions between the compounds $M[N(SiMe_3)_2]_2 \cdot 2THF$ *and cyclic ethers*

Crown ethers form 1 : 1 complexes with alkali metal silylamides[10] but have been reported to stabilize the ionic products of the disproportionation equilibria said to be present in solutions of dialkylmagnesium and diorganoaluminium halides.[11] The reactions of the alkaline earth bis-silylamides, **2**–**4**, with the cyclic ethers, 12-crown-4, 15-crown-5 and 18-crown-6, in a 1 : 1 molar ratio, were explored in the expectation that similar equilibrium products might be detected. The reactions in fact proceeded with elimination of the silylamine, $(Me_3Si)_2NH$, and the formation of species containing an alkoxide ligand bearing the vinyl ether function, presumably, $—O(CH_2CH_2O)_nCH{=}CH_2$, n = 3–5. The reactions were followed by ^{1}H NMR spectroscopy, where the appearance of the vinyl ether residue was an unmistakable feature in every case. The elimination of silylamine was confirmed by a trapping experiment. For the most part the products were isolated as pentane-insoluble, colourless oils having free cyclic ether, as well as the ring-opened ether product present, and these were not further purified. An extremely air-sensitive, colourless solid, however, was obtained from the 18-crown-

* D. C. Bradley and M. B. Hursthouse, unpublished results.

Table 1. Crystal data, intensity data, collection parameters and details of refinement

	1	5
Stoichiometry	$C_{20}H_{52}N_2O_2Si_4Mg$	$C_{20}H_{52}N_2O_2Si_4Mn$
Mol. wt.	489.292	519.925
a (Å)	14.043(3)	14.057(3)
b (Å)	12.099(2)	12.182(2)
c (Å)	18.574(3)	18.646(3)
α (°)	90	90
β (°)	97.46(1)	97.06(1)
γ (°)	90	90
V (Å^3)	3129.13(1.2)	3168.78(1.2)
System	Monoclinic	Monoclinic
Space group	$P2_1/c$	$P2_1/c$
D_c (g cm^{-3})	1.039	1.090
Z	4	4
$F(000)$	1080	1132
Radiation	Cu-K_α	Mo-K_α
λ (Å)	1.5418	0.71069
μ (cm^{-1})	21.059	5.64
θ min/max	3.0, 65	1.5, 25
Temperature	R.T.	R.T.
Total data measured	5396	5048
Total data unique	5286	4934
Total data observed	3126	4321
Significance test	$F_o > 3\sigma(F_o)$	$F_o > 3\sigma(F_o)$
Number of parameters	300	300
g^a (weighting scheme)	0.000253	0.000350
Final $R = \Sigma\|\Delta F\|/\Sigma\|F_o\|$	0.0603	0.0532
Final RG	0.0600	0.0620

[a] $1/[\sigma^2(F_o)+gF_o^2]$.

Table 2. Selected structural data for $M[N(SiMe_3)_2]_2 \cdot 2THF$, M = Mg (1), M = Mn (5)

	1	5
	Bond lengths (Å)	
M—N	2.015(5)	2.033(5)
	2.027(5)	2.048(5)
M—O	2.086(5)	2.226(5)
	2.101(5)	2.249(5)
N—Si	1.702(5)–1.709(5)	1.699(5)–1.715(5)
Si—C	1.869(7)–1.893(7)	1.862(7)–1.888(7)
	Bond angles (°)	
N—M—N	127.9(2)	131.7(2)
O—M—O	89.8(2)	86.6(2)
O—M—N	100.7(2)–116.4(2)	98.40(2)–117.3(2)
Si—N—Si	120.2(3)	121.6(2)
	121.7(3)	123.5(2)
N—Si—C	110.9(3)–115.6(3)	110.6(3)–115.2(3)
	Dihedral angle (°)	
OMO/NMN	100.8	105.6

6/barium silylamide reaction and this was recrystallized from toluene, affording very solvent dependent needle-like crystals. The ^{1}H NMR spectrum indicated the presence of a species containing the pentaoxoduodeca-1-ene oxide along with silylamide and cyclic ether, to which we tentatively assigned the composition $[(Me_3Si)_2N][BaO(CH_2CH_2O)_5CH{=}CH_2]$[18-crown-6]. The isolation of polyoxaalkane-eneoxide-containing products suggested a mechanism (Scheme 1) involving proton abstraction from coordinated crown-ether by the silylamide anion, with subsequent C—O bond cleavage and generation of the vinyl ether

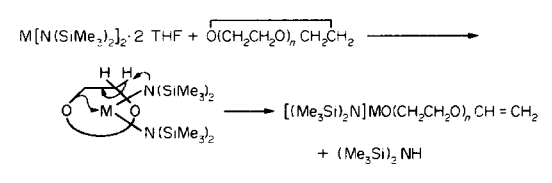

Scheme 1.

residue and donor alkoxide linkage. The free silylamide anion has not been isolated or detected but a linear structure is probably the most stable conformation for this species. The potassium compound $KN(SiMe_3)_2(dioxane)_2$ adopted a structure with the widest observed Si—N—Si angle (136.3°) suggesting a high degree of ionic character, although the K—N distance (2.70 Å) suggested that this species may at best be viewed as a tight ion pair.[8] The related free amide ion, $[Ph_3SiNSiPh_3]^-$, has an Si—N—Si angle of 154.9(3)°.[20] This type of ring-opening reactivity is to our knowledge unprecedented for crown ethers but similar base-promoted ring-opening has recently been observed for a range of crown-thioether complexes, $[M([9]aneS_3)_2]^{3+}$, M = Co, Rh, Ir.[12]

The THF solvated alkaline earth silylamides, **2–4**, were recovered unchanged from solutions in dioxane. There was, in addition, no apparent reaction between mercuric silylamide and 18-crown-6 ether. Implicit in these observations, and the fact that alkali metal silylamides form 1 : 1 complexes with crown ethers, is that the ring opening reaction requires a multidentate coordinating ether and a metal silylamide which is at least divalent and has a high degree of ionic character.

Reactions with 3-ethyl-3-pentanol

Metal silylamides are widely used as precursors for a range of other metallo-organic species including metal alkoxides.[13,14] Group II metal alkoxides are generally obtained by direct reaction with primary alcohols, but reaction with tertiary alcohols is sluggish.[15] The availability of the group 2 bis-silylamides offered a convenient route to the corresponding metal tertiary alkoxides and this was demonstrated by their reactions with 3-ethyl-3-pentanol. The series of compounds $[M(OCEt_3)_2]$, M = Ca, Sr and Ba (**6–8**), was isolated as colourless (Ca and Sr) or pale orange (Ba) solids. Their ^1H NMR spectra showed pronounced second-order effects at 80 MHz, but simple first-order spectra were obtained at 250 MHz and these indicated a single alkoxide environment. The single magnetic environment persisted at −10°C, below which temperature solubility problems were encountered.

EXPERIMENTAL

Synthetic work was carried out using standard Schlenk procedures. Solvents were dried over and distilled from the sodium ketyl of benzophenone, or molecular sieves. The spectroscopically pure silylamides consistently gave low carbon and nitrogen analyses despite several attempts to obtain these in each case from two different analytical services. Microanalytical data were obtained from the Butterworth and University College London services. Instruments: NMR, Bruker WP80 and WM-250, data were referenced to the C_6D_5H signal at 7.2 ppm, or the C_3D_5HO signal at 2.05 ppm, or the C_7D_5H signal at 2.1 ppm; Mass spectrometer, Kratos MS-902, E I, recorded at 70 eV; IR, Perkin–Elmer Grating Infrared spectrometer 225 and FTIR 1720 × (selected data are given in Table 3); UV–vis, Beckman DK 2 spectrometer.

Table 3. Selected IR data (cm^{-1}) for compounds $M[N(SiMe_3)_2]_2 \cdot 2THF$ (as Nujol mulls) (M = Mg, Ca, Sr, Ba, Mn)

M	$\nu_{as}(MN_2)$	$\nu_{as}(NSi_2)$	$\nu_{as}(COC)$
Mg	360(s)	988(vs)	1022(s)
Ca	367(s)	931(vs)	1050(s)
Sr	361(s)	1078(vs)	1021(s)
Ba	360(s)	1085(vs)	1036(s)
Mn	364(m)	1000(s)	1072(m)

$Na[N(SiMe_3)_2] \cdot THF$[16] *from* $Hg[N(SiMe_3)_2]_2$ *and sodium metal*

Freshly cleaned sodium metal (0.26 g, 11.3 mmol) was treated with a solution of mercuric silylamide (3.03 g, 5.82 mmol) in THF (25 cm^3). The stirred reaction mixture was held at room temperature for several hours and mercury metal was deposited from the resultant green solution. After 18 h the mixture was filtered and the solvent evaporated. The residual white solid was crystallized from a toluene–pentane mixture giving the white microcrystalline product (1.06 g, 37%). ^1H NMR (C_6D_6): 0.15 [s, 18H, $N(SiMe_3)_2$], 1.2 (m, 4H, THF), 3.54 (m, 4H, THF).

$Mg[N(SiMe_3)_2]_2 \cdot 2THF$ (**1**)

This compound was prepared from magnesium turnings (0.37 g, 15.02 mmol) and mercuric silylamide (4.02 g, 7.68 mmol) in refluxing THF (25 cm^3). The work-up given for sodium silylamide above afforded large transparent flakes from toluene–hexane (1 : 2) (2.8 g, 75%). ^1H NMR (C_6D_6): 0.27 [s, 36H, $N(SiMe_3)_2$], 1.2 (m, 8H, THF) 3.54 (m, 8H, THF). Mass spectrum: *m/z* 488 (1%) $[M-THF]^+$, 344 (2.3 %) $[Mg(N(SiMe_3)_2)(N(SiMe_3))]^+$.

$Ca[N(SiMe_3)_2]_2 \cdot 2THF$ (**2**)

This compound was prepared from mercuric silylamide (7.8 g, 15 mmol) and calcium metal (0.65 g,

16 mmol) in refluxing THF (100 cm^3) over 10 h. The solvent was evaporated and the pentane-soluble product filtered twice. The concentrated solution was cooled at −25°C affording colourless needles (6.6 g, 86%), m.p. 151–153°C. ^1H NMR (C_6D_6): 0.38 [s, 36H, $N(SiMe_3)_2$], 1.2 (m, 8H, THF), 3.6 (m, 8H, THF). Found: C, 45.5; H, 10.2; N, 5.3; Ca, 8.7. Calc. for $CaN_2Si_4C_{20}H_{52}O_2$: C, 47.5; H, 10.4; N, 5.5; Ca, 7.9%.

$Sr[N(SiMe_3)_2]_2 \cdot 2THF$ (**3**)

Prepared in the manner described for **2**, from mercuric silylamide (5.93 g, 11.4 mmol) and strontium metal (1 g, 11.4 mmol) in refluxing THF (150 cm^3). Isolated as colourless needles from pentane at −25°C (4.8 g, 76%), m.p. 128–130°C. ^1H NMR (C_6D_6): 0.38 [s, 36H, $N(SiMe_3)_2$], 1.32 (m, 8H, THF), 3.6 (m, 8H, THF). Found: C, 40.7; H, 9.5; N, 4.4; Sr, 17.1. Calc. for $SrN_2Si_4C_{20}H_{52}O_2$: C, 43.4; H, 9.5; N, 5.0; Sr, 16.0%.

$Ba[N(SiMe_3)_2]_2 \cdot 2THF$ (**4**)

Prepared in the manner described for **2**, from mercuric silylamide (3.64 g, 7 mmol) and barium metal (1 g, 7.3 mmol) in refluxing THF. Isolated as colourless needles (2.63 g, 53%), m.p. 88–90°C. ^1H NMR (C_6D_6): 0.33 [s, 36H, $N(SiMe_3)_2$], 1.32 (m, 8H, THF), 3.6 (m, 8H, THF). Found: C, 37.7; H, 8.5; N, 4.7; Ba, 23.1. Calc. for $BaN_2Si_4C_{20}H_{52}O_2$: C, 39.9; H, 8.7; N, 4.7; Ba, 22.8%.

$Mn[N(SiMe_3)_2]_2 \cdot 2THF$ (**5**)

The procedure described[5] for the synthesis of the dimer $\{Mn[N(SiMe_3)_2]\}_2$ was followed and the bis-tetrahydrofuranate was obtained on recrystallization of the product from THF. Mass spectra: *m/z* 578 (12%) $[M-H]^+$. UV–vis cm^{-1} (dm^3 mol^{-1} cm^{-1}) (THF): 20,400 (sh), 22,200 (0.5); 23,700, 25,600 (0.25), 27,300, 30,100. Magnetic susceptibilities (Gouy balance) over a temperature range (298–123 K) obeyed the Curie–Weiss law ($\theta = -12$ K) with average $\mu_{eff} = 6.06 \pm 0.02$ BM.

$Ca[N(SiMe_3)_2]_2 \cdot 2pyridine$

To a stirred solution of **2**, in THF at room temperature, was added pyridine (excess). This mixture was stirred for 2 h and the solvents removed under reduced pressure. Pale yellow leaf-like crystals were obtained from pentane solutions of the product. ^1H NMR (C_6D_6): 0.4 [s, 36H, $N(SiMe_3)_2$], 6.7 (m, C_5H_5N), 6.86 (m, C_5H_5N), 8.72 (m, C_5H_5N). Found: C, 49.3; H, 8.9; N, 9.9. Calc. for $CaN_4Si_4C_{22}H_{46}$: C, 50.9; H, 8.9; N, 10.8%.

*Reactions with crown-ethers**

Typically, a THF solution of the metal silylamide, $M[N(SiMe_3)_2]_2 \cdot 2THF$ (M = Ca, Sr or Ba) (0.5 g in 50 cm^3), was treated with one molar equivalent of crown-ether (one of 12-crown-4, 15-crown-5 or 18-crown-6) in THF (25 cm^3). The resultant mixture was stirred at room temperature for approximately 2 days. The volatiles were removed under reduced pressure and the residual material washed several times with pentane. Oils were generally obtained but a solid product was isolated from the reaction between 18-crown-6 ether and compound **4**. This solid was recrystallized from toluene giving colourless solvent-dependent needles; proposed composition $[(Me_3Si)_2N]BaO(CH_2CH_2O)_5CH{=}CH_2$(18-crown-6). ^1H NMR (C_7D_8) of (18-crown-6/compound **4** reaction product): 0.3 [s, 18H, $N(SiMe_3)_2$], 3.4–3.95 [m, 44H, $-O(CH_2CH_2O)_5$ and $\overline{O(CH_2CH_2O)_5CH_2CH_2}$],

3.95 (dd, 1H, 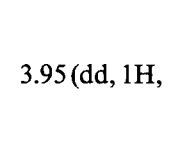),

4.2 (dd, 1H, 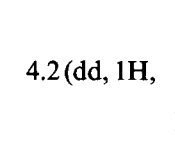),

6.43 (q, 1H, 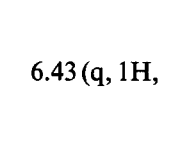)

$^3J_{ac} = 14$ Hz, $^3J_{ab} = 7$ Hz, $^2J_{bc} = 2$ Hz.

$[Ca(OCEt_3)_2]$ (**6**)

A stirred solution of **2** (2.9 g, 5.7 mmol) in benzene (200 cm^3) was treated with 3-ethyl-3-pentanol (1.33 g, 11.4 mmol). The mixture was held at the reflux temperature for 10 h and subsequently stirred at room temperature for 48 h. The solvent was evaporated and the colourless residual solid washed several times with pentane affording the product (1.2 g, 74%), m.p. > 350°C dec. ^1H NMR (C_3D_6O): 0.83 (t, 18H, $-CH_3$), 1.4 (q, 12H, $-CH_2$). Found: Ca, 15.0. Calc. for $CaO_2C_{14}H_{30}$: Ca, 14.8%.

*A full account of this work will be presented elsewhere.

$[Sr(OCEt_3)_2]$ (7)

This compound was prepared in the manner described for the calcium compound above from **3** (3.0 g, 5.4 mmol) and 3-ethyl-3-pentanol (1.27 g, 11.0 mmol) giving a white solid (1.3 g, 77%), m.p. > 300°C. ^{1}H NMR (C_3D_6O): 0.85 (t, 18H, —CH_3), 1.45 (q, 12H, —CH_2). Found: Sr, 28.7. Calc. for $SrO_2C_{14}H_{30}$: Sr, 27.5%.

$[Ba(OCEt_3)_2]$ (**8**)

This compound was prepared as described for the calcium derivative above from **4** (3 g, 4.9 mmol) and 3-ethyl-3-pentanol (1.2 g, 10.3 mmol) giving an orange solid (1.32 g, 72%). ^{1}H NMR (C_3D_6O): 0.85 (t, 18H, —CH_3), 1.43 (q, 18H, —CH_2). Found: C, 43.7; H, 8.3; Ba, 37.2. Calc. for $BaO_2C_{14}H_{30}$: C, 45.7; H, 8.2; Ba, 37.3%.

Crystallography

Measurements were made on crystals sealed under nitrogen in glass capillaries using a CAD4 diffractometer operating in the ω–2θ scan mode with graphite-monochromated Mo-K_α radiation ($\lambda = 0.71069$ Å) as previously described.[17] The intensity data were corrected for absorption empirically using psi-scan profiles. The structures were solved using standard heavy-atom procedures and refined using full-matrix least-squares methods[18] with scattering factors calculated from data obtained from reference 19. Non-hydrogen atoms were refined with anisotropic displacement factors; hydrogen atoms were included in idealized positions and refined with group isotropic displacement factors.

Acknowledgements—We thank the SERC and Queen Mary and Westfield College for grants and equipment and one of us (A.C.S.) thanks the SERC for an Advanced Fellowship. The Sudan Government and the British Council are thanked for support to A.A.I. We are also grateful to Mr Greg Coumbarides for the NMR spectra, and Mr Peter Cook for mass spectra.

REFERENCES

1. G. B. Deacon and A. J. Goplick, *J. Organomet. Chem.* 1978, **146**, C43; J. Vicento, J. A. Abad and J. F. Guttierrez-Jugo, *J. Chem. Soc., Dalton Trans.* 1989, **11**, 2241.
2. H. Burger, W. Sawodny and U. Wannagat, *J. Organomet. Chem.* 1965, **3**, 113.
3. H. Autzen, H. Kuckertz, H. J. Wismar and W. Wannagat, *Z. Anorg. Allg. Chem.* 1972, **394**, 254.
4. T. Fjeldberg and R. A. Andersen, *J. Molec. Struct.* 1984, **125**, 287.
5. D. C. Bradley, M. B. Hursthouse, K. M. Abdul Malik and R. Möseler, *Transition Met. Chem.* 1978, **3**, 253.
6. W. J. Evans, D. K. Drummond, H. Zhang and J. L. Atwood, *Inorg. Chem.* 1988, **27**, 575.
7. R. Grüning and J. L. Atwood, *J. Organomet. Chem.* 1977, **137**, 101.
8. A. M. Domingos and G. M. Sheldrick, *Acta Cryst.* 1974, **B30**, 517.
9. J. S. Ghotra, M. B. Hursthouse and A. J. Welch, *J. Chem. Soc., Chem. Commun.* 1973, 669.
10. P. P. Power and Xu Xiaojie, *J. Chem. Soc., Chem. Commun.* 1984, 358.
11. H. G. Richey Jr and G. L. BergStresser, *Organometallics* 1988, **7**, 1459.
12. A. J. Blake, A. J. Holder, T. I. Hyde, H-J. Kuppers, M. Schröder, S. Stötzel and K. Wieghardt, *J. Chem. Soc., Chem. Commun.* 1989, 1400.
13. M. Bochmann, M. B. Hursthouse and G. Wilkinson, *J. Chem. Soc., Dalton Trans.* 1980, 1863.
14. D. Barr, R. A. Bartlett, D. Decker, M. M. Olmstead and P. P. Power, *Inorg. Chem.* 1987, **26**, 1773.
15. D. C. Bradley, R. C. Mehrotra and D. P. Gaur, *Metal Alkoxides*. Academic Press, London (1978).
16. U. Wannagat, *Adv. Inorg. Chem. and Radiochem.* 1964, **6**, 225.
17. R. A. Jones, M. B. Hursthouse, K. M. A. Malik and G. Wilkinson, *J. Am. Chem. Soc.* 1979, **101**, 4128.
18. G. M. Sheldrick, SHELX-76, Program for crystal structure determination. University of Cambridge, U.K. (1976).
19. *International Tables for X-Ray Crystallography*, Vol. 4. Kynoch Press, Birmingham, U.K. (1974).
20. H. Chen, R. A. Bartlett, H. V. Rasika Dias, M. M. Olmstead and P. P. Power, *J. Am. Chem. Soc.* 1989, **111**, 4338.

Polyhedron Vol. 9, No. 24, pp. 2965–2969, 1990
Printed in Great Britain

0277–5387/90 $3.00+.00
Pergamon Press plc

REACTION OF THE TETRASULPHIDOMOLYBDENUM(IV) COMPLEX LMo(NCS)(S_4) WITH DICARBOMETHOXYACETYLENE: X-RAY STRUCTURE OF LMo(NCS){$S_2C_2(CO_2Me)_2$} [L = HYDROTRIS(3,5-DIMETHYLPYRAZOLYL)BORATE]

ASTON A. EAGLE and CHARLES G. YOUNG*

Department of Chemistry, La Trobe University, Bundoora, Victoria 3083, Australia

and

EDWARD R. T. TIEKINK

Department of Physical and Inorganic Chemistry, University of Adelaide, Adelaide, South Australia 5000, Australia

(*Received* 14 *May* 1990; *accepted* 13 *August* 1990)

Abstract—The reaction of {$HB(Me_2pz)_3$}Mo(NCS)(S_4) [$HB(Me_2pz)_3^-$ = hydrotris(3,5-dimethylpyrazolyl)borate anion] with dicarbomethoxyacetylene in refluxing toluene results in the formation of the brown, diamagnetic complex {$HB(Me_2pz)_3$}Mo(NCS){$S_2C_2(CO_2Me)_2$} (**1**) (the reactants above also yield **1** upon prolonged reaction in dichloromethane at 25°C), which has been characterized by X-ray crystallography. The mononuclear pseudo-octahedral complex contains a facially tridentate $HB(Me_2pz)_3^-$ ligand, a monodentate N-bound NCS^- ligand, and a bidentate $S_2C_2(CO_2Me)_2^{2-}$ ligand having a near planar MoS_2C_4 fragment and a SC=CS bond distance of 1.342(15) Å. Solutions of **1** are unstable in air and decompose to produce {$HB(Me_2pz)_3$}MoO_2(NCS) and {$HB(Me_2pz)_3$}MoO$(NCS)_2$.

The reactions of *cis*-{$HB(Me_2pz)_3$}MoO_2X (X = F^-, Cl^-, Br^-, NCS^-) complexes with sulphiding agents result in the formation of the tetrasulphidomolybdenum(IV) complexes {$HB(Me_2pz)_3$}$MoX(S_4)$.[1] NMR and X-ray crystallographic studies of these complexes indicate that the S_4^{2-} ligand possesses a degree of dithiolene-like character unprecedented in tetrasulphidomolybdenum complexes. Thus, in {$HB(Me_2pz)_3$}$MoCl(S_4)$ the S_4^{2-} ligand is planar with very short Mo—S bond distances and alternating S—S distances, indicative of $d\pi$–$p\pi$ bonding between molybdenum and sulphur and multiple bonding between the two uncoordinated sulphur atoms. In all the complexes, a methyl group on one of the pyrazole rings resides near and perpendicular to the centroid of the MoS_4 ring; this group exhibits a very shielded ^{1}H NMR signal (δ *ca* 0) due to its residence within a shielding zone presumably associated with the MoS_4 fragment. Previously characterized tetrasulphidomolybdenum complexes exhibit puckered MoS_4 rings which possess varying degrees of bond distance alternation.[1] Due mainly to their biological relevance, the reactions of polysulphido ligands with cyanide, phosphines and activated acetylenes have received considerable attention. Polysulphido complexes of Ti,[2] V,[2] Mo[3] and Fe[4] react with activated acetylenes to produce 1,2-dithiolene complexes. These reactions are reminiscent of the first synthesis of a dithiolene complex from diphenylacetylene and nickel sulphide.[5,6] In one case, the reaction of $[Mo_2O_2(\mu\text{-}S)_2(S_2)_2]^{2-}$ with dicarbomethoxyacetylene, an unusual molybda-2,3-dithiacyclopent-4-ene ring complex was formed.[7] We have now explored the reactivity of the tetra-

* Author to whom correspondence should be addressed.

sulphido ligand of $\{HB(Me_2pz)_3\}Mo(NCS)(S_4)$ with dicarbomethoxyacetylene and our results are reported herein.

EXPERIMENTAL

Materials and methods

The complex $\{HB(Me_2pz)_3\}Mo(NCS)(S_4)$ was prepared according to the method of Young *et al.*[1] Dicarbomethoxyacetylene was used as obtained from Aldrich Chemical Company. All solvents used were carefully dried, distilled and deoxygenated prior to use. Unless otherwise stated, all reactions were performed under an atmosphere of pure dinitrogen, employing standard Schlenk line techniques. Microanalyses were performed by Atlantic Microlabs. IR spectra were obtained on a Perkin–Elmer 1430 Ratio Recording IR spectrophotometer using pressed KBr discs with polystyrene as reference. NMR spectra were obtained using a Jeol JNM FX-200 Fourier transform spectrometer and were referenced against chloroform. Mass spectra were provided courtesy of Dr Sydney Middleton of Monash University. Column chromatography was performed on a 50 cm column using Merck Art. 7734 Kieselgel 60. TLCs were run on Merck Art. 5735 DC-Plastikfolien Kieselgel 60 F_{254}.

Synthesis of $\{HB(Me_2pz)_3\}Mo(NCS)\{S_2C_2(CO_2Me)_2\}$ (1)

A solution of $\{HB(Me_2pz)_3\}Mo(NCS)(S_4)$ (0.2 g, 0.345 mmol) and dicarbomethoxyacetylene (0.21 cm^3, 1.71 mmol) in toluene (10 cm^3) was heated at 60°C for 1 day. The fine brown crystals formed were filtered in air, washed with toluene (5 cm^3) and dried *in vacuo*. Yield 0.151 g (66.8%).

Found: C, 40.0; H, 4.2; N, 14.9; S, 14.6. Calc. for $C_{22}H_{28}BMoN_7O_4S_3$: C, 40.2; H, 4.3; N, 14.9; S, 14.6%. IR (KBr): 2960m, 2565m, 2040vs, 1730s, 1720s, 1535s, 1460s, 1440s, 1430s, 1415s, 1385s, 1355s, 1230s, 1185s, 1065s, 1045s, 1025s, 965m, 900m, 855s, 810s, 790m, 755m, 705m, 690m, 645m, 465m, 370m and 295m cm^{-1}. ^1H NMR ($CDCl_3$): δ 2.38 and 2.60 [s, 2 × 3H, 2 × CH_3 of $HB(Me_2pz)_3^-$], 2.39 and 2.63 [s, 2 × 6H, 4 × CH_3 of $HB(Me_2pz)_3^-$], 3.86 (s, 6H, 2 × CH_3 of ester groups), 5.57 [s, 1H, CH of $HB(Me_2pz)_3^-$], 5.88 [s, 2 × 1H, 2 × CH of $HB(Me_2pz)_3^-$]. Electronic spectrum (CH_2Cl_2) λ_{max}, nm (ε, M^{-1} cm^{-1}): 655 (900), 520 (1960), 403 (6730), 330 (12,000, sh), 285 (16,850). Mass spectrum, *m/z* (%) for $[1]^+$: 652 (8), 653 (48), 654 (21), 655 (53), 656 (74), 657 (84), 658 (79), 659 (100), 660 (37), 661 (42), 663 (13), 664 (5).

Reaction of $\{HB(Me_2pz)_3\}Mo(NCS)(S_4)$ *and* $C_2(CO_2Me)_2$ *in dichloromethane*

A solution of $\{HB(Me_2pz)_3\}Mo(NCS)(S_4)$ (0.15 g, 0.26 mmol) and dicarbomethoxyacetylene (0.035 cm^3, 0.28 mmol) in dichloromethane (20 cm^3) was stirred for a period of 2 months. The green coloration slowly dissipated and a brown solution was produced. TLC showed a good yield (estimated 70%) of **1** was present. Further stirring for 3 months led to a red solution. Column chromatography yielded a single orange fraction. Yield 0.09 g. The substance was shown to be a mixture of $\{HB(Me_2pz)_3\}MoO(NCS)_2$[8] (*ca* < 5%) and $\{HB(Me_2pz)_3\}MoO_2(NCS)$[9] by comparison with spectroscopic data from authentic samples.

Crystal structure determination of 1

Crystals suitable for X-ray diffraction studies were grown anaerobically by slow diffusion of hexane into a saturated dichloromethane solution of complex. Intensity data were measured at room temperature on an Enraf–Nonius CAD-4F diffractometer fitted with Mo-K_α radiation, $\lambda = 0.7107$ Å. The ω–2θ scan technique was employed to measure

Table 1. Experimental details of the crystal structure determination for **1**

Chemical formula	$C_{22}H_{28}BMoN_7O_4S_3$
fw	657.44
Crystal colour	Black–brown
Crystal system	Monoclinic
Space group	$P2_1/n$ (No. 14)
a (Å)	11.080(1)
b (Å)	14.052(1)
c (Å)	19.438(2)
β (°)	101.15(1)
V (Å^3)	2969.3
Z	4
ρ_{calc} (g cm^{-3})	1.471
$F(000)$	1343
μ (cm^{-1})	6.4
θ limits (°)	1.5–23.5
Scan technique	ω–2θ
Temperature (K)	295
Data measured	4856
hkl range	$\pm h, +k, +l$
Unique data	4329
Data with $I > 2.5\sigma(I)$	2405
Number of parameters	234
R	0.063
R_w	0.062
Max/min residual electron density (eÅ^{-3})	+0.80; −0.61

Table 2. Selected bond distances (Å) and angles (°) for **1**

Bond distances			
Mo—N(1)	2.067(10)	N(1)—C(1)	1.169(14)
Mo—S(2)	2.349(3)	C(1)—S(1)	1.577(14)
Mo—S(3)	2.365(3)	S(2)—C(2)	1.753(11)
Mo—N(11)	2.173(8)	S(3)—C(3)	1.704(10)
Mo—N(21)	2.179(8)	C(2)—C(3)	1.342(15)
Mo—N(31)	2.166(8)		

Bond angles			
S(2)—Mo—S(3)	83.5(1)	N(1)—Mo—S(2)	98.3(3)
N(1)—Mo—S(3)	92.7(3)	N(1)—Mo—N(11)	165.1(3)
N(1)—Mo—N(21)	86.7(3)	N(1)—Mo—N(31)	84.9(3)
S(2)—Mo—N(11)	93.9(2)	S(2)—Mo—N(21)	92.9(2)
S(2)—Mo—N(31)	176.8(3)	S(3)—Mo—N(11)	97.2(2)
S(3)—Mo—N(21)	176.2(2)	S(3)—Mo—N(31)	96.7(2)
N(11)—Mo—N(21)	84.1(3)	N(11)—Mo—N(31)	82.9(3)
N(21)—Mo—N(31)	87.0(3)	Mo—N(1)—C(1)	170.8(9)
N(1)—C(1)—S(1)	178.7(12)	Mo—S(2)—C(2)	106.5(4)
Mo—S(3)—C(3)	106.5(4)	S(2)—C(2)—C(3)	120.1(8)
S(3)—C(3)—C(2)	122.6(8)	S(2)—C(2)—C(4)	113.7(9)
S(3)—C(3)—C(6)	115.1(8)	C(2)—C(3)—C(6)	122.3(10)
C(3)—C(2)—C(4)	126.1(10)		

the intensities of 4856 reflections (θ_{max} 23.5°); the data were corrected for Lorentz and polarization effects but not for absorption. Of the reflections measured, 4329 were unique of which 2405 satisfied the $I > 2.5\sigma(I)$ criterion of observability and were used in the subsequent analysis. Relevant crystal data and details of the refinement are listed in Table 1. The structure of **1** was solved from the interpretation of the Patterson synthesis and refined by a full-matrix least-squares procedure based on F.[10] Non-carbon, non-hydrogen atoms were refined with anisotropic thermal parameters and hydrogen atoms were included in the model at their calculated positions. After the introduction of a weighting scheme of the form $w = k/[\sigma^2(F)+g|F|^2]$ (k = 1.55, g = 0.0011), the refinement was continued until convergence. Refinement was performed with the SHELX 76[10] suite of programs installed on a SUN4/280 computer. Selected interatomic parameters are given in Table 2 and the numbering scheme employed (drawn with ORTEP II[11]) is shown in Fig. 1. Scattering factors for neutral molybdenum corrected for f' and f'' were from ref. 12 and those for the remaining atoms were as incorporated in the SHELX 76 program. Material deposited comprises fractional atomic coordinates, thermal parameters, hydrogen atom parameters, all bond lengths and angles and structure factor tables.

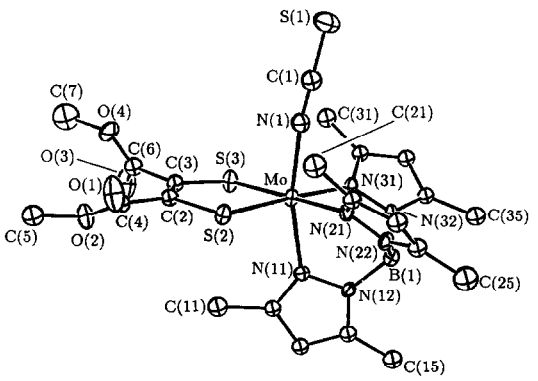

Fig. 1. Molecular structure and crystallographic numbering scheme employed for **1**.

RESULTS AND DISCUSSION

We have explored the reaction of $\{HB(Me_2pz)_3\}$ $Mo(NCS)(S_4)$ and dicarbomethoxyacetylene under various conditions and have thoroughly characterized the major product thereof as $\{HB(Me_2pz)_3\}Mo(NCS)\{S_2C_2(CO_2Me)_2\}$ (**1**). At room temperature in dichloromethane a very slow reaction took place and after a period of months the initial green solution had changed to brown. Chromatographic investigation of the reaction mixture indicated a *ca* 70% yield of **1**. Column chromatography of the reaction mixture after 6 months yielded an orange fraction which

contained $\{HB(Me_2pz)_3\}MoO_2(NCS)$[9] contaminated by a small amount of intensely coloured $\{HB(Me_2pz)_3\}MoO(NCS)_2$.[8] The source of the oxygen in the final product must arise from adventitious air, consistent with the independent observation that solutions of **1** are air sensitive. The reaction of $\{HB(Me_2pz)_3\}Mo(NCS)(S_4)$ with dicarbomethoxyacetylene, in refluxing toluene, results in the relatively rapid formation of **1**, which precipitates as brown crystals from the reaction mixture. The above reactions result in the formation of a dithiolene ligand, $S_2C_2(CO_2Me)_2^{2-}$, and sulphur (initially) through reaction of the tetrasulphido ligand with the activated acetylene. The possible mechanisms of this type of reaction have been discussed,[3b] but our observations shed no light on the mechanism of our reaction. We have been unable, for example, to prepare $\{HB(Me_2pz)_3\}MoX(S_2)$ complexes in order to test their reactivity with dicarbomethoxyacetylene, as support for the conversion of S_4^{2-} to S_2^{2-} (plus sulphur) prior to the concerted reaction of the S_2^{2-} ligand with acetylene. Examination of space-filling molecular models indicates that although sterically encumbered due to the $HB(Me_2pz)_3^-$ ligand, the coordinated sulphurs of the S_4^{2-} ligand are also able to undertake direct nucleophilic attack on the acetylenic carbons prior to expulsion of sulphur.

Complex **1** has been characterized by elemental analysis, IR, electronic and ^1H NMR spectroscopy, mass spectrometry and X-ray crystallography. Besides the many bands characteristic of the $HB(Me_2pz)_3^-$ ligand, the IR spectrum of **1** exhibits a strong band at 2040 cm^{-1}, which may be assigned to the NCS^- ligand, and bands at 1730, 1720 and 1230 cm^{-1}, which may be assigned to the bidentate $S_2C_2(CO_2Me)_2^{2-}$ ligand.[3] The ^1H NMR spectrum of **1** indicates that the molecule has C_s symmetry in solution, with the methyl and methine resonances of the facially coordinated $HB(Me_2pz)_3^-$ ligand having intensity ratios of 3 : 3 : 6 : 6 and 1 : 2, respectively. Only one resonance is observed for the methyl groups of the $S_2C_2(CO_2Me)_2^{2-}$ ligand. Thus, the mirror plane bisects the dithiolene ligand and contains the molybdenum atom and NCS^- ligand. The electronic spectrum of **1** is dominated by intense bands assigned to charge-transfer transitions. The mass spectrum of **1** exhibits a parent $[1]^+$ ion cluster with m/z 659.0; the calculated isotope pattern for $[1]^+$ closely matches that of the observed parent ion.

The X-ray crystal structure of **1** has been determined. The pseudo-octahedral complex (Fig. 1) is composed of a facially tridentate $HB(Me_2pz)_3^-$ ligand, a bidentate $S_2C_2(CO_2Me)_2^{2-}$ ligand and a monodentate N-bound thiocyanate ligand. The equatorial girdle composed of the S(2), S(3), N(21) and N(31) atoms is co-planar with the molybdenum atom with a maximum atom deviation of 0.10(1) Å [for N(31)] in the five-atom equatorial plane. The N(1) and N(11) atoms are 2.05(1) and 2.151(8) Å, respectively, from the equatorial plane, and the Mo—N(1,11) vectors are both tilted away from the dithiolene ligand; consequently, the N(1)—Mo—N(11) angle is only 165.1(3)°. The Mo—S distances are an average 2.357 Å and the average Mo—S—C angle is 106.5(4)°. The S—C bond distances of the dithiolene ligand are 1.75(1) and 1.70(1) Å and the C(2)—C(3) distance is 1.342(15) Å. The $S_2C(CO_2Me)_2$ fragment of the dithiolene ligand is planar with a maximum atom deviation from the plane of 0.07 Å [for C(4) and C(6)]; the molybdenum atom is 0.2376(9) Å out of the plane of this fragment and the dihedral angle between the ligand plane and the Mo,S(2),S(3) plane is 7.78°. The geometry and metrical parameters for the dithiolene ligand are very similar to those reported for related molybdenum dithiolene complexes.[3,5,13,14] The Mo—N bond distances of the $\{HB(Me_2pz)_3\}Mo$ fragment are identical within experimental error and average 2.173 Å. The metrical data for the NCS^- and $HB(Me_2pz)_3^-$ ligands are similar to those reported for related complexes.[15,16]

Acknowledgement—The financial support of the Australian Research Council is gratefully acknowledged.

REFERENCES

1. C. G. Young, I. P. McInerney, M. A. Bruck and J. H. Enemark, *Inorg. Chem.* 1990, **29**, 412.
2. C. M. Bolinger and T. B. Rauchfuss, *Inorg. Chem.* 1982, **21**, 3947.
3. (a) M. Draganjac and D. Coucouvanis, *J. Am. Chem. Soc.* 1983, **105**, 139; (b) D. Coucouvanis, A. Hadjikyriacou, M. Draganjac, M. G. Kanatzidis and O. Ileperuma, *Polyhedron* 1986, **5**, 349.
4. M. G. Kanatzidis and D. Coucouvanis, *Inorg. Chem.* 1984, **23**, 403.
5. G. N. Schrauzer and V. P. Mayweg, *J. Am. Chem. Soc.* 1962, **84**, 3221.
6. J. A. McCleverty, *Prog. Inorg. Chem.* 1968, **10**, 49.
7. T. R. Halbert, W.-H. Pan and E. I. Steifel, *J. Am. Chem. Soc.* 1983, **105**, 5476.
8. W. E. Cleland Jr, K. M. Barnhart, K. Yamanouchi, D. Collison, F. E. Mabbs, R. B. Ortega and J. H. Enemark, *Inorg. Chem.* 1987, **26**, 1017.
9. S. A. Roberts, C. G. Young, C. A. Kipke, W. E. Cleland Jr, K. Yamanouchi, M. Carducci and J. H. Enemark, *Inorg. Chem.* 1990, **29**, 3650.

10. G. M. Sheldrick, SHELX 76, Program for Crystal Structure Determination. University of Cambridge, U.K. (1976).
11. C. K. Johnston, ORTEP II, Report ORNL-3794, revised. Oak Ridge National Laboratory, Tennessee, U.S.A. (1976).
12. J. A. Ibers and W. C. Hamilton, *International Tables for X-ray Crystallography*, Vol. 4, pp. 99, 149. Kynoch Press, Birmingham, U.K. (1974).
13. A. E. Smith, G. N. Schrauzer, V. P. Mayweg and W. Heinrich, *J. Am. Chem. Soc.* 1965, **87**, 5798.
14. G. F. Brown and E. I. Stiefel, *Inorg. Chem.* 1973, **12**, 2140.
15. S. A. Roberts, R. B. Ortega, L. M. Zolg, W. E. Cleland Jr and J. H. Enemark, *Acta Cryst.* 1987, **43C**, 51.
16. C. G. Young, S. A. Roberts, R. Ortega and J. H. Enemark, *J. Am. Chem. Soc.* 1987, **109**, 2938.

Polyhedron Vol. 9, No. 24, pp. 2971–2979, 1990
Printed in Great Britain

0277–5387/90 $3.00+.00
© 1990 Pergamon Press plc

HIGH-SPIN ↔ LOW-SPIN TRANSITION IN [Fe(NCS)$_2$(4,4′-BIS-1,2,4-TRIAZOLE)$_2$](H$_2$O). X-RAY CRYSTAL STRUCTURE AND MAGNETIC, MÖSSBAUER AND EPR PROPERTIES

WIM VREUGDENHIL,* JOHN H. VAN DIEMEN, RUDOLF A. G. DE GRAAFF, JAAP G. HAASNOOT† and JAN REEDIJK

Gorlaeus Laboratories, Leiden University, P.O. Box 9502, 2300 RA Leiden, The Netherlands

and

ADRI M. VAN DER KRAAN

Interfacultair Reactor Instituut, Delft University of Technology, Delft, The Netherlands

and

OLIVIER KAHN and JACQUELINE ZAREMBOWITCH

Laboratoire de Chimie Inorganique, URA 420, Université Paris-Sud, 91405 Orsay, France

(*Received* 24 *May* 1990; *accepted* 13 *August* 1990)

Abstract—The Fe^{II} ion in [Fe(NCS)$_2$(4,4′-bis-1,2,4-triazole)$_2$](H$_2$O) has distorted tetragonal symmetry with two *trans*-oriented NCS$^-$ ligands. It shows a very abrupt high-spin ↔ low-spin transition at 123.5 K on cooling and 144.5 K on warming. The compound is rather stable *in vacuo* at room temperature; however, samples which have passed the spin transition once lose their water of hydration above 240 K *in vacuo*. The dehydrated substance does not show a spin transition; it is high spin in the whole temperature range. Mössbauer ligand-field spectra and magnetic behaviour of both the hydrated and non-hydrated compounds are discussed.

The spin transition has been followed by EPR measurements with the aid of traces of Cu^{2+} ions which could be substituted for Fe^{2+} in the tetragonal structure. In the high-spin phase the EPR signal is very broad and featureless; in the diamagnetic low-spin phase it is very sharp and resolved in hyperfine and superhyperfine structures. This unusual method to follow the spin transition was shown to be quite generally applicable.

In the crystal structure of Fe(NCS)$_2$(C$_4$H$_4$N$_6$)$_2$(H$_2$O) the distances Fe—NCS are 2.125(3) Å, and Fe—N(ligand) 2.180(3) and 2.188(2) Å. The water molecule is connected to the non-coordinating ligand N-atom by hydrogen bonding.

Thermally induced high-spin ↔ low-spin transitions of six-coordinated Fe^{II} and a few other first-row transition metal ions with d^4 to d^7 electron configurations, have been studied for many years. Several techniques are available to investigate this phenomenon. Mössbauer spectroscopy, magnetic measurements, heat capacity data, X-ray diffraction techniques and UV–vis and IR spectrometries, have been mainly used and the results were discussed in several review articles on the subject.[1–4]

Until now, only a few examples of iron compounds with triazole ligands, exhibiting a spin-crossover, have been described. [Fe(trz)

*Present address: Research Centre Amsterdam, AKZO Chemicals, P.O. Box 15, 1000 AA Amsterdam, The Netherlands.

† Author to whom correspondence should be addressed.

$(Htrz)_2](BF_4)$ (Htrz = 1,2,4-triazole)[5] is a low-spin iron compound at room temperature. A transition to high-spin occurs upon heating to 105–107°C. A hysteresis of 32 K was observed. A polynuclear structure was proposed for this complex.

$[Fe_3(4\text{-ethyl-}1,2,4\text{-triazole})_6(H_2O)_6](CF_3SO_3)_6$ contains differently coordinated iron atoms.[6] It has been shown that only the central iron atom, having a N(6) coordination, shows a spin transition.[7] Several other iron(II) compounds showing spin transition with 1,2,4-triazole and 4-amino-1,2,4-triazole as ligands have been described by Larionov and coworkers.[8]

Furthermore, a series of iron(II) compounds with the chelating bidentate ligand 5-(2′-pyridyl)-1,2,4-triazole has been described.[9] These compounds also exhibit a temperature-induced spin transition.

Recently, a series of isomorphous compounds has been described with general formula $[M(NCS)_2(btr)_2](H_2O)$ (M = Fe, Co or Ni, btr = 4,4′-bis-1,2,4-triazole).[10] A crystal structure determination, carried out on the cobalt compound,[11] revealed that the compounds have a two-dimensional structure with the metal atoms bridged by the btr ligands, coordinating through their N(1) and N(1′) atoms. Two *trans*-oriented thiocyanate anions form the axial ligands. With manganese, a similar two-dimensional structure has been observed for the nitrate: $[Mn(btr)_2(H_2O)_2](NO_3)_2$.[12] Surprisingly, $Mn(NCS)_2$ does not give a two-dimensional structure with btr. A compound of composition $[Mn(NCS)_2(btr)(H_2O)_2]\cdot 2H_2O$ appeared to be a btr-1,1′-linked linear chain.[13]

The iron compound, $[Fe(NCS)_2(btr)_2](H_2O)$, was reported to show a spin transition.[11] This spin transition is highly unusual because the ligand btr is not a very strong ligand; it is, for instance, weaker than 2,2′-bipyridine (bipy) or 1,10-phenanthroline (phen). $[Fe(btr)_6]^{2+}$ in the three-dimensional lattice of $[Fe(btr)_3](CF_3SO_3)_2$ is high-spin at all temperatures[14] (Dq = 1120 cm^{-1}). Moreover, there is no report so far on a spin transition in iron(II) compounds with *trans*-oriented thiocyanate groups. In contrast, numerous iron(II) compounds with *cis*-oriented NCS^- groups are well known to exhibit such a spin transition from high-spin to low-spin on cooling, e.g. $Fe(NCS)_2L_2$, L = bipy or phen.[1,2] The very few iron(II) *trans*-thiocyanate compounds which are known[15–18,34,35] do not exhibit a spin transition, they are high-spin in the whole temperature range. It also appears that $[Fe(NCS)_2(btr)_2](H_2O)$ is the first spin transition compound with a two-dimensional structure.

The ligand field of $[Fe(NCS)_2(btr)_2](H_2O)$ shows a Dq value of 1160 cm^{-1}, which is at the lower limit of the range of Dq values (1160 < Dq < 1340 cm^{-1}), given by Robinson *et al.*[19] for iron(II) compounds in which spin-crossover should occur.

Since the iron atoms in this compound have a site symmetry close to D_{4h}, it seemed appropriate to prepare a copper(II) dope in the iron compound. It has been shown that it is quite possible to detect the HS–LS transition in an iron compound by focusing on the variable temperature EPR spectra of doped species, which acts as a probe to get information about the spin state of the host lattice.[20–22]

In the present paper this method of detecting spin transitions in iron compounds will be described in more detail. A preliminary communication about the detection of the spin transition was published before.[21] The spin transition of $[Fe(NCS)_2(btr)_2](H_2O)$ will be discussed first.

These investigations on the compound made it more desirable to carry out the X-ray structure determination on the iron compound itself, since it is clear that there might be some differences with the isomorphous cobalt compound. Unfortunately, low-temperature single-crystal structure determination will not be possible since the crystals disintegrate upon passing the spin transition. The room temperature single crystal structure determination of the compound is described at the end of this paper.

EXPERIMENTAL

Synthesis

The synthesis of the compound and the dopes containing Cu^{II} and Mn^{II} have been described elsewhere.[11,20] The elemental analyses for the doped substances were done by using atomic absorption. The copper dope gave Fe–Cu = 1 : 0.011 and the manganese dope Fe–Mn = 1 : 0.010.

Measurements

Magnetic measurements have been carried out on polycrystalline samples weighing about 6 mg with a Faraday type magnetometer equipped with a helium continuous-flow cryostat from Oxford Instruments working in the 2–295 K temperature range (Orsay) or on an automatic Faraday balance in the temperature range 80–295 K operating *in vacuo* (Leiden).

The variable temperature EPR spectra of the copper-doped $[Fe(NCS)_2(btr)_2](H_2O)$ were obtained from a Bruker ER 200D spectrometer equipped with an Oxford Instruments continuous-flow cryostat.

Mössbauer spectra were obtained with a constant

Table 1. Crystallographic data[a] for $[Fe(NCS)_2(btr)_2](H_2O)$

Chemical formula $C_{10}H_{10}FeN_{14}OS_2$	$T = 20°C$
$f_w = 462.259$	λ(Mo-K_α) = 0.71073 Å
Space group $C2/c$	$\rho_{obs} = 1.60(2)$ Mg m^{-3} $\rho_{calc} = 1.59$ Mg m^{-3}
$a = 11.130(1)$ Å	Crystal dimensions $0.65 \times 0.22 \times 0.07$ mm
$b = 13.191(3)$ Å	$\mu = 10.18$ cm^{-1}
$c = 13.101(1)$ Å	Transmission coefficient = 0.84–1.07
$\beta = 91.82(4)°$	$R = 0.039$, $R_w = 0.049$
$V = 1923.0(8)$ Å^3	θ Range 2–27.5°
$Z = 4$	Range of indices h −14 to 14
$F(000) = 930$	k 0 to 17
	l 0 to 17
	Number of measured reflections 4393
	Number of independent reflections 4389
	Number of significant reflections 1368

[a] Estimated standard deviations in the least significant digits are given in parentheses.

acceleration spectrometer, which uses a ^{57}Co in Rh source. Isomer shifts are reported relative to the NBS standard $Na_2[Fe(CN)_5NO](H_2O)_2$. The measured spectra were fitted with calculated subspectra consisting of Lorentzian-shaped lines by varying the Mössbauer parameters in a non-linear, iterative minimization routine. UV–vis spectra were obtained using a Perkin–Elmer 330 spectrophotometer, applying the diffuse reflectance technique at room temperature with MgO as a reference.

Collection and reduction of X-ray intensity data

A bar shaped single crystal of $[Fe(btr)_2(NCS)_2](H_2O)$, btr = $C_4H_4N_6$, was selected and mounted on an Enraf-Nonius CAD-4 automatic four-circle diffractometer (graphite-monochromated Mo-K_α radiation; $\lambda = 0.71073$ Å), applying the ω–2θ scan technique at room temperature. The obtained diffraction data, which showed no systematic decay of intensity due to deterioration of the crystal (checked periodically every 90 min by using selected intensity standards), were corrected for Lorentz and polarization effects. Absorption correction, using the Monte Carlo method,[23] led to a value for R_{int} of 0.01. Atomic scattering factors for neutral atoms were taken from the literature.[24] Details on crystal data and intensity collection are listed in Table 1.

Solution and refinement of the structure

The structure was solved in space group $C2/c$. For the refinement, the atomic parameters of the non-hydrogen atoms of the isomorphous cobalt compound were used.[11] Successive cycles of least-squares refinement and difference Fourier syntheses based on 1368 significant reflections (with $I > 2\sigma_I$) did not yield the hydrogen positions, therefore the ligand hydrogens were placed at 0.98 Å and refined in the subsequent cycles with one overall isotropic temperature factor. The function minimized was $\Sigma[w(|F_o| - |F_c|)^2]$ with $w = 1/\sigma_{F^2}$ (σ_{F^2} from counting statistics). All non-hydrogen atoms were given individual anisotropic thermal parameters in the refinement. None of the remaining electron densities could be assigned to the water hydrogen atoms due to hydrogen bonding.

The final values for the discrepancy indices defined by $R = \Sigma(|F_o| - |F_c|)/\Sigma|F_o|$ and $R_w = [\Sigma w(|F_o| - |F_c|)^2/\Sigma w|F_o|^2]^{1/2}$ where $R = 0.039$ and R_w 0.049 with the significant set of reflections. The atomic positional parameters, and listings of F_o and F_c values and anisotropic thermal parameters for the non-hydrogen atoms are available as supplementary material.[25]

RESULTS AND DISCUSSION

Spin-crossover observations

The high-spin ↔ low-spin transition in $[Fe(NCS)_2(btr)_2](H_2O)$ has been followed by measuring the molar magnetic susceptibilities χ_M as a function of temperature T.

At first, the data were recorded from 80 to 295 K, and vice versa, under helium atmosphere at 10 mm Hg (1.3 kPa) pressure. A very broad hysteresis of more than 30 K was found *initially*, i.e. $T_c\downarrow = 123$ K, $T_c\uparrow \approx 153$ K, but after heating up to room temperature a second time and subsequently cooling down again no transition occurred. Nevertheless, the transition could be repeated many times in a test tube at normal pressure when the sample is cooled down in liquid nitrogen and heated up again. In this experiment the transition can be detected

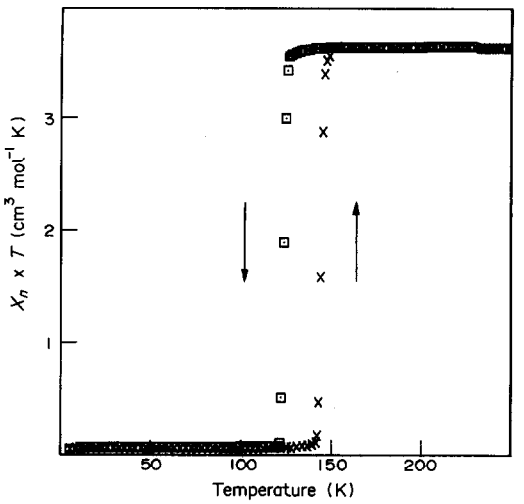

Fig. 1. The χT vs T curves of $Fe[(MCS)_2(btr)_2](H_2O)$ at increasing (×) and decreasing (⊡) temperatures, 0–250 K.

visually, because of the white-to-purple and vice versa colour change associated with the spin transition. The basic difference between this simple experiment and the magnetic measurements is the difference in pressure.

Analysis of the weight of the sample during the magnetic measurements revealed a loss of 3.9% of weight in the temperature region from 240 to 280 K. This loss closely corresponds to one mole of water per molecular unit. Afterwards, the weight remained constant. Therefore it is concluded that, at temperatures above 240 K and at 10 mmHg (1.3 kPa) pressure, the compound looses its non-coordinated water molecule. The loss of water became also clear from the disappearance of the bands characteristic of water in the IR spectra recorded after the magnetic measurements.

Subsequently, the magnetic measurements have been carried out on another sample in the temperature range 10–240 K, and under the same pressure conditions. The $\chi_M T$ vs T curves are given in Fig. 1. The weight of the sample remains constant over the whole temperature range. A hysteresis of 21 K appeared for this sample, $T_c\downarrow = 123.5$ K, $T_c\uparrow = 144.5$ K.

It is clear from these results that the loss of the water molecules present in the lattice induces the disappearance of the spin-crossover phenomenon in the system under investigation.

The high-spin ↔ low-spin transition of this compound was also studied by Mössbauer spectroscopy. At 295 K the isomer shift and the quadrupole splitting are 1.30 and 2.83 mm s^{-1}, respectively. Below the transition temperature the isomer shift is fairly constant at 0.76 mm s^{-1}, and any quadrupole splitting was not observed (line width 0.32 mm s^{-1}). The hysteresis effect can be seen from Fig. 2 in which Mössbauer spectra at various temperatures around T_c are presented. The transition temperature and the hysteresis are in good agreement with the results obtained from magnetic data. It is remarkable that the quadrupole splitting in the low-spin phase is (close to) 0 mm s^{-1}.

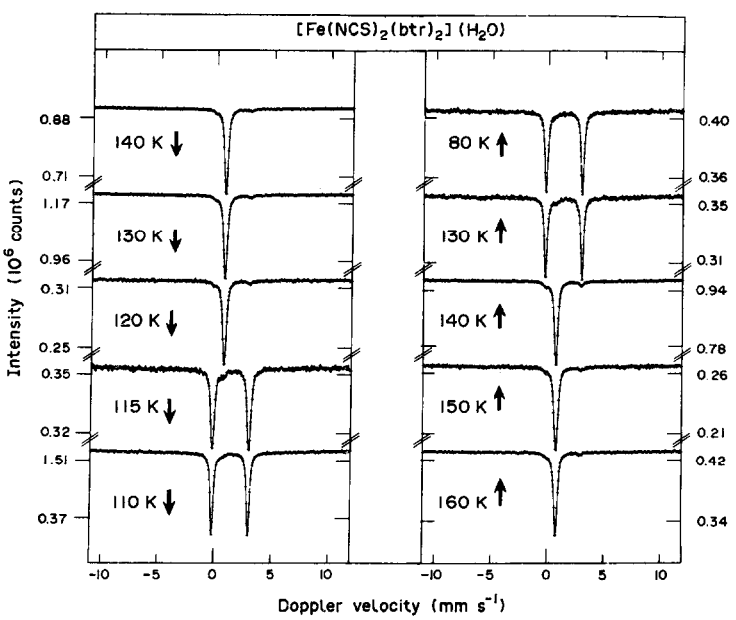

Fig. 2. Mössbauer spectra of $Fe[(MCS)_2(btr)_2](H_2O)$ at indicated temperatures: ↓ indicates decreasing temperatures, ↑ indicates increasing temperatures.

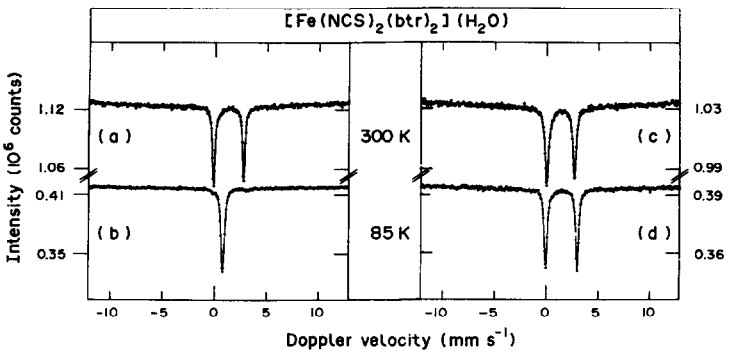

Fig. 3. Mössbauer spectra of $Fe[(MCS)_2(btr)_2](H_2O)$ at indicated temperatures: (a) and (b) unperturbed samples, (c) and (d) dehydrated samples.

Such small values are to be expected for iron(II) in a highly symmetric coordination sphere, e.g. hexakisligand systems.[3] Apparently, the tetragonal distortion of octahedral symmetry is rather small in the low-spin phase.

Dehydrated compound

Mössbauer spectra of a dehydrated sample have been recorded at room temperature and at 85 K (Fig. 3). No low-spin species could be detected at low temperature. The isomer shift (1.33 mm s^{-1} at 295 K, 1.43 mm s^{-1} at 85 K) and the quadrupole splitting (2.62 mm s^{-1} at 295 K, 2.99 mm s^{-1} at 85 K) of the dehydrated samples differ from those for the non-evacuated sample. This indicates a change in the local symmetry of the iron atom upon dehydration. Differences have also been observed in the ligand-field spectra of these samples. The *Dq* value of the dehydrated sample is 80 cm^{-1} lower than that of the hydrated one. This is clearly below the before mentioned range to give spin-crossover phenomena.[1,2,19] A further broadening of the ligand-field absorption is observed in the dehydrated sample indicating a tetragonal distortion of the iron atoms.

The previously reported partial spin transition of $[Fe(NCS)_2(btr)_2](H_2O)$[11] can now be explained by the above described disappearance of the spin transition upon dehydration. The partial dehydration of a sample apparently results in a partial overall spin transition.

EPR measurements

The above applied techniques, as well as other methods used to investigate HS–LS transitions all focus either on the metal species, which undergoes the transition, i.e. its electronic and magnetic properties, or on species which are present in the compound, i.e. ligands and eventually counterions and solvent molecules, or on structural changes accompanying the spin crossover, as revealed by heat capacity data and X-ray diffraction and/or spectral absorption patterns. It has been shown that it is possible to introduce a guest species in the compound, the behaviour of which is drastically changed when the host compound undergoes the spin transition, and to focus on that species with variable temperature physical measurements to detect the spin transition. In this way the crossover phenomenon can be observed indirectly.

$[Fe(NCS)_2(btr)_2](H_2O)$ is the first spin-transition iron compound with *trans*-oriented thiocyanate groups and ligand-bridged iron atoms. Because weak magnetic interaction might exist between the metal ions, it is to be expected that the spin transition of the iron ions will affect the magnetic properties of doped metal ions, such as Cu^{II} and Mn^{II} and thus, the EPR spectrum of the compound. A copper dope and a manganese dope of $[Fe(NCS)_2(btr)_2](H_2O)$ have therefore been synthesized. The doped species exhibit the same magnetic behaviour as observed for the undoped species, i.e. a very abrupt and complete spin transition and a large hysteresis.

The EPR spectra of the copper-doped iron compound recorded at variable temperatures have been reported previously.[20] It was shown that in the paramagnetic phase above T_c the EPR spectrum is very poorly resolved due to exchange broadening. In contrast, at T_c and below, a beautifully resolved spectrum was observed corresponding to a magnetically isolated Cu^{II} ion in an elongated tetragonal environment with hyperfine as well as superhyperfine structures. See Fig. 4.

To confirm that the features in the EPR spectra appeared because of the spin transition, EPR spectra have been recorded of the sample after dehydration, which induces the loss of the spin tran-

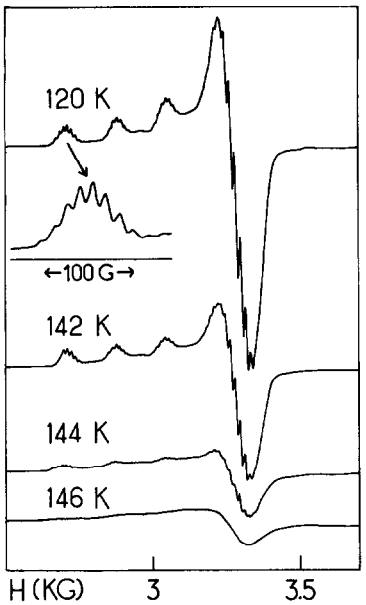

Fig. 4. EPR spectra of copper-doped Fe[$(MCS)_2(btr)_2$] (H_2O), at increasing temperatures.

sition behaviour as described above. Both at room temperature and at 77 K only a broad signal was observed around $g = 2$. At 77 K only very weak hyperfine splitting was observed, as shoulders on the broad signal, with $g = 2.3$ and $A = 165$ G. Furthermore an absorption appears at $g = 4.3$, which has also been observed in the unperturbed sample at room temperature.

These results clearly confirm the conclusion that the superhyperfine and hyperfine structures can be observed in the EPR spectra of the copper dope of $[Fe(NCS)_2(btr)_2](H_2O)$, because of the diamagnetic character due to the low-spin state of the host lattice.

The magnetic susceptibility curves for the manganese(II)-doped sample also closely resemble those of the pure compound. $T_c\downarrow$ is slightly lower, 120.5 K, and the hysteresis effect seems to be larger. A lowering of T_c is generally observed for doped compounds exhibiting a temperature-induced spin transition.[1,26–29] The variable temperature powder EPR spectra of the manganese(II) dope show only very broad signals above T_c, whereas small but abrupt changes occur at T_c. The spectrum is sharpened, though still not well resolved, in the diamagnetic phase and is essentially constant in the whole temperature range below T_c.

Rao *et al.*[30] detected the HS ↔ LS transition with EPR spectroscopy on a guest ion, by preparing manganese-doped $[Fe(phen)_2(NCS)_2]$ and $[Fe(pic)_3]Cl_2 \cdot EtOH$ [pic = 2-(amino-methyl)pyridine]. A broadening of the EPR resonance lines at the transition temperature was observed. A linewidth vs temperature curve for the composition $[Mn_{0.01}Fe_{0.99}(pic)_3]Cl_2 \cdot EtOH$ yielded a maximum at the transition temperature. This effect was explained by assuming a longer lifetime for iron(II) high-spin states in the critical temperature region.

The present study shows that it is quite possible to detect the HS–LS transition in an iron compound by focusing on the EPR spectrum of a doping ion, which acts as a "spy" to get information about the spin state of the host lattice. Both divalent copper and manganese appeared to be useful, although the effect in the copper dope expressed more pronounced.

As is shown by Ozarowski *et al.*[21] this doping technique is also useful for the study of other systems. So, a comparable effect was described for copper(II) and manganese(II) dopes in [Fe(1-propyltetrazole)$_6$]$(BF_4)_2$, known to exhibit high-spin ↔ low-spin transition as well.[31,32] The changes of the EPR spectra indicated the existence of two different diamagnetic phases, depending on the cooling rate.

DESCRIPTION OF THE STRUCTURE

The description of the isomorphic analogous cobalt compound,[11] already showed that the coordination around iron is a distorted octahedron with two thiocyanate N atoms *trans* to each other. The now found distances are Fe—NCS 2.125(3) Å and Fe—N(ligand) 2.180(3) and 2.188(2) Å (Table 2). These last distances are at the lower part of the range of high-spin Fe^{II}—N(triazole ligand) distances (2.29–2.167 Å)[14] and in fact in the range (2.1–2.2 Å) of values of compounds of high-spin Fe^{II} that change to low-spin upon cooling.[33] An ORTEP drawing of the structure showing the relative position of the iron atoms in the two-dimensional grid, the numbering of the atoms in the asymmetric unit and the hydrogen bonding between the water molecule and the ligand is shown in Fig. 5.

Compared with the isomorphic cobalt(II) compound the Fe—N distances are 0.03–0.05 Å longer which is quite normal. Compared with other two-dimensional iron(II) compounds of triazoles with *trans*-NCS^- ions, it is found that the mean distance is about the same or less: in $[Fe(NCS)_2(1,2,4\text{-triazole})_2]$[34] 2.15 and 2.24 Å, in $[Fe(NCS)_2(tp_2)]$ (tp = [1,2,4]triazolo[1,5-*a*]pyrimidine)[35] 2.25 and 2.33 Å. These two compounds do not change their spin state on cooling, although geometry and ligand type are the same. The difference can be explained by the fact that in these two compounds the triazole rings are *bidentate*, whereas in the btr compounds each triazole ring coordinates to only one metal

Table 2. Relevant bond distances (Å) and angles (°) for $[Fe(NCS)_2(btr)_2](H_2O)$ with ESDs in parentheses

Bond distances			
Fe—N	2.125(3)	N(14)—C(15)	1.351(4)
Fe—N(11)[a]	2.180(3)	C(15)—N(11)	1.296(4)
Fe—N(21)	2.188(2)	N(14)—N(24)	1.379(3)
N—C	1.149(4)	N(21)—N(22)	1.389(4)
C—S	1.620(4)	N(22)—C(23)	1.298(4)
N(11)—N(12)	1.388(4)	C(23)—N(24)	1.358(5)
N(12)—C(13)	1.297(4)	N(24)—C(25)	1.355(4)
C(13)—N(14)	1.356(4)	C(25)—N(21)	1.294(4)
Bond angles			
N—Fe—N(11)[a]	92.1(1)	Fe—N—C	153.7(3)
N—Fe—N(21)	89.1(1)	N—C—S	178.6(4)
N(21)—Fe—N(11)[a]	90.7(1)		
Fe—N(11)—N(12)	123.6(2)	Fe—N(21)—N(22)	124.0(2)
Fe—N(11)—C(15)	127.6(2)	Fe—N(21)—C(25)	127.2(2)
C(15)—N(11)—N(12)	108.6(3)	C(25)—N(21)—N(22)	108.6(3)
N(11)—N(12)—C(13)	106.5(3)	N(21)—N(22)—C(23)	106.7(3)
N(12)—C(13)—N(14)	109.7(3)	N(22)—C(23)—N(24)	109.5(3)
C(13)—N(14)—C(15)	106.6(3)	C(23)—N(24)—C(25)	106.6(3)
N(14)—C(15)—N(11)	108.6(3)	N(24)—C(25)—N(21)	108.6(3)
C(13)—N(14)—N(24)	128.0(3)	C(15)—N(14)—N(24)	125.4(3)
C(23)—N(24)—N(14)	127.6(3)	C(25)—N(24)—N(14)	125.7(3)
Hydrogen bridging system			
Distances		Angles	
Ow—N(12)[b]	3.782(3)	Ow—N(22)—N(21)	138.3(2)
Ow—N(12)[c]	3.616(3)	Ow—N(22)—C(23)	111.0(2)
Ow—N(22)	3.135(5)		

[a] $x, -y, -\frac{1}{2}+z$.
[b] $\frac{1}{2}+x, \frac{1}{2}-y, \frac{1}{2}+z$.
[c] $\frac{1}{2}+x, -\frac{1}{2}+y, z$.

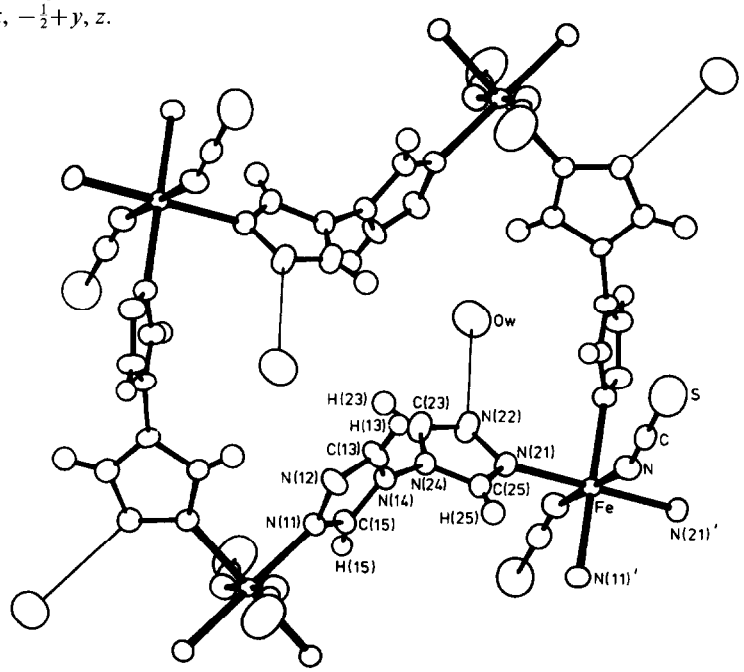

Fig. 5. ORTEP drawing of the structure of $Fe[(NCS)_2(btr)_2](H_2O)$ showing the relative position of the iron atoms in the two-dimensional grid, the numbering of the atoms in the asymmetric unit and the hydrogen bonding between the water molecule and the ligand as thin lines.

ion. The electronic effect of a second metal ion diminishes the strength of the ligand just enough to prevent spin change.

The compound differs further from the isomorphous cobalt compound by the fact that the sulphur atoms of the thiocyanate groups are not disordered. The Fe—N—C angle is 153.7(3)°, which deviates even more from 180° than in the cobalt compound. However, in all other characteristics the two structures are essentially the same, even in the hydrogen bonding system between the water molecule and the non-coordinating nitrogens of the btr ligand. As the cobalt compound is not easily dehydrated *in vacuo* one may conclude that the easy dehydration of the iron compound is caused by a structural phase change accompanying the spin transition that causes the crystals to crack and on warming up to pulverize. The dehydration occurs from the pulverized high-spin phase.

CONCLUDING REMARKS

As already observed with several compounds[1,36,37] the spin transition vanishes upon removal of lattice water of crystallization. As discussed above, removal of part of the water molecules results in partial spin transition.

To obtain more insight into the mechanism of the spin transition, the cooperative effect playing a rôle in it, it would be worthwhile to further investigate this compound. One might study the influence of Co^{2+} substitution on the transition behaviour. Insight into the interaction of the water molecules with the bridging ligands might be obtained if (crystalline) preparations of the same compound without water or with other solvent molecules (methanol, ethanol) were successful.

It appeared to be possible to get monocrystals seemingly intact through the spin transition into the low-spin phase, however, when mounted for a single crystal experiment no single crystal reflections could be obtained. On warming up to room temperature the crystals appear to be transformed to powder. This behaviour indicates that a crystalline phase transition accompanies the spin transition. At the same time it does not exclude that an intermediate unstable diamagnetic phase may be present for a short time after (rapid) cooling as suggested by Ozarowski *et al.*[21]

As shown above, detecting spin transition via EPR spectroscopy was not restricted to ligand-bridged compounds. In fact, the limiting factor seems to be the preparation of real dopes of the probe ions (Cu^{2+}, Mn^{2+}) in the iron compound lattice; the existence of compounds of copper(II) or manganese(II) isomorphous to the iron(II) compound to be doped is not essential. It is worthwhile to investigate whether this technique is also valid for iron thiocyanate compounds with the more common *cis*-configuration of the thiocyanate anions, especially of those of which detailed crystal structure analyses above and below T_c are available. If the EPR spectrum changes at T_c this method might give valuable information on the environment of the iron atoms above and below the transition temperature.

Acknowledgements—This work was sponsored by the Leiden Materials Science Centre (Werkgroep Fundamenteel Materialenonderzoek). The present investigations were carried out with support from the Netherlands Foundation for Chemical Research (SON) and with financial aid from the Netherlands Organization for Pure Research (ZWO) through project 333-17.

REFERENCES

1. P. Gütlich, *Structure and Bonding* 1981, **44**, 83.
2. E. König, G. Ritter and S. K. Kulshreshtha, *Chem. Rev.* 1985, **85**, 219.
3. P. Gütlich, in *Mössbauer Spectroscopy Applied to Inorganic Chemistry* (Edited by G. J. Long), Vol. 1, *Modern Inorganic Chemistry* series. Plenum Press, New York (1984).
4. M. Bacci, *Coord. Chem. Rev.* 1988, **86**, 245.
5. J. G. Haasnoot, G. Vos and W. L. Groeneveld, *Z. Naturforsch.* 1977, **32b**, 1421.
6. G. Vos, R. A. G. de Graaff, J. G. Haasnoot, A. M. van der Kraan, P. de Vaal and J. Reedijk, *Inorg. Chem.* 1984, **23**, 2905.
7. G. Vos, J. G. Haasnoot, G. C. Verschoor, J. Reedijk and P. E. L. Schaminee, *Inorg. Chim. Acta* 1985, **105**, 31.
8. L. G. Lavrenova, V. I. Ikorskiĭ, V. A. Varnek, I. M. Oglezneva and S. V. Larionov, *Koordinationnaya Khimiya* 1986, **12**, 207.
9. P. Stupik, J. H. Zhang, M. Kwiecien, W. M. Reiff, J. G. Haasnoot, R. Hage and J. Reedijk, *Hyperfine Interact.* 1986, **28**, 725.
10. J. G. Haasnoot and W. L. Groeneveld, *Z. Naturforsch.* 1979, **34b**, 1500.
11. W. Vreugdenhill, S. Gorter, J. G. Haasnoot and J. Reedijk, *Polyhderon* 1985, **4**, 1769.
12. W. Vreugdenhil, J. G. Haasnoot, R. A. G. de Graaff, H. A. Nieuwenhuis, D. Reefman and J. Reedijk, *Acta Cryst.* 1987, **C43**, 1527.
13. M. Biagini-Cingi, private communication.
14. W. Vreugdenhil, Ph.D. thesis, Leiden University (1987).
15. I. Sötofte and S. E. Rasmussen, *Acta Chem. Scand.* 1967, **21**, 2028.
16. G. Valle, U. Rosso and S. Calogero, *Transition Met. Chem.* 1980, **5**, 26.
17. M. G. B. Drew, H. bin Othman and S. M. Nelson, *J. Chem. Soc.* 1976, 1394.

18. G. J. Long, G. Galeazzi, U. Rosso, G. Valle and S. Calogero, *Inorg. Chem.* 1983, **22**, 506.
19. M. A. Robinson, J. D. Curry and D. H. Busch, *Inorg. Chem.* 1963, **2**, 1178.
20. W. Vreugdenhil, J. G. Haasnoot, O. Kahn, P. Thuéry and J. Reedijk, *J. Am. Chem. Soc.* 1987, **109**, 5272.
21. A. Ozarowski and B. R. McGarvey, *Inorg. Chem.* 1989, **28**, 2262.
22. A. Ozarowski, B. R. McGarvey, A. B. Sarkar and J. E. Drake, *Inorg. Chem.* 1988, **27**, 628.
23. R. A. G. de Graaff, *Acta Crystallogr.* 1973, **A29**, 298.
24. *International Tables for X-Ray Crystallography*, Vol. IV. Kynoch Press, Birmingham (1974).
25. Supplementary material deposited at the Cambridge Crystallographic Data Centre, comprising observed and calculated structure factors, and a last least-squares refinement.
26. M. S. Haddad, W. D. Federer, M. W. Lynch and D. N. Hendrickson, *Inorg. Chem.* 1981, **20**, 131.
27. I. Scanner, E. Meissner, H. Köppen, H. Spiering and P. Gütlich, *Chem. Phys.* 1984, **85**, 227.
28. R. Jakobi, H. Spiering, L. Wiehl, E. Gmelin and P. Gütlich, *Inorg. Chem.* 1988, **27**, 1823.
29. P. Adler, L. Wiehl, E. Meissner, C. P. Köhler, H. Spiering and P. Gütlich, *J. Phys. Chem. Solids* 1987, **48**, 517.
30. P. S. Rao, A. Reuveni, B. R. McGarvey, P. Gangüli and P. Gütlich, *Inorg. Chem.* 1981, **20**, 204.
31. P. L. Franke, J. G. Haasnoot and A. P. Zuur, *Inorg. Chim. Acta* 1982, **59**, 5.
32. S. Decurtins, P. Gütlich, C. P. Köhler and H. Spiering, *Chem. Phys. Lett.* 1984, **105**, 1.
33. E. König, in *Progress in Inorganic Chemistry* (Edited by S. J. Lippard), Vol. 35. Wiley–Interscience, New York (1987).
34. D. W. Engelfriet and G. C. Verschoor, *Acta Cryst.* 1981, **B37**, 237.
35. M. Biagini-Cingi, A. M. Manotti-Lanfredi, A. Tiripicchio, J. P. Cornelissen, J. G. Haasnoot and J. Reedijk, *Inorg. Chim. Acta* 1987, **127**, 189.
36. E. König, R. Schnakig, G. Ritter, W. Irler, B. Kanellakopulos and B. Powietzka, *Inorg. Chim. Acta* 1979, **35**, 239.
37. R. Claude, M. Philoche-Levisalles and J. Zarembowitch, to be published.

Polyhedron Vol. 9, No. 24, pp. 2981–2985, 1990
Printed in Great Britain

0277–5387/90 $3.00+.00
© 1990 Pergamon Press plc

TRANSITION METAL COMPLEXES OF THE SCHIFF BASES DERIVED FROM S-ALKYLDITHIOCARBAZATE WITH 2-PYRIDINECARBOXALDEHYDE N-OXIDE—I. SYNTHESIS, PROPERTIES AND STRUCTURE OF FOUR-COORDINATE COPPER(II) COMPLEXES

SHAOHUA GOU,* XIAOZENG YOU and ZHENG XU

Coordination Chemistry Institute, Nanjing University, Nanjing, P.R.C.

and

KAIBE YU and ZHONGYUAN ZHOU

Chengdu Center of Analysis and Determination, Academia Sinica, Chengdu, P.R.C.

(*Received* 23 *April* 1990; *accepted* 6 *August* 1990)

Abstract—Two new Schiff bases (SMPDH and SBPDH) of S-methyl- and S-benzyl-dithiocarbazate with 2-pyridinecarboxaldehyde N-oxide were prepared and confirmed by elemental analyses and IR spectra. Four copper(II) complexes of the above two Schiff base ligands with imidazole and pyridine were obtained and characterized spectroscopically. The crystal structure of $[Cu(SMPD)ImH]ClO_4$ was determined by X-ray diffraction analysis. The geometry of the copper atoms in these complexes is square planar with an unsymmetrical environment.

Transition metal ion complexes of ligands containing sulphur and nitrogen as donor atoms in Schiff bases were extensively studied, owing to their certain antitumour, antimalarial and antibacterial activity.[1–3] These types of ligand are commonly the products derived from the Schiff base condensations of S-alkylhydrazine carbodithioate and S-alkyldithiocarbazate with some ketones and aromatic aldehydes.[4] Here we report two new tridentate ligands of the above class via the condensation of S-R-dithiocarbazate with 2-pyridinecarboxaldehyde N-oxide (R = methyl, L = SMPDH; R = benzyl, L = SBPDH). A number of metal complexes with these two ligands were prepared and characterized by magnetic properties, UV and IR spectra, as well as elemental analyses, and crystal structures of some complexes have been determined by X-ray diffraction. As part of our series, four copper(II) complexes are studied in this paper.

* Author to whom correspondence should be addressed.

EXPERIMENTAL

Preparation

(1) *Ligands.* 2-Pyridinecarboxaldehyde N-oxide,[5] S-methyldithiocarbazate[6] and S-benzyldithiocarbazate[7] were prepared and confirmed by elemental analyses.

A solution of S-R-dithiocarbazate (20 mmol) in absolute ethanol (50 cm^3) was added to a hot solution of 2-pyridinecarboxaldehyde N-oxide (20 mmol) in absolute ethanol (50 cm^3). The mixture was stirred and refluxed for 30 min, then cooled to room temperature and filtered. Yellow crystals were obtained and recrystallized from hot ethanol.

(2) *Complexes.* All copper(II) complexes were prepared by the following method: a solution of ligand (1 mmol) and $Cu(ClO_4)_2 \cdot 6H_2O$ in ethanol (60 cm^3) was refluxed for 5 min, then imidazole or pyridine (2 mmol) in ethanol (10 cm^3) was added. After refluxing for 10 min, the mixture was filtered when hot. The filtrate was then kept at room temperature and green crystals were obtained.

Table 1. Elemental analyses and yields

Number	Compound	Formula	Yield (%)	Analyses (%) (Found/Calc.) C	H	N
1	SMPDH	$C_8H_9N_3OS_2$	82	42.0	3.8	18.0
				42.3	4.0	18.5
2	SBPDH	$C_{14}H_{13}N_3OS_2$	65	55.3	4.4	13.1
				55.4	4.3	13.9
3	[Cu(SMPD)ImH]ClO_4	$CuC_{11}H_{12}N_5ClO_5S_2$	79	28.7	2.5	14.8
				28.9	2.6	15.3
4	[Cu(SMPD)Py]ClO_4	$CuC_{13}H_{13}N_4ClO_5S_2$	71	33.0	2.7	11.6
				33.3	2.8	12.0
5	[Cu(SBPD)ImH]ClO_4	$CuC_{17}H_{16}N_5ClO_5S_2$	51	37.6	2.7	13.5
				38.3	3.0	13.1
6	[Cu(SBPD)Py]ClO_4	$CuC_{19}H_{17}N_4ClO_5S_2$	30	41.7	2.8	10.8
				41.9	3.1	10.3

Measurements

UV spectra were recorded using a Shimadzu 240 spectrophotometer. IR absorption spectra from 4000 to 400 cm^{-1} were obtained on a 170SX FT–IR instrument, with samples prepared as solid KBr pellets. Magnetic susceptibility measurements were carried out in the solid state at room temperature (283.2 K) using a Gouy balance with $[Ni(en)_3]S_2O_3$ as calibrant. Table 1 gives the elemental analyses and yields of the ligands and copper(II) complexes. Selected spectroscopic data and magnetic moments for the complexes are shown in Table 2.

Crystallographic analysis

Single cystals of [Cu(SMPD)ImH]ClO_4 were obtained by a diffusion method in an acetonitrile and ether system. A dark green crystal ($0.2 \times 0.4 \times 0.6$ mm) was used for data collection. Unit cell and intensity data were obtained using a R3M/E four-circle diffractometer and graphite-monochromatized Mo-K_α radiation, ω–2θ scan mode. Data correction for Lorentz and polarization factors was made, but not for absorption effects. The structure was solved by direct methods, refinement was by full-matrix least-squares cal-

Table 2. (a) Selected IR data for ligands

Number	ν(N—H)	ν(C=N)	ν(C=S) (cm^{-1})	ν(N—O)	δ(N—O)
1	3102m	1480vs	1087m	1221vs	877s
2	3106m	1485vs	1093m	1231vs	880s

Table 2. (b) Magnetic moments, UV and IR spectral data for the complexes

Number	Colour	μ_{eff} (R.T., BM)	*d–d* band[a] (cm^{-1})	ν(C=N)	ν(C—S)	ν(N—O) (cm^{-1})	ν(N—H)	ν(Cl—O)
3	Green	1.79	16,949	1431vs	1046w	1204m	3333m	1069vs
4	Green	1.67	17,241	1434vs	1046w	1199m		1090vs
5	Green	1.75	16,666	1429vs	1038w	1200m	3270m	1069vs
6	Green	1.65	16,806	1431vs	1045w	1202m		1088vs

[a] In acetonitrile.

Table 3. Crystallographic data for [Cu(SMPD)ImH]ClO_4

Formula	$CuC_{11}H_{12}N_5ClO_5S_2$
Mr	457.36
Space group	Monoclinic, $P2_1/n$
a (Å)	9.863(3)
b (Å)	11.155(3)
c (Å)	16.057(5)
β (°)	99.59(2)
V (Å)^3	1742.0(9)
Z	4
D_c (g cm^{-3})	1.74
μ (cm^{-1})	16.69
$F(000)$	891.81
Temperature	Room temperature
Radiation	λ(Mo-K_α) = 0.71073 Å
Maximum Bragg angle	22.5
Number of independent reflections	2654
Number of observed reflections	1953
Number of refined parameters	274
R and R_w	0.0278 and 0.0356

culations, initially with isotropic and later with anisotropic thermal parameters. All hydrogen atoms were located on the difference Fourier map. Crystal data are given in Table 3.

Lists of atomic coordinates, thermal parameters, calculated hydrogen coordinates and torsion angles have been deposited as supplementary material with the Editor, from whom copies are available on request.

RESULTS AND DISCUSSION

The corrected magnetic moments for all of the complexes at room temperature are within the normal values for copper(II) complexes in a square planar tetracoordinated environment. The *d–d* bands in the electronic spectra exhibit broad absorptions in the range 16,660–17,250 cm^{-1}, consistent with those of the square copper(II) complexes reported by Ali and Tarafdar,[7,8] the other absorptions at approx. 19,000 cm^{-1} may be shielded by the charge-transfer absorptions of the ligands.

In the IR spectra of two ligands, medium bands at 3100–3106 cm^{-1} are assigned to ν(N—H). Due to the existence of conjugation in the molecule, the vibration of the C=N bond moves to lower wavenumbers compared with that of the C=N bond in general Schiff bases; both SMPDH and SBPDH have a very strong band at 1480–1485 cm^{-1} assigned to ν(C=N). Two strong bands appearing in the ranges 1221–1231 cm^{-1} and 870–880 cm^{-1} are assigned to the ν(N—O) and δ(N—O) modes, which are in agreement with those of similar ligands.[9] Bands which are considered to derive some intensity from the C=S bond appear at approx. 1090 cm^{-1}.

In the IR spectra of the complexes, the ν(C=N) and ν(N—O) frequencies of the ligands decreased by *ca* 45–56 cm^{-1} and 17–31 cm^{-1}, respectively, upon complex formation, indicating the co-ordinated nitrogen atom of the C=N bond and oxygen atom of the N—O bond. In comparison with the free ligands, ν(C=S) disappears, whereas ν(C—S) appears at approx. 1045 cm^{-1}, which shows the coordinated ligand is in the thiolate form, similar to analogous ligands.[6,10] All complexes have a very strong ν(Cl—O) absorption in the region 1060–1090 cm^{-1}. Complexes **3** and **5** produce a band at 3270–3335 cm^{-1}, which is assigned to ν(N—H) of the additive imidazole, different from that of the ligand which disappears when the complex forms.

The structure of [Cu(SMPD)ImH]ClO_4 is shown in Fig. 1, together with the atomic numbering scheme. Figure 2 is a view of the unit cell illustrating the molecular packing. Selected bond lengths and bond angles are given in Table 4.

The copper atom in one molecule is planar, tetracoordinated by the S(1), N(4) and O(1) atoms of the ligand and one nitrogen atom of the imidazole. The Cu—S, Cu—N and Cu—O distances fall in the normal range, and the N(1)—Cu—O(1), O(1)—Cu—N(4), N(4)—Cu—S(1) and S(1)—Cu—N(1) bond angles are 87.5, 91.1, 86.2 and 95.1°, respectively.

Like other copper(II) complexes of pyridine N-oxide, the O(1) atom is not only coplanar with the binding pyridine group, but also has a normal O(1)–

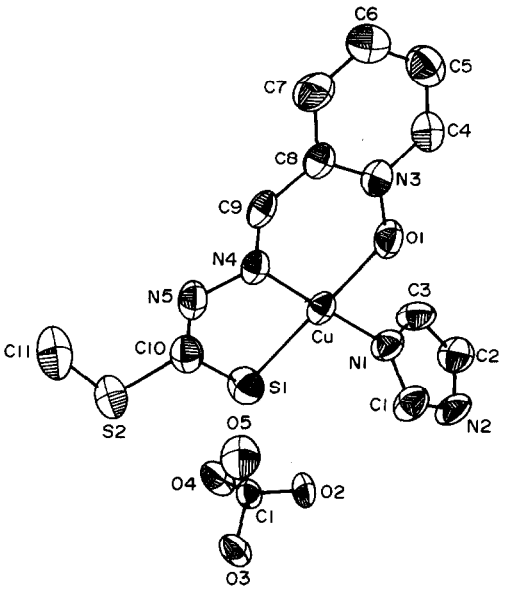

Fig. 1. The structure of $[Cu(SMPD)ImH]ClO_4$.

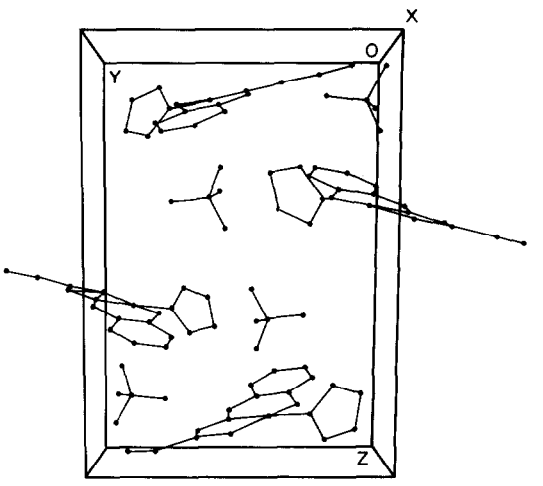

Fig. 2. View of the unit cell illustrating the molecular packing.

N(3) bond length (1.312 Å).[11] The O(1)—N(3), N(3)—C(8), C(8)—C(9), C(9)—N(4), N(4)—N(5), N(5)—C(10) and C(10)—S(1) bond lengths indicate that all these atoms are conjugated with each other via the pyridine group. Two least-squares planes composed of CuN(4)C(8)C(9)N(3)O(1) and CuN(4) N(5)C(10)S(1) are parallel to each other, but almost perpendicular to the imidazole ring to decrease spatial repulsion. The whole molecule has low symmetry, resulting from the presence of the large imidazole group which leads to a longer distance between molecules and prevents possible

Table 4. Selected bond lengths (Å) and bond angles (°)

Cu—S(1)	2.251(1)	Cu—N(1)	1.956(4)
Cu—N(4)	1.945(4)	Cu—O(1)	1.935(3)
S(1)—C(10)	1.737(5)	S(2)—C(10)	1.743(5)
N(3)—O(1)	1.312(5)	S(2)—C(11)	1.795(8)
N(1)—C(1)	1.303(6)	N(1)—C(3)	1.354(7)
N(2)—C(1)	1.323(7)	N(2)—C(2)	1.349(7)
N(3)—C(4)	1.364(6)	N(3)—C(8)	1.365(6)
N(4)—N(5)	1.391(5)	N(4)—C(9)	1.272(6)
N(5)—C(10)	1.299(7)	C(2)—C(3)	1.327(7)
C(8)—C(9)	1.443(6)		
S(1)—Cu—N(4)	86.2(1)	S(1)—Cu—N(1)	95.1(1)
S(1)—Cu—O(1)	175.7(1)	N(1)—Cu—N(4)	177.7(2)
N(4)—Cu—O(1)	91.1(1)	N(1)—Cu—O(1)	87.5(1)
C(10)—S(2)—C(11)	102.9(3)	Cu—S(1)—C(10)	93.6(2)
Cu—N(1)—C(1)	128.0(3)	Cu—O(1)—N(3)	127.5(3)
C(1)—N(1)—C(3)	105.0(4)	Cu—N(1)—C(3)	127.0(3)
O(1)—N(3)—C(4)	116.0(4)	C(1)—N(2)—C(2)	107.5(4)
C(4)—N(3)—C(8)	120.4(4)	O(1)—N(3)—C(8)	123.6(4)
Cu—N(4)—C(9)	125.2(3)	Cu—N(4)—N(5)	120.8(3)
N(4)—N(5)—C(10)	112.8(4)	N(5)—N(4)—C(9)	113.9(4)
N(2)—C(2)—C(3)	105.8(5)	N(1)—C(1)—N(2)	111.3(4)
N(3)—C(4)—C(5)	121.4(5)	N(1)—C(3)—C(2)	110.5(4)
N(3)—C(8)—C(9)	122.3(4)	N(3)—C(8)—C(7)	118.1(4)
N(4)—C(9)—C(8)	127.4(4)	C(7)—C(8)—C(9)	119.5(4)
S(1)—C(10)—S(2)	113.6(3)	S(2)—C(10)—N(5)	119.8(4)
		S(1)—C(10)—N(5)	126.6(4)

dimer formation via the potential bridging group O(1) atom or S(1) atom of the ligand.

It is expected that the ligand is deprotonated to be uninegative on complex formation and the crystal structure of the complex confirms this.

REFERENCES

1. D. L. Klayman, J. P. Scovill, J. F. Bartosevich and J. Bruce, *J. Med. Chem.* 1983, **26**, 35 and refs therein.
2. J. P. Scovill, D. L. Klayman and C. F. Franchino, *J. Med. Chem.* 1982, **25**, 1261.
3. J. P. Scovill, D. L. Klayman, C. Lambros, G. E. Childs and J. D. Nortsh, *J. Med. Chem.* 1984, **27**, 87.
4. M. A. Ali and S. E. Livingstone, *Coord. Chem. Rev.* 1974, **13**, 101.
5. D. Jerchel, J. Heider and H. Wagner, *Justus Liebigs Annln Chem.* 1958, **613**, 155.
6. M. Das and S. E. Livingstone, *Inorg. Chim. Acta* 1976, **19**, 5.
7. M. A. Ali and M. T. H. Tarafdar, *J. Inorg. Nucl. Chem.* 1977, **39**, 1785.
8. M. T. H. Tarafdar, M. A. Miah, R. N. Bose and M. A. Ali, *J. Inorg. Nucl. Chem.* 1981, **43**, 3151.
9. A. E. Landers and D. J. Phillips, *Inorg. Chim. Acta* 1984, **85**, 77.
10. D. X. West and L. K. Pannell, *Transition Met. Chem.* 1989, **14**, 457.
11. N. M. Carayannis, L. L. Pylewski and C. M. Mikulski, *Coord. Chem. Rev.* 1973, **11**, 93.

Polyhedron Vol. 9, No. 24, pp. 2987-2991, 1990
Printed in Great Britain

0277-5387/90 $3.00+.00
© 1990 Pergamon Press plc

SOME ACTINIDE COMPLEXES OF PYRIDIN-, PYRROL-, FURAN- AND THIOPHEN-ALDAZINE SCHIFF BASES*

MAHMOUD M. DAWOD, FAWWAZ I. KHALILI and AFIF M. SEYAM†

Department of Chemistry, University of Jordan, Amman, Jordan

(*Received* 11 *April* 1990; *accepted* 29 *August* 1990)

Abstract—Actinide chloride complexes with pyridinaldazine (PAA), pyrrolaldazine (PyAA-H_2), furanaldazine (FAA), and thiophenaldazine (TAA): $An(L)Cl_n \cdot m\text{-}H_2O$, where An = Th, UO_2; L = PAA, PyAA-H_2, FAA, TAA; $n = 2, 4$; $m = 0, 2, 3, 5$ (also, mononuclear with 2L, dinuclear and trinuclear complexes) have been prepared by the reaction of $ThCl_4$, UO_2Cl_2 or $UO_2(Ac)_2 \cdot 2H_2O$ with PAA, PyAA-H_2, FAA or TAA and characterized by spectral data, electrical conductance, thermal and elemental analysis.

Recently, we reported the synthesis and characterization of some lanthanide chloride complexes of pyridinaldazine and pyrrolaldazine Schiff bases.[1] It has been found that pyridinaldazine (PAA) and pyrrolaldazine (PyAA-H_2) form metal complexes of different stoichiometries.[1,2] Transition metal complexes of PAA[2], furanaldazine (FAA)[3,4] and thiophenaldazine (TAA)[4] are reported. In the complexes of FAA and TAA with transition metals, they behave in a monodentate fashion.[4] In this paper, we report the synthesis and characterization of some actinide complexes of PAA, PyAA-H_2, FAA and TAA.

EXPERIMENTAL

Physical and analytical measurements

Proton nuclear magnetic resonance (^{1}H-NMR) spectra were recorded on a varian T-60A spectrometer in methanol-d_4. Chemical shifts are reported relative to internal $Si(CH_3)_4$. IR spectra were recorded on a Perkin–Elmer (577) spectrometer as KBr discs or Nujol mulls pressed between two NaCl discs or two polyethylene sheets. Conductivity measurements were carried out using 10^{-3} M solution in methanol on a Philips PW 9059 digital conductivity meter at 25°C. UV–vis spectra were recorded on a Beckman Du-7 spectrophotometer. Thermogravimetric analyses (TGA) were recorded on a Mettler TG 10A TA processor using a Mettler Tg-50 thermobalance. Microanalyses were performed by Dr Franz Pascher/ Ellen Pascher Microanalysis laboratory (Bonn, F.R.G.). Thorium analyses were determined by titration with EDTA[5] after decomposition of the sample with HNO_3. The titration method was confirmed by analyses of the metals as the corresponding oxide. Uranium was determined as U_3O_8 using the ammonia method.[6] Chloride was determined gravimetrically as AgCl.[6]

Materials and methods

All procedures were performed using techniques for air sensitive compounds. Pyrrole-2-carboxyaldehyde (BDH) was purified by stirring over active carbon in methanol; pyridine-2-carboxyaldehyde (Fluka) and furan-2-carboxyaldehyde (Kock-Light) were purified as in the literature;[1,7] thiophene-2-carboxyaldehyde and hydrazine (Riedel- de- Haen) thorium tetrachloride, uranyl acetate dihydrate and uranyl chloride (BDH) were used without further purification. The ligands PAA, PyAA-H_2, FAA and TAA were prepared according to Stratton's method.[8]

Complexes with PAA, I

To a filtered solution of the metal salt, $ThCl_4$ or $UO_2(Ac)_2 \cdot 2H_2O$ (4.76 mmol) in methanol (15 cm^3), a solution of PAA (1.0 g, 4.76 mmol) in methanol (30 cm^3) was added (only 0.5 g, 2.38 mmol

* This paper is part of the MSc thesis of M. M. Dawod.
† Author to whom correspondence should be addressed.

Table 1. Yields, analytical and TGA data for the actinide complexes

Complex/Colour	Decomposition point (°C) (Yield, %)	Calculated/Found (%) C	H	N	Cl	M	TGA T^a (°C)	Weight loss (%)	Assignment
$[Th(PAA)Cl_4(H_2O)_2]$, **Ia**	200	23.2	2.3	9.0	22.9	37.4	91	1.45	—
Light yellow	(76)	23.5	2.6	9.0	22.7	37.7			
$[(UO_2)_2(PAA)(OH)_3Ac(H_2O)]$, **Ib**	280	19.1	2.1	6.4	—	54.5	—	—	—
Yellow	(87)	19.3	2.0	6.2	—	54.8			
$[Th_3(OH)_2(PyAA)_2Cl_4(H_2O)_{10}]Cl_2 \cdot 4H_2O$, **IIa**	230	15.4	3.0	7.2	13.6	44.5	95	4.84	$4H_2O$
Yellow	(60)	15.4	2.7	7.0	13.8	44.4			
$[UO_2(PyAA\text{-}H_3)_2Cl_2(H_2O)]Cl_2$, **IIb**	210	29.9	3.0	13.9	17.6	29.6	—	—	—
Yellow	(45)	29.6	2.8	13.8	17.5	29.0			
$[Th(FAA)Cl_2(H_2O)_3]Cl_2 \cdot 0.5THF$, **IIIa**	100	22.1	2.8	4.3	21.8	35.6	97	5.07	0.5THF
Yellowish-brown	(84)	21.4	2.4	4.4	21.8	36.0			
$[UO_2(FAA)Cl]Cl \cdot 0.5Et_2O$, **IIIb**	160	25.5	2.3	5.0	12.6	42.1	97	4.63	$0.5Et_2O$
Yellowish-brown	(80)	25.4	2.4	4.9	12.6	42.1			
$[Th(TAA)Cl_2(H_2O)_3]Cl_2 \cdot 2H_2O$, **IVa**	170	17.6	2.6	4.1	20.7	33.5	95	5.39	$2H_2O$
Brownish-yellow	(87)	17.4	2.2	4.0	20.8	33.5			
$[(UO_2)_3(TAA)_2Cl_4(H_2O)_6]Cl_2 \cdot 2H_2O$, **IVb**	220	14.9	2.0	3.5	13.2	44.4	97	2.21	$2H_2O$
Brownish-yellow	(83)	15.0	1.9	3.4	13.4	44.7			

[a] Starting temperature 45°C.

of PAA in the case of U^{VI} salt). The mixture was stirred for 48 h in the case of Th^{IV}, and 3 h in the case of U^{IV} at room temperature to give the complex as a precipitate. The precipitate was filtered, washed with cold methanol and diethyl ether, and dried *in vacuo* over P_4O_{10}. Both complexes are insoluble in most common solvents but hydrolyse in water.

Complexes with PyAA-H_2, **II**

To a stirred solution of the metal salt, $ThCl_4$ or UO_2Cl_2 (2.38 mmol) in a mixture of methanol–acetone (1:4; 15 cm^3), a solution of the ligand PyAA-H_2 (2.38 mmol) in a mixture of methanol–diethyl ether (1:10; 30 cm^3) was added. The reaction mixture was stirred overnight to give the complex as a precipitate. The complex was filtered, recrystallized from a mixture of methanol–acetone–diethyl ether (1:3:5), washed with acetone and diethyl ether and dried *in vacuo* over P_4O_{10}. Both complexes are soluble in methanol and ethanol, and partially soluble in acetone, THF, DMF and water.

Complexes with FAA *and* 2-TAA, **III** *and* **IV**

To a hot solution of the metal salt, $ThCl_4$ or UO_2Cl_2 (3.54 mmol) in methanol (80 cm^3), FAA or TAA (3.54 mmol) was added. The reaction mixture was refluxed for 3 h in the case of FAA, and 48 h in the case of TAA, then cooled to 40°C and the solvent was removed *in vacuo*. The residue was washed with diethyl ether (2 × 50 cm^3). The residue was extracted with THF (4 × 50 cm^3) at 40°C and the solvent was removed *in vacuo* to give the complex. The complexes are soluble in DMF, methanol and ethanol, and partially soluble in THF and acetone, but hydrolyse in water.

RESULTS AND DISCUSSION

The new actinide complexes of PAA, PyAA-H_2, FAA and TAA (Table 1) were prepared and characterized. Work-up procedures involved filtration and crystallization; yields are generally high (45–87%). The complexes gave satisfactory analytical data (Table 1). The complexes are air stable, usually yellow-coloured microcrystalline solids, complexes **II–IVa,b** are soluble in methanol and ethanol, and partially soluble in tetrahydrofuran and acetone, whilst complexes **Ia,b** are insoluble in most common solvents. Complexes **Ia,b**, **IIIa,b** and **IVa,b** hydrolyse in water, whilst **IIa,b** are soluble in water. Elemental analysis showed that the ratio of metal–ligand in the complexes is 1:1, except in complex **IIb** it is 1:2, and in complexes **IIa** and **IVb** it is 3:2.

TGA data (Table 1) show that water of hydration is lost around 95°C and helps in assigning the number of water molecules of hydration in these complexes. Conductivity data (Table 2) show that these

Table 2. Conductivity data, UV–vis and ^1H NMR spectroscopy for the actinide complexes

Complex	Λ_m(methanol) (ohm^{-1} cm^2 mol^{-1})	λ_{max} (nm) ($\varepsilon \times 10^{-4}$ dm^3 mol^{-1} cm^{-1})	^1H NMR (CD_3OD) δ (ppm)[a]
PAA	—	262(0.5761), 298(1.2618), 307(1.1754)	7.2–8.2(m), 8.9(s)
Ia	—[b]	—[b]	—[b]
Ib	—[b]	—[b]	—[b]
PyAA-H_2	—	266(0.6827), 269(0.6781), 356(4.0766)	6.2–7.2(m), 7.6(s), 8.3(d), 11.6(br)
IIa	230	270(0.2285), 305(0.2046), 385(sh), 403(0.4266), 421(sh)	6.3–7.7(m), 8.1(s), 8.4(s)
IIb	204	270(2.6909), 278(2.5066), 303(2.5345), 404(6.1066), 409(5.9635), 411(5.5911), 416(5.7849), 421(5.6806)	6.1–7.6(m), 7.9(s), 8.2(s), 11.9(br)
FAA	—	334(4.4835)	6.5–7.8(m), 8.4(s)
IIIa	158	229(0.3684), 335(2.8445), 418(sh)	1.8(m, 4H, THF), 3.7(m, 4H, THF), 6.5–7.7(m), 8.4(s)
IIIb	80	228(0.7473), 250(0.7473), 333(2.8183), 435(sh)	1.3(q, 6H, Et_2O), 6.6–7.8(m), 8.4(s)
TAA	—	271(4.2364), 341(4.5366)	7.1–7.5(m), 8.8(s)
IVa	172	263(sh), 271(sh), 278(2.1419), 342(4.7962)	7.1–7.7(m), 8.8(s)
IVb	206	252(sh), 256(1.2131), 262(sh), 270(1.0347), 278(1.1951), 341(2.2304)	7.0–7.6(m), 8.7(s)

[a] (s) = Singlet, (d) = doublet, (m) = multiplet, (br) = broad.
[b] Hydrolyses in water and is insoluble in other solvents.

Table 3. IR data (cm^{-1})[a]

Complex	ν(C═N)	Ring breathing	ν(N—H)/γ(N—H)	ν(C—Y—C)[b]	ν(N—N)	ν(O═U═O)	Others
PAA	1630(vs)	990(vs), 970(vs)			955(vs), 950(vs)		
Ia	1625(sh), 1615(vs)	1060(vs), 1025(vs)			970(w)		465(s), 450(sh), 425(w), 405(m), 370(m), 330(m)
Ib	1625(sh), 1610(vs)	1060(vs), 1015(vs)			970(w)	915(vs)	1550(m), 1445(vs), 1325(vs), 485(vs), 445(vs), 420(s), 400(vs), 260(vs)
PyAA-H_2·HCl	1650(vs,br), 1615(vs,br)	1055(vs), 1045(vs)	3300(s,br), 3200(s,br)/780(s,br)		975(s), 960(vs)		
PyAA-H_2	1630(vs,br)	1055(sh), 1040(vs)	3230(s,br)/690(m)		970(w), 960(s)		
IIa	1650(vs), 1610(vs)	1055(sh), 1045(vs)	—/—		960(s)		500(m,br), 400(w,br), 335(w), 225(w)
IIb	1655(vs), 1620(vs)	1055(vs), 1035(sh)	3400(vs), 3250(s)/700(vs)		980(s), 965(vs)	915(vs)	495(s), 470(m), 360(m), 330(s), 255(s)
FAA	1645(vs)	1030(vs)		1280(vs)	955(vs), 940(vs)		
IIIa	1665(vs), 1620(vs)	1030(vs,br)		1295(m,br)	965(w), 940(s)		520(m), 390(m,br), 310(w)
IIIb	1650(vs), 1620(vs)	1045(vs), 1030(vs)		1315(s), 1295(m)	970(s), 940(vs)	928(vs)	500(s,br), 475(s,br), 345(w)
TAA	1610(vs)	1045(vs)		725(vs)	955(vs)		
IVa	1645(vs), 1590(vs)	1070(s), 1060(sh)		745(s), 735(sh)	970(s)		450(w), 390(m,br), 325(w), 240(w)
IVb	1635(vs), 1590(vs)	1060(vs)		740(vs)	975(m)	928(vs)	500(m,br), 445(w), 430(w), 325(w)

[a] (s) = Strong, (vs) = very strong, (m) = medium, (w) = weak, (br) = broad, (sh) = shoulder.
[b] Y = O, S.

complexes behave as 1 : 2 electrolytes in methanol, whilst complex **IIIb** behaves as a 1 : 1 electrolyte.

^{1}H NMR (Table 2) of the complexes shows that the resonances are as expected for diamagnetic Th^{IV} and U^{VI} species. The presence of tetrahydrofuran in complex **IIIa** was confirmed by ^{1}H NMR as a multiplet at δ 3.7 ppm and a multiplet at δ 1.8 ppm, whilst complex **IIIb** shows a quartet at δ 1.3 ppm (methyl protons of Et_2O) indicating the presence of diethyl ether.

UV–vis data (Table 2) show that the electronic spectra of the complexes are dominated by ligand absorption bands with a hyperchromic effect, this is similar to what has been observed with Ln^{3+}[1] with PAA and PyAA-H_2.

IR data (Table 3) for the complexes **Ia**, **IIIa**, **IIIb** and **IVa** show a distinct splitting of the C=N group stretching bands and of the ring breathing vibrational bands characteristic of the tridentate ligand. The ligand is coordinated through the heteroatoms of the two rings and one nitrogen of the C=N groups. In complex **Ib**, the ligand PAA acts as a tetradentate one, to two uranyl ions, and due to the different environment around each uranyl ion {a bidentate acetate group to one uranyl ion [ν_{as}(COO) at 1550, ν_s(COO) at 1445 cm^{-1}] is suggested which is in accord with the literature[9]}, a splitting of the C=N group stretching bands and of the ring breathing vibrational bands occurs. A similar situation exists in complexes **IIa** and **IVb**, but the environment of the two heterocycles in each ligand is the same, so there are no changes in the ring breathing vibrational bands. The uranium complex of PyAA-H_2 (**IIb**) shows a splitting of the C=N vibrational bands similar to PyAA-H_2·HCl, with changes in the ring breathing vibrational band and the N—H stretching vibrational band. All this suggests that the ligand PyAA-H_3^+ is acting as a monodentate ligand probably through the pyrrole nitrogen.

The uranyl stretching vibration of complexes **I**–**IVb** gave rise to a very strong-intensity absorption at 928 or 915 cm^{-1}.[10] In the U^{VI} complex (**Ib**) a very strong band is observed at 1325 cm^{-1} which can be assigned to a bridging hydroxyl group,[11] and this might explain at least the dimeric nature of this complex.

Therefore, suggested formulae (Table 1), based on spectral data, electrical conductance, thermal and elemental analysis, show that in complexes **II**–**IVa** and **IVb** the coordination number is eight, whilst for complexes **Ia** it is nine, **Ib** and **IIb**, seven, and for **IIIb** it is six, and this is expected for the actinides.[12]

Acknowledgement—The authors thank the University for financial help (M.M.D.).

REFERENCES

1. M. M. Dawod, F. I. Khalili and A. M. Seyam, *Polyhedron* 1989, **8**, 21, and references therein.
2. C. J. O'Conner, R. J. Romananch, D. M. Robertson, E. E. Edudk and F. F. Fronczek, *Inorg. Chem.* 1983, **22**, 449; T. C. Woon, L. K. Thompson and Ph. Robichaud, *Inorg. Chim. Acta* 1984, **90**, 201.
3. G. K. Kornienko, V. I. Mar'in and A. D. Shebaldova, *Kim. Farm. Zh.* 1983, **17**, 318.
4. V. K. Gupta, N. C. Jain and D. K. Sharma, *Current Sci.* 1980, **49**, 459.
5. F. J. Welecher, *The Analytical Uses of EDTA*. Van Nostrand, New York (1965).
6. A. I. Vogel, *Quantitative Inorganic Analysis*, 3rd edn. Longmans, London (1961).
7. A. I. Vogel, *Quantitative Organic Analysis*, 3rd edn. Longmans, London (1961).
8. W. J. Stratton, *Inorg. Chem.* 1970, **9**, 518.
9. D. G. Karraker, *J. Inorg. Nucl. Chem.* 1969, **31**, 2833.
10. T. J. Marks, A. M. Seyam and J. R. Kolb, *J. Am. Chem. Soc.* 1973, **95**, 5529; A. M. Seyam, *Inorg. Chim. Acta* 1982, **58**, 71.
11. M. G. Kuzina and A. A. Lipovskii, *Russ. J. Inorg. Chem.* 1972, **17**, 569.
12. L. E. Schock, A. M. Seyam, M. Sabat and T. J. Marks, *Polyhedron* 1988, **7**, 1517.

VOLUME 8

SUBJECT INDEX

(Compiled by Peter Thornton)

A

Acetaldehyde complexes
  tungsten(IV), 1261
Acetates and acetato complexes
  cobalt(II), 51
  copper(II), 659,1077
  lanthanides, 555
  manganese(III), 1029
  molybdenum(II), 1751,1770,2359
  nickel(II), 2551
  osmium(I), 1537
  rhodium(II), 1117
  ruthenium(II), 597,1149
  ruthenium(II,III), 577,2571
  yttrium, 1923
Acetic acid complexes
  vanadium(II), 1823
Acetoin, 1213
Acetone, 653
Acetonethiosemicarbazonate
  nickel(II), 727
Acetonitrile, solvent for
  complexation, 2251
Acetonitrile complexes
  cobalt(III), 275,415,2389
  molybdenum, 1625
  molybdenym(0), 2119
  molybdenum(II), 1770,2599
  molybdenum(III), 545
  niobium(V), 549
  rhenium(I), 1872
  rhenium(III), 1689
  rhenium(V), 959
  rhodium(I), 2193
  ruthenium(II), 1223
  tantalum(V), 549
  titanium(IV), 311
  tungsten(II), 351,2587
  vanadium(IV), 87
N-Acetylglycinate, -leucinate,
  -phenylalaninate, Ni(II), 1329
Acetylsalicylate complexes
  copper(II), 2777
Actinides
  coordination numbers, 2431
  diketonate hydroxide complexes,
    2071
Acyl complexes
  iron(0), 603
Adipate, copper(II), 1239
Adsorption isotherms, adsorption
  of metal complexes on silica
  gel, 2901
Alanine complexes
  cobalt(III), 1015,1205,1227
Alcohols, oxidations catalysed by
  Ru(III) complex, 2813
Alcohol complexes
  cadmium, calcium, 1953
  copper(II), 769,2469
  iron(II), 1335
  molybdenum(IV), 29
  nickel(II), 2321
  vanadium(III), 1782
Aldehyde, hydrogenation, 121
Aldehyde complexes
  lanthanides, 2109
Alkene complexes
  tungsten(IV), 1261
Alkenyl complexes
  molybdenum(II), 1859
  platinum(II), 433
  ruthenium, 695
  tungsten, 695,1807
Alkoxides
  chromium(0), 653
  copper(II), 769,873
  molybdenum(IV), 29,123,129
  molybdenum(IV,V), 123
  molybdenum(V), 669
  molybdenum(V,VI), 537
  molybdenum(VI), 1213,2473,2915
  neodymium, 2183
  niobium(V), 1848
  osmium(VI), 597
  rhenium(V), 559
  titanium(IV), 2893
  tungsten(0), 653
  zinc, 1913
Alkyls
  aluminium, 831,1279,1497
  hafnium(IV), 2189
  indium, 763
  lanthanum, lutetium, 1850
  molybdenum(II), 1804,2599
  molybdenum(IV), 1802
  nickel(II), 285,585,1069,2449
  niobium(III), 2189.
  niobium(V), 1607
  phosphorus(V), 731,2623
  platinum(II), 57,551
  platinum(IV), 551
  rhenium(V), 959
  rhodium(III), 2689
  silicon, 427
  tantalum(III), 2189
  tantalum(V), 341,1607
  tin(II), 1891
  tin(IV), 1413,1753,2047,2557,
    2755
  titanium(IV), 1717,1838,2817

tungsten, 1807
tungsten(II), 1804
tungsten(III), 2035
vanadium(III), 1339,1767
zirconium, 77,1601
zirconium(III), 1758
zirconium(IV), 1758,1760,2189
Alkylamides
chromium(III), 1457
molybdenum(IV), 129,1419
molybdenum(VI), 2947
phosphorus(V), 2623
rhenium(VII), 2657
tantalum(V), 341
titanium(III), 1457
tungsten(VI), 2947
vanadium(III), 1339,1457
zirconium, 1601
Alkylidyne complexes
chromium, 179
cobalt, 1939
iron, 179
molybdenum, 179,2265,2271
platinum, 2265,2271
tungsten, 179,2271
tungsten(III), 2035
Alkylimido complexes
molybdenum(VI), 2947
niobium(V), 1819
rhenium(V), 1689
rhenium(VI),(VII), 2657
tantalum(V), 341
tungsten(IV), 1261
tungsten(VI), 1788,2947
Alkylphosphido complexes
Hf(III),(IV), Zr(III),(IV), 1774
Alkylphosphinidene complexes
tungsten(II), 2671
Alkyne complexes
molybdenum(0),(II), 1810
ruthenium, 1123
tungsten(II), 351,2587
Alkynyl complexes
electrophilic addition, 1595
Os, Ru, W, 2003
Allene complexes
electrophilic addition, 1595
Allyls
molybdenum(II), 2599
molybdenum(III),(IV), 203
nickel(II), 285,2449
platinum(II), 551
tungsten(II), 1859
Allyl alcohol complex
tungsten(IV), 1261
Aluminium
chloride complexes, 325,533
chloride dioxygen hydrocarbon complex, 533
chloride diphosphine methyl phosphine oxide complexes, 1497
chromium oxide, 1765
diaminoimine methyl complex, 1279
edta fluoride thio complexes, 2057
methyl phosphine complexes, 831
triazenide, 1909
Aluminophosphates, Co,Cr,Mg,Mn,Ni, 819
Americium(III)
diketonate hydroxide complexes, 2071
Amide(NH_2^-) complexes
Co(I), Fe(I), 1401
molybdenum, 1653
palladium(II), 1979
platinum(II), 1979
rhodium(I), 1401
tungsten, 1653
Amide($RCONH_2$) complexes
cadmium, 1093
copper(II), 1
mercury, zinc, 1093
1-Amidino-*O*-alkylurea complexes
copper(II), nickel(II), 757
Amido($RCONH^-$) complexes
antimony(III), 581
Amidoamine complexes
platinum(II), 2943
Amidodiphosphine complexes
iridium(I), 2291
Amine complexes
aluminium, 1279
chromium(0), 2681
cobalt(III), 491
copper(II), 659,909,991,2593, 2749,2837
indium, 633
iron(III), 491
lanthanides, 2459
molybdenum(0), 1857
molybdenum(III),(IV), 1971
molybdenum(VI), 2947
nickel(II), 25,909,1243,2837
palladium(II), 25
platinum(II), 25
rhodium(II), 1157
silver(I), 2951
tungsten(VI), 2947
uranium(VI), 2251
Aminoacid complexes
beryllium, 2017
cobalt(III), 1015,1205 ,1227
copper(II), 1,739,1019,2131
iron, 1865
lanthanides, 2139
molybdenum(VI), 2225
nickel(II), 1329
phosphorus(V), 731
thorium(IV), uranium(VI), 2233
vanadium(IV), 1173,1745
Aminoalcohol complexes
Mo(VI), U(VI), 977
2-Aminobenzenethiolates
molybdenum, 1033
titanium(IV), 2893
4-Aminobenzophenone complex
copper(II), 991
Aminocarbyne complexes
molybdenum, 1595,1653
rhenium, tungsten, 1595
2-Aminocyclopentene-1-dithiocarboxylate complexes, In, 633
2-Aminoethanethiol complexes
nickel(II), 2837
vanadium(III), 1723
2-Aminoethanol complexes
Mo(VI), U(VI), 977
3-Aminoisoxazole complexes, copper(II), 935
2-Aminophenol complexes
Th, U(VI), 977
2-Aminophenol Schiff base complexes, Co(III), 2677

Aminopolycarboxylates
thorium, 2385
titanium(III), 577
Aminopyridine complexes
Co, Cu, Ni, 2901
vanadium(IV), 2611
zinc, 2901
Aminothiolates
vanadium(III), 1723
Ammonia, from dinitrogen, 1463
Ammonia complexes
cobalt(II,III),(III), 2023
ruthenium(III), 577
Aniline Schiff base complexes
palladium(II), 2725
Anthracene, dioxygen halide complexes, 533
Antimonic acid, core - shell particles with silicic acid, 2577
Antimony(III)
amido aryl azole complexes, 581
chloride iron(0) molybdenum(0) tungsten(0) complexes, 2495
diimine halide complexes, 2937
dithiocarbamates, 1891
Arabinose complexes
cobalt(II,III),(III), 2023
Arene complexes
chromium, 1135,1589,1641
hafnium(0), 1641
molybdenum(0), 1641,1810
niobium(0),(I), 1641
ruthenium(I), 2803
Ti(0), W(0), Y(0), Zr(0), 1641
Arsenic(III) hydride imine, 1461
Arsine complexes
copper(II), 2469
molybdenum(II), 917
ruthenium(II), 1149
Arsine oxide complexes
thorium, zirconium, 109
Aryls
antimony(III), 581
carbaboranes, 805
copper(III), 1039
lanthanides, 17
mercury, 1085
nickel(II), 285,1069
palladium(II), 2209
phosphorus(V), 731,1445,2623
platinum(II), 2209
rhenium(VI),(VII), 2657
rhodium(III), 2727
tin(II), 1861
tin(IV), 1753,1897
titanium(III), 1457,1717
vanadium(III), 1339,1457,1767
Arylamido complexes
bismuth(III), 1579
nickel, 2603
platinum(II), 2507
tantalum(V), 341
Arylimido complexes
molybdenum, 1033
tantalum(V), 341
tungsten(IV), 1261
tungsten(VI), 1788
Arylphosphonium salts, 1039
Asparagine, aspartic acid complexes, copper(II), 1
Aspartate complexes
beryllium, 2017
copper(II), 1019
thorium(IV), uranium(VI), 2233
Attractive forces in transition metal complexes, 1742
Azide complexes
cobalt(II),(III), 641
Cu(II), Mn(II), 1523
mercury, 2731
molybdenum(0), 1471
molybdenum(II), 371
Pd(II), Pt(II), 897
tungsten(0), 1471
2,2'-Azobipyridine complexes
molybdenum(0), 921
Azole complexes
antimony(III), 581
cobalt(II), 1965
copper(II), 157,659,769,935, 1345,1965,2313,2777
lanthanides, 555
manganese(II), 1965
molybdenum, 1033
molybdenum(II), 371
molybdenum(VI), 541,2225
nickel(II), 1965
palladium(II), 1345
rhodium(II), 1157
ruthenium(II), 851
vanadium(IV), 1835
Azoresorcinol complexes
palladium(II), 197

B

Barium
cryptand complex, 1143
diaminepolycarboxylate complex, 2693
mixed metal oxides, 1615
tetracycline complexes, 189
Benzene complexes
chromium, 1589
chromium(0), 1135
Benzenethiolate, indium, 763
Benzil complexes
molybdenum(VI), 2915
Benzoates
cobalt(II), copper(II), 2395
lanthanides, 555
molybdenum(VI), 2915
nickel(II), 2395
titanium(IV), 1844,1846
Benzo-15-crown-5 complex
thallium(I), 2115
Benzohydroxamate complexes
molybdenum(IV), 29
Benzoin complexes
molybdenum(VI), 2915
Benzoin oxime complexes
molybdenum(VI), 2473
Benzonitrile complexes
rhenium(I), 1872
Benzophenone, 653
Benzoquinonedioxime complexes
ruthenium(II),(III), 851
Benzotriazole complexes
antimony(III), 581
N-Benzoylalaninate, -glycinate, -leucinate, -valinate complexes, nickel(II), 1329
Benzyls
nickel(II), 285,2449

tantalum(V), 341
zirconium, 77
6-Benzyl-2,2'-dipyridyl, 6-benzyl-4,4'-dimethyl-2,2'-dipyridyl complexes, zirconium, 77
Benzylisocyanide complexes
tungsten(II), 827
6-Benzyl-1,10-phenanthroline complexes, zirconium, 77
Beryllium
aminoacid hydroxide complexes, 2017
iodate water complex, 357
tetracycline complexes, 189
Bicarbonate complexes
cobalt(III), 2389
Bicyclo-2,2,1-hepta-2,5-diene complexes, rhodium(I), 167
Biguanidine complexes
copper(II), 7
Binucleating pentadentate ligand, copper(II) complex, 2513
Biomineralisation, iron oxides, 149
Biphasic catalysis, review, 407
2,2'-Bipyrazine complexes
molybdenum(0), 921
ruthenium(II), 2615
3,3'-Bipyridazine complexes
molybdenum(0), 921
ruthenium(II), 2615
2,2'-[&4,4'-]Bipyrimidine complexes, molybdenum(0), 921
1,4-Bis(2-butyltellurophenyl)-2,3-diazabuta-1,3-diene complexes
Pd(II), Pt(II), 2769
1,6-Bis(2-butyltellurophenyl)-2,5-diazahexa-1,5-diene complexes
Pd(II), Pt(II), Rh(I), 2769
Bis(3-dicyclohexylphosphino)propyl(phenyl)phosphine complexes
iridium, 1903
Bis(2-diethylaminoethyl)amido complexes, Cr(III), Ti(III), V(III), 1457
1,2-Bis(diethylphosphino)ethane complexes, Cr(II), 1821
Bis(2-diethylphosphinoethyl)-amido complexes
vanadium(III), 1339,1767
zirconium(IV), 1767
Bis(2-diethylphosphinoethyl)phosphido complexes, Zr(IV), 1767
1,2-Bis(dimethylarsino)benzene complexes, osmium(I), 1537
Bis(2-dimethylarsinoethyl)amido complexes, zirconium(IV), 1767
Bis-3-(dimethylphosphino)dipropylamine complexes
Ni(II), Pd(II), Pt(II), 25
1,2-Bis(dimethylphosphino)ethane complexes
chromium(II), 1821
nickel(II), 1069
niobium(I), 1784
rhenium(V), 959
technetium(V), 1879
titanium(0), 1611
vanadium(II),(IV), 1784
zirconium, 1601
Bis(2-dimethylphosphinoethyl)-amido complexes
vanadium(III), 1339,1767
zirconium(IV), 1767
Bis(2-dimethylphosphinoethyl)-phosphido complexes
zirconium(IV), 1767
Bis(4,6-dimethylpyridylimino)isoindoline complexes, Mo(II), 2359
1,2-Bis(diphenylarsino)ethane complexes, Re(II),(III), 1733
Bis(diphenylphosphino)amine complexes, palladium(I), 1045
1,2-Bis(diphenylphosphino)benzene complex, rhenium(V), 1689
1,4-Bis(diphenylphosphino)butane complexes
nickel(0), 13
platinum(II), 433
1,2-Bis(diphenylphosphino)ethane complexes
cobalt(II), 749
molybdenum, 1595
molybdenum(0), 1463,1810,2599
molybdenum(II), 1751,2599
molybdenum(III), 545
molybdenum(IV), 1870
nickel(0), 13
nickel(II), 585
niobium(I), 1784
osmium(I), 1537
palladium(II), 835,1979
platinum(II), 91,433,835,1979, 2507
rhenium, 1595
rhenium(I), 1872
ruthenium, 695
technetium(I), 1201
tungsten, 1595
vanadium(II),(IV), 1784
Bis(2-diphenylphosphinoethyl)phenylphosphine complexes, molybdenum(II),(IV), 1756
1,1'-Bis(diphenylphosphino)ferrocene complexes, Pt(II), 433
Bis(diphenylphosphino)methane complexes
aluminium, 1497
cobalt(II), 749
molybdenum(0), 1810
nickel(0), 13
osmium(I), 1537
platinum(II), 433
rhenium(II),(III),(IV), 1689
1,3-Bis(diphenylphosphino)propane complexes
cobalt(II), 749
nickel(0), 13
platinum(II), 433
Bis(diphenylphosphinoyl)methane complexes, aluminium, 1497
Bis[(diphenylphosphinyl)methyl]-phenylphosphine oxide complexes, Mo(0), W(0), 627
1,2-Bis(di-*i*-propylphosphino)ethane complex, Ir(III), 1945
Bis(2-di-*i*-propylphosphinoethyl)-amido complexes, Zr(IV), 1767
Bis(di-*i*-propylphosphino)methane complexes, platinum(II), 2169
1,3-Bis(2-hydroxyphenyl)propane-1,3-dionate complexes, Cd, Co(II), Ni(II), Zn, 2743
Bis(3-hydroxypropyl)thiourea, 1891
1,3-Bis(1-methylcyclohexyl)cyclopentadienyl complex, W(II), 1804

1,7-Bis(5-methyl-4-imidazolyl)2,6-dithiaheptane complexes, Co, Cu, Mn, Ni, 1965
Bis[2-(1-methylimidazolyl)methyl]-amine complex, copper(II), 659
Bismuth(III)
arylamide, 1579
carboxylate, 2941
diimine halide complexes, 2937
dithiocarbamates, 1891
dithiophosphate, 483
phosphonate complexes, 1307
Bis(phosphiranyl)oxide complexes
tungsten(0), 2671
Bis(pyridylimino)isoindoline complexes, molybdenum(II), 2359
2,3-Bis(2-pyridyl)pyrazine complexes, ruthenium(II), 2615
3,6-Bis(2'-pyridyl)-1,2,4,5-tetrazine complex, molybdenum(0), 921
1,9-Bis(2-pyridyl)-2,5,8-triazanonane complexes, copper(II), nickel(II), 909
Bis(triaza)diphosphine complexes
platinum(II), 2485
N-Bis(trifluoromethyl)nitroxyiminophosphine, 379
Bis(trimethylsilyl)cyclopentadienyl complexes,
hafnium(IV), 1774
niobium(IV), 1848
titanium(III), 1883
zirconium(III), 1882
zirconium(IV), 1774
Bis(trimethylsilyl)methyl complexes, La, Lu, 1850
Bis(triphenylphosphonium)methane salt, 1293
Book reviews
boron chemistry, 2011
general textbook, 705
organogermanium compounds, 1147
organolead compounds, 133
organometallic chemistry, 1361, 2735
rings, cages and clusters, 1147
semiconductor chemistry, 1361
Boraphosphene, 969
Borates, cadmium, mercury, 1567
Born - Haber cycle
iodoammonium salts, 2911
Borohydrides
titanium(III), 1883
zirconium, 1601
Boron
book review, 2011
capping agents, ruthenium(II) clathrochelates, 1391
halides, dioxygen hydrocarbon complexes, 533
Borylphosphinidene, 969
Bromate, 2791
Bromides
antimony(III), 2937
bismuth(III), 2937
cadmium, 1093
chromium(II), 1821
cobalt(II), 749,1545,1965
cobalt(III), 275,415,2389
copper(I), 1103
copper(II), 769,935,1545,1965, 2469,2593,2749
copper(III), 1039
iridium(III), 211
iron(II), 2425
manganese(II), 1965
mercury, 1085,1093
molybdenum(0), 1471
molybdenum(II), 1756,1876
molybdenum(III), 545
molybdenum(III,IV), 2785
molybdenum(IV), 1756
nickel(II), 285,1545,1965
niobium(IV),(V), 1848
palladium(I), 1045
palladium(II), 897,1485,2725
platinum(II), 897
platinum(IV), 893
rhenium(III), 1689
rhodium, 2565
rhodium(III), 211,2565
ruthenium(III), 2179
silver(I), 211
technetium(V), 1879
thallium(III), 2057
tin(IV), 2047
tungsten(0), 1471
tungsten(II), 1876,2587
tungsten(VI), 1675
vanadium(III), 1782
zinc, 1093
Bromine, oxidation of Ti(III) complexes, 2883
3-[&4-]Bromopyridine complexes
molybdenum(II), 917
Butadiene complexes
iridium(I), 2291
tungsten(IV), 1261
i-Butanol complex
iron(II), 1335
Butatriene complexes
chromium, manganese, 1589
i-Butyls
indium, 763
n-Butyls
tin(IV), 1891
t-Butyls
indium, 763
t-Butylamido complexes
molybdenum(VI), 2947
rhenium(VII), 2657
tungsten(VI), 2947
n-Butylamine complexes
chromium(0), 2681
t-Butylamine complexes
Mo(VI), W(VI), 2947
t-Butylcyclopentadienyls
molybdenum(III),(IV), 203
zirconium(IV), 1760
t-Butylimido complexes
molybdenum(VI), 2947
rhenium(VI),(VII), 2657
tungsten(IV), 1261
tungsten(VI), 1788,2947
t-Butylisocyanide complexes
molybdenum(II), 1786
platinum, 2271
titanium(IV), 1838
tungsten(II), 1786
tungsten(IV), 1261,1285
4-*t*-Butylphenoxide, zirconium, 845
t-Butylphosphido complexes
Hf(IV), Zr(III),(IV), 1774
t-Butylthiolates
Mo(IV), V(V), 1762
2-Butyne complexes

tungsten(II), 351,2587

C

Cadmium
amide cytosine halide phosphine oxide urea complexes,1093
chloride phosphinate phosphine oxide complexes, 2535
diamine malonate complexes, 2291
diaminopolycarboxylates, 1365 2693
diketonate pyridine complexes, 2743
mercury borates, 1567
nitrate pyrrolidone mercury complex, 1913
phosphonate, 1307
polyaminepolyphosphonate complexes, 453,2077
polyselenide complexes, 1995
vitamin D_3 complexes, 1953
Caesium
carboxylate carboxylic acid water complexes, 793
crown ether Fe(II) Ru(II) complexes, 879
Calcium
cryptand complex, 1143
diaminopolycarboxylates, 1365, 2693
tetracycline complexes, 189
vitamin D_3 complexes, 1953
Carbaboranes, 805
Carbaborane complexes
palladium(II), 1485
Carbazole complexes
antimony(III), 581
Carbazone complexes
molybdenum(VI), 677
Carbene complexes
chromium, 1589
hydride migrations, 1583
manganese, 1589
molybdenum(IV), 1583,1861,1863
ruthenium, tungsten, 2351
tungsten(IV), 1861
Carbohydrate complexes
cobalt(II,III),(III), 2023
Carbonate complexes
cobalt(III), 2389,2889
rhodium(III), 1163
Carbonyls
chromium, 179,1589
chromium(0), 653,887,1099,2125, 2681,2719
cobalt, 1625
cobalt(0), 2237
hafnium(0), 1611,1641
intermediates, 1637
iridium(I), 121
iron, 179,1885
iron(0), 479,603,1471,2237,2495, 2521
iron(II), 1503,2371,2425
manganese, 1589
manganese(0),(I), 1855
molybdenum, 179,2265,2271
molybdenum(0), 505,627,887,921, 1471,1810,1857,1876,2119,2333, 2495,2925
molybdenum(II), 505,917,1804, 1859,1876
molybdenum(IV), 1261,1589,1701, 1861,1863
nickel(0), 293,1351
niobium(III), 2189
osmium, 1437,2003
osmium(I), 1537
osmium(II), 1431
platinum, 2265,2271
platinum(0), 2521
platinum(II), 551
rhenium(II), 1689
rhodium(I), 167,2119,2193
rhodium(III), 1447
ruthenium, 695,1123,2003,2351
ruthenium(0), 2237
ruthenium(II), 597,1149,1431
ruthenium(III), 2199
tantalum(III), 2189
titanium(0), 1611
titanium(III), 1883
tungsten, 179,695,1807,2003, 2271,2351
tungsten(0), 505,627,653,827, 887,1471,1876,2125,2495,2671
tungsten(II), 351,505,827,1804, 1859,1876,2587,2671
tungsten(III), 2035
tungsten(IV), 1261,1589,1701, 1861
tungsten(VI), 1285
zirconium(0), 1611,1641
Carbonyl sulphide complexes
copper, 1447
ruthenium(II), 1149
Carboxyethyl complex
osmium(VI), 597
Carboxylate complexes
caesium, 793
chromium(III), 2941
cobalt(II), 39,51,2395
copper(II), 647,659,1077,2345, 2395,2777
iron(II), 1503
lanthanides, 555
manganese(III), 1029
molybdenum, 2265
molybdenum(II), 1751,1770,2359
molybdenum(V), 669
molybdenum(VI), 333,2915,2947
nickel(II), 39,2395,2551
osmium(I), 1537
platinum(II), 143
potassium, 2147
rhodium(I), 167
rhodium(II), 1117,1149
rhodium(III), 1085,2727
ruthenium(II), 597,1149
ruthenium(II,III), 577,2571
thallium(I), 793
titanium(IV), 1844,1846
tungsten(VI), 333,2947
vanadium(IV,V), 1723
yttrium, 1923
zirconium, 929
Carboxylic acid complexes
caesium, 793
potassium, 2147
thallium(I), 793
titanium(IV), 1846
vanadium(II), 1823
Carbyne complexes
Mo, Re, W, 1595

tungsten(VI), 1285
Catechol complexes
copper(II), 2345
tin(II), 2933
Catenand complex
copper(I), potassium, 1251
CD spectra
cobalt(II,III),(III) ammine arabinose hydroxide water complexes, 2023
cobalt(III) aminoacid chloride diaminopolycarboxylate water complexes, 1205
cobalt(III) aminoacid diamine nitrite complex, 1227
cobalt(III) carbonate chloride edda water complexes, 2889
rhodium(III) carbonate ethylenediamine hydroxide water complexes, 1163
vanadium(IV) aminoacid oxo complexes, 1173,1745
Cerium(III)
chloride pyridine pyrrole Schiff base water complexes, 21
crown ether complex, 1561
diketonate water complex, 1111
formylferrocene benzoylhydrazone complex, 2105
polyaminepolycarboxylates, 1425
Cerium(IV)
ether siloxide complex, 1001
Chemical vapour deposition,
platinum, 551
Chlorides and chloro complexes
aluminium, 325,1497
antimony(III), 2495,2937
bismuth(III), 2937
cadmium, 1093,2535
chromium(II), 1825
chromium(III), 1457,1770
cobalt(II), 427,1509,1965,2901
cobalt(III), 275,415,1205,2007, 2389,2889
copper(I), 325
copper(II), 427,769,909,935,991, 1345,1545,1965,2007,2469,2593, 2749,2901
gallium, 1053
germanium, 2641
indium, 2481
iridium, 1903
iridium(III), 211,2245
iron, 1865
iron(III), 135,1293
lanthanides, 21,1850
lanthanum, 2029
lutetium, 1850
manganese(II), 1965
mercury, 1085,1093,1913
molten, 325
molybdenum(0), 1471
molybdenum(II), 917,1756,1786, 2599
molybdenum(III,IV), 2785
molybdenum(IV), 25,1261,1717
molybdenum(V), 45,447,549,1705, 1833
molybdenum(VI), 549,1729,1736, 2947
nickel(II), 25,285,427,585,909, 1545,1965,2283,2901
niobium(IV), 1767
niobium(V), 549,1729,1736,1784, 1797,1819,1848
osmium(II), 1431
osmium(III), 2179
palladium(I), 1045
palladium(II), 25,91,161,897, 1345,1485,2151,2517,2769
phosphazenes, 1517
phosphorus(V), 2623
platinum(II), 25,143,551,897, 2169,2485,2769,2907,2943
platinum(IV), 997
rhenium, 1595
rhenium(I), 1778,1872
rhenium(II), 1689,1733
rhenium(III), 469,1689,1733
rhenium(IV), 469
rhenium(V), 959,1689
rhenium(VII), 1736,2657
rhodium(I), 1431,1575,2193,2769
rhodium(III), 211,613,1085,1447, 2689
ruthenium(I), 2803
ruthenium(II), 1149,1431
ruthenium(III), 2179,2813
silver(I), 211
tantalum(V), 549,1729
technetium(II),(V), 1879
thallium(III), 2057
tin(II), 917,1045,1085,1786
tin(IV), 1413,1753,2047
titanium(III), 1780,1883
titanium(IV), 311,1804,1846,2013
tungsten, 1807
tungsten(0), 1471
tungsten(II), 469,1261,1786
tungsten(III), 469
tungsten(IV), 1261
tungsten(VI), 549,1729,1788,2947
uranium(IV), 1767
vanadium(II), 1784,1823
vanadium(III), 1339,1723,1767, 1780
vanadium(IV), 87,1784
vanadium(IV,V), 1723
zinc, 1093,2593,2901
zirconium(III), 1758,1882
zirconium(IV), 929,1601,1767
N-Chloroacetylaminoacid complexes
nickel(II), 1329
4-Chloro-2,5-dimethylphenylthio-acetate complex, potassium, 2147
2-Chloroethyl(phenylamido)phosphine complexes, W(0), 2671
2-Chloroethylphosphinidene complexes, tungsten(II), 2671
Chlorogenic acid complexes
copper(II), 2345
2-Chloromethylbenzimidazole complexes, antimony(III), 581
4-(4-Chlorophenoxy)butanoate
nickel(II), 39
1-Chlorophosphirane complexes
tungsten(0), 2671
Chromium
alkylidyne carbonyl cyclopentadienyl diphosphine seleno selenoacyl thio thioacyl iron complexes, 179
arene carbene carbonyl triene complexes, 1589
oxycarbides, 1794
Chromium(0)

alkoxide carbonyl hydride complexes, 653
amine carbonyl complexes, 2681
arene complexes, 1641
arene cyclopentadienyl cyclopentaphosphorus complexes, 1135
carbonyl episulphide complexes, 887
carbonyl pentaoxapentaphosphorinane complexes, 2719
carbonyl phosphine complexes, 1099,2125
carbonyl phosphonite Mo(II) complexes, 2339
Chromium(II)
chloride phenylenediamine thiocyanate thiourea complexes, 1825
diphosphine halide complexes, 1821
oxidation, 469
Chromium(III)
alkylamido chloride complex, 1457
aluminium oxide, 1765
aluminophosphates, 819
carboxylate, 2941
chloride sulphonate thioether complexes, 1770
dipyridyl complex, 1453,1549
mixed metal oxides, 1615
oxidation by Mn(III), 1874
polyaminepolyphosphonate complexes, 453
Chromium(V)
oxo complexes, 1830
Citrate complexes
Hf(IV),Nb(V),Ta(V),Zr(IV), 1371
Clathrochelate complexes
ruthenium(II), 1391
Clay minerals, thermal decomposition, 2709
Cluster molecules, rearrangements, 1933
Cobalt
alkylidyne cyclopentadienyl hydride complexes, 1939
carbonyl thio molybdenum complex, 1625
disulphidothionitrate (NS_3^-) porphyrin complexes, 1447
phosphine thio complex, 801
Cobalt(0) carbonyls, 2237
Cobalt(I)
amide (NH_2^-) complexes, 1401
Cobalt(II)
acetate picolinate water complexes, 51
aluminophosphates, 819
azide complexes, 641
azole halide thiocyanate thioether complexes, 1965
bromide diphosphine complexes, 749
carboxylate morpholine piperazine piperidine complexes, 2345
carboxylate water complexes, 39
chloride pyridine complexes on silica gel, 2901
chloride siliconisothiocyanate complexes, 427
chloride tetramine - dioxime thiocyanate complexes, 1509
chloride, thiocyanate complexes on ion exchange media, 859
diaminopolycarboxylate complexes, 1365
diaminepolycarboxylate dicarboxylate complexes, 2693
diketonate pyridine complexes, 2743
dithiodipyridine halide complexes, 1545
oxo molybdenum(VI) complexes, 1675
phenoxide Schiff base copper(II) complexes, 2007
polyaminepolyphosphonate complexes, 453
pyridinedicarboxylate complexes, 745
Cobalt(II,III)
ammine arabinose hydroxide water complex, 2023
Cobalt(III)
acetonitrile halide oxyanion tetramine water complexes, 2389
acetonitrile halide polyamine complexes, 415
amine ammonia thiocyanate complexes, 775
aminoacid chloride diaminopolycarboxylate water complexes, 1205
aminoacid ethylendibiguanide complexes, 1015
ammine arabinose complex, 2023
azide complexes, 641
carbonate chloride edda water complexes, 2889
chloride phenoxide Schiff base copper(II) complexes, 2007
cyclopentadienyl salts, 1780
halide nitrile polyamine water complexes, 275
hexadentate complexes, 491
phenoxide salicylaldimine complexes, 2677
tetramine dioxime complexes, 1509
Conductimetric titrations
cobalt(II) bromide diphosphine complexes, 749
diaminopolycarboxylate complexes, 1365
phenylenediaminedisuccinate complexes, 2693
Controlled potential electrolysis
manganese(III) quinone complex, 1407
Copper
carbonyl sulphide disulphidothionitrate (NS_3^-) porphyrin complexes, 1447
Copper(I)
bromide phosphine complex, 1099
chloride complexes, 325
diimine catenand potassium complex, 1251
diisocyanide complexes, 317
polyselenide complexes, 1139
pyridine Schiff base complexes, 1321

Copper(I,II)
diisocyanide complexes, 317
Copper(II)
acetate oxime pyridine water complex, 1077
acetylsalicylate azole complexes, 2777
alcohol alkoxide azole halide thiocyanate complexes, 769
amide aminoacid hydroxide water complexes, 1
amidinoalkylurea complexes, 757
amine azole carboxylate complex, 659
amine chloride ketone complex, 991
amine halide theobromine complexes, 2593
aminoacid complexes, 1019
aminoacid salicylaldimine water complex, 2131
aminoacid sulphonyl complexes, 739
aminoethanethiol cystamine complexes, 2837
arsine halide methanol oxo phosphine stibine complexes, 2469
azide mepirizole thiocyanate complexes, 1523
azole chloride complex, 1345
azole dicyanamide tricyanomethyl complexes, 157
azole halide nitrate perchlorate complexes, 935
azole halide thiocyanate thioether complexes, 1965
azole thiocyanate complexes, 2313
biguanidine complexes, 7
carboxylate catecholate complexes, 2345
carboxylate morpholine piperazine piperidine complexes, 2395
chloride phenoxide Schiff base cobalt(II),(III) complexes, 2007
chloride polyamine pyridine complexes, 909
chloride pyridine complexes on silica gel, 2901
chloride silicon isothiocyanate complexes, 427
cyanamide dipyridyl complex, 2219
cyanate terpyridine complexes, 97
diamine hydroxide complex, 2645
diaminothioether halide complexes, 2749
dicarboxylates, 1239
dihydroxybenzoates, 647
diisocyanide complexes, 317
diketonates, 1549
diketonate ketoimine thiodiketonate complexes, 2305
dimethylglyoxime complexes, 2409
dithiodipyridine halide complexes, 1545
fluoride sulphate complexes, 457
hydroxide nitrate pyridone lanthanide complexes, 1531
hydroxide peptide complexes, 2463
hydroxide water binucleating complex, 2513
methoxide nitrate pyrrolidone mercury complex, 873
nitrate pyridine pyridine - *N*-oxide complex, 933
oxime complexes, 1957
oxime pyridine water complex, 301
polyaminepolyphosphonate complexes, 453
pyrazolinone - alkyldithioate complexes, 2723
pyridine salicylaldimine complexes, 2543
pyridinedicarboxylate complexes, 745
Copper(III)
aminoacid diamine nitrite complexes, 1227
aryl bromide diimine phosphine complex, 1039
diglycylethylenediamine oxime complexes, 2409
Crotonate, crotonic acid complexes
titanium(IV), 1846
Crown ether complexes
caesium, 879
lanthanum, 2029
potassium, 879,1251,2051
sodium, 879
thallium(I), 2115
uranium(VI), 2251
Cryptand complexes
barium, calcium, 1143
strontium, 1143,2797
Cubane clusters, review, 2843
Curium(III)
diketonate hydroxide complexes, 2071
Cyanamide complex, 2219
Cyanate complexes
copper(II), 97
Cyanide complexes
iron, 2627
iron(II), 361,419,941
iron(II,III),(III), 419
molybdenum, 1653,2897
molybdenum(IV), 1802
palladium(II), 897
platinum(II), 841,897
rhodium(I), 2415
ruthenium(II), 2091
silver(I), 361
tungsten(V), 2213
1-Cyano-2-(2,4,6-tri-t-butyl)phenyl-2-phosphaethene, 2087
Cyclic voltammetry
cadmium diamine malonate complexes, 2291
cobalt alkylidyne cyclopentadienyl hydride complexes, 1939
cobalt(III) chloride phenoxide Schiff base copper(II) complexes, 2007
cobalt(III) tetramine dioxime complexes, 1509
copper(I) pyridine Schiff base complexes, 1321
copper(II) amine azole

carboxylate complex, 6559
copper(II) chloride phenoxide Schiff base cobalt(III) complexes, 2007
copper(II) dimethylglyoxime complex, 2409
hafnium cyclopentadienyl halides, 1601
iron(0) carbonyl diene complexes, 479
iron(III) chloride Schiff base thiosemicarbazide complexes, 135
manganese(III) quinone complex, 1407
mercury thioether macrocyclic complex, 2041
metallocene alkali metal crown ether complexes, 879
molybdenum arylimide nitrosyl pyrazolylborate thiolate complexes, 1033
molybdenum complexes with multiply bonded ligands, 1653
molybdenum(II) azide nitrosyl pyrazolylborate thiocyanate complexes, 371
molybdenum(IV) cyclopentadienyl mercaptopyridine complexes, 2439
molybdenum(VI) imidazole oxo peroxide water complexes, 541
nickel(II) acetate polypyridine helical complex, 2551
nickel(II) methanol salicylaldimine complexes, 2321
nickel(II) salicylaldimine complexes, 113
rhenium(VI) alkylimido aryl complexes, 2657
ruthenium(II) arene chloride complex, 2803
ruthenium(II) diimine complexes, 2615
ruthenium(II) dioxime clathrochelates, 1391
ruthenium(III) carbonyl edta water complexes, 2199
ruthenium(III) chloride diketonate hydroxyketone phosphine complexes, 2813
silver(I) crown thioether complexes, 513
tungsten(IV) cyclopentadienyl mercaptopyridine complexes, 2439
vanadium(III),(IV) edta complexes, 1949
zirconium cyclopentadienyl halides, 1601
1,4-Cyclohexadiene complexes
iron(0), 479
1,4-Cyclohexadiene biepisulphide complexes, Cr(0), Mo(0), W(0), 887
1,2-Cyclohexanedione dioxime complexes, ruthenium(II), 1391
Cyclohexylisocyanide complexes
palladium(I), 1045
tungsten(II), 827
Cyclohexylthiolate
indium, 763
Cyclometallated complexes
nickel(II), 1069
niobium(V), 1607
palladium(II), 1485,2517,2725
tantalum(V), 1607
zirconium(III),(IV), 1758
1,5-Cyclooctadiene complex
iridium(I), 1431
platinum(0), 2521
platinum(II), 551
rhodium(I), 375,1431,1760
Cyclopentadienone complexes
molybdenum(0), 1810
Cyclopentadienyl complexes
chromium, 179,1135
cobalt, 1939
cobalt(III), 1780
hafnium, 1729
hafnium(III), 1774
hafnium(IV), 1774,2189
iron, 1135,1447
iron(0), 1471,2495
iron(II), 879,929,2265,2371, 2425,2459
lanthanides, 17,1007,1850,1983, 2109
lutetium, 1850
manganese, 1589
molybdenum, 179,2271
molybdenum(0), 2495
molybdenum(II), 1802,1859
molybdenum(III), 203
molybdenum(IV), 203,1589,1802, 1861,1863,1884,1999,2439
molybdenum(V), 1705
neodymium, 2109
nickel(II), 285,585
niobium(I), 1784
niobium(III), 2189
niobium(IV), 1762,1848
niobium(V), 1762,1784,1819,1848
platinum(II),(IV), 551
ruthenium(II), 879
samarium(II), 1007
tantalum(III), 2189
tantalum(V), 1729
titanium(0), 1611
titanium(III), 1780,1883
titanium(IV), 311,1729,1804, 1838,1844,2817
tungsten, 179,695,1807,2003, 2271
tungsten(0), 2495
tungsten(II), 1859
tungsten(III), 2035
tungsten(IV),1583,1861,1884, 2439
tungsten(VI), 1279
vanadium(II), 1784
vanadium(III), 1780,2763
vanadium(IV), 1784
ytterbium, 17,1983,2109
zirconium(III), 1758,1774,1882
zirconium(IV), 929,1601,1758, 1760,1774,2189
Cyclopentaphosphorus complexes
chromium, iron, 1135
Cyclotriphosphazenes, 1517
p-Cymene complexes
ruthenium(I), 2803
Cystamine complexes
copper(II), nickel(II), 2837
Cysteine, in ferrihydrite - goethite conversion, 149,2829

Cysteine complexes
cobalt(III), 1205
iron, 1865
vanadium(IV), 1745
Cytosine complexes
cadmium, mercury, zinc, 1093

D

Deuterium isotope effects, hydride cluster complexes, review, 383
Diacetamide complexes
cadmium, mercury, 1093
2,6-Diacetylpyridine Schiff base complexes, copper(I), 1321
Diallyl(phenyl)phosphine complexes
platinum(II), 897
Diaminato complexes
platinum(II), 143
Diamine complexes
cadmium, 2291
chromium(II), 1825
cobalt(III), 1227
copper(II), 2645
molybdenum, 2265
molybdenum(0), 1471
molybdenum(VI), 977
rhodium(III), 1163
ruthenium(II), 2091
thorium(IV), 977
tungsten(0), 1471
uranium(VI), 977,2251
1,4-Diaminobutane complexes
copper(II), 2645
3,3'-Diaminodipropylimido complexes, aluminium, 1279
Diaminopolycarboxylate complexes
barium, 2693
Ca, Cd, Co(II), 1365,2693
cobalt(III), 1205
Mg, Mn(II), Ni(II), 1365,2693
ruthenium(III), 463,2199
strontium, 2693
thorium, 109,2385
U(VI), W(VI), 109
zinc, 1365,2693
zirconium, 109
1,3-Diaminopropane complexes
cadmium, 2291
cobalt(III), 1227
1,3-Diaminopropane Schiff base complexes, Co(II),(III), Cu(II), 2007
Diarsine complexes
osmium(I), 1537
rhenium(II),(III), 1733
Diarsinoamido complexes
niobium(IV), 1767
Diazaphosphaphosphine complexes
platinum(0), 2485
2,10-Diaza-6-thiaundecane complexes, copper(II), 2749
Diazenide complexes
molybdenum(IV), 29
1,3-Diazinane-2-thione complexes
gold(I), 2823
Diazonium complexes
palladium(I), 1045
Dibromoacetate complexes
chromium(III), 2941
Dibromoacetic anhydride, 2941
3-(2,4-Dibromo-5-methylphenyl)-2,2'-dipyridyl complex, copper(III), 1039
Di-*n*-butylamine complexes
chromium(0), 2681
2,3,8,9-Di(2',4'-*t*-butylbenzo)-1,4,7,10-tetrathiadecane complexes, rhodium(III), 613
4,4'-Di-*t*-butyl-2,2'-dipyridyl complexes
nickel(II), 585
platinum(II), 57
Di-*i*-butyldithiocarbamates
Re(IV), V(IV), 1625
Di-*n*-butyldithiophosphate
manganese(II), 1853
2,6-Di-*t*-butyl-4-methylphenoxide
zirconium, 1601
2,6-Di-*t*-butylphenoxides
uranium(IV), 1247
zirconium, 77,1601
Di-*t*-Butylphosphido complexes
molybdenum(IV), 1419
2,5-Di-*t*-butyl-1,3,4-triphosphacyclopentadienyl, 849,2407
Dicarbomethoxyacetylene, reaction with disulphide complexes, 1705
Dicarboxylates
cadmium, 2291
cobalt(II), 745,2693
cobalt(III), 2389
copper(II), 745,1239
hafnium, 1371
iron(III), 813
lanthanides, 2367
manganese(II), 745
molybdenum(VI), 977
nickel(II), 745,2693
thorium, 109,977
uranium, 977
zinc, 745,2693
zirconium, 109,977,1371
1,4-Dichlorobut-2-yne complexes
tungsten(II), 2587
2,4-Dichloro-5-methylphenylthioacetate complexes, caesium, 793
Dicyanamide complexes
copper(II), 157
2,6-Dicyclohexylphenol, 1607
2,6-Dicyclohexylphenoxide
niobium(V), 1607
Dicyclohexylphosphine complexes
rhodium, 2565
Di(2,6-dimethoxyphenyl)phenylphosphine complexes, Ga, 1053
Diene complexes
iridium(I), 1431,2291
iron(0), 479
platinum(0), 2521
rhodium(I), 167,375,1431,1760
Dienolate complexes
molybdenum(VI), 2915
Diethoxy(ethyl)phosphine complexes
tungsten(0), 2671
Diethoxy(phenyl)phosphine complexes, rhenium(I), 1778
Diethylaminocarbyne complexes
tungsten(VI), 1285
Diethyldithiocarbamates
molybdenum, 1625
tin(IV), 2557
vanadium(IV), 1827
O,O'-Diethyldithiophosphates
bismuth(III), 483

manganese(II), 1853
Diethylenetriaminepentaacetate complexes, thorium, 2385
Diethylenetriaminepenta(methylenephosphonate) complexes,
cadmium, 453,2077
Co, Cr, Cu, Fe, 453
lead, 2077
nickel(II), 453
Diethylenetriamine-*N,N,N',N''*-tetraacetate-*N''*-propionate complexes, lanthanides, 1425
Di(2-ethylhexyl)phosphoric acid complexes,
cadmium, 2535
iron(III), 2099
Differential pulse polarography
ruthenium(III) carbonyl edta water complexes, 2199
2,6-Diformyl-4-methylphenol Schiff base complexes, Co(II),(III), Cu(II), 2007
Diglycylethylenediamine complexes
copper(III), 2409
Dihydropyran complexes
samarium(II), 1007
Dihydroxybenzoates
copper(II), 641
3,4-Dihydroxy-3-cyclobutene-1,2-dione complex, iron(II), 1335
3,4-Dihydroxyphenylcarboxylates
copper(II), 2345
Diimine, reaction with phosphine, 1039
Diimine complexes
antimony(III), 2937
bismuth(III), 2937
chromium(III), 1453,1549
copper(I), 1251
copper(II), 1523,2219
copper(III), 1039
manganese(II), 1523,1853
molybdenum(0), 921,1471
molybdenum(IV),(IV,V), 123
nickel(II), 585,689,925,2649
osmium(II), 367
palladium(II), 1989,2209
platinum(II), 57,2209
rhenium(III), 1689
rhenium(V), 959
rhodium(III), 83
ruthenium(II), 1223,2615
technetium(II),(V), 1879
titanium(IV), 2893
tungsten(0), 827,1471
tungsten(II), 827
vanadium(III), 1723
zirconium, 77
1,2-Diiminobenzene complexes
molybdenum, 1033
2,3-Diiminonaphthalene, 9,10-diiminophenanthrene complexes
nickel, 2603
Diisocyanide complexes
copper(I),(I,II),(II), 317
manganese(II), zinc, 317
1,2-Diisocyanoethane complexes
copper(I),(I,II),(II), 317
Diketal complexes
molybdenum(VI), 2915
Diketonates
actinides, 1111,2071
cadmium, 2743
cerium(III), 1111
cobalt(II), 2743
copper(II), 1549,2305
europium(III), 1111,2071
lanthanides, 1111,2071
lanthanum, 1111,2071
lutetium, 2071
neodymium, 2183
nickel(II), 2305,2743
osmium(III), 2179
platinum(IV), 551
rhodium(II), 1117
ruthenium(III), 2179,2813
thorium(IV), uranium(VI), 1111
vanadium(IV), 1827,2611
zinc, 2305,2743
2,3-Dimercaptosuccinic acid, 2809
1,2-Dimethoxyethane complex
cerium(IV), 1001
5,6-Dimethoxyindenyl complexes
molybdenum(III),(IV), 203
2,6-Dimethoxyphenyl(diphenyl)phosphine complexes, gallium, 1053
Di(2[&4-]-methoxyphenyl)(phenyl)-phosphine complexes,
gallium, 1053
rhenium(I), 1778
Dimethylacetamide complexes,
Cd, Hg, Zn, 1093
Dimethylacetylenedicarboxylate complexes, Mo(0),(II), 1810
Dimethylamides
molybdenum(IV), 129,1419
phosphorus(V), 2623
zirconium, 1601
Dimethylamine complexes
molybdenum(III),(IV), 1971
rhodium(II), 1157
2-Dimethylaminoethyl(polyfluorophenyl)amido complexes,
platinum(II), 2943
Dimethylamino(phenyl)carbene complexes, Ru, 2351
3-Dimethylamino-1-propanethiolate
nickel(II), 1253
4-*N,N*-Dimethylaminopyridine complexes, Cd,Co,Ni,Zn, 2743
9,10-Dimethylanthracene, dioxygen halide complexes, 533
6,7-Dimethylbis(2'-pyridyl)quinoxaline complexes, Ru(II), 2615
1,3-Dimethylcyclopentadienyl complexes, zirconium, 1601
2,5-Dimethyl-2,5-diisocyanohexane complexes, Cu, Mn, Zn, 317
2,9-Dimethyl-4,7-diphenyl-1,10-phenanthroline complexes,
platinum(II), 57
4,4'-Dimethyl-2,2'-dipyridyl complexes
nickel(II), 585
platinum(II), 57
zirconium, 77
Dimethyldithiocarbamate complexes
tin(IV), 1413,2557
Dimethylformamide complexes
Cd, Hg, Zn, 1093
N,N-Dimethylfurancarboselenoamide complexes, palladium(II), 2517
N,N-Dimethylglycine complexes
phosphorus(V), 731
Dimethylglyoxime complexes
copper(II),(III), 2409

ruthenium(II), 851,1391
1,2-Dimethylimidazole complexes
copper(II), 2777
1,3-Dimethylimidazolidine-2-thione complexes, vanadium(IV), 87
2,9-Dimethyl-1,10-phenanthroline complexes,
manganese(II), 1853
palladium(II), 1989
2,6-Dimethylphenoxides
tantalum(V), 341
2,6-Dimethylphenylisocyanide complexes, Pt, 2271
molybdenum(0), 2599
platinum, 2271
Dimethyl(phenyl)phosphine complexes
molybdenum(II), 1756
molybdenum(IV), 1701,1756
nickel(II), 585,1069
palladium(II), 897,1989,2151
platinum(II), 835,897,1979,2215, 2507,2907
platinum(IV), 997
rhenium(V), 959
rhodium(III), 2689
ruthenium, 1123
tin(IV), 2047
tungsten(IV), 1701
tungsten(VI), 1870
Dimethyl(phenyl)silylmethyl complexes,
nickel(II), 585
platinum(II), 57
Dimethylpiperazine complexes
Co(II), Cu(II), Ni(II), 2395
2,6-Dimethylpyrazine complex
iron(II), 941
2,6-Dimethylpyridine complexes
platinum(II), 143
Dimethylsulphoxide, as nucleophile, 941
Dimethylsulphoxide complexes
ruthenium(II), 851
N,N,-Dimethyl-*N'*-tetrafluoro-phenylethane-1,2-diaminato complexes, platinum(II), 143
Dimethylurea complexes
Cd, Hg, Zn, 1093
Dinitrogen complexes
molybdenum, 1653
molybdenum(0), 1463
rhenium(I), 1778
tungsten, 1653
Diolate complexes
Mo(VI), Os(VI), U(VI), W(VI), 519
DIOP complexes
nickel(II), 2449
Dioxygen, covalent halide - hydrocarbon complexes, 533
Diphenylacetylene complexes
tungsten(II), 351,2587
Diphenylamido complexes
bismuth(III), 1579
1,1-Diphenyl-3-azabut-2-ene complexes, zirconium, 1601
Diphenylcarbazone complexes
molybdenum(VI), 677
Diphenyl(2-ethylphenyl)phosphine complexes, Rh(I), 2193
Diphenyl(ethyl)phosphine complexes
molybdenum(IV), 1701
Diphenylglyoxime complexes
ruthenium(II), 1391
Diphenylmethoxides
Cr(0), W(0), 653
Diphenyl(2[&4-]-methoxyphenyl)-phosphine complexes, gallium, 1053
Diphenylmethyl complexes
zirconium, 1601
Diphenyl(methyl)phosphine complexes
manganese, 1589
molybdenum(IV), 1261,1701
nickel(0), 13
palladium(II), 897
platinum(II), 433,835,897,1979, 2507
rhodium(III), 2689
tungsten(II), (IV), 1261
4,7-Diphenyl-1,10-phenanthroline complexes
nickel(II), 585
platinum(II), 57
Diphenylphenoxides
Nb(V), Ta(V), 1607
Diphenylphosphido complexes
manganese(I), 1855
molybdenum(IV), 1419
tungsten, 1807
Diphenylphosphine complexes
manganese(0), 1855
Diphenylphosphinoacetate complex
iron(II), 1503
Diphenylphosphinomethyls
zirconium(III), 1758
zirconium(IV), 1758,1760
1-Diphenylphosphinomethyl-*o*-carba-borane, palladium(II), 1485
1,3-Diphenyl-1,3-propanedionate
ruthenium(III), 2179
Diphenylthiocarbazone complexes
molybdenum(VI), 677
1,3-Diphenyltriazenides
Al, Ga, In, 1909
Diphenyl(2,4,6-trimethoxyphenyl)-phosphine complexes, gallium, 1053
Diphenyl(vinyl)phosphine complexes
Pd(II), Pt(II), 897
Diphosphanato complexes
hafnium(IV), zirconium(IV), 1774
Diphosphine complexes
aluminium, 1497
chromium, 179
chromium(II), 1821
cobalt(II), 749
iridium(III), 1945
iron, 179
molybdenum, 179,1595
molybdenum(0), 293,1463,1810, 2599
molybdenum(II), 1751,2599
molybdenum(III), 545
molybdenum(IV), 1870
nickel(0), 13,293
nickel(II), 25,585,1069
niobium(I), 1784
osmium(I), 1537
palladium(I), 1045
palladium(II), 25,835
platinum(II), 25,91,433,835, 1979,2169,2507
rhenium, 1595

rhenium(I), 1872
rhenium(II),(III),(IV), 1689
rhenium(V), 959,1689
rhodium(I), 1575,1760
ruthenium, 695
technetium(I), 1201
technetium(V), 1879
titanium(0), 1611
tungsten, 179,1595
vanadium(II),(IV), 1784
zirconium, 1601
Diphosphinoamido complexes
U(IV), V(III),Zr(IV), 1767
Diphosphinophosphido complexes
zirconium(IV), 1767
Dipicolinates
niobium(V), tantalum(V), 1371
Di-*i*-propyldithiophosphate
manganese(II), 1853
1,2-Di(*i*-propylimino)ethene
complexes, Mo(IV),(V), 123
Di-*i*-propylmethanolates
molybdenum(IV), 129
2,6-Di-*i*-propylphenylimido
complexes, tantalum(V), 341
2,2'-Dipyrazyl complexes
platinum(II), 57
Dipyridinium perchlorate, 1557
2,2'-Dipyridyl complexes
antimony(III), 2937
bismuth(III), 2937
bridging, 2209
chromium(III), 1453,1549
copper(II), 2219
manganese(II), 1853
molybdenum(0), 921,1471
nickel(II), 585,689,925
osmium(II), 367
palladium(II), 2209
platinum(II), 57,2209
rhenium(V), 959
rhodium(III), 83
ruthenium(II), 1223,2615
technetium(II),(V), 1879
titanium(IV), 2893
tungsten(0), 827,1471
tungsten(II), 827
vanadium(III), 1723
zirconium, 77
2,2'-Dipyrimidyl complexes
nickel(II), 585
platinum(II), 57
Dissociation constants
dimercaptosuccinic acid, 2809
Disulphide [RSSR]complexes
copper(II), 2837
nickel(II), 2321,2837
Disulphide [S_2^{2-}] complexes
molybdenum(IV), 2419
molybdenum(V), 1705
vanadium(IV), 1625
Disulphidothionitrato [S_3N^-]
complexes, Co, Cu, 1447
Disulphurdiimide complexes
platinum(II), 841
Dithiobis(ethylene) [&phenylene]-
bis(salicylaldimine) complexes,
nickel(II), 2321
Dithiocarbamates
antimony(III), bismuth(III),
indium, 1891
molybdenum(IV), 1625
molybdenum(V), 1817
nickel(II), 2637
rhenium(IV), 1625
tin(IV), 1413,1891,2557
vanadium(IV), 1625,1827
zinc, 1891
Dithiocarboxylates
indium, 633
4,4'-Dithiodipyridine complexes
Co(II), Cu(II), Ni(II), 1545
Dithiolates
molybdenum, 1033
molybdenum(IV), 1625
molybdenum(V), 669
titanium(IV), 2893
vanadium(III),(IV), 1723
Dithiophosphates
bismuth(III), 483
manganese(II), 1853
Di(2,4,6-trimethoxyphenyl)phenyl-
phosphine complexes, gallium,
1053
Divinyl(phenyl)phosphine
complexes, Pd(II), Pt(II), 897
Dysprosium
amine ferrocene Schiff base
complex, 2459
crown ether complex, 1561
cyclopentadienyl ether indenyl
complexes, 17
formylferrocene benzoylhydrazone
complex, 2105
nitrate pyridone water
copper(II) complexes, 1531
oxalate pyrazolylborate, 2367
phosphonate complexes, 1307
polyaminepolycarboxylates, 1425
proline water complexes, 2139

E

EHMO calculations,
cyclopentaphosphorus complexes,
1135
Electric conductance
amidinoalkylurea complexes, 757
cobalt(II) chloride tetramine -
dioxime thiocyanate complexes,
1509
cobalt(III) aminoacid ethylene-
dibiguanide complexes, 1015
cobalt(III) tetramine dioxime
complexes, 1509
iron(II) cyclopentadienyl
lanthanide complexes, 2459
iron(III) chloride Schiff base
thiosemicarbazide complexes,
135
lanthanide amine ferrocenyl
ketone Schiff base complexes,
2459
lanthanide chloride pyridine
pyrrole Schiff base water
complexes, 21
lanthanide formylferrocene
benzoylhydrazone complexes,
2105
palladium(I) chloride
diphosphine isocyanide
complex, 1045
palladium(II), platinum(II)
chloride Schiff base telluro-
ether water complexes, 2769

potassium catenand complex, 1251
pyridinedicarboxylate complexes, 745
ruthenium(II) diimine complexes, 2615
yttrium formylferrocene benzoylhydrazone complex, 2105
Electric conductance (solid state)
nickel arylamido iodide complexes, 2603
Electrochromism, Mo(IV), Zr(IV) phthalocyanines, 1631
Electron diffraction
magnesium hydroxide nitrate, 1061
tetrasulphur tetranitride, 2631
Electronegativity, from XPE spectra, 1233
Electronic spectra
aluminium edta fluoride thio complexes, 2057
antimony(III), bismuth(III) diamine halide complexes, 2937
chromium(0) carbonyl phosphine complex, 1099
chromium(0) carbonyl phosphonite molybdenum(II) complexes, 2339
chromium(III) chloride sulphonate thioether complexes, 1770
cobalt(II) aluminophosphates, 819
cobalt(II) azole halide thiocyanate thioether complexes, 1965
cobalt(II) bromide diphosphine complexes, 749
cobalt(II) carboxylate morpholine piperazine piperidine complexes, 2395
cobalt(II) chloride silicon isothiocyanate complexes, 427
cobalt(II) chloride, thiocyanate complexes on ion exchange media, 859
cobalt(II) dithiodipyridine halide complexes, 1545
cobalt(II) pyridinedicarboxylate complexes, 745
cobalt(II,III) ammine arabinose hydroxide water complex, 2023
cobalt(III) acetonitrile halide oxyanion tetramine water complexes, 2389
cobalt(III) aminoacid chloride diaminopolycarboxylate water complexes, 1205
cobalt(III) aminoacid ethylene-dibiguanide complexes, 1015
cobalt(III) ammine arabinose complex, 2023
cobalt(III) azide complexes, 641
cobalt(III) carbonate chloride edda water complexes, 2889
cobalt(III) chloride phenoxide Schiff base copper(II) complex, 2007
cobalt(III) halide nitrile polyamine water complexes, 275
cobalt(III) hexadentate complexes, 491
cobalt(III) phenoxide salicyl-aldimine complexes, 2677
copper(I) pyridine Schiff base complexes, 1321
copper(II) acetate oxime pyridine water complex, 1077
copper(II) acetylsalicylate azole complexes, 2777
copper(II) alcohol alkoxide azole halide thiocyanate complexes, 769
copper(II) amidinoalkylurea complexes, 757
copper(II) amine azole carboxylate complex, 659
copper(II) amine chloride ketone complex, 991
copper(II) aminoacid salicylald-imine water complex, 2131
copper(II) aminoacid sulphonyl complexes, 739
copper(II) arsine halide methanol oxo phosphine stibine complexes, 2469
copper(II) azide mepirizole thiocyanate complexes, 1523
copper(II) azole dicyanamide tricyanomethyl complexes, 157
copper(II) azole halide thiocyanate thioether complexes, 1965
copper(II) azole thiocyanate complexes, 2313
copper(II) biguanidine complexes, 7
copper(II) carboxylate morpholine piperazine piperidine complexes, 2395
copper(II) chloride phenoxide Schiff base cobalt(III) complex, 2007
copper(II) chloride polyamine pyridine complexes, 909
copper(II) chloride silicon isothiocyanate complexes, 427
copper(II) cyanamide dipyridyl complex, 2219
copper(II) cyanate terpyridine complexes, 97
copper(II) cystamine complexes, 2837
copper(II) diaminehydroxide complex, 2645
copper(II) diaminothioether halide complexes, 2749
copper(II) dihydroxybenzoates, 647
copper(II) fluoride sulphate complexes, 457
copper(II) hydroxide peptide complexes, 2463
copper(II) hydroxide water binucleating complex, 2513
copper(II) pyrazolinone-alkyldi-thioate complexes, 2723
copper(II) pyridine salicylald-imine complexes, 2543
copper(II) pyridinedicarboxylate complexes, 745
dioxygen halide hydrocarbon complexes, 533
gallium heteropolymolybdate, 2739
gallium, indium edta fluoride thio complexes, 2057
ion - exchange supported

complexes, 859
iridium(III) chloride pyridine complex, 2245
iron(0) carbonyl cyclopentadienyl mercury complexes, 1471
iron(II) alcohol hydroxide squarate complex, 1335
iron(II) cyanide hydrazine complexes, 419
iron(II) cyclopentadienyl lanthanide complexes, 2459
iron(III) chloride Schiff base thiosemicarbazide complexes, 135
iron(III) cyanide complex on ion exchange media, 859
iron(III) hexadentate complexes, 491
iron(III) phosphine thio complex, 801
iron(III) salicylhydroxamate complexes, 1477
lanthanide amine ferrocenyl ketone Schiff base complexes, 2459
lanthanide chloride pyridine pyrrole Schiff base water complexes, 21
lanthanide crown ether complexes, 1561
lanthanide formylferrocene benzoylhydrazone complexes, 2105
lanthanide proline water complexes, 2139
manganese(II) azole halide thiocyanate thioether complexes, 1965
manganese(III) acetate hydroxyketoimine oxo thiocyanate complexes, 1029
manganese(III) quinone complex, 1407
mercury azide complex, 2731
molybdenum(0) carbonyl diamine diimine halide pseudohalide mercury complexes, 1471
molybdenum(0,II) carbonyl phosphonite complexes, 2339
molybdenum(II) acetate acetonitrile thioether complexes, 1770
molybdenum(III) bromide diphosphine complex, 545
molybdenum(III),(IV) edta thio complexes, 2791
molybdenum(IV) oxo phthalocyanine, 1631
molybdenum(V) chloride oxo phosphine complex, 447
molybdenum(V,VI) methoxide oxo isopolyanion, 537
molybdenum(VI) carbazone chloride oxo thiocarbazone complexes, 677
nickel(II) amidinoalkylurea complexes, 757
nickel(II) aminoacid water complexes, 1329
nickel(II) aminodiphosphine chloride complexes, 25
nickel(II) arylamides, 2603
nickel(II) azole halide thiocyanate thioether complexes, 1965
nickel(II) carboxylate morpholine piperazine piperidine complexes, 2395
nickel(II) chloride polyamine pyridine complexes, 909
nickel(II) chloride pyridine complexes, 2283
nickel(II) chloride silicon isothiocyanate complexes, 427
nickel(II) cystamine complexes, 2837
nickel(II) diimine hydrazinecarbodithioate complexes, 925
nickel(II) diketonate pyridine complexes, 2743
nickel(II) dithiocarbamates, 2637
nickel(II) dithiodipyridine halide complexes, 1545
nickel(II) methanol salicylaldimine complexes, 2321
nickel(II) nitrosonaphthol complexes, 473
nickel(II) pyrazolinone-alkyldithioate complexes, 2723
nickel(II) pyridinedicarboxylate complexes, 745
oxo complexes, polynuclear, 219
palladium(II) aminodiphosphine chloride complexes
palladium(II) azoresorcinol hexamethylenetetramine hydroxide complexes, 197
palladium(II) diimine phosphine complex, 1989
platinum(II) alkyl diimine pyridine complexes, 57
platinum(II) aminodiphosphine chloride complexes, 25
platinum(II) arylamide diphosphine phosphine complexes, 2507
praseodymium(III) on ion exchange media, 859
rhodium(II) amine azole carboxylate pyridine complexes, 1157
rhodium(III) carbonate ethylenediamine hydroxide water complexes, 1163
rhodium(III) diamine thiocyanate complexes, 775
ruthenium(II) acetate arsine carbonyl carbonyl sulphide chloride hydride phosphine thio thiocarbonyl complexes, 1149
ruthenium(II) azole oxime phosphine piperidine pyridine sulphoxide complexes, 851
ruthenium(II) cyanide ethylenediamine complex, 2091
ruthenium(II) diimine complexes, 2615
ruthenium(II) phosphine pyridine quinone oxime complexes, 103
ruthenium(II,III) acetate phosphine oxide complexes, 2571
ruthenium(III) carbonyl edta

water complexes, 2199
ruthenium(III) chloride diketonate hydroxyketone phosphine complexes, 2813
silver(II) crown thioether complexes, 513
sodium hyponitrite, 2621
thallium(III) edta halide thio complexes, 2057
tungsten(0) carbonyl diamine diimine halide pseudohalide mercury complexes, 1471
tungsten(0) carbonyl dipyridyl phosphite complexes, 827
tungsten(0) carbonyl phosphonite molybdenum(II) complexes, 2339
tungsten(III) chloride complex reduction, 469
tungsten(V) hydroxyquinoline oxo thio complexes, 947
uranium(VI) oxo salicylhydrazone complexes, 2527
vanadium(IV) acetonitrile chloride oxo thione water complexes, 87
vanadium(IV) aminoacid oxo complexes, 1173
yttrium formylferrocene benzoylhydrazone complex, 2105
zirconium phthalocyanine, 1631
Electron microscopy
aluminophosphates, 819
antimonic acid - silicic acid core - shell particles, 2577
ferrihydrite conversions, 149, 2829
magnesium hydroxide nitrate, 1061
titanium(III) chloride, 1867
Electron transfer reactions, 563
Electrophilic addition, complexes of unsaturated ligands, review, 1595
Enthalpy of activation
acid dissociations, 2809
adsorption of complexes on silica gel, 2901
aquation, cobalt(III) polyamine complexes, 275
fluxional behviour, mercury ketoimines, selenoneimines, thioneimines, 569
isomerization, chromium(0), tungsten(0) carbonyl phosphine complexes, 2125
oxidation, ruthenium(III) carbonyl edta water complexes, 2199
redox, chromium(III) - manganese(III), 1874
redox, cobalt(II) - periodate, 51
redox, silver(III) - sulphite, 1299
substitution, chromium carbonyl, 2681
substitution, cobalt(III) halide polyamine complexes, 415
substitution, ruthenium(II) oxime phosphine complexes, 851
substitution, ruthenium(III) edta water complex, 463
thermal analysis, vanadium(IV) diketonate oxo pyridine complexes, 2611
Enthalpy of formation
iodoammonium salts, 2911
thorium(IV) aminopolycarboxylate complexes, 2385
thorium(IV), uranium(VI) oxo, aspartate complexes, 2233
Enthalpy of sublimation
cadmium, mercury, zinc amide cytosine halide phosphine oxide urea complexes, 1093
Entropy of activation
acid dissociations, 2809
adsorption of complexes on silica gel, 2901
aquation, cobalt(III) polyamine complexes, 275
fluxional behaviour, mercury ketoimines, selenoneimines, thioneimines, 569
isomerization, chromium(0), tungsten(0) carbonyl phosphine complexes, 2125
oxidation, ruthenium(III) carbonyl edta water complexes, 2199
redox, chromium(III) - manganese(III), 1874
redox, cobalt(II) - periodate, 51
redox, silver(III) - sulphite, 1299
substitution, cobalt(III) halide polyamine complexes, 415
substitution, ruthenium(II) oxime phosphine complexes, 851
substitution, ruthenium(III) edta water complex, 463
Entropy of formation
thorium(IV) aminopolycarboxylate complexes, 2385
thorium(IV), uranium(VI) oxo, aspartate complexes, 2233
Eosin, anion for strontium cryptand complex, 2797
Episulphide complexes
Cr(0), Mo(0), W(0), 887
Equilibrium constants, cobalt(II) bromide diphosphine complex formation, 749
Erbium
cyclopentadienyl ether indenyl complexes, 17
formylferrocene benzoylhydrazone complex, 2105
phosphonate complexes, 1307
polyaminepolycarboxylates, 1425
Erythritol complex
molybdenum(VI), 1571
ESR spectra
clay minerals pyrolyses, 2709
copper(I,II) diisocyanide complexes, 317
copper(II) acetate oxime pyridine water complex, 1077
copper(II) acetylsalicylate azole complexes, 2777
copper(II) amine azole carboxylate complex, 659
copper(II) aminoacid salicylaldimine water complex, 2131
copper(II) aminoacid sulphonyl

complexes, 739
copper(II) azide mepirizole thiocyanate complexes, 1523
copper(II) azole dicyanamide tricyanomethyl complexes, 157
copper(II) azole halide nitrate perchlorate complexes, 935
copper(II) azole halide thiocyanate thioether complexes, 1965
copper(II) biguanidine complexes, 7
copper(II) carboxylate catecholate complexes, 2345
copper(II) carboxylate morpholine piperazine piperidine complexes, 2395
copper(II) cyanamide dipyridyl complex, 2219
copper(II) cyanate terpyridine complexes, 97
copper(II) dihydroxybenzoates, 647
copper(II) diisocyanide complexes, 317
copper(II) hydroxide peptide complexes, 2463
copper(II) methoxide nitrate pyrrolidone mercury complex, 873
copper(II) polyaminepolyphosphonate, 453
iron acyl carbonyl complexes, 603
manganese(II) diisocyanide complexes, 317
manganese(II) doped in cadmium complex, 1913
molybdenum(V) chloride oxo pyrazolylborate, 1833
molybdenum(V) dithiocarbamate in zeolite, 1817
neodymium diketonate hydroxide complex, 2183
oxo complexes, 1830
rhenium(VI) alkylimido aryl complexes, 2657
ruthenium(III) chloride diketonate hydroxyketone phosphine complexes, 2813
silver(II) crown thioether complexes, 513
sodium phosphine oxide thiocyanate complex formation intermediates, 215
titanium(III) alkylamido phenyl complexes, 1457
titanium(III) chloride cyclopentadienyl complex, 1780
titanium(III) chloride ether complex, 2013
vanadium in nitrogenase, 1695
vanadium(IV) acetonitrile chloride oxo thione water complexes, 87
vanadium(IV) aminoacid oxo complexes, 1173
vanadium(IV) azole oxo complexes, 1835
vanadium(IV) diketonate dithiocarbamate oxo pyrazolylborate complexes, 1827
vanadium(IV) oxo Schiff base complexes, 1748
yttrium(0) arene complex, 1641
zirconium(III) chloride cyclopentadienyl ether phosphine complexes, 1882
zirconium(III) cyclopentadienyl hydride phosphinoalkyl complexes, 1758
Ester - alkyl complexes
tin(IV), 1413
1,2-Ethanedithiolate
molybdenum(IV), 1625
titanium(IV), 2893
vanadium(III),(IV), 1723
Ethanethiolates
iron, molybdenum, 1865
palladium(II), 2151
Ethanol complexes
molybdenum(IV), 29
vanadium(III), 1782
Ethene complexes
tungsten(IV), 1261
Ethenyldimethylsilylmethyl complexes, platinum(II), 433
Ether complexes
cerium(IV), 1001
lanthanides, 17,1001,1007,1850, 2109
molybdenum(0), 1857,2925
molybdenum(III), 545
samarium(II), 1007
tin(II), 2933
titanium(IV), 1838,2013
zirconium, 1717
zirconium(III), 1882
Ethoxides
molybdenum(IV), 29
niobium(V), 1848
rhenium(V), 559
1-Ethoxyphosphirane complexes
tungsten(0), 2671
Ethylamine complexes
copper(II), 2593
N,N'-Ethylenebis(2,4-pentanedioneiminato) complexes, molybdenum(IV), titanium(III), 1717
N,N'-Ethylenebis(salicylideneiminato) complexes,
titanium(IV), 1717
vanadium(III), 1782
vanadium(IV), 1753
Ethylenediamine complexes
molybdenum(0), 1471
rhodium(III), 1173
ruthenium(II), 2091
tungsten(0), 1471
Ethylenediamine-α-propionate complexes, cobalt(III), 1205
Ethylenediaminedi-*i*-butylate complexes, cobalt(III), 2889
Ethylenediamine Schiff base complexes, lanthanides, 2459
Ethylenediaminetetraacetate complexes
Al, Ga, In, 2057
molybdenum(III),(III,IV), 2791
ruthenium(III), 463,2199
thallium(III), 2057
thorium, 109,2385
titanium(III), 2883
Th, W(VI), U(VI), 109
vanadium(III),(IV), 1949

zirconium, 109
N,N'-Ethylenedibiguanide complexes
cobalt(III), 1015
N-Ethylglyoxylanilide oxime
complexes, Cu(II), Ni(II), 1957
2-Ethylhexylhydrogenphenylphos-
phonate complexes, Bi(III), Cd,
lanthanides, Zn, 1307
Ethylidyne complexes
cobalt, 1939
3-Ethyl-2,4-pentanedionate
ruthenium(III), 2179
Europium(III)
carboxylate pyrazolylborate, 555
crown ether complex, 1561
diketonate, 1111
diketonate hydroxide complexes,
2071
formylferrocene benzoylhydrazone
complex, 2105
polyaminepolycarboxylate, 1425
tetramine thiocyanate
macrocyclic complex, 2157
EXAFS
molybdenum(V) chloride oxo
complexes, 45
nitrogenases, 1649,1695

F

Fenske - Hall calculations, iron
carbonyl thio complex, 1885
Ferrihydrite, 149,2829
Ferrocenylformyl acetone Schiff
base complexes, lanthanides,
2459
Fluorescence, chromium(III)
dipyridyl complex, 1453
Fluorides and fluoro complexes
aluminium, 2057
cobalt(III), 275,415,2389
copper(II), 457
gallium, indium, 2057
phosphorus(V), 731
titanium(IV), 311
Fluoroenyl complexes
molybdenum(III),(IV), 203
2-[&3-,4-]Fluorophenoxides
zirconium, 845
Fluxional behaviour
benzyl complexes, 285
mercury ketoimines, selenon-
imines, thionimines, 569
nickel(II) alkyls, 585
platinum(II) alkenyl diphosph-
inoferrocene complex, 433
platinum(II) aminodiphosphine
chloride complexes, 25
polynuclear carbonyls, 2237
Force constants
Mo, W carbonyl phosphinyl
complexes, 627
Formation constants
actinide diketonate hydroxide
complexes, 2071
aluminium edta fluoride thio
complexes, 2057
beryllium aminoacid hydroxide
complexes, 2017
cadmium chloride phosphinate
phosphine oxide complexes,
2535
cadmium diamine malonate
complexes, 2291
cadmium, calcium vitamin D_3
complexes, 1953
cobalt(II) thiocyanate complex,
859
cobalt(III) azide complexes, 641
copper(II) amide aminoacid
hydroxide water complexes, 1
copper(II) aminoacid complexes,
1019
copper(II) aminoacid sulphonyl
complexes, 739
copper(II) carboxylate
catecholate complexes, 2345
copper(II) diamine hydroxide
complexes, 2645
copper(II) dicarboxylates, 1239
copper(II) dihydroxybenzoates,
647
copper(II) oxime complex, 1957
diaminepolycarboxylate
complexes, 1365
gadolinium phosphate complexes,
1315
gallium edta fluoride thio
complexes, 2057
group 2 tetracycline complexes,
189
indium edta fluoride thio
complexes, 2057
iron(III) malonate complexes,
813
iron(III) phosphonate complexes,
2099
iron(III) salicylhydroxamate
complexes, 1477
isopolyvanadates, 1800
lanthanide crown ether
complexes, 1561
lanthanide diketonate hydroxide
complexes, 2071
lanthanide polyaminepolycar-
boxylates, 1425
lanthanum chloride crown ether
complexes, 2029
neodymium hydroxide water
complexes, 2701
nickel(II) nitrosonaphthol
complexes, 473
nickel(II) oxime complexes, 1957
palladium(II) azoresorcinol
hexamethylene tetramine
complexes, 197
phenylenediaminedisuccinate
complexes, 2693
praseodymium hydroxide
complexes, 983
ruthenium(II) cyanide
ethylenediamine complex, 2091
thallium(I) crown ether
complex, 2115
thallium(III) edta halide thio
complexes, 2057
thorium aminopolycarboxylate
complexes, 2385
thorium aspartate complex, 2233
uranium(VI) amine crown ether
diamine oxo polyether
complexes, 2251
uranium(VI) aspartate oxo
complexes, 2233
vanadium(IV) aminoacid oxo

complexes, 1173,1745
zinc insulin complexes, 2065
Formylferrocene benzoylhydrazone complexes, lanthanides, yttrium, 2105
N-Formylleucinate, -phenylalaninate, -valinate complexes, nickel(II), 1329
Free energy of activation
acid dissociations, dimercaptosuccinic acid, 2809
adsorption of metal complexes on silica gel, 2901
fluxional behaviour, mercury ketoimines, selenonimines, thionimines, 569
substitution, ruthenium(III) edta water complex, 563
Free energy of formation
thorium aminopolycarboxylate complexes, 2385
Fulvalenide complexes
zirconium(III),(IV), 1758
Furan complexes
Ba, Ca, Sr, 1143
Furfuralkoxides, lanthanides, 2109

G

Gadolinium
amine ferrocenylketone Schiff base complex, 2459
formylferrocene benzoylhydrazone complex, 2105
nitrate pyridone copper(II) complexes, 1531
phosphate complexes, 1315
phosphonate complexes, 1307
polyaminepolycarboxylate, 1425
Gallium
chloride phosphine complexes, 1053
edta fluoride thio complexes, 2057
heteropolymolybdate, 2739
triaminetricarboxylate, 2481
triazenide, 1909
Gas sensors, 1615
Germanium
chloride thiocyanate complexes, 2641
organo compounds, book review, 1147
tetrafluoride dioxygen hydrocarbon complex, 533
Germyls, titanium(0), 1611
Glutamic acid complexes
copper(II), 1019
Glutarate, copper(II), 1239
Glycolate
molybdenum(VI), 977
Glycollates
niobium(V), tantalum(V), 1371
Glycylpeptide complexes
copper(II), 2463
Goethite, 149,2829
Gold
hydride phosphine iridium complex, 1903
Gold(I)
thiocyanate thione complexes, 2823

H

Haematite, 2829
Hafnium
cyclopentadienyl metallathiazenes, 1729
Hafnium(0)
arene carbonyl complexes, 1641
carbonyl triphosphine complexes, 1611
Hafnium(III)
alkylphosphido cyclopentadienyl complexes, 1774
Hafnium(IV)
alkylphosphido cyclopentadenyl diphosphonato triphosphonato complexes, 1774
alkoxide cyclopentadienyl methyl Nb(III) Ta(III) complexes, 2189
hydroxycarboxylate oxalate peroxide complexes, 1371
Helical complex, nickel(II), 2551
Heteropolymolybdate, 2739
Hexadentate complexes
cobalt(II),(III), 1509
yttrium, 1923
Hexafluoropentanedionates
Os(III), Ru(III), 2179
Hexamethylbenzene complexes
chromium, 1589
covalent halide dioxygen , 533
Hexamethyldisilthiane, 549
Hexamethylenetetramine complexes
palladium(II), 197
Hexamethylphosphoramide, 2623
Hexamethylphosphoramide complexes
cadmium, mercury, 1093
sodium, 215
zinc, 1093
1,4,7,10,13,16-Hexathiacycloctadecane complexes
molybdenum(0),(II), 505
silver(I),(II), 513
tungsten(0),(II), 505
1-Hexene, hydroformylation, 1760
Hexyl complexes
zirconium(IV), 1758
HF/6 -31G** calculations, boron - phosphorus compounds, 969
Histidine complexes
cobalt(III), 1015
molybdenum(VI), 2225
Holmium
cyclopentadienyl ether indenyl complexes, 17
formylferrocene benzoylhydrazone complex, 2105
polyaminepolycarboxylates, 1425
proline water complexes, 2139
"Hot" ions, 447
Hydrazide complexes
molybdenum(II), 1756
niobium(V), vanadium(IV), 1784
Hydrazine
from dinitrogen, 1463
oxidation, 419
Hydrazine complexes
iron(II),(II,III),(III), 419
Hydrazinecarbodithioate complexes
nickel(II), 925
Hydrazone complexes
uranium(VI), 2527

Hydride, migration to carbene
molybdenum(IV), 1863
review, 1583
Hydride complexes
arsenic(III), 1461
chromium(0), 653
cobalt, 1939
gold, iridium, 1903
iridium(III), 1945
manganese(I), 1855
molybdenum(II), 1751,1756,1802
molybdenum(IV), 1583,1701,1756, 1870,1884
niobium(V), 1607,1762
osmium(II), 1431
platinum, 2271
polynuclear, 383
rhenium(IV), 1689
rhodium(III), 613
ruthenium(II), 1149,1431
tungsten, 2271
tungsten(0), 653
tungsten(IV), 1583,1701,1884
tungsten(VI), 1870
zirconium(III), 1758
Hydrocarbons, dioxygen halide complexes, 533
Hydrocinnamate complexes
rhodium(II), 1157
Hydrodesulhpurisation, catalysis by molybdenum complexes, 1705
Hydroformylation, hexene, 1760
Hydrogen bonding, hydroxamic acids, 2255
Hydrogen chloride, reactions with phosphorus(V) complexes, 2623
Hydrogen sulphate complexes
cobalt(III), 2389
Hydrosulphide, carbaborane, 805
Hydrotelluride, 531
Hydrotris(3,5-dimethylpyrazolyl)-borate complexes
molybdenum, 1033,1675,1669
molybdenum(II), 371
molybdenum(V), 1833
vanadium(IV), 1827
zirconium, 845
Hydrotris(pyrazolylborate) complexes,
lanthanides, 2367
molybdenum, 2265
titanium(0), 1611
ytterbium, 117
Hydroxamate complexes
iron(III), 1477
molybdenum(IV), 29
Hydroxide complexes
americium(III), 2071
beryllium, 2017
cobalt(II,III), 2023
copper(II), 1,1531,2463,2513, 2645
curium(III), 2071
dysprosium(III), 1531
europium(III), 2071
gadolinium(III), 1531
iron(II), 1335
iron(III), 149,2829
La, Lu, 2071
magnesium, 1061
molybdenum(VI), 1387,2915
neodymium(III), 2183
palladium(II), 197
praseodymium(III), 983
rhodium(III), 1163
silver(III), 1299
titanium(IV), 1838
tungsten(VI), 1387,1675
vanadium(V), 1379
N-Hydroxyalkyldithiocarbamates
Bi(III),In,Sb(III),Sn(IV),Zn, 1891
Hydroxamic acids, 2255
Hydroxybenzylbenzimidazole complexes, copper(II), 769
Hydroxycarboxylates
Hf(IV), Nb(V), Ta(V), Zr(IV), 1371
N-(2-Hydroxyethyl)ethylenediamine-triacetate complexes,
thorium, 2385
titanium(III), 577
Hydroxyiminopentane-2,4-dionate complex, iron(II), 175
Hydroxyketoimine complexes
manganese(III), 1029
Hydroxyketone complexes
ruthenium(III), 2813
Hydroxylamine, reaction with $[W(CN)_8]^{3-}$, 2213
2-Hydroxy-1-naphthalidene Schiff base complexes
vanadium(IV), 1748
8-Hydroxyquinoline complexes
phosphorus(V), 731
tungsten(V), 947
2-Hydroxypyridine complexes
Cu(II), Dy(III), Gd(III), 1531
3-Hydroxypyridine complexes
Cd, Co, Ni, Zn, 2743
Hyponitrite, sodium, 2621
Hypophosphorus acid, 527

I

IEH calculations, boron phosphorus compounds, 969
Illite, thermal decomposition, 2709
Imidazidine-2-thione complexes
vanadium(IV), 87
Imidazole complexes
copper(II), 2777
molybdenum(VI), 541,2225
rhodium(II), 1157
vanadium(IV), 1835
Imidazoline-2-thione complexes
gold(I), 2823
Imide $[NH^{2-}]$ complexes
Mo, W, 1653
Iminato, phosphorane, complexes, review, 707
Imine complexes
aluminium, 1279
tantalum(V), 341
Iminoacyl complexes
rhenium(VII), 2657
tantalum(V), 341
Iminoalkene complexes
zirconium, 1601
Iminoarsines, 1461 ,2331
4-Imino-2-pentanonate complexes
copper(II), nickel(II), 2305
Iminophosphine, 379
Indazole complexes

Cu(II), Pd(II), 1345
Indenyl complexes
lanthanides, 17
molybdenum(III), 203
molybdenum(IV), 203,1861
titanium(0), 1611
tungsten(IV), 1861
Indium
alkyl thiolates, 763
amine dithiocarboxylate thioester complexes, 633
chloride triaminetricarboxylate complex, 2481
dithiocarbamates, 1891
edta fluoride thio complexes, 2057
pyridine selenophenoxide thiophenoxide complexes, 865
triazenide, 1909
Inner sphere processes, 563
Insulin complexes
zinc, 2065
Iodate complex
beryllium, 357
Iodic acid, 357
Iodides and iodo complexes
antimony(III), bismuth(III), 2937
cadmium, 1093
chromium(II), 1821
cobalt(II), 1545
copper(II), 769
mercury, 1085,1093
molybdenum(0), 1471
molybdenum(IV), 1802,1861
nickel(II), 1545,2603
niobium(IV),(V), 1848
palladium(II), 897,1485
phosphorus(V), 1445
platinum(II), 143,897,2943
rhodium(III), 1085
thallium(III), 2057
tungsten(0), 1471
tungsten(II), 351,2587
tungsten(IV), 1861
tungsten(VI), 1285
vanadium(III), 1782
zinc, 1093
Iodoammonium salts, 2911
Ion exchange media, metal complexes in, 859
IR spectra
acetaldehyde cmplex, 1261
acetone solvate, 1045
acyls, 603
alcohol complex, 1335
aldehyde complexes, 2109
alkoxides, 1213,1571,2893,2915
alkyls, 57,585,1413
alkylimido complexes, 2657
alkyne complexes, 351
allyls, 203,2599
amide complexes, 1
amidinoalkylurea complexes, 757
amido(RCONH$^-$) complexes, 581
amido(RNH$^-$) complexes, 1979
amine, 1045
amine complexes, 491,633,1971, 2395,2459,2593,2837
aminoacid complexes, 1,739,1205
aminoacid Schiff base complexes, 2131
ammines, 2023
arsine oxide complexes, 109
aryls, 17,1339
arylamido complexes, 2507,2603
arylimide complexes, 1033
azide complexes, 371,1471
azole complexes, 371,541,659, 769,935,1345,1523
borates, 1567
bromides, 203,935,1545,2593
carbazone complexes, 677
carbohydrate complexes, 2023
carbonyls, 167,179,351,505,597, 603,627,653,695,827,917,1085, 1149,1261,1285,1351,1447,1471, 1503,1537,1804,1857,2035,2119, 2193,2265,2271,2371,2495,2587, 2719
carbonyl intermediates, 1637
carbonyl sulphide complexes, 1149,1447
carboxylates, 143,167,597,659, 745,977,1029,1077,1085,1157, 1503,1537,1751,1844,1923,2131, 2395,2571,2777,2915
carboxymethyls, 597
carbyne complexes, 1285
chlorides, 29,87,91,135,143,161, 211,909,935,991,1045,1085, 1149,1345,1545,2013,2179,2245, 2517,2593,2599,2769,2813
clathrochelates, 1391
cyanamide complex, 2219
cyanate complexes, 97
cyanide complexes, 841,1802,2091
cyclopentadienyls, 1447,1810, 1844,2109,2371,2439
diaminato complexes, 143
diamine complexes, 2091
diazenide complexes, 29
dicarboxylates, 109,2367
dicyanamide complexes, 157
diene complexes, 167
diimine complexes, 925,2615
diisocyanide complexes, 317
diketal complexes, 2915
diketonates, 1111,2179,2183, 2305,2813
diolate complexes, 519
dioxime complexes, 1391
disulphide complexes, 2321,2419
disulphidothionitrate, 1447
disulphurdiimide complexes, 841
dithiocarbamates, 1413,1891, 2557,2637
dithiocarboxylate complexes, 633
edta complexes, 109
esters, 2557
ether complexes, 2109
ethylenedibiguanide complexes, 1015
fluorides, 457
guanyl complexes, 1015
heterocyclic S, Se, Te compounds, 2817
heteropolymolybdate, 2739
hexafluorophosphates, 491,1945, 2439,2571
hydrates, 457,739,745,935,1217, 2091
hydrazinecarbodithioates, 925
hydrazone complexes, 2105
hydrides, 613,1149,1461,1751, 1945

hydroxamate complexes, 29
hydroxide complexes, 1,1061, 1335,2023
hydroxyiminopentanedionate, 175
hydroxyketoimine complexes, 1029
hydroxyketone complexes, 2813
hydroxyquinoline complexes, 947
iminoarsines, 1461,2331
iminophosphine, 379
iodate complexes, 357
iodides, 1545
isocyanide complexes, 1045,1285, 1802
ketoimine complexes, 491,2305
ketone complexes, 2459
macrocyclic complexes, 1243
mercaptopyridine complexes, 2439
nitrates, 689,935,1061,1217
nitrile complexes, 87,311,1045, 2193,2389,2587
nitroaromatics, 2507
nitrosyls, 371,1033,1447,2897
nitroxyimines, 1461
oxime complexes, 1077,1391,1509
oxo complexes, 87,109,240,375, 519,537.541,597,669,677,947, 959,977,1029,1213,1379,1571, 1753,1782,1810,2469,2527,2915
perchlorate, 935
peroxo complexes, 109,541,977, 1371,1379
phenoxide complexes, 2513
phenylhydrazine complexes, 29
phosphaalkene, 2087
phosphazenes, 1517
phosphine, 379
phosphine complexes, 161
phosphine oxide complexes, 109, 977,1983,2571
phosphinyl complexes, 627
phosphorane iminato complexes, 720
polyamine complexes, 1509
polyaminepolyphosphonates, 453
purine complexes, 2593
pyrazolylborate complexes, 371, 1033
pyrazolinone - alkyldithioate complexes, 2723
pyridines on silica gel, 2901
pyridine complexes, 21,211,977, 1217,1321,1545,2245,2543,2743
pyridinedicarboxylates, 745
pyridine-*N*-oxide complexes, 977
pyrrole complexes, 21
quinone oxime complexes, 103
salicylidene complexes, 135,491
Schiff base complexes, 21,135, 491,1217,1321,1509,1753,1923, 2131,2157,2459,2513,2527,2755, 2769
selenoamide, 2517
silicon isothiocyanate complexes, 427
squarate, 1335
sulphates, 457
sulphonyl complexes, 739
sulphurdiimide complexes, 91
sulphur dioxide complexes, 1447
tetrafluoroborate, 1045
tetraphenylborate, 1045
thio complexes, 947
thiocarbazone complexes, 677
thiocarbonyl, 1149
thiocyanates, 775
thiocyanate complexes, 371,769, 1029,1471,1523,2157,2313,2823
thiodiketonates, 2305
thioester complexes, 633
thioether complexes, 505
thiolates, 2893
thione complexes, 87,1103,2823
thionitrosyls, 1447
thionylimino complexes, 835
thiosemicarbazide complexes, 135,2371
thiosemicarbazone complexes, 2371
triamine complexes, 2333
triazenides, 1909
tricyanomethyl complexes, 157
trifluoromethyl compound,379
water complexes, 1,87,357,2023, 2131,2769
Iridium
chloride hydride triphosphine gold complex, 1903
Iridium(I)
amidodiphosphine butadiene complex, 2291
carbonyl perchlorate phosphine complex, 121
diene phosphine complexes, 1431
Iridium(III)
chloride pyridine complex, 2245
diphosphine hydride complex, 1945
halide pyridine complexes, 211
Iron
alkoxide carbonyl thio tungsten complex, 127
alkylidyne carbonyl diphosphine seleno selenoacyl thio thioacyl heterobinuclear complexes, 179
carbonyl thio complex, 1885
chloride cysteinate thio thiolate molybdenum complexes, 1865
cyanide nitrosyl complex, 2627
cyclopentadienyl nitrosyl porphyrin sulphur dioxide thionitrosyl complexes, 1447
Iron(0)
acyl carbonyl complexes, 603
carbonyls, 2237
carbonyl cyclopentadienyl antimony complexes, 2495
carbonyl cyclopentadienyl mercury complexes, 1471
carbonyl diene complexes, 479
Iron(I)
amide (NH_2^-) complexes, 1401
Iron(II)
alcohol hydroxide squarate complex, 1335
bromide carbonyl cyclopentadienyl complex, 2425
carbonyl carboxylate phosphine complex, 1503
carbonylcyclopentadienyl thiosemicarbazide thiosemicarbazone complexes, 2367
cyanide hydrazine complex, 419
cyanide nitrosyl complexes, 361
cyanide pyrazine complex, 941
cyclopentadienyl complex, 929
cyclopentadienyl alkali metal

complexes, 879
cyclopentadienyl cyclopenta-phosphorus complexes, 1135
cyclopentadienyl lanthanide complexes, 2105,2459
cyclopentadienyl molybdenum platinum complexes, 2265
cyclopentadienyl yttrium complexes, 2105
hydroxyiminopentane-2,4-dionate complex, 175
polyaminepolyphosphonate complexes, 453
Iron(III)
chloride complex, 1293
chloride Schiff base thiosemicarbazide complexes, 135
cyanide complex, on ion exchange media, 859
hexadentate complexes, 491
hydroxide oxide, 149,2829
malonate complexes, 813
mixed metal oxides, 1615
oxo molybdenum(VI) complexes, 1675
phosphine thio complex, 801
phosphonate complexes, 2099
salicylhydroxamate complexes, 1477
Isocyanide complexes
electrophilic addition, 1595
molybdenum(0), 2599
molybdenum(II), 1762,1786
molybdenum(IV), 1802
palladium(I), 1045
platinum, 2271
platinum(II), 551
rhenium(I), 1778
titanium(IV), 1838
tungsten(II), 827,1786
tungsten(IV), 1261
tungsten(VI), 1285
Isoindoline complexes
molydenum(II), 2359
Isonitrosoketone oxime complexes
cobalt(II),(III), 1509
Isopolymolybdate, 537
Isopolyvanadates, 1800
Isotope effects, hydride cluster complexes, review, 383

J

Jaeger complexes
nickel(II), 1243
Jahn - Teller effect, second - order, in clusters, 1933

K

Ketoimine complexes
cobalt(III), 491
copper(II), 2305
mercury, 569
molybdenum(IV), 1717
nickel(II), 2305
titanium(III), 1717
Ketone complexes
copper(II), 991
lanthanides, 2459
Ketophosphonate complexes
uranium(VI), 1357
Kinetic deuterium isotope effects, hydride cluster complexes, review, 383
Kinetic studies
complexation, iron(II) hydroxy-iminopentanedionate complex, 175
complexation, iron(III) salicyl-hydroxamate complexes, 1477
complexation, molybdenum(VI) histidine imidazole oxo complexes, 2225
dissociation, ruthenium(II) cyanide ethylenediamine complex, 2091
ferrihydrite conversions, 149, 2829
fluxional behaviour, mercury ketoimines, selenoneimines, thioneimines, 569
hydrolysis, cobalt(III) polyamine complexes, 275
isomerisation, chromium(0), tungsten(0) carbonyl phosphine complexes, 2125
oxidation, ruthenium(III) carbonyl edta water complexes, 2199
radiation effects, molybdenum(V) chloride oxo phosphine complex, 447
redox, bromine - titanium(III) edta, water complexes, 2883
redox, chromium(III) - manganese(III), 1874
redox, cobalt(II) - periodate, 57
redox, copper(II) dimethylgly-oxime - copper(III) diglycyl-ethylenediamine complexes, 2409
redox, $[Fe(CN)_5]^{3-}$ - hydrazine, 419
redox, molybdenum edta thio complexes - bromate, vanadium(V), 2791
redox, ruthenium(II,III),(III) - titanium(III), 577
redox, silver(III) - sulphite, 1299
substitution, chromium carbonyl - amine reactions, 2681
substitution, cobalt(III) halide polyamine complexes, 415
substitution, iron(II) cyanide pyrazine complex, 941
substitution, rhodium(III) carbonate ethylenediamine hydroxide water complexes, 1163
substitution, ruthenium(II) acetonitrile dipyridyl nitrate pyridine complexes, 1223
substitution, ruthenium(II) oxime phosphine complexes, 851
substitution, ruthenium(III) edta water complex, 463
thermal analysis, vanadium(IV) diketonate oxo pyridine complexes, 2611
Kojic acid complexes
ruthenium(III), 2813

L

Lanthanides
alkyl cyclopentadienyl chloride ether complexes, 1850
amine ferroceneketone Schiff base complexes, 2459
carboxylate pyrazolylborates, 555
chloride crown ethercomplexes, 2029
chloride pyridine pyrrole Schiff base water complexes, 21
coordination numbers, 2431
crown ether complexes, 1561
cyclopentadienyl ether indenyl complexes, 17
cyclopentadienyl furfuralkoxide salicylaldehydate complexes, 2109
diketonate hydroxide complexes, 2071
diketonate water complexes, 1111
formylferrocene benzoylhydrazone complexes, 2105
nitrate pyridone water copper(II) complexes, 1531
oxalate pyrazolylborate, 2367
phosphonate complexes, 1307
polyaminepolycarboxylate, 1425
proline water complexes, 2139
tetramine thiocyanate macrocyclic complex, 2157
Lanthanum
alkyl cyclopentadienyl ether complexes, 1850
amine ferroceneketone Schiff base complex, 2459
chloride crown ether complexes, 2029
crown ether complex, 1561
diketonate hydroxide complexes, 2071
diketonate water complex, 1111
formylferrocene benzoylhydrazone complex, 2105
phosphonate complexes, 1307
polyaminepolycarboxylate, 1425
Lapachol complex
manganese(III), 1407
Lead(II)
polyaminepolyphosphonates, 2077
tetraselenide complex, 1995
Leden's function, cobalt(III) azide complexes, 641
Lepidocrocite, 2829
Leucine complexes
cobalt(III), 1015
Ligand effective radius, f-block elements, 2431
Ligand synthesis
amidinoalkylureas, 757
amine thioether macrocycle, 2951
binucleating pentadentate, 2513
bis(imidazolyl)amine, 659
bis(triaza)diphosphine, 2485
clathrochelates, 1391
diacetylpyridine Schiff bases, 1321
diaminate (1-), 143
diaminepolycarboxylic acid, 1365
diaminothioether, 2749
diketones, 1549
diphosphines, 293
dithiocarbamates, 2637
ethylenediaminedicarboxylate, 2889
furan Schiff base cryptand, 1143
Jaeger complexes, 1243
pentaoxapentaphosphirane, 2719
phosphinoalkylamines, 1339
phosphirane, 2671
selenoamide, 2517
silylsulphurdiimides, 91
tetrahydroxyfurane, 1213
Lutetium
alkyl cyclopentadienyl chloride ether complexes, 1850
amine ferroceneketone Schiff base complex, 2459
carboxylate pyrazolylborates, 555
diketonate hydroxide complexes, 2071
formylferrocene benzoylhydrazone complex, 2105
oxalate pyrazolylborate, 2367
polyaminepolycarboxylate, 1425
3,5-Lutidine complexes
vanadium(IV), 2611
Lyxose complexes
Mo(VI), W(VI), 333

M

Macrocyclic complexes
Co(II),(III), Cu(II), 2007
europium, 2157
mercury, 2041
molybdenum(0), 1857
nickel(I), 1243
silver(I), 2951
yttrium, 1217,1923,2157
Magnesium
aluminophosphates, 819
diaminopolycarboxylate complexes, 1365,2693
hydroxide nitrate, 1061
tetracycline complexes, 189
Magnetic moments
chromium(II) diphosphine halide complexes, 1821
chromium(II) thiocyanate thiourea complex, 1825
cobalt(II) carboxylate morpholine piperazine piperidine complexes, 2395
cobalt(II) chloride silicon isothiocyanate complexes, 427
cobalt(II) chloride tetramine - dioxime thiocyanate complexes, 1509
cobalt(II) dithiodipyridine halide complexes, 1545
cobalt(II) oxo molybdenum(VI) complexes, 1675
cobalt(II) pyridinedicarboxylate complexes, 745
cobalt(II,III) ammine arabinose hydroxide water complex, 2023
copper(I,II), diisocyanide complexes, 317
copper(II) acetylsalicylate azole complexes, 2777
copper(II) alcohol alkoxide

azole halide thiocyanate complexes, 769
copper(II) amidinoalkylurea complexes, 757
copper(II) amine azole carboxylate complex, 659
copper(II) amine theobromine complexes, 2593
copper(II) aminoacid salicylaldimine water complex, 2131
copper(II) azide mepirizole thiocyanate complexes, 1523
copper(II) azole dicyanamide tricyanomethyl complexes, 157
copper(II) carboxylate morpholine piperazine piperidine complexes, 2395
copper(II) chloride, polyamine pyridine complexes, 909
copper(II) chloride silicon isothiocyanate complexes, 427
copper(II) diaminothioether halide complexes, 2749
copper(II) diisocyanide complexes, 317
copper(II) dithiodipyridine halide complexes, 1545
copper(II) fluoride sulphate complexes, 457
copper(II) pyridinedicarboylate complexes, 745
iron(II) alcohol hydroxide squarate complex, 1335
iron(III) hexadentate complexes, 491
iron(III) oxo molybdenum(VI) complexes, 1675
lanthanide chloride pyridine pyrrole Schiff base water complexes, 21
manganese(II) azide mepirizole thiocyanate complexes, 1523
manganese(II) diisocyanide complexes, 317
manganese(II) pyridinedicarboxylate complexes, 745
nickel(II) aminoacid water complexes, 1329
nickel(II) aminodiphosphine complexes, 25
nickel(II) carboxylate morpholine piperazine piperidine complexes, 2395
nickel(II) chloride, polyamine pyridine complexes, 909
nickel(II) chloride silicon isothiocyanate complexes, 427
nickel(II) diimine nitrate water complexes, 689
nickel(II) dithiodipyridine halide complexes, 1545
nickel(II) methanol salicylaldimine complexes, 2321
nickel(II) pyridinedicarboxylate complexes, 745
niobium(I) arene complexes, 1641
oxo complexes, 237
polyamine polyphosphonate complexes, 453
ruthenium(II,III) acetate phosphine oxide complexes, 2571
titanium(III) alkylamido phenyl complexes, 1457
titanium(III) chloride ether complex, 2013
tungsten(V) hydroxyquinoline oxo thio complexes, 947
vanadium(III) alkylamido phenyl complexes, 1457
vanadium(III) aryl chloride methyl phosphinoalkylamide complexes, 1339
vanadium(III) cyclopentadienyl thio complex, 2763
Malate complexes
Hf, Nb, Ta, Zr, 1371
Malonate complexes
cadmium, 2291
cobalt(II), 2693
copper(II), 1239
iron(III), 813
molybdenum(VI), 977
nickel(II), 2693
uranium(VI), 977
zinc, 2693
Maltol complexes
ruthenium(III), 2813
Manganese
carbene carbonyl cyclopentadienyl phosphine phosphinidene phosphite silyl vinylidene complexes, 1589
Manganese(0)
carbonyl phosphine complexes, 1855
Manganese(I)
carbonyl hydide phosphido complexes, 1855
Manganese(II)
aluminophosphates, 819
azide mepirizole thiocyanate complexes, 1523
azole halide thiocyanate thioether complexes, 1965
diaminopolycarboxylate complexes, 1365,2693
diimine dithiophosphate complexes, 1853
diisocyanide complexes, 317
doped in cadmium complex, 1913
pyridinedicarboxylate complexes, 745
Manganese(III)
acetate hydroxyketoimine oxo thiocyanate complexes, 1029
oxidation of chromium(III), 1874
quinone complex, 1407
Mannose complexes
molybdenum(VI), 333
Mass spectra
alkali metal crown ether metallocene complexes, 879
amide (NH_2-) complexes, 1401
chromium(0) arene complexes, 1641
cobalt alkylidyne cyclopentadienyl hydride complexes, 1939
cobalt(III) hexadentate complexes, 491
field desorption, 1939
heterocyclic S, Se, Te compounds, 2817
iminophosphine, 379
iron(II) cyclopentadienyl complexes, 2459

iron(III) hexadentate complexes, 491
lanthanide cyclopentadienyl ether indenyl complexes, 17
lanthanide cyclopentadienyl furfural oxide salicylaldehydate complexes, 2109
lanthanide oxalate pyrazolylborate, 2367
metallocene alkali metal crown ether complexes, 879
molybdenum arylimide nitrosyl pyrazolylborate thiolate complexes, 1033
molybdenum(0) carbonyl macrocyclic aminoether complex, 1857
molybdenum(0) carbonyl cyclopentadienyl antimony complexes, 2495
molybdenum(0) diphosphine complexes, 293
molybdenum(II) nitrosyl pyrazolylborate thiocyanate complexes, 371
nickel(0) carbonyl diphosphine complexes, 293
nickel(0) carbonyl phosphine complexes, 1351
nickel(II) acetate polypyridine helical complex, 2551
niobium(V) alkylimide chloride cyclopentadienyl complex, 1819
nitroxyiminoarsines, 1461
phosphacyclopentadienyls, 849
platinum(II) arylamide diphosphino phosphine complexes, 2507
potassium catenand complex, 1251
rhodium(I) carbonyl chloride phosphine complexes, 2193
rhodium(III) chloride hydride phosphine thioether thiolate complexes, 613
technetium(I) diphosphine phosphite complexes, 1201
tin(IV) methyl salicylaldimine complexes, 2755
tungsten(0) carbonyl cyclopentadienyl antimony complexes, 2495
tungsten(VI) carbonyl carbyne cyclopentadienyl iodide isocyanide complexes, 1285
MCD spectra
vanadium in nitrogenase, 1695
Mepirizole complexes
copper(II), manganese(II), 1523
Mercaptoacetate, Mo(V), 669
2-Mercaptobenzthiazole complexes
antimony(III), 581
2-Mercaptopyridine complexes
Mo(IV), W(IV), 2439
Mercury
amide cytosine halide phosphine oxide urea complexes, 1093
azide complex, 2731
cadmium borates, 1567
chloride nitrate pyrrolidone cadmium zinc complexes, 1913
halide phenyl rhodium(III) complexes, 1085
iron(0) molybdenum(0) tungsten(0) complexes, 1471
ketoimines, 569
polyselenide complexes, 1995
pyrrolidone Cu(II) complex, 873
reactions with thiocyanate complexes, 775
selenoneimines, 569
thioether macrocyclic complex, 2041
thioneimines, 569
2,4,6-Mesityl complexes
nickel(II), 285
rhenium(VI),(VII), 2657
titanium(III), 1717
Mesitylene complexes
chromium, 1589
dioxygen halides, 533
2,3,6-Mesitylmethyls
zirconium(IV), 1601
Metallaheterocycles
review, 1729
titanium(IV), 2817
Metallaphosphazenes,1729,1736
Methanol complexes
copper(II), 2469
nickel(II), 2321
vanadium(III), 1782
Methionine complexes
beryllium, 2017
Methionine Schiff base complexes
copper(II), 2131
Methoxides
copper(II), 873
molybdenum(V), 669
molybdenum(V,VI), 537
molybdenum(VI), 2915
niobium(V), 1848
osmium(VI), 597
zinc, 1913
2-Methoxyethyl ether complexes
molybdenum(0), 2925
2-Methoxyindenyl complexes
molybdenum(III),(IV), 203
2-Methoxysalicylideneiminobenzene, 1897
Methyls
aluminium, 831,1279,1497
hafnium(IV), 2189
molybdenum(II), 1804,2599
molybdenum(IV), 1802
niobium(V), 1607
platinum(II),(IV), 551
rhenium(V), 959
rhodium(III), 2689
silicon, 427
tantalum(V) 341,1607
tin(IV), 1753,2047,2755
titanium(IV), 1717,1838
tungsten(II), 1804
vanadium(III), 1339,1767
zirconium(IV), 77,1601,2189
Methylcyclopentadienyl complexes
cobalt, 1939
manganese, 1589
molybdenum(III),(IV), 203
zirconium(IV), 1601
S-Methylcysteine complexes
cobalt(III), 1205
Methyleneamido complexes
Mo, Re, W, 1595
Methylenebis[diphenylphosphine oxide] complexes, Mo(0), W(0), 627

S-Methylhydrazinecarbodithioate
complexes, nickel(II), 925
1-Methylimidazole complexes
copper(II), 2777
ruthenium(II), 851
2-Methylimidazole complexes
antimony(III), 581
rhodium(II), 1157
Methylimide complexes
niobium(V), 1819
2-Methylindenyl complexes
molybdenum(III),(IV), 203
Methylisocyanide complexes
molybdenum(II),(IV), 1802
platinum(II), 551
rhenium(I), 1778
Methylisonicotinate complexes
Cd, Co, Ni, Zn, 2743
4-Methylmorpholine complexes
Co, Cu, Ni, 2395
4-Methyl-2-nitrophenyldiazonium
complexes, Pd(I), 1045
3-Methyl-2,4-pentanedionates
ruthenium(III), 2179
2-Methyl-2-phenylpropyl complexes
nickel(II), 585,1069
Methylpiperazines, methylpiperidines complexes, Co,Cu,Ni, 2395
2-Methyl-2-(2'-pyridyl)ethylcyclopentadienyls
Mo(II), Ti(IV), W(II), 1804
N-2-(Methylpyridyl)-5-methoxysalicylaldiminates, Cu(II), 2543
3-Methyl-2-pyrrolidone complex
copper(II), mercury, 873
2-Methylquinoline complexes
tungsten(V), 947
2-Methylthiobenzenethiolate
complexes, Rh(III), 627
Methylthiocarbaboranes, 805
Methyltriazopyrimidine complexes
copper(II), 2313
Methylurea complexes
Cd, Hg, Zn, 1093
Microscopy, titanium(III)
chloride, 1867
Modulus of rupture, aluminium
chromium(III) oxide, 1765
Moessbauer spectra
clay minerals pyrolysis, 2709
iron(II) alcohol hydroxide
squarate complex, 1335
iron(II) carbonyl cyclopentadienyl thiosemicarbazide thiosemicarbazone complexes, 2371
iron(II) cyclopentadienyl
lanthanide complexes, 2459
iron(III) hexadentate complexes,
491
tin(II) catechol ether
complexes, 2933
Molecular graphics
molybdenum sulphide, 1814
molybdenum(V) dithiocarbamate in
zeolite, 1817
Molecular mechanics, copper(II)
diketonates, 1549
Molecular orbitals
boron - phosphorus compounds,
969
chromium(0) arene cyclopentadienyl cyclopentaphosphorus
complexes, 1135
cubane clusters, 2847ff
iron carbonyl thio complex, 1885
iron(II) cyclopentadienyl
cyclopentaphosphorus
complexes, 1135
trinuclear complexes, 2785
Molecular sieves, 819
Molybdenum
acetonitrile dithiocarbamate
thio cobalt complex, 1625
alkylidyne carbonyl carboxylate
diamine pyrazolylborate
Fe(II) Pt complexes, 2265
alkylidyne carbonyl
cyclopentadienyl platinum
complexes, 2271
aminocarbyne carbyne diphosphine
methyleneamido vinyl
complexes, 1595
arylimide nitrosyl
pyrazolylborate thiolate
complexes, 1033
cyanide nitrosyl complexes, 2897
diphosphine seleno selenoacyl
thio thioacyl iron complexes,
179
multiply bonded ligand
complexes, 1653
in nitrogenase, 1649
nitrosyl pyrazolylborate
complexes, 1669
oxycarbides, 1794
sulphide (MoS_2), 1814
thio thiolate iron complexes,
1865
Molybdenum(0)
acetonitrile carbonyl
triphosphine complex, 2119
alkyne arene carbonyl
cyclopentadienone diphosphine
complexes, 1810
arene complexes, 1641
carbonyl crown thioether
complexes, 505
carbonyl cyclopentadienyl
antimony complexes, 2495
carbonyl diamine diimine halide
pseudohalide mercury
complexes, 1471
carbonyl diglyme complex, 2925
carbonyl diimine complexes, 921
carbonyl episulphide complexes,
887
carbonyl macrocyclic aminoether
complex, 1857
carbonyl phosphine thioether
complexes, 1876
carbonyl phosphinyl complexes,
627
carbonyl phosphonite
molybdenum(II) complexes, 2339
carbonyl triamine complexes,
2333
dinitrogen diphosphine complex,
1463
diphosphine complex, 293
diphosphine isocyanide complex,
2599
Molybdenum(II)
acetate acetonitrile thioether
complexes, 1770
acetate isoindoline pyridine
complexes, 2359

acetonitrile alkyl allyl chloride diphosphine complexes, 2599
alkyne cyclopentadienone oxo complex, 1810
allyl carbonyl cyclopentadienyl phosphine complex, 1859
arsine carbonyl chloride phosphine pyridine stibine trichlorostannate complexes, 917
azide nitrosyl pyrazolylborate thiocyanate complexes, 371
bromide carbonyl phosphine thioether complexes, 1876
carbonyl cyclopentadienyl methyl complexes, 1804
carbonyl iodide crown thioether complexes, 505
carboxylate diphosphine hydride oxyimide complexes, 1751
chloride isocyanide phosphine tin(II) complexes, 1786
cyclopentadienyl isocyanide complex, 1802
halide hydrazide hydride phosphine complexes, 1756
isocyanide thio niobium(V) complex, 1762
phosphonite heteropolynuclear complexes, 2339

Molybdenum(III)
allyl cyclopentadienyl complexes, 203
amine phenoxide complexes, 1971
bromide diphosphine ether nitrile complexes, 545
edta thio complexes, 2791

Molybdenum(III,IV)
edta thio complexes, 2791
halide oxo complexes, 2785

Molybdenum(IV)
alkoxide alkylamide complexes, 129
alkoxide chloride diazenide ethanol hydroxamate phenylhydrazine complexes, 29
alkoxide diimine complexes, 123
alkylamido phosphido complexes, 1419
allyl cyclopentadienyl complexes, 203
amine phenoxide complexes, 1971
bromide hydride phosphine complexes, 1756
carbene carbonyl cyclopentadienyl hydride complexes, 1583,1863
carbene carbonyl cyclopentadienyl iodide tin(II) complexes, 1861
carbonyl chloro oxo hosphine complex, 1261
carbonyl hydride phosphine phosphite pyridine thiophenoxide complexes, 1701
chloride ketoimine complex, 1717
cyanide cyclopentadienyl hydride iodide isocyanide methyl complexes, 1802
cyclopentadienyl hydride phosphine stannene tin(II) complexes, 1884
cyclopentadienyl mercaptopyridine complexes, 2439
cyclopentadienyl tetraselenide complex, 1999
diphosphine hydride complex, 1870
disulphide thio complex, 2419
dithiolate thio complex, 1625
oxo phthalocyanine, 1631
oxo thio complexes, 2785
thio thiolate niobium(IV),(V) complexes, 1762

Molybdenum(IV,V)
alkoxide diimine complexes, 123

Molybdenum(V)
alkoxide dithiolate mercaptocarboxylate oxo complexes, 669
chloride oxo complexes, 45
chloride oxo phosphine complex, 447
chloride oxo pyrazolylborate, 1833
chloride thio compound, 549
dithiocarbamate in zeolite, 1817
oxo complexes, 1830
oxo polysulphide thio vinyl disulphide complexes, 1705

Molybdenum(V,VI)
methoxide oxo isopolyanion, 537

Molybdenum(VI)
alkoxide carboxylate dienolate diketal hydroxide oxo complexes, 2915
alkoxide oxo complex, 1213
alkylamide alkylimido amine carboxylate chloride sulphonate tetrafluoroborate complexes, 2947
aminoalcohol diamine dicarboxylate glycol oxo peroxide water complexes, 977
benzoin oxime oxo salicylaldoxime salicylhydroxamate complexes, 2473
carbazone chloride oxo thiocarbazone complexes, 677
carbohydrate complexes, 333
chloride metallaphosphazenes, 1729,1736
chloride oxo thio compounds, 549
diolate complex, 519
erythritol oxo complexes, 1571
heteropolyanion, 2739
histidine imidazole oxo complexes, 2225
hydroxo oxo complex, substitutions, 1387
imidazole oxo peroxide water complexes, 541
oxo triamine cobalt(II) iron(III) complexes, 1675
tetrathio-, reactions, 1625

Montmorillonite, thermal decomposition, 2709

N

Naphthalene-2,3-diolate complexes, 519
1,2-Naphthoquinone-1-[&2-]oxime complexes, ruthenium(II), 103

1,8-Naphthyridine-*N*-oxide complex
copper(II), 933
Neodymium
alkoxide diketonate hydroxide oxo complexes, 2183
amine ferrocene Schiff base complex, 2459
chloride pyridine pyrrole Schiff base water complexes, 21
crown ether complex, 1561
cyclopentadienyl furfuralkoxide salicylaldehydate complexes, 2109
formylferrocene benzoylhydrazone complex, 2105
hydroxide water complexes, 2701
phosphonate complexes, 1307
polyaminepolycarboxylates, 1425
Nickel(0)
carbonyl diphosphine complexes, 293
carbonyl phosphine complexes, 1351
phosphine complexes, 13
Nickel(II)
acetate polypyridine helical complex, 2551
alkyl aryl phosphine pyridine cyclometallated complexes, 1069
alkyl chloride cyclopentadienyl diimine diphosphine phosphine complexes, 585
aluminophosphates, 819
amidinoalkylurea complexes, 757
aminoacid water complexes, 1329
aminodiphosphine chloride complexes, 25
aminoethanethil cystamine complexes, 2837
aryl benzyl cyclopentadienyl halide phosphine complexes, 285
arylamido iodide complexes, 2603
azole halide thiocyanate thioether complexes, 1965
benzyl phosphine complexes, 2449
carboxylate morphoine piperazine piperidine complexes, 2395
carboxylate water complexes, 39
chloride polyamine pyridine complexes, 909
chloride pyridine complexes, 2283,2901
chloride silicon isothiocyanate complexes, 427
diaminopolycarboxylate complexes, 1365
diaminepolycarboxylate dicarboxylate complexes, 2693
diimine hydrazinecarbodithioate complexes, 925
diimine nitrate water complexes, 689
diketonate ketoimine thiodiketonate water complexes, 2305
diketonate pyridine complexes, 2743
dithiocarbamates, 2637
dithiodipyridine halide complexes, 1545
macrocyclic tetradentate complexes, 1243
methanol salicylaldimine complexes, 2321
nitrate oxime pyridine complexes, 305
nitrosonaphthol complexes, 473
oxime complexes, 1957
phenanthroline complex, 2649
polyaminepolyphosphonates, 453
polyselenide complexes, 1995
pyrazolinine - alkyldithioate complexes, 2723
pyridinedicarboxylate complexes, 745
salicylaldimine complexes, 113
thiolate, 1253
Ninhydrin complexes
molybdenum(VI), 2915
Niobium(0) arene complexes, 1641
Niobium(I)
arene complexes, 1641
cyclopentadienyl diphosphine complex, 1784
Niobium(III)
alkyl carbonyl cyclopentadienyl Hf(IV), Zr(IV) complexes, 2189
Niobium(IV)
chloride diarsineamido complex, 1767
cyclopentadienyl halides, 1848
cyclopentadienyl thio molybdenum(IV) complex, 1762
Niobium(V)
alkoxide cyclopentadienyl halides, 1848
alkyl hydride phenoxide cyclometallated complexes, 1607
alkylimide chloride cyclopentadienyl complex, 1819
chloride cyclopentadienyl hydrazide complexes, 1784
chloride nitrile thio complexes, 549
chloride oxo metallaphosphazene, 1729,1736
chloride thio thiophenoxide complexes, 1797
cyclopentadienyl hydride thio thiolate molybdenum(II),(IV) complexes, 1762
dipicolinate hydroxycarboxylate peroxide complexes, 1371
peroxide complexes, 1379
Nitrate complexes
cadmium, 1913
cobalt(III), 2389
copper(II), 873,933,935,1531
dysprosium, gadolinium, 1531
magnesium, 1061
mercury, 1913
nickel(II), 305,689
rhodium(III), 2565
ruthenium(II), 1223
vanadium(IV,V), 1723
yttrium, 1217
zinc, 1913
Nitride complexes
technetium(V), 1879
Nitrile complexes
cobalt(III), 275,415,2389
electrophilic addition, 1595
molybdenum, 1625

molybdenum(0), 2119
molybdenum(II), 1770,2599
molybdenum(III), 545
niobium(V), 549
rhenium(I), 1872
rhenium(III), 1689
rhenium(V), 959
rhodium(I), 2193
ruthenium(II), 1223
tantalum(V), 549
titanium(IV), 311
tungsten(II), 341 ,2587
uranium(VI), 1357
vanadium(IV), 87
Nitrilotriacetates
thorium, 2385
Nitrite complexes
cobalt(III), 1227
palladium(II), 161
Nitrobenzoates
Co,Cu,Ni, 2395
4-Nitrocatechol complexes
tin(II), 2933
4-Nitro-1,2-diamidobenzene complexes, Pt(II), 2507
Nitrogen - sulphur compound, 2631
Nitrogenases, 1649,1695
3-[&4-]Nitrophenoxides
zirconium, 845
Nitroprusside, 2627
1-[&2-]Nitrosonaphtholsulphonate complexes, nickel(II), 473
Nitrosothiourea, reactions with metal compounds, 953
Nitrosyls
iron, 1447,2627
iron(II), 361
molybdenum, 1033,1669,2897
molybdenum(II), 371
rhodium, 2565
Nitroxyimine, arsenic(III), 1461
NMR(^{1}H) spectra
acetaldehyde complexes, 1261
alkene complexes, 1261
alkenyl complexes, 433,695
alkoxides, 597,2893
alkyls, 57,77,341,585,763,959, 1069,1413,2035,2557,2689,2755
alkylamido complexes, 341
alkylidyne complexes, 179,1939
alkylimido complexes, 341,1819, 2657
alkyne complexes, 351,1123,2587
alkynyl complexes, 2003
allyls, 203,2599
amido ($RCONH^-$) complexes, 581
amidoamine complexes, 2943
amidodiphosphine complex, 2291
amine complexes, 491,633,775, 1971,2459
aminoacid complexes, 731,1865
aminodiphosphine complexes,25
aryls, 1039,1069
arylamido complexes, 341,1579, 2507
arylimido complexes, 341,1033
benzyls, 285,2449
carbaborane complexes, 1485
carbazone complexes, 677
carbene complexes, 2351
carboxylates, 585,1117,1157, 1503,1537,2359
carbyne complexes, 1285
catenand complex, 1251
clathrochelate complexes, 1391
crown ether complexes, 879
cryptand complex, 1143
cyclometallated complexes, 1069, 1285,1485
cyclopentadienyls, 311,585,879, 1774,1780,1802,1819,1844,1939, 2003,2265,2371,2459
diaminato complexes, 143
diaminopolycarboxylate complexes, 1205,2889
diarsine complexes, 1537
diene complexes, 167,2291
diimine complexes, 57,77,83,959, 1039
diketonates, 1111,1117,2305,2743
diketones, 1549
diolate complexes, 519
dioxime complexes, 1391
diphosphine complexes, 179,293, 433,835,959,1069,1537,1945, 2169
diphosphinoamines, 1339
diphosphonato complexes, 1774
dithiocarbamates, 1413,2557
dithiocarboxylates, 633
episulphide complexes, 887
hydride complexes, 613,1607, 1751,1802,1903,1945,2271
hydroxyiminopentanedionate, 175
imine complexes, 341
iminoacyl complexes, 341,2657
iodoammonium salts, 2911
isocyanide complexes, 1285,1802
isoindoline complexes, 2359
ketoimine complexes, 491,569, 2305
ketone complexes, 2459
macrocyclic complexes, 1217,1243
mercaptocarboxylate, 669
mercaptopyridine complexes, 2439
nitrile complexes, 311,2587
oxime complexes, 1509
pentaoxapentaphosphorinane complex, 2719
phenoxides, 77,1247,1971
phosphaalkene, 2087
phosphacyclopentadienyls, 849
phosphazenes, 1517
phosphido complexes, 1774
phosphidophosphine complexes, 2169
phosphine complexes, 285,433, 835,959,1039,1053,1069,1261, 1351,1485,1503,1537,1903,2047, 2151,2193,2449
phosphonium salt, 1039
phosphorus(III) oxyacids, 527
polyamine complexes, 1509
polyaminepolycarboxylates, 2481
polyaminepolyphosphonates, 2077
pyrazolinone - alkyldithioate complexes, 2723
pyrazolylborate complexes, 371, 1033,2367
pyridine complexes, 21,1069, 1117,1217,1321,2359,2743, 2893,2943
pyrrole complexes, 21
quinaldinate complexes, 167
salicylaldimine complexes, 491
Schiff base complexes, 21,491,

569,1217,1321,1509,2459,2755,
2769
selenoamide, 2517
selenoneimine complexes, 569
siloxide, 2657
sulphonate complexes, 2943
thiaboranes, 2089
thiocarbazone complexes, 677
thiodiketonates, 2305
thioester complexes, 633
thioether complexes, 505,613,
887,2041
thiolates, 763,1865,2151,2893
thione complexes, 1103
thioneimine complexes, 69
thiophenoxides, 1033
thiosemicarbazide, thiosemicar-
bazone complexes, 2371
thiourea complexes, 351
triazenides, 1909
triphosphine complexes, 1903
triphosphonato complexes, 1774
ureas, 293
urea complexes, 351
water complex, 1111
NMR(^{2}H) spectra
phosphine complex, 2193
NMR(^{11}B) spectra
borohydrides, 1601
carbaborane complexes, 1485
thiaboranes, 2089
NMR(^{13}C) spectra
acetaldehyde complexes, 1261
alkene complexes, 1261
alkenyl complexes, 433,695
alkoxides, 97
alkyls, 57,585,763,959,1069,
1413,2755
alkylidyne complexes, 179,1939,
2035,2265,2271
alkylimido complexes, 2657
alkyne complexes, 351,2587
alkynyl complexes, 2003
amide complexes, 1
amidodiphosphine complex, 2291
amine complexes, 633
aminoacid complexes, 1
aminodiphosphine complexes, 25
aryls, 1069
arylamido complexes, 1579
benzyls, 285
bicarbonates, 2389
carbohydrate complexes, 333
carbonates, 2389
carbonyls, 179,351,505,695,1261,
1285,1503,2003,2035,2265,2271,
2333,2587,2925
carboxylates, 1503,1844
carboxymethyl, 597
carbyne complexes, 1285
crown ether complexes, 879
cryptand complex, 1143
cyanide reactions, 2627
cyclometallated compounds, 1069
cyclopentadienyls, 585,879,1007,
1285,1844,1939,2003,2035,2265
diene complex, 2291
diimine complexes, 57,77,83
diketonates, 2305
diketones, 1549
diolate complexes, 519
diphosphine complexes, 179,433,
695,959,1069,1611
dithiocarbamates, 1413,1891
dithiocarboxylate complexes, 633
ether complexes, 2925
hydroxycarboxylates, 1371
isocyanide complexes, 827,1261,
1285,2271
ketoimine complexes, 2305
nitrile complexes, 2587
oxalate complexes, 2389
oxime complexes, 1509
phosphaalkene, 2087
phosphacyclopentadienyls, 849
phosphazenes, 1517
phosphine complexes, 28,433,959,
1069,1503,2047
phosphinyl complexes, 627
polyamine complexes, 1509
pyridine complexes, 57,1069,1321
pyrazolylborate complexes, 2265
Schiff base complexes, 1321,
1509,2755
selenoamide complexes, 2517
tetramine complexes, 2389
thiodiketonates, 2305
thioester complexes, 633
thioether complexes, 505,2041
thiolates, 763
thione complexes, 2823
thiourea complexes, 351
triamine complexes, 2333
urea complexes, 351
NMR(^{14}N) spectra
phosphorane iminato complexes,
722
thiocyanates, 2641
NMR(^{17}O) spectra
heteropolymolybdate, 2739
oxo complexes, 240
NMR(^{19}F) spectra
amidoamine complexes, 2943
diaminato complexes, 143
diphosphine complexes, 293
fluoride, 311
fluorophosphine complex, 2485
fluorophosphoranes, 731
ureas, 293
NMR(^{27}Al) spectra
aluminium triazenides, 1909
NMR(^{31}P) spectra
aminodiphosphine complexes, 25,
2291
bis(triaza)diphosphine
complexes, 2485
diazatriphosphine complex, 2485
diphosphine complexes, 13,91,
179,293,433,585,695,835,959,
1045,1069,1537,1611,1751,1979,
2169,2507
diphosphinoamines, 1339
diphosphonato complexes, 1774
diphosphoxane complex, 1575
pentaoxapentaphosphorinane
complex, 2719
phosphaalkene, 2087
phosphacyclopentadienyls, 849
phosphazenes, 1517
phosphido complexes, 1774
phosphidophosphine complexes,
2169
phosphine complexes, 13,91,167,
285,433,585,835,893,897,959,
997,1039,1045,1053,1069,1085,
1261,1351,1485,1503,1537,1575,

1855,1903,1945,1979,1989,2047, 2151,2193,2215,2449,2485,2507, 2671,2689,2907
phosphinyl complexes, 627
phosphirane complexes, 2671
phosphite complexes, 819,2415
phosphonite complexes, 2339
phosphonium salt, 1039
phosphoranes, 731
phosphorane iminato complexes, 722
phosphorus(III) oxyacids, 527
phosphorus(V) chloride dimethylamido methyl phenyl complexes, reactions with HCl, 2623
polyaminepolyphosphonates, 2077
triphosphine complexes, 1903, 2119
triphosphonato complexes, 1774
ureas, 293
NMR(^{45}Sc, ^{49}Ti) spectra, 1657
NMR(^{51}V) spectra
peroxovanadates, 1379
review, 1657
vanadium(V) phosphorane iminato complexes, 722
NMR(^{53}Cr, ^{55}Mn) spectra, 1657
NMR(^{71}Ga) spectra
heteropolymolybdate, 2739
NMR(^{73}Ge) spectra
germanium chloride thiocyanate complexes, 2641
NMR(^{89}Y, ^{91}Zr, ^{93}Nb) spectra
review, 1657
NMR(^{95}Mo) spectra
molybdenum(0) carbonyl diimine complexes, 921
molybdenum(VI) carbohydrate complexes, 333
molybdenum(VI) phosphorane iminato complexes, 722
review, 1657
NMR(^{99}Tc) spectra
review, 1657
technetium(I) diphosphine phosphite complex, 1201
NMR(^{119}Sn) spectra
tin(II) chloride Mo(II), W(II) complexes, 1786
tin(IV) alkyl chloride dithiocarbamate complexes, 1413
tin(IV) butyl dithiocarbamates, 1891
tin(IV) halide methyl phosphine complexes, 2047
tin(IV) methyl salicylaldimine complexes, 2755
NMR(^{125}Te) spectra
telluroether complexes, 2769
NMR(^{139}La) spectra
lanthanum chloride crown ether complexes, 2029
review, 1657
NMR(^{181}Ta, ^{183}W, ^{187}Re) spectra, 1657
NMR(^{195}Pt) spectra
platinum alkylidyne carbonyl iron(II) molybdenum complex, 2265
platinum(II) bis(triaza)diphosphine chloride phosphine complexes, 2485
platinum(II) chloride Schiff base telluroether complexes, 2769
platinum(II) phosphine complexes, 897
NMR(^{199}Hg) spectra
mercury ketoimine selenoneimine thioneimine complexes, 569
NMR(2-D) spectra
germanium chloride thiocyanate complexes, 2641
iridium(I) amidodiphosphine butadiene complex, 2291
platinum(II) alkenyl phosphine complexes, 433
platinum(II) bis(triaza)diphosphine chloride phosphine complexes, 2485
NMR(DEPT) spectra
crown ether, cyclopentadienyl complexes, 879
NMR(solid state) spectra
molybdenum(0) carbonyl diglyme complex, 2925
molybdenum(0) carbonyl triamine complexes, 2333
NMR titrations
alkali metal - crown ether complexes, 879

O

Organometallics, book reviews, 1361,2735
Osmium
alkynyl carbonyl tungsten complexes, 2003
carbonyl thio cluster complexes, 1437
Osmium(I)
acetate carbonyl diarsine diphosphine phosphine complexes, 1537
Osmium(II)
carbonyl chloride hydride phosphine complex, 1431
diimine complex, 367
Osmium(III)
chloride diketonate phosphine complexes, 2179
Osmium(VI)
diolate oxo complexes, 519
carboxymethyl methoxide oxo complex, 597
Oxalate complexes
cobalt(II), 2693
cobalt(III), 2389
copper(II), 1239
hafnium(IV), 1371
lanthanides, 2367
nickel(II), zinc, 2693
zirconium(IV), 1371
Oxazolidine-2-thione, 1891
Oxides
Al-Cr, 1765
Ba-Fe-Ta, 1615
Cr-Ti, 1615
iron(III), 149,2829
Oxime complexes
cobalt(II),(III), 1509

copper(II), 301,1957,2409
copper(III), 2409
molybdenum(VI), 2473
nickel(II), 305,1957
ruthenium(II),(III), 851
Oxo complexes
chromium(V), 1830
cobalt(II), 1675
copper(II), 2469
iron(III), 1675
molybdenum(II), 1810
molybdenum(III,IV), 2785
molybdenum(IV), 1631,1653,2785
molybdenum(V), 45,447,669,1653, 1705,1830,1833
molybdenum(V,VI), 537,1653
molybdenum(VI), 519,541,549,677, 1213,1387,1571,1653,1656,2225, 2473,2915
neodymium, 2183
niobium(V), 1729
osmium(VI), 519,597
polynuclear, review, 219
rhenium(V), 559
rhenium(VII), 375
thorium, 109
titanium(IV), 1804,1846
tungsten, 1653,1807
tungsten(IV), 1261,1653,2785
tungsten(V), 1653
tungsten(VI), 109,519,549,1387, 1653,1675,1788
uranium(VI), 109,519,1357,2233, 2251,2527
vanadium(III), 1723
vanadium(III,IV), 1782
vanadium(IV), 87,1173,1723,1745, 1748,1753,1790,1830,1835,2611
vanadium(V), 1379,2791
zirconium, 109
1-Oxoethyl complexes
Nb(III), Ta(III), 2189
4-Oxoferrocenebutanoyloxy complex
zirconium, 929
Oxycarbides, Cr, Mo, W, 1794
Oxyimide complexes
molybdenum(II), 1751

P

Palladium(I)
diazonium diphosphine halide isocyanide phosphine sulphur dioxide tin(II) complexes, 1045
Palladium(II)
aminodiphosphine chloride complexes, 25
aryl diimine complexes, 2209
azole chloride complex, 1345
azoresorcinol hexamethylenetetramine hydroxide complexes, 197
bromide Schiff base cyclometallated complex, 2725
carbaborane halide phosphine cyclometallated complexes, 1485
chloride nitrite phosphine complexes, 161
chloride phosphine thiolate complexes, 2151
chloride Schiff base telluroether water complexes, 2769
chloride selenoamide cyclometallated complexes, 2517
chloride sulphurdiimide complexes, 91
diimine phosphine complex, 1989
diphosphine thionylimino complex, 835
dipyridyl thiocyanate complexes, 775
polytelluride complex, 701
PE spectra
carbaboranes, 805
Penicillamine complexes
vanadium(IV), 1745
Pentafluorophenyls
antimony(III), 581
Pd(II), Pt(II), 2209
Pentamethylcyclopentadienyl complexes,
hafnium, 1729
hafnium(IV), 1774
lanthanides, 1007,1850
lanthanum, 1850
lutetium, 1850
molybdenum(III), 203
molybdenum(IV), 203,1861
samarium(II), 1007
tantalum(V), 1729
titanium(IV), 1729,1838
tungsten, 2003
tungsten(IV), 1861
zirconium(IV), 1774
Pentamethylphenylmethyls
zirconium, 1601
2,4-Pentanedionates
copper(II), 2305
neodymium, 2183
nickel(II), 2305
osmium(III), 2179
platinum(IV), 551
ruthenium(III), 2179,2813
vanadium(IV), 1827,2611
zinc, 2305
2,4-Pentanedithionate
nickel(II), 2305
Pentaoxapentaphosphorinane complexes, chromium(0), 2719
Pentaphenylcyclopentadienyls
iron(II), 2425
Pentaselenide [Se_5^{2-}] complexes
copper(I), silver(I), 1139
Pentasulphide [S_5^{2-}], 2379
Peptide complexes
copper(II), 2463
copper(III), 2409
Perchlorate complex
copper(II), 935
iridium(I), 121
Periodate oxidations, 51
Peroxide complexes
hafnium, 1371
molybdenum(VI), 977
niobium(V), 1371,1379
polynuclear, review, 267
tantalum(V), 1371,1379
thorium, 109,977
tungsten(VI), 109
uranium(VI), 109
vanadium(V), 1379

zirconium, 977,1371
Perrhenate complex
rhodium(I), 375
Phase transfer catalysis, review, 407
Phenanthrenequinone complexes
molybdenum(VI), 2915
1,10-Phenanthroline complexes
manganese(II), 1853
molybdenum(0), 1471
nickel(II), 689,925,2649
palladium(II), 2209
platinum(II), 57,2209
titanium(IV), 2893
tungsten(0), 1471
Phenoxides
cobalt(II),(III), 2007
cobalt(III), 2677
copper(II), 647,2007,2513
lanthanides, 2109
molybdenum(III),(IV), 1971
molybdenum(VI), 2473
nickel(II), 113
niobium(V), 1607
tantalum(V), 341,1607
uranium(IV), 1247
zirconium, 77,845,1601
4-Phenoxybutanoates
cobalt(II), nickel(II), 39
Phenyls
antimony(III), 5581
carbaboranes, 805
mercury, 1085
phosphorus(V), 731,1445,2623
rhenium(VII), 2657
rhodium(III), 2727
tin(II), 1861
tin(IV), 1753,1897
titanium(III), 1457
vanadium(III), 1339,1457,1767
Phenylacetylene complexes
ruthenium, 1123
3-Phenyl-4-acetyl-5-isoxazolone complexes, lanthanides, thorium(IV), uranium(VI), 1111
Phenylalanine methyl ester Schiff base complexes, copper(I), 1321
Phenylalanylglycine complexes
copper(II), 2463
Phenylcyanamide complexes
copper(II), 2219
1-Phenyl-3,4-dimethylphosphole complexes, Pd(II), Pt(II), 897
3,3′-[1,3-Phenylenebis(methylene)-bis(2,4-pentanedionate)], copper(II), 1549
N,N′-o-Phenylenebis(salicylidene-iminato) complex, Zr, 1717
1,2-Phenylenediamine complexes
chromium(II), 1825
Mo(VI), Th(IV), U(VI), 977
1,3-Phenylenediamine-*N,N′*-disuccinate complexes, 2693
2-Phenylethynyl complexes
Os, Ru, W, 2003
Phenylhydrazide complexes
Nb(V), V(IV), 1784
Phenylhydrazine complexes
molybdenum(IV), 29
vanadium(III), 1782
Phenylimido complexes
tungsten(IV), 1261
tungsten(VI), 1788
2-Phenylindenyl complexes
molybdenum(III),(IV), 203
Phenylisocyanide complexes
tungsten(II), 827
2-Phenylphenoxide complexes
molybdenum(III),(IV), 1971
Phenylphosphido complexes
manganese(I), 1855
1-Phenylpiperazine complexes
Co, Cu, Ni, 2395
1-Phenylprop-2-yne complexes
tungsten(II), 2587
Phenylthioacetate, phenylthioacetic acid complexes, Cs, Tl, 793
N-Phenylthiourea, 2219
Phosphaalkene, 2087
Phosphacyclopentadienyls, 849,2407
Phosphate complexes
gadolinium, 1315
Phosphazenes, 1517
Phosphido [R_2P^-] complexes
manganese(I), 1855
molybdenum(IV), 1419
tungsten, 1807
Phosphidophosphine complexes
platinum(II), 2169
Phosphinate complexes
cadmium, 2535
Phosphine, reaction with diimine, 1039
Phosphine complexes
aluminium, 831
chromium(0), 1099,2125
cobalt, 801
copper(I), 1103
copper(II), 2469
copper(III), 1039
gallium, 1053
gold, 1903
iridium(I), 121,1431
iron(II), 1503
iron(III), 801
manganese, 1589
manganese(0), 1855
molybdenum(0), 1876
molybdenum(II), 1756,1786,1859, 1876
molybdenum(IV), 1261,1701,1756, 1884
molybdenum(V), 447
nickel(0), 13,1351
nickel(II), 285,585,1069,2449
osmium(I), 1537
osmium(II), 1431
osmium(III), 2179
palladium(I), 1045
palladium(II), 161,897,1485, 1989,2151
platinum, 2271
platinum(0), 2485
platinum(II), 91,143,433,701, 835,897,1979,2215,2485,2507, 2907
platinum(IV), 893,997
rhenium(I), 1778
rhenium(V), 959
rhodium, 2565
rhodium(I), 167,1431,1575,2193
rhodium(III), 613,1085,2565, 2689,2727
ruthenium, 1123
ruthenium(II), 103,851,1149,1431
ruthenium(III), 851,2179,2813

tin(IV), 2047
tungsten(0), 1876,2125,2671
tungsten(II), 1261,1786,1859, 1876
tungsten(IV), 1261,1701,1884
tungsten(VI), 1870
zirconium(III), 1882
Phosphine oxide complexes
aluminium, 1497
cadmium, 1093,2535
mercury, 1093
ruthenium(II,III), 2571
sodium, 215
thorium, 109,977
ytterbium, 1983
zinc, 1093
zirconium, 109,977
Phosphinidene complex, Mn, 1589
Phosphineiminate complexes
vanadium(IV), 1784
Phosphinoalkenyl complexes
tungsten, 1807
Phosphinoalkyl complexes
zirconium(III),(IV), 1758
Phosphinoalkylamido complexes
vanadium(III), 1339
Phosphinoborene, 969
Phosphinyl complexes
Mo(0), W(0), 627
Phosphirane complexes
tungsten(0), 2671
Phosphite complexes
manganese, 1589
rhenium(I), 1778
rhodium(I), 2415
technetium(I), 1201
tungsten(0), 827
Phosphonate complexes
Bi,Cd, 1307
iron(III), 2099
lanthanides, Zn, 1307
Phosphonium salt, 1293
Phosphoranes, 731
iminato-, complexes, review, 707
Phosphorescence, chromium(III)
dipyridyl complex, 1453
Phosphorous acid, 527
Phosphorus(V)
alkyl aminoacid fluoride hydroxyquinoline phenyl complexes, 731
chloride dimethylamido methyl phenyl complexes, 2623
iodo phenyl complex, 1445
Photoacoustic calorimetry
chromium(0) arene carbonyl complexes, 2681
Photochemistry, titanium(IV), vanadium(III) oxalate complexes, 1792
Photodecomposition, mercury azide complex, 2731
Phthalates
thorium, zirconium, 977
Phthalimido complexes
antimony(III), 581
Phthalocyanines
Mo(IV), Zr(IV), 1631
Picolinate complexes
cobalt(II), 51
rhodium(III), 1085
Picoline complexes
Cd, Co(II), Ni(II), 2743
thorium(IV), uranium(VI), 977
vanadium(IV), 2611
zinc, 2743
Piperazine complexes
Co, Cu, Ni, 2395
Piperidine complexes
chromium(0), 2681
Co, Cu, Ni, 2395
ruthenium(II), 851
Platinum
alkylidyne carbonyl iron(II) molybdenum complex, 2265
alkylidyne carbonyl isocyanide phosphine molybdenum tungsten complex, 2271
Platinum(0)
carbonyl diene iron(0) complexes, 2521
diaminodiphosphine phosphine complex,2485
Platinum(II)
alkenyl phosphine complexes, 433
alkyl diimine pyridine complexes, 57
allyl carbonyl chloride cyclopentadienyl diene isocyanide methyl complexes, 551
amidoamine halide pyridine sulphoxide complexes, 2943
amido phosphine complexes, 1979
aminodiphosphine chloride complexes, 25
arylamide diphosphine phosphine complexes, 2507
aryl diimine complexes, 2209
bis(triaza)diphosphine chloride phosphine complexes, 2485
carboxylate diaminato halide phosphine pyrazine pyridine complexes, 143
chloride diphosphine phosphido-phosphine complexes, 2169
chloride phosphine sulphur - nitrogen complex, 2907
chloride Schiff base telluroether water complexes, 2769
cyanide disulphurdiimide complexes, 841
halide phosphine pseudohalide complexes, 897
phosphine selenium - nitrogen complexes, 2215
phosphine sulphurdiimide complexes, 91
phosphine telluro complex, 701
phosphine thionylimino complexes, 835
Platinum(IV)
bromide phosphine complexes, 893
chloride phosphine sulphur - nitrogen complex, 997
cyclopentadienyl diketonate methyl compounds, 551
Polarography
vanadium(III),(IV) ethylenediaminetetraacetate complexes, 1949
Polyalkoxide, molybdenum(VI), 1571
Polyamine complexes
cobalt(II), 1509
cobalt(III), 275,415,1509

europium, yttrium, 2157
Polyaminepolycarboxylates
lanthanides, 1425
Polyaminepolyphosphonates
cadmium, lead, 2077
Polyaminopolycarboxylates
gallium, indium, 2481
thorium, 2385
Polymetallaphosphazenes, 1729
Polyphosphine complexes
Mo(0),(II), W(0),(II), 1876
Polypyridine complexes
nickel(II), 2551
Polyselenide complexes
cadmium, 1995
copper(I), 1139
lead, mercury, 1995
molybdenum(IV), 1999
nickel(II), 1995
silver(I), 1139
tin(IV), 1999
zinc, 1995
Polysulphide, Ag(I), 2379
Polytelluride, Pd(II), 701
Porphyrins
Co, Cu, Fe, Rh, 1447
Potassium
crown ether complex, 2051
crown ether copper(I) complex, 1251
crown ether Fe(II), Ru(II) complexes, 879
thioethercarboxylate, 2147
Potentiometric titrations
cobalt(III) azide complexes, 641
copper(II) diamine hydroxide complexes, 2645
group 2 - tetracycline complexes, 189
neodymium hydroxide water complexes, 2701
phenylenediaminedisuccinate complexes, 2693
ruthenium(III) carbonyl edta water complexes, 2199
zinc insulin complexes, 2065
Praseodymium(III)
crown ether complex, 1561
formylferrocene benzoylhydrazone complex, 2105
hydroxide complexes, 983
on ion exchange media, 859
phosphonate complexes, 1307
polyaminepolycarboxylate, 1425
Pressure effects on electronic spectra, 801
Proline complexes
dysprosium, holmium, 2139
Propanedithiolate complexes
molybdenum(V), 669
titanium(IV), 2893
Propanethiolates
indium, 763
palladium(II), 2151
Propargyloxyphosphazenes, 1517
i-Propoxides
chromium(0), 653
molybdenum(IV),(IV,V), 123
titanium(IV), 2893
tungsten(0), 653
Propene complexes
tungsten(IV), 1261
Propenoyl complexes
tungsten(II), 1859
i-Propoxides
neodymium, 2183
niobium(V), 1848
n-Propoxides
molybdenum(IV), 29
i-Propylcyclopentadienyl complexes, Mo(III),(IV), 203
Propylene, polymerization, 1867
Propylene carbonate, solvent for complexation studies, 2251
n-Propylimido complexes
rhenium(V), 1689
Propyne complexes
tungsten(IV), 1261
Protein complexes
zinc, 2065
Purine complexes
copper(II), zinc(II), 2593
Pyrazine complexes
iron(II), 941
platinum(II), 143
Pyrazolinone - alkyldithioate complexes, Cu, Ni, 2723
Pyrazolylborates
lanthanides, 117,555,2367
molybdenum, 1033,2265
molybdenum(II), 371
molybdenum(V), 1833
titanium(0), 1611
vanadium(IV), 1827
ytterbium, 117
zirconium, 845
Pyridinaldazine complexes
lanthanides, 21
Pyridine complexes
cadmium, 2743
cobalt(II), 51,1545,2743,2901
copper(I), 1321
copper(II), 301,909,933,1077, 1531,1545,2543,2901
dysprosium, 21,1531
europium, 2157
gadolinium, 21,1531
indium, 865
iridium(III), 211,2245
lanthanides, 21,1531,2157
molybdenum(0), 1857
molybdenum(II), 917,2359
molybdenum(IV), 1701,2439
nickel(II), 305,909,1069,1545, 2283,2743,2901
platinum(II), 57,143,2943
rhodium(I), 167
rhodium(II), 1117,1157
rhodium(III), 211,1085,2727
ruthenium(II), 103,851,1223
ruthenium(III), 577,2179
titanium(IV), 1804,2893
tungsten(IV), 1701,2439
vanadium(III), 1723
vanadium(IV), 2611
yttrium, 1217,1923,2157
zinc, 2743,2901
Pyridine-2-amidoxime complexes
copper(II), 301
nickel(II), 305
2,6-Pyridinedicarboxylate complexes, Co, Cu, Mn, Ni, Zn, 745
Pyridine-*N*-oxide complexes
copper(II), 933
zirconium, 977

Pyridine-2[&4-]-thione complexes
copper(I), 1103
N-2-Pyridinylcarbonyl-2-pyridine-carboximidate complex,
copper(II), 1077
Pyrimidine complexes
Cd, Hg, Zn, 1093
Pyrophosphate
cobalt(III), 2389
Pyrrolaldizine complexes
lanthanides, 21
Pyrrole complexes
iron(III), 491
lanthanides, 21
Pyrrolidone complex
cadmium, 1913
copper(II), 873
mercury, 873,1913
zinc, 1913

Q

2-Quinaldinate complexes
rhodium(I), 167
rhodium(III), 2727
Quinoline hydrogenation, 1431
Quinoline complexes
nickel(II), 2283
Quinone complex
manganese(III), 1407
Quinone oxime complexes
ruthenium(II), 103
Quinquepyridine complexes
nickel(II), 2551

R

Radiation effects, molybdenum(V) chloride oxo phosphine complex, 447
Raman spectra
carbonyls, 627
carboxylates, 1157
chlorides, 325,2245,2813
diketonates, 2813
diolate complexes, 519
dirhodium(II) complexes, 1157
disulphide, 2837
disulphide complex, 2419
hydroxyketone complexes, 2813
iodoammonium salts, 2911
oxo complexes, 240,519,1379, 2527
peroxide complexes, 1371,1379
polyiodides, 2603
pyridine complexes, 2245
sulphurdiimide complexes, 91
thio complex, 3419
Repulsive forces in transition metal complexes, 1742
Resonance Raman, *see* Raman
Rhamnose complexes
Mo(VI), W(VI), 333
Rhenium
aminocarbyne carbyne chloride diphosphine methyleneamido vinyl complexes, 1595
Rhenium(I)
chloride dinitrogen isocyanide phosphine phosphite complexes, 1778
chloride diphosphine nitrile complexes, 1872
Rhenium(II)
carbonyl chloride diphosphine complexes, 1689
chloride diarsine complex, 1733
Rhenium(III)
chloride complexes, 469
chloride diarsine complex, 1733
diimine diphosphine halide nitrile complexes, 1689
Rhenium(IV)
chloride complexes, 469
diphosphine hydride complex, 1689
dithiocarbamate thio complex, 1625
Rhenium(V)
acetonitrile chloride dipyridyl methyl oxo phosphine complexes, 959
alkoxide oxo Schiff base thioether complexes, 559
alkylimido chloride diphosphine complex, 1689
Rhenium(VI)
alkylimido aryl complexes, 2657
Rhenium(VII)
alkylamido alkylimido aryl chloride iminoacyl siloxide complexes, 2657
chloride metallaphosphazanes, 1736
oxo rhodium(I) complex, 375
Rhodanese, 2627
Rhodium
bromide nitrosyl phosphine complex, 265
Rhodium(I)
acetonitrile carbonyl chloride phosphine complexes, 2193
amide (NH_2^-) complexes, 1401
carbonyl chloride complex, 2119
carbonyl diene phosphine quinaldinate complexes, 167
chloride diene phosphine complexes, 1431
chloride diphosphine phosphine complex, 1575
chloride Schiff base telluroether complexes, 2769
cyanide phosphite complex, 2415
diene diphosphine zirconium(IV) complex, 1760
diene perrhenate complex, 375
Rhodium(II)
acetate diketonate pyridine complex, 1117
amine azole carboxylate pyridine complexes, 1157
carbonyl chloride triphosphine complex, 2119
Rhodium(III)
amine thiocyanate complexes, 775
bromide nitrate phosphine complex, 2565
carbonate ethylenediamine hydroxide water complexes, 1163
carbonyl chloride porphyrin complexes, 1447
chloride hydride phosphine thioether thiolate complexes, 613

chloride methyl phosphine complexes, 2689
dipyridyl complex, 83
halide phophine picolinate mercury tin(II) complexes, 1085
halide pyridine complexes, 211
phenyl phosphine quinaldinate trifluoroacetate water complex, 2727
Ruthenium
alkyne carbonyl phosphine thio complexes, 1123
alkynyl carbonyl tungsten complexes, 2003
carbene carbonyl thio tungsten complexes, 2351
carbonyl diphosphine vinyl tungsten complex, 695
Ruthenium(0)
carbonyls, 2237
Ruthenium(I)
arene chloride complex, 2803
Ruthenium(II)
acetate arsine carbonyl carbonyl sulphide chloride hydride phosphine thio thiocarbonyl complexes, 1149
acetate carbonyl compllex, 597
acetonitrile dipyridyl nitrate pyridine complexes, 1223
azole oxime phosphine piperidine pyridine sulphoxide complexes, 851
carbonyl chloride hydride phosphine complexes, 1431
cyanide ethylenediamine complex, 2091
cyclopentadienyll alkali metal complexes, 879
diimine complexes, 2615
dioxime clathrochelates, 1391
phosphine pyridine quinone oxime complexes, 103
Ruthenium(II,III)
acetate complex, 577
acetate phosphine oxide complexes, 2571
Ruthenium(III)
ammonia pyridine complex, 577
carbonyl edta water complexes, 2199
chloride diketonate hydroxyketone phosphine complexes, 2813
diketonate halide phosphine pyridine complexes, 2179
edta thiourea complex, 463
oxime phosphine complex, 851

S

S_3N^- complexes
cobalt, copper, 1447
$S_4N_4^{2-}$ complexes
platinum(II), 2907
platinum(IV), 997
Salicylaldehydate complexes
lanthanides, 2109
Salicylaldimines
cobalt(III), 491,2677
copper(II), 2131,2543
iron(III), 135,491
nickel(II), 113,2321
rhenium(V), 559
tin(IV), 2755
titanium(IV), 1717
uranium(VI), 2527
vanadium(IV), 1748,1753
zirconium(IV), 1717
Salicylaldoximes
molybdenum(VI), 2473
Salicylhydroxamates
iron(III), 1477
molybdenum(VI), 2473
Samarium(II)
cyclopentadienyl ether complexes, 1007
Samarium(III)
carboxylate pyrazolylborate, 555
chloride pyridine pyrrole Schiff base water complexes, 21
cyclopentadienyl ether indenyl complexes, 17
formylferrocene benzoylhydrazone complexes, 2105
oxalate pyrazolylborate, 2367
phosphonate complexes, 1307
polyaminepolycarboxylates, 1425
Scandium
coordination numbers, 2431
SCCC - EH calculations
trinuclear complexes, 2785
Schiff base complexes
barium, calcium, 1143
cobalt(II), 2007
cobalt(III), 491,2007,2677
copper(I), 1321
copper(II), 2007,2131,2409,2513, 2543
copper(III), 2409
early transition metals, review, 1717
iron(III), 135,491
lanthanides, 21,2157,2459
lanthanum, 2157
mercury, 569
molybdenum(IV); 1717
nickel(II), 113,1243,2321
palladium(II), 2725,2769
platinum(II), rhodium(I), 2769
rhenium(V), 559
strontium, 1143
tin(IV), 2755
titanium(III),(IV), 1717
uranium(VI), 2527
vanadium(III),(III,IV), 1782
vanadium(IV), 1748,1753,1790
yttrium, 1217,1923,2157
zirconium, 1717
Second order Jahn - Teller effect, 1933
Sedimentation coefficients, antimonic acid - silicic acid core - shell particles, 2577
Selenides, electronic structures, 1619
Selenium heterocyclic compounds, 2817
Selenium nitrogen complexes
platinum(II), 2215
Seleno complexes
Cr, Fe, Mo, W, 179
vanadium(IV), 1723
Selenoacyl complexes

Cr, Fe, Mo, W, 179
Selenoamide complexes
palladium(II), 2517
Selenoneimines, mercury, 569
Selenophenoxide, In(III), 865
Semiconducting oxides, 1615
Semiconductor chemistry, book review, 1361
Serine complexes
vanadium(IV), 1173
SERS spectra
iron(II) cyanide nitrosyl complexes, 361
Serylglycine complexes
copper(II), 2463
Silica gel, adsorption of metal complexes, 2901
Silicic acid, core -shell particles with antimonic acid, 2577
Silicon
methyls, 427
tetrachloride, dioxygen hydrocarbon complex, 533
thiocyanates, complexes, 427
Siloxides
cerium(IV), 1001
rhenium(VII), 2657
vanadium(IV), 1723
vanadium(V), 1736
Silver(I)
amine thioether macrocyclic complex, 2951
bromide complex, 211
crown thioether complexes, 513
cyanide complexes, 361
polyselenide complexes, 1139
polysulphide complex, 2379
Silver(II)
crown thioether complexes, 513
Silver(III)
hydroxide complex, 1299
Silylimido complexes
tungsten(IV), 1261
Silylsulphurdiimide complexes
Pd(II), Pt(II), 91
Sodium
crown ether Fe(II), Ru(II) complexes, 879
hyponitrite, 2621
pentacyanonitrosylferrate(2-), 2627
phosphine oxide thiocyanate complexes, 215
Solubility, cobalt(III) phenoxide salicylaldimine complexes, 2677
Solvent extraction
actinide diketonate hydroxide complexes, 2071
cadmium chloride phosphinate phosphine oxide complexes, 2535
copper(II) oxime complexes, 1957
gallium chloride phosphine complexes, 1053
iron(III) phosphonate complexes, 2099
lanthanide diketonates, 1111
lanthanide diketonate hydroxide complexes, 2071
nickel(II) oxime complexes, 1957
palladium(II) azoresorcinol hexamethylenetetramine hydroxide complexes, 197
phosphonate complexes, 1307
strontium cryptand complex, 2797
Th(IV), U(VI) diketonates, 1111
uranium(VI) ketophosphonate nitrate oxo complexes, 1357
Spectrophotometric titrations
cobalt(II) bromide diphosphine complexes, 749
edta fluoride thio complexes, 2057
iron(III) salicylhydroxamate complexes, 1477
lanthanide crown ether complexes, 1561
Spin crossover complex, chromium(II) diphosphine halide, 1821
Stannene complexes
molybdenum(IV), 1884
Stannyl complexes
titanium(0), 1611
Steric coordination number, 2431
Stibine complexes
copper(II), 2469
molybdenum(II), 917
Strontium
cryptand complexes, 1143,2797
diaminepolycarboxylate complexes, 2693
tetracycline complexes, 189
Styrene oligomerization, catalysis by nickel(II) complexes, 2449
Succinate complexes
cobalt(II), 2693
copper(II), 1239
nickel(II), 2693
thorium, 109
zinc, 2693
zirconium, 109
Succinimido complexes
antimony(III), 581
Sulphate complexes
cobalt(III), 2389
copper(II), 457
Sulphides
electronic structures, 1619
molybdenum, 1814
Sulphite, oxidation by silver(III), 1299
Sulphonates
chromium(III), 1770
Mo(VI), W(VI), 2947
Sulphonyl complexes
copper(II), 739
Sulphoxide complexes
platinum(II), 2943
ruthenium(II), 851
Sulphur, heterocyclic compounds, 2817
Sulphurdiimide complexes
Pd(II), Pt(II), 91
Sulphur dioxide complexes
iron, 1447
palladium(I), 1045
Sulphur nitrogen compounds
2631
Sulphur nitrogen complexes
cobalt, copper, 1447
Pd(II), Pt(II), 91
platinum(IV), 997

T

Tantalum(III)
alkyl carbonyl cyclopentadienyl Hf(IV) Zr(IV) complexes, 2189
Tantalum(V)
alkyl amido imido imine imino-acyl phenoxide complexes, 341
alkyl phenoxide cyclometallated complexes, 1607
chloride cyclopentadienyl nitride complexes, 1729
chloride nitrile thio complexes, 549
dipicolinate hydroxycarboxylate peroxide complexes, 1371
mixed metal oxides, 1615
peroxide complexes, 1379
Tartrate complexes
Hf, Nb, Ta, Zr, 1371
Technetium(I)
diphosphine phosphite complexes, 1201
Technetium(II) chloride diimine complexes, 1879
Technetium(III)-(VI), review, 1683
Technetium(V) diimine diphosphine halide nitride complexes, 1879
Tellurides, electronic structures, 1619
Tellurium, heterocyclic compounds, 2817
Tellurium(-I)
hydrotelluride (HTe^-), 531
Telluro (Te^{2-}) complex
platinum(II), 701
Telluroether complexes
Pd(II), Pt(II), Rh(I), 2769
Template reaction, octaaza macrocycle, 1825
Terbium
formylferrocene benzoylhydrazone complex, 2105
polyaminepolycarboxylates, 1425
2,2′:6′,2″-Terpyridine complexes
copper(II), 97
Tetracycline complexes
group 2, 189
Tetrafluorobenzoate, Pt(II), 143
Tetrafluoroborate complexes
Mo(VI), W(VI), 2947
Tetrahydrofuran complexes
lanthanides, 17,1850
molybdenum(III), 545
tin(II), 2933
titanium(IV), 1838,2013
zirconium, 1717
zirconium(III), 1882
Tetrahydropyran complexes
samarium(II), 1007
Tetrahydroxyltetramethylfurane complex, molybdenum(IV), 1213
Tetrakis(2-nitrophenyl)porphyrinate, cobalt, 1447
Tetramethylethylenediamine complexes, Mo, 2265
3,4,7,8-Tetramethyl-1,10-phenanthroline complexes
nickel(II), 585
platinum((II), 57
Tetramethylthiourea complexes
tungsten(II), 351
Tetramethylurea complexes
Cd, Hg, Zn, 1093
Tetramine complexes
cobalt(III), 2389
copper(III), 2409
Tetraphenylcyclopentadienone complexes
molybdenum(0),(II), 1810
Tetraphenyldiphosphoxane complex
rhodium(I), 1575
Tetraphenylporphyrinate complexes
Co, Cu, Fe, Rh(III), 1447
Tetraselenide[Se_4^{2-}] complexes
cadmium, 1995
copper(I), 1139
lead, mercury, 1995
molybdenum(IV), 1999
nickel(II), 1995
silver(I), 1139
tin(IV), 1999
zinc, 1995
Tetrasulphide[S_4^{2-}] complexes
molybdenum(V), 1705
Tetrasulphur tetranitride, 2631
1,4,8,11-Tetrathiacyclotetradecane complexes, Mo(0),(II), W(0),(II), 505
Thallium(I)
crown ether complex, 2115
Thallium(III)
edta halide thio complexes, 2057
Thenoyltrifluoroacetonates
actinides, lanthanides, 2071
Theobromine complexes
Cu(II), Zn, 2593
Thermal analysis
aluminophosphates, 819
cadmium mercury borates, 1567
copper(II) acetate oxime pyridine water complex, 1077
copper(II) amine chloride ketone complex, 991
ferrihydrite - goethite conversion, 149
iridium(III) chloride pyridine complex, 2245
iron(II) cyclopentadienyl lanthanide complexes, 2459
lanthanide amine ferrocenyl ketone Schiff base complexes, 2459
lanthanide chloride pyridine pyrrole Schiff base water complexes, 21
lanthanum formylferrocene benzoylhydrazone complex, 2105
magnesium hydroxide nitrate, 1061
manganese(III) acetate hydroxyketoimine oxo thiocyanate complexes, 1029
nickel arylamido iodide complexes, 2603
polyaminepolyphosphonate complexes, 453
pyridinedicarboxylate complexes, 745
silicon isothiocyyanate complexes, 427
uranium(VI) oxo salicylhyrazone complexes, 2527
vanadium(IV) diketonate oxo pyridine complexes, 2611

yttrium formylferrocene benzoylhydrazone complex, 2105
Thiaboranes, 2089
Thianaphthene hydrogenation, 1431
Thiazolidine-2-thione, 1891
Thio complexes
aluminium, 2057
chromium, 179
cobalt, 801,1625
cubane, review, 2843
gallium, indium, 2057
iron, 179,1865,1885
iron(III), 801
molybdenum, 179,1625,1865
molybdenum(II), 1762
molybdenum(III), 2791
molybdenum(III,IV), 2785,2791
molybdenum(IV), 1625,1762,2419, 2785
molybdenum(V), 549,1705
molybdenum(VI), 549,1625
niobium(IV), 1762
niobium(V), 549,1797
osmium, 1437
rhenium(IV), 1625
ruthenium, 1123,2351
ruthenium(II), 1149
tantalum(V), 549
tin(IV), 2557
tungsten, 179,2351
tungsten(IV), 1261
tungsten(V), 947
tungsten(VI), 549
vanadium(III), 2763
vanadium(IV), 1723
vanadium(V), 1762
Thioacyl complexes
Cr, Fe, Mo, W, 179
Thiocarbazone complexes
molybdenum(VI), 677
Thiocarbonyl complexes
ruthenium(II), 1149
Thiocyanate, 2627
formation from nitrosothiourea, 953
Thiocyanate complexes
chromium(II), 1825
cobalt(II), 1509,1965
cobalt(III), 775
copper(II), 769,1523,1965,2313
europium, 2157
germanium, 2641
gold(I), 2823
manganese(II), 1523,1965
manganese(III), 1029
molybdenum(0), 1471
molybdenum(II), 371
nickel(II), 1965
Pd(II), Rh(III), 775
sodium, 215
tin(IV), 1897
tungsten(0), 1471
yttrium, 2157
Thiocyanates (organo), reactions with CF_3CO_2H, 775
Thiodiketonates
Cu(II), Ni(II), Zn, 2305
Thioester complexes
indium, 633
Thioether complexes
carbaboranes, 805
chromium(0), 887
chromium(III), 1770
cobalt(II), 1965
cobalt(III), 491
copper(II), 1965,2749
iron(III), 491
manganese(II), 1965
mercury, 2041
molybdenum(0), 505,887,1876
molybdenum(II), 505,1770,1876
nickel(II), 1965
potassium, 2147
rhenium(V), 559
rhodium(III), 613
silver(I), 513,2951
silver(II), 513
thallium(I), 793
tungsten(0), 505,887,1876
tungsten(II), 505,1876
Thiolates
indium, 763
iron, molybdenum, 1865
molybdenum(IV), 1762,2439
nickel(II), 1253,2837
palladium(II), 2151
rhodium(III), 613
tungsten(IV), 2439
vanadium(III), 1723
vanadium(V), 1762
Thione complexes
copper(I), 1103
gold(I), 2823
vanadium(IV), 87
Thioneimine complexes
mercury, 569
Thionitrosyl complexes
iron, 1447
Thionylimino [NSO^-] complexes
Pd(II), Pt(II), 835
Thiophene-2-carboxylate complexes
vanadium(IV,V), 1723
Thiophenoxides
indium(III), 865
molybdenum, 1033
molybdenum(IV), 1701
niobium(V), 1797
tungsten(IV), 1701
Thiosemicarbazide complexes
iron(II), 2371
iron(III), 135
Thiosemicarbazone complexes
iron(II), 2371
nickel(II), 727
Thiourea, formation from nitrosothiourea, 953
Thiourea complexes
chromium(II), 1825
ruthenium(III), 463
tungsten(II), 351
4-Thioxo-2-pentanonates
Cu(II), Ni(II), Zn, 2305
Thorium
aminophenol diamine dicarboxylate oxo peroxide phosphine oxide picoline complexes, 977
aminopolycarboxylate complexes, 2385
arsine oxide edta peroxide phosphine oxide succinate complexes, 109
aspartate complex, 2233
diketonate, 1111
Threonine complexes
vanadium(IV), 1173

Threonylglycine complexes
copper(II), 2463
Thulium
formylferrocene benzoylhydrazone complex, 2105
polyaminepolycarboxylates, 1425
Tin(II)
alkyl chloride Mo(IV), W(IV) complexes, 1884
catechol ether complex, 2933
chloride molybdenum(II) complexes, 917,1786
chloride palladium(I) complexes, 1045
chloride rhodium(III) complexes, 1085
chloride tungsten(II) complexes, 1786
phenyl Mo(IV), W(IV) complexes, 1861
Tin(IV)
alkyl chloride dithiocarbamate complexes, 1413
alkyl dithiocarbamate thio complexes, 2557
butyl dithiocarbamates, 1891
chloride dioxygen hydrocarbon complex, 533
chloride methyl phenyl vanadium(IV) complexes, 1753
halide methyl phosphine complexes, 2047
methyl salicylaldimine complexes, 2749
phenyl thiocyanate complex, 1897
tetraselenide complex, 1999
Titanium(0)
arene complexes, 1641
carbonyl cyclopentadienyl diphosphine pyrazolylborate stannyl triphosphine complexes, 1611
Titanium(III)
alkylamido phenyl complexes, 1457
aminopolycarboxylate complex, 577
aryl ketoimine complex, 1717
borohydride carbonyl chloride cyclopetadienyl dienyl complexes, 1883
chloride, 1867
chloride cyclopentadienyl complexes, 1780
chloride ether complex, 2013
edta water complexes, 2883
Titanium(IV)
acetonitrile cyclopentadienyl halide complexes, 311
alkoxide diimine dithiolate pyridine complexes, 2893
alkyl cyclopentadienyl metallocyclic compounds, 2817
alkyl salicylaldimine complex, 1717
carboxylate carboxylic acid chloride oxo complexes, 1846
carboxylate cyclopentadienyls, 1844
chloride cyclopentadienyl oxo pyridine complex, 1804
chloride, dioxygen hydrocarbon complex, 533
chloride tetrahydrofuran complex, 2013
chromium(III) oxide, 1615
cyclopentadienyl ether hydroxide isocyanide methyl water complexes, 1838
cyclopentadienyl imide nitride complex, 1729
oxalate oxo complex, 1792
2,5-Toluenediamine-*N,N'*-disuccinate complexes, 1365
Toluene-3,4-dithiolates
molybdenum, 1033
titanium(IV), 2893
4-Toluenethiolates
titanium(IV), 2893
2-Tolyl complexes
rhenium(VII), 2657
vanadium(III), 1339,1767
4-Tolylimido complexes
tungsten(IV), 1261
4-Tolylisocyanide complexes
palladium(I), 1045
rhenium(I), 1778
4-Tolylmethyl complexes
Nb(V), Ta(V), 1607
N-Tosylasparagine complexes
copper(II), 739
N-Tosylglutamine complexes
copper(II), 739
Transfer chemical potentials
cobalt(III) phenoxide salicylaldimine complexes, 2677
Triamine complexes
molybdenum(0), 2333
Mo(VI), W(VI), 1675
1,4,7-Triazacyclononane complexes
tungsten(VI), 1675
1,4,7-Triazacyclononanetriacetates
gallium, indium, 2481
Triazatrimetallabenzenes, 1729
Triazenide complexes
Al, Ga, In, 1909
Tribenzylphosphine complexes
platinum(II), 897
Tribenzylphosphine oxide complexes
zinc, 1093
Tri-*n*-butylamine complexes
chromium(0), 2681
1,3,5-Tri-*t*-butylbenzene complexes
Cr(0),Hf(0),Mo(0), Nb(0),(I), W(0),Y(0),Zr(0), 1641
2,4,5-Tri-*t*-butyl-1,3-diphosphacyclopentadienyl, 849,2407
Tri-*n*-butylphosphine complexes
chromium(0), 1099
nickel(0), 1351
nickel(II), 585
platinum(II), 835
tin(IV), 2047
Tributylphosphite complexes
ruthenium(II), 851
N-Trichloroacetylalaninate complexes, nickel(II), 1329
Trichlorostannate(II) complexes
molybdenum(II), 917,1786
palladium(I), 1045
rhodium(III), 1085
tungsten(II), 1786
Tricyanomethyl complexes
copper(II), 157
Tricyclohexylphosphine complexes
nickel(II), 585

platinum(II), 433
Tri(2,6-dimethoxyphenyl)phosphine complexes, gallium, 1053
Triene complexes
chromium, manganese, 1589
Triethylenetetramine oxime complexes, Co(II),(III), 1509
Triethylphosphine complexes
cobalt, 801
iron(III), 801
nickel(II), 585
platinum(II), 433,835,897,1979, 2507
tin(IV), 2047
Triethylphosphine oxide complexes
Cd, Hg, Zn, 1093
Triethylphosphite complexes
Mo(IV), W(IV), 1701
Trifluoroacetates
molybdenum, 2265
molybdenum(VI), 2947
rhodium(III), 2727
tungsten(VI), 2947
Trifluoroacetic acid, reactions with organothiocyanates, 775
N-Trifluoroacetylalaninate, -glycinate, -valinate complexes, nickel(II), 1329
Trifluoromethanesulphonates
Mo(VI), W(VI), 2947
N-Trifluoromethyliminoarsine, 2331
Trifluoromethylsulphonate
chromium(III), 1770
1,1,1-Trifluoro-2,4-pentanedionate complexes,
osmium(III), 2179
rhodium(II), 1117
ruthenium(III), 2179
Trifluorophosphine complexes
chromium(0), tungsten(0), 2125
Trimethylacetate
titanium(IV), 1846
2,4,6-Trimethylphenylthiophenoxides, Mo(IV), W(IV), 1701
Trimethylphosphine complexes
molybdenum(II), 1786
nickel(0), 1351
nickel(II), 285,585,1069
platinum(II), 433,835,1979
tungsten(II), 1786
tungsten(IV), 1261
zirconium(III), 1882
Trimethylphosphite complexes
molybdenum(IV), 1701
rhenium(I), 1770
rhenium(V), 959
technetium(I), 1201
tungsten(0), 827
tungsten(IV), 1701
3,4,5-Trimethylpyrazole complexes
copper(II), 157
Trimethylsiloxides
rhenium(VII), 2657
vanadium(IV), 1723
vanadium(V), 1736
Trimethylsilylcyclopentadienyls
niobium(IV),(V), 1848
Trimethylsilylimido complexes
tungsten(IV), 1261
Trimethylsilylmethyls
molybdenum(II), 2599
N,N',N''-Trimethyl-1,4,7-triazacyclononane complexes,
Mo(VI), W(VI), 1675
Trinuclear clusters, molecular orbitals, 2785
Trioctylphosphine oxide complexes
cadmium, 2535
Triphenylarsine complexes
copper(II), 2469
molybdenum(II), 917
ruthenium(II), 1149
Triphenylarsine oxide complexes
thorium, 109
Triphenylgermyl complexes,
titanium(0), 1611
Triphenylphosphine complexes
aluminium, 831
copper(I), 1103
copper(II), 2469
copper(III), 1039
gold, 1903
iridium(I), 121,1431
molybdenum(II), 917,1859
molybdenum(V), 447
nickel(0), 13
nickel(II), 585,2449
osmium(I), 1537
osmium(II), 1431
osmium(III), 2179
palladium(I), 1045
platinum(0), 2485
platinum(II), 91,143,433,701, 835,2485
platinum(IV), 893
rhenium(I), 1770
rhodium(I), 1431,1575
rhodium(III), 613
ruthenium(II), 103,851,1149,1431
ruthenium(III), 851,2179,2813
tungsten(II), 1859
Triphenylphosphine oxide complexes
cadmium, mercury, 1093
ruthenium(II,III), 2571
thorium, 109,977
ytterbium, 1983
zinc, 1093
Triphenylphosphineiminate
vanadium(IV), 1784
Triphenylphosphite complexes
manganese, 1589
molybdenum(II), 917
rhodium(I), 2415
Triphenylsiloxide complex
cerium(IV), 1001
Triphenylstannyl complexes
molybdenum(IV), 1861
titanium(0), 1611
tungsten(IV), 1861
Triphenylstibine complexes
copper(II), 2469
molybdenum(II), 917
Triphosphanate complexes
hafnium(IV), zirconium(IV), 1774
Triphosphine complexes
gold, 1903
hafnium(0), 1611
molybdenum(0), 2119
molybdenum(II),(IV), 1756
rhodium(I),(II), 2119
Ti(0), Zr(0), 1611
2,4,6-Tri-*i*-propylphenylthiophenoxide complexes, Mo(IV), W(IV), 1701
Tri-*i*-propylphosphine complexes
platinum, 2271

Tri-*n*-propylphosphine
complexes
palladium(II), 161
platinum(II), 835
Tris(3-aminopropyl)amine complexes
cobalt(III), 275,415,2389
Tris(4-chlorophenyl)phosphine
complexes
nickel(0), 13
rhodium(I), 167
rhodium(III), 1085
Tris(4-chlorophenyl)phosphine oxidecomplexes, Ru(II,III), 2571
Tris(4-dimethylaminophenyl)phosphine complexes, nickel(0), 13
1,1,1-Tris(dimethylphosphinomethyl)ethane complexes, Hf, Ti, Zr, 1611
Tris(diphenylphosphino)methane complexes, Mo(0),Rh(I),(II), 2119
Tris(4-fluorophenyl)phosphine
complexes
rhodium(I), 167
rhodium(III), 1085,2727
Tris(4-fluorophenyl)phosphine oxide complexes, Ru(II,III), 2571
Tris(2-methoxyphenyl)phosphine
complexes, gallium, 1053
Tris(4-methoxyphenyl)phosphine
complexes
gallium, 1053
nickel(0), 13
rhodium(I), 167
rhodium(III), 1085
Tris(4-methoxyphenyl)phosphine
oxide complexes, Ru(II,III), 2571
Tris(*m*-tolyl)phosphine
complexes
rhodium(I), 167
Tris(*o*-tolyl)phosphine complexes
aluminium, 831
rhodium(I), 167
Tris(*p*-tolyl)phosphine complexes
nickel(0), 13
rhodium(I), 167
rhodium(III), 1085
1,4,7-Trithiacyclononane complexes
chromium(III), 1770
mercury, 2041
molybdenum(II), 1770
silver(II), 513
Tri(2,4,6-trimethoxyphenyl)phosphine complexes, gallium, 1053
Tropolonates
ruthenium(III), 2813
ytterbium, 117
Tungsten
alkenyl alkyl carbonyl chloride
cyclopentadienyl oxo phosphido
phosphinoalkenyl complexes, 1807
alkoxide pyridine thio iron
complex, 127
alkylidyne carbonyl
cyclopentadienyl hydride
platinum complexes, 2271
alkynyl carbonyl
cyclopentadienyl osmium
ruthenium complexes, 2003
aminocarbyne carbyne diphosphine
methyleneamido vinyl complexes, 1595
carbonyl cyclopentadienyl vinyl
ruthenium complex, 695
carbonyl thio ruthenium complex, 2351
diphosphine seleno selenoacyl
thio thioacyl iron complexes, 179
multiply - bonded ligands with, 1653
oxycarbides, 1794
Tungsten(0)
alkoxide carbonyl hydride
complexes, 653
arene complexes, 1641
carbonyl crown thioether
complexes, 505
carbonyl cyclopentadienyl
antimony complexes, 2495
carbonyl diamine diimine halide
pseudohalide mercury
complexes, 1471
carbonyl dipyridyl phosphite
complexes, 827
carbonyl episulphide complexes, 887
carbonyl phosphine complexes, 2125
carbonyl phosphine phosphirane
complexws, 2671
carbonyl phosphine thioether
complexes, 1876
carbonyl phosphinyl complexes, 627
carbonyl phosphonite Mo(II)
complexes, 2339
Tungsten(II)
acetonitrile alkyne carbonyl
halide complexes, 2587
alkylphosphinidene carbonyl
complex, 2671
alkyne carbonyl iodide thiourea
urea complexes, 351
bromide carbonyl phosphine
thioether complexes, 1876
carbonyl cyclopentadienyl methyl
complexes, 1804
carbonyl cyclopentadienyl
phosphine vinyl complex, 1859
carbonyl dipyridyl isocyanide
complexes, 827
carbonyl iodide crown thioether
complexes, 505
chloride complexes, 469
chloride isocyanide phosphine
tin(II) complexes, 1786
chloride phosphine complex, 1261
Tungsten(III)
alkylidyne carbonyl
cyclopentadienyl methyl
complexes, 2035
chloride complexes, 469
Tungsten(IV)
acetaldehyde alkene alkylimido
alkyne arylimido carbonyl
chloride isocyanide oxo
phosphine silylimido thio
complexes, 1261
carbene carbonyl
cyclopentadienyl hydride
complexes, 1583
carbene carbonyl
cyclopentadienyl iodide

tin(II) complexes, 1861
carbonyl hydride phosphine phosphite pyridine thiophenoxide complexes, 1701
cyclopentadienyl hydride phosphene tin(II) complexes, 1884
cyclopentadienyl mercaptopyridine complexes, 2439
oxo thio complexes, 2785
Tungsten(V)
cyanide complex, reaction with NH_2OH, 2213
hydroxyquinoline oxo thio complexes, 947
Tungsten(VI)
adsorption on carbon, 71
alkylamide alkylimido amine carboxylate chloride sulphonate tetrafluoroborate complexes, 2947
alkylimido arylimido chloide oxo complexes, 1788
bromide hydroxide oxo triamine complexes, 1675
carbohydrate complexes, 333
carbonyl carbyne cyclopentadienyl iodide isocyanide complexes, 1285
chloride metallaphosphazenes, 1729,1736
chloride oxo thio compounds, 549
diolate oxo complex, 519
edta oxo peroxide phosphine oxide succinate complexes, 109
hydride phosphine complexes, 1870
hydroxo oxo complex, substitutions, 1387
Tyrosine ethyl ester, Schiff base complexes, copper(I), 1321

U

Uranium(IV)
chloride diphosphinoamido complex, 1767
phenoxide, 1247
Uranium(VI)
amine crown ether diamine oxo polyether complexes, 2251
aminoalcohol aminophenol diamine dicarboxylate oxo picoline water complexes, 977
aspartate oxo complexes, 2233
diketonate oxo complex, 1111
diolate oxo complex, 519
edta oxo peroxide complex, 109
ketophosphonate nitrate oxo complexes, 1357
oxo salicylhydrazone complexes, 2527
Ureas, difluorophosphine-, 293
Urea complexes
cadmium mercury, 1093
tungsten(II), 351
zinc, 1093

V

Valine complexes
cobalt(III), 1015
Vanadium
nitrogenase component, 1649,1695
Vanadium(II)
acetic acid chloride water complexes, 1823
chloride cyclopentadienyl diphosphine complexes, 1784
oxidation, 469
Vanadium(III)
alcohol halide phenylhydrazine Schiff base complexes, 1782
alkylamido phenyl complexes, 1457
aminothiolate chloride dipyridyl dithiolate oxo pyridine thiolate complexes, 1723
aryl chloride diphosphinoamido methyl complexes, 1767
aryl chloride methyl phosphinoalkylamido complexes, 1339
chloride cyclopentadienyl complexes, 1780
cyclopentadienyl thio complex, 2763
ethylenediaminetetraacetate complex, 1949
oxalate oxo complex, 1792
Vanadium(III,IV)
oxo Schiff base complex, 1782
Vanadium(IV)
acetonitrile chloride oxo thione water complexes, 87
aminoacid oxo complexes,1173, 1745
azole oxo complexes, 1835
chloride cyclopentadienyl diphosphine hydrazide phosphineiminate complexes, 1784
diketonate dithiocarbamate oxo pyrazolylborate complexes, 1827
diketonate oxo pyridine complexes, 2611
disulphide dithiocarbamate complex, 1625
dithiolate oxo seleno siloxide thio thiolate complexes, 1723
ethylenediaminetetraacetate complex, 1949
oxo complexes, 1830
oxo salicylaldimine tin(IV) complexes, 1753
oxo Schiff base complexes, 1748, 1790
Vanadium(IV,V)
carboxylate chloride nitrate complexes, 1723
Vanadium(V)
chloride metallaphosphazenes, 1736
isopolyanions, 1800
oxo water complex, 2791
peroxide complexes in water, 1379
Vinyl complexes
molybdenum, 1595
molybdenum(II), 1859
rhenium, 1595
ruthenium, 695
tungstem, 695,1595
Vinyl disulphide complexes
molybdenum(V), 1705
Vinylidene complexes

electrophilic addition, 1595
manganese, 1589
Vitamin D_3 complexes
cadmium, calcium, 1953

W

Water complexes
beryllium, 357
caesium, 793
cobalt(II), 39,51
cobalt(II,III), 2023
cobalt(III), 1205,2389,2889
copper(II), 1,301,1077,2131,2513
lanthanides, 21,1111,1531,2139
molybdenum(VI), 541,977
nickel(II), 39,689,1329,2305
palladium(II), 2769
platinum(II), 2769
rhodium(III), 1163,2727
ruthenium(III), 463
thorium, 1111
titanium(III), 2883
titanium(IV), 1838
uranium(VI), 977,1111
vanadium(II), 1823
vanadium(IV), 87
vanadium(V), 1379,2791
yttrium, 1217,1923
zinc, 2305
Weibull modulus, aluminium chromium(III) oxide, 1765

X

XANES, molybdenum(V) chloride oxo complexes, 45
XPE spectra
electronegativity and, 1233
lanthanide cyclopentadienyl furfuralkoxide salicylaldehyde complexes, 2109
rhodium(II) amine azole carboxylate pyridine complexes, 1157
X-ray crystal structures
aluminium chloride diphosphine methyl phosphine oxide complexes, 1497
aluminium diaminoimine methyl complex, 1279
aluminium methyl phosphine complexes, 831
aluminium triazenide, 1909
bismuth(III) arylamide, 1579
bismuth(III) dithiophosphate, 483
cadmium diketonate pyridine complex, 2743
cadmium nitrate pyrrolidone mercury complex, 1913
caesium carboxylate carboxylic acid water complex, 793
carboxylic acids, 39
cerium(IV) ether siloxide complex, 1001
chromium(0) carbonyl episulphide complex, 887
chromium(III) dipyridyl complex, 1549
cobalt alkylidyne cyclopentadienyl hydride complexes, 1939
cobalt(II) azole thiocyanate thioether complex, 1965
cobalt(II) carboxylate water complexes, 39
cobalt(II) oxo molybdenum(VI) complexes, 1675
cobalt(III) aminoacid diamine nitrite complex, 1227
cobalt(III) cyclopentadienyl salts, 1780
copper(I) bromide phosphine thione complexes, 1103
copper(I) polyselenide complexes, 1139
copper(II) acetate oxime pyridine water complex, 1077
copper(II) alcohol alkoxide azole halide thiocyanate complexes, 769
copper(II) amine azole carboxylate complex, 659
copper(II) amine chloride ketone complex, 991
copper(II) aminoacid salicylaldimine water complex, 2131
copper(II) azole chloride complex, 1345
copper(II) azole thiocyanate complexes, 2313
copper(II) chloride, polyamine pyridine complexes, 909
copper(II) cyanamide dipyridyl complex, 2219
copper(II) cyanate terpyridine complexes, 97
copper(II) diaminothioether halide complexes, 2749
copper(II) hydroxide nitrate pyridone lanthanide complexes, 1531
copper(II) hydroxide water binucleating complex, 2513
copper(II) methoxide nitrate pyrrolidone mercury complex, 873
copper(II) nitrate pyridine pyridine-N-oxide complex, 933
copper(II) oxime pyridine water complex, 301
copper(II) pyridine salicylaldimine complexes, 2543
dysprosium nitrate pyridone water copper(II) complex, 1531
dysprosium proline water complex, 2139
europium tetramine thiocyanate macrocyclic complex, 2157
furan Schiff base cryptand, 1143
gadolinium nitrate pyridone water copper(II) complex, 1531
holmium proline water complex, 2139
hydrotelluride, 531
indium chloride triaminetricarboxylate, 2481
indium(III) pyridine selenophenoxide thiophenoxide complexes, 865
iridium(I) amidodiphosphine butadiene complex, 2291
iron alkoxide carbonyl thio tungsten complex, 127

iron carbonyl thio complex, 1885
iron(0) carbonyl platinum(0) complexes, 2521
iron(II) bromide carbonyl cyclopentadienyl complex, 2425
iron(II) carbonyl cyclopentadienyl thiosemicarbazide thiosemicarbazone complexes, 2371
iron(II) cyclopentadienyl molybdenum platinum complexes, 2265
iron(II) cyclopentadienyl potassium complex, 879
iron(III) hexadentate complexes, 491
iron(III) oxo molybdenum(VI) complexes, 1675
lanthanum alkyl cyclopentadienyl complex, 1850
manganese(0) carbonyl phosphine complex, 1855
manganese(II) phenanthroline complex, 1853
mercury chloride nitrate pyrrolidone cadmium zinc complexes, 1913
mercury pyrrolidone copper(II) complex, 873
mercury thioether macrocyclic complex, 2041
mercury thioneimine complex, 569
molybdenum alkylidyne carbonyl carboxylate diamine pyrazolylborate iron(II) platinum complexes, 2265
molybdenum(0) carbonyl cyclopentadienone complex, 1810
molybdenum(0) carbonyl cyclopentadienyl antimony complex, 2495
molybdenum(0) carbonyl macrocyclic aminoether complex, 1857
molybdenum(0) carbonyl triamine complexes, 2333
molybdenum(0,II) carbonyl phosphonite complex, 2339
molybdenum(II) acetate isoindoline pyridine complexes, 2359
molybdenum(II) chloride isocyanide phosphine complex, 1786
molybdenum(III) allyl cyclopentadienyl complexes, 203
molybdenum(III) amine phenoxide complexes, 1971
molybdenum(III) bromide diphosphine complex, 545
molybdenum(IV) alkoxide alkylamide complexes, 129
molybdenum(IV) alkoxide chloride diazenide ethanol hydroxamate phenylhydrazine complexes, 29
molybdenum(IV) alkoxide diimine complexes, 123
molybdenum(IV) alkylamido phosphido complex, 1419
molybdenum(IV) allyl cyclopentadienyl complexes, 203
molybdenum(V) alkoxide dithiolate mercaptocarboxylate oxo complexes, 669
molybdenum(IV) amine phenoxide complex, 1971
molybdenum(IV) cyclopentadienyl mercaptopyridine complex, 2439
molybdenum(IV) cyclopentadienyl tetraselenide complex, 1999
molybdenum(IV) thio niobium(IV) complex, 1762
molybdenum(V,VI) methoxide oxo isopolyanion, 537
molybdenum(VI) alkoxide carboxylate dienolate diketal hydroxide oxo complexes, 2915
molybdenum(VI) alkoxide oxo complex, 1213
molybdenum(VI) benzoin oxime oxo salicylaldoxime salicylhydroxamate complexes, 2473
molybdenum(VI) carbazone chloride oxo thiocarbazone complexes, 677
molybdenum(VI) diolate oxo complex, 519
molybdenum(VI) erythritol oxo complexes, 1571
molybdenum(VI) oxo peroxide water complexes, 541
molybdenum(VI) oxo triamine cobalt(II) iron(III) complexes, 1675
neodymium diketonate hydroxide complex, 2183
nickel(0) carbonyl phosphine complex, 1351
nickel(II) acetate polypyridine helical complex, 2551
nickel(II) alkyl pyridine cyclometallated complex, 1069
nickel(II) aminoacid water complexes, 1329
nickel(II) aminoethanethiolate, 2837
nickel(II) benzyl phosphine complexes, 2449
nickel(II) carboxylate water complexes, 39
nickel(II) diimine nitrate water complexes, 689
nickel(II) methanol salicylaldimine complex, 2321
nickel(II) nitrate oxime pyridine complex, 305
nickel(II) phenanthroline complex, 2649
nickel(II) thiolate, 1253
nickel(II) thiosemicarbazonate, 727
niobium(IV) cyclopentadienyl thio molybdenum(IV) complex, 1762
niobium(V) alkylimide chloride cyclopentadienyl, 1819
niobium(V) hydride phenoxide complex, 1607
niobium(V) thio thiophenoxide complex, 1797
osmium alkynyl carbonyl tungsten complex, 2003
osmium carbonyl thio complex, 1437
osmium(II) diimine complex, 367
osmium(VI) carboxymethyl methoxide oxo complex, 597

palladium(I) chloride diphosphine complex, 1045
palladium(II) chloride nitrite phosphine complexes, 161
palladium(II) chloride phosphine thiolate complexes, 2151
palladium(II) chloride sulphurdiimide complex, 91
palladium(II) diimine phosphine complex, 1989
palladium(II) polytelluride complex, 701
phosphaalkene, 2087
phosphonium salts, 1039,1293
phosphorane iminato complexes, 716
phosphorus(V) aminoacid fluoride phenyl compounds, 731
platinum alkylidyne carbonyl Fe(II) Mo complex, 2265
platinum(0) carbonyl diene iron(0) complexes, 2521
platinum(II) amido phosphine complexes, 1979
platinum(II) aryl dipyridyl binuclear complex, 2209
platinum(II) arylamide phosphine complex, 2507
platinum(II) bis(triaza)diphosphine chloride phosphine complex, 2485
platinum(II) chloride diphosphine phosphidophosphine complexes, 2169
platinum(II) cyanide disulphurdiimide complexes, 841
platinum(II) phosphine selenium - nitrogen complexes, 2215
platinum(II) phosphine telluro complex, 701
platinum(II) phosphine thionylimino complex, 835
platinum(IV) bromide phosphine complex, 893
platinum(IV) chloride phosphine sulphur - nitrogen complex, 997
polyselenide complexes, 1995
potassium crown ether complex, 2051
potassium crown ether iron(II) complex, 879
potassium thioethercarboxylate, 2147
rhenium(I) chloride diphosphine nitrile complex, 1872
rhenium(II),(III) chloride diarsine complexes, 1733
rhenium(V) chloride methyl oxo phosphine complex, 959
rhenium(VI) alkylimide, 2657
rhenium(VII) alkylimido aryl chloride siloxide complexes, 2657
rhodium(I) carbonyl chloride complex, 2119
rhodium bromide nitrosyl phosphine complex, 2565
rhodium(I) chloride diphosphine phosphine complex, 1575
rhodium(I) cyanide phosphite complex, 2415
rhodium(I) diene diphosphine zirconium(IV) complex, 1760
rhodium(I) diene perrhenate complex, 375
rhodium(II) acetate diketonate pyridine complex, 1117
rhodium(II) carbonyl chloride triphosphine complex, 2119
rhodium(III) bromide nitrate phosphine complex, 2565
rhodium(III) chloride hydride phosphine thioether thiolate complexes, 613
rhodium(III) phenyl phosphine quinaldinate trifluoroacete water complex, 2727
ruthenium alkyne carbonyl phosphine thio complexes, 1123
ruthenium alkynyl carbonyl tungsten complex, 2003
ruthenium carbene carbonyl thio tungsten complex, 2351
ruthenium carbonyl diphosphine vinyl tungsten complex, 695
ruthenium(II) acetate carbonyl complex, 597
ruthenium(II) pyridine quinone oxime complex, 103
ruthenium(II,III) acetate phosphine oxide complex, 2571
samarium(II) cyclopentadienyl ether complexes, 1007
silver(I) amine thioether macrocyclic complex, 2951
silver(I) crown thioether complexes, 513
silver(I) polyselenide complexes, 1139
silver(I) polysulphide complex, 2379
sodium phosphine oxide thiocyanate complexes, 215
tantalum(V) alkyl amido imido imine iminoacyl phenoxide complexes, 341
technetium(II) chloride diimine complexes, 1879
technetium(V) diimine diphosphine halide nitride complexes, 1879
thallium(I) carboxylate carboxylic acid thioether complex, 793
tin(II) catechol ether complex, 2933
tin(IV) alkyl chloride dithiocarbamate complex, 1413
tin(IV) chloride phenyl vanadium(IV) complexes, 1753
tin(IV) phenyl thiocyanate complex, 1897
tin(IV) tetraselenide complex, 1999
titanium(III) carbonyl chloride complex, 1883
titanium(III) chloride cyclopentadienyl complexes, 1780
titanium(III) chloride ether complex, 2013
titanium(IV) carboxylate carboxylic acid chloride oxo complexes, 1841
titanium(IV) chloride

cyclopentadienyl oxo pyridine complex, 1804
titanium(IV) cyclopentadienyl ether hydroxide methyl water complexes, 1838
tungsten carbonyl chloride cyclopentadienyl phosphinoalkenyl complex, 1807
tungsten carbonyl cyclopentadienyl vinyl ruthenium complex, 695
tungsten carbonyl thio ruthenium complex, 2351
tungsten(0) carbonyl cyclopentadienyl antimony complex, 2495
tungsten(0) carbonyl phosphine thioether complex, 1876
tungsten(0) carbonyl phosphirane complex, 2671
tungsten(II) chloride phosphine complex, 1261
tungsten(III) alkylidyne carbonyl cyclopentadienyl methyl complex, 2035
tungsten(IV) alkene arylimido carbonyl chloride oxo phosphine complex, 1261
tungsten(VI) alkylimido amine sulphonate complex, 2947
tungsten(VI) alkylimido arylimido chloride oxo complexes, 1788
tungsten(VI) bromide hydroxide oxo triamine complexes, 1675
uranium(IV) phenoxide, 1247
uranium(VI) ketophosphonate nitrate oxo complexes, 1357
vanadium(II) acetic acid chloride water complexes, 1823
vanadium(III) alkylamido phenyl complex, 1457
vanadium(III) cyclopentadienyl thio complex, 2763
vanadium(IV) chloride oxo thione water complex, 87
vanadium(IV) oxo salicylaldimine tin(IV) complexes, 1753
ytterbium benzoate pyrazolylborate, 551
ytterbium cyclopentadienyl phosphine oxide complex, 1983
yttrium acetate hexadentate macrocycle water complexes, 1923
yttrium tetramine thiocyanate macrocyclic complex, 2157
zinc methoxide nitrate pyrrolidone mercury complexes, 1913
zirconium alkyl alkylamido borohydride chloride cyclopentadienyl diphosphine iminoalkene phenoxide complexes, 1601
zirconium alkyl cyclopentadienyl rhodium(I) complex, 1760
zirconium carboxylate chloride cyclopentadienyl complex, 929
zirconium diimine phenoxide complex, 77
zirconium phenoxide pyrazolylborate complex, 845
X-ray diffraction
aluminophosphates, 819
beryllium iodate water complex, 357
cadmium mercury borates, 1567
clay minerals pyrolysis, 2709
copper(II) acetate oxime pyridine water complex, 1077
ferrihydrite - goethite conversion, 149
iridium(III) chloride pyridine complex, 2245
magnesium hydroxide nitrate, 1061
molybdenum cyanide nitrosyl complexes, 2897
vanadium(IV) oxo Schiff base complexes, 1790
2,6-Xylylmethylidyne complexes
Cr, Fe, Mo, W, 179

Y

Ytterbium
carboxylate pyrazolylborate, 555
chloride pyridine pyrrole Schiff base water complexes, 21
crown ether complex, 1561
cyclopentadienyl ether indenyl complexes, 17
cyclopentadienyl furfuralkoxide salicylaldehydate complexes, 2109
cyclopentadienyl phosphine oxide complex, 1983
formylferrocene benzoylhydrazone complex, 2105
oxalate pyrazolylborate, 2367
polyaminepolycarboxylate, 1425
pyrazolylborate tropolonate complexes, 117
Yttrium(0)
arene complexes, 1641
Yttrium(III)
acetate hexadentate macrocycle water complexes, 1923
carboxylate pyrazolylborate, 555
coordination numbers, 2431
formylferrocene benzoylhydrazone complex, 2105
nitrate pyridine Schiff base water macrocyclic complex, 1217
oxalate pyrazolylborate, 2367
tetramine thiocyanate macrocyclic complex, 2157

Z

Zeolite, molybdenum(V)
dithiocarbamate in, 1817
Ziegler - Natta catalysis, 1867
Zinc
amide cytosine halide phosphine oxide urea complexes, 1093
chloride pyridine complexes on silica gel, 2901
chloride theobromine complex, 2593
diaminepolycarboxylate dicarboxylate complexes, 2693
diisocyanide complex, 317

diketonate pyridine complexes, 2743
diketonate thiodiketonate water complexes, 2305
dithiocarbamates, 1891
insulin complexes, 2065
methoxide nitrate pyrrolidone mercury complex, 1913
phosphonate complexes, 1307
polyselenide complexes, 1995
pyridinedicarboxylate complexes, 745
Zirconium(0)
arene carbonyl complexes, 1641
carbonyl triphosphine complexes, 1611
Zirconium(III)
alkyl chloride cyclopentadienyl fulvalenide hydride phosphinoalkyl complexes, 1758
alkylphosphido cyclopentadienyl complexes, 1774
chloride cyclopentadienyl ether phosphine complexes, 1882
Zirconium(IV)
alkoxide cyclopentadienyl methyl Nb(III) Ta(III) complexes, 2189
alkyl alkylamido borohydride chloride cyclopentadienyl diphosphine iminoalkene phenoxide complexes, 1601
alkyl cyclopentadienyl phosphinoalkyl complex, 1758
alkyl cyclopentadienyl rhodium(I) complex, 1760
alkyl diimine phenoxide complexes, 77
alkylphosphido cyclopentadienyl diphosphanate triphosphanate complexes, 1774
carboxylate chloride cyclopentadienyl complex, 929
chloride diphosphinoamido diphosphinophosphido complexes, 1767
chloride ether salicylaldimine complex, 1717
cyclopentadienyl metallathiazenes, 1729
diaminopolycarboxylate complexes, 1365
dicarboxylate peroxide pyridine-*N*-oxide complex, 977
edta peroxide phosphine oxide succinate complexes, 109
hydroxycarboxylate oxalate peroxide complexes, 1371
phenoxide pyrazolylborate complexes, 845
phthalocyanine, 1631

AUTHOR INDEX

Abbott, R. G. 1821
Abdul Malik, K. M. 2959
Abel, E. W. 703
Abu-Elenien, M. H. 99
Adams, R. D. 2385
Adams, S. 1297
Agarwal, D. D. 487, 1401, 1405
Agarwala, U. C. 863, 2153
Agrawal, S. 1065
Akashi, H. 1671
Akbar Ali, M. 1017
Akiyama, T. 1123
Al-Ansi, T. Y. 2029
Al-Masoudi, E. A. 847
Al-Obaidi, Y. N. 1141
Al-Rubaie, A. Z. 847, 1141
Al-Shatti, N. I. 99
Alam, F. 891
Ali, N. J. 999
Allen, D. W. 129, 681
AlObaidi, N. J. 693
Alyea, E. C. 739, 1059, 2393, 2463
Amin, R. R. 2029
Andjelkovic, K. 2149
Ang, H. G. 1479, 2189
Angelici, R. J. 1883
Angelova, O. 2597
Anisuzzaman, A. K. M. 891
Antelo, J. M. 665
Aravamudan, G. 2879
Arce, F. 665
Archer, C. M. 1497
Arif, A. M. 1573, 1677
Armstrong, E. M. 801
Armstrong, R. S. 2815
Arnold, D. P. 1331
Arriortua, M. I. 2693
Askham, F. R. 1317
Aslanidiś, P. 981, 2833
Astruc, D. 2727
Atkinson, N. 2641
Atwood, J. L. 309
Au-Yeung, B. W. 2901

Babaian-Kibala, E. 1689
Bachrach, M. 1775
Backer-Dirks, J. D. J. 1423
Bader, D. S. 2619
Baerends, E. J. 1919
Baghurst, D. R. 893
Baker, P. K. 801, 2135, 2233, 2507
Ballester, L. 1341
Ballester-Reventos, L. 2163
Banbery, H. J. 615, 2549
Banks, M. A. 335
Baran, E. J. 1383
Bariz, R. 2663
Barral, M. C. 1723
Barron, A. R. 149, 233
Barsuaskas, G. 773
Basolo, F. 1503
Basto, M. C. R. M. P. 713, 2035
Bates, R. S. 1113
Baumgart, F. 1199
Baumgartner, M. 1155
Bayo, K. 1087
Beachley, O. T. Jr 335
Beauchamp, A. L. 2733
Becalska, A. 581
Becker, B. 1659
Beddoes, R. L. 2483
Bedel-Cloutour, C. H. 1297
Bedia Erim, F. 1537
Beer, P. D. 1091, 1747
Begley, M. J. 1113
Bell, N. A. 681
Bell, T. 2815
Beltran-Porter, D. 2699
Benet, E. 2839
Benetollo, F. 1411
Benlian, D. 1087
Benn, R. 11, 23
Bennett, A. M. A. 2823
Bernhard, P. 1095
Bertoncello, K. 2867
Bhardwaj, C. 1243
Bhardwaj, R. C. 1243
Bhatnagar, R. P. 1405
Bhattacharjee, C. R. 1653
Bhattacharjee, M. 1653
Bhattacharya, P. K. 2239
Bilewicz, R. 2353
Bin, L. 2019
Biner, M. 1095
Bisi Castellani, C. 939, 1639, 2061
Blake, A. J. 2641, 2911, 2919, 2925, 2931
Block, E. 1429
Bochmann, M. 2097

Bodini, M. E. 1181
Boeyens, J. C. A. 975
Bombieri, G. 1411
Boone, S. R. 2267
Bott, A. W. 1769
Bott, S. G. 309
Bradley, D. C. 343, 719, 1423, 2959
Bradley, J. S. 1809
Braga, D. 53
Bravo-Zhivotovskii, D. A. 227
Bremard, C. 2663
Bright, T. A. 1573
Brock, T. H. 11, 23
Brown, S. J. 2809
Bruce, D. W. 687
Bruno, G. 2591
Buck, E. A. 743
Buffin, B. P. 2887
Buhro, W. E. 611
Bulychev, B. M. 387
Bursten, B. E. 1781, 2001
Buslaev, Yu. A. 1379, 2803
Butler, A. R. 913, 2399
Byers, J. J. 2205

Cabral, M. F. 2847
Cai, S. 957
Calsy, A. M. 913
Calvet, T. 1729
Cameron, T. S. 1683
Campagna, S. 2591
Campbell, M. J. M. 1065
Campora, J. 1107
Cano, M. 619, 2863
Carlton, L. 2717
Carmona, E. 757, 1447
Carugo, O. 939, 1639, 2061
Casabo, J. 2839
Casals, I. 763, 769
Casassas, E. 1191
Casella, L. 1469
Castellano, E. E. 2937
Caulton, K. G. 1867, 2319
Cesarotti, E. 639
Cetinkaya, B. 239
Chadha, P. 487, 1401
Chaffee, A. L. 2815
Chan, C. B. 901
Chang, C. S. J. 1965
Chao, Y.-W. 2709
Chapelle, S. 1225
Chardon, C. 1867
Charrier, C. 1363
Chatterjee, D. 2681
Chaudhry, S. C. 2171
Chaudhuri, M. K. 1653
Chebi, D. E. 839, 969
Chen, G. 2385
Chen, H. 875, 2469, 2901
Chen, H.-M. 2689
Chen, J. 1883
Cheng, M.-C. 2579
Cherifi, K. 831
Chesnut, R. W. 1051
Chi, Y. 1491
Chiang, M. Y. 611
Chisholm, M. H. 253, 1271, 1829, 2941
Chongwu, N. 2019
Choudhury, S. 1653, 2251
Chow, F. L. 875, 2469, 2901
Christiansz, G. I. 921
Chudzynska, H. 719, 1423
Ciavatta, L. 1263
Clark, H. C. 1683
Clarkson, L. M. 2533
Clemenson, P. I. 2053
Clevette, D. J. 151
Coe, B. J. 687
Coker, E. N. 813
Cole-Hamilton, D. J. 1107, 1235
Collison, D. 2483
Colson, S. F. 1637
Colwell, S. M. 1035
Connolly, J. W. 1337
Constable, E. C. 1613, 1621, 1939
Cook, J. 2221
Cooper, S. R. 893
Copenhaver, A. S. 1783
Costa Pessoa, J. 81, 2101
Costa, J. 2847
Costello, M. T. 573
Cotton, F. A. 1217, 1221, 1689, 1821, 2553
Cotton, S. 627
Cowley, A. H. 1337
Crane, R. A. 1893
Crayston, J. A. 1741
Crisponi, G. 789
Cropper, P. E. 129
Curtis, M. D. 1855
Cusumano, M. 2591
Czuchajowska, J. 1217, 1221, 2553

Dai, A.-B. 1849

Dallin, P. 2759
Daniels, L. M. 1883
Danopoulos, A. A. 1009, 2413, 2625
Danovich, D. K. 1249
Daran, J-C. 1305
Dartiguenave, M. 1867
Das, S. K. 2705
Dash, K. C. 1011
Davies, A. G. 147, 2191
Davies, G. 2319
Davison, N. 2273
Dawes, H. M. 343
Dawod, M. M. 2987
De Almeida-Santos, R. H. 2699
De Simone, C. A. 2937
Deacon, G. B. 921
Deb, A. K. 2251
Debad, J. D. 581
Deeming, A. J. 623
Dei, A. 1729
DeKock, R. L. 1919
Del Valle, M. A. 1181
Delgado, R. 2847
Deng, D. 1453
Dengel, A. C. 1751
Denner, L. 975
Derringer, D. R. 573, 743
Desbois, M.-H. 2727
Dhingra, S. 1389
Di Vaira, M. 2477
Dias, M. C. F. B. 11
Diaz, C. 1045
Dickson, R. S. 921
Diebold, M. P. 75
Dieman, J. H. van 2971
Dilworth, J. R. 1323, 1497, 2751
DiStasi, V. F. 253
Do Prado-Gambardella, M. T. 2699
Dobson, G. R. 2511
Dohaidel, M. K. 1633
Domingos, A. 69, 1645
Dong, W. 2285
Dossett, S. J. 2953
Douglas, T. 329
Drager, M. 1297
Drake, S. R. 455
Dreos Garlatti, R. 2057
Drew, M. G. B. 2751
Drozdzynski, J. 2175
Druzina, B. 47
Dubler, E. 1155
Duesler, E. N. 773, 1127
Dunbar, K. R. 1695
Duran, I. 2693
Dziegielewski, J. O. 645

Eagle, A. A. 2965
Edwards, P. G. 2413
Eisenstein, O. 1867
El-Asmy, A. A. 2029
El-Dissouky, A. 2443
El-Ezaby, M. S. 629
El-Hendawy, A. M. 1751, 2309
El-Sonbati, A. Z. 2443
El-Zaru, R. A. 113, 2299
Elias, A. J. 1433
Ellis, A. B. 1913
Ellis, D. 2221
Enemark, J. H. 1965
Eng, G. 653
Engelhardt, L. M. 1079
Engles, B. 2549
English, R. B. 1589
Ernst, L. 1463
Errington, R. J. 899
Escuer, A. 1729
Esjornson, S. M. V. 743, 1165
Esmadi, F. T. 1633
Evans, D. F. 813
Evans, I. G. 2549
Ewing, K. J. 1209

Fallon, G. D. 777, 2867
Falvello, L. R. 1821
Fanwick, P. E. 565, 573, 743, 839, 963, 969, 1051, 1165, 1487, 1617, 2651
Farrugia, L. J. 2533
Fedotov, M. A. 1249
Fehlner, T. P. 1955
Feng, Q. 1555
Fenton, D. E. 2239
Ferguson, G. 739, 2393, 2463
Fernandez, J. J. 2741
Ferreira, M. J. P. 2035
Field, L. D. 2139
Filippou, A. C. 727
Fischer, B. 2199
Fisher, K. J. 2393
Fitzmaurice, J. C. 1561
Flower, K. R. 2135, 2233, 2507
Folgado, J.-V. 2699
Fonda, K. K. 949, 1411
Font-Bardia, M. 769
Fordon, K. J. 1079, 275
Fornies, J. 2181

Forsyth, G. A. 1603
Foulds, G. A. 2823
Frausto da Silva, J. J. R. 2847
Frigo, D. M. 719, 897, 1779
Fujii, S. 361
Fujiwara, M. 2491

Gabe, E. G. 653
Gagne, M. R. 1867
Gamasa, M. P. 2603
Ganadu, M. L. 789
Ganguly, S. 2517
Garcia Montelongo, F. 501
Garcia-Granda, S. 2603
Garvey, N. 63
Gatter, M. G. 2001
Gayoso, M. 2741
Gebreyes, K. 545
George, A. V. 2139
George, T. A. 545
Ghodsian, R. 629
Ghosh, S. 881
Giannetto, A. 2591
Gibson, J. F. 1593
Gibson, V. C. 2293
Gillard, R. D. 81, 2101, 2127
Gillespie, P. A. 999
Gimeno, J. 2603
Glidewell, C. 1741, 2399
Glidewell, S. M. 2399
Gochev, G. 2597
Goel, S. C. 611
Goldberg, K. I. 2001
Gonzalez-Duarte, P. 763, 769
Goodgame, D. M. L. 491, 1765
Gossage, R. A. 1059, 2393
Goswami, S. 2251
Gou, S. 2981
Gould, R. O. 2919
Graaff, R. A. G. de 2971
Granifo, J. 1187
Grassi, M. 639
Gray, H. B. 1949
Green, L. M. 35
Green, M. L. H. 2763
Greene, D. L. 893
Grepioni, F. 53
Griffith, W. P. 1751
Grimes, R. N. 949
Grybos, R. 1397
Grzybek, R. 645
Grzybkowski, W. 1375, 2257
Gullotti, M. 1469
Guofa, L. 2019
Gupta, C. 2449
Gutierrez, A. 2081
Gutierrez-Alonso, A. 1341, 2163
Gutierrez-Puebla, E. 1341

Ha, T. B. T. 2647
Haasnoot, J. G. 2971
Hadzija, O. 2895
Haefner, S. C. 1695
Hagen, K. 1603
Haggerty, B. S. 329
Hailiang, Z. 859
Hall, L. A. P. M. 2575
Hall, M. B. 1799
Haller, K. J. 1893
Hambley, T. W. 2139
Hamilton, E. J. M. 2407
Hammond, C. E. 1829
Hammond, M. E. 719
Hamon, J.-R. 2727
Hamor, T. A. 615, 2549
Hampden-Smith, M. J. 773, 1127
Han, R. 1775, 2655
Hanna, J. V. 1331
Hanton, L. R. 2127
Hanusa, T. P. 1345
Hanuza, J. 659
Hardcastle, K. I. 623
Harlan, C. J. 669
Harris, S. 1809
Hartmann, U. 353
Harvey, P. D. 1949
Hastings, J. J. 143
Hay-Motherwell, R. S. 931, 2071
Heaton, D. E. 1573
Hefford, S. 2221
Hefter, G. T. 901, 2429
Herak, R. 2149
Heras, J. V. 619
Herrmann, W. A. 2211
Hetherington, A. 1609
Hill, E. W. 1809
Hill, J. E. 1617
Hill, R. H. 581
Hirayama, N. 223
Hitchcock, P. B. 239, 245
Hodali, H. A. 113, 2299
Hoffman, D. M. 957
Hoffmann, R. 1901

Holder, A. J. 2919
Holt, E. M. 2319
Holwerda, R. A. 2433
Hor, T. S. A. 2305
Horvat, J. 2895
Horvat, S. 2895
Houlton, A. 2751
Hountas, A. 981, 2833
Housecroft, C. E. 1939
Howarth, O. W. 143
Hrncir, D. C. 2205
Hu, Y.-P. 2747
Huang, S.-P. 1389
Huang, T.-C. 1147
Hubbard, J. L. 1783
Huber, B. 283
Hubert-Pfalzgraf, L. G. 1305
Huffman, J. C. 1051, 1271, 1829, 1867 2941
Hugh-Jones, D. 1769
Hursthouse, M. B. 343, 535, 541, 719, 931, 1323, 1423, 2071,2081,2097, 2625, 2959
Huskowska, E. 659
Hussain, A. 2681
Hussain, B. 931
Hussain, W. 2549
Hussain-Bates, B. 2071, 2081, 2625
Hussein, M. A. 99

Ibrahim, A. A. 1423, 2959
Ibrahim, S. K. 1323
Ikeda, S. 1717
Indrasenan, P. 795
Iuliano, M. 1263
Izod, K. J. 535
Izquierdo-Ridorsa, A. 1191

Jackson, G. E. 163, 505
Jackson, S. A. 1867
Jaggar, A. J. 2097
Jain, R. 1405
Jasim, H. A. 239, 245
Jemmis, E. D. 2359
Jennings, M. C. 739, 2393, 2463
Jensen, D. 1199
Jezowska-Trzebiatowska, B. 2567
Jiaxi, L. 1625
Jimenez, F. 501
Jimenez-Aparicio, R. 1723
Jing, S.-P. 1849
Jinshun, H. 1625
Jobanputra, P. 1497
Johnson, B. F. G. 75, 1035, 1769, 2221, 2759
Johnson, I. L. 913
Johnson, N. P. 2647
Johnston, R. L. 1901
Jolliffe, J. M. 1751
Jolly, P. W. 11, 23
Jones, A. C. 1483
Jones, C. J. 527, 615, 619, 687, 693, 697, 1119, 2185 2549
Jones, R. A. 669, 1573
Juranic, N. 2149

Kabesova, M. 1029
Kabir-ud-Din 2437
Kahn, O. 2971
Kajitani, M. 1123
Kanatzidis, M. G. 1389
Kanaya, K. 361
Kapanadze, T. Sh. 1379, 2803
Kaplan, M. L. 751
Karagiannidis, P. 981, 2833
Karaulov, A. A. 1323
Karim, M. 623
Kaukorat, T. 1463
Kee, T. P. 2293
Kelly, J. D. 1497
Kelly, P. F. 1567, 2659
Kennard, C. H. L. 1667
Kerschner, J. L. 839
Khaled, A. M. 1765
Khalil, R. A. 2239
Khalili, F. I. 2987
Khan, M. A. 2613
Khan, O. F. Z. 541
Khan, S. R. 1323
Khandelwal, B. L. 495, 851, 2041
Khatoon, Z. 2437
Khoo, L. E. 653
Kibala, P. A. 1689
Kikuchi, R. 1123
Kimura, Y. 371
Kiprof, P. 2211
Kiss, A. 831
Kiss, T. 189
Kitao, T. 371
Kitchen, S. J. 2239
Klahn, A. H. 1131
Klang, J. A. 1271
Klaui, W. 2549
Klein, S. I. 2937
Klinszporn, L. 1375

Kobayashi, A. 2053
Kobayashi, H. 2053
Koczon, L. M. 545
Koh, C. H. 2189
Kokunov, Yu. V. 1379, 2803
Koley, A. P. 881
Koschmieder, S. U. 669
Kostic, N. M. 1975
Kozisek, J. 1029
Koziskova, Z. 1029
Kozlowski, H. 831
Kraan, A. M. van der 2971
Kramer, K. S. 611
Krannich, L. K. 289
Kravtsov, D. N. 1
Kresinski, R. A. 2185
Ku, Y.-T. 2023
Kubiak, C. P. 1487, 2651
Kufelnicki, A. 2567
Kugita, T. 2263
Kumar, R. 409
Kumar, V. 2879
Kunchandy, S. 795
Kunyuan, M. 2019
Kura, G. 511, 2177
Kuroya, H. 1671
Kwag, C.-Y. 319
Kwik, W. L. 1293, 1479

Lacoste, M. 2727
Lakshman, S. V. J. 1475
Lakshmana Rao, J. 1475
Lalor, F. J. 63
Lamanna, W. M. 301
Lambert, R. J. 1741
Lamoureux, M. 589
Laneman, S. A. 1317
Lappert, M. F. 239, 245
Larramendi, J. I. R. 2693
Larson, J. W. 1071
Laschi, F. 1469
Lastra, E. 2603
Lau, P. T. 1479
Lavery, A. J. 2641, 2919
Lawrance, G. A. 2227
Laxma Reddy, K. 805, 1703
Layh, M. 277
Le Floch, P. 991
Lee, B. 313
Lee, F. L. 653
Lee, G.-H. 1491
Leese, T. A. 1613
Legendziewicz, J. 659
Lei, D. 773, 1127
Leung, W.-H. 2625
Levason, W. 1609
Lewis, J. 75
Li, B. 1453, 2463
Li, P. 2873
Li, X. 2285
Li, Y. 479
Lichtenberger, D. L. 1783, 1965
Linden, A. 1683
Lindsay, A. J. 1561
Lingaiah, P. 805
Lippert, B. 2199
Liu, B.-Y. 2023
Liu, S. 1541, 2375, 2463
Liu, S.-T. 2579
Looney, A. 265
Lopez, C. 763
Lopez, X. 2839
Loumrhari, H. 907
Lovely, C. J. 527
Lubinu, G. 789
Ludi, A. 1095
Luks, E. 475
Lukyanenko, N. G. 1369
Lyons, A. M. 751

Ma, L. 545, 1541
Mabbs, F. E. 2483
MacDougall, J. K. 1235
Machado, A. A. S. C. 713, 2035
Macherone, D. 1429, 2375
Macicek, J. 2597
Madhok, K. L. 2449
Maeder, M. 2227
Mague, J. T. 2635
Maigrot, N. 1363
Majumder, S. M. M. H. 1017
Mak, T. C. W. 1667, 2469, 2901
Malhotra, K. C. 2171
Malinar, M. J. 2149
Malito, J. 1059
Maloney, J. D. 335
Manchanda, V. K. 2455
Mandair, A.-P. S. 517, 1709
Manojlovic-Muir, L. 2767
Manzur, C. 1131
Marcalo, J. 1645
March, L. A. 681
Marcos, D. 2699
Marinelli, G. 1867
Marques, N. 69
Marques, R. L. 81
Marseglia, E. A. 2759
Martell, A. E. 171
Martin, J. D. 1829

Martin, R. B. 189, 193
Martinez, F. 2181
Maruoka, K. 223
Marzilli, P. A. 1079
Masters, A. F. 2809, 2815
Mathey, F. 991, 1363, 2193, 2859
Matsuda, H. 361
Matsuda, J. 2491
Mauclaire, L. 1297
Mauro, A. E. 2937
Mazid, M. A. 535, 541, 719, 2097
Mazurek, W. 777
McCleverty, J. A. 527, 615, 619 687, 693, 2185, 2549
McCrudden, K. 2533
McCurry, J. D. 2527
McElfresh, M. W. 1843
McFarlane, H. C. E. 1757
McFarlane, W. 1757
McGowty, D. 1541
McGregor, K. 921
McPartlin, M. 75, 1497
McPhail, A. T. 319
McQuillan, F. S. 615
McWhinnie, W. R. 517, 999, 1709, 2273
Means, C. M. 309
Meek, D. W. 35
Meider, H. 1099
Menezes, J. C. 1237
Mentzafos, D. 981, 2833
Mercier, F. 2859
Mesa, J. L. 2693
Meullemeestre, J. 2613
Meyer, D. 1311
Michael, P. J. 517
Milicev, S. 47
Miller, S. M. 63
Milletti, M. C. 1855
Milne, J. 589
Mingos, D. M. P. 893
Minyu, T. 859, 2371
Mishra, A. 863, 2153
Mishra, K. 863
Mishra, R. L. 2153
Mitchell, S. H. 2127
Mizuno, H. 1287
Mochida, K. 2263
Modrick, M. A. 1809
Mohanty, R. N. 1011
Mohapatra, P. K. 2455
Moiz, M. A. 2681
Monzyk, M. M. 2433
Moran, J. K. 597
Morrison, E. A. 1331
Moseler, R. 2959
Moss, M. A. J. 697, 1119
Motekaitis, R. J. 171
Motevalli, M. 541, 1423, 2959
Moulines, F. 2727
Mounir, M. 2029
Mountford, P. 2763
Muir, A. S. 1757
Muir, K. W. 2767
Muller, G. 283
Munir, Z. A. 1059
Murata, K. 1717
Murphy, C. J. 1913
Murray, K. S. 2867
Music, S. 2895

Nagasawa, A. 215
Nageswara Rao, G. 2497
Nakadaira, Y. 2263
Nakashima, T. 2609
Narahari Sastry, G. 2359
Narendra, G. L. 1475
Nash, J. M. 1617
Navarro, R. 2181
Nazarova, N. Yu. 1369
Nehete, D. T. 2013
Neves, E. A. 1257
Newmark, R. A. 301
Newnham, S. 491
Nicholas, A. M. 1683
Nichols, P. J. 777
Nielson, A. J. 603
Nieuwenhuyzen, M. 2315
Ning, T. 859, 2371
Nomura, R. 361
Nonoyama, M. 1287
Norman, N. C. 2533
Nowak, R. 283
Nowell, I. W. 681
Nowogrocki, G. 2663
Nunn, C. M. 669, 1337, 1573
Nurchi, V. 789
Nyeki, O. 825

O'Brien, P. 119, 541, 1175, 1483
O'Leary, M. A. 2227
O'Mahoney, C. A. 491, 1765
Ochiai, R. 1123
Ogorodnikova, N. A. 1
Ohman, L.-O. 199
Okubo, M. 1123
Oliver, J. P. 409

Olmstead, M. M. 257
Orrell, K. G. 703
Ortigueira, J. M. 2741
Orvig, C. 151
Osborn, J. A. 1311
Ostropolska, L. 1021
Ouedraogo, G. V. 1087

Padmaja, N. 2497
Pain, G. N. 921
Pallanza, G. 1469
Palma, P. 757, 1447
Palma-Ramirez, P. 1107
Pandey, D. S. 2153
Pandey, K. K. 2013
Panizo, M. 2863
Papastefanou, S. 981, 2833
Parkin, G. 265, 1775, 2655
Parkin, I. P. 987, 2941
Parr, J. 813
Passand, M. A. 2483
Pasynkiewicz, S. 429
Pavan Kumar, P. N. V. 2359
Paw, W. 1397
Penedo, F. J. 665
Peng, S.-M. 1491, 2579
Pennington, W. T. 313, 2205
Perales, A. 907
Pereira, E. F. A. C. 2035
Pereyre, M. 1297
Perez-Garcia, V. 2163
Perpinan, M. F. 1341
Pertsikov, B. Z. 1249
Peters, E.-M. 1659
Peters, K. 1659
Peters, M. P. 1257
Peterson, M. A. 1919
Petrilli, L. 1457
Phang, L.-T. 2305
Pierpont, C. G. 2267
Pietraskiewicz, M. 2353
Pilarczyk, M. 1375
Pilkington, M. J. 987
Pilotti, M. U. 2953
Pires de Matos, A. 69, 1645
Pitt, C. G. 319
Planinic, P. 1099
Pogorzelec, P. 1107
Polo, A. 1411
Polson, S. 2709
Pompeo, M. P. 2385
Poncelet, O. 1305
Pons, J. 2839
Poole, A. G. R. 527
Poon, W. C-K. 2759
Porto, R. 1263
Poveda, M. L. 757, 1447
Povey, D. C. 1497, 2041
Powell, H. 2959
Powell, H. R. 75
Powell, N. I. 623
Power, M. B. 233
Power, P. P. 257
Prabhakar, B. 805
Prakash, S. 2705
Prati, L. 639
Prelesnik, B. V. 2149
Preut, H. 2199
Price, A. C. 573
Pruchnik, F. P. 1135
Puche, R. S. 1383
Puddephatt, R. J. 2767
Pulcinelli, S. H. 2699
Purdy, A. P. 319
Purohit, S. 881

Qi, J.-S. 565
Qian, C. 479, 1453
Qianer, Z. 1625
Quillevere, A. 1695
Quiros, M. 2733
Qureshi, K. B. 703

Radecka-Paryzek, W. 475
Radomska, B. 825
Rahman, K. M. M. 1017
Rai-Chaudhuri, A. 1965
Raja Rao, A. V. S. 2171
Ramachandraiah, A. 1703
Ramana, K. V. 2497
Raos, N. 1277, 2419
Ratcliff, K. S. 1487
Ratliff, K. S. 2651
Ray, R. K. 2245
Reder, A. S. 1369
Reedijk, J. 2971
Reid, G. 2641, 2925, 2931
Rey, F. 665
Reynolds, S. M. 893
Rheingold, A. L. 329, 1209
Rial, C. 1723
Ribas, J. 1729
Ribas, X. 2675
Ricard, L. 991, 1363, 2193, 2859
Rice, D. A. 1603
Ricevuto, V. 2591
Richmond, T. G. 1677, 2887
Rivera, M. I. 573
Rizzi, M. 2061

Roberts, J. E. 2527
Roberts, R. M. G. 2751
Robinson, G. H. 313, 205
Robinson, S. D. 1737
Robinson, W. T. 2315
Rodger, A. 1035, 1769
Rogers, R. D. 335, 751
Rojo, T. 2693
Romao, C. C. 1237
Romero, M. A. 2733
Ros, J. 907
Rothwell, I. P. 839, 963, 969, 1051, 1617
Roundhill, D. M. 597, 2517
Rovai, D. 2477
Rowe, R. S. 921
Royer, E. 1723
Rubio Gonzalez, J. M. 2603
Rufinska, A. 11, 23
Ruiz-Valero, C. 1341, 2163
Runnacles, J. D. 2959
Rushworth, S. A. 1483
Russo, U. 2721
Rzepa, H. S. 107

Sabolovic, J. 1277, 2419
Sachinidis, J. I. 2809
Saito, K. 215
Salam, S. S. 527
Salas, J. M. 2733
Saldana, J. S. 2937
Salvado, V. 2675
Sambasiva Rao, R. 2497
Sanati, H. K. 581
Sanchez, F. J. 2839
Sanchez, M^{a}. J. 501
Sangokoya, S. A. 313
Santana, B. 501
Santos, I. 1645
Saratchandra Babu, M. 2497
Sargent, A. L. 1799
Sarojini, T. 1703
Sattelberger, A. P. 1843
Saucedo, M. J. 1723
Saum, S. E. 1317
Sauvage, J. P. 1225
Scheiber, E. 573
Schmalle, H. 1155
Schmidbaur, H. 283
Schmutzler, R. 1463
Schnering, H. G. von 1659
Schollhorn, H. 2199
Schomburg, D. 1463
Schon, I. 825
Schroder, M. 2641, 2911, 2919, 2925, 2931
Schroepfer, J. N. 301
Schroth, G. 11, 23
Schugart, K. A. 1935
Schulte, H.-J. 2549
Schumann, H. 353, 1677
Schwellnus, A. H. 975
Schwing, M. J. 2613
Seevogel, K. 11
Seleznev, A. V. 227
Self, M. F. 313
Sellers, N. B. 119, 1175
Seshasayee, M. 2879
Seyam, A. M. 2987
Shaikh, S. N. 545, 1429
Sharma, N. 2171
Sharma, R. B. 2013
Sharma, U. 1065
Shaw, A. 2293
Shibahara, T. 1671
Shirai, M. 367
Shuaib, N. M. 629
Shupack, S. I. 1209
Siedle, A. R. 301
Sik, V. 703
Sikanyika, H. 1091, 1747
Silver, J. 2751
Simard, M. 2733
Singh, A. K. 495, 851, 2041
Singh, J. D. 943
Singh, M. 505
Singh, N. 1441
Singh, N. B. 557
Singh, N. K. 1065, 1441
Singh, P. 125
Singh, P. P. 557
Singh, R. 1027
Siurek III, E. W. 573
Skelton, B. W. 1079
Slawin, A. M. Z. 987, 1561, 1567, 2659
Smith, F. E. 653, 1017
Smith, G. 1667
Smith, G. W. 1497, 2041
Smith, L. M. 343
Smith, R. M. 171
Smout, G. J. 2763
Sola, J. 769
Solans, X. 763, 769, 1729
Soloway, A. H. 891
Soria, J. 1383
Souchard, J.-P. 2647
Sovago, I. 189, 825, 831
Speel, S. R. 2763

Spicer, M. D. 1609
Spychala, J. 831
Srivastava, D. K. 289
Srivastava, P. C. 125
Srivastava, S. 487, 1401, 1405
Srivastava, S. K. 943
Srivastava, T. N. 943
Srivastava, V. 495, 851, 2041
Stanley, G. G. 1317
Steffey, B. D. 839, 963
Steudel, R. 1199
Stone, F. G. A. 2953
Stoppioni, P. 2477
Streib, W. E. 253, 1867, 2941
Suarez, A. 2741
Sudheendra Rao, M. N. 1433
Sueur , S. 2663
Sugihara, G. 2609
Sugimori, A. 1123
Sulfab, Y. 99
Sullivan, A. C. 1423, 2959
Sun, S. 2385
Szterenberg, L. 2585
Szymaszek, A. 1135

Takacs, J. 2211
Takats, J. 1867
Tanaka, H. 2609
Tanimoto, S. 371
Taqui Khan, M. M. 1243, 2681
Tarli, F. 1457
Tattershall, B. W. 553
Tauzher, G. 2047
Tay, A. W. N. 1293
Taylor, A. 2911
Taylor, M. J. 207
Teixidor, F. 2839
Teo, B. K. 1985
Terzian, G. 1087
Terzis, A. 981, 2833
Theopold, K. H. 329
Thewalt, U. 2199
Thompson, R. M. 1497
Thornton, D. A. 2823
Thornton, P. 535
Thornton-Pett, M. 343
Tiekink, E. R. T. 2965
Timmer, L. K. 1919
Tioh, N. H. 901
Tisdale, R. C. 545
Tocher, D. A. 1613
Tomar, B. S. 2705
Tomic, Z. 2149
Tomkinson, J. 2759
Tongbu, L. 2371
Tonkovic, M. 2895
Torres, M. R. 907
Toscano, P. J. 1079, 2375
Tran Huy, N. H. 2193
Tregloan, P. A. 2809
Treichel, P. M. 1893
Trivedi, A. 125
Trofimenko, S. 619
Truong, N. 839
Tsai, T.-H. 1147
Tsao, C.-L. 2579
Tsintsadze, G. V. 1379
Tuck, D. G. 377
Turnbull, M. M. 2619

Uhl, W. 277
Ullah, M. R. 2239
Underhill, A. E. 2053
Urbanos, F. A. 1723
Urbanska, J. 831
Urriolabeitia, E. P. 2181

Vakul'skaya, T. I. 227
Valiente, M. 2675
Vallarino, L. M. 1411
Van Der Sluys, W. G. 1843
Varghese, B. 1433
Varnagy, K. 831
Varret, F. 2727
Vasca, E. 1263
Vaughan, O. J. 1593
Vender, M. 2809
Verchere, J. F. 1225
Verma, R. 1441
Vernooijs, P. 1919
Vetrogon, N. I. 1369
Vetrogon, V. I. 1369
Via, J. 2693
Vicente, R. 1729
Vidali, M. 2721
Vierling, F. 2613
Vila, J. M. 2741
Vilas Boas, L. F. 81, 2101
Vilhena, M. F. 2847
Vives, J. 769
Vogt, A. 2567
Volavsek, B. 47
Voronkov, M. G. 227
Vreugdenhil, W. 2971

Waggoner, K. M. 257

Waki, H. 511, 1555, 2609
Wakita, H. 2491
Walsh, J. R. 1483
Walton, R. A. 565, 573, 743, 1165
Wang, B. 2873
Wang, R.-J. 2469, 2901
Wang, X. 479, 2023
Wanyan, H. 2285
Ware, D. C. 603
Wassermann, W. 353
Wassmuth, B. 11
Watkins, C. L. 289
Wayda, A. L. 751
Welch, A. J. 2407
Wells, R. L. 319
Wendan, C. 1625
Wesolek, M. 1311
West, B. O. 777, 921
White, A. H. 1079
White, D. 2717
Whittaker, A. 2221
Wierda, D. A. 957
Wigley, D. E. 2709
Wilkins, C. J. 2315
Wilkinson, G. 931, 1009, 2071, 2081, 2625
Wille, K. 597
Williams, D. J. 491, 987, 1561, 1567, 1765, 2659
Williams, H. D. 239, 245
Williams, M. A. 2815
Williams, P. A. M. 1383
Wills, A. R. 2413
Wimmer, F. L. 2647
Wojnowski, W. 1659
Wong, W.-K. 875, 2469, 2901
Woollins, J. D. 107, 987, 1561, 1567, 2659
Woon, F.-H. 2227
Wright, A. H. 1113
Wu, J. 2873
Wu, W.-Z. 1849
Wu, Z. 2143

Xie, G.-Y. 2023
Xin, W. 783
Xinmin, G. 859, 2371
Xu, Z. 137, 739, 2463, 2981

Yamaguchi, O. 367
Yamamoto, E. 1717
Yamamoto, H. 223
Yamane, H. 371
Yamashita, S. 1717
Yang, R. 2285
Yang, W.-D. 2747
Yaokun, Z. 783
Ye, C. 479
Ying, Z. 783
Yip, W.-H. 1667
Yordanov, N. D. 2597
You, X. 1849, 2463, 2981
Young, C. G. 2965
Yousif, L. Z. 1141
Yu, J. S. 1051
Yu, K. 2981

Zacharias, P. S. 1703
Zanello, P. 1469
Zarembowitch, J. 2971
Zarli, B. 2721
Zhang, H. 137, 1985, 2873
Zhang, S. 2511
Zhao, F. 2143
Zheng, P. 2873
Zhiqiang, W. 783
Zhou, X. Y. 1975
Zhou, Y.-K. 2689
Zhou, Z. 2143, 2981
Zubieta, J. 545, 1429, 1541, 2375
Zukerman-Schpector, J. 2937
Zych, E. 2175